 © 1988 The Chemical Society of Japan Bull. Chem. Soc. Jpn., 61, 1—11 (1988)

Invited Paper

Is Accurate X-Ray Analysis Worthwhile?

Jack D. DUNITZ

Organic Chemistry Laboratory, Swiss Federal Institute of Technology,
ETH-Zentrum, CH-8092 Zürich, Switzerland
(Received August 3, 1987)

Following a brief introduction to X-ray analysis, three areas are discussed where accurate measurements can lead to results of interest to chemistry. These areas are: (a) molecular geometry, (b) molecular motions in the solid state, (c) experimental electron density distributions. As the technical possibilities for accurate X-ray analysis improve, important developments in all three areas can be expected.

Most chemists nowadays are aware that the last two decades or so have seen a remarkable increase in the *ease* and *rapidity* with which X-ray crystal structure analyses can be accomplished; for this is a development that has transformed the tactics and strategies of preparative chemistry, both in the organic and organometallic areas. Almost as well known is the impressive increase in the *complexity* of the structures that can be elucidated at atomic or near atomic resolution, a development which is beginning to provide the structural basis for understanding and controlling many biochemical processes, with obvious implications for biology and medicine. Less well known, perhaps, is the remarkable improvement in the *accuracy* attainable in modern X-ray structure analysis. This particular improvement is due to instrumental and computational developments but also to the increased attention that has been paid to various sources of systematic error in the diffraction experiment.[1] Another most important factor is the sheer increase in the number of available diffractometers, thanks to which it no longer necessary to make the measurements in a hurry.

In this paper I shall mention three areas where this improved accuracy can lead to results of interest in chemistry: (a) small differences in bond length can be correlated with differences in chemical reactivity; (b) anisotropic displacement parameters can provide information about molecular motions in crystals and also about internal molecular motions; (c) electron density measurements provide an experimental approach to questions of chemical bonding. Before we discuss these developments, we first require a very brief introduction to X-ray crystallography in general.[2]

X-Ray Analysis in a Nutshell

When X-rays pass through matter they are scattered by the extra-nuclear electrons. In a crystal the electron density $\rho(\boldsymbol{X})$ is periodic and can therefore be represented as a Fourier series.

$$\rho(\boldsymbol{X}) = (1/V)\sum|F(\boldsymbol{H})|\cos[2\pi\boldsymbol{H}\cdot\boldsymbol{X}-\alpha(\boldsymbol{H})], \quad (1)$$

where V is the volume of the unit cell. The coefficients $|F(\boldsymbol{H})|$ of this series can be shown to correspond to the amplitudes of the diffracted beams in the directions of the scattering vector $\boldsymbol{H}(h_1, h_2, h_3)$. These amplitudes can be measured in an X-ray diffraction experiment. In order to reconstruct the electron density $\rho(\boldsymbol{X})$, we also need the corresponding phase angles $\alpha(\boldsymbol{H})$, as expressed in Eq. 1, that is, we need to know whether each Fourier wave starts at the origin with a maximum ($\alpha=0$) or a minimum ($\alpha=\pi$) or some intermediate value. This is the well known "phase problem," and methods are available for solving it.[3] For centrosymmetric crystals α is limited to the values 0 or π. Since $|F(\boldsymbol{H})|$ can be measured and $\alpha(\boldsymbol{H})$ can be obtained indirectly, there is nothing to stop us from evaluating the electron density $\rho(\boldsymbol{X})$ at each point $\boldsymbol{X}(x_1, x_2, x_3)$ of the unit cell by summation of the Fourier series in Eq. 1. Since the atomic nuclei are located at the points of maximum density (or, more correctly, at the centroids of the individual density peaks), the atomic arrangement can then be read off directly from $\rho(\boldsymbol{X})$. This is the way most crystal structures are solved.

Unfortunately, the electron density obtained from Eq. 1 is not quite true. In order to build up a faithful image of $\rho(\boldsymbol{X})$ we would need an infinite number of terms in the Fourier series. With a finite number of terms, the image is flawed by what is called "termination of series error," which consists mainly of spurious, more or less spherical, ripples of electron density emanating outwards from the atomic peaks. In most modern structure analyses, the set of atomic positions derived from $\rho(\boldsymbol{X})$ serves merely as a starting point for a series of non-linear least-squares refinements. Essentially, the parameters describing the atomic arrangement are adjusted to obtain optimal agreement with measured values of $|F(\boldsymbol{H})|$. The passage from the continuous electron density function $\rho(\boldsymbol{X})$ to the parametrized discrete-atom model runs something along the following lines.

By inversion of Eq. 1 we can express the complex structure amplitudes $F(\boldsymbol{H})$ as the Fourier transform of the continuous electron density within a unit cell,

$$F(\boldsymbol{H}) = \int \rho(\boldsymbol{X}) \exp[2\pi i\boldsymbol{H}\cdot\boldsymbol{X}]\mathrm{d}\boldsymbol{X}. \quad (2)$$

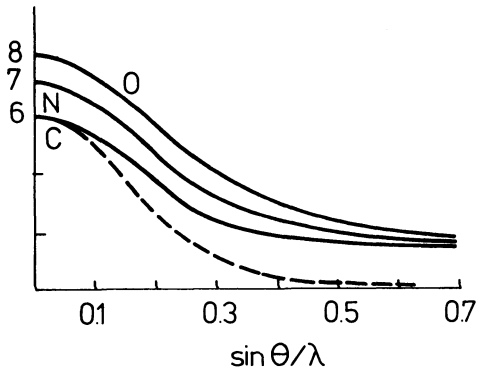

Fig. 1. Atomic scattering factors (form factors) for C, N, and O atoms at rest. The scattering factor is also shown for a C atom with mean-square displacement amplitude of 0.1 Å².

We now approximate $\rho(\boldsymbol{X})$ as a superposition of spherical density peaks associated with a set of non-interacting atoms at the positions $\boldsymbol{X}_j$ to obtain

$$\begin{aligned} F(\boldsymbol{H}) &= \int \Sigma \rho_j(\boldsymbol{X}-\boldsymbol{X}_j) \exp[2\pi i \boldsymbol{H}\cdot\boldsymbol{X}] \mathrm{d}\boldsymbol{X} \\ &= \Sigma \int \rho_j(\boldsymbol{X}-\boldsymbol{X}_j) \exp[2\pi i \boldsymbol{H}\cdot(\boldsymbol{X}-\boldsymbol{X}_j)] \\ &\qquad \times \exp[2\pi i \boldsymbol{H}\cdot\boldsymbol{X}_j] \mathrm{d}\boldsymbol{X} \\ &= \Sigma f_j(\boldsymbol{H}) \exp[2\pi i \boldsymbol{H}\cdot\boldsymbol{X}_j], \end{aligned} \tag{3}$$

where

$$f_j(\boldsymbol{H}) = \int \rho_j(\boldsymbol{X}) \exp[2\pi i \boldsymbol{H}\cdot\boldsymbol{X}] \mathrm{d}\boldsymbol{X}.$$

Since the atoms are assumed to have spherical symmetry, this integral can be written as

$$f_j(R) = 4\pi \int r^2 \rho(r) \frac{\sin 2\pi Rr}{2\pi Rr} \mathrm{d}r, \tag{4}$$

where r and R are radial distances in real and reciprocal space, respectively. The quantity $f_j(R)$ is the scattering power of the jth atom and is independent of the atomic position $\boldsymbol{X}_j$. Atomic scattering factors (form factors) for isolated neutral and ionic atoms have been calculated by many authors using various quantum mechanical models to obtain the appropriate electron densities; standard tabulations are given in International Tables for X-Ray Crystallography.[4] At zero scattering angle ($\boldsymbol{H}=0$), all electrons scatter in phase, so $f_j(0)$ equals the total number of electrons in the respective atom or ion. As the scattering angle increases ($|H|=2\sin\theta/\lambda$), interference between different regions of the electron cloud reduces the net scattering power, but even at large angles the inner core electrons are still scattering in phase (Fig. 1.)

Atomic Motion in Crystals

The atoms in a crystal are not stationary. From diffraction studies it is possible to obtain information not only about the mean atomic positions but also about the probability density functions (pdf's) of the atoms resulting from the time-averaged motion, averaged again over all unit cells in the crystal. In small molecule crystallography, the atomic pdf's are usually taken as trivariate Gaussian probability functions, except for hydrogen atoms which are taken as isotropic because their weak scattering power precludes the use of too many parameters in the description of their averaged motion. The atomic ellipsoids in the ORTEP diagrams[5] used to illustrate so many crystal structures are bounding surfaces that enclose some specific probability, usually 0.5, hence "50% probability ellipsoids." With these assumptions each atomic scattering factor has to be multiplied by the Fourier transform of the corresponding pdf, often referred to as the "anisotropic temperature factor," $T_j(\boldsymbol{H})$, which may be written in a compact form as

$$T(\boldsymbol{H}) = \exp(-2\pi^2 \boldsymbol{H}^T \boldsymbol{U} \boldsymbol{H}), \tag{5}$$

where $\boldsymbol{U}$ is a symmetric matrix, the matrix of second moments of the pdf. The second moment of the pdf in a given direction defined by a unit vector $\boldsymbol{n}$, i.e. the mean-square displacement of the atom in that direction, is then $\boldsymbol{n}^T\boldsymbol{U}\boldsymbol{n}$. The six components of $\boldsymbol{U}$ (or only one in the isotropic case) for each atom are included (as anisotropic displacement parameters or ADP's, together with the usual atomic positional parameters) in the least-squares analysis. In principle, higher cumulants of non-Gaussian pdf's can also be determined — 10 cubic terms, 15 quartic, and so on — but there are difficulties. The main problem is that these higher terms are only likely to be important when the second moments of the atomic pdf's are very large; however, the larger the second moments, the more rapidly the scattering from the atomic centre in question falls off with scattering angle. Thus, it is just when the higher terms become important that they become virtually impossible to measure.

Accuracy in Atomic Positions from X-Ray Diffraction

Atomic positions determined by X-ray diffraction correspond to centroids of distributions obtained by convoluting the atomic charge distributions with the corresponding pdf's. For small to medium sized molecules, these centroids are obtainable with nominal standard deviations of the order of a few thousandths of an Å, an uncertainty range that is usually considerably smaller than the built-in uncertainties involved in the derivation of averaged molecular structural parameters in systems where the

atoms are undergoing vibration. Since the relative phases of the vibrating atoms are generally unknown, separations between atomic centroids cannot be interpreted directly as interatomic distances.[6] The larger the mean-square displacements, the larger the uncertainties. In addition, atomic positions from X-ray analyses of molecular crystals based on low-angle[7] diffraction data are prone to systematic errors arising from asphericity in the distribution of the valency electrons. These errors can be reduced somewhat by appropriate weighting of the observations in the least-squares analysis.[8] However, it is much better to cool the crystals as far as possible to reduce the vibrational motion and try to measure the diffracted intensity at higher scattering angles. Atomic positions obtained from least-squares refinement of sufficiently extensive high-angle, low-temperature X-ray data can be expected to correspond closely to nuclear positions (as obtained from neutron diffraction data) and should be relatively free from systematic error. Indeed, for a small molecule, 2-aminopropenenitrile, atomic positions from 97 K X-ray diffraction data yield rotational constants very close to those obtained from a microwave spectroscopic study of the molecule in the gas phase.[9]

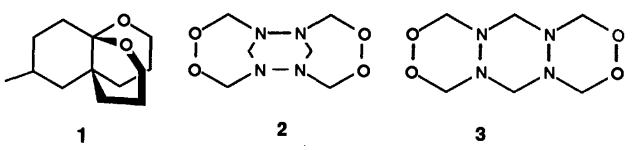

1 2 3

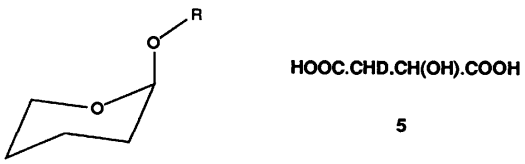

4

HOOC.CHD.CH(OH).COOH

5

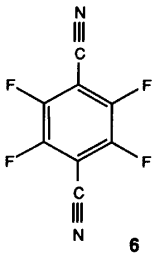

6

Accurate X-ray analysis can reveal subtle structural expressions of stereo-electronic effects.[10] In the dioxapropellane ketal **1** the two oxygen atoms O5 and O14 are chemically similar[11] but conformationally different (Fig. 2). From a crystal structure analysis at 98 K[12] the only pair of chemically equivalent bonds that shows an appreciable (>0.003 Å) difference in bond length is C6—O5, 1.412 Å, and C6–O14, 1.438 Å, difference 0.026 Å, with estimated standard deviation (esd) less than 0.003 Å. As seen in Fig. 2, the longer bond C6–O14 is synclinal (*sc*) to O5–C4 and hence antiperiplanar (*ap*) to a tetrahedral lone pair on O5, whereas the shorter bond C6—O5 is *ap* to O14—C13. The observed difference of 0.026 Å is in pleasing agreement with results of calculations on methanediol and methoxymethanol in the *sc,ap* conformation, which predict a relative lengthening by 0.025—0.030 Å of the C–O bond *ap* to a lone pair.[13]

Very similar results are observed for the tetraaza-tetraoxa-tricyclic molecule **2** from a crystal structure analysis at 96 K.[14] From the stereoview of the molecular conformation in Fig. 3, it is seen that the molecule as a whole is centrosymmetric and that the two sides of each seven-membered ring are conformationally different. The exocyclic N1–C1 bond is 0.025 Å shorter than N2–C2, while C1–O1 is 0.017 Å longer than C2–O2, differences that again clearly depend on stereoelectronic factors, the lone pair at N1 being *ap* to the C1–O1 bond while the lone pair at N2 is anticlinal (*ac*) to C2–O2. It is interesting that **2** must be thermodynamically more stable than the isomeric structure **3**, with which the compound was previously identified.[15] In the seven-membered ring the torsion angle about the O–O bond is 100°, close to the value in hydrogen peroxide.[16] In a six-membered ring, however, with normal bond lengths and approximately tetrahedral bond angles, it is impossible to obtain a torsion angle much greater than about 60°.

Bond-length differences of the magnitude we have been discussing may be associated with significant

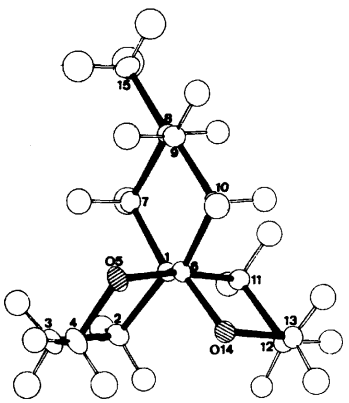

Fig. 2. View of molecule **1** at 98 K down the central C–C bond and showing atom numbering.[12]

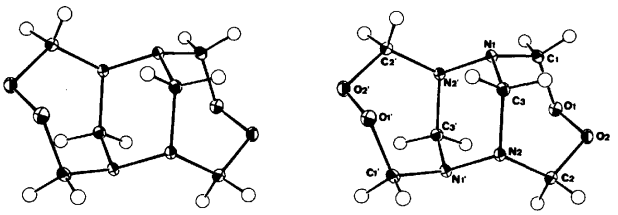

Fig. 3. Stereoview of molecule **2** at 96 K showing 50% probability ellipsoids and atomic numbering.[14]

changes in chemical reactivity. By combining crystallographic and kinetic data for acetals and related molecules, Kirby and Jones[17] found a linear relationship between the extension of a C–O bond (relative to some standard bond length) and the free energy of activation for heterolytic fission of the bond. For these reactions, and also for others,[18] it would appear that differences in the transition state are unimportant compared with differences in ground state structure. For axial aryl tetrahydropyranyl acetals **4** and for phosphate monoester anions $(ROPO_3)^{2-}$ the slope $\delta\Delta G^{\ddagger}/\delta r$ was found to be about 250 kcal mol^{-1} Å^{-1}. Thus, an increase of 0.02 Å in equilibrium bond length would correspond to a decrease of 5 kcal mol^{-1} in activation energy or to a 4000-fold increase in rate at room temperature. This astonishingly sharp sensitivity of activation energy of bond-breaking processes to quite small changes in ground-state structure can be accounted for in terms of a model involving a simple modification of the Morse equation, which is known to provide a good approximation to the potential energy of many classes of bonds.[19]

These results underline the need for accurate bond length measurements in structural studies bearing on questions of chemical reactivity.

Accuracy of Atomic Displacement Parameters from X-Ray Diffraction

Atomic displacement parameters (U values or ADP's) are calculated for thousands of crystal structure analyses each year, but the results do not seem to be generally regarded as being of any particular interest, at any rate not interesting enough to justify their publication in scientific journals. In fact, ADP's have practically disappeared from the published literature.[20] While one can sympathize with the reluctance of Journal Editors to publish long lists of numbers (six per atom for the usual Gaussian ADP's), the virtual disappearance of these data seems a pity because ADP's from reasonably careful routine analyses based on modern diffractometer measurements may often yield physically significant information about the atomic motions. Indeed, there is an ironical twist to the circumstance that most ADP's to be found in the literature are of poor quality. The reason for this is that just about the time when routine analyses were beginning to produce reasonably reliable numbers for these quantities, Editorial Boards were deciding against them. For the last few years ADP's have mostly been relegated to the category of supplementary information to be deposited and filed away in the vaults of scientific societies, publishing houses, libraries and similar depositaries.[21]

In the meantime, however, several studies have shown that ADP's from diffraction studies can yield important information not only about the molecular rigid-body motion but also about the internal molecular motion and other dynamical processes in crystals.[22] It is clear that for every pair of atoms A,B in a perfectly rigid grouping the mean-square displacements of both atoms must be exactly equal along the interatomic direction;

$$\Delta(\mathrm{A,B}) = \boldsymbol{n}^T\boldsymbol{U}_\mathrm{A}\boldsymbol{n} - \boldsymbol{n}^T\boldsymbol{U}_\mathrm{B}\boldsymbol{n} = 0, \qquad (6)$$

where $\boldsymbol{n}$ is the unit vector in the A,B direction. This condition is in effect a definition of rigidity, and if it is not satisfied within experimental accuracy there must be a relative motion of the atoms in the A,B direction. Note that the converse does not hold; Δ(A,B) may be zero if the relative motion of the atoms is perpendicular to the A,B direction. Thus, for example, the Δ values will not deviate significantly from zero for the out-of-plane vibrations of a planar molecule. Subject to this reservation, Eq. 6 provides a simple method of testing whether or not the ADP's obtained for a given molecule or molecular fragment are compatible with rigid-body behaviour.[23] Since bond-stretching vibrations typically have negligible amplitudes compared with other internal motions,[24] Eq. 6 should be valid for bonded pairs of atoms even in non-rigid molecules. Thus, evaluation of Δ(A,B) over all bonded pairs of atoms provides a useful estimate of the overall quality of the ADP's.[25] Failures of the rigid-bond criterion in certain structures have been used as a diagnostic to detect disorder among similarly shaped molecules with different bond lengths for corresponding bonds, e.g. different orientations of Jahn–Teller distorted complexes, and different spin-states of otherwise similar molecules.[26]

A visual impression of internal molecular motions can sometimes be gained simply from looking at ORTEP diagrams. Inspection of the matrix of Δ(A,B) values can reveal relative motion of rigid subgroups more objectively. Within the subgroups the Δ values should not differ significantly from zero, while relative motion of the subgroups will be manifested by much larger values of some of the inter-group Δ's. An example is given in Table 1, where Δ values for triphenylphosphine oxide in its orthorhombic crystal modification at 100 K[27] are shown. The triangles labelled A,B,C contain Δ values for the three phenyl groups (Fig. 4); the three blocks AB, AC, BC contain Δ values for pairs of atoms belonging to different rings. The esd's of the Δ's are about 7 units (Å$^2\times10^{-4}$) and the root-mean-square (rms) Δ's for the three individual rings are 11, 6, and 8 units respectively. Thus, the rings can be regarded as being essentially rigid. On the other hand, there is clear evidence of significant motion of the rings relative to one another, especially of ring A relative to rings B and C; the rms Δ values for blocks AB and AC are four or five times as large as those within the rings.

Two main methods for estimating amplitudes of

internal motion of non-rigid molecules, superimposed on the overall molecular motion,[28] have been proposed: (1) the segmented-body model, involving a network of coupled rigid bodies;[29] (2) addition of contributions from specified internal librations to those from rigid-body motion.[30] Although problems arise in connection with the correlations among internal and overall molecular librations,[31] mean-square amplitudes for torsional vibrations about bonds can be estimated reasonably well, especially when they are large compared with the overall molecular librations, and from this information (plus a knowledge of the crystal temperature) quadratic force constants for the motions in question can be derived.[32] A survey of ADP's from more than 125 crystal structures has shown that force constants estimated in this way for various librating groups are at least in the same range as those obtained by other techniques.[33]

Provided one is prepared to make a guess about the shape of the potential barrier hindering rotation of assumedly rigid groups, barrier heights can also be estimated from a knowledge of the mean-square libration amplitude $\langle\phi^2\rangle$ and the crystal temperature.

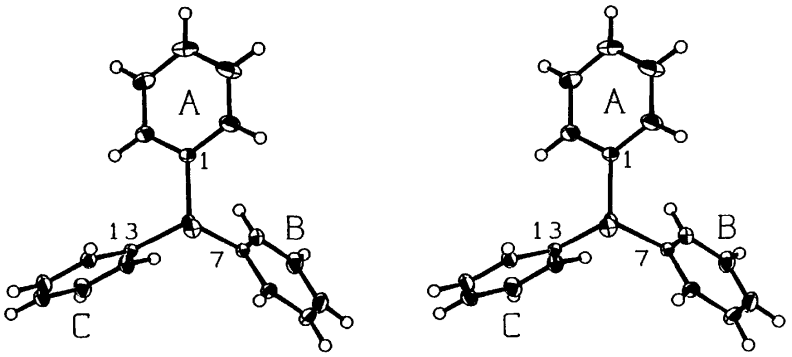

Fig. 4. Stereoview of triphenylphosphine oxide (orthorhombic modification)[27] at 100 K showing ring labels and atoms numbered 1, 7, and 13.

Table 1. Matrix of Δ values (in units of 10^{-4} Å^2) for triphenylphosphine oxide at 100 K. Each Δ is the mean-square displacement amplitude (MSDA) of the atom at the head of the column minus the MSDA for the atom at the left of the row, both MSDA's being taken along the interatomic vector. Atoms C1–C6 comprise ring A, C7–C12 ring B, C13–C18 ring C (see Fig. 4).

ATOM	C18	C17	C16	C15	C14	C13	C12	C11	C10	C9	C8	C7	C6	C5	C4	C3	C2	C1	P1
O1	0	−8	−15	−6	−6	−19	18	8	10	35	32	9	2	−15	−22	9	48	−10	−20
P1	33	31	23	25	31	10	38	32	22	31	35	22	29	25	16	24	41	13	
C1	48	28	−2	−11	−5	−9	40	44	11	−5	−3	0	11	5	5	10	21		
C2	15	5	−23	−44	−46	−34	−73	−89	−100	−77	−57	−61	−2	−7	5	−6			
C3	49	26	−22	−45	−38	−20	−21	−31	−74	−78	−57	−42	−11	−22	2				
C4	56	12	−53	−59	−34	−25	36	67	12	−31	−29	−15	−10	−16		A			
C5	14	−32	−78	−68	−41	−47	−25	2	−25	−40	−29	−33	−11						
C6	17	−10	−34	−32	−18	−30	−50	−34	−51	−49	−32	−44							
C7	35	42	23	20	19	3	2	−1	0	1	−6								
C8	19	13	−19	−23	−23	−36	8	−9	−9	1									
C9	19	12	−27	−32	−30	−36	5	−5	−3										
C10	27	44	13	4	−1	−12	−5	−8		B									
C11	−2	21	1	−3	−5	−17	−7												
C12	6	24	4	−1	−1	−11													
C13	7	16	13	7	3														
C14	0	5	7	2															
C15	−8	−13	−11																
C16	2	4		C															
C17	−5																		

For example, rotation barriers estimated from ADP analysis for the cyclopentadienyl rings in crystalline metallocenes with the assumption of a fivefold sinusoidal potential agree well with those derived by solid-state NMR and other spectroscopic methods.[34]

Further developments in this direction could well lead during the next decade or so to an intrusion by crystallographers into the study of low-energy, large-amplitude molecular motions, a field that has traditionally been regarded as a preserve of molecular spectroscopy and gas-phase electron diffraction.

One possible use of accurate displacement parameters is to distinguish protium from deuterium in specifically labelled molecules by X-ray diffraction. This is no problem as far as neutron diffraction is concerned, since the neutron scattering powers of the two nuclei are very different, but neutron diffraction facilities are by no means so widely available. The problem with the distinction by means of X-rays is that the X-ray scattering powers of the two kinds of atom are identical. However, the heavier isotope is associated with a smaller vibrational amplitude. For a -CHD- methylene group, the difference between isotropic U_H and U_D can be estimated to be about 0.0035 Å^2, roughly double the standard deviation attainable today from low-temperature (liquid nitrogen) X-ray data of the highest quality.[35] In a practical test, it was possible to establish the relative configuration of the two stereogenic centres in deuterium-labelled malic acid **5** obtained by enzymatic addition of D_2O to fumaric acid.[36] The experiment was actually made with the crystalline mono ammonium salt and gave the same configuration as that established by neutron diffraction of the corresponding phenylethylammonium salt.[37] While it is clear that the X-ray method cannot possibly compete with neutron diffraction as far as isotope discrimination is concerned, its potentialities in this respect should not be altogether dismissed.

Another area where analysis of ADP's might be important includes studies of the nature and mechanism of phase changes, especially those involving order/disorder transformations. In ferrocene, for example, the cyclopentadienyl rings in the monoclinic high-temperature crystal modification are orientationally disordered down to the phase transition at 164 K.[38] Below this temperature the structure becomes triclinic, and the rings librate about well defined equilibrium orientations.[39]

Electron Density Maps

Electron density maps have been used for years to give images of molecules in crystals, and it has always been realized that such maps might also tell us something about the fundamental problem of the nature of the chemical bond. If only we could make those maps accurate enough they might help to illuminate for us the problem of how atoms are held together in molecules and crystals.

It was fortunate for the development of crystal structure analysis that the electron density in a molecular or ionic crystal is very closely similar to the superposition of the densities of the separated atoms, placed at the positions they occupy in the crystal. This similarity made it possible to use standard, spherically symmetric scattering factors (as expressed in Eq. 4 and Fig. 1) in solving crystal structures and also in refining them by least-squares methods. In fact, when crystallographers take pride in their low R factors,[40] they pay tribute to the goodness of the pro-crystal approximation as well as to the accuracy of their measurements. The difference $\Delta\rho(\boldsymbol{X})=\rho(\boldsymbol{X})-\rho_M(\boldsymbol{X})$ between the actual density and the pro-molecule density is known as the deformation density. It can be interpreted as representing the reorganization in the electron density that occurs when a collection of independent, isolated, spherically averaged atoms is combined to form a molecule in a crystal. Since $\Delta\rho$ is only a very small fraction of ρ in the region of the atoms, it is very susceptible to experimental error in the X-ray measurements and to inadequacies in the model (errors in the assumed atomic positions and ADP's).

The deformation density $\Delta\rho$ is conveniently obtained as:

$$\Delta\rho(\boldsymbol{X}) = (1/V)\sum\{|F(\boldsymbol{H})| - |F_M(\boldsymbol{H})|\} \times \cos[2\pi\boldsymbol{H}\cdot\boldsymbol{X} - \alpha_M(\boldsymbol{H})], \quad (7)$$

by analogy with Eq. 1, where $F_M(\boldsymbol{H})$ is calculated for the pro-crystal according to Eq. 3, suitably modified to allow for the atomic temperature factors (Eq. 5). The positions $\boldsymbol{X}_j$ and corresponding $\boldsymbol{U}_j$ components of the atoms in the pro-molecule (or pro-crystal) need to be estimated as accurately as possible by least-squares analysis, preferably using high-angle, low-temperature data, as described earlier in this article, or in a separate neutron-diffraction experiment.[41] Since the observed density $\rho(\boldsymbol{X})$ and the pro-molecule density $\rho_M(\boldsymbol{X})$ are both smeared by the vibrational motion of the atoms, so is the difference density obtained by subtracting one from the other.

In an alternative procedure, the deformation density is expressed in parametric form as the sum of a number of suitably designed functions, usually chosen as a set of multipoles, each multiplied by a radial function and centred at an atomic position. The Fourier transforms of the deformation functions are then added to the free-atom form factors with variable coefficients, which are refined, together with the atomic coordinates and ADP's, by least-squares analysis. The deformation density obtained in this way is, of course, restricted by the particular choice of deformation functions included in the model. Gen-

erally, it looks smoother than the difference density. The deformation density calculated with the multipole model is often called the static deformation density[42] since it represents the charge density reorganization in going from the vibrationless promolecule to the vibrationless molecule. This makes it more suitable for direct comparison with deformation densities obtained by quantum-mechanical calculations.

As recently discussed by Seiler,[1] it is becoming increasingly clear that dependable deformation densities require an expenditure in experimental time and effort far in excess of that involved in routine X-ray analysis. If the parameters describing the promolecule are to be obtained from X-ray data, accurate and extensive measurements of high-order reflections are required. To obtain such data, the atomic vibrations must be reduced as far as possible. It is therefore advisable to carry out the diffraction measurements with the crystal held at liquid nitrogen temperature or lower. And finally, even when all these conditions are fulfilled, the significant features of the deformation density are only a small fraction of the total density. We can maximize this ratio by dealing with light-atom structures. Indeed, until we understand how to obtain physically meaningful and interpretable maps for light-atom structures, it seems prudent to avoid crystals containing heavy elements as far as possible.

We mention here two examples of recent deformation density studies which have led to results of some chemical interest. The first example concerns tetrafluoroterephthalonitrile **6**. The molecule occupies a site of C_{2h} symmetry in the crystal, so that the asymmetric unit consists of only two atoms (C and F) in general positions plus three atoms (two C and one N) on a crystallographic mirror plane. For the deformation density study,[43] the intensities of *all* reflections within a limiting sphere of radius $\sin\theta/\lambda=1.15$Å^{-1} were measured with Mo $K\alpha$ radiation at 98 K; most reflections were measured in all symmetry-equivalent orientations, leading to a total of 17740 measurements. After averaging equivalent reflections, 2387 independent observations were left, nearly 700 per atom in the asymmetric unit. The difference map in the molecular plane, calculated with 1269 reflections with $F>20\sigma(F)$ is shown in Fig. 5. Prominent peaks occur close to the mid-points of the ring C–C bonds ($\approx$0.6 e Å^{-3}), of the exocyclic C–C bond ($\approx$0.4 e Å^{-3}), and of the C≡N triple bond ($\approx$0.75 e Å^{-3}), as well as in a region that is clearly associated with the *sp* lone pair of the N atom ($\approx$0.25 e Å^{-3}).[44] In contrast, the difference density along the polar C–F bond does not exceed 0.1 e Å^{-3}. Difference maps calculated with slightly different atomic form factors or with pro-crystal models obtained by varying details of the least-squares refinement were not significantly different from that shown in Fig. 5.

The static deformation density map calculated on the basis of the same experimental data is shown in Fig. 6A.[45] Compared with Fig. 5, the density peaks are of slightly different shapes and heights, but, allowing for the differences in the underlying assumptions, the main qualitative features of the two maps are remarkably similar.[46] There is also a close agreement between the experimental deformation

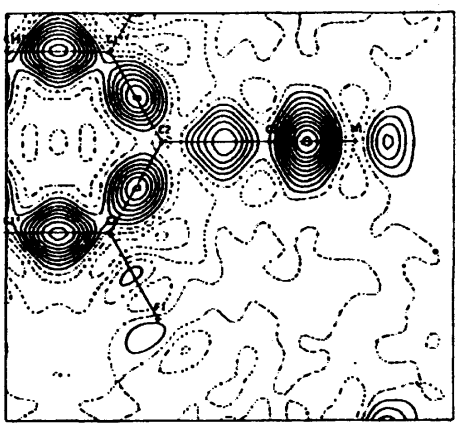

Fig. 5. Tetrafluoroterephthalonitrile. Electron density difference map $\Delta\rho$ in the molecular plane. Contour interval 0.075 e Å^{-3}, zero and negative contours broken.[43]

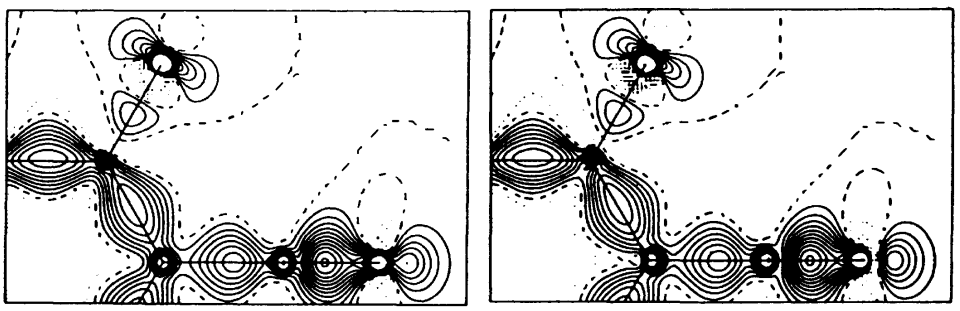

Fig. 6. Tetrafluoroterephthalonitrile. Static deformation density map in the molecular plane from (A) unconstrained, and (B) Hellmann-Feynman constrained refinements.[48] Contour interval 0.1 e Å^{-3}.

density and that calculated by density functional theory,[47] the main differences being in the lone-pair densities, which are somewhat smaller in the experimental map.

The Hellmann-Feynman theorem states that if the correct charge density is available, the forces on the atomic nuclei can be calculated by classical electrostatics; for a stable atomic arrangement, these forces must be zero. Hirshfeld has shown[48] that this condition is not fulfilled for the static deformation density shown in Fig. 6A. In particular, the electric field at the F nucleus was found to be strongly repulsive. The condition of zero net-force was then included as a constraint in the least-squares refinement with the same set of multipole terms, leading to the deformation map shown in Fig. 6B. At a first glance, the two maps look almost identical, and it may seem remarkable that one corresponds to appreciable forces on the atomic nuclei, the other to electrostatic equilibrium. The main difference is that sharp dipoles (core polarization) are produced at the nuclei, coupled with very small changes (less than 0.001 Å) in the atomic positions. Clearly, the electric field at the nuclear positions is extremely sensitive to features of the static deformation density close to the nuclei, features that are not easily determined from the X-ray data alone. The problem here is not so much the quality of the data as the strong correlation between the core polarization functions and the atomic coordinates.

For peroxides, difference maps show a density deficit at the mid-point of the O–O bond.[49,50] For example, Fig. 7 shows the difference density along the O–O bond in molecule **2**. The negative density along the bond axis contrasts with the positive density peaks corresponding to other bonding features seen in the Figure, such as the C–O and C–H bonds, as well as the O lone pairs.

In fact, from these and other studies, experimental "bonding density" seems to decrease in the order C–C>C–N>C–O≈N–N>C–F≈N–O>O–O, i.e., with increase in the number of valency electrons. This trend can be explained by comparing the tetrahedrally hybridized orbital occupation numbers for the bonded atoms with those of the spherically averaged atoms that are subtracted out.[51] It is also clear that the choice of reference states is to some extent arbitrary and that other kinds of trend could be produced by assuming non-spherical charge distributions for the atoms in the pro-molecule. Nevertheless, it may seem disturbing that the deformation-density results seem to contradict (or at least modify) the conventional wisdom about the nature of the chemical bond, namely that a build up of charge between the nuclei is necessary.[52,53] Indeed, the use of spherically averaged atoms to define the pro-molecule has come in for considerable criticism from theoreticians.[54,55] Difference densities more in line with theoretical views of chemical bonding could certainly be obtained by subtracting out suitably oriented ground-state or valence-state atoms, although such a procedure is also not without its difficulties. The choice of the reference state is clearly to some extent arbitrary. It can hardly be denied, however, that the spherically averaged density is the only choice that allows fully for the reduction in symmetry that occurs when a free atom becomes part of a molecule.

Our final example concerns the question: are ionic solids really built from ions? As Slater pointed out many years ago, the difference in charge distribution between the superposition of neutral atoms and the superposition of ions is "small and subtle, and difficult to determine by examination of the total density."[56] The main problem is that the difference between the charge densities of individual neutral atoms and corresponding ions only become appreci-

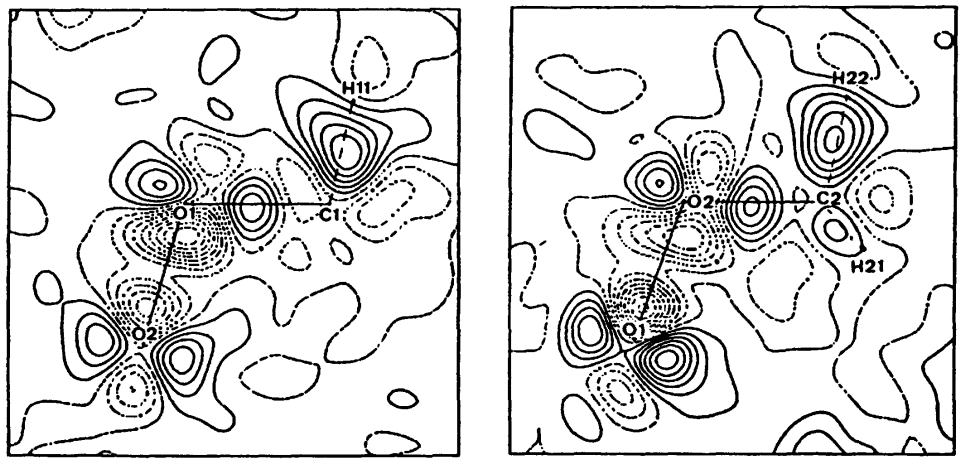

Fig. 7. Electron density difference maps $\Delta\rho$ in sections passing through the C–O–O planes of molecule **3**. Contour interval 0.075 e Å^{-3}, zero and negative contours broken.[50]

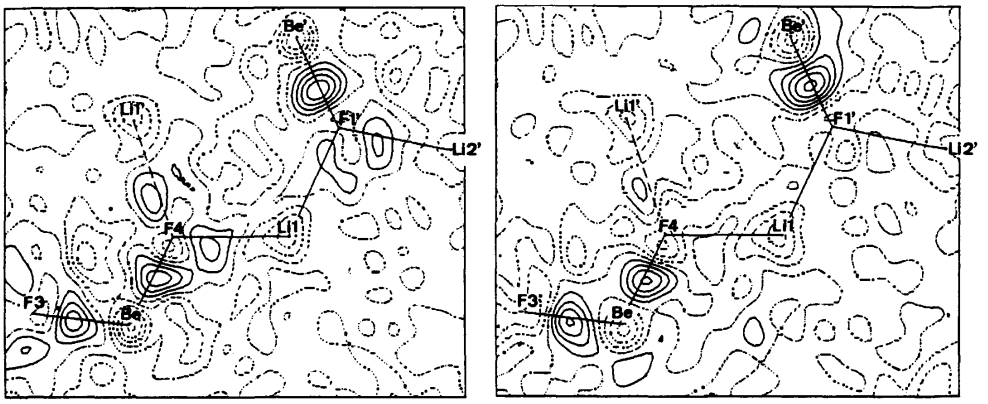

Fig. 8. Electron density difference maps $\Delta\rho$ for a chain of atoms in the Li_2BeF_4 crystal structure, based on the neutral-atom pro-crystal (left) and the ionic one (right). Contour interval 0.045 e Å^{-3}, zero and negative contours broken.[57]

able at large distances from the respective nuclei. In a crystal, where densities of neighbouring atoms overlap, this diffuse difference density cannot be unequivocally assigned to one atom or another. At these large distances, even if the density associated with a given atom may be quite small, the contribution of the spherical shell to the integrated charge may be considerable. The problem can also be expressed in terms of the respective form factors: the scattering powers (Eq. 4) of neutral atoms and of their corresponding ions differ appreciably only in a small region of reciprocal space close to the origin.

Indeed, in a new, accurate analysis of lithium tetrafluoroberyllate, Li_2BeF_4, at 81 K, both models yielded almost identical R factors[40] of 0.015 for all 6345 independent reflections out to $\sin\theta/\lambda$=1.35 Å^{-1}, an indication that the charge distribution is almost equally compatible with a superposition of neutral atom charge distributions and a superposition of ionic charges.[57] The two distributions are so similar that they can hardly be distinguished by examining the corresponding difference densities, shown in Fig. 8. Both maps show peaks of up to 0.2 e Å^{-3} along the Be–F bonds of the tetrahedral BeF_4 "anions" and still weaker ones along the Li–F directions.

Since the form factors of the neutral and ionic species differ only in the low-angle region, the intensities of the low-order reflections were re-measured in a separate experiment with a smaller crystal and with particular attention to the avoidance of systematic errors. When attention is focussed on 22 weak reflections in the region ($\sin\theta/\lambda$<0.25 Å^{-1}) where the form factors still show detectable differences, the neutral atom model reproduces the observed intensities better than the ionic one. This indicates that the diffuse charge density far from the nuclei is better represented by the superposition of outer tails of spherical distributions centred at the Li and Be atoms than by the tails of F-centred distributions.

However, since the charge distribution of the ionic model is so very similar to that of the neutral atom model, the two distributions must correspond to very similar energies. Thus, the cohesive energy estimated for an ionic model with integral charges will still be close to the correct result — and much simpler to calculate — even if the actual charge distribution happens to be slightly closer to that of the neutral atom model.[58] The fact that it is easier to calculate many properties of solids with integral point charges than with atomic charge distributions certainly makes the ionic model more convenient, but it does not necessarily make it more correct.

This work has been supported over the years by the Swiss National Foundation for Scientific Research. It has been made possible only through the dedicated collaboration of many students and colleagues, whose names are mentioned in the text and footnotes.

References

1) P. Seiler, *Chimia*, **41**, 104 (1987).

2) For a more extensive treatment along similar lines, see J. D. Dunitz, "X-Ray Analysis and the Structure of Organic Molecules," Cornell, Ithaca NY (1979).

3) J. Karle, *Science*, **232**, 837 (1986); H. Hauptman, *ibid.*, **233**, 178 (1986).

4) "International Tables for X-Ray Crystallography," Kynoch Press, Birmingham (1974), Vol. IV.

5) C. K. Johnson, ORTEP II: A Fortran Thermal-Ellipsoid Plot Program for Crystal Structure Illustrations. Report ORNL-5138, Oak Ridge National Laboratory, Oak Ridge TE (1976).

6) W. R. Busing and H. A. Levy, *Acta Crystallogr.*, **17**, 142 (1964).

7) In this context, low-angle means roughly within the limit of Cu $K\alpha$ radiation, say $\sin\theta/\lambda$ less than 0.65 Å^{-1}.

8) J. D. Dunitz and P. Seiler, *Acta Crystallogr., Sect. B*, **29**, 589 (1973).

9) P. Seiler and J. D. Dunitz, *Helv. Chim. Acta*, **68**, 2093 (1985).

10) P. Deslongchamps, "Stereoelectronic Effects in Or-

ganic Chemistry," Pergamon, Oxford (1983); A. J. Kirby, "The Anomeric Effect and Related Stereoelectronic Effects at Oxygen," Springer, Berlin (1983).

11) They would be equivalent but for their relationship to the methyl group in the third ring.

12) K. L. Brown, G. L. Down, J. D. Dunitz, and P. Seiler, *Acta Crystallogr., Sect. B*, **38**, 1241 (1982).

13) G. A. Jeffrey, J. A. Pople, and L. Radom, *Carbohydr. Res.*, **38**, 81 (1974); J. M. Lehn, G. Wipff, and H. B. Bürgi, *Helv. Chim. Acta*, **57**, 493 (1974); J. O. Williams, J. N. Scarsdale, L. Schäfer, and H. J. Geise, *J. Mol. Struct.*, **76**, 11 (1981).

14) S. N. Whittleton, P. Seiler, and J. D. Dunitz, *Helv. Chim. Acta*, **64**, 2614 (1981).

15) A. R. Katritzky, V. J. Barker, F. M. S. Brito-Palma, J. M. Sullivan, and R. B. Finzel, *J. Chem. Soc., Perkin Trans. 2*, **1979**, 1133.

16) R. M. Hunt, R. A. Leacock, C. W. Peters and K. T. Hecht, *J. Chem. Phys.*, **42**, 1931 (1965).

17) A. J. Kirby and P. G. Jones, *J. Am. Chem. Soc.*, **106**, 6207 (1984).

18) For example, hydrolysis of $[Ni(en)_n(H_2O)_{6-2n}]^{2+}$ and $[Ni(tach)_m(H_2O)_{6-3m}]^{2+}$ complexes (en=ethylenediamine, n= 0,1,2,3; tach=*cis,cis*-1,3,5-triaminocyclohexane, m=0,1,2) leads to analogous linear relationships $\delta\Delta G^*/\delta r \approx 60$ kcal mol^{-1} Å^{-1} for the rate-determining bond rupture and $\delta\Delta G^*/\delta r \approx 40$—50 kcal mol^{-1} Å^{-1} for the water-exchange reaction. G. Schwarzenbach, H. B. Bürgi, W. P. Jensen, G. A. Lawrence, L. Monsted, and A. M. Sargeson, *Inorg. Chem.*, **22**, 4029 (1983).

19) H. B. Bürgi and J. D. Dunitz, *J. Am. Chem. Soc.*, **109**, 2924 (1987).

20) Acta Crystallographica is no exception.

21) From which they can in principle be retrieved, but often only at the cost of considerable delay, inconvenience, and expense. The main problem is that supplementary data that are not printed are rarely checked. As a result, deposited ADP's, when they can be found at all, are riddled with errors that are difficult to detect and sometimes impossible to correct. Some journals lack a deposition scheme altogether, so that data supplementary to papers published in them are simply lost.

22) For a recent, more detailed account of the potentialities and limitations of interpreting ADP's, see J. D. Dunitz, V. Schomaker, and K. N. Trueblood, *J. Phys. Chem.* in press.

23) R. E. Rosenfield, K. N. Trueblood, and J. D. Dunitz, *Acta Crystallogr., Sect. A*, **34**, 828 (1978).

24) Except where the masses of the atoms involved differ greatly.

25) F. L. Hirshfeld, *Acta Crystallogr., Sect. A*, **32**, 239 (1976).

26) J. H. Ammeter, H. B. Bürgi, E. Gamp, V. Meyer-Sandrin, and W. P. Jensen, *Inorg. Chem.*, **18**, 733 (1979); K. Chandrasekhar and H. B. Bürgi, *Acta Crystallogr., Sect. B*, **40**, 387 (1976). M. Stebler and H. B. Bürgi, *J. Am. Chem. Soc.*, **109**, 1395 (1987).

27) C. P. Brock, W. B. Schweizer, and J. D. Dunitz, *J. Am. Chem. Soc.*, **107**, 6964 (1985).

28) Usually estimated in terms of the **T, L, S** model: V. Schomaker and K. N. Trueblood, *Acta Crystallogr., Sect. B*, **24**, 63 (1968).

29) C. K. Johnson in "Thermal Neutron Diffraction," ed by B. T. M. Willis, Oxford (1970), p. 132.

30) J. D. Dunitz and D. N. J. White, *Acta Crystallogr., Sect. A*, **29**, 93 (1973).

31) V. Schomaker and K. N. Trueblood, *Acta Crystallogr., Sect. A*, Supplement **40**, C-339 (1984).

32) For a vibrating particle in a quadratic potential, $V(x)=fx^2/2$, the classical Boltzmann distribution leads to an expression for the mean-square displacement, $\langle x^2\rangle = RT/f$. The possibilities, limitations, and dangers of using such mean-field potentials in the interpretation of atomic ADP's are discussed in the article mentioned in Ref. 22.

33) K. N. Trueblood and J. D. Dunitz, *Acta Crystallogr., Sect. B*, **39**, 120 (1983).

34) E. Maverick and J. D. Dunitz, *Mol. Phys.*, **62**, 451 (1987).

35) Standard deviations in U components attainable for heavier elements such as carbon are many times smaller than this.

36) P. Seiler, B. Martinoni, and J. D. Dunitz, *Nature (London)*, **309**, 435 (1984).

37) R. Bau, I. Brewer, M. Y. Chiang, S. Fujita, J. Hoffman, M. I. Watkins, and T. F. Koetzle, *Biochem. Biophys. Res. Commun.*, **115**, 1048 (1984).

38) P. Seiler and J. D. Dunitz, *Acta Crystallogr., Sect. B*, **35**, 1068 (1979).

39) P. Seiler and J. D. Dunitz, *Acta Crystallogr., Sect. B*, **35**, 2020 (1979).

40) The crystallographic R factor, sometimes called the agreement factor, sometimes the disagreement factor, is usually defined as $R=\sum|F_H(\text{obs})-F_H(\text{calc})|/\sum F_H(\text{obs})$.

41) The use of neutron diffraction to obtain the parameters describing the pro-molecule completely avoids the bias associated with the use of isolated-atom form factors. Difference densities obtained in this way are known as X−N densities. The main disadvantage, apart from the extra work and inconvenience, is that one has to contend with two sets of experimental error instead of one. For investigations where the electron density around hydrogen atoms is of special interest, e.g., in studies of hydrogen bonding, etc., the additional work and complications involved in the double experiment are certainly justified.

42) A useful account of the concepts and terms used in experimental charge density studies has been provided by P. Coppens, "Electron Distributions and the Chemical Bond," ed by P. Coppens and M. B. Hall, Plenum, New York (1982), p. 61.

43) J. D. Dunitz, W. B. Schweizer, and P. Seiler, *Helv. Chim. Acta*, **66**, 123 (1983).

44) For comparison, the highest peak in the total electron density amounts to about 40 e Å^{-3} (at the F atom).

45) L. Hirshfeld, *Acta Crystallogr., Sect. B*, **40**, 484 (1984).

46) The main difference is that the static density (Fig. 6A) shows two lobes of a p-orbital like density at the F atom, whereas this feature is absent in the vibrationally smeared density (Fig. 5). Related to this difference, the U component of the F atom in the p-orbital direction is larger in the refinement without deformation density terms. Because of the high correlation in the least-squares calculation between vibrational and deformation parameters, this difference is not particularly serious.

47) B. Delley, *Chem. Phys.*, **110**, 329 (1986).

48) F. L. Hirshfeld, *Acta Crystallogr., Sect. B*, **40**, 613 (1984).

49) J. M. Savariault and M. S. Lehmann, *J. Am. Chem.*

Soc., **102**, 1298 (1980).

50) J. D. Dunitz and P. Seiler, *J. Am. Chem. Soc.*, **105**, 7056 (1983).

51) K. Angermund, K. H. Klaus, R. Goddard, and C. Krüger, *Angew. Chem.*, **97**, 241 (1985); *Angew. Chem., Int. Ed. Engl.*, **24**, 237 (1985).

52) For a criticism of the conventional view, see M. A. Spackman and E. N. Maslen, *Acta Crystallogr., Sect. A*, **41**, 347 (1985).

53) The hydrogen molecule H_2 may not, after all, be a suitable prototype for the chemical bond in general; the H atom is atypical in that it lacks an inner core, and the molecule is atypical in that it contains only two electrons.

54) W. H. E. Schwarz, P. Valtazanos, and K. Ruedenberg, *Theor. Chim. Acta*, **68**, 471 (1985); W. H. E. Schwarz, L. Mensching, P. Valtazanos, and W. von Niessen, *Int. J. Quantum Chem.*, **29**, 909 (1986).

55) K. L. Kunze and M. B. Hall, *J. Am. Chem. Soc.*, **108**, 5122 (1986).

56) J. C. Slater, "Quantum Theory of Molecules and Solids," McGraw-Hill, New York (1965), Vol. 2, p. 113.

57) P. Seiler and J. D. Dunitz, *Helv. Chim. Acta*, **69**, 1107 (1986).

58) W. A. Harrison, "Electronic Structure and the Properties of Solids," Freeman, San Francisco (1980).

 © 1988 The Chemical Society of Japan Bull. Chem. Soc. Jpn., 61, 13—15 (1988)

Invited Paper

Compensation Effects in the Activation Parameters for the Homolytic Dissociation of Transition Metal-Alkyl Bonds

Jack HALPERN
Department of Chemistry, The University of Chicago, Chicago, Illinois 60637, U.S.A.
(Received August 14, 1987)

Determining the activation enthalpies of the homolytic dissociation of transition metal-alkyl bonds constitutes one of the most useful methods of deducing such bond dissociation energies. For several series of organocobalt compounds it has been found that trends of increasing enthalpies of activation for homolytic cobalt-carbon bond dissociation (i.e., of cobalt-carbon bond dissociation energies) are accompanied by partially compensating trends of increasingly positive entropies of activation. Evidence is advanced that these compensation effects are genuine. A suggested explanation is that, with increasing endothermicity of the bond dissociation process, the transition state becomes more "product-like," i.e., further along the path to dissociation.

In 1982[1] we described a method for the determination of transition metal-alkyl bond dissociation energies (D_{M-R}) based on determining the activation enthalpies of the bond-dissociation reaction (Eq. 1) and using the relation of Eq. 2.

$$L_NM\text{-}R \underset{k_{-1}}{\overset{k_1}{\rightleftharpoons}} L_NM\cdot + R\cdot \quad (1)$$

$$D_{M-R} = \Delta H_1^{\ddagger} - \Delta H_{-1}^{\ddagger} \quad (2)$$

In several cases where this has been tested, the reverse reaction of Eq. 1, i.e., the recombination of $L_NM\cdot$ and $R\cdot$, has been found to be diffusion-controlled.[2,3] Thus, $\Delta H_{-1}^{\ddagger}$ may be approximated by the value of the activation ethalpy for a diffusion-controlled reaction which, in organic solvents of low viscosity such as acetone or toluene, corresponds to about 2 kcal mol^{-1}. Accordingly, in practice, only $\Delta H_1^{\ddagger}$ needs to be determined in such solvents and D_{M-R} may be deduced from the relation,

$$D_{M-R} \approx \Delta H_1^{\ddagger} - 2 \text{ kcal mol}^{-1} \quad (3)$$

This approach has subsequently been extensively applied by ourselves and others and, indeed, has become one of the most successful and widely used methods for determining transition metal-alkyl bond dissociation energies in solution.[4-8] We have been interested in elucidating the factors that influence such bond energies and that could contribute to the enzyme-induced cobalt-carbon bond weakening and dissociation of coenzyme B_{12} that triggers the latter's biological role. For this purpose we have determined the Co-C bond dissociation energies of an extensive array of octahedral organocobalt(III) compounds [R-Co(Chel)B] (**1**) in which the alkyl group (R), the tetradentate equatorial ligand (Chel) and the trans-axial ligand (B) have been systematically varied.[1,3,8,9]

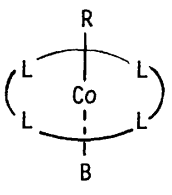

1 (L_4=Chel)

Results and Discussion

Our studies have encompassed various combinations of: R=$C_6H_5CH_2$, $C_6H_5CH(CH_3)$, $CH_3CH_2CH_2$, $(CH_3)_3CCH_2$; Chel=Bis(dimethylglyoximato) $(DH^-)_2$, *N,N'*-bis(salicylidene)-*o*-phenylenediamine (Saloph^{2-}), Octaethylporphyrin (OEP^{2-}); B=pyridine, 4-CN-pyridine, 4-CH_3-pyridine, 4-NH_2-pyridine, PMe_2Ph, PEt_2Ph, PBu_3^n, P(*cyclo*-C_6H_{11})$_3$ and PPh_3. The results of these measurements are summarized in Table 1.

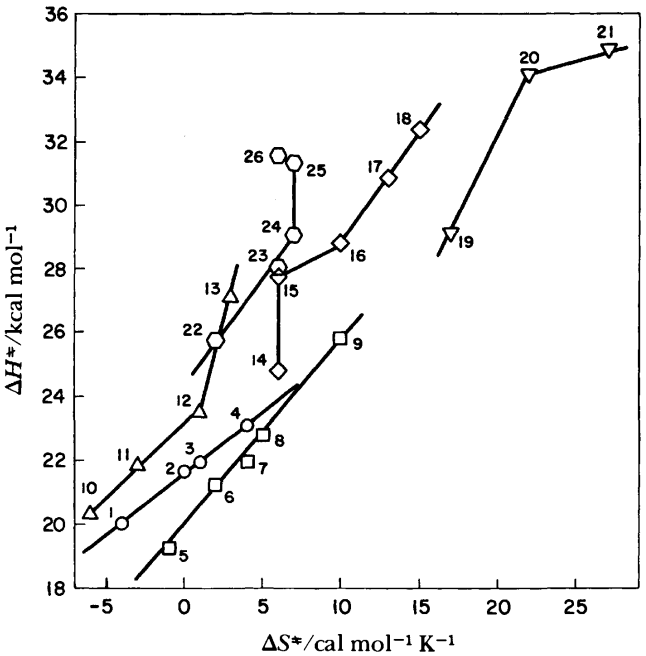

Fig. 1. Relations between enthalpies and entropies of activation for homolytic cobalt-carbon bond dissociation reactions. Numbers refer to entries in Table 1.

Examination of these data reveals that for each series of compounds with a given equatorial ligand, (Chel), variation of either R or B results in a systematic partial "compensation" of the activation parameters such that ΔS^* becomes increasingly positive as ΔH^* increases. The trends are depicted in Fig. 1.

There are well recognized grounds for treating such "compensation" effects with suspicion since they commonly have an artifactual origin reflecting the interdependence of ΔH^* and ΔS^*.[11-15] Thus, random errors in the determination of ΔH^* for a series of reactions, in which the variation of ΔG^* is small, will automatically be reflected in compensating variations in the interdependent variable ΔS^* through the relation, $\Delta G^*=\Delta H^*-T\Delta S^*$; hence for $\Delta\Delta G^*\approx 0$,

$$\Delta\Delta H^* \approx T\Delta\Delta S^* \tag{4}$$

or

$$\Delta H^* \approx \Delta H_0^* + T\Delta S^* \tag{5}$$

Several considerations, cited below, lead us to conclude that the trends of dependence of ΔS_1^* on ΔH_1^*, identified in Table 1 and Fig. 1, are genuine and not of such artifactual origin.

1. The variation of ΔH_1^* (and, correspondingly, of ΔS_1^*) in each series is not random but increases monotonically with ΔG^*. This is contrary to what would be expected if the compensating variations of ΔH_1^* and ΔS_1^* had their origins in random errors in the determination of ΔH_1^*.

2. According to Eq. 4 the slopes of plots of ΔH^* vs. ΔS^* should approximate the mean temperatures ($\overline{T}$) of the measurements. In fact, the slopes of the approximately linear plots of ΔH_1^* vs. ΔS_1^* in Fig. 1 are consistently significantly higher than $\overline{T}$. Thus, for the series [PhCH(CH_3)-Co(DH)$_2$(4-X-pyridine)] the slope is ca. 375 K whereas $\overline{T}$=298 K. Similarly, for the series [PhCH(CH_3)-Co(DH)$_2$(PR_3)] the slope is ca. 600 K whereas $\overline{T}$=293 K.

3. Similar trends of dependence of ΔH_1^* on ΔS_1^* are observed for several different series of compounds, namely for those in which (Chel)=(DH^-)$_2$, ($Saloph^{2-}$) and (OEP^{2-}) and for different procedures used to determine ΔH_1^*. Furthermore, for one of these series, [PhCH(CH_3)-Co(DH)$_2$(4-X-pyridine)], the validity of

Table 1. Kinetic Data for Cobalt-Alkyl Bond Dissociation Reactions

No.	R	Chel	B	Solvent	Temp range °C	ΔH_1^* kcal mol^{-1}	ΔS_1^* cal mol^{-1} K^{-1}	Ref.
1	$CH(CH_3)C_6H_5$	$(DH)_2$	4-CN-pyridine	Acetone	14—36	20.1	−4	2
2	$CH(CH_3)C_6H_5$	$(DH)_2$	Pyridine	Acetone	15—35	21.6	0	2
3	$CH(CH_3)C_6H_5$	$(DH)_2$	4-CH_3-pyridine	Acetone	15—35	21.8	1	2
4	$CH(CH_3)C_6H_5$	$(DH)_2$	4-NH_2-pyridine	Acetone	20—35	23.1	4	2
5	$CH(CH_3)C_6H_5$	$(DH)_2$	PPh_3	Acetone	5—25	19.3	−1	9
6	$CH(CH_3)C_6H_5$	$(DH)_2$	$PEtPh_2$	Acetone	25—46	21.3	2	9
7	$CH(CH_3)C_6H_5$	$(DH)_2$	$P(CH_2CH_2CN)_3$	Acetone	10—25	22.1	4	9
8	$CH(CH_3)C_6H_5$	$(DH)_2$	PBu_3^n	Acetone	15—35	22.8	5	9
9	$CH(CH_3)C_6H_5$	$(DH)_2$	PMe_2Ph	Acetone	10—25	25.9	10	9
10	$CH_2C(CH_3)_3$	Saloph	Pyridine	Pyridine	54—69	20.3	−6	1
11	$CH(CH_3)_2$	Saloph	Pyridine	Pyridine	43—63	21.8	−3	1
12	$CH_2C_6H_5$	Saloph	Pyridine	Pyridine	55—65	23.6	1	1
13	$CH_2CH_2CH_3$	Saloph	Pyridine	Pyridine	77—97	27.1	3	1
14	$C_6H_5CH_2$	$(DH)_2$	$P(c\text{-}C_6H_{11})_3$	Toluene	10—46	24.8	6	8
15	$C_6H_5CH_2$	$(DH)_2$	PPh_3	Toluene	47—75	27.8	6	8
16	$C_6H_5CH_2$	$(DH)_2$	$PEtPh_2$	Toluene	50—82	28.8	10	8
17	$C_6H_5CH_2$	$(DH)_2$	PBu_3^n	Toluene	62—100	30.9	13	8
18	$C_6H_5CH_2$	$(DH)_2$	PMe_2Ph	Toluene	66—100	32.4	15	8
19	$C_6H_5CH_2$	$(DH)_2$	$P(c\text{-}C_6H_{11})_3$	Ethylene glycol	35—64	29.1	17	9
20	$C_6H_5CH_2$	$(DH)_2$	PPh_3	Ethylene glycol	47—75	34.1	22	9
21	$C_6H_5CH_2$	$(DH)_2$	$PEtPh_2$	Ethylene glycol	60—88	34.8	27	9
22	$C_6H_5CH_2$	OEP	PPh_3	Toluene	50—70	25.8	2	8
23	$C_6H_5CH_2$	OEP	$PEtPh_2$	Toluene	55—90	28.1	6	8
24	$C_6H_5CH_2$	OEP	PMe_2Ph	Toluene	55—90	29.1	7	8
25	$C_6H_5CH_2$	OEP	PBu_3^n	Toluene	65—100	31.3	7	8
26	$C_6H_5CH_2$	OEP	$P(c\text{-}C_6H_{11})_3$	Toluene	73—91	31.6	6	8

the ΔH_1^* values has been supported, using Eq. 2, by independent determinations of D_{Co-R} based on *thermodynamic* measurements.[3]

All of the above argue against the trends of compensating variations of ΔH_1^* and ΔS_1^*, in Table 1 and Fig. 1, having their origin in errors in the determination of ΔH_1^*. Accordingly, we conclude that these partial compensation effects are genuine and reflect systematic dependencies of structural features of the transition state on ΔH_1^*. The bond dissociation process associated with ΔH_1^* is substantially endothermic and the activation barrier (ΔH_{-1}^*) associated with the reverse (recombination) is small. Thus, the transition state for the dissociation reaction is anticipated to be "product-like" and to become more so with increasing endothermicity, i.e., with increasing D_{Co-R} and ΔH_1^* (Hammond postulate[16]). Since the entropy of the overall dissociation process is substantially positive, it is expected that this should be accompanied by an increase in the entropy of activation, ΔS_1^*, possibly associated with increasing relaxation of the originally octahedral configuration to the more product-like, less rigid, structure **2**. This provides a plausible explanation for the compensating dependence of ΔH_1^* on ΔS_1^* that we have identified as a general feature of such transition metal-alkyl bond dissociation reactions.

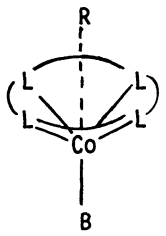

2

In this connection, it is of interest that for the series of complexes, $[C_6H_5CH_2\text{-}Co(OEP)PR_3]$, containing the octaethylporphyrin ligand, which we have previously concluded to be less flexible than the other equatorial ligands,[8] ΔS_1^* does indeed exhibit the smallest variation.

Thus it is seen that the relation between the bond dissociation rate and bond dissociation energy is not entirely simple. This is of some interest in the context of understanding the nature and origin of the "bond weakening" that is involved in the enzyme-induced Co-C bond dissociation of coenzyme B_{12}.[17] Clearly, entropic as well as enthalpic factors may contribute to such bond weakening.

Support of this research by grants from the National Institutes of Health, the National Science Foundation and the Petroleum Research Fund, administered by the American Chemical Society, is gratefully acknowledged.

References

1) T. T. Tsou, M. Loots, and J. Halpern, *J. Am. Chem. Soc.*, **104**, 623 (1982).
2) J. Halpern, *Accts. Chem. Res.*, **15**, 238 (1982).
3) F. T. T. Ng, G. L. Rempel, and J. Halpern, *J. Am. Chem. Soc.*, **104**, 621 (1982).
4) R. G. Finke, B. L. Smith, B. J. Mayer, and A. A. Molinero, *Inorg. Chem.*, **22**, 3677 (1983).
5) R. G. Finke and B. P. Hay, *Inorg. Chem.*, **23**, 3041 (1984); B. P. Hay and R. G. Finke, *J. Am. Chem. Soc.*, **108**, 4820 (1986).
6) J. Halpern, S. H. Kim, and T. W. Leung, *J. Am. Chem. Soc.*, **106**, 8317 (1984).
7) J. P. Collman, L. McElwee-White, P. J. Brothers, and R. Rose, *J. Am. Chem. Soc.*, **108**, 1332 (1986).
8) M. K. Geno and J. Halpern, *J. Am. Chem. Soc.*, **109**, 1238 (1987).
9) M. K. Geno and J. Halpern, *J. Chem. Soc., Chem. Commun.*, **1987**, 1052.
10) F. T. T. Ng, G. L. Rempel, and J. Halpern, *Inorg. Chim. Acta*, **77**, L165 (1983).
11) Such grounds for concern are especially cogent with respect to claims of precisely linear dependence of ΔH^* on ΔS^*, i.e., manifestations of the so-called "isokinetic relationship," $\Delta H^* = \Delta H_0^* + \beta \Delta S^*$, particularly when the value of β is close to the temperature range of measurement. Indeed, there is reason to question the physical plausibility of such an isokinetic relation since it implies reversal of reactivity trends in passing through the "isokinetic temperature." For the purpose of the issues addressed in this paper the precise form of the dependence of ΔH^* on ΔS^* is not of primary importance and we have been careful to avoid claims of "isokinetic" behavior. We do, however, attach relevance to the qualitative monotonic dependence of ΔH^* on ΔS^* that we have observed consistently in the course of these measurements and that we conclude to be genuine.
12) J. E. Leffler, *J. Org. Chem.*, **20**, 1202 (1955).
13) R. C. Peterson, *J. Org. Chem.*, **29**, 3133 (1964).
14) O. Exner, *Progr. Phys. Org. Chem.*, **10**, 411 (1973) and references therein.
15) O. Exner, *Coll. Czech. Chem. Comm.*, **40**, 2762 (1975).
16) G. S. Hammond, *J. Am. Chem. Soc.*, **77**, 334 (1955).
17) J. Halpern, *Science*, **227**, 869 (1985).

 © 1988 The Chemical Society of Japan Bull. Chem. Soc. Jpn., 61, 17—24 (1988)

Invited Paper

Electrogenerated Chemiluminescence. 50. Electrochemistry and Electrogenerated Chemiluminescence of Micelle Solubilized $Os(bpy)_3^{2+}$

Jiangbo OUYANG and Allen J. BARD*
Department of Chemistry, The University of Texas Austin, TX 78712, U.S.A.
(Received August 20, 1987)

The oxidative electrochemistry and electrogenerated chemiluminescence (ECL) of $Os(bpy)_3^{2+}$ were studied in the presence of sodium dodecyl sulfate (SDS), Triton X-100, and cetyltrimethylammonium bromide (CTAB) in aqueous solutions. Variation of supporting electrolyte (NaCl) concentration affected the interaction between $Os(bpy)_3^{2+}$ and the surfactants. The measurement of oxidation peak current (i_{pa}) and ECL intensity at different NaCl concentrations suggested a strong interaction of $Os(bpy)_3^{2+}$ with SDS. Above the critical micelle concentration (cmc) the strong hydrophobic interaction of $Os(bpy)_3^{2+}$ and the SDS micelle core greatly suppresses both i_{pa} and the ECL intensity. The interaction of $Os(bpy)_3^{2+}$ with CTAB micelle is much weaker because of electrostatic effects. Triton X-100 micelles do not interact with $Os(bpy)_3^{2+}$.

We report studies of the effect of micelle-forming surfactants on the oxidative electrochemistry of $Os(bpy)_3^{2+}$ and its ECL in the presence of oxalate. Surfactants have been used in polarographic experiments and other electrochemical experiments. Most experiments deal with $E_{1/2}^{i}$ shifts and homogeneous electron-transfer kinetics of the substances solubilized in micelles.[1-3] Micelles have also been of interest in micellar catalysis and micellar models of biological membranes.[4] Micelles are dynamic aggregates of amphiphilic molecules and possess regions of hydrophilic and hydrophobic character.[5] The interactions that are operative between soluble substances and host micelles include electrostatic attractions,[6] surface adsorption,[7] pseudophase extraction,[8] and substrate/amphiphile coassembly to yield a unique micelle composition.[9] The specific nature of the interaction between a soluble species and the host micelle governs the effect of micellar microenvironment on the behavior of the substrate. This study was mainly motivated by our interest in the application of $Ru(bpy)_3^{2+}$ and other emitting centers as tags for analysis of species at low concentration.[10] In certain samples, e.g., biological fluids, the addition of surfactants can be helpful in suppressing the effects of interferences.

The present experiment was designed to elucidate the microenvironment effects of micelles on the electrochemical and ECL behavior of $Os(bpy)_3^{2+}$, which is a reasonably good luminescor.[11,12] The one-electron oxidation near +0.6 V vs. SCE allows the study of these compounds in aqueous solutions. Sodium dodecyl sulfate (SDS), Triton X-100, and cetyltrimethylammonium bromide (CTAB) were used as the representatives of anionic, neutral and cationic micelles, respectively. We also show that the electrolyte concentration affects the electrochemical and ECL behavior.

SDS = $CH_3(CH_2)_{11}OSO_3^-Na^+$

CTAB = $CH_3(CH_2)_{15}N^+(CH_3)_3Br^-$

Triton X-100 = $CH_3(CH_2)_7(OCH_2CH_2)_{9.5}$- 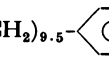 -OH

Structures of Surfactants

Experimental

SDS, CTAB, and Triton X-100 were obtained from Aldrich Chemicals (Milwaukee, WI) and were used without further purification. Sodium chloride was purchased from MCB (reagent grade, Cincinnati, OH) and Milli-Q water (Millipore Corp. El Paso, TX) was used to prepare all solutions. $Os(bpy)_3(PF_6)_2$ was prepared according to the procedure of Gaudiello et al.[13] The surface active compounds were dissolved in a very small volume of acetone to assist the solubility in water.

A three compartment cell was used to carry out all experiments. Electrochemical measurements were performed with a Princeton Applied Research (PAR) (Princeton, NJ) Model 175 universal programmer, a Model 173 potentiostat and a Model 179 digital coulometer equipped with positive feedback circuitry for IR compensation. Voltammograms were recorded on a Houston Instruments Model 2000 X-Y recorder. A BAS-100 electrochemical analyzer (Bioanalytical Systems, Lafayette, IN) was also used in the electrochemical measurements. ECL spectra were recorded on an Aminco-Bowman Spectrometer with a Hamamatsu R928 photomultiplier tube. Absorption spectra were obtained with a Hewlett-Packard Model 8450A dual-beam spectrophotometer.

Most of the experiments were performed under a purified nitrogen atmosphere. The electrochemical cell was adapted to a Schlenk line. Glassy carbon electrodes (0.07 cm^2) (BAS, Lafayette, IN) were employed as working electrodes for voltammetry and ECL. The electrodes were polished with a 0.05 μm alumina/water slurry on a felt surface and sonicated. A platinum mesh was used as counter electrode and all potentials were recorded against a saturated calomel electrode (SCE).

Results

Cyclic Voltammetry. Cyclic voltammetry (CV) experiments were carried out to study the effect of

SDS, Triton X-100, and CTAB micelles on the redox potentials and peak currents (i_p) for the oxidation of $Os(bpy)_3^{2+}$. The cyclic voltammogram of a 0.2 mM† aqueous solution of $Os(bpy)_3^{2+}$ in 50 mM NaCl in the absence and presence of surfactants is shown in Fig. 1. The waves observed are due to the one-electron oxidation[12] of $Os(bpy)_3^{2+}$, and, on reversal, the reduction of the +3 species:

$$Os(bpy)_3^{2+} \rightleftharpoons Os(bpy)_3^{3+} + e^- . \quad (1)$$

CV waves were observed in all three micellar solutions as shown in Fig. 1b—d. The value of ΔE_p, the separation between anodic and cathodic peak potentials ($E_{pa}-E_{pc}$), shows that the waves are essentially reversible in all solutions. ΔE_p is listed in Table 1 for all media. There are variations in the redox potentials associated with half reaction 1 in SDS media. In the presence of SDS, the $E_{1/2}$ (formal standard potential)

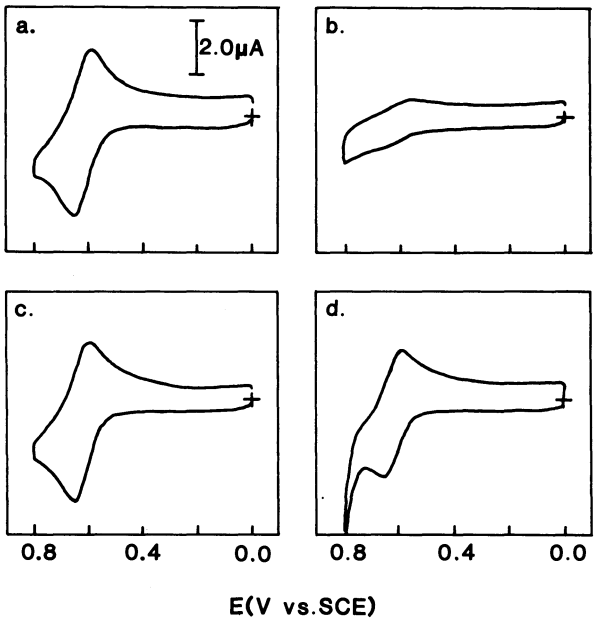

Fig. 1. Cyclic voltammogram for the oxidation of 0.2 mM $Os(bpy)_3^{2+}$, 50 mM NaCl, at a GC electrode. Scan rate, 100 mV s^{-1}. (a) Aqueous solution; (b) 70 mM SDS; (c) 5% (w/v) Triton X-100; (d) 70 mM CTAB.

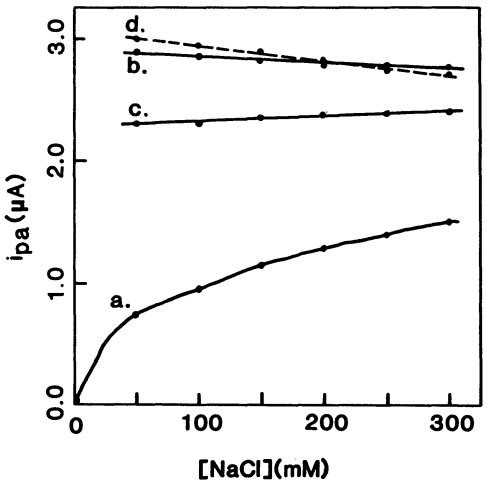

Fig. 2. Electrolyte (NaCl) concentration dependence of peak current for the oxidation of 0.2 mM $Os(bpy)_3^{2+}$ at GC electrode. Scan rate, 100 mV s^{-1}. (a) 70 mM SDS; (b) 5% (w/v) Triton X-100; (c) 70 mM CTAB; (d) pure aqueous.

Table 1. Variations of Half-Wave Potentials for $Os(bpy)_3^{3+}/Os(bpy)_3^{2+}$ ($C=0.2$ mM) in Different Media at Different NaCl Concentrations

	50 mM				100 mM				150 mM			
	E_{pa} a)	E_{pc} a)	ΔE_p b)	$\frac{E_{pa}+E_{pc}}{2}$	E_{pa}	E_{pc}	ΔE_p	$\frac{E_{pa}+E_{pc}}{2}$	E_{pa}	E_{pc}	ΔE_p	$\frac{E_{pa}+E_{pc}}{2}$
Aqueous	0.655	0.590	65	0.623	0.650	0.585	65	0.618	0.650	0.585	65	0.618
70 mM SDS	0.650	0.580	70	0.615	0.656	0.590	66	0.623	0.680	0.610	70	0.645
70 mM CTAB	0.655	0.588	67	0.622	0.650	0.580	70	0.615	0.648	0.580	68	0.614
5% (w/v) Triton X-100	0.655	0.595	60	0.625	0.652	0.590	62	0.621	0.648	0.582	66	0.615
	200 mM				250 mM				300 mM			
	E_{pa}	E_{pc}	ΔE_p	$\frac{E_{pa}+E_{pc}}{2}$	E_{pa}	E_{pc}	ΔE_p	$\frac{E_{pa}+E_{pc}}{2}$	E_{pa}	E_{pc}	ΔE_p	$\frac{E_{pa}+E_{pc}}{2}$
Aqueous	0.645	0.585	60	0.615	0.640	0.580	60	0.610	0.640	0.580	60	0.610
70 mM SDS	0.690	0.618	72	0.654	0.695	0.625	70	0.660	0.705	0.630	75	0.668
70 mM CTAB	0.640	0.578	62	0.609	0.638	0.576	62	0.607	0.638	0.572	66	0.605
5% (w/v) Triton X-100	0.640	0.580	60	0.610	0.645	0.582	63	0.614	0.642	0.578	64	0.610

a) E_{pa} and E_{pc} in V vs. SCE. b) ΔE_p in mV.

† 1 M=1 mol dm^{-3}.

shifted to slightly more positive values (see Table 1), especially at higher supporting electrolyte concentration; e.g., $E_{1/2}$ was 0.668 V vs. SCE at 300 mM NaCl with 70 mM SDS compared to 0.610 V in 300 mM NaCl alone. Both i_{pc} and i_{pa} were depressed about four times in the presence of SDS (50 mM NaCl in solution) and reduced slightly in the presence of Triton X-100 micelles and of CTAB micelles compared to that in an aqueous solution in the absence of surfactant (Fig. 2).

The supporting electrolyte concentration affects the oxidation of $Os(bpy)_3^{2+}$ as shown by i_{pa} vs. concentration of NaCl plots in Fig. 2. The variation of electrolyte concentration caused different responses for the three different micellar solutions. In 70 mM SDS (Fig. 2a), when the concentration of NaCl increased from 50 mM to 300 mM, the formal standard potential shifted from 0.615 to 0.688 V vs. SCE and the i_{pa} increased from 0.75 to 1.5 μA. In the absence of added NaCl, a solution with 0.2 mM $Os(bpy)_3^{2+}$ shows an i_{pa}=1.6 μA (with positive feedback iR compensation). However, under the same conditions in the presence of 70 μm SDS, no oxidation wave is seen ($i_{pa}\approx 0$). This indicates that all of the $Os(bpy)_3^{2+}$ in the SDS micelles becomes completely electrochemically inactive in the absence of supporting electrolyte. The peak current increased slightly upon the successive addition of NaCl with CTAB micelles, as shown in Fig. 2c. In the presence of Triton X-100 micelles, as well as without any surfactant added, the peak current decreased slightly as the concentration of NaCl increased.

The voltammetry was also studied at various concentrations of SDS. A plot of peak current vs. concentration of SDS is shown in Fig. 3a. SDS was gradually added to an aqueous solution containing 0.2 mM $Os(bpy)_3^{2+}$ and 50 mM NaCl. The oxidation peak current dropped from 3.0 to 1.9 μA upon the addition of 1.7 mM SDS, then continued decreasing, roughly linearly proportional to the SDS concentration, up to about 12 mM. Addition of more SDS depressed the peak current further until 30 mM SDS had been added. The peak current then leveled at 0.55 μA for SDS concentration up to 50 mM. The same phenomenon is observed for MV^+ reduction at different concentrations of SDS,[14] where the reduction current was depressed continually as the SDS concentration was raised above the critical micelle concentration (cmc) (which is 2.25 mM at 50 mM NaCl).

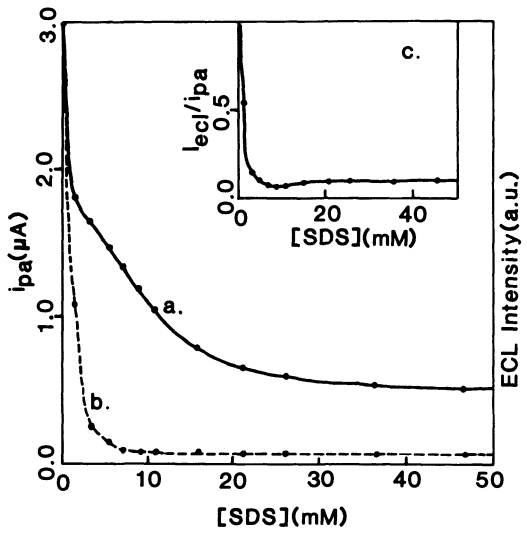

Fig. 3. (a) SDS concentration dependence of peak current for 0.2 mM $Os(bpy)_3^{2+}$ in 50 mM NaCl solution at GC electrode. Scan rate, 100 mV s^{-1}. (b) SDS concentration dependence of ECL intensity of $Os(bpy)_3^{2+}$ in 50 mM NaCl, 20 mM $C_2O_4^{2-}$; (c) ratio of the ECL intensity by the current at corresponding SDS concentration.

Diffusion Coefficients. The diffusion coefficient, D_o, is a measure of the association of electroactive molecules with the surfactant and micelles. Plots of i_{pa} vs. the square root of the sweep rate ($v^{1/2}$) in different media (Fig. 4) are linear, indicating that the electrode reaction of $Os(bpy)_3^{2+}$ is diffusion-controlled in the absence and presence of surfactant. This suggests that the electrochemically active species in the presence of SDS is the micelle-solubilized $Os(bpy)_3^{2+}$ in the bulk solution, since the slope of the i_{pa} vs. $v^{1/2}$ line corresponding to the SDS solution is significantly smaller than those corresponding to the other media. This observation is also clear from the decreased i_{pa} value in CV for a 0.2 mM solution of $Os(bpy)_3^{2+}$ in the presence of SDS micelles as compared to i_{pa}-values in the other media. D_o was 7.3×10^{-6} cm^2 s^{-1} in 50 mM NaCl aqueous solution, while D_o was 3.3×10^{-7} cm^2 s^{-1} in a 70 mM SDS and 50 mM NaCl solution. The decrease in D_o agrees with previous results of other species due to association with surfactants and in micellar assemblies[1a,3a,15] and an increase in the effective radius of the substrate.[16]

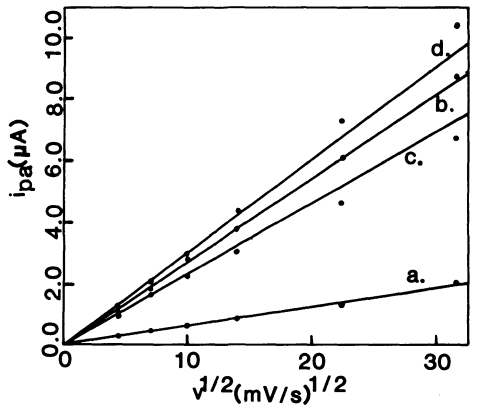

Fig. 4. Scan rate dependence of the anodic peak current for the oxidation of 0.2 mM $Os(bpy)_3^{2+}$. (a) 50 mM NaCl +70 mM SDS; (b) 50 mM NaCl +5% Triton X-100; (c) 50 mM NaCl +70 mM CTAB; (d) 50 mM NaCl aqueous.

The slopes of the i_p vs. $v^{1/2}$ lines in the presence of CTAB and Triton X-100 (50 mM NaCl) deviate little from those in aqueous solution and yield D_o-values of 4.4×10^{-6} and 5.9×10^{-6} $cm^2 s^{-1}$ for $Os(bpy)_3^{2+}$, respectively.

In general, the addition of electrolytes increases the size of ionic micelles.[17] As shown by other experiments[18] with no added salt, the SDS micelles are monodisperse with an aggregation number of 55. The aggregation numbers are 98.6 with 0.189 M NaCl and 162 with 0.424 M NaCl. The larger size of the micelles would suggest a smaller value for D_o. This is contrary to what is shown in Fig. 5, where the slopes of the i_p vs. $v^{1/2}$ line become steeper at higher concentration of NaCl in the presence of SDS micelles. The magnitude of i_{pa} in CV also increases with an increase in NaCl concentration in the presence of SDS. Thus, for example, the diffusion coefficient increased from 3.3×10^{-7} to 1.3×10^{-6} $cm^2 s^{-1}$ when the NaCl concentration increased from 50 to 300 mM. An explanation for this effect is proposed in the Discussion section. In all other media (surfactant-free solution, CTAB and Triton X-100 micellar solution), the addition of more NaCl caused only sight changes in the slopes of i_p vs. $v^{1/2}$ lines; i.e., diffusion coefficients showed only minor changes at higher concentrations of NaCl.

Electrogenerated Chemiluminescence. ECL of $Os(bpy)_3^{2+*}$ has been observed[12] upon the annihilation reaction between electrogenerated $Os(bpy)_3^{3+}$ and $Os(bpy)_3^{+}$ in acetonitrile solution. Because of the limited potential range of water, an alternative method, using oxalate oxidation,[19] to generate the ECL of $Os(bpy)_3^{2+*}$ was tried. When the potential was scanned to positive values in solutions of $Os(bpy)_3^{2+}$ and $C_2O_4^{2-}$, $Os(bpy)_3^{2+}$ was oxidized to $Os(bpy)_3^{3+}$ and $C_2O_4^{2-}$ generated CO_2^{-}, which in turn produced $Os(bpy)_3^{2+*}$.[19] Figure 6 shows the ECL intensity-potential profile for the system of 0.2 mM $Os(bpy)_3^{2+}$, 20 mM $C_2O_4^{2-}$, 50 mM NaCl in aqueous solution. ECL was first observed at the potential where $Os(bpy)_3^{2+}$ is oxidized. No emission was observed at this sensitivity in the absence of $Os(bpy)_3^{2+}$ (Fig. 6a). The addition of 70 mM SDS reduced the ECL intensity twenty-fold. When 5% (w/v) Triton X-100 or 70 mM CTAB was added (50 mM NaCl in solution), the ECL intensity decreased to two-thirds the value found in the absence of surfactant.

The effect of electrolyte concentration on the ECL intensity is shown in Fig. 7. In the SDS micellar media, increasing the NaCl concentration resulted in more intense ECL (Fig. 7a), in the same way that the

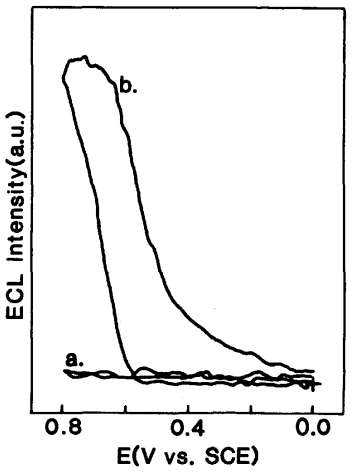

Fig. 6. Potential dependence of ECL intensity. (a) Background, 50 mM NaCl + 20 mM $(NH_4)_2C_2O_4$; (b) system (a) +0.2 mM $Os(bpy)_3^{2+}$.

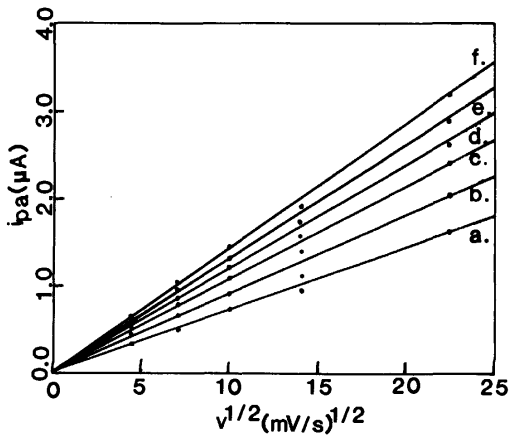

Fig. 5. Scan rate dependence of the anodic peak current for the oxidation of 0.2 mM $Os(bpy)_3^{2+}$ at GC electrode in the presence of 70 mM SDS at the concentration of (a) 50 mM NaCl; (b) 100 mM NaCl; (c) 150 mM NaCl; (d) 200 mM NaCl; (e) 250 mM NaCl; (f) 300 mM NaCl.

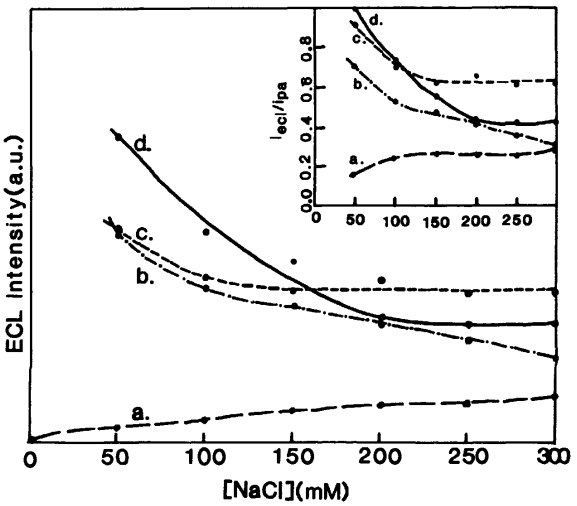

Fig. 7. NaCl concentration dependence of ECL intensity of 0.2 mM $Os(bpy)_3^{2+}$, 20 mM $C_2O_4^{2-}$. (a) 70 mM SDS; (b) 5% Triton X-100; (c) 70 mM CTAB; (d) pure aqueous.

i_{pa}-value increased with the electrolyte concentration. A zero ECL intensity was obtained by extrapolation to zero electrolyte concentration, which is expected from the zero peak current at zero electrolyte concentration (Fig. 2a). For CTAB solutions, the ECL intensity decreased as the NaCl concentration increased from 50 mM to 100 mM and reached a constant value at higher NaCl concentration (Fig. 7c). Similarly the ECL intensity decreased with an increase in NaCl concentration in the Triton X-100 micellar solution (Fig. 7b), which was similar to the ECL intensity change in aqueous solution (Fig. 7b).

The ratio of ECL intensity to peak current (I/i_{pa}) is much lower in an SDS solution than that in all other media at lower NaCl concentration as shown by the insert in Fig. 7. As the NaCl concentration increased, the I/i_{pa} ratio increased at higher NaCl concentration in SDS micellar solution. The ratio decreased for all other media as the NaCl concentration increased, except in the CTAB micellar solution, where the ratio reached a constant value and was larger than that in all other media at higher NaCl concentrations.

The ECL intensity vs. SDS concentration dependence is shown in Fig. 3b. It shows the same trend as the i_{pa}-SDS concentration plot. The presence of 1.7 mM SDS greatly reduced the ECL intensity. The greater the SDS concentration, the weaker was the ECL intensity. At an SDS concentration of 7 mM or higher, only very weak ECL was observed, and the intensities became essentially independent of SDS concentration. Figure 3c is a plot of the ratio of ECL intensity (Fig. 3b) to i_{pa} (Fig. 3a) at each SDS concentration.

Absorption and Luminescence Spectra. The spectroscopic properties of molecules are usually influenced by the environment. Since micelle formation produces a different environment for the solubilized $Os(bpy)_3^{2+}$, the spectroscopic behavior of $Os(bpy)_3^{2+}$ should change upon addition of SDS. Figure 8 shows the absorption spectra of $Os(bpy)_3^{2+}$ in different media. The spectra in CTAB and Triton X-100 micellar solutions were essentially the same as those in the pure aqueous solution. The absorption spectrum changed slightly upon addition of SDS, with the minimum at 460 nm becoming flat. The absorption spectra did not change when the NaCl concentration was varied.

The luminsecence spectra (Fig. 9) were also affected to a greater extent in the presence of SDS. The emission spectra of $Os(bpy)_3^{2+*}$ in 70 mM CTAB and 5% (w/v) Triton X-100 micelle solution were identical to that in aqueous solution with a maximum at about 730 nm. The position of the emission peak was shifted to 765 nm in a 70 mM SDS micellar solution. Since the concentration of $Os(bpy)_3^{2+}$ was the same in all of the solutions of different surfactants and in a 50 mM NaCl aqueous solution alone, and because the absorbances were the same, the fact that the emission intensities were about the same indicates that the quantum yields are about the same in different solutions. Variation of concentration of NaCl did not change the absorption or luminescence spectra in any of the solutions, nor did it affect the absorbance or emission intensities.

The shift in the emission peak for $Os(bpy)_3^{2+}$ in the SDS solution clearly shows an interaction between these species. The effect on the $Os(bpy)_3^{2+}$ emission depends upon whether the SDS concentration is above or below the cmc. The spectrum has a peak at 730 nm in pure aqueous solution. Addition of up to 3.4 mM SDS shifted the peak to 710 nm (a blue shift) (Fig. 9b). The turning point concentration of SDS for the large red spectral shift was near the critical micelle concentration of SDS (2.25 mM); i.e., when the concentration of SDS changed from below the cmc to above it, a large shift in peak position towards longer wavelengths (to 765 nm) resulted. As a comparison, the luminescence spectrum of $Os(bpy)_3^{2+}$ in hexane

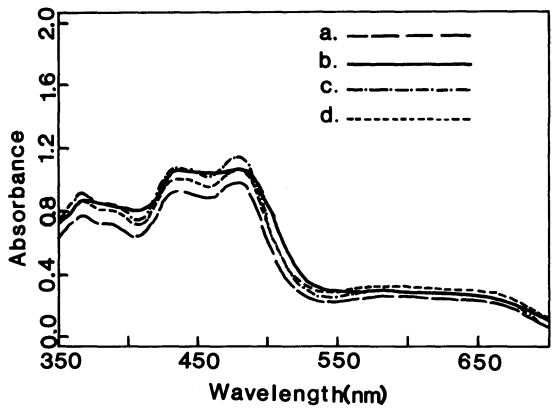

Fig. 8. Absorption spectra of $Os(bpy)_3^{2+}$, in (a) aqueous solution, (b) 70 mM SDS solution; (c) 5% Triton X-100 solution; (d) 70 mM CTAB solution. 1 cm path length cell.

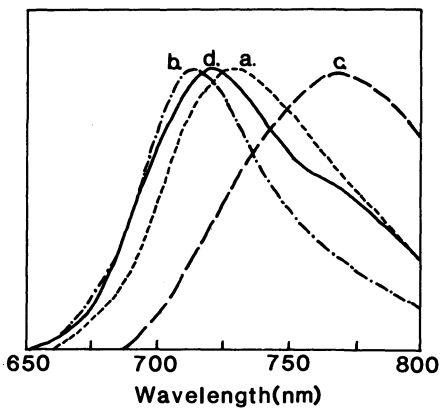

Fig. 9. Luminescence spectra of $Os(bpy)_3^{2+}$, in (a) pure aqueous, or 70 mM CTAB or 5% Triton X-100 solutions; (b) 2 mM SDS solution; (c) 70 mM SDS solution; (d) hexane solution. λ_{exc}=470 nm.

was measured; a shoulder appeared at 767 nm in addition to a peak at 720 nm. Note that a similar emission spectrum shift was reported for [11-(3-hexyl-1-indolyl)undecyl]trimethylammonium bromide around the cmc in an aqueous solution.[20]

Discussion

Dissolved species associate with surfactant molecules in different ways at different surfactant concentrations.[21] Below the critical micelle concentration (cmc), complexes can be formed between dissolved species and surfactant molecules (premicellar aggregates).[14,21] Above the cmc the surfactant exists in solution as micelles, and dissolved species, A, can partition between the micellar and the water phase. Scheme 1 is often used to describe a redox couple in which the oxidized and reduced forms interact with micellar aggregates (when the surfactant concentration is above the cmc).[1a]

$$\begin{array}{ccc} A_M^{(z+1)+} & \underset{-e}{\overset{+e}{\rightleftharpoons}} & A_M^{z+} \\ K_O \uparrow\downarrow & & \uparrow\downarrow K_R \\ A_W^{(z+1)+} + \text{Micelle} & \underset{-e}{\overset{+e}{\rightleftharpoons}} & A_W^{z+} + \text{Micelle} \end{array}$$

Scheme 1.

$K_O=[A_W^{(Z+1)+}][\text{micelle}]/[A_W^{(Z+1)+}]$ and $K_R=[A_W^{Z+}][\text{micelle}][A_M^{Z+}]$ are equilibrium constants, the subscripts M and W indicate the micellar and aqueous phases, respectively; and O and R indicate constants appropriate for the oxidant and reductant, respectively. For a simple reversible one-electron process, the formal standard potential can be represented as $E_W^\circ+(RT/F)\ln K_O(1+K_R)/K_R(1+K_O)$. When $A^{(Z+1)+}$ and A^{Z+} exist predominantly in the micelles, K_O, $K_R \ll 1$, the formal standard potential becomes $E_W^\circ+(RT/F)\ln[K_O/K_R]$. When $A^{(Z+1)+}$ and A^{Z+} exist predominantly in the water phase, K_O, $K_R \gg 1$, the logarithmic term disappears and the potential is E_W°, which represents the formal standard potential of the redox couple in the absence of micelles. The electrochemical evidence presented here indicates predominant existence of $A^{(Z+1)+}$ and A^{Z+} in the SDS micelles. The positive potential shift implies that $K_O > K_R$ and SDS micelles associate more strongly with $Os(bpy)_3^{2+}$ than with $Os(bpy)_3^{3+}$. Higher electrolyte concentrations resulted in a more positive potential shift, which indicates that the association of SDS with $Os(bpy)_3^{2+}$ was enhanced relative to that of $Os(bpy)_3^{3+}$; i.e., $(K_O/K_R)' > K_O/K_R$ where the prime denotes a higher electrolyte concentration. Two types of interactions can be considered between the Os-species and the SDS molecules: electrostatic and hydrophobic. The stronger interaction of the Os(II) species suggests that the hydrophobic interaction, involving the bpy ligands and the hydrocarbon chains on the SDS, is important. A similar phenomenon has been observed for association of SDS with methyl viologens of different oxidation states;[14,15] i.e., SDS associates more strongly with MV^+ than with the MV^{2+} form. Similarly $Ru(bpy)_3^{2+}$ is bound into Nafion more strongly than $Ru(bpy)_3^{3+}$.[22] This was also explained by the importance of hydrophobic interactions between the complex and the nonpolar regions of the Nafion.

The observed depression of the peak current for the oxidation of $Os(bpy)_3^{2+}$ at SDS levels below the cmc indicates that $Os(bpy)_3^{2+}$–surfactant aggregates are formed. By the same argument that has been applied to explain, for example, the shift in standard potential for 10-methylphenothiazine at premicellar concentrations of SDS,[21] the near independence of peak potentials for the oxidation of $Os(bpy)_3^{2+}$ at these levels of SDS indicates that $Os(bpy)_3^{2+}$–SDS and $Os(bpy)_3^{3+}$–SDS complexes have essentially equal formation constants.

At concentrations of SDS above the cmc, the aggregation number of the micelles can be altered by changing the electrolyte concentration in solution.[18] In general, both theoretical treatments[23] and experimental studies[18] show that higher electrolyte concentrations result in larger aggregation numbers. Thus with an increase of electrolyte (e.g., NaCl) concentration, the size of the micelle should increase and its diffusion coefficient should decrease. If the $Os(bpy)_3^{2+}$ contained in the micelle was reduced directly at the electrode, one would predict that the oxidation peak current and the measured D_R would decrease with an increase in NaCl concentration. However, the experimental results showed that i_{pa} (Fig. 2a) and D_R (Fig. 5) both increased with an increase of NaCl concentration. This finding can be explained, however, using the same model as that of Saji et al.,[24] for a similar finding for the oxidation of (11-ferrocenylundecyl)trimethylammonium bromide in the presence of SDS micelles. These authors showed that the ferrocenyl moiety incorporated in the micelle is not electroactive in the absence of added electrolyte. Earlier studies of others, given in this paper,[24] have similarly found that a species incorporated in a micelle could become electroinactive. In the case described here, when $Os(bpy)_3^{2+}$ penetrates the micellar surface, it associates strongly with the hydrocarbon core via hydrophobic interactions. This $Os(bpy)_3^{2+}$ would not be electroactive, since the micelle would prevent it from coming within electron transfer distance to the electrode and small anions would not be available to maintain electroneutrality. These micelle-bound $Os(bpy)_3^{2+}$ species would make no contribution to the anodic current. As found here, increasing the NaCl concentration increases the electroactivity of the micelle-bound $Os(bpy)_3^{2+}$, presumably because of a greater availability of anions to

balance the positive charge formed during the electrode reaction and maintain electroneutrality.

The decrease in i_{pa} in the presence of CTAB, as well as the effect of NaCl concentration on i_{pa}, is much smaller than for SDS. This suggests a much weaker interaction, perhaps because of the electrostatic repulsion between CTAB and $Os(bpy)_3^{2+}$, with the bulk of the current observed in the presence of CTAB originating from $Os(bpy)_3^{2+}$ present in solution. By similar arguments, the interaction of $Os(bpy)_3^{2+}$ and Triton X-100 is even weaker or absent.

In the present experiment, ECL was generated by the following mechanism:[19]

$$Os(bpy)_3^{2+}{}_{(W\text{ or }M)} \longrightarrow Os(bpy)_3^{3+}{}_{(W\text{ or }M)} + e^-, \quad (2)$$

$$Os(bpy)_3^{3+}{}_{(W\text{ or }M)} + C_2O_4^{2-} \longrightarrow CO_2^{-} + CO_2 + Os(bpy)_3^{2+}{}_{(W\text{ or }M)}, \quad (3)$$

$$CO_2^{-} + Os(bpy)_3^{3+}{}_{(W\text{ or }M)} \longrightarrow CO_2 + Os(bpy)_3^{2+*}{}_{(W\text{ or }M)}, \quad (4)$$

$$Os(bpy)_3^{2+*}{}_{(W\text{ or }M)} \longrightarrow Os(bpy)_3^{2+}{}_{(W\text{ or }M)} + h\nu, \quad (5)$$

where the subscripts W and M represent the aqueous and micellar phases, respectively. If we assume the luminescence yields of $Os(bpy)_3^{2+*}$ in the water and micellar phases are the same, there are two main factors affecting the ECL intensities: the amount of $Os(bpy)_3^{2+}$ oxidized to $Os(bpy)_3^{3+}$ and the nature of the environment of the reaction of CO_2^- with $Os(bpy)_3^{3+}$ to generate $Os(bpy)_3^{2+*}$. In aqueous solution in the absence of surfactant and in Triton X-100 micellar solution, the NaCl concentration strongly affected the observed ECL intensity (Fig. 7). While we have not investigated the mechanism of this decrease in intensity with NaCl concentration, it probably involves perturbation of the reaction of CO_2^- with $Os(bpy)_3^{3+}$ [or $Os(bpy)_3^{2+}$]. The ECL intensity of $Os(bpy)_3^{2+*}$ emission in an acetonitrile solution produced by generation of the +1 and +3 species, increases 2.5 times with an increase in tetrabutylammonium hexafluorophosphate from 50 mM to 200 mM. In SDS micellar solution the ECL intensity was lower than that in the other media. As discussed above, the amount of $Os(bpy)_3^{3+}$ generated, i.e., the oxidation current, is decreased in the presence of SDS. This leads to a strong decrease in the ECL intensity. The oxidation current was larger at higher NaCl concentrations, and in addition, the reaction of CO_2^- with $Os(bpy)_3^{3+}$ may take place in an environment that is less strongly perturbed by increases in ionic strength. This can account for the increase in ECL intensity as the NaCl concentration increased. The addition of CTAB decreased the intensity of ECL in 50 mM NaCl. In this case this decreased with added NaCl. The rate of decrease with increasing NaCl was not as high in the presence of CTAB as in aqueous NaCl solutions alone (Fig. 7), so that at NaCl concentrations above 200 mM, the ECL intensity in the presence of CTAB was larger than in its absence.

The luminescence spectra also indicate an interaction of $Os(bpy)_3^{2+}$ and SDS; the spectra strongly depend upon the SDS concentration. At the pre-cmc concentration level, the luminescence spectrum shows a peak wavelength at 710 nm, which is blue-shifted with respect to that at 730 nm in an aqueous solution without SDS. We ascribe this spectrum to an $Os(bpy)_3^{2+}$–SDS aggregate. When the SDS concentration was increased above the cmc, the spectrum showed a red shift with the peak wavelength at 765 nm. This apparently indicates a different type of interaction of $Os(bpy)_3^{2+}$ with SDS micelles than in premicellar aggregates. While the luminescence spectrum has only one peak at 730 nm in aqueous solution, there is additional shoulder at 767 nm in a hexane solution of $Os(bpy)_3^{2+}$. Thus the observed emission peak in SDS micelles at 765 nm can probably be attributed to a hydrophobic interaction.

Conclusion

Electrochemical techniques and ECL were used to study the interactions of the surfactants SDS, CTAB, and Triton X-100 with $Os(bpy)_3^{2+}$ at different concentrations of electrolyte. The $Os(bpy)_3^{2+}$ interacted most strongly with SDS, and at concentrations of SDS above the cmc and in the absence of added electrolyte (NaCl), both the electrochemical response and ECL (in the presence of oxalate) were suppressed. Addition of NaCl caused increases in both anodic current and ECL emission, although the levels remained below those under similar conditions in the absence of SDS. The interaction of $Os(bpy)_3^{2+}$ with CTAB was much weaker, while that with Triton X-100 was almost absent.

The support of this research by the Army Research Office is gratefully acknowledged.

References

1) a) Y. Ohsawa, Y. Shimazaki, and S. Aoyagui, *J. Electroanal. Chem.*, **114**, 235 (1980); b) Y. Ohsawa and S. Aoyagui, *J. Electroanal. Chem.*, **136**, 353 (1982); c) P. Yeh and T. Kuwana, *J. Electroanal. Chem.*, **123**, 1334 (1976).

2) G. Meyer, L. Nadjo, and J. M. Savéant, *J. Electroanal. Chem.*, **119**, 417 (1981).

3) G. L. McIntire, D. M. Chiappardi, R. L. Casselberry, and H. N. Blount, *J. Phys. Chem.*, **86**, 2632 (1982).

4) I. V. Berezin, K. Martinek, and A. K. Yatsimirskii, *Russ. Chem. Rev. (Engl. Transl.)*, **42**, 787 (1973).

5) J. H. Fendler and E. J. Fendler, "Catalysis in Micellar and Macromolecular Systems," Academic Press, New York (1975).

6) F. H. Quina, M. J. Politi, J. M. Cuccoria, E. Baumgarten, S. M. Martins-Franchetti, and H. Chairmorich, *J. Phys. Chem.*, **84**, 361 (1980).

7) J. C. Eriksson and G. Gillberg, *Acta Chem. Scand.*, **20**, 2019 (1966).

8) C. A. Bunton, L. S. Romsted, and G. Savelli, *J. Am. Chem. Soc.*, **101**, 1253 (1979).
9) N. Funasuki and S. Hada, *J. Phys. Chem.*, **84**, 736 (1980).
10) D. Ege, W. G. Becker, and A. J.Bard, *Anal. Chem.*, **56**, 2413 (1984).
11) E. M. Kober, B. P. Sulliran, W. J. Dressick, J. V. Caspar, and T. J. Meyer, *J. Am. Chem. Soc.*, **102**, 7383 (1980).
12) H. D. Abruna, *J. Electroanal. Chem.*, **175**, 321 (1984).
13) J. G. Gaudiello, P. G. Bradley, K. A. Norton, W. H. Woodruff, and A. J. Bard, *Inorg. Chem.*, **23**, 3 (1984).
14) J. W. Park and H. L. Nam, *Bull. Korean Chem. Soc.*, **5**, 182 (1984).
15) A. E. Kaifer and A. J. Bard, *J. Phys. Chem.*, **89**, 4876 (1985).
16) M. Stackelberg, M. Pilgram, and V. Toome, *Z. Elektrochem.*, **57**, 342 (1953).
17) K. Granath, *Acta Chem. Scand.*, **7**, 297 (1953).
18) G. G. Warr, F. Griser, and D. F. Evans, *J. Chem. Soc., Faraday Trans. 1*, **82**, 1829 (1986).
19) a) M. M. Chang, T. Saji, and A. J. Bard, *J. Am. Chem. Soc.*, **99**, 5399 (1977); b) I. Rubinstein and A. J. Bard, *J. Am. Chem. Soc.*, **103**, 512 (1981).
20) N. E. Schore and N. J. Turro, *J. Am. Chem. Soc.*, **96**, 306 (1974).
21) G. L. McIntire and H. N. Blount, *J. Am. Chem. Soc.*, **101**, 7720 (1979).
22) C. R. Martin, I. Rubinstein, and A. J. Bard, *J. Am. Chem. Soc.*, **194**, 4817 (1982).
23) G. G. Warr and F. Griser, *J. Chem. Soc., Faraday Trans. 1*, **82**, 1813 (1986).
24) K. Hoshino, K. Suga, and T. Saji, *Chem. Lett.*, **1986**, 979.

 © 1988 The Chemical Society of Japan Bull. Chem. Soc. Jpn., 61, 25—27 (1988)

Invited Paper

Heat Capacity of CH_3D Adsorbed on Graphite at Monolayer Coverages between 0.3 and 7 K

Akira INABA[†,*] and (the late) James Alexander MORRISON[††]
Department of Chemistry, McMaster University, Hamilton, Ontario L8S 4M1, Canada
(Received August 28, 1987)

Heat capacity measurements have been made on CH_3D adsorbed on exfoliated graphite (Grafoil MAT) over the temperature range $0.3<T<7$ K at two surface coverages near a monolayer, to evaluate predictions of the energy states of the adsorbed molecules, based on earlier studies of the properties of bulk solid CH_3D and other isotopic methanes. Two Schottky-type anomalies are observed with maxima at 2 and 0.1 K; these are consistent with the predictions in a general way.

The heat capacities of bulk solid isotopic methanes have been studied over the years with the fundamental object of understanding molecular energy states—especially those associated with hindered rotational motion of the molecules in the solids. In addition to the original publications, several reviews of the studies are available in papers devoted to the discussion of molecular orientational ordering and related matters. For example, Bloom and Morrison published one such review[1] in 1973. More recently, Yamamoto et al. produced a summary of the theoretical and experimental investigation of solid methane[2] in terms of a specific quantum mechanical model, developed from a classical study.[3] The model is particularly valuable in showing how complicated and difficult the methane "problem" is from both the experimental and theoretical points of view. The methane system shows all of the features of the better-known example of the hydrogen/deuterium system[1] but with more solid phases and phase transitions and a greater number of nuclear spin symmetry species. Finally, a pertinent book on single particle rotations in molecular crystals should be mentioned.[4]

It is obvious that no one technique—either experimental or theoretical—will provide sufficient information to describe orientational motion in solids fully. In the case of the rotational energy of molecules, the characteristic temperature for rotation is generally low, e.g. $\theta_{rot}<87.5$ K for solid methane. (This can be worked out easily from data in Table 1 of Ref. 1.) Thus, contributions which rotational (orientational) motions make to thermodynamic properties and to the magnitude or separation of energy states depend upon θ_{rot}/T. In practical terms, this means that to exploit measured properties, such as heat capacities, to learn about quantum states of molecular solids, we need to make measurements at low temperatures, typically in the region $T<20$ K. Full details can be found in Refs. 1 and 2.

The so-called Schottky anomaly[5] has long been used to deduce information about arrays of energy levels from measured heat capacities and has been widely exploited for this purpose for the solid isotopic methanes.[6] The resulting energies have often been compared and correlated with estimates obtained from measurements of inelastic neutron scattering. In one extensive study[7] of the sequence of molecules, CH_4, CH_3D, CH_2D_2, CHD_3, and CD_4, expected results were obtained for CH_4 and CD_4 but not for the partially deuterated compounds in one of the solid phases, — viz. in phase III. It is the lowest temperature phase that exists under the equilibrium vapour pressure and is thought to have at least three different site symmetries,[8] but that is still not established in fact.[9] The investigation of the discrepancy brought out the following important conclusion which is contained in a direct quotation from Ref. 7.

> "The importance of the partial deuteration is that it defines a molecular axis. Thus, when the molecules interact with sites of lower symmetry, a distinction can be made between orientational levels, where the splitting stems from the change of the molecular axis relative to the site symmetry axes, and tunneling levels, where the splitting arises from overlap between equivalent molecular orientations. It turns out that the neutron scattering and thermodynamic experiments sample the manifolds of energy states in different ways. This is exploited through a model to yield a picture of orientational and tunneling states that is broadly consistent with experimental observation for all of the deuterated methanes including CD_4."

In other words, the combination of heat capacity and neutron scattering data for the solid methanes significantly refined our understanding of orientational and tunneling behaviour in them over what was obtainable from one type of data alone.

The work was extended by Maki in a theoretical study[10] of the much more anisotropic example of a monolayer of CH_3D adsorbed on the surface of a graphite crystallite. Information became available from neutron scattering measurements[11,12] to characterize vibrational/librational/orientational motion of

---

[†] Permanent address: Department of Chemistry, Faculty of Science, Osaka University, Toyonaka, Osaka 560, Japan.

[††] Professor J. A. Morrison passed away on October 20, 1987. This became his last paper. (Editor)

the CH_3D molecules in this system. With that and his model for the bulk solid methanes, Maki was able to calculate the low temperature heat capacity to be expected for CH_3D on graphite.[10] He made a challenge to experimentalists to test his calculations and the present short paper is about a response to that challenge. The agreement between theory and experiment that is found is remarkably good and very satisfying.

For now, we are content to show that the Maki predictions are borne out by experiment. It will be possible in later publications to report the results of more detailed comparisons. There is also information contained in our measurements about conversion between nuclear spin symmetry species of CH_3D but we shall not deal with it here. The dynamics and mechanism of that process are still not known for certain.[13]

Experimental

The calorimeter assembly was installed in a rebuilt Mark V helium dilution refrigerator[14] (Oxford Instruments Ltd.). The calorimeter vessel was constructed of copper and contained graphite adsorbent in it. It carried a small specially designed needle valve[15] through which the gas to be adsorbed could be filled or emptied quantitatively. The germanium thermometer used had been calibrated by the supplier between 0.05 and 8 K based on the T-76[16] from 0.5 to 8 K and on the CMN magnetic scale below 0.5 K.

An exfoliated graphite called Grafoil MAT from Union Carbide was used after purification and outgassing as the adsorbent for the present measurements. It has a specific surface of 24 $m^2 g^{-1}$ and a bulk density of 0.3 g cm^{-3}.[17] The preparation and analyses of CH_3D of high isotopic purity by gas chromatography have been fully described.[18] The amount of the gas put into the calorimeter vessel was measured volumetrically with uncertainty of about ±0.2%.

One of the main experimental difficulties usually encountered in the heat capacity measurements for such adsorbed system or for small particles is long equilibrium time caused by poor thermal contact between adsorbent/sample and the calorimeter vessel. However, rather unexpectedly, it was found that our calorimeter system could be operated very satisfactorily as experienced many years ago in the heat capacity measurement of small particles of MgO.[19]

The heat capacity of two sub-monolayer samples with 3.014 and 2.590 mmol of the actual amount of CH_3D gas was measured between 0.3 and 7 K. The former corresponds to a coverage of 0.94 monolayer, which slightly exceeds a capacity of the commensurate ($\sqrt{3}\times\sqrt{3}$) structure, and the latter corresponds to a coverage of 0.81 monolayer. The contribution of the monolayer CH_3D to the total heat capacity including the calorimeter vessel was at least 7% at 7 K and amounted up to 95% at 0.3 K.

Results and Discussion

The after-drifts of all of the heat capacity measurements were fitted to an exponential time

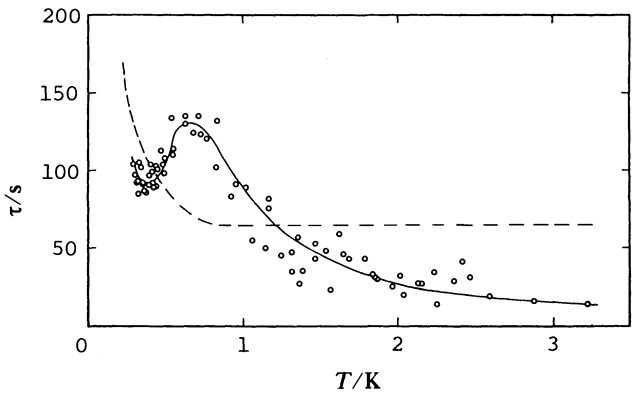

Fig. 1. Relaxation times for thermal equilibration as a function of temperature. ——, the present results for CH_3D/graphite; ------, for the bulk CH_3D.[21]

dependence in order to derive characteristic relaxation times that are plotted as a function of temperature in Fig. 1. About 3 K, they approached those obtained for the calorimeter vessel with graphite alone. The results for the two sets of measurements were indistinguishable and they had a structure with a maximum around 0.7 K, which is different from the behaviour of the bulk CH_3D as investigated by nuclear magnetic resonance[13] as well as by thermal measurements.[20,21]

Two sets of heat capacity measurements at different coverages are essentially indistinguishable from each other below 3 K. The shape of the Schottky anomalies observed is totally different from that of the bulk CH_3D.[20,21] The heat capacity has a broad maximum around 2 K and probably another one at 0.1 K. It means that the manifold of low-lying energy levels in CH_3D on graphite must be considerably different from that known for the bulk CH_3D.[7]

Complete understanding of the shape of the heat capacity curve would require to work out the energy levels of CH_3D molecules on the surface of graphite. Neutron scattering experiments which are being undertaken will certainly provide useful information toward that end, but the present experimental results alone are sufficient to give an insight into the structure of the energy level manifold. Fuller analysis of the heat capacities together with the experimental details will be reported elsewhere when the neutron scattering results have been rationalized.

The research was supported by a grant from the Natural Sciences and Engineering Research Council of Canada and, in part, by a Grant-in-Aid for Scientific Research administered by the Ministry of Education, Science and Culture of Japan. We are grateful to Dr. M. B. Dowell of the Union Carbide Corporation for the preparation of the Grafoil MAT. We thank Mr. W. Scott for supplying liquid helium efficiently. We also thank Dr. R. K. Thomas and Dr. K. Maki for stimulating discussions and helpful

correspondence. One of us (A.I.) would like to thank Professor H. Chihara and Professor M. L. Klein for their continuing advice and encouragement. The other (J.A.M.) wishes to express his long admiration for the high quality of the scientific contributions of Professor Tsunenobu Yamamoto of Kyoto University to our understanding of the methane "problem".

References

1) M. Bloom and J. A. Morrison, "Surface and Defect Properties of Solids," The Chemical Society, London (1973), Vol. 2, p. 140.

2) T. Yamamoto, Y. Kataoka, and K. Okada, *J. Chem. Phys.*, **66**, 2701 (1977).

3) H. M. James and T. A. Keenan, *J. Chem. Phys.*, **31**, 12 (1959).

4) W. Press, "Springer Tracts of Modern Physics," Springer, Berlin (1981), Vol. 92.

5) See for example R. H. Fowler and E. A. Guggenheim, "Statistical Thermodynamics," Cambridge University Press, New York (1949).

6) See Ref. 2. A number of references to details is contained in the reference list of Ref. 7.

7) K. J. Lushington, K. Maki, J. A. Morrison, A. Heidemann, and W. Press, *J. Chem. Phys.*, **75**, 4010 (1981).

8) K. Maki, Y. Kataoka, and T. Yamamoto, *J. Chem. Phys.*, **70**, 655 (1979).

9) W. Press, University of Kiel, private communication (1987).

10) K. Maki, *J. Chem. Phys.*, **74**, 2049 (1981).

11) G. Bomchil, A. Hüller, T. Rayment, S. J. Roser, M. V. Smalley, R. K. Thomas, and J. W. White, *Philos. Trans. R. Soc. London, Ser. B*, **290**, 537 (1980).

12) M. W. Newberry, T. Rayment, M. V. Smalley, R. K. Thomas, and J. W. White, *Chem. Phys. Lett.*, **59**, 461 (1978).

13) J. Higinbotham, B. M. Wood, and R. F. Code, *Can. J. Phys.*, **57**, 1752 (1979).

14) A. Inaba and J. A. Morrison, *J. Phys. Soc. Jpn.*, **54**, 3815 (1985).

15) J. A. Morrison and P. R. Norton, *J. Chem. Phys.*, **56**, 1457 (1972).

16) The 1976 Provisional 0.5 to 30 K Temperature Scale, *Metrologia*, **15**, 65 (1979).

17) A. Inaba, Y. Koga, and J. A. Morrison, *J. Chem. Soc., Faraday Trans. 2*, **82**, 1635 (1986).

18) P. R. Norton, *J. Chromatog. Sci.*, **8**, 411 (1970).

19) W. H. Lien and N. E. Phillips, *J. Chem. Phys.*, **29**, 1415 (1958).

20) J. H. Colwell, *J. Chem. Phys.*, **51**, 3820 (1969).

21) K. J. Lushington and J. A. Morrison, *J. Chem. Phys.*, **69**, 4214 (1978).

 © 1988 The Chemical Society of Japan Bull. Chem. Soc. Jpn., 61, 29—38 (1988)

Invited Paper

Chemical Reaction Dynamics—The Study of Molecular Reactivity and Disequilibrium

Rephael David LEVINE

The Fritz Haber Research Center for Molecular Dynamics, The Hebrew University, Jerusalem 91904, Israel

(Received September 16, 1987)

Recent progress in molecular reaction dynamics is discussed with special reference to the selectivity in the reactivity and the specificity in product formation. Topics considered in some detail include dynamical aspects of stereochemistry, rotational state distributions in reactive collisions and intramolecular dynamics of larger molecules. The conceptual foundations of the thermodynamic-like approach to molecular disequilibrium are considered.

1. Introduction

On the molecular level, a chemical reaction occurs when atoms or groups of atoms rearrange themselves so as to result in a new configuration. The process can be intramolecular as in a unimolecular isomerization in the gas phase. It can be intermolecular as in a bimolecular reaction. It can involve several species as in a reaction in a liquid which may require some reorganization of the solvent molecules or as in a reaction catalysed by some surface site. Chemical reaction dynamics[1-15] seeks to understand the motions which occur during the chemical reaction. It asks what are the primary factors which govern these motions. When some understanding has been achieved it seeks to apply the new concepts. The question then becomes which factors are under our experimental control and how can we best manipulate these factors so as to influence the outcome of the chemical reaction on the molecular level.

It is the study of reactions on the elementary level of the isolated chemical act which makes dynamics distinct from its older sister, chemical kinetics. An example will perhaps best serve to illustrate the point. Chemical kinetics studies reactions under bulk conditions. In general, we find that increasing the temperature of the reagents will often increase the reaction rate. This general observation is also correct for example for the reaction

$$H_2 + OH \rightarrow H_2O + H$$

which is of importance in combustion.[16,17] The very concept of 'the temperature of the reagents' is a macroscopic one valid under special bulk conditions when the rate of the chemical reactions is slow as compared to the rate of inelastic energy transfer, collisions. One can then assume that the rapid inelastic collisions maintain the system in a state of thermal (but not chemical) equilibrium. For rapid chemical reactions and particularly so for very exothermic reactions, one typically needs to add to the mixture an excess of buffer gas whose role is to rapidly dissipate any deviations from equilibrium. In a real combustion process, the reagents will often be in marked deviation from thermal equilibrium. We are then faced with the need for dynamics for the following reason. As long as the reagents are in thermal equilibrium there is only one way of changing their energy and that is by heating the system. Temperature is the only relevant factor. Increasing the temperature leads to an increase in the energy content of each degree of freedom of the reagents. At higher temperatures we have the classical 'equipartition' result that each degree of freedom has an energy of $(1/2)RT$ where R is the gas constant ($\simeq$2 cal deg^{-1} mol^{-1}). At low temperatures, the energy content of the vibrational degrees of freedom will be somewhat below the classical value but can be readily computed, if need be, from equilibrium statistical mechanics. The key point is that for chemical kinetics, temperature is the only relevant operational variable for governing the distribution of the reagents over their different energy states (which are electronic, vibrational, rotational, and translational). One cannot selectively increase, say, the vibrational energy content of the reagents. Thermal heating is a democratic process where every degree of freedom receives on equal footing.

Once we need to deal with reagents not in thermal equilibrium, the required understanding changes in an essential way. One will now have to consider different ways in which the energy of the reagents can be changed. Putting a given amount of energy into the relative motion of the reagents (so that they collide with a higher relative velocity) need not change the rate of the reaction to the same extent as putting the same amount of energy in the vibrational excitation. Indeed, there are two modes of vibrational motion, that of H_2 and that of OH. We now know that vibrational excitation of H_2 is much more conducive to reaction than that of OH[18] and we have an interpretation of that selectivity based on the nature of the forces that operate during the collision.[19] One can consider many other types of selectivity. Even for our simple example, recall that OH is a radical with a lone electron in a p orbital. This orbital can be

aligned in space. Equally, OH as a rotating diatomic molecule has a plane of rotation. The p orbital can lie within that plane (a, so called, Π^- state) or be perpendicular to it (a Π^+ state). Are the two states equally reactive? My guess is that the Π^+ state is much more reactive. Much more so than the slight energy difference between the two states (Π^- is lower in energy) would suggest. As far as I know, there is not yet a definite answer but I am fairly certain about my intuitive guess. Yet another selectivity concerns the angle of approach. What is the optimal orientation for the molecular axes of H_2 and OH for reaction to take place. Here too, chemical intuition would lead one to expect that not all orientations are equally reactive and such stereoselectivity[10] can again be related to the nature of the forces during the reactive collision,[20] Fig. 1.

Chemical reaction dynamics is concerned not only with reagents in selected states. Equally of interest is the probing of the state of the products. Of course, this need be done immediately after the reactive collision prior to any secondary collisions. Otherwise the subsequent collisions will rapidly equilibrate the products. In chemical kinetics we characterize the reaction as, say, exothermic. In chemical dynamics we need to know in which modes of motion the excess energy will be found in the receeding products of the reaction. Historically, it was often experimentally easier to probe the products than to select the reagents. Hence much of our initial evidence came from product's analysis.[4] It should however be stressed that the two are obverse to one another. This can be best seen by considering microscopic reversibility as in the following analogy: Imagine a movie showing the motion of the atoms during the collision of the reagents. Repeat the movie many times by using reagents in different energy states. Sometimes, the collision will end up in a reaction having taken place. Other times, the reagents will separate, the collision being nonreactive. Say most of the reactive collisions originated from vibrationally excited reagents. Now run all those movies backwards. Those reactive collisions are now seen to preferentially produce vibrationally excited products. (Recall that for a reactive collision, the roles of reagents and products is reversed when the movie is run in the opposite direction in time). Hence, if the reaction of $OH+H_2$ proceeds preferentially from vibrationally excited H_2 molecules, the reverse reaction, that of $H+H_2O$ will preferentially produce vibrationally excited H_2 products.

It is important to bear in mind that dynamics studies not only scalar quantities such as energy but also vectors such as momenta. Indeed, one of the earliest questions asked in molecular reaction dynamics is what is the disposal of the momentum of the

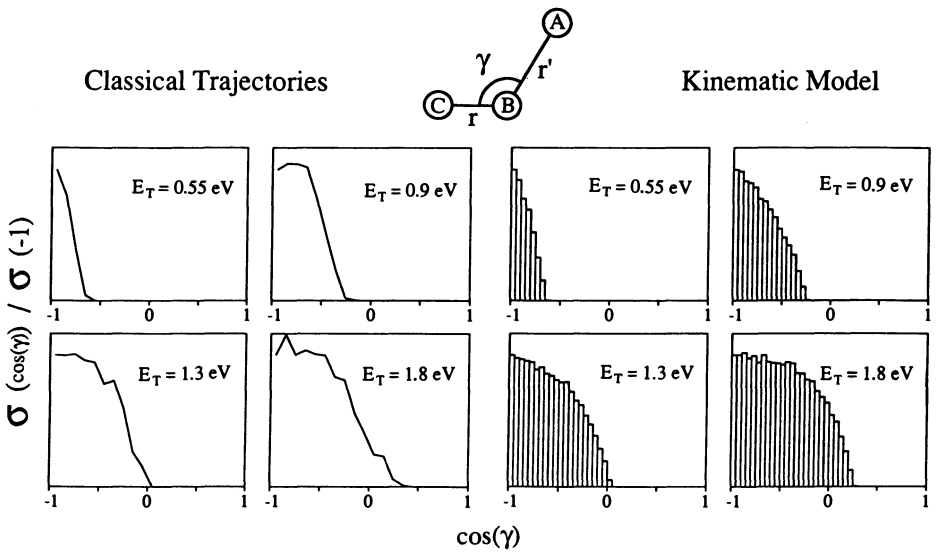

Fig. 1. An example of stereoselectivity. The reactivity in the $D+H_2 \rightarrow DH+H$ elementary reaction as a function of the angle of approach γ of the D atom to the axis of the H_2 molecule (see insert). Left panels: The reactivity computed using the method of classical trajectories[1] at a number of collision energies. Note how the 'cone of acceptance' for reaction opens up at higher collision energies. [For further details, see I. Schechter and R. D. Levine, *Int. J. Chem. Kinet.*, **18**, 1023 (1986)]. Right panels: The reactivity computed using a simple model where reaction takes place if the reactants can cross the barrier for reaction at the angle γ. [For further details, see I. Schechter, M. Prisant and R. D. Levine, *J. Phys. Chem.*, (1987)]. The success of the model shows that the cone of acceptance is governed primarily by the dependence of the height of the barrier to reaction on the angle of approach.

products. In particular, what is the direction of this momentum. To examine the question in detail we need to bear in mind that the motion of the systems' center of mass is unchanged during a chemical process in the gas phase. Hence it is the relative motion that we are really concerned with. So the issue is whether the (relative) momentum is distributed isotropically in space (suggesting that the collision has no memory of any preferred direction as would be the case for a long living collision complex), or not. One of the early indications of nonrandom dynamics was the observation that for many elementary reactions, the angular distribution of the products was strongly anisotropic indicating a very direct, brief process. It was indeed awhile before clear-cut examples of longer-duration reaction processes were discovered.[21] Nor is the study of products' angular distribution usful only for pure gas phase processes. Consider, for example, a beam of molecules incident on a surface at a given angle is the scattering mostly specular, with the angle of scattering about equal to the angle of incidence or is there a wide distribution in scattering angles? The latter is evidence for a trapping-desorption process where the scattered molecules spend some time at the surface prior to their 'evaporation' from the surface.

The study of the orientation dependence of

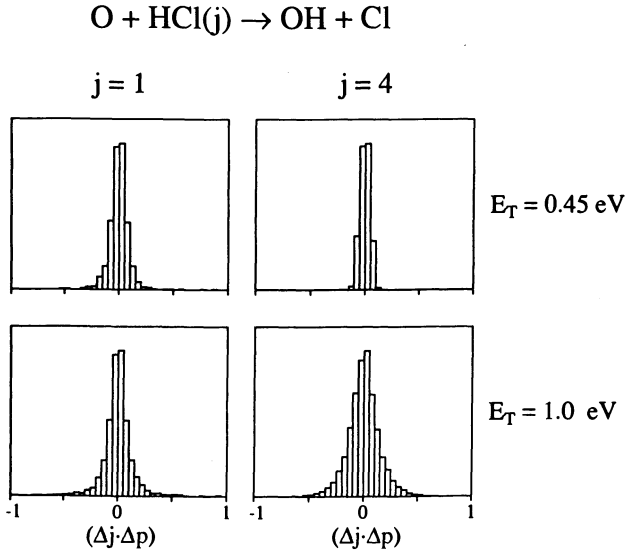

Fig. 2. Angular momentum correlations in the O+HCl→OH+Cl reaction. $\Delta\mathbf{j}$ is the change in the rotational angular momentum (j of OH minus j of HCl). $\Delta\mathbf{p}$ is the change in the linear momentum (momentum of the Cl-OH motion minus momentum of the O-HCl motion). The plot is vs. the scalar product of the unit vectors $\Delta\hat{\mathbf{j}}=\Delta\mathbf{j}/|\Delta j|$ and $\Delta\hat{\mathbf{p}}=\Delta\mathbf{p}/|\Delta p|$. The figure shows that for most collisions that result in reaction $\Delta\mathbf{j}$ is perpendicular to $\Delta\mathbf{p}$. This need *not* be the case in general and can be shown due to the lighter mass of the exchanged H atom. (I. Schechter and R. D. Levine, to be published).

chemical reactivity[10] also belongs to vector dynamics. More recently, the correlation amongst different vectors is also receiving much attention,[22,23] Fig. 2.

Experiments will typically select the reagents before the collision and/or probe the products after the collision. Theory is needed to bridge between these two ends. In their infancy are new experiments which use spectroscopic techniques to monitor the very process of the reactive collision.[24] Here, however, the need for theory is even more acute.

A generation ago, when I began work, the number of theorists actively interested in the field was so small that I could summarize everything I knew in one volume.[25] Less than ten years later two volumes were needed[26] and four volumes were required for a 1985 survey of the theory.[9] It is therefore no longer possible to overview the wide range of theoretical activity in the field. Instead, I have chosen to very briefly discuss one particular approach with which I have been closely associated.

2. The Distribution of Final States

Figure 3 shows the fraction of the total energy, E, carried by a CH_3 group as kinetic energy when an energy rich $Cd(CH_3)_2$ molecule dissociates.[27] The balance of the energy is in the other Cd–CH_3 bond and we have a distribution because a given total energy E can be partitioned in many different ways between the two bonds. Seemingly, the distribution is very asymmetic with the CH_3 group departing preferentially with either very little or with most of the available energy. Yet the theoretical analysis[27] suggested that

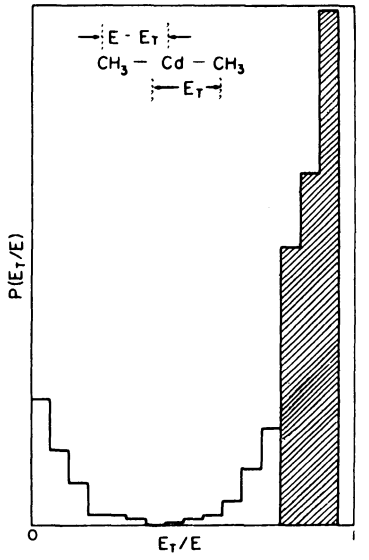

Fig. 3. The distribution of kinetic (E_T) and internal ($E-E_T$, see insert) energies in the dissociation of energy rich $Cd(CH_3)_2$.[27] The shaded region are those dissociating molecules where enough energy is taken by the dissociating CH_3 that $CdCH_3$ is stable.

this is *not* an example of specific energy disposal. Rather, this is what one should expect in the absence of specific effects. A uniform distribution, say, would have been much more surprising. It is not the shape of the distribution *per se* which one takes as evidence of specificity. What then is a disequilibrium distribution?

To answer this question we consider the complementary one: What is an equilibrium (or equipartition) distribution? The answer has been known in thermodynamics for a long time. At a given total energy, equilibrium is when all final quantum states are equally probable. It will take too much time to show that for the system of Fig. 3, the equilibrium distribution in kinetic energy E_T is [27]

$$P(E_T|E) \propto [E_T(E-E_T)]^{-1/2}, \tag{1}$$

which is indeed highly asymmetric. Instead, we consider a simpler case, say the products of the 'simplest' chemical exchange reaction

$$H + H_2 \rightarrow H_2(v=0,j) + H.$$

Here v and j are the vibrational and rotational quantum numbers of the product H_2 molecule. If the total energy is not too high only H_2 molecules in the ground vibrational state (i.e., $v=0$) can be formed. Of course, if reaction readily takes place then there need be enough energy to overcome the barrier along the reaction path.[28] In the products this energy is distributed between the rotation of H_2 about its center and the kinetic energy E_T of the motion of the H atom and the H_2 molecule. If we had to deal only with the H_2 molecule, the computation would be real simple: When H_2 is in the j'th rotational state it corresponds to $2j+1$ distinct quantum states. These correspond to the $2j+1$ distinct orientations in space of the angular momentum vector **j**. Another way of saying this is that a single rotational quantum state of a diatomic molecule is specified by two quantum numbers j and m_j and m_j can take up all integer values from $-j$ to $+j$ inclusive, i.e., $2j+1$ distinct values. When H_2 is in the rotational state j it has a rotational energy, E_j, which at lower j's is given by

$$E_j = Bj(j+1), \tag{2}$$

where B is the rotational constant. The energy which is then available for translation is $E_T=E-E_j$. The higher is the rotational energy of H_2, the less kinetic energy is available for the (relative) motion of H and H_2. Now the translational motion is also quantized. Just as for rotation, the larger the momentum **p**, the more quantum states are accessible. Since however the translational energy is, for all practical purposes, continuously varying, one typically speaks not of the number of such states but of their density, $\rho(E_T)$. It is defined so that there are $\rho(E_T)\delta E_T$ quantum states when the translational energy is confined to the short interval from E_T to $E_T+\delta E_T$. One shows that[1]

$$\rho(E_T) = A_T(E_T)^{1/2}, \tag{3}$$

where A_T depends on the mass. For the H+H_2 reaction we thus have that the density of final quantum states at the total energy E is

$$\begin{aligned}\rho(j,E) &= (2j+1)\rho(E_T) \\ &= A_T(2j+1)(E-E_j)^{1/2}\end{aligned} \tag{4}$$

At low j values, the dominant variation of $\rho(j,E)$ with j is the linear increase with j. As j increases, E_j increases even faster, (cf. (2)) and sooner or later E_j becomes a large fraction of E (Of course, $E_j \leq E$). When that happens, the square root term in (4) becomes rapidly variable and $\rho(j,E)$ decrease and becomes zero at $E_j=E$.

When the reaction is non-specific in its energy disposal we expect that the fraction $P^o(j)$ of H_2 product molecules in the state $(v=0,j)$ be proportional to $\rho(j,E)$

$$P^o(j) = (2j+1)(E-E_j)^{1/2}/\sum_j (2j+1)(E-E_j)^{1/2} \tag{5}$$

The denominator in (5) is simply there to insure normalization, i.e., that H_2 be found in some final j state

$$\sum_j P^o(j) = 1. \tag{6}$$

In both (5) and (6), the value of j is restricted by the

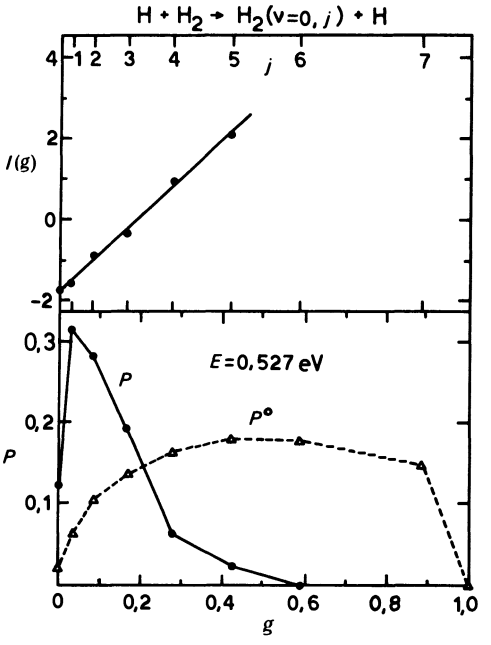

Fig. 4. Specificity of energy disposal. Bottom panel: Quantum mechanical computations (dots, from Ref. 29) and prior distribution (triangles, from Eq. 5) for the product H_2 rotational states vs. the reduced variable $g=E_j/E$. The two are quite different showing that lower rotational states are specifically populated by the reaction. Upper panel: The rotational surprisal, Eq. 7 vs. g. The line corresponds to $\theta_R=8$.

conservation of energy in a single collision, i.e., $E_j \leq E$.

How well does our equilibrium result (5) agree with the observed (or computed[29-32]) results? Not very well. Higher j values, as seen in Fig. 4 are far less probable than their fraction as given by (5). The reaction clearly selectively populates the final rotational states.

One can readily provide also an essentially quantitative characterization of the deviance from equilibrium. As in thermodynamics proper, a system can fail to reach complete equilibrium if it is subject to constraints. A simple example is compressed gas in a cylinder which is constrained from expansion by a piston which is firmly in place. If we free the piston, the gas will expand until its pressure equals the external pressure. A constraint can maintain a system in disequilibrium. This state of disequilibrium is really very simple to characterize: but for the constraint, the system is in equilibrium.

We find that precisely the same holds for disequilibrium in single collisions. The one difference is that the constraint(s), if any, is due to the preparation of the initial state and to the dynamics. The unexpected finding is that the dynamics gives rise to rather simple constraints. To see this, we shall return to the example of the $H+H_2$ reaction, and many others, in section 4.

As in thermodynamics proper we shall characterize the fraction of molecules in any given state by the chemical potential. This means that we regard the H_2 molecules in different quantum states as different and distinct chemical species. This give rise to no essential problem for it is known that a distinct chemical species is any molecule that can be distinguished from others and there are numerous spectroscopic and other methods whereby H_2 molecules in different rotational states can be sorted out. Even the $2j+1$ degenerate m_j states can be distinguished (e.g., by a Stern-Gerlach type experiment). Finally, the different orientations of the momentum $\mathbf{p}$ of the relative motion of H and H_2 can be studied by measuring the angular distribution of the products. Indeed, even in conventional, macroscopic thermodynamics it is sometimes useful to regard molecules in different states as distinct species.[33] Here however we are concerned with the nascent products of a single collision. We discuss the thermodynamics of a single collision in section 3 returning to our main theme in section 4. The reader willing to accept thermodynamic concepts can proceed directly to section 4.

3. Thermodynamics of Collision Processes

A single collision is a system of very finite number of degrees of freedom. Not only finite but often quite small (e.g., six for the three atom H_3 system, including the rotation). There is therefore a question of principle: Are we allowed to use thermodynamics for such a system? Is thermodynamics not a theory or systems of very many degrees of freedom? We have devoted considerable attention[33-38] to this question. Our starting point was information theory,[39] Thereby we have been able to extend the usual machinery of thermodynamics to small dynamical systems. Finally, we have been able to show[37,38] that exact quantum dynamics can be formulated as a thermodynamical theory. We shall return to this point in section 5 below.

The thermodynamical approach to dynamics that we have pioneered enables us to provide a dynamical justification to the procedures discussed section 4. One can wonder however, why do textbooks emphasize the 'large size' of thermodynamics systems. To clarify this point we need to discuss two conceps from probability theory. Since this is a point that many people are concerned about we would like to clarify it in some detail. We do this since the ideas are simple and the source of the confusion is semantic, that is the failure to properly distinguish between two, strictly distinct, concepts.

In the application of thermodynamics to finite, isolated systems it is essential to properly distinguish between the probability of an event (which is what is provided by the theory) and the frequency of an event (which is what is measured in an experiment). As an example we examine the most familiar example, that of tossing a coin. Take an honest coin. We assign a probability of 1/2 to each face. Let us call the two faces A and B. Now let us do an experiment-one tossing of the coin. Say the results is that face A is up. In our experiment the frequency of 'event A' is one and the frequency of 'event B' is zero. The frequency and the probability are quite distinct and both are well defined. Now consider another experiment: The coin is tossed twice. A possible outcome is that the coin fell 'face A up' in the first toss and 'face B up' in the second toss. In this experiment the frequency of 'event A' is 1/2 and so is the frequency of 'event B.' In this experiment the *numerical value* of the frequencies and the probabilities is the same. *However, an equally likely* outcome in our experiment is that the coin fell 'face A up' in both tosses. Then the numerical values of the frequencies and the probabilities would be quite different. Let us now toss the coin three times. A moment's reflection shows that whatever the outcome is, there is just no way for the *observed* frequency in such an experiment to be numerically equal to the *theoretical* probability. Indeed, it rapidly emerges that for any experiment where the coin is tossed an *odd* number of times, the frequency cannot equal the probability! The coin is but the simplest example. Take an honest die with six distinct but equivalent faces. The probability of each face coming up is 1/6. Unless we roll the die $6n$, n integer, times we will *never*

observe frequencies equal to the probabilities. Even if we do roll the die $6n$ times, there is no guarantee that all six faces will show up with exactly equal frequencies. In the great majority of all possible experiments with a die, the experimental frequency is not exactly equal to the probability.

Frequency and probability are thus two, quite distinct, concept which differ not only in their definition but also in their possible numerical values. What then gives rise to the confusion? The blame is on the law of large numbers. This theorem, very loosely stated, says that upon very many repetitions of an experiment, the observed frequencies will have numerical values very close to the theoretical probabilities. Hence the pragmatic result that the numerical value of the probability of an event can be determined as its frequency observed in a very large number of independent repetitions of the experiment. It must clearly however be understood that what the law of large numbers provides is a practical route to the assignment of a numerical value to the probability.

The purpose of the theory is to predict and explain observed results. What the law of large numbers tells us is that for the purpose of comparing observed frequencies with theoretical probabilities we require many repetitions. This is automatically insured if we carry an experiment on the distribution of H_2 rotational states on a macroscpic gaseous sample. Such a sample contains the order of Avogadro's number of molecules. We are thus assured that the observed frequency will be very close to the theoretical probability. The necessary conditions for the validity of the law of large numbers can also however be insured if the experiment is on the H_2 rotational state distribution after a single, isolated $H+H_2$ reactive collision. All that is necessary is that one observes many reactive collisions, each one isolated from the others. The experimenter knows this very well for if too few collisions are observed, the signal will not rise above the noise. The theorist is equally aware of this point on the pragmatic level. An instructive illustration is provided by the very common method — that of the study of the dynamics using classical trajectories.[40] Each one classical trajectory has a definite outcome. To simulate the inherent quantal uncertainty in the initial conditions and the resulting distribution of final states one needs to compute 'many' classical trajectories. How do we know how many is 'many'—by increasing the number of trajectories until the frequencies of the final states settles down to within the desired tolerance.

As a side comment we note the following implication. The method of classical trajectories is very extensively applied. However, as our experiments are reaching for higher and higher resolution we need to run more and more classical trajectories to achieve the corresponding computational resolution. We are already at a level where so many trajectories need be computed that fully quantal methods will soon become computationally more feasible!

4. Surprisal Analysis

As in thermodynamics, we characterize the observed distribution of products in terms of its deviance from a reference. Since we are typically dealing with collisions at a given value of the total energy, the typical reference is that of all final quantum states being equally probable. As discussed in section 2, one seldom fully resolves the final quantum states. Hence one needs to count the number of final states that correspond to the event of interest. For the $H+H_2 \rightarrow H_2(v=0,j)+H$ reaction we have performed the count in section 2 leading to Eq. (5) for $P^o(j)$, the reference or *prior* distribution of H_2 rotational states. We denote by $P(j)$ the actual, observed distribution. The corresponding thermodynamical potential known in this context as the *surprisal* is defined by

$$I_j = -\ln[P(j)/P^o(j)], \tag{7}$$

or

$$I_j = \ln[P^o(j)] - \ln[P(j)]. \tag{8}$$

Figure 4 shows a plot of I_j vs. the rotational energy of the H_2 molecule for a quantum mechanical computation of $P(j)$.[29–31] As is very clear, I_j is linearly dependent on E_j

$$I_j = \theta_o + \theta_R(E_j/E). \tag{9}$$

θ_o and θ_R are two constants, but θ_o is a function of θ_R as can be seen by combining (8) and (9)

$$P(j) = P^o(j) \exp(-\theta_o - \theta_R(E_j/E)). \tag{10}$$

Here $P^o(j)$ is given by (5) and since

$$\Sigma_j P(j) = 1, \tag{11}$$

it follows from (10) that θ_o can be computed from θ_R

$$\exp(\theta_o) = \sum_j P^0(j) \exp(-\theta_R(E_j/E)). \tag{12}$$

Hence the distribution of rotational states is fully characterized by the value of one (intensive) parameter, θ_R.

As in ordinary thermodynamics, one can use either θ_R or the corresponding (extensive) parameter, the mean value, $\langle E_j \rangle$,

$$\langle E_j \rangle = \sum_j E_j P(j), \tag{13}$$

of the rotational energy of the H_2 molecules. Since at a given total energy E, we have $E_j \leq E$, it is advantageous to work with the dimensionless reduced parameter $g \equiv E_j/E$ which spans the range from zero to

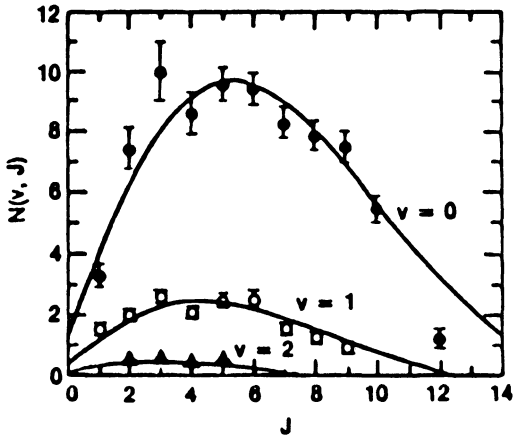

Fig. 5. The observed (points with error bars, from Ref. 41) HD vibrotational populations in the $H+D_2$ reaction using hot H atoms and the fit (curves) to the data using the functional forms (10) and (18) with a prior distribution given by (15). Note that the population scale is linear.

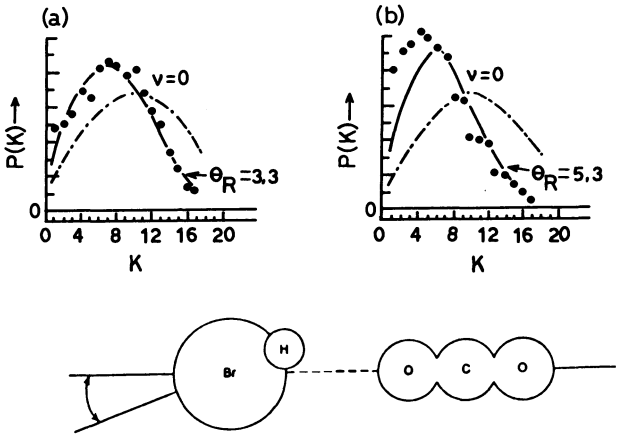

Fig. 6. The OH(v=0) rotational state distribution from the $H+CO_2 \rightarrow HO+CO$ reaction: (a) For a random approach; (b) For a geometry limited approach. Points are experimental data from Ref. 44. The line is Eq. 10 and the dashed line is the prior distribution. K is the OH rotational quantum number. The insert shows the principle of the geometry limited experiment. The $CO_2 \cdot HBr$ van der Waals adduct is photolyzed to yield hot H atoms. The angle of the HBr axis with respect to the CO_2 axis is largely confined to within the range indicated by a (weak, van der Waals) bending potential. Upon photolysis of HBr the H atom approaches CO_2 preferentially collinearly.

one. From (13) and (12) we see that there is a one-to-one relation between $\langle E_j\rangle/E$ and θ_R,

$$\langle (E_j/E)\rangle = \sum_j (E_j/E)P^o(j)\exp(-\theta_R(E_j/E))/\sum_j P^o(j)\exp(-\theta_R(E_j/E)). \quad (14)$$

If $\theta_R>0$ the population of the higher rotational states is below that expected on prior grounds and the value of $\langle E_j\rangle/E$ computed from (14) is below the value computed for $\theta_R=0$ which is the prior limit. If $\theta_R<0$, the higher rotational states are preferentially populated.

This distribution (10) provides an accurate fit for both quantal and classical computations[29-32] of product H_2 rotational distributions. More recently[41,42] using hot (i.e., fast) H atoms generated by laser-pulse photolysis of HBr, it was possible to experimentally resolve the H_2 product rotational states, Fig. 5. It is interesting to comment on the technique used to insure that the nascent products of a single collision are detected. This was achieved by using a second probe laser which is fired after the photolysis laser within a time short compared to the time between collisions. This second laser detects the H_2 products. The prior distribution used in Fig. 5 is not (5) but rather

$$P^o(j,v) \propto (2j+1)(E-E_v-E_j)^{1/2}. \quad (15)$$

The reason is that the hot H atoms carry sufficient energy for the H_2 products to be formed in excited vibrational states. When the H_2 molecule is in the vibrational state v,v=0,1$\cdots$ with an energy E_v, the energy released as kinetic energy is not $E-E_j$ but rather $E-E_v-E_j$. Hence (cf. (4)) is the change between (5) and (15). Otherwise, a single value of θ_R suffices to reproduce the experimental distribution.†

It is only recently that using laser probing, reliable nascent products' rotational distribution became available. Such results have been extensively analyzed using (10). A particularly interesting case, shown in Fig. 6 is the

$$H + CO_2 \rightarrow CO + OH(v,j)$$

reaction. This has been studied both for H atoms approaching CO_2 from all possible directions[43] and for H atoms confined to approach with a cone along the (linear) CO_2 axis. The geometry-limited initial state is achieved[44] by photolyzing the HBr bond in the van der Waals adduct[1] $BrH \cdot CO_2$ formed via a supersonic expansion of an HBr/CO_2 mixture. As can be seen in Fig. 6, both initial states give rise to an OH final rotational distribution which is well described by (10). The value of θ_R is higher for the geometry-limited initial state indicating a stronger preference for rotationally unexcited OH molecules.

Highly exoergic reactions can populate several products vibrational states. Much of the earlier work (reviewed in Ref. 45) in surprisal analysis examined these vibrational distributions which are more readily

† Note that since now $E_j \leq E-E_v$, the reduced variable in (10) is not (E_j/E) but $E_j/(E-E_v)$.

available from experiment. The prior distribution of vibrational states $P^o(v)$ is obtained by summing over all final quantum states where the vibrational state is v. From (15)

$$P^o(v) = \sum_j P^o(v,j) \propto \sum_j (2j+1)(E-E_v-E_j)^{1/2} \quad (16)$$

where summation is over all those rotational states allowed by conservation of energy, i.e., such that $E_j \leq E-E_v$. When the rotational constant B defined (in (2)) is very small compared to $E-E_v$ so that many terms contribute to the sum in (16) we can replace summation over j by an integration over E_j to get

$$P^o(v) \propto \int_0^{E-E_v} dE_j (E-E_v-E_j)^{1/2} \propto (E-E_v)^{3/2}. \quad (16')$$

The observed vibrational state distribution $P(v)$ defines the vibrational surprisal by

$$I_v = -\ln [P(v)/P^o(v)]. \quad (17)$$

Here too it is often the case that the surprisal is a linear function of the vibrational energy so that $P(v)$ can be well represented as

$$P(v) = P^o(v) \exp(-\lambda_0 - \lambda_v (E_v/E)). \quad (18)$$

A recent example, that of the

$$D_2 + F \rightarrow D + DF(v),$$

exoergic reaction at a well defined energy[46] is shown in Fig. 7. Here, as in many other reactions λ_v is negative showing a preferential disposal of the reaction exoergicity into the products vibration.

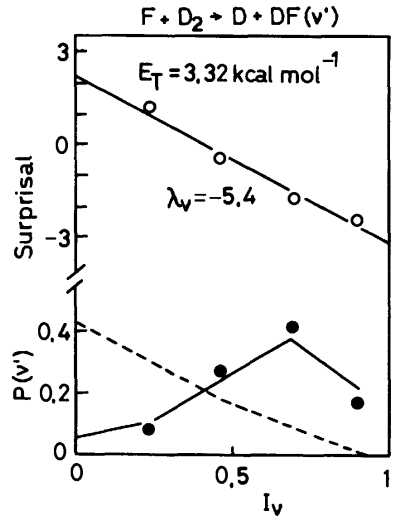

Fig. 7. Surprisal plot for the vibrational energy disposal in the F+D_2 reaction vs. $f_v \equiv E_v/E$. [Adapted from Y. M. Engel and R. D. Levine, *Chem. Phys. Lett.*, **123**, 42 (1986) using the experimental data (points) from Ref. 46]. The distribution (18) is shown as a solid line and the prior distribution (16) is the dashed line. $\lambda_v = -5.4$ as there is specific population of the higher vibrational states.

Microscopic reversibility, as discussed in section 1, can be used to show that the surprisal of the energy disposal equals the surprisal of the energy requirements in the reverse reaction.

Laser probing[7] of the states of molecules after a single collision has also provided much new information on inelastic, energy-transfer collisions. Typically, at energies in the chemical range such processes are constrained by the inefficient conversion of translational to internal energy.[47] Such an 'exponential gap'[1] behavior is illustrated in Fig. 8 for the

$$Xe + HgBr(v=52) \rightarrow Xe + HgBr(v')$$

process,[48] using thermal Xe atoms and HgBr in the $B^2\Sigma$ electronic state. The system 'resists' the change in the internal energy and the surprisal is linearly dependent on the magnitude of the 'gap' in vibrational energy $E_{v'}-E_v$ which is provided from the translation. Note that if $v'>v$, energy is taken out of the initial kinetic energy and the gap is positive, while if $v'<v$, energy is put into the final kinetic energy and the gap is negative. The surprisal which reflects the constraint on a change in energy is however a function of the absolute value of the gap, Fig. 8, and not on its sign.

We have centered attention on bimolecular, intermolecular processes. One can equally discuss intramolecular dynamics. Here we consider a particular aspect, that of optical excitation. When we excite the fundamental vibrational modes of a polyatomic molecule or the lower overtones, we have the limiting behavior familiar from spectroscopy. There are strong selection rules which limit the possible transitions and every spectral line can be assigned to a particular mode of excitation of the molecule. Newer experiments (e.g., Refs. 8 and 49) are preparing molecules with considerable excess energy.

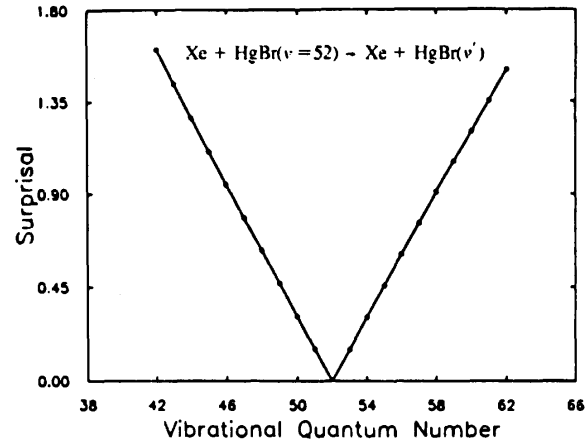

Fig. 8. Surprisal vs. the energy gap for the inelastic collision Xe+HgBr(v)→Xe+HgBr(v'). The surprisal is seen to be a function of the absolute value of the gap. From Ref. 48.

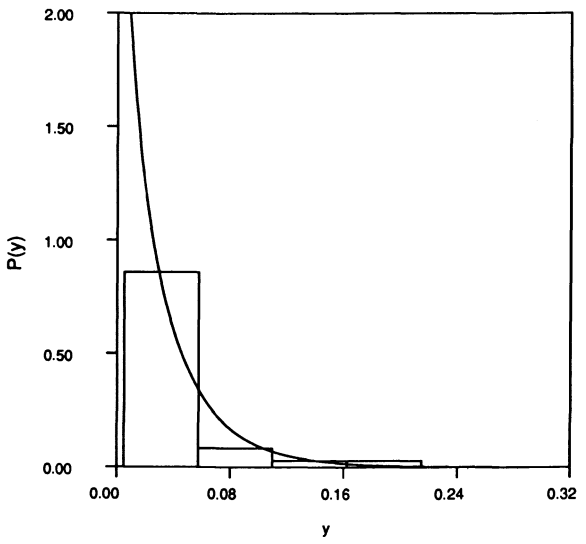

Fig. 9. The distribution of absorption intensities (data of Ref. 51) plottd as a histogram, for a fully resolved spectrum of pyrazine. The smooth curve is the corresponding prior distribution showing that the classical dynamics is chaotic.

There are numerous lines in the spectrum and it is by no means clear that the energy distribution in the optically excited molecule is very selective. It remains the case however that the intensity of lines in the spectrum gives the probabilities of the different transitions. Very recently[50] the thermodynamic approach has been applied to the distribution of intensities in optical spectra. Figure 9 shows the observed distribution[51] for pyrazine near the origin of the $^1Ag0_o^o \rightarrow {}^1B_{3u}$ transition. The coupling of the excited singlet $^1B_{3u}$ state to lower-lying triplet $^3B_{3u}$ states leads to vibrational energy redistribution, which, as shown by the analysis in Fig. 9 is totally non-selective (i.e., chaotic).

5. Thermodynamics

Surprisal analysis is used to quantitatively characterize the selectivity and specificity of chemical reactions and to identify the relevant variables. Can one however *predict* these variables and the parameters (e.g., θ_R, λ_v) directly from the forces that operate during the collision without computing the distributions first? It turns out[37,38] that this can be done if we center attention on the dynamics in phase space.[52,53] That is, we traceout the evolution of the distribution in phase space during the collision. The technical details will require too much space to be spelled out. The essential idea is that it proves possible to use the exponential forms as in (10) or (18) not only after the collision but also in the interaction region. The point of view we suggested earlier namely, that the state of a system is always one of equilibrium subject however to constraints is thereby shown to be equally valid for systems which evolve with time. It thus follows that thermodynamics is indeed also a theory of dynamics and not only of static equilibrium states.

References

1) R. D. Levine and R. B. Bernstein, "Molecular Reaction Dynamics and Chemical Reactivity," Oxford University Press, N. Y. (1987). Japanese translation by H. Inouye, Tokyo University Press. Many of the general references cited below have appeared since this book was prepared. Older references will be found in Ref. 1.

2) K. J. Laidler, "Chemical kinetics," 3rd ed, Harper & Row, New York (1987).

3) M. S. Child, *Sci. Prog., Oxf.*, **70**, 73 (1986).

4) J. C. Polanyi, *Science*, **236**, 680 (1987) and in Nobel Lectures 1986, Elsevier, Amsterdam (1987).

5) D. R. Herschbach in Nobel Lectures 1986, Elsevier, Amsterdam (1987).

6) Y. T. Lee in Nobel Lectures 1986, Elsevier, Amsterdam (1987).

7) S. R. Leone, *Science*, **227**, 889 (1985).

8) W. D. Lawrence, C. B. Moore, and H. Petek, *Science*, **227**, 895 (1985).

9) "Theory of Chemical Reaction Dynamics," ed by M. Baer, CRC Press, Florida (1985).

10) R. B. Bernstein, D. R. Herschbach, and R. D. Levine, *J. Phys. Chem.*, **91**, 5365 (1987).

11) Faraday Discussion 84: Dynamics of Elementary Gas Phase Reactions.

12) Faraday Discussion 82: Dynamics of Molecular Photofragmentation.

13) "Molecular Photodissociation Dynamics," ed by J. E. Baggolt and M. N. R. Ashfold, Royal Society of Chemistry, London (1987).

14) "The Evolution of Size Effects in Chemical Dynamics," ed by J. Jortner, R. D. Levine, and S. A. Rice, Wiley, New York (1987).

15) Chemical Dynamics: *Chem. Rev.*, **87**, 1—288 (1987).

16) G. P. Glass and B. K. Chaturvedi, *J. Chem. Phys.*, **75**, 2749 (1981).

17) R. Zellner and W. Steinert, *Chem. Phys. Lett.*, **81**, 568 (1981).

18) G. C. Schatz, *J. Chem. Phys.*, **74**, 113 (1981).

19) T. H. Dunning, Jr., E. Kraka, and R. A. Eades, in Ref. 11.

20) K. Fukui, "Theory of Orientation and Stereoselection," Springer Verlag, Berlin (1970).

21) W. B. Miller, S. A. Safron, and D. R. Herschbach, *Discuss. Faraday Soc.*, **44**, 108 (1967).

22) J. P. Simons, *J. Phys. Chem.*, **91**, 5378 (1987).

23) P. L. Houston, *J. Phys. Chem.*, **91**, 5388 (1987).

24) P. Hering, S. L. Cunha, and K. L. Kompa, *J. Phys. Chem.*, (1987); P. R. Brooks, R. F. Curl, S. Kaesdorf, and T. C. Maguire, in Ref. 11; D. Imre, J. L. Kinsey, A. Sinha, and J. Krenos, *J. Phys. Chem.*, **88**, 3956 (1984); P. D. Kleiber, A. M. Lygra, K. M. Sando, V. Zafiropolos, and W. C. Stwalley, *J. Chem. Phys.*, **85**, 5493 (1986); J. K. Ku, G. Inoue, and D. W. Setser, *J. Phys. Chem.*, **87**, 2989 (1983); H. J. Foth, J. C. Polanyi, and H. H. Telle, *J. Phys. Chem.*, **86**, 5027 (1982).

25) R. D. Levine, "Quantum Mechanics of Molecular Rate Processes," Clarendon Press, Oxford (1969).

26) "Dynamics of Molecular Collisions," ed by W. H. Miller, Plenum, New York (1976).
27) M. Tamir, U. Halavee, and R. D. Levine, *Chem. Phys. Lett.*, **25**, 38 (1974).
28) K. Fukui, *Acc. Chem. Res.*, **14**, 368 (1981).
29) R. E. Wyatt, *Chem. Phys. Lett.*, **34**, 167 (1975).
30) G. C. Schatz and A. Kuppermann, *J. Chem. Phys.*, **65**, 4668 (1976).
31) C. Lesech, R. K. Nesbet, and R. B. Walker, *Chem. Phys. Lett.*, **59**, 1 (1978); D. C. Clary and R. K. Nesbet, *J. Chem. Phys.*, **71**, 1101 (1978).
32) E. Zamir, R. D. Levine, and R. B. Bernstein, *Chem. Phys. Lett.*, **107**, 217 (1983).
33) R. D. Levine, *Chem. Phys. Lett.*, **39**, 205 (1976); W. C. Gardiner, Jr. and R. D. Levine, *J. Chem. Phys.*, **68**, 4524 (1978); R. D. Levine, Proc. 12th Intl. Symp. on Shock Tubes and Waves, Jerusalem 1979, ed by A. Lifshitz and J. Rom, Magness Press, Jerusalem (1980).
34) R. D. Levine and R. B. Bernstein, in Ref. 26.
35) R. D. Levine and A. Ben-Shaul, "Chemical and Biochemical Applications of Lasers," ed by C. B. Moore (1977), Vol. II, p. 145.
36) "The Maximum Entropy Formalism," ed by R. D. Levine and M. Tribus, MIT Press, Cambridge (1979).
37) R. D. Levine, *Adv. Chem. Phys.*, **47**, 239 (1981).
38) R. D. Levine, in Ref. 9.
39) A. Katz, "Principles of Statistical Mechanics," Freeman, San Francisco (1967).
40) D. G. Truhlar and J. T. Muckerman, "Atom-Molecule Collision Theory," ed by R. B. Bernstein, Plenum, New York (1979).
41) D. P. Gerrity and J. J. Valentini, *J. Chem. Phys.*, **81**, 1298 (1984); **82**, 1323 (1985).
42) E. E. Marrinero, C. T. Rettner, and R. N. Zare, *J. Chem. Phys.*, **80**, 4142 (1984).
43) J. Wolfrum, *J. Phys. Chem.*, **89**, 2525 (1985).
44) S. Buelow, M. Noble, G. Radhakrishnan, H. Reisler, C. Wittig, and G. Hancok, *J. Phys. Chem.*, **90**, 1015 (1986).
45) R. D. Levine, *Ann. Rev. Phys. Chem.*, **29**, 59 (1978).
46) D. M. Neumark, A. M. Wodtke, G. N. Robinson, C. C. Hayden, K. Shobatake, R. K. Sparks, T. P. Schafer, and Y. T. Lee, *J. Chem. Phys.*, **82**, 3067 (1985).
47) K. Takayanagi, *Prog. Theor. Phys. Supp.*, **25**, 1 (1963).
48) N. H. Cheung, T. A. Cool, and A. C. Eerlandson, *J. Chem. Phys.*, **86**, 6203 (1987).
49) C. E. Hamilton, J. L. Kinsey, and R. W. Field, *Ann. Rev. Phys. Chem.*, **37**, 493 (1986).
50) R. D. Levine, *Adv. Chem. Phys.*, **70**, 53 (1987).
51) I. W. M. van Herpen, W. L. Meerts, K. E. Drabe, and J. Kommandeur, *J. Chem. Phys.*, **86**, 4396 (1987).
52) Y. Alhassid and R. D. Levine, *Phys. Rev. C*, **20**, 1775 (1979).
53) K. Takatsuka and H. Nakamura, *J. Chem. Phys.*, **82**, 2573 (1985).

 © 1988 The Chemical Society of Japan Bull. Chem. Soc. Jpn., 61, 39—45 (1988)

Invited Paper

Role of the Interface in Solvent Extraction Processes

Henry FREISER
Strategic Metals Recovery Research Facility, Department of Chemistry,
University of Arizona, Tucson, AZ 85721, U.S.A.
(Received July 20, 1987)

This paper reviews 25 years' investigation of kinetics of metal chelate extraction systems under high speed stirring conditions. Values of chelate formation rate constants for both analytical and hydrometallurgical extractants derived from such measurements using the assumption that the rate-determining step(s) occur in bulk aqueous phase, have been shown to be in reasonable agreement with expectations. Nevertheless, the introduction of the microporous Teflon phase separator in extraction kinetics resulted in clear evidence of reaction pathways involving the interface, as well as the bulk aqueous phase, even for simple chelating extractants.

For the first twenty years of our research into the kinetics and mechanisms of reactions of metal chelate formation and dissociation using solvent extraction techniques,[1] we did not believe that the liquid–liquid (L–L) interface played any significant role. At first, frankly, we simply did not give the matter too much thought. Using high speed stirring, which we believed would eliminate the need to consider mass transfer steps as rate determining, our results led us to conclude that the rate-determining step (rds) was the formation of an intermediate (usually a 1:1) metal chelate complex in the bulk aqueous phase.[2] This conclusion was greatly reinforced by the generally good agreement between the rate constants we calculated for such reactions with those in the literature obtained by a variety of experimental approaches. Since its introduction in 1962, Zangen[3] has successfully employed this technique for the kinetics of formation of Hg(II) complexes, Haraguchi et al. for the study of various Ni(II) complexes,[4,5] and it has also been utilized with kinetic studies of two organic chemical reactions, ester hydrolysis[6] and carbonium ion reactions.[7] While the technique we developed is uniquely useful for systems involving highly insoluble metal chelates, it was especially gratifying to note that it gave results that were in good agreement with those obtained by stopped-flow and other methods in at least two systems, Ni(II)–1,10-phenanthroline[8] and Ni(II)–8-quinolinol.[4]

The introduction of higher molecular weight chelating extractants for large scale, hydrometallurgical metal recoveries in the nineteen sixties and the subsequent study of some of the fundamentals of the behavior of these interesting reagents, served to focus attention on the interesting questions about the role of the interface in such extraction systems. For this reason, we conducted a detailed study of the kinetics of extraction of Cu(II) with aromatic (e.g. LIX 65N) and aliphatic (e.g. LIX 63) hydroxy oximes which were introduced in the 1960s by General Mills for the large scale extraction of copper.[9]

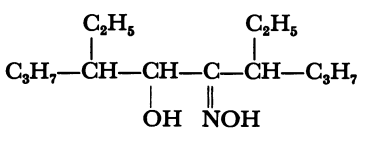

4,7-Diethyl-6-hydroxy-5-decanone oxime
LIX 63

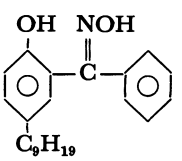

2-Hydroxy-5-nonylbenzophenone oxime
LIX 65N

Previous workers, pointing to the low aqueous solubility of the LIX reagents, intuitively discarded the possibility of chelate formation in the aqueous phase and proposed that interfacial reaction kinetics, rather than homogeneous chemically controlled rates, are dominant.[10–12] Thus, in a review of the kinetics and mechanisms of Cu(II) extraction by LIX reagents, Flett[13] asserted that because these reagents are "so hydrophobic", their aqueous phase solubility could be totally ignored! Having taken this view, when chemical parameters appeared in the extraction rate expressions, these investigators had no choice but to invoke an "interfacial reaction" as the rate-determining step.

A key aspect of the extraction mechanism controversy lies in the nature of the experimental configuration used by various investigators. Under conditions of vigorous shaking[14,15] or high speed stirring,[16,17] mass transfer rates in metal chelate solvent extraction processes are much higher than chemical reaction rates. It is axiomatic that, in any multistep process, the overall kinetics of the process gives information about the slowest, i.e., the rate-determining step. Our high speed stirring apparatus is based on the classical Morton flask assembly[18] and is capable of speeds up to 20000 rpm. Our apparatus[16] is always operated at a stirring speed beyond the level at which the extraction rate becomes independent of the stirring speed. The plateau is a consequence of the balance between dispersion and coalescence, i.e., where further stirring energy does not reduce drop size of the dispersed phase, but simply contributes to overall convective movement in the reaction flask. The data we obtain are highly reproducible and

almost always result in simple experimental rate expressions having very nearly integral reaction orders. Furthermore, the values of chelation rate constants derived from the data are generally in accord with those expected for the substitution rates of metal ions in aqueous media and, where available, in good agreement with published values from studies utilizing independent methods.

In contrast, most others interested in mass transfer kinetics in liquid–liquid distribution systems start by considering diffusion as the primary source of "resistance" and then include slow chemical reaction kinetics as added "resistances", usually without attempting to account quantitatively for the reaction rate constants. These workers tend to favor experiments in which the interfacial area is well known but relatively small. Fixed interfacial area designs[19–24] are rooted in the assumption that the reaction is either diffusion or interfacially controlled. Inasmuch as rate constraints of such reactions must be expressed in terms of unit interfacial area, fixed-interface experiments permit this measurement to be made. Until recently, this has not been considered to be possible with high dispersion experiments because the interfacial contact area is unknown. Most fixed-interface experiments have been performed with either a series of single drops in a continuous phase or a Lewis cell. In the drop method, droplets of one phase are allowed to rise (or fall) through a column containing the second phase. This approach has been criticized for not overcoming diffusion effects in the droplet. The Lewis cell is designed so that both phases stand in contact with each other while each phase is stirred separately. Stirring supposedly overcomes diffusion problems by replenishing the interface with reactant from each bulk phase. Nevertheless, since the vigor of the stirring must be severely limited to avoid vortex formation, it is doubtful that diffusion effects totally eliminated.

We initiated our study of hydroxy oxime extractants with the LIX 65N-copper system. First, we determined the distribution equilibrium of LIX 65N between chloroform and water to be $10^{4.6\pm0.3}$,[17] which means that LIX 65N is significantly less hydrophobic than dithizone. The rate expression obtained from our kinetic data for the extraction of copper by LIX 65N can be quantitatively described by Eq. 1.

$$-\frac{d[Cu^{2+}]}{dt} = k'\frac{[Cu^{2+}][HL]_o^{2.0}}{[H^+]^{1.0}} \tag{1}$$

where HL represents LIX 65N.

From the observed kinetics, a reasonable mechanism for this system identifies the rds as the reaction of CuL^+ with HL (Eq. 4)

$$HL(o) \overset{K_{DR}}{\rightleftharpoons} HL \qquad \text{fast} \quad (2)$$

$$Cu^{2+} + HL \overset{\beta_1 K_a}{\rightleftharpoons} CuL^+ + H^+ \qquad \text{fast} \quad (3)$$

$$CuL^+ + HL \xrightarrow{k_1} CuL_2 + H^+ \qquad \text{slow} \quad (4)$$

$$CuL_2 \overset{K_{DC}}{\rightleftharpoons} CuL_2(o) \qquad \text{fast} \quad (5)$$

where K_{DR} and K_{DC} represent the distribution constants of ligand and chelate, K_a the acid dissociation constant of LIX 65N, and β_1 the equilibrium formation constant of CuL^+ from Cu^{2+} and L^-. The kinetic expression for the rds, Eq. 4, is

$$-\frac{d[Cu^{2+}]}{dt} = k_1[CuL^+][HL] \tag{6}$$

By substituting appropriately from Eqs. 2 and 3 into 6, one obtains Eq. 7, with which the observed dependence on metal ion, ligand, and pH are consistent.

$$-\frac{d[Cu^{2+}]}{dt} = \frac{k_1\beta_1 K_a[Cu^{2+}][HL]_o^2}{K_{DR}^2[H^+]} \tag{7}$$

The extraction of copper by LIX 65N is unusual in that the observed second-order dependence on ligand concentration contrasts sharply with the nearly universally observed first-order ligand dependencies.[25] This behavior is not unique, however, since for d^9 metal ions, the rate constants for the 1:1 and 1:2 complexes are not as different as they are for most other transition metal ions. Further, the observed reaction rate constant, k', is seen to be given in Eq. 8:

$$k' = k_1\beta_1 K_a/K_{DR}^2 \tag{8}$$

Together with the value of K_{DR} as $10^{4.6}$ and k' of 1.37, k_1 for LIX 65N is seen to be 2.2×10^7 M^{-1} s^{-1}, a value that is quite similar to rate constants for typical substitution reactions of Cu^{2+} (the corresponding rate constant for Cu and phenanthroline is only 3 times larger).[26]

Further proof of the mechanism described above was obtained by testing the validity of Eq. 8, using a series of organic solvents in parallel rate studies. Thus, Akiba and Freiser[27] found the observed rate of extraction of copper with LIX 65N, k', to vary by 3 orders of magnitude when seven organic solvents ranging from trichloromethane to heptane were used. The variation of log k' with log K_{DR} was linear and had a slope of -2, as required by Eq. 7. Similarly, in the case of the extraction kinetics of nickel with LIX 65N, which was found to be first order in ligand, the value of the slope of the log–log line of k' vs. K_{DR} is unity, in keeping with the mechanism having as the rate-determining step the formation of NiL^+ in the aqueous bulk phase.[27] The exact correspondence of variation of the observed rates to inverse first (with Ni) and second (with Cu) orders of the ligand distribution constants with the same set of solvents would seem to rule out any influence of interfacial effects in these systems.

Although all of our work to this point convinced us of the primary importance of the bulk aqueous phase

as the site of the rds, the chemical reaction of metal complex formation, this should not be taken to mean that an interfacial influence on extraction kinetics conducted under high-speed stirring conditions will **never** occur. Indeed, in collaboration with Watarai, we set about to search for systems in which just effects could occur by preparing and studying a series of symmetrically dialkylated dithizones, from methyl (HMeDz) to hexyl (HHxDz). An automated solvent extraction apparatus was developed,[28] of which a microporous teflon phase separator (MTPS) is a key element. With the MTPS, bulk organic phase is cleanly separated from a fine dispersion of the two phases in the flask, circulated through a spectrophotometric flow cell, and returned. It seemed appropriate to start with derivatives of dithizone, the extractant having the highest K_{DR} of all of the extractants studied to date. With use of the automated extraction apparatus, at high pH values, a drop in the alkylated dithizone concentration in chloroform was observed; this decrement increased with stirring speed up to a plateau region. The extent of the decrease in concentration varied with pH at stirring speeds in the plateau region in a manner parallel to the nonstirring experiment. The (stirring vs. nonstirring) difference in $pH_{1/2}$ values, $\Delta pH_{1/2}$, (pH at which 50% of the ligand remains in the organic phase) increased from 0.16, 0.66, 3.0, and 5.0 as the alkyl group varied from methyl to ethyl, butyl, and hexyl. No observable change was obtained with dithizone itself.

Interfacial tension (γ_i) measurements were carried out with aqueous phases at two pH values, 3.5 and 12.0, and the following organic phases: HDz in $CHCl_3$, HBuDz in CCl_4, and HBuDz in $CHCl_3$. In the acidic systems, there was no change in γ_i value that could be attributed to the presence of the solute. In the alkaline systems, however, a decrease in γ_i was observed which became linear with an increase of the logarithm of the solute concentration. The slopes of these curves were used to estimate the surface area occupied by one solute molecule, a_m, by means of one form of the Gibbs adsorption isotherm

$$a_m = -kT/(\delta\gamma_i/\delta \ln C)_T \qquad (9)$$

where K is the Boltzmann constant and C is the concentration of solute. The estimated values for a_m (Å^2 molecule^{-1}) were 90 for HDz in $CHCl_3$, 70 for HBuDz in CCl_4, and 150 for HBuDz in $CHCl_3$. The minimum solute concentration required for interfacial saturation, C_m, can also be estimated; the values for $\log C_m$ were -2.2 for HDz in $CHCl_3$, -3.7 for HBuDz in CCl_4, and -2.8 for HBuDz in $CHCl_3$. As might be expected, the greater effect is observed in the poorer solvent. The decrease in interfacial tension under alkaline but not acid conditions suggests that it is the reagent anion rather than the nonionized reagent that is surface active.

The reversible concentration change in organic phase, which was caused by stirring, suggests a significant participation of the liquid–liquid interface in the equilibrium. The interfacial component is less than 3% for dithizone and then rises rather rapidly from 26% in HMeDz to 82% in HEtDz, to 99.9% in HBuDz, and to all but 7×10^{-4}% in HHxDz. These changes are indicative of the dramatic change in the heterogeneous acid–base equilibrium constant (up to a factor of 10^5) that occurs because the anionic alkyldithizonate (but not the neutral ligand) is surface active and is adsorbed into the interfacial region.[29]

The extraction kinetics of nickel and zinc with the alkyldithizonates[29] closely resembled those with dithizone and its analogues studied earlier,[30] in that the rate was first order each in metal and ligand and inverse first order in hydrogen ion. If one were to assume that the mechanism remained the same, however, i.e., that the rds is the formation of the 1:1 complex from metal and ligand anion in the aqueous phase, the resulting second-order reaction rate constants increase with the size of alkyl group until, with the hexyldithizone, the values for both Ni and Zn would exceed the diffusion-limited rate constant for bimolecular reaction!

This unrealistic conclusion is avoided by accounting for the adsorption of the ligand anion in the interface, which is the probable locus for the formation of the 1:1 complex. Calculating the correct value of the ligand anion concentration in the interface from the observed differences in $pH_{1/2}$ values (vide supra) and assuming that since the metal ion is not surface active, its concentration in the interface is the same as it is in the bulk aqueous phase, we obtained values for rate constants that were eminently reasonable, i.e., essentially constant values for all the alkylated dithizones. Log k_1 for Ni and Zn are 5.13 and 8.80, respectively. These are consistent with those obtained from these metals in a broad cross section of ligand-substitution reactions. Essentially the entire cause of the unusual kinetic behavior, as well as of the unusual extraction equilibrium behavior, is the excess concentration of the ligand anion in the interfacial region, which is greatly enlarged by high-speed stirring.

From interfacial tension measurements, together with the use of MTPS, we were now able to interpret the variation of rates of extraction with stirring speed. We wished particularly to understand why, when the ligand anion was adsorbed into the interface, the rates reached maximum values at stirring speeds above 5000—6000 rpm. Combining the interfacial tension measurement of a particular system with the decrements in absorbance, ΔA, observed under stirring conditions, yields the expression:[31]

$$\Gamma a_i = \frac{\Delta A}{\varepsilon} V_o \left(1 + \frac{1}{K_D}\right) \sim \frac{\Delta A}{\varepsilon} V_o \qquad (10)$$

in which Γ is the surface excess in mol cm^{-2} (calculated using Eq. 9 with R instead of k), a_i the interfacial area, ΔA the absorbance decrement obtained with stirring, ε and K_D the molar absorbance and distribution constant of the extractant, and V_o the volume of the organic phase. Since every other parameter in Eq. 10 is experimentally determined, this now serves to evaluate, a_i, the interfacial area. Figure 1 summarizes the results of a study of the variation of interfacial area (recalculated as average drop size) with stirring speed for aqueous–$CHCl_3$ systems containing the extractant bis(*p*-butylphenyl)thiocarbazone (HBuDz), seen previously to function as an anionic surfactant, a neutral surfactant, either Triton X-45 (TX-45) or Triton X-100 (TX-100), or a cationic surfactant *N*-cetylpyridinium chloride (CPC).

As seen in Fig. 1, the average drop size (d) decreases with increasing stirring rate (ω), reaching a minimum at rates of about 80—100 rps, reflecting a balance between breakup and coalescence. It is interesting to note that while the minimum average drop size observed for the butyldithizone and the two Triton X systems was about the same, namely 210±10 μm, that for CPC, a more active surfactant, a measurably smaller average drop size, 160 μm, was achieved.

An interesting question arises about the fate of the adsorbed species when the droplets of organic phase pass through the MTPS. As the organic drops hit and penetrate the MTPS membrane, does the adsorbed species, in many cases relatively hydrophobic, accompany the organic phase, or is it desorbed and returned to be equilibrated with the two phase mixture in the flask? Our standard procedure cannot serve to decide this question because such a small fraction of the droplets of organic phase and their accompanying adsorbed material are removed at any point in time so that the fate of this adsorbate cannot be deduced from this experiment. If, instead of returning the separated organic phase to the reaction flask as before, the return stream goes to waste, however, the organic phase volume will be continuously reduced and the question can be resolved.

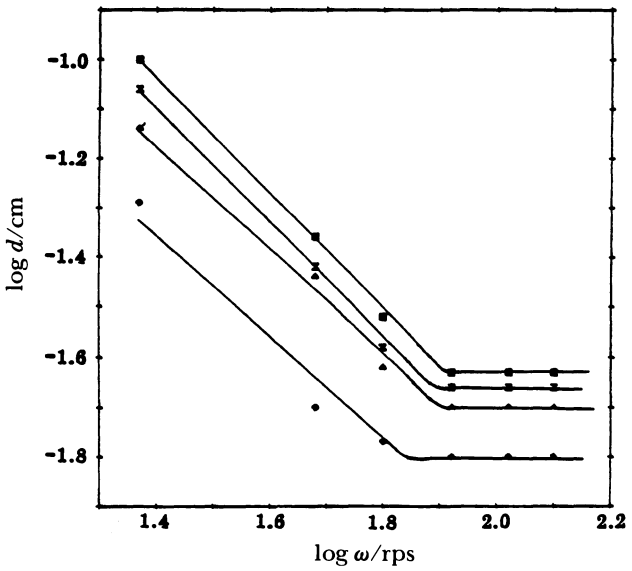

Fig. 1. Drop size as a function of stirring rate. (□) BuDz, (×) TX-100, (◆) TX-45 (▲) CPC.

If the first of the two possibilities described above occurs, the observed absorbance should remain constant throughout the experiment. Alternatively, if the adsorbed species were stripped from the interface and returned to the reaction flask as the total organic phase volume and total interfacial area decreased, the absorbance should rise during the course of the experiment.

From such experiments conducted on three systems (LIX 65N in heptane–water, 7-dodecenyl-8-quinolinol [KELEX 100] in xylene–water, and 4,7-diphenyl-1,10-phenanthroline in $CHCl_3$–water) it was evident that the species adsorbed on the interface during the initial phase of the experiment, i.e., before any filtered organic phase is removed, is essentially all retained in the reaction flask.[32] This would be consistent with the positioning of the polar end of the adsorbed species in the aqueous side of the interface and the non-polar position in the organic side. As the phases separate on the MTPS, the adsorbed species are not retained in the aqueous interfacial region. This probably can be attributed to an energetically more unfavorable dehydration of the polar portion of the molecule than desolvation of the nonpolar portion required when the species leaves the organic interfacial region.

Armed with this technique, enabling us to measure and control reliably the interfacial area, we are now in the process of studying the effect of the interface on the overall extraction kinetics in a variety of chelate extraction systems. To begin with, we selected the system, Ni(II)–7-(5,5,7,7-tetramethyl-1-octen-3-yl)-8-quinolinol (KELEX 100) (B)[33] and NI(II)–8-quinolinol (A), because previous studies[34,35] have demonstrated that nickel extraction by 8-quinolinol (oxine) (A) occurs via two reaction pathways: (1) reaction between nickel and neutral oxine and (2) reaction of metal with ligand anion.

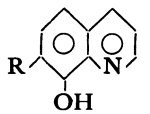

(A) R=H

(B) R=-CH(CH=CH$_2$)-CH$_2$-C(CH$_3$)$_2$-CH$_2$-C(CH$_3$)$_3$

In each case, it has been postulated in earlier studies that these rate-determining reactions occur in the bulk aqueous phase. Recent work in this laboratory[25,29] has revealed that, in cases where the ligand anion is a surface active species, the extraction may, at least partially, proceed through a reaction path involving

the interfacial region. Haraguchi and Freiser[36] have found that for KELEX 100 (B), the pH value is affected by high speed stirring, indicating that the distribution of the ligand anion is sensitive to changes in interfacial area. To help answer the question of whether the rate-determining steps for the extraction of nickel by oxine and its higher molecular weight analog, KELEX 100, are taking place in the bulk aqueous phase or in the interfacial region, this system has been studied with the MTPS apparatus.

The rates of extraction of nickel with oxine and KELEX 100 were found to be dependent on hydrogen ion concentration raised to a fractional power,[34,35] indicating two concurrent pathways whose rate determining steps involve either neutral and anionic forms of the ligand. These two paths had been previously presumed to occur strictly in the bulk aqueous phase. Finding that an increase in interfacial area can cause a drop in absorbance of the neutral reagent in the bulk organic phase under alkaline conditions, however, suggests that the ligand anion is surface active.[29] This leads to the possibility that the reaction of nickel with ligand anion may, at least in part, involve an interfacial reaction mechanism.

It was determined from the drop in absorbance of the species in the organic phase upon stirring, that at pH 11.3, the oxine anion exhibited an interfacial excess of 3×10^{-12} mol cm^{-2}, while for KELEX 100 the excess by 6×10^{-12} mol cm^{-2}, twice that of oxine. Even in the case of KELEX 100, the value of Γ is equivalent to each molecule occupying about 2800 Å^2 of interface, a value much larger than that expected for an interface saturated with a monolayer of the molecules. The rather small Γ values indicate that these species are only weakly surface active, yet even this leads to the kinetic effects observed.

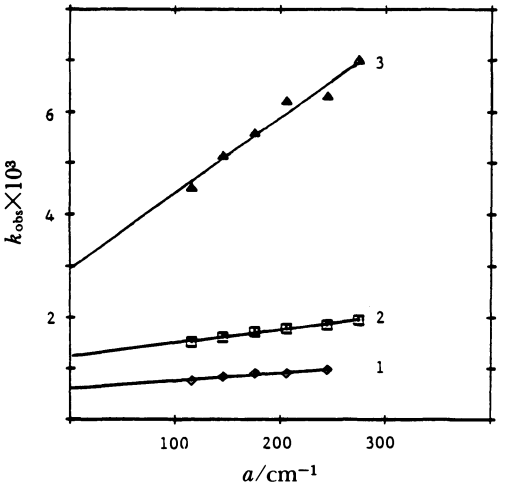

Fig. 2. Specific interfacial area dependency of nickel extraction by KELEX 100. (1) pH 7.27; (2) pH 7.7; (3) pH 8.45, Conditions: (KELEX)=1×10^{-2} M; ($NaClO_4$)=0.1 M; (Ni)=1×10^{-4} M.

In order to evaluate the role of the interface in the extraction kinetics of nickel with 8-quinolinols, the rates of reaction were measured as a function of specific interfacial area (interfacial area per unit volume of the organic phase). The results are illustrated in Fig. 2 for KELEX 100. The experiments were run over a range of pH values to see how the ratio of neutral to ligand anion would affect the balance between the two possible pathways (bulk and interfacial). The results, which indicate that the pH of extraction is very important in determining what combination of mechanisms is operative, can be rationalized by the reaction scheme illustrated in Fig. 3.

This scheme allows for three distinct concurrent reaction pathways: Path 1: Reaction between metal and neutral ligand in the bulk aqueous phase. Path 2: Reaction of metal with ligand anion in the bulk aqueous phase. Path 3: Reaction of metal and ligand anion in the interface.

Evidence in support of this reaction scheme is seen in Fig. 2. In the low pH range, the rate constants are relatively independent of specific interfacial area. In this range the neutral form of the ligand predominates, and its reaction with nickel ion occurs in the bulk (path 1). Inasmuch as the neutral ligand shows no observable surface activity lends support to the likelihood of a purely bulk phase reaction.

With increasing pH, increases in both slopes and intercepts is observed, indicating the dual anion mechanisms (paths 2 and 3). The significance of the increasing intercept is that, in the limit of zero interfacial area, the rate increases with pH, as required by a bulk phase reaction of the ligand anion.

The increase of the observed rate with interfacial area is heightened with increasing pH, demonstrating that the ligand anion participates in a rate-determining step at the interface (path 3).

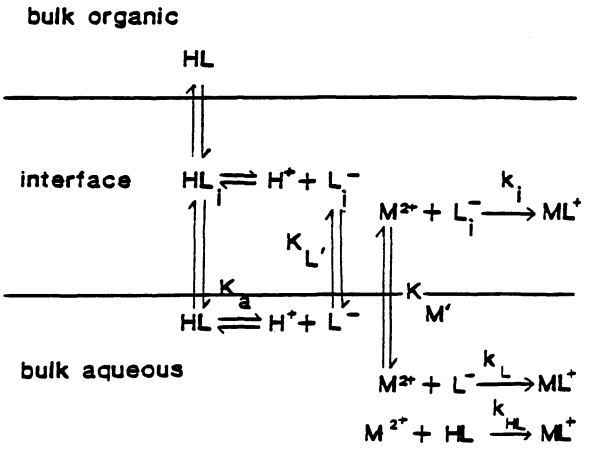

Fig. 3. Schematie mechanism of Ni(II)-8-quinolinol extraction system.

These findings can be represented quantitatively by the following derived relations:

$$-\frac{d[Ni]}{dt} = k_{obs}[Ni] \tag{11}$$

$$-\frac{d[Ni]}{dt} = \left(k_{HL} + k_L \frac{K_a}{[H^+]}\right)\frac{[HL]_o[Ni]}{K_D} + k_i K_{M'} K_{L'} ad \frac{K_a}{[H^+]} \frac{[Ni][HL]_o}{K_D} \tag{12}$$

$$k_{obs} = \left(k_{HL} + k_L \frac{K_a}{[H^+]}\right)\frac{[HL]_o}{K_D} + k_i K_{M'} K_{L'} ad \frac{K_a}{[H^+]} \frac{[HL]_o}{K_D} \tag{13}$$

where k_{obs} is the observed pseudo-first-order rate constant, k_{HL} is the second-order rate constant of metal plus neutral ligand in the bulk aqueous phase, k_L is the second-order rate constant for metal plus ligand anion in the bulk aqueous phase, k_i is the interfacial rate constant, K_a is the acid dissociation constant (pK_a 9.90 and 10.40 for oxine and KELEX 100, respectively[36]), K_D is the distribution constant of the neutral ligand ($10^{2.6}$ and $10^{5.52}$ for oxine and KELEX, respectively[39]), K_M is the distribution constant of the metal between the interface and bulk aqueous phase, K_L is the distribution constant of the ligand anion between the interface and the bulk aqueous phase, d is the thickness of the interface, and a is the specific interfacial area. A plot of k_{obs} vs. a (Fig. 2) permits the evaluation of all the rate constants, provided the other values are known. The excellent linearity seen in the plots confirms the applicability of Eq. 13.

The only unknown values in Eq. 13 are $K_{M'}$, $K_{L'}$, and d, since it is assumed that the metal is not surface active, $K_{M'}$ is taken as unity. The values of the produce of (K_L, d) can be obtained by measurement of $\Delta pH_{1/2}$. This relation[29] is

$$10^{\Delta pH_{1/2}} - 1 = K_{L'} ad \tag{14}$$

The $\Delta pH_{1/2}$ value for oxine was 0.03±0.01 and that for KELEX 100 was 0.8±0.6, yielding the values from Eq. 14 of ($K_{L'}$ ad) as $10^{-3.6\pm0.2}$ for oxine and $10^{-1.7\pm1.0}$ for KELEX 100.

The values of the slopes and intercepts of the lines in Fig. 2 can be used to evaluate all three rate constants, as well as the degrees of contribution of the three pathways. Results are tabulated in Table 1 along with values from other studies. A similar ligand, 8-mercaptoquinoline, is included for comparative purposes.

Table 1. Summary of Rate Constants for Nickel Extraction With Oxine and Its Analogs

Extractant	Log k_{HL} / $M^{-1}s^{-1}$	Log k_L / $M^{-1}s^{-1}$	Log k_i / $M^{-1}s^{-1}$
Oxine[a]	2.97	5.46	6.7±0.2
Oxine[b]	3.55	5.73	
Thiooxine[c]	3.45	5.45	
KELEX 100[a]	4.4	6.8	6.7±1.0
KELEX 100[d]	3.74		6.92

a) Present work. b) Reference 34. c) Reference 38. d) Reference 35.

These results are in fairly good agreement with Yamada et al.[34] for the Ni(II)-system, dispite the different assumptions about the reaction mechanism. The 10 fold higher interfacial rate constant we reported[33] can be accounted for in terms of the different environment in the bulk and interfacial phases. For example, the dielectric constant at the interface may be somewhere between that of the bulk solvents, and hence lower than that of bulk water. This would be expected to be a more conducive environment for the reaction involving charge neutralization, as is the case here. Also, the number of degrees of freedom for the adsorbed ligand should be lower at the interface, than the free anion in bulk water, resulting in a more positive entropy change. In addition, the geometric orientation of the weakly surface active chelating agent may be affected by the different environment that the interface provides. The polar chelating group is expected to be pointing towards the aqueous phase which will also enhance the chances of reaction. These factors would all lead to the observed larger interfacial rate constant found for oxine.

Although the more hydrophobic KELEX 100 anion is more highly adsorbed into the interfacial region than is the 8-quinolinolate (i.e., K'_L is higher) and thus a greater proportion of the reaction of the anion with Ni^{2+} takes place in that region, it is interesting to note that the corresponding rate constants, k_L and k_i, are not different. Thus, the interfacial region would seem to have an essentially aqueous character. Further investigation is necessary to obtain a general answer to the question of how the interfacial and bulk rate constants compare to one another.

The finding in this study of a three path reaction mechanism for the extraction of a well-known, simple, chelating system indicates the complexity that may be involved. The usefulness of the new extraction kinetics apparatus as a diagnostic tool for evaluating the role of the liquid–liquid interface in solvent extraction systems has been demonstrated. The ability to differentiate between bulk phase and interfacial reactions can be very important in the design of improved extractants, as well as in the understanding of the fundamental chemical properties of the liquid–liquid interface.

The interest in the role of the interface in solvent extraction processes will almost certainly result in significantly improved understanding of the details of the fundamental nature of such processes which will have positive benefits in practical applications of the

technique of solvent extraction, as well as to other fields of research involving surface forces.

Much of the research described here was conducted with the support of the National Science Foundation. In addition, I would like to express my appreciation to my Japanese coworkers for their great contributions to this and other aspects of my research.

References

1) H. Freiser, *Acc. Chem. Res.*, **17(4)**, 126—131 (1984).
2) C. B. Honaker and H. Freiser, *J. Phys. Chem.*, **66**, 127 (1962).
3) M. Zangen, *Isr. J. Chem.*, **2**, 91 (1964).
4) K. Yamada, K. Nakagawa, K. Haraguchi, and S. Ito, *Nippon Kagaku Kaishi*, **1975**, 1431.
5) S. Ito, K. Haraguchi, K. Nakagawa, and K. Yamada, *Nippon Kagaku Kaishi*, **1973**, 948.
6) K. Nanda and R. Sharma, *Chem. Eng. Sci.*, **22**, 769 (1967).
7) G. Hoogeveen, *Chem. Commun.*, **1967**, 634.
8) G. Colovos, A. Yokoyama, and H. Freiser, *Anal. Chem.*, **47**, 2441 (1975).
9) R. R. Swanson, U. S. Patents 3131998, May 1964; 3224873, Dec. 1965; 3428449, Feb. 1969.
10) D. S. Flett, D. N. Okuhara, and D. R. Spink, *J. Inorg. Nucl. Chem.*, **35**, 2471 (1973).
11) D. S. Flett, J. A. Hartlage, D. R. Spink, and D. N. Okuhara, *J. Inorg. Nucl. Chem.*, **37**, 1967 (1975).
12) D. S. Flett, M. Cox, and J. D. Heels, *J. Inorg. Nucl. Chem.*, **37**, 2533 (1975).
13) D. S. Flett, *Acc. Chem. Res.*, **10**, 99 (1977).
14) C. B. Honaker and H. Freiser, *J. Phys. Chem.*, **66**, 127 (1962).
15) B. E. McClellan and H. Freiser, *Anal. Chem.*, **36**, 2262 (1964).
16) S. P. Carter and H. Freiser, *Anal. Chem.*, **51**, 1100 (1979).
17) S. P. Carter and H. Freiser, *Anal. Chem.*, **52**, 511 (1980).
18) A. A. Morton and J. Fallwell, *J. Am. Chem. Soc.*, **60**, 1429 (1938).
19) L. Farber, H. A. C. McKay, and A. Wain, *Proc. Int. Solvent. Extr. Conf.*, 1974.
20) R. J. Whewell, C. Hanson, and M. A. Hughes, *J. Inorg. Nucl. Chem.*, **37**, 2303 (1975).
21) R. L. Atwood, D. N. Thatcher, and J. D. Miller, *Metall. Trans. B*, **6**, 465 (1975).
22) C. A. Fleming, N. I. M. Report No. 1793. Johannesburg, South Africa, 1976.
23) J. B. Lewis, *Chem. Eng. Sci.*, **3**, 284 (1954).
24) H. R. C. Pratt, *Ind. Chem.*, **1955**, 63.
25) H. Watarai and H. Freiser, *J. Am. Chem. Soc.*, **105**, 189 (1983).
26) R. G. Wilkins, "The Study of Kinetics and Mechanism of Reactions of Transition Metal Complexes," Allyn and Bacon, Boston (1974).
27) K. Akiba and H. Freiser, *Anal. Chim. Acta*, **136**, 329 (1982).
28) H. Watarai, L. Cunningham, and H. Freiser, *Anal. Chem.*, **54**, 2390 (1982).
29) H. Watarai and H. Freiser, *J. Am. Chem. Soc.*, **105**, 191 (1983).
30) J. Oh and H. Freiser, *Anal. Chem.*, **39**, 22 (1967).
31) E. Aprahamian, F. F. Cantwell, and H. Freiser, *Langmuir*, **1**, 79 (1985).
32) V. G. Chamupathi and H. Freiser, *Langmuir*, **3**, 0000 (1987).
33) E. Aprahamian and H. Freiser, *Sep. Sci. Technol.*, **22(2 & 3)**, 233 (1987).
34) K. Yamada, K. Nakagawa, K. Haraguchi, and S. Ito, *Nippon Kagaku Kaishi*, **1975**, 294.
35) S. Ito, K. Haraguchi, and K. Yamada, *Nippon Kagaku Kaishi*, **1977**, 8, 1137.
36) K. Haraguchi and H. Freiser, *Inorg. Chem.*, **22**, 1187 (1983).
37) S. P. Bag and H. Freiser, *Anal. Chim. Acta*, **135**, 319 (1982).
38) K. Haraguchi and H. Freiser, *Anal. Chem.*, **55**, 656 (1983).

 © 1988 The Chemical Society of Japan Bull. Chem. Soc. Jpn., 61, 47—57 (1988)

Invited Paper

Manganese "Picnic Basket" Porphyrins: Cytochrome P-450 Active Site Analogues

James P. COLLMAN,* John I. BRAUMAN, Jeffrey P. FITZGERALD, Philip D. HAMPTON, Yoshinori NARUTA,† and Takashi MICHIDA††

A Contribution from The Department of Chemistry, Stanford University, Stanford, CA, 94305, U.S.A.

†The Department of Chemistry, Kyoto University, Kyoto 606, Japan

††Faculty of Pharmaceutical Sciences, Kobe-Gakuin University, Kobe 673, Japan

(Received August 4, 1987)

This paper describes studies of a new class of cytochrome P-450 model compounds called the "picnic basket porphyrins." The picnic basket porphyrins are unsymmetrical porphyrins with one face sterically protected by a superstructure and the other unhindered. The manganese(III) porphyrins have been investigated as shape selective catalysts using oxygen atom donors in the presence of a sterically bulky imidazole. This paper presents ligand binding studies and competitive olefin epoxidations which lead to the surprising conclusion that catalysis by the manganese picnic basket porphyrins occurs exclusively on the sterically unhindered face indicating reaction by the minor catalyst component and not the selective major catalyst component.

Synthetic metalloporphyrins have received considerable attention as olefin epoxidation and alkane hydroxylation catalysts, and, thus, as models of the enzyme cytochrome P-450.[1,2,11,26,28] As catalysts metalloporphyrins are sometimes limited by their low turnover numbers and difficult syntheses, yet some have shown good shape selectivity (cis versus trans olefins) and modest asymmetric induction in olefin epoxidation.[2]

Most studies of catalysis have utilized oxygen atom donors including iodosylbenzene, hypochlorite, hydrogen peroxide, alkyl hydroperoxides, or amine *N*-oxides to generate the metalloporphyrin-based oxidant. In addition, several examples of apparent activation of dioxygen to oxidize substrates employing reducing agents and metalloporphyrins have been reported.[3] In most of these examples, however, it is not clear if metal-bound dioxygen is actually being activated or if catalysis is mediated by free hydrogen peroxide or peracids formed under these conditions.

While metalloporphyrins have limited practical applications, studies of oxygenations by metalloporphyrins and their selectivity have been useful in understanding the mechanism of cytochrome P-450 activity. This family of heme containing monooxygenases catalyze the oxygenation of organic substrates using dioxygen and NADH. Many key steps in the activation of oxygen by cytochrome P-450 and the subsequent oxidation of substrates are still not well-understood.

In an attempt to learn more about this important enzyme, we have prepared a new family of porphyrins called the "picnic basket" porphyrins, which are designed to exclude bulky axial ligands and yet allow small molecules like dioxygen to bind within the pocket.

In our investigation of these porphyrins we were particularly interested in probing the selectivity of the pocket toward axial ligands and olefin structure in catalytic epoxidations. Since we hope eventually to use the picnic basket porphyrins to activate dioxygen, information about the substrate selectivity within the pocket would allow us to determine whether bound dioxygen was activated in this cavity or whether catalysis was mediated by a free oxygen atom donor as discussed earlier. This paper describes the synthesis of the picnic basket porphyrins, ligand binding studies, and results from competitive olefin epoxidation. These studies led to unexpected conclusions about catalysis by manganese derivatives of the picnic basket porphyrins.

Experimental

Materials: Methylene dichloride, chloroform, tetrahydrofuran, 30% hydrogen peroxide and basic alumina (activity I) were purchased from J. T. Baker Chemical Company and used without further purification. Anhydrous manganese(II) bromide, 1-methylimidazole, (diacetoxyiodo)benzene, and *N*,*N*-dimethylformamide were purchased from Aldrich Chemical Co. and used as received. 2,6-Lutidine was purchased from Aldrich Chemical Co. and was dried by stirring over KOH and distilling from BaO. Manganese tetraphenylporphyrin (TPP) and tetramesitylporphyrin (TMP) were prepared as described in the literature. Iodosylbenzene was prepared from the diacetate by basic hydrolysis. 1,5-Diphenylimidazole was prepared by a modified literature procedure.[4] $\alpha,\alpha,\alpha,\alpha$-Tetrakis(*o*-aminophenyl)porphyrin was prepared as reported in the literature.[5] Manganese(III) porphyrin salts of various counterions were prepared from the corresponding bromide using the method of Bruice et al.[25]

Methods: Visible spectra were recorded either on a Varian Cary 219 Spectrometer or with a Hewlett Packard 8450A Diode Array Spectrometer with 7470A Plotter. In order to obtain reproducible spectral titrations, all glassware was treated with 5% aqueous NaOH for 12 h, rinsed, and then soaked in dilute aqueous HBr for 12 h. Spectra were recorded of CH_2Cl_2 solutions, at 25.0±0.5 °C, from 700 to

300 nm in a 1 cm pathlength cell. The concentration of Mn(PBP)Br was approximately 2×10^{-5} M and the imidazole concentration ranged from 0 to 20 mM. *N*-Substituted imidazoles were added to the cuvette from standard stock solutions via microliter syringe. Data were analyzed by the method of Dolphin and James.[6] Cyclic voltammograms were obtained using a Princeton Applied Research wave generator and a Hewlett Packard x-y recorder. $E_{1/2}$ values were measured for CH_2Cl_2 solutions containing 0.2 M tetrabutylammonium perchlorate (TBAP) as electrolyte at a glassy carbon electrode and are referenced to SSCE. All measured $E_{1/2}$ values are for reversible (ΔE_p=60—80 mV) or quasireversible waves (ΔE_p=80—110 mV). Epoxide production was monitored on a Hewlett Packard Model 5880A gas chromatograph fitted with a 15′×1/8″ column of OV-101 on Supelcoport. Chiral shift ^{1}H NMR was accomplished by adding Tris[3-(heptafluoropropylhydroxymethylene) (+)-camphorato]europium(III) [Eu(hfc)$_3$] (Aldrich) to a NMR sample of the isolated epoxide until the epoxide signals were resolved.[2a]

Synthesis: Bis(5-nitroisophthalamido)-α,α,α,α-tetrakis-(*o*-aminophenyl)porphyrin (2). The reaction was carried out under a rigorously dry nitrogen atmosphere using oven-dried glassware. 5-Nitroisophthaloyl chloride (3.968 g, 16.0 mmol) in dry CH_2Cl_2 (100 mL distilled from P_2O_5) was slowly added, with stirring, to a solution of α,α,α,α-TAMPP (340 mg, 0.50 mmol) in CH_2Cl_2 (1.0 L) containing pyridine (10 mL) in an ice bath. After stirring for 12 h at 0 °C the solution was treated with aqueous $NaHCO_3$ solution. The solution was filtered through a celite pad and the pad was washed with 9:1 EtOH-$CHCl_3$. After separation of the organic layer, the aqueous layer was extracted with two 100 mL portions of $CHCl_3$. The combined organic layers were washed with two 100 mL portions of saturated $NaHCO_3$ and with two 100 mL portions of water, reduced to a small volume, and purified by chromatography on a silica-gel column, eluting with $CHCl_3$ to 20:1 EtOH-$CHCl_3$. A purple band was cleanly separated. The product was crystallized by addition of EtOH and slow evaporation of the solvent and dried in vacuo (10^{-6} Torr) to yield 500 mg (24.4%) of purple crystals. ^{1}H NMR (CF_3CO_2D-$CDCl_3$) δ=9.06 (s, 4H), 8.81 (s, 4H), 8.57 (d, 4H), 8.43 (d, 4H), 8.16 (m, 4H), 7.97 (t, 4H), 7.72 (d, 4H), 7.01 (s, 2H). UV-vis (5% EtOH-$CHCl_3$) λ 449, 512 (sh), 545, 582, 618, 674 nm. IR (KBr) 3411 (vs), 1690 (vs), 1582 (s), 1526 (vs), 1449 (s), 1347 (m), 1313 (s), 967 (m), 812 (m), 800 (m), 759 (s), 723 (s) cm^{-1}. MS *m/z* 1025 (M+H).

Bis(5-aminoisophthalamido)-α,α,α,α-tetrakis(*o*-aminophenyl)porphyrin (3). The dinitro compound **2** (1.375 g, 1.34 mmol) was dissolved in a mixture of trifluoroacetic acid (20 mL) and acetic acid (50 mL) cooled in an ice bath. To this solution was added a concentrated hydrochloric acid solution (7.5 mL) of $SnCl_2\cdot2H_2O$ (9.07 g, 40.2 mmol); the mixture was then stirred for 6 h in an ice bath. The reaction mixture was slowly poured into aqueous $NaHCO_3$ in an ice bath. The resulting mixture was filtered through a celite pad. After removal of the water the celite pad was washed with 40% EtOH-$CHCl_3$ (about 500 mL) until the filtrate was nearly colorless. The organic solution was washed with saturated aqueous $NaHCO_3$ and then with water and dried over $MgSO_4$. The solution was concentrated in vacuo and the fine purple crystals which precipitated were centrifuged and washed with EtOH. After drying (10^{-6} Torr, 60—70 °C, 12 h) solvent-free diamine was obtained in 68% yield (884 mg). ^{1}H NMR (CF_3CO_2D-$CDCl_3$) δ=8.89 (s, 4H), 8.58 (s, 4H), 8.39 (d, 4H), 8.14 (m, 8H), 8.01 (t, 4H), 6.94 (s, 2H). UV-vis (5% EtOH-$CHCl_3$) λ 428, 490 (sh), 524, 563, 598, 653 nm. IR (KBr) 3453 (m), 3411 (s), 1681 (vs), 1579 (vs), 1520 (vs), 1446 (vs), 1341 (s), 1298 (s), 1239 (m), 964 (s), 884 (m), 806 (s), 791 (s), 757 (vs) cm^{-1}. MS *m/z* 964 (M−1).

General Method for the Synthesis of Amide-Strapped "Picnic Basket" Porphyrins 4a—e. The following reaction was carried out under a rigorously dry nitrogen atmosphere. To a dry $CHCl_3$ solution (50 mL) containing dry pyridine (0.5 mL), both a DMF solution (3 mL) of the diamine **3** (20 mg, 0.0207 mmol) and a CH_2Cl_2 solution (3 mL) of the diacid chloride (0.03 mmol) were added at the rate of about 10^{-2} mL min^{-1} by means of a syringe pump. After the addition was complete the mixture was stirred for an additional two hours. The reaction mixture was washed with two 20 mL portions of saturated $NaHCO_3$ and with two 20 mL portions of water. After the solvent was evaporated in vacuo, the residue was chromatographed on silica gel, eluting with 5% MeOH-CH_2Cl_2 (or EtOH-$CHCl_3$). A bright purple band was cleanly isolated. The fine red-purple crystals obtained on slow evaporation of the solvent were washed with EtOH and dried in vacuo (10^{-6} Torr, 60 °C, 12 h) to give the amide-strapped picnic basket porphyrins (**4a—e**).

***n*-C8-PBP (4a).** ^{1}H NMR (CF_3CO_2D-$CDCl_3$) δ=9.08 (s, 4H), 8.76 (s, 4H), 8.55 (d, 4H, *J*=7.8 Hz), 8.41 (d, 4H, *J*=7.5 Hz), 8.13 (t, 4H, *J*=7.8 Hz), 7.94 (t, 4H, *J*=7.5 Hz), 7.44 (s, 4H), 6.60 (s, 2H), 2.03 (br, t, 4H, *J*=6.7 Hz), 1.05 (br, t, 4H), 0.72 (br, 4H). UV-vis (5% EtOH-$CHCl_3$) λ 425, 487 (sh), 521, 556, 594, 648 nm. IR (KBr) 3411 (s), 2927 (m), 2857 (w), 1690 (vs), 1678 (vs), 1579 (s), 1520 (vs), 1462 (sh), 1449 (vs), 1338 (s), 1239 (s), 964 (s), 890, 797 (s), 757 (s) cm^{-1}. MS *m/z* 1102 (M).

***n*-C9-PBP (4b).** ^{1}H NMR (CF_3CO_2D-$CDCl_3$) δ=9.05 (s, 4H), 8.78 (s, 4H), 8.51 (d, 4H, *J*=7.9 Hz), 8.41 (d, 4H, *J*=7.3 Hz), 8.14 (t, 4H, *J*=7.9 Hz), 7.96 (t, 4H, *J*=7.3 Hz), 7.47 (s, 4H), 6.48 (s, 2H), 2.12 (br, t, 4H, *J*=5 Hz), 1.26 (br, s, 4H), 0.63 (br, 2H), 0.62 (br, 4H). UV-vis (5% EtOH-$CHCl_3$) λ 427, 523, 562, 596, 652 nm. IR (KBr) 3411 (s), 2927 (m), 2857 (m), 1687 (vs), 1672 (vs), 1579 (s), 1520 (vs), 1462 (sh), 1446 (vs), 1341 (m), 1319 (sh), 1242 (m), 964 (m), 806, 797 (m), 757 (m) cm^{-1}. MS *m/z* 1116 (M).

***n*-C10-PBP (4c).** ^{1}H NMR (CF_3CO_2D-$CDCl_3$) δ=9.02 (s, 4H), 8.79 (s, 4H), 8.50 (d, 4H, *J*=7.9 Hz), 8.39 (d, 4H, *J*=7.6 Hz), 8.15 (t, 4H, *J*=7.9 Hz), 7.97 (t, 4H, *J*=7.6 Hz), 7.51 (s, 4H), 6.54 (s, 2H), 2.13 (br, 4H), 1.27 (br, 4H), 0.78 (br, 8H). UV-vis (5% EtOH-$CHCl_3$) λ 428, 525, 563, 597, 653 nm. IR (KBr) 3411 (s), 2927 (m), 2850 (m), 1690 (vs), 1672 (sh), 1579 (vs), 1520 (vs), 1462 (sh), 1446 (vs), 1341 (s), 1316 (s), 1242 (s), 964 (s), 800 (m), 757 (s) cm^{-1}. MS *m/z* 1130 (M).

***n*-C11-PBP (4d).** ^{1}H NMR (CF_3CO_2D-$CDCl_3$) δ=9.05 (s, 4H), 8.77 (s, 4H), 8.56 (d, 4H, *J*=7.9 Hz), 8.39 (d, 4H, *J*=7.6 Hz), 8.15 (t, 4H, *J*=7.9 Hz), 7.96 (t, 4H, *J*=7.6 Hz), 7.56 (s, 4H), 6.53 (s, 2H), 2.16 (bt, 4H), 1.30 (br, 4H), 0.85 (br, 8H), 0.69 (br, 2H). UV-vis (5% EtOH-$CHCl_3$) λ 429, 488 (sh), 523, 561, 597, 642 nm.

General Procedure for Metallation of H_2(PBP) with Mn. Unmetallated picnic basket porphyrin (100 μmol), anhydrous $MnBr_2$ (215 mg, 1 mmol) and 20 drops of 2,6-lutidene were heated at reflux in 25 mL DMF under air in a 50 mL round bottom flask fitted with a magnetic stirrer and

a condenser. After 5 h at reflux, UV-vis spectral analysis indicated complete metallation. The reaction mixture was cooled to room temperature and poured into 600 mL deionized water. The precipitate was collected by filtration through a Celite pad and washed liberally with deionized water. The crude product was extracted from the Celite with $CHCl_3$ and the filtrate reduced on a rotovap. The green residue was dissolved in 20 mL CH_2Cl_2 and loaded onto a basic activity I Al_2O_3 column (3.5 cm diameter×8 cm) prepared from CH_2Cl_2 slurry. The desired green band was obtained by elution with $CHCl_3$. The $CHCl_3$ layer was washed three times with 100 mL saturated aqueous KBr in a separatory funnel and passed through crystalline KBr. Removal of solvent and drying the residue provided the desired Mn(PBP)Br in 80—85% yield.

Mn(C10-PBP)Br, 5. UV-vis (CH_2Cl_2) λ 376, 400 (sh), 420 (sh), 489 (Soret), 534, 591, 628. MS m/z=1158 (M+1−Br) for $C_{70}H_{54}N_8O_6MnBr$ (LSIMS$^+$). Calcd for $C_{70}H_{54}N_8O_6MnBr$: C, 67.90; H, 4.40; N, 9.05%. Found: C, 67.65; H, 4.63; N, 8.72%.

Mn(C8-PBP)Br, 6. UV-vis (CH_2Cl_2) λ 377, 400 (sh), 489 (Soret), 534, 592, 628. MS m/z 1130 (M+1−Br) for $C_{68}H_{50}N_8O_6MnBr$ (LSIMS$^+$). Calcd for $C_{68}H_{50}N_8O_6MnBr$: C, 67.49; H, 4.17; N, 9.26%. Found: C, 66.32; H, 4.19; N, 8.71%.

Mn(C6-PBP)Br, 7. UV-vis (CH_2Cl_2) λ 376, 404 (sh), 489 (Soret), 532, 590, 628. MS m/z 1102 (M+1−Br) for $C_{66}H_{46}N_8O_6MnBr$ (LSIMS$^+$). Calcd for $C_{66}H_{46}N_8O_6MnBr$: C, 67.06; H, 3.93; N, 9.48%. Found: C, 66.99; H, 3.67; N, 9.28%.

Mn(PXY-PBP)Br, 8. UV-vis (CH_2Cl_2) λ 376, 400 (sh), 488 (Soret), 532, 590, 628. MS m/z 1121 (M+1−Br) for $C_{68}H_{42}N_8O_6MnBr$ (LSIMS$^+$). Calcd for $C_{68}H_{42}N_8O_6MnBr$: C, 67.94; H, 3.53; N, 9.32%. Found: C, 65.33; H, 3.55; N, 8.85%.

Mn(BN-PBP)Br, 9. UV-vis (CH_2Cl_2) λ 377, 396 (sh), 490 (Soret), 524, 590, 628. CD(CH_2Cl_2) λ 380, 400, 495, 600, 630.

Results and Discussion

The "Picnic Basket" Approach: Our approach to a new cytochrome P-450 model compound is illustrated in Scheme 1. This approach utilizes synthetic porphyrins that are sterically protected on one face of the porphyrin macrocycle. A bulky ligand, which cannot fit into the pocket should block the axial site on the unhindered side of the porphyrin and force molecules such as O_2 or oxygen atom donors to bind within the cavity. Activation of bound dioxygen or O-atom transfer would then generate the metal oxo inside the pocket. A smaller (or cis) olefin, which has greater access to the sterically hindered metal oxo moiety, should then be epoxidized in preference to a larger (or trans) olefin. If R were made chiral catalytic, asymmetric epoxidation might be realized.

In the design of a sterically protected oxidation catalyst several factors must be considered. The cavity must be sufficiently hindered to prevent coordination of the bulky axial ligand but not so hindered as to exclude the oxidant or substrate. Since most of the sterically protected porphyrins reported to date were prepared as hemoglobin or myoglobin active site analogues, they were designed to bind dioxygen within very tight cavities. The cavities hinder coordination of ligands as small as 1-methylimidazole and even carbon monoxide. A crystal structure of Baldwin's capped porphyrin, for example, shows a separation of less than 4 Å between the phenyl "cap" and the porphyrin ring.[7] Porphyrins containing hindered pockets have also been prepared by Momenteau[8a] and Traylor.[8b] While the cavities in these porphyrins can control axial ligand coordination they can also restrict access of a substrate to the active site. In addition, several groups have observed the oxidation of alkyl groups on a porphyrin that are accessible to the metal oxo. Thus a sterically protected porphyrin was needed which had a large, permanent cavity within which O_2 could be bound and activated without oxidation of the superstructure.

We previously reported[9] good yields for the high dilution coupling of two equivalents of isophthaloyl chloride and the 4:0 atropisomer of tetrakis(*o*-aminophenyl)porphyrin (TAMPP) (Scheme 2). The

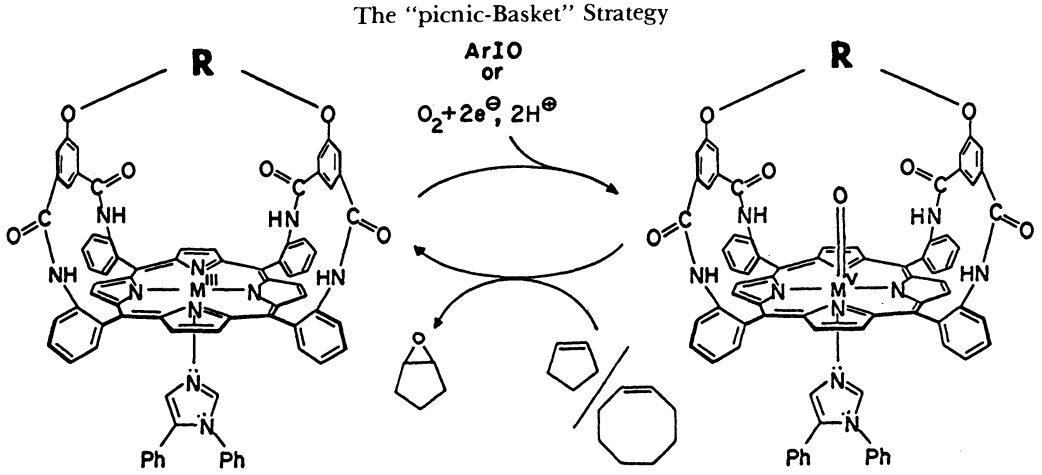

Scheme 1. Strategy for catalysis by "picnic-basket" porphyrins.

high yield was attributed to the complementary geometries of the isophthaloyl bridge and the aminophenyl groups on adjacent meso positions. No trans aminophenyl-bridged species were detected. Although the iron(II) derivative of **1** proved to be unsuccessful as a hemoglobin or myoglobin model it satisfied the above criteria since the rigid isophthalamido walls extend away from the porphyrin, forming a molecular cleft of large volume. By linking the 5 and 5′ positions the size of the cavity can be varied. Because of their shape we have given this class of molecules the trivial name "picnic basket" porphyrins.

Ligand Synthesis. The first picnic basket porphyrins were synthesized via the route outlined in Scheme 3. High dilution coupling of the 4:0 atropisomer of tetrakis(*o*-aminophenyl)porphyrin with 5-nitroisophthaloyl chloride yielded **2**, the 5,5′-dinitro derivative of **1**. Tin(II) chloride reduction to the 5,5′-diamino derivative **3** followed by high dilution coupling with a series of α,ω-diacid chlorides produced a family of porphyrins of general structure **4**. Derivatives with eight to twelve carbon atoms in the strap were synthesized in overall yields ranging from 10 to 22% based on the amount of 4:0 TAMPP used.

The solubility of these amide-strapped picnic basket porphyrins is very poor in nonprotic polar solvents such as methylene dichloride. This low solubility appears to result from intermolecular hydrogen bonding involving the amides in the strap. In addition to the solubility problem, this synthesis requires two high dilution reactions which severely limit reaction scale and introduce the most expensive

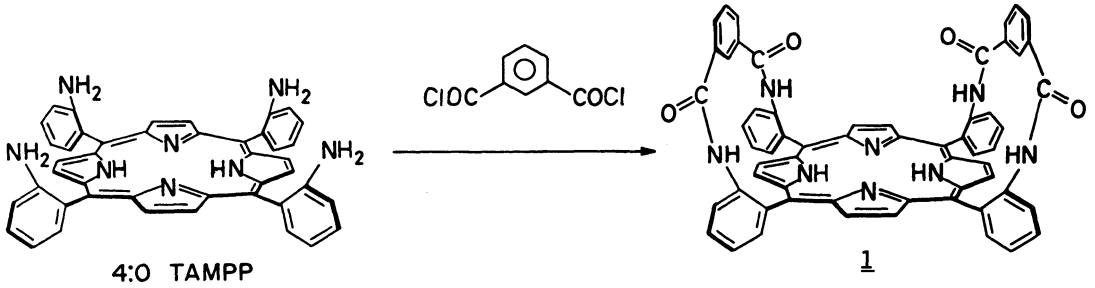

Scheme 2. Picnic basket precursor demonstrating complementary geometries between 4:0 TAMPP and isophthaloyl chloride.

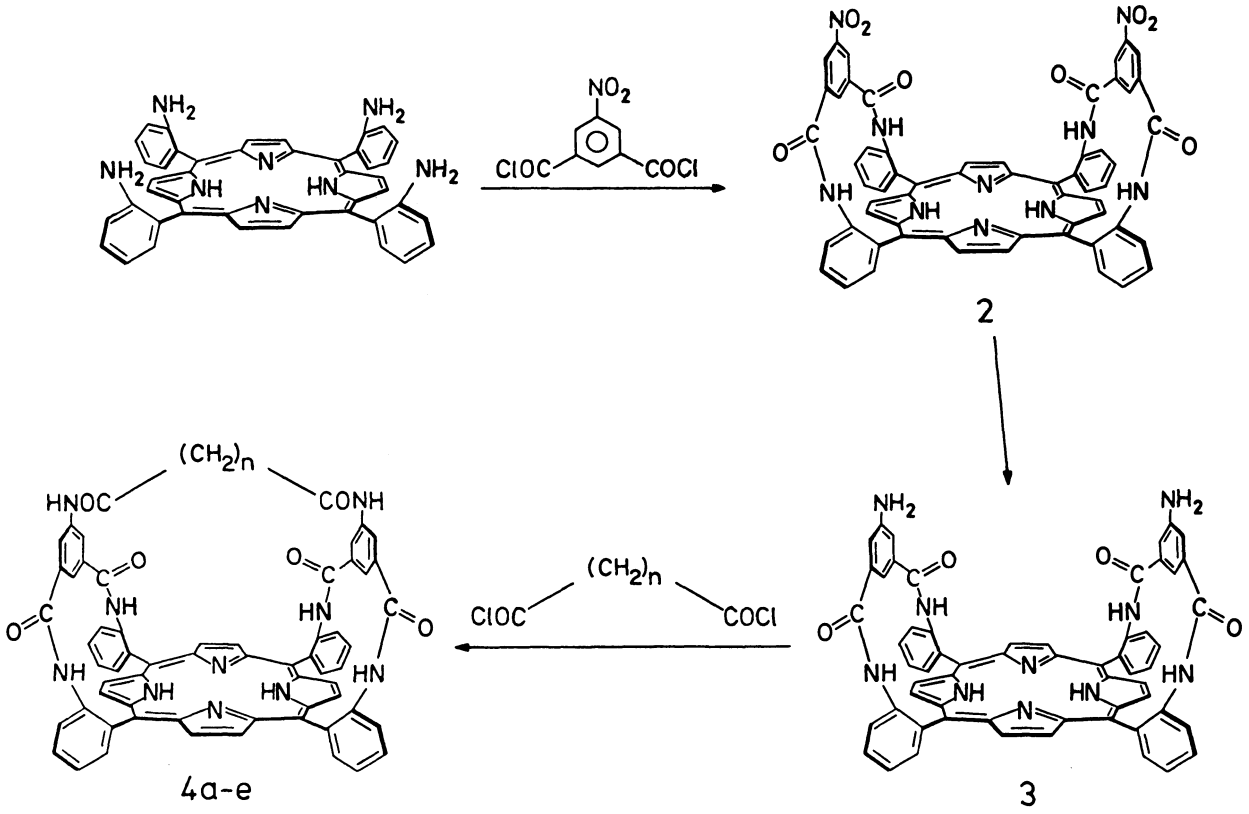

Scheme 3. Synthesis of amide-strapped porphyrins **4a—e**.

reagent, the 4:0 TAMPP, three steps from the final product. In spite of these difficulties, the synthesis outlined in Scheme 3 has proven to be a viable route to this class of porphyrins.

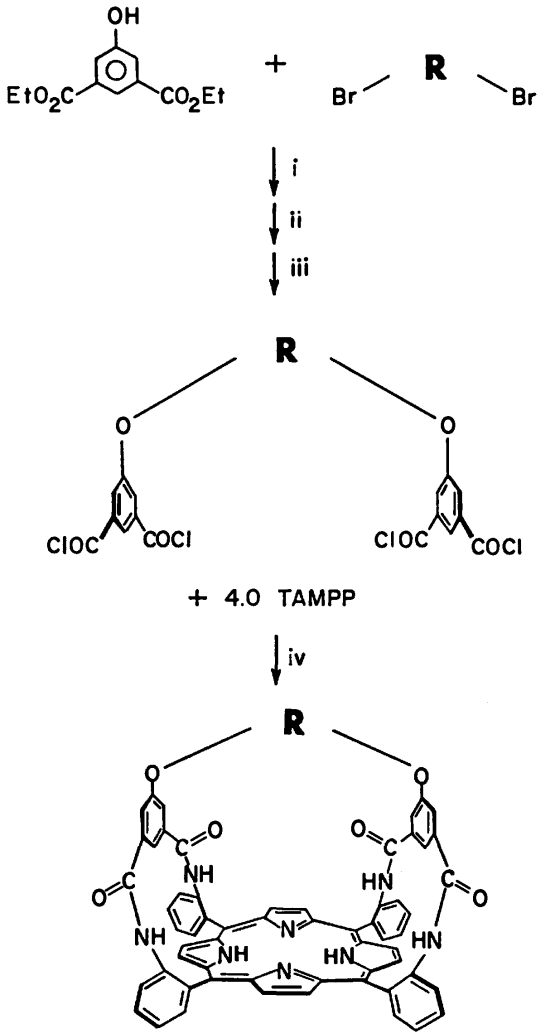

Scheme 4. Synthesis of ether-strapped porphyrins **5**—**9**.

Both of these problems were solved by replacing the amide linkages with ether linkages and through the use of a convergent synthesis as outlined in Scheme 4. This general synthesis has several advantages over that outlined in Scheme 3 in that it contains only one high dilution step and introduces the 4:0 TAMPP in the final step. The eight compounds depicted in Fig. 1 are available by this route. All of the following studies were performed on the ether strapped porphyrins whose synthesis and characterization have been described in detail.[10b] The various complexes of these ligands are specified by the following notation in this paper:

$$Mn(R\text{-}PBP)(L)_{in}(L')_{out}$$

where R=bridging group
C_n=normal alkane
PXY=*p*-xylene
DMB=2,6-dimethylbenzoate
BN=binaphthyl
PBP=picnic basket porphyrin
$(L)_{in}$=ligand coordinated within protected cavity
$(L)_{out}$=ligand bound on unencumbered porphyrin face

Manganese(III) Picnic Basket Porphyrins. Several recent studies have documented the beneficial effects of nitrogenous axial ligands in both Fe(III) and Mn(III) metalloporphyrin catalysts. Meunier[11a] and our group[11b] have observed dramatic increases in reaction rate, catalyst stability, epoxide yield, and stereospecificity in the epoxidation of alkenes by hypochlorite ion catalyzed by Mn(III) porphyrins with imidazoles and pyridine. Although the origin of these effects is not fully understood, they have been shown to result from nitrogenous base ligation.[12] Manganese porphyrin catalyzed epoxidations using

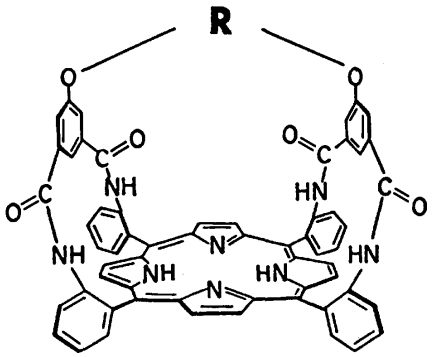

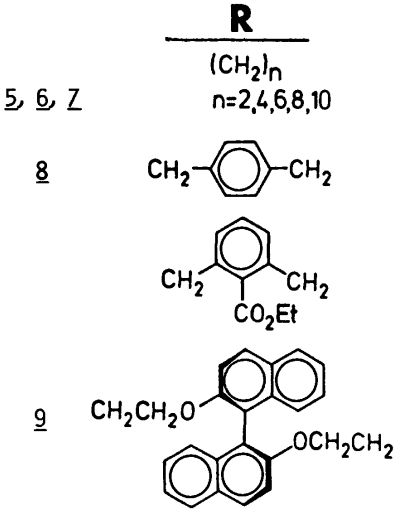

Fig. 1. Structures of ether-strapped porphyrins **5**—**9**.

other oxygen atom sources, such as iodosylbenzene[12] and peroxides,[13] are similarly affected by nitrogenous axial ligands. Since manganese porphyrins are well-behaved catalysts in the presence of nitrogenous ligands, we decided to investigate the selectivity of Mn(III) picnic basket porphyrins.

Metallation was accomplished by heating a DMF solution of the unmetallated picnic basket porphyrin with manganese bromide and the noncoordinating base, 2,6-lutidene, to give a compound with a visible spectrum similar to Mn(TPP)Br. The ^{1}H NMR spectrum shows severe paramagnetic broadening as is expected for a high spin d^4 system. Mass spectral analysis shows a molecular ion peak for Mn(PBP)$^+$. Loss of bromide ion is a result of the ionization method. Thus, the presence of a bromide counterion was inferred from the visible spectrum which is known to be counterion dependent.[24]

Ligand Binding. Since the picnic basket approach requires that the sterically unencumbered face of the porphyrin be made catalytically inactive by blocking that side of the porphyrin with a coordinated nitrogenous base, it is important to understand the thermodynamics and regiochemistry of nitrogenous base ligation. Unlike Mn(II) porphyrins, where crystallographic[14a] and solution[14b] studies have shown formation of only the mono-ligated complex, axial ligation to Mn(III) porphyrins is more complicated. Treatment of a five-coordinate Mn(III) porphyrin with an exogenous neutral ligand, L, can be expected to produce either a mono-L complex or a six coordinate bis-L complex, depending on the concentration of L and the relative magnitudes of the equilibrium binding constants K_L and $K_L{}^L$. The mono-ligated complex may be overall five or six-coordinate depending on the coordination properties of the counterion, X^-. This situation is depicted in Fig. 2. As the scheme in Fig. 2 suggests, equilibrium binding constants for neutral ligands will depend on the nature of the counterion. This has been demonstrated by isolation and structure determination of six-coordinate Mn(III) mono-L adducts with tightly coordinating anions such as azide[15a] or chloride,[15b] but only bis-L complexes have been isolated when a poorly coordinating counterion, perchlorate,[16] is present. Gravimetric analysis also indicates that a single pyridine binds to Mn(etioporphyrin)OAc.[17]

The spectral changes observed when a CH_2Cl_2 solution of Mn(PXY-PBP)Br is titrated with 1-methylimidazole are illustrated in Fig. 3. Six sharp isosbestic points indicate only two species, one of which is the starting material, are present over the course of the titration. The spectral changes are linear with the concentration of imidazole to the first power indicating that only one imidazole binds to each Mn(PXY-PBP)Br with an equilibrium constant of 2.7×10^3 M^{-1}. No evidence was found for binding of a

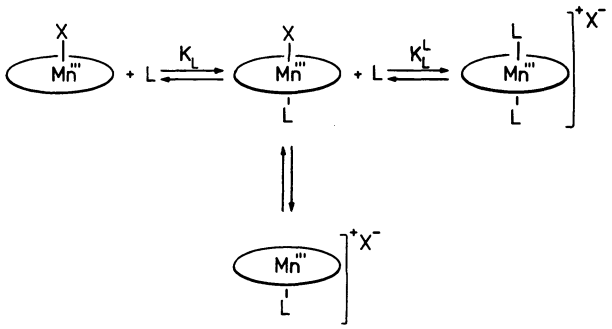

Fig. 2. Ligand binding to Mn(III) porphyrins.

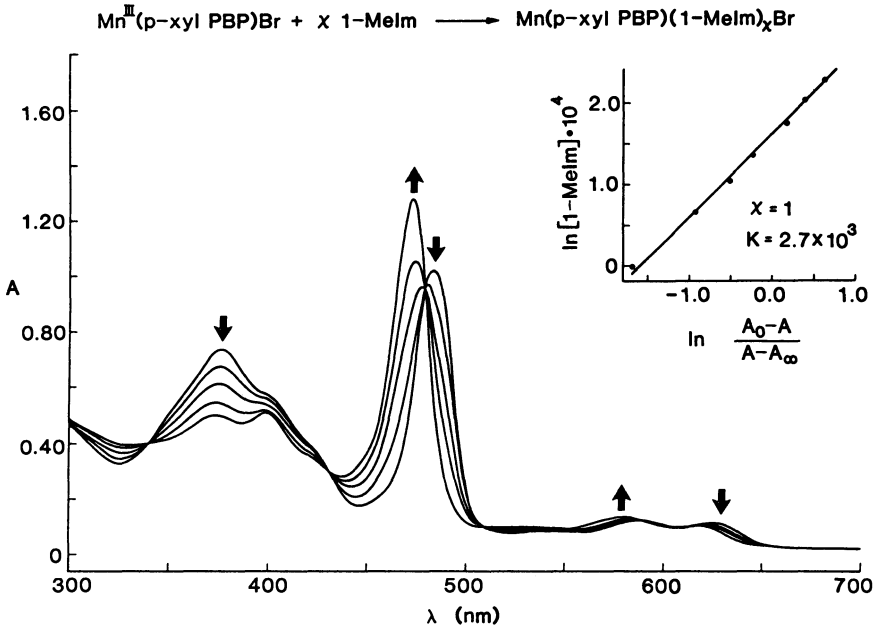

Fig. 3. Spectral titration of Mn(PXY-PBP)Br (**8**) with 1-methylimidazole.

second imidazole.

Similar changes are observed for a spectral titration using the bulky 1,5-diphenylimidazole but are complicated by two factors, that the ligand absorbs below 450 nm and, at high ligand concentrations, slow reduction to Mn(II) occurs. Reduction of Fe(III) porphyrins by excess nitrogenous ligand is well recognized. Despite these complications, the above analysis shows that a single 1,5-diphenylimidazole binds to each Mn(PXY-PBP)Br with an equilibrium constant estimated at $1.2\times10^3\ M^{-1}$.

In order to obtain spectral titrations which maintained sharp isosbestic points and did not change with time, all glassware had to be treated as described in the Experimental Section. Titrations performed in untreated glassware maintained isosbestic points only for the early part of the titration and showed spectral changes over time without addition of imidazole. As mentioned above, the visible spectrum of Mn(III) porphyrins depends strongly on the counterion. The behavior observed in untreated glassware is attributed to exchange of the bromide counterion for another counterion (probably chloride) adsorbed on the cuvette walls. Thus, the treatment described in the Experimental Section was designed to replace any anions which had leached into the glass with bromide.

Boucher studied the visible spectroscopy of Mn(III) porphyrins but reported no quantitative measure of equilibrium binding constants.[18] He does report that in the presence of excess ligand, Mn(III) porphyrins have the same visible spectrum, independent of the counterion in the starting material. Since the spectra of the starting materials do depend on the counterion, Boucher concludes a reaction with the neutral ligand has occurred and the anion is no longer coordinated. The product could be either the five-coordinate mono-L complex or the six-coordinate bis-L species.

La Mar has reported nonisosbestic spectral changes when Mn(III) porphyrins are treated with pyridine or 1-methylimidazole, and concluded that more than two species were present.[19]

Recently, Bruice has derived consecutive binding constants for 1-methylimidazole coordination to Mn(tpp)Cl from a spectral titration.[20] The lack of rigorous isosbestic points was considered evidence for the simultaneous presence of unligated, mono-L and bis-L species. K_L was determined to be $96.3\pm8.4\ M^{-1}$ and $K_LK_L^L$ to be $8530\pm330\ M^{-2}$ using Walker's method of analysis.[21] This analytical method, however, rests upon an unwarranted assumption — that the absorption coefficients of the mono-L and bis-L species are the same at the wavelength chosen for analysis. Several authors[22] have questioned this assumption in Walker's analysis. Thus, the results of Bruice, although consistent with those reported herein, must be considered questionable.

The present spectral study demonstrates that a single imidazole coordinates to Mn(PBP)Br and allows determination of the equilibrium binding constant but does not establish the site of ligation. To show that the hindered face of the picnic basket porphyrin can exclude a bulky axial ligand, an electrochemical study similar to that of Kadish[23] was undertaken.

Kadish examined nitrogenous base ligation to Mn(TPP)X complexes (X=N_3, Cl, ClO_4) by monitoring the Mn(II/III) half wave potential as a function of ligand concentration. For X=Cl or ClO_4, a cathodic shift in the half wave potential was observed as the concentration of pyridine increased. The magnitude of the shift, 53 mV per tenfold increase in pyridine concentration, is consistent with loss of a coordinated pyridine on reduction of Mn(III) to Mn(II), as shown in Eq. 1.

$$(1)\quad Mn^{III}(Por)(L)_n \xrightarrow{e^-} Mn^{II}(Por)(L)_{n-1} + L$$

Kadish concluded that the Mn(III) porphyrin is a bis(pyridine) adduct which, on reduction, becomes a monopyridine complex. The alternative explanation, that Mn(III) binds a single pyridine which is lost upon reduction to Mn(II), can be ruled out since Mn(II) porphyrins are known to exist as monopyridine complexes at these concentrations.[14b,24]

We repeated this experiment using Mn(TPP)Br or Mn(C8PBP)Br and varying concentrations of 1-methylimidazole or 1,5-diphenylimidazole. The results are plotted in Fig. 4. For two porphyrin/imidazole combinations, Mn(TPP)Br with the bulky 1,5-diphenylimidazole and the hindered Mn(C8PBP)-Br with 1-methylimidazole, no steric hindrance to imidazole coordination is expected by molecular models. For these combinations the Mn(II/III) half wave potential shifts cathodically 65 mV per tenfold increase in the imidazole concentration. This is consistent with the loss of a coordinated imidazole on reduction as observed by Kadish.[23]

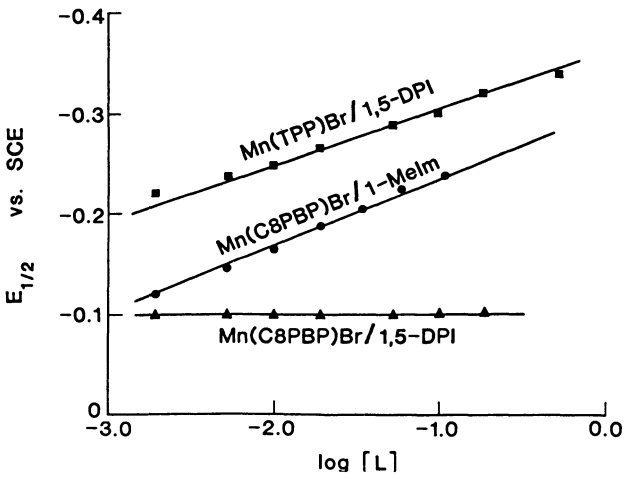

Fig. 4. Electrochemical study of Mn(III/II) half wave potential as a function of log[L].

For the porphyrin/imidazole combination where binding of a second imidazole is sterically disfavored, Mn(C8-PBP) with 1,5-diphenylimidazole, the Mn(II/III) half wave potential is independent of the imidazole concentration. Thus both the Mn(III) and the Mn(II) picnic basket porphyrins bind a single imidazole. This is direct evidence that the cavity in the picnic basket porphyrins will not accommodate 1,5-diphenylimidazole.

The electrochemical results indicate the binding of two imidazoles to Mn(III) in the unhindered cases while the spectral titrations indicate only one imidazole is bound. This apparent inconsistency can be explained by the fact that the electrochemical titration requires a supporting electrolyte, in this case tetrabutylammonium perchlorate, which supplies the perchlorate anion in concentrations 200 times that of the Mn(III) porphyrin. Under these conditions Bruice[25] and Kadish[23] have observed exchange of perchlorate for the counterion in the starting material. Thus, the manganese complex in the electrochemical titration is the perchlorate salt not the bromide salt used in the spectral titration. Since perchlorate is a weakly coordinating anion, perchlorate salts of Mn(III) porphyrins will bind two imidazoles unless sterically prevented from doing so.

Competitive Epoxidations. With knowledge of the regiochemistry and binding constant for imidazole ligation, we examined the substrate selectivity of the picnic basket porphyrin. Examination of molecular models showed that the unhindered face of the picnic basket porphyrin should be like TPP and the hindered pocket should resemble the sterically hindered TMP. As we have reported earlier,[26] Mn(TMP)Br is very selective for the epoxidation of cis olefins versus trans olefins. Mn(TPP)Br exhibits equal reactivity with cis and trans olefins. Table 1 shows the observed epoxide ratios for the hypochlorite oxidation of 1:1 olefin mixtures when catalyzed by Mn(TPP)Cl and Mn(TMP)Cl.[26] Thus, epoxidations of 1:1 mixtures of a cis and trans olefin, for example *cis*-2-octene and *trans*-β-methylstyrene, could be used to assay the

Table 1. Cis/Trans Olefin Selectivity of Mn(TMP)Cl vs. Mn(TPP)Cl in 1:1 Competitions

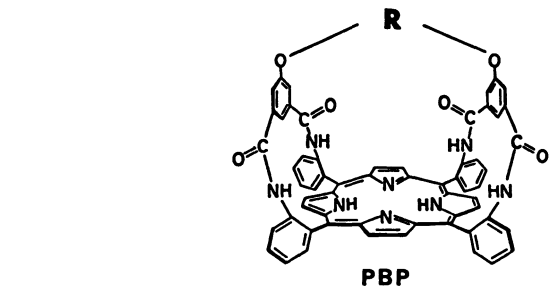

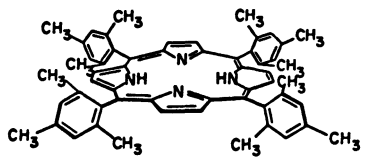

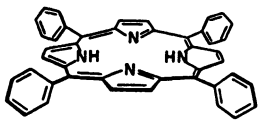

	epoxide ratio from 1:1 competition	
	Mn(TMP)Cl	Mn(TPP)Cl
	>20	1.3
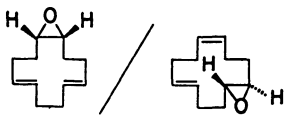	15	1.4

amount of catalytic oxygen atom transfer that occurs inside the pocket of the picnic basket porphyrin.

The epoxide ratios for several competitive oxygenations are listed in Table 2. Despite changes in the pocket size, counter-ion, the 1,5-diphenylimidazole concentration, and the nature of the oxidant, the ratio of epoxides was similar to Mn(TPP)Cl. Control experiments with each oxidant catalyzed by Mn(TPP)Cl and Mn(TMP)Cl showed dramatic changes in epoxide ratios as discussed above. In all cases the yield of total epoxide or the conversion of olefin to epoxide was in the range reported in the literature. Rates of Mn(PBP)Br catalyzed reactions were never less than 60% of the rate for the Mn(TPP)Br catalyzed reaction. The epoxide ratio did not vary significantly over the course of the catalytic reaction. The Mn(PBP)Br was also more stable than Mn(TPP)Br under the same reaction conditions as determined by decay of their visible bands.

These observations all indicate that catalytic reaction is occurring on the unhindered, sterically nonselective face of the porphyrin despite the presence of a large excess of nitrogenous base. The alternative explanation, that all or some fraction of the catalytic reaction is occurring inside the pocket and the pocket is sterically unselective, seems unlikely given the demonstrated steric sensitivity of competitive oxygenation by Mn(TMP)Cl. Similar results were obtained for the competitive oxygenation of *cis,trans, trans*-cyclododecatriene supporting this conclusion. We have attributed the lack of shape selectivity to failure to control the regiochemistry of high-valent metal-oxo formation, as illustrated in Fig. 5.

Studies of the kinetics of ligand exchange on Mn(III) porphyrins, although limited, show extremely fast exchange rates. Jordan has determined rate constants of 1.5×10^7 and 6.4×10^7 s^{-1} respectively for the exchange of free methanol or *N,N*-dimethylformamide for ligand coordinated to Mn(III)(protoporphyrin IX dimethyl ester)(ClO_4).[27] Bruice has also shown rapid exchange of anionic ligands.[25]

In contrast, oxygen atom transfer to manganese porphyrins appears to be a much slower process.[28] Bimolecular rate constants for oxygen atom transfer from alkyl hydroperoxides to Mn(TPP)Cl, in the presence of 1-methylimidazole, are reported in the range of 200—300 M^{-1} s^{-1}.[20] Thus, interconversion of the Mn(III) porphyrins, **I** and **II** (Fig. 5), is probably rapid relative to conversion to the postulated oxo complexes, **III** and **IV**. The Mn(III) species, **I** and **II**, are therefore always in equilibrium; the ratio being given by the concentration of 1,5-diphenylimidazole and the equilibrium binding constant, which was determined spectrally. For the competitive alkene epoxidations, the ratio of species **II** to **I** is calculated to be 60:1.

The lack of shape selectivity in the competitive oxygenations must be due to the relative rates of formation of the high-valent manganese species, **III** and **IV**. Perhaps oxygen atom transfer to the minor Mn(III) component, **I**, is so much faster than transfer to the major component, **II**, as to outweigh the concentration difference. This rate difference may arise from the larger steric hindrance of the pocket encountered by the oxygen atom donor in reacting with **II**. As we have previously reported,[10] we have observed rate constants which differ by at least two orders of magnitude for reactions occurring inside versus outside the picnic basket porphyrin cavity. The possibility that species **IV**, which has the oxo ligand bound within the cavity, is formed but reacts with olefin much more slowly than does **III** is inconsistent with the constant rate of epoxidation by Mn(PBP)Br, which is similar to that of Mn(TPP)Br. Under these conditions **IV** should accumulate with time and the

Table 2. Cis/Trans Olefin Selectivity of Mn(PBP)X Under a Variety of Reaction Conditions

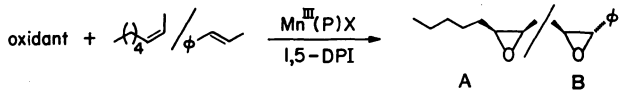

Oxidant	P	X⁻	[1,5-DPI]	A/B
C_6H_5IO	TPP	Br	50 mM	1.0
C_6H_5IO	TMP	Br	50 mM	25.0
C_6H_5IO	C6-PBP	Br	50 mM	1.9
NaOBr	C6-PBP	Br	50 mM	1.1
H_2O_2	C6-PBP	Br	50 mM	0.9
H_2O_2	PXY-PBP	Br	50 mM	0.8
H_2O_2	PXY-PBP	ClO_4	50 mM	0.8
H_2O_2	PXY-PBP	ClO_4	500 mM	0.8
C_6H_5IO	C8-PBP	Ph_3CCO_2	0 mM	1.6

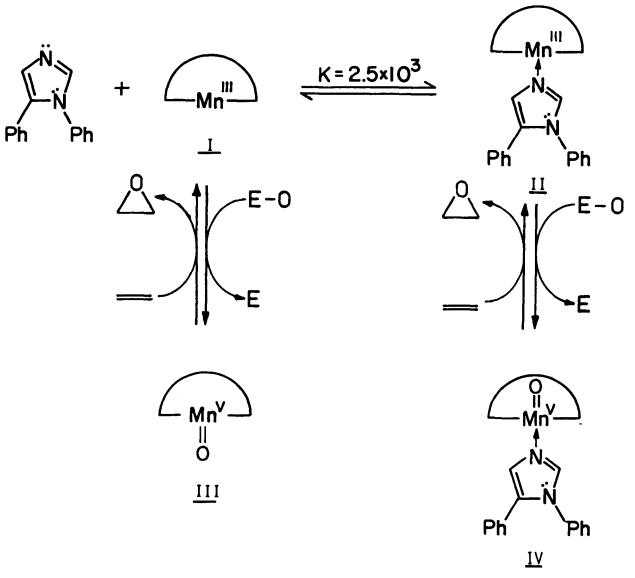

Fig. 5. Regiochemistry of metal oxo formation with Mn(PBP)X.

catalyst should exhibit reduced activity. Thus **IV**, if it is formed, must be able to revert to **II** at a fairly rapid rate. Thus, the lack of shape selectivity is probably due to the minor, unselective component in the catalyst mixture being the more active catalyst.

Studies of the Chiral Picnic Basket Mn(BN-PBP)Br, 9. The chiral binaphthyl picnic basket porphyrin **9** was studied under conditions similar to those reported above with 1-octene or styrene as substrates and LiOCl/phase transfer agent or hydrogen peroxide as the oxygen atom donors in the presence of 1,5-diphenylimidazole. Since circular dichroism spectra of **9** showed bands in the 300—700 nm region the synthesis and Mn metallation did not racemize the porphyrin. Within experimental error no asymmetric induction was observed in the product epoxides by chiral shift ^{1}H NMR using Eu(hfc)$_3$; this result is consistent with oxo formation occurring on the unhindered, achiral face of the porphyrin as observed above and not within the chiral pocket.

Conclusion

While modest regio and enantioselectivities have previously been observed for oxygenations catalyzed by Mn(III) and Fe(III) porphyrins, the porpyrins used in these studies are symmetric with respect to the porphyrin plane. No attempts to observe reaction within the pocket of an unsymmetrical porphyrin have been reported. Studies on the unsymmetrical Mn(PBP)X have shown that metal oxo formation appears to occur only on the unhindered and unselective porphyrin face. Metal oxo formation must occur inside the cavity before shape selective oxygenations can be observed with the picnic basket porphyrins.

While we were unable to observed any olefin selectivity with oxygen atom donors that would indicate epoxidation within the pocket, we felt that dioxygen could still be bound and activated within the pocket. Both ruthenium(II)[10a] and iron(II) picnic basket porphyrins and similar iron(II) pocket porphyrins[29] exhibit reversible binding of dioxygen in the presence of a bulky axial ligand, but preliminary attempts to activate dioxygen using two reducing agent/metalloporphyrin systems provided no evidence for oxygen activation.[3a,c]

We are continuing to study other routes to dioxygen activation including a well-characterized ruthenium(II) picnic basket porphyrin O_2 adduct.[10a] Another possibility is to use oxygen atom donors with a kinetically less labile combination of metalloporphyrin and bulky ligand. One promising candidate is a ruthenium picnic basket porphyrin phosphine complex.

Support from the National Institutes of Health (Grants NIH GM17880-16,17) and the National Science Foundation (Grant NSF CHE83-18512) is gratefully acknowledged. The Nicolet NMC-300 and Varian XL-400 spectrometers were purchased with funds from the National Science Foundation (Grants NSF CHE81-09064 and NSF CHE84-14329). Ms. Patricia Bethel and the University of California, San Francisco Mass Spectrometry Facility supported by the National Institutes of Health (Grant RR01614) obtained all the mass spectral data reported. Dr. Ruth Records (Stanford) obtained the circular dichroism spectra. Mr. Ronald Nelson is gratefully acknowledged for synthetic help.

References

1) J. T. Groves, W. J. Kruper, T. E. Nemo, and R. S. Myers, *J. Mol. Catal.*, **7**, 169 (1980); J. T. Groves and T. E. Nemo, *J. Am. Chem. Soc.*, **105**, 5786 (1983); B. R. Cook, T. J. Reinert, and K. S. Suslick, *ibid.*, **108**, 7281 (1986).

2) a) T. G. Groves and R. S. Myers, *J. Am. Chem. Soc.*, **105**, 5791 (1983); b) D. Mansuy, P. Battioni, J. P. Renaud, and P. Guerin, *J. Chem. Soc., Chem. Commun.*, **1985**, 155.

3) a) S. E. Creager, S. A. Raybuck, and R. W. Murray, *J. Am. Chem. Soc.*, **108**, 4225 (1986); b) P. Battioni, J. F. Bartoli, P. Leduc, M. Fontecave, and D. Mansuy, *J. Chem. Soc., Chem. Commun.*, **1987**, 791; E. I. Karasevich, A. M. Khenkin, and A. E. Shilov, *ibid.*, **1987**, 731; I. Tabushi, M. Kodera, and M. Yokoyama, *J. Am. Chem. Soc.*, **107**, 4466 (1985); I. Tabushi, and M. Kodera, *ibid.*, **108**, 1101 (1986).

4) A. M. van Leusen, J. Wildeman, and O. H. Oldenziel, *J. Org. Chem.*, **42**, 1153 (1977).

5) T. N. Sorrell, *Inorg. Synth.*, **20**, 161 (1980); C. M. Elliott, *Anal. Chem.*, **52**, 666 (1980); J. Lindsey, *J. Org. Chem.*, **45**, 5215 (1980).

6) S. Ariel, D. Dolphin, G. Domazetis, B. R. James, T. W. Leung, S. J. Rettig, J. Trotter, and G. M. Williams, *Can. J. Chem.*, **62**, 755 (1984).

7) G. B. Jameson and J. A. Ibers, *J. Am. Chem. Soc.*, **102**, 2823 (1980).

8) a) L. Ricard, R. Weiss, and M. Momenteau., *J. Chem. Soc., Chem. Commun.*, **1986**, 818; b) T. G. Traylor, N. Koga, L. A. Deardurff, P. N. Swepston, and J. A. Ibers, *J. Am. Chem. Soc.*, **106**, 5132 (1984).

9) J. P. Collman, R. R. Gagne, C. A. Reed, T. R. Halbert, G. Land, and W. T. Robinson., *J. Am. Chem. Soc.*, **97**, 1427 (1975).

10) a) J. P. Collman, J. I. Brauman, J. P. Fitzgerald, J. W. Sparapany, J. A. Ibers, *J. Am. Chem. Soc.*, (in press); b) J. P. Collman, J. I. Brauman, J. P. Fitzgerald, P. D. Hampton, Y. Naruta, J. W. Sparapany, and J. A. Ibers, *ibid.*, (in press).

11) a) E. Guilmet and B. Meunier, *Nouv. J. Chim.*, **6**, 511 (1982); b) J. P. Collman, T. Kodadek, S. A. Raybuck, and B. Meunier, *Proc. Natl. Acad. Sci. U.S.A.*, **80**, 7039 (1983).

12) B. Meunier, E. Gulmet, M. E. De Carvalho, and R. Poilblanc, *J. Am. Chem. Soc.*, **106**, 6668 (1984).

13) D. Mansuy, P. Battioni, and J. P. Renaud, *J. Chem. Soc., Chem. Commun.*, **1984**, 1255; J. P. Renaud, P. Battioni, and J. F. Bartoli, and D. Mansuy, *ibid.*, **1985**, 888; P. Battioni, J. P. Renaud, J. F. Bartioni, and D. Mansuy, *ibid.*, **1986**, 341.

14) a) J. F. Kirner, C. A. Reed, and W. R. Scheidt, *J. Am.*

Chem. Soc., **99**, 2557 (1977); b) R. D. Jones, D. A. Summerville, and F. Basolo, *ibid.*, **100**, 4416 (1978).

15) a) V. W. Day, B. R. Stults, E. L. Tasset, R. O. Day, and R. S. Marianelli, *J. Am. Chem. Soc.*, **96**, 2650 (1974); b) J. F. Kirner and W. R. Scheidt, *Inorg. Chem.*, **14**, 2081 (1975).

16) C. L. Hill and M. M. Williamson, *Inorg. Chem.*, **24**, 2836 (1985).

17) A. Yamamoto, L. K. Phillips, and M. Calvin, *Inorg. Chem.*, **7**, 847 (1968).

18) L. J. Boucher, *J. Am. Chem. Soc.*, **90**, 6640 (1968); L. J. Boucher, *Coord. Chem. Rev.*, **7**, 289 (1972).

19) G. N. La Mar and F. A. Walker, *J. Am. Chem. Soc.*, **97**, 5103 (1975).

20) Y. C. Yuan and T. C. Bruice, *J. Am. Chem. Soc.*, **108**, 1643 (1986).

21) F. A. Walker, M. W. Lo, and M. T. Ree, *J. Am. Chem. Soc.*, **98**, 5552 (1976).

22) D. Burdige and D. A. Sweigart, *Inorg. Chim. Acta*, **28**, L131—L133 (1978); K. M. Adams, P. G. Rasmussen, W. R. Scheidt, and K. Hatano, *Inorg. Chem.*, **18**, 1892 (1979); R. S. Drago, "Physical Methods in Chemistry," W. B. Saunders Co. (1977), p. 91.

23) S. L. Kelly and K. M. Kadish, *Inorg. Chem.*, **21**, 3631 (1982).

24) K. M. Kadish and S. L. Kelly, *Inorg. Chem.*, **18**, 2968 (1979).

25) M. F. Powell, E. F. Pai, and T. C. Bruice, *J. Am. Chem. Soc.*, **106**, 3277 (1984).

26) J. P. Collman, J. I. Brauman, B. Meunier, S. A. Raybuck, and T. Kodadek, *Proc. Nat. Acad. Sci. U.S.A.*, **81**, 3245 (1984); J. P. Collman, J. I. Brauman, B. Meunier, T. Hayashi, T. Kodadek, and S. A. Raybuck, *J. Am. Chem. Soc.*, **107**, 2000 (1985).

27) L. Rusnak and R. B. Jordan, *Inorg. Chem.*, **11**, 196 (1972).

28) L. C. Yuan and T. C. Bruice, *Inorg. Chem.*, **24**, 986 (1985); C. L. Hill, J. A. Smegal, and T. J. Henley, *J. Org. Chem.*, **48**, 3277 (1983).

29) K. Suslick and T. J. Reinert, *J. Chem. Ed.*, **62**, 974 (1985).

 © 1988 The Chemical Society of Japan Bull. Chem. Soc. Jpn., 61, 59—69 (1988)

Invited Paper

Pentaamminechromium(III) t_{2g}^3 Level Properties as Determined from Vibronic Spectra and Crystal Field Calculations

Hans-Herbert SCHMIDTKE,* Heribert ADAMSKY, and Thomas SCHÖNHERR
Institut für Theoretische Chemie der Universität Düsseldorf, D-4000 Düsseldorf 1, F.R.G.
(Received August 7, 1987)

Low temperature (~5 K) absorption and emission spectra of various halogenopentaamminechromium(III) salts have been recorded at high sensitivity in the intercombination region from pure microcrystalline powders and doped into corresponding rhodium complexes. Zero phonon and vibrational side bands are better resolved than reported in earlier investigations. They depend on the crystal lattice and allow a more detailed analysis of the vibrational fine structure. For carrying out reliable assignments to vibronic energy levels, the influence of the crystalline environment in different salts is found to be of major importance. Ligand field and angular overlap calculations are very helpful for solving the assignment problem, they can reproduce the proposed energy level scheme if symmetry adapted π-orbital expansion coefficients are introduced into the electron repulsion terms.

Since the pioneering work of A. E. Becquerel[1] who reported the luminescence lifetime of ruby in 1867, chromium(III) ion lattices and complexes have become the subject of increasing research activity in the field of photophysics and photochemistry. In particular, the theoretical work of Tanabe and Sugano[2] has greatly stimulated the understanding of processes which are connected with light absorption and emission of these systems. At present, the discovery of the room temperature tunable alexandrite laser[3] and the potential use of chromium(III) doped glass ceramics as solar concentrators[4,5] have additionally focused attention on electronic and vibrational properties of d^3 complexes. Whereas, in general, most of the properties of ionic systems are determined by their particular lattices formed on crystallization, common coordination compounds as $[Cr(NH_3)_6]^{3+}$ or $Cr(acac)_3$ are better described by isolated molecular species in the solid using theoretical methods which are appropriate for investigating chemical bondings.[6,7] For examining the photochemical reaction pathways, starting from the optical spectra as a basis, in the past twenty years predominantly chromium ammine compounds have been extensively used as sample cases.[8,9]

In an early attempt, Schläfer[10] related the energy gap between the ^2E_g and $^4T_{2g}$ levels (in O_h notation) derived from spectroscopically obtained ligand field (LF) parameters to the type of photophysical activity (fluorescence or phosphorescence), an observation which later has been named as Schläfer's rule. In an alternative point of view, the various ways of metal–ligand bonding have been considered for rationalizing the experimental results by classifying the ligands according to their extent of σ- and π-interactions towards the central metal.[11] More recently, this idea has been taken over for use in the angular overlap model (AOM) by which photosubstitution processes could be investigated calculating metal–ligand strengths in the excited state.[12] Although this procedure seems to account for the majority of results obtained from low symmetry chromium(III) ammine complexes, the predictions on photosubstitution concerning the leaving group have been claimed to be incorrect for some of the acidopentaammines.[13] Forster and coworkers have examined the emission spectra of more than 40 tetragonal ammine complexes.[14,15] They classified these compounds, by inspection of band shapes obtained, into ^2E_g and $^2T_{1g}$ emitters and expressed the energies of the lowest excited states by AOM antibonding parameters derived from level splittings as measured for spin-allowed transitions into quartet states. In addition, the doublet transition energy has been found to be of major influence on the nonradiative decay rate, and even a slight modification of the second coordination sphere could lead to drastic changes of luminescence properties.[16] "Although a considerable body of data has been collected···the relative importance of changes in electronic and vibrational factors that accompany ligand substitution is not yet clear" (quoted from Ref. 17). Compared to the amount of experimental results reported in the literature, theoretical investigations on electronic states arising from t_{2g}^3 electron configuration are more rare. For instance, the magnitude of the splitting of the lowest excited ^2E_g level due to lower symmetry is not clear and has been an object of controversy;[18–20] also information on the location of the spin-orbit split components of $^2T_{1g}$ and $^2T_{2g}$ is very scarce[21] and explanations for the in various complexes[22–24] anomalously large $^4A_{2g}$ ground state splitting is still unsatisfactory. On the other hand, since much of the experimental work cited above was performed on glassy solutions yielding poorly resolved spectra, the amount of information which can be obtained from these results is very limited.

Therefore, we want to report in the following some low temperature absorption and emission spectra of microcrystalline materials of pure halogenopentaammine complexes and doped in crystal lattices of

similar composition yielding much better resolved band patterns as obtained earlier. The characterization of zero phonon bands different from vibrational side bands supplies an improved basis for carrying out band assignments and determining level splittings due to the lower symmetry; it contributes to investigate the role of spin-orbit coupling and covalent bonding effects on the energy level scheme and transition probabilities. Distortions of the nuclear framework in the excited state and, eventually, changes of potential energy surfaces close to the equilibrium geometry may be obtained from an analysis of the vibrational fine structure yielding evidence on the strength of vibronic coupling, important for the energy transfer and reactivity of the molecule. Parallel to the experiments various calculations have been carried out using common theoretical models as LF theory and the AOM, introducing only minor modifications when proved to be necessary. The results supply important contributions to the discussion of the assignment problem.

Experimental

Preparation of Compounds. The chromium(III) complexes were synthesized according to methods given in the literature.[25] The chloro- and bromopentaammine salts, abbreviated by $[Cl]Y_2$ and $[Br]Y_2$, were purified by metathesis from saturated solutions in respective acids HY. Preparation of iodopentaammine is interfered by rapid hydrolysis processes which prevent further recrystallization. The quality of these samples was checked by recording their luminescence spectra which are very sensitive to decomposition. Deuterated materials were obtained by repeated treatment of saturated D_2O solutions with DY. Small single crystals (0.2—0.5 mm diameter) of $[Cl]Cl_2$ were grown from hot (60 °C) acidified aqueous solutions within several hours. Analogous rhodium(III) compounds for use as suitable host crystals were prepared from $[Rh(NH_3)_5Cl]Cl_2$ which was recrystallized following given procedures.[26]

Spectroscopic Measurements. Visible and ultraviolet spectra were recorded using an appropriately modified Cary 17 spectrophotometer equipped with an RCA 4832 photomultiplier. Polarized spectra obtained from a specially designed microscopic optical device[27] gave additional information only on the splittings of the broad quartet bands. Absorption and emission spectra due to intercombination transitions were measured using a McPherson 0.5 m double monochromator model 285 fitted with a 1200 lines/mm grating and a red sensitive GaAs photomultiplier. For comparing peak intensities the emission spectra are corrected for apparative response. Further parts of the equipment have been an argon laser and a helium flow cryostat allowing temperature to be reached at the sample down to 5 K. Low excitation intensities were necessary to prevent photodecomposition of the compounds. The 20 K Raman spectrum of $[Cl](NO_3)_2$ was recorded by T. Woike[28] using the 620 nm line of an optically pumped dye laser. Under these mild conditions the spectrum can be reproducibly recorded avoiding photodecomposition to a large extent.

Energy Levels

Electronic States. Octahedral complex compounds of transition metal ions with t_{2g}^3 electron configuration have $\binom{6}{3}=20$ electronic levels which due to the molecular symmetry are in part degenerate leading to the multiplet states $^4A_{2g}$ (ground state), ^2E_g, $^2T_{1g}$, and $^2T_{2g}$. At lower symmetry these states are split into a maximum of 10 energy levels leaving a residual twofold degeneracy (Kramers doublets) if magnetic fields are absent. For C_{4v} point symmetry pertinent for the present compounds, the level symbols and level splittings due to the various interactions considered are indicated in Fig. 1.

Electron transitions between these states exhibit, at least for helium temperature spectra of crystalline solids, well resolved vibrational fine structure which can be compared to the IR and/or Raman spectra, vibrational quanta in the t_{2g}^3 excited states being similar to those in the ground state since chemical bonding will not be changed very much on excitation into levels arising from the same electron configuration. An analysis of the fine structure identifying particular vibrational side bands is, nevertheless, not easy because band superpositions will occur to a large extent due to several electron transitions being located close to each other. In particular, the positions of the low symmetry spin-orbit levels arising from $^2T_{1g}$ and $^2T_{2g}$ are difficult to localize in the energy level scheme

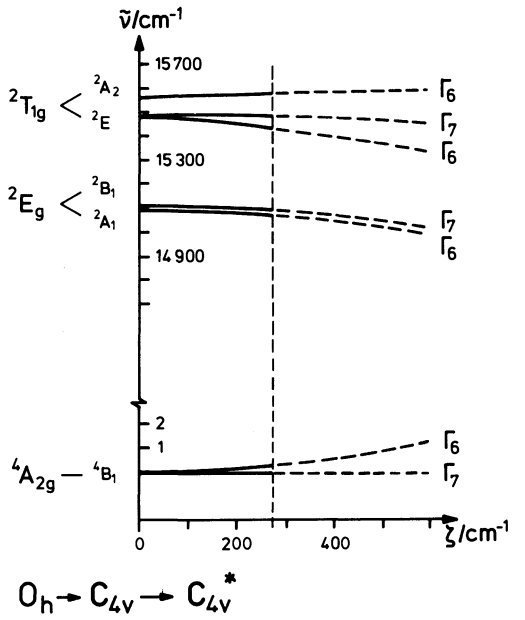

Fig. 1. Electronic t_{2g}^3 LF level scheme for C_{4v} symmetry chromium(III) complexes depending on the spin-orbit coupling coefficient ζ, for heavier ligands exceeding the parameter of the free ion (dotted lines). Model parameters chosen are σ_N= 7500, π_N=0, σ_X=5000, π_X=750, B=600, C=3500, all in cm^{-1}.

(see below); as far as the first excited ^2E_g level is concerned a splitting between 20 cm^{-1} for $[H_2O](ClO_4)_3$ and about 200 cm^{-1} for halogenopentaammine complexes [X] have been reported.[18,19] The latter result cannot be reproduced by conventional LF calculations[18,20] although level schemes of similar mixed halogeno-amine complexes of Cr(III) are explained very well by applying this model.[29] A substantial increase of ^2E_g level splitting is, however, calculated when different nephelauxetic effects are assumed for $b_2(d_{xy})$ and $e(d_{xz},d_{yz})$ orbitals of C_{4v} symmetry (see below). Since no crystal structural data had been available, earlier calculations could not use actual molecular geometries. Recently, however, the room temperature crystal structure of $[Cl]Cl_2$ has been reported[30] according to which the chromium ions occupy equivalent sites with approximately C_{4v} symmetry. The exact site symmetry is only C_s and the space group $D_{2h}^{16}\equiv Pnma$.

By spin-orbit coupling the multiplet levels are split by different amounts (see Fig. 1), the $^4B_1(C_{4v})$ ground state splitting being very small which cannot be resolved by electronic spectroscopy. ESR results report zero field splittings of the ground state of some 0.2 (chloro complex) to 0.9 cm^{-1} (iodo complex).[22,31,32] The experimental splittings thus obtained for the heavier halogeno complexes turn out to be much larger than those predicted from conventional LF calculations from which it was concluded that the effective spin-orbit coupling constants should be increased to unusual high values.[22] To what extent this assumption can be justified will be discussed when describing the LF calculations.

Vibrational Levels. In the infrared spectrum only vibrations of a_1 and e symmetry type will be expected on the basis of C_{4v} selection rules, in the Raman spectrum on the other hand all vibrational transitions of CrN_5X chromophore are allowed. Figure 2 illustrates the 20 K Raman spectrum of $[Cl](NO_3)_2$ which due to the easy photodecomposition of the compound is only obtained by a careful wave length selection of incident light. Assignments to internal complex vibrations were made on the basis of available infrared data, normal coordinate analyses,[33]

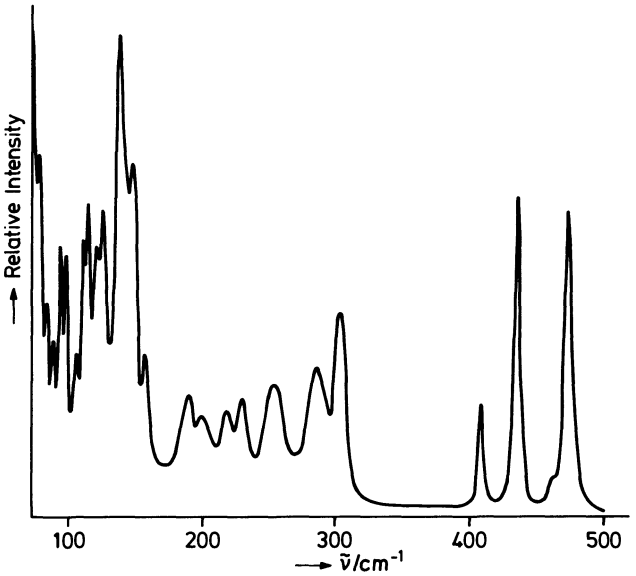

Fig. 2. Raman spectrum of $[Cr(NH_3)_5Cl](NO_3)_2$ at 20 K obtained from a 620 nm dye laser excitation.

Table 1. Normal Vibrations and Observed Frequencies for $[Cl]Y_2$ Compounds Obtained for $Y=NO_3$ from Raman and Emission Spectra and for Y=Cl from the Emission Spectrum only

No.	Symmetry	Atomic group vibrations (approximate)	Observed frequency $[Cl]Y_2$		$\nu(H)/\nu(D)$
			$Y=NO_3$	Y=Cl	Y=Cl
ν_1	a_1	$\sigma(Cr\text{-}NH_3)_{ax}$	471	477	1.06
ν_2	a_1		434	438	
ν_3	b_1	$\sigma(Cr\text{-}NH_3)_{eq}$	406	415	1.08
ν_4	e		460	465	
ν_5	a_1	$\sigma(Cr\text{-}X)$	301	309	1.02
ν_6	a_1		215	214	1.11
ν_7	b_1		189	187	1.08
ν_8	b_2	$\delta(H_3N\text{-}Cr\text{-}NH_3)$	285	276	1.11
ν_9	e		252	254	1.10
ν_{10}	e		125	115	1.10
ν_{11}	e	$\delta(H_3N\text{-}Cr\text{-}X)$	147	141	1.00
ν_{12}	a_1		805	806	1.30
ν_{13}	a_2		745	751	1.27
ν_{14}	b_1	$\delta(Cr\text{-}N\text{-}H)_{eq}$	660	667	1.30
ν_{15}	b_2		680	687	1.32
ν_{16}	e		766	771	1.28
ν_{17}	e		700	702	1.32
ν_{18}	e	$\delta(Cr\text{-}N\text{-}H)_{ax}$	—	652	1.31

and results obtained from the present vibronic spectra. Table 1 compiles all normal vibrations of given symmetry type involving the chromium central atom; also an assignment of all vibrational frequencies together with their deuterium shifts measured for the chloro complex is given.

Results and Discussion

^2E_g and $^2T_{1g}$ Spectrum. In Fig. 3 the crystalline powder absorption spectra of three halogenopentaammine complexes recorded at low temperature (~5 K) in the $^4A_{2g} \rightarrow {}^2E_g$, $^2T_{1g}$ (O_h notation) energy region are illustrated. The dominating band peaks indicated by A, B, and C are assigned in agreement with earlier works[18-20] to zero phonon transitions; on deuteration they exhibit isotope shifts which are negligible compared to the other bands. The vibronic side band pattern can be explained in terms of σ(Cr-NH_3), σ(Cr-X), δ(H_3N-Cr-NH_3), and δ(Cr-N-H) atomic group vibrations of the chromophore (cf. Table 1). Assignment of zero phonon peaks to their octahedral parent states ^2E_g and $^2T_{1g}$ is, however, in dispute[18-20] (see above).

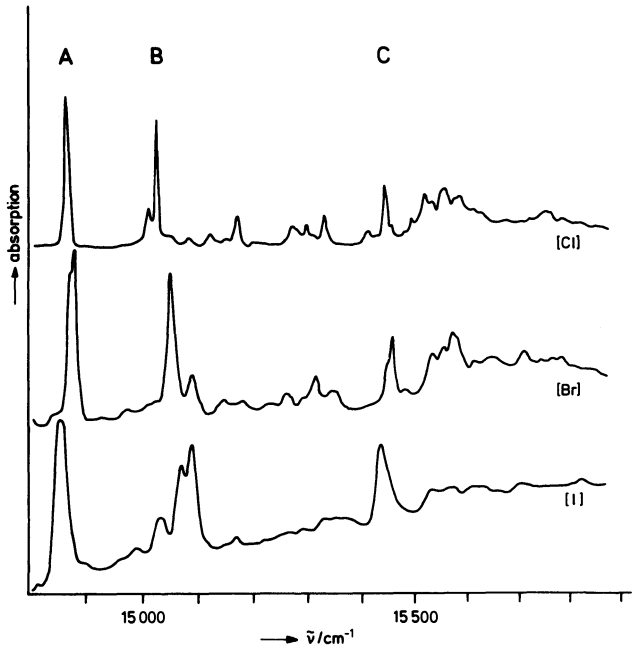

Fig. 3. Overall 5 K absorption spectra in the ^2E_g and $^2T_{1g}$ region of micro crystalline $[Cr(NH_3)_5X](NO_3)_2$.

The relative intensities of vibronic side bands obviously decrease in the series from [Cl] to [I] which may be explained by the larger perturbation of the octahedral symmetry by heavier halogen ligands breaking the d-d parity selection rule more efficiently and making pure electronic transitions allowed. It is further noticed that the band A belonging to the lowest transition energy is not much affected by the hetero ligands Cl, Br, or I which seems to be surprising in view of the fact that the energy gap to the ground state, approximately given by Racah parameters 9B+3C, ought to be subject to a varying nephelauxetic effect in this series of compounds. Also the energy difference between A and C peaks is almost unchanged in the spectra, only the position of the B bands varies to a certain amount. On the other hand crystalline effects are much larger than expected which becomes apparent from changing the anions of the salts, they even dominate the band shifts resulting from a variation of the hetero ligand (cf. Table 2).

$^2E_g(O_h)$ Splitting. The spectrum of crystalline $[Cl]Cl_2$ recorded with high resolution (better than 2 cm^{-1}) exhibits a splitting of the A band into two components A_I and A_{II} of different intensities (cf. Fig. 4). Half widths (8—10 cm^{-1}) and peak separations (12 cm^{-1}) are measured equally well for the deuterated complex (separation 14 cm^{-1}). In the emission spectrum the two peaks are found at almost identical frequencies, the intensity of the peak at higher energy increasing with temperature. For different counter ions the band profile changes, however, significantly. This applies for the degree of splitting and for the

Table 2. Zero Phonon Bands (in cm^{-1}) of $[Cr(NH_3)_5X]Y_2$ due to t_{2g}^3 Transitions Obtained from Low Temperature Absorption Spectra. I Refers to the Main Peak, II to a Satellite Peak or Shoulder

Compound	A_I	A_{II}-A_I	B-A_I	C_I-A_I	C_{II}-C_I
$[Cl](NO_3)_2$	14866	+6	160	580	—
$[Cl]Cl_2$	14826	−12	179	598	−7
$[Cl]Br_2$	14782	—[a]	188	589	—[a]
$[Cl]I_2$	14719	<0	192	617 (537)[b]	15 (−20)[b]
$[Br](NO_3)_2$	14888	−7	170	575	−9
$[Br]Br_2$	14780	−13	224	602	−10
$[I](NO_3)_2$	14853	+11	237	585	+10
$[I]I_2$	14656	—[a]	307	600	—[a]
Proposed Assignment:	$^2A_1(^2E_g)$		$^2B_1(^2E_g)$	$^2A_2(^2T_{1g})$	

a) Broad band, splitting not resolved. b) Alternative assignment possible.

relative intensities of the peaks as well (see Table 2) which may have different explanations depending on the assignment made to the low symmetry level scheme (see later). Ligand field theory using common model parameters predicts the transition into the $\Gamma_6(^2A_1)$ component (cf. Fig. 1) to be lowest in energy. In addition, for some of the complex salts, e.g. $[Cl](NO_3)_2$, in this zero phonon region another much weaker transition is detected which in the absorption spectrum is observed as a shoulder.

The corresponding doublet band patterns could not be resolved in the case of $[NCO](NO_3)_2$[20] and $[I]I_2$ (Table 2), on the other hand in the spectra of most of the compounds investigated two transitions are observed which are located closely together in energy, one (A_I) with a higher intensity than the other (A_{II}). It is tempting to assign these peaks to the C_{4v} symmetry splitting of $^2E_g(O_h)$, i.e. to $^2A_1$ and $^2B_1$ which would be in agreement with the assignment proposed for the $[H_2O]$ and [OH] perchlorate.[19] However, pair interactions of paramagnetic Cr^{3+} centers could also give rise to additional peaks in the intercombination spectra.[34] Since these pair states are essentially determined by Cr–Cr distances we also investigated doped materials (0.1—3%Cr^{3+}) in corresponding Rh(III) complex salts. The spectra of these samples show, however, a quite similar A band pattern by which the occurrence of pair spectra can be excluded.

A further, more probable explanation is offered by the presence of different sites for Cr positions in the crystal. The space group *Pnma* obtained at room temperature for the $[Cl]Cl_2$ has only equivalent sites available for Cr atoms,[30] however, a temperature dependent X-ray investigation carried out on a powder sample distinctly reveals a structural phase transition between 220 and 230 K which cannot be detected in the electronic spectrum due to the lack of appropriate fine structure at these temperatures. Consequently we prefer to assign the band at A to only one of the ^2E_g split levels, the pair character being due to different sites; the other ^2E_g component then gives rise to the B band 150 to 300 cm^{-1} higher in energy. This interpretation would also explain the doublet structure of the zero phonon band C (cf. Table 2) although a similar pattern for B which equally well should be expected as a pair of bands could not be resolved. The varying band profile of A observed when changing the counter ion is then due to different environmental effects on crystalline Cr sites.

$^2T_{1g}(O_h)$ Splitting. From the six-fold degenerate $^2T_{1g}$ level which in octahedral complexes is located some 550 to 600 cm^{-1} higher than ^2E_g, at maximum three Kramers doublets can result (cf. Fig. 1) from which in tetragonal symmetry the $^2E(^2T_{1g})$ levels are appreciably decreased in energy due to interaction with the higher $^2E(^2T_{2g})$ levels of the same symmetry. The change in energy can be estimated from the AOM perturbation matrix by

$$\Delta E(^2E) = \frac{(\pi_L - \pi_X)^2}{6B + 2C} \quad (1)$$

with antibonding parameters π_L and π_X for the ligands L and X of a ML_5X chromophore. Since this expression is a negative contribution to the energy for any parameters associated to the ligands, $^2E(C_{4v})$ resulting from $^2T_{1g}(O_h)$ is always stabilized. On the other hand, the second $^2T_{1g}$ component, i.e. $^2A_2$, is almost unchanged on symmetry reduction since except for smaller spin-orbit coupling effects no interactions of neighboring levels are possible by symmetry reasons. As band C remains at almost equal position, e.g. in the series [Cl], [Br], and [I] of nitrate salts (see Table 2) for which π_X should essentially change, an assignment of this zero phonon band to $^2A_2$ seems to be straightforward (see crystal field calcula-

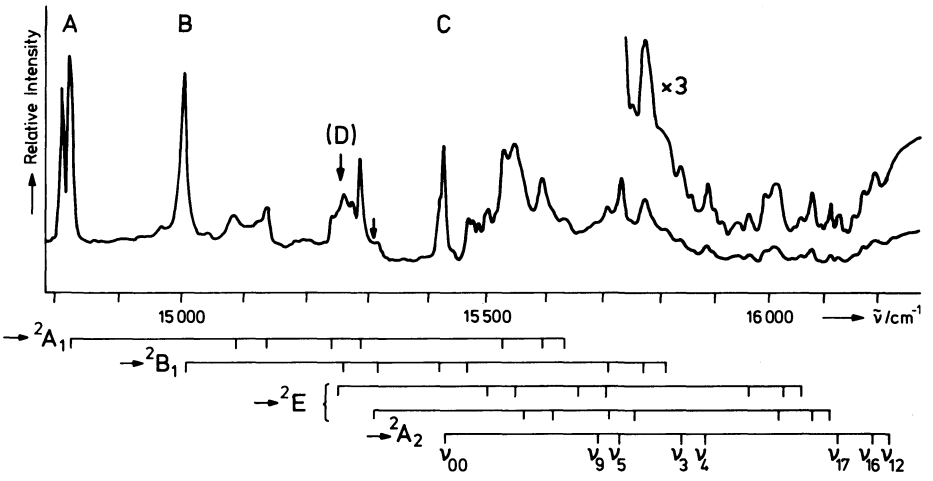

Fig. 4. High resolution absorption spectrum of $[Cr(NH_3)_5Cl]Cl_2$ at 5 K and vibronic assignments to C_{4v} symmetry levels (in the neighboring energy region narrow line spectra cannot be resolved).

tions).

Reliable assignments of $^4B_1 \rightarrow \Gamma_6, \Gamma_7(^2E)$ transitions in absorption spectra of low symmetry Cr(III) ammine complexes have not been carried out as yet because corresponding peaks are usually superimposed by vibrational side bands of $\Gamma_6(A_1)$ and $\Gamma_7(B_1)$ transitions arising from $^2E_g(O_h)$, the zero phonon peaks of which we have assigned to the A and B band. For localizing hidden zero phonon transitions in this region a vibronic band analysis must be performed assigning all vibronic intervals to normal vibrations known from Raman and luminescence spectra. In Fig. 4 the result of this analysis obtained for the [Cl]Cl_2 spectrum is presented by indicating the normal modes which give rise to absorption peaks in the side band spectrum. For this assignment only those vibrational quanta are used which are measured in the luminescence spectrum as main bands; by this virtually all satellite peaks can be explained. The same procedure is applied also to the corresponding deuterated compound which allows for checking each of the band assignments by regarding the expected isotope shifts of Table 1. As a result we conclude that a further zero phonon transition (D) should be present at 15246 cm^{-1} that is calculated from vibrational intervals belonging to ν_3, ν_5, ν_9, and ν_{16} to ν_{18} quanta. Indications for another zero phonon transition in this region also lower in energy than $^2A_2$ are found at a position marked by an arrow in Fig. 4 which could originate from the second split component of $^2E(C_{4v})$. However, these assignments are less certain.

$^2T_{2g}$ Spectrum. In Fig. 5 the spectrum of [Br]Br_2 is presented which includes also quartet transitions. Superimposed to one of these quartets the highest t_{2g}^3 intraconfigurational transitions can be detected with unusually large intensity. A similar band pattern has been reported[35] in this region for tr[Cr en_2Br_2](ClO_4) which was explained being due to the D_{4h} components ^2E_g and $^2B_{2g}$ of $^2T_{2g}(O_h)$. Güdel and co-workers, on the other hand, have assigned two narrow band shoulders they detected on the short wave length flank of the first quartet band of [OH]$(ClO_4)_2$ to the Γ_6 and Γ_7 components of $^2E(^2T_{2g})$, however, did not find any other fine structure close to these absorptions.[19] The present band profile obtained for [Br]Br_2 (similar features can be observed at high resolution also in the other halogenopentaammine spectra) with a relatively slowly decreasing progression of about 240 cm^{-1} is detected only at low temperatures. It cannot be assigned to a spin allowed transition, since quartet bands remain essentially unchanged on cooling to liquid helium temperatures. Higher intensities (extinction coefficients $\varepsilon \sim 10$) and larger band widths (~ 50 cm^{-1}) can be well explained from the interacting electronic energy level scheme considering spin-orbit coupling. Relevant finite off-diagonal perturbation matrix elements intermixing ^2E and $^4B_2$ wave functions of C_{4v} are

$$\langle \Gamma_6(^2E) | H_{SO} | \Gamma_6(^4B_2) \rangle = -\frac{\zeta}{2}$$

$$\langle \Gamma_7(^2E) | H_{SO} | \Gamma_7(^4B_2) \rangle = -\frac{\zeta}{\sqrt{12}} \qquad (2)$$

ζ being the one-electron spin-orbit coupling coefficient, while the corresponding matrix element with the second $^2T_{2g}(O_h)$ component, i.e. $\Gamma_7(^2B_2)$, is vanishing.[36] Other interactions of this kind involving the $^4E(C_{4v})$ state of $^4T_{2g}$ are small due to the energy denominator which is several thousand wavenumbers larger than for interactions with $^4B_2(C_{4v})$. Due to the larger mixing coefficient of $\Gamma_6(^4B_2)$ into $\Gamma_6(^2E)$ functions the transition into the $\Gamma_6(^2E)$ state should

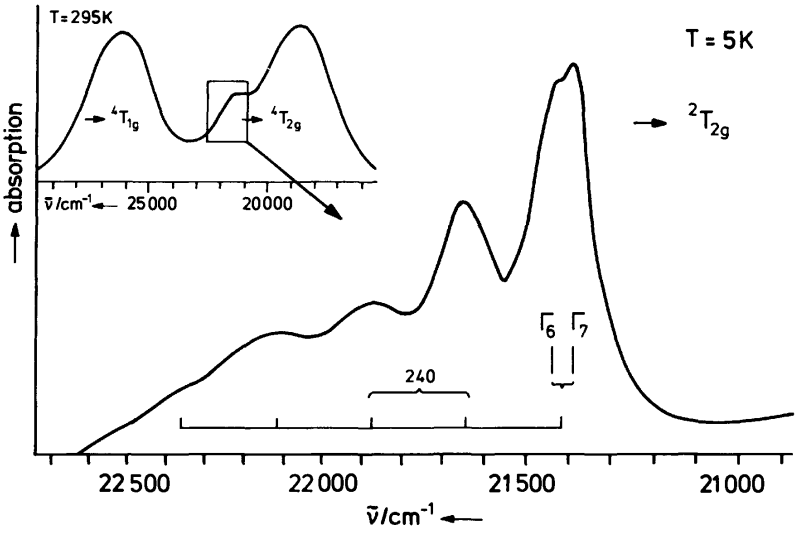

Fig. 5. Room temperature quartet absorption spectrum and 5 K high resolution $^2T_{2g}$ spectrum.

obtain higher intensity than for $\Gamma_7(^2E)$; the total splitting into Γ_6 and Γ_7 of ^2E is computed by a complete ligand field calculation to be some 50 cm^{-1} which is in good accordance with the assignment given in Fig. 5. The band widths, which are increased compared to usual doublet transitions of Cr(III), also indicate a higher contribution of quartet character which accounts for the occurrence of a vibrational progression due to larger nuclear distortions with respect to the ground state geometry.

The Fluoro Complex. In the series of halogenopentaammines of chromium(III) the fluoro complex spectrum obviously occupies a particular position. In the region of $^4A_{2g} \rightarrow {}^2E_g$ zero phonon transitions the absorption spectrum shows six intensive peaks, some with different half widths (cf. Fig. 6). In the emission spectrum corresponding bands are located at equal energies, their intensities being strongly temperature dependent which partly can be explained by Boltzmann distribution. The band pattern is repeated a few times shifted towards smaller wavenumbers into the vibrational side band region. These findings are best accounted for by the presence of a bunch of zero phonon transitions which arise from several nonequivalent sites in the crystal. Unfortunately no structural data is available for the fluoropentaamminechromium complex (as is not for other central metal ions). A preliminary powder X-ray recording at room temperature indicates a complicated super structure which is not unusual for perchlorate lattices. This would be in agreement with the given interpretation assuming nonequivalent chromium positions. A possible explanation may be given by the smaller size of the fluoride ion compared to NH_3 ligands preventing the hetero-ligand to favor a certain coordinate direction in the crystal lattice (the complex is considered to be built into the holes of the anion lattice) that would lead to a formation of different sites in the crystal.

An analysis of the vibrational side bands similar to the discussion carried out for the other halogeno complexes is not possible due to large band superpositions and a lack of sufficient peak resolution in this spectrum. Therefore also the zero phonon lines arising from $^2T_{1g}(O_h)$ split levels cannot be located. However, the slowly decreasing progressions in 530 cm^{-1} quanta clearly identified in the emission spectrum are explained being due to the metal-halogen stretching vibration $\nu_5(a_1)$ which is also observed in the spectra of the other pentaammine complexes. The intensity distribution in these progressions will be used for determining the geometric distortion of the emitting state (see below).

Crystal Field Calculations. Conventional LF and AOM calculations are, in general, able for the present compounds to account for the electronic energy level scheme verified from the experiment.[19,20,36] There are, however, some exceptions: e.g., the size of the low symmetry splitting of the $^4A_{2g}(O_h)$ ground and first excited state ^2E_g cannot be reproduced, i.e. in the experiment they are found about one order of magnitude larger than from theory even though when complete LF calculations are carried out considering all possible $\binom{10}{3}=120$ wave functions of the d^3 electron configuration. The highest level splittings calculated from usual model parameters which hold also for other chromium(III) complexes are ~0.3 cm^{-1} for $^4A_{2g}$ and ~50 cm^{-1} for ^2E_g. The results do not change very much if various improvements are implemented in the computer program:[21] consideration of the real

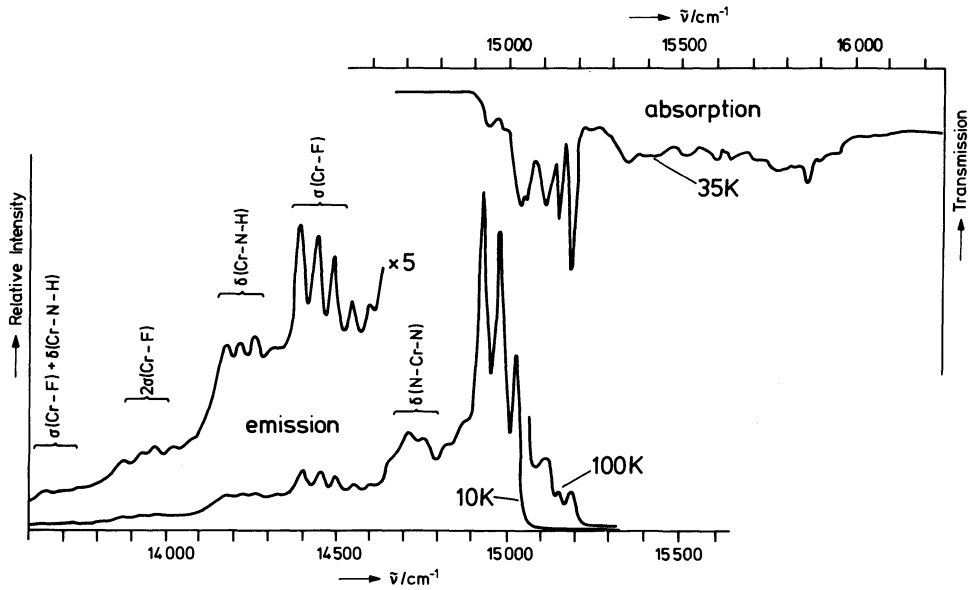

Fig. 6. Vibronic absorption spectrum (35 K) in the intercombination region and emission spectrum (10 K and 100 K, λ_{exc}=514.5 nm) of $[Cr(NH_3)_5F](ClO_4)_2$.

geometry, introduction of Trees correction, distinction of nephelauxetic effects for e_g and t_{2g} orbitals ($\beta_{55} \neq \beta_{35} \neq \beta_{33}$ according to Jørgensen[37]), and inclusion of potential interactions to the second coordination sphere by considering for hexacoordinated systems σ bonds between t_{2g} metal- and p-functions of the anions.[16] We have undertaken to check in detail all these influences by performing extensive ligand field calculations varying parameters within ranges being of physical significance which reproduce the correct quartet level sequences as derived from the polarized spectra, with the result that all these effects are not capable to explain the large ^2E_g splitting of these compounds. This is in agreement with earlier investigations.[16,18-20,36]

The incomplete treatment of the electron repulsion part that uses only parameters adapted to spherical symmetry has been criticized already earlier[18,37] and some founded extensions of the original models have been proposed to remove this shortcoming. A consequent consideration of electron repulsion leads, however, even at cubic symmetry to an inflation of parameters,[38] by which the convenient relations between theory and experiment, very useful in practice within the conventional models, are lost. The way out of this problem may be shown by the Stevens delocalization coefficients,[37] which in O_h symmetry consider differences in the LCAO expansion coefficients μ for e_g and t_{2g} orbitals,[39] i.e.

$$\psi = \mu\varphi_M + \lambda\varphi_L \qquad (3)$$

At this symmetry only two sets of μ,λ-coefficients are possible. The neglect of more center integrals justified by the strong localization of d-orbitals on the metal atom leads to various electron repulsion terms differing in symmetry

$$\mu_a\mu_b\mu_c\mu_d\langle ab|1/r_{12}|cd\rangle \qquad (4)$$

(each $\mu_i<1$) which can be expressed again by linear combinations of spherical Slater-Condon or Racah parameters.

For C_{4v} complexes the corresponding symmetry adapted μ-coefficients may be denoted by τ_ζ of d_{xy}, $\tau_\xi=\tau_\eta$ of d_{yz}, $d_{xz}(t_{2g})$ and ε_u of $d_{x^2-y^2}$, ε_v of $d_{z^2}(e_g)$. Since NH_3 ligands do not contribute to π-bonding ($\pi_N=0$), for present pentaammine complexes the corresponding π-coefficient is $\tau_\zeta=1$. A complete AOM calculation performed with a significant set of parameters shows that already a very small deviation of the other τ parameters from unity has a large effect on the ^2E_g splitting (cf. Fig. 7), the size of the ε-expansion coefficients chosen for e_g orbitals is found to be of minor importance for the splitting pattern of ^2E_g and $^2T_{1g}$ levels. Thus, a parameter value of $\tau_\xi=\tau_\eta=0.992$ can reproduce a level spacing of $\sim$200 cm^{-1} for ^2E_g determined from experiment.

The variation of level differences with the π-expansion parameter $\tau(=\tau_\xi=\tau_\eta)$ as demonstrated in Fig. 7 can be estimated also from the diagonal elements of the LF perturbation matrix of tetragonal symmetry given in terms of Racah parameters A, B, and C

$$\begin{aligned}
&^2E_g \text{ splitting} \quad \Delta E(^2B_1-{}^2A_1) = 2\tau^2(1-\tau^2)(3B+C)>0,\\
&^2T_{1g}-{}^2E_g \text{ separation} \quad \Delta E(^2A_2-{}^2A_1) = 0,\\
&^2T_{1g} \text{ splitting} \quad \Delta E(^2A_2-{}^2E) = (-0.5\tau^4+\tau^2-0.5)A\\
&\qquad + (2.5\tau^4-0.5\tau^2-2)B + 1.5(\tau^2-1)C<0,\\
&^4A_{2g} \text{ (ground state) splitting} \quad \Delta E(\Gamma_6-\Gamma_7) = 0. \qquad (5)
\end{aligned}$$

It is seen that for $\tau<1$ the ^2E_g level splitting is increased, the $^2T_{1g}-{}^2E_g$ spacing and ground state splitting remain unchanged but the $^2T_{1g}$ splitting tends to be smaller than calculated from conventional LF theory (cf. Eq. 1). The appearence of the A-parameter in the expression for the $^2T_{1g}$ splitting in Eq. 5, which in the spherically symmetric model cancels for any of the transition energies, does not cause difficulties: since its contribution to $\Delta E(^2A_2-{}^2E)$ is relatively small due to its coefficient dependent on τ even for large values of A the qualitative aspects of the results will not be changed.

As seen from the full LF calculation (Fig. 7) the total energy separation $\Delta E(^2A_2-{}^2A_1)$ is changed only slightly with varying τ which agrees with the observed positions of band C being at constant energy difference compared to A ($\sim$600 cm^{-1}) for all compounds considered as well as for the hexaammine complex.[7] Due to the avoided crossing of Γ_6 levels arising from $^2A_2$ and ^2E these states are strongly

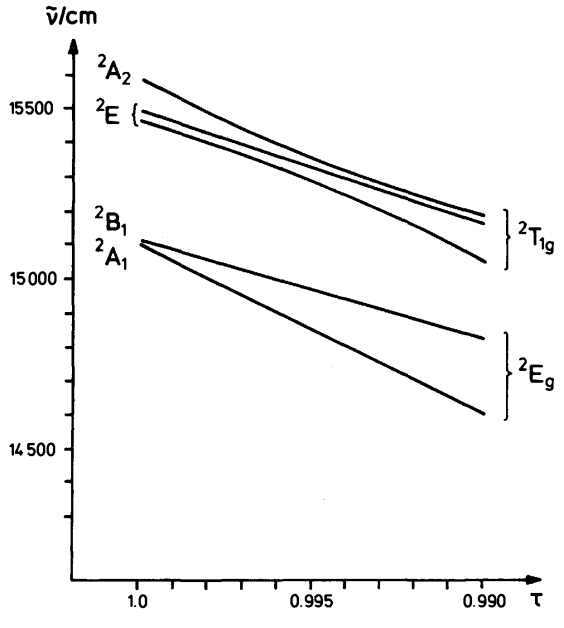

Fig. 7. Low symmetry ligand field splitting of ^2E_g, $^2T_{1g}$ levels depending on the π-orbital expansion factor τ (see text). Parameters are chosen as in Fig. 1 and ζ=200 cm^{-1}; $\varepsilon_u=\varepsilon_v$=1.0.

intermixed at $\tau<0.995$ by which the transition giving rise to band C should obtain an increased $^4B_1 \rightarrow {}^2E$ character. The situation is further complicated by a possible occurrence of a pseudo Jahn-Teller effect in the ^2E state[40] shifting the zero phonon transitions by virtue of vibronic coupling which has not been considered in the present model. A final decision on the assignment of band C can only be made on the basis of more detailed theoretical investigations.

Concerning the ground state $^4A_{2g}$, symmetry adapted expansion coefficients will not be able to calculate increased values for the splitting of this level since both Kramers doublets resulting from spin-orbit interaction have essentially identical orbital wave functions which hardly are affected differently by neighboring atoms that could lead to unequal energies. The large splittings for metal compounds with heavier halogen ligands observed from ESR spectra,[22-24] therefore, are only explained by a relativistic nephelauxetic effect which is described within the framework of LCAO theory in a similar way as Stevens expansion coefficients which allow the spin-orbit coupling parameters to be increased up to values higher than obtained for the free ions.[22,37]

Luminescence Intensity Analysis. The molecular structure of excited electronic states can be determined if in the vibronic spectrum at least partially resolved band profiles are obtained. For an analysis, the relative band intensities in the progression, e.g., of an emission spectrum

$$\nu_n = \nu_{00} - \nu_{pr} - n \cdot \nu_{ac} \tag{6}$$

are used where ν_{00} represents the zero phonon band gap, ν_{pr} a promoting mode which makes the transition electric dipole allowed, and ν_{ac} denotes the accepting mode forming the actual series of equally spaced band peaks.[41] If the pure electronic (zero phonon) transition is allowed, in general, some normal modes of given symmetry (which are totally symmetric if Jahn-Teller effects are absent) may act as promoting and accepting mode as well, a situation which leads to a rather complicated theoretical description of relative transition probabilities. In the Herzberg-Teller coupling scheme of electron-nuclear interaction the vibronic transition moment for g→a is expressed by

$$M^{ga} \approx \langle M_e^{ga} \rangle \langle \chi_v | \chi_{v'} \rangle + \sum_k \frac{\langle M_e^{gk} \rangle}{E_e^a - E_e^k} \sum_\mu \left\langle \left| \frac{\partial H_e}{\partial Q_\mu} \right|^{ka} \right\rangle \langle \chi_v | Q_\mu | \chi_{v'} \rangle + \cdots \tag{7}$$

where χ_v and $\chi_{v'}$ are total nuclear wave functions of the molecule in the ground and excited state, respectively, $\frac{\partial H_e}{\partial Q_\mu} Q_\mu$ is the linear vibronic coupling operator and E_e^k the energy of the wave function mixing into the states considered.[42] Due to the lack of appropriate electronic wave functions the size of these integrals are not known. Therefore relative Franck-Condon factors can only be compared to the spectra if some of the terms of Eq. 7 can be neglected, i.e., either the first contribution is zero if the pure electronic transition is strictly forbidden or χ_v refers to the zero phonon excitation and $\chi_{v'}$ belongs to a nontotally symmetric representation or the second and all higher terms are vanishingly small compared to the first term in the case of an allowed transition.

In the emission spectra of [X] complexes, apart from side bands assigned to fundamental vibrations, we can identify intensive transitions in combination with the Cr-halogen stretching vibration $\nu_5(a_1)$ as well as progressions in the same mode. Figure 8 depicts the luminescence spectrum of the $[Cl]Cl_2$ complex doped into the corresponding Rh(III) compound. This

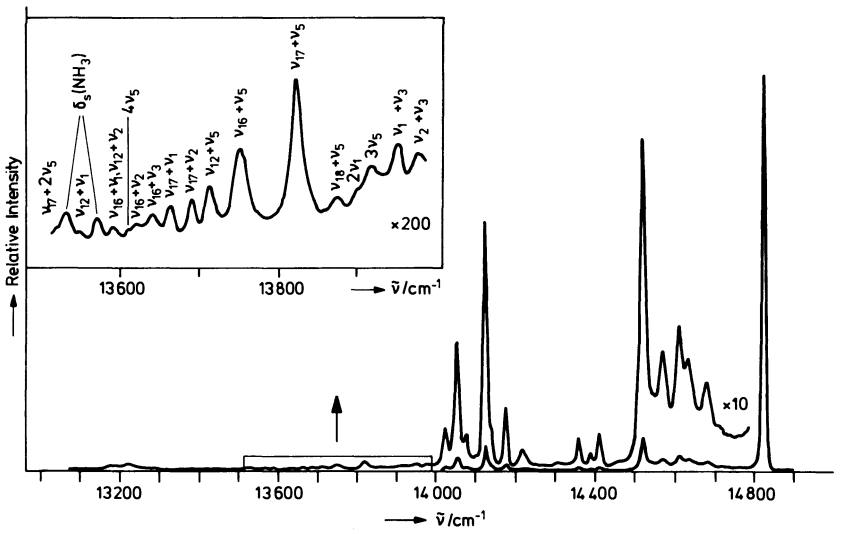

Fig. 8. ^2E_g emission spectrum of Cr^{3+} doped in $[Rh(NH_3)_5Cl]Cl_2$ at 5 K exhibiting low intensity members in the vibrational progression (λ_{exc}=514.5 nm).

Table 3. Intensity Relations in Vibrational Progressions and Nuclear Equilibrium Distortions in the First Excited State

X	σ_X/cm^{-1}	ν_5/ν_{00}	$2\nu_5/\nu_5$	$(\nu_{pr}^{a)}+\nu_5)/(\nu_{pr})$	ΔR(Cr-X)/pm
F	7400	0.11	0.12	0.08	≈ 3
Cl	5500	0.086[b)]	0.050[b)]	0.029[b)]	≈ 2
Br	5000	0.118[b)]	0.054[b)]	0.044[b)]	$\lesssim 1.5$[c)]
I	4500	0.12	0.06	0.07	$\lesssim 1.5$[c)]

a) $\nu_{pr}=\nu_{16}$ or ν_{17}, i.e. δ(Cr-N-H) of e-symmetry. b) Obtained from doped compounds (Rh-host). c) σ(Cr-X) is strongly mixed with the totally symmetric bending mode δ(N-Cr-N).

system has been chosen since intensity relations differing up to four orders of magnitude (1:10^4) could be determined in this case. Some of the intensity relations obtained are compiled in Table 3. Since ν_5 is at the same time promoting and accepting mode, the different numbers calculated for the two progressions considered are explained by the result of the discussion following Eq. 7. For a Franck-Condon analysis, therefore only the intensity relations in the ν_5-progression in combination with the nontotally symmetric vibrational modes δ(Cr-N-H), i.e. ν_{16} and ν_{17}, are evaluated since in these cases the first term in Eq. 7 vanishes for symmetry reasons. The fitting of experimental band intensities in the progression to a theoretical band profile function allows an intramolecular distribution function $I(n,\Delta,\beta)$ to be determined from which the parameter Δ is calculated containing the geometric distortion coordinates in the excited state.[43] The frequency factor $\beta=\nu_g/\nu_a$ is approximately unity since vibrational frequencies ν_a measured from the absorption spectra are almost equal to corresponding values ν_g obtained from IR and Raman data applying to the ground state.

Due to the rapidly decaying band intensities in the progression which moreover is obscured by many other vibrational side bands, a Franck-Condon analysis of the absorption spectrum cannot be carried out. On the other hand are emission spectra by far less perturbed by superpositions since transitions from only one or two of the lowest excited electronic states are involved; therefore they are more appropriate for these analyses. In the present spectra of halogenopentaammines, including the [F] compound, the most intense progressions are found to be due to the $\nu_5(a_1)$ mode which for [F] and [Cl] is an almost pure metal-halogen stretching vibration, but for [Br] and [I] it is appreciably mixed with the $\nu_6(a_1)$ bending mode (cf. Table 1).[33] As indicated in Table 3 the degree of the excited potential curve shift ΔR(Cr-X) proceeds with the size of the σ-antibonding parameter σ_X of the halogen ligand which is to be expected due the increased geometric distortion if the d_{z^2}-orbital (the hetero atom is located on the z-axis) is partially occupied on excitation.

From the distinctly longer progression observed in the $^2E(^2T_{2g})$ absorption spectrum (see Fig. 5) it can be concluded that this state exhibits a larger geometric distortion due to the intermixing of higher energy levels belonging to electron configurations which involve e_g orbitals. Actual numbers cannot be given since normal coordinates for the excited state would be required.

Conclusions

Since for many of the most common complex compounds, as the present halogenopentaammines of chromium(III), the electronic and vibrational energy level schemes are not known in detail, it is recommended to look more closely into well resolved vibronic spectra, i.e. to record low temperature crystalline absorption and emission spectra at high sensitivity. The measured band patterns are strongly dependent on the geometric properties of the crystals, possibly yielding in some instances more detailed information on local distortions than can be obtained from common X-ray investigations. In addition the analysis of the vibronic side bands, if vibrational fine structure is sufficiently well resolved, allows the geometry of some of the excited states to be determined which contributes for characterizing the emitting states being important for explaining photochemical processes.

Conventional ligand field and angular overlap calculations are very useful for carrying out band assignments but they are not in all cases appropriate models for reproducing values of energy levels derived from the experiment. However, small extension or variation of these models, e.g. as presently including symmetry restricted π-orbital expansion factors into the electron repulsion part, may lead to a satisfactory description of experimental results. It is these possible extensions of the model which should be considered in the near future in order to obtain a theory which is generally applicable to a larger variety of cases.

The authors are grateful to Dr. M. A. Atanasov, Sofia, for making us aware of the large level splittings due to orbital expansion factors, to Dr. T. Woike, Jülich, for recording the Raman spectrum, to Prof. R. Kniep and Mr. R. Seidel, Düsseldorf, for carrying out the X-ray investigations. We also appreciate the aid of

Degussa Company, Hanau, supplying us with the rhodium material.

References

1) A. E. Becquerel, "La lumière, ses causes et ses effects," Gauthier-Villars, Paris (1867).
2) Y. Tanabe and S. Sugano, *J. Phys. Soc. Jpn.*, **9**, 753, 766 (1954).
3) J. C. Walling, H. P. Jenssen, R. C. Morris, E. W. O'Dell, and O. G. Peterson, *Opt. Lett.*, **4**, 182 (1979).
4) R. Reisfeld and C. K. Jørgensen, *Struct. and Bondg.*, **49**, 1 (1982).
5) L. J. Andrews, G. H. Beall, and A. Lempicki, *J. Lumin.*, **36**, 65 (1986).
6) A. Ceulemans, M. Dendoven, and L. G. Vanquickenborne, *Inorg. Chem.*, **24**, 1153 (1985).
7) A. Urushiyama, T. Schönherr, and H.-H. Schmidtke, *Ber. Bunsenges. Phys. Chem.*, **90**, 1195 (1986).
8) V. Balzani and V. Carassiti, "Photochemistry of Coordination Compounds," Academic Press, London (1970).
9) "Concepts in Inorganic Photochemistry," ed by E. Zinato and A. W. Adamson, Wiley, New York (1975).
10) H. L. Schläfer, *Z. Chem.*, **10**, 9 (1970).
11) M. Wrighton, H. B. Gray, and G. S. Hammond, *Mol. Photochem.*, **5**, 165 (1973).
12) L. G. Vanquickenborne and A. Ceulemans, *Coord. Chem. Rev.*, **48**, 157 (1983).
13) A. D. Kirk, S. Arunachalam, and D. Kneeland, *Inorg. Chem.*, **25**, 3551 (1986).
14) L. S. Forster, J. V. Rund, and A. F. Fucaloro, *J. Phys. Chem.*, **88**, 5012 (1984).
15) A. F. Fucaloro, L. S. Forster, S. G. Glover, and A. D. Kirk, *Inorg. Chem.*, **24**, 4242 (1985).
16) P. E. Hoggard in "Proc. 7th International Symposium on the Photochemistry and Photophysics of Coordination Compounds," Springer Verlag, Heidelberg (1987) in press.
17) L. S. Forster and O. Monstedt, *J. Chem. Phys.*, **90**, 5131 (1986).
18) C. D. Flint and A. P. Matthews, *J. Chem. Soc., Faraday Trans. 2*, **69**, 419 (1973).
19) S. Decurtins, H. U. Güdel, and K. Neuenschwander, *Inorg. Chem.*, **16**, 796 (1977).
20) T. Schönherr and H.-H. Schmidtke, *Inorg. Chem.*, **18**, 2726 (1979).
21) P. E. Hoggard, *Coord. Chem. Rev.*, **70**, 85 (1986).
22) E. Pedersen and S. Kallesoe, *Inorg. Chem.*, **14**, 85 (1975).
23) T. Schönherr, G. Eyring, and R. Linder, *Z. Naturforsch., a*, **38**, 736 (1983).
24) A. Hauser, M. Mäder, W. T. Robinson, R. Murugesan, and J. Ferguson, *Inorg. Chem.*, **26**, 1331 (1987).
25) Gmelin, "Handbuch der Anorganischen Chemie," Vol. 52, Part C, 8 ed, Verlag Chemie, Weinheim (1965).
26) S. N. Anderson and F. Basolo, *Inorg. Synth.*, **7**, 214 (1963).
27) U. Teutsch and H.-H. Schmidtke, *J. Chem. Phys.*, **84**, 6034 (1986).
28) T. Woike, KFA Jülich, private communication.
29) C. D. Flint and A. P. Matthews, *J. Chem. Soc., Faraday Trans. 2*, **1974**, 1307.
30) T. W. Hambley and P. A. Lay, *Inorg. Chem.*, **25**, 4553 (1986).
31) W. T. M. Andriessen and J. Meuldijk, *Inorg. Chem.*, **15**, 2044 (1976).
32) B. B. Garrett, M. T. Holbrook, and J. A. Stanko, *Inorg. Chem.*, **16**, 1159 (1977).
33) H.-H. Schmidtke and M. Rosner, to be published.
34) H. van den Boom, A. J. J. van Dijsseldonk, and J. C. M. Henning, *J. Chem. Phys.*, **66**, 2368 (1977).
35) L. Dubicki and P. Day, *Inorg. Chem.*, **10**, 2043 (1971).
36) P. E. Hoggard, *Z. Naturforsch., a*, **36**, 1276 (1981).
37) C. K. Jørgensen, *Struct. and Bondg.*, **1**, 3 (1966).
38) J. C. Eisenstein, *J. Chem. Phys.*, **34**, 1628 (1961).
39) W. M. Wallace and P. E. Hoggard, *Inorg. Chem.*, **22**, 491 (1983).
40) A. Ceulemans, N. Bongaerts, and L. G. Vanquickenborne, *Inorg. Chem.*, **26**, 1566 (1987).
41) K. Hakamata, A. Urushiyama, J. Degen, H. Kupka, and H.-H. Schmidtke, *Inorg. Chem.*, **22**, 3519 (1983).
42) H.-H. Schmidtke, "Quantenchemie," VCH-Verlag, Weinheim (1987), p. 277.
43) R. Wernicke, H. Kupka, W. Enßlin, and H.-H. Schmidtke, *Chem. Phys.*, **47**, 235 (1980).

 © 1988 The Chemical Society of Japan Bull. Chem. Soc. Jpn., 61, 71—77 (1988)

Invited Paper

Metal Complexes with Tetrapyrrole Ligands. 47.[1] Yttrium(III) Bis(octaalkylporphyrinate)s: Synthesis and Electron Spin Resonance Spectra of Earth Metal Porphyrin Sandwich Compounds

Johann Walter BUCHLER,* Jürgen HÜTTERMANN,† and Jürgen LÖFFLER
Institut für Anorganische Chemie, Technische Hochschule Darmstadt, D-6100 Darmstadt, F.R.G.
†Fachgebiet Biophysik und Physikalische Grundlagen der Medizin, Fachbereich Theoretische Medizin, Universität des Saarlandes, D-6650 Homburg/Saar, F.R.G.
(Received August 10, 1987)

Reaction of tris(2,4-pentanedionato)yttrium(III) with octaethylporhyrin, H_2oep in refluxing 1,2,4-trichlorobenzene (TCB) produces a trace (2%) of the double-decker, Y(oep)$_2$ (**3A**) besides major amounts (72%) of the yttrium(III) monoporphyrinate, Y(oep)(acac) which are separated by chromatography. Appreciable yields of Y(oep)$_2$ (**3A**) (25%) are obtained from dilithium octaethylporphyrinate, Li_2(oep), formed in situ and Y(oep)(acac) in refluxing TCB. The constitution of the double-decker **3A** is proved by UV/VIS, IR, ^{1}H NMR, ESR, ENDOR, and mass spectra. The well-defined composition Y(oep)$_2$ requires that one of the porphyrin rings is electron-deficient, i.e. the charge of the Y^{III} ion is compensated by the normal porphyrinate dianion and a porphyrinate monoanion radical. The magnetic moment in the solid state, μ_{eff}=1.5 B.M. (5—100 K), demonstrates the radical nature of **3A** as well. Under the time resolution of the methods used, the unpaired electron is delocalized between the two porphyrin rings. The wavenumber of the internal charge transfer absorption band in the near infrared (λ_{CTI} 1175 nm) agrees well with the value expected for the ionic radius of Y^{III} according the linear relationship of the energy of the CTI band and the ionic radius which has been established for the series of lanthanoid octaethylporphyrinates, Ln(oep)$_2$ (Ln=La···Lu). **3A** can be reduced to the diamagnetic sandwich anion, [Y(oep)$_2$]$^-$. Y^{III} double-decker radicals Y(omp)$_2$ (**3B**; λ_{CTI} 1100 nm) or Y(hbp)$_2$ (**3C**, λ_{CTI} 1100 nm) containing octamethylporphyrin or hexadecahydrotetrabenzoporphyrin have also been prepared.

Sandwich like metal bis(tetrapyrrole)s are known since the first description of tin(IV) bis(phthalocyaninate), Sn(pc)$_2$,[2,3] and the sandwich nature was demonstrated by crystallography in the case of Sn(pc)$_2$ and the actinoid sandwich systems, An(pc)$_2$ (An=Th, U),[4] or the lanthanoid double-deckers, Ln(pc)$_2$.[5] The latter compounds are intensively studied as prospective materials for electrical devices such as semiconductors or color displays.[6]

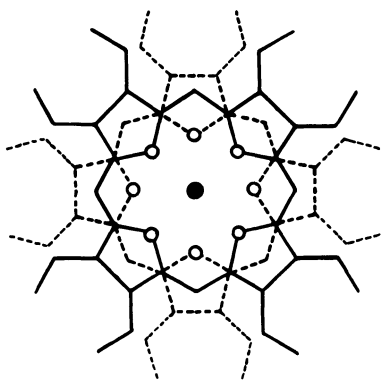

A

●=M, central metal
○=N, nitrogen atom

No.	1	2	3	4	5	6
M	Ce	Eu	Y	Ho	Er	Lu

Synthetic investigations on the corresponding porphyrin sandwich systems have been initiated with the cerium(IV) bis[tetra(*p*-tolyl)porphyrinate], Ce(ttp)$_2$, and praseodymium(III) hydrogen bis[tetra(*p*-tolyl)-porphyrinate], PrH(ttp)$_2$.[7] Due to the limited solubility of the former species, the further investigation of the corresponding octaethylporphyrin derivatives M(oep)$_2$ (**A**; M=Ln; Ln=La···Lu save Pm) has been undertaken.[8] The diamagnetic parent compound, the Ce^{IV} sandwich Ce(oep)$_2$ (**1A**) has been fully described and the square antiprismatic geometry shown in **A** demonstrated by X-ray crystallography.[9]

The same geometry obtains for the paramagnetic Eu^{III} sandwich, Eu(oep)$_2$ (**2A**).[1] As in **2A**, the porphyrin rings in all the Ln^{III} double-deckers Ln(oep)$_2$ occur in two different oxidation states: There is a normal $(oep)^{2-}$ dianion, and an electron-deficient radical anion, $(oep\cdot)^{1-}$. These two rings show an internal charge transfer absorption band (CTI band) in the near infrared the energy of which is solely dependent on the ionic radius of the Ln^{III} ion.[10,11] As the radius of the Ln^{III} ion at coordination number 8 increases, the energy of the CTI band decreases,[11] and the redox potential of reaction (1) decreases likewise.[10,12]

$$Ln(oep)_2 + e^- \rightleftharpoons [Ln(oep)_2]^- \quad (1)$$

Obviously, interelectronic repulsion is less pronounced when the two porphyrin rings have a larger

distance. Hence, the electron-rich reduced species is the more stable the larger the Ln^{III} ion is.

The importance of the ionic radius in these double-deckers led to the hypothesis that yttrium(III) derivatives, e.g. $Y(oep)_2$ (**3A**), should be accessible and have redox potentials and energies of CTI bands close to those of $Ho(oep)_2$ (**4A**) or $Er(oep)_2$ (**5A**), because the ionic radii of these metal(III) ions are very similar: Y, 101.5 pm; Ho, 102 pm; Er, 100 pm.[13] Indeed, this idea has been realised. The synthesis and spectral properties of the yttrium(III) porphyrin sandwich compounds $Y(oep)_2$ (**3A**), $Y(omp)_2$ (**3B**), and $Y(hbp)_2$ (**3C**)[3] are described in this paper.

Experimental

Material and Methods. Chemicals and instruments used were the same as previously described[9] if not stated below. $Y(acac)_3 \cdot H_2O$ was prepared following literature methods.[14] Octamethylporphyrin, H_2omp, was a gift of Professor R. Guilard, Dijon. Hexadecahydrotetrabenzoporphyrin, H_2hbp, was prepared as described by Fuhrhop.[15] Near infrared spectra (Fig. 1) were taken with a Zeiss spectrophotometer DMR 21. The ESR spectra [Fig. 2; Varian X-band, E-line spectrometer; 9.25 GHz; diphenylpicrylhydrazyl (g=2.0036) as calibrant] and the magnetic susceptibility of $Y(oep)_2$ (5—100 K; vibrating reed magnetometer[16]) were obtained by Mr. Weißenberger and Mr. F. Arenz at the Institut für Festkörperphysik, Technische Hochschule Darmstadt (courtesy of Professor B. Elschner). A 0.25 M (1 M=1 mol dm^{-3}) solution of sodium anthracenide in THF was prepared as described elsewhere.[17]

Synthesis of 2,4-Pentanedionato(2,3,7,8,12,13,17,18-octaethylporphyrinato)yttrium(III), Y(oep)(acac). 300 mg (0.56 mmol) octaethylporphyrin and 500 mg $Y(acac)_3 \cdot H_2O$ (1.25 mmol) are heated to reflux in 50 ml TCB under a stream of nitrogen. After 5 h, the cherry-red solution is freed from TCB in vacuo, the residue dissolved in toluene, filtered and chromatographed at alumina (grade I, basic, column 4×6 cm). Elution with toluene yields Fraction 1: traces of Y(oep)(acac) and TCB. A second, red-brown Fraction 2 is eluted with toluene/methanol (100:1) and consists of H_2oep and $Y(oep)_2$. The alumina column is now deactivated with water,[8] dried and eluted with THF, whereupon the main product Y(oep)(acac) is obtained as Fraction 3 (bright red). This THF solution is diluted with dichloromethane and extracted several times with water for removal of THF. The dichloromethane phase is filtered, the solvent removed in vacuo and the red-violet powder of Y(oep)(acac) (290 mg, 72%) dried in vacuo. UV/VIS [λ_{max}]: 574 (I), 538 (II), 404 (III), 334 (IV) nm; rel. intens. III>IV≈I>II.[18] IR (KBr): 1605 and 1510 cm^{-1} (bands of the coordinated acetylacetonate ligand[19]). MS (FD): Calcd for Y(oep)(acac), M=720, Found M=720, Calcd for Y(oep)(OAc): M=680, Found M=680. (This peak is due to thermolysis of the coordinated acetylacetonate as observed previously with Sc(oep)(acac).[19])

Fraction 2 is rechromatographed at alumina (grade I, basic, 2×6 cm). With toluene, some H_2oep is eluted. With toluene–methanol (200:1), a brownish-red fraction containing 10 mg (2%) of $Y(oep)_2$ (**3A**; see below) is obtained.

Synthesis of Bis(2,3,7,8,12,13,17,18-octaethylporphyrinato)yttrium(III), Y(oep)$_2$ (3A). 4 ml of a 1.6 molar solution of butyllithium in hexane[8] is added dropwise to a solution of 135 mg (0.25 mmol) of H_2oep in 50 ml of TCB under argon. After stirring for 1 h at 20 °C, 180 mg (0.25 mmol) Y(oep)(acac) are added and heated to reflux under a rapid stream of argon. The color of the initially red-violet reaction mixture changes to brown after 5 h. The TCB is then removed in a high vacuum at 50 °C. The residue is chromatographed at an alumina column (grade I, basic, 4×8 cm) with toluene. After an orange-yellow forerun of unknown composition, a brown main fraction is eluted which at its end is increasingly contaminated with H_2oep. This eluate is evaporated to dryness and rechromatographed as above in order to remove the large amounts of H_2oep. The obtained solid is fractionately dissolved in benzene–TCB (5:1) leaving undissolved H_2oep which is filtered. Crystallization of the solution yields small black rhombs of **3A** (72 mg, 25%) which are dried in vacuo at 50 °C. Found: C, 74.12; H, 7.58; N, 9.68%. Calcd for **3A**, $C_{72}H_{88}N_8Y$: 1154.52: C 74.91; H 7.68; N, 9.70%. IR (KBr): 1535 cm^{-1} (oxidation state marker band[20]). MS(FD): Found, M=1154, Calcd for ^{89}Y, M=1153.6. UV/VIS [λ_{max}, (log ε), cyclohexane]: 674 (3.38), 538 (3.88), 374 (5.10), 340 (4.96). NIR [λ_{max} (log ε), cyclohexane]: 1175 (3.83). See also Fig. 1. TLC-R_f value: 0.68 (toluene).

Sodium Bis(2,3,7,8,12,13,17,18-octaethylporphyrinato)yttriate(III) in toluene/tetrahydrofurane. A solution of 5 mg (0.004 mmol) $Y(oep)_2$ (dried in vacuo at 50 °C) in 0.5 ml toluene-d_8 containing a trace of TMS was placed under Ar into a dry NMR tube and seald with a septum cap and Nescoe film. With a Hamilton syringe, 15 µl of 0.25 M sodium anthracenide in THF was added and a ^1H NMR spectrum taken (see Table 1); apart from the signals of $[Y(oep)_2]^-$, stronger signals of THF and weaker signals of anthracene, toluene, TMS, and H_2oep were noted. Afterwards, the red-brown solution was transferred (under air) to a cuvette for absorption spectroscopy. It did not show any absorption in the near infrared (900—2000 nm). UV/VIS (λ_{max}, toluene): 586 (I), 542 (II), 492 (III), 390 (IV) nm; rel. intens. IV>I>III>II. The relatively high intensity of band III is due to the presence of some H_2oep.

Synthesis of 2,4-Pentanedionato(2,3,7,8,12,13,17,18-octamethylporphyrinato)yttrium(III), Y(omp)(acac), and Bis(2,3,7,8,12,13,17,18-octamethylporphyrinato)yttrium(III), Y(omp)$_2$ (3B). As described for Y(oep)(acac), 300 mg (0.71 mmol) H_2omp and 600 mg (1.5 mmol) $Y(acac)_3 \cdot H_2O$ are reacted and the reaction products separated. After 5 h, besides the expected Y(omp)(acac) (170 mg, 40%) a notable part of the reaction product consisted of **3B**. After chromatography, **3B** (98 mg, 16%) was obtained as a dark brown powder which could not be recrystallized due to its very limited solubility. UV/VIS [λ_{max}], Y(omp)(acac) [dichloromethane]: 574 (I), 538 (II), 404 (III), 334 (IV) nm; rel. intens. III>IV≈I>II. $Y(omp)_2$ [toluene]: 670 (I), 536 (II), 374 (III), 340 (IV) nm, rel. intens. III>IV>II>I. NIR [λ_{max}, toluene]: $Y(omp)_2$, 1100 nm (about the same intensity as the VIS band II). MS (FD), Y(omp)(acac): Found, M=608, Calcd ^{89}Y, M=608; $Y(omp)_2$: Found, M=929, Calcd ^{89}Y, M=929. A TLC-R_f value could not be determined for $Y(omp)_2$: A spot of $Y(omp)_2$ was not visible on attempted chromatography with toluene.

Synthesis of 2,4-Pentanedionato(hexadecahydrotetrabenzo[*b,g,l,q*]porphyrinato)yttrium(III), Y(hbp)(acac). As described for Y(oep)(acac), 300 mg (0.57 mmol) H_2hbp and

500 mg (1.25 mmol) $Y(acac)_3 \cdot H_2O$ are reacted and the products separated. Fraction 2 yields 20 mg (3%) $Y(hbp)_2$, Fraction 3 270 mg (66%) Y(hbp)(acac).—UV/VIS (λ_{max}, dichloromethane): 572 (I), 536 (II), 404 (III), 334 (IV); rel. intens. III>IV≈I>II.—MS(FD): Found, M=712; Calcd ^{89}Y, M=712.

Synthesis of Bis(hexadecahydrotetrabenzo[*b,g,l,q*]porphyrinato)yttrium(III), Y(hbp)$_2$ (3C). As reported for **3A**, 135 mg (0.25 mmol) H_2hbp, 4 ml of a 1.6 molar solution of butyllithium, and 180 mg (0.25 mmol) Y(hbp)(acac) are reacted and the products separated. The resulting **3C** is less soluble than **3A** in all usual organic solvents and is obtained as a dark brown powder (51 mg; 18%) by recrystallization from toluene. UV/VIS (λ_{max}, toluene): 670 (I), 536 (II), 374 (III), 340 (IV) nm; rel. intens. III>IV>II>I. NIR (λ_{max}, toluene): 1100 nm (about the same intensity as the VIS band II). TLC-R_f: see note for $Y(omp)_2$.

ENDOR Spectroscopy. A Bruker ER 420 spectrometer was attached to a Dietz 621 computer and equipped with an ENDOR facility described previously[21]. Measurements between 1 and 20 MHz were performed at about 10 K and a ESR frequency of 9.4804 GHz with a sample of $Y(oep)_2$ in frozen toluene solution and recorded in the first derivative mode. The pattern of the weakly coupled proton signals (10—20 MHz; see Fig. 3) was not significantly changed when the measurement were not done at g=2.002(4), but at the tails of the ESR signal.

Results and Discussion

(a) Chemistry. The reaction of lanthanoid acetylacetonates $Ln(acac)_3$ with porphyrins H_2p is normally achieved by heating the reactants in boiling trichlorobenzene for 1—4 h and then produces the monoporphyrin complexes Ln(p)(acac)[22] according Eq. 2.

$$Ln(acac)_3 + H_2p \longrightarrow Ln(p)(acac) + 2Hacac \quad (2)$$

Prolonged heating (up to 20 h) yields the double-deckers in the tetraarylporphyrin series, e.g. $Ce(ttp)_2$[7] or the double-deckers $Ln(oep)_2$ with Ln=La···Tb[8-10,23] (Eqs. 3, 4).

$$Ln(p)(acac) + H_2p \longrightarrow LnH(p)_2 + Hacac \quad (3)$$

$$4LnH(p)_2 + O_2 \longrightarrow Ln(p)_2 + 2H_2O \quad (4)$$

The latter are accompanied by triple-deckers $Ln_2(oep)_3$[8-10,23] for Ln=La···Gd which emerge from reaction (5).

$$LnH(p)_2 + Ln(p)(acac) \longrightarrow Ln_2(p)_3 + Hacac \quad (5)$$

Obviously, the tendency to form double- and triple-deckers decreases with decreasing ionic radius of the lanthanoid ion and increasing bulkiness of the porphyrin. The later members of the series $Ln(oep)_2$ where Ln=Dy···Lu are not accessible from $Ln(acac)_3$. They have to be prepared by a modified "raise-by-one-story" reaction sequence 6—7 similar to Eqs. 3 and 4 using the monoporphyrin Ln(oep)(acac) and the dilithium complex of octaethylporphyrin, $Li_2(oep)$, which is an unstable material but easily obtained in situ from H_2oep and an excess of butyllithium in inert solvents.[8,24]

$$Ln(oep)(acac) + Li_2(oep) \longrightarrow LnLi(oep)_2 \quad (6)$$

$$4LnLi(oep)_2 + O_2 \longrightarrow 4Ln(oep)_2 + 2Li_2O \quad (7)$$

Other feasible starting materials for the synthesis of lanthanoid sandwich complexes would be the lanthanoid dialkylamides. While a uranium(IV) double-decker cannot be made from $U(oep)(acac)_2$ and $Li_2(oep)$,[8] $U(tpp)_2$ has been prepared from $U(NEt_2)_4$ and H_2tpp in refluxing toluene.[25]

Yttrium being similar to Holmium and Erbium as regards their ionic radii, the formation of a double-decker in the reaction of $Y(acac)_3$ with any porphyrin H_2p was not expected. At first, therefore, the monoporphyrinates Y(p)(acac) where prepared from octaethylporphyrin, octamethylporphyrin, and hexadecahydrotetrabenzoporphyrin.[15] However, when $Y(acac)_3$ is reacted with the octaalkylporphyrins, surprisingly, small amounts of double-deckers $Y(p)_2$ (**3A—3C**) are found besides the monoporphyrins Y(p)(acac) [(p)=(oep), (omp), (hbp)]: 2% for **3A**, 16% for **3B**, 3% for **3C**. The obtained yield of **3B** was sufficient to characterize the compound. Therefore, only the synthesis of **3A** and **3C** was performed with the "butyllithium raise-by-one-story" method (Eqs. 3 and 4).[8]

The monoporphyrins Y(p)(acac) are formed in reasonable yields, but have not been fully characterized because Y(tpp)(acac)[26] and Y(oep)(acac)[18] have already been described. It is more probable, however, that all the monoporphyrinates Ln(p)(acac) rather have the composition $Ln(p)(acac)(H_2O)_2$ or similar octacoordinate geometries in view of the known crystal structures[5,27] of lanthanoid phthalocyanines with bidentate acetate or acetylacetonate ligands. Furthermore, bridged binuclear structures may be formed from these monoporphyrinates in solution which still show the molecular ion of Ln(p)(acac) in the mass spectrum after crystallization but give inconsistent elemental analyses for this composition.[28] Therefore, the formula Y(p)(acac) is only used for simplicity.

Equations 4 and 7 imply that an oxidation is involved in the formation of the double-deckers $Ln(p)_2$. For an earth metal ion like Y^{III}, no other oxidation state is available. The oxidation must then involve the porphyrin ligand. Evidence for the presence of a porphyrin radical in $Y(p)_2$ is presented in the later sections.

All the properties of the porphyrin radical vanish in $Y(oep)_2$ when it is reduced to the diamagnetic anion $[Y(oep)_2]^-$. This reduction according Eq. 1[1,8] is done with sodium anthracenide in THF and easily followed by NMR spectroscopy. The oxidation-reduction potential for the pair $Y(oep)_2/[Y(oep)_2]^-$ is −0.21 V (cyclic voltammetry, SCE, DMF, NBu_4PF_6).[10,12]

$Y(oep)_2$ closely resembles its cerium analog: **3A** is

rather soluble even in alkanes. However, **3B** and **3C** only have a very limited solubility, like their parent porphyrins and the other metal complexes of the latter. This has precluded a more thorough investigation of **3B** and **3C**.

(b) Identification. $Y(oep)_2$ (**3A**), $Y(omp)_2$ (**3B**), and $Y(hbp)_2$ (**3C**) are identified by optical absorption (UV/VIS and NIR) and mass spectra. The optical absorption spectra of **3A—3C** do not have the "normal" appearence[29] of their cerium(IV) analogs, but are typical for species in which the porphyrin ligand is oxidized to a π-radical.[30] Specifically, the bands at 670 nm are reminiscent to strong absorption occurring in $Mg(oep)ClO_4$ (**7**) at about 660 nm.[30b] The bands found in **3A—3C** correspond well with those found with all compounds $Ln(oep)_2$ containing Ln^{III} ions.[11]

Furthermore, infrared spectra showing all the typical bands of octaethylporphyrin complexes lacking axial ligands, magnetic measurements and elemental analyses fully identify **3A**. As in the case of $Lu(pc)_2$[5a,31] and $Lu(oep)_2$ (**6A**),[8] the magnetic moment measured in the solid state clearly demonstrates the radical nature of $Y(oep)_2$: μ_{eff}=1.46—1.52 B. M. between 5.4 and 100 K (Curie-Weiss behavior, θ=1.5 K).

The most characteristical property of these double-decker radicals consisting of a noninteracting central metal ion M^{III} or M^{IV}, a porphyrinate dianion $(p)^{2-}$ and a porphyrinate monoanion radical $(p\cdot)^-$ is the NIR absorption band which occurs, e.g., for $La(oep)_2$ at 1480 nm,[10,11] $Eu(oep)_2$ at 1280 nm,[10,11,23] $Lu(oep)_2$ at 1135 nm,[10,11] $[Ce(oep)_2]^+$ at 1270 nm,[32] and $[Ce(ttp)_2]^+$ at 1340 nm.[32] This band is due to an internal charge-transfer complex (electron donor acceptor complex)[33] which is formed between the donor, $(p)^{2-}$, and the acceptor, $(p\cdot)^-$.[1,11] Donor and acceptor are combined in the same molecule. In an alternative view, these radicals could be "inverse mixed valence complexes," the mixed valencies not residing on two metals, but rather on two ligands.[1,11] The yttrium doubledeckers clearly fall into this class with their NIR bands for $Y(oep)_2$ (**3A**) at 1175 nm and $Y(omp)_2$ as well as $Y(hbp)_2$ at 1100 nm (see Fig. 1). The value for **3A** indeed coincides with the value for $Er(oep)_2$ (**5A**) at 1175 nm[11] and is very close to the value of $Ho(oep)_2$ (**4A**) at 1180 nm.[11]

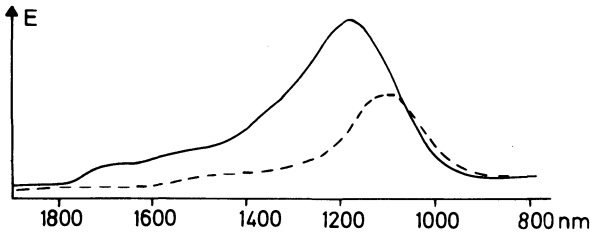

Fig. 1. Near infrared absorption spectra of $Y(oep)_2$ (**3A**) and $Y(omp)_2$ (**3B**) (extinction arbitrary).

A working hypothesis for a explanation of the lower wavelength found with **3B** and **3C** as compared with **3A** is the following: In the octamethyl or hexadecahydrotetrabenzo porphyrin sandwiches, the steric inter-ring repulsion is smaller than in the octaethyl porphyrin sandwich. Hence, the distance of the $C_{20}N_4$ mean planes is also smaller, and the electronic properties more closely resemble $Lu(oep)_2$ in which due to the smaller Lu^{III} ion the rings are forced more closely together.

The NIR band found in these double-deckers is reminiscent to the oxidized form $[(BChl)_2]^+$ of the "special pair" of bacteriochlorophyll b molecules $(BChl)_2$. $[(BChl)_2]^+$ is formed on illumination and has a NIR absorption at 1300 nm in Rhodopseumonas viridis.[34] The redox pair $[(BChl)_2]^+/(BChl)_2$ corresponds to the redox pairs $[Ce(oep)_2]^+/Ce(oep)_2$[32] or $Y(oep)_2/[Y(oep)_2]^-$ (see above). This relationship to the photosynthetic reaction center makes further studies of these double-deckers quite attractive.

(c) ^{1}H NMR Spectroscopy. The ^{1}H HMR spectrum of $Y(oep)_2$ (**3A**, data in Table 1) is much more complicated than the spectrum of $Ce(oep)_2$ (**1A**). This is seen in the chemical shifts and the linewidths of the signals. Most notable is a strong very broad peak at δ 3. This is reminiscent to a very broad peak in the spectrum of $[Ce(oep)_2]^+$[32] at δ 2.25 and a similar peak in the spectrum of $Lu(oep)_2$ (**6A**) at δ 3.06. In fact, these two peaks are the only ones in the spectra of **3A** and **6A** which point to paramagnetism of the compounds. All the other signals appear in regions where the proton signals occur in the diamagnetic reference **1A**. A detailed interpretation of the NMR spectra of **1A** and **2A** is given elsewhere.[1,8,9]

Even the methine signals of **3A** are duplicated, indicating a sandwich system in which one porphyrin ring is slightly different from the other, a situation which is also found in the diamagnetic anions, $[Y(oep)_2]^-$ and $[Lu(oep)_2]^-$.[8] In the latter, the duplication of the methine signals is due to the formation of an ion pair with a THF-solvated Na^+ counter ion which is thought to coordinate to the pyrrole nitrogen atoms on one side of the sandwich system. In the absence of any charges and ions, the diamagnetic species present in **3A** could be a centrally vacant quadruple-decker $[M(p)_2]_2$ formed in an association equilibrium (8):

$$2\,M(p)_2 \rightleftharpoons [M(p)_2]_2 \qquad (8)$$

Monoporphyrin π-radicals, e.g. $[Zn(oep)]ClO_4$,[35] tend to dimerize as well in concentrated solutions and thus form diamagnetic π-π-dimers. The diamagnetic component in the solution of **3A** (and **6A**[8]) can be removed by addition of the radical di-*t*-butyl nitroxide $(t\text{Bu})_2NO$, which otherwise acts as a "spin relaxer".[36] Generally, the line width of the NMR spectra of organic radicals is reduced in the presence of

Table 1. ^{1}H NMR Data (300 MHz) of Y(oep)$_2$ (**3A**), Its Reduction Product Na[Y(oep)$_2$], and Lu(oep)$_2$ (**6A**) Together with the Reference Data of Ce(oep)$_2$ (**1A**)

Compound	Chemical shifts δ, coupling constants J, or line widths $w(1/2)$[a]						
	CH= (e)[b]	CH= (i)[c]	CH_2 (i)	CH_2 (e, 1)[d]	CH_2 (e, 2)[d]	CH_3 (i)	CH_3 (e)
Ce(oep)$_2$	9.11			4.20	3.86		1.68
[Y(oep)$_2$]$_2$[e]	9.14	9.05	4.17	3.85		1.72	1.62
Y(oep)$_2$							3.00
Y(oep)$_2$[f]	26.8			22.3	14.5		3.16
$w(1/2)$	*125*			*150*	*110*		*68*
δ_{iso}(rad)[g]	17.7			18.3[h]	10.5[h]		1.48
[Lu(oep)$_2$]$_2$[e]	9.11	9.07	4.23	3.87		1.69	1.61
Lu(oep)$_2$[f]	30.1			23.0	15.0		3.06
$w(1/2)$	*702*			*414*	*234*		*68*
δ_{iso}(rad)[g]	21.0			19.0[h]	11.0[h]		1.38
[Y(oep)$_2$]$^-$ M[i]	9.21 s	9.07 s	4.42; 4.02 m m	4.30 m	3.90 m	1.77 t	1.60 t

a) δ [ppm] vs. int. TMS; J [Hz] or half widths $w(1/2)$ [Hz] (in italics). b) Methine protons of external (e) ring (outwards of the molecule). c) Methine protons of internal (i) ring (inwards to the molecule). d) 1 and 2 denote exo and endo methylene protons, respectively (assignment arbitrary). e) Presumed dimer present in the concentrated solution. f) Compound measured in presence of spin relaxer (tBu)$_2$NO. g) Isotropic shift of the radical $\delta_{iso}(rad)=\delta_{obs}-\delta_{ref}$ [Ce(oep)$_2$]. h) Reference is $1/2[\delta CH_2(e,1)+\delta CH_2(e,2)]$ because of ambiguity of assignment. i) Multiplicity of the signals observed.

other paramagnetic molecules acting as "spin relaxers". Hence, in the presence of (tBu)$_2$NO, the NMR spectrum of the radical **3A** alone becomes visible with all its four broad peaks that are to be expected in comparison to the diamagnetic **1A**. The assignments indicated in Table 1 are based on integrated intensity ratios. The multiplicity of the signals indicates only one set of methyl and two sets of diastereotopic methylene protons. On the NMR timescale, therefore, the two porphyrin rings are identical, and the π-electron hole seems to be delocalized.

The equilibrium (8) for **3A** obviously exists only in solution. Solid **3A** consists of paramagnetic monomers. Otherwise it should be diamagnetic (as is the solid phase of La(oep)$_2$[8]) and not exhibit an ESR spectrum as microcrystalline material in frozen matrices like **7**.[30b]

The isotropic shifts of the radical **3A** using **1A** as a diamagnetic reference are given in Table 1 as $\delta_{iso}(rad)=\delta_{obs}-\delta_{dia}$, along with the corresponding values of **6A**[8] and those calculated for the porphyrin radical contribution from the spectrum of **2A**.[1]

(d) Electron Spin Resonance and Electron Nuclear Double Resonance Spectra. ESR spectra of Y(oep)$_2$ at various temperatures in toluene or frozen toluene are shown in Fig. 2. With g=2.002(4), this is a typical signal of an organic radical. The line width ΔH_{pp} does not change very much on cooling to 70 K ($\Delta H_{pp}\simeq$4.11 G at 70 K, 3.52 G at 290 K), but on cooling below 40 K, shoulders appear causing an increase of total spectral extent to ~28 G at 4.2 K together with a slight increase in ΔH_{pp}(≃4.76) of the central line (see Fig. 2). The

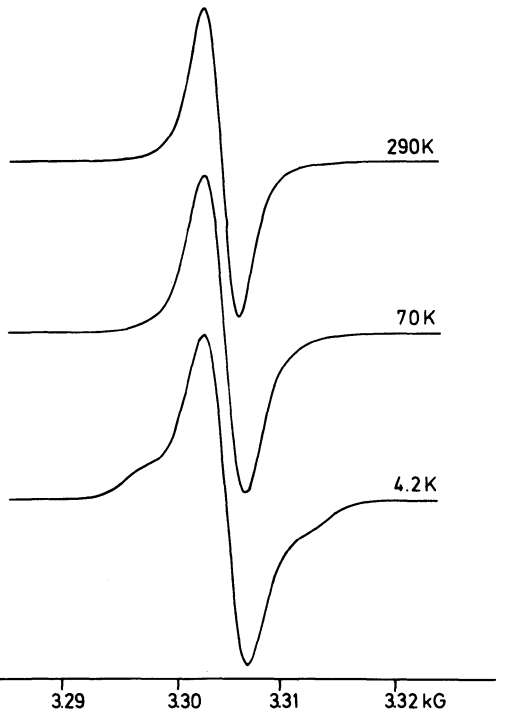

Fig. 2. Electron spin resonance spectrum of Y(oep)$_2$ (**3A**) (derivative mode).

reason for the additional lines is unclear. The slight asymmetry of the shoulders with respect to the central line could be indicative of the presence of a second, chemically different species. ΔH_{pp} at 70 K is slightly larger than that of the signal of the monoporphyrin radical [Mg(oep)]ClO$_4$ (**7**) [g=2.0025 at 223 K; $\Delta H_{pp}\approx$ 3.5 G].[30b]

While the spectrum of **7** shows a proton hyperfine structure (HFS) due to the methine H atoms [a_H=1.48 G=0.148 mT], such a fine structure is not distinguishable in the spectrum of **3A**. Under the assumption that the unpaired electron is delocalized between the two rings on the ESR time scale, a_H should be smaller for each contributing nucleus, and the total linewidth be reduced as compared with **7** although the number of contributing nuclei is doubled. The observed somewhat larger width of the signal of **3A** points to a coupling of the electron spin with another nucleus not present in **7**. This could be the ^{89}Y nucleus (100% natural abundance; spin 1/2; μ/μ_N=−0.237). Radicals derived from oep complexes, like **7**, bear the unpaired electron in the A_{1u} molecular orbital[30b] which has nodal planes at the four porphyrin nitrogen atoms. There is no spin density at these atoms and hence no ^{14}N-HFS seen. Likewise, in **3A** a ^{14}N hyperfine splitting is not observable. Hence, **3A** is probably also an A_{1u} radical. This is consistent with the visible absorption spectrum.[30b] Further investigations with meso-deuterated **3A** or Y(tpp)$_2$ would be useful, but the latter compound is hitherto not accessible via the butyllithium raise-by-one-story reaction.

The proton ENDOR spectrum is shown in Fig. 3. Three types of interaction can be distinguished. One is a sharp "matrix proton" line at the free nuclear frequency ν_n≃14.5 MHz; it gives no structural information. Next is a pair of lines displaced symmetrically about ν_n with a coupling of 0.45 MHz; its line shape indicates a dominantly isotropic interaction. The third coupling involves a broad, more powder-type anisotropic pair with 1.1 to 2.0 MHz. The absence of any larger interaction corroborates the notion of a distribution of spin density between the two porphyrin rings. The methine-H coupling in the monoporphyrin radical **7** translates into about 2.64 MHz for the double-decker **3A** whereas twice this value would be expected for the monoporphyrin radical.

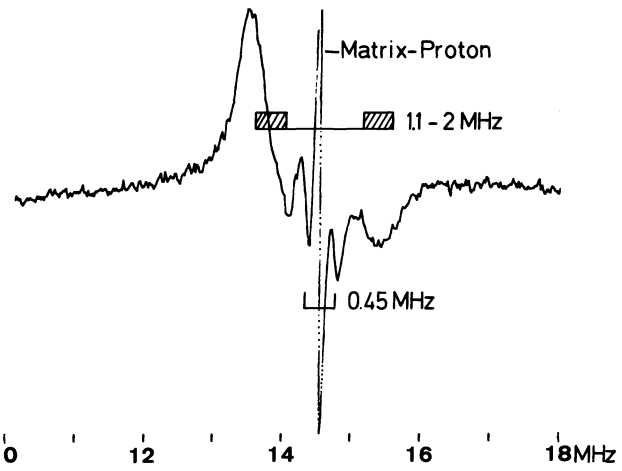

Fig. 3. Electron nuclear double resonance spectrum of Y(oep)$_2$ (**3A**) (proton range, 10—18 MHz).

If we assign the broad line pair in **3A** to the methine protons, the even lower observed (1.1—2.0 MHz) interaction again points to a contribution of the ^{89}Y nucleus onto which some spin density should be transferred. Such an interaction was looked for in the 1—10 MHz frequency region, but the data so far are not interpretable with reliability. The 0.45 MHz proton interaction could be due to the methylene protons of the ethyl groups.

(e) Conclusion. In view of the existence of yttrium(III) phthalocyaninate double-deckers Y(pc)$_2$[37] and probably also triple-deckers Y$_2$(pc)$_3$,[38] it is promising for further investigations to have the corresponding porphyrin sandwich **3A** which is much better soluble. With its NIR absorption, any redox reactions can be very easily followed. Indeed, not only the energies of the NIR absorption bands, but also the oxidation reduction potentials for the following steps (9a)—(9c) have been determined accurately in the

$$[M(oep)_2]^+ \underset{(a)}{\rightleftharpoons} M(oep)_2 \underset{(b)}{\rightleftharpoons} [M(oep)_2]^- \underset{(c)}{\rightleftharpoons} [M(oep)_2]^{2-} \quad (9)$$

porphyrin series for M=Ln (Ln=La···Lu save Pm) and for M=Y (**3A**).[10,12] The redox potentials associated with reactions (9a) [which is reaction (1) for M=Ln], (9b), and (9c) as well as the energy of the NIR band each lie on a straight line in the series M=La···Lu as the ionic radius decreases. The corresponding values obtained with **3A** fall onto these lines between Ho(oep)$_2$ (**4A**) and Er(oep)$_2$ (**5A**), demonstrating the importance of the ionic radius and the ring-ring distance in these sandwich systems.[10–12]

This work was supported by the Deutsche Forschungsgemeinschaft (Bonn), the Fonds der Chemischen Industrie (Frankfurt), and the Vereinigung von Freunden der Technischen Hochschule Darmstadt. We thank Professor Dr. B. Elschner, Mr. F. Arenz, and Mr. S. Weißenberger for magnetic and ESR measurements, Priv.-Doz. Dr. M. Veith and M. Fischer for the mass spectra, Dr. S. Braun for advice on the measurement of the NMR spectra, and Professor Dr. R. Guilard for a gift of octamethylporphyrin.

References

1) Paper 46: J. W. Buchler, A. de Cian, J. Fischer, M. Kihn-Botulinski, and R. Weiss, *Inorg. Chem.*, **27**(1), (1988) (in press).

2) P. A. Barrett, C. E. Dent, and R. J. P. Linstead, *J. Chem. Soc.*, **1936**, 1719.

3) Abbreviations used: M, metal; (p)$^{2-}$, (oep)$^{2-}$, (pc)$^{2-}$, (tpp)$^{2-}$, (ttp)$^{2-}$, (omp)$^{2-}$, (hbp)$^{2-}$: dianions of a general porphyrin, 2,3,7,8,12,13,17,18-octaethylporphyrin, phthalocyanine, 5,10,15,20-tetraphenylporphyrin, 5,10,15,20-tetra-

(*p*-tolyl)porphyrin, octamethylporphyrin, hexadecahydrotetrabenzoporphyrin, respectively; Ln: lanthanoid metal; Hacac, acetylacetone; DMF: *N,N*-dimethylformamide; HOAc, acetic acid; TCB, 1,2,4-trichlorobenzene; TLC, thin-layer chromatography; NIR, near-infrared; MS(FD), mass spectrum in the field ion desorption mode; THF: tetrahydrofuran; SCE: saturated calomel electrode.

4) A. Gieren and W. Hoppe, *J. Chem. Soc., Chem. Commun.*, **1971**, 413.

5) a) A. De Cian, M. Moussavi, J. Fischer, and R. Weiss, *Inorg. Chem.*, **24**, 3162 (1985). b) K. Kasuga, M. Tsutsui, R. C. Petterson, K. Tatsumi, N. van Opdenbosch, G. Pepe, and E. F. Meyer, Jr., *J. Am. Chem. Soc.*, **102**, 4836 (1980).

6) a) G. A. Corker, B. Grant, and N. J. Clecak *J. Electrochem. Soc.*, **126**, 1339 (1979). b) G. C. S. Collin and D. J. Schiffrin, *J. Electroanal. Chem. Interfacial Electrochem.*, **139**, 335 (1982). c) J. J. André, K. Holczer, P. Petit, M. T. Riou, C. Clarisse, R. Even, M. Fourmige, and J. Simon, *Chem. Phys. Lett.*, **115**, 463 (1985).

7) J. W. Buchler, H. G. Kapellmann, M. Knoff, K. L. Lay, and S. Pfeifer, *Z. Naturforsch., B*: Anorg. Chem., Org. Chem., **38B**, 1339 (1983).

8) M. Kihn-Botulinski (formerly Knoff), Doctoral Dissertation, Technische Hochschule Darmstadt (1986).

9) J. W. Buchler, A. de Cian, J. Fischer, M. Kihn-Botulinski, H. Paulus, and R. Weiss, *J. Am. Chem. Soc.*, **108**, 3652 (1986).

10) J. W. Buchler and B. Scharbert, *J. Am. Chem. Soc.*, submitted.

11) J. W. Buchler, K. Elsässer, M. Kihn-Botulinski, B. Scharbert, and S. Tansil, *ACS Symposium Series*, **321**, 94 (1986).

12) J. W. Buchler, M. Kihn-Botulinski, and B. Scharbert, *Recl. Trav. Chim. Pays-Bas*, **106**, 321 (1987).

13) R. D. Shannon and C. T. Prewitt, *Acta Crystallogr., Sect. B*, **25**, 925 (1969).

14) J. G. Stites, C. N. McCarty, and L. L. Quill, *J. Am. Chem. Soc.*, **79**, 3142 (1948).

15) J.-H. Fuhrhop and D. Hosseinpour, *Justus Liebigs Ann. Chem.*, **1985**, 689.

16) K.-H. Unterreiner, Doctoral Dissertation, Technische Hochschule Darmstadt (1969).

17) J. W. Buchler and L. Puppe, *Justus Liebigs Ann. Chem.*, **740**, 142 (1970).

18) M. Gouterman, C. D. Schumaker, T. S. Srivastava, and T. Yonetani, *Chem. Phys. Lett.*, **40**, 456 (1976).

19) J. W. Buchler, G. Eikelmann, L. Puppe, K. Rohbock, H. H. Schneehage, and D. Weck, *Justus Liebigs Ann. Chem.*, **745**, 135 (1971).

20) E. T. Shimomura, M. A. Philippi, H. M. Goff, W. F. Scholz, and C. A. Reed, *J. Am. Chem. Soc.*, **103**, 6778 (1981).

21) a) R. Kappl, M. Höhn-Berlage, J. Hüttermann, N. Bartlett, and M. C. R. Symons, *Biochim. Biophys. Acta*, **827**, 327 (1985); b) M. Höhn, J. Hüttermann, J. C. W. Chien, and L. C. J. Dickinson, *J. Am. Chem. Soc.*, **105**, 109 (1983).

22) C.-P. Wong, R. F. Venteicher, and W. DeW. Horrocks, Jr., *J. Am. Chem. Soc.*, **96**, 7149 (1974).

23) J. W. Buchler and M. Knoff, "Optical Spectra and Structure of Tetrapyrroles," ed by G. Blauer and H. Sund, de Gruyter: Berlin (1985), pp. 91—105.

24) J. W. Buchler and M. Kihn-Botulinski, manuscript in preparation.

25) G. S. Girolami, S. N. Milam, and K. N. Suslick, *Inorg. Chem.*, **26**, 343 (1987).

26) L. P. Wong and W. DeW. Horrocks, Jr., *Tetrahedron Lett.*, **1975**, 2637.

27) H. Sugimoto, T. Higashi, A. Maeda, M. Mori, H. Masuda, and T. Taga, *J. Chem. Soc., Chem. Commun.*, **1983**, 1234.

28) P. Hammerschmitt, Diplomarbeit, Technische Hochschule Darmstadt (1987).

29) M. Gouterman, "The Porphyrins," ed by D. Dolphin, Academic Press: New York (1978), Vol. 3, pp. 1—165.

30) a) D. Dolphin, Z. Muljiani, K. Rousseau, D. C. Borg, J. Fajer, and R. H. Felton, *Ann. New York Acad. Sci.*, **206**, 177 (1973). b) J. Fajer, D. C. Borg, A. Forman, D. Dolphin, and R. H. Felton, *J. Am. Chem. Soc.*, **92**, 3451 (1970).

31) A. T. Chang and J. C. Marchon, *Inorg. Chim. Acta*, **53**, L241 (1981).

32) J. W. Buchler, K. Elsässer, M. Kihn-Botulinski, and B. Scharbert, *Angew. Chem.*, **98**, 257 (1986); *Angew. Chem., Int. Ed. Engl.*, **25**, 286 (1986).

33) G. Briegleb, "Elektronen-Donator-Akzeptor-Komplexe," Springer, Berlin (1961).

34) M. S. Davis, A. Forman, L. K. Hanson, J. P. Thornber, and J. Fajer, *J. Phys. Chem.*, **83**, 3325 (1979).

35) J. H. Fuhrhop, P. Wasser, D. Riesner, and D. Mauzerall, *J. Am. Chem. Soc.*, **94**, 7996 (1972).

36) F. Yamauchi and R. W. Kreilick, *J. Am. Chem. Soc.*, **91**, 3429 (1969).

37) a) P. N. Moskalev and I. S. Kirin, *Russ, J. Inorg. Chem.*, **15**, 7 (1970); b) K. Kasuga, M. Ando, and H. Morimoto, *Inorg. Chim. Acta*, **112**, 99 (1986).

38) K. Kasuga, M. Ando, H. Morimoto, and M. Isa, *Chem. Lett.*, **1986**, 1095.

 © 1988 The Chemical Society of Japan Bull. Chem. Soc. Jpn., 61, 79—85 (1988)

Invited Paper

Atom Trapping Atomic Absorption Spectrometric Determination of Some Trace Elements in Soils, Natural Waters, Seawater, and Bovine Liver

C. M. LAU, A. M. URE, and T. S. WEST*
Macaulay Land Use Research Institute, Aberdeen, AB9 2QJ, U.K.
(Received August 10, 1987)

The operational conditions for the determination of Ag, As, Au, Bi, Cd, Cu, Mn, Pb, Sb, Se, Tl, and Zn by atom trapping atomic absorption spectrometry are summarised. With this technique some of these trace elements can be determined in soils, natural waters, seawater and bovine liver at concentrations that are not possible by the conventional technique of flame AAS. For example, seawater is diluted ten-fold with distilled water to overcome nebulisation problems due to salt concentrations and the trace elements are collected for 2 min in situ in the air-acetylene flame before release and measurement. The attack of sodium on the hot silica atom trap tube in the flame gases is prevented by pre-aspiration of aluminium chloride into the flame, thus depositing a protective film of Al_2O_3. X-Ray diffraction, infrared spectroscopy, scanning electron microscopy, and spark source mass spectrometry are used to show that the protective alumina film consists of mainly σ alumina with a small amount of θ alumina spheroids of varying sizes <1 μm diameter and is highly pure. The nature of a similarly deposited Fe_2O_3 film is shown to be a more closely packed and irregular form of hematite with a small content of metallic iron. The results obtained by this simple new technique compare well with those obtained by spark source mass spectrometry and electrothermal AAS with a graphite furnace.

The development of atom trapping atomic absorption spectrometry[1] as a potential analytical technique for ultratrace element determination has been described in previous papers.[2-7] The surface of a water-cooled 4 mm o.d. silica tube traps and preconcentrates atomic species, or their precursors, within the body of an air–acetylene flame. When a sufficient amount has been collected (e.g. after 30 s—5 min) the trapped species are released into the flame subsequently by ejecting the water with a blast of air. The skin temperature of the silica tube attains that of the flame gases within 5—10 seconds. The trapped analyte is then atomised normally as a transient cloud of atoms within the flame. The tube is mounted permanently in the flame. Because of the uniquely low coefficient of thermal expansion of silica, the tube withstands the repeated thermal shocks produced by switching cold water back through the hot silica tube for the next trapping cycle for at least one hundred experiments before the surface becomes seriously etched. The atom trapping technique preserves the inherent simplicity, element-specificity and reliability of conventional flame AAS, as well as its ease of operation. In addition, it offers considerably higher sensitivity than the conventional technique whilst preserving most of its relative freedom from matrix interference when compared to other analytical methods of similar capacity. Hence we found it possible directly to determine selenium in plants,[4] and also lead and cadmium[5] in soils which would have been impossible by conventional flame AAS because of the low levels involved. This paper further explores the analytical applications of atom trapping AAS for the determination of some trace elements in fresh water, seawater, liver and soil samples, with particular attention to those containing very low analyte element concentrations. It also collates and summarises operational conditions for atom trapping AAS of Ag, As, Au, Bi, Cd, Cu, Mn, Pb, Sb, Se, Tl, and Zn.

Experimental

Equipment: The atom trapping AAS measurements were made with a Varian Techtron Model AA6 atomic absorption spectrophotometer equipped with background correction as described previously.[6] Instrumental parameters for each of the elements were optimised using standard solutions; these are summarised in Table 1. The possibility of background absorption and scattering effects occurring during atomic absorption measurements was examined in each case; only for elements with resonance lines below 240 nm was background correction necessary.

An Instrumental Laboratories Model 751 atomic absorption spectrophotometer fitted with a Model 555 controlled-temperature graphite furnace was used for electrothermal AAS determinations of some fresh water samples for the purposes of comparison.

Sample Preparation: Six Scottish top-soils (1 g samples) were digested with three 10 ml aliquots of aqua regia and taken to dryness each time on a steam bath, as previously described.[5] The final solutions were made up to 25 ml in 0.5 M nitric acid (1 M=1 mol dm^{-3}) and the arsenic concentrations in these solutions were measured by atom trapping AAS.

A nitric acid–hydrogen peroxide dissolution method was applied to the liver sample. In this method, a 1 g sample of the freeze-dried, powdered liver was digested with 10 ml of concentrated nitric acid on a steam bath and another 10 ml portion of the acid was added before the mixture was evaporated to less than 5 ml. The procedure was repeated with two 10 ml portions of 20 vol.(6%) hydrogen peroxide. The final mixture was filtered on Whatman No. 542 filter paper and the filtrate made up to 10 ml with 0.5 M nitric

Table 1. Instrumental Parameters for Atom Trapping AAS Determination of Twelve Elements

Working condition	Element											
	Ag	As	Au	Bi	Cd	Cu	Mn	Pb	Sb	Se	Tl	Zn
H. C. lamp current/mA	1	4	4	3	2	3	5	3	4	7	6	2
Band width/nm	0.2	1.00	0.2	0.2	0.5	0.5	0.2	1.00	0.2	1.00	0.5	0.5
Wavelength/nm	328.1	193.6	242.8	223.1	228.8	324.8	279.5	217.0	217.6	196.0	276.8	213.9
Distance between collector tube (base) and the burner head/mm	5	21	7	5	7	5	9	5	5	10	6	12
% obscuration of optical path by tube/%[a]	50	35—40	25	10—15	50	50	35—40	50	35—40	25	35—40	50
Flame mixture[b]	A-A	A-B	A-A	A-A	A-A	A-A	A-A	A-A	A-A	A-A	A-A	A-A
Flame condition[c]	R	O	O	R	O	O	S	R	R	O	R	O
Background correction	No	Yes	No	Yes	Yes	No	No	Yes	Yes	Yes	No	Yes

a) % obscuration figures are approximate. b) A-A=Air-acetylene. A-B=Air-butane. c) Flame Condition: R=reducing, O=oxidizing, S=stoichiometric.

acid.

Fresh water samples were collected and stored in polypropylene bottles and were acidified with 1% nitric acid prior to use. The samples were stored in a cold room (4 °C) and warmed up to room temperature for an hour before analysis.

The sea water was first filtered through a 50 μm sintered glass filter to remove suspended material and acidified with 1% hydrochloric acid before storing in a polypropylene bottle.

Standard Solutions: Stock solutions for the analyte elements were prepared from analytical reagent grade chemicals. Standard solutions with concentrations appropriate to the analysis were diluted from the stock solutions immediately before use. These standard solutions were prepared with an acid strength and matrix similar to the samples so that any interference effects of matrix elements on nebulisation of the solution or the trapping or release of the analyte could be minimised.

Preparation of Coated Tubes: The pre-deposited alumina and iron oxide coatings on the silica atom trap tubes were prepared by aspirating a 5000 μg ml^{-1} solution of aluminium (5 min) or iron(III) chloride (30 s) into the flame, and collecting the oxide formed on the surface of the water-cooled silica atom trap tube.

Procedure for Measurement. Arsenic in Aqua Regia Digests of Soils: Standard arsenic solutions were prepared in the range 0.1 to 0.5 μg ml^{-1} As and were made up in 0.5 M nitric acid with 200 μg ml^{-1} each of sodium and iron added to the solutions to match the approximate content of soil digests. Both the sample digests and standard solutions were collected for four minutes on an iron oxide-on-alumina-coated tube prior to atomic absorption measurement. The standard solutions were measured before and after the sample to ensure no change in sensitivity as a result of tube surface alteration. The concentrations of arsenic in the digests found from the standard calibration curve were checked by a standard addition method. Arsenic, 25 μg equivalent to 1.0 μg ml^{-1} arsenic in the digest, was added to the sample soils before the digestion procedure. The amount of arsenic recovered from the digest was measured as above.

Zinc in Seawater: Standard zinc solutions (0.8—8 ng ml^{-1} Zn^{2+}) were prepared by diluting from a zinc stock solution. The solutions were made up in 0.05 M hydrochloric acid and with the addition of 1000 μg ml^{-1} NaCl to simulate the main matrix constituent of seawater. The seawater sample was diluted ten times with double distilled water. The zinc in this diluted sample and the standard solutions were collected on an alumina coated tube for a period of 1 minute prior to atomic absorption measurement. The accuracy of the measurement was checked by testing the recovery of added zinc (2, 4, and 6 ng) to aliquots of the diluted seawater sample.

Trace Elements in a Bovine Liver Sample: Ag. Bi, Cd, and Pb were determined in nitric acid-hydrogen peroxide digests of freeze-dried bovine liver. Standard solutions of these elements were prepared to contain 500 μg ml^{-1} Fe, and 200 μg ml^{-1} each of Ca, K, and Na approximately to match the matrix of the sample digests. The sample and standard solutions were collected for a period of 2 min (except for Cd which required only 30 s) on an iron oxide-on-alumina-coated silica atom trap before atomic absorption measurements were made. The accuracy of the method was checked by calculating the % recovery of lead added to the liver sample solution, and also by comparing the values with previous spark source mass spectrometry results.

Trace Elements in Fresh Water Samples: Several elements (Ag, Cd, Cu, Mn, Pb, Tl, and Zn) were analysed in water samples. The standard solutions were prepared by freshly diluting from stock solutions and making up in 0.05 M nitric acid. Both the standard and sample solutions were collected on alumina coated tubes, usually with a four or five min. collection time, depending on the concentration of the elements in the samples, except for zinc where the concentration was adequate for conventional flame AAS. The accuracy of the method was checked by graphite furnace atomic absorption spectrometry in some cases.

Results and Discussion

The twelve elements (Ag, As, Au, Bi, Cd, Cu, Mn, Pb, Sb, Se, Tl, and Zn) were first determined by atom trapping AAS using a silica atom trap tube according to the instrumental conditions outlined in Table 1.

Table 2. Comparisons of Characteristic Concentration[a] and Detection Limits[b] of Twelve Elements Determined by Conventional Flame AAS and Atom Trapping AAS

	Ag	As	Au	Bi	Cd	Cu	Mn	Pb	Sb	Se	Tl	Zn
Conventional Flame AAS												
Characteristic concentration[a] /μg ml^{-1}	0.036	0.92	0.22	0.25	0.012	0.088	0.037	0.12	0.44	0.38	0.28	0.01
Detection limit[b] /μg ml^{-1}	0.025	0.85	0.018	0.05	0.004	0.044	0.011	0.04	0.65	0.4	0.15	0.005
Relative standard deviation (%) (12 results)	1.5	7	4	5	3	5	2.5	3.5	5.5	8	4	5
Atom Trapping AAS (Silica Atom Trap)												
Characteristic Concentration[a] /μg ml^{-1} 30 s collection	0.003	0.087	0.049	0.022	0.0013	0.015	0.010	0.010	0.038	0.050	0.043	0.002
1 min collection	0.0016	0.045	0.037	0.012	0.0007	0.0075	0.005	0.0057	0.021	0.028	0.022	0.001
2 min collection	0.0009	0.024	0.028	0.006	0.00046	0.004	0.003	0.0029	0.011	0.015	0.015	0.0005
3 min collection	0.0006	0.019	0.022	0.004	0.00037	0.0028	0.002	0.0020	0.007	0.0088	0.012	0.00036
Detection limit[b] /μg ml^{-1} (2 min collection)	0.0005	0.05	0.020	0.010	0.0001	0.004	0.002	0.005	0.036	0.030	0.009	0.001
Relative standard deviation/% (12 results)	2.9	10	8.7	8	7.4	5	4.2	6.8	8.3	14	5	6.3

a) Sometimes called sensitivity (μg ml^{-1} required for 1% absorption). b) Signal/Noise ratio 2/1.

Table 3. Characteristic Concentration and Detection Limits of the Twelve Elements Determined by Atom Trapping AAS Using Alumina and Iron Oxide Coated Tubes

	Ag	As	Au	Bi	Cd	Cu	Mn	Pb	Sb	Se	Tl	Zn
Alumina Coated Tube (2 min collection)												
Characteristic concentration /μg ml^{-1}	0.0015	0.072	0.039	0.010	0.0005	0.008	0.008	0.0026	0.044	0.023	0.024	0.0005
Detection limit/μg ml^{-1}	0.0008	0.15	0.035	0.030	0.0003	0.019	0.010	0.0011	0.048	0.05	0.011	0.0017
Relative standard deviation/% (12 results)	4	10	9	10	8	7	7	7.5	12	12	6	4
Iron Oxide Coated Tube (2 min collection)												
Characteristic concentration /μg ml^{-1}	0.0022	0.095	Not applicable	0.012	0.0002	Not applicable	Not applicable	0.003	0.090	0.022	0.027	0.0002
Detection limit/μg ml^{-1}	0.001	0.19		0.040	0.0001			0.015	0.10	0.045	0.012	0.0005
Relative standard deviation/% (12 results)	6	11		10	8			7	11	13	5	5

The characteristic concentration (μg ml^{-1} for 1% absorption) and detection limit for each element obtained by atom trapping AAS are compared with those of conventional flame AAS in Table 2. For all of these elements, even for Mn which has a relatively high melting point of 1244 °C, the atom trapping technique increased the sensitivity (characteristic concentration) considerably when ca. 2 min trapping periods were used. However, the loss of hollow cathode lamp signal due to partial obscuration of the optical path by the silica tube and light scattering noise on the tube surface, led to a somewhat poorer relative standard deviation. It will be seen that for elements with resonance lines below 200 nm, e.g. As and Se, this factor resulted in % relative standard deviations >10%. All the elements were determined using an air–acetylene flame except for arsenic which required the cooler air–butane flame to minimise volatilization losses of arsenic during the trapping cycle.

In order to minimise interference arising from the co-deposition of major matrix or chemically active species on the silica tube during the trapping of analyte species, alumina or iron oxide was pre-deposited on the silica tube before the sample solutions were analysed.[5] The determination of these elements by atom trapping AAS was, therefore, also made on alumina and iron oxide coated silica atom trap tubes. Table 3 summarises the results. Most elements were less sensitive when collected on these surfaces except for Cd, Pb, and Zn. The signals for Au, Cu, and Mn were depressed on the alumina coated tube and no signals were obtained from an iron oxide coated tube.

Nature and Structure of Alumina and Iron(III) Oxide Coating Materials: Investigations were made to identify the nature and structure of the alumina and iron oxide coatings, formed by rapid condensation of the vaporized products from an aluminium or iron(III) chloride solution on the ca. 200 °C silica

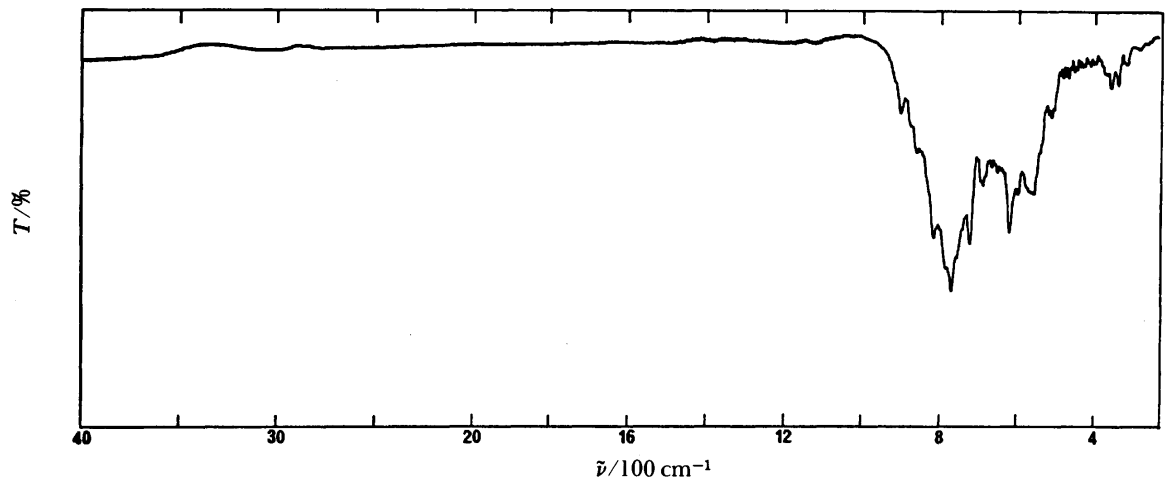

Fig. 1. Infrared absorption spectrum of alumina deposited on 'cold' surface of silica atom trap in air–acetylene flame. The Al_2O_3 is mainly δ but with a small amount of θ alumina.

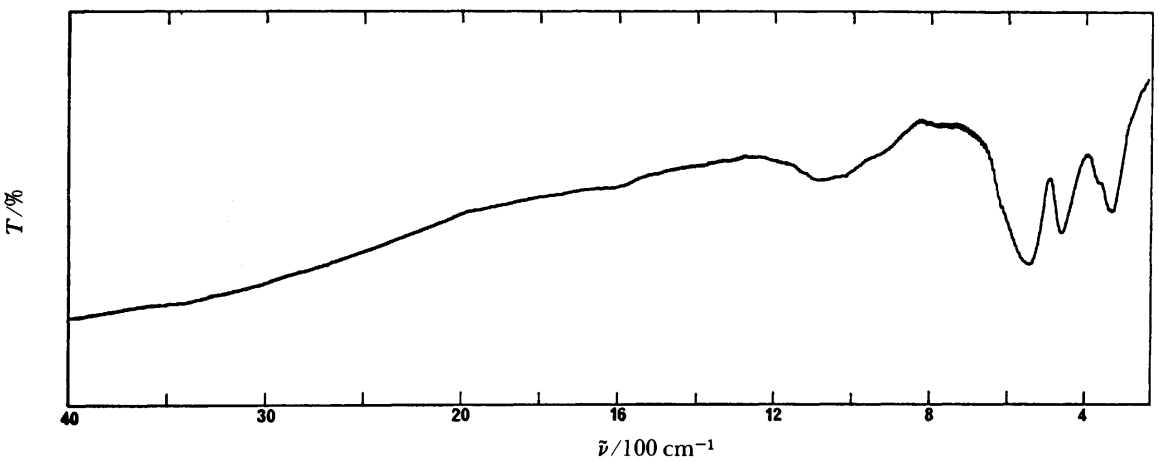

Fig. 2. Infrared absorption spectrum of iron oxide deposited on 'cold' surface of silica atom trap in air–acetylene flame. The deposit is mainly hematite with a small amount of metallic iron.

surface from flame gases ca. 3000 °C. Several techniques were employed, including infrared spectroscopy, X-ray diffraction, spark source mass spectrometry and scanning electron microscopy. The infrared spectra (Figs. 1 and 2) of the two coating materials showed that the alumina coating had a complicated absorption spectrum, but the iron oxide coating spectrum was identical to that of hematite.[8]

The X-ray diffraction pattern showed the alumina deposit to be dominated by delta (δ) alumina with a small amount of theta (θ) alumina. The same technique confirmed that the iron oxide coating was hematite with a trace of Fe metal. The spark source mass spectrometric analysis indicated that except for Cl, P, and Si, most other elements are present at less than the $\mu g\,g^{-1}$ level in the alumina coating material. This coating can, therefore, be considered relatively free from contamination for trace element analysis.

Further studies of the coatings were made using scanning electron microscopy to examine their microstructure. Under high magnification (×10000), Figs. 3 and 4, the alumina coating is seen to consist of loosely packed spheroids. Although the spheres were of different sizes, the largest was less than 1 μm in diameter. The iron oxide coating, however, was more compact, and more irregular in size and shape. Although the pre-deposition of these coating materials on the silica atom trap surface was an efficient way of minimising interference, the sensitivity for most elements was slightly decreased relative to collection on a clean silica tube surface. Broad peak signals were also observed for some elements when collected on the coated surface. It seems probable that these coatings greatly increased the surface area whilst simultaneously allowing some of the analyte species to become sequestered in the interstitial spaces of the coating, thus protracting the release time as shown by the broader release peaks and correspondingly lower peak heights.

Effects of Extraneous Elements: Interference effects in atom trapping AAS are more complicated than in conventional flame AAS. The presence of an extraneous element in the analyte solution may influence the proportion of free analyte atoms formed in the flame as in the conventional flame technique, but additionally cause physical alteration of the tube surface or alloy formation on the trap and subsequently affect the efficiency of trapping and/or release of analyte from the collector tube.

More than ten extraneous elements of concentrations up to $500\,\mu g\,ml^{-1}$ were added to each of the analyte solutions and their effects on the analyte signal were determined by atom trapping AAS with an alumina coated tube. According to the effects they produced on the analyte signal, the extraneous elements could be classified into two groups. For alkali and alkaline earth metals and other volatile elements, the highest concentration added caused less than ±30% interference on the analyte signal. The presence of the alumina on the collector tube prevented chemical attack (vitrification) of the silica surface by alkali metals and the volatile nature of the

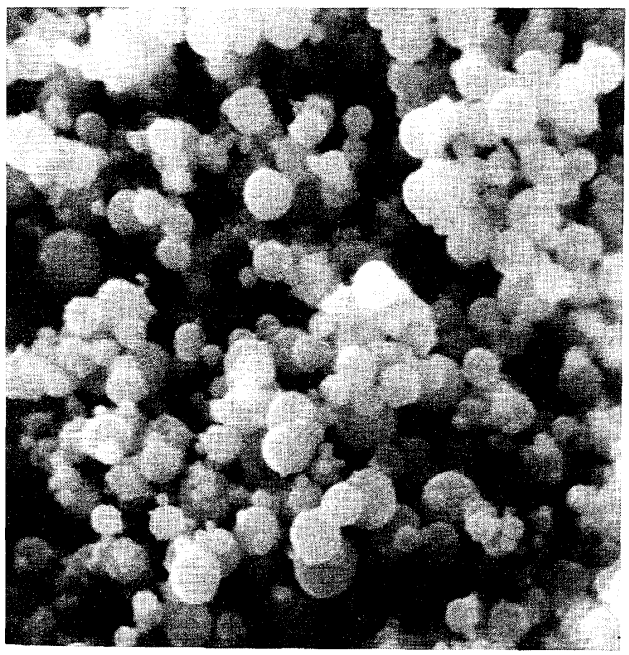

Fig. 3. Electron micrograph (×10000) of alumina deposited on 'cold' surface of silica atom trap following aspiration of $AlCl_3$ into air-acetylene flame.

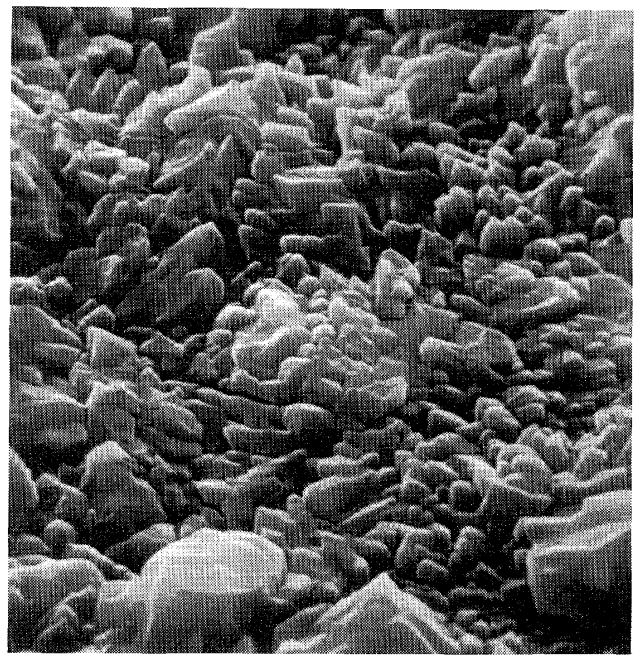

Fig. 4. Electron micrograph (×10000) of hematite deposited on 'cold' surface of silica atom trap following aspiration of $FeCl_3$ into air-acetylene flame.

metals also ensured their instant release together with the trapped analyte as the surface of the collector tube became hot without affecting the analyte signal to any marked extent. Such interference as occurred from these elements could be minimised by matrix matching and pre-conditioning of the tube with these elements before analysis.

The interference effects were more severe for involatile extraneous elements such as Fe, Co, Ni, Cu, Mn. For example, the presence of 500 μg ml^{-1} Fe, 500 μg ml^{-1} Co, or 500 μg ml^{-1} Ni reduced the copper signal by 40, 50, and 60% respectively. The effects of these elements were mainly due to their virtually permanent deposition on the alumina surface resulting in a gradual alteration in physical structure of the surface for the trapping of the analyte species. In the case of iron, the effect could be eliminated by pre-deposition of iron oxide on top of the alumina coated tube, and then collecting the high iron-containing analyte solutions on this modified tube surface. However, for *high* concentrations of other non-volatile elements such as Co and Ni, pre-deposition of these elements or their oxides on the tube surface did not lead to elimination or compensation. Alternative methods must, therefore, be used for samples containing *high* levels of Co or Ni in their matrix.

Sample Analysis. The results reported in Tables 4—7 are those of single individual determinations.

Arsenic in Aqua Regia Digests of Soils: The presence of the extremely toxic element arsenic in the environment is mainly of geological origin, although industrial processes have also made contributions. A recent survey gave the average content of arsenic of over 1000 soils to be 11.3 mg kg^{-1}.[9] A content of >50 mg kg^{-1} arsenic in a soil is regarded as potentially toxic to susceptible plants.[10] Several acid mixtures have been used for the extraction of arsenic from soil; these include nitric and sulphuric acids,[11] aqua regia,[12] perchloric and nitric,[13] and hydrofluoric and perchloric acids.[14] Aqua regia was used in this work because it is widely used for monitoring heavy metals in polluted soils.[15]

The arsenic contents of the six Scottish top-soils analysed in this study were found to range from 5—10 μg g^{-1}. The % recovery of added arsenic was 100% (±10%), Table 4.

Zinc in Seawater: The direct determination of trace elements in sea water by conventional AAS is difficult because of their low concentrations and the high salt matrix. One common procedure frequently used is preconcentration/separation by solvent extraction followed by electrothermal atomization AAS for analysis,[16] However, the sensitivity of the atom trapping method permits direct analysis of sea water diluted 10-fold to reduce nebulisation problems. The results of the analysis by atom trapping AAS are shown in Table 5. The concentration of zinc in the sample was found to be 9 μg l^{-1} compared to a literature value of 10 μg l^{-1}.[18] The % recovery of zinc added to the sample was also 100±10%.

Trace Elements in a Bovine Liver Sample: Flame atomic absorption spectrometry is often employed for the determination of trace elements in bovine liver tissue but, because of the high organic content in the sample, special sample treatments are required. Some

Table 4. Results of the Analysis of Arsenic in the Aqua Regia Digests of Six Scottish Top-Soils by Atom Trapping AAS, by (A) Direct Determination, and (B) Standard Addition, Reported in μg g^{-1} of Soil

Sample	(A)	(B)
1	11.3	10.3
2	10.2	10.4
3	5.7	7.5
4	5.2	4.5
5	11.5	12.5
6	7.5	6.8

Table 5. Replicate Determination of Zinc in Seawater by Atom Trapping AAS

Aliquots of seawater sample (10× dilution)	1	2	3	4
Concentration of zinc added/μg l^{-1}	0	2.0	4.0	6.0
Concentration of zinc found/μg l^{-1}	0.9	3.1	5.1	7.0
Actual concentration of zinc/μg l^{-1}	0.9	1.1	1.1	1.0
Concentration of zinc in undiluted seawater/μg l^{-1}	9	11	11	10

Table 6. The Determination of Ag, Bi, Cd, and Pb in a Bovine Liver Sample by (A) Atom Trapping AAS, Compared to (B) Spark Source Mass Spectrometry Results
(Values Reported Are in μg g^{-1} Freeze-Dried Liver)

Element	(A)	(B)
Ag	0.05	0.06
Bi	0.48	0.14
Cd	0.27	0.27
Pb	0.35	0.34

Table 7. The Concentration (μg l^{-1}) of Several Trace Elements in Three Fresh Water Samples Determined by Atom Trapping AAS, and by Electrothermal Atomization AAS[a] (Mn and Pb) for Comparison

Element	Sample 1	Sample 2	Sample 3
Ag	<1	<1	<1
Cd	4	<1	<1
Cu	<5	<5	<5
Mn	7; 8.3[a]	<2; 0.2[a]	4; 2.8[a]
Pb	69; 55[a]	<2; 0.4[a]	23; 10[a]
Tl	<5	<5	<5
Zn	500	1.5	50

of the reported methods of sample preparation suitable for analysis by flame AAS included low temperature ashing (RF-excited oxygen plasma),[19] enzyme digestion,[20] or wet-oxidative digestion.[21] Amongst these, wet-oxidative digestion offers two main advantages over the other procedures. It is generally faster and, as it requires lower working temperatures (50—250 °C), the risk of losing volatile elements is reduced. The nitric acid–hydrogen peroxide procedure employed here was first tested by checking the recovery of lead added to the freeze-dried, powdered liver sample before digestion. The recovery was 100±10% of the quantity of the added lead. The concentrations of lead, cadmium, silver, and bismuth were then found by the method described, and the values were compared with those from previous spark source mass spectrometry results, Table 6. Apart from bismuth the other three elements showed consistent results by the two methods.

Trace Elements in Fresh Water Samples: Atomic absorption spectrometry is ideally suited to the analysis of fresh water for a wide range of elements. However, the extremely low levels of some elements in fresh water samples prevent their direct determination by conventional flame AAS, except for a few such as sodium, potassium, magnesium, calcium, and occasionally zinc. Several of these ultra-trace elements can, however, be determined directly by atom trapping AAS, e.g. in the three fresh water samples, featured in Table 7. Two elements (Mn and Pb) were also measured directly by electrothermal atomization AAS, which showed fair agreement with atom trapping.

Conclusion

Atom-trapping AAS can be applied to determine a wide range of elements with significant enhancement in sensitivity compared to conventional flame AAS. The successful analysis of trace elements in different types of sample showed the technique to be reliable for a range of matrices.

One of us (CML) is indebted to the Council of Management of this Institute for a grant in partial support of this work. We also thank M. J. Wilson, W. J. McHardy, A. R. Fraser, and C. A. Shand for assistance with the data on X-ray diffraction, electron microscopy, infrared absorption, and spark source mass spectrometry.

References

1) C. Lau, A. Held, and R. Stephens, *Can. J. Spectroscopy*, **21**, 100 (1976).
2) J. Khalighie, A. M. Ure, and T. S. West, *Anal. Chim. Acta*, **107**, 191 (1979).
3) J. Khalighie, A. M. Ure, and T. S. West, *Anal. Chim. Acta*, **117**, 257 (1980); **134**, 271 (1982); **131**, 27 (1981).
4) C. M. Lau, A. M. Ure, and T. S. West, *Anal. Chim. Acta*, **141**, 213 (1982).
5) C. M. Lau, A. M. Ure, and T. S. West, *Anal. Chim. Acta*, **146**, 171 (1983).
6) C. M. Lau, A. M. Ure, and T. S. West, *Anal. Proc.*, **20**, 114 (1983).
7) C. Hallam and K. C. Thompson, *Analyst*, **110**, 497 (1985).
8) "The Infrared Spectra of Minerals," ed by V. C. Farmer, Mineralogical Society (1974), p. 19.
9) A. M. Ure and M. L. Berrow, "Environmental Chemistry," Vol. 2, Royal Society of Chemistry (1982), p. 189.
10) A. W. McPhee, D. Chisholm, and C. R. MacEachern, *Can. J. Soil Sci.*, **40**, 59 (1970).
11) A. J. Thompson and P. A. Thoresby, *Analyst*, **102**, 9 (1977).
12) J. Rubeska and V. Hlavinkova, *At. Absorpt. Newsl.*, **18**, 5 (1979).
13) P. N. Vijan, A. C. Rayner, D. Sturgis, and G. R. Wood, *Anal. Chim. Acta*, **82**, 329 (1976).
14) S. Bajo, *Anal. Chem.*, **50**, 649 (1978).
15) M. L. Berrow and W. M. Stein, *Analyst*, **108**, 277 (1983).
16) R. E. Sturgeon, S. S. Berman, A. Desaulniers, and D. S. Russell, *Talanta*, **27**, 85 (1980).
17) R. Guevremont, R. E. Sturgeon, and S. S. Berman, *Anal. Chim. Acta*, **115**, 163 (1980).
18) B. Mason, "Principles of Geochemistry," 3rd ed, Wiley, N. Y. (1966), p. 195.
19) J. Locke, *Anal. Chim. Acta*, **104**, 255 (1979).
20) R. C. Carpenter, *Anal. Chim. Acta*, **175**, 209 (1981).
21) J. Flanjak and H. Y. Lee, *J. Sci. Food Agric.*, **30**, 503 (1979).

 © 1988 The Chemical Society of Japan Bull. Chem. Soc. Jpn., 61, 87—92 (1988)

Invited Paper

Mass Spectrometry of Molecular Adsorbates Using Laser Desorption/Laser Multiphoton Ionization

Richard N. Zare,* Jong Hoon Hahn, and Renato Zenobi
Department of Chemistry, Stanford University, Stanford, CA 94305, U.S.A.
(Received August 20, 1987)

Current and potential applications of a new mass spectrometric technique for the analysis of nonvolatile and thermally labile substances are reviewed. The method is compared to other approaches and its advantages are discussed.

For the purposes of chemical analysis, gas chromatography combined with mass spectrometry (GC–MS) is often the method of choice for volatile compounds.[1] Here one relies on GC to separate components in a complex mixture and MS to identify them in terms of parent mass and daughter fragments. The GC–MS combination allows quantitation over a wide range of concentrations down to the parts per billion level. For nonvolatile compounds or compounds which decompose upon heating, one generally relies on liquid chromatography (LC) or electrophoresis. However, these techniques are not easily interfaced to mass spectrometers so that they generally do not partake of the identification powers of GC–MS. One effort to overcome this difficulty is to apply mass spectrometry to the analysis of molecular surface overlayers. Often this is accomplished by a one-step process in which molecules are ionized and ejected from the surface by bombardment with energetic particles, such as by electrons (ESD),[2] ions (SIMS),[3] fast neutral atoms (FAB),[4] fission fragments (plasma desorption),[5–7] and photons (laser desorption).[8–14] Compounds of major interest include peptides, proteins, polynucleotides, porphyrins, oligosaccharides, and biomolecules having strong acidic, basic, or polar side groups. However, it is necessary to understand in detail the ejection and ionization mechanism at the surface in order to relate the observed mass spectrum to the nature of the molecular adsorbate. Often this is obscured by matrix-dependent ionization as well as extensive fragmentation. We are exploring an alternative approach in which the desorption step is separated in time and in space from the ionization step.[15,16] This method has first been applied to the trace detection of atoms from surfaces,[17–22] then molecules from surfaces.[23–26] Many variations are possible, but our preferred embodiment of this method involves an infrared laser to desorb essentially intact molecules from a substrate opaque to this wavelength followed, after a suitable delay, by an ultraviolet laser to cause resonance-enhanced multiphoton ionization (REMPI) of those species absorbing the second wavelength. In comparison with other mass spectrometric methods, the two-step laser desorption/laser multiphoton ionization method has the advantages:

- short analysis time
- high sensitivity
- high selectivity in ionization
- no matrix ionzation effects
- simple mass spectrum often dominated by the parent ion peak
- large dynamic range of quantitation

In what follows we discuss these features and review our present efforts to develop this new mass spectrometric technique.

Two-Step Laser Desorption/Multiphoton Ionization Mass Spectrometry

A. Laser Desorption. Our two-step methodology has been described previously.[15,16] As a first step (Fig. 1a), a CO_2 laser pulse (10.6 μm; ca. 10 mJ pulse^{-1}; 10 μs pulse width; 10 Hz repetition rate) is directed onto a thin film of molecular adsorbate deposited on the surface of a suitable solid substrate, e.g., glass or machinable ceramic (MACOR). The substrate is rapidly heated and neutral molecules are desorbed from the surface (Fig. 1b).

The rate of heating induced by the CO_2 laser pulse is approximately 10^8 K s^{-1}. This should be compared to heating rates of 10 K s^{-1} or less, which can be obtained by traditional resistive heating. For adsorbates that undergo extensive molecular decomposition on the surface at a conventional heating rate, the rapid laser induced heating rates can favor desorption over decomposition.[27,28] It has been proposed[29] that the van der Waals type bonds between the physisorbed molecules and a solid substrate may serve as a "bottleneck" for energy transfer from a rapidly heated surface to the internal degrees of freedom of the adsorbed molecules, causing internally lukewarm intact molecules to be desorbed. There is much experimental evidence to support the claim that relatively cold molecules escape from a hot surface by laser-induced thermal desorption (LITD).[30–33] The same type of behavior in which evaporation dominates over decomposition has also been observed for large molecules desorbing from surfaces following

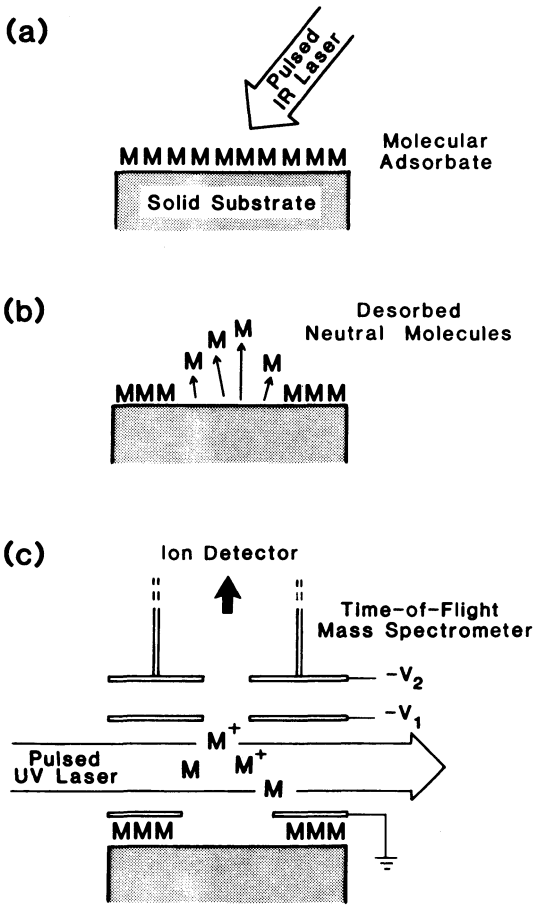

Fig. 1. Procedure for two-step laser desorption/laser multiphoton ionization mass spectrometry: (a) a CO_2 laser pulse is directed onto a film of molecular adsorbate; (b) neutral molecules escape from the surface by rapid thermal desorption; and (c) after a suitable time delay, the fourth harmonic of a Nd:YAG laser selectively ionizes neutral molecules, and the ions are then detected by a time-of-flight mass spectrometer.

pulsed laser heating.[8,9,15,16,26,27,34–37] Moreover, nonvolatile large molecules tend to desorb by LITD rather than by a resonant infrared absorption. For example, we have found that the parent ion signal of protoporphyrin IX dimethyl ester evaporated from a glass surface by a CO_2 laser pulse is 3×10^5 times stronger than that from a NaCl surface (which is transparent at the CO_2 laser wavelength).

B. Multiphoton Ionization. In the second step (Fig. 1c) of our methodology, desorbed molecules are ionized by 1+1 REMPI with the fourth harmonic (266 nm) of a Nd:YAG laser (ca. 1 mJ pulse^{-1}; 10 ns pulse width; 10 Hz repetition rate). The appropriate delay (70—90 μs) between the desorbing CO_2 laser and the ionizing Nd:YAG laser pulse is chosen so that the ionizing laser pulse intercepts as many molecules as possible.

In 1+1 REMPI, one photon causes a molecule to make a transition to an electronically excited state and a second photon ionizes the excited molecule. Wavelength selectivity results from the photon energy being resonant with an intermediate state while such selectivity is lost in the direct one-photon ionization process.[38] REMPI has other important attributes for mass spectrometry; it can provide very efficient "soft ionization"[15,16,34–42] in which the parent molecular ion dominates the mass spectrum. This is in sharp contrast to electron impact ionization where soft ionization can be obtained only with a significant decrease in ionization efficiency. In our experiments the Nd:YAG laser was slightly focused by a quartz lens to a 6 mm diameter spot size, resulting in a power density of about 10^6 W cm^{-2} in the ionization volume.

In contrast to direct one-step ionization of molecular adsorbates, the two-step laser methodology where the desorption and ionization processes are spatially and temporally separated allows a much larger fraction of the molecules to be converted to parent ions by optimizing separately the two laser sources. In addition, this technique avoids the variations of the ionization efficiency with surface substrate (matrix effect).

C. Ion Detection. Because the ion production is pulsed, it is natural to carry out mass analysis in a linear time-of-flight (TOF) system[15,16,26] or in a reflectron TOF mass spectrometer.[35–37,43] High-resolution Fourier-transform ion cyclotron resonance (FI-ICR) mass spectrometers may also be used as detectors.[44,45]

In our setup, the ions are mass-separated in a 30 cm flight tube and detected by an electron multiplier connected to two preamplifiers which feed a transient digitizer. Our typical mass resolution with this arrangement is about 100; we are presently modifying the TOF instrument into a reflectron configuration to provide much higher mass resolution.

D. Sample Preparation. In order to achieve the quantitative analysis of molecular adsorbates, it is essential to make a homogeneous film on a solid substrate. Figure 2a shows a schematic drawing of the system for preparing a thin sample film. Application of about 200 μl of the sample solution to a glass cup provides a convenient sample size for quantitative analysis. After application of the solution, the glass cup is spun horizontally by a motor and the solution spreads out as a layer over the inner cylindrical surface. A vacuum is applied to evaporate the solvent, resulting in a dry homogeneous film with known thickness. The glass cup is then mounted onto the tip of a 1/2 inch diameter Teflon rod, directly introduced into the main vacuum chamber (ca. 10^{-7} Torr) through a gate valve without breaking high vacuum, and placed in the center of the first electrode of our TOF instrument. The direct sample introduction

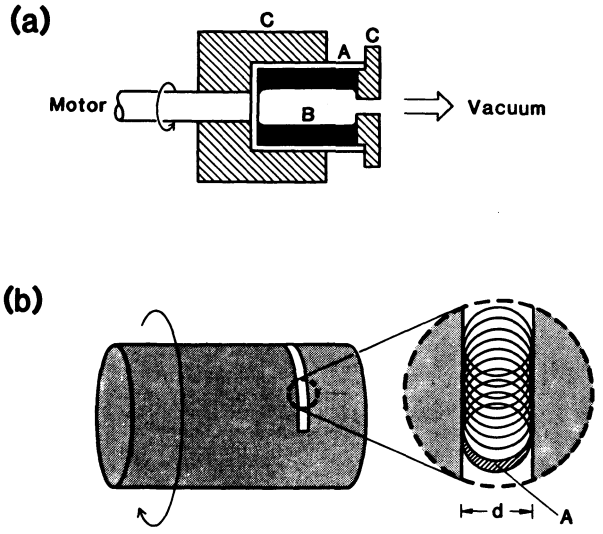

Fig. 2. (a) Apparatus for making a thin homogeneous sample film. Here A is a glass cup (12 mm×20 mm), B represents the sample solution layer formed as the glass cup is spun horizontally and by a motor, C is a Teflon clamp and cap assembly. (b) A CO_2 laser desorption track on the inner surface of the glass cup: d is the diameter of the desorption laser spot (ca. 1 mm) and A is the new area exposed in consecutive laser shots (ca. 5×10^{-2} mm^2).

method takes about one minute, and the mass spectrum can be recorded without further delay.

Representative Applications

Figure 3 shows typical laser desorption/laser multiphoton ionization mass spectra of a purine base, a dipeptide, a steroid, and a porphyrin. Common properties of these molecules are low volatility, high polarity, and a UV chromophore allowing for 1+1 REMPI (in the form of an aromatic or π-conjugated system). The most important features of these spectra are dominant parent ion peaks in all cases. Almost complete absence of fragmentation in Fig. 3c and 3d demonstrates the desorption of intact parent molecules in the laser evaporation step as well as the soft ionization capabilities of the REMPI process. The amount of fragmentation depends on the ionization laser fluence. For adenine, e.g., almost no fragmentation occurs at lower laser fluence.[16] Of course, fragmentation can also be a virtue in the identification of large molecules, and controlled fragmentation is easily achieved by increasing the fluence of the laser used in the ionization step. To some extent, fragmentation also depends on the nature of the surface/adsorbate bond: For gly-phe (Fig. 3b) and other dipeptides fairly intense fragments show up in the mass spectrum.[34] On the other hand, it is possible to observe parent ions of a decapeptide (MW=1295 amu)[36] and of proteins up to a mass of 23000 amu

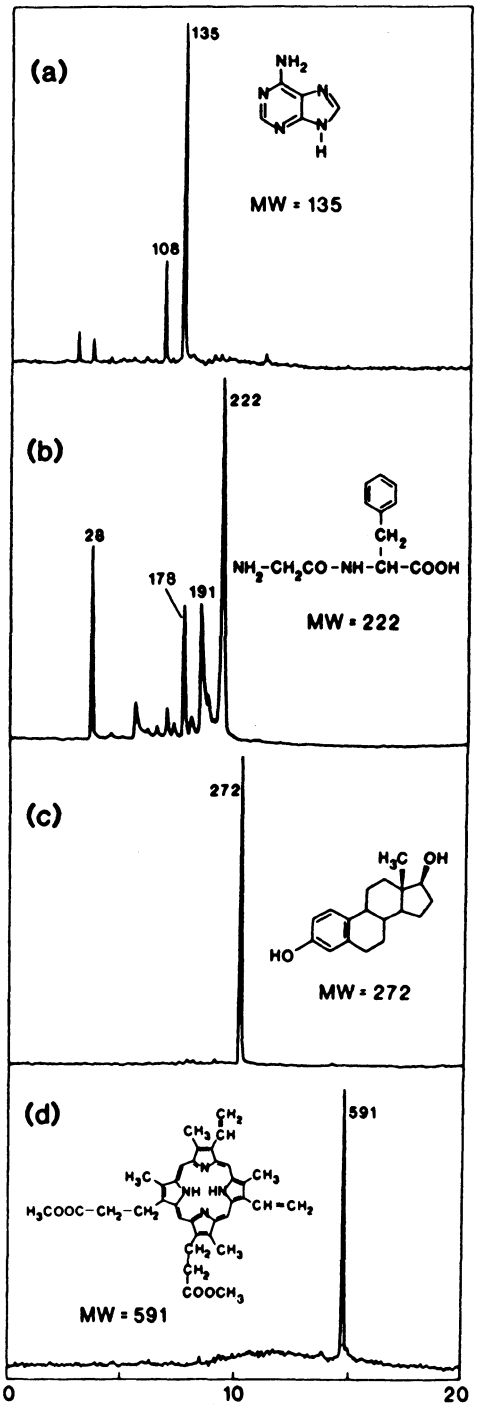

Fig. 3. Laser desorption/laser multiphoton ionization mass spectra of (a) adenine, (b) glycyl-L-phenylalanine (gly-phe), (c) β-estradiol, and (d) protoporphyrin IX dimethyl ester. Each mass spectrum represents an average over 200 laser shots.

(using ^{252}Cf bombardment).[6] We still lack a thorough understanding of various desorption mechanisms, and the examples above indicate that we need a better theoretical description in order to optimize the two-step process.

Higher-mass compounds are also tractable with our technique, as shown in Fig. 4. These two synthetic porphyrins again exhibit single parent ion peaks at 1132 and 1232 amu, respectively. This class of compounds is readily ionized by the fourth harmonic of the Nd:YAG laser. For protoporphyrin IX dimethyl ester (Fig. 3d) we have found[16] a detection limit of 4×10^{-17} mol.

Dominant parent ion peaks enable us to record spectra of mixtures. Figure 5 shows an example of an equimolar mixture of 5 phenylthiohydantoin (PTH)-amino acids. These compounds are the final products of the Edman degradation method used in protein sequencing. In our original work, all the 20 PTH-amino acids, corresponding to the 20 naturally occurring amino acids could be analyzed.[15] We were even able to distinguish between the leucine and isoleucine isomers owing to a difference in the fragmentation pattern. An example of a different sort is provided by the analysis of a meteorite sample.[46] Figure 6 shows a mass spectrum of material from Murchison, a meteorite rich in organic carbon compounds.[47] By spiking the sample with various standards, it was possible to identify a series of polynuclear aromatic compounds in the mass range from 120—300 amu, which is consistent with previous results.[48] Please note by its conspicuous absence the lack of porphyrins in this meteorite sample. This is now an accepted fact, but was the subject of a scientific debate for a long time.[49]

A particularly useful feature of our methodology is the linear quantitation we have achieved using the sampling technique described above. From experiments, where we exposed the same spot to the

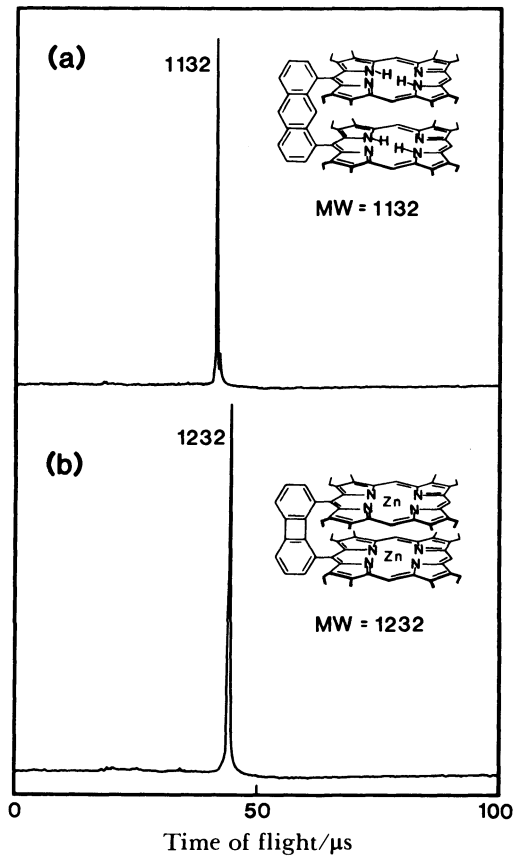

Fig. 4. Laser desorption/laser multiphoton ionization TOF mass spectra of (a) H_4(DPA) and (b) Zn_2(DPB).
DPA=1,8-bis(3,7,13,17-tetraethyl-2,8,12,18-tetramethyl-5-porphyrinyl)anthracene; DPB=1,8-bis(....)biphenylene.

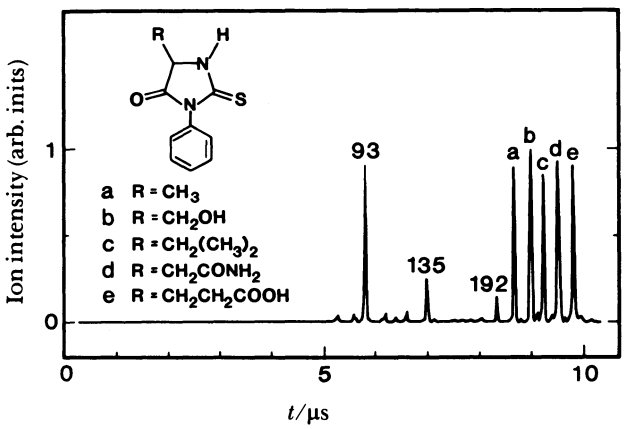

Fig. 5. A mixture of equimolar amounts of (a) PTH-alanine, (b) PTH-serine, (c) PTH-valine, (d) PTH-asparagine, and (e) PTH-glutamic acid analyzed by laser desorption/laser multiphoton ionization mass spectrometry. The peaks labeled a—e are the parent ions; some fragments of the compounds in the mixture superimpose in the lower mass region and give rise to the signals at 93, 135, and 192 amu.

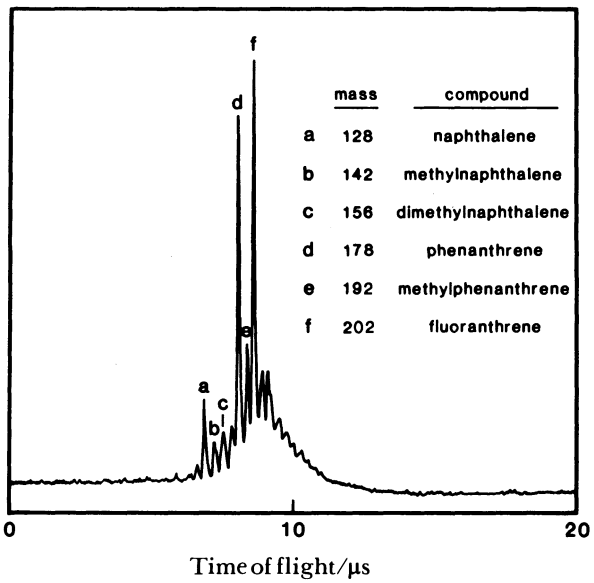

Fig. 6. Laser desorption/laser multiphoton ionization mass spectrum obtained from 1 μg of the Murchison meteorite.

desorption laser twice, we found that the desorption of the adsorbate is essentially complete after the first shot. Spectra taken for quantitative studies represent an average over many shots. Here we rotate the sample and expose a small surface area, A, to each new laser shot. This area can be calculated from a knowledge of the repetition rate of the desorption laser, the rotation speed of the sample, and the measured laser track width (cf. Fig. 2b). The amount of adsorbate which is removed per laser shot, n, is then calculated by

$$n = n_{tot} \cdot (A/A_{tot})$$

where n_{tot} is the total of amount of adsorbate deposited on A_{tot}, the total area covered. By monitoring how the signal height of the parent ion peak varies with adsorbate concentration, we found a linear dependence of n over a range of 5 orders of magnitude, as shown in Fig. 7.[16] The amount of adsorbate desorbed per laser shot ranges from nanomoles (100 monolayers) to femtomoles (10^{-4} monolayers).

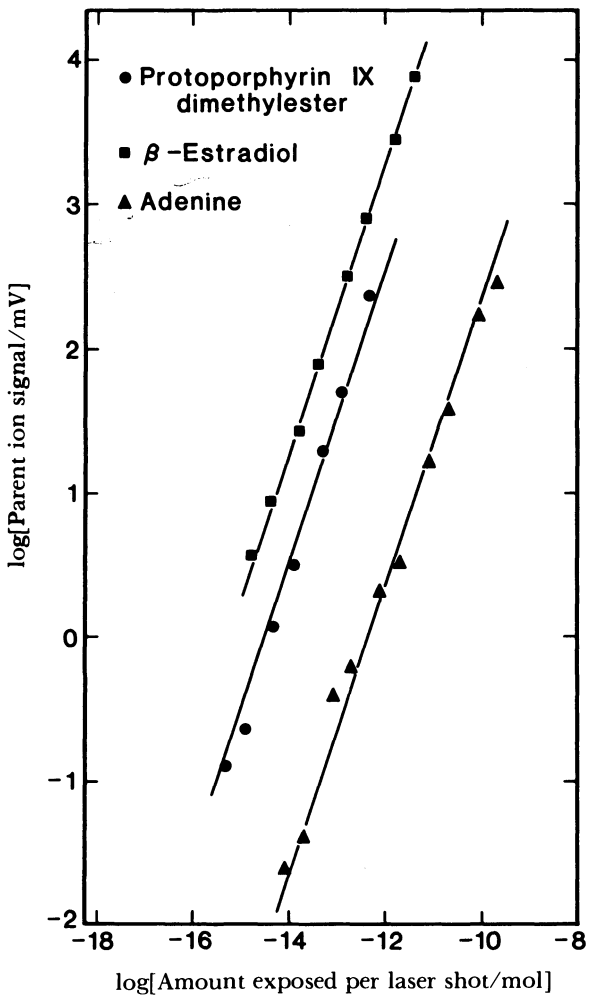

Fig. 7. Quantitation: Parent ion signal of protoporphyrin IX dimethyl ester, β-estradiol, and adenine vs. surface concentration.

Concluding Remarks

Laser desorption/laser multiphoton ionization has a number of appealing advantages for the mass spectrometric analysis of molecular adsorbates: high sensitivity, controlled fragmentation, selective ionization, rapid quantitation, and negligible matrix effects. This technique is in its early infancy but the applications to large biomolecules and other thermally labile and/or nonvolatile compounds are quite encouraging. More needs to be known about the desorption mechanism involving the adsorbate/substrate interaction before this method can be routinely applied. Nevertheless, this method has particular promise for the analysis of samples of limited availability, suggesting that some of its most dramatic uses may be in the analysis of rare samples, such as, fossils, lunar soils, meteorites, cosmic dust, and other cosmogeochemical materials.

References

1) W. L. Budde and J. W. Eichelberger, "Organics Analysis Using Gas Chromatography Mass Spectrometry," Ann Arbor Science Publishers, Inc., Ann Arbor (1979).

2) T. E. Madey, *Science*, **234**, 316 (1986).

3) A. Benninghoven, R. J. Colton, D. S. Simons, and H. W. Werner, "Secondary Ion Mass Spectrometry SIMS V," Springer-Verlag, Berlin (1986).

4) C. Fenselau, "Ion Formation from Organic Solids," ed by A. Benninghoven, Springer-Verlag, Berlin (1983), pp. 90—100.

5) R. D. Macfarlane, "Ion Formation from Organic Solids," ed by A. Benninghoven, Springer-Verlag, Berlin (1983), pp. 32—46.

6) R. D. Macfarlane, J. C. Hill, D. L. Jacobs, and R. G. Phelps, "Mass Spectrometry in the Analysis of Large Molecules," ed by C. J. McNeal, John Wiley & Sons Ltd., New York (1986), pp. 1—12.

7) M. Alai, P. Demirev, C. Fenselau, and R. J. Cotter, *Anal. Chem.*, **58**, 1303 (1986).

8) M. A. Posthumas, P. G. Kistemaker, H. L. C. Meuzelaar, and M. C. Ten Noever de Brauw, *Anal. Chem.*, **50**, 985 (1978).

9) P. G. Kistemaker, G. J. Q. van der Peyl, and J. Haverkamp, "Soft Ionization Biological Mass Spectrometry," ed by H. R. Morris, Heyden, London (1981).

10) R. Stoll and F. W. Röllgen, *Org. Mass Spectrom.*, **14**, 642 (1979).

11) D. M. Hercules, R. J. Day, K. Balasanmugam, T. A. Dang, and C. P. Li, *Anal. Chem.*, **54**, 280A (1982).

12) M. Karas and U. Bahr, *Trends Anal. Chem.*, **5**, 90 (1986).

13) F. Hillenkamp, "Ion Formation from Organic Solids," ed by A. Benninghoven, Springer-Verlag, Berlin (1983), pp. 190—205.

14) R. J. Conzemius and J. M. Capellen, *Int. J. Mass Spectrom. Ion Phys.*, **34**, 197 (1980).

15) F. Engelke, J. H. Hahn, W. Henke, and R. N. Zare, *Anal. Chem.*, **59**, 909 (1987).

16) J. H. Hahn, R. Zenobi, and R. N. Zare, *J. Am. Chem.*

Soc., **109**, 2842 (1987).
17) N. Winograd, J. P. Baxter, and F. M. Kimock, *Chem. Phys. Lett.*, **88**, 581 (1982).
18) F. M. Kimock, J. P. Baxter, and N. Winograd, *Surf. Sci. Lett.*, **124**, L41 (1983).
19) F. M. Kimock, J. P. Baxter, and N. Winograd, *Nucl. Instrum. Methods Phys. Res.*, **218**, 287 (1983).
20) S. Mayo, T. B. Lucatorto, and G. G. Luther, *Anal. Chem.*, **54**, 553 (1982).
21) C. H. Becker and K. T. Gillen, *Anal. Chem.*, **56**, 1671 (1984).
22) C. H. Becker and K. T. Gillen, *J. Opt. Soc. Am. B*, **2**, 1438 (1985).
23) V. S. Antonov, S. E. Egorov, V. S. Letokhov, and A. N. Shibanov, *JETP Lett.*, **38**, 217 (1983).
24) S. E. Egorov, V. S. Letokhov, and A. N. Shibanov, *Chem. Phys.*, **85**, 349 (1984).
25) H. V. Weyssenhoff, H. L. Selzle, and E. W. Schlag, *Z. Naturforsch.*, **40a**, 674 (1985).
26) R. Tembreull and D. M. Lubman, *Anal. Chem.*, **58**, 1299 (1986).
27) M. G. Sherman, J. R. Kingsley, R. T. McIver, Jr., and J. C. Hemminger, "Catalyst Characterization Science; ACS Symposium Series No. 288," ed by M. L. Deviney and J. L. Gland, American Chemical Society, Washington, D. C. (1985), pp. 238—251.
28) A. A. Deckert and S. M. George, *Surf. Sci.*, **182**, L215 (1987).
29) R. N. Zare and R. D. Levine, *Chem. Phys. Lett.*, **136**, 593 (1987).
30) D. Burgess, Jr., R. Viswanathan, I. Hussla, P. C. Stair, and E. Weitz, *J. Chem. Phys.*, **79**, 5200 (1983).
31) D. Burgess, Jr., D. A. Mantell, R. R. Cavanagh, and D. S. King, *J. Chem. Phys.*, **85**, 3123 (1986).
32) G. Wedler and H. Ruhmann, *Surf. Sci.*, **121**, 464 (1982).
33) C. J. S. M. Simpson and J. P. Hardy, *Chem. Phy. Lett.*, **130**, 175 (1986).
34) R. Tembreull and D. M. Lubman, *Anal. Chem.*, **59**, 1003 (1987).
35) J. Grotemeyer, U. Boesl, K. Walter, and E. W. Schlag, *J. Am. Chem. Soc.*, **108**, 4233 (1986).
36) J. Grotemeyer, U. Boesl, K. Walter, and E. W. Schlag, *Org. Mass Spectrom.*, **21**, 595 (1986).
37) J. Grotemeyer, U. Boesl, K. Walter, and E. W. Schlag, *Org. Mass Spectrom.*, **21**, 645 (1986).
38) D. M. Lubman, *Anal. Chem.*, **59**, 31A (1987).
39) A. N. Shibanov, "Laser Analytical Spectrometry," ed by V. S. Letokhov, IOP Publishing Ltd., Bristol (1986), pp. 353—404.
40) R. N. Zare, *Science*, **226**, 298 (1984).
41) D. A. Lichtin, L. Zandee, and R. B. Bernstein, "Lasers in Chemical Analysis," ed by G. M. Hieftje, J. C. Travis, and F. E. Lytle, The Humana Press, Clifton (1981), pp. 125—141.
42) D. A. Gobeli, J. J. Yang, and M. A. El-Sayed, *Chem. Rev.*, **85**, 529 (1985).
43) M. Yang and J. P. Reilly, *Int. J. Mass Spectrom. Ion Phys.*, **75**, 209 (1987).
44) M. G. Sherman, J. R. Kingsley, D. A. Dahlgren, J. C. Hemminger, and R. T. McIver, Jr., *Surf. Sci.*, **148**, L25 (1985).
45) C. L. Wilkins, D. A. Weil, C. L. C. Yang, and C. F. Ijames, *Anal. Chem.*, **57**, 520 (1985).
46) In collaboration with Prof. Jeffrey L. Bada, Scripps Institution of Oceanography, University of California, San Diego, La Jolla, CA 92093.
47) F. Mullie and J. Reisse, *Topics in Current Chemistry*, **139**, 83 (1987).
48) K. L. Pering and C. Ponnamperuma, *Science*, **173**, 237 (1971).
49) E. Anders and R. Hayatsu, *Topics in Current Chemistry.*, **99**, 1 (1981).

 © 1988 The Chemical Society of Japan Bull. Chem. Soc. Jpn., 61, 93—100 (1988)

Invited Paper

Chiral Synthesis via Organoboranes. 11. Hydroboration. 82. Asymmetric Hydroboration of 1-Heteroarylcycloalkenes with Monoisopinocampheylborane. Synthesis of *trans*-2-Heteroarylcycloalkyl Boronates and Derived Alcohols of Very High Enantiomeric Purity

Herbert C. BROWN,* Ashok K. GUPTA, and J. V. N. VARA PRASAD[1]
H. C. Brown and R. B. Wetherill Laboratories of Chemistry, Purdue University,
West Lafayette, Indiana 47907, U.S.A.
(Received May 28, 1987)

The hydroboration of representative 1-heteroarylcycloalkenes with monoisopinocampheylborane ($IpcBH_2$) was investigated systematically to establish the degree of asymmetric induction during hydroboration. The hydroboration of 1-heteroarylcyclopentene with $IpcBH_2$ at −25 °C proceeded cleanly to afford the corresponding dialkylboranes. These dialkylboranes, upon treatment with acetaldehyde and then oxidation, afforded the corresponding *trans*-2-heteroarylcycloalkanols of 85—86% ee. Similarly, 1-heteroarylcyclohexenes, upon hydroboration with $IpcBH_2$, followed by acetaldehyde treatment and oxidation, gave the corresponding alcohols in ca. 90% ee. The dialkylboranes or alkylboronic acids derived from 1-heteroarylcyclopentenes and $IpcBH_2$ can be recrystallized to furnish materials approaching 100% ee. From such dialkylboranes or alkylboronic acids, the corresponding boronates of ca. 100% ee were prepared and isolated. These are proving to be highly versatile synthetic intermediates for organic synthesis.

Asymmetric hydroboration, since its discovery in 1961,[2] proved to be a highly efficient reaction in synthetic organic chemistry.[3] Recently there has been intense interest in developing efficient methods for the preparation of organic compounds of high enantiomeric purities.[4] Of these procedures, asymmetric hydroboration is highly promising as a method for preparation of chiral compounds containing various functional groups.[5]

Monoisopinocampheylborane (**1**, $IpcBH_2$) hydroborates *trans*- and trisubstituted olefins with optical induction ranging from 53% to 100% ee.[6] The dialkylboranes derived from $IpcBH_2$ and trisubstituted olefins were crystallized to materials approaching 100% ee.[7] Recently heterocyclic olefins containing a double bond inside the ring were hydroborated with diisopinocampheylborane (**2**, Ipc_2BH) with quantitative asymmetric induction.[8,9a] Masamune and coworkers[10] have recently synthesized an asymmetric hydroborating agent, *trans*-2,5-dimethylborolane (**3**)

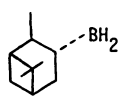

1

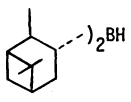

2

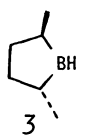

3

possessing a C_2 symmetry, which hydroborates *cis*-, *trans*- and trisubstituted olefins with an asymmetric induction ranging from 93—97% ee.

The wide range of biological activity, e.g., antitumor, carcinogenic, microbial growth inhibitor, plant growth inhibitor, antifeedant and antiflammatory displayed by a number of compounds possessing the furan and thiophene moiety has stimulated considerable effort to synthesize them.[11] In continuation of our studies on the asymmetric hydroboration of heterocyclic olefins,[8,9] various 1-heteroarylcycloalkenes were selected for study. This paper describes a systematic study of the hydroboration of 1-heteroarylcycloalkenes with $IpcBH_2$ to synthesize various chiral heterocyclic compounds.

Results and Discussion

In this study we consistently used monoisopinocampheylborane ($IpcBH_2$, 100% ee) from 92% ee (+)-α-pinene. A stock solution of $IpcBH_2$ was prepared from the TMED adduct of $IpcBH_2$ and boron trifluoride etherate in ethyl ether.[12] Representative 1-heteroarylcycloalkenes (**4**) were selected for the

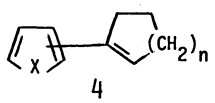

4

X = O or S

n = 1, 2 or 3

study. These alkenes, **4**, hitherto unreported, were prepared by the dehydration of the corresponding tertiary alcohols obtained from the addition of the heteroaryllithium to the cyclic ketone (Scheme 1). The olefins thus obtained were characterized by spectra and were 97—100% pure by GC examination.

Hydroboration of 1-Heteroarylcycloalkenes with $IpcBH_2$. All of these representative olefins were hydroborated with an equimolar quantity of $IpcBH_2$. The reaction was monitored by quenching aliquots with methanol, followed by ^{11}B NMR spectra of the sample.

Hydroboration of 1-(2-Furyl)cycloalkenes. 2-Furylcycloalkenes of varying ring size were hydroborated

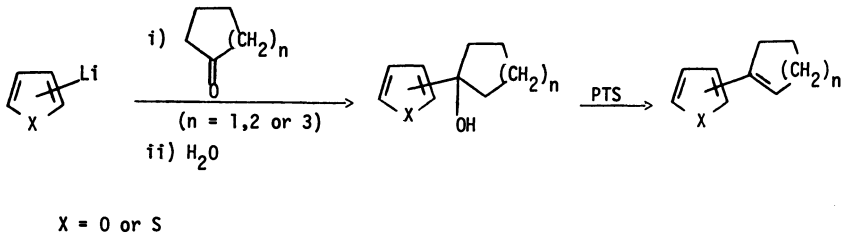

Scheme 1.

with $IpcBH_2$ in order to study the effect of ring size on asymmetric induction during hydroboration. The hydroboration of 1-(2-furyl)cyclopentene with (−)-$IpcBH_2$ [derived from (+)-α-pinene] proceeded smoothly at −25 °C in ethyl ether. The dialkylborane obtained was treated with acetaldehyde, then oxidation with alkaline hydrogen peroxide afforded *trans*-2-(2-furyl)cyclopentanol in excellent yield (Eq. 1, X=O).

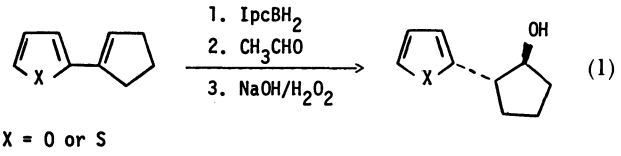

(1)

The optical purity of the alcohol by capillary GC analysis of its corresponding MTPA ester[13] was found to be of 86%.

The hydroboration of 1-(2-furyl)cyclohexene with (−)-$IpcBH_2$ proceeded slowly at −25 °C, achieving a 65% conversion in 10 days. The dialkylborane thus obtained was treated with acetaldehyde, followed by oxidation, affording *trans*-2-(2-furyl)cyclohexanol in 90% ee (Eq. 2). By increasing the temperature, i.e., to

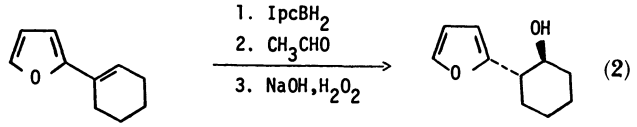

(2)

0 °C, employed during hydroboration, 80% of the olefin could be hydroborated. However, the optical purity of the alcohol obtained after oxidation is lower, i.e., 80% ee. Similarly, 1-(2-furyl)cycloheptene could be hydroborated at −25 °C easily. Treatment with acetaldehyde, followed by oxidation, gave *trans*-2-(2-furyl)cycloheptanol in excellent yield (Eq. 3), with an

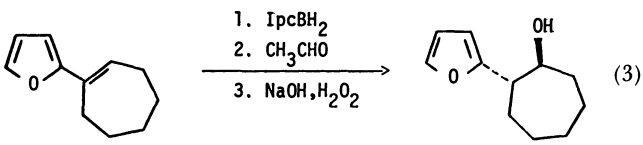

(3)

optical purity of the alcohol of 86%.

The asymmetric induction during hydroboration of 1-heteroarylcycloalkenes with $IpcBH_2$ increases slightly from the five-membered ring to the six-membered ring. The asymmetric induction in the seven-membered ring is, as expected, similar to that of the five-membered ring. Since the hydroboration of these cyclopentenes and cyclohexenes gave products with excellent asymmetric induction, various 1-heteroarylcyclopentenes and -cyclohexenes were hydroborated with $IpcBH_2$.

Hydroboration of 1-Heteroarylcyclopentenes. The hydroboration of 1-(3-furyl)cyclopentene with $IpcBH_2$ could be achieved at −25 °C. The dialkylborane obtained on treatment with acetaldehyde and then oxidation afforded *trans*-2-(3-furyl)cyclopentanol in 85% ee (Eq. 4, X=O). Similarly, 1-(2-thienyl)cyclopentene and 1-(3-thienyl)cyclopentene were hydroborated with $IpcBH_2$. The asymmetric induction during hydroboration was found to be 86% ee in both cases (Eqs. 1 and 4, X=S).

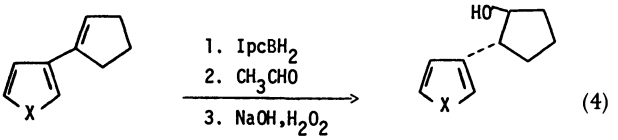

(4)

The hydroboration of 1-(2-benzofuryl)cyclopentene proceeded slowly at −25 °C. The dialkylborane was treated with acetaldehyde, followed by oxidation with alkaline hydrogen peroxide, giving *trans*-2-(2-benzofuryl)cyclopentanol in 85% ee (Eq. 5).

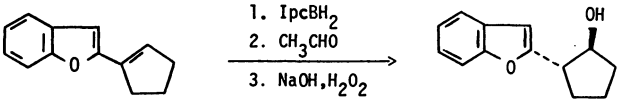

(5)

These results demonstrate the remarkable consistency in the asymmetric induction of these heterocyclic cyclopentenes during hydroboration with $IpcBH_2$. No significant change was observed in the asymmetric induction achieved during hydroboration with $IpcBH_2$, either by changing the heteroatom in the heterocycle (O or S), or by changing the position of the cyclopentene ring (2- or 3-position), or by altering substituents on the heteroaryl ring.

Hydroboration of 1-Heteroarylcyclohexenes. The hydroboration of 1-(3-furyl)cyclohexene proceeded similar to that of 1-(2-furyl)cyclohexene at −25 °C. The dialkylborane was treated with acetaldehyde and then oxidized to obtain *trans*-2-(3-furyl)cyclohexanol in 90% ee (Eq. 6, X=O). Similarly, 1-(3-thienyl)-

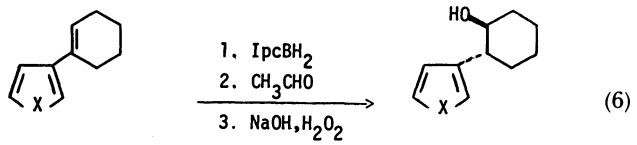

(6)

X = O or S

cyclohexene (Eq. 6, X=S) upon hydroboration with $IpcBH_2$, followed by acetaldehyde treatment, gave the boronic ester. Oxidation then afforded the corresponding *trans*-alcohol in 83% ee. The results are summarized in Table 1.

The absolute configuration of all product alcohols is not known. It was already established that $IpcBH_2$ attacks preferentially from one enantiotopic face of the alkene, realizing the alcohols of the same absolute configuration. Thus, the remarkable consistency of $IpcBH_2$ providing alcohols of the same absolute configuration was used to assign the absolute configurations of all of these alcohols. They are shown in Table 1.

Upgrading the Optical Purities of Boranes. In all of the above examples, only 83—90% of asymmetric induction could be achieved. It is highly desirable to have materials approaching 100% ee. We selected the 2-heteroarylcyclopentylboranes to study upgrading to materials of essentially 100% ee.

The above mentioned *trans*-2-heteroarylcyclopentylisopinocampheylboranes[14] were found to be solids at −25 °C in ethyl ether. For example, *trans*-2-(2-furyl)cyclopentylisopinocampheylborane (**4**), obtained via hydroboration of 1-(2-furyl)cyclopentene with $IpcBH_2$ at −35 °C, crystallized in a well-defined form in 65% yield. The dialkylborane on oxidation produced *trans*-2-(2-furyl)cyclopentanol of essentially 100% optical purity.

Similarly, the selective crystallization of *trans*-2-(3-furyl)cyclopentylisopinocampheylborane (**5**) at −35 °C provided material of only 90% ee. However, a second crystallization in ethyl ether at 0 °C gave material approaching 100% ee.

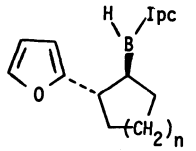

4, n = 1
8, n = 2
9, n = 3

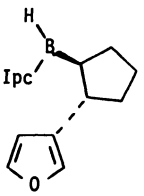

5

trans-2-(2-Thienyl)cyclopentylisopinocampheylborane (**6**) from 1-(2-thienyl)cyclopentene and $IpcBH_2$ showed unusual behavior. Although it is a dimer like the others (as evidenced by IR absorption at 1542 cm^{-1}), the major enantiomer accumulated in the mother liquor. The crystallized dialkylborane, **6**, showed reduced optical purity of only 7%. The dialkylborane in the mother liquor showed an optical purity of only 90%. It was further upgraded to 94% by cooling the reaction mixture to −78 °C, followed by the removal of crystalline borane. However, a

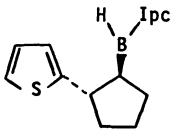

6

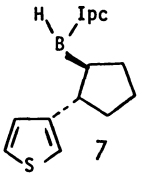

7

Table 1. Asymmetric Hydroboration of 1-Heteroarylcycloalkenes with (−)-$IpcBH_2$[a]

Olefin	Product	Reaction temp °C	Reaction time Days	Isolated yield[b] %	$[\alpha]_D$ in degrees	% ee[c]	Absolute configuration
1-(2-Furyl)cyclopentene	*trans*-2-(2-Furyl)cyclopentanol	−25	4	82	+75.6 (*c* 2.2, MeOH)	86	1S, 2S
1-(2-Furyl)cyclohexene	*trans*-2-(2-Furyl)cyclohexanol	−25	10	70	+53.04 (*c* 1.8, MeOH)	90	1S, 2S
1-(2-Furyl)cycloheptene	*trans*-2-(2-Furyl)cycloheptanol	−25	4	80	+30.04 (*c* 2.4, MeOH)	86	1S, 2S
1-(3-Furyl)cyclopentene	*trans*-2-(3-Furyl)cyclopentanol	−25	4	84	+52.3 (*c* 2.2, MeOH)	85	1S, 2R
1-(3-Furyl)cyclohexene	*trans*-2-(3-Furyl)cyclohexanol	−25	10	77	+37.6 (*c* 2.1, MeOH)	90	1S, 2R
1-(2-Thienyl)cyclopentene	*trans*-2-(2-Thienyl)cyclopentanol	−25	4	86	+60.95 (*c* 2.3, MeOH)	86	1S, 2S
1-(3-Thienyl)cyclopentene	*trans*-2-(3-Thienyl)cyclopentanol	−25	3	89	+63.7 (*c* 2.05, MeOH)	86	1S, 2R
1-(3-Thienyl)cyclohexene	*trans*-2-(3-Thienyl)cyclohexanol	−25	10	84	+31.93 (*c* 1.45, MeOH)	83	1S, 2R
1-(2-Benzofuryl)cyclopentene	*trans*-2-(2-Benzofuryl)-pentanol	−25	10	71	+48.6 (*c* 2.74, MeOH)	85	1S, 2S

a) The reagent was prepared from (+)-α-pinene $[\alpha]_D^{25}$ +47.2 (neat), 92% ee and BMS. b) Based on the amount of olefin. c) Determined by capillary GC analysis of the corresponding Mosher ester.

material of ca. 99% optical purity could be obtained by crystallizing its *trans*-2-(2-thienyl)cyclopentylboronic acid. *trans*-2-(3-Thienyl)cyclopentylisopinocampheylborane (**7**) crystallized at −35 °C, similar to **4**, to produce a material approaching 100% ee.

Further, in the case of *trans*-2-(2-furyl)cyclohexylisopinocampheylborane (**8**) and *trans*-2-(2-furyl)cycloheptylisopinocampheylborane (**9**), the dimer, $(R^*BHIpc)_2$, was not crystalline. The products are readily converted into boronic acid, $R^*B(OH)_2$, by treatment with acetaldehyde, followed by hydrolysis. A simple crystallization of these boronic acids in ether/pentane provided material of high optical purity. The corresponding *trans*-alcohols obtained after oxidation of these pure dialkylboranes or alkyl boronic acid were characterized and the results are summarized in Table 2.

Isolation of *trans*-3-Heteroarylcycloalkylboronates of High Enantiomeric Purities. Chiral alkylboronic esters containing only one alkyl group attached to boron are highly promising intermediates for asymmetric synthesis proceeding through boron

Table 2. *trans*-2-Heteroarylcycloalkanols of High Enantiomeric Purity

Heterocycloalkanols	Yield %	$[\alpha]_D$ in degree	% ee[a]	Absolute configuration
trans-2-(2-Furyl)cyclopentanol	70	+88.2 (*c* 2.325, MeOH)	99	1S, 2S
trans-2-(3-Furyl)cyclopentanol	60	+60.6 (*c* 2.29, MeOH)	99	1S, 2R
trans-2-(2-Thienyl)cyclopentanol	64	+70.6 (*c* 2.35, MeOH)	99	1S, 2S
trans-2-(3-Thienyl)cyclopentanol	65	+73.01 (*c* 2.32, MeOH)	99	1S, 2R
trans-2-(2-Furyl)cyclohexanol	55	+58.2 (*c* 1.8, MeOH)	98	1S, 2S
trans-2-(2-Furyl)cycloheptanol	70	+34.9 (*c* 2.4, MeOH)	99	1S, 2S

a) Determined by capillary GC analysis of the corresponding Mosher ester.

Table 3. Diethyl *trans*-2-Heteroarylcycloalkylboronates of High Enantiomeric Purity

Boronic ester $R^*B(OEt)_2$	Yield %	$[\alpha]_D$ in degree	% ee	Absolute configuration	^{11}B NMR chemical shift δ[a]
Diethyl *trans*-2-(2-furyl)cyclopentylboronate	60	+51.58 (*c* 2.52, EtOH)	99	1S, 2S	+31.4
Diethyl *trans*-2-(3-furyl)cyclopentylboronate	50	+41.34 (*c* 2.38, EtOH)	99	1S, 2R	+31.4
Diethyl *trans*-2-(2-thienyl)cyclopentylboronate	64	+36.10 (*c* 2.535, EtOH)	99	1S, 2S	+30.9
Diethyl *trans*-2-(3-thienyl)cyclopentylboronate	50	+46.72 (*c* 2.50, EtOH)	99	1S, 2R	+31.4
Diethyl *trans*-2-(2-furyl)cyclohexylboronate	35	+36.2 (*c* 2.10, EtOH)	98	1S, 2S	+31.3
Diethyl *trans*-2-(2-furyl)cycloheptylboronate	45	+24.6 (*c* 2.40, EtOH)	99	1S, 2S	+31.7

a) Relative to $EE\cdot BF_3$ ($\delta=0$).

Table 4. Diethanolamine *trans*-2-Heteroarylcycloalkylboronates of High Optical Purity

Boronic ester 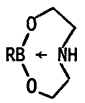	Yield %	Mp θ_m/°C	% ee	Absolute configuration	*m/z* M^+ 1
Diethanolamine *trans*-2-(2-furyl)-cyclopentylboronate	80	101—102	99	1S, 2S	250
Diethanolamine *trans*-2-(3-furyl)-cyclopentylboronate	85	160—161	99	1S, 2R	250
Diethanolamine *trans*-2-(2-thienyl)-cyclopentylboronate	85	128—130	99	1S, 2S	250
Diethanolamine *trans*-2-(3-thienyl)-cyclopentylboronate	86	153—154	99	1S, 2R	250
Diethanolamine *trans*-2-(2-furyl)-cyclohexylboronate	87	152—153	98	1S, 2S	264
Diethanolamine *trans*-2-(2-furyl)-cycloheptylboronare	90	157—158	99	1S, 2S	278

chemistry.[5,15,16] Previously, Brown, Jadhav and Desai[17] established the clean elimination of α-pinene from Ipc_2BR^* and IpcBHR* by treatment with acetaldehyde, giving $R^*B(OEt)_2$ without loss of optical activity (Eq. 7). A similar procedure provided

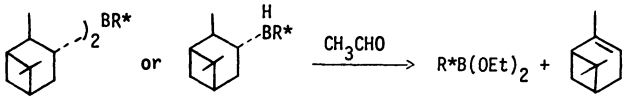

(7)

trans-2-heteroarylcycloalkylboronates. Simple distillation provided a pure boronate, characterized by ^{11}B NMR and ^1H NMR. The results are summarized in Table 3. From these esters, optically pure crystalline chelate esters stable in air were prepared by treating the ethyl boronates with diethanolamine (Eq. 8). From such derivatives, the corresponding boronic

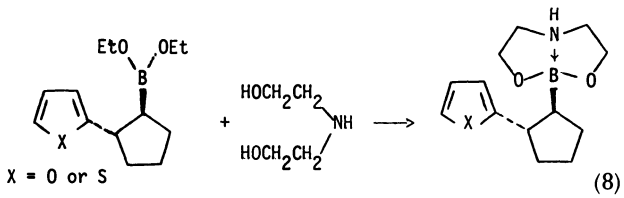

(8)

acid can be easily regenerated by treating with hydrochloric acid.[18] These crystalline compounds showed a correct M^+ ion in the mass spectra. The results are summarized in Table 4.

Conclusion

The present method provides a simple and efficient method for the preparation of various *trans*-2-heteroarylcycloalkanols of high enantiomeric purity. Due to the availability of both enantiomers of α-pinene, both enantiomers of the heterocycles can be synthesized. The chiral auxiliary, α-pinene, can be recovered and recycled. The isolation of heterocyclic boronates of 100% ee provides a simple route to synthesize various heterocycles containing different functional groups in essentially 100% ee. The synthetic implications of such optically pure boronates are described elsewhere.[5] Moreover, using the known chemistry, these heterocycles can be converted to various other compounds.

Experimental

The reaction flasks and other glass equipment were stored in an oven at 150 °C overnight and assembled in a stream of dry nitrogen gas. Syringes were assembled and fitted with needles while hot and cooled in a stream of dry nitrogen gas. Special experimental techniques used in handling air-sensitive materials are described in detail elsewhere.[19]

Spectra. ^{11}B NMR spectra were recorded on a Varian FT-80A instrument. The chemical shifts are in δ relative to $BF_3 \cdot OEt_2$. ^1H NMR (60 MHz) were recorded on a Varian T-60. IR and mass spectra were recorded on Perkin-Elmer 137 and Finnegan GC/mass spectrometers respectively. Optical rotations were measured on a Rudolph polarimeter Autopol III.

GC Analysis. All GC analyses were carried out with a Hewlett Packard 5750 chromatograph using (a) 12 ft×0.125 in column packed with 10% Carbowax 20 M on Chromosorb W (100—120 mesh) or (b) 12 ft×0.125 in column packed with 10% SE-30 on Chromosorb W (100—120 mesh). For preparative GC, either (c) a 6 ft×0.5 in column packed with 20% Carbowax 20 M on Chromosorb W (60—80 mesh) or (d) a 6 ft×0.5 in column packed with 20% SP-2100 on Chromosorb W (60—80 mesh) was used.

Materials. Borane-methyl sulfide (BMS) purchased from Aldrich Chemical Company was estimated according to the standard procedure.[19] (+)-α-Pinene $[\alpha]_D^{23}$ +47.2° (neat) was purchased from Aldrich Chemical Company and distilled from a small excess of LAH. Anhydrous ethyl ether available from Mallinckrodt, Inc. was used directly. *N,N,N',N'*-Tetramethylethylenediamine (TMED) was distilled over excess calcium hydride. Tetrahydrofuran (THF) was distilled over anhydrous benzophenone ketyl and stored under nitrogen atmosphere in an ampule. The bis adduct of monoisopinocampheylborane with tetramethylethylenediamine (TMED·2IpcBH$_2$) and generation of (−)-IpcBH$_2$ of 100% ee from it was done as reported in the literature.[12]

Preparation of 1-Heteroarylcycloalkenes. Preparation of Tertiary Alcohols. Tertiary alcohols were prepared according to a similar procedure reported in the literature.[20] To a cooled (0 °C) solution of 16.32 g (240 mmol) of furan and ether (200 mL) was added *n*-BuLi in hexane, 76.8 mL (176 mmol) dropwise. The resulting mixture was stirred at 0 °C for 1 h, after which was added an ethereal solution of the corresponding ketone (152 mmol). After being stirred overnight, the reaction mixture was quenched with water (10 mL). The ether layer was decanted, dried ($MgSO_4$) and the solvent was removed under reduced pressure.

Preparation of 1-Heteroarylcycloalkenes. The crude alcohol taken in 100 mL benzene was treated with catalytic amount of *p*-toluenesulfonic acid for about 30 min at 40—50 °C. The benzene layer was dried over anhydrous K_2CO_3 and distilled to give the required olefins in 80—90% overall yield and >97% GC pure.

1-(2-Furyl)cyclopentene. Bp 60—61°/3.5 mmHg, n_D^{21} 1.5400, IR (neat in cm^{-1}) 2953, 2928, 2847, 1481, 1331, 992, 950, 914, 793, 732. ^1H NMR ($CDCl_3$) δ=1.75—2.80 (6H, m), 5.90—6.45 (3H, m), 7.35 (1H, m). Mass spectrum *m/z* 134 (M^+).

1-(2-Furyl)cyclohexene. Bp 76—77°/2.5 mmHg, n_D^{21} 1.5242, IR (neat in cm^{-1}), 2931, 2860, 2837, 1490, 1437, 1154, 1021, 1005, 793, 732. ^1H NMR ($CDCl_3$) δ=1.40—2.60 (8H, m), 6.10—6.60 (3H, m), 7.30 (1H, m). Mass spectrum *m/z* 148 (M^+).

1-(2-Furyl)cycloheptene. Bp 70—72 °C/1.0 mmHg, n_D^{21} 1.5380, IR (neat in cm^{-1}) 2920, 2851, 1447, 1354, 1156, 1015, 790, 730. ^1H NMR ($CDCl_3$) δ=1.40—2.45 (10H, m), 6.05—6.40 (3H, m), 7.30 (1H, m). Mass spectrum *m/z* 162 (M^+).

1-(2-Thienyl)cyclopentene. Bp 68—70°/0.2 mmHg, n_D^{21} 1.5940, IR (neat in cm^{-1}) 2951, 2925, 2894, 2844, 1434, 1330, 1256, 852, 822, 798, 694. ^1H NMR ($CDCl_3$) δ=1.80—2.80 (6H, m), 6.0 (1H, m), 6.80—7.15 (3H, m). Mass spectrum *m/z* 150 (M^+).

1-(2-Benzofuryl)cycloheptene. Mp 72—73 °C, IR (KBr in cm^{-1}) 2948, 2945, 2891, 1446, 1437, 1251, 791, 746. ^1H NMR ($CDCl_3$) δ=1.8—2.25 (2H, m), 2.30—2.90 (4H, m), 6.3—6.6

(2H, bs), 7.1—7.7 (4H, m). Mass spectrum *m/z* 184 (M^+).

Preparation of 1-(3-Furyl/3-Thienyl)cycloalkenes. Following the general procedure used to prepare 3-furyl- or 3-thienyl-substituted cycloalkenes, 3-bromofuran or 3-bromothiophene (120 mmol) was taken in a 250-mL flask along with 150 mL of ether. It was cooled to −78 °C under N_2 and *n*-BuLi (144 mmol) was added dropwise. The reaction mixture was stirred at −78 °C for 1 h after which was added the corresponding ketone (120 mmol) slowly. It was further stirred 1 h at −78 °C, warmed to room temperature and quenched with water (10 mL). The ether layer was decanted, dried ($MgSO_4$) and the solvent was removed under reduced pressure. The crude product directly taken in benzene (100 mL) and treated with catalytic amount of *p*-toluenesulfonic acid for 30 min at 40—50 °C. The benzene layer was dried over anhydrous K_2CO_3 and distilled to give the corresponding olefins in 75—90% overall yield.

1-(3-Furyl)cyclopentene. Bp 88—90°/3.0 mmHg, n_D^{21} 1.5080, IR (neat on cm^{-1}) 2955, 2871, 1732, 1506, 1449, 1157, 1046, 1022, 1005, 905, 873, 784. ^1H NMR ($CDCl_3$) δ=1.35—2.80 (6H, m), 5.90 (1H, m), 6.55 (1H, m), 7.40 (2H, m). Mass spectrum *m/z* 134 (M^+).

1-(3-Furyl)cyclohexene. Bp 58—60°/0.3 mmHg, n_D^{21} 1.5100, IR (neat in cm^{-1}) 2990, 2920, 1580, 1480, 1190, 1170, 1090, 1070, 1000, 950, 905, 810, 760. ^1H NMR ($CDCl_3$) δ=1.30—2.40 (8H, m), 6.0 (1H, m), 6.50 (1H, m), 7.30 (2H, m). Mass spectrum *m/z* 148 (M^+).

1-(3-Thienyl)cyclopentene. Mp 59—60 °C. IR (Nujol in cm^{-1}) 2904, 2676, 1745, 1716, 1515, 1464, 1419, 1377, 1318, 1294, 1083, 1035, 954, 866, 838, 770, 722. ^1H NMR ($CDCl_3$) δ=1.80—2.80 (6H, m), 5.95 (1H, m), 6.80—7.25 (3H, m). Mass spectrum *m/z* 150 (M^+).

1-(3-Thienyl)cyclohexene. Bp 78—84°/0.05 mmHg, n_D^{21} 1.5650. IR (neat in cm^{-1}) 2927, 2857, 2833, 1447, 1435, 869, 841, 770, 714, 633. ^1H NMR ($CDCl_3$) δ=1.30—2.50 (8H, m), 6.15 (1H, m), 6.90—7.30 (3H, m). Mass spectrum *m/z* 164 (M^+).

Hydroboration of 1-(2-Furyl)cyclopentene. In a 250-mL flask equipped with septum inlet, magnetic stirring bar and a connecting tube leading to a mercury bubbler was placed 30 mL (25 mmol) of $IpcBH_2$ in ethyl ether and this was cooled to −25 °C. To the reaction flask was added with stirring 3.35 g (25 mmol) of 1-(2-furyl)cyclopentene over a period of 5 min. The reaction mixture was allowed to stir at −25 °C for 4 days. After completing the reaction (^{11}B NMR), the reaction flask was brought to 0 °C and 5.6 mL (10 mmol) of acetaldehyde was added dropwise and stirred at 25 °C for 6 h. Excess acetaldehyde was removed under reduced pressure (25 °C, 15 mmHg, 1 h) and to it 10 mL of THF was added. The boronate thus obtained was oxidized with 25 mL of 3 M sodium hydroxide and 3.7 mL of 30% H_2O_2. The reaction mixture was stirred at 25 °C for 5 h. The aqueous layer was saturated with potassium carbonate and extracted with 3×25 mL of ether, dried over $MgSO_4$ and the ether evaporated. The residue was passed through silica-gel column. The pentane eluent removed α-pinene, 5% ether in pentane removed unreacted olefins whereas the ether·pentane (20:80) afforded the alcohol, which, upon distillation, yielded 3.1 g of (1*S*,2*S*)-*trans*-2-(2-furyl)cyclopentanol, by 67—70°/0.02 mmHg, 82% isolated yield. GC purity >98%. It was further purified by preparative GC column c to furnish a GC pure material $[\alpha]_D^{23}$ +76.66° (*c* 2.215, MeOH), n_D^{21} 1.5065, 86% ee by capillary GC of its Mosher ester. IR (neat in cm^{-1}) 3358, 2959, 2975, 1594, 1504, 1451, 1147, 1069, 1045, 1010, 992, 800. ^1H NMR ($CDCl_3$) δ=1.80 (6H, m), 2.40 (1H, s), 3.0 (1H, m), 4.20 (1H, m), 6.0 (1H, m), 6.2 (1H, m), 7.25 (1H, m). Mass spectrum *m/z* 152 (M^+).

Hydroboration of 1-(2-Furyl)cyclohexene. With the usual experimental setup, 3.70 g (25 mmol) of 1-(2-furyl)cyclohexene was added dropwise to 35 mL (25 mmol) of $IpcBH_2$ in ethyl ether at −25 °C. The contents were stirred for 10 days at −25 °C and (5.6 mL) of acetaldehyde was added dropwise and stirred further for 6 h at room temperature. The boronate thus obtained was oxidized, worked up as usual, and purified by column chromatography as described in earlier cases to give 2.9 g of pure (1*S*,2*S*)-(+)-*trans*-2-(2-furyl)cyclohexanol, bp 75—80°/0.02 mmHg, 70% isolated yield. It was further purified by preparative GC column c to give GC pure material $[\alpha]_D^{23}$ +53.04 (*c* 1.795, MeOH), n_D^{21} 1.5080, 90% ee by capillary GC of its Mosher ester. IR (neat in cm^{-1}) 2931, 2858, 1591, 1448, 1170, 1146, 1122, 1060, 1009, 921, 802, 730. ^1H NMR ($CDCl_3$) δ=1.30—2.25 (8H, m), 2.40 (2H, m), 3.60 (1H, m), 6.0—6.40 (2H, m), 7.35 (1H, m). Mass spectrum *m/z* 166 (M^+).

Hydroboration of 1-(2-Furyl)cycloheptene. With the usual experimental setup, 4.05 g (25 mmol) of 1-(2-furyl)cycloheptene was added dropwise to 35 mL (25 mmol) of (−)-$IpcBH_2$ at −25 °C. The reaction mixture was stirred at −25 °C for 4 days. To the dialkylborane thus obtained was added 5.6 mL of acetaldehyde and the contents stirred 5 h at 25 °C. The excess of acetaldehyde was pumped off and the reaction mixture oxidized and worked up as described above to give 3.6 g of (1*S*,2*S*)-(+)-*trans*-2-(2-furyl)cycloheptanol, bp 78—80°/0.01 mmHg, 80% isolated yield. $[\alpha]_D^{21}$ +30.04 (*c* 2.43, MeOH), n_D^{21} 1.5115, 86% ee by capillary GC of its Mosher ester. IR (neat in cm^{-1}) 3400, 2928, 2860, 1502, 1457, 1444, 1146, 1046, 1024, 1010, 729. ^1H NMR ($CDCl_3$) δ=1.70 (10H, m), 2.0 (1H, s), 2.80 (1H, m), 3.85 (1H, m), 6.10 (1H, m), 6.30 (1H, m), 7.30 (1H, m). Mass spectrum *m/z* 180 (M^+).

Hydroboration of 1-(2-Thienyl)cyclopentene. With the usual experimental setup, 3.75 g (25 mmol) of 1-(2-thienyl)cyclopentene was added dropwise to 35 mL (25 mmol) of (−)-$IpcBH_2$ at −25 °C. The reaction mixture was stirred for 4 days at −25 °C. The dialkylborane thus obtained was worked up as usual, as described above, to give 3.6 g of distilled (1*S*,2*S*)-(+)-*trans*-2-(2-thienyl)cyclopentanol, bp 88—91°/0.02 mmHg, 86% isolated yield. n_D^{21} 1.5600. It was further purified by preparative GC to give pure product $[\alpha]_D^{22}$ 60.95 (*c* 2.3, MeOH), 86% ee by capillary GC of its Mosher ester. IR (neat in cm^{-1}) 3363, 2956, 2872, 1439, 1339, 1237, 1081, 1037, 824, 694. ^1H NMR ($CDCl_3$) δ=1.70—2.40 (7H, m), 3.10 (1H, m), 4.10 (1H, m), 6.80—7.30 (3H, m). Mass spectrum *m/z* 168 (M^+).

Hydroboration of 1-(3-Furyl)cyclopentene. With the usual experimental setup, 3.35 g of 1-(3-furyl)cyclopentene was added dropwise to 35.7 mL (25 mmol) of (−)-$IpcBH_2$ in ethyl ether at −25 °C. The contents after stirring for 4 days at −25 °C were worked up as usual and purified as described above to give 3.17 g of (1*S*,2*R*)-(+)-*trans*-2-(3-furyl)cyclopentanol, bp 75—80°/0.05 mmHg, 84% isolated yield. $[\alpha]_D^{22}$ +52.3 (*c* 2.2, MeOH), 85% ee by capillary GC of its Mosher ester. IR (neat in cm^{-1}) 3357, 2956, 2874, 1500, 1468, 1450, 1340, 1161, 1090, 1064, 1025, 814, 726. ^1H NMR ($CDCl_3$) δ=1.60—2.30 (6H, m), 2.70 (2H, m), 4.05 (1H, m), 6.35 (1H,

bs), 7.40 (2H, m). Mass spectrum *m/z* 152 (M^+).

Hydroboration of 1-(3-Thienyl)cyclopentene. With the usual experimental setup, 3.75 g (25 mmol) of 1-(3-thienyl)cyclopentene (in 5 mL of ether) was added dropwise to 30 mL (25 mmol) of (−)-IpcBH$_2$ at −25 °C. After stirring for 3 days at −25 °C, it was treated with acetaldehyde and worked up as described above to give 3.75 g of (1*S*,2*S*)-(+)-*trans*-2-(3-thienyl)cyclopentanol, bp 90—91 °C/0.04 mmHg, 89% isolated yield. It was further purified by preparative GC column c to give GC pure product n_D^{21} 1.5620, $[\alpha]_D^{22}$ +63.7 (*c* 2.05, MeOH), 86% ee by capillary GC of its Mosher ester. IR (neat in cm^{-1}) 3357, 2955, 2871, 1449, 1411, 1082, 1045, 844, 776, 645. ^{1}H NMR ($CDCl_3$) δ=1.4—2.35 (7H, m), 2.90 (1H, m), 4.0 (1H, m), 6.70—7.30 (3H, m). Mass spectrum *m/z* 168 (M^+).

Hydroboration of 1-(2-Benzofuryl)cyclopentene. With the usual experimental setup, 4.6 g (25 mmol) of 1-(2-benzofuryl)cyclopentene in 5 mL of ether was added dropwise to 30 mL (25 mmol) of (−)-IpcBH$_2$ at −25 °C. The reaction mixture was stirred at −25 °C for 10 days and worked up as described above to give 3.6 g of (1*S*,2*S*)-(+)-*trans*-2-(2-benzofuryl)cyclopentanol, bp 115—120 °C/0.02 mmHg isolated yield 71%, $[\alpha]_D^{22}$ +48.6° (*c* 2.74, MeOH), 85% ee by capillary GC of its Mosher ester. IR (neat in cm^{-1}) 3381, 2954, 2872, 1476, 1450, 1439, 1260, 1177, 1054, 787, 768, ^{1}H NMR ($CDCl_3$) δ=1.40—2.40 (6H, m), 2.90—3.40 (2H, m), 4.10—4.70 (2H, m), 6.60—7.10 (4H, m).

Hydroboration of 1-(3-Furyl)cyclohexene. With the usual experimental setup, 3.7 g (25 mmol) of 1-(3-furyl)cyclohexene was added dropwise to 35 mL (25 mmol) of (−)-IpcBH$_2$ at −25 °C. The reaction mixture was stirred at −25 °C for 10 days and worked up, purified as described above to give 3.2 g of (1*S*,2*R*)-(+)-*trans*-2-(3-furyl)cyclohexanol, bp 85—90 °C/0.02 mmHg, 77% isolated yield. It was further purified by capillary GC column c to give GC pure alcohol $[\alpha]_D^{22}$ +37.6° (*c* 2.11, MeOH), 90% ee by capillary GC of its Mosher ester. IR (neat in cm^{-1}) 3427, 2929, 2856, 1498, 1447, 1344, 1159, 1119, 1059, 1025, 736. ^{1}H NMR ($CDCl_3$) δ=1.20—2.0 (9H, m), 2.15 (1H, s), 4.0 (1H, m), 6.45 (1H, bs), 7.40 (2H, m). Mass spectrum *m/z* 166 (M^+).

Hydroboration of 1-(3-Thienyl)cyclohexene. With the usual experimental setup, 4.1 g (25 mmol) of 1-(3-thiethyl)-cyclohexene was added dropwise to 35 mL (25 mmol) of (−)-IpcBH$_2$ in ether at −25 °C. The contents, after being stirred for 10 days at −25 °C, were treated with excess acetaldehyde, worked up as usual to give 3.82 g of (1*S*,2*R*)-(+)-*trans*-2-(3-thienyl)cyclohexanol, bp 95—100 °C/0.02 mmHg, 84% isolated yield. It was further purified by preparative GC to give GC pure product $[\alpha]_D^{20}$ +31.93° (*c* 1.450, MeOH), 83% ee by capillary GC of its Mosher ester. IR (Nujol in cm^{-1}) 3272, 2928, 1465, 1378, 1350, 1232, 1063, 787, 722. ^{1}H NMR ($CDCl_3$) δ=1.30—2.0 (8H, m), 2.20 (1H, s), 2.60 (1H, m), 3.50 (1H, m), 6.80—7.45 (3H, m). Mass spectrum *m/z* 182 (M^+).

General Procedure for Upgrading and Isolation of Boronic Esters of High Optical Purity. Diethyl *trans*-2-(2-Furyl)cyclopentylboronate. A 250-mL round-bottom flask equipped with a sidearm, magnetic stirring bar and gas lead was flushed with nitrogen. In this flask 70 mL (50 mmol) of (−)-IpcBH$_2$ was taken and cooled to −35 °C. To it was added 6.7 g (50 mmol) of 1-(2-furyl)cyclopentene dropwise with magnetic stirring. The flask was maintained at −35 °C without stirring for 4 days. A white crystalline solid separated out. The supernatant liquid was removed by double-ended needle and the crystals were washed with cold ether (3×20 mL). The solid was dried under vacuum (ca. 15 mmHg) at 0 °C. It was then suspended in 20 mL of ether and treated with excess acetaldehyde (6 mL). The reaction mixture was stirred at room temperature for 5 h and (^{11}B NMR δ=30.97) showed the absence of dialkylborane. The excess of acetaldehyde pumped off and the residue distilled to give (+)-diethyl (1*S*,2*S*)-*trans*-2-(2-furyl)cyclopentylboronate, 7.05 g, bp 65—70°/0.02 mmHg, 60% isolated yield. $[\alpha]_D^{22}$ +51.58° (*c* 2.52, EtOH), >99% ee. ^{1}H NMR ($CDCl_3$) δ=1.20 (6H, m), 1.60—2.25 (7H, m), 3.25 (1H, m), 3.85 (4H, q), 5.90 (1H, m), 6.20 (1H, m), 7.25 (1H, m). A part of the sample was oxidized with NaOH, H_2O_2 to give the *trans*-2-(2-furyl)cyclopentanol which was further purified by preparative GC. $[\alpha]_D^{23}$ +88.2° (*c* 2.325, MeOH), >99% ee by capillary GC of its Mosher ester.

Diethyl *trans*-2-(3-Furyl)cyclopentylboronate. With the usual experimental setup, 6.7 g (50 mmol) of 3-furylcyclopentene was added dropwise to 70 mL (50 mmol) of IpcBH$_2$ at −35 °C. The flask was maintained at −35 °C without stirring for 4 days. The white crystalline solid separated out. The supernatant liquid was removed by double-ended needle and the crystals were washed with (3×20 mL) of cold ether. The solid was redissolved in 25 mL of ether at room temperature in about 10 min. A part of the solution (0.5 mL) was oxidized with NaOH and H_2O_2 and the optical purity checked by capillary GC of its Mosher ester showed 90% ee. The remaining whole solution was kept in a cold room for slow crystallization at 0 °C for 24 h. The white crystalline needles separated out. The supernatant liquid was removed by double-ended needle and the crystals washed with ice cold ether (3×5 mL). The crystals were dried under vacuum and treated with excess acetaldehyde. The usual workup as described above gave 5.9 g required boronate, bp 76—80°/0.04 mmHg, 50% yield. $[\alpha]_D^{22}$ +41.34° (*c* 2.38, EtOH), >99% ee. ^{1}H NMR ($CDCl_3$) δ=0.9—1.3 (6H, m), 1.4—2.0 (7H, m), 3.0 (1H, m), 3.8 (4H, q), 6.25 (1H, m), 7.20 (2H, m). A part of the diethyl *trans*-2-(3-furyl)cyclopentylboronate was oxidized to give the corresponding alcohol $[\alpha]_D^{22}$ +60.6° (*c* 2.29, MeOH), >99%ee by capillary GC of its Mosher ester.

Diethyl *trans*-2-(3-Thienyl)cyclopentylboronate. With the usual experimental setup as described above, diethyl *trans*-2-(3-thienyl)cyclopentylboronate was obtained bp 90—91°/0.05 mmHg, 50% isolated yield. $[\alpha]_D^{24}$ +46.72° (*c* 2.5, EtOH), >99% ee. ^{11}B NMR δ=31.42, ^{1}H NMR ($CDCl_3$) δ=0.9—1.4 (6H, m), 1.6—2.40 (7H, m), 3.15 (1H, m), 3.80 (4H, m), 6.8—7.4 (3H, m) its corresponding alcohol $[\alpha]_D^{22}$ +73.01° (*c* 2.3175, MeOH), >99% ee.

Diethyl *trans*-2-(2-Thienyl)cyclopentylboronate. With the usual experimental setup, 7.5 g (50 mmol) of 1-(2-thienyl)cyclopentene was added dropwise to 70 mL (50 mmol) of IpcBH$_2$ at −35 °C. The flask was maintained at −35 °C for 4 days without stirring and further kept at −78 °C for 5 h. The mother liquor containing the pure enantiomer was removed carefully without any crystalline particle and treated with excess of acetaldehyde (8 mL). The reaction mixture was stirred at room temperature for 5 h (^{11}B NMR δ=30.78) showed the absence of dialkylborane. The excess acetaldehyde and solvent was pumped off and the residue was taken up in 100 mL of pentane. The pentane layer was extracted with 3×25 mL of ether. The ether layer

was washed with water, dried over anhydrous $MgSO_4$ and the solvent removed to give *trans*-2-(2-thienyl)cyclopentylboronic acid, 7.15 g, 80% yield, 94% ee. It was crystallized with ether pentane at room temperature to give 5.7 g of pure boronic acid, 64% yield, which, upon treatment with ethanol, afforded the corresponding boronate, bp 85—90°/0.25 mmHg, 64% yield, $[\alpha]_D^{23}$ +36.10° (*c* 2.54, EtOH), 99% ee. ^1H NMR ($CDCl_3$) δ=0.9—1.4 (6H, m), 1.5—2.5 (7H, m), 3.20 (1H, m), 3.90 (4H, m), 6.7—7.10 (3H, m). The above boronate, upon oxidation, gave *trans*-2-thienylcyclopentanol $[\alpha]_D^{21}$ +70.6° (*c* 2.30, MeOH) >99% ee.

Diethyl *trans*-2-(2-Furyl)cyclohexylboronate. With the usual experimental setup, 7.4 g (50 mmol) of 1-(2-furyl)-cyclohexene was added dropwise to 70 mL (50 mmol) of $IpcBH_2$ in THF at −25 °C. The contents were stirred for 10 days at −25 °C and acetaldehyde (11.2 mL) was added dropwise and stirred further for 6 h at room temperature. The excess acetaldehyde and solvent were pumped off and the residue taken up in 100 mL of pentane. The pentane layer was extracted with 3×20 mL of 3 M sodium hydroxide. The alkaline solution was neutralized with 6 M HCl and extracted with 3×25 mL of ether. The ether layer was washed with water, dried over anhydrous $MgSO_4$ and solvent removed to afford 5.82 g of *trans*-2-(2-furyl)cyclohexylboronic acid, 60% yield, $[\alpha]_D^{22}$ +40.0° (*c* 1.05, CH_2Cl_2), 90% ee. The white crystalline boronic acid dissolved in ether pentane (2:3), 25 mL and kept at room temperature for slow crystallization. The supernatant liquid was removed by double-ended needle and crystals washed with cold ether pentane mixture (3×5 mL). After the usual workup, it gave 3.8 g of boronic acid, yield, 40%. $[\alpha]_D^{22}$ +44.5° (*c* 1.1, CH_2Cl_2). It was treated with ethanol to give its diethyl *trans*-2-(2-furyl)cyclohexylboronate, bp 100—105°/0.8 mmHg, $[\alpha]_D$ +36.2° (*c* 2.1, EtOH). ^1H NMR ($CDCl_3$) δ=0.9—1.35 (6H, m), 1.50—2.3 (9H, m), 3.2 (1H, m), 3.6—4.0 (4H, m), 6.2 (2H, q), 7.2 (1H, m). The boronate was oxidized to give the corresponding alcohol $[\alpha]_D^{22}$ +58.2° (*c* 1.8, MeOH) >98% ee by capillary GC of its Mosher ester.

Diethyl *trans*-2-(2-Furyl)cycloheptylboronate. With the usual experimental setup as described above, *trans*-2-(2-furyl)cycloheptylboronic acid was obtained 9 g, 87% yield. The solid was dissolved in ether pentane (2:3) 25 mL at room temperature. A part of the solution (0.5 mL) was oxidized with $NaOH/H_2O_2$ and the optical purity checked by capillary GC of its Mosher ester showed 86% ee. The remaining solution was crystallized and recrystallized at 0 °C for 24 h. The white crystalline needles separated out. The crystals were filtered and washed with pentane to give pure boronic acid, 4.7 g, 45% yield. It was treated with ethanol to give diethyl *trans*-2-(2-furyl)cycloheptylboronate, bp 120—125°/0.9 mmHg, $[\alpha]_D^{22}$ +24.6 (*c* 2.4, EtOH). ^1H NMR ($CDCl_3$) δ=0.9—1.3 (6H, m), 1.4—2.0 (11H, m), 3.1 (1H, m), 3.65—4.0 (4H, q), 5.9 (1H, m), 6.2 (1H, m) and 7.3 (1H, m). A part of the diethyl *trans*-2-(2-furyl)cycloheptylboronate was oxidized to give the corresponding alcohol $[\alpha]_D$ +34.9° (*c* 2.4, MeOH) >99% ee by capillary GC of its Mosher ester.

General Procedure for the Preparation of Diethanolamine *trans*-2-Heteroarylcycloalkylboronate. Ethyl heteroarylcycloalkylboronate (5 mmol) prepared as described above was taken in 15 mL of ether. To it 0.52 mL (5.4 mmol) of diethanolamine in 5 mL of 2-propanol was added and the reaction mixture was stirred at 25 °C for 1 h. A crystalline solid formed. It was filtered and removed by filtration and washed with 5 mL of cold ether. The results are shown in Table 4.

We wish to thank the National Institutes of Health (GM 10937-23) for their financial support.

References

1) Postdoctoral research associates on grant GM 10937-23 from the National Institutes of Health.

2) H. C. Brown and G. Zweifel, *J. Am. Chem. Soc.*, **83**, 486 (1961).

3) H. C. Brown and P. K. Jadhav, "Asymmetric Synthesis," ed by J. D. Morrison, Academic Press, New York (1983), Vol. 2.

4) "Asymmetric Synthesis," ed by J. D. Morrison, Academic Press, New York (1983).

5) H. C. Brown, P. K. Jadhav, and B. Singaram, "Modern Synthetic Methods," ed by R. Scheffold, Springer-Verlag, Berlin-Heidelberg (1986), Vol. 4, pp. 307—356.

6) H. C. Brown, P. K. Jadhav, and A. K. Mandal, *J. Org. Chem.*, **47**, 5074 (1982).

7) H. C. Brown and B. Singaram, *J. Am. Chem. Soc.*, **106**, 1797 (1984).

8) H. C. Brown and J. V. N. Vara Prasad, *J. Am. Chem. Soc.*, **108**, 2049 (1986).

9) H. C. Brown, J. V. N. Vara Prasad, and A. K. Gupta, *J. Org. Chem.*, **51**, 4296 (1986). a) H. C. Brown and J. V. N. Vara Prasad, *Heterocycles*, **25**, 641 (1987).

10) S. Masamune, B. M. Kim, J. S. Peterson, T. Sato, S. Veenstra, and T. Imai, *J. Am. Chem. Soc.*, **107**, 4549 (1985).

11) A. R. Katritzky and C. S. Rees, "Comprehensive Heterocyclic Chemistry," Pergamon Press (1984), Vol. 1.

12) H. C. Brown, J. R. Schwier, and B. Singaram, *J. Org. Chem.*, **43**, 4395 (1978).

13) J. A. Dale and H. S. Mosher, *J. Am. Chem. Soc.*, **95**, 511 (1973).

14) These organoboranes actually exist in solution as the dimers, that is, as derivatives of diborane molecule. For the sake of convenience, they are referred to as simple borane derivatives.

15) H. C. Brown, R. G. Naik, R. K. Bakshi, C. Pyun, and B. Singaram, *J. Org. Chem.*, **50**, 5586 (1985) and references cited therein.

16) D. S. Matteson and D. S. Majumdar, *J. Am. Chem. Soc.*, **102**, 7588 (1980).

17) H. C. Brown, P. K. Jadhav, and M. C. Desai, *J. Am. Chem. Soc.*, **104**, 4303 (1982).

18) D. S. Matteson, R. Ray, R. R. Rocks, and D. J. Tsai, *Organometallics*, **2**, 1536 (1983).

19) H. C. Brown, G. W. Kramer, A. B. Levy, and M. M. Midland, "Organic Syntheses via Boranes," Wiley-Interscience, New York (1975).

20) G. A. Olah, A. L. Berrier, and G. K. Surya Prakash, *J. Org. Chem.*, **47**, 3903 (1982).

 © 1988 The Chemical Society of Japan Bull. Chem. Soc. Jpn., 61, 101—106 (1988)

Invited Paper

Reactivity† of Hypervalent Species: Reactions of Anionic Penta-Coordinated Silicon Complexes towards Nucleophiles

Alain BOUDIN, Geneviève CERVEAU, Claude CHUIT, Robert J. P. CORRIU,* and Catherine REYE

Institut de Chimie Fine, Université des Sciences et Techniques du Languedoc, Unité Associée CNRS UA N° 1097, Place E. Bataillon 34060 Montpellier Cedex, France

(Received July 17, 1987)

The reactivity of anionic penta-coordinated silicon complexes $[RSi(O_2C_6H_4\text{-}o)_2]^-Na^+$ **1** with nucleophilic reagents has been studied. **1** can be reduced to organosilanes $RSiH_3$ by metallic hydrides. Reactions with an excess of Grignard or organolithium reagents (R'MgX or R'Li) gave tetraorganosilanes $RSiR'_3$. When only two molar equivalents of Grignard reagents (R'MgX) or lithium reagents (R'Li) are added to complexes **1** functional silanes RR'_2SiX can be prepared.

It has been known for a long time that silicon can expand its valence shell and several types of penta- and hexa-coordinated silicon compounds have been reported, in which silicon is surrounded by electronegative ligands[2-4] and more recently by nonelectronegative ones.[5] Numerous structural studies of hexa- and penta-coordinated silicon complexes have been reported[2,3,5,6] but little attention has been paid to the fundamental chemical behaviour of these species. Some reports which are in the literature suggested that these complexes may have unusual properties compared with those of their tetra-coordinated analogues. Kummer et al.[7] have observed that cationic bis(2,2'-bipyridine), 1,10-phenantroline, and pyridine *N*-oxide silicon complexes have unexpected properties. For instance $[SiX_2(bipy)_2]\,Cl_2$ may be dissolved in water or methanol without reaction of the SiX bond (X=Cl,Br). Kumada[4,8,9] has shown the unique reactivity of the carbon-silicon bond in organopentafluorosilicates and has exploited these properties in organic synthesis. Muller[10] has reported that reaction is possible between an organopentafluorosilicate and strong nucleophiles such as Grignard reagents:

$$[CH_3SiF_5]M_2 + 3C_2H_5MgBr \longrightarrow CH_3Si(C_2H_5)_3 \quad 25\%$$

Finally 1-hydrosilatrane has been shown to have some potential uses as a reducing agent.[11] All these examples illustrate very well the difference between the chemical behaviour of hypervalent silicon species and the tetra-coordinated ones. Moreover mechanistic studies of nucleophilic substitution at silicon performed in our laboratory[12] have established the nucleophilic activation of nucleophilic substitution at silicon. To explain these results, a mechanism has been proposed in which the rate-determining step is attack of the nucleophile, Nu, at a penta-coordinated silicon centre. This mechanism is now given further support by some recent results:

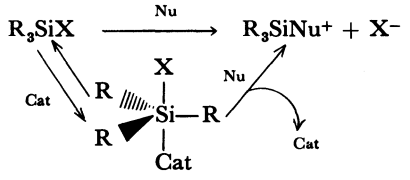

1) Reactivity of the Si–H bonds[13] in penta-coordinated silicon dihydrides towards nucleophiles is markedly greater than that of the corresponding tetra-coordinated species. For example these penta-coordinated silicon dihydrides react with carbonyl compounds without any catalyst as shown in the following reaction:

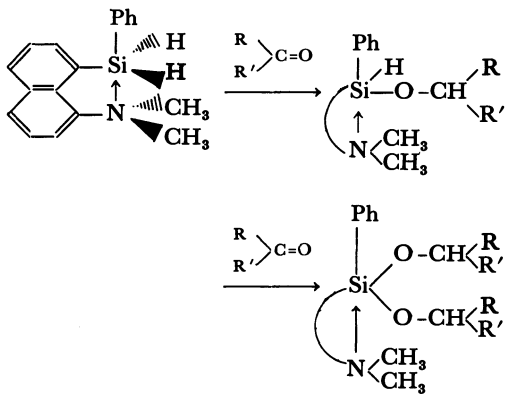

2) Other very recent experiments[14] have confirmed that penta-coordinated anionic trifluorosilicates $R_2SiF_3^-$ and difluorosilicates $R_3SiF_2^-$ react with nucleophiles faster than the corresponding fluorosilanes R_2SiF_2 and R_3SiF.

In this paper we describe the reactivity towards nucleophiles of anionic penta-coordinated silicon complexes of catechol $\left[RSi\left(\begin{smallmatrix}O\\O\end{smallmatrix}\!\!\bigcirc\right)_2\right]^-Na^+$ **1**. These derivatives have been prepared by Frye[15] and the structure of tetramethylammonium (1,2-benzenediolato)phenylsilicate has been determined by X-ray diffraction,[6a] but the chemistry of theses anions however has not yet been explored.

† Preliminary Communication Ref. 1.

Results and Discussion

Synthesis of Anionic Penta-Coordinated Silicon Complexes of Catechol. The anionic penta-coordinated silicon complexes **1** have been synthesized according to the method described by Frye,[15]

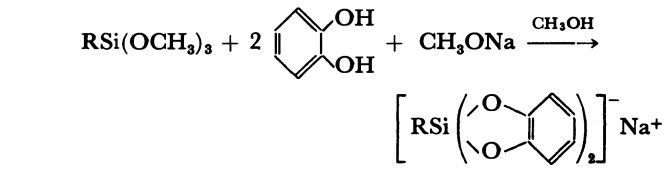

1a : R=Ph, **1b** : R=CH_3, **1c** : R=1-naphthyl

The complex **1b** can be also prepared with 90% yield from the polymer polymethylhydrosiloxane (PMHS):

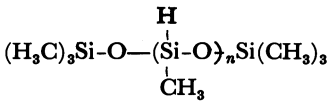

PMHS is obtained from methyldichlorosilane which is itself a by-product of the "direct synthesis" of dimethyldichlorosilane

Reactivity of Anionic Penta-Coordinated Silicon Complexes of Catechol towards Metal Hydrides. The reactivity of the anionic complexes **1a** and **1c** towards metal hydrides such as lithium aluminium hydride, diisobutylaluminium hydride and triethylaluminium/sodium hydride was investigated. The only product obtained is the monoorganosilane $RSiH_3$ in quite a good yield (Table 1).

Reactivity of Anionic Penta-Coordinated Silicon Complexes of Catechol towards Grignard and Organolithium Reagents. The reactivity of anionic complexes **1** with organometallic compounds (R'MgX and R'Li) has been studied. First, we have investigated the influence of the ratio complex/organometallic compound on the reaction products in order to examine the possible selectivty of the reaction.

Table 1. Reactions of Metalhydrides with Complexes **1**

Complex	Hydride	Reaction condition			Product (yield/%)[a]	
		Solvent	T/°C	t/h		
1a	$LiAlH_4$(excess)	Ether	20	2	$PhSiH_3$	(72)
1a	NaH/Et_3Al 4eq/3eq	Hexane	20	1	$PhSiH_3$	(68)
1a	i-Bu_2AlH(5eq)	CH_2Cl_2	0	1	$PhSiH_3$	(65)
1c	$LiAlH_4$(excess)	Ether	35	4	1-$NpSiH_3$	(73)
1c	NaH/Et_3Al 4 eq/3 eq	Hexane	20	1	1-$NpSiH_3$	(65)

a) Yield of isolated product.

Table 2. Reaction of Methyllithium and Methylmagnesium Bromide with Complex **1a**. Influence of the Ratio Complex **1a**/Organometallic Compound on the Reaction Products[a]

CH_3M	Reaction condition			$PhSiH_3$	$PhCH_3SiH_2$	$Ph(CH_3)_2SiH$	$PhSi(CH_3)_3$
	Solvent	T/°C	t/h				
CH_3MgBr(1eq)	Ether	0	2, 5	79	9	12	0
CH_3MgBr(1eq)	Ether	35	2	56	7	36	0
CH_3MgBr(1eq)	THF	60	2	54	5	41	0
CH_3MgBr(2eq)	Ether	35	2	6	6	85	3
CH_3MgBr(3eq)	Ether	35	2	0	4	58	38
CH_3Li(1eq)	Ether	35	2	48	7	44	0
CH_3Li(2eq)	Ether	35	2	12	4	81	4
CH_3Li(2eq)	THF	60	2	9	10	49	32
CH_3Li(3eq)	Ether	35	2	0	0	0	100

a) The ratio of the different reaction products was determined by GLC after reduction of the reaction mixture with $LiAlH_4$.

The results obtained after reduction of the reaction mixture with an excess of lithium aluminium hydride are reported in Table 2. It appears that:

1) The addition of 1 or 2 molar equivalents of organometallic reagents R'MgX or R'Li results mainly in the formation of two Si–C bonds whatever the reaction conditions (solvent, temperature, nature of the organometallic compound). This implies that the first substitution is rate-determining step.

2) The reaction of 2 molar equivalents of organometallic reagents (R'MgX or R'Li) followed by reduction with lithium aluminium hydride gives mainly organosilanes of type RR'_2SiH.

3) 3 molar equivalents of organolithium reagent R'Li lead only to the tetra-substituted silanes $RSiR'_3$ while the reaction with 3 molar equivalents of Grignard reagent R'MgX followed by reduction with lithium aluminium hydride gives a mixture of RR'_2SiH and $RSiR'_3$. The results of the reactions carried out with 2 or 3 molar equivalents of organometallic reagents are summarised in Tables 3 and 4 respectively. The great reactivity of the allylic and alkynyl Grignard reagents towards complexes **1a** and **1b** should be pointed out in that the tetra-substituted compounds $RSi(CH_2CH{=}CH_2)_3$ or $RSi(C{\equiv}CR')_3$ are the main products whatever the stoichiometry of the reactants. It is worth noting the preparation in one step of 1-methyl-2,5-diphenylsilacyclopentadiene and 1,2,5-triphenylsilacyclopentadiene with satisfactory yield (Table 3). The reactivity of *t*-butylmagnesium bromide towards **1a** is low. One molar equivalent of *t*-butylmagnesium bromide in the

Table 3. Reactions in Ether of 2 Molar Equivalents of Organometallic Reagents (RMgX, RLi) with Complexes **1** Followed by Reduction of the Reaction Mixture with an Excess of $LiAlH_4$[a)]

Complex	Organometallic reagent	Reaction condition		Product (yield/%)	
		T/°C	*t*/h		
1a	MeLi	35	1	$PhMe_2SiH$	(37)
1a	EtMgBr	20	3	$PhEt_2SiH$	(40)
1a	EtLi	20	3	$PhEt_2SiH$	(43)
1a	*i*-PrMgBr	20	3	$Ph(i\text{-}Pr)_2SiH$	(45)
1a	*n*-BuLi	20	3	$Ph(n\text{-}Bu)_2SiH$	(57)
1a	*t*-BuMgBr[b)]	35	15	$Ph(t\text{-}Bu)SiH_2$	(16)
1a	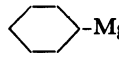	20	15	$Ph(C_6H_{11})_2SiH$	(83)
1a	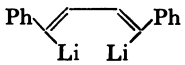	20	16	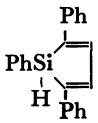	(50)
1b	PhLi	35	2	$MePh_2SiH$	(60)
1b	$PhCH_2MgBr$	35	6	$Me(PhCH_2)_2SiH$	(86)
1b	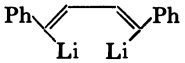	20	16	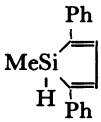	(51)

a) The reaction mixture has been heated about 4 hours at 35 °C after addition of an excess of $LiAlH_4$.
b) Only 1 molar equivalent of *t*-BuMgBr in presence of the cryptand TDA-1 was used to obtain $Ph(t\text{-}Bu)SiH_2$.

Table 4. Reactions of 3 Equivalents of Organometallic Reagents (RMgX,RLi) with Complexes **1** in Ether

Complex	Organometallic reagent	Reaction condition		Product (yield/%)	
		T/°C	*t*/h		
1a	MeLi	35	3	$PhSiMe_3$	(78)
1a		35	1	$PhSi(\text{ })_3$	(53)
1a	*n*-BuLi	35	2	$PhSi(n\text{-}Bu)_3$	(85)
1a	PhMgBr	20	3	Ph_4Si	(76)
1b	*n*-BuLi	35	2	$MeSi(n\text{-}Bu)_3$	(43)
1b		35	1	$MeSi(\text{ })_3$	(62)
1b	PhLi	35	2	$MeSi(Ph)_3$	(63)
1b	$PhC{\equiv}CMgBr$	35	4	$MeSi(C{\equiv}CPh)_3$	(82)

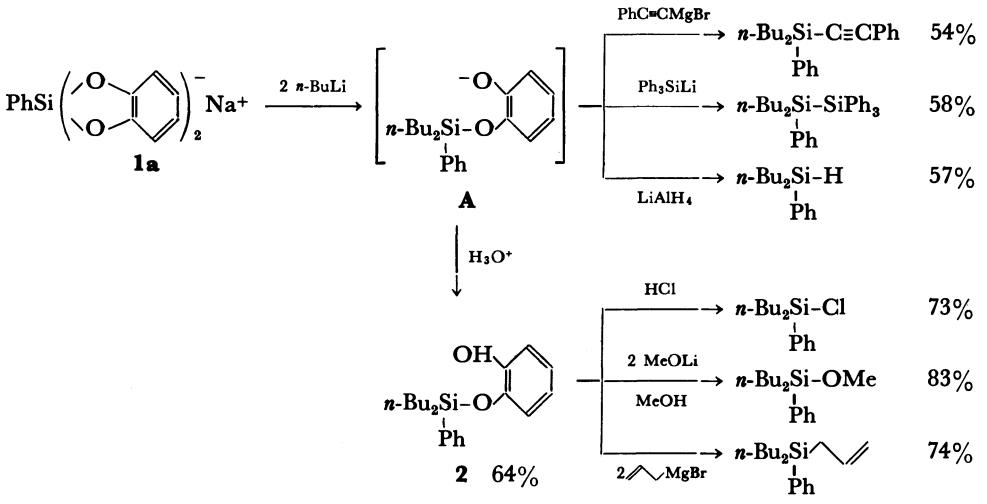

Scheme 1.

presence of one molar equivalent of the cryptand tris(3,6-dioxaheptyl)amine[16] (TDA-1) results in the formation of only one new Si–C bond giving after reduction with lithium aluminium hydride phenyl-*t*-butylsilane as the major product but in poor yield (16%) (Table 3) (without TDA-1 no reaction product at all was isolated). 3 molar equivalents of *t*-butylmagnesium bromide in the presence of 3 molar equivalents of TDA-1, react with **1a** to give after reduction with an excess of lithium aluminium hydride the unexpected product diphenyl-*t*-butylsilane in 31% yield.

$$\mathbf{1a} \xrightarrow[\text{2) } LiAlH_4]{\text{1) 3eq } t\text{-BuMgBr, 3eq TDA-1}} Ph_2SiH(t\text{-Bu})\ (31\%)$$

The formation of this product can be explained by a disproportionation of phenyl-*t*-butylsilane induced by $LiAlH_4$/TDA-1. Indeed other examples of disproportionation of silanes promoted by $LiAlH_4$/TDA-1 have been observed.[17]

$$PhSiH_3 \xrightarrow[\text{TDA-1}]{LiAlH_4} Ph_2SiH_2 \longrightarrow Ph_3SiH$$

Two different substituents can be introduced in successive steps into the complex **1a** without isolating the intermediate **A** (Scheme 1). This one can react with different nucleophilic reagents to give further organosilicon compounds with moderate to good yield. However in some cases, for purification purposes, it is better to hydrolyze the intermediate **A** and isolate **2** before adding the second nucleophile. Analogous results have been obtained with the dianionic hexa-coordinated silicon complex $\left[Si\left(O_2C_6H_4\right)_3\right]^{2-}\ 2Na^+$.[18]

In conclusion this work describes a new route to organosilicon compounds from penta-coordinated anionic species. From a mechanistic point of view the products obtained are the result of the reaction of a nucleophilic reagent with a negatively charged species. The mechanistic details of these nucleophilic reactions have yet to be elucidated. However these results open some new synthetic possibilities exploiting the reactivity of hypervalent silicon species.

Experimental

Reactions have been carried out under nitrogen. All solvents were purified by standard techniques before use. (All the compounds described in this paper have been characterized by usual techniques and analysis: CPV (Girdel,SE30). NMR spectra have been recorded with a Varian EM 360A spectrometer for ^1H, with a Bruker WP-80 for ^{13}C, with a Bruker WP-200 SY for ^{29}Si. All ^1H, ^{13}C, and ^{29}Si chemical shifts reported in ppm are relative to Me_4Si. IR spectra have been recorded with a Perkin Elmer 298 spectrophotometer, mass spectra with a JEOL JMS-DX 300 Mass Spectrometer. Microanalyses have been carried out by CNRS laboratories (Lyon).

Preparation of Complexes: Sodium Bis(1,2-benzenediolato)methylsilicate (1b) from $MeSi(OMe)_3$. A solution of $MeSi(OMe)_3$ (0.0475 mol) in 10 ml of MeOH was added at room temperature to a solution of MeONa (0.0475 mol) in 15 ml of MeOH. Then 10.34 g of catechol dissolved in 20 ml of MeOH were added dropwise at 25 °C. The mixture was heated for about 4 hours at 45 °C. MeOH was removed under vacuum. Complex was washed twice with ether and dried under vacuum at 100 °C for one day. 12 g (90%) of **1b** were obtained as a white powder. ^1H NMR (DMSO-d_6) δ=−0.1 (3H, s), 6.5—6.8 (8H,m); ^{13}C NMR (DMSO-d_6) δ=151.6, 120.8, 113.2, 1.2; ^{29}Si NMR (CD_3OD) δ=−73.77; IR (KBr) 1590, 1475, 1345, 1240, 1095, 1010, 895, 830, 750 cm^{-1}.

Sodium Bis(1,2-benzenediolato)methylsilicate (1b) from PMHS. 0.2 mol of catechol (22 g) and 0.2 mol of PMHS (12 g) were dissolved in about 50 ml of MeOH. 0.1 mol of MeONa dissolved in about 30 ml of MeOH was added slowly at room temperature. The reaction of MeONa with PMHS was exothermic. The mixture was stirred overnight during which time a precipitate from the polymer appeared. Then the solution was filtered and the solid washed twice

with methanol. The methanol was removed from the whole filtrate; 25.3 g (90%) of a grey powder was obtained. The spectral data were the same as those of the complex prepared from $MeSi(OMe)_3$.

Sodium Bis(1,2-benzenediolato)phenylsilicate (1a). The preparation of **1a** from $PhSi(OMe)_3$ was the same as that of **1b** from $MeSi(OMe)_3$. ^1H NMR (DMSO-d_6) δ=6.28—6.78 (8H, m), 6.95—7.22 (3H, m), 7.28—7.60 (2H, m); ^{13}C NMR (DMSO-d_6) δ=150.6, 140.8, 135.4, 129.4, 127.9, 119.9, 112.0; ^{29}Si NMR (DMSO-d_6) δ=−87.4; IR (KBr) 1600, 1475, 1340, 1240, 1220, 1110, 1100, 1010, 890, 825, 730, 700 cm^{-1}.

Sodium Bis(1,2-benzenediolato)-1-napthylsilicate (1c). The complex **1c** was prepared from $1\text{-}NpSi(OMe)_3$ as **1a** from $MeSi(OMe)_3$. ^1H NMR (DMSO-d_6) δ=6.1—6.7 (8H, m), 7.0—7.35 (3H, m), 7.35—7.78 (3H, m), 8.35—8.8 (1H, m); ^{13}C NMR (DMSO-d_6) δ=150.2, 132.7, 131.6, 130.1, 127.7, 127.1, 124.8, 124.6, 117.5, 110.1; ^{29}Si NMR (DMSO-d_6) δ=−84.64; IR (KBr) 1600, 1480, 1395, 1240, 1100, 1010, 890, 820, 740, 700 cm^{-1}.

Synthesis of Tetraorganosilanes $RSiR'_3$. The following is given as an example. **Methyltri(phenylethynyl)silane.** An excess of $PhC{\equiv}CMgBr$ (40 mmol) was added to a suspension of **1b** (10 mmol) in anhydrous ether (60 ml) at 20 °C. The mixture was stirred at 35 °C for about 4 hours, then hydrolyzed with aqueous 4M HCl. After 3 extractions with ether, the organic layer was washed 3 times with aqueous 2M NaOH then twice with water and once with brine. Evaporation of the solvent gave the crude $MeSi(C{\equiv}CPh)_3$ which was purified by recrystallization from pentane. 2.83 g (82%) of pure $MeSi(C{\equiv}CPh)_3$ was obtained, mp 125—6 °C (lit,[19] 126 °C).

The following products similarly prepared were: **Trimethylphenylsilane** (75%) bp 75—77 °C/30 Torr (lit,[20] 170.6 °C/760 Torr). **Triallylphenylsilane** (53%) bp 85—88 °C/0.4 Torr (lit,[21] 90—92 °C/0.8 Torr). **Tributylphenylsilane** (85%) bp 89—92 °C/0.05 Torr (lit,[22] 116—118 °C/0.9 Torr). **Tetraphenylsilane** (76%) mp 232—233 °C (lit,[23] 236.5—237 °C). **Tributylmethylsilane** (63%) bp 110—113 °C/14 Torr (lit,[24] 101—104 °C/9 Torr). **Triallylmethylsilane** (62%) bp 78—82 °C/35 Torr (lit,[25] 180.3 °C/745 Torr). **Methyltriphenylsilane** (63%) bp 150—160 °C/0.2 Torr (lit,[26] 196—200 °C/9 Torr). ***t*-Butylphenylsilane** (16%) bp 87 °C/30 Torr (lit,[27] 186—188 °C/760 Torr).

Synthesis of Triorganosilanes RR'_2SiH. The following is given as an example. **Dibutylphenylsilane.** Two molar equivalents of a molar solution of *n*-BuLi in ether were added to a suspension of **1a** (40 mmol) in 100 ml of ether at room temperature. The mixture was stirred at 20 °C about one hour then a suspension of 20 mmoles of $LiAlH_4$ in ether was added. The mixture was heated at 35 °C about 2 hours then hydrolyzed and extracted in the same way as for the isolation of $RSiR'_3$. 2.5 g (57%) of pure product was distilled at 75—79 °C/0.5 Torr (lit,[28]).

Similarly prepared were: **Dimethylphenylsilane** (37%) bp 89—91 °C/100 Torr (lit,[29] 159.3 °C/760 Torr). **Diethylphenylsilane** (40%) bp 115 °C/25 Torr (lit,[30] 97—100 °C/25 Torr). **Diisopropylphenylsilane** (45%) bp 120 °C/17 Torr (lit,[31] 58—60 °C/1.2 Torr). **Dicyclohexylphenylsilane** (83%) bp 145 °C/0.08 Torr (lit,[31] 124 °C/0.03 Torr). **Methyldiphenylsilane** (60%) bp 90—95 °C/1 Torr (lit,[32] 93.5 °C/1 Torr). **Dibenzylmethylsilane** (86%) bp 90—92 °C/0.05 Torr (lit,[33] 130—140 °C/3 Torr). **1-Methyl-2,5-diphenylsilacyclopentadiene** (51%) mp 97—99 °C (lit,[34] 97—98 °C). **1,2,5-Triphenylsilacyclopentadiene** (50%) mp 176—178 °C (lit,[35] 180—181 °C).

***t*-Butyldiphenylsilane.** 3 molar equivalents of *t*-BuMgCl in ether were added dropwise to a mixture of 20 mmoles of **1a** and 60 mmoles of TDA-1 in 100 ml of anhydrous ether. The pasty mixture was refluxed for 24 hours, then a suspension of 40 mmoles of $LiAlH_4$ in ether was added. The mixture was stirred at room temperature for one day, then hydrolyzed and extracted with ether. After the usual work-up the product was purified by silica-gel column chromatography to give 1.48 g of *t*-butyldiphenylsilane (31%). ^1H NMR (CCl_4) δ=1.0 (9H, s), 4.5 (1H, s), 7.05—7.55 (10H, m); IR (CCl_4) 2120 (SiH) cm^{-1} (lit,[36]).

Dibutylphenyl(2-hydroxyphenoxy)silane 2. 2 equivalents of *n*-BuLi in ether were added to a suspension of **1a** (20 mmol) in 150 ml of anhydrous ether at 20 °C. The mixture was stirred at room temperature for about one hour, then hydrolyzed with an aqueous solution of 4M HCl and extracted with ether three times. The combined organic extracts were washed 4 times with 2M NaOH, then with brine, dried ($MgSO_4$) and concentrated. The product was purified by distillation to give 4.2 g of **2** (64%). bp 153—5 °C/0.01 Torr. ^1H NMR (CCl_4) δ=0.42—2.02 (18H, m), 5.5 (1H, s), 6.5—7.0 (4H, m), 7.02—7.78 (5H, m); IR (CCl_4) 3560 (OH) cm^{-1}; Found: C, 73.21; H, 8.54; Si, 8,51%. Calcd for $C_{20}H_{28}O_2Si$: C, 73.17; H, 8.53; Si, 8.53%.

Dibutylphenyl(phenylethynyl)silane. 2 molar equivalents of *n*-BuLi in ether were added to a suspension of **1a** (20 mmol) in 150 ml of anhydrous ether at 20 °C. The mixture was stirred at room temperature for one hour then one equivalent of $PhC{\equiv}CMgBr$ was added at 20 °C. The mixture was heated at reflux about 6 hours then hydrolyzed with an aqueous solution of 4M HCl, and extracted with ether; the extracts were washed with 2M NaOH four times then with brine, dried ($MgSO_4$) and concentrated. The product was distilled to give 3.5 g (54%) of dibutylphenyl (phenylethynyl)silane, bp 150—153/0.01 Torr. ^1H NMR (CCl_4) δ=0.15—1.90 (18H, m), 6.65—7.90 (10H, m); IR (CCl_4) 2150 (-C≡C-) cm^{-1}; Found C, 82.39; H, 8.77; Si, 8.74%. Calcd for $C_{22}H_{28}Si$: C, 82.50; H, 8.75; Si, 8.75%.

Allyldibutylphenylsilane. An excess of allylmagnesium bromide was added to a solution of 15 mmoles of the organosilane **2** in 50 ml of anhydrous ether at 20 °C. The mixture was heated about 20 hours at reflux then hydrolyzed with an aqueous solution of 4 M HCl and extracted with ether three times. The combined organic extracts were washed with 2M NaOH four times then with brine, dried ($MgSO_4$) and concentrated. The product was distilled to give 2.8 g (74%) of allyldibutylphenylsilane; bp 167 °C/13 Torr; ^1H NMR (CCl_4) δ=0.63—1.67 (18H, m), 1.87 (2H, d), 4.60—6.05 (3H, m), 7.05—7.70 (5H, m); IR (CCl_4) 1625 (C=C) cm^{-1}; Found: C, 78,38; H, 10.74; Si, 10.77%. Calcd for $C_{17}H_{28}Si$: C, 78.46; H, 10.76; Si, 10.76%.

Dibutylphenylmethoxysilane. 2 molar equivalents of MeOLi dissolved in 15 ml of MeOH were added to a solution of 9.1 mmoles of the organosilane **2** in 100 ml of MeOH. The mixture was stirred about 1.5 h at 20 °C, then MeOH was removed. The residue was extracted with pentane, the salts were filtered and the solvent was removed under vacuum. The product was distilled to give 2.9 g of dibutylphenylmethoxysilane (83%); bp 113 °C/0.02 Torr; ^1H NMR (CCl_4) δ=0.8—1.8 (18H, m), 3.6 (3H, s), 7.3—7.8 (5H, m); Found: C, 72.11; H, 10.43; Si, 11.18%. Calcd for

$C_{15}H_{26}OSi$: C, 72.00; H, 10.40; Si, 11.20%.

Dibutylphenylchlorosilane. 5 molar equivalents of HCl diluted in ether (100 ml) were added to a solution of 15 mmoles of the organosilane **2** in 50 ml of ether. The mixture was stirred at 20 °C for about 15 hours, then the solvent was removed and the residue taken up in pentane. The catechol was filtered and the product was purified by distillation; bp 164 °C/13 Torr (yield 73%); ^{1}H NMR (CCl_4) δ: 0.45—1.90 (18H, m), 6.95—7.82 (5H, m); Found: C, 66.11; H, 9.02, Cl, 13.92; Si, 10.97%. Calcd for $C_{14}H_{23}ClSi$: C, 66.01; H, 9.03; Cl, 13.94; Si, 11.00%.

1,1-Dibutyl-1,2,2,2-tetraphenyldisilane. 2 equivalents of *n*-BuLi were added to a suspension of **1a** (10 mmol) in 50 ml of anhydrous ether at 20 °C. The mixture was stirred at room temperature for one hour, then 10 mmoles of Ph_3SiLi[37] in 30 ml of THF were added at 20 °C. The mixture was stirred under reflux during 36 hours. After this time the reaction mixture was completely colourless. The salts were filtered and washed with ether. The combined ether extracts were washed with water until the aqueous layer was colourless. The ethereal solution was dried over anhydrous $MgSO_4$ and concentrated. The solid residue was recrystallized from ethanol to give white crystals [2,77 g (58%)] of 1,1-dibutyl-1,2,2,2-tetraphenyldisilane; mp 108—110 °C; ^{1}H NMR (CCl_4) δ=0.75—1.65 (18H, m), 7.25—7.7 (20H, m); Found: C, 80.26; H, 7.98; Si, 11.75%. Calcd for $C_{32}H_{38}Si_2$: C, 80.33; H, 7.95; Si, 11.70%.

References

1) A. Boudin, G. Cerveau, C. Chuit, R. J. P. Corriu, and C. Reye, *Angew. Chem., Int. Ed. Engl.*, **25**, 473 (1986).

2) R. J. P. Corriu, C. Guerin, J. J. E. Moreau, *Top. Stereochem.*, **15**, 158 (1984) and references cited therein.

3) a) R. R. Holmes, R. O. Day, J. J. Harland, A. C. Sau, J. M. Holmes, *Organometallics*, **3**, 341 (1984); b) R. R. Holmes, R. O. Day, J. J. Harland, and J. M. Holmes, *Organometallics*, **3**, 347 (1984); c) R. R. Holmes, R. O. Day, V. Chandrasekhar, and J. M. Holmes, *Inorg. Chem.*, **24**, 2009 (1985); d) R. R. Holmes, R. O. Day, V. Chandrasekhar, and J. J. Harland, *Inorg. Chem.*, **24**, 2016 (1985).

4) K. Tamao, J. Yoshida, H. Yamamoto, T. Kakui, H. Matsumoto, M. Takahashi, A. Kurita, M. Murata, and M. Kumada, *Organometallics*, **1**, 355 (1982) and references cited therein.

5) J. J. Harland, J. S. Payne, R. O. Day, and R. R. Holmes, *Inorg. Chem.*, **26**, 760 (1987) and references cited therein.

6) a) F. P. Boer, J. J. Flynn, and J. W. Turley, *J. Am. Chem. Soc.*, **90**, 6973 (1968); J. J. Flynn and F. P. Boer, *ibid.*, **91**, 5756 (1969); b) J. J. Harland, R. O. Day, J. F. Vollano, A. C. Sau, and R. R. Holmes *ibid.*, **103**, 5269 (1981).

7) a) D. Kummer and H. Koster, *Z. Anorg. Allg. Chem.*, **398**, 279 (1973); b) D. Kummer and H. Koster *ibid.*, **402**, 297 (1973); c) D. Kummer, K. E. Gaiper, and T. Seshadri, *Chem. Ber.*, **110**, 1977 (1950); d) D. Kummer and T. Seshadri, *Z. Anorg. Allg. Chem.*, **428**, 129 (1977); e) D. Kummer and T. Seshadri, *Chem. Ber.*, **110**, 2355 (1977); f) D. Kummer and T. Seshadri, *Z. Anorg. Allg. Chem.*, **432**, 147 (1977).

8) J. Yoshida, K. Tamao, T. Kakui, A. Kurita, M. Murata, K. Yamada and M. Kumada, *Organometallics*, **1**, 369 (1982).

9) J. Yoshida, K. Tamao, H. Yamamoto, T. Kakui, T. Uchida, and M. Kumada, *Organometallics*, **1**, 542 (1982).

10) R. Muller, *Z. Chem.*, **24**, 41 (1984) and references cited therein.

11) M. T. Attar-Bashi, C. Eaborn, J. Vencl, and D. R. M. Walton, *J. Organomet. Chem.*, **117**, C87 (1976).

12) a) R. J. P. Corriu, G. Dabosi, and M. Martineau, *J. Chem. Soc., Chem. Commun.*, **1977**, 649; b) R. J. P. Corriu, G. Dabosi, and M. Martineau, *J. Organomet. Chem.*, **154**, 33 (1978); c) R. J. P. Corriu, G. Dabosi, and M. Martineau, *ibid.*, **186**, 25 (1980); d) R. J. P. Corriu and C. Guerin, *Adv. Organomet. Chem.*, **20**, 265 (1982).

13) J. Boyer, C. Breliere, R. J. P. Corriu, A. Kpoton, M. Poirier, and G. Royo, *J. Oranomet. Chem.*, **311**, C39 (1986).

14) R. J. P. Corriu, C. Guerin, B. Henner, and W. W. C. Wong Chi Man to be published.

15) a) C. L. Frye, *J. Am. Chem. Soc.*, **86**, 3170 (1964); b) C. L. Frye, DBP 1493601 (1964).

16) G. Soula, *J. Org. Chem.*, **50**, 3717 (1985).

17) B. Becker, R. J. P. Corriu, C. Guerin, and B. Henner to be published.

18) A. Boudin, G. Cerveau, C. Chuit, R. J. P. Corriu, and C. Reye., *Angew Chem., Int. Ed. Engl*, **25**, 474 (1986).

19) H. Hartmann, H. Wagner, B. Karlstein, M. K. E. A'ssar, and W. Reiss, *Naturwissenschaften*, **51**, 215 (1964).

20) H. Freiser, M. V. Eagle, and J. L. Speier, *J. Am. Chem. Soc.*, **75**, 2821 (1953).

21) R. H. Meen and H. Gilman, *J. Org. Chem.*, **22**, 684 (1957).

22) H. Gilman and F. L. Marshall, *J. Am. Chem Soc.*, **71**, 2066 (1949).

23) L. Spialter, D. C. Priest, and C. W. Harris, *J. Am. Chem. Soc.*, **77**, 6227 (1955).

24) E. Larsson, E. Van Gilse. Van der Pals, *Svensk. Kem. Tid.*, **63**, 179 (1951). *Chem. Abstr.*, **46**, 2516h (1952).

25) R. A. Bazhulin, Yu P. Egorov, and V. F. Mironov, *Doklady Akad. Nauk. SSSR*, **92**, 515 (1953); *Chem. Abstr.*, **48**, 6831i (1954).

26) H. Gilman and H. W. Jr. Melvin, *J. Am. Chem. Soc.*, **71**, 4050 (1949).

27) M. B. HuGhes, *Diss. Abstr.*, **19**, 1921 (1959).

28) This compound is reported without physical characteristics by P. E. Rakita and L. S. Worshmam, *J. Organomet. Chem.*, **137**, 145 (1977).

29) R. A. Benkeser and D. J. Foster, *J. Am. Chem. Soc.*, **74**, 5314 (1952).

30) W. H. Nebergall, *J. Am. Chem. Soc.*, **72**, 4702 (1950).

31) M. C. Harvey, W. H. Nebergall, and J. S. Peake, *J. Am. Chem. Soc.*, **79**, 2762 (1957).

32) H. Gilman, G. D. Lichtenwalter, and D. Wittenberg, *J. Am. Chem. Soc.*, **81**, 5320 (1959).

33) J. W. Jenkins and H. W. Post, *J. Org. Chem.*, **15**, 552 (1950).

34) F. Carre, E. Colomer, J. Y. Corey, R. J. P. Corriu, C. Guerin, B. J. L. Henner, B. Kolani, and W. W. C. Wong Chi Man, *Organometallics*, **5**, 910 (1985).

35) V. Hagen and K. Ruehlmann, *Z Chem.*, **8**, 262 (1968); *Chem. Abstr.*, **69**, 59323k (1969).

36) This compound is reported without physical characteristics by M. B. Lacout-Loustalet, J. P. Dupin, F. Metras, and J. Valade, *J. Organomet. Chem.*, **31**, 187 (1971).

37) H. Gilman and G. D. Lichtenwalter, *J. Am. Chem. Soc.*, **80**, 608 (1958).

Invited Paper

Chemical Chameleons. Organosulfones as Synthetic Building Blocks

Barry Martin Trost
Department of Chemistry, University of Wisconsin-Madison, 1101 University Avenue, Madison, WI 53706, U.S.A.
(Received July 29, 1987)

An overview of the duality of function of organosulfones as nucleophiles in basic media and electrophiles in Lewis acidic media, a change of reactivity for which they have been dubbed "chemical chameleons," is presented. In the first phase, transition metal catalysts activate allyl sulfones towards displacements. Use of palladium, molybdenum, and nickel catalysts allow stabilized anions to effect displacement; copper catalysts allow non-stabilized nucleophiles to be used. The use of the anion stabilizing and leaving group abilities of sulfones created a novel three carbon intercalation and a novel cyclocontraction-spiroannulation in which β-hydroxy sulfones participate in a Lewis acid catalyzed pinacol rearrangement. The lability of allyl and tertiary sulfones towards Lewis acids creates a wide array of electrophilic reactions such as Friedel-Crafts type cyclizations, intermolecular alkylations with organoalanes and enol silyl ethers, and ring expansions. The ability to design novel reagents for synthesis based upon this dual reactivity of organosulfones is illustrated by the use of an alkoxy-bis(phenylsulfonyl)methane as a synthon for a carbonyl 1,1-dipole.

The utility of organosulfones for organic synthesis emerged with the evolution of non-nucleophilic strong bases like lithium dialkylamides and *n*-butyllithium which permit formation of a carbanion[1] (pK_a methyl phenyl sulfone 29[2]). The resulting organometallic appears to be enolate like (**1a**←→**1b**) based on both theoretical[3] and experimental data.[4] A notable discrepancy arises in the case of the organometallic generated from allyl phenyl sulfone where the carbanion center appears to be pyramidilized.[5] In contrast to enolates, sulfone stabilized anions have little propensity to react at oxygen.[6] Thus, treatment with electrophiles normally leads to smooth addition to carbon to give **2**. Since the sulfone functionality is rarely present in the final synthetic target, the major obstacle then becomes removal of the sulfone.

Early Applications. The early applications of organosulfones relied upon extrusions of sulfur dioxide in the base treatment of α-halo sulfones to give olefins (Ramberg-Bäcklund rearrangement)[7] or thermally in the case of sulfolenes as in a recent synthesis of farnesene (Eq. 2).[8]

A major advance arose by the recognition of

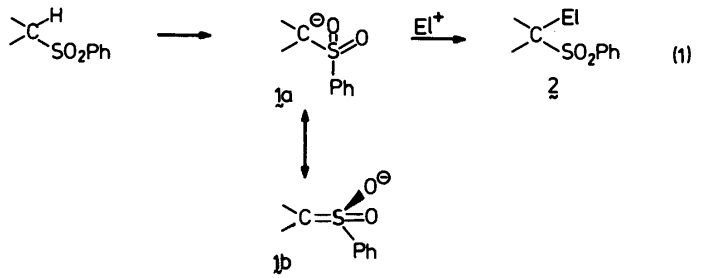

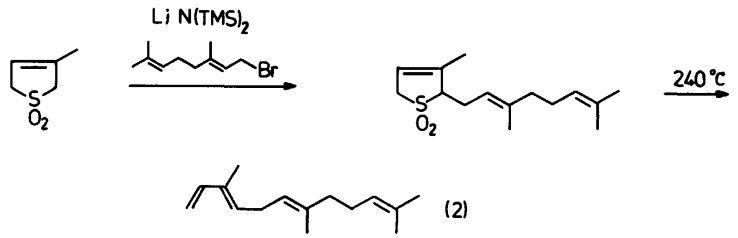

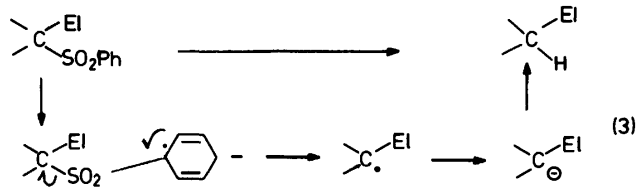

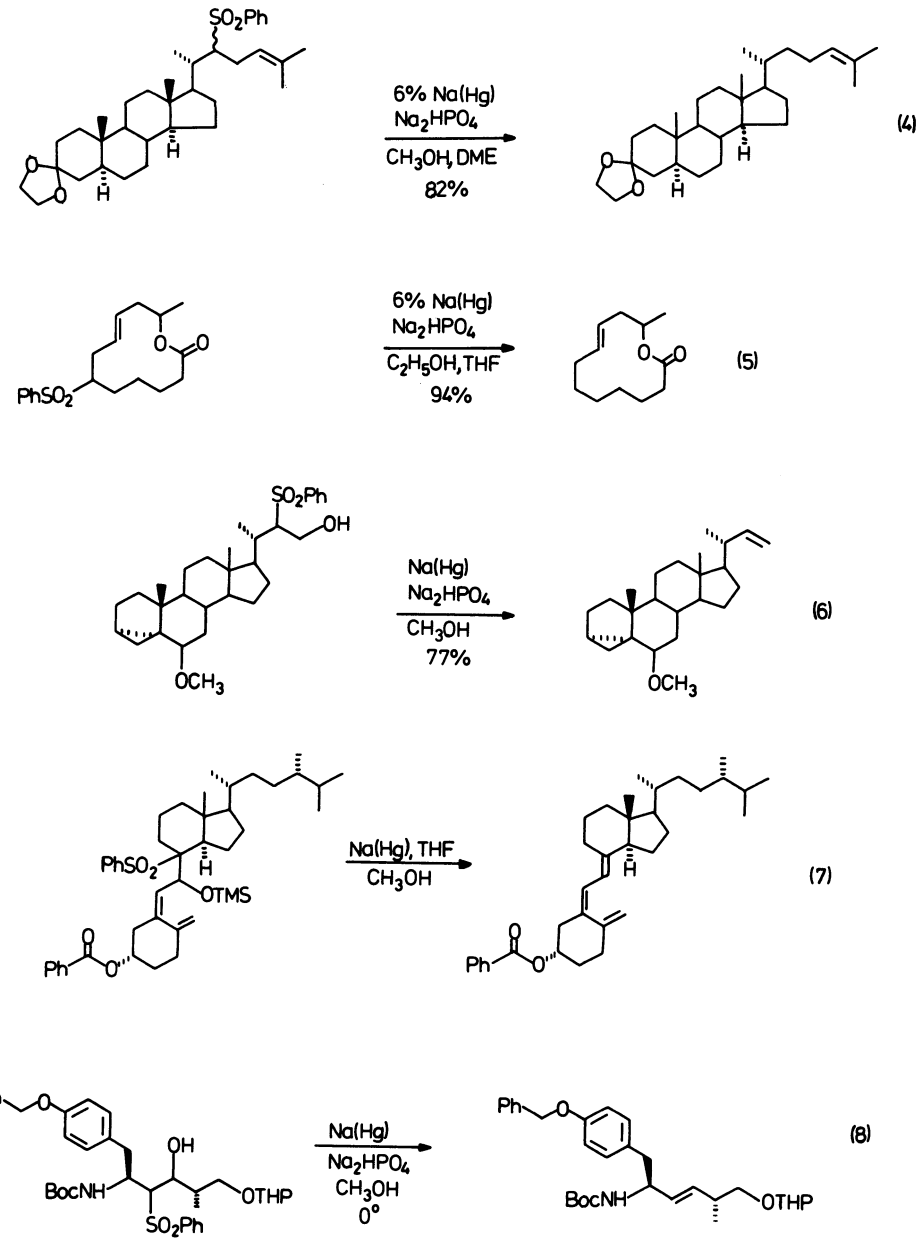

reductive desulfonation of aryl sulfones using dissolving metal reductions which permits the overall transformation shown in Eq. 3. Sodium amalgum in alcoholic solvents buffered with disodium hydrogenphosphate is a particularly mild way to effect such cleavages[9] (Eqs. 4[10] and 5[11]). In this reaction, the cleavage presumably occurs from the radical anion as depicted in Eq. 3. Its efficacy, therefore, depends upon the reduction potential of the sulfone and the stability of the resulting carbon radical. Thus, both "activated" sulfones, as in the case of an allyl system, and "unactivated" sulfones, represented by the saturated alkyl systems as in Eqs. 4 and 5, successfully cleave.

If the carbon β to the sulfones bears a potential leaving group, the reaction can be diverted to elimination to an olefin[12,16] (Eqs. 6[13] and 7[14]). Frequently, this method, originally introduced by Julia,[12] provides an olefin geometry complementary to that produced by Wittig type processes (cf. Eq. 8).[15]

An alternative stereocontrolled introduction of an olefin via organosulfones, also introduced by Julia, relies on the steric bulk of the sulfone to direct placement of the larger alkyl group on the β-carbon of an α,β-unsaturated sulfone to be trans as in Eq. 9.[16] Stereocontrolled replacement of the C–S bond by a C–H using basic dithionite completes a stereoselective approach to (Z)-olefins.

The base-catalyzed elimination of aryl sulfones has also served as a useful approach to olefins. A synthesis

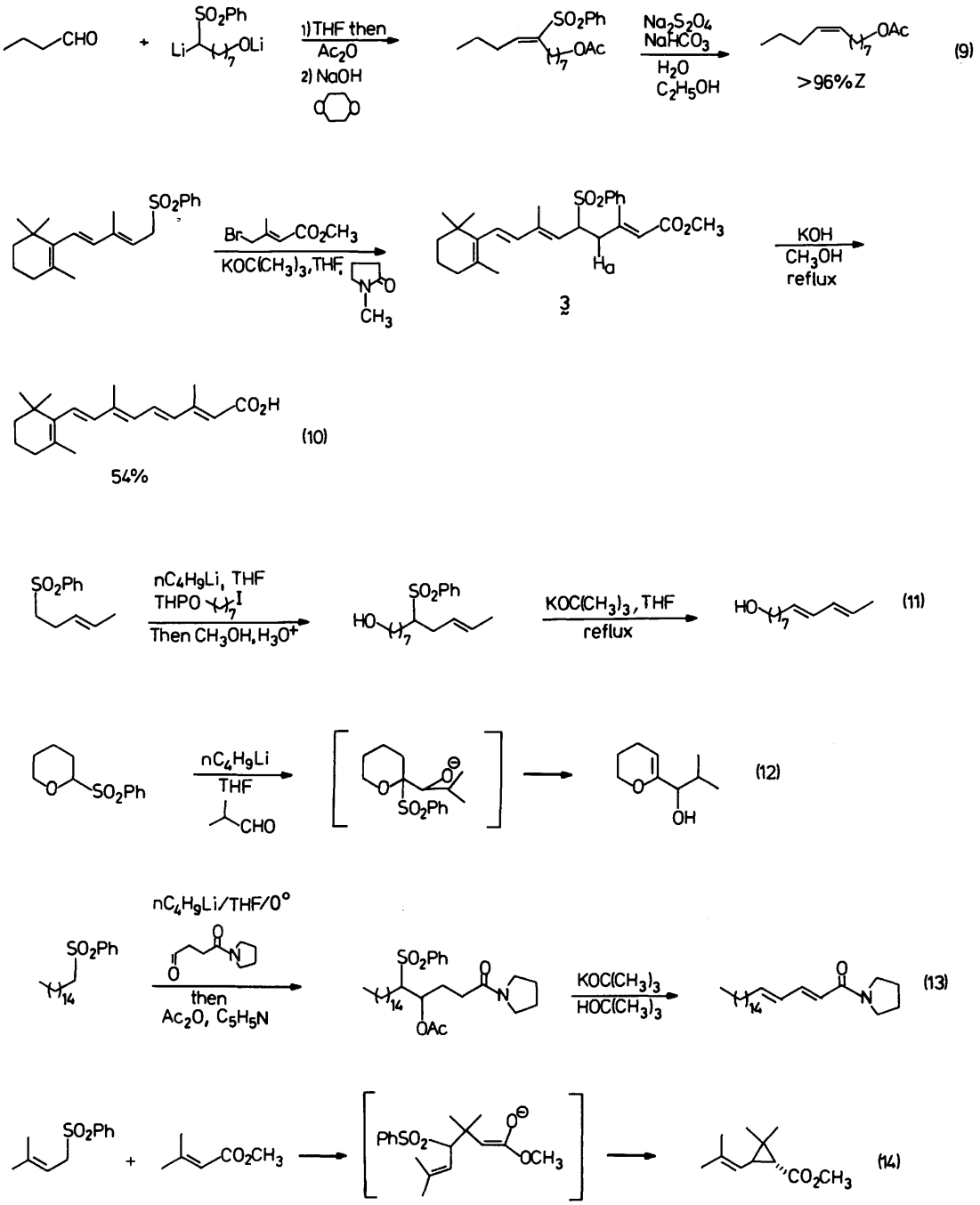

of vitamin A acid illustrates the alkylation-elimination sequence (Eq. 10).[17] The acidification of the proton to be removed (i.e. H_a in **3**) by virtue of its being vinylogously alpha to the ester facilitates the elimination but is not required. An allylic proton proved sufficient in a synthesis of a pheromone constituent of the false coddling moth (Eq. 11) but this elimination requires much harsher base conditions.[18] Activation of the sulfone as a leaving group by placing an electron donating group α to the sulfone has also proven effective (Eq. 12).[19] An interesting variant is a double elimination of β-acetoxy sulfones (Eq. 13)[20] which relies upon 1) facilitation of elimination of the elements of acetic acid by the sulfone, 2) the ease of converting a vinyl sulfone to an allyl sulfone and 3) the vinylogous elimination of the elements of benzenesulfinic acid.

The elimination of the elements of arenesulfinic acid to form olefins relies upon the leaving group ability of sulfones. Although a phenylsulfonyl group has been estimated[21] to be a poorer leaving group than chloride by 10^9, it still functions viably in such a role. We became intrigued with the question of substituting the sulfone—a type of reaction which was

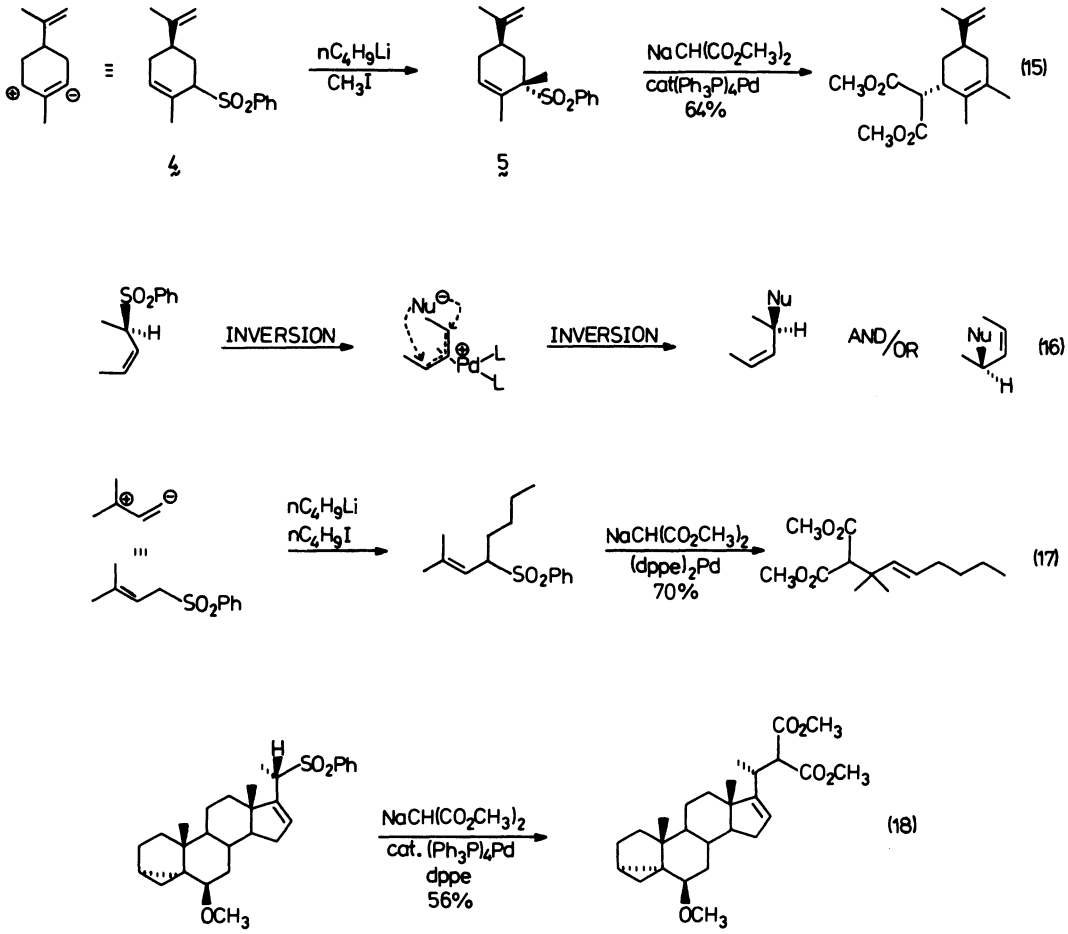

almost unprecedented. The earliest documented case involved formation of a cyclopropane[22] which evolved into a practical synthesis of methyl chrysanthemate according to Eq. 14.[23] Such a cyclopropanation proves to be rather limited and no other types of rings have been produced.

Transition Metal Promoted Substitutions. The poor leaving ability of an arylsulfonyl group has led to the exploitation of the trifluoromethylsulfonyl group which is 10^7 times better as a leaving group.[24] An alternative approach to overcome this lack of reactivity is to use a transition metal to activate the sulfone. The excellent ability of low valent palladium complexes to facilitate displacements of poor leaving groups at allylic positions led us to explore the reactions of allyl sulfones. Diastereoselective alkylation of allyl sulfone **4** leads predominately (88:12) to **5**.[25] Subjecting sulfone **5** to dimethyl sodiomalonate in the presence of a catalytic amount of a Pd(0) complex leads to regio- and diastereoselective substitution as depicted in Eq. 15. Since Pd(0) catalyzed alkylations involves initial substitution of the leaving group by palladium followed by displacement of the palladium by the nucleophile, the overall stereochemistry is net retention of configuration (Eq. 16). In principle, attachment can occur at either terminus of the allyl system independent of the original location of the sulfone. While formation of the new C–C bond at the less substituted position as depicted in Eq. 15 is most common, unhindered nucleophiles like malonate anion preferentially form the new C–C bond to the more substituted carbon when the competition is between a primary and a tertiary center or between a secondary and a tertiary center in an acyclic case (Eq. 17). This method has been employed to introduce a steroid side chain in a stereocontrolled manner (Eq. 18).[26]

The chemoselectivity of this approach for C–C bond formation is highlighted by a short synthesis of the dimethyl ester of the sex pheromone of the Monarch butterfly (**9b**).[25] The keto sulfone **6** was a substrate for the palladium reaction, without the need to protect the carbonyl group, to give **7** with excellent regioselectivity. On the other hand, use of a typical carbonyl reagent, a phosphonate anion, led to the olefination product **8** without complications from the allyl sulfone. Addition of the sterically less demanding catalyst, $Pd(dppe)_2$, and dimethyl sodio-

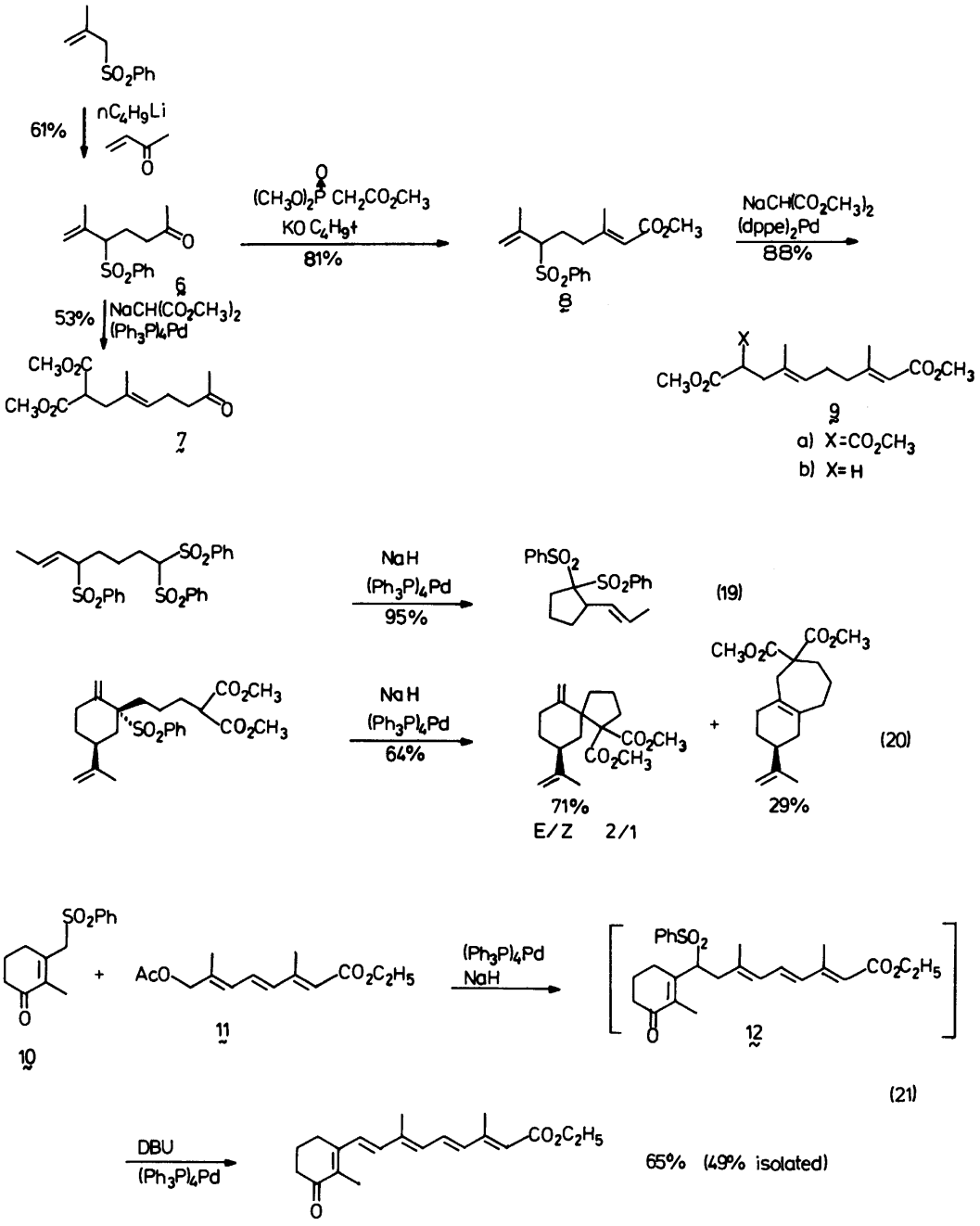

malonate led in a regioselective alkylation to **9a** which has been previously decarbomethoxylated to the pheromone ester **9b**.

Whereas, all of the foregoing examples involve intermolecular alkylations, intramolecular alkylations also succeed as shown in Eqs. 19 and 20.[27] The choice of nucleophile may determine the regioselectivity. Thus, as Eq. 20 shows, the sterically undemanding malonate prefers to attack the sterically congested tertiary carbon although the selectivity is only moderate. In the absence of a nucleophile, eliminations to dienes occur. The ability of sulfone stabilized anions to serve as nucleophiles in palladium catalyzed alkylations of allylic acetates combined with the palladium catalyzed eliminations of allylic sulfones has led to a useful one pot alkylative elimination to polyenes according to Eq. 21.[25] In a model to vitamin A metabolites, the anion derived from allyl sulfone **10** is smoothly alkylated by allylic acetate **11** in the presence of a Pd(0) catalyst in DMSO at room temperature to give the intermediate **12**. DBU is added directly to the reaction mixture and the temperature raised to 80 °C to complete the sequence. Both steps, alkylation and elimination, require Pd(0) activation.

Molybdenum catalysts also activate allylic sulfones

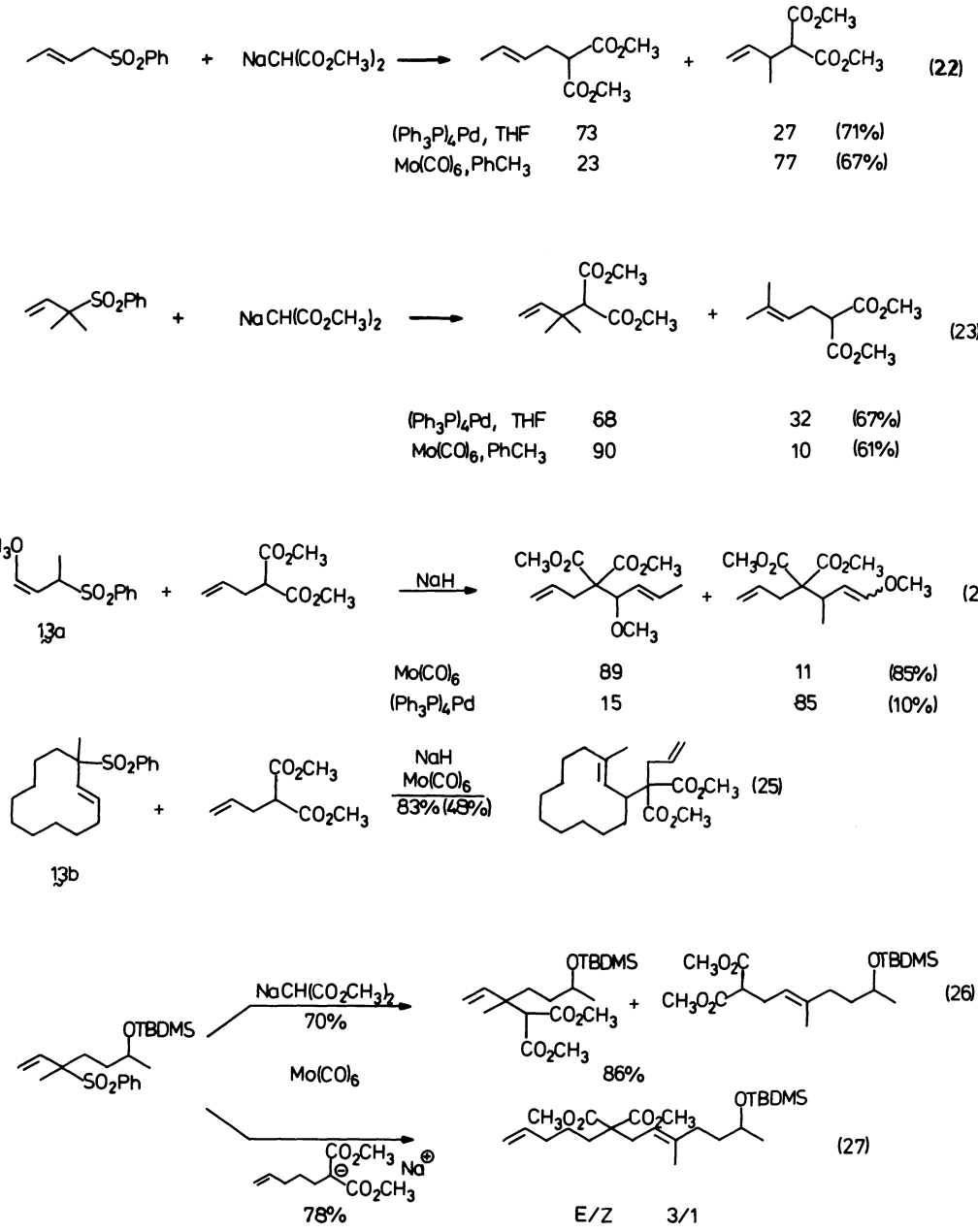

for alkylation.[27] Such catalysts usually complement the regiochemistry of the palladium catalyzed reactions as shown in Eq. 22. In the case of α,α-dimethylallyl phenyl sulfone, the propensity for alkylation at the tertiary position shown by the palladium catalyst is further enhanced by the molybdenum catalyst. In some cases, an allylic sulfone participates poorly in a Pd(0) catalyzed reaction but quite well in the Mo(0) version as in the case of **13a** and **13b** (Eqs. 24 and 25). In the case of Eq. 25, no reaction was observed with the Pd(0) catalyst; whereas, the Mo(0) catalyst gave an 83% yield at about 50% conversion. Normally, however, the Pd(0) catalyzed reaction is the more general.

Good diastereoselectivity may accompany these reactions as shown in Eq. 26 where only one diastereomeric product was observed although we have no basis for making an assignment of stereochemistry as yet. Increasing the steric bulk of the nucleophile by simply switching from the anion of dimethyl malonate (Eq. 26) to that derived from an alkylated malonate (Eq. 27) changes the regioselectivity from one dominated by the electronic distribution in the intermediate π-allylmolybdenum system to one dominated by the steric demands of the attacking nucleophile.

Combining alkylation of sulfone stabilized anions with molybdenum catalyzed reactions leads to a synthesis of 1,1-disubstituted cycloalkanes (Eqs. 28 and 29). As in all cases, use of a sterically more

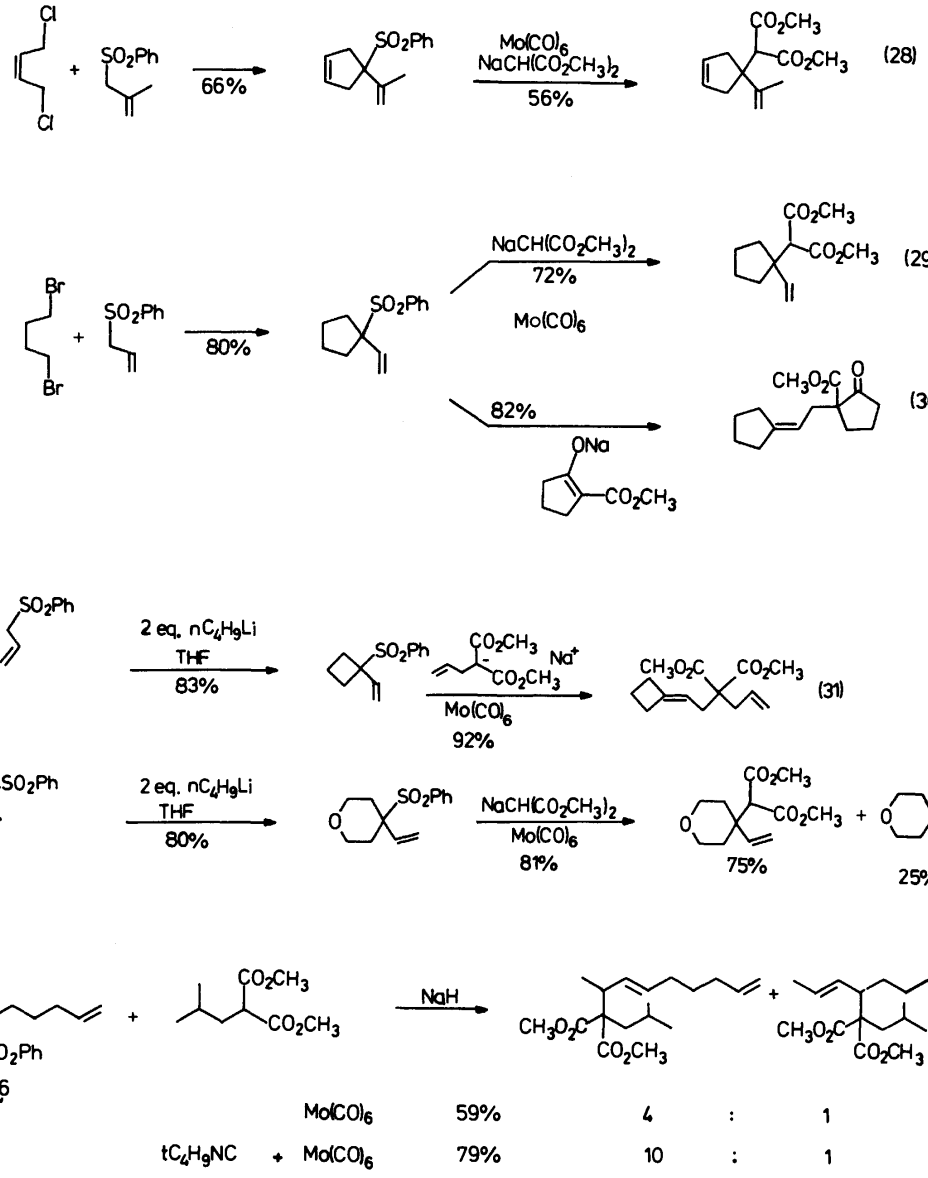

crowded nucleophile leads to attack at the primary carbon (Eq. 30). Both four membered rings (Eq. 31) and heterocycles (Eq. 32) can be made. Unlike other examples, dimethyl sodiomalonate gives poor regioselectivity in the four-membered ring case. This two step sequence illustrates the equivalency of an allyl sulfone to a 1,1,1-(i.e. **14**) or 1,1,3-(i.e. **15**) tripole.

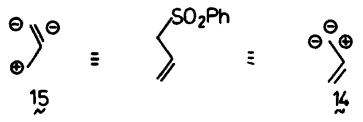

The lability and volatility of the CO ligands limits the lifetime of the molybdenum hexacarbonyl catalysts. In a preliminary examination, we found that addition of a catalytic amount of *t*-butyl isocyanide indeed enhances the catalyst lifetime.[27] For example, the yield in the alkylation of allyl sulfone **16** increased substantially as did the degree of regioselectivity upon adding 3 eq. of *t*-butyl isocyanide per molybdenum.

Nickel catalysts also promote substitutions of allyl sulfones[28] but with lower regioselectivity than observed with either palladium or molybdenum catalysts. For example, the alkylation of α,α-dimethylallyl sulfone with dimethyl sodiomalonate gave a 91% yield of the two alkylation products depicted in Eq. 23 in almost a 2:3 ratio (with the major product derived from attack at the primary carbon) using $(dppe)_2Ni$.[27]

In all of the cases discussed, stabilized anions, were employed as nucleophiles. Substitutions by non-stabilized carbon nucleophiles occur smoothly using copper catalyzed additions of Grignard reagents. For example, a chemo- and regioselective displacement of

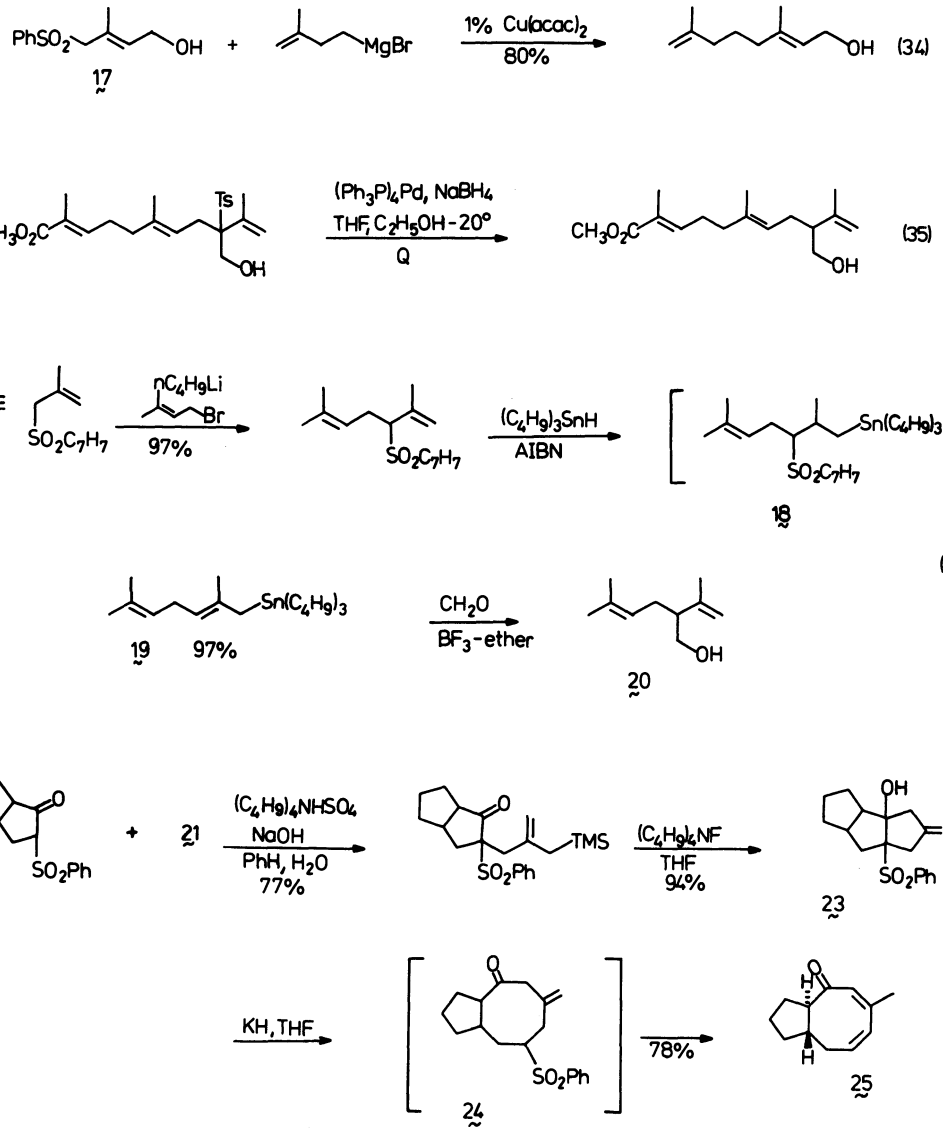

the sulfone moiety of the hydroxy sulfone **17** occurs as shown in Eq. 34.[29]

Reductive desulfonylations can also be achieved by using a hydride equivalent in metal catalyzed reactions. As shown in Eq. 35,[30] a synthesis of dehydrohelepuberinic acid ester took advantage of the sulfone stabilized anions to construct the carbon skeleton and then reductively cleaved the sulfone using Pd(0) catalysis in which the hydroxyl group dictated the regioselectivity.

Radical Substitutions. An alternative way to overcome the sluggishness of sulfones to substitution takes advantage of the radicals bearing a β-sulfone. Thus, the allyl sulfone **18** undergoes radical substitution, presumably by an addition-elimination sequence, by tributyltin radical as depicted in Eq. 36.[31] The resulting allylstannane undergoes carbonyl addition to give the monoterpene lavandulol (**20**). In this case, the umpolung associated with converting an allyl sulfone **18** to an allylstannane **19** equates the starting methallyl phenyl sulfone to a 1,1-dianion.

A Three Carbon Intercalation. The bifunctional conjunctive reagent **21** serves as a synthon for a 1,3-dipole **22**.[32] As depicted in Eq. 37, this zwitterionic

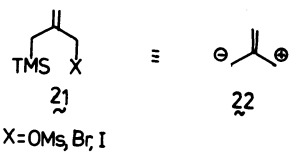

behavior allows straightforward methylenecyclopentane annulation.[33] By employing a β-keto sulfone as the starting meterial, the annulation creates a β-hydroxy sulfone **23**. Due to the anion stabilizing ability of the sulfone, converting the hydroxyl group into a "naked" alkoxide causes the common bond to cleave to create a ring enlarged β-keto sulfone **24**. Under the basic conditions for ring cleavage, the exocyclic double bond migrates into conjugation with the carbonyl group and, by so doing, facilitates the

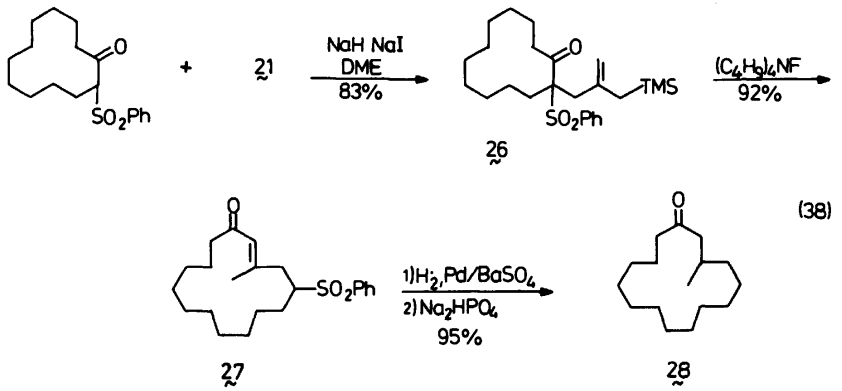

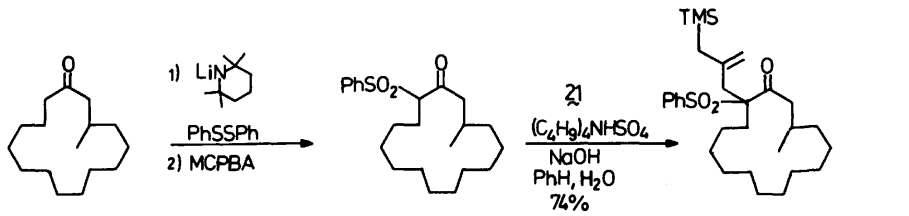

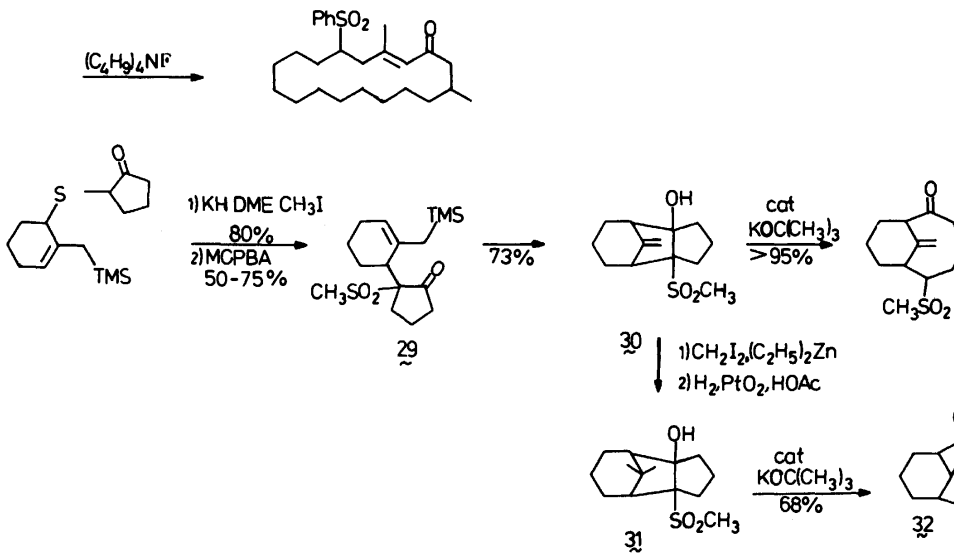

base catalyzed elimination of the elements of benzenesulfinic acid to produce the eight membered ring dienone **25**.

The facility of fragmentation of the β-hydroxy sulfone **23** is related to ring size. If the starting β-keto sulfone is either acyclic or a cyclic system of more than seven carbons, cyclization of the allylsilane to create the methylenecyclopentane is accompanied by fragmentation as depicted for the 12-membered case **26** (Eq. 38). Thus, fluoride promoted cyclization leads directly to the enone **27** whereby fragmentation of the methylenecyclopentane and double bond migration occur concomitant with initial cyclization. Catalytic hydrogenation and desulfonylation complete a synthesis of muscone in an outstanding 62% overall yield from cyclododecanone, the precursor of the β-keto sulfone. This sequence lends itself to an iterative process. As shown in Eq. 39, muscone has been grown to an 18-membered ring.[34]

This method can also be used to create bridged bicyclic systems. In a model directed toward the bridged bicyclic portion of taxanes, the keto sulfone **29** was prepared by a sigmatropic rearrangement followed by oxidation (Eq. 40).[35] Fluoride initiated cyclization of the allylsilane led to substantial protodesilylation. On the other hand, ethylaluminum dichloride induces cyclization to the bridged bicyclic hydroxy sulfone **30**. Fragmentation occurred most smoothly with a catalytic amount of potassium *t*-butoxide in DMSO. More pertinent, the gem-

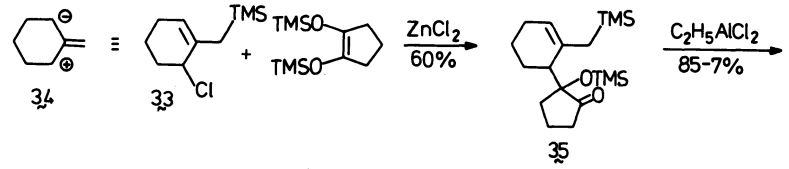

34 33 35

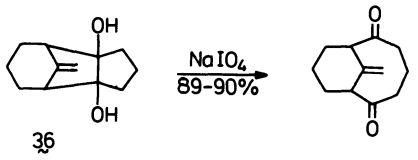

36 (41)

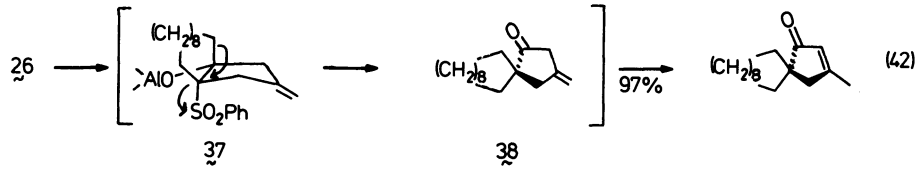

37 38 (42)

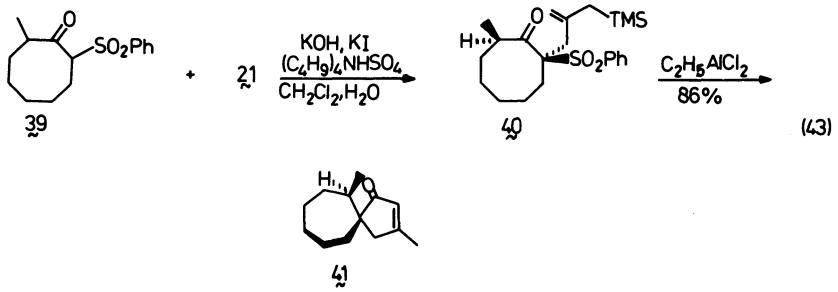

39 40 (43) 41

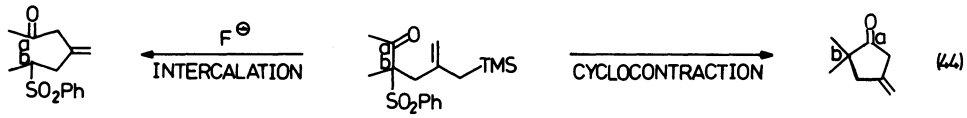

(44)

dimethyl compound **31**, available by hydrogenolysis of the cyclopropane derived from methylenation of the olefin of **30**, also fragments to the desired bicyclo-[5.3.1]undecane skeleton.[36]

In this version, the silyl chloride **33** serves directly as the 1,3-dipole synthon **34**. Lewis acids reveal both types of reactivity by, first, activating the allyl chloride **33** in its reaction with the enediol bis(silyl ether) and, second, by activating the carbonyl group of **35** towards addition by the allylsilane. Diol cleavage then completes the sequence.

The use of ethylaluminum chloride to cyclize the allylsilanes as in the cases of **29** and **35** proved limited. Applying the reaction to substrate **26** led to a totally different process as shown in Eq. 42.[37] In the presence of the Lewis acid, the initial cyclization product **37** apparently suffers a pinacol-type rearrangement to produce the ring contracted spiro ketone **38**. Isomerization of the exocyclic double bond into conjugation completes the sequence of this cyclocontraction-spiroannulation.

Excellent diastereoselectivity accompanies this novel approach to form spirocycles. Alkylation of the eight-membered ring keto sulfone **39** gives a single diastereomer **40** (Eq. 43). Ethylaluminum dichloride leads to cyclization and ring contraction to give the spirocycle **41** in which the migrating carbon completely retains its stereochemistry. Thus, depending upon the nature of the catalyst, two quite disparate reactions reflecting the multifaceted properties of sulfones can occur. As summarized in Eq. 44, a nucleophilic trigger promotes intercalation and an electrophilic trigger diverts the intermediate via a pinacol type rearrangement to a 2,2-disubstituted 4-

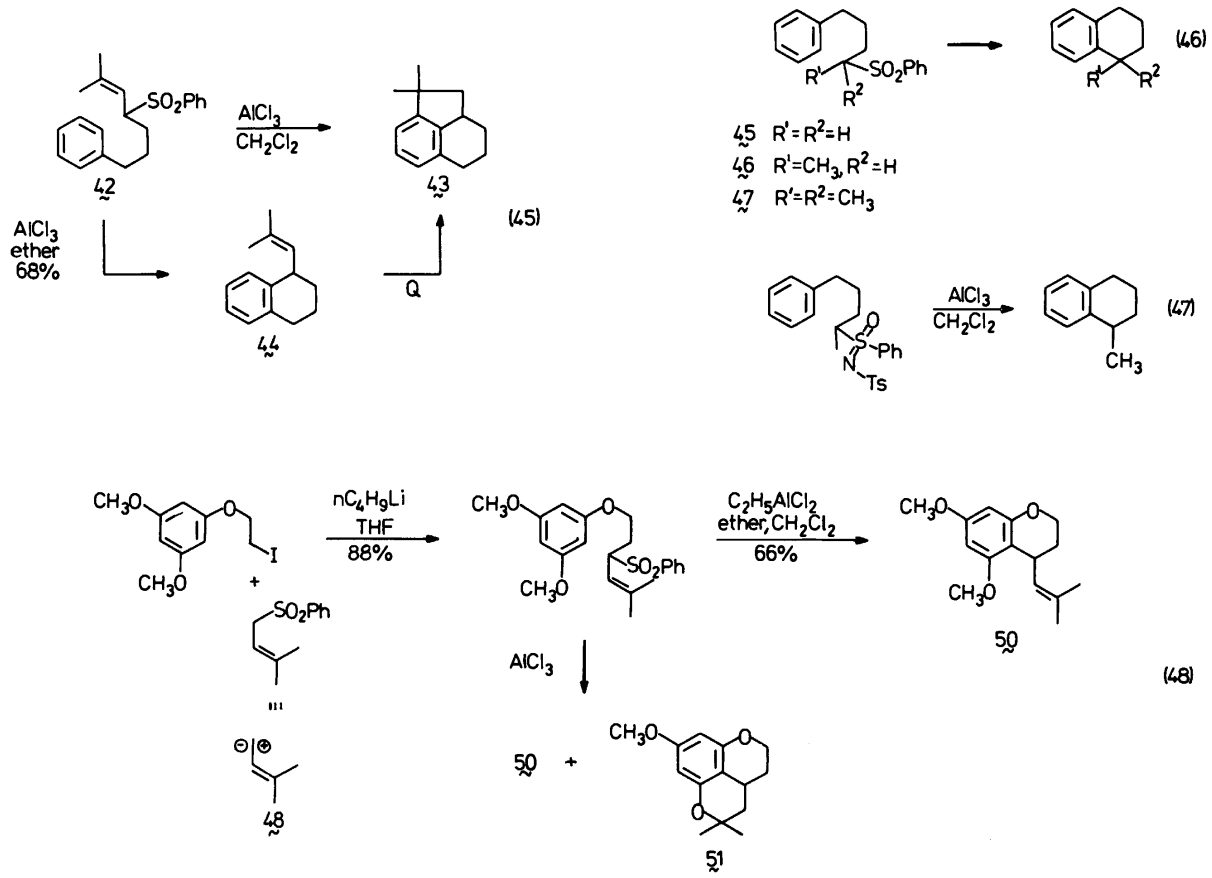

methylenecyclopentanone. The sensitivity of the β-hydroxy sulfone toward Lewis acid promoted rearrangement is quite remarkable considering the absence of any prior indication that Lewis acids induce ionization of organosulfones.[38]

Lewis Acid Induced Cyclizations. The ability to effect a pinacol-type rearrangement in which a phenylsulfonyl group ionizes in the presence of as weak a Lewis acid as ethylaluminum dichoride led to an investigation of the ionizing ability of simple organosulfones. Strikingly, the allyl sulfone **42** cyclized to the tricycle **43** even at −78°C in the presence of aluminum chloride in methylene dichloride.[39] Attenuating the reactivity of the aluminum chloride by using ether as a solvent requires 35°C for reaction, but the product is cleanly that of the simple cyclization **44**. Subsequent treatment with either aluminum chloride in methylene dichloride or trifluoroacetic acid quantitatively cyclizes the latter to the tricycle **43**.

To determine how good a cation is necessary for ionization, the substrates **45**—**47** were treated with aluminum chloride (Eq. 46). Neither **45** nor **46** satisfactorily cyclizes; however, the tertiary sulfone **47** smoothly produces 1,1-dimethyltetralin in 70—80% yield with aluminum chloride in methylene dichloride. Increasing the Lewis basicity of the sulfone by using the sulfoximine extends the cyclization to secondary carbon centers (Eq. 47).[40] Competition studies indicate the sulfoximines are about twice as reactive as the corresponding sulfones.

The chameleon-type behavior of sulfones is readily apparent by the source of the cyclization substrates as revealed by a model study related to robustadials[41] and euglobals[42] (Eq. 48). The first step takes advantage of the nucleophilic properties of sulfone stabilized anions and the second step utilizes the propensity of allyl sulfones to ionize to the corresponding cations. In this way, prenyl sulfone serves as a synthon for the 1,1-dipole **48**. The choice of Lewis acid and solvent may be important. For example, aluminum chloride effects a second cyclization to **51** in competition with formation of the simple cyclization product **50**. By using ethylaluminum dichloride and further attenuating the Lewis acidity by using ether as a cosolvent, the second cyclization can be suppressed. Eqs. 49 and 50 reveal some of the generality of this cyclization strategy for both carbo- and heterocyclic cases. Equation 49 illustrates the further cyclization of the initial tricyclic product. Equation 50 reveals that the acid labile pyrrole ring survives when a HCl scavenger, ethylaluminum dichloride, is also employed although the benzofuran system of Eq. 51 does not require it.

Equation 52 shows the utility of the adducts from the metalated sulfone and an aldehyde participating

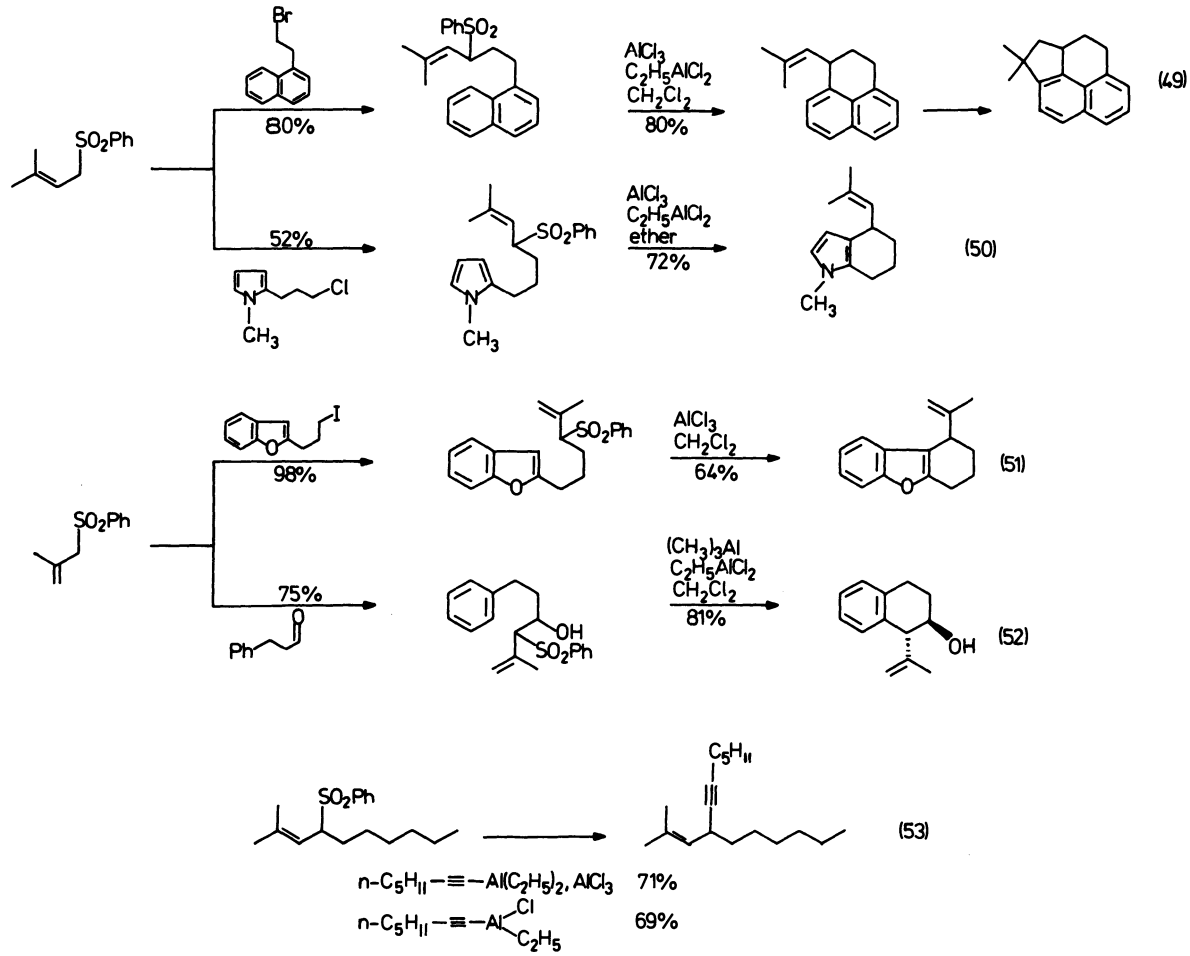

in the cyclization.[43] The alcohol is first reacted with trimethylaluminum before subjecting it to the stronger Lewis acid. Cyclization proceeds in excellent chemical yield and diastereoselectivity with only the (E)-product produced. The excellent diastereoselectivity is not limited to the hydroxyl substituent since the substrate bearing a methyl group in lieu of the hydroxyl group shows similar stereocontrol.[44] Viewing the cation generated upon ionization of the sulfone in a chair-type conformation suggests that placing this substituent in a pseudoaxial position as in **52** is less favorable than placing it in a pseudoequatorial one as in **53**.

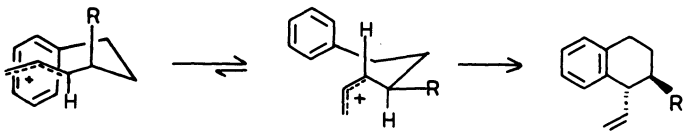

52 53

Lewis Acid Induced Condensations. The success of cyclization reactions led to a search of intermolecular condensations which require nucleophiles compatible with Lewis acids. Organoalanes have proven themselves as nucleophiles in the presence of Lewis acids and, in some cases, as both Lewis acid and nucleophile.[45]

Alkynylalanes, prepared by treating the lithiated alkyne with an appropriate chloroalane, smoothly condense with allyl sulfones. As shown in Eq. 53, use of a diethylalkynylalane requires aluminum chloride as a catalyst; whereas, an alkynylethylchloroalane serves as both the Lewis acid and nucleophile.[43] Unfortunately, the latter did not prove to be general and reactions frequently proceeded with only low conversions.

The high reactivity of the allyl sulfone is highlighted by the compatibility of the benzyl alcohol in the case of Eq. 54. As previously, smooth reaction requires initial treatment of the hydroxy sulfone with trimethylaluminum.

Even though the reaction proceeds through allyl cations, good regioselectivity normally accompanies this reaction. In the case of an unsymmetrical allyl system, competing a primary or secondary terminus with a tertiary one, very high selectivity for formation of the new C–C bond at the less substituted carbon occurs (cf. Eq. 53). In a primary versus secondary case, the selectivity for attack at the less substituted carbon

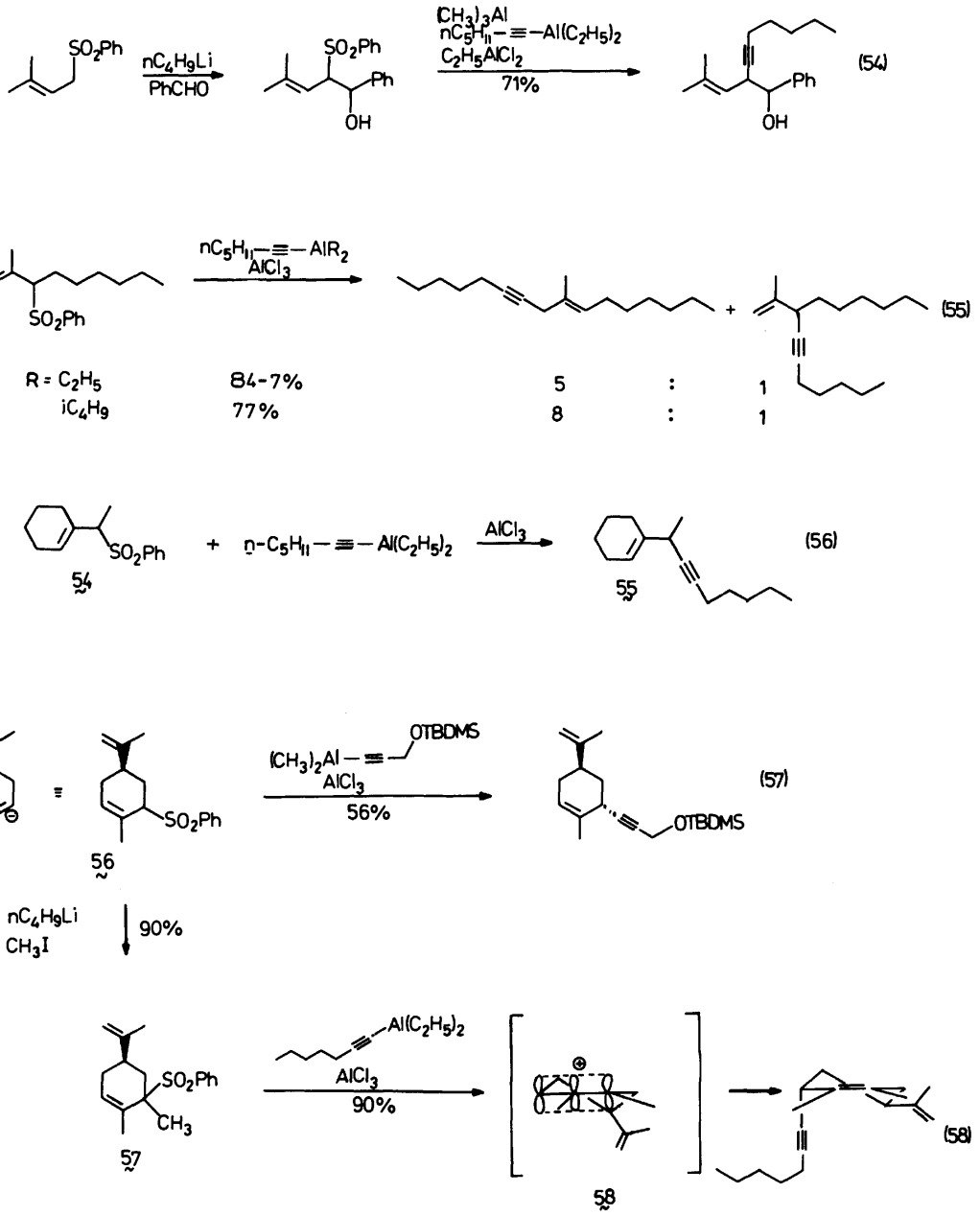

is somewhat lower (Eq. 55). By increasing the steric demands of the organoalane such as replacing ethyl by isobutyl, some improvement for attack at the primary terminus occurs. Allyl sulfone **54** competes two secondary carbons. The preference for the double bond to be endocyclic and the lower steric hindrance associated with attack at the exocyclic position leads to **55** as the dominant product (6:1, Eq. 56).

Good diastereoselectivity is obtained with cyclohexenyl phenyl sulfones (Eqs. 57 and 58). The preference for axial attack presumably derives from stereoelectronic factors.[46] Pseudoaxial attack on the intermediate allyl cation **58** allows the ring to directly distort toward the favorable half-chair conformation while maintaining good orbital overlap. Attack by the organoalane leading to the equatorial product requires distortion of the ring towards a boat—a less favorable process. The regioselectivity as shown in Eq. 58 demonstrates the preference for attack at the less hindered terminus of the allyl system regardless of the initial position of the sulfone. Since **57** arises by the methylation of the lithiated sulfone **56**, the latter is a synthetic equivalent to a 1,3-dipole **56a**.

Alkenylalanes, prepared by hydroalumination of acetylenes, behave in exactly analogous fashion as shown by Eqs. 59 and 60. Note that the intrinsically higher steric demands of an alkenylalane compared to an alkynylalane leads to higher regioselectivity (cf. Eqs. 55 versus 59).

The success of enol silanes as the nucleophilic

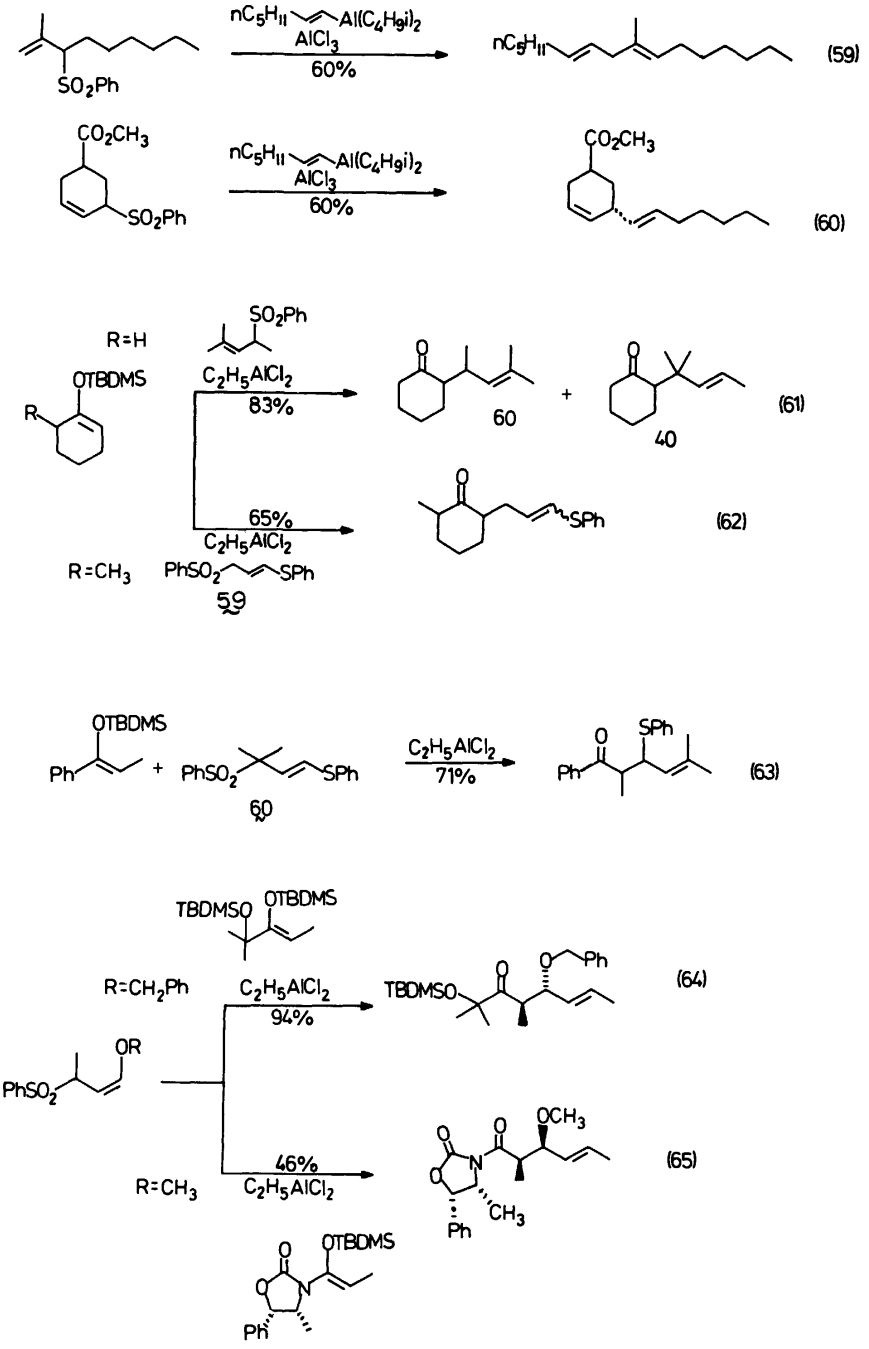

partners in Friedel–Crafts types of alkylations[47] led to their exploration as nucleophiles towards allyl sulfones. The most striking difference from the alkynyl- and alkenylalanes is the lower regioselectivity (cf. Eq. 61) unless the allyl sulfone has a strongly directing substituent (Eq. 62).[44] The regiochemistry in the latter case appears dictated by steric effects since the dimethyl analog **60** of the above sulfone **59** now proceeds by formation of the new C–C bond at the carbon bearing sulfur.

Modest diastereoselectivity accompanies this reaction. Whereas, the enol silyl ether of a ketone shows anti selectivity (Eq. 64, anti/syn 92/8); the enol silyl ether of an imide shows syn selectivity (Eq. 65, syn/anti 80/20).

The range of nucleophiles compatible with the conditions required for ionization of a sulfone remains yet to be defined. The success of organoalanes and enol silyl ethers indicated that we have reason to be optimistic that a rather broad variety will be feasible.

Lewis Acid Induced Ring Expansion. The duality of function of organosulfones corresponds to the type of reactivity necessary for ring expansions according to Eq. 66. The excellent acidifying properties of the sulfone should make this process feasible for

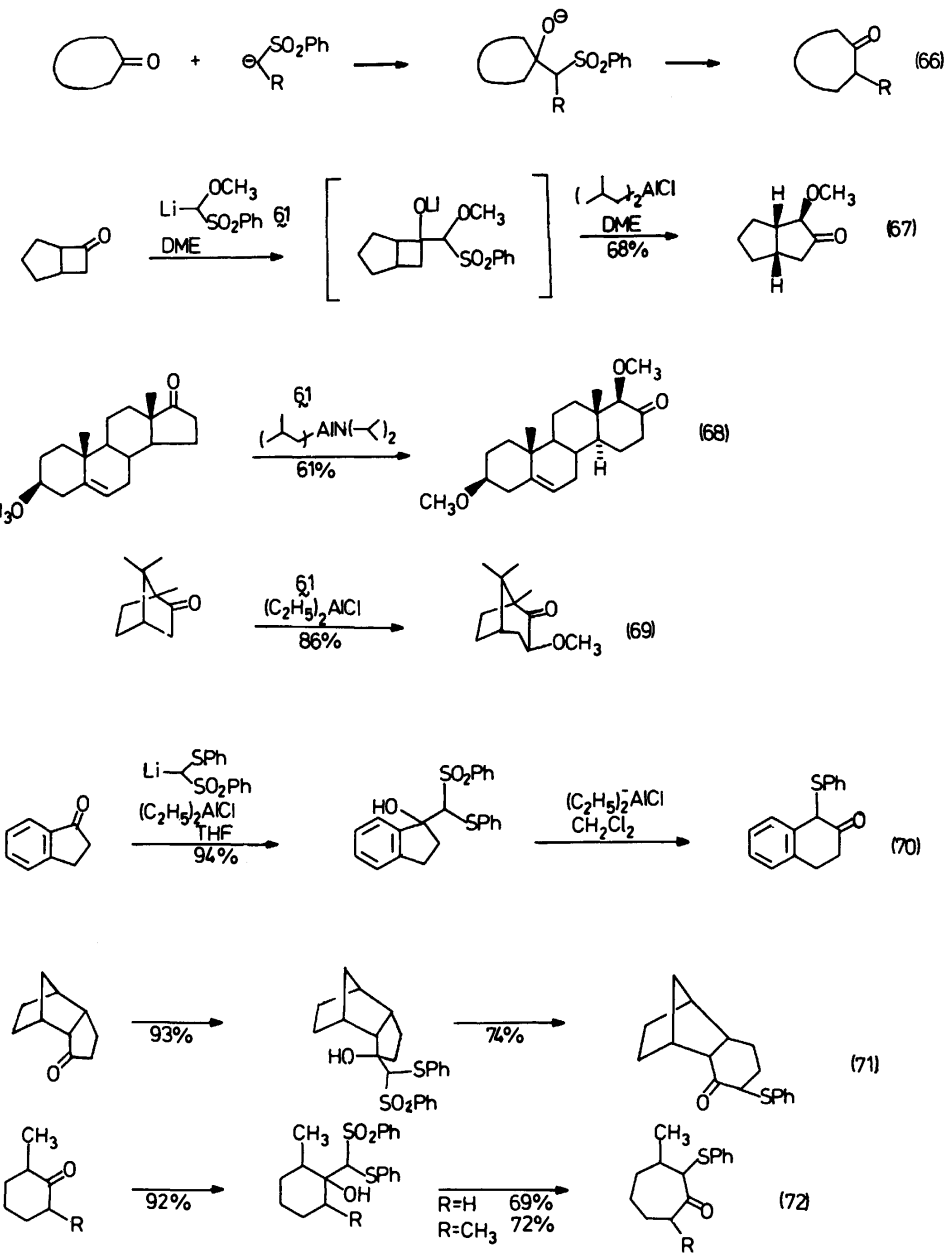

substrates in which R is a very poor anion stabilizing group or even anion destabilizing. Since few methods exist to expand rings directly to α-heteroatom substituted cycloalkanones, use of R=SPh and OCH_3 were first considered.[48]

As Eqs. 67—69 show, four- and five-membered ring ketones smoothly add methoxy(phenylsulfonyl)-methyllithium (**61**) in DME. Direct addition of a dialkylaluminum chloride to the lithium alkoxide effects ring enlargement in a one pot operation. While dialkylaluminum chlorides are normally employed (Eqs. 67 and 69), the steroid example required a milder Lewis acid which turned out to be diisobutylaluminum diisopropylamide (Eq. 68). As a carbonium ion process, the carbon α to the original carbonyl group that can best stabilize positive charge normally preferentially migrates (Eqs. 67 and 68). The case of camphor is an exception. Since migration of the bridgehead tertiary carbon would involve a boat-type transition state, the normally less favorable methylene group migrates since a favorable chair conformation can now be accomodated.[49]

Extension of the above ring expansion to the phenylthio series proved problematic due to the fact that the equilibrium for carbonyl addition of phenylthiophenylsulfonylmethyllithium in THF was unfavorable. However, addition of diethylaluminum chloride to the THF solution resolves this problem and gives the simple carbonyl adducts without rearrangement (Eqs. 70—72). Subjecting the hydroxy sulfones to the same aluminum reagent but in methylene dichloride effects smooth rearrangement.

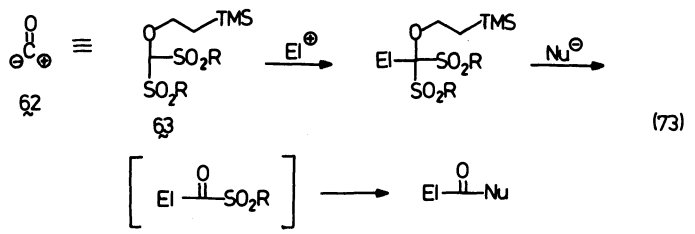

(73)

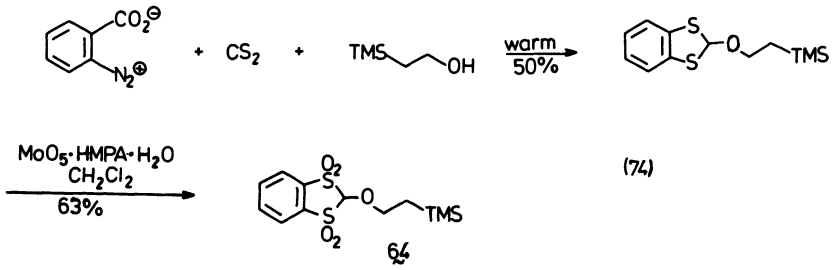

(74)

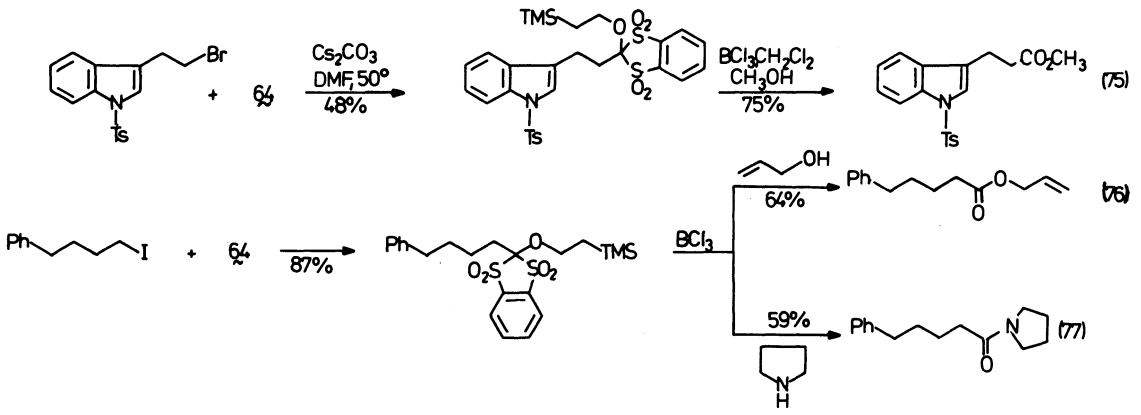

(75)

(76)

(77)

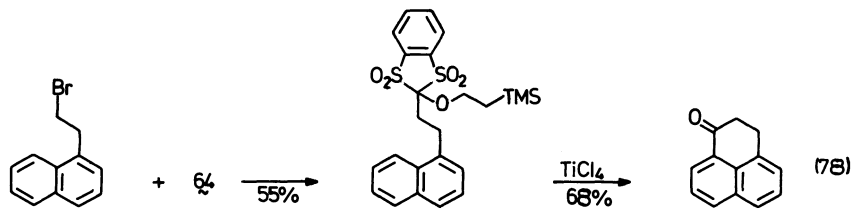

(78)

The migrating aptitude follows precisely the same pattern found for the methoxy reagent. The carbon that best stabilizes a positive charge normally migrates (Eqs. 70 and 72). On the other hand, conformational factors can overcome this electronic bias (Eq. 71). The ring expansion of the phenylthio reagent appears more general than that of the methoxy reagent **61**. Notably, ring expansion of six to seven (Eq. 72) occurs smoothly with the phenylthio reagent in contrast to the attempted reactions with **61**.

A Carbonyl 1,1-Dipole. The general importance of carbonyl compounds led to the extension of the above concepts to develop a controlled synthon for a carbonyl 1,1-dipole **62**. As revealed in Eq. 73, an alkoxy-bis(sulfone) **63** may be able to serve such a role. Such a reagent, **64**, was prepared as outlined in Eq. 74.[50]

The lability of the anion derived from **64** led to its formation in the presence of the appropriate electrophile. The examples of Eqs. 75—79 demonstrate that cesium carbonate in warm DMF best effects the alkylation. Exposure of the alkylation products to a Lewis acid such as boron trichloride followed by adding heteroatom nucleophiles such as an alcohol (Eqs. 75 and 76) or an amine (Eq. 77) completes the sequence. In these examples, a carbon group served as the electrophile and a heteroatom group served as the nucleophile. Thus, an ester and an amide synthesis is

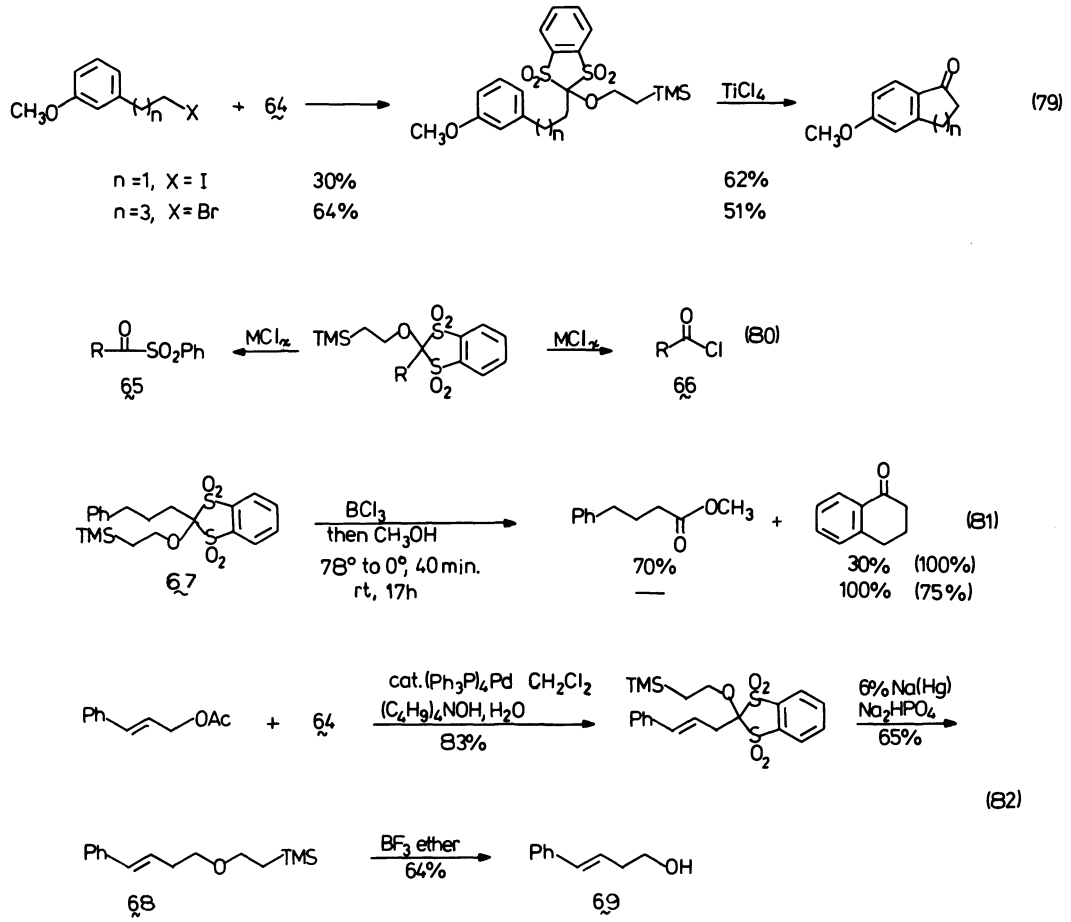

available.

By using carbon groups as both nucleophile and electrophile, ketones are available. Equations 78 and 79 show how a carbonyl group can be stitched into place with appropriate arylalkyl halides. The demonstrated examples illustrate formation of five-, six-, and seven-membered rings.

The nature of the reactive electrophile in all of the above cases remains undefined. While it is tempting to speculate that acyl sulfones **65** may be involved, an acid chloride **66** may also be postulated (Eq. 80). That a reactive intermediate is indeed produced is strongly supported by treating **67** with boron trichloride at −78 to 0 °C followed by addition of methanol (Eq. 81) whereby the corresponding methyl ester and tetralone are both produced. Increasing the reaction time and temperature before adding methanol produces only tetralone.

The reductive desulfonylation of sulfones opens yet another avenue for application of this alkoxy-bis(sulfone) as shown in Eq. 82. The 2-(trimethylsilyl) ethyl group of **68** can be cleaved to produce the free saturated alcohol **69**. The overall transformation of Eq. 82 constitutes a homologation of an allyl alcohol to a homoallyl alcohol and corresponds to employment of the anion derived from **64** as a hydroxymethyl anion equivalent.

Conclusion

While it is always tempting to believe that a well explored path offers little opportunity for innovation, the tremendous subtleties that control reactivity undermine any such notion. Although the chemistry of sulfones extends back for over one hundred years, their utility as synthetic building blocks based upon their facilitation of carbanion formation strongly emerged in the 1960's. In spite of this extensive work, their high sensitivity to ionization to carbocations in the presence of Lewis acids, especially those derived from aluminum, had gone unnoticed. This reactivity of an inverse electronic sense opens new vistas. Their ability to function as nucleophiles in a basic environment and as electrophiles in a Lewis acidic environment aptly allows them to be called "chemical chameleons" from which many new applications and new synthetic reagents remain to be discovered.

We wish to thank the National Science Foundation and the National Institutes of Health for their generous support of our programs.

References

1) a) P. D. Magnus, *Tetrahedron*, **33**, 2019 (1977); b) P. J. Kocienski, *Chem. Ind. (London)*, **1981**, 548; c) F. Vogtle and L. Rossa, *Angew. Chem., Int. Ed. Engl.*, **18**, 515 (1979).

2) W. S. Matthews, J. E. Bares, J. E. Bartmess, F. G. Bordwell, F. J. Gornforth, G. E. Drucker, Z. Margolin, R. J. McCallum, G. J. McCollum, and N. R. Vanier, *J. Am. Chem. Soc.*, **97**, 7007 (1975). Also see F. G. Bordwell, M. Van Der Puy, and N. R. Vanier, *J. Org. Chem.*, **41**, 1883 (1976).

3) D. A. Bors and A. Streitwieser, Jr., *J. Am. Chem. Soc.*, **108**, 1397 (1986); S. Wolfe, A. Stolow, and L. A. La John, *Tetrahedron Lett.*, **24**, 4071 (1983).

4) a) R. Lett, G. Chassaing, and A. Marquet, *J. Organomet. Chem.*, **111**, C17 (1976); b) G. Boche, M. Marsch, K. Harms, and G. M. Sheldrick, *Angew. Chem., Int. Ed. Engl.*, **24**, 573 (1985); c) H. J. Gais, H. J. Lindner, and J. Vollhardt, *ibid.*, **24**, 859 (1985).

5) H. J. Gais, J. Vollhardt, and H. J. Lindner, *Angew. Chem., Int. Ed. Engl.*, **25**, 939 (1986).

6) For an example of O-silylation see U. Rheude and W. Sundermeyer, *Chem. Ber.*, **114**, 3378 (1981).

7) L. A. Paquette, *Org. Reactions*, **25**, 1 (1977).

8) T. Chou, H. H. Tso, and L. J. Chang, *J. Chem. Soc., Chem. Commun.*, **1984**, 1323.

9) B. M. Trost, H. C. Arndt, P. E. Strege, and T. R. Verhoeven, *Tetrahedron Lett.*, **1976**, 3477; M. Julia and D. Uguen, *Bull. Soc. Chim. France*, **1976**, 513; G. H. Posner and D. J. Brunelle, *J. Org. Chem.*, **38**, 2747 (1973).

10) B. M. Trost and T. R. Verhoeven, *J. Am. Chem. Soc.*, **100**, 3435 (1978).

11) B. M. Trost and T. R. Verhoeven, *Tetrahedron Lett.*, **1978**, 2275; *J. Am. Chem. Soc.*, **102**, 4743 (1980).

12) M. Julia and J. M. Paris, *Tetrahedron Lett.*, **1973**, 4833.

13) B. M. Trost and Y. Matsumura, *J. Org. Chem.*, **42**, 2036 (1977).

14) P. C. Kocienski, B. Lythgoe, and S. Ruston, *J. Chem. Soc., Perkin Trans. 1*, **1980**, 1290, 1400.

15) A. Spaltenstein; P. A. Carpino, F. Miyake, and P. B. Hopkins, *Tetrahedron Lett.*, **27**, 2095 (1986).

16) M. Julia and J. P. Stacino, *Tetrahedron*, **42**, 2469 (1986).

17) D. Arnould, P. Chabardes, G. Farge, and M. Julia, *Bull. Soc. Chim. France*, **1985**, 130.

18) C. Herve du Penhoat and M. Julia, *Tetrahedron*, **42**, 4807 (1986).

19) S. V. Ley, B. Lygo, and A. Wonnacott, *Tetrahedron Lett.*, **26**, 535 (1985).

20) T. Moriyama, T. Mandai, M. Kawada, J. Otera, and B. M. Trost, *J. Org. Chem.*, **51**, 3896 (1986).

21) X. Creary, *J. Org. Chem.*, **50**, 5080 (1985).

22) W. L. Parker and R. B. Woodward, *J. Org. Chem.*, **34**, 3085 (1969).

23) R. V. M. Campbell, L. Crombie, D. A. R. Findley, R. W. King, G. Pattenden, and D. A. Whiting, *J. Chem. Soc., Perkin Trans. 1*, **1975**, 897; M. Julia and A. Guy-Rouault, *Bull. Soc. Chim. France*, **1967**, 1411.

24) J. B. Hendrickson, D. D. Sternbach, and K. W. Bair, *Acc. Chem. Res.*, **10**, 306 (1977). For a recent application of the triflone leaving group in a version of the Ramberg-Bäcklund see J. B. Hendrickson, G. J. Boudreaux, and P. S. Palumbo, *J. Am. Chem. Soc.*, **108**, 2358 (1986).

25) B. M. Trost, N. R. Schmuff, and M. J. Miller, *J. Am. Chem. Soc.*, **102**, 5979 (1980).

26) N. R. Schmuff, Ph. D. Thesis, University of Wisconsin, 1982.

27) C. A. Merlic, unpublished results in these laboratories.

28) T. Cuvigny and M. Julia, *J. Organomet. Chem.*, **250**, C21 (1983).

29) M. Julia and J. N. Verpeaux, *Tetrahedron*, **39**, 3289 (1983).

30) K. Inomata, Private communication. Cf. K. Inomata, S. Igarashi, M. Mohri, T. Yamamoto, H. Kinoshita, and H. Kotake, *Chem. Lett.*, **1987**, 707.

31) Y. Ueno, S. Aoki, and M. Okawara, *J. Chem. Soc., Chem. Commun.*, **1980**, 683.

32) Cf. B. M. Trost, *Angew. Chem., Int. Ed. Engl.*, **25**, 1 (1986).

33) B. M. Trost and J. E. Vincent, *J. Am. Chem. Soc.*, **102**, 5680 (1980).

34) J. Vincent, unpublished work in these laboratories.

35) B. M. Trost and H. Hiemstra, *J. Am. Chem. Soc.*, **104**, 886 (1982).

36) B. M. Trost and M. J. Fray, *Tetrahedron Lett.*, **25**, 4605 (1984).

37) B. M. Trost and B. R. Adams, *J. Am. Chem. Soc.*, **105**, 4849 (1983).

38) Cf. C. G. M. Janssen and E. F. Godefroi, *J. Org. Chem.*, **47**, 3274 (1982).

39) B. M. Trost and M. R. Ghadiri, *J. Am. Chem. Soc.*, **106**, 7260 (1984).

40) R. Matsuoka, unpublished work in these laboratories.

41) R. Xe, J. K. Snyder, and K. Nakanishi, *J. Am. Chem. Soc.*, **106**, 734 (1984).

42) M. Kozuka, *Chem. Pharm. Bull.*, **30**, 1952, 1964 (1982).

43) B. M. Trost and M. R. Ghadiri, *J. Am. Chem. Soc.*, **108**, 1098 (1986).

44) M. R. Ghadiri, Ph. D. Thesis, University of Wisconsin, 1986.

45) T. Mole and E. A. Jeffrey, "Organoaluminum Compounds," Elsevier, Amsterdam (1972); G. Bruno, "The Use of Aluminum Alkyls in Organic Synthesis," Ethyl Corp., Baton Rouge, 1970, 1973, 1980; H. Yamamoto and H. Nozaki, *Angew. Chem., Int. Ed. Engl.*, **17**, 169 (1978); E. Negishi "Organometallics in Organic Synthesis," Wiley, New York (1980), Vol. 1, pp. 286—393; K. Maruoka and H. Yamamoto, *Angew. Chem., Int. Ed. Engl.*, **24**, 668 (1985).

46) Cf. M. T. Reetz, P. Walz, F. Hubner, S. H. Huttenhain, H. Heimbach, and K. Schwellnus, *Chem. Ber.*, **117**, 322 (1984).

47) M. T. Reetz and W. F. Maier, *Angew. Chem., Int. Ed. Engl.*, **17**, 48 (1978); M. T. Reetz and K. Schwellnus, *Tetrahedron Lett.*, **1978**, 1455; M. T. Reetz and S. H. Huttenhain, *Synthesis*, **1980**, 941.

48) B. M. Trost and G. K. Mikhail, *J. Am. Chem. Soc.*, **109**, 4124 (1987).

49) Cf. R. R. Sauers and J. A. Beisler, *J. Org. Chem.*, **29**, 210 (1964); R. R. Sauers and G. P. Ahearn, *J. Am. Chem. Soc.*, **83**, 2759 (1961).

50) B. M. Trost and P. Quayle, *J. Am. Chem. Soc.*, **106**, 2469 (1984).

 © 1988 The Chemical Society of Japan Bull. Chem. Soc. Jpn., 61, 125—132 (1988)

Invited Paper

Cathodic Addition of Benzylidyne Trichloride to Ketones and Aldehydes[1)]

Michael STEINIGER and Hans J. SCHÄFER*
Organisch-Chemisches Institut der Universität, Correns-Str 40, D-4400 Münster, F.R.G.
(Received August 3, 1987)

Ketones are converted to homologated enones **7a—g** in good yields by cathodic addition of benzylidyne trichloride (**1d**). As intermediates α-chlorooxiranes **6** are assumed, which rearrange via α-keto carbenium ions **9** to enones. The intermediacy of **9** is supported by the addition of **1d** to norcamphor, where the products indicate equilibrating norbornyl cations as intermediates. α,β-Unsaturated ketones lead depending on steric shielding of the double bond to the cyclopropane **23** as 1,4-adduct or the enone **26** as 1,2-adduct. With aldehydes and **1d**, α-chloro or α-hydroxy ketones, the conversion products of 2-chlorooxiranes, are obtained.

The electrochemical reduction of organic *gem*-trihalides **1** (Eq. 1) proceeds in two consecutive one-electron transfer steps and results in cleavage of the C–Halo bond to carbanions **2**,[2)] which can react with electrophiles. As electrophiles, protons,[3)] Michael acceptors,[4)] and carbonyl compounds[5)] have been used.

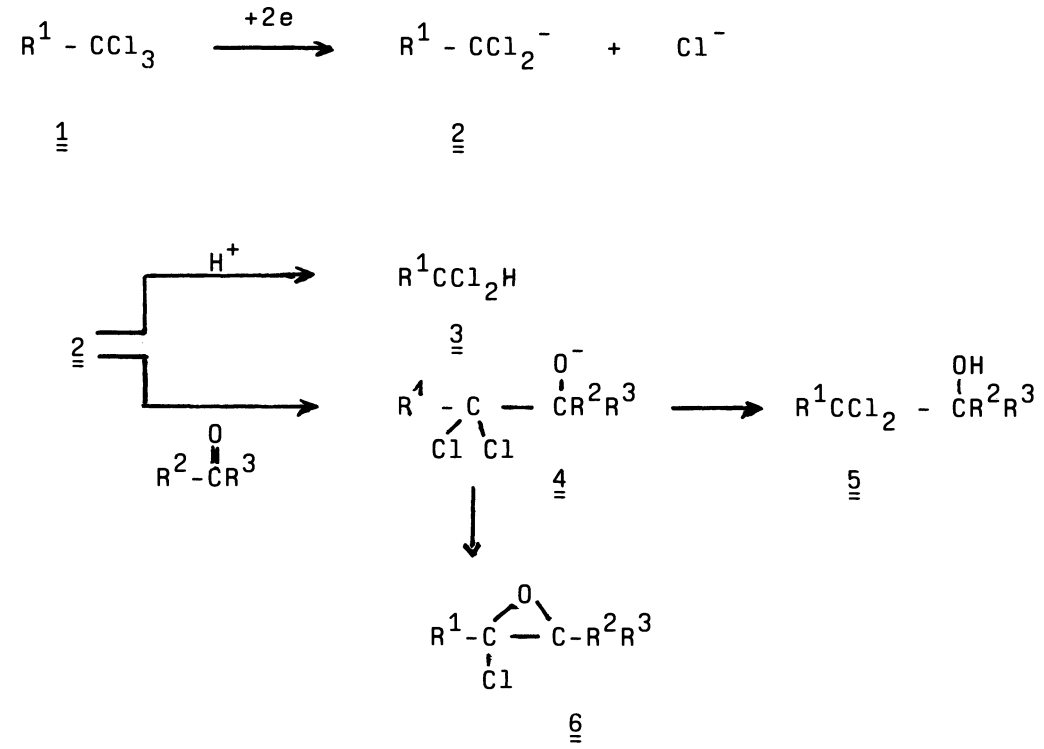

(1)

	R^1
a	Cl
b	CH_3
c	CO_2Et
d	C_6H_5

The electrochemical reduction of tetrachloromethane (**1a**) in the presence of carbonyl compounds produces trichloromethylcarbinols **5**[5a,b] and trichloroethane (**1b**) also forms analogous adducts in 19 to 34% yield.[6] The cathodic addition of ethyl trichloroacetate (**1c**) to cyclopentanone leads to a ring expansion to 2-chloro-2-(ethoxycarbonyl)cyclohexanone,[5a,6] this rearrangement points to 2-chlorooxirane **6** as intermediate. When **1c** is reduced in the presence of 2-methylpentanal 69% **6** (R^1=CO_2Et, R^2=H, R^3=$CH(CH_3)$-C_3H_7) can be isolated.[7] These results indicate, that the further reaction of **4** depends on R^1. For R^1=Cl, CH_3, **4** is not appreciably further converted. For R^1=CO_2Et an intramolecular nucleophilic substitution seems to be facilitated by the π-bond of the carbonyl group,[8] so that cyclization to **6** becomes the main reaction. To examine this assumption benzylidyne trichloride (**1d**) was reduced in the presence of carbonyl compounds. The addition of the benzyl anion **2d** should lead to **4d**, whose cyclization to **6d** should be favoured by the phenyl group.[8]

Results and Discussion

Cathodic Addition of Benzylidyne Trichloride (1d) to Ketones.[9] The reduction potential of **1d** was polarographically determined to be −0.8 V vs. Marple (−1.5 V vs. SCE). This is 0.5 V more cathodic than that of **1c**, which indicates that **2d** is more reactive than **2c** and therefore should add also to less reactive ketones. 5 to 10 mmol **1d** were electrolyzed at −0.8 V vs. Marple in the presence of 2 equiv of ketone until total conversion. After usual work up, the α,β-unsaturated ketones **7a—g** (Eq. 2) are isolated in good yields by LC (Table 1). Seen from the point of synthetic methodology, this reaction is a nucleophilic acylation with subsequent dehydration. Ketones are converted in this way to homologated enones.[10] The formation of **3d** at the expense of the wanted **7** is most probably due to protons of the anolyte passing the diaphragm. Addition of NaH to the anolyte and catholyte decreases the formation of **3d** and raises the yield to **7** significantly. The formation of the ketones **7** can be best explained with the 2-chlorooxirane **6d** as intermediate, which subsequently rearranges and eliminates HCl. The carbinol **5d** could be detected in 4% yield at the most. The exclusive cyclization of **4d** to **6d** is promoted besides by the phenyl group by the high nucleophilicity of the tertiary alcohol and the relief of its "back strain". Thermally or Lewis-acid catalyzed rearrangement of 2-halooxiranes to 2-halo ketones was accompanied mostly by migration of halogen. This can occur in a synchronous process via the transition state **8**[11] or via a α-keto carbenium ion **9**.[12] This means **6d** can be converted to **7** either via **8** or **9** and subsequent elimination of HCl (Eq. 3). A

Table 1. Cathodic Addition of Benzylidyne Trichloride (**1d**) to Ketones[a]

Ketone	Addition product **7**		Yield/%[b] **7**	Yield/%[b] **3d**
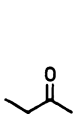	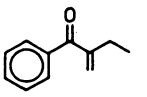	**a** (40)[c]	(48)	(40)
	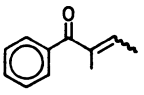	**b** (60)		
	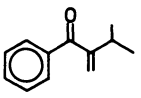	**c** (70)	59	16
	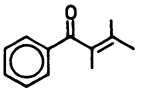	**d** (30)		
	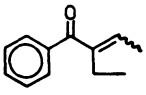	**e**	65 (34)	23 (59)
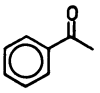	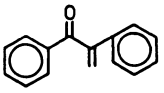	**f**	58 (28)	29 (56)
	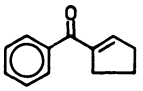	**g**	64 (38)	22 (58)

a) Reduction at −0.8 V vs. Marple-electrode in 0.5 mol dm^{-3} $LiClO_4$ in THF with addition of NaH. b) Isolated yields; numbers in parenthesis are yields without addition of NaH. c) Relative yields.

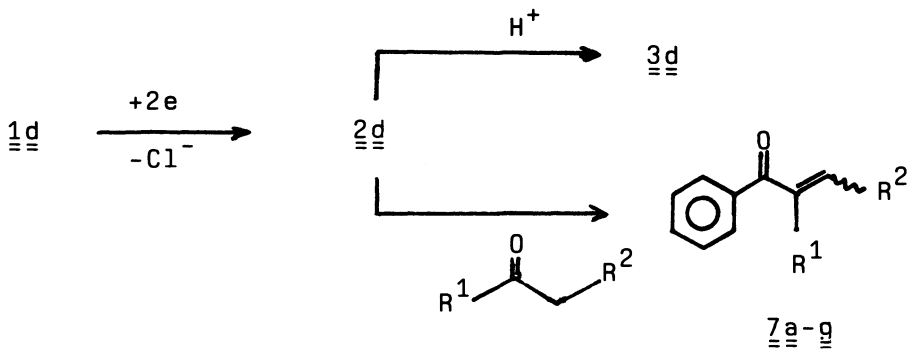

(2)

probe for the intermediacy of **9** should be the addition to norcamphor, where the intermediate 2-oxonorbornyl cation should lead to rearranged products. Reductive addition of **1d** to norcamphor produces the products **13**—**17**. Their formation supports the three equilibrating norbornyl cations **10**—**12** as intermediates (Eq. 4). A synchronous rearrangement of the

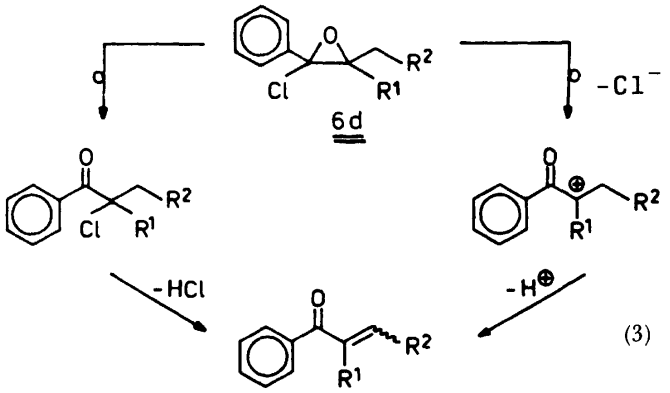

(3)

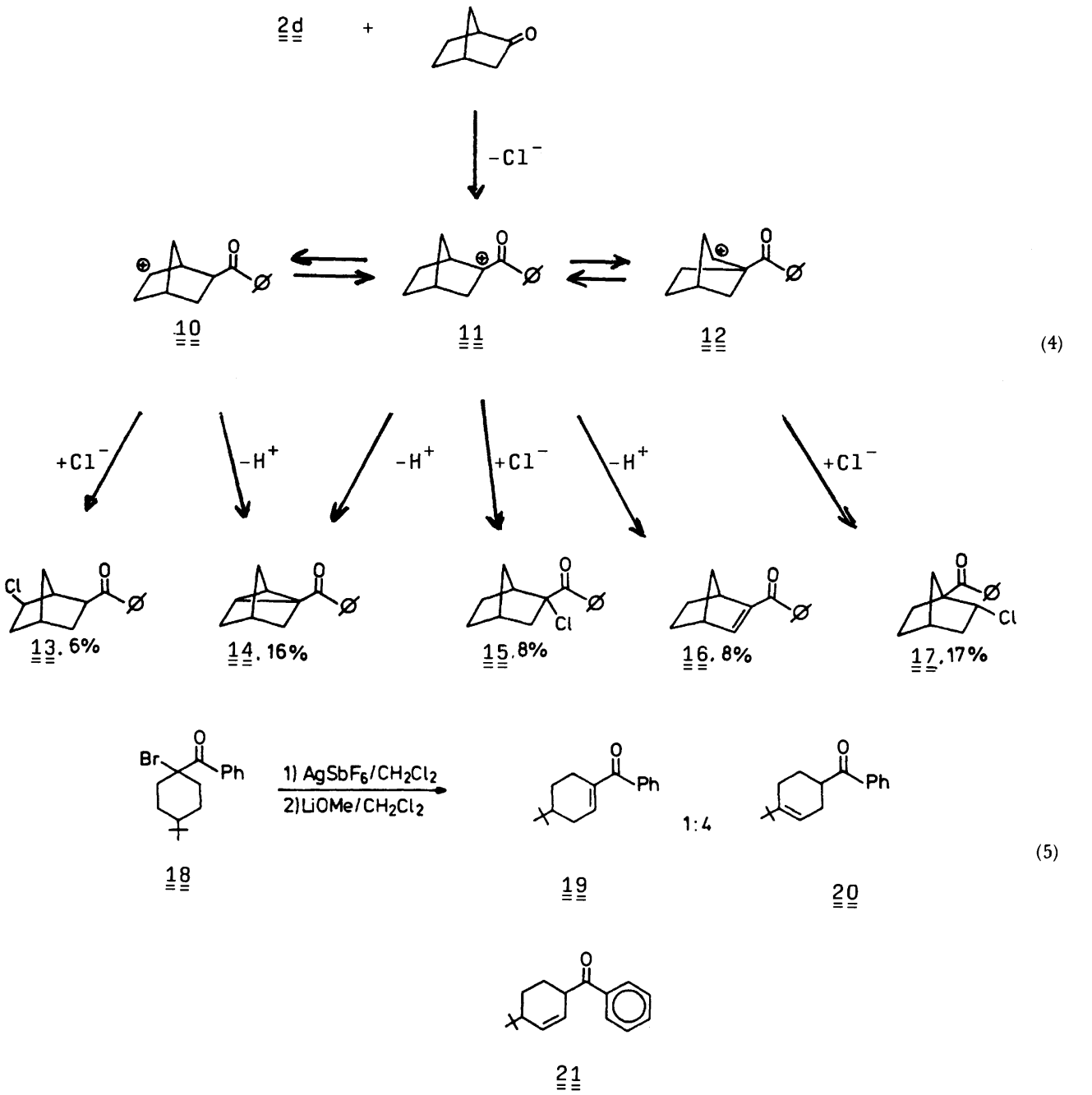

(4)

(5)

2-chlorooxirane should have led to **15** and **16** only. The intermediacy of the cations **10** to **12** is further supported by the acetolysis of *exo*-2-benzoyl-*endo*-2-norbornyl mesylate, where via an intermediate 2-benzoylnorbornyl cation acetates, corresponding to **13**, **14**, and **17**, are yielded.[13] A α-keto carbenium ion has been generated from **18** with $AgSbF_6$, its quenching with LiOMe leads to the ketones **19** and **20**.[14] The latter is formed by a transannular hydride shift, which converts the keto carbenium ion to a more stable tertiary carbocation (Eq. 5). Reductive addition of **1d** to 4-*t*-butylcyclohexanone formed, depending on the electrolyte, 21—36% **19**. Two minor products of about 5% yield were detected by GC/MS, whose structures are probably those of the isomers **20** and **21**. The different reaction behaviors could be attributed to the longer lifetime of the 2-keto carbenium ion in the first case, which favors the 1,4-hydride shift prior to deprotonation.

Structure Proofs: The MS spectra of all compounds exhibit besides the base peak *m/z* 105 ($C_6H_5CO^+$) intense M^+ ions. In the IR spectra the carbonyl group conjugated to a phenyl group and a double bond appears between 1660 and 1635 cm^{-1}. The chemical shifts of the olefinic protons in the ^1H NMR are found in the typical region of δ 5.45 to 6.65. The E/Z-isomers of **7b** were assigned using increments,[15] according to which the resonance of the olefinic proton in (*E*)-**7b** is found at higher δ-values. The ^1H NMR of **14** is due to the symmetry of the molecule and small coupling constants without much conclusiveness, but by its ^{13}C NMR the structure could be unambigously assigned. The chlorinated norbornyl compounds **13**, **15**, and **17** are isomers. Here the position of the chloro and the benzoyl substituent could be determined by ^1H NMR.

Cathodic Addition of 1d to α,β-Unsaturated Ketones. When **1d** is reduced as before in 0.1 mol dm^{-3} $LiClO_4$/DMF in the presence of methyl vinyl ketone, besides 8% **3d** the adducts **22** and **23** are isolated in the ratio 1:2 (Eq. 6). The low yields of adduct in spite of minor protonation of **2d** is possibly due to losses through extensive oligomer formation. **22** can be rationalized by 1,2-addition of **2d**, whilst **23** appears to be formed by 1,4-addition and subsequent cyclization. For the cathodic addition of **1c** to acrylonitrile or ethyl acrylate, the formation of analogous cyclopropane derivatives has been reported.[4] To decrease the 1,4-addition by steric shielding of the double bond **1d** was added to mesityl oxide. Although 2F(1F=96480C) mol^{-1} of charge had been passed, 20% of **1d** were recovered on work up, which indicated current consumption in a follow-up reduction of the product. The expected dienones **24**, **25** could be detected in only about 6% yield, main product with 30% was the enone **26** (44% by GLC). The 1,4-adduct **27** decreased to 6% as intended (Eq. 7). The enone **26** originates presumably from either **24**, **25**, or the chlorides **29**, **30**. They should be easily reducible at the applied potential to yield the carbanion **28**, which is protonated to **26** (Eq. 8).

Structure Proofs: For **23** the IR absorption of the carbonyl group at 1710 cm^{-1} and the base peak *m/z*=43 in the mass spectrum indicate the acetyl group. (*Z*)- and (*E*)-**23** can be distinguished by their ^1H NMR. The characteristic changes in the shifts for the E- and Z-isomer can be rationalized by the anisotropy effect of the phenyl ring. The correct

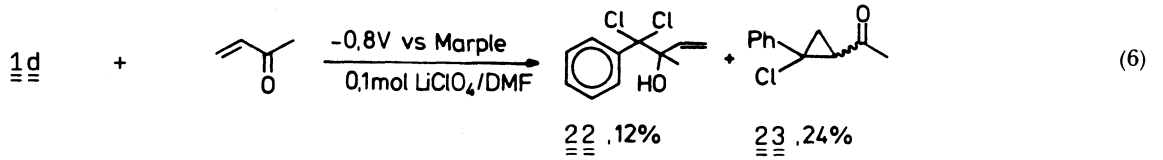

22 ,12% 23 ,24% (6)

24 25

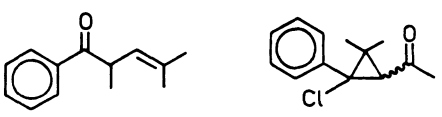

26 27 (7)

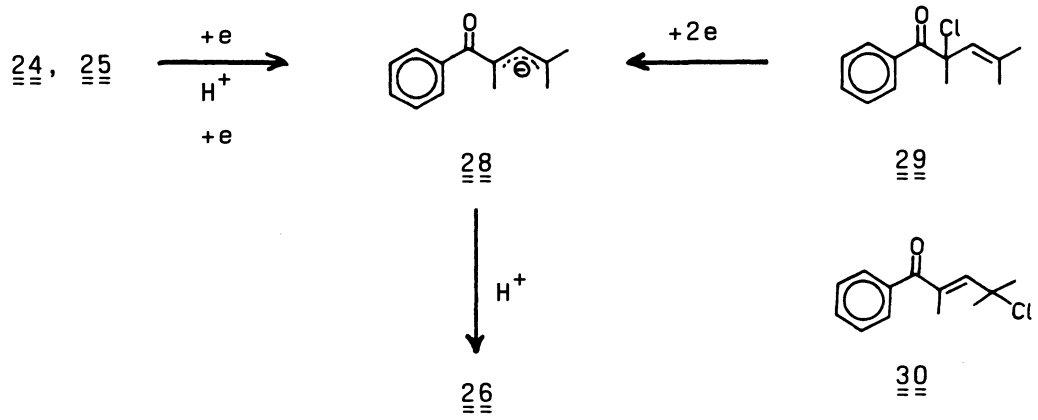

(8)

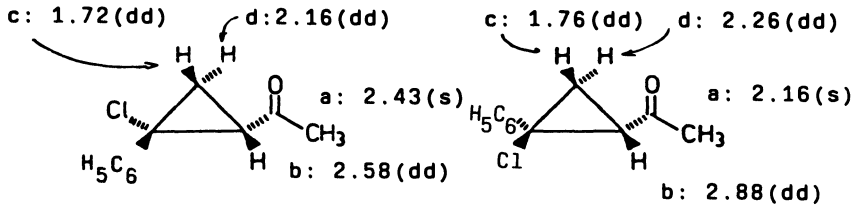

(*Z*)-**23** (*E*)-**23**

assignment was further checked by NOE. The IR spectrum of **26** with the carbonyl absorption at 1680 cm^{-1} indicates that the double bond is not conjugated with the benzoyl group. The assignment is supported by the appearance of two allylic methyl groups at δ 1.65 and 1.70 in the ^1H NMR.

Reductive Addition of 1d to Aldehydes. Reductive additions of **1d** to pentanal yielded the alcohol **31** and the chloro ketone **32** (Eq. 9). The suppressed formation of **3d** (9%) reflects the high reactivity of the aldehyde. The results further demonstrate that not only the π-system of the phenyl group,[8] but also "back strain" in **4** is necessary for the formation of the 2-chlorooxirane. It was therefore expected, that the addition to an α-branched aldehyde should lead to a higher portion of **6**. This proved indeed to be the case. Reduction of **1d** in the presence of 2-methylpentanal led besides a small amount of **3d** to the 2-chloro-oxirane **33** as a main product. Its structure was indicated by the mass spectrum and conversion to **34** and **35** (Eq. 10). Attempts to purify crude **33** by filtration over silica gel let to the α-chloro ketone **34** and the α-hydroxy ketone **35**. This conversion is not surprising, as 2-chlorooxiranes are easily hydrolyzed to mixtures of α-chloro and α-hydroxy ketones.[11b]

Structure Proofs: **31** shows in the mass spectrum the fragment ion m/z=160 from McLafferty-rearrangement. The other part of the molecule can be deduced from an α-cleavage to m/z=87. The structure of **32** is established from its carbonyl absorption at 1685 cm^{-1} in the IR, by the base peak of m/z=105 ($C_6H_5CO^+$) in the MS and the triplet for the chloromethine proton at δ 5.15 in the ^1H NMR. The ^1H NMR spectra for **34** and **35** are very similar. For **34** the chloromethine proton appears as doublet at δ 4.92, the hydroxymethine proton as multiplett between δ 4.87 and 5.16.

(9)

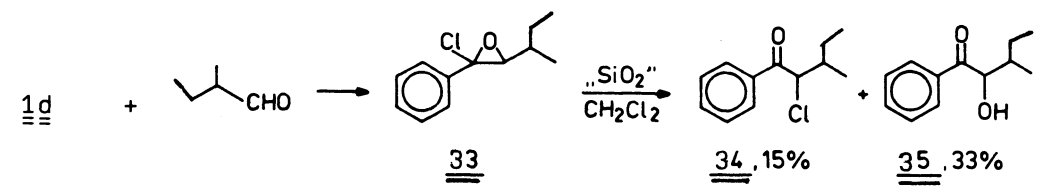

(10)

Experimental

IR spectra were obtained on Perkin-Elmer spectrometers 177 and 421. ^{1}H NMR spectra were recorded on a JEOL PMX 60, Varian HA 100 and Bruker WM 300. ^{13}C NMR spectra were measured on Bruker WH 90 and WM 300 spectrometers. Mass spectra were taken with the Varian instruments SM 1 and CH 7 at 70 eV ionization energy. Combined GC/MS-spectra were taken with the Varian instrument MAT 111. Elemental analyses were performed by M. Beller, Göttingen and on a Perkin-Elmer CHN-analyser. Gas chromatographic analyses were done with a Varian 1400 instrument, a Kipp & Zonen BD 7 recorder and the Minigrator Autolab of Spectra Physics. The following glass columns were used: 1.7 m, d=2 mm, 4% SE 30 on Chromosorb W, and 1.7 m, d=2 mm, 4% OV 225 on Chromosorb W. For TLC silica-gel plates 60 F 254 of Merck were used. HPLC was performed with a Waters 6000 A pump and an U6K injector together with a steel column (d=8 mm, l=50 cm) filled with LiChromosorb Si 60 (7 µm, Fa. Merck). For detection the Knauer differential refractometer type 51.78 coupled with a Abimed recorder Modell 300 was used. Eluent was in all cases CH_2Cl_2. Polarographic measurements were performed with the Bruker polarograph E 310, glass equipment and drop controller E 354 S from Metrohm and the Hewlett-Packard XY-recorder 7045 A; the following conditions were applied: drop time: 1 s, scan time: 10 mV s^{-1}, puls amphitude 50 mV. Preparative electrolyses at controlled potential were performed with the Wenking-potentiostat (3A/60 V). The electrolyses were operated in a double-walled glass cell (150 ml) with a Teflon stopper. Through this the anode compartment (glass tube with G4-frit), Luggin capillary, current feeder for the mercury pool cathode (d=4.5 cm) and nitrogen inlet were inserted. Reference electrode was the Marple electrode.[16] All electrolyses were conducted at 0 °C under nitrogen. The following electrolytes were used for polarography and preparative electrolyses: Electrolyte A: 0.2 mol dm^{-3} $LiClO_4$/DMF; electrolyte B, catholyte: 0.5 mol dm^{-3} $LiClO_4$/THF, 10 mg NaH, anolyte: 0.2 mol dm^{-3} $LiClO_4$/DMF, 10 mg NaH; electrolyte C: as B, but without NaH. For the work-up of the electrolyses, the catholyte was poured into the threefold amount of water, neutralized, extracted with ether (3×50 ml), the ether extracts were washed with water, dried ($MgSO_4$) and the ether was rotaevaporated. Benzene dried *N,N*-dimethylformamide (DMF) was stirred 24 h with P_2O_5, distilled at 18 Torr under nitrogen and stored over molecular sieve (4 Å).

Electrolysis of Benzylidyne Trichloride (1d) in Presence of 2-Butanone. 5 mmol (1.00 g) **1d** and 10 mmol (0.7 g) 2-butanone are electrolyzed in electrolyte A at −0.8 V vs. Marple until total conversion (10 mF). LC-separation of the crude product yielded 330 mg (2 mmol, 40%) **3d** and 390 mg (2.4 mmol, 48%) **7a, b**, which could be separated by analytical HPLC into **7a**, (*Z*)-**7b** and (*E*)-**7b**.

2-Ethyl-1-phenyl-2-propen-1-one (7a): Oil; IR and ^{1}H NMR spectra corresponded to those in the literature.[17]

(*Z*)-2-Methyl-1-phenyl-2-buten-1-one ((*Z*)-7b): Colorless oil; IR (neat 1655 (C=O) cm^{-1}; ^{1}H NMR (60 MHz, $CDCl_3$) δ=1.54 (d, 3H, ^4J=2 Hz), 1.95 (s, 3H, ^4J=1.5 Hz), 5.77 (q, 1H, ^4J=2 Hz), 7.15—8.05 (m, 5H); MS (70 eV) *m/z* (%) 160 (M$^+$; 32), 159 (28), 145 (38), 105 (100).

(*E*)-2-Methyl-1-phenyl-2-buten-1-one ((*E*)-7b): Oil; IR (neat) 1640 (C=O) cm^{-1}; ^{1}H NMR ($CDCl_3$) δ=1.87 (d, 3H), 1.97 (s, 3H), 6.41 (q, 1H), 7.34—7.8 (m, 5H). **7b** is reported as E/Z-mixture in lit.[18]

Electrolysis of 1d in Presence of 3-Methyl-2-butanone. 5 mmol **1d** and 10 mmol (0.86 g) 3-methyl-2-butanone are electrolyzed in electrolyte B under efficient stirring at −0.8 V vs. Marple until 10 mF had been consumed. The catholyte is poured into ice water controlling the pH between 6—7 and worked-up. HPLC of the crude product yielded 130 mg (0.8 mmol, 16%) **3d**, 350 mg (2 mmol, 41%) **7c** and 160 mg (0.9 mmol, 18%) **7d**.

2-Isopropyl-1-phenyl-2-propen-1-one (7c): Colorless oil; IR (neat) 1655 (C=O) cm^{-1}; ^{1}H NMR (60 MHz, $CDCl_3$) δ=1.15 (d, 6H), 2.70—3.30 (m, 1H), 5.45 (s, 1H), 5.70 (s, 1H), 7.2—7.9 (m, 5H); MS (70 eV) *m/z* (%) 174 (M$^+$; 15), 173 (22), 159 (20), 105 (100); Found: C, 82.55; H, 8.15%. Calcd for $C_{12}H_{14}O$ (174.24): C, 82.72; H, 8.09%.

2,3-Dimethyl-1-phenyl-2-buten-1-one (7d): Oil; IR and ^{1}H NMR spectra agree with those in lit.[19]

Electrolysis of 1d in Presence of 3-Pentanone. 5 mmol (1.0 g) **1d** and 10 mmol (0.84 g) 3-pentanone are electrolyzed in electrolyte B or C at −0.8 V vs. Marple until 10 mF are consumed. Work-up of the crude product (1.1 g) and preparative HPLC yielded 490 mg (59%) **3d** and 300 mg (34%) **7e** (electrolyte C) or 190 mg (23%) **3d** and 580 mg (65%) **7e** (electrolyte B). **7d** was a 2:1 E/Z-mixture.

2-Ethyl-1-phenyl-2-buten-1-one (7d): Colorless oil; IR (neat) 1645 (C=O) cm^{-1}; ^{1}H NMR (60 MHz, $CDCl_3$) δ=1.00 (t, 3H), 1.80 (d, 3H), 2.45 (q, 2H), 6.25 (q, 1H), 7.25—7.75 (m, 5H); MS (70 eV) *m/z* (%) 174 (M$^+$; 20), 173 (20), 145 (81), 105 (100); Found: C, 82.64; H, 8.12%. Calcd for $C_{12}H_{14}O$ (174.24): C, 82.72; H, 8.09%.

Electrolysis of 1d in Presence of Acetophenone: As described above 5 mmol (1.0 g) **1d** were reduced in presence of 10 mmol (1.2 g) acetophenone to yield after HPLC 450 mg (56%) **3d** and 290 mg (28%) **7f** (electrolyte A) or 230 mg (29%) **3d**, 600 mg (58%) **7f** (electrolyte B). To prevent polymer formation solvents were rotaevaporated at room temp. The IR and ^{1}H NMR data of **1,2-diphenyl-2-propen-1-one (7f)**, oil, correspond to those in lit.[20]

Electrolysis of 1d in Presence of Cyclopentanone: 5 mmol (1 g) **1d** and 10 mmol (0.85 g) cyclopentanone are electrolyzed as above to afford after HPLC 450 mg (56%) **3d** and 310 mg (36%) **7g** (electrolyte A) or 170 mg (22%) **3d** and 550 mg (64%) **7g** (electrolyte B).

1-Benzoyl-1-cyclopentene (7g): Oil; IR and ^{1}H NMR spectra agree with those reported in lit.[21]

Electrolysis of 1d in Presence of Norcamphor: 10 mmol (2.0 g) **1d** and 20 mmol (2.2 g) norcamphor are electrolyzed in electrolyte B as above until 20 mF were consumed. HPLC yielded in order of elution: 500 mg (31%) **3d**, 200 mg (8%) **15**, 140 mg (6%) **13**, 400 mg (17%) **17**, 150 mg (8%) **16** and 320 mg (16%) **14**.

2-Benzoyl-6-chlorobicyclo[2.2.1]heptane (13): Oil; IR (neat) 1655 (C=O) cm^{-1}; ^{1}H NMR (300 MHz, $CDCl_3$) δ=0.98—1.75 (m, 4H), 2.1—2.28 (m, 2H), 2.46—2.57 (m, 1H), 2.68—2.80 (m, 1H), 3.92—4.04 (m, 1H), 4.54—4.66 (m, 1H), 7.40—7.62 (m, 3H), 7.83—8.04 (m, 2H); MS (70 eV) *m/z* (%): 234 (M$^+$; 4), 198 (17), 105 (100); Anal. by high resolution MS: Found: *m/z* 234.0811. Calcd for $C_{14}H_{15}ClO$: M, 234.0811.

1-Benzoyltricyclo[2.2.1.0^{2,6}]heptane (14): Oil; IR (neat)

1655 (C=O) cm^{-1}; ^1H and ^{13}C NMR correspond to lit;[12] MS (70 eV) *m/z* (%) 198 (M^+; 55), 105 (100); Found: C, 84.60; H, 7.10%. Calcd for $C_{14}H_{14}O$ (198.28): C, 84.81; H, 7.11%.

2-Benzoyl-2-chloro-bicyclo[2.2.1]heptane (15): Oil; IR (neat) 1675 (C=O) cm^{-1}; ^1H NMR (300 MHz, $CDCl_3$) δ=1.05—1.20 (m, 2H), 1.42—1.56 (m, 3H), 2.08—2.20 (m, 1H), 2.20—2.29 (m, 1H), 2.37—2.45 (m, 1H), 2.74—2.83 (m, 1H), 3.00—3.06 (m, 1H), 7.40—7.58 (m, 3H), 8.11—8.18 (m, 2H); MS (70 eV) *m/z* (%) 234 (M^+; 4), 105 (100); Found: C, 71.79; H, 6.68; Cl, 14.92%. Calcd for $C_{14}H_{15}ClO$ (234.7): C, 71.64; H, 6.82; Cl, 15.10%.

2-Benzoylbicyclo[2.2.1]hept-2-ene (16): Oil; IR (neat) 1635 (C=C, C=O) cm^{-1}; ^1H NMR (60 MHz, $CDCl_3$) δ=1.0—2.1 (m, 6H), 3.0—3.25 (m, 1H), 3.40—3.65 (m, 1H), 6.65 (d, 1H), 7.3—7.6 (m, 3H), 7.6—7.8 (m, 2H); MS (70 eV) *m/z* (%) 198 (M^+; 20), 170 (51), 105 (100); Anal. by high resolution MS: Found: *m/z* 198.1041. Calcd for $C_{14}H_{14}O$: M, 198.1044.

1-Benzoyl-2-chlorobicyclo[2.2.1]heptane (17): Oil; IR (neat) 1658 (C=O) cm^{-1}; ^1H NMR (300 MHz, $CDCl_3$) δ=1.28—1.48 (m, 1H), 1.65—2.46 (m, 8H), 4.34—4.50 (m, 1H), 7.35—7.58 (m, 3H), 7.78—7.96 (m, 2H); MS (70 eV) *m/z* (%) 234 (M^+; 7), 105 (100); Found: C, 71.70; H, 6.49; Cl, 14.88%. Calcd for $C_{14}H_{15}ClO$ (234.7): C, 71.64; H, 6.82; Cl, 15.10%.

Electrolysis of 1d in Presence of 4-*t*-Butylcyclohexanone. 5 mmol (1.0 g) **1d** and 10 mmol (1.3 g) 4-*t*-butylcyclohexanone were electrolyzed as above until total conversion in electrolyte A or B. LC (silica gel) afforded 250 mg (21%) **19** in electrolyte A or 430 mg (36%) **19** in electrolyte B. GLC shows about 5% of two double bond isomers of **19** with similar MS spectra.

1-Benzoyl-4-*t*-butyl-1-cyclohexene (19): Oil; IR (neat) 1635 (C=O) cm^{-1}; ^1H NMR (300 MHz, $CDCl_3$) δ=0.92 (s, 9H), 1.15—1.40 (m, 2H), 1.95—2.10 (m, 2H), 2.18—2.38 (m, 2H), 2.65—2.75 (m, 1H), 6.55—6.65 (m, 1H), 7.35—7.55 (m, 3H), 7.60—7.67 (m, 2H); MS (70 eV) *m/z* (%) 242 (M^+; 32), 185 (30), 105 (100); Found: C, 84.00; H, 9.27%. Calcd for $C_{17}H_{22}O$ (242.4): C, 84.25; H, 9.15%.

Electrolysis of 1d in Presence of Methyl Vinyl Ketone. 5 mmol (1.0 g) **1d** and 10 mmol (0.7 g) methyl vinyl ketone are electrolyzed in electrolyte A. Considerable loss of product (40%) during column filtration indicates polymer formation. HPLC yields 80 mg (10%) **3d**, 140 mg (12%) **22**, 80 mg (8%) (*E*)-**23** and 150 mg (16%) (*Z*)-**23**.

1,1-Dichloro-2-methyl-1-phenyl-3-buten-2-ol (22): Oil; IR (neat) 3500 (OH), 1635 (C=C), 995, 935 (C=CH_2) cm^{-1}; ^1H NMR (60 MHz, $CDCl_3$) δ=1.46 (s, 3H), 2.4 (s, 1H), 5.15—5.45 (m, 2H), 6.15 (dd, 1H), 7.20—7.90 (m, 5H); MS (70 eV) *m/z* (%) 159 ($M^+-C_4H_7O$; 8), 71 ($C_4H_7O^+$; 100); Found: C, 57.31; H, 5.51; Cl, 30.13%. Calcd for $C_{11}H_{12}Cl_2O$ (231.1): C, 57.17; H, 5.23; Cl, 30.68%.

1-Acetyl-2-chloro-2-phenylcyclopropane (23): Oil; IR (neat) 3060, 3030 (CH), 1710 (C=O) cm^{-1}; ^1H NMR (*E*-isomer, 300 MHz, $CDCl_3$) δ=1.76 (dd, 1H, *J*=6.3 Hz, *J*=8.5 Hz), 2.16 (s, 3H), 2.26 (dd, 1H, *J*=6.3 Hz, *J*=7.5 Hz), 2.88 (dd, 1H, *J*=7.5 Hz, 8.4 Hz), 7.24—7.40 (m, 5H); ^1H NMR (*Z*-isomer, 300 MHz, $CDCl_3$) δ=1.72 (dd, 1H, *J*=6.5 Hz, 8.6 Hz), 2.16 (dd, 1H, *J*=6.5 Hz, 7.5 Hz), 2.43 (s, 3H), 2.58 (dd, 1H, *J*=7.5 Hz, 8.6 Hz), 7.28—7.50 (m, 5H); MS (70 eV) *m/z* (%) 194 (M^+; 1), 159 (55), 43 (100); Found: C, 68.24; H, 5.76; Cl, 18.77%. Calcd for $C_{11}H_{11}ClO$ (194.7): C, 67.86; H, 5.70; Cl, 18.21%.

Electrolysis of 1d in Presence of 4-Methyl-3-penten-2-one. 7.5 mmol (1.5 g) **1d** and 15 mmol 4-methyl-3-penten-2-one are electrolyzed in electrolyte A until 15 mF are consumed. HPLC yielded 400 mg **1d** and **3d**, 528 mg (44%) **26** and 152 mg of a 1:1:1-mixture of **24**, **25**, **27**.

2,4-Dimethyl-1-phenyl-3-penten-1-one (26): Oil; IR (neat) 1680 (C=O) cm^{-1}; ^1H NMR spectrum corresponds to that reported in lit.[22]

4-Methyl-2-methylene-1-phenyl-3-penten-1-one (24): MS (70 eV) *m/z* (%) 186 (M^+; 23), 185 (20), 105 (100).

2,4-Dimethyl-1-phenyl-2,4-pentadien-1-one (25): MS (70 eV) *m/z* (%) 186 (M^+; 23), 185 (50), 171 (100), 105 (81).

1-Acetyl-2-chloro-3,3-dimethyl-2-phenylcyclopropane (27): MS (70 eV) *m/z* (%) 186 (M^+-HCl; 31), 179 (65), 43 (100).

Electrolysis of 1d in Presence of Pentanal. 10 mmol (2.0 g) **1d** are electrolyzed in presence of 20 mmol (1.72 g) pentanal. HPLC of the crude product (1.63 g) led to 140 mg (8.5%) **3d**, 480 mg (23%) **32** and 600 mg (24%) **31**.

1,1-Dichloro-1-phenyl-2-hexanol (31): Oil; IR (neat) 3400 (OH) cm^{-1}; ^1H NMR (300 MHz, $CDCl_3$) δ=0.84 (t, 3H), 1.16—1.44 (m, 4H), 1.44—1.66 (m, 2H), 4.10 (dd, 1H), 7.32—7.80 (m, 5H); MS (70 eV) *m/z* 210 (M^+-HCl; 5); **31** (+TMS−H) MS (70 eV) *m/z* (%) 303 (M^+-15; 1); Anal. by high resolution MS, Found: *m/z* 303.0739. Calcd for $C_{15}H_{24}Cl_2OSi$: $M-CH_3$ 303.0739.

2-Chloro-1-phenyl-1-pentanone (32): Oil; IR (neat) 1685 (C=O) cm^{-1}; ^1H NMR (60 MHz, $CDCl_3$) δ=0.93 (t, 3H), 1.28—1.67 (m, 4H), 1.83—2.30 (m, 2H), 5.15 (t, 1H), 7.28—8.20 (m, 5H); MS (70 eV) *m/z* (%) 210 (M^+; 3), 105 (100); Found: C, 68.49; H, 7.21; Cl, 16.97%. Calcd for $C_{12}H_{15}ClO$ (210.7): C, 68.40; H, 7.18; Cl, 16.82%.

Electrolysis of 1d in Presence of 2-Methylpropanal. 10 mmol (2.0 g) **1d** and 20 mmol (1.4 g) isobutyraldehyde were electrolyzed until conversion. GLC shows besides a small amount of **3d** about 60% **33**, attempted purification of **33** by filtration over silica converts it into **34** and **35**. HPLC afforded 130 mg (8%) **3d**, 290 mg (15%) **34**, and 590 mg (33%) **35**.

2-Chloro-3-methyl-1-phenyl-1-butanone (34): Oil; IR and ^1H NMR spectra agree with those in lit.[23] Found: C, 67.31; H, 6.64; Cl, 18.18%. Calcd for $C_{11}H_{13}OCl$ (196.7): C, 67.18; H, 6.66; Cl, 18.03%.

2-Hydroxy-3-methyl-1-phenyl-1-butanone (35): Oil; IR (neat) 3450 (OH), 1675 (C=O) cm^{-1}; ^1H NMR spectrum agreed with this in lit.[24]

1-Chloro-2-isopropyl-1-phenyloxirane (33): MS (70 eV) *m/z* (%) 196 (M^+; 3), 124 ($M^+-C_4H_8O$; 40), 105 (100).

We thank the Arbeitsgemeinschaft Industrieller Forschungsvereinigungen e.V. and the Fonds der Chemischen Industrie for financial support, H. Luftmann for interpretation of the mass spectra and H. Rennefeld for technical assistance.

References

1) Electroorganic synthesis, 36; Part 35: R. Michaelis, U. Müller, and H. J. Schäfer, *Angew. Chem., Int. Ed. Engl.*, **26**, 1023 (1987).

2) J. Casanova and L. Eberson, "Chemistry of the Carbon-Halogen Bond," ed by S. Patai, Interscience, New York (1974), Chapt. 15.

3) M. Nagao, N. Sato, T. Akashi, and T. Yoshida, *J. Am. Chem. Soc.*, **88**, 3447 (1966).

4) M. M. Baizer and J. L. Chruma, *J. Org. Chem.*, **37**, 1951 (1972).

5) a) F. Karrenbrock and H. J. Schäfer, *Tetrahedron Lett.*, **1978**, 1521; b) T. Shono, N. Kise, and T. Suzumoto, *J. Am. Chem. Soc.*, **106**, 259 (1984); T. Shono, N. Kise, M. Masuda, and T. Suzumoto, *J. Org. Chem.*, **50**, 2527 (1985). c) F. Karrenbrock, H. J. Schäfer, and I. Langer, *Tetrahedron Lett.*, **1979**, 2915; J. M. van Tilborg and C. J. Smit, *Recl. Trav. Chim. Pays-Bas*, **99**, 202 (1980).

6) M. Steiniger, Masters thesis, Universität Münster 1980.

7) M. Steiniger, Ph. D. Thesis, Universität Münster, 1984.

8) R. W. Alder, R. Baker, and J. M. Brown, "Mechanism in Organic Chemistry," Wiley (1971), p. 198.

9) Preliminary Communication: M. Steiniger and H. J. Schäfer, *Angew. Chem., Int. Ed. Engl.*, **21**, 79 (1982); *Angew. Chem. Suppl.*, **1982**, 137.

10) For other procedures effecting this conversion see D. F. Taber and B. P. Gunn, *J. Org. Chem.*, **44**, 450 (1978) and there Ref. 1.

11) a) A. Kirrmann, P. Duhamel, and R. Nouri-Bimorghi, *Bull. Soc. Chim. Fr.*, **1964**, 3264; *Justus Liebigs Ann. Chem.*, **691**, 33 (1966); b) A. Kirrmann and R. Nouri-Bimorghi, *Bull. Soc. Chim. Fr.*, **1968**, 3213.

12) R. N. McDonald, "Mechanisms of Molecular Migrations," Wiley, New York (1971); Vol. 3, p. 67; R. N. McDonald and Th. E. Tabor, *J. Am. Chem. Soc.*, **89**, 6573 (1967); J. P. Begue and M. Charpentier-Morize, *Acc. Chem. Res.*, **13**, 207 (1980).

13) X. Creary and C. C. Geiger, *J. Am. Chem. Soc.*, **104**, 4151 (1982).

14) J. P. Begue, M. Charpentier-Morize, and C. Pardo, *Tetrahedron*, **31**, 1919 (1975).

15) U. E. Matter, C. Pascual, E. Pretsch, A. Pross, W. Simon, and S. Sternhell, *Tetrahedron*, **25**, 691 (1969).

16) L. W. Marple, *Anal. Chem.*, **39**, 844 (1967).

17) H. O. House, W. C. McDonald, R. F. Sieloff, and D. Vanderweer, *J. Org. Chem.*, **43**, 4316 (1978).

18) G. Dana, Sa le Thi Thuan, and J. Gharbi Benarous, *Bull. Soc. Chim. Fr.*, **1974**, 2089.

19) L. E. Friedrich and R. A. Fiato, *J. Am. Chem. Soc.*, **96**, 5783 (1974).

20) L. E. Friedrich and R. A. Fiato, *J. Org. Chem.*, **39**, 416 (1974).

21) A. B. Smith III and W. C. Ajosta, *J. Am. Chem. Soc.*, **95**, 4313 (1973).

22) A. J. A. van der Weerdt and H. Certontain, *J. Chem. Soc., Perkin Trans. 2*, **1980**, 592.

23) G. A. Russell, B. Mudryk, M. Jawdosink, and Z. Wrobel, *J. Org. Chem.*, **47**, 1879 (1982).

24) S. Hünig and G. Wehner, *Chem. Ber.*, **112**, 2062 (1979).

 © 1988 The Chemical Society of Japan Bull. Chem. Soc. Jpn., 61, 133—139 (1988)

Invited Paper

Use of Monoclonal Antibodies in the Study of the Conformation and Conformational Alterations in Proteins

Ephraim KATCHALSKI-KATZIR* and Dan KENETT
Department of Biotechnology, Faculty of Life Science, Tel-Aviv University, Tel Aviv, Israel, and Department of Biophysics, Weizmann Institute of Science, Rehovot, Israel
(Received August 7, 1987)

The conformational flexibility of many of the native proteins facilitates their attainment of new reversible three-dimensional structures under well-specified conditions. Such structures appear to be of great importance in biological processes involving biologically active proteins, such as enzymes, receptors or protein hormones. Recently it was shown that the above conformational alterations can be followed not only by physicochemical methods but also immunochemically by the use of monoclonal antibodies (mAbs). mAbs are specific proteins, each capable of recognizing a corresponding well-characterized region (epitope) on the surface of a protein antigen. They are thus useful as tools in the study of the structure and properties of protein surfaces. Of particular interest is the fact that it is possible to prepare mAbs with predetermined specificities towards the different epitopes of a given protein. Such mAbs can thus be used to detect conformational alterations occurring at the different segments of a protein antigen. In the present review article we describe our own work and that of others on the use of mAbs as probes to detect the conformation and conformational alterations occurring in proteins exposed to different conditions, such as heat, adsorption onto solid surfaces, interaction with ligands and protein-protein interaction. The use of mAbs in the detection of protein folding intermediates is also described.

Powerful X-ray diffraction techniques developed for protein analysis have made it possible to elucidate the three-dimensional structure of approximately 300 proteins to date. In all of them it was noticed that the bending of the polypeptide backbone, leading to the formation of α-helices, β-pleated sheets and characteristic loops, brings about contact between amino acid residues located originally at relatively large distances from one another along the peptide chain. Because of the tertiary structure thus obtained, native protein molecules possess a characteristic "topography" when surveyed from the outside and a characteristic core when surveyed from the inside. The characteristic three-dimensional structure of a native protein seems to be derived from the primary amino acid sequence of the protein, since polypeptides possessing this primary sequence can coil, under appropriate conditions, into the native three-dimensional structure. Exposure of proteins to extreme conditions (high temperatures, extreme pH values or denaturating agents) is usually accompanied by disruption of the three-dimensional structure characterizing the native protein. The resulting denatured proteins possess physical, chemical, and biological properties which differ markedly from those of the native protein. Recently accumulated evidence shows that the three-dimensional structure of proteins is not rigid, but undergoes subtle reversible conformational fluctuations. Flexibility of amino acid side chains, mobility of peptide segments, and movement of structural domains as rigid bodies, have been demonstrated.[1] Physical methods (X-ray or neutron diffraction, NMR, fluorescence spectroscopy, hydrogen-deuterium exchange) have proved particularly useful in the determination of the amplitudes, time spans, and energies involved in these conformational oscillations. The conformational flexibility of many of the native proteins facilitates their acquisition of new reversible three-dimensional structures under well-specified conditions. Such structures seem to be of great importance in biological processes involving biologically active proteins, such as enzymes, receptors or protein hormones in which the conformational alterations in solution can be readily followed, not only by physicochemical methods but also immunochemically by the use of monoclonal antibodies (mAbs).

In the present review we describe the work of ourselves and others on the use of mAbs as probes to detect the conformation and conformational alterations occurring in proteins exposed to different conditions (heat, adsorption onto solid surfaces, interaction with ligands, protein-protein interaction). The use of mAbs in the detection of protein folding intermediates is also described.

Monoclonal Antibodies as Conformational Probes

The cell hybridization technique developed by Köhler and Milstein[2] enables the preparation of murine monoclonal antibodies (mAbs) capable of recognizing corresponding single well-characterized regions (epitopes) on the surface of the protein antigens used to elicit the immunological response. It thus seems that mAbs might serve as useful tools in the study of the structure and properties of protein surfaces. All antigenic determinants of proteins appear to be topographical, i.e., composed of

structures on the protein surface which may be contained within a single segment of the amino acid sequence or assembled from residues far apart in the amino acid sequence but brought together on the surface by the folding of the protein in its native conformation.[3] It is thus pertinent to note that mAbs are not only directed towards corresponding amino acid residues of the antigen, but seem also to recognize well-defined conformations of protein segments. Any alteration in the conformation of such a segment is usually accompanied by a marked change in the characteristic binding of the mAb with its protein antigen. It is obvious, however, that the use of mAbs as conformational probes of proteins will be reliable only if general information is available as to the antigenic determinant recognized by the mAb, and if no conformational alterations are induced in the antigen as a result of its interaction with the mAb.

The three-dimensional structure of an antigen-antibody complex was recently determined for the first time by X-ray crystallography using hen egg white lysozyme (HEL) and the Fab fragment of a mAb (D1.3) at a resolution of 2.8 Å.[4] The antigenic determinant was shown to be topographic, with the interface between antigen and antibody extending over an area having maximum dimensions of 30×20 Å. Complex formation with the mAb D1.3 did not produce any significant distortion in the structure of the lysozyme. This was also confirmed by the simultaneous binding of two different mAbs to the lysozyme[5] and the retention of enzymatic activity by the HEL-mAb D1.3 complex.[6] It is worth noting that mAbs towards different enzymes have been obtained which do not affect their catalytic activity.[7]

The three-dimensional structure of the HEL-D1.3 Fab complex suggests that the interaction between the enzyme and the mAb can be described by a "lock and key" model, in which complex formation is essentially an association between two rigid molecules. An absence of marked conformational changes (>2 Å) upon complex formation is, in fact, characteristic of nearly all protein-protein complexes studied to date at high resolution, in which the structure of the unbound form of at least one of the component proteins is also known. These complexes include bovine trypsin–pancreatic trypsin inhibitor;[8] porcine kallikrein A–bovine pancreatic trypsin inhibitor,[9] and carboxypeptidase A–potato inhibitor.[10]

The three-dimensional structure of another enzyme antibody complex, that formed between neuraminidase and a corresponding mAb, was recently elucidated by X-ray crystallography.[11] Unlike in the case of HEL mAb D1.3 Fab, the specific interaction was accompanied here by significant conformational changes in both the antigen and antibody. Conformational changes in proteins as a result of interaction with their corresponding antibodies have also been reported by others.[12] It is reasonable to assume that such changes occur in a region of the protein characterized by significant flexibility. If this is the case, one might explain the observed conformational alterations by assuming an "induced fit mechanism," whereby the antigen and/or the antibody achieve greater complementarity by undergoing conformational changes.

It is still too early to predict, on theoretical grounds, when the interaction between a protein antigen and its corresponding mAb proceeds according to the lock and key mechanism, and when it favors the induced fit mechanism. It is obvious, however, that determination of the parameters characterizing the binding of a protein antigen with its mAb in solution should supply valuable information on the conformational characteristics of the interacting protein antigen epitopes.

Recognition of the region of interaction of a protein antigen with a given mAb is necessary if the conformational alterations occurring under various conditions in that region are to be detected. Antigenic determinats can be delineated by means of a physical approach using X-ray diffraction methods as illustrated above, or by an immunochemical approach in which direct or competitive assays are used to determine the reactivity of the mAb with isoenzymes or natural variants, and with natural or synthetic fragments of the target proteins. It has recently become clear that antibodies against most regions of a protein can be induced by immunization with short synthetic peptides. This has permitted the generation of mAbs with predetermined specificity[13] which constitute excellent tools for probing surface conformations of proteins at precise locations.

Detection of Conformational Changes Induced by Ligands

The activity of many enzymes, and particularly of allosteric enzymes, is drastically modified by the binding of coenzymes, ligands, modulators, cofactors or inhibitors. Coenzymes are involved in many transfer reactions and may act by changing the molecular dynamics of specific biocatalysts.

Conformational alterations resulting from the binding of the β_2-subunit of *Escherichia coli* tryptophan synthase with its ligands were detected and analyzed by Djavadi-Ohaniance et al.[14] using mAbs as specific probes. Five mAbs recognizing five different epitopes of the β_2-subunit of *E. coli* tryptophan synthase were prepared and their apparent binding constants with the enzyme subunit determined in solution. Fixation of the coenzyme pyridoxal 5-phosphate and the substrate L-serine by the β_2-subunit modified the affinity constants of most of the mAbs for the enzyme, thus demonstrating the existence of extended conformational rearrangements of the

protein. Association of the α-subunit with the β_2-subunit, brought about an increase of the tryptophan synthase activity and abolished the serine deaminase activity of β_2; this was accompanied by important conformational changes readily detected with appropriate mAbs. The above changes are not limited to a small region near the ligand binding site of the protein but rather affect an extended area of the protein surface, as shown by the observation that each ligand modifies the association constant of at least four mAbs recognizing distinct and non-overlapping epitopes.

Conformational transitions induced by the binding of metal ions to specific sites of proteins have been monitored by various physicochemical methods. These transitions can also be localized by immunochemical methods. Specific mAbs directed against the calcium-stabilized structure of human prothrombin have been prepared and characterized by Lewis et al.[15] One of the mAbs was found to bind with prothrombin only in the presence of $CaCl_2$. It did not interact with abnormal prothrombin lacking the γ-carboxy-glutamate residues known to interact with metal ions. Replacement of the calcium cation by Mn^{2+}, Mg^{2+}, and Co^{2+} promoted binding. The conformational transitions in prothrombin occurring as a result of the metal binding have been monitored using circular dichroism and fluorescence techniques.[16,17] The above findings were corroborated by the earlier studies of Tai et al.[18] who used polyclonal antibodies in their immunochemical studies. Antigenic differences could be detected in bovine prothrombin in the presence or absence of Ca^{2+} with antibodies raised in rabbits and fractionated by affinity chromatography.

The value of mAbs as conformational probes is further illustrated by their use in the detection of the calcium-induced conformational change(s) in a C-reactive protein (a protein appearing in the serum in the acute phase of certain infections). Three out of four mAbs against C-reactive protein bind to the protein antigen in the presence of Ca^{2+}, but not in the presence of EDTA, indicating that the conformation of the antigenic determinant recognized by these mAbs is calcium-dependent. The Ca^{2+}-independent binding of the fourth mAb, however, suggests that the conformation of the epitope recognized by this mAb is independent of bound calcium.

Monoclonal antibodies possessing similar binding characteristics to those described above, and directed towards the various domains of protein C have been recently described by Wakabayashi et al.[19] The three mAbs which react with protein C only in the presence of Ca^{2+} were found to bind to the light chain of protein C, i.e. the chain possessing γ-carboxy-glutamic acid residues. Other mAbs which recognize the conformation of a protein in a medium devoid of Ca^{2+}, but not that in a medium containing Ca^{2+}, have been described by Dixit et al.,[20] who prepared and studied the characteristic of two such mAbs directed against thrombospondin.

The induction of different calcineurin conformations by metal ions could also be demonstrated by suitable mAbs.[21] The experimental data showed that the active conformational states of calcineurin are metal-ion-dependent, that the mAb VA_I affects the Ni^{2+}-induced conformational change of the enzyme, and that the β-subunit of calcineurin plays a critical role in the expression of Ni^{2+}-stimulated phosphatase activity. Conformational changes induced in myosin by Ca^{2+} could also be detected with appropriate mAbs. Particularly useful in the studies of Shimizu et al.[22] was a mAb capable of detecting conformational alteration in the light chain of myosin LC2.

Three mAbs that interact with carboxypeptidase-A with relatively high binding constants but without affecting the enzyme activity, were used in our laboratory[23] for the detection of subtle conformational alterations occurring in the enzyme molecule when exposed to various conditions. Of particular interest was the finding that the three mAbs can detect subtle reversible conformational alterations occurring on removal of zinc from the active site of the enzyme by 1,10-phenanthroline. Reconstitution of the enzymatic activity by addition of zinc to the apoenzyme led to full recovery of the antigenic characteristics of carboxypeptidase-A recognized by the three mAbs.

Use of Monoclonal Antibodies in the Detection of Protein Folding Intermediates

The "translation" of the amino acid sequence of a newly synthesized polypeptide chain into the well-ordered "native" three-dimensional structure of a functional protein is commonly referred to as "protein folding." This was clearly illustrated by the classical experiment of Anfinsen et al.[24] who demonstrated that reduced and urea-denatured pancreatic ribonuclease readily undergoes renaturation in an oxygen containing solution on removal of the denaturing agent. It should be pointed out, however, that the detailed mechanism involved in molecular renaturation and denaturing is still only poorly understood, though obviously of great interest to the molecular biologist. Up to quite recently the conformational processes occurring during renaturation or denaturation were studied mainly from a theoretical point of view as very few experimental techniques were available to tackle the problem. Rapid developments in the various physical methods, particularly X-ray and NMR, as well as the recently developed capacity for substituting different amino acid residues in proteins by site directed mutagenesis, have opened up new possibilities for the experimental study of the

process and the intermediate conformers appearing during protein renaturation and denaturation. Protein folding seems to proceed through a series of structural intermediates from short stretches of local, barely stable, secondary structures to compact "domains" that interact to yield the final tertiary structure. At each step on this pathway, the structural intermediates appear to undergo conformational rearrangements. In these protein folding studies mAbs can contribute as probes for detection of the early intermediates. The potential usefulness of mAbs in this connection was illustrated by the pioneer work of Blond and Goldberg[25] on the β_2 subunit of *E. coli* tryptophan synthase. Two mAbs were directed against the native β_2-subunit of the enzyme, and their association with either the intact β_2-subunit or its isolated domains was investigated using fluorescence energy transfer between the tryptophan residues of the antibodies and a dansyl group covalently linked to the antigen. Denaturation of the β_2-subunit was induced by a concentrated guanidine hydrochloride solution, and renaturation initiated by extremely rapid dilution of the denaturating agent. Association of both mAbs with the antigen occurred within a few seconds of intitiating the renaturation, while complete refolding of the β_2 subunit required several minutes. It was concluded that immunoreactive intermediates appear to be formed at an early stage of the folding process.

The β_2-subunit of *E. coli* tryptophan synthase is composed of two independently folding domains; F_1 (N-terminal) and F_2 (C-terminal) which can be isolated following mild proteolytic treatment of β_2 by trypsin. The effects of domain assembly on the conformations of the F_1 and F_2 domains were analyzed using six mAbs which recognize six different epitopes of the native β_2-subunit.[26] It was found that the association of the F_1 and F_2 domains within β_2 is accompanied by structural changes within the two domains, as detected by variations in their affinity constants for the mAbs.

The building of the quaternary structure of proteins composed of several protein subunits is often accompanied by corresponding subtle conformational changes in each of the subunits. Monoclonal antibodies can be used here to detect suspected conformational alterations. Such alterations have been observed, for example, in the case of glutamine synthetase, an enzyme composed of 12 identical subunits. Some of the mAbs prepared against this enzyme[27] were found to bind only to the monomeric form, whereas others recognize the full dodecameric form.

An interesting use of mAbs is in the detection of the assembly of mouse muscle acetylcholine receptors in vivo.[28] The receptor consists of α, β, γ, and δ subunits. With the aid of the mAbs prepared, one α-subunit species that may be an assembly intermediate has been identified.

Detection of Conformational Changes Induced by Heat and Absorption onto Solid Supports

The susceptibility of the tertiary structure of proteins to heat, to denaturants such as urea and guanidine hydrochloride, and to extreme pH value, is well-known. Such conformational alterations have been readily detected by means of polyclonal antibodies directed either to the native or to the denatured corresponding protein antigen. There is also considerable evidence that the binding of proteins to plastic surfaces, or to other organic or inorganic surfaces, may cause partial denaturation and lead to changes in protein conformation and antigenicity.[29–33] One might even predict that the specific environment to which enzymes, receptors and other biologically active proteins are exposed when embedded in native membranes could affect their conformation. Milne et al.[34] have recently demonstrated that mAbs can also be used to distinguish between the lipid dependent and reversible conformational states of human apolipoprotein B.

Vaidya et al.[32] reported marked modifications in the antigenic behavior of creatine kinase (CK) and lactate dehydrogenase (LDH) after their adsorption onto polystyrene plates, as revealed by their corresponding mAbs. Hybridomas producing anti-CK and anti-LDH antibodies were screened by an enzyme-linked immunosorbent assay (ELISA) with antigen coated onto plastic wells. Of seven antibodies that were positive for each isoenzyme of CK, four failed to bind to the native enzyme in solution. Moreover, none of the mAbs prepared against the various LDH isoenzymes, interacted with the corresponding enzyme in solution. These results strongly support the suggestion made that the conformation of protein-antigen in the solid phase may differ from that in solution. Observations similar to those of Vaidya et al.[32] were recorded in our own laboratory where it has been found that the mAb MF 30 against human lactate dehydrogenase isoenzyme 5 (HLDH5) was found to interact with HLDH5 adsorbed onto the polystyrene microtiter plate, but not with the enzyme in solution.[35] In contrast, mAb 2/66 prepared against porcine lactate dehydrogenase 5 (PLDH5) reacted equally well with HLDH5, when in solution and when adsorbed onto polystyrene. Following its denaturation by heating to 70 °C HLDH5 no longer reacted with mAb 2/66. The findings obtained are summarized in Table 1. Our data obtained suggest that the mAbs MF30 and 2/66 recognize two different antigenic sites of HLDH5. The antigenic site which is recognized by 2/66, and is present in the native enzyme both in solution and when adsorbed onto polystyrene, disappears on heating. The other antigenic determinant is recognized by mAb MF30 when the enzyme is adsorbed onto a polystyrene surface both before and after heat treatment.

Table 1. Qualitative Description of the Binding of the mAbs 2/66 and MF30 with Native and Heat Treated Human or Porcine Lactate Dehydrogenase Isoenzyme 5 (HLDH5 or PLDH5) when in Solution or Adsorbed onto Polystyrene

Monoclonal antibody	Solution[a]				Adsorbed onto polystyrene surface[b]			
	HLDH5		PLDH5		HLDH5		PLDH5	
	Nat.[d]	Ht.[d]	Nat.	Ht.	Nat.	Ht.	Nat.	Ht.
2/66[c]	+	−	+	−	+	−	+	−
MF30[c]	−	−	−	−	+	+	−	+

a) The native and heat-treated enzymes were allowed to interact with the corresponding monoclonal antibodies in solution. b) Interaction was allowed to take place between the native or heat-treated enzymes adsorbed onto polystyrene and corresponding antibodies kept in solution. c) 2/66 and MF30 denote the monoclonal antibodies obtained against porcine and human LDH5 isoenzymes, respectively. d) Nat. stands for native enzyme; Ht. stands for enzyme heated in PBS, pH 7.5, for 45 s at 70 °C (see Ref. 35).

Subtle conformational alterations in the antigenic region of carboxypeptidase-A(CPA) between the amino acid residues 209—218 following the adsorption of CPA onto polystyrene were also detected by our group with the aid of three mAbs directed towards this antigenic region.[23,36] The mAbs interacted with CPA with relatively high binding constants without affecting the enzyme's activity. Binding of the three mAbs with CPA adsorbed onto the polystyene plates was characterized by apparent binding constants which were higher by one or two orders of magnitude than the corresponding binding constants characterizing their interaction in solution. The conformational alterations occurring in CPA following its treatment with urea were also readily detectable by the mAbs employed.

Detection by mAbs of subtle conformational changes in proteins following their physical adsorption to solid supports has also been reported by the French school. Friguet et al.,[30] using mAbs directed against different epitopes of the β_2-subunit of *E. coli* tryptophan synthase, have shown that some of the antibodies bind very slowly to the native β_2-subunit in solution, but recognize the antigen quite rapidly when adsorbed onto a microtiter plate. Their observation imply that the ELISA test commonly used in screening for specific hybridomas may lead to the retention of antibodies not specific for the native conformation of the antigen.

Also investigated by our group was the interaction of mAbs raised against native hen egg white lysozyme (HEL) with the enzyme after its partial irreversible denaturation by heating. This antigen/antibody system was chosen because it has been well-characterized by the Pasteur group.[4] Irreversibly heat-denatured HEL (D. Kenett, unpublished results) was recognized by the mAbs D44.2 directed against the "loop" region of the native enzyme and by the mAb D1.3 directed against the amino and carboxyl termini of the enzyme. The mAb D74.3, which binds to an

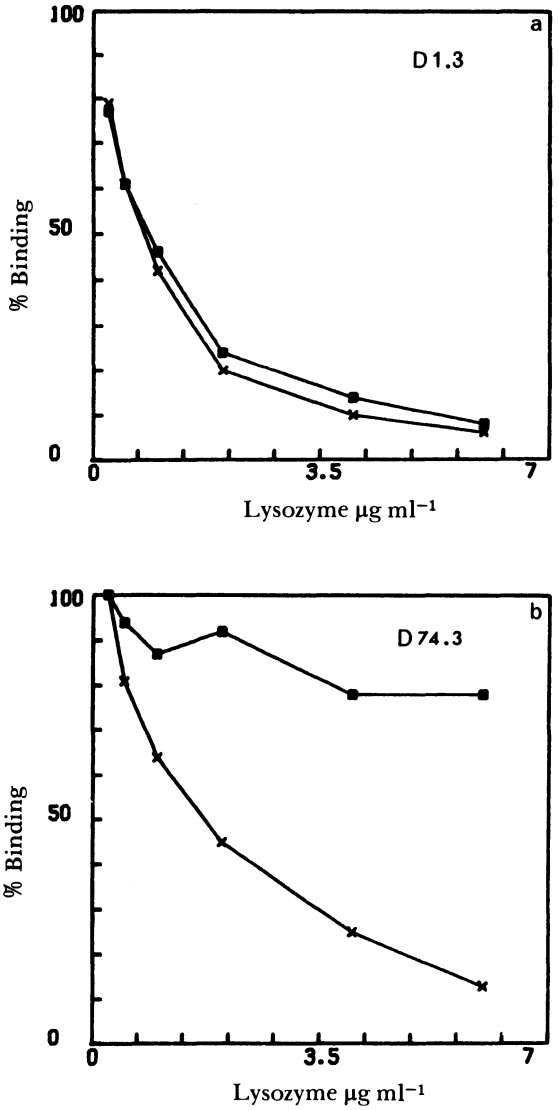

Fig. 1. Binding of the mAb D 1.3 (Fig. 1a) or mAb D 74.3 (Fig. 1b) onto HEL adsorbed on microtiter polystyrene plates in the presence of increasing concentrations of native (-X-X-) or partially heat denatured (-□-□-) (120 min at 95 °C, pH 5) enzyme.

epitope within the active site region of HEL, reacted only weakly with the denatured enzyme which lost most of its catalytic activity after heating (see Fig. 1). The active site of lysozyme is located in a cleft between two globular lobes which oscillate btween an open and a closed conformation during the catalytic cycle. As revealed by the mAbs, the active site appears to be more prone to conformational change than the rest of the molecule probably because of the hinge bending motion.

Monoclonal Antibodies as Topographical Probes

Monoclonal antibodies usually recognize a single well-characterized "surface" of a protein antigen. One might, therefore, expect to find them useful in building up a topographic picture of protein antigens, providing information about their orientation, attachment, ligand binding sites and carbohydrate attachment sites. They might be particularly useful in the elucidation of the molecular "surfaces" involved in subunit assembly, and the protein "surfaces" involved in the binding of a given protein with other proteins or with macro- or micro-environmental components.

The use of mAbs in the study of subunit assembly may be illustrated by the work of Moradi-Amel et al.[37] on the structure of mitochondrial F_1-ATPase. Four stable mAbs against pig heart mitochondrial F_1-ATPase were prepared. Three of them interact with the β-subunits and one binds strongly to the α-subunits. Quantitative analysis of the interaction of these mAbs with their corresponding subunits led to the prediction that mitochondrial F_1-ATPase consists of three α- and three β-subunits.

As an example of the use of mAbs in the topographical analysis of proteins, we might cite the elucidation of the position of the immunoglobulin (IgD) molecules within lymphocyte membranes using mAbs.[38,39] Treatment of intact cells with trypsin abolished the binding of mAb 11-6.3, but did not affect the binding of mAb 10-4.22. The mAb 11-6.3 was found to bind to the Fab portion of IgD, while mAb 10-4.22 bound to the Fc portion. It was thus conculded that IgD is enclosed within the lymphocyte cell membrane via its Fc portion.

The use of mAbs against subunits of human chorionic gonadotropin (hCG) in order to examine the orientation of the hormone in its complex with gonadal receptors, has been illustrated by Moyle et al.[40] hCG is a glycoprotein composed of α- and β-subunits which interact with gonadal receptors to stimulate steroid synthesis. The purified mAbs obtained were iodinated and used to determine which antigenic sites on hCG remained free in the hCG-receptor complexes. The resulting data indicated that portions of the β-subunit were buried (i.e. failed to bind with radiolabeled antibody), whereas other portions remained exposed (i.e., they bound with radiolabeled antibody). Those antibodies which interacted with portions of hCG that became inaccessible in the hCG-receptor complex also blocked the biological action of hCG, whereas those that interacted with exposed sites had little or no effect on its activity. A similar approach was used in order to determine the orientation of a human leukocyte interferon molecule on its cell surface.[41] Using a mAb against a synthetic interferon fragment, it was possible to show that the carboxyl terminus of the interferon remains accessible to the mAb even after its interaction with the corresponding cell surface receptor.

The use of mAbs as probes of the α-bungarotoxin (αBTx) and cholinergic-binding regions of the acetylcholine receptor (AcChR)[42] revealed the non-equivalence of the two αBTx binding regions of the AcChR molecule. Furthermore, it was possible to identify epitopes on the αBTx binding region that, when bound, produce differential effects on the binding of the agonist carbamyl-choline and the antagonist d-tubocurarine.

Concluding Remarks

We have shown here that mAbs might serve as useful probes in the detection of given protein conformations and conformational alterations. The high specificity of mAbs towards given antigen determinant conformations was recently illustrated by the preparation of "abzymes," i.e. mAbs that can catalyze a chemical reaction because they have been made to recognize the transition state of the reaction under consideration.[43] The value of mAbs as conformational probes will no doubt increase as more detailed information is acquired as to the structure of the antigenic epitopes which they recognize. In this respect, the production of mAbs of predetermined specificity by means of selected peptides might be of considerable importance.

Since mAbs prepared against a given protein recognize different antigenic sites of the antigen, it should be possible to use them in detecting the effect of amino acid substitution by site-directed mutagenesis on the conformation of different molecular regions. They may thus pave the way for the preparation of highly stable proteins under selected conditions.

In the section dealing with the use of mAbs as topographical probes, we have shown that they can be used in the elucidation of the quaternary structure of proteins, receptors and more complex biological systems. Their application in this area will undoubtedly increase in the future.

The use of mAbs as conformational probes is relatively new. Their use in conjunction with other methods in studies on structure and function is promising.

References

1) R. Huber, S. William, and J. R. Bennett, *Biopolymers*, **22**, 261 (1983).

2) G. Köhler and C. Milstein, *Nature (London)*, **256**, 495 (1975).

3) D. C. Benjamin, J. A. Berzofsky, I. J. East, F. R. Gurd, C. Hannum, S. Leach, E. Margoliash, G. Michael, A. Miller, E. M. Prager, M. Reichlin, E. E. Sercarz, S. J. Smith-Gill, P. E. Todd, and A. C. Wilson, *Ann. Rev. Immunol.*, **2**, 67 (1984).

4) A. Amit, R. Mariuzza, S. Phillips, and R. Poljak, *Science*, **233**, 747 (1986).

5) M. Harper, F. Lema, G. Boulot, R. Poljak, *Mol. Immunol.*, **24**, 97 (1987).

6) D. Kenett, G. Fleminger, E. Katchalski-Katzir, and R. Poljak, *Mol. Immunol.*, **24**, 313 (1987).

7) E. A. Kabat, "Structural Concepts in Immunology and Immunochemistry," 2nd ed, Holt, Rinehart, and Winston, New York (1986), p. 440.

8) R. Huber, D. Kukla, W. Bode, P. Schwager, K. Bartels, J. Deisenhofer, and W. Steigemann, *J. Mol. Biol.*, **89**, 73 (1974).

9) Z. Chen and W. Bode, *J. Mol. Biol.*, **164**, 283 (1983).

10) D. C. Rees and W. N. Lipscomb, *J. Mol. Biol.*, **160**, 475 (1982).

11) P. M. Colman, W. G. Laver, J. N. Varghese, A. T. Baker, P. A. Tulloch, G. M. Air, and R. G. Webster, *Nature (London)*, **326**, 358 (1987).

12) A. G. Diamond, G. W. Butcher, and J. C. Howard, *J. Immunol.*, **132**, 1169 (1984).

13) P. De la Paz, B. Sutton, M. Parsley, and A. Rees, *EMBO J.*, **5**, 415 (1986).

14) L. Djvadi-Ohaniance, B. Friguet, and M. Goldberg, *Biochemistry*, **25**, 2502 (1986).

15) R. Lewis, B. Furie, and B. Furie, *Biochemistry*, **22**, 948 (1983).

16) J. W. Bloom and K. G. Mann, *Biochemistry*, **17**, 4430 (1978).

17) F. G. Prendergast and K. G. Mann, *J. Biol. Chem.*, **252**, 840 (1977).

18) M. Tai, B. Furie, and B. Furie, *J. Biol. Chem.*, **255**, 2790 (1980).

19) K. Wakabayashi, Y. Sakata, and N. Aoki, *J. Biol. Chem.*, **261**, 11097 (1986).

20) V. Dixet, N. Galvin, K. Orourke, and W. Frazier, *J. Biol. Chem.*, **261**, 1962 (1986).

21) H. Matsui, C. Pallen, A. Adachi, J. Wang, and P. Lam, *J. Biol. Chem.*, **260**, 4174 (1985).

22) T. Shimizu, F. Reinach, T. Masaki, and D. Fishman, *J. Mol. Biol.*, **183**, 271 (1985).

23) B. Solomon and R. Kopel, *Biochemistry*, submitted for publication.

24) C. Anfinsen, E. Haber, M. Sela, and F. H. White, *Proc. Natl. Acad. Sci. U. S. A.*, **47**, 1309 (1961).

25) S. Blond and M. Goldberg, *Proc. Natl. Acad. Sci. U. S. A.*, **84**, 1147 (1987).

26) B. Friguet, L. Djavadi-Ohaniance, and M. Goldberg *Eur. J. Biochem.*, **160**, 593 (1986).

27) H. Chung, S. Park, and S. Rhee, *J. Biol. Chem.*, **259**, 11756 (1984).

28) J. P. Merlie and J. Lindstrom, *Cell*, **34**, 747 (1983).

29) R. C. Mireldorf, Jr. and R. L. Dimond, *Anal. Biochem.*, **135**, 221 (1983).

30) B. Friguet, L. Djavadi-Ohaniance, and M. E. Goldberg, *Mol. Immunol.*, **21**, 673 (1984).

31) Z. Al Moudallal, J. P. Briand, and M. H. V. Van Regenmortel, *EMBO J.*, **1**, 1005 (1982).

32) H. C. Vaidya, D. N. Dietzer, and J. H. Ladenson, *Hybridoma*, **4**, 271 (1985).

33) K. C. McCullough, J. R. Crowther, and R. N. Butcher, *J. Immunol. Met.*, **82**, 91 (1985).

34) R. Milne, L. Blanchette, R. Theolis, P. Weech, and Y. Marcel, *Mol. Immunol.*, **24**, 435 (1987).

35) Z. Hollander and E. Katchalski-Katzir, *Mol. Immunol.*, **23**, 927 (1986).

36) B. Solomon, R. Kopel, D. Kenett, and G. Fleminger, *Biochemistry*, submitted for publication.

37) M. Moradi-Amel, and G. Godinot, *Proc. Natl. Acad. Sci. U. S. A.*, **80**, 6167 (1983).

38) S. W. Kessler, V. L. Woods, F. D. Finkelman, and I. Scher, *J. Immunol.*, **123**, 2772 (1979).

39) J. W. Goding, *J. Immunol.*, **124**, 2082 (1980).

40) W. R. Moyle, P. H. Ehrlich, and R. E. Canfield, *Proc. Natl. Acad. Sci. U. S. A.*, **79**, 2245 (1982).

41) H. Arnheiter, M. Ohno, M. Smith, B. Gutte, and K. Zoon, *Proc. Natl. Acad. Sci. U. S. A.*, **80**, 2539 (1983).

42) M. Mihovilovic and D. P. Richman, *J. Biol. Chem.*, **262**, 4978 (1987).

43) S. J. Pollack, J. W. Jacobs, and P. G. Schultz, *Science*, **234**, 1570 (1986).

 © 1988 The Chemical Society of Japan Bull. Chem. Soc. Jpn., 61, 141—148 (1988)

Invited Paper

Synthesis of Three Acyclic All-*trans*-Tetraterpene Diols, Putative Precursors of Bacterial Lipids

Bertrand CHAPPE,* Hélène MUSIKAS, Dominique MARIE, and Guy OURISSON
Institut de Chimie des Substances Naturelles du CNRS, 91198-Gif-sur-Yvette, France
(Received August 10, 1987)

Three acyclic all-*trans*-tetraterpene diols, **A**, **B**, and **C** have been synthesized from geraniol (**1**), by a convergent scheme involving six different C_{10} synthons derived from geraniol, and coupling by known reactions of three different types: substitution of allylic chlorides by carbanions α to sulfones, duplication of allylic alcohols, and Pd(0)-catalyzed coupling of allylic carbonates with doubly stabilized carbanions. **A**, **B**, and **C** represent postulated phylogenetic precursors of known membrane reinforcers, and are the three possible distally dihydroxylated dimers of geranylgeraniol: tail-to-tail, head-to-head, and head-to-tail.

We describe below the syntheses of three acyclic all-*trans*-tetraterpene diols **A**, **B**, and **C**, representing the three possible modes of coupling geranylgeraniol units (**A**: tail-to-tail, **B**: head-to-head, and **C**: head-to-tail). The diols thus obtained are distally dihydroxylated polyterpene chains about 40 Å long, and should therefore be able to form transmembrane inserts in normal biological phospholipid bilayers; they have been postulated[1] to be phylogenetic precursors of bacterial membrane-spanning carotenoids,[2] of the tricyclopolyprenols assumed from their known molecular fossils to be bacterial membrane lipids,[3] and of the known archaebacterial phospholipids.[4] **A**, **B**, and **C** are thus not known *per se* as natural products. We plan, and have begun, to test their membrane properties, either as such or as part of phospholipids or of other highly polar derivatives (phosphates, glucosides, ···), and also to test their effect on some lipid-dependent microorganisms.

The syntheses so far carried out have been limited to the all-trans substances; we plan to complete them later with syntheses of some of their Z-isomers, at least for the head-to-tail diol **C**: biologically important regular polyterpenols are often partially Z.

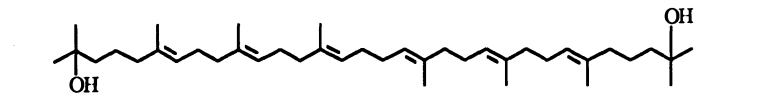

A

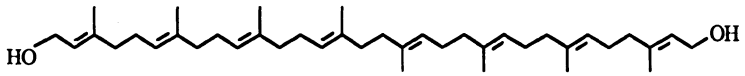

B

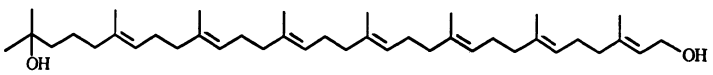

C

Methods and Results

The syntheses of carotenoids have illustrated the various ingenious ways to reach C_{40} by all possible arithmetic combinations of smaller units. We have chosen for our syntheses to start from the readily available geraniol (**1**), which was first modified in three ways to obtain the C_{10} properly functionnalized derivatives **5**, **7**, and **9**; the chloride **5** is the potential source of an allylic carbenium ion on one of the "head" methyl groups, and sulfones **7** and **9** function as potential sources of allylic carbanions on C-1, the "tail" of the geraniol unit, with different hydroxylation patterns at the "head". The practical synthetic problems have revolved around the proper choice of temporary protecting groups and of efficient coupling methods.

The protecting groups used have been chosen to permit selective removals; they include THP (tetrahydropyranyl), MEM (2-methoxyethoxymethoxy) and tBDMS (*t*-butyldimethylsilyl) ethers. The coupling methods involve base-catalyzed reaction of allylic chlorides with allylic sulfones, reductive dimerization of allylic alcohols with Ti(III), and Pd(0)-catalyzed reaction of allylic carbonates with allylic carbanions

Dedicated respectfully and with admiration to Professor Edgar Lederer, on the occasion of his approaching 80th birthday (G.O.).

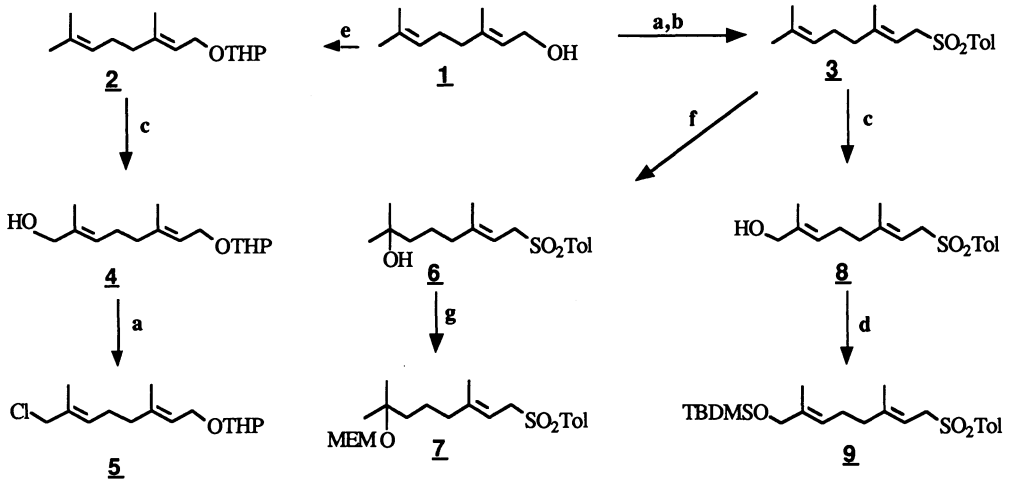

Scheme 1. a: TsCl, DMAP, TEA/CH_2Cl_2; b: *p*-$MeC_6H_4SO_2Na$/DMF; c: SeO_2, TBHP/CH_2Cl_2; d: tBDMSCl, DIPEA/DMF; e: DHP, PPTS/CH_2Cl_2; f: $(AcO)_2Hg$, NaOH, $NaBH_4$/THF, H_2O; g: MEMCl, DIPEA/CH_2Cl_2.

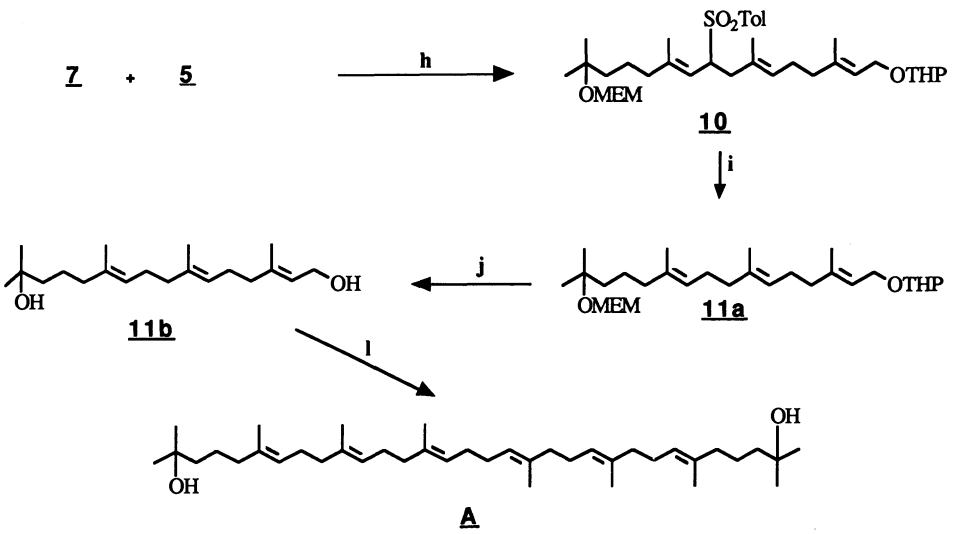

Scheme 2. h: *n*-BuLi/THF; i: Na/Hg, Na_2HPO_4/MeOH; j: TsOH/EtOH; l: $TiCl_3$, *n*-BuLi/Dimethoxyethane.

(in this case, with additional stabilization of the carbanion by a methoxycarbonyl group geminated with the sulfone).

Chloride **5** was obtained by reaction of the THP-protected hydroxygeraniol **4** by reaction with tosyl chloride and triethylamine/4-dimethylaminopyridine.[5] The allylic oxidation of geranyl-THP ether **2** was efficiently achieved with *t*-butyl hydroperoxide with selenium dioxide as a catalyst;[6] this method is known to oxidize selectively the (E)-methyl group. Geraniol (**1**) itself gave, by the same chlorination method, geranyl chloride which was directly transformed into the *p*-tolyl sulfone **3** by reaction with sodium *p*-toluenesulfinate in DMF.[7] Geranyl *p*-tolylsulfone (**3**) was converted into the alcohols **6** and **8**, respectively by Brown's mercuration-reduction sequence,[8] and by the SeO_2-catalyzed allylic oxidation already mentioned.

The C_{10} sulfone **7** has next been converted with butyllithium into its carbanion, which reacted with the chloride **5** to give the C_{20} sulfone **10**; this was desulfonated by mild reduction with sodium amalgam in methanol, in the presence of disodium hydrogenphosphate.[9] After acid-catalyzed deprotection, the allylic alcohol **11b** was reductively duplicated with titanium trichloride and butyllithium,[10] to give the first C_{40} diol wanted, the tail-to-tail tetraterpenediol **A**.

The second goal, the head-to-head diol **B**, was similarly obtained, by identical reactions, from the same chloride **5** and the other sulfone **9**. In this case, the use of a tBDMS-ether permitted the selective deprotection with tetrabutylammonium fluoride (TBAF) of the silyl ether,[11] to unmask one only of the two allylic groups of the C_{20} chain, before the allylic

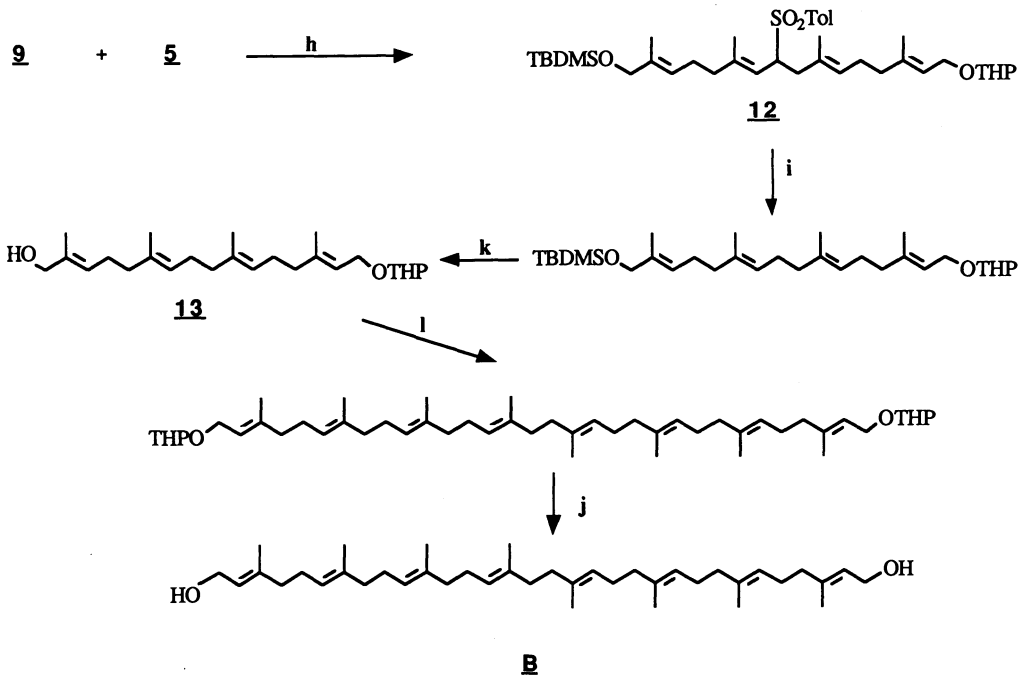

Scheme 3. h: *n*-BuLi/THF; i: Na/Hg, Na_2HPO_4/MeOH; j: TsOH/EtOH; k: TBAF/THF; l: $TiCl_3$, *n*-BuLi/Dimethoxyethane.

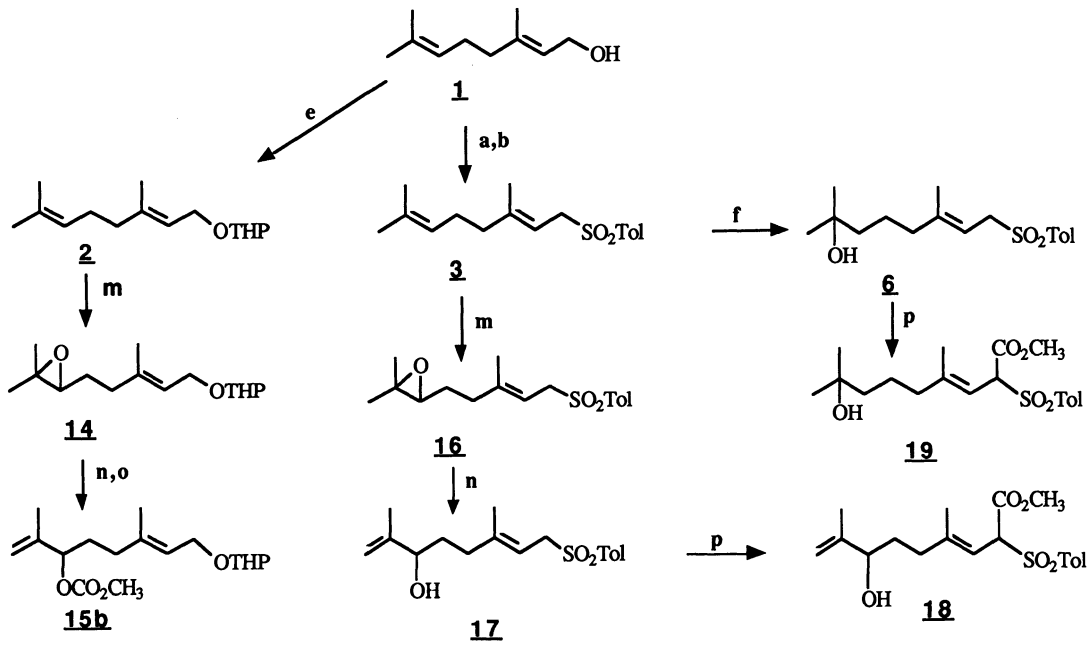

Scheme 4. a: TsCl, DMAP, TEA/CH_2Cl_2; b: *p*-$MeC_6H_4SO_2Na$/DMF; f: $(AcO)_2Hg$, NaOH, $NaBH_4$/THF, H_2O; m: mCPBA/CH_2Cl_2; n: $(C_3H_7O)_3Al$/*i*-PrOH/Tol; o: $ClCO_2Me$, Py/Tol; p: Me_2CO_3, *t*-BuOK/DMF.

alcohol **13** was coupled as before.

The third tetraterpene diol, **C**, has a regular head-to-tail polyprenyl chain. It was synthesized by iteration, according to a C_{10}–C_{20}–C_{30}–C_{40} sequence. The coupling reaction used was that developed by Keynan.[12] This required first the construction of the new C_{10} building blocks **15b**, **18**, and **19**; the known isomerization of epoxides into allylic alcohols with aluminium isopropoxide[13] paved the way for condensation, with the help of Pd(0) as its triphenylphosphine tetracoordinated complex, of the corresponding allylic carbonate. The demethoxycarbonylation was

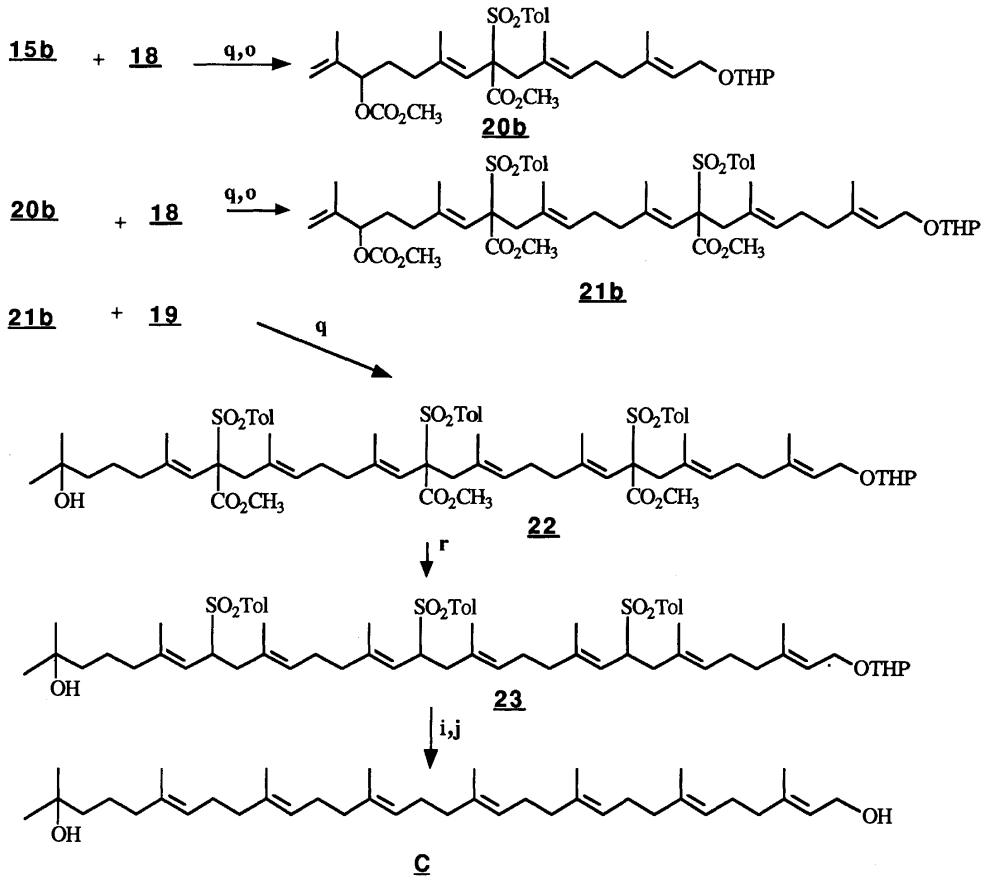

Scheme 5. i: Na/Hg, Na_2HPO_4/MeOH; j: TsOH/EtOH; o: $ClCO_2Me$, Py/Tol; q: $(Ph_3P)_4Pd/Et_2O$; r: PATP, $CsCO_3$/DMF.

achieved with 4-aminothiophenol (PATP) and cesium carbonate, and the removal of the sulfone residues as above with sodium amalgam.

The convergent nature of this synthesis has made it possible to obtain sufficient amounts for the physical studies, which will be reported later.

Experimental

General Methods: NMR spectra were recorded in deuterochloroform with tetramethylsilane as internal standard on Bruker 80, 200 or 400 MHz spectrometers and are expressed as δ. Mass spectra: Kratos MS-80 or MS-9 spectrometers; expressed as m/z. Infrared spectra: chloroform solutions, Perkin-Elmer 297 spectrophotometer; date in agreement with the structures, available on request. Elemental analyses were carried out in the microanalytical laboratory of ICSN by Mlle C. Muller. Thin-layer chromatography (TLC): on Merck silica gel 60-F254 glass plates. Column chromatography: on Chromatogel 60ACC, 70—230 mesh or (for flash chromatography) 230—400 mesh silica gel. All solvents were freshly distilled; tetrahydrofuran (THF) was dried by distillation over sodium-benzophenone, ether by distillation over lithium aluminium hydride, *N,N*-dimethylformamide (DMF) by distillation over calcium hydride, methylene chloride by distillation over calcium chloride. All the substances obtained are oils, which gave however in general good analytical results after purification by flash chromatography monitored by TLC.

General Treatment of Ether Extracts: The usual treatment of ether extracts was to wash them successively with water, if necessary with dilute acid or alkali and again with water, and with saturated brine; they were then dried over anhydrous sodium sulfate and evaporated in vacuo.

General Procedure for Removal of *p*-Tolylsulfonyl Groups: To a mixture of sulfone (1 mol) and disodium hydrogenphosphate (4 mol) in anhydrous methanol, was added at 0 °C an excess of freshly prepared 6% sodium amalgam. Stirring was continued at 0 °C until the starting material had disappeared (TLC), and excess amalgam was destroyed with cold water. The ether extract of the reaction mixture was treated as usual and chromatographed on silica gel.

General Procedure for Terminal Allylic Oxidation: To a solution of selenium dioxide (0.03 mol) in methylene chloride, was added 70% *t*-butyl hydroperoxide (3 mol). The mixture was stirred at 25 °C for 30 min, then the substrate (1 mol) was introduced as a solution in methylene chloride, and stirring was continued for 20 h at 25 °C. Toluene was added, and the solvents were removed in a rotatory evaporator in vacuo. The residue was extracted three times with ether. The ether extract was treated as usual. The residue was dissolved in ethanol and treated with sodium borohydride at 0 °C for 1 h. Cold water was added, the

reaction mixture was extracted with ether, and the ether extract was treated as usual. Flash chromatography was used to isolate the allylic alcohol.

Geranyl Tetrahydropyranyl Ether (2). To a solution of geraniol (**1**) (15.4 g, 0.1 mol) in dry methylene chloride, were added dihydropyran (12.6 g, 0.15 mol) and *p*-toluenesulfonic acid (2.5 g, 0.01 mol). The mixture was stirred for 3 h at room temperature, and evaporated in vacuo. The ether extract of the residue was treated as usual. Filtration on silica gel gave the ether **2** (23.7 g, 99.5%). R_f=0.95 (hexane/ether 1/1). ^{1}H NMR: 5.39 (t, 1H), 5.10 (m, 1H), 4.65 (s, 1H), 4.31 (m, 2H), 3.60 (m, 2H), 2.08 (m, 4H), 1.73 (s, 6H), 1.60 (s, 9H); MS 238 (M^+), 137 (M^+−OTHP). Found: C, 75.4; H, 10.8; O, 13.5%. Calcd for $C_{15}H_{26}O_2$: C, 75.63; H, 10.92; O, 13.45%.

Geranyl *p*-Tolyl Sulfone (3). To a stirred solution of geraniol (**1**) (15.6 g, 0.101 mol) in dry methylene chloride (30 ml), were added at room temperature under an argon atmosphere 4-(dimethylamino)pyridine (DMAP, 7.15 g, 0.06 mol), *p*-toluenesulfonyl chloride (23.2 g, 0.12 mol) and triethylamine (14.09 ml, 0.1 mol). Stirring was maintained during 3 h, and methylene chloride was removed in vacuo. The ether extract of the residue was first washed with 10% $CuSO_4$, then with 10% $NaHCO_3$, and finally treated as usual, and purified by flash chromatography to give geranyl chloride (17.03 g, 97%), characterized by its ^{1}H NMR and mass spectra (*m/z* 172—174 M^+). R_f=0.96 (hexane/ether 1/1). Geranyl chloride (3.8 g, 22 mmol) in dry DMF (50 ml) was treated overnight at 25 °C with sodium *p*-toluenesulfinate (4.3 g, 24 mmol) under nitrogen. After evaporation of the solvent, addition of water and extraction with ether, the extract was treated as usual, and purified by flash chromatography (hexane/ether 1/1) to give geranyl *p*-tolyl sulfone (**3**) (5.6 g, 86%) as a colorless oil, apparently crystallizable at low temperature, but which we could not further purify (cf. analysis below). R_f 0.97 (ether). ^{1}H NMR 7.62 (d, 2H), 7.13 (d, 2H), 5.07 (m, 2H), 3.77 (m, 2H), 2.35 (s, 3H), 2.00 (d, 4H), 1.73 (s, 3H), 1.63 (s, 3H), 1.40 (s, 3H). MS 292 (M^+), 137 (M^+−$TolSO_2$). Found: C, 70.2; H, 8.5; S, 10.6%. Calcd for $C_{17}H_{24}O_2S$: C, 69.22; H, 8.5; S, 10.96%.

(2*E*,6*E*)-1-(Tetrahydro-2-pyranyloxy)-3,7-dimethyl-2,6-octadien-8-ol (4). Geranyl tetrahydropyranyl ether (**2**) (4.05 g, 17 mmol) was oxidized with *t*-BuOOH/SeO_2 according to the general procedure. After purification by flash chromatography on silica gel (hexane/ether 1/1), the mono THP-ether **4** was obtained (2.46 g, 57%). R_f 0.17 (hexane/ether 1/1). ^{1}H NMR 5.25 (m, 2H), 4.52 (s, 1H), 4.15—3.70 (m, 6H), 2.83 (s, 1H), 2.08 (m, 4H), 1.63 (m, 12H). MS 254 (M^+), 236 (M^+−H_2O), 153 (M^+−OTHP). Found: C, 70.6; H, 10.2; O, 19.2%. Calcd for $C_{15}H_{26}O_3$: C, 70.87; H, 10.24; O, 18.90%.

(2*E*,6*E*)-8-Chloro-1-(tetrahydro-2-pyranyloxy)-3,7-dimethyl-2,6-octadiene (5). To a solution of the mono THP-ether **4** (4.2 g, 16 mmol) in dry methylene chloride (40 ml) were added sequentially under nitrogen at 25 °C 4-(dimethylamino)pyridine (1.21 g, 10 mmol), tosyl chloride (3.8 g, 20 mmol) and triethylamine (2.22 ml, 16 mmol). The reaction mixture was stirred for 3 h, and methylene chloride was removed was removed in vacuo. The residue, diluted with water, was extracted 4 times with ether, with gentle magnetic stirring. Purification on silica gel afforded 4.55 g of pure chloride **5** (95%) as a colorless oil which could not be obtained analytically pure. R_f 0.97 (hexane/ether 1/1). ^{1}H NMR 5.27 (m, 2H), 4.50 (s, 1H), 4.15—3.70 (m, 6H), 2.08 (m, 4H), 1.67 (s, 3H), 1.57 (s, 3H), 1.67—1.57 (m, 6H). MS 274—272 (M^+), 236 (M^+−HCl).

(2*E*)-1-(*p*-Tolylsulfonyl)-3,7-dimethyl-2-octen-7-ol (6). To a magnetically stirred solution of sulfone **3** (3.1 g, 10.6 mmol) in THF (40 ml) and water (10 ml), was added with ice cooling mercuric acetate (3.38 g, 10.6 mmol). After 2 h, the reaction was completed by addition of 3 M sodium hydroxide (10 ml) and 0.5 M sodium borohydride in 3 M sodium hydroxide (10 ml). Stirring was continued for 30 min. The reaction mixture was saturated with potassium carbonate and extracted with ether. The extract was treated as usual, evaporated and purified on silica gel to give the hydroxy sulfone **6** (2.95 g, 89%). R_f 0.50 (ether). ^{1}H NMR 7.71 (d, 2H), 7.29 (d, 2H), 5.16 (t, 1H), 3.76 (d, 2H), 2.44 (s, 3H), 2.08 (m, 2H), 1.37 (s, 3H), 1.52—1.30 (m, 5H), 1.22 (s, 6H). MS 310 (M^+), 292 (M^+−H_2O). Found: C, 65.7; H, 8.7; O, 15.6; S, 10.05%. Calcd for $C_{17}H_{26}O_3S$: C,65.80; H, 8.38; O, 15.48; S, 10.32%.

(2*E*)-1-(*p*-Tolylsulfonyl)-7-(2-methoxyethoxymethoxy)-3,7-dimethyl-2-octene (7). To a stirred solution of the hydroxy sulfone **6** (2.8 g, 9 mmol) in dry methylene chloride (30 ml), were added at 25 °C *N,N*-diisopropylethylamine (DIPEA, 2.4 ml, 13.9 mmol) and MEM-chloride (1.6 ml, 14 mmol). Stirring was continued for 4 h (disappearance of the starting material, TLC), water and ether were added and the ether extract was treated as usual. Purification on silica gel afforded the MEM-ether **7** (3.45 g, 96%). R_f 0.72 (ether). ^{1}H NMR: 7.65 (d, 2H), 7.23 (d, 2H), 5.13 (m, 1H), 4.72 (s, 2H), 3.78 (d, 2H), 3.73—3.42 (m, 4H), 3.30 (s, 3H), 2.43 (s, 3H), 2.08—1.83 (m, 2H), 1.48—1.31 (m, 4H), 1.37 (s, 3H), 1.22 (s, 6H). MS 398 (M^+), 367 (M^+−31). Found: C, 63.0; H, 8.5; S, 7.74%. Calcd for $C_{21}H_{34}O_5S$: C, 63.31; H, 8.54; S, 8.04%.

(2*E*,6*E*)-1-(*p*-Tolylsulfonyl)-3,7-dimethyl-2,6-octadien-8-ol (8). Sulfone **3** (2.52 g, 8.6 mmol) was oxidized with *t*-BuOOH/SeO_2 in methylene chloride according to the general procedure, which afforded the hydroxy sulfone **8** (1.75 g, 66%). R_f 0.54 (ether). ^{1}H NMR 7.72 (d, 2H), 7.29 (d, 2H), 5.25 (m, 2H), 4.00 (s, 2H), 3.83 (d, 2H), 2.45 (s, 3H), 2.08 (m, 4H), 1.66 (s, 4H), 1.42 (s, 3H). MS 308 (M^+), 153 (M^+−$TolSO_2$). Found: C, 66.3; H, 7.8; O, 15.5; S, 10.2%. Calcd for $C_{17}H_{24}O_3S$: C, 66.23; H, 7.79; O, 15.58; S 10.39%.

(2*E*,6*E*)-1-(*p*-Tolylsulfonyl)-8-(*t*-butyldimethylsilyloxy)-3,7-dimethyl-2,6-octadiene (9). A stirred mixture of the hydroxy sulfone **8** (4.21 g, 13.6 mmol), *N,N*-diisopropylethylamine (3.56 ml, 20.5 mmol) and disodium hydrogenphosphate (7.75 g, 54.6 mmole) in dry DMF was treated at 25 °C with *t*-butyldimethylsilyl chloride (2.46 g, 16.4 mmol). Stirring was continued for 3 h at room temperature, water and ether were added and the ether extract was teated as usual. After evaporation in vacuo and flash chromatography on silica gel, the TBDMS-ether **9** was obtained (5.55 g, 96%). ^{1}H NMR 7.70 (d, 2H), 7.25 (d, 2H), 5.25 (m, 2H), 3.98 (s, 2H), 3.75 (d, 2H), 2.42 (s, 3H), 2.07 (m, 4H), 1.57 (s, 3H), 1.35 (s, 3H), 0.90 (s, 9H), 0.08 (s, 6H). MS (CI, NH_3) 423 (M^++1), 291 (M^++1−*t*-BuDMSiOH). Found: C, 65.5; H, 8.75%. Calcd for $C_{23}H_{38}O_3SiS$: C, 65.40; H, 9.00%.

(2*E*,6*E*,10*E*)-1-(Tetrahydro-2-pyranyloxy)-9-(*p*-tolylsulfonyl)-15-(2-methoxyethoxymethoxy)-3,7,11,15-tetramethyl-2,6,10-hexadecatriene (10). To a stirred solution of the MEM-sulfone **7** (3.35 g, 8.42 mmol) in dry THF (40 ml) and HMPA (10 ml), was added at −78 °C, under nitrogen, a solution of

n-BuLi (6.6 ml, 9.25 mmol). After 2h, was added at −78 °C, over 1 h a solution of the THP-chloride **5** (2.52 g, 9.25 mmol) in dry THF (8 ml) and HMPA (2 ml). The mixture was stirred overnight and worked up as usual. The crude product, after flash chromatography (ether/hexane 1/1) gave the triene **10** (3.2 g, 58%). R_f 0.3 (ether/hexane 1/1). ^{1}H NMR 7.70 (d, 2H), 7.26 (d, 2H), 5.57—4.98 (m, 3H), 4.78 (s, 2H), 4.58 (s, 1H), 4.37—3.78 (m, 5H), 3.78—3.45 (m, 4H), 3.38 (s, 3H), 2.43 (s, 3H), 2.32—1.78 (m, 8H), 1.75—1.46 (m, 6H), 1.67 (s, 9H), 1.46—1.32 (m, 4H), 1.22 (s, 6H). MS 634 (M^+), 603 (M^+-31). Found; C, 68.3; H, 9.0; O, 17.8; S, 4.8%. Calcd for $C_{36}H_{58}O_7S$: C, 68.14; H, 9.15; O, 17.67; S, 5.04%.

(2*E*,6*E*,10*E*)-1-(Tetrahydro-2-pyranyloxy)-15-(2-methoxyethoxymethoxy)-3,7,11,15-tetramethyl-2,6,10-hexadecatriene (11a). Elimination of the *p*-tolylsulfonyl group of the preceding product **10** (3.1 g, 4.9 mmol) was carried out according to the general procedure to give the THP-MEM-protected triene **11a** (2.12 g, 90%). R_f 0.55 (hexane/ether 1/1). ^{1}H NMR 5.47—4.95 (m, 3H), 4.78 (s, 2H), 4.58 (s, 1H), 4.37—3.80 (m, 4H), 3.80—3.46 (m, 4H), 3.38 (s, 3H), 2.22—1.80 (m, 10H), 1.75—1.55 (m, 15H), 1.55—1.38 (m, 4H), 1.22 (s, 6H). MS 480 (M^+), 404 ($M^+-HOCH_2CH_2OCH_3$), 374 ($M^+-HOMEM$). Found: C, 72.7; H, 11.0; O, 16.4%. Calcd for $C_{29}H_{52}O_5$: C, 72.50; H, 10.83; O, 16.67%.

(2*E*,6*E*,10*E*)-3,7,11,15-Tetramethyl-2,6,10-hexadecatriene-1,15-diol (11b). The THP-MEM ether **11a** (1.3 g, 2.7 mmol) was treated with *p*-toluenesulfonic acid in ethanol at 55 °C for 3 h. The solvent was removed in vacuo and water was added. The rection mixture was taken in ether and treated as usual. Flash chromatography afforded the diol **11b** (0.3 g) and two partially deprotected products, which were treated again with *p*-TsOH in the same conditions, to give 0.218 g more of the diol **11b**. Total yield 0.518 g (62%). ^{1}H NMR 5.52—4.95 (m, 3H), 4.11 (d, 2H), 2.63 (s, 1H), 2.26—1.83 (m, 10H), 1.68 (s)+1.60 (s)+1 OH (10H), 1.52—1.28 (m, 4H), 1.21 (s, 6H). MS (CI, NH_3): 291 (MH^+-H_2O), 273 (MH^+-2H_2O). Found: C, 78.1; H, 11.5; O, 10.6%. Calcd. for $C_{20}H_{36}O_2$: C, 77.92; H, 11.69; O, 10.39%.

(6*E*,10*E*,14*E*,18*E*,22*E*,26*E*,)-2,6,10,14,19,23,27,31-Octamethyl-6,10,14,18,22,26-dotriacontahexaene-2,31-diol (A). To a stirred solution of titanium trichloride (75 mg, 0.49 mmol) in dry 1,2-dimethoxyethane (2 ml), was added at −78 °C *n*-BuLi (1.1 ml, 1.40 mmol). After 5 min, alcohol **11b** (300 mg, 0.97 mmol) was added, and the reaction mixture was warmed to room temperature and retained for 15 min before addition of water and ether. The ether extract was treated as usual and silica gel chromatography gave the desired diol **A** (100 mg, 35%). ^{1}H NMR 5.25—4.91 (m, 6H), 2.60 (s, 2H), 2.17—1.87 (m, 24H), 1.62 (m, 18H), 1.47—1.31 (m, 8H), 1.22 (s, 12H). MS 582 (M^+), 564 (M^+-H_2O), 546 (M^+-2H_2O). Found: C, 82.1; H, 11.9%. Calcd for $C_{40}H_{70}O_2$: C, 82.47; H, 12.02%.

(2*E*,6*E*,10*E*,14*E*)-1-(*t*-Butyldimethylsilyloxy)-8-(*p*-tolylsulfonyl)-16-(tetrahydro-2-pyranyloxy)-2,6,10,14-tetramethyl-2,6,10,14-hexadecatetraene (12). The allylic cross-coupling reaction between the sulfone **9** (5.55 g, 13.15 mmol) and the chloride **5** (4.29 g, 15.77 mmol) was carried out in the same manner as for the synthesis of **10** from **5** and **7**. Yield: 6.85 g (72%). ^{1}H NMR 7.65 (d, 2H), 7.23 (d, 2H), 5.37—4.75 (m, 4H), 4.58 (s, 1H), 4.18—3.30 (m, 5H), 3.98 (s, 2H), 2.43 (s, 3H), 2.00—1.91 (m, 10H), 1.64 (s, 3H), 1.58 (s, 3H), 1.64—1.48 (m, 6H), 1.23 (s, 6H), 0.90 (s, 9H) 0.08 (s, 6H). MS 658 (M^+), 573 (M^+-THP), 557 (M^+-OTHP). Found: C, 69.2; H, 9.6; S, 4.9%. Calcd for $C_{38}H_{62}O_5SSi$: C, 69.30; H, 9.42; S, 4.86%.

(2*E*,6*E*,10*E*,14*E*)-16-(Tetrahydro-2-pyranyloxy)-2,6,10,14-tetramethyl-2,6,10,14-hexadecatetraen-1-ol (13). The TBDMS-THP ether **12** (3.07 g, 4.66 mmol) was treated with sodium amalgam according to the general procedure for sulfone removal. The reaction mixture was purified on silica gel and afforded the desulfonated product (2.05 g, 87%; R_f=0.9 in hexane/ether 7/3).

This product (1.84 g, 3.65 mmol) was treated for 3 h at 25 °C with N (*n*-Bu)$_4$NF in THF (10.7 ml, 3 equiv). The solvent was removed and the crude product, obtained from the ether extract in the usual way, was purified on sillica gel (hexane/ehter 7/3), to give the THP-monoprotected diol **13** (1.14 g, 81%). ^{1}H NMR 5.47—4.91 (m, 4H), 4.60 (s, 1H), 4.23—3.30 (m, 6H), 2.33—1.92 (m, 12H), 1.78—1.42 (m, 19H). MS (CI, NH_3) 408 ($M+NH_4^+$), 373 (MH^+-H_2O). Found: C, 76.75; H, 10.75; O, 12.3%. Calcd for $C_{25}H_{42}O_3$: C, 76.92; H, 10.77; O, 12.31%.

(2*E*,6*E*,10*E*,14*E*,18*E*,22*E*,26*E*,30*E*)-3,7,11,18,22,26,30-Octamethyl-2,6,10,14,18,22,26,30-dotriacontaoctaene-1,32-diol (B). The allylic coupling of the THP-monoprotected diol **13** (1 g, 2.56 mol) to give diol **B** was carried out with the same procedure as for the conversion of **11b** into **A**. The crude product was purified on silica gel (hexane/ether 7/3) to give the C_{40}-bis-THP-ether (0.22 g, 23%). This (0.18 g) was treated with *p*-TsOH in ethanol at 55 °C for 3 h. The solvent was evaporated in vacuo, the residue was extracted 4 time with ether and purified on silica gel (hexane/ether 1/1) to give the C_{40}-diol **B** (97 mg, 70%). ^{1}H NMR 5.55—4.98 (m, 8H), 4.72 (s, 2H), 4.17 (d, 4H), 2.32—1.91 (m, 28H), 1.70 (s, 12H), 1.62 (s, 12H). MS (CI, NH_3) 596 (MNH_4^+), 561 (MH^+-H_2O), 543 (MH^+-2H_2O). Found: C, 82.8; H, 11.6; O, 5.6%. Calcd for $C_{40}H_{66}O_2$: C, 83.04; H, 11.41; O, 5.53%.

(2*E*)-6,7-Epoxy-1-(tetrahydro-2-pyranyloxy)-3,7-dimethyl-2-octene (14). To a stirred solution of the THP-ether **2** (15 g, 63 mmol) in methylene chloride (100 ml), was added at 0 °C a solution of *m*-chloroperbenzoic acid (12 g) in the same solvent (100 ml). After 1 h, the reaction mixture was washed with a saturated solution of sodium hydrogencarbonate, water and brine, and was dried over sodium sulfate. The crude product was chromatographed on silica gel to give the epoxide **14** (12.3 g, 77%). R_f=0.83 (hexane/ether 1/1). ^{1}H NMR 5.30 (t, 1H), 4.52 (s, 1H), 4.30—3.23 (m, 4H), 2.60 (t, 1H), 2.11 (m, 2H), 1.62 (s, 3H), 1.96—1.30 (m, 8H), 1.22 (s, 3H), 1.18 (s, 3H). MS 254 (M^+), 169 (M^+-THP), 153 (M^+-OTHP). Found: C, 71.0; H, 10.15; O, 19.1%. Calcd for $C_{15}H_{26}O_3$: C, 70.87; H, 10.23; O, 18.90%.

(2*E*)-1-(Tetrahydro-2-pyranyloxy)-3,7-dimethyl-2,7-octadien-6-ol (15a). To a solution of the epoxide **14** (12.3 g, 48.4 mmol) in dry toluene (100 ml), was added a solution of aluminium isopropoxide in 2-propanol. The mixture was heated under reflux for 24 h, cooled, washed with N HCl (50 ml), water and brine, and dried over sodium sulfate. Flash chromatography (hexane/ether 1/1) on silica gel gave the allylic alcohol **15a** (10.7 g, 87%). R_f=0.45 (hexane/ether 1/1). ^{1}H NMR 5.31 (t, 1H), 4.85 (s, 1H), 4.76 (s, 1H), 4.52 (s, 1H), 4.32—3.26 (m, 5H), 2.35—1.87 (m, 2H), 1.87—1.35 (m, 3H+s, 6H at 1.68). MS 254 (M^+), 236 (M^+-H_2O), 170 (M^+-THP), 153 (M^+-OTHP). Found: C, 71.15; H, 10.1; O, 18.7%. Calcd for $C_{15}H_{26}O_3$: C, 70.87; H, 10.24; O, 18.90%.

(2*E*)-6-(Methoxycarbonyloxy)-1-(tetrahydro-2-pyranyloxy)-3,7-dimethyl-2,7-octadiene (15b). To a stirred solution of the alcohol **15a** (4.2 g, 16.5 mmol) in dry toluene (40 ml), were added at 25 °C, over 1 h, dry pyridine (2 ml) and methyl chloroformate (2 ml). Stirring was maintained for 12 h. The reaction mixture was washed with a dilute solution of ammonium chloride, water, a solution of copper sulfate, water and saturated brine, dried over sodium sulfate, evaporated and purified by chromatography over silica gel to give the mixed carbonate **15b** (5.06 g, 98%). ^{1}H NMR 5.31 (t, 1H), 4.97 (s, 1H), 4.88 (s, 1H), 4.58 (s, 1H), 4.37—3.31 (m, 5H), 3.75 (s, 3H), 2.20—1.42 (m, 10H), 1.73 (s, 3H), 1.67 (s, 3H). MS (CI, NH_3) 313 (MH^+), 237 (MH^+-HOCO_2Me), 211 ($MH^+-HOTHP$). Found: C, 65.4; H, 9.04; O, 25.45%. Calcd for $C_{17}H_{28}O_5$: C, 65.38; H, 8.97; O, 25.64%.

(2*E*)-6,7-Epoxy-1-(*p*-tolylsulfonyl)-3,7-dimethyl-2-octene (16) Epoxidation of sulfone **3** (6 g, 19.5 mmol) was carried out in the same manner as for the THP-ether **2** to give epoxide **16** (4.73 g, 75%). R_f=0.30 (hexane/ether 1/1). ^{1}H NMR 7.72 (d, 2H), 7.30 (d, 2H), 5.22 (t, 1H), 3.78 (d, 2H), 2.67 (t, 1H), 2.44 (s, 3H), 2.30—1.83 (m, 2H), 1.72—1.47 (m, 2H), 1.42 (s, 3H), 1.32 (s, 3H), 1.27 (s, 3H). MS 308 (M^+), 153 ($M^+-TolSO_2$), 135 ($M^+-TolSO_2-H_2O$).

(2*E*)-6-Hydroxy-1-(*p*-tolylsulfonyl)-3,7-dimethyl-2,7-octadiene (17). Isomerization of **16** was achieved in the same way as for **14** to afford sulfone **17** (1.8 g, 84%), identical with the known product.[12] R_f=0.30 (hexane/ether 1/1). ^{1}H NMR 7.73 (d, 2H), 7.32 (d, 2H), 5.21 (t, 1H), 4.49 (s, 1H), 4.85 (s, 1H), 3.99 (t, 1H), 3.79 (d, 2H), 2.43 (s, 3H), 2.11—1.95 (m, 2H), 1.71 (s, 4H), 1.66—1.48 (m, 2H), 1.35 (s, 3H). MS 308 (M^+), 153 ($M^+-TolSO_2$), 135 ($M^+-TolSO_2-H_2O$).

Methyl (3*E*)-7-Hydroxy-2-(*p*-tolylsulfonyl)-4,8-dimethyl-3,8-nonadienoate (18). This was prepared in 72% yield according to published procedures.[12] ^{1}H NMR 7.70 (d, 2H), 7.30 (d, 2H), 5.28 (d, 1H), 4.90 (s, 1H), 4.82 (s, 1H), 4.73 (d, 1H), 3.97 (t, 1H), 3.73 (s, 3H), 2.43 (s, 3H), 2.25—1.95 (m, 2H), 1.82—1.50 (m, 3H), 1.71 (s, 3H), 1.55 (s, 3H). MS (CI, NH_3) 349 (MH^+-H_2O), 309 ($MH^+-C_2H_2O_2H$).

Methyl (3*E*)-8-Hydroxy-2-(*p*-tolylsulfonyl)-4,8-dimethyl-3-nonenoate (19) Tertiary alcohol **6** (2 g, 6.5 mmol) was treated in the same manner as allylic alcohol **17** to give the sulfone carboxylate **19** (1.7 g, 65%). ^{1}H NMR 7.69 (d, 2H), 7.28 (d, 2H), 5.25 (d, 1H), 4.75 (d, 1H), 3.70 (s, 3H), 2.44 (s, 3H), 2.25—1.91 (m, 2H), 1.82 (s, 1H), 1.55 (s, 3H), 1.50—1.30 (m, 4H), 1.22 (s, 6H). MS (CI, NH_3) 351 (MH^+-H_2O), 293 ($MH^+-H_2O-C_2H_2O_2$), 197 ($MH^+-H_2O-C_7H_6O_2S$), 195 ($MH^+-H_2O-C_7H_8O_2S$). Found: C, 61.7; H, 7.5; O, 21.9; S, 8.7%. Calcd for $C_{19}H_{28}SO_5$: C, 61.96; H, 7.60; O, 21.74; S, 8.70%.

(2*E*,6*E*,10*E*)-9-Methoxycarbonyl-14-methoxycarbonyloxy-1-(tetrahydro-2-pyranyloxy)-9-(*p*-tolylsulfonyl)-3,7,11,15-tetramethyl-2,6,10,15-hexadecatetraene (20b). To a mixture of the THP-ether **15b** (1.45 g, 4.1 mmol) and the allylic alcohol **18** (1.70 g, 4.65 mmol) in dry THF (6 ml), was added at 25 °C 0.268g of tetrakis(triphenylphosphine)palladium(0). After 2 h, ether and water were added, the ether extract was washed with N sodium cyanide, and treated as usual. The crude product was dissolved in dry toluene (20 ml); pyridine (0.5 ml, 6.5 mmol) and methyl chloroformate (0.5 ml, 6.5 mmol) were added. Stirring was continued overnight, and the mixture was washed with dilute ammonium chloride, water, dilute copper sulfate, water, and saturated brine, then dried over sodium sulfate, evaporated and chromatographed (hexane/ether 1/1) to give product **20b** (1.9 g, 62%). R_f=0.45 (hexane/ether 1/1). ^{1}H NMR 7.72 (d, 2H), 7.30 (d, 2H), 5.35 (s, 1H), 5.31 (t, 1H), 5.15 (m, 1H), 5.00 (s, 1H), 4.95 (s, 1H), 4.61 (s, 1H), 4.11 (m, 2H), 3.88 (t, 1H), 3.78 (s, 3H), 3.70 (s, 3H), 3.51 (m, 2H), 3.10 (d, 1H), 2.90 (d, 1H), 2.44 (s, 3H), 2.17—1.95 (m, 6H), 1.83—1.53 (m, 8H, incl. 1.73 s, 1.65 s, 1.57 s), 1.48 (s, 3H). MS (CI, NH_3) 661 (MH^+), 559 ($MH^+-HOTHP$), 505 ($MH^+-C_7H_8O_2S$), 483 $MH^+-HOTHP-HOCO_2Me$), 403 ($MH^+-HOTHP-C_7H_8O_2S$). Found: C, 65.3; H, 8.0; O, 21.9; S, 4.9%. Calcd for $C_{36}H_{52}O_9S$: C, 65.45; H, 7.88; O, 21.82; S, 4.85%.

(2*E*,6*E*,10*E*,14*E*,18*E*)-1-(Tetrahydro-2-pyranyloxy)-9-17-bis(methoxycarbonyl)-22-methoxycarbonyloxy-9,17-bis(*p*-tolylsulfonyl)-3,7,11,15,19,23-hexamethyl-2,6,10,14,18,23-tetracosahexaene (21b). The Pd(0)-catalyzed coupling between the allylic carbonate **20b** (1.7 g, 2.6 mmol) and the allylic alcohol **18** (1.1 g, 3.0 mmol) was run as above to give the expected product **21b** (1.6 g, 61%) and starting materials. R_f=0.26 (hexane/ether 3/7). ^{1}H NMR 7.69 (d, 4H), 7.28 (d, 4H), 5.31 (m, 2H), 5.25—5.06 (m, 3H), 4.95 (s, 2H), 4.61 (s, 1H), 4.41—3.90 (m, 3H), 3.78 (s, 3H), 3.68 (s, 6H), 3.52 (m, 2H), 3.20—2.90 (m, 4H), 2.44 (s, 6H), 2.20—1.92 (m, 10H), 1.82—1.52 (m, 23H, incl. s 1.75, 1.65, 1.60), 1.49 (s, 3H). MS (FAB, NaCl) 1031 (MNa^+), 907 ($MH^+-HOTHP$), 853 ($MH^+-TolSO_2$), 751 ($MH^+-TolSO_2-HOTHP$), 675 ($MH^+-TolSO_2-HOTHP-MeOCOOH$) Found: C, 65.6; H, 7.6; O, 20.7; S, 6.6%. Calcd for $C_{55}H_{76}O_{13}S_2$: C, 65.47; H, 7.54; O, 20.63; S, 6.35%.

(2*E*,6*E*,10*E*,14*E*,18*E*,22*E*,26*E*)-31-Hydroxy-1-(tetrahydro-2-pyranyloxy)-9,17,25-tris(methoxycarbonyl)-9,17,25-tris(*p*-tolylsulfonyl)-3,7,11,15,19,23,27,31-octamethyl-2,6,10,14,18,22,26-dotriacontaheptaene (22). The same Pd(0)-catalyzed coupling was achieved between substrates **19** (1 g, 2.7 mmol) and **21b** (1.5 g, 1.5 mmol) to give the expected product **22** (1.7 g, 88%). ^{1}H NMR 7.73 (d, 6H), 7.30 (d, 6H), 5.37—5.08 (m, 7H), 4.62 (s, 1H), 4.27—3.41 (m, 4H), 3.68 (s, 9H), 3.25—2.66 (m, 6H), 2.44 (s, 9H), 2.15—1.82 (m, 14H), 1.70—1.25 (m, 32H, incl. s 1.64, 1.60, 1.58, 1.56, 1.46, 1.25), 1.22 (s, 6H). MS (FAB, NaCl) 1323 (MNa^+), 1167 (MNa^+-HSO_2Tol), 1013 ($MNa^+-HSO_2Tol-TolSO_2$). Found: C, 66.2; H, 7.6; O, 18.5; S 7.35%. Calcd for $C_{72}H_{100}O_{15}S_3$: C, 66.46; H, 7.69; O, 18.64; S, 7.38%.

(2*E*,6*E*,10*E*,14*E*,18*E*,22*E*,26*E*)-31-Hydroxy-1-(tetrahydro-2-pyranyloxy)-9,17,25-tris(*p*-tolylsulfonyl)-3,7,11,15,19,23,27,31-octamethyldotriaconta-2,6,10,14,18,22,26-heptaene (23). To a solution of the above tricarboxylate **22** (400 mg, 0.3 mmol) in dry DMF (10 ml), were added *p*-aminothiophenol (230 mg, 1.85 mmol) and cesium carbonate (100 mg). The mixture was stirred at 85 °C for 3 h, poured into water and extracted with ether. The usual treatment gave, after purification on silica gel the decarboxylated product **23** (203 mg, 60%). ^{1}H NMR 7.73 (m, 6H), 7.31 (d, 6H), 5.43—4.86 (m, 7H), 4.60 (s, 1H), 4.36—3.46 (m, 7H), 2.46 (s, 9H), 2.11—1.78 (m, 20H), 1.63—1.43 (m, 6H), 1.43—1.30 (m, 4H), 1.65 (s, 4H), 1.51 (s, 9H), 1.25 (s, 9H), 1.21 (s, 6H). MS (FAB, NaCl) 1149 (MNa^+), 993 (MNa^+-HSO_2Tol). Found: C,70.15; H, 8.4; O, 12.8; S, 8.3%. Calcd for $C_{66}H_{94}O_9S_3$: C, 70.34; H, 8.35; O, 12.79; S, 8.52%.

(2*E*,6*E*,10*E*,14*E*,18*E*,22*E*,26*E*)-3,7,11,15,19,23,27,31-Octamethyl-2,6,10,14,18,22,26-dotriacontaheptaene-1,31-diol (C). Desulfonation of the preceding substance **23** (200 mg, 1.18 mmol) by the general procedure gave the THP-ether of diol **C**, which was prepared irectly by treatment with

a trace of *p*-TsOH in ethanol at 55 °C for 3 h, to give after purification the desired product **C** (60 mg, 58%). ^{1}H NMR 5.58—4.92 (m, 7H), 4.18 (d, 2H), 3.05—2.92 (m, 2H), 2.54—1.83 (m, 24H), 1.67—1.65 (m, 21H), 1.51—1.33 (m, 6H), 1.24 (s, 6H). MS (CI, NH_3) 598 (MNH_4^+), 563 (MH^+-H_2O), 545 (MH^+-2H_2O). Found: C, 82.7; H, 11.9; O, 5.75%. Calcd for $C_{40}H_{68}O_2$: C, 82.75; H, 11.72; O, 5.52%.

One of us (H. M.) thanks Ecole Normale Supérieure for a fellowship-at-large. We thank CNRS (PIRMED programme) for a partial grant. We thank Dr. B. Das and his staff for the mass spectra and Mlle C. Muller for the microanalyses.

References

1) G. Ourisson, P. Albrecht, and M. Rohmer, *Trends Biochem. Sci.*, **7**, 236, (1982).

2) A. Milon, G. Wolff, G. Ourisson, and Y. Nakatani, *Helv. Chim. Acta*, **69**, 12 (1986).

3) D. Heissler, R. Ocampo, P. Albrecht, J.-J. Riehl, and G. Ourisson, *J. Chem. Soc., Chem. Commun.*, **1984**, 496.

4) M. de Rosa and A. Gambacorta, *System. Appl. Microbiol.*, **7**, 278 (1986).

5) C. K. Hwang, W. S. Li, and K. C. Nicolaou, *Tetrahedron Lett.*, **25**, 2295 (1984).

6) M. A. Umbreit and K. B. Sharpless, *J. Am. Chem. Soc.*, **99**, 5526 (1977).

7) P. A. Grieco and Y. Masaki, *J. Org. Chem.*, **39**, 2135 (1974).

8) H. C. Brown, P. J. Geoghegan, G. J. Lynch, and J. T. Kurek, *J. Org. Chem.*, **37**, 1941 (1977).

9) K. Sato, S. Inoue, A. Onishi, N. Uchida, and N. Minowa, *J. Chem. Soc., Perkin Trans. 1*, **1981**, 761.

10) K. B. Sharpless, R. P. Hanzlik, and E. E. van Tamelen, *J. Am. Chem. Soc.*, **90**, 209 (1968).

11) E. J. Corey and A. Venkateswarlu, *J. Am. Chem. Soc.*, **94**, 6190 (1972).

12) E. Keynan and D. Eren, *J. Org. Chem.*, **51**, 3165 (1986) and private communication.

13) S. Terao, M. Shiraishi, and K. Kato, *Synthesis*, **1979**, 467.

 © 1988 The Chemical Society of Japan Bull. Chem. Soc. Jpn., 61, 149—154 (1988)

Invited Paper

Radical Cyclization in the Control of Regio- and Stereochemistry

Gilbert STORK
Department of Chemistry, Columbia University, New York, New York 10027, U.S.A.
(Received August 25, 1987)

This article presents a review of the control of regio- and stereochemistry which is now possible by the use of the recently introduced haloacetal and the related halosilyl ether cyclizations, starting from a cyclohexenol or a cyclopentenol. The hydroxyl group is the control element which permits the addition of two carbon chains to the double bond of the allylic alcohol system, with complete regiospecificity and stereospecificity at the near end of the double bond, and with complete regiospecificity and high stereoselectivity at the far end of the bond. Examples of the use of the new methodology from the field of alkaloid, steroid and prostaglandin synthesis are given.

It is remarkable that the long-known radical-mediated cyclization of 6-bromo-1-hexene to methylcyclopentane[1] has not seen much application to specific problems of synthesis. Perhaps this is because the process is intrinsically limited to the construction of structures which specifically include a substituted cyclopentane (or, less frequently, a substituted cylcohexane).[2]

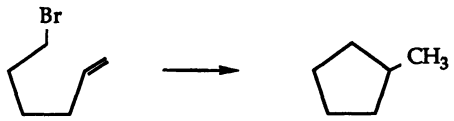

A potentially much broader field of application opened up with the introduction of the vinyl radical cyclization,[3] since the resulting five- or six-membered ring now contains a double bond in a predetermined position, where it can serve as the basis for subsequent synthetic elaboration. A further increase in scope followed the discovery[4] that the vinyl radical which leads to ring formation can be produced not only by the classical removal of a halogen atom, but also by selective addition of a stannyl radical to an alkyne.

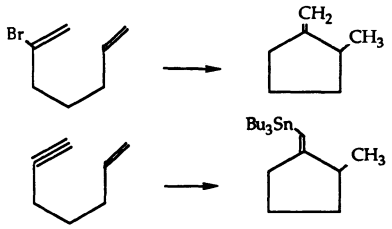

These developments have been important. What I wish to review here, however, are radical-mediated cyclizations which we believe to be of much wider application. The new methodology followed the realization that the stereochemistry of the hydroxyl group of a cyclic allylic alcohol, most commonly a cyclopentenol or a cyclohexenol (cf. 1), could be used to add functional carbon chains at the near (α), as well as at the far (β) end of the double bond. And this proceeds with *complete* regiospecificity and stereospecificity at the α end, as well as complete regiospecificity and high stereoselectivity at the β end. In other words, any of the four possible arrangements of two functional chains on adjacent carbon atoms could be produced at will.

The principle of the method involves *connecting to the allylic hydroxyl a detachable radical precursor capable of cyclizing to a five-membered ring.*[5] The *regiospecificity* at the α-center follows because of the great preference (magnified here, for obvious reasons) for the formation of a five-membered ring. The *stereospecificity* at the α-center follows from the Bürgi-Dunitz-like[6] ($\sim 109^{\circ}_{\pm}$) approach of the radical center to the plane of the double bond.[7] When the olefinic double bond is in a six-membered or smaller ring, this necessarily results in the cis fusion of the new ring. Eventual removal of the detachable connection concludes the regio- and stereospecific attachment of the α-chain, cis to the controlling hydroxyl group.

This is illustrated, using an acetal link as the detachable connector.

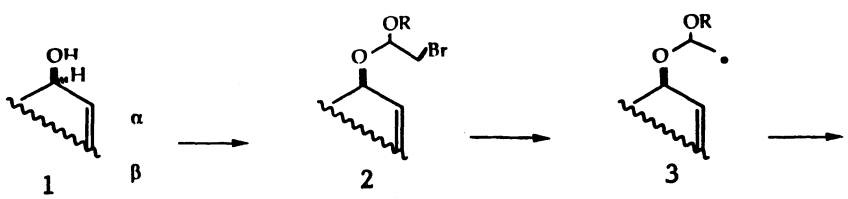

Obviously, the epimeric stereochemical attachment of the α-chain is accessible by starting with the epimeric allylic alcohol.

Not only can regio- and stereospecific addition of a functional chain be accomplished at the α-center, it can simultaneously be achieved at the β-center. Three requirements had to be met to make this a useful process: a) The radical generated at the β-center by the initial cyclization has to be trapped in an *intermolecular* reaction within the lifetime of that radical. This is not a problem when the required β-substituent is a hydrogen (e.g. from a stannane). It becomes a problem when the trap must be a functional carbon atom or a functional carbon chain. Such a trap should not be so efficient that it would trap the initiator itself (e.g. $Bu_3Sn\cdot$) or the initial primary radical before it cyclizes, but efficient enough to trap the β-center (which may be secondary or tertiary) faster than the latter either acquires a hydrogen from some component of the medium, or disproportionates. b) The species capable of trapping the β-center must be as versatile as possible. The most useful trap would result in the delivery of a one carbon functional species. c) The stereochemistry must be controlled.

We eventually concluded that *t*-butyl isocyanide would answer the second requirement by transferring a cyano group to the β-center.[8] That this proved successful is fortunate because isocyanides are known to react with stannyl radicals, as shown.[9]

$$R_3Sn\cdot + R'\text{-}N{=}C \rightarrow R_3Sn(C{\equiv}N) + R'\cdot$$

This process is, however, considerably slower than reaction of the stannyl radical with the halo acetal (**2**→**3**). It is, of course, necessary to keep the stannane concentration low enough if one wishes to deliver a carbon species, rather than a hydrogen, at the β-center.

A convenient way to achieve the required low concentration involves producing the necessary stannane by conducting the radical cyclization-trapping in the presence of sodium cyanotrihydroborate in refluxing *t*-butyl alcohol.[10] This procedure regenerates tributylstannane from the small concentration of tributylstannyl halide produced as the reaction proceeds. An important added advantage is that only ~0.1 equiv of halostannane needs to be added to carry out the whole process.

Note that the use of *t*-butyl isocyanide cannot lead to telomer formation because the adduct once formed loses its radical nature simply by ejection of a *t*-butyl radical.

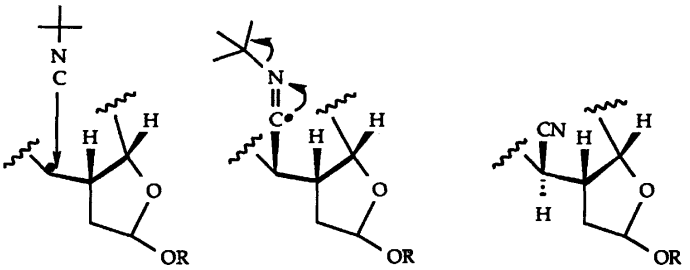

With respect to the final requirement of stereoselectivity at the β-center, we made use of the fact that the cis fusion of the five-membered acetal ring would produce a molecule with a clear-cut differentiation between its convex and its concave faces. As we anticipated, attachment of the trap takes place on the more accessible convex face with high selectivity.

The result of this cyclization-trapping process, therefore, is that the allylic hydroxyl controls the attachment of the vicinal substituent (an acetaldehyde equivalent in the bromo acetal version of the general

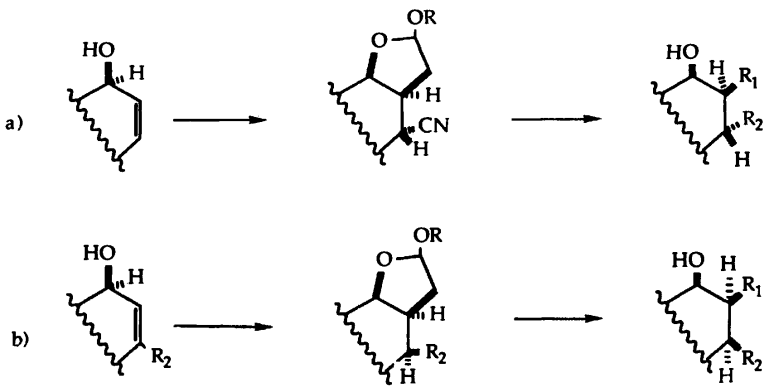

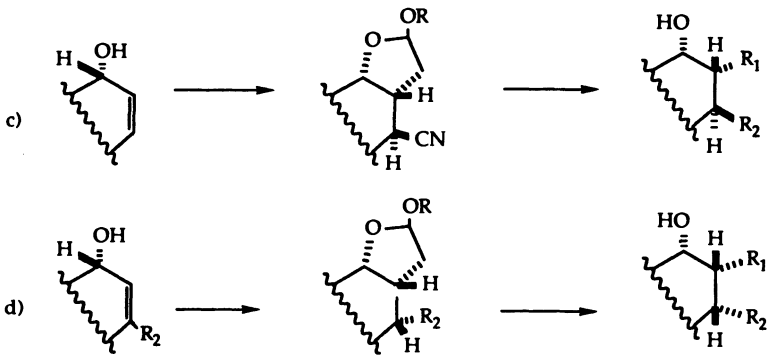

scheme) cis, and that of the substituent at the far end of the double bond trans to it. Because the far end substituent can be either a functional carbon (e.g. cyano group) or a hydrogen (in the absence of carbon trap), all four possible arrangements at the site of the original double bond can be produced at will. This is shown in a)—d) above. Of course, after it has served its control function, the hydroxyl can eventually be kept, inverted, oxidized or removed entirely, as the situation requires.

Note also that the halo acetal sequence delivers the acetaldehyde chain in a protected acetal form. This allows various organometallic transformations to be carried out on the substituent (e.g. cyano) before liberating and elaborating the acetaldehyde chain.

The synthesis of prostaglandins,[11] which is illustrated below, is one of the simplest and most obvious applications of the general principles that have just been outlined.

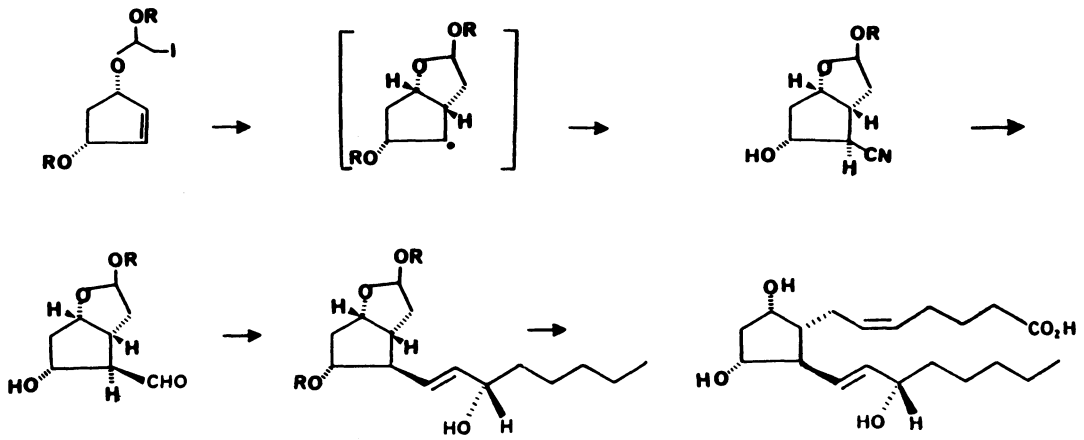

This is an archetype for this type of construction since it simply requires the addition of two chains of defined stereochemistry to the double bond of a cyclic allyl alcohol. One further illustration, in a less obvious situation, will serve to emphasize the generality of this reaction sequence. Consider the problem of constructing the hydrindan **4** a useful starting material for the synthesis of calcitriol (**5**) and other D vitamins.

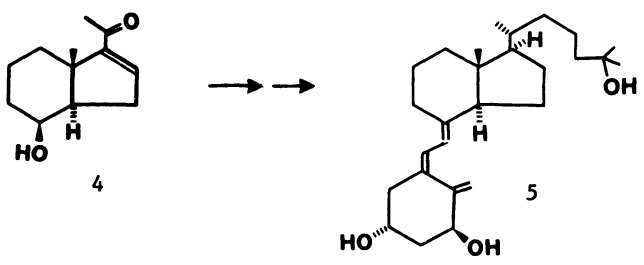

4 5

This requires the assembly of a *trans*-hydrindan system, and it is not immediately obvious that this target could, nevertheless, be reached easily by the general bromo acetal route. This is, however, again simply a matter of controlling the regio- and stereochemistry of two vicinal functional chains: only four steps are required to make **4**, starting with 3-methyl-2-cyclohexenol,[12] as is shown below.

In this particular construction, we see again the protection afforded by the acetal function during the transformation (reaction of **6** with LDA, then with oxygen) of the functional chain trapped at the far center (methacrylonitrile, rather than t-butyl isocyanide, was used as the trap in this particular case, as a convenient precursor of the required acetonyl residue).

This is not the only way that the problem of ring junction stereochemistry can be solved using the

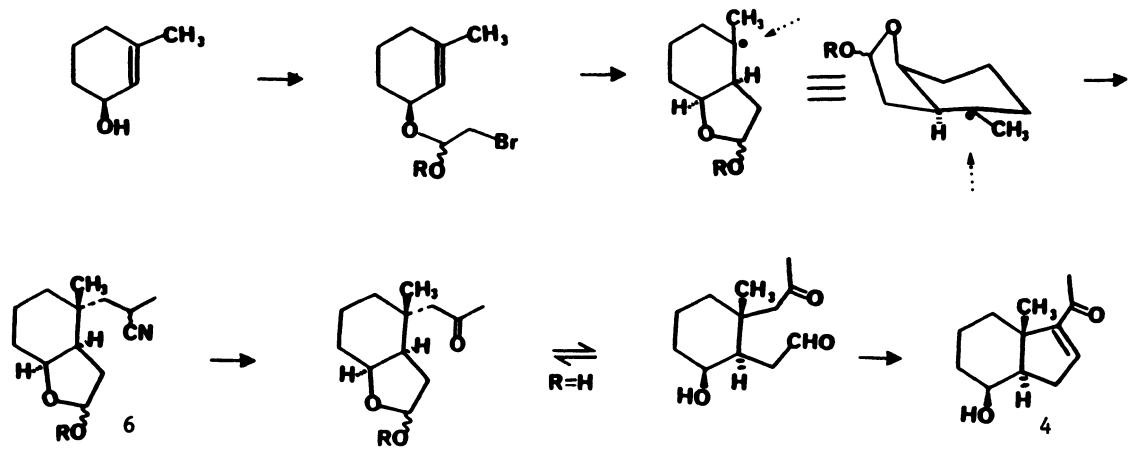

principles outlined here. The trapping from the convex side at the far center means that if it is a hydrogen atom which is delivered at that center (no carbon trap present), it will be delivered anti to the controlling allylic hydroxyl (cf. b) and d) above). An important corollary of that simple fact is that cis or trans ring fusions can be generated at will.[13] An example[14] is shown below.

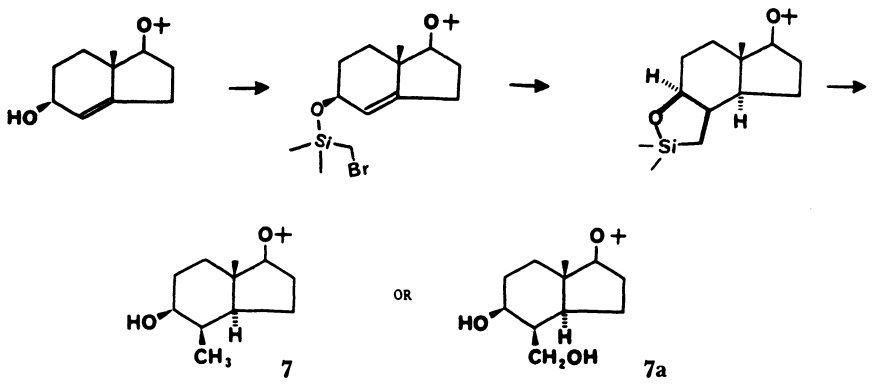

Note that the cis junction would be produced, if desired, merely by starting with the epimeric alcohol.

This particular case illustrates the use of a silyl ether rather than an acetal as the detachable connection. This is a useful variant when either a one carbon functional group[15] (cf. **7a**), or even a methyl group, is required adjacent to the original allylic hydroxyl, rather than an acetaldehyde chain.

Two special features should be pointed out here: 1) The ring junction is produced, cis or trans at will, by a process which does not depend on the thermodynamic stability of the particular bicyclic system. Either cis- or trans-hydrindans can thus be produced, as well as cis or trans decalins. 2) The regio- and stereochemistry of the newly added substituent, either hydroxymethyl or methyl, is also kinetically determined so that, in the trans series, it ends up axial even if, as in **7** and **7a** this happens to produce a 1,3-diaxial interaction with an angular methyl group.[16] This is particularly useful because it is often a simple matter to invert the axial substituent to the more stable epimeric position, via the adjacent ketone.

Let us end by showing an example which further emphasizes the variety of synthetic targets which can take advantage of the features that we are illustrating here. This concerns again setting up vicinal stereochemistry on a double bond via the bromo acetal route, but it now involves a homoallylic rather than an allylic alcohol as we see in **8**. This raises a new problem because abstraction of the starred allylic hydrogen by the radical derived from the bromo acetal would now compete with cyclization. This is circumvented by increasing the cyclization rate, in this particular case by making the olefin more electron poor by conjugation with the carbonyl group.

The radical cyclization-trapping process (trapping at the far center is now by a hydrogen; cf. case b above) thus controls the last two centers in ring E of the alkaloid reserpine. That these are correctly placed, as anticipated, is shown by transformation of the major cyclization product **9** to reserpinol.[17]

There are other processes which make use of the stereochemistry of an allylic hydroxyl to direct the formation of a carbon-carbon bond. The best known of these is the Claisen rearrangement (cf. A below). This very important reaction transfers

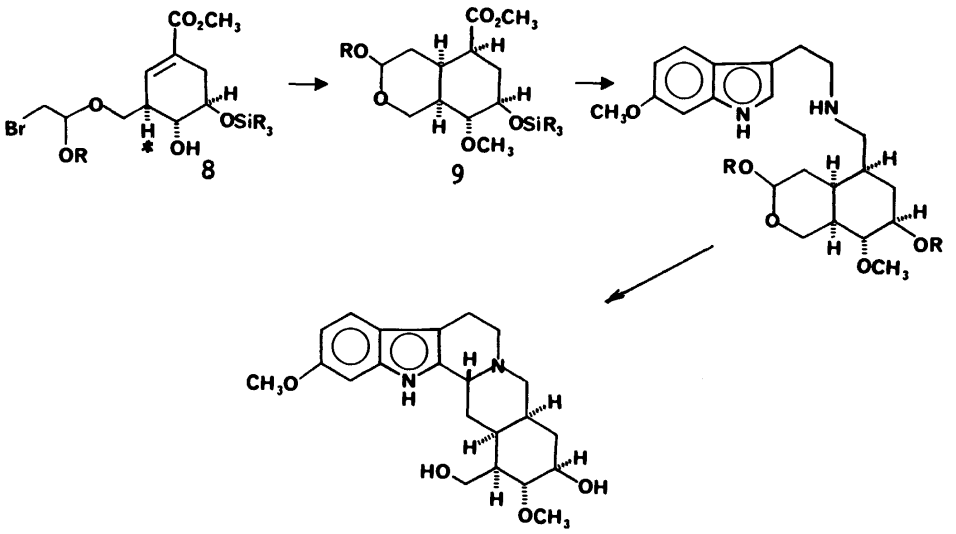

stereochemistry from an allylic hydroxyl to the far end of the related double bond, but loses the hydroxyl in the process. There are multiple-step schemes which can control two adjacent centers, as the bromo acetal radical process can. The Diels-Alder reaction, for instance, using a conjugated cyclic ketone, leads to a cyclohexene which can be cleaved to give two different chains adjacent to the carbon oxygen bond (cf. **B**). The stereochemistry is, however, not broadly controllable in this special application of a reaction which

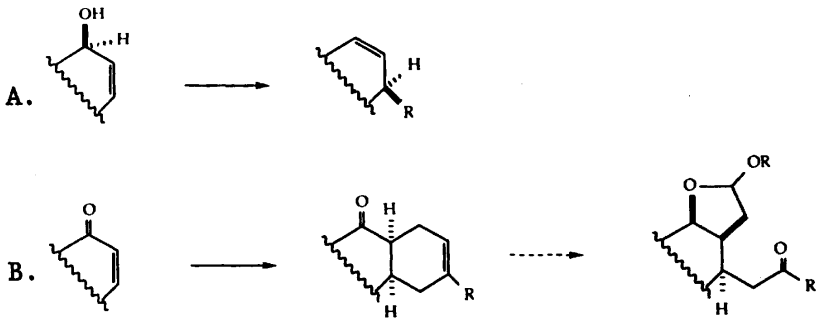

has, of course, many other important uses. We believe, however, that the concise transformations we have just discussed (cf. a)—d) above) have considerable potential in synthesis.

I want to acknowledge my indebtedness to the members of my group, some cited here, some not, who have helped shape the work described here. I am also pleased to thank the United States National Science Foundation and the National Institutes of Health for their financial support, without which this work would not have been possible.

References

1) C. Walling, J. H. Cooley, A. A. Ponaras, and E. J. Racah, *J. Am. Chem. Soc.*, **88**, 5361 (1966); R. C. Lamb, P. W. Ayers, and M. K. Toney, *ibid.*, **85**, 3483 (1963); C. Walling and A. Cioffari, *ibid.*, **94**, 6059 (1972) and A. L. J. Beckwith and K. U. Ingold, "Rearrangements in Ground and Excited States," ed by P. de Mayo, Academic Press, New York (1980) pp. 182—220.

2) Imaginative application of this "simple" radical cyclization has, however, recently been made by Curran: D. Curran and S. C. Kuo, *J. Am. Chem. Soc.*, **108**, 1106 (1986).

3) G. Stork and N. H. Baine, *J. Am. Chem. Soc.*, **104**, 2321 (1982).

4) G. Stork and R. Mook, Jr., *J. Am. Chem. Soc.*, **109**, 2829 (1987).

5) G. Stork, R. Mook, S. D. Biller, and S. D. Rychnovsky, *J. Am. Chem. Soc.*, **105**, 3741 (1983).

6) H. B. Bürgi, J. D. Dunitz, J. M. Lehn, and G. Wippf, *Tetrahedron*, **30**, 1563 (1974), and earlier papers.

7) Cf. M. J. S. Dewar and S. Olivella, *J. Am. Chem. Soc.*, **100**, 5290 (1978); A. L. J. Beckwith and C. H. Schiesser, *Tetrahedron*, **41**, 3925 (1985); K. N. Houk, M. N. Paddon-Row, D. C. Spellmeyer, N. G. Rondan, and S. Nagase, *J. Org. Chem.*, **51**, 2874 (1986).

8) G. Stork and P. M. Sher, *J. Am. Chem. Soc.*, **105**, 6765 (1983).

9) Cf. D. H. R. Barton, G. Bringmann, and W. B. Motherwell, *Synthesis*, **1980**, 68.

10) G. Stork and P. M. Sher, *J. Am. Chem. Soc.*, **108**, 303 (1986).

11) G. Stork, P. M. Sher, and H. L. Chen, *J. Am. Chem.*

Soc., **108**, 6384 (1986).
12) Unpublished work by T. Zebovitz from this laboratory.
13) G. Stork and M. Kahn, *J. Am. Chem. Soc.*, **107**, 500 (1985).
14) G. Stork and M. J. Sofia, *J. Am. Chem. Soc.*, **108**, 6826 (1986).
15) Cf. K. Tamao, N. Ishida, and M. Kumada, *J. Org. Chem.*, **48**, 2120 (1983).
16) A. J. Burgstahler and I. C. Nordin, *J. Am. Chem. Soc.*, **81**, 3151 (1959); see also R. K. Hill and A. G. Edwards, *Tetrahedron Lett.*, **1964**, 3239.
17) Unpublished work by M. Casey and P. C. Tang from this laboratory.

 © 1988 The Chemical Society of Japan Bull. Chem. Soc. Jpn., 61, 155—163 (1988)

Invited Paper

Syntheses and Dynamic Behavior of Chiral Heptalenes

Klaus HAFNER,* Günter L. KNAUP, and Hans Jörg LINDNER
Institut für Organische Chemie der Technischen Hochschule Darmstadt,
Petersenstrasse 22, D-6100 Darmstadt, F.R.G.
(Received August 31, 1987)

Cycloaddition reactions of azulenes with dimethyl acetylenedicarboxylate afford an excellent access to a large variety of substituted dimethyl 1,2-heptalenedicarboxylates. These can be converted into various methylheptalenes, which proved to be remarkably stable. This allowed for the first time a separation of the bond shift isomers as well as an optical resolution of derivatives of this axial chiral 12π-electron system. Kinetic studies of bond shifting and ring inversion provide information on the transition states of these dynamic processes.

Since Hückel introduced his famous rule[1] that a monocyclic planar π-electron system should be aromatic if it contains $[4n+2]$ π-electrons, a large number of neutral and ionic ring systems[2] had been prepared in order to test the validity of this aromaticity concept. The investigations verified a clear distinction in the chemical and physical properties between the $[4n+2]$ and $4n$ π-electron systems and completely justified Hückels rule. For instance, the two species differ characteristically in the ^{1}H NMR spectra. While the outer protons of the $[4n+2]$ π-systems show a low field shift caused by a diamagnetic ring current,[3] those of the $4n$ π-systems show a high field shift, which could be attributed to a paramagnetic contribution arising from the mixing of excited states with the ground state.[4] Whereas the HMO-theory originally only predicted that $[4n+2]$ π-systems should be more stable than $4n$ π-systems, later theories suggested that the $4n$ π-systems should be destabilized by delocalization and should be in fact antiaromatic.[5] This is valid not only for annulenes, but also for bicyclic systems derived from annulenes bridged by an essential single bond. Indeed, the smallest members of the mono- and bicyclic annulenes, cyclobutadiene[2] and pentalene,[6] are so reactive, that they can not be isolated. Another significant difference is the fact that mono- and bicyclic systems with $4n$ π-perimeters possess localized double bonds in the ground states. Therefore, the structures with delocalized bonds are only transition states on the potential surfaces which connect the localized bond systems with one another. This could be established for tetra-*t*-butylcyclobutadiene,[7] 1,3,5-tri-*t*-butylpentalene,[8] cyclooctatetraene,[9] and heptalene.[10] In contrast to cyclobutadiene and pentalene, the higher homologues, cyclooctatetraene and heptalene, are characterized by nonplanar structures. Thus, from each of these systems exist four isodynamic structures, which are, via bond shifting and ring inversion, in a dynamic equilibrium with one another. A study of both dynamic processes should provide information on their transition states and, therefore, also on the antiaromaticity of the delocalized systems. Assuming planar delocalized transition states for the bond shift and planar localized transition states for the ring inversion, the difference between the activation enthalpies of both processes should be equal to the delocalization energies for the planar ring systems. For cyclooctatetraene, Oth[9] determined by NMR measurements of the ethoxy derivative a difference of 3.5 kcal mol^{-1}, which he attributed to the energy required for the delocalization of the planar 8π-perimeter. A similar value was calculated by Paquette et al.[11] from the differences of the activation enthalpies of methyl-substituted cyclooctatetraenes taking into account different steric strains in the assumed planar localized and delocalized transition states. In the case of the 1,2,3-tri- and 1,2,3,4-tetramethylcyclooctatetraenes, even a separation of the bond shift isomers and an enrichment of the enantiomers was possible.[12]

Syntheses and Physical Properties of Heptalenes

Dauben and Bertelli[13] demonstrated in 1961 that the dihydroheptalenes **2** and **3** can be transformed into heptalene **5** by hydride abstraction and subsequent

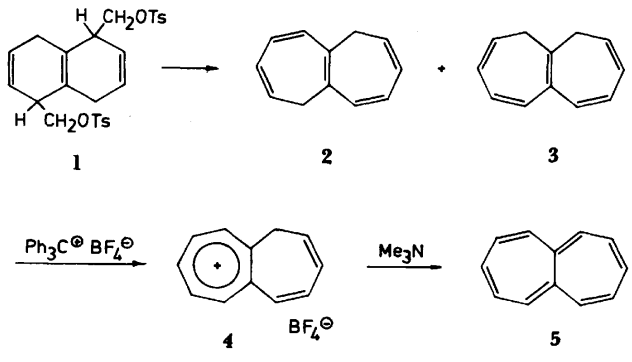

Scheme 1.

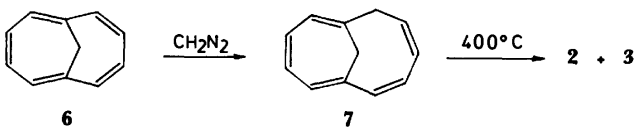

Scheme 2.

deprotonation of the resulting heptalenium salt **4** (Scheme 1). Since then, additional syntheses of the bicyclic 12π-system **5** were published[14] using this method. While Dauben and Bertelli[15] prepared a mixture of **2** and **3** by solvolytic rearrangement of the isotetralin **1**, Vogel et al.[10] obtained a similar mixture by pyrolysis of **7**, which was prepared by ring expansion of 1,6-methano[10]annulene **6** (Scheme 2).

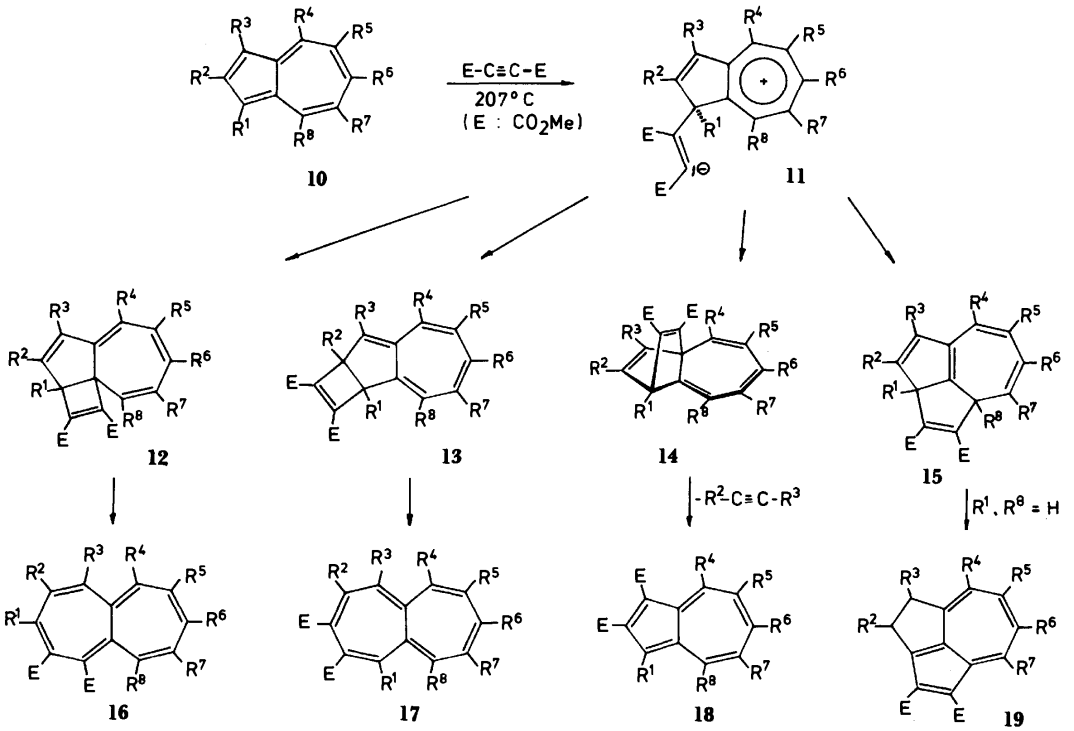

Scheme 3.

10—19	R^1	R^2	R^3	R^4	R^5	R^6	R^7	R^8	Yield/%			
									16	**17**	**18**	**19**
a	H	H	H	H	H	H	H	H	25	—	2	1
b	H	H	Me	H	H	H	H	H	23	17	3[a]	1
c	H	H	*t*-Bu	H	H	H	H	H	2	1	21	—
d	H	H	H	H	H	H	H	Me	35[b]	—	2[b]	—[b]
e	Me	H	Me	H	H	H	H	H	—	—	40	—
f	H	H	Me	Me	H	H	H	H	—	—	42	—
g	H	H	Me	H	H	H	H	Me	53	—	10	—
h	H	H	H	Me	H	H	H	Me	44	—	3	—
i	H	H	H	Me	H	Me	H	Me	56	—	8	—
j	H	H	Me	Me	H	H	H	Me	32	—	55	—
k	H	H	Me	Me	H	Me	H	Me	40	2	21	—
l	H	Me	H	Me	H	Me	H	Me	56	—	3	—
m	H	*i*-Pr	H	Me	H	Me	H	Me	56	—	6	—
n	H	*t*-Bu	H	Me	H	Me	H	Me	55	—	—	—
o	H	H	*i*-Pr	Me	H	Me	H	Me	7	—	53	—
p[21]	H	H	Me	H	*i*-Pr	H	H	Me	63	—	6	—
q	H	H	$-(CH_2)_2-$		H	H	H	H	—	—	—	—[c]
r	H	H	$-(CH_2)_3-$		H	H	H	H	8	5	—	—
s	H	H	$-(CH_2)_4-$		H	H	H	H	35	23	—	1
t	H	H	$-(CH_2)_4-$		H	Me	H	Me	51	1	—	—
u	H	H	H	Me	H	OMe	H	Me	43	—	10	—
v	H	H	H	H	H	CO_2Et	H	H	10	—	—	—

a) and 1% dimethyl 3-methylazulene-1,2-dicarboxylate b) and 3% dimethyl 6-methylheptalene-1,2-dicarboxylate, 1% dimethyl 4-methylazulene-2,3-dicarboxylate, 4% dimethyl 5-methyl-3,4-dihydrocyclopent[*cd*]azulene-1,2-dicarboxylate c) and 7% dimethyl 3,4-dihydrocyclopent[*cd*]azulene-1,2-dicarboxylate.

In 1979, both Vogel et al.[16] and Paquette et al.[17] developed heptalene syntheses based on dibromocarbene additions to isotetralin. Similarly 3,8-dibromoheptalene **8**[18] and dimethyl heptalene-3,8-dicarboxylate **9**[19] can be prepared. In contrast to these multistep

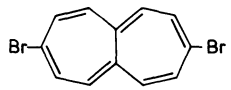

8

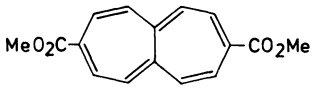

9

syntheses, we developed an extremely simple, onepot synthesis, which allows the preparation of numerous substituted heptalene-1,2-dicarboxylates.[20] Cycloaddition of dimethyl acetylenedicarboxylate to azulenes **10** in boiling tetralin affords the dimethyl heptalene-1,2-dicarboxylates **16** in yields up to 64%. Side products of these reactions are the dimethyl heptalene-2,3-dicarboxylates **17**, the dimethyl azulene-1,2-dicarboxylates **18** and the dimethyl 3,4-dihydrocyclopent[*cd*]azulene-1,2-dicarboxylates **19** in varying yields (Scheme 3). The formation of all these compounds can be rationalized by invoking **11** as an intermediate formed by an electrophilic attack of the electron-deficient alkyne to the azulene. Ring closure of **11** should lead to the adducts **12**—**15**, which then isomerize to the heptalenes **16**, **17**, and the azulene derivatives **18**, **19**, respectively. The drastic reaction conditions required for the cycloaddition did not allow the detection of the proposed intermediates. However, if the reaction is carried out at 7 kbar and 50 °C, the [4+2] adduct **14** becomes the main product.[22]

In contrast to the parent compound **5**, the 3,8-disubstituted derivatives **8**, **9**, and the heptalenedicarboxylates **16**, **17** are remarkably stable. However, in boiling tetralin **16** undergoes a slow irreversible rearrangement to heptalene-1,3-dicarboxylates **20** and a ring contraction to the azulene derivatives **18**, **21**, and **22**. The rate of this reaction and the ratio of the products depend strongly on the substituents.[23] While the thermolysis of the dimethyl heptalene-1,2-dicarboxylate **16a** yields predominantely the azulenes **18a**, **21a**, and **22a**, and only traces of the heptalene-1,3-dicarboxylate **20a**, compounds of this type become the main products by the thermolyses of methyl-substituted heptalenedicarboxylates (Scheme 4). As we could show, the stability of heptalenes not only increases by electron-withdrawing substituents in the 1- or 3-position (the positions with high electron densities) but also by alkyl substituents in the peri-positions. Therefore, reduction of the dimethyl heptalenedicarboxylates **16** with diisobutylaluminum hydride (DIBAH) afford the 1,2-bis(hydroxymethyl)-heptalenes **23** as thermally and air-stable yellow crystals[24,25] (Scheme 5). Due to the chiral heptalene system, the diastereotopic hydroxymethyl groups appear in the ^{1}H NMR spectra as AB spin systems with vicinal coupling constants around 15 Hz. The tetramethyl derivative **23k** can be converted into the dichloride **24b**, which can be reduced with lithium triethylborohydride to the hexamethylheptalene **26**.[24] In contrast to **24b**, the trimethyl derivative **24a** is unstable at room temperature but rather eliminates HCl spontaneously to the dimethylidene compound **25**[25] (Scheme 6). Similarly to the HCl elimination of **24a**, the diols **23** can be dehydrated by treatment with catalytic amounts of *p*-toluenesulfonic acid in boiling benzene.[25] These reactions lead (probably via an enolic structure similar to **25** to the heptalene-2-carbaldehydes **27**. Decarbonylation of **27** with chlorotris(triphenylphosphin)rhodium(I) yields the methylheptalenes **28** as thermally and airstable compounds[25] (Scheme 7). In addition to **28a**—**d** we also synthesized 1,6-dimethylheptalene **31** by an

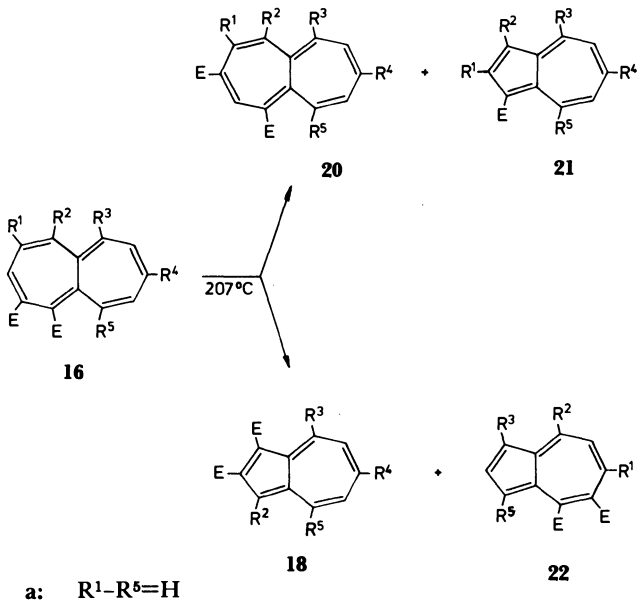

a: R^1-R^5=H
d: R^1-R^4=H, R^5=Me
i: R^1,R^2=H, R^3-R^5=Me
k: R^1=H, R^2-R^5=Me
l: R^2=H, R^1,R^3-R^5=Me

Scheme 4.

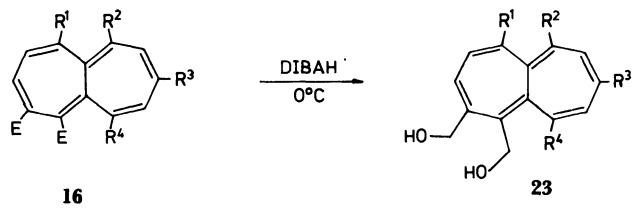

b: R^1=Me, R^2-R^4=H
d: R^1-R^3=H, R^4=Me
i: R^1=H, R^2-R^4=Me
j: R^3=H, R^1,R^2,R^4=Me
k: R^1-R^4=Me

Scheme 5.

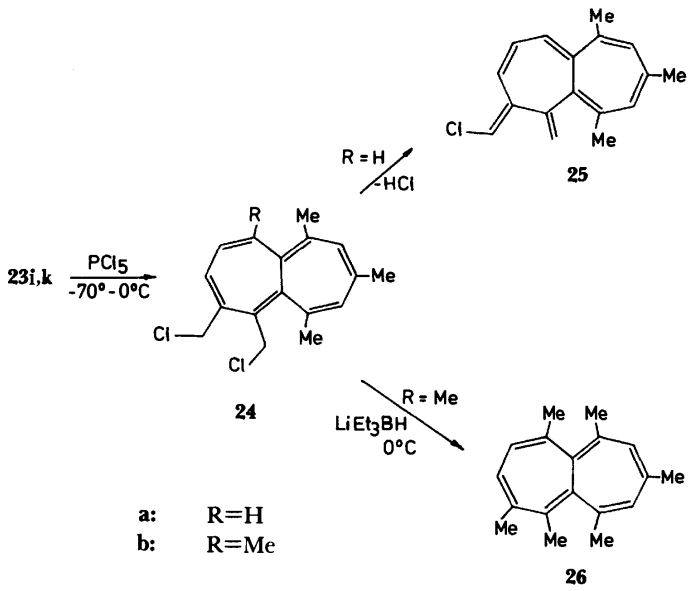

Scheme 6.

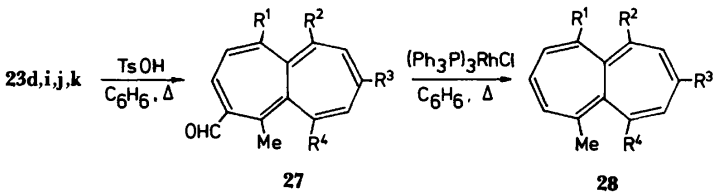

a: R^1-R^3=H, R^4=Me
b: R^1=H, R^2-R^4=Me
c: R^1,R^2,R^4=Me, R^3=H
d: R^1-R^4=Me

Scheme 7.

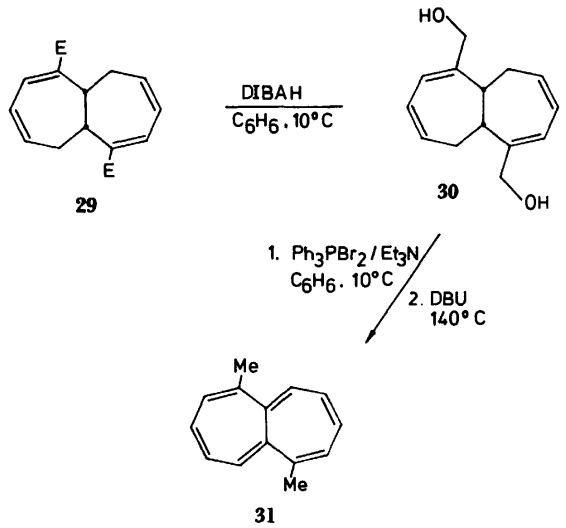

Scheme 8.

entirely different pathway after the dimethyl *cis*-1,5a,6,10a-tetrahydroheptalenedicarboxylate **29** became readily available by a new rearrangement reaction.[26]

Reduction of **29** with DIBAH and subsequent twofold dehydration of the resulting alcohol **30** affords the heptalene **31** as a yellow oil[25] (Scheme 8). In contrast to the extremely air-sensitive and thermally unstable parent compound **5**, the described methylheptalenes — even the dimethyl derivatives **28a** and **31** — are surprisingly stable. This could not only be a result of a kinetic stabilization due to a steric shielding of the heptalene system, but rather to an enhancement of twisting of the nonplanar 12π-perimeter caused mainly by the steric interaction of the substituents in the peri-positions. This reduces the cyclic conjugation and increases the HOMO-LUMO gap and, therefore, reduces the reactivity of the $4n$ π-system.

Resolution and Chiroptical Properties of Chiral Heptalenes

Heptalenes, as most other $4n$ π-systems, show in the ground state π-bond fixation. Therefore, from unsymmetrically substituted heptalenes exist two nonequivalent bond shift isomers. The ratio of these isomers depends on the substituents. For the un- and

monosubstituted dimethyl heptalene-1,2-dicarboxylates **16a—d** and the bridged derivatives **16r—t** only the bond shift isomers with a single bond between the ester groups can be observed in the ^{1}H NMR spectra. However, for **16g—o**, which have two or three alkyl substituents in the peri-positions, 10—30% of the other bond shift isomers can be detected. The preference of the isomers with a single bond between the ester groups can be explained by the tendency of the carboxylate groups to assume a coplanar arrangement to the adjacent double bonds of the ring system, which is sterically hindered in the other isomers. In contrast to some heptalene-1,2-dicarboxylates **16**, both bond shift isomers of the diols **23**, the 2-carbaldehydes **27** as well as the methylheptalenes **26** and **28** can be detected in varying ratios in the ^{1}H NMR spectra. Although a unique trend has not been found so far, an effect is evident. The isomer with the lowest number of substituents in the peri-positions having a double bond to the bridge atoms C-5a and C-10a is thermodynamically more stable than the other. This might be due to a smaller steric interaction across the peri-positions in this bond shift isomer.

X-Ray analyses[27] of the heptalene dicarboxylates **9** and **16a** confirmed a C_2-geometry for the heptalene system with the two annelated seven-membered rings in boat conformations. Therefore, for heptalenes should, according to Oth et al.,[28] exist four isodynamic axial chiral structures which are, via bond shift (BS) and ring inversion (RI), in a dynamic equillibrium with one another (Scheme 9). So far, π-bond shift has been investigated in heptalene itself (E_a=3.5 kcal mol^{-1}),[10] heptalene-1,6-dicarbaldehyde ($\Delta G^{\ddagger}$=9.9 kcal mol^{-1}),[16] dimethyl heptalene-1,6-dicarboxylate ($\Delta G^{\ddagger}$=14 kcal mol^{-1}),[16] and dimethyl 6,8,10-trimethylheptalene-1,2-dicarboxylate **16i** ($\Delta G^{\ddagger}$=21.7 and 21.0 kcal mol^{-1}, respectively).[29] For the latter, the bond shift isomers can even be separated by low temperature chromatography. As these results indicate, the energy barrier for the bond shift increases with the number of substituents in the peri-positions of the heptalenes. In fact, for the dimethyl 5,6,8,10-tetramethylheptalene-1,2-dicarboxylate **16k** we succeeded for the first time in isolating in pure form all four isomers (+)-M-**A**, (+)-M-**B**, (−)-P-**A**, and (−)-P-**B** of a $4n$ π-system.[30,31] The bond shift isomers rac-**A** and rac-**B** of **16k** can be separated by simple chromatography on alumina at room temperature. Both bond shift isomers differ characteristically in their NMR and UV spectra. While the protons H-3 and H-4 of **16kA** show a coupling constant of 6.9 Hz, those of **16kb** appear as an AB spin-system with a coupling constant of 11.8 Hz. These values are characteristic for coupling constants via single and double bonds in substituted heptalenes and allow a simple assignment of the positions of the double bonds. The structures of the bond shift isomers A and B of **16k** were also established by X-ray analyses.[30] Although the optical resolution can be carried out by HPLC on triacetylcellulose,[32] for a preparative scale separation we prefered the classic method of fractional crystallization of diastereomeric salts. For that the diesters **16kA**

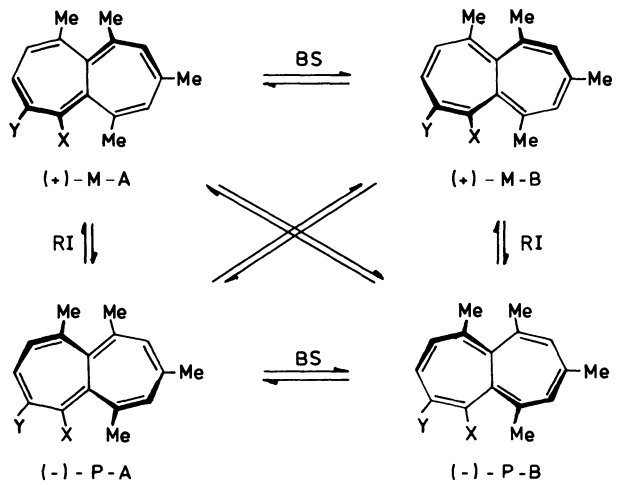

	16k	23k	24b	26	32
X	CO_2Me	CH_2OH	CH_2Cl	Me	CO_2Me
Y	CO_2Me	CH_2OH	CH_2Cl	Me	CO_2H

Scheme 9.

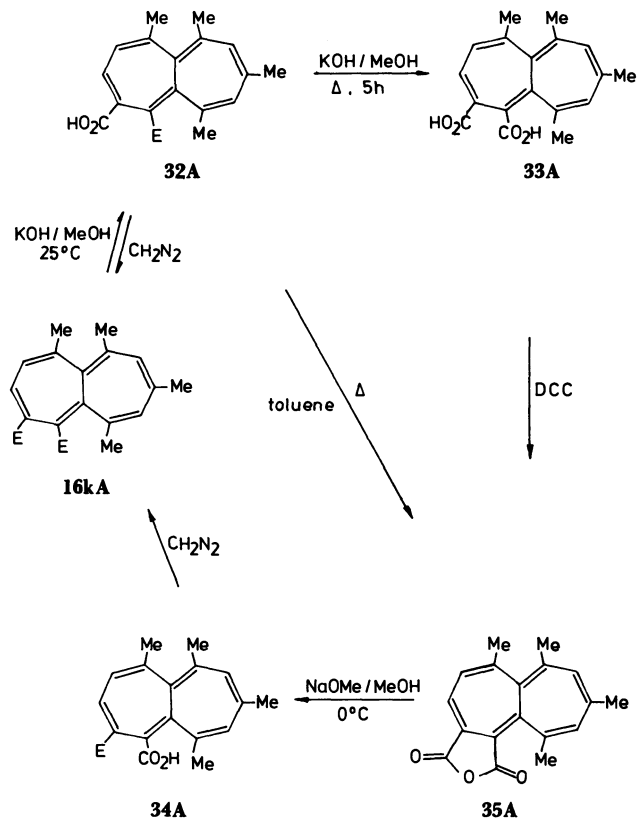

Scheme 10.

and **16kB** were converted into the free acids with potassium hydroxide in methanol. If the reactions are carried out at room temperature, selectively **32A** and **32B** with the carboxylic acid group in 2-position are obtained without bond shift isomerization. On the other hand, the preparation of the dicarboxylic acid **33A** requires considerably higher temperatures. Both the mono-**32A** and the dicarboxylic acid **33A** can be converted into the anhydride **35A**, which selectively affords the 1-carboxylic acid **34A** by treating with sodium methoxide (Scheme 10). The selectivity of the saponification of **16k** and the esterification of **35A** might be due to a steric shielding of the carboxylate group in the 1-positions caused by the methyl groups in the 8-position. In fact, heptalene-1,2-dicarboxylates without substituents in the 8-position, i.e. **16a**—**d**, yield under the same reaction conditions mixtures of the corresponding 1- and 2-carboxylic acids. By our experience, the best optically active amines suitable for the resolution of the 2-carboxylic acids **32** are cinchonine and (+)-1-phenylethylamine for **32A** and (+)- and (−)-ephedrine for **32B**. With these amines, the heptalenes (+)-M-**32A**, (+)-M-**32B**, (−)-P-**32A**, and (−)-P-**32B** were obtained with an enantiomeric purity of greater than 98%, as determined by NMR spectroscopy of the diastereomeric ephedrine salts. The optically active heptalenecarboxylic acids **32** and the diesters **16k**, prepared from **32** with diazomethane without racemization, have very high specific optical rotations (Table 1), typical for systems with helical chiral chromophores. The absolute configuration of the chiral heptalenes was achieved by X-ray analysis of the (+)-ephedrine salt of (+)-M-**32A**. Since both bond shift isomers of (+)-M-**32** show very similar CD-spectra (characterized by two positive Cotton effects at 358, 321 nm, and 380, 312 nm, respectively, and two negative Cotton effects at 280, 252 nm, and 278, 224 nm, respectively) (Fig. 1), the two bond shift isomers must have the same absolute configuration. Although the bond shift isomers of the dimethyl 6,8,10-trimethylheptalene-1,2-dicarboxylate **16i** undergo at room temperature in solution a fast interconversion, they are stable in the crystalline form. NMR spectra taken of solutions of these crystals show each to be isomerically pure. While crystallization from hexane/ether of **16i** and the 4-isopropyl- and 4-*t*-butyl derivatives **16m** and **16n** affords selectively the thermodynamically more stable isomers (single bond between the ester groups), the tetramethyl derivative **16l** crystallizes to give only the other isomer. So far, all attempts for an optical resolution, or at least an enrichment of one of the enantiomeres, of **16i** by fractional crystallization of salts of the carboxylic acid **36** with optically active amines have failed. This is probably due to the existence of both bond shift isomers of **16i** in solution. Nevertheless, a resolution could be achieved with the (−)-menthyl ester **38**, prepared from the anhydride **37** with (−)-menthol and subsequent esterification with diazomethane (Scheme 11). Crystallization at room temperature leads selectively to the (−)-menthyl-(−)-P-heptalene diastereomer (−)-**38A**. However, the ^{1}H NMR spectra at room temperature clearly show that the four diastereomers (−)-**38A**, (+)-**38A**, (−)-**38B**, and (+)-**38B** exist in the equilibrium in a ratio of 5.5:3.3:1.2:1. Reduction of the enantiomerically pure diesters (−)-P-**16kA** and (−)-P-**16kB** with diisobutylaluminium hydride affords the alcohols (−)-P-**23kA** and (−)-P-**23kB** with enantiomeric purities of greater than 98%, as shown by ^{1}H NMR spectra using the chiral shift reagent Eu(hfc)$_3$. Since these optically active alcohols, which have no electron-withdrawing substituents, show CD-spectra very similar to the heptalene-1,2-

Table 1. Specific Optical Rotations of the Heptalenes (+)-M-**16k**, (−)-P-**23k**, (+)-M-**32**, and (−)-P-**28c** in $CHCl_3$

Heptalene	$[\alpha]^{20}_{546}$	$[\alpha]^{20}_{578}$
(+)-M-**16kA**	+1930 (c=1.03)	+1460 (c=1.03)
(+)-M-**16kB**	+1860 (c=0.92)	+1310 (c=0.92)
(+)-M-**32A**	+2550 (c=1.00)	+1910 (c=1.00)
(+)-M-**32B**	+2140 (c=0.51)	+1430 (c=1.03)
(−)-P-**23kA**	−1270 (c=0.99)	−980 (c=0.99)
(−)-P-**23kB**	−1420 (c=0.98)	−1100 (c=0.98)
(−)-P-**28c**	−1670 (c=0.10)	−1290 (c=0.10)

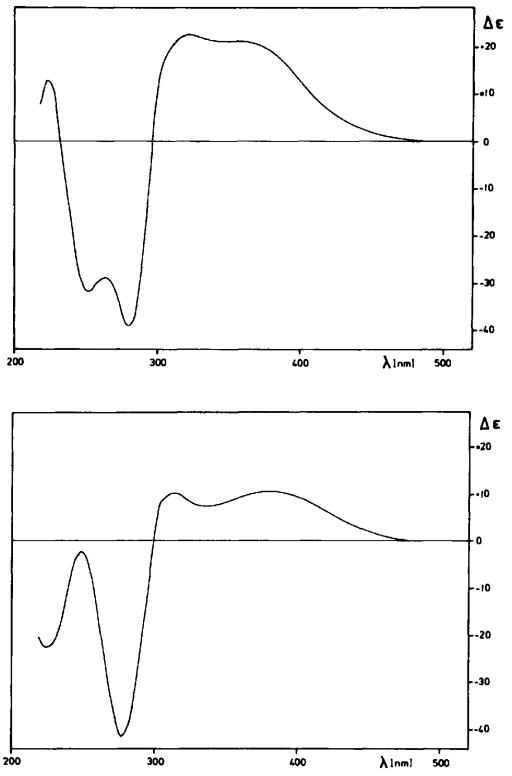

Fig. 1. CD-spectra of the heptalenes (+)-M-**32A** (top) and (+)-M-**32B** (bottom) in $CHCl_3$.

dicarboxylates **16k** and **27**, the chiroptical properties of the chiral heptalenes are caused mainly by the inherent chiral heptalene system and depend, only to a small degree, on the substituents.

The reaction of a mixture of rac-**23kA** and **B** with phosphorus pentachloride and subsequent reduction of the resulting dichloride rac-**24b** affords a mixture of the hexamethylheptalenes rac-**26A** and **B** in good yields. However, all attempts to prepare the enantiomerically pure (−)-P-**26** starting with the pure (−)-P-**23kA** or (−)-P-**23kB** have failed. Instead of the pure compounds, only mixtures of the bond shift isomers of **24k** and of **26** were obtained with specific optical rotations of at most 50, equivalent to an ee of at most 5%. A possible explanation for these results is that the chlorination of **23k** proceeds via an almost planar tropylium cation, which may also be responsible for the instability of the trimethyl derivative **24a**. In fact, the chlorination of **23kA** leads selectively to the bond shift isomer **24kB**, which then is acid-catalyzed equilibrated with the isomer **24bA**. This was shown by isolating the pure isomer **24bB** after quenching the reaction at −60 °C with $NaHCO_3$. A similar tropylium cation may also be responsible for the readily acid-catalyzed dehydration of the alcohols **23** to the aldehydes **27**. This reaction is also accompanied by a racemization. Thus, it is not possible to prepare enantiomerically pure methylheptalenes by this reaction sequence, starting with enantiomerically pure heptalene-1,2-dicarboxylates.[24,25] However, it has been shown recently that the optical resolution of the 1,5,6,10-tetramethylheptalene rac-**28c** can be carried out in good yields by HPLC on triacetylcellulose.[34] As expected, the chiroptical properties of the enantiomers of **28c** are very similar to those of the corresponding optically active heptalene carboxylates and diols.

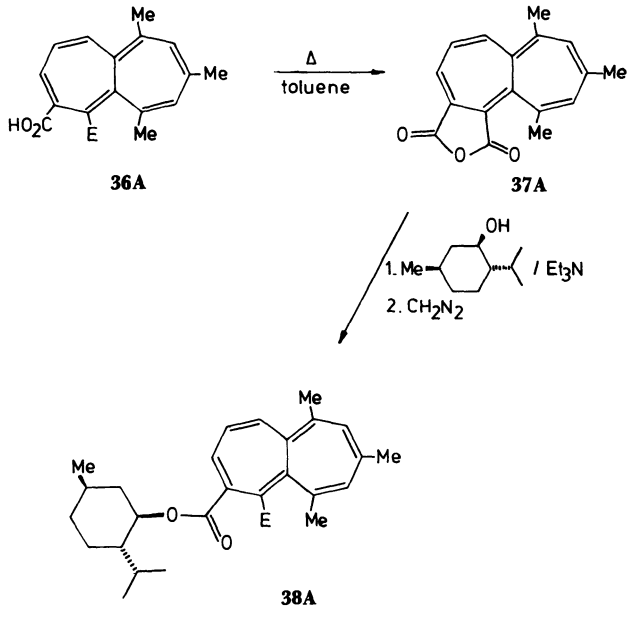

Scheme 11.

The Dynamic Behavior of Chiral Heptalenes

The separation of the bond shift isomers and the resolution of the enantiomers of the dimethyl 5,6,8,10-tetramethylheptalene-1,2-dicarboxylate **16k** allowed for the first time a determination of the kinetic parameters of both the bond shift and the ring inversion of a substituted heptalene. According to the corresponding studies of cyclooctatetraenes,[9,11,12] this should provide information about the delocalized heptalene system and, therefore, about the antiaromaticity of this 12π-system. However, the energy barrier for the ring inversion of **16k** is considerably higher than that for the bond shift (Table 2). These results are inconsistent with planar transition states for both processes as proposed for the dynamic behavior of all cyclooctatetraenes investigated so far.[9,11] Rather the bond shift must occur via a nonplanar, helical chiral transition state. Therefore, it seems impossible to determine the delocalization energy for the antiaromatic systems from the difference of the activation enthalpies of both processes as done by Oth[9] and Paquette et al.[11] for cyclooctatetraene. Also for the hexamethylheptalene **26** the bond shift occurs with retention of the configuration, but both energy barriers are higher than those for the corresponding dicarboxylate **16k** (Table 2). This might be due to a larger steric hindrance of the spherical methyl groups in comparison with the ester groups. This assumption is corroborated by the fact that the value for the ring inversion, which requires an almost planar transition state, increases more than those for the bond shift. In order to obtain more detailed information about the geometries of the transition states, we calculated the dynamics of both processes for the substituted heptalenes **39**, **40**, **28a**, and **28c** having methyl groups in the peri-positions and also for the parent compound **5** by π-SCF-force field calculations.[35] According to these calculations, the bond shift of the

Table 2. Kinetic Parameters for the Bond Shift (BS) and the Ring Inversion (RI) of the Heptalenes **16k**, **26**, **28c**, and **38**.

Dynamic process	$\Delta H^{\ddagger}_{35°C}$/kcal mol^{-1}	$\Delta S^{\ddagger}_{35°C}$/e.u.
BS **16kB** → **16kA**	22.8±0.6	−11.1±2.0
BS **16kA** → **16kB**	25.7±0.6	−7.8±1.7
RI [(−)-**16kA** ⇌ (−)-**16kB**] → [rac-**16kA** ⇌ rac-**16kB**]	28.3±0.4	−11.6±0.9
RI [(−)-**38A** ⇌ (−)-**38B**] → [rac-**38A** ⇌ rac-**38B**]	20.4±0.3	−10.7±1.0
BS **26A** → **26B**	26.7±1.2	−4.4±3.3
RI [(−)-**26A** ⇌ (−)-**26B**] → [rac-**26A** ⇌ rac-**26B**]	36.7±2.1	1.9±4.6
RI (−)-**28c** → rac-**28c**	31.8±1.2	−4.9±2.6

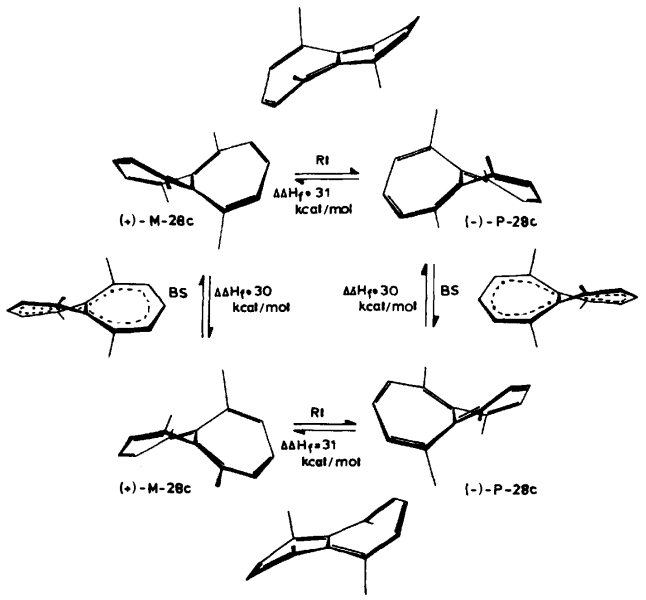

Fig. 2. Dynamic processes of 1,5,6,10-tetramethylheptalene **28c** (π-SCF-force field calculation).

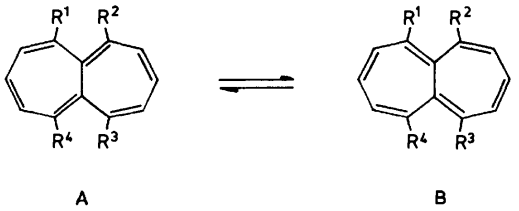

	R¹	R²	R³	R⁴
5	H	H	H	H
28a	Me	Me	H	H
28c	Me	Me	Me	Me
39	Me	H	H	H
40	Me	H	H	Me

Scheme 12.

1,5,6,10-tetramethylheptalene **28c** should occur via helical chiral, delocalized transition states with an activation enthalpy of 30 kcal mol^{-1}. On the other hand, the ring inversion should occur via partly planar, localized transition states with an activation enthalpy of 31 kcal mol^{-1} (Fig. 2). This value is in good agreement with recent experimental results (Table 2).[36] In contrast to this, planar transition states for both processes should require activation enthalpies of 62 and 72 kcal mol^{-1}, respectively. Therefore, the calculated conformations of the transition states seem to represent a good model for the dynamic behavior of highly substituted heptalenes. As the calculated values for the activation enthalpies for the dynamic processes (Table 3) indicate, the bond shift of the methylheptalenes **39**, **40**,

Table 3. π-SCF-Force Field Calculations[35] of the Activation Enthalpies [kcal mol^{-1}] for Ring Inversion (RI) and Bond Shift (BS)

	Planar transition state		Nonplanar transition state	
	ΔH_{RI}	ΔH_{BS}	ΔH_{RI}	ΔH_{BS}
5	0.2	8.4	—[a]	—[a]
28a	23.9	33.0	19.4	19.6
28c	62.2	72.0	31.3	30.1
39	2.9[b]	13.6[d]	—[a]	13.2[d]
	6.2[c]	15.1[e]		14.6[e]
40	12.7[b]	20.8[d]	—[a]	18.4[d]
	14.4[c]	23.4[e]		21.1[e]

a) The planar transition state is energetically more favorable. b) (−)-P-A→(+)-M-A, c) (−)-P-B→(+)-M-B, d) A→B, e) B→A.

and **28a** should also occur via nonplanar transition states. However, the difference of the activation enthalpies of both processes should decrease with the number of substituents. Furthermore, for heptalenes with two or less substituents in the peri-positions the ring inversion should be faster than the bond shift. While we could demonstrate that the bond shift of the (−)-menthyl heptalenecarboxylate **38** is not accompanied by racemization, we have not yet investigated the lower substituted heptalenes. However, the necessary data can be obtained by NMR measurements of heptalenes with diastereotopic substituents, i.e. the hydroxymethylheptalenes **23**. Similarily, Paquette et al.[11,12] found that the activation enthalpies of both dynamic processes for methyl-substituted cyclooctatetraenes were also dependend on the degree of substitution. While these authors explained this exclusively by the different steric interaction of the substituents in the assumed planar localized and delocalized transition states, our results for substituted heptalenes suggest that this may be due to different conformations of the transition states and, therefore, different steric strains of the ring system. In fact, calculations by Dewar et al.[37] suggest that the bond shift of cyclooctatetraene also proceeds via a nonplanar transition state.

Conclusion

Our investigations of the dynamic behavior of chiral heptalenes established that the ring inversion and the bond shift, at least of highly substituted heptalenes, occur via nonplanar transition states with different conformations. Thus, it seems very questionable to determine the delocalization energies of heptalenes (even of the parent compound) from the difference of the activation parameters of both dynamic processes. The same should be valid for cyclooctatetraenes.

This work was generously supported by the Deutsche Forschungsgemeinschaft, the Fonds der Chemischen Industrie, and the Degussa A. G., Frankfurt/Main.

References

1) E. Hückel, *Z. Phys.*, **70**, 204 (1931); E. Hückel, *Z. Elektrochem.*, **43**, 752 (1937); E. Hückel, "Grundzüge der Theorie ungesättigter und aromatischer Verbindungen," Verlag Chemie, Berlin (1938).

2) D. Lloyd, "Nonbenzenoid Conjugated Carbocyclic Compounds," Elsevier, Amsterdam (1984); P. J. Garratt, "Aromaticity," J. Wiley & Sons, New York (1986).

3) J. A. Pople, *J. Chem. Phys.*, **24**, 111 (1956).

4) H. C. Longuet-Higgins, *Chem. Soc. Spec. Publ.*, No. 21, 109, (1967); J. A. Pople and K. G. Untch, *J. Am. Chem. Soc.*, **88**, 4811 (1966); F. Baer, H. Kuhn, and W. Regel, *Z. Naturforschung*, **22a**, 103 (1967).

5) R. Breslow, *Acc. Chem. Res.*, **6**, 393 (1973); M. J. S. Dewar, *Adv. Chem. Phys.*, **8**, 121 (1965).

6) K. Hafner, *Nachr. Chem. Tech. Lab.*, **28**, 222 (1980).

7) H. Irngartinger and M. Nixdorf, *Angew. Chem.*, **95**, 415 (1983); *Angew. Chem., Int. Ed. Engl.*, **22**, 403 (1983), and references cited therein.

8) B. Kitschke and H. J. Lindner, *Tetrahedron Lett.*, **1977**, 2511; P. Bischof, R. Gleiter, K. Hafner, K. H. Knauer, J. Spanget-Larsen, and H. U. Süss, *Chem. Ber.*, **111**, 932 (1978).

9) J. F. M. Oth, *Pure Appl. Chem.*, **25**, 573 (1971).

10) E. Vogel, H. Königshofen, J. Wassen, K. Müllen, and J. F. M. Oth, *Angew. Chem.*, **86**, 777 (1974); *Angew. Chem., Int. Ed. Engl.*, **13**, 732 (1974).

11) L. A. Paquette and J. M. Gardlik, *J. Am. Chem. Soc.*, **102**, 5033 (1980); L. A. Paquette, *Pure Appl. Chem.*, **54**, 987 (1982); L. A. Paquette, J. M. Gardlik, K. J. McCullough, R. Samodral, G. DeLucca, and R. J. Ouellette, *J. Am. Chem. Soc.*, **105**, 7649 (1983).

12) L. A. Paquette and J. A. Gardlik, *J. Am. Chem. Soc.*, **102**, 5016 (1980); L. A. Paquette, J. A. Gardlik, L. K. Johnson, and K. J. McCullough, *J. Am. Chem. Soc.*, **102**, 5026 (1980).

13) H. J. Dauben and D. J. Bertelli, *J. Am. Chem. Soc.*, **83**, 4659 (1961).

14) For reviews see: L. A. Paquette, *Isr. J. Chem.*, **20**, 233 (1980); G. Becker and H. Kolshorn in Houben-Weyl, "Methoden der Organischen Chemie," Vol. 5, part 2c, p. 418, Georg Thieme Verlag Stuttgart 1985.

15) H. J. Dauben and D. J. Bertelli, *J. Am. Chem. Soc.*, **83**, 4657 (1961).

16) E. Vogel, D. Kerimis, N. T. Allison, R. Zellerhoff, and J. Wassen, *Angew. Chem.*, **91**, 579 (1979); *Angew. Chem., Int. Ed. Engl.*, **18**, 545 (1979).

17) L. A. Paquette, A. R. Browne, and E. Chamot, *Angew. Chem.*, **91**, 581 (1979); *Angew. Chem., Int. Ed. Engl.*, **18**, 546 (1979); L. A. Paquette, A. R. Browne, E. Chamot, and J. F. Blount, *J. Am. Chem. Soc.*, **102**, 643 (1980).

18) E. Vogel and J. Ippen, *Angew. Chem.*, **86**, 778 (1974); *Angew. Chem., Int. Ed. Engl.*, **13**, 734 (1974).

19) E. Vogel and F. Hogrefe, *Angew. Chem.*, **86**, 779 (1974); *Angew. Chem., Int. Ed. Engl.*, **13**, 735 (1974).

20) K. Hafner, H. Diehl, and H. U. Süss, *Angew. Chem.*, **88**, 121 (1976); *Angew. Chem., Int. Ed. Engl.*, **15**, 104 (1976); W. Ude, Ph. D. thesis, TH Darmstadt 1980; G. L. Knaup, Ph. D. thesis, TH Darmstadt 1985.

21) W. Bernhard, H.-R. Zumbrunnen, and H.-J. Hansen, *Chimia*, **33**, 324 (1979).

22) F.-G. Klärner, B. Dogan, W. R. Roth, and K. Hafner, *Angew. Chem.*, **94**, 721 (1982); *Angew. Chem., Int. Ed. Engl.*, **21**, 701 (1982).

23) K. Hafner and G. L. Knaup, *Tetrahedron Lett.*, **27**, 1673 (1986); see also: 21) and W. Bernhard, P. Brügger, J. J. Daly, G. Englert, P. Schönholzer, and H.-J. Hansen, *Helv. Chim. Acta*, **68**, 1010 (1985).

24) K. Hafner and G. L. Knaup, *Tetrahedron Lett.*, **27**, 1665 (1986).

25) K. Hafner, N. Hock, G. L. Knaup, and K.-P. Meinhardt, *Tetrahedron Lett.*, **27**, 1669 (1986).

26) K. Hafner and K.-P. Meinhardt, unpublished results.

27) H. J. Lindner and B. Kitschke, *Angew. Chem.*, **88**, 123 (1976); *Angew. Chem., Int. Ed. Engl.*, **15**, 106 (1976); J. Stegemann and H. J. Lindner, *Tetrahedron Lett.*, **1977**, 2515.

28) J. F. M. Oth, K. Müllen, H. Königshofen, J. Wassen, and E. Vogel, *Helv. Chim. Acta*, **57**, 2387 (1974).

29) F. G. Klärner, private communication; B. M. J. Dogan, Ph. D. thesis, Bochum 1983.

30) K. Hafner, G. L. Knaup, H. J. Lindner, and H.-C. Flöter, *Angew. Chem.*, **97**, 209 (1985); *Angew. Chem., Int. Ed. Engl.*, **24**, 212 (1985).

31) The bond shift isomers **16kA** and **16kB** were also synthesized and seperated by H.-J. Hansen et al. (W. Bernhard, P. Brügger, J. J. Daly, P. Schönholzer, R. H. Weber, and H.-J. Hansen, *Helv. Chim. Acta*, **68**, 415 (1985); W. Bernhard, P. Brügger, P. Schönholzer, R. H. Weber, and H.-J. Hansen, *Helv. Chim. Acta*, **68**, 429 (1985), but these authors originally postulated the structure of dimethyl 3,6,8,10-tetramethylheptalene-1,2-dicarboxylate for **16kB** and a new rearrangement of the heptalene skeleton for the interconversion **A**⇄**B** (H.-J. Hansen, lecture at the ETH Zürich, January 21, 1985; W. Bernhard, Ph. D. thesis, Fribourg/Switzerland 1982; P. Brügger, Ph. D. thesis, Fribrourg/Switzerland 1983).

32) A. Manschreck, unpublished results.

33) G. L. Knaup and K. Hafner, unpublished results; see also R. H. Weber, P. Brügger, T. A. Jenny, and H.-J. Hansen, *Helv. Chim. Acta*, **70**, 742 (1987).

34) G. Blaschke, unpublished results.

35) H. J. Lindner, *Tetrahedron*, **30**, 1127 (1974); Program PIMM82, unpublished, TH Darmstadt, 1982; H.-C. Flöter, Ph. D. thesis, TH Darmstadt 1987.

36) K. Hafner and N. Hock, unpublished results.

37) M. J. S. Dewar, A. Harget, and E. Haselbach, *J. Am. Chem. Soc.*, **91**, 7521 (1969).

 © 1988 The Chemical Society of Japan Bull. Chem. Soc. Jpn., 61, 165—170 (1988)

Invited Paper

Antioxidants

Gerald SCOTT
Polymer Group, Aston University, Birmingham, B4 7ET, U.K.
(Received September 3, 1987)

Antioxidants can be classified by the way in which they interfere with the process of autoxidation. Two main types can be identified; the chain-breaking antioxidants which either reduce the alkylperoxyl radical or oxidise the alkyl radical and the preventive antioxidants which either retard the breakdown of hydroperoxides (metal deactivators, UV absorbers) or destroy them by non-radical mechanisms. Synergism results from the complementary action of antioxidants when used together. Recent studies of antioxidant mechanisms have led to the discovery of "stable" redox systems which are able to catalytically scavenge alkyl and alkylperoxyl radicals in competition with the normal reactions of these species in autoxidation. The physical behaviour (solubility, volatility etc.) of antioxidants can dominate their behaviour under certain conditions and the development of polymer-bound antioxidants is believed to be a solution to antioxidant migration and loss.

The Significance of Autoxidation in Technological and Biological Processes. Most carbon-based materials deteriorate as a result of chemical reaction with oxygen of the environment. During the past century autoxidation has been shown to be a common factor in the loss of physical properties of rubbers and plastics, in the rancidification of fats and oils, in the deterioration of lubricating properties of hydrocarbon oils[1] and more recently reactive species involved in autoxidation have been implicated in a variety of diseases in vivo.[2–12]

The phenomenon of rubber "ageing" and the effects of very small amounts of added chemicals which were given the name "antioxygens" or "antioxidants" in inhibiting this process were observed at an early stage in the development of rubber as a technological material. Ageing of rubber was recognized by Ostwald to be associated with the absorption of oxygen in the early 1900's.[13] However, the understanding of the mechanism of oxidative deterioration remained obscure until the free radical chain reaction of autoxidation was proposed by Bäckström for benzaldehyde in the mid 1920's.[14] A key feature of the process (reactions (1)—(6)) is the formation of an intermediate peroxide[15] since this provided an explanation for the autoaccelerating oxidation rate curve which had first been observed by Genthe in 1906 in a study of the autoxidation of linseed oil.[16] The rate of autoxidation is now known to be directly related to the concentration of this species in many organic substrates and once it is present in the autoxidising system, no other initiator is required (reaction (1)).

Initiation

$$\mathrm{ROOH} \xrightarrow[(a)]{\Delta,\,h\nu} \mathrm{RO}\cdot + \cdot\mathrm{OH} \qquad (1)$$

$$\mathrm{RH} + \left.\begin{matrix}\cdot\mathrm{OH}\\ \cdot\mathrm{OR}\end{matrix}\right] \xrightarrow[(b)]{} \mathrm{R}\cdot + \left.\begin{matrix}\mathrm{H_2O}\\ \mathrm{ROH}\end{matrix}\right]$$

Propagation

$$\mathrm{R}\cdot + \mathrm{O_2} \longrightarrow \mathrm{ROO}\cdot \qquad (2)$$

$$\mathrm{ROO}\cdot + \mathrm{RH} \longrightarrow \mathrm{ROOH} + \mathrm{R}\cdot \qquad (3)$$

Termination

$$2\mathrm{R}\cdot \longrightarrow \mathrm{R\text{-}R} \qquad (4)$$

$$\mathrm{R}\cdot + \mathrm{ROO}\cdot \longrightarrow \mathrm{ROOR} \qquad (5)$$

$$2\mathrm{ROO}\cdot \longrightarrow \text{Disproportionation products} \qquad (6)$$

Since reaction (3) is normally rate determining, termination generally occurs by reaction (6) but important exceptions to this will be discussed below.

The oxidation of fats and oils has been studied by chemists for almost as long as polymeric materials. The pure linoleate esters were frequently used as chemical models of more complex oils and fats and indeed the understanding of the chemistry of cross-linking of drying oils and the deterioration of food stuffs resulted from early observations of the effects of oxygen on the 1,4 unsaturated fatty acids and their esters.[17,18] In recent years the full significance of this chemistry has begun to be appreciated by biologists and biochemists and to the scientist concerned with the durability of relatively stable systems it is a cause of wonder that nature has been able to develop such highly effective antioxidant systems in vivo. The chemical constituents of the lipids when isolated from their natural antioxidants undergo oxidative breakdown and cross-linking extremely rapidly and it is clear that man has much to learn from nature about the preservation of organic materials. Nevertheless, evidence is accumulating that the natural antioxidant defences of the body become less effective with age.[11] This results in increasing free radical activity in the cells and associated loss of elasticity of the cell tissues. There is strong evidence too that many of the diseases of old age, notably Alzheimer's disease,[10] Parkinsons disease,[12] artherio-sclerosis[12] and cancer[12] are associated with decreased oxidation resistance of the organisms involved.

There is clearly then a powerful motivation on the

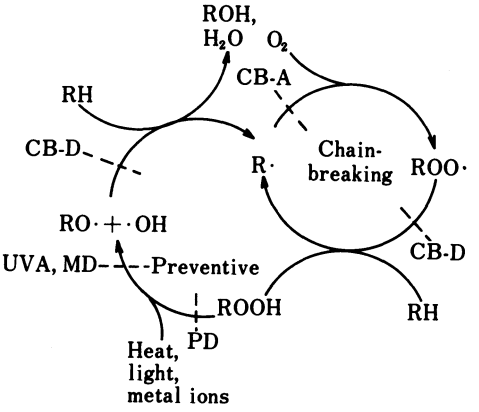

CB-A	Chain-breaking acceptor
CB-D	Chain-breaking donor
PD	Peroxide decomposer
UVA	UV absorber
MD	Metal deactivator

Scheme 1. Antioxidant mechanisms.

part of both technologists and biologists to a better understanding of how destructive oxidation processes may be inhibited. The following review aims to bring together the most important developments in antioxidant mechanisms that have occurred during the past thirty years.

Inhibition of Autoxidation. The autoxidation chain reaction outlined in reactions (1)—(6) can be conveniently reformulated in a way (Scheme 1) that illustrates in principle the means by which the kinetic chain can be inhibited.[19] It is clear from Scheme 1 that the process of autoxidation involves two distinct but interacting cyclical processes. The primary kinetic chain reaction involves the continuous regeneration of the chain propagating species, R· and ROO· but this cycle is continually replenished with new alkyl radicals as a result of homolysis (which may be light or metal ion catalysed) of hydroperoxides. From this formulation antioxidants may be broadly categorised into those which intercept the primary chain reaction, the chain breaking (CB) antioxidants, or those which prevent or retard the formation of initiating radicals, the preventive (P) antioxidants.[20]

Chain-Breaking Mechanism of Antioxidant Action. The alkyl and alkylperoxyl radicals display complementary behaviour.[21] Alkylperoxyl, ROO·, is an electron acceptor and can be readily reduced by hydrogen (or electron) donors. Provided the radical species produced by oxidation is stable and cannot continue the kinetic chain, this constitutes the chain-breaking hydrogen (or electron) donor (CB-D) mechanism of antioxidant action. Most CB-D antioxidants are hindered phenols or aromatic amines and representative examples used in technological systems are the 2,6-di-tert-butyl phenols (**1**) or diphenylamine derivatives (**2**).

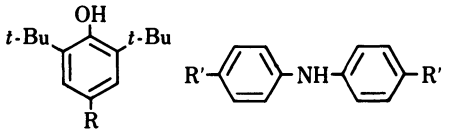

1 **2**

In the former, -R varies from a simple alkyl group as in BHT (R=methyl) to the much more complex multifunctional group (e.g. $C(CH_2OCOCH_2CH_2-)_4$ designed to meet the physical requirements (solubility, low volatility) of a polymeric substrate. In the diphenylamines, again the group -R′ varies widely and is frequently attached through nitrogen or oxygen.

A large amount of semiempirical information based on studies in hydrocarbon substrates has provided the following generalisation on the relationship between CB–D activity and structure.[20]

1. Electron releasing groups in the aromatic ring increase antioxidant activity, whereas electron attracting groups decrease it.

2. Substituents that delocalise the electron in the aryloxyl or arylaminyl radicals increase antioxidant activity.

These "rules" can be rationalised on the basis of the transition state (**3**) involved in hydrogen abstraction

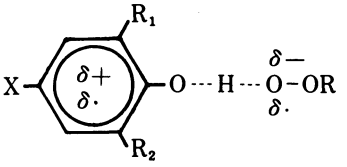

3

by alkylperoxyl. There is both partial separation of charge between the alkylperoxyl and the aromatic ring and partial delocalisation of the electron in the π bond system. Thus, groups in X and R_1,R_2 which release electrons or delocalise the impaired electron decrease the transition state energy.

A third generalization which has proved useful is that bulky groups which hinder the group from which hydrogen abstraction occurs improve antioxidant activity. This has been related to the steric stabilisation (non-reactivity) of the radical produced.[22]

The biological antioxidants, the tocopherols

Tocopherols	R_1	R_2	R_3
α	CH_3	CH_3	CH_3
β	CH_3	H	CH_3
γ	H	CH_3	CH_3
δ	H	H	CH_3

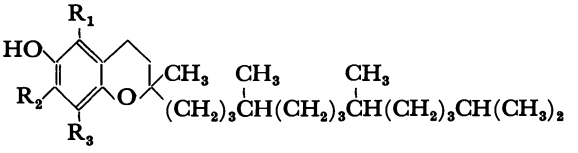

4

Ascorbic acid

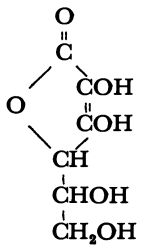

5

(Vitamin E) (**4**) and ascorbic acid (**5**) both act by the CB–D mechanism.

Although the aryloxyl derived from α-tocopherol is not as stable as many hindered phenoxyls, there is evidence that it can be readily reduced back to the parent phenol by ascorbic acid[23,24] and this cooperative interaction is believed to account for the synergism that has been obseved between these two CB–D antioxidants in the unsaturated fatty esters. Similar synergism has been observed in technological media.[25]

Although the chain-breaking donor mechanism of antioxidant action has been known for many years following the pioneering studies in the 1930s of Lowry and his co-workers,[26] very little attention was paid to the complementary chain-breaking acceptor mechanism until relatively recently. The main reason for this is that any oxidising agent for alkyl radicals is in competition with oxygen (see Scheme 2) and the CB–A process will only occur if alkyl radicals are present in the system at a concentration that makes this competition possible. CB–A antioxidants involve essentially the same radical trapping chemistry as polymerization inhibition in the absence of oxygen.[27] Among the more effective are quinones, nitro compounds and "stable" radicals; they are effective electron acceptors. These are precisely the species now recognised to be important as CB–A antioxidants.[28,29]

It was suggested some years ago[30] that an antioxidant which was capable of reversible oxidation and reduction could in principle behave as a catalytic antioxidant. The example quoted was the Cu^{2+}/Cu^{+} system since cupric salts were known to be antioxidants in some substrates. This antioxidant mechanism was subsequently shown to occur in paint media[31] where cupric acetate, which is used as a blue-green pigment, was shown to lead to the formation of conjugated polyunsaturation and brown discolouration in the paint medium.

The mechanism proposed is summarized in reactions (7) and (8) and was subsequently shown to

$$R\cdot + Cu^{2+} \longrightarrow [RCu^{+}] \longrightarrow \text{>C=C<} + Cu^{+} + H^{+} \quad (7)$$

$$ROO\cdot + Cu^{+} + H^{+} \longrightarrow ROOH + Cu^{2+} \quad (8)$$

operate in polypropylene subjected to oxidation in a high shearing mixer when the oxygen concentration is low.[32] A side reaction which competes with this process and limits its practical usefulness at higher oxygen pressures when the hydroperoxide concentration is appreciable, is the well-known redox sequence involving hydroperoxide.

$$Cu^{+} + ROOH \longrightarrow Cu^{2+} + RO\cdot + OH^{-} \quad (9)$$

$$Cu^{2+} + ROOH \longrightarrow Cu^{+} + ROO\cdot + H^{+} \quad (10)$$

Nevertheless, the catalytic cycle summarised in reactions (7) and (8) has proved to be a useful model to explain the behaviour of a variety of oxidising species as antioxidants in oxygen deficient systems. Particularly interesting is the very high efficiency of "stable" oxyl radicals as melt stabilisers for polypropylene.[27] Galvinoxyl (**6**) and the nitroxyls derived from "hindered" piperidines (**7**) have been studied in

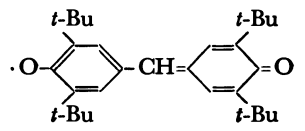

6

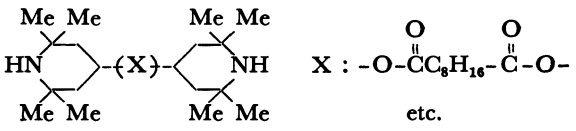

7

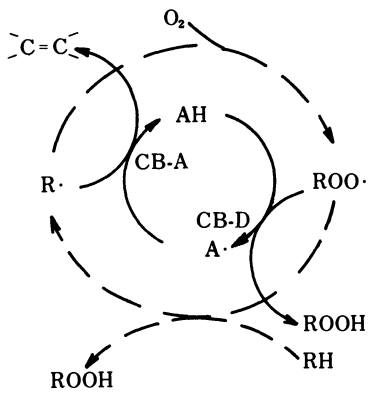

A· = Phenoxyl, nitroxyl, quinone, Cu^{2+}, I_2, ETC

Scheme 2. The chain-breaking antioxidant mechanisms.

Scheme 3. Mechanism of catalytic chain-breaking antioxidants.

some detail.[28,33–35] and the mechanism proposed is generalised in Scheme 3. Scheme 3 shows the competition between oxygen and the CB–A antioxidant (A·) for alkyl radicals and between the CB–D antioxidant (AH) and the substrate for alkylperoxyl radicals. The catalytic CB–A/CB–D mechanism has been shown to occur in polymeric substrates when the diffusion of oxygen into the system is limited and the oxygen concentration is therefore low.[28] The general conditions for its operation are:

(i) The antioxidant has two relatively stable oxidation states which can coexist in the substrate. These include aryloxyl and their cognate phenols, nitroxyls and their cognate hydroxylamines, quinones and their cognate semiquinones, iodine and hydrogen iodide and cupric, and cuprous ions.

(ii) Termination can occur through alkyl. It has been known for many years, since the pioneering studies of Bateman and his co-workers,[36] that hydrocarbons which oxidise to give resonance stabilised radicals terminate in part by reactions (4) and (5) up to relatively high oxygen concentrations. Limitation of oxygen diffusion which occurs widely in polymeric substrates also increases termination through alkyl radicals so that in photo-oxidation at ambient oxygen pressure, termination of macroalkyl by nitroxyl can readily occur.[28,37] A high rate of initiation by UV light may also lead to a higher macroalkyl concentration, again favouring the CB–A/CB–D process.

Nitroxyl radicals can be generated in situ in polymers by the spin trapping procedure.[38] Mechanical shear in polyolefins during processing gives rise to macroalkyl radicals which subsequently react with spin traps.[39,40] Thus 2-methyl-2-nitrosopropane (NTB) processed into polypropylene is an effective light stabiliser. Its photoantioxidant activity is directly related to the amount of nitroxyl produced in the polymer.[40]

The Preventive Mechanism. Scheme 1 indicates three main mechanisms of preventive antioxidant action. Two of these, the deactivation of metal ions and the absorption of UV light, are palliative and are therefore of limited effectiveness since they retard rather than inhibit the generation of free radicals from hydroperoxides. Many such compounds are in commercial use but most of them operate by more than one mechanism, thus displaying the phenomenon of autosynergism (i.e. they contain two complementary inhibitory functions in the same molecule). Thus the copper deactivator, **8**[41] and the UV stabiliser, **9**[42] are both CB–D antioxidants and the

8

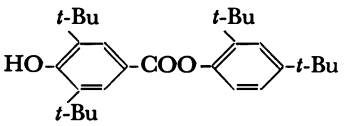

9

copper deactivator **10**[43] and the UV stabiliser **11**[44] are

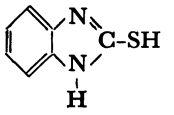

10

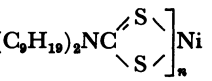

11

both effective peroxide decomposers. The decomposition of hydroperoxides by chemical reactions which do not lead to the formation of free radicals is by far the most important preventive mechanism of antioxidant action. It was first observed in hydrocarbon oils[45] and most modern lubricating oils contain a zinc dialkyl dithiophosphate (**12**) as a key stabilizing component. The mechanism of the metal dithiolates of which the dithiocarbamates (**11**) dithiophosphates (**12**) are typical has been extensively investigated in recent years[44] and they have been shown to function by being oxidised by hydroperoxides formed in the substrate to sulfur acids which in turn act as ionic catalysts for the further and complete destruction of hydroperoxides. Simple aliphatic sulphides (**13**) also act

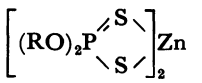

12

$(ROCOCH_2CH_2)_2S$

13

in the same way.[46] The chemistry is complex and the generation of the antioxidant species is preceded by the formation of intermediates which destroy hydroperoxides in a free radical process (Scheme 4). The early stages of the action of peroxide decomposing antioxidants are therefore often associated with prooxidant effects. Other sulphur antioxidants including the dithiolates, generate sulphinic, sulphonic and sulphuric acids in analogous processes.[44] Prior oxidation of the sulphur precursors has been shown in some cases to give rise to more effective stabilising systems.[47,48] Glutathione peroxidase (**14**) is a

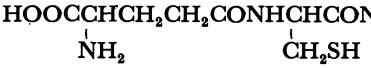

14

biological antioxidant with a formal resemblance to the synthetic peroxidases. However, it seems that its hydroperoxide decomposing mechanism is quite different from the latter, involving coupled single electron-transfer steps which reduce hydroperoxides to alcohols.[49]

Synergism. Reference to Scheme 1 suggests that preventive antioxidants and chain-breaking antioxidants should have a mutual protective effect on one another. This phenomenon, commonly referred to as

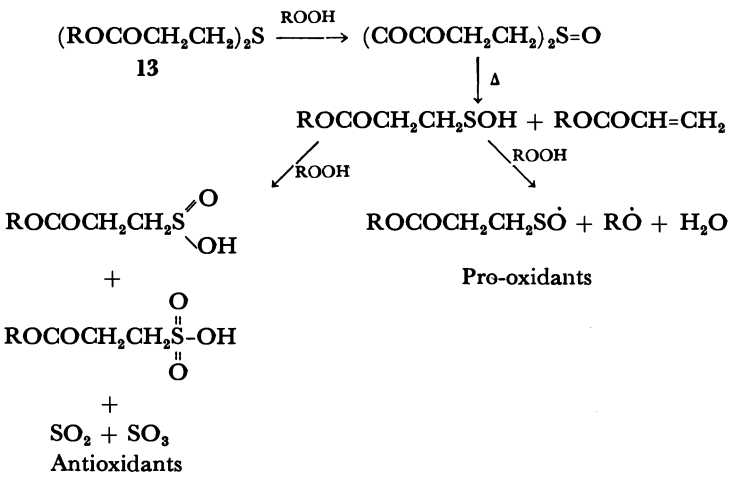

Scheme 4. Mechanism of sulfide antioxidants.

"synergism" has in practice proved to be of considerable importance in technological systems. A typical synergist used in the thermal-oxidative stabilisation of polypropylene is a combination of a typical high molecular weight hindered phenol (**1**) and a 3,3′-thiodipropionate ester.[50] However, synergism can also occur between preventive antioxidants. Thus, for example, it is known that the primary initiator in photo-oxidation is the hydroperoxide which is inevitably present as a result of the processing operation.[51] The generation of radicals by this process (reaction (1)) places a very severe strain on other antioxidants present. However, many peroxide decomposers and chain-breaking antioxidants are photolytically unstable and cannot survive for very long unless they are themselves protected against UV light.[52] UV absorbers have the ability to protect chain-breaking and peroxidolytic antioxidants against photo-oxidation and some of the most effective systems condtain a combination of peroxide decomposer, chain-breaking antioxidant (sometimes as in the case of the nitroxyls, catalytic) and a UV absorber.[53]

Physical Aspects of Antioxidant Action. In recent years, attention has turned from the organic chemistry to the physical chemistry of antioxidant behaviour. Homologous antioxidants containing the same functional group frequently behave very differently in technological systems and this phenomenon can be related to their physical behaviour, particularly solubility and volatility which determine their effectiveness.[54] In order to minimise such effects a good deal of attention is being directed to the chemical attachment of antioxidants and UV stabilisers to the polymer backbone. This can be done conveniently by copolymerization or by grafting of antioxidants to the polymer chain.[55,56] Considerable success has been achieved in producing polymers which are much less susceptible to high-temperature oxidation but which will also stand up to the rigorous conditions of oil or solvent extraction to which rubbers and plastics are often exposed in the technological environment.[56,57]

An important by-product of research into polymer-bound antioxidants is the discovery that in rubber modified plastics (e.g. ABS), antioxidants chemically attached to the more oxidisable rubber phase are several times more effective than conventional antioxidants. This is due to the fact that the antioxidants are located in much higher concentration in the rubber domains where they are required to act.[57]

Future Perspective. The study of antioxidants which began as an empirical art has now become a systematic scientific discipline to interpret disparate technological phenomena by unified chemical and physical concepts. The mechanisms elaborated over the past twenty years permit the selection of antioxidants to solve specific technological problems.

As polymers and other technological media are used under more and more severe conditions, it seems inevitable that durability will in the future be an important design factor. In the field of biology too, the prevention of random oxidation is seen to be increasingly desirable in the fight against disease. In the design of synergistic antioxidant mixtures and in the targeting of antioxidants to specific sites, the biochemist can profit from research in vitro. However, man has yet to learn how to mimic the complex single electron transfer peroxidases developed by nature.

References

1) G. Scott, "Atmospheric Oxidation and Antioxidants," Elsevier (1965).

2) P. O. P. Ts'o, W. J. Caspary, and R. J. Lorentzen "Free Radicals in Biology," Vol. III., ed by W. A. Pryor, Acad. Press, New York (1977), p. 251.

3) B. Halliwell and J. M. C. Gutteridge, *Mol. Aspects Med.*, **8**, 89 (1985).

4) L. A. Witting and M. K. Horwitt, *Lipids*, **2**, 89, 99 (1962).
5) J. Green, A. T. Diplock, J. Bunyan, I. R. Muthy, and D. McHale, *Bri. J. Nutr.*, **21**, 497 (1967).
6) J. M. C. Gutteridge, D. A. Rowley, E. Griffiths, and B. Halliwell, *Clin. Sci.*, **68**, 463 (1985).
7) R. P. Mason, W. G. Harrelson, B. Kalyanaraman, C. Mottley, F. J. Peterson, and J. T. Holtzman, "Free Radicals, Lipid Peroxidation and Cancer," ed by D. C. H. McBrien and T. F. Slater, Acad. Press. London, New York (1982), p. 377.
8) B. Halliwell and J. M. C. Gutteridge, *Trends Neurosci.*, **8**, 22 (1985).
9) M. K. Horwith, *Fed. Proc.*, **24**, 68 (1965).
10) D. Harman, "Free Radicals in Biology," Vol. V, ed by W. A. Pryor, Acad. Press (1982), p. 255.
11) R. S. Sohal and R. G. Allen, *Adv. Free Rad. Biol. and Med.*, **2**, 117 (1986).
12) R. J. Melhorn and G. Cole, *Adv. Free Rad. Biol. and Med.*, **1**, 165 (1985).
13) W. Ostwald, *J. Soc. Chem. Ind.*, **32**, 179 (1913).
14) H. L. J. Backstrom, *J. Am. Chem. Soc.*, **49**, 1460 (1927).
15) Ref. 1, Chaps. 1, 2.
16) A. Genthe, *Z. Angew, Chem.*, **19**, 2087 (1906).
17) H. S. Olcott and H. A. Mattill, *Chem. Rev.*, **29**, 257 (1941).
18) C. Golumbic, *Oil and Soap*, **23**, 184 (1946).
19) N. Grassie and G. Scott, "Polymer Degradation and Stabilisation," Cambridge University Press (1985), Chap. 5.
20) Ref. 1, Chaps. 4 and 5.
21) Ref. 1, p. 164 et seq.
22) J. K. Becconsall, S. Clough, and G. Scott, *Trans. Farad. Soc.*, **56**, 459 (1960).
23) C. Golumbic, *Oil and Soap*, **19**, 181 (1942), **20**, 105 (1943).
24) J. E. Packer, T. F. Slater, and R. L. Willson, *Nature (London)*, **278**, 737 (1979).
25) Ref. 1, p. 204 et seq.
26) C. D. Lowry, G. Egloff, J. C. Morrell, and C. G. Dryer, *Ind. Eng. Chem.*, **25**, 804 (1933).
27) T. J. Henman, "Developments in Polymer Stabilisation-1," ed by G. Scott, App. Sci. Pub., London (1979), p. 39.
28) G. Scott, "Developments in Polymer Stabilisation-7," ed by G. Scott, Elsevier App. Sci., London (1984), p. 65.
29) H. Berger, T. A. B. M. Bolsman, and D. M. Brouwer, "Developments in Polymer Stabilisation-6," App. Sci. Pub., London (1983), p. 1.
30) G. Scott, *Brit. Polym. J.*, **3**, 24 (1971).
31) F. Rasti and G. Scott, *Eur. Polym. J.*, **16**, 1153 (1980).
32) R. Bagheri, K. B. Chakraborty, and G. Scott, *Polym. Deg. and Stab.*, **11**, 1 (1985).
33) R. Bagheri, K. B. Chakraborty, and G. Scott, *Chem. Ind.*, **1980**, 865; *Polym. Deg. and Stab.*, **5**, 145 (1983).
34) A. A. Katbab and G. Scott, *Eur. Polym. J.*, **17**, 559 (1981).
35) R. Bagheri, K. B. Chakraborty, and G. Scott, *Polym. Deg. and Stab.*, **4**, 1 (1982).
36) L. Bateman and A. L. Morris, *Trans. Farad. Soc.*, **49**, 1026 (1953).
37) D. J. Carlsson, A. Garton, and D. M. Wiles, "Developments in Polymer Stabilisation-1," ed by G. Scott, App. Sci. Pub., London (1979), p. 219.
38) K. B. Chakraborty and G. Scott, Brit. Pat. App., 8,326,238/Sept. 1983.
39) K. B. Chakraborty and G. Scott, *J. Polym. Sci., Polym. Lett.*, **22**, 553 (1984).
40) K. B. Chakraborty, H. Yaghmour, and G. Scott, *J. App. Polym. Sci.*, **30**, 189 (1985).
41) Z. Osawa, "Developments in Polymer Stabilisation-7," ed by G. Scott, App. Sci. Pub., London (1984), p. 193.
42) F. Gugumus, "Developments in Polymer Stabilisation-1," ed by G. Scott, App. Sci. Pub., London (1979), p. 261.
43) Ref. 1, p. 405.
44) S. Al-Malaika, K. B. Chakraborty, and G. Scott, "Developments in Polymer Stabilisation-6," ed by G. Scott, App. Sci. Pub., London (1983), p. 73.
45) Ref. 1, p. 264 et seq.
46) G. Scott, "Developments in Polymer Stabilization-6, ed by G. Scott, App. Sci. Pub., London (1983), p. 29.
47) S. Al-Malaika and G. Scott, *Polym. Deg. and Stab.*, **5**, 415 (1983).
48) S. Al-Malaika, M. Coker, and G. Scott, *Polym. Deg. and Stab.*, **10**, 173 (1985).
49) L. Flohe, "Free Radicals in Biology," Vol. V, ed by W. A. Pryor, Acad. Press (1982), p. 223.
50) G. Scott, *Europ. Polym. J. Supplement*, **1969**, 189.
51) G. Scott, "Developments in Polymer Degradation-1," ed by N. Grassie, App. Sci. Pub., London (1977), p. 205.
52) G. Scott, *Pure App. Chem.*, **52**, 365 (1980).
53) G. Scott, *Brit. Polym. J.*, **16**, 271 (1984).
54) G. Scott, *J. App. Polym. Sci.*, **35**, 123 (1979).
55) D. Munteanu, "Developments in Polymer Stabilisation-8," ed by G. Scott, Elsevier App. Sci., London (1987), p. 179.
56) G. Scott, "Developments in Polymer Stabilisation-4," ed by G. Scott, App. Sci. Pub., London, p. 181.
57) G. Scott, "Developments in Polymer Stabilisation-8," ed by G. Scott, Elsevier App. Sci., London (1987), p. 209.

 © 1988 The Chemical Society of Japan Bull. Chem. Soc. Jpn., 61, 171—180 (1988)

Invited Paper

Insertion of Carbon-Heteroatom Multiple Bonds into Bis(η^5-cyclopentadienyl)titanacyclobutenes

James Douglas MEINHART and Robert Howard GRUBBS*
Contribution No. 7667 from the Arnold and Mabel Beckman Laboratory of Chemical Synthesis, California Institute of Technology, Pasadena, California, 91125, U.S.A.
(Received September 17, 1987)

Titanacyclobutenes that are readily produced by the reaction of Tebbe reagent with disubstituted acetylenes react with a variety of heteroatom multiple bonds. The reaction with aldehydes and ketones is particularly clean and has been studied mechanistically. The aldehyde or ketone carbonyl oxygen coordinates to the titanium center in a preequilibrium step before ring expansion to the product metallaoxacyclohexenes.

Introduction

Insertion of unsaturated organic molecules into transition-metal carbon bonds has received much attention during the past thirty years. Insertion of carbon-carbon multiple bonds into transition-metal alkyl .complexes has been the focus of many laboratories due to the economic importance of polyolefins.[1] Carbon-heteroatom multiple bonds (i.e. ketone, ester, nitrile, and imine) also insert into transition-metal alkyl complexes.[2] Application of transition-metal alkyl complexes rather than main group complexes for nucleophilic addition to carbon-heteroatom bonds has the potential to alter the reactivity and selectivity by the appropriate combination of ancillary ligands.

Organic chemistry contains many examples of metal alkyl addition to carbon-heteroatom multiple bonds. The Grignard reaction is a classic example of this type of reaction. Alkyl and aryl compounds derived from Li, Na, Al, and Cd are commonly used in organic synthesis.[3] The reactivity of these complexes is generally 1,2 addition to carbonyl groups, with varying selectivity.

Few transition-metal organometallic reagents have been developed for addition to carbon-heteroatom functionality. Dialkylcuprate complexes (R_2CuLi) add to α,β-unsaturated ketones in a 1,4 sense to yield a γ-alkylated ketone.[4] In contrast, an alkyllithium reagent adds in a 1,2 sense to the same ketone to yield an alcohol. This modified selectivity of a main group complex via a transition metal may provide new methods for regio- and stereo-controlled reactions.

Likewise, $(Pr^iO)_3TiCl$, when treated with a Grignard reagent, forms an alkyl titanium derivative, which is selective for aldehydes in the presence of ketones and nitriles.[5] Thus, the need for protection-deprotection of sensitive functionality may be reduced. This same titanium reagent also reacts in a highly diastereoselective manner with ketones and aldehydes. Transition-metal alkyl complexes from the left half of the transition block are highly reactive toward carbonyl compounds due to the oxophilicity of the metal.

Several reactions are known where a transition metal complex serves as a catalyst, transferring or coupling alkyl groups from a donor complex to the unsaturated substrate.[6]

Recently, 1,2-addition of carbonyl compounds to metallacyclobutane complexes has been postulated by product analysis.[7]

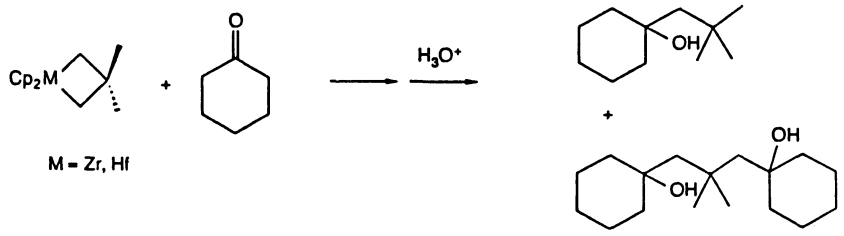

Due to the lack of methylene transfer chemistry of titanacyclobutenes, the reactivity of titanacyclobutenes with carbon-heteroatom bonds was investigated. Titanacyclobutenes[8] offer a unique template for the study of insertion into titanium-carbon bonds.

Results

Treatment of a solution of 2,3-diphenyltitanocenacyclobutene, **1a**, with acetone at room temperature for 2 days yields titanocenaoxacyclohexene, **2a**, in quantitative yield (Eq. 1). The reaction is greatly accelerated by warming the sample to 80 °C for

approximately 10—15 minutes. The 3-methyl-2-phenyltitanacyclobutene, **1b**, works equally well.[9] The titanaoxacyclohexenes, **2**, are isolated as yellow solids.

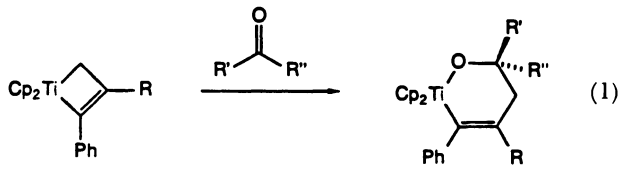

(1)

1a : R = Ph
1b : R = CH_3

2

The reaction is general for a variety of organic ketones (Table 1). Methylene transfer reaction to the ketone is not observed. Enolization of the ketone by the titanacyclobutene is not a significant side reaction.

However, titanacyclobutenes with β-hydrogens do not insert ketones to an appreciable extent. The metallacycle begins to react, and the insertion product decomposes rapidly at room temperature.

The kinetics of the insertion reaction of acetone into **1a** was monitored by NMR (Eq. 2). The rate expression was first order in metallacycle and ketone, second order overall. At 50 °C a second-order rate constant was calculated, $k_{323}=5.94(3)\times10^{-4}\ M^{-1}\ s^{-1}$.

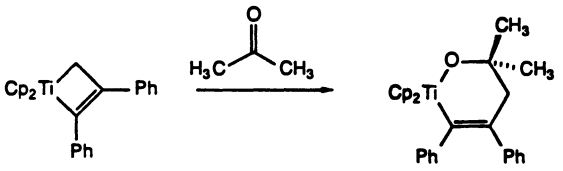

(2)

1a **2a**

Table 1. Ketone Insertion into Titanacyclobutenes

Ketone	Titanacycle	Product		Ketone	Titanacycle	Product	
	1a	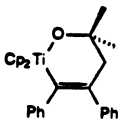	**2a**	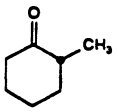	**1a**	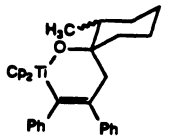	**2i**
	1a	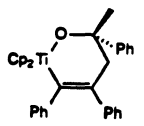	**2b**	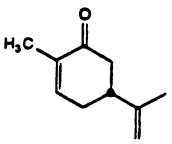	**1a**	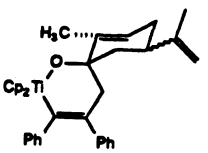	**2j**
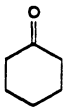	**1a**	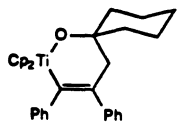	**2c**	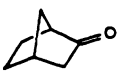	**1a**	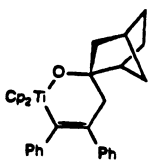	**2k**
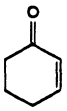	**1a**	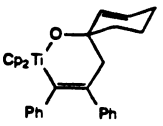	**2d**	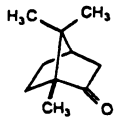	**1a**	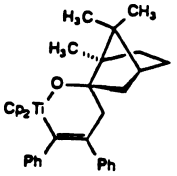	**2l**
	1a	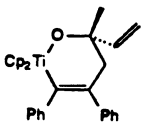	**2e**	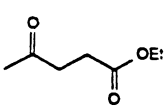	**1a**	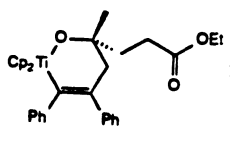	**2m**
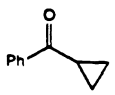	**1a**	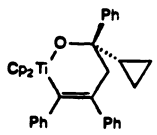	**2f**	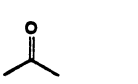	**1b**	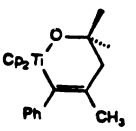	**2n**
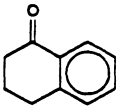	**1a**	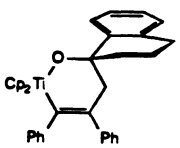	**2g**	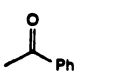	**1b**	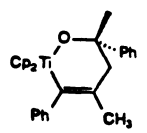	**2o**
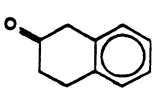	**1a**	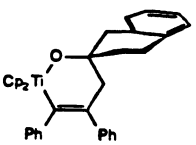	**2h**				

The activation parameters were determined by Eyring analysis of the rate constants over a 40 °C temperature range (Table 2).

The NMR of the reaction solution at room temperature shows sharp signals for the metallacycle but a broad signal for the acetone. Upon cooling, the acetone signal broadens and disappears at ca. −40 °C at 90 MHz. Upon further cooling to −80 °C, the acetone signal begins to sharpen but does not split into a resolved doublet.

Aldehydes also insert cleanly into titanacyclobutenes (Eq. 3). Treatment of a solution of **1a** with *p*-tolualdehyde at room temperature cleanly results in disappearance of the starting material. Examination of the reaction mixture by NMR reveals the formation of two products in a 2:1 ratio. The major product is the expected isomer **3a** containing a titanium-oxygen bond. However, the second product appears to be a regioisomer, **3b**, in which the aldehyde has inserted in the opposite sense, forming a titanium-carbon bond. The dialkyl-substituted oxatitanacyclohexene, **3b**, is much less stable than **3a**. The titanaoxacyclohexenes are moderately air-stable and may be chromatographed on silica. The dialkyl isomers, **3b**, are air-sensitive and decompose upon warming to 80 °C. Insertion of acetaldehyde also yields two isomeric insertion products **4a** and **4b** in a nearly 1:1 ratio.

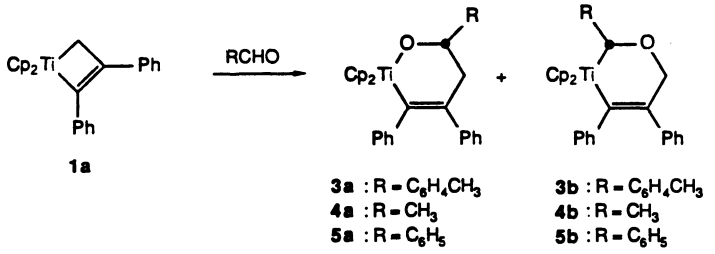

1a

3a : R = $C_6H_4CH_3$ **3b** : R = $C_6H_4CH_3$
4a : R = CH_3 **4b** : R = CH_3
5a : R = C_6H_5 **5b** : R = C_6H_5

(3)

The insertion of benzaldehyde into **1a** has also been studied by Brown-Wensley.[9] Again, two products **5a** and **5b** were observed in a 2:1 ratio. The isomers were physically separated and hydrolyzed with HCl. The organic products were identified and are consistent with proposed regiochemistry.

Several other carbon-heteroatom multiple bonds add to titanacycles **1a**. Tetramethylguanidine inserts to yield an azatitanacyclohexene **6** (Eq. 4). The 90 MHz ^{1}H NMR exhibits a broad singlet for the $N(CH_3)_2$ groups at room temperature. The signal passes through coalescence at +15 °C, and becomes two singlets ($\Delta\nu$=47.8 Hz) at −80 °C. The η^5-cyclopentadienyl resonance also is a singlet until −47 °C when it passes through coalescence and becomes two singlets ($\Delta\nu$=73.5 Hz) at −80 °C.

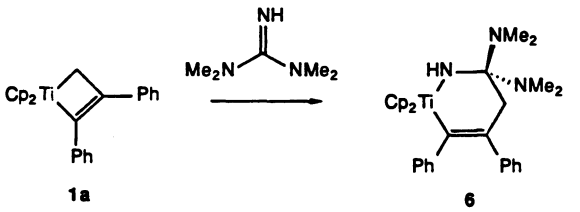

1a **6**

(4)

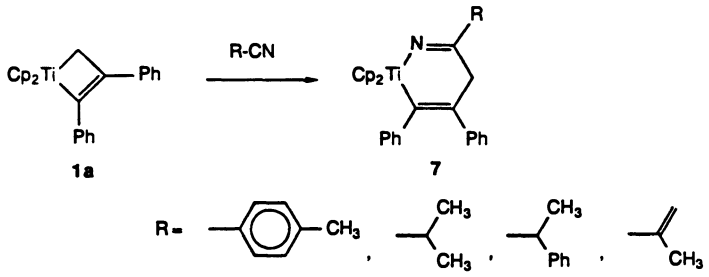

1a **7**

(5)

Table 2. Rate Constants and Activation Parameters for Acetone Insertion into **1a**

Temperature/K	k/$M^{-1}s^{-1}\times10^4$
293	3.51(7)
301	5.9(1)
313	16.8(2)
323	29.5(4)

$\Delta G^{\ddagger}_{301}$ = 22.0(5) kcal mol^{-1}. $\Delta H^{\ddagger}$ = 13.1(4) kcal mol^{-1}. $\Delta S^{\ddagger}_{301}$ = −29(1) eu.

Nitriles also react with titanacyclobutenes (Eq. 5); however, the reactions are not as clean as ketone insertions, and the products are not as stable. Treatment of a solution of **1a** in 400 μL of C_6D_6 with one equivalent of benzonitrile yielded, over 24 hours, a 1-aza-2-titanacyclohexa-3,6-diene complex, **7**. The product was stable for days in solution but eventually decomposed. The insertion reaction works for a variety of nitriles: *p*-tolyl, 1-methylpropyl, 1-phenylpropyl, and methacrylonitrile. Acetonitrile yielded

several products that decomposed rapidly at room temperature. Insertion of nitriles into titanacycle **1b** was also facile. Hydrolysis of the insertion products yields the corresponding ketones (Eq. 6).

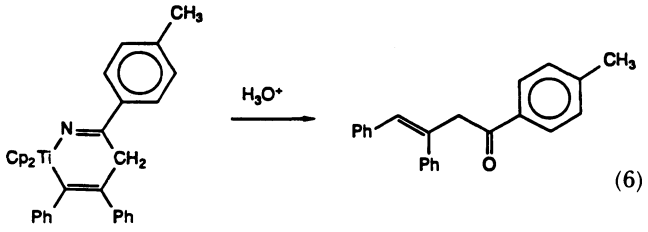

(6)

A variety of substrates do not react with the titanacyclobutenes: esters, carbonates, CO_2, CS_2, and imines.

The titanaoxacyclohexenes **2a** can be removed from the metal fragment by hydrolysis with HCl to yield a homoallylic alcohol in high yield (Eq. 7).

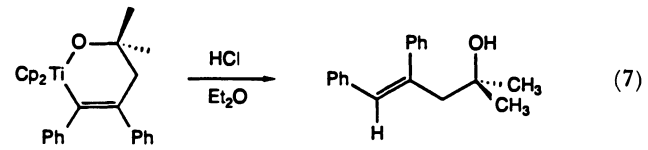

(7)

We had hoped to insert CO into the remaining titanium–carbon bond of **2a** to eventually yield a lactone (Eq. 8). However, all attempts to react **2a** with CO either thermally or photochemically failed.

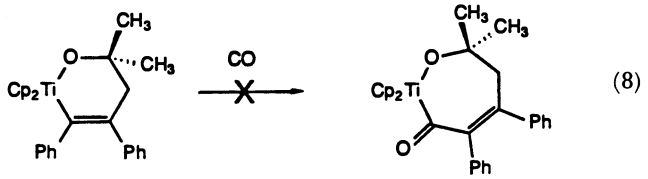

(8)

2a

Lewis acids are known to accelerate migratory insertions of CO into metal–carbon bonds.[10,11] Treatment of **2a** with one equivalent of dimethylaluminum chloride results in immediate formation of a new complex. The new complex was dark-red and the NMR spectrum was very complex. Treatment of this complex with CO yield starting material **2a**. The deep-red color of the reaction mixture and analysis of the NMR spectrum suggest that the Ti–O bond transmetallates to the dimethylaluminum chloride, forming a titanocene alkenyl chloride and aluminum alkoxide (Eq. 9). Trimethyltin chloride did not react with **2a**.

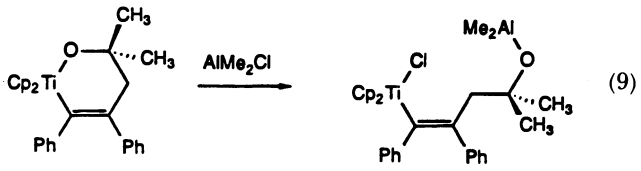

(9)

Discussion

Titanocenacyclobutenes readily insert ketones to yield titanocenaoxacyclohexenes. The reaction is quite general for many ketones, and a few examples deserve mention.

The insertion shows very little facial selection for cyclohexenone derivatives. Insertion of 2-methylcyclohexanone yields two diastereomeric products in nearly equal ratios. Insertion of *l*-carvone gives two diastereomeric products in a 62:38 ratio. The lack of diastereoselection reflects both a lack of adverse steric interactions at the transition state and the relatively high reaction temperature. Attempting to increase the diastereoselection by reducing the temperature is impractical because of the slow reaction rate at room temperature.

Titanacyclobutenes will add very sterically crowded ketones, such as *d*-camphor, although the reaction is much slower. The NMR data and difference NOE experiments suggest that the metallacycle adds to the *endo*-face of the camphor molecule (Eq. 10).[12]

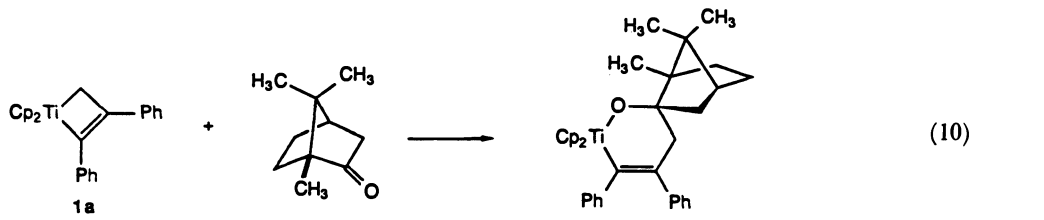

(10)

Phenyl cyclopropyl ketone inserts without any rearrangement to produce a single product in high yield. If the insertion mechanism involved a one-electron reduction or oxidation of the ketone, the cyclopropyl carbinyl radical could open.[13] Although rearrangement is not observed, this experiment does not conclusively rule out a radical mechanism.

Ethyl levulinate reacts exclusively at the methyl ketone to yield the expected oxacyclohexene, **2m**. Simple esters such as methyl benzoate do not react with the titanacyclobutenes. This selectivity for ketones over esters may arise from two factors. Esters are slightly weaker bases than ketone (1–2 pK_a units).[14] The carbonyl carbon of an ester is less electrophilic compared to a ketone, due to resonance from the other oxygen atom.[15] Both factors, the less

basic carbonly oxygen and the less electrophilic carbon, contribute to the selectivity. Steric factors are not significant. Unlike ketones, which display an exchanged broadened NMR signal for the ketone during reaction, the NMR signals of the ester remain sharp.

The NMR spectra during the reaction suggest that the ketone is associated with the metallacycle prior to reaction. Titanacyclobutenes are formally 16-electron complexes and have a vacant orbital into which the carbonyl may coordinate. Variable temperature NMR experiments confirm a dynamic process with a very low activation barrier, possibly ketone coordination, occurs. Kinetic data and activation parameters (Table 2) are consistent with a second-order reaction. A rapid pre-equilibrium does not change the observed rate analysis.[16]

The regiochemistry of aldehyde insertion also provides information about the mechanism. Formation of a titanium–carbon bond compared to a more thermodynamically stable titanium-oxygen bond is very unusual. The estimated energy difference of a Ti–C and Ti–O bond is ca. 50 kcal mol^{-1}.[17] The formation of a Ti–C bond has been observed in the head-to-tail coupling of diphenylketene units in a titanium diphenylketene complex.[18]

A possible explanation for the product distribution is kinetic control of the insertion proceeding via a π-bound aldehyde complex. An organic carbonyl group can coordinate either in a π-sense or σ-sense to the metallacycle. A $Cp_2V(acetone)^+$ complex in which the acetone molecule is η^1-coordinated through the sp^2 lone pair of the oxygen atom has been structurally characterized.[19] The variable temperature NMR results may be explained, by a reversible coordination of the carbonyl group in either geometry. However, a π-complex is the necessary transition state for the insertion due to orbital overlap constraints.[20] If η^1-coordination of the oxygen atom lead directly to product, then only **3** should be formed because the carbon would never interact with the titanium. A π-complex could give two isomeric complexes, one with the oxygen atom toward the metallacycle and one with the oxygen away from the metallacycle. Due to steric interactions, ketones react only with the alkyl substituents directed away from the η^5-cyclopentadienyl rings, resulting in the observed regiospecificity. Since aldehydes have only one alkyl group, they can twist slightly to accommodate reaction in either direction (Fig. 1). Larger substituents on the aldehyde

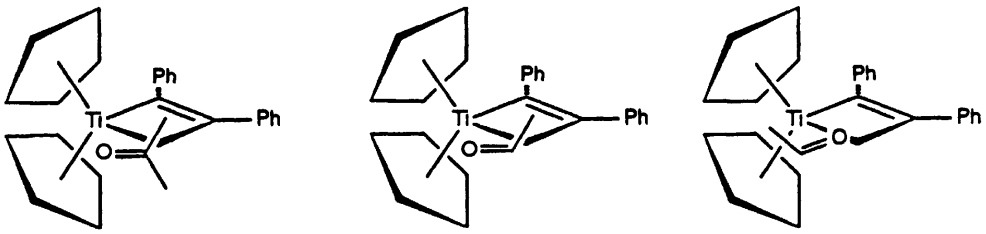

Fig. 1. Proposed carbonyl complexes of **2a**.

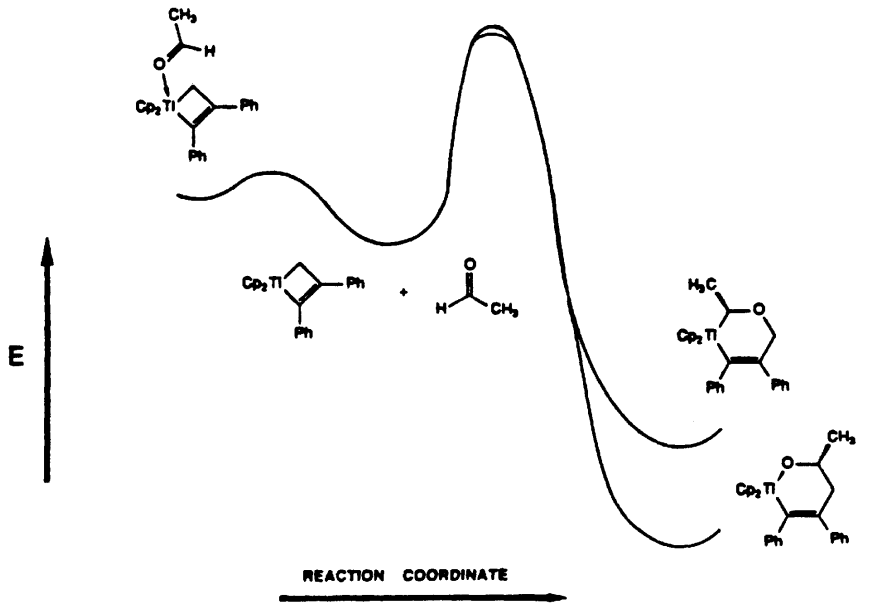

Fig. 2. Proposed energy profile for aldehyde and ketone insertion.

favor the Ti–O product as predicted. The metal center is d^0, and a rotation barrier resulting from back-bonding to the π^* orbital should not exist.

The products are also consistent with an early transition state. Based on the Hammond postulate, an early transition state should be "reactant-like" and not reflect the relative stability of the products.[21] A substituents-effect study of the kinetics may provide information about the polarization of the transition state. A proposed reaction coordinate is shown in Fig. 2.

Insertion of nitriles is analogous to insertion of ketones. However, the products appear to be less stable. The remaining methylene group at the γ-position may be quite acidic due to resonance delocalization (Eq. 11), and deprotonation could lead to decomposition. Nitrile insertions into zirconocene hydride and alkyl complexes yield stable complexes.[22] If the nitrile insertion product is immediately hydrolyzed, the expected ketone is isolated in low yield.

(11)

The most unusual substrate that inserts into titanacyclobutenes is tetramethylguanidine. The insertion product, **6**, has two fluxional processes by NMR.[23] The higher-energy process coalesces at +15 °C at 90 MHz, yielding a $\Delta G^*=14.2\pm0.3$ kcal mol^{-1}. This process is attributable to hindered rotation of the $N(CH_3)_2$ groups. The lower-energy process coalesces at −47 °C, yielding a $\Delta G^*=10.9\pm0.3$ kcal mol^{-1}. This process is attributable to the inversion of the NH group bonded to the titanium. The nitrogen pair presumably interacts with the vacant LUMO on the metal (Eq. 12).[24] This interaction would lead to inequivalent η^5-cyclopentadienyl rings, if the rate were slowed below the NMR time scale.

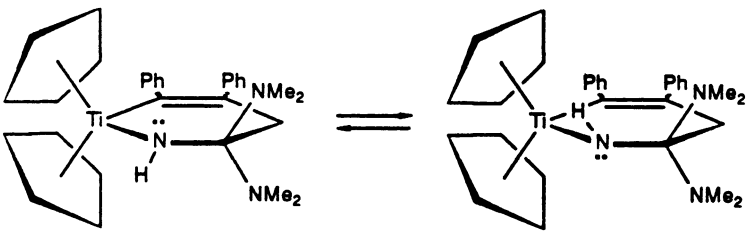

(12)

The lack of carbonylation of **2a** is consistent with other titanium and zirconium alkyl alkoxide complexes. The lack of carbonylation is usually explained by invoking donation of the oxygen lone pair into the LUMO on the titanium. Dative interaction from the oxygen fills the orbital, which would be used for coordination of the CO. This π-donation from the oxygen of titanium alkoxides has been structurally verified.[25] Attempts to complex the oxygen to another Lewis acid failed. Dimethylaluminum chloride appeared to transmetallate the Ti–O bond, although the resulting complex did not react with CO.

Conclusion

Titanacyclobutenes readily insert ketones, aldehydes, and nitriles to form new organometalic complexes. These reactions proceed in good yield with titanacyclobutenes that have a phenyl grouped at the α-position. Titanacyclobutenes that have alkyl substituents at the α-position form unstable products.

The reaction is general for many ketones and highly selective for ketones and aldehydes over esters. Aldehydes yield two products, the predicted Ti–O bound isomer but also the Ti–C bound isomer. The product distribution is consistent with a π-bound carbonyl group at the rate-determining transition state. A detailed kinetics study of the insertion, including substituent effects, would be useful in understanding the mechanism.

Insertion of nitriles forms an analogous product; however, they are less stable than the ketone products.

The titanaoxacyclohexenes, **2**, may be hydrolyzed to the corresponding homoallylic alcohols in high yield. Unfortunately, the titanaoxacyclohexenes would not insert CO under any of the conditions used. Extensions of this work utilizing functionalized titanacyclobutenes and different Lewis acids may find use in organic synthesis.

Experimental

General Considerations. All manipulations were performed with the use of standard Schlenk techniques under argon or in a Vacuum Atmospheres Co. glovebox under nitrogen. Argon was purified by passage through columns of BASF R3-11 (Chemalog) and Linde 4 Å molecular sieves. Carbonylations were performed in Lab-Glass pressure bottles (60 or 100 mL) fitted with two inlet valves and a pressure gauge. Toluene, benzene, THF, and diethyl ether were vacuum-transferred from sodium benzophenone ketyl and stored in Teflon-valve sealed vessels under argon. Pentane and hexane were stirred over concentrated H_2SO_4, dried, vacuum-transferred from sodium benzophenone ketyl and stored in Teflon-valve sealed vessels under argon.

Methylene chloride was vacuum-transferred from P_2O_5 or CaH_2 and stored under argon. Benzene-d_6, toluene-d_8, and THF-d_8 were vacuum-transferred from sodium benzophenone ketyl. Carbon monoxide (CP) was obtained from Matheson. ^{13}C-enriched carbon monoxide (90% ^{13}C) was obtained from Monsanto-Mound Laboratories. Trimethylphosphine was obtained from Strem Chemicals. Acetylenes were obtained from Aldrich, Farchan Laboratory, or Wiley Organics and dried or distilled before use.

Instrumentation. Infrared spectra were recorded on either a Beckman 4240, Shimadzu IR-435, or Perkin-Elmer 1310 spectrophotometer. ^{1}H NMR were recorded on a Varian EM-390, JEOL FX-90Q, Varian XL-200, JEOL GX-400, or Brüker WM-500 and referenced to residual solvent (C_6D_6, δ 7.15; C_7D_8, δ 2.09; THF-d_8, δ 3.58 or 1.73; $CDCl_3$, δ 7.24). ^{31}P{^{1}H} NMR were recorded on a JEOL FX-90Q and referenced to external 85% H_3PO_4 (positive δ, lower field). ^{13}C{^{1}H} NMR were recorded on a JEOL FX-90Q, Varian XL-200, or JEOL GX-400. Difference NOE spectra were recorded on a JEOL GX-400 or a Brüker WM-500 at the Southern California Regional NMR Facility located at the California Institute of Technology. Reaction kinetics were performed on the JEOL FX-90Q using an automated routine. Elemental analyses were performed by Dornis and Kolbe, Mulheim, West Germany, and the analytical facility of the California Institute of Technology.

Kinetics. The rates of the reaction were determined by NMR in septum capped tubes. At least 12 data points were taken by integration of the methylene signals in the starting material and products. The complex **1a** varied in concentration from 0.12 to 0.24 M and the acetone was always in excess varying from 0.17—0.34 M in C_6D_6. Probe temperature was determined at each temperature by a standard second order kinetic calculation.

Materials. Titanacyclobutenes were synthesized as previously described.[8] Ketones, aldehydes, and nitriles were purchased from Aldrich Chemical Co. and used as received. Tetramethylguanidine was obtained from Kodak and dried over 4 Å molecular sieves.

Insertion of Ketones into Titanacyclobutenes 1a and 1b. All reactions were performed by the same general procedure. A stirred solution or suspension of the titanacyclobutene (typically 0.5 M in toluene) was treated with the ketone. The mixture was stirred for 24—48 hours at room temperature, at which time the solution was clear orange. As an alternate method, the reaction mixture was heated to 80 °C for 10—15 minutes and cooled to room temperature. The orange solution was filtered and the volatiles removed, the solid washed with pentane or ether, and dried in vacuo to yield the product.

3,3-Dimethyl-5,6-diphenyl-2-oxa-titanocenecyclohex-5-ene, 2a. Yield: 93%. ^{1}H NMR (90 MHz, C_6D_6) δ=7.08—6.64 (m, 10H), 5.77 (s, 10H), 2.67 (s, 2H), 1.21 (s, 6H). ^{13}C{^{1}H} NMR (22.5 MHz, C_6D_6) δ=190.32, 154.32, 147.23, 134.30, 129.82, 127.55, 124.68, 122.87, 113.64 (Cp), 88.16, 58.79, 28.64. IR (KBr, cm^{-1}) 3010 (w), 2960 (m), 2920 (m), 1650 (w), 1155 (s), 995 (s), 800 (s). Anal. Calcd for $C_{28}H_{28}OTi$: C, 78.50; H, 6.59%. Found: C, 78.50; H, 6.72%.

3-Methyl-3,5,6-triphenyl-2-oxa-titanocenecylohex-5-ene, 2b. Yield: 87%. ^{1}H NMR (400 MHz, C_6D_6) δ=7.267—6.789 (m, 15H), 5.954 (s, 5H), 5.591 (s, 5H), 3.089 (d, J=15.4 Hz, 1H), 2.962 (d, J=15.4 Hz, 1H), 1.578 (s, 3H). Difference NOE experiments: irradiation of δ 5.954 enhances δ 7.220, 6.789, 5.591, 3.089; irradiation of δ 5.591 enhances δ 6.789, 5.954. ^{13}C{^{1}H} NMR (22.5 MHz, C_6D_6) δ=190.7, 154.2, 150.6, 147.3, 133.9, 129.8, 128.3, 127.7, 126.4, 124.9, 123.1, 114.9 (Cp), 113.2 (Cp), 90.8, 58.3, 29.3. IR (KBr, cm^{-1}) 3025 (m), 2975 (m), 1600 (w), 1090 (s), 1068 (s), 1000 (s), 804 (s). Anal. Calcd for $C_{33}H_{30}OTi$: C, 80.81; H, 6.16%. Found: C, 79.70; H, 6.06%.

Reaction of Cyclohexanone with 1a, 2c. Yield: 90%. ^{1}H NMR (400 MHz, C_6D_6) δ=7.029 (m, 6H), 6.883 (t of t, J=7.0, 2.0 Hz, 1H), 6.767 (m, 3H), 5.775 (s, 10H), 2.646 (s, 2H), 1.710 (m, 2H), 1.472 (m, 5H), 1.349 (m, 2H), 1.239 (m, 1H). Difference NOE experiments: irradiation of δ 5.775 enhances δ 6.767, 2.646, 1.710; irradiation of δ 2.646 enhances δ 5.775, 1.349. ^{13}C{^{1}H} NMR (50 MHz, C_6D_6) δ=189.4, 154.7, 147.6, 133.6, 129.9, 128.3, 124.6, 122.8, 113.5 (Cp), 89.9, 57.1, 37.8 (×2), 26.6, 23.6 (×2). IR (KBr, cm^{-1}) 3030 (m), 2925 (s), 1068 (s), 995 (s), 800 (s).

Reaction of 2-Cyclohexen-1-one with 1a, 2d. Yield: 57%. ^{1}H NMR (400 MHz, C_6D_6) δ=7.062—7.046 (m, 6H), 6.868 (m, 1H), 6.804 (m, 3H), 6.044 (d, J=10.0 Hz, 1H), 5.841 (s, 5H), 5.742 (s, 5H), 5.74 (d, overlapping Cp, 1H), 2.838 (d, J=15.4 Hz, 1H), 2.750 (d, J=15.4 Hz, 1H), 1.932—1.755 (m, 3H), 1.641—1.518 (m, 3H). Difference NOE experiments: irradiation of δ 5.841 enhances δ 6.84, 2.838; irradiation of δ 5.742 enhances δ 6.044, 2.750. ^{13}C{^{1}H} NMR (50 MHz, C_6D_6) δ=190.7, 154.2, 147.2, 133.3, 133.6, 129.9, 128.7, 128.3, 127.8, 124.8, 122.9, 113.9 (Cp), 113.7 (Cp), 87.4, 57.8, 36.6, 25.9, 25.4, 20.3. IR (KBr, cm^{-1}) 3015 (w), 2920 (m), 1068 (s), 993 (s), 805 (s).

3-Cyclopropyl-3,5,6-triphenyl-2-oxa-titanocenecyclohex-5-ene, 2e. Yield: 77%. ^{1}H NMR (400 MHz, C_6D_6) δ=7.23—6.76 (m, 15H), 5.842 (s, 5H), 5.673 (s, 5H), 3.381 (d, J=15.4 Hz, 1H), 3.283 (d, J=15.4 Hz, 1H), 1.472 (m, 1H), 0.430 (m, 2H), 0.295 (m, 1H), 0.198 (m, 1H). Difference NOE experiments: irradiation of δ 5.842 enhances δ 7.06, 6.77, 3.28; irradiation of 5.673 enhances δ 6.77, 1.47, 0.43, 0.198. ^{13}C{^{1}H} NMR (22.5 MHz, C_6D_6) δ=189.3, 154.4, 147.6, 146.7, 133.7, 130.1, 127.5, 127.7, 126.4, 124.9, 123.0, 115.1 (Cp), 112.8 (Cp), 91.7, 57.1, 22.8, 2.19, 1.47. IR (KBr, cm^{-1}) 3010 (m), 2930 (w), 1030 (s), 810 (s).

Reaction of α-Tetralone with 1a, 2f. Yield: 96%. ^{1}H NMR (400 MHz, C_6D_6) δ=7.940 (d, J=7.6 Hz, 1H), 7.237 (m, 1H), 7.108 (m, 1H), 7.044 (m, 8H), 6.860 (m, 2H), 6.796 (m, 1H), 5.998 (s, 5H), 5.673 (s, 5H), 3.150 (d, J=16.1 Hz, 1H), 2.920 (s, J=16.1 Hz, 1H), 2.643 (m, 1H), 2.588 (m, 1H), 2.320 (m, 1H), 1.923 (m, 1H), 1.815 (m, 2H). Difference NOE experiments: irradiation of δ 5.998 enhances δ 7.940, 6.860, 5.673, 3.150; irradiation of δ 5.673 enhances δ 6.860, 5.998, 2.920, 1.923.

Reaction of β-Tetralone with 1a, 2g. Yield: 77%. ^{1}H NMR (400 MHz, C_6D_6) δ=7.236—6.911 (m, 14H), 5.961 (s, 1H), 5.561 (s, 5H), 3.270 (d, J=16.3 Hz, 1H), 2.942 (m, 1H), 2.920 (d, J=15.6 Hz, 1H), 2.880 (d, J=16.6 Hz, 1H), 2.722 (d, J=15.6 Hz, 1H), 1.825 (m, 1H), 1.780 (m, 1H). Difference NOE experiments: irradiation of δ 5.961 enhances δ 6.91, 5.561, 2.920; irradiation δ 5.561 enhances δ 6.91, 5.961, 3.270.

3-Methyl-5,6-diphenyl-3-vinyl-2-oxa-titanocenecylohex-5-ene, 2h. Yield: 62%. ^{1}H NMR (400 MHz, C_6D_6) δ=7.03—6.76 (m, 10H), 5.97 (d of d, J=10.5, 17.1 Hz, 1H), 5.938 (s, 5H), 5.612 (s, 5H), 5.100 (d of d, J=17.1, 2.2 Hz, 1H), 4.970 (d

of d, J=10.5, 2.2 Hz, 1H), 2.910 (d, J=15.4 Hz, 1H), 2.58 (d, J=15.4 Hz, 1H), 1.34 s 3. Difference NOE experiments: irradiation of δ 5.940 and 5.970 enhances δ 6.76, 5.61, 2.91; irradiation of δ 5.61 enhances δ 6.76, 5.94; irradiation of δ 1.34 enhances 7.02, 5.97, 5.61, 5.10, 2.58. $^{13}C\{^1H\}$ NMR (22.5 MHz, C_6D_6) δ=190.7, 154.3, 147.0, 146.1, 133.4, 129.9, 127.6, 124.8, 123.0, 114.5, 113.4, 110.3, 89.7, 57.0, 26.2. IR (KBr, cm^{-1}) 3005 (m), 2910 (s), 1015 (s), 987 (s), 800 (s).

Reaction of Ethyl Levulinate with 1a. Synthesis of 2m. ^1H NMR (400 MHz, C_6D_6) δ=7.02—6.69 (m, 6H), 6.88 (t of t, J=7.0, 2.0 Hz, 1H), 6.75 (m, 3H), 5.901 (s, 5H), 5.596 (s, 5H), 4.010 (m, 2H), 2.720 (d, J=15.4 Hz, 1H), 2.460 (d, J=15.4 Hz, 1H), 2.315 (m, 2H), 2.138 (m, 1H), 2.01 (m, 1H), 1.77 (m, 1H), 1.134 (s, 3H), 1.020 (t, J=7.1 Hz, 3H). Difference NOE experiments: irradiation of δ 5.901 enhances δ 6.75 and 2.72; irradiation of δ 5.596 enhances δ 6.75. $^{13}C\{^1H\}$ NMR (22.5 MHz, C_6D_6) δ 190.52, 173.51, 154.27, 147.18, 133.85, 129.84 (CH), 127.62 (CH), 124.75 (CH), 122.96 (CH), 114.19 (Cp), 113.59 (Cp), 89.38 (quat), 60.07 (CH_2), 57.52 (CH_2), 37.53 (CH_2), 30.11 (CH_2), 24.64 (CH_3) 14.34 (CH_3).

Reaction of *l*-Carvone with 1a. Synthesis of 2j. Major isomer: ^1H NMR (400 MHz, C_6D_6) δ=7.31—6.75 (m, 10H), 6.076 (s, 5H), 5.441 (s, 5H), 5.32 (br s, 1H), 5.05 (t, J=1.0 Hz, 1H), 4.91 (t, J=1.0 Hz, 1H), 3.16 (d of d, J=15.8, 1.7 Hz, 1H), 2.70 (m, 1H), 2.69 (d, J=15.8 Hz, 1H), 2.50 (m, 2H), 1.95 (m, 1H), 1.83 (br s, 3H), 1.79 (s, 3H). Difference NOE experiments: irradiation of δ 6.074 enhances δ 6.880, 5.441, 3.16; irradiation of δ 5.441 enhances δ 6.076. $^{13}C\{^1H\}$ NMR (22.5 MHz, C_6D_6) δ 190.95, 154.22, 149.51, 147.45, 140.13, 134.34, 130.11, 129.95, 127.67, 125.94, 125.40, 124.08, 123.18, 123.07, 113.37 (Cp), 114.51 (Cp), 109.71, 93.33, 53.68, 40.89, 39.27, 31.89, 20.52, 19.22.

Minor isomer: ^1H NMR (400 MHz, C_6D_6) δ=7.31—6.75 (m, 10H), 6.032 (s, 5H), 5.665 (s, 5H), 5.44 (br d, J=12 Hz, 1H), 5.01 (t, J=1.0 Hz, 1H), 4.89 (t, J=1.0 Hz, 1H), 3.35 (d, J=15.6 Hz, 1H), 2.41 (d, J=15.6 Hz, 1H), 2.70 (m, 1H), 2.50 (m, 2H), 1.95 (m, 1H), 1.88 (br s, 3H), 1.78 (s, 3H). Difference NOE experiments: irradiation of δ 6.032 enhances δ 6.75, 5.665, 3.35; irradiation of δ 5.665 enhances δ 6.75, 6.032. $^{13}C\{^1H\}$ NMR (22.5 MHz, C_6D_6) δ=190.14, 154.44, 149.78, 147.12, 137.86, 134.23, 130.11, 129.95, 127.67, 125.94, 125.40, 124.08, 123.18, 123.07, 114.51 (Cp), 113.48 (Cp), 109.64, 91.00, 56.06, 41.81, 38.72, 32.33, 20.95, 19.54. (Some signals of the isomers overlap.)

Reaction of Norcamphor with 1a. Synthesis of 2k. ^1H NMR (400 MHz, C_6D_6) δ=7.05—6.99 (m, 6H), 6.86 (t of t, J=7.1, 2.0 Hz, 1H), 6.78 (m, 3H), 5.825 (s, 5H), 5.692 (s, 5H), 2.84 (d, J=15.4 Hz, 1H), 2.73 (d, J=15.4 Hz, 1H), 2.18—2.15 (m, 2H), 1.81 (m, 1H), 1.73 (m, 1H), 1.53 (m, 1H), 1.35—1.15 (m, 4H), 0.93 (m, 1H). Difference NOE experiments: irradiation of δ 5.825 enhances δ 6.78, 5.692, 2.84; irradiation of δ 5.692 enhances δ 6.78, 5.825, 2.73, 1.35. $^{13}C\{^1H\}$ NMR (22.5 MHz, C_6D_6) δ=190.30, 154.92, 147.34, 134.12, 129.90, 127.62, 127.51, 124.70, 122.85, 113.59 (Cp), 113.48 (Cp), 97.45, 57.52, 48.26, 45.44, 38.24, 37.42, 29.29, 22.85.

Reaction of *d*-Camphor with 1a. Synthesis of 2l. ^1H NMR (400 MHz, C_6D_6) δ=7.14—6.99 (m, 6H), 6.86—6.78 (m, 4H), 5.961 (s, 10H), 5.641 (s, 10H), 2.940 (d, J=15.4 Hz, 1H), 2.360 (d, J=15.4 Hz, 1H), 2.195 (d of t, J=12.9, 1.5, 1H), 1.72 (t, J=4.6 Hz, 1H), 1.68 (d, J=13.2 Hz, 1H), 1.56 (m, 2H), 1.32 (m, 2H), 1.017 (s, 3H), 0.932 (s, 3H), 0.852 (s, 3H). Difference NOE experiments: irradiation of δ 5.961 enhances δ 5.641, 2.96, 1.72, 0.932; irradiation of δ 5.641 enhances δ 5.961, 2.360, 2.195, 1.017. $^{13}C\{^1H\}$ NMR (22.5 MHz, C_6D_6) δ 190.57, 154.82, 147.77, 134.39, 129.95, 128.49, 127.67, 127.57, 124.75, 122.96, 113.64 (Cp), 113.37 (Cp), 100.80, 54.65, 54.43, 49.40, 45.88, 31.57, 27.51, 21.55, 21.39, 12.12.

Reaction of 2-Methylcyclohexanone with 1a. Synthesis of 2i. First isomer: ^1H NMR (400 MHz, C_6D_6) δ=7.06—6.75 (m, 10H), 6.000 (s, 5H), 5.644 (s, 5H), 2.80 (d, J=15.6 Hz, 1H), 2.56 (d, J=15.6 Hz, 1H), 2.01 (m, 1H), 1.56—1.10 (m, 8H), 0.995 (d, J=6.6 Hz, 3H). Second isomer: ^1H NMR (400 MHz, C_6D_6) δ=7.06—6.75 (m, 10H), 5.943 (s, 5H), 5.601 (s, 5H), 2.96 (d, J=15.6 Hz, 1H), 2.53 (d, J=15.6 Hz, 1H), 2.01 (m, 1H), 1.56—1.04 (m, 8H), 0.950 (d, J=7.1 Hz, 3H). Difference NOE experiments: irradiation of δ 6.000 enhances δ 6.75, 2.80; irradiation of δ 5.943 enhances δ 6.75, 2.96; irradiation of δ 5.664 enhances δ 6.75, 2.56, 2.01, 1.53; irradiation of δ 5.601 enhances δ 6.75, 2.53, 2.01. $^{13}C\{^1H\}$ NMR (22.5 MHz, C_6D_6) δ 189.60, 189.27, 154.82, 154.55, 147.94, 147.61, 134.45, 134.28, 129.95, 127.62, 124.75, 122.91, 114.19, 114.02, 113.32, 113.05, 93.4, 92.52, 55.68, 50.15, 41.76, 41.43, 35.25, 31.79, 24.53, 24.42, 24.09, 23.94, 16.46.

3,3-Bis(dimethylamino)-5,6-diphenyl-2-aza-titanocenecyclohex-5-ene, 6. Yield: 92%. ^1H NMR (90 MHz, C_7D_8) δ=7.30—6.24 (m, 10H), 5.72 (s, 10H), 2.56 (br s, 6H), 2.45 (s, 3H). $^{13}C\{^1H\}$ NMR (22.5 MHz, C_7D_8) δ=178.70, 161.09, 158.76, 150.15, 129.29, 127.88, 127.34, 127.07, 124.09, 121.71, 110.28 (Cp), 39.20 (br), 30.96. IR (KBr, cm^{-1}) 3060 (w), 3020 (w), 2920 (m), 2870 (m), 1570 (s), 1485 (s), 1455 (s), 1425 (s), 1360 (s), 1122 (s), 1022 (s), 805 (s). Anal. Calcd for $C_{30}H_{35}N_3Ti$: C, 74.21; H, 7.27; N, 8.65%. Found: C, 74.05; H, 7.18; N, 8.52%.

3,3,5-Trimethyl-6-phenyl-2-oxa-titanocenecyclohex-5-ene, 2n. Yield: 74%. ^1H NMR (90 MHz, C_6D_6) δ=7.38—6.87 (m, 5H), 5.74 (s, 10H), 2.26 (s, 2H), 1.64 (s, 3H), 1.13 (s, 6H). $^{13}C\{^1H\}$ NMR (22.5 MHz, C_6D_6) δ=186.8, 155.0, 123.0, 113.6, 88.0, 57.4, 28.5, 24.2. IR (KBr, cm^{-1}) 3020 (w), 2980 (m), 2910 (m), 1000 (s), 805 (s). Anal. Calcd for $C_{23}H_{26}OTi$: C, 75.41; H, 7.15%. Found: C, 75.16; H, 7.03%.

3,5-Dimethyl-3,6-diphenyl-2-oxa-titanocenecyclohex-5-ene, 2o. Yield: 85%. ^1H NMR (90 MHz, C_6D_6) δ=7.33—6.95 (m, 10H), 5.88 (s, 5H), 5.62 (s, 5H), 2.83 (d of d, J=15.3, 1.0 Hz, 1H), 2.42 (d, J=15.3 Hz, 1H), 1.70 (d, J=1.0 Hz, 3H), 1.42 (s, 3H). $^{13}C\{^1H\}$ NMR (22.5 MHz, C_6D_6) δ=187.05, 154.87, 150.81, 128.27, 126.54, 126.37, 124.91, 123.40, 114.67 (Cp), 113.10 (Cp), 90.78, 56.82, 28.64, 24.42. IR (KBr, cm^{-1}) 3060 (w), 2990 (m), 2890 (m), 1100 (s), 1070 (s), 808 (s).

Acidolysis of 2a. A stirred suspension of **2a** (115 mg, 0.268 mmol) in 2 ml of diethyl ether at 0 °C was treated with anhydrous HCl gas (15 ml, 0.67 mmol). The mixture immediately turned red and a red precipitate formed. The reaction was warmed to room temperature over 15 minutes, diluted with 10 ml more diethyl ether, filtered through a 1-inch plug of silica gel and the filtrate concentrated at reduced pressure to yield an orange residue. The residue was extracted with petroleum ether: ether (3:1), the extract filtered through glass wool, and concentrated at reduced pressure to yield the product 2-methyl-4,5-diphenyl-4-penten-2-ol (61 mg, 0.242 mmol, 90%) as yellowish crystals. ^1H NMR (400 MHz, $CDCl_3$) δ=7.279—7.198 (m, 5H), 7.100—7.052 (m, 3H), 6.940—6.921 (m, 2H), 6.522 (s, 1H),

2.768 (s, 2H), 1.497 (br s, 1H), 1.155 (s, 6H). $^{13}C\{^1H\}$ NMR (22.5 MHz, $CDCl_3$) δ=141.41, 139.35, 137.13, 130.68, 129.00, 128.63, 127.82, 127.11, 126.35, 71.53, 53.71 (CH_2), 29.76 (CH_3).

Reaction of *p*-Tolualdehyde with 1a. To a stirred suspension of titanacyclobutene **1a** (365 mg, 0.986 mmol) in 2 ml toluene at room temperature was added *p*-tolualdehyde (140 ml, 1.18 mmol). The mixture was stirred at room temperature for 12 hours, then the volatiles removed in vacuo to yield a red-orange form. The foam was triturated with diethylether, the yellow precipitate filtered from the red solution, and both fractions taken to dryness. The yellow fraction (150 mg, 0.307 mmol) was the insertion product **10a**: ^1H NMR (90 MHz, C_6D_6) δ=7.37—6.67 (m, 14H), 6.06 (s, 5H), 5.59 (s, 5H), 5.48 (m, 1H), 3.05 (s, 1H), 2.97 (d, J=3.2 Hz, 1H), 2.18 (s, 3H). ^1H NMR (400 MHz, C_6D_6) δ=7.29—6.95 (m, 10H), 6.89 (t of t, J=7.1, 0.8 Hz, 2H), 6.78 (t, of t, J=7.1, 0.8 Hz, 2H), 6.119 (s, 5H), 5.610 (s, 5H), 5.53 (d of d, J=10.1, 2.8 Hz, 1H), 3.07 (d of d, J=16.6, 2.9 Hz, 1H), 2.985 (d of d, J=16.6, 10.2 Hz, 1H), 2.18 (s, 3H). $^{13}C\{^1H\}$ NMR (22.5 MHz, C_6D_6) δ=191.44, 153.03, 146.71, 136.51, 136.29, 130.06, 129.08, 128.43, 127.62, 125.72, 124.97, 123.28, 114.35 (Cp), 113.86 (Cp), 88.67, 57.09, 21.11. The diethyl ether-soluble fraction revealed a 2:1 ration of products. The major product was the same as the yellow precipitate; the minor product had ^1H NMR η^5-cyclopentadienyl resonances at δ 5.91, 5.82.

Reaction of Acetaldehyde with 1a. To a stirred suspension of titanacyclobutene **1a** (320 mg, 0.864 mmol) in 3 ml of toluene at room temperature was added acetaldehyde (60 ml, 1.07 mmol) via syringe. The reaction vessel was wrapped in Al foil and the mixture stirred for 12 hours. The reaction mixture was taken to dryness and the red-orange solid was extracted with 2 ml toluene at −78 °C. Both fractions were dried in vacuo. The extract was red-orange and the residue was dark-red. The red-orange extract material was a 2:1 ratio of the Ti-O product. Orange isomer: ^1H NMR (90 MHz, C_6D_6) δ=7.34—6.57 (m, 10H), 5.98 (s, 5H), 5.60 (s, 5H), 4.66—4.29 (m, 1H), 2.70 (s, 1H), 2.64 (d, J=2.9 Hz, 1H), 1.06 (d, J=5.8 Hz, 3H). ^1H NMR (400 MHz, C_6D_6) δ=7.406—6.728 (m, 10H), 5.982 (s, 5H), 5.592 (s, 5H), 4.498 (m, 1H), 2.70 (d of d, J=16.4, 2.8 Hz, 1H), 2.60 (d of d, J=16.4, 9.5 Hz, 1H), 1.06 (d, J=5.9 Hz, 3H). $^{13}C\{^1H\}$ NMR (22.5 MHz, C_6D_6) δ=191.11, 153.30, 136.18, 130.49, 130.06, 128.33, 127.57, 124.91, 123.12, 114.19 (Cp), 113.54 (Cp), 83.25, 55.95, 23.77. Red isomer: ^1H NMR (400 MHz, C_6D_6) δ=7.336—6.944 (m, 10H), 5.890 (s, 5H), 5.883 (s, 5H), 5.641 (q, J=6.35 Hz, 1H), 4.470 (d of d, J=10.0, 4.2 Hz, 1H), 1.48 (d, J=9.8 Hz, 1H), 1.215 (d, J=6.35 Hz, 3H). $^{13}C\{^1H\}$ NMR (22.5 MHz, C_6D_6) δ=181.76, 148.32, 146.09, 144.63, 143.06, 130.44, 130.00, 128.27, 127.57, 126.05, 125.67, 113.54 (Cp), 111.29 (Cp), 87.97, 59.42, 22.41.

Reaction of Benzonitrile with 1a. A solution of titanacycle **1a** (34 mg, 0.092 mmol) in 400 μL of C_6D_6 in an NMR tube was treated with benzonitrile (10 μL, 0.098 mmol). After 24 hours the solution was dark orange and NMR analysis revealed a new compound: ^1H NMR (90 MHz, C_6D_6) δ=7.50—6.80 (m, 15H), 5.64 (s, 10H), 4.03 (s, 2H).

Reaction of *p*-Tolunitrile with 1a. A solution of titanacyclobutene **1a** (38 mg, 0.103 mmol) in 400 μL of C_6D_6 in an NMR tube was treated with *p*-tolunitrile. After 18 hours the color had changed to dark-orange, and the NMR spectrum revealed the reaction as 90% complete: ^1H NMR (90 MHz, C_6D_6) δ=7.50—6.80 (m, 14H), 5.66 (s, 10H), 4.01 (s, 2H), 2.13 (s, 3H).

Reaction of α-Phenylpropionitrile with 1a. A solution of **1a** (38 mg, 0.103 mmol) in 400 μL of C_6D_6 in an NMR tube was treated with α-phenylpropionitrile (14 μL, 0.105 mmol) at room temperature. The color changed slowly over 24 hours from red to dark-orange. NMR analysis revealed a single product and some remaining starting materials: ^1H NMR (90 MHz, C_6D_6) δ=7.15—6.60 (m, 15H), 5.63 (s, 5H), 5.61 (s, 5H), 3.54 (br s, 2H), 3.08 (q, J=7.0 Hz, 1H), 1.32 (d, J=7.0 Hz, 3H).

Reaction of α-Methylpropionitrile with 1a. A solution of **1a** (38 mg, 0.103 mmol) in 400 μL of C_6D_6 in an NMR tube was treated with α-methylpropionitrile (10 μL, 0.11 mmol) at room temperature. The color changed slowly over 24 hours from red to dark-orange. NMR analysis revealed a single product and some remaining starting materials: ^1H NMR (90 MHz, C_6D_6) δ=7.15—6.60 (m, 10H), 5.60 (s, 10H), 3.51 (s, 2H), 1.94 (septet, J=7.1 Hz, 1H), 0.93 (d, J=7.1 Hz, 6H).

Reaction of Methacrylonitrile with 1a. A solution of **1a** (26 mg, 0.071 mmol) in 400 μL of C_6D_6 was treated with methacrylonitrile (6 μL, 0.071 mmol) at room temperature. After 12 hours the reaction was ca. 60% complete by NMR analysis: ^1H NMR (90 MHz, C_6D_6) δ=7.16—6.50 (m, 10H), 5.60 (s, 5H), 5.58 (s, 5H), 5.03 (m, 2H), 3.87 (s, 2H), 1.82 (br s, 3H).

Hydrolysis of the Insertion Product of 1a and *p*-Tolunitrile. To a stirred solution of metallacycle **1a** (200 mg, 0.54 mmol) in 3 ml of THF was added *p*-tolunitrile (75 μL, 0.627 mmol) at room temperature. The reaction was stirred at room temperature for 24 hours. The volatiles were removed in vacuo and the solid suspended in diethyl ether and hydrolyzed with 5% aqueous HCl for 30 minutes. The aqueous phase was separated and extracted with diethyl ether 3×5 ml, the organic phases combined, dried over $MgSO_4$, and concentrated in vacuo. The product was flash-chromatographed ($CHCl_3$) to yield 41 mg of the product ketone: ^1H NMR (90 MHz, $CDCl_3$) δ=7.80—7.00 (m, 14H), 6.55 (br s, 1H), 4.11 (d, J=1.2 Hz, 2H), 2.37 (s, 3H).

Reaction of *p*-Tolunitrile with 1b. A solution of metallacycle **1b** (97 mg, 0.315 mmol) in 500 μL of C_6D_6 was treated with *p*-tolunitrile (36 μL, 0.32 mmol) at room temperature. The reaction was complete within 4 hours to yield a dark-orange solution: ^1H NMR (90 MHz, C_6D_6) δ=7.50—6.80 (m, 9H), 5.70 (s, 10H), 3.68 (s, 2H), 2.20 (s, 3H), 1.65 (s, 3H).

The author wishes to acknowledge the financial support of the National Science Foundation (CHE 8520517) and the National Institute of Health (GM 31332).

References

1) W. Keim, A. Behr, and M. Röper, "Comprehensive Organometallic Chemistry," Vol. 8, Chap. 52, pp. 371—46, ed by G. Willkinson, Permagon Press, Oxford (1982).

2) "Comprehensive Organic Chemistry," ed by D. Barbon et al., Permagon Press, Oxford (1982), Vol. 3, Part

15, pp. 941—1126.

3) a) "Transition Metals in Organic Synthesis," ed by H. Alper, Academic Press, New York (1978), Vol. II, Chap 3. b) "Organic Synthesis by Means of Transition Metal Complexes, J. Tsuji in "Reactivity and Structure Concepts in Organic Chemistry," ed by K. Hafner et al., Springer-Verlag, Berlin (1975), Vol. 1.

4) A. E. Jukes, *Adv. Organomet. Chem.*, **12**, 215 (1974).

5) a) M. T. Reetz, *Top. Curr. Chem.*, **106**, 1 (1982). b) B. Weidmann and D. Seebach, *Angew. Chem., Int. Ed. Engl.*, **22**, 31 (1983).

6) a) W. F. Goure, M. E. Wright, P. D. Davis, S. S. Labadie, and J. K. Stille, *J. Am. Chem. Soc.*, **106**, 6417 (1984). b) R. F. Heck, *Acc. Chem. Res.*, **12**, 146 (1979). c) J. Schwartz, M. J. Loots, and H. Kosugi, *J. Am. Chem. Soc.*, **102**, 1333 (1980).

7) J. W. F. L. Seetz, B. J. J. Van de Heisteeg, G. Schat, O. S. Akkerman, and F. Bickelhaupt, *J. Mol. Cat.*, **28**, 71 (1985).

8) a) F. N. Tebbe, G. W. Parshall, and D. W. Ovenall, *J. Am. Chem. Soc.*, **101**, 5074 (1979). b) F. N. Tebbe and R. L. Harlow, *ibid.*, **102**, 6149 (1980). c) R. J. McKinney, T. H. Tulip, T. H. Thorn, T. S. Coolbaugh, and F. N. Tebbe, *ibid.*, **103**, 5584 (1981). d) J. D. Meinhart, B. D. Santarsiero, and R. H. Grubbs, *ibid.*, **108**, 3318 (1986).

9) K. A. Brown-Wensley, Ph. D. Thesis, California Institute of Technology, 1981.

10) T. G. Richmond, F. Basolo, and D. F. Shriver, *Inorg. Chem.*, **21**, 1272 (1982).

11) R. M. Waymouth, K. R. Clauser, and R. H. Grubbs, *J. Am. Chem. Soc.*, **108**, 6385 (1986).

12) A preliminary X-ray crystal structure confirms this assignment.

13) a) D. D. Tanner, G. E. Diaz, and A. Potter, *J. Org. Chem.*, **50**, 2149 (1985). b) "Rearrangements in the Ground and Excited States," ed by P. de Mayo, Academic Press, New York (1980), Vol. 1.

14) The Proton: "Applications to Organic Chemistry," R. Stewart, Academic Press, New York (1985).

15) F. A. Carey and R. J. Sundberg, "Advanced Organic Chemistry," Part A, Plenum Press, New York (1984).

16) "Kinetics and Mechanism," J. W. Moore and R. G. Pearson, Wiley and Sons, New York (1981).

17) M. F. Lappert, D. S. Patil, and J. B. Pedley, *J. Chem. Soc., Chem. Commun.*, **1975**, 830.

18) G. Fachenetti, C. Biran, C. Floriani, A. Cheisi-Villa, and D. Guastini, *Inorg. Chem.*, **17**, 2995 (1978).

19) S. Gambaroota, M. Pasquali, C. Floriani, A. Cheisi-Villa, and C. Guastini, *Inorg. Chem.*, **20**, 1173 (1981).

20) J. E. Baldwin, *J. Chem. Soc., Chem. Commun.*, **1976**, 738.

21) J. March, "Advanced Organic Chemistry," Wiley and Sons, New York (1985).

22) a) W. Froemberg and G. Erker, *J. Organomet. Chem.*, **280**, 343 (1985). b) G. Erker, W. Froemberg, J. L. Atwood, and W. E. Hunter, *Angew. Chem., Int. Ed. Engl.*, **23**, 68 (1984).

23) "Dynamic Nuclear Magnetic Resonance," ed by L. M. Jackman and F. A. Cotton, Academic Press, New York (1975).

24) a) J. W. Lauher and R. Hoffmann, *J. Am. Chem. Soc.*, **98**, 1729 (1976). b) G. L. Hillhouse and J. E. Bercaw, *J. Am. Chem. Soc.*, **98**, 1729 (1976). c) G. L. Hillhouse and J. E. Bercaw, *J. Am. Chem. Soc.*, **106**, 5472 (1984). d) S. J. Simpson and R. A. Andersen, *Inorg. Chem.*, **20**, 3627 (1981).

25) a) J. A. Marsella, K. G. Moloy, and K. G. Cauton, *J. Organomet. Chem.*, **201**, 389 (1980). b) J. C. Huffman, K. G. Moloy, J. A. Marsella, and K. G. Caulton, *J. Am. Chem. Soc.*, **102**, 3009 (1980).

 © 1988 The Chemical Society of Japan Bull. Chem. Soc. Jpn., 61, 181—186 (1988)

An ESR Study of 5-Formazanyl Copper(II) Complexes as an Analogy to Three Types of Copper-Containing Proteins

Yoshiko KAWAMURA, Yasuo DEGUCHI,* Jun YAMAUCHI, and Hiroaki OHYA-NISHIGUCHI†
Department of Chemistry, College of Liberal Arts and Sciences, Kyoto University, Kyoto 606
†Department of Chemistry, Faculty of Science, Kyoto University, Kyoto 606
(Received May 18, 1987)

The Electron Spin Resonance(ESR) spectra of ten 5-formazanyl copper(II) complexes in toluene solutions have been observed at room temperature and at that of liquidnitrogen. The ESR($g_{//}$ and $A_{//}$) and bonding(α^2) parameters of the copper ion were greatly affected by substituting several groups at the ortho position of 1-phenyl ring of formazan. Based on these results, the complexes are classified into three groups: Group I, in which $A_{//}\simeq 0.012$—$0.013\,cm^{-1}$ and $\alpha^2\simeq 0.5$; Group II, in which $A_{//}\simeq 0.017\,cm^{-1}$ and $\alpha^2\simeq 0.7$, and Group III, in which two copper ions are interacting. It is clarified that they correspond nicely to three types of copper-containing proteins previously investigated.

Since Kuhn and Jerchel studied the tetrazolium salts of formazan in a program of research on invert soap,[1] these compounds, with their remarkable biological potentialities, have been extensively investigated. Especially, formazans obtained by the reduction of the corresponding tetrazolium salts have been widely utilized to check enzyme activity in plant and animal tissues.[2]

Formazans have been known to form complexes with some transition metals having the stoichiometries of 2:1 and 1:1.[3-5] Previously, we ourselves reported that some copper complexes of formazan show small isotropic splitting constants of the copper ion in the ESR spectra of these complexes and that their magnetic properties change drastically with different kinds of substituents to the 1-phenyl ring of 1,3,5-triphenyl-5-formazan (Fig. 1).[6] These results have motivated us to undertake a thorough examination of the substituent effects on the electronic states and magnetic properties of these complexes.

Many studies of copper complexes have established that the structural configuration around the copper ion is affected by the inductive property of the substituent group,[7,8] the distortion due to the bulky substituents,[9,10] and the apical coordination of the solvent molecules, in addition to the symmetry of the ligand field.[11,12] The change in the ESR parameters has been discussed in relation to various kinds of binding sites of copper proteins. A comparison of ESR data of the binding sites of copper proteins with those of well-defined model complexes enables us to suppose micro-structural information about the area around the copper ion in proteins.[13-17] Thus, the copper ions in the various copper proteins thus far investigated have been classified into three types, based on ESR spectroscopic studies.[18-21]

The effects of the substituent groups on the copper complexes mentioned above have thus far been found in the range of a perturbation within each type of copper-containing protein. However, we have now found that the copper-ion environment in 5-formazanyl copper(II) complexes is much affected by the introduction of different substituent groups into formazan and that the change in the spectroscopic behavior due to these substituents extends over all three types. Therefore, we have attempted to establish the micro-structural details of the present complexes and the analogy to the binding site of copper-containing proteins.

In this paper, we will report the results of our ESR spectroscopic study of copper complexes of formazan with several kinds of substituents. The results obtained are examined based on the inductive, distortional, and coordinational effects. Finally, the configulational change suggested by the ESR and bonding parameters will be discussed in relation to three types of copper-containing proteins.

Experimental

Preparation of Samples. 1,3,5-Triphenyl-5-formazan, which has no substituent in the 1-phenyl ring, is shown in Fig. 1. Formazans with a para or ortho substituent in the 1-phenyl ring were obtained by the reaction of the diazonium salts of para- or ortho-substituted aniline with benzaldehyde phenylhydrazone by a method described elsewhere.[22] (Hereafter, we will abbreviate the substituent as X.) The copper complex was prepared by mixing ethanol solutions of formazan and copper acetate monohydrate.[4] The precipitate was obtained by the addition of water to the ethanol solution. Recrystallization was also carried out in the ethanol solution. The complexes obtained consisted of a fine powder and so could not be submitted to X-ray crystallographic measurements. The analytical data of the complexes prepared for the present study are listed in Table 1. The complexes obtained are abbreviated as *p*-X-Cu (2:1) for bis[1-(*p*-X phenyl)-3,5-diphenyl-5-formazanyl]copper and *o*-X-Cu (1:1) for bis[1-(*o*-X phenyl)-3,5-diphenyl-5-formazanyl]dicopper.

Physical Measurements. The X-band (9 GHz) ESR spectra were obtained in the toluene solutions of the

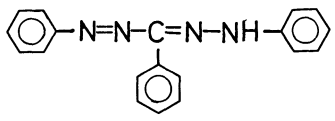

Fig. 1. 1,3,5-Triphenyl-5-formazan.

Table 1. Analytical Data of the 5-Formazanyl Copper(II) Complexes

Complex	Molecular formula	Found(%)				Calcd(%)			
		C	H	N	Halogen	C	H	N	Halogen
1, *p*-H-Cu(2:1)	$C_{38}N_8H_{30}Cu$	68.8	4.6	16.6		68.9	4.5	16.4	
2, *p*-Cl-Cu(2:1)	$C_{38}N_8H_{28}Cl_2Cu$	61.7	3.9	14.8	9.9	62.4	3.9	15.3	9.7
3, *p*-Br-Cu(2:1)	$C_{38}N_8H_{28}Br_2Cu$	55.6	3.4	13.5	19.3	55.7	3.4	13.7	19.5
4, *p*-NO_2-Cu(2:1)	$C_{38}N_{10}O_4H_{28}Cu$	60.5	3.7	18.6		60.7	3.7	18.6	
5, *p*-CH_3-Cu(2:1)	$C_{40}N_8H_{34}Cu$	70.0	4.9	15.2		69.6	4.9	16.2	
6, *o*-CH_3-Cu(2:1)	$C_{40}N_8H_{34}Cu$	69.7	4.9	16.2		69.6	4.9	16.2	
7, *o*-Cl-Cu(2:1)	$C_{38}N_8H_{28}Cl_2Cu$	61.8	3.6	14.1	10.7	62.4	3.9	15.3	9.7
8, *o*-Br-Cu(2:1)	$C_{38}N_8H_{28}Br_2Cu$	55.2	3.4	13.9	19.3	55.7	3.4	13.7	19.5
9, *o*-COOH-Cu(1:1)	$C_{40}N_8O_4H_{28}Cu_2$	59.0	3.6	13.5		59.2	3.5	13.8	
10, *o*-OH-Cu(1:1)	$C_{38}N_8O_2H_{28}Cu_2$	60.6	3.9	14.8		60.4	3.7	14.8	

complex at room temperature and in frozen glasses at 77 K with a JEOL ME-3X spectrometer equipped with 100 KHz field modulation. The Mn^{2+} in MgO was used as a standard sample for the calibration of the magnetic field. The optical spectra of the complexes were measured in toluene solutions at room temperature by the use of a Shimazu Double-beam Spectrophotometer, UV200, in the range of 300—700 nm and by the use of a Shimazu Multi-purpose Spectrophotometer, MPS50L, in the range of 600—2000 nm.

Results

The 5-formazanyl copper complexes obtained are classified into two categories on the basis of the stoichiometry of formazan and the copper ion from the results of the elemental analyses; one is of a 2:1 stoichiometry of formazan and the copper ion, while the other is of 1:1. Based on the ESR parameters to be described below, the former is further divided into two groups, Group I and Group II; the latter is abbreviated as Group III. The molecular structures of the complexes tentatively suggested by the elemental analyses are shown in Fig. 2(a) for the complexes in Groups I and II and in Fig. 2(b) for those in Group III. The latter shows the dimer structures of the complex. The complexes belonging to each group are listed in Table 2.

Group I. The ESR spectrum of *p*-H-Cu (2:1), **1**, in a toluene solution at room temperature is shown in Fig. 3(a) as a typical example of the spectra of the complexes belonging to Group I. The spectra of the complexes of Group I consisted of four ill-resolved resonance lines attributable to one copper ion (I=3/2). In some complexes, further splittings around 0.0005 cm^{-1} were observed at the absorption line in the highest field; they were unambiguously assigned to the superhyperfine interaction between the unpaired electron of the copper ion and the ligand-nitrogen nuclei. The isotropic copper splitting constants, A_{iso}(Cu), are around 0.004 cm^{-1}. These values are extremely small compared with those of the ordinary copper complexes with a planar configuration.[23,24]

The ESR spectrum of **1** obtained in a frozen toluene solution at 77 K is shown in Fig. 3(b), which is also typical of monomeric copper species. The g values, g_1, g_2, and g_3, which were experimentally determined in the ESR spectra at 77 K, are tabulated in Table 2. The g_1 clearly corresponds to the usual notation, $g_{//}$.

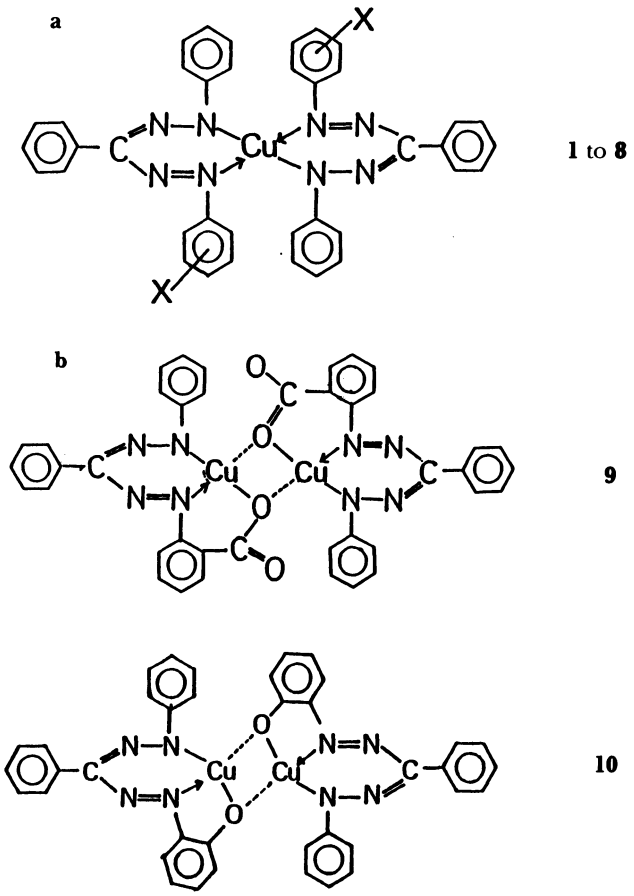

Fig. 2. **a**, Bis[1-(*p*-X phenyl)-3,5-diphenyl-5-formazanyl]copper, **1**: X=H; **2**: X=Cl; **3**: X=Br; **4**: X=NO_2; **5**: X=CH_3. Bis[1-(*o*-X phenyl)-3,5-diphenyl-5-formazanyl]copper, **6**: X=CH_3; **7**: X=Cl; **8**: X=Br. **b**, **9**, Bis[1-(*o*-carboxyphenyl)-3,5-diphenyl-5-formazanyl]-dicopper, and **10**, bis[1-(*o*-hydroxy)-3,5-diphenyl-5-formazanyl]dicopper.

Table 2. ESR and Bonding Parameters, and Visible Absorptions of *p*-X-Cu and *o*-X-Cu in Toluene

Complex	g_1	g_2	g_3	g_{ave}	A_1(Cu)	A_2	A_3	A_{iso}(Cu)	α^2	Absorption maxima
					10^{-4} cm^{-1}					nm
1, *p*-H-Cu	2.114	2.032	1.991	2.043	115	8.5	—	38	0.47	440, 470(sh)[a], 590, 790
2, *p*-Cl-Cu	2.115	2.034	1.984	2.045	121	6.5	—	38	0.49	440, 580, 780
3, *p*-Br-Cu	2.113	2.032	1.985	2.044	120	7.9	8.2	38	0.49	450. 590, 780
4, *p*-NO_2-Cu	2.111	2.031	1.985	2.043	121	5.6	—	38	0.49	480, 600, 780
5, *p*-CH_3-Cu	2.121	2.032	1.984	2.046	120	7.4	—	38	0.49	440, 560, 800
6, *o*-CH_3-Cu	2.122	2.035	1.983	2.049	132	6.9	—	41	0.55	420, 500, 540, 750
7, *o*-Cl-Cu	2.120	2.031	1.991	2.048	169	15.4	15.4	77	0.60	485, 590
8, *o*-Br-Cu	2.125	2.019		2.054	175	16.5		77	0.63	485, 590
9, *o*-COOH-Cu	2.192	2.054	1.986	2.077	163	18.5	—	65	0.69	555, 580(sh), 820
10, *o*-OH-Cu	2.143	2.026	1.978	2.049	179	16.0	18.6	71	0.68	580, 820

a) "sh" designates shoulder.

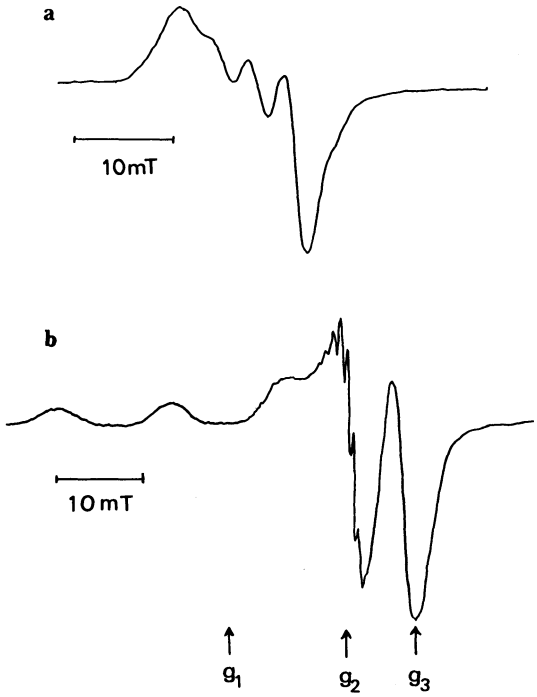

Fig. 3. ESR spectra of **1** in toluene solution at (a) room temperature and (b) liquid-nitrogen temperature. Further splittings were not observed in (a).

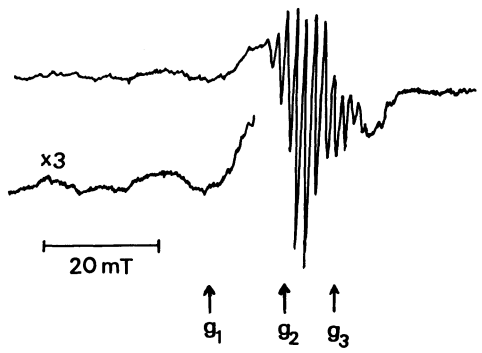

Fig. 4. ESR spectrum of **7** in toluene solution at liquid-nitrogen temperature.

The g_2 and g_3 can not, however, be uniquely assigned to g_x and g_y. The splitting of 0.012 cm^{-1} at the g_1 position, A_1(Cu), can reasonably be assigned to the parallel component of the copper hyperfine splittings, $A_{//}$(Cu). This value is also small compared with those of the usual planar copper complexes. Further splitting constants at the g_2 and g_3 positions are represented as A_2 and A_3 respectively. These can not be uniquely assigned to the splittings due to the x and y components of the copper ion, for the splittings due to the four equivalent nitrogen nuclei may overlap. However, in view of the apparent intensity ratios of the absorption lines at the g_2 and g_3 positions, the assignment of these splittings to the ligand nitrogens seems most plausible. The ESR parameters of the other complexes of Group I, **2**, to **6**, are also tabulated in Table 2. These parameters of Group I are almost all the same in spite of the various kinds of substituents.

Group II. Figure 4 shows the ESR spectrum of *o*-Cl-Cu (2:1), **7**, in a toluene solution at 77 K. The ESR spectral patterns of this complex at room temperature and 77 K were similar with those of Group I except for the fact of the larger values of A_1(Cu), A_2, A_3, and A_{iso}(Cu). A_1(Cu) and A_{iso}(Cu) are 0.017 cm^{-1} and 0.0077 cm^{-1} respectively. A_2 and A_3 are 0.0015 cm^{-1}. These are usual values in copper complexes with planar or pseudo-planar configurations.[23,24] Their g values are also similar to those of the complexes of Group I. In the ESR spectrum of *o*-Br-Cu (2:1), **8**, in a toluene solution at 77 K, the splitting constants of the copper ion and the g values are similar with those of **7** except for the property of the axial symmetry with $g_2=g_3$ and $A_2=A_3$.

Group III. As has previously been reported, the ESR of *o*-COOH-Cu (1:1), **9**, in a toluene solution showed only one sharp single line and did not reveal any hyperfine structure at either room temperature or

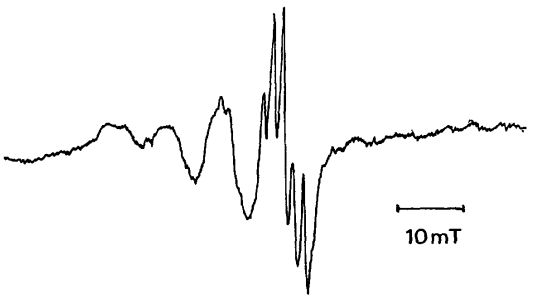

Fig. 5. ESR spectrum of **10** in toluene solution at room temperature. Superhyperfine splittings due to ligand nitrogens are observed in the absorption line at the highest field.

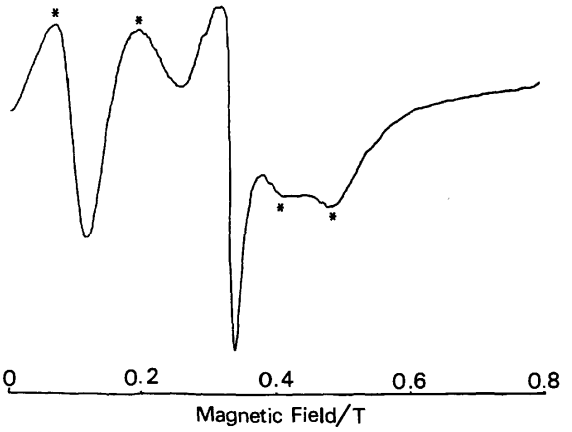

Fig. 6. ESR spectrum of **10** in microcrystalline state at room temperature. The asterisks in the spectrum show the absorptions due to the excited triplet state of the dimer. These disappear at liquid-nitrogen temperature. The central part of the spectrum is due to the monomeric species.

the temperature of liquidnitrogen. The temperature dependence of the magnetic susceptibility of the powdered sample could well be interpreted on the basis of the ground triplet-excited singlet model for the dimeric species of the copper ions.[25] Therefore, one absorption line was attributed to the exchange interaction between two copper ions. In order to get further information about the copper monomer, the addition of pyridine to the toluene solution was attempted. As a result, the hyperfine structure due to the copper monomer appeared at room temperature and that of liquidnitrogen. The data in Table 2 are what were obtained in this way: The g_{ave}(Cu) of **9** is slightly larger than those of Group II, but A_{iso}(Cu) and A_1(Cu) are similar to those of Group II. These values of **9** might, by the addition of pyridine, have been varied from those without the solvation of pyridine.[26] However, the visible absorptions did not show any appreciable change by the addition of pyridine. Therefore, it is conceivable that the configurational change around the copper ion may be small in the pyridine-added toluene solution.

The ESR spectrum of *o*-OH-Cu (1:1), **10**, in the toluene solution at room temperature consisted of four lines attributable to the copper monomer (Fig. 5). Further splittings to five lines at the absorption in the highest field provide firm evidence that the two nitrogens of the ligand take part in the superhyperfine interaction. At the temperature of liquidnitrogen the typical spectrum of the usual copper ion with an anisotropy was observed. The ESR parameters of the monomer were similar to those of Group II. In the microcrystalline state, on the other hand, the ESR spectrum of the triplet state was observed at room temperature on both sides of the absorption line attributable to the monomeric species of the copper ion, as is shown in Fig. 6. The absorption line without the asterisk around 0.3 T corresponds to that of the copper monomeric species. The signal intensity of the triplet state became too weak to be recognized at 77 K. It is obvious from these facts that the two copper ions are interacting with each other through exchange interaction. The details of the triplet state, including the estimation of the zero-field-splitting parameter, D, will be reported elsewhere.

Discussion

Table 2 indicates that the unsubstituted 5-formazanyl copper, **1**, and all of the complexes with para substituent groups, **2** to **6**, belong to Group I. The symmetry around the copper ion in these complexes can plausibly be considered to be planar or pseudo-planar, based upon the g values and the hypothetical molecular structures. On the other hand, the complexes with ortho substituent groups belong to all three groups, suggesting that the substitution results in a different ligand configuration around the copper ion.

The change in the electronic state of the copper ion has been discussed on the basis of: 1) The electron-inductive effect caused by the substituent groups, 2) the distortional effect caused by the substituent groups, and 3) the apical coordination effect, caused mainly by the solvent molecules. The effects of the increased electron-donating ability of the substituent groups on the ESR parameters are to decrease $g_{//}$ and to increase $A_{//}$(Cu). The ESR behavior of Group I did not depend upon the electron-donating ability of the para substituent groups. The trend of the change in $g_{//}$ and $A_{//}$(Cu), expected from the increase in the electron-donating ability (-Cl, -Br, -H, and -CH_3), was not observed in the complexes with the ortho substituent groups. Therefore, the electron-inductive effect of the substituent groups is not dominant in the para and ortho substituents. Yokoi et al. reported that the distortional effect becomes dominant when the substituent groups are bulkier.[9] In such a case, $A_{//}$(Cu) decreases and $g_{//}$ increases with the degree of

distortion from the plane containing the copper ion. The facts that *o*-H-Cu (2:1), **1**, and *o*-CH_3-Cu (2:1), **6**, are in Group I, while *o*-Cl-Cu (2:1), **7**, and *o*-Br-Cu (2:1), **8**, are in Group II obviate the importance of the distortional effect caused by the substituent groups on the electronic state of the copper ion. The apical coordination of the solvent molecules is weak in the case of the toluene solution. Therefore, it may be concluded that the three effects mentioned above are not adequate to interpret the drastic change in the ESR parameters shown in Table 2.

For the probable structure with the square-planar symmetry and with the ground orbital of $d_{x^2-y^2}$,[27] Kivelson and Neiman defined a bonding parameter, α^2.[28] Here we will use α^2 expressed semiempirically by Bryce:[29]

$$\alpha^2 = \frac{A_{//}}{P} + (g_{//}-2.0023) + \frac{3}{7}(g_{\perp}-2.0023) + 0.04$$

where P=0.04 cm^{-1}. In order to ascertain the bonding characters of the copper ion under the assumption of the square-planar symmetry around the copper ion, the bonding parameters of Group I and II are compared. In a previous paper, the square-planar structure around the copper ion in the microcrystalline state of **1** was presumably adopted with reference to the *g* values of the other copper complexes with the square-planar symmetry.[6] Though the three different values of the *g* component in the frozen toluene solutions of the present complexes suggest a deviation from the square-planar symmetry around the copper ion, the structure is presumed not to be much changed from the planarity, for the difference between g_2 and g_3 is not very large. Under these assumptions, the bonding parameters, α^2, of Group I and II were calculated; they are tabulated in the last column of Table 2.

The deviation from 1.0 shows the degree of covalency of the bonding. The fact that α^2 in Group I, about 0.5, is extremely small indicates the strong covalency in the bonding between the copper ion and the ligands. Such small values have previously been reported with respect to the complexes with sulfur coordination and to plastocyanine, in which the sulfur coordination was determined by means of X-ray analyses.[30,31] On the other hand, the α^2 around 0.7 of Group II is not so small and is comparable to those of Cu-phthalocyanine (0.73) and Cu-tetraphenylporphyrine (0.79).[21] Therefore, it may be concluded that the bonding conditions of Group I and Group II differ considerably.

The toluene solution of **9** showed only a single line, without any hyperfine splitting, at room temperature and at that of liquidnitrogen. These results can be well-interpreted by assuming that, even in a toluene solution, the dimeric structure shown in Fig. 2(b) is retained and that the exchange interaction between the two copper ions in the dimer smears out the lines caused by the hyperfine splittings. Upon the addition of one drop of pyridine, however, the ESR spectrum characteristic of the monomeric copper ion was observed. Therefore, it is adequate to mention that the addition of pyridine to the toluene solution of **9** has led to the dissociation of the dimer to the monomer, probably ligated by the pyridine molecule, as is shown in Scheme 1. Previously it has been shown that the

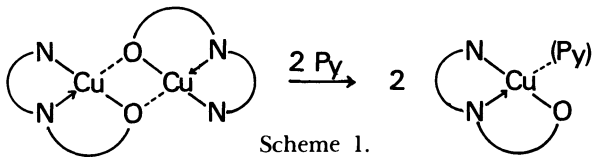

Scheme 1.

temperature dependence of the magnetic susceptibility of **9** could be well-interpreted by the dimeric model with ferromagnetic exchange interaction of the order of 20 K. Therefore, it is plausible to consider that **9** retains the dimeric structure even in the toluene solution. On the other hand, the ESR spectrum of the triplet state observed in **10**, indicates that **10** makes a dimer in the microcrystalline state. However, the ESR spectrum of **10** in the toluene solution showed the hyperfine structure characteristic of the monomeric copper ion at room temperature and at that of liquidnitrogen. The half-field resonance giving one evidence of the dimeric interaction was not observed in the toluene solution, even at the temperature of liquidnitrogen. These results suggest that the dimer of the **10** formed in the microcrystalline state dissociates into two monomeric species in the toluene solution, as is shown in Scheme 1. Such a difference between **9** and **10** in the toluene solutions may be due to the difference in ligation ability between -COOH and -OH. Consequently, the complexes belonging to Group III can be characterized as those in which the complexes have the dimeric structure in the solid state.

Unfortunately, we could not obtain the useful information from the ESR spectra of **9** and **10**, about the circumstances of the copper ions in the dimer. However, the fact that the ESR parameters of the dissociated species of **9** and **10** are very similar to those of the complexes in Group II indicates that the ligand configurations of the copper ions in the dimers are not so different as those of the copper ions belonging to Group II. The substituents of formazan, -COOH and -OH, can be regarded as bases, $-COO^-$ and $-O^-$. On the other hand, the substituent groups in Group I and II can not be bases, though they are electronegative. Therefore. only the ortho substituents, which can be bases for the copper ion, have the possibility of forming magnetically interacted dimeric species.

It is interesting to compare the α^2 and $A_{//}$(Cu) of the present complexes with those of copper-containing proteins. Copper-containing proteins have been classified into three types from the spectroscopic point of view:[20]

Type I: Blue copper proteins. $A_{//}$(Cu) is less than

0.008 cm^{-1}, and there is an abnormally strong absorption maximum around 600 nm.

Type II: Normal copper proteins. The copper splitting constants are of the order of 0.017 cm^{-1}, and the other spectroscopic parameters are similar to those of the copper complexes with a planar structure.

Type III: ESR nondetectable copper proteins. It is generally said that a strong antiferromagnetic or ferromagnetic coupling between two copper ions leads to the ESR spectra becoming nondetectable.

X-Ray analyses were carried out in several kinds of **Type I** copper proteins; the sulfur coordination was thus authenticated.[30,31] Their bonding conditions have become clear.[32] Though sulfurs do not exist in the ligands of the present complexes, the ESR parameters and α^2 values of Group I correspond well to those of **Type I** copper proteins. Therefore, the nitrogens of formazan would constitute strong covalent bondings with the copper ion in the complexes of Group I, as in the case of **Type I** copper proteins. The α^2 values of the ordinary copper complexes with peptide bondings, in which the copper ions have the square-planar symmetry, are in the range from 0.81 to 0.82. The α^2 and $A_{/\!/}$(Cu) values of the complexes of Group II are 0.7 and 0.017 cm^{-1} respectively. Therefore, the complexes of Group II correspond well to the **Type II** copper proteins. It had been considered that the two copper ions were so strongly coupled in the **Type III** copper proteins that ESR observation was difficult. However, the observation of the ESR of the triplet state was accomplished first in the Met derivative of hemocyanine copper, showing clear evidence of the interaction of the two copper ions. As has previously been mentioned in the Results section, the exchange-narrowing was observed in **9** and the ESR spectrum of the triplet state was observed in **10**, in each microcrystalline state. They are characterized as the species with the dimeric interaction, corresponding to **Type III**.

The most characteristic point of these results is that the three types of ESR behaviour, depending upon the different substituent groups to the ortho position of 1-phenyl ring, correspond to the three types of copper proteins. These results may be useful in elucidating the micro-structural details around the copper ions in **Types I, II,** and **III** copper proteins. The 5-formazanyl copper(II) complexes with a flexible molecular structure have the possibility of being plausible model compounds of copper-containing proteins.

The authors wish to thank Dr. Takaharu Matsubara for the measurements of the absorption spectra and also Professor Noboru Hirota for his valuable discussions. This work was partially supported by the Grant-in-Aid for Scientific Research on Priority Area of "Macromolecular Complexes (No. 62612005)" from the Ministry of Education, Science and Culture.

References

1) R. Kuhn and D. Jerchel, *Ber.*, **74**, 949 (1941).
2) A. W. Neinham, *Chem. Rev.*, **55**, 355 (1954). Other references are cited herein, for example: A. M. Mattson, C. O. Jensen, and R. A. Dutcher, *Science*, **106**, 274 (1947).
3) R. Kuhn and D. Jerchel, *Ber.*, 74, 941 (1949).
4) R. W. Zinger and V. Biro, *Helv. Chim. Acta*, **27**, 901 (1949).
5) P. Price, *J. Chem. Soc. A*, **1971**, 3371.
6) Y. Kawamura, Y. Deguchi, J. Yamauchi, and H. Ohya-Nishiguchi, *Bull. Chem. Soc. Jpn.*, **57**, 1441 (1984).
7) H. A. Kuska and M. T. Rogers, *J. Chem. Phys.*, **43**, 1744 (1965).
8) H. Yokoi and T. Kishi, *Chem. Lett.*, **1973**, 749.
9) H. Yokoi, *Bull. Chem. Soc. Jpn.*, **47**, 3037 (1974).
10) H. Yokoi and A. W. Addison, *Inorg. Chem.*, **16**, 1341 (1977).
11) J. I. Zink and R. S. Drago, *J. Am. Chem. Soc.*, **94**, 4559 (1972).
12) H. Yokoi, M. Sai, and T. Isobe, *Bull. Chem. Soc. Jpn.*, **43**, 1078 (1970).
13) Y. Sugiura, Y. Hirayama, H. Tanaka, and K. Ishizu, *J. Am. Chem. Soc.*, **97**, 5577 (1975).
14) D. E. Wilcox, J. R. Long, and E. I. Solomon, *J. Am. Chem. Soc.*, **106**, 2186 (1984).
15) V. McKee, M. Zvagulis, J. V. Dagdigian, M. G. Patch, and C. A. Reed, *J. Am. Chem. Soc.*, **106**, 4765 (1984).
16) K. D. Karlin, R. W. Cruse, Y. Gultney, J. C. Ayes, and J. Zubieta, *J. Am. Chem. Soc.*, **106**, 3372 (1984).
17) V. McKee, M. Zvagulis, and C. A. Reed, *Inorg. Chem.*, **24**, 2914 (1985).
18) J. A. Fee, *Struct. Bonding (Berlin)*, **23**, 1 (1975).
19) H. Beinert, *Coord. Chem. Rev.*, **33**, 55 (1980).
20) E. I. Solomon, "Copper Proteins," ed by T. G. Spiro, Wiley: New York (1981).
21) S. G. Malmstrom, B. Reinhammer, and T. Varnngard, *Biochim. Biophys. Acta*, **205**, 48 (1970).
22) J. N. Ashley, B. M. Davis, A. W. Nineham, and R. Stack, *J. Chem. Soc.*, **1953**, 3381.
23) S. E. Harrison and J. M. Assour, *J. Chem. Phys.*, **49**, 365 (1964).
24) J. M. Assour, *J. Chem. Phys.*, **43**, 2477 (1963).
25) J. J. Mooiji, A. A. Klassen, and E. de Boer, *Mol. Phys.*, **32**, 879 (1976).
26) J. I. Zink and R. S. Drago, *J. Am. Chem. Soc.*, **94**, 4550 (1972).
27) B. R. McGarvey, *J. Phys. Chem.*, **71**, 51 (1967); Other references are cited herein.
28) D. Kivelson and R. Neiman, *J. Chem. Phys.*, **35**, 149 (1961).
29) G. F. Bryce, *J. Phys. Chem.*, **79**, 3549 (1966).
30) P. M. Colmann, H. C. Freeman, J. M. Guss, M. Marata, V. A. M. Rawshow, and M. P. Penkatappa, *Nature (London)*, **272**, 319 (1978).
31) a) E. T. Adman, R. E. Stenkamp, L. C. Sieken, and L. H. Jensen, *J. Mol. Biol.*, **123**, 35 (1978). b) E. T. Adman and L. H. Jensen, *Isr. J. Chem.*, **21**, 8 (1981).
32) K. W. Penfield, A. A. Gewirth, and E. I. Solomon, *J. Am. Chem. Soc.*, **107**, 4519 (1985).

 © 1988 The Chemical Society of Japan Bull. Chem. Soc. Jpn., 61, 187—190 (1988)

Removal of Phosphates from Aqueous Solution by Active Charcoal Electrode

Masao Ichinose, Takashi Yasuoka,* Shunmei Mitsuzawa, and Tsunetaka Sasaki
Department of Chemistry, Faculty of Science, Tokai University,
1117 Kitakaname, Hiratsuka-shi 259-12
(Received June 4, 1987)

The electrolytic removal of phosphoric acid and mono-, di-, and tripotassium phosphates from aqueous solution was attemped using improved active charcoal electrodes which proved more effective in removing these electrolytes than the previous one. The degree of removal of phosphoric acid and phosphates exceeded 90% after 80 min's electrolysis, tending to 100% after sufficient time of electrolysis. The mechanism of removal of phosphoric acid and potassium phosphates was confirmed to be the entrapment and concentration of these substances as potassium hydroxide and phosphoric acid in the pores of the active charcoal. The processes of removal of phosphoric acid and phosphates were found to be complicated due to hydrogen and hydroxide ions formed by the dissociation of phosphoric acid and hydrolysis of phosphates respectively which explained the initial rate of removal of these substances decreasing in the order of phosphoric acid through potassium dihydrogen- to tripotassium phosphate. Regeneration of active charcoal electrode was further inferred.

Present authors have reported in a previous paper that alkali and sulfate ions were effectively removed from alkali sulfate solution by the electrolysis using active charcoal electrodes.[1] In the present paper, the removal of potassium phosphates and phosphoric acid from an aqueous solution by this technique was reported. These salts require detailed study from the viewpoints of both water pollutant[2] and the complicated behavior exhibited during their removal by electrolysis, due mainly to the hydrolysis of polybasic phosphate salts and dissociation of phosphoric acid. The improvement of the electrodes used for the measurement of removal of electrolytes was also devised in comparison with the former one.[1]

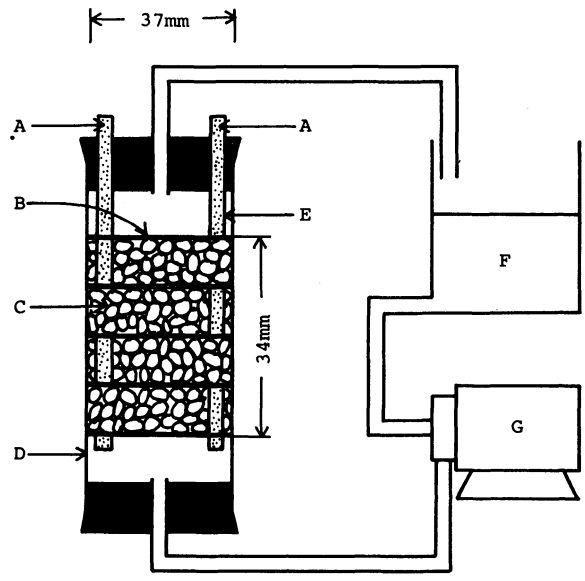

Fig. 1. Apparatus.
A: Graphite electrode, B: perforated plastic plate, C: active charcoal, D: glass tube, E: tape-insulated part, F: sample reservoir G: circulation pump.

Experimental

Materials. The phosphoric acid and potassium phosphates used were guaranteed-grade products of Wako Pure Chemical Co. Ltd. which were used without further purification. The active charcoal used as electrodes was a guaranteed-grade product of Wako, charcoal activated, granulated, the size being about 4 mm in diameter and 4 to 10 mm in length, which was washed with conductivity water until it showed no increase in electric conductance.

Apparatus and Procedure. The apparatus used is similar as a whole to that used in a previous paper:[1] It consists of three parts, an electrode chamber, a circulation pump, and a reservoir, as shown in Fig. 1. But the electrode chamber is different from the former one. The electrode consists of four layers of packed charcoal granules, 15 g in total weight. The layers are separated from each other by perforated plastic plates of 2 mm in pore diameter and 1 mm in thickness, perforated portion covering two third of the area of plastic plate. The electrode is constructed by alternately connecting charcoal layers to a cathode and an anode carbon rods.

To carry out the electrolytic removal of phosphoric acid and potassium phosphates, each 1 dm^3 solution of phosphoric acid, potassium dihydrogenphosphate, dipotassium hydrogenphosphate, and tripotassium phosphate containing 20 ppm of phosphate ions as PO_4^{3-} was introduced in the apparatus. The solution was circulated at the rate of 7.9 $dm^3\ min^{-1}$ † and a direct current was applied. The voltage was controlled so as to keep a constant current of 50 mA. During the electrolysis, small portions of the solution were withdrawn from the reservoir at intervals of 20 min, and the concentrations of phosphate and potassium ions were measured by Shimazu LC-5A Liquid Chromatograph and by Hitachi 508 type Atomic Absorption Spectrophotometer respectively. From the concentration thus obtained the degree of removal of each ions was calculated as a percent of initial concentration and was plotted against the time of electrolysis to study the rate of

† The degree of removal was found nearly the same for the flow rate down to 3 $dm^3\ min^{-1}$: 4 $dm^3\ min^{-1}$ may be sufficient for practical application of 80 min's electrolysis.

removal. Further, in order to study the mechanism and to obtain the optimum conditions of electrolytic removal of phosphoric acid and potassium phosphates, measurements of electrolytic removal were carried out in detail.

Results and Discussion

Performance of Electrode. In the former case of removal of potassium sulfate from an aqueous solution by using active charcoal electrode,[1] the porous porcelain septum used consumed a large electric power due to a large electric resistance between the electrodes. To confirm the efficiency of the improved electrode used to overcome this loss, aqueous dipotassium hydrogenphosphate solution was electrolyzed under the conditions mentioned above and the results obtained were compared with those obtained using previous electrode for the same amount of active charcoal and current conditions. The degree of removal vs. time curves agreed with each other up to 93% removal within the difference of 2% for the period of 80 min while the applied voltage was markedly reduced in the present measurement as shown in Fig. 2: Electric power consumed during this period was calculated to be about 24 to 31 Wh for the former electrode and about 3 Wh for the present electrode. The marked reduction of electric power consumption proved the effectiveness of the improved electrode used in the present study.

The degree of removal of phosphate ions obtained for phosphoric acid, and potassium phosphates was plotted against time of electrolysis as shown by solid lines in Fig. 3. The broken lines show the degree of removal by active charcoal without electrolysis.

Mechanism of Removal without Electrolysis. In the case of phosphate ions without electrolysis, the degree of removal was low as a whole compared with the case of electrolysis. The degree of removal was most marked for phosphoric acid and gradually decreased from potassium dihydrogenphosphate to tripotassium phosphate. As regards such an adsorption of phosphate ions, it may be pertinent to refer to the fact that the addition of hydrogen ions to the salt of weak acid strongly increase the adsorption of corresponding anion.[3] In the present case, as shown later in Fig. 4, hydrogen ion concentration of aqueous solutions decreased from phosphoric acid through potassium dihydrogenphosphate to tripotassium phosphate. This fact together with the above mentioned tendency of adsorption explain the order of adsorption of phosphate ion shown in Fig. 3.

Mechanism of Removal by Electrolysis. In the case of removal by electrolysis both initial rate and maximum value of the degree of removal were larger than those obtained without electrolysis as shown in Figs. 3 and 5. The removal of phosphate ions after 80 min was 100% for phosphoric acid and was least value of 90% for tripotassium phosphate. The degree of removal after sufficient time of electrolysis tended towards 100%, irrespective of the salts used. The difference between the removals with and without electrolysis is evident since the latter is affected by the

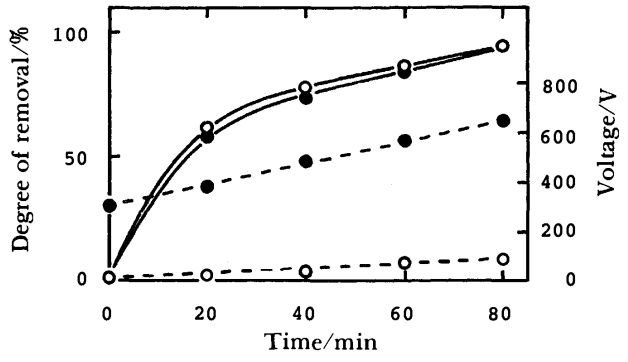

Fig. 2. Degree of removal of phosphate ions and applied voltage.
O: Present electrode, ●: previous electrode. ——: Degree of removal of phosphate ions, ------: applied voltage.

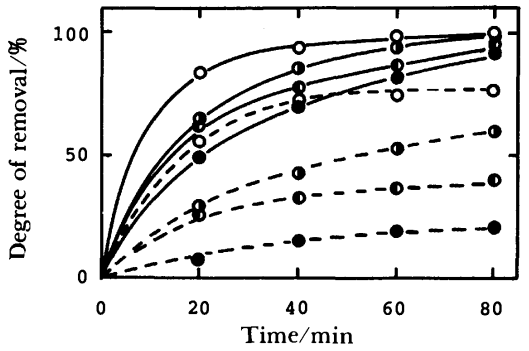

Fig. 3. Degree of removal of phosphate ions.
O: Phosphoric acid, ◑: potassium dihydrogenphosphate, ◐: dipotassium hydrogenphosphate, ●: tripotassium phosphate.
——: With electrolysis (current 50 mA), ------: without electrolysis.

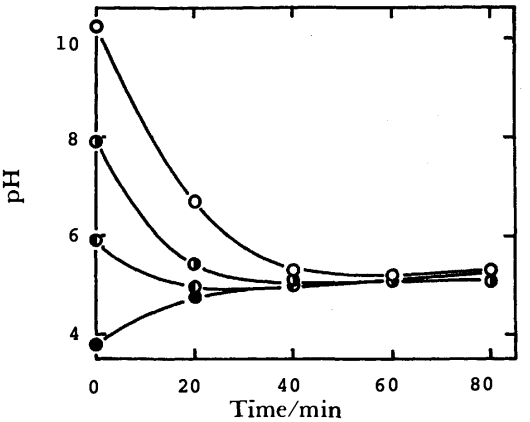

Fig. 4. Change of pH with time of electrolysis.
O: Tripotassium phosphate, ◑: dipotassium hydrogen phosphate, ◐: potassium dihydrogenphosphate, ●: phosphoric acid.

hydrogen ion concentration as mentioned above while the former is determined mainly by the movement of ions in the solution in an electric field mentioned as follows.

Hydrolysis and Dissociation of Phosphates and Phosphoric Acid: As for the initial rate of removal of phosphate ions, decreasing order of phosphoric acid, potassium dihydrogen-, dipotassium hydrogen-, and tripotassium phosphates was confirmed which is considered to be closely related to hydroxide and hydrogen ions produced respectively by the hydrolysis of phosphates and dissociation of phosphoric acid since these ions are expected to remarkably influence the transference of both potassium and phosphate ions. This was confirmed by the measurement of pH change of the solution against time of electrolysis as shown in Fig. 4.

In this figure pH value after 80 min agreed with pH value of distilled water after sufficient time of electrolysis. As was evident from a high initial value of pH and its rapid decrease in the initial stage of electrolysis of tripotassium salt, high electric mobility of hydroxide ions[††] produced by hydrolysis and their discharge at the anode was dominant which reduced both the initial ionic transport and the rate of removal of potassium and phosphate ions.[4] As seen in Fig. 4 such a tendency was most marked for tripotassium phosphate, less marked for dipotassium hydrogenphosphate and almost negligible for potassium dihydrogenphosphate. Initial rate of removal of phosphate ions is explained to increase in parallel with this. The decreasing order of initial concentration of potassium ions from tripotassium phosphate to potassium dihydrogenphosphate is also in accord with this increase. In the case of potassium dihydrogenphosphate, both hydrolysis and dissociation of phosphate ions are calculated to be negligible, and the salt simply dissociate to form potassium and dihydrogenphosphate ions which migrate towards electrodes with the least hindrance by hydroxide ions. A slight decrease of pH after sufficient time of electrolysis, as mentioned above may come from dissolved carbon dioxide which could not be removed from distilled water used. The larger initial rate of removal of phosphate ions in the case of phosphoric acid than that of potassium salts may be due to the overlapping of a large initial rate of adsorption exhibited even without electrolysis which was already shown by the broken line in Fig. 3. Thus, phosphate ions both in the form of free acid and in various forms of potassium salts can be confirmed to be removed effectively by the electrolysis using active charcoal electrode.

The degree of removal of potassium ions was measured at the same time with phosphate ions and was plotted against the time of electrolysis as shown in Fig. 5, together with the degree of removal without electrolysis. As seen, initial rate of removal increased from tripotassium phosphate through dipotassium hydrogen- to potassium dihydrogenphosphate and about 95% of potassium ions was removed after 80 min's electrolysis of these salts similarly to the degree of removal of phosphate ions. The order of the initial rate of removal of potassium ions mentioned above may be similarly explained by taking account of hydrolytic formation of hydroxide ions of large ionic mobility and resulting decrease of the transference number of potassium ion.[4] No removal of potassium ions by the circulation of solution without electrolysis is distinctly shown in Fig. 5. The phenomena may have some relation with the negative adsorption of potassium hydroxide towards charcoal[3] but it was not studied in detail in the present paper.

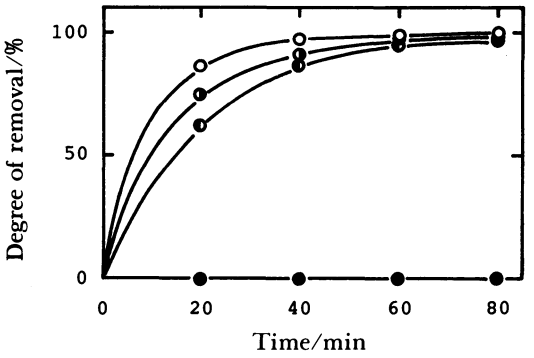

Fig. 5. Degree of removal of potassium ions.
With electrolysis (current 50 mA). ○: Potassium dihydrogenphosphate, ◑: dipotassium hydrogenphosphate, ◐: tripotassium phosphate.
Without electrolysis. ●: Tripotassium dipotassium hydrogen-, and potassium dihydrogenphosphates.

Up-Take of Ions by Charcoal Electrode: Phosphoric acid and potassium phosphates removed from the solution are considered to be entrapped and concentrated in the pores of active charcoal electrodes similarly to the case of the removal of potassium sulfate reported in a previous paper.[1]

To confirm this, extraction of potassium and phosphate ions from active charcoal electrodes which are considered to entrap these ions was carried out by treating the charcoal with acid or alkali. The amount of ions extracted was expressed as the percentage of the total amount of each ions entrapped. The results showed that from active charcoal used as the anode for the removal of potassium dihydrogenphosphate, phosphate ions could not be extracted with acid solution but more than 90% was extracted with concentrated potassium hydroxide, and nearly 100% of potassium ions were extracted from the cathode with concentrated hydrochloric acid. Further, active

[††] Mobility of ions at 25 °C (unit in $S\,cm^2\,mol^{-1}$); OH^- 198.3, $H_2PO_4^-$ 36, HPO_4^{2-} 57, PO_4^{3-} 69.0, K^+ 73.5.

charcoal electrode used for removing potassium dihydrogenphosphate was put in conductivity water together with a platinum wire electrode, and the direct current was applied in the reverse direction to that applied during the removal experiment. The amounts of potassium and phosphate ions thus extracted were nearly 100% and 65% of the amount entrapped respectively.

These results confirmed the fact similar to the case of potassium sulfate[1] that phosphate and potassium ions were entrapped respectively as phosphoric acid and potassium hydroxide in each electrode. But different from the case of alkali sulfate, polyvalency of phosphate ion and formation of hydroxide ions due to its hydrolysis complicated the process of electrolytic removal as mentioned. However, even under such conditions, complete removal could be established after sufficient time of electrolysis, irrespective of the phosphates used.

Regeneration of Active Charcoal Electrodes. As mentioned above phosphate and potassium ions taken up by the charcoal electrodes can be easily released by treating them with acid, alkali, and by electrolysis. These facts may suggest the possibility of regeneration and repeated use of active charcoal as the electrode. The problem should be paid attention when the present method is applied for the practical problem, details of which are under study.

References

1) M. Ichinose, T. Yasuoka, S. Mitsuzawa, and T. Sasaki, *Bull. Chem. Soc. Jpn.*, **59**, 3347 (1986).

2) L. E. Kuentzel, *Environ. Lett.*, **2**, 101 (1971); D. W. Schindler, *J. Phycol.*, **7**, 321 (1971).

3) H. Freundlich, "Kapillarchemie," Akademische Verlag, Bd **I**, Leipzig (1930), pp. 131, 290.

4) R. A. Robinson and F. A. A. Stokes, "Electrolyte Solutions," 2nd ed., Butterworths Sci. Pub., London (1959), p. 44.

Excitation Wavelength Dependence of Phosphorescence and Hydrogen-Bonding Formation of Thioxanthone and 2,4-Diisopentylthioxanthone

Hiroshi MORITA,* Shigeyasu MORI, and Tsuguo YAMAOKA
Department of Image Science and Technology, Faculty of Engineering, Chiba University, Yayoi-cho, Chiba 260
(Received June 8, 1987)

Phosphorescence spectra of the ethanol solutions of thioxanthone(TX) and 2,4-diisopentylthioxanthone (DITX) exhibited excitation wavelength dependence at 77 K. In addition to the normal phosphorescence observed at 450 nm for TX and at 460 nm for DITX, a new red-shifted phosphorescence was resolved at 470 nm and 485 nm, respectively, when TX and DITX were excited at the absorption tail. The lifetimes and excitation spectra of the red-shifted phosphorescence were found to differ from those of the normal phosphorescence. Based on the study on UV absorption spectra and phosphorescence spectra measured with hydrated species of TX and DITX in ethanol–water solution at 77 K, the red-shifted phosphorescence is ascribed to the hydrogen-bonded species with water. In 2-methyltetrahydrofuran, phosphorescences of TX and DITX shift to the longer wavelengths and the lifetimes become longer when excited at the longer absorption tail, although the phosphorescence excitation spectra do not change appreciably.

In polymer photochemistry, thioxanthone[9*H*-thioxanthen-9-one](TX) and its derivatives are effective sensitizers in radical polymerization of vinyl monomers,[1–3] in photocrosslinking of polyacrylates and polystyrenes,[4,5] and in photocuring of coating systems.[6] In order to understand the sensitization mechanisms, photophysical and photochemical properties of TX and its derivatives have been studied extensively.[1,3,5,7,8] As is widely recognized in aromatic carbonyl compounds,[9–12] TX has close-lying $S_1(\pi\text{-}\pi^*)$ and $S_2(n\text{-}\pi^*)$, and $T_1(\pi\text{-}\pi^*)$ and $T_2(n\text{-}\pi^*)$ states.[13–15] Due to the proximity of the S_1 and S_2 states, S_1–S_0 internal conversion rate of TX is influenced significantly by the solvent polarity, and hence fluorescence intensity, peak position, and lifetime largely change depending on solvents.[16]

Nature of the triplet state of TX and its derivatives is of particular interest in relation to the photochemical behavior as a sensitizer. Because the T_1 state of TX is assigned to $\pi\text{-}\pi^*$ state even in nonpolar solvents,[13–15] the phosphorescent behavior of TX and its derivatives is not expected to change significantly depending on solvents in contrast to the case of xanthone.[12]

Recently, however, we have observed that the phosphorescence spectra observed with the ethanol and 2-methyltetrahydrofuran (MTHF) solutions of TX and 2,4-diisopentylthioxanthone (DITX) change significantly depending on excitation wavelengths. To investigate this in detail, we have measured in the present paper, the phosphorescence and UV absorption spectra of TX and DITX in ethanol, in ethanol–water, and in MTHF at 77 K, and found that TX and DITX form hydrogen-bonded(H-bonded) species with water even in freshly distilled ethanol solution.

Experimental

TX (Kanto G.R. grade) and DITX (Toshin Kayacure) were purified by repeated recrystallization from benzene three times and finally by vacuum sublimation. Ethanol (Wako G.R. grade) used as a solvent was purified by fractional distillation, and MTHF (Tokyo Kasei G.R. grade), by fractional distillation immediately before use in the dark. Degassed solutions of TX and DITX were prepared by freeze-pump-thaw cycles under a background pressure of 6×10^{-3} Pa.

Phosphorescence spectra and phosphorescence excitation spectra were measured at 77 K with the combination of a phosphoroscope, a monochromator (JASCO CT-50), and a photomultiplier tube (EMI 6256S), exciting light from a 150 W xenon arc lamp (Ushio UXL-150D) being monochromatized with a monochromator (Nikon G250). Phosphorescence decay curves were recorded with the use of a transient memory (Kawasaki Electronica MR100E). UV absorption spectra were measured at 77 K and at room temperature with a Hitachi 200-20 and a Hitachi 330 recording spectrophotometers in cells of 1 and 10 mm light path lengths. The effect of photoproducts[5,7] of the ethanol and MTHF solutions of TX and DITX on phosphorescence lifetimes and spectra, and on UV spectra is negligible under the present experimental conditions.

Results and Discussion

Phosphorescence of TX and DITX in Ethanol. Phosphorescence spectrum observed with the ethanol solution of TX (2.4×10^{-4} M†) excited at 380 nm is shown in Fig. 1A. Observed spectrum is broad and has a peak at 450 nm and a shoulder at ≈480 nm (hereafter this phosphorescence is called the normal phosphorescence). Phosphorescence excitation spectra of TX monitored at 450 and 480 nm are shown in Fig. 1B; the excitation spectrum monitored at 450 nm has peaks at 384, 366, and 299 nm, and coincides well with the UV absorption spectrum of TX measured at 77 K (Fig. 1C). On the other hand, the excitation spectrum monitored at 480 nm shows an additional new band at ≈400 nm. Hence, phosphorescence spectrum was further measured by exciting TX at

† 1 M=1 mol dm^{-3}.

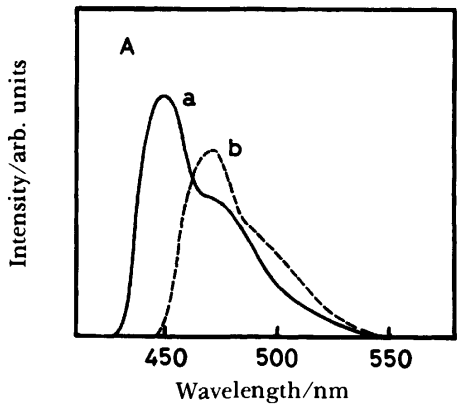

Fig. 1A. Phosphorescence spectra measured with the ethanol solution of TX (2.4×10^{-4} M) excited at (a) 380 nm and (b) 400 nm. The phosphorescence spectra in this and the following other figures are not corrected for the detector responce of a monochromator and photomultiplier tube unless otherwise stated.

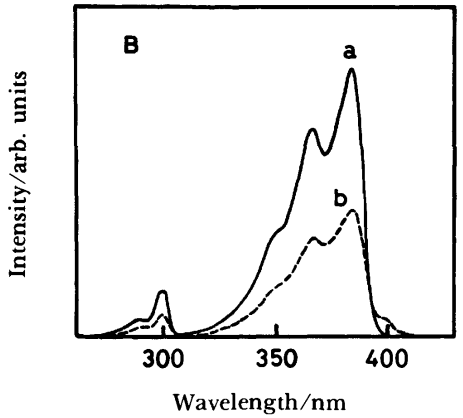

Fig. 1B. Phosphorescence excitation spectra measured with the ethanol solution of TX (2.4×10^{-4} M) monitored at (a) 450 nm and (b) 480 nm. The excitation spectra in this and the following other figures are not corrected for the spectral intensity of an exciting light source unless otherwise stated.

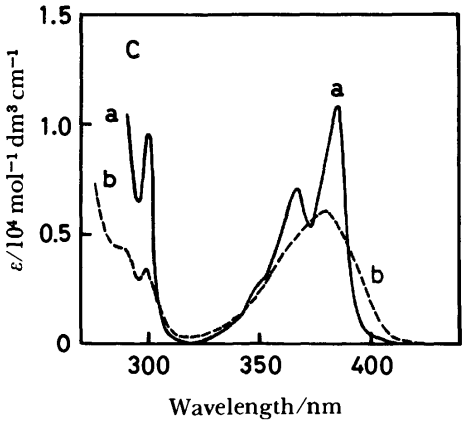

Fig. 1C. UV absorption spectra measured with the ethanol solutions of (a) TX (5.5×10^{-5} M) at 77 K and (b) TX (2.0×10^{-3} M) at room temperature.

400 nm; the result is also shown in Fig. 1A. The weak and broad phosphorescence spectrum with a peak at ≈470 nm and a shoulder at ≈500 nm was observed (referring to the normal phosphorescence, this is called the red-shifted phosphorescence). The red-

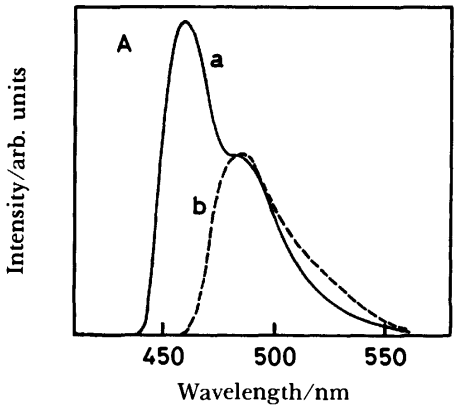

Fig. 2A. Phosphorescence spectra measured with the ethanol solution of DITX (4.4×10^{-4} M) excited at (a) 392 nm and (b) 410 nm.

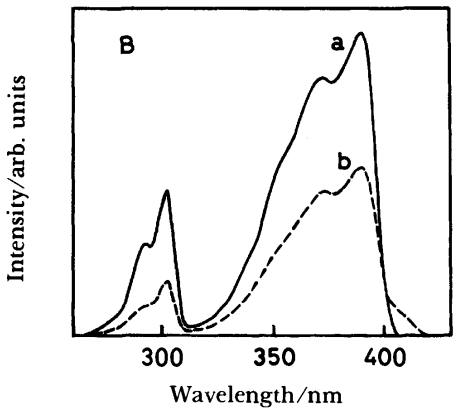

Fig. 2B. Phosphorescence excitation spectra measured with the ethanol solution of DITX (4.4×10^{-4} M) monitored at (a) 460 nm and (b) 490 nm.

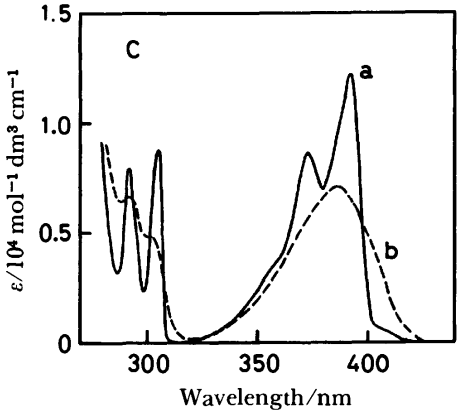

Fig. 2C. UV absorption spectra measured with the ethanol solutions of (a) DITX (7.3×10^{-5} M) at 77 K and (b) DITX (8.3×10^{-5} M) at room temperature.

shifted phosphorescence monitored at 480 nm decays single-exponentially, and the lifetime is 213 ms. This is longer than the one (160 ms) of the normal phosphorescence monitored at 450 nm and also at 475 nm which decays single-exponentially. From the lifetime measurement, the normal and the red-shifted phosphorescences can be assigned to different species of TX.

As in the case of TX, phosphorescence observed with the ethanol solution of DITX exhibits excitation wavelength dependence. Phosphorescence spectrum of DITX excited at 392 nm (near an absorption maximum) has a peak at 460 nm and a shoulder at ≈490 nm, whereas the one excited at 410 nm has a peak at 485 nm and a shoulder at ≈520 nm (Fig. 2A). The lifetime of the latter (i.e., of the red-shifted phosphorescence) is 226 ms and is longer than the one (173 ms) of the former (i.e., of the normal phosphorescence). In phosphorescence excitation spectrum, a new 410 nm band was observed when monitored at ≈490 nm (Fig. 2B). From these results, the normal and the red-shifted phosphorescences can be assigned to different species of DITX.

It is worthwhile to notice that the red-shifted phosphorescence can be observed with the ethanol solution of such a low concentration as 6×10^{-6} M of TX. The extra 400 nm(or 410 nm) band in the excitation spectrum of TX(or DITX) corresponds to the tail of the strong UV absorption measured at 77 K (Figs. 1C and 2C). Intensity of the absorption tail (in terms of apparent extinction coefficient) is rather unaffected by the concentration change of TX from 6×10^{-5} M to 2×10^{-3} M. These results indicate that the new chemical species which gives rise to the red-shifted phosphorescence is neither an associate such as a dimer or an aggregate, nor triplet excimer state which is suggested in naphthoquinones and anthraquinones.[17] Furthermore, the phosphorescence lifetimes were measured with degassed solutions. The lifetimes for the normal and the red-shifted phosphorescences of TX and DITX agree well with the values of the corresponding aerated solutions. The result suggests that a radical species and a light-absorbing transient (LAT) therefrom[7,18,19] are not responsible for the observation of the red-shifted phosphorescence. Judging from the experimental results mentioned above, formation of a hydrated species due to a little dissolved water in ethanol as an impurity is suggested.

Hydrogen-Bonded Species of TX and DITX. To investigate the nature of the hydrated species of TX and DITX in ethanol, UV absorption spectra of TX and DITX were measured at 77 K in ethanol-water mixed solutions; the results are shown in Fig. 3. As the water content is increased, a new band appears at ≈398 nm in the spectrum of TX and at ≈405 nm in the spectrum of DITX with isosbestic points.

The spectral change can be analysed on the basis of

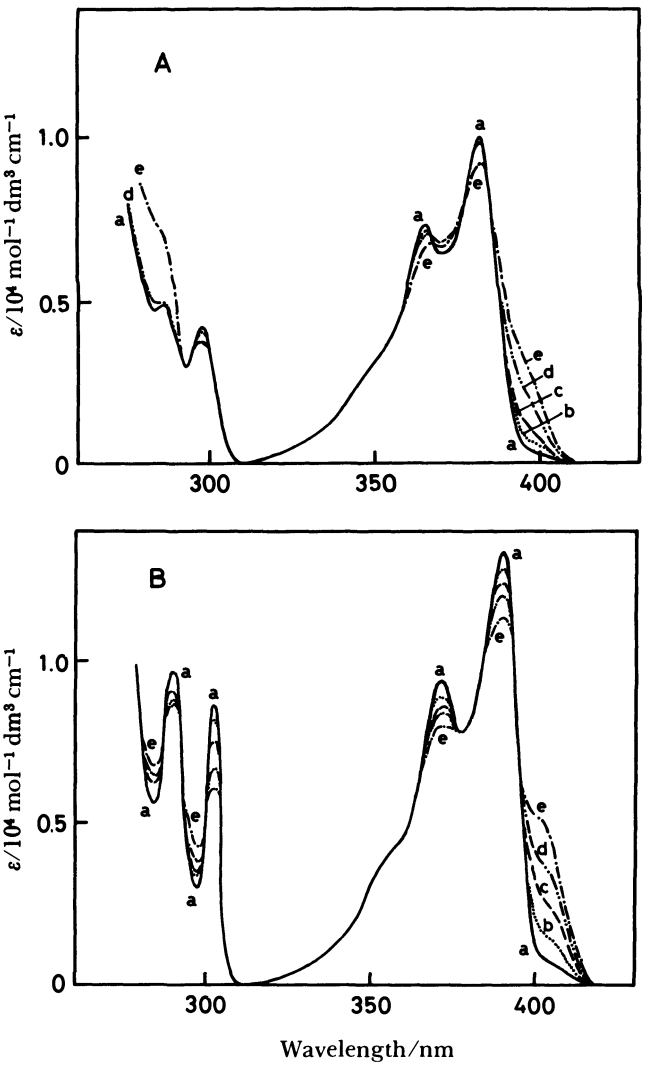

Fig. 3. UV absorption spectra measured with the ethanol-water solutions of (A) TX (9.0×10^{-5} M) and (B) DITX (9.7×10^{-5} M) at 77 K. Water content is (A):(a) 0, (b) 1, (c) 2, (d) 4, and (e) 6 vol%; and (B):(a) 0, (b) 1, (c) 2.5, (d) 4, and (e) 6 vol%.

formation of an associate between TX(or DITX) (A) and water (B):A+B→AB(or C). The association constant, K, was evaluated by the use of the equation;[20,21]

$$(d/[A]_0-\varepsilon_A)^{-1} = ((\varepsilon_C-\varepsilon_A)K[B]_0)^{-1} + (\varepsilon_C-\varepsilon_A)^{-1}, \quad (1)$$

where d is the apparent absorbance (per 1 cm light path length) for the system, ε_A and ε_C, the molar extinction coefficients of TX(or DITX) and the associate, respectively, and $[A]_0$ and $[B]_0$, the initial concentrations of TX(or DITX) and water, respectively. The equation is applicable to the case where $[B]_0 \gg [A]_0$ and $\varepsilon_B \approx 0$ are satisfied. Taking into account of the volume change of ethanol-water mixed solution at 77 K, $(d/[A]_0-\varepsilon_A)^{-1}$ was plotted against $[B]_0^{-1}$ at several wavelengths; the results are shown in Fig. 4. Linear relationship holds for both TX and

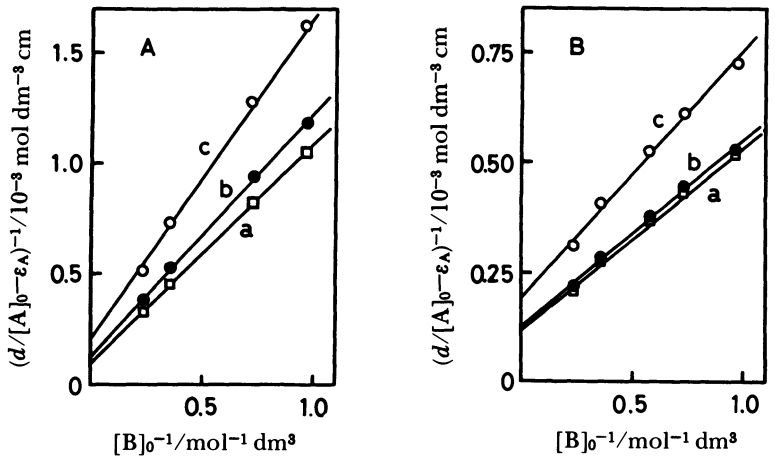

Fig. 4. Plots of $(d/[A]_0-\varepsilon_A)^{-1}$ against $[B]_0^{-1}$ for (A) TX at (a) 392.5 nm, (b) 397.5 nm, and (c) 400 nm; and (B) DITX at (a) 402 nm, (b) 404 nm, and (c) 408 nm in ethanol-water solution at 77 K.

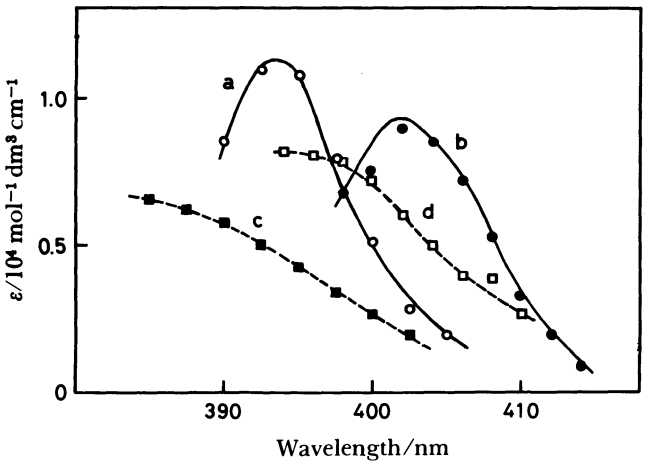

Fig. 5. UV absorption spectra of H-bonded species in ethanol-water solution of (a) TX and (b) DITX at 77 K, and (c) TX and (d) DITX at room temperature. For a detailed procedure, see the text.

DITX, indicating that the 1:1 associated species between TX(or DITX) and water is predominantly formed in ethanol. From the slopes and intercepts of the straight lines in Fig. 4, K and ε_C values were evaluated; the average of K's evaluated for TX-water in 392.5—400 nm region is 0.11±0.03, and the one evaluated for DITX-water in 400—408 nm region is 0.29±0.05. The observed K values are small in ethanol. In the case of xanthone in ethanol-water mixed solvent, a strongly hydrated species in which water molecule is H-bonded to carbonyl group was also reported from the measurement of time-resolved EPR spectrum at 77 K.[22] Considering the similarity between TX(or DITX) and xanthone in H-bond formation, and also considering the small K values in protic solvents being characteristic for H-bond formation,[23,24] the associate between TX(or DITX) and water may be assigned to the H-bonded species. By the use of the ε_C values, absorption spectra of the H-bonded species are shown in Fig. 5. The H-bonded species of TX-water has an absorption maximum at ≈394 nm, and the one of DITX-water, at ≈402 nm. It is noticed that as the water content is decreased, a slight shift to the longer wavelengths was observed with the absorption peak as is easily seen in Fig. 3.

The electronic structure of TX was calculated theoretically by the Pariser-Parr-Pople method in π-electron approximation.[25,26] The first π-π^* state (i.e., 384 nm band in ethanol) of TX is rich in intramolecular charge-transfer character from sulfur atom to carbonyl group as in the case of xanthone.[27] In the calculation procedure of π-electron structure, H-bond formation with water mainly affect the core Coulomb integral, α_P, of the H-bonded atom.[25] In TX, the H-bond, =O···H-O, between the carbonyl oxygen and water is thought to be more stable than the H-bond, S···H-O, between the sulfur atom and water.[23] Actual calculations have been done for the above two cases; theoretical results predict that the first π-π^* band shifts to longer wavelengths for =O···H-O H-bonding formation and to shorter wavelengths for S···H-O H-bonding formation. The observed longer wavelength shift of the first π-π^* band in Fig. 5 qualitatively supports the =O···H-O H-bond formation between TX and water.

The hydrated species between TX(or DITX) and water is also formed at room temperature as is shown in Fig. 6. The UV spectral change can be attributed to the formation of H-bonded species as in the case at 77 K, and K and ε_C values were evaluated from Eq. 1. The average K value is 0.26±0.03 for TX-water and 0.16±0.04 for DITX-water. By the use of the ε_C values, absorption spectra of the H-bonded species are also shown in Fig. 5.

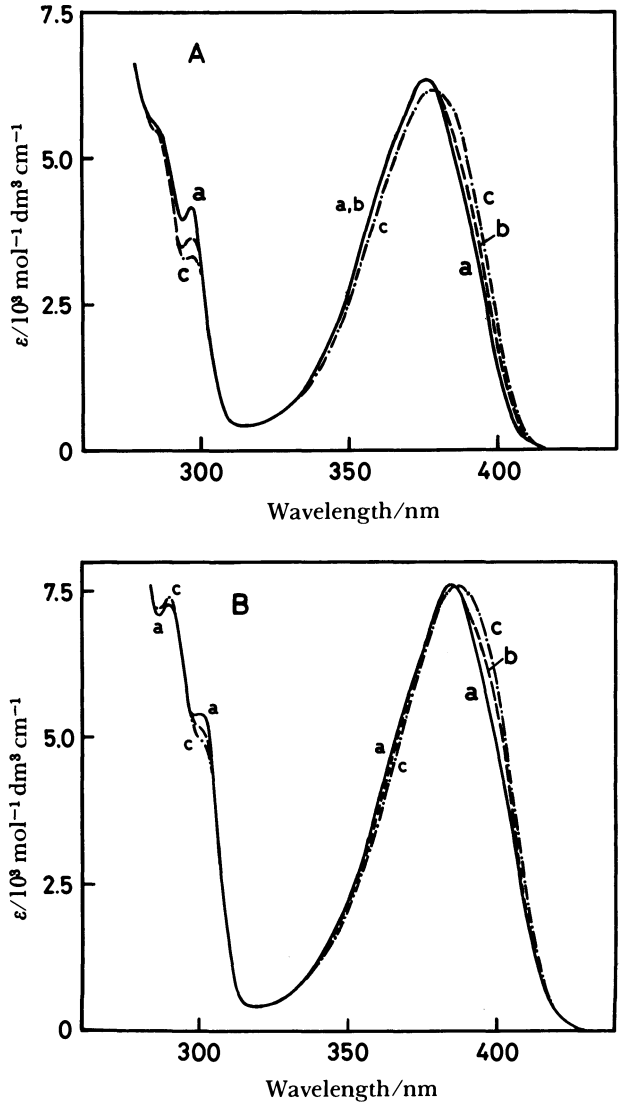

Fig. 6. UV absorption spectra measured with the ethanol-water solutions of (A) TX (7.2×10^{-5} M) and (B) DITX (7.9×10^{-5} M) at room temperature. Water content is (A):(a) 0, (b) 2, and (c) 10 vol%, and (B):(a) 0, (b) 4, and (c) 10 vol%.

Phosphorescence of TX and DITX in Ethanol-Water Solution. Phosphorescence spectra observed with the ethanol-water mixed solution of TX excited at 385 nm are shown in Fig. 7A. As the water content is increased, ≈470 nm and ≈442 nm regions increase their intensities relative to the 452 nm band. This result suggests that at least two phosphorescent species coexist in ethanol-water solution. This is confirmed by measuring the excitation wavelength dependence of phosphorescence spectrum (Fig. 7B) and also by observing excitation spectrum at several monitoring wavelengths (Fig. 7C). In Fig. 7B, besides the normal phosphorescence observed at 452 nm, ≈470 nm phosphorescence was resolved by exciting TX at 400 nm. The ≈470 nm phosphorescence increases its intensity as the water content is increased.

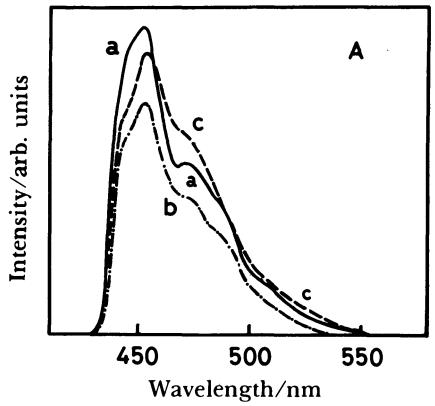

Fig. 7A. Phosphorescence spectra measured with the ethanol-water mixed solutions of TX (2.0×10^{-4} M) excited at 385 nm. Water content is (a) 1.0, (b) 4.8, and (c) 9.1 vol%.

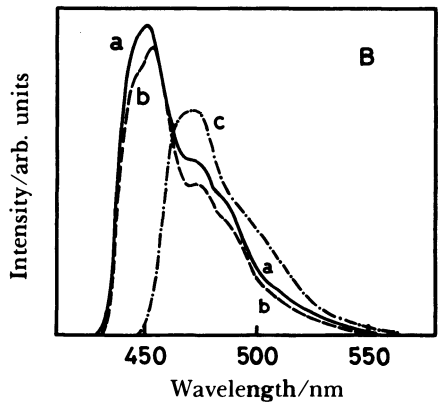

Fig. 7B. Phosphorescence spectra measured with the ethanol-water (100:1 by volume) solution of TX (2.7×10^{-4} M) excited at (a 350 nm, (b) 385 nm, and (c) 400 nm.

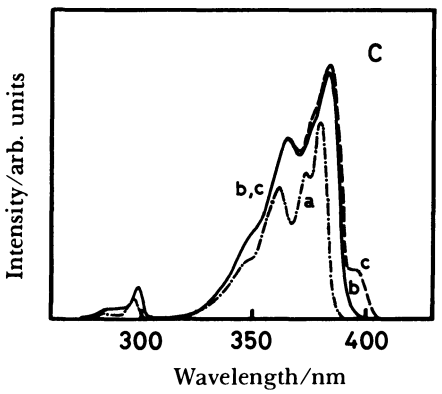

Fig. 7C. Phosphorescence excitation spectra measured with the ethanol-water (100:1 by volume) solution of TX (2.7×10^{-4} M) monitored at (a) 433 nm, (b) 450 nm, and (c) 475 nm.

The same intensity increase was also observed for 397 nm band in the excitation spectrum. Referring to the UV absorption spectrum of TX in ethanol-water at 77 K (Fig. 3), the ≈470 nm phosphorescence is safely

assigned to the hydrated (H-bonded) species. The phosphorescences monitored at 475 nm and at 450 nm decay single-exponentially, and the lifetimes are 212 ms and 160 ms, respectively, in good agreement with the corresponding values of the red-shifted and the normal phosphorescences of TX in pure ethanol. From these results, the red-shifted phosphorescence observed weakly in ethanol can be assigned to the H-bonded species between TX and water.

To understand the phosphorescent behavior in the 442 nm region, the phosphorescence excitation spectra were measured at several monitoring wavelengths; the result monitored at 433—435 nm (Fig. 7C) shows a new distinct band at 374 nm, revealing that the 442 nm phosphorescence can be ascribed to another (i.e., the third) chemical species. Coexistence of three chemical species in ethanol-water solution was also reported in the case of xanthone.[22]

In Fig. 7C, ≈380 nm band in the excitation spectrum shifts to shorter wavelengths (from 384 nm to 380 nm) as the monitoring wavelength becomes shorter (from 475 nm to 433 nm). This may suggest that the normal phosphorescence of TX shows inhomogeneous broadening by solute-solvent interaction.

Phosphorescent behavior of DITX in ethanol-water solution is similar to the one of TX mentioned above. In addition to the normal phosphorescence at 458 nm,

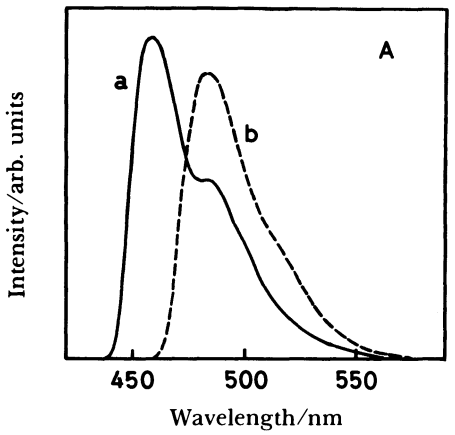

Fig. 8A. Phosphorescence spectra measured with the ethanol-water (100:1 by volume) solution of DITX (3.0×10^{-4} M) excited at (a) 392 nm and (b) 410 nm.

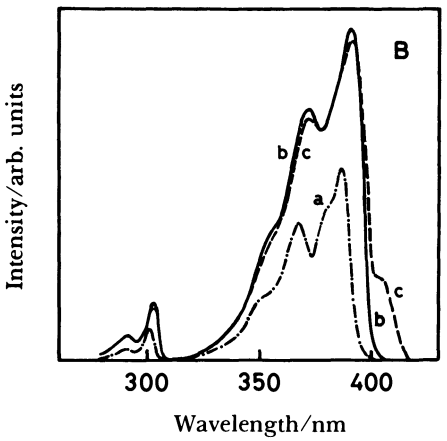

Fig. 8B. Phosphorescence excitation spectra measured with the ethanol-water (100:1 by volume) solution of DITX (3.0×10^{-4} M) monitored at (a) 442 nm, (b) 458 nm, and (c) 490 nm.

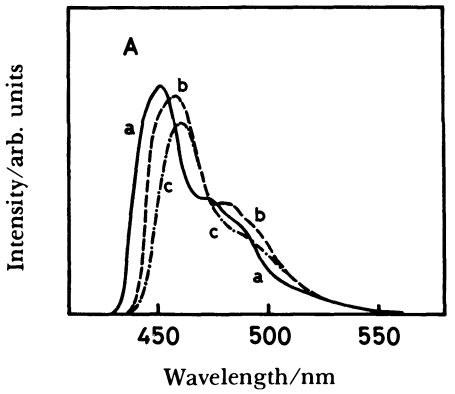

Fig. 9A. Phosphorescence spectra measured with the MTHF solution of TX (3.1×10^{-4} M) excited at (a) 385 nm, (b) 395 nm, and (c) 398 nm.

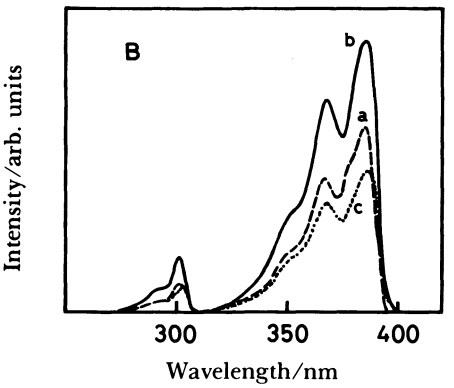

Fig. 9B. Phosphorescence excitation spectra measured with the MTHF solution of TX (3.1×10^{-4} M) monitored at (a) 440 nm, (b) 450 nm, and (c) 475 nm.

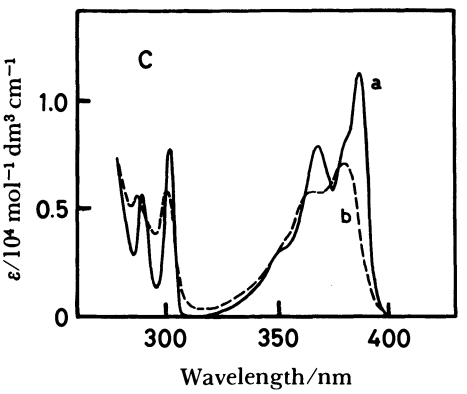

Fig. 9C. UV absorption spectra measured with the MTHF solutions of (a) TX (5.2×10^{-5} M) at 77 K and (b) TX (1.6×10^{-4} M) at room temperature.

phosphorescence due to the H-bonded species is resolved at 485 nm by exciting DITX at 410 nm (Fig. 8A). Furthermore, excitation spectrum monitored at 442 nm shows a new band at ≈380 nm as a shoulder

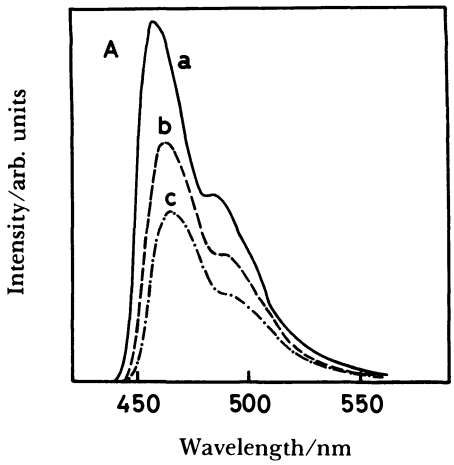

Fig. 10A. Phosphorescence spectra measured with the MTHF solution of DITX (1.7×10^{-4} M) excited at (a) 394 nm, (b) 400 nm, and (c) 403 nm.

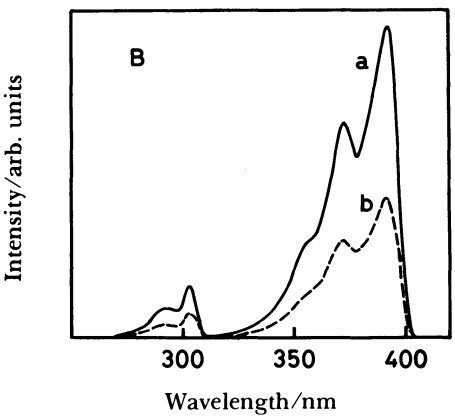

Fig. 10B. Phosphorescence excitation spectra measured with the MTHF solution of DITX (1.7×10^{-4} M) monitored at (a) 458 nm and (b) 490 nm.

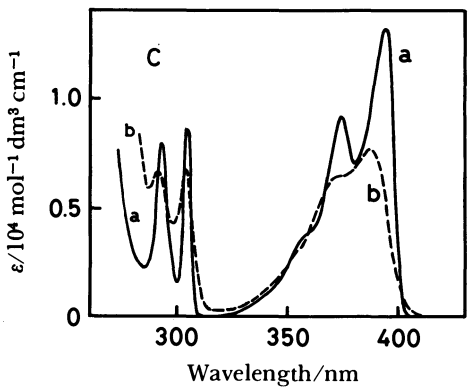

Fig. 10C. UV absorption spectra measured with the MTHF solution of DITX (8.6×10^{-5} M) at (a) 77 K and (b) room temperature.

(Fig. 8B), revealing that the third chemical species exists and phosphoresces in shorter wavelength region of the normal phosphorescence.

As in the case of TX, ≈390 nm band in the excitation spectrum shifts to shorter wavelengths (from 391 nm to 386 nm) as the monitoring wavelength becomes shorter (from 490 nm to 442 nm), suggesting that phosphorescence of DITX exhibits inhomogeneous broadening by solute–solvent interaction.

Phosphorescence of TX and DITX in MTHF. Phosphorescence spectra being excited at several wavelengths were measured with the MTHF solutions of TX and DITX. The results are shown in Figs. 9A and 10A. As the longer excitation wavelength is used, the phosphorescence shifts to the longer wavelengths (by ≈10 nm for TX, and by ≈6 nm for DITX), and the longer is the phosphorescence lifetime. The lifetime of TX varies from 150 ms (excited at 385 nm) to 177 ms (excited at 398 nm), and the one of DITX, from 163 ms (excited at 394 nm) to 186 ms (excited at 403 nm). In phosphorescence decay of DITX excited at 403 nm, a slight deviation from a single-exponential decay was observed. Although the phosphorescence excitation spectra and UV absorption spectra in MTHF (Figs. 9B, 9C, 10B, and 10C) did not exhibit any new band in ≈400 nm region in contrast to the cases of TX and DITX in ethanol, these results may suggest that another chemical species, phosphorescence of which can be resolved poorly in the present study, may coexist in MTHF, too.

References

1) G. Amirzadeh and W. Schnabel, *Makromol. Chem.*, **182**, 2821 (1981).

2) A. Hult and B. Ranby, "Primary and Secondary Reactions in Photoinitiated Free-Radical Polymerization of Organic Coatings," in "ACS Symposium Series, No. 266," American Chemical Society, Washington, D. C. (1984), Chap. 23, pp. 457—472.

3) J. P. Fouassier, P. Jacques, D. L. Lougnot, and T. Pilot, *Polym. Photochem.*, **5**, 57 (1984).

4) M. F. Molaire, *J. Polym. Sci.*, **20**, 847 (1982).

5) Y-C. Zhang, H. Morita, and T. Yamaoka, *J. Appl. Polym. Sci.*, **32**, 6005 (1986).

6) V. D. McGinniss, *J. Radiat. Curing*, **5**, 35 (1978); *Photogr. Sci. Eng.*, **23**, 124 (1979).

7) S. F. Yates and G. B. Schuster, *J. Org. Chem.*, **49**, 3349 (1984).

8) R. W. Yip, A. G. Szabo, and P. K. Tolg, *J. Am. Chem. Soc.*, **95**, 4471 (1973).

9) H. Hayashi and S. Nagakura, *Mol. Phys.*, **24**, 801 (1972); **27**, 969 (1974).

10) C. R. Jones, A. H. Pappano, A. H. Maki, and D. R. Kearns, *Chem. Phys. Lett.*, **13**, 521 (1972).

11) M. Batley and R. Bramley, *Chem. Phys. Lett.*, **15**, 337 (1972).

12) J. C. Scaiano, *J. Am. Chem. Soc.*, **102**, 7747 (1980).

13) K. Suga and M. Kinoshita, *Bull. Chem. Soc. Jpn.*, **54**,

1651 (1981).
14) H. J. Griesser and R. Bramley, *Chem. Phys. Lett.*, **86**, 144 (1982).
15) J. C. Dalton and F. C. Montgomery, *J. Am. Chem. Soc.*, **96**, 6230 (1974).
16) T. Lai and E. C. Lim, *Chem. Phys. Lett.*, **73**, 244 (1980); **84**, 303 (1981).
17) A. Kuboyama, Y. Kojima, and S. Y. Matsuzaki, *Bull. Chem. Soc. Jpn.*, **56**, 2572 (1983); A. Kuboyama and S. Y. Matsuzaki, *ibid.*, **58**, 73 (1985).
18) J. Chilton, L. Giering, and C. Steel, *J. Am. Chem. Soc.*, **98**, 1865 (1976).
19) J. C. Scaiano, E. B. Abuin, and L. C. Stewart, *J. Am. Chem. Soc.*, **104**, 5673 (1982).
20) J. A. A. Ketelaar, C. van de Stolpe, A. Goudsmidt, and W. Dzcubas, *Recl. Trav. Chim. Pays-Bas*, **71**, 1104 (1952).
21) H. Nakanishi, H. Morita, and S. Nagakura, *J. Mol. Spectrosc.*, **65**, 295 (1977).
22) M. Minami, H. Murai, Y. I'Haya, T. Imamura, and K. Obi, 49th National Meeting of the Chemical Society of Japan, Tokyo, April 1984, Abstr. No. 1B03; H. Murai, M. Minami, and Y. J. I'Haya, Preprint submitted to J. Phys. Chem.
23) G. C. Pimentel and A. L. McClellan, "The Hydrogen Bond," W. H. Freeman & Co., London (1960), pp. 365—386.
24) D. R. Cartwright and C. B. Monk, *J. Chem. Soc.*, **1955**, 2500.
25) R. Pariser and R. G. Parr, *J. Chem. Phys.*, **21**, 466 (1953); **21**, 767 (1953).
26) J. A. Pople, *Proc. Phys. Soc., London, Sect. A*, **68**, 81 (1955).
27) T. Minegishi, T. Hoshi, H. Hiratsuka, and Y. Tanizaki, *Bull. Chem. Soc. Jpn.*, **50**, 3140 (1977).

 © 1988 The Chemical Society of Japan Bull. Chem. Soc. Jpn., 61, 199—205 (1988)

Photoacoustic Study of 280 nm Band of Acetone Vapor

Takefumi OKA,* Humiyo KOBAYASHI, Naoki OGUMA, and Makoto MOROHASHI
Department of Electrical Engineering, Nagaoka Technical College, 888 Nishikatakai Nagaoka, Niigata 940
(Received June 8, 1987)

Relaxation of the energy absorbed by acetone vapor (200 Torr) on excitation with UV (230—340 nm) was investigated by the photoacoustic technique. The presence of two relaxation paths was found by their difference in heat production rates: The faster path is $S_0 \rightarrow S_1 \rightarrow T_1 \rightarrow S_0$ and the slower path is $S_0 \rightarrow$ radicals→recombination products. The PA spectra corresponding to these paths were determined separately. The spectrum for the T_1 path has a peak around 295 nm and extends to longer wavelengths beyond 310 nm. The spectrum for the decomposition path has a peak around 275 nm and overlaps with the spectrum for the T_1 path in the region of $\lambda<310$ nm. The study of frequency dependences of PA signals showed the presence of faster and slower heat releasing steps in each path. In the T_1 path, the faster and the slower steps are due to vibrational deactivation of hot T_1 formed from S_1 and of hot S_0 formed from T_1 respectively. In the radical path, the faster and slower steps are the deactivation of the hot radicals and the recombination of the thermalized radicals respectively. The addition of O_2 to the system accelerated the heat release process via the relaxed T_1 and also converted the slow heat release process of recombination into a fast process of addition reactions of O_2 to the radicals.

When a gas in a closed space is irradiated with intensity modulated radiation, generally some of the energy absorbed is released as modulated heat. This in turn produces a modulated pressure change, an acoustic wave. This is known as Photo Acoustic Effect (PA hereafter).

The frequency of the PA signal is the same as that of the excitation radiation but the PA signal has a phase lag behind the radiation. The phase lag as well as the amplitude of the PA signal bears information about the relaxation of the absorbed energy to heat.

By comparison of in-phase and out-of-phase PA spectra which are observed at phase angles separated by 90°, we can distinguish parts of an absorption band relaxing at different rates. Biacetyl,[1] azabenzenes,[2] and aromatic ketones[3] have been studied in this way. If the PA spectrum and the absorption spectrum of a particular gas are different, it also indicates the presence of different relaxation processes in that absorption band. This kind of technique has been used to determine the fluorescence quantum yield of benzene[4] and to investigate nonradiative processes of benzene.[5]

The frequency dependence of the phase lag provides chance to determine the rate constant of the relaxation process involved. Hunter et al. have developed a multi-state relaxation model[6] and have determined the triplet lifetimes of biacetyl,[7] benzenes,[8] and alkyl iodides[9,10] by applying the model to the frequency dependence of phase lag and/or amplitude.

In the present study, acetone is investigated by the PA technique measuring the PA spectra and the frequency dependence of the phase lag.

Acetone has an absorption band ranging from 220 nm to 330 nm with a maximum around 275 nm. The fluorescence quantum yield is very low (<0.002)[11] and nonradiative processes dominate the decay process. For low vibrational levels of S_1, the quantum yield of the $S_1 \rightarrow T_1$ intersystem crossing is 1 and $k_{isc}=3.8\times10^8\ s^{-1}$.[12] The intersystem crossing $S_1 \rightarrow T_1$ should form a hot triplet. On decreasing the excitation wavelength below 310 nm, k_{isc} decreases but the decomposition rate constant k_d increases.[13] Recently, Copeland and Crosley have reported the barrier height for decomposition into CH_3 and $COCH_3$ to be 385 kJ mol^{-1} above the ground state S_0 (50 kJ mol^{-1} above T_1). They have also shown the vibrational deactivation rate constant of the hot triplet by S_0 to be 7.59×10^{10} mol^{-1} dm^3 s^{-1} ($\approx10^9\ s^{-1}$ with 200 Torr of acetone (1 Torr=133.322 Pa)) and the lifetime of the thermal triplet to be 0.225 ms.[14] Since the quantum yield of the phosphorescence is small (≈0.02),[15] the lifetime of T_1 is ascribed to intersystem crossing to S_0.

Therefore we expect two paths of heat production in acetone: fast heat ($\approx50+\alpha$ kJ mol^{-1}) followed by slow ($\tau\approx0.2$ ms) heat (≈335 kJ mol^{-1}) for the $S_0 \rightarrow S_1 \rightarrow T_1 \rightarrow S_0$ path and fast heat ($\approx50+\alpha$ kJ mol^{-1}) followed by very slow heat (≈335 kJ mol^{-1})[16] for the $S_0 \rightarrow$ radicals→recombination products path. The α depends on the excess energy above the barrier. T_1 is quenched by oxygen with the rate constant of 8.4×10^9 mol^{-1} dm^3 s^{-1} ($5\times10^7\ s^{-1}$ with 100 Torr of O_2). Consequently the rate of heat production due to T_1 should increase in the presence of O_2.

Method

In order to analyze the PA spectra and the frequency dependence of the phase lag, equations to describe them are derived below. We assume a sinusoidally amplitude modulated light beam:

$$I(\lambda) = I_0(\lambda)(\delta+\sin\omega t)$$

where $I_0(\lambda)$ is the beam intensity at a wavelength of λ, ω is the angular frequency of modulation and δ is the relative intensity of the DC component. The light absorption process is expressed as

$$S_0 + h\nu \xrightarrow{I(\lambda)A(\lambda)} S_1$$

where $A(\lambda)$ is the fraction of the absorption over the full path length divided by the path length, and S_0 and S_1 refer to the ground and excited state respectively.

First, we shall deal with the PA spectra for a system which has two heat production processes with different rate constants. We assume two paths for heat production characterized by $\{r_1(\lambda),X_1,k_1,q_1\}$ and $\{r_2(\lambda),X_2,k_2,q_2\}$ as shown in the equations below.

$$\begin{array}{l} S_1 \xrightarrow{r_1(\lambda)} X_1 \xrightarrow{k_1} S_0 + q_1 \\ S_1 \xrightarrow{r_2(\lambda)} X_2 \xrightarrow{k_2} S_0 + q_2 \end{array}$$

where r_1 and r_2 refer to branching ratios from S_1 to the states X_1 and X_2 respectively, and X_1 and X_2 are only symbolic. They may or may not be real states. The point is that there are two parallel processes producing heat q_1 with a rate constant k_1 and heat q_2 with k_2. The heat production process may not be a single step in each path, but we assume so here. This assumption is adequate for the purpose of spectral analysis. Later we will employ a two-step model for the analysis of the frequency dependence.

The acoustic pressure $p(t)$ expected for the above scheme is as follows.

$$p(t) = K\frac{I_0(\lambda)}{\sqrt{\omega^2+k_t^2}}\{A_1(\lambda)b_1(\omega)\sin(\omega t-\phi_a-\phi_1) + A_2(\lambda)b_2(\omega)\sin(\omega t-\phi_a-\phi_2)\}$$

where $A_i(\lambda)=A(\lambda)r_i/(r_1+r_2)$, $b_i(\omega)=k_iq_i/\sqrt{\omega^2+k_i^2}$, $\phi_i=\tan^{-1}(\omega/k_i)$, k_t is a reciprocal of the time of thermal relaxation of the heated gas onto the cell walls and ϕ_a represents a phase lag due to the apparatus including a phase lag due to a thermal diffusivity effect. K is a constant independent of t, ω, and λ.

Then, the output of a lock-in amplifier $p(\lambda)$ is

$$p(\lambda) = K\frac{I_0(\lambda)}{\sqrt{\omega^2+k_t^2}}\{A_1(\lambda)b_1(\omega)\cos(\phi_r-\phi_a-\phi_1) + A_2(\lambda)b_2(\omega)\cos(\phi_r-\phi_a-\phi_2)\} \quad (1)$$

where ϕ_r is an adjustable phase lag of a reference signal. The in-phase spectrum with respect to the heat q_1 can be obtained by setting $\phi_r=\phi_a+\phi_1$:

$$p_{in}(\lambda) = K\frac{I_0(\lambda)}{\sqrt{\omega^2+k_t^2}}\{A_1(\lambda)b_1(\omega) + A_2(\lambda)b_2(\omega)\cos(\phi_1-\phi_2)\}. \quad (2)$$

The out-of-phase spectrum is given by setting $\phi_r=\phi_a+\phi_1+90°$ as

$$p_{out}(\lambda) = K\frac{I_0(\lambda)}{\sqrt{\omega^2+k_t^2}}\{0-A_2(\lambda)b_2(\omega)\sin(\phi_1-\phi_2)\}. \quad (3)$$

Since we know the shape of $I_0(\lambda)$ from a PA spectrum of carbon black,[18] the shape of the spectrum $A_2(\lambda)$ can be obtained from the out-of-phase spectrum of Eq. 3. Generally, the other spectrum $A_1(\lambda)$ can not be determined from $p_{in}(\lambda)$ of Eq. 2 even if the shape of $A_2(\lambda)$ is known. In the present study, however, we can find the shape of $A_1(\lambda)$ because $A_2(\lambda)b_2(\omega)$ term in $p_{in}(\lambda)$ is negligibly small compared to $A_1(\lambda)b_1(\omega)$ at particular frequencies.

Next we shall deal with the frequency dependence of the PA signal. In the spectrum analysis (Eqs. 1—3), we assumed for simplicity a single step, and consequently one rate constant for each heat producing path. The frequency analysis is only effective for a single path mechanism. Usually, a real path has many steps in series.

Here we assume a single path model consisting of two steps in series which are characterized by different rate constants as shown in Fig. 1. This model is essentially the same as the one used by Hunter et al.[6] In the first step, the fast heat F is released with a rate constant of $1/\tau_f$ and the slow heat S is released with a rate constant of $1/\tau_s$ in the second step.

When $\tau_f \ll \tau_s$, the PA signal can be approximated by

$$p(t) = K\frac{I_0(\lambda)}{\sqrt{\omega^2+k_t^2}}A(\lambda)b(\omega)\sin(\omega t-\phi_a-\phi) \quad (4)$$

where

$$b(\omega) = S\sqrt{(F/S)^2+\{1+2(F/S)\}/\{1+(\omega\tau_s)^2\}} \quad (5)$$

$$\phi = \mathrm{Tan}^{-1}\frac{\omega\tau_s}{(F/S)\{1+(\omega\tau_s)^2\}+1} \quad (6)$$

ϕ_a: a phase lag of the apparatus including that due to the thermal diffusivity effect. The $b(\omega)$ can be interpreted as the effective heat detected at ω. If this two-step model is applicable to each path in the previous model for spectral analysis, then the $b_i(\omega)$ terms in Eqs. 1—3 must be replaced by $b(\omega)$ of Eq. 5. Of course, S, F, and τ_s are different for each path.

To use frequency dependence of the PA amplitude, a logarithmic function of the amplitude, excluding the thermal diffusivity factor, is useful:

$$\log\{b(\omega)/S\} = \frac{1}{2}\log\left\{(F/S)^2+\frac{1+2(F/S)}{1+(\omega\tau_s)^2}\right\}. \quad (7)$$

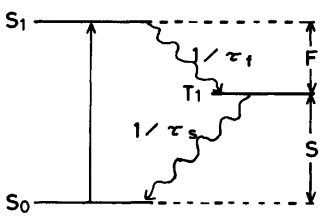

Fig. 1. A model of a relaxation path consisting of two steps in series. τ_f and F refer to the lifetime and the heat released in the first(fast) step; τ_s and S those in the second (slow) step. T_1 is not necessarily a triplet state and can be any state.

This quantity decreases as the frequency increases. The limiting values at lower frequencies and at higher frequencies are $\log\{1+(F/S)\}$ and $\log(F/S)$ respectively. Therefore we can determine the ratio of the fast heat(F) to the slow heat(S) if the relative amplitudes are obtained over a wide frequency range.

The phase lag ϕ is a more sensitive function of ω than the amplitude. To extract information on the relaxation due to the sample gas from the experimentally observed phase lag ($\phi+\phi_a$), ϕ_a must be determined and be subtracted. This can be done using a gas which has no slow heat, i.e. $S=0$ and consequently no phase lag, i.e. $\phi=0$. With this gas the observed phase lag is equal to ϕ_a.

The function ϕ of Eq. 6 has a maximum of $\tan^{-1}\frac{1}{2\sqrt{(F/S)\{1+(F/S)\}}}$ at $\omega=\{1+(S/F)\}/\tau_s$ and takes small values at lower and higher frequencies. When we observed this maximum, we can determine both the ratio F/S and the lifetime τ_s.

Experimental

The apparatus used is schematically shown in Fig. 2. The light source was a 500W xenon arc lamp (Ushio, UXL500D). The light beam was modulated at a frequency between 10 and 1000 Hz by a rotating disk chopper (Scetic Instruments, 300C) and then was passed through a 20 cm scanning monochromator (Ritsu, MC-20L) with a bandpass of 4.2 nm. The modulated monochromatic light beam was passed through a cylindrical PA cell (18 mm diameter, 70 mm long) along its axis to a solar blind phototube (HTV R1384).

The body of the PA cell was made of Pyrex, and two quartz windows were attached to the cell with epoxy resin. This cell also had two gas ports with greaseless stop cocks. PA signals were sensed by an electret microphone with a built-in FET preamplifier. The microphone was mounted in a small cavity adjacent to the cell body at its middle by using electron wax. The back side of the microphone was sealed with epoxy resin to make it vacuum tight. The microphone was polarized by a battery (9 V).

The output of the microphone (or of the phototube) was sent to a lock-in amplifier (Stanford Research Inc., SR 510) where a signal from a photocoupler on the chopper was used as a reference signal. The output of the lock-in amplifier was fed into a strip chart recorder.

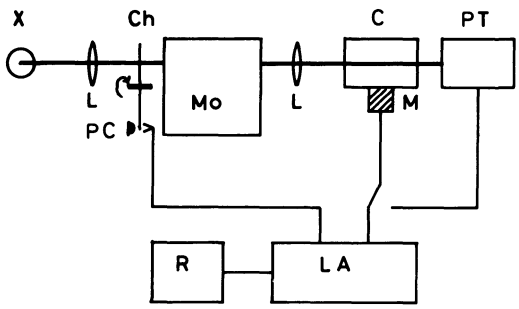

Fig. 2. Block diagram of the apparatus.
X, Xe lamp; L, lens; Ch, chopper; Mo, monochromator; C, cell; M, microphone; PT, photo tube; PC, photo coupler; LA, lock-in amplifier; R, recorder.

Sample gases were mixtures of acetone 200 Torr and a buffer gas (Ar or air) 560 Torr. The cell was filled on a conventional vacuum line. Filling and pumping of the cell was done slowly ($\approx$1 Torr s^{-1}) to prevent rupturing the diaphragm of the microphone.

To test the performance of this cell, measurements were made on mixtures of benzene vapor and a buffer gas (Ar or air). The cell showed no resonance below 1.5 kHz. The phase lag obtained with the mixtures showed chopping frequency dependence, but this was used as a phase lag of the apparatus (ϕ_a in Eq. 4).

To obtain corrected PA spectra, apparent PA spectra were divided by a PA spectrum of carbon black.[18] The spectra in Figs. 5, 9, and 10 are so corrected.

Three kinds of measurements were done in the present work.

1. PA spectra were measured by scanning the wavelength with a fixed chopping frequency at two fixed phase angles separated by 90° from each other.
2. The frequency dependence of the phase lag was obtained by a null reading at various chopping frequencies between 10 and 1000 Hz at a fixed wavelength.
3. Optical absorption spectra were obtained by division of a spectrum of the transmitted light intensity with a sample gas mixture in the cell by that with a buffer gas alone.

All the measurements were done at room temperature.

Results and Discussion

PA Spectra in Ar. The PA spectra of acetone (200 Torr) with Ar as a buffer gas at a frequency of 20 Hz are shown in Fig. 3. The out-of-phase spectrum (ϕ=90° in Fig. 3) was taken with the phase angle to null PA signal at 310 nm. The in-phase spectrum (ϕ=0°) was taken with a phase lead of 90° in front of the phase angle of the out-of-phase spectrum. At wavelengths longer than 310 nm, the signal appears

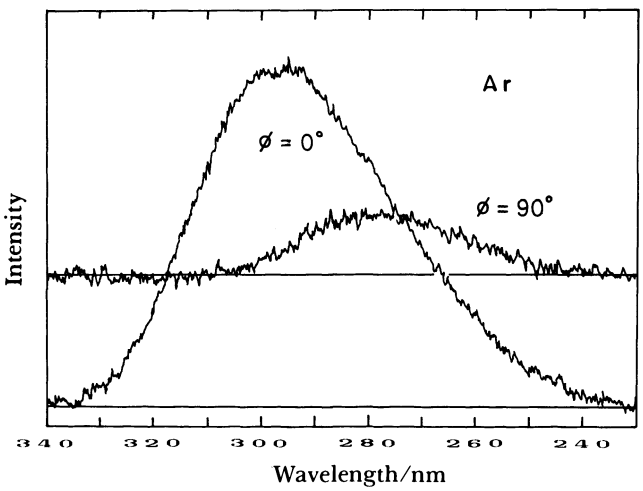

Fig. 3. PA spectra of acetone with Ar as a buffer gas (f=20 Hz). Acetone 200 Torr and Ar 560 Torr. Phase angles are of relative values.

only in the in-phase spectrum. This means that at $\lambda>310$ nm, there is only one relaxation process. On the other hand, there are two processes at $\lambda<310$ nm. In other words, the situation of Eqs. 2 and 3 is achieved in Fig. 3; Eq. 2 corresponds to the in-phase spectrum in the figure and Eq. 3 to the out-of-phase spectrum. The out-of-phase spectrum represents the spectral shape of one ($I_0(\lambda)A_2(\lambda)$ in Eq. 3) of two relaxation processes, which is a relatively slower one because the positive value of the out-of-phase spectrum results in $\phi_2>\phi_1$ in Eq. 3.

According to Eq. 2, the in-phase spectrum should be a mixture of two spectra $I_0(\lambda)A_2(\lambda)$ and $I_0(\lambda)A_1(\lambda)$. To confirm this interpretation, we examined the PA spectra at various frequencies (20—700 Hz). When the frequency was increased, the out-of-phase spectrum quickly decreased its relative intensity to that of the in-phase spectrum. This is consistent with the out-of-phase spectrum being that of slower relaxation: in Eqs. 2 and 3 the amplitude ratio $b_2(\omega)/b_1(\omega)$ is mathematically expected to become smaller as ω increases in the range of $k_1>\omega>k_2$.

In order to confirm the presence of a relatively faster heat releasing process and to determine its spectral shape $I_0(\lambda)A_1(\lambda)$, a trial spectrum for the faster process is tested in Fig. 4. Actually the trial spectrum is the in-phase spectrum at 35 Hz. In Fig. 4, the trial spectrum was so adjusted in its intensity to fit the long wavelength part of the mixture spectrum (the in-phase spectrum at 20 Hz) and was then subtracted from the latter. The difference between the mixed and the trial (the solid line in Fig. 4) reproduces the shape of the spectrum of the slower process which is actually the out-of-phase spectrum at 20 Hz. Therefore this trial spectrum is the spectrum of the faster process ($I_0(\lambda)A_1(\lambda)$ in Eq. 2).

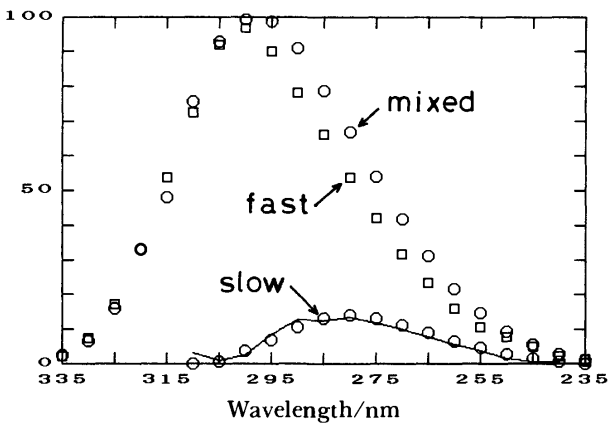

Fig. 4. Decomposition of the in-phase PA spectrum of Fig. 3 into a faster and a slower components. ○ (upper): the in-phase (ϕ=0°) PA spectrum in Fig. 3 (normalized to 100 at the peak).
□: trial spectrum for a faster component. ○ (lower): the out-of-phase (ϕ=90°) PA spectrum in Fig. 3 (height adjusted to fit the solid curve).
Solid curve: difference of ○ (upper) and □.

The corrected spectra of the slower ($A_2(\lambda)$) and the faster ($A_1(\lambda)$) heat releasing processes are shown in Fig. 5. Their shapes are frequency independent but their relative intensities in the in-phase and out-of-phase spectra depend on the frequency.

Since the slower process is absent at 310 nm, we can determine the rate constant for the faster process by measuring phase lags ϕ_1 at 310 nm as a function of frequency. Figure 6 shows the results. It is seen in Fig. 6 that the curve calculated by using Eq. 6 with τ_s=0.2 ms and F/S=0.2 fits the data well. The lifetime of the relaxed triplet state (T_1) of acetone has been reported to be 0.225 ms.[14] The expected values for F and S are 50 and 335 kJ mol^{-1} respectively for the relaxation path $S_1\rightarrow T_1\rightarrow S_0$ (excited at 310 nm). Therefore we assign the faster heat releasing process to

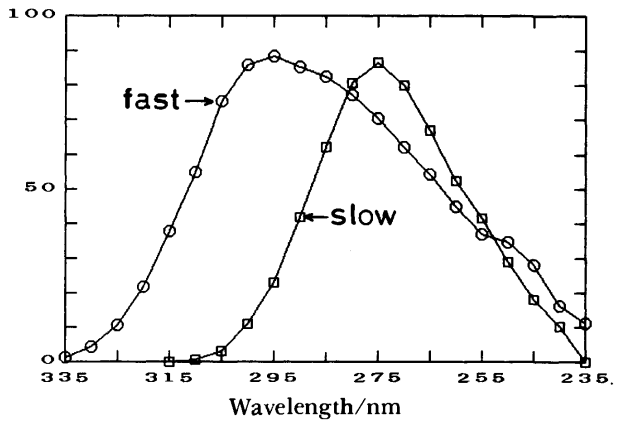

Fig. 5. Corrected PA spectra corresponding to the faster (T_1) and the slower (radicals) heat releasing processes. Normalized at their peaks. The correction was made by division with PA spectrum of carbon black.

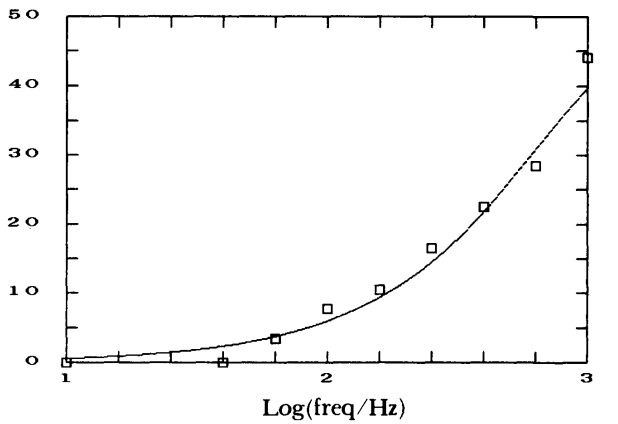

Fig. 6. Frequency dependence of phase lag of the heat released by T_1 observed at 310 nm.
Correction was made for the phase lag due to the apparatus. The solid line is the curve of Eq. 6 with τ_s=0.2 ms and F/S=0.2.

the relaxation path via the triplet state (T_1).

On the other hand, the slower process can be assigned to the heat release on the recombination of radicals formed by photolysis of acetone because its heat releasing rate is slower than that of T_1 and its excitation wavelength ($\lambda<310$ nm) corresponds to the energy above the barrier height of decomposition, i.e. 385 kJ mol^{-1}.[14]

This slower process can not be studied directly in the same manner as the faster one, because its entire spectrum overlaps with that of the faster one. However, we can get some idea about the frequency dependence of the slower process indirectly from analyses of the PA spectra obtained at various frequencies. It should be mentioned here that in the following analysis of the slower process, we approximate second order recombination reactions by a pseudo first order reaction assuming a constant steady state concentration of the radicals.

We now know the spectral shape of the faster process $A_1(\lambda)$ and the slower $A_2(\lambda)$ as well as the phase lag of the faster process $\phi_1(\omega)$. We should therefore be able to determine $\phi_2(\omega)$ and $b_2(\omega)/b_1(\omega)$ of Eq. 1 by decomposing the in-phase spectrum into the two components (as done in Fig. 4) and comparing the resulting component spectra and the out-of-phase spectrum. To calculate the relative values of $b_2(\omega)$ from the ratio $b_2(\omega)/b_1(\omega)$, we used $b_1(\omega)$ calculated by using Eq. 5 with $F/S=0.2$ and $\tau_s=0.2$ ms for we did not measure $b_1(\omega)$. The calculated $b_1(\omega)$ is constant between 10 and 200 Hz and then gradually decreases down to 0.4 of the constant value as the frequency increases to 1000 Hz. The values of $\log\{b_2(\omega)\}$ and $\phi_2(\omega)$ thus obtained are shown in Fig. 7 (circles) as a function of $\log f$.

These curves are typical forms of the theoretical Eqs. 6 and 7; and are indications of the presence of two steps in the heat production process due to radicals. We estimate $F/S\lesssim 0.35$ from the highest and the lowest values of $\log\{b_2(\omega)\}$ and the approximate frequency of $\phi_2(\omega)$ peak of 35 Hz. These values lead to a very slow lifetime of $\tau_s\gtrsim 6$ ms. Equation 6 with these parameter values can reproduce the shape of $\phi_2(\omega)$ curve in Fig. 7 but predicts the peak of $\phi_2(\omega)\gtrsim 30°$. This discrepancy in the peak value of ϕ_2 may be due to the large errors in the determination of ϕ_2 by the spectrum subtraction method.

The two steps found in the heat production process due to radicals are interpreted as follows: heat release during the primary photodecomposition is the faster step remaining even at high frequencies ($f\leqq 100$ Hz) while the heat release on radical recombination is the slower one, present only at low frequencies ($f\leqq 20$ Hz).

PA Spectra in Air. PA spectra at 20 Hz with air as a buffer gas are shown in Fig. 8. As the PA spectra in Ar at 20 Hz (Fig. 3), these spectra also have two components. We decomposed the in-phase spectrum into a faster and a slower component spectra and found that the shapes of both component spectra were the same as those in Ar. Therefore we assign the out-of-phase spectrum to that due to radicals and the in-phase spectrum to a mixture of spectra due to radicals and to T_1.

The phase lags at 310 nm were found to be null in the frequency range of 10 to 1000 Hz. This indicates that the lifetime of T_1 is shortened (<20 μs) by the presence of about 100 Torr of O_2.

The frequency dependences of ϕ_2 and $\log b_2$ determined by spectral subtraction method as before are shown in Fig. 7 (squares). We used $\phi_1=0$ and $b_1=1$ for the heat production rate of T_1 in air because the rate is supposed to be much larger than that in Ar. A tail of a peak is observed in the ϕ_2 curve.

Therefore the heat production process due to radicals also has two steps: A faster one and a slower

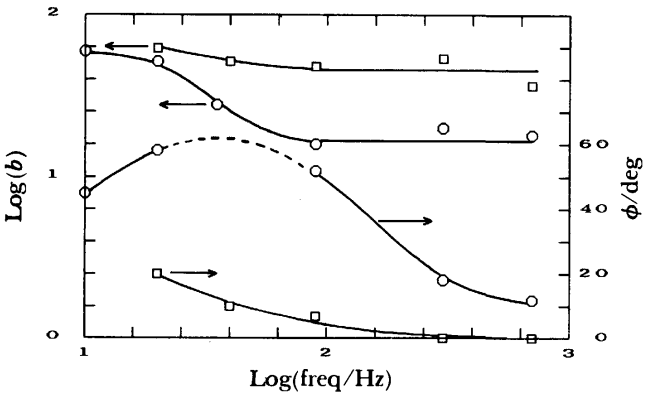

Fig. 7. Frequency dependences of PA signals due to the heat released by radicals.
O: Ar as a buffer gas, □: air as a buffer gas. ϕ: phase lag, b: amplitude. All the data were obtained indirectly from frequency dependence of spectral shape.

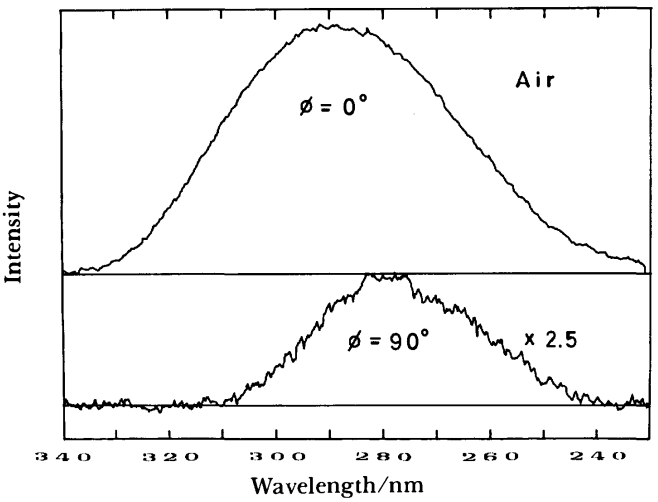

Fig. 8. PA spectra of acetone with air as a buffer gas (f=20 Hz).
Acetone 200 Torr and air 560 Torr. Phase angles are of relative values.

one. The faster step remaining at high frequencies (f>100 Hz) may be the primary photodecomposition and the reactions of the radicals so produced with O_2. For example, the pseudo first order rate constant of CH_3 with 100 Torr of O_2 is calculated to be 5×10^7 s^{-1} according to the literature.[19] The slower step observed at very low frequencies (f<20 Hz) could be heat release on recombination reactions of heavier radicals which are formed by addition of O_2 to primary radicals such as CH_3O_2.

Comparison of PA Spectra (PAS) with Absorption Spectra (ABS). In Fig. 9 the in-phase PAS at 423 Hz and the ABS with Ar as a buffer gas are compared. In Fig. 10 the in-phase PAS at 508 Hz and the ABS with air as a buffer gas are compared. The same sample was used in the measurements of the corresponding PAS and ABS. These PAS are corrected for $I_0(\lambda)$.

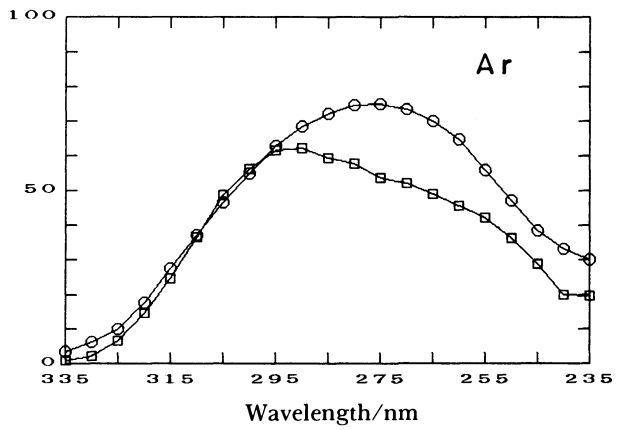

Fig. 9. Comparison of the absorption spectrum and the corrected PA spectrum of acetone with Ar as a buffer gas (f=423 Hz).
Acetone 200 Torr and Ar 560 Torr. The absorption-(○) is in % unit. PAS(□) is normalized to fit ABS at longer wavelengths.

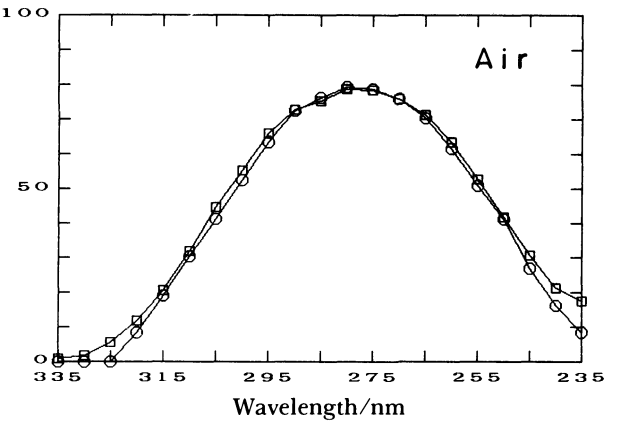

Fig. 10. Comparison of the absorption spectrum and the corrected PA spectrum of acetone with air as a buffer gas (f=508 Hz). See the legend of Fig. 9.

An ABS represents energy absorbed but a PAS represents energy released as heat. The heat defect in Fig. 9 can be considered due to failure to observe the slowly released heat at the high frequency.

The ABS in Fig. 10 as well as in Fig. 9 is proportional to $A(\lambda)$ in Eq. 2: $A(\lambda)=A_1(\lambda)+A_2(\lambda)$. The PAS in air (Fig. 10) can be also expressed by Eq. 2 as $A_1(\lambda)b_1(f=508)+A_2(\lambda)b_2(f=508)\cos(0)$. The effective heat at 508 Hz for T_1 path, i.e. $b_1(f=508)$ is equal to the total energy absorbed because the total energy of T_1 is released by the faster process in the presence of O_2: $b_1(508)$=430 kJ mol^{-1} at 280 nm. Judging from Fig. 7, $b_2(508)$ is the heat released by the faster process in the radical path: $b_2(508)=100+Q$ kJ mol^{-1} at 280 nm. Here the Q represents a sum of the heat released by the addition reactions of the two primary radicals to O_2. The coincidence of ABS and PAS in air (Fig. 10) requires Q to be about 330 kJ mol^{-1}.

Summary

It was found that there are two heat production paths in the 280 nm absorption band of acetone: one via T_1 and the other via radicals.

The spectral shapes for T_1 formation and photodecomposition were determined (Fig. 5).

The assignments of the heat observed in PA signals are summarized in Table 1 and the following reaction scheme.

$$S_0 \longrightarrow S_1$$
$$S_1 \longrightarrow T_1 + q_1$$
$$S_1 \longrightarrow \text{decomposition}(R_1+R_2) + q_2$$
$$T_1 \longrightarrow S_0 + q_3$$
$$R_1, R_2 \text{ recombination} \longrightarrow \text{products} + q_4$$
$$T_1 + O_2 \longrightarrow S_0 + O_2 + q_3' \quad (q_3=q_3')$$
$$R_1 + R_2 + 2O_2 \longrightarrow R_1O_2 + R_2O_2 + q_5$$
$$R_1O_2 + R_2O_2 \longrightarrow \text{products} + q_6$$

where q_i refers to heat released.

Table 1. Assignments of the Heat Observed[a]

Buffer	Path via T_1		Path via radicals	
	Fast	Slow	Fast	Slow
Ar	q_1 (50+α)	q_3 (335)	q_2 (50+α)	q_4 (335)
air	q_1+q_3' (385+α)	—	q_2+q_5 (385+α)	q_6

a) The numbers in parentheses are rough estimates of the amount of heat released in kJ mol^{-1} unit. $\alpha=1.2\times10^5/\lambda-385$ kJ mol^{-1}. λ is the excitation wavelength in nm.

References

1) K. Kaya, W. R. Harshbarger, and M. B. Robin, *J. Chem. Phys.*, **60**, 4231 (1974).
2) K. Kaya, C. L. Chatelain, M. B. Robin, and N. A. Kuebler, *J. Am. Chem. Soc.*, **97**, 2153 (1975).
3) M. B. Robin and N. A. Kuebler, *J. Am. Chem. Soc.*, **97**, 4822 (1975).
4) M. G. Rockley, *Chem. Phys. Lett.*, **50**, 427 (1977).
5) H. Nakamura, Y. Hiura, K. Tsubouchi, and N. Mikoshiba, *Jpn. J. Appl. Phys.*, **23**, L430 (1984).
6) T. F. Hunter, D. Rumbles, and M. G. Stock, *J. Chem. Soc., Faraday Trans. 2*, **70**, 1010 (1974).
7) T. F. Hunter and M. G. Stock, *J. Chem. Soc., Faraday Trans. 2*, **70**, 1022 (1974).
8) T. F. Hunter and M. G. Stock, *J. Chem. Soc., Faraday Trans. 2*, **70**, 1028 (1974).
9) T. F. Hunter and K. S. Kristjansson, *J. Chem. Soc., Faraday Trans. 2*, **78**, 2067 (1982).
10) T. F. Hunter, S. Lunt, and K. S. Kristjansson, *J. Chem. Soc., Faraday Trans. 2*, **79**, 303 (1983).
11) G. M. Breuer and E. K. C. Lee, *J. Phys. Chem.*, **75**, 989 (1971).
12) D. A. Hansen and E. K. C. Lee, *J. Chem. Phys.*, **62**, 183 (1975).
13) A. Gandini and P. A. Hackett, *J. Am. Chem. Soc.*, **99**, 6195 (1977).
14) R. A. Copeland and D. R. Crosley, *Chem. Phys. Lett.*, **115**, 362 (1985).
15) T. Heicklen, *J. Am. Chem. Soc.*, **81**, 3863 (1959).
16) $2CH_3 \rightarrow C_2H_6 + 335\ kJ\ mol^{-1}$, $2COCH_3 \rightarrow (CH_3CO)_2 + 293\ kJ\ mol^{-1}$.
17) H. J. Groh, G. W. Luckey, and W. A. Noyes, *J. Chem. Phys.*, **21**, 115 (1953).
18) W. R. Harshbarger and M. B. Robin, *Acc. Chem. Res.*, **6**, 329 (1973).
19) H. E. Van der Bergh and A. B. Callear, *Trans. Faraday Soc.*, **67**, 2017 (1971).

 © 1988 The Chemical Society of Japan Bull. Chem. Soc. Jpn., 61, 207—210 (1988)

Design of Novel Mesomorphic Compounds: *N,N′,N″*-Trialkyl-1,3,5-benzenetricarboxamides

Yoshio MATSUNAGA,* Nobuhiko MIYAJIMA, Yuichi NAKAYASU, Satoshi SAKAI, and Michihiro YONENAGA
Department of Chemistry, Faculty of Science, Hokkaido University, Sapporo 060
(Received June 12, 1987)

N,N′-Dialkyl-1,4-benzenedicarboxamides melt with anomalously small enthalpy changes. The 1,3-analogs behave similarly but at lower temperatures. These observations provide a clue to design novel mesomorphic compounds; *N,N′,N″*-trialkyl-1,3,5-benzenetricarboxamides. The compounds carrying pentyl to octadecyl groups melt at temperatures between 49 and 119 °C depending upon the alkyl chain length. The clearing points are located above 200 °C. The unoriented liquid crystals show X-ray diffraction patterns consisting of two major peaks. The inner sharp peak gives a spacing, which increases as the series is ascended, from 1.40 to 2.26 nm. The outer one is sharp in the pentyl and hexyl derivatives but diffuse in the higher homologous members. The second moments of the broad-line proton NMR spectra measured above the melting points are as small as a few hundredths G^2 and firmly establish the liquid-like characteristics of the alkyl chains.

Our earlier study on the phase diagrams of a number of binary systems composed of *N*-(4-propoxybenzylidene)-4-hexylaniline and *N*-alkyl-4-nitrobenzamide or *N*-(4-nitrophenyl)alkanamide revealed that these *p*-disubstituted benzenes would form smectic liquid crystals near room temperature if the melts were sufficiently supercooled.[1] Thus, the substituents $CONHC_nH_{2n+1}$ and $NHCOC_nH_{2n+1}$ appeared to be outstandingly efficient to promote the thermal stability of liquid crystals. This conclusion is in accordance with the placement of the $NHCOCH_3$ group by Gray at the top of the order of efficiency in promoting both nematic and smectic liquid crystals.[2] He suggested that hydrogen bonding is possibly of importance in this case in retaining the molecular order in the mesophases. Therefore, we have looked into the thermal properties of benzene derivatives carrying two or more $CONHC_nH_{2n+1}$ or $NHCOC_nH_{2n+1}$ groups with the hope of finding new ways to design mesomorphic compounds.[3,4] The present paper records details of our work on *N,N′*-dialkyl-1,4- and 1,3-benzenedicarboxamides and *N,N′,N″*-trialkyl-1,3,5-benzenetricarboxamides.

Experimental

Materials. The isophthaloyl dichloride, terephthaloyl dichloride, 1,3,5-benzenetricarbonyl trichloride, and alkylamines were obtained from commercial sources. The condensation reaction between the acyl chloride and the amine was carried out in boiling benzene by the addition of pyridine. The products were purified by repeated recrystallizations from appropriate solvents and were carefully dried. For example, Found: C, 68.91; H, 9.43; N, 10.08%. Calcd for $C_6H_3(CONHC_5H_{11})_3$: C, 69.03; H, 9.41; N, 10.06%. Found: C, 77.43; H, 11.93; N, 5.10%. Calcd for $C_6H_3(CONHC_{15}H_{31})_3$: C, 77.36; H, 11.90; N, 5.01%.

Measurements. Calorimetric, X-ray, and NMR measurements were made as described in our previous papers.[3-5]

Results and Discussion

Thermal Properties of *N,N′*-Dialkylbenzenedicarboxamides. As ordinary liquid crystals are known to be formed by elongated molecules, the compounds initially examined by us were *N,N′*-dialkyl-1,4-benzenedicarboxamides (**1**). Their transition temperatures and associated enthalpies are presented in Table 1. It must be noted that the enthalpy of melting decreases as the series is ascended and also that the values are rather small. For comparison, dioctadecyl terephthalate, which is closely-related in molecular structure to the octadecyl derivative, melts at 86 °C with an enthalpy change of 136 kJ mol^{-1}. This value is 2.2 times the corresponding one of octadecane, 62 kJ mol^{-1}. These observations imply that the *N,N′*-dialkyl-1,4-benzenedicarboxamide crystal is considerably disordered just below the melting point. In other words, the high-temperature form is in a stage

Table 1. Transition Temperatures (°C) and Enthalpy Changes (kJ mol^{-1}) of Compounds **1**[a]

n[b]	Solid-solid	Solid-liquid
12	121 (33)	187 (69)
	173 (9)	
14	116 (10)	179 (62)
	123 (17)	
	160 (16)	
16	117 (14)	164 (48)
	124 (26)	
	136 (2)	
	155 (42)	
18	105 (3)	171 (45)
	129 (15)	
	151 (10)	
	157 (7)	

a) The latter quantities are in parentheses. b) The number of carbon atoms in the alkyl group.

Table 2. Transition Temperatures (°C) and Enthalpy Changes (kJ mol^{-1}) of Compounds **2**[a]

n[b]	Solid-solid	Solid-liquid
12	101 (37)	129 (36)
	123 (15)	
14	89 (4)	128 (43)
	101 (31)	
	123 (10)	
16	57 (1)	129 (48)
	96 (5)	
	112 (44)	
	124 (18)	
18	69 (2)	128 (54)
	102 (5)	
	112 (50)	
	124 (20)	

a) The latter quantities are in parentheses. b) The number of carbon atoms in the alkyl group.

Table 3. Transition Temperatures (°C) and Enthalpy Changes (kJ mol^{-1}) of Compounds **3**[a]

n[b]	K_2	K_1	M	I
4	· 98 (8)	·	226 (17)	·
5	· 75 (6)	· 119 (10)	· 206 (6)	·
6		· 99 (12)	· 205 (22)	·
7		· 116 (16)	· 208 (12)	·
8		· 102 (19)	· 204 (17)	·
9		· 65 (17)	· 215 (15)	·
10		· 49 (47)	· 208 (20)	·
11		· 72 (32)	· 216 (15)	·
12	· 21 (11)	· 88 (36)	· 212 (16)	·
13	· 32 (7)	· 81 (27)	· 216 (13)	·
14		· 61 (59)	· 209 (15)	·
15		· 88 (56)	· 214 (14)	·
16	· 73 (68)		· 205 (12)	·
17		· 87 (66)	· 211 (9)	·
18		· 78 (68)	· 206 (12)	·

a) The latter quantities are in parentheses. b) The number of carbon atoms in the alkyl group.

intermediate between the isotropic liquid and the well-organized solid state. The compound is not very soluble in most organic solvents. Moreover, the endothermic peaks are broadened in a second and subsequent heatings indicating that the compound is prone to thermal decomposition.

We extended our examination to *N,N'*-dialkyl-1,3-benzenedicarboxamides (**2**) expecting depression of melting points and also improved solubilities. These compounds are polymorphic (see Table 2). The enthalpies of melting are as small as those of the 1,4-analogs; however, the value increases with the increase of alkyl chain length in contrast to the aforementioned series. The compounds dissolve well in benzene and are easily recrystallized from mixtures of benzene and ethanol. Thus, both compounds **1** and **2** are promising as starting materials to obtain mesomorphic compounds but the latter are easiler to handle. Our next step to approach the emergence of liquid crystals was the introduction of an extra $CONHC_nH_{2n+1}$ group into the *N,N'*-dialkyl-1,3-benzenedicarboxamide molecule. As will be described in the following paragraphs, *N,N',N''*-trialkyl-1,3,5-benzenetricarboxamides (**3**) are truly mesomorphic.

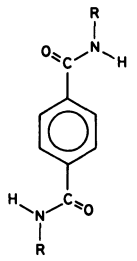

1

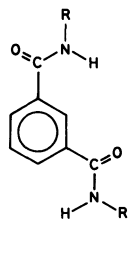

$R = C_nH_{2n+1}$

2

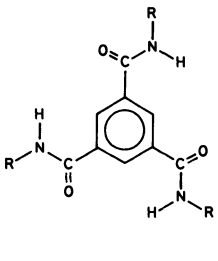

3

Thermal Properties of *N,N',N''*-Trialkyl-1,3,5-benzenetricarboxamides. The thermal properties are summarized in Table 3. Here, K, M, and I stand for crystal, mesophase, and isotropic liquid respectively. The stable form of the hexadecyl derivative melts at about 90 °C. As this form is always contaminated by the metastable form melting at 73 °C which is easily crystallized from the melt, the data for the latter are presented in this table. Most of the compounds exhibit two transitions above room temperature. The pentyl derivative and higher homologs form viscous birefringent fluids upon the transition located between 49 and 119 °C. The enthalpy change associated with the transition increases on ascending the series. The presence of a large difference between the nonyl and decyl derivatives must be noted. The mesophase covers a wide temperature range and the transformation into an isotropic liquid occurs above 200 °C in all cases. The transition is accompanied by enthalpy changes from 6 to 22 kJ mol^{-1}. The supercooling of the isotropic liquid is not detectable at a cooling rate of 5 K s^{-1}. The odd-even alternation of clearing point is found in the whole series and is particularly remarkable when the alkyl group is octyl or longer.

The butyl derivative shows a solid-solid transition in the temperature range where the higher homologs are transformed into liquid crystals and melts at a temperature higher than the clearing points of any other members. It may be added that trioctadecyl 1,3,5-benzenetricarboxylate melts at 79 °C with an enthalpy change of 133 kJ mol^{-1}. Therefore, the mesophase of the octadecyl derivative appears in the temperature range where the corresponding ester is liquid.

No identifiable texture is shown by the liquid crystals when the crystals melt. However, the texture observed for liquid crystals of low homologous members appearing by slow cooling of the isotropic liquid is likely to be fan or broken fan shaped.

X-Ray Diffraction. Figure 1 presents plots of spacings against the number of carbon atoms in an alkyl group, n. The longest spacing given by the butyl derivative is 1.20 nm at room temperature. No abrupt change is found at the solid-solid transition located at 98 °C. The spacing increases gradually upon further heating and reaches 1.26 nm at 150 °C. The higher members in the crystalline state can be classified into three groups by the alkyl chain length dependence. The pentyl and hexyl derivatives give nearly the same values, 1.67 and 1.68 nm. From the heptyl to decyl derivatives, the spacing increases by 0.17 nm per methylene group. There is an abrupt increase between the decyl and undecyl derivatives. Then, the spacing changes again linearly with n by as much as 0.20 nm per methylene group. The tetradecyl derivative is the only exception to this group.

The diffraction patterns recorded at 150±10 °C for the "unoriented" liquid crystals consist of two major peaks. In fact, the specimen spread in the form of a thin film over an aluminum holder cannot be free from orientation; therefore, "unoriented" here means not intentionally oriented. The inner peak is sharp and strong and gives a spacing of 1.63 nm for the heptyl derivative and 2.26 nm for the octadecyl derivative. The outer peak is diffuse in these homologous members. The maximum remains at the same Bragg angle throughout the series as shown in Fig. 1. This feature is consistent with not only a nonordered smectic phase but also a hexagonal disordered columnar structure. The enthalpy changes at the clearing points, 6 to 22 kJ mol^{-1}, are in the range of values for the nonordered smectic-isotropic transitions collected by Demus et al.[6] They are also comparable with the enthalpy changes given at the hexagonal disordered columnar-isotropic transitions of hexakis(alkanoyloxy)benzenes but appreciably smaller than the corresponding values of *N,N'*-dialkanoyl-2,3,5,6-tetrakis(alkanoyloxy)-1,4-benzenediamines.[5,7,8]

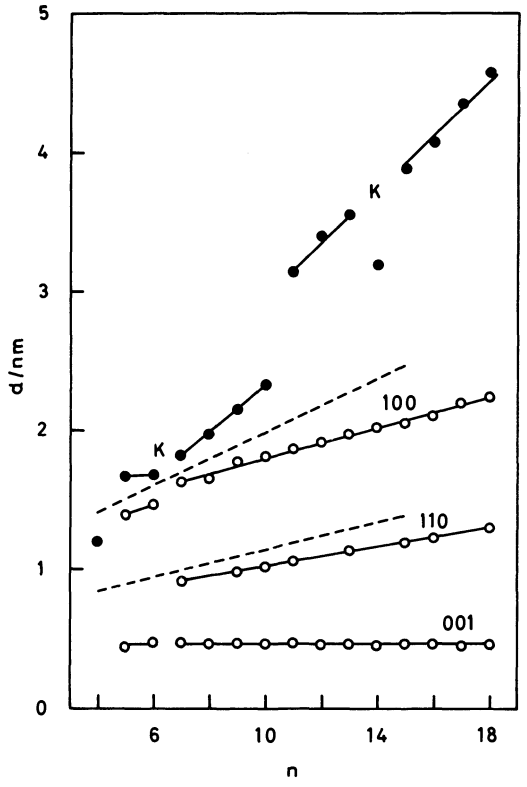

Fig. 1. Plots of spacings against the number of carbon atoms in the alkyl group of compounds **3**. The open circles show the spacings measured in mesophases. Broken lines indicate the corresponding spacings of *N,N'*-dialkanoyl-2,3,5,6-tetrakis(alkanoyloxy)-1,4-benzenediamines in the hexagonal disordered columnar phase.

Levelut has assumed that a disk-like molecule must be made of a planar rigid core surrounded by a more or less planar ring of aliphatic chains.[9] According to this view, the paraffinic crown of the *N,N',N''*-trialkyl-1,3,5-benzenetricarboxamide molecule cannot be considered to be dense enough to form columnar liquid crystals. However, a careful examination of many diffraction patterns revealed the presence of a peak, although not in all the cases, the spacing of which is about $1/\sqrt{3}$ times the longest one. The peak is very weak possibly due to the unfavorable orientation of the liquid crystals. This ratio is characteristic of a hexagonal columnar structure. The longest spacing may be assigned to the first order 100 reflection and the other one to 110 reflection. In Fig. 1, broken lines show the spacings d_{100} and d_{110} in the mesophase of *N,N'*-dialkanoyl-2,3,5,6-tetrakis(alkanoyloxy)-1,4-benzenediamines taken from our previous work.[5] Compared with them, not only the spacings themselves but also the increments per methylene group of compound **3** are shorter suggesting that the alkyl chains are more liquid-like and/or more interdigitated. Because the molecule carries only three alkyl groups, the chains attached to neighboring molecules must be differently oriented in order to achieve hexagonal packing of the columns. The molecules in each column are irregularly spaced. The average distance 0.47 nm agrees well with the values estimated for the above-mentioned hexasubstituted benzenes.[5,7,8]

While the d_{100} value in the heptyl to octadecyl derivatives varies linearly with n, the longest spacings exhibited by the pentyl and hexyl derivatives are smaller by about 0.1 nm than those expected by a linear relationship. The two compounds give sharp outer peaks and the whole diffraction patterns bear

strong resemblances to those reported for smectic B phase. The intermolecular distance (d) is estimated to be 0.47 nm by Bragg's formula and 0.54 nm when one employs the formula $2d \sin\theta = 1.1547\lambda$ proposed by de Vries specifically for smectic B phase.[10] The latter value is slightly longer than those reported for ordinary smectic B liquid crystals. If this identification is accepted, the longer spacing is assigned to the 001 reflection and the shorter one to the overlap of the 110 and 200 reflections. The molecules must be in a high degree of rotational disorder around the axis in the plane of the benzene ring and are in hexagonal packing within the layers. Such a motion may be possible only when the alkyl chains are not long. One might assume that the mesophases exhibited by these two are also hexagonal columnar. As the outer peak is sharp, the molecules in each column are equally spaced. It must be noted that the observed distance between parallel molecules, 0.47 nm, is unusually large compared with those known for some ordered columnar phases; namely, 0.36 nm of hexaalkoxytriphenylenes and hexaalkoxytruxenes.[11,12] Evidently, further studies are required to yield precise information regarding the molecular arrangement in these mesophases.

NMR Spectra. The liquid-like characteristics of alkyl chains in the mesophases are well demonstrated by small second moments of broad-line proton NMR spectrum (the mean-square width of the resonance line), $\langle \Delta H^2 \rangle$, above the melting point. Values of the order of 0.01 G^2 ($G=10^{-4}$ T) for the mesophases of the octyl and hexadecyl derivatives are almost indistinguishable from those of isotropic liquids because of the resolution limit of our spectrometer. The increase in the enthalpy change of melting with the increase of alkyl chain length is clearly manifested by the magnitude of the second moment decrease at the transition temperature; that is, about 2 G^2 at 116 °C and about 6 G^2 at 90 °C. The depression of the moment by about 2 G^2 in the non-mesogenic butyl derivative occurs in a temperature range higher by 10 to 20 °C than the calorimetric transition point located at 98 °C, indicating that the chains are not moving fast enough on an NMR time scale at the transition temperature. Moreover, the moment remains at about 3 G^2 in the high-temperature form.

The molecules examined in the present work are neither rod-like nor disk-like; nevertheless, the behavior reported above fully confirms the formation of liquid crystals. The primary requirement for the appearance of liquid crystals is not the specific geometrical anisotropy of the molecules but the anisotropy of the intermolecular forces maintaining order in the crystal and liquid crystals. The interaction between the benzenetricarboxamide units keeps the molecules in columns or layers up to relatively high temperatures. The N–H stretching vibrational band is shifted by 15 to 35 cm^{-1} to the lower wavenumber by melting and the C=O band slightly to the opposite direction, suggesting that the hydrogen bonding is strengthened upon the transition. On the other hand, the long flexible alkyl chains are conformationally disordered at lower temperatures. This molecular feature seems sufficient to fulfill the above-mentioned requirement.

Finally, it must be added that mesomorphic 1,3,5-trisubstituted benzenes are not entirely new. However, the compounds so far reported carry substituents such as cholesteryloxycarbonyloxy groups or 4-alkyl- and 4-alkoxybenzoyl groups.[13–15] They are not as simple as the present compounds and may be classified into different families of liquid crystal materials.

This work was supported by a Grant-in-Aid for Scientific Research No. 60470001 from the Ministry of Education, Science and Culture.

References

1) E. Chino, Y. Matsunaga, and M. Suzuki, *Bull. Chem. Soc. Jpn.*, **57**, 2371 (1984).
2) G. W. Gray, *Mol. Cryst.*, **1**, 333 (1966).
3) Y. Matsunaga and M. Terada, *Mol. Cryst. Liq. Cryst.*, **141**, 321 (1986).
4) Y. Matsunaga, Y. Nakayasu, S. Sakai, and M. Yonenaga, *Mol. Cryst. Liq. Cryst.*, **141**, 327 (1986).
5) Y. Kobayashi and Y. Matsunaga, *Bull. Chem. Soc. Jpn.*, **60**, 3515 (1987).
6) D. Demus, S. Diele, S. Grande, and H. Sackmann, "Advances in Liquid Crystals," Vol. 6, ed by G. H. Brown, Academic Press, New York (1983) p. 65.
7) S. Chandrasekhar, B. K. Sadashiva, K. A. Suresh, N. V. Madhusudana, S. Kumar, R. Shashidhar, and G. Venkatesh, *J. Phys. (Paris)*, **40**, C3-120 (1979).
8) S. Chandrasekhar, "Advances in Liquid Crystals," Vol. 5, ed by G. H. Brown, Academic Press, New York (1982) pp. 53—54.
9) A. M. Levelut, *J. Chim. Phys.*, **80**, 149 (1983).
10) A. de Vries, *Mol. Cryst. Liq. Cryst.*, **131**, 125 (1985).
11) A. M. Levelut, *J. Phys. (Paris)*, **40**, L-81 (1979).
12) P. Foucher, C. Destrade, Nguyen Huu Tinh, J. Malthete, and A. M. Levelut, *Mol. Cryst. Liq. Cryst.*, **108**, 219 (1984).
13) E. Schadendorff and A. Verdino, *Monatsh. Chem.*, **65**, 338 (1934).
14) K. Nishimura, S. Takenaka, and S. Kusabayashi, *Mol. Cryst. Liq. Cryst.*, **104**, 347 (1984).
15) S. Takenaka, K. Nishimura, and S. Kusabayashi, *Mol. Cryst. Liq. Cryst.*, **111**, 227 (1984).

 © 1988 The Chemical Society of Japan Bull. Chem. Soc. Jpn., 61, 211—216 (1988)

Pressure-Induced Phase Transition and Superconductivity in Phosphorus

Ichimin SHIROTANI,* Haruki KAWAMURA,† Kazuhiko TSUJI,†† Kazuhiko TSUBURAYA, Osamu SHIMOMURA,††† and Kyoji TACHIKAWA††††

Muroran Institute of Technology, 27-1, Mizumoto, Muroran 050
†Himeji Institute of Technology, 2167, Shosha, Himeji 671-22
††Faculty of Science and Technology, Keio University, Hiyoshi, Yokohama 223
†††National Institute for Research in Inorganic Materials, Sakura, Niihari, Ibaraki 305
††††National Research Institute for Metals, Sakura, Niihari, Ibaraki 305
(Received June 17, 1987)

The pressure-induced superconductivity in black phosphorus was measured along five different paths in a P–T phase diagram. The effect of the pressure on the superconducting transition temperature-(T_c) depends strongly on the path in the P–T phase diagram. The results for several paths were compared with those obtained by Wittig et al. If black phosphorus was pressurized at the temperature of liquid helium, the T_c went up to 10.7 K and the onset temperature of transition was beyond 13 K at very high pressures. When red phosphorus was used as the starting material and pressurized at 4.2 K, T_c steeply increased with an increase in the pressure; it increased up to 13 K, while the onset temperature of transition reached 18 K at 30 GPa. This is the highest superconducting transition temperature among the elements. Pressure-induced phase transitions have also been studied by the X-ray techniques using synchrotron radiation at the temperature of liquid nitrogen. The pressure of the transition at 77 K was higher than that at room temperature. Two or three phases coexisted in a wide pressure (6—14 GPa) at 77 K.

The anomalous superconductivities of black phosphorus (black P) have been investigated at low temperatures and high pressures.[1-4] The superconducting transition temperature (T_c) of black P reaches to about 11 K under very high pressures. The T_c vs. pressure curve depends on the path in the P–T phase diagram.[1,2] Wittig et al. have found double maxima in the T_c–P curve.[3] Yokovlev et al. have studied the superconductivity under pressure using a red phosphorus as the starting material.[4]

Black P is transformed from an orthorhombic structure to a rhombohedral structure, and then further to a simple cubic form, with the increase in the pressure at room temperature.[5] The transition from the orthorhombic form to the rhombohedral one is very slow, and these phases coexist over a wide pressure range. The simple cubic form is very stable under pressure and exists at least up to 60 GPa.[6] The mechanism of phase transitions in black P has already been discussed by many authors.[7-12] Iwasaki et al. have determined the P–T phase diagram of black P above room temperature by means of X-ray study with synchrotron radiation.[13] However, the phase diagram has not yet been studied below room temperature. An X-ray beam of synchrotron radiation is quite suitable for high-pressure experiments because of such excellent characteristics as brightness, a small divergence, and a constant energy.[14] By using synchrotron radiation, we have investigated the pressure-induced phase transitions of black P at the temperature of liquid nitrogen.

In this paper we wish to report our results on the pressure-induced superconductivity and phase transitions in black P obtained by the use of new high-pressure apparatuses that can continuously change the pressure at low temperatures.

Experimental

In determining the pressure dependence of T_c by the resistive method, we used the apparatus described in a previous paper.[15] The system consists of a diamond-anvil pressure cell mounted on a booster which is actuated by helium gas. The pressure can continuously be changed at the temperature of liquid helium.

Figure 1 illustrates the sample assembly for the measurement of the resistance. Each diamond anvil was convered by polyvinyl chloride films to a thickness of about 25 μm; these films were used as a pressure medium. Copper electrical leads with a thickness of 10 μm were set between two anvils. The gap width between two electrodes was about 30 μm. This configuration is similar to that is Sakai's method.[16]

A thin rectangular plate of black P was cut from a single crystal in the air and put on the gap between electrodes. The resistance was measured along the *ac* plane of the crystal. The measurement of the resistance under high pressure was carried out along the five different paths depicted in Fig. 2. Path (A1): After the sample was transformed into the simple

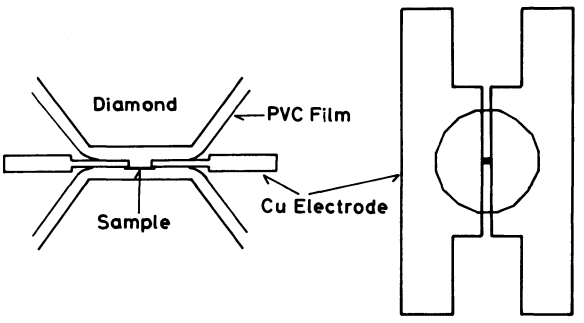

Fig. 1. Sample assembly used for the measurement of the electrical resistance.

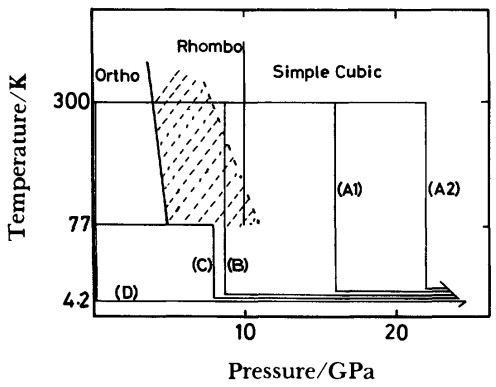

Fig. 2. Schematic phase diagram of black phosphorus: Hatched region shows the pressure range where two or three phases coexist. Five paths along which T_c was measued are also illustrated.

cubic phase by a pressure of 16 GPa at room temperature, the pressure cell was cooled to the temperature of liquid helium, keeping the pressure constant. Then, the pressure was raised further at the temperature of liquid helium. The T_c's were measured at constant pressures. Path (A2): After pressure was applied up to 22 GPa at room temperature, the cell was cooled. Then, the T_c was measured by the same procedure as above. Path (B): Pressure was applied up to 8.7 GPa at room temperature, whereupon the sample was trans formed into the rhombohedral phase. Then, it was cooled to the temperature of liquid helium. Path (C): Pressure was increased to 8 GPa at the temperature of liquid nitrogen. Both orthorhombic and rhombohedral phases coexist under this condition. Then, the cell was cooled to the temperature of liquid helium. Path (D): After the sample had been cooled to the temperature of liquid helium at almost the ambient pressure, pressure was applied. The T_c's were measured at constant pressures. The resistance of the high-purity red phosphorus was also measured along this path. The red P was provided by the Mitsubishi Metal Corporation; its purity was over 99.9999%.

The pressure was determined by means of fixed points for the Bi, ZnS, and GaP transitions at room temperature. To estimate the pressure at low temperatures, we adopted the calibration curve between the generated pressure and the applied force, as determined at room temperature.

A new diamond-anvil pressure cell was developed for X-ray measurement which makes possible a continuous change in the pressure at low temperatures. The details of the high-pressure system have been reported elsewhere.[17] The X-ray measurement at high pressures and 77 K was carried out using a bending-magnet beam line at the Photon Factory (Synchrotron Radiation Laboratory) in Tsukuba. An energy-dispersive X-ray diffraction system was adopted in this experiment. The diffraction patterns of black P and NaCl were recorded at $2\theta=21°$. The diffraction lines of NaCl were used to determine the pressure value according to Decker's scale.

Single crystals of black P were grown at about 1100 °C and at 1 GPa using a wedge-type cubic anvil high-pressure apparatus.[18]

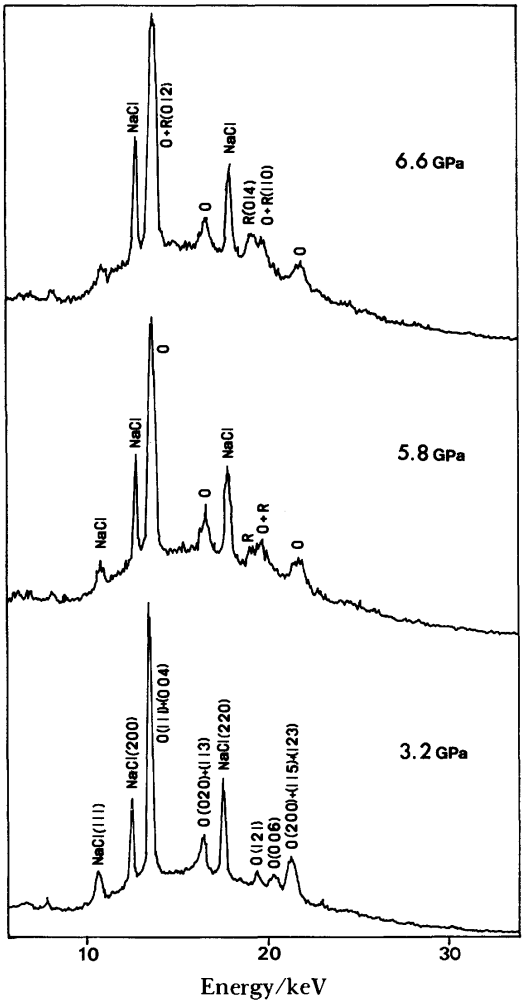

Fig. 3. Energy dispersive X-ray diffraction profiles of black phosphorus in the pressure range 0—7 GPa at 77 K, O: orthorhombic, R: rhombohedral, C: simple cubic.

Results and Discussion

1. Pressure-Induced Phase Transitions at 77 K.

X-Ray diffraction for black P under quasi-hydrostatic conditions has already been studied using a cubic anvil press at room temperature. A cube made of a mixture of boron and epoxy resin is used as the pressure-transmiting medium. The transition from the orthorhombic form to the rhombohedral one begins to occur at about 4.5 GPa. A rate of the transition is very slow. Both phases coexist between 4.5 and 8.1 GPa under quasi-hydrostatic condition.[2] Recently, we have obtained some results on the phase transition in black P under hydrostatic pressure at room temperature by means of an X-ray study with synchrotron radiation.[14] When a 4:1 solution of methanol to ethanol was used as the pressure-transmitting medium, the phase transition occured sharply at around 4.6 GPa, and the pressure range of the coexistence became narrow under hydrostatic

conditions. The phase transition from orthorhombic to rhombohedral is very sensitive to the degree of hydrostaticity of the solid and liquid pressure media, even at room temperature.

Figure 3 shows the energy-dispersive X-ray diffraction profiles of black P in the pressure range of 0—7 GPa at 77 K. The pressure was continuously increased at 77 K under quasi-hydrostatic conditions. The (*hkl*) of the diffraction lines for P and NaCl is indicated in Fig. 3. A single-phase pattern of the orthorhombic form was observed at 3.2 GPa. The five peaks in the phase shifted to higher energies with the increase in the pressure. The transition from orthorhombic to rhombohedral started at around 6 GPa. The two diffraction lines of the rhombohedral black P, (014) and (110), were clearly observed at around 6.6 GPa. The diffraction lines of the orthorhombic phase did not disappear at this pressure.

Figure 4 shows energy-dispersive X-ray diffraction patterns in the pressure range of 8—14 GPa at 77 K. The diffraction lines of the orthorhombic and rhombohedral structures were also found to coexist at 8.5 GPa. The transition to the cubic phase appeared at around 10 GPa. The intensity of the (110) line in the simple cubic phase increased with an increase in the pressure. The pattern of the simple cubic became dominant above 13 GPa at 77 K. The coexistence of two or three phases was observed in the pressure range of 6—14 GPa at 77 K under quasi-hydrostatic conditions.

Figure 5 exhibits the X-ray diffraction patterns at 77 K under a decrease in the pressure. As the pressure was reduced to 11.7 GPa at 77 K, the simple cubic phase began to be transformed into the rhombohedral structure, which became dominant at around 10 GPa. The simple cubic rhombohedral transition was nearly reversible with either an increase or a decrease in the pressure at 77 K. The rhombohedral phase was stable on a decrease in the pressure. The diffraction line of the orthorhombic structure could not be observed, even in the very low pressure region, at 77 K.

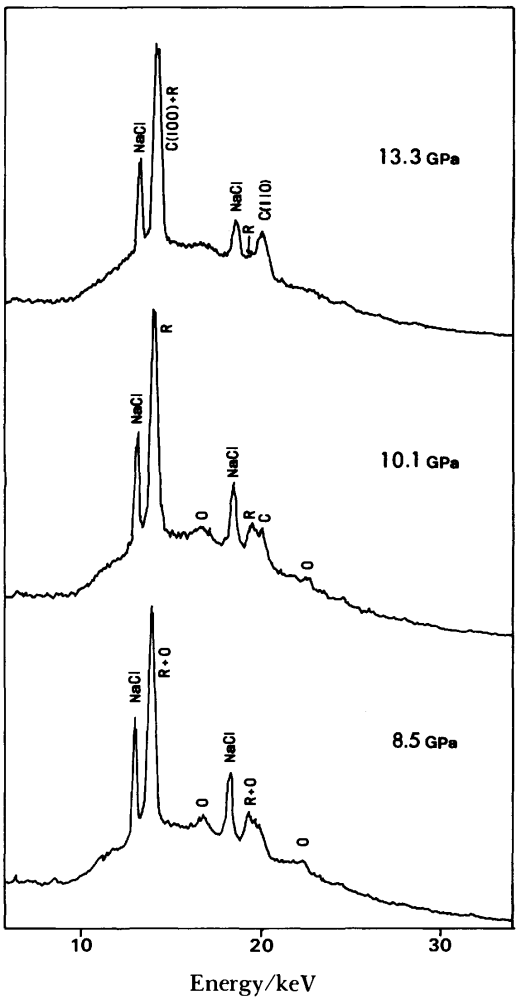

Fig. 4. Energy dispersive X-ray diffraction profiles of black Phosphorus in the pressure range 8—14 GPa at 77 K.

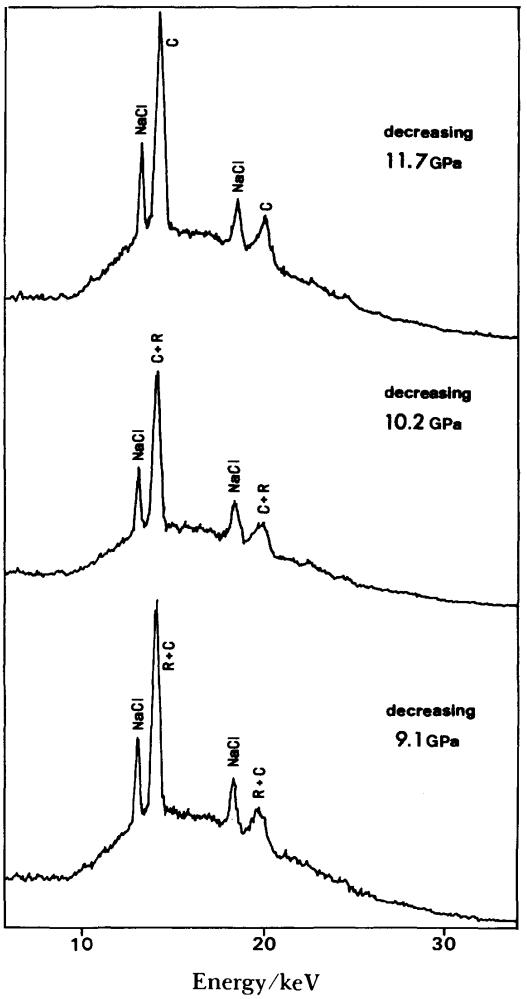

Fig. 5. X-Ray diffraction patterns at 77 K under decreasing pressure.

2. Superconductivity. Figure 6 depicts the pressure-dependence of the T_c along five different paths. Path (A1): Black P shows the metallic behavior at 16 GPa. The ratio of the resistance at room temperature to that just above T_c is about 2.5. The element becomes a superconductor at the T_c of about 6 K at this pressure. The T_c slightly increases with an increase in the pressure. Path (A2): After pressure was raised to 22 GPa at room temperature, the sample was cooled to the temperature of liquid helium at this pressure. The superconductivity of the simple cubic phase was observed at 8.1 K under 22 GPa. The T_c is increased from 5.9 K at 16 GPa in Path (A1) to 8.1 K at 22 GPa in Path (A2) by applying pressure at room temperature. The T_c at 27 GPa was 8.7 K when the pressure was increased from 22 GPa to 27 GPa at 4.2 K. Wittig et al. have reported that the T_c of the simple cubic phase is increased to 10 K at very high pressure.[3] In their experiment, the pressure was always changed at room temperature, and the pressure cell was cooled only for the measurement of T_c. The results for Path (A2) and Wittig's path are shown in Fig. 7. The T_c of the simple cubic phase rapidly increased with the increase in the pressure. On the other hand, the T_c is not sensitive to pressure, as it is pressurized at 4.2 K. The origin of this difference can not be elucidated at present. Path (B): The superconductivity was observed around 5.7 K at 9 GPa. The T_c–P curve along Path (B) is similar to that along Path (A1). Path (C): As is shown in Fig. 4, both orthorhombic and rhombohedral phases coexist at 8 GPa and the temperature of liquid nitrogen. The sample was cooled to the temperature of liquid helium from this condition. The superconductivity was found at around 5.2 K under about 10 GPa. It should be noted that the T_c is higher than that along Path (D) at this pressure. Path (D): The T_c rapidly increased with the increase in the pressure; it went up to 10.7 K, and the onset temperature of the transition was beyond 13 K at very high pressures.

Figure 8 shows the critical current at 4.2 K and at 29 GPa. The value of dI_c/dT along Path (A1) is about one order of magnitude higher than that along Path (D). The pressure dependence of the residual resistance greatly differs from Path (A1) to Path (D). These results suggest that systems along the paths do not coincide with each other, even under the same pressure.

A red phosphorus (red P) is directly transformed to a black modification at around 8 GPa at room temperature.[20] Yakovlev et al. have studied the superconductivity of black P converted from red P at room temperature and high pressures; they have thus obtained a high superconducting transition temperature.[4] We have also measured the resistance of the high-purity red P along Path (D). The resistance suddenly decreased at about 7 GPa and 4.2 K. The red P had to be converted to the black P under these

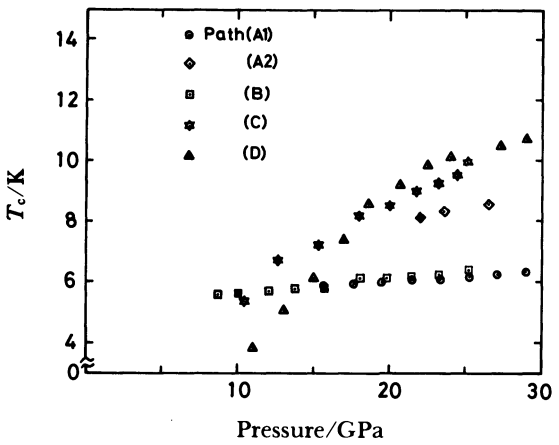

Fig. 6. Pressure dependence of the T_c along five different paths depicted in the Fig. 1.

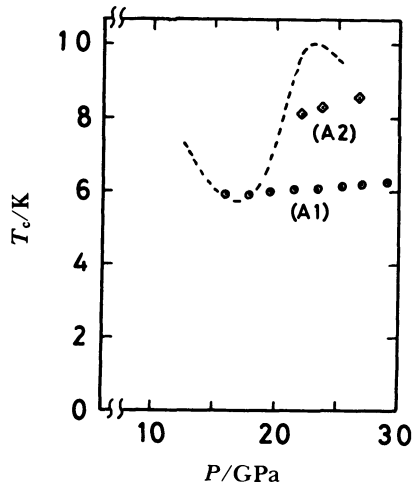

Fig. 7. T_c–P curves of the simple cubic phase: The dashed curve is obtained by Wittig et al.

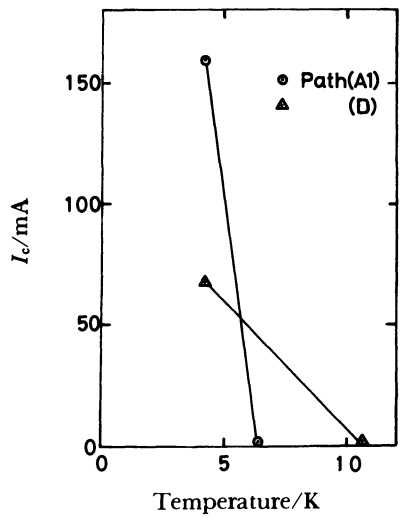

Fig. 8. Critical current of black phosphorus along the path (A1) and (D) at 4.2 K and 29 GPa.

conditions. The superconductivity was observed at around 10 GPa. Figure 9 shows the superconducting transition curves along Path (D). The T_c steeply increased with the increase in the pressure; it went up to 13 K, and the onset temperature of transition reached 18 K at 30 GPa. The T_c somewhat differed for several samples. The transition from superconductivity to the normal state does not readily terminate on the high-temperature side. The width of this transition was 6—7 K. This is very broard compared with the results of black P along Path (D). Figure 10 shows the T_c–P curves along Path (D) when the red P and black P were used as the starting materials. The T_c of the "red P" is much higher than that of black P at very high pressures. Here, the value of the superconducting transition temperature is the highest among the elements. The T_c of the phosphorus along Path (D) is higher than that of the simple cubic phase

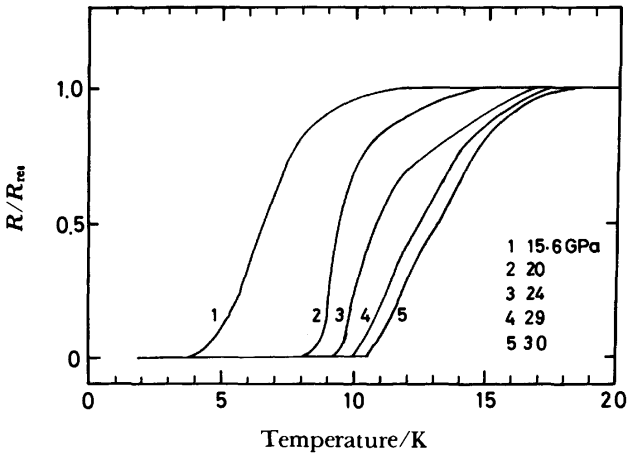

Fig. 9. The superconducting transition curves for the "red phosphorus" along the path(D). The red P was converted to the black P at about 7 GPa and 4.2 K.

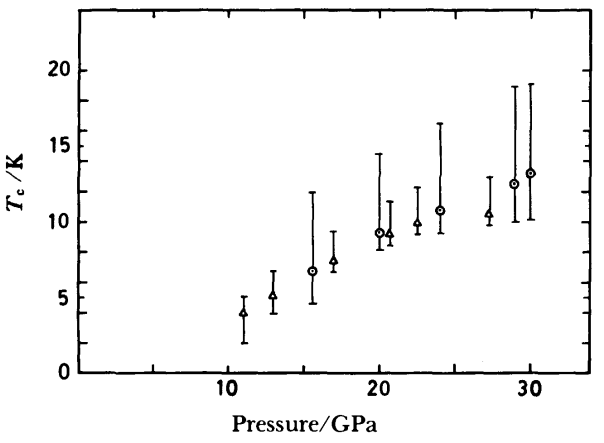

Fig. 10. T_c–P curves along the path (D) when the red P and black P as the starting materials were used; O: red P, Δ: black P. Vertial arrow heads shows the transition width.

obtained by Wittig et al.

The X-ray diffraction of black P with synchrotron radiation has been studied at the temperature of liquid helium and at high pressures. We thus obtained some preliminary results: The orthorhombic form began to be transformed to the rhombohedral form at about 10 GPa; several phases coexist in a wider pressure range.[21]

These experimental results suggest that the high T_c-superconductivity observed when pressure is applied at 4.2 K is not due to the simple cubic phase only.

The present work was partly supported by a Grant-in-Aid for Scientific research from the Ministry of Education, Science and Culture.

References

1) H. Kawamura, I. Shirotani, and K. Tachikawa, *Solid State Commun.*, **49**, 879 (1984).

2) H. Kawamura, I. Shirotani, and K. Tachikawa, *Solid State Commun.*, **54**, 775 (1985).

3) J. Wittig, B. Bireckoven, and T. Weidlich, "Solid State Physics under Pressure," ed by S. Minomura, KTK Scientific Publisher, Tokyo (1985), p. 217.

4) T. V. Valyanskaya, G. N. Stepanov, and E. N. Yakovlef, *Sov. Phys. Solid State*, **28**, 665 (1986).

5) J. C. Jamieson, *Science*, **139**, 1291 (1963).

6) I. Shirotani, A. Fukizawa, H. Kawamura, T. Yagi, and S. Akimoto, "Solid State Physics under Pressure," ed by S. Minomura, KTK Scientific Publisher, Tokyo (1985), p. 207.

7) D. Schiferl, *Phys. Rev. B*, **19**, 806 (1979).

8) Y. Yamada, Y. Fujii, Y. Akahama, S. Endo, S. Narita, J. D. Axe, and D. B. McWhan, *Phys. Rev. B*, **30**, 2410 (1984).

9) T. Kikegawa and H. Iwasaki, *Acta Crystallogr., Sect. B*, **39**, 158 (1983).

10) H. Asahina, A. Morita, and K. Shindo, *J. Phys. Soc. Jpn., Suppl. A*, **49**, 85 (1980).

11) M. Yoshizawa, I. Shirotani, and T. Fujimura, *J. Phys. Soc. Jpn.*, **55**, 1196 (1986).

12) K. J. Chang and M. L. Cohen, *Phys. Rev. B*, **33**, 6177 (1986).

13) H. Iwasaki, T. Kikegawa, T. Fujimura, S. Endo, Y. Akahama, T. Akai, O. Shimomura, S. Yamaoka, T. Yagi, S. Akimoto, and I. Shirotani, *Physica*, **139 & 140B**, 301 (1986); H. Iwasaki and T. Kikegawa, *Phys. Monthly (in Japanese)*, **6**, 414 (1985).

14) O. Shimomura, Y. Yamaoka, T. Yagi, M. Wakatsuki, K. Tsuji, O. Fukunaga, H. Kawamura, K. Aoki, and S. Akimoto, *Mat. Res. Soc. Symp. Proc.*, **22**, 17 (1984), Published by Elsevier Science Publishing Company.

15) H. Kawamura, O. Shimomura, and K. Tachikawa, *Rev. Sci. Instrum.*, **56**, 1903 (1985).

16) N. Sakai, T. Kajiwara, K. Tsuji, and S. Minomura, *Rev. Sci. Instrum.*, **53**, 499 (1982).

17) K. Tsuji, "Solid State Physics under Pressure," ed by S. Minomura, KTK Scientific Publisher, Tokyo (1985), p. 375.

18) I. Shirotani, R. Maniwa, H. Sato, A. Fukizawa, N. Sato, Y. Maruyama, T. Kajiwara, H. Inokuchi, and S.

Akimoto, *Nippon Kagaku Kaishi*, **1981**, 1604; I. Shirotani, *Mol. Cryst. Liq. Cryst.*, **86**, 1943 (1982); S. Akimoto, N. Hamaya, and I. Shirotani, "Material Science of Earth's Interior," ed by I. Sunagawa, Terra Scientific Publishing Company, Tokyo (1984), p. 131; I. Shirotani, *Phys. Monthly (in Japanese)*, **6**, 380 (1985).

19) I. Shirotani, Zhi-Dong Hao, O. Shimomura, K. Itakura, H. Kawamura, S. Fukushima, and S. Akimoto, *Photon Factory Activity Report (National Laboratory for High Energy Physics in Japan)*, **3**, 123 (1984/1985).

20) P. W. Bridgman, *Proc. Am. Acad. Arts Sci.*, **62**, 207 (1927); **70**, 71 (1935); **76**, 55 (1948).

21) I. Shirotani et al., Annual Meeting of Chemical Society of Japan, Tokyo (1987).

 © 1988 The Chemical Society of Japan Bull. Chem. Soc. Jpn., 61, 217—221 (1988)

Structural Studies of Liquid 1,1,1-Trichloroethane by Means of X-Ray Diffraction[1)]

Keiko NISHIKAWA* and Takao IIJIMA
Department of Chemistry, Faculty of Science, Gakushuin University, Mejiro, Toshima-ku, Tokyo 171
(Received July 8, 1987)

The X-ray scattering intensities from liquid 1,1,1-trichloroethane (TCE) were measured at room temperature by the energy-dispersive method. By the use of the real space expansion and the reciprocal space expansion based on the local lattice structure model, structure simulation studies for TCE were carried out. A bcc model with a random orientation of the methyl group reproduces the experimental intensities well. The number of molecules in the structure region, n, was determined by a trial-and-error method, and a least-squares refinement was carried out to determine the following four parameters; the lattice constant of the bcc cell, a; the Prins parameter, D; the radius up to the continuous region, R_c; and its damping factor, l_c. The refined parameters with the standard deviations in parentheses are: a=6.78 (0.11) Å, D=0.049 (0.009) Å, R_c=12.70 (0.48) Å, and l_c=1.76 (1.22) Å with n=51.

In order to understand the orientational correlation of molecular liquids, it has been proved to be useful to construct a local lattice structure model[2-4)] and to test it against the experimental intensity. The present authors previously reported that the scattering intensities of tetrahedral molecular liquids, such as carbon tetrachloride[3-5)] and neopentane,[6)] were reproduced well by the bcc (body-centered cubic) local-lattice-structure model.

In the bcc model, a chlorine atom (or a methyl group) of one molecule lies in a hollow formed by three off-axis chlorine atoms (or methyl groups) of the neighboring molecule, and the three-fold axes of these molecules are aligned. This packing has been named "head-tail head-tail packing." By the repetition of the packing over a three-dimensional space, a bcc lattice is obtained.[3)]

In the present work a structural study of 1,1,1-trichloroethane (TCE) has been carried out. A molecule of TCE is a quasi- tetrahedral molecule; it is obtained by replacing one of the chlorine atoms of carbon tetrachloride by a methyl group. Because the radius of the van der Waals spheres of a methyl group is almost equal to that of a chlorine atom, an appropriate structure model for liquid TCE can be expected to be similar to that of liquid carbon tetrachloride[3-5)] or liquid neopentane.[6)]

Both the real space expansion and the reciprocal space expansion are applied in the simulation study. The former expansion is a traditional calculation. However, it has the limitation that it is difficult to simulate scattering intensities in the small-s region because of the inevitable appearance of ghosts. The reciprocal space expansion was previously pesented by the present authors to overcome this difficulty in the real space expansion.[5,7)]

It is reported that the scattering intensities of liquid TCE can be simulated well by the same bcc model as is used for liquid carbon tetrachloride, where one of the chlorine atoms of carbon tetrachloride is replaced at random by a methyl group. This random replacement of a methyl group is called "random orientation of a methyl group" in the present paper.

Experimental

The sample, TCE (Kanto Kagaku), was purified by careful distillation. The scattering intensities from liquid TCE were measured at 20 °C. An energy-dispersive diffractometer with a horizontal scattering plane and a θ—2θ scanning system was used. A fine-focus X-ray tube with a tungsten target was used under the operating condition of 47.5 kV and 25 mA (or 20 mA). The scattered photons were detected by means of a pure Ge SSD (ORTEC) equipped with a multichannel pulse height analyzer (NAIG). The transmission method was applied to the collection of the data at the scattering angles (2θ) of 2.5, 5, 10, 20, and 40°. The details of the experimentation by the energy-dispersive method and the analysis of the intensity data have been reported elsewhere.[8)]

Intensity Simulation of Liquid TCE

In constructing a local lattice structure model,[2,4)] we assume a certain nearest-neighbor configuration around a central molecule and repeat this structural unit by some specific rule. According to this model the average molecular positions, as viewed from the location of a given central molecule, conform to a certain lattice structure and any molecule in the liquid can be a central molecule. Unlike the crystalline case, however, the repetition of the structural unit is imperfect and is, therefore, accompanied by a rapid loss of positional correlation as the distance between the central molecule and the surrounding ones increases. This loss of correlation may be embodied in the model in the form of a mean-square deviation of the distribution of the separation between atoms, which increases rapidly with the distance. At least beyond a few molecular radii away from any starting point, the structure can be regarded as a continuum. This distance is denoted by R_c in the present paper.

By using the group scattering factor for a methyl group introduced by Narten,[9)] a methyl group is

treated as an "atom" in the following calculations.

The coherent scattering intensity per molecule from liquid TCE in the form of the real-space expansion[4] is given by:

$$I(s) = \sum_i \sum_m f_i f_m j_0(s r_{im}) \exp(-l_{im}^2 s^2/2) + I_c \quad (1)$$

where $j_0(x)$ is given by $\sin(x)/x$, f_i is the atomic scattering factor of the i-th atom and l_{im} is the root mean-square deviation of the mean interatomic distance, r_{im}. The notation s is the scattering parameter defined by $4\pi\sin\theta/\lambda$ (2θ: scattering angle, λ: wavelength of X-rays). The summation for i is over all the atoms of the central TCE molecule, while the summation for m is over all the atoms in the discrete structure region within the radius R_c. I_c is the contribution from the region where the structure is regarded as a continuum. The expression of I_c is given by:

$$I_c = \sum_i f_i \langle F \rangle n \frac{3[sR_c\cos(sR_c) - \sin(sR_c)]}{(sR_c)^3} \exp(-l_c^2 s^2/2) \quad (2)$$

where $\langle F \rangle$ is the mean scattering amplitude of a molecule given by:

$$\langle F \rangle = \sum_i f_i \quad (3)$$

and n is the number of molecules within the discrete-structure region.[4] For the mean-square deviation the Prins relation:[2,10]

$$l_{im}^2 = 2Dr_{im} \quad (4)$$

was employed.

By the application of the Poisson summation formula,[11] we can obtain the following expression as the reciprocal space expansion:

$$I(s) = \frac{1}{v}\sum_{\nu}{}' \frac{2\pi D s}{b_\nu} \left[\frac{1}{(Ds^2)^2 + (s-b_\nu)^2} - \frac{1}{(Ds^2)^2 + (s+b_\nu)^2}\right] \times \sum_\alpha \sum_\beta f_\alpha f_\beta \exp(-i\boldsymbol{b}_\nu \cdot \boldsymbol{a}_{\alpha\beta}) + \sum_{\alpha \neq \beta} \sum f_\alpha f_\beta [\exp(-l_{\alpha\beta}^2 s^2/2) - \exp(-Dr_{\alpha\beta} s^2)] j_0(s r_{\alpha\beta}) \quad (5)$$

where $\boldsymbol{b}_\nu$ is the reciprocal-lattice-point vector. The notation α indicates the α-th atom and $\boldsymbol{a}_{\alpha\beta}$ is the vector between α and β atoms. The summation for α in the first term is carried out over all the atoms in a molecule and the summation for β over all the atoms in a unit cell. The second term in Eq. 5 is the correction term due to the mean-square deviations of intramolecular distances which are not given by the Prins relation. The summation for α and β in the second term is carried out over all the atoms in a molecule. The notation $l_{\alpha\beta}$ is the root mean-square amplitude of the intramolecular distance, $r_{\alpha\beta}$. The details of the derivation of Eq. 5 has been described in the previous papers.[5,7]

Results and Discussion

The experimental total coherent intensity, $I(s)$, from liquid TCE is shown in Fig. 1 by a solid curve, with the calculated self-scattering intensity shown by a broken curve. The weighted structure function is shown in Fig. 2; it is defined by:

$$si(s) = s(I(s) - \sum_i f_i(s)^2). \quad (6)$$

The weighted structure function for a free TCE

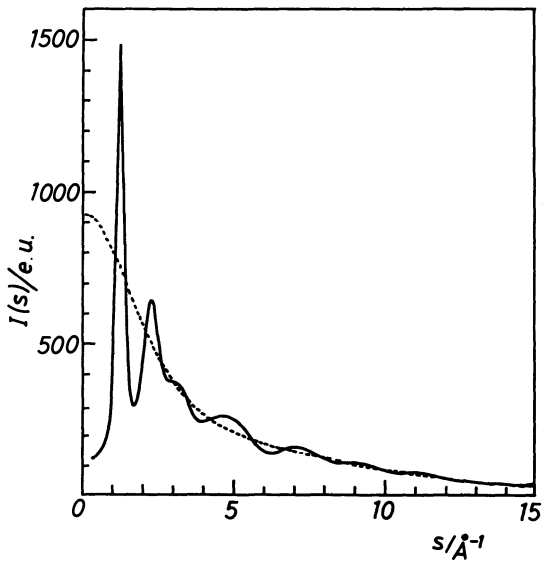

Fig. 1. The observed total coherent intensity $I(s)$ for liquid TCE (solid curve) and the self-scattering intensity from the constituent atoms (dotted curve).

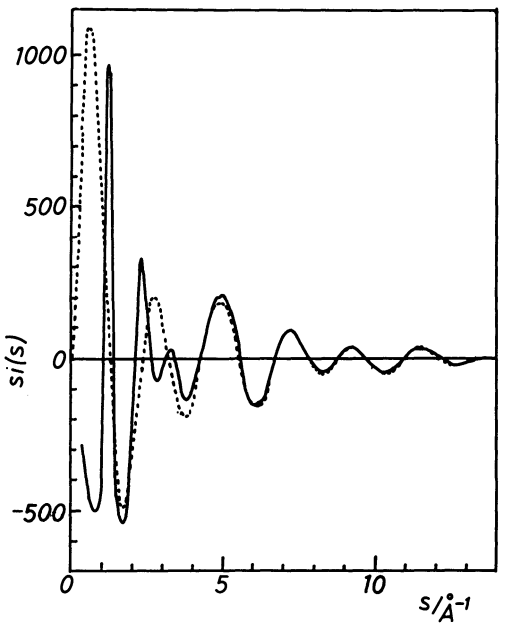

Fig. 2. Observed weighted structure function $si(s)$ for liquid TCE (solid curve) and the calculated one for a free molecule of TCE (dotted curve).

molecule is shown by a broken curve. For the intramolecular parameters, r_{ij} and l_{ij}, the data for a gaseous molecule[12] were utilized. The experimental weighted structure function is in good agreement with the calculated one for the free molecule in the range of $s>6$ Å^{-1}. The pattern of the scattering intensity from liquid TCE is very similar to that from liquid carbon tetrachloride,[3,4,8] i.e., a very sharp peak at $s\approx1.3$ Å^{-1} the successive peak at $s\approx2.3$ Å^{-1} and a small peak at $s\approx3.2$ Å^{-1}. However, the relative intensity of the second peak of TCE at $s\approx2.3$ Å^{-1} is lower.

The Fourier transform of the weighted structure function, $si(s)$, as defined by:

$$4\pi r^2(\rho-\rho_0)=\frac{2r}{\pi\sum_i Z_i^2}\sum si(s)\sin sr\cdot\Delta s \qquad (7)$$

gives the distribution function, including the weight of the electron cloud of each atom. The distribution function is shown in Fig. 3. The peaks at $r\approx1.8$ Å and 2.9 Å are attributed to the intramolecular distances of the carbon and chlorine atoms and of the chlorine and chlorine atoms, respectively. The peak at $r\approx3.9$ Å shows the nearest distance between the atoms belonging to the neighboring molecules. The peaks with respect to the long-range correlation of the molecular arrangement appear at integral multiples of about 5.9 Å; i.e., r=6.3, 11.5, 16.5, and 21.5 Å. This may show that the TCE molecules are arranged linearly. The peak at $r\approx3.9$ Å is a probe to know the distance of the neighboring molecules. When the head-tail head-tail packing is assumed, the distance of the centers of neighboring molecules is obtained as 5.9 Å by using the value of 3.9Å; the second nearest neighbor distance is 6.8 Å, which corresponds to the lattice constant of the bcc lattice. The pile of the first nearest neighbors at 5.9 Å and the second nearest neighbors at 6.8 Å forms a large peak centered at 6.3 Å in the distribution function of Fig. 3.

As has been mentioned above, the most probable packing for the molecules of liquid TCE is the head-tail head-tail packing. In fact, the calculated intensity based on the bcc model with the random orientation of a methyl group has reproduced the experimental intensity well. The intensity calculation for the random orientation of a methyl group was performed as follows; a central molecule was placed on the lattice point of the bcc, four possible arrangements of a methyl group being considered. The first nearest neighbor molecules were put on the next lattice points with the four arrangements of a methyl group in the same way. The intensities for the 16 ways of molecular arrangement were calculated by the use of Eq. 1, and then the total was divided by 16. For molecules farther than the first nearest neighbors, similar calculations were carried out.

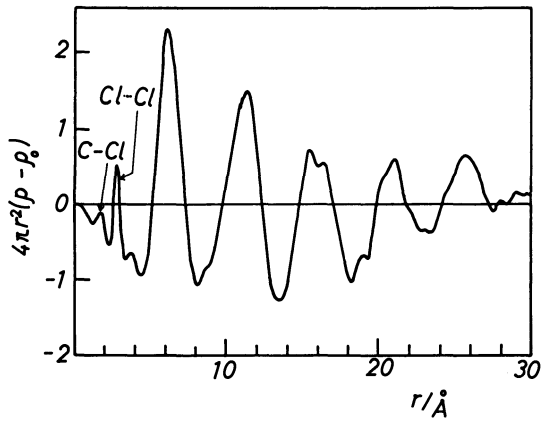

Fig. 3. The radial distribution function of liquid TCE.

Next, the least-squares refinements for the weighted structure function $si(s)$, based on the bcc local-lattice structure with the random orientation of a methyl group were carried out. The refined parameters were as follows; the number of molecules (n) in the discrete structure region, the lattice constant of the bcc cell (a), the Prins parameter (D) which gives the mean-square deviation of the distance of atoms belonging to different molecules (see Eq. 4) and the radius of the discrete-structure region (R_c) and its damping factor (l_c) (see Eq. 2). For the determination of the number n, a trial-and-error method was applied. The other four parameters were refined by the least-squares method. The weighted structure function obtained by the use of the following values showed the best agreement with the experimental values: n is 51, which corresponds to the inclusion up to the fourth nearest neighbors, a=6.78 (0.11) Å, D=0.049 (0.009) Å, R_c= 12.70 (0.48) Å and l_c=1.76 (1.22) Å, where the numerals in the parentheses are the standard deviations. The reliability factor, $\mathscr{R}$, as defined by:

$$\mathscr{R}=\left[\frac{\sum w(s)[si(s)_{exp}-si(s)_{calc}]^2}{\sum w(s)[si(s)_{exp}]^2}\right]^{\frac{1}{2}} \qquad (8)$$

was 0.23, where $w(s)$ was the weight function. The values of $w(s)$ were chosen as 0.1 for $0<s\leqslant1$ Å^{-1} and 1.0 for $s>1$ Å^{-1}. From the refined value of a, the distance of the first nearest neighbors becomes 5.87 Å. The weighted-structure function calculated by the use of these refined values is shown in Fig. 4 by the solid curve together with the experimental one (broken curve). The calculated intensity is in good agreement with the experimental one in the region of $s\geqslant1$ Å^{-1}.

The discrepancy in the region of $s<1$ Å^{-1} originates from the sudden onset of the continuum region to the discrete-structure region.[5,7] In order to overcome the difficulty of the real space expansion, the reciprocal space expansion was carried out. Because it is impossible to simulate the intensity for the random orientation exactly in the case of the reciprocal space expansion, the following approximation was adopted: the bond distance between a centered carbon atom

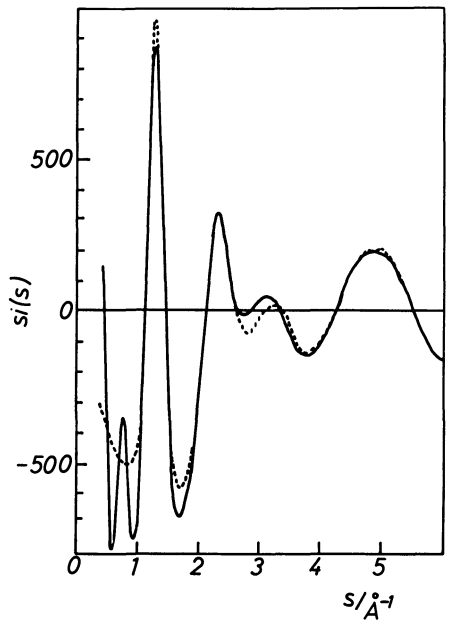

Fig. 4. The weighted structure function $si(s)$ for liquid TCE. The solid curve is the calculated one for the bcc model with the random orientation of the methyl group and the dotted curve is the experimental one.

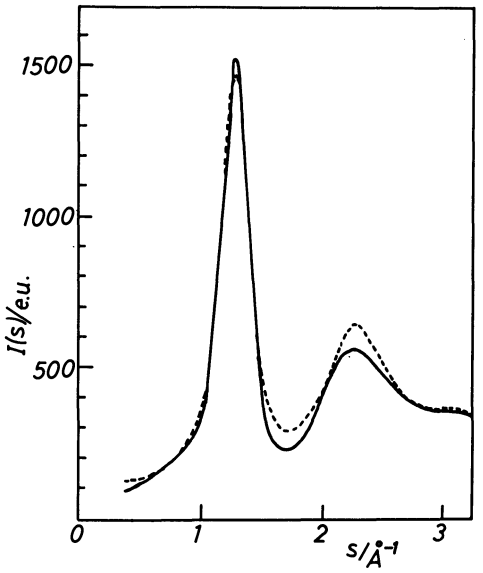

Fig. 5. The total coherent intensity of liquid TCE. The solid curve is the calculated intensity based on the bcc model by the use fo the "reciprocal space expansion." The broken curve is the experimental intensity.

and a methyl group (1.54 Å) was changed to that between the carbon atom and a chlorine atom (1.77 Å) and hypothetical atoms with the scattering factor of $(3f_{Cl}+f_{Me})/4$ were equally placed at the positions of chlorine atoms and a methyl group. The other structural parameters used in the reciprocal-space expansion were identical with those obtained by the least-square refinement in the real-space expansion. Reciprocal lattice points up to $\nu=(600)$ ($b_\nu=5.56$ Å^{-1}) were included. The results of the application to TCE based on the bcc local-lattice structure shows an excellent agreement of the calculated intensity with the experimental value in the region of s smaller than 2 Å^{-1} (see Fig. 5). The total coherent intensity is shown in Fig. 5, because it demonstrates the discrepancy between the experimental and the simulated intensities in the small-s region. Contrary to the real space expansion, the convergence becomes worse with an increase in the s. By the use of both the real space and the reciprocal space expansion, the observed scattering intensity of liquid TCE in the whole range of s is satisfactorily accounted for on the basis of the bcc local-lattice model.

Molecules with an octupole moment, such as carbon tetrachloride and neopentane, are highly stabilized by the head-tail head-tail packing.[13] Because a TCE molecule has a dipole moment, the bcc model in the liquid TCE with the random orientation of a methyl group is not consistent with the electrostatic interaction of the molecule. Some of the other orientations of the methyl group were, therefore, attempted in the simulation study. As was shown in the structure study of the plastic crystal of carbon tetrachloride,[14] the calculated intensity curve for packings other than the head-tail head-tail packing has peaks and valleys at entirely different positions from the experimental curve. Therefore, we can restrict the model for liquid TCE to the head-tail head-tail packing. The head-tail head-tail packing with the parallel orientation of a methyl group gives the same pattern, but the first peak at $s\approx1.3$ Å^{-1} becomes much higher than the experimental one and the reliability factor becomes worse. Of course, the parallel orientation of the methyl group can not be permitted physically because of the unstabilization caused by the interaction between the dipole moments. However, the fact mentioned above shows that the height of the first peak in the intensity curve is fairly sensitive to the orientation of the methyl groups. Next, the intensity for another model was calculated, where molecular arrangements with a parallel dipole moment to that of the central molecule are omitted in the arrangements of the first neighbors and molecules farther than the first nearest neighbors have the random orientation for the methyl groups. The intensity curve for this model was in very good agreement with that for the random orientation of the methyl group, and the reliability factor was 0.235 (cf. 0.230 in the random orientation.)

Though the TCE molecules may be arranged so as to stabilize the dipole interaction, the information on the orientation of the methyl group is smeared in the

liquid; it may, however, be said that the orientation is random in the liquid on the average. In the case of liquid TCE, the agreement between the experimental intensity and the calculated one based on the bcc model is of the same degree as in liquid carbon tetrachloride or liquid neopentane.

TCE has two plastic crystal phases, i.e., a fcc phase and a rohmbohedral phase,[15] just like carbon tetrachloride. In the structure analysis of Phase Ia (plastic crystal fcc) of carbon tetrachloride, it has been shown that the head-tail head-tail packing is dominant.[14] The simulation study in the plastic crystal is easier than in the liquid, because the nearest neighbor distance of molecules can be determined from the unit-cell dimensions and so only the orientational correlation needs to be investigated. The structure study of plastic crystal of TCE is now under way and it will give further information on the structure of liquid TCE. It will be reported in the near future.

References

1) A portion of the present work was published as a preliminary communication: K. Nishikawa, K. Nagano, and T. Iijima, *Nippon Kagaku Kaishi*, **1986**, 1479.

2) J. A. Prins and H. Petersen, *Physica*, **3**, 147 (1936).

3) K. Nishikawa and Y. Murata, *Bull. Chem. Soc. Jpn.*, **52**, 293 (1979).

4) K. Nishikawa and T. Iijima, *Bull. Chem. Soc. Jpn.*, **58**, 1215 (1985).

5) K. Nishikawa and T. Iijima, *Bull. Chem. Soc. Jpn.*, **59**, 117 (1986).

6) K. Nishikawa, *Bull. Chem. Soc. Jpn.*, **59**, 2920 (1986).

7) T. Iijima and K. Nishikawa, *Chem. Phys. Lett.*, **115**, 522 (1985).

8) K. Nishikawa and T. Iijima, *Bull. Chem. Soc. Jpn.*, **57**, 1750 (1984).

9) A. H. Narten, *J. Chem. Phys.*, **70**, 299 (1979).

10) J. Frenkel, "Kinetic Theory of Liquids," Dover Publications, New York (1955).

11) P. M. Morse and H. Feshbach, "Method of Theoretical Physics," McGraw-Hill, New York (1953).

12) J. R. Durig, M. M. Chen, and Y. S. Li, *J. Mol. Struct.*, **15**, 37 (1972); T. Iijima and R. Wada, Symposium on Structure Chemistry, November 1986, Osaka.

13) T. Kihara, "Intermolecular Force," Iwanami, Tokyo (1976).

14) K. Nishikawa, K. Tohji, and Y. Murata, *J. Chem. Phys.*, **74**, 5817 (1981).

15) R. Rudman and B. Post, *Mol. Cryst.*, **5**, 95 (1968); R. Rudman, *Mol. Cryst. Liq. Cryst.*, **6**, 427 (1970).

 © 1988 The Chemical Society of Japan Bull. Chem. Soc. Jpn., 61, 223—228 (1988)

Why Does the Hückel Rule Hold for a Variety of Monocyclic Conjugated Systems?

Jun-ichi AIHARA* and Hiroshi ICHIKAWA†
Department of Chemistry, Faculty of Science, Shizuoka University, Oya, Shizuoka 422
†Hoshi College of Pharmacy, Shinagawa, Tokyo 142
(Received July 9, 1987)

Hückel's $4n+2$ rule is shown to be applicable to diverse monocyclic π systems by means of graph theory and frontier orbital theory. All monocyclic $(4n+2)$-π-electron systems are proved to have both kinetic and thermodynamic stabilities. They are predicted to be diatropic in nature.

In 1931 Hückel presented so-called Hückel molecular orbital (HMO) theory.[1] He applied it to annulene π systems, and established the well-known Hückel rule for aromaticity, according to which all annulenes with $4n+2$ π electrons are predicted to be chemically stable or aromatic, and all annulenes with $4n$ π electrons are predicted to be rather reactive or antiaromatic. The Hückel rule is applicable not only to neutral annulenes but also to annulene ions.[1-3] Hückel suggested that it is also applicable to such heteroconjugated systems as pyridine and pyrrole.[1] As a matter of fact, the Hückel rule has been successfully applied to many monocyclic heteroconjugated systems and their ions.[4]

Hückel pointed out that the highest occupied molecular orbitals (HOMO's) of [$4n+2$]annulene are completely filled.[1] He then associated the closed-shell π system with the stability or aromaticity of an entire conjugated system. The HOMO's of [$4n+3$]annulene cations and [$4n+1$]annulene anions are also completely filled. In contrast to them, the HOMO's of [$4n$]annulene are relatively high in energy, and not completely filled. Hückel predicted that it must be reactive for this reason.[1]

A number of attempts have been made to test the validity of the Hückel rule. Various perturbational MO methods have been used to explain stabilization or destabilization of annulenes due to cyclic conjugation.[5-8] Breslow compared the energy of a cyclic π system with that of an open-chain reference system.[9] The applicability of the Hückel rule to annulenes has been confirmed by these attempts.

Dewar et al. devised an olefinic reference system of the same geometry as a real π system, using such bonds as scissored off from acyclic π systems,[10] and evaluated the so-called Dewar resonance energy relative to the energy of such a reference system. Hess and Schaad defined this type of resonance energy within the framework of HMO theory.[11,12] Aihara found that for monocyclic π systems Dewar resonance energy is definable using π bond energies of infinitely large cyclic π systems.[13] Two research groups formulated the Dewar resonance energy graph-theoretically.[14-18] All these attempts revealed that very many heterocyclic compounds obey the Hückel rule.

However, it has not been clarified yet whether or not the Hückel rule is applicable to all monocyclic π systems conceivable. There has been no general proof for the validity of the Hückel rule. This paper aims at elucidating the applicability and the physical meaning of the Hückel rule by means of graph theory[14-20] and frontier orbital theory.[7,21-23] The HMO model is used throughout this paper. Arbitrary integers are represented by N, m, n, p, or q.

Kinetic Aspect of the Hückel Rule

First, an aromatic molecule must be chemically stable or preferably unreactive. This kind of stability has been referred to as kinetic stability. We show below that the Hückel rule can be used reasonably to predict the kinetic stability of any monocyclic π system.

A given monocyclic π system formed by N conjugated atoms is denoted by G. We assume that there is no substituent in G. A characteristic polynomial $P_G(X)$ for G can be obtained by means of Sachs graph theory.[14-20] A reference polynomial $R_G(X)$ is a characteristic polynomial constructed graph-theoretically for a hypothetical olefinic reference structure of G.[14-18] Both $P_G(X)$ and $R_G(X)$ are the polynomials of degree N. The reference structure defined by $R_G(X)$ is assumed to have exactly the same geometry as G. However, the π bonds in it are tacitly assumed to have the same π bond energies as the analogous π bonds in acyclic polyenes.

For monocyclic π systems, $P_G(X)$ is obtainable simply by subtracting a constant from $R_G(X)$, namely,[14-18]

$$P_G(X) = R_G(X) - K_G, \tag{1}$$

where $K_G > 0$ is the constant given by

$$K_G = 2\prod_{(ij)}^{G} k_{ij}. \tag{2}$$

Here, k_{ij} is the Hückel parameter for the i-j π bond, and (ij) runs over all π bonds in G. The curves $Y=P_G(X)$ and $Y=R_G(X)$ coincide exactly in the X-Y plane by displacing the former curve upward by K_G. There are N zeroes in $P_G(X)$ and $R_G(X)$, which represent the energies of N molecular orbitals (MO's)

in G and its reference structure, respectively.[14-18] For example, K_G is 1.3122 for 1,4-dihydropyrazine, and $P_G(X)$ and $R_G(X)$ are

$$P_G(X) = X^6 - 3X^5 - 2.99X^4 + 10.86X^3 + 2.3644X^2 - 7.86X - 0.3744, \quad (3)$$

$$R_G(X) = X^6 - 3X^5 - 2.99X^4 + 10.86X^3 + 2.3644X^2 - 7.86X + 0.9378. \quad (4)$$

Here, the Hückel parameters of Hess, Schaad, and Holyoke[11] were used. The curves $Y=P_G(X)$ and $Y=R_G(X)$ for this eight-π-electron system are drawn in Fig. 1.

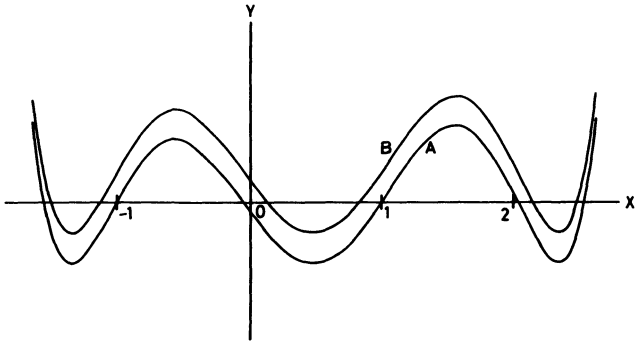

Fig. 1. The curves $Y=P_G(X)$ (A) and $Y=R_G(X)$ (B) for 1,4-dihydropyrazine.

Fikui et al.[7,21-23] named the HOMO and the lowest unoccupied molecular orbital (LUMO) frontier MOs, the energies and phases of which are closely related to the reactivity of the molecule. The HOMO and the LUMO contribute much more to such reactivity indices as superdelocalizabilities than any other MO's.[22] Therefore, it is instructive to examine the locations of these MO's in the energy scale.

The mth largest root X_m of the equation $P_G(X)=0$ represents the energy of the mth MO in G. The mth largest root X_m° of the equation $R_G(X)=0$ represents the energy of the mth MO in an olefinic reference system of G.[14-18] In general, positive and negative roots correspond to bonding and antibonding MOs, respectively. As can be seen from Fig. 1, the following two inequalities hold:

$$\begin{aligned} X_m &> X_m^\circ \text{ for } m = 2p+1 \\ X_m &< X_m^\circ \text{ for } m = 2p \end{aligned} \quad (5)$$

It is clear from Eq. 5 that the HOMO of a monocyclic $(4n+2)$-π-electron system is always lower in energy than that of the olefinic reference system, but that the LUMO is always higher in energy than that of the reference system. Such a $(4n+2)$-π-electron system must have much smaller superdelocalizabilities than its olefinic reference system defined by $R_G(X)$. This indicates that a $(4n+2)$-π-electron system must be much more resistant both to electrophilic and nucleophilic substitutions than a hypothetical olefinic system of the same geometry (i.e., the reference system). On the other hand, a monocyclic $4n$-π-electron system has a higher HOMO and a lower LUMO, both of which contribute much to the increase in reactivity. It has thus been confirmed that the Hückel rule holds in a kinetic sense for all kinds of monocyclic π systems. Therefore, it is very possible that most monocyclic species classified as aromatics are less reactive than those classified as antiaromatics.

Figure 1 shows that even if the $(2p)$th and $(2p+1)$th MO's of a monocyclic π system are degenerate in energy, the $(2p+1)$th and $(2p+2)$th MO's are never degenerate. If the $(2p+1)$th and $(2p+2)$th MO's were degenerate, the corresponding roots of the equation $R_G(X)=0$ would become complex numbers. This never occurs since the realness of these roots has been proved mathematically.[24] Therefore, a monocyclic conjugated species with $4n+2$ π electrons always has a closed-shell π system with a doubly occupied HOMO. As mentioned, Hückel showed that [$4n+2$]annulene has a closed-shell π system.[1] The present graph-theoretical analysis happens to constitute an extension of this viewpoint to all monocyclic conjugated systems. There is no open-shell $(4n+2)$-π-electron system as far as monocyclic conjugated molecules are concerned.

A singly occupied molecular orbital (SOMO) is also one of the frontier orbitals.[7,22,23] As seen above, Hückel's original interpretation of aromaticity is based on the kinetic instability of an open-shell π system with SOMO's.[1] It is very true that an open-shell π system is very reactive. Aside from [$4n$]annulenes, however, there are few monocyclic systems with SOMO's. Even in [$4n$]annulenes the degeneracy of the SOMO's are in fact lifted by the introduction of bond-length alternation. Since most heterocyclic systems with $4n$ π electrons have no degenerate SOMO's, the interpretation of antiaromaticity in terms of SOMO's is of limited use.

Thermodynamic Aspect of the Hückel Rule

Ideally, an aromatic molecule must exhibit not only kinetic but also thermodynamic stabilities.[3-9] Haddon and Fukunaga showed that [$4n+2$]annulenes meet the thermodynamic and kinetic criteria of aromatic character.[25] We next prove that any monocyclic $(4n+2)$-π-electron system is thermodynamically stabilized by cyclic conjugation. Fukui's frontier MO theory[7] is again useful for this purpose.

The Schrödinger equation defined in HMO theory for a linear π system is essentially of one-dimensional character, and can formally be reduced to the one-dimensional form:

$$-\frac{\hbar^2}{2m}\frac{d^2}{dX^2}\Psi(X) + \{V(X) - E\}\Psi(X) = 0, \quad (6)$$

where $\Psi(X)$ is the eigenfunction (i.e., the MO), E is the

eigenvalue (i.e., the energy of the MO), $V(X)$ is the electrostatic potential felt by an electron, m is the mass of an electron, and $\hbar$ is the Planck constant divided by 2π. The interatomic distances and the form of $V(X)$ can in principle be chosen in such a manner that Eq. 6 yields the Hückel secular determinant for a given linear π system. In other words, $V(X)$ may be an unrealistic function as far as Eq. 6 reproduces the Hückel matrix elements within the Hückel approximation. $V(X)$ may be assumed to be a differentiable function. In this treatment, we tacitly use hypothetical one-dimensional AO analogues as the LCAO basis functions.

Such a Schrödinger equation is mathematically identical with the eigenvalue problem of the Sturm-Liouville type.[26] The mth eigenfunction obtained by solving this problem has $m-1$ zeroes in the defined region. In the present case, the mth eigenfunction corresponds to the mth MO of a linear π system, which necessarily has $m-1$ nodes. The number of nodes increases one by one on going to higher MOs. Accordingly, LCAO coefficients of the $(2p+1)$th MO have the same sign at the two edge atoms, whereas those of the $(2p)$th MO at the edge atoms differ in sign. This sign rule holds for all kinds of linear π systems.

Fukui indicated that any conceivable division of benzene into two fragments produces segments whose HOMO and LUMO overlap in-phase at the original two junctions.[7] HOMO–LUMO interactions then give rise to stabilization by cyclic conjugation. We adopt this way of reasoning. An arbitrarily chosen monocyclic π system is first divided into two segments, both of which are linear conjugated subsystems. These two segments are assumed to have an even number of π electrons. Figure 2 shows the case in which a monocyclic aromatic molecule is divided into two segments, the one with two conjugated atoms and two π electrons and the other with the remaining conjugated atoms and π electrons.

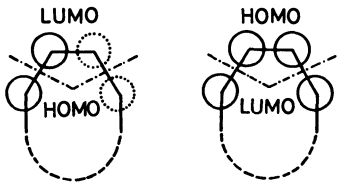

Fig. 2. Stabilizing HOMO–LUMO interactions in a monocyclic $(4n+2)$-π-electron system.

It follows that if the HOMO and the LUMO concerned are the $(2p+1)$th MO of one segment and the $(2q+1)$th MO of the other segment, respectively, both MO's overlop in-phase at the original two junctions. If the HOMO and the LUMO are the $(2p)$th MO of one segment and the $(2q)$th MO of the other segment, respectively, both MO's overlap in-phase, too. Then, the entire cyclic π system is predicted to gain stabilization energy by HOMO–LUMO interactions. Such a situation occurs only if the entire cyclic system has $4n+2$ π electrons.

On the other hand, if the HOMO and the LUMO concerned are the $(2p)$th MO of one segment and the $(2q+1)$th MO of the other segment, respectively, both MO's do not overlap in-phase at one of the junctions. In this case, the HOMO of the latter segment necessarily does not overlap in-phase with the LUMO of the former segment, either. The entire cyclic π system is predicted not to be stabilized by HOMO–LUMO interactions. Such a situation occurs only if the entire cyclic π system have $4n$ π electrons.

We can also assume that an odd number of π electrons reside at each segment.[5,7] This time the SOMO's of the two segments become interacting frontier MO's. Exactly the same proof can be achieved for the thermodynamic aspect of the Hückel rule by examining whether or not a phase dislocation occurs between the SOMO's at the original two junctions. Unless the total number of π electrons is equal to $4n+2$, the two SOMO's do not overlap in-phase at one of the junctions.

The above frontier MO analyses apply not only to all neutral monocyclic species but also to all charged ones. It is monocyclic $(4n+2)$-π-electron systems alone that are stabilized by HOMO–LUMO interactions. This is the very reason why the Hückel rule can be interpreted in thermodynamic terms. We can safely say on this basis that all kinds of $(4n+2)$-π-electron systems are thermodynamically stable.

Thermodynamic stability of a molecule due to cyclic conjugation is given numerically by the graph-theoretically defined resonance energy, RE.[14–18] It is defined as the difference in total π-electron energy between a given conjugated system and its reference system. RE is expressed explicitly as

$$\mathrm{RE} = \sum_{m=1}^{N} g_m(X_m - X_m^\circ), \tag{7}$$

where g_m is the occupation number for the mth MO. The mth orbital resonance energy, ORE_m, is defined as[27]

$$\mathrm{ORE}_m = X_m - X_m^\circ. \tag{8}$$

Since Eq. 5 holds, ORE_m is positive if $m=2p+1$, and negative otherwise. Therefore, the HOMO resonance energy of a $(4n+2)$-π-electron system is positive, whereas that of a $(4n)$-π-electron system is negative. RE is obtainable by adding up twice the orbital resonance energies of all occupied MO's.[27]

Figure 1 indicates that $P_G(X)$, in general, has a rather steep gradient at $X=X_1$ and X_N, compared to those at other zeroes of $P_G(X)$. This implies that the absolute values of ORE_1 and ORE_N are in general smaller than those of other orbital resonance energies. ORE_1 always has a small positive value. ORE_m is

positive in sign if m=even, and negative otherwise. Except the cases of m=1 and N, the absolute values of the orbital resonance energies are rather comparable with each other. This might be understandable from Fig. 1. Since any monocyclic π system behaves as such, the sign of the overall resonance energy (i.e., RE) is determined primarily by the sign of the HOMO resonance energy, i.e., the orbital resonance energy of the HOMO.

We have calculated RE's of many monocyclic heteroconjugated systems.[14,18] Resonance energies and orbital resonance energies for four typical monocyclic π systems are listed in Table 1. Here, the Hückel parameters determined by Hess, Schaad, and Holyoke were employed.[11] For all these molecules, the sign of RE is really determined by the sign of HOMO resonance energy. No exceptions were found in accordance with the above frontier MO analyses. As predicted by the frontier MO analyses, monocyclic $(4n+2)$-π-electron systems alone have positive RE due to cyclic conjugation. There seems to be no monocyclic aromatic species which has a destabilized HOMO and no monocyclic antiaromatic species which has a stabilized HOMO.

For most neutral monocyclic systems, all bonding MO's are filled, and all antibonding MOs vacant. For these systems, aromaticity can be estimated by comparing the values of $|P_G(i)|$ and $|R_G(i)|$, where $i=\sqrt{-1}$.[15,28] If $|P_G(i)|>|R_G(i)|$ for a given species G, it is aromatic thermodynamically. Logarithms of $|P_G(i)|$ and $|R_G(i)|$ are roughly proportional to the total π-electron energies of G and its olefinic reference structure, respectively.[15] K_G increases or decreases the value of $|P_G(i)|$ according to the Hückel rule. If G has $2n+1$ bonding MO's with $4n+2$ π electrons, K_G makes $|P_G(i)|$ larger than $|R_G(i)|$, and positive RE results. There are no exceptions.

Table 1. Orbital Resonance Energies of Monocyclic π Systems

m	X_m	X_m°	ORE$_m/\beta$[a]
A. 1,4-Dihydropyrazine (RE=−0.132β)			
1	2.547	2.494	0.053
2	2.034	2.146	−0.112
3	1.000	0.833	0.167
4	−0.047	0.127	−0.174
5	−1.000	−1.121	0.121
6	−1.534	−1.479	−0.055
B. Imidazole (RE=0.196β)			
1	2.366	2.334	0.032
2	1.064	1.270	−0.206
3	0.633	0.361	0.272
4	−0.892	−0.706	−0.186
5	−1.292	−1.380	0.088
C. Pyrimidine (RE=0.193β)			
1	1.749	1.704	0.045
2	0.961	1.248	−0.287
3	0.915	0.578	0.337
4	−0.535	−0.268	−0.267
5	−0.727	−0.923	0.196
6	−1.604	−1.578	−0.026
D. Azepine (RE=−0.288β)			
1	2.398	2.381	0.017
2	1.600	1.719	−0.119
3	1.247	1.057	0.190
4	−0.021	0.210	−0.231
5	−0.445	−0.653	0.208
6	−1.476	−1.374	−0.102
7	−1.802	−1.841	0.039

a) β is an absolute value of β.

Magnetotropic Aspect of the Hückel Rule

It has widely been accepted that aromatic and antiaromatic annulenes are diatropic and paratropic, respectively.[29] Magnetotropism of annulens is simply determined by the number of π electrons. Therefore, it is predictable from the Hückel rule. Let us examine whether or not the magnetotropism of an arbitrarily chosen monocyclic π system is predictable from the Hückel rule.

When the magnetic field is applied to a monocyclic π system, only the term K_G in $P_G(X)$ changes.[16,27,30] All coefficients of $R_G(X)$ are not dependent upon the external field. If the field is perpendicular to the molecular plane, K_G is expressed as

$$K_G = 2\cos\left(\frac{eSB}{\hbar}\right)\prod_{(ij)}^{G} k_{ij}, \tag{9}$$

where B is the field strength, S is the area of the ring, and e is the charge of an electron.

Since K_G slightly decreases in the magnetic field, $P_G(X)$ displaces slightly downward toward the location of $R_G(X)$. Accordingly, every MO with positive orbital resonance energy is destabilized by the field, whereas every MO with negative orbital resonance energy is stabilized by the field. The former MO contributes to the exaltation of molecular diamagnetism.[27,31] The latter MO is paramagnetic in nature, decreasing molecular diamagnetism. The HOMO of a monocyclic system with $4n+2$ π electrons is always diamagnetic or diatropic in nature. These magnetic effects arise from the ring current induced in a cyclic system.

Haddon[32] and Aihara[33] proved that the ring current intensity is proportional to the product of the resonance energy and the ring area for all aromatic annulenes and annulene ions. Aihara extended this idea to all monocyclic π systems, and found that the induced ring current is approximately proportional to the resonance energy, multiplied by the area of the ring.[34] Since it has been proved that monocyclic systems with $4n+2$ π electrons have positive RE, they all are necessarily diatropic. Those with $4n$ π electrons have negative RE, so they must be paratropic. Thus, magnetotropism is an excellent index for determining the degree of aromatic

stabilization. Conversely, the Hückel rule can be used assuredly to determine the sign of magnetropism for all monocyclic π systems.

Concluding Remarks

The Hückel rule has been used successfully to identify innumerable monocyclic π systems as aromatic or antiaromatic species. The above treatments based on graph theory and frontier orbital theory revealed novel physical implications of the Hückel rule, and justified well the use of it. It has been established that any monocyclic $(4n+2)$-π-electron system has not only kinetic but also thermodynamic stabilities. The sign of the overall resonance energy is determined simply by the number of π electrons. Ichikawa and Ebisawa[35] recently found a nice correlation between the Hückel resonance energy[11] and the kinetic energy of π electrons.

If a given monocyclic molecule has a singly twisted π system (i.e., a Möbius ring system),[36] the sign of K_G in Eq. 2 becomes negative.[17,37] The curve $Y=P_G(X)$ for a Möbius system displaces upward from the curve $Y=R_G(X)$. When a $(4n+2)$-π-electron Möbius system is divided into two segments, a phase dislocation occurs between the frontier MO's of the two segments. For a $(4n)$-π-electron Möbius system, however, it does not occurs. The Hückel rule is thus reversed. Any Möbius system with $4n+2$ π electrons then becomes antiaromatic, and any Möbius system with $4n$ π electrons aromatic.

The Hückel rule and the above explanation of it do not apply to highly charged molecules since electrostatic interactions are far from being balanced. Thus, such species as tetraanions and tetracations of monocyclic π systems may be very unstable even if they have $4n+2$ π electrons. We might say that the Hückel rule is universally applicable as far as intramolecular electrostatic interactions are well-balanced.

If the Hückel rule seems not to be applicable to a given neutral molecule, the validity of its bonding scheme, rather than that of the Hückel rule, should be questioned. For example, phosphole does not behave like an aromatic molecule although it appears to be iso-π-electronic with pyrrole.[4] Cyclophosphazene of any size is neither aromatic nor antiaromatic.[38] Its diamagnetic susceptibility can be estimated additively with respect to constituent atoms and bonds.[39] There must be no cyclic conjugation in these compounds, and the Hückel rule is not applicable.

We are grateful to Professor Haruo Moriguchi (Shizuoka University) for helpful discussions.

References

1) E. Hückel, *Z. Phys.*, **70**, 204 (1931); "Grundzüge der Theorie Ungesättigter und Aromatischer Verbindungen," Verlag Chemie, Berlin (1938).

2) F. Sondheimer, *Acc. Chem. Res.*, **5**, 81 (1972).

3) For recent accounts of aromaticity and aromatic compounds, see: D. Lloyd, "Non-Benzenoid Conjugated Carbocyclic Compounds," Elsevier, Amsterdam (1984); P. J. Garratt, "Aromaticity," Wiley, New York (1986).

4) See, e.g.: M. J. Cook, A. R. Katritzky, and P. Linda, *Adv. Heterocycl. Chem.*, **17**, 255 (1974).

5) M. J. S. Dewar, *J. Am. Chem. Soc.*, **74**, 3345 (1952); "Molecular Orbital Theory of Organic Chemistry," McGraw-Hill, New York (1969), Chap. 5.

6) K. Fukui, A. Imamura, T. Yonezawa, and C. Nagata, *Bull. Chem. Soc. Jpn.*, **33**, 1591 (1960).

7) K. Fukui, *Angew. Chem., Int. Ed. Engl.*, **21**, 801 (1982).

8) J. P. Malrieu, "Localization and Delocalization in Quantum Chemistry," ed by O. Chalvet, R. Daudel, S. Diner, and J. P. Malrieu, Reidel, Dordrecht-Holland (1975), Vol. I, pp. 335—343.

9) R. Breslow and E. Mohacsi, *J. Am. Chem. Soc.*, **85**, 431 (1963); W. D. Hobey, *J. Org. Chem.*, **37**, 1137 (1972).

10) M. J. S. Dewar and G. J. Gleicher, *J. Am. Chem. Soc.*, **87**, 685 (1965); M. J. S. Dewar and C. de Llano, *ibid.*, **91**, 789 (1969); M. J. S. Dewar, A. J. Harget, and N. Trinajstić, *ibid.*, **91**, 6321 (1969); M. J. S. Dewar and N. Trinajstić, *Theor. Chim. Acta*, **17**, 235 (1970).

11) B. A. Hess, Jr. and L. J. Schaad, *J. Am. Chem. Soc.*, **93**, 305 (1971); B. A. Hess, Jr., L. J. Schaad, and C. W. Holyoke, Jr., *Tetrahedron*, **28**, 3657 (1972); **31**, 295 (1975).

12) B. A. Hess, Jr., L. J. Schaad, and M. Nakagawa, *J. Org. Chem.*, **42**, 1669 (1977).

13) J. Aihara, *Bull. Chem. Soc. Jpn.*, **48**, 517,1501 (1975); **49**, 1427 (1976).

14) J. Aihara, *J. Am. Chem. Soc.*, **98**, 2750, 6840 (1976).

15) J. Aihara, *J. Org. Chem.*, **41**, 2488 (1976); *Bull. Chem. Soc. Jpn.*, **53**, 1751 (1980).

16) J. Aihara, *Bull. Chem. Soc. Jpn.*, **51**, 1788 (1978).

17) J. Aihara, *Pure Appl. Chem.*, **54**, 1115 (1982).

18) M. Milun, I. Gutman, and N. Trinajstić, *J. Am. Chem. Soc.*, **99**, 1692 (1977); A. Graovac, I. Gutman, and N. Trinajstić, "Topological Approach to the Chemistry of Conjugated Molecules," Springer, Berlin (1977), Chap. 4.

19) H. Sachs, *Publ. Math. (Debrecen)*, **11**, 119 (1964).

20) A. Graovac, I. Gutman, N. Trinajstić, and T. Živković, *Theor. Chim. Acta*, **26**, 67 (1972); A. Graovac, O. E. Polansky, N. Trinajstić, and N. Tyutyulkov, *Z. Naturforsch., A*, **30**, 1696 (1975); M. J. Rigby, R. B. Mallion, and A. C. Day, *Chem. Phys. Lett.*, **51**, 178 (1977).

21) K. Fukui, T. Yonezawa, and H. Shingu, *J. Chem. Phys.*, **20**, 722 (1952); K. Fukui, T. Yonezawa, C. Nagata, and H. Shingu, *ibid.*, **22**, 1433 (1954).

22) K. Fukui, T. Yonezawa, and C. Nagata, *Bull. Chem. Soc. Jpn.*, **27**, 423 (1954); *J. Chem. Phys.*, **27**, 1247 (1957).

23) K. Fukui, *Bull. Chem. Soc. Jpn.*, **39**, 498 (1966); *Acc. Chem. Res.*, **4**, 57 (1971); "Theory of Orientation and Stereoselection," Springer, Berlin (1970).

24) C. D. Godsil and I. Gutman, *Z. Naturforsch., A*, **34**, 776 (1979); I. Gutman, *Croat. Chem. Acta*, **54**, 75 (1981).

25) R. C. Haddon and T. Fukunaga, *Tetrahedron Lett.*, **21**, 1191 (1980).

26) See, e.g.: E. A. Coddington and N. Levinson, "Theory of Ordinary Differential Equations," McGraw-Hill, New

York (1955), Chap. 8; F. B. Hildebrand, "Advanced Calculus for Applications," Prentice-Hall, Englewood Cliffs, N. J. (1963), Chap. 5.

27) J. Aihara, *J. Am. Chem. Soc.*, **101**, 5913 (1979).

28) H. Hosoya, K. Hosoi, and I. Gutman, *Theor. Chim. Acta*, **38**, 37 (1975).

29) See, e.g.: R. C. Haddon, V. R. Haddon, and L. M. Jackman, *Top. Curr. Chem.*, **16**, 103 (1970/1971); K. Müllen, *Chem. Rev.*, **84**, 603 (1984).

30) J. Aihara, *J. Am. Chem. Soc.*, **101**, 558 (1979).

31) See, e.g.: H. J. Dauben, Jr., J. D. Wilson, and J. L. Laity, *J. Am. Chem. Soc.*, **90**, 811 (1968); **91**, 1991 (1969).

32) R. C. Haddon, *J. Am. Chem. Soc.*, **101**, 1722 (1979).

33) J. Aihara, *Bull. Chem. Soc. Jpn.*, **53**, 1163 (1980).

34) J. Aihara, *J. Am. Chem. Soc.*, **103**, 5704 (1981).

35) H. Ichikawa and Y. Ebisawa, *J. Am. Chem. Soc.*, **107**, 1161 (1985).

36) E. Heilbronner, *Tetrahedron Lett.*, **1964**, 1932.

37) A. Graovac and N. Trinajstić, *J. Mol. Struct.*, **30**, 416 (1976).

38) D. P. Craig and N. L. Paddock, "Nonbenzenoid Aromatics," ed by J. P. Snyder, Academic Press, New York (1971), Vol. II, Chap. 5; S. S. Krishnamurthy, A. C. Sau, and M. Woods, *Adv. Inorg. Chem. Radiochem.*, **21**, 41 (1978).

39) D. P. Craig, M. L. Heffernan, R. Mason, and N. L. Paddock, *J. Chem. Soc.*, **1961**, 1376.

 © 1988 The Chemical Society of Japan Bull. Chem. Soc. Jpn., 61, 229—235 (1988)

Raman Spectral Characteristics of Cobalt(III) Complexes with Quadridentate Ligands

Tatsuya KAWAMOTO,* Jinsai HIDAKA, and Hisahiko EINAGA†
Department of Chemistry, University of Tsukuba, Tsukuba, Ibaraki 305
†Institute of Materials Science, University of Tsukuba, Tsukuba, Ibaraki 305
(Received April 16, 1987)

The Raman spectra of cobalt(III) complexes with quadridentate ligands such as triethylenetetramine (trien), ethylenediamine-*N*,*N*′-diacetate (edda), tris(2-aminoethyl)amine (tren), and *N*-(2-aminoethyl)iminodiacetate (aeida), were measured for the skeletal vibration region of 200—700 cm^{-1} in order to obtain general information on the relation between the spectra and the structures of these complexes. The Raman bands can be classified into four vibration modes; a totally symmetric stretching vibration mode in the 420—670 cm^{-1} region, a stretching vibration mode excluding the totally symmetric one in the 390—450 cm^{-1} region, a metal-ligand skeletal bending deformation mode in the 300—420 cm^{-1} region, and the chelate ring deformation mode in the 240—290 cm^{-1} region. The skeletal vibrations of cis-α and cis-β isomers of the cobalt(III) complexes with linear quadridentate ligands correspond to those of the tris(bidentate)cobalt(III) and the mer isomers of bis(terdentate)cobalt(III) complexes, respectively. In addition, the skeletal vibrations of the cobalt(III) complexes with tripodlike quadridentate ligands also correspond to those of the mer isomers of bis(terdentate)cobalt(III) complexes. The Raman spectra of the present complexes depend primarily on the configuration of the quadridentate ligands and the effect due to the bidentate ligands is of secondary importance.

In the last few years, it has been recognized that Raman spectra in the skeletal vibration region can be applied successfully to the differentiation of geometrical isomers of cobalt(III) complexes.[1] The main interest has been focused on the low frequency region where the Raman bands for the skeletal vibrations appear. However, little systematic investigations had been reported at this time concerning the relation between the Raman spectra and the structural characteristics of the metal complexes.

In the previous papers, we reported the Raman spectral characteristics of the $[Co(gly)_x(ox)_y(en)_z]$-type complexes (gly, glycinate; ox, oxalate; and en, 1,2-ethanediamine),[2] the $[Co(ida)_n(dien)_{2-n}]$-type complexes (ida, iminodiacetate and dien, diethylenetriamine),[3] and the cobalt(III) complexes containing the six-membered chelate ring.[4] The Raman spectra of the $[Co(gly)_x(ox)_y(en)_z]$-type complexes have been treated in terms of the effective symmetry,[2] which was mainly specified by the arrangement of the coordinated atoms around the cobalt(III). It has been found that the striking differences in the Raman spectral characteristics of the mer and fac isomers of the $[Co(ida)_n(dien)_{2-n}]$-type complexes reflect the structural distortion in the isomeric pairs.

In this paper, the Raman spectra in the skeletal vibration region of the cobalt(III) complexes with quadridentate ligands, triethylenetetramine (trien), ethylenediamine-*N*,*N*′-diacetate (edda), tris(2-aminoethyl)amine (tren), and *N*-(2-aminoethyl)iminodiacetate (aeida), are measured and the relation between the stereochemical properties and Raman spectra of these complexes is discussed in relation to the Raman spectral characteristics of the tris(bidentate)- and bis(terdentate)cobalt(III) complexes.

Experimental

Complexes. The following complexes were prepared and characterized according to procedures in the literature *cis*-α-[Co(en)(trien)]I_3,[5] *cis*-β-[Co(en)(trien)]Cl_3,[5,6] *cis*-α-[Co(edda)(en)]ClO_4,[7] *cis*-β-[Co(edda)(en)]ClO_4,[7] *cis*-α-[Co(edda)$(NH_3)_2$]NO_3,[7] *cis*-α-[Co(edda)(gly)],[8] and *cis*-α-Na[Co(edda)(ox)].[9]

[Co(ox)(trien)]Cl. *cis*-α- and *cis*-β-[Co(ox)(trien)]I, which were prepared in the same way as has been reported,[10] were converted to the chloride by passing the solution through a column of Dowex 1-X8 anion-exchange resin in the chloride form. Found for the cis-α isomer: C, 28.27; H, 5.63; N, 16.47%. Calcd for $[Co(ox)(trien)]Cl \cdot 1/2H_2O = CoC_8H_{18}N_4O_4Cl \cdot 1/2H_2O$: C, 28.46; H, 5.67; N, 16.59%. Found for the cis-β isomer: C, 25.98; H, 5.92; N, 15.18%. Calcd for $[Co(ox)(trien)]Cl \cdot 9/4H_2O$: C, 26.03; H, 6.14; N, 15.18%.

[Co(en)(tren)]Cl_3. This complex was prepared by a procedure alternative to that described in the literature.[11] To a solution of $[CoCl_2(tren)]Cl$[12] (3.3 g) in 20 cm^3 of water on a steam bath was added 1,2-ethanediamine (0.6 g). Heating was continued for 30 min. After cooling, [Co(en)(tren)]Cl_3 was isolated by the column chromatographic method using SP-Sephadex C-25 (Na^+ form, 4 cm×20 cm) and a 0.2 mol dm^{-3} aqueous solution of NaCl as an eluent. Found: C, 23.47; H, 7.48; N, 20.50%. Calcd for $[Co(en)(tren)]Cl_3 \cdot 2H_2O = CoC_8H_{26}N_6Cl_3 \cdot 2H_2O$: C, 23.57; H, 7.42; N, 20.62%.

[Co(ox)(tren)]Cl. This complex was prepared by a procedure similar to that used for $[Co(ox)(trien)]^+$. A solution containing $[CoCl_2(tren)]Cl$ (0.5 g) and oxalic acid (0.4 g) in 10 cm^3 of water was warmed on a steam bath for 30 min. After cooling, the resulting red solution was passed through a column of SP-Sephadex C-25 (Na^+ form, 3 cm×40 cm) with a 0.05 mol dm^{-3} aqueous solution of NaCl as an eluent. The red eluate was concentrated and then cooled in an ice bath in order to obtain [Co(ox)(tren)]Cl. Found: C, 27.69; H, 5.88; N, 16.23%. Calcd for $[Co(ox)(tren)]Cl \cdot H_2O = CoC_8H_{18}N_4O_4Cl \cdot H_2O$: C, 27.72; H,

5.82; N, 16.16%. Absorp. max. $10^{-3}\sigma/cm^{-1}$($\log \varepsilon/mol^{-1}$ $dm^3\,cm^{-1}$): 20.12 (2.13) and 28.17 (2.16).

[Co(edda)(tn)]ClO_4. The preparation procedure was identical with that of [Co(edda)(en)]$^{+}$[7] except that 1,3-propanediamine (tn) was used instead of en. The reaction mixture was poured onto a column of Dowex 50W-X8 (200—400 mesh, Na^+ form, 3 cm×60 cm) and the three main red bands were eluted. It was found that the second eluate was *cis*-*α*-[Co(edda)(tn)]$^+$ and the third one was *cis*-*β*-[Co(edda)(tn)]$^+$ from their absorption, ^1H NMR, and ^{13}C NMR spectra. Found for the cis-*α* isomer: C, 26.48; H, 4.87; N, 13.61%. Calcd for [Co(edda)(tn)]ClO_4=$CoC_9H_{20}N_4O_8Cl$: C, 26.58; H, 4.96; N, 13.78%. Found for the cis-*β* isomer: C, 25.43; H, 5.18; N, 13.00%. Calcd for [Co(edda)(tn)]-$ClO_4\cdot H_2O$: C, 25.45; H, 5.22; N, 13.19%. Absorp. max. $10^{-3}\sigma/cm^{-1}$ ($\log \varepsilon/mol^{-1}dm^3cm^{-1}$): the cis-*α* isomer: 18.59 (2.00), 21.69sh (1.73), 27.55 (2.18) and the cis-*β* isomer: 19.92 (2.14), 27.86 (2.23).

***cis*-α-[Co(edda)(β-ala)].** This complex has been prepared by Nakazawa et al.,[13] but the synthesis in the present work was carried out according to the procedure of the complex with the glycinate ligand,[8] except that *β*-alanine was used in place of glycine. Found: C, 32.02; H, 5.24; N, 12.67%. Calcd for [Co(edda)(*β*-ala)]$\cdot 3/4H_2O$=$CoC_9H_{16}N_3O_6\cdot 3/4H_2O$: C, 32.30; H, 5.27; N, 12.56%. Absorp. max. $10^{-3}\sigma/cm^{-1}$ ($\log \varepsilon/mol^{-1}dm^3cm^{-1}$): 17.99sh (1.99), 19.69 (2.05), and 26.74 (2.09).

[Co(aeida)(en)]Cl. Two isomers were separated by an SP-Sephadex C-25 column chromatography using an aqueous solution of NaCl in place of that of $NaClO_4$ as an eluent given in literature.[14] Found for the trans(O) isomer: C, 25.00; H, 6.27; N, 14.70%. Calcd for [Co(aeida)(en)]Cl$\cdot 3H_2O$=$CoC_8H_{18}N_4O_4Cl\cdot 3H_2O$: C, 25.11; H, 6.32; N, 14.64%. Found for the cis(O) isomer: C, 26.27; H, 5.91; N, 15.29%. Calcd for [Co(aeida)(en)]Cl$\cdot 2H_2O$: C, 26.35; H, 6.08; N, 15.36%.

Measurements. The Raman spectra were recorded on a JASCO Laser Raman spectrometer, which was constructed specially with a double monochromator, model CT-25, a He-Ne laser, model NEC GLG-8500, and a data processor, model DP-500, as the main components. The sample solution was excited at 632.8 nm, and the Raman spectra were calibrated with indene. The electronic absorption spectra were recorded with JASCO UVIDEC-1 and -610 spectrophotometers, and the ^1H NMR and ^{13}C NMR spectra were recorded in deuterium oxide on a JEOL JNM-FX-100 NMR spectrometer at the probe temperature. Sodium 2,2-dimethyl-2-silapentane-5-sulfonate (DSS) was used as internal reference.

Results and Discussion

General Aspect. [Co(quadridentate)(bidentate)]-type complexes used in this work for Raman spectral study are depicted in Fig. 1. The Raman spectral data in the skeletal vibration region of the cobalt(III) complexes with quadridentate ligands such as trien, tren, edda, and aeida, are summarized in Table 1, together with those of $[Co(NH_3)_6]^{3+}$,[2] $[Co(en)_3]^{3+}$,[2] *unsym-fac*-$[Co(dien)_2]^{3+}$,[3] and *trans*(O)-$[Co(gly)_2(en)]^{+}$[2] for comparison.

Figure 2 shows the Raman spectrum of *cis*-*α*-

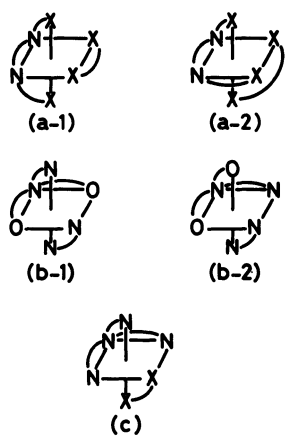

Fig. 1. Structures of [Co(quadridentate)(bidentate)]-type complexes. Cis-*α* (a-1) and cis-*β* (a-2) isomers of the complexes with trien (X=N) and edda (X=O), trans(O) (b-1) and cis(O) (b-2) isomers of [Co(aeida)-(en)]$^+$, and the complexes with tren (c).

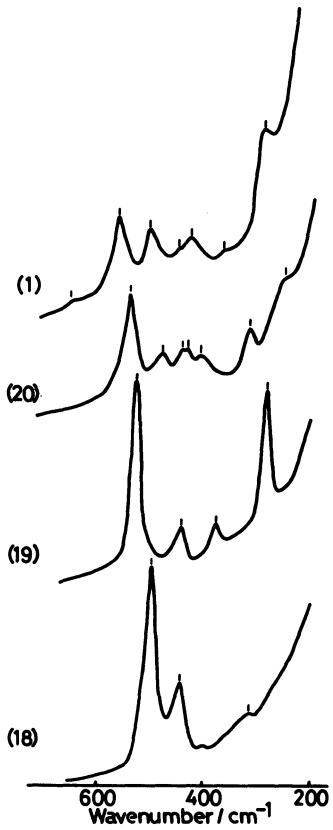

Fig. 2. Raman spectra of *cis*-*α*-[Co(en)(trien)]$^{3+}$, *unsyn-fac*-$[Co(dien)_2]^{3+}$ (Ref. 3), $[Co(en)_3]^{3+}$ (Ref. 2), and $[Co(NH_3)_6]^{3+}$ (Ref. 2). Numbers in parentheses correspond to those in Table 1.

[Co(en)(trien)]$^{3+}$ as a typical example of the cobalt(III) complexes with quadridentate ligand, together with those of *unsym-fac*-$[Co(dien)_2]^{3+}$, $[Co(en)_3]^{3+}$, and $[Co(NH_3)_6]^{3+}$. These complexes all possess an O_h

Table 1. Raman Spectral Data of the Cobalt(III) Complexes with Quadridentate Ligands

No.	Complex	Raman frequency/cm^{-1} [a]			
1	*cis*-α-[Co(en)(trien)]$^{3+}$	646 vw(−) 555 s(p) 498 m(p)	446 w(−) 421 m(dp)	354 vw(−)	282 m(p)
2	*cis*-β-[Co(en)(trien)]$^{3+}$	575 m(p) 531 s(p) 507 s(p) 465 w(−) 433 s(p)		385 vw(−) 349 w(−) 318 vw(−)	
3	*cis*-α-[Co(ox)(trien)]$^{+}$	649 vw(−) 570 s(p) 510 w(p)	429 m(dp)		282 vw(−)
4	*cis*-β-[Co(ox)(trien)]$^{+}$	589 w(p) *539 s(p)* *457 m(p)*	428 m(dp)	370 vw(−) *342 w(−)*	
5	[Co(en)(tren)]$^{3+}$	605 w(p) 531 s(p) 514 m(p)		442 m(p)[d] 419 w(−) 383 w(dp)	265 m(p)
6	[Co(ox)(tren)]$^{+}$	606 w(p) 542 s(p) 475 vw(−)		453 m(p)[d] 418 w(−) 370 w(dp)	242 w(−)
7	*cis*-α-[Co(edda)(en)]$^{+}$	617 m(p) 525 m(p) 461 m(p)	421 vw(dp)	349 w(−)	262 m(−)
8	*cis*-β-[Co(edda)(en)]$^{+}$	660 w(p) 594 vw(−) 530 m(p) 465 m(p)	438 w(−) 405 w(−)	346 vw(dp) 308 vw(−)	
9	*cis*-α-[Co(edda)(tn)]$^{+}$	613 m(p) 521 m(p) 478 sh(−) 448 m(p)	390 vw(−)	350 w(−)	
10	*cis*-β-[Co(edda)(tn)]$^{+}$	655 w(p) 556 vw(−) 530 w(−) 485 s(p) 425 m(p)		313 w(−)	
11	*cis*-α-[Co(edda)(NH_3)$_2$]$^{+}$	620 m(p) 522 m(p) 470 sh(−) 452 m(p)	398 vw(−)	349 m(−)	260 vw(−)
12	*cis*-α-[Co(edda)(gly)]	621 s(p) 537 m(p) 473 w(−)	429 w(−)	385 vw(−) 347 w(−)	265 m(−)
13	*cis*-α-[Co(edda)(β-ala)]	615 m(p) 529 w(p) 452 vw(−)		354 vw(−)	
14	*cis*-α-[Co(edda)(ox)]$^{-}$	618 m(p) 533 w(p)	417 w(−)	373 vw(−)	
15	*cis*-β-[Co(edda)(ox)]$^{-}$	662 vw(−) 570 vw(−)	425 vw(−)		

Table 1. (continued)

No.	Complex	Raman frequency/cm^{-1} [a]			
16	*trans*(O)-[Co(aeida)(en)]$^+$	546 w(p) 494 w(−) 449 vw(−)		400 m(p)[d]	
17	*cis*(O)-[Co(aeida)(en)]$^+$	550 m(p) 505 vw(−) 450 m(p)		409 m(−)[d]	245 vw(−)
18	$[Co(NH_3)_6]^{3+}$ [b]	495 s(p)	440 m(dp)	320 w(dp)	
19	$[Co(en)_3]^{3+}$ [b]	525 s(p)	440 w(dp)	378 w(dp)	283 s(p)
20	*unsym-fac*-$[Co(dien)_2]^{3+}$ [c]	546 s(p)	485 m(dp) 444 m(dp) 434 m(dp)	409 w(p)[d] 321 m(dp)	255 vw(−)
21	*trans*(O)-$[Co(gly)_2(en)]^+$ [b]	596 m(p) 523 m(p)	504 sh(dp) 458 w(dp)	368 w(dp)	275 s(p)
	Assignment[e]	ν_{ts}(Co–L)	ν(Co–L)	δ_{sbd}(L–Co–L)	$\delta_{crd}(Co\lessdot^{L}_{L})$

a) The following abbreviations are used: s, strong; m, medium; w, weak; vw, very weak; sh, shoulder; p, polarized; dp, depolarized. b) Ref. 2. c) Ref. 3. d) These bands correspond to the breathing vibration mode which is characteristic for the bis(terdentate)cobalt(III) complexes. e) ν_{ts} denotes the totally symmetric stretching vibration mode; ν, the stretching vibration mode excluding the totally symmetric one; δ_{sbd}, the metal-ligand skeletal bending deformation mode; δ_{crd}, the chelate ring deformation mode, and L, the donor atom (N and/or O).

symmetry with respect to the coordinated atoms. From their Raman frequencies and intensities, it seems that the Raman bands at 555, 420—500, 354, and 282 cm^{-1} of *cis*-α-$[Co(en)(trien)]^{3+}$ correspond to those at 546, 430—490, 321, and 255 cm^{-1} of *unsym-fac*-$[Co(dien)_2]^{3+}$ and to those at 525, 440, 378, and 283 cm^{-1} of $[Co(en)_3]^{3+}$, respectively. However, the depolarization ratio of the Raman band at 498 cm^{-1} of *cis*-α-$[Co(en)(trien)]^{3+}$ is different from that of the corresponding Raman bands of *unsym-fac*-$[Co(dien)_2]^{3+}$ (485 cm^{-1}), $[Co(en)_3]^{3+}$ (440 cm^{-1}), and $[Co(NH_3)_6]^{3+}$ (440 cm^{-1}) (Table 1, Fig. 2); the band at 498 cm^{-1} of *cis*-α-$[Co(en)(trien)]^{3+}$ is polarized, while the band at 485 cm^{-1} of *unsym-fac*-$[Co(dien)_2]^{3+}$ and the bands at 440 cm^{-1} of $[Co(en)_3]^{3+}$ and $[Co(NH_3)_6]^{3+}$ are depolarized. This spectral feature is unique for the cobalt(III) complexes with quadridentate ligands: The polarized Raman bands at 440—510 cm^{-1} are regarded as characteristic of the cobalt(III) complexes with quadridentate ligands, because they were not observed for bis(terdentate)- and tris(bidentate)cobalt(III) and related complexes.[2,3] On the contrary, the polarized Raman bands around 400 cm^{-1}, characteristic for the cobalt(III) complexes with terdentate ligands, could not be observed for the cobalt(III) complexes with quadridentate ligands.

It is evident from Fig. 2 and Table 1 that the Raman spectral characteristic of *cis*-α-$[Co(en)(trien)]^{3+}$ is similar to that of $[Co(en)_3]^{3+}$ rather than that of *unsym-fac*-$[Co(dien)_2]^{3+}$. Accordingly, the Raman spectrum of *cis*-α-$[Co(en)(trien)]^{3+}$ can be assigned on the basis of the Raman spectrum of $[Co(en)_3]^{3+}$ except for the Raman band at 498 cm^{-1}. This deduction is supported by comparison of *cis*-α-$[Co(edda)(en)]^+$ with *trans*(O)-$[Co(gly)_2(en)]^+$ which have a D_{4h} symmetry with respect to the coordinated atoms; that is, Table 1 shows that the Raman bands at 520—620, 420—470, 349, and 262 cm^{-1} of *cis*-α-$[Co(edda)(en)]^+$ correspond to those at 520—600, 450—510, 368, and 275 cm^{-1} of *trans*(O)-$[Co(gly)_2(en)]^+$, except for the difference in the depolarization ratio between the Raman band at 461 cm^{-1} of the former and that at 504 cm^{-1} of the latter. Furthermore, taking the Raman frequency and the depolarization ratio into account, it is considered that the polarized bands at 498 cm^{-1} of *cis*-α-$[Co(en)(trien)]^{3+}$ and at 461 cm^{-1} of *cis*-α-$[Co(edda)(en)]^+$ can be assigned to the totally symmetric vibration mode.

On the basis of the above discussion and the Raman spectral characteristics summarized in Table 1, it can be concluded that the Raman spectra of the cobalt(III) complexes with quadridentate ligands can be classified into four categories similar to those of tris(bidentate)cobalt(III) complexes;[2] polarized bands in the 420—670 cm^{-1} region, depolarized ones in the 390—450 cm^{-1} region, depolarized ones in the 300—420 cm^{-1} region, and polarized ones in the 240—290 cm^{-1} region. These can be assigned to the totally symmetric stretching vibration mode, the stretching vibration mode excluding the totally symmetric one, the metal-ligand skeletal bending deformation mode, and the chelate ring deformation mode, respectively.

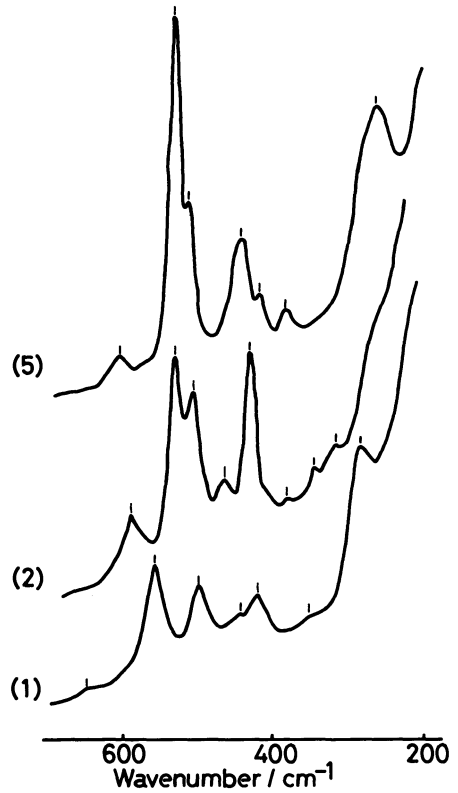

Fig. 3 Raman spectra of *cis*-α- and *cis*-β-[Co(en)(trien)]$^{3+}$ and [Co(en)(tren)]$^{3+}$. Numbers in parentheses correspond to those in Table 1.

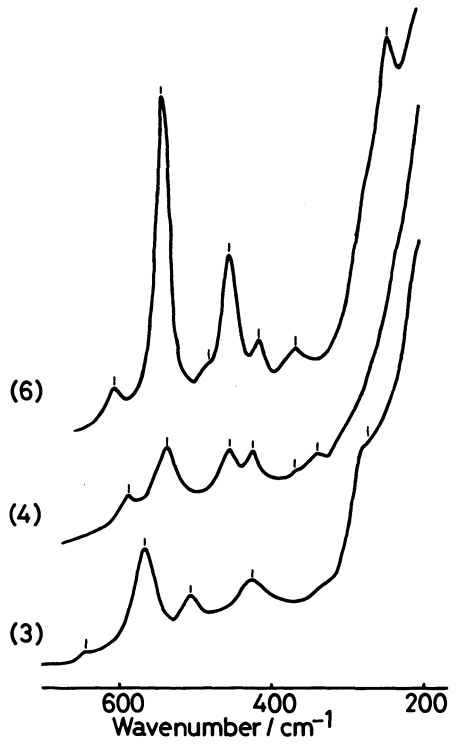

Fig. 4. Raman spectra of *cis*-α- and *cis*-β-[Co(ox)(trien)]$^{+}$ and [Co(ox)(tren)]$^{+}$. Numbers in parentheses correspond to those in Table 1.

Raman Spectra of [Co(trien)(bidentate)]- and [Co(tren)(bidentate)]-type Complexes. It can be seen from Fig. 3 and Table 1 that *cis*-α- and *cis*-β-[Co(en)(trien)]$^{3+}$ show different Raman spectral feature in each skeletal vibration region; the Raman spectrum of *cis*-β-[Co(en)(trien)]$^{3+}$ is similar to that of [Co(en)(tren)]$^{3+}$ rather than that of the cis-α isomer. The significant aspect in structures of *cis*-β-[Co(en)(trien)]$^{3+}$ and [Co(en)(tren)]$^{3+}$ is that the coordinated N-N-N portion of the quadridentate ligands (trien and tren) have equally meridional configuration toward the central metal atom. It is obvious that this meridional configuration greatly influences the normal vibration modes in the skeletal vibration region of the Raman spectra of *cis*-β-[Co(en)(trien)]$^{3+}$ and [Co(en)(tren)]$^{3+}$, because the mer isomers of the bis(terdentate)cobalt(III) complexes have shown the Raman spectral feature quite different from that of the fac isomers.[3] This type of Raman spectral feature can also be observed for the two geometrical isomers of [Co(ox)(trien)]$^{+}$ and [Co(ox)(tren)]$^{+}$; the Raman spectrum of *cis*-β-[Co(ox)(trien)]$^{+}$ can not be correlated to that of cis-α isomer, but, that of [Co(ox)(tren)]$^{+}$ (Fig. 4).

As shown in Figs. 3 and 4, the cobalt(III) complexes with quadridentate ligands, *cis*-β-[Co(en)(trien)]$^{3+}$, *cis*-β-[Co(ox)(trien)]$^{+}$, [Co(en)(tren)]$^{3+}$, and [Co(ox)(tren)]$^{+}$, which have equally meridional configuration with respect to the coordinated N-N-N portion in the quadridentate ligands, exhibit multiple polarized bands in the stretching vibration region, which is characteristic for the mer isomers of bis(terdentate)-cobalt(III) complexes.[3] These findings suggest that their Raman spectra are mainly regulated by the normal vibrational modes of the meridional configuration of the quadridentate ligands. Especially, the polarized Raman bands around 450 cm^{-1} are regarded as characteristic for cis-β isomers of the [Co(trien)-(bidentate)]- and [Co(tren)(bidentate)]-type complexes since the corresponding bands could not be observed in the spectra of the tris(bidentate)cobalt(III) complexes and the fac isomers of the bis(terdentate)-cobalt(III) complexes.

Hence, in the cobalt(III) complexes with trien and tren ligands, so far as skeletal vibrations are concerned, the Raman spectra of the cis-α isomers can be correlated with those of the tris(bidentate)cobalt-(III) complexes, and those of the cis-β isomers and the complexes with the tripodlike quadridentate ligands can be correlated with those of the mer isomers of the bis(terdentate)cobalt(III) complexes, respectively.

Raman Spectra of [Co(edda)(bidentate)]-type and [Co(aeida)(en)]$^{+}$ Complexes. Figure 5 shows the Raman spectra of cis-α and cis-β isomers of [Co(edda)(en)]$^{+}$ and [Co(edda)(tn)]$^{+}$. In view of the Raman spectra of the tris(bidentate)cobalt(III)[2] and

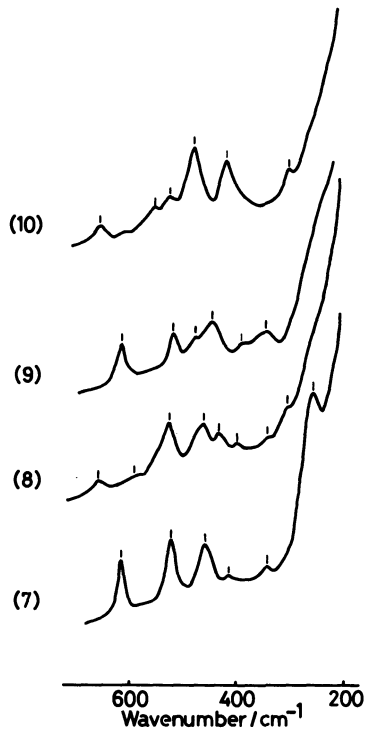

Fig. 5. Raman spectra of cis-α and cis-β isomers of $[Co(edda)(en)]^+$ and of $[Co(edda)(tn)]^+$. Numbers in parentheses correspond to those in Table 1.

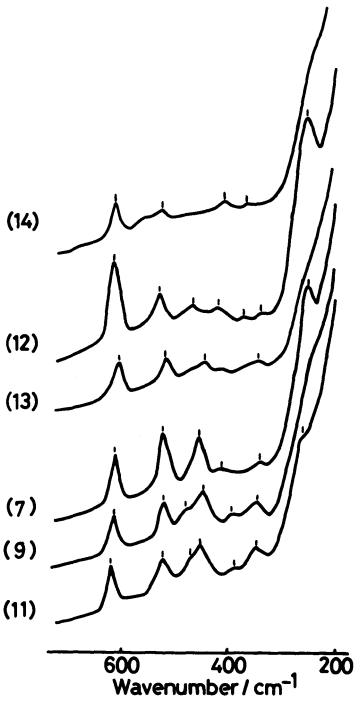

Fig. 6. Raman spectra of cis-α isomers of $[Co(edda)(ox)]^-$, $[Co(edda)(gly)]$, $[Co(edda)(\beta\text{-ala})]$, $[Co(edda)(en)]^+$, $[Co(edda)(tn)]^+$, and $[Co(edda)(NH_3)_2]^+$. Numbers in parentheses correspond to those in Table 1.

bis(terdentate)cobalt(III)[3] complexes, the Raman band at 617 cm^{-1} of the cis-α isomer of $[Co(edda)(en)]^+$ and that at 660 cm^{-1} of the cis-β isomer are closely associated with the coordinated oxygen atom. Furthermore, the shift of these bands is most prominent for the Raman spectra of *cis*-α- and *cis*-β-$[Co(edda)(en)]^+$ and is useful for differentiation between the cis-α and cis-β isomers. A similar feature is also observed for the Raman spectra of the cis-α and cis-β isomeric pairs of $[Co(edda)(tn)]^+$ (Fig. 5) and $[Co(edda)(ox)]^-$ (Table 1).

The Raman spectra of *trans*(O)- and *cis*(O)-$[Co(aeida)(en)]^+$ exhibit unique differences around 400 cm^{-1} from the Raman spectrum of *cis*-β-$[Co(edda)(en)]^+$ with the different chelate ring structure (Table 1). The trans(O) and cis(O) isomers of $[Co(aeida)(en)]^+$ show polarized bands at 400 and 409 cm^{-1}, respectively, but the cis-β isomer of $[Co(edda)(en)]^+$ shows no polarized band in the corresponding region. These polarized bands around 400 cm^{-1} can be assigned to the skeletal breathing mode on the basis of the Raman spectral characteristics of the mer isomers of $[Co(ida)(dien)]^+$, $[Co(mida)(mdien)]^+$, $[Co(ida)(mida)]^-$, and $[Co(mida)_2]^-$,[3] where mida and mdien denote *N*-methyliminodiacetate and *N*,*N*-bis(2-aminoethyl)methylamine, respectively. The skeletal breathing mode of the cobalt(III) complexes with a tripodlike quadridentate ligand, $[Co(en)(tren)]^{3+}$ and $[Co(ox)(tren)]^+$, are also detectable at 442 and 453 cm^{-1} by comparison with the mer isomers of $[Co(dien)_2]^{3+}$, $[Co(ida)(dien)]^+$, and $[Co(mida)(mdien)]^+$.[3]

Role of Bidentate Ligands. It can be seen by comparison of Figs. 3 and 4 that *cis*-α-$[Co(en)(trien)]^{3+}$ and $[Co(en)(tren)]^{3+}$ exhibit Raman spectral characteristics similar to *cis*-α-$[Co(ox)(trien)]^+$ and $[Co(ox)(tren)]^+$, respectively. Furthermore, the Raman spectral behavior of the same geometrical isomers of the cobalt(III) complexes with edda ligand in the higher frequency region resemble each other as shown in Figs. 5 and 6. Accordingly, it is evident that the Raman spectra of the [Co(quadridentate)(bidentate)]-type complexes depend mainly on the configuration of the quadridentate ligands and the role of the bidentate ligands is of minor importance.

References

1) a) K. Kanamori and K. Kawai, *Bull. Chem. Soc. Jpn.*, **53**, 2520 (1980); b) K. Kanamori, T. Morikawa, and K. Kawai, *Bull. Chem. Soc. Jpn.*, **53**, 2787 (1980); c) K. Kanamori and K. Kawai, *Bull. Chem. Soc. Jpn.*, **55**, 764 (1982); d) K. Kanamori, I. Ichinose, and K. Kawai, *Bull. Chem. Soc. Jpn.*, **55**, 1315 (1982); e) K. Kanamori, Y. Nunomura, M. Takashima, K. Nagata, K. Kawai, and J. Hidaka, *Bull. Chem. Soc. Jpn.*, **58**, 92 (1985); f) K. Kanamori, I. Bansho, K. Kawai, K. Akamatsu, and Y. Shimura, *Bull. Chem. Soc. Jpn.*, **58**, 943 (1985); g) K. Kanamori and K. Kawai, *Inorg. Chem.*, **25**, 3711 (1986).

2) T. F. Maruyama, K. Okamoto, J. Hidaka, and H. Einaga, *Bull. Chem. Soc. Jpn.*, **56**, 2610 (1983).
3) T. Kawamoto, T. F. Maruyama, T. Yasui, K. Okamoto, J. Hidaka, and H. Einaga, *Bull. Chem. Soc. Jpn.*, **59**, 2393 (1986).
4) T. Kawamoto, H. Einaga, and J. Hidaka, *Bull. Chem. Soc. Jpn.*, **60**, 919 (1987).
5) D. P. Schaefer and G. R. Brubaker, *Inorg. Chem.*, **8**, 1794 (1969).
6) Y. Yoshikawa, N. Kato, Y. Kimura, S. Utsuno, and G. N. Natu, *Bull. Chem. Soc. Jpn.*, **59**, 2123 (1986).
7) J. I. Legg and D. W. Cooke, *Inorg. Chem.*, **4**, 1576 (1965).
8) J. I. Legg, D. W. Cooke, and B. E. Douglas, *Inorg. Chem.*, **6**, 700 (1967).
9) P. F. Coleman, J. I. Legg, and J. Steele, *Inorg. Chem.*, **9**, 937 (1970).
10) G. R. Brubaker and D. P. Schaefer, *Inorg. Chem.*, **10**, 968 (1971).
11) a) G. A. Bottomley, L. G. Glossop, B. W. Skelton, and A. H. White, *Aust. J. Chem.*, **32**, 285 (1979); b) K. Akamatsu, T. Komorita, and Y. Shimura, *Bull. Chem. Soc. Jpn.*, **54**, 3000 (1981).
12) E. Kimura, S. Young, and J. P. Collman, *Inorg. Chem.*, **9**, 1183 (1970).
13) H. Nakazawa, H. Ohtsuru, and H. Yoneda, *Bull. Chem. Soc. Jpn.*, **60**, 525 (1987).
14) K. Akamatsu, T. Komorita, and Y. Shimura, *Bull. Chem. Soc. Jpn.*, **55**, 2390 (1982).

Azoxy- and Azoferrocenes, and *N*-(Ferrocenylarylmethylene)anilines Formed via Aryliminodimagnesium(IDMg) Procedure. Effect of Ferrocenyl Group on IDMg Reaction and Molecular Structures of Products[1)]

Toshiki TSUTSUMI, Masao ŌKUBO,* Noritake YASUOKA,† and Yukiteru KATSUBE††
Department of Chemistry, Faculty of Science and Engineering, Saga University, Honjō-machi, Saga 840
†Basic Research Laboratory, Himeji Institute of Technology,
2167, Shosha, Himeji 671-22
††Institute for Protein Research, Osaka University,
Suita, Osaka 565
(Received March 13, 1987)

Some unsymmetrical azoxy- and azoferrocenes and *N*-(ferrocenylarylmethylene)anilines were obtained by the reactions of aryliminodimagnesium reagents ($ArN(MgBr)_2$) with nitro- and aroylferrocenes. The types of products were same as those obtained in the similar reactions with nitrobenzenes and benzophenones. The different distribution of products arising from quite mild reactions was understood by the effect of bulky and electron-rich ferrocenyl group which retards the initial coordination and electron transfer processes, in comparison with that of phenyl group. The characteristic molecular structures of the new ferrocene compounds were studied by means of electronic absorption, ^1H NMR, and X-ray crystallography. The results were summarized and discussed.

In the electron transfer initiated fifteen reactions of various magnesium reagents with aromatic nitro and carbonyl compounds, the distribution of normal and abnormal (radical) products was recently correlated with the combination of electron-donating and -accepting abilities (EDA and EAA) of reactants,[2)] which represent the efficiency of electron transfer, and was estimated by the difference (ΔE) between the oxidation and reduction potentials of reactants.

Among the fifteen reactions, the deoxygenative condensation of aryliminodimagnesium reagents

a) $Ar^1NO_2 + ArN(MgBr)_2 \rightarrow Ar^1N(O)=NAr + Ar^1N=NAr + \underline{ArN=NAr}$

b) $Ar^1COAr^2 + ArN(MgBr)_2 \rightarrow Ar^1CAr^2 + Ar^1CHAr^2$
$\quad\quad\quad

2) and benzoylferrocenes (Scheme 3), the types of products are same as those in the reactions 1a and 1b. The product distribution in the reactions 2 and 3 is noticeably different reflecting their much milder natures due to the retarding effect of bulky and electron rich ferrocenyl group in comparison with that of phenyl group: Some modification of the EDA-EAA concept is necessary. The azoxy- and azoferrocenes as well as *N*-(ferrocenylarylmethylene)-anilines are new compounds, and the molecular structures were studied by means of ^{1}H NMR, electronic absorption, and X-ray crystallography. The results will be summarized and discussed.

Results and Discussion

The EDA-EAA concept deals with the efficiency of initial processes essential to the reactions, i.e., the σ-complex formation and the subsequent electron transfer.[2] The product distributions in reactions 2 and 3 will be elucidated partly by the simple concept and additionally by modifying it by the effect of ferrocenyl group on the two processes. The phenyl-IDMg reagents used are *p*-MeO-, *p*-Me-, and *p*-Cl-substituted ones: The normalized oxidation peak potentials measured in THF–Bu_4NClO_4 system are 0.912V, 0.941V, and 1.056V, respectively.[8] The large positive value indicates a weak EDA.

IDMg Reaction with Nitroferrocene. The product distribution in reaction 2 under fixed conditions is given in Table 1 (Runs 1—5); the two previous results of reaction 1a with *p*-MeO-nitrobenzene[3] are listed for comparison (Runs 6 and 7). The unavoidable formation of symmetrical (*sym*-) azoarene (**3**) indicates involvement with electron transfer.[3,9] The reactivity of azoxyarenes in the IDMg deoxygenation, influencing on the relative yields of azoxy and unsymmetrical azo compounds, was also correlated to EDA and EAA.[5]

For discussing the character of reaction 2, some normalized reduction potentials of nitro and azoxy substrates are given below. The large negative value indicates weak EAA. The ΔE value of 2.6—2.8, estimated from the potential of nitroferrocene, corresponds to the borderline of "electron transfer"

(Fc=ferrocenyl)

$FcNO_2$	−1.693V
$FcN(O)=NC_6H_4Cl$-*p*	−1.604V
p-$MeOC_6H_4NO_2$	−1.508V
p-$MeOC_6H_4N(O)=NC_6H_4Cl$-*p*	−1.563V

and "coordination" controlled reactions.[2] The hybrid character may be one of the reasons of the small effect of EDA indicated by slight variation of yields of azoxy- and azoferrocenes (**1** and **2**) and **3** (Runs 1, 2, 4, and 5). The weaker EAA of nitroferrocene than that of *p*-MeO-nitrobenzene, as shown by remarkably different (185 mV) potentials, seems responsible for the noticeably different yields between Runs 2 and 6 using *p*-MeC_6H_4-IDMg. The small EDA effect, including the almost same yields in Runs 5 and 7 using *p*-ClC_6H_4-IDMg, is understood by the nature of **1** which is resistant to deoxygenation as described below.

Even in Runs 1 and 2 using 5.0 mol of IDMg's having stronger EDA's the yield of **1** is still higher than that of **2**: A larger amount of IDMg is needed for effective deoxygenation (Run 3). The sluggish deoxygenation is in accord with weaker EAA of **1** than that of azoxybenzene (vide supra), but is not in accord with noticeably stronger EAA of **1** than that of nitroferrocene. The neighboring bulky ferrocenyl group of **1** will cause steric repulsion against the attack of anionic IDMg nitrogen on the positive azoxy nitrogen.[5] However, as shown in the final section, the planar molecular structure of **1** is the most reliable reason for the sluggish deoxygenation.

IDMg Reaction with Benzoylferrocenes. The yields of *N*-(ferrocenylarylmethylene)anilines (**4**, anils)[4] and amounts of recovered substrates in reaction 3 are summarized in Table 2 (Runs 1—30). Benzoylferrocenes have weaker EAA than that of benzophenone (reduction potential: −1.989V[2]): their potentials were undetermined, because they are over the potential window of THF–Bu_4NClO_4 system.[2] The ΔE value of reaction 3 is larger than 3.1, suggesting the "coordination controlled" character[2,5] accompanying a much milder electron transfer. This is supported by the almost negligible formation of radical products, ferrocenylarylmethanol and *sym*-azoarene. The

Table 1. Product Distribution in IDMg Reaction with Nitroferrocene and *p*-MeO-nitrobenzene

Run No.	*p*-RC_6H_4-IDMg R	$ArNO_2$ Ar	[IDMg]/[Substr]	Yield/%[a] **1** Azoxy	**2** *unsym*-Azo	**3** *sym*-Azo
1	MeO	Fc[b]	5	53	34	12
2	Me	Fc	5	52	18	8
3	Me	Fc	10	20	50	16
4	H	Fc	5	71	9	4
5	Cl	Fc	5	73	15	3
6	Me	*p*-MeO-Ph[c]	6.2	24	52	4
7	Cl	*p*-MeO-Ph	6.2	73	15	5

a) Yields obtained after heating at 55 °C for 3 h. b) Fc=ferrocenyl. c) Cf. Ref. 1).

former, formed via hydrogen abstraction from the solvent by ketyl radical,[3] was detected by ^{1}H NMR (see Experimental). The formation of the latter will be discussed later. The reaction 3 is clean as shown by high combined amounts of anil and the recovery, and it proceeds very slowly (vide infra). By comparing the relative yields of **4** (Table 2), reflecting the reactivity of reactants, some new type substituent effects depending on the molar ratio were disclosed in the field of Grignard and IDMg reactions.

By use of 1.2 mol of IDMg and unsubstituted benzoylferrocene, the conversion was quite low after treating at 55 °C for 2 h (Runs 1, 6, and 11) and at room temperature (8—12 °C) for 16 h (Runs 16, 21, and 26). In contrast to the reaction 1b giving sufficient conversion at 55 °C for 2 h,[4] reaction 3 is notably sluggish and leads to disclosure of an expected but new type substituent effect of reagent. At both the temperatures, the conversion becomes greater as the substituent changes from MeO via Me and H to Cl. Thus the conversion manner indicates the substituent effect on positive charge of the reagent's Mg atom; the strong charge of Cl reagent is favorable for the σ-complex formation. For estimating the acceleration by temperature elevation, the conversion per 1 h at 55 °C was compared with that at room temperature. A rough estimate, 33-, 13-, and 11-folds for accelerations by MeO, Me, and Cl reagents, respectively, indicates the "coordination controlled" character of reaction 2.

By use of 2.4 mol of IDMg, the conversion became fairly high, and the substituent effect of reagent was unobservable. These facts suggest a cooperation of two IDMg molecules;[10] the σ-complex is formed by one and electron-donating addition of the other, in which substituent effect may compensate with each other. Instead, the effect of substrate appears in a novel U-shaped manner shown in Fig. 1 by the typical results of Runs 2—5 using MeO-substituted IDMg. The conversion is higher in the cases of MeO and Cl substrates and is lower in the cases of Me and H substrates. The U-shaped variation is common to almost all the runs using fixed substituent of IDMg at both the temperatures (Runs 7—10, 12—15, 17—20, 22—25, and 26—30). The variation is conceivable if

Table 2. Product Distribution in IDMg Reaction with Benzoylferrocenes

Run No.	*p*-R^{1}C$_6$H$_4$COFc R^1	*p*-R^{2}C$_6$H$_4$-IDMg R^2	[IDMg]/[Substr.]	Reacn. condn.[a]	Yield/% Anil	Recov.	*sym*-Azo
1	H	MeO	1.2	A	4	94	Trace
2	H	MeO	2.4	A	32	61	1
3	MeO	MeO	2.4	A	58	37	0
4	Me	MeO	2.4	A	33	65	0
5	Cl	MeO	2.4	A	62	36	0
6	H	Me	1.2	A	16	85	1
7	H	Me	2.4	A	50	49	Trace
8	MeO	Me	2.4	A	59	39	0
9	Me	Me	2.4	A	36	59	0
10	Cl	Me	2.4	A	58	34	0
11	H	Cl	1.2	A	27	67	Trace
12	H	Cl	2.4	A	44	50	Trace
13	MeO	Cl	2.4	A	57	31	0
14	Me	Cl	2.4	A	33	57	0
15	Cl	Cl	2.4	A	58	39	0
16	H	MeO	1.2	B	1	95	2
17	H	MeO	2.4	B	53	42	3
18	MeO	MeO	2.4	B	59	26	Trace
19	Me	MeO	2.4	B	26	69	5
20	Cl	MeO	2.4	B	60	35	0
21	H	Me	1.2	B	10	90	5
22	H	Me	2.4	B	49	44	7
23	MeO	Me	2.4	B	58	38	3
24	Me	Me	2.4	B	38	54	6
25	Cl	Me	2.4	B	46	46	0
26	H	Cl	1.2	B	20	75	3
27	H	Cl	2.4	B	61	31	Trace
28	MeO	Cl	2.4	B	46	50	3
29	Me	Cl	2.4	B	35	59	Trace
30	Cl	Cl	2.4	B	69	28	2

a) The condition A: at 55 °C for 3 h; B: at room temperature for 16 h.

we assume that the σ-complex formed at the most essential process of reaction 3 is a "loose" one due to steric repulsion by the ferrocenyl group with reference to that expected in reaction 1b. As the substituent changes from MeO via Me and H to Cl, the EAA becomes stronger,[2] while the σ-complex becomes more loose. Thus the high reactivity of the Cl substrate is ascribed to its strong EAA, whereas the reactivity of the MeO substrate is ascribed to formation of a fairly tight σ-complex which assists the substrate in accepting electrons.[7]

The formation of small amount of *sym*-azoarene, observed also for the first time among IDMg reactions of type 1b, becomes appreciable at lower temperatures. The formation, in spite of the much milder electron transfer, is not unexpected according to the mechanism of two electron oxidation of IDMg molecules proposed recently.[9] At lower temperatures favorable for accumulating the "loose" σ-complex, a small part of which tends to dissociate, after electron transfer, into ketyl and arylaminyl radicals due to steric repulsion. The latter radicals produced in proximity to each other undergo disproportionation and dimerization affording *sym*-azoarenes.[9]

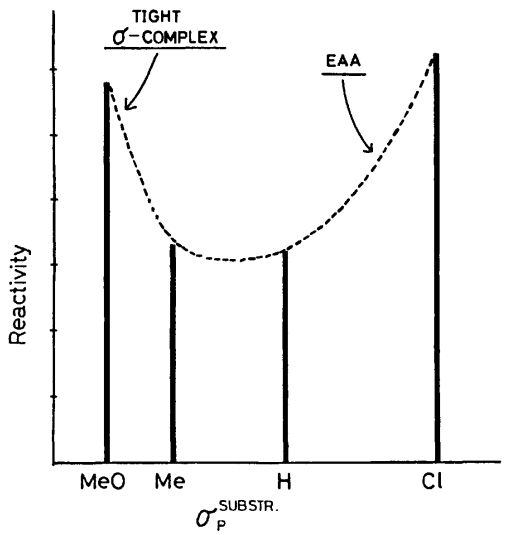

Fig. 1. Schematic diagram for the relative reactivities of *p*-substituted benzoylferrocenes.

Electronic Absorption of Deeply Colored Azoxy- and Azoferrocenes. The azoxy- and azoferrocenes (**1** and **2**) form deep-red crystals. The electronic absorption maxima obtained by measurements in 1,4-dioxane are summarized in Table 3; those of azoxy- and azobenzenes are listed for comparison. The deep color of **1** and **2** is ascribed to the d-d transition[11] as shown below.

The azoxyferrocenes have two absorption maxima: λ^A in the region of 320—350 nm and λ^B in that of 475—495 nm. As shown in Table 3, λ^A shifts toward red depending on the electron-repelling resonance effect of the substituent in the manner similar to that of λ^C of azoxybenzenes; both λ^A and λ^C are assigned to the $\pi\rightarrow\pi^*$ transition. In contrast, λ^B shifts toward blue depending on the inductive effect of the substituent, and is assigned to the d-d transition.

The azoferrocenes have also two absorption maxima: λ^D in the region of 320—340 nm and λ^E in that of 520—540 nm. As shown in the table, λ^D as well as λ^F of azobenzenes shift in the manner similar to λ^A and λ^C, and is assigned to the $\pi\rightarrow\pi^*$ transition. While λ^G of azobenzene in the region of 430—440 nm is assigned to the $n\rightarrow\pi^*$ transition, λ^E shifts in the manner similar to λ^B and is assigned to the d-d transition. The possibility that the λ^E band overlaps with the $n\rightarrow\pi^*$ band can, however, not be excluded.

Molecular Structures of Azoxyferrocene (1), Azoferrocene (2), and *N*-(Ferrocenylarylmethylene)aniline (4). An unexpected chemical shift of cyclopentadienyl protons was disclosed from comparison of azoxy- and azoferrocenes (**1** and **2**, Fig. 2). Usually in *p*-substituted azoxybenzenes, both the two doublets of AB-quartet appear at lower magnetic fields compared to those of the corresponding azobenzenes.[3] In a similar manner, one of the two narrow triplets of cyclopentadienyl protons of **1** appears at a lower field

Table 3. Electronic Absorption Maxima of Azoxy- and Azoferrocenes

Fc-N(O)=N-C$_6$H$_4$-R(*p*)				Fc-N=N-C$_6$H$_4$-R(*p*)			
R	λ^A/nm		λ^B/nm	R	λ^D/nm		λ^E/nm
MeO	347		476	MeO	341		520
Me	329	$\pi\rightarrow\pi^*$	480 d-d	Me	328	$\pi\rightarrow\pi^*$	522 d-d
H	322		483	H	321		528 ($n\rightarrow\pi^*$)
Cl	328		493	Cl	328		539
(*p*)R-C$_6$H$_4$-N(O)=N-C$_6$H$_4$-R(*p*)				(*p*)R-C$_6$H$_4$-N=N-C$_6$H$_4$-R(*p*)			
R	λ^C/nm			R	λ^F/nm		λ^G/nm
MeO	354		—	MeO	356		430
Me	329	$\pi\rightarrow\pi^*$	—	Me	328	$\pi\rightarrow\pi^*$	440 $n\rightarrow\pi^*$
H	323		—	H	320		440
Cl	335		—	Cl	331		440

(δ 5.21—5.27) compared to that of **2** (δ 4.99—5.11, See Table 4). However, the other triplet of **1** appears at a higher field (δ 4.36—4.40) compared to that of **2** (δ 4.48—4.57). In order to understand the reason for this anomaly, the X-ray structure determination of **1** and **2** was carried out. The single crystals of sufficient size were obtained only in a few cases, and *p*-MeO-substituted azoxyferrocene ($\mathbf{1}^{MeO}$, 1-ferrocenyl-*ONN*-4-methoxybenzene) and *p*-Cl-substituted azoferrocene ($\mathbf{2}^{Cl}$, 4-chlorophenylazoferrocene) were submitted to the analyses (Table 4). The structure analysis of an anil ($\mathbf{4}^{MeO}{}_{H}$, *N*-(ferrocenylphenylmethylene)-4-methoxy-

Table 4. Analytical Data of Azoxy- and Azoferrocenes

R	Mp θ_m/°C	Found (Calcd)/% C	H	N	^{1}H NMR data /δ		
Fc-N(O)=N-C_6H_4-R(*p*) (**1**)							
MeO	113—113.5	60.82 (60.73)	4.61 (4.80)	8.37 (8.34)	6.94(2H, d), 4.38(2H, t),	8.18(2H, d), 4.23(5H, s),	5.21(2H, d), 3.85(3H, s).
Me	137.5—138.5	63.92 (63.77)	5.09 (5.04)	8.76 (8.75)	8.05(2H, d), 4.40(2H, t),	7.29(2H, d), 4.24(5H, s),	5.27(2H, d), 2.40(3H, s).
H	98.5—99	62.84 (62.77)	4.57 (4.61)	9.27 (9.15)	8.08(2H, m), 4.36(2H, t),	7.44(3H, m), 4.23(5H, s).	5.26(2H, d),
Cl	120.5—121	56.71 (56.42)	3.86 (3.83)	8.24 (8.23)	8.05(2H, d), 4.38(2H, t),	7.40(2H, d), 4.22(5H, s).	5.21(2H, d),
Fc-N=N-C_6H_4-R(*p*) (**2**)							
MeO	138—138.5	63.86 (63.77)	4.95 (5.04)	8.78 (8.75)	7.76(2H, d), 4.48(2H, t),	6.96(2H, d), 4.19(5H, s),	4.99(2H, d), 3.81(3H, s).
Me	139—140	67.09 (67.12)	5.30 (5.30)	9.25 (9.12)	7.70(2H, d), 4.49(2H, t),	7.25(2H, d), 4.20(5H, s),	5.03(2H, d), 2.36(3H, s).
H	104—104.5	66.58 (66.23)	4.94 (4.86)	9.73 (9.66)	7.82(2H, m), 4.57(2H, t),	7.50(2H, d), 4.23(5H, s).	5.11(2H, d),
Cl	165—165.5	59.24 (59.20)	3.84 (4.04)	8.65 (8.63)	7.72(2H, d), 4.57(2H, t),	7.43(2H, d), 4.23(5H, s).	5.06(2H, d),

Table 5. Analytical Data of Aroylferrocene Anils

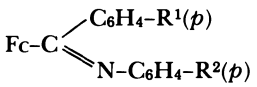

(**4**)

R^1	R^2	Mp θ_m/°C	Found (Calcd)/% C	H	N	^{1}H NMR data /δ
MeO	MeO	173.5—174	70.82 (70.61)	5.50 (5.45)	3.26 (3.29)	7.38—6.30(8H, m), 4.65(2H, d), 4.35(2H, t), 4.21(5H, s), 3.72(3H, s), 3.68(3H, s).
Me	MeO	129.5—130	73.25 (73.37)	5.72 (5.52)	3.32 (3.65)	7.16—7.06(4H, m), 6.70—6.60(4H, m), 4.70(2H, d), 4.43(2H, t), 4.25(5H, s), 3.65(3H, s), 2.32(3H, s).
H	MeO	176—176.5	72.12 (72.09)	5.38 (5.52)	3.77 (3.65)	7.23—7.20(5H, m), 6.60—6.58(4H, m), 4.53(2H, d), 4.38(2H, t), 4.20(5H, s), 3.63(3H, s).
Cl	MeO	152—153	66.28 (66.13)	4.69 (4.83)	3.20 (3.35)	7.23—7.16(4H, m), 6.66—6.56(4H, m), 4.62(2H, d), 4.20(5H, s), 3.72(3H, s).
MeO	Me	139—140	73.21 (73.37)	5.62 (5.67)	3.40 (3.42)	7.35—6.45(8H, m), 4.69(2H, d), 4.39(2H, t), 4.18(5H, s), 3.73(3H, s), 3.23(3H, s).
Me	Me	96—97	76.21 (76.36)	5.75 (5.90)	3.65 (3.56)	7.14—7.05(4H, m), 6.87(2H, d), 6.52(2H, d), 4.65(2H, d), 4.38(2H, t), 4.21(5H, s), 2.28(3H, s), 2.18(3H, s).
H	Me	139—139.5	75.65 (75.23)	5.62 (5.77)	3.63 (3.81)	7.26—7.20(5H, m), 6.89(2H, d), 6.56(2H, d), 4.65(2H, d), 4.40(2H, t), 4.21(5H, t), 2.19(3H, s).
Cl	Me	129—130	68.89 (68.77)	5.17 (5.02)	3.53 (3.44)	7.25—7.20(4H, m), 6.92(2H, d), 6.55(2H, d), 4.65(2H, d), 4.42(2H, t), 4.22(5H, s), 2.23(3H, s).
MeO	Cl	172.5—173	66.08 (66.13)	4.96 (4.83)	3.42 (3.35)	7.35—6.50(8H, m), 4.70(2H, d), 4.44(2H, t), 4.24(5H, s), 3.83(3H, s).
Me	Cl	151.5—152	68.66 (68.77)	5.00 (5.02)	3.55 (3.49)	7.16—6.96(4H, m), 6.60(2H, d), 4.60(2H, d), 4.44(2H, t), 4.21(5H, s), 2.33(3H, s).
H	Cl	148.5—149	68.29 (68.15)	4.78 (4.68)	3.72 (3.61)	7.36—7.24(5H, m), 7.05(2H, d), 6.54(2H, d) 4.64(2H, d), 4.38(2H, t), 4.18(5H, s).
Cl	Cl	140.5—141	62.67 (62.54)	4.00 (4.06)	3.20 (3.32)	7.20—6.95(6H, m), 6.47(2H, d), 4.62(2H, d), 4.42(2H, t), 4.19(5H, s).

aniline, Table 5) was also carried out.

The structure of the three molecules is shown in Fig. 3; the numbering schemes of atoms and the definition of planar groups are given in the figure. The structures are viewed from the direction perpendicular to the plane passing through C(1), N(1), and N(2) atoms in $\mathbf{1}^{MeO}$ and $\mathbf{2}^{Cl}$, whereas C(1), C(41), and N atoms in $\mathbf{4}^{MeO}_{H}$. The dihedral angles between the planar groups are shown in Table 6. Crystal data, selected bond lengths and angles are summarized in Tables 7—9. Tables of atomic coordinates, thermal parameters, and observed and calculated structure factors are kept at the Chemical Society of Japan, Document No. 8767.

A common structural feature of the three molecules is that cyclopentadiene and -dienyl rings in ferrocenyl moiety are in an eclipsed conformation, which was reported previously in the case of ferrocenecarboxylic acid.[12] The presence of oxygen atom attached to diazo group in $\mathbf{1}^{MeO}$ seems to have a little effect on the overall conformation of molecule (vide infra), judging from the tabulated values of molecular dimensions. The effective delocalization of π-electrons of diazo and phenyl groups in $\mathbf{1}^{MeO}$ and $\mathbf{2}^{Cl}$ is shown by the

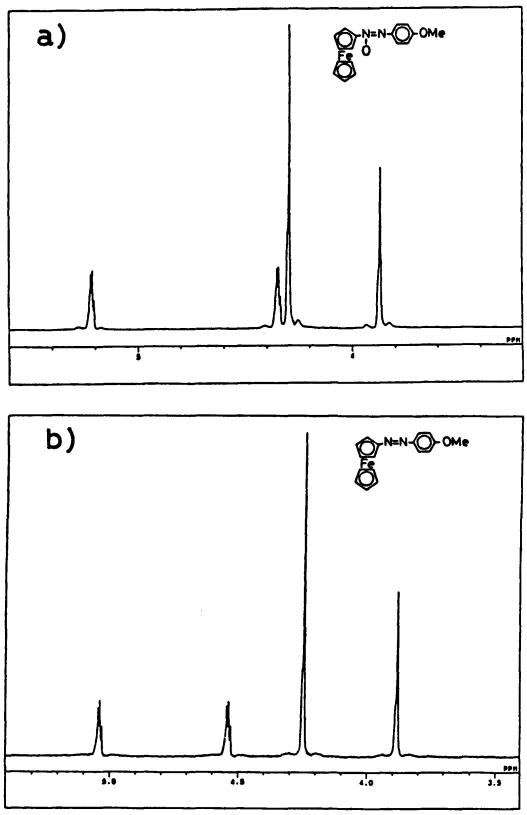

Fig. 2. Cyclopentadienyl proton chemical shift of azoxy- and azoferrocenes.

Table 6. Dihedral Angles between Planes Defined in Each Molecule

	$\mathbf{1}^{MeO}$	$\mathbf{2}^{Cl}$	$\mathbf{4}^{MeO}_{H}$
1-2	1.4	1.1	3.3
1-3	6.1	6.2	1.7
1-4	6.2	3.5	86.5
2-3	6.3	6.5	3.3
2-4	6.4	4.1	88.6
3-4	0.3	9.3	88.0
3-5			85.5
4-5			69.7

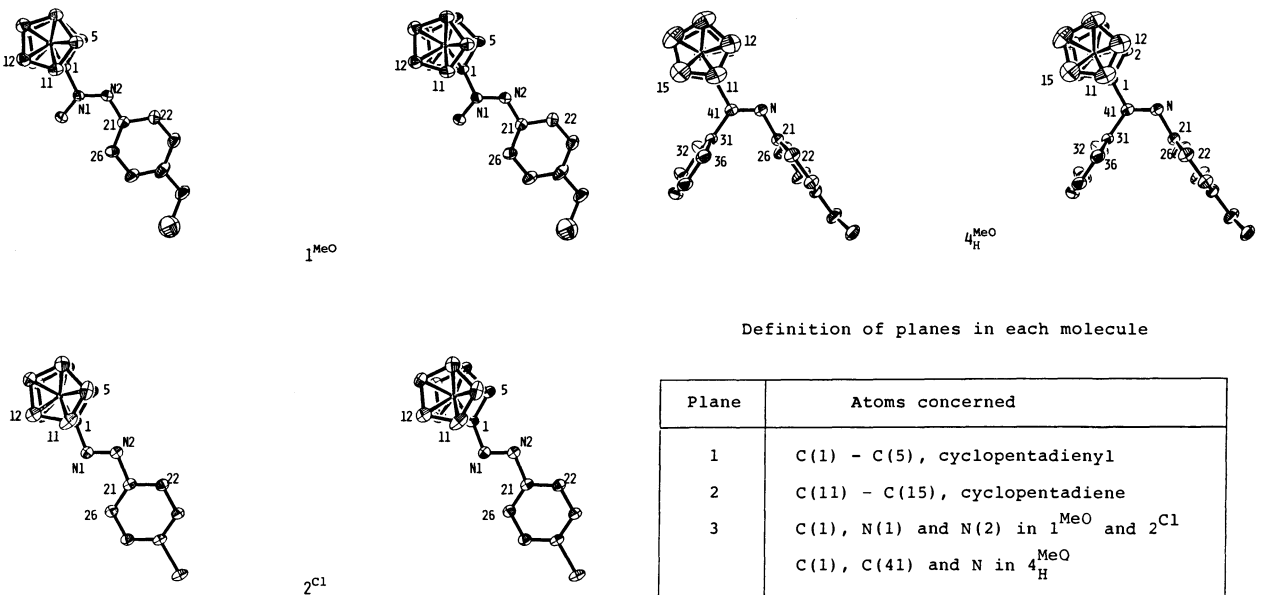

Definition of planes in each molecule

Plane	Atoms concerned
1	C(1) - C(5), cyclopentadienyl
2	C(11) - C(15), cyclopentadiene
3	C(1), N(1) and N(2) in 1^{MeO} and 2^{Cl} C(1), C(41) and N in 4^{MeO}_{H}
4	C(21) - C(26), benzene
5	C(31) - C(36), benzene only in 4^{MeO}_{H}

Fig. 3. Molecular structures of azoxyferrocene, azoferrocene, and benzoylferrocene anil.

tabulated values of bond length.

The structure of 4^{MeO}_{H} is quite different from those of 1^{MeO} and 2^{Cl}, mainly because of the steric repulsion between the two phenyl rings. These rings are perpendicular to C(1), C(41), and N planes. No delocalization of π-electrons is indicated by the

Table 7. Crystal Data and Experimental Conditions

	1^{MeO}	2^{Cl}	4^{MeO}_{H}
Formula	$C_{17}H_{17}FeN_2O_2$	$C_{16}H_{13}ClFeN_2$	$C_{24}H_{21}FeNO$
Mol. wt.	337.2	314.6	395.3
Space group	$P2_1/c$	$P2_1/c$	$P2_1/n$
a/Å	16.952(9)	12.239(3)	8.486(2)
b/Å	7.652(4)	10.681(2)	17.630(4)
c/Å	11.710(4)	11.605(2)	13.347(3)
β/°	98.26(4)	115.41(2)	106.66(2)
Dc/g cm^{-3}	1.49	1.53	1.37
Z	4	4	4
Abs. coeff./cm^{-1} (Mo $K\alpha$)	10.4	14.0	8.2
Crystal size/mm^3	0.5×0.4×0.05	0.3×0.3×0.2	0.3×0.2×0.2
No. of reflections	2476	2922	3145
R	0.078	0.063	0.051

Table 8. Selected Bond Lengths with Estimated Standard Deviations in Parentheses

Bond		1^{MeO}	2^{Cl}	4^{MeO}_{H}
C(1)	- C(2)	1.418(11)	1.443(8)	1.433(6)
C(2)	- C(3)	1.443(12)	1.430(8)	1.426(6)
C(3)	- C(4)	1.451(11)	1.448(8)	1.418(6)
C(4)	- C(5)	1.432(11)	1.442(8)	1.426(6)
C(5)	- C(1)	1.447(11)	1.458(8)	1.428(5)
C(1—5)	- Fe av.	2.049(8)	2.053(6)	2.040(4)
C(11)	- C(12)	1.432(10)	1.439(9)	1.418(9)
C(12)	- C(13)	1.434(11)	1.424(9)	1.431(10)
C(13)	- C(14)	1.440(11)	1.436(9)	1.399(9)
C(14)	- C(15)	1.434(11)	1.433(11)	1.437(9)
C(15)	- C(11)	1.447(10)	1.438(11)	1.424(8)
C(11—15)	- Fe av.	2.053(8)	2.058(6)	2.039(4)
C(1)	- N(1)	1.449(10)	1.428(7)	
C(1)	- C(41)			1.470(5)
N(1)	- O(1)	1.258(8)		
N(1)	- N(2)	1.267(8)	1.247(6)	
C(41)	- N			1.272(5)
C(41)	- C(31)			1.495(5)
N(2)	- C(21)	1.409(9)	1.456(7)	
N	- C(21)			1.436(6)
C(21)	- C(22)	1.410(11)	1.387(8)	1.367(6)
C(22)	- C(23)	1.371(12)	1.397(8)	1.403(6)
C(23)	- C(24)	1.410(14)	1.397(8)	1.360(6)
C(24)	- C(25)	1.399(14)	1.391(8)	1.369(8)
C(25)	- C(26)	1.395(12)	1.411(8)	1.383(9)
C(26)	- C(21)	1.406(11)	1.402(8)	1.365(8)
C(24)	- O(2)	1.377(12)		
C(24)	- O			1.386(6)
C(24)	- Cl		1.744(5)	
O(2)	- Me	1.651(18)		
O	- Me			1.430(7)
C(31)	- C(32)			1.369(7)
C(32)	- C(33)			1.390(9)
C(33)	- C(34)			1.374(9)
C(34)	- C(35)			1.364(9)
C(35)	- C(36)			1.391(8)
C(36)	- C(31)			1.386(6)

Table 9. Selected Bond Angles with Estimated Standard Deviations in Parentheses

Bond angle	1^{MeO}	2^{Cl}	4_H^{MeO}
C(1) -N(1) -N(2)	115.7(6)	111.1(5)	
C(1) -C(41)-N			118.0(4)
C(1) -N(1) -O(1)	116.5(6)		
C(1) -C(41)-C(31)			117.5(4)
N(2) -N(1) -O(1)	127.8(6)		
N -C(41)-C(31)			124.4(4)
N(1) -N(2) -C(21)	121.2(6)	112.4(5)	
C(41)-N -C(21)			120.6(4)

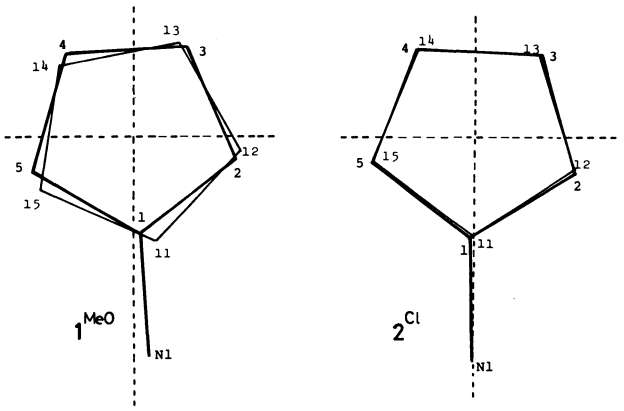

Fig. 4. Projection of plane 2 on plane 1.

C(41)-N bond length of 1.272(5) Å which is comparable to the value of the pure C=N bond.

The projection of diene plane(2) on dienyl plane(1) of 1^{MeO} and 2^{Cl} is shown in Fig. 4. In contrast to almost completely eclipsed conformation of 2^{Cl}, the plane 2 in 1^{MeO} is slightly twisted from the plane 1 seemingly due to steric repulsion with the negative azoxy oxygen caused by planarity. The twist, however, does not provide any clue to elucidation of the abnormal chemical shift of 3- and 4-protons of dienyl ring observed in solution (vide supra), because the singlet signal of the diene protons (δ 4.22—4.24, Fig. 2 and Table 4) indicates the free rotation. The low barrier to internal rotation of diene planes in ferrocene was reported.[13] It is significant that both the pairs of narrow triplets of 1^R and 2^R have almost the same centers at δ 4.73—4.84, and that the splitting by ca. 0.43 ppm from the center of 1^R is notably larger than that by ca. 0.26 ppm of 2^R. The large splitting suggests a participation of polarized resonance structure of the dienyl ring of 1^R caused by positive azoxy nitrogen. The polarization may be the true reason causing the ^1H NMR anomaly (Fig. 2) as well as the twist (Fig. 4).

Data of ^1H NMR summarized in Tables 4 and 5 are similar to each other. Thus it may be concluded that all the products, 1^R, 2^R, and $4^{R^1}{}_{R^2}$, have the molecular structures same as those described above.

General Discussion. The simple EDA-EAA concept, useful for understanding the reactions of magnesium reagents with noncrowded benzene derivatives,[2] seems unsuitable for extending directly to the IDMg reactions with somewhat bulky and electron rich ferrocene derivatives. However, new type substituent effects were disclosed and elucidated, in line with the previous discussion,[2] by modifying the concept based on the effect of ferrocenyl group retarding two initial processes of the reactions.

The elucidation of the results of reactions is compatible with the structure analyses of products. The coplanar structure of 1^R is distinct from twisted ones of azoxybenzenes; an example of the latter having the dihedral angle of ca. 23 degree between the two phenyl rings was reported.[14] The planarity and effective π-electron delocalization of 1^R lead to reduction of the positive charge on azoxy nitrogen making it unfavorable to the attack of anionic IDMg nitrogen (vide supra).[9] Thus the quite sluggish deoxygenation of 1^R in reaction 2 is most plausibly ascribed to its planar structure involving the electron rich ferrocenyl group. The perpendicular twist between ferrocenyl and phenyl planes in $4^{R^1}{}_{R^2}$ reflects the steric repulsion responsible for the sluggishness of reaction 3.

The synthetic aspect of formation of **1**, **2** (reaction 2), and **4** (reaction 3) should be noted, though the optimum conditions for preparing them were undetermined. Azo-substituted ferrocene is so far difficult to access because of the instability of ferrocene ring under diazotization conditions. The symmetrical diferrocenyl diazene is known,[15] and only one phenylazo derivative was prepared in a low yield by treating an equimolar mixture of phenylazo- and unsubstituted cyclopentadienyllithiums with iron(II) chloride.[16] Neither symmetrical nor unsymmetrical azoxyferrocene has been reported. Thus the IDMg procedure will provide a convenient route for preparing unsymmetrical azoxy- and azoferrocenes if the method for preparing nitroferrocene (See Experi-

mental) is improved. Concerning the condensation of diaryl ketones with anilines, a Lewis acid catalyst (e.g., BF_3) gives sufficient yields of anils only when the carbonyl component is a strong electrophile, e.g., fluorenone and its nitro derivatives.[3] In contrast, the IDMg procedure applied to the moderate electrophiles such as benzophenones can be extended to the extremely weak electrophile, i.e., benzoylferrocenes.

Experimental

Materials and Reaction Procedures. Nitroferrocene was obtained in yields lower than 20% by lithiation of ferrocene with BuLi followed by nitration with N_2O_4.[17] Benzoylferrocenes were prepared in good yields by Fridel-Crafts method using appropriate aroyl chlorides.[18] The IDMg reactions were carried out by adding the substrate (1.3 mmol) dissolved in THF (10 ml) to a solution of reagent in THF (35 ml) at 0 °C, and the resulting mixture was stirred at 55 °C or at room temperature (8—12 °C); the reaction times are given in Tables 1 and 2. The products were separated by column chromatography on silica gel (Wako Gel C-200 and C-300). The melting points, the elemental analysis results, and ^1H NMR data are summarized in Tables 4 and 5. The melting points are uncorrected. The trace amount of ferrocenylarylmethanols in reaction 3 was confirmed by ^1H NMR signal of benzylic proton appearing at δ 4.05—4.25.

Crystallographic Analyses. The three dimensional structures of $\mathbf{1}^{MeO}$, $\mathbf{2}^{Cl}$, and $\mathbf{4}^{MeO}{}_H$ were established by X-ray diffraction. The intensity data were collected on an automated single-crystal diffractometer by use of graphite-monochromated Mo $K\alpha$ radiation. The structure was solved by combined use of the direct method with MULTAN 78 and heavy atom method, and then refined by the block-diagonal least-squares procedure. Anisotropic temparature factors are assigned for non-hydrogen atoms except for methyl carbon atom in $\mathbf{1}^{MeO}$. Hydrogen atoms were not considered in structure factor calculation for $\mathbf{1}^{MeO}$ and $\mathbf{2}^{Cl}$, whereas they could be located in the difference map for $\mathbf{4}^{MeO}{}_H$ and were included in the least-squares computations. Absorption correction was not applied; it may limit the accuracy of the present structure analyses. Crystal data and some indices concerning the results of structure determination were listed in Tables 7—9.

The authors wish to thank Dr. Shuji Emori, Saga University, for his helpful discussion on the molecular structures of azoxy- and azoferrocenes. The authors are grateful to the Ministry of Education, Science and Culture for a financial support by a Grant-in-Aid for Scientific Research (No. 60470026).

References

1) Aryliminodimagnesium Reagents. XIII; Part XII: M. Ōkubo, K. Asao, and H. Hyakutake, *Bull. Chem. Soc. Jpn.*, **60**, 3781 (1987).
2) M. Ōkubo, T. Tsutsumi, and K. Matsuo, *Bull. Chem. Soc. Jpn.*, **60**, 2085 (1987).
3) M. Ōkubo, T. Takahashi, and K. Koga, *Bull. Chem. Soc. Jpn.*, **56**, 199 (1983).
4) M. Ōkubo and S. Ueda, *Bull. Chem. Soc. Jpn.*, **53**, 281 (1980); M. Ōkubo, S. Hayashi, M. Matsunaga, and Y. Uematsu, *ibid.*, **54**, 2337 (1981).
5) M. Ōkubo and K. Koga, *Bull. Chem. Soc. Jpn.*, **56**, 203 (1983); M. Ōkubo, C. Sugimori, M. Tokisada, and T. Tsutsumi, *ibid.*, **59**, 1664 (1986).
6) M. Ōkubo, M. Yoshida, K. Horinouchi, H. Nishida, and Y. Fukuyama, *Bull. Chem. Soc. Jpn.*, **56**, 1196 (1983).
7) M. Ōkubo, *Bull. Chem. Soc. Jpn.*, **58**, 3108 (1985).
8) M. Ōkubo, T. Tsutsumi, A. Ichimura, and T. Kitagawa, *Bull. Chem. Soc. Jpn.*, **57**, 2679 (1984).
9) M. Ōkubo, S. Yoshida, and K. Matsuo, *Bull. Chem. Soc. Jpn.*, **60**, 1741 (1987).
10) K. Maruyama and T. Katagiri, *J. Am. Chem. Soc.*, **108**, 6263 (1986); M. Ōkubo, *Bull. Chem. Soc. Jpn.*, **48**, 2057 (1975).
11) D. R. Scott and R. H. Becker, *J. Chem. Phys.*, **35**, 516 (1961).
12) G. J. Palenik, *Inorg. Chem.*, **6**, 2744 (1969).
13) A. Haaland, *Acc. Chem. Res.*, **12**, 415 (1979).
14) W. R. Krigbaum, Y. Chatani, and P. G. Barber, *Acta Crystallogr., Sect. B*, **26**, 97 (1970).
15) A. N. Nesmeyanov, E. G. Perevalova, and T. V. Nikitina, *Tetrahedron Lett.*, **1960**, 1.
16) D. R. Knox, *Proc. Chem. Soc.*, **1959**, 56.
17) D. W. Mayo, P. D. Shaw, and M. Rausch, *Chem. Ind.*, **1957**, 1388.
18) N. Welky and E. S. Gould, *J. Am. Chem. Soc.*, **79**, 2742 (1957).

 © 1988 The Chemical Society of Japan Bull. Chem. Soc. Jpn., 61, 247—253 (1988)

Water-Soluble Acylating Agents: Preparation of 2-Acylthio-1-alkylpyridinium Salts and Acylation of Phenols, Acids, and/or Amines with These Salts in an Aqueous Phase

Tohru SAKAKIBARA,* Yukie WATABE,† Masahide YAMADA,† and (the late) Rokuro SUDOH†
Department of Chemistry, Yokohama City University, Seto, Kanazawa-ku, Yokohama 236
†Department of Chemistry, Faculty of Science, Tokyo Institute of Technology, Ookayama, Meguro-ku, Tokyo 152
(Received June 9, 1987)

Reaction of phenols, amines, and acids with 2-benzoylthio-1-methylpyridinium chloride prepared in situ from benzoyl chloride and 1-methyl-2(1*H*)-pyridinethione, afforded the corresponding benzoyl derivatives in good yields. In the reaction of *p*-nitrophenol, even a catalytic amount of 1-methyl-2(1*H*)-pyridinethione proved to be effective. Similar reactions of *p*-nitrophenol with isobutyryl chloride and acetyl chloride in the presence of 1-methyl-2(1*H*)-pyridinethione afforded *p*-nitrophenyl isobutyrate and *p*-nitrophenyl acetate in 63 and 44% yields, respectively. 2-Benzoylthio-, 2-acetylthio-, and 2-isobutyrylthio-1-ethylpyridinium tetrafluoroborates were prepared by treatment of the corresponding 2-acylthiopyridines with triethyloxonium tetrafluoroborate. These pyridinium salts also acted as acylating agents in an aqueous phase. Some competitive reactions of 2-aminoethanol and phenols with 2-benzoylthio-1-methylpyridinium chloride were also investigated.

Conversion of the reaction medium from a nonaqueous phase into an aqueous phase can be useful, especially for treatment of enzymes or proteins, because they are generally more or less denatured in organic solvents. On the other hand, esters of carbothioic *S*-acids are much more reactive than the corresponding carboxylic acid esters and frequently serve as acylating agents in biological reactions, e.g., acetyl-CoA.[1] As one of the candidates for water-soluble acylating agents, we chose 2-acylthio-1-alkylpyridinium salts;[2] the pyridinium moiety should not only activate the *S*-thioester but also make the compounds water-soluble.[3]

Results and Discussion

Treatment of 1-methyl-2(1*H*)-pyridinethione (**1**) with benzoyl chloride (**2a**) in refluxing acetonitrile for 2 h afforded 2-benzoylthio-1-methylpyridinium chloride (**3a**) as a highly hygroscopic precipitate. Its ^{1}H NMR spectrum showed that the salt **3a** was stable in D_2O, at least for 1 h, suggesting that it might act as a benzoylating agent in an aqueous layer. In fact, addition of sodium *p*-nitrophenoxide (**4**) to an aqueous solution containing a crude **3a** gave *p*-nitrophenyl benzoate (**5a**) in 50% yield. The salt **3a**, however, was in equilibrium with the starting materials (**3a**:**1**=ca. 1:4) in chloroform-*d*.

When **1** and **2a** were mixed in $CDCl_3$–D_2O, it is shown later that the salt **3a** formed in the organic layer is selectively extracted into the aqueous layer. This led to a more convenient 'one-pot' procedure; without isolation of **3a**, direct addition of water-soluble sodium *p*-nitrophenoxide (**4**) to a chloroform–water solution of **1** and **2a** afforded the ester **5a** in 81% yield. Similar treatment of phenol, 2,4-dinitrophenol, and 2-aminoethanol in the presence of an equimolar amount of 1 M NaOH (1 M=1 mol dm^{-3}) gave phenyl benzoate (**6**), 2,4-dinitrophenyl benzoate (**7**), and *N*-(2-hydroxyethyl)benzamide (**8**) in 83, 73, and 67% yields, respectively.

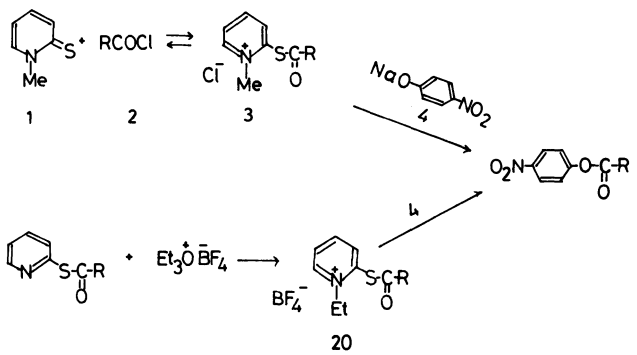

a: R=Ph, b: R=CHMe$_2$, c: R=Me, d: R=OEt

Since 1-methyl-2(1*H*)-pyridinethione (**1**) regenerates after benzoylation, a catalytic amount of **1** might promote the reaction.[4] Benzoylation of **4** was performed, therefore, in changing the amounts of **1**. As shown in Table 1, benzoylation was accelerated with the increase of **1**, but even 0.01 equimolar amount of **1** was found to be effective, giving **5a** in 65% yield.

If a product formed in an aqueous phase is extracted smoothly into an organic phase, a heterogeneous system is applicable for the preparation of such a fairly water-sensitive compound as an acid anhydride. Sodium acetate, therefore, was added to a chloroform–water solution of **1** and **2a**, providing acetic benzoic anhydride **10** in 83% yield as estimated from ^{1}H NMR spectroscopy. Formation of acetanilide (59%) by addition of aniline to the crude product proved that acid anhydride **10** had been generated. Similar reactions of **3a** with several acids in the

Table 1. The Effect of the Amounts of **1** in Benzoylation of **4**

Relative amount of **1** to **2a** and **4**	Reaction time/min	Yield of **5a**[c]/%
0[a]	70	4
0[a]	480	24
0.01[a]	420	65
0.05[a]	70	26
0.1[a]	70	41
0.2[a]	70	69
1[a]	70	81
0[b]	70	7
0.1[b]	20	71
0.1[b]	40	77

a) Compound **2a** (1 mmol) and **4** (1 mmol) were treated in H_2O (5 ml)–$CHCl_3$ (5 ml). b) Compound **2a** (5 mmol) and **4** (5 mmol) were treated in H_2O (5 ml)–$CHCl_3$ (5 ml). c) Isolated yields.

Table 2. Benzoylation of Phenols, Acids, and Amines with **3a**[a]

Substrate	Base[b]	Product(s)	Yield/%
Sodium *p*-nitrophenoxide		**5a**	81
Phenol	NaOH	**6**	82
2,4-Dinitrophenol	NaOH	**7**	73
Sodium Acetate		**10**	83[c] (59)
3-Phenylpropionic acid	$NaHCO_3$	**11**	82[c] (62)
Phenoxyacetic acid	$NaHCO_3$	**12**	79[c] (63)
Isobutyric acid	NaOH	**13**	61[c] (21)
Toluic acid	NaOH	**14**	91[c] (23)
Cinnamic acid	NaOH	**15**	66[c]
2-Aminoethanol	NaOH	**8**	75[d]
p-Aminobenzoic acid	$NaHCO_3$	**17**	79
Glycine	$NaHCO_3$	**18**	19

a) Prepared in situ from **1** and **2a** in $CHCl_3$–H_2O. The reaction mixture was stirred for 1.5 h at room temperature, except for the case of sodium *p*-nitrophenoxide (2 h). b) Equimolar amount of base was used. c) Estimated by ^1H NMR spectroscopy; figures in parentheses showed the yields isolated as the corresponding anilides; besides the anilides, benzanilide was obtained in 6, 18, trace, 26, and 55% yields, respectively, from **10**—**14**. d) Small amounts (5%) of dibenzoyl derivative **9** was isolated.

presence of an equimolar amount of sodium hydrogencarbonate or sodium hydroxide afforded the corresponding mixed acid anhydrides in moderate to good yields (Table 2). Furthermore addition of sodium hydroxide to a chloroform-water solution of **1** and **2a** yielded benzoic anhydride (**16**) in 79% yield. This reaction should involve hydrolysis of **2a**, followed by nucleophilic attack of the benzoic acid thus produced on **3a**. Under the same conditions, but in the absence of **1**, hydrolysis of **2a** occurred predominantly to give benzoic acid together with small amounts of benzoic anhydride and benzoyl chloride.

When **3a** was similarly treated with trifluoroacetic acid, only the hydrolysis was observed. This is reasonable because benzoic trifluoroacetic anhydride was hydrolyzed within 10 min by stirring it in a benzene-water solution.

Reaction of *p*-aminobenzoic acid with **3a** gave the *N*-benzoyl derivative **17** in 75% yield, whereas benzoylation of glycine yielded the *N,O*-dibenzoyl derivative **18** (19%), which was partially converted into *N*-benzoylglycine during column chromatography or recrystallization.

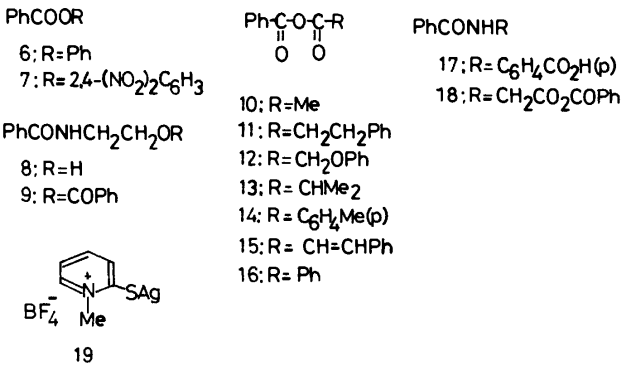

19

An aqueous solution of sodium *p*-nitrophenoxide (**4**) was added to a chloroform–water solution of **1** and isobutyryl chloride, giving the ester **5b** in 63% yield based on isobutyryl chloride. Similar reaction of **4** with acetyl chloride provided the acetate **5c** in 44% yield. Under the same conditions, but in the absence of **1**, the acetate **5c** could not be obtained.

In order to obtain some information about the partition of **3** between chloroform and water as well as the stability of **3**, the following ^1H NMR spectral investigation was performed. (i) In a NMR sample

Table 3. The Ratios of **3** to **1** in Chloroform-*d* and Partition of **3** between Chloroform-*d* and Deuterium Oxide

Acyl(Sulfonyl) chloride	Product	The ratios of **3** to **1**+**3**/% in $CDCl_3$[a]	The estimated amount of **3**/%[b] in $CDCl_3$		in D_2O	
			After 5 min	After 2 h	After 5 min	After 2 h
PhCOCl	**3a**	22 (δ=4.80)[c]	0	0	77	71
$Me_2CHCOCl$	**3b**	16 (δ=4.65)[c]	0	0	49	11[d]
AcCl	**3c**	18 (δ=4.65)[c]	0	0	28	3[d]
EtOCOCl	**3d**	49 (δ=4.88)[c]	4.0	3.4	53	58
p-$MeC_6H_4SO_2Cl$		0	0	0	0	0

a) In the absence of D_2O: Calculated by method (i). b) Calculated by method (ii). c) The chemical shift of the 1-methyl signal of **3**. d) Most acyl chloride was hydrolyzed, since strong signals of the methyl groups of isobutyric acid and acetic acid were observed, respectively.

tube, **1** (0.2 mmol) and acyl chloride (0.2 mmol) were dissolved in $CDCl_3$ (0.2 ml) and the reaction was monitored by ^1H NMR spectroscopy; the ratio of **1** and **3** was calculated on the basis of area-ratios due to the 1-methyl signal of **1** (δ=4.00) and that of **3** (see, Table 3). (ii) After 1 h, D_2O (0.2 ml) was added to the sample tube and the ratios of **1** to **3** in both the layers were determined by comparing the integration of the methyl signals due to **1** and **3** with that of toluene (added as an internal standard). The results are shown in Table 3. The salts **3a**—**c** were formed immediately and equilibrated with the starting material within 10 min, whereas formation of **3b** was slow and even after 1 h, equilibrium was not attained. Under the same conditions, however, *p*-toluenesulfonyl chloride did not afford the corresponding salt. The salts **3a** and **3d** were fairly stable in an aqueous layer, but the salt **3c** was sensitive to water. In accord with expectation, the stability of **3b** stood between **3a** and **3c**.

Treatment of sodium *p*-nitrophenoxide with ethyl chloroformate in the presence of **1** afforded the carbonate **5d** in 32 and 70% yields, respectively, after 1.5 h and 5 h. In the absence of **1**, however, the carbonate **5d** formed in 61% yield after 5 h.

Several attempts to purify **3a** failed, mainly owing to its reversibility in solution. Therefore, the counter ion was changed to a less nucleophilic tetrafluoroborate. After reflux of an acetonitrile solution of **1** and **2a** for 2 h, silver tetrafluoroborate was added to give water-insoluble precipitates. Its IR and/or ^1H NMR spectra indicated the absence of a carbonyl group, but the presence of a *N*-methyl group (δ=4.07, DMSO-d_6) and the characteristic absorption band for tetrafluoroborate (1000—1150 cm^{-1}). The same compound was obtained by treatment of **1** with silver tetrafluoroborate, as judged by IR spectroscopy. From these results the product was tentatively assigned to **19**.

The intending tetrafluoroborate **20a** was prepared by *N*-ethylation of 2-benzoylthiopyridine with triethyloxonium tetrafluoroborate in 85% yield. The salt **20a** is fairly stable at room temperature even in an open vessel and is soluble in chloroform as well as in water. Similar treatment of 2-isobutyrylthiopyridine and 2-acetylthiopyridine afforded the corresponding salts **20b** and **20c** as a syrup, respectively. The latter two salts gradually turned yellow even in a desiccator over phosphorus pentaoxide and they were soluble in water but insufficiently soluble in chloroform. By this route water-soluble acylating agents could be synthesized from carboxylic acid, since 2-acylthiopyridines were prepared by treatment of the corresponding carboxylic acid with 2-pyridinethiol in the presence of di-2-pyridyl sulfide-triphenylphosphine[5] or dicyclohexylcarbodiimide.[6]

Treatment of the phenoxide **4** with the salts **20a**—**c** in water yielded the corresponding esters in 95, 80, and 73% yields, respectively.

Addition of an equimolar amount of 1 M sodium hydroxide and either methanol or benzyl alcohol to a chloroform–water solution of **1** and **2a** gave the corresponding esters in only 2.4 and 10% yields, respectively. These results suggested that it may be possible to achieve selective benzoylation of the phenolic hydroxyl group, if the compounds have both alcoholic and phenolic hydroxyl groups. In fact benzoylation of *p*-hydroxybenzyl alcohol with **3a** afforded *p*-(hydroxymethyl)phenyl benzoate (**21**) (49%) and dibenzoate **22** (3%).[7] Similar reaction of pyridoxol hydrochloride gave 3,α^4-dibenzoate **23** in 36% yield. Since migration of the acyl group from C-3 to C-4 was known to occur,[8] two equimolar amounts of **3a** were used; the yield of **23** was raised to 75%, together with the perbenzoate **24** (7%).

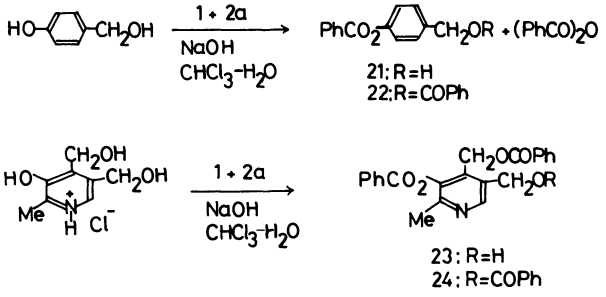

Addition of an equimolar amount of sodium *p*-nitrophenoxide and 2-aminoethanol to **3a** (generated in situ) provided the benzoate **5a** and benzamide **8**

(isolated as the acetate) in 56 and 25% yields, respectively. On the other hand, in the absence of **1** similar heterogeneous or homogeneous reactions with **2a** gave **5a** and **8** in 13 and 73% or 16 and 70% yields, respectively. In similar competitive reactions between 2-aminoethanol and 2,4-dinitrophenol or *p*-ethylphenol, predominant benzoylation of phenolic hydroxyl groups was also observed in the presence of **1**.

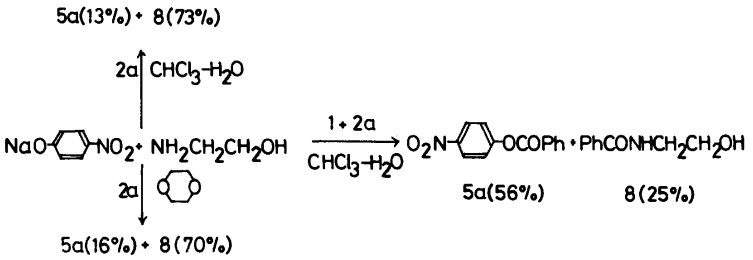

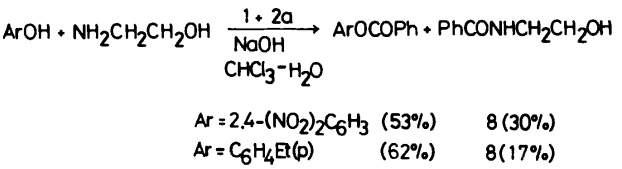

Contrary to the competitive reactions described above, benzoylation of tyramine, having both amino and phenolic hydroxyl groups in the same molecule, with **3a** preponderant gave the *N*-benzoyl derivative **25** (64%) together with the *N,O*-dibenzoyl derivative **26** (13%) and unreacted tyramine (11%, recovery).[9]

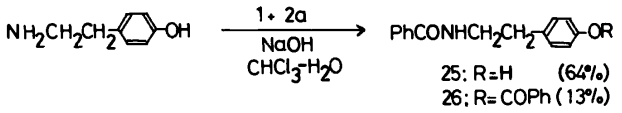

Such a difference may be explained as follows. The amino group might be more reactive than the phenoxide ion towards **3a**. Benzoylation of phenoxide ion, however, should be entropically favorable, since the phenoxide ion could become the counter ion of the pyridinium salt, but 2-aminoethanol could not. But, in the case of tyramine, which should be captured as the counter ion of pyridinium salt, such an entropical predominance seems to be negligible and the more reactive amino group would be preferentially benzoylated.

Experimental

General. All melting points are uncorrected. ^{1}H NMR spectra were recorded with a Varian EM-360A Spectrometer in $CDCl_3$ and D_2O solution with tetramethylsilane and DSS, respectively, as an internal standard. IR Spectra were determined with a Hitachi 285 Infrared Spectrophotometer. Column chromatography was performed on silica gel (Wako, C-300). The organic solutions were dried over magnesium sulfate and distilled under reduced pressure.

2-Benzoylthio-1-methylpyridinium Chloride (3a). A solution of 1-methyl-2(1*H*)-pyridinethione (**1**) (1.81 g, 14.5 mmol) and benzoyl chloride (**2a**) (2.04 g, 14.5 mmol) in acetonitrile (15 ml) was heated under reflux for 2 h and cooled at room temperature. Addition of diethyl ether to the mixture caused hygroscopic precipitates; ^{1}H NMR ($CDCl_3$) δ=4.00 (s, N-Me), 4.80 (s, N^+-Me), 6.70 (d, pyridine ring proton at 6), and 7.10—8.85 (m, ring protons); ^{1}H NMR (D_2O) δ=4.05 (s, N-Me), 4.37 (s, N^+-Me), 7.35—8.80 (m, ring protons), and 9.18 (d, pyridinium ring proton at 6). Attempts to purify the precipitate failed. The ^{1}H NMR spectrum in $CDCl_3$ showed that the salt **3a** attained an equilibrium with the starting material (**3a**:**1**=ca. 1:4).

Benzoylation of Sodium *p*-Nitrophenoxide with 3a. (a) The precipitate of **3a** (61 mg) and sodium *p*-nitrophenoxide (**4**) (37 mg, 0.23 mmol) was dissolved in water (2 ml). After being stirred for 30 min at room temperature, the mixture was extracted with chloroform. The extracts were combined and evaporated. The residue was chromatographed with dichloromethane to afford 28 mg (50%) of *p*-nitrophenyl benzoate (**5a**). (b) To an ice-cooled solution of the pyridinethione **1** (126 mg, 1.01 mmol) and benzoyl chloride (142 mg, 1.01 mmol) in chloroform (5 ml) was added water (5 ml) and the mixture was stirred for 5 min. After addition of **4** (163 mg, 1.01 mmol) at 0 °C, the mixture was stirred for 2 h at room temperature and extracted with chloroform. Similar processing as described above afforded 199 mg (81%) of **5a**.

Benzoylation of Phenol. To a solution of **1** (136 mg, 1.09 mmol) and benzoyl chloride (153 mg, 1.09 mmol) in chloroform (5 ml) was added water (3 ml) and the mixture was stirred for 5 mim and cooled with ice-water. A solution of phenol (103 mg, 1.09 mmol) in water (8 ml) containing 1 M NaOH (1.09 ml) was added over 15 min and the mixture was stirred for an additional 1.5 h at room temperature and then extracted with chloroform. The combined extracts were dried, and evaporated to a syrup, which was chromatographed with dichloromethane, to give 178 mg (82%) of phenyl benzoate (**6**).

Similar treatment of 2,4-dinitrophenol (201 mg, 1.09 mmol) gave 2,4-dinitrophenyl benzoate (**7**) in 73% (229 mg) yield.

Benzoylation of 2-Aminoethanol. Similar treatment of 2-aminoethanol (67 mg, 1.1 mmol) described for the pre-

paration of **6** afforded a syrup, which was chromatographed with chloroform, to give successively 17 mg (7%) of benzoic anhydride, 15 mg (5%) of the *N,O*-dibenzoyl derivative **9**, and 38 mg (21%) of the *N*-benzoyl derivative **8**. The residue obtained by evaporation of the aqueous layer was extracted with chloroform and the extracts were evaporated to give 83 mg of **8** (total yield 67%).

Typical Procedure for the Preparation of Acid Anhydride; Acetic Benzoic Anhydride (10): To an ice-cooled solution of **1** (179 mg, 1.43 mmol) and **2a** (201 mg, 1.43 mmol) in chloroform (10 ml) were added 5 ml of water and the solution was stirred for 5 min. To the mixture was added sodium acetate (117 mg, 1.43 mmol) at 0 °C. After being stirred for 1.5 h at room temperature, the mixture was extracted with chloroform and the combined extracts were dried, and evaporated to a syrup. The yield of acetic benzoic anhydride (83%) was deduced on the basis of signals due to the 1-methyl group of **1** (δ=4.00) and the acetyl group of **10** (δ=2.35). In its spectrum, the acetyl signals of acetic acid (δ=2.09) and acetic anhydride (δ=2.20) were negligible. Purification by column chromatography with benzene provided 61 mg (26%) of **10**, together with 87 mg (50%) of benzoic acid. Sublimation of the anhydride was found to be unsuitable because of the co-sublimation of **1**. To a chloroform solution (2 ml) of the crude product was added aniline (133 mg, 1.43 mmol). The mixture was kept for 3.5 h at room temperature, diluted with chloroform and washed successively with dilute HCl, aq $NaHCO_3$, and water, dried, and evaporated. The syrup was chromatographed with dichloromethane to yield acetanilide (114 mg, 59%) and benzanilide (17 mg, 6%).

Similar treatment of the acid, except for the addition of an equimolar amount of sodium hydrogencarbonate, afforded the corresponding acid anhydride. The estimated yield of benzoic 3-phenylpropionic anhydride (**11**) (based on the ethylene signals at δ=3.00) and benzoic phenoxyacetic anhydride (**12**) (methylene signals at δ=4.91) were 82 and 79%, respectively.

Similar treatment of the acid, except for the use of sodium hydroxide instead of sodium hydrogencarbonate, provided benzoic isobutyric anhydride (**13**) (61%, methyl signals at δ=1.36 and 1.25), benzoic *p*-toluic anhydride (**14**) (91%, methyl signal at δ=2.45), benzoic cinnamic anhydride (**15**) (66%, signals of olefinic proton at δ=6.70 and 6.43).

Benzoic Anhydride (16). To a stirred solution of **1** (1.12 mmol) and **2a** (1.12 mmol) in 10 ml of chloroform was added 4 ml of water at room temperature and the solution was stirred for 5 min. To the solution was added over 5 min 1 M NaOH (1.12 ml) and the mixture was stirred for 1.5 h and extracted with chloroform. The extracts were evaporated and the residue was chromatographed with chloroform, to give 100 mg (79%) of **16**.

Benzoylation of *p*-Aminobenzoic Acid and Glycine. Similar treatment of *p*-aminobenzoic acid (196 mg, 1.43 mmol) described for the preparation of **11** afforded 259 mg (75%) of **17**.

Glycine (107 mg, 1.43 mmol) was similarly benzoylated. After chromatography with dichloromethane, the *N,O*-dibenzoyl derivative **18** was isolated in 77 mg (19%); IR (KBr) 1810, 1655, and 1450 cm^{-1}; ^1H NMR ($CDCl_3$) δ=4.42 (4H, s, $-CH_2-$), 7.35—7.75 and 7.90—8.25 (10H, m, 2×Ph). Purification of **18** failed because of partial hydrolysis to *N*-benzoylglycine during recrystallization from benzene.

Acylation of Sodium *p*-Nitrophenoxide. (a) To an ice-cooled solution of **1** (120 mg, 0.96 mmol) and isobutyryl chloride (102 mg, 0.96 mmol) in chloroform (5 ml) and water (5 ml) was added sodium *p*-nitrophenoxide (**4**) (155 mg, 0.96 mmol). After being stirred for 1 h at room temperature, the mixture was extracted with chloroform. The combined extracts were dried, and evaporated. The residue was chromatographed with chloroform to give 126.4 mg (63%) of **5b**.

(b) Similar treatment of acetyl chloride (75 mg, 0.96 mmol) with **4** (0.96 mmol) afforded 76 mg (44%) of *p*-nitrophenyl acetate (**5c**).

Ethyl *p*-Nitrophenyl Carbonate (5d). Similar treatment of ethyl chloroformate (104 mg, 0.96 mmol) with **4** as described above gave **5d** in 32% yield. When the reaction time was extended to 5 h, the yield was raised to 70%.

Similar treatment in the absence of **1** for 5 h afforded **5d** in 61% yield.

Attempt at Preparation of 20a by Exchange of the Counter Ion. Compound **1** (2.06 mmol) and **2** (2.06 mmol) was stirred for 5 min in chloroform (10 ml)–water (10 ml) and the organic layer was drawn off. To the aqueous layer was added silver tetrafluoroborate (2.06 mmol). After filtration of the precipitates, the filtrate was freeze-drying to give 230 mg of hygroscopic powder; IR (KBr) 1620, 1540, 1490, 1420, 1400, 1260, 1050, 760, and 700 cm^{-1}.

The same product, as judged from IR spectroscopy, was obtained by treatment of **1** with silver tetrafluoroborate.

2-Benzoylthio-1-ethylpyridinium Tetrafluoroborate (20a). A suspension of benzoic acid (3.66 g, 30 mmol) and 2-pyridinethiol (3.33 g, 30 mmol) in dry ethyl acetate (18 ml) was cooled with ice-ethanol (ca. −12 °C). To the solution was added over 10 min a solution of dicyclohexylcarbodiimide (6.18 g, 30 mmol) in dry ethyl acetate (15 ml) with stirring. After being cooled at ambient temperature, the mixture was kept overnight at room temperature . After filtration, the filtrate was evaporated and the residue was purified by bulb to bulb distillation, bp 145 °C (oven temperature)/0.1 Torr (1 Torr=133.322 Pa), to afford 5.03 g (78%) of 2-benzoylthiopyridine. The same compound was also prepared from sodium 2-pyridinethiolate with benzoyl chloride.[10]

To an ice-cooled solution of triethyloxonium tetrafluoroborate (190 mg, 1 mmol) in dichloromethane (1 ml) was added a solution of 2-benzoylthiopyridine (210 mg, 0.98 mmol) in dichloromethane (1.5 ml) with stirring. The mixture was stirred overnight at room temperature and filtered (14 mg of a precipitate was obtained, which had no ethyl group). The filtrate was washed with diethyl ether (decantation). Reprecipitation from acetone–diethyl ether afforded 276 mg (85%) of **20a**, mp 79—80 °C; IR (KBr) 1695, 1600, 1490, and 1060 cm^{-1}; ^1H NMR ($CDCl_3$) δ=1.58 (3H, t, J=7.0 Hz, Et), 4.90 (2H, q, Et), 7.35—8.90 (8H, m, Ph and H-3, H-4, and H-5 of the pyridine ring), and 9.36 (1H, d, J=7.0 Hz, H-6 of the pyridine ring). Found: C, 50.38; H, 4.17; N, 4.22; S, 9.98%. Calcd for $C_{14}H_{14}NOSBF_4$: C, 50.78; H, 4.26; N, 4.23; S, 9.68%.

1-Ethyl-2-isobutyrylthiopyridinium Tetrafluoroborate (20b). Similar treatment of isobutyrylthiopyridine with triethyloxonium tetrafluoroborate as described above afforded a syrup. It was partially purified by repeated decantation with dichloromethane–diethyl ether (ca. 70%), but complete purification was unsuccessful, because it

gradually turned yellow in a desiccator containing phosphorus pentaoxide, IR(KBr) 1740 and 1060 cm^{-1}; ^1H NMR (CD_3COCD_3) δ=1.36 (6H, d, J=7.0 Hz, $CHMe_2$), 1.68 (3H, t, J=7.0 Hz, Et), 3.30 (1H, m, $CHMe_2$), 5.03 (2H, q, Et), 8.30—9.05 (3H, m, ring protons), and 9.51 (1H, q, ring proton).

2-Acetylthio-1-ethylpyridinium Tetrafluoroborate (20c). Similar treatment of 2-acetylthiopyridine with triethyloxonium tetrafluoroborate gave **20c** as a syrup in ca. 88% yield, which also gradually turned yellow and failed to purify, IR (KBr) 1745, 1615, and 1060 cm^{-1}; ^1H NMR (CD_3COCD_3) δ=1.62 (3H, t, J=7.0 Hz, Et), 2.82 (3H, s, COMe), 4.98 (2H, q, Et), 8.22—9.05 (3H, m, ring protons), and 9.47 (1H, q, ring proton).

Acetylation of Sodium *p*-Nitrophenoxide with 2-Acylthio-1-ethylpyridinium Tetrafluoroborate. To a stirred solution of **20a** (166 mg, 0.53 mmol) was added sodium *p*-nitrophenoxide (81 mg, 0.50 mmol). After being stirred for 1 h at room temperature, the mixture was extracted with chloroform and the extracts were evaporated. The syrup was chromatographed with chloroform, to afford the ester **5a** in 95% yield.

Similar treatment of **20b** and **20c** with sodium *p*-nitrophenoxide provided the corresponding esters **5b** and **5c** in 80 and 73% yields, respectively.

Benzoylation of *p*-Hydroxybenzyl Alcohol. To an ice-cooled solution of **1** (2.86 mmol) and **2a** (2.86 mmol) in chloroform (10 ml) was added 10 ml of water and the mixture was stirred for 10 min. To the solution was added over 20 min a solution of *p*-hydroxybenzyl alcohol (355 mg, 2.86 mmol) and 1 M NaOH (2.86 ml) in 10 ml of water. After being stirred for 1.5 h at room temperature, the mixture was extracted with chloroform and the extracts were dried and evaporated. The residue was chromatographed with dichloromethane, to give successively benzoic anhydride (22% based on **2a**), *p*-(hydroxymethyl)phenyl benzoate (**21**) (320 mg, 49%), and *p*-[(benzoyloxy)methyl]phenyl benzoate (**22**) (29 mg, 3% based on the alcohol).

Benzoylation of Pyridoxol. Similar treatment of pyridoxol hydrochloride (588 mg, 2.86 mmol) as described above, but using two equimolar amounts of NaOH, yielded 389 mg (36%) of 3,α^4-dibenzoate (**23**). When two equimolar amounts of **1** and **2a** were used, the yield of **23** was raised to 75%, together with the tribenzoate **24** (7%).

Hydrogen chloride was bubbled into a solution of **23** in methanol-diethyl ether to give white crystals of the salt of **23**, mp 151—152 °C (lit, 152—153 °C).[8] The tribenzoate was recrystallized from ethanol; mp 120—121 °C (lit, 122 °C).[11]

Competitive Benzoylation between 2-Aminoethanol and Sodium Phenoxide. (a) In the Presence of 1. To a solution of **1** (1.96 mmol) and **2a** (1.96 mmol) in chloroform (10 ml) was added over 15 min a solution of sodium *p*-nitrophenoxide (**4**) (1.96 mmol) and 2-aminoethanol (1.96 mmol) in 10 ml of water at room temperature. After being stirred for an additional 1 h, the mixture was extracted with chloroform and the extracts were evaporated to a syrup, which was chromatographed with dichloromethane, to give 267 mg (56%) of **5a**. To the residue obtained by evaporation of the aqueous layer was added acetic anhydride (10 ml) and 0.5 ml of BF_3 etherate and the mixture was stirred overnight. After conventional work up, the residue was chromatographed with chloroform, to provide 101 mg (25%) of 2-(benzamido)ethyl acetate. An analytical sample was prepared by recrystallization from cyclohexane, mp 50—51 °C; IR(KBr) 3350 (NH), 1715 (CO), 1617 and 1513 cm^{-1} (NHCO). Found: C, 63.78; H, 6.36; N, 6.70%. Calcd for $C_{11}H_{13}NO_3$: C, 63.75; H, 6.32; N, 6.76%.

(b) In the Absence of 1. To a solution of **4** (1.96 mmol) and 2-aminoethanol (1.96 mmol) in 10 ml of water was added benzoyl chloride (**2a**) (1.96 mmol) in 10 ml of dichloromethane and the mixture was stirred for 24 h. Processing as described above afforded the ester **5a**, amide **8**, and 2-(benzamido)ethyl acetate in 13, 52, and 21% yields, respectively.

Similar benzoylation in 1,4-dioxane afforded **5a**, **8**, and 2-benzamidoethyl acetate in 16, 40, and 30% yields, respectively.

To a solution of **1** (2.07 mmol) and **2a** (2.07 mmol) in chloroform (20 ml)–water (4 ml) at ca. 5 °C was added an aqueous solution (24 ml) of 2,4-dinitrophenol (2.07 mmol), sodium hydroxide (2.07 mmol), and 2-aminoethanol (2.07 mmol). After being stirred for 1.5 h, the mixture was worked up as described above, to give the ester **7** (53%) and 2-(benzamido)ethyl acetate (30%).

Similar competitive reaction of 2-aminoethanol (2.02 mmol) and *p*-ethylphenol yielded *p*-ethylphenyl benzoate (62%) and 2-benzamidoethyl acetate (17%).

The possibility of benzoyl migration from *p*-nitrophenyl benzoate to 2-aminoethanol was excluded as follows. To a chloroform solution of **5a** (2.23 mmol) was added an aqueous solution (10 ml) of 2-aminoethanol (2.23 mmol) and the solution was stirred for 24 h. The organic layer separated was evaporated to afford the unchanged **5a** in 95% yield.

Benzoylation of Tyramine. To a solution of **1** (0.97 mmol) and **2a** (0.97 mmol) in chloroform (10 ml) was added a solution of tyramine (133 mg, 0.97 mmol) containing 1 M NaOH (0.97 ml) in water (10 ml) at room temperature. After being stirred for 1 h, the mixture was diluted with chloroform. The organic layer was washed with water and evaporated to a syrup, which was chromatographed with chloroform, to give 44 mg (13%, based on tyramine) of the dibenzoate **26** as the first fraction, mp 171—172 °C (lit, 172 °C).[12] The second fraction (150 mg, 64%) was the *N*-benzoyl derivative **25**, which was recrystallized from acetonitrile, mp 163—164 °C (lit, 162 °C).[13]

The aqueous layer was evaporated and the residue (870 mg) was acetylated to give 24 mg (11%) of the *N,O*-diacetyl derivative of tyramine, which was isolated by column chromatography with chloroform. The acetate was recrystallized from benzene, mp 97—98 °C; IR (KBr) 3300 (NH), 1770 and 1760 (CO), and 1643 (NHCO) cm^{-1}. Found: C, 64.86; H, 6.81; N, 6.29%. Calcd for $C_{12}H_{15}NO_3$: C, 65.14; H, 6.83; N, 6.33%.

The present work was partially supported by a Grant-in-Aid for Scientific Research from the Ministry of Education.

References

1) For example, I. S. Kleiner and J. M. Orten, "Biochemistry," 7th ed., ed by C. V. Mosby, Saint Louis (1966), p. 385.

2) For reviews on the onium salts of aza-arenes: T. Mukaiyama, *Angew. Chem., Int. Ed. Engl.*, **18**, 707 (1979).

3) Preparation of **3a** and benzoylation of some acids, amines, and phenols with **3a** had been reported in a preliminary form; M. Yamada, Y. Watabe, T. Sakakibara, and R. Sudoh, *J. Chem. Soc., Chem. Commun.*, **1979**, 179.

4) If the acylation was slow, hydrolysis of acyl chloride should be the major reaction path, since these reactions compete each other.

5) E. J. Corey and K. C. Nicolaou, *J. Am. Chem. Soc.*, **96**, 5614 (1974).

6) K. Lloyd and G. T. Young, *J. Chem. Soc. C*, **1971**, 2890.

7) Since *p*-hydroxybenzyl alcohol was insufficiently soluble in both water and chloroform, the alcohol was partially recovered under the employed conditions.

8) W. Korytryk and B. Paul, *J. Org. Chem.*, **32**, 3791 (1967).

9) When tyramine and *N,O*-dibenzoyltyramine were kept for 1 h in chloroform or for 3 h in acetone or ethanol, no change was observed in TLC, suggesting that intermolecular benzoyl migration was negligible.

10) S. Ueno, S. Asakawa, and E. Imoto, *Nippon Kagaku Zassi*, **89**, 101 (1968).

11) T. Matukawa, *J. Pharm. Jpn.*, **60**, 551 (1940).

12) E. F. Gale, *Biochem. J.*, **34**, 846 (1949).

13) G. Barger, *J. Chem. Soc.*, **95**, 1123 (1909).

The Chiral Recognition of Optically Active Poly(triphenylmethyl methacrylate) Derivatives as Stationary Phases for HPLC[1)]

Yoshio Okamoto,* Eiji Yashima,† Motoshi Ishikura, and Koichi Hatada
Department of Chemistry, Faculty of Engineering Science, Osaka University, Toyonaka, Osaka 560
(Received June 30, 1987)

Four *meta*-halogen- or *meta*-methyl-substituted optically active poly(triphenylmethyl methacrylate) [poly(TrMA)] derivatives with a one-handed helical structure were coated on macroporous silica gel and their chiral-recognition abilities as stationary phases for high-pherformance liquid chromatography were investigated with methanol or hexane–2-propanol (95:5(v/v)) as the eluent. The chiral-recognition abilities of poly(*m*-fluorophenyldiphenylmethyl methacrylate) and poly(*m*-chlorophenyldiphenylmethyl methacrylate) were slightly low compared with that of poly(TrMA) when methanol was used as the eluent. Poly[tris(*m*-chlorophenyl)methyl methacrylate] [poly(*m*-Cl_3TrMA)] showed no resolving ability, although poly[tris(*m*-tolyl)methyl methacrylate] [poly(*m*-Me_3TrMA)] had an effective chiral recognition ability and resolved some racemates more efficiently than poly(TrMA). When hexane–2-propanol (95/5) was used as the eluent, the optical-resolution abilities of all these chiral polymers except for poly(*m*-Cl_3TrMA) were rather similar to that of poly(TrMA) under the same eluent system. The chiral-adsorbing sites are considered to be the chiral triarylmethyl propellers in the methanol system; carbonyl groups may also be involved in the hexane–2-propanol system. The difference in the chiral-recognition abilities of the two tri-substituted chiral polymers were ascribed to their different propeller structures and/or the different conformations of their carbonyl groups. The optical-resolution abilities of poly[TrMA-*co*-(*m*-Cl_3TrMA)] and poly[TrMA-*co*-(*m*-Me_3TrMA)] were also investigated. From the results, the mechanism of the separation of enantiomers on poly(TrMA) was discussed.

Optically active poly(TrMA) is a unique polymer whose chirality is caused only by helicity; it is directly prepared by the asymmetric polymerization of TrMA with chiral anionic initiators, such as (−)-sparteine-butyllithium[2)] and (+)-(2*S*,3*S*)- or (−)-(2*R*,3*R*)-dimethoxy-1,4-bis(dimethylamino)butane (DDB)–lithium amide complexes[3)] in toluene at a low temperature. The polymer, especially when coated on macroporous silica gel,[4)] can resolve many racemic compounds, including hydrocarbons, esters, amides, and alcohols, most of which were first resolved on a poly(TrMA) column.[5)] As eluents, polar solvents like methanol are more effective than nonpolar solvents like hexane, indicating that the nonpolar interaction between the polymer, probably triphenylmethyl groups, and nonpolar groups of enantiomers plays an important role in chiral recognition.[5)] However, when methanol is used as the eluent, the ester groups of poly(TrMA) are slowly solvolyzed to form methyl triphenylmethyl ether.[6)] In order to improve this defect, we prepared (*m*-fluorophenyl)diphenylmethyl methacrylate (*m*-F_1TrMA), (*m*-chlorophenyl)diphenylmethyl methacrylate (*m*-Cl_1TrMA), tris(*m*-chlorophenyl)methyl methacrylate (*m*-Cl_3TrMA), tris(*m*-tolyl)methyl methacrylate (*m*-Me_3TrMA), and tris(*p*-chlorophenyl)methyl methacrylate (*p*-Cl_3TrMA), and then measured the rates of methanolysis by means of ^{1}H NMR spectroscopy.[7)] The methacrylates with electron-withdrawing substituents like halogen were much more stable against methanolysis than those with electron-donating substituents like the methyl group. All the methacrylates except for *p*-Cl_3TrMA gave optically active isotactic one-handed helical polymers with chiral anionic initiators in toluene at −78 °C.[7)] The CD spectra of these chiral polymers were greatly different from each other. We assumed that the difference is attributable to the different propeller structures and/or conformations of ester groups, including carbonyl groups.

In this article, we will investigate the optical-resolution abilities of these chiral polymers and chiral copolymers of TrMA; we will also discuss the mechanism of enantiomer recognition.

Experimental

Materials. Optically active poly(triphenylmethyl methacrylate) derivatives were prepared by the asymmetric polymerization of the corresponding monomer with chiral lithium initiators in toluene at −78 °C;[3,7)] the $[\alpha]_D^{25}$ values of the polymer in tetrahydrofuran (THF) were +343° [poly(TrMA)], +330° [poly(*m*-F_1TrMA)], +356° [poly(*m*-Cl_1TrMA)], −284° [poly(*m*-Cl_3TrMA)], and $[\alpha]_{546}^{25}$ −310° [poly(*m*-Me_3TrMA)]. The fractions which were soluble in THF and insoluble in benzene–hexane (1:1(v/v)) were used for the preparation of the chiral stationary phases.

Poly(TrMA-*co*-*m*-Cl_3TrMA) and poly(TrMA-*co*-*m*-Me_3TrMA) were prepared by asymmetric copolymerization with (+)- or (−)-DDB and *N*,*N*′-diphenylethylenediamine monolithium amide complex in toluene at −78 °C, as previously reported.[7)]

Most racemic compounds were commercially available or were prepared by the usual procedures.

Preparation of Stationary Phase. Macroporous silica gels, (Merck, LiChrospher SI 1000 (diameter, 10 μm; pore size, 100 nm) and SI 4000 (10 μm; 400 nm)), were treated

† Present address: Department of Applied Chemistry, Faculty of Engineering, Kagoshima University, Korimoto, Kagoshima 890.

with a large excess of dichlorodiphenylsilane in toluene at 110 °C for 24 h and with (3-aminopropyl)triethoxysilane in benzene at 80 °C for 24 h respectively. After the reaction, the silica gels were poured into methanol, filtered, and dried. Found for SI 1000: C, 2.93; H, 0.54%. Found for SI 4000: C, 0.23; H, 0.07%.

A chiral polymer (0.75 g) was dissolved in 10 ml of THF and the silanized silica gel (3.0 g) was wetted with the polymer solution (ca. 5 ml) as uniformly as possible. Then, the solvent was evaporated under reduced pressure. This process was repeated with the remaining polymer solution. The stationary phases contained 20—24.5 wt% of polymer on silica gel, judging from the elemental analyses. The packing materials thus obtained were packed in a stainless-steel column (25×0.46 (i.d.) cm) at 300 kg cm^{-2} by means of a slurry method using methanol. The plate number of a column was 3000—4500 for acetone when methanol (0.5 ml min^{-1}) was the eluent at 15 °C. The void volume (V_0) of the column was estimated to be 3.3 ml, with water as a non-retained compound.

Measurements. Chromatographic resolution was accomplished on a JASCO TRIROTAR-II chromatograph equipped with UV (JASCO UVIDEC-100-III) and polarimetric (JASCO DIP-181C) detectors. The optical rotation was followed in a flow cell (5×0.2 (i.d.) cm) at full lamp (mercury) intensity without filters. Resolution was carried out with methanol or a hexane-2-propanol (95:5 (v/v)) mixture at a flow-rate of 0.5 ml min^{-1} at 15 °C, unless otherwise stated.

Results and Discussion

Figure 1 shows the chromatogram of the resolution of *trans*-2,3-diphenyloxirane (**1**) on a poly(*m*-F$_1$TrMA) column. The enantiomers were eluted at the retention volumes, V_1 and V_2. The capacity factors, k_1' and k_2', were determined to be 0.66 and 1.20 respectively by using the following relations:

$$k_1' = \frac{(V_1 - V_0)}{V_0} \qquad k_2' = \frac{(V_2 - V_0)}{V_0}$$

The separation factor, α, and the resolution factor, R_s, were estimated to be 1.82 and 2.51 respectively from these equations:

$$\alpha = \frac{k_2'}{k_1'} \qquad R_s = \frac{2(V_2 - V_1)}{(W_1 + W_2)}$$

Table 1 shows the results of the optical resolution of racemates **1**, *trans*-cyclopropanedicarboxylic acid dianilide (**2**), the Tröger base (**3**), benzoin (**4**), 2,2′-dihydroxy-1,1′-binaphtyl (**5**), 2,2′-(2,2-dimethyl-2-silapropane-1,3-diyl)-1,1′-binaphthalene (**6**),[8] and tris(acetylacetonato)cobalt(III) (Co(acac)$_3$), with methanol as the eluent. All the compounds were almost completely resolved by the use of a (+)-poly(TrMA) column. When a polar solvent like methanol was used as the eluent, the driving force for the separation of the enantiomers on (+)-poly(TrMA) has been considered to be nonpolar interaction between the polymer, probably the chiral propeller of the triphenylmethyl group, and nonpolar groups of

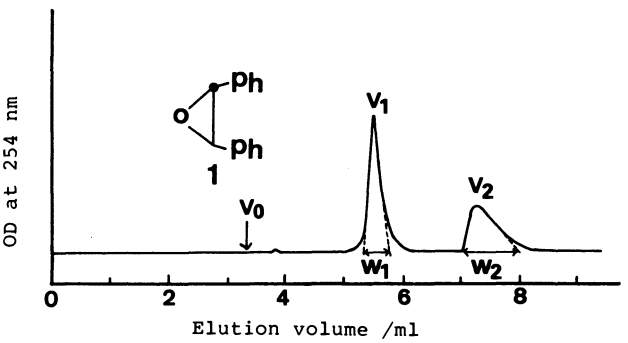

Fig. 1. Chromatographic resolution of *trans*-2,3-diphenyloxirane (**1**) on (+)poly(*m*-F$_1$TrMA) column. (Column: 25 cm×0.46 (i.d.) cm, eluent: methanol (0.5 ml min^{-1}), 15 °C).

Table 1. Resolution of Racemic Compounds on Optically Active Polymers[a]

Racemate	(+)-Poly(TrMA)			(+)-Poly(*m*-F$_1$TrMA)			(+)-Poly(*m*-Cl$_1$TrMA)		
	k_1'(±)	α	R_s	k_1'(±)	α	R_s	k_1'(±)	α	R_s
1	0.82(−)	5.21	5.30	0.66(−)	1.81	2.51	0.48(−)	1.44	0.75
2	0.22(−)	1.24	0.50	0.53	1	0	0.17	1	0
3	0.59(+)	1.75	3.38	0.61(+)	1.51	1.71	0.72(+)	1.43	1.19
4	0.39(−)	1.34	1.30	0.27(−)	1	0	0.20	1	0
5	0.50(+)	2.37	3.83	0.47(+)	1.63	1.65	0.47(+)	1.60	1.23
6	2.47(−)	1.78	2.46	2.15(−)	1.26	1.14	2.24(−)	1.23	0.59
Co(acac)$_3$	0.46(+)	1.32	0.88	0.52(+)	1.09	0.26	0.72(+)	>1	0
	(−)-Poly(*m*-Cl$_3$TrMA)			(−)-Poly(*m*-Me$_3$TrMA)					
	k_1'(±)	α	R_s	k_1'(±)	α	R_s			
1	0.44(+)	>1	0	0.59(+)	1.76	1.47			
2	0.10	1	0	0.11	1	0			
3	0.60	1	0	0.54(−)	1.14				
4	0.14	1	0	0.14	1	0			
5	0.31	1	0	0.23	1	0			
6	2.27	1	0	1.40(+)	1.49	2.07			
Co(acac)$_3$	0.57	1	0	0.24	1	0			

a) Operating conditions: column, 25×0.46 (i.d.)cm; eluent, methanol; flow rate, 0.50 ml min^{-1}; temperature, 15 °C.

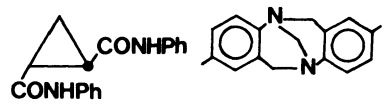

2 3

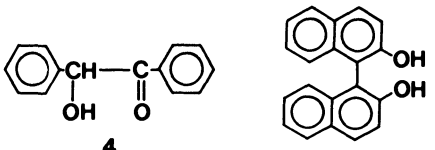

4 5

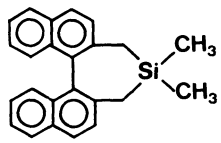

6

enantiomers.[5] The capacity factors (k_1') and the chiral-recognition abilities (α) decrease with an increase in the size and number of halogen substituents of the stationary phases. Poly(*m*-Cl_3TrMA) having a specific rotation as high as those of other chiral polymers, could not resolve any racemic compounds. However, poly(*m*-Me_3TrMA) showed a complete separation for Compounds **1** and **6** and a partial separation of **3**. Moreover, poly(*m*-Me_3TrMA) resolved 1,2,2,2-tetraphenylethanol (**7**, α=1.16) and methyl 2-(1-carbazolyl)propionate (**8**, α=1.45) more effectively than poly(TrMA) by using a mobile phase of methanol-H_2O=85/15 (v/v). These results indicate that the effects of the halogen and methyl substituents are greatly different from each other; this will be discussed later.

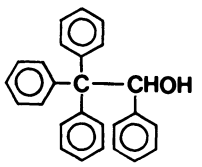

7

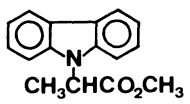

8

In the resolution of **1**, all the (+)-polymers adsorbed the (+)-isomer more strongly than the (−)-isomer, while the two negative polymers adsorbed the (−)-isomer more strongly. Similar results were also obtained for the other compounds, indicating that the sign of the optical rotation of polymers reflects the helicity of the polymer chains.

In Table 2 are collected the results of the resolution of racemates **1**, **3**, **4**, and Co(acac)$_3$ on the chiral polymers, using hexane-2-propanol (95:5 (v/v)) as the eluent at 15 °C. Poly(TrMA) resolved all the racemates with a slightly low separation factor in comparison to that with the methanol eluent. The chiral-recognition abilities of the other polymers did not always decrease in hexane-2-propanol, and **3**, **4**, and Co(acac)$_3$ were more effectively resolved on the poly(*m*-F_1TrMA) and poly(*m*-Cl_1TrMA) columns than on the poly(TrMA) column. In this non-polar system, the ester group (COO) and the triarylmethyl group may both more effectively participate in chiral discrimination. This might bring about the similar optical resolving powers of poly(TrMA), poly(*m*-F_1TrMA), poly(*m*-Cl_1TrMA), and poly(*m*-Me_3TrMA). The extremely low chiral-recognition ability of poly(*m*-Cl_3TrMA) in both the eluent systems may be attributed to a different structure of the triarylmethyl group.

Previously, we proposed that the triphenylmethyl groups on the optically active poly(TrMA) may take either left- or right-handed propeller structures, accompanied by the formation of a one-handed helical polymer chain.[9] (+)-Poly(TrMA) has been considered to possess a right-handed helix on polymer chains and a left-handed propeller on the triphenylmethyl group, based on the results of the optical resolution of various racemic compounds.[5,9] Such a chiral propeller structure of the triphenylmethyl group has been demonstrated by Empirical Force Field Calculations,[10,11] while perchlorotriphenylamine has been

Table 2. Resolution of Racemic Compounds on Optically Active Polymers with Hexane-2-Propanol (95/5)[a]

Racemate	(+)-Poly(TrMA)			(+)-Poly(*m*-F_1TrMA)			(+)-Poly(*m*-Cl_1TrMA)		
	$k_1'(\pm)$	α	R_s	$k_1'(\pm)$	α	R_s	$k_1'(\pm)$	α	R_s
1	0.76(−)	1.54	1.96	0.82(−)	1	0	0.54(−)	1.38	1.19
3	0.66	1.44	1.30	0.57(+)	1.50	1.57	0.61(+)	1.43	0.84
4	1.88	1.13	0.59	1.33(−)	1.17	1.11	1.41	1.32	1.22
Co(acac)$_3$	2.21(+)	1.26	1.25	3.51(+)	1.19	1.00	4.40(+)	1.34	0.99
	(+)-Poly(*m*-Cl_3TrMA)			(−)-Poly(*m*-Me_3TrMA)					
	$k_1'(\pm)$	α	R_s	$k_1'(\pm)$	α	R_s			
1	0.31(+)	1	0	0.18(+)	1.25	0.15			
3	0.38	1	0	1.15(−)	1.32	0.96			
4	0.95	1	0	0.68(+)	1.16	0.56			
Co(acac)$_3$	3.58	>1	0	1.18	>1	0			

a) Operating conditions: see Table 1.

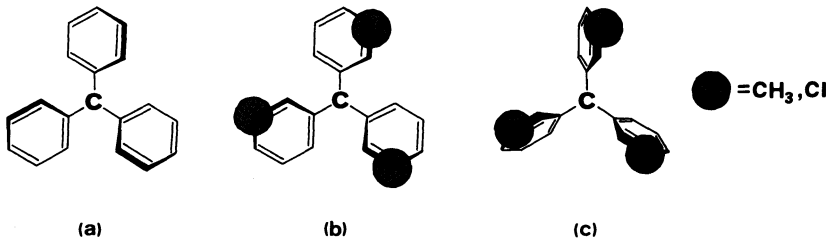

Fig. 2. Possible propeller structures of triphenylmethyl group (a), tris(*m*-tolyl)methyl group (b), and tris(*m*-chlorophenyl)methyl group (c).

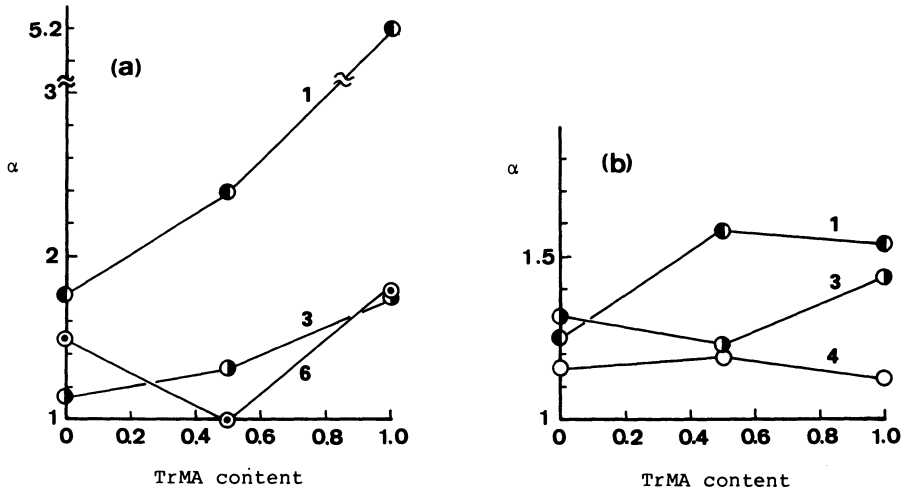

Fig. 3. Influence of TrMA content on separation factor (α) of poly(TrMA-*co*-*m*-Me$_3$TrMA). Eluent: (a), methanol; (b), hexane–2-propanol (95/5).

proved to take a stable propeller structure by its optical resolution.[12]

Figure 2 shows the possible left-handed propeller structures of the triphenylmethyl group and its derivatives. Three phenyl rings are likely to be twisted at some intermediate angle to each other for steric hindrance (Fig. 2(a)); the dihedral angle formed by the planes of the phenyl rings was calculated to be 35.7° for the most stable structure of triphenylmethane.[10] These chiral propeller faces must play the most important role in recognizing enantiomers, at least when methanol is used as the eluent. The three *m*-tolyl rings may also be twisted (Fig. 2(b)), because poly(*m*-Me$_3$TrMA) showed an effective chiral-recognition ability, similar to that of poly(TrMA) to some enantiomers. On the other hand, three *m*-chlorophenyl rings seem to be more upright, as is illustrated in Fig. 2(c). Therefore, enantiomers can not interact with chiral propeller faces and will be less retained in the stationary phase. This must lead to a poor separation of the enantiomers, regardless of the eluents.

The chiral recognition of the poly(triarylmethylmethacrylate)s must be governed not only by a single triarylmethyl propeller but also by adjacent propellers. In order to investigate this, copolymers of TrMA and *m*-Cl$_3$TrMA or *m*-Me$_3$TrMA were prepared[7] and used as chiral stationary phases in the same manner as homopolymers. All the copolymers in our experiments showed almost the same optical rotation, regardless of the molar ratios, as has previously been reported.[7] Figure 3 shows the relationships between the TrMA content in poly(TrMA-*co*-*m*-Me$_3$TrMA) and the separation factors (α) for the three racemates **1**, **3**, and **4**. When methanol was used as the eluent (Fig. 3(a)), the α values for **1** and **3** were nearly equal to the average values of those on the two homopolymers. These compounds may be recognized on a single propeller unit. The copolymer could not resolve Compound **6**, although both the homopolymers resolved it well, indicating that continuous, same monomer units in polymer chains are necessary for the separation of **6**. On the other hand, **1** and **4** were better resolved on the copolymer than on either of the homopolymers in the hexane–2-propanol system (Fig. 3(b)). Those compounds seem to be recognized more effectively on chiral sites lying between TrMA and *m*-Me$_3$TrMA units.

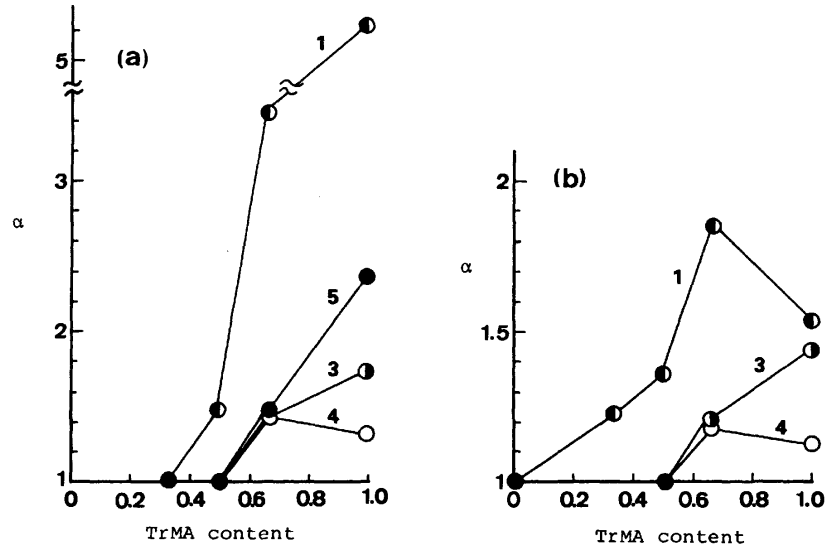

Fig. 4. Influence of TrMA content on separation factor (α) of poly(TrMA-*co*-*m*-Cl_3TrMA). Eluent: (a), methanol; (b), hexane–2-propanol (95/5).

Figure 4 shows the relationships between the TrMA content in poly(TrMA-*co*-*m*-Cl_3TrMA) and the α values for the four racemates **1**, **3**, **4**, and **5**. In both eluent systems, all of the racemates except **1** were not resolved on the copolymers containing less than 50% TrMA units; the resolution of **1** could be attained on the copolymers containing 50 and 33% TrMA units. These results suggest that two or more continuous TrMA units are necessary for the resolution of **3**, **4**, and **5**, while **1** can be resolved by only one TrMA unit in the copolymer.

The authors are grateful to Professor Ryoji Noyori of Nagoya University and Professor C. G. Overberger of the University of Michigan for providing the two racemic compounds **6** and **8** respectively. This work was partially supported by a Grant-in-Aid for Scientific Research on Priority Area, Advanced Molecular Conversion, from the Ministry of Education, Science and Culture.

References

1) Chromatographic Resolution XVIII. Part XVII: Y. Okamoto, R. Aburatani, T. Fukumoto, and K. Hatada, *Chem. Lett.*, **1987**, 1857.

2) Y. Okamoto, K. Suzuki, K. Ohta, K. Hatada, and H. Yuki, *J. Am. Chem. Soc.*, **101**, 4763 (1979).

3) Y. Okamoto, H. Shohi, and H. Yuki, *J. Polym. Sci., Polym. Lett. Ed.*, **21**, 601 (1983).

4) Y. Okamoto, S. Honda, I. Okamoto, H. Yuki, S. Murata, R. Noyori, and H. Takaya, *J. Am. Chem. Soc.*, **103**, 6971 (1981).

5) Y. Okamoto and K. Hatada, *J. Liq. Chromatogr.*, **9**, 369 (1986).

6) Y. Okamoto, S. Honda, K. Hatada, and H. Yuki, *J. Chromatogr.*, **350**, 127 (1985).

7) Y. Okamoto, E. Yashima, M. Ishikura, and K. Hatada, *Polym. J.*, **19**, 1183 (1987).

8) R. Noyori, N. Sano, S. Murata, Y. Okamoto, H. Yuki, and T. Ito, *Tetrahedron Lett.*, **23**, 2969 (1982).

9) Y. Okamoto, S. Honda, E. Yashima, and H. Yuki, *Chem. Lett.*, **1983**, 1221.

10) J. D. Andose and K. Mislow, *J. Am. Chem. Soc.*, **96**, 2168 (1974).

11) K. Mislow, *Acc. Chem. Res.*, **1976**, 26.

12) Y. Okamoto, E. Yashima, K. Hatada, and K. Mislow, *J. Org. Chem.*, **49**, 557 (1984).

A Twin-TCNQ-Type Acceptor. Synthesis of 11,11,12,12,13,13,14,14-Octacyano-1,4:5,8-anthradiquinotetramethane and Structures of the Tetraethylammonium Salts of Its Mono- and Dianion

Tsutomu MITSUHASHI,* Midori GOTO,† Kazumasa HONDA,† Yusei MARUYAMA,††
Tamotsu INABE,†† Tadashi SUGAWARA,††† and Tokuko WATANABE††††
Department of Chemistry, Faculty of Science, The University of Tokyo, Bunkyo-ku, Tokyo 113
†National Chemical Laboratory for Industry, Tsukuba, Ibaraki 305
††Institute for Molecular Science, Myodaiji, Okazaki 444
†††Department of Pure and Applied Sciences, College of Arts and Sciences, The University of Tokyo, Meguro-ku, Tokyo 153
††††Laboratory of Chemistry, Tokyo University of Fisheries, Minato-ku, Tokyo 108
(Received July 1, 1987)

The title compound (OCNAQ) was synthesized. Treatment of 1,2,3,4,5,6,7,8-octahydroanthracene with *N*-bromosuccinimide (NBS) under irradiation using a 100-W light bulb in refluxing CCl_4 followed by dicyanomethylation with excess of $NaCH(CN)_2$ in Me_2SO gave an isomeric mixture of 1,4,5,8-tetrakis(dicyanomethyl) derivatives. The mixture was subjected by repetition of the successive bromination-dehydrobromination procedure giving OCNAQ in 20% overall yield. The cyclic voltammogram of OCNAQ exhibits four redox waves ($E_{1/2}^1$ 0.26, $E_{1/2}^2$ 0.05, $E_{1/2}^3$ −0.44, and $E_{1/2}^4$ −0.53 V vs. SCE in MeCN), indicating that OCNAQ is a stronger acceptor than tetracyanoquinodimethane (TCNQ, $E_{1/2}^1$ 0.17 V vs. SCE). Both 1:1 and 2:1 salts, (Et_4N)(OCNAQ) and $(Et_4N)_2$(OCNAQ), were obtained from reactions of Et_4NI with potassium and lithium salts of OCNAQ, respectively. The X-ray crystal analyses of these salts indicate that the TCNQ moieties are boat-shaped bent to opposite directions. With the 1:1 salt, which behaves as a semiconductor (4×10^{-4} Ω^{-1} cm^{-1} at room temperature, E_a 0.22 eV), the OCNAQ molecules are arrayed in the segregated stacking mode, while the 2:1 salt (10^{-7} Ω^{-1} cm^{-1}) has no columnar structure of the OCNAQ molecules.

A large number of tetracyanoquinodimethane (TCNQ) derivatives have appeared in the past few decades; however, twin-TCNQ-type acceptors had not as yet been presented.[1] The compound **1** (abbreviated as OCNAQ) is one of the simplest examples of this

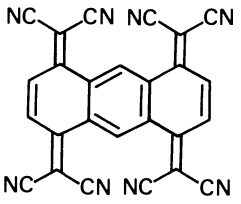

OCNAQ
1

type in which a pair of TCNQ nuclei are linked together through two methylidyne (-CH=) groups. The simple Hückel molecular orbital theory predicts that the lowest unoccupied molecular orbitals (LUMO) of OCNAQ and TCNQ are equal in energy and upon introduction of an electron into the OCNAQ molecule, the charge density is shared equally by both TCNQ nuclei.[2] Such charge dispersal would result in the reduction of on-site Coulomb repulsion and thus OCNAQ is expected to accept a second electron more easily than TCNQ.

Another factor that is not expected from TCNQ is the nonbonded interaction between cyano groups at positions 11 and 14 or 12 and 13 as well as that between a cyano group and a methylidyne group at position 9 or 10. Such a steric interaction

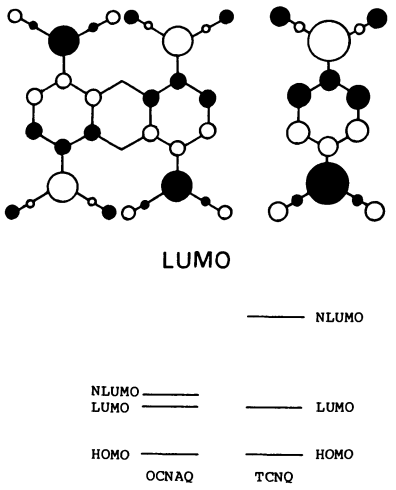

undoubtedly affects not only the molecular and crystal structures of the OCNAQ salts but also their electronic states.

In view of these considerations, it seems worthwhile to synthesize OCNAQ and to compare its physical and chemical properties with those of TCNQ which have been accumulated numerously since this intriguing acceptor was reported by Du Pont chemists.[3] This paper describes the synthetic route to OCNAQ and its fundamental properties obtained mainly from the mono- and dianion tetraethylammonium salts, a part of which has recently been reported in preliminary form.[4]

Results and Discussion

Synthesis. A number of synthetic strategies have been developed in order to construct the TCNQ-type-framework.[3,5-18] Survey of literature procedures suggested 1,4,5,8-tetrakis(cyanomethyl)anthracene and 1,4,5,8-tetrachloroanthraquinone to be most promising starting materials of the OCNAQ synthesis;[8] however, such approaches were unsuccessful. One of the key intermediates would be 1,4,5,8-tetrakis-(dicyanomethyl)-1,2,3,4,5,6,7,8-octahydroanthracene (**4**). It has been found that **4** is obtainable by simple substitution reactions and can be converted into OCNAQ by repetition of the successive bromination-dehydrobromination procedure in an overall yield of 20% as outlined in Scheme 1. The starting material, 1,2,3,4,5,6,7,8-octahydroanthracene (**2**), is readily available in one step from cheap, commercial compounds.[19] A mixture of **2** and *N*-bromosuccinimide (NBS) in refluxing carbon tetrachloride was irradiated with a 100-W unfrosted light bulb to afford an isomeric mixture of the 1,4,5,8-tetrabromo derivatives **3** as a white solid in 81% yield. The bromides **3** are unexpectedly stable at room temperature and can be stored in a freezer (−20 °C) without decomposition for a couple of days. Although **3** underwent dehydrobromination on treatment with sodium acetate in refluxing acetic acid to give anthracene in ca. 80% yield, the satisfactory dicyanomethylation of **3** was achieved by the use of a large excess of the sodium salt of malononitrile in Me_2SO to afford an isomeric mixture of **4** in 95% yield.

The active hydrogen atom of dicyanomethyl groups of **4** was easily replaced by bromine on treatment with NBS in MeCN in the presence of acetic acid. A difficulty with which the present procedure was confronted was the subsequent dehydrobromination, since even the action of such a weak base as pyridine led to the formation of polymerized products. One way out of the difficulty might be to carry out the dehydrobromination using a very weak base under slightly acidic conditions. A combination of *N*,*N*-dimethylformamide (DMF), acetic acid, and a small amount of ethanol was found to be suitable for the conversion of the bromination product from **4** into the tetrakis(dicyanomethylene) derivative **5** although the yield was moderate (35% based on **4**). The treatment of **5** with pyridine in MeCN followed by the addition of a solution of excess of bromine in 50% acetic acid gave OCNAQ as a yellow powder in 75% yield. The resulting crude product is sparingly soluble in MeCN but can be used directly for the preparation of charge-transfer complexes. OCNAQ reacted easily with potassium iodide in MeCN to afford the potassium salt of OCNAQ, which was then treated with tetraethylammonium iodide in refluxing MeCN giving the (Et_4N)(OCNAQ) salt (**6**) as black needles. Oxidation of **6** with bromine followed by recrystallization from MeCN gave an analytically pure sample of

$$\mathbf{1} \xrightarrow{KI} K^+OCNAQ^- \xrightarrow{Et_4NI} \underset{\mathbf{6}}{Et_4N^+OCNAQ^-} \xrightarrow{Br_2} \mathbf{1}$$

OCNAQ as fine golden yellow plates, which did not melt upon heating up to 400 °C but gradually turned brown above 180 °C. The infrared spectrum of OCNAQ as well as that of **5** exhibits a very strong absorption band due to the cyano stretching vibration at 2225 cm^{-1} indicating the presence of conjugated cyano groups.

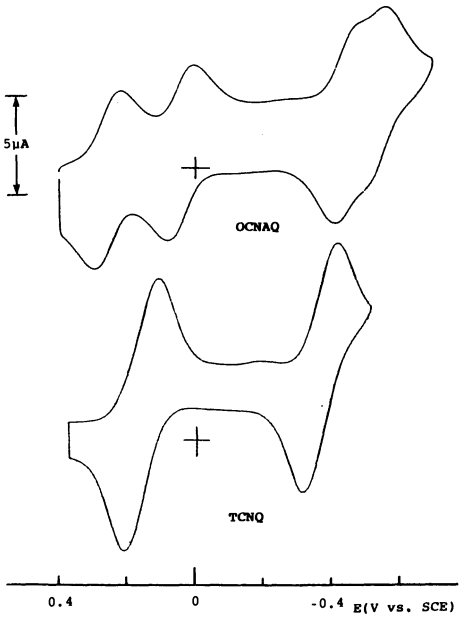

Fig. 1. Cyclic voltammograms of OCNAQ and TCNQ: solvent, MeCN; supporting electrolyte, Et_4NClO_4 (0.1 mol dm^{-3}); reference electrode, calomel; working electrode, platinum; sweep, 250 mV s^{-1}.

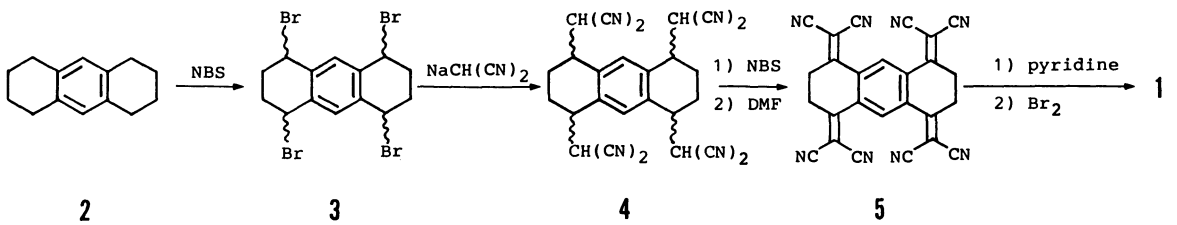

Scheme 1.

Electrochemical Studies. Figure 1 shows the cyclic voltammogram of OCNAQ with tetraethylammonium perchlorate as the supporting electrolyte in MeCN together with that of TCNQ measured under the same conditions. Four reversible redox waves appear at the potentials ($E_{1/2}$) 0.26, 0.05, −0.44, and −0.53 V vs. SCE. A comparison of the first redox potential of OCNAQ with that of TCNQ ($E_{1/2}$ 0.17 V vs. SCE)[20] reveals that OCNAQ is a stronger electron acceptor than TCNQ and thus the result is not exactly in accord with the expectation based on the simple Hückel molecular orbital calculation. Considerable deformation observed in the OCNAQ framework as described below as well as the stabilization due to charge dispersal present in the actual anion radical would result in such a discrepancy. Another interesting feature is that the second redox potential of OCNAQ is close to the first rather than the second redox potential of TCNQ ($E_{1/2}$ −0.36 V vs. SCE).[20] As mentioned in the introductory part, such a higher value of the second redox potential can be predicted by the simple Hückel MO theory combined with a consideration of Coulomb repulsive interaction.[21] In consequence, it is evident that the electron affinity of the anion radical $OCNAQ^{\cdot-}$ is stronger than that of $TCNQ^{\cdot-}$.

ESR Spectrum of the Radical Anion $OCNAQ^{\cdot-}$. A highly resolved ESR spectrum was obtained from the salt (Et_4N)(OCNAQ) **6** in MeCN with a *g*-factor of 2.0044. Figure 2 shows the observed spectrum and its simulation. The salt is completely ionic, because no hyperfine splitting due to the tetraethylammonium moiety has been observed. The hyperfine data derived from the spectrum together with the modified McLachlan calculation[22] provides the following coupling constants for the radical anion $OCNAQ^{\cdot-}$: a_H(2,3,6,7), 0.054±0.002 mT; a_H(9,10), −0.053±0.004 mT; a_N, 0.047±0.002 mT. Since a pair of acceptors are linked together through a conjugated system in OCNAQ, the charge in its anion radical $OCNAQ^{-\cdot}$ is expected to be highly delocalized. In fact, compared with the coupling constants for the radical anion $TCNQ^{\cdot-}$ [a_H (mT), 0.142[22] or 0.144;[23] a_N (mT), 0.099[22] or 0.102[23]], the value for the protons at positions 2,3,6,7 is about one-third and the value for the nitrogen atoms half as much.

X-Ray Structure of the (Et_4N)(OCNAQ) Salt (6). The structure of the OCNAQ framework was definitely confirmed by X-ray diffraction analysis of the salt **6** (Fig. 3). The crystal data are collected in Table 1. The final atomic parameters are listed in Table 2.[24] It is noteworthy that a quinonoid structure still remains in the OCNAQ framework of the salt, since the C–C distances between positions 2 and 3 and between positions 6 and 7 (1.33 Å) are shorter than those of aromatic rings and $TCNQ^{\cdot-}$ (1.38 Å;[25] 1.36 Å[26]) but are close to the corresponding distances of the neutral TCNQ (1.35 Å),[27] benzo-TCNQ (1.35 Å),[28] and $(Me)_4$TCNQ (1.34 Å)[17] in which the delocalization of π electrons of the bonds is depressed as a result of deformation from planarity. The result

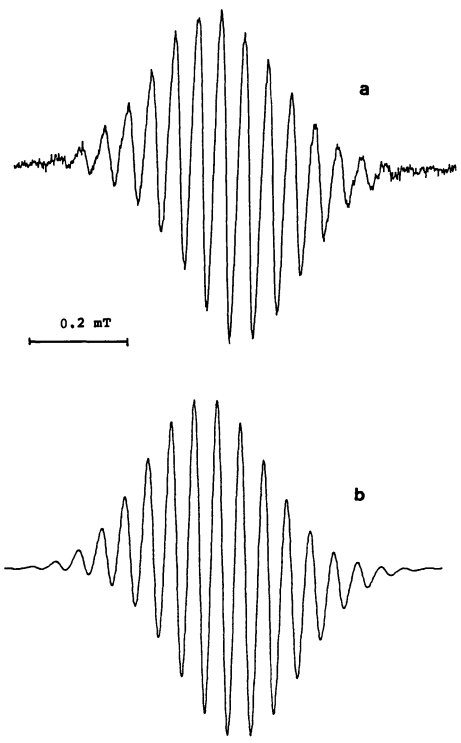

Fig. 2. ESR spectrum of $Et_4N^+OCNAQ^{\cdot-}$, **6**, in acetonitrile: (a) experimental; (b) computer simulation.

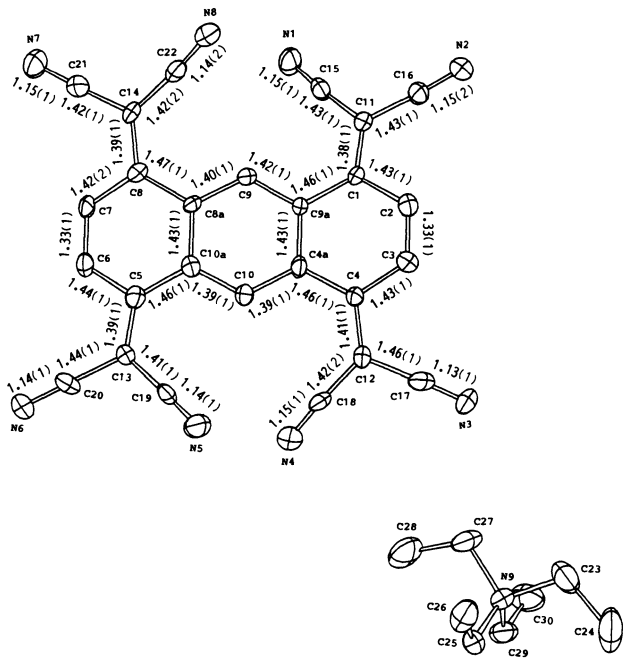

Fig. 3. ORTEP view of (Et_4N)(OCNAQ), **6**, showing the atom numbering scheme and bond lengths (Å).

Table 1. Crystal Data for $(Et_4N)(OCNAQ)$ (**6**) and $(Et_4N)_2(OCNAQ)$ (**7**)

	6	**7**
Molecular formula	$C_{34}H_{26}N_9$	$C_{42}H_{46}N_{10}$
M_w	560.65	690.91
Crystal size/mm	0.6×0.05×0.1	0.3×0.05×0.1
a/Å	7.800 (1)	12.383 (3)
b/Å	12.435 (1)	19.240 (5)
c/Å	16.004 (1)	9.090 (2)
α/deg	97.17 (1)	
β/deg	86.50 (1)	114.89 (2)
γ/deg	112.23 (1)	
U/Å^3	1425.5 (1)	1964.5 (9)
Z	2	2
D_c/g cm^{-3}	1.306	1.168
Space group	Triclinic, $P\bar{1}$	Monoclinic, $P2_1/n$
Absorption coeff/cm^{-1}	7.90	5.97

Table 2. Atomic Parameters (×10^4) and Their Equivalent Isotropic Temperature Factors for $(Et_4N)(OCNAQ)$ (**6**)

Atom	x	y	z	B_{eq}/Å^{2} [a]
C1	8373(11)	2467(7)	−680(4)	2.1(3)
C2	7793(13)	3142(8)	−16(6)	3.0(3)
C3	7343(14)	2826(8)	758(6)	3.1(3)
C4	7439(12)	1773(7)	977(5)	2.5(3)
C4A	7632(11)	926(7)	298(5)	2.5(3)
C5	7179(12)	−2236(7)	−79(5)	2.9(3)
C6	7654(13)	−2931(8)	−775(6)	3.1(3)
C7	7889(13)	−2627(8)	−1557(6)	3.0(3)
C8	7758(12)	−1593(7)	−1790(5)	2.7(3)
C8A	7689(11)	−742(6)	−1077(4)	2.4(3)
C9	8033(12)	411(7)	−1205(5)	2.6(3)
C9A	8060(11)	1270(6)	−531(4)	2.2(3)
C10	7345(13)	−218(8)	408(6)	2.7(3)
C10A	7379(11)	−1068(7)	−239(5)	2.7(3)
C11	9113(12)	2973(7)	−1409(5)	2.8(3)
C12	7350(12)	1648(7)	1841(5)	2.9(3)
C13	6521(12)	−2740(7)	663(5)	2.7(3)
C14	7646(12)	−1491(7)	−2639(5)	2.9(3)
C15	9986(13)	2514(7)	−2099(5)	3.0(3)
C16	9097(12)	4086(8)	−1534(5)	3.2(3)
C17	7110(15)	2561(8)	2451(6)	3.9(4)
C18	7692(13)	791(8)	2241(5)	3.2(3)
C19	5685(13)	−2309(7)	1358(6)	2.8(3)
C20	6534(12)	−3873(8)	768(5)	3.3(3)
C21	7923(14)	−2318(8)	−3272(6)	3.7(3)
C22	7207(13)	−619(8)	−2975(5)	3.5(3)
C23	5317(22)	3932(11)	5711(8)	5.7(5)
C24	4747(30)	4376(13)	6567(13)	8.3(7)
C25	4335(14)	1855(7)	6040(6)	3.3(3)
C26	2617(18)	1393(11)	5519(8)	4.7(4)
C27	6445(19)	2596(11)	4821(6)	4.9(4)
C28	7171(23)	1624(13)	4718(9)	6.3(6)
C29	7502(15)	3166(9)	6306(6)	4.0(4)
C30	9276(20)	4154(11)	6097(9)	5.7(5)
N1	10740(12)	2230(7)	−2668(5)	4.9(3)
N2	9020(13)	4956(7)	−1663(5)	5.1(4)
N3	6914(13)	3245(7)	2942(5)	5.0(3)
N4	8027(11)	174(7)	2625(5)	4.2(3)
N5	4932(11)	−2023(7)	1921(5)	4.1(3)
N6	6512(12)	−4769(7)	861(5)	4.5(3)
N7	8127(14)	−2977(7)	−3799(5)	5.6(4)
N8	6790(14)	7(7)	−3302(5)	5.4(4)
N9	5927(11)	2892(6)	5727(4)	3.3(2)

a) $B_{eq}=4/3(\sum_i\sum_j\beta_{ij}a_i\cdot a_j)$.

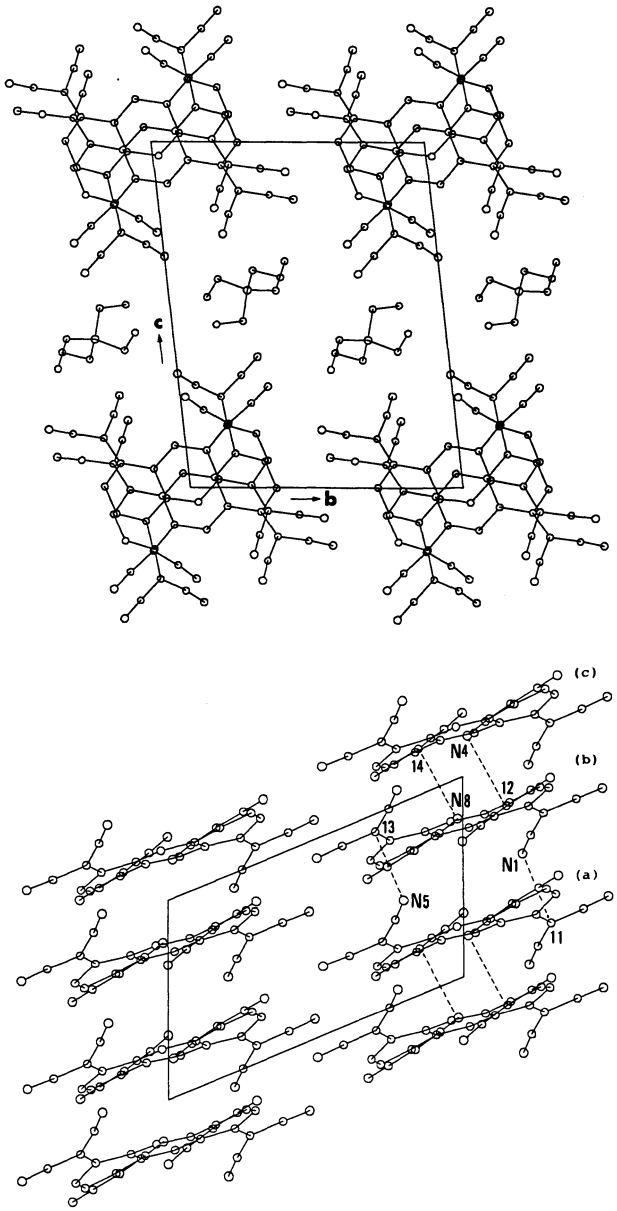

Fig. 4. Crystal structure of **6**: a-axis projection (upper) and drawing of the OCNAQ molecules projected on the [001] direction (lower).

Table 3. Dihedral Angles for Salts **6** and **7**

Plane I	Central benzene ring (e.g., C9, C9a, C4a, C10, C10a, C8a for **6**)		
Plane II	C2, C3, C4a, C9a	Plane III	C6, C7, C8a, C10a
Plane IV	C1, C2, C9a	Plane V	C3, C4, C4a
Plane VI	C7, C8, C8a	Plane VII	C5, C6 C10a
Plane VIII	C11, N1, N2	Plane IX	C12, N3, N4
Plane X	C14, N7, N8	Plane XI	C13, N5 N6

Angle between the planes A and B

Salt **6**			Salt **7**		
A	B	Angle (ϕ/°)	A	B	Angle (ϕ/°)
I	II	10.5(3)	I	II	10.4(4)
I	III	9.7(3)			
II	IV	12.0(9)	II	IV	12.4(13)
II	V	10.6(10)	II	V	10.6(14)
III	VI	10.3(9)			
III	VII	10.2(9)			
IV	VIII	10.2(4)	IV	VIII	9.8(12)
V	IX	9.7(8)	V	IX	14.3(10)
VI	X	10.5(6)			
VII	XI	11.0(7)			

suggests that OCNAQ has the ability to accept a second electron more easily than TCNQ, in agreement with a higher value of the second redox potential of OCNAQ. The benzene ring is essentially planar but the TCNQ nuclei are distorted into boat forms, and the bows and sterns of the two boats face in opposite directions. The $C(CN)_2$ groups are twisted about the exo CC axes (10—11°). The boat forms are bent by 10—12° and the dihedral angles between the plane of the benzene ring and that of the bottom of the boat form are ca. 10° (Table 3).[24]

Figure 4 shows the crystal structure. Clearly, the OCNAQ molecules stack nearly along a-axis to form a column with an alternate arrangement of slightly different interplanar spacings between the benzene rings of the adjacent molecules; the longer one (3.81 Å) appears between molecules (a) and (b) in Fig. 4, and the shorter (3.70 Å) between molecules (b) and (c), both of which are longer than the sum of the van der Waals radii (3.40 Å)[29] and thus much longer than those of the usual TCNQ columns (3.2—3.3 Å). In contrast, the shortest and the next shortest interatomic distances between nitrogens of the inside cyano groups of one molecule and exo-methylene carbons of the adjacent molecule, i.e., 3.05 (1) and 3.14 (1) Å, are shorter than the sum of the van der Waals radii (3.25 Å).[29] Interestingly the interatomic distances N(a)5···C(b)13 and C(a)11···N(b)1, which are placed between a pair of the molecules showing the longer interplanar spacing, are the shortest (3.05 Å), and hence the next shortest distance (3.14 Å) is allocated to the distances N(b)8···C(c)14 and C(b)12···N(c)4 belonging to a pair of the molecules with the shorter interplanar spacing.[30] This fact implies that the intermolecular charge delocalization in the column is

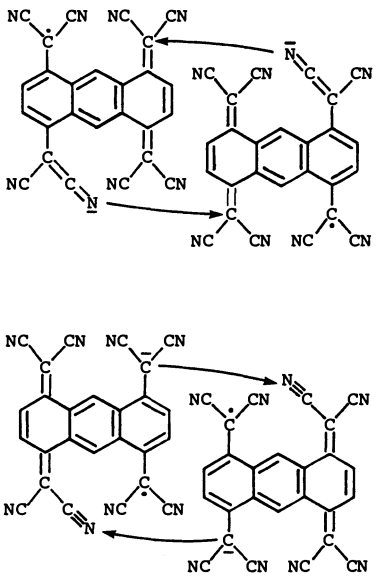

Scheme 2.

mainly caused by overlapping of orbitals of thses nitrogen and carbon atoms rather than that of the carbon atoms constituting anthracene nuclei, as can be illustrated by Scheme 2.

Solid State ESR Measurements of 6. Generally the ground state of the TCNQ salts is singlet and the singlet-triplet energy difference J ranges from 0.03 to 0.4 eV.[31-35] To evaluate the extent of intermolecular interaction in the OCNAQ column, the temperature dependence of ESR absorption intensity of the powdered salt was examined. As shown in Fig. 5, the intensity is increased by a factor of 10 on changing the temperature from −166 °C to −19 °C and the

equation[31,36] $I \propto [\exp(-J/kT)]/T$ holds in this temperature range, giving J=0.052 eV. The result suggests that there exist distinct intermolecular attractive forces other than those of the van der Waals type, which hold the columnar structure of the OCNAQ molecules and lead to the ground state singlet.

Electrical Conductivity of 6. The single crystal resistivity of **6** was measured with a two-probe technique. The room-temperature conductivity is ca. $4\times10^{-4}\,\Omega^{-1}\,cm^{-1}$. Unfortunately no information on the single crystal conductivities of 1:1 TCNQ ammonium salts is available. However, their compacted powder pellets exhibit much lower conductivities ($\sigma \leqq 10^{-6}\,\Omega^{-1}\,cm^{-1}$).[3,37] It seems reasonable to assume that the reduction of on-site Coulomb repulsion in $OCNAQ^{-}$ is responsible for the high conductivity of **6** as compared with those of simple TCNQ ammonium salts. The salt **6** behaves as a semiconductor. Figure 6 shows the temperature dependence of the resistivity. The conductivity is increased by a factor of 8 on changing the temperature from 300 to 400 K with an activation energy of 0.22 eV.

X-Ray Structure of the $(Et_4N)_2$(OCNAQ) Salt (7). The action of Et_4NI on the lithium salt of

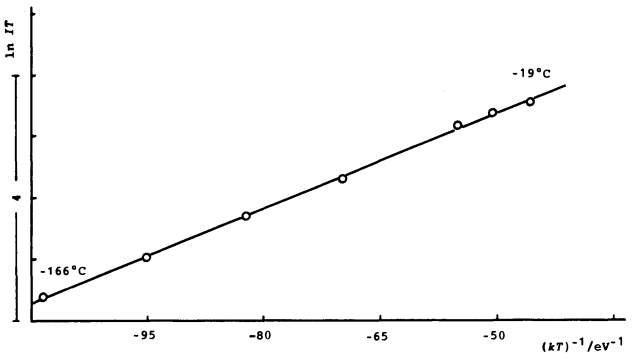

Fig. 5. Temperature dependence of ESR absorption intensity of powdered $Et_4N^{+}OCNAQ^{-\cdot}$, **6**.

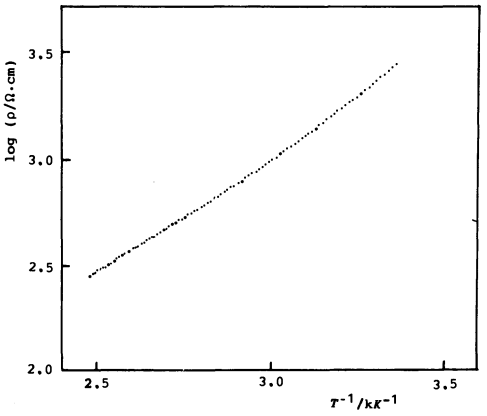

Fig. 6. Temperature dependence of the single-crystal resistivity of **6**.

Table 4. Atomic Parameters ($\times10^4$) and Their Equivalent Isotropic Temperature Factors for $(Et_4N)_2$(OCNAQ) (**7**)

Atom	x	y	z	B_{eq}/Å$^{2a)}$
C1	1109(7)	−1100(5)	−965(13)	5.1(4)
C2	551(9)	−1329(5)	−2577(14)	6.2(4)
C3	−340(8)	−949(4)	−3725(15)	5.7(4)
C4	−717(7)	−296(5)	−3352(15)	5.2(4)
C4A	−341(7)	−127(5)	−1712(14)	4.7(4)
C9	865(9)	−384(6)	1150(18)	4.9(4)
C9A	581(7)	−534(4)	−422(15)	4.5(4)
C11	2212(8)	−1434(5)	72(13)	5.7(4)
C12	−1399(7)	144(5)	−4694(14)	5.3(4)
C15	3007(10)	−1239(5)	1600(15)	6.9(5)
C16	2648(9)	−1993(7)	−567(15)	7.8(5)
C17	−1827(8)	−91(5)	−6290(14)	5.5(4)
C18	−1587(9)	863(7)	−4531(13)	7.3(5)
C23	6070(13)	−1701(9)	6625(22)	9.8(6)
C24	6579(16)	−1324(16)	5597(26)	13.3(8)
C25	5989(8)	−649(5)	8228(19)	8.0(6)
C26	4652(11)	−550(10)	7271(30)	12.2(7)
C27	5771(12)	−1852(9)	9096(30)	9.6(7)
C28	5928(18)	−1611(14)	10783(30)	12.6(8)
C29	7722(7)	−1367(6)	9299(21)	8.0(5)
C30	8340(12)	−2073(8)	9507(37)	13.7(10)
N1	3689(8)	−1067(5)	2872(14)	9.6(5)
N2	3024(8)	−2433(5)	−1085(15)	10.8(6)
N3	−2163(7)	−264(5)	−7596(11)	7.7(4)
N4	−1741(10)	1446(5)	−4463(15)	11.2(6)
N9	6371(6)	−1397(4)	8277(13)	6.7(4)

a) $B_{eq}=4/3(\sum_i\sum_j \beta_{ij} a_i \cdot a_j)$.

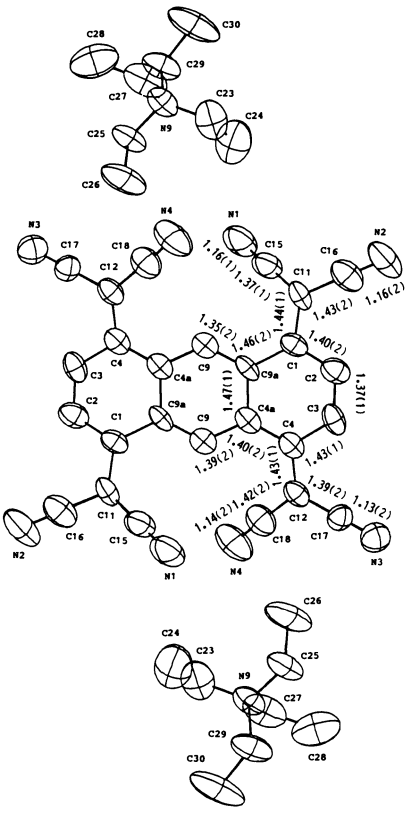

Fig. 7. ORTEP view of $(Et_4N)_2$(OCNAQ), **7**, showing the atom numbering scheme and bond lengths (Å).

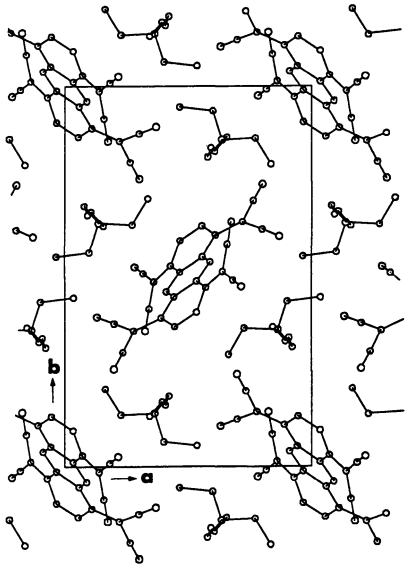

Fig. 8. Crystal structure of **7** (c-axis projection).

OCNAQ in hot methanol gave the 2:1 $(Et_4N)_2$-(OCNAQ) salt (**7**) as blue-black needles, reflecting a higher value of the second redox potential or the presence of a pair of TCNQ moieties. The salt **7** is readily soluble in hot methanol in which the salt **6** is insoluble. Its conductivity ($1.2\times10^{-7}\,\Omega^{-1}\,cm^{-1}$ at room temperature) is much lower than that of the 1:1 salt **6**. The crystal data and final atomic parameters of the salt are listed in Tables 1 and 4,[24] respectively. The salt has a center of symmetry in the OCNAQ molecule (Fig. 7). In contrast to the monoanion salt **6**, the C(2)-C(3) distance (1.37 Å) is within the range of the above-mentioned values of $TCNQ^-$ (1.35—1.38 Å), suggesting that the quinonoid geometry of the acceptor seems almost lacking. Such a geometrical change implies much difficulty in introducing a third electron into the OCNAQ molecule, in agreement with a considerably lower value of the third redox potential of OCNAQ, and would be responsible for a dramatic change in the crystal structure of the salt in which a columnar structure of the OCNAQ molecules is no longer present (Fig. 8). Deformation of the anthracene framework of **7** is, however, similar to that of **6**: The boat-shaped TCNQ nuclei in **7** are bent by 10—12° and the dihedral angle between the plane of the benzene ring and that of the bottom of the boat form is ca. 10° (Table 3).[24]

Experimental

Instruments. The following spectrometers were used: IR, Hitachi 260-30; ^1H NMR, Varian EM-390; ESR, Varian E-112/V 7800 for an MeCN solution, which was degassed in a quartz tube (4 mm o.d.) by three freeze-thaw cycles, and JEOL FE1X for a solid sample; Cyclic voltammograms were measured by a potentiostat (Yanaco V8-3010PG) equipped with a function generator (NF FG-121B) and an XY recorder (Watanabe WX 4401). MeCN (special grade) was distilled over P_2O_5 and subsequently over K_2CO_3. Resistivity measurements were performed by a two-probe (gold paste electrodes) technique.

X-Ray Structure Analyses. The structure analyses were made with a Rigaku Denki AFC-4 automatic four-circle diffractometer [Cu $K\alpha$ radiation (1.54184 Å), graphite monochromator, ω—2θ scan technique, $2\theta\leqq120°$, scan speed 4° min^{-1} (θ), scan range (1.1+0.5 tan θ)°]. Three standard reflections measured every 50 reflections showed no significant X-ray damage or crystal decay. Of 2595 (for **6**) and 2166 (for **7**) independent reflections observed, unique 1647 (for **6**) and 1007 (for **7**) reflections with $|F_o|>3\sigma(|F_o|)$ were used for structure determination. The structure was solved by direct methods with MULTAN 78[38] (with atomic scattering factors from International Tables for X-ray Crystallography)[39] and refined by full-matrix least squares (UNICS III)[40,41] with anisotropic thermal parameters for non-hydrogen atoms and isotropic for hydrogen atoms. **6**: $R=0.064$ and $R_w=0.074$, where $w=(4.155-0.274|F_{obs}|+0.006F_{obs}^2)^{-1}$. **7**: $R=0.072$ and $R_w=0.070$, where $w=(2.343-0.092|F_{obs}|+0.004F_{obs}^2)^{-1}$.

Elemental analyses were performed by Mses Toshiko Seki and Kimiyo Saeki of the analytical section of the Department of Chemistry, The University of Tokyo.

Preparation of 1,4,5,8-Tetrabromo-1,2,3,4,5,6,7,8-octahydroanthracenes (3). 1,2,3,4,5,6,7,8-Octahydroanthracene (**2**) was prepared by the action of $AlCl_3$ on a mixture of tetralin and 1,4-dichlorobutane (special grade) according to the literature procedure[19] and was recrystallized repeatedly from ethanol: mp 71.5 °C [lit,[19] mp 72 °C]. A solution of **2** (5.0 g, 26.8 mmol) in 250 ml of CCl_4 was placed in a 500-ml round-bottomed pyrex flask, and NBS (21 g, 117 mmol) was added. The flask was immersed in an oil bath preheated at 90 °C. The mixture was refluxed with stirring and was exposed to the light of an ordinary 100-W unfrosted bulb placed 1 cm from the flask. Vigorous reaction took place within 5 min. After irradiation for 45 min, the reaction mixture was cooled with water and filtered. The isolated solid mass was washed with CCl_4 and the washings were combined with the filtrate. The solid was then washed with water and ethanol to remove succinimide, and the residue was washed finally with hexane to give the first crop of the bromide **3** as a white solid (2.5 g, 19%), which was rather stable and decomposed only very slowly with loss of HBr at room temperature; IR (KBr, cm^{-1}) 2950 w, 2900 w, 1630 w, 1495 w, 1430 s, 1345 w, 1225 s, 1190 s, 1000 w, 985 w, 915 s, 895 m, 765 w, 740 m, 630 s, 520 m; ^1H NMR ($CDCl_3$) δ=2.3—2.8 (m, 8H), 5.4—5.8 (m, 4H), 7.33 (s, 2H). Found: C, 33.14; H, 2.57%. Calcd for $C_{14}H_{14}Br_4$: C, 33.50; H, 2.81%. The filtrate and the CCl_4 washings were concentrated under reduced pressure, and the viscous residue was triturated with 10 ml of $CHCl_3$, diluted with 10 ml of hexane, and cooled in a refrigerator. The resulting precipitate was isolated by filtration and washed with ethanol and hexane, affording the second crop of the bromide **3** as a white solid (8.3 g, 62%), which showed satisfactory elemental analysis after recrystallization from benzene. Found: C, 33.64; H, 2.60%. Calcd for $C_{14}H_{14}Br_4$: C, 33.50; H, 2.81%. These two crops of the crude bromide were combined, pulverized in a mortar, and used in the next step.

Preparation of 1,4,5,8-Tetrakis(dicyanomethyl)-1,2,3,4,5,6,7,8-octahydroanthracenes (4). To a mechanically stirred suspension of 20 g (0.5 mol) of sodium hydride (60% oil dispersion) in 60 ml of Me_2SO, which was placed in a 1000-ml three-necked flask, was added a solution of 35 g (0.53 mol) of malononitrile in 40 ml of Me_2SO at 25 °C under an atmosphere of nitrogen. After the addition was complete, stirring was continued for 15 min. To the resulting homogeneous solution was added 10.8 g (21.5 mmol) of the above powder of the bromide **3** in one portion and stirring was continued for 3 h. To the reaction mixture was added 500 ml of 10% aqueous acetic acid with stirring. The resulting light brown paste was collected, washed successively with water, benzene, and hexane and treated with 100 ml of hot acetic acid followed by addition of 500 ml of water. The resulting precipitate was isolated by filtration, washed with water and hexane, and dried in vacuo, affording a white solid (9.0 g, 19.2 mmol, 95%). The NMR spectrum in MeCN showed the solid to be an isomeric mixture of **4**. In a separate experiment under the same conditions, the bromide obtained as the first crop described above gave only one isomer of **4**: colorless needles from MeCN (dried at 80 °C in vacuo); mp 355 °C decomp; IR (KBr, cm^{-1}) 2900 s, 2245 m (CN), 2200 w (CN), 1620 m, 1510 m, 1440 m, 1400 w, 1320 m, 1260 w, 1230 m, 1145 m, 1040 w, 1000 w, 980 m, 920 m, 905 m, 795 m, 760 w, 720 m. ^1H NMR (Me_2SO-d_6) δ=1.5—2.6 (m. 8H), 3.6—3.9 (m, 4H), 5.56 (d, 4H, J=4.5 Hz), 7.52 (s, 2H). Found: C, 70.71; H, 4.04; N, 25.47%. Calcd for $C_{26}H_{18}N_8$: C, 70.57; H, 4.10; N, 25.33%. The second crop of the bromide afforded an isomeric mixture of **4**.

Preparation of 1,4,5,8-Tetrakis(dicyanomethylene)-1,2,3,4,5,6,7,8-octahydroanthracene (5). To a mixture of 60 ml of MeCN and 10 ml of acetic acid were added **4** (9.0 g) and NBS (20 g, 112 mmol), and the mixture was stirred at room temperature for 1 h and at 45 °C for 2 h and then filtered. To the well-stirred and water-cooled filtrate a mixture of 50 ml of DMF, 25 ml of acetic acid, and 3 ml of ethanol was added dropwise over a period of 1 h. The reaction mixture was stirred overnight and diluted with 100 ml of 50% aqueous acetic acid. The dark brown mixture was stirred for an additional 1 h. The product was separated by filtration and washed with MeCN until the filtrate became bright yellow. The yield of **5** was 3.1 g (7.1 mmol, 35%): mp 320—325 °C decomp, as yellow crystals from MeCN; IR (KBr, cm^{-1}) 3065 w, 2920 m, 2225 vs (CN), 1640 m, 1590 s, 1560 s, 1550 s, 1480 m, 1440 m, 1410 w, 1350 w, 1320 m, 1295 m, 1220 m, 1205 m, 1100 w, 980 w, 970 w, 915 m, 880 m, 800 s, 775 w. Found: C, 71.74; H, 2.44 N, 25.69%. Calcd for $C_{26}H_{10}N_8$: C, 71.88; H, 2.32; N, 25.80%.

Preparation of 11,11,12,12,13,13,14,14-Octacyano-1,4:5,8-anthradiquinotetramethane (1).[42] To a stirred suspension of 3.1 g of **5** in 100 ml of MeCN was added a solution of 3 g of pyridine in 50 ml of MeCN under an atmosphere of nitrogen. After 30 min, the dark blue-black mixture was ice-cooled and then an ice-cooled solution of 3.5 g of bromine in 250 ml of 50% aqueous acetic acid was added in one portion and stirred for 5 min. The product was separated by filtration and washed successively with 50% aqueous acetic acid, water, ethanol, and finally MeCN until the filtrate became bright yellow. The yield of **1** thus obtained was 2.3 g (5.3 mmol, 75%) as a yellow powder, and the overall yield starting from **2** was therefore 20%. This crude product was used without further purification. An analytical sample of **1** was obtained by two recrystallizations (from MeCN) of **1** regenerated from the bromine oxidation of the salt **6** as described below: fine golden yellow plates; mp>400 °C (its appearance gradually turned brown above 180 °C and dark brown above 380 °C); IR (KBr, cm^{-1}) 3060 w, 2930 vw, 2225 vs (CN), 1640 m, 1590 w, 1555 vs, 1480 w, 1335 w, 1300 m, 1260 vw, 1205 m, 1100 w, 970 w, 935 vw, 895 m, 800 m, 775 w. Found: C, 72.85; H, 1.40; N, 26.20%. Calcd for $C_{26}H_6N_8$: C, 72.56; H, 1.41; N, 26.04%.

Preparation of the Salt (Et_4N)(OCNAQ)(6) To a suspension of 0.5 g of OCNAQ in 40 ml of MeCN was added 0.5 g of potassium iodide and the mixture was stirred for 2 h. The black deposit was separated by filtration and washed with MeCN. A mixture of the crude potassium salt (0.55 g) and tetraethylammonium iodide (0.4 g) in 20 ml of MeCN was refluxed for 5 min. The resulting precipitate (0.58 g) was recrystallized twice from MeCN to give **6** as black needles. Found: C, 73.04; H, 4.43; N, 22.56%. Calcd for $C_{34}H_{26}N_9$: C, 72.84; H, 4.67; N, 22.49%. OCNAQ was regenerated upon addition of excess of an aqueous bromine solution to a suspension of **6** in MeCN.

Preparation of the Salt (Et_4N)$_2$(OCNAQ)(7). The crude lithium salt of OCNAQ, which was prepared analogously as described above, was dissolved in methanol and filtered. To the dark blue filtrate was added an excess of Et_4NI (more than 2.5 equiv) and the mixture was heated to boiling, filtered, and then the filtrate was cooled. The resulting precipitate was collected and recrystallized from methanol to give **7** as blue-black needles. Found: C, 73.02; H, 6.55; N, 20.42%. Calcd for $C_{42}H_{46}N_{10}$: C, 73.01; H, 6.71; N, 20.27%. A 1:1 mixture of **7** and OCNAQ was heated in MeCN to yield **6**.

We are grateful to Drs. Gaku Yamamoto, Akiko Kobayashi, and Shigeru Murata for many helpful discussions.

References

1) F. Wudl, "The Physics and Chemistry of Low Dimensional Solids," ed by L. Alcácer and D. Reidel, Dordrecht, Holland (1980), p. 272.

2) The parameters used here for the dicyanomethylene groups (h_N=1.0, k_{CN}=2.0, and k_{C-CN}=0.9) are those reported in the literature: F. Gerson, R. Heckendorn, D. O. Cowan, A. M. Kini, and M. Maxfield, *J. Am. Chem. Soc.*, **105**, 7017 (1983).

3) D. S. Acker and W. R. Hertler, *J. Am. Chem. Soc.*, **84**, 3370 (1962); L. R. Melby, R. J. Harder, W. R. Hertler, W. Mahler, R. E. Benson, and W. E. Mochel, *ibid.*, **84**, 3374 (1962).

4) T. Mitsuhashi, M. Goto, K. Honda, Y. Maruyama, T. Sugawara, T. Inabe, and T. Watanabe, *J. Chem. Soc., Chem. Commun.*, **1987**, 810.

5) S. Chatterjee, *J. Chem. Soc.*, **1967**, 1170.

6) J. Diekmann, W. R. Hertler, and R. E. Benson, *J. Org. Chem.*, **28**, 2719 (1963).

7) D. J. Sandman and A. F. Garito, *J. Org. Chem.*, **39**, 1165 (1974).

8) R. C. Wheland and E. L. Martin, *J. Org. Chem.*, **40**, 3101 (1975).

9) W. R. Hertler, *J. Org. Chem.*, **40**, 1412 (1976).

10) A. W. Addison, N. S. Dalal, Y. Hoyano, S. Huizinga, and L. Weiler, *Can. J. Chem.*, **55**, 4191 (1977).
11) E. Aharon-Shalom, J. Y. Becker, and I. Agranat, *Nouv. J. Chim.*, **3**, 643 (1979).
12) M. R. Maxfield, D. O. Cowan, A. N. Bloch, and T. O. Poehler, *Nouv. J. Chim.*, **3**, 647 (1979).
13) M. R. Maxfield, S. M. Willi, D. O. Cowan, A. N. Bloch, and T. O. Poehler, *J. Chem. Soc., Chem. Commun.*, **1980**, 947.
14) N. Acton, D. Hou. J. Schwarz, and T. J. Katz, *J. Org. Chem.*, **47**, 1011 (1982).
15) A. Aumüller and S. Hünig, *Liebigs Ann. Chem.*, **1984**, 618; B. S. Ong and B. Keoshkerian, *J. Org. Chem.*, **49**, 5002 (1984).
16) A. M. Kini, D. O. Cowan, F. Gerson, and R. Möckel, *J. Am. Chem. Soc.*, **107**, 556 (1985); S. Yamaguchi, G. Tatemitsu, Y. Sakata, and S. Misumi, *Chem. Lett.*, **1983**, 1229; S. Hotta, T. Tosaka, N. Sonoda, and S. Shimotsuma, European Patent Applied EP 61 264, Sept 1982; *Chem. Abstr.*, **98**, 99701n (1983): Matsushita Electric Industrial Co., Ltd. Japanese Patent 58 10554, Jan 1983; *Chem. Abstr.*, **98**, 197809y (1983): S. Hotta, T. Tosaka, N. Sonoda, and S. Shimotsuma, European Patent Applied EP 76 639, Apr 1983; *Chem. Abstr.*, **99**, 105013d (1983).
17) B. Rosenau, C. Krieger, and H. A. Staab, *Tetrahedron Lett.*, **26**, 2081 (1985).
18) Y. Yamashita, T. Suzuki, T. Mukai, and G. Saito, *J. Chem. Soc., Chem. Commun.*, **1985**, 1044.
19) D. Hausigk and G. Kölling, *Chem. Ber.*, **101**, 469 (1968).
20) These data are compatible with those reported: M. R. Suchanski, *J. Electrochem. Soc.*, **123**, 181C (1976). See also Ref. 15.
21) An alternative explanation is that a second electron may be lifted up on NLUMO to advantage in reducing on-site Coulomb repulsion because the energy difference between the LUMO and NLUMO of OCNAQ seems small.
22) P. Devolder, *Tetrahedron*, **35**, 1307 (1979).
23) P. H. H. Fischer and C. A. McDowell, *J. Am. Chem. Soc.*, **85**, 2694 (1963).
24) The lists of structure factors, atomic parameters for hydrogen atoms, anisotropic thermal parameters for non-hydrogen atoms, bond lengths and angles, and dihedral angles are deposited at Bull. Chem. Soc. Jpn. (Document No. 8774).
25) H. Kobayashi, Y. Ohashi, F. Marumo, and Y. Saito, *Acta Crystallogr., Sect. B*, **26**, 459 (1970).
26) P. Goldstein, K. Seff, and K. N. Trueblood, *Acta Crystallogr., Sect. B*, **24**, 785 (1968).
27) R. E. Long, R. A. Sparks, and K. N. Trueblood, *Acta Crystallogr.*, **18**, 932 (1965).
28) F. Iwasaki, *Acta Crystallogr., Sect. B*, **27**, 1360 (1971).
29) L. Pauling, "The Nature of the Chemical Bond," 3rd ed, Cornell University Press, Ithaca, N. Y. (1960), p. 260; A. Bondi, *J. Phys. Chem.*, **68**, 441 (1964).
30) As a necessary consequence of the zigzag arrangement (Fig. 4), the other corresponding distances are much longer: N(a)8···C(b)14 and C(a)12···N(b)4, 3.92 Å; N(b)5···C(c)13 and C(b)11···N(c)1, 3.81 Å.
31) D. B. Chesnut and W. D. Phillips, *J. Chem. Phys.*, **35**, 1002 (1961).
32) D. B. Chesnut and P. Arthur, Jr., *J. Chem. Phys.*, **36**, 2969 (1962).
33) M. T. Jones and D. B. Chesnut, *J. Chem. Phys.*, **38**, 1311 (1963).
34) M. T. Jones, *J. Chem. Phys.*, **40**, 1837 (1964).
35) J. C. Bailey and D. B. Chesnut, *J. Chem. Phys.*, **51**, 5118 (1969).
36) D. Bijl, H. Kainer, and A. C. Rose-Innes, *J. Chem. Phys.*, **30**, 765 (1959).
37) H. Kusakawa and K. Akashi, *Bull. Chem. Soc. Jpn.*, **42**, 263 (1969).
38) P. Main, S. E. Hull, L. Lessinger, G. Germain, J.-P. Declercq, and M. M. Woolfson, MULTAN 78. A System of Computer Programs for the Automatic Solution of Crystal Structures from X-Ray Diffraction Data. Univs. of York (England) and Louvain (Belgium)(1978).
39) "International Tables for X-Ray Crystallography," Vol. IV, ed by J. A. Ibers and W. C. Hamilton, Birmingham, Kynoch press (1974).
40) T. Sakurai and K. Kobayashi, *Rep. Inst. Phys. Chem. Res.*, **55**, 69 (1979).
41) C. K. Johnson, ORTEP. Report ORNL-3794. Oak Ridge National Laboratory, Tennessee (1965).
42) 2,2′,2″,2‴-(1,4,5,8-Tetrahydroanthracene-1,4,5,8-tetrayl-idene)tetrakis(propanedinitrile) according to the Chemical Abstracts Index name.

 © 1988 The Chemical Society of Japan Bull. Chem. Soc. Jpn., 61, 271—279 (1988)

Conductive Salts of Tropylium Ions with Tetracyanoquinodimethan Anion Radical ($TCNQ^{-}$) and Bisthiadiazolotetracyanoquinodimethan Anion Radical (BTDA-$TCNQ^{-}$)

Yoshiro YAMASHITA,* Koji HAGIYA, Gunzi SAITO,† and Toshio MUKAI
Department of Chemistry, Faculty of Science, Tohoku University, Aramaki, Sendai 980
†Institute for Solid State Physics, The University of Tokyo, Roppongi, Tokyo 106
(Received July 2, 1987)

Tropylium ions have been found to be good cations for forming highly conductive salts of $TCNQ^{-}$. Tropylium ions with different reduction potentials were prepared. The first reduction potentials which are correlated with the substituent constants σ_p^+ control the formation of the salts. The cations with higher reduction potentials underwent a reaction with $TCNQ^{-}$ to give neutral TCNQ and coupling products. The molar ratios of the initially formed salts are also dependent on the reduction potentials. The simple salts are only formed when the reduction potentials are lower than −0.43 V. This fact is rationalized by the difference in the ease of electron transfer from $TCNQ^{-}$ to tropylium ions which is determined by the reduction potentials. Some simple salts show significantly low electrical resistivities compared with usual $TCNQ^{-}$ simple salts. BTDA-$TCNQ^{-}$ also gave conductive salts of tropylium ions, indicating that BTDA-TCNQ is useful for forming organic semiconductors.

Recently much attention has been focused on organic conductors and the requirements for them have been proposed.[1] In the tetrathiafulvalene (TTF)-tetracyanoquinodimethan (TCNQ) system, the redox potentials are the most important factors to determine conductivity, where the difference between the first oxidation potentials for donors [E_1^{ox}(D)] and the first reduction potentials for acceptors [E_1^{red}(A)] is $-0.02<E_1^{ox}(D)-E_1^{red}(A)<0.34$ V for giving organic metals.[2] The difference in the redox potentials is related to the degree of charge transfer.[3] On the other hand, simple $TCNQ^{-}$ salts of cations usually exhibit low conductivity because of the complete charge transfer.[3,4] Therefore, the systematic study on the factors governing the conductivities of simple $TCNQ^{-}$ salts has not been done although the effect of the reduction potentials of cations has been pointed out by Torrance.[3] *N*-Methylphenazinium (NMP) which has a higher reduction potential compared with those for other cations is an exceptional cation whose 1:1 $TCNQ^{-}$ salt is an organic metal.[5] Tropylium ion whose reduction potential is close to that of NMP[6] has been reported to undergo a reaction with $TCNQ^{-}$ without formation of salts.[7] However, its derivatives still seemed attractive cations for preparing highly conductive salts as well as for the systematic study on the substituent effects for the following reasons. First, they are stable aromatic cations and can be easily functionalized to change electron affinity. Second, they have high polarizability which is related to the high conductivities of the complex salts of $TCNQ^{-}$ with heterocyclic cations.[8] Third, they are desirable cations for the investigation of substituent effects since substituents are directly attached to the delocalized cation ring. Finally, heteroatoms which increase intra- and interstack interactions for stabilizing the metallic state are easily introduced in the substituents. From these viewpoints, we have investigated the salt formation of tropylium ions with $TCNQ^{-}$ [9] as well as bis[1,2,5]thiadiazolotetracyanoquinodimethan anion radical (BTDA-$TCNQ^{-}$) which we prepared recently.[10]

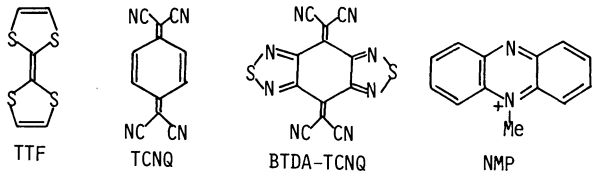

Results and Discussion

Preparation of Tropylium Ions. Monocyclic tropylium ions **1a,b,g,j,k,o,r** are new compounds which were prepared by the following methods.[11] Reaction of 5-bromo-2-methoxytropone with trimethyloxonium tetrafluoroborate in nitromethane gave **1a** and **1b** in 12% and 61% yields, respectively. The similar reaction of 4-methoxytropone and 2-aminotropone led to the formation of **1k** and **1r** in 85% and 36% yields, respectively. Methylthio derivatives **1g,j,o** were synthesized by the reaction of the corresponding tropothiones with methyl iodide in ether in 70%, 25%, and 48% yields, respectively. Bicyclic cations **2a,b** were synthesized by deprotonation of the corresponding cycloheptatriene derivatives **3a**[12] and **3b**[13] with $NOBF_4$ in 72% and 80% yields, respectively. This method using $NOBF_4$ is useful for the deprotonation of cyclic cycloheptatrienes to give tropylium ions.[14] Tricyclic cations **4b—f** whose structures are analogous to that of NMP were prepared from the corresponding heterocycles, cyclohepta[*b*][1,4]benzothiazine (**5a**),[15] cyclohepta[*b*][1,4]benzoxazine (**5b**),[16] and *N*-methylcyclohepta[b][1,4]benzodiazine (**5c**)[17] by protonation with hydrogen chloride or methylation with methyl iodide. Cation **4a** was prepared as the BF_4^{-} salt according to Nozoe's method.[15b] Heterocyclic cation **6**

with two sulfur atoms were prepared as the BF_4^- salt by deprotonation of heterocycle **7**[12] in acetonitrile.

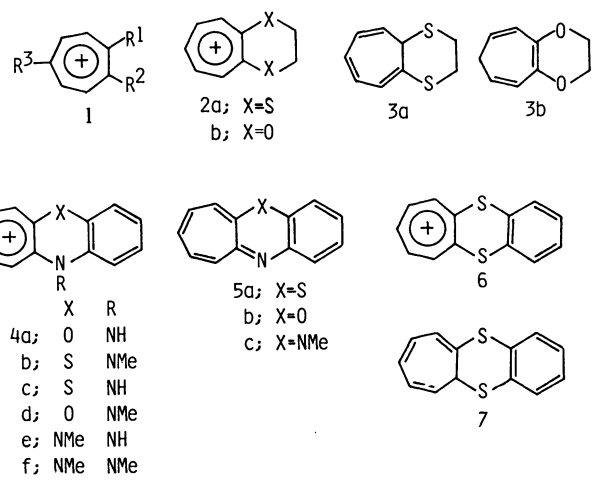

Reduction Potentials for Tropylium Ions. The first reduction potentials (E_1^{red}) for tropylium ions were measured by cyclic voltammetry. The data for monocyclic tropylium ions summarized in Table 1 show that electron-donating substituents lower the first reduction potentials. The values are linearly correlated with the sum of the substituent constants σ_p^+ as shown in Fig. 1.[18] This linear relationship means the presence of the additive properties of substituent effects on the reduction potentials. Introduction of an SMe group decreases the reduction potentials by −0.10—−0.15 V, while introduction of an OMe group decreases them by −0.20—−0.26 V.[19] The reduction potentials for bicyclic cations **2a,b** are also shown in Table 1. Their higher reduction potentials compared with those for the corresponding monocyclic cations

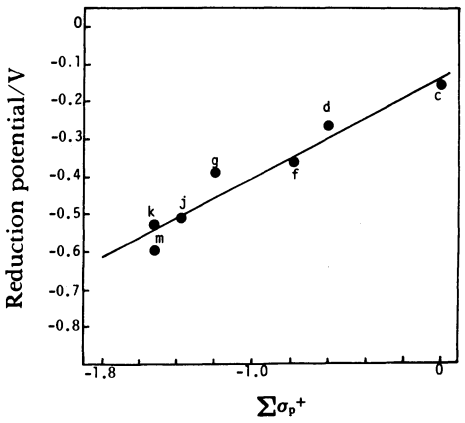

Fig. 1. Plots of first reduction potentials vs. the sum of the substituent constants σ_p^+.
$E_1^{red}=-0.14+0.27\ \Sigma\sigma_p^+$ $r=0.944$.

Table 2. Redox Potentials of Tricyclic Cations **4** and **6**[a]

Cation	E_1^{ox}/V vs. SCE[b]	E_1^{red}/V vs. SCE[c]
4a-BF_4^-	1.44	−0.43
4b-BF_4^-	1.54	−0.45
4c-BF_4^-	1.41	−0.47
4d-I^-	1.65	−0.55
4e-BF_4^-	1.10	−0.58
4f-BF_4^-	1.15	−0.85
6-BF_4^-	1.86	−0.13

a) 0.1 M Et_4NClO_4 in MeCN, Pt electrode, scan rate 100 mV s^{-1}. b) Irreversible. Calculated as E_{pa} (anodic peak potential)−0.03. c) Irreversible. Calculated as E_{pc} (cathodic peak potential)+0.03.

Table 1. Reduction Potentials of Tropylium Ions **1** and **2**[a]

Cation	R^1	R^2	R^3	Counter Ion	E_1^{red}/V vs. SCE[b]
1a	OMe	OH	Br	BF_4^-	−0.06
1b	OMe	OMe	Br	BF_4^-	−0.13
1c	H	H	H	BF_4^-	−0.16
1d	SMe	H	H	ClO_4^-	−0.26
1e	OMe	OH	H	Cl^-	−0.33
1f	OMe	H	H	ClO_4^-	−0.36
1g	SMe	SMe	H	ClO_4^-	−0.38
1h	*p*-$NMe_2C_6H_4$	H	H	ClO_4^-	−0.40
1i	1,3,5-Trimethyl			BF_4^-	−0.42
1j	OMe	SMe	H	I^-	−0.51
1k	OMe	H	OMe	BF_4^-	−0.53
1l	1,2,4,5-Tetramethyl			BF_4^-	−0.55
1m	OMe	OMe	H	BF_4^-	−0.55
1n	NHMe	H	H	BF_4^-	−0.64
1o	NH_2	SMe	H	I^-	−0.64
1p	-NMePh	H	H	ClO_4^-	−0.73
1q	NMe_2	H	H	BF_4^-	−0.80
1r	NHMe	OMe	H	BF_4^-	−0.90
2a	$-SCH_2CH_2S-$		H	BF_4^-	−0.29
2b	$-OCH_2CH_2O-$		H	BF_4^-	−0.51

a) 0.1 M Et_4NClO_4 (1 M=1 mol dm^{-3}) in MeCN, Pt electrode, scan rate 100 mV s^{-1}. b) These peaks are all irreversible. Calculated as E_{pc} (cathodic peak potential)+0.03.

1g,m by 0.09 V may be attributed to the nonplanar structures of **2a,b**. The redox potentials for the tricyclic cations **4** are shown in Table 2. The values are higher than those for the corresponding monocyclic or bicyclic cations and even oxidation potentials are observed. These results show that tropylium ions with different reduction potentials can be readily prepared.

Reaction of Tropylium Ions with $TCNQ^{-}$. When a boiling ethanol or acetonitrile solution of the salts of monocyclic tropylium ions **1** was treated with $TCNQ^{-}$ lithium salt in boiling ethanol, **1j,k,l,m,n,q** gave simple salts and **1d,f,g,h,p** gave complex salts. The molar ratios are shown in Table 3. Cation **1g** which formed a complex salt by direct mixing gave a simple salt when the metathesis was carried out in the presence of lithium iodide. Treatment of the simple salts with TCNQ in boiling acetonitrile gave their complex salts. These salts are the first $TCNQ^{-}$ salts of tropylium ion species.

In contrast, nonsubstituted one **1c** underwent a reaction with $TCNQ^{-}$ to give **8** (R=H) and neutral TCNQ without the formation of salts as reported by Melby.[7] Tropylium ions **1b,i** underwent the same type of reaction to give **8** and neutral TCNQ. The bicyclic cations **2a** also underwent the same type of reaction, while **2b** gave a complex salt. In the case of tricyclic cations, **4a,c—f** gave simple salts and **4b** gave a 1:2 salt by metathesis, while **6** underwent the reaction with $TCNQ^{-}$. It should be noted that the cations **1b,c,i,2a** and **6** which underwent the reaction have higher reduction potentials. This fact shows that the reduction potentials strongly affect the formation of salts. The molar ratios of the initially formed salts are also related to the reduction potentials. Figure 2 clearly shows the effects of the reduction potentials. The tropylium ions in region I ($E_1^{red}>-0.2$ V) underwent the reaction. The ions in region II (-0.43 V$<E_1^{red}<-0.2$ V) formed complex salts, while the ions in region III ($E_1^{red}<-0.43$ V) formed simple salts. There are some exceptions, indicating that the salt formation is also affected by other factors. For example, the bicyclic cation **2a** in region II underwent the reaction and **2b** in region III formed a complex salt. This can be attributed to the nonplanar structures which make it difficult to form salts. The reason for the formation of the complex salt of **1p** which is in region III may be attributed to the large size of **1p**. Decrease in the Coulomb force due to the low electron affinity of **1r** may be the reason for the formation of the complex salt of **1r**.

These findings suggest the reaction mechanism shown in Scheme 1. When the salt formation takes place faster than the coupling reaction or electron transfer, simple salts are formed. When electron transfer competes with the salt formation, complex salts are formed since electron transfer leads to the formation of neutral TCNQ which reacts with simple salts to give complex salts. The effect of lithium

Table 3. Properties of $TCNQ^{-}$ Salts

Cation	Molar ratio	ν/cm^{-1}	ρ/Ω cm[a]
1d	1:2	2187	9.4
1f	2:3	2184	3.7×10
1g	1:1[b]	2184	1.3×10^{2}
	2:3	2183	1.6×10
1h	1:2:$(H_2O)_{0.5}$	2188	9.6
1j	1:1	2187	5.2×10^{2}
	1:1:H_2O	2188	3.8×10^{2}
1k	1:1	2173	2.7×10^{7}
	1:2[c]	2194	9.2×10^{3}
1l	1:1	2167	1.1×10^{6}
	1:2[c]	—[d]	1.1×10^{2}
1m	1:1	2182	5.8×10
	1:2[c]	2187	2.9×10
1n	1:1:H_2O	2189	3.3×10^{2}
	2:3[c]	2188	7.4
1p	1:2	2189	4.8×10
1q	1:1	2160	5.1×10^{6}
	1:2[c]	2188	2.4
1r	1:2:$(H_2O)_2$	2188	9.1
2b	2:3	2184	2.8×10^{4}
4a	1:1	2170	1.9×10^{3}
	1:2[c]	2190	4.0
4b	1:2	2190	1.3×10
4c	1:1	2178	2.8×10
	1:2[c]	2188	4.3
4d	1:1	2178	1.4×10^{3}
	1:2[c]	2192	5.2
4e	1:1	2173	7.1×10^{7}
4f	1:1	2167	7.4×10^{7}
	1:2[c]	2193	9.0

a) Measured at room temperature as compressed pellets by two probe technique. The electrical resistivity of the TTF-TCNQ complex measured by this method was 0.37. b) In the presence of LiI. c) Obtained by reaction of 1:1 salts with TCNQ. d) No measurement.

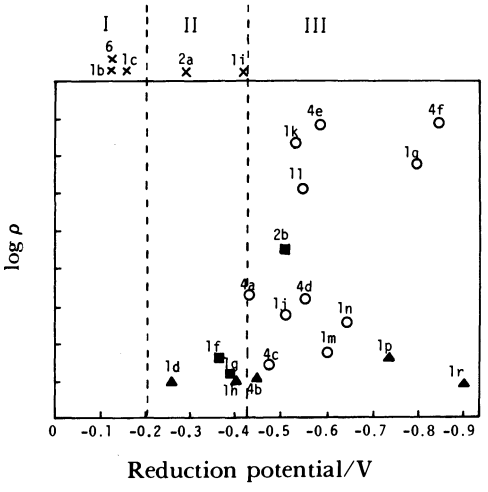

Fig. 2. Relationship between reduction potentials of cations and electrical resistivities (ρ) and molar ratios of the initially for med salts. 1: salt (○); 1:2 salt (▲); 2:3 salt (■); reaction (×).

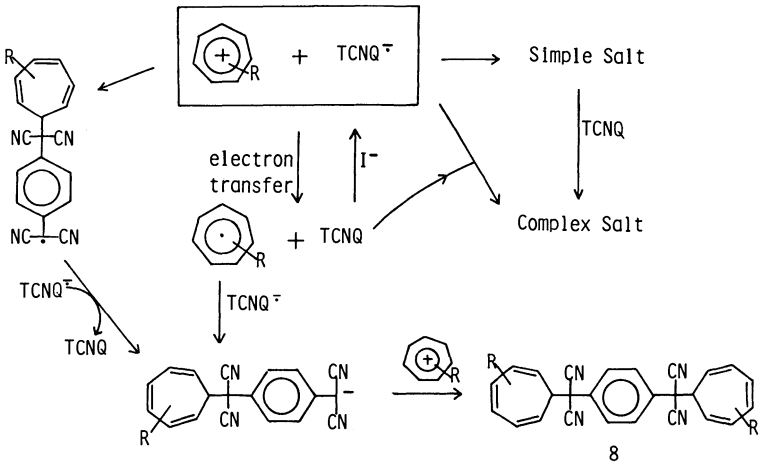

Scheme 1.

iodide can be explained by considering that neutral TCNQ which was formed by the electron transfer reaction was reduced by I^- to give $TCNQ^-$. On the other hand, highly reactive tropylium ions undergo the reaction to give the adducts **8** by the mechanism shown in Scheme **1** instead of the salt formation. The reduction potentials for the cations play an important role in determining the reactivities, since the reduction potentials of tropylium ions are related to their pK_R^+ values and electron affinities.[19]

This mechanism is supported by the following results. When each ethanol solution of cations and Li^+TCNQ^- (1 equiv) at low concentration (ca. 10^{-4} M) were mixed, the green color due to $TCNQ^-$ immediately disappeared in the case of cations which belong to region I and II, while in the case of cations which belong to region III the green color remained. The molar ratios of the cations to TCNQ can be determined by measuring the intensity ratios of the absorbance at 400 nm to that at 842 nm in the absorption spectra in which those for the simple salts are shown to be 0.5.[5,20] In fact, ratios in the above green solutions were about 0.5. The ratios for the **1p,r** which belong to region III but form complex salts were 0.50 and 0.54, respectively, indicating that the cations **1p,r** as well as other cations which belong to region III are stable under these conditions. These findings suggest that the reactivity of cations to $TCNQ^-$ is determined by the reduction potentials, but the salt formation is also affected by the factors other than the reactivity of cations.

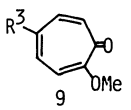

9

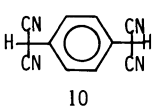

10

On the other hand, hydroxy derivatives **1a,e** underwent a proton transfer to give tropone derivatives **9** and dihydrodihydroxy-TCNQ **10**, indicating that hydroxy derivatives cannot be used for the formation of salts.

The properties of $TCNQ^-$ salts are summarized in Table 3. Electrical resistivities are relatively low, indicating that tropylium ions are good cations for forming highly conductive $TCNQ^-$ salts. It is interesting that even alkyl derivative **11** forms conductive $TCNQ^-$ salts. The 1:2 salts are more conductive than the corresponding 1:1 salts as found in usual $TCNQ^-$ salts.[3,4] It should be noted here that the simple salts of **1m** and **4c** show significantly low resistivities compared with those for $TCNQ^-$ simple salts of other cations except NMP.[3,4] Resistivities of the simple salts seem to be related to the structures of cations as well as the reduction potentials as shown in Fig. 2. For example, the resistivity of 1,4-dimethoxy derivative **1k** is higher than that of 1,2-dimethoxy derivative **1m**. This can be accounted for by the nonplanar structure of **1k** which is deduced from the higher reduction potential compared with that for **1m**. The high resistivity of the $TCNQ^-$ simple salt of tetramethyl derivative **11** may also be explained in terms of the steric factor. In addition, the fact that the cations **1q** and **4f** having lower reduction potentials form lower conductive salts indicates that there is a lower limit of the reduction potentials for the cations to show good conductivities. In the salts of cations having lower reduction potentials, the ions seem to be completely charged due to the poor electron affinity of the cations. This is supported by the finding that the anion radical of $TCNQF_4$ which is a strong electron acceptor than TCNQ forms a low conductive simple salt with tricyclic cation **4c** (ρ; $1.8\times10^5\ \Omega$ cm).

Another interesting feature is that the nitrile stretching frequencies for 1:1 salts are lower than those for the metal salts[21] even if the salts show high conductivities. Nitrile stretching frequencies for TCNQ complexes or salts are reported to be linearly correlated with the degree of charge transfer[22] and are

conventionally used for determining it. It has recently been reported that when a salt or a complex takes a mixed stack, there is no linear correlation between them.[23] Our result shows that even in the case of good conductive salts which are considered to form segregated stacks, nitrile stretching frequencies are not always linearly correlated with the degree of charge transfer.

BTDA-TCNQ$^-$ Salts of Tropylium Ions. Bis-[1,2,5]thiadiazolotetracyanoquinodimethan (BTDA-TCNQ) has been found to afford highly conductive charge transfer (CT) complexes with some donors.[10,24] BTDA-TCNQ which forms a two dimensional network by a strong S···N≡C interaction[25] is expected to give two- or three-dimensional CT complexes or anion radical salts. The first reduction potential of BTDA-TCNQ (−0.02 V vs. SCE) is a little lower than that of TCNQ (+0.18 V vs. SCE), indicating that the electron transfer from BTDA-TCNQ$^-$ to cations more easily takes place than that from TCNQ$^-$. On the other hand, the nucleophilicity of BTDA-TCNQ$^-$ is considered to be weaker than that of TCNQ$^-$ since negative charge is delocalized in the thiadiazole rings.[26]

When a boiling ethanol or acetonitrile solution of monocyclic tropylium ions was treated with Li$^+$ BTDA-TCNQ$^-$ in boiling ethanol, salts whose molar ratios are shown in Table 4 precipitated. Most of salts contain water, indicating that BTDA-TCNQ$^-$ tends to uptake water. It should be noted that the cations **1b** and **1i** which underwent the coupling reaction with TCNQ$^-$ gave salts with BTDA-TCNQ$^-$. Bicyclic cation **2a** which underwent the coupling reaction with TCNQ$^-$ also formed a salt with BTDA-TCNQ$^-$. These facts can be explained in terms of the low nucleophilicity of BTDA-TCNQ$^-$ which reduces the reactivity for the coupling reaction. The electrical resistivities of the BTDA-TCNQ$^-$ salts summarized in Table 4 show that these salts are conductive, indicating the usefulness of BTDA-TCNQ$^-$ for forming organic semiconductors with cations. The nitrile stretching frequencies are lower than those for the metal salts.[27] This may be accounted for by the strong S···N≡C interaction.

Table 4. Properties of TCNQ$^-$ Salts

Cation	Molar ratio	ν/cm^{-1}	ρ/Ω cm[a]
1b	3:4	2173	3.7×10^2
1d	1:1	2172	2.5×10^3
1f	1:3:H_2O	2177	9.7×10^3
1g	1:1:H_2O	2172	7.6×10^2
1h	1:1.5:H_2O	2170	1.4×10
1i	2:3:H_2O	2167	4.5×10
1j	1:1:$(H_2O)_{1.5}$	2170	9.4×10
1l	1:2:H_2O	2173	8.5×10
1m	2:3	2174	4.0×10
1n	1:1:$(H_2O)_2$	2166	2.9×10^2
1p	3:4	2177	3.0×10
1q	1:1:H_2O	2167	4.4×10^3
1r	2:3:$(H_2O)_3$	2167	3.0×10^3

a) Measured under the same conditions as those of TCNQ$^-$ Salts

Conclusion

Tropylium ions with different reduction potentials were prepared. The first reduction potentials are correlated with the substituent constants σ_p^+ and the substituent effects are additive. The tropylium ions were found to form conductive salts with TCNQ$^-$. The reduction potentials for cations affect the salt formation. The tropylium ions with higher reduction potentials (E_1^{red}>−0.2 V) undergo the reaction with TCNQ$^-$. When the reduction potentials are between −0.2 V and −0.43 V, complex salts are formed. When they are lower than −0.43 V, simple salts are formed. Electrical resistivities of the salts are relatively low and particularly, those of the simple salts of **1m** and **4c** are much lower than those of usual TCNQ$^-$ simple salts. The nitrile stretching frequencies for the salts are not linearly correlated with the degree of charge transfer. BTDA-TCNQ$^-$ also gave conductive salts of tropylium ions. Due to the low nucleophilicity, BTDA-TCNQ$^-$ formed salts with even tropylium ions which have high reduction potentials and underwent the reaction with TCNQ$^-$.

Experimental

General Methods. IR spectra were taken on a Shimadzu IR-27G spectrometer or a Shimadzu IR-435 spectrometer equipped with a Shimadzu DR-1 data recorder. UV spectra were measured with a Hitachi 340 spectrophotometer and mass spectra with a Hitachi M-52 mass spectrometer. ^{1}H NMR spectra were obtained at 60 MHz on a Varian EM-360, at 90 MHz on a Varian EM-390, at 200 MHz on a Varian XL-200 spectrometer. Redox potentials were measured on a Yanako Voltammetric Analyzer p-1000. All reaction solvents were distilled prior to use. Melting points were measured on a Laboratory Devices MEL-TEMP apparatus and are uncorrected.

Preparation of 5-Bromo-1-hydroxy-2-methoxytropylium Tetrafluoroborate and 5-Bromo-1,2-dimethoxytropylium Tetrafluoroborate. A solution of 900 mg (4.19 mmol) of 5-bromo-2-methoxytropone and 743 mg (7.03 mmol) of trimethyloxonium tetrafluoroborate in 5 ml of anhydrous nitromethane was stirred under nitrogen for 58 h at room temperature. After 1 ml of methanol was added to quench the excess of the methylating reagent, addition of 15 ml of absolute ether precipitated pale yellow crystals which were collected by filtration followed by washing with absolute ether to give 810 mg (61% yield) of the BF_4^- salt of **1b**. From the filtrate, pale yellow crystals were precipitated on cooling. Filtration followed by washing with absolute ether gave 150 mg (12% yield) of the BF_4^- salt of **1a**. **1a**-BF_4^-: mp 155—158 °C; IR (KBr) 3400—3300, 3100—3000, 1592, 1570, 1500, 1450, 1350, 1275, 1150—980, 830, 530 cm^{-1}; ^{1}H NMR (CD_3CN, 90 MHz) δ=4.05 (s, 3H), 5.75—5.95 (brs, 1H), 7.31 (d, 1H, J=12 Hz), 7.41 (d, 1H, J=12 Hz), 8.10 (d, 2H,

J=12 Hz). **1b**-BF_4^-: mp 157—159 °C; IR (KBr) 3100, 1530, 1475, 1445, 1280, 1150-950, 923, 840, 700 cm^{-1}; MS m/z 316 (M^+); ^1H NMR (CD_3CN, 90 MHz) δ=4.28 (s, 6H), 8.07 (d, 2H, J=12 Hz), 8.73 (d, 2H, J=12 Hz).

Preparation of 1,4-Dimethoxytropylium Tetrafluoroborate. A solution of 80 mg (0.588 mmol) of 4-methoxytropone and 100 mg (0.647 mmol) of trimethyloxonium tetrafluoroborate in 3 ml of dichloromethane was stirred under nitrogen for 12 h. Addition of 50 ml of absolute ether precipitated 80 mg (85% yield) of **1k**-BF_4^- as colorless crystals which were used for the salt formation without further purification due to the deliquescent property. **1k**-BF_4^-: mp 93—95 °C; IR (KBr) 3100—2950, 1570, 1490, 1431, 1305, 1205, 1150—950, 862, 682 cm^{-1}; MS m/z 150 (M^+-BF_4); ^1H NMR (CD_3CN, 90 MHz) δ=4.12 (s, 6H), 7.95 (d, 2H, J=11 Hz), 8.11 (s, 2H), 8.70 (t, 1H, J=11 Hz).

Preparation of 1-Methylamino-2-methoxytropylium Tetrafluoroborate. 300 mg (2.83 mmol) of 2-aminotropone and 460 mg (3.11 mmol) of trimethyloxonium tetrafluoroborate in 5 ml of anhydrous nitromethane was stirred at room temperature for 82 h. After methanol was added to quench the excess of trimethyloxonium salt, addition of 30 ml of absolute ether precipitated yellow crystals. Filtration followed by washing with absolute ether gave 225 mg (36% yield) of **1r**-BF_4^- which was used without further purification due to the strongly deliquescent property. **1r**-BF_4^-: mp 93—98 °C, IR (KBr) 3200—2900, 1640, 1590, 1500, 1440, 1275, 1218, 1150—950, 940, 745 cm^{-1}; MS m/z 150 (M^+-BF_4); ^1H NMR (CD_3CN, 90 MHz) δ=4.19 (s, 3H), 4.73 (s, 3H), 7.40—7.95 (m, 5H).

Preparation of Methylthio Derivatives 1g,j,o. These tropylium ions were prepared by the reaction of corresponding tropothiones with methyl iodide. 2-Methyltropothione[28] and 2-aminotropothione[29] were prepared according to Nozoe's method. 2-Methoxytropothione was synthesized by the following method. To a suspension of 1.63 g (7.35 mmol) of phosphorus pentasulfide and 0.800 g (8.09 mmol) of triethylamine in 50 ml of carbon disulfide, a solution of 1.00 g (7.35 mmol) of 2-methoxytropone in 50 ml of carbon disulfide was added and stirred under nitrogen for 12 h at room temperature. The precipitated deep orange crystals were separated by decantation and washed with 10 ml of carbon disulfide 3 times. The combined carbon disulfide solution was evaporated under reduced pressure below 20 °C to give 670 mg (60% yield) of 2-methoxytropothione which was used without further purification. The structure of 2-methoxytropothione was confirmed by the ^1H NMR spectrum. ($CDCl_3$, 60 MHz) δ=3.90 (s, 3H), 6.5—7.0 (m, 4H), 8.15 (d, 1H, J=12 Hz).

When a solution of tropothiones and methyl iodide (10—30 equiv) in absolute ether was stirred under nitrogen for 12—15 h at room temperature, red solids deposited. Filtration followed by washing with absolute ether gave the iodides of tropylium ions **1g,j,o** in 70%, 25%, and 48% yields, respectively. **1g**: mp 178—180 °C; IR (KBr) 3100—2900, 1490, 1472, 1400, 1389, 1320, 1278, 1240, 1090, 1045, 735, 550 cm^{-1}; MS m/z 183 (M^+-I); ^1H NMR (CD_3CN, 90 MHz) δ=2.92 (s, 6H), 8.13—8.47 (m, 5H). **1j**: mp 93—95 °C; IR (KBr) 3000—2950, 1510, 1488, 1450, 1420, 1280, 1220, 1020, 938, 750, 560 cm^{-1}; ^1H NMR (CD_3CN, 90 MHz) δ=2.79 (s, 3H), 4.40 (s, 3H), 8.2—8.5 (m, 5H). **1o**: mp 130 °C (decomp); ^1H NMR (CD_3CN, 90 MHz) δ=2.78 (s, 3H), 7.6—8.1 (m, 5H).

Since the solubility of the iodide of **1g** in ethanol or acetonitrile was too low to be used for the salt formation, the counter anion was substituted for BF_4^-. To a solution of 200 mg of the iodide in 5 ml of absolute acetonitrile, 126 mg (0.645 mmol) of $AgBF_4$ was added. After the solution was stirred at room temperature for 1 h, the deposited AgI was filtered off and washed with absolute acetonitrile. The combined acetonitrile solution was evaporated to give 147 mg (84% yield) of the BF_4^- salt: mp 205—210 °C (decomp).

Preparation of Bicyclic Tropylium Ions 2. These ions were prepared by the deprotonation of the corresponding cycloheptatrienes **3a**[12] and **3b**.[13] To a solution of 200 mg (0.338 mmol) of bicyclic cycloheptatriene **3a** in 10 ml of anhydrous acetonitrile, 236 mg (2.02 mmol) of $NOBF_4$ in 5 ml of anhydrous acetonitrile was added with nitrogen bubbling. After the solution was stirred at room temperature for 15 min, addition of 50 ml of absolute ether precipitated yellow crystals. Filtration followed by washing with absolute ether gave 65 mg of **2a**-BF_4^-. The residue which was obtained by evaporation of the filtrate was treated with absolute ethanol. From the soluble part in ethanol, 130 mg of **2a**-BF_4^- was obtained by removal of the solvent. The total yield was 72%. **2a**-BF_4^-: mp 138—140 °C, IR (KBr) 3050—2950, 1500, 1470, 1425, 1285, 1150—950, 730 cm^{-1}; ^1H NMR (CD_3CN, 90 MHz) δ=3.61 (s, 4H), 8.02 (d, 2H, J=11 Hz), 8.10 (t, 1H, J=11 Hz), 8.45 (dd, 2H, J=11, 11 Hz).

Similarly, the reaction of 150 mg (1 mmol) of bicyclic cycloheptatriene **3b** with $NOBF_4$ (2 equiv) gave 189 mg (80% yield) of ethylenedioxytropylium ion **2b**: mp 128—130 °C; IR (KBr) 3100—3000, 1480, 1468, 1284, 1185, 1150—950, 750, 700 cm^{-1}; ^1H NMR (CD_3CN, 90 MHz) δ=4.70 (s, 4H), 8.40 (s, 5H).

Preparation of 5-Methyl-5*H*-cyclohepta[*b*]quinoxaline. A solution of 4.69 g (33.4 mmol) of 2-chlorotropone and 4.50 g (36.9 mmol) of *N*-methyl-1,2-phenylenediamine[30] in 60 ml of absolute ethanol was refluxed under nitrogen for 48 h. Removal of the solvent gave black tarry matter to which 2 M hydrochloric acid was added. The solution was washed with benzene to remove the recovered 2-chlorotropone, made basic with 2 M sodium hydroxide, and extracted with 100 ml of benzene 3 times. The extract was washed with sat. aqueous $NaHCO_3$ and dried over Na_2SO_4. Evaporation of the solvent followed by column chromatography on alumina (2:1 ether-hexane) gave 2.38 g of dark green crystals which were recrystallized from pentane-hexane to give 1.80 g (26% yield) of **5c** as dark green needles: mp 92—93 °C; IR (KBr) 3050, 2900, 1620, 1570, 1480, 1330, 720 cm^{-1}; MS (25 ev)(relative intensity) 208 (M^+, 92), 193 (M^+,$-CH_3$); ^1H NMR ($CDCl_3$, 200 MHz) δ=2.74 (s, 3H), 4.42 (ddd, 1H, J=9.5, 2.0, 0.8 Hz), 5.29 (dddd, 1H, J=11.0, 8.0, 2.9, 2.0 Hz), 5.57 (ddd, 1H, J=12.0, 2.9, 1.0 Hz), 5.85 (dddd, 1H, J=12.0, 8.0, 1.2, 0.8 Hz), 5.86 (dddd, 1H, J=11.0, 9.5, 1.2, 1.0 Hz), 6.19 (dd, 1H, J=8.0, 1.2 Hz), 6.63 (ddd, 1H, J=10.0, 7.0, 1.2 Hz), 6.66 (dd, 1H, J=10.0, 2.3 Hz), 6.73 (ddd, 1H, J=8.0, 7.0, 2.3 Hz). Found: C, 80.74; H, 5.81; N, 13.45%. Calcd for $C_{14}H_{12}N_2$: C, 80.46; H, 5.81; N, 13.51%.

Preparation of Tricyclic Cation 4b,d,f by Methylation of the Corresponding Heterocycles 5. Methylation of **5a** using methyl iodide or dimethyl sulfate gave a complex mixture of products. However, reaction of **5a** with trimethyloxonium tetrafluoroborate gave the methylated

Table 5. Decomposition Points, Crystal Forms, and Analytical Data of $TCNQ^-$ Salts

Cation	Decomp °C	Crystal form	Molar ratio	Anal. Calcd / Found C/%	H/%	N/%
1d	208—210	Black needles	1:2	70.43	3.14	20.54
				70.14	2.88	20.00
1f	185—188	Violet needles	2:3	73.06	3.54	19.00
				73.15	3.32	19.55
1g	206—208	Black needles	1:1	65.09	3.90	14.46
				64.95	3.86	15.02
	202—205	Black needles	2:3	66.23	3.50	17.17
				65.38	3.47	17.15
1h	205—210	Black powder	$1:2:(H_2O)_{0.5}$	74.63	3.85	20.08
				74.90	3.80	19.75
1j	203—205	Black needles	1:1	67.91	4.08	15.08
				67.58	3.92	15.79
	203—205	Black needles	$1:1:H_2O$	64.76	4.40	14.39
				65.09	4.27	14.25
1k	205—208	Black needles	1:1	70.98	4.25	15.77
				70.66	4.72	15.88
	208—210	Black needles	1:2	70.83	3.42	20.03
				70.84	3.48	19.55
1l	>120	Green powder	1:1	78.83	5.18	15.99
				78.99	5.38	15.87
	158—160	Black needles	1:2	75.80	4.00	20.20
				75.76	4.05	20.05
1m	172—174	Violet needles	1:1	70.98	4.25	15.77
				70.71	4.83	15.18
	210—213	Black powder	1:2	70.83	3.42	20.03
				71.07	3.29	20.59
1n	135—140	Blue-violet powder	$1:1:H_2O$	70.58	4.15	20.58
				70.40	4.15	19.93
	180—185	Black needles	2:3	73.23	3.78	22.99
				73.00	3.45	23.24
1p	210—220	Violet powder	1:2	75.48	3.67	20.86
				75.13	3.30	20.03
1q	204—206	Violet needles	1:1	74.54	4.77	20.70
				74.29	4.56	20.48
	>350	Black needles	1:2	73.05	3.92	23.23
				73.41	3.49	23.03
1r	>350	Violet needles	$1:2:(H_2O)_2$	66.66	4.07	21.20
				67.16	3.55	20.57
2b	>350	Black needles	2:3	71.20	3.32	18.45
				70.79	3.30	18.04
4a	195—200	Violet needles	1:1	74.99	3.52	17.49
				75.19	3.42	17.14
	>350	Violet needles	1:2	73.50	3.00	20.85
				72.66	2.91	21.29
4b	229—231	Violet needles	1:2	71.91	3.18	19.86
				71.42	3.02	19.16
4c	198—200	Blue-violet needles	1:1	72.10	3.39	16.82
				71.39	3.29	16.47
	>350	Violet plates	1:2	71.60	2.92	20.31
				70.65	2.94	19.69
4d	208—210	Red-violet needles	1:1	75.35	3.89	16.90
				74.70	3.56	17.13
	251—255	Violet needles	1:2	73.28	3.26	20.38
				72.95	3.12	20.62
4e	157—160	Green columns	1:1	75.53	4.14	20.33
				74.94	3.87	20.22
4f	226—227	Blue-violet needles	1:1	75.86	4.48	19.66
				76.18	4.34	19.41
	264—266	Blue-violet needles	1:1	74.16	3.67	22.17
				74.11	3.43	22.19

Table 6. Decomposition Points, Color, and Analytical Data of BTDA-TCNA$^-$ Salts

Cation	Decomp °C	Color	Molar ratio	Anal. Calcd / Found C/%	H/%	N/%
1b	310—315	Blue-black	3:4	45.69	1.53	22.73
				46.15	1.71	22.53
1d	265—270	Violet	1:1	52.04	2.84	24.28
				51.15	1.76	24.68
1f	230—260	Black	1:3:H_2O	48.04	1.01	30.56
				47.38	0.78	30.49
1g	265—270	Black	1:1:H_2O	48.35	2.41	21.48
				48.22	1.98	21.48
1h	219—224	Black	1:1.5:H_2O	55.92	2.56	25.69
				56.33	2.11	24.95
1i	155—158	Black	2:3:H_2O	53.23	1.57	26.60
				53.79	2.34	26.63
1j	252—255	Black	1:1:$(H_2O)_{1.5}$	49.02	2.74	21.78
				48.62	1.98	22.32
1l	204—205	Violet	1:2:H_2O	54.11	2.35	26.11
				53.42	2.40	25.54
1m	295—310	Violet	2:3	50.62	1.88	26.24
				51.16	1.86	25.78
1n	238—240	Violet	1:1:$(H_2O)_2$	50.47	2.96	26.45
				50.57	2.78	26.49
1p	215—218	Violet	3:4	57.80	2.26	26.21
				57.63	2.35	26.16
1q	250—252	Violet	1:1:H_2O	53.38	2.99	26.68
				53.55	2.49	26.24
1r	238—240	Violet	2:3:$(H_2O)_3$	49.30	2.29	27.68
				49.26	1.96	26.71
2a	277—280	Brown	—[a]	—	—	—
				48.88	2.40	16.28

a) The molar ratio could not be determined on the basis of the analytical data.

compound **4b**. 99 mg (0.711 mmol) of trimethyloxonium tetrafluoroborate was added under nitrogen to a solution of 150 mg (0.711 mmol) of **5a** in 5 ml of dichloromethane. Stirring at room temperature for 24 h gave 180 mg (80% yield) of **4b**-BF_4^-: mp 158—160 °C (decomp); ^{1}H NMR (CD_3CN, 60 MHz) δ=3.67 (s, 3H), 6.97—7.67 (m, 9H).

Methylation of **5b** with methyl iodide in absolute ether readily gave **4d**-I^-: mp 196—198 °C (decomp); ^{1}H NMR (CD_3CN, 90 MHz) δ=3.33 (s, 3H), 6.67—9.96 (m, 9H).

Methylation of **5c** with methyl iodide in absolute ether gave deep green crystals which were recrystallized from ethanol to give **4f**-I^- in 75% yield as deep green plates: mp 267—268 °C (decomp); ^{1}H NMR (DMSO-d_6, 90 MHz) δ=3.13 (s, 6H), 6.46 (m, 2H), 6.55 (m, 1H), 6.67—7.10 (m, 4H), 7.30 (m, 2H). Found: C, 51.26; H, 4.36; N, 7.94%. Calcd for $C_{15}H_{15}N_2I$: C, 51.45; H, 4.32; N, 8.00%.

Preparation of Heterocyclic Cation 6. In a similar manner as the preparation of bicyclic cations **2a,b**, heterocyclic cation **6** was prepared by the dehydrogenation of heterocycle **7**[12] with $NOBF_4$. The reaction of 100 mg (0.434 mmol) of **7** with 51 mg (0.434 mg) of $NOBF_4$ in anhydrous acetonitrile gave 51 mg (37% yield) of **6**-BF_4^-: mp 40—42 °C; IR (KBr) 3020, 1604, 1510, 1457, 1440, 1270, 1100—980, 755, 730, 560 cm^{-1}; MS *m/z* 230 (M^+-BF_4) ^{1}H NMR (CD_3CN, 90 MHz) δ=7.4—7.9 (m, 4H), 8.3—8.7 (m, 5H). Found: C, 47.40; H, 3.48; S, 19.82%. Calcd for $C_{13}H_{10}S_2BF_4(H_2O)_{0.5}$: C, 48.02; H, 3.10; S, 19.72%.

Preparation of TCNQ$^-$ salts. The following is a general procedure to prepare salts. A boiling saturated absolute ethanol or acetonitrile solution of cations and a boiling saturated absolute ethanol solution of Li$^+$TCNQ$^-$ were mixed. The solution was allowed to stand at room temperature until crystals precipitated. Filtration followed by washing with a small amount of absolute ethanol and then absolute ether gave salts. The reaction of 1:1 salts with another equivalent of TCNQ in boiling acetonitrile gave their complex salts. Melting points, forms of crystals, and analytical data of salts are shown in Table 5.

Preparation of BTDA-TCNQ$^-$ Salts. BTDA-TCNQ$^-$ of tropylium ions were prepared by metathesis of tropylium ions and Li$^+$BTDA-TCNQ$^-$ in a similar manner as TCNQ$^-$ salts. The properties along with analytical data are shown in Table 6.

References

1) D. O. Cowan and F. M. Wiygul, *Chem. Eng. News*, **1986**, July 21, 28; M. R. Bryce and L. C. Murphy, *Nature (London)*, **309**, 119 (1984).

2) R. C. Wheland, *J. Am. Chem. Soc.*, **98**, 3926 (1976); G. Saito and J. P. Ferraris, *Bull. Chem. Soc. Jpn.*, **53**, 2141 (1980).

3) J. B. Torrance, *Acc. Chem. Res.*, **12**, 79 (1979).

4) J. H. Perlstein, *Angew. Chem., Int. Ed. Engl.*, **16**, 519 (1977).

5) L. R. Melby, *Can. J. Chem.*, **43**, 1448 (1965); D. J. Sandman, *J. Am. Chem. Soc.*, **100**, 5230 (1978).

6) The reduction potential ($E_{1/2}^{red}$) of $MeSO_4^-$ salt of NMP is −0.12 V vs. SCE which was measured under the con-

ditions shown in Table 1 (that of tropylium ion is −0.16 V vs. SCE).

7) L. R. Melby, R. J. Harder, W. R. Hertler, W. Mahler, R. E. Benson, and W. E. Mochel, *J. Am. Chem. Soc.*, **84**, 3374 (1962).

8) B. H. Klanderman and D. C. Hoesterey, *J. Chem. Phys.*, **51**, 377 (1969).

9) A report concerning $TCNQ^-$ salts of heterocyclic cations containing a tropylium ion skeleton has been published as a communication. Y. Yamashita, K. Hagiya, G. Saito, and T. Mukai, *Chem. Lett.*, **1986**, 537.

10) Y. Yamashita, T. Suzuki, T. Mukai, and G. Saito, *J. Chem. Soc., Chem. Commun.*, **1985**, 1044.

11) Other cations were prepared according to the following reports. **1d,f,h**; B. Föhlisch and E. Haug, *Chem. Ber.*, **104**, 2324 (1971). **1i,l**; K. Takeuchi, Y. Yokomichi, T. Kurosaki, Y. Kimura, and K. Okamoto, *Tetrahedron*, **35**, 949 (1979). **1m**; K. Hafner, H. W. Riedel, and M. Danielisz, *Angew. Chem.*, **75**, 344 (1963). **1p**; C. Juty and F. Voithenleitner, *Chem. Ber.*, **97**, 29 (1964). **1n,q**; H. J. Dauben, Jr., and D. F. Rhoades, *J. Am. Chem. Soc.*, **89**, 6764 (1967).

12) M. Cavazza, G. Morganti, and F. Pietra, *Rec. J. Roy. Net. Chem. Soc.*, **98**, 165 (1979).

13) T. Fukunaga, T. Mukai, Y. Akasaki, and R. Suzuki, *Tetrahedron Lett.*, **1970**, 2975.

14) Other methods of the deprotonation failed to give the cations **2**.

15) a) T. Nozoe, T. Asao, and K. Takahashi, *Bull. Chem. Soc. Jpn.*, **34**, 146 (1961); b) K. Shindo, S. Ishikawa, and T. Nozoe, *ibid.*, **58**, 165 (1985).

16) T. Nozoe, H. Okai, and T. Someya, *Bull. Chem. Soc. Jpn.*, **51**, 2185 (1978).

17) K. Shindo, S. Ishikawa, and T. Nozoe, The 47th National Meeting of the Chemical Society of Japan, Kyoto, April, **1983**, Abstr., 4F 34.

18) Amino and hydroxy derivatives are removed since the σ_p^+ substituent constant for amino and hydroxyl substituents are uncertain. H. C. Brown and Y. Okamoto, *J. Am. Chem. Soc.*, **80**, 4979 (1958).

19) The additivity of the methyl substituent effect has been already pointed out by Okamoto's group. K. Takeuchi, T. Kurosaki, Y. Yokomichi, Y. Kimura, Y. Kubota, H. Fujimoto, and K. Okamoto, *J. Chem. Soc., Perkin Trans. 2*, **1981**, 670.

20) R. Buvet, P. Dupuis, J. Neel, and J. Perichon, *Bull. Soc. Chim. Fr.*, **1969**, 3991.

21) The nitrile stretching frequencies of Li^+, Na^+, and K^+ were measured to be 2197, 2185, and 2188 cm^{-1}, respectively, under the same conditions as those for tropylium ion salts.

22) J. S. Chappell, A. N. Bloch, W. A. Bryden, M. Maxfield, T. O. Poehler, and D. O. Cowan, *J. Am. Chem. Soc.*, **103**, 2442 (1981).

23) M. Meneghetti, A. Girlando, and C. Pecile, *J. Chem. Phys.*, **83**, 3134 (1985).

24) Y. Yamashita, T. Suzuki, G. Saito, and T. Mukai, *Chem. Lett.*, **1985**, 1759.

25) C. Kabuto, T. Suzuki, Y. Yamashita, and T. Mukai, *Chem. Lett.*, **1986**, 1433.

26) X-Ray analyses of tetraalkylammonium salts of BTDA-$TCNQ^-$ show the delocalization of the negative charge. Dianion of BTDA-TCNQ can be isolated as stable Na^+ salts due to the delocalization in contrast to the dianion of TCNQ. These results will be soon reported elsewhere.

27) The nitrile stretching frequencies of neutral BTDA-TCNQ, and Li^+, Na^+, K^+ salts were 2225, 2195, 2185, and 2183 cm^{-1}, respectively.

28) T. Nozoe, M. Sato, and K. Matsui, *Proc. Jpn. Acad.*, **29**, 22 (1953).

29) T. Nozoe and K. Matsui, *Bull. Chem. Soc. Jpn.*, **34**, 1382 (1961).

30) G. W. H. Cheeseman, *J. Chem. Soc.*, **1955**, 3308.

The Solubility of Peptide Intermediates in Organic Solvents.[1] Solubilizing Potential of Hexafluoro-2-propanol

Mitsuaki NARITA,* Shinya HONDA, Hiroshi UMEYAMA, and Satoshi OBANA
Department of Industrial Chemistry, Faculty of Technology, Tokyo University of Agriculture and Technology, Koganei 184
(Received July 29, 1987)

The solubility of peptides to be insoluble in EtOH, MeOH, DMF, DMA, NMP, DMSO, and HMPA was examined in HFIP, sulfolane, TMP, PC, and a mixture of 5—10% HFIP-CH_2Cl_2 (v/v). HFIP has the highest solubilizing potential, followed by HMPA and DMSO, while the solubilizing potential of sulfolane, TMP, and PC is lower than that of HMPA, DMSO, DMF, and NMP and is close to that of MeOH and EtOH. The solubility of the peptides in the mixture of HFIP-CH_2Cl_2 marvelously is as high as that in HFIP alone. The solvent-titration study in CH_2Cl_2-polar solvents clearly indicated that the solubility of peptides having a β-sheet structure in organic solvents was independent of the polarity of the solvents but was strongly dependent on their hydrogen donating and accepting ability. The conformation of the peptides in the mixture of HFIP-CH_2Cl_2 and in HFIP alone was examined using the IR and CD spectroscopies, respectively.

The search for effective solvents for peptide and protein synthesis is of practical significance since the insolubility of peptide intermediates, protected peptides, is a serious problem for peptide and protein synthesis.[2] In many cases, the insolubility of peptide intemediates in high-polar organic solvents, namely, DMA, DMF, NMP, DMSO, and HMPA is caused by a β-sheet aggregation consisting of peptide chains equal to or larger than an octa- or nonapeptide sequence.[3-10] Therefore, it is of paramount significance to elucidate what plays an important role in disrupting a β-sheet aggregation.

1. Boc-Ser(Bzl)ValSer(Bzl)Thr(Bzl)ValLeu-OBzl
2. Boc-Leu6-OBzl
3. Boc-AlaSer(Bzl)LeuAsp(OBzl)Lys(Z)PheLeu-OPac
4. Boc-AlaSer(Bzl)ValSer(Bzl)Thr(Bzl)ValLeu-OPac
5. Boc-Glu(OBzl)AlaGlu(OBzl)Asp(OBzl)LeuGlnValGly-OPac
6. Boc-LeuAlaLeuGlu(OBzl)GlySer(Bzl)LeuGln-OPac
7. Boc-GlnValGlyGlnValGlu(OBzl)LeuGly-OPac
8. Boc-LeuAlaSer(Bzl)ValSer(Bzl)Thr(Bzl)ValLeu-OBzl
9. Boc-ValValLeuGlyAlaAlaIleVal-OBzl
10. Boc-Leu9-OBzl
11. Boc-Asp(OBzl)Lys(Z)PheLeuAlaSer(Bzl)ValSer(Bzl)Thr(Bzl)ValLeu-OBzl
12. Boc-ValAlaValLeuValValLeuGlyAlaAlaIleVal-OBzl
13. Boc-Leu12-OBzl
14. Boc-Glu(OBzl)AlaGlu(OBzl)Asp(OBzl)LeuGlnValGlyGlnValGlu(OBzl)LeuGly-OPac
15. Boc-AlaSer(Bzl)LeuAsp(OBzl)Lys(Z)PheLeuAlaSer(Bzl)ValSer(Bzl)Thr(Bzl)ValLeu-OBzl

Fig. 1. The peptides **1**—**15** used in this study.

Table 1. Solubility Properties[a] of the Peptides **1**—**15** (c=1.0 g dl^{-1})

Peptide ( )[c]	Solvent[b] HFIP	Sulfolane	TMP	PC	HMPA	DMSO	DMF DMA NMP	EtOH MeOH	AN	5% HFIP-CH_2Cl_2	10% HFIP-CH_2Cl_2	CH_2Cl_2
1 (6)	A	B	A	B	A	A	A	B	B	A	A	A
2 (6)	A	D	D	C	A	B	A	C, B	D	A	A	D
3 (7)	A	A	A	A	A	A	A	A	A	A	A	A
4 (7)	A	C	D	C	A	A	A	B	D	A	A	B
5 (8)	A	A	B	B	A	A	A	C	D	A	A	C
6 (8)	A	B	B	D	A	A	A	B	D	A	A	C
7 (8)	A	D	D	D	A	A	A	D	D	A	A	D
8 (8)	A	D	D	C	B	B	B	D	D	A	A	D
9 (8)	A	D	C	D	A	C	D	D	D	A	A	D
10 (9)	A	D	D	C	C	C	D	D	D	A	A	D
11(11)	A	D	D	D	C	D	D	D	D	D	A	D
12(12)	A	D	D	D	C	D	D	D	D	B	A	D
13(12)	C	D	D	D	D	D	D	D	D	D	D	D
14(13)	A	D	D	D	D	D	D	D	D	D	D	D
15(14)	C	D	D	D	C	D	D	D	D	D	D	D

a) Symbols of A, B, C, and D: see text. b) The dielectric constant of each solvent: HFIP, —; sulfolane, 43.3; TMP, —; PC, 65.1; HMPA, 30.0; DMSO, 46.7; DMF, 36.7; DMA, 37.8; NMP, 32.0; EtOH, 24.6; MeOH, 32.7; AN, 37.5; CH_2Cl_2, 8.9. c) Value in parenthesis: number of amino acid residues of peptides.

In this paper, we first examine the solubility of the peptides **1—15** (Fig. 1) in high-polar organic solvents shown in Table 1. Next using a solvent-titration technique, we exemplify that the hydrogen donating and accepting ability of solvent plays an important role in disrupting a β-sheet aggregation.

The peptides **1—15** have a β-sheet structure in the solid state, and their solubility was already examined in low-, medium-, and high-polar solvents such as benzene, carbon tetrachloride, ethyl acetate, tetrahydrofuran, dichloromethane, chloroform, AN, EtOH, MeOH, DMF, DMA, NMP, DMSO, and HMPA.[3-6] Generally, the solubility of peptides having a β-sheet structure in medium-polar solvents decreases extremely at a hexa- or heptapeptide level and their solubility in high-polar solvents, at an octa- or nonapeptide level.

Experimental

Materials. The samples of the peptides **1—15** are those prepared before.[3-6] The purity of the peptides was confirmed by elemental and amino acid analyses. The peptides soluble in DMF gave a single peak on high-performance liquid chromatography.

IR Measurements. The IR absorption spectra of the samples in dichloromethane were recorded at room temperature with a JEOL Model JIR-100 FT-IR spectrometer by employing 0.5 mm-path length cells with sodium chloride windows. The concentration of the peptides was kept 1.0×10^{-3} M (1 M=1 mol dm^{-3}).

CD Measurements. The CD spectra were recorded using a JASCO model J-40AS recording spectropolarimeter. Experimental details have been reported elsewhere.[11] The concentration of the peptides was kept 1.0 mg ml^{-1}.

Results and Discussion

The Solubility of the Peptides 1—15 in High-Polar Organic Solvents. The solubility of the peptides **1—15** was examined in the high-polar solvents shown in Table, namely, HFIP, sulfolane, PC, TMP, and a mixture of 5—10% HFIP-CH_2Cl_2 (v/v). The results are summarized in Table together with the solubility of the peptides **1—15** in HMPA, DMSO, DMF, DMA, NMP, EtOH, MeOH, AN, and CH_2Cl_2.[3-6] The solubility (c=1.0 g dl^{-1}) was divided into the following four classes: (A) completely soluble at room temperature, (B) completely soluble at 80°, (C) partially soluble at 80° and (D) nearly insoluble at 80°. In the cases of HFIP, EtOH, MeOH, 5% and 10% HFIP-CH_2Cl_2 mixtures, and CH_2Cl_2, the classes (B), (C), and (D) were decided at refluxing temperature. As shown in Table, among the solvents examined, HFIP has the highest solubilizing potential, followed by the second class of HMPA and DMSO and the third one of DMF, DMA, and NMP, while the solubilizing potential of sulfolane, TMP, and PC is lower than that of DMF, DMA, and NMP and is close to that of EtOH and MeOH. It is marvelous that the solubilizing potential of the mixture of HFIP-CH_2Cl_2 is higher than that of HMPA and DMSO and is close to that of HFIP alone. The last result is of great significance for peptide and protein synthesis since it suggests that we can use a mixture of HFIP and CH_2Cl_2 instead of quite expensive HFIP for further peptide-chain elongation.

Solvent-Titration Study of Boc-Val-Gly-Phe-Gly-Leu-Ile-Leu_2-OBzl 16. Octapeptides having a β-sheet structure in the solid state are usually insoluble

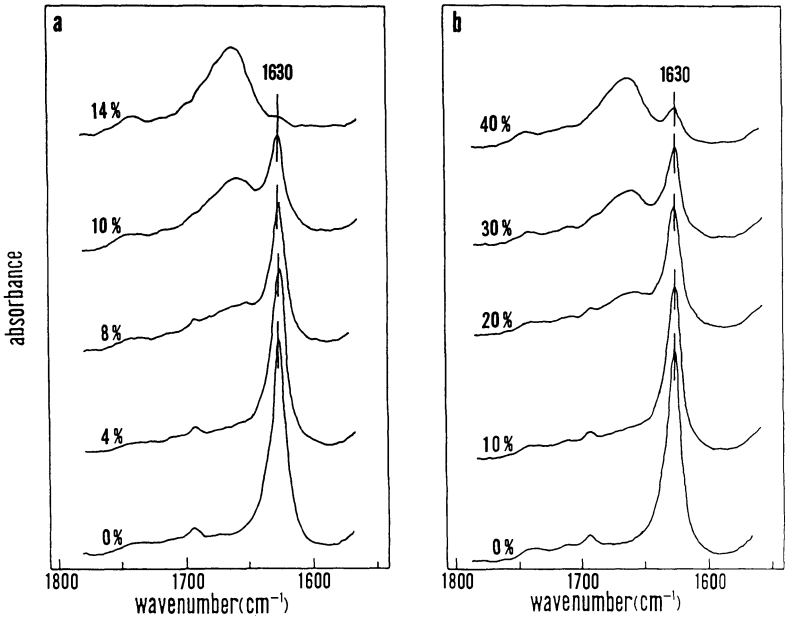

Fig. 2. Typical IR absorption spectra in the amide I region of the peptide **16** in CH_2Cl_2-DMSO (a) and CH_2Cl_2-TMP (b). The percentages in Fig. 2 indicate v/v-%.

in CH_2Cl_2,[3-6] but the octapeptide **16** is a novel one to be soluble in CH_2Cl_2. It has an antiparallel β-sheet structure in CH_2Cl_2 solution.[4] Figure 2 shows typical IR absorption spectra of the peptide **16** in CH_2Cl_2–DMSO and CH_2Cl_2–TMP solutions in the amide I region. Weak and strong bands at 1690 and 1630 cm^{-1} in CH_2Cl_2 solution, respectively, are assigned to an antiparallel β-sheet structure.[12] Successive addition of DMSO or TMP to the CH_2Cl_2 solution induces a dramatic decrease in the strong band at 1630 cm^{-1} and an increase in the broad band at 1660 cm^{-1}, indicating that the β-sheet aggregation of the peptide **16** is easily disrupted by increasing amounts of DMSO and TMP. Both solvents are known to function as hydrogen acceptor and to form effective hydrogen bonds with peptide N–H bonds, thereby disrupting the β-sheet aggregation. Figure 3 illustrates the solvent-titration curves of the peptide **16** in the CH_2Cl_2 solution. By adding increasing amounts of the high-polar solvents, namely, HFIP, HMPA, DMSO, TMP, and PC, similar trends as a function of solvent composition are observed among the high-polar solvents. These solvent-titration curves indicate that, among the solvents examined, HFIP has the highest potential for disrupting a β-sheet aggregation in the CH_2Cl_2 solution, followed by the second class of HMPA and DMSO, and the third one of TMP and PC. The similar trends were also observed among DMSO, HMPA, and TMP in the solvent-titration study of N-protected C-terminal sequences of substance P.[13] PC has the highest polarity (see footnotes in Table), but its solubilizing potential is low, while the polarity of HFIP is estimated to be similar to that of HMPA and DMSO, but its solubilizing potential is the highest. Similarly, AN with higher polarity than HMPA has remarkably lower solubilizing potential than HMPA. These results distinctly denote that the solubility of the peptides **1**—**15** in the high-polar solvents is independent of the polarity of solvent but is strongly dependent on the hydrogen donating and accepting ability of solvent.

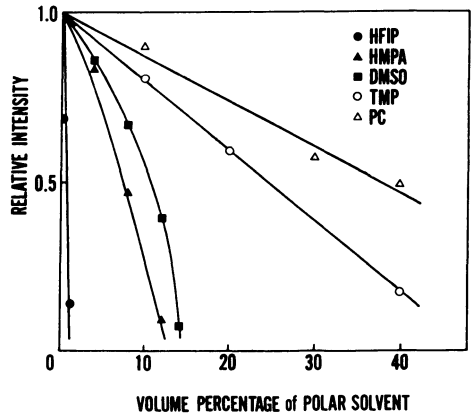

Fig. 3. Relative intensity of the amide I carbonyl stretching 1630-cm^{-1} band related to the β-sheet structure in the IR absorption spectra of the peptide **16** in CH_2Cl_2–HFIP (●) CH_2Cl_2–HMPA (▲), CH_2Cl_2–DMSO (■), CH_2Cl_2–TMP (○), and CH_2Cl_2–PC (△).

Conformation of the Peptides 6, 8—10, and 12 in 5% HFIP–CH_2Cl_2 (v/v) Solution and in HFIP Solution. Figure 4 presents the IR absorption spectra of the peptides **6**, **8—10**, and **12** in a 5% HFIP–CH_2Cl_2 solution in the amide I region. These spectra show that the 1630-cm^{-1} band disappears completely and the strong 1660-cm^{-1} band appears. These results distinctly indicate that HFIP having a strong proton donating ability effectively disrupts a β-sheet aggrega-

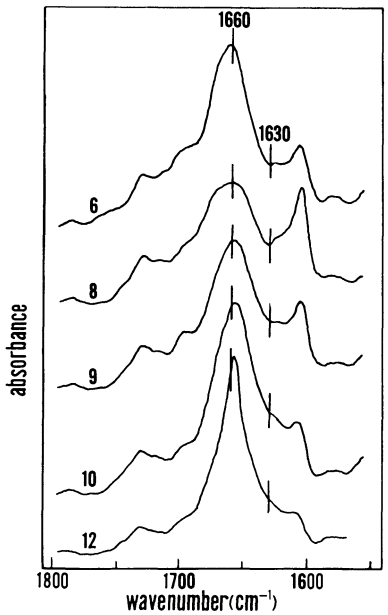

Fig. 4. IR absorption spectra in the amide I region of the peptides **6**, **8—10**, and **12** in 5% HFIP–CH_2Cl_2 solution.

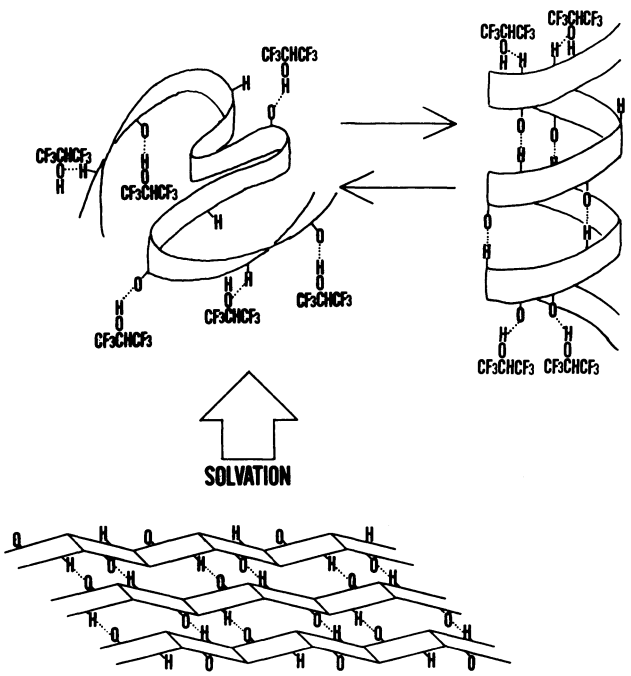

Fig. 5. Scheme in eqeuilibrium between unordered and helix structures.

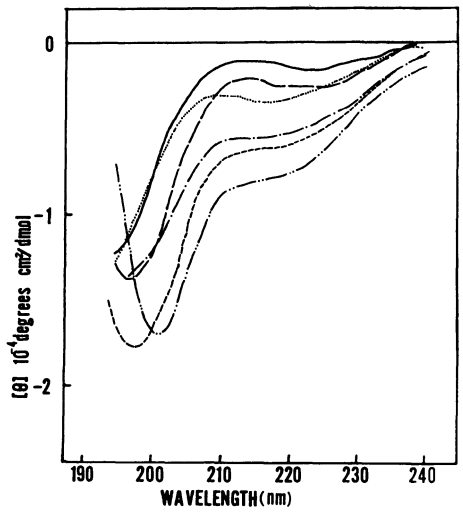

Fig. 6. CD spectra of the peptides **8**—**12** and **14** in HFIP solution. **8**, ——; **9**, ··; **10**, ------; **11**, —— **12**, —·—·—; **14**, —··—··—.

tion formed by peptide chains equal to or smaller than a dodecapeptide sequence. Since HFIP is known to promote helical folding of peptide chains, the conformation of the peptides **6**, **8**—**10**, and **12** in the 5% HFIP-CH_2Cl_2 solution might be in equilibrium between helical and unordered structures (Fig. 5), and the peptide to have unordered structures is justly subjected to solvation to form hydrogen bonds effectively shown in Fig. 5. As shown in Fig. 6, the CD spectra of the peptides **8**—**12** and **14** in HFIP practically indicate these peptides to be in equilibrium between helix and unordered structures. The equilibrium constant is properly dependent on the nature of amino acid sequences.

Conclusion

The solubilizing potential of high-polar organic solvents for peptide intermediates was in fairly good agreement with the hydrogen donating and accepting ability of solvents. Namely, the solubilizing potential was in the following order: HFIP≫HMPA and DMSO>DMF, DMA, and NMP≫TMP, PC, EtOH, and MeOH≫AN, while the hydrogen donating and accepting ability was also in the following order: HFIP≫HMPA>DMSO≫TMP>PC. The solubility of peptides equal to or larger than octapeptides having a β-sheet structure in the solid state in the mixture of 5—10% HFIP-CH_2Cl_2 (v/v) was marvelously close to their solubility in HFIP alone, indicating that HFIP behaves itself like a denaturant in CH_2Cl_2 solution although HFIP has a high potential as a promoter of helical folding of peptides. The results obtained in this paper afford the powerful basis for exploration of effective solvents for peptide and protein synthesis. Use of a mixture of HFIP and CH_2Cl_2 as a solvent in peptide chain elongation, in many cases, will also overcome the serious problem for peptide and protein synthesis, namely, the insolubility of peptide intermediates. Now, we are working on the peptide chain elongation in a mixture of HFIP-CH_2Cl_2.

The authors wish to thank Central Glass Co., Ltd., for the generous gift of HFIP.

References

1) This paper forms Part X of "Designs of Three-dimensional Structures of Peptides and Proteins and the Synthetic Route for Peptides and Proteins" series. For part IX of this series, see M. Narita, S. Honda, and H. Umeyama, *Bull. Chem. Soc. Jpn.*, to be submitted. The abbreviations for amino acids are those recommended by the IUPAC-IUB Commission on Biochemical Nomenclature, *J. Biol. Chem.*, **247**, 977 (1972). Amino acid symbols except for Gly denote the L-configuration. Additional abbreviations used are the following: EtOH, ethanol; MeOH, methanol; DMF, *N*,*N*-dimethylformamide; DMA, *N*,*N*-dimethylacetamide; NMP, *N*-methylpyrrolidone; DMSO, dimethyl sulfoxide; HMPA, hexamethylphosphoric triamide; HFIP, 1,1,1,3,3,3-hexafluoro-2-propanol; sulfolane, tetrahydrothiophene 1,1-dioxide; TMP, trimethyl phosphate; PC, propylene carbonate; AN, acetonitrile; IR; infrared; CD, circular dichroism; Boc, *t*-butoxycarbonyl; Bzl, benzyl; Z, benzyloxycarbonyl; Pac, phenacyl.

2) M. Narita, K. Ishikawa, J.-Y. Chen, and Y. Kim, *Int. J. Peptide Protein Res.*, **24**, 580 (1984).

3) M. Narita, T. Fukunaga, A. Wakabayashi, K. Ishikawa, and H. Nakano, *Int. J. Peptide Protein Res.*, **23**, 306 (1984).

4) M. Narita, J.-Y. Chen, H. Sato, and Y. Kim, *Bull. Chem. Soc. Jpn.*, **58**, 2494 (1985).

5) M. Narita, T. Ogura, K. Sato, and S. Honda, *Bull. Chem. Soc. Jpn.*, **59**, 2433, 2439, 2445 (1986).

6) M. Narita, M. Doi, and T. Nakai, *Int. J. Peptide Protein Res.*, to be submitted; M. Narita, M. Doi, and T. Nakai, *Bull. Chem. Soc. Jpn.*, in press; M. Narita, M. Doi, and H. Takegahara, *Bull. Chem. Soc. Jpn.*, in press.

7) M. Narita, S. Nagasawa, J.-Y. Chen, H. Sato, and Y. Tanaka, *Makromol. Chem.*, **185**, 1069 (1984); M. Narita, N. Ohkawa, S. Nagasawa, and S. Isokawa, *Int. J. Peptide Protein Res.*, **24**, 129 (1984); S. Isokawa, T. Asakura, and M. Narita, *Macromolecules*, **18**, 871 (1985); S. Isokawa, I. Tominaga, T. Asakura, and M. Narita, *ibid.*, **18**, 878 (1985).

8) M. Narita, M. Doi, H. Sugasawa, and K. Ishikawa, *Bull. Chem. Soc. Jpn.*, **58**, 1473 (1985); M. Narita, K. Ishikawa, H. Sugasawa, and M. Doi, *ibid.*, **58**, 1731 (1985).

9) M. Narita, M. Doi, K. Kudo, and Y. Terauchi, *Bull. Chem. Soc. Jpn.*, **59**, 3553 (1986).

10) M. Narita, S. Honda, and H. Umeyama, *Bull. Chem. Soc. Jpn.*, to be submitted.

11) M. Narita, K. Ishikawa, H. Nakano, and S. Isokawa, *Int. J. Peptide Protein Res.*, **24**, 14 (1984).

12) T. Miyazawa and E. J. Blout, *J. Am. Chem. Soc.*, **83**, 712 (1961); M. Narita, S. Isokawa, Y. Tomotake, and S. Nagasawa, *Polym. J.*, **15**, 25 (1983), and references cited therein.

13) C. Toniolo, G. M. Bonora, G. Stavropoulos, P. Cordopatis, and D. Theodoropoulos, *Biopolymers*, **25**, 281 (1986).

 © 1988 The Chemical Society of Japan Bull. Chem. Soc. Jpn., 61, 285—289 (1988)

Novel Sulfur-Containing Phytoalexins from the Chinese Cabbage *Brassica campestris* L. ssp. *pekinensis* (Cruciferae)[1]

Mitsuo TAKASUGI,* Kenji MONDE, Nobukatsu KATSUI, and Akira SHIRATA†,††
Department of Chemistry, Faculty of Science, Hokkaido University, Sapporo 060
†National Institute of Agro-Environmental Sciences, Yatabe-machi, Tsukuba 305
(Received July 29, 1987)

The first isolation and structure elucidation of four sulfur-containing indole phytoalexins from Chinese cabbage inoculated with *Pseudomonas cichorii* are described.

Accumulation of phytoalexins, antimicrobial compounds synthesized by plants after their exposure to micro-organisms,[2] has been described from over 20 plant families,[3] Because of their antimicrobial properties, an important role of phytoalexins in host defense mechanisms has been suggested.[4] We recently reported the isolation of two sesquiterpenoids,[5] a bibenzyl,[6] and two polyacetylenes[7] as phytoalexins from lettuce (*Lactuca sativa* var. *capitata*, Compositae), Chinese yam (*Dioscorea batatas*, Dioscoreaceae), and burdock (*Arctium lappa*, Compositae), respectively. The plant family Cruciferae includes many vegetables of economic importance such as cabbage, Chinese cabbage, radish, turnip, and so on.[8] However, no phytoalexins have been reported from this family. We reported, in a preliminary communication,[9] on the isolation and structures of three cruciferous phytoalexins, named methoxybrassinin (**1**), brassinin (**2**), and cyclobrassinin (**3**), from Chinese cabbage (*Brassica*

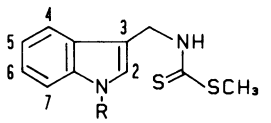

1 : R=OCH3
2 : R=H

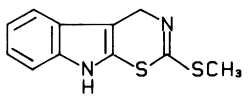

3

campestris L. ssp. *pekinensis*) inoculated with the bacterium *Pseudomonas cichorii*. In this paper we describe the details of the study and the isolation of an additional new phytoalexin, methoxybrassitin (**4**), together with a related compound **5**.

Results and Discussion

Sliced heads of Chinese cabbage were inoculated with the suspension of the bacterium *Pseudomonas cichorii* and incubated at 20 °C for 3 days. After being dried, the incubated tissue was extracted with acetone. Two-dimensional TLC bioassay[9] of the extracts revealed the presence of several antifungal compounds not detected in uninoculated control tissue. The acetone extracts from the inoculated tissue were submitted to sequential chromatography on silica gel and Sephadex LH-20 columns, giving five antifungal compounds **1**, **2**, **3**, **4**, and **5** in the yields (based on dry weight of the tissue) of 0.018%, 0.0022%, 0.0098%, 0.0011%, and 0.00047%, respectively.[10]

Methoxybrassinin (**1**) was obtained as a viscous oil. The molecular formula of **1** was determined to be $C_{12}H_{14}N_2OS_2$ by high-resolution mass spectrometry (HR-MS), together with ^1H and ^{13}C NMR spectral information. Its UV [λ_{max} (CH_3OH) 218 and 267 nm] spectrum suggested the presence of an *N*-methoxyindole nucleus[11] in **1**. The ^1H NMR spectrum ($CDCl_3$) showed signals for five aromatic protons, of which four [δ 7.60 (d, J=8 Hz, 4-H), 7.17 (ddd, J=8, 8, and 2 Hz, 5-H), 7.30 (ddd, J=8, 8, and 2 Hz, 6-H), and 7.45 (d, J=8 Hz, 7-H)] were assigned successively by spin-decoupling experiments and their locations were confirmed by nuclear Overhauser enhancement (NOE) difference experiments. Irradiation of N-OCH_3 protons at δ 4.10 resulted in enhancements of both the signals at δ 7.45 (7-H) and 7.34 (2-H), indicating that the position 2 of the indole nucleus is unsubstituted. Therefore, the position 3 of the nucleus should have a substituent. The ^1H and ^{13}C NMR spectra further indicated that the substituent contains one each of $-CH_2-$ [δ_H 5.02 (d, J=4 Hz) and δ_C 42.8], >NH [δ_H 7.0 (br s)], >C=S (δ_C 198.3), and $-SCH_3$ [δ_H 2.65 (s) and δ_C 18.2]. Its mass spectrum showed a base peak at *m/z* 160.0733 $(M-C_2H_4NS_2)^+$, indicating that the methylene in the substituent is attached to C-3 of the nucleus. Since ^1H NMR signals of the methylene changed from a doublet to a singlet on exchange with D_2O, it is further connected to the >NH leading to the whole structure **1**. The dithiocarbamate structure in **1** was further supported by the presence of a minor rotational isomer [δ 2.75 (s, $-SCH_3$), 4.75 (br d, J=4 Hz, $-CH_2-$), and 7.6 (br s, >NH)] due to hindered C-N rotation.[12] 1-Methoxyindole derivatives are rather rare as natural products[11] although the occurrence of indole alkaloids has been observed in many plants.[13]

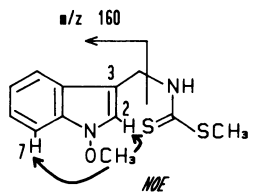

1

†† Present address: Sericultural Experiment Station, Yatabe-machi, Tsukuba 305.

Brassinin (**2**), mp 132—133 °C, has the molecular formula $C_{11}H_{12}N_2S_2$ by HR-MS. Its spectral data indicated **2** as a demethoxy derivative of **1**. The ^{1}H NMR spectrum was similar to that of **1** except that **2** showed a signal due to an indolic NH (δ 8.16) in place of the methoxyl group. The IR spectrum showed a sharp absorption (ν_{max} 3490 cm^{-1}) due to the indolic NH. The UV spectrum [λ_{max} (CH_3OH) 218 and 268 nm] was similar to that of **1**. The mass spectrum showed a base peak at *m/z* 130.0679 $(M-C_2H_4NS_2)^+$ and implied that the indole ring of **2** is connected to a methylene group of a side chain as in **1**. Similarly, NOE experiment confirmed the position of the side chain at C-3. Namely, irradiation of the indolic NH induced the enhancements of signals at δ 7.25 (2-H) and 7.42 (7-H). The side chain was shown to be the same as that of **1** based on ^{1}H and ^{13}C NMR spectra [δ_H 5.07 (d, J=4 Hz) and δ_C 43.2 (t), $-CH_2-$; δ_H 7.0 (br), >NH; δ_C 198.2, >C=S; δ_H 2.65 (s) and δ_C 18.2 (q), $-SCH_3$]. Therefore, the whole structure of brassinin should be represented by **2**. The structure of **2** was confirmed by the following synthesis. Treatment of 3-(aminomethyl)indole[14] with carbon disulfide in the presence of pyridine and triethylamine gave a dithiocarbamate salt, which was methylated with methyl iodide to give **2** in 66% yield. The both synthetic and natural specimens were identical in all respects.

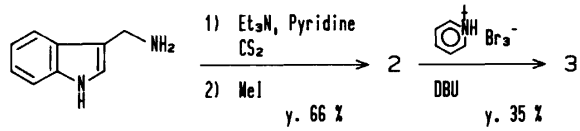

Cyclobrassinin (**3**), mp 136—137 °C, has the molecular formula $C_{11}H_{10}N_2S_2$ by HR-MS and showed a slightly different UV [λ_{max} (CH_3OH) 204, 227, 284, and 294 nm] spectrum from those of **1** and **2**. Its ^{1}H NMR spectrum showed signals for 2,3-disubstituted indole. In NOE difference experiment, irradiation of an indolic NH at δ 7.91 caused enhancement of the only one proton signal at δ 7.33 (7-H, indole numbering). Consecutive spin-decoupling experiments assigned the three remaining indole ring protons [δ 7.18 (6-H), 7.14 (5-H), and 7.49 (4-H)]. The spectrum further showed the presence of a methylene (δ 5.09, 2H, s) and a methylthio (δ 2.56, 3H, s) groups. The presence of nine sp^2 carbon atoms in the ^{13}C NMR spectrum, together with eight degrees of unsaturation implied a tricyclic structure of **3**. Its mass spectrum showed two peaks at *m/z* 161 $(M-C_2H_3NS)^+$ and 73 (C_2H_3NS), which suggested a retro-Diels-Alder fission of the third ring in **3**. This fragmentation and the presence of a >C=N- group (δ_c 152.0; ν_{max} 1600 cm^{-1}) suggested that **3** contained a 4*H*-1,3- or a 4*H*-1,2-thiazine moiety. The former was preferred when we considered the low carbon chemical shift (δ 48.8) of the methylene and the co-occurrence of **3** with **2** in the inoculated Chinese cabbage tissue. In NOE difference experiment irradiation of the indole ring proton at δ 7.49 (4-H) resulted in the signal enhancement of the methylene protons and supported the proposed structure **3**. The structure was confirmed by transforming brassinin (**2**) to **3**. Bromination of **2** with pyridinium bromide perbromide, followed by dehydrobromination, gave **3** in 35% yield, which was identical with natural cyclobrassinin.

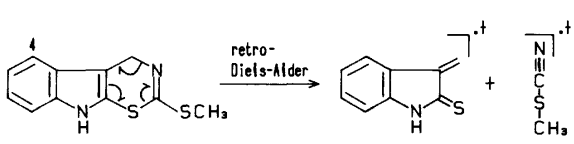

Methoxybrassitin (**4**). mp 94—96 °C, has a molecular formula of $C_{12}H_{14}N_2O_2S$. Comparison of its ^{1}H NMR spectral feature [δ 7.60 (4-H), 7.15 (5-H), 7.28 (6-H), 7.43 (7-H), 7.25 (2-H), and 4.07 (1-OCH_3)] with those of **1** suggested that **4** was also a 3-substituted *N*-methoxyindole. This view was supported by spin-decoupling and NOE difference experiments. Irradiation of the methoxyl protons and of the aromatic proton at δ 7.60 (4-H) caused signal enhancements of 2-H and 7-H protons, and methylene protons at δ 4.61 (d, J=5 Hz), respectively. The mass spectrum of **4** showed a base peak at *m/z* 160 $(M-C_2H_4NOS)^+$, indicating that the *N*-methoxyindole nucleus links a methylene group as in **1**. Since the methylene proton signals changed from a doublet to a singlet on exchange with D_2O, the methylene was further connected to a >NH. Namely, methoxybrassitin (**4**) differs from **1** in a substituent at the >NH. The substituent (C_2H_3OS) was assigned $-(C=O)SCH_3$ based on IR (1662 cm^{-1}, >C=O) and ^{13}C NMR [δ 167.6 (s), >C=O; 12.4 (q), $-SCH_3$] spectral data giving the structure **4**.

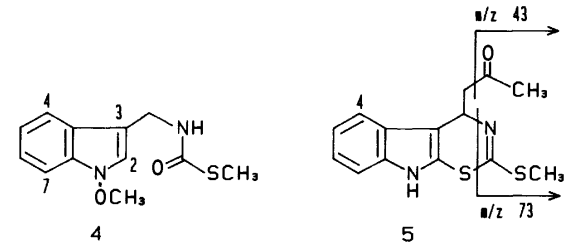

The fifth compound **5**, amorphous solid, has a molecular formula of $C_{14}H_{14}N_2OS_2$ and showed a very similar UV [λ_{max} (CH_3OH) 202, 227, 282, and 294 nm] spectrum to that of cyclobrassinin (**3**). The ^{1}H NMR spectrum [δ 7.59 (4-H), 7.14 (5-H), 7.17 (6-H), 7.31 (7-H), and 7.96 (br s, indole NH)] of **5** also showed characteristic of 2,3-disubstituted indole. The same ring system as in **3** was postulated when the IR (**5**: 1598 cm^{-1}; **3**: 1600 cm^{-1}) and ^{13}C NMR (**5**: δ_c 151.8; **3**: δ_c 152.0) absorptions of >C=N- groups were compared

with those of **3**. The NMR spectra of **5** further showed the presence of a methylthio group (δ_H 2.51 and δ_C 15.1) attached probably to the above >C=N- and also of a moiety CH_3COCH_2- [δ_H 2.21 (3H, s) and δ_C 30.9, $-CH_3$; δ_C 206.5, >C=O; δ_H 2.87 (dd, J=8 and 15 Hz) and 2.99 (dd, J=6 and 15 Hz), and δ_C 49.0, $-CH_2-$] attached to a methine group [δ_H 6.00 (dd, J=6 and 8 Hz) and δ_C 56.0]. In NOE difference experiments, irradiation of the proton at δ 7.59 (4-H) resulted in enhancements of signals due to both the methine and the methylene protons. Therefore, the structure **5** was proposed. Two diagnostic mass fragments at m/z 43 (C_2H_3O) and 73 (C_2H_3NS) were reasonably explainable by the structure **5**. The compound **5** may be an artefact derived from **3**, since it showed no optical activity and acetone was used as a solvent for extraction. The artefact-forming process, however, requires an oxidation step. Long time stirring of **3** with acetone in the presence of air showed no indication of the formation of **5**. Therefore, **5** might be a condensation product of

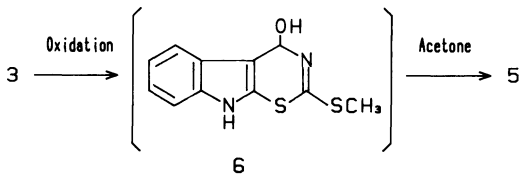

6

acetone with a hydroxy derivative **6** produced in the inoculated tissue, although such compound has not been isolated to date.

Cruciferous plants, including Chinese cabbage, contain thioglucosides called glucosinolates,[15] which undergo enzymic hydrolysis on crushing of the plant tissues to give isothiocyanates. Since Chinese cabbage contains neoglucobrassicin and glucobrassicin (**7** and **8**, respectively)[15] the formation of methoxybrassinin (**1**) and brassinin (**2**) might be explained by reactions of the respective isothiocyanates (**9** and **10**) derived from the glucosinolates (**7** and **8**) with methanethiol

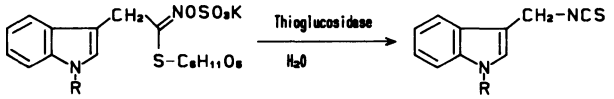

7: R=OCH₃
8: R=H

9: R=OCH₃
10: R=H

possibly generated in the course of cutting the tissue. This possibility was ruled out, however, from the following experiments: i) crushed uninoculated Chinese cabbage tissue gave none of these compounds when they were incubated for 0, 1, 2, 3, and 4 days at 20 °C; ii) none of these compounds **1** to **4** were detected when the excised Chinese cabbage tissue without the bacterium inoculation was incubated under the same conditions as those of the inoculated tissue (20 °C, 3 days); iii) production of these compounds was also induced by ultraviolet irradiation. In this case, tissue is not mechanically injured.

It is interesting to note that Nomoto and Tamura reported the isolation of 1-methoxyindoleacetonitrile from clubroots of Chinese cabbage.[11] They supposed it to be a metabolite of the roots infected with *Plasmodiophora brassicae*. We have also observed the presence of this compound in *P. cichorii*-inoculated daikon (*Raphanus sativus* L. var. *hortensis*).[16]

These four compounds **1**, **2**, **3**, and **4** exhibited broad, moderate antifungal activity against over 31 plant pathogenic fungi, e. g. *Pyricularia orizae*, with complete inhibition at 400 ppm, and moderate inhibition at 100 ppm.

Although many phytoalexins (over 200 compounds) have been isolated to date,[3] this is the first report of sulfur-containing phytoalexins.

Experimental

All the melting points were uncorrected. IR spectra were recorded with a JASCO A-120 spectrometer, UV spectra with Shimadzu UV 240 spectrometer, ^1H and ^{13}C NMR spectra with JEOL JNX-GX400 or JEOL JNM-FX200 spectrometer in deuteriochloroform solution containing tetramethylsilane as an internal standard, low and high resolution mass spectra with a JEOL JMS-D300 spectrometer, with direct inlet system operating at 70 eV. HPLC separation was performed with a Hitachi 635S equipped with a JASCO UVIDEC-100V detector, using an analytical or a preparative μ-Porasil column (Waters Associates).

Method of Bioassay. For two-dimensional TLC bioassay, developed silica-gel sheet (i, Et_2O; ii, CH_2Cl_2-CH_3OH, 98:2) was sprayed with a dense conidial suspension of *Bipolaris leersiae* in a potato-glucose medium, and incubated in a moist box at 25 °C for 2 days. Fungitoxic spots appeared white against a dark gray background. Antifungal activity of each chromatographic fraction was monitored by one-dimensional TLC bioassay using the solvent system i or ii.

Induction and Isolation of the Phytoalexins. Chinese cabbage heads (*Brassica campestris* L. ssp. *pekinensis*) were cut into small pieces and kept in a moist chamber at 20 °C for 1 day, and then inoculated with *Pseudomonas cichorii* (ca. 10^8 cells ml^{-1}). After being incubated at 20 °C for 3 days they were air-dried at 60 °C. The dried tissue (1418 g) was extracted twice with acetone at room temperature. The extracts were evaporated under reduced pressure below 35 °C to give an acetone extract (20.0 g), which was triturated with ethyl acetate to remove inactive insoluble material (2.27 g). The filtered ethyl acetate solution was passed through a short silica-gel column and the column was eluted with ethyl acetate. The eluate (14.15 g) from the column was separated into three fractions by chromatography on silica gel: F-1-1 (0.97 g), inactive fraction eluted with CH_2Cl_2-CH_3OH (99.5:0.5); F-1-2 (4.55 g), less polar active fraction eluted with the above eluent; F-1-3 (8.87 g), more polar active fraction eluted with CH_2Cl_2-CH_3OH (99.5:0.5, and 7:3). Further fractionation of F-1-3 will be reported in future.

Fraction F-1-2 was separated into five fraction (F-2-1—F-2-5) by chromatography on Sephadex LH-20 with CH_3OH-EtOAc (1:1). Fraction F-2-3 (525 mg) was further separated

into 6 fractions (F-3-1—F-3-6) by chromatography on silica gel with hexane-diethyl ether (4:1). Fraction F-3-2 (265 mg) was further purified by chromatography on silica gel with CH_2Cl_2-CH_3OH (99.5:0.5) to give methoxybrassinin **1**, 250 mg). Fraction F-3-4 (15.8 mg) was purified by three sequential preparative HPLC on a μ-Porasil column using CH_2Cl_2-CH_3OH (99.5:0.5), benzene-EtOAc (20:1), and hexane-diethyl ether (4:1) to give a compound **5** (6.7 mg). Fraction F-3-5 (40.2 mg) was purified by a silica-gel column with benzene-EtOAc (10:1), followed by preparative HPLC on a μ-Porasil column using CH_2Cl_2-hexane-CH_3OH (800:200:1), yielding methoxybrassitin (**4**, 15.9 mg). Fraction F-2-4 (226 mg) was fractionated by chromatography on silica gel with CH_2Cl_2 to give cyclobrassinin (**3**, 139.1 mg) and brassinin (**2**, 30.8 mg).

Characterization of the Compounds 1—5. Methoxybrassinin (1): $C_{12}H_{14}N_2OS_2$ (*m/z* 266.0550, M^+); viscous oil; IR ($CHCl_3$) 3380, 1475, 1452, 1352, 1298, 1088, 958, and 922 cm^{-1}; UV (CH_3OH) 218 (ε 37300), 241 (trough, 11500), 267 (15800), 287 (sh, 9470), and 297 (sh, 5740) nm; ^1H NMR δ=2.65 (s, $-SCH_3$), 4.10 (s, $-OCH_3$), 5.02 (d, *J*=4 Hz, $-CH_2-$), 7.0 (br, >NH), 7.17 (ddd, *J*=8, 8, and 2 Hz, 5-H), 7.30 (ddd, *J*=8, 8, 2 Hz, 6-H), 7.34 (s, 2-H), 7.45 (d, *J*=8 Hz, 7-H), and 7.60 (d, *J*=8 Hz, 4-H). The spectrum showed minor signals (1/4 intensity of the major signals) due to a rotamer at δ= 2.75 (s, $-SCH_3$), 4.75 (br d, *J*=4 Hz), and 7.6 (br, >NH); ^{13}C NMR δ=18.2 (q, $-SCH_3$), 42.8 (t, $-CH_2-$), 66.0 (q, $-OCH_3$), 106.4 (s), 108.6 (d), 119.0 (d), 120.5 (d), 122.7 (d), 123.0 (s), 123.1 (d), 132.3 (s), and 198.3 (s, >C=S); MS *m/z* (%) 266 (4, M^+), 235 [54, $(M-OCH_3)^+$], 218 [16, $(M-SCH_3-H)^+$], 160 (100, $C_{10}H_{10}NO$), 145 (28), 129 (57), and 91 (23, $C_2H_3S_2$).

Brassinin (2): $C_{11}H_{12}N_2S_2$ (*m/z* 236.0418, M^+); mp 132—133 °C (CH_2Cl_2-hexane); IR ($CHCl_3$) 3490, 3380, 1480, 1455, 1092, and 922 cm^{-1}; UV (CH_3OH) 218 (ε 38300), 236 (trough, 8740), 268 (16100), and 287 (9070) nm; ^1H NMR δ=2.65 (s, $-SCH_3$), 5.07 (d, *J*=4 Hz, $-CH_2-$), 7.0 (br, >NH), 7.18 (ddd, *J*=8, 8, and 1 Hz, 5-H), 7.25 (ddd, *J*=8, 8, and 1 Hz, 6-H overlapped with 2-H), 7.42 (d, *J*=8 Hz, 7-H), 7.64 (br d, *J*=8 Hz, 4-H), 8.16 (br s, 1-H), and minor signals (1/4 intensity of the major ones) due to a rotamer at δ=2.75 (s, $-SCH_3$), 4.80 (d, *J*=4 Hz, $-CH_2-$), and 7.6 (br, >NH); ^{13}C NMR δ=18.2 (q, $-SCH_3$), 43.2 (t, $-CH_2-$), 110.9 (s), 111.5 (d), 118.7 (d), 120.4 (d), 122.8 (d), 124.0 (d), 126.5 (s), 136.3 (s), and 198.2 (s, >C=S); MS *m/z* (%) 236 (46, M^+), 188 [3, $(M-SCH_3-H)^+$], 162 (16, C_9H_8NS), and 130 (100, C_9H_8N).

Synthesis fo Brassinin (2): To a mixture of 3-(aminomethyl)indole[14] (730 mg), pyridine (2.0 ml), and triethylamine (0.70 ml) was added carbon disulfide (330 µl) at 0 °C and the mixture was kept at the temperature for 1 h. The reaction mixture was then treated with methyl iodide (312 µl), kept at 3 °C for 24 h, and poured into 1.5 M H_2SO_4 (1 M=1 mol dm^{-3}) (50 ml).[17] The crude product extracted from the reaction mixture with diethyl ether was crystallized from CH_2Cl_2-hexane to yield **2** (782 mg), mp 132—133 °C, in 66% yield.

Cyclobrassinin (3): $C_{11}H_{10}N_2S_2$ (*m/z* 234.0264, M^+); mp 136—137 °C (CH_2Cl_2-hexane); IR ($CHCl_3$) 3450, 1600, 1450, 1430, 1338, 980, and 910; UV (CH_3OH) 204 (ε 24700), 227 (34000), 259 (trough, 6330), 284 (7830), and 294 (8170) nm; ^1H NMR δ=2.56 (3H, s, $-SCH_3$), 5.09 (2H, s, $-CH_2-$), 7.14 (1H, ddd, *J*=7, 7, and 2 Hz, 5-H), 7.18 (1H, ddd, *J*=7, 7, and 2 Hz, 6-H), 7.33 (1H, dd, *J*=7 and 2 Hz, 7-H), 7.49 (1H, dd, *J*=7 and 2 Hz, 4-H), and 7.91 (1H, br, 1-H); ^{13}C NMR δ=15.2 (q, $-SCH_3$), 48.8 (t, $-CH_2-$), 103.9 (s), 110.7 (d), 117.2 (d), 120.3 (d), 122.0 (d), 122.4 (s), 125.2 (s), 136.7 (s), and 152.0 (s, >C=N); MS *m/z* (%) 234 (10, M^+), 161 (100, C_9H_7NS), 117 (47, C_8H_7N), and 73 (6, C_2H_3NS).

Synthesis of Cyclobrassinin (3): To a solution of **2** (237 mg) in CH_2Cl_2 (24 ml) was added pyridinium bromide perbromide (336 mg) in small portions at room temperature and the mixture was kept at the temperature for 20 min and then basified with 1,8-diazabicyclo[5.4.0]undec-7-ene (DBU) and refluxed for 10 min. The reaction mixture was evaporated and the residue was applied on a silica-gel column and eluted with CH_2Cl_2 to give crystalline material (107 mg), which on recrystallization from CH_2Cl_2-hexane gave **3** (81 mg) in 35% yield, indistinguishable from natural cyclobrassinin.

Methoxybrassitin (4): $C_{12}H_{14}N_2O_2S$ (*m/z* 250.0772, M^+); mp 94—96 °C (Et_2O-EtOH); IR ($CHCl_3$) 3430, 1662, 1482, 1455, and 1182 cm^{-1}; UV (CH_3OH) 219 (ε 32100), 247 (trough, 2360), 273 (5200), 287 (5200), 295 (sh, 4250) nm; ^1H NMR δ=2.38 (3H, s, $-SCH_3$), 4.07 (3H, s, $-OCH_3$), 4.61 (2H, d, *J*=5 Hz, $-CH_2-$), 5.51 (1H, br s, >NH), 7.15 (1H, ddd, *J*=8, 8, and 1 Hz, 5-H), 7.25 (1H, s, 2-H), 7.28 (1H, ddd, *J*=8, 8, and 1 Hz, 6-H), 7.43 (1H, br d, *J*=8 Hz, 7-H), and 7.60 (1H, br d, *J*=8 Hz, 4-H); ^{13}C NMR δ=12.4 (q, $-SCH_3$), 36.8 (t, $-CH_2-$), 65.9 (q, $-OCH_3$), 108.0 (s), 108.5 (d), 119.1 (d), 120.3 (d), 122.1 (d), 122.8 (s), 123.0 (d), 132.5 (s), and 167.6 (s, >C=O); MS *m/z* (%) 250 (42, M^+), 219 (33), 202 [43, $(M-SCH_3-H)^+$], 176 (48), 171 [33, $(M-SCH_3-OCH_3-H)^+$], 160 [100, $(M-NHCOSCH_3)^+$], 145 (36), 129 (57), 102 (31), 75 (54), and 47 (66).

Compound 5: $C_{14}H_{14}N_2OS_2$ (*m/z* 290.0550, M^+); IR ($CHCl_3$) 3460, 1705, 1598, 1445, 1423, 1355, 1338, 1260, 1158, 965, and 918 cm^{-1}; UV (CH_3OH) 202 (ε 18900), 227 (28000), 259 (trough, 5740), 282 (6490), and 294 (6690) nm; ^1H NMR δ=2.21 (3H, s, $-COCH_3$), 2.51 (3H, s, $-SCH_3$), 2.87 (1H, dd, *J*=15 and 8 Hz), 2.99 (1H, dd, *J*=15 and 6 Hz), 6.00 (1H, dd, *J*=8 and 6 Hz, >CH-), 7.14 (1H, ddd, *J*=7, 7, and 2 Hz, 5-H), 7.17 (1H, ddd, *J*=7, 7, and 2 Hz, 6-H), 7.31 (1H, dd, *J*=7 and 2 Hz, 7-H), 7.59 (1H, dd, *J*=7 and 2 Hz, 4-H), and 7.96 (1H, br, >NH); ^{13}C NMR δ=15.1 (q, $-SCH_3$), 30.9 (q, $\underline{C}O\underline{C}H_3$), 49.0 (t, $-CH_2-$), 56.0 (d, >CH-), 106.3 (s), 110.7 (d), 117.8 (d), 120.6 (d), 122.2 (s), 122.3 (d), 124.8 (s), 136.6 (s), 151.8 (s, >C=N-), and 206.5 (s, >C=O); MS *m/z* (%) 290 (21, M^+), 275 (14), 217 (31), 199 (31), 184 (74), 175 (100, $C_{10}H_9NS$), and 73 (32, C_2H_3NS), and 43 (62).

References

1) Part 7 in the series "Studies on Stress Metabolites." For part 6, see M. Takasugi, K. Monde, N. Katsui, and A. Shirata, *Chem. Lett.*, **1987**, 1631.

2) J. D. Paxton, *Phytopath. Z.*, **101**, 106 (1981).

3) N. T. Keen and B. Bruegger, "Host Plant Resistance to Pests," ed by P. A. Hedin, ACS Symposium Series No. 62, American Chemical Society, Washington D. C. (1977), Chap. 1; D. T. Coxon, "Phytoalexins," ed by J. A. Bailey and J. W. Mansfield, Blackie, Glasgow and London (1982), Chap. 4; C. J. W. Brooks and D. G. Watson, *Natural Product Reports*, **1985**, 427.

4) N. T. Keen, "Plant Disease Control: Resistance and Susceptibility," ed by R. C. Staples and G. H. Toenniessen, Wiley-Interscience, New York (1981), pp. 155—177.

5) M. Takasugi, S. Okinaka, N. Katsui, T. Masamune,

A. Shirata, and M. Ohuchi, *J. Chem. Soc., Chem. Commun.*, **1985**, 621.

6) M. Takasugi, S. Kawashima, K. Monde, N. Katsui, T. Masamune, and A. Shirata, *Phytochemistry*, **26**, 371 (1987).

7) M. Takasugi, S. Kawashima, N. Katsui, and A. Shirata, *Phytochemistry*, **26**, 2957 (1987).

8) U. Mizushima, *Kagaku To Seibutsu*, **10**, 78 (1972).

9) M. Takasugi, N. Katsui, and A. Shirata, *J. Chem. Soc., Chem. Commun.*, **1986**, 1077.

10) Yields from smaller amounts of the inoculated tissue were recorded in Ref. 9.

11) R. Gmelin and A. I. Virtanen, *Acta Chem. Scand.*, **16**, 1378 (1962); H. Morimoto and H. Oshio, *Justus Liebigs Ann. Chem.*, **682**, 212 (1965); S. R. Johns, J. A. Lamberton, and J. L. Occolowitz, *Aust. J. Chem.*, **20**, 1737 (1967); M. Nomoto and S. Tamura, *Agric. Biol. Chem.*, **34**, 1590 (1970); T. Kinoshita, S. Tatara, and U. Sankawa, *Chem. Pharm. Bull.*, **33**, 1770 (1985).

12) A. Lidén and J. Sandström, *Acta Chem. Scand.*, **27**, 2567 (1973).

13) K. Nakanishi, T. Goto, S. Ito, S. Natori, and S. Nozoe ed "Natural Products Chemistry," Kodansha, Tokyo (1975), Vol. 2, Chap. 10, pp. 365—421.

14) J. Schallenberg and E. Meyer, *Z. Naturforsch.*, **38b**, 108 (1983).

15) M. E. Daxenbichler, C. H. VanEtten, and P. H. Williams, *J. Agric. Food Chem.*, **27**, 34 (1979); C. H. VanEtten and H. L. Tookey, "Herbivores," ed by G. A. Rosenthal and D. H. Janzen, Academic Press, New York (1979), Chap. 13, pp. 471—500.

16) Unpublished observation (K. Monde).

17) J. C. Crawhall and D. F. Elliot, *J. Chem. Soc.*, **1952**, 3094.

An Ab Initio Molecular Orbital Study of Pyridyl Radicals

Osamu KIKUCHI,* Yuji HONDO, Kenji MORIHASHI, and Mitsunobu NAKAYAMA
Department of Chemistry, The University of Tsukuba, Tennodai, Tsukuba 305
(Received July 4, 1987)

Synopsis. Open-shell RHF and UHF ab initio calculations were carried out for 2-, 3-, and 4-pyridyl radicals in order to determine their molecular structures and relative energies. The minimal STO-3G basis set was used for the structure optimization, while the 4-31G basis set was used for the energy evaluation. The 2-pyridyl radical has the lowest energy, although the energy differences among these three isomers were very small. The possibility of a Π-ground state in pyridyl radicals was rejected.

Pyridyl radicals are typical aryl radicals and are derived formally from the homolytic cleavage of the CH bond of pyridine. Three isomers, 2-, 3-, and 4-pyridyl radicals, have been detected by ESR,[1,2] and the reactivity of 2-pyridyl has recently been discussed.[3] An interesting aspect from the theoretical point of view is the relative energies of the three isomers, since the interaction between the singly-occupied molecular orbital (SOMO) and the nonbonding orbital at the nitrogen atom can be expected to affect the stability of

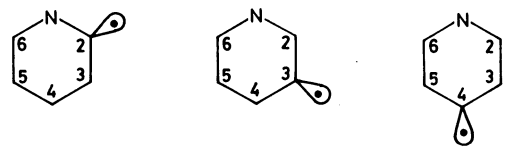

2 3 4

these radicals. Another interesting point is to examine the possibility of the Π-ground state, in which the π_4 orbital is occupied by the unpaired electron, although ESR has suggested the Σ-ground states for these radicals.[2] There have been only a few theoretical studies of pyridyl radicals;[2,4] all of them are semiempirical calculations applied to idealized or assumed molecular structures. In the present study, the molecular structures of three pyridyl radicals, **2**—**4** were optimized by ab initio MO methods, and their relative energies were compared.

The open-shell RHF and UHF methods were employed. The RHF orbitals are appropriate for understanding the orbital shape, while the UHF orbitals involve the spin-polarization effect. The molecular structures were optimized with the STO-3G basis set,[5] and the energies were calculated with the 4-31G basis set.[6]

The RHF calculation showed that the SOMO of each radical is localized mainly on the carbon atom at the radical center; the atomic-spin populations at the carbon atoms in **2**, **3**, and **4** are 0.879, 0.918, and 0.916 respectively. The molecular structures optimized by RHF and UHF (in parentheses) calculations are shown in Fig. 1. The CC and CN bonds calculated by the UHF method are longer than those calculated by the RHF method by 0.02—0.05 Å. The RHF N–C(2) bond length in **2**, 1.323 Å, is very short in comparison with those in **3** and **4**, which are in the range of 1.35—1.36 Å. This is caused by the interaction between the nitrogen nonbonding orbital and the unpaired electron at the adjacent carbon atom in **2**. This interaction is also reflected in the calculated orbital energies of the SOMO and the nonbonding orbital. As may be seen from Fig. 2, the SOMO energy of **2** is higher than those of **3** and **4**, while the nonbonding orbital of **2** lies lower than those of **3** and **4**. These facts indicate an appreciable interaction between the two orbitals in 2-pyridyl.

The 2-pyridyl radical has the lowest energy of the three isomers, as is shown in Table 1. The energy differences among the three isomers, however, are not large. The origin of the stability of **2** is not clear, although the interaction between SOMO and the nonbonding orbital may contribute to some extent.

Since the SOMO of **2** lies higher than those of **3** and **4**, the Π state of 2-pyridyl, in which the σ_{18} electron is

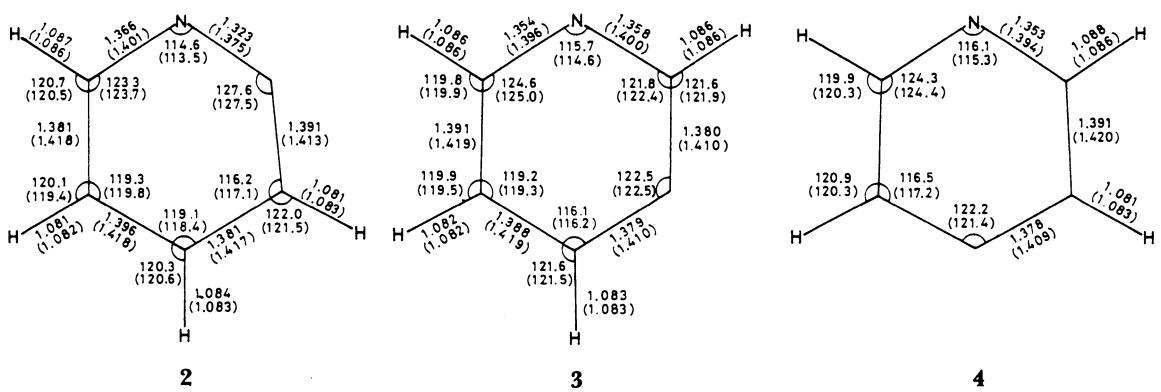

2 3 4

Fig. 1. Molecular structures of pyridyl radicals optimized by open-shell RHF and UHF methods with STO-3G basis set. The UHF values are in parentheses. The optimization was performed under restriction of the planarity of molecular structure. Bond lengths are shown in Å, and bond angles are in degrees.

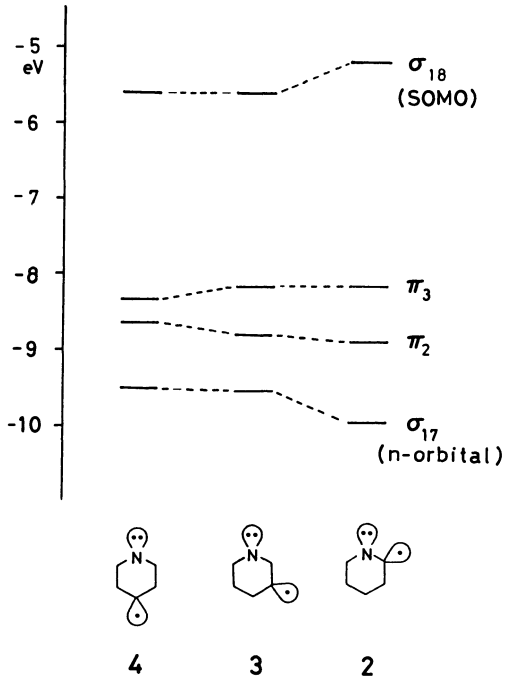

Fig. 2. Higher four occupied molecular orbitals of pyridyl radicals calculated by open-shell RHF method with STO-3G basis set. The σ_{18} orbital is the singly-occupied orbital.

Table 1. Calculated Energies (au) of Three Isomers of Pyridyl Radicals[a)]

	RHF 4-31G//STO-3G	UHF 4-31G//STO-3G
2-Pyridyl (**2**)	−245.67930(0.0)	−245.68987(0.0)
3-Pyridyl (**3**)	−245.67319(16.0)	−245.68667(8.4)
4-Pyridyl (**4**)	−245.67617(8.2)	−245.68804(4.8)

a) Values in parentheses are relative energies in kJ mol^{-1}.

excited to the π_4 orbital, may be expected to lie low. The Π state of 2-pyridyl was thus examined. The optimized structure is shown in Fig. 3. The structure of the Π state of 2-pyridyl is very different from that of the Σ state in Fig. 1. The N–C_2 bond, 1.221 Å, is extremely short, while the N–C_2–C_3 bond angle is very large. These facts suggest that the N–C_2 bond may be written formally as a triple bond, $-N^+{\equiv}C-$. The Π state was calculated to lie 376 kJ mol^{-1} above the Σ-ground state (STO-3G energy difference). It is thus concluded that the Π state is not expected for the

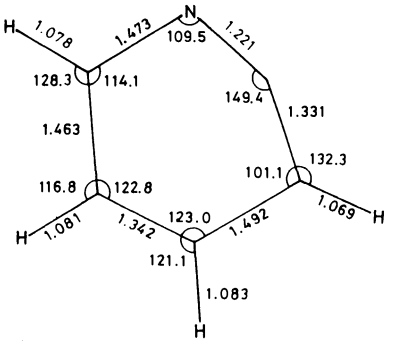

Fig. 3. Molecular structure of the excited Π state of 2-pyridyl radical optimized by open-shell RHF method with STO-3G basis set.

ground state of 2-pyridyl, even if the substitution and/or environmental effects are changed.

The calculated spin distribution of pyridyl radicals did not agree with the experimental values estimated from the ESR spectra. The proton hyperfine coupling constants[7)] of 2-pyridyl, for example, were calculated by means of the RHF method to be very small (0.4—2.1 G (1G=10^{-4} T)); experiments have shown the coupling constants of 10 and 6 G to two protons.[2)] The UHF method gave larger values: $a(H_3)$=36, $a(H_4)$=−30, $a(H_5)$=33, $a(H_6)$=−33. The disagreement may come from the method of calculation. The UHF values are generally larger than the experimental values because of the failure of the spin-polarization contribution.[8)]

All the calculations were carried out with the ABINIT program written by our group. The work was supported by the University of Tsukuba Project Research.

References

1) H. J. Bower, J. A. McRae, and M. C. R. Symons, *Chem. Commun.*, **1967**, 542; *J. Chem. Soc. A*, **1968**, 2696.
2) P. H. Kasai and D. McLeod, Jr., *J. Am. Chem. Soc.*, **92**, 6085 (1970); **94**, 720 (1972).
3) J. A. Zoltewicz and G. A. Locko, *J. Org. Chem.*, **48**, 4214 (1983).
4) K. Sakaguchi and K. Inuzuka, *Nippon Kagaku Kaishi*, **1976**, 1343.
5) W. J. Hehre, R. F. Stewart, and J. A. Pople, *J. Chem. Phys.*, **51**, 2657 (1969).
6) W. J. Hehre, R. Ditchfield, and J. A. Pople, *J. Chem. Phys.*, **56**, 2257 (1972).
7) Estimated by the use of $a(H)=507\times\rho_H$.
8) K. Ohta, H. Nakatsuji, K. Hirao, and T. Yonezawa, *J. Chem. Phys.*, **73**, 1770 (1980).

Effects of Crown-Type Host-Guest Complexation on Electrochemical Profiles of Pb^{2+} Ion

Hiroshi Tsukube,* Kentaro Takagi, Tatsuo Higashiyama, Tadashi Iwachido, and Naomi Hayama
Department of Chemistry, College of Liberal Arts & Science, Okayama University, Okayama 700
(Received July 6, 1987)

Synopsis. Crown ethers, cryptands, and related synthetic host molecules modified electrochemical profiles of Pb^{2+} ion by host-guest complexations. The reduction potentials of the Pb^{2+} complexes were significantly correlated with their complex stabilities.

Crown ethers, cryptands, and other synthetic host molecules specifically bind guest cations and often modify their physicochemical properties and chemical reactivities. For example, solubility, spectroscopic profile, and catalytic activity of the guest cation were demonstrated to be varied by host-guest complexation.[1]

Here we examined electrochemical properties of a series of Pb^{2+} complexes with tripodes, crown ethers, double armed crowns, and cryptand molecules, and revealed an interesting relationship between thermodynamic stabilities and reduction potentials of Pb^{2+} complexes. Since electrochemical properties of the Pb^{2+} complexes were significantly influenced by the natures and the structures of ligating host molecules, the present study may provide further possibilities in controlling redox chemistry of active guest species at will.

Results and Discussion

We employed a series of tripodes, crown ethers, and cryptands, which had various distributions, numbers, and types of donor groups (Fig. 1).[2,3] Typical cyclic voltammograms for aqueous solutions of Pb^{2+} ion in the presence and absence of double armed crown ether **8** are shown in Fig. 2. When 0.5 equiv of double armed crown ether **8** was added to a solution of Pb^{2+} ion, new reduction peak B appeared at more negative potential than that of initially observed peak A. Then peak A disappeared in the presence of ca. 1.0—2.0 equiv of **8** to Pb^{2+} ion, and only peak B remained in the presence of excess of **8**. Similar successive changes were observed in the other examined systems, and crown-type host-guest complexation may be essentially involved in such a heterogeneous electrochemical reaction.[4] Although free Pb^{2+} ion showed more positive reduction peak potential (−0.51 V) than Cd^{2+} and Zn^{2+} ions (−0.83 and −1.27 V) under the employed conditions (see Experimental), double armed crown ether **8**, and cryptands **10** and **11** modified Pb^{2+} ion less reducible than Cd^{2+} ion.

Figure 3 shows relationship between induced shifts of reduction peak potentials by complexation and stability constants for corresponding Pb^{2+} complexes.[5] It clearly indicates that redox reaction of

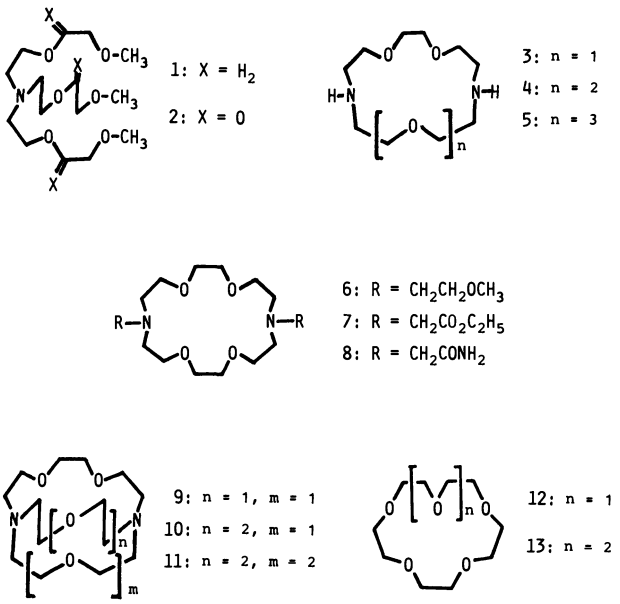

Fig. 1. Examined tripodes, crown ethers, and cryptands.

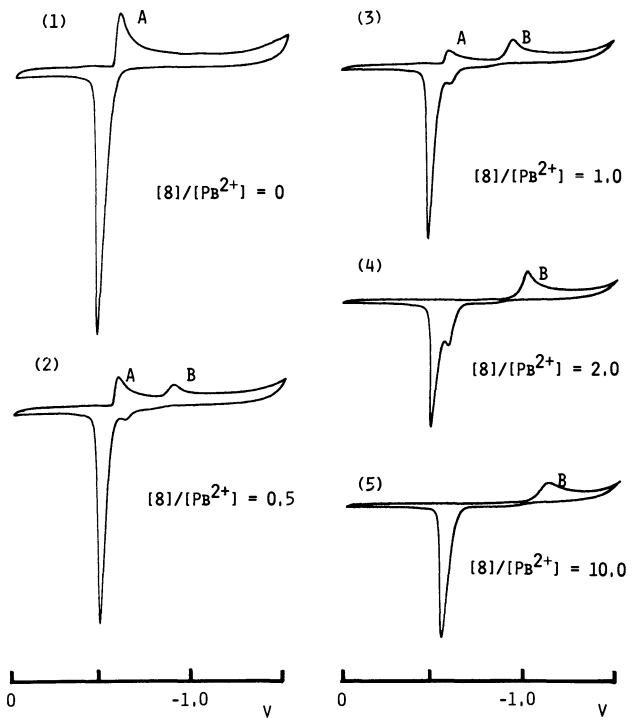

Fig. 2. Cyclic voltammograms for Pb^{2+}/Pb^0 couple in the (1) absence, (2) presence of 0.5 equiv, (3) presence of 1.0 equiv, (4) presence of 2.0 equiv, and (5) presence of 10.0 equiv of double armed crown ether **8**. $Pb(ClO_4)_2$, 6.1×10^{-4} M.

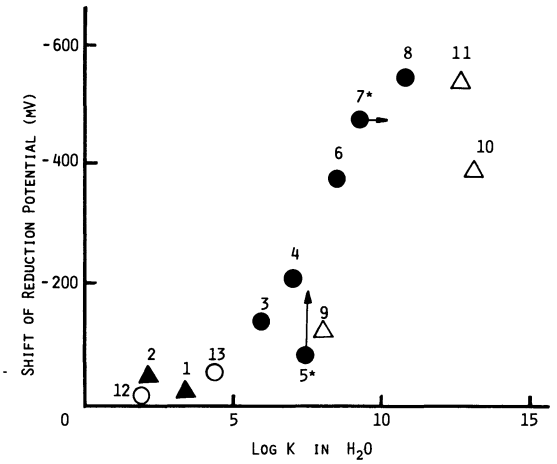

Fig. 3. Relationship between induced shift in reduction potential of Pb^{2+} complex and its stability constant in H_2O.
▲ tripodes **1** and **2**, ● aza-crown ethers **3**—**8**, △ crystands **9**—**11**, ○ oxa-crown ethers **12** and **13**.
*Log K for aza-crown ether **7** was obtained as higher than 8.7.
Since aza-crown ether **5** and/or its Pb^{2+} complex were suspended under the employed electrochemical conditions. The shift value indicated was estimated as smaller.

Pb^{2+} complex largely depended on the nature and the structure of the ligating molecule. The relationship is almost sigmoidal and provides some indication of the structures of the Pb^{2+} complexes with the various ligands. Interestingly, double armed crown ethers **6**—**8** and cryptands **10**—**11** showed greater induced shifts in the reduction potentials than tripodes and simple crown ethers. Since ^{13}C NMR studies have strongly suggested that these host molecules could completely wrap around the electroactive Pb^{2+} ion and effectively shield it from the surroundings,[6] they markedly inhibited electron transfer reaction and offered much negative reduction potentials. These observations offer an interesting method for correlating the stability constants and electrode potentials for the Pb^{2+} ion, and further possibilities that electrochemistry of other kinds of guest species may be controlled by appropriate choice of crown ethers and/or related host molecules.

Experimental

1. Host Molecules. Host molecules **2**, **6**, **7**, and **8** were prepared by the literature methods,[2,3] and showed satisfactory mass, ^1H NMR, and IR spectroscopic data as well as physical properties.

Other employed host molecules and reagents were commercially available and used as received.

2. Cyclic Voltammetry Experiments. Electrochemical measurements were conducted under an Ar in a buffered aqueous solution (0.1 M CH_3CO_2H/0.1 M CH_3CO_2Na, 1 M=1 mol dm^{-3}, pH=6.22). A standard H-cell, glassy carbon (working electrode), and a platinum wire (counter-electrode) were used. All the cyclic voltammograms were recorded at room temperature after several scans (scan rate; 20 mV s^{-1}), and reduction peak potentials were obtained vs. Ag/AgCl electrode.

3. Determination of Stability Constant for Pb^{2+} Complex. Stability constants of host molecules **1**, **2**, **5**, and **7** for Pb^{2+} ion were determined potentiometrically at 17 °C by a modification of the Frensdorff method:[7] log K=3.6 for **1**; 2.1 for **2**; 7.4 for **5**; and >8.7 for **7**. Pb^{2+} ion specific electrode (Denki Kagaku Keiki, Model 7180) was used to ascertain stability constants, and the reference electrode was Ag/AgCl (Orion, Model 90-01). The activities of Pb^{2+} ion were measured in an aqueous solution of $Pb(ClO_4)_2$ both in the absence and presence of each host molecule: $Pb(ClO_4)_2$, 1.0×10^{-3} M; host, 3.0×10^{-3} M. The stability constants for other host molecules were found in the literature:[5] Log K=5.85 for **3**; 6.90 for **4**; 8.39 for **6**; 10.70 for **8**; 7.93 for **9**; 13.12 for **10**; 12.72 for **11**; 1.85 for **12**; and 4.27 for **13**.

The authors are grateful to Drs. Nakao (Okayama Univ.) and Satoh (Osaka Prefectural Univ.) for helpful discussion.

References

1) Recent review: E. Weber and F. Vögtle, "Topics in Current Chemistry," Springer-Verlag, Berlin (1981), Vol. 98, p. 1. Electrochemistry of crown-type complex: E. L. Yee, O. A. Gansow, and M. J. Weaver, *J. Am. Chem. Soc.*, **102**, 2278 (1980); C. Boudon, M. Gross, and F. Peter, *J. Electroanal. Chem.*, **145**, 181 (1983).

2) U. Heimann, M. Herzhoff, and F. Vögtle, *Chem. Ber.*, **112**, 1392 (1979); H. Tsukube, K. Takagi, T. Higashiyama, T. Iwachido, and N. Hayama, *Chem. Lett.*, **1986**, 1079.

3) S. Kulstad and L. A. Malmsten, *Acta Chem. Scand.*, **1979**, 469.

4) Although a detailed mechanism is not clear, the following electrochemical and complexation processes may be possible:

$$Pb^{2+} + 2e^- \rightleftharpoons \underline{Pb^0}$$
$$Pb^{2+} + Host \rightleftharpoons (Pb^{2+} \cdot Host)$$
$$(Pb^{2+} \cdot Host) + 2e^- \rightleftharpoons \underline{(Pb^0 \cdot Host)}$$
$$\underline{(Pb^0 \cdot Host)} \rightleftharpoons \underline{Pb^0} + Host$$

The species underlined are deposited on electrode surface. It is noted that Pb^0 is much weakly bound to the each host.

5) Stability constants of **3**, **4**, **6**, **8**, **9**, **10**, **11**, **12**, and **13**: See R. M. Izatt, J. S. Bradshaw, S. A. Nielsen, J. D. Lamb, J. J. Christensen, and D. Sen, *Chem. Rev.*, **85**, 271 (1985).

6) H. Tsukube, K. Takagi, T. Higashiyama, T. Iwachido, and N. Hayama, XXV International Conference on Coordination Chemistry, Abstract C2-468, Nanjing, 1987.

7) H. K. Frensdorff, *J. Am. Chem. Soc.*, **93**, 600 (1971).

Effect of Pore Diffusion in Liquid-Phase Enantioselective Hydrogenation with Ni-SiO_2 Catalysts

Yuriko NITTA* and Toshinobu IMANAKA
Department of Chemical Engineering, Faculty of Engineering Science, Osaka University, Toyonaka, Osaka 560
(Received June 5, 1987)

Synopsis. A series of Ni-SiO_2 catalysts, having a constant Ni loading and different Ni crystallite sizes, were prepared by using series of silica supports with controlled wide-pore structure. The crystallite size effect in enantioselective hydrogenation was found to hold also for the reactions controlled by the pore diffusion.

Since Izumi et al.[1] developed the modified Raney-Ni catalysts for the enantioselective hydrogenation of methyl acetoacetate (MAA) to optically active methyl 3-hydroxybutyrate (MHB), much effort has been devoted to the understanding of the reactions on metal catalysts.[2-5] The reaction is known to be highly sensitive to the catalyst-surface structure and modifying conditions. As to unsupported Ni catalysts modified under fixed conditions, we reported that amorphous catalysts have only low enantioselectivity and that the selectivity increased with increasing crystallite size of Ni up to around 10 nm.[6] Harada et al.[7] also suggested that amorphous and crystalline parts of H_2-reduced catalysts obtained from NiO provides nonselective and selective sites, respectively. With SiO_2-supported Ni catalysts, the observation that higher Ni loadings result in higher enantioselectivities was also explained by the crystallite size effect similarly to the case of unsupported catalysts.[8,9]

On the other hand, Sachtler interpreted the effect of Ni loading in terms of pore diffusion during catalyst modification.[5] He suggested that, to verify the crystallite size effect, one should change the size of Ni crystallites while keeping the Ni loading of the catalyst constant. Woerde et al.[10] reported that the liquid-phase hydrogenation is also a pore-diffusion process. Therefore, in order to establish the crystallite size effect, we should clarify the effect of pore diffusion on the apparent enantioselectivity, although we have already confirmed the crystallite size effect with Ni-SiO_2 catalysts having constant Ni loading.[9,11,12] For this purpose, the use of a series of wide-pore silica with controlled pore structure looks promising. The preparation of Rh catalysts using these silica supports provided series of Rh-SiO_2 catalysts with desired metal particle size.[13]

In this work, we prepared a series of Ni-SiO_2 catalysts, which have a constant Ni loading and different Ni crystallite sizes, by using a series of silica supports with controlled pore structure and examined the enantioselective hydrogenation of MAA with these catalysts under different reaction conditions.

Experimental

The Ni-SiO_2 catalysts were prepared by the pore-filling procedure with aqueous solution of nickel nitrate and a series of silica (Super Micro Bead Silica Gel, Fuji-Davison Chemical Ltd.) having different pore diameters. The Ni loading was kept constant at 7.5 wt% unless otherwise stated. The samples were dried in air at 383 K for 16 h. Two grams of a sample were reduced in flowing hydrogen at 673 K for 3 h and then modified with aqueous (2*R*,3*R*)-tartaric acid solution (pH=5.1). The enantioselective hydrogenation of MAA was carried out for 17 h either with a glass autoclave (No. 1) (TEM-U-50, Taiatsu Glass Industry Co.) equipped with a vigorous-stirring system under an initial H_2 pressure of 10 kg cm^{-2} at 333 K, or with a stainless-steel autoclave (No. 2) (TVS-2, Taiatsu Glass Industry Co.) attached to a shaking apparatus of 100 times per minute under an H_2 pressure of ca. 100 kg cm^{-2} at 350 K. The detailed procedures of the catalyst modification and the hydrogenation reaction were described elsewhere.[8]

The hydrogenation activity of the catalyst was determined from the pressure decrease during the initial 15 min of the reaction. The optical yield (OY) of (−)-MHB determined from the optical rotation of the distilled product was used as a measure of the enantioselectivity of the catalyst. The mean crystallite size of Ni (D_c) in the catalyst was obtained from the half-width of the peak on (111) plane of Ni metal in the X-ray diffraction pattern of the catalyst.

Results and Discussion

The physical properties of the silica supports employed here are listed in Table 1. These wide-pore supports were found to provide a series of suitable catalysts for studying the effects of pore diffusion and the Ni crystallite size.

The silica support (Silica Gel No. 1, Nakarai Chemicals, Ltd.) having been employed in our previous works[8,11,14] had only micropores with a

Table 1. Physical Properties of Silica Supports[a]

Support	Mean pore diameter	Pore volume	Surface area
	nm	$cm^3\ g^{-1}$	$m^2\ g^{-1}$
S-1	16.3	1.28	212
S-2	27.8	1.06	135
S-3	52.8	0.96	65
S-4	72.8	1.11	50

a) Data were furnished by Fuji-Davison Chemical Ltd.

Table 2. Catalytic Properties of 7.5wt% Ni-SiO_2 Catalysts

Support	D_c[a]	r_0[b]	OY[c]
	nm	mmol·min^{-1} g Ni^{-1}	%
S-1	7.2	1.56	18.9
S-2	8.9	1.30	16.8
S-3	11.3	0.98	13.8
S-4	13.5	1.02	8.7

a) Mean crystallite size of Ni determined from the XRD measurement. b) Initial hydrogenation rate. c) Optical yield of (−)-MHB.

mean diameter of 3 nm,[9] and the supported catalysts were prepared by the precipitation method. Under these conditions, the contribution of Ni in pores to the overall reaction was negligible.[9] In such a case, the hydrogenation reactions carried out under vigorous stirring (i.e., in autoclave No. 1) were controlled by the surface reaction, whereas the diffusion process was not neglected in the reactions carried out under mild stirring (i.e., in autoclave No. 2).[14]

With the catalysts prepared here by the pore-filling method using the wide-pore supports, Ni particles are regarded to exist mainly in the pores, based on the models proposed by Dorling et al.[15,16] and Dafler.[17] When the Ni loading was kept constant, the mean crystallite size of Ni increased with an increase in the pore diameter of the silica support as shown in Table 2. This tendency is the same as that observed in the preparation of Rh-SiO_2 catalysts with desired metal-particle size.[13]

The apparent enantioselectivity of these Ni-SiO_2 catalysts observed in the reactions carried out in the autoclave No. 1 decreased with an increase in the pore diameter of silica support in spite of an increase in the mean crystallite size of Ni in these catalysts. On the other hand, when hydrogenations were carried out by using another autoclave (No. 2) with a mild shaking system, the enantioselectivity of the catalysts increased with an increase in the mean crystallite size of Ni just as with the catalysts reported previously (Fig. 1). In this case, the reactions are regarded to be diffusion controlled as already pointed out,[10,14] probably because of the slow mass transfer from gas-liquid interface to the catalyst surface under a low stirring intensity. Accordingly, the higher selectivity of the catalyst with the larger Ni crystallites reflects the increase in the fraction of selective sites in the catalyst surface.

As shown in Fig. 1, the catalysts with different Ni loadings (4.1 to 11.3 wt%), prepared by using S-4 silica with the widest pore (72.8 nm) as the support, exhibited an increased enantioselectivity with an increase in the mean crystallite size of Ni even in the case using the autoclave No. 1. Therefore, the results shown in Table 1 suggest that the reaction on the catalysts with narrower pores is retarded by the pore diffusion. Since the surface reaction rate on nonselective sites is higher than that on selective sites under our reaction conditions,[14] the reaction on nonselective sites becomes more limited when the concentration of reactants in pores is lowered by the slow diffusion, which leads to a higher enantioselectivity of the catalyst with narrower pores.

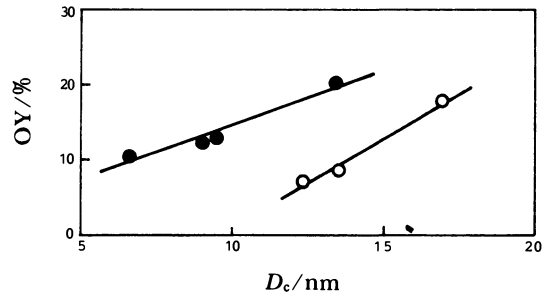

Fig. 1. Enantioselectivity of modified Ni-SiO_2 catalysts as a function of the mean crystallite size of Ni. Reactions were carried out either with the catalysts having different Ni loadings in autoclave No. 1 (○) (surface reaction controlled), or with 7.5 wt% Ni-SiO_2 catalysts in autoclave No. 2 (●) (pore diffusion controlled).

In the liquid-phase reaction carried out by using autoclave No. 1 with a vigorous-stirring system, the rate of mass transfer of H_2 from gas phase to the pellet surface is fast enough and the concentration ratio MAA/H_2 is in the order of 10^2. Under these conditions the modulus Φ can be estimated as follows:[18]

$$\Phi = \eta\phi^2 = R_p^2 \frac{r_{obs}}{D_{eff} C_{H2}}$$

where η is the effectiveness factor, ϕ is the Thiele modulus, R_p is the radius of the spherical catalyst pellet (5 μm), and D_{eff} is the effective diffusion coefficient of H_2. With $D_{eff}=3.5\times10^{-4}$ cm^2 s^{-1} and $C_{H_2}=3.6\times10^{-5}$ mol cm^{-3} at 333 K in ethyl acetate, Φ was calculated from the observed highest rate and found to be in the order of 10^{-4}. Since Φ is so small, the effectiveness factor for mass transfer inside the catalyst particle is essentially unity and so the reaction is essentially intrinsic. However, D_{eff} in liquid phase is difficult to estimate especially in narrower pores with relatively large Ni particles in them and might be much smaller than the value assumed above. Even values in the order of 10^{-10} to 10^{-14} have been reported for D_{eff} in Zeolites.[18] Therefore, the possibility that the pore diffusion interferes with the reactions on the catalysts with narrower pores cannot be denied.

These findings and discussion strongly suggest that the crystallite size effect holds for the reactions controlled by either the surface reaction or the pore diffusion. However, we should be careful in estimating the surface properties of supported

catalysts from the apparent enantioselectivities when the rate determining step varies with the catalysts.

The authors are greatly obliged to the Fuji-Davison Chemical Ltd. for presenting them with a series of silica supports, Super Micro Bead Silica Gel, and the data of their physical properties.

References

1) Y. Izumi, M. Imaida, H. Fukawa, and S. Akabori, *Bull. Chem. Soc. Jpn.*, **36**, 21 (1963).
2) Y. Izumi, *Adv. Catal.*, **32**, 215 (1983).
3) A. Tai and T. Harada, "Tailored Metal Catalysts," ed by Y. Iwasawa, D. Reidel Publishing Co., The Netherlands (1986), p. 265.
4) M. Bartók, "Stereochemistry of Heterogeneous Metal Catalysis," John Willey & Sons, New York (1985), p. 511.
5) W. M. H. Sachtler, "Catalysis of Organic Reactions," ed by R. L. Augustine, Marcel Dekker Inc., New York (1985), p. 189.
6) Y. Nitta, F. Sekine, T. Imanaka, and S. Teranishi, *Bull. Chem. Soc. Jpn.*, **54**, 980 (1981).
7) T. Harada, Y. Imachi, A. Tai, and Y. Izumi, *Stud. Surf. Sci. Catal.*, **11**, 377 (1982).
8) Y. Nitta, F. Sekine, T. Imanaka, and S. Teranishi, *J. Catal.*, **74**, 382 (1982).
9) Y. Nitta, O. Yamanishi, F. Sekine, T. Imanaka, and S. Teranishi, *J. Catal.*, **79**, 475 (1983).
10) H. M. Woerde, L. J. Bostelaar, A. Hoak, and W. M. H. Sachtler, *J. Catal.*, **76**, 316 (1982).
11) Y. Nitta, T. Imanaka, and S. Teranishi, *J. Catal.*, **96**, 429 (1985).
12) Y. Nitta, M. Kawabe, H. Kajita, and T. Imanaka, *Chem. Express*, **1**, 631 (1986).
13) H. Hamada, R. Funaki, Y. Kuwahara, Y. Kintaichi, K. Wakabayashi, and T. Ito, *Appl. Catal.*, **30**, 177 (1987).
14) Y. Nitta, T. Imanaka, and S. Teranishi, *J. Catal.*, **80**, 31 (1983).
15) T. A. Dorling and R. L. Moss, *J. Catal.*, **7**, 378 (1967).
16) T. A. Dorling, B. W. J. Lynch, and R. L. Moss, *J. Catal.*, **20**, 190 (1971).
17) J. R. Dafler, *J. Am. Oil Chemist's Soc.*, **54**, 17 (1977).
18) C. N. Satterfield, "Mass Transfer in Heterogeneous Catalysis," Colonial Press, Clinton, Massachusetts (1970).

Terplex Formation in the Excited Triplet State. The Chloranil and Mesitylene System

Harumichi KOBASHI,* Ken-ichi HIRATSUKA, and Kazuaki MOTEGI
Department of Chemistry, Faculty of Engineering, Gunma University, Kiryu, Gunma 376
(Received July 1, 1987)

Synopsis. The enthalpy and entropy changes have been estimated for the formation of a triplet-state (1:2) terplex as well as an ordinary (1:1) exciplex between triplet chloranil (^{3}CA) and mesitylene (M) in carbon tetrachloride. Results indicate that the terplex is energetically less stable than the bimolecular exciplex, while the stabilization of the terplex is compensated by the positive entropy change associated with transformation from the exciplex to the terplex.

There are many reports on the formation of a ternary component exciplex (terplex) in the excited singlet state of electron donor-acceptor systems.[1-4] On the other hand, only little is known the terplex formation in the excited triplet state.[5] In addition, it was reported recently that not only termolecular interaction but also the existence of an ordinary triplet exciplex could not be reconfirmed for some systems such as the zinc etioporphyrin I and *p*-nitrotoluene system, which had been believed for a long time as a representative of a locally excited (LE-type) triplet exciplex.[6] Under these circumstances, it will be very important to study a triplet-state terplex as well as ordinary (1:1) exciplex and the contribution of the terplex to a dynamic behavior of the exciplex.

In a previous paper,[7] one of us reported both spectroscopic and kinetic results concerning the formation of the LE-type triplet exciplex between ^{3}CA and M, ^{3}(CA-M), which is an intermediate for the hydrogen atom transfer from M to ^{3}CA in 1,2-dichloroethane (DCE). During the course of our study concerning solvent effects on the reactivity of this triplet exciplex,[8] we have found that a termolecular interaction occurs between the exciplex and the exess donor M in less polar solvents.[9]

In this paper, we describe results of thermodynamic and kinetic properties of the terplex ^{3}(CA-M_2) as well as the exciplex ^{3}(CA-M) in the nonpolar solvent CCl_4. This is, to our knowledge, the first report presenting thermodynamic data of a terplex formed in the excited triplet state. After this work had been completed, we knew a report concerning the (1:1) exciplex formation for the same system in CCl_4.[10] However, there was no information concerning the terplex formation.

Experimental

A nanosecond laser photolysis was carried out using the same ruby laser as used previously.[7] A transient signal was memorized to a strage oscilloscope (Iwatu, TS-8123) and displayed on a recorder (Rikadenki, RW-11T). Temperature was varied in the range 5—55 °C by circulating water into a sample cell holder using a thermostat (Taitec, Jr-80) combined with a cooling pipe (Taitec, 150L). Chloranil (tetrachloro-*p*-benzoquinone) and mesitylene (1,3,5-trimethylbenzene) were purified by the same methods as used before.[7,11] Carbon tetrachloride (*Cica*-Merk, Uvasol) as a solvent was fractionally distilled after purification through an alumina column. All samples were carefully degassed by the usual freeze-pump-thaw method.

Results and Discussion

Figure 1 shows transient absorption spectra observed for a CCl_4 solution of CA (0.0025 mol dm^{-3}) and M (0.030 mol dm^{-3}). A broad band in the wavelength region longer than 800 nm is attributed to the CT band of the LE-type triplet exciplex ^{3}(CA-M).[7] The relative intensity of this band to the band at 510 nm increased apparently for the case [M]=0.60 mol dm^{-3}, although no other new band was observed. The band around 510 nm, which is due to both free ^{3}CA and ^{3}(CA-M), decays rapidly and the bands attributable to chloranil semiquinone radical (CAH·) emerge at 427.5 and 360 nm. The rise time of CAH· followed at 427.5 nm was identical to the decay time of the triplet species monitored at 510 nm as well as at 1000 nm. These spectral features are quite similar to those observed in DCE. Namely, the hydrogen atom transfer from M to ^{3}CA proceeds through the exciplex;

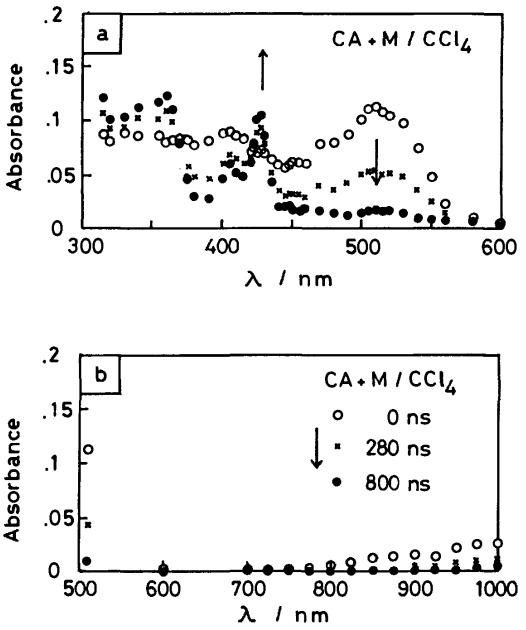

Fig. 1. Transient absorption spectra for the CCl_4 solution containing CA(0.0025 mol dm^{-3}) and M(0.030 mol dm^{-3}) in the wevelength regions of (a) 320—600 nm measured using an R636 photomultiplier and (b) 510—1000 nm measured using an R406 photomultiplier. Time after the pulsing: (○) 0, (×) 280, and (●) 800 ns. The absorbances of the 0 ns spectra in (a) and (b) were normalized to each other at 510 nm.

the same mechanism as revealed previously in DCE.[7]

Figure 2 shows the dependence of the decay rate (τ^{-1}) at the 510 nm band on [M] ranging from 0.0025 to 1.2 mol dm^{-3}. The decay rates were not dependent on the laser power for excitation (ca. 3—15 mJ). In the low concentration region of [M] less than ca. 0.1 mol dm^{-3}, the quenching curve bends downward with an increase of [M], while in the more concentrated region the decay rate becomes slow gradually passing through the maximum value with increasing [M]. The decay features can not be interpreted only by taking into account the (1:1) exciplex formation. This finding suggests that there exists the interaction between the exciplex and another M molecule. Since the triplet species at 510 nm decays exactly with a single exponential function, it is reasonable to consider that a dynamic equilibrium may be established rapidly among triplet species including a terplex under the present experimental conditions. The reaction scheme is written as follows:

$$^3CA + M \underset{}{\overset{K_1}{\rightleftharpoons}} {}^3(CA^{\delta-} - M^{\delta+}) \underset{-M}{\overset{+M}{\rightleftharpoons}} {}^3(CA^{\delta'-} - M_2^{\delta'+})$$

$$\downarrow k_0 \qquad \downarrow k_1 \qquad \downarrow k_2$$

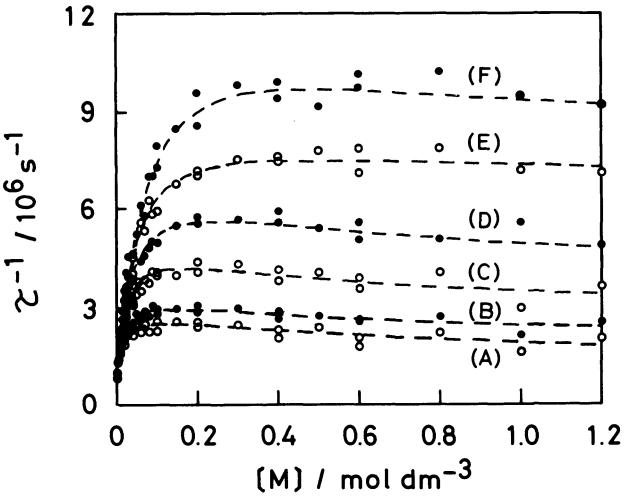

Fig. 2. Relations of τ^{-1} vs. [M] ranging from 0.0025 to 1.2 mol dm^{-3} at several temperatures: (○) and (●) Observed values measured at (A) 10, (B) 15, (C) 25, (D), 35, (E) 45, and (F) 55 °C. (----) Calculated curves.

In this case, the decay rate of ^{3}CA can be expressed by the following Eq. 1.

$$\tau^{-1} = \frac{k_0 + k_1K_1[M] + k_2K_1K_2[M]^2}{1 + K_1[M] + K_1K_2[M]^2} \quad (1)$$

where k_0, k_1, and k_2 are the decay rate parameters of free ^{3}CA, ordinary exciplex ^{3}(CA-M) and terplex ^{3}(CA-M$_2$), respectively, and K_1 and K_2 are the equilibrium constants for formation of the exciplex and terplex, respectively.

As exemplified in Fig. 2, the calculated curve according to Eq. 1 reproduces well the experimental values. Then, five parameters k_0, k_1, k_2, K_1, and K_2 can be estimated by a nonlinear least-square regression analysis using a combination of damping Gauss-Newton and Marquardt methods for 32 experimental points. Results are listed in Table 1. The k_1 and K_1 values are obtained with a good accuracy at each temperature. The corresponding parameters for the terplex, k_2 and K_2, are also estimated although the errors are relatively large. The k_0 values have large errors in the present 5-parameters fitting and tend to be estimated somewhat largely; e.g., the decay rate of ^{3}CA in the absence of M is ca. 0.1×10^6 s^{-1} at 25 °C. The van't Hoff plots for K_1 and K_2 values in Table 1 yield the enthalpy (ΔH) and entropy (ΔS) changes for the formation of both (1:1) and (1:2) exciplexes. These thermodynamic parameters together with equilibrium constants (K_e) and lifetimes (τ_e) of both exciplexes are summarized in Table 2.

The noticeable results in Table 2 are the positive enthalpy and entropy changes for the terplex formation. That is, the terplex formation from the

Table 2. Properties of Triplet Exciplexes in CCl_4

	Exciplex	
	(1:1)	(1:2)
K_e/dm^3 mol^{-1}[a]	49±1	1.7±1.3
ΔG/kJ mol^{-1}[a,b]	−9.6±0.1	$-1.3\pm^{1.4}_{3.6}$
ΔH/kJ mol^{-1}[c]	−32±3	15±3
ΔS/J K^{-1} mol^{-1}[c]	−74±11	52±9
τ_e/ns[a]	197±4	391±121

a) At 25 °C. b) Calculated using the relation $\Delta G = -RT\ln K_e$. c) The errors were estimated by a linear least-square regression treatment of the relation of $\ln K_e$ vs. $1/T$ including the experimental deviations of K_e as weight.

Table 1. Results of 5-Parameters Fitting by Nonlinear Least-Square Regression Analysis

T	k_0	k_1	k_2	K_1	K_2
°C		10^6 s^{-1}		dm^3 mol^{-1}	
10	0.78±0.81	2.8±0.5	0.8±1.0	90±1	0.9±0.6
15	0.63±0.69	3.3±0.4	1.5±0.8	80±1	0.9±0.5
25	0.34±0.12	5.1±0.1	2.6±0.8	49±1	1.7±1.3
35	0.59±0.08	7.0±0.1	3.6±1.2	29±1	1.4±1.2
45	0.65±0.29	8.7±0.5	6.6±1.6	23±5	1.5±3.1
55	1.04±0.10	13.0±0.4	8.0±0.6	11±1	2.1±1.0

bimolecular exciplex is energetically unfavorable but the positive entropy change contributes largely to decreasing the free energy change. The latter result may be attributed to an increase in entropy of solvation on going from the exciplex state to the terplex state or attributed to a conformational change between ^{3}(CA–M) and ^{3}(CA–M_2) accompanied by a solvent reorientation. A similar discussion about such contribution of entropy has been given for the stabilization of an ordinary (1:1) triplet exciplex[12] and the conformational change has been suggested for a terplex formed in the excited singlet state.[2]

Other results are summarized as follows: 1) The triplet-state terplex formation becomes significant in a concentrated solution of M over ca. 0.2 mol dm^{-3}, although no distinct absorption due to the terplex was observed. 2) The deactivation rate of the terplex is smaller than that of the ordinary exciplex. This fact suggests that H-atom transfer in the terplex takes place more slowly than that in the exciplex, because it is considered that the reaction rate of H-atom transfer must depend on the mutual orientation between ^{3}CA and M in each exciplex but a competing deactivation, i.e., intersystem crossing, would be relatively unaffected. 3) The thermodynamic quantities for the (1:1) exciplex are similar to those for an usual electron donor–acceptor complex in the ground state.[13] 4) The lifetime of ^{3}(CA–M) in CCl_4 is considerably longer than that in DCE (32 ns at 25 °C).[7] It is presumed from this result that the solvent polarity affects significantly on the H-atom transfer reaction.

This work was financially supported in part by the Gunma University Foundation for Science and Technology. The authors also thank to Professor Haruo Shizuka for his interest and manuscript reading.

References

1) H. Beens and A. Weller, *Chem. Phys. Lett.*, **2**, 140 (1968).

2) K. H. Grellmann and U. Suckow, *Chem. Phys. Lett.*, **32**, 250 (1975).

3) T. Mimura and M. Itoh, *J. Am. Chem. Soc.*, **98**, 1095 (1976); *Bull. Chem. Soc. Jpn.*, **50**, 1739 (1977); T. Mimura, M. Itoh, T. Ohta, and T. Okamoto, *ibid.*, **50**, 1665 (1977); M. Itoh, N. Takita, and M. Matsumoto, *J. Am. Chem. Soc.*, **101**, 7363 (1979).

4) R. A. Beecroft, R. S. Davidson, and D. Goodwin, *Tetrahedron*, **41**, 3853 (1985).

5) J. K. Roy, F. A. Carroll, and D. G. Whitten, *J. Am. Chem. Soc.*, **96**, 6349 (1974).

6) I. V. Renge, V. A. Kuzmin, and Yu. E. Borsevich, *J. Photochem.*, **31**, 67 (1985).

7) H. Kobashi, T. Okada, and N. Mataga, *Bull. Chem. Soc. Jpn.*, **59**, 1975 (1986).

8) H. Kobashi, K. Motegi, and H. Shizuka, Preprint for the 52nd Annual Meeting of Chem. Soc. Jpn. (Kyoto, April 1986), Abstr. No. I-2F31; H. Kobashi, K. Hiratsuka, and H. Shizuka, Symposium on Molecular Structure (Osaka, October 1986), Abstr. No. 2B05.

9) Partly presented in the 54th Annual Meeting of Chem. Soc. Jpn. (Tokyo, April 1987), Abstr. No. I-3IIIQ11.

10) P. P. Levin and V. A. Kuzmin, *Bull. Acad. Sci. USSR, Div. Chem. Sci.*, **35**, 1303 (1986).

11) H. Kobashi, H. Gyoda, and T. Morita, *Bull. Chem. Soc. Jpn.*, **50**, 1731 (1977).

12) E. I. Kapinus, M. M. Aleksankina, and I. I. Dilung, *Chem. Phys. Lett.*, **114**, 507 (1985).

13) G. Briegleb, "Elektron-Donor-Acceptor-Komplexe," Springer-Verlag, Berlin (1962).

Determination of a Small Amount of a Biological Constituent by the Use of Chemiluminescence. XII. Highly Sensitive Immunoaffinity Chromatography

Tadashi HARA,* Kazuhiko TSUKAGOSHI, Akihiro ARAI, and Takeshi IHARADA
Department of Chemical Engineering, Faculty of Engineering, Doshisha University, Karasuma Imadegawa, Kamigyo-ku, Kyoto 602
(Received June 16, 1987)

Synopsis. Highly sensitive immunoaffinity chromatography was established by combining a micro-bore affinity column with a chemiluminescence detector for protein monitored by a flow-injection method using a 1,10-phenanthroline–hydrogen peroxide–copper(II) system. After having optimized the bed volume of a column, the flow rate of a buffer solution which was used for an immune reaction, and the time necessary for an immune reaction in a column, human serum albumin in the range of 3×10^{-4}—1×10^{-1} g dm^{-3} could be determined, with the detection limit of 15 ng as the injected amount. Human serum γ-globulin and bovine serum γ-globulin showed somewhat nonspecific adsorption onto an affinity column with values of 0.16 and 0.14 based on the specific adsorption 1.00 of human serum albumin onto a column, whereas bovine serum albumin, bovine serum α-globulin, and ovalbumin showed no nonspecific adsorption.

Cyclic immunoaffinity chromatography was previously established by the authors by combining an affinity column with a chemiluminescence (CL) detector for protein using the chemiluminescent reaction of a 5-amino-2,3-dihydro-1,4-phthalazinedione (luminol)–hydrogen peroxide (H_2O_2)–copper(II) (Cu(II)) system.[1,2] According to this method, a small amount of protein could be determined continuously and selectively without using a labeling procedure. However the sensitivity of this method was not yet satisfactory for the determination of a trace amount of α-fetoprotein (AFP) as a tumor marker. Furthermore, some problems as to both nonspecific adsorption onto an immunoaffinity column and the cycling of a sample solution still remained undissolved.

On the other hand, a highly sensitive CL detector for protein monitored by a flow-injection method using a 1,10-phenanthroline (phen)–H_2O_2–Cu(II) system was established by the authors in the previous paper[3]. This method was 40 times superior to the previous one using a luminol–H_2O_2–Cu(II) system in their detection limits of protein.

In the present study, the above mentioned CL detector using a phen–H_2O_2–Cu(II) system was used for the determination of protein together with a micro-bore immunoaffinity column which required no cycling of the sample solution. Experimental conditions such as the bed volume of an affinity column, the flow rate of a buffer solution which was used for an immune reaction, and the time necessary for an immune reaction in a column were optimized, followed by the determination of human serum albumin. The result showed that marked improvement could be achieved compared with the previous work in the following points: The detection limit of protein, the nonspecific adsorption onto a column, the time necessary for a measurement, and the durability of a column.

Experimental

All reagents were of commercially available special grade. Ion exchanged water was distilled for use. A phen solution, a H_2O_2 solution, and a Cu(II) catalyst solution containing L-arginine hydrochloride were prepared as in the previous paper.[3] Human serum albumin (HSA) (Miles Laboratories, Inc.), bovine serum albumin (BSA) (Nakarai Chemicals, Ltd.), human serum γ-globulin (HγG) (Sigma Chemical Co.), bovine serum γ-globulin (BγG) (Sigma Chemical Co.), bovine serum α-globulin (BαG) (ICN Pharmaceuticals, Inc.), ovalbumin (Ova) (Sigma Chemical Co.), and human control serum (Q-PAK-Chemistry Control Serum I; Hyland) were diluted with a 8.34×10^{-3} mol dm^{-3} phosphate buffer solution (Buff-A, pH 7.3) consisting of a 2.78×10^{-3} mol dm^{-3} potassium dihydrogenphosphate solution and a 5.56×10^{-3} mol dm^{-3} disodium hydrogenphosphate solution.

Rabbit anti-HSA (DAKO) was immobilized onto CNBr-Activated Sepharose 4B (Pharmacia Fine Chemicals) in accordance with the instruction paper. About 5 mg of antibody was immobilized onto 1 cm^3 of support. This value was obtained by the measurement of the remaining antibody by the UV monitor (Hitachi, Ltd., wavelength-

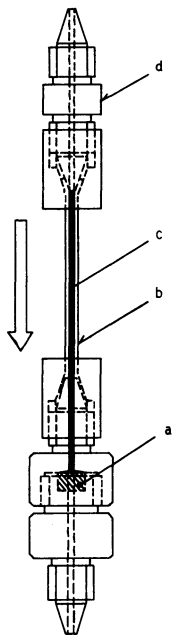

Fig. 1. Structure of a micro-bore column.
a: 10 μm Teflon filter, b: 2 mm o.d.×1 mm i.d. Teflon tube, c: immunosorbent, and d: joint (0.6 mm i.d.).

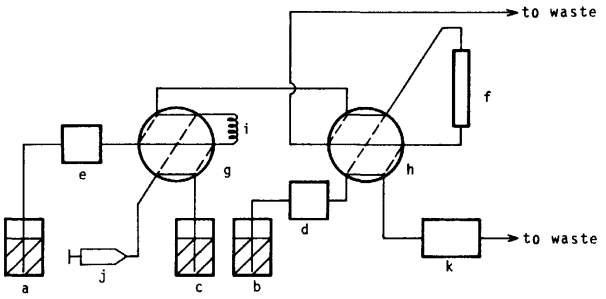

Fig. 2. Schematic flow diagram of the immunoaffinity chromatography system equipped with a CL detector.
a: Buffer solution (Buff-A), b: eluent (Buff-B), c: sample solution, d and e: pump, f: column, g and h: six-way cock, i: sampling loop, j: syringe, and k: CL detector.

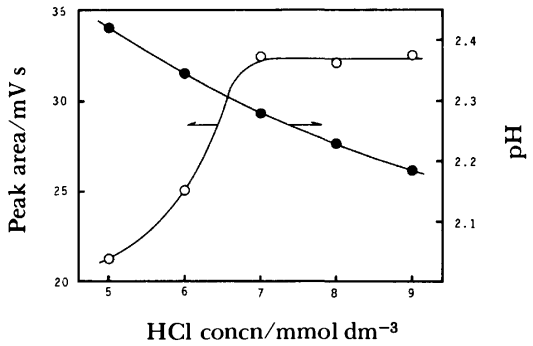

Fig. 3. Effect of HCl concn on liberation.
○: peak area and ●: pH of eluent. Conditions: 2.5×10^{-2} mol dm^{-3} KCl and 1.0×10^{-1} g dm^{-3} HSA.

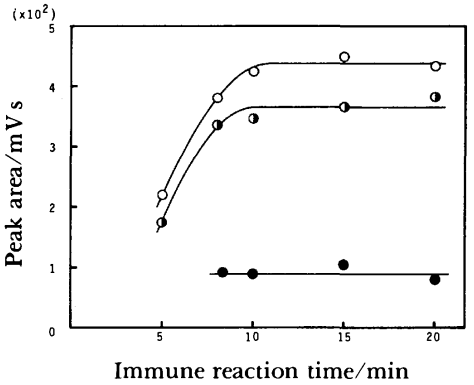

Fig. 4. Relationship between the immune reaction time and the peak area of liberated protein.
○: 1 mm i.d.×50 mm, ◑: 1 mm i.d.×30 mm, ●: 1 mm i.d.×15 mm column. Condition: 4.0×10^{-3} g dm^{-3} HSA.

tunable effluent monitor, 634A). This immunosorbent was packed in a micro-bore column (1 mm i.d. ×50 mm) which was manufactured using a Teflon tube (2 mm o.d. ×1 mm i.d.) and a Teflon line-filter (Nishio Kogyo, Ltd.) (Fig. 1).

A flow diagram of the immunoaffinity chromatography system equipped with the CL detector devised by the authors is shown in Fig. 2. A buffer solution which was used for an immune reaction (Buff-A) (a) was fed at the flow rate of 0.2 cm^3 min^{-1} by the pump (e) (Atto, SJ1211), and an eluent (Buff-B, pH 2.2) (b) consisting of a 8.0×10^{-3} mol dm^{-3} hydrochloric acid solution and a 2.5×10^{-2} mol dm^{-3} potassium chloride solution was fed at the flow rate of 1.0 cm^3 min^{-1} by the pump (d) (Pharmacia Fine Chemicals, High-precision Pump, P-500). A 50 mm^3 portion of HSA solution was injected into the Buff-A line through a sampling loop (i) and a six-way cock (g), and passed through an affinity column (f). The immune reaction was performed by feeding Buff-A to the column for 10 min after the injection of a sample solution. Then Buff-B was fed to the column to liberate HSA by operating a six-way cock (h). HSA in the eluate from the column was detected by the CL detector (k). Subsequently Buff-A was fed again to the column for 2 min to regenerate it by operating a six-way cock (h).

Results and Discussion

The optimum pH value of an eluent was determined so as to liberate sufficient HSA from an affinity column (Fig. 3). The gel immobilized with antibody was packed in a column (3 mm i.d. ×50 mm, Omnifit), and to it, 200 mm^3 of 1.0×10^{-1} g dm^{-3} HSA solution was loaded. Then HSA was liberated by feeding the eluent at various concentrations of hydrochloric acid (the concentration of potassium chloride was constant: 2.5×10^{-2} mol dm^{-3}). HSA in the eluate from the column was detected by means of the UV monitor, and the peak area was measured by use of an integrator (Shimadzu Chromatopac E1A). Judging from Fig. 3, 8.0×10^{-3} mol dm^{-3} hydrochloric acid–2.5×10^{-2} mol dm^{-3} potassium chloride buffer solution (pH 2.2) was employed as an eluent.

In the previous work, the equipment and the procedure for analysis were complicated since it required the cycling of a sample solution for an immune reaction. Moreover, the cycling of a sample solution was thought to badly influence the time necessary for a measurement, the durability of the column, the coefficient of variation, and nonspecific adsorption onto the column. Therefore, a micro-bore immunoaffinity column in the present study was manufactured using a Teflon tube (1 mm i.d.) and a Teflon line-filter (pore size=10 μm) which required no cycling of a sample solution (Fig. 1). The flow rate of Buff-A was selected to be 0.2 cm^3 min^{-1}, the minimum flow rate achieved by the pump used, so as to perform the immune reaction sufficiently on a column during a single passage of a sample solution. Using this flow rate, the bed volume of a column and the reaction time (the time of feeding Buff-A) required were investigated using a 4.0×10^{-3} g dm^{-3} HSA solution. The relationship between the immune reaction time and the peak area of the liberated protein is shown in Fig. 4 using several columns of various bed volume (1 mm i.d. ×15, 30, and 50 mm). In case of a 1 mm i.d. ×70 mm column, the blank value was so large that the measurement was disturbed. Therefore a 1 mm i.d. ×50 mm column was employed so as to reduce the blank value and to obtain the maximum peak area at the same time. The immune reaction time was

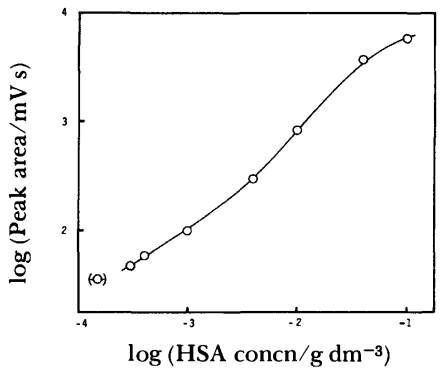

Fig. 5. Calibration curve of HSA.
(—O—): Blank value.

Table 1. Selectivity of an Affinity Column

Protein	Selectivity
HSA	1.00
HγG	0.16
BSA	0.00
BγG	0.14
BαG	0.00
Ova	0.00

Protein concn = 1.0×10^{-2} g dm^{-3}.

selected to be 10 min. A 1.0×10^{-1} g dm^{-3} BSA solution was analyzed under the above mentioned conditions, but no protein peak was observed. Liberation of HSA was performed by feeding Buff-B at the flow rate of 1.0 cm^3 min^{-1}. HSA less than 1.0×10^{-2} g dm^{-3} could be completely eluted within 5 min. Then the column was regenerated for 2 min at the flow rate of 1.0 cm^3 min^{-1} by feeding Buff-A corresponding to the volume of 50 times as large as the bed volume. The time necessary for an overall measurement (immune reaction-liberation-regeneration) was 17 min.

Under the condition mentioned above, the calibration curve of HSA obtained by the present method is shown in Fig. 5. As can be seen from Fig. 5, HSA in the range of 3×10^{-4}—1×10^{-1} g dm^{-3} could be determined with the lower limit of 15 ng. The coefficient of variation for six analyses of 4.0×10^{-3} g dm^{-3} HSA was 4.0%, and the affinity column was durable for about 40 replicate analysis.

The selectivity of the affinity column is indicated on the basis of the analytical value of HSA (Table 1). Each 1.0×10^{-2} g dm^{-3} of protein was used throughout this experiment. HγG and BγG showed somewhat nonspecific adsorption with values of 0.16 and 0.14 based on the specific adsorption 1.00 of HSA, whereas BSA, BαG, and Ova showed no nonspecific adsorption. The determination of HSA in a serum sample was next examined. Various amounts of HSA were estimated in either the presence or absence of a definite amount of control serum (containing about 6×10^{-3} g dm^{-3} HSA, diluted to a volume of 5000 times with a buffer solution), and the relationship between HSA concentration and the analytical value was obtained by the use of the calibration curve shown in Fig. 5

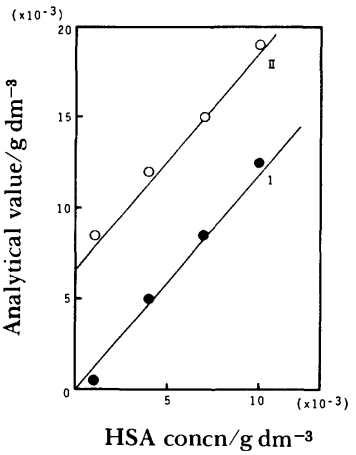

Fig. 6. Relationship between HSA concn and analytical value.
●: HSA and O: HSA+control serum.

(Fig. 6). The difference between straight lines I and II in the graph was approximately equal to the amount of HSA in the added control serum. This means that the present method was applicable to the selective determination of protein in a serum sample.

According to the previous cyclic immunoaffinity chromatography using a luminol-H_2O_2-Cu(II) chemiluminescence system, the detection limit of protein, nonspecific adsorption onto a column, the time necessary for a measurement, durability of a column, and the coefficient of variation were 100 ng, 0.00—0.63 (5 kinds of protein, on the basis of the analytical value of HSA), 34 min, about 20 times, and 5.7% (n=5, 1.0×10^{-2} g dm^{-3} HSA) respectively. In the present study, they were as follows; 15 ng, 0.00—0.16, 17 min, about 40 times, and 4.0% (n=6, 4.0×10^{-3} g dm^{-3} HSA) respectively.

Recently a small amount of protein such as AFP has attracted public attention as a tumor marker. As for AFP, Single Radial Immunodiffusion method and Reverse Passive Haemagglutination method have been generally used for simple screening. Their detection limits are 5000 and 200 ng cm^{-3} respectively, and the latter method is only qualitative.[4] Though HSA was analyzed in the present study by immobilizing anti-HSA on agarose gel, a trace amount of protein such as AFP might be analyzed continuously and selectively with the sensitivity required for practical use if suitable antibody should be immobilized.

References

1) T. Hara, M. Toriyama, and K. Tsukagoshi, *Bull. Chem. Soc. Jpn.*, **57**, 1551 (1984).
2) T. Hara, M. Toriyama, T. Ebuchi, and M. Imaki, *Bull. Chem. Soc. Jpn.*, **59**, 2368 (1986).
3) T. Hara, T. Ebuchi, A. Arai, and M. Imaki, *Bull. Chem. Soc. Jpn.*, **59**, 1833 (1986).
4) I. Urushizaki and N. Hattori, "Tumor Markers," Igakushoin Ltd., Tokyo (1986).

^{17}O NMR Study of Metal Carbonyl Cluster Compounds. III.[1] ^{17}O NMR Spectra of Mixed Metal Carbonyl Cluster Compounds, $R_2Sn[M(CO)_x][M'(CO)_y]$, $R_2Sn[M(CO)_x][M'(CO)_yCp]$, and $ClSn[Mn(CO)_5][Fe(CO)_2Cp]_2$

Satoru ONAKA* and Yoshio KATO
Department of Chemistry, Nagoya Institute of Technology, Gokiso-cho, Showa-ku, Nagoya 466
(Received July 6, 1987)

Synopsis. A series of mixed metal carbonyl cluster compounds of $R_2Sn[M(CO)_x][M'(CO)_y]$ and $R_2Sn[M(CO)_x][M'(CO)_yCp]$ were synthesized and their ^{17}O NMR spectra were measured to demonstrate how ^{17}O NMR spectroscopy is superior to IR spectroscopy to study the electronic nature of the oxygen atoms in CO groups. For these mixed metal clusters, ^{17}O NMR spectral assignments were easily made and the electron distribution around the O atoms was concluded to be only slightly changed compared with those of homo-dinuclear $R_2Sn[M(CO)_x]_2$ and $R_2Sn[M'(CO)_yCp]_2$.

In previous papers,[1] we have demonstrated that ^{17}O NMR is an eligible alternative to ^{13}C NMR or IR (ν(CO) region) for elucidating the change of electron distribution and/or structures of metal carbonyl cluster derivatives. This trait of ^{17}O NMR spectroscopy is now applied to a series of $R_2Sn[M(CO)_x]_2$, $R_2Sn[M'(CO)_yCp]_2$, $R_2Sn[M(CO)_x][M'(CO)_y]$, and $R_2Sn[M(CO)_x][M'(CO)_yCp]$ type derivatives. The present paper reports the syntheses of a series of $R_2Sn[M(CO)_x][M'(CO)_y]$, $R_2Sn[M(CO)_x][M'(CO)_yCp]$ type compounds and $ClSn[Mn(CO)_5][Fe(CO)_2Cp]_2$ and the results of ^{17}O NMR measurements for a sereis of aforementioned homo-dinuclear and hetero-dinuclear or hetero-trinuclear metal carbonyl derivatives.

Experimental

All the manipulations were made under a purified nitrogen atmosphere. Solvents were distilled from benzophenone ketyl under N_2 before use. Literature methods were employed to obtain the following homo-dinuclear metal carbony derivatives, $Me_2Sn[Mn(CO)_5]_2$ (**1**),[2] $Ph_2Sn[Mn(CO)_5]_2$ (**2**),[3] $Me_2Sn[Re(CO)_5]_2$ (**3**),[3] $Me_2Sn[Co(CO)_4]_2$ (**4**),[4] $Ph_2Sn[Co(CO)_4]_2$ (**5**),[4] $Cl_2Sn[Co(CO)_4]_2$ (**6**),[5] $Me_2Sn[Mo(CO)_3Cp]_2$ (**7**),[6] $Me_2Sn[Fe(CO)_2Cp]_2$ (**8**)[7], and $Cl_2Sn[Fe(CO)_2Cp]_2$ (**9**).[7]

Synthesis of $Me_2Sn[Mn(CO)_5][Re(CO)_5]$ (10). A 850 mg sample (2 mmol) of $BrMe_2SnMn(CO)_5$[8] was allowed to react with an equimolar amount of $NaRe(CO)_5$ in THF at room temperature and the reaction mixture was stirred overnight. Then the solvent was vacuum-stripped from the yellow-orange solution to leave yellow solid. This solid was recrystallized from hexane to yield 620 mg of pale yellow sample (yield 46%). Found: C, 21.77; H, 0.95%. Calcd for $C_{12}H_6MnO_{10}ReSn$: C, 21.52; H, 0.90%. ν(CO) (ligroine solution): 2117 (w), 2095 (w), 2080 (m), 2077 (m, sh), 2010 (vs), and 1982 (s) cm^{-1}.

Synthesis of $Ph_2Sn[Mn(CO)_5][Co(CO)_4]$ (11). A similar method as the above was employed; a 960 mg (2 mmol) sample of $ClPh_2Sn$-$Co(CO)_4$[9] was allowed to react with an equimolar amount of $NaMn(CO)_5$ in THF at room temperature. Similar treatment as the above and recrystallization from pentane to give 300 mg (yield 23%) of pale yellow crystals. Found: C, 39.53; H, 1.52%. Calcd for $C_{21}H_{10}CoMnO_9Sn$: C, 39.48; H, 1.56%. ν(CO) (Nujoll mull): 2105 (w), 2100 (w), 2080 (s), 2030 (m), 2018 (s), 2010 (vs), and 1985 (m) cm^{-1}.

Synthesis of $Me_2Sn[Mn(CO)_5][Mo(CO)_3Cp]$ (12). A 0.76 g (2 mmol) sample of $ClMe_2Sn$-$Mn(CO)_5$[10] was treated with an equimolar amount of $NaMo(CO)_3Cp$ in THF as above described and recrystallization from petroleum ether gave 0.90 g sample of pure product (yield 76%). The purity of this sample was checked by spectroscopic data (IR, and ^1H NMR)[11].

Synthesis of $ClSn[Mn(CO)_5][Fe(CO)_2Cp]_2$ (13). A 220 mg (0.55 mmol) sample of $Mn_2(CO)_{10}$ was dissolved into 50 ml of THF and the solution was stirred over 1% Na amalgam for 2 h. After filtration of this solution, a THF solution (50 ml) which contains a 400 mg (1.1 mmol) sample of $Cl_2Sn[Fe(CO)_2Cp]_2$ was added to this filtrate and the reaction mixture was stirred overnight at room temperature. From the resulting red solution, the solvent was vacuum-stripped and red-orange residue was extracted three times with each 20 ml of benzene. From the combined extracts, the solvent was partially vacuum-distilled off and 20 ml of petroleum ether was added. Storage of this solution in a refrigerator for a few days gave orange-red crystals (220 mg; yield 28%). So far analytically pure sample has not yet been obtained. However, several spectroscopic data suggest that this sample is spectroscopically pure. ν(CO) (CCl_4 solution): 2089 (s), 2060 (vw), 2025 (m, sh), 2010 (vs), 2000 (s), 1990 (s), and 1949 (m) cm^{-1}. ^1H NMR: δ=4.5 (C_5H_5).

Spectral Measurements. ^{17}O NMR spectra were recorded on a Varian XL-200 spectrometer operated at 27.12 MHz for ca 0.5 mol dm^{-3} THF, benzene, and/or chloroform solutions at 30 °C with Fourier transform mode for naturally abundant level (0.037%). The spectra were measured using a 10 mm o.d. sample tube with 0.01 s acquisition time and 90° pulse. Chemical shifts were measured in parts per million with reference to external $H_2{}^{17}O$ standard contained in a 1 mm capillary. IR spectra were recorded on a Jasco 701G spectrometer and proton NMR spectra were obtained with a Hitachi-Perkin-Elmer R-24A spectrometer (60 MHz). Absorption spectra were recorded on a Hitachi 220A double-beam spectrophotometer with a 1.0 mm quartz cell in cyclohexane. All the spectral results are tabulated in Table 1.

^{17}O NMR Spectral Results and Assignment

The manganese and rhenium carbonyl unit, $M(CO)_5$ (M=Mn and Re) has four equatorial and one axial carbonyls. Therefore, two peaks wth relative intensity of 4:1 are observed for compounds **1**—**3** (Fig. 1a). The cobalt carbonyl unit, $Co(CO)_4$, has three equatorial and one axial carbonyls. However, compounds **4**—**6** show unresolved ^{17}O NMR spectra. Molybdenum cyclopentadienyl derivative **7** has two carbonyl groups (Scheme) and therefore two peaks with relative intensity of 2:1 are observed (Fig. 1b). Two carbonyls in iron cyclopentadienyl derivatives **8** and **9** are equivalent and only one resonance is

detected in ^{17}O NMR spectra of these derivatives. With all these assignments in mind for homodinuclear metal carbonyl derivatives, **1—9**, ^{17}O NMR spectral assignments are easily made for hetero-

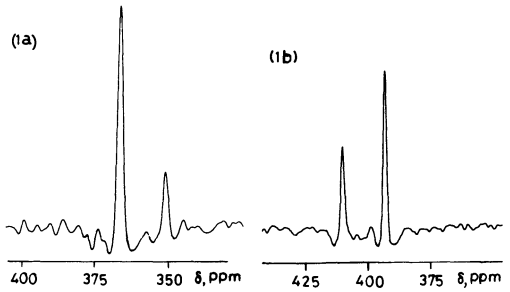

Fig. 1. ^{17}O NMR spectra of: (1a) $Me_2Sn[Re(CO)_5]_2$ and (1b) $Me_2Sn[Mo(CO)_3Cp]_2$.

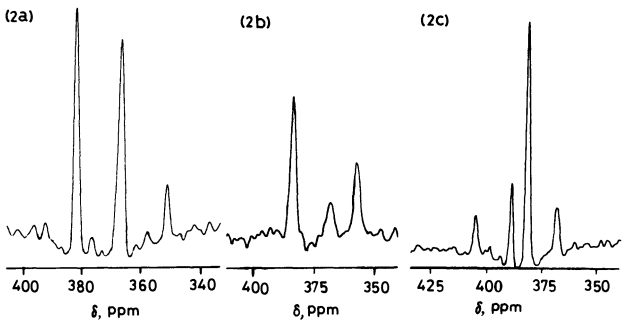

Fig. 2. ^{17}O NMR spectra of: (2a) $Me_2Sn[Mn(CO)_5]$-$[Re(CO)_5]$, (2b) $Ph_2Sn[Mn(CO)_5][Co(CO)_4]$, and (2c) $Me_2Sn[Mn(CO)_5][Mo(CO)_3Cp]$.

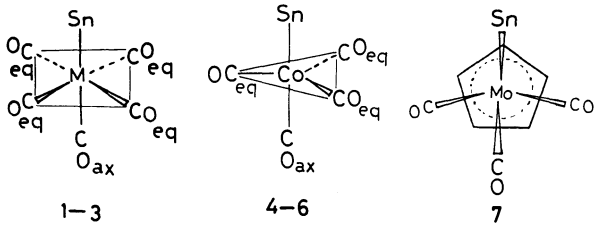

Scheme

dinuclear or hetero-trinuclear metal carbonyl derivatives **10—13**; $Me_2Sn[Mn(CO)_5][Re(CO)_5]$ (**10**) shows two intense and one weak resonances (Fig. 2a) and the most intense peak is assigned to the equatorial carbonyls in the $Mn(CO)_5$ moiety. The line width of the next intense peak at δ 366.8 is broader than that of the most intense peak at δ 382.1 and the chemical shift is quite close to the resonance of the axial carbonyls in $Me_2Sn[Mn(CO)_5]_2$ (**1**) at δ 365.9. Therefore, this peak is assigned to the equatorial carbonyls in the $Re(CO)_5$ moiety and the axial carbonyl in the $Mn(CO)_5$ moiety. The weak peak at 351.5 ppm is assigned to the axial carbonyl in the $Re(CO)_5$ moiety. $Ph_2Sn[Mn(CO)_5][Co(CO)_4]$ shows three peaks at δ 383.0, 367.5, and 357.1 in THF (Fig. 2b). The most intense peak at δ 383.0 is assigned to the four equatorial carbonyls and the weakest peak at δ 367.5 is assigned to the axial carbonyl in the $Mn(CO)_5$ moiety. The medium intensity peak at δ 357.1 is assigned to the carbonyls in the $Co(CO)_4$ moiety. Here again the resonance due to the three equatorial carbonyls and the resonance due to the axial carbonyl in the $Co(CO)_4$ moiety are not resolved. Although the most complex

Table 1. Spectral Data

Compound		^{17}O NMR chemical shift, δ/ppm	λ_{max}/nm (ε/M^{-1} cm^{-1})	ν(CO)/cm^{-1}
$Me_2Sn[Mn(CO)_5]_2$	(**1**)	381.5(eq), 365.9(ax)[a]	320(17000)	2099, 2074, 2019, 2004,[d] 2002, 1984, 1961
$Ph_2Sn[Mn(CO)_5]_2$	(**2**)	383.1(eq), 366.7(ax)[a]	328(20400)	2100, 2078, 2029, 2009,[d] 2006, 2002, 1986, 1961
$Me_2Sn[Re(CO)_5]_2$	(**3**)	365.9(eq), 350.8(ax)[a]	328(15600)	2114, 2092, 2070, 2044,[d] 2010, 2009, 1998, 1987
$Me_2Sn[Co(CO)_4]_2$	(**4**)	359.7[b]	310(sh)	2095, 2078, 2031, 2024,[e] 2013, 2002, 1992
$Ph_2Sn[Co(CO)_4]_2$	(**5**)	357.4[a]	320(13300)	2095, 2080, 2033, 2029,[e] 2018, 2009, 1995
$Cl_2Sn[Co(CO)_4]_2$	(**6**)	362.9[b]	355(2000)	2114, 2097, 2056, 2052,[f] 2040, 2023, 2016
$Me_2Sn[Mo(CO)_3Cp]_2$	(**7**)	410.3(tr), 393.1(cis)[c]	323(4000)	2004, 1988, 1937, 1925,[g] 1910, 1894
$Me_2Sn[Fe(CO)_2Cp]_2$	(**8**)	356.3[b]	332(10200)	2002, 1990, 1945, 1936[h]
$Cl_2Sn[Fe(CO)_2Cp]_2$	(**9**)	367.9[a]	355(2000)	2040, 2025, 1993[h]
$Me_2Sn<^{Mn(CO)_5}_{Re(CO)_5}$	(**10**)	382.1(eq), 366.8(ax)[b] 366.8(eq), 351.5(ax)	322(16200)	2117, 2095, 2080,[i,j] 2077, 2010, 1982
$Ph_2Sn<^{Mn(CO)_5}_{Co(CO)_4}$	(**11**)	383.0(eq), 367.5(ax)[a] 357.1	325(10200)	2105, 2100, 2080, 2030,[i,k] 2018, 2010, 1985
$Me_2Sn<^{Mn(CO)_5}_{Mo(CO)_3Cp}$	(**12**)	381.7(eq), 367.8(ax)[c] 405.6(tr), 388.8(cis)	312(12200)	2092, 2088, 2076, 2020,[i,l] 2002, 1990, 1930, 1903
$ClSn<^{Mn(CO)_5}_{[Fe(CO)_2Cp]_2}$	(**13**)	382.1(eq), 367.2(ax)[a] 367.2	340(15300)	2089, 2060, 2025, 2010,[i,m] 2000, 1990, 1949

a) THF solution. b) $CHCl_3$ solution. c) C_6H_6 solution. d) Ref. 3. e) Ref. 4. f) Ref. 5. g) Ref. 6. h) Ref. 7. i) This work. j) Ligroine solution. k) Nujoll mull. l) Cyclohexane solution. m) CCl_4 solution.

spectrum is displayed for $Me_2Sn[Mn(CO)_5][Mo(CO)_3Cp]$ (**12**) (Fig. 2c), spectral assignment is easily made with reference to the assignments of (**1**) and (**7**). The weak peak at δ 405.6 is assigned to the trans CO with respect to Sn and the medium intensity peak at δ 388.8 to the two cis CO with respect to Sn on the $Mo(CO)_3Cp$ moiety. The most intense peak at δ 381.7 is assigned to the equatorial four CO and the weak peak at δ 367.8 to the axial CO in the $Mn(CO)_5$ moiety. $ClSn[Mn(CO)_5][Fe(CO)_2Cp]_2$ (**13**) shows two intense peaks at δ 382.1 and δ 367.2. The peak at δ 382.1 is assigned to the four equatorial carbonyls in the $Mn(CO)_5$ moiety and the peak at δ 367.2 is assigned to the axial CO in the $Mn(CO)_5$ moiety and the four carbonyls in the two $Fe(CO)_2Cp$ units.

Discussion

As for absorption spectra, we have previously suggested that the absorption between 300 and 400 nm is assignable to $\sigma \rightarrow \sigma^*$ transition of the Sn–Mn bonds in $Me_2Sn[Mn(CO)_5]_2$ and $MeSn[Mn(CO)_5]_3$.[2] To supplement this suggestion, absorption spectral measurements are examined for a present series of derivatives, **1**—**13**. All these derivatives exhibit absorptions between 300 and 400 nm and these absorptions are assignable to $\sigma \rightarrow \sigma^*$ transition of the Sn–M bonds in the present series of derivatives.

As is shown in the Table 1, all the derivatives which are employed for the present study show very complex IR spectra in the ν(CO) region. On the other hand ^{17}O NMR spectra for these derivatives are generally simpler than the corresponding ν(CO) spectra and the ^{17}O NMR spectral assignments are easily achieved as is mentioned in the previous section. The investigation for the change of electron distribution around the oxygen atom(s) of interest are easily made in terms of the ^{17}O chemical shift, whereas normal coordinate treatments by use of a computer are necessary in order to make similar investigation in terms of force constants for IR spectroscopy in the ν(CO) region.[12] In this sense, the superiority of ^{17}O NMR spectroscopy to IR spectroscopy is again demonstrated for present more complex systems than those simpler systems which were demonstrated in the previous studies.[1]

Then, ^{17}O NMR spectroscopy is applied to investigate the effect of substitution of one of the $M(CO)_x$ or $M'(CO)_yCp$ unit in the homo-dinuclear $R_2Sn[M(CO)_x]_2$ or $R_2Sn[M'(CO)_yCp]_2$ system with other metal carbonyl unit, $M'(CO)_y$ on the electron distribution around the O atom(s) of interest; that is, ^{17}O-chemical shifts for **10**—**13** are compared with those for **1**—**3**, **5**, **7**, and **9**. The substitution, however, causes only slight changes of the chemical shifts except for $Me_2Sn[Mo(CO)_3Cp]_2$ (**7**); several ppm shifts are observed for the $Mo(CO)_3Cp$ moiety by substitution of one of the $Mo(CO)_3Cp$ unit with a $Mn(CO)_5$ unit. The fact that the substituent is on the third atom from the O atoms of interest explains this range of small shift. Todd et al. reported a larger down-field shift, that is, 14.4 ppm, in the substitution of bromine atoms for triphenylphosphines in $Mn_2(CO)_8(PPh_3)_2$;[13] in this system, the substituent is on the second atom from the O atoms of interest. The effect of the substituents, R, on the ^{17}O-chemical shift is also studied for a series of $R_2Sn[Co(CO)_4]_2$ (R=Me, Ph, and Cl) (**4**—**6**) and $R_2Sn[Fe(CO)_2Cp]_2$ (**8**, **9**) (R=Me and Cl). For a series of Co derivatives, 5.5 ppm lower-field shift is observed by substitution of Ph with Cl and 11.6 ppm lower-field shift is observed by substitution of Me with Cl for a series of Fe derivatives. Here again, the substituent is on the third atom from the O atoms of interest and only slight lower-field shifts are observed. These lines of evidence suggest that ^{17}O-chemical shift of CO groups is sensitive to the metal atom to which the CO groups are coordinated and the effect of the substituent on the ^{17}O-chemical shift, that is, on the electron distribution around the oxygen atom(s), is small, if any, in the case that the substitution is made on the third atom from the O atoms of interest. We are now applying this trait of ^{17}O NMR spectroscopy for higher nuclearity mixed metal carbonyl clusters.

We would like to express our gratitude to professor Kensuke Takahashi of this Institute for his kind help to get ^{17}O NMR spectra.

References

1) Part 1: S. Onaka, T. Sugawara, Y. Kawada, and H. Iwamura, *J. Chem. Soc., Dalton Trans.*, **1982**, 257. Part 2: S. Onaka, T. Sugawara, Y. Kawada, Y. Yokoyama, and H. Iwamura, *Bull. Chem. Soc. Jpn.*, **59**, 3079 (1986).
2) S. Onaka, Y. Kondo, N. Furuichi, K. Toriumi, and T. Ito, *Bull. Chem. Soc. Jpn.*, **56**, 87 (1983).
3) J. A. J. Thompson and W. A. G. Graham, *Inorg. Chem.*, **6**, 1365 (1967).
4) D. J. Patmore and W. A. G. Graham, *Inorg. Chem.*, **6**, 981 (1967).
5) D. J. Patmore and W. A. G. Graham, *Inorg. Chem.*, **5**, 1405 (1966).
6) H. R. H. Patil and W. A. G. Graham, *Inorg. Chem.*, **5**, 1401 (1966).
7) F. Bonati and G. Wilkinson, *J. Chem. Soc. A*, **1964**, 179.
8) S. Onaka, T. Miyamoto, and Y. Sasaki, *Bull. Chem. Soc. Jpn.*, **44**, 1851 (1971).
9) D. J. Patmore and W. A. G. Graham, *Inorg. Chem.*, **7**, 771 (1968).
10) R. D. Gorsich, *J. Am. Chem. Soc.*, **84**, 2486 (1962).
11) H. R. H. Patil and W. A. G. Graham, *J. Am. Chem. Soc.*, **87**, 673 (1965).
12) S. Onaka, *Bull. Chem. Soc. Jpn.*, **44**, 2135 (1971).; S. Onaka, *ibid.*, **46**, 2444 (1973).
13) R. L. Kump and L. J. Todd, *J. Organomet. Chem.*, **194**, C43, (1980).

Novel Racemization of Atropisomeric Flavins and 5-Deazaflavins via Adduct Formation[1)]

Seiji SHINKAI,*, Hideki NAKAO, Toshiro YAMAGUCHI, and Osamu MANABE
Department of Industrial Chemistry, Faculty of Engineering, Nagasaki University, Nagasaki 852
(Received April 18, 1987)

Synopsis. The molecular structures of covalent adducts derived from flavins and 5-deazaflavins are discussed on the basis of racemization of atropisomeric flavins and 5-deazaflavins. The 5-adducts with SO_3^{2-} and CN^- underwent facile racemization, indicating that the molecular structure changes from the "tense" planar state to the "relaxed" bent state. On the other hand, the 4a-adduct prepared by the photo-alkylation method did not racemize at room temperature. This indicates that the structure of the 4a-adduct is different from the bent 5-adduct. These results provide an information useful to discuss the reduced state of flavoproteins.

A number of papers have reported on the synthesis and the resolution of optical isomers caused by restricted rotation about a C–C single bond.[2–7)] The typical examples are sterically-hindered binaphthyls and biphenyls.[3–5)] In contrast, only a few precedents exist for such optical isomers including restricted rotation about a C–N single bond,[8–11)] and the characteristics arising from the C–N axis are not understood well. We recently synthesized several isoalloxazines (**1NR** and **2NR**) and 5-deazaisoalloxazines (**1CHR** and **2CHR**) with restricted rotation about the C(1′)–N(10) single bond.[12,13)] They were optically resolved by a liquid chromatographic method using a chiral packing column. It was found that these atropisomers did not recemize thermally (below 70 °C) or by visible light irradiation (at 30 °C) but the (5-deaza)isoalloxazines with a 2′-substituted phenyl group or a naphthyl group at N(10) racemized invariably when they were reduced to 1,5-dihydro forms.[13,14)] Detailed examination established that the facile rotation in the reduced state is due to conversion of the "planar" oxidized forms to the "bent" reduced forms by which the steric restriction is partically relaxed:[14)] that is, reduction changes the molecular geometry from the "tense" steric state to the "relaxed" steric state.

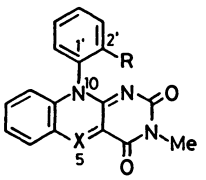

1XR

1NPh: X=N, R=phenyl
1CHPh: X=CH, R=phenyl

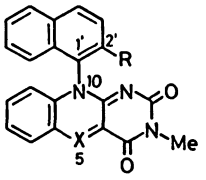

2XR

2NH: X=N, R=H
2NOMe: X=N, R=OMe
2CHOMe: X=CH, R=OMe

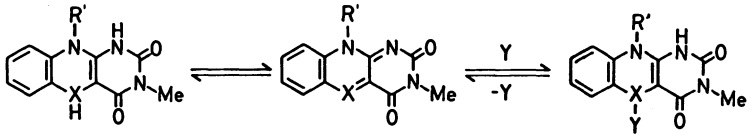

1,5-dihydro form — Y=CN^-, SO_3^{2-} (1)

It is known that flavins and 5-deazaflavins reversibly form covalent adducts (i.e., 5-adducts) with nucleophiles such as CN^- and SO_3^{2-} at 5-position.[14)] It would be of value to examine whether the racemization is also induced by the adduct formation. If they recemize, it provides unambiguous evidence for the bent structure. With this object in mind, we treated optically-pure **1XR** and **2XR** with the nucleophiles and checked whether recovered (5-deaza)isoalloxazines recemized.

Experimental

Materials. Preparations of 3-methyl-10-(2-phenylphenyl)isoalloxazine (**1NPh**), 3-methyl-10-(2-phenylphenyl)-5-deazaisoalloxazine (**1CHPh**), 3-methyl-10-(1-naphthyl)isoalloxazine (**2NH**), 3-methyl-10-(2-methoxy-1-naphthyl)isoalloxazine (**2NOMe**), and 3-methyl-10-(2-methoxy-1-naphthyl)-5-deazaisoalloxazine (**2CHOMe**) were described previously.[12,13)] The method of optical resolution was also described.[12,13)]

Reactions with KCN or K_2SO_3. The aqueous reactions of (5-deaza)isoalloxazines with KCN or K_2SO_3 were conducted aerobically in the quartz cuvette at 30 °C. The concentrations of the reactants are recorded in footnotes to Table 1. The progress of the reactions was followed spectrophotometrically by monitoring the disappearance of the absorption band at around 440 nm for isoalloxazines and 400 nm for 5-deazaisoalloxazines. The reaction of 5-deazaisoalloxazines and K_2SO_3 was finished immediately after mixing. Other reactions took 1—2 h. After completion of the reactions the solution (5 ml) was acidified with concd HCl (15 ml) and stirred for 1 h at room temperature. By this treatment the adducts decomposed to the oxidized forms, which were easily monitored by the recovery of the yellow solution color. Then, the solution was adjusted to pH 4 with 0.1 M Na_2HPO_4 (1 M=1 mol dm^{-3}) and extracted with chloroform. The chloroform solution was concentrated in vacuo and the residue (about 1 ml) was analyzed by HPLC using a chiral packing column (Sumipax OA-2000). The results are summarized in Table 1. We confirmed in a separate experiment that in the absence of the nucleophiles these (5-deaza)isoalloxazines do not racemize by the treatment described above.

Photo-Alkylation. (+)-**1NPh** (6.17×10^{-5} M) and ammonium phenylacetate (5.44×10^{-2} M) were dissolved in a mixed solvent of methanol–water (1.3:2.0 v/v). The solution pH was 7.1. The anaerobic solution in a Thunberg cuvette was photoirradiated by a 17-W flourescent lamp for 30 min at

room temperature. The absorption spectra taken every 5 min were very similar to those reported in Ref. 20 in which "pure" 4a-benzyl-4a,5-dihydroflavin resulted: That is, the absorption maximum (440 nm) decreased with photoirradiation with an isosbestic point (315 nm) giving rise to a new absorption maximum (350 nm). The solution was diluted with water and then extracted with chloroform. The chloroform layer was separated and dried over Na_2SO_4. The solution was concentrated in vacuo to dryness. The residue (dissolved in 0.5 ml chloroform) was subjected to HPLC analysis using a chiral packing column (Sumipax OA-2000) connected to a photo-diode array UV-VIS detector (Shimadzu SPD-M1A). In a separate study, we confirmed that photoirradiation in the absence of ammonium phenylacetate at room temperature does not induce racemization.

Results and Discussion

It is clearly seen from Table 1 that **1NPh**, **1CHPh**, and **2NH** racemize when they form the 5-adducts. It is firmly established by X-ray crystallographic studies that oxidized flavins are planar, whereas reduced 1,5-dihydroflavins are folded along a line through N(5) and N(10) like butterfly wings.[15,16] This is because the nitrogen atoms N(5) and N(10) have a high degree of tetrahedral sp^3 hybridization in the reduced state.[15,16] Although there exists no firm evidence for the molecular structure of 5-adducts, it has been expected that 5-adducts would be bent like 1,5-dihydro forms on the basis of the spectral similarity. Our finding that the 5-adducts derived from chiral (5-deaza)isoalloxazines with a 2′-phenylphenyl group or a naphthyl group easily racemize at room temperature clearly supports that the 5-adducts employ the bent structure which can relax the steric restriction (Eq. 2).

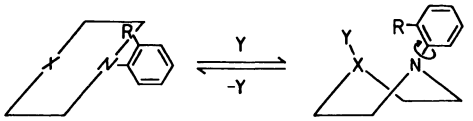

(2)

In contrast, the optical purities of 2NOMe and 2CHOMe are essentially unaffected by this treatment, indicating that racemization does not occur either in the 5-adduct state or in the transition state.[17] We have found that the redox treatment of these (5-deaza)isoalloxazines (Y=H in Eq. 2) does not change the optical purities.[12,13] This means that the steric bulkiness of the 2′-methoxy-1′-naphthyl group (but not of Y) is responsible for the retention of the optical purities. Therefore, the difference between the 2′-methoxy-1′-naphthyl group and the 2′-substituted phenyl group can be explained as follows: In the 2′-methoxy-1′-naphthyl group which would be comparable sterically with the 2′,6′-disubstituted phenyl group both 2′-methoxyl group and 8′-hydrogen provide steric hindrance to restrict the rotation, whereas in the 2′-substituted phenyl group the steric bulkiness is not enough to suppress the rotation.

The foregoing racemization trend is completely in accord with that observed for the redox treatment of the chiral (5-deaza)flavins.[12,13] Therefore, the 5-adducts should employ the bent structure with butterfly-like wings similar to the 1,5-dihydro forms.

Racemization may also take place via 4a-adducts (covalent adducts at 4a-position) if they employ the bent structure. The thermal nucleophilic attack usually occurs at 5-position of the isoalloxazine ring except a few cases.[18,19] It is known, on the other hand, that light-induced alkylation occurs at 4a-position.[20] By means of this photo-alkylation method we examined whether racemization takes place via 4a-adducts.

Accoding to Bruice et al.,[18,19] λ_{max} for 5-adducts characteristically appears between 296 and 330 nm and λ_{max} for 4a-adducts appears between 360 and 370 nm. In photo-alkylation of 6,7-dimethyl-10-(tetra-*O*-acetylribityl)isoalloxazine by phenylacetate, Walker et al.[20]

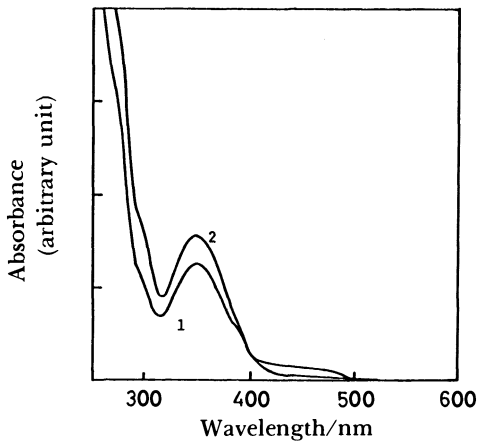

Fig. 1. Absorption spectra of the first peak (1) and the second peak (2) measured by a photo-diode array UV-VIS detector connected to a chiral peaking column.

Table 1. Racemization via Adduct Formation

Flavin[a]	Optical purity of (+)-Isomer/e.e.%	Nucleophile[b]	Recovered flavin	
			(+)-Isomer/%	(−)-Isomer/%
1NPh	100	K_2SO_3	46.6	52.4
1CHPh	100	K_2SO_3	55.0	45.0
1CHPh	100	KCN	54.4	45.6
2NH	100	K_2SO_3	52.8	47.2
2NOMe	98.0	K_2SO_3	98.0	2.0
2CHOMe	100	K_2SO_3	100	0
2CHOMe	100	KCN	100	0

a) [1NPh]=6.20×10^{-5} M, [1CHPh]=4.74×10^{-5} M. The concentrations of other flavins were 5.00×10^{-5} M. b) [K_2SO_3]=0.752 M for isoalloxazines and 0.125 M for 5-deazaisoalloxazines, [KCN]=1.10×10^{-3} M. The reaction between 5-deazaisoalloxazines and KCN was not completely reversible because in the HPLC analysis we detected a small amount of some unknown products in addition to recovered 5-deazaisoalloxazines.

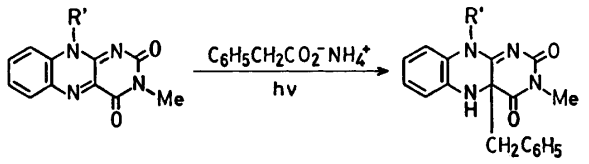

(3)

observed a new absorption maximum at 364 nm which was attributed to the 4a-adduct. In HPLC we observed two large peaks which gave the identical absorption spectra (λ_{max} 350 nm: Fig. 1). Therefore, these two peaks are attributed to the optically-isomeric 4a-adducts of 1NPh. The peak intensity ratio of the first vs. the second peak was 1.0:2.1. The ratio was affected neither by heating in chloroform for 2 h at 60 °C nor by keeping at room temperature in the dark for 3 days. These results suggest that the C(1')–N(10) axis in the 4a-adduct cannot racemize at room temperature and that the peak separation in HPLC is due to the chirality at 4a position. The absolute configuration of (+)-1NPh is not determined yet. If it could be drawn as in Eq. 4, it would result in two optical isomers, A and B. The attack from the 2'-phenyl side results in A while that from the 6'-hydrogen side results in B. Presumably, the attack from the sterically-crowded 2'-phenyl side is less advantageous. If so, the first weak peak (32%) is attributed to A and the second strong peak (68%) is attributed to B.

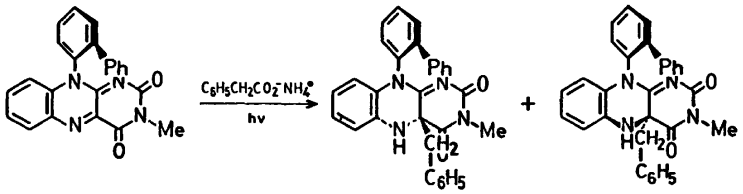

A B

(4)

Recently, Yoneda et al.[21] reported an X-ray crystallographic structure of 4a,5-dihydro-4a-hydroxy-3,10-dimethyl-5-deazaisoalloxazine, a 4a-adduct of 5-deazaisoalloxazine. The picture shows that N(10) with sp^2 nitrogen is almost planar while C(5) with sp^3 carbon is bent to the chair-like form, totally resulting in a half-chair conformation. On the other hand, almost nothing is known with certainty as to the 4a-adduct of isoalloxazine. If it is bent along the N(5)–N(10) like butterfly wings, the 4a-adduct of (+)-1NPh should racemize easily at room temperature. Thus, the present result suggests that N(10) in the 4a-adduct should be planar with sp^2 nitrogen which does not allow facile racemization.

According to Massey and Hemmerich,[22] a large number of flavoproteins may be classified into two groups from a viewpoint of their regiospecific reactivities, a 5-activated group and a 4a-activated group. The first group which uses the N(5) in the redox reactions is characterized by red semiquinone, high sulfite affinity, and *bent structure of reduced form*, whereas the second group which uses the C(4a) in the redox reactions is characterized by blue semiquinone, low sulfite affinity, and *almost planar structure of reduced form*. As demonsrated in the present study, the 5-adduct employs the bent structure while the 4a-adduct employs the almost planar N(10). The difference is well-correlated with the classification in flavoenzymes: that is, the reactions including N(5) take the bent intermediates while those including C(4a) take the planar intermediates not only in the flavoenzymes but also in the model systems. Therefore, the present results could provide a significant cross-link between enzymic reactions and model organic reactions.

References

1) Coenzyme Models. 49.
2) J. L. A. Webb, *J. Org. Chem.*, **18**, 1413 (1935).
3) E. L. Eliel, "Stereochemistry of Carbon Compounds," McGraw-Hill, New York (1962), p. 156.
4) R. Adams and H. C. Yuan, *Chem. Rev.*, **12**, 261 (1933).
5) M. Ōki, *Acc. Chem. Res.*, **17**, 154 (1984).
6) A. Luttrighaus and H. Gralheer, *Justus Liebigs Ann. Chem.*, **550**, 67 (1941).
7) T. H. Sidall and W. E. Stewart, *J. Org. Chem.*, **34**, 233 (1969).
8) W. H. Patterson and R. Adams, *J. Am. Chem. Soc.*, **55**, 1069 (1933).
9) C. Kashima and A. Katoh, *J. Chem. Soc., Perkin Trans. 1*, **1980**, 1599.
10) J. C. Jochims, H. von Voithenberg, and G. Wegner, *Chem. Ber.*, **111**, 1693, 2745 (1978).
11) M. Mintas, Z. Orhanovic, K. Jakopcic, H. Koller, G. Stühler, and A. Mannschreck, *Tetrahedron*, **41**, 229 (1985) and references cited therein.
12) S. Shinkai, H. Nakao, and O. Manabe, *Tetrahedron Lett.*, **26**, 5183 (1985).
13) S. Shinkai, H. Nakao, I. Kuwahara, M. Miyamoto, T. Yamaguchi, and O. Manabe, *J. Chem. Soc., Perkin Trans. 1*, in press.
14) P. Hemmerich, V. Massey, and H. Fenner, *FEBS Lett.*, **84**, 5 (1977).
15) L. Tauscher, S. Ghisla, and P. Hemmerich, *Helv. Chim. Acta*, **56**, 630 (1973) and references cited therein.
16) P. Kierkegaard, R. Norrestam, P. Werner, I. Csoregh, M. Glehn, R. Karlsson, M. Leijionmarch, O. Ronnquist, B. Sternland, O. Tillberg, and L. Torbjornsson, "Flavins and Flavoproteins," University Park Press, Baltimore (1971), p. 1.
17) M. Ōki, *Top. Stereochem.*, **14**, 1 (1983).
18) L. Hevesi and T. C. Bruice, *J. Am. Chem. Soc.*, **94**, 8277 (1972).
19) T. C. Bruice, L. Hevesi, and S. Shinkai, *Biochemistry*, **12**, 2083 (1973).
20) W. H. Walker, P. Hemmerich, and V. Massey, *Eur. J. Biochem.*, **13**, 258 (1970).
21) F. Yoneda, K. Tanaka, Y. Sakuma, H. Yoshino, and M. Takamoto, *Chem. Pharm. Bull.*, **32**, 3761 (1984).
22) V. Massey and P. Hemmerich, *Biochem. Soc. Trans.*, **8**, 246 (1980).

A Facile Synthesis of 3-Hydroxymethyl- and 3-Formylindoles from *o*-Nitrotoluene

Hideo TANAKA, Yasuo MURAKAMI, Koichi OKAMOTO, Takao AIZAWA, and Sigeru TORII*
Department of Industrial Chemistry, School of Engineering, Okayama University, Okayama 700
(Received July, 3, 1987)

Synopsis. A synthesis of 3-hydroxymethyl- and 3-formylindoles has been performed by manipulation of the side chain of 3-hydroxymethylindoline derived from *o*-nitrotoluene. Electro-reductive cyclization of 2-(2-nitrophenyl)-1,3-bis(methylsulfonyloxy)propane to 3-(benzyloxymethyl)indole, is also discussed.

The conversion of readily available *o*-nitrotoluene (**1**) into useful 3-substituted indoles **6** is of current interest.[1] We have recently reported an efficient electrogenerated base (EG Base) induced double hydroxymethylation of the methyl group of *o*-nitrotoluene (**1**) with formaldehyde.[2] The adduct **2a** (R^1=H) possesses all of the framework elements required for the formation of 3-hydroxymethyl- or 3-formylindole (**6a**, **6b**), which are intermediates for the synthesis of useful indole derivatives.[3] Herewith, we describe a convenient synthesis of **6a** (Y=CH_2OH, Z=Ms) and **6b** (Y=CHO, Z=Ms) by manipulation of the C(3)-side chain of indolines **4**, derived from **2a**, together with electroreductive transformation of **2b** (R^1=Ms) to **6c** (Y=CH_2OCH_2Ph, Z=H).

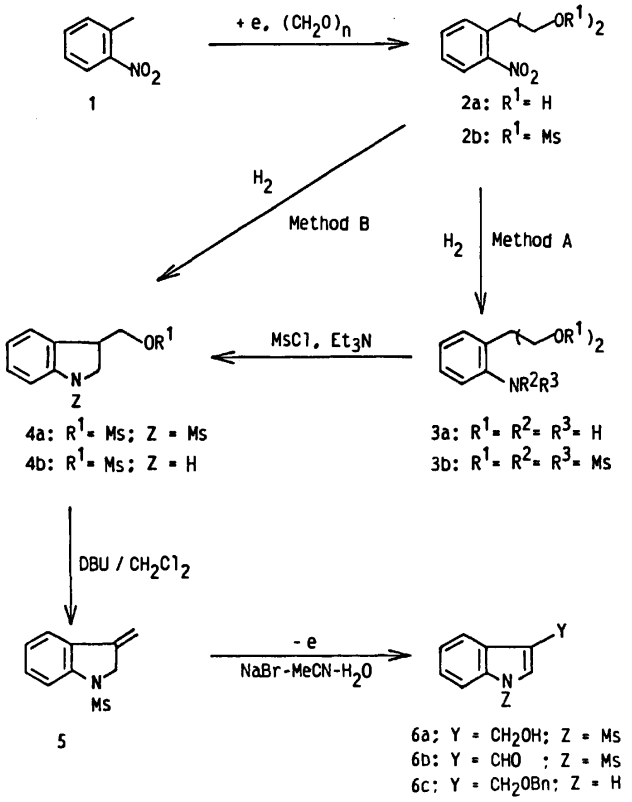

Scheme 1.

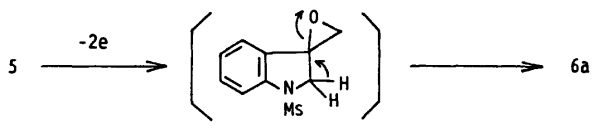

Scheme 2.

Our approach to indoles **6** is outlined in Scheme 1. The key intermediate **4a** (R^1=Z=Ms) was prepared by two different pathways (Methods A and B).[4,5] Thus, hydrogenation of **2a** over Pd/C catalyst gave amine **3a** (R^1=R^2=R^3=H; 96%) which, upon treatment with methanesulfonyl chloride (MsCl) and Et_3N in CH_2Cl_2, was converted to indoline **4a** (85%) along with **3b** (R^1=R^2=R^3=Ms, 3%) (Method A).[4] Cyclization of the by-product **3b** to **4a** was successfully performed in 91% yield by the electroreduction in DMF containing ascorbic acid and anthracene.[6] Alternatively (Method B), hydrogenation of methanesulfonate **2b** over PtO_2 in benzene containing K_2CO_3 afforded indoline **4b** (R^1=Ms, Z=H) exclusively (80%).[5] Treatment of **4b** with MsCl/Et_3N in CH_2Cl_2 afforded **4a** (88%).

Next task is the introduction of the C=C double bond at the C(2)-position of indoline **4a**. At first, we investigated the direct dehydrogenation of **4a** using catalysts, e.g., PtO_2 and Pd/C. All attempts, however, resulted in the formation of a complex mixture and failed in obtaining an appreciable amount of the desired products **6**.[7] Finally, we found a new route involving two-step operation (**4a**→**5**→**6a**); heating **4a** with diazabicyclo[5.4.0]undec-7-ene (DBU) in CH_2Cl_2 afforded 3-methyleneindoline (**5**) (94%), which was, in turn, electrolyzed in an aqueous CH_3CN solution containing NaBr to give indole **6a** (Y=CH_2OH) in 85% yield. The electrochemical transformation (**5**→**6a**) can be explained by assuming that the intermediary epoxide **7** (Scheme 2), formed by an electrolytic epoxidation of **5**,[8] is isomerized to **6a** in the electrolysis media. In fact, treatment of **5** with *m*-chloroperbenzoic acid and CH_2Cl_2 also afforded alcohol **6a** (49%). Aldehyde **6b** was obtained in 89% yield by oxidation of **6a** under O_2 (1 atm) in the presence of $RuCl_2(PPh_3)_3$ catalyst.[9]

As an alternative route to 3-substituted indoles, transformation of **2b** (R^1=Ms) to indole **6c** was performed by electroreduction of **2b** (R^1=Ms) in a benzyl chloride/Et_4NBr/DMF (Pt electrodes) system, affording **6c** (60%) after passage of 3.2 F mol^{-1} (1 F=96480C) of electricity. The presence of benzyl chloride in the electrolysis media is indispensable since absence of benzyl chloride resulted in the formation of a complex mixture. Although the mechanism is still unclear, it is likely that anion species, generated from electroreduction of the nitro group,[10] attack the methylsulfonyloxy group on the side chain.

Experimental

Apparatus and Procedures. IR spectra were recorded on a JASCO IRA-1 grating spectrometer. ^{1}H NMR spectra were measured at 60 MHz with a Hitachi R-24 spectrometer and ^{13}C NMR spectra were recorded with a JEOL FX-100 (25.05 MHz) spectrometer. Melting and boiling points are uncorrected. Column chromatography was carried out using Wako C-200 (silica gel) with hexane–EtOAc as an eluent. Elemental analysis were performed in our laboratory.

2-(2-Nitrophenyl)-1,3-bis(methylsulfonyloxy)propane (2b). To a mixture of **2a** (2.27 g, 11.5 mmol)[2] and Et_3N (10 ml) in CH_2Cl_2 (20 ml) was added MsCl (5 ml) at 0 °C. After stirring for 2 h at room temperature, usual workup of the mixture followed by chromatography (3:1 hexane–EtOAc) afforded **2b** (3.92 g, 97%) as colorless crystals: mp 90—91 °C (from benzene–CH_2Cl_2); IR (Nujol) 1355, 1175 cm^{-1}; ^{1}H NMR ($CDCl_3$) δ=2.89 (3H, s, CH_3SO_3), 3.9—4.2 (1H, m, CH), 4.56 (4H, d, J=5 Hz, CH_2O), 7.4—7.9 (4H, m, Ar). Anal. ($C_{11}H_{15}NO_8S_2$) C, H.

2-(2-Aminophenyl)-1,3-propanediol (3a). A mixture of **2a** (1.02 g, 5.2 mmol) and 5% Pd/C (100 mg) in EtOAc (20 ml) was stirred at room temperature under H_2 (1 atm) for 15 h. After the catalysts were removed by filtration, evaporation of the solvent afforded **3a** (840 mg, 96%) as colorless crystals: mp 72—75 °C (from benzene–CH_2Cl_2); IR (Nujol) 3360, 3330, 3300, 3200 cm^{-1}; ^{1}H NMR ($CDCl_3$–acetone-d_6) δ=3.0—3.4 (1H, m, CH), 3.6—4.1 (8H, m, NH_2, CH_2OH), 6.4—7.1 (4H, m, Ar). Anal. ($C_9H_{13}NO_2$) C, H.

1-Methylsulfonyl-2-(methylsulfonyloxymethyl)indoline (4a). Method A: To a mixture of **3a** (179 mg, 1.1 mmol) and Et_3N (0.6 ml, 4.3 mmol) in dry CH_2Cl_2 (4 ml) was added MsCl (0.18 ml, 2.3 mmol) at −10 °C. After being stirred at room temperature for 2 h, MsCl (0.08 ml, 1.0 mmol) was added at 10 °C and stirring was continued for an additional 1 h at room temperature. Usual workup of the mixture followed by chromatography (4:1 hexane–EtOAc) afforded **4a** (278 mg, 85%) as colorless crystals along with **3b** (16 mg, 3%). Compound **4a**: mp 99—101 °C (from benzene–CH_2Cl_2); IR ($CHCl_3$) 1370, 1355, 1175, 1160 cm^{-1}; ^{1}H NMR ($CDCl_3$) δ=2.89 (3H, s, CH_3SO_2N), 2.95 (3H, s, CH_3SO_3), 3.6—4.1 (3H, m, $CHCH_2N$), 4.32 (2H, dd, J=6, 1 Hz, CH_2O), 7.0—7.4 (4H, m, Ar). Anal. ($C_{11}H_{15}NO_5S_2$) C, H. Compound **3b**: mp 184—186 °C (from benzene–CH_2Cl_2); IR (Nujol) 3330—3380, 1190, 1185, 1170, 1160 cm^{-1}; ^{1}H NMR ($CDCl_3$–acetone-d_6) δ=2.95 (6H, s, CH_3SO_3), 3.51 (6H, s, CH_3SO_2N), 3.8—4.1 (1H, m, CH), 4.53 (4H, d, J=6 Hz, CH_2O), 7.4—7.7 (4H, m, Ar). Anal. ($C_{13}H_{21}NO_{10}S_4$) C, H.

Method B: To a solution of **2b** (1.13 g, 3.2 mmol) in benzene (80 ml) were added K_2CO_3 (800 mg) and $PtO_2 \cdot 3H_2O$ (120 mg). After stirring at room temperature under H_2 (1 atm) for 4 h, the catalysts were removed by filtration. Evaporation of the solvents followed by chromatography (2:1 hexane–EtOAc) afforded **4b** (580 mg, 80%): IR (neat) 3360, 1360, 1180 cm^{-1}; ^{1}H NMR ($CDCl_3$) δ=2.90 (3H, s, SO_2CH_3), 3.3—3.8 (2H, m, CH_2N), 3.55 (1H, br. s, H, NH), 3.3—3.8 (1H, m, CH), 4.1—4.4 (2H, m, CH_2O), 6.5—7.3 (4H, m, Ar). The structure of **4b** was confirmed by the following transformation into **4a**. To a mixture of **4b** (39 mg, 0.17 mmol) and Et_3N (0.2 ml) in CH_2Cl_2 (3 ml) was added MsCl (0.06 ml, 1.43 mmol) at −10 °C. After stirring for 3 h at room temperature, usual workup of the mixture followed by chromatography (3:1 hexane–EtOAc) afforded **4a** (46 mg, 88%), whose IR spectra and ^{1}H NMR were fully identical with those of **4a** described above.

1-Methylsulfonyl-3-methyleneindoline (5). A mixture of **4a** (125 mg, 0.41 mmol) and 1,8-diazabicyclo[5.4.0]undec-7-ene (0.25 ml, 1.67 mmol) in CH_2Cl_2 (4 ml) was heated at reflux for 15 h. Usual workup of the mixture followed by chromatography (3:1 hexane–EtOAc) afforded **5** (81 mg, 94%) as colorless crystals: mp 114—116 °C (from benzene); IR ($CHCl_3$) 1640, 1355, 1160 cm^{-1}; ^{1}H NMR ($CDCl_3$) δ=2.83 (3H, s, CH_3SO_2N), 4.55 (1H, dd, J=3 Hz, HC=C), 6.8—7.5 (4H, m, Ar). Anal. ($C_{10}H_{11}NO_2S$) C, H.

3-Hydroxymethyl-1-(methylsulfonyl)indole (6a). A solution of **5** (35 mg, 0.17 mmol) in MeCN (10 ml)–H_2O (2 ml) contaning NaBr (27 mg, 0.26 mmol) was electrolyzed under a constant current density of 3.3 mA cm^{-2} at room temperature in a beaker type cell fitted with two platinum electrodes (3 cm^2).[12] After passage of 3 F mol^{-1} of electricity (2.8 h), workup of the electrolytes followed by chromatography (4:1 hexane–EtOAc) afforded **6a** (33 mg, 85%) as colorless crystals: mp 117—120 °C (from benzene–CH_2Cl_2); IR ($CHCl_3$) 3400, 1370, 1170, 1110 cm^{-1}; ^{1}H NMR ($CDCl_3$) δ=2.45 (1H, br. s, OH), 3.02 (3H, s, CH_3SO_2N), 4.79 (2H, br. s, CH_2O), 7.2—7.9 (5H, m, Ar, HC=C). Anal. ($C_{10}H_{11}NO_3S$) C, H.

3-Formyl-1-(methylsulfonyl)indole (6b). A mixture of **6a** (240 mg, 1.1 mmol) and $RuCl_2(PPh_3)_3$ (310 mg, 0.3 mmol)[10] in CH_2ClCH_2Cl (10 ml) was stirred under O_2 (1 atm) at 50—60 °C for 4 h. After evaporation of the solvent, the residue was passed through short Florisil column (hexane–EtOAc). The eluents were concentrated and chromatographed (4:1 hexane–EtOAc), affording colorless crystals **6b** (192 mg, 80%): mp 170—171 °C (from benzene–CH_2Cl_2); IR (Nujol) 1690, 1380, 1185 cm^{-1}; ^{1}H NMR ($CDCl_3$) δ=3.25 (3H, s, CH_3SO_2N), 7.4—8.4 (4H, m, Ar), 8.04 (1H, s, HC=C), 10.07 (1H, s, CHO). Anal. ($C_{10}H_9NSO_3$) C, H.

Electroreductive Cyclization of 2-[2-[Bis(methylsulfonyl)-amino]phenyl]-1,3-bis(methylsulfonyloxy)propane (3b). Electrolysis was carried out in an H-shaped divided cell fitted with Pt-cathode (3 cm^2) and Pt-anode (3 cm^2).[12] Into both anode and cathode compartments was charged a DMF solution of Et_4NOTs (6 ml/133 mg each). To the catholyte were added **3b** (48 mg, 0.1 mmol), ascorbic acid (35 mg, 0.2 mmol), and anthracene (18 mg, 0.1 mmol). The mixture was electrolyzed under a constant current density of 3.3 mA cm^{-2} at room temperature for 2.4 h (4.5 F mol^{-1}). The catholyte was worked up in the usual manner, yielding colorless crystals **4a** (28 mg, 90%), whose IR and ^{1}H NMR spectra were fully identical with those of **4a** described above.

3-(Benzyloxymethyl)indole (6c). Electrolysis was carried out in the same cell as described above. Into both the anode and cathode compartments was placed a DMF solution of Et_4NBr (6 ml, 315 mg each). To the catholyte were added **2b** (107 mg, 0.3 mmol) and benzyl chloride (0.17 ml, 1.48 mmol). The mixture was electrolyzed under a constant current (1.7 mA cm^{-2}) at room temperature for 5.2 h (3.2 F mol^{-1}). Usual workup of the catholyte followed by chromatography on Florisil (10:1 hexane–EtOAc) afforded 3-(benzyloxymethyl)indole (**6c**)[13] (43 mg, 60%): IR (neat) 3340, 1455, 1105 cm^{-1}; ^{1}H NMR ($CDCl_3$) δ=1.86 (1H, br. s, NH), 4.67 (2H, s, C=CCH_2O), 5.07 (2H, s, OCH_2Ph), 6.9—7.7 (5H, m, Ar, NCH=C), 7.29 (4H, s, Ph); ^{13}C NMR ($CDCl_3$) δ=56.8 (t), 80.2 (t), 108.6 (d), 111.5 (s), 119.2 (d), 120.0 (d), 122.6 (d), 122.8 (d), 122.8 (s), 128.6 (d), 129.1 (d), 129.5 (d), 132.9 (s), 134.6 (s).

References

1) For example, see: P. N. James and H. R. Synder, *Org. Synth.*, Coll. Vol. 4, 539 (1963); W. E. Noland and F. G. Baude, *ibid.*, Coll. Vol. 5, 567 (1973); G. M. Coppola, G. E. Hardtmann, and B. S. J. Huegi, *J. Heterocycl. Chem.*, **1974**, 51; J. Bakke, E. B. Heikmann, and E. B. Hellgren, *Acta Chem. Scand.*, **B28**, 393 (1974); M. G. Saulnier and G. W. Gribble, *J.*

Org. Chem., **47**, 758 (1982); R. D. Clark and D. B. Repke, *Heterocycles*, **22**, 195 (1984); Y. Tsuji, K. T. Huh, Y. Yokoyama, and Y. Watanabe, *J. Chem. Soc., Chem. Commun.*, **1986**, 1575 and references cited therein.

2) S. Torii, Y. Murakami, H. Tanaka, and K. Okamoto, *J. Org. Chem.*, **51**, 3143 (1986).

3) For example, see: P. Magnus, T. Gallagher, P. Brown, and J. C. Huffman, *J. Am. Chem. Soc.*, **106**, 2105 (1984); G. W. Gribble, M. G. Saulnier, M. P. Sibi, and J. A. Obaza-Nutaitis, *J. Org. Chem.*, **49**, 4518 (1984); K.-F. Cheng, Y.-F. Kong, and T.-Y. Chan, *J. Chem. Soc., Chem. Commun.*, **1985**, 48; H. Muratake and M. Natsume, *Heterocycles*, **23**, 1111 (1985); J. P. Dirlam, D. A. Clark, and S. J. J. Hecker, *J. Org. Chem.*, **51**, 4920 (1986).

4) T. Kametani, S. Asagi, S. Nakamura, M. Satoh, N. Wagatsuma, and S. Takano, *Yakugaku Zasshi*, **86**, 107 (1966).

5) W. J. Wierenga, *J. Am. Chem. Soc.*, **103**, 5621 (1981).

6) Reductive C–N bond fission of sulfonamide in the same electrolysis media has been reported: K. Oda, T. Ohnuma, and Y. Ban, *J. Org. Chem.*, **49**, 953 (1984).

7) Dehydrogenative cyclization[1] of **3a** to **6** (Y=CH_2OH; Z=H) with $RuCl_2(PPh_3)_3$ failed.

8) S. Torii, K. Uneyama, H. Tanaka, T. Yamanaka, T. Yasuda, M. Ono, and Y. Kohmoto, *J. Org. Chem.*, **46**, 3312 (1981).

9) M. Matsumoto and S. Ito, *J. Chem. Soc., Chem. Commun.*, **1981**, 907.

10) J. H. J. Wagenknecht, *J. Org. Chem.*, **42**, 1836 (1977); C. Degrand, P.-L. Compagnon, G. Belot, and D. Jacquin, *J. Org. Chem.*, **45**, 1189 (1980).

11) P. S. Hallman, T. A. Stephenson, and G. Wilkinson, *Inorg. Synth.*, **12**, 238 (1970).

12) Details on the electrolysis cell: S. Torii, T. Inokuchi, and T. Sugiura, *J. Org. Chem.*, **51**, 155 (1986); see also Ref. 2.

13) The structure of **6c** was confirmed by hydrogenation of **6c** over Pd/C into 3-(hydroxymethyl)indole, whose IR and ^1H NMR spectra were fully identical with those of the authentic sample: R. M. Silverstein, E. E. Ryskiewicz, and S. W. Chaikin, *J. Am. Chem. Soc.*, **76**, 4485 (1954).

The Infrared Spectrum of Dioxygen Bound to the Synthetic Porphinatoiron in an Aqueous Medium

Makoto YUASA, Kimiko YAMAMOTO, Hiroyuki NISHIDE, and Eishun TSUCHIDA*
Department of Polymer Chemistry, Waseda University, Tokyo 160
(Received June 29, 1987)

Synopsis. A highly concentrated aqueous solution of heme ([heme]=25 mM) was prepared by embedding the 5,10,15,20-tetrakis(α,α,α,α-*o*-(2′,2′-dimethyl-20′-(2″-trimethylammonio)ethylphosphonatoxy)eicosanamido)phenyl)porphinatoiron(II) complex of 1-dodecylimidazole in bilayer of polymerized 1,2-bis(2,4-octadecadienoyl)-*sn*-glycero-3-phosphocholine liposome (poly-lipid liposome/heme). The dioxygen-binding mode of the poly-lipid liposome/oxy-heme in the aqueous medium was then measured by means of infrared difference spectroscopy: The ν_{O-O} value at 1161 cm^{-1} was found to correspond to those of the oxy picket-fence heme in Nujol mulls, oxy myoglobin, and oxy hemoglobin in an aqueous medium.

The present authors previously found and reported that the heme derivatives incorporated into a bilayer of natural, synthetic, or polymerized lipid liposome could bind dioxygen reversibly under physiological conditions.[1-3] We could also prepare a highly concentrated aqueous heme solution by embedding the 5,10,15,20-tetrakis(α,α,α,α-*o*-(2′,2′-dimethyl-20′-(2″-trimethylammonioethylphosphonatoxy)eicosanamido)phenyl)porphinatoiron(II) complex of 1-dodecylimidazole in bilayer of polymerized 1,2-bis(2,4-octadecadienoyl)-*sn*-glycero-3-phosphocholine liposome (abbreviated as poly-lipid liposome/heme). In this note, we described the dioxygen-binding mode of the poly-lipid liposome/oxy-heme in an aqueous medium, as measured by means of infrared difference spectroscopy and discussed it in comparison with those of the picket-fence oxy-heme[4] in Nujol mulls, and of oxy myoglobin (oxy-Mb) and oxy hemoglobin (oxy-Hb) in an aqueous medium.

Experimental

Meterials. The heme derivative and 1-dodecylimidazole were synthesized as previously reported.[2] The lipid derivative was prepared according to the procedure in the literature.[5] The Mb from Horse Skeletal Muscle was purchased from Sigma (special grade). The $^{18}O_2$ gas was purchased from the Takachiho Shouji Co., Ltd.

Preparation of samples. A mixture (methanol-benzene) of the heme (1.45 g), the imidazole (0.354 g), and the lipid (3.91 g) (molar ratio 1/3/10) was freeze-dried to give a reddish powder. Oxygen-free distilled water (pH 7, adjusted with a dil. NaOH solution, 10 ml) was then added, and the mixture was shaken by means of a Vortex mixer. It was ultrasonicated and homoginized in an ice-water bath under a nitrogen atmosphere (60 W×1 h, using a probe-type sonicator; Nihon-Seiki US-600) to yield a deep red-colored and concentrated liposome/heme solution ([heme]=25 mM†). The solution thus prepared was allowed to stand under ultraviolet (UV) irradiation (Rika-Seiki UVL-32LB, 64 W×3 day) at 40 °C under a nitrogen atmosphere in order to polymerize the lipid and to give a concd poly-lipid liposome/deoxy-heme solution. The pH and volume of the aqueous solution were adjusted to pH 7 and 20 ml with a dil. NaOH solution and oxygen-free distilled water. The reduction of the Fe(III)-heme derivative to the deoxy-heme spontaneously occurred during the polymerization. The complete polymerization and reduction were confirmed by means of UV and Vis absorption and ^{13}C NMR spectroscopical measurements, as has been reported previously.[3] The poly-lipid liposome/heme looked like a small unilammelar vesicle (SUV), and its diameter was estimated to be ca. 350 A by means of transmission electron microscopic measurements.

The oxy- and carboxy-Mb solutions were prepared as reported in the literature.[6] ([Mb]=20 mM, pH 9, 0.1 M Tris buffer solution).

Measurements. The infrared difference spectra were measured for the poly-lipid liposome/heme and Mb in the aqueous media at 10 °C under $^{16}O_2$ vs. $^{18}O_2$, $^{16}O_2$ vs. $^{12}C^{16}O$, and $^{12}C^{16}O$ vs. a nitrogen atmosphere. The cells used were precisely matched in terms of path-length (25 μm) and calcium fluoride (CaF_2) window thickness. The spectra were recorded with a Japan Spectroscopic Co., ltd. Model IR-810-type infrared spectrophotometer in the absorbance mode, using a double beam, an expanded ordinate and abscissa, and a resolution of 2 cm^{-1}, with a data processor.

The UV and Vis absorption spectra were measured with a double- beam UV and Vis absorption spectroscophotometer (Shimazu MPS-2000). The cells with CaF_2 windows could be used for both the UV and Vis and infrared absorption spectroscopy, recorded in the same cell.

Results and Discussion

The values of the O-O and C-O stretching frequencies (ν_{O-O} and ν_{C-O}) of oxy- and carboxy-Mb were 1103 cm^{-1} (band width at 1/2 height=ca. 10 cm^{-1}) and 1944 cm^{-1} (ca. 16 cm^{-1}) respectively: these values were consistent with those reported

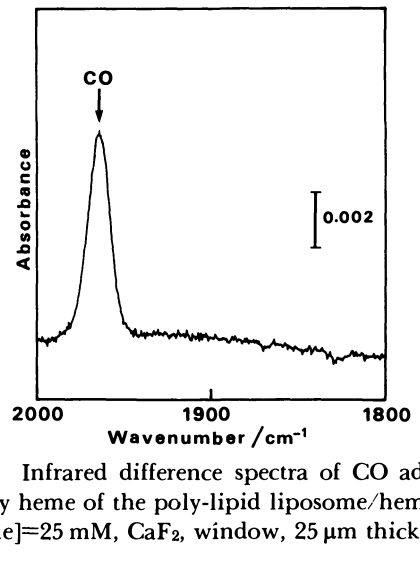

Fig. 1. Infrared difference spectra of CO adduct vs. deoxy heme of the poly-lipid liposome/heme. [heme]=25 mM, CaF_2, window, 25 μm thickness.

† 1 M=1 mol dm^{-3}.

previously.[6] The intensity relative to the CO band was also similar to the reference data. The UV and Vis absorption spectra of oxy- and carboxy-Mb did not change before and after infrared absorption spectroscopic measurements and agreed with those reported in the literature.[7] This result supports the validity of the measuring procedure used in the present experiment.

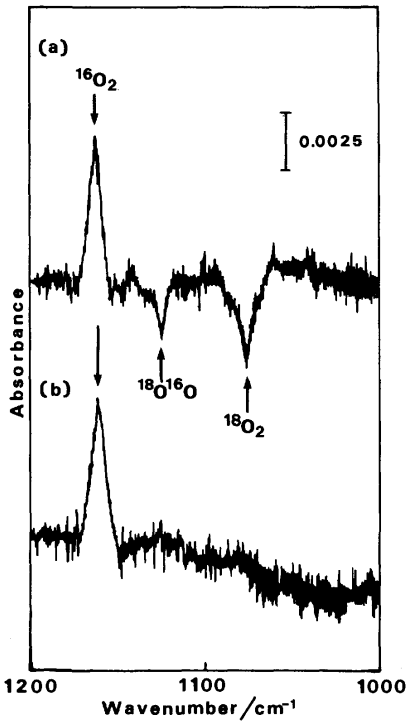

Fig. 2. Infrared difference spectra of $^{16}O_2$ vs. $^{18}O_2$ adducts (a) and $^{16}O_2$ vs. $^{12}C^{16}O$ adducts (b) of the poly-lipid liposome/heme. [heme]=25 mM, CaF_2 window, 25 μm thickness.

The UV and Vis absorption spectrum (λ_{max}; 426, 535 and 562 nm) of the poly-lipid liposome/deoxy-heme changed to the spectrum that was assigned to the oxygen adduct (λ_{max}; 422 and 544 nm) upon exposure to oxygen. The spectrum of the oxygen adduct changed to that of the carbon monoxide (CO) adduct (423 and 540 nm) on bubbling through CO and then returned to that of the deoxy-heme on bubbling through nitrogen. The half-lifetime of the oxygen adduct was ca. 30 hr in the aqueous medium 10 °C.

Figure 1 shows the infrared spectrum of the CO adduct of the poly-lipid liposome/heme, as corrected with the spectrum of the corresponding deoxy-heme in the reference cell. The intense band with a maximum at 1966 cm^{-1} is similar to that of the picket-fence heme-CO complex of 1-methylimidazole in Nujol mulls (ν_{CO}=1969 cm^{-1}).[8] Similarly, the difference spectrum of the CO vs. the $^{16}O_2$ adducts of the poly-lipid liposome/heme showed an intense bond at 1966 cm^{-1}.

The difference spectrum (Fig. 2a) of the $^{16}O_2$ adduct vs. the CO adduct of the poly-lipid liposome/heme shows an intense band at 1161 cm^{-1} with a band-width of 14 cm^{-1} at 1/2 height, a value which agrees with those of the picket-fence heme complex in Nujol mulls and of oxy-Mb and oxy-Hb in aqueous media.[6,8,9] The intensity ralative to be CO band of the poly-lipid liposome/heme was similar to those of Mb and Hb. For the difference spectra of the $^{16}O_2$ vs. the $^{18}O_2$ adducts of the poly-lipid liposome/heme, the $^{16}O_2$ adduct shows an intense band at 1161 cm^{-1} while the $^{18}O_2$ adduct shows prominent bands at 1125 and 1076 cm^{-1} based on the frequency of ^{16}O–^{18}O and ^{18}O–^{18}O respectively (Fig. 2b). The UV and Vis absorption spectra supported the gaseous molecule-binding ability of the ploy-lipid liposome/heme after

Table 1. Infrared and Ultraviolet-Visible Absorption Spectral Data of the Poly-Lipid Liposome/Heme

Heme	Ligand	Solvent	O_2			
			$\nu_{16O-16O}$	$\Delta\nu_{1/2}$	$\nu_{18O-18O}$	λ_{max}
			cm^{-1}	cm^{-1}	cm^{-1}	nm
Poly-lipid liposome/heme	LIm	H_2O	1161	(11)	1076	544
Picket-fence heme	MIm	Nujol	1159	(—)	1075	548
Myoglobin	—	H_2O	1103	(8±1)	1065	542, 580
Hemoglobin	—	H_2O	1107	(9±1)	1065	541, 577
O_2 or CO gas	—	—	1556	(—)	—	—
O_2^-	—	—	1145	(—)	—	—

Heme	CO			Intensity ratio $A(O_2)/A(CO)$ (—)	Ref.
	ν_{C-O}	$\Delta\nu_{1/2}$	λ_{max}		
	cm^{-1}	cm^{-1}	nm		
Poly-lipid liposome/heme	1966	(14)	540	0.15	This work
Picket-fence heme	1969	(—)	542	—	8
Myoglobin	1944	(12)	540, 579	0.10	6
Hemoglobin	1951	(8)	540, 569	0.19	9
O_2 or CO gas	2143	(—)	—	—	10, 11
O_2^-	—	(—)	—	—	10

LIm; 1-laurylimidazole, MIm; 1-methylimidazole. $\Delta\nu_{1/2}$; band width ar 1/2 height, $A(O_2)/A(CO)$; intensity ratio between O_2 and CO bands.

the infrared-spectroscopic measurement.

The data of the infrared and UV and Vis absorption spectra are summarized in Table 1. The O–O stretching frequency of the poly-lipid liposome/oxy-heme differs from that of the gaseous oxygen molecule (ν_{O-O}=1556 cm^{-1}),[10] but is similar to that of superoxide (O_2^-, 1145 cm^{-1}).[10] Metal dioxygen complexes with both oxygen atoms bound to a metal (side-on type) have an O–O stretch between 800 and 900 cm^{-1} [12,13] and an O–O bond order of about 1.0. On the other hand, both cobalt dioxygen complexes with a configuration such as the bent end-on type[14] and an O–O bond order of 1.5 exhibit an O–O stretching frequency between 1000 and 1500 cm^{-1}.[15,16] Thus, it may be concluded that molecular dioxygen obviously coordinates to the synthetic lipid-heme, even in an aqueous medium, and that its coordination structure is a bent end-on type one similar to oxy-Mb, oxy-Hb, and the oxygen adduct of the picket-fence heme.

This work was partially supported by Grant-in-Aids for Scientific Research on Priority Area of Macromolecular Complexes, and Encouragement of Young Scientists from the Ministry of Education, Science and Culture.

References

1) E. Tsuchida, H. Nishide, M. Yuasa, E. Hasegawa, and Y. Matsushita, *J. Chem. Soc., Dalton Trans.*, **1984**, 1147.

2) E. Tsuchida, H. Nishide, M. Yuasa, E. Hasegawa, Y. Matsushita, and K. Eshima, *J. Chem. Soc., Dalton Trans.*, **1985**, 275.

3) E. Tsuchida, E. Hasegawa, Y. Matsushita, K. Eshima, M. Yuasa, and H. Nishide, *Chem. Lett.*, **1985**, 969.

4) J. P. Collman, R. R. Gagne, C. A. Reed, T. R. Halbert, G. Lang, and W. T. Robinson, *J. Am. Chem. Soc.*, **97**, 1427 (1975).

5) B. Hupfer, H. Ringsdorf, and H. Schupp, *Makromol. Chem.*, **182**, 247 (1981); B. Hupfer, H. Ringsdorf, and H. Schupp, *Chem. Phys. Lipids*, **33**, 355 (1983).

6) J. C. Maxwell, J. A. Volpe, C. H. Barlow, and W. S. Caughey, *Biochem. Biophys. Res. Commun.*, **58**, 166 (1974).

7) E. Antonini and M. Brunori, "Hemoglobin and Myoglobin in their Reaction with Ligands," Nor-Holland Pub., Amsterdam (1970).

8) J. P. Collman, J. I. Brauman, T. R. Halbert, and K. S. Suslick, *Proc. Natl. Acad. Sci. U.S.A.*, **73**, 3333 (1976).

9) C. H. Barlow, J. C. Maxwell, W. J. Wallace, and W. S. Caughey, *Biochem. Biophys. Res. Commun.*, **55**, 91 (1973).

10) G. Herzberg, "Molecular Spectra and Molecular Structure I. Spectra of Diatomic Molecules," Van Nostrand Co., New York (1950), p. 560.

11) K. Nakamoto, "Infrared Spectra of Inorganic and Coordination Compounds," Wiley-Interscience, New York (1970), p. 78.

12) J. A. McGinnety, R. J. Doedens, and J. A. Ibers, *Inorg. Chem.*, **6**, 2243 (1967).

13) A. Nakamura, Y. Tatsuno, M. Yamamoto, and S. Otsuka, *J. Am. Chem. Soc.*, **93**, 6052 (1971).

14) L. Pauling, "Hemoglobin," ed by F. J. W. Roughton and J. C. Kendrew, Butterworths, London (1949), pp. 57—65.

15) A. L. Crumbliss and F. Basolo, *J. Am. Chem. Soc.*, **92**, 55 (1970).

16) J. D. Landels and G. A. Rodley, *Syn. Inorg. Metal-Org. Chem.*, **2**, 65 (1972).

Structures of New [4+2]-Cycloadducts from Diels-Alder Reactions of Methyl 2-Oxo-2*H*-pyran-5-carboxylate with 2-Methyl- and 2-Methoxy-1,3-butadienes[1)]

Takanao MATSUI,* Shinji KITAJIMA, and Mitsuru NAKAYAMA†
Faculty of Engineering, Miyazaki University, Kumano, Miyazaki 889-21
†Department of Agricultural Chemistry, College of Agriculture, University of Osaka Prefecture, Sakai, Osaka 591
(Received July 2, 1987)

Synopsis. A Diels-Alder reaction of methyl 2-oxo-2*H*-pyran-5-carboxylate (**1**) with isoprene gave two stereoisomers, methyl 8-methyl-8-vinyl- and 8-isopropenyl-3-oxo-2-oxabicyclo[2.2.2]oct-5-ene-6-carboxylates. On the other hand, only a stereoisomer from a reaction of **1** with 2-methoxy-1,3-butadiene, methyl 8-methoxy-8-vinyl-3-oxo-2-oxabicyclo[2.2.2]oct-5-ene-6-carboxylate was obtained. The stereostructures of these adducts were determined by NMR spectral data and single-crystal X-ray analyses.

Diels-Alder reactions[2)] using 2-pyrones can be used to prepare such versatile products as various [4+2]-cycloadducts, polycyclic compounds, and benzene derivatives since 2-pyrones might serve as either dienes or dienophiles and the primary adducts undergo succeeding thermal conversions through their secondary reactions, e.g., decarboxylation, hydrogen migration, and intramolecular cycloaddition. In the course of our study on the thermal cycloaddition reactions of enone compounds, we became interested in the use of methyl 2-oxo-2*H*-pyran-5-carboxylate (**1**) as a substrate bearing two enone systems with the expectation that it might selectively react as a diene or a dienophile to the reaction partner and that the products potentially serve as synthetic intermediates. Previous papers[3)] have demonstrated that the Diels-Alder reactions of **1** with 2-substituted 1,3-butadienes **2** afford tetrahydrocoumarins **3**—**5** and that they can be used as one approach to the synthesis of trichothecane sesquiterpenes.[3b,4)] In addition to the documented products resulting from the reaction of **1** acting as a dienophile, we have tried to isolate hitherto unidentified cycloadducts of **1** as a diene. We now report on the structures of the newly isolated [4+2]-cycloadducts **6**, **7**,[5)] and **8**.

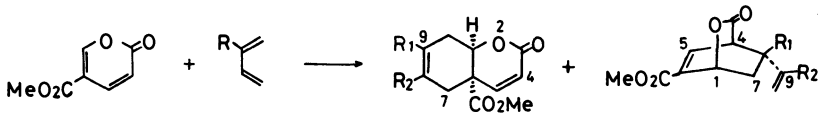

1 **2** R=Me, OMe

3 R_1=Me, R_2=H
4 R_1=H, R_2=Me
5 R_1=OMe, R_2=H

6 R_1=Me, R_2=H
7 R_1=H, R_2=Me
8 R_1=OMe, R_2=H
9 R_1=H, R_2=OMe

Cycloadditions of **1** with isoprene or 2-methoxy-1,3-butadiene were carried out at 90—114 °C in an autoclave. The crude products were repeatedly column-chromatographed and recrystallized to afford three pure bicyclic lactones **6**—**8**, along with some other known products **3**—**5**. However, in the present reactions the regioisomer (**9**) of **8** could not be detected.[6)] The combined yield and the ratio of **6** to **7** were seriously effected by the reaction temperature since further conversions of these initial adducts occurred under applied conditions.[7)] As shown in Table 1, the IR and ^{1}H NMR spectra of the three compounds indicated characteristic of absorption bands (1635—1640 and 950—990 cm^{-1}) and signals

Table 1. IR and ^{1}H NMR Spectral Data for Cycloadducts

	6	**7**	**8**
IR/cm^{-1}	1750, 1715, 1635, 990, 970	1750, 1720, 1640, 990, 960	1760, 1720, 1640, 970, 950
NMR/δ			
C_1-H	5.46—5.77(m)	5.61—5.74(m)	5.44—5.66(m)
C_4-H	3.42(d, J=6)	3.78(dd, J=6, 2)	3.80(d, J=6)
C_5-H	7.26(dd, J=6, 2)	7.18(dd, J=6, 2)	7.17(dd, J=6, 2)
C_7-H	1.94(d, J=2)	2.42(dd, J=10, 4)	1.83(dd, J=14, 2)
	2.00(d, J=4)	2.67—2.84(m)	2.40(dd, J=14, 4)
C_8-H		1.62(ddd, J=10, 4, 2)	
C_9-H	5.46—5.77(m)		5.44—5.66(m)
C_{10}-H	4.84(dd, J=8, 2)	4.58(bs)	5.10(dd, J=8, 2)
	5.08(d, J=2)	4.79(bs)	5.32(d, J=2)
C-Me	1.32(s)	1.73(s)	
O-Me	3.79(s)	3.78(s)	3.69(s), 3.00(s)

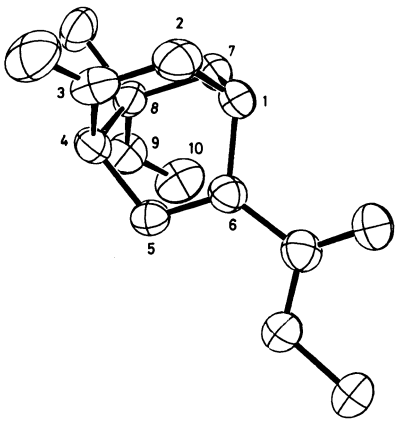

Fig. 1. ORTEP drawing of the molecular structure of **6**.

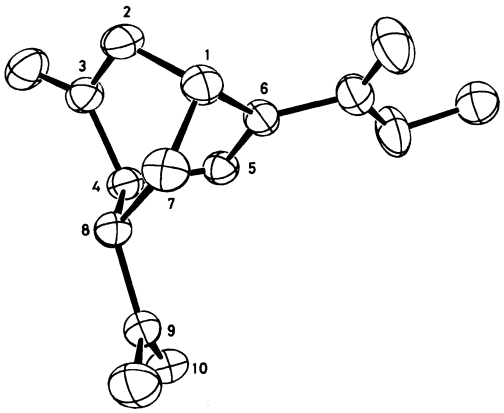

Fig. 2. ORTEP drawing of the molecular structure of **7**.

due to vinyl and isopropenyl groups. The ^{1}H NMR spectra also revealed the presence of one olefinic proton (C_5-H) at the lowest field with the splitting pattern of a doublet of doublets (J=6 and 2 Hz) and two methine protons (C_1-H and C_4-H) at positions α to the oxygen and carbonyl of the lactone. The similality of these spectral data indicates that they possess the same structural skeleton formed presumably by an endo addition; however, they differed in regiochemistry. Furthermore, the stereochemistry of **6** and **7** could be confirmed by X-ray crystal structure analyses; these were performed with single crystals prepared from methanol solutions. Perspective views are depicted in Figs. 1 and 2.[8] Thus, their structures were determined to be **6**, **7**, and **8**. The results obtained here show that **1** can react both as a dienophile and a diene toward 2-methyl- and 2-methoxy-1,3-butadienes to furnish [4+2]-cycloadducts **3**—**5** and **6**—**8**.

Experimental

Melting points are uncorrected. IR spectra were measured in $CHCl_3$ with a Hitachi 260-50 spectrometer. NMR spectra were obtained with JEOL JNM MH-100, JEOL JNM-PMX 60, and JEOL JNM-FX 60 spectrometers for ^{1}H and ^{13}C in $CDCl_3$, respectively. Chemical shifts are given in δ values (ppm) downfield from the internal TMS reference. Mass spectra were measured with a JEOL JMS-D 300S spectrometer. Column chromatography was performed with Fuji-Davison BW-300 silica gel.

Methyl 8-Methyl-8-vinyl- and 8-Isopropenyl-3-oxo-2-oxabicyclo[2.2.2]oct-5-ene-6-carboxylates (6 and 7). A mixture of 1.0 g (6.5 mmol) of **1** and 2.2 g (32 mmol) of isoprene in 100 ml of benzene was heated at 110—114 °C for 10 h in an autoclave under a nitrogen atmosphere. After removing the solvent and excess diene, the residue was chromatographed on silica gel with hexane-ethyl acetate (19:1) as an eluent to give a mixture of **6** and **7** (0.56 g; 50% yield based on **1** consumed) along with a mixture of **3** and **4** (0.32 g), and **1** (0.22 g). A mixture of **6** and **7** was repeatedly column-chromatographed and finally recrystallized from methanol to afford each pure compound (ratio of **6**/**7** was about 1:3); the elevation of the reaction temperature (above ca. 120 °C) led to a decrease of a total yield of **6** and **7**, and to change of the isomer ratio. The high reaction temperature also improved the yield of the known product, tricyclo[3.2.1.0^{2,7}]-octene compound.[3a] **6**: Mp 115—116 °C (methanol); MS: m/z 222 (M^+) and 223 [M+1]$^+$); Found: C, 64.65; H, 6.24%. Calcd for $C_{12}H_{14}O_4$: C, 64.85; H, 6.35%. **7**: Mp 106—106.5 °C (methanol); MS: 222 (M^+) and 223 [M+1]$^+$); Found: C, 64.80; H, 6.43%. Calcd for $C_{12}H_{14}O_4$: C, 64.85; H, 6.35%.

Methyl 8-Methoxy-8-vinyl-3-oxo-2-oxabicyclo[2.2.2]oct-5-ene-6-carboxylate (8) and the Related Adducts. A mixture of 5.0 g (32 mmol) of **1** and 5.1 g (60 mmol) of 2-methoxy-1,3-butadiene in 50 ml of toluene was heated at 90—100 °C for 3 h in an autoclave under a nitrogen atmosphere. Removing the solvent and excess diene gave 9.5 g of a yellow viscous oil. The crude products were column-chromatographed on silica gel using hexane-ethyl acetate (4:1) as an eluent to afford 9-methoxy-6-methoxycarbonyl-2-oxabicyclo-[4.4.0]deca-4,8-dien-3-one (**5**; 5.0 g), and its 9,10-dehydro isomer (0.78 g). The other fractions were further chromatographed under similar conditions to give **8** as a colorless solid (ca. 10% yield) together with unidentified materials. **5**: Mp 104.5—105.5 °C (hexane-acetone) (lit,[3b] mp 96—98 °C); IR: 1730—1740 and 1675 cm^{-1}; ^{1}H NMR: 2.15—2.95 (4H, m, 2X-CH_2-), 3.50 (3H, s, -OCH_3), 3.78 (3H, s, -CO_2CH_3), 4.67 (1H, m, -$CH_2\underline{C}\underline{H}O$-), 5.02 (1H, dd, J=7 and 2 Hz, -$C\underline{H}$=$\underline{C}OCH_3$), 6.04 and 6.94 (each 1H, d, J=11 Hz, -CH=CH-); ^{13}C NMR: 29.6, 31.4, 46.2, 53.0, 54.2, 77.0, 89.9, 121.0, 149.3, 152.2, 163.1, and 171.5; MS: m/z 238 (M^+). 9,10-Dehydro isomer of **5**: Mp 100—103 °C (hexane-ethyl acetate); IR: 1730—1740 and 1675 cm^{-1}; ^{1}H NMR: 1.72—2.24 (4H, m, 2X-CH_2-), 3.49 (3H, s, -OCH_3), 3.70 (3H, s, -CO_2CH_3), 4.72 (1H, d, J=5 Hz, =$CH\underline{C}\underline{H}O$-), 5.38 (1H, d, J=5 Hz, =$C\underline{H}\underline{C}HO$-), 5.91 and 6.57 (each 1H, d, J=11 Hz, -CH=CH-); MS: m/z 238 (M^+); Found: C, 60.41; H, 5.82%. Calcd for $C_{12}H_{14}O_5$: C, 60.49; H, 5.92%. This enol compound was transformed into the corresponding keto compound, 6-methoxycarbonyl-2-oxabicyclo[4.4.0]dec-4-ene-3,9-dione through the column chromatography using silica gel; mp 128—129 °C (ether) (lit,[3b] 121—122 °C); IR: 1730—1740 cm^{-1}; ^{1}H NMR: 2.00—2.89 (6H, m, 3X-CH_2-), 3.90 (3H, s, -CO_2CH_3), 5.18 (1H, t, J=4 Hz, -$CH_2\underline{C}\underline{H}O$-), 6.09 and 7.00 (each 1H, d, J=11 Hz, -CH=CH-); ^{13}C NMR: 29.5, 37.3, 43.7, 46.8, 53.6, 78.7, 121.3, 148.0, 162.0, 171.1, and 205.0; MS: m/z 224 (M^+); Found: C, 58.79; H, 5.46%. Calcd for $C_{11}H_{12}O_5$: C, 58.92; H, 5.40%. **8**: Mp 105—106.5 °C (hexane-methanol); MS: m/z 208 ([M+1]$^+$−31) and 207 (M^+−31); Found: C, 60.70; H, 6.01%. Calcd for $C_{12}H_{14}O_5$: C, 60.50; H, 5.92%.

X-Ray Analyses of 6 and 7.[9] The single crystals used for X-ray analyses were recrystallized from methanol solutions. The diffraction data for compounds **6** and **7** were collected on an Enraf-Nonius CAD-4 automated four-circle diffractometer with graphite-monochromated Mo $K\alpha$ radiation (λ=0.71073 Å). The unit-cell constants and diffraction intensities were measured by the ω-2θ scan method. The intensities were corrected for the Lorentz and polarization factors, but no corrections were made for the absorption. The structures were solved by direct method using the program MULTAN 82[10] and the refinement were done by full-matrix least-squares method with anisotropic temperature factors for the non-H atoms and isotropic temperature factors, B=5, for the H atoms. The atomic-scattering factors taken from the International Tables for Crystallography[11] were used on a SDP program package.[12] The crystal data are as follows.

6: $C_{12}H_{14}O_4$, M=222.24, colorless single-crystal size 0.4×0.1×0.05 mm^3, monoclinic, space group $P2_1/n$, a=6.150(6), b=6.7759(8), c=26.680(3) Å, γ=95.91(3)°, V=1106(1) Å^3, Z=4, D_C=1.335 g cm^{-3}, μ(Mo $K\alpha$)=0.936 cm^{-1}. A total of 3228 reflections in the range $2°<2\theta<60°$ were collected for the structure analysis. The final R value was R=0.049, R_W=0.053 for 145 valiables and 1007 reflections with $I>3.0\sigma(I)$.

7: $C_{12}H_{14}O_4$, M=222.24, colorless single-crystal size 0.8×1.0×0.3 mm^3, triclinic, space group $P\bar{1}$, a=6.234(2), b=7.91(1), c=12.248(5) Å, α=101.93(5), β=97.41(3), γ=107.76(4)°, V=551(1) Å^3, Z=2, D_C=1.340 g cm^{-3}, μ(Mo $K\alpha$)=0.985 cm^{-1}. A total of 4827 reflections in the range $2°<2\theta<70$ were collected for the structure analysis. The final R value was R=0.104, R_W=0.136 for 144 valiables and 3074 reflections with $I>3.0\sigma(I)$. The molecules of **7** take randomly one of the two possible conformations which differ in the methyl group orientation around the C–O ester linkage.

The authors wish to thank Professor Kiyohisa Imada for X-ray crystallographic analyses and correcting this manuscript, and to Miss Kimiko Tanabe for mass spectral measurements. We are also thankful to the Research Center for Material Analysis in Miyazaki University for the use of the NMR, MS, and X-ray apparatus.

References

1) This work is Part 4 of "Cycloadditions in Pyrones," Part 3: T. Matsui, T. Morooka, and M. Nakayama, *Bull. Chem. Soc. Jpn.*, **60**, 417 (1987).

2) For some examples of the reactions with acetylenes and olefins, see: J. A. Reed, C. L. Schilling, Jr., R. F. Tarvin, T. A. Rettig, and J. K. Stille, *J. Org. Chem.*, **34**, 2188 (1969); T. A. Bryson and D. M. Donelson, *J. Org. Chem.*, **42**, 2930 (1977); H. E. Zimmerman, G. L. Grunewald, R. M. Paufler, and M. A. Sherwin, *J. Am. Chem. Soc.*, **91**, 2330 (1969); T. Imagawa, T. Nakagawa, M. Kawanisi, and K. Sisido, *Bull. Chem. Soc. Jpn.*, **52**, 1506 (1979).

3) a) T. Imagawa, N. Sueda, and M. Kawanisi, *Tetrahedron*, **30**, 2227 (1974). b) Y. Nakahara and T. Tatsuno, *Chem. Pharm. Bull.*, **28**, 1981 (1980). c) T. Matsui, T. Inoue, M. Nakayama, and J. D. White, *Bull. Chem. Soc. Jpn.*, **56**, 647 (1983); M. Nakayama, J. Kuramoto, T. Matsui, and J. D. White, *ibid.*, **58**, 3051 (1985). d) B. A. Brown and E. W. Colvin, *J. Chem. Soc., Chem. Commun.*, **1984**, 1514.

4) G. A. Kraus and K. Frazier, *J. Org. Chem.*, **45**, 4820 (1980); J. D. White, T. Matsui, and J. A. Thomas, *J. Org. Chem.*, **46**, 3376 (1981).

5) Preparation of **7** has been reported, but no description on the stereochemistry has been found, see: Ref. 3d.

6) The addition in which **1** functions as a diene is predicted to occur at its 3,6-positions with both 2,1- and 3,4-positions of isoprene and 2-methoxy-1,3-butadiene on the basis of their molecular orbital coefficients (HOMO for **1**, LUMO for dienes) by the Hückel method.

7) The conversion reactions of the primary adducts are under investigation and the results will be described in detail elsewhere.

8) C. K. Johnson, ORTEP. Oak Ridge National Laboratory Report ORNL-3794 (1965).

9) The tables of anisotropic thermal parameters, coordinates of hydrogen atoms, bond lengths and angles, and Fo and Fc values are deposited as Document No. 8768 at the Office of the Editor of Bull. Chem. Soc. Jpn.

10) P. Main, MULTAN 11/82 (1982).

11) D. T. Cromer and J. T. Waker, "International Tables for X-Ray Crystallography," Kynoch Press, Birmingham (1974), Vol. IV.

12) B. A. Frenz and Enraf-Nonius, SDP, Structure Determination Package (1982).

Diastereoselective Hydrogenation of Methyl 2-[α-(Methoxycarbonylamino)-benzyl]acrylate Catalyzed by Ru(II) or Rh(I) Complexes[1]

Keiji YAMAMOTO,* Masatoshi TAKAGI, and Jiro TSUJI
Department of Chemical Engineering, Tokyo Institute of Technology, Meguro, Tokyo 152
(Received July 16, 1987)

Synopsis. The title compound was prepared and hydrogenated by using a Ru(II)- or Rh(I)-phosphine catalyst precursor with excellent *anti*-selectivity, the results indicating that a ligating group, $NHCO_2Me$, may direct the addition of hydrogen to an olefinic diastereoface proximate to this group which binds the catalyst.

Recently, highly anti-selective preparation of the Aldol-type α-substituted β-hydroxy esters has been reported[2] via diastereoselective hydrogenation of α-(hydroxyalkyl)acrylates, and the selectivity stems from the hydroxyl-directed olefin hydrogenation of these chiral allylic alcohols.[3]

We report here that a ligating group, $NHCO_2Me$ in an allylic position of certain olefinic substrates, can bind the catalyst and direct effectively addition of hydrogen from one olefinic diastereoface of the molecule.

Very recently, Brown et al.[4] have reported the same directed hydrogenation of N-substituted α-(aminoalkyl)acrylates closely related to the present substrate, even with the kinetic resolution by using a chiral rhodium(I)–phosphine complex.

Results and Discussion

Methyl 2-[α-(methoxycarbonylamino)benzyl]acrylate (**1**) was readily prepared from methyl benzylidenecarbamate[5] and methyl acrylate (Eq. 1).

$$PhCH{=}NCO_2Me + H_2C{=}CHCO_2Me \xrightarrow{DABCO} \underset{\displaystyle CH_2}{\overset{\displaystyle \overset{\displaystyle NHCO_2Me}{|}}{PhCHCCO_2Me}}{\overset{\displaystyle \|}{}} \quad (1)$$

We have found that the amine-catalyzed reaction of acrylates with the imine compound is much faster than that with common aldehydes[6] at room temperature in the presence of 1,4-diazabicyclo[2.2.2]octane (DABCO) to give **1** in ca. 80% yield.

Acrylate **1** thus obtained was hydrogenated under various conditions by using 1 mol% of $Ru(OCOCF_3)_2(PPh_3)_2$ (**2**) or $[Rh(cod)(dppe)]^+ClO_4^-$ (**3**) as a catalyst precursor. The Ru(II) complex **2** was prepared by a reported procedure with slight modification.[7] All data for conversion and selectivity of the present hydrogenation of **1** are given in Table 1.

Hydrogenation of **1** was markedly dependent on the solvent used, less polar solvent such as dichloromethane, benzene or THF being found to behave either inhibitive or a little less selective (Entries 1—3, 8 and 9).

Methanol was generally the best solvent. Hydrogen pressure also played a crucial role for acceptable rate of hydrogenation (at 25 °C in two days) and 30 atm or above of hydrogen pressure was necessary for both catalysts **2** and **3** (Entries 4—6 and 10) or $[Rh(cod)(dppb)]^+ClO_4^-$ (**5**) (Entries 11 and 12). Thus, under selected conditions, excellent diastereoselective hydrogenation was achieved in two cases (99.1% anti

Table 1. Hydrogenation of Methyl 2-[α-(Methoxycarbonylamino)benzyl]acrylate (**1**)

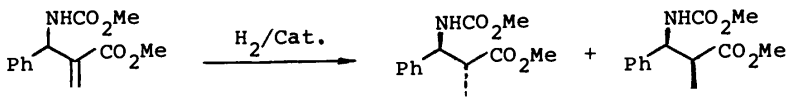

1 **4a** (anti) **4b** (syn)

Entry	Catalyst[a] (1 mol%)	Solvent (5 mL)	H_2 atm	Temp °C	Time h	Conversion[b] %	Selectivity[c] anti/%
1	**2**	CH_2Cl_2	30	50	33	0	
2	**2**	PhH	30	50	34	8	
3	**2**	THF	30	50	48	40	58.3
4	**2**	MeOH	30	25	65	100	99.1
5	**2**	MeOH	5	25	48	8	
6	**2**	MeOH	10	25	48	50	87.5
7	**2**	MeOH	75	25	40	100	97.9
8	**3**	CH_2Cl_2	30	25	48	30	98.9
9	**3**	THF	30	25	48	99	95.0
10	**3**	MeOH	30	25	40	100	98.0
11	**5**	MeOH	30	25	17	100	97.0
12	**5**	MeOH	10	25	16	20	
13	**6**	MeOH	10	25	3	100	30.3—35.7

a) Substrate **1** (1 mmol, 0.2 M) was used. b) GLC analysis (Silicone DC-550, 3 m×3 mm, at 200 °C). c) Determined by capillary GLC (HR-20M, 30 m×0.2 mm, at 200 °C).

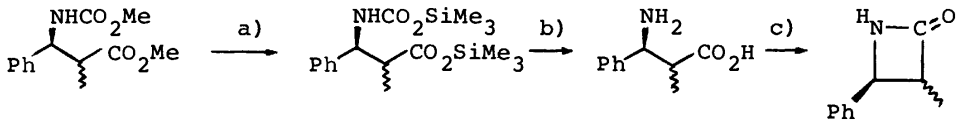

4 7

Scheme 1. a) 2 Me_3SiI/MeCN, Δ. b) Silica gel/MeOH. c) I^-/Et_3N/MeCN, Δ.

in Entry 4 and 98.0% anti in Entry 10, respectively).

As is seen in Entry 13, 5% palladium on charcoal (**6**) was active enough for complete hydrogenation of **1** under 10 atm of hydrogen in 3 h, to result in low but reverse selectivity.

Since stereochemistry of the diastereomeric hydrogenation products **4** was hardly determined on the basis of coupling constants of vicinal protons (5.9 and 6.4 Hz, respectively), they were converted to the corresponding 2-azetidinone derivatives in the following manner: Two samples of **4** obtained from Entries 10 and 13 were independently converted into 3-methyl-4-phenyl-2-azetidinone (**7**) by unambiguous three-step procedures as depicted in Scheme 1.

A sample of **4** from Entry 10 (diastereomer ratio=50:1) afforded *trans*-**7** in exclusive preference (trans:cis=70:1), indicating that the present hydrogenation of **1** proceeded with anti-selectivity.

A plausible explanation of the observed selectivity could derive from the presence of a ligating $NHCO_2Me$ group in **1**, which directs efficiently the attack of the hydrogenation catalyst, Ru(II) or Rh(I)/H_2/MeOH, on one diastereoface of the molecule proximate to the directing group.

It should be noted that an *N*-tosylated analog of **1**[8] was found to be very reluctant to the hydrogenation under conditions employed.

Furthermore, the alkyl analogs of **1**, i.e. methyl (**8**), isopropyl (**9**), isobutyl (**10**), and *t*-butyl (**11**) instead of phenyl group in **1**, were prepared (see **Experimental**). However, these analogs were found, at the present time, to undergo hydrogenation under the comparable conditions with much inferior anti-selectivity (54—93%).

Experimental

General Comments. All boiling and melting points are uncorrected. ^1H and $^{13}C\{^1H\}$ NMR spectra were obtained on a JEOL FX-90Q spectrometer with Me_4Si as an internal standard in $CDCl_3$. IR spectra (mostly neat) were recorded on JASCO IRA-2 spectrophotometer.

Catalyst Precursors. $Ru(OCOCF_3)_2(PPh_3)_2$ (**2**)[7], [Rh(dppe)(cod)]$^+ClO_4^-$ (**3**)[9] (dppe=1,2-bis(diphenylphosphino)ethane, cod=1,5-cyclooctadiene), and [Rh(dppb)(cod)]$^+ClO_4^-$ (**5**)[9] (dppb=1,4-bis(diphenylphosphino)butane) were prepared according to the reported procedures, respectively. Complex **2** was prepared by the reaction of $RuCl_2(PPh_3)_3$ with $AgOCOCF_3$ in acetone.

Preparation of Methyl 2-[α-(Methoxycarbonylamino)benzyl]acrylate (1). Methyl benzylidenecarbamate[5] (7.23 g, 44 mmol) and DABCO (1.00 g, 9 mmol, 20 mol%) were dissolved in methyl acrylate (5 mL) and the mixture was stirred overnight at room temperature. Excess acrylate was removed by evaporation and crystalline materials remained were dissolved in $CHCl_3$ (150 mL). The $CHCl_3$ solution was washed with 3 M† HCl, aq $NaHCO_3$, and water to remove DABCO, and dried ($MgSO_4$). Solvent was removed and fairly clean product (80% yield) was recrystallized (hexane-$CHCl_3$) to give analytically pure **1**: Mp 120—121 °C; ^1H NMR (90 MHz) δ=3.67 and 3.70 (s, MeO×2), 5.67 (br. s, NH and CH-N), 5.91 (br. s, =CH), 6.37 (d, *J*=0.9 Hz, =CH), and 7.28 (br. s, Ph). IR (KBr) 1715 and 1690 cm^{-1}; Found: C, 62.49; H, 6.01; N, 5.53%. Calcd for $C_{13}H_{15}NO_4$: C, 62.64; H, 6.07; N, 5.62%.

Preparation of Methyl 2-[α-(Methoxycarbonylamino)alkyl]acrylates (8—11). In a typical reaction, methyl (1-ethoxyethyl)carbamate (2.50 g, 17 mmol), obtained from acetaldehyde diethyl acetal and methyl carbamate, and methyl 3-(dimethylamino)propionate (2.22 g, 17 mmol) were treated with 2 equiv. of lithium diisopropylamide (LDA) (40 mmol) in hexane-THF (1:2, 75 mL) at −78 °C for 15 min.[10] The whole mixture was allowed to warm up to 0 °C and stirred for additional 2 h. Usual workup and removal of the solvents afforded a precursor of the requisite acrylate.

The crude precursor (17 mmol) was treated overnight with excess MeI (90 mmol) in MeOH (5 mL) and the resulting ammonium salt was then treated with 1,8-diazabicyclo-[5.4.0]undec-7-ene (DBU) (20 mmol) in acetone (15 mL). Workup and distillation as usual gave methyl 2-[α-(methoxycarbonylamino)ethyl]acrylate (**8**) (1.40 g, 43% overall yield): Bp 82—84 °C/2 Torr††; ^1H NMR δ=1.35 (d, *J*=7 Hz, Me), 3.65 and 3.77 (s, MeO×2), 4.60 (m, CH), 5.10 (br. d, NH), 5.76 (s, =CH), and 6.17 (d, *J*=0.9 Hz, =CH); IR (neat) 1715 and 1695 cm^{-1}; Found: C, 51.39; H, 7.30; N, 7.31%. Calcd for $C_8H_{13}NO_4$: C, 51.33; H, 7.00; N, 7.48%.

In exactly the same manner as above, isopropyl (**9**), isobutyl (**10**), and *t*-butyl (**11**) analogs were prepared starting with respective acetals of *i*-PrCHO, *i*-BuCHO, and *t*-BuCHO. (**9**) (61% yield): Bp 98—100 °C/2 Torr; ^1H NMR δ=0.84 and 0.95 (d, *J*=6.6 Hz, 3H×2), 1.95 (m, 1H), 3.66 (s, 3H), 3.76 (s, 3H), 4.08 (t, *J*=9 Hz, 1H), 5.42 (br. d, 1H), 5.71 (br. s, 1H), and 6.22 (d, *J*=1.1 Hz, 1H); Found: CHN. (**10**) (74% yield): Bp 75—78 °C/2 Torr; ^1H NMR δ=0.94 and 0.96 (d, *J*=6.4 Hz, 3H×2), 1.54 (m, 3H), 3.65 (s, 3H), 3.76 (s, 3H), 4.50 (q, *J*=9 Hz, 1H), 5.33 (br. d, 1H), 5.75 (br. s, 1H), and 6.18 (d, *J*=1.1 Hz); Found: CHN. (**11**) (53% yield): Bp 112—113 °C/2 Torr; ^1H NMR δ=0.90 (s, 9H), 3.66 (s, 3H), 3.76 (s, 3H), 4.39 (d, *J*=10 Hz, 1H), 5.65 (br. s, 1H), 5.90 (br. d, 1H), and 6.28 (d, *J*=1.1 Hz, 1H); Found: CHN.

Hydrogenation Procedures. In a 50-mL micro autoclave containing a glass lining tube and a stirring magnetic bar, under an argon atmosphere, were placed a catalyst precursor (1×10^{-2} mmol) and the substrate **1** (1 mmol) dissolved in a given solvent (5 mL). The inert atmosphere was replaced with hydrogen, the initial pressure of hydrogen being adjusted to 5—30 atm in each run. The reaction mixture was stirred at room temperature for 15—48 h depending on the other reaction conditions. The mixture was then filtered

† 1 M=1 mol dm^{-3}.

†† 1 Torr=133.322 Pa.

through a short plug of silica gel to remove the catalyst complex and the filtrate was evaporated to leave an oil. Conversion of the reaction was determined by capillary GLC (HR-20M, 30 m×0.2 mm, at 200 °C). Purification of the product by column chromatography (silica gel, hexane–ether) afforded a major component (**4a**) from the diastereomeric mixtures. ^{1}H NMR δ=1.23 (d, J=7.0 Hz, Me), 2.93 (qd, J=7.0 and 5.9 Hz, CH), 3.58 and 3.65 (s, MeO×2), 4.84 (dd, J=9.4 and 5.9 Hz, CHN), 6.00 (br. d, J=9.4 Hz, NH), and 7.26 (br. s, Ph). The vicinal coupling of the minor component (**4b**), J=6.4 Hz. Data of hydrogenation of **1** were given in Table 1. Hydrogenation of alkyl analogs of **1** (**8**—**11**) was also carried out in essentially the same procedure as described above (in methanol). Antiselectivity in each analog was given in parentheses: **8** (93%), **9** (69%), **10** (54%), and **11** (77%).

Preparation of 3-Methyl-4-phenyl-2-azetidinone (7). Iodine (0.76 g, 3 mmol) and hexamethyldisilane (0.51 g, 3.5 mmol) were stirred at 70 °C for 30 min. To trimethylsilyl iodide thus formed was added **4** (obtained from Entry 10) (1 mmol) dissolved in MeCN (5 mL) and the mixture was heated under reflux for 4 h. All volatile materials but disilylated product were evacuated under 2 Torr, and the residue was treated through a short silica gel column with MeOH. The eluent was evaporated to leave crude β-amino acid, $PhCH(NH_2)CHMeCO_2H$. The latter was treated with 2-chloro-1-methylpyridinium iodide (0.28 g, 1.1 mmol) and Et_3N (0.3 mL, 2.2 mmol) in dry MeCN (100 mL) under reflux for 8 h.[11] After evaporation of the solvent, the residue was extracted with ether and the extracts were washed with water and dried ($MgSO_4$). The crude product was purified by column chromatography (silica gel, hexane–ether) to give **7** (86.6 mg, 54% overall yield). The ratio of cis/trans=1/70 was determined by capillary GLC (HR-20M, 30 m×0.2 mm at 200 °C): T_R(trans) 18 min, T_R(cis) 23 min.

In the same manner as above, a sample of **4** from Entry 13 was converted into **7**. In this case, the cis/trans ratio was 80/20, and the isomers were separated by column chromatography. NMR spectral data of *cis*- and *trans*-**7**[12] were given below. *cis*-**7**: ^{1}H NMR δ=0.82 (d, J=7.5 Hz, 3H), 3.58 (ddq, J=1.8, 5.5, and 7.5 Hz, 1H), 4.88 (d, J=5.5 Hz, 1H), 6.14 (br., 1H), and 7.13—7.48 (m, 5H). ^{13}C NMR (22.5 MHz) δ=10.1, 51.0, 55.2, 126.6, 127.9, 128.6, 137.6, and 173.8. *trans*-**7**: ^{1}H NMR δ=1.42 (d, J=7.5 Hz, 3H), 3.06 (dq, J=2.2 and 7.5 Hz, 1H), 3.61 (d, J=2.2 Hz, 1H), 6.20 (br., 1H), and 7.35 (br. s, 5H). ^{13}C NMR δ=13.0, 56.5, 59.3, 125.5, 128.0, 128.8, 140.3, and 171.7.

Appendix

Elemental Analyses for 2-[α-(Methoxycarbonylamino)-alkyl]acrylates.

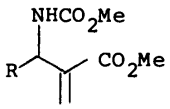

R=*i*-Pr (**9**) Found: C, 55.60; H, 8.07; N, 6.77% Calcd for $C_{10}H_{17}NO_4$: C, 55.80; H, 7.96; N, 6.51%

R=*i*-Bu (**10**) Found: C, 57.46; H, 8.45; N, 6.36% Calcd for $C_{11}H_{19}NO_4$: C, 57.63; H, 8.35; N, 6.11%

R=*t*-Bu (**11**) Found: C, 57.82; H, 8.60; N, 6.26% Calcd for $C_{11}H_{19}NO_4$: C, 57.63; H, 8.35; N, 6.11%

Support of this work by a Grant-in-Aid for Scientific Research (No. 61225005) from the Ministry of Education, Science and Culture is gratefully acknowledged.

References

1) Part of this work was presented at the 54th National Meeting of the Chemical Society of Japan, Tokyo, April 1987, Abstr. 2IIIO42.

2) J. M. Brown and I. Cutting, *J. Chem. Soc., Chem. Commun.*, **1985**, 578.

3) J. M. Brown and R. G. Naik, *J. Chem. Soc., Chem. Commun.*, **1982**, 348; J. M. Brown and S. A. Hall, *J. Organomet. Chem.*, **285**, 333 (1985); R. H. Crabtree and M. W. Davis, *Organometallics*, **2**, 681 (1983); R. H. Crabtree and M. W. Davis, *J. Org. Chem.*, **51**, 2655 (1986); G. Stork and D. E. Kahne, *J. Am. Chem. Soc.*, **105**, 1072 (1983); D. A. Evans and M. M. Morrissey, *Tetrahedron Lett.*, **25**, 4637 (1984); D. A. Evans and M. DiMare, *J. Am. Chem. Soc.*, **108**, 2476 (1986).

4) J. M. Brown, A. P. James, and L. M. Prior, *Tetrahedron Lett.*, **28**, 2179 (1987).

5) A. V. Stavrovskaya, T. V. Protopopova, A. P. Skoldinov, *Zh. Org. Khim.*, **6**, 19 (1970).

6) The DABCO catalyzed reaction of acrylates with aldehydes is amply precedented: For latest work on the related reaction of phenyl vinyl sulfone with aldehydes, see P. Anuray, P. Knochel, and J. F. Normant, *Tetrahedron Lett.*, **27**, 5095 (1986) and references therein.

7) R. A. Sanches-Delgado, J. S. Bradley, and G. Wilkinson, *J. Chem. Soc., Dalton Trans.*, **1976**, 399. Also, R. W. Mitchell, A. Spencer, and G. Wilkinson, *ibid.*, **1973**, 846. The trans configuration of the complex was assigned in the former literature.

8) P. Perlmutter and C. C. Teo, *Tetrahedron Lett.*, **25**, 5951 (1984).

9) D. Sinou and H. B. Kagan, *J. Organomet. Chem.*, **114**, 325 (1976).

10) T. Shono, N. Kise, F. Sanda, and Y. Arai, 54th National Meeting of the Chemical Society of Japan, Tokyo, April 1987, Abstr. 3IIIG43.

11) H. Huang, N. Iwasawa, and T. Mukaiyama, *Chem. Lett.*, **1984**, 1465.

12) E. J. Moriconi and J. F. Kelly, *Tetrahedron Lett.*, **1968**, 1435; T. R. Durst, R. Van den Elzen, and R. Legault, *Can. J. Chem.*, **52**, 3206 (1974).

A Novel Chiral Stationary Phase for Optical Resolution of Amino Acids and Their Derivatives by Ligand-Exchange High-Performance Liquid Chromatography

Kazuhiko SAIGO,* Yoichi YUKI,† Hiroki KIMOTO, Toru NISHIDA, and Masaki HASEGAWA
Department of Synthetic Chemistry, Faculty of Engineering, The University of Tokyo, Hongo, Bunkyo-ku, Tokyo 113
†Research Center, Daicel Chemical Industries Ltd., Shinzaike, Aboshi-ku, Himeji, Hyogo 671-12
(Received July 28, 1987)

Synopsis. A novel chiral stationary phase, [(1*R*,2*S*)-2-hydroxy-1-methyl-2-phenylethylamino]acetic acid, was prepared from (−)-norephedrine, and its sodium salt was bound to silica gel pretreated with [3-(glycidyloxy)propyl]trimethoxysilane. The chiral stationary phase was found to be effective for the optical resolution of amino acids and their derivatives by ligand-exchange high-performance liquid chromatography using aq copper(II) sulfate solution as an eluent.

The chromatographic resolution of amino acids is achieved by ligand-exchange chromatography using copper(II) complexes of chiral stationary phases (CSPs). Gübitz and his co-workers developed practically useful packings for high-performance liquid chromatography (HPLC), in which copper(II) complexes of various amino acids are covalently bonded to silica gel pretreated with [3-(glycidyloxy)-propyl]trimethoxysilane.[1–5] Among these CSPs, L-hydroxyproline shows the best chiral recognition ability. Moreover, recently we developed and reported new CSPs consisting of optically active *erythro*- and *threo*-2-carboxymethylamino-1,2-diphenylethanol moieties.[6,7] These results indicate that hydroxyl group in the chiral amino acid moieties may play an important role for the chiral recognition and that optically active 2-aminoalkanols would be applicable as chiral moieties for CSPs.

On the basis of this consideration, we prepared a novel CSP, [(1*R*,2*S*)-2-hydroxy-1-methyl-2-phenylethylamino]acetic acid, from (−)-norephedrine and applied it for ligand-exchange HPLC.

Sodium [(1*R*,2*S*)-2-hydroxy-1-methyl-2-phenylethylamino]acetate (sodium salt of N-carboxymethylated norephedrine) (**2**) was easily prepared by ethoxycarbonylmethylation of (−)-norephedrine (**1**) with ethyl bromoacetate, followed by hydrolysis with aq NaOH solution. Without further purification, the sodium salt was allowed to react with silica gel pretreated with [3-(glycidyloxy)propyl]trimethoxysilane to give a new covalently-bonded CSP (**3**). The CSP was converted to copper(II) complex (**4**) by treatment with aq $CuSO_4$ solution. The silica gel, bonded with the CSP, was packed in a stainless steel column by the ascending slurry technique.

A number of amino acids and *N*-benzyloxycarbonylated (Z-) amino acids could be resolved on the copper(II) complex of this CSP by means of ligand-exchange HPLC using an aq copper(II) sulfate solution as a mobile phase. But, this CSP could not resolve amino acids such as alanine, leucine, methionine, phenylglycine, glutamine, glutamic acid, citrulline, and histidine. Typical chromatograms for the resolution of amino acids by HPLC are shown in Fig. 1, and the corresponding chromatographic parameters are given in the Table 1.

The CSPs, derived from *erythro*- and *threo*-2-amino-1,2-diphenylethanol, have quite different chiral recognition ability each other for amino acids and their derivatives, namely, amino acids and their derivatives resolved can be devided into two groups.[6,7] But, **4** could resolve amino acids and their derivatives of the two groups, although the scope of application and the α values obtained are smaller than those showed when *erythro*- and *threo*-2-amino-1,2-diphenylethanol moieties were used as CSPs.[6,7] This difference in the chiral recognition should result from the difference of the substituent at C2. In the case of *erythro*- and *threo*-2-amino-1,2-diphenylethanol, the

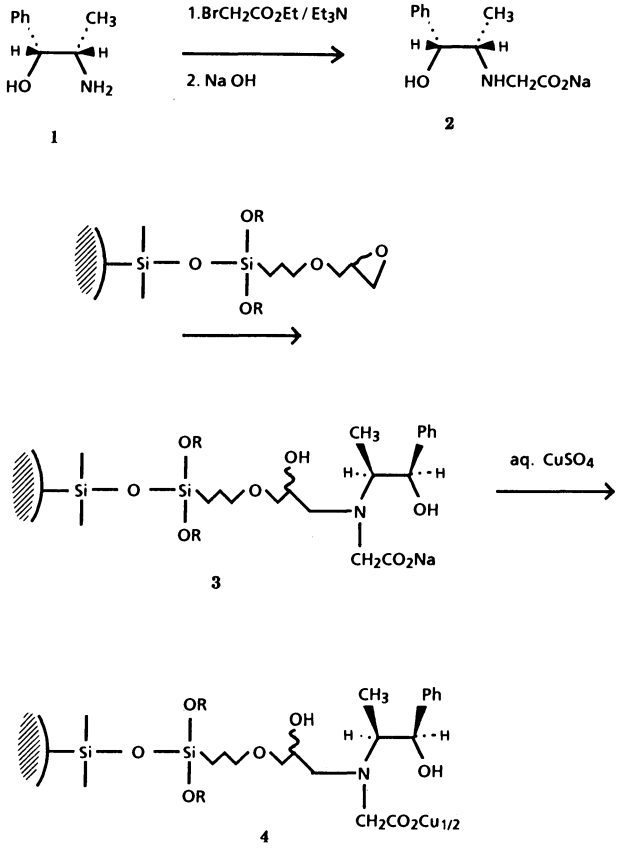

Table 1. Chromatographic Parameters for the Resolution of Amino Acids and N-Benzyloxycarbonylated Amino Acids

Racemate	Capacity factor k'_L	Capacity factor k'_D	Separation factor α	Resolution factor R_s
Valine	7.50	8.28	1.10	1.10
Isoleucine	8.94	9.90	1.11	1.15
tert-Leucine	6.58	7.65	1.16	1.00
Phenylalanine	10.18	11.60	1.14	1.15
Tyrosine	8.28	10.13	1.22	1.51
Proline	9.73	8.74	1.11	0.87
Asparagine	4.39	3.75	1.17	1.38
Aspartic acid	5.22	6.05	1.16	1.06
Serine	4.40	4.72	1.07	0.56
Threonine	4.61	5.04	1.09	0.83
Tryptophan	16.20	18.67	1.15	0.83
Arginine HCl	9.05	9.75	1.08	0.55
Lysine HCl	7.43	7.15	1.04	—
Z-Phenylalanine	9.92	9.10	1.09	—
Z-Alanine	3.56	3.34	1.07	—
Z-Valine	4.74	4.36	1.09	—
Z-Asparagine	3.50	3.17	1.10	0.95

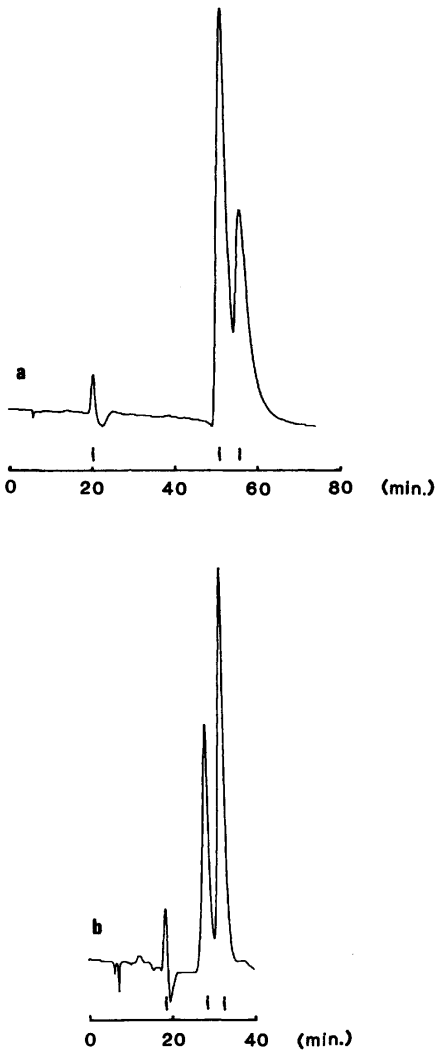

Fig. 1. The HPLC Chromatograms of (a) valine and (b) asparagine (D/L=1/2).

π–π interaction between the phenyl groups at C1 and C2 play an important role to fix the comformation of the copper(II) chelates. On the other hand, the chelate of **4**, in which the π–π interaction is absent, would be flexible. The flexibility would result in the samller α values for amino acids and their derivatives in the two groups.

Moreover, the CSP, derived from (*R*)-2-amino-2-phenylethanol showed no chiral recognition ability, indicating that the phenyl group at C1 plays also an important role for the chiral recognition.

Experimental

Materials. (−)-Norephedrine was purchased from Aldrich Chemical Company, silica gel, Develosil 100-5 from Nomura Chemical Co., [3-(glycidyloxy)propyl]trimethoxysilane from Shin-Etsu Chemical Co., amino acids from the Peptide Institute, and *N*-benzyloxycarbonylated amino acids from Sigma Chemical Company.

All solvents were of reagent grade.

Instruments. Melting point was measured by a Laboratory Devices MEL-TEMP apparatus and is uncorrected. IR spectra were recorded on a JASCO IR-810 spectrometer. ^{1}H NMR was recorded on a JOEL JNM-PMX60 at 60 MHz using TMS as an internal standard. A JASCO TRIROTAR-V, a Rheodyne 7125 injector, a JASCO UVIDEC-100-IV UV detector, and a NIHON CROMATO CDS 86 Ver. 2.7 data processor were used for HPLC. The column temperature was maintained at 35 °C by a JASCO TU-100 column oven.

Ethyl [(1*R*,2*S*)-2-Hydroxy-1-methyl-2-phenylethylamino]-acetate. To a solution of (−)-norephedrine (1.21 g, 8 mmol) in dichloromethane (10 ml) was added drop by drop a solution of ethyl bromoacetate (1.50 g, 9 mmol) in dichloromethane (10 ml) in a period of 30 min at room temperature. After stirring at the temperature for additional 2.5 h, triethylamine (1.2 ml, about 9 mmol) was added to the solution, and the reaction mixture was stirred for 2.5 h. Then, the solvent was evaporated, and benzene (ca. 100 ml) was added to the residue. The benzene solution was washed with water and sat. NaCl solution and dried with Na_2SO_4. After evaporation of the solvent under reduced pressure, crude product was purified by silica-gel chromatography

(eluent: hexane/ethyl acetate=1/1) to give ethyl [(1*R*,2*S*)-2-hydroxy-1-methyl-2-phenylethylamino]acetate in 78% yield. Glassy oil. $[\alpha]_D^{22.4}$ +2.4° (*c* 0.414, EtOH). IR (KBr): 3470, 1747, 1455, 1241, 1148, and 703 cm^{-1}. ^1H NMR ($CDCl_3$): 0.78 (d, 3H, *J*=7 Hz), 1.22 (t, 3H, *J*=7 Hz), 2.74 (m, 3H), 3.30 (s, 2H), 4.08 (q, 2H, *J*=7 Hz), 4.57 (d, 1H, *J*=4 Hz), and 7.23 (s, 5H).

Calcd for $C_{13}H_{19}NO_3$: C, 65.80; H, 8.07; N, 5.90%. Found: C, 65.43; H, 8.02; N, 5.94%.

Sodium [(1*R*,2*S*)-2-Hydroxy-1-methyl-2-phenylethylamino]-acetate (2). To a solution of ethyl [(1*R*,2*S*)-2-hydroxy-1-methyl-2-phenylethylamino]acetate (1.66 g, 7 mmol) was added 7.2 ml of 1 $mol \cdot dm^{-3}$ NaOH solution at room temperature, and the solution was stirred overnight at room temperature. Evaporation of the solvent gave 1.60 g of slightly yellow-colored solid mass. The mass was identified to be **2** by IR spectroscopy. IR (KBr): 3400, 1600, 1415, 1000, 760, 700 cm^{-1}.

Coating on Silica Gel. A suspension of silica gel (50 g), dried for 3 h at 120 °C, in dry benzene (500 ml) was refluxed, and the benzene (ca. 50 ml) was distilled off. Then, [3-(glycidyloxy)propyl]trimethoxysilane (25 ml) was added to the suspension. The suspension was refluxed for 8 h with removal of methanol formed from the mixture. After cooling, the benzene was removed by filtration, and the silica gel was thoroughly washed with dichloromethane. To a solution of **2** in methanol (20 ml) was added the silica gel (7.0 g), and the mixture was stirred for 6 d at 30 °C. The CSP-bonded silica gel was collected by filtration, washed with methanol, and poured into 1 w/v% $CuSO_4$ solution (150 ml). The copper(II)-loaded silica gel was collected by filtration and washed thoroughly with 2.5×10^{-4} $mol \cdot dm^{-3}$ $CuSO_4$ solution. Elemental analysis for the copper-loaded silica gel gave C, 6.00; H, 1.35; N, 0.32% (C, 4.20; H, 1.25% for the silanized silica gel).

Chromatography. The copper-loaded silica gel, suspended in 2.5×10^{-4} $mol \cdot dm^{-3}$ $CuSO_4$ solution, was packed in a stainless steel column (25×0.46 (i.d.) cm) by the slurry technique under the pressure of 250 $kg \cdot cm^{-2}$.

The chromatography was carried out at 35 °C at a flow-rate of 0.5 $ml \cdot min^{-1}$ using 2.5×10^{-4} $mol \cdot dm^{-3}$ $CuSO_4$ solution as a mobile phase. The dead volume of the column was estimated to be 3.00 cm^3 with water.

The *k'* values of unresolved amino acids were as follows; alanine (5.96), leucine (9.35), methionine (7.95), phenylglycine (8.77), glutamine (10.53), glutamic acid (9.68), citrulline (6.10), and histidine (13.67).

References

1) G. Gübitz, W. Jellenz, G. Löfler, and W. Santi, *J. High Resolut. Chromatogr. Commun.*, **2**, 145 (1979).

2) G. Gübitz, W. Jellenz, and W. Santi, *J. Liq. Chromatogr.*, **4**, 701 (1981).

3) G. Gübitz, W. Jellenz, and W. Santi, *J. Chromatogr.*, **203**, 377 (1981).

4) G. Gübitz, F. Juffmann, and W. Jellenz, *Chromatographia*, **16**, 103 (1982).

5) G. Gübitz and S. Mihellyes, *Chromatographia*, **19**, 257 (1984).

6) Y. Yuki, K. Saigo, K. Tachibana, and M. Hasegawa, *Chem. Lett.*, 1347 (1986).

7) Y. Yuki, K. Saigo, H. Kimoto, K. Tachibana, and M. Hasegawa, *J. Chromatogr.*, **400**, 65 (1987).

Cobalt-Catalyzed Hydrohydroxymethylation of Formaldehyde: Effect of $Ru_3(CO)_{12}$ and Phenol

Kazuhisa MURATA,* Akio MATSUDA, and Takashi MASUDA
National Chemical Laboratory for Industry, Yatabe, Tsukuba, Ibaraki 305
(Received July 1, 1987)

Synopsis. A catalyst system, containing $Co_2(CO)_8$, $Ru_3(CO)_{12}$, and phenol, was found to be effective for the hydrohydroxymethylation of formaldehyde to give ethylene glycol with the yield of ca.65%, better than those previously reported.

The hydrohydroxymethylation, by which ethylene glycol(EG) is produced directly from formaldehyde, is receiving increasingly wider attention as an attractive route to C_2 compounds.[1] So far, stoichiometric,[2] and catalytic[3] hydroformylation of formaldehyde to glycolaldehyde(GLA) has been achieved by using cobalt and rhodium catalysts with reasonable selectivity. However, these require a successive hydrogenation of GLA to obtain EG. Recently, the hydrohydroxymethylation of CH_2O has been reported with moderate EG yield(ca. 25%) using rhodium-cobalt system.[4]

In the course of our study on a syngas conversion to EG, where cobalt catalyst is employed under high pressure, we have found that the addition of $Ru_3(CO)_{12}$ is effective for enhancing the glycol productivity,[5] in addition to the effectiveness of phenol as solvent.[6] In this study, the effects of addition of $Ru_3(CO)_{12}$ and phenol on the cobalt-catalyzed hydrohydroxymethylation of CH_2O will be described.

Results and Discussion

In the preliminary stage of our study, we examined the behavior of cobalt catalyst under the conditions of 200 atm at 180 °C. The results are given in Table 1. Ethylene glycol was produced in ca. 20% yield after the reaction in dioxane solvent for 7 h, where 37% formaldehyde aqueous solution was used as formaldehyde source (Run 1): Methanol (9%) was obtained as by-product and small amounts of ethanol (1.5%) and methyl cellosolve (18%) were detected. The addition of phosphine (1,2-bis(diphenylphosphino)-ethane (dpe), P/Co=0.5(molar ratio)) caused the EG yield to be slightly enhanced (Run 2). Paraformaldehyde was less favorable than CH_2O (aq.) (Run 3), but

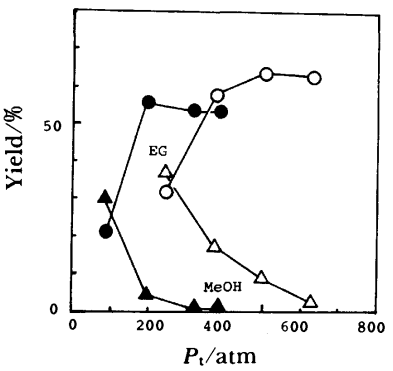

Fig. 1. Effect of total pressure.
○△ $Co_2(CO)_8$ 2.5 mmol, $Ru_3(CO)_{12}$ 0.167 mmol, CH_2O(aq) 40 mmol, PhOH 106 mmol, toluene 12 ml, H_2/CO=4, 180 °C, 2 h. ●▲ $Co_2(CO)_8$ 2 mmol, dpe 1.5 mmol, AcOH 50 mmol, CH_2O(aq) 50 mmol, dioxane 50 ml, H_2/CO=1, 180 °C, 4.5 h.

Table 1. Effects of Solvents and Organic Acids on the Cobalt-Catalyzed Hydrohydroxymethylation of Formaldehyde[a]

Run No.	Time/h	dpe[b] / mmol	Solvent	Acid / mmol	EG	Yield/%[c] totalEG	MeOH
1	7	—	Dioxane	—	19.4	—	9.0
2	7	1.0	Dioxane	—	22.4	—	6.4
3[d]	7	1.0	Dioxane	—	8.0	—	8.0
4[e]	7	1.0	Dioxane	—	15.0	—	15.4
5	7	1.0	EtOH	—	1.6	57.6[f]	4.6
6	7	1.0	*i*-PrOH	—	9.0	45.0[g]	3.0
7	7	1.5	AcOH	—	11.4	28.2[h]	6.8
8[i]	—	1.0	Dioxane	—	43.2	43.8[j]	6.2
9	4.5	—	Dioxane	AcOH(50)	45.8	49.2[k]	10.0
10	4.5	—	Dioxane	HCOOH(50)	33.8	44.0[l]	4.2
11	4.5	—	Dioxane	PhCOOH(50)	48.4	51.4[m]	5.2
12	4.5	—	Dioxane	PhOH(50)	46.0	—	5.0
13	4.5	1.5	Dioxane	AcOH(50)	44.6	55.8	4.8
14	4.5	1.5	Dioxane	AcOH(75)	35.4	47.0	4.6

a) Conditions: $Co_2(CO)_8$ 2 mmol, solvent 50 ml, CH_2O(aq.) 5 mmol, 180 °C, 200atm(H_2/CO=1). b) $Ph_2P(CH_2)_2PPh_2$. c) Based on CH_2O initially added(50 mmol). d) Paraformaldehyde(50 mmol). e) Paraformaldehyde(50 mmol)/H_2O(60 mmol). f) EG+$EtOCH_2CH_2OH$. g) EG+*i*-$PrOCH_2CH_2OH$. h) EG+$AcOCH_2CH_2OH$+$AcOCH_2CH_2OAc$. i) Two-stage reaction: 60 °C, 6 h→190 °C, 2.5 h. j) EG+$HOCH_2CHO$. k) EG+$AcOCH_2CH_2OH$. l) EG+$HCOOCH_2CH_2OH$. m) EG+$PhCOOCH_2CH_2OH$.

the addition of H_2O, in this case, raised the EG yield(Run 4). By use of alcohol solvents, alkyl cellosolves[7] were produced in high yields with a small amount of EG (Runs 5,6). In case of acetic acid solvent, ethylene glycol and its acetate esters were formed in ca. 28% yield, but a partial decomposition of $Co_2(CO)_8$ occurred (Run 7).

When organic acids were used as additives but not solvent, the enhancement of the EG yield was also observed (Table 1, Runs 9—14). The yield decreased by the addition of excess acid (Run 14). Also the yield was influenced by total pressure and temperature: the yield increased with the increases in pressure up to 200 atm (Fig. 1,● and in temperature to 180 °C (Fig. 2,●), whereas methanol formation decreased with the increase in pressure (Fig. 1,▲) and increased with the increase in temperature (Fig. 2,▲).

We have found the Co-Ru system, which is active for syngas conversion to EG;[5] so, effect of ruthenium was examined using cobalt-phenol system, the results of which are given in Table 2. The EG yield as well as MeOH increased with the increase in Ru concentration: EG and MeOH accounts for up to ca. 88% of products (Runs 4,5). Other metal carbonyls such as $Re_2(CO)_{10}$, $Mo(CO)_6$, $Fe(CO)_5$, and $Cr(CO)_6$ were unfavorable.

Figure 2 (○) shows the effect of reaction temperature. The maximum EG yield of ca. 65%, which is the highest value of those previously reported,[1a] was achieved at 180 °C: The yield of MeOH increased with the increase in temperature. As shown in Fig. 1, the pressure effect of Co-Ru-PhOH system was analogous to that of Co-AcOH system: The EG yield increased with the increase in pressure up to 500 atm (○). The effect of H_2 pressure was similar to that of total pressure (Fig. 3) and the EG yield was little affected by CO pressure (Fig. 3,●).

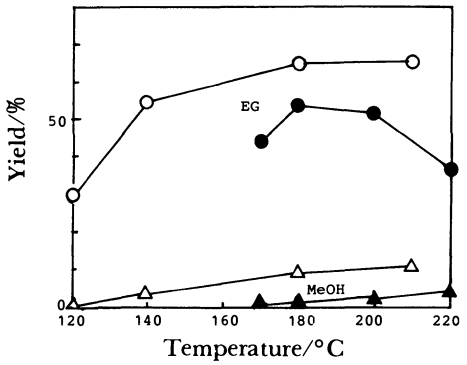

Fig. 2. Effect of temperature.
○△ $Co_2(CO)_8$ 2.5 mmol, $Ru_3(CO)_{12}$ 0.167 mmol, PhOH 106 mmol, CH_2O(aq) 40 mmol, toluene 12 ml, 500 atm(H_2/CO=4), 2 h. ●▲ $Co_2(CO)_8$ 2 mmol, dpe 1.5 mmol, AcOH 50 mmol, CH_2O(aq) 50 mmol, dioxane 50 ml, 390 atm(H_2/CO=1), 4.5 h.

Table 2. Effects of $Ru_3(CO)_{12}$[a]

Run No.	$Ru_3(CO)_{12}$/mmol	Yield/%[b] (Sel./%[c]) EG	MeOH
1	—	26.5(27.4)	1.93(2.0)
2	0.083	41.4(43.5)	12.2(12.8)
3	0.133	46.7(48.7)	14.2(14.8)
4	0.20	55.9(60.8)	25.5(27.7)
5	0.233	56.8(60.4)	26.1(27.8)

a) Conditions: $Co_2(CO)_8$ 2.5 mmol, CH_2O(aq.) 40 mmol, PhOH 106 mmol, Toluene 12 ml, 500 atm(H_2/CO=9), 140 °C, 2 h. b) See footnote (c) of Table 1. c) Selectivity=Product(mol)×100/Converted CH_2O(mol).

In the absence of organic acid and ruthenium, the EG yield was ca. 20% (Table 1, Runs 1,2). The low EG yield might be that the aldol condensation of CH_2O and/or GLA takes place to form higher molecular weight by-products.[3] Glycolaldehyde was produced in ca. 70% yield[2] after the hydroformylation of CH_2O at 60 °C for 6 h: When the resulting solution was further treated at 190 °C for 2.5 h, the EG formed was ca. 43% (Table 1, Run 8), indicating that the condensation as well as hydrogenation of GLA could occur. Therefore, in order to increase the yield of EG formed by one-batch process at 180 °C, it seems to be important that the hydrohydroxymethylation of CH_2O predominates over the condensation at temperature as high as 180 °C.

Considering the schemes of syngas conversion[6-8] and of Rh-catalyzed hydroformylation of CH_2O,[3] this cobalt-catalyzed reaction may be assumed to proceed by the Scheme 1, in which hydroxymethylcobalt complex a,[9] the formation of which might be prompted by phenol,[10,11,12] (steps I—III), is involved as a key intermediate: The complex a thus formed undergoes CO insertion(IV) and subsequent hydrogenation(V) to give GLA, which is reduced to EG(VI) by catalysis of cobalt and/or ruthenium. MeOH could be produced via hydrogenolysis of methoxycobalt complex b(VIII) as well as of the complex a(IX).

An acceleration of MeOH formation as well as EG formation was observed in the presence of Ru (Table 2). So, ruthenium, at least, appears to be responsible for the reduction of GLA and/or CH_2O.[13] The Halcon Group suggested that Ru-phosphine complex could be a catalyst effective for the reduction of GLA to EG.[14] In hydrocarbonylation of MeOH to EtOH, it

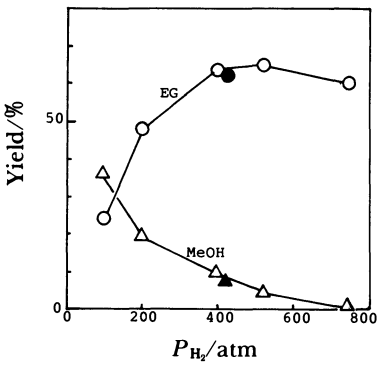

Fig. 3. Effect of hydrogen pressure.
$Co_2(CO)_8$ 2.5 mmol, $Ru_3(CO)_{12}$ 0.167 mmol, PhOH 106 mmol, CH_2O(aq) 40 mmol, toluene 12 ml, Pco=100 at, 180 °C, 2 h. ●▲ Pco=75 atm.

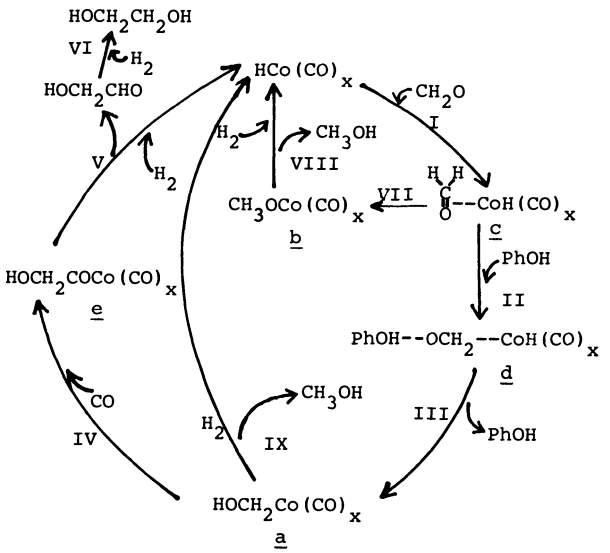

Scheme 1.

has been reported that hydrogenation of CH_3CHO occurs readily by Ru catalysis.[15]

The hydroformylation of CH_2O occurs even at 60 °C (Table 1, Run 8) and also the hydrohydroxymethylation activity is little affected by CO pressure (Fig. 3,●), indicating that CO insertion step(IV) is rapid under the conditions employed. Therefore, it is probable that the EG formation could be accelerated by an increased hydrogen pressure (Fig. 3).

Experimental

Materials. $Ru_3(CO)_{12}$, solvents, and organic acids were obtained commercially and used with no further purification. $Co_2(CO)_8$ was prepared according to an usual procedure. Aqueous 37% formaldehyde solution and paraformaldehyde were commercial products.

Reaction Procedure. A typical experiment can be described as follows: A catalyst solution containing $Co_2(CO)_8$, $Ru_3(CO)_{12}$, PhOH, and CH_2O(aq) in solvent (50 ml) was placed in a stainless steel autoclave (100 ml), which was subsequently charged with syngas (H_2/CO=4). When the system was heated to a desired temperature, the total pressure was adjusted to a desired pressure by introducing more syngas mixture. After the reaction, the vessel was cooled to room temperature and the solution was analyzed by GLC.

The two-stage reaction was carried out, first at 60 °C for 6 h to produce glycolaldehyde, then by increasing the temperature to 190 °C for another period of 2.5 h giving EG.

This work is a part of "C_1 Chemistry Project," a National Research and Development Program of Agency of Industrial Science and Technology, Ministry of International Trade and Industry (M.I.T.I.), Japan.

References

1) a) T. Onoda, Jpn. Patent 51-128903(1976); b) T. Suzuki, K. Kudo, and N. Sugita, S56 Meeting of the Catalysis Society of Japan, Okayama, October 1981, Abstr., No. 2V20.

2) J. A. Roth and M. Orchin, *J. Organomet. Chem.*, **172**, C27 (1979).

3) A. Spencer, *J. Organomet. Chem.*, **194**, 113 (1980); T. Suzuki, K. Kudo, and N. Sugita, *Nippon Kagaku Kaishi*, **1982**, 1357; A. S. C. Chan, W. E. Carroll, and D. E. Willis, *J. Mol. Catal.*, **19**, 377 (1983); M. Marchionna and G. Longoni, *Organometallics*, **6**, 606 (1987).

4) M. Marchionna and G. Longoni, *J. Mol. Catal.*, **35**, 107 (1986).

5) K. Murata, A. Matsuda, T. Masuda, M. Ishino, and M. Tamura, *Bull. Chem. Soc. Jpn.*, **60**, 438 (1987).

6) T. Masuda, K. Murata, T. Kobayashi, and A. Matsuda, *Nippon Kagaku Kaishi*, **1986**, 171.

7) $CH_2O+2ROH \rightarrow CH_2(OR)_2 \xrightarrow{CO/H_2} ROCH_2CHO \xrightarrow{H_2} ROCH_2CH_2OH$ J. F. Knifton, *J. Mol. Catal.*, **30**, 281 (1985).

8) T. Masuda, K. Murata, and A. Matsuda, *Bull. Chem. Soc. Jpn.*, **59**, 1287 (1986).

9) An alternative route, in which acyloxymethyl complex ($RCOOCH_2$-$Co(CO)_x$) is involved, is also likely, because EG monoacetate or monoformate was detected on adding AcOH or HCOOH (Table 2, Runs 2,3). B. D. Dombek, *J. Am. Chem. Soc.*, **102**, 6855 (1980).

10) The acid-catalyzed reaction of formaldehyde, the first step of which is formation of a carbonium ion ($CH_2O+H^+ \rightarrow CH_2OH$), will aid in considering Scheme I (steps I—III). A. C. Hopkinson, N. K. Holbrook, K. Yates, and I. G. Csizmadia, *J. Chem. Phys.*, **49**, 3596 (1968).

11) No infrared spectral changes were observed in the metal carbonyl region on adding phenol to the cobalt-toluene solution.

12) It also seems likely that another role of these acids is to depress a concomitant condensation of CH_2O and/or GLA. J. F. Walker, "Formaldehyde," 3rd ed, ed by R. E. Krieger Publishing Company, Huntington, New York (1975), pp. 55, 345.

13) Under the conditions employed in Table 2, the use of $Ru_3(CO)_{12}$(0.133 mmol) alone resulted in the formation of MeOH (ca. 80% yield, based on CH_2O) with no detectable amount of EG.

14) L. C. Costa, Jpn. Patent 57-75940(1982).

15) G. Jenner and P. Andrianary, *J. Catal.*, **88**, 535 (1984).

Development and Applications for the Simulater of Intermolecular Potentials. II.† Hydration Effects on the Conformation of Tyramine

Tatsuya TAKAGI,* Akito TANAKA, Mika TANI, Hironobu MAEZAKI, Hideaki FUJIWARA, and Yoshio SASAKI
Faculty of Pharmaceutical Sciences, Osaka University, 1-6 Yamada-Oka, Suita, Osaka 565
(Received May 22, 1987)

Conformational energy maps of the tyramine monocation and its hydrated species were calculated using the SIMP system. The populations of the trans conformer were calculated to be 18% and 53% for the isolated monocation and the hydrated one respectively. The computational results was supported by the results of conformational analysis based on ^{1}H NMR spectroscopy.

Recently, the conformations of compounds which possess physiological activity have been studied widely in order to estimate the structural requirements for the active compounds and to reveal the chemical environments around the active sites of receptors.[2,3] For example, Pullman et al.[2] reported PCILO calculations in connection with conformational studies of the derivatives of phenethylamine, which is a basic skeleton of biological and medicinal interest. They concluded that the phenethylamines exist as a mixture of two nearly equally populated conformers in vacuo. Chuman[3] also reported, from a computational analysis of molecular mechanics, that the active form of enkephaline was similar to that proposed by Hudson et al.[4] However, these analyses have a common defect that the compounds are treated in vacuo and not in solution. Indeed, Chuman's active conformer of enkephaline was calculated to be located 25 kcal mol^{-1} above the global minimum. He claimed that such an energy difference was understandable if the computational accuracy, the conformational change by an induced fitting, and the differences in surroundings were considered (the virtual molecules for these calculations are in vacuo, whereas practical molecules are dissolved in solution). To overcome this defect, Pullman et al.[5] attempted conformational analyses of some hydrated models, which resemble actual states more closely in surroundings than do the molecules in vacuo, using the semiempirical PCILO and ab initio MO methods. Nevertheless, the PCILO method was not accurate enough with respect to the interaction energy, and the CPU time was not sufficient for a full ab initio MO calculation.

In a previous report,[1] we ourselves have developed the SIMP (Simulater of Intermolecular Potentials) system for the calculation of intermolecular interactions with sufficient accuracy and within a reasonably short CPU time. In the present study, we have estimated the preferred conformations of hydrated tyramine by this method and have compared them with those from NMR measurements. Tyramine has the ability to displace noradrenaline from a cytoplasmic mobile pool in adrenergic nerve terminals, leading to sympathomimetic effects. A similar displacement can also occur from granular storage sites. Since the structural specificity of this displacement is quite distinct[6] from that reported for the α-and β-receptors,[7] the preferred conformations of tyramine in an aqueous solution have attracted much attention.

We also explored the applicability of SIMP to the estimation of solvent effects on the conformational energies of this molecule.

Experimental

D_2O, $CDCl_3$, and CD_2Cl_2 (Uvasol reagents from E. Merck) were used as received. Tyramine (a special grade reagent) was used without any special purification. The saturated solutions of tyramine in the above solvents were used for the NMR measurements. The ^{1}H NMR spectra were observed with a HITACHI R-900M FT NMR spectrometer operating at 90 MHz and at 35 °C using 16k data points. Satisfactory signal-to-noise ratios were obtained after the accumulation of 128 transients for the D_2O solution, 5036 transients for the $CDCl_3$ solution, and 1024 transients for the CD_2Cl_2 solution. Programs for the SIMP and MNDO MO[8] calculations were the same as those in previous reports.[1,9] The MOPAC program system,[10] as updated by us for the SIMP calculations, was also used. The ^{1}H NMR spectra were analyzed by the use of the LAOCN5 program.[11] The numerical computations were done with the NEAC S1000 plus SX-1 system at the Computation Center Osaka University, with the M-780 plus VP-200 system at the Data Processing Center Kyoto University, and with the M680H plus S810/10 system at the Computer Center of the Institute for Molecular Science.

Results and Discussion

Since tyramine is known to take a monocation form in the neighbourhood of pH7, we have made computations with the monocation form. The structural parameters used for the MNDO MO calculations were taken from the X-ray crystallographic structures,[12] except for those relating to the hydrogen atoms. The distance of O-H, the angle of C-C-H, etc. were optimized using the MNDO MO method. The numbering of atoms in the tyramine monocation and the structural parameters are shown in Fig. 1 and Table 1 respectively. Tyramine has three flexible dihedral angles, as is defined in Fig. 1. Since the dihedral angles of θ_1 and

† See Ref. 1 for I.

Table 1. Bond Lengths, Bond Angles, and Dihedral Angles of Tyramine Used in This Work

Bond length/Å		Bond angle/°		Dihedral angle/°	
1-2	1.4246	1-2-3	120.00	1-b-a-H	120.00
4-O	1.3672	3-4-O	120.00	N-a-b-H	120.00
1-b	1.5272	2-1-b	120.00	3-4-O-H	90.00
b-a	1.5272	1-b-a	113.54		
a-N	1.5500	b-a-N	115.88		
2-H	1.0887	1-2-H	120.00		
O-H	0.9489	4-O-H	111.07		
b-H	1.1132	1-b-H	110.90		
a-H	1.1132	b-a-H	110.90		
N-H	1.0258	a-N-H	111.42		

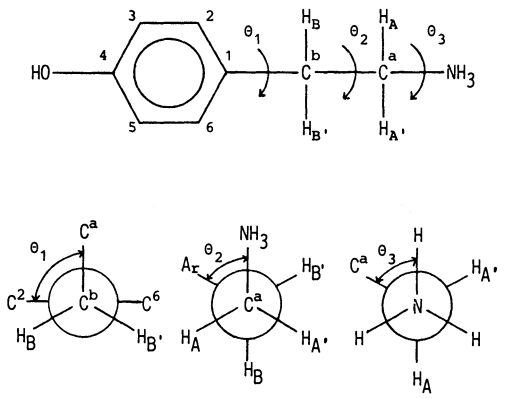

Fig. 1. The numbering of atoms and the definition of dihedral angles for tyramine.

θ_2 are considered to be more significant than that of θ_3 with respect to the overall molecular shape, we varied θ_1 and θ_2 for the computation of the conformational energy maps, while θ_3 was optimized in order to minimize the conformational energy for each set of θ_1 and θ_2 values. The other structural parameters were kept unchanged from the monomer values throughout the computations. Here, we will define the two regions of the conformations of tyramine. One is a gauche region which is defined by θ_2 being equal to 0°—120° or 240°—360°. The other is a trans region defined by θ_2=120°—240°, which is considered to be a structure similar to that of noradrenaline in an aqueous solution.[13]

The conformational energy map for the tyramine monocation obtained is shown in Fig. 2. Although the 'bulk repulsive concept,'[14] which is the basis of organic stereochemistry, would lead to a trans conformer as the preferred one, this map shows that the gauche conformer is more preferable than the trans one. In fact, the most stable values of θ_1 and θ_2 were calculated to be in a gauche region (75° and 57° respectively), though the conformational energy for the most stable conformation in the trans region was higher than the global minimum by only 3.9 kJ mol^{-1}. This profile is qualitatively consistent with that of the conformational energy map obtained by Pullman et al.[2] We have previously reported[15] that alkyl/aryl interac-

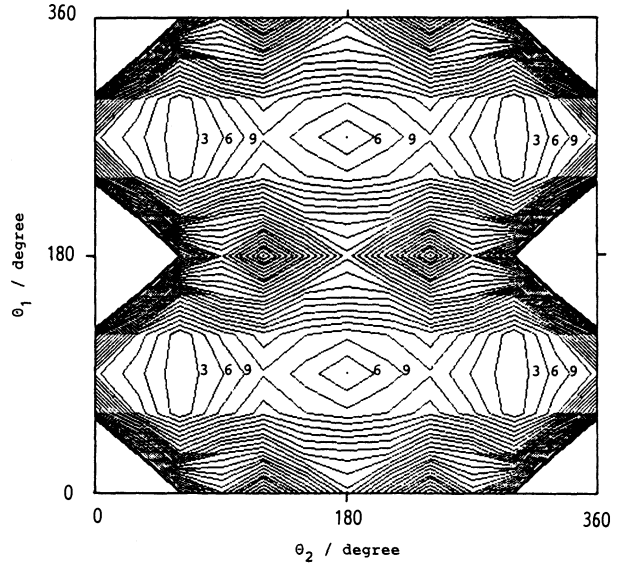

Fig. 2. The conformational energy map of tyramine monocation (kJ mol^{-1} with respect to the global minimum).

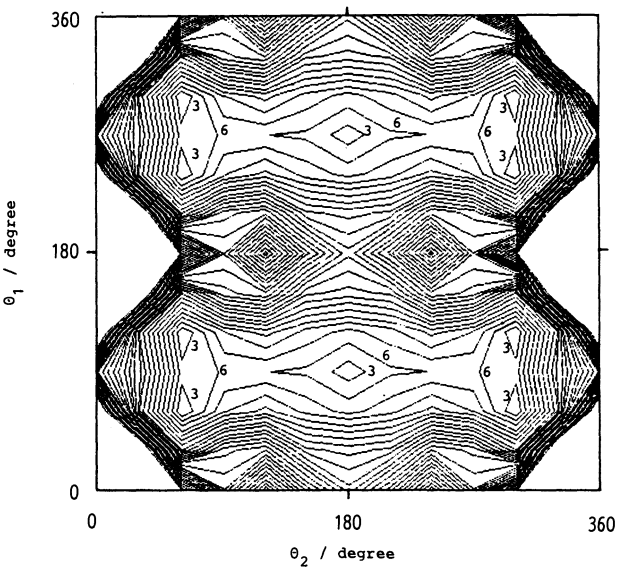

Fig. 3. The conformational energy map of hydrated tyramine monocation (kJ mol^{-1} with respect to the global minimum).

tions, called CH/π interactions by Nishio et al.,[16] can dominate the conformation of molecules, leading to a gauche conformer with respect to the alkyl and aryl groups. We have also reported, on the basis of the results of the energy decomposition analysis proposed by Kitaura et al.,[17] that the CH/π intramolecular interactions resemble the weak hydrogen bondings, as exemplified by the OH/π interactions. Since the most strong intramolecular interaction for the tyramine monocation in nature is an NH/π interaction, which is thought to be much stronger than the CH/π interaction, the preference of the gauche conformer may be reasonable.

In order to explore the hydration effects on the conformational energy map, four H_2O molecules were placed around the two polar sites of OH and NH_3. The angle of θ_3 and the distances between the polar sites and the H_2O molecules were optimized. The resulting conformational energy map of hydrated tyramine is shown in Fig. 3. Although the total profile of the energy map for the hydrated system was similar to that for the isolated system, the difference in energies was sufficiently large to change the population of each conformer. The difference in energies of the most stable conformations in the gauche and trans regions was calculated to be 2.4 kJ mol^{-1}, about half of that for the isolated system calculated above. In addition, the conformational energy increases around the regions of the global minimum more abruptly for the hydrated system than for the isolated system. In order to compare the population of trans and gauche conformers in detail, the populations were calculated by defining the trans conformer as θ_2=120°—240°, and the gauche one, as θ_2=0°—120° and θ_2=240°—360°. Under these conditions, the following equations hold:

$$P_t = \frac{1}{P_0} \int_{\frac{2}{3}\pi}^{\frac{4}{3}\pi} \int_0^{2\pi} \exp\{-\Delta E(\theta_1, \theta_2)/RT\} \, d\theta_1 \, d\theta_2 \quad (1)$$

$$P_g = 1 - P_t \quad (2)$$

$$P_0 = \int_0^{2\pi} \int_0^{2\pi} \exp\{-\Delta E(\theta_1, \theta_2)/RT\} \, d\theta_1 \, d\theta_2 \quad (3)$$

where P_t is the population of the trans conformer and P_g is that of the gauche conformer. The double integrations and the necessary interpolation of ΔE (θ_1, θ_2) were carried out using spline functions. The resultant populations at 35 °C are shown in Table 2. From these results, the trans conformer of tyramine is estimated to be more preferable in an aqueous solution than in vacuo. The reason for this populational change should be as follows: the NH/π interactions, which are considered to be the main origin of the preference of the gauche conformer, are replaced by the stronger interactions of the NH/H_2O interactions.

In order to confirm these computational results, we have analyzed the ^{1}H NMR spectra of tyramine in an aqueous solution as well as in several organic solvents. Examples of the calculated and observed NMR spectra of tyramine are shown in Fig. 4. The shift values and the vicinal coupling constants obtained using the LAOCN5 program are listed in Table 3. The rms errors between the observed and calculated coupling constants for tyramine in H_2O, CD_2Cl_2, and $CDCl_3$ are 0.11, 0.14, and 0.11 Hz respectively. As is shown in Fig. 5, the observed coupling constants, J_{AB} and $J_{AB'}$, may be represented by the following equations:

$$J_{AB} = P_t J_t + P_g J_g + \varepsilon \quad (4)$$

$$J_{AB'} = P_t J_g + \frac{1}{2} P_g (J_g + J_t) + \varepsilon' \quad (5)$$

$$P_t + P_g = 1 \quad (6)$$

where J_g and J_t are the ideal coupling constants for the gauche conformer and the trans conformer respectively, and where ε and ε' are the error terms. The values of J_g and J_t were assumed to be 2.0 and 13.0 Hz

Table 2. Rotamer Populations of Tyramine at 35 °C as Calculated by SIMP

System	Trans/%	Gauche/%
Isolated	18	82
Hydrated	53	47

Table 3. ^{1}H NMR Parameters for the AA'BB' Part of Tyramine

Solvent	$\nu_A - \nu_B$/Hz	J_{AB}/Hz	$J_{AB'}$/Hz
CD_2Cl_2	21.12	6.70	6.68
$CDCl_3$	22.61	6.80	6.53
D_2O	23.40	9.17	2.84

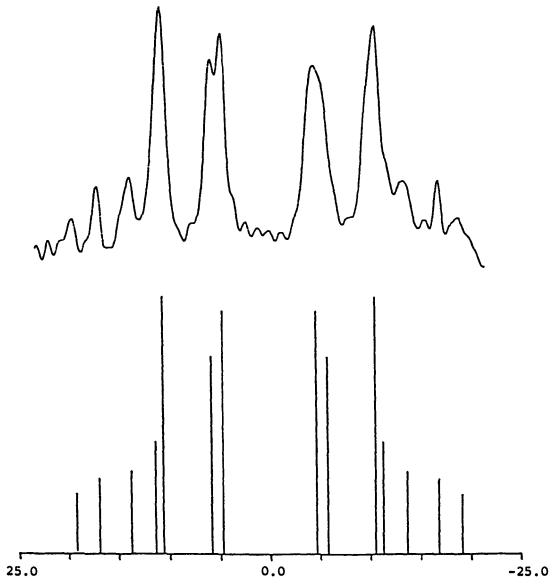

Fig. 4. The observed (upper) and the calculated (lower) NMR spectra of tyramine in CD_2Cl_2. The AA'BB' part from the alkyl side chain is shown. Lines at the higher field side are broadened by the small couplings with the aromatic protons.

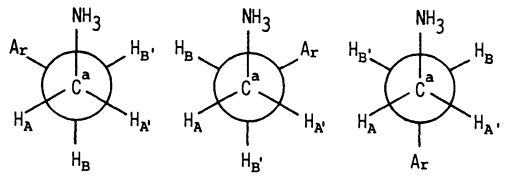

Fig. 5. Three possible conformations relating to the dihedral angle of θ_2.

Table 4. Rotamer Populations of Tyramine in Various Solvents

Solvent	Trans/%	Gauche/%
CD_2Cl_2	37	63
$CDCl_3$	38	62
D_2O	69	31

respectively, these values were cited from the literature.[18] When the value of $\varepsilon^2+\varepsilon'^2$ was minimized, P_t and P_g are determined experimentally as follows:

$$P_t = \frac{4J_{AB} - 2J_{AB'} + J_t - 3J_g}{5(J_t - J_g)} \quad (7)$$

$$P_g = 1 - P_t \quad (8)$$

Note from the definition (Fig. 5) that J_{AB} is larger than $J_{AB'}$ in Eq. 7. The resulting populations are listed in Table 4, which indicates that the trans conformer is preferable in D_2O, this is in agreement with the above SIMP calculations. In this way, our SIMP system is expected to offer a powerful method for determining hydration effects on the conformations of biologically significant molecules.

In Table 4, populations are also determined experimentally in CD_2Cl_2 and $CDCl_3$. The preference for the gauche conformer, which is indicated by the calculation for the isolated system in Table 2, is supported by the experiments.

The authors wish to thank the Institute of Molecular Science for allotting them CPU time on the HITAC M-680H plus S810/10 computer system. This investigation was supported as one of the Special Projects for Program Development at the Computation Center Osaka University using the NEAC S-1000 plus SX-1 computer system.

References

1) T. Takagi, A. Tanaka, S. Maeda, S. Matsuo, H. Fujiwara, and Y. Sasaki, *Bull. Chem. Soc. Jpn.*, **59**, 1317 (1986).

2) B. Pullman, J.-L. Coubeils, Ph. Courriere, and J.-P. Gervois, *J. Med. Chem.*, **15**, 17 (1972).

3) H. Chuman and A. Tomonaga, "Structure-activity Relationships-Quantitative Approaches. The Applications to Drug Design and Mode-of-Action Studies," ed by T. Fujita, Nankodo, Tokyo (1982), p. 277.

4) D. Hudson, R. Sharpe, and M. Szelke, *Int. J. Peptide Res.*, **15**, 122 (1980).

5) B. Pullman, "Molecular and Quantum Pharmacology (Proceedings of the 7th Jerusalem Symposium)," ed by E. D. Bergmann and B. Pullman, D. Reidel Publishing Company, Dordrecht (1975), p. 9; B. Pullman, "Environmental Effects on Molecular Structure and Properties (Proceedings of the 8th Jerusalem Symposium)," ed by B. Pullman, D. Reidel Publishing Company, Dordrecht (1976), p. 55.

6) J. D. Deupree and R. H. Kennedy, *Biochim. Biophys. Acta*, **582**, 470 (1979).

7) D. C. U'Prichard and S. H. Snyder, *Life Sci.*, **20**, 527 (1977); D. C. U'Prichard and S. H. Snyder, *J. Biol. Chem.*, **252**, 6450 (1977); D. B. Bylund and S. H. Snyder, *Mol. Pharmacol.*, **12**, 568 (1976).

8) M. J. S. Dewar and W. Thiel, *J. Am. Chem. Soc.*, **99**, 4899, 4907 (1977).

9) W. Thiel, QCPE #353; Y. Beppu and I. Ninomiya, QCPE #409.

10) M. J. S. Dewar, QCPE #455.

11) L. Cassidei and O. Sciacovelli, QCPE #458.

12) A. Podder, J. K. Dattagupta, N. N. Saha, and W. Seanger, *Acta Crystallogr., Sect. B*, **35**, 649, (1979).

13) R. R. Ison, P. Partington, and G. C. K. Roberts, *Mol. Pharmacol.*, **9**, 756 (1973).

14) D. J. Cram and F. A. A. Elhafez, *J. Am. Chem. Soc.*, **74**, 5828 (1952); D. H. Barton, *Experimentia*, **6**, 316 (1950).

15) T. Takagi, A. Tanaka, S. Matsuo, H. Maezaki, M. Tani, H. Fujiwara, and Y. Sasaki, *J. Chem. Soc., Perkin Trans. 2*, **1987**, 1015.

16) Y. Iitaka, Y. Kodama, K. Nishihata, and M. Nishio, *J. Chem. Soc., Chem. Commun.*, **1974**, 389; K. Nishihata and M. Nishio, *Tetrahedron Lett.*, **1977**, 1041; M. Hirota, Y. Takahashi, M. Nishio, and K. Nishihata, *Bull. Chem. Soc. Jpn.*, **51**, 2358 (1978); M. Hirota, K. Abe, H. Tashiro, and M. Nishio, *Chem. Lett.*, **1982**, 777; M. Nishio, *Kagaku No Ryoiki*, **31**, 998 (1977); M. Nishio, *ibid.*, **33**, 422 (1979); M. Nishio, *ibid.*, **37**, 243 (1983); Y. Kodama, K. Nishihata, M. Nishio, and N. Nakagawa, *Tetrahedron Lett.*, **1977**, 2105.

17) K. Morokuma, *J. Chem. Phys.*, **55**, 1236 (1971); K. Kitaura and K. Morokuma, *Int. J. Quant. Chem.*, **10**, 325 (1976).

18) G. A. Neville, R. Deslauriers, B. J. Blackburn, and I. C. P. Smith, *J. Med. Chem.*, **14**, 717 (1970); S. Sternhell, *Quart. Rev.*, **23**, 247 (1969).

 © 1988 The Chemical Society of Japan Bull. Chem. Soc. Jpn., 61, 333—339 (1988)

Relationship between Solubility and Micellization of Surfactants; Micelle Temperature Range (MTR) Instead of Krafft Point

Yoshikiyo Moroi* and Ryohei Matuura
Department of Chemistry, Faculty of Science, Kyushu University, Higashi-ku, Fukuoka 812
(Received June 5, 1987)

In order to clarify the relation between the solubility and micellization of surfactants, the micellar temperature range (MTR) is proposed instead of the usually used Krafft point. The physicochemical meaning of cmc defined by Phillips was examined from a mathematical point of view. As a result, it became clear that the temperature range for MTR is based on the concentration range for cmc, which in turn results from the polydispersity of micelles. The mass-action model of multiple association can be used to explain these facts. The MTR, thus determined by solubility and by cmc, was found to be able to explain a leveling of the MTR for homologous surfactants with an increase of the alkyl chain length and its increase of sodium dodecyl sulfate with increasing concentration of added sodium chloride.

In a previous paper,[1] the authors discussed the dissolution, micellization of surfactants, and solubilization in their aqueous solution from the viewpoint of degrees of freedom based on the phase rule and reached the conclusion that the mass action model for micelle formation can perfectly elucidate the above phenomena of surfactant solutions. It was also found from a series of studies on anionic surfactants with divalent cationic gegenions[2-5] that the Krafft point is not a single point but is a diffuse temperature range which might be called the micelle temperature range (MTR) or the Krafft range.[3] That is, the MTR is a narrow temperature range over which the surfactant solubility as monomer becomes sufficiently high for monomers to start micellization notably; it is consistent with the mass-action model of micelle formation.

Up to now, two concepts have been reported concerning the Krafft point: one is a phase transition at the Krafft point and the other is a solubility increase up to the cmc for micellization at the Krafft point. Recent examples of the former concept are a melting point model of hydrated surfactant solid,[6,7] and the phase transition from a stable coagel to a composite state of gel and micelles.[8] As for the latter, the most direct approach to the Krafft point absolutely rests on the solubility and cmc measurements of surfactants with temperature, as was often pointed out in our preceding papers. From the measurements, the concept of the Krafft point can be made clear.

The authors have studied the effects of both the alkyl chain length of a surfactant ion[3] and the extent of charge separation of divalent genenion on dissolution and micelle formation[5] of surfactants and have concluded that the Krafft point should be replaced by the new term "MTR" of surfactants, which is physicochemically correct. In this study, the technical terms and concepts which had been presented in order to relate the dissolution of surfactants with their micellization are reviewed. Also, it is confirmed that the term "MTR" can be used to successfully elucidate various phenomena concerning the dissolution and micellization of surfactants, not only from a view point of the phase rule but also experimentally.

Progress of Concepts of the Krafft Point

Since 1895, Krafft and Wiglow[9] have worked with soap solutions and have used the term "Ausscheidungstemperatur" which means the temperature at which a new phase separates from the soap solutions upon cooling, colloid chemists have studied the problem with deep concern. Above all, McBain and Elford[10] have studied the potassium oleate-water system and drew a phase diagram in which the minimum temperature at which heterogeneous systems just turned into a homogeneous isotropic liquid was recorded. Also, Lawrence[11] in 1935 called this transition temperature the "Krafft point" for the first time and showed that the Krafft point represents a phase change of the adhesion between hydrocarbon chains throughout the micelle (from solid to liquid). Shinoda and Hutchinson[6]

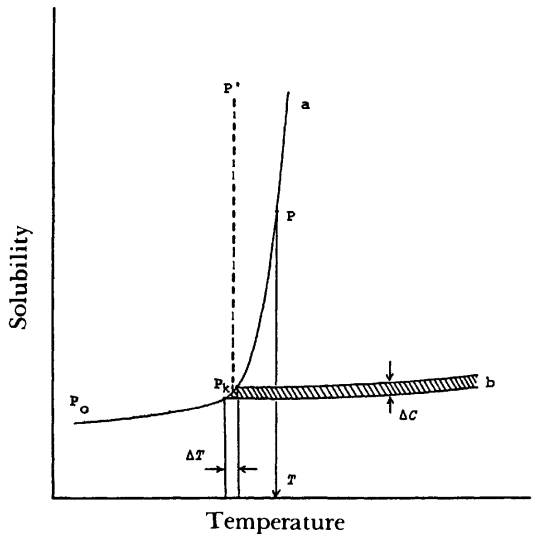

Fig. 1. Changes of solubility and cmc with temperature: (a) solubility curve, (b), cmc curve, ΔC narrow concentration range of cmc, ΔT narrow temperature range of MTR, $P_o \rightarrow P_k \rightarrow P'$ solubility for phase separation model.

presented an interpretation that the Krafft point represented a freezing of micelles or the melting point of a hydrated solid of surfactants; they said "the Krafft point now can be interpreted as a point at which solid hydrated agent and micelles are in equilibrium with monomers: in terms of phase, with two components the equilibrium hydrated solid⇄monomers⇄micelles is univariant, so that at given pressure the point is fixed."

On the other hand, in 1951 Eggenberger and Harwood[12] performed conductometric studies on the solubility and micelle formation of dodecylammonium chloride and found a point on the solubility curve corresponding to a very sharp break in the solubility vs. temperature curve which could be attributed to the "Krafft effect" or a solubilization of the undissociated molecule by the micelle. Significantly, the cmc vs. temperature curve intersected the precipitation curve at this point. Thereafter, a view of the Krafft point seemed to have been established as described in a paper by Phillips,[13] in which the Krafft point was defined as the temperature at which the cmc is equal to the saturation solubility. Alexander and Johnson[14] interpreted the "Krafft phenomenon" as an unusual property in that the solubility of soaps increased enormously over a small temperature range (Krafft point). Other technical terms, "critical solution temperature (cst)[15]" and "critical micellar temperature (cmt),[16]" appeared to designate this characteristic phenomenon.

As mentioned in the above review, the concept of the Krafft point can be divided into two different aspects: a phase transition of solid surfactant and a solubility increase up to cmc for micellization. Then, the Krafft point becomes a definite temperature, a point, for the former concept and a small temperature range for the latter. The existence of two different views concerning the same phenomenon is quite confusing. Therefore, it is very necessary to solve the present conflict.

Physicochemical Meaning of Critical Micelle Concentration (cmc)

The striking characteristic of a surfactant solution is the fact that monomeric surfactant molecules aggregate to form micelles above a certain concentration, leading to an abrupt change in such solution properties as the surface tension, osmotic pressure, intensity of scattered light, electrical conductivity, and so on. The narrow concentration range for these changes is called the critical micelle concentration.[17,18] There have been reported a number of methods for determining the cmc, all of which, of course, depend on abrupt changes in the concentration dependence of several properties of surfactant solutions. Taking the changes into consideration, Phillips defined the cmc as being the concentration corresponding to the maximum change in the gradient in the property-concentration (ϕ–C_t) curve:[13]

$$\left(\frac{d^3\phi}{dC_t^3}\right)_{C_t=cmc} = 0 \quad (1)$$

where

$$\phi = \alpha[S] + \beta[M] \quad (2)$$

α and β are proportionality constants, and [S] and [M] are the concentrations of the monomeric surfactant and the micelle, respectively. In reality, however, the property of a solution can not be expressed so simply as in Eq. 2, although Eq. 1 is correct.

Suppose that a surfactant molecule ($G_{\nu_g}S_{\nu_s}$) is composed of ν_g counterions (G) with charge z_g and ν_s surfactant ions (S) with charge z_s. For the electrical neutrality condition to be satisfied,

$$z_g\nu_g + z_s\nu_s = 0 \quad (3)$$

As is well-known, micelles are not monodisperse but polydisperse; thus, the following equilibria between counterions and surfactant ions can be given for micellization:

$$\begin{aligned} m_1G + n_1S &\overset{K_1}{\rightleftharpoons} M_1 \\ m_2G + n_2S &\overset{K_2}{\rightleftharpoons} M_2 \\ &\cdots\cdots\cdots\cdots \\ m_iG + n_iS &\overset{K_i}{\rightleftharpoons} M_i \end{aligned} \quad (4)$$

Also, the electroneutrality of a solution holds:

$$z_g[G] + z_s[S] + \sum_i (z_g m_i + z_s n_i)[M_i] = 0 \quad (5)$$

where the brackets refer to the concentration of chemical species. From Eq. 4 the micellization constant can be written as

$$K_i = [M_i]/([G]^{m_i}[S]^{n_i}) \quad (6)$$

It is important at present to examine the number of degrees of freedom using Gibbs' phase rule ($f = C-P+2-r$) for the succeeding discussion. The total number of components (C) is $i+3$ (solvent, G, S, M_1, M_2, $\cdots$ M_i), the number of phases (P) is one (surfactant solution), and the number of equilibrium equations (r) is $i+1$ (Eqs. 5 and 6). Therefore, the degrees of freedom becomes three, and the total surfactant concentration (C_t) determines the concentrations of every chemical species at constant temperature and pressure. The mass balance for the counterion and surfactant ion can be expressed, respectively, as

$$\nu_g C_t = [G] + \sum_i m_i[M_i] \quad (7)$$

$$\nu_s C_t = [S] + \sum_i n_i[M_i] \quad (8)$$

From an analogy with Eq. 2 the solution property (ϕ) becomes a composite of the contributions from every chemical species:

$$\phi = \alpha_1[S] + \alpha_2[G] + \sum_i \beta_i[M_i] \quad (9)$$

where α_1, α_2, and β_i are the contribution factors of each chemical species. Their magnitudes depend on the solution properties used for a cmc determination. The solvent contribution is omitted here, since the surfac-

tant concentration is relatively small and the solution property without a solvent contribution is usually employed. Equations 8 and 9 can be rewritten in terms of the concentrations of the monomeric surfactant ion and counterion with the help of Eq. 6;

$$\nu_s C_t = [S] + \sum_i n_i K_i [G]^{m_i} [S]^{n_i} \quad (10)$$

$$\phi = \alpha_1 [S] + \alpha_2 [G] + \sum_i \beta_i K_i [G]^{m_i} [S]^{n_i} \quad (11)$$

From Eqs. 6, 7, 8, and 10, C_t and ϕ turn out to be functions of common variable [S] or [G]. The next step for a cmc determination is to obtain a solution of Eq. 1, in which the derivative of ϕ with respect to C_t can be calculated through a common variable [S]. Then, cmc (C_t) can be automatically determined from the [S] value thus determined. What must be stressed here is that the cmc value determined as a solution of Eq. 1 is a function of the contribution factors: α_1, α_2, and β_i. In other words, cmc depends on the solution property employed for a cmc determination and is naturally different, depending on a method used. Therefore, the cmc turns out to have a value with a narrow concentration range. As a matter of fact, the cmc values obtained from the solution properties mainly due to a monomeric surfactant contribution are less than those due to a surfactant micelle contribution,[17,18,19] as can be seen in Figs. 2a and 2b. In this case random errors are taken into account for the cmc determination methods. For example, the cmc from the surface tension is less than that from turbidity.[20] Contrary to the above expectation, however, the cmc has often come to be presented as a definite concentration,[21,22] especially after the appearance of a phase-separation model for micellization.[6] It is pertinent to

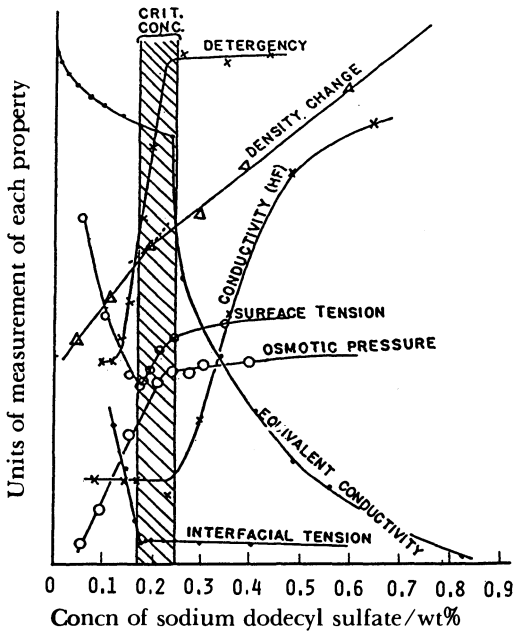

Fig. 2a. Physical property curves for sodium dodecylsulfate. Temperature=25—38°C.[17]

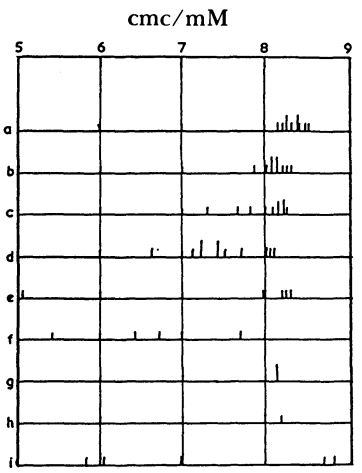

Fig. 2b. Variation of cmc of sodium dodecyl sulfate at temperature between 20 and 30°C by various experimental methods.[19] a) Specific conductivity, b) equivalent conductivity, c) other conductance, d) surface tension vs. logarithm of concentration, e) other relationships between surface tension and concentration, f) absorbance, g) solubilization of OT dye, h) light scattering, i) other methods such as refractive index, emf, vapor pressure, sound velocity, and viscosity.

demonstrate in this paper, therefore, the fact that the cmc can vary for a narrow concentration range in terms of the above discussion.

Monodisperse Micelle of Nonionic Surfactant. The most simplified example is monodisperse micelle of a nonionic surfactant, in which $\nu_g=0$, $z_s=0$, and $n_i=n$. Then, Eqs. 10 and 11 become, respectively,

$$C_t = [S] + nK_n[S]^n \quad (12)$$

and

$$\phi = \alpha[S] + \beta K_n [S]^n. \quad (13)$$

The third derivative of ϕ with respect to C_t becomes

$$\frac{d^3\phi}{dC_t^3} = (\beta - \alpha n)\, n(n-1) K_n [S]^{n-3} \times \{(n-2)(1+n^2 K_n [S]^{n-1}) - 3n^2(n-1)K_n[S]^{n-1}\} / (1+n^2 K_n [S]^{n-1})^5. \quad (14)$$

The solution of $d^3\phi/dC_t^3=0$ gives

$$[S] = \left\{\frac{n-2}{(2n^3-n^2)K_n}\right\}^{1/(n-1)} \quad (15)$$

and

$$C_t = \left\{\frac{n-2}{(2n^3-n^2)K_n}\right\}^{1/(n-1)} \times \frac{2n^2-2}{2n^2-n}. \quad (16)$$

The two important implications of the above are (1) cmc (C_t) does not depend on the contribution factors and (2) the micellization constant (K_n) can be estimated in terms of the values of cmc and the aggregation number of the micelle. The former clear-cut result

Table 1. Micellization Constant (K_n) of Nonionic Surfactants of Oxyethylene Type Based on Monodisperse Micelle

Lipophile	Oxyethylene unit	cmc / μmol dm^{-3}	n	log K_n
1-Dodecanol[24]	8	110	123	478
	12	93	81	318
	18	83	51	200
	23	91	40	154
Nonylphenol[25]	15	110	80	309
	20	140	62	231
	30	185	44	157
	50	280	20	65
1-Tridecanol[26]	10	125	88	335
	15	150	38	138
	22	196	28	97

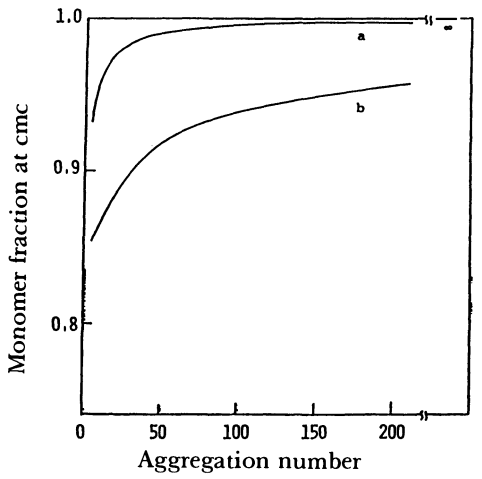

Fig. 3. Monomer fraction at cmc with aggregation number for monodisperse micelle of nonionic surfactant: a Eq. 17, b Eq. 18.

arises from the monodispersity of micelles, and cmc becomes independent of the method used for a cmc determination. In Table 1 are given many K_n values evaluated using Eq. 16 for nonionic surfactants of the oxyethylene type whose cmc and aggregation number are known.[23-26] As expected, K_n values increase with increasing aggregation number. From Eqs. 15 and 16 the fraction of nomomeric surfactants against the total surfactant concentration at cmc becomes

$$\frac{[S]}{C_t} = 1 - \frac{n-2}{2n^2-2}. \tag{17}$$

This fraction is illustrated against n in Fig. 3. On the other hand, Desnoyers et al. have already and independently presented the monomer fraction at the cmc and obtained a different expression from the same standpoint; he derived it in terms of the second derivative of the monomer fraction with respect to the total surfactant concentration.[27] However, the reason why the cmc can be defined as the total concentration at an inflection point of the monomer fraction is not clear. The fraction by Desnoyers,

$$\frac{[S]}{C_t} = \frac{n}{n-1} \times \{1 - (1/2n)^{1/2}\}, \tag{18}$$

is also shown in Fig. 3. The monomeric fraction has been found to be more than 99% at the cmc for the usual nonionic surfactant micelles with aggregation numbers greater than 50.

Monodisperse Micelle of Ionic Surfactant. Next, we consider the monodisperse micelle of an ionic surfactant. From the electroneutrality of a solution (eq. 5), the micelle concentration $[M_n]$ becomes

$$[M_n] = K_n[S]^n[G]^m = -x[S] - y[G] \tag{19}$$

where

$$x = z_s/(z_g m + z_s n) \tag{20}$$

and

$$y = z_g/(z_g m + z_s n) \tag{21}$$

Then, the equations corresponding to Eqs. 10 and 11 read, respectively, as

$$\nu_s C_t = (1-nx)[S] - ny[G] \tag{22}$$

and

$$\phi = (\alpha_1 - \beta x)[S] + (\alpha_2 - \beta y)[G] \tag{23}$$

The third derivative of ϕ with respect to C_t can likewise be obtained as

$$\frac{1}{\nu_s^3}\frac{d^3\phi}{dC_t^3} = (\alpha_2 - \beta y - \alpha_2 nx - \alpha_1 ny + 2\beta nxy) \times \{G'''(1 - nx - nyG') - 3nyG''^2\}/(1 - nx + nyG')^5 \tag{24}$$

where G′, G″, and G‴ are, respectively, the first, second, and third derivatives of [G] with respect to [S]. The solution then becomes

$$G'''(1 - nx + nyG') - 3nyG''^2 = 0 \tag{25}$$

In this case, too, the monomer concentration at the cmc turns out not to include any contribution factor at all. Hence, it becomes evident that the cmc theoretically does not depend on the method of cmc determination, regardless of whether an ionic or nonionic micelle is considered, as long as micelles are monodispersed. Experimentally, however, there must be random errors for the cmc values. In other words, the cmc values coincide with one another, independent of the cmc determination method, whether it is based on a solution property due to the surfactant monomer or due to the micelle. In reality, however, cmc's have been determined within a narrow concentration range.[18] This experimental fact means that the micelles formed in a surfactant solution are not monodisperse but, rather, polydisperse.

Polydisperse Micelle of Nonionic Surfactant. Now

that monodisperse micelles have been considered, the succeeding discussion should be about polydisperse micelles. Consider the simplest example in which micelles having only two kinds of aggregation numbers (n_1 and n_2) are formed in a solution. In this case, Eqs. 10 and 11 become, respectively,

$$C_t=[S]+n_1K_1[S]^{n_1}+n_2K_2[S]^{n_2} \quad (26)$$

and

$$\phi=\alpha_1[S]+\beta_1K_1[S]^{n_1}+\beta_2K_2[S]^{n_2} \quad (27)$$

Thus, from Eqs. 26 and 27,

$$\frac{d^3\phi}{dC_t^3}=N/(1+n_1^2K_1[S]^{n_1-1}+n_2^2K_2[S]^{n_2-1})^5, \quad (28)$$

where the numerator is given by

$$\begin{aligned}N &=(\beta_1-\alpha_1n_1)n_1(n_1-1)K_1[S]^{n_1-3}\times\{n_1-2\\ &+n_1^2(1-2n_1)K_1[S]^{n_1-1}\\ &+n_2^2(1+n_1-3n_2)K_2[S]^{n_2-1}\}\\ &+(\beta_2-\alpha_1n_2)n_2(n_2-1)K_2[S]^{n_2-3}\times\{n_2-2\\ &+n_1^2(1-3n_1+n_2)K_1[S]^{n_1-1}+n_2^2(1-2n_2)K_2[S]^{n_2-1}\}\\ &+n_1n_2(n_1-n_2)(\beta_1n_2-\beta_2n_1)K_1K_2[S]^{n_1+n_2-4}\\ &\times\{n_1+n_2-3+n_1^2(-2n_1+n_2)K_1[S]^{n_1-1}\\ &+n_2^2(n_1-2n_2)K_2[S]^{n_2-1}\} \quad (29)\end{aligned}$$

It turns out from Eq. 29 that the monomer concentration [S] satisfying $d^3\phi/dC_t^3=0$ depends on the contribution factors: α_1, β_1, and β_2. That is, the cmc value (C_t) obtained from the monomer concentration depends on a method for cmc determination. Thus, the cmc difference due to the method of determination is a systematic difference, just as systematic errors are different from random errors. The micelle aggregation number in a real system is much more dispersed than in the present case: two kinds of aggregation numbers.[28-33] Therefore, as a matter of fact, the cmc depends on the method used for a cmc determination and the cmc value should be defined as a narrow concentration range. From the above discussion, the relationship between the solubility and the cmc can be schematically illustrated (Fig. 1). The solubility is determined only by the temperature at atmospheric pressure and the cmc is given by a narrow concentration range, even at a specified temperature. As for the phase rule on a solubility curve, an excess surfactant phase coexists in the system and the number of phases becomes two. Thus, the number of degrees of freedom turns out to be two, as should be clear from the above discussion. The temperature determines the concentration of every chemical species at a specified pressure. This fact is in total agreement with the experimental fact that the solubility is determined only by the temperature at atmospheric pressure. For more details, reference to the literature[1] is recommended. The cmc change with temperature, on the other hand, is due to the variation of K_n, α, and β with temperature. As a result, the micelle temperature range (MTR) must be defined as the temperature within a narrow temperature range, for which the solubility vs. temperature curve intersects the cmc range vs. temperature curve although a single temperature within the MTR can be obtained from one cmc determination method. In other words, MTR is determined by balancing between the cmc range and the solubility and by their dependence on the temperature. In this sense, MTR is a phenomenological temperature range rather than a strict physical quantity.

Elucidation of MTR Changes

At present, it is very important to show that some experimental facts can be elucidated by the above definition of MTR, since the validity of the definition should be examined by this approach. The following are two typical examples of MTR changes.

Leveling of MTR for Homologous Surfactants with an Increase in Their Alkyl Chain Length. The Krafft point of homologous ionic surfactants has been reported to increase with an increase in the alkyl chain length of a surfactant ion.[3,34-36] The important feature is that MTR does not increase linearly with the carbon number of an alkyl chain, but with gradual leveling. On the other hand, the logarithms of both the solubility and the cmc decrease linearly with an increase in the carbon number.[3] Of course this applies for cases in which the logarithm of the solubility is less than that of the cmc at low temperature. In addition, the heat of dissolution below MTR becomes more positive with an increasing carbon number of surfactant ions; the rate of solubility increase with temperature is more rapid for a surfactant ion with a longer alkyl chain.[3] On the contrary, the cmc change with temperature is relatively small, irrespective of the alkyl chain length (Fig. 4). From the definition of MTR, in which solubility and cmc curves should intersect each other,

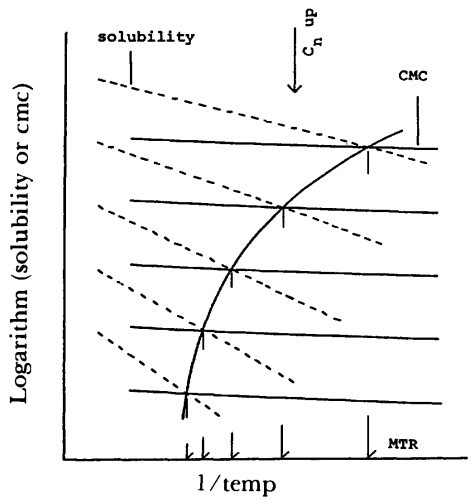

Fig. 4. Schematic illustration of MTR change with increase of carbon number of surfactant ion.

the leveling of MTR is easily understood from the figure.

MTR Increase of Sodium Dodecyl Sulfate (SDS) with Increase of Counterion Concentration. The addition of a salt having an ion in common with a counterion into an ionic surfactant solution leads to both a decrease in the cmc and an increase in the aggregation number of micelles. The presence of excess counterions also leads to a solubility decrease of the surfactant due to the constant solubility product of the counterion and the surfactant ion, as long as an excess surfactant phase coexists in the system, even when the surfactant concentration is above the cmc. Then, an MTR change is expected from an addition of excess salt into the system. In fact, the MTR of sodium dodecylsulfate increases with an increase in the concentration of sodium chloride in the solution. The aim of this section is to elucidate the movement of the MTR to higher temperature from the viewpoint of the present concept as to MTR and to compare the evaluated results with the reported ones.[16]

Let us suppose a monodisperse micelle formation, sicne the mass-action model of a single micellar size has been well applied to ionic surfactants.[37] The relation between the cmc and the counterion concentration then, according to Eq. 6, becomes

$$\ln \text{cmc} = -\frac{m}{n}\ln[\text{G}] - \frac{1}{n}\ln K_n + \frac{1}{n}\ln[\text{M}_n] \qquad (30)$$

since the concentration of the monomeric surfactant ion at the cmc can be replaced by the total surfactant concentration with more than 99% confidence, according to Phillips' definition of cmc.[37] In the usual case ($n > 50$; $K_n \gg [\text{M}_n]$) the last term on the right-hand side is less than a few percent of the constant term of association constant, and Eq. 30 can be well approximated by

$$\ln \text{cmc} = -\frac{m}{n}\ln[\text{G}] + \text{constant}. \qquad (31)$$

Here, m/n is the association degree of gegenion to the micelle. The linear relataionship between ln cmc and ln [G] has been ascertained from a number of experiments; this indicates that the above approximation is correct. The cmc of SDS is 8.4×10^{-3} mol dm^{-3} and m/n was extrapolated to be 0.72—0.75[38] at its MTR (9 °C).[39] The value of the constant was evaluated to be −8.22 and −8.36 for 0.72 and 0.75 of m/n, respectively. On the other hand, the solubility of SDS decreases with an increase in the counterion concentration, while maintaining the solubilty product constant at 9 °C;

$$C(C + C_{\text{Na}^+}) = (8.4\times10^{-3})^2, \qquad (32)$$

where C is the concentration of the surfactant or the solubility. From Eqs. 31 and 32 the difference between ln cmc and ln C at 9 °C can be evaluated at different C_{Na^+} concentrations. A cmc change with temperature

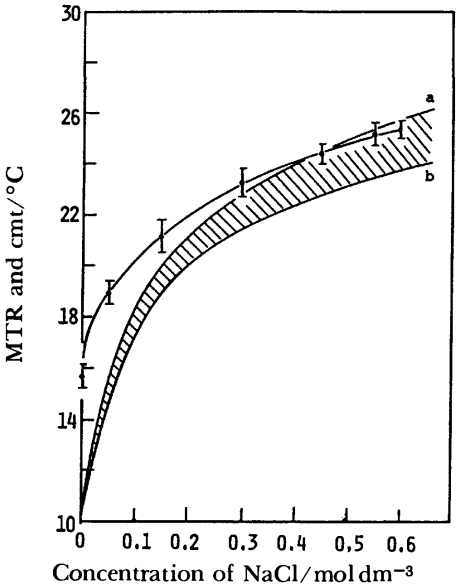

Fig. 5. MTR increase of sodium dodecylsulfate with increase of sodium chloride concentration: ⊖ cmt change, a m/n=0.72, b m/n=0.75.

is negligibly small compared with a solubility change. Then, it can be presumed that the difference ln cmc—ln C can be made zero only by a solubility increase with temperature. Then, MTR is the temperature at which the above difference becomes zero. The heat of dissolution (Δh) is necessary for the present calculation; Δh was estimated to be 50 kJ mol^{-1} from the solubility data of Nakayama and Shinoda.[40] The range of MTR thus obtained from two m/n values, 0.72 and 0.75, is shown in Fig. 5 together with the experimental results. The difference is less than a few degrees between the MTR and the critical micellar temperature (cmt)[16] by Mazer and Benedek; this is quite reasonable, judging from the definition of cmt. In spite of the difference between MTR and cmt, the present agreement can be said to be excellent.

The conclusions reached from the above discussion are (1) the micelle temperature range (MTR) is a better technical term than the Krafft point for expressing the relation between the solubility and micelle formation, (2) MTR can be determined only by balancing between the cmc range and the solubility and their dependence on temperature, and (3) these can be well explained by the mass-action model of micelle formation and the size distribution of micelles.

The work was supported in part by a Grant-in-Aid for Scientific Research from the Ministry of Education, Nos. 60104005 and 60470011.

References

1) Y. Moroi, R. Sugii, and R. Matuura, *J. Colloid Interface Sci.*, **98**, 184 (1984).

2) Y. Moroi, N. Ikeda, and R. Matuura, *J. Colloid Inter-*

face Sci., **101**, 285 (1984).
3) Y. Moroi, R. Sugii, C. Akine, and R. Matuura, *J. Colloid Interface Sci.*, **108**, 180 (1985).
4) R. Matuura and Y. Moroi, "Surfactants in Solution," ed by K. L. Mittal, Plenum Press, New York (1986), Vol. 4, pp. 289—298.
5) Y. Moroi, R. Matuura, T. Kuwamura, and S. Inokuma, *J. Colloid Interface Sci.*, **113**, 225 (1986).
6) K. Shinoda and E. Hutchinson, *J. Phys. Chem.*, **66**, 577 (1962).
7) K. Shinoda, *J. Phys. Chem.*, **85**, 3311 (1981).
8) M. Kodama and S. Seki, *Netsu Sokutei*, **11**, 104 (1984).
9) F. Krafft and H. Wiglow, *Ber. Dtsch. Chem. Ges.* **28**, 2566 (1895).
10) J. W. McBain and W. J. Elford, *J. Chem. Soc.*, **129**, 421 (1926).
11) A. S. C. Lawrence, *Trans. Faraday Soc.*, **31**, 206 (1935).
12) D. N. Eggenberger and H. J. Harwood, *J. Am. Chem. Soc.*, **73**, 3353 (1951).
13) J. N. Phillips, *Trans. Faraday Soc.*, **51**, 561 (1955).
14) A. E. Alexander and P. Johnson, "Colloid Science," Oxford University Press, London (1949), pp. 683—685.
15) K. Kon-no, T. Jin-no, and A. Kitahara, *J. Colloid Interface Sci.*, **49**, 383 (1974).
16) A. M. Mazer and G. B. Benedek, *J. Phys. Chem.*, **80**, 1075 (1976).
17) W. C. Preston, *J. Phys. Chem.*, **52**, 84 (1948).
18) P. Mukerjee and K. J. Mysels, *Natl. Stand. Ref. Data Ser. (U. S., Matl. Bur. Stand.)*, No. 36 (1971).
19) F. Franks, "Water; A Comprehensive Treatise, Vol. 4 Aqueous Solutions of Amphiphiles and Macromolecules," Plenum Press, New Nork (1975), p. 97.
20) P. Debye, *J. Phys. Chem.*, **53**, 1 (1949).
21) H. Lange, *Parfumerie u. Kosmet.*, **46**, 129 (1965).
22) D. J. show, "Introduction to Colloid and Surface Chemistry," Butterworth, London (1970), 2nd ed, p. 65.
23) P. Becher, "Nonionic Surfactants," ed by M. J. Schick, Marcel Dekker, New York (1967), Chap. 15, pp. 478—515.
24) P. Becher, *J. Colloid Sci.*, **16**, 49 (1961).
25) M. J. Schick, S. M. Atlas, and F. R. Eirich, *J. Phys. Chem.*, **66**, 1326 (1962).
26) P. Becher, "Proc. 4th Intern. Cong. on Surface Active Substances," Brussels 1964, ed by J. Th. G. Overbeek, Vol. 2, p. 621.
27) J. E. Desnoyers, G. Caron, R. DeLisi, D. Roberts, A. Roux, and G. Perron, *J. Phys. Chem.*, **87**, 1397 (1983).
28) Y. Moroi and R. Matuura, *J. Phys. Chem.*, **89**, 2923 (1985).
29) D. C. Poland and H. A. Scheraga, *J. Phys. Chem.*, **69**, 2431 (1965).
30) C. Tanford, *J. Phys. Chem.*, **78**, 2469 (1974).
31) P. Mukerjee, "Micellization, Solubilization, and Microemulsions," Vol. 1, ed by K. L.Mittal, Plenum Press (1977), p. 171.
32) E. Ruckenstein and R. Nagarajan, *J. Phys. Chem.*, **85**, 3010 (1981).
33) A. Ben-Naim and F. H. Stillinger, *J. Phys. Chem.*, **84**, 2872 (1980).
34) H. Lange and M. J. Schwuger, *Kolloid Z. und Z. Polym.*, **223**, 145 (1967).
35) K. Ogino and Y. Ichikawa, *Bull. Chem. Soc. Jpn.*, **49**, 2683 (1976).
36) M. Saito, Y. Moroi, and R. Matuura, *J. Colloid Interface Sci.*, **88**, 578 (1982).
37) Y. Moroi, *J. Colloid Interface Sci.*, accepted for publication.
38) Y. Moroi, N. Nishikido, H. Uehara, and R. Matuura, *J. Colloid Interface Sci.*, **50**, 254 (1975).
39) Y. Moroi, T. Oyama, and R. Matuura, *J. Colloid Interface Sci.*, **60**, 103 (1977).
40) H. Yamanaka and K. Shinoda, *Bull. Chem. Soc. Jpn.*, **40**, 1797 (1967).

 © 1988 The Chemical Society of Japan Bull. Chem. Soc. Jpn., 61, 341—345 (1988)

The Preparation of Organo Colloidal Precious Metal Particles

Kenjiro MEGURO, Makoto TORIZUKA, and Kunio ESUMI*
Department of Applied Chemistry, Institute of Colloid and Interface Science, Science University of Tokyo, Kagurazaka, Shinjuku-ku, Tokyo 162
(Received June 17, 1987)

Platinum particles were prepared by reducing the hydrogen hexachloroplatinate extracted in organic solvents from an aqueous solution by these extractants:dioctadecyldimethylammonium chloride(DDAC), trioctylmethylammonium chloride(TMAC), and trioctylphosphine oxide(TOPO). The extraction ratio of platinum(IV) increased in chloroform, isobutyl methyl ketone, and cyclohexane with an increase in the concentrations of the extractants, and then approached a constant state. The extracts were reduced by formaldehyde or benzaldehyde in the presence of water and a base (sodium hydroxide or triethylamine) for several hours at 65 °C. The platinum particles obtained in chloroform and isobutyl methyl ketone were very stable; their diameters were 15—25 Å.

The preparation of colloidal metals has long been studied extensively.[1-4] Recently, many investigations of the preparation of particles have concentrated upon precious metals because of their many applications, e.g., as catalysts.[5,6] The greater part of the experiments have been made in an aqueous solution in the presence of surfactants or polymers in order to stabilize the colloidal particles.[5-7] Further, it has been reported[8,9] that the precious metal particles can be prepared in water in oil microemulsions. However, there have been only a few reports on the preparation of precious metal particles in organic solvents, since the solubility of most particle precursors is very low in organic solvents.

On the other hand, metal salts can be transferred into organic solvents by means of solvent extraction.[10-13] This method allows precious metal salt to be extracted in organic solvents as particle precursors of organic precious metal.

The aim of the present work was to prepare platinum metal particles from their salts extracted into organic solvents.

Experimental

Materials. Hexachloroplatinic(IV) acid was supplied by Tanaka Kikinzoku Kogyo K.K. as a hexahydrate ($H_2PtCl_6 \cdot 6H_2O$). As extractants, dioctadecyldimethylammonium chloride (DDAC), trioctylmethylammonium chloride (TMAC), and trioctylphosphine oxide (TOPO) were employed. The DDAC was obtained from the Lion Co., Ltd., and was purified once by recrystallization from 2-propanol. The TMAC and TOPO were commercial, extra pure grades from the Tokyo Chemical Industry Co., Ltd., and were used without further purification. The other chemicals were commercial, extra pure grades from Wako Pure Chemical Industries, Ltd. The water used in this experiment was deionized by means of the MILLI-Q Water Purification System.

Procedure. For the extraction, two kinds of solutions were mixed; one was a 10 ml aqueous solution of 0.5 mmol dm^{-3} hexachloroplatinic(IV) acid, while the other was 0—3.0 mmol dm^{-3} of the extractant in chloroform, isobutyl methyl ketone (MIBK), or cyclohexane (in the case of TOPO, 0—2.0 mol dm^{-3} HCl was used). Then, the mixed solution was shaken at 25°C for 12 h to attain an equilibrium of extraction. After the extraction, the concentration of platinum(IV) remaining in the aqueous solution was determined photometrically by means of the tin chloride method. The extraction ratio was calculated from the difference between the initial concentration of Pt(IV) and that remaining in the aqueous phase.

In order to obtain Pt particles, each of the platinum(IV) salts extracted in an organic solvent was directly reduced by several reductants: formaldehyde, benzaldehyde in the presence of sodium hydroxide, triethylamine (TEA) and water, hydrazine, and hydrogen (through bubbling). The subsequent refluxing of the solution under nitrogen gas on a water bath (65 °C) between 15 min and 10 h gave a homogeneous dark brown solution of platinum sols.

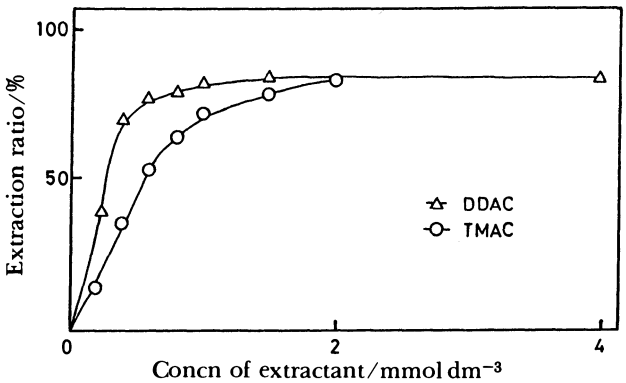

Fig. 1. Effect of concentration of DDAC and TMAC in chloroform on the extraction of platinum(IV).

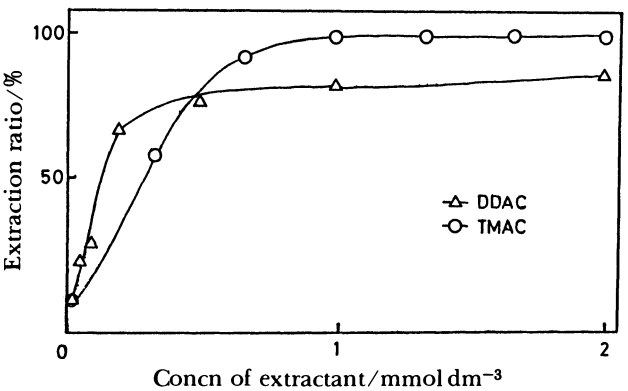

Fig. 2. Effect of concentration of DDAC and TMAC in MIBK on the extraction of platinum(IV).

The Pt-particle sizes were determined by means of transmission electron microscopy with a Hitachi H-800 microscope. The magnification of the electron microscope was 70000—200000. The particle size distribution and the average diameter of the Pt particles were obtained on the basis of these enlarged electron-microscope photographs.

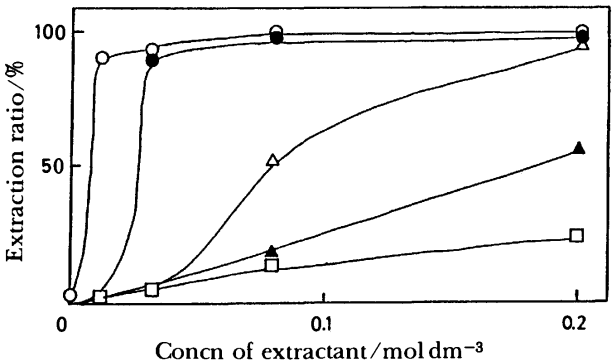

Fig. 3. Effect of concentration of TOPO in cyclohexane on the extraction of platinum(IV): HCl concentration; (□) 0, (▲) 0.1, (△) 0.5, (●) 1.0, (○) 2.0 mol dm^{-3}.

Results and Discussion

The effect of the extractant concentration on the transfer of platinum(IV) salt to an organic solvent was studied. The efficiency of extraction is usually defined as the ratio of the platinum(IV) concentration in an organic solvent against the total platinum(IV) concentration: This is named the "extraction ratio." The extraction ratios of platinum(IV) to chloroform by

Table 1. Properties of Precursors of Platinum Sols by Extraction

Initial concn of Pt	Extractant and concn	Organic solvent	Extraction ratio	Concn of Pt in organic phase
mmol dm^{-3}	mmol dm^{-3}		%	mmol dm^{-3}
0.5	DDAC 1.5	Chloroform	83.6	0.42[D/C]
	TMAC 2.0		82.6	0.42[T/C]
	DDAC 0.5	MIBK	77.0	0.39[D/M]
	TMAC 1.0		98.6	0.49[T/M]
	TOPO 50	Cyclohexane	99.8	0.50[T/H]

Table 2. Properties of Platinum Sols Prepared in Chloroform

Extractant	Reducing agent	Base/H_2O	Reduction	Dispersion
DDAC	Formaldehyde	—	×	—
		NaOH+H_2O	○	Stable
		TEA+H_2O	○	Stable
	Benzaldehyde	—	×	—
		NaOH+H_2O	○	Stable
		TEA	×	—
		TEA+H_2O	○	Stable
	Hydrazine	—	○	Instable
	Hydrogen	—	×	—
TMAC	Formaldehyde	—	×	—
		NaOH+H_2O	○	Stable
		TEA+H_2O	○	Stable
	Benzaldehyde	—	×	—
		NaOH+H_2O	○	Stable
		TEA	×	—
		TEA+H_2O	○	Stable

○: complete reduction, ×: incomplete reduction.

Table 3. Properties of Platinum Sols Prepared in MIBK

Extractant	Reducing agent	Base/H_2O	Reduction	Dispersion
DDAC	Formaldehyde	—	×	—
		NaOH+H_2O	○	Instable
		TEA+H_2O	○	Instable
	Benzaldehyde	—	×	—
		NaOH+H_2O	○	Instable
		TEA	×	—
		TEA+H_2O	○	Instable
TMAC	Formaldehyde	—	×	—
		NaOH+H_2O	○	Stable
		TEA+H_2O	○	Stable
	Benzaldehyde	—	×	—
		NaOH+H_2O	○	Stable
		TEA	×	—
		TEA+H_2O	○	Stable

○: complete reduction, ×: incomplete reduction.

DDAC and TMAC are plotted against the concentration of the extractant in Fig. 1. It can be seen that the extraction ratios for both extractants increase with an increase in the concentration of the extractant and then approach to a constant state. In the case of DDAC, the extraction ratio reaches above 85% above the concentration of 1.5 mmol dm^{-3}, while the concentration of more than 2 mmol dm^{-3} of TMAC gave a

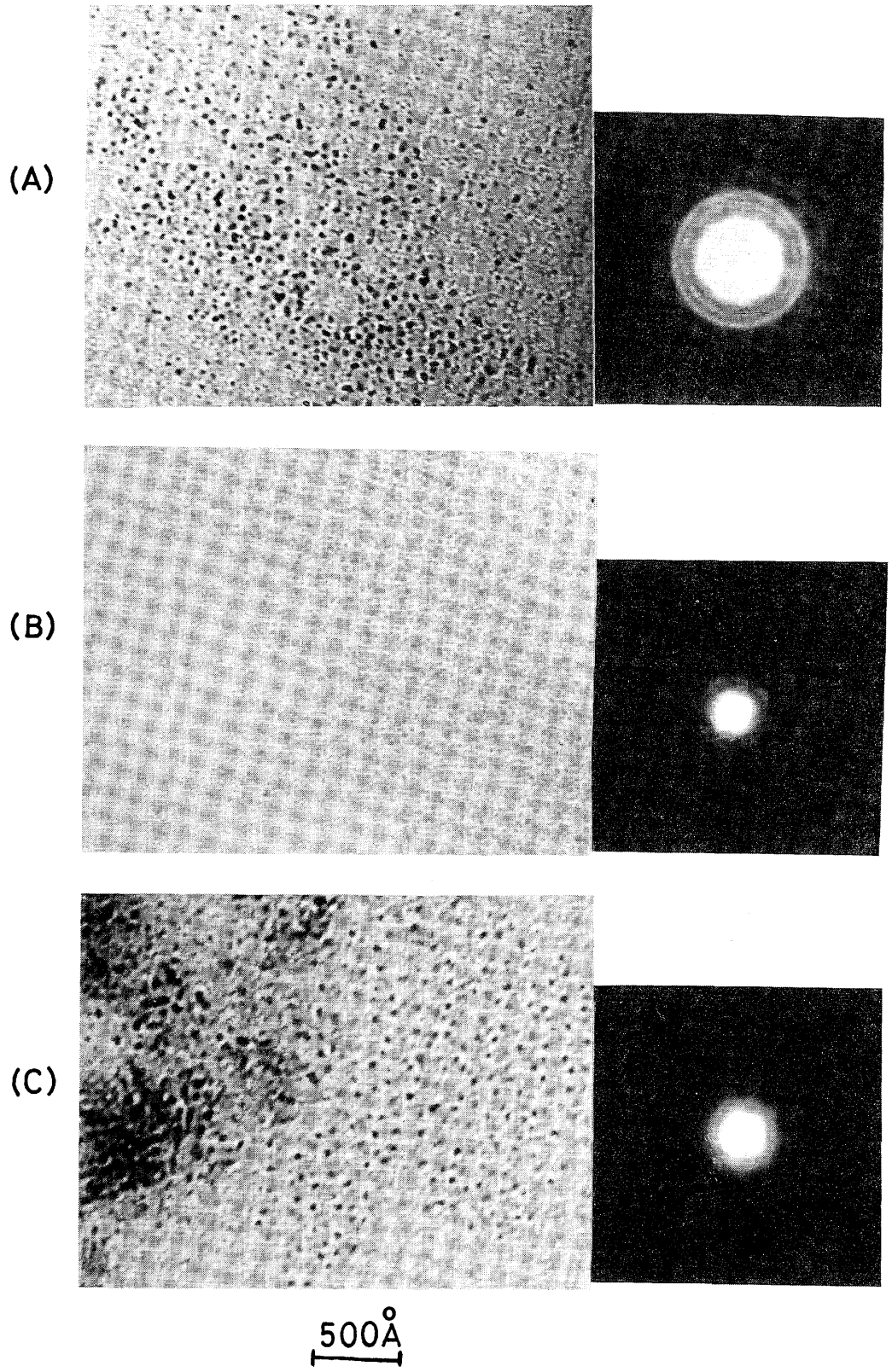

Fig. 4. Electron micrograph and electron diffractogram of platinum sols reduced with formaldehyde from various extracts: (A) D/C, (B) T/M, (C) T/H.

ratio of more than 83%. Similarly, the extraction ratios of platinum(IV) to MIBK by DDAC and TMAC are shown in Fig. 2. When the DDAC and TMAC concentrations were above 1 mmol dm^{-3}, the extraction ratio for the former became more than 80%, while that for the latter was almost 100%. Figure 3 shows the extraction ratio of platinum(IV) in cyclohexane as a function of the concentration of TOPO. It is found that the extraction ratio of platinum(IV) increases with an increase in the concentration of TOPO without any addition of hydrochloric acid, but it is still very low. Upon the addition of hydrochloric acid, however, the extraction ratio increased remarkably: it was almost 100% when the TOPO concentration was 0.05 mol dm^{-3} in the presence of 1.0 mol dm^{-3} hydrochloric acid in water. Thus, it was confirmed that the platinum(IV) salt in an aqueous solution is efficiently transferred to an organic solvent by using adequate extractants.

The particle precursors were prepared under the conditions shown in Table 1. Table 2 shows the conditions of sols preparation from extracts in chloroform and the stability of the sols. The extracts of platinum salt were not reduced by only formaldehyde or benzaldehyde, without any base or water. However, upon the addition of a base and water, very stable Pt sols were obtained. From Table 3 it is apparent that the extracts in MIBK are reduced by formaldehyde or benzaldehyde in the presence of a base and water and that the sols obtained are stable for TMAC, but not for DDAC. In the case of extracts with TOPO in cyclohexane, the sols were also obtained only upon the addition of a base and water, but they were not stable.

The platinum sols particles prepared by the reduction with formaldehyde or benzaldehyde were almost spherical. The extracts obtained by DDAC in chloroform, TMAC in chloroform, DDAC in MIBK, TMAC in MIBK, and TOPO in cyclohexane are abbrevated D/C, T/C, D/M, T/M, and T/H respectively. The electron micrograph and electron diffractogram of particles formed by the reduction of D/C with formaldehyde and sodium hydroxide are shown in Fig. 4(A); their particle-diameter distribution is shown in Fig. 5(A), where the mean particle diameter is 17.5 Å, with a standard deviation of 3.23 Å. Similarly, Figs. 4(B) and 5(B) show the electron micrograph, the electron diffractogram, and the diameter distribution of the platinum particles prepared by the reduction of T/M with formaldehyde and sodium hydroxide; the mean particle diameter was 19.3 Å, with a standard deviation of 3.99 Å. The mean particle diameter of the platinum prepared by the reduction of T/H with formaldehyde and sodium hydroxide was 19.0 Å, and the standard deviation was 4.94 Å, as is shown in Figs. 4(C) and 5(C). The platinum particles prepared by the above method are crystalline, with a diffraction pattern corresponding to the fcc structure of platinum.

The effect of the reaction time on the particle-diameter distribution of the platinum particles produced by the reduction of T/C with benzaldehyde,

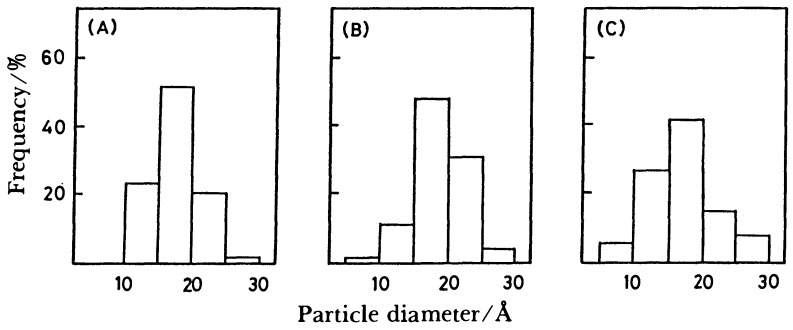

Fig. 5. Particle diameter distribution of platinum sol particle: (A) D/C, (B) T/M, (C) T/H.

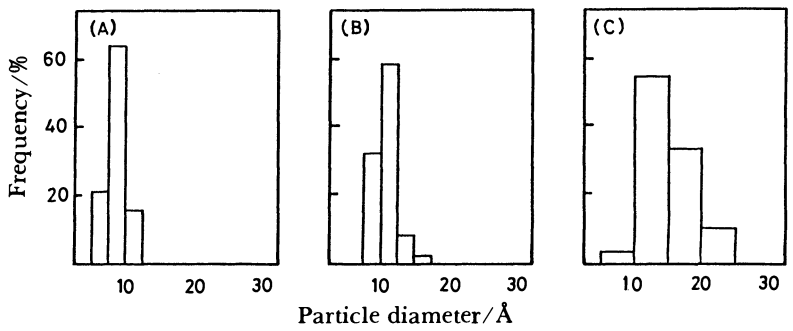

Fig. 6. Particle diameter distribution of platinum sol particles by reduction of T/C with benzaldehyde, triethylamine and water: reaction time; (A) 15, (B) 30, (C) 120 min.

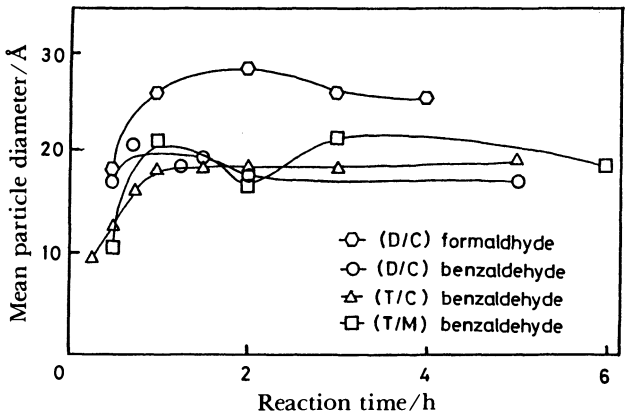

Fig. 7. Relationship between reaction time and mean particle size of platinum sol.

triethylamine, and water was also studied. In Fig. 6 it can be seen that the size of the platinum particles increases with an increase in the reaction time; the mean particle diameters are 8.3, 10.5, and 15.1 Å for 15, 30, and 120 min respectively, while the corresponding deviations are 1.39, 1.62, and 3.07 Å. Further, the plots of the mean particle diameter vs. the reaction time for the four systems are shown in Fig. 7. It is found that the mean particle diameter increases with an increase in the reaction time until about 1 h, and then becomes constant, suggesting that the nucleation of the platinum particle occurs and that the nucleus has grown into a certain constant value during the initial hour. Compared with the reduction of D/C by formaldehyde and benzaldehyde, the former provides larger platinum particles than the latter. This result is, presumably, attributably to the difference between the solubilities of benzaldehyde and formaldehyde in chloroform; benzaldehyde has a higher solubility than formaldehyde.

As a conclusion, it can be said that the preparation of platinum particles in an organic solvent needs water to facilitate the reduction of platinum(IV) with formaldehyde or benzaldehyde. It seems that the reduction of platinum(IV) occurs at the interface between the water and the organic solvent and that the platinum nucleus is produced and grows quickly (in about one hour) at this interface. As a result, platinum particles with diameters in the range of 15—25 Å are obtained. This method can also be used in the preparation of other precious metal particles in organic solvents.

References

1) J. Turkevich, R. C. Stevenson, and J. Hiller, *Discuss. Faraday Soc.*, **11**, 55 (1951).
2) K. Takiyama, *Bull. Chem. Soc. Jpn.*, **31**, 944 (1958).
3) B. V. Enustun and J. Turkevich, *J. Am. Chem. Soc.*, **85**, 3317 (1963).
4) R. M. Wilenzick, D. C. Russell, R. H. Morriss, and S. W. Marshall, *J. Chem. Phys.*, **47**, 533 (1967).
5) H. Hirai, K. Ishihara, and I. Shinohara, *Makromol. Chem. Rapid Commun.*, **2**, 99 (1981).
6) T. Toshima, T. Takahashi and H. Hirai, *Chem. Lett.* **1985**, 1245.
7) J. Kiwi and M. Grätzel, *J. Am. Chem. Soc.*, **101**, 7214 (1979).
8) M. Boutonnet, J. Kizling, and P. Stenius, *Colloids and Surfaces*, **5**, 209 (1982).
9) K. Kurihara, J. Kizling, P. Stenius, and J. H. Fendler, *J. Am. Chem. Soc.*, **105**, 2574 (1983).
10) M. A. Khattak and R. J. Magee, *Talanta*, **12**, 733 (1965).
11) M. J. Cleare, P. Charlesworth, and D. J. Bryson, *J. Tech. Biotechnol.*, **29**, 210 (1979).
12) M. Majski, *J. Radioanal. Chem.*, **46**, 239 (1978).
13) T. Sekine and Y. Hasegawa, *Bunseki*, 1978, 627.
14) I. Maziekien, L. Ermanis and T. J. Walsh, *Anal. Chem.*, **32**, 645 (1960).

The Preparation of Colloidal Precious Metal Particles Using Copolymers of Vinyl Alcohol-*N*-Vinylpyrrolidone

Kenjiro MEGURO, Yukari NAKAMURA, Yoshihiro HAYASHI, Makoto TORIZUKA, and Kunio ESUMI*

Department of Applied Chemistry, Institute of Colloid and Interface Science, Science University of Tokyo, Kagurazaka, Shinjuku-ku, Tokyo 162

(Received June 18, 1987)

Precious metal particles of platinum and silver have been prepared by the reduction of metal salts dissolved in an aqueous solution of a copolymer of vinyl alcohol and *N*-vinylpyrrolidone with methanol. The stable platinum sols were obtained in the presence of poly(vinyl alcohol), poly(*N*-vinylpyrrolidone), and their copolymers, but their particle sizes hardly changed with the ratio of *N*-vinylpyrrolidone in the copolymer. On the other hand, colloidal stable silver sols were obtained only in the presence of a copolymer. Further, with an increase in the ratio of *N*-vinylpyrrolidone in the copolymer, the particle size of silver became small.

Precious metal particles have been attractive as catalysts[1-3] when it is desirable to use fine monodispersed particles. On the preparation of fine particles, precious metal ions have often been reduced in a mixture of precious metal ions, protective colloids, and a reducing agent. As protective colloids, poly(vinyl alcohol), poly(*N*-vinylpyrrolidone), and poly(methyl vinyl ether)[4-9] have been employed. However, homopolymers are not easily adsorbed on precious metal particles, so monodispersed particles are hard to obtain when they are used.

The objective of this work was to prepare fine monodispersed precious metal particles using copolymers of vinyl alcohol-*N*-vinylpyrrolidone.

Experimental

Materials. The $H_2PtCl_6 \cdot 6H_2O$ was supplied by Tanaka Kikinzoku K.K., while the $AgNO_3$ was obtained from the Tokyo Kasei Co. Ltd. The poly(vinyl alcohol)(PVA) and poly (*N*-vinylpyrrolidone)(PVP) were obtained from Kishida Chemicals Co., Ltd., and the Tokyo Kasei Co., Ltd., respectively. As monomers, vinyl acetate (VAc) and *N*-vinylpyrrolidone(VP) were obtained from Wako Chemical Industries: They were distilled under reduced pressure before use. The other chemicals were of extra pure grades. The water used was purified through the Milli-Q Reagent Water System.

Preparation of Copolymers: Mixtures of VAc and VP in various ratios were added to acetone, and the polymerization was carried out under a nitrogen gas atmosphere at 70 °C, using α,α'-azobisisobutyronitrile as the initiator. Then, the products, as purified with petroleum ether, were dissolved into methanol and saponified upon the addition of sodium methoxide at 40 °C under a nitrogen-gas atmosphere. The samples thus obtained were purified with diethyl ether and acetone.

Measurements: The molecular weights of the samples were determined by means of gel permeation chromatography (Japan Optical Co.) with a column of Shodex OH Pak B800P and B804 (Showa Denkou Co.): Pullulan was used as the standard sample, and a mixture of methanol and water (1 : 1) was used as the solvent.

Determination of the Content Ratio of the Copolymer of Vinyl Alcohol-*N*-Vinylpyrrolidone: Some VAc-VP copolymers were dissolved into acetone, and then sodium hydroxide was added for saponification. After the complete saponification, the remaining sodium hydroxide was back-titrated with hydrochloric acid. From the results of a subsequent titration, the ratio of VA-VP in the copolymers was determined.

Preparation of Colloidal Particles: A polymer (7.5—200 mg) as a protective colloid and a metal salt (0.033 mmol dm^{-3}) were dissolved in a mixed solvent consisting of methanol (25 ml) and water (25 ml). The resulting solution was refluxed to prepare a colloidal dispersion of the metal. In the case of silver nitrate, the concentrations ranged between 0.033 and 0.33 mmol dm^{-3}.

The particle sizes of the precious-metal particles obtained were determined by means of transmission electron microscopy with a Hitachi H 800 microscope.

Results and Discussion

Platinum Sol. Figure 1 shows the relationship between the amount of PVP added and the number-average particle size of platinum. When the amount of PVP was 75 mg, the particle size was smallest in the case of the highest molecular weight of PVP. However, upon the addition of 150—200 mg of PVP, the particle size increased with an increase in the molecular weight of PVP. Similar experiments were also carried out in the case of PVA. It was found that the

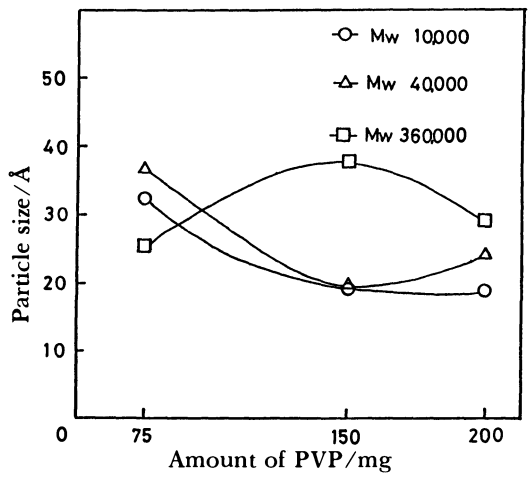

Fig. 1. Mean particle size of platinum sols as a function of molecular weight of PVP.

particle size hardly changed with an increase in the amount of PVA added (M.W.=20000). Further, using PVA (M.W.=88000), stable platinum sols were obtained, but their particle size could not be determined by transmission electron microscopy because extensive coagulation resulted from the evaporation of the solvent from a drop of solution on the support. Accordingly, in order to study the effect of copolymers on the particle size of platinum particles, the molecular weight of the copolymer was controlled to within the range of 30000—60000. The pertinent properties of the copolymers are given in Table 1.

Figure 2 shows the number-average particle size of platinum with the molar ratio of VA or VP in the copolymers. Here, the amount of the copolymers added was 150 mg. From Fig. 2 it can be seen that, except for PVA, the particle sizes of platinum are almost the same for the other copolymers, indicating that the copolymers of VA-VP do not provide a different colloidal protective action from homopolymers (PVA or PVP).

Silver Sol. Keeping constant the amount of copolymers added (150 mg), silver sols were prepared as a function of the amount of silver nitrate. In the case of PVA alone, stable silver sols were not obtained and the

Table 1. Pertinent Properties of Copolymers

Copolymer	Molar ratio in copolymer		Molecular weight
	VA	VP	
A2	0.15	0.85	4.4×10^4
A4	0.35	0.65	6.4×10^4
A8	0.74	0.26	3.1×10^4

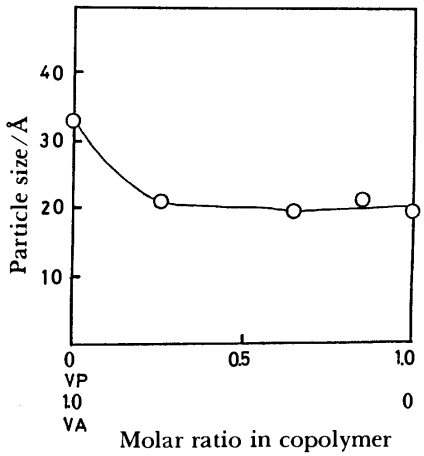

Fig. 2. Mean particle size of platinum sols as a function of molar ratio of VA or VP in copolymers.

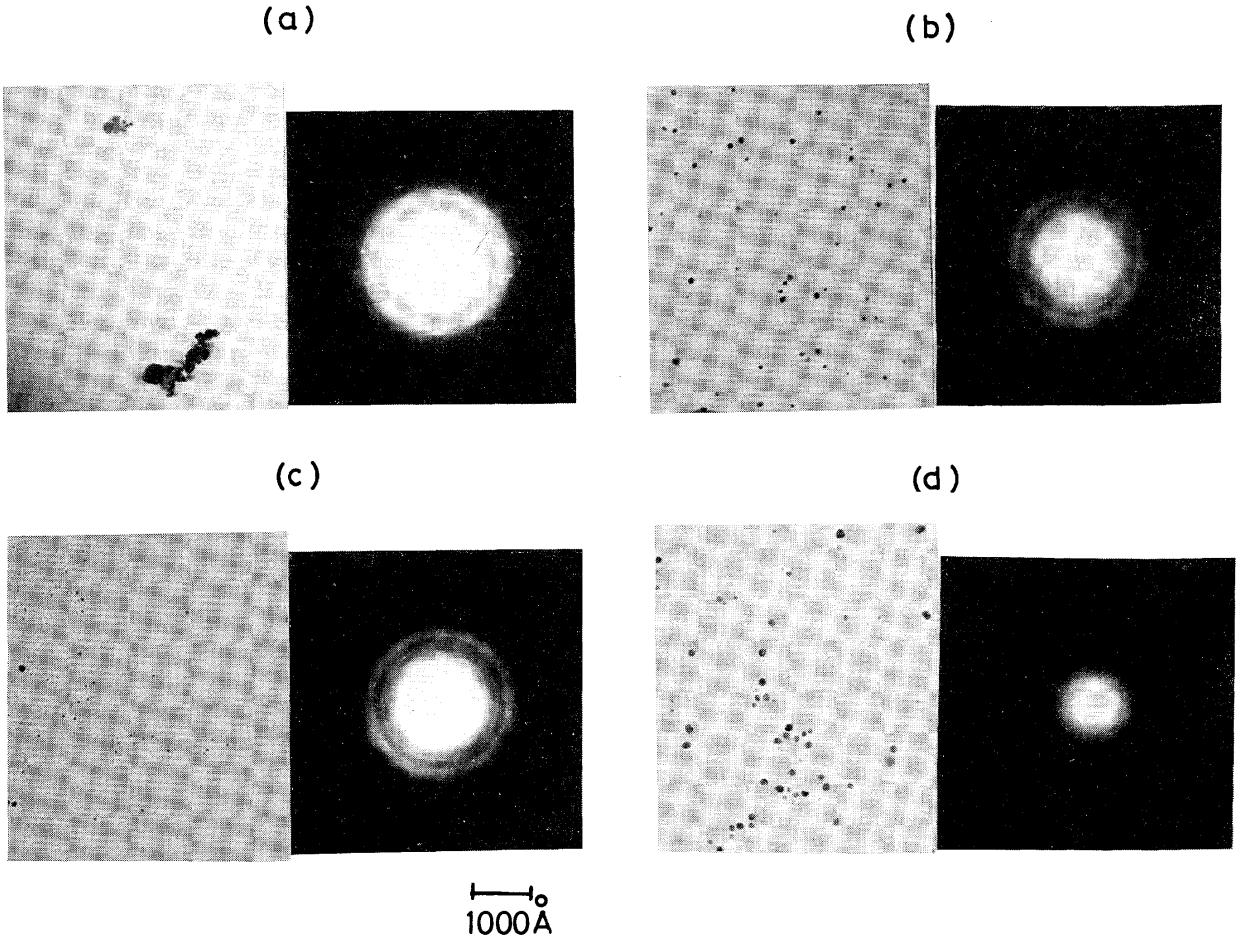

Fig. 3. Electron micrograph and electron diffractogram of colloidal silver sols: (a) PVP, (b) A2, (c) A4, (d) A8.

colloidal dispersions were turbid. This result coincided with that obtained by Hirai et al.[8] Similarly, PVP alone did not provide any stable silver sols. The electron photograph and electron diffractogram of these particles are shown in Fig. 3(a), where their particle sizes range from 300 to 400 Å.

On the other hand, with the copolymers of VA-VP, a transparent silver dispersion was obtained, where the copolymers of A2 and A8 gave yellow sols, and the others, red sols. The electron photograph and electron diffractogram of these stable sols are shown in Fig. 3(b), (c), and (d). The particle size of the silver sols prepared with the copolymers of A2 and A8 was rather monodispersed, being 80—170 Å of diameter, while those of the sols prepared with the copolymer of A4 were both large and small; the former was about 150 Å, and the latter, 50 Å. From the electron diffractogram, the particles can be said to be crystalline, with a diffraction pattern corresponding to the f.c.c. structure of silver.

Thus, the above results confirm that stable silver sols are obtained only by the use of the copolymer of VA-VP.

In order to elucidate the effect of the copolymer on the formation of silver sols, the silver sols were prepared as a function of the amount of copolymer added. In the case of the copolymer A2 (shown in Table 2), yellow silver sols were obtained in the range of 7.5—200 mg. When 15 and 7.5 mg portions were added, the particle sizes were divided into two regions; one was 100—200 Å, and the other, 30—40 Å. In the case of the copolymer A4 (shown in Table 3), the color of sols changed with the amount of the copolymer added; the red sols were obtained in the range of 100—200 mg and 7.5—15.0 mg, and the yellow sols, in the range of 25—75 mg. The electron microscopy shows that, upon the addition of 37.5—75 mg, and 200 mg of the copolymer A4, monodispersed sols are prepared, but the addition of 100—175 mg of the copolymer A4 leads to a broad particle size distribution. Table 4 shows the properties of the silver sols prepared in the presence of the copolymer A8. Upon the addition of less than 37.5 mg of the copolymer A8, no stable sols were obtained, but the addition of 75 mg of the copolymer A8 allowed the preparation of monodispersed sols. Upon the further addition of the copolymer A8, the stable sols were still obtained. Thus, with an increase in the ratio of *N*-vinylpyrrolidone in the copolymers, the particles of silver sols became smaller.

Table 2. Color, Dispersion, and Particle Size of Colloidal Silver with the Copolymer A2

Added amount/mg	Color	Dispersion	Particle size/Å
200	Yellow	Stable	70—120
175	Yellow	Stable	50—200
150	Yellow	Stable	100—160
100	Yellow	Stable	60—150
75	Yellow	Stable	80—150
37.5	Yellow	Stable	70—100
15	Yellow	Stable	100—180, 30—40
7.5	Yellow	Stable	150—200, 30

Table 3. Color, Dispersion, and Particle Size of Colloidal Silver with the Copolymer A4

Added amount/mg	Color	Dispersion	Particle size/Å
200	Red	Stable	60—110
175	Red	Stable	20—180
150	Red	Stable	100—200, 50
100	Red	Stable	100—200
75	Yellow	Stable	60—110
37.5	Yellow	Stable	60—110
25	Yellow	Stable	30—150
15	Red	Stable	20—150
7.5	Red	Stable	100—300, 30—70

Table 4. Color, Dispersion, and Particle Size of Colloidal Silver with the Copolymer A8

Added amount/mg	Color	Dispersion	Particle size/Å
200	Yellow	Stable	50—110, 250
175	Yellow	Stable	50—130
150	Yellow	Stable	80—150
100	Red	Stable	60—170
75	Yellow	Stable	60—110
37.5	Gray	Instable	20—300
25	Gray	Instable	Coagulate
15	Gray	Instable	Coagulate
7.5	Gray	Instable	Coagulate

Consequently, it can be summarized that, upon the addition of the copolymer A2 in the range of 0.5—4 wt%, rather monodispersed silver sols are prepared, while the addition of the copolymer A4 or A8 also leads to the formation of monodispersed silver sols, although the additive concentration is restricted to some degree.

Protective colloids, such as PVA, and PVP, have been used to prepare colloidal precious metal particles because they adsorb on metal particles, resulting in stable sols. In this study, PVA and PVP are found to be effective as a protective colloid for the preparation of colloidal platinum sols. Although Jirgensons et al.[10] have reported that decreasing the degree of the polymerization of PVP results in a depression of the aggregation of precious metal particles, an opposite result is obtained in this study.

In the case of the preparation of silver sols, the copolymers of VA-VP give rather monodispersed silver sols, suggesting that the copolymers of VA-VP are adsorbed effectively on the silver sols. In fact, Ueno[11] has reported that the surface tension of the copolymers of VA-VP decreases with an increase in the VP content and is lower than that of each homopolymer. This result leads to the conclusion that the copolymers of VA-VP can adsorb on a solid surface more easily than

homopolymers, resulting in the formation of monodispersed particles as an effective protective colloid.

References

1) H. Hirai, K. Ishihara, and I. Shinohara, *Makromol. Chem. Rapid Commun.*, **2**, 99 (1981).
2) T. Toshima, T. Takahashi, and H. Hirai, *Chem. Lett.*, **1985**, 1245.
3) I. Tabushi, K. Kurihara, and K. Morimitsu, *Yuki Gosei Kagaku, Kyokai Shi*, **43**, 323 (1985).
4) W. P. Dunworth and F. F. Nord, *Adv. Cat.*, **6**, 125 (1954).
5) J. Kiwi and M. Grätzel, *J. Am. Chem. Soc.*, **101**, 7214 (1979).
6) P. A. Brugger, P. Cuendet, and M. Grätzel, *J. Am. Chem. Soc.*, **103**, 2923 (1981).
7) H. Hirai, *J. Macromol. Sci., Chem.*, **A13**, 633 (1979).
8) H. Hirai, Y. Nakao, and N. Toshima, *J. Macromol. Sci., Chem.*, **A13**, 727 (1979).
9) J. Westerhausen, A. Henglein, and J. Lilie, *Ber. Bunsenges. Phys. Chem.*, **85**, 181 (1981).
10) B. Jirgensons and M. E. Straumanis, "A Short Textbook of Colloid Chemistry," 2nd ed, Pergamon Press, London (1962).
11) Y. Ueno, Master's Thesis of Science University of Tokyo (1964).

 © 1988 The Chemical Society of Japan Bull. Chem. Soc. Jpn., 61, 351—358 (1988)

Electronic Structure of Poly(dimethylsilane) and Polysilane Studied by XPS, UPS, and Band Calculation

Kazuhiko SEKI,* Takehiko MORI,† Hiroo INOKUCHI,† and Kentaro MURANO††
Department of Materials Science, Faculty of Science, Hiroshima University, Hiroshima 730
†Institute for Molecular Science, Myodaiji, Okazaki 444
††The National Institute for Environmental Studies, Yatabe-cho, Tsukuba, Ibaraki 305
(Received June 22, 1987)

The valence electronic structures of poly(dimethylsilane)(PDMS) $(Si(CH_3)_2)_n$ and polysilane $(SiH_2)_n$ were studied. PDMS was experimentally studied by X-ray photoelectron spectroscopy (XPS) and UV photoelectron spectroscopy (UPS), and band calculations were performed for both compounds. The observed spectral features and calculated band structures were assigned and discussed through a comparison with theoretical and experimental results for oligomers and other polymers. These analyses have demonstrated how the electronic structures of these compounds are correlated through factors such as (i) change in the chain length, (ii) methylation, and (iii) the substitution of Si by C. PDMS has a small ionization energy (5.9 eV) almost as low as that of poly(*p*-phenylene) (5.6 eV). This small value comes from the combined contribution from the small electronegativity of silicon, σ-conjugation, and the inductive effect of methyl groups. The small ionization energy and large σ-conjugation explain the reported high conductivity of PDMS and its derivatives upon acceptor doping.

Recently the electronic properties of polysilane $(SiH_2)_n$ and their derivatives have attracted considerable interest from various viewpoints such as the strong delocalization of σ-electrons (σ-conjugation),[1-3] a new class of conducting polymers,[1,4,5] photoresists,[1] photoinitiators for polymerization,[1] and species found in the films of plasma-deposited Si:H alloy.[6,7] The permethylated or other organo-substituted compounds are used for protecting the polysilane backbone from unstability to air.

The elucidation of the electronic structures of polysilane and poly(dimethylsilane) $(SiMe_2)_m$ (PDMS), which is the simplest poly(organosilane), is the basis for such studies. However, the electronic structures of these compounds have not been investigated experimentally, although shorter members of silanes Si_nH_{2n+2} $(n \leqslant 5)$[8,9] and permethylated silanes $Si_m(CH_3)_{2m+2}$ $(m \leqslant 5)$[8,10] have been extensively studied by gas phase UV photoelectron spectroscopy (UPS). On the theoretical side, there have been several band calculations for polysilane and their derivatives.[11-13] A recently reported UPS study of polysilanes with complex pendants[14] clarified several important points such as the dominant contribution of the large pendants to their electronic structure and the relation of chain-pendant interaction with their ability as photoresists. Unfortunately, however, the topmost part of the valence band could not be studied in detail, and there is a large uncertainty in the energy axis due to sample charging.

In this paper we report on a study of the whole valence electronic structures of PDMS and polysilane. PDMS is studied by X-ray photoelectron spectroscopy (XPS) and UPS. Such experiments could not be performed on unstable unsubstituted polysilane, but band calculations were performed on both compounds; the results are discussed in terms of the relevant data for oligomers. A comparison is also made with polyethylene $(CH_2)_n$, the carbon analogue of polysilane, and conducting polymers with π-conjugated carbon chains.

Furthermore, in the process of sample preparation we found that thin films of PDMS can be prepared by vacuum-evaporation, a technique which has been successfully applied to other polymers such as polyethylene and polypropylene.[15] This technique may also be applicable for the thin-film preparation of other polysilanes.

Experimental

The PDMS powder was supplied from Shinnisso-Kako Co. Ltd., and used without further purification. The XPS spectra were measured on a VG ESCALAB 5 photoelectron spectrometer using Al $K\alpha$ radiation ($h\nu$=1486.6 eV). The sample powder was supported on a Nichiban double-sided adhesive tape.

The UPS spectra were measured using two photoelectron spectrometers with different light sources, i.e. (i) rare-gas resonance lines (He I, $h\nu$=21.2 eV; Ne I, $h\nu$=16.8 eV, and Ar I, $h\nu$=11.7 eV), and (ii) the combination of a Hinteregger-type hydrogen discharge lamp with a 0.5-m Seya-Namioka-type monochromator ($h\nu$=7.7—10.5 eV). The base pressure of the chamber was ca. 5×10^{-8} Pa and ca. 2×10^{-4} Pa for spectrometers (i) and (ii), respectively. In both cases, the energy analyzer of photoelectrons was a retarding-potential type one. The photoelectron spectra were obtained using an ac moduation technique,[16,17] with a modulation of 0.2 V peak to peak.

One advantage of the retarding-potential-type analyzer is that we could accurately determine the absolute binding energy.[16,17] In order to use this advantage for insulators, however, a thin film of several tens nm thickness was necessary for avoiding sample charging. Such a film was obtained by in-situ vacuum-evaporation in the photoelectron spectrometer to a thickness of 25 nm, which was monitored by a quartz oscillator.

The evaporated film was examined by IR spectroscopy.

The IR spectrum of PDMS before evaporation was measured with a KBr pellet, and agreed well with the reported spectrum.[18] It exhibits bands due to adsorbed water at 3440 cm^{-1} and 1650 cm^{-1}, and a band due to Si-O bond at 1035 cm^{-1}. We also observed a weak oxygen 1s peak in the XPS spectrum of the powder, which corresponds to a few per cent of O atom per Si atom. Such a small amount of oxygen is not expected to affect the observed UPS and valence-XPS spectra. A weak band due to the Si-H stretching also appears at 2100 cm^{-1}. In the spectrum of a film evaporated onto a KBr disk, water-derived bands are completely removed and the Si-O band becomes weak. On the other hand, the Si-H band becomes stronger, and the band around 700 cm^{-1}, which is related to the Si-C bonds, becomes weaker. From these results, we conclude that some of the CH_3 groups are replaced by H atoms upon evaporation: however, main structure of PDMS is preserved.

The evaporated film did not sublime away, even after a long storage in high vacuum. This indicates that the molecular weight of PDMS in the evaporated film is much larger than those of the short oligomers ($n \leqslant 5$) studied in gas-phase UPS experiments.[8,10]

Calculation

The band structure calculations were performed with an extended Hückel approximation using a program described elsewhere.[19] Parameters by Nguyen et al.[20] (Table 1) were used.

The validity of this method was examined by comparing the observed gas phase UPS spectra of small silanes[8] and methylated silanes[10] with the calculated energy levels by this method without Si 3d orbitals. The calculated results compare reasonably well with the observed UPS spectra, when we shift the calculated results by about 2 eV to the lower-energy side. The character of calculated levels also agree well with the experimentally assigned ones by Bock et al.[8-10] These results indicate that we can use this rather primitive method for discussing the gross features of the electronic structures of polysilane and PDMS.

We also calculated the molecular orbitals of Si_2H_6 with (i) the use of a slightly smaller orbital exponent ζ=1.2 for Si and (ii) an extended basis set including the Si 3d orbital. The results showed that these changes have little effect on the calculated results. Since the calculated band structures of PDMS and polysilane are also little affected by these changes, we report here only the results without 3d orbitals and ζ=1.383.

Band structure calculations of polymers were performed for polysilane, PDMS, and polyethylene. All three polymers were taken to be in a planar-zigzag conformation: The bond angles and bond lengths are listed in Table 1(b). This conformation has not yet been experimentally verified for polysilane and PDMS, and other possibilities are also suggested.[23] However, UPS and XPS experiments on crystalline and gaseous alkanes[24] indicate only a minor difference of the density-of-states between extended planar-zigzag and random-coil conformations. Therefore, the results for an adopted conformation will be at least a good first-

Table 1. Parameters for Band Calculations.

(a) Extended Hückel Parameters[20]

	$-H_{ii}$/eV	Exponent ζ
H 1s	13.60	1.000
C 2s	21.40	1.625
C 2p	11.40	
Si 3s	17.31	1.383
Si 3p	9.20	
Si 3d	6.00	

(b) Bond Lengths (in pm) and Bond Angles (in Degrees)

Si-Si	226.4[a]
Si-C	186.7[b]
C-C	152.93[c]
Si-H	149.3 (polyethylene)[a]
C-H	106.89 (polyethylene)[c]
	112.7 (PDMS)[b]
<SiSiSi	118.97[a]
<CSiC	110.5[b]
<HSiH	100.39[a]
<HCH	110.3 (PDMS)[b]
	107.0 (polyethylene)[c]
<CCC	112.0[c]

a) From the optimized geometry in Ref. 12. b) From the molecular structure of hexadimethylsilane.[21] c) From the X-ray geometry cited in Ref. 22.

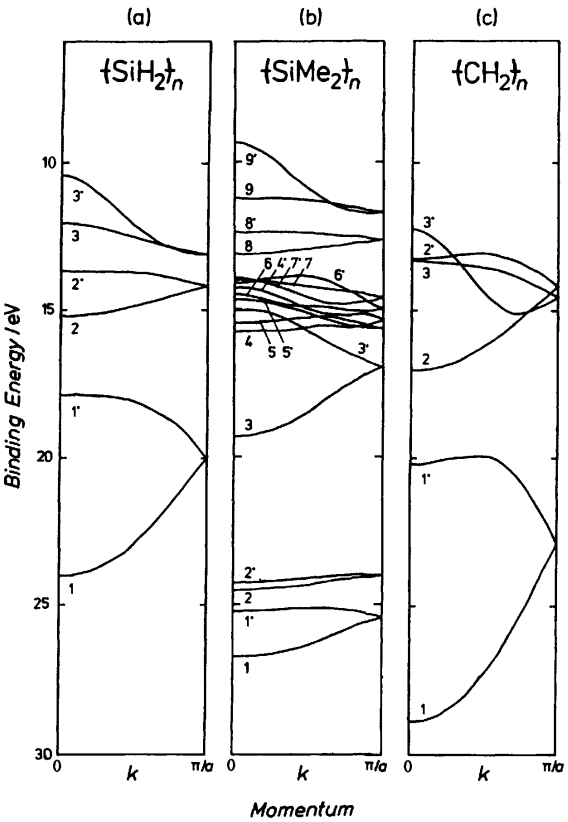

Fig. 1. Calculated enegy band structures of (a) polysilane, (b) poly(dimethylsilane), and (c) polyethylene by extended Hückel method. The results of polyethylene is the same as that by McCubbin and Manne.[25]

order approximation to the real systems.

Results and Discussion

Polysilane. The calculated band structure of polysilane is shown in Fig. 1(a). Due to the assumption of a planar-zigzag conformation, the bands form pairs degenerate at the edge of the Brillouin zone ($k=\pi/a$), where a is the lattice constant. The same kind of pairing also occurs in the results for other polymers in Figs. 1(b) and (c). The Si 3s orbitals form a broad band 1+1′. Si-H and Si-Si bonds form separated bands 2+2′ and 3+3′, respectively. These results agree with other calculations,[11-13] except that some of them indicate an overlap of the bands 2+2′ and 3+3′. We discuss this point later.

This band structure is fairly similar to that of polyethylene (Fig. 1(c)), which is the same as that by McCubbin and Manne.[25] However, the bands in polysilane show lower binding energies than corresponding ones in polyethylene. This should be due to the smaller electronegativity of Si (1.8 in Pauling scale[26]) than that of C (2.5), which appear as the smaller H_{ii} of Si 3p than that of C 2p in Table 1. Another difference is the overlap of the C-H and C-C bands (2+2′ and 3+3′) in polyethylene, which is well verified by photoemission experiments[27] and other calculations.[22]

In Fig. 2(c) we show the density of states (DOS) of polysilane derived from Fig. 1(a). The peaks in the DOS correspond to the bands in Fig. 1(a); their characters are also shown. For a comparison, in Figs. 2(a) and (b) we show the reported gas-phase UPS spectra of SiH_4[28,29] and Si_5H_{12}.[8] The peak energies in these spectra are listed in Table 2. In this comparison, the calculated DOS is rigidly shifted by 2.0 eV as described in Calculation. The studies of Si_nH_{2n+2} from n=1 to 5 by Bock et al.[8] revealed that the spectra of these compounds consist of (i) a largely unchanged intense peak due to the SiH bonds and (ii) split levels below and above the SiH peak, which are derived from interacting Si3s orbitals and SiSi bonds, respectively. These characters are shown in the figure.

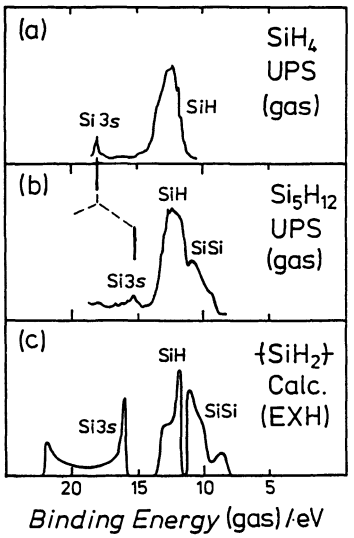

Fig. 2. Gas phase UPS spectra of SiH_4[35] (a) and Si_5H_{12}[8] (b) compared with the calculated density of states of polysilane derived from Fig. 1(a).

Since previous studies have shown that electronic structures of oligomers of 5 units already resemble that of a polymer,[30-32] a comparison between the theory and the spectrum of Si_5H_{12}, the longest silane oligomer so far measured, is meaningful for the discussion of polysilane. In Fig. 2 a good correspondence can be seen between these two, as well as an agreement of the peak assignments.

We also see a good correspondence between the band calculation and the n-dependence reported by Bock et al.[8] The large shift of the uppermost Si3s level from n=1 to 5 (2.86 eV) corresponds to the wide dispersion of the Si 3s band in Fig. 1(a), which reflects the strong interaction between the directly bonded Si atoms. Further, the insensitivity of the SiH peak to the chain length corresponds to the narrow width of the calculated SiH bands in Fig. 1(a), which indicates a weak interaction among the SiH bonds. These results support the absence of an overlap between the SiSi and

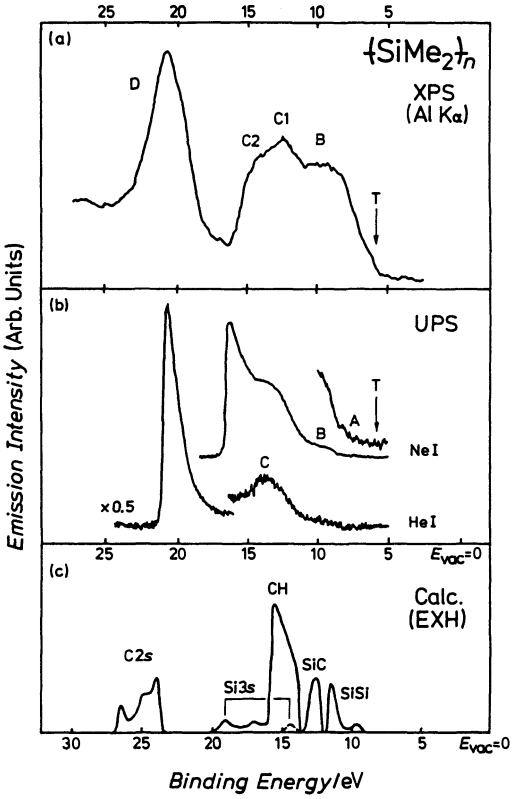

Fig. 3. X-Ray (a) and ultraviolet (b) photoelectron spectra of poly(dimethylsilane) solid compared with (c) the density of states deduced from the extended Hückel calculation in Fig. 1(b) by making a histogram of 0.5 eV steps. The abscissa is 2.5 eV shifted as described in the text. The ionization threshold and peaks are labelled T and A—D, respectively.

SiH bands in the present calculation. This absence also agrees with a recent calculation using realistic semiempirical parameters.[13] In contrast to this, the UPS spectra of short alkanes[33] show no stationary peak, because of the mixing among the electronic states derived from the CH and CC bonds.

Thus we can conclude that the important aspects of the electronic structure of polysilane are reproduced in the calculated band structure in Fig. 1(a).

Poly(dimethylsilane). In Figs. 3(a) and (b), we show the XPS and UPS spectra of PDMS. The abscissa is the binding energy relative to the vacuum level. The absolute energy scale could be accurately determined for the UPS spectra by taking the left-hand cutoff of each spectrum to be zero kinetic energy of photoelectrons.[17] The absence of charging is verified; by the sharpness of this cutoff. The energy scale of the XPS spectrum is adjusted to fit the spectral features with those in the UPS spectra.

In the XPS spectra we can see four features labelled B, C1, C2, and D. In the UPS spectra, three valence band features (A, B, and C) can be seen. Feature C corresponds to the broad band formed by C1 and C2 in the XPS spectrum. The sharp intense peak near the left-hand cutoff in the UPS spectra are due to secondary electrons. The topmost part of the valence band is not clearly seen in the UPS spectra in Fig. 3, possibly due to an incomplete cleanliness of the sample surface. Fortunately, this part (feature A) can be more clearly seen in the UPS spectra at lower photon energies (Fig. 4) with a clear onset T at 5.9±0.1 eV corresponding to the ionization threshold. The binding energies of these spectral features are listed in Table 2.

We now analyze these spectra with the aid of the calculated band structure of PDMS and the theoretical and experimental results of the relevant compounds.

The calculated band structure of PDMS is shown in Fig. 1(b). The highest occupied bands 9+9′ originate from interacting Si-Si bonds, as in polysilane. The

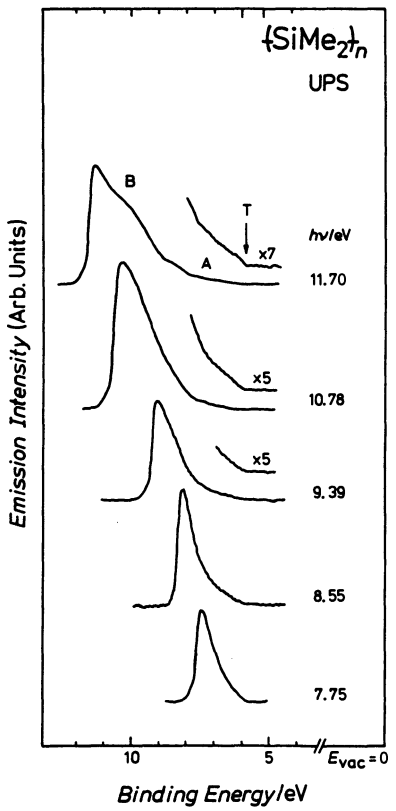

Fig. 4. Ultraviolet photoelectron spectra of poly(dimethylsilane) solid at low photon energies.

Table 2. Observed Binding Energies of the Spectral Features in the Photoelectron Spectra (in eV)

Feature	PDMS				$SiMe_4$		Si_2Me_6	Si_4Me_{10}	SiH_4	Si_5H_{12}
	XPS (solid)	label	UPS (solid)	label	XPS (gas)	UPS (gas)	UPS (gas)	UPS (gas)	UPS (gas)	UPS (gas)
Threshold	—	T	5.9	T	—	9.42[a] 9.79[a]				
SiSi			6—9	A	—	—	8.69	7.98 8.76	—	9.36 [10.1] [10.6] [10.9]
SiC	9.5	B	9.5	B	10.4	10.57	10.4	10.5	—	—
SiH	—	—	—	—	—	—	—	—	12.82	[11.8] [12.2] [12.5]
CH	12.6	C1	13.6	C	11.5 13.2	13.06	13.5	Not shown	—	—
	14.1	C2			14.1	14.08				
Si3*s*	12.6	C1	Not obsd.		15.5	15.58	Not obsd.	Not shown	18.16	15.3
C2*s*	20.7 22.8	D			21.72 24.0				—	—
Ref.	This work		This work		34	35	10	10	28,29	8

Values in the brackets are estimated from the deconvolution of the observed spectrum.
a) Values reported in two works in Ref. 35 obtained by different ways of extrapolation. Energies of other spectral features are almost the same.

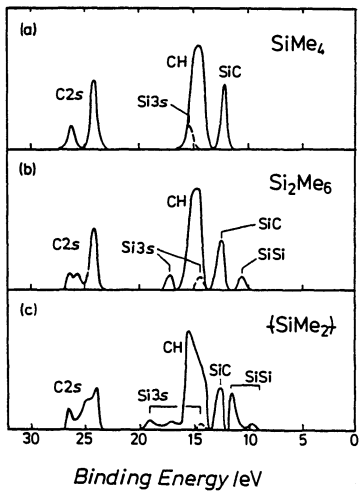

Fig. 5. Calculated density of states of $Si(CH_3)_4$ (a), $Si_2(CH_3)_6$ (b), and poly(dimethylsilane) (c).

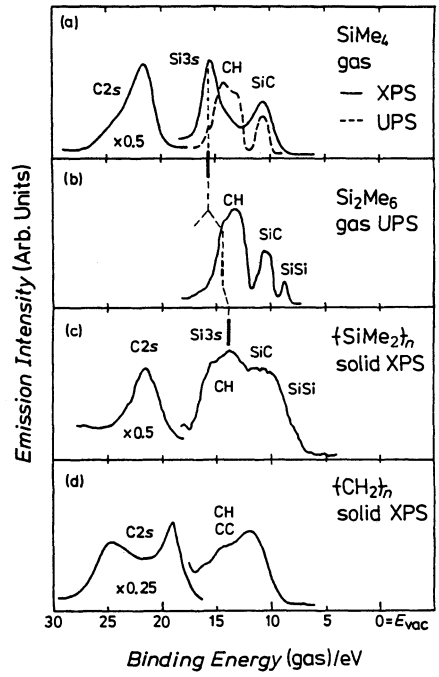

Fig. 6. Photoelectron spectra of permethylated silanes[10,34,35] and n-$C_{36}H_{74}$.[36] Solid state spectra are shifted by 1.0 eV for compensating the polarization energy. The location of the upper edge of the Si3s band is indicated.

dispersion is also farily similar to that of polysilane. The next bands 8+8′ are derived from the Si-C bonds. The next four pairs of narrow bands 4+4′—7+7′ at 15 eV originate mainly from the C-H bonds. The linear combination of Si3s orbitals form the wide band 3+3′ at ca. 17 eV. The character analysis of the bands revealed that the top of the Si band is not in 3′ at k=0 but in 6′ at k=0. This splitting originates from the avoided crossing with the CH bands with the same symmetry. Finally, the two pairs of bands 2+2′ and 1+1′ around 25 eV are derived from the C2s orbitals.

The DOS of PDMS obtained from this band calculation is shown in Fig. 3 (c) with the characters of the contributing bands. Further, in Fig. 5 we compare this DOS with those of $Si(CH_3)_4$ and $Si_2(CH_3)_6$. For the latter two, the functions located at MO binding energies are convoluted with a Gaussian function of 0.7 eV FWHM for simulating the photoelectron spectra.

As a counterpart from experimental observations, in Fig. 6 we compare our XPS and UPS spectra with the reported photoelectron spectra of permethylated silanes[10,34,35] and a long alkane n-$C_{36}H_{74}$,[36] a good model compound of polyethylene. The binding energies of the features in these spectra are listed in Table 2. The characters of each band in the reported spectra are taken from the original papers.

It is known that the photoelectron spectrum of a molecular solid fits well with the gas phase spectrum of a constituent molecule, when due allowance is made for a shift in the binding energy scale and for peak broadening.[37] Thus we can compare the observed XPS and UPS results of solid state with the gas-phase spectra and theoretical calculations (for an isolated chain) by rigidly shifting the energy scale. Since the shift comes from the polarization of the molecules surrounding the cation, it is called the polarization energy.[38] In Fig. 6, the solid spectra are shifted by 1.0 eV, which is a common value observed for other compounds.[39] In Fig. 5, the calculated DOS is shifted by 2.5 eV for the best overall fit with the XPS and UPS results. This shift contains contributions from the polarization energy and from the shift described in Calculation.

From Figs. 5 and 6, the intense feature D in the XPS spectrum can be easily assigned to the calculated C2s bands 2+2′ and 1+1′, the latter probably corresponding to the tail at the higher-binding-energy side. The observed width (FWHM 3.3 eV) is much smaller than that of polyethylene (7.6 eV at half height) (Fig. 6(d)). Correspondingly, the calculated total width of the 1+1′ and 2+2′ bands are much smaller than that of the 1+1′ band of polyethylene. This difference can be explained by the fact that the interaction among the C2s orbitals is small in PDMS where the carbon atoms are not directly bonded, while the interaction is strong in the directly-bonded carbon chain of polyethylene.

In discussing the lower binding energy region, we at first note that the photoionization cross section of the Si3s orbital is almost negligible in the UPS region, as can be seen from a comparison of the XPS and UPS spectra of $Si(CH_3)_4$ in Fig. 6(a). Thus, we can analyze the UPS spectra in terms of the bands derived from the CH-, SiC-, and SiSi-bonds.

The calculation shown in Fig. 1(b) indicates that these bands do not overlap. In particular, each CH- and SiC-derived band shows a small dispersion. Reflecting this situation, the energies of the DOS peaks of CH and SiC character in Fig. 5 are almost

independent of the silicon number, m.

The trends in the UPS spectra of $Si(CH_3)_4$ and $Si_2(CH_3)_6$ in Fig. 6 verify this theoretical expectation. The CH-, SiC-, and SiSi-peaks are well separated, and the energies of the former two are almost the same. We can thus assign peaks C, B, and A in the UPS spectra of PDMS to the CH-, SiC-, and SiSi-bands, respectively.

Next we discuss the levels derived from the Si 3s orbitals. The band calculation of PDMS in Fig. 1(b) shows a large dispersion of the Si3s-derived bands 3+3′, which corresponds to the strong 3s-3s interaction by the Si-Si bonds. This situation can also be seen as an increasing splitting of the DOS peaks in Fig. 5 with increasing m (note that the upper edge of the Si3s band is at 6′ at k=0). Thus, we expect a significant overlap of the CH- and Si3s-derived bands.

By comparing the UPS and XPS spectra in Figs. 2(a) and (b), we find that the upper-binding-energy part of peak C in the UPS spectrum becomes enhanced as C1 in the XPS spectrum. Thus. we can assign this enhanced peak to the upper edge of the Si3s band, and the broad background peak C1+C2 to the CH bands. The shift of the Si3s level from that of $Si(CH_3)_4$ (ca. 2 eV) due to the band formation is a little smaller than the corresponding value for polysilane (ca. 3 eV), in accordance with the calculation. The lower edge of the Si3s band is difficult to distinguish, even in the XPS spectrum. It may be buried in the tail of the intense C2s band on the low-energy side.

Finally, we discuss the inductive effect of the methyl groups. It shifts the Si-Si and Si3s levels of PDMS to a lower binding energy than those of polysilane. This shift is evaluated to be 1.6 eV from a comparison of the observed spectra of oligomers, while calculations in Fig. 1 gives a value of about 1 eV. A similar shift is also found in a recent calculation on alkyl-substituted polysilanes.[13]

Ionization Thresholds and Electrical Conductivity. Two important parameters of the uppermost band in discussing the electrical conductivity of polymers are (i) the energy of the upper edge (ionization threshold energy) and (ii) the bandwidth. The former is related to the feasibility of carrier (hole) generation by acceptor doping, while the latter is a measure of the degree of delocalization in a single chain.

In Table 3, we compare the solid ionization thresholds I_s^{th} and the widths of the highest occupied bands of PDMS, polysilane, and polyethylene.[40] Relevant data of poly(p-phenylene)[32] and polyacetylene[41] are also included as representatives of conduct-

Table 3. Ionization Threshold Energies and Bandwidths of Polysilane, PDMS, and Related Polymers (in eV)

Polymer	I_s^{th}/eV	Width of the highest occupied band
PDMS	5.9	2.0[e]
Polysilane	(7.5)[a]	2.0[e]
Polyethylene	8.5[b]	4.0[f]
Polyacetylene	5.24[c]	5—6[c]
Poly(p-phenylen)	5.6$_5$[d]	3.9[d]

a) Estimated from the value of PDMS assuming a shift of 1.6 eV. b) Ref. 40. c) Ref. 41. d) Ref. 32. e) Estimated from the UPS spectra of oligomers. f) Ref. 27.

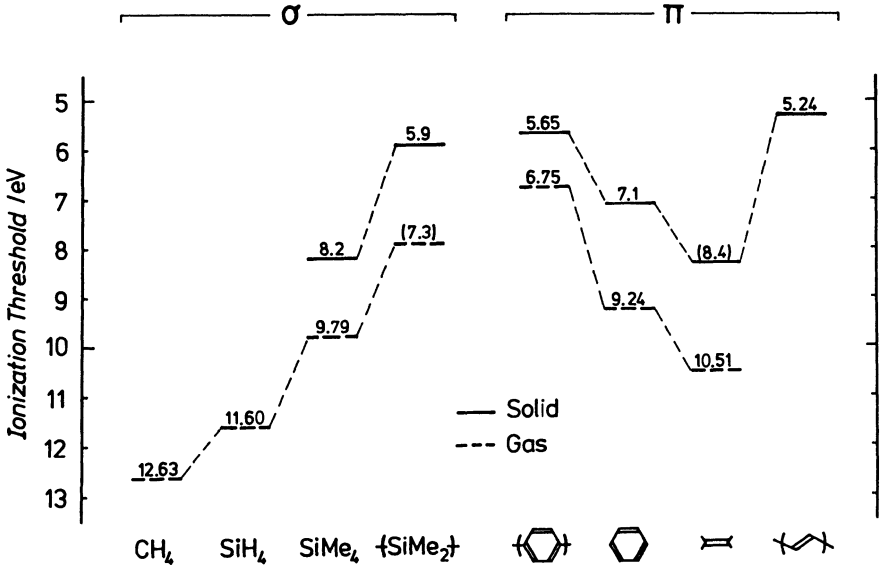

Fig. 7. Ionization thresholds of σ-conjugated silanes and π-conjugated hydrocarbons. For comparison, the data of CH_4 is included in the σ-system. The data in the parentheses are estimated by assuming a gas-to-solid difference in the adjacent compound in the figure. Values not listed in Tables 2 and 3 are taken from the following: CH_4: Ref. 43 (gas); $Si(CH_3)_4$: Ref. 44 (solid); poly(p-phenylene): Ref. 32 (gas); benzene: Refs. 43 (gas) and 45 (solid); ethylene: Refs. 43 (gas) and 46 (solid).

ing polymers with a π-conjugated carbon principal chain. The ionization threshold of polysilane is estimated from the value of PDMS, assuming a 1.6-eV shift due to the inductive effect by the methyl groups. Although a precise determination of the band widths is difficult for PDMS and polysilane, we can still estimate them to be of the order of ca. 2 eV from the spectra of PDMS (Fig. 4) and oligomers. The value of polyacetylene was also deduced from the data of oligomers.[42]

In Table 3 we can see that the threshold of polysilane is 1 eV smaller than that of polyethylene due to the smaller electronegativity of Si than C (as discussed above). Further, the value of PDMS is 1.6 eV smaller than that of polysilane by the inductive effect of methyl groups, and almost comparable to that of poly(*p*-phenylene). However, it is still significantly larger than that of polyacetylene, which can be doped with iodine. This is consistent with the experimental results that doping of PDMS needs strong acceptors, such as AsF_5 and SbF_5.[1]

In Fig. 7 the change of ionization thresholds of σ-conjugated systems from CH_4 to PDMS are compared with analogous change in π-conjugated hydrocarbon systems. In the latter, the orbital energies of the highest occupied orbital is lowered by a strong (4 to 5 eV bandwidth) π conjugation. Note that the ionization threshold of the solid polymers are smaller than the value of gas phase due to the polarization energy.

The bandwidths of polysilane and PDMS are less than those of π-conjugated polymers. However, such bandwidths should still be sufficient for realizing a good intrachain conductivity, since they are already much larger than the bandwidths of conducting molecular complexes.[47] Therefore, the origin of the limited conductivity of doped PDMS (7×10^{-3} S cm^{-1})[1] may be a small interchain conductivity. Although permethylation is advantageous for a high intrachain conductivity by lowering the ionization threshold, the methyl groups hinder the hole transport from chain to chain. The increased conductivity of photo-crosslinked polymers[1] supports this idea. Another possible way of increasing the interchain conductivity will be the partial substitution of PDMS by some pendant group which can "shake hands" to transport the holes. However, the conductivities of doped phenyl-substituted PDMS are lower than that of doped PDMS.[1] Therefore, the choice of an appropriate pendant for such a purpose needs further consideration.

Concluding Remarks

In this paper we reported a combined theoretical and experimental study of polysilane and poly(dimethylsilane) (PDMS). Observed XPS and UPS spectra of PDMS could be analyzed in a detailed way by theoretical band calculations. Further, a comparison with oligomers confirmed the assignments and also revealed how the electronic structures of these polymers evolve from those of constituent units. Such a successful use of oligomers for studying the Si-backboned polymers is an extension of similar studies for polymers with carbon-derived backbones, where the usefulness of oligomers has been already well demonstrated.[27,30-32]

Polysilane and PDMS have rather small ionization energies due to the small electronegativity of Si, σ-delocalization and the inductive effect of methyl groups. Although the one-dimensional delocalization makes the ionization energy still larger than that of a three-dimensionally connected Si solid (5.35 eV),[48] the value of PDMS is already comparable to those of π-conjugated carbon-derived polymers. This fact explains the good conductivity to PDMS and its derivatives upon doping. Further, the linear structure offers useful properties such as the solubility to organic solvents.

Thus, the introduction of Si as a constituent atom of the principal chain offers an exciting prospect for designing materials of interesting electronic properties. Although in this work we have dealt with the most basic two polymers of this group, other interesting derivatives, e.g. with π-pendants, have also been synthesized.[1] A study of the electronic structures of such polymers will give more insight into the full possibilities of polysilanes. The work of Loubriel and Zeigler[14] pioneered this direction, and recently we have also examined the chain-pendant interaction in poly(methylphenylsilane) in some detail.[49]

We thank Dr. Kyozaburo Takeda of Nippon Telegram and Telephone Corporation for helpful discussions. This work was partly supported by the Grant-in-Aid for Scientific Research (No. 60104006) and the Grant-in-Aid for Scientific Research on Priority Area "Dynamic Interactions and Electronic Processes of Macromolecular Complexes" (No. 62612003) from the Ministry of Education, Science and Culture.

References

1) For a review, see, for example, R. West, *J. Organomet. Chem.*, **300**, 327 (1986).
2) V. F. Traven and R. West, *J. Am. Chem. Soc.*, **95**, 6824 (1973).
3) H. Sakurai, M. Kira, and T. Uchida, *J. Am. Chem. Soc.*, **95**, 6826 (1973).
4) P. John, I. M. Odeh, and J. Wood, *J. Chem. Soc., Chem. Commun.*, **1983**, 1496.
5) R. West, L. D. David, P. I. Djurovich, K. L. Stearley, K. S. V. Shrinivasan, and H. Yu, *J. Am. Chem. Soc.*, **103**, 7352 (1981).
6) M. H. Brodsky, M. Cardona, and J. J. Cuomo, *Phys. Rev. B*, **16**, 3556 (1977).
7) S. Furukawa and N. Matsumoto, *Phys. Rev. B*, **31**, 2114 (1985).
8) H. Bock, W. Ensslin, F. Fehler, and R. Freund, *J. Am. Chem. Soc.*, **98**, 668 (1976).

9) W. Ensslin, H. Bergmann, and S. Ebel, *J. Chem. Soc., Faraday Trans. 2*, **71**, 913 (1975).
10) H. Bock and W. Ensslin, *Angew. Chem., Int. Ed. Engl.*, **10**, 404 (1971).
11) P. N. Dyachkov, N. V. Ioslovich, and A. A. Levin, *Theoret. Chim. Acta*, **40**, 237 (1975).
12) H. Teramae, T. Yamabe, and A. Imamura, *Theoret. Chem. Acta*, **64**, 1 (1983).
13) K. Takeda, N. Matsumoto, and M. Fukuchi, *Phys. Rev.*, **30**, 5871 (1984); K. Takeda and N. Matsumoto, *J. Phys. C*, **18**, 6121 (1985).
14) G. Loubriel and J. Zeigler, *Phys. Rev. B*, **33**, 4203 (1986).
15) M. Ashida, Y. Ueda, and T. Watanabe, *J. Polym. Sci., Polym. Phys. Ed.*, **16**, 179 (1978) and references therin.
16) R. C. Eden, *Rev. Sci. Irstrum*, **41**, 252 (1970); T. Hirooka, K. Tanaka, K. Kuchitsu, M. Fujihira, H. Inokuchi, and Y. Harada, *Chem. Phys. Lett.*, **18**, 390 (1973).
17) See, for example, G. F. Derbenwick, D. T. Pierce, and W. E. Spicer, "Methods of Experimental Physics," ed by L. Marton, Vol. 11, Academic Press, N. Y. (1974), p. 67.
18) J. P. Wesson and T. C. Williams, *J. Polym. Sci., Polym. Chem. Ed.*, **17**, 2833 (1979).
19) T. Mori, Ph D Thesis, Univ. Tokyo (1985).
20) T. A. Nguyen, M. Elian, and R. Hoffmann, *J. Am. Chem. Soc.*, **100**, 110 (1978).
21) B. Beagley, J. J. Monaghan, and T. G. Hewitt, *J. Mol. Struc.*, **8**, 401 (1971).
22) A. Karpfen, *J. Chem. Phys.*, **95**, 238 (1981), and references therein.
23) J. R. Damewood and R. West, *Macromolecules*, **18**, 158 (1985); J. R. Damewood, *Macromolecules*, **18**, 1793 (1985).
24) K. Seki and H. Inokuchi, *Chem. Phys. Lett.*, **89**, 268 (1982).
25) W. L. McCubbin and R. Manne, *Chem. Phys. Lett.*, **2**, 230 (1968).
26) L. Pauling, "The Nature of the Chemical Bond," 3rd ed, Cornell Univ. Press, Ithaca (1960).
27) K. Seki, U. Karlsson, R. Engelhardt, and E. E. Koch, *Chem. Phys. Lett.*, **103**, 343 (1984); N. Ueno, W. Gädeke, E. E. Koch, R. Engelhardt, R. Dudde, L. Laxhuber, and H. Möhwald, *J. Mol. Electron.*, **1**, 19 (1985); K. Seki, N. Ueno, U. O. Karlsson, R. Ergelhardt, and E. E. Koch, *Chem. Phys.*, **105**, 247 (1986).
28) S. Cradock, *J. Chem. Phys.*, **55**, 980 (1971); A. W. Potts and W. C. Price, *Proc. R. Soc. London*, **326**, 165 (1972).
29) B. P. Pullen, T. A. Carlson, W. E. Moddeman, G. K. Schweitzer, W. E. Bull, and F. A. Grin, *J. Chem, Phys.*, **53**, 768 (1970).
30) J. J. Pireaux and R. Caudano, *Phys. Rev.*, **B15**, 2242 (1977); J. J. Pireaux, S. Svensson, E. Basilier, P.-A. Malmqvist, U. Gelius, R. Caudano, and K. Siegbahn, *Phys. Rev.*, **A14**, 2133 (1976).
31) C. B. Duke and A. Paton, "Conductive Polymers," ed by R. B. Seymour, Plenum Press, N. Y. (1981), p. 155.
32) K. Seki, U. O. Karlsson, R. Ergelhardt, E. E. Koch, and W. Schmidt, *Chem. Phys.*, **91**. 459 (1984).
33) A. W. Potts and D. G. Streets, *J. Chem. Soc., Fradady Trans. 2.*, **70**, 875 (1974).
34) W. B. Perry and W. L. Jolly, *J. Electron Spectrosc.*, **4**, 219 (1974).
35) S. Evance, J. C. Green, P. Joachim, A. F. Orchard, D. W. Turner, and J. P. Maier, *J. Chem. Soc., Faraday Trans. 2*, **68**, 905 (1972); A. Jonas, G. K. Schweitzer, F. A. Grimm, and T. A. Carlson, *J. Electron Spectrosc.*, **1**, 29 (1972/73).
36) J. J. Pireaux, R. Caudano, and J. Verbist, *J. Electron Spectrosc.*, **5**. 267 (1974).
37) K. Seki, H. Inokuchi, and Y. Harada, *Chem. Phys. Lett.*, **20**, 197 (1973).
38) L. E. Lyons, *J. Chem. Soc.*, **1961**, 5001.
39) N. Sato, K. Seki, and H. Inokuchi, *J. Chem. Soc., Faraday Trans.* **2**, 77, 1621 (1981).
40) M. Fujihira and H. Inokuchi, *Chem. Phys. Lett.*, **17**, 554 (1972).
41) J. Tanaka, M. Tanaka, H. Fujimoto, M. Shimizu, N. Sato, and H. Inokuchi, *J. de Phys.*, **C3**, 279 (1983).
42) M. Beez, G. Bieri, H. Bock, and E. Heilbronner, *Helv. Chim. Acta*, **56**, 1028 (1973).
43) D. W. Turner, C. Baker, A. D. Baker, and C. R. Brundle, "Molecular Photoelectron Spectroscopy," John Wiley, London (1970).
44) K. Seki and H. Inokuchi, *Bull. Chem. Soc. Jpn.*, **56**, 2212 (1983).
45) K. Seki, unpublished.
46) J. E. Demuth and D. E. Eastman, *Phys. Rev. Lett.*, **32**, 1123, (1974).
47) For example, S. Shitzkovsky, M. Wegner, and H. Gutfreund, *J. de Phys. (Paris)*, **39**, 711 (1978).
48) C. Sebenne, D. Bolmont, G. Guichar, and M. Balkanski, *Phys. Rev.*, **B12**, 3280 (1975).
49) M. Takeda, M. Fujino, K. Seki, and H. Inokuchi, *Phys. Rev. B*, **15**, 8129 (1987).

The Photocatalytic Activity of a Platinized Titanium Dioxide Catalyst Supported over Silica

Kazunari DOMEN, Yoshihisa SAKATA, Akihiko KUDO, Ken-ichi MARUYA, and Takaharu ONISHI*
Research Laboratory of Resources Utilization, Tokyo Institute of Technology,
4259 Nagatsuta, Midori-ku, Yokohama 227
(Received July 4, 1987)

The effect of the amount of TiO_2 loading on the photocatalytic activity of H_2 evolution from aqueous methanol solution over a platinized TiO_2/SiO_2 catalyst was studied. UV diffuse reflectance spectra of TiO_2/SiO_2 showed the blue shift of absorption edge for the catalyst of lower amount of TiO_2 loading, which suggested the higher dispersion of TiO_2 on SiO_2. The activity decreased monotonously with the decrease of the amount of TiO_2 loading over SiO_2, i.e. with the increase of the dispersion.

Various photo-induced reactions over TiO_2 powder have been studied by many workers. For example the photo-oxidation of hydrocarbons by O_2,[1,2] photo-adsorption and desorption of O_2,[3-5] and hydrogenation of unsaturated hydrocarbons[6,7] were reported. On the other hand, the platinized TiO_2 powder is known as an effective photocatalyst for some reactions, such as photo-Kolbe reaction[8,9] and the H_2 evolution from aqueous solutions containing organic compounds.[10,11] In the latter system, the catalyst is generally regarded as a micro-photoelectrochemical cell. In that model, both the electron in the conduction band and the hole in the valence band are produced by the band gap irradiation, and then the excited electron reduces a reactant over the platinum surface, and the hole oxidizes a reactant over the TiO_2 surface. Therefore the electron and the hole have to be separated and to migrate to those reaction sites. On such "charge-separation" type reactions, the effects of the particle size[12,13] and also the crystal structures of TiO_2 (anatase, rutile, or amorphous)[14,15] upon the photocatalytic activities were reported.

Recently Anpo et al. studied the photocatalytic activities of hydrogenation of unsaturated hydrocarbons with H_2O over titanium-silicon oxides[16] and titanium oxide anchored onto porous Vycol glass.[17] They concluded that the high dispersion of titanium oxide resulted in the high activity for the reaction. In their system, localized electron-hole pair excited by photon seems to be an active species. For the "charge-separation" type reaction, however, the effect of the loading of the photoactive materials over an insulator with a large surface area has been scarcely studied.[18,19] In this paper, the activity of platinized TiO_2 supported over SiO_2 for the H_2 evolution from aqueous methanol solution is reported.

Experimental

A titanium sulfate solution (24.0% as $Ti(SO_4)_2$) was purchased from Kanto Chemical Co. and hexachloroplatinic acid was obtained from Wako Pure Chemical Ind. SiO_2 with ca. 200 $m^2 g^{-1}$ of BET surface area (Degussa) was used. A TiO_2/SiO_2 catalyst was prepared by an impregnation method: SiO_2 powder impregnated with aqueous titanium sulfate solution was stirred for 1 h and then it was dried by a rotary evaporator, followed by calcination at various temperatures for 2 h in air.

The reaction was carried out using a closed gas circulation system (ca. 300 ml) attached with a vacuum line. A reaction vessel (200 ml) made of Pyrex glass was irradiated through a flat window. An aqueous methanol solution suspended with the catalyst was stirred magnetically. The measurement of the activity of the H_2 evolution was carried out as follows. The aqueous methanol solution (typically 100 ml of methanol and 100 ml of water) containing TiO_2/SiO_2 and H_2PtCl_6 was degassed until no air peaks were detected in the gas phase by gas chromatography. Then, the solution was irradiated by an Xe lamp (USHIO, UXL 500D-O, 500 W), which was used at 300 W for obtaining a stable intensity of light for a long time. The amount of evolved H_2 was measured by gas chromatography (MS 5A column, Ar carrier) attached directly to the closed circulation system.

Catalysts were characterized using X-ray diffraction (Rigaku), X-ray photoelectron spectroscopy (Shimadzu, ESCA-750) and UV diffuse reflectance spectroscopy (JASCO UVIDEC-505). The surface area of the catalyst was determined by BET measurement. The quantum yield at 365 nm was measured using a monochrometer (H. 20, ISA JOBIN YVON Instrument) and thermopile (The Eppley Laboratory Inc.)

Results and Discussion

Characterization of TiO_2/SiO_2 Calcined at Various Temperatures. SiO_2 impregnated with aqueous $Ti(SO_4)_2$ solution was dried and calcined at various temperatures. Titanium sulfate began to decompose at about 673 K. In Table 1, the BET surface areas and

Table 1. BET Surface Areas and Ratios of XPS Peak Area of TiO_2(5 wt%)/SiO_2 Calcined at Various Temperatures

Calcination temperature	BET surface area	Ratio of peak area	
K	$m^2 \cdot g^{-1}$	Ti/Si	O/Si
673	126	0.61	0.73
833	170	0.61	0.70
998	180	0.56	0.70
1073	170	0.55	0.72

The surface area of SiO_2 used in the experimental was 202 $m^2 \cdot g^{-1}$.

the results of XPS of TiO_2(5 wt%)/SiO_2 calcined at various temperatures are shown. The surfase area increased with the increase of calcination temperature from 673 K to 833 K and it was almost constant above 833 K. Sulfur was observed on the sample calcined at 673 K by XPS, while no sulfur remained on those calcined above 998 K.

The signal intensity ratio of Ti(2p3/2)/Si(2s), decreased ca. 10% at high calcination temperatures (998 K and 1073 K), probably due to the sintering of supported TiO_2, which resulted in the decrease of the surface area. In the X-ray diffraction (XRD) pattern, no clear peak of TiO_2 was observed in TiO_2 (5 wt%)/SiO_2 at any calcination temperatures.

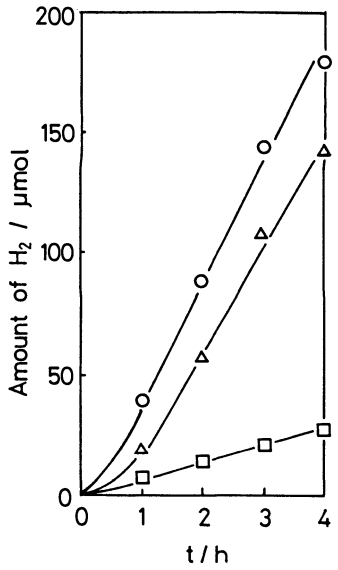

Fig. 1. H_2 evolution from aqueous methanol solution (50 vol%) over Pt-TiO_2/SiO_2 catalysts. ○: Pt(1 wt%)-TiO_2(2 wt%)/SiO_2, △: Pt(0.5 wt%)-TiO_2(2 wt%)/SiO_2, □: Pt(0.1 wt%)-TiO_2(2 wt%)/SiO_2, catalyst: 0.5 g, solution: 200 ml, an Xe lamp (500 W) was used at 300 W.

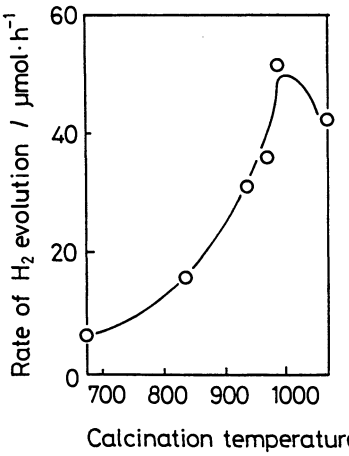

Fig. 2. Dependence of the rate of H_2 evolution from aqueous methanol solution (50 vol%) over Pt-(1 wt%)-TiO_2(5 wt%)/SiO_2 upon the calcination temperature for TiO_2/SiO_2. Catalyst: 0.5 g, solution: 200 ml.

Dependence of the Activity upon the Calcination Temperature of TiO_2/SiO_2. Typical H_2 evolution behaviours are shown in Fig. 1. The rate of the H_2 evolution was a little slower at the beginning than that at the steady state, probably due to the reduction of platinum. Therefore, the rate of the H_2 evolution at the steady state was regarded as the activity of the catalyst.

The dependence of the activity of the Pt (1 wt%)-TiO_2 (5 wt%)/SiO_2 catalyst upon the calcination temperature of TiO_2/SiO_2 is shown in Fig. 2. Pt (1 wt%)-TiO_2 (5 wt%)/SiO_2 denotes the catalyst which contains 1 wt% of Pt against TiO_2, and 5 wt% of TiO_2 against SiO_2. The activity increased markedly with the increase of the calcination temperature up to 998 K, and decreased slightly at higher temperature. Thus, in this study all the catalysts were calcined at 998 K.

UV Diffuse Reflectance Spectra of TiO_2/SiO_2. In Fig. 3, UV diffuse reflectance spectra of TiO_2/SiO_2 samples calcined at 998 K are shown. With the decrease of the amount of TiO_2, the absorption edge shifted monotonously to shorter wavelength. Similar blue shifts were previously reported in TiO_2/SiO_2 mixed oxide[16] and TiO_2 anchored on porous Vycor glass.[17] This phenomenon is interpreted by the so-called quantization effect,[20,21] which arises from the confinement of charge carriers in a semiconductor of a small volume. Thus, the blue shift of absorption spectra shown in Fig. 3 could be attributed to the change of the dispersion of supported TiO_2 on SiO_2, i.e. for the lower loading of TiO_2, higher dispersion

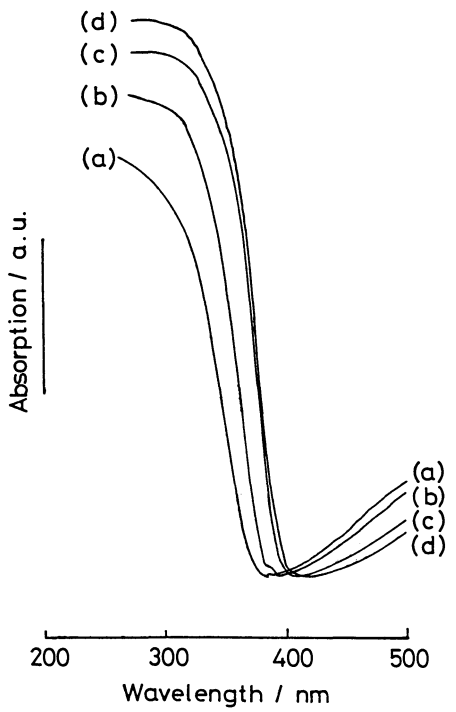

Fig. 3. UV diffuse reflectance spectra of various TiO_2/SiO_2 catalysts calcined at 998 K. (a); TiO_2(0.5 wt%)/SiO_2, (b); TiO_2(2 wt%)/SiO_2, (c); TiO_2(10 wt%)/SiO_2 (d); TiO_2(20 wt%)/SiO_2.

was achieved and, electrons and holes were confined in a smaller volume of TiO_2. Thus, it is concluded that TiO_2 is supported on SiO_2 and that the degree of the dispersion is controlled by changing the amount of the loading of TiO_2.

Dependence of the Activity upon the Amount of Pt Supported on TiO_2/SiO_2. The dependence of the activities upon the amounts of supported Pt over several kinds of TiO_2/SiO_2 catalysts are shown in Fig. 4. The activities increased in proportion to the amounts of supported platinum in the region of small platinum loading on TiO_2. This may suggest that most part of Pt, added as H_2PtCl_6, was reduced and worked as the catalyst for the H_2 evolution on TiO_2. In the higher loading region, the activities decreased gradually with the increases of the amounts of platinum. Since the color of the catalyst changed from gray to dark gray or black with the increase of Pt loading, one of the reasons for the decrease of the activity is due to the decrease of the amount of photons absorbed in TiO_2 because of the absorption of UV photons by Pt metal particles. Another one is the increase of the possibility of the recombination of an electron and a hole over platinum.

The optimum amount of Pt was different in each catalyst, as shown in Fig. 4. With the decrease of the amount of supported TiO_2 over SiO_2, the optimum ratio of Pt to TiO_2 increased.

Comparison of the Intrinsic Photocatalytic Activities of the H_2 Evolution among Pt-TiO_2/SiO_2 Catalysts. To compare the intrinsic photocatalytic activities, the amount of Pt loading was fixed at the value

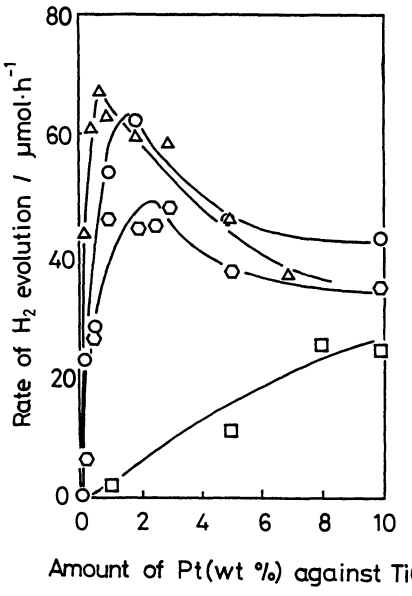

Fig. 4. Dependence of the rates of H_2 evolution from aqueous methanol solution (50 vol%) over various TiO_2/SiO_2 catalysts calcined at 998 K upon the amounts of loaded platinum. □: TiO_2(0.5 wt%)/SiO_2, ○: TiO_2(2 wt%)/SiO_2, ○: TiO_2-(5 wt%)/SiO_2, △: TiO_2(10 wt%)/SiO_2, catalyst: 0.5 g, solution: 200 ml.

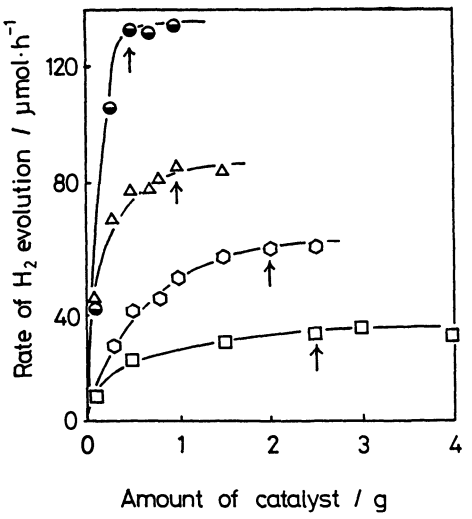

Fig. 5. Dependence of the rates of H_2 evolution from aqueous methanol solution (50 vol%) over various Pt-TiO_2/SiO_2 upon the amounts of catalysts. □: Pt(10 wt%)-TiO_2(0.5 wt%)/SiO_2, ○: Pt(2.5 wt%)-TiO_2(2 wt%)/SiO_2, △: Pt(0.5 wt%)-TiO_2(10 wt%)/SiO_2, ◒: Pt(0.25 wt%)-TiO_2(20 wt%)/SiO_2, solution: 200 ml. Arrows indicate minimum amounts of the catalysts by which the maximum rates of H_2 evolution were shown.

which each catalyst showed the maximum activity as indicated in Fig. 4. Figure 5 depicts the dependence of the rates of the H_2 evolution upon the amounts of catalysts in aqueous methanol solution. For all catalysts, the activity increased with the increase of the amount of the catalyst and reached the value which was almost independent of the amount of the catalyst. Under the condition of the saturated amount of catalyst, almost all photons, which had larger energy than the band gap of TiO_2 and entered into the reaction vessel, should be absorbed by TiO_2 although a small part of photons might go out by scattering. Therefore, the rate at the saturated amount of the catalyst was regarded as the intrinsic activity for the Pt-TiO_2/SiO_2 catalyst, which was normalized by the number of the absorbed photons. It should be noted that the number of the absorbed photons is different in each catalyst, because the UV absorption edge shifted to the shorter wavelength region with the decrease of TiO_2 loading as shown in Fig. 3. It was estimated that TiO_2 (0.5 wt%)/SiO_2 absorbed by about 30% smaller number of photons than TiO_2 (20 wt%)/SiO_2 did. On the other hand, the activity of TiO_2 (20 wt%)/SiO_2 was higher by ca. 3 times than that of TiO_2 (0.5 wt%)/SiO_2 under the same irradiation condition as shown in Fig. 5.

Thus, it is concluded that the activity of the H_2 evolution decreased monotonously with the decrease of the amount of supported TiO_2 over SiO_2. In other words, a higher dispersion catalyst exhibited the quantum efficiency of H_2 evolution lower than the lower dispersion catalyst did. In Table 2, the quantum yields are also summarized. This result is seemingly contra-

Table 2. Comparison of the Maximum Activities over Various TiO_2/SiO_2 Catalysts

Catalysts	Amounts of catalyst[a)]	Pt wt%	Amounts of TiO_2 on SiO_2	Rate of H_2 evolution	Quantum yield
	g/200 ml	wt%/TiO_2	g/200 ml	10^{-6} mol · h^{-1}	% at 365 nm
TiO_2(0.5wt%)/SiO_2	2.5	10	0.0125	29	8
TiO_2(2wt%)/SiO_2	2	2.5	0.04	58	16
TiO_2(10wt%)/SiO_2	1	0.5	0.1	86	23
TiO_2(20wt%)/SiO_2	0.5	0.25	0.1	132	35

a) The amounts of catalysts are indicated by arrows in Fig. 5.

dictory to those previously reported, i.e. the high efficiency of highly dispersed TiO_2 in SiO_2[16] and also anchored onto porous Vycor glass[17] for hydrogenation of alkyne with water. The active species for alkyne hydrogenation was regarded as localized electron-hole pairs. On the other hand, in the present case, electrons and holes have to be separated well enough to react with substrates at different sites, i.e. Pt and TiO_2 surfaces. As the detailed structure of the catalyst, Pt-TiO_2/SiO_2, is not clear one can only surmise the explanation of the result. One of the interpretations for the decrease of the activity at low TiO_2 loading region may be the low efficiency of the electron transfer from the conduction band of TiO_2 into Pt particles, which might be caused by the formation of mixed oxide of TiO_2 and SiO_2 due to the calcination at 998 K. If a part of loaded TiO_2 formed the mixed oxide with SiO_2, the diffusion length of the conduction band electron could be reduced and the effect would be more dominant for the lower TiO_2 loading catalyst.

Thus, the high dispersion of a photoactive material over an inert material with a large surface area does not simply result in the increase of the efficiency of the photocatalytic reaction for the "charge-separation" type reaction. To reveal the reason for the low efficiency of the highly dispersed TiO_2 on SiO_2, the detailed structual study of the catalyst will be of importance.

We thank Prof. Yasuhiro Iwasawa and Dr. Tetsuya Aruga, Faculty of Science, The University of Tokyo, for the measurements of UV diffuse reflectance spectroscopy.

References

1) M. Formenti, F. Juillet, and S. J. Teichner, *C. R. Acad. Sci.*, **C270**, 138 (1970).

2) M. Formenti, F. Juillet, P. Meriaudeau, and S. J. Teichner, *Chem. Tech.*, **1971**, 680.

3) R. I. Bickley, G. Munuera, and F. S. Stone, *J. Catal.*, **31**, 398 (1973).

4) G. Munuera, V. Rives-Arnau, and A. Saucedo, *J. Chem. Soc., Faraday Trans. 1*, **75**, 736 (1979).

5) G. Munuera, A. G. Gonzalez-Elipe, and J. Soria, *J. Chem. Soc., Faraday Trans. 1*, **76**, 1535 (1980).

6) A. H. Boonstra and C. A. H. A. Matsaers, *J. Phys. Chem.*, **79**, 2025 (1975).

7) M. Anpo, N. Aikawa, S. Kodama, and Y. Kubokawa, *J. Phys. Chem.*, **88**, 2569 (1984).

8) B. Kraeutler and A. J. Bard, *J. Am. Chem. Soc.*, **100**, 2239 (1978).

9) B. Kraeutler and A. J. Bard, *J. Am. Chem. Soc.*, **100**, 5985 (1978).

10) T. Kawai and T. Sakata, *Nature (London)*, **286**, 474 (1980).

11) M. R. St. John, A. J. Furgala, and A. F. Sammells, *J. Phys. Chem.*, **87**, 801 (1983).

12) T. Sakata, T. Kawai, and K. Hashimoto, *Chem. Phys. Lett.*, **88**, 50 (1982).

13) H. Harada and T. Ueda, *Chem. Phys. Lett.*, **106**, 229 (1984).

14) S. Sato, *J. Phys. Chem.*, **87**, 3531 (1983).

15) S. Nishimoto, B. Ohtani, H. Kajiwara, and T. Kagiya, *J. Chem. Soc., Faraday Trans. 1*, **79**, 2685 (1983).

16) M. Anpo, H. Nagaya, S. Kodama, Y. Kubokawa, K. Domen, and T. Onishi, *J. Phys. Chem.*, **90**, 1633 (1986).

17) M. Anpo, N. Aikawa, Y. Kubokawa, M. Che, C. Louis, and E. Giamello, *J. Phys. Chem.*, **89**, 5017 (1985).

18) N. Kakuta, K. H. Park, M. F. Finlayson, A. Ueno, A. J. Bard, A. Campion, M. A. Fox. S. E. Webber, and J. M. White, *J. Phys. Chem.*, **89**, 732 (1985).

19) A. Ueno, N. Kakuta, K. H. Park, M. F. Finlayson, A. J. Bard, A. Campion, M. A. Fox, S. E. Webber, and J. M. White, *J. Phys. Chem.*, **89**, 3828 (1985).

20) A. J. Nozik, F. Williams, M. T. Nenadovic, T, Rajh, and O. I. Micic, *J. Phys. Chem.*, **89**, 397 (1985).

21) A. J. Nozik, B. R. Thacker, J. A. Turner, and J. M. Olson, *J. Am. Chem. Soc.*, **107**, 7805 (1985).

 © 1988 The Chemical Society of Japan Bull. Chem. Soc. Jpn., 61, 363—368 (1988)

A Consideration of the Charge Density of Polyelectrolytes Based on a Layer Model in Solution

Tetsuo KANEKO
1-16, Kogane, Kazusa-cho, Matsudo-shi, Chiba-ken 270
(Received July 10, 1987)

In a model system where layers formed by aggregations of polyelectrolyte molecules are mutually parallel in a solvent, the surface-charge density of the layers is estimated by solving the one-dimensional Poisson-Boltzmann equation. The surface-charge density at a over temperature, T, can be determined depending on the number, n_g, of charged groups per unit of the volume in a layer of polyelectrolytes and on the thickness, Δx, of the layer, if the distance between layers of polyelectrolyts is sufficiently large. This surface-charge density is evaluated by assuming that n_g is given by the reciprocal of the cubed mean length between neighboring charged groups in a polyelectrolyte molecule and that Δx is of the order of an ion diameter, possibly including the hydration sheath. The surface-charge density given by the layer model agrees well with that semiempirically given by a rod-like polyelectrolyte model. Also, the ratio of the total charge of a layer to the total charge of the charged groups in the layer agrees well with the degree of the ionic dissociation of ionene polymers in a salt-free solution.

Polyelectrolytes in aqueous solutions form a strong electric field which attracts counter ions, because the molecules of the polyelectrolytes have ionizable groups with high densities. Because of the strong electric field, counter ions may condense in the charged macromolecules, and counter ions condensed in polyions may affect the charge density of the polyions. In order to interpret some properties of polyelectrolyte solutions as exhibited in the phenomenon of osmotic pressure, it is important to know the charge density of polyions. The phenomenon of the condensation of counter ions due to polyions is well-known,[1] although the charge density of polyions after the condensation of counter ions has not yet been obtained obviously on a priori grounds. Lately, Manning deduced that the condensation of counter ions on polyions composed of wormlike chains depended on the charge (of charged groups) per unit of length in a chain of polyelectrolytes.[2] If the solution of the Poisson-Boltzmann equation can be obtained in a system consisting of not freely mobile charges and freely mobile ions, the charge density of the polyion should be given. Manning noted that the statistical-mechanical phase integral for an infinite line-charge model diverges for all values of a uniform linear-charge density greater than the critical value, and he was able to estimate the condensation of counter ions on a polyion,[2] although he did not solve the Poisson-Boltzmann equation.

The purpose of the investigation in this paper is to determine the polyion-charge density by solving the Poisson-Boltzmann equation. Although the Poisson-Boltzmann equation is not readily solved, an analytically rigorous solution of the one-dimensional Poisson-Boltzmann equation for two parallel charged plates in a solution containing only counter ions has been given by Engström and Wennerström.[3]

The polyelectrolyte solution model treated in this investigation is a system in which the layers formed by aggregations of polyelectrolyte molecules are immersed in a solvent and in which the layers are parallel to each other. The charge density of the polyions in this investigation is taken as the surface-charge density on these layers; this surface-charge density is obtained by using an analytically rigorous solution given by Engström and Wennerström. The magnitute of the surface-charge density in this paper is determined from the electrostatic interaction between a polyion and counter ions. Knowledge with respect to its magnitude determined by means of the contribution of the electrostatic interaction would be useful in ascertaining the dominant factor which determines polyion-charge density. Thus, it would be valuable to estimate the surface-charge density attributable to the electrostatic contribution, although the surface-charge density in the rod-like polyelectrolyte model of Lifson and Katchalsky[4] can be estimated by using an experimentally given osmotic coefficient.

The density, n_g, of charged groups of polyelectrolytes taken into the model used in this paper is the number of charged groups per unit of volume in an aggregation of polyelectrolytes. A net-like polyelectrolyte, an ion-permeable membrane (which contains ionizable groups in its structure), etc. can be regarded as aggregations of the chains of polyelectrolytes. Therefore, their surface-charge density in water may be readily estimated if the surface-charge density of an aggregation of polyelectrolytes can be determined as a function of n_g. In addition, the thickness of a layer formed by the aggregation of polyelectrolytes must be determined in order to estimate the surface-charge density. It is considered, becuase of the size of the charged groups, that this layer thickness should have a minimum value which is not zero. The surface-charge density of a layer is estimated by assuming the minimum thickness of a layer and a sufficiently large distance between layers. As a result, it is found that the ratio of this surface-charge density to the charges attributed to charged groups in the layer is comparable with the degree of the ionic dissociation of ionene

polymers.[5]

Model

Structure of a Layer Model. A model which represents polyelectrolyte solutions as charged plates immersed in a simple salt solution has been used in order to describe the properties of polyelectrolyte solutions.[6] In this investigation, instead of the charged plates, layers consisting of polyelectrolytes are placed in a solvent, and layers of a salt-free solution interleave the layers of polyelectrolytes, as is shown in Fig. 1. This polyelectrolyte-solution model of the layer structure may be described as follows:

1) A model system is comprised of many layers consisting of layers of polyelectrolytes and layers of the solution, and these layers are parallel to each other.

2) The distances between the layers of polyelectrolytes equal $2a$.

3) All the layers of polyelectrolytes are Δx thick.

4) The number of charged groups per unit of volume in all layers of polyelectrolytes is n_g.

Electrostatic Potential. The electrostatic potential, ψ, in this layer model is described by the one-dimensional Poisson-Boltzmann equation. In accordance with the assumption of a salt-free solution, the Poisson-Boltzmann equation (SI units) within the layer of polyelectrolyte (Region 1 : $0 \leqq x \leqq \Delta x/2$) is:

$$\frac{d^2\psi_1}{dx^2} = -\frac{1}{\varepsilon}\cdot\{-z'e n_g + z e n_0 \exp[-ze\psi_1/kT]\}, \quad (1)$$

while outside the layer of polyelectrolytes (Region 2: $\Delta x/2 \leqq x \leqq 2a+\Delta x/2$) it is:

$$\frac{d^2\psi_2}{dx^2} = -\frac{z e n_0}{\varepsilon}\cdot \exp[-ze\psi_2/kT], \quad (2)$$

where ze is the charge of a counter ion, $-z'e$ is the charge of a charged group, n_0 is a normalization constant, ε is the dielectric constant of the pure solvent, k is Boltzmann's constant, and T is the absolute temperature. In addition, it has been assumed that the dielectric constant within a layer of polyelectrolytes is the same as that outside.

The boundary conditions for Eq. 2 are:

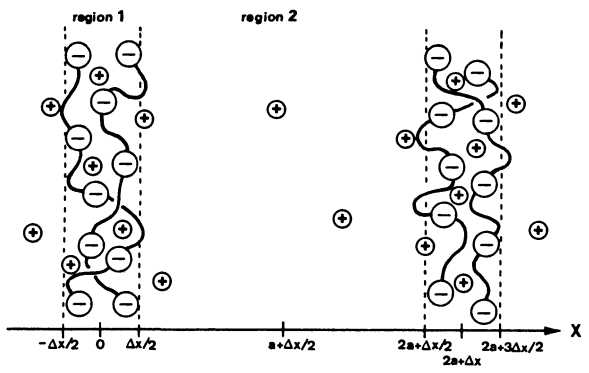

Fig. 1. Layer model of polyelectrolyte solution. Charged groups and counter ions are represented by (−) and (+) respectively.

$$\psi_2(a+\Delta x/2) = 0, \quad -\left.\frac{d\psi_2}{dx}\right|_{x=a+\Delta x/2} = 0,$$

and:

$$-\left.\frac{d\psi_2}{dx}\right|_{x=\Delta x/2} = \left.\frac{d\psi_2}{dx}\right|_{x=2a+\Delta x/2} = -\frac{\sigma}{\varepsilon}, \quad (3)$$

where $-\sigma$ is the surface-charge density on a polyelectrolyte layer.

A rigorous solution for Eq. 2 can be obtained analytically by integrating Eq. 2 twice in a manner similar to that in which a rigorous solution for two parallel charged plates was given by Engström and Wennerström.[3] As a result, the electrostatic potential in the Region 2 ($\Delta x/2 \leqq x \leqq a+\Delta x/2$) is given as follows:

$$\psi_2 = \frac{2kT}{ze}\cdot \ln\{\cos\frac{s}{a}\cdot((a+\frac{\Delta x}{2})-x)\}, \quad (4)$$

where $$s \equiv a\cdot\left(\frac{n_0 z^2 e^2}{2kT\varepsilon}\right)^{1/2}$$

On the basis of Eq. 3 and the first derivative of Eq. 4, the dimensionless parameter s can also be represented as:

$$s\tan s = \frac{\sigma z e a}{2kT\varepsilon}, \quad (5)$$

and for a sufficiently large value of the right side of Eq. 5, s approaches $\pi/2$; then the above formula becomes:

$$\tan s = \frac{\sigma z e a}{\pi kT\varepsilon}. \quad (6)$$

On the other hand, it is difficult to solve Eq. 1 analytically and rigorously. On the basis of a perturbation method used by Lifson in order to obtain an approximate analytical solution for the electrostatic potential of spherical polyelectrolytes,[7] an approximate solution of Eq. 1 can, however, be obtained.

A first approximation, v, to ψ_1 in this perturbation method means that the total charge density is zero everywhere; v must satisfy:

$$\frac{d^2v}{dx^2} = 0, \quad (7)$$

Moreover, in order to satisfy Eq. 1 v should be:

$$v = -\frac{kT}{ze}\ln f, \quad (8)$$

where:

$$f \equiv \frac{z' n_g}{z n_0}.$$

A correction function, w, for v is defined as satisfying the following equation:

$$\psi_1 = v + w. \quad (9)$$

If Taylor's expansion is carried out as follows:

$$\exp[-\frac{ze\psi_1}{kT}] = \exp[-\frac{ze}{kT}v] - \frac{ze}{kT}\cdot \exp[-\frac{ze}{kT}v]\cdot w + \cdots,$$

when Eq. 9 is substituted into Eq. 1, by considering Eqs. 7 and 8 the following differential equation for w is obtained:

$$\frac{d^2w}{dx^2} = \mu^2 w, \tag{10}$$

where $\mu^2 \equiv zz'e^2n_g/\varepsilon kT$. An approximation of w is given by solving Eq. 10.

The continuity of the electrostatic potential at $x=\Delta x/2$ and the continuity of the electrostatic field at $x=\Delta x/2$ require the following conditions, based on Eqs. 3 and 4:

$$\psi_1(\frac{\Delta x}{2}) = \frac{kT}{ze} \cdot \ln(\cos^2 s) \tag{11}$$

$$-\frac{d\psi_1}{dx}\Big|_{x=\Delta x/2} = -\frac{\sigma}{\varepsilon}.$$

The electrostatic potential, ψ_1, which is obtained by substituting the solution of w from Eq. 10 into Eq. 9 and which satisfies the above conditions, is given as follows:

$$\psi_1 = -\frac{kT}{ze}\cdot\ln f + \frac{kT}{ze}\cdot\{\frac{1}{2}(\ln(\cos^2 s)+\ln f)+\frac{\Lambda\sigma}{\sqrt{2}}\}\cdot \exp[-\mu(\frac{\Delta x}{2}-x)] + \frac{kT}{ze}\cdot\{\frac{1}{2}(\ln(\cos^2 s)+\ln f) - \frac{\Lambda\sigma}{\sqrt{2}}\}\cdot\exp[\mu(\frac{\Delta x}{2}-x)], \tag{12}$$

where $\Lambda^2 \equiv z/(2z'kT\varepsilon n_g)$.

Surface-Charge Density. The demand of electrostatic field continuity in Region 1 ($-\Delta x/2<x<\Delta x/2$) imposes a restriction on the exponential coefficients in Eq. 12. The demand is:

$$-\frac{d\psi_1}{dx}\Big|_{x=0} = 0, \tag{13}$$

because the sign of the electrostatic field at $x>0$ differs from that at $x<0$ in the region close to $x=0$ if the distribution of counter ions on the right side of a layer equals that on the left side of the layer. Equation 13 requires that the exponential coefficients in Eq. 12 satisfy the following equation:

$$\ln f = \sqrt{2}\Lambda\sigma\cdot\{\tanh[\mu\Delta x/2]\}^{-1} - \ln\cos^2 s. \tag{14}$$

The continuity of counter-ion distribution in all regions of the system leads to a formula independent of Eq. 14 on the basis of the electrostatic potential at $x=\Delta x/2$, the second derivative of the potential, and the definition of f. By considering Eq. 11, the density of counter ions $n(x)$ at $x=\Delta x/2$ is:

$$n(\Delta x/2) = n_0\cdot\exp[-\frac{ze\psi_1(\Delta x/2)}{kT}] = \frac{n_0}{\cos^2 s}. \tag{15}$$

On the other hand, by considering Eq. 5, the second derivative of $\psi_2(x)$ given by Eq. 4 yields:

$$n(\Delta x/2) = \frac{\sigma^2}{2kT\varepsilon} + \frac{2kT\varepsilon s^2}{(zea)^2}. \tag{16}$$

If the magnitude of a is of the order of 10^2 Å and the magnitude σ is of the order of 10^{-2} C·m^{-2}, even though the magnitude of s is the maximum $\pi/2$, the second term on the right side of Eq. 16 is much smaller than the first term. Hence, under the condition that the second term can be neglected, the following equation is obtained:

$$n(\Delta x/2) = \frac{\sigma^2}{2kT\varepsilon}. \tag{17}$$

By substituting Eq. 17 into Eq. 15, the following formula is obtained:

$$n_0 = \frac{\sigma^2}{2kT\varepsilon}\cdot\cos^2 s. \tag{18}$$

When, Eq. 18 is substituted into the definition of f,

$$\ln f = -2\ln\Lambda\sigma - \ln\cos^2 s. \tag{19}$$

By equating Eq. 14 with Eq. 19, we obtain the following formula for the surface-charge density of the layer of polyelectrolytes:

$$\frac{\Lambda\sigma}{\ln\Lambda\sigma} = -\sqrt{2}\tanh[\mu\Delta x/2]. \tag{20}$$

In addition, in accordance with the sign on the right side of Eq. 20 and its magnitude, the magnitude of $\Lambda\sigma$ is close to 1 and must satisfy $\Lambda\sigma<1$. Therefore, $\ln\Lambda\sigma$ may be represented approximately as follows:

$$\ln\Lambda\sigma = -2(1-\sqrt{\Lambda\sigma}).$$

On the basis of this approximation and Eq. 20, the surface-charge density can be described as:

$$-\sigma = -\frac{Y}{2\Lambda}\{(Y+2)-\sqrt{(Y+4)Y}\}, \tag{21}$$

where: $Y \equiv 2\sqrt{2}\tanh[\mu\Delta x/2]$.

Parameters in $-\sigma$. Both the surface-charge density, $-\sigma$, given by Eq. 20 and that given approximately by Eq. 21 depend on only three parameters: n_g, Δx, and T, when Eq. 17 is satisfied. f depends on four parameters: n_g, Δx, a, and T, as may be seen in both Eq. 14 and Eq. 19 because s depends on four parameters: n_g, Δx, a, and T, as may be seen in Eq. 5. Hence, the electrostatic potential, the electrostatic field, and the density of counter ions at a certain position x depend on four parameters: n_g, Δx, a, and T.

In order to estimate $-\sigma$, the n_g and Δx parameters must be determined. It is considered that the density n_g must be equivalent to the density of charged groups in a polyion dispersed in a solution, if we are to describe the charged circumstance of the polyion according to the layer model, and it is assumed that, while the distance, b, between neighboring charged groups in a polyion dispersed in a salt-free solution is held constant, charged groups in polyelectrolyte molecules are packed in a layer of polyelectrolytes. Thus, n_g is given as follows:

$$n_g = 1/b^3. \tag{22}$$

The density n_g given by Eq. 22 is regarded as the density approximately equivalent to the density of charged groups in a polyion. In addition, Fujii has found[5] that the distance between neighboring charged groups (obtained by substituting the degree of ionic dissociation, ξ^{-1}, of polyions found experimentally in a sufficiently dilute salt-free solution of ionene polymers into the formula given by Manning: $\xi^{-1}=(e^2/\varepsilon kTb)^{-1}$ (CGS-esu)) is approximately equal to the mean distance between neighboring charged groups in the polyion chain, which is regarded as a freely rotating methylene chain. Therefore, the density n_g, obtained on the basis of Eq. 22 by assuming that the distance, b, between neighboring charged groups in a flexible polyelectrolyte can be taken as the mean distance between neighboring ionizable groups in a freely rotating methylene chain, is used to calculate $-\sigma$ when a polyelectrolyte solution described by the layer model is a sufficiently dilute salt-free solution.

The thickness, Δx, of a layer is another parameter affecting $-\sigma$ and must be determined in order to calculate $-\sigma$. This thickness, Δx, should have a minimum which is not zero because of the size of the charged groups. The most dilute condition in the layer model system corresponds to the condition that Δx is at its minimum and the distance between layers is infinite. Therefore, it is considered that $-\sigma$, compared with the charge density of a polyion in a sufficiently dilute salt-free solution, should be calculated under the condition that Δx is at its minimum; in order to calculate this surface-charge density, $-\sigma$, it is assumed that Δx is at its minimum and that Δx is of the order of an ion diameter, possibly including the hydration sheath, when the polyelectrolyte is flexible.

Results and Discussion

Surface-Charge Density. The electrostatic potential, the electrostatic field, and the density of counter ions in the layer model treated here depend on these parameters: n_g, Δx, a, and T.

The surface-charge density $-\sigma$ depends on these parameters: n_g, Δx, and T, when the magnitude of a is larger than the order of 10^2 Å. Moreover, when the magnitude of Δx is larger than several angstroms, the $-\sigma$ value given by Eq. 21 becomes independent of, Δx, as is shown in Fig. 2. This independence from Δx is hardly affected by the magnitute of n_g, and it is interesting that the magnitude of Δx at which the independence begins to appear nearly equals the order of an ion diameter, possibly including the hydration sheath. The behavior of $-\sigma$, which become independent of Δx, suggests that, although several polyelectrolytes are associated with one another, the charge density of polyions may be invariable in a sufficiently dilute solution.

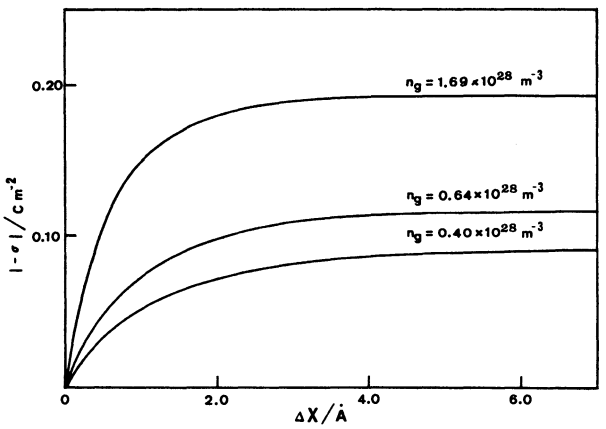

Fig. 2. The dependence of $-\sigma$ on Δx at 298 K on the basis of Eq. 21. The physical meaning of $-\sigma$ is incomplete at the magnitude of Δx which is smaller than a minimum thickness.

Electrostatic Potential. The dependence of the electrostatic potential on a may be seen from the following formulae, which are obtained from Eq. 4 and Eq. 12 by considering Eqs. 6 and 19, when a is sufficiently large: at $0 \leqq x < \Delta x/2$ (in a layer of polyelectrolytes):

$$\psi_1(x) = -\frac{2kT}{ze}\cdot\ln\left(\frac{\sqrt{2}}{\pi}\mu a\right) - \frac{kT}{ze}\cdot\left\{\left(\frac{\Delta\sigma}{\sqrt{2}}+\ln\Delta\sigma\right)\cdot\exp\left[\mu\left(\frac{\Delta x}{2}-x\right)\right] - \left(\frac{\Delta\sigma}{\sqrt{2}}-\ln\Delta\sigma\right)\cdot\exp\left[-\mu\left(\frac{\Delta x}{2}-x\right)\right]\right\} \quad (23)$$

and at $\Delta x/2 \leqq x$ (in the vicinity of the layer surface where $\{\pi(x-\Delta x/2)/2a\}^2 \ll 1$ is satisfied):

$$\psi_2(x) = -\frac{2kT}{ze}\cdot\ln\left(\frac{\sqrt{2}}{\pi}\Delta\sigma\mu a\right)+\frac{2kT}{ze}\cdot \ln\left\{1+\frac{1}{\sqrt{2}}\Delta\sigma\mu\left(x-\frac{\Delta x}{2}\right)\right\}. \quad (24)$$

The increase in the absolute value of the potential in accordance with the increase in a, as noted by Engström and Wennerström,[3] is shown in Eqs. 23 and 24. Equations 23 and 24, however, indicate that the difference in potential $\psi(x_1)-\psi(x_2)$ between the x_1 and x_2 positions which satisfies $\{\pi(x-\Delta x/2)/2a\}^2 \ll 1$ is independent of a.

Electric Field. As is suggested by the property of the potential mentioned above, when a is sufficiently large the electrostatic field $-\varepsilon\,d\psi/dx$ at a position which satisfies $\{\pi(x-\Delta x/2)/2a\}^2 \ll 1$ is independent of a, as is shown in the following formulae:
at $0 \leqq x < \Delta x/2$ (in a layer of polyelectrolytes):

$$-\varepsilon\cdot\frac{d\psi_1}{dx} = \frac{-1}{\sqrt{2}\Delta}\cdot\left\{\frac{\Delta\sigma}{\sqrt{2}}+\ln\Delta\sigma\right\}\cdot\exp\left[\mu\left(\frac{\Delta x}{2}-x\right)\right] - \frac{1}{\sqrt{2}\Delta}\cdot\left\{\frac{\Delta\sigma}{\sqrt{2}}-\ln\Delta\sigma\right\}\cdot\exp\left[-\mu\left(\frac{\Delta x}{2}-x\right)\right], \quad (25)$$

and at $\Delta x/2 \leqq x$ (where $\{\pi(x-\Delta x/2)/2a\}^2 \ll 1$ is satisfied):

$$-\varepsilon\cdot\frac{d\psi_2}{dx} = -\sigma\cdot\left\{1+\frac{1}{\sqrt{2}}\cdot\Delta\sigma\mu\left(x-\frac{\Delta x}{2}\right)\right\}^{-1}. \quad (26)$$

The property of this electrostatic field suggests that the number of counter ions which are distributed within a closed surface covering a polyion and close to the polyion itself is independent of the concentration of polyelectrolytes in a sufficiently dilute salt-free solution.

Density of Counter Ions. As is suggested by the property of the electrostatic field mentioned above, when a is sufficiently large the density of counter ions $n(x)$ at a position which satisfies $\{\pi(x-\Delta x/2)/2a\}^2 \ll 1$ is independent of a, and $n(x)$ is given by the following formulae: at $0 \leqq x < \Delta x/2$ (in a layer of polyelectrolytes):

$$n(x) = \frac{z'}{z} \cdot n_g \cdot \exp\left[\left\{\frac{\Delta\sigma}{\sqrt{2}} + \ln \Delta\sigma\right\} \cdot \exp\left[\mu\left(\frac{\Delta x}{2} - x\right)\right]\right.$$
$$\left. - \left\{\frac{\Delta\sigma}{\sqrt{2}} - \ln \Delta\sigma\right\} \cdot \exp\left[-\mu\left(\frac{\Delta x}{2} - x\right)\right]\right], \quad (27)$$

and at $\Delta x/2 \leqq x$ (where $\{\pi(x-\Delta x/2)/2a\}^2 \ll 1$ is satisfied):

$$n(x) = \frac{1}{\sqrt{2}} \cdot \Delta\sigma\mu \cdot \left(\frac{\sigma}{e}\right) \cdot \left\{1 + \frac{1}{\sqrt{2}} \cdot \right.$$
$$\left. \Delta\sigma\mu \cdot \left(x - \frac{\Delta x}{2}\right)\right\}^{-2}. \quad (28)$$

Equation 27 is given by substituting Eq. 23 into $n_0 \cdot \exp[-ze\psi/kT]$ and by considering Eqs. 6 and 18. Similarly, Eq. 28 is obtained by substituting Eq. 24 into $n_0 \cdot \exp[-ze\psi/kT]$. The property of $n(x)$ mentioned here suggests that the density of counter ions close to a polyion is independent of the concentration of polyelectrolytes in a sufficiently dilute salt-free solution.

Evaluation of $-\sigma$. The surface-charge density $-\sigma$ and the $\sigma/(en_g\Delta x/2)$ ratio, calculated under the conditions that Δx is the minimum thickness and a is sufficiently large, agree well with the polyion-charge density[8] (given by the rod-like model of a polyelectrolyte) and the degree of ionic dissociation[5] of a polyelectrolyte (found experimentally in a sufficiently dilute salt-free solution) respectively, as may be seen in Tables 1 and 2. These results suggest that the layer model is a good approximate description of a polyelectrolyte solution. Also, the charged-groups packing density n_g assumed in the Model and the determination of Δx mentioned in the Model both seem reasonable when a sufficiently dilute salt-free solution of flexible polyelectrolytes is described according to the layer model. As a result, although the layer model is a one-dimensional model system, it seem that this model can lead to a quantitative description of the charged circumstance of a polyion.

The values of $-\sigma$ and σ shown in Tables 1 and 2 were calculated by determining n_g from Eq. 22 and by using Eq. 21, at 298 K. It is assumed that the minimum thickness of a layer of polyelectrolytes is 3 Å,[3] regarded as the order of an ion diameter, possibly including its hydration sheath. $-\sigma_{rod}$ in Table 1 is the surface-charge density given by the rod-like model of a polyelectrolyte. $-\sigma_{rod}$ is obtained by using the dimensionless parameter λ[8] in CGS-esu as follows:

$$-\sigma_{rod} = -(\varepsilon kT/2\pi re) \cdot \lambda,$$

where r is the radius of the rod-like model. λ may be calculated[4] on the basis of the osmotic coefficient of a salt-free polyelectrolyte solution. The λ calculated as described here is $\lambda_{effective}$[8] in Table 1. The $\sigma/(en_g\Delta x/2)$ ratio, shown in Table 2, represents the charged rate of a layer of polyelectrolytes, because σ is the total charge within a cylinder of unit cross section; it ends at $x=0$ and $x=\Delta x/2$ and is parallel to the x-axis.

In the layer model, counter ions permeate into a layer of polyelectrolytes. Consequently, the condensation of counter ions implies that counter ions are condensed between charged groups. The counter ions located between charged groups contribute to the relaxation of the positive electrostatic energy and to the relaxation of tension induced in a methylene chain by the repulsion between charged groups. If it is noted that the $\sigma/(en_g\Delta x/2)$ ratio agrees well with the degree of dissociation ξ^{-1} given experimentally, it may be considered that the counter ions mentioned above are located between the charged groups, even though a

Table 1. $-\sigma_{rod}$ and $-\sigma$ for Polyacrylate at 298 K

α[a]	r / Å	$\lambda_{effective}$	$-\sigma_{rod}$[c] / C·m^{-2}	$-\sigma$[d] / C·m^{-2}
0.8	6	4	−0.24	−0.17
0.3	6	2.4	−0.14	−0.10
0.1	6	1.25	−0.07	−0.05
1	6	3.0[b]	−0.18	−0.19

a) Degree of ionization b) $\lambda_{effective}$ for the vinylic polyelectrolytes at sufficiently high degrees of ionization is found to be about twice the magnitude calculated for the wholly stretched chain.[8] This value of λ is represented as:

$$\lambda_{stretched} = \alpha e^2/\varepsilon k\, Tl \text{ (CGS-esu)},$$

where l is the distance between neighboring charged groups. For polyacrylate, $l \fallingdotseq 4.9$ Å and so $\lambda_{stretched}=1.5$. c) Values reduced to SI units d) Values calculated by means of Eq. 21 (the mean distance between neighboring -COOH's in the polyacrylate molectule is taken as 3.9 Å and considering the degree of ionization: $n_g=\alpha/(3.9)^3/\text{Å}^{-3}$.)

Table 2. The Degree of the Ionic Dissociation[5] of Ionene Bromide and the Change Density on a Layer of This Polyelectrolyte at 298 K

Polyelectrolyte	b[a] / Å	ξ^{-1}[b]	σ[c] / C·m^{-2}	$\sigma/en_g\Delta x/2$
3.3-ionene bromide	3.9	0.576	0.189	0.47
4.4-ionene bromide	4.5	0.628	0.149	0.56
6.6-ionene bromide	5.4	0.745	0.109	0.71
8.8-ionene bromide	6.3	0.876	0.081	0.84

a) The mean distance between neighboring ionizable groups in a freely rotating methylene chain. b) The measured degree of ionic dissociation.[5] c) The values given by Eq. 21.

polyelectrolyte solution is a sufficiently dilute salt-free solution.

Conclusion

The layer model of a polyelectrolyte solution treated here has a structure in which layers of polyelectrolytes are arranged in a parallel manner in a solvent. The electrostatic potential, the electrostatic field, and the density of counter ions within and outside the layers are determined on the basis of solutions of the one-dimensional Poisson-Botzmann equation; they depend on the thickness, Δx, of the layers; the distance, $2a$, between the layers; the density, n_g, of charged groups in the layers; and the absolute temperature T. When a is sufficiently large, the electrostatic field and the density of counter ions within a layer of polyelectrolytes become independent of a. Outside the layer also, the electrostatic field and the density of counter ions become independent of a at positions which satisfy $\{\pi(x-\Delta x/2)/2a\}^2 \ll 1$. These results suggest not only that the charge density of a polyion is independent of the concentration of polyelectrolytes in a sufficiently dilute salt-free solution, but also that the distribution of counter ions close to a polyion is independent of thier concentration.

The surface-charge density $-\sigma$ on a layer of polyelectrolytes in the layer model depends only on Δx, n_g, and T, as determined from the properties of the electrostatic field when a is sufficiently large. The surface-charge density $-\sigma$ given by Eq. 21 for polyacrylate when a is sufficiently large is comparable to the $-\sigma_{rod}$ value semiempirically givien by the rod-like model of polyelectrolytes. Also, the charged rate, $\sigma/(en_g\Delta x/2)$, of layers of polyelectrolytes calculated by using the σ value given by Eq. 21 agrees with degree of dissociation of counter ions in salt-free solutions of ionene bromides at an infinite dilution. In addition, it has been assumed that the methylene chain of polyelectrolyte rotates freely and that n_g is given by the reciprocal of the cubed mean length between neighboring ionizable groups in the chain in calculating $-\sigma$ and $\sigma/(en_g\Delta x/2)$; also, it has been assumed that Δx is of the order of an ion diameter, possibly including the hydration sheath.

The surface-charge density $-\sigma$ comparable to $-\sigma_{rod}$ and the $\sigma/(en_g\Delta x/2)$ ratio comparable to the degree of the ionic dissociation of the ionene polymer suggest that, although the layer model is one-dimensional, the charged circumstance of a polyion may be quantitatively described according to the layer model. Therefore, it may be concluded that the layer model can lead to a quantitative estimation of the charged circumstance of a polyion, while $-\sigma$ in the layer model can be determined from Δx, n_g, and T when the solution of polyelectrolytes is salt-free and is sufficiently dilute.

Appendix

The mean distance, $(\overline{d^2})^{1/2}$, between the neighboring ionizable groups in a freely rotating methylene chain is given by the following formula:

$$\overline{d^2} = n l^2 \cdot \left\{\frac{1-\cos\theta}{1+\cos\theta} + \frac{2-\cos\theta}{n} \cdot \frac{1-(-\cos\theta)^n}{(1+\cos\theta)^2}\right\},$$

where n is the number of bonds between neighboring ionizable groups, l is the bond length, and θ is the bond angle. $\overline{d^2}$ is calculated by assuming that both C-C and C-N bond lengths are 1.5 Å, while both C-C-C and C-C-N bond angles are 109.5°.

The author wished to express his thanks to Dr. Kazumi Kogure for her many helpful discussion and to Hideo Mizutani for his valuable discussion.

References

1) A. Katchalsky, Z. Alexandrowicz, and O. Kedem, "Polyelectrolyte Solutions," in "Chemical Physics of Ionic Solutions," ed. by B. E. Conway and R. G. Barradas, John Wiley & Sons, New York (1966), Chap. 15, pp. 318—321.

2) G. S. Manning, *J. Chem. Phys.*, **51**, 924 (1969).

3) S. Engström and H. Wennerstörm, *J. Phys. Chem.*, **82**, 2711 (1978).

4) S. Lifson and A. Katchalsky, *J. Polym. Sci.*, **13**, 43 (1953).

5) M. Fujii, *J. Polym. Sci.*, **24**, 39 (1986).

6) J. Th. G. Overbeek, *Prog. Biophys. Biophys. Chem.*, **6**, 57 (1956).

7) S. Lifson, *J. Chem. Phys.*, **27**, 700 (1957).

8) Z. Alexandrowicz and A. Katchalsky, *J. Polym. Sci., Part A*, **1**, 3231 (1963).

 © 1988 The Chemical Society of Japan Bull. Chem. Soc. Jpn., 61, 369—373 (1988)

Solution Structure and Preferred Orientation of 3,7-Dibromo-10*H*-phenothiazine Dissolved in Nematic Liquid Crystal†

Hideaki FUJIWARA*, Masayuki WATANABE, Iwao YAMANAKA, Tatsuya TAKAGI, and Yoshio SASAKI
Faculty of Pharmaceutical Sciences, Osaka University, 1-6 Yamadaoka, Suita, Osaka 565
(Received August 14, 1987)

The NMR spectrum of the title compound has been measured in nematic phase ZLI1167 and analyzed to obtain the direct couplings. The direct couplings were interpreted by assuming a folded structure of the tricyclic framework. The dihedral angle of the two phenyl rings is determined to be 149.1±2.5° and a value of 170±3° is obtained for the angle of S···N-H. The NH proton is concluded to occupy a "equatorial" position on the central ring in a boat form. The preferred orientation of the molecule in ZLI1167 is discussed by comparing the principal axes of order tensor with those of the moment of inertia.

NMR studies of molecules oriented in liquid crystals provide important information on the molecular structure and preferred orientation in mobile state. These studies for some tricyclic compounds **1** folded along a symmetry axis have proved that the angle of

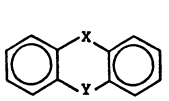

1
The tricyclic framework

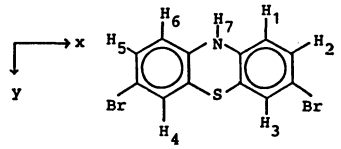

2
3,7-Dibromo-10*H*-phenothiazine

folding (dihedral angle) changes depending on the state of compound investigated.[1-5] For example, dihedral angles of 131.4° in gaseous state,[6] 128° in crystals,[7,8] and 141.6°[2] and 140.6°[1] in solution (of nematic liquid crystals) have been reported for thianthrene (X=Y=S in **1**). These facts stimulate systematic works on structural parameters including the dihedral angle in the mobile state. In the present study, 3,7-dibromo-10*H*-phenothiazine (**2**) is taken up among derivatives of the phenothiazines. The tricyclic compounds phenothiazines are interested because they include a number of important drugs with tranquilizing, antihistaminic, and antiemetic activities.

Experimental

3,7-Dibromo-10*H*-phenothiazine was synthesized by the bromination of 10*H*-phenothiazine.[9] The raw product was

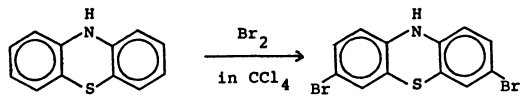

recrystallized from toluene after decolorizing by sodium dithionite $Na_2S_2O_4$. Melting point of the final product (pale green) was 206—209 °C (lit, 197—198 °C,[9] 190—196 °C,[10] and 206—207 °C[11]).

3,7-Dibromo-10*H*-phenothiazine was dissolved in nematic solvent ZLI1167 (Merck) by 5.2 wt%. ^{1}H NMR spectrum was measured on a XL-200 NMR spectrometer operating at 200 MHz. The temperature of measurement was 34.1 °C. Fids of 5000 transients were accumulated using a 40° (4 μs) pulse at an interval of 0.4 s and Fourier transformed to obtain a spectral width of 8 kHz for the data point of 16k. A convolution difference was taken to remove very broad background signals originating from the solvent. The resulting line width was ca. 10 Hz in the center and ca. 20 Hz at the edges of the spectrum. The preliminary spectra were considerably broadened probably because of a contamination with some metallic or radical impurities, and hence a small amount of 1,10-phenanthroline was added to obtain the final sharp spectrum. Normal spectrum in an isotropic medium was taken on a Hitachi R-22 NMR spectrometer in CW mode at 90 MHz and at the probe temperature of 34.1 °C. The solvent used was a mixture (20/80 in volume) of dimethyl sulfoxide and carbon tetrachloride which was suited for a better separation in chemical shifts.

Analysis of NMR spectra obtained in the nematic phase was made by the programs LAO3D9 and LAO3D9D. These programs are modified versions of LAOCN3 and applicable up to 9 spins. These versions have been written in double precision and LAO3D9D includes a damping route as reported by the authors.[5] The resulting direct couplings were analyzed by the program SHAPE[12] to obtain structural and order parameters. Only the variance in LAOCN calculation was input for the error analysis. All the above calculations were done on NEAC S-1000 and SX-1 computers at the Computation Center in Osaka University.

Results

3,7-Dibromo-10*H*-phenothiazine has C_s symmetry and exhibits spectra with the seven spin system of AA'BB'CC'D. It includes four chemical shifts (δ_1, δ_2, δ_3, and δ_7) and twelve direct couplings (D_{12}, D_{13}, D_{14}, D_{15}, D_{16}, D_{17}, D_{23}, D_{24}, D_{25}, D_{27}, D_{34}, D_{37}) besides the twelve indirect couplings J_{ij} as independent variables. Among these parameters the indirect couplings were fixed at the values observed in an isotropic medium as usually done[13] when the indirect couplings show no discernible solvent dependency. The values used were J_{12}=8.20 and J_{23}=2.20 Hz observed in the mixed solvent above mentioned, other indirect couplings being negligibly small. The LAOCN iteration calculation has given rms error of 1.35 Hz for the ninety seven of the observed and the simulated transition frequencies.

† NMR Study of Molecules in Anisotropic Systems. VI.

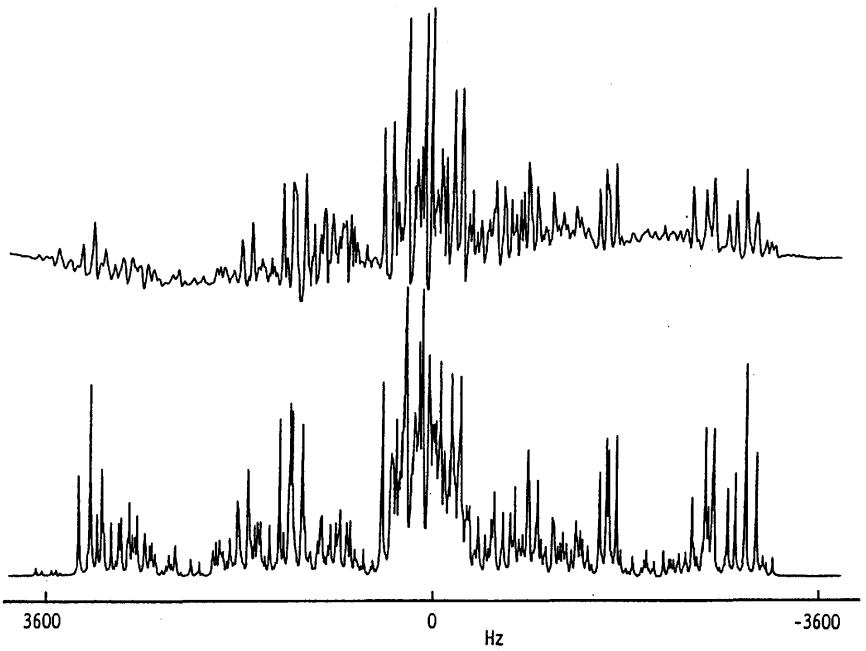

Fig. 1. Experimental(upper) and simulated(lower) NMR spectra of ^1H for 3,7-dibromo-10*H*-phenothiazine dissolved in nematic solvent ZLI1167.

Table 1. NMR Parameters of 3,7-Dibromo-10*H*-phenothiazine Dissolved in Nematic Phase ZLI1167

Direct coupling/Hz:			
D_{12}	822.91±0.14	D_{34}	97.82±0.17
D_{13}	58.97±0.22	D_{37}	56.17±0.21
D_{14}	32.65±0.24		
D_{15}	45.97±0.19	Chemical shift/Hz:[a]	
D_{16}	161.49±0.40	ν_1	−67.32±0.25
D_{17}	1026.67±0.15	ν_2	48.01±0.24
D_{23}	98.65±0.20	ν_3	68.36±0.23
D_{24}	23.77±0.21	ν_7	331.08±0.35
D_{25}	21.77±0.29		
D_{27}	135.22±0.22		

a) Given in Hz at 200 MHz relative to the carrier frequency. Positive toward the low field side.

The simulated spectrum is shown in Fig. 1 together with that observed. The experimental line width is broader at the edges of the spectrum. This is caused by a temperature fluctuation on the sample and also probably by a trace amount of impurities which remain unmasked even on addition of 1,10-phenanthroline. The NMR parameters determined are listed in Table 1. The chemical shifts of H_2 and H_3 are reversed in order in the nematic phase compared to those in an isotropic medium where $\delta_2-\delta_1=0.356$ ppm, $\delta_3-\delta_1=0.267$ ppm, and $\delta_7-\delta_1=1.889$ ppm have been obtained in the above mixed solvent. This may be due to a solvent effect. The direct couplings obtained are analyzed by the program SHAPE. The resulting order parameters and the structural parameters are listed in Table 2 (case 1).

Table 2. Structural Parameters and Order Parameters of 3,7-Dibromo-10*H*-phenothiazine Dissolved in ZLI1167

	Case 1[a]	Case 2[a]	10*H*-phenothiazine[a]
Distance ratio			
r_{13}/r_{12}	2.089±0.014	2.092±0.013	1.979
r_{14}/r_{12}	2.943±0.017	2.958±0.013	2.860
r_{15}/r_{12}	2.856±0.024	2.854±0.025	2.835
r_{16}/r_{12}	1.907±0.019	1.904±0.018	1.902
r_{17}/r_{12}	1.003±0.014	1.003±0.013	0.969
r_{23}/r_{12}	1.943±0.039	1.952±0.045	1.750
r_{24}/r_{12}	3.497±0.044	3.525±0.055	3.368
r_{25}/r_{12}	3.753±0.036	3.753±0.036	3.697
r_{27}/r_{12}	1.927±0.019	1.929±0.020	1.858
r_{34}/r_{12}	2.253±0.022	2.296±0.041	2.240
r_{37}/r_{12}	2.171±0.025	2.175±0.027	2.248
Angle			
ϕ_0[b]	150.6±2.1	149.1±2.5	158.5
θ_0[c]	172.7±3.1	170.5±3.4	181.9
	(171.4±3.1)	(169.3±3.4)	
Order parameter[d]			
S_{xx}	−0.1219±0.0003	−0.1223±0.0009	
S_{zz}	0.1798±0.0023	0.1834±0.0013	
S_{yz}	0.0672±0.0177	0.0659±0.0234	

a) Case 1: The ring inversion motion is not included in the SHAPE calculation. Case 2: The ring inversion motion is included. 10*H*-phenothiazine: Crystal data are cited for the parent compound(orthorhombic)[19] because such data are lacking for the dibromo derivative. b) The dihedral angle. c) The angle of S···N-H. See text for detail. d) $r_{12}=2.356$ Å assumed.[19]

Discussion

The framework of phenothiazine is known to be

folded and to interconvert very rapidly between two equivalent structures:

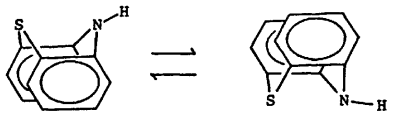

The barrier to inversion is reported to be 2.87[14] and 2.4[15] kcal mol^{-1} for 10*H*-phenothiazine from dielectric relaxation studies, but no data are available for the dibromo derivative. In the above calculation (case 1 in Table 2), the barrier to this inversion is assumed to be so high that only the ground state is occupied at the measurement temperature. In this regard, correlation between the internal motion and the overall molecular reorientation[16-18] can affect the calculation. When the barrier to internal motion is very low and the rate of internal motion is much faster than that of the whole molecular reorientation, only a set of the order parameters is sufficient to describe the orientational behavior of the molecule and the molecular structure reflects a statistical average of the fast internal motion. This is the case for the internal rotation of methyl group. But when the rate of internal motion is comparable to or slower than that of the whole molecular reorientation, order parameters can differ in each step of the internal motion and in principle an infinite number of the order parameters are needed. In the present study, calculations were also attempted under the fast inversion limit: a potential function of Eq. 1 was adopted,

$$V=V_0\{(\psi/\psi_0)^4-2(\psi/\psi_0)^2\},\quad \psi=(\pi-\phi)/2 \qquad (1)$$

where V_0 is the inversion barrier and ϕ is the dihedral angle between the two phenyl rings, ϕ_0 being this angle at ground state. An alternative function is proposed by Higashi et al.,[15] which has a singular point at $\phi=\pi$ and is not used here. Statistical averaging of the direct couplings under such inversion motion can be achieved by following equation

$$\langle D_{ij}\rangle=\int D_{ij}(\psi)P(\psi)\,d\psi \qquad (2)$$

where $\langle\ \rangle$ means the statistical average and where $D_{ij}(\psi)$ and $P(\psi)$ are the direct coupling and the distribution function, respectively, calculated under a dihedral angle of ϕ. This distribution function is given by Eq. 3.

$$P(\psi)\,d\psi=\exp(-V/RT)\,d\psi/\int\exp(-V/RT)\,d\psi \qquad (3)$$

To perform the integration in above equations, ϕ was changed from 80° to 180° in 0.1° step and integrated numerically. Subroutines were added to SHAPE for this calculation: DIHED to calculate the dihedral angle for the ground state, XYZIM to give new coordinates for the dihedral angles changed stepwise, and CALCUD to derive the direct couplings for the variable dihedral angles. Only one set of the order parameters are defined since the very rapid rate of the inversion motion is assumed. The barrier was set equal to 2.4 kcal mol^{-1}. An effort to determine this barrier from the simulation of the direct couplings was unsuccessful. The results of calculation are also summarized in Table 2 (case 2). The weighted rms error between the observed and the simulated direct couplings was almost the same in the two cases, i.e., 0.240 Hz (case 1) and 0.239 Hz (case 2). In fact, the recalculated values of D_{ij} were the same in the two cases, and only those of D_{15}, D_{24}, and D_{25} deviated from the experimental values by slightly more than their probable errors, i.e., D_{15}=46.45, D_{24}=23.30, and D_{25}=21.19 Hz. Therefore, it may be concluded that the experimental values of D_{ij} have failed to distinguish between the two cases because of their relatively large errors coming from the line broadening in the spectrum. A more elaborate analysis of the direct couplings assuming a correlation between the inversion and the whole molecular reorientation was not attempted, since the barrier to inversion was not known for the dibromo derivative and the experimental values of D_{ij} were not so accurately obtained as to make the barrier determinable in that analysis. However, the structural parameters and the order parameters derived above deserve further discussion as described below.

Molecular Structure of 3,7-Dibromo-10*H*-phenothiazine Dissolved in ZLI1167. The dihedral angle (ϕ_0) and the angle of S···N-H (θ) in the ground state are listed in Table 2. The latter angle is determined assuming that N and S atoms lie just on the coplanar line made by the two planes of phenyl ring and assuming that r_{NH}=1.09 Å.[19] This angle is also determined for the case when N and S stoms deviate from the coplanar line by 0.03 and 0.18 Å, respectively, and r_{SN} equals 3.03 Å as reported in crystal.[19] This value is listed in parenthesis in Table 2. Also listed in the Table are structural parameters in an orthorhombic crystal of 10*H*-phenothiazine for reference. The dihedral angle in a little smaller in the dibromo derivative than that in the parent molecule in Table 2. This angle in the latter compound is also reported to be 153.3°[20] in monoclinic crystal and 144±7°[21] in solution. Hitherto, much effort has been devoted to study the conformation of phenothiazines. However, some controversies still remain unresolved especially regarding the conformation of the NH proton. For 10*H*-phenothiazine a molecular orbital calculation predicted superiority of the "H-intra" conformer in the stability compared to the "H-extra" one,[22] and this

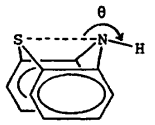

"H-intra" form

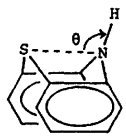

"H-extra" form

was proved in crystal.[19,20] However, the conformation in the crystal does not necessarily indicate the stability of a molecule in itself since the molecule is embedded

in a rigid lattice in the crystal. In solution a molecular Kerr constant study supported the "H-intra" conformation[21] and NMR chemical shifts did not conflict with this conclusion.[23] However, coexistence of "H-intra" and "H-extra" conformers was suggested from a dipole moment study.[24] In the present case of 3,7-dibromo-10*H*-phenothiazine, the angle of S ··· N-H is less than 180° and might indicate the "H-extra" conformation.[25] However, in a pure "H-extra" conformation, the angle of S ··· N-H needs to be in close vicinity to 90° since the proton is situated at an "axial" position of the central ring in the boat form. In this sense, discussion of the stability of the two conformers made on the basis of the S ··· N-H angle is confusing.[26] This angle lies between 150° and 185° in various phenothiazines[25] including the present case. These values deviate far from 90° and it may be said that the phenothiazine derivatives are supported to be in the "equatorial" conformation irrespective of the substituent attached to nitrogen, although the position of the substituent is changed from one derivative to another. With regard to the dihedral angle and the conformation of NH proton, a similar NMR study using liquid crystal solvent is interested for 10*H*-phenothiazine itself. However, some special techniques such as multiple quantum NMR spectroscopy or high power decoupling for some deuterated compounds are needed to simplify the spectrum.

Preferred Orientation of 3,7-Dibromo-10*H*-phenothiazine Dissolved in ZLI1167. The authors have demonstrated on an interrelation between the principal axes for the order tensor and those for the moment of inertia in the studies of hexachlorocyclohexane isomers.[27,28] In the present case, principal axes x',y',z' for the order tensor can be derived as follows. The axis x' coincides with x from symmetry. The axes y' and z' are those which makes $S_{y'z'}$ equal to zero. $S_{y'z'}$ is expressed as in Eq. 4,

$$S_{y'z'}=\sum_{p,q}\cos\theta_q^{z'}S_{pq},\quad p,q=x,y,z \tag{4}$$

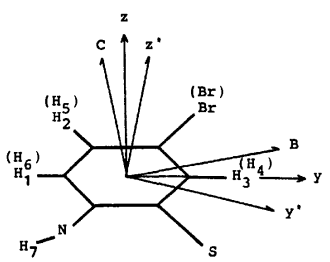

Fig. 2. Principal axis systems for the order tensor (x',y',z') and for the moment of inertia(A,B,C) in 3,7-dibromo-10*H*-phenothiazine (side view).
The x' and A axes coincide with the x axis from the C_s symmetry, but these three axes are abbreviated in the Figure for simplicity. The x, y, and z axes are defined so as to place the protons of H_1, H_3, H_4, and H_6 on the xy plane. Angles of rotation are −11.7° for y' and z' axes and 11.3° for B and C axes with regard to the y and z axes.

where $\theta_p^{y'}$ means the angle between axes p and y'. From this equation, an angle of rotaion ω which moves y and z on to y' and z', respectively, can be obtained as,

$$\tan(2\omega)=2S_{yz}/(S_{yy}-S_{zz}) \tag{5}$$

and also the relevant principal values turn out to be: $S_{x'x'}=S_{xx}$ and $S_{z'z'}=\sin^2\omega S_{yy}+\cos^2\omega S_{zz}-\sin(2\omega)S_{yz}$. From these equations, $\omega=-11.7$, $S_{x'x'}=-0.1223$, and $S_{z'z'}=0.1995$ are reached (Fig. 2). Principal axes A, B, C for the moment of inertia were determined by the program XYZ[29] modified by the present author, principal values being $I_A=513.0$, $I_B=5671.3$, and $I_C=6003.7$ amu·Å^2. In this calculation, bond lengths obtained in a crystal,[19] bonding angles of 120° for carbons, an angle of 170.5° for S ··· N-H, and the dihedral angle of 149.1° were used together with the angles of 66.0° for <S-N-C and 54.0° for <N-S-C. The B and C axes are seen to be rotated by 11.3° from y and z axes (Fig. 2). Therefore, the two principal axis systems differ 23° from each other, suggesting a special steric effect of Br atoms on the phenyl rings as observed[27,28] for Cl stoms in hexachlorocyclohexane.

The author (H. F.) is grateful to Professor Kensuke Takahashi of Nagoya Institute of Technology for facilities for the NMR measurements

References

1) G. Fronza and E. Ragg, *J. Chem. Soc., Perkin Trans. 2*, **1982**, 1209.
2) H. Fujiwara, A. Kawamura, T. Takagi, and Y. Sasaki, *J. Am. Chem. Soc.*, **105**, 125 (1983).
3) G. Fronza and E. Ragg, *J. Chem. Soc., Perkin Trans. 2*, **1982**, 291.
4) H. Fujiwara, T. Hirota, M. Watanabe, and Y. Sasaki, unpublished results.
5) H. Fujiwara, I. Yamanaka, and Y. Sasaki, *Nippon Kagaku Kaishi*, **1986**, 1566.
6) K. L. Gallaher and S. H. Bauer, *J. Chem. Soc., Faraday Trans. 2*, **71**, 586 (1968).
7) H. Lynton and E. G. Cox, *J. Chem. Soc.*, **1956**, 4886.
8) I. Rowe and B. Post, *Acta Crystallogr.*, **11**, 372 (1958).
9) Y. Ikeda, T. Shimura, and E. Manda, *Nippon Kagaku Kaishi*, **1979**, 437.
10) J. Barbe and A. M. Chauvet-Monges, *Compt. Rend. Acad. Sci., Ser. C*, **279**, 935 (1974).
11) C. Bodea and M. Raileanu, *Ann. Chim. (Paris)*, **631**, 194 (1960).
12) P. Diehl, P. M. Henrichs, and W. Niederberger, *Mol. Phys.*, **20**, 139 (1971).
13) H. Fujiwara and Y. Sasaki, *J. Chem. Soc., Chem. Commun.*, **1981**, 35.
14) M. Davies and J. Swain, *Trans. Faraday Soc.*, **67**, 1637 (1971).
15) Y. Koga, H. Takahashi, and K. Higashi, *Bull. Chem. Soc. Jpn.*, **46**, 3359 (1973).
16) E. E. Burnell and C. A. DeLange, *J. Magn. Reson.*, **39**, 461 (1980).
17) J. W. Emsley and G. R. Luckhurst, *Mol. Phys.*, **41**, 19

(1980).
18) D. S. Stephenson and G. Binsch, *Mol. Phys.*, **43**, 697 (1981).
19) J. J. H. McDowell, *Acta Crystallogr., Sect. B*, **32**, 5 (1976).
20) J. D. Bell, J. F. Blount, O. V. Briscoe, and H. C. Freeman, *J. Chem. Soc., Chem. Commun.*, **1968**, 1656.
21) M. J. Aroney, G. M. Hoskins, and R. J. W. LeFevre, *J. Chem. Soc., B*, **1968**, 1206.
22) J.-P. Malrieu and B. Pullman, *Theor. Chim. Acta*, **2**, 293 (1964).
23) G. Fronza, R. Mondelli, G. Scapini, G. Ronsisvalle, and F. Vittorio, *J. Magn. Reson.*, **23**, 437 (1976).
24) C. Levayer, A.-M. Galy, and J. Barbe, *J. Pharm. Sci.*, **69**, 116 (1980).
25) J.-P. Reboul and B. Cristau, *J. Chim. Phys.*, **75**, 1109 (1978).
26) Bonding angles around the N atom change considerably reflecting the degree of conjugation of N with the phenyl rings. And so, the two conformers are better differentiated from whether the H atom is located closer to the phenyl rings ("H-intra") or the lone pair electrons are ("H-extra"). This condition is well judged on a basis of the angle between the N-H bond and the plane made by the N atom and the two phenyl carbons attached to it.
27) H. Fujiwara, N. Shimizu, T. Takagi, and Y. Sasaki, *Magn. Reson. Chem.*, **24**, 71 (1986).
28) H. Fujiwara, N. Shimizu, T. Takagi, and Y. Sasaki, *Bull. Chem. Soc. Jpn.*, **58**, 2285 (1985).
29) QCPE No. 178, Indiana University.

 © 1988 The Chemical Society of Japan Bull. Chem. Soc. Jpn., 61, 375—377 (1988)

Emission Spectrum of Acetylene by Controlled Electron Impact

Toshifumi YOSHIDOME, Masaharu TANIGUCHI, Keiji NAKASHIMA, Hirofumi KAWAZUMI, and Teiichiro OGAWA*

Department of Molecular Science and Technology, Kyushu University, Kasuga-shi, Fukuoka 816

(Received September 10, 1987)

Emission spectra of C_2H_2 and C_2D_2 excited by collisions with electrons of 7—20 eV show a broad and diffuse band in the 240—400 nm region and this band was assigned to the S_1(lower vibrational levels)-S_0 transition of acetylene on the basis of its wavelength, excitation function (threshold: 5.5 eV) and lifetime (323±30 ns). Their emission cross sections are on the order of 10^{-19} cm^2. Among intense fragment emissions at higher electron energies, band of C_2H has also been observed and its lifetime is 3.9±0.8 μs.

Fluorescence of acetylene is very weak. A discrete fluorescence was observed in a high frequency discharge,[1] in a matrix[2] and in the gas phase under a laser excitation.[3,4] These fluorescence was assigned to the transition from the lowest excited state to the ground state. The fluorescence quantum yield in the gas phase was estimated to be 10^{-4}, and it decreased sharply with decreasing exciting wavelength.[5]

The electron is an efficient excitation source and is able to excite both optically-allowed and forbidden transitions.[6] Aromatic molecules exhibit characteristic emission upon excitation by electrons similar to optical fluorescence.[7] However, their vibrational structure is different and optically-forbidden vibrational levels are predominant in the benzene spectrum.[8] Meanwhile, emission spectrum of acetylene excited by electrons showed only bands of fragments and no parent emission was detected in the previous investigation.[9]

In order to clarify spectroscopic properties of acetylene, we have again measured emission spectrum of acetylene under controlled electron-impact excitation and analyzed its decay curve.

Experimental

The apparatus is similar with the one described previously.[7] In brief, the collision chamber (8″) was evacuated with a 4″ oil-diffusion pump with a liquid nitrogen trap. The base pressure was of the order 10^{-6} Torr (1 Torr=133 Pa) and the operating pressure was about 1×10^{-3} Torr. The sample gas was jetted into the collision region through a mass flow controller (Standard Tech. 400MKII) and a multichannel nozzle, and was collided with the electron beam from a tungsten filament.

The optical emission was observed through a quartz window at an angle of 45° with respect to the electron beam. The spectrum was obtained with a SPEX 1670 monochromator equipped with a 1200 grooves/mm grating blazed at 300 nm and a Hamamatsu R585 photomultiplier and with an NF PC545 photoncounter. The electron beam was pulsed so as to subtract the stray radiation from the hot filament.

The instrumental response of the optical system was calibrated with a Hamamatsu L591 standard deuterium lamp. The corrected spectrum was expressed in units of relative number of photons per wavenumber. The electron energy was calibrated with the peak of N_2^* (337.1 nm) at 14.5 eV and its energy resolution was 0.8 eV at 10 eV.

Fluorescence decay was measured with an Ortec 457 time-to-amplitude converter, an Ortec 473A constant-fraction discriminator, a Norland Ino-tech 5300 multichannel analyzer, and an NEC PC 9801VF microcomputer. The pulse width of the electron beam was 1 μs, and its repetition rate was 50 kHz. The system was calibrated with the lifetime (1.7 ns) of the 3^1P-2^1S transition of He (501.4 nm).

C_2H_2 was commercially obtained (Eto Sanso, 99.6%) and was used as supplied. C_2D_2 was prepared from CaC_2 and D_2O, and its isotopic purity was > 96% according to a mass spectrometric analysis.

Results and Discussion

There are bands of H (Balmer lines), CH (the A-X and B-X transitions), CH^+ (the B-A and b-a transitions) and C_2 (the d-a transition) on the emission spectrum by controlled electron impact on acetylene, as are reported previously.[9,10] But no feature assignable to C_2H_2 was observed previously,[9] partly because measurements were carried out at higher electron energies. Typical emission spectra of C_2H_2 and C_2D_2 excited at electron energies of 14 and 7 eV are shown in Fig. 1;

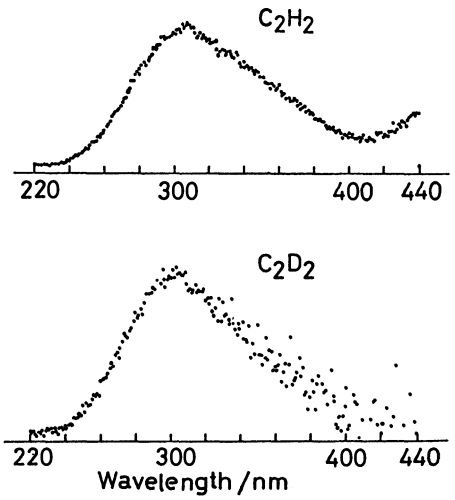

Fig. 1. Emission spectra of C_2H_2 and C_2D_2 by controlled electron impact. Electron energy: 14 eV (C_2H_2) and 7 eV (C_2D_2). Optical resolution: 5 nm.

the optical resolution was 5 nm and the optical response of the instrument was corrected. The spectra are broad and diffuse, and the peak appears at 307 nm for C_2H_2 and at 300 nm for C_2D_2.

The similarity of the observed spectra with those by the optical excitation[2-4] shows that the observed emission is due to the transition from the lowest excited state ($^1\Sigma_u$) to the ground state($^1\Sigma_g$), as is optical fluorescence. However, the present spectrum was measured at a much lower pressure than that in the laser excitation and collisional effects can be ignored. The spectrum of C_2H_2 shifts to the red than that of C_2D_2, probably because the vibrational spacing of the latter in the ground electronic state is smaller.

There is no contribution of any fragment species at 7 eV and only C_2H and CH(C) may appear at 14 eV, because the calculated dissociation limits of C_2H(B) and CH(C) are 9.29[11,12] and 13.91[11,13] eV, respectively. The increase at 400 nm region toward longer wavelength in the C_2H_2 spectrum can be assigned to the band of C_2H*.

The excitation function of C_2H_2 measured at 280 nm is shown in Fig. 2. A peak at 14.5 eV is due to N_2 (the C-B transition) measured together for a calibration of the electron energy. The rise toward higher electron energy is due to fragments such as C_2H* and CH(C-X). The excitation function above 9.0 eV was obtained by subtracting the contribution from the fragment emission, and is shown by triangles. It has a maximum at about 10 eV and decreases smoothly to higher electron energies. The C_2H_2* emission was not distinguishable from the fragment emissions at higher electron energies. The threshold energy is found to be 5.5±0.6 eV. The 0-0 transition of C_2H_2 is located at 5.23 eV,[14] and this agreement is consistent with the assignment. Because this threshold energy is much lower than the dissociation limit of any fragment, the observed emission is certainly not due to any fragment species.

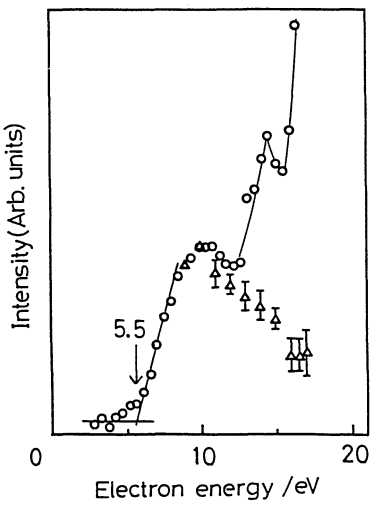

Fig. 2. Excitation function of C_2H_2 at 280 nm.
O: Total optical emission. Δ: C_2H_2* above 10 eV.
Total optical emission should be due to C_2H_2* below 9.5 eV.

The electron excitation is nonresonant in principle and many vibrational levels may be excited together. Thus, the acetylene spectra may be diffuse, though it exhibits banded fluorescence under a dye-laser excitation. The peak of the spectra seems to locate in the identical region with that excited at the 0-0 transition by the laser,[3] if we take instrumental response into consideration. However, the present spectrum is broader than the 0-0 fluorescence by the laser excitation, and this finding indicates that not only the 0 level but also some lower vibrational states are also excited by controlled electron impact.

The 0-0 transition is forbidden due to the geometry change between the ground and the excited states, and excitation to the higher vibrational levels had larger intensity in the optical excitation.[3,14] Nevertheless, the 0-0 transition seems to be prominent under electron excitation. This is also the case in benzene.[8] The higher intensity of the 0-0 transition should be due to a specific interaction between the molecule and the electron.

The emission cross sections of acetylene emission were determined by measuring the band areas relative to that of the C-B transition of N_2; the emission cross section of the latter was determined to be 1.6×10^{-18} cm^2 at 12.4 eV.[15] They were 2.2×10^{-19} cm^2 for C_2H_2 and 3.2×10^{-19} cm^2 for C_2D_2 at the incident electron energy of 12.4 eV. Uncertainty of these values would be 50% mainly due to uncertainty in the pressure measurements; however, relative values of C_2H_2 and C_2D_2 should be more accurate.

The decay curve of the C_2H_2 emission at 300 nm is

Table 1. The Lifetime of C_2H_2* by Controlled Electron Impact at an Electron Energy of 17 eV

Wavelength/nm	Lifetime/ns
280	313±26
290	322±20
300	336±30
315	319±41

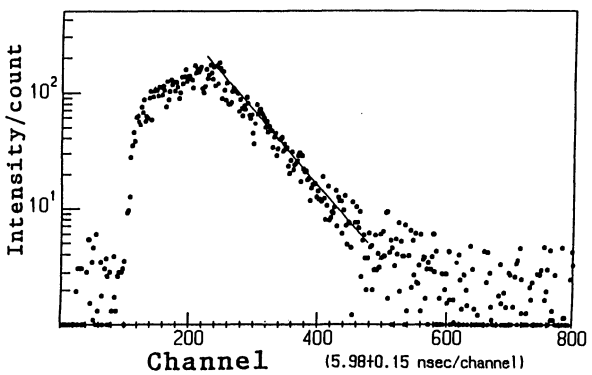

Fig. 3. Fluorescence decay curve for C_2H_2 at 300 nm.
The electron energy: 10 eV.

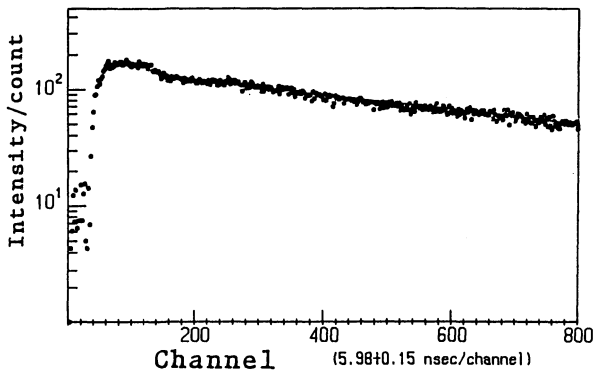

Fig. 4. Fluorescence decay curve for C_2H at 500 nm. The electron energy: 50 eV.

Table 2. The Lifetime of C_2H^* by Controlled Electron Impact

Wavelength /nm	Lifetime at 19eV/μs	Lifetime at 50 eV/μs
300		3.5±0.5
450	3.6±1.0	3.9±0.7
500	3.9±0.8	4.4±0.7

shown in Fig. 3; the incident electron energy was 10 eV. The lifetime of the excited state was determined to be 328±50 ns by a least-square fitting of the decay curve. The results of the decay curve analysis is shown in Table 1. The lifetime was independent of the electron energy between 10 and 50 eV and of the wavelength between 280 and 315 nm within experimental uncertainties. Then, we can conclude that the lifetime of $C_2H_2^*$ is 323±30 ns by taking the average of all data. This lifetime agrees with that to lower vibrational levels measured by laser excitation[3] within experimental uncertainties, and disagree with that to higher vibrational levels.[4] This finding confirms the assignment that the observed emission arises mainly from the lower vibrational levels of the A state of acetylene.

There is another band above 410 nm in Fig. 1(a). This band is also broad and diffuse and is extended to longer wavelength region. Since its threshold is about 10 eV and the calculated threshold for C_2H is 9.29 eV, this band can be assigned to C_2H^*, as was reported by a VUV photolysis of acetylene.[16] The decay curve of the C_2H emission at 500 nm is shown in Fig. 4 and the lifetime was determined to be 4.4±0.7 μs. The lifetimes measured are shown in Table 2; lifetime does not vary with wavelength within experimental uncertainties. The lifetime of C_2H was determined to be 3.9±0.8 μs by taking an average of these results. This lifetime is approximately in agreement with those obtained in a VUV photolysis;[16] however, the latter values were measured at higher pressures by extraporating observed lifetime to zero pressure. Since the present measurements were carried out at 10^{-3} Torr, our values should be more accurate.

The electron excitation is a useful technique to investigate the molecular excited state at a very low pressure where collisional effect can be ignored.

The authors thank to professor Yukio Nishimura for the use of his standard deuterium lamp and to Dr. Teijiro Ichimura of Tokyo Institute of Technology for his comments.

References

1) P. J. Dyne, *Can. J. Phys.*, **30**, 79 (1952).
2) L. E. Bruss, *J. Mol. Spectrosc.*, **75**, 245 (1979).
3) J. C. Stephenson, J. A. Blazy, and D. S. King, *Chem. Phys.*, **85**, 31 (1984).
4) E. Abramson, C. Kittrell, J. L. Kinsey, and R. W. Field, *J. Chem. Phys.*, **76**, 2293 (1982); E. Abramson, R. W. Field, D. Imre, K. K. Innes, and J. L. Kinsey, *J. Chem. Phys.*, **83**, 453 (1985).
5) S. Hamai and F. Hirayama, *J. Chem. Phys.*, **71**, 2934 (1979).
6) T. Ogawa, *Eng. Sci. Repts. Kyushu Univ.*, **7**, 231 (1986); Y. Hatano, *Comments At. Mol. Phys.*, **13**, 259 (1983).
7) T. Ogawa, N. Yamami, M. Tsuji, and Y. Nishimura, *Bull. Chem. Soc. Jpn.*, **54**, 1203 (1981).
8) H. Kawazumi, T. Oomori, N. Yamami, and T. Ogawa, *Chem. Phys. Lett.*, **106**, 351 (1984).
9) M. Tsuji, T. Ogawa, Y. Nishimura, and N. Ishibashi, *Bull. Chem. Soc. Jpn.*, **49**, 2913 (1976).
10) M. Tsuji, T. Ogawa, Y. Nishimura, and N. Ishibashi, *Chem. Lett.*, **1975**, 317.
11) "Kagaku Binran, Kiso-hen (Handbook of Chemistry, Basic Data)" 3rd ed, ed by Chemical Society of Japan, Maruzen, Tokyo (1984), Chap. 9.
12) H. Okabe, *J. Chem. Phys.*, **62**, 2782 (1975).
13) R. W. B. Pearse and A. G. Gaydon, "The Identification of Molecular Spectra," 3rd ed, Chapman & Hall, London (1965), p. 101.
14) C. K. Ingold and G. W. King, *J. Chem. Soc.*, **1953**, 2725.
15) M. Imami and W. L. Borst, *J. Chem. Phys.*, **61**, 1115 (1974).
16) Y. Saito, T. Hikida, T. Ichimura, and Y. Mori, *J. Chem. Phys.*, **80**, 31 (1984).

The Thermal Decomposition and Hydrolysis of Calcium Carbamoyl Phosphate

Choichiro SHIMASAKI* and Hiroki SUZUKI
Department of Industrial Chemistry, Faculty of Engineering, Toyama University, Gofuku, Toyama 930
(Received May 18, 1987)

Calcium carbamoyl phosphate (**1**) was prepared by adding an aqueous calcium chloride solution to a reaction solution of KH_2PO_4 with KOCN. **1** was unstable at room temprature. **1** was dehydrated to make anhydrous salt and thermally decomposed to liberate ammonia, cyanic acid, and carbon dioxide, finally resulting in the formation of calcium pyrophosphate in air. The apparent activation energies for the three endothermic peaks of the DTA curve were estimated to be 50.0, 83.9, and 148.3 kJ mol^{-1} respectively. The hydrolysis of **1** in an aqueous solution apparently obeyed the first-order kinetics. The activation parameters for the hydrolysis of **1** were evaluated by using the ^{31}P NMR spectra of **1** with the lapse of the reaction time. The activation energy was 92.2 kJ mol^{-1}; the activation enthalpy, 89.7 kJ mol^{-1}, and the activation entropy, −6.3 e.u.

Some phosphor-nitrogen compounds are already used as industrial materials and obtained as industrial products. There are a series of phosphorus-nitrogen compounds which have amino groups on a P atom. There compounds have the potential for use as new flameproofing and glow-retardant agents on a large number of cellulosic materials; further, they can be used as the starting materials in the preparation of many organic and inorganic phosphorus compounds.

In our previous papers,[1-3] the thermal behavior of many phosphoramidates were reported. This paper will describe the synthesis, thermal behavior, and hydrolysis of calcium carbamoyl phosphate (**1**) containing nitrogen and carbon. This compound was instable even at room temperature, and its thermal product resulted in calcium pyrophosphate. It was found by ^{31}P NMR measurements that the hydrolysis of **1** apparently obeys the first-order kinetics.

Experimental

Preparation of Calcium Carbamoyl Phosphate. **1** was synthesized by reference to the method described in the literature.[4] Potassium dihydrogenphosphate (0.1 mol) and potassium cyanate (0.1 mol) were dissolved in 100 cm^3 of water. To the resulting mixture, which had been cooled in an ice bath, two solutions of 60 ml of 1 mol dm^{-3} $BaCl_2$ and 50 ml of 1 mol dm^{-3} NaOH were slowly added, drop by drop with continuous stirring. During the treatment, the pH of the solution was kept at 9.0—9.3. The resulting cream-colored precipitate of barium monohydrogenphosphate was removed by suction filtration. The filtrate was transferred to a flask, and 50 ml of 1 mol dm^{-3} $CaCl_2$ was added, drop by drop. To the resulting solution was slowly added 100 ml of ethanol. The resulting white precipitate was collected by suction filtration, washed with several small portions of water, ethanol, and acetone, air-dried, and finally dried in a vacuum over diphosphorus pentaoxide for 48 h.

Chemical Analysis. The phosphorus in a sample was determined colorimetrically by the molybdenum-blue method. The calcium in a sample was estimated by the atomic-absorption-analysis technique. The nitrogen, carbon, and hydrogen in a sample were determined by using a Hitachi C, H, N analyser-026 at the Toyama Medical and Pharmacy University.

Measurements. The thermal analysis measurements were made in air by using a Rigakudenki TG-DTA, DSC apparatus, at the heating rates of 3, 5, 6, 8, and 10 K min^{-1} for TG-DTA and 5 K min for DSC respectively. The IR spectra of the sample were recorded on a Nipponbunko IR-810 apparatus using the KBr-disc method. For the ^{31}P NMR spectra, a sample of about 100 mg was put in 5.0 cm^3 of a 6% EDTA deuterated-water solution and stirred for several minutes. A JNM-FX 90 Fourier transform spektrometer was used to measure the ^{31}P NMR spectra. An X-ray diffraction diagram of a powder sample was taken with nickel-filtered Cu $K\alpha$ radiation using a Shimazu X-ray diffractometer XD-5, XD-3A, and a Rigaku RAD-RVB apparatus.

Results and Discussion

Thermal Behavior. The DTA and TG curves of **1** are shown in Fig. 1. The DTA curve indicated four endothermic peaks in this range: r.t.—362, 362—430, 430—465, and 465—541 K, while the TG curve indicated a slow decrease in the weight. For each type of peak (E_{D1}, E_{D2}, E_{D3}, and E_{D4}) shown in Fig. 1, two temperatures are recorded; the first one is the point of departure from the base line, while the second one is the end point of the peak temperature. The indication of "temperature" on the DTA curve in Fig. 1 means the temperature at which samples were removed from a furnace prior to being cooled in a silicagel desiccator and subjected to further research. The results of the elemental analyses of the thermal products are shown in Table 1. It can be seen from Table 1 that the nitrogen, carbon, and hydrogen contents of the thermal product decreased in the heating process and that the

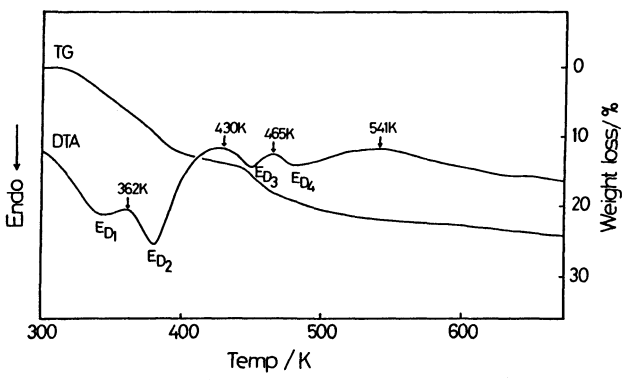

Fig. 1. DTA and TG curves of CaCAP·1.5H_2O. Heating rate: 5 K min^{-1}.

thermal product at 541 K contained no nitrogen and hydrogen. These data on the reduction in weight after 30 min at each endothermic peak temperature were not always in agreement with those calculated from the TG curve. The results showed that carbon dioxide, ammonia, and cyanic acid are exhausted in the case of the thermal condensation of **1**.

The IR spectra of the thermal products are shown in Fig. 2. For the IR spectrum of **1**, the absorption band at about 3400 cm^{-1} is assigned to the N-H stretching vibration; those at 1680 and 1730 cm^{-1}, to the C=O stretching vibration; those at 1610 and 1630 cm^{-1}, to the N-H deformation vibration; that at 1400 cm^{-1}, to the C-N stretching vibration; that at 1150 cm^{-1}, to the P=O stretching vibration; that at 980 cm^{-1}, to the P-O-C stretching vibration, and that at 570 cm^{-1}, to the $(PO_2)^-$ or $(PO_3)^{2-}$ deformation vibration. These absorptions grew weaker with an increase in the temperature, and they disappeared in the thermal product at 430 K. At about 910 cm^{-1}, the absorption band attributed to the P-O-P antisymmetric stretching vibration grew strong. This showed that the condensation polymerization was proceeding. For the thermal product at 362—673 K, the absorption band of carbon dioxide was observed at 2350 cm^{-1}. Also, for the thermal product at 1073 K, the absorption observed at 900—1250 cm^{-1} was very complex, with strong peaks. This complexity of absorption was attributed to the progress of the crystallization.

Table 1. Elemental Analysis of the Thermal Products of $CaCAP \cdot 1.5H_2O$

Sample	Ca/%	P.%	N/%	C/%	H/%
r.t.[a]	19.1	15.0	6.2	5.4	2.3
	(19.4)	(15.0)	(6.8)	(5.8)	(2.5)
362 K	21.5	16.1	5.4	5.1	2.1
430 K	25.2	19.3	3.4	3.1	1.3
465 K	25.4	20.9	2.1	2.9	0.5
541 K	27.2	21.7	0.0	2.1	0.0
673 K	30.1	23.7	0.0	1.6	0.0
1273 K[b]	32.5	24.5	0.0	0.0	0.0
	(32.8)	(25.4)			

a) Calculated values in parentheses as $CaCAP \cdot 1.5H_2O$.
b) Calculated values in parentheses as $Ca_2P_2O_7$.

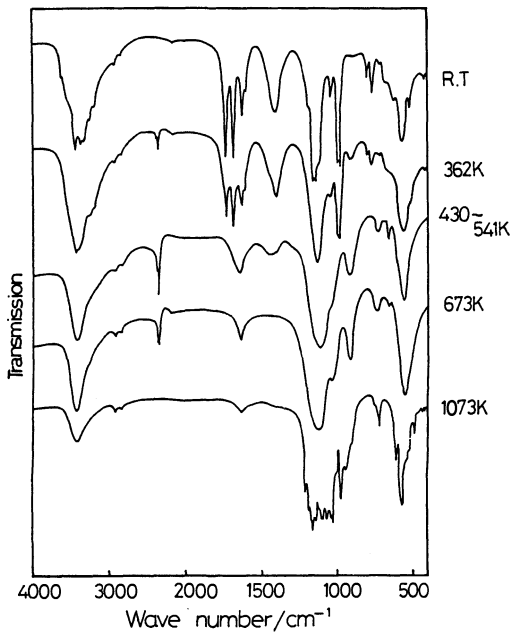

Fig. 2. IR spectra of the thermal products of $CaCAP \cdot 1.5H_2O$.

The ^{31}P NMR spectra of the thermal products are shown in Fig. 3. As has been mentioned previously, **1** is very instable at room temperature; therfore, the

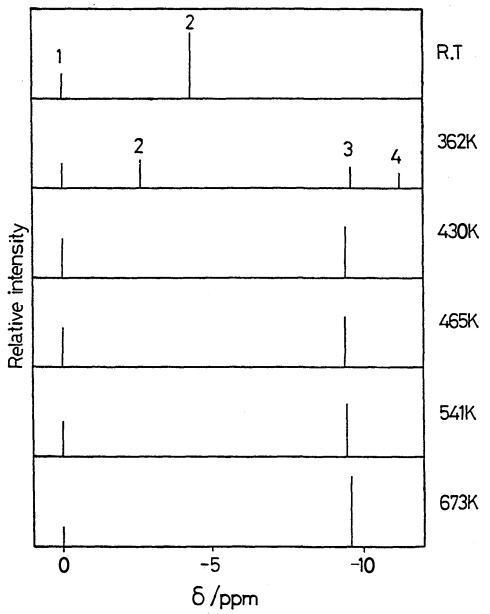

Fig. 3. ^{31}P NMR spectra of the thermal products of $CaCAP \cdot 1.5H_2O$. 1: Orthophosphate, 2: carbamoylphosphate, 3: diphosphate, 4: end PO_4 group of intermediate polyphosphate ($n>3$).

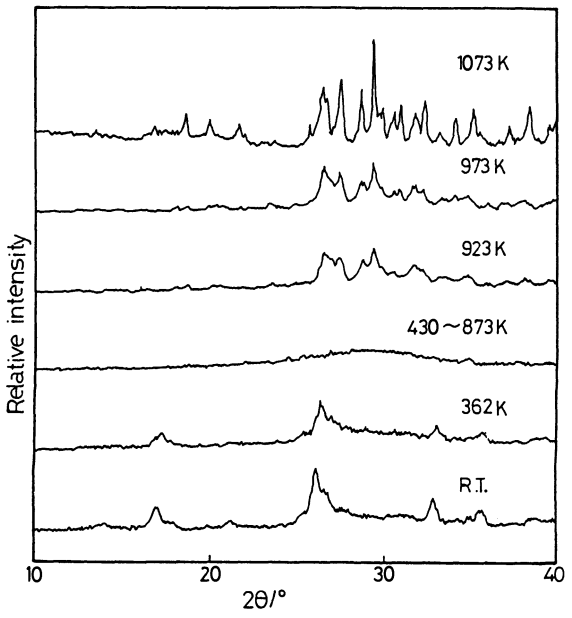

Fig. 4. X-Ray diffraction diagrams of the thermal products of $CaCAP \cdot 1.5H_2O$. Heating rate: 2 K min^{-1}.

^{31}P NMR spectrum of **1** indicated peaks caused by a carbamoyl phosphate (CAP) and an orthophosphate (PO_4). The molar ratio CAP/(CAP+PO_4), is calculated by means of the signal area, was 0.88 for **1**. The ^{31}P NMR spectrum of the thermal product at 362 K indicated peaks attributable to a PO_4, a CAP, a diphosphate (P_2O_7), and an intermediate of the thermal condensation. The thermal product at 430 K indicated no CAP peak, but peaks of PO_4 and P_2O_7 were both registered. These results agreed with those of the IR spectra. The peak of P_2O_7 grew stronger above 430 K.

The X-ray diffractions of the thermal product at a given isothermal temperature, as obtained by using XD-3A, are shown in Fig. 4. No diffraction patterns on the thermal products were observed at room temperature at 430—873 K. The X-ray diffraction of the thermal product at 973 K indicated weak patterns, but these patterns were much clearer than those at 923 K. The X-ray diffraction patterns of the thermal products at the temperature interval from 465 to 673 K, as obtained using the Rigaku RAD-RVB apparatus, were similar to the amorphous solid compositions, as is shown in Fig. 4. The thermal product at 1073 K showed strong X-ray diffraction patterns of α-$Ca_2P_2O_7$.[5]

Decomposition at Room Temperature. The stability of **1** was checked at room temperatue (283—303 K) in air. Figure 5 should the IR and ^{31}P NMR spectra of the decomposition of **1** at room temperature. **1** was very instable at room temperature. At 910 cm^{-1}, the absorption of the P-O-P antisymmetric stretching vibration appeared, and its intensity increased with the lapse of the reaction time. Therefore, either the polymerization or the condensation of **1** seemed to be progressing. This agrees with the results of the IR and ^{31}P NMR spectra. A peak attributable to P_2O_7 appeared after the lapse of 8 dyas, and its intensity increased with the lapse of the reaction time. A peak due to CAP decreased with the lapse of the reaction time. A peak due to CAP decreased with the lapse of the reaction time, on the other hand, and disappeared at 133 days.

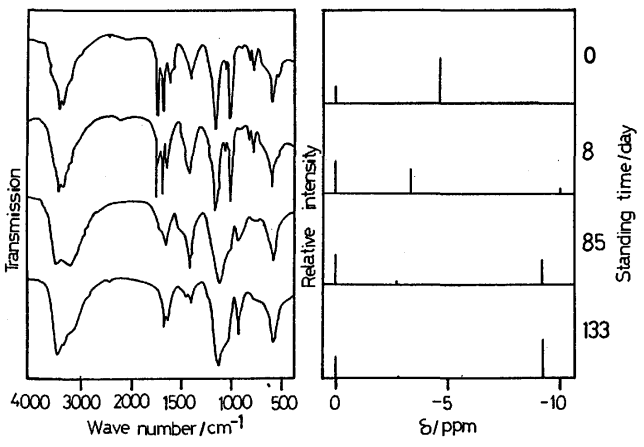

Fig. 5. IR and ^{31}P NMR spectra of the decomposition of CaCAP·1.5H_2O at room temperature.

Kinetic Studies of Thermal Process. Kinetic studies of the pyrolysis (i.e., dehydration and condensation) of **1** were done by the Kissinger method[6] on the basis of the DTA peaks E_{D1}—E_{D4}, as is shown in Fig. 1. As the heating rate increased, both the initial transition and the peak maximum for dehydration and condensation were shifted to higher temperatures. The theoretical work of Kissinger indicated that the activation energy of the pyrolysis process of **1** was defined by the following form:

$$\frac{d \ln (\phi/T_m^2)}{d(1/T_m)} = -E/R$$

where ϕ stands for the heating rate; T_m, for the temperature of the DTA-maximum, E, for the activation energy, and R, for the gas constant. These plots of $\ln(\phi/T_m^2)$ against $1/T_m$ are linear, the slop being equal to $-E/R$. Thus, the apparent activation energies of each pyrolysis process were obtained from this slop. The apparent activation energies for the three endothermic peaks (=E_{D1}, E_{D2}, and E_{D3}) were estimated to be 50.0, 83.9, and 148.3 kJ mol^{-1} respectively. The results are shown in Fig. 6 and Table 2. As the heating rate increased, the peak maximum for E_{D4} was not appreciably shifted. It was found that the E_{D4} peak was caused by the heat of crystallization.

According to these results, the pyrolysis mechanism of **1** may be written as Scheme 1. **1** is dehydrated to

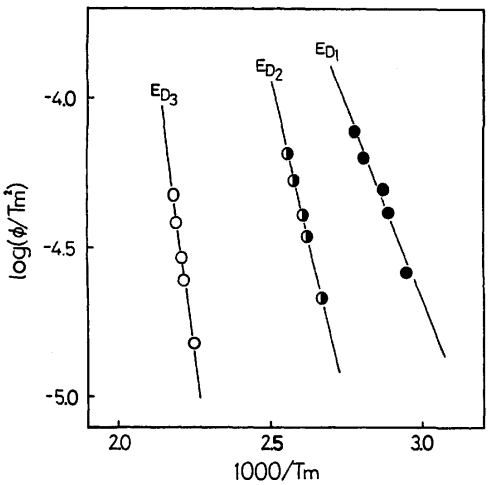

Fig. 6. The Kissinger's plots for E_{D1}, E_{D2}, and E_{D3} in DTA curves for CaCAP·1.5H_2O.

Table 2. Kinetic Data for the Pyrolysis of CaCAP·1.5H_2O

DTA peak	Equation of straight line	$r^{a)}$	E/kJ·mol^{-1}
E_{D1}	$\log(\phi/T_m^2)=-2.609\cdot1000/T_m+3.147$	0.985	50.0
E_{D2}	$\log(\phi/T_m^2)=-4.378\cdot1000/T_m+7.019$	0.996	83.9
E_{D3}	$\log(\phi/T_m^2)=-7.735\cdot1000/T_m+12.550$	0.999	148.3

a) Linear correlation coefficient.

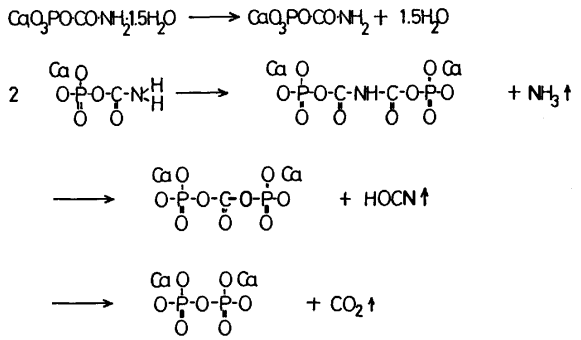

Scheme 1.

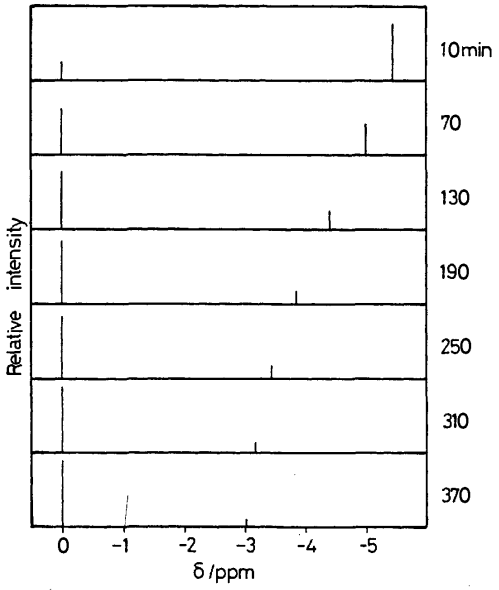

Fig. 7. ^{31}P NMR spectra of CaCAP·1.5H$_2$O with the elapse of the reaction time at 302.6 K.

make anhydrous salts. Next, the anhydrous salts are bimolecularly condensed to liberate ammonia, cyanic acid, and carbon dioxide. Finally, calcium pyrophosphate is formed.

Hydrolysis of Calcium Carbamoyl Phosphate in an Aqueous Solution. The hydrolysis of **1** in an aqueous solution seems to progress as follows:

$$OPO_3 \cdot CO \cdot NH_2^{2-} + H_2O \rightarrow PO_4H_2^- + CO_2NH_2^-,$$

$$CO_2NH_2^- + PO_4H_2^- + H_2O \rightarrow CO_3H^- + NH_4^+ + PO_4H^{2-}.$$

^{31}P NMR measurement was used to investigate the hydrolysis reaction of **1** at temperatures from 299.0 to 315.2 K. The ^{31}P NMR spectra of **1** with the lapse of the reaction time at 302.6 K are shown in Fig. 7. These spectra indicated peaks attributable to CAP and PO_4; the former decreased and shifted to a low magnetic field with the lapse of the reaction time. The chemical shifts of the ^{31}P NMR spectra at various temperatures, taken at intervals, are shown in Fig. 3. Smooth curves were obtained at all temperatures. The speed of shifting grew rapidly with the rise in the temperature. After the lapse of an infinite time, the peak due to CAP was shifted by about −2.6 ppm. This phenomenon is independent of the pH, as was shown in the pH measurement of a solution[7] with the lapse of the reaction time over a period of 307 min. As Fig. 7 shows, the peak attributable to CAP decreased and that attributable to PO_4 increased with the lapse of the reaction time (apparently obeying the first-order kinetics). The first-order kinetics can represented as follows:

$$kt = \ln \frac{a_o - a_\infty}{a_t - a_\infty},$$

where a_o and a_∞ are the CAP/(CAP+PO_4) molar ratios at the beginning and when the reaction is complete respectively; a_t, the value after time t, and k, the rate constant. a_o, a_∞, and a_t were determined by measuring the integral intensities of the ^{31}P NMR spectrum for CAP and PO_4 respectively. The first-order kinetic

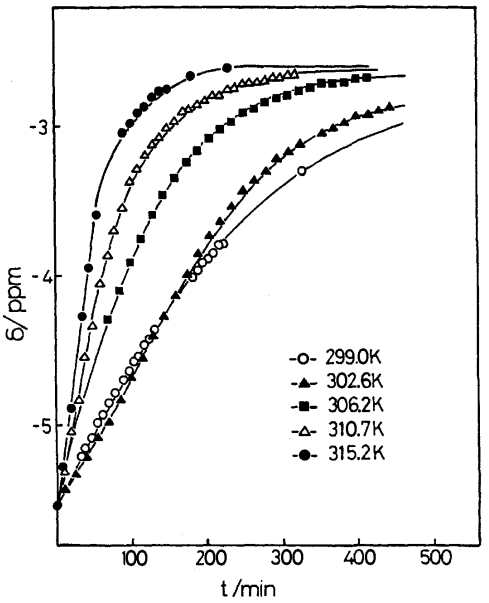

Fig. 8. The chemical shift of ^{31}P NMR spectra at various temperatures.

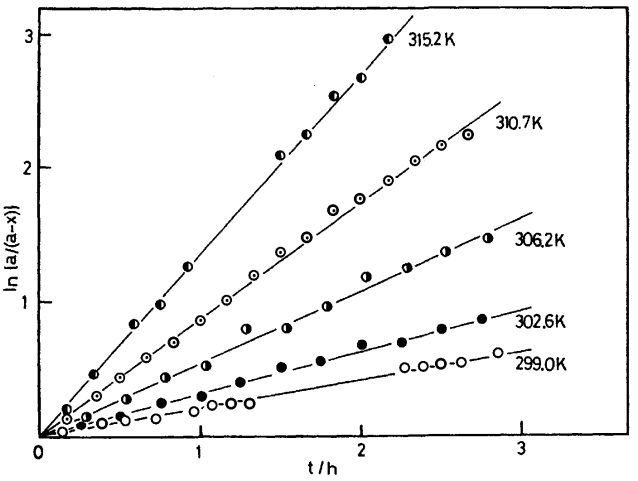

Fig. 9. The first order kinetic plots of ln $a/(a-x)$ vs. t for the hydrolysis of CaCAP·1.5H$_2$O in aqueous solution.

plots of $\ln[(a_0-a_\infty)/(a_t-a_\infty)]$ vs. t at various temperatures were found to be linear, as is shown in Fig. 9. The rate constants for the hydrolysis of **1** are shown in Table 3. Arrhenius plots (Fig. 10) give us the activation energy and the frequency factor. The activation enthalpy and entropy were obtained by using the values of the activation energy and the frequency factor. These kinetic data are tabulated in Table 4.

One of the most significant treatments of the theory of reaction rates is based on the concept of the existence of an activated complex as an intermediate stage in all chemical reactions. In a reaction involving two or more molecules, the reactants, possessing sufficient energy, must approach one another closely. Since in any bimolecular reaction except in the dissociation of two molecules, a reaction with $A \fallingdotseq 10^{11}\,M^{-1}\cdot s^{-1}$ is generally regarded as a standard bimolecular reaction,[8] the value of the frequency factor in this paper suggests a bimolecular reaction. Even in a unimolecular reaction, in which a single molecule takes part in each chemical act, it is necessary for some rearrangement of atoms and energy to occur, thus giving the requisite activated complex, before a reaction can take place. From the results of Table 4, the value of the activation energy can be said to be approximately identical to that of the activation enthalpy. By supposing that an equilibrium exists between the reacting molecules and the activated complex, which decompose at a definite rate, it has been found possible to estimate the apparent ΔS^* value for the hydrolysis reaction. Such a ΔS^* value suggests that mechanism of the hydrolysis reaction consists of two main complicating steps which can be described by the above chemical equations.

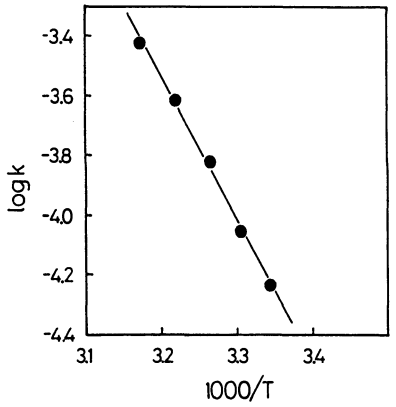

Fig. 10. Arrehenius plots of the first order rate constants for the hydrolysis of CaCAP·1.5H_2O in aqueous solution.

Table 3. Rate Constants for the Hydrolysis of CaCAP·1.5H_2O in an Aqueous Solution

T/K	Rate constant k/s^{-1}	$r^{a)}$
299.0	5.82×10^{-5}	0.997
302.6	8.83×10^{-5}	0.998
306.2	1.51×10^{-4}	0.996
310.7	2.42×10^{-4}	0.999
315.2	3.78×10^{-4}	0.999

a) Linear correlation coefficient.

Table 4. Kinetic Data for the Hydrolysis of CaCAP·1.5H_2O in an Aqueous Solution

A/$s^{-1}\,mol^{-1}$	E_a/kJ mol^{-1}	ΔH^*/kJ mol^{-1}	ΔS^*/e.u.
7.02×10^{11}	92.2	89.7	−6.3

We wish to thank Professor Ikuya Matsuura and Mr. Akira Matsui for the X-ray diffraction analysis, Mr. Kiyoshi Terayama for the DTA-TG, and Mr. Yoshiharu Yoneyama for the NMR spectra.

References

1) C. Shimasaki, Y. Oono, F. Takai, M. Shoji, and M. Yoshizawa, *Nippon Kagaku Kaishi*, **1982**, 376.

2) C. Shimasaki, S. Ookawa, and R. Ishizaka, *Bull. Chem. Soc. Jpn.*, **58**, 592 (1985).

3) C. Shimasaki and M. Hara, *Bull. Chem. Soc. Jpn.*, **58**, 3613 (1985).

4) F. Seel and F. Schineeling, *Z. Naturforsch.* **33b**, 374 (1978).

5) "Index (inorganic) to the powder diffraction file," American Society for Testing Materials (1968). Jcpds Cards 9-345.

6) H. E.Kissinger, *Anal. Chem.*, **29**, 1702 (1957).

7) CaCAP 1.5H_2O (0.4 g) was dissolved in 50 ml of a 6% EDTA deuterated-water solution.

8) T. Fueno, "Kagaku Hannoron," Asakura, Tokyo (1975), p. 123.

 © 1988 The Chemical Society of Japan Bull. Chem. Soc. Jpn., 61, 385—391 (1988)

Pressure and Temperature Effects on Octahedral-Tetrahedral Equilibria in 4-Methylpyridine and 2-Methylpyridine Solutions of Some Cobalt(II) Halides

Kazuo KOJIMA
Department of Chemistry, Faculty of Science and Engineering, Ritsumeikan University, Kita-ku, Kyoto 603
(Received May 18, 1987)

The visible absorption spectra of CoX_2 (X=Cl, Br) in solutions of both 4-methylpyridine (4-Me-py) and 2-methylpyridine (2-Me-py) have been measured in the pressure range of 1 bar —3 kbar at room temperature, and in the temperature range of ≈6—≈75 °C at 1 bar. In the 4-Me-py solution system, the configuration equilibrium, $[CoX_2(4\text{-Me-py})_2]$ (tetrahedral) $+2(4\text{-Me-py}) \rightleftarrows [CoX_2(4\text{-Me-py})_4]$ (octahedral), was found to exist over the experimental pressure range. Increasing the pressure shifted the equilibrium toward the octahedral species side with volume changes of -26 cm^3 mol^{-1} for the chloro complex and -25 cm^3 mol^{-1} for the bromo complex at 1 bar. The above equilibrium held fairly well over the whole experimental temperature range for the chloro complex, but in the restricted temperature range for the bromo complex. Increasing the temperature tended to increase the formation of the tetrahedral species, the heats of reaction, being 53.3 kJ mol^{-1} and 62.6 kJ mol^{-1} for the chloro and bromo complexes, respectively. On the other hand, in the 2-Me-py solution system, increasing the pressure or temperature could hardly confirm the existence of the octahedral-tetrahedral configuration equilibrium. A charge-transfer band between the solvent molecule 2-Me-py and the free ion X^- decreased in intensity with increasing temperature. The above results in the 4-Me-py and 2-Me-py systems were compared with those of the pyridine (py) and 3-methylpyridine (3-Me-py) systems mentioned in the literature.

As a typical configuration equilibrium between the tetrahedral and octahedral complexes of Co(II), the following reaction is known in some nonaqueous solvents

$$[CoX_2(R\text{-py})_2] + 2(R\text{-py}) \overset{K}{\rightleftarrows} [CoX_2(R\text{-py})_4], \quad (1)$$
(tetrahedral) (octahedral)

where K is the equilibrium constant, X=Cl, Br, or I, and R-py=py or methylpyridines.

By means of spectrophotometric measurements of the $CoCl_2$-py system, Katzin[1] could study the temperature effect on the equilibrium and determined the value of ΔH. Using a series of R-py, Nelson et al.[2,3] have obtained thermodynamic data related to the equilibrium by means of spectroscopic, electrical, and calorimetric measurements. They interpreted the data in terms of the dative π-bonding from Co(II) to the pyridine base, which depends first on the kind of X^- and R-py and, secondly, on the hydrogen bond between the ligand and the solvent molecule. However, Libus et al.[4] have pointed out the importance of the hydrogen bond. Sawada et al.[5,6] have spectrophotometrically investigated the equilibrium of Eq. 1 for 1,2-dihaloethane solutions and found a linear correlation between the strength of the Co(II)-N bond and pK_b of R-py. On the other hand, the kinetic parameters related to the equilibrium have been determined by using nitrogen-14 NMR[7] and the temperature-jump method.[8,9]

All of the above reports, except for Katzin's,[1] have dealt with the equilibrium of Eq. 1 at atmospheric pressure and near room temperature. On the other hand, the effects of pressure and temperature on the equilibrium of Eq. 1 in the systems of R-py=py and 3-Me-py have been reported in previous papers.[10-12] There have been many studies[13] of high-pressure effects on inorganic reactions which involve ionic species. In these reactions, the contribution of electrostriction to the reaction volume or the activation volume is significant. However, the reaction of Eq. 1 involves no ionic species; therefore, the effect of electrostriction seems to be negligible.

Both the py[10,11] and 3-Me-py[12] systems under high pressures favored the octahedral species; however, at high temperatures the tetrahedral species was favored. Thus, from the variation of K with pressure and temperature, the values of ΔV and ΔH could be estimated. In the 3-Me-py system,[12] the 400-nm band which becomes stronger with increasing temperature was assigned to a charge-transfer transition between the solvent molecule (3-Me-py) and X^- arising from a dissociation of the tetrahedral species $[CoX_2(3\text{-Me-py})_2]$.

In the present paper, the pressure and temperature effects on the equilibrium of Eq. 1 (X=Cl, Br, R-py=4-Me-py, 2-Me-py) are described. The results are discussed in comparison with those of the py[10,11] and 3-Me-py[12] systems.

Experimental

$CoCl_2$ and $CoBr_2 \cdot 6H_2O$ were used after drying and 4-Me-py and 2-Me-py were used after drying and distillation. Sample solutions of CoX_2 in 4-Me-py or in 2-Me-py were prepared just before spectroscopic measurements.

High-pressure spectra were recorded at room temperature on a Shimadzu UV-365 spectrophotometer equipped with a clamp-type cell[14] (optical path length: 1.6 cm). High-temperature spectra were recorded at atmospheric pressure on a Shimadzu MPS-2000 instrument equipped with a pair of thermostated quartz cells (optical path length: 0.98 cm).

The experimental details were described in a previous paper.[10]

Results and Discussion

Spectra at Atmospheric Pressure and Room Temperature. The positions of the visible absorption spectra of CoX_2 in 4-Me-py and 2-Me-py solutions at atmospheric pressure and room temperature are listed in Table 1 together with those of the py[10,11] and 3-Me-py[12] systems. In the 4-Me-py system, the spectra are composed of both the O- and T-bands. This feature is similar to that in the py[10,11] or 3-Me-py[12] system. The O-band is due to the $^4T_{1g}(F) \rightarrow {}^4T_{1g}(P)$ electronic transition of the octahedral complex and the T-band is due to the $^4A_2(F) \rightarrow {}^4T_1(P)$ transition of the tetrahedral complex. On the other hand, in the spectra of the 2-Me-py system, a strong T-band is observed, but an O-band is hardly found. Similar results have been mentioned in the earlier reports[2,5,6,15-17] which described how the $[CoX_2(2\text{-Me-py})_4]$ complex seems to be little formed owing to a steric hindrance by the methyl group in 2-Me-py.

It can be seen in Table 1 that for octahedral or tetrahedral halo complexes having different ligands of amine bases, the energy of the strongest peak decreases in the order: py $\geqslant$ 4-Me-py > 3-Me-py > 2-Me-py. The position of the strongest peak could be a rough measure for the strength of the ligand field, though the position of the center of a band should be an exact measure of that. Therefore, the above order of R-py also reveals roughly a decreasing order of the ligand-field strength. This dependence of the ligand-field strength on R-py may result from a steric effect. This result is in contrast with earlier results.[5,6,16-18] The positions of the T-band have been reported to remain almost unchanged regardless of ligand R-py, namely, $[CoX_2(4\text{-Me-py})_2]$ or $[CoX_2(2\text{-Me-py})_2]$ in chloroform[16] and $[CoX_2(py)_2]$ or $[CoX_2(2\text{-Me-py})_2]$ in py or 2-Me-py solution.[17] Sawada et al.[5,6] have also found that the peak positions of $[CoX_2(R\text{-py})_2]$ in 1,2-dihaloethane solutions do not depend on the kind of ligand R-py. As for octahedral complexes, Goodgame and Hayward[18] have shown that for solid complexes the O-band of $[CoBr_2(4\text{-Me-py})_4]$ lies at longer wavelength than that of $[CoBr_2(3\text{-Me-py})_4]$.

Table 1. Positions of the Visible Absorption Spectra

Complex	Position[a] (in nm)	Reference
	O-band	
$[CoCl_2(py)_4]$	524, 500	10
$[CoCl_2(4\text{-Me-py})_4]$	525, 503, 557^{sh}, 571^{sh}	This work
$[CoCl_2(3\text{-Me-py})_4]$	530, 503, 560^{sh}	12
$[CoBr_2(py)_4]$	522, 539, 492^{sh}	10
$[CoBr_2(4\text{-Me-py})_4]$	520, 543, 570^{sh}, 505, 483	This work
$[CoBr_2(3\text{-Me-py})_4]$	526, 543, 570^{sh}, 490^{sh}	12
	T-band	
$[CoCl_2(py)_2]$	608, 637^{sh}, 571, 664^{sh}	10
$[CoCl_2(4\text{-Me-py})_2]$	610, 636, 575, 664^{sh}	This work
$[CoCl_2(3\text{-Me-py})_2]$	613, 640, 578, 665^{sh}	12
$[CoCl_2(2\text{-Me-py})_2]$	615, 634, 581, 662^{sh}	This work
$[CoBr_2(py)_2]$	643, 629^{sh}, 593, 711^{sh}	10
$[CoBr_2(4\text{-Me-py})_2]$	646, 628^{sh}, 595, 671^{sh}	This work
$[CoBr_2(3\text{-Me-py})_2]$	648, 626^{sh}, 597, 675^{sh}	12
$[CoBr_2(2\text{-Me-py})_2]$	650, 630^{sh}, 597	This work

sh: shoulder.
a) In each complex, the peaks and shoulders are aligned in the order of decreasing intensity on going from left to right.

Pressure Effect. Figure 1 shows the pressure dependence of the spectra of $CoCl_2$ in 4-Me-py. For both chloro and bromo (not shown) complexes, the intensities of the T-band decrease, but those of the O-band increase with increasing pressure. Therefore, it can be concluded that the equilibrium of Eq. 1 shifts toward the octahedral species $[CoX_2(4\text{-Me-py})_4]$ with increasing pressure. A similar feature has been also found in the py[10] or 3-Me-py[12] system.

The absorption spectra of $CoCl_2$ in 2-Me-py at various pressures are shown in Fig. 2. Two bands were found in addition to the T-band: a weak band at about 510 nm, and a weak, broad band ranging from $\approx$360 to $\approx$410 nm (see also Fig. 5). These two bands are discussed below in the section concerning the tempera-

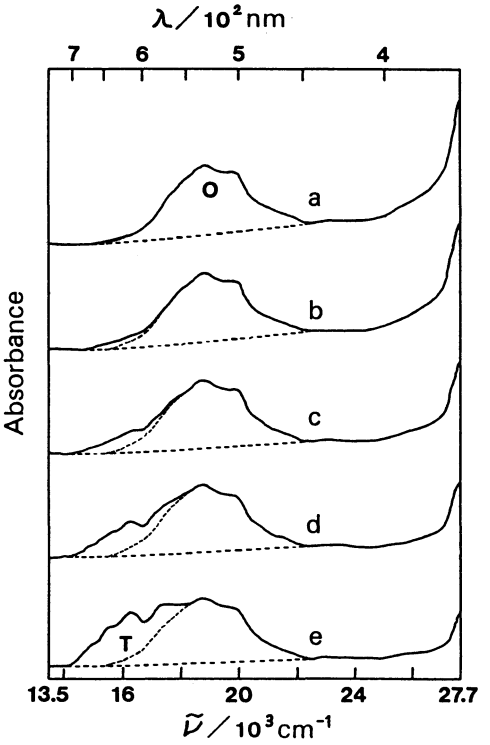

Fig. 1. Absorption spectra of $CoCl_2$ in 4-Me-py at high pressures (28.2°C), uncorrected for compression of solution. Each broken line shows the separation of the bands. Concn: 8.16×10^{-4} mol dm^{-3}. a: 3.0 kbar, b: 2.1 kbar, c: 1.0 kbar, d: 0.5 kbar, e: 1 bar.

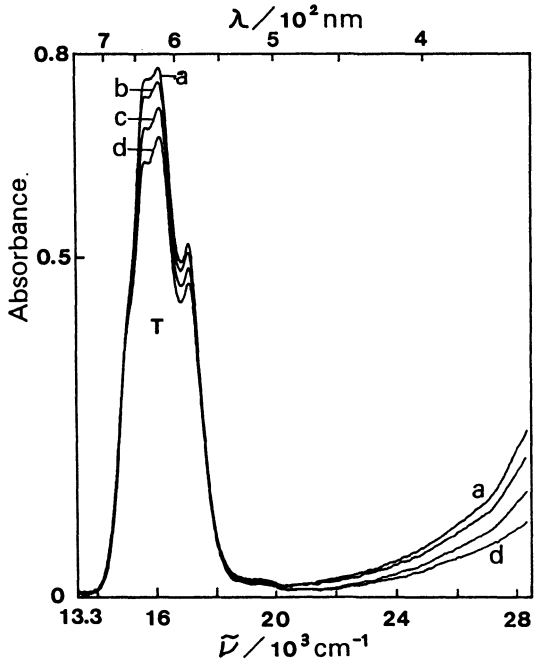

Fig. 2. Absorption spectra of $CoCl_2$ in 2-Me-py at high pressures (27.7°C), uncorrected for compression of solution. Concn: 7.70×10^{-4} mol dm^{-3}. a: 3.0 kbar, b: 2.0 kbar, c: 1.1 kbar, d: 1 bar.

ture effect. Contrary to the 4-Me-py system, the T-band in the 2-Me-py system apparently becomes stronger with increasing pressure. This tendency has also been observed in the high-pressure spectra of the tetrahedral complex $[CoCl_4]^{2-}$ in CH_3NO_2.[19] Even if the spectra are corrected for a compression of the solution, the T-band intensity changes little with pressure. Therefore, in the 2-Me-py system, the equilibrium of Eq. 1, if it exists, may be scarcely affected by the pressure.

Consider the equilibrium of Eq. 1 in the 4-Me-py system described above. When the pressure increases, the equilibrium shifts toward the octahedral complex side with a volume change (ΔV) of the system. ΔV is calculated by the equation[10]

$$\Delta V = -RT\frac{d}{dP}\ln(I_o/I_T), \qquad (2)$$

where R is the gas constant and I_o and I_T are the integrated intensities of the O- and T-bands, respectively.

As described in Ref. 10, Eq. 2 is derived by assuming that the molar absorption coefficients of both the $[CoX_2(4\text{-Me-py})_4]$ and $[CoX_2(4\text{-Me-py})_2]$ complexes hardly depend on the pressure at relatively low pressures.[20] The activity coefficient of solvent 4-Me-py is also assumed to be independent of pressure; this seems to be reasonable at relatively low pressures.

The plots of $\ln(I_o/I_T)$ vs. pressure in Fig. 3 were fitted to the following equations by a least-squares method:

$$\ln(I_o/I_T) = 0.565 + 1.017P, \text{ for the chloro complex, and}$$
$$\ln(I_o/I_T) = 0.0254 + 0.995P - 0.209P^2 + 0.0211P^3, \text{ for the bromo complex.} \qquad (3)$$

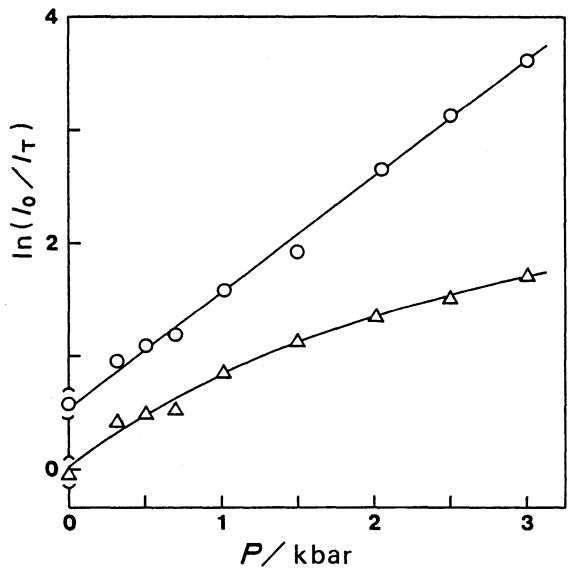

Fig. 3. Logarithm of the integrated-intensity ratio of the O-band to the T-band (I_o/I_T) vs. pressure in the 4-Me-py solution system. O: $CoCl_2$, Δ: $CoBr_2$, ——: calculated fitting lines.

Table 2. ΔV for the Reaction of $[CoX_2(R\text{-py})_2]+2(R\text{-py}) \rightleftarrows [CoX_2(R\text{-py})_4]$ at Various Pressures

P / kbar	$-\Delta V$ / cm^3 mol^{-1}						
	4-Me-py[a]		3-Me-py[b]		py		
	Cl	Br	Cl	Br	Cl[c]	Br[c]	I[d]
0.001	26	25	18	19	41	29	6
0.5	26	20	21	19	35	31	6
1.0	26	16	24	19	29	31	6
1.5	26	13	27	19	24	28	6
2.0	26	10	29		18	23	6
2.5	26	9	32		13	16	6
3.0	26	8	34		7	6	6

a) This work. b) Ref. 12. c) Ref. 10. d) Ref. 11.

From Eqs. 2 and 3, the values of ΔV were estimated to be all negative; these are listed in Table 2 together with those of the py[10,11] and 3-Me-py[12] systems.

From Eq. 1, ΔV equals $V_{oct}-(V_{tet}+2V_{sol})$, where V_{oct}, V_{tet}, and V_{sol} are the intrinsic molar volumes of the octahedral species, the tetrahedral species, and the solvent, respectively. The values of V_{oct} and V_{tet} are not available, but the molar volumes of some related complexes in solutions have been reported. Libus et al. have estimated the molar volumes of $[ZnCl_2(py)_2]$ and $[NiCl_2(py)_4]$ in py solutions to be 198.7 ± 1.3 cm^3 mol^{-1} [21] and 333 ± 10 cm^3 mol^{-1},[22] respectively. Narbutt and Siekierski[23] have obtained the molar volume of $[Co(NCS)_2(4\text{-Me-py})_4]$ in benzene solutions as 428 ± 15 cm^3 mol^{-1}. The molar volumes of py and methylpyridines can be estimated from their densities to be of the order of 80 and 100 cm^3 mol^{-1}, respectively. On the basis of the above values, the magnitude of $|\Delta V|$ at 1 bar (Table 2) seems reasonable.

The values of $|\Delta V|$ at 1 bar were found to decrease

according to the ligand sequence py>4-Me-py>3-Me-py. This sequence shows that V_{oct} relative to the sum of V_{tet} and $2V_{sol}$ becomes large in the order, py<4-Me-py<3-Me-py, owing to the steric hindrance of R-py ligands in each octahedral complex.

The differences in $|\Delta V|$ at 1 bar between the chloro and bromo complexes are large in the py system, but are small in the 4-Me-py and 3-Me-py systems. This fact suggests that the contribution of X to both V_{oct} and V_{tet} is smaller in the methylpyridine systems than in the py system.

It can be seen in Table 2 that for both the chloro and bromo complexes the ratios of the values of $|\Delta V|$ at high pressures to those at 1 bar increase in the order, py<4-Me-py<3-Me-py. It is impossible to discuss further this pressure dependence of $|\Delta V|$, since the activities and compressibilities of solvents R-py were not obtained at high pressures.

Temperature Effect. The absorption spectra of $CoCl_2$ in 4-Me-py at various temperatures are shown in Fig. 4. The intensity of the T-band increases steeply with increasing temperature. Although the change in the O-band with temperature could be obscured due to the intense T-band, the equilibrium of Eq. 1 probably shifts toward the tetrahedral species $[CoCl_2(4\text{-Me-py})_2]$ with increasing temperature, contrary to the pressure effect described above. A similar result was obtained

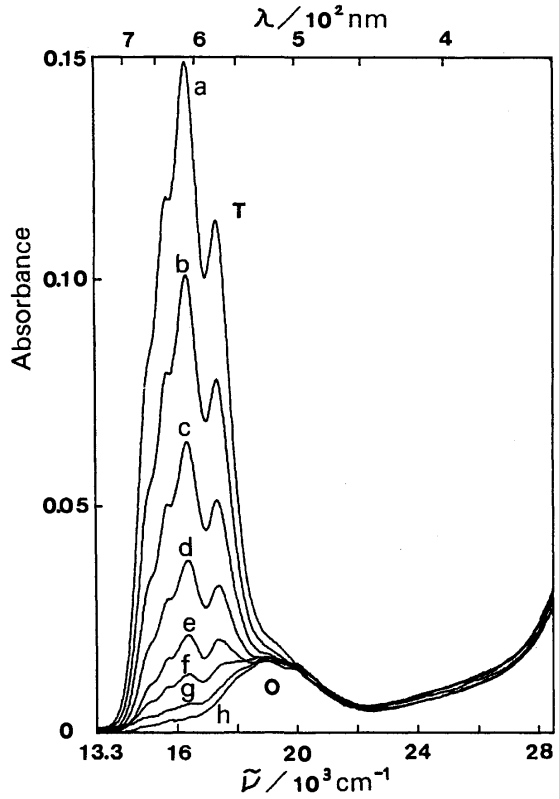

Fig. 4. Absorption spectra of $CoCl_2$ in 4-Me-py at various temperatures, uncorrected for thermal expansion of solution. Concn: 7.39×10^{-4} mol dm^{-3}. a: 74.8°C, b: 64.4°C, c: 54.6°C, d: 44.8°C, e: 35.2°C, f: 25.0°C, g: 14.9°C, h: 5.8°C.

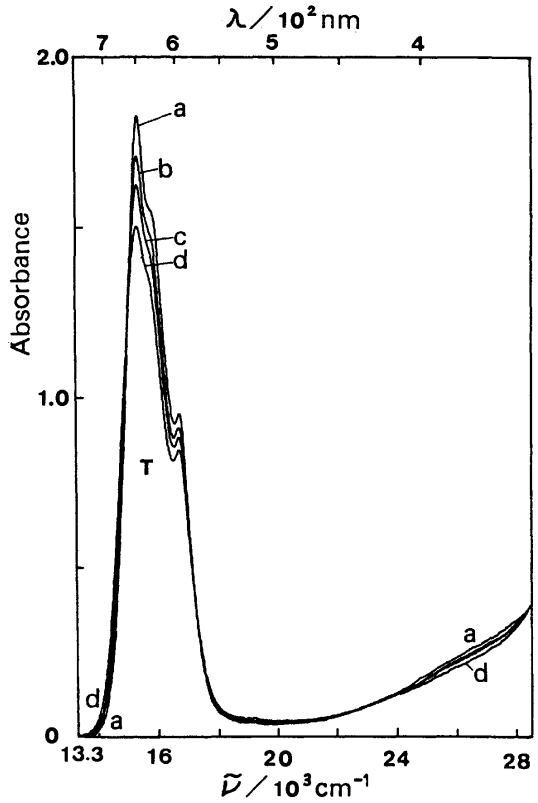

Fig. 5. Absorption spectra of $CoBr_2$ in 2-Me-py at various temperatures, uncorrected for thermal expansion of solution. Concn: 2.18×10^{-3} mol dm^{-3}. a: 5.5°C, b: 26.3°C, c: 44.5°C, d: 75.3°C.

for the bromo complex (not shown). Such a tendency is similar to that of the py[10] or 3-Me-py[12] system.

Figure 5 shows the absorption spectra of $CoBr_2$ in 2-Me-py at various temperatures. Contrary to the 4-Me-py system, the intensity of the T-band apparently decreases slightly with increasing temperature. Therefore, the equilibrium of Eq. 1 in the 2-Me-py system may be hardly shifted with increasing temperature.

In the 4-Me-py system, the heat of reaction for $[CoX_2(4\text{-Me-py})_4] \rightleftarrows [CoX_2(4\text{-Me-py})_2]+2(4\text{-Me-py})$, ΔH, can be obtained by the method described in Ref. 10: The variation of the equilibrium constant for the reaction of $[CoX_2(4\text{-Me-py})_4] \rightleftarrows [CoX_2(4\text{-Me-py})_2]+2(4\text{-Me-py})$ with temperature can be approximately followed by the change of the T-band intensity. As the intensity of the T-band, the absorbance of the 664-nm shoulder for the chloro complex and that of the 646-nm peak for the bromo complex are used. In Fig. 6, the logarithm of the corrected absorbance A' is plotted against the reciprocal absolute temperature. In order to obtain A', the observed absorbance is corrected by use of the thermal expansion coefficient for solvent 4-Me-py (1.038×10^{-3} K^{-1}[24]). The plots in Fig. 6 can be fitted to straight lines, indicating that each value of ΔH is constant over each temperature range. The slopes of the lines give ΔH as follows: 53.3 kJ mol^{-1} for the chloro complex over the range of 5.8—74.8 °C and 62.6 kJ mol^{-1} for the bromo complex over the range of

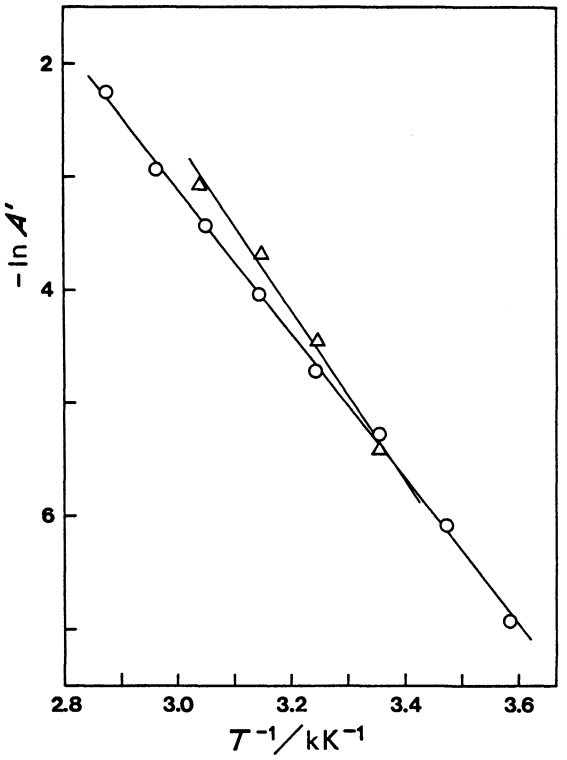

Fig. 6. Logarithm of the corrected absorbance A' vs. reciprocal absolute temperature in the 4-Me-py solution system. O: $CoCl_2$, Δ: $CoBr_2$, ——: calculated fitting lines.

Table 3. ΔH for the Reaction of $[CoX_2(R\text{-}py)_4] \rightleftarrows [CoX_2(R\text{-}py)_2]+2(R\text{-}py)$

R-py (ligand)	Solvent	ΔH / kJ mol^{-1}			Reference
		Cl	Br	I	
py	py	57.3	60.7	65.3	10, 11
	$CHCl_3$	63.6	65.3	69.5	2
4-Me-py	4-Me-py	53.3	62.6		This work
	$CHCl_3$	65.7			3
3-Me-py	3-Me-py	56.7	58.6		12
	$CHCl_3$	56.1			3

25.0—55.8 °C These values are listed in Table 3 together with the values for the py and 3-Me-py complexes in each R-py solution[10-12] and in $CHCl_3$ solutions.[2,3]

As described above, the values of ΔH are determined by the same method as that described in the literature,[1,8,9,25] by assuming that the concentration of the octahedral complex is constant in the experimental temperature range.[10] This assumption seems reasonable when the concentration of the octahedral complex is much larger than that of the tetrahedral complex. In order to examine the validity of this assumption, in the $CoCl_2$-4-Me-py system (Fig. 4), for example, the decrease in the concentration of $[CoCl_2(4\text{-}Me\text{-}py)_4]$ with increasing temperature was attempted to be taken into account by subtracting the concentration of $[CoCl_2(4\text{-}Me\text{-}py)_2]$ from the total concentration of Co(II). The concentration of $[CoCl_2(4\text{-}Me\text{-}py)_2]$ was determined by using the molar absorption coefficient at 615 nm of 663 dm^3 mol^{-1} cm^{-1} for $[CoCl_2(4\text{-}Me\text{-}py)_2]$ in $CHCl_3$-4-Me-py mixtures,[16] since the value in the 4-Me-py solution could not be obtained. Using the spectral data in Fig. 4, the above procedure gives a ΔH which is larger by 2.5 kJ mol^{-1} than 53.3 kJ mol^{-1} in Table 3.

In spectroscopic studies of solution equilibrium, few studies have taken into account the temperature dependence of the activity of the solvent. Exceptionally, in an aqueous solution system, Swaddle and Fabes[26] regarded the relative density $\rho_r(=\rho_{T,P}/\rho_{298\,K,1\,bar})$ as an activity of the solvent water at high temperatures and high pressures on the basis of the solvent effect on the oscillator strength of the absorption band. In addition to the above consideration concerning the concentration of $[CoCl_2(4\text{-}Me\text{-}py)_4]$, taking the activity of solvent 4-Me-py into account with the method by Swaddle and Fabes,[26] the value of ΔH is 53.8 kJ mol^{-1}. This is only by 0.5 kJ mol^{-1} larger than 53.3 kJ mol^{-1} in Table 3.

Since the above procedures give similar effects concerning the values of ΔH in the other CoX_2-R-py systems, the values of ΔH in Table 3 seem to be reasonable.

It seems to be difficult at present to determine the values of the absorption coefficients of the octahedral and tetrahedral complexes in solutions of py, 3-Me-py, and 4-Me-py and the values of the activities of solvents at high temperatures. However, the method for determining ΔH used in the present and previous[10-12] reports seems to be reasonable.

As Table 3 shows, ΔH of the 4-Me-py system is larger for ligand Br^- than for ligand Cl^-, which is similar to the py,[10,11] 3-Me-py,[12] and $CHCl_3$[2,3] solution systems. This trend seems to be explained in terms of the dative π-bonding from Co(II) to the pyridine base proposed by King et al.:[2] Charge is readily transferred from ligand X^- to Co(II) in the order $Cl^- < Br^- < I^-$. This enhances the release of non-bonding d-electrons of Co(II) to antibonding pyridine base π-orbitals, thereby strengthening the Co(II)-N bond in the order $Cl^- < Br^- < I^-$.

The heats of dissociation of the solid complexes $[CoX_2(R\text{-}py)_4]$ in the reaction, $[CoX_2(R\text{-}py)_4](solid) \rightleftarrows [CoX_2(R\text{-}py)_2](solid)+2(R\text{-}py)(gas)$, have been reported to increase in the order $I^- < Br^- < Cl^-$ for the 4-Me-py[3,27] and 3-Me-py[3] complexes. The fact that this order for the heats of dissociation is opposed to the order for ΔH seems to be important in a further discussion of the X^- dependence of the dative π-bonding in solutions.

In the $CoBr_2$-R-py systems ΔH decreases in the order of ligand R-py: 4-Me-py > py > 3-Me-py (Table 3). This order agrees with that of the $CoCl_2$-$CHCl_3$ systems.[2,3] Cabral et al.[3] have pointed out that 3-Me-py

is the weakest π-acceptor since the charge densities on the 2-, 4-, and 6-positions, on which charges from Co(II) are concentrated, increase through a 3-methyl substituent. Therefore, the smallest ΔH for the 3-Me-py complex is mainly due to the dative π-bonding from Co(II) to ligand 3-Me-py. However, the largest ΔH for the 4-Me-py complexes may not be interpreted only in terms of the dative π-bonding, since 4-Me-py is a weaker π-acceptor than py; nevertheless, ΔH is larger for the 4-Me-py complexes than for the py ones. In the $CoCl_2$-R-py systems, the dependence of ΔH on ligand R-py is not the same as that of the $CoBr_2$-R-py systems. Especially, ΔH in the $CoCl_2$-4-Me-py system seems to be comparatively small (Table 3).

Lastly, temperature effects for the 2-Me-py solution system are discussed. As stated above, the intensity of the T-band for $CoBr_2$ in 2-Me-py apparently decreases with increasing temperature (Fig. 5). A similar result has been observed for $CoCl_2$ (not shown). Even if the intensity was corrected for the thermal expansion coefficient (1.123×10^{-3} K^{-1} [24]), it decreases with increasing temperature (not shown). The temperature effect on broadening the T-band is found to be small; thus, the oscillator strength of the T-band may decrease slightly with increasing temperature. This fact is interesting from the view point of the temperature dependence of the oscillator strength of the T-band.

Assuming that only the tetrahedral complex $[CoX_2(2\text{-Me-py})_2]$ exists in the CoX_2-2-Me-py solutions at room temperature and atmospheric pressure, the molar absorption coefficient is estimated to be ε_{615}=537 $dm^3 mol^{-1} cm^{-1}$ for the chloro complex and ε_{650}=800 $dm^3 mol^{-1} cm^{-1}$ for the bromo complex. In the literature, the values of ε_{615} (693[16] and 610 $dm^3 mol^{-1} cm^{-1}$ [17]) and those of ε_{650} (853[16] and 832 $dm^3 mol^{-1} cm^{-1}$ [17]) have been reported; these values seem to be too large compared with those of this work. It is interesting that the inconsistency among the values of ε is large not for the bromo complex but for the chloro one. There are two possible explanations for this inconsistency. One is that no subtraction of the base lines for the T-bands was taken into account by Graddon and Watton[16] and by Libus et al.;[17] the other is that a partial dissociation of $[CoX_2(2\text{-Me-py})_2]$ probably occurs in the 2-Me-py solutions. This possible dissociation may be supported by the existence of both a weak band centered at about 510 nm and a weak, broad band ranging from ≈360 to ≈410 nm (Fig. 5).

The 510-nm band may be due to an ionic octahedral species of the type $[CoX_x(2\text{-Me-py})_{6-x}]^{2-x}$ [2,3] (x=0 or 1). According to a previous paper,[12] the band ranging from ≈360 to ≈410 nm may be assigned to a charge-transfer band arising in a contact pair of solvent molecule 2-Me-py with free ion X^-. $[CoX_x(2\text{-Me-py})_{6-x}]^{2-x}$ and free X^- may result from a dissociation of the tetrahedral complex $[CoX_2(2\text{-Me-py})_2]$.

As Fig. 5 shows, the intensity of the CT band in the 2-Me-py system decreases with increasing temperature, which is contrary to that of the 3-Me-py system.[12] An explanation may be that in the 2-Me-py system the concentration of the free X^- ion decreases with increasing temperature, probably because of the formation of such an ionic tetrahedral species as $[CoX_3(2\text{-Me-py})]^-$ by a reaction between X^- and $[CoX_2(2\text{-Me-py})_2]$ at high temperatures.

The intensity of the CT band in the 2-Me-py system is less than that of the 3-Me-py system[12] at room temperature and the CT band is hardly observed in the py[10] and 4-Me-py systems. From these results, it is concluded that free ion X^- can be easily formed in solvents in the order 4-Me-py, py $\ll$ 2-Me-py $<$ 3-Me-py.

Referring to the literature[28,29] showing structures of the ion pairs as

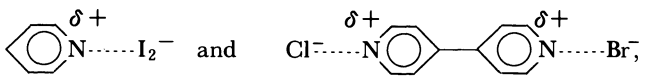

the structure of the CT complex in the present study may be:

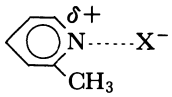

where X^- is a donor and nitrogen is an acceptor.

The author would like to express his sincere thanks to Professor Jiro Matsuda of Ritsumeikan University for valuable discussions, critical reading of the manuscript, and continuous encouragements. The author also wishes to thank Professor Ikuji Tsujikawa and Dr. Norimichi Kojima of Kyoto University for their encouragement. Thanks are due to Mr. Hajime Taguchi and Mr. Toshiro Nakada of Ritsumeikan University for their support during the experiment.

References

1) L. I. Katzin, *J. Chem. Phys.*, **35**, 467 (1961).
2) H. C. A. King, E. Körös, and S. M. Nelson, *J. Chem. Soc., A*, **1963**, 5449.
3) J. de O. Cabral, H. C. A. King, S. M. Nelson, T. M. Shepherd, and E. Körös, *J. Chem. Soc., A*, **1966**, 1348.
4) W. Libus, K. Chachulska, and M. Mecik, *Inorg. Chem.*, **19**, 2259 (1980).
5) K. Sawada and T. Suzuki, *J. Inorg. Nucl. Chem.*, **43**, 2301 (1981).
6) K. Sawada, K. Miura, and T. Suzuki, *Bull. Chem. Soc. Jpn.*, **55**, 780 (1982).
7) G. D. Howard and R. S. Marianelli, *Inorg. Chem.*, **9**, 1738 (1970).
8) R. D. Farina and J. H. Swinehart, *J. Am. Chem. Soc.*, **91**, 568 (1969).
9) R. D. Farina and J. H. Swinehart, *Inorg. Chem.*, **11**, 645 (1972).
10) K. Kojima, M. Saida, M. Donoue, and J. Matsuda, *Bull. Chem. Soc. Jpn.*, **56**, 684 (1983).
11) K. Kojima, T. Miyashita, and J. Matsuda, *Bull. Chem.*

Soc. Jpn., **57**, 879 (1984).

12) K. Kojima, *Bull. Chem. Soc. Jpn.*, **60**, 603 (1987).

13) "Inorganic High Pressure Chemistry," ed. by R. van Eldik, Elsevier, Amsterdam (1986).

14) K. Suzuki and M. Tsuchiya, *Bull. Chem. Soc. Jpn.*, **48**, 1701 (1975).

15) D. P. Graddon, R. Schultz, E. C. Watton, and D. G. Weeden, *Nature (London)*, **198**, 1299 (1963).

16) D. P. Graddon and E. C. Watton, *Aust. J. Chem.*, **18**, 507 (1965).

17) W. Libus, H. Berek, and M. Kluczkowski, *Bull. Acad. Pol. Sci., Ser. Sci. Chim.*, **27**, 509 (1979).

18) M. Goodgame and P. J. Hayward, *J. Chem. Soc., A*, **1971**, 3406.

19) K. Kojima and J. Matsuda, unpublished result.

20) H. D Lüdemann and E. U. Frank, *Ber. Bunsenges. Phys. Chem.*, **71**, 455 (1967); **72**, 514 (1968); S. Rodriguez and H. Offen, *Inorg. Chem.*, **10**, 2086 (1971).

21) W. Libus, K. Chachulska, and J. Stangret, *J. Sol. Chem.*, **12**, 529 (1983).

22) W. Libus, B. Janaszewski, R. Pastewski, and H. Twardowska, *J. Sol. Chem.*, **9**, 737 (1980).

23) J. Narbutt and S. Siekierski, *Roczniki Chem.*, **48**, 1777 (1974).

24) The thermal expansion coefficient of 4-Me-py, $1.038\times10^{-3}\,K^{-1}$, is evaluated from the slope of the least-square fitting straight line for the plots of the reciprocals of densities of 4-Me-py vs. temperatures. Those densities are given in "Beilsteins Handbuch der Organishen Chemie," ed. by Deutschen Chemischen Gesellschaft, Springer-Verlag, Berlin (1935), Hauptwerk Band XX, p. 240 and *ibid.*, ed. by Beilstein-Institut für Literatur der Organischen Chemie, Springer-Verlag, Berlin (1978), Ergänzungswerk III/IV, Band XX, p. 2734. By the same manner, the thermal expansion coefficients of the other amine bases are estimated as follows: $1.084\times10^{-3}\,K^{-1}$ for py, $0.875\times10^{-3}\,K^{-1}$ for 3-Me-py, and $1.123\times10^{-3}\,K^{-1}$ for 2-Me-py. In Refs. 10 and 12, the values of ΔH for the py and 3-Me-py systems (X=Cl, Br) have been obtained by using the approximate thermal expansion coefficient $1\times10^{-3}\,K^{-1}$. The values of ΔH estimated by using the above new coefficients are found to agree with those in the previous reports[10,12] within the experimental error.

25) D. E. Scaife and K. P. Wood, *Inorg Chem.*, **6**, 358 (1967); K Mizutani and K. Sone, *Z. Anorg Allg. Chem.*, **350**, 216 (1967).

26) T. W. Swaddle and L. Fabes, *Can J. Chem.*, **58**, 1418 (1980).

27) G. Beech, C. T. Mortimer, and E. G. Tyler, *J. Chem Soc., A*, **1967**, 925.

28) Z. Pawelka and L. Sobczyk, *J. Sol. Chem*, **12**, 355 (1983).

29) T. Nishijima, T. Nagamura, and T. Matsuo, *J. Polym. Sci., Polym. Lett. Ed.*, **19**, 65 (1981).

The Crystal and Molecular Structure of Scandium(III), Yttrium(III), and Some Lanthanoid(III) *p*-Toluenesulfonates, $[Sc(C_7H_7SO_3)_2(H_2O)_4](C_7H_7SO_3)\cdot 2H_2O$ and $[M(C_7H_7SO_3)_2(H_2O)_6](C_7H_7SO_3)\cdot 3H_2O$ (M=Y, Sm, Gd, Dy, Ho, Er, Yb); and Yttrium(III) and Dysprosium(III) 2-Naphthalenesulfonates, $[M(C_{10}H_7SO_3)_2(H_2O)_6]\text{-}(C_{10}H_7SO_3)\cdot 3H_2O$ (M=Y, Dy)

Yoshiyuki Ohki,† Yasuo Suzuki,† Toshio Takeuchi,†† and Akira Ouchi*

Department of Chemistry, College of Arts and Sciences, The University of Tokyo, Komaba, Meguro-ku, Tokyo 153
†Department of Industrial Chemistry, Faculty of Engineering, Meiji University, Higashi-Mita, Tama-ku, Kawasaki-shi, Kanagawa 214
††Department of Natural Sciences, Faculty of Science and Technology, Sophia University, Kioi, Chiyoda-ku, Tokyo 102

(Received May 20, 1987)

Scandium(III) *p*-toluenesulfonate hexahydrate, as well as the isomorphous yttrium(III) and six lanthanoid(III) (Sm, Gd, Dy, Ho, Er, and Yb) *p*-toluenesulfonate enneahydrates, were synthesized and their structures were determined by the single-crystal X-ray diffraction technique. The scandium salt was monoclinic with the space group $P2_1/a$, $Z=4$ (the cell constants were $a=23.672(16)$, $b=15.792(6)$, $c=7.7543(12)$ Å, $\beta=92.86(3)°$, and the final R value was 0.059). The central metal atom is hexa-coordinated, being in an octahedral geometry, in which two unidentate sulfonate oxygen atoms (in cis-configuration) and four water oxygen atoms are ligated. The latter seven salts were also monoclinic with a space group of $P2_1/n$, and $Z=4$ (the cell constants of the holmium salt, for example, were $a=25.058(19)$, $b=7.476(2)$, $c=17.802(10)$ Å, $\beta=98.80(8)°$, and its final R value was 0.039). The central metal atom of these complexes are octa-coordinated, being in a square-antiprism geometry in which two unidentate sulfonate and six water oxygen atoms are ligated. In both types of complexes, no ligand bridgings were found, and one in three sulfonate ions was not coordinated to the metal atom. In the respective lanthanoid(III) complexes, M-O(sulfonato) bonds are shorter than the M-O(water) ones. The corresponding M-O bonds of the respective complexes decrease, almost proportional to the sum of the Shannon's ionic radii of the metal and oxygen, with the metal atomic numbers. Each M-O bond length of the yttrium(III) *p*-toluenesulfonate and 2-naphthalenesulfonate had the value expected from the corresponding bond lengths of the series of the respective isomorphous lanthanoid(III) salts, referring to its metal ionic radius.

Since only a few structural data concerning lanthanoid sulfonates have been published, the coordination behavior of such a hard base to a hard acid metal is very interesting. The structures of the lanthanoid 2-naphthalenesulfonates had already been elucidated,[1] but since the ligand is large, we should also examine the other arenesulfonates in order to reveal the common structure of the group of complexes. In the rare earth ethyl sulfates (La—Yb), all the coordination positions around the metal atom were occupied not by the sulfato but by the water oxygen atoms[2,3] On the other hand, in crystals of the lanthanoid(III) (Pr—Yb) 2-naphthalenesulfonates two in three anions as well as six water molecules act as unidentates. Since no bridging or chelating of the ligand was found, the coordination geometry around the metal atom is not so deformed as the carboxylato complexes.[4-8]

Recently, we could synthesize the scandium(III), yttrium(III), and some lanthanoid(III) (Sm through Yb) *p*-toluenesulfonates approximately by the same synthetic method. It is interesting to compare their structures with each other, especially those of the scandium and yttrium salts with the lanthanoid(III) ones.

We have relatively small numbers of structural data concerning the scandium(III) and yttrium(III) complexes. Regarding the scandium(III) carboxylates studied, the central metal atom was always hexa-coordinated and the high coordination number found in the yttrium or lanthanoid complexes were not recognized.[9,10] However, it was reported that tris(cyclopentadienyl)scandium and -lutetium have the same type chain structure, probably due to their similar atomic radii.[11] Therefore, the hexa-coordination of scandium is thought not to be always assured in all kinds of the complexes.

From the structural data, it was found that yttrium(III) formate,[12] acetate,[13] chloroacetate,[10] hexafluoroacetylacetonate,[14] and some acetylacetonates,[15,16] are isomorphous with the corresponding salts of lanthanoid(III). As the energy levels of the 4f orbitals in the yttrium(III) ion are thought to be too high to make any hybrid orbitals,[17] the orbitals are not likely used in the coordination bonds of its complexes. Although Cotton already wrote that 4f electrons hardly contribute to the formation of hybrid orbitals,[18] this fact can be more clearly proved if any isomorphous yttrium and lanthanoid complexes of the same ligand are found to always have the same geometrical environment around the respective metal atoms.

From this point of view, it is desirable to compare more structural data concerning their same ligand complexes, especially those which are obtained by the same synthetic technique and are isomorphous with each other.

The present study of the series of the rare earth *p*-

toluenesulfonates was aimed at investigating: 1) how the arenesulfonate ions are coordinated with the metal atoms, 2) if the scandium(III) and yttrium(III) salts have the same structures as those of the lanthanoid salts, and 3) how the M-O bond strength (which is related to the bond length observed) changes with the atomic number and with the metal ionic radius.

Therefore, we studied their crystal and molecular structures by the single-crystal X-ray diffraction technique. Their structures, bond lengths and angles were examined comparatively; especially their observed M-O bond lengths were compared with the standard values (the respective sums of the Shannon's ionic radii).[19]

The structures of the series of the rare-earth 2-naphthalenesulfonates,[1] including the newly obtained yttrium(III) and dysprosium(III) salts, have been examined comparatively, in order to clarify whether the relation between the observed M-O bond lengths and the sums of Shannon's ionic radii is the same as the *p*-toluenesulfonates.

Table 1. Analyses of the Rare Earth *p*-Toluenesulfonates and 2-Naphthalenesulfonates[a)]

	Chemical formula	Analysis(n/%)		
		M	C	H
$ScL_3{\cdot}3H_2O$[b,c)]	$ScC_{21}H_{27}O_{12}S_3$	7.20 (7.34)	41.00 (41.17)	4.19 (4.44)
$YL_3{\cdot}9H_2O$	$YC_{21}H_{39}O_{18}S_3$	11.69 (11.63)	32.99 (32.99)	4.98 (5.14)
$SmL_3{\cdot}9H_2O$	$SmC_{21}H_{39}O_{18}S_3$	18.13 (18.20)	30.24 (30.52)	4.57 (4.76)
$GdL_3{\cdot}9H_2O$	$GdC_{21}H_{39}O_{18}S_3$	18.80 (18.88)	30.26 (30.28)	4.42 (4.72)
$DyL_3{\cdot}9H_2O$	$DyC_{21}H_{39}O_{18}S_3$	19.48 (19.51)	30.09 (30.09)	4.55 (4.69)
$HoL_3{\cdot}9H_2O$	$HoC_{21}H_{39}O_{18}S_3$	19.62 (19.62)	29.93 (30.00)	4.52 (4.68)
$ErL_3{\cdot}9H_2O$	$ErC_{21}H_{39}O_{18}S_3$	19.77 (19.84)	29.77 (29.92)	4.48 (4.66)
$YbL_3{\cdot}9H_2O$	$YbC_{21}H_{39}O_{18}S_3$	20.40 (20.39)	29.59 (29.72)	4.41 (4.63)
$YL'_3{\cdot}9H_2O$[d)]	$YC_{30}H_{39}O_{18}S_3$	10.25 (10.19)	41.28 (41.29)	4.46 (4.50)
$DyL'_3{\cdot}9H_2O$[d)]	$DyC_{30}H_{39}O_{18}S_3$	17.05 (17.17)	37.99 (38.08)	4.20 (4.15)

a) The calculated values are shown in parentheses. b) HL=*p*-toluenesulfonic acid. c) Three in six water molecules of the original crystal $ScL_3{\cdot}6H_2O$ were lost by the drying process before the elemental analysis (lost water; Found 8.03%; Calcd 8.11%). d) HL'=2-naphthalenesulfonic acid.

Experimental

Syntheses of [Tetraaquabis(*p*-toluenesulfonato)scandium(III)] *p*-Toluenesulfonate Dihydrate. Into an aqueous solution of scandium(III) cholride (prepared by dissolving Sc_2O_3 (0.14 g, 1.0 mmol) into an excess of hydrochloric acid), excess of sodium hydroxide was added. Precipitated scandium(III) hydroxide was separated and dissolved in 10 cm^3 of water and *p*-toluenesulfonic acid hydrate (1.14 g, 6.0 mmol). The aqueous solution was left standing for several days until about two thirds of the water was evaporated off. Crystals of the title complex were deposited and were used for an X-ray structure analysis. Yield: 0.78 g (59%). Elemental analyses

Table 2. Crystallographic Data and Some Experimental Conditions to Obtain their Intensity Data of Scandium, Yttrium and Lanthanoid *p*-Toluenesulfonates: $[Sc(C_7H_7SO_3)_2(H_2O)_4](C_7H_7SO_3){\cdot}2H_2O$ (Monoclinic, Space Group $P2_1/a$, Z=4); and $[M(C_7H_7SO_3)_2(H_2O)_6](C_7H_7SO_3){\cdot}3H_2O$ (M=Y, Sm, Gd, Dy, Ho, Er, and Yb) (Monoclinic, Space Group $P2_1/n$, Z=4)

M=	Sc	Y	Sm	Gd	Dy	Ho	Er	Yb
F. W.	666.14	764.09	825.58	832.43	837.68	840.11	842.44	848.22
a(*l*/Å)	23.672(16)	25.034(12)	25.150(12)	25.122(9)	25.073(7)	25.058(19)	25.031(11)	24.981(13)
b(*l*/Å)	15.792(6)	7.477(2)	7.515(2)	7.499(1)	7.481(1)	7.476(2)	7.473(3)	7.457(2)
c(*l*/Å)	7.7543(12)	17.815(8)	17.898(7)	17.862(5)	17.833(4)	17.802(10)	17.796(8)	17.774(6)
β(ϕ/°)	92.86(3)	98.84(4)	99.00(4)	98.94(3)	98.90(2)	98.80(5)	98.77(4)	98.75(3)
U(v/Å^3)	2895(2)	3295(2)	3340(2)	3324.2(17)	3304.7(13)	3296(3)	3290(2)	3273(2)
D_m(d/Mg m^{-3})	1.51(3)	1.52(3)	1.62(3)	1.65(3)	1.68(3)	1.69(3)	1.69(3)	1.69(3)
D_x(d/Mg m^{-3})	1.53	1.54	1.64	1.66	1.68	1.69	1.70	1.72
μ(Mo $K\alpha$) (n/mm^{-1})	0.53_9	2.09	2.04	2.31	2.61	2.75	2.91	3.27
Number of reflections measured	6262	6311	7528	7496	7454	7433	7423	7186
Reflections used for the calculation[e)]	4153	3839	5038	5010	5587	5402	5235	5250
Measured range (2θ/°)	3—52	3—50	3—53	3—53	3—53	3—53	3—53	3—53
R[f)]	0.059	0.064	0.045	0.049	0.038	0.039	0.047	0.040
Size of crystal used (v/mm^3)	0.50×0.30 ×0.20	0.25×0.25 ×0.25	0.30×0.30 ×0.20	0.20×0.10 ×0.10	0.35×0.35 ×0.30	0.31×0.30 ×0.28	0.30×0.35 ×0.15	0.30×0.30 ×0.32
Slit width (θ/°)	1.02+ 0.5tanθ	1.01	1.00	1.00	1.00	1.01	1.01	1.01

e) Reflections with $|F_o|>3\sigma(|F_o|)$ were used. f) $R=\sum||F_o|-|F_c||/\sum|F_o|$

Table 3. Crystallographic Data and Some Experimental Conditions to Obtain Intensity Data of Yttrium and Dysprosium 2-Naphthalenesulfonates: $[M(C_{10}H_7SO_3)_2(H_2O)_6](C_{10}H_7SO_3)\cdot 3H_2O$ (M=Y, Dy) (Monoclinic, Space Group $P2_1$, Z=2)

M=	Y	Dy
F. W.	872.8	976.4
a(*l*/Å)	18.117(8)	18.111(7)
b(*l*/Å)	7.446(2)	7.452(3)
c(*l*/Å)	14.034(3)	14.049(5)
β(ϕ/°)	107.80(2)	107.78(3)
U(v/Å^3)	1802.5(10)	1805.4(12)
D_m(d/Mg m^{-3})	1.61(3)	1.73(3)
D_x(d/Mg m^{-3})	1.61	1.74
μ(Mo $K\alpha$)(n/mm^{-1})	1.92	2.40
Number of reflections measured	5572	4505
Reflections used for the calculation[e]	4203	3284
Measured range (2θ/°)	3—60	3—55
R[f]	0.057[g]	0.058[g]
Size of crystal used (v/mm^3)	0.15×0.15 ×0.25	0.20×0.10 ×0.15
Slit width (θ/°)	1.08+ 0.5tanθ	1.10+ 0.5tanθ

e, f) See footnotes of Table 2. g) Their R values with inverse chirality were 0.069 and 0.059 respectively.

revealed that a sample dried for 24h in a vacuum desiccator over silica gel lost three water molecules per one metal atom. The results of the elemental analyses are shown in Table 1.

Syntheses of [Hexaaquabis(*p*-toluenesulfonato)yttrium-(III)] *p*-Toluenesulfonate Trihydrate and the Isomorphous. Lanthanoid(III) (Sm, Gd, Dy, Ho, Er, and Yb) Salts. An aqueous solution of the yttrium(III) salt was obtained almost in the same way as for the scandium(III) salt, starting with 0.23 g (1.0 mmol) of yttrium(III) oxide (Y_2O_3) and the acid hydrate (1.14 g, 6 mmol). It was left standing for several days in open air at room temperature until about four fifths of the water was removed. Crystals of the yttrium(III) complex were depositied. Yield: 1.12 g (72%). Isomorphous lanthanoid(III) (Sm, Gd, Dy, Ho, Er, Yb) salts were also obtained by an analogous method; their yields were between 70 and 80%.

All of the obtained salts did not show a mass loss beyond the experimental error after being left standing for two days in a vacuum silica gel desiccator at ambient temperature. However, when they were kept for several months under the conditions, some part of water was lost especially in the case of the samarium(III), and to a smaller extent, in the case of the gadolinium(III) salt. When these crystals were dipped into methanol, ethanol, or 1- or 2-propanol medium, crystals of the samarium salt were destroyed immediately, and those of the gadolinium salt after a few minutes. Althouth the heavier lanthanoid salts did not decompose soon, they also lost water while being kept in the medium longer. When all of these salts, after being kept for a long time in alcohol, were dried in a vacuum silica gel desiccator, dehydrated salts were obtained. The stability of these hydrated crystals probably increases depending on the atomic number of the metal. Analyses of these salts are shown in Table 1.

Attempts to obtain a lighter isomorphous lanthanoid(III) (La—Nd) *p*-toluenesulfonates by the same synthetic method were not successful; their salts in the triclinic system, which effloresce very rapidly, were obtained alternatively.

Syntheses of [Hexaaquabis(2-naphthalenesulfonato)yttrium(III)] 2-Naphthalenesulfonate Trihydrate. The synthetic technique for isomorphous lanthanoid(III) complexes previously reported[1] was used, starting with yttrium(III) chloride ($YCl_3\cdot 6H_2O$) (0.30 g, 1.0 mmol) and 2-naphthalenesulfonic acid (0.70 g, 3.4 mmol). Yield: 0.45 g (52%). Their analyses are shown in Table 1.

Single Crystal X-Ray Structure Analysis. The crystal and molecular structures of the ten titled complex crystals were examined by the single-crystal X-ray diffraction method. Their crystallographic data, experimental conditions for obtaining intensity data, and their final R values calculated after applying anisotropic thermal parameters to all non-hydrogen atoms are shown in Tables 2 and 3.

During the intensity data collection, the crystals of samarium(III) and gadolinium(III) complexes were destroyed through irradiation by X-rays in open air. Consequently, the crystals of the samarium and gadolinium salts used for the X-ray diffraction study were sealed into borosilicate glass capillaries. Since the decomposition rate decreases rapidly, depending on the atomic number of the metal, practically no trouble was found regarding measurements of the heavier lanthanoid complexes.

The reflections were collected on a Rigaku AFC-6A automated four-circle X-ray diffractometer with graphite-monochromated Mo $K\alpha$ (λ=0.71073 Å) radiation, with a scan speed of 4° (θ) min^{-1}. The ω-2θ scan technique was used for scandium *p*-toluensulfonate and both of the 2-naphthalenesulfonates, while the ω-scan method was applied for the other *p*-toluenesulfonates. The intensities were corrected for Lorentz and polarization factors, but not for absorption and extinction.

Structure Determination. The structure of the scandium(III) and yttrium(III) *p*-toluenesulfonates were solved by the heavy-atom method. The positions of the metal and sulfur atoms were, respectively, deduced from three dimensional Patterson maps. The positions of the other atoms were succesively located by Fourier syntheses. Their positional and thermal parameters were repeatedly refined by the block-diagonal least-squares method. In the end, all non-hydrogen atoms were found.

The structures of the isomorphous lanthanoid(III) *p*-toluenesulfonates were refined by starting with the parameters of the isomorphous yttrium complex. The structures of yttrium(III) and dysprosium(III) 2-naphthalenesulfonates were obtained starting with the final parameters of the isomorphous erbium(III) salt, $[Er(C_{10}H_7SO_3)_2(H_2O)_6](C_{10}H_7SO_3)\cdot 3H_2O$, and refined as usual.[1] In these cases, the positions of the naphthalene-ring hydrogen atoms were calculated assuming the C-H bond lengths to be 1.08 Å and their B_{iso}'s to be 6.0 Å^2. The parameters of the hydrogen atoms were fixed during the refinement. Since their crystals have no center of symmetry, refinements using the inverse chirality were also carried out; the one giving a lower R value was adopted for each complex. Both of them were found to have the same chirality as the erbium salt. All calculations were carried out on a HITAC M-682H appara-

Table 4. Final Atomic Coordinates ($\times 10^4$) of the Non-Hydrogen Atoms and Their Equivalent Isotropic Temperature Factors of the Complexes (Estimated Standard Deviations in Parentheses)

(4.1) Scandium(III) *p*-Toluenesulfonate Hexahydrate

Atom	*x*	*y*	*z*	B_{eq}/Å^{2} [h]
Sc	−11.4(4)	1788.9(5)	3301.6(11)	1.9_5
S(1)	694(1)	1505(1)	7204(2)	2.6_3
S(2)	709(1)	3707(1)	2873(2)	3.9_7
S(3)	1338(1)	−867(1)	2471(2)	2.5_7
O(11)	518(2)	1400(2)	5349(4)	3.2_3
O(12)	472(2)	801(2)	8180(4)	3.2_6
O(13)	560(2)	2316(2)	7856(5)	4.5_8
O(21)	386(1)	2907(2)	2993(4)	3.2_1
O(22)	530(2)	4156(3)	1346(8)	7.9_5
O(23)	681(2)	4191(3)	4408(8)	8.2_7
O(31)	1357(2)	−1697(2)	3258(5)	4.2_3
O(32)	1032(2)	−263(2)	3508(4)	3.1_5
O(33)	1117(2)	−869(3)	690(4)	3.9_1
O(W1)	−538(2)	708(2)	3598(4)	3.2_0
O(W2)	490(1)	995(2)	1790(4)	2.8_5
O(W3)	−468(1)	2042(2)	972(4)	3.1_6
O(W4)	−573(1)	2415(2)	4920(4)	3.0_1
O(W5)	−317(2)	3956(3)	6097(6)	5.7_6
O(W6)	−388(2)	3491(3)	−434(7)	6.9_4
C(11)	1432(2)	1387(3)	7278(6)	2.6_3
C(12)	1686(2)	703(3)	8145(6)	2.9_6
C(13)	2274(2)	637(3)	8221(7)	3.2_3
C(14)	2602(2)	1247(4)	7456(6)	3.1_5
C(15)	2341(2)	1925(4)	6594(7)	3.5_2
C(16)	1756(2)	2003(3)	6513(7)	3.2_8
C(17)	3247(2)	1176(4)	7561(8)	4.6_8
C(21)	1416(2)	3397(3)	2676(6)	2.8_0
C(22)	1838(2)	3845(3)	3567(7)	3.4_8
C(23)	2396(3)	3626(4)	3359(7)	3.8_7
C(24)	2533(2)	2959(4)	2285(7)	3.4_2
C(25)	2102(2)	2507(4)	1402(7)	3.4_5
C(26)	1537(2)	2731(3)	1592(7)	3.2_1
C(27)	3151(3)	2740(5)	2051(10)	5.6_1
C(31)	2041(2)	−508(3)	2440(6)	2.4_0
C(32)	2441(2)	−1028(3)	1741(6)	3.0_8
C(33)	2999(2)	−762(4)	1690(7)	3.8_0
C(34)	3158(2)	37(4)	2320(7)	3.4_0
C(35)	2749(2)	548(4)	3023(7)	3.6_7
C(36)	2193(2)	276(3)	3095(7)	3.3_2
C(37)	3766(3)	330(5)	2253(9)	5.3_9

(4.2) Yttrium(III) *p*-Toluenesulfonate Enneahydrate

Atom	*x*	*y*	*z*	B_{eq}/Å^{2} [h]
Y	2506.0(3)	−165.3(10)	4707.9(4)	2.2_9
S(1)	1453(1)	−3160(3)	3867(1)	3.4_3
S(2)	3387(1)	3414(3)	4240(1)	2.9_7
S(3)	3439(1)	2235(3)	7721(1)	3.2_3
O(11)	1820(2)	−2229(8)	4467(3)	3.6_2
O(12)	1526(2)	−5076(9)	3921(4)	5.6_8
O(13)	1502(2)	−2520(10)	3127(3)	5.2_2
O(21)	3078(2)	1751(7)	4148(3)	3.0_9
O(22)	3219(2)	4638(7)	3621(3)	3.9_7
O(23)	3377(2)	4219(7)	4979(3)	3.9_9
O(31)	3147(2)	3899(8)	7502(4)	5.2_0
O(32)	3420(2)	1773(8)	8506(3)	4.1_9
O(33)	3218(2)	794(8)	7217(3)	4.7_1
O(W1)	2099(2)	2589(8)	4890(3)	3.9_8
O(W2)	2017(2)	642(7)	3503(3)	3.7_8
O(W3)	2108(2)	−415(7)	5835(3)	3.8_3
O(W4)	2937(2)	−2596(7)	5360(3)	3.4_3
O(W5)	3117(2)	1161(7)	5694(3)	3.2_4
O(W6)	2908(2)	−1871(7)	3826(3)	3.5_8
O(W7)	2192(2)	3832(8)	2730(3)	4.4_0
O(W8)	2160(2)	3460(9)	6386(3)	5.3_5
O(W9)	3216(3)	−2783(9)	6864(3)	7.3_6
C(11)	802(3)	−2695(11)	4046(4)	3.4_2
C(12)	418(4)	−2062(14)	3462(5)	5.3_7
C(13)	−111(4)	−1764(15)	3611(6)	6.3_7
C(14)	−241(4)	−2026(17)	4321(6)	6.7_3
C(15)	145(4)	−2749(25)	4872(7)	10.9_6
C(16)	672(4)	−3026(21)	4741(5)	8.1_3
C(17)	−829(4)	−1688(24)	4462(8)	11.4_8
C(21)	4058(3)	2794(10)	4215(4)	2.8_6
C(22)	4186(4)	2015(15)	3567(5)	5.2_3
C(23)	4730(4)	1469(15)	3563(6)	6.0_9
C(24)	5121(3)	1779(13)	4189(6)	5.3_7
C(25)	4979(4)	2571(17)	4816(6)	7.0_9
C(26)	4448(4)	3116(15)	4845(5)	5.6_3
C(27)	5711(4)	1182(17)	4181(8)	8.4_5
C(31)	4108(3)	2538(11)	7606(4)	3.2_8
C(32)	4236(3)	3626(12)	7030(4)	4.0_1
C(33)	4783(4)	3805(13)	6929(5)	4.6_0
C(34)	5185(4)	2858(13)	7402(5)	5.0_6
C(35)	5050(4)	1801(14)	7973(5)	5.3_7
C(36)	4514(4)	1587(13)	8087(5)	4.8_5
C(37)	5782(4)	3041(17)	7284(7)	7.3_7

tus at the Computer Center of the University of Tokyo using a local version of the UNICS program.[20] The atomic scattering factors were taken from Ref. 21.

Other Measurements. Their infrared spectra were obtained by a JASCO A-202 grating infrared spectrophotometer using liquid paraffin and hexachloro-1,3-butadiene mull. Simultaneous thermogravimetric (TG) and differential thermal analyses (DTA) were carried out with a Rigaku Denki "Thermoflex" M-8075 using samples weighing about 10 mg each, at a heating rate of 10 °C min^{-1} in air, α-alumina as the reference.

Results and Discussion

The final atomic parameters and the equivalent isotropic temperature factors of the scandium(III), yttrium(III), and lanthanoids(III) (Sm, Gd, Dy, Ho, Er, Yb) *p*-toluenesulfonates, as well as those of the yttrium(III) and dysprosium(III) 2-naphthalenesulfonates are shown in Table 4. Their selected bond lengths and bond angles are tabulated in Tables 5, 6, and 7.[22] A perspective drawings of the scandium(III) and yttrium(III) *p*-toluenesulfonates around their central metals, together with the numbering scheme, are shown in Figs. 1 and 2. The crystal packing diagrams of the scandium(III) and yttrium(III) *p*-toluenesulfonates, together with the nomination of the toluene rings, are shown in Figs. 3 and 4 respectively.

In the scandium(III) *p*-toluenesulfonate, the central metal atom is hexa-coordinated and is in an octahedral geometry, where two unidentate sulfonato oxygen

Table 4. (Continued)

(4.3) Samarium(III) *p*-Toluenesulfonate Enneahydrate

Atom	*x*	*y*	*z*	B_{eq}/Å^{2} [h]
Sm	2505.1(1)	−179.6(4)	4703.1(2)	2.2_2
S(1)	1432(1)	−3185(3)	3860(1)	3.4_1
S(2)	3401(1)	3414(2)	4227(1)	3.0_3
S(3)	3429(1)	2242(2)	7718(1)	3.1_7
O(11)	1795(2)	−2268(7)	4455(3)	3.7_3
O(12)	1497(2)	−5099(8)	3901(4)	6.3_3
O(13)	1474(2)	−2514(9)	3123(3)	5.3_8
O(21)	3086(2)	1769(6)	4130(3)	3.2_7
O(22)	3232(2)	4620(6)	3602(3)	3.8_8
O(23)	3394(2)	4227(7)	4962(3)	4.3_4
O(31)	3152(2)	3879(7)	7491(4)	5.2_7
O(32)	3422(2)	1798(8)	8497(3)	4.4_9
O(33)	3227(2)	811(7)	7222(3)	4.5_9
O(W1)	2092(2)	2668(7)	4893(3)	4.3_5
O(W2)	2011(2)	636(7)	3469(3)	3.9_8
O(W3)	2102(2)	−405(7)	5858(3)	4.1_7
O(W4)	2943(2)	−2664(6)	5377(3)	3.6_5
O(W5)	3132(2)	1206(6)	5708(3)	3.4_4
O(W6)	2908(2)	−1929(6)	3796(3)	3.8_2
O(W7)	2189(2)	3830(7)	2745(3)	4.3_7
O(W8)	2161(2)	3477(8)	6390(3)	5.2_2
O(W9)	3230(3)	−2805(8)	6875(3)	7.0_1
C(11)	786(3)	−2714(10)	4036(4)	3.3_0
C(12)	401(3)	−2105(13)	3469(5)	5.5_0
C(13)	−125(4)	−1772(14)	3621(6)	6.7_3
C(14)	−259(4)	−2050(16)	4302(6)	6.8_4
C(15)	131(4)	−2733(26)	4859(7)	11.3_6
C(16)	659(4)	−3077(20)	4737(5)	8.7_7
C(17)	−835(4)	−1681(23)	4449(8)	10.8_0
C(21)	4069(3)	2795(8)	4213(4)	2.7_8
C(22)	4196(3)	1969(13)	3578(5)	5.1_3
C(23)	4733(4)	1454(14)	3577(5)	6.1_4
C(24)	5119(3)	1741(12)	4188(5)	5.3_5
C(25)	4981(4)	2564(16)	4802(6)	6.8_1
C(26)	4454(3)	3123(13)	4829(5)	5.5_4
C(27)	5712(4)	1152(16)	4173(7)	8.4_0
C(31)	4104(3)	2544(10)	7607(4)	3.1_8
C(32)	4229(3)	3651(10)	7032(4)	3.7_0
C(33)	4770(3)	3790(11)	6935(5)	4.6_0
C(34)	5176(3)	2893(12)	7406(5)	4.8_2
C(35)	5040(3)	1788(13)	7967(5)	5.5_3
C(36)	4509(3)	1612(12)	8078(5)	4.7_5
C(37)	5769(3)	3071(15)	7286(6)	6.6_8

(4.4) Gadolinium(III) *p*-Toluenesulfonate Enneahydrate

Atom	*x*	*y*	*z*	B_{eq}/Å^{2} [h]
Gd	2505.8(1)	−174.9(4)	4704.3(2)	2.2_4
S(1)	1441(1)	−3178(3)	3865(1)	3.4_3
S(2)	3396(1)	3409(3)	4232(1)	3.0_4
S(3)	3429(1)	2240(3)	7720(1)	3.1_9
O(11)	1808(2)	−2263(8)	4455(3)	3.7_7
O(12)	1510(3)	−5094(9)	3909(4)	6.1_0
O(13)	1488(2)	−2479(10)	3125(3)	5.1_3
O(21)	3081(2)	1765(7)	4139(3)	3.4_3
O(22)	3231(2)	4623(7)	3611(3)	3.9_9
O(23)	3385(3)	4227(7)	4965(3)	4.3_8
O(31)	3150(3)	3872(8)	7495(4)	5.2_5
O(32)	3427(2)	1772(9)	8501(3)	4.5_6
O(33)	3223(3)	791(8)	7223(3)	4.8_0
O(W1)	2096(2)	2636(8)	4882(3)	4.1_9
O(W2)	2011(2)	634(8)	3488(3)	3.9_8
O(W3)	2102(2)	−416(8)	5846(3)	4.1_7
O(W4)	2940(2)	−2644(7)	5370(3)	3.4_0
O(W5)	3122(2)	1188(7)	5704(3)	3.4_0
O(W6)	2908(2)	−1906(7)	3805(3)	3.6_3
O(W7)	2188(2)	3831(8)	2738(3)	4.2_5
O(W8)	2163(3)	3457(9)	6388(4)	5.2_9
O(W9)	3228(4)	−2792(9)	6872(4)	7.2_6
C(11)	788(3)	−2705(11)	4039(4)	3.2_1
C(12)	411(4)	−2076(15)	3460(6)	5.6_3
C(13)	−111(4)	−1752(16)	3618(7)	6.6_4
C(14)	−259(4)	−2049(18)	4288(7)	6.8_6
C(15)	129(5)	−2707(28)	4855(7)	10.6_4
C(16)	665(4)	−3040(22)	4742(6)	8.3_6
C(17)	−838(4)	−1734(26)	4443(10)	11.1_9
C(21)	4071(3)	2798(10)	4212(4)	3.0_0
C(22)	4193(4)	1937(14)	3573(5)	4.9_2
C(23)	4732(4)	1461(16)	3573(6)	5.9_8
C(24)	5128(4)	1748(13)	4201(6)	5.3_3
C(25)	4976(4)	2588(18)	4809(7)	7.0_6
C(26)	4446(4)	3116(16)	4831(6)	5.9_0
C(27)	5710(4)	1159(19)	4179(9)	8.5_6
C(31)	4107(3)	2543(11)	7610(4)	3.3_2
C(32)	4237(3)	3658(11)	7031(4)	3.7_3
C(33)	4772(4)	3796(13)	6933(5)	4.5_5
C(34)	5185(4)	2882(13)	7405(5)	4.9_7
C(35)	5046(4)	1801(15)	7972(6)	5.6_0
C(36)	4507(4)	1605(13)	8080(5)	4.7_3
C(37)	5777(4)	3043(17)	7287(7)	6.6_8

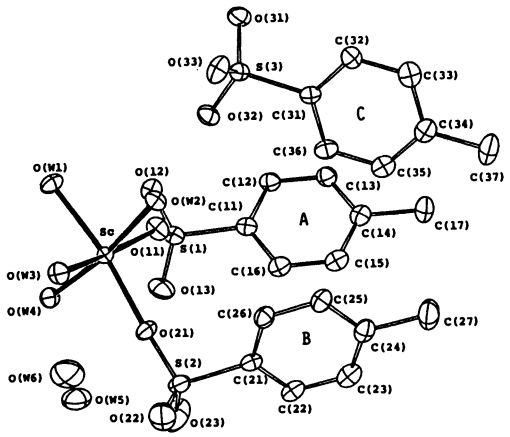

Fig. 1. A perspective drawing of scandium(III) *p*-toluenesulfonate hexahydrate with the numbering scheme.

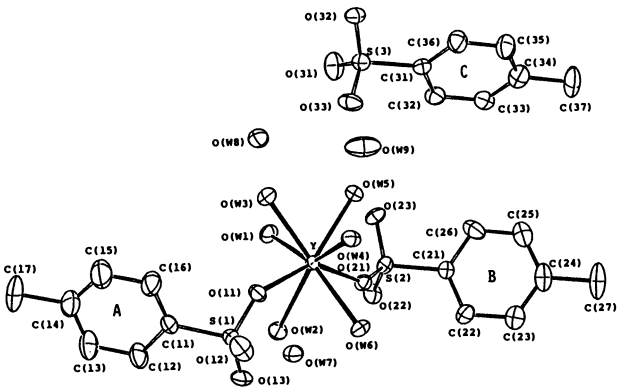

Fig. 2. A perspective drawing of yttrium(III) *p*-toluenesulfonate enneahydrate with the numbering scheme.

Table 4. (Continued)

(4.5) Dysprosium(III) *p*-Toluenesulfonate Enneahydrate

Atom	*x*	*y*	*z*	B_{eq}/Å^{2} [h]
Dy	2506.4(1)	−167.2(3)	4707.2(1)	2.2_0
S(1)	1449(1)	−3168(2)	3868(1)	3.3_3
S(2)	3392(1)	3415(2)	4236(1)	2.9_2
S(3)	3429(1)	2239(2)	7721(1)	3.1_7
O(11)	1816(2)	−2239(6)	4464(2)	3.5_7
O(12)	1516(2)	−5082(7)	3925(4)	5.7_5
O(13)	1493(2)	−2490(8)	3123(3)	5.1_6
O(21)	3080(2)	1757(6)	4141(2)	3.3_1
O(22)	3227(2)	4638(6)	3612(3)	3.8_1
O(23)	3385(2)	4229(6)	4973(3)	4.0_7
O(31)	3153(2)	3885(7)	7500(3)	5.2_7
O(32)	3425(2)	1776(7)	8503(2)	4.1_2
O(33)	3220(2)	796(7)	7223(3)	4.6_6
O(W1)	2104(2)	2602(6)	4890(3)	4.0_6
O(W2)	2019(2)	654(6)	3505(3)	3.7_5
O(W3)	2106(2)	−417(6)	5835(3)	3.9_3
O(W4)	2933(2)	−2609(6)	5366(2)	3.4_6
O(W5)	3121(2)	1171(6)	5697(2)	3.2_2
O(W6)	2904(2)	−1881(6)	3820(2)	3.6_1
O(W7)	2193(2)	3819(7)	2733(3)	4.3_8
O(W8)	2162(2)	3457(7)	6387(3)	5.2_0
O(W9)	3226(3)	−2782(8)	6865(3)	7.1_8
C(11)	796(3)	−2692(9)	4041(4)	3.2_0
C(12)	414(3)	−2064(12)	3468(5)	5.5_4
C(13)	−108(3)	−1763(14)	3615(6)	6.6_5
C(14)	−249(3)	−2020(14)	4295(6)	6.5_5
C(15)	133(4)	−2734(26)	4861(6)	11.6_5
C(16)	664(3)	−3070(18)	4737(5)	8.0_4
C(17)	−834(4)	−1664(22)	4441(8)	10.9_8
C(21)	4064(2)	2796(8)	4215(3)	2.8_5
C(22)	4186(3)	1976(12)	3580(4)	4.8_5
C(23)	4730(3)	1479(14)	3571(5)	6.1_6
C(24)	5123(3)	1753(11)	4198(5)	4.9_1
C(25)	4979(3)	2567(16)	4806(5)	6.9_8
C(26)	4452(3)	3140(13)	4829(5)	5.4_8
C(27)	5707(3)	1189(16)	4167(7)	8.0_5
C(31)	4105(3)	2532(9)	7603(3)	3.1_4
C(32)	4232(3)	3636(10)	7038(4)	3.8_2
C(33)	4775(3)	3775(11)	6939(4)	4.6_7
C(34)	5184(3)	2858(11)	7408(4)	4.8_1
C(35)	5042(3)	1784(12)	7974(5)	5.2_4
C(36)	4511(3)	1597(11)	8081(4)	4.6_1
C(37)	5779(3)	3034(15)	7289(6)	6.9_8

(4.6) Holmium(III) *p*-Toluenesulfonate Enneahydrate

Atom	*x*	*y*	*z*	B_{eq}/Å^{2} [h]
Ho	2506.5(1)	−163.1(3)	4708.1(1)	2.1_5
S(1)	1452(1)	−3162(2)	3869(1)	3.2_7
S(2)	3389(1)	3417(2)	4239(1)	2.8_8
S(3)	3428(1)	2237(2)	7722(1)	3.1_0
O(11)	1818(2)	−2225(6)	4467(2)	3.5_8
O(12)	1522(2)	−5071(7)	3920(3)	5.7_1
O(13)	1498(2)	−2502(8)	3125(2)	5.0_5
O(21)	3079(2)	1763(5)	4145(2)	3.3_0
O(22)	3223(2)	4634(6)	3615(3)	3.7_9
O(23)	3381(2)	4224(6)	4978(3)	4.0_7
O(31)	3156(2)	3892(7)	7505(3)	5.3_3
O(32)	3422(2)	1774(7)	8505(2)	4.2_5
O(33)	3219(2)	799(7)	7222(3)	4.6_5
O(W1)	2102(2)	2590(6)	4893(3)	4.0_5
O(W2)	2019(2)	650(6)	3508(2)	3.8_3
O(W3)	2106(2)	−416(6)	5831(2)	3.8_5
O(W4)	2935(2)	−2590(5)	5363(2)	3.3_8
O(W5)	3120(2)	1160(6)	5695(2)	3.2_3
O(W6)	2897(2)	−1868(5)	3819(2)	3.4_6
O(W7)	2194(2)	3825(7)	2729(2)	4.2_7
O(W8)	2161(2)	3454(7)	6385(3)	5.2_3
O(W9)	3222(3)	−2800(7)	6862(3)	7.1_7
C(11)	797(2)	−2686(8)	4044(3)	3.1_3
C(12)	417(3)	−2055(12)	3467(5)	5.5_6
C(13)	−109(3)	−1762(13)	3621(6)	6.4_5
C(14)	−251(3)	−2058(15)	4303(6)	7.2_7
C(15)	143(4)	−2741(24)	4869(6)	11.1_7
C(16)	669(3)	−3064(17)	4738(5)	7.8_1
C(17)	−832(4)	−1699(21)	4442(8)	10.9_3
C(21)	4061(2)	2802(7)	4217(3)	2.6_8
C(22)	4191(3)	1981(12)	3577(4)	5.0_3
C(23)	4731(3)	1488(13)	3568(5)	6.0_2
C(24)	5122(3)	1743(10)	4191(5)	5.0_8
C(25)	4978(3)	2576(15)	4808(5)	7.0_5
C(26)	4448(3)	3118(12)	4835(4)	5.5_1
C(27)	5710(3)	1178(15)	4163(7)	8.2_1
C(31)	4107(2)	2531(8)	7599(3)	3.1_6
C(32)	4234(3)	3623(9)	7036(4)	3.9_3
C(33)	4779(3)	3784(10)	6939(4)	4.5_7
C(34)	5188(3)	2860(11)	7404(4)	4.7_9
C(35)	5047(3)	1804(12)	7968(5)	5.2_6
C(36)	4510(3)	1595(11)	8080(4)	4.7_1
C(37)	5784(3)	3027(14)	7284(6)	7.0_5

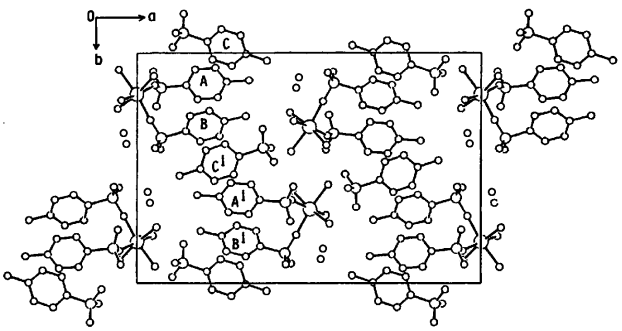

Fig. 3. A projection of the unit cell to the ab plane of scandium(III) *p*-toluenesulfonate hexahydrate. Key to the symmetry operations: i, 0.5−*x*, 0.5+*y*, 1−*z*.

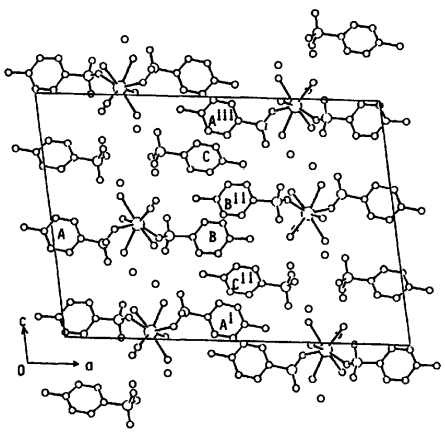

Fig. 4. A projection of the unit cell to the ac-plane of yttrium(III) *p*-toluenesulfonate enneahydrate. Key to the symmetry operations: i, 0.5−*x*, 0.5+*y*, 0.5−*z*; ii, 1−*x*, 1−*y*, 1−*z*; iii, 0.5+*x*, 0.5−*y*, 0.5+*z*.

Table 4. (Continued)

(4.7) Erbium(III) *p*-Toluenesulfonate Enneahydrate

Atom	*x*	*y*	*z*	B_{eq}/Å^{2} [h]
Er	2506.9(1)	−162.3(4)	4708.9(2)	2.2_2
S(1)	1456(1)	−3159(3)	3872(1)	3.3_0
S(2)	3387(1)	3417(3)	4241(1)	2.9_6
S(3)	3427(1)	2235(3)	7723(1)	3.2_6
O(11)	1820(2)	−2215(8)	4463(3)	3.6_4
O(12)	1526(3)	−5070(8)	3923(4)	5.7_0
O(13)	1498(2)	−2501(10)	3126(3)	4.9_7
O(21)	3075(2)	1768(7)	4145(3)	3.1_8
O(22)	3222(2)	4639(7)	3618(3)	3.8_6
O(23)	3377(2)	4218(8)	4979(3)	4.2_0
O(31)	3153(2)	3887(8)	7505(4)	5.1_7
O(32)	3421(2)	1771(8)	8506(3)	4.2_1
O(33)	3219(3)	789(8)	7218(3)	4.5_7
O(W1)	2107(2)	2601(8)	4898(3)	4.2_3
O(W2)	2021(2)	643(8)	3518(3)	3.8_8
O(W3)	2107(2)	−403(7)	5823(3)	3.6_1
O(W4)	2932(2)	−2591(7)	5363(3)	3.5_1
O(W5)	3120(2)	1157(7)	5693(3)	3.2_4
O(W6)	2900(2)	−1859(7)	3826(3)	3.6_0
O(W7)	2198(2)	3813(9)	2732(3)	4.4_7
O(W8)	2164(2)	3454(9)	6390(4)	5.0_9
O(W9)	3220(4)	−2807(9)	6856(4)	7.4_4
C(11)	801(3)	−2686(11)	4049(5)	3.3_8
C(12)	423(4)	−2041(14)	3457(6)	5.3_2
C(13)	−107(4)	−1757(16)	3612(7)	6.6_2
C(14)	−250(4)	−2029(17)	4305(6)	6.3_7
C(15)	129(5)	−2757(28)	4856(7)	10.7_0
C(16)	669(4)	−3075(21)	4747(6)	7.7_9
C(17)	−836(4)	−1688(24)	4433(9)	10.1_3
C(21)	4063(3)	2794(10)	4218(4)	2.7_3
C(22)	4187(4)	2008(15)	3576(5)	5.1_3
C(23)	4731(4)	1506(16)	3565(6)	6.1_6
C(24)	5117(4)	1780(13)	4193(6)	5.2_0
C(25)	4972(4)	2559(18)	4817(7)	7.0_9
C(26)	4443(4)	3124(15)	4838(6)	5.5_5
C(27)	5711(4)	1180(18)	4157(9)	8.3_0
C(31)	4103(3)	2545(11)	7602(4)	3.3_6
C(32)	4234(3)	3620(12)	7033(5)	3.9_7
C(33)	4781(4)	3769(13)	6936(5)	4.6_5
C(34)	5185(4)	2854(13)	7403(5)	4.5_5
C(35)	5050(4)	1795(15)	7969(6)	5.4_7
C(36)	4513(4)	1586(13)	8082(5)	4.8_0
C(37)	5784(4)	3016(17)	7277(7)	6.7_7

(4.8) Ytterbium(III) *p*-Toluenesulfonate Enneahydrate

Atom	*x*	*y*	*z*	B_{eq}/Å^{2} [h]
Yb	2507.0(1)	−158.9(3)	4710.2(1)	2.1_0
S(1)	1463(1)	−3160(3)	3874(1)	3.1_7
S(2)	3383(1)	3420(2)	4244(1)	2.8_2
S(3)	3426(1)	2234(2)	7723(1)	3.0_6
O(11)	1826(2)	−2213(7)	4469(3)	3.4_1
O(12)	1533(2)	−5072(7)	3928(4)	5.5_3
O(13)	1509(2)	−2490(9)	3128(3)	4.8_1
O(21)	3066(2)	1764(6)	4146(3)	3.2_0
O(22)	3218(2)	4646(6)	3619(3)	3.5_8
O(23)	3375(2)	4230(6)	4984(3)	4.0_3
O(31)	3152(2)	3894(7)	7510(4)	5.1_8
O(32)	3418(2)	1753(7)	8504(3)	4.0_8
O(33)	3218(2)	796(7)	7216(3)	4.4_6
O(W1)	2103(2)	2562(7)	4896(3)	4.0_2
O(W2)	2028(2)	660(7)	3528(3)	3.5_2
O(W3)	2104(2)	−426(7)	5820(3)	3.7_9
O(W4)	2930(2)	−2563(6)	5351(3)	3.3_1
O(W5)	3112(2)	1138(6)	5686(2)	3.0_4
O(W6)	2896(2)	−1833(6)	3832(2)	3.3_0
O(W7)	2198(2)	3826(7)	2726(3)	4.2_2
O(W8)	2162(2)	3443(8)	6381(3)	4.8_6
O(W9)	3219(3)	−2793(8)	6859(3)	6.8_9
C(11)	807(3)	−2670(9)	4048(4)	3.1_5
C(12)	429(3)	−2049(13)	3460(5)	5.2_0
C(13)	−103(4)	−1733(14)	3618(6)	6.6_1
C(14)	−248(3)	−2055(16)	4308(6)	6.4_4
C(15)	140(4)	−2731(27)	4864(6)	11.2_7
C(16)	674(4)	−3036(19)	4751(5)	7.8_5
C(17)	−832(4)	−1699(21)	4452(8)	10.0_3
C(21)	4058(3)	2806(8)	4220(4)	2.8_2
C(22)	4182(3)	2011(12)	3566(4)	4.6_6
C(23)	4731(3)	1503(14)	3561(6)	5.9_8
C(24)	5120(3)	1773(11)	4200(5)	5.1_5
C(25)	4974(4)	2561(17)	4817(5)	6.7_0
C(26)	4440(3)	3116(14)	4847(5)	5.5_0
C(27)	5711(4)	1206(16)	4171(7)	7.9_7
C(31)	4105(3)	2519(9)	7605(4)	3.0_8
C(32)	4232(3)	3629(10)	7028(4)	3.8_6
C(33)	4783(3)	3765(11)	6930(4)	4.2_7
C(34)	5191(3)	2852(11)	7407(5)	4.6_0
C(35)	5055(3)	1778(13)	7979(5)	5.2_9
C(36)	4513(3)	1582(12)	8090(4)	4.5_7
C(37)	5787(3)	3022(15)	7282(6)	6.8_1

atoms are ligated in the cis-configuration; the other four coordinating positions are occupied by water oxygen atoms.

Both of the Sc-O (sulfonato) (2.044 Å, on the average (hereafter, shown by av.)) are shorter than the Sc-O (water) (2.117 Å av.), and the average of all the Sc-O bond lengths is 2.092 Å; this is approximately the same as the sum of the Shannon's ionic radii of Sc (Valence (Val)=3+, Coordination number (CN)=6) and O (Val=2−, CN=2), 2.10 Å.[19] The angle of Sc-O(11)-S(1) (147.2(2)°) is about the same as any M-O-S angles of lanthanoid *p*-toluenesulfonates and 2-naphthalenesulfonates,[1] but the other angle Sc-O(21)-S(2) (175.6(2)°) is much larger. This is probably due to a steric hindrance of the ligand coordinated at the cis-position. The third sulfonate ion is not coordinated to the metal atom, although it is bridged by hydrogen bondings to the coordinated water oxygen atoms. All three S-O bond lengths of the non-coordinated anion are not much different from each other (1.445, 1.452, and 1.462 Å). While in the coordinated anions, the S-O bond lengths of the ligated oxygen atoms (1.485 Å av.) are longer than the other two to the non-ligated oxygen atoms (1.431 Å av.). However, the average of all three S-O bond lengths of the coordinated and non-coordinated ions are not much different from each other (1.453 and 1.449 Å, respectively).

In the crystal, the metal atoms are approximately on the (200) planes. The hydrophobic layers of the tolyl groups of the ligands intercalate between respective pairs of hydrophilic metal complex planes. No ligand bridgings have been found between any neighboring

Table 4. (Continued)

(4.9) Yttrium(III) 2-Naphthalenesulfonate Enneahydrate

Atom	x	y	z	B_{eq}/Å^{2} h)
Y	7225.9(4)	7500	5032.8(5)	1.7_0
S(1)	6088(1)	4487(3)	3199(1)	2.2_3
S(2)	7000(1)	10993(3)	6760(1)	2.2_4
S(3)	9581(1)	5023(3)	3341(1)	2.5_2
O(1)	6785(3)	5559(8)	3717(4)	2.6_6
O(2)	6138(3)	2674(10)	3594(4)	3.4_7
O(3)	5381(3)	5371(8)	3186(4)	2.9_5
O(4)	6824(3)	9419(8)	6104(4)	2.6_7
O(5)	6367(3)	12271(9)	6489(4)	3.3_7
O(6)	7738(3)	11807(8)	6801(4)	3.1_1
O(7)	8809(3)	4476(9)	3321(4)	3.4_6
O(8)	9851(4)	6578(9)	3965(4)	4.4_6
O(9)	10141(3)	3564(9)	3607(4)	4.1_0
O(W1)	8230(3)	7194(9)	4272(4)	3.5_3
O(W2)	8350(3)	8890(8)	6119(4)	2.6_6
O(W3)	7969(3)	5056(8)	5875(4)	3.1_2
O(W4)	5930(3)	8401(7)	4180(4)	2.7_9
O(W5)	7314(3)	10225(8)	4226(4)	3.7_1
O(W6)	6422(3)	5740(8)	5723(4)	3.1_2
O(W7)	4837(3)	6352(9)	5350(4)	3.5_1
O(W8)	9477(3)	4911(9)	6176(6)	5.4_8
O(W9)	8783(3)	11072(10)	4260(4)	4.3_6
C(1)	5491(4)	4887(11)	1200(5)	2.1_7
C(2)	6110(4)	4317(10)	1960(5)	2.2_2
C(3)	6765(4)	3537(11)	1788(6)	2.7_2
C(4)	6781(4)	3303(11)	830(5)	2.5_8
C(5)	6142(4)	3874(11)	2(5)	2.4_3
C(6)	6141(4)	3606(12)	−993(5)	3.0_2
C(7)	5509(5)	4114(13)	−1769(6)	3.5_5
C(8)	4855(5)	4831(13)	−1586(6)	3.2_2
C(9)	4836(5)	5113(11)	−646(6)	2.9_4
C(10)	5505(4)	4627(11)	199(5)	2.3_1
C(11)	7734(4)	10557(11)	8739(5)	2.5_5
C(12)	7080(4)	10173(11)	7962(5)	2.4_1
C(13)	6459(4)	9153(12)	8083(6)	2.8_3
C(14)	6502(4)	8556(12)	9023(6)	3.0_4
C(15)	7142(5)	8959(11)	9859(5)	3.0_1
C(16)	7166(5)	8404(13)	10841(6)	4.0_1
C(17)	7808(6)	8880(14)	11629(6)	4.6_5
C(18)	8426(5)	9834(14)	11479(6)	4.0_4
C(19)	8426(5)	10366(13)	10571(6)	3.6_5
C(20)	7771(4)	9937(12)	9712(5)	2.6_6
C(21)	8906(4)	5203(12)	1329(6)	2.9_0
C(22)	9538(4)	5691(11)	2126(5)	2.4_8
C(23)	10157(4)	6663(11)	1979(6)	2.7_9
C(24)	10131(4)	7174(12)	1030(6)	3.2_6
C(25)	9496(4)	6710(11)	194(6)	2.7_0
C(26)	9457(5)	7192(13)	−806(6)	3.7_3
C(27)	8829(6)	6689(14)	−1570(6)	4.6_7
C(28)	8207(5)	5763(14)	−1426(6)	3.6_9
C(29)	8221(5)	5264(13)	−496(6)	3.6_9
C(30)	8869(4)	5715(12)	345(5)	2.8_1

(4.10) Dysprosium(III) 2-Naphthalenesulfonate Enneahydrate

Atom	x	y	z	B_{eq}/Å^{2} h)
Dy	7226.6(4)	7500	5036.8(5)	1.7_1
S(1)	6088(2)	4509(6)	3194(3)	2.2_6
S(2)	7000(2)	11020(6)	6772(3)	2.3_1
S(3)	9582(2)	5049(6)	3339(3)	2.5_1
O(1)	6779(6)	5596(16)	3731(8)	2.9_5
O(2)	6127(6)	2730(25)	3586(7)	3.1_8
O(3)	5382(6)	5388(16)	3177(8)	2.9_7
O(4)	6841(6)	9523(17)	6105(7)	2.9_4
O(5)	6367(6)	12244(18)	6503(7)	2.8_9
O(6)	7733(6)	11823(14)	6811(7)	2.5_9
O(7)	8807(6)	4486(17)	3315(8)	3.0_9
O(8)	9874(8)	6573(18)	3987(9)	4.6_3
O(9)	10138(6)	3604(18)	3604(9)	4.1_5
O(W1)	8248(6)	7200(21)	4274(7)	3.3_7
O(W2)	8339(6)	8913(16)	6128(8)	3.2_3
O(W3)	7986(6)	5123(15)	5911(8)	2.9_8
O(W4)	5930(6)	8446(14)	4166(7)	2.5_6
O(W5)	7318(6)	10252(16)	4225(9)	3.4_4
O(W6)	6424(6)	5757(14)	5754(8)	2.9_0
O(W7)	4839(6)	6376(18)	5345(8)	3.3_4
O(W8)	9474(7)	4922(18)	6167(13)	6.3_4
O(W9)	8787(7)	11112(19)	4273(9)	4.5_6
C(1)	5484(8)	4900(23)	1201(11)	2.3_8
C(2)	6090(8)	4313(18)	1956(10)	1.8_1
C(3)	6781(9)	3545(21)	1803(12)	2.8_1
C(4)	6782(8)	3335(23)	834(11)	2.5_9
C(5)	6143(9)	3865(23)	−5(12)	2.8_4
C(6)	6133(9)	3642(24)	−1004(12)	3.0_0
C(7)	5531(10)	4069(25)	−1757(12)	3.2_0
C(8)	4859(11)	4830(27)	−1579(13)	3.8_5
C(9)	4838(9)	5113(21)	−664(11)	2.4_7
C(10)	5489(8)	4671(20)	207(12)	2.4_1
C(11)	7730(10)	10552(23)	8740(12)	2.8_0
C(12)	7088(9)	10226(23)	7964(10)	2.3_8
C(13)	6450(8)	9217(24)	8092(12)	2.6_4
C(14)	6506(8)	8602(24)	9025(12)	2.8_0
C(15)	7124(10)	8996(24)	9864(12)	3.5_1
C(16)	7198(11)	8462(24)	10856(13)	3.8_1
C(17)	7787(11)	8887(26)	11651(12)	3.7_8
C(18)	8444(11)	9907(27)	11492(11)	3.5_0
C(19)	8425(11)	10381(26)	10562(12)	3.7_2
C(20)	7785(9)	9980(23)	9713(11)	2.9_8
C(21)	8896(9)	5260(22)	1328(12)	2.7_2
C(22)	9519(8)	5691(21)	2126(11)	2.2_4
C(23)	10159(10)	6724(25)	1981(12)	3.2_1
C(24)	10130(9)	7161(22)	1039(12)	2.8_5
C(25)	9512(10)	6789(22)	180(12)	2.9_8
C(26)	9445(10)	7159(23)	−805(11)	3.1_8
C(27)	8831(12)	6724(27)	−1579(13)	4.5_0
C(28)	8213(11)	5764(30)	−1419(15)	4.3_7
C(29)	8229(10)	5259(24)	−472(13)	3.4_2
C(30)	8866(9)	5740(21)	361(11)	2.3_9

h) The equivalent isotropic temperature factors were computed using the following expression: $B_{eq}=4/3(B_{11}a^2+B_{22}b^2+B_{33}c^2+B_{13}ac\cos\beta)$. The B_{ij}'s are defined by $T=\exp[-(h^2B_{11}+k^2B_{22}+l^2B_{33}+2klB_{23}+2hkB_{12}+2hlB_{13}]$.

metal complexes, though they are bridged by hydrogen bondings via interposed crystalline water molecules and free anions. In the c-axis direction, hydrogen bond bridgings are found between any pairs of side-by-side metal complexes; however, in the b-axis direction, the respective pairs of the neighboring metal complexes are bridged or non-bridged alternately. Therefore, the hydrogen bond network in the crystal is extended like a belt in the c-axis direction.

As shown in Fig. 3, both tolyl groups of the ligands coordinated to the same metal atom are in the same side hydrophobic layer: Their methyl groups are

extended toward the same direction.

All toluene rings of the ligands are laid approximately perpendicular to the bc-plane, and A^i, B, C, as well as A, C^i, B^i, planes (i=0.5−*x*, 0.5+*y*, 1−*z*) are accumulated approximately in parallel, respectively: The dihedral angles between the ab-plane and the both group planes are about −30° and +30°, respectively.[22]

In yttrium(III) *p*-toluenesulfonate and, accordingly, in the isomorphous lanthanoid(III) salts as well the central metal atom is octa-coordinated, being in a square-antiprism geometry in which the oxygen atoms of the unidentate *p*-toluenesulfonate ions take positions on the different squares while keeping the maximum separation from each other. The general feature of the coordination geometry around the metal atom resembles that of the lanthanoid(III) 2-naphthalenesulfonates.[1]

Table 5. Selected Bond Lengths and Bond Angles of Scandium(III) *p*-Toluenesulfonate Hexahydrate

Bond length (*l*/Å)			
Sc-O(11)	2.067(4)	Sc-O(21)	2.021(4)
Sc-O(W1)	2.132(4)	Sc-O(W2)	2.119(4)
Sc-O(W3)	2.097(4)	Sc-O(W4)	2.118(4)
S(1)-O(11)	1.487(4)	S(1)-O(12)	1.457(4)
S(1)-O(13)	1.419(4)	S(2)-O(21)	1.482(4)
S(2)-O(22)	1.427(6)	S(2)-O(23)	1.419(6)
S(3)-O(31)	1.445(4)	S(3)-O(32)	1.462(4)
S(3)-O(33)	1.452(4)		
Bond angle (*φ*/°)			
Sc-O(11)-S(1)	147.2(2)	Sc-O(21)-S(2)	175.6(2)

The Y-O (sulfonato) bond lengths (2.326 Å av.) are shorter than the Y-O (water) (2.361 Å). The average of the all Y-O bond lengths is 2.352 Å, which is a little shorter than the sum of the Shannon's ionic radii, 2.369 Å.[19] The Y-O-S angles are 144.8 and 144.9°. These values are not much different from the corresponding ones of the yttrium and lanthanoid(III) 2-naphthalenesulfonates. As in the case of the scandium salt, the bond from the sulfur to the ligating oxygen atoms (1.467 Å av.) are longer than the bonds to the non-ligating oxygen atoms (1.442 Å av.), while three S-O bonds of the non-coordinated sulfonate ion are not much different from each other (1.453, 1.445, and 1.449 Å). As shown in Table 6, the same bond length relations are also found in the respective lanthanoid(III) salts.

The metal complex cores are located approximately on the planes parallel to (100), which cross the a-axis at 1/4 and 3/4. The metal complexes are connected with each other by two-dimensional hydrogen bonds, as shown schematically in Fig. 5. Each pair of the neighboring hydrophilic layers of the complex cores is intercalated by the hydrophobic layer of the tolyl groups of the anions. As shown in Fig. 4, the arrangement of the tolyl groups in the crystal is different from that in the scandium complex. Both of the toluene rings of the coordinating ligands are in the hydrophobic layers on both sides of the metal atoms; their methyl groups are extended toward the opposite directions from each other.

Table 6. Selected Bond Lengths and Bond Angles of Yttrium(III) and Lanthanoid(III) (Sm, Gd, Dy, Ho, Er, and Yb) *p*-Toluenesulfonate Enneahydrates

Bond length (*l*/Å) M=	Y	Sm	Gd	Dy	Ho	Er	Yb
M-O(11)	2.300(5)	2.366(5)	2.341(6)	2.305(4)	2.305(4)	2.297(5)	2.281(5)
M-O(21)	2.352(8)	2.409(7)	2.383(9)	2.362(7)	2.362(7)	2.354(8)	2.333(7)
M-O(W1)	2.342(6)	2.426(6)	2.388(7)	2.349(5)	2.340(5)	2.341(7)	2.312(6)
M-O(W2)	2.380(12)	2.438(11)	2.408(13)	2.378(10)	2.372(10)	2.355(13)	2.336(11)
M-O(W3)	2.382(13)	2.446(13)	2.422(14)	2.390(11)	2.378(11)	2.361(13)	2.355(12)
M-O(W4)	2.331(7)	2.396(7)	2.373(7)	2.340(6)	2.329(6)	2.324(8)	2.294(7)
M-O(W5)	2.363(10)	2.432(9)	2.402(10)	2.376(8)	2.367(8)	2.360(9)	2.330(8)
M-O(W6)	2.365(11)	2.429(10)	2.406(11)	2.373(9)	2.358(9)	2.348(11)	2.324(9)
$M\text{-}O(S)_{av.}$[j]	2.326	2.388	2.362	2.341	2.334	2.326	2.307
$M\text{-}O(W)_{av.}$[k]	2.361	2.428	2.400	2.368	2.357	2.348	2.325
$M\text{-}(all)_{av.}$[l]	2.352	2.418	2.390	2.368	2.357	2.348	2.325
S(1)-O(11)	1.472(11)	1.463(10)	1.460(11)	1.469(9)	1.470(9)	1.463(11)	1.465(9)
S(1)-O(12)	1.445(7)	1.448(6)	1.448(7)	1.444(6)	1.439(5)	1.440(7)	1.437(6)
S(1)-O(13)	1.426(13)	1.431(17)	1.444(18)	1.443(16)	1.435(15)	1.435(18)	1.437(16)
S(2)-O(21)	1.461(5)	1.464(5)	1.460(6)	1.462(4)	1.456(4)	1.456(5)	1.462(5)
S(2)-O(22)	1.445(12)	1.451(10)	1.445(12)	1.450(9)	1.447(9)	1.448(11)	1.449(10)
S(2)-O(23)	1.451(14)	1.453(13)	1.451(14)	1.451(12)	1.450(11)	1.446(14)	1.450(12)
S(3)-O(31)	1.453(7)	1.441(6)	1.436(7)	1.437(6)	1.437(6)	1.436(7)	1.436(6)
S(3)-O(32)	1.445(16)	1.437(15)	1.441(17)	1.438(13)	1.439(13)	1.438(16)	1.436(14)
S(3)-O(33)	1.449(11)	1.437(9)	1.446(10)	1.443(9)	1.442(9)	1.450(11)	1.446(9)
Bond angle (*φ*/°)							
M-O(11)-S(1)	144.8(6)	144.7(5)	145.4(6)	145.0(5)	145.0(5)	145.6(6)	145.2(5)
M-O(21)-S(2)	144.9(7)	144.7(7)	145.1(8)	144.6(6)	144.8(6)	144.8(7)	144.7(7)

j) Average of the M-O lengths of the ligated sulfonato oxygen atoms. k) Average of the M-O lengths of the ligated water oxygen atoms. l) Average of the M-O length of the all ligated oxygen atoms.

Table 7. Selected Bond Lengths and Bond Angles of Yttrium(III) and Dysprosium(III) 2-Naphthalenesulfonate Enneahydrates

Bond length (l/Å) M=	Y	Dy
M-O(1)	2.287(9)	2.27(2)
M-O(4)	2.344(10)	2.38(2)
M-O(W1)	2.383(10)	2.42(2)
M-O(W2)	2.374(6)	2.373(14)
M-O(W3)	2.354(6)	2.347(13)
M-O(W4)	2.381(5)	2.399(10)
M-O(W5)	2.351(9)	2.377(17)
M-O(W6)	2.373(9)	2.389(17)
M-O(S)$_{av.}$[j]	2.316	2.321
M-O(W)$_{av.}$[k]	2.369	2.383
M-O(all)$_{av.}$[l]	2.356	2.368
S(1)-O(1)	1.483(6)	1.488(13)
S(1)-O(2)	1.451(9)	1.43(2)
S(1)-O(3)	1.435(7)	1.432(13)
S(2)-O(4)	1.464(9)	1.429(19)
S(2)-O(5)	1.448(6)	1.423(13)
S(2)-O(6)	1.452(7)	1.441(13)
S(3)-O(7)	1.446(7)	1.456(14)
S(3)-O(8)	1.443(9)	1.451(19)
S(3)-O(9)	1.455(6)	1.444(13)
Bond angle (ϕ/°)		
M-O(1)-S(1)	140.4(7)	142.2(14)
M-O(4)-S(2)	147.1(6)	150.5(12)

j, k, l) See footnotes of Table 6.

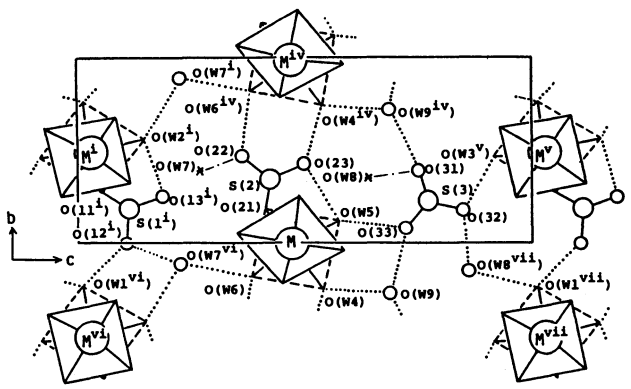

Fig. 5. Schematic presentation of the bridgings between the metal(III) complex molecules of yttrium(III) or lanthanoid(III) (Sm, Gd, Dy, Ho, Er, Yb) p-toluenesulfonate enneahydrates. As four two-fold screw axes are perpendicular to the ac-plane (crossing the plane at; 1/4, 0, 1/4; 1/4, 0, 3/4; 3/4, 0, 1/4; and 3/4, 0, 3/4), the same type of the linkage network exists also in the upper plane. Key to the symmetry operations: i, 0.5−x, 0.5+y, 0.5−z; ii, 1−x, 1−y, 1−z; iv, x, 1+y, z; v, 0.5−x, 0.5+y, 1.5−z; vi, 0.5−x, −0.5+y, 0.5−z; vii, 0.5−x, −0.5+y, 1.5−z.

The toluene rings of the anions are not perpendicular to the bc-plane, nor parallel with each other, and the dihedral angles between the bc-plane, and the A[i], B, C, planes are about 75, 79, and 84°, respectively.[22]

Generally, in the complexes of 3d-metals, the hard-base ligands such as the sulfonates cannot make strong coordination bonds, and the M-O bonds are usually longer than those by the common ligands.[23]

Table 8. Dihedral Angles between the Planes in the Square-Antiprism Geometry around Metal Atoms of Yttrium(III) and Lanthanoid(III) (Sm, Gd, Dy, Ho, Er, Yb) p-Toluenesulfonate Enneahydrates (θ/°)

M=	a—b[m]	c—d[m]
Y	1.78	44.34
Sm	1.74	44.64
Gd	1.87	44.29
Dy	1.70	44.53
Ho	1.42	44.51
Er	1.62	44.70
Yb	1.50	44.59

m) Respective least squares planes, a, b, c, and d, include atoms written as follows: a, O(11), O(W3), O(W1), O(W2); b, O(21), O(W5), O(W4), O(W6); c, O(11), M, O(W1); d, O(21), M, O(W4). The numbering of the atoms is the same as Fig. 3.

On the other hand, in these rare earth p-toluenesulfonates as well as in the 2-naphthalenesulfonates, the M-O (sulfonato) bond lengths are shorter than the standard M-O bond longths, the sum of the Shannon's ionic radii.[19] In cases of the other lanthanoid(III) complexes, their carboxylates, for example, have the M-O (carboxylato) bond lengths, which are almost the same as the respective sums of the Shannon's ionic radii.[4–10,12,13,24] Although in some lanthanoid(III) β-diketonates, the M-O (ligand) bond lengths are shorter than the respective sums,[25–27] it is rather due to the chelating effect of the ligand.

Since the title complexes have only unidentate ligands, sulfonato ions and water molecules, the square-antiprism geometry around the central metal atom is not much deformed from the ideal shape, as shown in Table 8. On the contrary, in carboxylato complexes, which have many chelating and bridging ligands, the geometry is much deformed. This is an expected result from the structural consideration by Kepert.[28,29]

As shown in Table 2, in the series of the isomorphous lanthanoid(III) p-toluenesulfonates, the cell-dimensions as well as the cell volume decrease, and the crystal density increases with the atomic number of the central metal atom. However, the size and shapes of the hydrocarbon part of the ligands stay approximately the same.

From a comparison of the atomic parameters of the corresponding atoms of the respective isomorphous complexes, those of the oxygen atom (sulfonato and water) and, to a smaller extent, those of the sulfur atoms change with the metal atomic number. However, the arene-carbon atoms also move to some extent, which may be caused by the larger standard deviations of their parameters. The largest observed deviations of

atomic parameters in the series of complexes are: the *x*-coordinate of O(12) (from 0.1497(2) (Sm) to 0.1533(2) (Yb)); the *y*-coordinate of O(W4) (from −0.2664(6) (Sm) to −0.2563(6) (Yb)); the *z*-coordinate of O(W2) (from 0.3469(3) (Sm) to 0.3528(3) (Yb)). All of these values change with the atomic number of the central metal atom.

Thus, the change of the packing in the unit cell due to a decrease in the metal ionic size occurs mainly around the coordination sphere. Consequently, it is important to clarify the relation between the observed M-O lengths and the respective standard value (now the sum of the Shannon's ionic radii[19] was adopted for the purpose) of the series of the isomorphous lanthanoid(III) complexes, which are shown graphically in Fig. 6.

In this figure, lines 1 and 2 show the average M-O (sulfonato) and M-O (water) bond-lengths of the complexes, respectively, while lines 3 to 6 are examples of the M-O bond lengths to the individual oxygen atoms. Line 7 is a reference line which shows the sum of the Shannon's ionic radii.

All of the observed M-O values do not deviate much from the respective lines (1—6), although the points of lines 3—6 are distributed over the wider range than those of lines 1 and 2.

All M-O bond lengths of the yttrium complex were found to be situated not far from the respective corresponding lines if the sum of its Shannon's ionic radii (2.37 Å) was taken as their abscissa value.

Although the same relation was found between the observed M-O bond lengths and the sums of the Shannon's ionic radii in the series of the yttrium and lanthanoid 2-naphthalenesulfonates, more detailed results were not obtained owing to the larger standard deviations of their final atomic parameters.

From these results, not only the carboxylates or β-diketonates, but also the arenesulfonates of yttrium were found to have the same coordination geometry and coordination number of the central metal atom as the corresponding salts of lanthanoids, especially which have approximately the same ionic radii.

Although scandium is also a member of the same group element of the periodic table, since its tervalent ionic radius is much smaller than those of yttrium or lanthanoids, it takes a different coordination number.

As shown in the former section, at ambient temperature, enneahydrated *p*-toluenesulfonates of samarium and gadolinium lost their water more easily. To clarify this dehydration process, we have examined simultaneous TG and DTA measurements of all the synthesized *p*-toluenesulfonates. Curves of the scandium and the gadolinium salts are shown in Fig. 7, as the examples, and the results of all the salts are tabu-

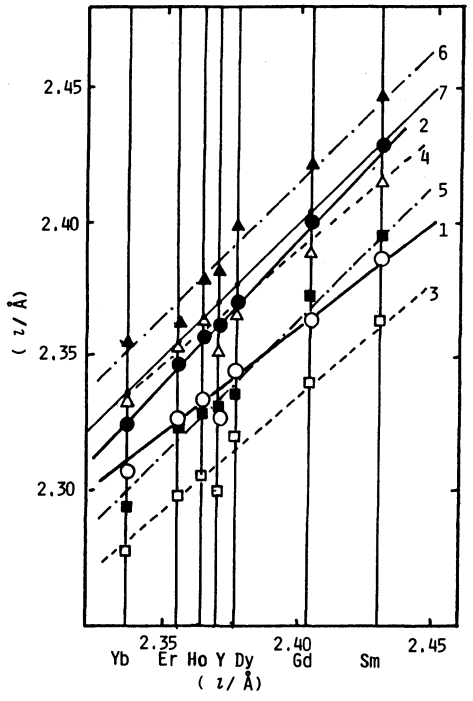

Fig. 6. The relation between the calculated (abscissa) and the observed (ordinate) M-O bond lengths of the yttrium and lanthanoids (Sm—Yb) *p*-toluenesulfonate enneahydrates. 1, —○—, the average of the M-O(sulfonato); 2, —●—, the average of the M-O(water); 3, –□–, M-O(11); 4, –△–, M-O(21); 5, –■–, M-O(W4), 6, –▲–, M-O(W3), 7, —●—, sum of the Shannon's ionic radii (calculated value).[22]

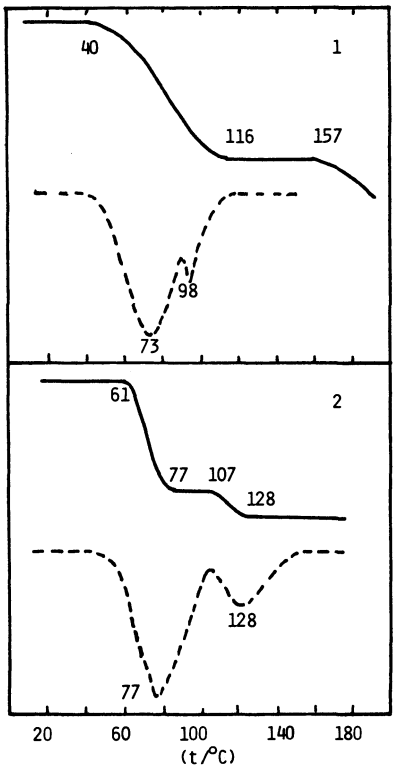

Fig. 7. TG(——) and DTA(----) curves of the *p*-toluenesulfonates; 1, $ScL_3 \cdot 6H_2O$, 2, $GdL_3 \cdot 9H_2O$ (HL=*p*-toluenesulfonic acid). Mass loss of TG was taken downward, and the exothermal change of DTA was taken upward.

Table 9. Thermal Analytical Data of Rare Earth *p*-Toluenesulfonates, $ScL_3 \cdot 6H_2O$ and $ML_3 \cdot 9H_2O$ (HL=*p*-Toluenesulfonic Acid, M=Y, Sm, Gd, Dy, Ho, Er, and Yb)

M=	Sc	Sm	Gd	Dy	Y	Ho	Er	Yb
First mass loss of TG (t/°C)[n]	40	53	61	57	58	57	58	56
Second mass loss (t/°C)[n]		105	107	109	108	104	110	103
Lost water at first step (n/mol)[o]	6.0	7.3	7.4	7.5	7.6	7.6	7.7	7.8
Lost water at second step (n/mol)[o]		1.7	1.6	1.5	1.4	1.4	1.3	1.2
First peak of DTA (t/°C)[p]	73	70	77	84	85	85	86	86
Second peak of DTA (t/°C)[p]	(98)	127	128	127	126	128	128	126

n) The temperature where each TG curve is going down was read (the starting point of each mass loss). o) The mol numbers of the lost water at respective steps were calculated from the TG curves. p) The temperatures of respective endothermic peaks of the DTA curves.

lated in Table 9.

From the TG curves, it was found that the water molecules of the scandium salt were removed in one step, while those of the gadolinium through ytterbium as well as the yttrium complexes in two steps. On their DTA curves, all complexes show two endothermic peaks, the first big one and the second small one; both of them seem to correspond to the respective two steps of the mass loss of the TG curve, except for the scandium salt, which also shows a small second peak at a much lower temperature. The general feature of the respective TG and DTA curves of the isomorphous lanthanoid (Sm—Yb) complexes are approximately the same, though there are some continuous variations depending on the increase of the central metal atomic number:

i) All the hydrated water molecules in the crystals were lost in two steps: the ratio of the first step mass loss to the second one increases. (from 7.3(Sm) to 7.8(Yb) molecules of water).

ii) The temperature of the first endothermic peak of the DTA curve is elevated (from 70 (Sm) to 86 (Yb) (t/°C).

iii) The observed corresponding values of the yttrium complex took positions approximately between those of the dysprosium and holmium salts, while the metal ionic radius of yttrium was between those of the latter two metals.

Although we could clearly recognize that water in the crystals could be removed more easily from complexes of the lighter lanthanoid(III) complexes than those of the heavier ones at ambient temperature, the respective TG and DTA curves were not much different from each other.

As the coordination number of lanthanoid(III) is always high (commonly 8 or 9 except when the ligand is very large[30]) it does not decreased even when the hydrated water molecules are removed from the crystal. The sulfonate anions must move and act as multidentates forming more M-O bonds in place of the removed water oxygen atoms. From their unit cell size, as well as from their density, we can imagine that the anion can move more easily in samarium and gadolinium complexes, since there is more free space in the unit cell. Moreover, since we could not obtain isomorphous members of neodymium or lighter lanthanoid salts when the same synthetic process was applied, the crystal structures of the light lanthanoid elements may not be so stable as the heavier metal salts. However, the energy barrier to keep the hydrated water molecules in the respective positions is probably not high in all of these crystals, although they are effective in the heavier metal complexes at ambient temperature.

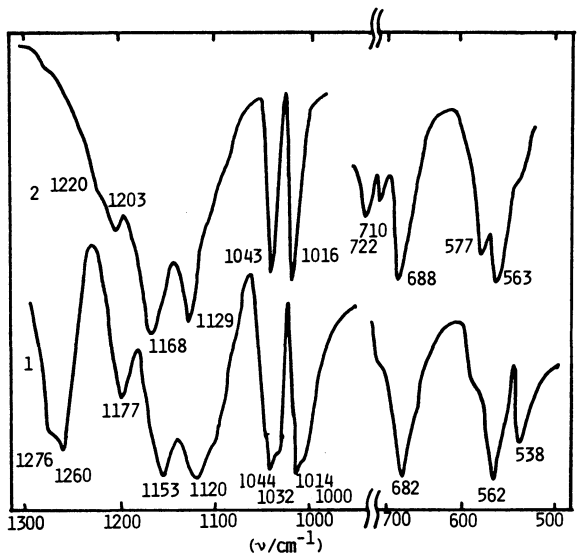

Fig. 8. Infrared spectra of 1, scandium(III) and 2, yttrium(III) *p*-toluenesulfonates, $ScL_3 \cdot 6H_2O$, and $YL_3 \cdot 9H_2O$ (HL=*p*-toluenesulfonic acid).

From their thermal analyses, it was shown that, when the temperature is elevated, all water molecules of even the heavier metal salts obtain sufficient kinetic energy to jump over the barrier and to move in the crystal easily. The dehydration rates of all the member salts are much more accerelated than those at room temperature, and are not much different from each other.

The infrared spectra of the scandium, yttrium, and lanthanoid (Sm, Gd, Dy, Ho, Er, Yb) *p*-toluenesulfonates were examined; the spectra of the former two in the 1100—1300 cm^{-1} as well as 500—700 cm^{-1} regions are shown in Fig. 8, where the characteristic bands of the sulfonato group are expected to appear.

The scandium salt, which is in a hexa-coordination geometry, gave an infrared spectrum that is a little different from those of the other salts, while the isomorphous lanthanoid as well as yttrium salts almost gave the same pattern spectra in these regions. Therefore, there are almost no differences between the bonding character of the sulfonato ions in the series of the latter complexes.

The authors wish to thank the Shin-Etsu Chemical Ind. Co., Ltd., for presenting us with the highly pure rare earth oxides.

References

1) Y. Ohki, Y. Suzuki, M. Nakamura, M. Shimoi, and A. Ouchi, *Bull. Chem. Soc. Jpn.*, **58**, 2968 (1985).
2) R. W. Broach and J. M. Williams, *Acta Crystallogr., Sect. B*, **35**, 2317 (1979).
3) J. Albertsson and I. Elding, *Acta Crystallogr., Sect. B*, **33**, 1460 (1977).
4) M. C. Favas, D. L. Kepert, B. W. Skelton, and A. H. White, *J. Chem. Soc., Dalton Trans.*, **1980**, 454.
5) Y. Koizumi, H. Sawase, Y. Suzuki, T. Takeuchi, M. Shimoi, and A. Ouchi, *Bull. Chem. Soc. Jpn.*, **57**, 1809 (1984).
6) S. Kondo, M. Shimoi, A. Ouchi, and T. Takeuchi, *Bull. Chem. Soc. Jpn.*, **55**, 2840 (1982).
7) T. Imai, M. Shimoi, and A. Ouchi, *Bull. Chem. Soc. Jpn.*, **60**, 159 (1987).
8) Y. Sugita and A. Ouchi, *Bull. Chem. Soc. Jpn.*, **60**, 171 (1987).
9) M. K. Guseinova, A. S. Antsyshkina, and M. A. Porai-Koshits, *Zh. Strukt. Khim.*, **9**, 1040 (1968).
10) Y. Sugita, Y. Ohki, Y. Suzuki, and A. Ouchi, *Bull. Chem. Soc. Jpn.*, **60**, 3441 (1987).
11) S. H. Eggers, H. Schultze, J. Kopf, and R. D. Fischer, *Angew. Chem., Int. Ed. Engl.*, **25**, 656 (1986).
12) H. R. Wenk, *Z. Kristallogr.*, **154**, 137 (1981).
13) A. S. Antsyshkina, M. A. Porai-Koshits, I. V. Arkhangel'skii, V. N. Ostrikova, and A. Z. Amanov, *Dokl, Akad, Nauk. Az. SSR*, **34**, 22 (1978).
14) M. J. Bennett, F. A. Cotton, P. Legzdins, and S. J. Lippard, *Inorg. Chem.*, **7**, 1770 (1968).
15) J. A. Cunningham, D. E. Sands, and W. F. Wagner, *Inorg. Chem.*, **6**, 499 (1967).
16) W. H. Watson, R. J. Williams, and N. R. Stemple, *J. Inorg. Nucl. Chem.*, **34**, 501 (1972).
17) J. C. Slater, "Quantum Theory of Matters," 2nd ed, McGraw-Hill, New York (1968), p. 137.
18) F. A. Cotton and G. Wilkinson, "Advanced Inorganic Chemistry," 4th ed, Wiley, New York (1980), p. 987.
19) R. D. Shannon, *Acta Crystallogr., Sect. A*, **32**, 751 (1976). The ionic radii shown in the reference are: O(Val=2−, CN=2), 1.35 Å; Sc(Val=3+, CN=6), 0.745 Å; the other metal ions (Val=3+, CN=8), Y, 1.019; Sm, 1.079; Gd, 1.053; Dy, 1.027; Ho, 1.015; Er, 1.004; and Yb, 0.985 Å.
20) "Universal Crystallographic Computation Program System *(UNICS)*," ed by T. Sakurai, Crystallographic Society of Jpn., Tokyo (1968).
21) "International Tables for X-Ray Crystallography," Kynoch Press, Birmingham, (1974), Vol. IV. pp. 72, 150.
22) The positions of the hydrogen atoms, the final thermal parameters, the final F_o-F_c tables, some additional data of the bond lengths and bond angles, and the packing projection of the toluene rings of the ligands of the scandium and yttrium *p*-toluenesulfonates are deposited as Document No. 8770 at the Office of the Editor of Bull. Chem. Soc. Jpn.
23) G. A. Lawrance, *Chem. Rev.*, **86**, 17 (1986).
24) M. S. Khiyalov, I. R. Amiraslanov, Kh. S. Mamedov, and E. M. Movsumov, *Koord, Khim.*, **7**, 1255 (1981).
25) L. A. Aslanov, M. A. Porai-Koshits, and M. O. Dekaprilevich, *Zh. Strukt. Khim.*, **12**, 470 (1971).
26) T. Phillips, D. E. Sands, and W. F. Wagner, *Inorg. Chem.*, **7**, 2295 (1968).
27) M. Nakamura, R. Nakamura, K. Nagai, M. Shimoi, S. Tomoda, Y. Takeuchi, and A. Ouchi, *Bull. Chem. Soc. Jpn.*, **59**, 332 (1986).
28) D. L. Kepert, *Prog. Inorg. Chem.*, **23**, 1 (1977); **24**, 179 (1978); **25**, 41 (1979).
29) M. C. Favas and D. L. Kepert, *Prog. Inorg. Chem.*, **27**, 325 (1980); **28**, 309 (1981).
30) T. Moeller, "Comprehensive Inorganic Chemistry," ed by J. C. Bailer, H. J. Emeléus, Sir R. Nyholm, and A. F. Trotman-Dickenson, New York (1973), Vol. 4, p. 22.

 © 1988 The Chemical Society of Japan Bull. Chem. Soc. Jpn., 61, 407—411 (1988)

The pH Titration Study of Lithium Ion Adsorption on λ-MnO_2

Kenta Ooi,* Yoshitaka Miyai, Shunsaku Katoh, Hiroshi Maeda,† and Mitsuo Abe††
Government Industrial Research Institute, Shikoku, 2-3-3 Hananomiya-cho, Takamatsu 761
†Department of Chemistry, Faculty of Science, Nagoya University, Furo-cho, Chikusa-ku, Nagoya 464
††Department of Chemistry, Faculty of Science, Tokyo Institute of Technology, 2-12-1, Ookayama, Meguro-ku 152
(Received June 18, 1987)

The pH titration curves of λ-MnO_2 showed apparently dibasic acid character toward Li^+ ions, but a monobasic acid character toward Na^+, K^+, Rb^+, and Cs^+ ions. The adsorptive capacities of alkali metal ions increased in the order; K^+, Rb^+, $Cs^+ < Na^+ \ll Li^+$ at pH 10. Overall equilibrium constants were calculated by a simplified Gaines-Thomas equation from the titration curves based on the ion-exchange mechanism. Thermodynamic data were derived for the system of (0.1-M LiCl+LiOH)(1 M=1 mol dm^{-3}) at different temperatures. Effects of ionic strength and adsorption temperature on the lithium ion adsorptivity were studied using (LiCl+LiOH) and (KCl+LiOH) solutions.

Ion-sieve type manganese oxides show excellent selectivities for certain ions or group of ions.[1-7] They are prepared by a crystallization of manganese hydroxide containing metal ions, followed by a topotactic extraction of the metal ions with mineral acid. Their adsorptive properties depend on the kind of metal ions introduced as precursors into the manganese hydroxide.[2,6] When lithium and magnesium ions were used as introducing ions, the manganese oxides obtained show a remarkably high selectivity for lithium ions.[6,7] Their lithium-selective properties are closely related to the formation of such spinel-type materials as $LiMn_2O_4$ and $MgMn_2O_4$ during thermal crystallization while being prepared.

Recently, Hunter prepared spinel-type manganese oxide (λ-MnO_2) by extracting lithium from pure $LiMn_2O_4$ with acid.[8] Because of its uniform character, λ-MnO_2 is very suitable as a model compound for a fundamental study of the ion-sieve effect for metal ions extracted from the aqueous phase. In a previous paper, its adsorptive properties for various metal ions showed a remarkably high selectivity for lithium ions in a range above pH 2.5.[9] The metal-ion uptake at pH 10 reached about 5 meq·g^{-1} for lithium ions but less than 0.2 meq·g^{-1} for potassium and cesium ions. The distribution coefficients (K_d's) of metal ions at pH 4 were in the order $Na^+ < K^+ < Rb^+ < Cs^+ \ll Li^+$ for alkali metal-, $Mg^{2+} < Ca^{2+} < Sr^{2+} < Ba^{2+}$ for alkaline earth metal-, and $Ni^{2+} < Zn^{2+} < Co^{2+} < Cu^{2+}$ for transition metal-ions. These results are readily explained if we recognize that the tetrahedral vacant sites in λ-MnO_2 are too narrow for metal ions other than lithium to enter. The only species which can enter these sites are H^+ and dehydrated Li^+ ions.

The present paper describes a pH titration study on λ-MnO_2 for alkali metal ions. The selectivity constants and overall thermodynamic constant were evaluated from the titration data based on the ion-exchange model. Acid-base properties have been investigated for different types of manganese oxides from electrochemical[10,11] and geochemical[12-14] interests and for the fundamental study of the adsorption phenomena.[15,16]

Experimental

Ion-Exchange Material and Characterization. The λ-MnO_2 used was the same as that described in a preceding paper.[8] It was prepared by the acid treatment of $LiMn_2O_4$ with a 1-M HNO_3 solution. The lithium content of the acid-treated sample was 0.12 meq·g^{-1}, indicating that more than 97% of the lithium was extracted from the $LiMn_2O_4$ by the acid treatment. A powdered X-ray diffraction analysis showed λ-MnO_2 of a spinel type structure with an 0.800-nm lattice constant on a cubic unit cell.

pH Titration Curve. A weighed amount (0.100 g) of the λ-MnO_2 was immersed into a mixed solution (10 cm^3) of (MCl+MOH) (M=Li, Na, K, Rb, Cs) in varying ratios with intermittent shaking at 25 °C. The concentration of MCl was adjusted to 0.1 M. After shaking for 3 weeks, the pH of the supernatant solution was determined in a decarbonated atmosphere. The kinetic study showed that three weeks were sufficient to attain a constant pH value. The metal ion concentration in the supernatant solution was determined by atomic absorption spectrometry. The metal ion uptake by λ-MnO_2 was evaluated from the difference between the initial and equilibrium concentrations of the metal ion in the solution or from determining metal ions after dissolving metal ion-adsorbed λ-MnO_2 with a mixed solution of concentrated HNO_3 and HCl. The chloride ion uptake was determined by ion chromatography after dissolving the λ-MnO_2 with a mixed solution of H_2O_2 and H_2SO_4.

In the case of lithium ion adsorption, the effects of ionic strength and adsorption temperature were examined in (KCl+LiOH) and (LiCl+LiOH) systems in addition to the above titration.

Apparatus. X-Ray diffraction analysis was carried out with a Rigaku Denki X-ray diffractometer (model Rad II) using Ni filtered Cu $K\alpha$ radiation(graphite monochrometer). A Perkin-Elmer atomic absorption spectrophotometer (model 403) was employed for atomic absorption spectrometry and a Horiba M8s pH meter for pH measurement. A Dionex Ion Chromatograph apparatus (model 10) was used for ion chromatography.

Reagents. All the chemicals were of an analytical grade from Wako Pure Chemical Ind. Ltd., except for RbCl, RbOH, and CsOH which were obtained from Merck Ltd. These were used without further purification.

Results and Discussion

pH Titration Curves. The pH titration curves and pH dependences of metal ion uptakes are shown in Fig. 1. A remarkable difference was obtained between a (LiCl+LiOH) system and the other metal salt systems on the pH titration curve. The pH titration curve in the (LiCl+LiOH) system (Fig. 1, top right) showed a dibasic acid charactor. The apparent capacity of Li^+ was found to be about 5 meq·g^{-1} on the pH titration curve. The supernatant solutions at pH>8 had a slightly purplish color due to the presence of a small amount of Mn(VII) ions. Their concentration was less than 5×10^{-4} M by atomic absorption spectrometry. Smaller differences than the Li-system were observed between the pH titration curves for the other systems and for the blank experiment. A small apparent capacity of 0.2 meq·g^{-1} was obtained even on the system of (NaCl+NaOH). The supernatant solutions were colorless over the pH ranges studied.

The apparent capacities determined by metal ion uptakes were nearly equal to those obtained by the differences between the blank run and each titration curve (Fig. 1(B)). This suggests that the metal ion adsorption proceeds by an ion-exchange mechanism. The apparent adsorptive capacity increased in the order: Na, K, Rb, Cs≪Li at pH values below 7. The affinity order changed to K, Rb, Cs<Na≪Li above pH 7, probably due to the large steric effect for large unhydrated cations (K, Rb, Cs) at higher pH. The chloride ion uptakes were found to be less than 0.01 meq·g^{-1} over the pH range studied. The affinity orders in the present study showed large differences from those on other types of manganese oxides. For example, cryptomelane-type hydrous manganese(IV) oxide(CRYMO) shows the affinity orders; Li< Na<Cs<Rb<K at pH 2 and Cs<Rb<Na<Li<K at pH 10,[16] and the layered hydrous manganese oxide ($H_4Mn_9O_{18}\cdot7H_2O$) Li<Na<K at pH<4 and K< Na<Li at pH>5.[5]

The difference in the affinity order between λ-MnO_2 and CRYMO can well be understood based on the difference in crystal structure. Cryptomelane-type manganese oxide has [2×2] tunnels of edge-shared MnO_6 octahedra.[17] Tsuji and Abe have pointed out that these [2×2] tunnels are very suitable to fix the metal ions with an effective ionic radius of 0.14 nm (K^+, Rb^+, Ba^{2+}).[4] Our result agrees in showing that the manganese oxides with [2×2] tunnels have high selectivities for Rb^+ and K^+ ions.[6] The λ-MnO_2 in H^+ form can be derived from the spinel structure of $LiMn_2O_4$.[18] The cubic $LiMn_2O_4$ spinel (lattice parameter a_0) contains eight formula units and has its close-packed array of

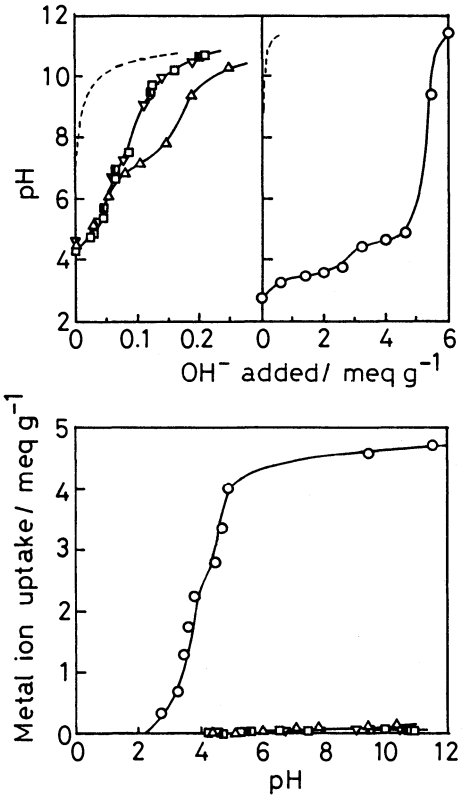

Fig. 1. pH titration curves of λ-MnO_2 by various bases and the pH dependences of metal ion uptake. λ-MnO_2: 0.100 g, soln: (0.1-M MCl+MOH) (M=Li(○), Na(△), K(□), Rb(▽), and Cs(◧)), total vol. of soln: 10 cm^3, temp: 25 °C. The dotted lines describe blank titrations.

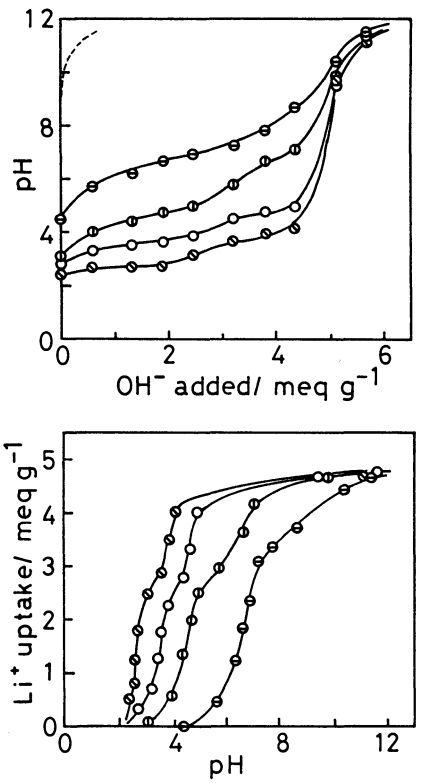

Fig. 2. pH titration curves of λ-MnO_2 toward lithium ions and the pH dependences of lithium ion uptakes. λ-MnO_2: 0.100 g, soln: (LiCl+LiOH) (concn of LiCl: 0 M(⊖), 0.01 M(Φ), 0.1 M(○), 1 M(⊗)), total vol. of soln: 10 cm^3, temp: 25 °C.

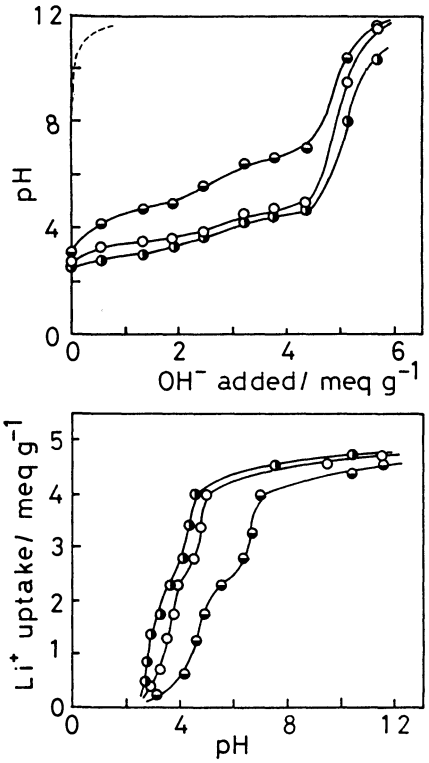

Fig. 3. pH titration curves in (0.1-M LiCl+LiOH) solution and the pH dependences of lithium ion uptakes. The experimental conditions are the same as those in Fig. 2 except for adsorption temperature. Temp: 10°C(◒), 25°C(○), 40°C(◑).

oxygens located at the 32e positions of the space group $Fd3m(O_h^7)$.[19] The Mn^{3+} and Mn^{4+} ions occupy half the octahedral sites, and the Li^+ ions an eighth of the tetrahedral sites. The acid treatment of $LiMn_2O_4$ causes the removal of nearly all of the lithium from the tetrahedral sites while maintaining a spinel structure.[8] Therefore, λ-MnO_2 has a structure that is related to spinel but with vacant tetrahedral sites. Since the size of the vacant sites is markedly smaller than the width of the [2×2] tunnels, it is reasonable to consider that the vacant sites are too narrow to hold the alkali metal ions except lithium even in a dehydrated state. Therefore, the pH titration curves for Na^+, K^+, Rb^+, and Cs^+ ions suggests that the ion-exchange reactions proceed only at the surface of the λ-MnO_2 particles.

The pH Titration Curves in (LiCl+LiOH) Solutions. Figure 2 illustrates the pH titration curves in (LiCl+LiOH) solutions with different LiCl concetrations. The pH titration curve shifts to lower pH range with increasing LiCl concentration. Figure 3 showed that the titration curve shifted to lower pH range with increasing adsorption temperature in the system of the (0.1-M LiCl+LiOH). The maximum lithium ion uptake can be estimated to be 4.75 meq · g^{-1} from Figs. 2 and 3, which is somewhat smaller than the value that is expected from the chemical formula of $LiMn_2O_4$ (5.7 meq · g^{-1}).

The previous paper indicated that the lattice constant (a_0) of the spinel structure increased by adsorption of lithium ions.[9] A similar tendency was also observed in the present study. The a_0 value calculated from the d_{111} peak of the X-ray diffraction pattern is plotted against $\overline{X}_{Li}$ ($\overline{X}_{Li}$ in Fig. 4: Equivalent fraction of lithium ions in λ-MnO_2=lithium ion uptake/ maximum lithium ion uptake). There was a difference in a_0 vs. $\overline{X}_{Li}$ curves between $\overline{X}_{Li}<0.5$ and $\overline{X}_{Li}>0.5$. The curve was sigmoidal at $\overline{X}_{Li}<0.5$ with steep slope around $\overline{X}_{Li}=0.25$. The a_0 value increased gradualy with increasing $\overline{X}_{Li}$ in a range of $\overline{X}_{Li}>0.5$. The lithium ion uptake vs. pH curves (Fig. 2) showed a pH rise at the boundary of the two curves ($\overline{X}_{Li}=0.5$). These results suggest that the mode of the insertion reaction of lithium ions differed slightly between $\overline{X}_{Li}<0.5$ and $\overline{X}_{Li}>0.5$. The presence of a stable $Li_{0.5}Mn_2O_4$ species has been observed in the case of the electrochemical removal of lithium from $LiMn_2O_4$; the removal of lithium proceeds easily to $Li_{0.5}Mn_2O_4$ but further electrochemical extraction becomes more difficult.[19]

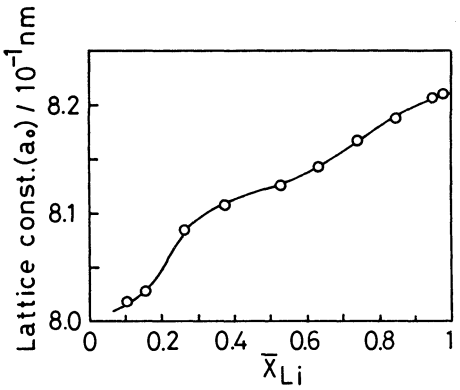

Fig. 4. Lattice constant of spinel structure as a function of $\overline{X}_{Li}$. Ion-exchanged λ-MnO_2 are obtained from (1-M LiCl+LiOH) solution at 25°C.

The pH Titration Curves in (KCl+LiOH) Solutions. Figure 5 illustrates pH titration curves in (KCl+LiOH) solutions with different KCl concentrations. The pH titration curve and the lithium ion uptake curve were scarcely influenced by the addition of KCl in a range below pH 7. This indicates that the sites for lithium ion adsorption are very specific and are scarcely influenced by the presence of potassium ions. In the range above pH 7, the pH titration curve showed a tendency to shift to lower pH values by the addition of KCl, and the lithium ion uptake to increase. The increase of the lithium ion uptake may not be due to a Li^+-K^+ exchange, because the lithium ion uptake decreases with KCl concentration in the case of competing exchange between lithium and potassium ions. The pH titration curves suggest that the λ-MnO_2 has negative charge at pH>5. Therefore, both the decrease of the pH value and the increase of the lithium ion uptake may be due to a decrease of the negative potential at the surface of λ-MnO_2 by the addition of KCl. The decrease of pH with increasing

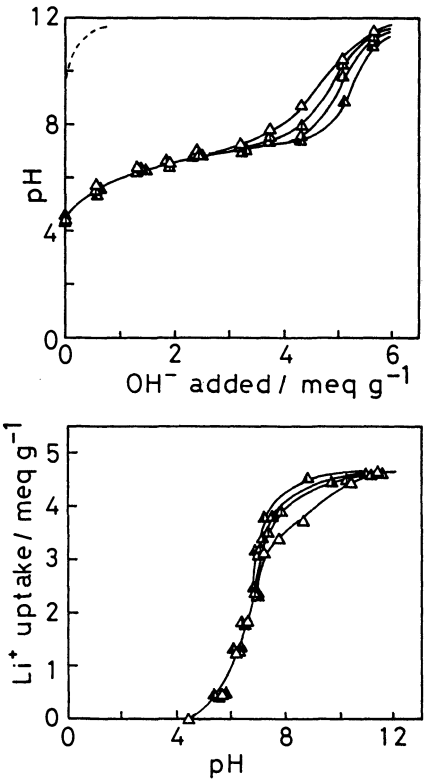

Fig. 5. pH titration curves in (KCl+LiOH) solutions and the pH dependences of lithium ion uptakes. The experimental conditions are the same as those in Fig. 2 except for KCl concentration. KCl concn: 0 M(△), 0.03 M(▲), 0.1 M(▲), and 1 M(▲).

salt concentration usually occurs in aqueous phase for negatively charged metal oxides owing to a decrease of the surface negative charge.[14,20]

Analysis Based on the Model of Ion-Exchange Reaction. The pH titration data can be analyzed on the basis of the ion-exchange mechanism as follows,

$$\bar{H}^+ + M^+ \rightleftarrows \bar{M}^+ + H^+ \quad (1)$$

where bar refers to H^+ or M^+ in λ-MnO_2 and M^+ is monovalent alkali metal ions. The equilibrium constant, K, of the above reaction is defined as,

$$K=[a_H(\bar{f}_M\bar{X}_M)]/[a_M(\bar{f}_H\bar{X}_H)]=K_C(\bar{f}_M/\bar{f}_H) \quad (2)$$

where a_H and a_M are activities of protons and metal ions in solution, respectively, $\bar{X}_H$ and $\bar{X}_M$ are the equivalent fractions of H^+ and M^+ in the λ-MnO_2, respectively, and $\bar{f}_H$ and $\bar{f}_M$ are the activity coefficients of H^+ and M^+ in the λ-MnO_2 phase, respectively. K_c is the selectivity constant including the activity coefficient of the metal ions in solution. It can be evaluated from the pH titration data as follows,

$$pK_C=-\log K_C = -\log[(a_H\bar{X}_M)/(a_M\bar{X}_H)] = pH-\log[\bar{X}_M/(1-\bar{X}_M)]+\log a_M. \quad (3)$$

In the case of a uni-univalent ion-exchange system, the contribution of the activity coefficient term in aqueous solution does not deviate seriously even over a temperature range from 283 to 313 K. Therefore, Eq. 3 can be related to the concentration term of metal ions (C_M) of Eq. 4,

$$pK_C \doteqdot pH-\log[\bar{X}_M/(1-\bar{X}_M)]+\log C_M. \quad (4)$$

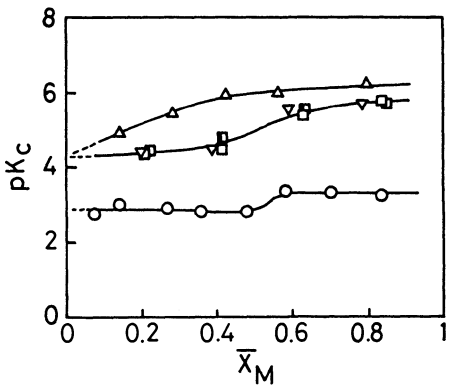

Fig. 6. pK_c vs. $\bar{X}_M$ plots calculated from Fig. 1. The symbols are the same as those in Fig. 1.

The K value and standard free energy change ($\Delta G°$) can be evaluated by using the simplified treatment of the Gaines-Thomas equation, assuming that the change of water content in the exchanger and the entrance of anion from the solution phase are negligible,[21]

$$pK = -\log K = \int_0^1 pK_C\, d\bar{X}_M \quad (5)$$

$$\Delta G° = (2.303\,RT)\,pK \quad (6)$$

pK_c vs. $\bar{X}_M$ Plots. Figure 6 illustrates a plot of pK_c vs. $\bar{X}_M$ in (MCl+MOH) system using Eq. 4. The maximum uptakes ($\bar{X}_M$ =1) of the metal ions were estimated as 4.75 meq·g^{-1} for Li^+, 0.18 meq·g^{-1} for Na^+, and 0.10 meq·g^{-1} for K^+, Rb^+, and Cs^+, respectively. The pK_c value was nearly constant (2.9) for Li^+/H^+ exchanges in the range below $\bar{X}_{Li}<0.5$ while it increased to 3.4 at $\bar{X}_{Li}>0.5$. This indicates the presence of two types of adsorption sites with slightly different affinities for lithium ions. The pK_c values showed a tendency to increase with increasing $\bar{X}_M$ for the other M^+/H^+ exchanges, probably due to an increase of negative surface charge with $\bar{X}_M$. The selectivity constant at $\bar{X}_M=0$ (pK_0) could be estimated by extrapolating pK_c value to $\bar{X}_M=0$ (Table 1).

Figure 7 illustrates the pK_c vs. $\bar{X}_{Li}$ plots in (LiCl+LiOH) and (KCl+LiOH) solutions. The pK_0 values were nearly equal (2.9—3.2) regardless of the salt species and salt concentration (Table 1). In the range above $\bar{X}_{Li}>0.5$, the pK_c value showed a tendency to decrease with increasing salt concentration. Since the decrease of pK_c in the (KCl+LiOH) system corresponds to the decrease of the pH with KCl concentration, the decrease may be partly due to the decrease of surface negative potential by the addition of neutral salt.

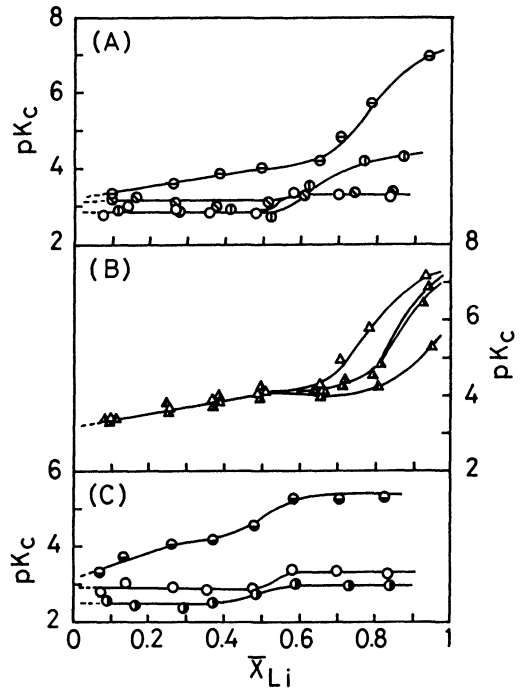

Fig. 7. pK_c vs. $\bar{X}_{Li}$ plots. Figures 8(A), 8(B), and 8(C) are calculated from Figs. 2, 5, and 3, respectively. The symbols are the same as those in the corresponding figures.

Table 1. Values of pK_0, pK, and $\Delta G°$ for λ-MnO_2

System	Concentration of added salt / mol dm^{-3}	T / °C	pK_0	pK	$\Delta G°$ / 10^3J mol^{-1}
LiCl+LiOH	0	25	3.23	4.53	25.9
	0.01	25	2.96	3.40	19.4
	0.1	25	2.91	3.13	17.9
	0.1	10	3.08	4.64	26.5
	0.1	40	2.58	2.74	16.4
	1	25	3.11	3.24	18.5
KCl+LiOH	0.03	25		4.33	24.7
	0.1	25	3.23	4.29	24.5
	1	25		4.01	22.8
NaCl+NaOH	0.1	25	4.2	5.8	33
KCl+KOH	0.1	25	4.2	5.1	29
RbCl+RbOH	0.1	25	4.2	5.1	29
CsCl+CsOH	0.1	25	4.2	5.1	29

Calculation of Equilibrium Constant. The pK values calculated using Eq. 5 and the $\Delta G°$ values are given in Table 1. The $\Delta G°$ value for Li^+/H^+ exchange showed tendencies to decrease with salt concentration and to decrease with adsorption temperature. The standard enthalpy and entropy changes ($\Delta H°$ and $\Delta S°$) at 298 K could be evaluated from the temperature dependence of $\Delta G°$ by the usual method. The $\Delta H°$ value, estimated with least square method, was 120 kJ per mole of lithium and a corresponding $\Delta S°$ 300 J K^{-1} mol^{-1}. Both of the $\Delta H°$ and $\Delta S°$ values were positive and were larger than those of Li^+/H^+ exchanges on another type of inorganic ion exchangers.[22,23] The positive $\Delta G°$ values may possibly arise from the increase of the volume of the unit cell and of water transfer to the aqueous solution from the exchanger with increasing adsorption of lithium ions at the tetrahedral vacant sites. Further study may be needed to determine the alternative contribution for $\Delta S°$ in this system.

References

1) V. V. Vol'khin, G. V. Leont'eva, and S. A. Onorin, *Neorg. Mater.*, **9**, 1041 (1973).
2) G. V. Leont'eva and V. V. Vol'khin, *Zh. Prikl. Khim.*, **44**, 2615 (1971).
3) S. Xiang-mu and W. Xue-yuan, *Acta Chim. Sin.*, **39**, 711 (1981).
4) M. Tsuji and M. Abe, *Solv. Extr. Ion Exch.*, **1**, 97 (1984).
5) S. Xiang-mu and A. Clearfield, *J. Solid State Chem.*, **64**, 270 (1986).
6) K. Ooi, Y. Miyai, and S. Katoh, *Sep. Sci. Technol.*, **21**, 755 (1986). K. Ooi, Y. Miyai, and S. Kato, *Sep. Sci. Technol.*, **22**, 1779 (1987).
7) Y. Miyai, K. Ooi, and S. Katoh, Paper Presented at the 37th Meeting of Sea Water Science of Japan, Tokyo, June 1986.
8) J. C. Hunter, *J. Solid State Chem.*, **39**, 142 (1981).
9) K. Ooi, Y. Miyai, and S. Katoh, *Solv. Extr. Ion Exch.*, **5**, 561 (1987).
10) I. Tari and T. Hirai, *Denki Kagaku*, **52**, 498 (1984).
11) H. Tamura, M. Mitsuta, and M. Nagayama, *Denki Kagaku*, **54**, 250 (1986).
12) T. W. Healy, A. P. Herring, and D. W. Fuerstenau, *J. Colloid Interface Sci.*, **21**, 435 (1966).
13) J. W. Murray, *J. Colloid Interface Sci.*, **46**, 357 (1974).
14) L. S. Balistrieri and J. W. Murray, *Geochim. Cosmochim. Acta*, **46**, 1041 (1982).
15) M. Abe and T. Ito, *Nippon Kagaku Zasshi*, **86**, 1259 (1965).
16) M. Tsuji and M. Abe, *Bull. Chem. Soc. Jpn.*, **58**, 1109 (1985).
17) R. G. Burns and V. M. Burns, "Manganese Dioxide Symposium Vol. 2," ed by B. Schumm, Jr., H. M. Joseph, and A. Kozawa, MnO_2 Sample Office, Cleveland (1981), p. 97.
18) D. G. Wickham and W. J. Croft, *J. Phys. Chem. Solids*, **7**, 351 (1958).
19) J. B. Goodenough, M. M. Thackeray, W. I. F. David, and P. G. Bruce, *Rev. Chim. Minerale*, **21**, 435 (1984).
20) R. O. James, "Adsorption of Inorganics at Solid-Liquid Interface," ed by M. A. Anderson and A. J. Rubin, Ann Arbor Sci., Michigan (1981), p. 219.
21) G. L. Gaines, Jr. and H. C. Thomas, *J. Chem. Phys.*, **21**, 714 (1953).
22) A. Clearfield and D. A. Tuhtar, *J. Phys. Chem.*, **80**, 1302 (1976).
23) M. Abe and N. Furuki, *Solv. Extr. Ion Exch.*, **4**, 547 (1986).

 © 1988 The Chemical Society of Japan Bull. Chem. Soc. Jpn., 61, 413—416 (1988)

Synthesis of the Cyclohexylammonium Form of α-Zirconium Phosphate and Its Application to Nickel(II) Ion Exchange[1)]

Yoshitsugu HASEGAWA,* Kaname SASAKI, and Hiroe TANAKA
Department of Industrial Chemistry, Faculty of Technology, Tokyo University of Agriculture and Technology, Nakamachi, Koganei, Tokyo 184
(Received June 22, 1987)

The uptake of cyclohexylamine with α-zirconium phosphate was studied by means of the pH-titration method. Cyclohexylamine was loaded up to 75% of the ion-exchange capacity of α-zirconium phosphate. Chemical analysis, thermal analysis, infrared spectroscopy, and X-ray diffractometry were used to characterize the product obtained at the final step of pH titration, which was referred to as the cyclohexylammonium form. The chemical composition can be presented as $Zr(C_6H_{11}NH_3)_{1.5}(H)_{0.5}(PO_4)_2 \cdot H_2O$. The interlayer distance of the exchanger expanded to 18.4 Å upon the uptake of cyclohexylamine. The cyclohexylammonium ion was exchanged easily with the nickel(II) ion in a solution.

α-Zirconium phosphate, having a layered structure, has been investigated not only as an inorganic ion exchanger but also as the host of an intercalate.[2)] Generally, the intercalate obtained has a larger interlayer distance than that of α-zirconium phosphate, and it can be expected to show a specific reaction toward a large cation.

Primary alkylamines, such as methyl- and ethylamine, have also been studied, and the relationship between the alkyl-chain length and the interlayer distance of the product has been discussed.[3)] Clearfield and Tindwa have found that the butylamine intercalate of α-zirconium phosphate can be ion-exchanged with a large cation.[4)] Recently, the electric conductivity was measured by using the intercalation compounds of α-zirconium phosphate with propylamine.[5)] Among the compounds with a ring system, benzylamine has been studied, but the details of the work have not been published.[2)]

Since cyclohexylamine is more strongly basic in an aqueous solution than is ammonia,[6)] the ion-exchange reaction can be expected to proceed easily. In this work cyclohexylamine is selected as an intercalant (guest) and the uptake of the amine was investigated by means of the pH-titration method. The cyclohexylammonium form of α-zirconium phosphate (ZP-Cy) obtained was then used in nickel(II) ion exchange.

Experimental

Reagents. The α-zirconium phosphate was prepared according to the literature.[6)] Reagent-grade cyclohexylamine (Wako Pure Chemical Industries, Ltd.; guaranteed) was used without further purification. Reagent-grade nickel(II) dichloride hexahydrate (Koso Chemical Co., Ltd.) was also used.

pH Titration. A weighed amount of α-zirconium phosphate was equilibrated with a mixture of 0.1 mol dm^{-3} cyclohexylamine and its hydrochloride solution. The composition of the solution was adjusted so that the total amount of the cyclohexylammonium ion was always equal to 0.1 mol dm^{-3} while the ratio of cyclohexylamine to its chloride was varied in the range from 1 to 0. The mixture was shaken continuously at 25 °C for a specified period of time, and then the pH value of the supernatant was measured on a pH meter.

A slight excess of cyclohexylamine to the ion-exchange capacity of α-zirconium phosphate was added to a weighed amount of the exchanger, and the mixture was shaken at 25 °C for 48 h. Then, the solid was separated with centrifugation and dried at room temperature in air. The product thus obtained is referred to as ZP-Cy (the cyclohexylammonium form of zirconium phosphate).

Nickel(II) Ion Exchange. The ion exchange was carried out by the batch method. The nickel(II) ion was exchanged by adding a weighed amount of ZP-Cy to a solution of 0.03 mol dm^{-3} nickel chloride. The amount of nickel was equal to 150% of the total ion-exchange capacity of the α-zirconium phosphate. The mixture was shaken continuously at 25°C for 48 h. After the reaction, the solid was separated from the solution and then washed with distilled water until it was free from chloride ions. The nickel-ion content in a solution was determined by an EDTA titration using PAN (1-(2-pyridylazo)-2-naphthol) as an indicator.

Analytical Procedure. The change in the crystal structure was studied by means of X-ray diffractometry using Ni-filtered Cu $K\alpha$ radiation (λ=1.542 Å)(Rigaku Geigerflex RAD-2B). Thermogravimetric (TG) and differential thermal analysis (DTA) data were obtained on a Shimadzu thermal analyzer at the heating rate of 10 °C min^{-1} in static air. The infrared (IR) spectra were measured on a A-302 spectrophotometer (Japan Specroscopic Co., Ltd.).

The chemical composition of the nickel form was analyzed according to the method in the literature.[8)] In this work, zirconium was separated as an mandelate and then ignited to zirconium oxide and weighed. The carbon, hydrogen, and nitrogen contents of ZP-Cy and the nickel form were determined by means of elemental analysis.

Results and Discussion

To determine the equilibration time, the pH value in the solution was measured after a given period of time by adding cyclohexylamine of 4.5 meq g^{-1} α-zirconium phosphate to the samples. Since equilibrium was attained within 12 h, the reaction time of 48 h was chosen.

Figure 1 shows the titration curve of α-zirconium

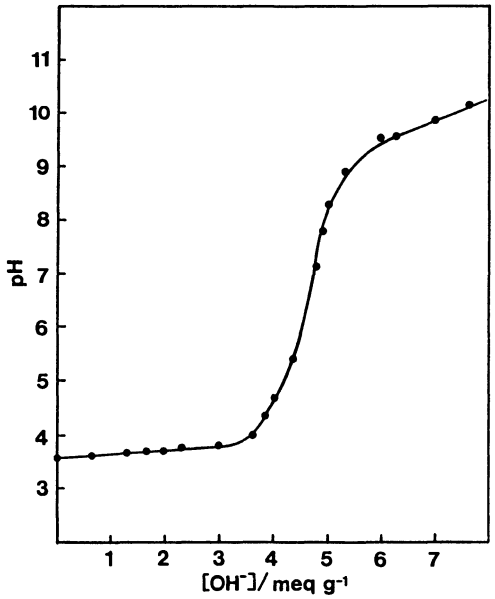

Fig. 1. pH titration curve.

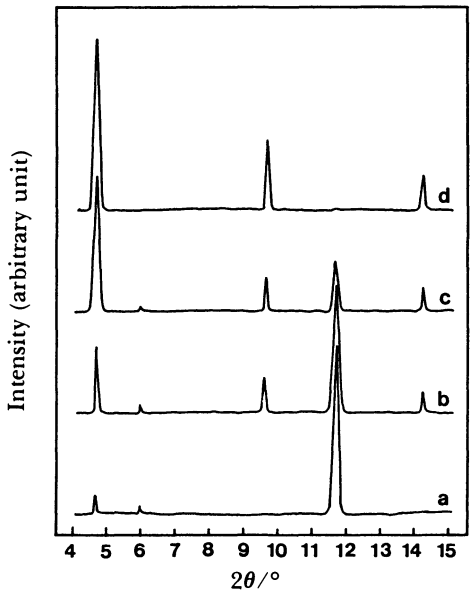

Fig. 2. Schematic diagram of X-ray powder diffraction at the lowest angle region. The percentage of ion exchange: a 15; b 30; c 45; d 60%.

phosphate with cyclohexylamine. Cyclohexylamine was taken up at a low pH value. The end point corresponded to 75% of the total ion-exchange capacity of α-zirconium phosphate.

Figure 2 shows the change in the crystal structure of the exchanger. Since α-zirconium phosphate has a layered structure, the change in the interlayer distance can be observed at the lowest angle region of the X-ray diffractogram. At the beginning of the ion-exchange reaction, only the α-zirconium phosphate phase (α-phase) was present. Between the loading from 10 to 55% of the total ion-exchange capacity of the exchanger, two phases, Phase I (interlayer distance

Table 1. The Intensity of Peaks for Dried Phases

Percentage loading/%	Interplanar spacing (d/Å)					
	18.4[a]	17.8[b]	14.7	9.2[a]	8.9[b]	7.6[c]
			I/I_0			
15		2	53			100
30		65	100		10	67
45		100	61		13	20
55		100	32		14	1
60		100	20		17	
65	100			9	24	
70	100			15		
75	100			11		

a), b): The pair of peaks originated from one phase, as was observed in the intercalation compounds of α-$Sn(HPO_4)_2 \cdot H_2O$.[9] c): The interlayer distance of α-zirconium phosphate.

18.4 Å) and the α-phase, were present. The ratio of Phase I to α-phase increased with an increase in the exchange process. In the region of 60—75% of the loading, however, only phase I was present.

It is possible for cyclohexylamine to form two conformations, chair and boat. Since the chair conformation is more stable than the boat one,[10] it can be assumed that the cyclohexylamine is present as the chair conformation between the layers. While the bond length of C-C and the ∠CCC bond angle are 1.54 Å and 111° respectively in the molecule of cyclohexane, the length and the angle are 1.53 Å and 114° in the butane molecule.[11] If the angle and the distnce of the bond between the carbon and amino groups are almost identical in the butylamine and cyclohexylamine molecules, the lengths of the two molecules can be estimeted to be equal. Since the interlayer distance is equal to 19.0 Å in the butylamine intercalate of α-zirconium phosphate[12] and equal to 18.4 Å in the cyclohexylamine ones, the above assumption is reasonable. The estimation also suggests that the orientation of cyclohexylamine is similar to that of butylamine between the layers of zirconium phosphate. The sizes of benzylamine and cyclohexylamine can also be estimated based on the molecular sizes of cyclohexane and toluene. In consideration of the size of the amino group, the length of cyclohexylamine is calculated to be 8.7 Å, and that of benzylamine, to be 9.3 Å. Hence, the interlayer distance of the cyclohexylamine intercalates is comparable with that of the benzylamine form, having the interlayer spacing of 19.2 Å.[2]

The solid phases formed in the exchange process tend to lose hydrated water(s). After the solid has been exposed to room air on a sample holder, the X-ray diffractogram was different from that recorded under wet conditions. For example, the solid obtained at a 45% loading showed three peaks—at 18.4 Å (2θ=4.79°), 17.8 Å (2θ=4.96°), and 14.7 Å (2θ=5.96°)— after a short exposure. Table 1 shows the intensities of the peaks obtained after drying at room temperature. The intensity of the peak at 14.7 Å reached a maximum at about

Table 2. Interplanar Spacings (d-Values) of ZP-Cy

d/Å	I/I_0	d/Å	I/I_0
18.4	100	3.68	1
9.17	11	3.54	*
6.12	6	3.38	2
5.51	*	3.25	*
4.57	1	3.12	*
4.39	*	2.98	*
4.24	2	2.87	*
4.13	1	2.75	*
3.98	1	2.65	1
3.82	3	2.61	*

"*" means that the intensity is less than unity.

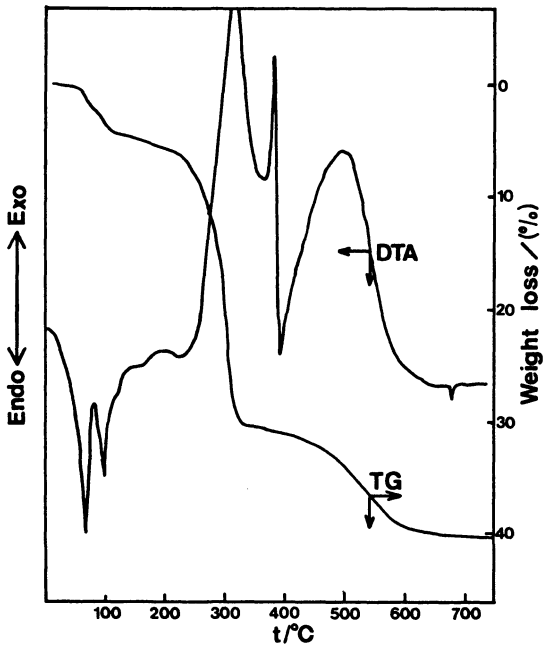

Fig. 3. Thermoanalytical curves.

a 20% loading. The intensity of the 17.8 Å peak increased up to a 60% loading. No change in the interlayer distance was observed above the 60% loading. These facts indicate that the hydrated water(s) play(s) an important role in expanding and maintaining the interlayer distance of the exchanger and that, at higher loadings, cyclohexylamine itself acts as a "pillar." Also, it is suggested that, when the intercalate compound with the amine lose hydrated water(s), the orientation of cyclohexylamine must change in the solid.

Characterization of ZP-Cy. The interplanar spacings (d-values) of ZP-Cy are shown in Table 2. The interlayer distance was comparable with those of the butylamine and benzylamine intercalate of α-zirconium phosphate described above.

Figure 3 shows the TG and DTA curves of ZP-Cy. The decomposition took place in three steps. In the first, the dehydration ocurred. In the temperature region of 200—300 °C, a weight loss and exothermic

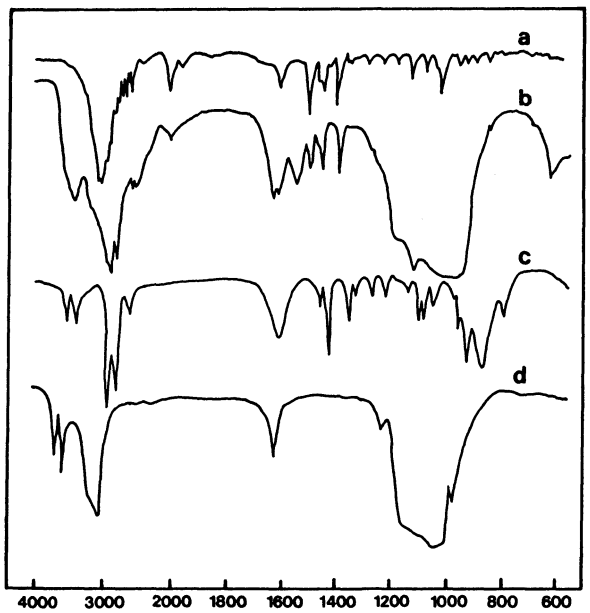

Fig. 4. Infrared spectrum of a cyclohexylamine hydrochloride, b ZP-Cy, c cyclohexylamine, and d α-zirconium phosphate.

peaks were observed. The weight loss was, however, smaller than that to be expected from the chemical formula (see below). These facts indicate that, in this step, the cyclohexylamine was evolved, decomposed, and oxidized partially on the surface of a platinum pan, and that a small amount of a residue (presumably carbon) was formed. The decomposition temperature was higher than that observed for the ammonium form, reflecting the basicity of cyclohexylamine.[13] In the temperature region of 400—500 °C, a weight loss was observed caused by the dehydration associated with the condensation of $(HPO_4)_2$ to P_2O_7. The reaction was supposed to be endothermic, but an exothermic peak appeared. This was caused by the oxidation of the residue formed at the second step, since the weight loss was larger than that to be expected from the chemical formula.

The IR spectra of ZP-Cy and related compounds are shown in Fig. 4. It is clear that the spectrum of ZP-Cy was almost identical with that of cyclohexylammonium chloride in the region of 1800—3500 cm^{-1}. Especially, the absorption was found at 2000 cm^{-1} only for the hydrochloride and ZP-Cy. This absorption is assigned to the group of NH_3^+. The absorption due to -OH stretching was present near 3500 cm^{-1} in the spectrum of ZP-Cy. These facts indicate that the cyclohexylamine was present as the cyclohexylammonium ion between the layers and that the unexchanged protons appear as $-HPO_4$, similarly to the situation in α-zirconium phosphate.

The contents of carbon, hydrogen, and nitrogen were as follows: Found: C, 24.0: H, 5.3: N, 4.3%. Calcd

for $Zr(C_6H_{11}NH_3)_{1.5}(H)_{0.5}(PO_4)_2 \cdot H_2O$: C, 24.0; H, 5.3; N, 4.3%.

It is concluded that α-zirconium phosphate uptakes cyclohexylamine up to 75% of the total ion-exchange capacity and that the cyclohexylamine is present as the cyclohexylammonium ion between the layers.

Nickel(II) Ion Exchange. The determination of nickel(II) showed that all the cyclohexylammonium ions in ZP-Cy were exchanged with Ni(II) in a solution. This also indicates that the cyclohexylamines are present as quartarnary ammonium ions between the layers of zirconium phosphate. The ion-exchange reaction did not proceed further, even if the solid phase after the first ion exchange was immersed in a nickel (II) solution. Thus, the nickel(II) in a solution can be exchanged easily only with the cyclohexylammonium ion in the solid. The product was pale green. The X-ray diffraction pattern of the product agreed well with that reported for $ZrNi(PO_4)_2 \cdot 4H_2O$. The chemical composition was as follows: Zr, 23.6; Ni, 11.6; PO_4, 47.5; H, 1.8: ignition loss, 17.4%. Calcd for $ZrNi_{0.75}H_{0.5}(PO_4)_2 \cdot 3.5H_2O$: Zr, 23.5; Ni, 11.3; PO_4, 48.9; ignition loss, 17.4%. The contents of carbon and nitrogen were within the background limit indicated by the elemental analysis.

The authors wish to express their thanks to Professor Isao Tomita, Ochanomizu University, for the measurement of the thermal analysis.

References

1) A part of this work was presented at the 54th National Meeting of the Chemical Society of Japan, Tokyo, April, 1987, Abstr. No. 2VIB 44.

2) G. Alberti, *Acc. Chem. Res.*, **11**, 163 (1978).

3) G. Alberti and U. Costantino, "Intercalation Chemistry," ed by M. S. Whittingham and A. J. Jacobson, Academic Press, New York (1982), Chap. 5, pp. 147—180.

4) A. Clearfield and R. M. Tindwa, *Inorg. Nucl. Chem. Lett.*, **15**, 251 (1979).

5) M. Casciola, U. Costantino, and S. D'Amico, *Solid State Ionics*, **22**, 127 (1986).

6) "Lange's Handbook of Chemistry," 13th ed, ed by J. A. Dean, McGraw-Hill Book Company, New York (1985), pp. 5—30.

7) Y. Hasegawa and M. Kuwayama, *Bull. Chem. Soc. Jpn.*, **51**, 3485 (1978).

8) Y. Hasegawa and G. Yamamine, *Bull. Chem. Soc. Jpn.*, **56**, 3765 (1983).

9) E. Rodriguez-Castellon, A. Rodriguez-Garcia, and S. Bruque, *Inorg. Chem.*, **24**, 1187 (1985).

10) T. W. G. Solomons, "Organic Chemistry," 2nd ed, John Wiley & Sons, New York (1980), pp. 102—105.

11) "Kagaku Binran," 3rd ed, ed by the Chemical Society of Japan, Maruzen, Tokyo (1984), pp. II—655, 659—660.

12) S. Yamanaka, Y. Horibe, and M. Tanaka, *J. Inorg. Nucl. Chem.*, **38**, 323 (1976).

13) Y. Hasegawa, *Bull. Chem. Soc. Jpn.*, **46**, 3296 (1973).

14) S. Alluli, C. Ferragina, A. La Ginestra, M. A. Massuci, and N. Tomassini, *J. Chem. Soc., Dalton Trans.*, **1976**, 2115.

 © 1988 The Chemical Society of Japan Bull. Chem. Soc. Jpn., 61, 417—421 (1988)

Oxygen Evolution by Means of Water Oxidation Catalyzed by Mononuclear Ruthenium-Ammine Complexes

Masao KANEKO,* Ramasamy RAMARAJ, and Akira KIRA
Solar Energy Science Research Group, The Institute of Physical and Chemical Research, Wako, Saitama 351-01
(Received August 3, 1987)

Water oxidation was achieved catalytically by the use of mononuclear ruthenium-ammine complexes and using Ce(IV) as an oxidant. Cyclic voltammetric studies of the mononuclear ruthenium-ammine complexes $[Ru(NH_3)_5Cl]^{2+}$ and $[Ru(NH_3)_5(H_2O)]^{3+}$, have been carried out using Basal Plane Pyrolytic Graphite (BPG) coated with poly(*p*-styrenesulfonate), Nafion, or Kaolin clay. The electrochemical properties of these ruthenium-ammine complexes show that they can be used as two-electron oxidants for water oxidation. It has also been found that these complexes oxidize water to evolve oxygen in the presence of excess Ce(IV) under homogeneous as well as heterogeneous conditions. The oxygen evolution by means of water oxidation was confirmed by using the $H_2{}^{18}O$ isotope in the reaction medium. The water oxidation process was found to be dependent on the ionic strength of the medium. Higher acidic conditions gave higher O_2 yields. Heterogeneous catalysis with the Ru complex adsorbed in Kaolin clay was as effective as the homogeneous one. The water oxidation reaction catalyzed by ruthenium-ammine complexes was also discussed.

The oxidation of water to molecular oxygen is of great importance as a means of converting light energy into chemical energy, because, among the possible methods of solar energy storage, its conversion into the energy of chemical fuels seems to be one of the most promising.[1,2] In order to realize such light-to-chemical energy conversion systems, the use of water as an electron donor, i.e., water oxidation, is a crucial point, as in the photosynthesis in nature. Oxygen evolution is significantly more difficult to accomplish than hydrogen evolution because four electrons must be transferred in the reaction (Eq. 1):

$$2H_2O \rightarrow O_2 + 4H^+ + 4e^- \quad (1)$$

The photogeneration of oxygen from water is an essential part of green-plant photosynthesis, where the oxygen evolves as a result of water photooxidation in the active center of the photosystem II, with the participation of Mn ions.[3] However, the mechanism of Mn catalytic action is still unclear. The difficulty of creating such models lies in the need to couple the four-electron oxidation of water (Eq. 1) with the one-electron chemistry of the photoredox process.[4] Several types of oxygen evolving catalysts have been identified,[5] but these catalysts are far from ideal, and there are many problems associated with their use in model photochemical systems.[4-8] In recent reports,[9-13] it has been shown that the soluble polynuclear metal complexes work as homogeneous[9-11] as well as heterogeneous catalysts[12-14a] to oxidize water to oxygen.

Recently, Collin and Sauvage[15] have prepared several complexes of ruthenium(II) which contain two molecules of sterically hindering diimine as ligands; they have studied the catalytic activity of the complexes toward water oxidation. None of these complexes display catalytic activity for oxygen formation from water in the presence of excess cerium(IV). Based on their observations, they concluded that a multimetallic system is required to achieve water oxidation to oxygen. Until now it has seemed quite rational to think that only the polynuclear complexes are candidates for the water oxidation because the reaction is a four-electron process. However, the present authors have found, for the first time, that mononuclear ruthenium-ammine complexes catalyze oxygen evolution by means of water oxidation in the homogeneous[14b] as well as in the heterogeneous state; they wish to report their findings in this paper.

Experimental

$[Ru(NH_3)_5Cl]^{2+}$ (Aldrich Chemicals) was used as received, while $[Ru(NH_3)_5(H_2O)]^{3+}$ was prepared by modifying the reported procedure.[16] A hot solution of silver trifluoroacetate, prepared by dissolving 0.079 g of Ag_2O in a 4 ml aqueous solution of 2 M trifluoroacetic acid (1 M=1 mol dm^{-3}), was added to 0.1 g of $[Ru(NH_3)_5Cl]^{2+}$. The AgCl precipitate was digested by heating and stirring for several minutes. The AgCl precipitate was then removed by filtration, and the solution was cooled to room temperature. The pH of the solution was adjusted to about pH 3 by the drop-by-drop addition of 3 M NaOH. The solid $[Ru(NH_3)_5(H_2O)]^{3+}$ complex was isolated by adding solid NH_4PF_6 (about 0.5 g) to the solution, which was then filtered and washed with ethanol and finally with ether. The Kaolin clay (Nakarai Chemicals) was used in this investigation without further treatment. Kaolin clay with the $[Ru(NH_3)_5(H_2O)]^{3+}$ catalyst adsorbed was prepared by mixing the known amounts of the clay and the catalyst in deionized water. The mixture was stirred until complete adsorption was noticed. The clay was filtered after adsorption, washed with deionized water, and dried in air. The adsorbed complex was not desorbed upon dipping into fresh water.

Cyclic voltammograms were run using a Function Generator HB-104 model and a Potentiostat/Galvanostat HA-301 model of Hokuto Denko, Ltd. A basal plane pyrolytic graphite (BPG) electrode coated with poly(*p*-styrenesulfonate), Nafion, or Kaolin clay was used as the working electrode; platinum wire, as the counter electrode, and a Saturated Calomel Electrode (SCE), as the reference electrode. The supporting electrolyte was 0.5 M H_2SO_4.

A water oxidation experiment was carried out under an argon atmosphere by mixing the mononuclear ruthenium-ammine complex and excess ammonium cerium(IV) nitrate.[10,13] The gas evolved by the reaction was analyzed by the use of the Gas Chromatogram (Shimadzu GC 4C, 1.5-m column of Molecular Sieve 5A and an argon carrier). The amount of O_2 evolved was corrected by subtracting the amount of O_2 coming from the dissolved air. The water oxidation was confirmed by using $H_2{}^{18}O$ in the reaction medium, and a Quadrupole Mass Spectrometer from the Ulvac Corporation (MSQ-150A) was used to analyze the gas evolved.

Results and Discussion

The solution chemistry of ruthenium ammine complexes has been studied extensively.[17] These complexes are widely used as quenchers[18] for the excited state of $[Ru(bpy)_3]^{2+}$. The electrochemical behavior of the ruthenium-ammine complexes has also been investigated;[19] however, attention has not been focused on the redox chemistry involving the higher oxidation states, e.g., Ru(IV) and Ru(V).

Cyclic voltammograms obtained for $[Ru(NH_3)_5Cl]^{2+}$ and $[Ru(NH_3)_5(H_2O)]^{3+}$ are given in Fig. 1. When the uncoated BPG was used to record the cyclic voltammograms in the potential region from 0.5 to 1.5 V vs. SCE, a large catalytic current attributable to the electrochemical water oxidation was observed. However, a better cyclic voltammogram was obtained when the BPG was modified with poly(*p*-styrenesulfonate), Nafion, or Kaolin clay.

For both the ruthenium-ammine complexes, the $[Ru(NH_3)_5Cl]^{2+/+}$ and $[Ru(NH_3)_5(H_2O)]^{3+/2+}$ couples were observed in the potential region from −0.5 to 0.3 V vs. SCE (Fig. 1). Figure 1 shows that there are two oxidative peaks in the potential region from 0.5 to 1.5 V vs. SCE, peaks which are reversible in the reductive scan for the $[Ru(NH_3)_5Cl]^{2+}$ and $[Ru(NH_3)_5(H_2O)]^{3+}$ complexes. However, the reductive waves were not clear because of the larger catalytic current caused by water oxidation.

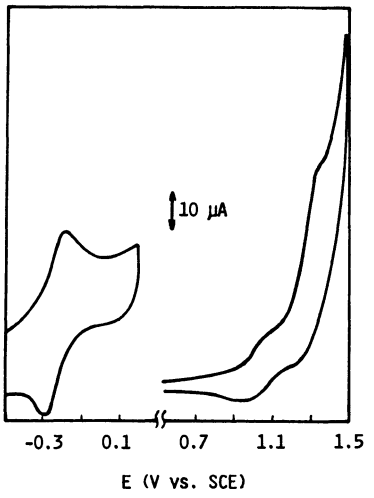

Fig. 1. Cyclic voltammogram of $[Ru(NH_3)_5Cl]^{2+}$ in 0.1 M H_2SO_4 at Nafion coated BPG at a scan rate of 50 mV s^{-1}.

The $[Ru(NH_3)_5Cl]^{2+/+}$ couple appears at −0.25 V vs. SCE. The other two peaks in the potential region from 0.5 to 1.5 V vs. SCE indicate the formation of $[Ru^{V}(NH_3)_5Cl]^{4+}$ by a series of one-electron oxidation of $[Ru^{III}(NH_3)_5Cl]^{2+}$ (Eq. 2). Similar results were observed for the $[Ru(NH_3)_5(H_2O)]^{3+}$ complex. However, the peak potentials are slightly shifted to less positive values than those for the $[Ru(NH_3)_5Cl]^{2+}$ complex. It has already been reported[19] that the formal potentials of the $[Ru(NH_3)_5Cl]^{2+/+}$ and $[Ru(NH_3)_5(H_2O)]^{3+/2+}$ couples are almost the same. Based on the present results, the various redox processes occurring in the chloropentammine ruthenium complex may be said to be as given in Eq. 2:

$$[Ru^{II}(NH_3)_5Cl]^{+} \underset{+e^-}{\overset{-e^-}{\rightleftharpoons}} [Ru^{III}(NH_3)_5Cl]^{2+} \underset{+e^-}{\overset{-e^-}{\rightleftharpoons}} \quad (-0.25\ \text{V}, \quad 1.06\ \text{V})$$

$$[Ru^{IV}(NH_3)_5Cl]^{3+} \underset{+e^-}{\overset{-e^-}{\rightleftharpoons}} [Ru^{V}(NH_3)_5Cl]^{4+} \quad (1.28\ \text{V}) \qquad (2)$$

For both the complexes, fairly large peak separations (100 mV) were observed. They may be caused by the rapid reduction of the higher-oxidation-state ruthenium by water or by the polymer coating rather than by electrochemical reduction. Such processes have already been observed in our own earlier works[10,11] with dinuclear ruthenium complexes. It has also been reported that the $[Ru(NH_3)_5Cl]^{+}$ complex undergoes rapid aquation with a rate constant of 4.7 s^{-1} (Eq. 3), which corresponds to a half-life of 0.15 s:[20]

$$[Ru(NH_3)_5Cl]^{+} + H_2O \rightarrow [Ru(NH_3)_5(H_2O)]^{2+} + Cl^{-} \qquad (3)$$

The monomeric ruthenium complexes easily form higher-oxidation-state Ru(V) complexes upon chemical oxidation, and the redox potentials of the ruthenium complexes show that they can be used as oxidants for water oxidation. These monomeric ruthenium complexes can act as two-electron oxidants and, therefore, might be able to bring about the four-electron oxidation of water to oxygen only on the surface of a suitable catalyst. However, oxygen evolution was observed visibly in a homogeneous solution upon the addition of excess Ce(IV) to the monomeric ruthenium complexes, without the addition of any external oxygen evolution catalyst. Gas bubbles were observed in solution soon after the addition of excess Ce(IV), and the chromatographic results (Fig. 2) show that the gas evolved is oxygen. Water oxidation was confirmed by mass spectrometry using water containing $H_2{}^{18}O$ isotopes. Oxygen was confirmed by the peaks at m/z=32, 34, and 36, which correspond to $^{16}O_2$, $^{18}O^{16}O$, and $^{18}O_2$ respectively. Both the gas-chromatograph and mass-spectral data clearly showed that oxygen is

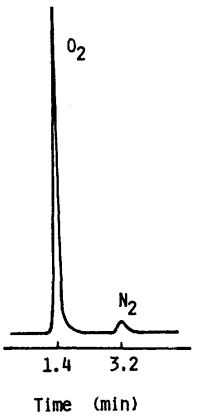

Fig. 2. Gas chromatogram of the gas evolved by reaction of $[Ru(NH_3)_5Cl]^{2+}$ in water in the presence of Ce(IV). Carrier gas, argon; column, Molecular Sieve 5A; 200 μl of the evolved gas was injected for the measurement.

Table 1. Oxygen Evolution by Water Oxidation under Homogeneous Conditions Using $[Ru(NH_3)_5Cl]^{2+}$ at 25 °C

Ru : Ce(IV) (molar ratio)	O_2 evolved	
	(μl)	Turnover number
1 : 50	26	1.04
1 : 100	56	2.29
1 : 200	166	6.86
1 : 300	203	8.36

$[Ru(NH_3)_5Cl]^{2+}$, 2 μmol. Solution volume, 10 ml; reaction time, 90 min.

Table 2. Oxygen Evolution by Water Oxidation under Homogeneous Conditions Using $[Ru(NH_3)_5Cl]^{2+}$ at 25 °C: Concentration Variation of the Catalyst

Ru complex (10^{-4} M)	O_2 evolved	
	(μl)	Turnover number
6.70	64	2.63
3.35	131	5.41
2.01	166	6.86

Ru: Ce(IV)=1 : 200 (molar ratio). $[Ru(NH_3)_5Cl]^{2+}$, 2 μmol; reaction time, 90 min.

evolved by the water oxidation. The experimental results of the homogeneous catalysis of water oxidation by monomeric ruthenium complexes were treated with great caution because the decomposition product of the compounds is often ruthenium oxide, which is catalytically active for water oxidation.[21,22] The Ru complex was stable in water, even in the presence of excess Ce(IV), as was confirmed by visible spectroscopy. Gas bubbles were observed immediately after Ce(IV) had been added to the complex solution. These results indicate that the Ru complex itself is active in the catalysis.

The amount of oxygen evolved in 90 minutes with different Ru : Ce(IV) ratios (molar ratio) under homogeneous conditions are given in Table 1. When the Ru: Ce(IV) (molar ratio) was changed from 1 : 50 to 1 : 300, the oxygen evolution increased with the increase in the Ce(IV) concentration. The results shown in Table 1 indicate that the monomeric ruthenium complex works as a catalyst in the water oxidation process. Table 2 shows that when the ruthenium complex concentration is decreased from 6.7×10^{-4} to 2.01×10^{-4} M the oxygen evolution is increased 2.6 times. However, Table 3 shows that the increase in the ionic strength leads to the decrease in the oxygen evolution. The four-electron oxidation of water must be realized through the interaction of two intermediate mononuclear ruthenium complexes. Such interaction would be hindered by increasing the ionic strength. It is clear that the effect of the concentration change on

Table 3. OxygenEvolution by Water Oxidation Using $[Ru(NH_3)_5Cl]^{2+}$ under Homogeneous Conditions at 25 °C: Ionic Strength Variation

Ionic strength[a]	O_2 evolved	
	(μl)	Turnover number
0.48	166	6.86
0.58	135	5.56
0.98	84	3.47
1.48	70	2.89
2.48	50	2.04

a) Adjusted with KNO_3. Ru : Ce(IV)=1 : 200 (molar ratio). $[Ru(NH_3)_5Cl]^{2+}$, 2 μmol; solution volume, 10 ml; reaction time, 90 min.

Table 4. Oxygen Evolution by Water Oxidation Using $[Ru(NH_3)_5Cl]^{2+}$ under Homogeneous Conditions at 25 °C

Ionic strength[a] : 2.11			Ionic strength[a] : 3.11		
Ru complex (10^{-4} M)	O_2 evolved		Ru complex (10^{-4} M)	O_2 evolved	
	(μl)	Turnover number		(μl)	Turnover number
6.67	64	2.64	6.67	40	1.66
3.33	56	2.31	3.33	45	1.84
2.0	67	2.76	2.0	45	1.84

a) Adjusted with KNO_3. $[Ru(NH_3)_5Cl]^{2+}$, 2 μmol; Ru: Ce(IV)=1 : 200 (molar ratio); reaction time, 90 min.

water oxidation shown in Table 2 is attributable to the ionic strength effect. The change in the concentration of the ruthenium complex did not have any important effect on the water oxidation process under a constant ionic strength (Table 4).

The effect of acid on the water-oxidation process was also studied; the data are given in Table 5. When the HNO_3 concentration was increased to 0.2 M, an increase in the oxygen evolution with the HNO_3 concentration was observed. In an acidic solution, $[Ru(NH_3)_5Cl]^{2+}$ readily undergoes aquation accompanied by the formation of the water-substituted pentammine ruthenium complex; the higher rate of oxygen evolution can be explained on the basis that the water molecule in the coordination sphere is involved in the water oxidation process. When $[(bpy)_2(H_2O)RuORu(H_2O)(bpy)_2]^{4+}$ was used as the catalyst for water oxidation,[9,23] it was explained that the water ligands in the dinuclear ruthenium complex take part in the water oxidation reaction.

As catalysts for water oxidation, the $[Ru(NH_3)_5(H_2O)]^{3+}$ complex was used in a homogeneous state, and the Kaolin clay-adsorbed complex, in a heterogeneous state. The amount of oxygen evolved in 90 minutes with different concentration of Ce(IV), using the homogeneous as well as the heterogeneous state $[Ru(NH_3)_5(H_2O)]^{3+}$ in water oxidation, are given in Table 6. The effect of the concentration of the complex adsorbed in the clay in the heterogeneous catalysis was also studied; the results are given in Table 7. A comparison of the results of Table 6 (homogeneous system) and Table 2 will show that the $[Ru(NH_3)(H_2O)]^{3+}$ is a better catalyst than the chloropentammineruthenium complex. One reason for the better catalytic activity of the aquapentammine complex can be the fact that the water molecules in the coordination sphere are involved in the water oxidation process, as has been explained before. It should also be noted that the $[Ru(NH_3)_5(H_2O)]^{4+/5+}$ couple is less positive than the chloropentammine complex and that the Ce(IV) will more readily oxidize the water complex than the chloro complex, thus producing the higher-oxidation-state ruthenium complex. From the electrochemical data, it is clear that the ruthenium-ammine complexes can act as a two-electron oxidants for water oxidation. In order to evolve one molecule of oxygen by water oxidation, two molecules of a ruthenium complex are needed. The addition of excess Ce(IV) to a solution of a mononuclear ruthenium-ammine complex should lead to the oxidation of the complex to give Ru(V) complex; then, the two molecules of the Ru(V) complex will oxidize water to oxygen.

When $[Ru(NH_3)_5Cl]^{2+}$ is used as a catalyst for water oxidation, the water will coordinate at first to the $[Ru^{V}(NH_3)_5Cl]^{4+}$ higher-oxidation-state complex, and then the two molecules of the water-coordinated intermediate should lead to oxygen evolution. Such a seven coordination in the intermediate step has been suggested for the Ru(IV) and Ru(III) complexes (d^4 and d^5 ions) in the oxidation-reduction reactions of monomeric ruthenium-ammine complexes.[24,25] It is probable that the Cl^- ligand will be oxidized by the Ru(V) metal center or by the Ce(IV), which will lead to the formation of the water substituted ruthenium complex. Considering that the coordinated water molecule is involved in the water-oxidation reaction, as has been reported for the dinuclear ruthenium complex,[7,19] the following reaction scheme is proposed to explain the oxygen evolution by the monomeric ruthenium-ammine complex. Two molecules of the water coordinated monomeric Ru(V) complex would lead to the formation of a peroxo-bridged dinuclear ruthenium complex, Ru-O-O-Ru, and then the intermediate would release one molecule of oxygen. Such a peroxo-bridged ruthenium intermediate complex is not known; however, the oxo-bridged dinuclear

Table 5. Oxygen Evolution by Water Oxidation under Homogeneous Conditions Using $[Ru(NH_3)_5Cl]^{2+}$ at 25 °C

HNO_3 (M)	O_2 evolved	
	(μl)	Turnover number
0.0	166	6.86
0.01	189	7.79
0.05	238	9.80
0.1	252	10.41
0.2	286	11.82

$[Ru(NH_3)_5Cl]^{2+}$, 2 μmol. Ru : Ce(IV)=1 : 200 (molar ratio); solution volume, 10 ml; reaction time, 90 min.

Table 6. Oxygen Evolution by Water Oxidation under Homogeneous and Heterogeneous Conditions at 25 °C with $[Ru(NH_3)_5(H_2O)]^{3+}$

$[Ru(NH_3)_5(H_2O)]^{3+}$ in water (homogeneous)			$[Ru(NH_3)_5(H_2O)]^{3+}$ in Kaolin clay (heterogeneous)		
Ru: Ce(IV) (molar ratio)	O_2 evolved		Ru: Ce(IV) (molar ratio)	O_2 evolved	
	(μl)	Turnover number		(μl)	Turnover number
1 : 100	243	10.04	1 : 200	362	14.96
1 : 200	287	11.87	1 : 400	378	15.58
1 : 300	308	12.73	1 : 500	436	18.01
1 : 400	358	14.77			

$[Ru(NH_3)_5(H_2O)]^{3+}$, 2 μmol; Kaolin clay, 100 mg; solution volume, 5 ml; reaction time, 90 min.

Table 7. Oxygen Evolution by Water Oxidation under Heterogeneous Conditions Using $[Ru(NH_3)_5(H_2O)]^{3+}$ Adsorbed on Kaolin Clay

Kaolin clay	O_2 evolved	
mg	(μl)	Turnover number
100	378	15.58
300	389	16.05
500	453	18.63

Ru : Ce(IV)=1 : 400 (molar ratio). $[Ru(NH_3)_5(H_2O)]^{3+}$, 2 μmol; solution volume, 5 ml; reaction time, 90 min.

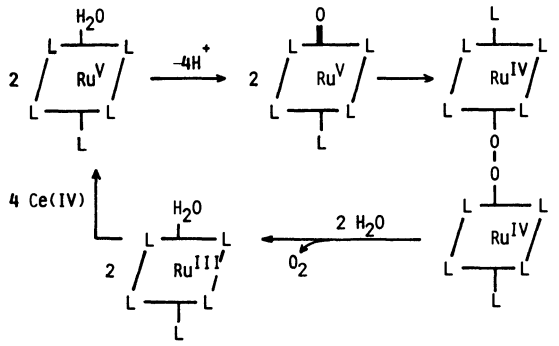

ruthenium complex, $[(NH_3)_5RuORu(NH_3)_5]^{4+}$, is known.[26]

Porter[27] suggested that manganese(IV) complexes of porphyrin might oxidize water and that this water-oxidation reaction might be expected to occur via an intermediate oxygen bridged dinuclear complex. So far, the generation of oxygen with such systems has remained ambiguous, and there are no substantiated reports in which a metalloporphyrin has been used to oxidize water to oxygen. The oxygen evolution in the photosystem II is expected to occur via oxygen-bridged dinuclear species.[3,28] Recently, the formation of an O-O bond as an intermediate has been proposed to explain the oxygen evolution by water oxidation using multimetal complex systems,[9,10,13,23] which would support the above mentioned intermediate formation.

The authors are thankful to the Grant-in-Aid (No. 62612002) for Scientific Resesarch on Priority Area of "Macromolecular Complex" from the Ministry of Education, Science and Culture.

References

1) "Energy Resources Through Photochemistry and Catalysis," ed by M. Graetzel, Academic Press, New York (1983).

2) "Photochemical Conversion and Storage of Solar Energy," ed by J. S. Connolly, Academic Press, New York (1981).

3) "The Oxygen Evolving System of Photosynthesis," ed by Y. Inoue, A. R. Crofts, Govindjee, N. Murata, G. Renger, and K. Satoh, Academic Press, New York (1983).

4) A. Harriman, *J. Photochem.*, **25**, 23 (1984).

5) K. I. Zamaraev and V. N. Parmon, "Energy Resources Through Photochemistry and Catalysis," ed by M. Graetzel, Academic Press, New York (1983), p. 123.

6) H. Nijs, M. I. Cruz, J. J. Fripiat, and H. Van Damme, *Nouv. J. Chim.*, **6**, 551 (1982).

7) G. Blondeel, A. Harriman, G. Porter, D. Urwin, and J. Kiwi, *J. Phys. Chem.*, **87**, 2432 (1979).

8) A. Mills and M. L. Zeeman, *J. Chem. Soc., Chem. Commun.*, **1981**, 948.

9) J. A. Gilbert, D. Eggleston, W. R. Murphy Jr., D. A. Geselowitz, S. W. Gersten, D. J. Hodgson, and T. J. Meyer, *J. Am. Chem. Soc.*, **107**, 3855 (1985).

10) R. Ramaraj, A. Kira, and M. Kaneko, *J. Chem. Soc., Faraday Trans. 1*, **82**, 3515 (1986).

11) R. Ramaraj, A. Kira, and M. Kaneko, *J. Chem. Soc., Faraday Trans. 1*, **83**, 1539 (1987).

12) R. Ramaraj, A. Kira, and M. Kaneko, *Angew. Chem., Int. Ed. Engl.*, **25**, 1009 (1986).

13) R. Ramaraj, A. Kira, and M. Kaneko, *Angew. Chem., Int. Ed. Engl.*, **25**, 825 (1986).

14) a) M. Kaneko, N. Takabayashi, Y. Yamauchi, and A. Yamada, *Bull. Chem. Soc. Jpn.*, **57**, 156 (1984); b) R. Ramaraj, A. Kira, and M. Kaneko, *Chem. Commun.*, **1987**, 227.

15) J. P. Collin and J. P. Sauvage, *Inorg. Chem.*, **25**, 135 (1986).

16) C. G. Kuehn and H. Taube, *J. Am. Chem. Soc.*, **98**, 689 (1976).

17) P. C. Ford, *Coord. Chem. Rev.*, **5**, 75 (1970).

18) K. Kalyanasundaram, *Coord. Chem. Rev.*, **46**, 159 (1982).

19) H. Lim, D. J. Barclay, and F. C. Anson, *Inorg. Chem.*, **11**, 1460 (1972).

20) J. H. Baxendale, A. J. Rogers, and M. D. Ward, *J. Chem. Soc. A*, **1970**, 1246.

21) K. Kalyanasundaram and M. Graetzel, *Angew. Chem., Int. Ed. Engl.*, **18**, 701 (1979).

22) J. P. Collin, J. M. Lehn, and R. Ziessel, *Nouv. J. Chim.*, **6**, 405 (1982).

23) M. Graetzel, "Homogeneous and Heterogeneous Photocatalysis," ed by E. Pelizzetti and N. Serpone, NATO ASI Series, D. Reidel Publishing Company, Dordrecht (1986), p. 108.

24) J. F. Endicott and H. Taube, *Inorg. Chem.*, **4**, 437 (1965).

25) H. Scheiddizer, J. Armor, and H. Taube, *J. Am. Chem. Soc.*, **90**, 5828 (1968).

26) J. A. Baumann and T. J. Meyer, *Inorg. Chem.*, **19**, 345 (1980).

27) G. Porter, *Proc. R. Soc. London, Ser. A*, **362**, 281 (1978).

28) Govindjee, T. Kambara, and W. Colman, *Photochem. Photobiol.*, **42**, 187 (1985).

Synthesis and Properties of 4*H*-Benzo[*hi*]pyrrolo[2,1,5-*cd*]indolizin-4-ones[1)]

Michihiko NOGUCHI,* Takashi YAMAMOTO, Shoji KAJIGAESHI, Keiji SAITO,† and Tsuyoshi ARAI†
Department of Industrial Chemistry, Faculty of Engineering, Yamaguchi University, Tokiwadai, Ube 755
†UBE Scientific Analysis Laboratory, Kogushi, Ube 755
(Received May 14, 1987)

3-Phenyl-4*H*-benzo[*hi*]pyrrolo[2,1,5-*cd*]indolizin-4-one (**5**) was prepared by saponification accompanied by the decarboxylation of the corresponding 1,2-bis(methoxycarbonyl) derivative, which was obtained by the DDQ oxidation of 5,6-dihydro one. Investigations concerning its spectral data and MO calculations revealed interesting electronic features for **5**, e.g., i) a highly polarized structure in the ground state, ii) the exsistence of a peripheral [12]annulene system in acidic media, and iii) a significant stabilization of the excited state by protonation.

Much attention has been paid to the chemistry of 1*H*-phenalen-1-one (**A**) owing to its unusual properties, e.g., high basicity, high dipole moment, low-frequency shift of carbonyl absorption, and so on. These properties have been ascribed to an important contribution of an ionic structure (**A'**) to the resonance hybrid.[2)] From synthetic and physicochemical viewpoints, much effort has been made to prepare the iso π-electronic analogs of **A**, e.g., 3*H*-benz[*cd*]azulen-3-one (**B**)[3)] and 2,14-dihydrotricyclo[7,3,2,$0^{5,13}$]tetradeca-1,3,5,7,9,11-hexaen-2-one (**C**).[4)] Their interesting properties have been elucidated during the last two decades.

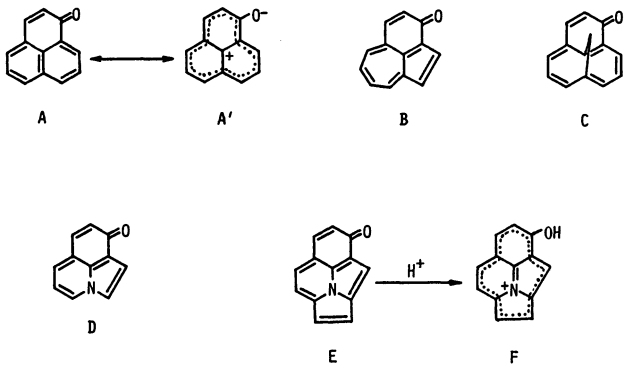

A more recent report[5)] on the synthesis and properties of 9*H*-pyrrolo[3,2,1-*ij*]quinolin-9-one (**D**) stimulated us to investigate 4*H*-benzo[*hi*]pyrrolo[2,1,5-*cd*]indolizin-4-one (**E**), which involves a peripheral 10 π-electronic [3.2.2]cyclazine system instead of the indolizine nuclei of **D**. Therein, the [12]annulene system **F**, perturbed by an internal azomethinium ion, would be provided by the protonation of **E**.

In a preliminary paper,[6)] we communicated a facile preparation of the derivatives of **E** and a few of their interesting electronic features. In the present paper, details concerning the syntheses of 3-aryl-4*H*-benzo[*hi*]pyrrolo[2,1,5-*cd*]indolizin-4-ones are described; also, their properties are discussed on the basis of spectral evidence and molecular orbital (MO) calculations.

Results and Discussion

Synthesis. According to the reported method for the introduction of a carbonyl function into the α-methylene moiety in azulene,[7)] 5,6-dihydro-1-methoxycarbonyl- and 5,6-dihydro-1,2-bis(methoxycarbonyl)-3-aryl-4*H*-benzo[*hi*]pyrrolo[2,1,5-*cd*]-indolizinenes (**1**) were oxidized with 2,3-dichloro-5,6-dicyano-*p*-benzoquinone (DDQ) (4 mol equiv.) in 10% aqueous dioxane to give selectively 4*H*-benzo-[*hi*]pyrrolo[2,1,5-*cd*]indolizin-4-one derivatives (**2**) (Scheme 1). The structures of **2** were confirmed on the basis of analytical data and spectral evidence. These results and spectral data for **2** are summarized in Tables 3 and 4, respectively.

For this regioselective oxidation leading to **2**, we proposed a reaction pathway which initiates a CT complex formation between DDQ and aryl groups at the 3-position of **1** (Fig. 1). This was supported by the following results; at an earlier stage of the reaction, a dark-green solution was observed, which was in accordance with CT complex formation.[8)] The progress of

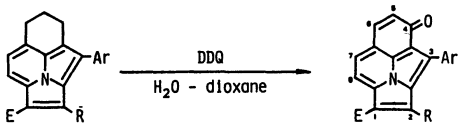

a: Ar=C_6H_5, R=H; b: Ar=C_6H_5, R=E; b-d_5: Ar=C_6D_5, R=E; c: Ar=C_6H_4-OMe(*p*), R=E; d: Ar=C_6H_4-Br(*p*), R=E; e: Ar=4-Biphenyl, R=E; f: 2-Naphthyl, R=E.

Scheme 1.

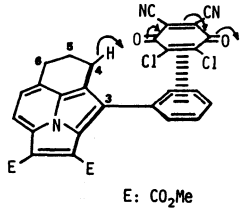

Fig. 1. CT complex formation between the phenyl group of **1a** and DDQ.

the oxidation was dependent upon the facility of the CT complex formation, which was also ascribed to the electron density of the aromatic ring at the 3-position.[9]

In order to prepare the 3-phenyl-4*H*-benzo[*hi*]-pyrrolo[2,1,5-*cd*]indolizin-4-one (**5**), the corresponding 5,6-dihydro derivative **3** was treated with 1.5 mol equiv. of DDQ to give 5,6-dihydro-3-phenyl-4*H*-benzo[*hi*]pyrrolo[2,1,5-*cd*]indolizin-4-one (**4**) in 42% yield. A similar treatment with 4.0 mol equiv. of DDQ gave the desired **5** and **4** in 33 and 16% yields, respectively. However, a successive oxidation of **4** to **5** was considerably sensitive to the reaction conditions employed; therefore, another synthetic approach to **5** was surveyed.

The saponification of **2b** with methanolic potassium hydroxide followed by acidification gave the corresponding dicarboxylic acid, which was decarboxylated in refluxing quinoline in the presence of copper dust to afford **5**. Similarly, the 3-pentadeuteriophenyl derivative **5**-d_5 was obtained from **2b**-d_5 (Scheme 2).

MO Calculations. In an attempt to obtain a better understanding of the properties of **5**, MO calculations using the MNDOA method[10] for the parent compound **E** were performed. All of its bond lengths and valence angles were reinvestigated using the structure optimization program therein (see Experimental section).

The results of these calculations indicate that there is no significant departure from planarity of molecule **E**. Among these results, the bond lengths and atomic charges for **E** are presented in Fig. 2. These suggest that the enone moiety attached to the peri position of [3.2.2]cyclazine nuclei is electron-withdrawing and that a considerable negative charge is located at the carbonyl oxygen atom. Consequently, the carbonyl group is highly polarized and the dipole moment was calculated to be 4.26 D, which is comparable to that of tropone.[11]

IR Spectra. The lower-frequency shift of 44 cm^{-1} for the carbonyl absorption was caused by a conversion of the 5,6-dihydro derivative **4** (1650 cm^{-1}) into fully conjugated **5** (1606 cm^{-1}). The carbonyl absorptions at the 4-position for **2** were also observed at 1624—1592 cm^{-1}, which were somewhat lower than those of the other systems: **A**, **B**, and **D**.[2,3,5] These results indicate that the carbonyl groups of **2** and **5** are highly polarized and that the ionic structure **E′** is important to the resonance hybrid in the ground state of **E** (Scheme 3).

^{13}C NMR Spectra. A full assignment of the ^{13}C NMR spectrum for **5** was accomplished by a comparison with the spectra for **2a**, **2b**, **2c**, and **5**-d_5 using several decoupling techniques (see Experimental section). The chemical shifts are presented in Fig. 3; these values for the benzopyrroloindolizinone moiety of **5** corresponded to the atomic charges of the 4*H*-

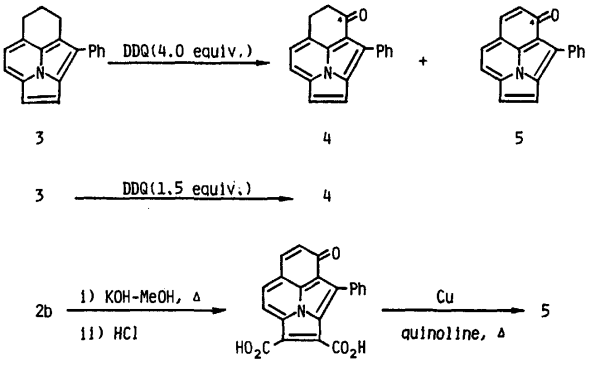

Scheme 2.

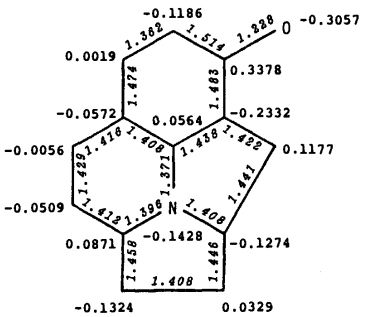

Fig. 2. Net atomic charge and atomic distance (Å) of **E** by MNDOA.

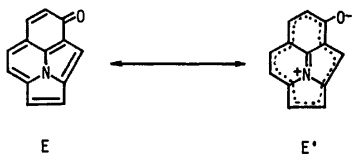

Scheme 3.

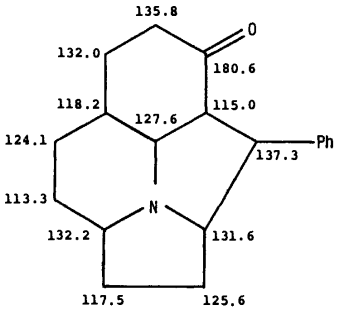

Fig. 3. Assignment of ^{13}C NMR spectrum of **5** in $CDCl_3$.

Table 1. ^{1}H NMR Spectral Data for **3**-d_5 and **5**-d_5 in $CDCl_3$

Compd	δ/ppm				*J*/Hz	
	1-H	2-H	7-H	8-H	$J_{1,2}$	$J_{7,8}$
3-d_5	7.18	7.65	7.35	7.82	3.9	7.8
5-d_5	7.02	7.57	7.51	7.67	4.6	7.8
Δδ[a]	0.16	0.08	−0.16	0.15		

a) Δδ=δ(**3**-d_5)−δ(**5**-d_5).

Table 2. ^{1}H NMR Spectral Data of **5**-d_5 in $CDCl_3$ and CF_3COOD

Solvent	δ/ppm						J/Hz		
	1-H	2-H	5-H	6-H	7-H	8-H	$J_{1\text{-}2}$	$J_{5\text{-}6}$	$J_{7\text{-}8}$
$CDCl_3$	7.02	7.57	6.44	7.29	7.51	7.67	4.6	9.6	7.8
CF_3COOD	7.06	7.48	7.06	7.82	7.69	8.29	5.2	9.1	8.4
Δδ[a]	−0.04	0.09	−0.62	−0.53	−0.18	−0.62			

a) $\Delta\delta=\delta(CDCl_3)-\delta(CF_3COOD)$.

benzo[*hi*]pyrrolo[2,1,5-*cd*]indolizin-4-one system (**E**) calculated by MNDOA (Fig. 2). This implies that the results from the MNDOA calculations for **E** are useful for a qualitative discussion of the electronic features for **2** and **5**.

^{1}H NMR Spectra. The assignment and discussion concerning the cyclazine ring protons of **5** were achieved by an analysis of the spectrum of the pentadeuteriophenyl derivative **5**-d_5. The chemical shifts[12] and coupling constants of **3**-d_5 and **5**-d_5 are tabulated in Table 1. Therein, the introduction of the enone moiety into [3.2.2]cyclazine caused a small upperfield shift for all protons other than 7-H. The spectral data for **5**-d_5 in deuteriochloroform ($CDCl_3$) and in trifluoroacetic acid-d_1 (CF_3CO_2D) are summarized in Table 2. The positive charge resulting from the protonation caused relatively small downfield shifts for the protons (Δδ: within −0.6); interestingly, a small upfield shift was observed for 2-H in CF_3CO_2D in comparison with that in $CDCl_3$. The differences among the coupling constants became smaller in CF_3CO_2D, which implied that the bond-alternation of the peripheral π-system was weakened by the protonation.

As is well-known, the protonation of other iso π-electronic systems caused considerable downfield shifts of all the ring protons, i.e., Δδ=−0.7—−1.8 for 1*H*-phenalen-1-one,[13] Δδ=0.0—−1.3 for 7,9-dimethyl-3*H*-benz[*cd*]azulen-3-one,[3b] and Δδ=−0.4—−0.9[14] for 2-ethoxycarbonyl-7-phenyl-9*H*-pyrrolo[3,2,1-*ij*]quinolin-9-one. On the other hand, 5*H*-cyclopenta[*cd*]-phenalen-5-one, a [13]annulenone perturbed by an internal vinyl π-system, exhibited both small up and downfield shifts for the ring protons on protonation (Δδ=−0.3—0.3), for which the existence of the paramagnetic ring current arising from the peripheral 12 π-electronic system has been proposed.[15]

The results in the present work are probably attributable to the ring current due to the peripheral [12]-annulene system, which is cross-linked by an azomethinium ion.

Electronic Spectra. The electronic spectra of **3**, **4**, and **5** are shown in Fig. 4. These reveal that the introduction of an enone moiety into the [3.2.2]cyclazine system causes a significant change in π-electronic features of the parent system. The solvent dependency of the spectra of **5** was also investigated. The spectra in chloroform, methanol, and methanol-sulfuric acid (100/1) do not show any solvent effect.[16]

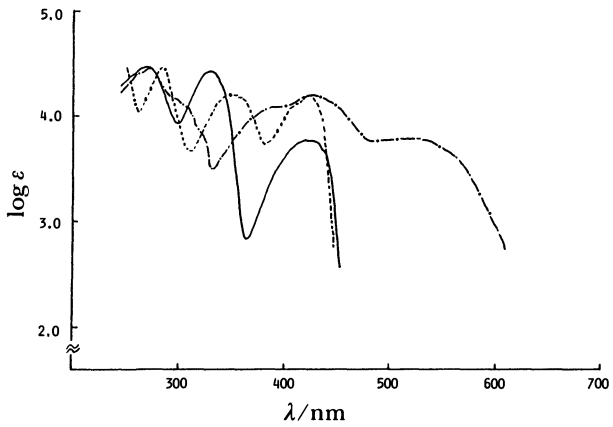

Fig. 4. Electronic spectra of **3** (——), **4** (----), and **5** (-·-·-) in $CHCl_3$.

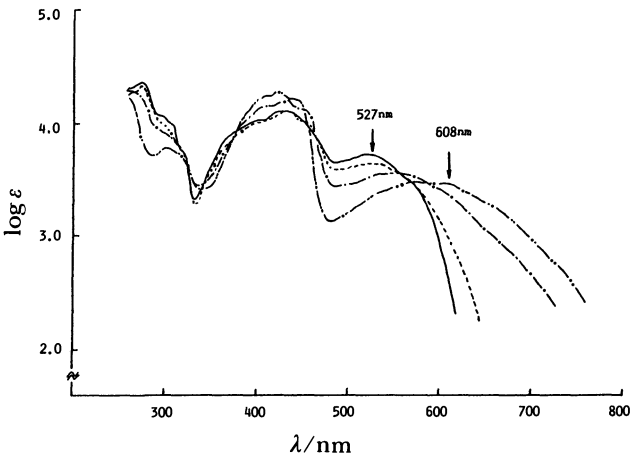

Fig. 5. Change of the electronic spectra of **5** with acid concentrations: (——) in $CHCl_3$; (----) in $CHCl_3$–CF_3COOH=100/1; (-·-·-) in 50/1; (-···-) in 3/2.

However, when the protonation of carbonyl oxygen atom of **5** was complete,[17] the absorption maximum due to the first electronic transition was shifted to a longer wavelength, and the spectra were changed as the acid concentrations decreased (Fig. 5). The longer wavelength shift by the protonation of **5** did not depend on the concentrations of substrate **5** in the range 8.0×10^{-7} to 3.6×10^{-6} M (1M=1 mol dm^{-3}). The addition of *p*-dimethoxybenzene or 1,4-dimethoxynaphthalene caused no changes of the spectra in acidic media. Also, the 1,2-bis(methoxycarbonyl) derivative

2a showed the same behavior under acidic conditions as those of **5**.

From these results, we suggest that the shift was not due to an intermolecular interaction, e.g., a CT complex formation between **5** and its protonated species, but due to inherent changes in the electronic system of **5** by protonation.[18]

On the other hand, the spectra of phenalenones[2] or 3*H*-benz[*cd*]azulen-3-one[3b] in acidic media exhibited considerable hypsochromic shifts, which were ascribed to a stabilization of their ground states. Accordingly, the present results indicate that protonation onto the carbonyl oxygen atom of **5** results in a more significant stabilization of its excited state, rather than of its ground state.

In order to confirm this point, MO calculations for **F**, the protonated species of **E**, were attempted. The HOMO and LUMO energy levels of **F** were calculated to be −8.52 and −3.98 eV, respectively. This means that a very small instabilization of the HOMO and a large stabilization of the LUMO are caused by the protonation, in comparison with those of **E** (HOMO: −8.62 eV; LUMO: −1.54 eV). Also, as shown in Fig. 6, the positive charge caused by the protonation was delocalized over the peripheral system of **F**, and the peripheral bond lengths were averaged, indicating the bond alternations of the π-system were less significant.

In conclusion, 4*H*-benzo[*hi*]pyrrolo[2,1,5-*cd*]-indolizin-4-one (**E**) has the following characteristic properties: i) a highly-polarized structure in the ground state and ii) a significant stabilization of the LUMO of **E** by protonation, which is considerably different from its π-electronic analogs, such as 1*H*-phenalen-1-one (**A**), 3*H*-benz[*cd*]azulen-3-one (**B**), and 9*H*-pyrrolo[3,2,1-*ij*]quinolin-9-one (**D**).

Experimental

General. All melting points are uncorrected. The IR spectra were measured on a JASCO IRA-1 spectrometer. The ^{1}H NMR spectra were obtained on JEOL FX-200 and/or JMN-MH-100 spectrometers and ^{13}CNMR spectra were recorded on a JEOL FX-200 spectrometer at 50.1 MHz. Chemical shifts are expressed in parts per million (ppm) downfield from tetramethylsilane. The mass spectra were determined with a JEOL JMS-D spectrometer at 75 eV using a direct inlet method. The electronic spectra were taken by a Hitachi 220 spectrophotometer. The elemental analyses were performed on a Hitachi 026 CHN analyzer. Most of the reactions were monitored by thin-layer chromatography (Silica gel 60F-254, Merck). The visualization was made with ultraviolet light (254 and 365 nm). Wakogel C-200 and C-300 (Wako Pure Chemical Industries LTD) and Aluminium Oxide 90 (Merck) were used for preparative column chromatography.

The unknown starting materials **1a**, **1c**, **1d**, **1e**, and **1f** were prepared from reactions of the corresponding benzo[*hi*]indolizines and acetylenes in a similar manner to the reported method.[19]

1a: Mp 140—141 °C. Found: C, 80.11; H, 5.50; N, 4.18%. Calcd for $C_{21}H_{17}NO_2$: C, 79.98; H, 5.43; N, 4.44%.

1c: Mp 153—154 °C. Found: C, 71.58; H, 5.32; N, 3.62%. Calcd for $C_{24}H_{21}NO_5$: C, 71.45; H, 5.25; N, 3.47%.

1d: Mp 194—195 °C. Found: C, 61.09; H, 4.07; N, 3.29%. Calcd for $C_{23}H_{18}BrNO_4$: C, 61.07; H, 4.01; N, 3.10%.

1e: Mp 224—225 °C. Found: C, 77.60; H, 5.20; N, 3.24%. Calcd for $C_{29}H_{23}NO_4$: C, 77.48; H, 5.16; N, 3.12%.

1f: Mp 201—203 °C. Found: C, 76.38; H, 5.03; N, 3.37%. Calcd for $C_{27}H_{21}NO_4$: C, 76.58; H, 5.00; N, 3.31%.

Oxidation of 1 with DDQ to 2. General Procedure: To a 10% aqueous dioxane solution (30 mL) of **1a** (500 mg, 1.59 mmol), DDQ (1.44 g, 6.36 mmol) was added portionwise at room temperature; the reaction mixture was heated under reflux for 6 h. The resultant hydroquinone was filtered off and the filtrate was evaporated to dryness. The residue was subjected to a short column chromatography (alumina-chloroform) in order to remove any unreacted DDQ. The chloroform elution was collected and concentrated to give a residue. The residue was chromatographed on silica gel to afford **2a** (359 mg, 69%) as a chloroform eluent.

2a: Red needles (ethanol); mp 274—275 °C. Found: C, 76.87; H, 4.15; N, 4.56%. Calcd for $C_{21}H_{13}NO_3$: C, 77.05; H, 4.00; N. 4.28%.

A similar oxidation of **1b—f** gave the corresponding 4*H*-benzo[*hi*]pyrrolo[2,1,5-*cd*]indolizin-4-one derivatives **2b—2f**.

2b: Red needles (ethanol); mp 189—190 °C. Found: C, 71.42; H, 4.09; N, 3.43%. Calcd for $C_{23}H_{15}NO_5$: C, 71.68; H, 3.92; N, 3.64%.

2c: Red needles (ethanol); mp 225—226 °C. Found: C, 69.16; H, 4.17; N, 3.35%. Calcd for $C_{24}H_{17}NO_6$: C, 69.39; H, 4.13; N, 3.37%.

2d: Deep red needles (ethanol); mp 227—229 °C. Found: C, 59.44; H, 3.18; N, 3.24%. Calcd for $C_{23}H_{14}BrNO_5$: C, 59.44; H, 3.18; N, 3.24%.

2e: Red needles (ethanol); mp 256—258 °C. Found: C, 75.56; H, 4.21; N, 3.28%. Calcd for $C_{29}H_{19}NO_5$: C, 75.48; H, 4.15; N, 3.04%.

2f: Deep red needles (ethanol); mp 219—220 °C. Found: C, 74.64; H, 4.11; N, 3.44%. Calcd for $C_{27}H_{17}NO_5$: C, 74.47; H, 3.93; N, 3.22%.

These results and the spectral data for **2** are presented in Tables 3 and 4, respectively.

Oxidation of 3 with DDQ to 4 and 5. A mixture of **3** (265 mg, 1.03 mmol) and DDQ (350 mg, 1.54 mmol) in 10% aqueous dioxane (10 mL) was stirred at room temperature for 18 h. After similar procedures as mentioned above, **4** was obtained in 42% yield. Also, the oxidation of **3** with DDQ (4.0 mol equiv.) in 10% aqueous dioxane under reflux for 12

Table 3. Oxidation of **1** with DDQ in Refluxing Dioxane Leading to **2**

Run	Molar ratio DDQ/**1**	Time / h	**2** Yield/%
a	4	6	69
b	4	6	68
b-d_5	4	6	72
c	4	6	96
d	4	45	Trace
	6	54	34
e	4	24	47
f	6	42	55

Table 4. Spectral Data for 4*H*-Benzo[*hi*]pyrrolo[2,1,5-*cd*]indolizin-4-ones **2**

Compd	IR ν(CO)	^{1}H NMR($CDCl_3$) δ	M^+ *m/z*
2a	1692 1600	4.02 (3H, s, $-OCH_3$), 6.52 (1H, d, J=8 Hz, 5-H), 7.42 (1H, d, J=8 Hz, 6-H), 7.5—7.6 (3H, m, phenyl), 7.84 (1H, d, J=10 Hz, 7-H), 8.06 (1H, d, J=10 Hz, 8-H), 8.25 (1H, s, 2-H), 8.69 (1H, d, J=8 Hz, phenyl)	327
2b	1740 1716 1618	3.98, 4.02 (3H each, 2s, $-OCH_3$), 6.48 (1H, d, J=9.8 Hz, 5-H), 7.42 (1H, d, J=9.8 Hz, 6-H), 7.5—7.6 (3H, m, phenyl), 7.87 (1H, d, J=8.3 Hz, 7-H), 8.09 (1H, d, J=8.3 Hz, 8-H), 8.2—8.8 (2H, m, phenyl)	385
2c	1742 1711 1600	3.93 (3H, s, $-OCH_3$), 4.01 (6H, s, $-OCH_3$), 6.50 (1H, d, J=10 Hz, 5-H), 7.1 (2H, m, phenyl), 7.42 (1H, d, J=10 Hz, 6-H), 7.85 (1H, d, J=8 Hz, 8-H), 8.05 (1H, d, J=8 Hz, 8-H), 8.3 (2H, m, phenyl)	415
2d	1739 1721 1624	3.99, 4.01 (3H each, 2s, $-OCH_3$), 6.50 (1H, d, J=10 Hz, 5-H), 7.44 (1H, d, J=10 Hz, 6-H), 7.7 (2H, m, phenyl), 7.92 (1H, d, J= 8 Hz, 7-H), 8.14 (1H, d, J=8 Hz, 8-H), 8.2 (2H, m, phenyl)	465 463
2e	1728 1706 1603	4.02, 4.03 (3H each, 2s, $-OCH_3$), 6.51 (1H, d, J=10 Hz, 5-H), 7.42 (1H, d, J=10 Hz, 6-H), 7.3—7.8 (7H, m, aromatic), 7.89 (1H, d, J=8 Hz, 7-H), 8.10 (1H, d, J=8 Hz, 8-H), 8.4 (2H, m, phenyl)	461
2f	1718 1707 1592	3.59, 4.03 (3H each, 2s, $-OCH_3$), 6.53 (1H, d, J=10 Hz, 5-H), 7.46 (1H, d, J=10 Hz, 6-H), 7.6 (2H, m, naphthyl), 7.91 (1H, d, J=8 Hz, 7-H), 7.8—8.1 (3H, m, naphthyl), 8.12 (1H, d, J=8 Hz, 8-H), 8.3 (1H, dd, J=8, 2 Hz, naphthyl), 8.91(1H, br s, naphthyl)	438

h gave a mixture of **4** (16%) and **5** (33%).

4: Yellow needles (hexane-benzene); mp 99—100 °C; IR (KBr) cm^{-1}: 1650 (CO) and 1625 (C=C); ^{1}H NMR ($CDCl_3$) δ=2.99 (2H, t, 6-H, J=6 Hz), 3.38 (2H, t, 5-H, J=6 Hz), 7.17 (1H, d, 1-H, J=4 Hz), 7.2—7.6 (6H, m, 2- and 7-H and phenyl), and 8.1—8.2 (2H, m, phenyl); MS *m/z* (rel intensity): 271 (M^+, base peak), 270 (M^+ −H, 46), and 241 (26). Found: C, 84.04; H, 4.88; N, 5.37%. Calcd for $C_{19}H_{13}NO$: C, 84.11; H, 4.83; N, 5.16%.

5: Red needles (hexane-benzene); mp 121—122 °C; IR (KBr) cm^{-1}: 1606 (CO) and 1593 (C=C); ^{1}H NMR ($CDCl_3$) δ=6.23 (1H, d, 5-H, J=10 Hz), 6.79 (1H, d, 1-H, J=4 Hz), 7.06 (1H, d, 6-H, J=10 Hz), 7.2—7.8 (6H, m, 2-, 7-, and 8-H and phenyl), and 8.3—8.5 (2H, m, phenyl); MS *m/z* (rel intensity): 269 (M^+, 96), 268 (M^+ −H, base peak), and 239 (46). Found: C, 84.47; H, 4.40; N, 5.12%. Calcd for $C_{19}H_{10}NO$: C, 84.74; H, 4.12; N, 5.20%.

Preparation of 5 from 2b. Compound **2b** (570 mg, 1.48 mmol) was heated under reflux in 5% methanolic potassium hydroxide (30 mL) for 12 h and the methanol was removed to give a residue. The residue was made acidic with concd hydrochloric acid. The resultant diacid was filtered, dried, and subjected to the next decarboxylation without further purification. A solution of the diacid in quinoline (30 mL) was refluxed for 0.5 h in the presence of copper dust (100 mg). The copper dust was filtered off and the filtrate was evaporated to give a residue. The residue was dissolved in benzene (50 mL) and washed with 0.5 M hydrochloric acid (50 mL×3) in order to completely remove the quinoline. The organic layer was collected, dried and evaporated to dryness. The residue was subjected to a chromatography on alumina to afford **5** (74% from **2b**) as a chloroform eluent.

Similarly, the pentadeuteriophenyl derivative **5**-d_5 was obtained from **2b**-d_5 in 80% yield.

MO Calculations. The calculations were carried out by using the ACOS system 1000 computer in the Computation Center of Osaka University. For an optimization of the

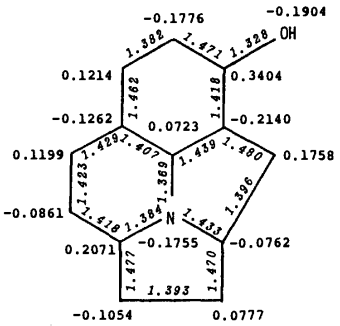

Fig. 6. Net atomic charge and atomic distance (Å) of **F** by MNDOA.

structure, the initial structure was taken as follows: for the geometries of the cyclazine moiety of **E**, the X-ray analytical data for 1,4-dibromopyrrolo[2,1,5-*cd*]indolizine[20] were used. Those of the enone part were estimated by using the molecular models fused by the above cyclazine system. The distance of the C=O bond was taken from that of acrylaldehyde (1.23 Å). A structure optimization was performed for the bond length and valence and dihedral angles of all the atoms of **E**, except for the hydrogen atoms. Among the results, the net atomic charge and bond length for **E** are demonstrated in Fig. 2. A structure optimization for the 3-phenyl derivative **5** was also performed. For the geometries of the benzopyrroloindolizinone moiety and of the phenyl one of **5**, the data for **E** obtained above and for biphenyl were taken, respectively. An optimization was performed for the C-C bond length and the dihedral angle between the mother nuclei and the phenyl one. The results showed that the dihedral angle was calculated to be 76.7°. This showed that the π-electronic system of the phenyl ring had little effect on the mother nuclei.

The structural optimization for **F**, the protonated species of **E**, was performed using the attained geometries for **E** as an

Table 5. The Full Assignments of ^{13}C NMR Spectra of **5** and **2b**

Assign	**5**/^{13}C		^{1}H	**2b**/^{13}C		
	δ	NON; J/Hz		δ	NON; J/Hz	Method
1	117.5	dd(177, 4)	6.90	118.0	s	b)
2	125.6	dd(174, 4)	a)	123.7	s	b)
2a	131.6	s		133.6	s	LPSEL
3	137.3			141.6	t(5)	NOE, SEL
3a	115.0			117.1	d(5)	LPSEL
4	180.6	d(10)		180.7	d(10)	
5	135.8	d(164)	6.34	136.1	d(164)	NOE, LPSEL
6	132.0	dd(164, 3)	7.15	132.6	dd(164, 4)	NOE, SEL
6a	118.2	dd(12, 8)		119.4	dd(12, 8)	LPSEL
7	124.1	d(163)	a)	125.8	d(164)	NOE, SEL
8	113.3	d(167)	a)	116.5	d(174)	NOE, SEL
8a	132.2	m		131.5	t(7)	LPSEL
8c	127.6			129.1	dd(9, 3)	LPSEL
1′	133.2	t(7)		131.7	t(10)	LPSEL
2′	128.7	dd(165, 7)	8.55	130.3	d(160)	NOE, SEL
3′	129.5	dt(161, 6)	a)	128.6	d(164)	SEL
4′	130.0	dt(162, 7)	a)	131.1	dt(161, 8)	SEL

a) Overlapped with each other. b) Assigned by the comparison with **2a**.

initial structure. The net atomic charge and bond length for **F** are presented in Fig. 6.

^{13}C NMR Spectra. On the basis of the ^{1}H NMR spectral data, assignments for the ^{13}C signals were made by using the nuclear Overhauser effect (NOE) and complete decoupling (COM), non-decoupling (NON), proton selective decoupling (SEL), and/or low-power selective proton decoupling techniques (LPSEL).[21]

It seemed to be difficult to directly assign the ^{13}C signals of **5**, since its ^{1}H signals were superimposed on each other; therefore, the relationships between the ^{1}H and ^{13}C signals were obscure. Thus, first the assignment for **2b** was attempted; the SEL technique for the ring protons accomplished the assignment for C-5, -6, -7, and -8, and the quartery C-3a, -6a, and -6b were confirmed by using LPSEL measurements. The assignments for C-1 and -2 were accomplished through comparisons with those of the 1-methoxycarbonyl derivative **2a**; also, the phenyl carbons (C-2′, -3′, and -4′) were assigned by the comparisons with those of the 3-(*p*-methoxyphenyl) derivative **2c**. On the basis of the above results for **2b**, the assignment for **5** was attained, except for the signals at δ=131.6, 132.2, and 133.2 due to C-2a, -8a, and -1′. The replacement of the phenyl group of **5** by pentadeuteriophenyl one, **5**-d_5, resulted in changes of the coupling patterns of the signal due to C-1′: the carbon signal at δ=133.2 (NON: t) for **5** was changed to a singlet (δ=132.9) for **5**-d_5, and, therefore, assigned to be C-1′. The LPSEL technique irradiating the 7-H (δ=7.57) of **5**-d_5 caused a simplification of the signal patterns at δ=132.3, and the signal at δ=132.2 of **5** was assignable to be C-8a. Consequently, the signal at δ=131.8 of **5** was deduced to be C-2a.

These assignments for **5** and **2b** are summarized in Table 5.

The authors wish to thank Professor Masashi Tashiro, Research Institute of Industrial Science, Kyushu University, for the elemental analyses. The author (M. N.) is grateful to the Ministry of Education, Science and Calture for financial support through a Grand-in-Aid for Scientific Research (No 59750691).

References

1) Studies on Nitrogen-bridged Heterocycles. VI. Part V in this series: M. Noguchi, N. Tanigawa, and S. Kajigaeshi, *Bull. Chem. Soc. Jpn.*, **58**, 3444 (1985).

2) For reviews: D. H. Reid, *Quart. Rev.*, **19**, 274 (1964); I. Murata, "Topics in Nonbenzenoid Aromatic Chemistry," ed by T. Nozoe, R. Breslow, K. Hafner, S. Ito, and I. Murata, Hirokawa, Tokyo (1973), Vol. 1, p. 159.

3) a) T. Nakadate, T. Morita, and K. Takase, *Chem. Lett.*, **1977**, 591; b) R. Neidlein and W. Kramer, *Helv. Chim. Acta*, **65**, 280 (1982); c) R. Neidlein, W. Kramer, and D. Scheutzow, *ibid.*, **65**, 1804 (1982).

4) I. Murata, T. Nakazawa, and T. Tatsuoka, *Tetrahedron Lett.*, **1971**, 1789; U. Kuffner and K. Schlogl, *Monatsh. Chem.*, **103**, 1320 (1972); R. Yahashi, H. Shimanouchi, and Y. Sasada, *Bull. Chem. Soc. Jpn.*, **46**, 1441 (1973); R. Neidlein and H. Zeiner, *Monatsh. Chem.*, **113**, 1151 (1982).

5) Y. Miki, N. Nishikubo, Y. Nomura, H. Kinoshita, S. Takemura, and M. Ikeda, *Heterocycles*, **22**, 2467 (1984).

6) M. Noguchi, N. Tanigawa, T. Yamamoto, and S. Kajigaeshi, *Chem. Lett.*, **1985**, 873.

7) T. Amemiya, M. Yasunami, and K. Takase, *Chem. Lett.*, **1977**, 587.

8) P. P. Fu and R. G. Harney, *Chem. Rev.*, **78**, 334 (1978), and references cited there.

9) Under similar conditions the DDQ oxidation of 3-(*p*-methoxyphenyl) derivative **1c** was carried out more easily than that of 3-phenyl one **1b**, and gave **2c** quantitatively. On the other hand, the DDQ oxidation of 3-(*p*-bromophenyl) derivative **1d** did not take place at the same conditions. More severer conditions were required in order to obtain **2d** (Table 3).

10) W. Thiel, *QCPE*, **11**, 353 (1978); Y. Beppu and I. Ninomiya, *ibid.*, **14**, 409 (1981); Y. Sasaki, T. Takagi, and R. Tokura, *Bull. Comput. Cent. Osaka Univ.*, **14**, 103 (1985).

11) Y. Kurita, S. Seto, T. Nozoe, and M. Kubo, *Bull. Chem. Soc. Jpn.*, **26**, 272 (1953).

12) Chemical shifts of the ring protons of **2**, **3**, and **5** were highly dependent on the concentrations of measuring samples, i.e., signals of the ring protons were observed at higher field as the concentration of sample was increased. Consequently, the considerations on chemical shifts were made using 0.10 M solution of the corresponding samples.

13) H. Prinzbach, V. Freudenberger, and U. Scheidegger, *Helv. Chim. Acta*, **50**, 1087 (1967).

14) These values were obtained after the addition of a few drops of CF_3CO_2D to the $CDCl_3$ solution.[5] Probably, the protonation onto the carbonyl oxygen atom at 9-position was incomplete at the point, and more downfield shift would be expected in CF_3CO_2D.

15) I. Murata, K. Yamamoto, T. Hirotsu, and M. Morioka, *Tetrahedron Lett.*, **1972**, 331.

16) The electronic spectrum in cyclohexane was somewhat different from those in these solvents. The absorption maxima were shifted wholly to shorter wavelength (ca. 10 nm), and fine structures were observed over the ranges of 480—570 nm.

17) No significant changes of its electronic spectra were observed at higher acid concentrations than $CHCl_3$-CF_3CO_2H (8/1). On the contrary, the downfield shifts of the ring protons on the ^1H NMR spectra were observed up to the acid concentration of $CDCl_3$-CF_3CO_2D (2/3).

18) Similar behaviors on the electronic spectra were found in 6*H*-benzo[*hi*]pyrrolo[2,1,5-*cd*]indolizin-6-one system, a regio-isomer of **E**. Those results would be published elsewhere.

19) M. Noguchi, N. Tanigawa, and S. Kajigaeshi, *J. Heterocycl. Chem.*, **22**, 1049 (1985).

20) A. W. Hanson, *Acta Crystallogr.*, **14**, 124 (1961).

21) H. Seto, T. Sasaki, H. Yonehara, and J. Uzawa, *Tetrahedron Lett.*, **1978**, 923.

 © 1988 The Chemical Society of Japan Bull. Chem. Soc. Jpn., 61, 431—434 (1988)

New Ferroelectric Liquid Crystal Materials: (+)-4-(2-Methylbutoxycarbonyl)-phenyl 4-(5-Alkyl-1,3-dioxan-2-yl)benzoate

Yuichiro HARAMOTO,* Katumasa KAWASHIMA, and Hiroyoshi KAMOGAWA
Department of Applied Chemistry, Yamanashi University, Takeda 4, Kofu 400
(Received May 30, 1987)

(+)-4-(2-Methylbutoxycarbonyl)phenyl 4-(5-alkyl-1,3-dioxan-2-yl)benzoate (**12**), (+)-4-(2-methylbutoxy)-phenyl 4-(5-alkyl-1,3-dioxan-2-yl)benzoate (**11**) and the corresponding 1,3-oxathiane (**13**, **14**) and 1,3-dithiane compounds (**15**, **16**) were synthesized. The mesomorphic behaviors of these compounds were measured. Compounds **12** exhibited the ferroelectric liquid-crystal behavior (R=*n*-$C_{11}H_{23}$: −4 SmC* 94 °C), while the corresponding 1,3-oxathiane (**13**, **14**) and 1,3-dithiane compounds (**15**, **16**) did not exhibit such behavior. Therefore, 1,3-dioxane compounds are more favorable for transition of SmA to SmC* than the 1,3-oxathiane or 1,3-dithiane analogs.

2,5-Disubstituted 1,3-dioxanes, 1,3-oxathianes, and 1,3-dithianes were synthesized recently as new types of nematic liquid crystal materials.[1-10] With increasing interests in liquid-crystal displays using ferroelectric liquid crystals, various ferroelectric liquid crystal compounds have been synthesized: the basic structure of optically active liquid-crystal compounds with a 1,3-dioxane, a 1,3-oxathiane, and a 1,3-dithiane ring have been synthesized.[11,12] In a previous letter,[12] we reported new ferroelectric liquid-crystal compounds with a 1,3-dioxane ring. This paper deals with the synthesis and the mesomorphic behavior of these compounds in detail.

Results and Discussion

(+)-4-(2-Methylbutoxy)phenyl 4-(5-alkyl-1,3-dioxan-2-yl)benzoate (**11**), (+)-4-(2-methylbutoxycarbonyl)phenyl 4-(5-alkyl-1,3-dioxan-2-yl)benzoate (**12**) and the corresponding oxathianes (**13**, **14**) and dithianes (**15**, **16**) were synthesized via the following route.

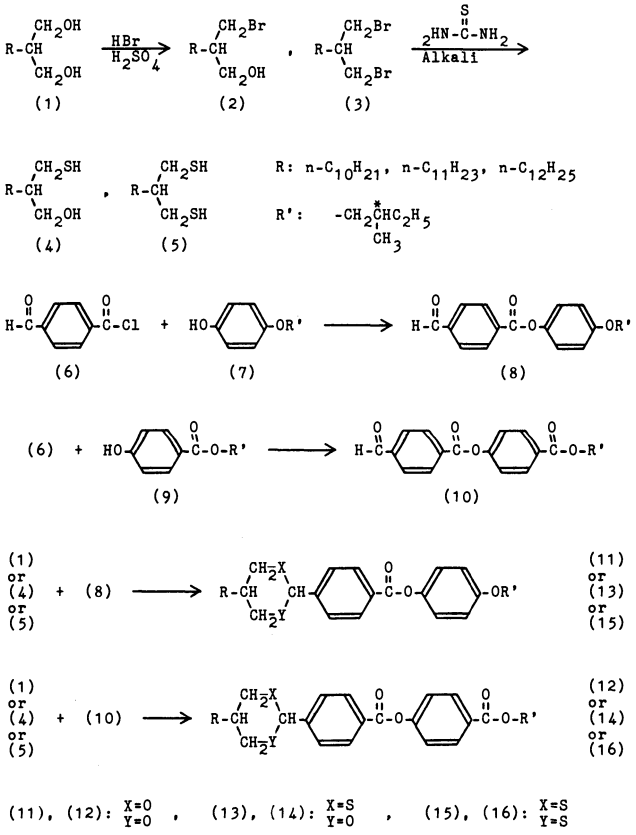

Fig. 1.

In step **1**→**2**, **3**, the reaction temperature of bromination was kept within the range 80 to 85 °C in order to obtain compounds **2** and **3** at nearly equal yields. In the conversion of **2**, **3** into **4**, **5** respectively, a mixture of compounds **2** and **3** was used. The mixture of compounds **4** and **5**, thus obtained, was separated by column chromatography. Compound **4** was eluted in an ether fraction and **5** in a hexane fraction. Compound **7** was synthesized by the monoetherification of hydroquinone.

Compound **9** was obtained by the esterification of *p*-hydroxybenzoic acid with (+)-2-methyl-1-butanol in the presence of an acid catalyst using a Dean-Stark trap. A two-day reaction is necessary to obtain a sufficient yield.

In steps **6**,**7**→**8** and **6**,**9**→**10**, 1,8-diazabicyclo[5.4.0]-undec-7-ene (DBU) was used as a base. Both compounds **8** and **10** were extracted with hexane.

Compounds **11**—**15**, and **16** were synthesized by ring-formation reactions of compounds **1**, **4**, and **5** with aldehydes (**8**, **10**), respectively. The products, **11**—**16**, were purified by column chromatography and recrystallized from hexane. The trans isomers of **11**, **13**, **15**, **16** were isolated by means of TLC (hexane: ether=5:2) of the cis and trans mixtures. In the ^{1}H NMR data of the 1,3-dioxane, 1,3-oxathiane, and 1,3-dithiane compounds, C-2 proton signals of the 1,3-dioxane, 1,3-oxathiane, and 1,3-dithiane rings for the trans and cis isomers are separated by about 0.05 ppm. For example, the C-2 proton of the trans isomers absorbs at δ=5.50 (compound **12-1**), 5.75 (**14-1**), and 5.20 (**16-1**) but that of the corresponding cis isomer absorbs at δ=5.55 (**12-1**), 5.80 (**14-1**), and 5.15 (**16-1**), respectively.

Table 1. Mesomorphic Ranges for Compounds **11**, **12**, **13**, **14**, **15**, and **16**

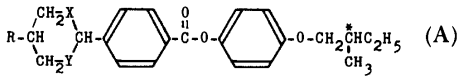

(A)

	R	X Y	Mesomorphic range/°C[a]
11-1	$C_{10}H_{21}$	O O	C $\overset{66}{\underset{22}{\rightleftarrows}}$ SmB $\overset{100}{\underset{100}{\rightleftarrows}}$ SmA $\overset{136}{\underset{136}{\rightleftarrows}}$ I
11-2	$C_{11}H_{23}$	O O	C $\overset{113}{\underset{94}{\rightleftarrows}}$ SmA $\overset{137}{\underset{137}{\rightleftarrows}}$ I
11-3	$C_{12}H_{25}$	O O	C $\overset{70}{\underset{22}{\rightleftarrows}}$ SmB $\overset{97}{\underset{97}{\rightleftarrows}}$ SmA $\overset{137}{\underset{137}{\rightleftarrows}}$ I
13-1	$C_{10}H_{21}$	S O	C $\overset{66}{\underset{-50}{\rightleftarrows}}$ SmB $\overset{111}{\underset{111}{\rightleftarrows}}$ SmA $\overset{134}{\underset{134}{\rightleftarrows}}$ I
13-2	$C_{11}H_{23}$	S O	C $\overset{64}{\underset{-50}{\rightleftarrows}}$ SmB $\overset{111}{\underset{111}{\rightleftarrows}}$ SmA $\overset{132}{\underset{132}{\rightleftarrows}}$ I
13-3	$C_{12}H_{25}$	S O	C $\overset{59}{\underset{-50}{\rightleftarrows}}$ SmB $\overset{117}{\underset{117}{\rightleftarrows}}$ SmA $\overset{132}{\underset{132}{\rightleftarrows}}$ I
15-1	$C_{10}H_{21}$	S S	C $\overset{104}{\underset{54}{\rightleftarrows}}$ SmB $\overset{136}{\underset{136}{\rightleftarrows}}$ SmA $\overset{153}{\underset{153}{\rightleftarrows}}$ I
15-2	$C_{11}H_{23}$	S S	C $\overset{109}{\underset{63}{\rightleftarrows}}$ SmB $\overset{140}{\underset{140}{\rightleftarrows}}$ SmA $\overset{153}{\underset{153}{\rightleftarrows}}$ I
15-3	$C_{12}H_{25}$	S S	C $\overset{87}{\underset{57}{\rightleftarrows}}$ SmA $\overset{139}{\underset{139}{\rightleftarrows}}$ I

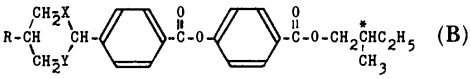

(B)

	R	X Y	Mesomorphic range/°C[a]
12-1	$C_{10}H_{21}$	O O	C $\overset{59}{\underset{14}{\rightleftarrows}}$ SmC* $\overset{93}{\underset{93}{\rightleftarrows}}$ SmA $\overset{137}{\underset{137}{\rightleftarrows}}$ I
12-2	$C_{11}H_{23}$	O O	C $\overset{62}{\underset{-4}{\rightleftarrows}}$ SmC* $\overset{94}{\underset{94}{\rightleftarrows}}$ SmA $\overset{136}{\underset{136}{\rightleftarrows}}$ I
12-3	$C_{12}H_{25}$	O O	C $\overset{66}{\underset{30}{\rightleftarrows}}$ SmC* $\overset{95}{\underset{95}{\rightleftarrows}}$ SmA $\overset{135}{\underset{135}{\rightleftarrows}}$ I
14-1	$C_{10}H_{21}$	S O	C $\overset{89}{\underset{-50}{\rightleftarrows}}$ SmA $\overset{134}{\underset{134}{\rightleftarrows}}$ I
14-2	$C_{11}H_{23}$	S O	C $\overset{70}{\underset{-50}{\rightleftarrows}}$ SmB $\overset{98}{\underset{98}{\rightleftarrows}}$ SmA $\overset{136}{\underset{136}{\rightleftarrows}}$ I
14-3	$C_{12}H_{25}$	S O	C $\overset{68}{\underset{20}{\rightleftarrows}}$ SmA $\overset{133}{\underset{133}{\rightleftarrows}}$ I
16-1	$C_{10}H_{21}$	S S	C $\overset{113}{\underset{94}{\rightleftarrows}}$ SmA $\overset{150}{\underset{150}{\rightleftarrows}}$ I
16-2	$C_{11}H_{23}$	S S	C $\overset{117}{\underset{99}{\rightleftarrows}}$ SmA $\overset{147}{\underset{147}{\rightleftarrows}}$ I
16-3	$C_{12}H_{25}$	S S	C $\overset{107}{\underset{90}{\rightleftarrows}}$ SmA $\overset{141}{\underset{141}{\rightleftarrows}}$ I

a) C: crystal; S: smectic; I: isotropic.

Measurements of the mesomorphic ranges and assignments of the mesophases were carried out by means of a micro melting point apparatus equipped with polarizers and a differential scanning calorimeter (DSC).

To determine the type of smectic phase, the observed smectic phases were compared with color photographs found in the literature.[13,14] Mesomorphic ranges of the synthesized compounds are given in Table 1. SmA, SmB, and SmC* mean smectic A, smectic B, and chiral smectic C phase, respectively.

Though SmC* of compounds **12** can be driven in homogenious cells (d=2 μm, applied voltage=20 V), other smectic phases can not. Therefore, compounds **12** are ferroelectric liquid-crystal compounds and others are not.

The 1,3-oxathiane and 1,3-dithiane compounds which correspond to compounds **12** did not exhibit a SmC* liquid-crystal phase. This must imply that 1,3-dioxane compounds are more favorable for the transition of SmA to SmC* than the corresponding 1,3-oxathiane or 1,3-dithiane compounds.

Though compounds **12** exhibit an SmC* phase, compounds **11** do not. The difference in these two compounds lies in the number of the carbonyl group. Therefore, a carbonyl group having a dipole moment in a vertical direction to the molecular axis must contribute to the transition from SmA to SmC*.

The transition temperatures of SmA to isotropic ($T_{S\text{-}I}$) for 1,3-oxathiane compounds are lower than those for the corresponding 1,3-dioxanes and 1,3-dithianes. In a smectic liquid crystal, the temperature of the isotropic to smectic transition ($T_{S\text{-}I}$) is affected by two factors: the molecular width and interactions of side substituens.[15] The 1,3-oxathiane compounds are bent at the 1,3-oxathiane ring, caused by a difference in the atomic size between sulfur and oxygen. Therefore, the width of 1,3-oxathiane compounds is wider than that of the corresponding 1,3-dioxane or 1,3-dithiane compounds. This must make $T_{S\text{-}I}$ for 1,3-oxathiane compounds lower than those for the corresponding 1,3-dioxane or 1,3-dithiane compounds.

The transition temperatures of SmA to isotropic ($T_{S\text{-}I}$) for compounds A are nearly equal to those for the corresponding compounds B. This difference in the terminal group hardly affects the thermal stability of smectic phase.

Textures of SmA and SmB are focal-conic fan texture.

At the transition temperatures of the SmA to SmB phase, pronounced transition bars appeared on the surface of the focal-conic fan texture. Textures of

SmC* are broken focal-conic fan texture.

Several properties as a ferroelectric liquid crystal compound were measured for compound **12-3**; the strength of the spontanious polarization=1.3 $nC\,cm^{-2}$ (85 °C), helical pich length=14.3 μm (85 °C), the response of the optical transmission=61 μs (85 °C, 20 V), tilt angle=13.5° (85 °C).

Though the strength of the spontanious polarization of compound **12-3** is smaller than that of (S)-2-methylbutyl *p*-(*p*-decyloxybenzylideneamino)cinnamate (DOBAMBC),[16] the helical pitch length of this compounds is longer than that of DOBAMBC.

The most remerkable feature of these new ferroelectric liquid crystal compounds is that, with the appearance of the supercooling state, they exhibit the ferroelectric liquid crystal behavior over a very wide range, including ordinary room temperature (**12-1**: 14 SmC* 93, **12-2**: −4 SmC* 94, **12-3**: 30 SmC* 95).

$\Delta H_{C\text{-}S}$ of compounds **11-3**, **12-3**, **13-3**, **14-3**, **15-3**, and **16-3** are 25.0, 34.1, 29.5, 19.5, 18.7, and 16.8 $kJ\,mol^{-1}$, respectively.

These values are somewhat smaller than those of other common liquid crystal materials.[17]

The $\Delta H_{S\text{-}I}$ of these compounds are 6.0, 5.8, 6.7, 6.5, 3.0, and 5.2 $kJ\,mol^{-1}$, respectively. Nearly the same values have been obtained for other common smectic liquid crystal compounds.[18]

Experimental

IR, ^{1}H NMR, and mass spectra were obtained with a Hitachi 215 spectrophotometer, a JNM-PMX 60 spectrometer, and a Hitachi M-80B spectrometer, respectively. Elemental analyses were carried out with a Perkin-Elmer 250 instrument. Transition temperatures and mesomorphic phases were determined by means of both a Mitamura Riken micro melting-point apparatus equipped with polarizers and a Rigaku Denki DSC CN8059L1, CN8208A2. The rate of cooling was fixed to 1 $°C\,min^{-1}$.

Mixtures of 2-alkyl-3-bromo-1-propanol (**2**) and 2-alkyl-1,3-dibromopropane (**3**) were prepared previously.[11]

2-Alkyl-3-mercapto-1-propanol (4) and 2-Alkyl-1,3-propanedithiol (5). The same procedure as that in the previous paper[11] was used. Compounds **4** were colorless transparent liquid and **5** were yellow transparent liquid.

IR ($CHCl_3$): Compounds **4**; 3600 (OH), 2800—3000 (alkyl) cm^{-1}. Compounds **5**; 2800—3000 (alkyl) cm^{-1}.

^{1}H NMR ($CDCl_3$): Compounds **4**; δ=0.6—2.0 (m, R-CH, SH), 2.5—2.8 (m, 2H, CH_2S), 3.4—4.0 (m, 3H, CH_2OH), Compounds **5**: δ=0.6—2.0 (m, R-CH, SH), 2.5—2.9 (m, 4H, CH_2S).

(+)-4-(2-Methylbutoxy)phenol(7). The Williamson synthesis was applied to hydroquinone and (+)-2-methylbutyl bromide. As the diether was produced as a side product, the crude product was purified by column chromatography. Compound **7** was eluted with benzene and the diether with hexane. Transparent liquid was obtained in a 30—40% yields.

IR ($CHCl_3$) 3600 (OH), 2800—3000 (alkyl), 1600 (Ar), 1260 (ether) cm^{-1}.

^{1}H NMR ($CDCl_3$) δ=0.6—2.3 (m, 9H, $OCH_2C_4\underline{H}_9$), 3.8 (d, 2H, OCH_2), 5.9 (s, 1H, OH), 6.8 (s, 4H, ArH).

(+)-2-Methylbutyl *p*-Hydroxybenzoate (9). A solution of *p*-hydroxybenzoic acid (0.1 mol) and 2-methylbutanol (0.1 mol) and *p*-toluenesulfonic acid (0.3 g) in anhyd. toluene (100 ml) was refluxed for 48 h with a Dean-Stark trap fitted. Then toluene was removed on a rotary evaporator. The residue was dissolved in diethyl ether (300 ml), washed with 5% aq. $NaHCO_3$ (200 ml), dried over anhyd. Na_2SO_4, and evaporated in vacuo.

Transparent liquid was obtained in a 85—90% yields.

IR ($CHCl_3$) 3600 (OH), 2800—3000 (alkyl), 1715 (C=O), 1600 (Ar) cm^{-1}.

^{1}H NMR ($CDCl_3$) δ=0.7—2.2 (m, 9H, $OCH_2C_4\underline{H}_9$), 4.2 (d, 2H, OCH_2), 7.5 (q, 4H, ArH), 8.5 (s, 1H, OH).

(+)-4-(2-Methylbutoxy)phenyl 4-Formylbenzoate (8). To a solution of compound **7** (0.03 mol), and 1,8-diazabicyclo-[5.4.0]undec-7-ene (0.03 mol) in anhyd. *N*,*N*-dimethylformamide (30 ml) was added compound **6** (0.03 mol) in a nitrogen atmosphere, followed by stirring at 40 °C for 18 h. The solution was poured into ice water and extracted twice with ether (each 200 ml). The extract was washed with cold 2% aq. HCl, dried over anhyd. Na_2SO_4, and evaporated in vacuo at 40 °C. The residue was extracted with hexane, and concentrated under reduced pressure. Light yellow liquid was obtained in a 50—55% yields.

IR ($CHCl_3$) 2800—3000 (alkyl), 1740, 1680 (C=O), 1600 (Ar), 1260 (ether) cm^{-1}.

^{1}H NMR ($CDCl_3$) δ=0.7—2.2 (m, 9H, $OCH_2C_4\underline{H}_9$), 3.75 (d, 2H, OCH_2), 6.7—8.5 (m, 8H, ArH), 10.05 (s, 1H, CHO).

(+)-4-(2-Methylbutoxycarbonyl)phenyl 4-Formylbenzoate (10). The same procedure as that for compound **8** was used for preparation of compounds **6** and **9**. Light yellow liquid was obtained in 50—60% yields.

IR ($CHCl_3$) 2800—3000 (alkyl), 1680—1740 (C=O), 1600 (Ar) cm^{-1}.

^{1}H NMR ($CDCl_3$) δ=0.6—2.2 (m, 9H, $OCH_2C_4\underline{H}_9$), 4.2 (d, 2H, OCH_2), 7.2—8.5 (m, 8H, ArH), 10.2 (s, 1H, CHO).

(+)-4-(2-Methylbutoxy)phenyl 4-(5-Alkyl-1,3-dioxan-2-yl)-benzoate (11). To a solution of compound **1** (0.004 mol) and compound **8** (0.004 mol) in anhyd. $CHCl_3$ (200 ml) cooled in an ice bath were added $BF_3\cdot(C_2H_5)_2O$ (0.5 g) and Molecular Sieves (3A, 1/15; 3 g). The mixture was stirred at 0—5 °C for 8 h and then at 20—25 °C for 16 h. The solution was washed with 10% aq. $NaHCO_3$ (400 ml), dried over anhyd. Na_2SO_4, and concentrated under reduced pressure at 40 °C. The crude product was purified by column chromatography and recrystallizations from hexane, then separetive TLC was used to remove cis isomer.

IR ($CHCl_3$) 2800—3000 (alkyl), 1730 (C=O), 1600 (Ar), 1260 (ether) cm^{-1}.

^{1}H NMR ($CDCl_3$) δ=0.7—2.3 (m, R-CH, $OCH_2\underline{R}''$), 3.3—4.5 (m, 6H, OCH_2), 5.50 (s, 1H, $\underset{O}{\underset{O}{CH}}$), 6.7—8.4 (m, 8H, ArH).

(+)-4-(2-Methylbutoxycarbonyl)phenyl 4-(5-Alkyl-1,3-dioxan-2-yl)benzoate (12). To a solution of compound **1** (0.004 mol) and compound **10** (0.004 mol) in anhyd. $CHCl_3$ (200 ml) cooled in an ice bath were added $BF_3\cdot(C_2H_5)_2O$ (0.5 g) and Molecular Sieves (3A, 1/15; 3 g). The mixture was stirred at 0—5 °C for 8h and then at 20—25 °C for 16h. The solution was washed with 10% aq. $NaHCO_3$ (400 ml), dried over anhyd. Na_2SO_4, and concentrated under reduced pressure at 40 °C. The crude product was purified by column chromatography and recrystallizations from hexane.

IR ($CHCl_3$) 2800—3000 (alkyl), 1700—1740 (C=O), 1600 (Ar) cm^{-1}.

^1H NMR ($CDCl_3$) δ=0.7—2.2 (m, R-CH, OCH_2R''), 3.3—4.5 (m, 6H, OCH_2), 5.50 (s, 1H, $\overset{O}{\underset{O}{}}CH$), 7.2—8.5 (m, 8H, ArH).

(+)-4-(2-Methylbutoxy)phenyl 4-(5-Alkyl-1,3-oxathian-2-yl)benzoate (13). Compounds **13** were synthesized according to the same procedure as that for compounds **11**.

IR ($CHCl_3$) 2800—3000 (alkyl), 1730 (C=O), 1600 (Ar), 1270 (ether) cm^{-1}.

^1H NMR ($CDCl_3$) δ=0.6—2.2 (m, R-CH, $OCH_2\underline{R}''$), 2.85 (d, 2H, CH_2S), 3.2—4.5 (m, 4H, OCH_2), 5.75 (s, 1H, $\overset{S}{\underset{O}{}}CH$), 6.75—8.5 (m, 8H, ArH).

(+)-4-(2-Methylbutoxycarbonyl)phenyl 4-(5-Alkyl-1,3-oxathian-2-yl)benzoate (14). Compounds **14** were synthesized according to the same procedure as that for compounds **12**.

IR ($CHCl_3$) 2800—3000 (alkyl), 1700—1740 (C=OO, 1600 (Ar) cm^{-1}.

^1H NMR ($CDCl_3$) δ=0.6—2.2 (m, R-CH, $OCH_2\underline{R}''$), 2.85 (d, 2H, CH_2S), 3.2—4.5 (m, 4H, OCH_2), 5.75 (s, 1H, $\overset{S}{\underset{O}{}}CH$), 7.2—8.5 (m, 8H, ArH).

(+)-4-(2-Methylbutoxy)phenyl 4-(5-Alkyl-1,3-dithian-2-yl)benzoate (15). Compounds **15** were synthesized according to the same procedure as that for compounds **11**.

IR ($CHCl_3$) 2800—3000 (alkyl), 1735 (C=O), 1600 (Ar), 1270 (ether) cm^{-1}.

^1H NMR ($CDCl_3$) δ=0.6—2.2 (m, R-CH, $OCH_2\underline{R}''$), 2.6—2.95 (m, 4H, CH_2S), 3.8 (d, 2H, OCH_2), 5.20 (s, 1H, $\overset{S}{\underset{S}{}}CH$), 6.75—8.5 (m, 8H, ArH).

(+)-4-(2-Methylbutoxycarbonyl)phenyl 4-(5-Alkyl-1,3-dithian-2-yl)benzoate (16). Compounds **16** were synthesized according to the same procedure as that for compounds **11**.

IR ($CHCl_3$) 2800—3000 (alkyl), 1700—17400 (C=O), 1600 (Ar).

^1H NMR ($CDCl_3$) δ=0.6—2.2 (m, R-CH, OCH_2R''), 2.7—3.0 (m, 4H, CH_2S), 4.2 (d, 2H, OCH_2), 5.20 (s, ^1H, $\overset{S}{\underset{S}{}}CH$), 7.2—8.5 (m, 8H, ArH).

11-1: Yield, 25%. Found: C, 75.57; H, 9.04%; M^+, 510. Calcd for $C_{32}H_{46}O_5$: C, 75.26; H, 9.08%; M, 510.

11-2: Yield, 33%. Found: C, 75.53; H, 9.09%; M^+, 524. Calcd for $C_{33}H_{48}O_5$: C, 75.53; H, 9.22%; M, 524.

11-3: Yield, 28%. Fond: C, 76.01; H, 9.33%; M^+, 538. Calcd for $C_{34}H_{50}O_5$: C, 75.80; H, 9.36%, M, 538.

12-1: Yield, 37%. Found: C, 73.96; H, 8.56%; M^+, 538. Calcd for $C_{33}H_{46}O_6$: C, 73.57; H, 8.61%; M, 538.

12-2: Yield, 36%. Found: C, 73.73; H, 8.76%; M^+ , 552. Calcd for $C_{34}H_{48}O_6$: C, 73.88; H, 8.75%; M, 552.

12-3: Yield, 31%. Found: C, 74.68; H, 8.64%; M^+ , 566. Calcd for $C_{35}H_{50}O_6$: C, 74.17; H, 8.89%; M, 566.

13-1: Yield, 24%. Found: C, 72.88; H, 8.80%; M^+, 526. Calcd for $C_{32}H_{46}O_4S_1$: C, 72.96; H, 8.80%; M, 526.

12-2: Yield, 27%. Fond: C, 73.33; H, 9.00%; M^+, 540. Calcd for $C_{33}H_{48}O_4S_1$: C, 73.29; H, 8.95%; M, 540.

13-3: Yield, 23%. Found: C, 73.86; H, 9.05%; M^+, 554. Calcd for $C_{34}H_{50}O_4S_1$: C, 73.60; H, 9.08%; M, 554.

14-1: Yield, 32%. Found: C, 71.34; H, 8.37%; M^+, 554. Calcd for $C_{33}H_{46}O_5S_1$: C, 71.44; H, 8.36%; M, 554.

14-2: Yield, 39%. Found: C, 71.41; H, 8.51%; M^+, 568. Calcd for $C_{34}H_{48}O_5S_1$: C, 71.79; H, 8.51%; M, 568.

14-3: Yield, 34%. Found: C, 72.16; H, 8.64%; M^+, 582. Calcd for $C_{35}H_{50}O_5S_1$: C, 72.12; H, 8.65%; M, 582.

15-1: Yield, 14%. Found: C, 70.62; H, 8.53%; M^+, 542. Calcd for $C_{32}H_{46}O_3S_2$: C, 70.80; H, 8.54%; M, 542.

15-2: Yield, 18%. Found: C, 71.35; H, 8.66%; M^+, 556. Calcd for $C_{33}H_{48}O_3S_2$: C, 71.18; H, 8.69%; M, 556.

15-3: Yield, 22%. Found: C, 71.43; H, 8.79%; M^+, 570. Calcd for $C_{34}H_{50}O_3S_2$: C, 71.53; H, 8.79%; M, 570.

16-1: Yield, 22%. Found: C, 69.57; H, 8.10%; M^+, 570. Calcd for $C_{33}H_{46}O_4S_2$: C, 69.43; H, 8.12%; M, 570.

16-2: Yield, 26%. Found: C, 69.83; H, 8.11%; M^+, 584. Calcd for $C_{34}H_{48}O_4S_2$: C, 69.82; H, 8.27%; M, 584.

16-3: Yield, 25%. Found: C, 70.02; H, 8.44%; M^+, 598. Calcd for $C_{35}H_{50}O_4S_2$: C, 70.19; H, 8.42%; M, 598.

References

1) Y. Haramoto and H. Kamogawa, *J. Chem. Soc., Chem. Commun.*, **1983**, 75.

2) Y. Haramoto, A. Nobe, and H. Kamogawa, *Bull. Chem. Soc. Jpn.*, **57**, 1966 (1984).

3) Y. Haramoto, K. Akazawa, and H. Kamogawa, *Bull. Chem. Soc. Jpn.*, **57**, 3173 (1984).

4) Y. Haramoto and H. Kamogawa, *Bull. Chem. Soc. Jpn.*, **58**, 477 (1985).

5) Y. Haramoto and H. Kamogawa, *Chem. Lett.*, **1985**, 79.

6) Y. Haramoto and H. Kamogawa, *Bull. Chem. Soc. Jpn.*, **58**, 1821 (1985).

7) Y. Haramoto and H. Kamogawa, *Mol. Cryst. Liq. Cryst.*, **131**, 101 (1985).

8) Y. Haramoto and H. Kamogawa, *Mol. Cryst. Liq. Cryst.*, **131**, 201 (1985).

9) Y. Haramoto, M. Sano, and H. Kamogawa, *Bull. Chem. Soc. Jpn.*, **59**, 1337 (1986).

10) D. Demus and H. Zaschke, (to V.E.W. Kombinat Mikroelectronic), Japan Pat. Appl. No 54-160916, Dec. (1979).

11) Y. Haramoto, Y. Tomita, and H. Kamogawa, *Bull. Chem. Soc. Jpn.*, **59**, 3877 (1986).

12) Y. Haramoto and H. Kamogawa, *Chem. Lett.*, **1987**, 755.

13) D. Demus and L. Richter, "Textures of Liquid Crystals," Verlag Chemie, Weinheim, New York (1978).

14) G. W. Gray and J. W. Goodby, "Smectic Liquid Crystals-Textures and Structures," Heyden & Son Inc., Philadelphia (1984).

15) G. W. Gray and B. M. Worrall, *J. Chem. Soc.*, **1959**, 1545.

16) R. B. Meyer, L. Liebert, L. Strzelecki, and P. Keller, *J. de Phys.*, **36**, 69 (1975).

17) G. W. Gray and P. A. Winsor, "Liquid Crystals & Plastic Crystals," Wiley, New York (1978), Vol. 2, p. 254.

18) G. W. Gray and J. W. Goodby, "Smectic Liquid Crystals-Textures and Structures," Heyden & Son Inc., Philadelphia (1984), p. 21.

 © 1988 The Chemical Society of Japan Bull. Chem. Soc. Jpn., 61, 435—439 (1988)

Mechanism of the Carboxylation of Cyclohexanone with Carbon Dioxide Catalyzed by 1,8-Diazabicyclo[5.4.0]undec-7-ene

Hisakazu MORI
Kyoritsu College of Pharmacy, Shibakoen, Minato-ku, Tokyo 105
(Received June 13, 1987)

The dependence of the rate of carboxylation upon the concentration of the reactant was investigated in dimethyl sulfoxide. The reaction rate depended upon the concentration of cyclohexanone and 1,8-diazabicyclo[5.4.0]undec-7-ene(DBU) in the first order, respectively. The reaction also followed first-order kinetics regarding the CO_2 pressure in the range 50—400 Torr. From these reaction characteristics, it is suggested that carboxylation proceeds via a reaction between CO_2 dissolved in dimethyl sulfoxide and the anion of cyclohexanone, rather than between the CO_2 adduct with DBU and cyclohexanone. The results of carboxylation by the CO_2 adduct with DBU and by CO_2 dissolved in dimethyl sulfoxide also support the above conclusion. The formation of the cyclohexanone anion by a reaction of cyclohexanone with DBU was verified by the UV spectrum of a solution of concentrated DBU and cyclohexanone.

A number of carbon dioxide fixation reactions catalyzed by a base is known in organic chemistry. In these reactions, compounds containing active methylene are transformed to carboxylic acids. The bases used as the

$$RH + CO_2 + B^- \rightarrow RCO_2^- + BH$$

catalyst are classified into two groups. One of them contains metal oxides such as sodium[1] or potassium[2,3] phenoxide or magnesium methoxide.[4] Another group includes nitrogen bases. Strong bases such as 1,8-diazabicyclo[5.4.0]undec-7-ene(DBU)[5] or tetramethylguanidine[6] are used in the absence of metal ions, and weak bases such as triethylamine[7] and 2-imidazolidinone[8] are used in the presence of metal ions.

We have investigated carboxylation using potassium phenoxide (PhOK).[2,3] With regard to the mechanism of this reaction, it was suggested[3] that the CO_2 complex with PhOK served as the CO_2 source of the carboxylate. We are now interested in the catalysis of nitrogen bases. Among nitrogen bases, DBU has been extensively studied by Haruki et al.[9] and was established as an effective carboxylating agent in synthetic chemistry. In a preliminary experiment, we found that the carboxylation of cyclohexanone using this base in dimethyl sulfoxide (DMSO) gives 2-oxocyclohexanecarboxylic acid in a homogeneous reaction system. We therefore selected this reaction system as a typical carboxylation by a nitrogen base, and studied it from a mechanistic view point. Iwatani et al.[10] studied this system under a high pressure of CO_2. In the present paper, the kinetics of carboxylation with CO_2 under a pressure lower than atmospheric are reported, and a reaction mechanism under this condition is proposed.

Experimental

Material and Glassware. DBU was dried with NaOH for several days at room temperature and distilled under nitrogen at a reduced pressure prior to use. Cyclohexanone was distilled under atmospheric pressure. DMSO was refluxed with CaH_2 for about 3 h, and distilled under a reduced nitrogen pressure. Well-dried glassware was used for the uptake of CO_2 by DBU and for carboxylation.

The Uptake of CO_2 by DBU. The uptake of CO_2 by DBU was investigated with a 0.2-M (1 M=1 mol dm^{-3}) DMSO solution at 20 °C in the vacuum system described in a previous paper.[3] The amount of CO_2 taken up by DBU was calculated by subtracting the amount dissolved in DMSO from the total amount taken up by the DMSO solution of DBU.

Carboxylation of Cyclohexanone with DBU and CO_2. CO_2 at atmospheric pressure was passed through a DMSO solution of DBU for 1 h at 20 °C. Then, cyclohexanone was added to this solution. A portion of the mixture was withdrawn at predetermined intervals, acidified with diluted HCl, and extracted with ether. The ethereal layer was dried with anhydrous sodium sulfate and treated with diazomethane. The methyl ester of the carboxylic acid was determined by means of gas chromatography. In a study of the dependence of the reaction rate upon the concentration of DBU, varying amounts of DBU in the ranges of 5—40 mmol and 10 mmol of cyclohexanone were used with 100 cm^3 of DMSO. Similarly, to study the dependence upon the concentration of cyclohexanone, 10 mmol of DBU and 5—40 mmol of cyclohexanone were used. In a study regarding the dependence upon the CO_2 pressure, mixtures of N_2 and CO_2 in varying ratios were used. The amounts of DBU and cyclohexanone used in this experiment were 20 and 10 mmol, respectively, with 100 cm^3 of DMSO.

Spectral Measurement. Infrared (IR) spectra were measured with a Hitachi EPI-G3 spectrophotometer, and electronic spectra, with a Hitachi 100-50 spectrophotometer.

Results and Discussion

Regarding carboxylation with PhOK, we suggested[3] that CO_2 complexed with PhOK plays the role of a CO_2 source. Accordingly, we first investigated the reaction between DBU and CO_2 in DMSO. After CO_2 was passed through a DMSO solution of DBU, a new absorption was observed at 1642 cm^{-1} in the IR spectrum. This fact indicates that CO_2 forms an adduct with DBU. In Fig. 1 is shown the uptake of CO_2 by

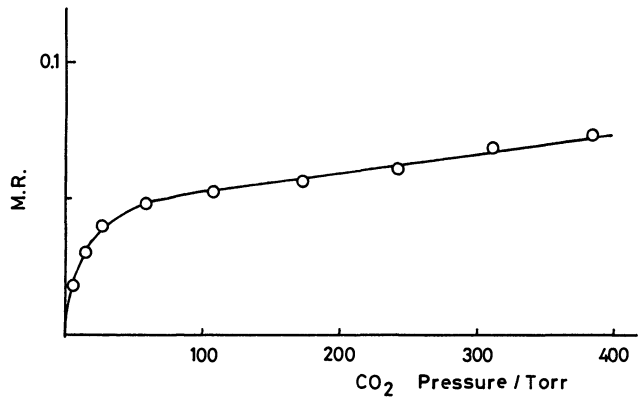

Fig. 1. The uptake of CO_2 by DBU at 20°C under various CO_2 pressure (0.2 M DMSO solution).

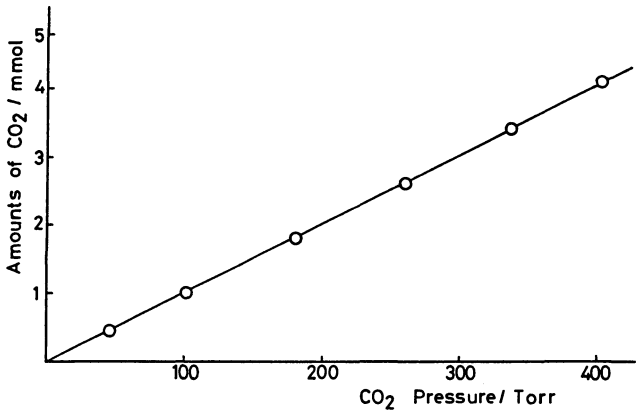

Fig. 2. The solubility of CO_2 in 50 cm^3 of DMSO at various CO_2 pressure at 20°C.

DBU in DMSO under various CO_2 pressures. The amount of CO_2 taken up by DBU was obtained by subtracting the amount of CO_2 dissolved in DMSO (Fig. 2, slope=2.05×10^{-4} mmol $Torr^{-1}$ cm^{-3}, 1 Torr= 133.322 Pa) from that dissolved in the DMSO solution of DBU. The ordinate indicates the M.R.: that is, the molar ratio of CO_2 adduct to the total amount of DBU. The value of M.R. was less than 0.1, even at a CO_2 pressure of about 400 Torr. On the contrary, the uptake by PhOK was extensive and the M.R. value amounted to more than 0.5 at 10 Torr.[3]

In Fig. 3, the time courses of the carboxylation with varying amounts of DBU are shown. The yields of carboxylate were calculated on the basis of the amount of cyclohexanone initially added (10 mmol). The yield of carboxylate increased almost linearly with the reaction time. The initial rates of carboxylate formation were calculated from the results. A plot of the initial rates of carboxylate formation against the initial concentration of DBU gave a straight line with a slope of 1.71 ± 0.07 (% min^{-1} M^{-1}). Thus, it was shown that the rate of carboxylation depended upon the concentration of DBU in the first order.

The dependence of the reaction rate upon the concentration of cyclohexanone was also studied. In this

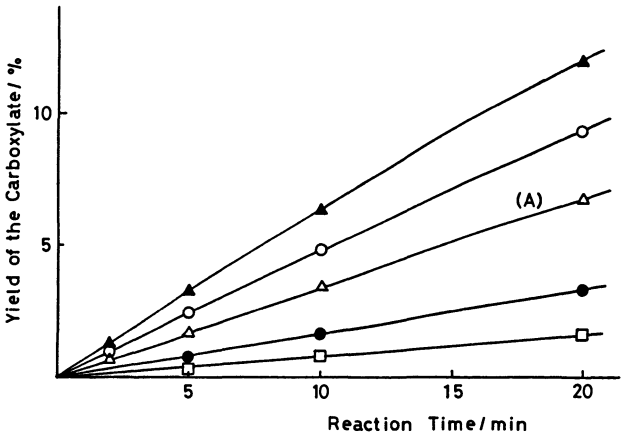

Fig. 3. The carboxylation with various amounts of DBU. —□—, 5 mmol; —●—, 10 mmol; —△—, 20 mmol; —○—, 30 mmol; —▲—, 40 mmol.

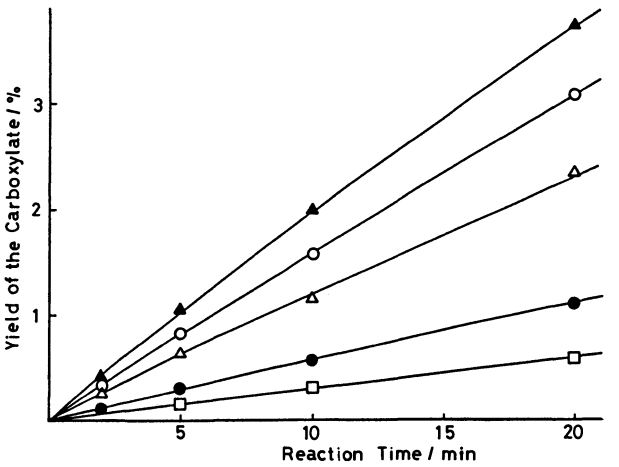

Fig. 4. The carboxylation with various CO_2 pressure. —□—, 47.5 Torr; —●—, 95 Torr; —△—, 190 Torr; —○—, 285 Torr; —▲—, 380 Torr.

case, the yield of carboxylate was calculated on the basis of the amount of DBU initially added. The rate of the carboxylation increased almost linearly with the increase in the concentration of cyclohexanone, with a slope of 1.67 ± 0.15 (% min^{-1} M^{-1}). Thus, the relationship between the reaction rate and the concentration of cyclohexanone showed a first-order dependence; the obtained slope was almost the same magnitude as that obtained in the study of the dependence upon the concentration of DBU. Thus, the slopes give a pseudo second-order rate constant of about 1.7 (% min^{-1} M^{-1}).

In Fig. 4, the time courses of carboxylation under various CO_2 pressures are shown. The yield of the carboxylate increased almost linearly with the reaction time. The initial rates of the carboxylate formation were obtained from the results. A plot of the initial rate against the CO_2 pressure gave a curve with a slight deviation from a straight line (Fig. 5).

With respect to carboxylation, two species can be considered as the possible CO_2 source of the carboxylate. They are the CO_2 adduct with DBU and CO_2

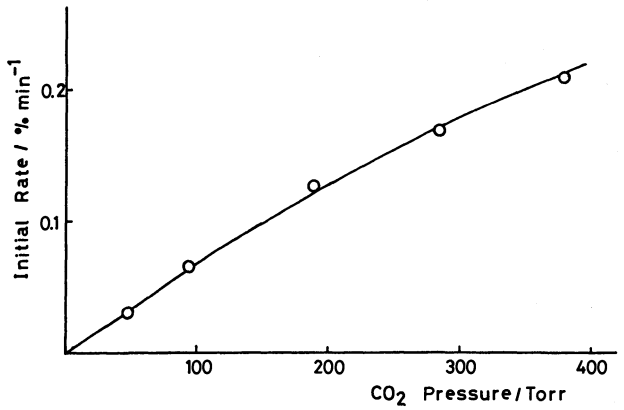

Fig. 5. The relationship between the initial rate of the carboxylation and CO_2 pressure.

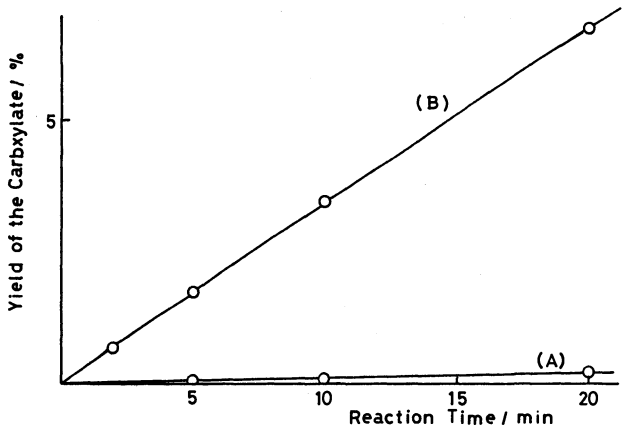

Fig. 6. The time courses of the carboxylation. (A) in the case of using CO_2 adduct with DBU, (B) in the case of using CO_2 dissolved in DMSO.

dissolved in DMSO. We now discuss the reaction mechanisms corresponding to the respective CO_2 species. The mechanism including CO_2 adduct with DBU is shown below, as is proposed by Iwatani et al.[10] Here,

$$\text{(A)} \quad \begin{cases} \text{DBU} + CO_2 \rightarrow \text{DBU} \cdot CO_2 & (1) \\ \text{DBU} \cdot CO_2 + \text{ChH} \rightarrow \text{ChCO}_2^- \cdot \text{DBUH}^+ & (2) \end{cases}$$

ChH designates cyclohexanone. In this mechanism, a CO_2 transfer occurs from the adduct to cyclohexanone to form the carboxylate (step (2)). Since the DMSO solution of DBU was preequilibrated with CO_2, step (1) might be in equilibrium. In such a case, the concentration of the adduct can be expressed by

$$c = aPK/(1+PK), \quad (3)$$

where P is the pressure of CO_2, K is the equilibrium constant of step (1), and a is the total concentration of DBU. This equation indicates that the concentration of the adduct increases proportionately with the initial concentration of DBU under a constant CO_2 pressure. In the carboxylation reaction, cyclohexanone was added to a CO_2 saturated DMSO solution of DBU. Therefore, the initial rate of carboxylation would be that of step (2). The rate of step (2) would show a first-order dependence upon the concentrations of both cyclohexanone and the adduct and, consequently, upon the concentration of DBU (as shown in Eq. 3). Experimental results were in accordance with the above discussion. The dependency of the rate upon the CO_2 pressure was assumed to be analogous to the curve shown in Fig. 1, since this curve indicates the dependence of the concentration of the adduct upon the CO_2 pressure. However, the experimental results (Fig. 5) were not in agreement with this assumption.

Another possible mechanism (B) is shown below:

$$\text{(B)} \quad \begin{cases} \text{ChH} + \text{DBU} \rightarrow \text{Ch}^- \cdot \text{DBUH}^+ & (4) \\ \text{Ch}^- \cdot \text{DBUH}^+ + CO_2 \rightarrow \text{ChCO}_2^- \cdot \text{DBUH}^+ & (5) \end{cases}$$

Cyclohexanone anion (Ch^-) is formed by the reaction between cyclohexanone and DBU (step (4)) and reacts with CO_2 dissolved in DMSO to form the carboxylate (step (5)). If step (5) was the rate-limiting step, the reaction rate would depend upon the respective concentrations of the anion and CO_2 to the first order. Cyclohexanone is a very weak acid (pK_a=16.9[11]), and DBU is a strong base with a pK_a of 11.5.[12] Thus, a small amount of cyclohexanone anion might be formed in step (4), and during the initial stage of carboxylation, the amount of formed cyclohexanone anion would be proportional to the amounts of the respective substrates. Though a part of DBU forms the adduct with CO_2 (as indicated in Eq. 3), the resultant concentration of DBU increases along with an increase in the initial concentration of DBU. Thus, the rate of carboxylation would show a first-order dependence upon the initial concentrations of both DBU and cyclohexanone. As shown in Fig. 2, the solubility of CO_2 in DMSO increased linearly in accordance with the increase in CO_2 pressure. Therefore, the rate of the reaction would increase linearly with an increase in the CO_2 pressure. Experimental results described previously seem to be consistent with this mechanism (B).

As discussed above, it is suggested that carboxylation proceeds via the reaction mechanism (B) rather than mechanism (A). In order to obtain further support for this mechanism, we studied carboxylation using only one CO_2 species. In the absence of the solvent, DBU (neat) was reacted with CO_2 at atmospheric pressure. It absorbed CO_2 in the molar ratio of 0.08. The carboxylation reaction was carried out with this mixture of the adduct and unreacted DBU.[13] The time course of the reaction is shown in Fig. 6 (curve (A)). A separate experiment[14] showed that CO_2 was scarcely transferred from the adduct to the solvent. If carboxylation proceeded via reaction mechanism (A), the initial rate of carboxylation with this adduct sample should have been the same as that of carboxylation for the case[15] in which atmospheric CO_2 was passed

through about a 0.2-M DMSO solution of DBU (Fig. 3 curve (A)). However, the initial rate of the former was considerably smaller than that of the latter (in the ratio of about 1 : 30). This result shows that the contribution of the adduct to the carboxylation was very small. As shown in Fig. 1, the concentration of the adduct, the low active species, increases with an increase in the CO_2 pressure, reducing the concentration of DBU. Thus, with respect to the curve shown in Fig. 5, the deviation from a straight line could be ascribed to the reduced amount of DBU at the starting point of carboxylation with the increased CO_2 pressure.

Carboxylation using CO_2 dissolved in DMSO was also carried out.[16] The time course of this carboxylation is given in Fig. 6 (curve (B)). This curve for carboxylate formation is very similar to that shown in Fig. 3 (curve (A)). It can therefore be pointed out that CO_2 dissolved in DMSO plays an important role in carboxylation by DBU.

The reaction between DBU and cyclohexanone was studied spectrophotometrically. Figure 7 shows the electronic absorption spectrum of a DMSO solution containing both 1 M DBU and 1 M cyclohexanone (spectrum (A)), which was measured with a 1-M DMSO solution of DBU as a reference. Since cyclohexanone does not have an absorption in this region of the spectrum, a new absorption with a maximum between 360 and 370 nm can be ascribed to the formation of the cyclohexanone anion. The spectrum of potassium salt of cyclohexanone (enolate)[17] in DMSO has a maximum at 362 nm (spectrum (B)). The results confirmed the reaction between cyclohexanone and DBU to form the cyclohexanone anion (step (4)).

The experimental results described above support the idea that carboxylation catalyzed by DBU proceeds via reaction mechanism (B). On the contrary, Iwatani et al. suggested[10] mechanism (A) for carboxylation under a higher CO_2 pressure and higher concentrations of DBU and cyclohexanone than ours. However, upon inspecting their data, it seems that mechanism (B) could not always be excluded as a possible mechanism. A further investigation may be necessary before the results of the two groups can be understood with consistency, considering the difference in the reaction conditions.

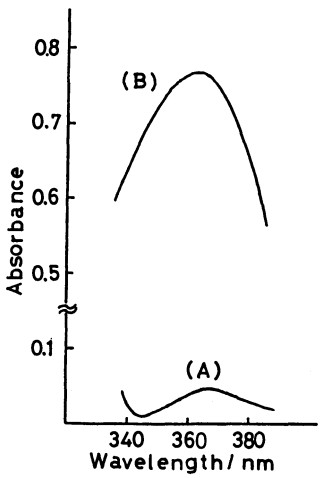

Fig. 7. Electronic absorption spectra. (A) DMSO solution containing both 1 M DBU and 1 M cyclohexanone, (B) DMSO solution of potassium salts of cyclohexanone.

Anyhow, the results obtained in our present work strongly suggest that the reaction proceeds mainly via reaction mechanism (B). This mechanism is in contrast with that of carboxylation catalyzed by PhOK, in which the CO_2 source of the carboxylate was considered to be CO_2 complexed with PhOK.[3] In the two reactions, the rate of the latter is, generally, much larger than that of the former, especially at a low CO_2 pressure. The dependence of the rate upon the CO_2 pressure is fairly different among the two reactions. It is noted that PhOK binds with CO_2 more strongly than DBU, in spite of its low pK_a (pK_a of phenol is 10.0). The formation of CO_2 species other than $CO_2 \cdot$ PhOK is suggested (data are not shown). Thus, the difference of the reactivity in carboxylation between PhOK and DBU may result from the unique reactivity of PhOK toward CO_2.

The author is very grateful to Professor Yoshikazu Matsushima (Kyoritsu College of Pharmacy) for helpful discussion.

References

1) G. Bottaccio and G. P. Chiusoli, *Chem. Commun.*, **1966**, 618; G. Bottaccio, G. P. Chiusoli, and M. G. Felicioli, *Gazz. Chim. Ital.*, **103**, 105 (1973).

2) H. Mori, H. Yamamoto, and T. Kwan, *Chem. Pharm. Bull.*, **20**, 2440 (1972); H. Mori, K. Mineta, and T. Kwan, *Chem. Pharm. Bull.*, **31**, 3002 (1983); H. Mori, M. Okubo, Y. Oke, N. Noguchi, M. Fukuda, and M. Ishihara, *Chem. Pharm. Bull.*, **32**, 2200 (1984).

3) H. Mori and Y. Satake, *Chem. Pharm. Bull.*, **33**, 3469 (1985).

4) H. L. Finkbeiner and M. Stiles, *J. Am. Chem. Soc.*, **85**, 616 (1963).

5) E. Haruki, M. Arakawa, N. Matsunuma, Y. Otsuji, and E. Imoto, *Chem. Lett.*, **1974**, 427.

6) E. L. Patmore, U. S. Patent 3694494, *Chem. Abstr.*, **78**, 4013q (1973).

7) N. Matsumura, Y. Yagyu, and E. Imoto, *Nippon Kagaku Kaishi*, **1977**, 1344.

8) H. Sakurai, A. Shirahata, and A. Hosomi, *Tetrahedron Lett.*, **21**, 1967 (1980).

9) E. Haruki, "Organic and Bio-organic Chemistry of Carbon Dioxide," ed. by S. Inoue and N. Yamazaki, Kodansha Ltd., Tokyo, 1981, pp. 14—34.

10) M. Iwatani, K. Kudo, N. Sugita, and Y. Takezaki, *Sekiyu Gakkaishi*, **21**, 290 (1978).

11) R. P. Bell and P. W. Smith, *J. Chem. Soc. B*, **1966**, 241.

12) K. Nakatani and S. Hashimoto, *Yuki Gosei Kagaku Kyokai Shi*, **33**, 925 (1975).

13) Twenty mmol of DBU(neat) was reacted with CO_2 of atmospheric pressure for 1 h, absorbing 1.6 mmol of CO_2

(gravimetrically determined). This sample was dissolved in 100 cm^3 of DMSO and reacted with 10 mmol of cyclohexanone.

14) The variation of the concentration of CO_2 adduct with DBU was observed in the IR spectra after the sample was dissolved in DMSO. The relative intensity of the absorption at 1642 cm^{-1} to that at 1610 cm^{-1} due to DBU was followed for 1 h. And no marked variation of the relative intensity was observed. It was also shown, by comparison with the spectrum of the DBU solution (in DMSO) which was saturated with CO_2 of atmospheric pressure, that most parts of the dissolved adduct retained the form of adduct in solution.

15) With respect to this solution, it was estimated by the gravimetric method that 100 cm^3 of DMSO dissolves 15.0 mmol of CO_2 and 20 mmol of DBU uptakes 1.8 mmol of CO_2, respectively.

16) CO_2 of atmospheric pressure was passed through the solution containing 100 cm^3 of DMSO and 10 mmol of cyclohexanone for 1 h. Then 20 mmol of DBU was added. In connection with this carboxylation reaction, the experiment as shown below was carried out. DBU was added to the CO_2 saturated DMSO solution and the IR spectrum of the solution was measured. The spectrum showed that only a small portion of CO_2 was present in the adduct form in the solution.

17) Potassium salt of cyclohexanone was prepared in THF by the reaction of cyclohexanone with potassium hydride (Ref. 18), and this solution was diluted with DMSO.

18) C. A. Brown, *J. Org. Chem.*, **39**, 1324 (1974).

 © 1988 The Chemical Society of Japan Bull. Chem. Soc. Jpn., 61, 441—447 (1988)

Studies of the Selective *O*-Alkylation and Dealkylation of Flavonoids. XI. A New Convenient Method for Synthesizing 3,5,7-Trihydroxy-8-methoxyflavones from 7-Hydroxy-3,5,8-trimethoxyflavones[1)]

Tokunaru HORIE,* Masao TSUKAYAMA, Yasuhiko KAWAMURA, Masamichi SENO, and Shigeo YAMAMOTO
Department of Applied Chemistry, Faculty of Engineering, Tokushima University, Minamijosanjima-cho, Tokushima 770
(Received July 4, 1987)

The 3- or 5-methoxyl group in the ditosylates of 5,7-dihydroxy-3,4′,8-trimethoxy- and 3,7-dihydroxy-4′,5,8-trimethoxyflavones was quantitatively demethylated with anhydrous aluminum bromide in acetonitrile to give the corresponding monohydroxyflavones, which were easily hydrolyzed into 3,5,7-trihydroxy-4′,8-dimethoxyflavone. On the basis of the results, the following convenient method for synthesizing 3,5,7-trihydroxy-8-methoxyflavones from 7-hydroxy-3,5,8-trimethoxyflavones was established. 7-Hydroxy-3,5,8-trimethoxyflavones or their tosylates were demethylated with 5% w/v anhydrous aluminum bromide in acetonitrile to give a mixture of the corresponding 3- and 5-hydroxyflavones. The mixture was tosylated and the resultant mixture was demethylated under the same conditions. The demethylated products were hydrolyzed with anhydrous potassium carbonate in methanol to give the desired 3,5,7-trihydroxy-8-methoxyflavones in high yields.

Generally, the selective cleavage of the 5-methoxyl group in flavones with free 3-hydroxyl and 8-methoxyl groups is not possible and the syntheses of 3,5,7-trihydroxy-8-methoxyflavones (**1**) from 7-hydroxy-3,5,8-trimethoxyflavones (**2**) by the selective demethylation have not also been successful.[2)] Therefore, the 3,5,7-trihydroxyflavones have been synthesized by the four following routes which bypassed the difficulty of the selective demethylation, albeit in low yields: (1) oxidative demethylation of the dibenzyl ether of 3,7-dihydroxy-5,8-dimethoxyflavones (**4**),[3)] (2) partial *O*-alkylation and dealkylation of 3,5,7,8-tetrahydroxyflavones,[4)] (3) Allan-Robinson reaction of ω-benzoyloxy-2,4,6-trihydroxy-3-methoxyacetophenone,[5)] and (4) nuclear oxidation of 3,7-bis(benzyloxy)-5-hydroxyflavones.[6)]

In previous papers, we reported that the demethylation of 7-hydroxy-3,5,8-trimethoxyflavones (**2**) with anhydrous aluminum bromide in acetonitrile afforded quantitatively a mixture of 5,7-dihydroxy-3,8-dimethoxyflavones (**3**) and 3,7-dihydroxy-5,8-dimethoxyflavones (**4**),[1)] and that 3-hydroxy-5,7,8-trimethoxyflavones were demethylated to 3,5-dihydroxy-7,8-dimethoxyflavones via the corresponding sulfonates.[7)] The results show that 3,5,7-trihydroxyflavones (**1**) are easily synthesized from **2** when the respective 3- and 5-methoxyl groups in tosylates of **3** and **4** are selectively cleaved and the tosyloxyl groups

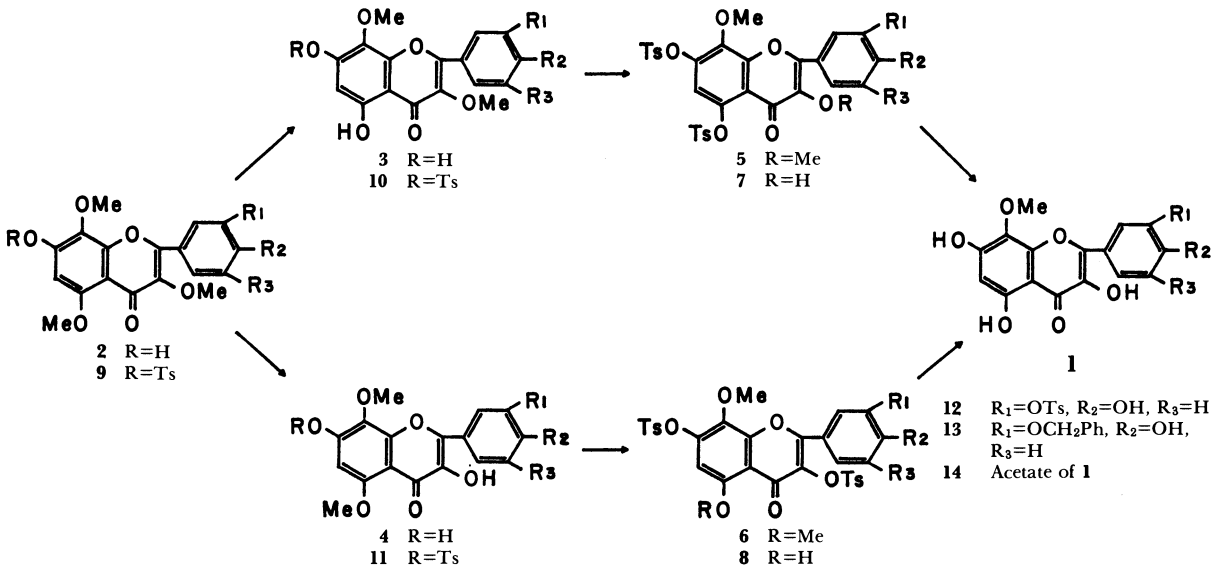

Scheme 1.

are easily hydrolyzed. Therefore, we studied the selective demethylation of ditosylates (**5a** and **6a**) of 5,7-dihydroxy-3,4′,8-trimethoxyflavone (**3a**) and 3,7-dihydroxy-4′,5,8-trimethoxyflavone (**4a**) and the hydrolysis of the resultant 3- and 5-hydroxyflavones, and consequently established a convenient method for synthesizing 3,5,7-trihydroxy-8-methoxyflavones (**1**) from 7-hydroxy-3,5,8-trimethoxyflavones (**2**). In this paper, we report on a general method for synthesizing **1** and their characterization.

Results and Discussion

Selective Demethylation of 5,7-Dihydroxy-3,4′,8-trimethoxyflavone (3a) and 3,7-Dihydroxy-4′,5,8-trimethoxyflavone (4a). The outline of the demethylation of the dihydroxyflavones **3a** and **4a** to **1a** was as follows. The 3-methoxyl group of the ditosylate **5a**, which was easily synthesized from **3a** by the tosylation, was selectively cleaved with 5% w/v anhydrous aluminum bromide in acetonitrile to give quantitatively 3-hydroxy-4′,8-dimethoxy-5,7-bis(tosyloxy)flavone (**7a**). The tosyloxyl groups in **7a** were smoothly hydrolyzed with potassium carbonate in methanol and the desired 3,5,7-trihydroxy-4′,8-dimethoxyflavone (**1a**) was easily obtained. On the other hand, the 3-hydroxyflavone **4a** was also demethylated to **1a** under similar conditions via the corresponding ditosylates **6a** and **8a**. All of the reactions proceeded quantitatively and no side reaction products were detected by TLC. The results show that **1a** was easily synthesized by the demethylation of 7-hydroxy-3,4′,5,8-tetramethoxyflavone (**2a**) as shown in Scheme 1.

A Method for Synthesizing 3,5,7-Trihydroxy-8-methoxyflavones (1). The demethylation of **2a** with anhydrous aluminum bromide in acetonitrile gave quantitatively a mixture of **3a** and **4a**.[1] The condensation of the mixture with *p*-toluenesulfonyl chloride in the presence of potassium carbonate afforded a mixture of tosylates **5a** and **6a**. The mixture of tosylates was selectively demethylated with anhydrous aluminum bromide in acetonitrile to give the monohydroxyflavones **7a** and **8a**, which were hydrolyzed to the desired **1a** with anhydrous potassium carbonate in methanol under nitrogen atmosphere. The overall yield of **1a** was 72%. The flavones **1b** and **1c** with no hydroxyl groups on the B ring were easily synthesized from the corresponding 7-hydroxyflavones **2b** and **2c** by this method.

On the other hand, the tosylates **9l** and **9m** of hydroxyflavones **2e** and **2g** as starting materials were used for syntheses of the 3,5,7-trihydroxyflavones **1e** and **1g** with hydroxyl groups on the B ring, since the selective demethylation of flavones with no hydroxyl group proceeded more smoothly than that of flavones with hydroxyl groups.[1,8] 3,4′,5,7-Tetrahydroxy-3′,8-dimethoxyflavone (**1e**) was easily synthesized from the tosylate **9l**. The tosylate **9m** of **2g** was also demethylated under similar conditions to give a mixture of two monohydroxyflavones **10m** and **11m**. The mixture was converted into a mixture of 3-hydroxy-8-methoxy-3′,4′,5,7-tetrakis(tosyloxy)flavone (**7m**) and 5-hydroxy-8-methoxy-3,3′,4′,7-tetrakis(tosyloxy)flavone (**8m**) by tosylation and subsequent demethylation. However, these tosylates were not easily hydrolyzed with potassium carbonate in methanol, and a mixture (ca. 1/1) of **1g** and its 3′-tosylate **12** was obtained in the hydrolysis for 10 h.

The results show that the 3-, 4′-, 5-, and 7-tosyloxyl groups which are associated with the carbonyl group in the flavone skeleton are easily hydrolyzed under mild conditions, but that hydrolysis of the tosyloxyl groups at the other positions is difficult. It is desired that the alkaline hydrolysis is carried out under as mild conditions as possible in the flavone synthesis, since the stability of flavones in alkaline media generally decreases with increasing the number of hydroxyl groups. Therefore, an alternative method for the protection of the hydroxyl groups on the B ring was studied in order to establish a general method for synthesizing 3,5,7-trihydroxy-8-methoxyflavones (**1**).

A General Method for Synthesizing 3,5,7-Trihydroxy-8-methoxyflavones (1) from 7-Hydroxy-3,5,8-trimethoxyflavones (2). In the demethylation, a benzyl group seems to be the most suitable protecting group of the hydroxyl groups when the 3- or 5-methoxyl group in the 3,5-dimethoxyflavone derivatives with benzyloxyl groups on the B ring is selectively cleaved without the cleavage of benzyloxyl groups. However, the demethylation of the 5-methoxyl group in the 5,7,8-trioxygenated flavones by anhydrous aluminum chloride in acetonitrile is generally more difficult than that in 5,6,7-trioxygenated flavones, and that the 5-methoxyl group in 8-hydroxy-5,7-dimethoxyflavones with benzyloxyl groups on the B ring is not demethylated selectively with anhydrous aluminum chloride because of the simultaneous cleavage of the benzyloxyl groups.[1,9] On the other hand, anhydrous aluminum bromide as a demethylating reagent can be expected to be much more selective than aluminum chloride.[7,10] Therefore, the demethylation of tosylates **9i** and **9k** of **2i** and **2k** was examined. The 3- or 5-methoxyl group in the tosylate **9i** with a benzyloxyl group on the B ring was selectively cleaved with 5% w/v anhydrous aluminum bromide in acetonitrile for 1 h at room temperature without debenzylation to give a mixture of the two monohydroxyflavones **10i** and **11i**, which was easily converted into **1i** via the corresponding tosylates by the demethylation and hydrolysis. The tosylate **9k** with two adjacent benzyloxyl groups on the B ring was also selectively demethylated under similar conditions, but a little amount of debenzylated products were detected by TLC. And the mixture of the tosylates of the demethylated products was converted into **1k** and a little

Table 3. UV Spectral Data for 3,5,7-Trihydroxy-8-methoxyflavones (**1**, **12**, and **13**) and Ditosylates of **1a** (**7a** and **8a**)[a)]

Compd.		λ_{max}/nm(log ε)			
1a	EtOH		274(4.31)	321(4.10)	377(4.19)
	EtOH-$AlCl_3$		271(4.31)	353(4.06)	435(4.28)
	EtOH-NaOAc		283(4.39)	307(4.15)	396(4.10)
1b	EtOH	257(4.25)	275(4.20)	335(4.05)	379(4.21)
	EtOH-$AlCl_3$		268(4.32)	362(4.01)	438(4.29)
	EtOH-NaOAc		284(4.31)	325(4.08)	398(4.10)
1c	EtOH		277(4.24)	315(4.11)	380(4.13)
	EtOH-$AlCl_3$		276(4.31)	355(4.05)	436(4.25)
	EtOH-NaOAc		286(4.36)	310(4.11)	415(4.13)
1d	EtOH		274(4.31)	325(4.09)	379(4.23)
	EtOH-$AlCl_3$		272(4.33)	355(4.09)	436(4.32)
	EtOH-NaOAc		282(4.40)	312(4.14)	401(4.14)
1e	EtOH	259(4.29)	270sh(4.26)	340i(4.00)	386(4.17)
	EtOH-$AlCl_3$		268(4.36)	365(4.03)	440(4.33)
	EtOH-NaOAc		284(4.30)	329(4.14)	408(4.01)
1f	EtOH	259(4.31)	274(4.25)	339i(4.04)	381(4.23)
	EtOH-$AlCl_3$		269(4.40)	365(3.97)	438(4.33)
	EtOH-NaOAc		283(4.37)	327(4.11)	397(4.15)
1g	EtOH	260(4.30)	272i(4.20)		383(4.28)
	EtOH-$AlCl_3$		270(4.37)	367(3.88)	443(4.36)
	EtOH-NaOAc	263sh(4.16)	281(4.25)	328(4.03)	394(4.15)
1h	EtOH		275(4.34)	320(4.16)	378(4.20)
	EtOH-$AlCl_3$		271(4.35)	353(4.14)	435(4.33)
	EtOH-NaOAc		283(4.42)	305sh(4.19)	404(4.12)
1i	EtOH	258(4.27)	276(4.25)	331(4.10)	380(4.22)
	EtOH-$AlCl_3$		266(4.38)	361(4.06)	438(4.34)
	EtOH-NaOAc		284(4.36)	324(4.13)	410(4.14)
1j	EtOH	258(4.28)	276(4.23)	332(4.07)	379(4.19)
	EtOH-$AlCl_3$		267(4.33)	360(4.04)	437(4.28)
	EtOH-NaOAc		284(4.34)	324(4.10)	395(4.12)
1k	EtOH	258(4.29)	277(4.25)	329(4.10)	382(4.18)
	EtOH-$AlCl_3$		265(4.37)	360(4.07)	438(4.31)
	EtOH-NaOAc		284(4.36)	322(4.12)	407(4.12)
12	EtOH		275(4.30)	320(4.10)	378(4.20)
	EtOH-$AlCl_3$		268(4.31)	353(4.07)	435(4.30)
	EtOH-NaOAc		282(4.32)	307i(4.07)	407(4.20)
13	EtOH	258(4.30)	275(4.25)	334(4.16)	381(4.23)
	EtOH-$AlCl_3$		269(4.40)	363(4.04)	438(4.34)
	EtOH-NaOAc		284(4.35)	325(4.10)	405(4.08)
7a	EtOH		262(4.27)		365(4.24)
	EtOH-$AlCl_3$		265sh(4.27)		437(4.40)
	EtOH-NaOAc		262(4.27)	366(4.13)	427(3.84)
8a	EtOH	268(4.31)	298(4.10)	332(4.23)	
	EtOH-$AlCl_3$	275(4.28)	320(4.20)	348(4.21)	410(3.89)
	EtOH-NaOAc	268(4.30)	300(4.17)	322(4.17)	

a) sh, shoulder; i, inflection point.

and **8a** show the presence of two tosyloxyl groups and the UV spectra exhibit the characteristic properties for 3- or 5-hydroxyflavones, suggesting that the structure of **7a** and **8a** are the 5,7- and 3,7-ditosylates of **1a**, respectively (Tables 1 and 3).

The properties of five of the synthesized flavones **1** agreed with those of the flavones **1a**,[3] **1d**,[6] **1e**,[5] **1g**,[4] and **1i**[5] which had been synthesized by the alternative routes, respectively. Also, the flavones **1a**—g afforded the corresponding acetates **14a**—g by the acetylation with acetic anhydride-pyridine. The ^{1}H NMR data for these flavones are shown in Tables 1 and 2. Signals of C_6-protons in **1** (in DMSO-d_6) are in the range of δ 6.23 to 6.28 and those in the acetates **14** (in $CDCl_3$) of **1** shift paramagnetically into the range of δ 6.75 to 6.82. The signals of C_6-protons in 5,7-

dihydroxy-3,8-dimethoxyflavones (**3**) and their acetates are appeared in a similar range,[1] respectively. The chemical shifts of the aromatic protons on the B ring are affected by the 3-hydroxyl or acetoxyl groups; these signals were similar to those in 3,7-dihydroxy-5,8-dimethoxyflavones (**4**) and their acetates.[1]

In the UV spectral data for **1**, Bands I and II are seen at 375 to 385 and 260 to 275 nm, respectively (Table 3). These Bands I shift bathochromically about 60 nm by the addition of aluminum chloride, but the bathochromic shift of Bands II is not observed. On the other hand, Bands I and II in all 3,5,7-trihydroxy-8-methoxyflavones shift bathochromically upon the addition of sodium acetate and the characteristic shift attributed to the 4′-hydroxyl group could not be found. These properties in the UV spectra are useful for a distinction from the other flavones, such as 3,5-dihydroxy-7,8-dimethoxyflavones,[7] but are shown to be applicable for the assignment of 4′-hydroxyl group in 3,5,7-trihydroxy-8-methoxyflavones in contrast to that in 5,7,8-trioxygenated flavones with no hydroxyl group at the 3-position.[9]

The ^{1}H NMR spectrum for **12** shows the presence of a methoxyl and a tosyloxyl group, suggesting that the structure is a monotosylate of **1g**. In a comparison of the ^{1}H NMR spectra for **1g** and **12**, the aromatic protons at 2′- and 6′-positions in **12** are more largely influenced by the tosyloxyl group than that at the 5′-position; both signals appeared at δ 8.00. The results show that the structure of **12** is the 3′-*O*-tosylate of **1g**. The ^{1}H NMR spectrum for **13** shows the presence of a benzyl group and the UV spectral data are similar to those for **12**, suggesting that the structure of **13** is the 3′-*O*-benzyl ether of **1g**.

Identification of a Natural Flavone (1f). During the survey of the flavonoids in the *Primulaceae*, Harborne proposed originally that the structure of Primula F 3A, which was isolated from an acid hydrolysate of several yellow-flowered Primula species, was a methyl ether of quercetagetin.[11] The author later revised its structure: Primula F 3A could be the as yet unknown 8,4′-dimethyl ether of gossypetin; however, further studies are required.[12] The UV spectral data for the flavone are essentially identical with those for the synthetic flavone (**1f**) and it shows that the proposed structure is correct. However, a direct comparison between the natural and synthetic flavones is required for a more accurate determination of the structure since the UV spectral data for the 3,5,7-trihydroxyflavones having 3,3′,4′,5,7,8-hexaoxygenated structure are similar to each other (Table 3).

Conclusion

The method for synthesizing 3,5,7-trihydroxy-8-methoxyflavones consists of the following three fundamental reactions which proceed quantitatively:

1. The 3- or 5-methoxyl group in 7-hydroxy-3,5,8-trimethoxyflavones (**2**) and their tosylates (**9**) was selectively cleaved with 5% w/v anhydrous aluminum bromide in acetonitrile at room temperature for 1—2 h to give a mixture of the corresponding 3- and 5-hydroxyflavones, and the benzyloxyl groups on the B ring were hardly cleaved under the conditions.
2. The respective 3- and 5-methoxyl groups in the 3-methoxy-5-tosyloxy- and 5-methoxy-3-tosyloxyflavone derivatives were also cleaved selectively under similar conditions.
3. The tosyloxyl groups at the 3-, 4′-, 5-, and 7-positions which are associated with the carbonyl group in the flavone skeleton, are hydrolyzed under mild conditions such as potassium carbonate in methanol.

It seems that the reactions can not be attributed to the characteristic properties for 3,5,7,8-tetraoxygenated flavones. Therefore, the method would be widely applied to the syntheses of 3,5-dihydroxyflavone derivatives.

Experimental

All melting points were determined in glass capillaries and are uncorrected. ^{1}H NMR spectra were recorded on a Hitachi R-24 spectrometer (60 MHz), using tetramethylsilane as an internal standard, and chemical shifts were given in δ values. UV spectra were recorded on a Hitachi 124 spectrometer. Thin-layer chromatography was carried out with silica-gel plates (Merck, Kiesel gel 60 F_{254}) using chloroform–ethyl acetate as an eluent. Elemental analyses were performed with a Yanaco CHN corder model MT-2.

7-Hydroxy-3,5,8-trimethoxyflavones (2). Flavones **2** were synthesized from 2,4-dihydroxy-3,6,ω-trimethoxyacetophenone by the Allan-Robinson reaction according to the method described in a previous paper.[1] 4′-Benzyloxy-7-hydroxy-3,5,8-trimethoxyflavone (**2h**): mp 238—240 °C (from ethyl acetate); (lit,[13] mp 240—242 °C); yield 55%. 3′-Benzyloxy-7-hydroxy-3,4′,5,8-tetramethoxyflavone (**2j**): mp 214—216 °C (from methanol); (lit,[14] mp 215—217 °C); yield 52%.

3-Hydroxy-4′,8-dimethoxy-5,7-bis(tosyloxy)flavone (7a). The flavone **5a** (85 mg) was dissolved in a solution of 5% w/v anhydrous aluminum bromide in acetonitrile (10 cm^3) and allowed to stand for 2 h. The mixture was poured into 2% hydrochloric acid and heated at 70—80 °C for 20 min and diluted with water. After the mixture was concentrated under reduced pressure, the crystals separated as yellow needles were collected, washed with water and dried to give **7a**: mp 173—174 °C; yield 80 mg (96%). Found: C, 58.15; H, 3.89%. Calcd for $C_{31}H_{26}O_{11}S_2$: C, 58.31; H, 4.08%.

5-Hydroxy-4′,8-dimethoxy-3,7-bis(tosyloxy)flavone (8a). The flavone **6a** (85 mg) was demethylated and treated under the same conditions as described above to give **8a** as pale yellow plates: mp 173—174 °C; yield 77 mg (93%). Found: C, 58.10; H, 3.89%. Calcd for $C_{31}H_{26}O_{11}S_2$: C, 58.31; H, 4.08%.

3,5,7-Trihydroxy-4′,8-dimethoxyflavone (1a). A mixture of **7a** (70 mg) and anhydrous potassium carbonate (0.5 g) in methanol (25 cm^3) was refluxed with stirring for 2 h. The mixture was acidified with diluted hydrochloric acid; then the methanol was evaporated under reduced pressure. The

separated crystals were recrystallized from aq methanol to give **1a** as yellow needles, yield 30 mg (83%). The flavone **1a** was also synthesized from **8a** (60 mg) by the hydrolysis described above, yield 25 mg (80%).

3,5,8-Trimethoxy-7-tosyloxyflavones 9a—c and 9h—k. A mixture of 7-hydroxy-3,5,8-trimethoxyflavone (**2**) with no hydroxyl groups on the B ring (1 mmol), *p*-toluenesulfonyl chloride (285 mg; 1.5 mmol), and anhydrous potassium carbonate (1.5—2 g; 8—11 mmol) in acetone (30—50 cm^3) was refluxed with stirring until the starting material disappeared (2—3 h). The cooled reaction mixture was poured into diluted hydrochloric acid and then concentrated under reduced pressure. The separated precipitate was collected, washed with water and a little amount of ether, and then recrystallized to give **9** as colorless prisms or needles. The results are shown in Table 4.

3,4′,8-Trimethoxy-5,7-bis(tosyloxy)flavone (5a), 4′,5,8-Trimethoxy-3,7-bis(tosyloxy)flavone (6a), and 3,3′,5,8-Tetramethoxy-4′,7-bis(tosyloxy)flavone (9l). A mixture of the flavone[1] (**3a**, **4a**, or **2e**) (0.3 mmol), *p*-toluenesulfonyl chloride (190 mg; 1 mmol), and anhydrous potassium carbonate (1.5 g; 10 mmol) in acetone (20—30 cm^3) was refluxed with stirring for 3—5 h. The reaction mixture was treated by the method described above to give the ditosylate as colorless needles or prisms (Table 4).

3,5,8-Trimethoxy-3′,4′,7-tris(tosyloxy)flavone (9m). The flavone **2g** (180 mg) was tosylated with *p*-toluenesulfonyl chloride (450 mg), and anhydrous potassium carbonate (2 g) in acetone to give **9k** as colorless needles (Table 4).

A General Method for Synthesizing 3,5,7-Trihydroxy-8-methoxyflavones (1) from 3,5,8-Trimethoxy-7-tosyloxyflavones (9). The flavone **9** (1 mmol) was dissolved in a solution of 5% w/v anhydrous aluminum bromide in acetonitrile (25—30 cm^3; 4.5—5.5 mmol) and the solution is allowed to stand at room temperature (25—28 °C) for 2 h. The reaction times in the demethylation of the flavones **1h—k** with benzyloxyl groups on the B ring were reduced to 1 h. The reaction mixture was poured into 2% hydrochloric acid

Table 4. 3,5,8-Trimethoxy-7-tosyloxyflavones (**9**) and 5,7- and 3,7-Ditosyloxyflavones (**5a** and **6a**)

Compd.	Mp	Recrystn. solvent	Yield	^1H NMR in $CDCl_3$		Formula	Found (%)		Calcd (%)	
	θ_m/°C		%	C_6-H	Ph-Me		C	H	C	H
9a	201—202	$CHCl_3$-MeOH	95	6.47s	2.45s	$C_{26}H_{24}O_9S$	60.94	4.61	60.93	4.72
9b	170—171	$CHCl_3$-MeOH	96	6.43s	2.45s	$C_{27}H_{26}O_{10}S$	59.50	5.02	59.77	4.83
9c	205—205.5	$CHCl_3$-MeOH	83	6.43s	2.46s	$C_{28}H_{28}O_{11}S$	58.52	5.06	58.73	4.93
9h	194—195	$CHCl_3$-MeOH	95	6.49s	2.45s	$C_{32}H_{28}O_9S$	65.05	4.69	65.29	4.80
9i	140—141	EtOAc-MeOH	90	6.43s	2.44s	$C_{33}H_{30}O_{10}S$	63.78	4.79	64.07	4.89
9j	134—136	Me_2CO-EtOAc	85	6.44s	2.44s	$C_{33}H_{30}O_{10}S$	64.29	4.81	64.07	4.89
9k	151—152	EtOAc-Et_2O	86	6.42s	2.42s	$C_{39}H_{34}O_{10}S$	67.32	4.89	67.42	4.93
9l	159—160	EtOAc-MeOH	85	6.51s	2.47s(6H)	$C_{33}H_{30}O_{12}S_2$	57.86	4.24	58.05	4.43
9m	149—150	EtOAc-MeOH	90	6.54s	2.46s(9H)	$C_{39}H_{34}O_{14}S_3$	56.64	4.04	56.92	4.16
5a	160—161	EtOAc-MeOH	87	6.86s	2.42s 2.46s	$C_{32}H_{28}O_{11}S_2$	58.60	4.12	58.88	4.32
6a	176—177	EtOAc	82	6.54s	2.39s 2.46s	$C_{32}H_{28}O_{11}S_2$	58.89	4.13	58.88	4.32

Table 5. 3,5,7-Trihydroxy-8-methoxyflavones (**1**, **12**, and **13**)

Compd.	Starting material	Mp	Recrystn. solvent	Yield	Formula	Found(%)		Calcd (%)	
		θ_m/°C		%		C	H	C	H
1a	**2a**	206—207	MeOH	72	$C_{17}H_{14}O_7$	61.53	4.48	61.82	4.27
	9a	(lit,[3] 207—208)		75					
1b	**2b**	246—248	aq MeOH	70	$C_{18}H_{16}O_8$	59.90	4.32	60.00	4.48
	9b			79					
1c	**2c**	220—221	EtOAc	75	$C_{19}H_{18}O_9$	58.54	4.57	58.46	4.65
	9c			76					
1d	**1h**	276—278	MeOH	97	$C_{16}H_{12}O_7$	60.82	3.71	60.76	3.82
		(lit,[6] 269—270)							
1e	**1i**	269—271	aq MeOH	85	$C_{17}H_{14}O_8$	59.10	4.11	58.96	4.08
	9l	(lit,[5] 269—271)		60					
1f	**1j**	242—243	AcOH	95	$C_{17}H_{14}O_8$	58.76	4.06	58.96	4.08
1g	**1k**	274—276	aq MeOH	91	$C_{16}H_{12}O_8$	57.71	3.62	57.83	3.64
		(lit,[4] 273—275)							
1h	**9h**	192—193	MeOH	88	$C_{23}H_{18}O_7$	68.07	4.53	67.97	4.46
1i	**9i**	238—240	AcOH	80	$C_{24}H_{20}O_8$	65.89	4.49	66.05	4.62
		(lit,[5] 247—249)							
1j	**9j**	187—189	MeOH	85	$C_{24}H_{20}O_8$	66.18	4.65	66.05	4.62
1k	**9k**	183—185	MeOH	75	$C_{30}H_{24}O_8$	70.21	4.78	70.30	4.72
12	**9m**	220—222	MeOH	25[a] 27	$C_{23}H_{18}O_{10}S$	56.47	4.02	56.79	3.73
13[b]	**9k**	228—230	MeOH	2	$C_{23}H_{18}O_8$	65.25	4.20	65.40	4.30

a) This is the yield of **1g**. b) This is a byproduct in the synthesis of **1k** from **9k**.

Table 6. Acetates **14** of 3,5,7-Trihydroxy-8-methoxyflavones (**1**)

Compd.	Mp θ_m/°C	Recrystn. solvent	Formula	Found (%) C	Found (%) H	Calcd (%) C	Calcd (%) H
14a	203—204	EtOAc-MeOH	$C_{23}H_{20}O_{10}$	60.41	4.38	60.52	4.42
14b	167—168	MeOH	$C_{24}H_{22}O_{11}$	59.27	4.52	59.26	4.56
14c	131—133	aq MeOH	$C_{25}H_{24}O_{12}$	57.99	4.73	58.14	4.68
14d	155—157	MeOH	$C_{24}H_{20}O_{11}$	59.22	4.12	59.50	4.16
14e	173—175 (lit,[15] 155—156)	MeOH	$C_{25}H_{22}O_{12}$	58.45	4.43	58.37	4.31
14f	199—200	$CHCl_3$-MeOH	$C_{25}H_{22}O_{12}$	58.12	4.28	58.37	4.31
14g	142—144 (lit,[4] 142—144)	MeOH	$C_{26}H_{22}O_{13}$	57.35	4.20	57.57	4.09

(50—60 cm^3), heated at 70—80 °C for 15—30 min, and diluted with water. After the solvent was evaporated under reduced pressure, the separated yellow crystals were collected, washed with water, and dried to give a mixture of **10** and **11**.

The mixture was refluxed with *p*-toluenesulfonyl chloride (285 mg; 1.5 mmol) and anhydrous potassium carbonate (2 g; 11 mmol) in acetone (40—50 cm^3) with stirring until the hydroxyflavones disappeared (3—6 h). The mixture was poured into diluted hydrochloric acid and the solvent was evaporated under reduced pressure. The separated precipitate was collected, washed with water and dried to give a mixture of **5** and **6**.

However, the precipitate obtained from the flavone **1h—k** with benzyloxyl groups on the B ring was extracted with ethyl acetate, and the extract was washed with water and then concentrated to give a mixture of **5** and **6**. The mixture was contaminated with a small amount of *p*-toluenesulfonyl chloride; however, the following demethylation was not affected by the chloride.

The mixture of **5** and **6** was demethylated with 5% w/v anhydrous aluminum bromide in acetonitrile under the same conditions as described in the demethylation of **9**. The demethylated product was extracted with ethyl acetate, and the extract was washed with water and then concentrated to give a mixture of **7** and **8**. To the mixture, methanol (40—50 cm^3) and anhydrous potassium carbonate (3—4 g; 21—28 mmol) were added. The mixture was refluxed with stirring under nitrogen atmosphere for 2—3 h, and then poured into diluted hydrochloric acid. The methanol was evaporated under reduced pressure and the separated yellow crystals were collected to give a crude product **1**. All products except for **12** and **13** were purified by recrystallization to give **1** as yellow needles. The flavone **13** was obtained from the mother liquor of **1k** by silica-gel chromatography with chloroform.

Only the mixture of **7m** and **8m** was hydrolyzed for 10 h under conditions similar to that described above, and the products were separated by the preparative HPLC, using a column (20×600 mm) packed with Hitachi gel #3019 and methanol as an eluent, to give **1g** and **12**. The results are shown in Table 5.

3,5-Dihydroxyflavones (**1a**, **1b**, and **1c**) were also synthesized from the corresponding 7-hydroxyflavones **2a**, **2b**, and **2c** by a method similar to that described above.

3,5,7-Trihydroxy-8-methoxyflavones (1d—g) with Hydroxyl Groups on the B Ring. The benzyloxyflavones **1h—k** (200 mg) were hydrogenated over palladium on charcoal (10%; 100 mg) in ethyl acetate-methanol (1/2 volume ratio; 300 cm^3) until the uptake of hydrogen ceased. After the catalyst was filtered off, the filtrate was evaporated and the residue was recrystallized to give **1** as yellow needles (Table 5).

Acetates (14a—g) of 1. The flavone **1** (40 mg) was dissolved in acetic anhydride (0.4 cm^3)-pyridine (0.04 cm^3), and allowed to stand at room temperature for 1 day and then treated with water to give **14** as colorless needles. The results are shown in Table 6.

References

1) Part X of this series: T. Horie, M. Tsukayama, Y. Kawamura, and M. Seno, *J. Org. Chem.*, **52**, 4702 (1987).

2) H. Wagner and L. Farkas, "The Flavonoids," ed by J. B. Harborne, T. S. Mabry, and H. Mabry, Chapman and Hall, London (1975), pp. 155—158.

3) M. Krishnamurti, T. R. Seshadri, and P. R. Shankaran, *Tetrahedron*, **22**, 941 (1966).

4) H. Wagner, R. Rüger, G. Maurer, and L. Farkas, *Chem. Ber.*, **110**, 737 (1977).

5) D. L. Dreyer, S. Tabata, and R. M. Horowitz, *Tetrahedron*, **20**, 2977 (1964).

6) K. J. Balakrishna and T. R. Seshadri, *Proc. Ind. Acad. Sci.*, **26A**, 234 (1947).

7) T. Horie, M. Tsukayama, Y. Kawamura, and S. Yamamoto, *Chem. Pharm. Bull.*, **35**, 4465 (1987).

8) T. Horie, H. Kourai, M. Tsukayama, M. Masumura, and M. Nakayama, *Yakugaku Zasshi*, **105**, 232 (1985).

9) T. Horie, H. Kourai, and N. Fujita, *Bull. Chem. Soc. Jpn.*, **56**, 3773 (1983).

10) T. Horie, M. Tsukayama, H. Kourai, C. Yokoyama, M. Furukawa, T. Yoshimoto, S. Yamamoto, S. Watanabe-Kohno, and K. Ohata, *J. Med. Chem.*, **29**, 2256 (1986).

11) J. B. Harborne, *Phytochemistry*, **4**, 647 (1965).

12) J. B. Harborne, *Phytochemistry*, **7**, 1215 (1968).

13) K. Fukui, T. Matsumoto, and S. Tanaka, *Bull. Chem. Soc. Jpn.*, **42**, 2380 (1969).

14) M. Krishnamurti, T. R. Seshadri, and P. R. Shankaran, *Indian J. Chem.*, **5**, 137 (1967).

15) R. M. Horowitz and B. Gentili, *J. Org. Chem.*, **61**, 2899 (1961).

 © 1988 The Chemical Society of Japan Bull. Chem. Soc. Jpn., 61, 449—454 (1988)

Reaction of Benzeneseleninyl Chloride with Olefins in the Presence of a Lewis Acid. A Novel One Step Vinylic Chlorination

Nobumasa KAMIGATA,* Takeshi SATOH, and Masato YOSHIDA
Department of Chemistry, Faculty of Science, Tokyo Metropolitan University, Fukazawa, Setagaya-ku, Tokyo 158
(Received July 9, 1987)

In the presence of aluminum chloride benzeneseleninyl chloride was found to be an excellent vinylic chlorinating reagent of olefins under mild conditions. However, such olefins as styrene, *trans*-stilbene, and *trans*-1-phenylpropene afforded dichloro adducts under similar conditions. A plausible reaction mechanism involving positive chlorine intermediate is proposed.

In recent years organic selenium reagents have become a very powerful tool in organic synthesis.[1] Of particular importance is the following discovery: a) Epoxides are converted into olefins by treatment with triphenylphosphine selenide in the presence of an acid,[2] b) selenoxides prepared by oxidation of selenides undergo clean syn elimination of selenenic acid to form olefins at or below room temperature,[3] c) epoxides are converted into allylic alcohols by ring opening with benzeneselenolate ion followed by selenoxide fragmentation and the intermediate β-hydroxy alkyl selenides are transformed into olefin,[4] d) selenium metal catalyze the reaction of amines and alcohols with carbon monoxide to give ureas and carbonates, respectively,[5] e) olefins are converted into ally alcohols by treatment with selenium dioxide,[6] and f) semicarbazones are transformed into 1,2,3-selenadiazoles by treatment with selenium dioxide which collapse at high temperatures to produce acetylenes.[7]

Benzeneseleninyl chloride (**1**) was first prepared by Ayrey et al. by the reaction of benzeneselenenyl chloride with ozone and is known to be highly hygroscopic and hydrolyzed to benzeneseleninic acid.[8] So far, little effort has been made to employ compound **1** as a synthetic tool; however, a few papers were found (reported by Czarny and Sosnovsky) in which aminodiphenylmethane and benzylamine were oxidized by **1** to give benzophenone and benzyl cyanide, respectively.[9,11] We found that a reaction of compound **1** with olefins in the presence of a Lewis acid gives chloro-substituted olefins at olefinic carbon. The results are described in this paper, and the mechanism is discussed.

Results and Discussion

The reaction of benzeneseleninyl chloride (**1**) with 1,1-diphenylethylene was carried out in dichloromethane in the presence of a Lewis acid at room temperature. When aluminum chloride was employed as a catalyst, the reaction occurred very smoothly and after stirring for 2 h at room temperature, 2-chloro-1,1-diphenylethylene (**2a**) was formed in 94% yield. However, such Lewis acids as iron(III) chloride and zinc chloride afforded the chlorinated compounds **2a** under similar conditions in 68 and 26% yield, respectively. The reaction proceeded very slowly when the reaction was carried out in the absence of a Lewis acid, and 2-chloro-1,1-diphenylethylene was obtained in 60% yield after 142 h at 40 °C.

When aluminum bromide was used as the catalyst instead of aluminum chloride in the reaction of **1** with 1,1-diphenylethylene, 2-bromo-1,1-diphenylethylene (**2b**) was obtained in 84% yield after stirring at room temperature for 1 h. The reaction of **1** with triphenylethylene in the presence of aluminum chloride and aluminum bromide under similar conditions afforded chlorotriphenylethylene (**2c**) and bromotriphenylethylene (**2d**) in quantitative yield, respectively. The results are summarized in Table 1.

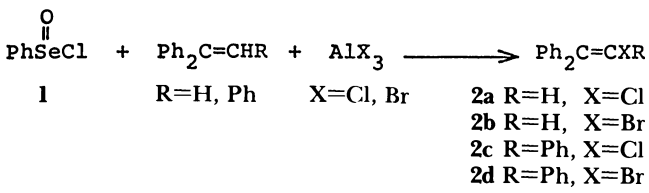

The present reaction seems to be an excellent halogenating method since a direct vinylic halogenation of olefins is hitherto unknown. A possible reaction mechanism shown in Scheme 1 accounts for these novel one-step vinylic chlorinations of olefins with **1**.

The aluminum catalyst abstracts chloride ion from benzeneseleninyl chloride to give benzeneseleninyl cation species **3** and aluminum tetrachloride anion species, as is known for the acylium ion intermediate in the Friedel-Crafts acylation of acyl chloride with aluminum chloride. The electrophilic addition of **3** to olefin affords cyclic selenoxonium ion intermediate **4a**, which is attacked by a chloride ion to give a ring-

Table 1. Reaction of Benzeneseleninyl Chloride with Vinyl-Substituted Arenes at Room Temperature

R in Ph_2C=CHR	Catalyst	Reaction time/h	Product	Yield/%
H	None	140[a]	**2a**	60
H	$AlCl_3$	2	**2a**	94
H	$FeCl_3$	2	**2a**	68
H	$ZnCl_2$	2	**2a**	26
H	$AlBr_3$	1	**2b**	84
Ph	$AlCl_3$	3	**2c**	100
Ph	$AlBr_3$	3	**2d**	97

a) The reaction was carried out at 40 °C.

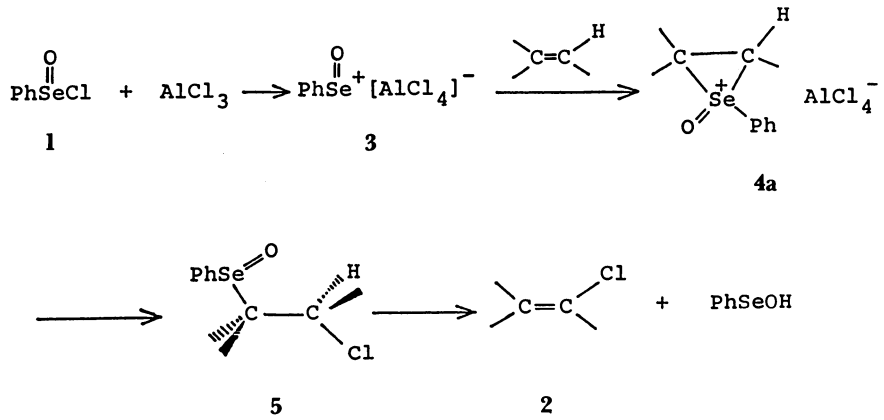

Scheme 1.

opening adduct **5**. The following syn-elimination of benzeneselenenic acid from **5** gives the final vinylic chlorination product **2**. The syn-elimination of benzeneseleninyl group with β-hydrogen is well-known and this method has been given much attention for the synthesis of olefins.[3] The reason why the reaction of **1** with 1,1-diphenylethylene in the absence of aluminum chloride is slow can be best accounted for by the fact that direct electrophilic reaction of **1** to the olefin forming cyclic selenoxonium intermediate **4b** is slow: meanwhile, the benzeneseleninyl cation species **3** reacts with olefin very smoothly.

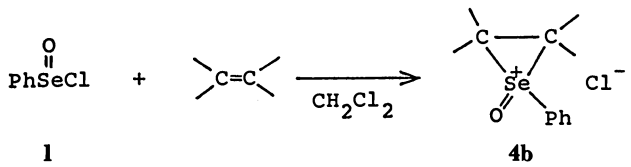

The reaction of **1** with phenyl-substituted ethylenes such as styrene, *trans*-stilbene, and *trans*-1-phenylpropene was carried out in the presence of aluminum chloride. In the reaction of **1** with styrene, styrene dichloride was isolated in 48% yield, and no formation of chloro-substituted styrene obtainable from substitution at olefinic hydrogen was observed.

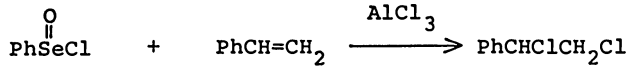

In the reaction of **1** with stilbene, *dl*- and *meso*-1,2-dichloro-1,2-diphenylethane **6a**, **6b** were isolated in 21 and 31% yield, respectively.

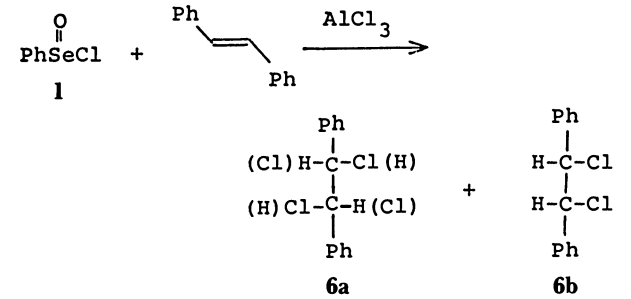

Table 2. α-Chlorination of α,β-Unsaturated Carbonyl Compounds **7** with Benzeneseleninyl Chloride Catalyzed by $AlCl_3$ at 40 °C

	Compound **7**			Reaction time/h	Product	Yield/%
	R_1	R_2	R_3			
7a	Me	H	H	2	**8a**	77
7b	Ph	H	H	55	**8b**	61
7c	Ph	Ph	H	71	**8c**	45
7d	Ph	H	Me	18	**8d**	50
7e	Ph	H	Ph	78	**8e**	30
7f	H	H	OEt	26	**8f**	70
7g	H	H	OBu^n	22	**8g**	46
7h	Me	H	OMe	23	**8h**	96
7i	Me	H	OEt	23	**8i**	88
7j	Ph	H	OMe	30	**8j**[a]	11
7k	Ph	H	OEt	26	**8k**[b]	17

a) The mixture of *threo*- and *erythro*-methy 2,3-dichloro-3-phenyl propionate was isolated in 33% yield together with **8j**. b) The mixture of *threo*- and *erythro*-ethyl 2,3-dichloro-3-phenyl propionate was isolated in 48% yield together with **8k**.

Similarly, in the reaction of *trans*-1-phenylpropene, *threo*- and *erythro*-1,2-dichloro-1-phenylpropane **6c**, **d** were obtained in 38 and 23% yield, respectively.

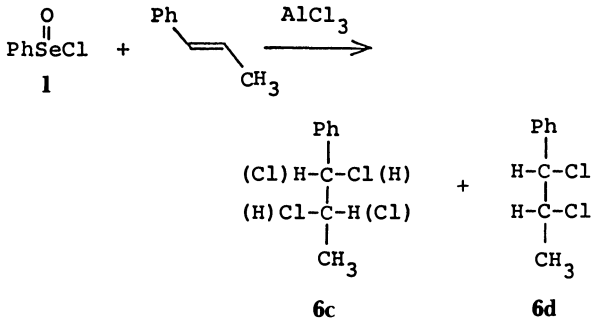

Against our expectations, the reaction of **1** with these phenyl-substituted ethylenes did not afford chloro-substituted arenes but formed dichloro adducts. It is difficult to explain these addition products by a reaction mechanism involving the cyclic selenoxonium ion intermediate shown in Scheme 1.

The reaction of **1** with α,β-unsaturated carbonyl

compounds in the presence of aluminum chloride was carried out at 40 °C. The chloro-substituted products at α-hydrogen were obtained in moderate to high yield. The structure of the products was determined by IR, ^{1}H NMR, ^{13}C NMR, and mass spectra (see experimental section). The results are summarized in Table 2.

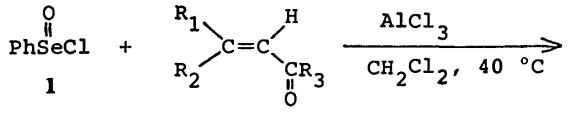

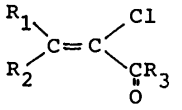

In the case of the reaction of **1** with methyl and ethyl cinnamate, dichloro adducts *threo*- and *erythro*-2,3-dichloro-3-phenylpropionic acid methyl ester (33%) and *threo*- and *erythro*-2,3-dichloro-3-phenylpropionic acid ethyl ester (48%) were formed together with chloro-substituted products **8j** and **8k**, respectively. The results mean that the addition and substitution occurr competitively.

The reaction of **1** with 2-cyclopenten-1-one (**9a**) in the presence of aluminum chloride at room temperature afforded 2-chloro-2-cyclopenten-1-one (**10a**) in 47% yield. Similarly, 2-cyclohexen-1-one (**9b**) and 2-cycloheptenone-1-one (**9c**) were chlorinated by **1** in the presence of aluminum chloride to give corresponding 2-chlorocycloalkenones **10b** and **10c** in moderate to good yield. 1,4-Benzoquinone was also chlorinated by **1** under similar conditions to give 2-chloro-1,4-benzoquinone (**10d**) in 44% yield. However, no chloro-

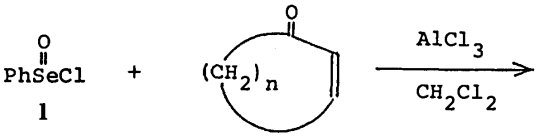

9a n=2
9b n=3
9c n=4

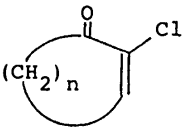

substituted product was obtained in the reaction of **1** with 1,4-naphthoquinone catalyzed by aluminum chloride under various reaction conditions. The results are summarized in Table 3.

Table 3. α-Chlorination of Cyclic α,β-Unsaturated Ketones

Ketone	Reaction temp/°C	Reaction time/h	Product	Yield/%
9a	Room temp	48	**10a**	47
9b	0	9	**10b**	41
9c	0	7	**10c**	56
1,4-Benzoquinone	40	22	**10d**	44

The results in the Tables 1, 2, and 3 show that the reaction of benzeneseleninyl chloride (**1**) with olefins catalyzed by aluminum chloride provides chloro-substituted compounds at vinyl position in one step in good yield; therefore, **1** can be regarded as an excellent vinylic chlorinating reagent and a new synthetic tool for chlorination.

The reaction mechanism shown in Scheme 1 can explain the vinylic chlorination products but can not

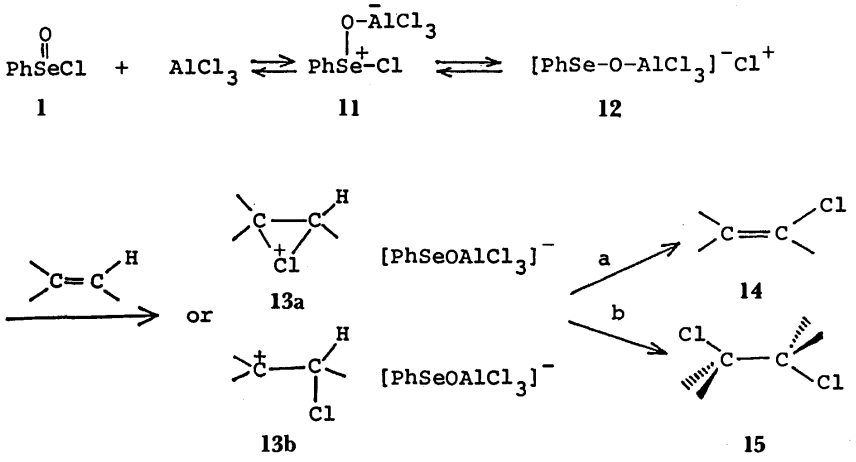

Scheme 2.

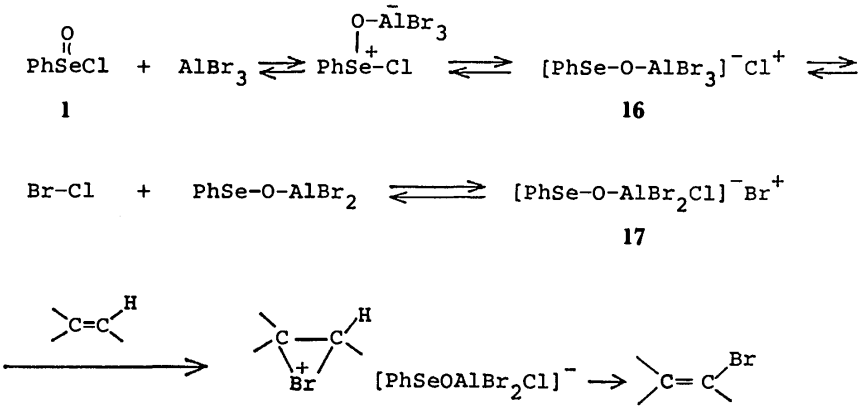

Scheme 3.

easily explain the dichloro-addition products observed in the reaction of **1** with such olefins as styrene, *trans*-1-phenylpropene, and *trans*-stilbene. An alternative mechanism shown in Scheme 2 interprets both the chloro-substituted products at the vinyl position and the dichloro-adducts from the common reactive intermediate.

Aluminum chloride does not abstract the chloride ion but reacts with the oxygen atom of the benzeneseleninyl chloride to form the intermediate **11** which easily converts to chloronium trichloro(phenylselenooxy)aluminate (**12**). The following electrophilic reaction of the chloronium ion with olefin gives either a chloronium ion **13a** or a carbocation intermediate **13b**. If the chloride ion of the trichloro(phenylselenooxy)aluminate species attacks the hydrogen atom of intermediate **13** (path a), chloro-substituted vinyl products **14** are obtained. On the other hand, when a chloride ion of the trichloro(phenylselenooxy)aluminate species attacks the carbon atom of intermediate **13a** or the carbocation intermediate **13b** (path b), dichloro adducts are obtained. The reaction of path a will occur in the following cases: a) the substituents of the olefin are a bulky group, b) the β-hydrogen of the cation intermediate **13a** or **13b** is relatively acidic. Case a) was observed in such olefins as 1,1-diphenylethylene and triphenylethylene, and case b) was observed in α,β-unsaturated carbonyl compounds. Such olefins as styrene, *trans*-1-phenylpropene, and *trans*-stilbene formed dichloro adducts since these olefins do not conform to these two cases.

When aluminum bromide was employed instead of aluminum chloride in the reaction of **1** with 1,1-diphenylethylene, 2-bromo-1,1-diphenylethylene was obtained in 84% yield, and no formation of 2-chloro-1,1-diphenylethylene was observed. This means that chloronium tribromo(phenylselenooxy)aluminate (**16**), formed by the reaction of **1** with aluminum bromide, transforms rapidly to bromonium dibromochloro-(phenylselenooxy)aluminate(**17**). The following electrophilic reaction of the bromonium ion with olefin gives the bromo-substituted products as shown in Scheme 3.

To justify the mechanism shown in Scheme 2, ^{77}Se NMR studies were carried out. The ^{77}Se NMR signal of benzeneseleninyl chloride in dichloromethane appeared at 850 ppm, shifted to 670 ppm when equimolar ammounts of aluminum chloride were added to a solution of **1** in dichloromethane (diphenyl diselenide was employed as the internal standard). The results suggest that the $PhSe^{+}[AlCl_4]^{-}$ species (**3**) is not formed by the addition of aluminum chloride to **1** (as shown in Scheme 1), since one can expect a down-field shift more than 850 ppm about such a benzeneseleninyl cation species **3** from diphenyl diselenide. Thus, we believe that the observation of the 180 ppm up-field shift can be attributed to the formation of chloronium trichloro(phenylselenooxy)aluminate intermediate (**12**).

Experimental

Measurement. Melting points and boiling points were uncorrected. The infrared absorption spectra were determined on a Hitachi Model 260-10 spectrometer with samples as either neat liquid or KBr disks. The proton magnetic resonance spectra were recorded at 60 MHz by using a JEOL JNM-PMX 60 SI spectrometer with Me_4Si as an internal standard in $CDCl_3$. The ^{13}C and ^{77}Se NMR spectra were recorded by using a JEOL JNM-FX 90Q spectrometer with Me_4Si and PhSeSePh as an internal standard, respectively. Gas chromatography was performed by using a Hitachi 163 and 263-30 gas chromatograph using SE 30 (10%), 1 m column. The gel-permeation chromatography was performed by using a JAI Model LC-08 liquid chromatograph with a JAIGEL-1H column (20×600 mm×2) using chloroform as an eluent. Mass spectra were determined with a JEOL JMX-DX 300 mass spectrometer with a JEOL JMA 5000 Mass Data System at an ionizing voltage of 20—70 eV.

Materials. Benzeneselenenyl chloride of Nakarai Chemicals was distilled prior to use; bp 82 °C/3 mmHg† (120 °C/20 mmHg).[10] Benzeneseleninyl chloride (**1**) was prepared by ozonization of benzeneselenenyl chloride with stirring in dry dichloromethane at −70 °C until the orange-red color faded

† 1 mmHg=133.322 Pa.

to a light yellow[8,11] by introducing ozone prepared by a Nippon Ozone Model 0-3-2 ozonizer. The prepared benzeneseleninyl chloride was used in reactions with olefins in situ since the compound is extremely hygroscopic and care must be taken to avoid moisture.

General Procedure for the Reaction of Benzeneseleninyl Chloride with Olefins. To a stirred solution containing 2.0 mmol of benzeneseleninyl chloride (**1**) in 20 cm^3 of dichloromethane under nitrogen bubbling in an ice bath was added 2 mmol of an olefin and 2 mmol of a Lewis acid. The mixture was stirred for an adequate time (until **1** has almost consumed by TLC analysis) at 0 °C or room temperature. Water (30 cm^3) was added to the reaction mixture, and the organic layer was separated and dried over anhydrous magnesium sulfate. The reaction products were isolated by gel-permeation chromatograph, and the structure was identified on the basis of their spectroscopic data.

2-Chloro-1,1-diphenylethylene (2a): Bp 118 °C/0.5 mmHg (298 °C);[12] IR (neat) 3070, 1600, 1500, 1445, 830, 755, and 695 cm^{-1}; ^1H NMR ($CDCl_3$) δ=6.57 (1H, s), 7.21 (5H, s), and 7.33 (5H, s); MS m/z 214 (^{35}Cl, M^+).

2-Bromo-1,1-diphenylethylene (2b): Bp 125—126 °C/1 mmHg (175—176 °C/11.5 mmHg);[13] IR (neat) 3065, 1590, 1500, 1445, 1220, 1075, 765, 740, and 695 cm^{-1}; ^1H NMR ($CDCl_3$) δ=6.70 (1H, s), 7.18 (5H, s), and 7.30 (5H, s); MS, m/z 258 (^{79}Br, M^+).

Chlorotriphenylethylene (2c): Mp 116—117 °C (117 °C);[14] IR (KBr) 3060, 1600, 1495, 1445, 750, and 695 cm^{-1}; ^1H NMR ($CDCl_3$) δ=6.81—7.47 (15H, m); MS m/z 290 (^{35}Cl, M^+).

1,2-Dichloro-1-phenylethane:[15] IR (neat) 3000, 1485, 1445, 1195, 1075, 940, 920, and 695 cm^{-1}; ^1H NMR ($CDCl_3$) δ=3.89 (2H, d, J=7.6 Hz), 4.95 (1H, t, J=7.6 Hz), and 7.29 (5H, s); MS m/z 174 (^{35}Cl, M^+).

***dl*-1,2-Dichloro-1,2-diphenylethane (6a):** Mp 93 °C (93 °C);[16] IR (KBr) 3070, 1490, 1450, 1230, 1205, 1070, 775, 745, and 700 cm^{-1}; ^1H NMR ($CDCl_3$) δ=5.18 (2H, s) and 7.09—7.28 (10H, m); MS m/z 250 (^{35}Cl, M^+).

***meso*-1,2-Dichloro-1,2-diphenylethane (6b):** Mp 190 °C (191 °C);[16] IR (KBr) 3010, 1490, 1440, 1225, 1175, 1065, 805, 760, and 685 cm^{-1}; ^1H NMR ($CDCl_3$) δ=5.17 (2H, s) and 7.36 (10H, s); MS m/z 250 (M^+).

2-Chloro-2-butenal (8a): Bp 147—148 °C (147—150 °C);[17] IR (neat) 1695 and 1175 cm^{-1}; ^1H NMR ($CDCl_3$) δ=2.06 (3H, d, J=6.6 Hz), 6.93 (1H, q, J=6.6 Hz), and 9.27 (1H, s); MS m/z 104 (^{35}Cl, M^+).

2-Chloro-3-phenylpropenal (8b): Bp 90—91 °C/1 mmHg (132—134 °C/8 mmHg);[17] IR (neat) 1685 and 1295 cm^{-1}; ^1H NMR ($CDCl_3$) δ=7.36—8.09 (6H, m) and 9.41 (1H, s); MS m/z 166 (^{35}Cl, M^+).

2-Chloro-3,3-diphenylpropenal (8c): Mp 117—119 °C; IR (KBr) 1685 and 1150 cm^{-1}. ^1H NMR ($CDCl_3$) δ=7.01—7.30 (10H, m) and 9.34 (1H, s); MS m/z 242 (^{35}Cl, M^+); Found: m/z 242.0492. Calcd for $C_{15}H_{11}OCl$: M, 242.0498.

3-Chloro-4-phenyl-3-buten-2-one (8d): IR (neat) 1695 and 1210 cm^{-1}; ^1H NMR ($CDCl_3$) δ=2.52 (3H, s) and 7.23—7.92 (6H, m); MS m/z 180 (^{35}Cl, M^+); Found: m/z 180.0346. Calcd for $C_{10}H_9OCl$: M, 180.0342.

2-Chloro-1,3-diphenyl-2-propen-1-one (8e): IR (neat) 1660 and 1250 cm^{-1}; ^1H NMR ($CDCl_3$) δ=7.27—7.91 (11H, m); ^{13}C NMR ($CDCl_3$) δ=128.39, 128.56, 129.48, 129.86, 130.34, 130.56, 132.46, 132.94, 136.84, 139.34, and 191.07; MS m/z 242 (^{35}Cl, M^+); Found: m/z 242.0497. Calcd for $C_{15}H_{11}OCl$: M, 242.0498.

Ethyl 2-Chloropropenoate (8f): IR (neat) 1745 and 1275 cm^{-1}; ^1H NMR ($CDCl_3$) δ=1.33 (3H, t, J=7.2 Hz), 4.28 (2H, q, J=7.2 Hz), 5.92 (1H, d, J=2.0 Hz), and 6.45 (1H, t, J=2.0 Hz); MS m/z 134 (^{35}Cl, M^+); Found: m/z 134.0139. Calcd for $C_5H_7O_2Cl$: M, 134.0134.

Butyl 2-Chloropropenoate (8g): IR (neat) 1745 and 1280 cm^{-1}. ^1H NMR ($CDCl_3$) δ=0.80—2.00 (7H, m), 4.20 (2H, t, J=7.2 Hz), 5.94 (1H, d, J=2.0 Hz), and 6.44 (1H, d, J=2.0 Hz); MS m/z 162 (^{35}Cl, M^+); Found: m/z 162.0452. Calcd for $C_7H_{11}O_2Cl$: M, 162.0447.

Methyl 2-Chloro-2-butenoate (8h): Bp 160—161 °C (161 °C);[18] IR (neat) 1745 and 1275 cm^{-1}; ^1H NMR ($CDCl_3$) δ=1.94 (3H, d, J=7.0 Hz), 3.78 (3H, s), and 7.10 (1H, q, J=7.0 Hz); MS m/z 134 (^{35}Cl, M^+).

Ethyl 2-Chloro-2-butenoate (8i): Bp 175—176 °C (176 °C);[18] IR (neat) 1725 and 1265 cm^{-1}; ^1H NMR ($CDCl_3$) δ=1.33 (3H, t, J=7.2 Hz), 1.94 (3H, d, J=7.2 Hz), 4.24 (2H, q, J=7.8 Hz), and 7.07 (1H, q, J=7.2 Hz); ^{13}C NMR ($CDCl_3$) δ=14.09, 14.91, 61.98, 125.96, 137.07, and 162.36; MS m/z 148 (^{35}Cl, M^+).

Methyl 2-Chloro-3-phenylpropenoate (8j): Mp 32—33 °C (33.0—33.5 °C);[19] IR (neat) 1730 and 1270 cm^{-1}; ^1H NMR ($CDCl_3$) δ=3.90 (3H, s) and 7.19—7.62 (6H, m); ^{13}C NMR ($CDCl_3$) δ=53.37, 121.84, 128.56, 130.24, 130.67, 132.95, 137.23, and 163.94; MS m/z 196 (^{35}Cl, M^+).

Ethyl 2-Chloro-3-phenylpropenoate (8k): Bp 104—105 °C/1 mmHg (209 °C/75 mmHg);[20] IR (neat) 1735 and 1265 cm^{-1}; ^1H NMR ($CDCl_3$) δ=1.36 (3H, t, J=7.4 Hz), 4.32 (2H, q, J=7.4 Hz), and 7.17—8.16 (6H, m); ^{13}C NMR ($CDCl_3$) δ=14.26, 62.58, 122.28, 128.51, 130.13, 130.62, 133.00, 136.90, and 163.39; MS m/z 210 (^{35}Cl, M^+).

Methyl *threo*-2,3-Dichloro-3-phenylpropionate:[21] ^1H NMR ($CDCl_3$) δ=3.57 (3H, s), 4.61 (1H, d, J=8.4 Hz), 5.42 (1H, d, J=8.4 Hz), and 7.33 (5H, s); MS m/z 232 (^{35}Cl, M^+).

Methyl *erythro*-2,3-Dichloro-3-phenylpropionate:[21] IR (KBr) 1750 and 1210 cm^{-1}; ^1H NMR ($CDCl_3$) δ=3.84 (3H, s), 4.54 (1H, d, J=10.8 Hz), 5.13 (1H, d, J=10.8 Hz), and 7.33 (5H, s); MS m/z 232 (^{35}Cl, M^+).

Ethyl *threo*-2,3-Dichloro-3-phenylpropionate:[21] ^1H NMR ($CDCl_3$) δ=1.06 (3H, t, J=7.4 Hz), 4.02 (2H, q, J=7.4 Hz), 4.63 (1H, d, J=8.6 Hz), 5.27 (1H, d, J=8.6 Hz), and 7.35 (5H, s); MS, m/z 246 (^{35}Cl, M^+).

Ethyl *erythro*-2,3-Dichloro-3-phenylpropionate:[21] IR (neat) 1750 and 1275 cm^{-1}; ^1H NMR ($CDCl_3$) δ=1.32 (3H, t, J=7.4 Hz), 4.28 (2H, q, J=7.4 Hz), 4.56 (1H, d, J=10.4 Hz), 5.17 (1H, d, J=10.4 Hz), and 7.31 (5H, s); MS m/z 246 (^{35}Cl, M^+).

2-Chloro-2-cyclopenten-1-one (10a): IR (neat) 1730 and 1300 cm^{-1}; ^1H NMR ($CDCl_3$) δ=2.35—2.86 (4H, m) and 7.51 (1H, t, J=2.8 Hz); MS, m/z 116 (^{35}Cl, M^+); Found: m/z 116.0032. Calcd for C_5H_5OCl: M, 116.0029.

2-Chloro-2-cyclohexen-2-one (10b): Mp 70—72 °C (70 °C);[22] IR (KBr) 1680 and 1320 cm^{-1}; ^1H NMR ($CDCl_3$) δ=1.78—2.75 (6H, m) and 7.07 (1H, t, J=4.8 Hz); MS, m/z 130 (^{35}Cl, M^+); Found: m/z 130.0192. Calcd for C_6H_7OCl: M, 130.0185.

2-Chloro-2-cyclohepten-1-one (10c): IR (neat) 1690 and 1350 cm^{-1}; ^1H NMR ($CDCl_3$) δ=1.34—2.91 (8H, m) and 6.95 (1H, t, J=6.8 Hz); MS m/z 144 (^{35}Cl, M^+); Found: m/z 144.0338. Calcd for C_7H_9OCl: M, 144.0342.

2-Chloro-1,4-benzoquinone (10d): Mp 55—56 °C (57 °C);[23] IR (KBr) 1655 and 1285 cm^{-1}; ^1H NMR ($CDCl_3$) δ=6.79 (2H, s) and 6.95 (1H, s); MS m/z 142 (^{35}Cl, M^+).

^{77}Se NMR Studies. A solution containing 1.92 g (10 mmol) of benzeneselenenyl chloride in 20 cm^3 of dry dichloromethane was ozonized at −50 °C. A part of the solution containing benzeneseleninyl chloride (**1**) was transferred to a NMR tube, and the ^{77}Se NMR spectrum was determined. The ^{77}Se NMR signal was observed at 850 ppm from diphenyl diselenide as the internal standard. Then, to a solution of benzeneseleninyl chloride prepared by the same manner described above was added 1.33 g (10 mmol) of aluminum chloride, and the mixture was stirred for 10 min at −50 °C. A part of the solution was transferred to a NMR tube, and the ^{77}Se NMR was determined. The ^{77}Se NMR signal was observed at 670 ppm from diphenyl diselenide as the internal standard.

References

1) For excellent reviews on organoselenium chemistry, see "Organic Selenium Compounds: Their Chemistry and Biology," ed by D. L. Klaymen and W. H. H. Grünther, John Wiley & Sons, New York (1973); "The Chemistry of Organic Selenium and Tellurium Compounds," ed by S. Patai and Z. Rappoport, John Wiley & Sons, New York (1986), Vol. 1; C. Paulmier, "Selenium Reagents and Intermediates in Organic Synthesis," ed by J. E. Baldwin, Pergamon Press, Oxford (1986); D. J. Clive, *Tetrahedron*, **34**, 1049 (1978); H. J. Reich, *Acc. Chem. Res.*, **12**, 22 (1979); K. C. Nicolaou, *Tetrahedron*, **37**, 4097 (1981); J. V. Comasseto, *J. Organomet. Chem.*, **253**, 131 (1983); D. Liotta, *Acc. Chem. Res.*, **17**, 28 (1984).

2) D. L. J. Clive and C. V. Denyer, *J. Chem. Soc., Chem. Commun.*, **1973**, 253.

3) D. L. J. Clive, *J. Chem. Soc., Chem. Commun.*, **1973**, 695; K. B. Sharpless, M. W. Young, and R. F. Lauer, *Tetrahedron Lett.*, **1973**, 1979; H. J. Reich, I. L. Reich, and J. M. Renga, *J. Am. Chem. Soc.*, **95**, 5813 (1973); H. J. Reich, J. M. Reng, and I. L. Reich, *ibid.*, **97**, 5434 (1975).

4) K. B. Sharpless, K. M. Gordon, R. F. Lauer, D. W. Patrick, S. P. Singer, and M. W. Young, *Chemica Scripta*, **8A**, 9 (1975); K. B. Sharpless and R. F. Lauer, *J. Am. Chem. Soc.*, **95**, 2697 (1973); P. A. Grieco, J. A. Noguez, and Y. Masaki, *Tetrahedron Lett.*, **1975**, 4213; W. Dumont, P. Bayet, and A. Krief, *Angew. Chem., Int. Ed. Engl.*, **13**, 806 (1974).

5) N. Sonoda, T. Yasuhara, K. Kondo, T. Ikehara, and S. Tsutsumi, *J. Am. Chem. Soc.*, **93**, 6344 (1971); K. Kondo, N. Sonoda, and H. Sakurai, *Chem. Lett.*, **1974**, 1429; K. Kondo, N. Sonoda, K. Yoshida, M. Koishi, and S. Tsutsumi, *Chem. Lett.*, **1972**, 401; K. Kondo, N. Sonoda, and S. Tsutsumi, *Tetrahedron Lett.*, **1971**, 4885; K. Kondo, N. Sonoda, and H. Sakurai, *Bull. Chem. Soc. Jpn.*, **48**, 108 (1975).

6) K. B. Sharpless and R. F. Lauer, *J. Am. Chem. Soc.*, **94**, 7154 (1972); D. Arigoni, A. Vasella, K. B. Sharpless, and H. P. Jensen, *ibid.*, **95**, 7917 (1973); H. P. Jensen and K. B. Sharpless, *J. Org. Chem.*, **40**, 264 (1975).

7) I. Lalezari, A. Shafiee, and M. Yalpani, *Tetrahedron Lett.*, **1969**, 5105; I. Lalezari, A. Shafiee, and M. Yalpani, *Angew. Chem., Int. Ed. Engl.*, **9**, 464 (1970); H. Meier and H. Gugel, *Synthesis*, **1976**, 338.

8) G. Ayrey, D. Barnard, and D. T. Woodbridge, *J. Chem. Soc.*, **1962**, 2089.

9) M. R. Czarny, *Synth. Commun.*, **6**, 285 (1976); G. Sosnovsky, J. A. Krogh, *Z. Naturforsch., B, Anorg. Chem., Org. Chem.*, **34B**, 511 (1979).

10) O. Behaghel and H. Seibert, *Ber.*, **66**, 708 (1933).

11) H. J. Reich, J. M. Renga, and I. L. Reich, *J. Am. Chem. Soc.*, **97**, 5434 (1975).

12) W. P. Bettenberg, *Justus Liebigs Ann. Chem.*, **279**, 324 (1894).

13) P. Lipp, *Ber.*, **56**, 567 (1923); G. Wittig and R. Kethur, *ibid.*, **69**, 2078 (1936).

14) E. Bergmann and A. Bondi, *Ber.*, **64**, 1455 (1931).

15) H. Bilz, *Justus Liebigs Ann. Chem.*, **296**, 263 (1897); G. H. Coleman and A. W. Campbell, *J. Am. Chem. Soc.*, **50**, 2754 (1928).

16) Th. Zincke, *Ber.*, **10**, 996 (1877); **12**, 115 (1879); P. Pfeiffer, *Ber.*, **45**, 1810 (1912); P. Pfeiffer and B. Eistert, *J. Pract. Chem.*, **124**, 168 (1930).

17) H. Hibbert, E. O. Houghton, and K. A. Taylor, *J. Am. Chem. Soc.*, **51**, 611 (1929).

18) F. D. Chattaway and H. Irving, *J. Chem. Soc.*, **1929**, 1038.

19) R. Stoermer and H. Kirchner, *Ber.*, **53**, 1289 (1920).

20) K. V. Auwers and E. Schmellenkamp, *Ber.*, **54**, 624 (1921).

21) C. Liebermann and H. Finkenbeiner, *Ber.*, **26**, 833 (1893); **28**, 2235 (1895).

22) A. Kotz and K. Richter, *J. Pract. Chem.*, **111**, 373 (1925).

23) E. Wöhler, *Justus Liebigs Ann. Chem.*, **51**, 145 (1844); G. Städeler, *ibid.*, **69**, 300 (1849).

 © 1988 The Chemical Society of Japan Bull. Chem. Soc. Jpn., 61, 455—459 (1988)

2-(Trifluoromethylsulfonyloxy)pyridine as a Reagent for the Ketone Synthesis from Carboxylic Acids and Aromatic Hydrocarbons

Takashi KEUMI,* Kiichiro YOSHIMURA, Masakazu SHIMADA, and Hidehiko KITAJIMA
Department of Applied Chemistry, Faculty of Engineering, Fukui University, Bunkyo, Fukui 910
(Received July 11, 1987)

A new reagent 2-(trifluoromethylsulfonyloxy)pyridine (**TFOP**) was prepared by the reaction of sodium salt of 2-pyridinol with trifluoromethylsulfonyl chloride in dioxane. The compound **TFOP** in trifluoroacetic acid has been found to intermolecularly dehydrate from benzoic acid and aromatic hydrocarbons to give the corresponding benzophenones in high yield. It was further elucidated, in the reaction of fluorene, that a variety of carboxylic acids can be used as the acyl precursor for the aromatic ketone synthesis in conjunction with the **TFOP/TFA** system. This acylation procedure has been applied to the synthesis of 2-acylthiophenes, which are hard to prepare in a satisfactory yield by the classical Friedel-Crafts reaction using aluminum chloride as the catalyst.

Acylation is one of the most important reaction in organic synthesis. Although various procedures for the acylation of hetero atoms of amines or alcohols, and for that of aliphatic carbons are available, only a few routes of acylation of aromatic carbons are known.[1] Among them, the Friedel-Crafts reaction using aluminum chloride as a catalyst is the most useful means.[2] However, we have encountered some inconveniences in the use of aluminum chloride as the catalyst. The acylation generally requires molar amounts of a catalyst which is a hygroscopic solid and forms complexes with the products. A consequent work-up is needed to decompose these complexes, and the catalyst is usually non-recoverable. A large amount of hydrochloric acid evolves during the reaction and during the hydrolysis of the complexes. In addition, the catalyst sometimes induces undesirable side reactions. For example, an acylation of thiophene with acid chloride and aluminum chloride is accompanied by a polymerization of the substrate.[3]

Recently, some procedures capable of acylating aromatic hydrocarbons without the use of the classical catalyst have been developed.[4-13] Above all the report by Effenberger that a carboxylic trifluoromethylsulfonic anhydride (I) has an ability to acylate aromatic hydrocarbons is very interesting.[4]

We have previously reported that an acyl group of 2-acyloxypyridines undergoes transacylation catalyzed by trifluoroacetic acid (**TFA**) to aromatic hydrocarbons existing in the solution to give aromatic ketones (Eq. 1).[8]

(1)

Analogously, the "transsulfonylation" could be expected to occur from 2-(trifluoromethylsulfonyloxy)pyridine (**TFOP**) to carboxylic acid in a **TFA** solution to give the mixed anhydride **I**, which is a good acylating agent of aromatic hydrocarbons.

In the present paper, we will report on the synthesis of **TFOP** and its application to a condensation reaction between carboxylic acids and aromatic hydrocarbons to give aromatic ketones.[14]

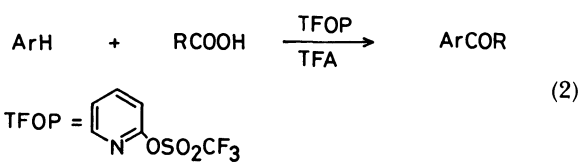

(2)

Results and Discussion

A new reagent, **TFOP**, was prepared by a reaction of the sodium salt of 2-pyridinol with trifluoromethylsulfonyl chloride in dioxane. The compound is a relatively stable and colorless liquid. Its physical data are shown in the experimental section.

The utility of **TFOP** as a dehydrating reagent between carboxylic acid and aromatic hydrocarbon to give aromatic ketones was investigated. First, a reaction involving some kinds of aromatic hydrocarbons with benzoic acid in the presence of **TFOP** has been carried out in **TFA** solution (Eq. 3). For example, durene was heated with benzoic acid and **TFOP** in a molar ratio of 1 : 1.1 : 1.1, respectively, in **TFA** under reflux for 5 h to give 2,3,5,6-tetramethylbenzophenone in a quantitative yield. In a similar procedure, reactions of some other aromatic hydrocarbons with benzoic acid were carried out. The results are summarized in Table 1. Dimethoxybenzenes, tri- and tetramethylbenzenes, anisoles, dibenzofuran, and diphenyl ether reacted with benzoic acid in the presence of **TFOP** in **TFA** to give the corresponding benzophenone derivatives in satisfactory yields. Alternatively, benzene, biphenyl, and *p*-xylene were not benzoylated by this method.

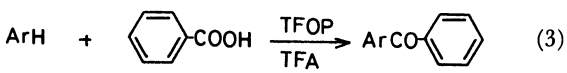

(3)

The validity of the **TFOP/TFA** system as a reagent leading carboxylic acids and aromatic hydrocarbons to

Table 1. The Results of Benzoylation of Aromatic Hydrocarbons with **TFOP** and Benzoic Acid[a]

Aromatic substrate	Product	Isolated yield %	Mp or Bp/°C/mmHg Found	Mp or Bp/°C/mmHg Reported	IR $\nu_{C=O}$/cm^{-1} (KBr or neat)
o-Dimethoxybenzene	3,4-Dimethoxy-BZ[b]	97	99—100	103—104[15]	1640
m-Dimethoxybenzene	2,4-Dimethoxy-BZ	97	86—88	87—88[15]	1660
p-Dimethoxybenzene	2,5-Dimethoxy-BZ	93	49—50	51[16]	1665
Dibenzofuran	2-Benzoyldibenzofuran	75	136—137	136—137[17]	1655
Durene	2,3,5,6-Tetramethyl-BZ	99	119—120	119[15]	1670
1,2,3,5-Tetramethylbenzene	2,3,4,6-Tetramethyl-BZ	99	60—61	62—63[15]	1665
o-Methylanisole	3-Methyl-4-methoxy-BZ	99	80—81	80[18]	1643
Anisole	4-Methoxy-BZ	97	61—63	61—62[15]	1650
Diphenyl ether	4-Phenoxy-BZ	99	66—67	71[19]	1650
Mesitylene	2,4,6-Trimethyl-BZ	96	156—157/6	189/17[15]	1670
m-Xylene	2,4-Dimethyl-BZ	95	186/12	186—190/15[15]	1660
p-Xylene	2,5-Dimethyl-BZ	19[c]	36	36[15]	1668
Biphenyl	4-Phenyl-BZ	31[c]	102—103	103[15]	1642
Benzene	BZ	17[c]	48	49[15]	1655

a) All the reactions were carried out under reflux of a solution of ArH (6 mmol), benzoic acid (7 mmol), and **TFOP** (7 mmol) in **TFA** (5 mL) for 5 h. b) BZ=Benzophenone. c) Determined by GLC.

Table 2. The Reaction of Acylation of Fluorene with a Carboxylic Acid and **TFOP**[a]

Entry	Carboxylic acid	2-Acylfluorene isolated yield/%	Mp[b]/°C	IR $\nu_{C=O}$/cm^{-1} (KBr)
1	CH_3COOH	81	130—131	1678
2	CH_3CH_2COOH	82	118—119	1675
3	C_6H_5COOH	93	122—123	1645
4	*p*-$CH_3OC_6H_4COOH$	82	155—156	1640
5	*m*-$CH_3OC_6H_4COOH$	67	99—100	1645
6	*p*-$CH_3C_6H_4COOH$	96	118—119	1645
7	*m*-$CH_3C_6H_4COOH$	80	115—116	1655
8	*o*-$CH_3C_6H_4COOH$	71	138—139	1660
9	*p*-ClC_6H_4COOH	81	177—179	1648
10	*m*-ClC_6H_4COOH	56	149—151	1650
11	*o*-ClC_6H_4COOH	75	133—134	1650
12[c]	*p*-$NO_2C_6H_4COOH$	34	184—185	1644

a) All the reactions were carried out under reflux of a solution of fluorene (6 mmol), carboxylic acid (7 mmol), and TFOP (7 mmol) in TFA (5 mL) for 5 h. b) The products were identified by the mixed melting point test with authentic samples previously reported in Ref. 9. c) Heterogeneous reaction due to the low solubility of *p*-nitrobenzoic acid in boiling TFA.

ketones was further investigated in a reaction of fluorene with a variety of carboxylic acids (Eq. 4). Reactions were also carried out in a manner similar to that described for the benzoylation of durene. The results are summarized in Table 2. Except for *p*-nitrobenzoic acid, aliphatic and aromatic carboxylic acids gave the corresponding 2-acylfluorenes in good isolated yields. Particularly, aliphatic carboxylic acids and benzoic acids, having an electron-donating group, resulted in a high yield of 2-acylfluorenes.

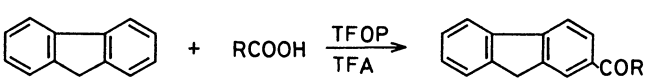

(4)

The combination of carboxylic acid with the **TFOP/TFA** system was applied to the acylation of thiophene (Eq. 5). A mixture of thiophene, *p*-chlorobenzoic acid, and **TFOP** was heated in **TFA** under reflux for 4 h to yield 2-(*p*-chlorobenzoyl)-thiophene in a quantitative yield. Other acylthiophenes were also obtained by the reaction of thiophene with **TFOP** and carboxylic acids in satisfactory yields. The results are given in Table 3.

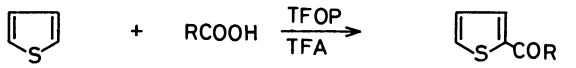

(5)

Thus, **TFOP** has been shown to serve as a condensation reagent between a variety of carboxylic acids and aromatic hydrocarbons to give aromatic ketones.

The classical catalyst aluminum chloride is not so suitable for an acylation of thiophene by Friedel-Crafts method since the catalyst partly induces a polymerization of thiophene. Although some improved procedures using less weak acids such as BF_3/MeOH complex,[24] $SnCl_4$,[3] 85% H_3PO_4,[21] or solid super acid Nafion-H,[12] and so on, have been used, the yields of acylthiophenes are still not very satisfactory. The

Table 3. The Results of Acylation of Thiophene with a Carboxylic Acid and **TFOP**[a]

Carboxylic acid	2-Acylthiophene Isolated yield/%	Mp or Bp/°C/mmHg		IR $\nu_{C=O}$/cm^{-1} (KBr or neat)
		Found	Reported	
CH_3COOH	99	107—110/30	89—91/9[3]	1662
CH_3CH_2COOH	95	115—116/33	116/20[20]	1662
C_6H_5COOH	99	55—56	56—57[21]	1630
p-$CH_3OC_6H_4COOH$	93	72—74	76—77[22]	1630
m-$CH_3OC_6H_4COOH$	92	146—148/3		1635
p-$CH_3C_6H_4COOH$	89	70—71	75—76[23]	1630
m-$CH_3C_6H_4COOH$	93	219—220/25		1632
o-$CH_3C_6H_4COOH$	95	145—147/5		1637
p-ClC_6H_4COOH	99	94—95	99—100[22]	1632
m-ClC_6H_4COOH	93	62—64		1635
p-FC_6H_4COOH	99	95—96		1630

a) All the reactions were carried out under reflux of a solution of thiophene (6 mmol), carboxylic acid (7 mmol), and **TFOP** (7 mmol) in **TFA** (5 mL) for 4 h.

Table 4. Effects of **TFA** and Solvent on the Benzoylation of Thiophene with Benzoic Acid and **TFOP**[a]

Entry	Solvent	Molar ratio of **TFA**/ thiophene	Yield of 2-benzoyl-thiophene/%[b]
1	1,2-Dichloroethane	10	99
2	1,2-Dichloroethane	5	99
3	1,2-Dichloroethane	2	86
4	1,2-Dichloroethane	1	29
5	1,2-Dichloroethane	0	0
6	Acetonitrile	5	62
7	Chloroform	5	11
8	Dichloromethane	5	2

a) All the reactions were carried out under reflux of a solution of thiophene (6 mmol), benzoic acid (7 mmol), and **TFOP** (7 mmol) in a given solvent (5 mL) for 4 h. b) Determined by GLC.

method described here directly gives the 2-acylthiophenes from carboxylic acid and thiophene in a quite high yield.

In light of the reaction mechanism, the effect of **TFA** on the ketone yields was investigated in the benzoylation of thiophene with benzoic acid and **TFOP** in a solvent. The results are shown in Table 4. As can be seen, the acylation reaction dose not occur without the addition of **TFA**. The reaction requires at least two equivalents of **TFA** to **TFOP** to result in a satisfactory yield of the ketone. An inert solvent with a relatively high boiling point, 1,2-dichloroethane, seems to be recommendable as a co-solvent for a ketone synthesis by the carboxylic acid/**TFOP**/**TFA** system.

If the acylation reaction proceeds via a cationic acyl species which attacks an aromatic nucleus in the rate-determining step, as in a usual Friedel-Crafts reaction, the ketone yields should increase with an electron-withdrawing group in the acylating species.[25] On the contrary the yields of 2-acylfluorenes by the substituted benzoic acid/**TFOP**/**TFA** system have resulted in a decrease with an electron-withdrawing group in the benzoic acid (entries 5 and 10 in Table 2). Hence, a direct electrophilic attack on the aromatic nucleus by the cationic acyl carbon dose not seem to be involved in the rate-determining step.

We have previously reported that the 2-acyloxypyridine/**TFA** system acylates fluorene to give 2-acylfluorene, in which a mechanism proceeding via the formation of pyridinium salt **A** followed by acyl trifluoroacetate (**II**) playing a role as the real acylating entities was assumed (shown in Scheme 1).[8] The substituent effects on acylation of fluorene by the substituted benzoic acids/**TFOP**/**TFA** system is similar to the trend observed in the acylation by the 2-acyloxypyridine/**TFA** system.

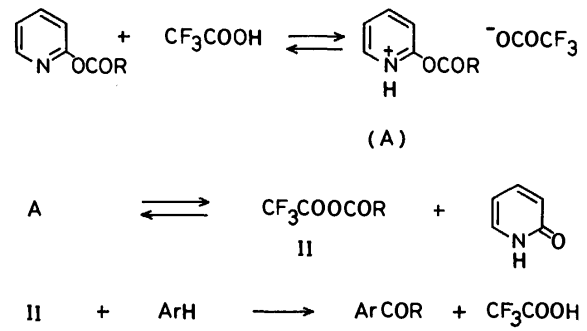

Scheme 1.

Effenberger had reported that the mixed anhydride **I** prepared from carboxylic acid chloride and silver trifluoromethylsulfonate can acylate an aromatic hydrocarbon. Here also, it can be considered that these kinds of mixed anhydrides could be formed via the activated pyridinium salt **B** in the course of the reaction. Thus, the transsulfonylation of the salt **B** to carboxylic acid would take place to give the anhydride **I**, and/or the salt **B** would generate the very reactive trifluoroacetic trifluoromethylsulfonic anhydride which reacts with carboxylic acid to give the mixed anhydride **II**. Either **I** or **II**, or both of them, seem to work as an acylating agent of aromatic compounds, as shown in Scheme 2. The formation of mixed anhydrides **I** and **II** might be involved in the rate-controlling step regarding the reaction. A significant substituent effect in the substi-

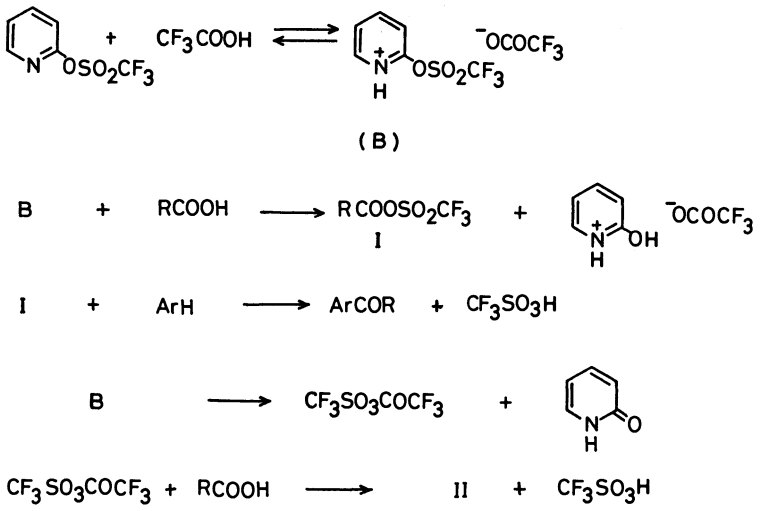

Scheme 2.

tuted benzoic acids, however, has not been observed in the acylation of thiophene which is more reactive than fluorene. Consequently, a cleavage of the carbon-oxygen bond between the acyl group and trifluoromethylsulfonate or trifluoroacetate, respectively, in **I** or **II** would be involved in the transition state, so that the yield of 2-acylfluorenes would be lower in the reaction with the benzoic acids containing an electron-withdrawing group, since the bond in such anhydrides is difficult to break.

In conclusion, we have now established that **TFOP** is useful as a reagent for a condensation between carboxylic acid and aromatic hydrocarbon to give aromatic ketones. Our method seems to have the following superior points. The ketones can be directly obtained by a reaction of aromatic compound with an equivalent mole of carboxylic acid in quite high yield. This system can acylate thiophene to give 2-acylthiophenes free from contamination by polymerization products. Trifluoroacetic acid is now popular and it has a moderate boiling point to make it easy to recover from the reaction mixture by distillation. If necessary, we can use 1,2-dichloroethane as the co-solvent to reduce a quantity of **TFA**. The reaction products can be easily separated by washing the mixture with water after distilling off **TFA**. Trifluoromethylsulfonic acid dissolved in the washing aqueous solution can be recoverd quantitatively as the barium salt.

Experimental

Materials and Measurements. All the acylated products were identified by comparing their physical data with those of authentic samples synthesized by classical Friedel-Crafts reactions, or by IR, ^{1}H NMR, and elemental analysis. Melting points are uncorrected. The IR spectra were recorded on a Hitachi EPI-S2 model infrared spectrophotometer. ^{1}H NMR spectra were recorded on a JEOL-FX 270 FT-NMR spectrometer in chloroform-*d* solution with tetramethylsilane internal standard. GLC analysis was carried out on a Hitachi GC Model 163 gas chromatograph equipped with a hydrogen flame ionization detector and a stainless steel column (length 3 m, i.d. 3 mm) packed with 3% Dexil 300 GC on Chromosorb W.

Preparation of TFOP. To a solution of 2-hydroxypyridine (14.07 g, 0.148 mol) in dry dioxane (100 mL), a suspension of sodium hydride (3.55 g, 0.148 mol) in dioxane (20 mL) was added with stirring at 40 °C over 15 min. Then, a solution of trifluoromethylsulfonyl chloride (25.0 g, 0.148 mol) in dry tetrahydrofuran (20 mL) was added slowly to the mixture with stirring over 1 h. After stirring at room temperature for 2 h, the reaction mixture was filtered, and the solvent of filtrate was evaporated under reduced pressure. The residue was distilled under reduced pressure to give **TFOP** (22 g, 65% yield); bp 108 °C/25 mmHg,† 105 °C/22 mmHg, 95 °C/19 mmHg; IR (neat) 1600, 1430, 1260, 1175, and 890 cm^{-1}; ^{1}H NMR ($CDCl_3$) δ=8.41 (dd, 1H, J=0.5 and 2 Hz), 7.92 (dt, 1H, J=0.72 and 3Hz), 7.38—7.43 (m, 1H), and 7.24 (d, 1H, J=7 Hz); MS *m/z* (rel intensity, %) 227 (M^+, 70), 163 (10), 135 (100), and 113 (20). Found: C, 31.65; H, 2.00; N, 6.18%. Calcd for $C_6H_4NO_3SF_3$: C, 31.72; H, 1.77; N, 5.17%.

Benzoylation of Durene. To a mixture of benzoic acid (7 mmol) and **TFOP** (7 mmol) in **TFA** (5 mL), durene (6 mmol) was added. After the mixture was heated under reflux for 5 h, it was poured into ice-water, and the resulting precipitate was filtered and washed with water and a dilute alkali solution to give the crude product of 2,3,5,6-tetramethylbenzophenone (mp 119 °C, 99% yield). Recrystallization of the crude product from methanol gave a product of mp 119—120 °C (85% yield).

***p*-Chlorobenzoylation of Fluorene.** To a mixture of fluorene (6 mmol), *p*-chlorobenzoic acid (7 mmol), and **TFOP** (7 mmol), **TFA** (5 mL) was added and the mixture was heated under reflux for 5 h. Then, after evaporating **TFA** under reduced pressure, unreacted fluorene was distilled off with steam to give 2-(*p*-chlorobenzoyl)fluorene as the residue (mp 172—176 °C, 81% yield). Recrystallization of the product from ethanol gave a product of mp 177—179 °C.

***o*-Methylbenzoylation of Thiophene.** To a mixture of thiophene (6 mmol), *o*-methylbenzoic acid (7 mmol), and

† 1 mmHg=133.322 Pa.

TFOP (7 mmol), **TFA** (5 mL) was added and the mixture was heated under reflux for 4 h. Then, the reaction mixture was poured into ice-water and was extracted by ether. The organic layer was washed with water, alkali, and water, and was dried over anhydrous sodium sulfate. After evaporation of the solvent, crude 2-(*o*-methylbenzoyl)thiophene was obtained as the oily product (95% yield). The distillation of the oil under reduced pressure gave a product of bp 145—147 °C/5 mmHg (85% yield); IR (Neat) 1637, 1410, 1305, 1276, 850, and 735 cm^{-1}; ^1H NMR ($CDCl_3$) δ=7.70 (d, 1H, J=2 Hz), 7.36—7.66 (m, 5H), 7.13—7.16 (m, 1H), and 2.42 (s, 3H, Me). Found: C, 71.21; H, 4.94%. Calcd for $C_{12}H_{10}OS$: C, 71.26; H, 4.98%.

By a similar procedure, the following 2-acylthiophenes were prepared.

2-(*m*-Methylbenzoyl)thiophene: 93% yield; bp 219—220 °C/25 mmHg; IR (neat) 1632, 1410, 1290, 1210, 775, and 730 cm^{-1}; ^1H NMR ($CDCl_3$) δ=7.70—7.72 (m, 4H), 7.29—7.42 (m, 2H), 7.08—7.25 (m, 1H), and 2.38 (s, 3H, Me). Found: C, 71.42; H, 4.99%. Calcd for $C_{12}H_{10}OS$: C, 71.26; H, 4.98%.

2-(*m*-Methoxybenzoyl)thiophene: 92% yield; bp 146—148 °C/3 mmHg; IR (neat) 1635, 1410, 1285, 890, and 730 cm^{-1}; ^1H NMR($CDCl_3$) δ=7.65—7.71 (m, 2H), 7.38—7.45 (m, 3H), 7.10—7.16 (m, 2H), and 3.85 (s, 3H, OMe). Found: C, 66.09; H, 4.58%. Calcd for $C_{12}H_{10}O_2S$: C, 66.03; H, 4.62%.

2-(*m*-Chlorobenzoyl)thiophene: 93% yield; Mp 62—64 °C (from hexane); IR (KBr) 1635, 1400. 1290, 890, and 730 cm^{-1}; ^1H NMR ($CDCl_3$) δ=7.41—7.83 (m, 6H) and 7.16—7.20 (m, 1H). Found: C, 9.49; H, 3.22%. Calcd for $C_{11}H_7OSCl$: C, 59.33; H, 3.17%.

2-(*p*-Fluorobenzoyl)thiophene: 99% yield; Mp 95—96 °C (from 60% EtOH); IR (KBr) 1630, 1412, 1295, 850, and 720 cm^{-1}; ^1H NMR ($CDCl_3$) δ=7.89—7.94 (m, 2H), 7.63—7.75 (m, 2H), and 7.15—7.25 (m, 3H). Found: C, 63.89; H, 3.21%. Calcd for $C_{11}H_7OSF$: C, 64.06; H, 3.42%.

References

1) S. R. Sandler and W. Karo, "Organic Functional Group Preparations," Academic Press, New York (1968), p. 245, 270; A. Buehler and D. E. Person, "Survey of Organic Syntheses," John Wiley and Sons, New York (1970), p. 801, 894; H. O. House, "Modern Synthetic Reactions," Benjamin, Menlo Park (1972), p. 734.

2) P. H. Gore, *Chem. Rev.*, **55**, 233 (1955); "Friedel-Crafts and Related Reactions," ed by G. A. Olah, John Wiley and Sons, New York (1964), Vol. 111, p. 1.

3) J. R. Johnson and G. E. May, *Org. Synth.*, Coll. Vol. II, 8 (1943).

4) F. Effenberger and G. Epple, *Angew. Chem., Int. Ed. Engl.*, **11**, 299 (1972).

5) F. Effenberger, G. Konig, and H. Klenk, *Angew. Chem., Int. Ed. Engl.* **17**, 695 (1978).

6) T. R. Forbus and J. C. Martin, *J. Org. Chem.*, **44**, 313 (1979).

7) C. Gall, *Synthesis*, **1979**, 303.

8) T. Keumi, R. Taniguchi, and H. Kitajima, *Synthesis*, **1980**, 139.

9) T. Keumi, H. Saga, and H. Kitajima, *Bull. Chem. Soc. Jpn.*, **53**, 1638 (1980).

10) G. A. Olah, R. Malhotra, S. C. Narang, and J. A. Olah, *Synthesis*, **1978**, 672.

11) K. Nomiya, Y. Sugaya, S. Saga, and M. Miwa, *Bull. Chem. Soc. Jpn.*, **53**, 2089 (1980).

12) H. Konishi, K. Suetzugu, T. Okano, and J. Kiji, *Bull. Chem. Soc. Jpn.*, **55**, 957 (1982).

13) T. Mukaiyama, H. Nagaoka, and M. Oshima, *Chem. Lett.*, **1986**, 165.

14) A part of the results have been preliminarily reported as communications: T. Keumi, H. Saga, R. Taniguchi, and H. Kitajima, *Chem. Lett.*, **1977**, 1099.

15) H. Heibron, "Dictionary of Organic Compounds," Maruzen, Tokyo (1965).

16) M. T. Bogert and H. P. Howell, *J. Am. Chem. Soc.*, **52**, 837 (1930).

17) T. Keumi, S. Shimakawa, and Y. Oshima, *Nippon Kagaku Kaishi*, **1977**, 1518.

18) W. Koenigs and R. W. Carl, *Ber.*, **24**, 3898 (1891).

19) H. Kipper, *Ber.*, **38**, 2492 (1905).

20) K. Krekeler, *Ber.*, **19**, 677 (1886).

21) A. I. Kosak and H. D. Hartough, U. S. Patent 2458519 (1949); *Chem. Abstr.*, **43**, 2643g (1949).

22) N. D. Buu-Hoi, Ng. Hoan, and Ng. D. Xuong, *Rec. Trav. Chem.*, **69**, 1083 (1950).

23) J. J. Spurlock, *J. Am. Chem. Soc.*, **75**, 1115 (1953).

24) H. D. Hartough and A. I. Kosak, *J. Am. Chem. Soc.*, **70**, 867 (1948).

25) P. J. Slootmaekers, A. Rasschaert, and W. Janssens, *Bull. Soc. Chim. Belges.*, **75**, 199 (1966).

 © 1988 The Chemical Society of Japan Bull. Chem. Soc. Jpn., 61, 461—465 (1988)

Synthesis and a Novel Fragmentation of 6-Alkoxy-5,6-dihydro-4*H*-1,2-oxazine 2-Oxide

Yasuo TOHDA,* Norihiko YAMAWAKI, Hiroko MATSUI, Toshihide KAWASHIMA, Masahiro ARIGA, and Yutaka MORI

Department of Chemistry, Osaka Kyoiku University, Minamikawahoricho 4-88, Tennoji-ku, Osaka 543

(Received July 28, 1987)

An electron-deficient nitro olefin, methyl α,*p*-dinitrocinnamate, reacts with vinyl ethers to give cyclic nitronic esters, which are stable as compared with those produced by reactions of nitro olefins with enamines. Stability of the cyclic nitronate depends on the properties of the substituents at 4- and 6-positions of the ring. The adducts undergo fragmentation by a catalytic amount of base to β,γ-unsaturated α-hydroxyimino esters.

A cyclic nitronic ester, 5,6-dihydro-4*H*-1,2-oxazine 2-oxide, has been known as an interesting intermediate which can be converted into nitroalkylated enamines,[1] 1,4-diones,[2] and so forth[3] via easy heterolytic cleavage of the O(1)-C(6) bond. Such cyclic compounds are easily obtainable by reactions of simple nitro olefins with enamines,[1] silyl enol ethers,[2] enolate anions,[4] or cyclohexene,[5] although little has been clarified on the chemical properties of them except for the O(1)-C(6) bond cleavage owing to their thermal and hydrolytic instability. In order to investigate further reactivities of the dihydrooxazine *N*-oxide, we wished to prepare stable cyclo adducts by reaction of nitro olefins with vinyl ethers. The dihydrooxazine *N*-oxide might be stable if the carbocation formed by the bond cleavage of the compound would be unstable (Scheme 1) or, in other words, if the substituent X in Scheme 1 would be less electron-donating. Direct reaction of simple nitro olefins with vinyl ethers failed, however, to give adducts because of low nucleophilicity of the latters. Another strategy to prepare the stable cycloadduct may be usage of highly electrophilic nitro olefins. We report here cycloaddition of an electron-deficient nitro olefin, methyl α,*p*-dinitrocinnamate (**1**), with vinyl ethers, and some properties of the cycloadducts.

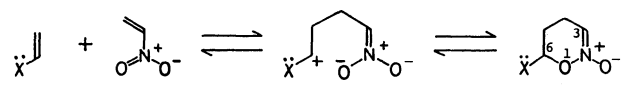

Scheme 1.

Results and Discussion

Reaction of **1** with ethyl vinyl ether in DMF at room temperature gave a diastereomeric mixture **2** of two cycloadducts in 92% yield. The ^{1}H NMR spectra of the isomers **2a** and **2b** reveal that they have cyclic structures rather than the alternative linear ones, methyl 5-ethoxy-2-nitro-3-(*p*-nitrophenyl)-2-, 3-, or 4-pentenoates. The ratio of the isomers **2a** and **2b** was about 4 : 1 regardless of the configurations of the nitro olefin. The results are consistent with the mechanism of the step wise cyclization shown in Scheme 1. The small coupling constants (ca. 3.5 Hz) between 6-H and 5- or 5′-H of both isomers show that the 6-ethoxyl group is in an axial position of a pseudo chair ring. The configuration may be rationalized by the strong anomeric effect of the ring.[6] A difference between the spectra of **2a** and **2b** lies in the coupling patterns of 4-H ($J_{4,5}$ and $J_{4,5'}$=3.5 Hz and 8.7 Hz for **2a**; $J_{4,5}$ and $J_{4,5'}$=8.7 Hz and 9.1 Hz for **2b**). This difference may arise from different configurations of the aryl group at C(4) of the ring. The aryl group of **2a** is in a pseudoaxial position, while that of **2b** is in a pseudoequatorial one. Another difference is observed in the ester stretching band (1705 cm^{-1} for **2a**; 1745 cm^{-1} for **2b**). The higher frequency of the carbonyl band of **2b** may be interpreted in terms of restricted conjugation between the ester and the nitronic ester groups due to steric repulsion between the ester and the aryl groups (Fig. 1). From these results the structures of **2a** and **2b** were assigned to *cis*- and *trans*-6-ethoxy-3-methoxycarbonyl-4-(*p*-nitrophenyl)-5,6-dihydro-4*H*-1,2-oxazine 2-oxide, respectively (Fig. 1).

Other substituted vinyl ethers also reacted with **1** at higher temperatures to give the similar cyclic adducts **3**—**6** (Eq. 1 and Table 1). These substituted vinyl ethers did not reacted at room temperature because of the bulkiness of the reagents. The ^{1}H NMR and IR spectra of the adducts show that they are also a mixture of diastereomers, although details of their stereochemistry are not clear yet.

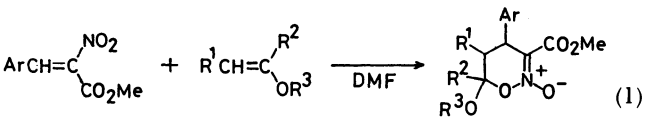

(1)

1 **2~6**

(Ar=*p*-$C_6H_4NO_2$)

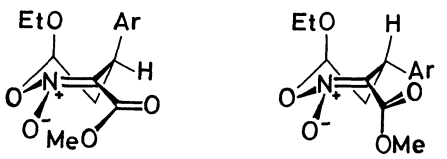

2a **2b**

Fig. 1. Structures of the adducts **2a** and **2b**. (Ar=$C_6H_4NO_2$-*p*)

Table 1. Cycloaddition of Methyl α,*p*-Dinitrocinnamate (**1**) with Vinyl Ethers

Vinyl ether	Reaction conditions		Product	Decomp temp/°C	Yield/%
	Temp./°C	Time/h			
Ethyl vinyl ether	r.t.	24	**2**	124—127	92
2,3-Dihydrofuran	60	12	**3**	148—153	80
3,4-Dihydro-2*H*-pyran	60	12	**4**	140—143	30
1-Methoxycyclopentene	50	12	**5**	141—144	84
1-Methoxycyclohexene	50	12	**6**	174—175	72

When **1** was reacted with 1-morpholinocyclohexene at 0 °C in benzene, an unstable adduct, which was assumed to be a dihydrooxazine *N*-oxide derivative, was precipitated. It spontaneously decomposed into the Michael adduct in benzene solution as well as other cyclic adducts of nitro olefins with enamines.[1] On the contrary, the adducts **2—6** were very stable even at 100 °C. This fact indicates that the stability of the dihydrooxazine *N*-oxide structure depends on the electronic properties of the substituents at C(6) as expected.

Reactions of methyl α-nitrocinnamate (**7**) or less electrophilic nitro olefins such as methyl β-methoxy-α-nitroacrylate or β,*p*-dinitrostyrene, with ethyl vinyl ether did not give the corresponding 1 : 1 cycloadducts even at higher temperatures. On the other hand, treatment of **7** with ethyl vinyl ether in the presence of acrylonitrile at 70 °C in DMF gave an 1 : 1 : 1 adduct **8** in 57% yield (Eq. 2). The role of the acrylonitrile is to trap an unstable dihydrooxazine *N*-oxide by 1,3-dipolar addition, because **2a** also reacted with acrylonitrile even in the presence of ethyl vinyl ether to give the corresponding 1 : 1 : 1 adduct **9** (Eq. 3). In the absence of acrylonitrile, the reaction of **2a** with ethyl vinyl ether gave an 1 : 2 adduct **10** at 70 °C in DMF. These reactions are consistent with the reactivity of nitronic esters as an electron-rich 1,3-dipole.[7] The 1 : 1 cycloadduct of **7** with ethyl vinyl ether (see Eq. 2) could not be isolated in contrast with the stable nitronate **2**. The fact implies that the stability of the dihydrooxazine *N*-oxide seems to be affected by the C(4)-substituent as well as the C(6)-one.

Methanolysis of **2a** and **2b** under acidic conditions gave the same product, methyl 5,5-dimethoxy-2-nitro-3-(*p*-nitrophenyl)pentanoate as a result of the common O(1)-C(6) bond cleavage.[1-4]

Treatment of **2a** by a catalytic amount of sodium hydroxide in DMSO-d_6 at room temperature gave ethyl formate and methyl 2-hydroxyimino-3-(*p*-nitrophenyl)-3-butenoate (**11**), immediately and quantitatively. Ammonia was a less efficient catalyst because of poor yield of **11**. Bulky triethylamine did not give any products even at a reflux temperature of THF. On the other hand, the stereoisomer **2b** gave neither **11** nor **8** under the corresponding reaction conditions. These results may be attributed to the steric hinderance around the nitronic ester moiety of **2b** as mentioned above. Although the adducts **2—6** are mixtures of diastereomers, they also gave the fragmentation products **11—15** in good to moderate yields by treatment with sodium methoxide (Eq. 4 and Table 2). The formation of the products **12** and **13** may proceed via easy hydrolysis of the initially formed formate given in Eq. 4. On the basis of these results, the rate-determinig step of the fragmentation may be deprotonation of 4-H of the ring. Such a reaction of the 5,6-dihydro-4*H*-1,2-oxazine 2-oxides has not been known yet, while the similar fragmentation of some related compounds, 5-thia analogues[8] or N-alkyl salts[9] of 5,6-dihydro-4*H*-1,2-oxazine have been reported. Most of the reported reactions of the dihydrooxazine *N*-oxides with strong bases also proceed via the O(1)-C(6) bond cleavage.[1a,4] Stability of the O(1)-C(6) bond may be one of the important factors of this fragmentation.

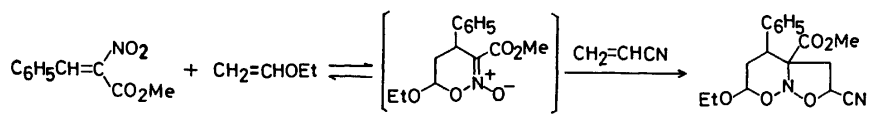

7 8 (2)

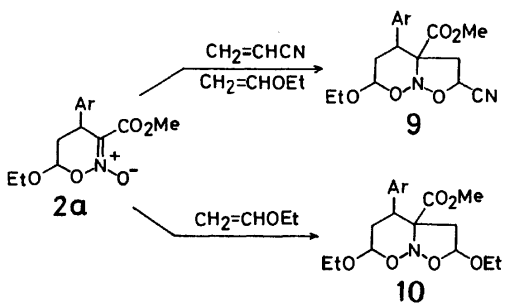

(3)

(Ar=$C_6H_4NO_2$-*p*)

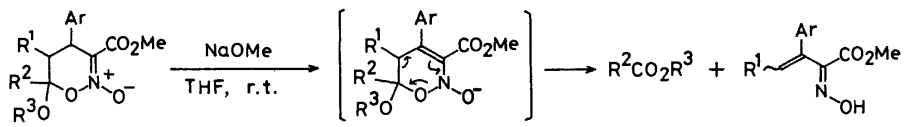

2~6 11~15 (4)

(Ar=$C_6H_4NO_2$-*p*)

Table 2. Fragmentation of 6-Alkoxy-5,6-dihydro-4*H*-1,2-oxazine 2-Oxides by Sodium Methoxide

Substrate	Product	R^1	Mp θ_m/°C	Yield/%
2	**11**	H	149.5—151.5	82
3	**12**	$(CH_2)_2OH$[a)]	140.5—144.5	25
4	**13**	$(CH_2)_3OH$[a)]	96.5—98.5	80
5	**14**	$(CH_2)_3CO_2Me$	98.5—99.0	78
6	**15**	$(CH_2)_4CO_2Me$	Oil	64

a) The isolated products were given by hydrolysis of the initial products [R^1=$[(CH_2)_nOCOH]$ under the reaction conditions.

Reduction of **2a** and **2b** by triethyl phosphite gave the corresponding isomers of 2-deoxygenated products, **16a** and **16b**, respectively. Treatment of **16a** with a catalytic amount of sodium methoxide in THF gave the other isomer **16b** in 42% yield probably via deprotonation of 4-H of the ring. However the similar fragmentation of **16b** shown by Eq. 4 did not occur at all. Reported transformations of other 5,6-dihydro-4*H*-1,2-oxazines[10] are also quite different from this fragmentation. Consequently the *N*-oxide function of the adducts must play a significant role in the fragmentation.

The present fragmentation is a unique reaction of stable 5,6-dihydro-4*H*-1,2-oxazine 2-oxides.

Experimental

The infrared spectra were measured in nujol by means of a Hitachi 260-10 spectrophotometer and the ^{1}H NMR spectra were taken on a Hitachi R-20B spectrometer.

Methyl α,*p*-Dinitrocinnamate (1). This nitro olefin was prepared by the method of Dornow[11] in 72% yield (E : Z=3 : 4 by ^{1}H NMR). Fractional recrystallization from CCl_4 gave each isomer. E Isomer: Pale yellow needles; mp 135—138 °C. ^{1}H NMR ($CDCl_3$) δ=3.96 (s, 3H), 7.69 (d, 2H, *J*=8.9 Hz), 8.12 (s, 1H), 8.31 (d, 2H, *J*=8.9 Hz). IR: 1740 cm^{-1} (C=O), 1520, 1350 cm^{-1} (NO_2). Found: C, 47.57; H, 3.21; N, 10.98%. Calcd for $C_{10}H_8H_2O_6$: C, 47.62; H, 3.20; N, 11.11%. Z Isomer: Pale yellow needles; mp 125—130 °C. ^{1}H NMR ($CDCl_3$) δ=3.97 (s, 3H), 7.60 (d, 2H, *J*=8.6 Hz), 7.63 (s, 1H), 8.28 (d, 2H, *J*=8.6 Hz). IR: 1720 cm^{-1} (C=O), 1550, 1535, 1340 cm^{-1} (NO_2). Found: C, 47.50; H, 3.14; N, 11.13%. Calcd for $C_{10}H_8N_2O_6$: C, 47.62; H, 3.20; N, 11.11%.

Reaction of 1 with Ethyl Vinyl Ether. A solution of 2.52 g (10 mmol) of **1** and 3.60 g (50 mmol) of ethyl vinyl ether in 20 ml of DMF was allowed to stand for 1 d. After the solvent was removed in vacuo the residual solid was recrystallized from benzene-hexane to give 2.98 g (92%) of a diastereomeric mixture (**2a** : **2b**=4 : 1) of 6-ethoxy-3-methoxycarbonyl-4-(*p*-nitrophenyl)-5,6-dihydro-4*H*-1,2-oxazine 2-oxide (**2**). Fractional recrystallization of **2** from benzene-hexane gave each isomer.

2a (cis isomer): Colorless prisms; mp 124—126 °C (decomp). ^{1}H NMR ($CDCl_3$) δ=1.18 (t, 3H, *J*=7.1 Hz), 2.26 (td, 1H, *J*=3.5 Hz and 14.3 Hz), 2.65 (ddd, 1H, *J*=3.5 Hz, 8.7 Hz, and 14.3 Hz), 3.70 (s, 3H), 3.8 (m, 2H), 4.50 (dd, 1H, *J*=3.5 Hz and 8.7 Hz), 5.48 (t, 1H, *J*=3.5 Hz), 7.46 (d, 2H, *J*=8.8 Hz), 8.16 (d, 2H, *J*=8.8 Hz). IR: 1705 cm^{-1} (C=O), 1595 cm^{-1} (C=N), 1520, 1345 cm^{-1} (NO_2). Found: C, 51.78; H, 4.93; N, 8.57%. Calcd for $C_{14}H_{16}N_2O_7$: C, 51.85; H, 4.97; N, 8.64%.

2b (trans isomer): Colorless prisms; mp 137—139 °C (decomp). ^{1}H NMR ($CDCl_3$) δ=1.29 (t, 3H, *J*=7.0 Hz), 2.34 (dd, 1H, *J*=9.1 Hz and 3.9 Hz), 2.40 (dd, 1H, *J*=8.7 Hz and 3.0 Hz), 3.70 (s, 3H), 3.77 (qd, 1H, *J*=7.0 Hz and 9.7 Hz), 4.07 (qd, 1H, *J*=7.0 Hz and 9.7 Hz), 4.54 (dd, 1H, *J*=8.7 Hz and 9.1 Hz), 5.50 (dd, 1H, *J*=3.0 Hz and 3.7 Hz), 7.44 (d, 2H, *J*=8.4 Hz), 8.20 (d, 2H, *J*=8.4 Hz). IR: 1745 cm^{-1} (C=O), 1590 cm^{-1} (C=N), 1520, 1350 cm^{-1} (NO_2). Found: C, 51.72; H, 4.95; N, 8.64%. Calcd for $C_{14}H_{16}N_2O_7$: C, 51.85; H, 4.97; N, 8.64%.

Reaction of 1 with 2,3-Dihydrofuran. A solution of 2,3-dihydrofuran (2.90 g, 41.4 mmol) and **1** (1.34 g, 5.3 mmol) in 6 ml of DMF was heated at 60 °C for 12 h. After removal of the solvent, residual solid was recrystallized from benzene-hexane to give 1.37 g (80%) of a diastereomeric mixture of **3** [mp 148—153 °C (decomp), IR: 1730 and 1700 cm^{-1}]. Recrystallization of **3** from ether gave one of the isomers **3b**; colorless prisms; mp 150—154 °C (decomp). ^{1}H NMR ($CDCl_3$) δ=1.8—2.7 (m, 2H), 3.1—3.6 (m, 1H), 3.91 (s, 3H), 3.9—4.3 (m, 2H), 4.63 (m, 1H), 5.94 (d, 1H, *J*=7.0 Hz), 7.50 (d, 2H, *J*=8.5 Hz), 8.20 (d, 2H, *J*=8.5 Hz). IR: 1730 cm^{-1} (C=O), 1580 cm^{-1} (C=N), 1520, 1355 cm^{-1} (NO_2). Found: C, 52.50; H, 4.40; N, 8.40%. Calcd for $C_{14}H_{14}N_2O_7$: C, 52.17; H, 4.38; N, 8.69%.

Reactionof 1 with 3,4-Dihydro-2*H*-pyran. A solution of 2.77 g (11 mmol) of **1** and 4.62 g (55 mmol) of dihydropyran in 5 ml of DMF was heated at 60 °C for 12 h. After removal of the solvent in vacuo, residual oil was column-chromatographed on solica gel. The first eluent (chloroform-benzene 1 : 1) gave 0.83 g (30%) of the recovered nitro olefin. The second eluent (chloroform-acetone 20 : 1) gave 1.11 g (30%) of a diastereomeric mixture of the adduct **4** [mp 140—143 °C (decomp), IR: 1730, 1710, 1695 cm^{-1}]. Recrystallization of **4** from benzene-hexane gave an isomer **4a**; colorless powder; mp 142—145 °C (decomp). ^{1}H NMR ($CDCl_3$) δ=1.4—1.8 (m, 4H), 2.2—2.7 (m, 1H), 3.63 (s, 3H), 3.7—4.1 (m, 2H), 4.74 (d, 1H, *J*=8.4 Hz), 5.85 (m, 1H), 7.31 (d, 2H, *J*=8.7 Hz), 8.19 (d, 2H, *J*=8.7 Hz). IR: 1690 cm^{-1} (C=O), 1580 cm^{-1} (C=N), 1515, 1360, 1345 cm^{-1} (NO_2). Found: C, 53.33; H, 4.82; N, 8.43%. Calcd for $C_{15}H_{16}N_2O_7$: C, 53.57; H, 4.80; N, 8.33%.

Reaction of 1 with 1-Methoxycyclopentene. A solution of 2.52 g (10 mmol) of **1** and 5.90 g (50 mmol) of 1-methoxycyclopentene in 10 ml of DMF was heated at 50 °C

for 12 h. After removal of the solvent in vacuo, the residue was recrystallized from benzene-hexane to give 2.93 g (83%) of the adduct **5**. Colorless needles; mp 141—144 °C (decomp). ^{1}H NMR ($CDCl_3$) δ=1.4—2.6 (m, 7H), 3.49 (s, 3H), 3.63 (s, 3H), 4.06 (d, 1H, J=4.5 Hz), 7.43 (d, 2H, J=8.8 Hz), 8.16 (d, 2H, J=8.8 Hz). IR: 1740, 1725 cm^{-1} (C=O), 1595 cm^{-1} (C=N), 1515, 1350 cm^{-1} (NO_2). Found: C, 54.91; H, 5.14; N, 7.95%. Calcd for $C_{16}H_{18}N_2O_7$: C, 54.85; H, 5.17; N, 7.99%. Similarly the adduct **6** was obtained from a reaction of **1** with 1-methoxycyclohexene. Colorless prisms; mp 174—175 °C (decomp). ^{1}H NMR ($CDCl_3$) δ=1.2—2.5 (m, 9H), 3.33 (s, 3H), 3.71 (s, 3H), 4.10 (s, 1H), 7.38 (d, 2H, J=9.0 Hz), 8.15 (d, 2H, J=9.0 Hz). IR: 1735 cm^{-1} (C=O), 1585 cm^{-1} (C=N), 1520, 1345 cm^{-1} (NO_2). Found: C, 56.15; H, 5.49; N, 7.55%. Calcd for $C_{17}H_{20}N_2O_7$: C, 56.04; H, 5.53; N, 7.69%.

Reaction of Methyl α-Nitrocinnamate (7) with Ethyl Vinyl Ether and Acrylonitrile. A solution of 0.41 g (2 mmol) of **7**, 0.32 g (6 mmol) of acrylonitrile, and 0.72 g (10 mmol) of ethyl vinyl ether in 5 ml of DMF was heated at 70 °C for 3 h. After removal of the solvent, residual oil was crystallized from benzene-hexane to give 0.38 g (57%) of 8-cyano-3-ethoxy-6-methoxycarbonyl-5-phenyl-2,9-dioxa-1-azabicyclo[4.3.0]nonane (**8**). Colorless needles; mp 165—174 °C. ^{1}H NMR ($CDCl_3$) δ=1.31 (t, 3H, J=7.0 Hz), 2.2 (ddd, 1H, J=13.0 Hz, 6.6 Hz, and 2.9 Hz), 2.5—4.2 (m, 6H), 3.42 (s, 3H), 5.02 (dd, 1H, J=7.7 Hz and 6.6 Hz), 5.31 (dd, 1H, J=10.2 Hz and 4.3 Hz), 7.0—7.4 (m, 5H). IR: 1740 cm^{-1} (C=O). Found: C, 61.13; H, 6.15; N, 8.40%. Calcd for $C_{17}H_{20}N_2O_5$: C, 61.43; H, 6.07: N, 8.43%.

Similarly, by a reaction of **2a** with acrylonitrile in the presence of ethyl vinyl ether, 8-cyano-3-ethoxy-6-methoxycarbonyl-5-(*p*-nitrophenyl)-2,9-dioxa-1-azabicyclo-[4.3.0]nonane (**9**) was obtained in 87% yield. Colorless powder; mp 210—218 °C. ^{1}H NMR (DMSO-d_6) δ=1.22 (t, 3H, J=7.2 Hz), 2.0—4.0 (m, 7H), 3.36 (s, 3H), 5.07 (t, 1H, J=7.3 Hz), 5.65 (dd, 1H, J=9.8 Hz and 4.7 Hz), 7.51 (d, 2H, J=8.9 Hz), 8.19 (d, 2H, J=8.9 Hz). IR: 1735 cm^{-1} (C=O), 1520, 1510, 1350, 1345 cm^{-1} (NO_2). Found: C, 54.30; H, 5.12; N, 11.03%. Calcd for $C_{17}H_{19}N_3O_7$: C, 54.11; H, 5.08; N, 11.14%.

Reaction of 2a with Ethyl Vinyl Ether. A solution of 0.65 g (2 mmol) of **2a** and 0.72 g (10 mmol) of ethyl vinyl ether in 5 ml of DMF was heated at 60 °C for 5 h. After removal of the solvent, residue was recrystallized from benzene-hexane to give 0.66 g (83%) of 3,8-diethoxy-6-methoxycarbonyl-5-(*p*-nitrophenyl)-2,9-dioxa-1-azabicyclo[4.3.0]nonane (**10**). Colorless needles; mp 174—175 °C. ^{1}H NMR ($CDCl_3$) δ=1.11 (t, 3H, J=7.0 Hz), 1.32 (t, 3H, J=7.0 Hz), 2.0—2.4 (m, 9H), 3.37 (s, 3H), 4.98 (t, 1H, J=7.0 Hz), 5.80 (d, 1H, J=6.0 Hz), 7.36 (d, 2H, J=8.6 Hz), 8.18 (d, 2H, J=8.6 Hz). IR: 1740 cm^{-1} (C=O), 1515, 1350 cm^{-1} (NO_2). Found: C, 54.33; H, 6.09; N, 7.01%. Calcd for $C_{18}H_{24}N_2O_8$: C, 54.55; H, 6.10; N, 7.10%.

Reaction of 1 with 1-Morpholinocyclohexene. To a solution of 1.66 g (6.6 mmol) of **1** in 60 ml of benzene, 1.10 g (6.6 mmol) of 1-morpholinocyclohexene in 10 ml of benzene was added at 0 °C. After 2 h, 0.55 g (20%) of colorless precipitate was obtained which was assumed to be a cyclo adduct. Decomp 80—81.5 °C. IR: 1730 cm^{-1} (C=O), 1565, 1520, 1345 cm^{-1} (NO_2). Residual benzene layer was crystallized from benzene-hexane to give 1.65 g (60%) of a mixture (1 : 1) of two diastereomers of methyl 3-(2-morpholino-2-cyclohexenyl)-2-nitro-3-(*p*-nitrophenyl)propanoate. Yellow powder; mp 120—124.5 °C. ^{1}H NMR ($CDCl_3$) δ=1.1—3.2 (m, 11H), 3.55 (s, 3H, ester methyl protons of one isomer), 3.80 (s, 3H, ester methyl protons of another isomer), 3.6—3.9 (m, 4H), 4.3 (m, 1H), 4.98 (t, 1H, J=3.9 Hz, an olefin proton of enamine), 5.86 (d, 1H, J=8.8 Hz, 2-H of one isomer), 6.02 (d, 1H, J=9.7 Hz, 2-H of another isomer), 7.44 (d, 2H, J=8.9 Hz, one isomer), 7.46 (d, 2H, J=8.9 Hz, another isomer), 8.11 (d, 2H, J=8.9 Hz). IR: 1745 cm^{-1} (C=O), 1650 cm^{-1} (C=C-N). Found: C, 57.28; H, 5.99: N, 9.87%. Calcd for $C_{20}H_{25}N_3O_7$: C, 57.27; H, 6.01; N, 10.02%.

Methanolysis of 2 by Acid Catalyst. A solution of 0.975 g (3 mmol) of **2a** and 0.057 g (0.3 mmol) of *p*-toluenesulfonic acid in 30 ml of dry methanol was refluxed for 4 h. After removal of the solvent, residual oil was dissolved in chloroform, washed with water, and dried over sodium sulfate. The crude product was recrystallized by benzene-hexane to give 0.72 g (70%) of one of the diastereomers of methyl 5,5-dimethoxy-2-nitro-3-(*p*-nitrophenyl)pentanoate. Colorless plates; mp 94—98 °C. ^{1}H NMR ($CDCl_3$) δ=1.9—2.3 (m, 2H), 3.22 (s, 3H), 3.26 (s, 3H), 3.89 (s, 3H), 3.7—4.2 (m, 2H), 5.47 (d, 1H, J=10.0 Hz), 7.51 (d, 2H, J=8.7 Hz), 8.24 (d, 2H, J=8.7 Hz). IR: 1760 cm^{-1} (C=O), 1565, 1520, 1350 cm^{-1} (NO_2). Found: C, 49.35; H, 5.29; N, 8.16%. Calcd for $C_{14}H_{18}N_2O_8$: C, 49.12; H, 5.30; N, 8.18%. The similar treatment of **2b** gave the same product in 67% yield.

Fragmentation of the Adduct 2 by Sodium Methoxide. To a solution of 0.65 g (2 mmol) of **2** in 30 ml of THF at −15 °C, 1 ml (0.35 mmol) of sodium methoxide in methanol solution was added. The solution turned to red and was allowed to stand at room temperature for 30 min. An equimolar amount of hydrogen chloride (methanol solution, 0.8 mol dm^{-3}) was added to the solution and the solvent was removed under reduced pressure. The residue was dissolved in chloroform, washed with water, and dried over magnesium sulfate. After removal of the solvent, residual solid was recrystallized from benzene-hexane to give 0.41 g (82%) of methyl 2-hydroxyimino-3-(*p*-nitrophenyl)-3-butenoate (**11**). Colorless prisms; mp 149.5—151.5 °C. ^{1}H NMR ($CDCl_3$) δ=3.85 (s, 3H), 5.59 (s, 1H), 5.68 (s, 1H), 7.46 (d, 2H, J=8.7 Hz), 8.13 (d, 2H, J=8.7 Hz), 8.54 (s, 1H). IR: 3320 cm^{-1} (O-H), 3120, 3090 cm^{-1} (vinyl C-H), 1730 cm^{-1} (C=O), 1510, 1345 cm^{-1} (NO_2). Found: C, 53.03; H, 4.07; N, 11.07%. Calcd for $C_{11}H_{10}N_2O_5$: C, 52.80; H, 4.03; N, 11.20%.

The similar treatment of the adducts **3**—**6** gave the oximes **12**—**15**, which were purified by column chromatography on silica gel. Acetone-chloroform elutes were recrystallized from benzene-hexane.

Methyl 6-Hydroxy-2-hydroxyimino-3-(*p*-nitrophenyl)-3-hexenoate (12): Colorless needles; mp 140.5—144.5 °C. ^{1}H NMR ($CDCl_3$) δ=2.4—2.8 (m, 3H), 3.69 (s, 3H), 3.7—4.0 (m, 2H), 6.41 (t, 1H, J=7.3 Hz), 7.51 (d, 2H, J=9.0 Hz), 8.21 (d, 2H, J=9.0 Hz), 11.6 (broad s, 1H). IR: 3250 cm^{-1} (O-H), 1740 cm^{-1} (C=O), 1510, 1350 cm^{-1} (NO_2). Found: C, 53.40; H, 4.87; N, 9.55%. Calcd for $C_{13}H_{14}N_2O_6$: C, 53.06; H, 4.80; N, 9.52%.

Methyl 7-Hydroxy-2-hydroxyimino-3-(*p*-nitrophenyl)-3-heptenoate (13): Colorless prisms; mp 96.5—98.5 °C. ^{1}H NMR ($CDCl_3$) A mixture of two configurational isomers A and B (A : B=3 : 2). A: δ=1.4—3.0 (m, 5H), 3.4—3.8 (m, 2H), 3.91 (s, 3H), 6.01 (t, 1H, J=7.7 Hz), 7.25 (d, 2H, J=8.7 Hz), 8.21 (d, 2H, J=8.7 Hz), 8.61 (s, 1H). B: δ=1.4—3.0 (m, 5H), 3.4—3.8 (m, 2H), 3.70 (s, 3H), 6.28 (t, 1H, J=8.0 Hz), 7.49 (d, 2H, J=8.7 Hz), 8.19 (d, 2H, J=8.7 Hz), 11.49 (s, 1H). IR: 3480, 3170 cm^{-1} (O-H), 1740, 1730 cm^{-1} (C=O), 1515,

1350 cm^{-1} (NO_2). Found: C, 54.79; H, 5.26; N, 9.12%. Calcd for $C_{14}H_{16}N_2O_6$: C, 54.54; H, 5.23; N, 9.09%.

Dimethyl 2-Hydroxyimino-3-(*p*-nitrophenyl)-3-octenedioate (14): Colorless prisms; mp 98.5—99 °C. ^1H NMR ($CDCl_3$) δ=1.5—2.5 (m, 6H), 3.59 (s, 3H), 3.88 (s, 3H), 5.95 (t, 1H, J=8.2 Hz), 7.31 (d, 2H, J=8.6 Hz), 8.20 (s, 1H), 8.22 (d, 2H, J=8.6 Hz). IR: 3300 cm^{-1} (O-H), 1735 cm^{-1} (C=O), 1520, 1350 cm^{-1} (NO_2). Found: C, 54.97; H, 5.23; N, 8.01%. Calcd for $C_{16}H_{18}N_2O_7$: C, 54.85; H, 5.17; N, 7.99%.

Dimethyl 2-Hydroxyimino-3-(*p*-nitrophenyl)-3-nonenedioate (15): Colorless oil. ^1H NMR ($CDCl_3$) δ=1.4—1.8 (m, 4H), 2.2—2.5 (m, 4H), 3.68 (s, 3H), 3.76 (s, 3H), 6.33 (t, 1H, J=7.5 Hz), 7.49 (d, 2H, J=9.1 Hz), 8.16 (d, 2H, J=9.1 Hz), 10.76 (s, 1H). IR: 3350 cm^{-1} (O-H), 1735 cm^{-1} (C=O), 1520, 1345 cm^{-1} (NO_2). Mass spectra: m/z 364 (M^+).

Reduction of 2 with Triethyl Phosphite. A solution of 0.65 g (2 mmol) of **2a** and 0.46 g (3 mmol) of triethyl phosphite in 10 ml of xylene was heated at 95 °C for 7.5 h under a nitrogen atmosphere. After removal of the solvent in vacuo, residue was recrystallized from benzene-hexane to give 0.47 g (76%) of *cis*-6-ethoxy-3-methoxycarbonyl-4-(*p*-nitrophenyl)-5,6-dihydro-4*H*-1,2-oxazine (**16a**): Colorless prisms; mp 91—92.5 °C. ^1H NMR ($CDCl_3$) δ=1.07 (t, 3H, J=7.0 Hz), 2.2—2.5 (m, 2H), 3.3—4.0 (m, 2H), 3.80 (s, 3H), 4.08 (dd, 1H, J=6.7 Hz and 4.0 Hz), 5.23 (t, 1H, J=3.2 Hz), 7.36 (d, 2H, J=9.1 Hz), 8.14 (d, 2H, J=9.1 Hz). IR: 1730 cm^{-1} (C=O), 1520, 1345 cm^{-1} (NO_2). Found: C, 54.44; H, 5.22; N, 8.97%. Calcd for $C_{14}H_{16}N_2O_6$: C, 54.54; H, 5.23; N, 9.09%.

Similarly, **16b** (trans isomer) was obtained by a reaction of **2b** with triethyl phosphite in 61% yield. Colorless powder; mp 101—103 °C. ^1H NMR ($CDCl_3$) δ=1.25 (t, 3H, J=6.9 Hz), 2.04 (ddd, 1H, J=13.6 Hz, 11.4 Hz, and 2.6 Hz), 2.38 (ddd, 1H, J=13.6 Hz, 7.8 Hz, and 2.6 Hz), 3.3—4.2 (m, 2H), 3.70 (s, 3H), 4.13 (dd, 1H, J=11.4 Hz and 7.8 Hz), 5.24 (t, 1H, J=2.6 Hz), 7.36 (d, 2H, J=9.0 Hz), 8.20 (d, 2H, J=9.0 Hz). IR: 1745 cm^{-1} (C=O), 1515, 1350 cm^{-1} (NO_2). Found: C, 54.33; H, 5.33; N, 8.89%. Calcd for $C_{14}H_{16}N_2O_6$: C, 54.54; H, 5.23; N, 9.09%.

Isomerization of 16a to 16b. Treatment of **16a** with sodium methoxide under the similar conditions of the fragmentation of **2a** with sodium methoxide gave **16b** in 42% yield.

References

1) a) S. Daneo, G. Pitacco, A. Risaliti, and E. Valentin, *Tetrahedron*, **38**, 1499 (1982); b) A. T. Nielsen and T. G. Archibald, *Tetrahedron*, **26**, 3475 (1970); R. S. Varma and G. W. Kabalka, *Heterocycles*, **24**, 2645 (1986).

2) M. Miyashita, T. Yanami, and A. Yoshikoshi, *J. Am. Chem. Soc.*, **98**, 4679 (1976); M. Miyashita, T. Yanami, T. Kumazawa, and A. Yoshikoshi, *ibid.*, **106**, 2149 (1984); A. Yoshikoshi and M. Miyashita, *Acc. Chem. Res.*, **18**, 284 (1985).

3) G. Barbarella, G. Pitacco, C. Russo, and E. Valentin, *Tetrahedron Lett.*, **24**, 1621 (1983); A. T. Nielsen and T. G. Archibald, *Tetrahedron*, **25**, 2393 (1969).

4) A. T. Nielsen and T. G. Archibald, *J. Org. Chem.*, **34**, 1470 (1969).

5) S. E. Denmark, C. J. Cramer, and J. A. Sternberg, *Tetrahedron Lett.*, **27**, 3693 (1986).

6) G. Casnati, A. Pochini, M. G. Terenghi, and R. Ungaro, *J. Org. Chem.*, **48**, 3783 (1983).

7) A. T. Nielsen, "The Chemistry of the Nitro and Nitroso Group," ed by H. Feuer, John Wiley & Sons, New York (1969), Chap. 7.

8) B. F. Bonini, E. Foresti, G. Maccagnani, G. Mazzanti, P. Sabatino, and P. Zani, *Tetrahedron Lett.*, **26**, 2131 (1985).

9) P. Gygax, T. K. Das Gupta, and A. Eshenmoser, *Helv. Chim. Acta*, **55**, 2205 (1972).

10) T. L. Gilchrist and T. G. Roberts, *J. Chem. Soc., Chem. Commun.*, **1979**, 1090; T. L. Gilchrist, G. M. Iskander, and A. K. Yagoub, *J. Chem. Soc., Chem. Commun.*, **1981**, 696.

11) A. Dornow and H. Menzel, *Justus Liebigs Ann. Chem.*, **588**, 40 (1954).

 © 1988 The Chemical Society of Japan Bull. Chem. Soc. Jpn., 61, 467—473 (1988)

The Asymmetric Diels-Alder Cycloaddition Using Ethyl (−)-(*Z*)-(*R*)$_S$-2-Methyl-3-(*p*-tolylsulfinyl)propenoate: Application to an Enantioselective Synthesis of (+)-*epi*-β-Santalene

Yoshitsugu ARAI, Masatoshi YAMAMOTO, and Toru KOIZUMI*
Faculty of Pharmaceutical Sciences, Toyama Medical and Pharmaceutical University, Sugitani 2630, Toyama 930-01
(Received July 31, 1987)

The Diels-Alder reaction of ethyl (−)-(*Z*)-(*R*)$_S$-2-methyl-3-(*p*-tolylsulfinyl)propenoate (**6**)[1] with cyclopentadiene gave the cycloadducts **7**, **8**, and **9** in a high diastereoselective manner. The cycloadduct **7** was transformed into the acetal (−)-**25**. The racemic **25** was used as an intermediate in the synthesis of (±)-β-santalol. Thus, the chiral acetal (−)-**25** should provide a route to (−)-β-santalol. The cycloadduct **8** was converted into (+)-*epi*-β-santalene in 11 steps.

East Indian sandalwood oil was obtained from the tree, *Santalum album* L., growing in the forest of Mysore, India.[2] The oil is prized for its woody sweet and very long-lasting odor. Recently, it was pointed[3] that the orfactory character was responsible mainly for two major components of the essential oil, (+)-α-santalol (**1**), and (−)-β-santalol (**2**). Of course, many of the minor components, e.g., (−)-β-santalene (**3**), (+)-*epi*-β-santalene (**4**), and (+)-*epi*-β-santalol (**5**) are also considered to contribute the perfume character. The structural relationship and absolute configuration of these sesquiterpenes were established by Money and co-workers.[4] Since the appearence of the pioneering work of Corey,[5] Brieger,[6] and Money,[7] a number of

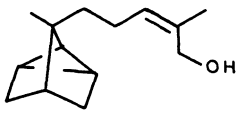

1

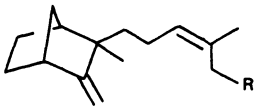

2 R = OH
3 R = H

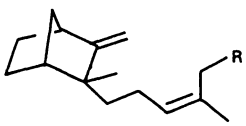

4 R = H
5 R = OH

syntheses of the santalols and santalenes have come on the scene.[8] However, there have been only two reports on the chiral synthesis of these sesquiterpenes: an elegant synthesis of (−)-**3** by Oppolzer[9] and a novel synthesis of some sesquiterpenes by Money.[4] Especially, the Oppolzer's synthesis involved an asymmetric Diels-Alder cycloaddition as a crucial step.

In the past few years, an asymmetric Diels-Alder reaction employing α,β-unsaturated sulfoxides has received a great deal of attention.[10] Because of the high diastereodifferentiation, the interpretation of the stereochemical course of the cycloadditions has been recently reported by Hehre from theoretical interest.[11] However, there have been few reports on the application to natural product synthesis, based upon the strategy of the asymmetric cycloaddition using chiral sulfoxides.[12]

As part of our investigation in this area, we reported that the Diels-Alder cycloaddition of the sulfoxides **6** and cyclopentadiene gave the cycloadducts **7**, **8**, and **9**

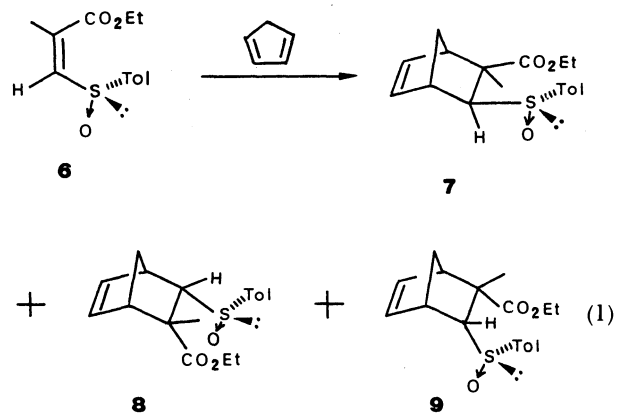

(1)

(ratio 32:66:2) in 92% combined yield. The diastereomeric excesses of the exo and endo adducts were proved to be 100 and 94% by HPLC analysis, respectively.[13] The absolute configuration of **7** was determined by chemical correlation. Although the absolute stereochemistry of the endo diastereomers was not clarified, we pointed out that the structure of **8** should be shown as depicted in Eq. 1, based upon our proposal of the steric course in the cycloaddition.

Since chirons[14] **7**—**9** derived from **6** possess functionalized bicyclo[2.2.1]heptane systems, the bicyclic sesquiterpenes such as **2** and **4** seemed to be attractive as a synthetic target molecule. In a preliminary communication,[15] we have described the use of the chirons **7** and **8** for the chiral synthesis of the bicyclic sesquiterpenes. In this paper we report in details these results.

Results and Discussion

Synthesis of (+)-*epi*-β-Santalene. At the outset, we undertook the transformation of the sulfinyl group in

8 into the carbonyl function (Scheme 1). Hydrogenation of **8** ($[\alpha]_D^{19}$ −4.8°) over Pd on carbon followed by reduction of the sulfinyl group gave the sulfide **10** ($[\alpha]_D^{26}$ −7.32°) in 92% yield. Transformation of **10** into the keto ester (−)-**11** ($[\alpha]_D^{26}$ −7.15°) proceeded smoothly by chlorination with *N*-chlorosuccinimide (NCS) and subsequent oxidative hydrolysis,[16] in 85% yield. The stereostructure of (−)-**11** was ascertained by the following experiment. (±)-Norcamphor was ethoxycarbonylated with ethyl cyanoformate[17] under kinetically controlled conditions affording ester (±)-**12** whose enolate was stereoselectively methylated on the less hindered exo face of the ester to give (±)-**11**. The spectral and gas chromatographic characteristics were identical with those of (−)-**11** derived from **8**. The enantiomeric excess of (−)-**11** was proved to be no less than 97% by ^{1}H NMR examination in the presence of Eu(hfc)$_3$.

The next stage was set for the introduction of the terminal olefin in (−)-**11**. Reaction of (−)-**11** with a Wittig type reagent (methylenetriphenylphosphorane or the carbanion generated from diethyl methylphosphonate) did not produce the desired product **13**. In order to introduce the terminal olefin at a later stage, we tried to protect the keto group in (−)-**11**. Several attempts under a variety of conditions were unsuccessful, probably due to the steric hindrance. Finally, methylenation of the hindered carbonyl in (−)-**11** was best carried out by the Nozaki's method[18] (CH_2Br_2/Zn/$TiCl_4$) to produce **13** ($[\alpha]_D^{29}$ −46.3°) in 40% yield.[19]

The procedure adopted for converting the ester group in **13** into the requisite 4-methyl-3-pentenyl side chain is as follows. Reduction of **13** with diisobutylaluminium hydride (DIBAL, 2 equiv) gave the alcohol **14** ($[\alpha]_D^{26}$ + 96.2°) in quantitative yield. Pyridinium chlorochromate (PCC) oxidation[20] of **14** yielded the unstable aldehyde **15** (90%), $[\alpha]_D^{18}$ +17.1°, which was subjected to the Emmons-Horner condensation (triethyl phosphonoacetate, *n*-BuLi) giving the unsaturated ester **16** (96%), $[\alpha]_D^{26}$ −136°, as a single *E*-isomer. Reaction of **16** with Li-NH_3 gave the alcohol **18** in low yields. Good yields of **18** were obtained by the following operations. Hydrosilylation of **16** with triethylsilane in the presence of Wilkinson catalyst ($(Ph_3P)_3RhCl$) followed by ethanolysis provided the ester **17**, $[\alpha]_D^{25}$ +25.8°, in quantitative yield.[21] The spectroscopic data were consistent with those reported previously by Christenson and Willis in their synthesis of racemic **4**,[8b] According to the procedure of Christenson,[22] **17** was converted into (+)-*epi*-β-santalene by a 3-step sequence in 51% overall yield; reduction (DIBAL), PCC oxidation, and Wittig reaction. The spectral data (NMR, IR) were identical with those of an authentic sample kindly supplied by Dr. P. Christenson and the optical rotation ($[\alpha]_D^{27}$ +26.4°) was in good agreement with that reported in the literature ($[\alpha]_D^{27}$ +26.9°).[4]

Synthesis of the Intermediate (−)-25 of (−)-β-Santalol. In a manner similar to the first step of the synthesis of (+)-**4** the exo sulfoxide **7** was converted into the keto ester **21**, $[\alpha]_D^{25}$ −93.7° (Scheme 2). The structure of **21** was confirmed by direct comparison with that independently obtained by ethoxycarbonylation of (±)-3-methylnorcamphor.[23] Because the methylenation of the hindered keto group in **21** had been proved to be difficult, we chose the transformation of the ester group. The ester **21** was reduced with lithium aluminium hydride (LAH) to give the diol **22** (63%), $[\alpha]_D^{25}$ −8.5°, as a single isomer. The coupling constant ($J_{1,2}$=4 Hz) of the NMR spectrum showed that the C-2 hydroxyl group was located in the endo configuration. Swern oxidation[24] of **22** afforded the unstable keto aldehyde **23** (96%), and the aldehydic group was then selectively acetalized[25] with trimethyl orthoformate in the presence of cerium trichloride giving the acetal (−)-**24** (72%), $[\alpha]_D^{24}$ −62.6°. The enantiomeric excess (ee) of (−)-**24** was proved to be >97% as judged by NMR spectroscopy using Eu(hfc)$_3$. The exocyclic methylene group was introduced by the Nozaki's method to give (−)-**25** , $[\alpha]_D^{24}$ −119°, in 30%

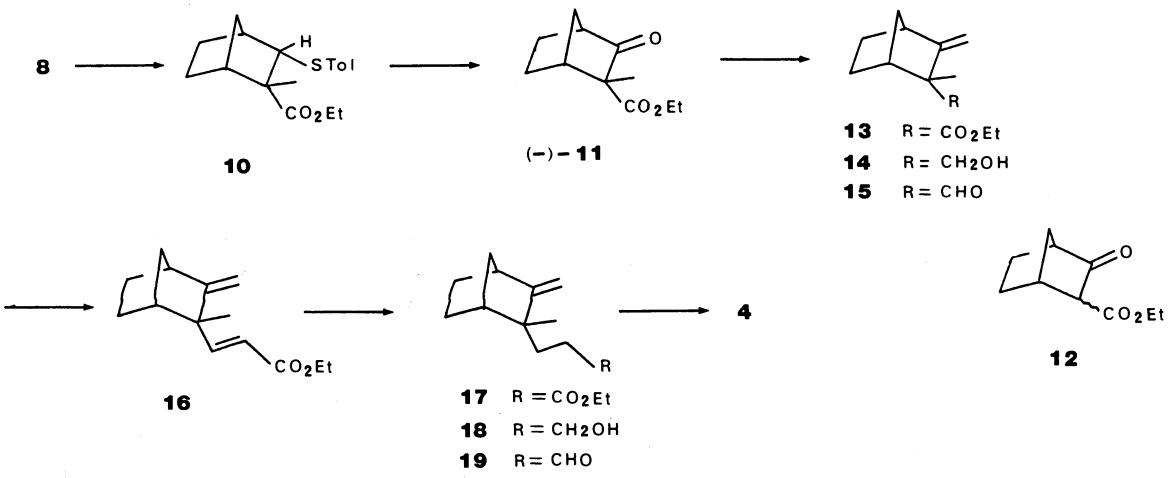

Scheme 1.

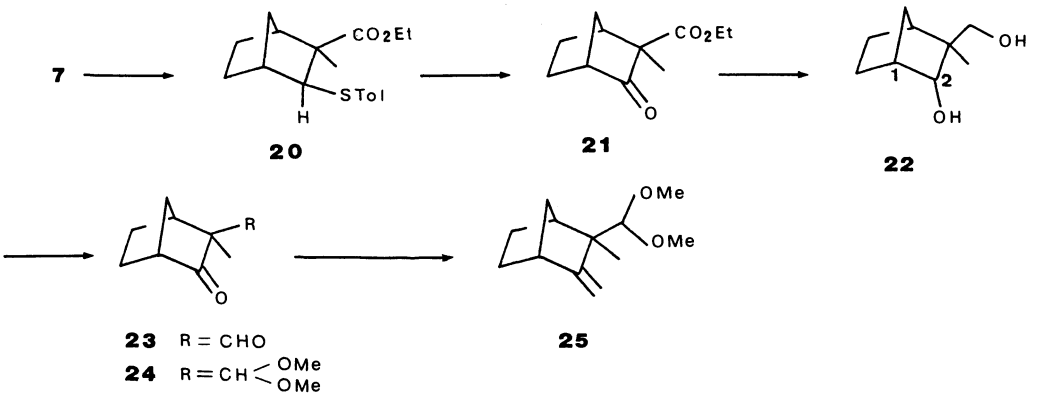

Scheme 2.

yield. Since the absolute configuration of a chiron **7** have been determined,[13] the absolute stereochemistry of (−)-**25** should be deduced as depicted in Scheme 2. Racemic **25** was employed as an intermediate in the synthesis of (±)-**2** by the BASF group.[26] Having chiral acetal (−)-**25** in hand, it will be possible to transform the intermediate into (−)-**2**.

In conclusion, the chiron **7** was converted into a key intermediate in the synthesis of (−)-β-santalol. The chiron **8** was transformed into (+)-*epi*-β-santalene in enantiomerically pure form. Therefore, the absolute stereochemistry of the cycloadduct **8** was proved to be depicted in this paper. Based on our proposal[13] in the cycloaddition of a chiral sulfoxide, it was found that absolute stereostructure of the adducts could be predictable. And, we believe that the chirons would serve as the chiral intermediates for the synthesis of other natural products by transformation of the functionality such as the olefin, sulfinyl group and ethoxycarbonyl groups.

Experimental

The melting points and boiling points are uncorrected. ^{1}H NMR spectra were determined on a JEOL PMX-60, a Varian XL-200 or a JEOL GX-270 spectrometer. IR spectra were recorded on a JASCO A-102. Mass determinations were obtained on a JEOL D-200 spectrometer. Optical rotations were taken with a JASCO DIP-140 digital polarimeter. Gas chromatography was carried out on a Shimadzu GC-4A instrument with a column packed with 10% SE-30.

All experiments were carried out under a slight positive pressure of argon. Column chromatography was performed with Nakarai Chemicals 70—230 mesh silica gel. Wako's precoated thin-layer silica $PF70_{254}$ plates were used for monitoring the reactions. MPLC (medium-pressure chromatography) was performed with a Michael-Miller column (Ace Glass Co.) packed with 230—400 mesh silica gel (Nakarai Chemicals). Analytical high performance liquid chromatography (HPLC) was carried out on a Waters Associates chromatograph by using a μ-Polasil column and monitoring at 254 nm. Peak areas were measured with a Shimadzu (Chromatopac C-R3A) integrator. Evaporation of the solvents was performed by a rotary evaporator below 15 °C.

Ethyl (−)-(*Z*)-(*R*)$_s$-2-Methyl-3-(*p*-tolylsufinyl)propenoate (6). To a stirred solution of diethyl *p*-tolylsulfinylmethylphosphonate[13] (4.74 g, 16.3 mmol), $[\alpha]_D^{24}$ +96.3° (*c* 1.3, $CHCl_3$) in dry THF (50 ml) was added dropwise 1.56 M (1 M=1 mol dm^{-3}) *n*-BuLi in hexane (21 ml, 32.8 mmol) at −80 °C over a period of 9 min. After stirring at the same temperature for 30 min freshly distilled ethyl pyruvate (3.5 ml, 31.9 mmol) in dry THF (20 ml) was added dropwise for 10 min. After an additional 10 min the orange-colored mixture was quenched with 3% hydrochloric acid to become slightly acidic. The solvent was removed by a rotary evaporator and the aqueous solution was extracted with $CHCl_3$ (3×100 ml). The extracts were washed with water (3×100 ml), dil. $NaHCO_3$ aq (2×100 ml), sat. brine (100 ml) and dried ($MgSO_4$). After evaporation of the solvent the crude oil was purified by MPLC (hexane-ethyl acetate 7:3). Initial fractions contained pure (*E*)-**6** (1.033 g, 25%). Late fractions gave pure (*Z*)-**6** (1.222 g, 33%). (*E*)-**6**: bp 125—130 °C/0.1 mmHg (1 mmHg=133.322 Pa); $[\alpha]_D^{25}$ −78.9° (*c* 1.26, $CHCl_3$); IR (neat) 1730, 1630, 1050 cm^{-1}; ^{1}H NMR ($CDCl_3$) δ=1.28 (t, *J*=7 Hz, 3H), 2.30 (d, *J*=2 Hz, 3H), 2.45 (s, 3H), 4.22 (q, *J*=7 Hz, 2H), 7.18 (m, 1H), 7.33, 7.58 (ABq, *J*=8 Hz, 2×2H). Found: C, 61.76; H, 6.24%. Calcd for $C_{13}H_{16}O_3S$: C, 61.87; H, 6.40%; MS *m/z* 253 (M^+ +1), 236, 204, 159. (*Z*)-**6**: bp 130—135 °C/0.1 mmHg; $[\alpha]_D^{24}$ −390.8° (*c* 1.18, $CHCl_3$); IR (neat) 1720, 1660, 1600, 1090 cm^{-1}; ^{1}H NMR ($CDCl_3$) δ=1.36 (t, *J*=7 Hz, 3H), 2.03 (d, *J*=2 Hz, 3H), 2.40 (s, 3H), 4.33 (q, *J*=7 Hz, 2H), 6.50 (m, 1H), 7.28, 7.72 (ABq, *J*=8 Hz, 2×2H). Found: C, 61.8; H, 6.2%. Calcd for $C_{13}H_{16}O_3S$: C, 61.87; H, 6.40%; MS *m/z* 253 (M^+ +1), 236, 204, 159.

If the reaction conditions (−80 °C) are not maintained throughout, partial racemization occurs, resulting in low optically active (*E*)- and (*Z*)-**6**.

As indicated in the preliminary communication,[13] a Emmons-Horner condensation using NaH as a base gave the (*E*)- and (*Z*)-**6** in 23 and 10% yields, respectively. A variety of conditions were explored to optimize the yields. Finally, it was found that the reaction conducted by the use of *n*-BuLi as a base, at low temperature, gave slight satisfactory yields of (*Z*)-**6** (33%) and (*E*)-**6** (25%).

Diels-Alder Reaction of (*Z*)-6 and Cyclopentadiene. A mixture of freshly distilled cyclopentadiene (240 ml, 2.9 mol) and (*Z*)-**6** (22.13 g, 87.8 mmol, $[\alpha]_D^{26}$ −337° (*c* 1.0, $CHCl_3$)) was heated at 90 °C for 5 h in a pressure bottle tightly sealed with a stainless steel cap. Unreacted cyclopentadiene was removed under reduced pressure to give crude material, which was filtered by a silica-gel column (6×40 cm) in hexane. Elution with the solvent gave dicyclopentadiene. Elu-

tion was continued with ethyl acetate giving a mixture of **7**—**9** and recovered **6**. The HPLC analysis (hexane-ethyl acetate 1 : 1) of the crude product showed a mixture of 32 : 66 : 2 (**7** : **8** : **9**). Thus, the diastereomeric excesses of exo and endo sulfoxides were determined to be 100% and 94%, respectively. The crude mixture was chromatographed on silica gel (MPLC, 350 g) with hexane-ethyl acetate (1 : 3) to afford (*Z*)-**6** (1.084 g). Elution with ethyl acetate gave **7** (8.772 g, 31%), **8** (16.011 g, 57%), and **9** (0.848 g, 3%).

Ethyl (+)-(*R*)$_S$-(1*R*,4*S*)-*endo*-2-Methyl-*exo*-3-(*p*-tolylsulfinyl)bicyclo[2.2.1]hept-5-ene-*exo*-2-carboxylate (7). mp 91 °C (hexane); $[\alpha]_D^{24}$ +60.2° (*c* 0.72, $CHCl_3$); IR (KBr) 1725, 1600, 1040 cm^{-1}; ^1H NMR ($CDCl_3$) δ=1.17 (s, 3H), 1.33 (t, *J*=7 Hz, 3H), 1.57 (br d, *J*=9 Hz, 1H), 2.23 (d, *J*=9 Hz, 1H), 2.25 (d, *J*=3 Hz, 1H), 2.45 (s, 3H), 3.1 (br s, 1H), 3.2 (br s, 1H), 4.24 (q, *J*=7 Hz, 2H), 6.12 (br s, 2H), 7.20, 7.47 (ABq, *J*=9 Hz, 2×2H). Found: C, 67.92; H, 6.94%. Calcd for $C_{18}H_{22}O_3S$: C, 67.88; H, 6.98%; MS *m*/*z* 319 (M^+ +1), 273, 179.

Ethyl (−)-(*R*)$_S$-(1*S*,4*S*)-*exo*-2-Methyl-*endo*-3-(*p*-tolylsulfinyl)bicyclo[2.2.1]hept-5-en-*endo*-2-carboxylate (8). mp 85—86 °C (hexane); $[\alpha]_D^{19}$ −4.82° (*c* 0.65, $CHCl_3$); IR (KBr) 1730, 1600, 1030 cm^{-1}; ^1H NMR ($CDCl_3$) δ=1.12 (*J*=8 Hz, 3H), 1.12 (s, 3H), 1.54 (s, 2H), 2.30 (s, 3H), 2.83 (s, 1H), 3.10 (d, *J*=4 Hz, 1H), 3.40 (s, 1H), 4.00 (m, 2H), 6.18 (dd, *J*=6, 3 Hz, 1H), 6.47 (dd, *J*=6, 3 Hz, 1H), 7.20, 7.70 (ABq, *J*=8 Hz, 2×2H). Found: C, 68.02; H, 6.98%. Calcd for $C_{18}H_{22}O_3S$: C, 67.88; H, 6.98%; MS *m*/*z* 319 (M^+ +1), 273, 179, 91.

Ethyl (+)-(*R*)$_S$-(1*R*,4*S*)-*exo*-2-Methyl-*endo*-3-(*p*-tolylsulfinyl)bicyclo[2.2.1]hept-5-ene-*endo*-2-carboxylate (9). mp 89—90 °C (hexane); $[\alpha]_D^{27}$ +184.10° (*c* 0.97, $CHCl_3$); IR ($CHCl_3$) 1730, 1590, 1030 cm^{-1}; ^1H NMR ($CDCl_3$) δ=1.34 (t, *J*=7 Hz, 3H), 1.42 (d, *J*=8 Hz, 1H), 1.62 (d, *J*=8 Hz, 1H), 1.70 (s, 3H), 2.24 (br s, 1H), 2.45 (s, 3H), 2.97 (br s, 1H), 3.06 (d, *J*=3 Hz, 1H), 4.26 (dq, *J*=7, 1 Hz, 2H), 6.18 (dd, *J*=6, 3 Hz, 1H), 6.32 (dd, *J*=6, 3 Hz, 1H), 7.38, 7.70 (ABq, *J*=8 Hz, 2×2H). Found: C, 67.63; H, 6.87%. Calcd for $C_{18}H_{22}O_3S$: C, 67.88; H, 6.98%; Exact mass Found: *m*/*z* 318.1311. Calcd for $C_{18}H_{22}O_3S$: M, 318.1288; MS *m*/*z* 319 (M^+ +1), 179, 151, 91.

Ethyl (−)-(1*R*,4*S*)-*exo*-2-Methyl-*endo*-3-(*p*-tolylthio)-bicyclo[2.2.1]heptane-*endo*-2-carboxylate (10). A mixture of **8** (3.59 g, 11.3 mmol) and 10% Pd on carbon (495 mg) in ethanol (45 ml) was evacuated, flushed with hydrogen and stirred vigorously under hydrogen atmosphere at room temperature for 7 h. The mixture was filtered through a short pad of Celite and the filter pad was washed with warm ethanol (4×25 ml). Solvent evaporation gave the dihydro sulfoxide (3.61 g, 100%). mp 67 °C (hexane); $[\alpha]_D^{26}$ −104.6° (*c* 1.01, $CHCl_3$); IR (melt) 1730, 1600 cm^{-1}; ^1H NMR ($CDCl_3$) δ=0.77 (s, 3H), 1.27 (t, *J*=7 Hz, 3H), 1.3—1.7 (m, 6H), 2.2 (br, 1H), 2.40 (s, 3H), 2.6 (m, 1H), 3.0 (br, 1H), 4.13 (q, *J*=7 Hz, 2H), 7.20, 7.67 (ABq, *J*=8 Hz, 2×2H). Found: C, 67.40; H, 7.53%. Calcd for $C_{18}H_{24}O_3S$: C, 67.47; H, 7.55%; MS *m*/*z* 321 (M^+ +1), 181, 153.

To a solution of the sufoxide obtained above (3.396 g, 10.6 mmol) in ethanol (30 ml) was added dropwise ca. 25% aq. $TiCl_3$ solution (8 ml, 13 mmol) at room temperature. The reaction mixture was stirred for 1 h and diluted with water (50 ml). Most of the ethanol was evaporated and the aqueous layer was extracted with ether (5×50 ml). Evaporation and purification by distillation afforded pure sulfide **10** (2.952 g, 92%). bp 110—113 °C/0.2 mmHg; $[\alpha]_D^{26}$ −7.32° (*c* 1.09, $CHCl_3$); IR (neat) 1725, 1500 cm^{-1}; ^1H NMR ($CDCl_3$) δ=1.2—1.8 (m, 6H), 1.30 (t, *J*=7 Hz, 3H), 1.38 (s, 3H), 2.2 (br s, 2H), 2.32 (s, 3H), 3.00 (dd, *J*=4, 2 Hz, 1H), 4.17 (q, *J*=7 Hz, 2H), 7.00, 7.27 (ABq, *J*=8 Hz, 2×2H). Exact mass Found: *m*/*z* 304.1462. Calcd for $C_{18}H_{24}O_2S$: M, 304.1497; MS *m*/*z* 304 (M^+), 236, 153, 91.

Ethyl (−)-(1*S*,4*R*)-*exo*-2-Methyl-3-oxobicyclo[2.2.1]-heptane-*endo*-2-carboxylate ((−)-11). A mixture of sulfide **10** (216 mg, 0.7 mmol) and NCS (513 mg, 3.8 mmol) in CCl_4 (6 ml) was refluxed for 30 min. The reaction mixture was filtered and the filtrate was concentrated to dryness. Without further purification the crude product was successively treated with $CuCl_2 \cdot 2H_2O$ (309 mg, 2 mmol), CuO (247 mg, 3.1 mmol), acetone (10 ml) and water (1 ml) to reflux for 20 min. The reaction mixture was then filtered through a short pad of Celite and the filtrate was concentrated. The residue was partitioned with ether (2×30 ml) and water (10 ml). The combined ether portions were washed with sat. brine, dried ($MgSO_4$) and concentrated. The crude product was purified by silica-gel chromatography(benzene and then ether) to give **11** (119 mg, 85%). A prolonged heating resulted in gradual decomposition of the product. **11**: bp 114—118 °C/7 mmHg; $[\alpha]_D^{26}$ −7.15° (*c* 1.55, $CHCl_3$); IR (neat) 1750, 1720 cm^{-1}; ^1H NMR (CCl_4) δ=1.0—2.0 (m, 6H), 1.27 (t, *J*=8 Hz, 3H), 1.27 (s, 3H), 2.53 (br, 2H), 4.13 (q, *J*=8 Hz, 2H). Exact mass Found: *m*/*z* 196.110. Calcd for $C_{11}H_{16}O_3$: M, 196.110. In the NMR spectrum of (±)-**11**, the two enantiotopic tertiary methyl hydrogens resonate at 3.17 and 3.28 ppm due to (+)- and (−)-enantiomer, respectively, by adding a chiral shift reagent, tris[3-(heptafluoropropylhydroxymethylene)-*d*-camphorato]europium(III) (Eu(hfc)$_3$). No such separation was observable under the same conditions (0.28 equiv used) in the spectrum of (−)-**11** derived from **10**.

Ethyl (−)-(1*R*,4*S*)-*exo*-2-Methyl-3-methylenebicyclo[2.2.1]-heptane-*endo*-2-carboxylate (13). A suspension of activated zinc dust (2.124 g, 32.5 mmol) and dibromomethane (1.2 ml, 17.1 mmol) in dry THF (10 ml) was treated with 1 M $TiCl_4$ solution in CH_2Cl_2 (3.8 ml, 3.8 mmol) at room temperature. Instantaneous reaction occurred under evolution of heat and the color changed to dark brown. After 20 min **11** (730 mg, 3.72 mmol) in dry THF (10 ml) was added by a syringe for 15 min. The suspension was stirred for 21 h at room temperature. The reaction mixture was diluted with ether (20 ml) and poured into 5% hydrochloric acid (15 ml). The aqueous layer was extracted with ether (5×20 ml). The extracts were washed with brine, dried ($MgSO_4$) and concentrated. Purification by chromatography on silica gel gave **13** (288 mg, 40%). bp 76—81 °C/13 mmHg; $[\alpha]_D^{29}$ −46.3° (*c* 0.75, $CHCl_3$); IR (neat) 1735, 1718, 1260, 1250 cm^{-1}; ^1H NMR ($CDCl_3$) δ=1.27 (t, *J*=7 Hz, 3H), 1.33 (s, 3H), 1.1—1.8 (m, 6H), 2.33 (br s, 1H), 2.73 (br s, 1H), 4.17 (q, *J*=7 Hz, 2H), 4.83 (s, 1H), 5.03 (s, 1H). Exact mass Found: *m*/*z* 194.1303. Calcd for $C_{12}H_{18}O_2$: M, 194.1306; MS *m*/*z* 194 (M^+), 149, 121, 93; R_f 0.44 (benzene).

(+)-(1*R*,4*S*)-*exo*-2-Methyl-3-methylenebicyclo[2.2.1]-heptane-*endo*-2-methanol (14). Diisobutylaluminium hydride (1 M in hexane, 3 ml, 3 mmol) was added slowly to a solution of **13** (288 mg, 1.48 mmol) in dry ether (5 ml) at −78 °C. The mixture was stirred for 1 h at that temperature and diluted with 5% hydrochloric acid (5 ml). The clear solution was extracted with ether (5×10 ml) and the extracts were washed with sat. brine and dried ($MgSO_4$). Evaporation gave **14** (226 mg, 100%) as an oil, which crystallized. bp 117—121 °C/63 mmHg; mp 74—79 °C (pentane); $[\alpha]_D^{24}$ +96.2° (*c* 0.85, $CHCl_3$); IR (neat) 3380, 1645 cm^{-1}; ^1H NMR

($CDCl_3$) δ=1.12 (s, 3H), 1.0—2.0 (m, 6H), 2.13 (br s, 1H), 2.72 (br s, 1H), 3.50 (s, 2H), 4.47 (s, 1H), 4.80 (s, 1H). Found: C, 79.01; H, 10.41%. Calcd for $C_{10}H_{16}O$: C, 78.90; H, 10.59%; MS *m/z* 152 (M^+), 121, 79; R_f 0.1 (benzene).

(+)-(1*R*,4*S*)-*exo*-2-Methyl-3-methylenebicyclo[2.2.1]-heptane-*endo*-2-carbaldehyde (15). A mixture of PCC (1.084 g, 5.03 mmol), **14** (226 mg, 1.48 mmol) and Molecular Sieves 4A (822 mg) in dry CH_2Cl_2 (5 ml) was stirred vigorously for 30 min. The mixture was diluted with ether (15 ml) and the ether layer was filtered through a short pad of Florisil. This work-up was repeated three times and the filtrates were concentrated to give the aldehyde **15** (158 mg, 90%). bp 113—117 °C/80 mmHg; $[\alpha]_D^{28}$ +17.1° (*c* 1.46, $CHCl_3$) ; IR (neat) 1715, 880 cm^{-1}; ^1H NMR ($CDCl_3$) δ=1.13 (s, 3H), 1.0—2.0 (m, 6H), 2.30 (br s, 1H), 2.83 (br s, 1H), 4.60 (s, 1H), 5.03 (s, 1H), 9.60 (s, 1H). Exact mass Found: *m/z* 150.1007. Calcd for $C_{16}H_{14}O$: M, 150.1043; MS *m/z* 150 (M^+), 149, 113, 57; R_f 0.52 (benzene).

(*E*)-Ethyl (−)-(1*R*,4*S*)-3-[*exo*-2-Methyl-3-methylene-bicyclo[2.2.1]hept-*endo*-2-yl]-2-propenoate (16). To a solution of triethyl phosphonoacetate (0.6 ml, 3.02 mmol) in dry THF (3 ml) was added 1.62 M *n*-BuLi in hexane (1.8 ml, 2.92 mmol) at −78 °C. After 45 min the reaction mixture was added to a stirred solution of **15** (158 mg, 1.05 mmol) in dry THF (2 ml) by a cannula. The mixture was stirred at that temperature for 30 min. Diluted hydrochloric acid was poured into the mixture and the aqueous layer was extracted with ether (5×10 ml). The combined extracts were washed with brine, dried ($MgSO_4$) and concentrated. The crude oil was purified by chromatography (ether/pentane 1 : 4) to give **16** (223 mg, 96%). bp 116—121 °C/15 mmHg; $[\alpha]_D^{28}$ −132.5° (*c* 1.12, $CHCl_3$); IR (neat) 1719, 1642, 1280, 1170 cm^{-1}; ^1H NMR ($CDCl_3$) δ=1.17 (s, 3H), 1.30 (t, *J*=7 Hz, 2H), 1.0—2.0 (m, 6H), 2.10 (br s, 1H), 2.77 (br s, 1H), 4.18 (q, *J*=7 Hz, 2H), 4.52 (s, 1H), 4.97 (s, 1H), 5.92 (d, *J*=16 Hz, 1H), 6.93 (d, *J*=16 Hz, 1H). Exact mass Found: *m/z* 220.1487. Calcd for $C_{14}H_{20}O_2$: M, 220.1462; MS *m/z* 220 (M^+), 191, 147, 91; R_f 0.50 (benzene).

Ethyl (+)-(1*R*,4*S*)-3-[*exo*-2-Methyl-3-methylenebicyclo-[2.2.1]hept-*endo*-2-yl]propanoate (17). A mixture of **16** (281 mg, 1.28 mmol), triethylsilane (0.3 ml, 1.9 mmol) and a catalytic amounts of tris (triphenylphosphine) chlororhodium was heated at 90 °C for 20 min. After cooling, ethanol (0.5 ml) was added to the mixture. The mixture was concentrated and the crude oil was chromatographed (ether-pentane 1 : 5) to give **17** (283 mg, 100%). bp 140—144 °C/15 mmHg; $[\alpha]_D^{26}$ +25.8° (*c* 2.45, $CHCl_3$); IR (neat) 1738 cm^{-1}; ^1H NMR ($CDCl_3$) δ=1.00 (s, 3H), 1.27 (t, *J*=7 Hz, 3H), 1.0—2.6 (m, 11H), 2.70 (br s, 1H), 4.16 (q, *J*=7 Hz, 2H), 4.53 (s, 1H), 4.78 (s, 1H). Exact mass Found: *m/z* 222.1588. Calcd for $C_{14}H_{22}O_2$: M, 222.1619; MS *m/z* 223, 222 (M^+), 93, 91; R_f 0.52 (benzene).

(+)-(1*R*,4*S*)-*exo*-2-Methyl-3-methylenebicyclo[2.2.1]-hept-2-ene-*endo*-3-propanol (18). To a solution of **17** (397 mg, 1.79 mmol) in dry ether (7 ml) was added 1 M DIBAL in hexane (5.4 ml, 5.4 mmol) at −78 °C and the mixture was stirred for 2.5 h. Diluted hydrochloric acid was added to the mixture and the aqueous layer was extracted with ether (5×10 ml). The combined extracts were dried ($MgSO_4$) and concentrated. The crude oil was purified by chromatography (ether/pentane 1 : 1) to give **18** (298 mg, 93%). bp 126—139 °C/11 mmHg; $[\alpha]_D^{25}$ +48.3° (*c* 1.13, $CHCl_3$); IR (neat) 3325, 1650 cm^{-1}; ^1H NMR ($CDCl_3$) δ=1.01 (s, 3H), 1.1—1.6 (m, 10H), 2.00 (br s, 1H), 2.69 (br s, 1H), 3.64 (m, 2H), 4.48 (s, 1H), 4.72 (s, 1H). Exact mass Found: *m/z* 180.1513. Calcd for $C_{14}H_{20}O_2$: M, 180.1513; MS *m/z* 180 (M^+), 136; R_f 0.10 (benzene).

(+)-(1*R*,4*S*)-*exo*-2-Methyl-3-methylenebicyclo[2.2.1]-hept-2-ene-*endo*-3-propanal (19). A mixture of PCC (981 mg, 4.55 mmol), **18** (298 mg, 1.66 mmol) and Molecular Sieves 4A (1 g) in dry CH_2Cl_2 (15 ml) was stirred vigorously for 1 h. The mixture was diluted with ether (45 ml) and the ether layer was filterd through a short pad of Florisil (ca. 10 g). The black residue was washed with ether (3×10 ml) and the combined filtrates were concentrated to give **19** (284 mg, 96%). bp 98—101 °C/15 mmHg; $[\alpha]_D^{25}$ +30.83° (*c* 1.10, $CHCl_3$); IR (neat) 1725, 1650 cm^{-1}; ^1H NMR ($CDCl_3$) δ=1.00 (s, 3H), 1.00—1.87 (m, 8H), 1.97 (br s, 1H), 2.27—2.70 (m, 2H), 2.70 (br s, 1H), 4.52 (s, 1H), 4.77 (s, 1H), 9.80 (t, *J*=1.5 Hz, 1H). Exact mass Found: *m/z* 178.1356. Calcd for $C_{14}H_{18}O_2$: M, 178.1356; MS *m/z* 178 (M^+), 163, 94, 93, 91; R_f 0.52 (benzene).

(+)-*epi*-β-Santalene (4). To a suspension of isopropyltriphenylphophonium bromide (358 mg, 0.93 mmol) in dry THF (7 ml) was added dropwise 1.62 M *n*-BuLi in hexane (1.7 ml, 2.75 mmol) at 0 °C. After an additional 10 min **19** (102 mg, 0.57 mmol) in dry THF (3 ml) was added to the red suspension. The mixture was stirred for 18 h at room temperature and poured into water (10 ml). The aqueous layer was extracted with petroleum ether (5×10 ml). The combined extracts were washed with water (10 ml), sat. brine and dried ($MgSO_4$). The solvent was evaporated and the crude oil was purified by chromatography (petroleum ether) to give (+)-*epi*-β-santalene (**4**)(67 mg, 57%). bp 94—115 °C/2—5 mmHg; $[\alpha]_D^{27}$ +26.35° (*c* 0.39, $CHCl_3$) (lit,[4] $[\alpha]_D^{22}$ +23.3° (*c* 4.12, $CHCl_3$), $[\alpha]_D^{27}$ +26.9° (*c* 2.6, $CHCl_3$)); IR (neat) 1655, 1445, 1375, 1103, 879 cm^{-1}; ^1H NMR ($CDCl_3$) δ=1.02 (s, 3H), 1.00—2.08 (m, 11H), 1.62 (s, 3H), 1.68 (s, 3H), 2.67 (br s, 1H), 4.46 (s, 1H), 4.70 (s, 1H), 5.12 (br t, *J*=7 Hz, 1H). Exact mass Found: *m/z* 204.1901. Calcd for $C_{15}H_{25}$: M, 204.1878; MS *m/z* 204 (M^+), 161, 105, 91; R_f 0.73 (petroleum ether).

Ethyl (+)-(1*S*,4*R*)-*endo*-2-Methyl-3-(*p*-tolylthio)bicyclo[2.2.1]heptane-*exo*-2-carboxylate (20). As described above for **8**→**10**, the cycloadduct **7** (415 mg, 1.31 mmol) in ethanol (12 ml) was hydrogenated to give the dihydro sulfoxide (420 mg, 100%). mp 95—96 °C (diisopropyl ether); $[\alpha]_D^{25}$ +28.14° (*c* 1.19, $CHCl_3$); IR (KBr) 1725, 1045 cm^{-1}; ^1H NMR ($CDCl_3$) δ=1.3—1.8 (m, 6H), 1.13 (s, 3H), 1.30 (t, *J*=7 Hz, 3H), 2.40 (s, 3H), 2.8 (br s, 1H), 2.0—3.0 (m, 2H), 4.17 (q, *J*=7 Hz, 2H), 7.27, 7.60 (ABq, *J*=8 Hz, 2×2H). Found: C, 67.26; H, 7.54%. Calcd for $C_{18}H_{24}O_3S$: C, 67.47; H, 7.55%; MS *m/z* 321 (M^+ +1), 304, 153.

The sulfoxide (439 mg, 1.37 mmol) was treated as decribed for **10**, giving the sulfide **20** (384 mg, 92%). mp 39—41.5 °C (sublimed); bp 123—125 °C/0.1 mmHg; $[\alpha]_D^{24}$ −14.87° (*c* 1.30, $CHCl_3$); IR (KBr) 1720 cm^{-1}; ^1H NMR ($CDCl_3$) δ=1.0—1.7 (m, 5H), 1.23 (t, *J*=7 Hz, 3H), 1.37 (s, 3H), 2.30 (s, 3H), 2.0—2.6 (m, 3H), 2.70 (d, *J*=2 Hz, 1H), 4.10 (q, *J*=7 Hz, 2H), 7.03, 7.27 (ABq, *J*=8 Hz, 2×2H). Found: C, 71.30; H, 7.87%. Calcd for $C_{18}H_{24}O_2S$: C, 71.07; H, 7.95%; MS *m/z* 304 (M^+), 143.

Ethyl (−)-(1*S*,4*R*)-*endo*-3-Oxobicyclo[2.2.1]heptane-*exo*-2-carboxylate (21). A mixture of sulfide **20** (398 mg, 1.29 mmol), NCS (886 mg, 6.64 mmol), and CCl_4 (25 ml) was heated to reflux for 2 h. After cooling, the reaction mixture was filtered and the filtrate was concentrated to dryness.

Without further purification, the crude product was successively treated with $CuCl_2 \cdot 2H_2O$ (941 mg, 6.17 mmol), CuO (935 mg, 11.8 mmol), acetone (17 ml) and water (1.7 ml) to reflux for 4 h. The mixture was filtered through a short pad of Celite and the filtrate was concentrated. The residue was partitioned with Et_2O and H_2O. The Et_2O layer was washed with satd brine, dried ($MgSO_4$) and concentrated. The residue was chromatographed on silica (PhH and then Et_2O) and distilled to give **21** (183 mg, 72%). bp 150—157 °C/5 mmHg; $[\alpha]_D^{25}$ −93.7° (*c* 0.87, $CHCl_3$); IR (neat) 2990, 1760, 1725, 1250 cm^{-1}; ^1H NMR ($CDCl_3$) δ=1.25 (s, 3H), 1.28 (t, *J*=7 Hz, 3H), 1.4—2.3 (m, 6H), 2.58 (br, 1H), 2.77 (br, 1H), 4.13 (q, *J*=7 Hz, 2H). Found: C, 66.86; H, 8.28%. Calcd for $C_{11}H_{16}O_3$: C, 67.32; H, 8.22%. Exact mass Found: *m/z* 196.1109. Calcd for $C_{11}H_{16}O_3$: M, 196.1099; MS *m/z* 196 (M^+), 168, 139, 95, 67.

(−)-(1*S*,4*R*)-*endo*-2-Hydroxy-*exo*-3-methylbicyclo[2.2.1]heptane-*endo*-2-methanol (22). A solution of keto ester **21** (2.328 g, 12 mmol) in dry Et_2O (10 ml) was added to a suspension of $LiAlH_4$ (1.163 g) in dry Et_2O (30 ml) at 0 °C. The mixture was stirred for 3 h at room temperature. The excess of reagent was destroyed by addition of a minimal amount of H_2O. The mixture was filtered and the filtrate was concentrated under vacuum. Purification by crystallization from *i*-Pr_2O afforded diol **22** (1.282 g, 69%). mp 108—110 °C; $[\alpha]_D^{25}$ −8.55° (*c* 0.52, $CHCl_3$); IR (KBr) 3320, 2975, 1470, 1355 cm^{-1}; ^1H NMR ($CDCl_3$) δ=0.92 (s, 3H), 1.0—2.0 (m, 7H), 2.32 (br, 1H), 2.55 (br, 2H, OH), 3.35 (s, 2H), 3.75 (d, *J*=4 Hz, 1H). Found: C, 69.43; H, 10.23%. Calcd for $C_9H_{16}O_2$: C, 69.19; H, 10.32%; MS *m/z* 138 (M^+ −18), 123, 107, 95, 69, 67.

(−)-(1*S*,4*R*)-*endo*-2-Methyl-3-oxobicyclo[2.2.1]heptane-*exo*-2-carbaldehyde (23). To a solution of CH_2Cl_2 (25 ml) and oxalyl dichloride (0.07 ml, 0.8 mmol) was added dropwise DMSO (0.12 ml, 1.7 mmol) in CH_2Cl_2 (0.5 ml) at −50—60 °C. The mixture was stirred for 3 min and the diol **22** (107 mg, 0.69 mmol) in CH_2Cl_2 (1 ml) was added dropwise over a period of 5 min. The reaction mixture was stirred for an additional 20 min. Triethylamine (4.5 ml, 32 mmol) was added and the mixture was stirred for 20 min. After diluting with H_2O (10 ml) the aqueous layer was extracted with CH_2Cl_2 (3×15 ml). The combined extracts were washed with dil HCl, sat. brine, dried ($MgSO_4$) and concentrated. Purification of the oily product by distillation gave keto aldehyde **23** (100 mg, 96%). bp 65—75 °C/6 mmHg; $[\alpha]_D^{24}$ −329.1° (*c* 0.43, $CHCl_3$); IR (neat) 2720, 1750, 1710 cm^{-1}; ^1H NMR (CCl_4) δ=1.20 (s, 3H), 1.3—2.1 (m, 6H), 2.57 (br, 1H), 2.83 (br, 1H), 9.36 (s, 1H). Found: C, 68.77; H, 8.03%. Calcd for $C_9H_{12}O_2$: C, 71.02; H, 7.95%. Exact mass Found: *m/z* 152.0841. Calcd for $C_9H_{12}O_2$: M, 152.0837; MS *m/z* 152 (M^+), 124, 109, 95, 67.

(−)-(1*S*,4*R*)-*endo*-2-Methyl-3-oxobicyclo[2.2.1]heptane-*exo*-2-carbaldehyde Dimethyl Acetal (24). Keto aldehyde **23** was dissolved in a 0.2 M methanolic solution of $CeCl_3 \cdot 7H_2O$ (1.5 ml, 0.3 mmol) and trimethyl orthoformate (0.166 ml, 1.5 mmol) was added to the solution. The reaction mixture was allowed to stand for 3 days at room temperature. After addition of sat. $NaHCO_3$ (3 ml), the mixture was extracted with Et_2O (3×15 ml) and the extracts were concentrated. Purification by distillation afforded acetal **24** (43 mg, 72%, purity >86% from vpc). An analytical sample was obtained by redistillation. bp 65—75 °C/3 mmHg; $[\alpha]_D^{24}$ −62.6° (*c* 0.71, $CHCl_3$); IR (neat) 1740, 1445, 1110, 1065 cm^{-1}; ^1H NMR (CCl_4) δ=0.95 (s, 3H), 1.12—1.87 (m, 6H), 2.37 (br, 1H), 2.62 (br, 1H), 3.32 (s, 3H), 3.38 (s, 3H), 4.12 (s, 3H). Found: C, 66.49; H, 9.24%. Calcd for $C_{11}H_{18}O_3$: C, 66.64; H, 9.15%; MS *m/z* 198 (M^+), 167, 139, 107, 75, 67.

In the ^1H NMR, racemic **24** (prepared from (±)-**21**) was resolved to a pair of singlets due to the tertiary methyl at 2.97 and 3.10 ppm using a chiral shift reagent Eu(hfc)$_3$ (1.67 equiv used). The acetal (−)-**24** showed the tertiary methyl signal at 2.97 ppm. The peak of the corresponding enantiomer was hardly observed within the limit of detection.

(−)-(1*S*,4*R*)-*endo*-2-Methyl-3-methylenebicyclo[2.2.1]heptane-*exo*-2-carbaldehyde Dimethyl Acetal (25). A suspension of activated Zn (129 mg, 2 mg atom) and CH_2Br_2 (0.04 ml, 0.57 mmol) in dry THF (0.5 ml) was treated with 1 M $TiCl_4$ in CH_2Cl_2 (0.4 ml, 0.4 mmol) at room temperature. During the reaction the color changed to dark brown. After 15 min, keto acetal **24** (72 mg, 0.36 mmol) in dry THF (0.5 ml) was added dropwise over a period of 15 min via a syringe. The mixture was stirred for 21 h at ambient temperature. The reaction mixture was partitioned with CH_2Cl_2 (5 ml) and sat. $NaHCO_3$ (5 ml). The aqueous layer was extracted with CH_2Cl_2 (3×10 ml). The combined extracts were concentrated to dryness. Purification by chromatography (pentane) afforded acetal **25** (43 mg, 60%, 51% purity from vpc). An analytical sample was obtained by a Kugelrohr distillation. bp 120—125 °C/42 mmHg; $[\alpha]_D^{24}$ −119.3° (*c* 0.91, $CHCl_3$); IR (neat) 1655, 1450, 1190, 1110, 1070, 985, 890 cm^{-1}; ^1H NMR ($CDCl_3$, 270 MHz) δ=1.08 (s, 3H), 1.0—1.9 (m, 6H), 2.32 (br, 1H), 2.69 (br, 1H), 3.49 (s, 3H), 3.48 (s, 3H), 4.01 (s, 1H), 4.73 (s, 1H), 4.84 (s,1H). Found: C, 70.40; H, 10.00%. Calcd for $C_{12}H_{20}O_2$: C, 73.43; H, 10.27%; MS *m/z* 167 (M^+ −29), 149, 93, 75.

We acknowledge financial support from the Japan Research Foundation for Optically Active Compounds and by the Grant-in-Aid for Scientific Research from the Ministry of Education, Science and Culture (No. 59570888).

We thank Dr. W. Gramlich (BASF, Germany) for sending copies of NMR and IR spectra of (±)-**25** and Dr. P. Christenson (Fritzche Dodge & Olcott Inc.) for NMR and IR spectra of (±)-*epi*-β-santalene.

References

1) The symbol $(R)_S$ given in this paper expresses that the chirality at sulfur is the *R* configuration.

2) For a review of the isolation and characterization of α-and β-santalenes and santalols, see: J. L. Simonsen and D. H. R. Barton, "The Terpenes," Vol. III, Cambridge University Press, England (1952), p. 178. For a review of the general chemistry of Sandalwood oil, see: G. T. Walker, Perf. Essent. Oil Record (London), 778 (1968).

3) E. J. Brunke, *Perfum+Kosmet.*, **63**, 73 (1981).

4) The absolute configuration of (−)-**3** and (+)-**4** was determined by Money et al.: C. R. Eck, G. L. Hodgson, D. F. MacSweeny, R. W. Mills, and T. Money, *J. Chem. Soc., Perkin Trans. 1*, **1974**, 1938. (−)-**3** was transformed into (−)-**2** by oxidation with selenium dioxide: V. M. Sathe, K. K. Chakravarti, M. V. Kadival, and S. C. Bhattacharyya, *Indian J. Chem.*, **4**, 393 (1966).

5) E. J. Corey, R. Hartmann, and P. A. Vatakencherry, *J. Am. Chem. Soc.*, **84**, 2611 (1962).

6) G. Brieger, *Tetrahedron Lett.*, **1963**, 1949.

7) G. L. Hodgson, D. F. MacSweeny, and T. Money, *J. Chem. Soc., Perkin Trans. 1*, **1973**, 2113.

8) a) "The Total Synthesis of Natural Products," ed by J. ApSimon, John Wiley & Sons, New York (1983), pp. 249—259. For syntheses of **2** after 1980, see: K. Sato, O. Miyamoto, S. Inoue, and K. Honda, *Chem. Lett.*, **1981**, 1183; D. Solas and J. Wolinsky, *J. Org. Chem.*, **48**, 1988 (1983). For syntheses of **4** after 1980, see: b) P. A. Christenson and B. J. Willis, *J. Org. Chem.*, **45**, 3068 (1980). c) R. L. Snowden, P. Sonnay, and G. Ohloff, *Helv. Chim. Acta*, **64**, 25 (1981).

9) W. Oppolzer and C. Chapuis, *Tetrahedron Lett.*, **24**, 4665 (1983).

10) For the first example of an asymmetric cycloaddition using a chiral sulfoxide, see: T. Koizumi, H. Hirai, and E. Yoshii, *J. Org. Chem.*, **47**, 4004 (1982). For recent examples of an asymmetric Diels-Alder reaction using an α,β-unsaturated sulfoxide, see: C. Maignan and R. A. Raphael, *Tetrahedron*, **39**, 3245 (1983); S. M. Proust and D. D. Ridley, *Aust. J. Chem.*, **37**, 1677 (1984); C. Maignan, A. Guessous, F. Rouessac, *Tetrahedron Lett.*, **25**, 1727 (1984); O. De Lucchi, V. Lucchioni, C. Marchioro, G. Valle, and G. Modena, *J. Org. Chem.*, **51**, 1457 (1986); Y. Arai, S. Kuwayama, Y. Takeuchi, and T. Koizumi, *Tetrahedron Lett.*, **26**, 6205 (1985); *idem, Synthetic Commun.*, **16**, 233 (1986); H. Takayama, A. Iyobe, and T. Koizumi, *J. Chem. Soc., Chem. Commun.*, **1986**, 771.

11) S. D. Kahn and W. J. Hehre, *J. Am. Chem. Soc.*, **108**, 7399 (1986); *idem, Tetrahedron Lett.*, **27**, 6041 (1986).

12) H. Takayama, K. Hayashi, and T. Koizumi, *Tetrahedron Lett.*, **27**, 5509 (1986); Y. Arai, Y. Hayashi, M. Yamamoto, H. Takayama, and T. Koizumi, *Chem. Lett.*, **1987**, 185; H. Takayama, A. Iyobe, and T. Koizumi, *Chem. Pharm. Bull.*, **35**, 433 (1987).

13) T. Koizumi, I. Hakamada, and E. Yoshii, *Tetrahedron Lett.*, **25**, 87 (1984)

14) S. Hanessian, "The Chiron Approach," Pergamon, New York (1984).

15) Y. Arai, M. Yamamoto, and T. Koizumi, *Chem. Lett.*, **1986**, 1225.

16) C. Maignan and R. A. Raphael, *Tetrahedron*, **39**, 3245 (1983).

17) L.N. Mander and S. P. Sethi, *Tetrahedron Lett.*, **24**, 5425 (1983).

18) K. Takai, Y. Hotta, K. Oshima, and H. Nozaki, *Bull. Chem. Soc. Jpn.*, **53**, 1698 (1980). The keto ester **11** is quite resistant not only to acetalization with a variety of reagent (ethylene glycol/PPTS, 2,2-dimethoxypropane/*p*-tolunesulfonic acid), but also to methylenation by a standard Wittig reagent($Ph_3P=CH_2$).

19) During the course of this study, the investigation of more reactive reagent($CH_2I_2/Zn/TiCl_4$) than the CH_2Br_2 system has been examined by Takai et al. We are thankful to Dr. Takai for making available to us some of his results in advance of publication. See also: J.-I. Hibino, T. Okazoe, K. Takai, and H. Nozaki, *Tetrahedron Lett.*, **26**, 5579 (1985). We attempted to improve the yield of this reaction using diiodomethane instead of dibromomethane but the yield did not exceed.

20) J. Herscovici, M.-J. Egron, and K. Antonakis, *J. Chem. Soc., Perkin Trans. 1*, **1982**, 1967.

21) E. Yoshii, Y. Kobayashi, T. Koizumi, and T. Oribe, *Chem. Pharm. Bull.*, **22**, 2767 (1974).

22) Although we have repeated the direct conversion (**17**→**19**) by DIBAL reduction described in the literature, we were unable to produce **19** exclusively, resulting in contamination with **18**.

23) For a convenient preparation of (±)-3-methylnorcamphor, see: W. Kreiser and L. Janitschke, *Chem. Ber.*, **112**, 408 (1979).

24) K. Omura and D. Swern, *Tetrahedron*, **34**, 1651 (1978).

25) A. L. Gemal and J.-L. Luche, *J. Org. Chem.*, **44**, 4187 (1979).

26) M. Baumann and W. Hoffmann, *Justus Liebigs Ann. Chem.*, **1979**, 743.

 © 1988 The Chemical Society of Japan Bull. Chem. Soc. Jpn., 61, 475—481 (1988)

Autoxidation of Solid Guaiazulene and of the Solution in DMF in the Presence of Base or Acid: A Comparative Study of the Product Distribution[1)]

Shin-ichi TAKEKUMA,* Yoshiharu MATSUBARA, Hiroshi YAMAMOTO,*,† and Tetsuo NOZOE††
Department of Applied Chemistry, Faculty of Science and Engineering, Kinki University, Kowakae, Higashi-Osaka 577
†Department of Chemistry, Okayama University, Okayama 700
††Tokyo Research Laboratories, Takasago Corporation, 5-36-31 Kamata, Ohta-ku, Tokyo 144
(Received August 17, 1987)

Autoxidation of guaiazulene was examined in detail under the following conditions: in a highly diluted DMF solution, in DMF in the presence of acid or base (at 80—100 °C), and as solid state under sunlight or in the dark (at 25—50 °C). In all cases a wide variety of products were obtained (33 separable compounds altogether), and a comparable study on the distribution of the products under the various reaction conditions was made to establish more precise reaction pathways for the formation of these interesting compounds.

In the past few years we have undertaken a detailed study on various azulenes in *N,N*-dimethylformamide (DMF) or hexamethylphosphoric triamide: e.g., guaiazulene (**1**),[2)] 4,6,8-trimethylazulene (**2**),[2b,3)] 3,3′-methylenebisguaiazulene (**3**),[4)] 1-methyl- and 1,3-dimethylazulene (**4**,**5**)[5)] as well as azulene itself.[6)] As a result, these azulenes gave a wide variety of products possessing interesting structures through such several types of reactions as oxidative dimerization, oxidation of side chains, azulenequinone formation, intermolecular one-carbon transfer reactions, and rearrangements to naphthalenoid, benzenoid, and 1*H*-inden-1-one derivatives. The product distribution of these oxidation and coupling reactions was found to heavily depend upon the type of the starting azulenes employed, although the facility of the radical attack of oxygen (or various other free radical species) on the C-1 and C-3 position of the azulene nucleus mostly exceeded that on various positions of the seven-membered ring, as in the cases of many other electrophilic reactions of azulenes.[7)]

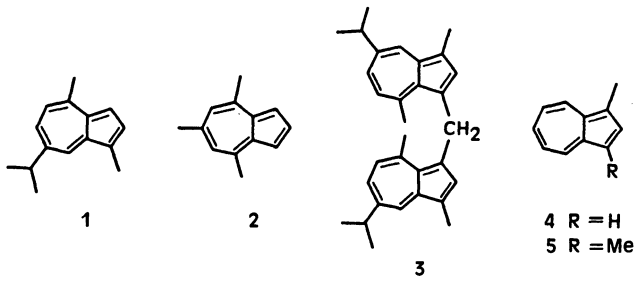

1 2 3 4 R = H 5 R = Me

We now wish to report in this paper the detailed study on autoxidation of guaiazulene (**1**) as a solid (at 25—50 °C) and in a DMF solution in the presence of base or acid (at 80—100 °C). This study was conducted to compare the mode of the oxidation under different reaction conditions to establish a further general aspect of the reaction mechanism of oxidation of azulenes by taking **1** as a representative, model compound.

Results and Discussion

Autoxidation of Guaiazulene (1). The oxidation was conducted under the conditions summarized in Table 1: namely, *A* (expt ii), in a much more dilute DMF solution than the previous experiment;[2)] *B* (expt iii), in a DMF solution in the presence of 1,4-diazabicyclo[2.2.2]octane (Dabco/DMF); *C* (expt iv), in a DMF solution in the presence of dilute sulfuric acid (H_2SO_4/DMF); *D* (expt v), as a solid under sunlight; *E* (expt vi) as a solid in a laboratory; *F* (expt vii), as a solid protected from light. The experiments in DMF solutions were carried out in a manner similar to that described previously[2)] by allowing finely bubbling oxygen to pass into a solution of the substrate **1** in DMF at 100 °C and the reaction was monitored by the use of the reversed phase high-pressured liquid chromatography (HPLC) or silica-gel TLC. The solid oxidation was conducted by impregnating **1** on a filter paper and allowing it to stand under the conditions shown in Table 1. The time-dependent HPLC diagrams of the expts ii—vii are shown in Fig. 1. Then, the reaction products were separated into each component by using chromatography, when about a half of the starting material was consumed. The products thus obtained as pure components [33 altogether besides the recovered starting material **1** (**1A**$_1$)] are referred to as Compounds **1A**—**S** according to the same

Table 1. Reaction Conditions of Autoxidation of **1**

Expt	Temp/°C	Time/d	Other condition	Recovered **1**/%
i[a)]	100	1	In 20 parts of DMF	41
ii	100	1	In 1000 parts of DMF	66
iii	85	6	In 20 parts of DMF +0.5 mol equiv of Dabco	70
iv	85	1	In 20 parts of DMF +0.5 M H_2SO_4	40
v	40—50	8.5	Solid, under sunlight	20
vi	25—35	134	Solid, in a laboratory	40
vii	25—35	127	Solid, protected from light	47

a) From Ref. 2.

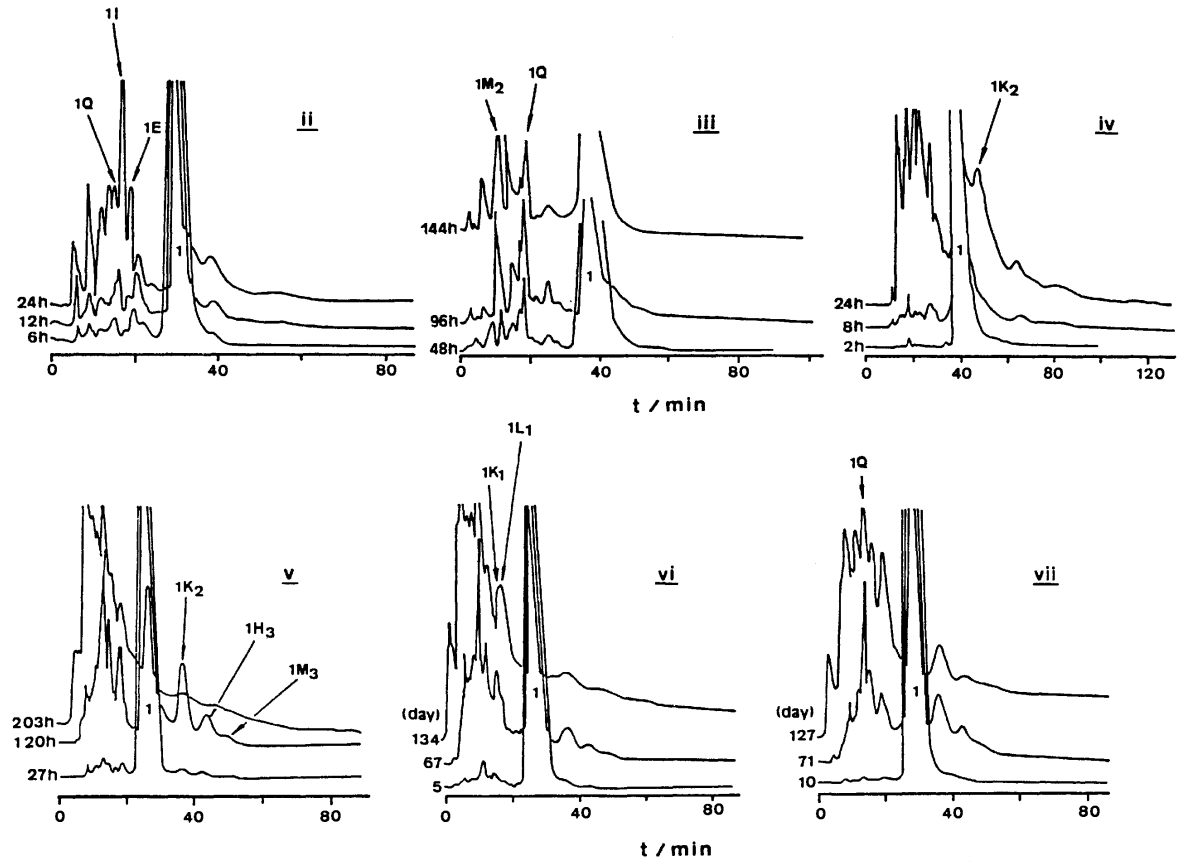

Fig. 1. The time-dependent HPLC diagrams of the autoxidation of **1** (expts ii—vii).

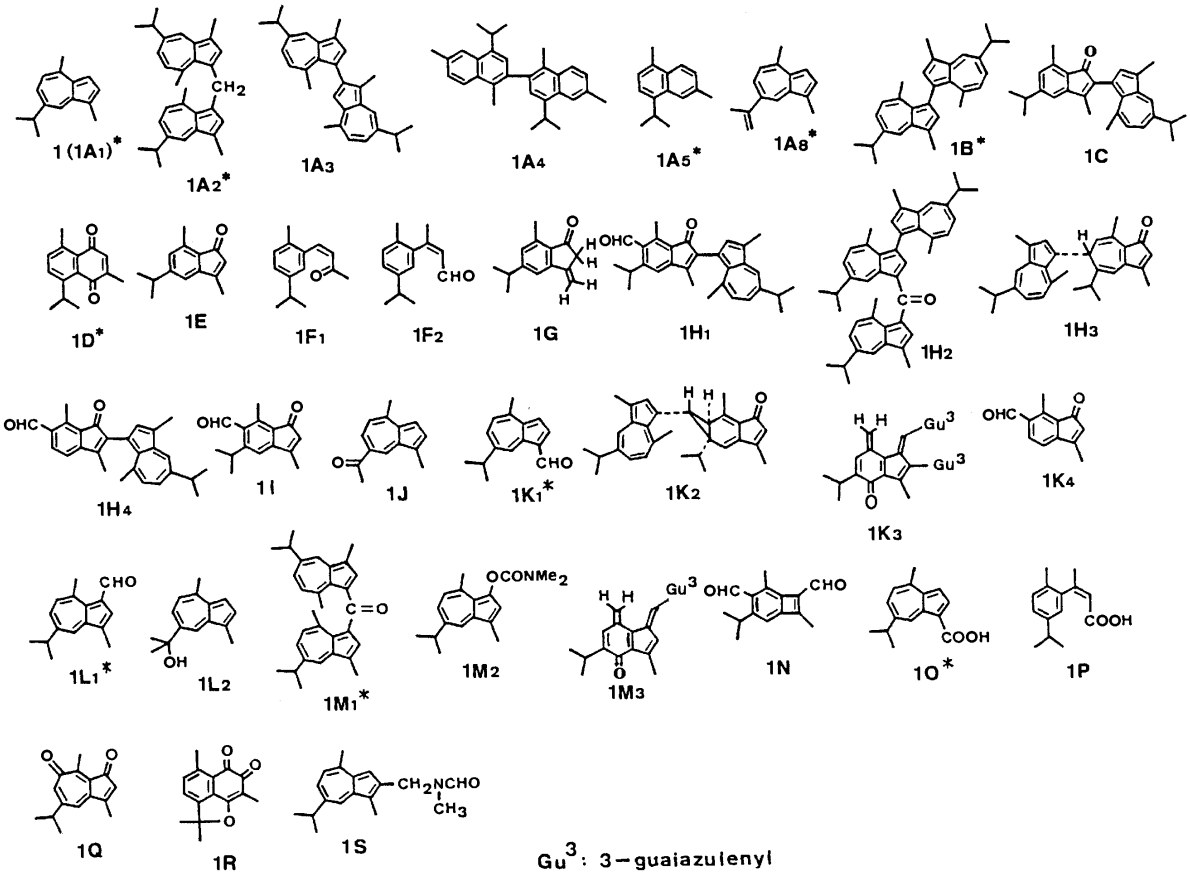

Chart 1. Structures of the autoxidation products from **1**; *previously known compounds.

definition employed in the previous study.[2-6]

In Chart 1 are summarized structures of these products which were established by spectroscopy and chromatography by taking into account the parameters established earlier[2-6] for similar compounds as will be explained below. Among these products, the followings were isolated for the first time in the present study: **1A**$_8$,[8] **1H**$_3$, **1H**$_4$, **1K**$_2$, **1K**$_3$, **1K**$_4$, **1L**$_2$, and **1M**$_3$; other products were identified as all known compounds.[9] The theoretical yields of these isolated products and of an unidentified resinous polar product of rather high molecular weights are summarized in Table 2.

Compounds **1A**$_8$ and **1M**$_3$ were shown to have compositions of $C_{15}H_{16}$ and $C_{15}H_{18}O$ by MS. Thus structures of 7-isopropenyl-[8] and 7-(1-hydroxy-1-methylethyl)-1,4-dimethylazulene were respectively assigned to these minor products by the careful comparison of the ^{1}H NMR spectral data (see the Experimental section) with those of the starting material **1**.

Compounds **1K**$_4$ and **1H**$_4$ showed similar UV and IR spectra to those[2] of **1I** and **1H**$_1$, respectively. The ^{1}H NMR spectra of **1K**$_4$ and **1H**$_4$ also closely resembled those[2] of **1I** and **1H**$_1$, respectively, except for the absence of 5-isopropyl group in **1K**$_4$ and **1H**$_4$. Therefore, the structures without the 5-isopropyl group were assigned to these newly isolated products and were confirmed by MS. Compound **1K**$_4$ appears to gradually dimerize on setting aside at 25 °C (after ca. 7 d).[10]

Compounds **1H**$_3$ and **1K**$_2$ (both $C_{30}H_{34}O$ by MS) were shown by ^{1}H NMR to be dimeric guaiazulenes having a 3-guaiazulenyl moiety ($C_{15}H_{17}$) attached to different nuclei that both consisted of $C_{15}H_{17}O$ containing a carbonyl group (1685—1680 cm^{-1}). By the careful analysis of the parameters of the ^{1}H NMR of these compounds as well as their reactivities (see below), structures of 6-(3-guaiazulenyl)-1(6*H*)-guaiazulenone (**1H**$_3$) and its norcaradiene isomer **1K**$_2$ were assigned to these products. When either of these compounds was kept in oxygen-free cyclohexane, a noticeable equilibrium was observed between them; the equilibrium ratio was 20/80 for **1H**$_3$/**1K**$_2$ at 25 °C. The reasons for the equilibrium in favor of **1K**$_2$ are assumed to be not only electronic and steric effects of the substituents on the cyclopropane ring but also the non-cyclopentadienone structure of the fused five-membered ring.[11] It is the first example, to the best of our knowledge, among carbocyclic compounds that both norcaradiene and cycloheptatriene forms have been separated as pure compounds and an equilibrium has been confirmed between them.[12]

Compounds **1M**$_3$ and **1K**$_3$ were found by MS to have dimeric ($C_{30}H_{32}O$) and trimeric ($C_{45}H_{48}O$) compositions, respectively. The ^{1}H NMR, UV, and IR spectra of both compounds showed the presence of a 3-guaiazulenyl group and a common non-azulenic nucleus containing a conjugated carbonyl; **1K**$_3$ contained another 3-guaiazulenyl group attached to the above nucleus. Combination of these spectral data led to 1-[(3-guaiazulenyl)methylene]-5-isopropyl-3-methyl-7-methylene-4,7-dihydro-4(1*H*)-indenone and its 2-(3-guaiazulenyl) derivative as the most likely structures

Table 2. Isolated Yield[a]/% of the Autoxidation Products from **1**

Reaction pathway[b]	Product	Expt (reaction condition)[c]						
		i	ii	iii	iv	v	vi	vii
[a]	**1B**	6.8	—	—	7.0	2.5	4.7	9.4
	1A$_3$	0.9	—	—	1.0	1.3	2.0	1.9
	1H$_2$	0.2	—	—	—	—	—	—
	total	7.9	—	—	8.0	3.8	6.7	11.3
[b]	**1K**$_1$	7.9	7.4	20.0	8.0	5.0	13.3	17.0
	1O	1.5	1.6	1.4	1.5	1.3	2.0	0.6
	1M$_3$	—	—	—	2.0	*	0.7	0.6
	1K$_3$	—	—	—	2.0	*	0.7	0.6
	1A$_8$	—	—	—	0.3	—	—	—
	1J	0.3	1.6	1.4	0.3	0.3	0.7	0.6
	1L$_3$	—	1.6	1.4	0.3	*	0.7	0.6
	total	9.7	12.2	24.2	15.3	6.6	18.1	20.0
[c]	**1A**$_2$	8.2	—	—	8.0	*	0.7	0.6
	1M$_1$	1.6	—	—	2.0	*	0.7	0.6
	1H$_3$	—	0.1	—	—	0.4	0.1	0.1
	1K$_2$	—	0.7	—	4.0	1.0	0.7	0.6
	1E	1.7	3.7	2.5	2.0	2.5	3.3	3.8
	1G	0.8	1.6	—	1.0	*	0.7	0.6
	1L$_1$	1.5	1.6	1.4	1.5	1.3	2.0	3.8
	1C	2.2	1.6	—	2.0	1.3	0.7	3.8
	1K$_4$	—	0.4	—	2.0	0.5	0.4	0.4
	1H$_4$	—	1.6	—	2.0	1.3	0.7	0.7
	total	16.0	11.2	3.9	24.5	8.3	10.0	15.0
[d]	**1Q**	1.5	7.4	10.0	1.5	3.8	6.7	18.9
[e]	**1I**	2.9	3.7	5.0	3.0	5.0	6.7	9.4
	1N	0.3	—	—	—	—	—	—
	1H$_1$	2.1	1.6	—	2.0	1.3	0.7	3.8
	total	5.3	5.3	5.0	5.0	6.3	7.4	13.2
[f]	**1D**	5.1	3.7	—	5.0	—	—	—
	1R	0.7	1.6	—	1.0	—	—	—
	1A$_5$	0.9	—	—	—	—	—	—
	1A$_4$	0.4	—	—	—	—	—	—
	total	7.1	5.3	—	6.0	—	—	—
[g]	**1F**$_1$	1.7	1.6	1.4	2.0	*	0.7	0.6
	1F$_2$	1.7	1.6	1.4	2.0	*	0.7	0.6
	1P	2.3	1.6	1.4	2.0	*	0.7	0.6
	total	5.7	4.8	4.2	6.0	*	2.1	1.8
[h]	**1F**$_2$	0.6	14.8	30.0	2.0	—	—	—
	1S	0.6	14.8	2.5	1.0	—	—	—
	total	1.2	29.6	32.5	3.0	—	—	—
	RS[d]	34.0	22.2	15.0	30.0	67.5	45.0	18.9

a) The yield of each product is based on the consumed **1** (see Table 1); *, Although the compound was detected by the HPLC and TLC checking during the oxidation, it was not isolable after the work-up owing to decomposition; —, the compound was not detected. b) [a]. Oxidative dimerization; [b], side-chain oxidation; [c], one-carbon-transfer reaction; [d], 1,7-azulenequinone formation; [e], rearrangement to indenone derivatives; [f], rearrangement to naphthalenoids; [g], rearrangement to benzenoids; [h], condensation with solvent. c) Expts i—vii correspond those in Table 1. d) Polar resinous substance.

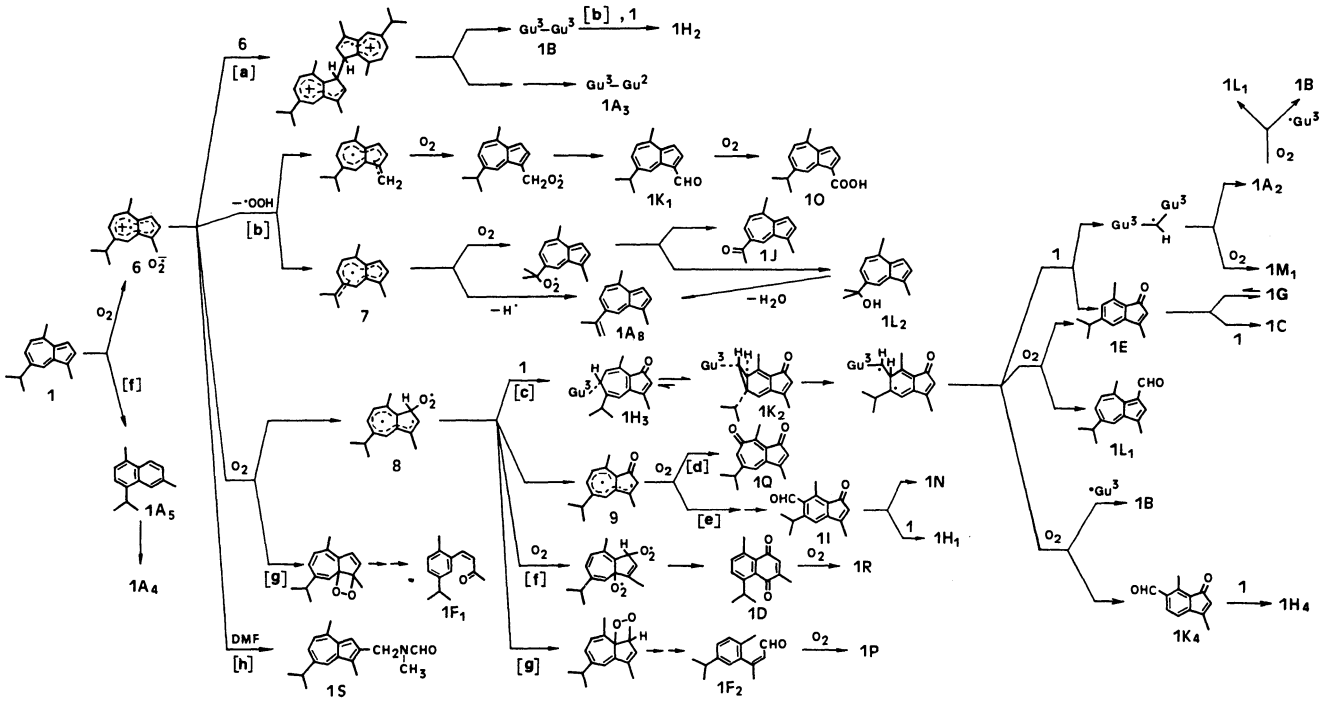

Scheme 1. Possible reaction pathways for the autoxidation products from **1**.

for $\mathbf{1M_3}$ and $\mathbf{1K_3}$, respectively;[13] the assignments for the NMR parameters are given in the Experimental section.

Possible Reaction Pathways for the Formation of Autoxidation Products of 1 and a Comparative Study of the Product Distribution. Autoxidation of **1** under various different conditions has resulted in the simultaneous formation of many kinds of complex products by competitive processes as was observed earlier.[2] In order to grasp an overall view of the autoxidation of **1** and other azulenes, an attempt will now be made here to consider the various reaction pathways as a whole and the product distribution under these different conditions. The possible reaction pathways are summarized in Scheme 1, although many of these intermediates in the Scheme have been presented previously.[2]

By attack of oxygen, guaiazulene (**1**) is considered to initially form an electron-transfer complex **6**, which in turn leads to the formation of various products mainly through the following six kinds of reaction pathways [a]—[g] as illustrated in Scheme 1. The yields of the products shown in Table 2 are grouped together by the reaction pathway and the total yield of each pathway is also given in the Table. Although the figures of these yields do not necessarily reflect the ease of the corresponding reaction pathway, they are listed for a comparative study of the product distribution and the reaction pathways under various conditions as will be explained below.

[a] Oxidative Dimerization: It is characteristic that this type of reaction does not take place in dilute DMF or Dabco/DMF. Dimerization of **6** thus appears to be retarded by the presence of the base. Under other conditions, the 3,3′-dimer **1B** is always obtained as one of the main products in the oxidation, whereas 2,3′-dimer $\mathbf{1A_3}$ is formed in a much smaller quantity.

[b] Side-Chain Oxidation: Under all conditions employed in the present study, the methyl group at C-1 of the azulene nucleus is preferentially oxidized, giving the aldehyde $\mathbf{1K_1}$ as one of the main products. Of particular, it is noted that the yield of this type of compound considerably increases in the case of the solid oxidation in the dark and in Dabco/DMF, under which conditions other reactions are presumed to be relatively suppressed due to the facile decomposition (by Dabco) of the secondarily formed various peroxide intermediates.

Compared with the oxidation of 1-methyl group, the α-hydrogen of the isopropyl group at C-7 of **1** is not readily oxidized in all cases on the evidence of the extremely low yields of the 7-acetyl derivative **1J**. In the present study minor quantities of compounds $\mathbf{1A_8}$ and $\mathbf{1L_2}$ which are apparently derived through the same reaction pathways as **1J** (via **7**, see Scheme 1) have been obtained as well.

Also newly isolated in the present study are small quantities of compounds $\mathbf{1M_3}$ and $\mathbf{1K_3}$. The former is most likely formed by further oxidation[4] of $\mathbf{1A_2}$ accompanied by rearrangement, and the latter ($\mathbf{1K_3}$) is derived by condendation of $\mathbf{1M_3}$ with another molecule of **1**. This indicates that the side chain at C-4 is also susceptible, to a small extent, to the autoxidation of **1** as solid or in H_2SO_4-DMF. Under all conditions examined in the present study, the side chain oxidation as a whole is apparently one of the main reactions in the autoxidation of **1**, by taking into consideration

the total yield of the reaction products of this type.

[c] Intermolecular One-Carbon-Transfer Reaction: This reaction path has been established by the following additional, experimental facts[1] as illustracted in Scheme 1: *1)* 6-(3-guaiazulenyl)-1(6*H*)-guaiazulenone (**1H**$_3$) was isolated and confirmed to become in an equilibrium with the norcaradiene isomer **1K**$_2$; *2)* in the presence of one equivalent of **1**, **1K**$_2$ afforded 3,3′-methylenebisguaiazulene (**1A**$_2$) and 5-isopropyl-3,7-dimethyl-1*H*-inden-1-one (**1E**) under nitrogen at 100 °C in DMF; *3)* on exposure to air, however, **1K**$_2$ yielded 3-formylguaiazulene (**1L**$_1$) and **1E** at 25 °C. It has become evident presently that in the presence of oxygen **1K**$_2$ and **1** afford **1B** as well as **1K**$_4$ and **1H**$_4$, an elimination of the 5-isopropyl group being accompanied in the last to compounds. Compound **1A**$_2$ has also been confirmed to yield **1B** and **1L** in the presence of air. The most likely intermediates and the reaction pathways of these transformation are shown in Scheme 1.

It is a characteristic feature that only a very small quantity of **1A**$_2$ was obtained by the autoxidation of solid **1** and in dilute DMF or Dabco/DMF, whereas **1A**$_2$ was isolated as a main product in a concentrated DMF solution and in H_2SO_4/DMF. In particular, the presence of Dabco suppresses the reaction path [c] considerably as a whole. It is also notable in the present study that the presence of dilute sulfuric acid in DMF resulted in the formation of **1K**$_2$ in as high as 4% yield, although the role of acid on the reaction mechanism is still under investigation.

[d] 1,7-Guaiazulenequinone (1Q) Formation: As for the reaction path for **1Q**, diradical **8** and then 3-oxoguaiazulenyl radical **9** shown in Scheme 1 were presumed[2] as possible intermediates. It should be noticed that the solid autoxidation at 25—30 °C in the dark and the oxidation in Dabco/DMF produce **1Q** in as high as 19 and 10% yield, respectively (see Table 2). This would be mainly due to the stability of **1Q** under the above reaction conditions compared with others, although the exact role of Dabco in this case has also remained to be clarified. However, the present result is of significance in view of exploitation of a convenient synthetic scheme for azulenequinones, which are currently drawing increasing interest in the potential utility of the physicochemical properties and biological activity.[14]

[e] Rearrangement to 6-formyl-1*H*-inden-1-one (1I) and its Derivatives: This type of reaction takes place under all reaction conditions examined, yielding **1I** and its 2-(3-guaiazulenyl) derivative **1H**$_1$ illustrated in Scheme 1. The solid oxidation of **1** in the dark gives the highest total yield of the products via path [e].

[f] Rearrangement to Naphthalenoids: These compounds have been presumed[2] to be derived through the pathways shown as path [f] in Scheme 1. It has become apparent by the present experiment that no skeletal rearrangement of this type takes place in Dabco/DMF and as a solid, the reason for which is not certain at this stage.

[g] Rearrangement to Benzenoids: Although in relatively small quantities, these compounds have been found to be always produced under all conditions. However, this reaction path (Scheme 1) can be regarded as a minor one.

[h] Condensation with Solvent DMF: It has become apparent in the present study that the product **1S** of this type considerably increases in a dilute DMF solution and in the presence of Dabco/DMF.

The polar resinous substances (R_f=0 on TLC) appears to relatively decrease in the autoxidation of **1** in Dabco/DMF and as solid state in the dark, under which conditions various oligomerization and polymerization reactions seem to be suppressed.

Autoxidation of guaiazulene and the product distributions under various conditions have been closely examined. As a result, complex reaction pathways of the autoxidation of a representative, naturally occurring azulene **1** have been made clarified to a considerable extent. Such information in turn gives important suggestion for the elucidation of exact mechanism of the oxidation of azulenes using various other oxidizing reagents.[15]

Experimental

Melting points were determined with a Yanagimoto MP-S3 instrument and are uncorrected. Column chromatography was performed with Wako C-300 silica gel. TLC was conducted on plates precoated with silica gel 60F-254 (0.25 mm, Merck) by using 15:85 AcOEt–hexane as eluant. HPLC was carried out with Hitachi gel #3011 packed in a Pyrex column (ϕ 5 mm, 500 mm length) with 1 : 9 hexane–MeOH as solvent.

UV and IR (in MeOH and $CHCl_3$, respectively, unless otherwise specified) spectra were taken on a Hitachi 323 spectrophotometer and a Nihonbunko IR-A-202 Grating spectrometer, respectively. NMR spectra were recorded in $CDCl_3$ (unless otherwise stated) with a JEOL-FX200 cryospectrometer (200-MHz for ^{1}H and 50-MHz for ^{13}C) at 27 °C. Chemical shifts are reported as δ values in parts per million rel to tetramethylsilane (δ 0.0) as the internal standard. The assignments of all signals were made by employing a first-order analysis with the aid of decoupling technique and the parameters were confirmed by a computer-assisted simulation analysis. Mass spectra were taken on a JEOL JMS-HX100 (with a JEOL JMA-DA5000 mass data system) high-resolution instrument and are given in terms of m/z (rel intensity) compared with the base peak.

Oxidation of Guaiazulene (1) in DMF. A. In Dilute DMF Solution (expt ii): A soln of **1**[16] (0.020 g) in freshly distilled HMPA (20 g) was placed in a Pyrex flask (ϕ 18 mm, 600 mm height) and subjected to autoxidation by allowing finely bubbling oxygen to pass through the soln (from the bottom of the flask) for 24h at 100 ±5 °C. Time-dependent HPLC diagrams of this reaction are given in Fig. 1. After cooling, the mixture was diluted with water (200 cm^3) and extracted with ether (4×50 cm^3). The combined organic layers were washed with water, dried (Na_2SO_4), and evaporated in vacuo,

giving a brown oil. This oil was preliminarily separated into five fractions by means of preparetive HPLC with Hitachi gel #3019 (100 g) using methanol as eluant. Then each fraction was carefully separated by silica-gel column or thin layer with AcOEt-hexane; when necessary, this chromatographic procedure was repeated. Thus, the 22 products were obtained as pure substances (**1A—S**), besides the recovered starting material **1** (**1A**$_1$: 13.2 mg (66%); R_f=0.95) and polar resinous substances [1.5 mg, 22.2% (w/w), R_f=0.0]. The yield of each product based on the consumed starting material (6.8 mg) is summarized in Table 2.

B. In the Presence of Dabco (expt iii): The same oxidation procedures as those shown above (expt ii) were employed. Thus, a solution of **1** (1.00 g) dissolved in DMF (20 g) containing Dabco (0.28 g, 0.5 mole equiv.) was oxidized at 85±5 °C for 6 d, and the yield of each product is summarized in Table 2; 70% of the starting material **1** was recovered.

C. In the Presence of Sulfuric Acid (expt iv): Similarly, a solution of **1** (1.00 g) in DMF (20 g) containing 0.5 M sulfuric acid (5 cm^3) was oxidized, and the yield of each product is summarized in Table 2.

Oxidation of Solid Guaiazulene (1). A. Under Sunlight (expt v): Solid **1** (0.10 g) dissolved in hexane (0.5 cm^3) was homogeneously impregnated into a filter paper (70×50 mm, 0.27 mm thickness), which was hanged on a wire in a Pyrex beaker (500 cm^3) covered with a thin layer of cotton and allowed to stand at 40—50 °C for 8.5 d under the sunlight. After the same work-up, the yield of each product isolated is summarized in Table 2.

B. In a Laboratory (expt vi): **1** (0.10 g) was similarly oxidized on exposure to air in an ordinary laboratory room (without protection from light) at 25—35 °C for 134 d, and the yield of each product is summarized in Table 2.

C. Under the Protection from Light (expt vii): **1** (0.10 g) was similarly oxidized in a dark room at 25—35 °C for 127 d; the time-dependent HPLC diagrams are shown in Fig. 1. The yield of each product is summarized in Table 2.

7-Isopropenyl-1,4-dimethylazulene (Lactarazulene,[8] 1A$_8$). Blue prisms: mp 22 °C (Ref. 8, 20—22 °C); R_f 0.95; UV λ_{max} nm (log ε) 243 (4.53), 290 (4.58), 354sh (4.08), 368 (4.11), 374sh (4.10), 604 (2.94), 630sh (2.93), and 650sh (2.92); MS m/z 196 (M$^+$; 100), 181 (49), 165 (56), and 28 (54); ^{1}H NMR δ=2.27 (3H, brs, CH$_3$-C-7), 2.66 (3H, s, Me-1), 2.83 (3H, s, Me-4), 5.15 (1H, dq, J=1.0 Hz, (*E*)-HC=C-7), 5.27 (1H, brs, (*Z*)-HC=C-7), 6.97 (1H, d, $J_{5,6}$=11.0 Hz, H-5), 7.23 (1H, d, $J_{2,3}$=4.0 Hz, H-3), 7.57 (1H, dd, $J_{6,8}$=2.0 Hz, H-6), 7.59 (1H, d, H-2), and 8.36 (1H, d, H-8); (Found: m/z 196.1281).

6-(3-Guaiazulenyl)-1(6*H*)-guaiazulenone (1H$_3$). Dark blue prisms: mp 137 °C (from hexane); R_f 0.64; UV λ_{max} (hexane) nm (log ε) 225sh (4.19), 249 (4.29), 290 (4.31), 307sh (4.20), 340sh (3.94), 355 (3.98), 373 (3.96), 624 (3.03), and 650sh (2.99); MS m/z 410 (M$^+$; 100), 395 (28), 367 (45), and 198 (66); IR 1685 cm^{-1} (C=O); ^{1}H NMR δ=1.08, 1.12 (3H each, d, J=7.0 Hz, *i*-Pr-5), 1.34 (6H, d, J=7.0 Hz, *i*-Pr-7′), 2.02 (3H, s, Me-4′), 2.26 (3H, d, $J_{2,Me}$=1.5 Hz, Me-3), 2.54 (1H, sept, HC-5), 2.67 (3H, s, Me-1′), 2.68 (3H, brs, Me-8), 3.01 (1H, sept, HC-7′), 4.66 (1H, d, $J_{6,7}$=6.0 Hz,H-6), 5.86 (1H, brd, H-7), 5.92 (1H, brq, H-2), 6.45 (1H, s, H-4), 6.79 (1H, d, $J_{5',6'}$=11.0 Hz, H-5′), 7.23 (1H, dd, $J_{6',8'}$=2.0 Hz, H-6′), 7.76 (1H, s, H-2′), and 8.09 (1H, d, H-8′), (DMSO-d_6) 1.07, 1.09 (3H each, d, J=7.0 Hz, *i*-Pr-5), 1.29 (6H, d, J=7.0 Hz, *i*-Pr-7′), 1.90 (3H, s, Me-4′), 2.26 (3H, d, $J_{2,Me}$=1.5 Hz, Me-3), 2.36 (3H, d, $J_{7,Me}$=1.5 Hz, Me-8), 2.63 (3H, s, Me-1′), 3.00 (1H, sept, HC-7′), 4.57 (1H, d, $J_{6,7}$=6.0 Hz, H-6), 5.89 (1H, dq, H-7), 5.95 (1H, qd, $J_{2,4}$≃0.3 Hz, H-2), 6.56 (1H, d, H-4), 6.83 (1H, d, $J_{5',6'}$=11.0 Hz, H-5′), 7.30 (1H, dd, $J_{6',8'}$=2.0 Hz, H-6′), 7.81 (1H, s, H-2′), and 8.05 (1H, d, H-8′).

Found: m/z 410.2620. Calcd for $C_{30}H_{34}O$: M, 410.2609.

2-(3-Guaiazulenyl)-3,7-dimethyl-1-oxo-1*H*-indene-6-carbaldehyde (1H$_4$). Dark red-violet prisms: mp 145 °C (from hexane); R_f 0.64; UV λ_{max} nm (log ε) 248 (4.15), 291 (4.15), 305sh (4.10), 351 (3.81), 368 (3.79), 384sh (3.73), and 526 (3.53); MS m/z 382 (M$^+$; 100) and 367 (23); IR 1700 and 1680 cm^{-1} (C=O); ^{1}H NMR δ=1.38 (6H, d, J=7.0Hz, *i*-Pr-7′), 2.38 (3H, s, Me-3), 2.64 (3H, s, Me-1′), 2.65 (6H, s, Me-7.4′), 3.08 (1H, sept, HC-7′), 6.96 (1H, d, $J_{5',6'}$=11.0 Hz, H-5′), 7.10 (1H, d, $J_{4,5}$=8.0 Hz, H-4), 7.38 (1H, dd, $J_{6',8'}$=2.0 Hz, H-6′), 7.39 (1H, s, H-2′), 7.82 (1H, d, H-5), 8.16 (1H, d, H-8′), and 10.63 (1H, s, OHC-6); ^{13}C NMR δ=197.27, 189.50, 151.43, 148.68, 145.70, 142.49, 141.15, 140.21, 139.63, 138.93, 135.78, 135.31, 133.79, 132.21, 131.16, 129.47, 128.07, 127.72, 125.03, 115.63, 37.96, 25.81, 24.70, 18.45, 17.81, and 12.96.

Found: m/z 382.1897. Calcd for $C_{27}H_{26}O_2$: M, 382.1933.

The Norcaradiene Isomer of 1H$_3$: 1-(3-Guaiazulenyl)-6a-isopropyl-2,5-dimethyl-1,1a,3,6a-tetrahydrocyclopropa[*f*]-inden-3-one (1K$_2$). Dark green prisms: mp 155 °C (from hexane); R_f 0.49; UV λ_{max} (hexane) nm (log ε) 228sh (4.18), 247 (4.27), 251 (4.28), 289 (4.25), 305sh (4.17), 364 (400), 385 (4.02), 638 (2.81), and 670sh (2.77); MS m/z 410 (M$^+$; 100), 395 (27), 367 (53), and 198 (78); IR 1680 cm^{-1} (C=O); ^{1}H NMR* δ=0.79, 0.87 (3H each, d, J=7.0 Hz, *i*-Pr-5), 1.11 (1H, sept, HC-5), 1.34 (6H, d, J=7.0 Hz, *i*-Pr-7′), 2.22 (3H, d, $J_{2,Me}$=1.5 Hz, Me-3), 2.46 (1H, d, $J_{6,7}$=5.5 Hz, H-7), 2.55 (1H, d, H-6), 2.58 (3H, s, Me-8), 2.63 (3H, s, Me-1′), 2.90 (3H, s, Me-4′), 3.01 (1H, sept, HC-7′), 6.08 (1H, q, H-2), 6.36 (1H, s, H-4), 6.84 (1H, d, $J_{5',6'}$=11.0 Hz, H-5′), 7.26 (1H, dd, $J_{6',8'}$=2.0 Hz, H-6′), 7.48 (1H, s, H-2′), and 8.05 (1H, d, H-8′), * the numbering of **1K$_2$** for the assignment of the NMR spectrum corresponds to that of **1H$_3$** for the purpose of comparison.

Found: m/z 410.2607. Calcd for $C_{30}H_{34}O$: M, 410.2609.

2-(3-Guaiazulenyl)-1-[(3-Guaiazulenyl)methylene]-5-isopropyl-3-methyl-7-methylene-4,7-dihydro-4(1*H*)-indenone (1K$_3$). A dark red-violet paste: R_f 0.49; UV λ_{max} nm (log ε) 246 (4.41), 288 (4.41), 305sh (4.34), 325sh (4.28), 392 (4.03), and 546 (4.10); MS m/z 604 (M$^+$; 62), 410 (100), and 44 (97); IR 1720, 1680, and 1620 cm^{-1} (C=O); ^{1}H NMR δ=1.14 (6H, d, J=7.0 Hz, *i*-Pr-5), 1.34 (6H, d, J=7.0 Hz, *i*-Pr-7′), 1.36 (6H, d, J=7.0 Hz, *i*-Pr-7″), 2.14 (3H, s, Me-3), 2.47 (1H, sept, HC-5), 2.57 (3H, s, Me-4″), 2.59 (3H, s, Me-1′), 2.64 (3H, s, Me-1″), 2.96 (3H, s, Me-4′), 3.00 (1H, sept, HC-7′), 3.06 (1H, sept, HC-7″), 6.12 [1H, d, $^2J_{H,H}$=1.0 Hz, (*E*)-HC=C-7], 6.79 [1H, dd, $^4J_{6,H}$≃0.5 Hz, (*Z*)-HC=C-7], 6.89 (1H, d, $J_{5'',6''}$=11.0 Hz, H-5″), 6.93 (1H, d, $J_{5',6'}$=11.0 Hz, H-5′), 7.23 (1H, d, H-6), 7.26 (1H, dd, $J_{6',8}$=2.0 Hz, H-6′), 7.34 (1H, s, HC=C-1), 7.34 (1H, dd, $J_{6'',8''}$=2.0 Hz, H-6″), 7.38 (1H, s, H-2″), 7.76 (1H, s, H-2′), 7.99 (1H, d, H-8′), and 8.14 (1H, d, H-8″).

Found: m/z 604.3721. Calcd for $C_{45}H_{48}O$: M, 604.3705.

3,7-Dimethyl-1-oxo-1*H*-indene-6-carbaldehyde (1K$_4$). Pale yellow prisms: mp 125 °C (from hexane); R_f 0.49; UV λ_{max} ($CHCl_3$) nm (log ε) 242 (3.97), 273 (3.96), 280sh (3.93), 315 (3.30), 342 (3.01), 355sh (2.97), and 370sh (2.86); MS m/z 186 (M$^+$; 100), 171 (2), 157 (25), 143 (3), 129 (34), and 115 (35); IR (KBr) 1700 and 1680 cm^{-1} (C=O); ^{1}H NMR δ=2.51 (3H, d, $J_{2,Me}$=1.5 Hz, Me-3), 2.59 (3H, s, Me-7), 5.88 (1H, brq, H-2), 7.13 (1H, brd, $J_{4,5}$=8.0 Hz, H-4), 7.77 (1H, d, H-5), and

10.53 (1H, s, OHC-6).

Found: *m/z* 186.0613. Calcd for $C_{12}H_{10}O_2$: M, 186.0681.

7-(1-Hydroxy-1-methylethyl)-1,4-dimethylazulene (1L$_2$). A blue paste: R_f 0.38; MS *m/z* 214 (M^+; 84), 199 (100), 196 (6), 181 (6), 171 (8), 165 (9), 157 (26), 155 (22), 152 (12), 141 (18), 128 (11), 115 (14), 92 (6), 77 (5), 43 (35), and 40 (20); ^{1}H NMR* δ=1.56 (1H, HO-C-7), 1.73 (6H, s, *i*-Pr-7), 2.69 (3H, s, Me-1), and 2.85 (3H, s, Me-4), * other signals were not observed due to a small quantity of the sample.

Found: *m/z* 214.1348. Calcd for $C_{15}H_{18}O$: M, 214.1357.

1-[(3-Guaiazulenyl)methylene]-5-isopropyl-3-methyl-7-methylene-4,7-dihydro-4(1*H*)-indenone (1M$_3$). A dark red-violet paste: R_f 0.35; UV λ_{max} nm (log ε) 243 (4.18), 282 (4.07), 329 (3.90), 386 (3.62), and 532 (3.94); MS *m/z* 408 (M^+; 100) and 44 (74); IR 1720, 1675, and 1615 cm^{-1} (C=O); ^{1}H NMR δ=1.10 (6H, d, *J*=7.0 Hz, *i*-Pr-5), 1.34 (6H, d, *J*=7.0 Hz, *i*-Pr-7′), 2.26 (3H, d, $J_{2,Me}$=1.0 Hz, Me-3), 2.40 (1H, sept, HC-5), 2.59 (3H, s, Me-1′), 2.95 (3H, s, Me-4′), 3.01 (1H, sept, HC-7′), 6.09 [1H, d, $^2J_{H,H}$=1.0 Hz, (*E*)-HC=C-7], 6.34 (1H, qd, $^4J_{2,H}$≃0.3 Hz, H-2), 6.80 [1H, dd, $^4J_{6,H}$≃0.5 Hz, (*Z*)-HC=C-7), 6.94 (1H, d, $J_{5',6'}$=11.0 Hz, H-5′), 7.13 (1H, d, H-6), 7.30 (1H, dd, $J_{6',8'}$=2.0 Hz, H-6′), 7.35 (1H, d, HC=C-1), 7.76 (1H, s, H-2′), and 8.03 (1H, d, H-8′).

Found: *m/z* 408.2502. Calcd for $C_{30}H_{32}O$: M, 408.2453.

References

1) A part of the results have been preliminarily presented: Y. Matsubara, S. Takekuma, K. Ueno, H. Yamamoto, and T. Nozoe, 52nd National Meeting of the Chemical Society of Japan, Kyoto, April 1986, Abstr. No. 2V27; Y. Matsubara, S. Takekuma, K. Kitajima, H. Yamamoto, and T. Nozoe, 53rd National Meeting of the Chemical Society of Japan, Nagoya, October 1986, Abstr. No. 3D07; Y. Mastubara, S. Takekuma, H. Yamamoto, and T. Nozoe, 31st Symposium on the Chemistry of Terpenes, Essential Oils, and Aromatics, Kyoto, September 1987, Abstr. p. 274; Y. Matsubara, S. Takekuma, H. Yamamoto, and T. Nozoe, *Chem. Lett.*, **1987**, 455.

2) a) T. Nozoe, S. Takekuma, M. Doi, Y. Matsubara, and H. Yamamoto, *Chem. Lett.*, **1984**, 627; b) Y. Matsubara, S. Takekuma, K. Yokoi, H. Yamamoto, and T. Nozoe, *Bull. Chem. Soc. Jpn.*, **60**, 1415 (1987).

3) Y. Matsubara, S. Takekuma, K. Yokoi, H. Yamamoto, and T. Nozoe, *Chem. Lett.*, **1984**, 631.

4) Y. Matsubara, S. Takekuma, K. Ibata, H. Yamamoto, and T. Nozoe, *Nippon Kagaku Kaishi*, **1987**, 1555.

5) S. Takekuma, Y. Matsubara, H. Yamamoto, and T. Nozoe, *Bull. Chem. Soc. Jpn.*, **60**, 3721 (1987).

6) S. Takekuma, Y. Matsubara, H. Yamamoto, and T. Nozoe, *Nippon Kagaku Kaishi*, **1988**, 105.

7) For reviews and monographs, see K. Hafner, *Angew. Chem.*, **70**, 419 (1958); *Angew. Chem., Int. Ed. Engl.*, **3**, 167 (1964); T. Nozoe and S. Ito, *Fortschr. Chem. Org. naturst.*, **19**, 33 (1961); A. G. Anderson and R. G. Anderson, *J. Org. Chem.*, **27**, 3578 (1962), and references cited therein; K. Takase and M. Yasunami, *Yuki Gosei Kagaku Kyokai Shi*, **39**, 1172 (1981); D. Lloyd, "Non-Benzenoid Conjugated Carbocyclic Compounds," Elsevier, Amsterdam (1984), pp. 351—377.

8) F. Sorm, V. Benesova, and V. Herout, *Chem. Listy*, **47**, 1856 (1953); *Collect. Czech. Chem. Commun.*, **19**, 357 (1954).

9) See Ref. 2 and references cited therein for the corresponding compounds.

10) A dimer: white prisms, mp >300 °C; UV λ_{max} (MeOH) nm (log ε) 229 (3.73), 255sh (3.60), 304sh (3.14), and 313 (3.16); MS *m/z* 372 (M^+; 24), 186 (100), 158 (14), 128 (14), and 115 (16); IR 1740—1690 cm^{-1} (C=O); Found: *m/z* 372.1367; Calcd for $C_{24}H_{20}O_4$: M, 372.1361. The structures of the dimers are under investigation.

11) More precise kinetic study for this equilibrium and investigation of reactivities of these two compounds are in progress. A temperature-dependent conformational analysis of **1H$_3$** is also under investigation to eliminate any unambiguousness of the NMR assignments. The results will be reported elsewhere.

12) For the norcaradiene-cycloheptatriene equilibrium systems confirmed in solution at low temperatures, see e.g., K. Takeuchi, Y. Senzaki, and K. Okamoto, *J. Chem. Soc., Chem. Commun.*, **1984**, 111; M. Balci, H. Fischer, and H. Günther, *Angew. Chem., Int. Ed. Engl.*, **19**, 301 (1980) and references, cited therein.

13) Related compounds, 8-(3-guaiazulenyl)-5-isopropyl-3,7-dimethyl-benzofulvenes, have been isolated by autoxidation of **1A$_2$** in DMF (Ref. 4).

14) a) L. T. Scott, M. D. Rozeboom, K. N. Houk, T. Fukunaga, H. J. Lindner, and K. Hafner, *J. Am. Chem. Soc.*, **102**, 5169 (1980), and references cited therein; b) L. T. Scott, *Pure Appl. Chem.*, **1983**, 363; c) L. T. Scott, P. Grutter, and R. Chamberlain, III, *J. Am. Chem. Soc.*, **106**, 4852 (1984); d) L. T. Scott and C. M. Adams, *ibid.*, **106**, 4857 (1984); e) T. Morita, M. Karasawa, and K. Takase, *Chem. Lett.*, **1980**, 197; f) T. Morita, F. Ise, and K. Takase, *ibid.*, **1982**, 1303.

15) Studies on more selective, aerobic, as well as anodic, oxidation of azulenes at lower temperatures are in progress.

16) **1** is commercially available from Konan Kako, Co. (Osaka): blue-violet prisms, mp 31 °C.

A New Type of Two-Dimensional Organic Conductors: Alkylammonium Bis[1,2,5]thiadiazolotetracyanoquinodimethanides

Takanori SUZUKI, Chizuko KABUTO,† Yoshiro YAMASHITA,*
Toshio MUKAI, Tsutomu MIYASHI, and Gunzi SAITO††
Department of Chemistry, Faculty of Science, Tohoku University, Aramaki, Sendai 980
†Instumental Analysis for Chemistry, Faculty of Science, Tohoku University, Aramaki, Sendai 980
††Institute for Solid State Physics, The University of Tokyo, Roppongi, Tokyo 106
(Received August 21, 1987)

Anion radical salts of bis[1,2,5]thiadiazolotetracyanoquinodimethan (BTDA) containing forty kinds of alkylammonium ions were prepared whose molar ratios are unique for each cation and changed from 1 : 1 (**2A**—**2L**) to 2 : 3 (**2M**—**2Z**), 1 : 2 (**2a**—**2m**), and 2 : 5 (**2n**) with elongation of the side chains. The electrical conductivities of the salts are largely affected by the molar ratio and the spatial requirement of cations (ρ_{RT} 3.1 Ω cm for **2a** and 4.2×10^6 Ω cm for **2L**), and some of the salts exhibit high electrical conductivities (ρ_{RT} 3.1—8.3 Ω cm for **2a**—**2e**) with small anisotropy ($\rho_{//}$ 1.7 Ω cm, $\rho_{\perp}$ 21.6 Ω cm for a single crystal of **2g**). Three salts (**2A**, **2M**, and **2g**) showed semiconducting temperature dependence of electrical conductivity with the activation energies of 0.12—0.20 eV. The X-ray study of three kinds of the salts (**2A**, **2g**, and **2m**) revealed that two-dimensional networks are formed by S-N≡C interactions (3.12—3.33 Å) of BTDA anion radicals. The crystals of **2A** and **2g** showing higher conductivities consist of two-dimensionally expanded "ribbon" networks accompanied with equally spaced columnar stackings while molecules are pairing to form dyads in **2m** which exhibits lower conductivity.

Bis[1,2,5]thiadiazolotetracyanoquinodimethan (BTDA, **1**) which forms highly conductive charge-transfer complexes with some donors[1] is a new type of electron acceptor designed in anticipation of the possible interheteroatom interactions as well as the decreased Coulomb repulsion by the annelation of thiadiazole rings. Recently **1** has been revealed to form a two-dimensional "sheet-like" network by strong transverse interactions of S-N≡C in the crystal.[2] In connection with the importance of such interactions[3] in the superconducting $(TMTSF)_2X$ and $(BEDT\text{-}TTF)_2X$ salts,[4] it is extremely intriguing to examine the anion radical salts of **1** in which two-dimensional networks are also expected to be formed. We report here the electrical properties and crystal structures of BTDA anion radical salts containing simple ammonium ions, from which the two-dimensional character of these salts and the relationship between the properties and crsytal structures are discussed.

Results

Preparation of Anion Radical Salts. Most of the anion radical salts were prepared by reaction of BTDA **1** with corresponding alkylammonium iodides[5] in acetonitrile and some were prepared by reaction of **1** with free amines followed by the hydrogen abstraction of aminium cation radicals.[5] These salts were obtained as black powder or microcrystals and the molar ratios were determined on the basis of elemental analyses. They are summarized in Table 1 along with the decomposion points and CN stretching frequencies. Interestingly, the molar ratios of the salts were unique for the kind of ammonium ions as shown in Table 1. Attempts to obtain the 1 : 1 salts which correspond to the complex salts **2M**, **2T**, **2a**, **2i**, and **2m** by metathesis of $Li^+(BTDA)^-$ with corresponding ammonium iodides in acetonitrile were unsuccessful. In addition, treatment of the 1 : 1 salts **2A**, **2G**, and **2K** with another equivalent of BTDA in acetonitrile did not give the 1 : 2 salts but only starting 1 : 1 salts were recovered. This result is in sharp contrast to the case of 7,7,8,8-tetracyanoquinodimethan (TCNQ)[5] whose 1 : 1 salts give the corresponding 1 : 2 salts by treatment with another equivalent of TCNQ. On the other hand, the molar ratios of $BTDA^-$ salts seem to depend on the size and shape of the cations, and gradually change from 1 : 1 to 2 : 3, 1 : 2, and 2 : 5 with elongation of the side chain of ammonium ions. Thus, ethyltrimethylammonium ion forms 1 : 1 salt **2A**, while diethyldimethyl one forms 2 : 3 salt **2T** and triethylmethyl one forms 1 : 2 salt **2f**.

Electrical Conductivities of Anion Radical Salts. Electrical resistivities measured on the compaction samples with a two-probe method are shown in Table 1. Some of the complex salts (**2a**—**2e**) exhibit high electrical conductivities because the partial charge-transfer state[6] is easy to be achieved in these complex salts. It should be noted here that ethyltrimethylammonium 1 : 1 salt **2A** in which the complete charge transfer occurs shows fairy good conductivity (ρ 82 Ω cm). Unfortunately, easy twinning of the crystals prevented the measurements of electrical conductivity on single crystals for many cations. However, we succeeded in preparing three kinds of single crystals (**2A**, triethylammonium 2 : 3 salt **2M**, and methyltributylammonium 1 : 2 salt **2g**) which afford the following electrical resistivities (ρ) and activation energies (E_a): **2A**, ρ 33 Ω cm (E_a 0.198 eV); **2M**, ρ 1.3 Ω cm (E_a 0.124 eV); **2g**, $\rho_{//}$ 1.7 Ω cm (E_a 0.14 eV) along the c axis in the crystal, $\rho_{\perp}$ 21.6 Ω cm along the a axis in the crystal. These single crystal conductivities are rather lower

Table 1. Decomposition Points, CN Stretching Frequencies and Electrical Resistivities[a] of $R_1R_2R_3R_4N^+$ $(BTDA)^{-}_{x}$ Salts **2A—2n**

Salt	R_1	R_2	R_3	R_4	Decomp/°C	ν_{CN}/cm^{-1}	$\rho_{RT}/\Omega cm$
1:1 salt (x=1)							
2A	Et	Me	Me	Me	269—271	2175	8.2×10
2B	H	H	H	H	290—295	2184	1.2×10^2
2C	$-(CH_2)_4-$		Me	H	243—244	2176	1.7×10^2
2D	$-(CH_2)_5-$		Me	Me	275—276	2173	2.5×10^3
2E	Me	Me	Me	Me	308—309	2171	2.8×10^3
2F	$-(CH_2)_4-$		H	H	245—247	2173	2.9×10^3
2G	*n*-Pr	Me	Me	Me	257—258	2172	3.0×10^3
2H	Me	Me	Me	H	262—270	2165	8.3×10^3
2I	$-(CH_2)_5-$		H	H	254—255	2178	1.6×10^4
2J	$-(CH_2)_5-$		Et	Me	266—267	2172	4.9×10^5
2K	$-(CH_2)_2-O-(CH_2)_2-$		Et	Me	259—260	2173	1.8×10^6
2L	$-(CH_2)_4-$		Me	Me	276—277	2175	4.2×10^6
2:3 salt (x=1.5)							
2M	Et	Et	Et	H	236—240	2167	1.2×10
2N	*i*-Pr	Me	Me	H	242—243	2174	1.9×10
2O	*i*-Pr	*i*-Pr	Et	H	225—226	2172	2.1×10
2P	Et	Me	Me	H	244—247	2174	4.1×10
2Q	$-(CH_2)_5-$		Me	H	253—256	2175	7.6×10
2R	*n*-Pr	*n*-Pr	*n*-Pr	Me	238—240	2177	8.2×10
2S	*n*-Bu	Et	Me	Me	253—255	2182	1.1×10^3
2T	Et	Et	Me	Me	262—263	2180	1.3×10^3
2U	*i*-Pr	Me	Me	Me	274—275	2177	3.6×10^3
2V	*n*-Bu	*i*-Pr	Me	Me	227—229	2184	3.7×10^3
2W	*i*-Pr	Et	Me	Me	269—270	2182	6.9×10^3
2X	*n*-Bu	Et	Et	Et	238—242	2183	8.8×10^3
2Y	$-(CH_2)_2-O-(CH_2)_2-$		Et	Et	265—266	2186	1.5×10^4
2Z	$-(CH_2)_4-$		Et	Me	263—265	2180	1.5×10^6
1:2 salt (x=2)							
2a	*n*-Bu	*n*-Bu	*n*-Bu	*n*-Bu	234—236	2172	3.1
2b	*n*-Pr	*n*-Pr	*n*-Pr	*n*-Pr	260—262	2166	3.7
2c	*n*-Bu	*n*-Pr	*n*-Pr	*n*-Pr	261—263	2177	4.5
2d	*n*-Pr	*n*-Pr	*n*-Pr	Et	261—263	2172	5.6
2e	*n*-Bu	*n*-Bu	*n*-Bu	*n*-Pr	247—248	2172	8.3
2f	Et	Et	Et	Me	254—260	2178	1.6×10
2g	*n*-Bu	*n*-Bu	*n*-Bu	Me	243—245	2175	1.6×10
2h	*n*-Bu	*n*-Bu	*n*-Bu	Et	229—235	2174	4.1×10
2i	*n*-Pen	*n*-Pen	*n*-Pen	*n*-Pr	218—220	2176	9.6×10
2j	*i*-Pr	Et	Et	Et	243—244	2182	1.3×10^2
2k	*n*-Pen	*n*-Pen	*n*-Pen	Et	194—196	2175	3.3×10^2
2l[b]	*n*-Hex	*n*-Hex	*n*-Hex	Et	174—180	2176	4.4×10^2
2m	Et	Et	Et	Et	278—280	2182	5.1×10^3
2:5 salt (x=2.5)							
2n	*n*-Pen	*n*-Pen	*n*-Pen	*n*-Bu	217—220	2177	4.1×10

a) Measured on compaction pellets by two-probe method at room temperature. b) Containing one molar of H_2O.

than expected from those for the compaction samples because 50- to 1000-fold conductivity is expected in usual pseudo one-dimensional organic solids.[7] The anisotropy of the conductivity is very small for the salt **2g** (1:13:140—700[8] along the c, a, and b axes in the crystal), which clearly shows the two-dimensional electrical character of this salt.

Crystal Structure of Ethyltrimethylammonium 1:1 Salt (2A). Three views of the crystal structure of **2A** are shown in Figs. 1—3. The crystal of **2A** consists of segregated layers of anion radicals and cations. The BTDA anion radicals form a two-dimensional "ribbon" network along the c axis (Fig. 1) and stack in a "zigzag" fashion along the b axis (Fig. 2). The cations are packed in the cavity of the alternately stacked anion radicals to separate the planar networks. It should be noted that this stacking motif is quite similar to those found isostructurally in the $(TMTSF)_2X$ salts.[9] According to the crystallographic requirement that the molecules must lie on the mirror planes, the completely planar BTDA anion radicals are structurally equivalent and equally spaced. The molecular overlapping is a familiar "ring-double bond" type[10] (Fig. 4) and the stacking distance of 3.24 Å (b/2) is short enough to be compared with those for the conductive TCNQ complexes (3.17—3.26 Å).[11] The nota-

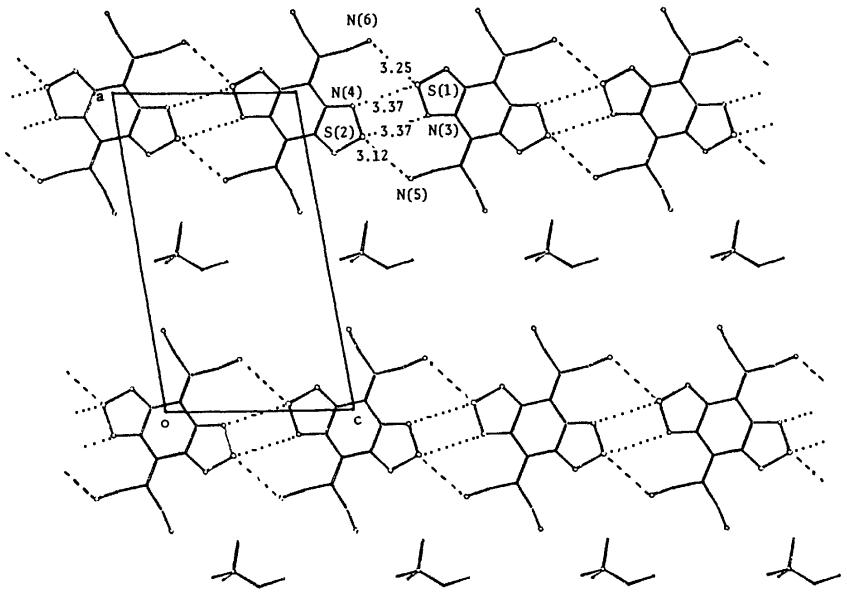

Fig. 1. "Ribbon" network of $BTDA^{-}$ in **2A**. S(1)-N(6)≡C(10) [3.25 Å] and S(2)-N(5)≡C(9) [3.12 Å] interactions are indicated by broken lines. Thiadiazole linkages of S(1)-N(4) [3.37 Å] and S(2)-N(3) [3.37 Å] are also indicated by dotted line.

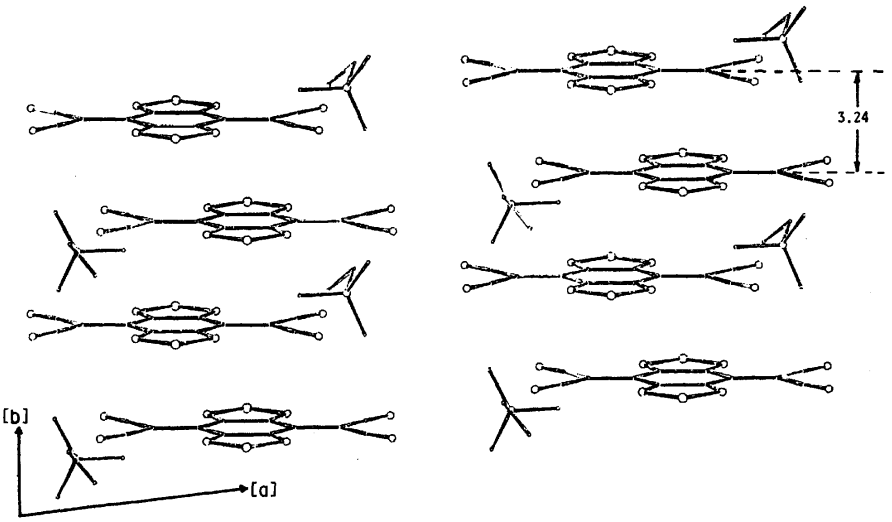

Fig. 2. "Zigzag" stacking in **2A** (tilted 10°). The ammonium N atoms locate on the same plane with the molecular plane of $BTDA^{-}$. Only one-sided mirror images are shown for the disordered ammonium ions.

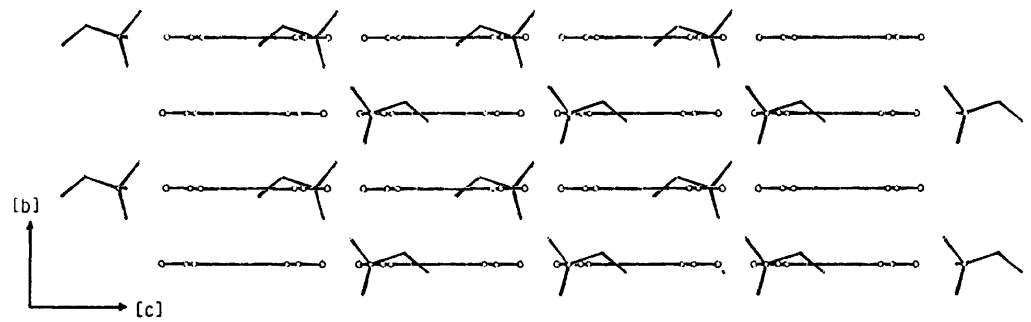

Fig. 3. Coplanar "ribbon" network in **2A** (side view). The interplanar distance is 3.24 Å. Only one-sided mirror images are shown for the disordered ammonium ions.

ble feature of this crystal is the two-dimensional "ribbon" network formed by two short S-N≡C interactions (3.12 and 3.25 Å) together with the thiadiazole linkages (3.37 Å) (Fig. 1). This network is also formed restrictedly in coplanar (Fig. 3), indicating the charge delocalization through the side-by-side network. The appearance of S-N linkage of fused rings, which does not exist in the crystal of neutral **1**,[2] is one of indications that the thiadiazole N atoms possess enhanced negative charge by delocalization since the S-N interaction between thiadiazole rings is caused by the polarized sulfur nitrogen bond.[12] The more definite indications appear in the molecular structure of $BTDA^{\cdot-}$ shown in Table 2 in which those of **1** and $TCNQ^{\cdot-}$[13] are also shown for comparisons. It should be pointed out that the dicyanomethylene C=C bond becomes shorter than that of $TCNQ^{\cdot-}$ (1.390 Å vs. 1.420 Å) and the thiadiazole C=N bond length is longer than that of **1** (1.346 Å vs. 1.330 Å).

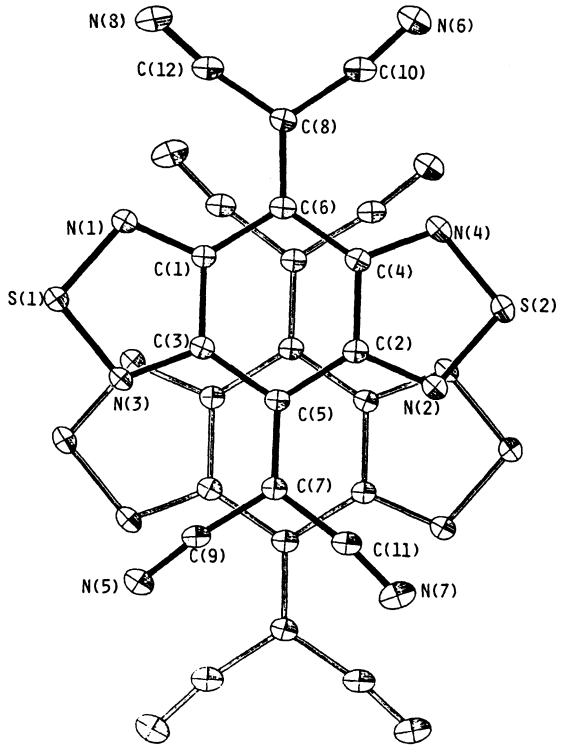

Fig. 4. "Ring-double bond" type overlapping in **2A**. Selected bond lengths: S(1)-N(1) 1.615(4), S(1)-N(3) 1.610(4), S(2)-N(2) 1.624(4), S(2)-N(4) 1.605(4), N(1)-C(1) 1.348(6), N(2)-C(2) 1.347(5), N(3)-C(3) 1.345(5), N(4)-C(4) 1.345(6), N(5)-C(9) 1.142(6), N(6)-C(10) 1.146(7), N(7)-C(11) 1.138(7), N(8)-C(12) 1.137(7), C(1)-C(3) 1.442(6), C(1)-C(6) 1.444(6), C(2)-C(4) 1.443(6), C(2)-C(5) 1.439(6), C(3)-C(5) 1.431(6), C(4)-C(6) 1.433(6), C(5)-C(7) 1.394(6), C(6)-C(8) 1.385(6), C(7)-C(9) 1.427(6), C(7)-C(11) 1.423(6), C(8)-C(10) 1.434(7), C(8)-C(12) 1.432(7) Å.

Crystal Structure of Methyltributylammonium 1:2 Salt (2g). Because of the positional disorder of the ammonium ions, the unit cell contains $Z=0.5$ for the formula of $MeBu_3N^+(BTDA)^{\cdot-}_2$. BTDA anion radicals are related by a center of symmetry at the origin of the unit cell. Similarly to the case of **2A**, the strong transverse interactions of S-N≡C (3.27 and 3.30 Å) connect the anion radicals to form a linear "ribbon" network along the a axis. The positionally disordered cations are packed between the "ribbon" networks along the b axis. An important difference from **2A** is that the networks are not coplanar but corrugated resulting in the formation of a three-dimensional "honeycomb" structure as shown in Fig. 5. Furthermore, the mode of stacking is a uniform type (not a zigzag type) in which BTDA anion radicals are structurally equivalent and equally spaced with the short interplanar distance of 3.24 Å (Fig. 6) and the "ring-double bond" type overlapping (Fig. 7). BTDA molecule possesses an almost planar conformation although the deviations of cyano groups from the molecular plane cause a slight twisting of the exo methylene double bond (1.6°). The bond lengths of dicyanomethylene C=C bond (1.379 Å) and thiadiazole C=N bond (1.340 Å) are intermediate between those in neutral **1** and those in 1 : 1 salt **2A** (Table 2), which reflect the fact that only a half of the negative charge is located on a BTDA molecule in 1 : 2 salt **2g**.

Crystal Structure of Tetraethylammonium 1:2 Salt (2m). Three views of crystal structure are shown in

Table 2. Comparison of Bond Lengths[a] (Å) in BTDA Molecule

Bond	$BTDA^{\cdot-}$ in **2A**	$BTDA^{1/2\cdot-}$ in **2g**	BTDA-1 in **2m**	BTDA-2 in **2m**	$BTDA^{\circ}$ [b]	$TCNQ^{\cdot-}$ [c]
a	1.390(6)	1.379(8)	1.372(12)	1.381(12)	1.356(7)	1.420(4)
b	1.437(6)	1.449(8)	1.454(12)	1.452(12)	1.457(6)	1.423(4)
c	1.433(5)	1.422(8)	1.428(12)	1.434(12)	1.422(6)	1.373(4)
d	1.429(7)	1.422(10)	1.443(13)	1.430(14)	1.438(6)	1.416(4)
e	1.140(6)	1.127(10)	1.128(14)	1.135(14)	1.143(5)	1.153(7)
f	1.346(6)	1.340(8)	1.336(12)	1.338(12)	1.330(4)	
g	1.614(4)	1.612(6)	1.615(8)	1.615(9)	1.617(6)	

a) Bond lengths are averaged over assumed mmm symmetry.
b) Ref. 2. c) These values are for $Rb^+TCNQ^{\cdot-}$, Ref. 13.

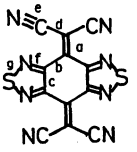

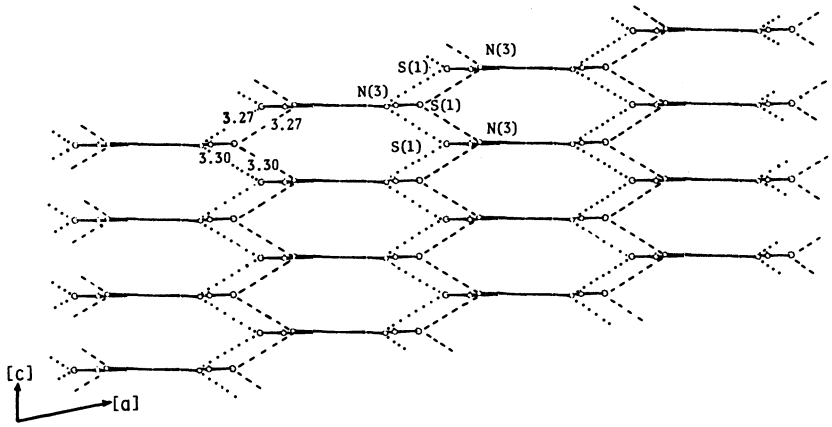

Fig. 5. "Honeycomb" network in **2g** (side view perpendicular to the molecular plane of BTDA). S(1)-N(3)≡C(5) [3.27 and 3.30 Å] interactions are indicated by broken lines. The interplanar distance is 3.24 Å. Disordered ammonium ions are not included for ease.

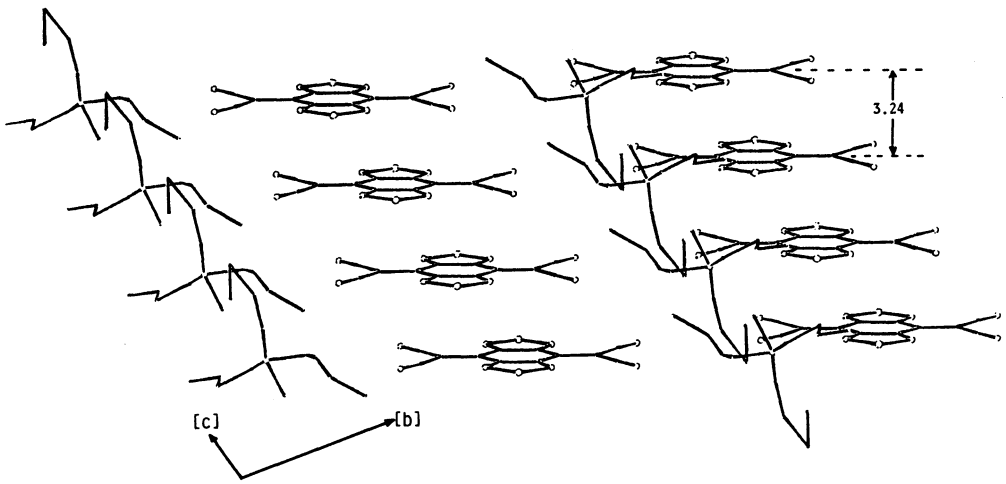

Fig. 6. Uniform segregated stacking in **2g** (tilted 10°). Ammonium ions are disordered along the stacking c axis (multiplicity 0.5), and also related by a center of symmetry which are not shown for ease.

Figs. 8—10. Because of $Z=2$ for the space group $P\bar{1}$, two different kinds of BTDA molecules exsist in the crystal (abbreviated as BTDA-1 and BTDA-2). Each molecule forms columnar stacks along the c axis in which molecules are not equally spaced but pairing to form dyads (Fig. 8). The interplanar distances are 3.17 and 3.39 Å for BTDA-1, and 3.26 and 3.41 Å for BTDA-2, respectively. Although each molecule forms corrugated "ribbon" networks along the a axis like **2g** (Figs. 9 and 10), these networks can not form the "honeycomb" because of the dyad formation as well as the ununiform overlapping patterns. That is, the molecular overlappings are "ring-double bond" type in the dyads for both BTDA-1 and BTDA-2, but molecules are slipped in parallel in the overlapping between the dyads (Figs. 11 and 12). Although both molecules are almost planar, slight twisting of dicyanomethylene C=C bond (2.8° and 1.4°) are observed for BTDA-2. Comparisons of molecular structure of BTDA-1 and BTDA-2 with those of neutral **1** and 1 : 1 salt **2A** indicate that BTDA-2 possesses the larger amount of negative charge than BTDA-1 (Table 2). For example, bond f for BTDA-2 is elongated [C(205)=C(207), 1.392 Å] which is nearly the same value with that for 1 : 1 salt **2A** [C(5)=C(7), 1.394 Å]. This charge distribution also affects the molecular packing. The cationic center of ammonium N atom is located on the same plane with the molecular plane of BTDA-2 (Fig. 10), while the molecular plane of BTDA-1 is shifted vertically (Fig. 9).

Discussion

The annelation of 1,2,5-thiadiazole rings to the TCNQ skeleton results in two significant differences from TCNQ itself. One of them is the two-dimensional electrical property and crystal structure formed by the strong interheteroatom interactions of

S-N≡C and the other is the decreased on-site Coulomb repulsion in the reduction form of **1**. The former is the most important characteristic of **1** since none of the organic electron acceptor have shown such a two-dimensional network so far.[14] The crystal structures described here are different from each other, indicating that the patterns of interactions are variable according to the spatial requirements of counter cations. This fact shows that the molecular interaction of BTDA is not only strong but also flexible. However, some common features are observed, which are the "ribbon" network and face-to-face columnar stacking. The "ribbon" is coplanar in **2A** and corrugated in **2g** and **2m**. The stacking pattern of **2A** is equally spaced "zig-zag" type like $(TMTSF)_2X$ salts and that of **2g** is equally spaced uniform type like TTF·TCNQ complex,[15] while molecules are dimerized in **2m** which is often observed in anion radical salts with low electrical conductivities. The fact that molar ratios of the salts are unique for each cation seems to be related with these networks since the ratios are gradually changed from 1:1 to 2:5 as the cations get larger. Cyclic ammonium ions tend to give 1:1 salts compared with corresponding acyclic cations as seen in a comparison of **2L** and **2J** with **2T** and **2S**. This fact also indicates that the spatial conditions play an important role in determining the molar ratios. This behavior is explained by considering that the cations locate between BTDA molecules which are connected in two directions of "ribbon" and stacking. Therefore, the larger the cation is, the more repeated units of "ribbon" and stacking are needed since the distances of the transverse S-N≡C interaction and the face-to-face overlapping are in some definite range of 3.12—3.33 and 3.17—3.41 Å, respectively. Once the molar ratio is determined with keeping this range of distances for a certain cation, the shape of the cation affects the mode of stacking and the "ribbon" network which reflect its electrical conductivity. These common features of the crystal structures make some difficulty in obtaining single crystals since disorder or twinning is very easy to occur in the direction where BTDA and cations are aligned alternately (the a axis for **2A**, the b axis for **2g** and **2m**). Whether the semiconducting properties of three salts (**2A**, **2M**, and **2g**) described here are attributed to this easy twinning or not is still ambiguous.

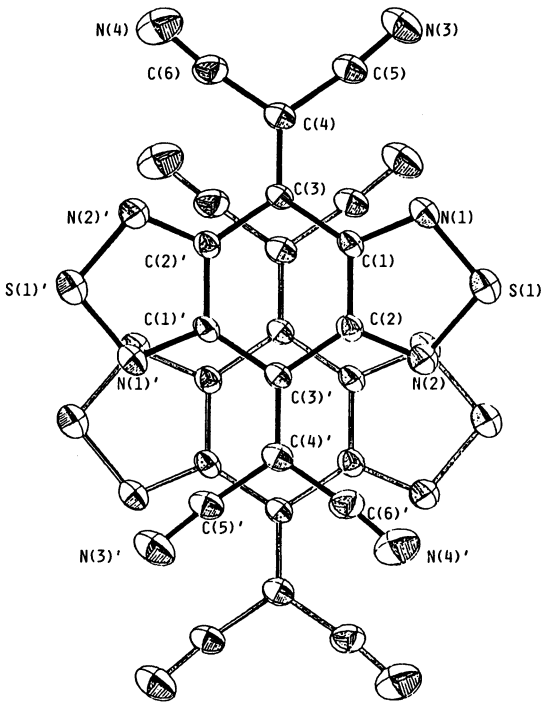

Fig. 7. "Ring-double bond" type overlapping in **2g**. Selected bond lengths: S(1)-N(1) 1.611(6), S(1)-N(2) 1.613(6), N(1)-C(1) 1.339(8), N(2)-C(2) 1.340(8), N(3)-C(5) 1.128(10), N(4)-C(6) 1.125(11), C(1)-C(2) 1.422(8), C(1)-C(3) 1.447(8), C(2)-C(3) 1.450(8), C(3)-C(4) 1.379(8), C(4)-C(5) 1.424(9), C(4)-C(6) 1.420(10) Å.

The second point is the decreased Coulomb repulsion in the reduction form of BTDA. This is first suggested by measuring the reduction potentials of **1**. The cyclic voltammogram of **1** shows four reversible reduction waves with the half wave potentials of −0.02, −0.49, −1.21, and −1.76 V vs. SCE.[1a,16] The

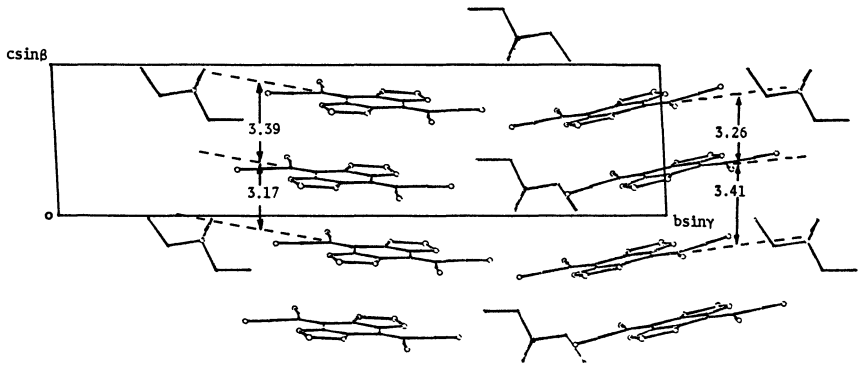

Fig. 8. Dimeric segregated columns in **2m** viewed along the a axis. The interplanar distances are 3.17 and 3.39 Å for BTDA-1 (left) and 3.26 and 3.41 Å for BTDA-2 (right), respectively.

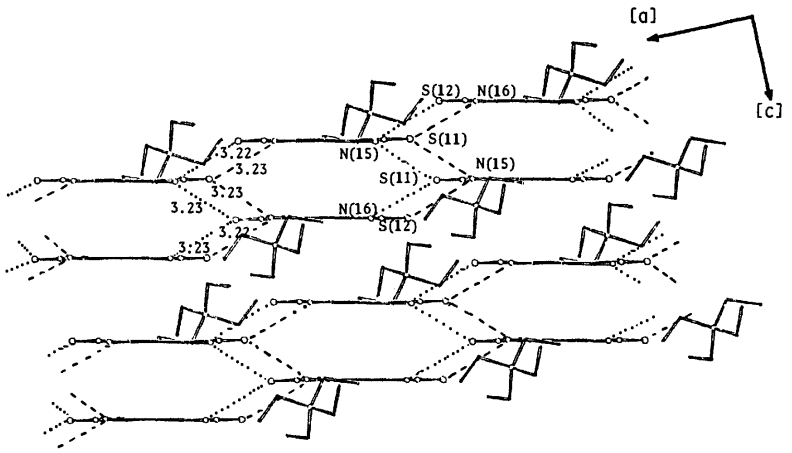

Fig. 9. Dimerized "ribbon" network of BTDA-1 in **2m** (side view). S(11)-N(15)≡C(109) [3.23 Å], S(11)-N(16)≡C(110) [3.23 Å], and S(12)-N(15)≡C(109) [3.22 Å] are indicated by broken lines.

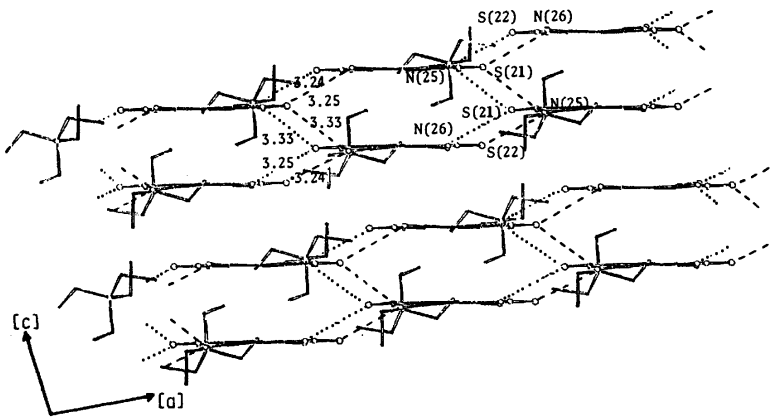

Fig. 10. Dimerized "ribbon" network of BTDA-2 in **2m** (side view). S(21)-N(25)≡C(209) [3.33 Å], S(21)-N(26)≡C(210) [3.25 Å], and S(22)-N(25)≡C(209) [3.24 Å] are indicated by broken lines.

semiquinone formation constant (K_{sem}) calculated using these values is 8.10 while that of TCNQ is 9.31. This contraction is attributed to the decreased Coulomb repulsion of $\mathbf{1}^{\cdot-}$ compared with $TCNQ^{\cdot-}$. This is also suggested by the fact that the dianion of BTDA is easily isolated as stable sodium salts[17] while the dianion of TCNQ is unstable and isolated only when special metal complex ions were used.[18] In this study, the comparisons of the molecular geometry in BTDA molecule show that the negative charge is delocalized to the fused thiadiazole rings. That is, the C=N double bond of thiadiazole (bond f in Table 2) is elongated by adding the negative charge on a BTDA molecule (1.330 Å in BTDA°, 1.340 Å in $BTDA^{1/2\cdot-}$ and 1.346 Å in $BTDA^{\cdot-}$), which is rationalized by considering the contribution of the structures **3b** and **3c** (Scheme 1) for the anion radical of BTDA **1**. The fact that 1 : 1 salt **2A** which is completely charge transferred exhibits higher electrical conductivity than usual Mott insulators[19] may be attributed to this decreased Coulomb repulsion of $\mathbf{1}^{\cdot-}$.

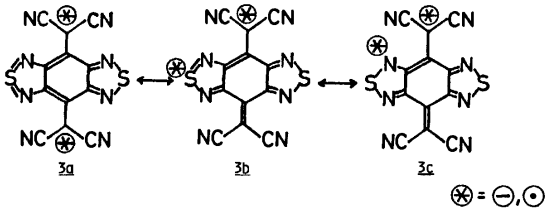

Scheme 1.

Conclusion

This study has revealed the novel properties of $BTDA^{\cdot-}$ which can construct the segregated columnar stacks with the face-to-face overlapping (uniform type or zigzag type) as well as the "ribbon" networks (coplanar or corrugated) by strong transverse interactions.[20] The modes of overlapping and transverse interactions in $BTDA^{\cdot-}$ are strongly affected by the spatial requirements of the cations, while these interactions also define the molar ratios of the salts since the ratios were unique for the cations. Although all of

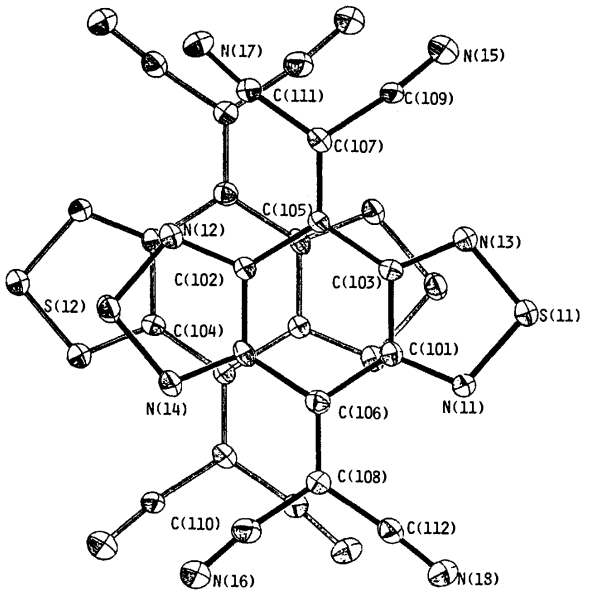

Fig. 11. Molecular overlapping of BTDA-1 in **2m** between the dyads. Selected bond lengths: S(11)-N(11) 1.609(8), S(11)-N(13) 1.608(9), S(12)-N(12) 1.612(8), S(12)-N(14) 1.630(8), N(11)-C(101) 1.322(12), N(12)-C(102) 1.339(11), N(13)-C(103) 1.351(12), N(14)-C(104) 1.332(12), N(15)-C(109) 1.122(13), N(16)-C(110) 1.128(15), N(17)-C(111) 1.133(14), N(18)-C(112) 1.128(15), C(101)-C(103) 1.419(12), C(101)-C(106) 1.462(13), C(102)-C(104) 1.437(12), C(102)-C(105) 1.455(12), C(103)-C(105) 1.443(12), C(104)-C(106) 1.454(13), C(105)-C(107) 1.382(12), C(106)-C(108) 1.362(13), C(107)-C(109) 1.445(13), C(107)-C(111) 1.438(13), C(108)-C(110) 1.442(13), C(108)-C(112) 1.445(14) Å.

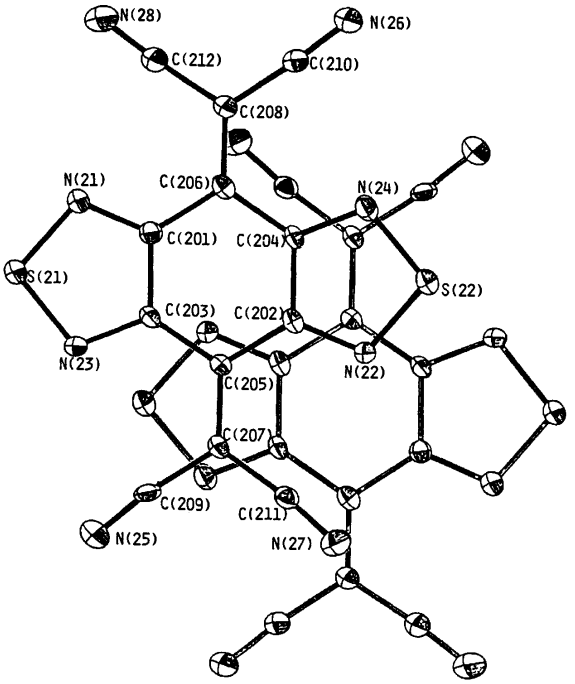

Fig. 12. Molecular overlapping of BTDA-2 in **2m** between the dyads. Selected bond lengths: S(21)-N(21) 1.613(9), S(21)-N(23) 1.624(9), S(22)-N(22) 1.612(8), S(22)-N(24) 1.611(9), N(21)-C(201) 1.330(12), N(22)-C(202) 1.343(12), N(23)-C(203) 1.346(12), N(24)-C(204) 1.333(12), N(25)-C(209) 1.134(14), N(26)-C(210) 1.140(15), N(27)-C(211) 1.140(13), N(28)-C(212) 1.126(16), C(201)-C(203) 1.437(12), C(201)-C(206) 1.457(12), C(202)-C(204) 1.430(12), C(202)-C(205) 1.439(12), C(203)-C(205) 1.434(12), C(204)-C(206) 1.477(12), C(205)-C(207) 1.392(12), C(206)-C(208) 1.370(13), C(207)-C(209) 1.433(13), C(207)-C(211) 1.433(13), C(208)-C(210) 1.423(14), C(208)-C(212) 1.432(15) Å.

three anion radical salts examined here were semiconductors with the activation energies of 0.12—0.20 eV, BTDA and analogous compounds[21] containing higher chalcogen atoms instead of sulfur atoms are promising electron acceptors to afford organic metals whose metallic states are stabilized by the novel two-dimensional structures as described here.

Experimental

General. IR spectra were measured in KBr disks on a Shimadzu IR-435 spectrometer with a DR-1 data recorder. The ν_{CN} values were determined as the minima of the transmittances measured by every 0.5 cm^{-1} using the ν_{max} of 1944 and 1871 cm^{-1} of the polystyrene film as standard. All the melting points are uncorrected. Electrical resistivities were measured by a conventional two-probe method for compaction samples at room temperature, and by a four-probe method for single crystals using the gold wire and gold paste for the connection.

Materials. Anion radical salts **2A—2n** were prepared by reaction of BTDA (0.4 mmol) with the corresponding ammonium iodides (3—5 equivalents) in boiling acetonitrile (30 ml) except for the case of **2C**, **2N**, **2O**, **2P**, and **2Q** in which free amines (1 equivalent) were used instead of the iodides. The salts showed correct elemental analyses for C, H, and N (±0.4%) without purification. Single crystals of **2A** and **2M** were prepared by electrochemical reduction (5—10 μA) of BTDA (10^{-3} mol dm^{-3}) containing $Me_3NEt^+MeSO_4^-$ or $Et_3NH^+BF_4^-$ as supporting electrolyte (10^{-1} mol dm^{-3}) in acetonitrile. Single crystals of **2g** were obtained when a hot acetonitrile solution of **1** and the iodide was cooled slowly, and those for **2m** were prepared by recrystallization from acetonitrile.

Structural Analysis of Ethyltrimethylammonium 1 : 1 Salt (2A). A needle-like crystal with dimensions of 0.08×0.30×0.15 mm^3 along the a, b, and c axes was used for the X-ray study. Crystal data are as follows: a=15.854(1), b=6.482(1), c=9.141(1) Å, β=100.07(1)°, V=924.9(2) $Å^3$, $P2_1/m$, Z=2, D_{calcd}=1.47 g cm^{-3}. A total of 1979 independent reflections was collected with graphite monochromated Cu $K\alpha$ radiation (λ=1.5418 Å) up to 2θ=128° using a Rigaku automated four circle diffractometer (AFC-6). The structure was solved by the direct method and refined by the block-diagonal least-squares method. Refinement was converged successfully for the space group $P2_1/m$ rather than the non-centrosymmetric $P2_1$. Therefore, the molecules are restricted in the way that all the atoms of BTDA molecule are located on the mirror planes of y=1/4 and y=3/4. The cations are disordered in the way that methylene C atoms are separated largely in two mirror images while others are slightly shifted. Most of hydrogen atoms are located by the difference

Table 3. Fractional Atomic Coordinates ($\times 10^4$) and Equivalent Temperature Factors (Å^2) of Ethyltrimethylammonium (1 : 1) Salt **2A**

Atom	X	Y	Z	BEQV[a)]
S1	1505(1)	2500(0)	7298(1)	3.1
S2	−142(1)	2500(0)	13837(1)	3.0
N1	2003(2)	2500(0)	8997(4)	3.1
N2	−643(2)	2500(0)	12129(4)	2.6
N3	524(2)	2500(0)	7542(4)	2.9
N4	836(2)	2500(0)	13591(4)	2.8
N5	−1463(3)	2500(0)	6003(5)	4.8
N6	2901(3)	2500(0)	15089(5)	4.1
N7	−2489(3)	2500(0)	9721(5)	4.5
N8	3821(3)	2500(0)	11244(5)	5.5
C1	1395(3)	2500(0)	9858(5)	2.5
C2	−34(3)	2500(0)	11270(4)	2.2
C3	536(3)	2500(0)	9017(5)	2.4
C4	824(3)	2500(0)	12116(4)	2.3
C5	−221(2)	2500(0)	9672(4)	2.2
C6	1583(3)	2500(0)	11462(5)	2.5
C7	−1047(3)	2500(0)	8843(5)	2.6
C8	2411(3)	2500(0)	12254(5)	2.7
C9	−1231(3)	2500(0)	7258(5)	3.1
C10	2624(3)	2500(0)	13845(5)	3.2
C11	−1818(3)	2500(0)	9438(5)	2.9
C12	3169(3)	2500(0)	11601(5)	3.6
N0	−3785(2)	2500(0)	12686(5)	3.8
C01	−2837(3)	2500(0)	13233(6)	4.5
C02	−4048(5)	561(15)	12036(9)	5.0
C03	−3981(5)	4202(15)	11480(9)	4.9
C04	−4267(5)	3259(0)	13915(8)	4.7
C06	−4021(6)	2003(0)	15325(9)	7.0

a) BEQV=(4/3) $\sum_{ij} \beta_{ij} (a_i \cdot a_j)$.

Table 4. Fractional Atomic Coordinates ($\times 10^4$) and Equivalent Temperature Factors (Å^2) of Methyltributylammonium (1 : 2) Salt **2g**

Atom	X	Y	Z	BEQV[a)]
S1	−2935(2)	1037(1)	−347(5)	4.2
N1	−2915(5)	71(4)	1364(13)	3.6
N2	−1207(6)	1391(4)	−1841(13)	3.5
N3	−4771(7)	−1751(5)	5500(17)	5.9
N4	−1396(9)	−3020(5)	5605(20)	6.9
C1	−1511(6)	−19(4)	804(13)	2.8
C2	−530(6)	741(4)	−1021(14)	2.8
C3	−1054(6)	−816(4)	1903(13)	2.8
C4	−2012(7)	−1561(4)	3631(15)	3.4
C5	−3556(7)	−1630(5)	4567(17)	4.1
C6	−1597(8)	−2361(5)	4642(18)	4.3
N100	8447(35)	4627(24)	−832(84)	7.7
C111	7349(47)	3763(22)	663(114)	7.6
C112	5757(39)	3949(21)	617(84)	5.5
C113	4717(54)	4190(35)	2345(130)	10.4
C114	3974(62)	3833(39)	5529(138)	10.5
C121	10176(42)	4722(29)	−131(125)	7.3
C122	11598(39)	5609(28)	−228(84)	6.5
C123	12812(36)	5084(29)	−151(112)	7.6
C124	14556(52)	5505(25)	−765(113)	8.4
C131	8497(50)	4815(37)	2910(102)	8.7
C141	7316(43)	4416(25)	−3840(100)	7.0
C142	6728(47)	4130(32)	−7162(105)	7.9
C143	6144(49)	4351(28)	−11177(89)	7.1
C144	5539(61)	5161(32)	−8859(149)	10.2

a) BEQV=(4/3) $\sum_{ij} \beta_{ij} (a_i \cdot a_j)$.

Table 5. Fractional Atomic Coordinates ($\times 10^4$) and Equivalent Temperature Factors (Å^2) of Tetraethylammonium (1:2) Salt **2m**

Atom	X	Y	Z	BEQV[a)]	Atom	X	Y	Z	BEQV[a)]
S11	−3121(3)	814(1)	−1911(4)	2.8	C107	−1665(10)	−674(3)	−1843(13)	2.3
S12	3209(3)	−237(1)	−3131(4)	2.7	C108	1758(10)	1262(3)	−3102(13)	2.1
S21	−8026(3)	5904(1)	4015(4)	2.9	C109	−3243(10)	−764(3)	−1476(13)	2.2
S22	−1649(3)	4997(1)	1818(4)	2.8	C110	3325(11)	1357(4)	−3496(15)	3.0
N11	−1443(8)	1070(3)	−2352(11)	2.4	C111	−1103(10)	−1132(3)	−1894(14)	2.4
N12	1531(8)	−493(3)	−2675(11)	2.5	C112	1151(10)	1714(4)	−3013(15)	3.0
N13	−2910(8)	247(3)	−1789(12)	2.6	C201	−5496(10)	5854(3)	3483(13)	2.0
N14	2995(8)	339(3)	−3248(11)	2.4	C202	−4172(9)	5040(3)	2459(13)	2.2
N15	−4437(10)	−878(3)	−1109(14)	3.9	C203	−6379(9)	5356(3)	3211(13)	2.0
N16	4537(10)	1481(3)	−3813(15)	4.4	C204	−3283(9)	5535(3)	2710(13)	2.0
N17	−794(10)	−1514(3)	−1905(15)	4.0	C205	−5765(9)	4927(3)	2716(12)	1.7
N18	785(10)	2085(3)	−2992(15)	4.3	C206	−3876(9)	5981(3)	3269(13)	2.1
N21	−6294(8)	6194(3)	3962(12)	2.6	C207	−6640(9)	4447(3)	2465(13)	2.0
N22	−3369(8)	4702(3)	1916(11)	2.4	C208	−3035(10)	6456(3)	3451(14)	2.5
N23	−7854(8)	5337(3)	3461(12)	2.6	C209	−8242(10)	4322(3)	2634(14)	2.4
N24	−1838(8)	5556(3)	2384(12)	2.7	C210	−1459(11)	6581(3)	3206(16)	3.0
N25	−9500(10)	4186(3)	2752(15)	4.2	C211	−6103(10)	4009(3)	1892(13)	2.4
N26	−201(10)	6711(3)	3035(15)	4.1	C212	−3686(11)	6884(3)	3837(16)	3.1
N27	−5807(10)	3639(3)	1420(14)	3.8	C501	2577(11)	6920(3)	−2076(15)	3.1
N28	−4111(11)	7238(3)	4131(17)	5.2	C502	2599(13)	6630(4)	−266(18)	4.2
N51	2536(8)	7472(3)	−1716(11)	2.5	C503	2477(12)	7688(4)	−3686(15)	3.4
C101	−628(10)	716(3)	−2415(13)	2.1	C504	2452(14)	8234(5)	−3650(20)	5.2
C102	729(9)	−129(3)	−2554(12)	1.7	C505	1145(11)	7525(4)	−723(16)	3.3
C103	−1462(9)	239(3)	−2126(12)	1.9	C506	−374(12)	7284(4)	−1807(19)	4.3
C104	1577(9)	351(3)	−2888(12)	2.0	C507	3927(12)	7737(4)	−339(16)	3.4
C105	−848(9)	−211(3)	−2147(12)	1.7	C508	5457(12)	7725(5)	−1043(19)	4.7
C106	957(10)	804(3)	−2826(13)	2.3					

a) BEQV=(4/3) $\sum_{ij} \beta_{ij} (a_i \cdot a_j)$.

Fourier map, which are included in the refinement together with the others calculated. The final R value is 0.049 for 1596 reflections with $|F_o|>1.5\sigma|F_o|$. The final atomic coordinates are given in Table 3.

Structural Analysis of Methyltributylammonium 1:2 Salt (2g). An almost twinning plate-like crystal with the dimensions of 0.10×0.30×0.30 mm^3 was used for the data collection on a Rigaku automated four circle diffractometer (AFC-5R) with rotating anode using graphite monochromated Mo $K\alpha$ radiation (λ=0.71069 Å). A total of 2850 reflections within 2θ=60° was collected. Although the Weissenberg photograph shows the disorder or twinning along the b and c axis, the most primitive cell was chosen for the structual determination. Thus obtained crystal data are as follows: a=8.943(2), b=14.756(3), c=3.991(1) Å, α=92.31(2), β=93.64(2), γ=110.27(2)°, V=492.0(2) Å^3, $P\bar{1}$, Z=0.5, D_{calcd}=1.42 g cm^{-3}. The structure was solved by the direct method and the parameters of BTDA molecule were obtained. After the block-diagonal least-squares refinement for these atoms with anisotropic temperature factors, the remaining atoms of ammonium ion were searched by the difference Fourier syntheses. By supposing the doubled unit cell along the stacking c axis, the positions of ammonium ions were proved to be disordered along this axis.[22] Furthermore, the N atom of the ammonium ion does not locate the center of symmetry, indicating that the cation is also orientationally disordered. Although these disordering made some difficulty, the atoms of the cation were successively picked up from the difference Fourier map. The final R value including these atoms is 0.097 for 1972 reflections with $|F_o|>3\sigma|F_o|$, and hydrogen atoms are not included in the refinement. The final atomic coordinates are given in Table 4.

Structural Analysis of Tetraethylammonium 1:2 Salt (2m). A needle-like crystal with dimensions of 0.15×0.15×0.25 mm^3 was used for the data collection. Crystal data are as follows: a=8.959(1), b=27.442(3), c=6.924(1) Å, α=92.78(1), β=97.24(1), γ=100.74(1)°, V=1654.6(4) Å^3, $P\bar{1}$, Z=2, D_{calcd}=1.55 g cm^{-3}. A total of 7199 reflections within 2θ=52° was collected on a Rigaku automated four circle diffractometer (AFC-5) using graphite monochromated Mo $K\alpha$ radiation (λ=0.71069 Å). The structure was solved by the direct method by supposing the space group to be noncentrosymmetric $P1$, and four kinds of BTDA molecules appeard in the Fourier map. These atoms were refined by the block-diagonal least-squares method followed by the difference Fourier syntheses from which the positions of two ammonium ions were determined. After refinement with isotropic temperature factors, two pairs of BTDA molecules and two ammonium ions were related by a center of symmetry indicating the space group to be centrosymmetric $P\bar{1}$ rather than $P1$. After transformation to the space group $P\bar{1}$ and successive refinement with anisotropic temperature factors, all the hydrogen atoms were located on the difference Fourier map. These are included in the refinement to give the final R value of 0.071 for the 3577 reflections with $|F_o|>3\sigma|F_o|$. The final atomic coordinates are given in Table 5.

For these three crystals, RANTAN 81 program[23] with some modification was used in the direct method. The atomic scattering factors from the International Tables for X-Ray Crystallography[24] were used. All the computation were carried out by an ACOS 1000 computer at Tohoku University using the applied library program of UNICS III system.[25]

Table of analytical values of anion radical salts **2A—2n**; listings of positional and thermal parameters, bond lengths and angles, and structural factors for **2A**, **2g**, and **2m** are kept at the Chemical Society of Japan (Document No. 8777).

The authors are grateful to Dr. Kokichi Oshima at Cryogenetic Center, The University of Tokyo for the temperature dependent resistivity measurement of **2g**.

References

1) BTDA **1**: 4,8-bis(dicyanomethylene)-4*H*,8*H*-benzo[1,2-*c*: 4,5-*c'*]bis[1,2;5]thiadiazole. (a) Y. Yamashita, T. Suzuki, T. Mukai, and G. Saito, *J. Chem. Soc., Chem. Commun.*, **1985**, 1044. (b) Y. Yamashita, T. Suzuki, G. Saito, and T. Mukai, *Chem. Lett.*, **1985**, 1759.

2) C. Kabuto, T. Suzuki, Y. Yamashita, and T. Mukai, *Chem. Lett.*, **1986**, 1433.

3) H. Kobayashi, A. Kobayashi, Y. Sasaki, G. Saito, T. Enoki, and H. Inokuchi, *J. Am. Chem. Soc.*, **105**, 297 (1983).

4) TMTSF and BEDT-TTF are abbreviations of tetramethyltetraselenafulvalene and bis(ethylenedithio)tetrathiafulvalene, and X represents monovalent anions. For a recent review: J. M. Williams, M. A. Beno, H. H. Wang, P. C. W. Leung, T. J. Emge, U. Geiser, and K. D. Carlson, *Acc. Chem. Res.*, **18**, 261 (1985).

5) L. R. Melby, R. J. Harder, W. R. Hertler, W. Mahler, R. E. Benson, and W. E. Mochel, *J. Am. Chem. Soc.*, **84**, 3374, (1962).

6) J. B. Torrance, *Acc. Chem. Res.*, **12**, 79 (1979).

7) For example, the resistivity of *N*-methylphenazinium TCNQ$^-$ salt at room temperature is 0.5 for a compaction sample while that for a single crystal is 0.007. L. R. Melby, *Can. J. Chem.*, **43**, 1448 (1965).

8) The single crystal of **2g** used for the conductivity measurement is very thin along the b axis which prevented the determination of the correct anisotropy along this axis but shows the range of the anisotropy.

9) N. Thorup, G. Rindorf, H. Soling, and K. Bechgaard, *Acta Crystallogr., Sect. B*, **37**, 1236 (1981).

10) C. J. Fritchie, Jr., *Acta Crystallogr.*, **20**, 892 (1966).

11) J. H. Perlstein, *Angew. Chem., Int. Ed. Engl.*, **16**, 519 (1977).

12) A. Gieren, V. Lamm, R. C. Haddon, and M. L. Kaplan, *J. Am. Chem. Soc.*, **101**, 7277 (1979); **102**, 5070 (1980).

13) A. Hoekstra, T. Spoelder, and A. Vos, *Acta Crystallogr., Sect. B*, **28**, 14 (1972).

14) TCNQ derivatives fused with thiophen units were reported to exhibit such an interaction of S-N≡C in the crystal of the neutral state. F. Iwasaki, N. Toyota, H. Mikami, N. Yamasaki, and K. Kobayashi, 54th National Meeting of the Chemical Society of Japan, Tokyo, April 1987, Abstr., No. 4IIIP33.

15) T. E. Phillips, T. J. Kistenmacher, J. P. Ferraris, and D. O. Cowan, *J. Chem. Soc., Chem. Commun.*, **1973**, 471.

16) Measured in CH_3CN containing 0.1 mol dm^{-3} Et_4NClO_4 as supporting electrolyte on platinum electrode with the scan rate of 100 mV s^{-1}. The reduction potentials of TCNQ measured under the same conditions are +0.18 and −0.36 V, and the oxidation potential of ferrocene is +0.38 V.

17) Y. Yamashita, T. Suzuki, and T. Mukai, *J. Chem. Soc., Chem. Commun.*, **1987**, 1184.

18) S. G. Clarkson, B. C. Lane, and F. Basolo, *Inorg. Chem.*, **11**, 662 (1972). M. Desbois, P. Michaud, and D. Astruc, *J. Chem. Soc., Chem. Commun.*, **1985**, 450.

19) J. B. Torrance, Y. Tomkiewicz, R. Bozio, C. Pecile, C. Wolfe, and K. Bechgaard, *Phys. Rev. B*, **26**, 2267 (1981).

20) Kobayashi et al. predicted in their papar that "However, if the interchain interaction is sufficiently strong, the column structure will be unfavorable and the conducting pathway will become more complicated." Ref. 3).

21) The preparation and crystal structures of BTDA analogues, TSDA and BSDA, containing selenium atoms are reported separatedly. T. Suzuki, C. Kabuto, Y. Yamashita, G. Saito, T. Mukai, and T. Miyashi, *Chem. Lett.*, **1987**, 2285.

22) Another total of 3326 reflections containing 2695 nonzero reflections was collected by supposing the doubled unit cell of a=8.948, b=15.134, c=7.988 Å, α=77.01, β=93.63, γ=110.78°, and Z=1, which was also used for the structural determination of **2g**.

23) Y. Jia-xing, *Acta Crystallogr., Sect. A*, **37**, 642 (1981); **39**, 35 (1983).

24) "International Tables for X-Ray Crystallography," Vol.III, Kynoch Press, Birmingham (1962), p. 202.

25) T. Sakurai and K. Kobayashi, *Rep. Inst. Phys. and Chem. Res.*, **55**, 69 (1979).

NAD(P)$^+$-NAD(P)H Models. 65. Photochemical Reductive Desulfonylation of β-Keto Sulfones with Hantzsch Ester

Masayuki Fujii,† Kaoru Nakamura, Hideyuki Mekata, Shinzaburo Oka, and Atsuyoshi Ohno*
Institute for Chemical Research, Kyoto University, Uji, Kyoto 611
(Received August 26, 1987)

A new procedure for the reductive desulfonylation of β-keto sulfones is described. The reaction proceeds under a photochemical conditions with the Hantzsch ester in pyridine in the presence of ruthenium(II). Various functional groups are unaffected under the reaction conditions. Application of the procedure to the syntheses of certain natural products is also described.

NAD(P)H and its model compounds have been widely studied from the viewpoint of mimeses of biochemical transformations. As a consequence, it has been succeeded in reducing certain activated carbonyl compounds with excellent stereospecificity.

However, on the other hand, little attention has been paid to apply dihydropyridine derivatives as reductants in organic synthesis, and the functional groups susceptible to the reduction with the model compounds are limited. Since the reactivity of NAD(P)H or its analogs is quite low, biological systems employ appropriate enzymes as catalysts for the transformations. Therefore, it is reasonable to expect that a dihydropyridine derivative may be an interesting reductant in organic reactions if an appropriate catalyst is found. Along this idea, we have studied to extend the scope and limitation of the reduction with dihydropyridine derivatives. The use of a dihydropyridine derivative as an organic reductant introduces interesting specificities into organic reactions. For example, α,β-unsaturated aldehydes and ketones are reduced into the corresponding saturated aldehydes and ketones with the Hantzsch ester (HEH) in the presence of silica gel, whereas α,β-unsaturated esters and nitriles are not affected at all. We recently found that desulfonylation of β-keto sulfone undergoes with HEH in the presence of ruthenium(II) without influencing many other functional groups. Since the α-position of β-keto sulfone is highly susceptible to the attack by an electrophile, β-keto sulfones are hopeful candidate as building blocks for organic syntheses, and we studied the scope of this desulfonylation.[4] In this paper, we would like to describe the details of the reaction and its application to the syntheses of natural products.

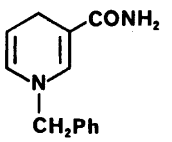

BNAH

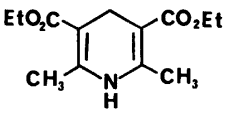

HEH

†Present address: Department of Industrial Chemistry, Faculty of Engineering, Kinki University, Iizuka, Fukuoka 820.

Results and Discussion

Alkylation. Alkylation of active methylene compounds has been studied extensively and many improved procedures have been reported.[5] Among these, it was found that the use of alkyl halide in benzene at room temperature in the presence of 1,8-diazabicyclo[5.4.0]undec-7-ene (DBU) is the best method for mono-alkylation of β-keto sulfones.[6] The results are summarized in Table 1.

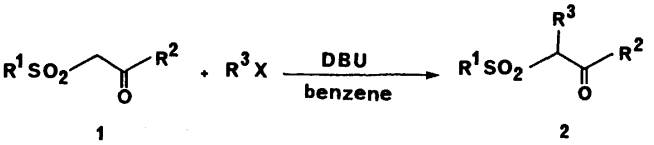

1 2

(1)

Desulfonylation. It is reported that α-nitro sulfones can be desulfonylated by *N*-benzyl-1,4-dihydronicotinamide (BNAH) in DMF into the corresponding nitro compounds.[7] We have proposed that the reduction with a dihydropyridine derivative is initiated by an electron transfer from the reductant to the substrate.[8] Although a strongly electron-defficient substrate such as an α-nitro sulfone may be reduced without a catalyst, the electron defficiency of a β-keto sulfone is not sufficient enough to undergo the desulfonylation spontaneously. Photo-irradiation is a method to activate a dihydropyridine derivative[9] and we first examined the efficiency of BNAH-DMF/*hν* system for the reduction of 4-phenyl-3-phenylsulfonyl-2-butanone (**2a**). However, the yield from this system was found to be quite low as shown in Table 2.

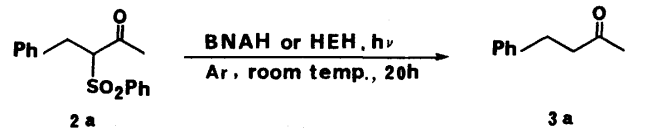

2a 3a

(2)

After several attempts, it was found that BNAH is sensitive to the photo-irradiation and self-decomposition proceeds rapidly. Therefore, HEH, which is less sensitive to the photodecomposition, is superior to BNAH for the purpose. Finally, we came to a conclu-

Table 1. Alkylation of β-Keto Sulfones[a)]

Reactant/g	Halide/g	Product/g	Yield/%
1-Phenylsulfonyl-2-propanone **1a** (1.98)	Benzyl bromide (1.71)	4-Phenyl-3-phenylsulfonyl-2-butanone **2a** (1.83)	64
1-Phenylsulfonyl-2-propanone **1a** (1.98)	Hexyl iodide (2.12)	3-Phenylsulfonyl-2-nonanone **2b** (2.43)	86
1-Phenylsulfonyl-2-propanone **1a** (1.52)	Cinnamyl bromide (1.68)	3-Phenylsulfonyl-6-phenyl-5-hexen-2-one **2c** (2.04)	65
Phenylsulfonylmethyl phenyl ketone **1b** (2.60)	Allyl bromide (1.21)	1-Phenyl-2-phenylsulfonyl-4-penten-1-one **2d** (2.19)	73
Methyl phenylsulfonylacetate **1c** (1.26)	Benzyl bromide (1.80)	Methyl 3-phenyl-2-phenylsulfonylpropionate **2f** (1.92)	62
Phenylsulfonylacetonitrile **1d** (2.14)	Benzyl bromide (1.71)	3-Phenyl-2-phenylsulfonylpropionate **2g** (2.79)	69[b)]
p-Nitrophenylsulfonylacetone **1e** (1.56)	Benzyl bromide (1.48)	3-*p*-Nitrophenylsulfonyl-4-phenyl-2-butanone **2h** (1.72)	89

a) Solvent; benzene (50 ml). Base; DBU (1.52 g). b) Solvent; benzene (20 ml). Base; DBU (0.66 g).

Table 2. Photo-Reduction of 4-Phenyl-3-phenylsulfonyl-2-butanone (**2a**)

Reducing agent[a)]	$h\nu$[b)]	Catalyst[c)]	Solvent	Yield/%[d)]
BNAH	None	None	DMF	0
BNAH	A	None	DMF	13
BNAH	B	None	DMF	5
BNAH	A	None	CH_3CN	17
BNAH	A	+	DMF	14
BNAH	A	+	Pyridine	2
HEH	B	+	Pyridine	13
HEH	A	+	DMF	Trace
HEH	A	+	CH_3CN	2
HEH	A	+	Pyridine	68
HEH	B	+	Pyridine	97
HEH[e)]	B	+	Pyridine	59
HEH[f)]	B	+	Pyridine	83

a) Three equivalent amounts were used unless otherwise indicated. b) A: 600 W high-pressure mercury lamp with a Pyrex filter. B: USHIO HALOGEN LAMP JCD (100 V-650 W). c) 1% mol of $RuCl_2(bpy)_3$ was used. d) Determined on VPC (OV 330, 1 m, 130 °C). e) 1.5 equivalent amounts. f) 2.0 equivalent amounts.

sion that the use of 3 equivalent amounts of HEH in pyridine in the presence of 1% mole of $RuCl_2(bpy)_3$, as a photosensitizer, with irradiation of visible light under an inert atmosphere affords the best result as listed in Table 2. The procedure was applied to the desulfonylation from various β-keto sulfones as summarized in Table 3. Interestingly, while a sulfonyl group at the α-position to the keto group can be substituted by a hydrogen in food to excellent yields under the present reaction conditions, those at the α-positions of an ester and a cyano group are not affected at all.

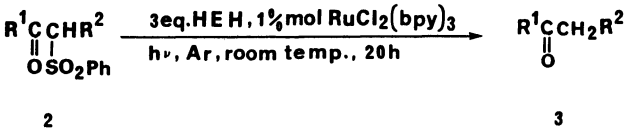

2 3 (3)

We believe that the present reaction proceeds through an electron-transfer from HEH to the substrate to form a radical ion intermediate and the process is mediated by the ruthenium complex. Indeed, it is known that Ru(II) is photochemically reduced into Ru(I)[10)] and Pac et al. proposed a Ru-mediated electron-transfer mechanism for the photochemical reduction of activated olefins with BNAH.[11)] As shown in the last example in Table 3, when the phenylsulfonyl group in the substrate is substituted by a *p*-nitrophenylsulfonyl group, the yield decreases remarkably to only 14%. Since the radical anion intermediate from the *p*-nitrophenylsulfonyl substrate is so stable under the reaction conditions due to the electron-withdrawing character of the *p*-nitro group that the cleavage of the C-S bond to form (probably) a carbon free radical and a sulfinate anion is inhibited here. Thus, the substituent on the sulfonyl group has to be electron-defficient but not too much in order to undergo the reaction smoothly.

Synthesis of Dihydrojasmone. Jasmones are im-

Table 3. Photo-Reduction of β-Keto Sulfones

	Substrate		Product	Yield/%
2a	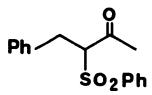	3a	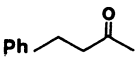	97
2b	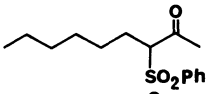	3b	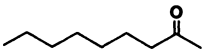	87
2c	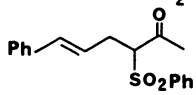	3c	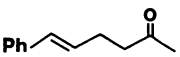	83
2d	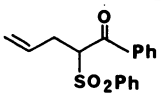	3d	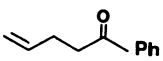	94
2e	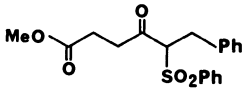	3e	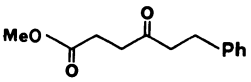	44
2f	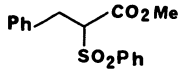	3f	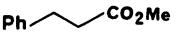	0
2g	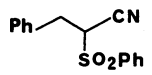	3g	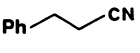	0
2h	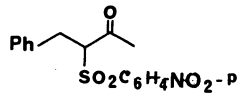	3h	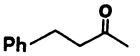	14

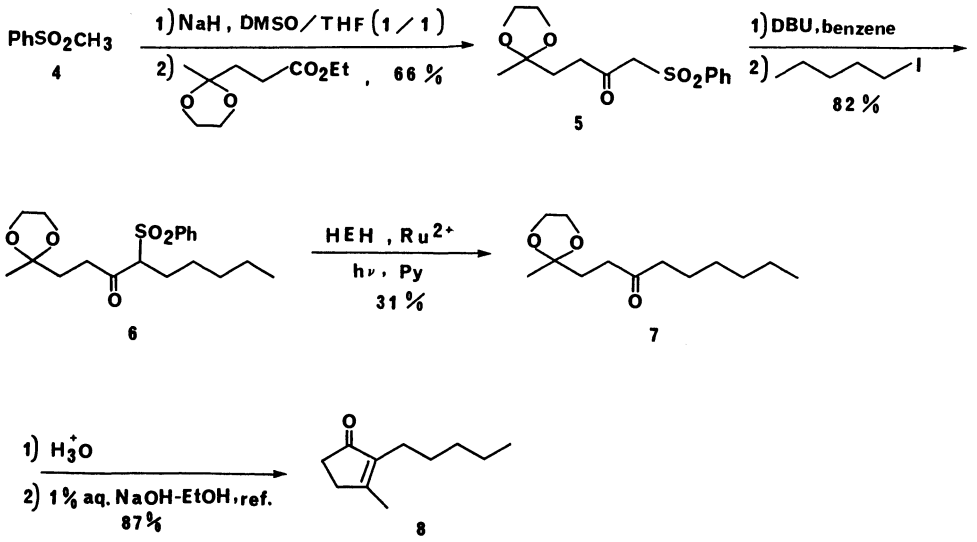

Scheme 1.

portant perfume components and have attracted a great attention of synthetic organic chemists.[12] We applied our alkylation-desulfonylation method to the synthesis of dihydrojasmone (**8**) along the process outlined in Scheme 1.

Methyl phenyl sulfone (**4**) was reacted with ethylene acetal of ethyl levulate in DMSO/THF (1/1) at 65 °C using sodium hydride as a base to afford the β-keto sulfone **5**, which was then alkylated with pentyl iodide in DBU/benzene system into the substituted β-keto sulfone **6**.

Desulfonylation of **6** was achieved with HEH in the presence of 1% mole of $RuCl_2(bpy)_3$ in pyridine under irradiation of visible light from a halogen lamp and the acetal **7** was isolated in 68% yield after purification on a column of silica gel. The acetal **7** was converted into dihydrojasmone (**8**) in 87% yield after an acid-catalyzed deprotection followed by reflux with 1% aq.

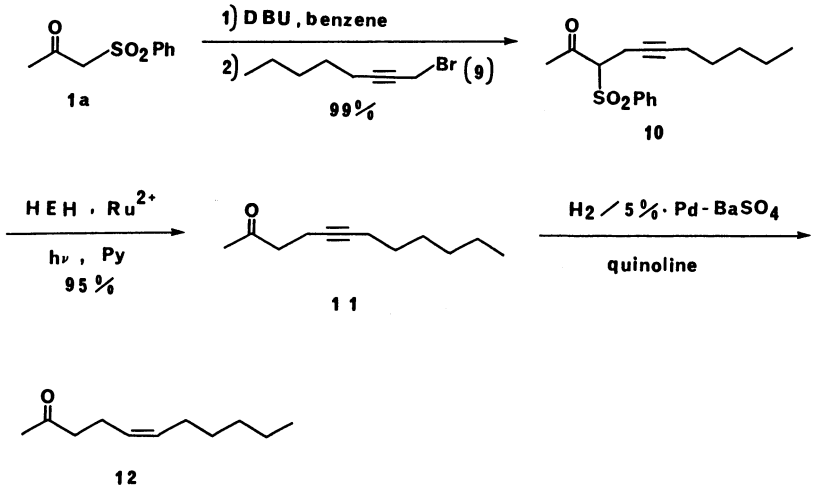

Scheme 2.

NaOH in EtOH.[13] Spectral data from **8** were identical with those reported in the literature[14] and the elemental analyses gave satisfactory results.

Synthesis of a Pheromone. (*Z*)-5-Undecen-2-one (**12**) was isolated as the principal volatile component of the pedal gland exudate of the bontebock, *Damaliscus dorcas dorcas*, by Burger et al.[15] They subjected the synthetic ketone **12** to the preliminary biological test as a mammalian pheromone and intense interest was shown by two captive animals. Application of our alkylation-desulfonylation method to the synthesis of this ketone provides a short (3 steps) and facile procedure and the ketone **12** was isolated in 79% overall yield (Scheme 2).

1-Phenylsulfonyl-2-propanone (**1a**) was regioselectively reacted with 1-bromo-2-octyne (**9**) in benzene with DBU to yield a β-keto sulfone **10** in 99% yield. Desulfonylation of **10** with the HEH-Ru(II)/*hν* system and subsequent purification on a column of silica gel afforded an acetylenic ketone, **11**, in 95% yield. Partial hydrogenation of **11** catalyzed by 5% Pd-$BaSO_4$ in the presence of quinoline gave the desired product **12** in 84% yield. The ^{1}H NMR spectrum indicated that the isolated product was consisted of the (Z)-isomer only. Other spectral data were also identical with those reported in the literature,[15] and the elemental analyses were satisfactory.

Experimental

Melting points were corrected with YANAGIMOTO MICRO MELTING POINT APPARATUS. Unless otherwise indicated, materials were purchaced from Nakarai Chemicals, Ltd.

Instruments. ^{1}H NMR spectra were measured at 100 MHz with a JEOL JN-FX100 fourier transform NMR spectrometer. IR spectra were recorded on a Hitachi EPI-S2 infrared spectrometer.

Elemental analyses were performed with a Yanaco MT-3 elemental analyzer. Gas chromatographic data were recorded on a Yanako G-1800 gas chromatograph (OV-330).

Alkylation: Preparation of 4-Phenyl-3-phenylsulfonyl-2-butanone (2a). A mixture of 1.98 g of 1-phenylsulfonyl-2-propanone (**1a**), 1.52 g of DBU, and 1.71 g of benzyl bromide in 50 ml of benzene was stirred at room temperature for 15 h. The reaction mixture was washed with three portions of each 50 ml of water and the organic layer was dried over anhydrous sodium sulfate. After removal of the solvent, the residue was purified by column chromatography on silica gel to give 1.83 g (64%) of 4-phenyl-3-phenylsulfonyl-2-butanone (**2a**), mp 92—93 °C.

^{1}H NMR ($CDCl_3$) δ=2.18 (s, 3H), 3.19 (q, 2H, *J*=14 Hz), 4.42, 4.45 (dd, 1H, *J*=11 Hz), 6.98—7.26 (m, 5H), and 7.52—7.90 (m, 5H). IR (KBr): 3000, 1723, 1320, and 1145 cm^{-1}. Found: C, 66.61; H, 5.52%. Calcd for $C_{16}H_{16}O_3S$: C, 66.64; H, 5.59%.

2b—g were obtained similarly. Results are summarized in Table 1.

2b: ^{1}H NMR ($CDCl_3$) δ=0.87 (t, 3H, *J*=7 Hz), 1.04—1.32 (m, 8H), 1.91 (q, 2H, *J*=7 Hz), 2.42 (s, 3H), 4.08 (t, 1H, *J*=7 Hz), and 7.29—7.88 (m, 5H). IR (neat): 3075 (m), 2930 (s), 1725 (s), 1305, and 1150 cm^{-1}(s). Found : C, 64.05; H, 7.88%. Calcd for $C_{15}H_{22}O_3S$: C, 63.80; H, 7.85%.

2c: ^{1}H NMR ($CDCl_3$) δ=2.34 (s, 3H), 2.79 (t, 2H, *J*=7 Hz), 4.30 (t, 1H, *J*=7 Hz), 5.80, 5.95 (dt, 1H, *J*=15, 7 Hz), 6.36 (d, 1H, *J*=15 Hz), 7.20 (m, 5H), and 7.42—7.85 (m, 5H). IR (KBr): 3000, 1723, 1315, and 1150 cm^{-1}. Found: C, 66.28; H, 5.49%. Calcd for $C_{18}H_{18}O_3S$: C, 66.43, H; 5.60%.

2d: ^{1}H NMR ($CDCl_3$) δ=2.76 (t, 2H, *J*=7 Hz), 4.93—5.22 (m, 3H), 5.40—5.80 (m, 1H), and 7.32—7.96 (m, 10H). IR (KBr): 3000, 1674, 1305, and 1145 cm^{-1}. Found: C, 68.30; H, 5.51%. Calcd for $C_{17}H_{16}O_3S$: C, 67.98; H, 5.37%.

2e: ^{1}H NMR ($CDCl_3$) δ=2.34—2.60 (m, 4H), 2.94—3.32 (m, 2H), 3.57 (s, H), 4.25 (q, 1H *J*=4 Hz), and 6.95—7.90 (m, 10H). IR (KBr): 3000 (m), 1740 (s, CO_2), 1715 (s, C=O), 1310, and 1140 cm^{-1} (s, SO_2). Found: C, 63.54; H, 5.54%. Calcd for $C_{19}H_{20}O_5S$: C, 63.32; H, 5.59%.

2f: Mp 92 °C. ^{1}H NMR ($CDCl_3$) δ=3.36 (d, 2H, *J*=4 Hz), 3.50 (s, 3H), 4.23 (dd, 1H, *J*=10, 4 Hz), 7.05—7.18 (m, 5H), and 7.48—7.97 (m, 5H). IR (Nujol): 2920 (s), 1735 (s, CO_2), 1310, and 1140 cm^{-1} (s, SO_2). Found: C, 63.06; H, 5.31%. Calcd for $C_{16}H_{16}O_4S$: C, 63.14; H, 5.30%.

2g: Mp 76—78 °C. ^{1}H NMR ($CDCl_3$) δ=3.18 (q, 2H, *J*=12 Hz), 4.04, 4.10, (dd, 1H, *J*=4 Hz), 7.20—7.38 (m, 5H), and

7.54—8.14 (m, 5H). IR (Nujol): 2930 (s), 2220 (w, CN), 1320, and 1160 cm^{-1} (s, SO_2). Found: C, 66.71; H, 4.69; N, 5.03%. Calcd for $C_{15}H_{13}NO_2S$: C, 66.40; H, 4.83; N, 5.16%.

Reductive Desulfonylation of β-Keto Sulfones: 4-Phenyl-2-butanone (3a). A solution of 288 mg (1 mmol) of **2a**, 750 mg of HEH (3 mmol) and 6.9 mg (0.01 mmol) of $RuCl_2(bpy)_3$ in 12 ml of pyridine was irradiated with visible light (USHIO HALOGEN LAMP JCD 100V-650W) at room temperature under an argon atmosphere for 20 h. The reaction mixture was poured into 100 ml of 2M hydrochloric acid (1 M=1 mol dm^{-3}) and extracted with ether. The organic layer was washed with water and brine, then dried on sodium sulfate. After removal of the solvent, the residue was chromatographed on silica gel with benzene as an eluent to give 143 mg (97%) of 4-phenyl-2-butanone (**3a**).

^{1}H NMR ($CDCl_3$) δ=2.12 (s, 3H), 2.60—3.04 (m, 4H), and 7.06—7.38 (m, 5H). IR (neat): 3000 (m) and 1715 cm^{-1} (s, C=O). Found: C, 80.94; H, 8.31%. Calcd for $C_{10}H_{12}O$: C, 81.04; H, 8.16%.

3b—e were obtained similarly. Results are summarized in Table 3.

3b: 87% yield. ^{1}H NMR ($CDCl_3$) δ=0.99 (t, 3H, *J*=6 Hz), 1.20—1.36 (m, 8H), 1.56 (t, 2H, *J*=7 Hz), 2.13 (s, 3H), and 2.43 (t, 2H, *J*=7 Hz). IR (neat): 3000 (s) and 1723 cm^{-1} (s, C=O). Found: C, 75.84; H, 12.91%. Calcd for $C_9H_{18}O$: C, 75.99; H, 12.76%.

3c: 83% yield. ^{1}H NMR ($CDCl_3$) δ=2.16 (s, 3H), 2.40—2.68 (m, 4H), 6.08, 6.23 (dt, 1H, *J*=6 Hz), 6.41 (d, 2H), and 7.20—7.36 (m, 5H). IR (neat): 3000 (m), 1710 (s, C=O), and 1600 cm^{-1} (m, C=C). Found: C, 82.90; H, 8.16%. Calcd for $C_{12}H_{14}O$: C, 82.72; H, 8.10%.

3d: 94% yield. ^{1}H NMR ($CDCl_3$) δ=2.36—2.60 (m, 2H), 3.04 (t, 2H, *J*=7 Hz), 4.90—5.16 (m, 2H), 5.68—6.08 (m, 1H), and 7.32—8.00 (m, 5H). IR (neat): 3000 (m), 1685 (s, C=O), and 1600 cm^{-1} (m, C=C). Found: C, 82.41; H, 7.75%. Calcd for $C_{11}H_{12}O$: C, 82.46; H, 7.55%.

3e: 44% yield. ^{1}H NMR ($CDCl_3$) δ=2.52—3.02 (m, 8H), 3.64 (s, 3H), and 7.10—7.28 (m, 5H). IR (neat): 3000 (m), 1740 (s, CO_2), and 1720 cm^{-1} (s). Found: C, 71.06; H, 7.54%. Calcd for $C_{13}H_{16}O_3$: C, 70.89; H, 7.32%.

Reduction of Methyl 3-Phenyl-2-phenylsulfonylpropionate (2f), 3-Phenyl-2-phenylsulfonylpropionitrile (2g), and 3-(*p*-Nitrophenylsulfonyl)-4-phenyl-2-butanone (2h). The reduction was carried out on 0.05 mmol scale of each substrate under the conditions as described for **2a**. The chemical yields of the corresponding reduction products were determined on GLC (OV330, 130 °C) employing hydroquinone dimethyl ether as an internal standard. No reduction product was detected from the reduction of **2f** and **2g**. 4-Phenyl-2-butanone was formed in 14% yield from **2h**.

Preparation of Dihydrojasmone (8) A mixture of 0.72 g (30 mmol) of sodium hydride, 4.68 g (30 mmol) of methyl phenyl sulfone (**4**) and 15 ml of dimethyl sulfoxide was heated to 65 °C with stirring until the evolution of hydrogen gas ceased (for about 30 min). The solution was cooled, diluted with 10 ml of tetrahydrofuran, and then a solution of 2.84 g (15 mmol) of ethyl levulate ethylene acetal in 5 ml of tetrahydrofuran was added. The resulting mixture was heated to 65 °C with stirring for 1 h, then cooled, poured into a mixture of ice and 2M hydrochloric acid, and extracted with six portions of chloroform. The combined organic extracts were washed successively with water, saturated aqueous sodium hydrogen carbonate, and brine, then dried and concentrated to leave the crude product which was column chromatographed on silica gel with hexane eluent to afford 2.60 g (66% yield) of 2-(4-phenylsulfonyl-3-oxobutyl)-2-methyl-1,3-dioxolane (**5**).

^{1}H NMR ($CDCl_3$) δ=1.28 (s, 3H), 2.00 (t, 2H, *J*=7 Hz), 2.73 (t, 2H, *J*=7 Hz), 3.85 (s, 4H), and 6.54—6.81 (m, 5H). IR (neat): 3000 (m), 1730 (s, C=O), 1310, and 1150 cm^{-1} (s, SO_2). Found: C, 56.63; H, 6.11%. Calcd for $C_{14}H_{18}O_5S$: C; 56.36, H; 6.08%.

A mixture of 2.12 g of **5**, 1.08 g of DBU and 1.40 g of pentyl iodide in 35 ml of dry benzene was stirred at room temperature for 15 h. The reaction mixture was worked up as described for **2a** to give 2.15 g (82%) of 2-methyl-2-(4-phenylsulfonyl-3-oxononyl)-1,3-dioxolane (**6**).

^{1}H NMR ($CDCl_3$) δ=0.81 (t, 3H, *J*=6 Hz), 1.15—1.36 (m, 6H), 1.28 (s, 3H), 1.74—2.09 (m, 4H), 2.72 (t, 2H, *J*=7 Hz), 3.88 (s, 4H), 4.15 (t, 1H, *J*=7 Hz), and 7.51—7.82 (m, 5H). IR (neat): 3000 (m), 1730 (s, C=O), 1310, and 1150 cm^{-1} (s, SO_2). Found: C, 61.82; H, 7.57%. Calcd for $C_{19}H_{23}O_5S$: C, 61.93; H, 7.66%.

A solution of 364 mg of **6**, 750 mg of HEH and 6.9 mg of $RuCl_2(bpy)_3$ in 12 ml of pyridine was irradiated with visible light at room temperature under an argon atmosphere for 20 h. The reaction mixture was worked up as described for **2a** to give 70 mg (31%) of 2-methyl-2-(3-oxononyl)-1,3-dioxolane (**7**).

^{1}H NMR ($CDCl_3$) δ=0.88 (t, 3H, *J*=6 Hz), 1.20—1.68 (m, 11H), 1.96 (t, 2H, *J*=7 Hz), 2.41 (t, 2H, *J*=7 Hz), 2.48 (t, 2H, *J*=7 Hz), and 3.92 (s, 1H). IR (neat): 2980 (m) and 1730 (s) cm^{-1}. Found: C, 71.53; H, 6.56%. Calcd for $C_{13}H_{14}O_3$: C, 71.54; H, 6.47%.

A solution of 228 mg (1 mmol) of **7** in 10 ml of acetone and a few drops of 2M hydrochloric acid was stirred at room temperature for 5 h. The reaction mixture was condensed in vacuo, diluted with 10 ml of ethanol and 2 ml of 1% aq. NaOH and then heated at 80 °C for 3 h. The solution was poured into 2M hydrochloric acid, extracted with dichloromethane and washed with water and brine. The organic layer was dried on sodium sulfate, condensed in vacuo, and purified by column chromatography on silica gel with hexane-ethyl acetate (2 : 1) mixture as an eluent. Dihydrojasmone (**8**) was obtained in 87% yield (144 mg) and showed satisfactory spectra compared with those reported in the literature.[12]

^{1}H NMR ($CDCl_3$) δ=0.88 (t, 3H, *J*=6 Hz), 1.20—1.36 (m, 6H), 2.04 (s, 3H), 2.20 (t, 2H, *J*=6 Hz), 2.34 (t, 2H, *J*=6 Hz), and 2.46 (t, 2H, *J*=7 Hz). IR (neat): 2930 (m), 1700 (s), and 1642 cm^{-1} (m). Found: C, 79.36; H, 11.03%. Calcd for $C_{11}H_{18}O$: C, 79.47; H, 10.91%.

Synthesis of a Pheromone, (*Z*)-5-Undecen-2-one (12). A mixture of 1.98 g of 1-phenylsulfonyl-2-propanone (**1a**), 1.52 g of DBU, 1.89 g of 1-bromo-2-octyne (**9**) in 50 ml of benzene was stirred at room temperature for 15 h. The reaction mixture was washed with water and the organic layer was dried over anhydrous sodium sulfate. After removal of the solvent, the residue was purified by column chromatography on silica gel to give 3.02 g (99%) of 3-phenylsulfonyl-5-undecyn-2-one (**10**).

^{1}H NMR ($CDCl_3$) δ=0.88 (t, 3H, *J*=6 Hz), 1.16—1.48 (m, 6H), 1.95—2.13 (m, 2H), 2.43 (s, 3H), 2.71—2.85 (m, 2H), 4.23 (t, 1H, *J*=8 Hz), and 7.44—7.91 (m, 5H). IR (neat): 2930 (s), 2212 (w), 1725 (s), 1310, and 1150 cm^{-1} (s). Found: C, 67.01; H, 7.27%. Calcd for $C_{17}H_{22}O_3S$: C, 66.63; H, 7.24%.

A solution of 305 mg (1 mmol) of **10**, 750 mg of HEH (3 mmol) and 6.9 mg (0.01 mmol) of $RuCl_2(bpy)_3$ in 10 ml of pyridine was irradiated with visible light at room temperature under an argon atmosphere for 20 h. The reaction mixture was poured into 100 ml of 2M hydrochloric acid and extracted with ether. The organic layer was washed with water and brine, and dried on sodium sulfate. After removal of the solvent, the residue was chromatographed on silica gel with benzene as an eluent to give 156 mg (95%) of 5-undecyn-2-one (**11**).

^{1}H NMR ($CDCl_3$) δ=0.88 (t, 3H, J=6 Hz), 1.20—1.60 (m, 6H), 2.02—2.20 (m, 2H), 2.13 (s, 3H), 2.18—2.28 (m, 2H), and 2.36—2.42 (m, 2H). IR (neat): 3000 (m) and 1715 cm^{-1} (s). Found: C, 79.30; H, 10.87%. Calcd for $C_{11}H_{18}O$: C, 79.46; H, 10.92%.

A mixture of 55 mg of **11**, 20 mg of 5% Pd/$BaSO_4$, 4 µl of quinoline in 10 ml of dry methanol under an atmosphere of hydrogen was stirred at room temperature for 6 h. The palladium catalyst was removed by filtration and the filtrate was concentrated in vacuo. The crude product was purified by column chromatography on silica gel with benzene as an eluent. The pure 5-undecen-2-one (**12**) was obtained in 84% yield and identified as the (*Z*)-isomer only by ^{1}H NMR analysis.

^{1}H NMR ($CDCl_3$) δ=0.88 (t, 3H, J=6 Hz), 1.20—1.40 (m, 6H), 2.02 (q, 2H, J=6 Hz), 2.11 (s, 3H), 2.29 (q, 2H, J=6 Hz), 2.41 (t, 2H, J=6 Hz), and 5.28 (qAB, 2H, J=6 Hz). IR (neat): 3000 (s), 1720 (s), and 1680 cm^{-1} (m). Found: C, 78.81; H, 12.32%. Calcd for $C_{11}H_{20}O$: C, 78.51; H, 11.98%.

References

1) A. Ohno, S. Ushida, "Mechanistic Models of Asymmetric Reductions," Lecture Notes in Bio-Organic Chemistry, Vol. 1, Springer-Verlag, Heidelberg (1986).

2) K. Nakamura, M. Fujii, S. Oka, and A. Ohno, *Chem. Lett.*, **1985**, 523.

3) K. Nakamura, M. Fujii, H. Mekata, S. Oka, and A. Ohno, *Chem. Lett.*, **1986**, 87.

4) For other methods of reductive desulfonylation, see E. E. van Tamelen and E. A. Grant, *J. Am. Chem. Soc.*, **81**, 2160 (1950); E. J. Corey and M. Chaykovsky, *J. Am. Chem. Soc.*, **86**, 1639 (1964); P. A. Grieco and Y. Masaki, *J. Org. Chem.*, **39**, 2135 (1974); J. B. Hendrickson, A. Giga, and J. Wareing, *J. Am. Chem. Soc.*, **96**, 2275 (1974); B. M. Trost, H. C. Arndt, D. E. Strege, and T. R. Verhoeven, *Tetrahedron Lett.*, **1976**, 3477.

5) For example, phase transfer method; E. V. Delmlow, *Angew. Chem., Int. Ed. Engl.*, **13**, 170 (1974); **13**, 493 (1977): and the method of ion pair extraction; A. Bröndstrom and U. Junggern, *Acta Chem. Scand.*, **23**, 2203 (1969); **23**, 2204 (1969); **23**, 3585 (1969); **25**, 1469 (1971).

6) N. Ono, T. Yoshimura, T. Saito, R. Tamura, R. Tanikaga, and A. Kaji, *Bull. Chem. Soc. Jpn.*, **52**, 1716 (1979).

7) N. Ono, R. Tamura, R. Tanikaga, and A. Kaji, *J. Chem. Soc., Chem. Commun.*, **1981**, 71.

8) A. Ohno, H. Yamamoto, and S. Oka, *J. Am. Chem. Soc.*, **103**, 2041 (1981).

9) Y. Ohnishi, M. Kagami, and A. Ohno, *Chem. Lett.*, **1975**, 125.

10) For a review on photoelectron transfer catalysis, see M. Julliard and M. Chanon, *Chem. Rev.*, **83**, 425 (1983).

11) C. Pac, M. Ihara, M. Yasuda, Y. Yamauchi, H. Sakurai, *J. Am. Chem. Soc.*, **103**, 6495 (1981); C. Pac, Y. Yamauchi, O. Ishitani, M. Ihara, M. Yasuda, and H. Sakurai, *J. Org. Chem.*, **49**, 26 (1984).

12) For reviews; R. A. Ellison, *Synthesis*, **1973**, 397; T.-L. Ho, Synth. *Commun.*, **4**, 265 (1974).

13) J. Tsuji and H. Yasuda, *Synth. Commun.*, **8**, 103 (1978).

14) F. Ogura, T. Otsubo, T. Sakamoto, and H. Yamaguchi, *Bull. Chem. Soc. Jpn.*, **57**, 1691 (1984).

15) B. V. Burger, M. leRoux, C. F. Garbers, H. S. C. Spies, R. G. Bigalke, K. G. R. Pachler, P. L. Wessels, V. Christ, and K. H. Mourer, *Z. Naturforsch.*, **31C**, 21 (1976).

 © 1988 The Chemical Society of Japan Bull. Chem. Soc. Jpn., 61, 501—504 (1988)

Anomalous Reaction of Arylmalononitriles with Nitric Acid. Para-Directing Nature of Dicyanomethyl Group and a Through-Ring Nitro/*aci*-Nitro Tautomerism of 4-Nitrophenylmalononitrile[1)]

Hitomi Suzuki,* Hideki Koide, and Takuji Ogawa*
Department of Chemistry, Faculty of Science, Ehime University, Bunkyo-cho, Matsuyama 790
(Received September 11, 1987)

Phenylmalononitrile reacts with nitric acid in dichloromethane at room temperature to afford 1,2-bis(4-nitrophenyl)-1,1,2,2-tetracyanoethane as an initial product, which readily suffers oxidative cleavage to give 4-nitrobenzoyl cyanide. Contrary to common understanding, dicyanomethyl group exhibits no meta-directing property. 4-Nitrophenylmalononitrile is found to exist in two stable tautomeric forms, which undergo a facile nitro/*aci*-nitro interconversion across aromatic ring depending on the nature of solvent employed.

Successive replacement of methyl hydrogen atoms in toluene by chlorine atoms changes the directing effect of methyl group from predominant ortho/para orientation to predominant meta orientation. Thus, benzyl chloride gives on nitration ortho, meta, and para nitro derivatives in 34, 14, and 53% yields, respectively,[2)] while the value is 7, 65, and 29% respectively for benzylidene trichloride.[3)] Since the cyano group is more strongly deactivating than chlorine atom, it is quite understandable that the substitution of two cyano groups into methyl group of toluene would change the directing nature of methyl group from ortho/para into meta. Indeed, Flürsheim and Holmes nitrated phenylmalononitrile (**1a**) with nitric acid in acetic anhydride and obtained 68 and 32% respectively of meta and (ortho plus para) nitration products.[4)] Their result has been taken as one of the examples of the substituent-dependent modification of the electron-releasing property of methyl group and no doubts seem to have been thrown for more than half a century.

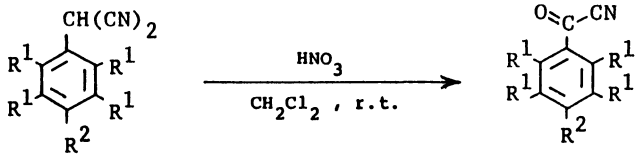

1 **2**

In the course of our continuing study on the non-conventional aromatic nitration,[5)] we had an occasion to reinvestigate the reaction of several arylmalononitriles with nitric acid under various conditions. Rather surprisingly, dinitrile **1a** underwent a facile reaction both on aromatic ring and on side chain, giving 4-nitrobenzoyl cyanide (**2c**) in a good yield. In contrast to the literature report,[4)] no 3-nitro isomer could be detected in the product mixture.

A close inspection of this unexpected result revealed a new chemistry. Thus, when the reaction was quenched with water immediately after the addition of nitrating agent to a solution of **1a** in dichloromethane at room temperature and the organic phase was worked up as usual, the product was a pale yellow crystalline solid which, after several recrystallization from THF and ether, melted at 156—157 °C with decomposition. On dissolving into THF and acetone, it developed a pale yellow and an orange color respectively. Its solution in DMSO had a deep red color. Elemental analysis of this compound was consistent with the empirical formula $C_{18}H_8N_6O_4$. The IR spectrum (KBr) demonstrated the presence of cyano (2275 cm^{-1}) and nitro groups (1535 and 1360 cm^{-1}), while its ^1H NMR spectrum (100 MHz; $(CD_3)_2SO$) showed signals at δ 8.50 and 7.70 (d; J=9.6 Hz), relative intensity 1 : 1, due to vicinal aromatic protons. The ^{13}C NMR spectrum (90 MHz; $(CD_3)_2SO$) indicated the presence of cyano groups (δ 110.0), substituted aromatic carbons (δ 129.4 and 149.5), unsubstituted aromatic carbons (δ 124.6 and 130.0), and sp^3 carbons (δ 52.8). These spectral evidences allowed for the compound the formulation of 1,2-bis(4-nitrophenyl)-1,1,2,2-tetracyanoethane (**3**). Its structure was further confirmed by direct comparison with an authentic specimen obtained from the oxidation of 4-nitrophenylmalononitrile (**1c**) with yellow mercury(II) oxide in dichloromethane at room temperature. When kept in contact with nitric acid in the same solvent, **3** was converted into benzoyl cyanide **2c**. Under similar conditions, 4-methylphenylmalononitrile (**1b**) and 2,3,5,6-tetrachloro-4-methylphenylmalononitrile (**1d**) afforded the corresponding benzoyl cyanide **2b** and **2d** as the respective single product. Interestingly, dinitrile **1c** with two electron-withdrawing groups on aromatic ring reacted more easily with nitric acid than unsubstituted dinitrile **1a** or methyl-substituted dinitrile **1b** to produce **2c** in high yields.

We also carried out the nitration of **1a** according to the procedure given in the literature.[4)] The reaction proceeded quite rapidly, giving after 30 min 58% of **2c** and 22% of 4-nitrobenzoic acid along with several minor products. No 3-nitro compounds could be obtained again. Although the reaction mechanism remains to be clarified, the oxidation of dinitrile **1c** to acyl cyanide **2c** most likely involves a nitrated *aci*-nitro compound **4**, which is formed via a S_E2' type process in which the attack of an electrophile occurs on the oxygen atom of nitro group with the loss of proton

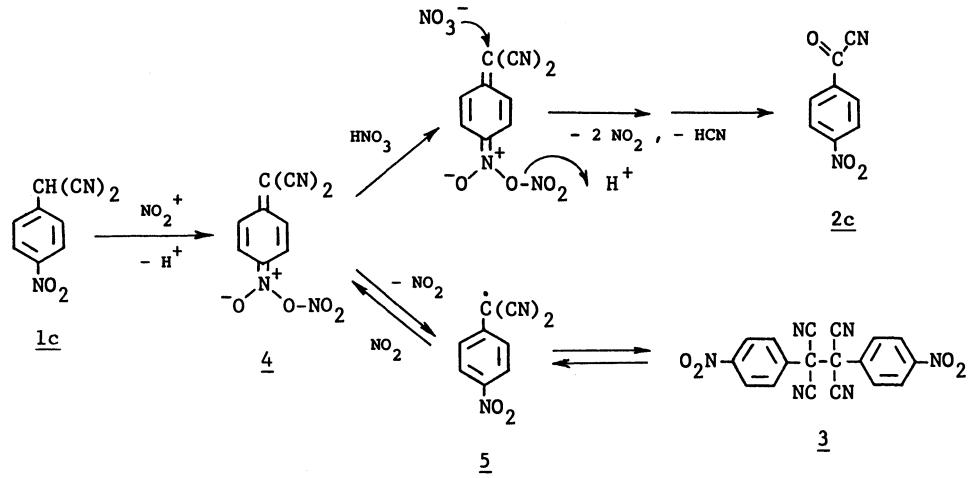

Scheme 1.

Table 1. Benzoyl Cyanides Obtained from the Reaction of Arylmalononitriles with Nitric Acid

	Arylmalononitrile **1**		Reaction time/h	Benzoyl cyanide **2**	
	R^1	R^2		Mp (θ_m/°C)	Yield/%[a]
a	H	H	6	116—117	77[b]
b	H	Me	8	50—51	74
c	H	NO_2	0.7	116—117	85
d	Cl	Me	6	126—129	72

a) Yields refer to the isolated compounds and are not optimized. b) Product was **2c**.

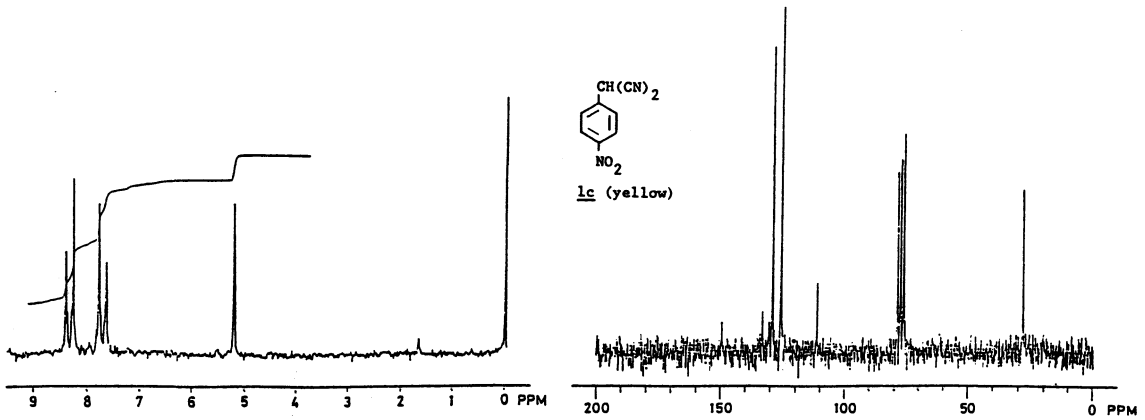

Fig. 1. ^1H and ^{13}C NMR spectra of **1c** in chloroform-*d*.

from the side chain. The intermediate **4** then undergoes attack of oxygen nucleophile on the electron-deficient exo-carbon to form acyl cyanide **2c** or dissociates into a radical **5** and nitrogen dioxide via the homolytic fission of a nitrogen-oxygen bond as sketched in Scheme 1. A stabilized radical **5** is expected to be in equilibrium with the dimer **3**.

Dinitrile **1c** is usually prepared by the action of cyanogen chloride on 4-nitrophenylacetonitrile anion[6] or by the arylation of malononitrile anion with 4-bromonitrobenzene.[7] It is described as pale yellow plates melting at 109—110 °C and characterized by its remarkable acidity.[7,8] When this compound was prepared by the literature method, there was obtained a pale yellow crystalline solid, mp 108.5—109.5 °C. Its IR, ^1H and ^{13}C NMR, and UV spectra were all consist-

Table 2. Spectroscopic Data of the Yellow and Red Forms of 4-Nitrophenylmalononitrile (**2c**)

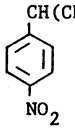 **1c**(yellow)	^1H NMR ($CDCl_3$): δ 5.21 (s, 1H), 7.76 (d, 2H; J= 8 Hz), 8.40 (d, 2H; J=8 Hz) ^{13}C NMR ($CDCl_3$): δ 27.9 (CH), 110.6 (CN), 125.0 (CH), 128.5 (CH), 129.8 (C), 148.9 (C) IR (KBr): 2255, 1610, 1590, 1525, 1350, 855 cm^{-1} UV ($CHCl_3$): λ_{max} 252 nm
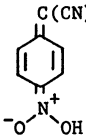 **6** (red)	^1H NMR (DMSO-d_6): δ 6.81 (d, 2H; J=9 Hz), 7.18 (s, variable; 1H), 7.90 (d, 2H; J=9 Hz) ^{13}C NMR (DMSO-d_6): δ 110.3 (CN), 119.5 (CH), 125.4 (CH), 130.3 (C), 138.0 (C), 149.3 (C) IR (KBr): 3340, 2190, 1520, 1345, 850 cm^{-1} UV ($CHCl_3$): λ_{max} 222, 262, 459 (vs) nm

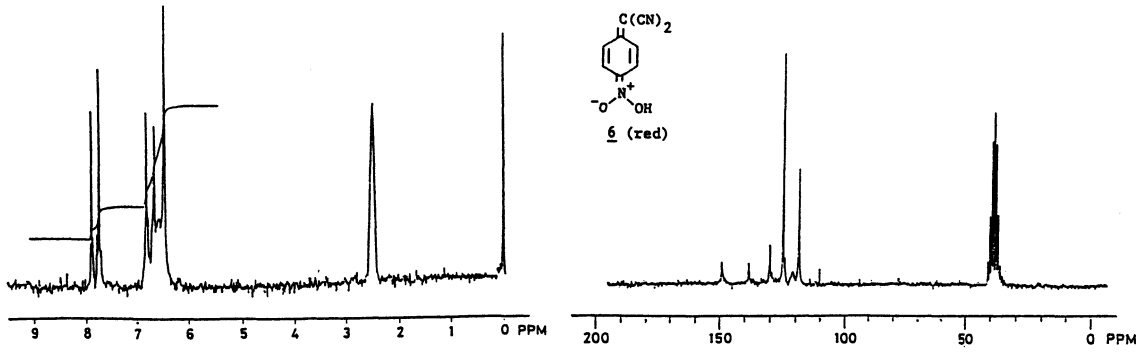

Fig. 2. ^{1}H and ^{13}C NMR spectra of **6** in DMSO-d_6.

ent with the aromatic structure **1c** (Table 2). When dissolved into methanol or DMSO, however, this yellow dinitrile developed a deep red color and the ^{1}H and ^{13}C NMR spectra of the solution thus obtained were completely different from those of chloroform or benzene solution (Figs. 1 and 2). A deep-colored methanolic solution was evaporated under reduced pressure to leave a dark red solid, which also exhibited an infrared spectrum very different from that of a pale yellow compound. The red dinitrile is soluble in acetone, DMSO, and methanol to form a red solution, but it is slightly soluble in benzene and chloroform to give a yellow solution. In contrast, the yellow dinitrile is soluble in most common organic solvents to give a yellow to deep red solution depending on the nature of solvent employed. Both dinitriles are interconvertible simply by choosing an appropriate solvent system. On the basis of spectroscopic and microanalytical data as well as their behaviors toward different solvent systems, a nitro structure **1c** was assigned to the yellow dinitrile and an *aci*-nitro structure **6** to the red one. Our finding represents an additional mode of nitro/*aci*-nitro tautomerism, which occurs through a long distance at the expense of aromatic stabilization of benzene nucleus.

Experimental

All melting points were determined on a hot-stage apparatus and are uncorrected. IR spectra were run as KBr pellets on a Hitachi 260-10 spectrophotometer and only prominent peaks are recorded. UV spectra were measured in chloroform with a Hitachi 220A spectrophotometer. ^{1}H and ^{13}C NMR spectra were obtained on Hitachi R-600 and JNM-FX-100 spectrometers using TMS as an internal standard. Unless otherwise stated NMR data refer to deuteriochloroform solutions. Mass spectra were determined on a Hitachi M-80B mass spectrometer with 70 eV ionizing current.

Arylmalononitriles were prepared by allowing the corresponding iodoarenes to react with malononitrile anion in the presence of copper(I) iodide in hot hexamethylphosphoric triamide (HMPA).[9] The following typical example illustrates the general procedure used in the synthesis of the dinitriles. In the preparation of **1c**, assistance by copper(I) catalyst is not necessary.

2,3,5,6-Tetrachloro-4-methylphenylmalononitrile (1d). A commercial 60% sodium hydride dispersion in mineral oil (ca. 4 g) was washed three times by decantation with hexane and the remaining solid was covered with dry HMPA (10 ml). A solution of malononitrile (3.3 g) in the same solvent (10 ml) was added with stirring under nitrogen. After the cease of gas evolution, 2,3,5,6-tetrachloro-4-iodotoluene (3.56 g) was added, followed by copper(I) iodide (2.0 g), and the mixture was gradually heated to 85 °C and kept at this temperature for 10 h. TLC monitoring of the reaction mixture at this time showed no unreacted iodide. The black mixture was then quenched with dilute hydrochloric acid and the organic phase was extracted several times with ether. The extracts were combined, washed with aqueous sodium sulfite, and evaporated under reduced pressure. The crude product was chromatographed on silica gel using a hexane-dichloromethane mixture as eluent to give dinitrile **1d** as a crystalline solid, mp 207—209 °C. Yield, 1.65 g (56%). MS (70 eV) *m/z* (rel intensity) 293 (M^+, 100), 264 (36), and 258 (37); ^{1}H NMR: δ=2.66 (s, 3H) and 6.11 (s, 1H); ^{13}C NMR: δ=20.67, 25.97, 109.20, 131.57, 132.22, 134.27, and 140.96; IR: 2240, 1550, 1440, 1400, 1385, 1360, 1135, and 1000 cm^{-1}. Found: C, 41.09; H, 1.39; N, 9.59%. Calcd for $C_{10}H_4N_2Cl_4$: C, 40.86; H, 1.37; N, 9.53%.

Phenylmalononitrile (1a): Mp 67—68 °C. ^{1}H NMR: δ= 5.06 (s, 1H) and 7.48 (s, 5H); IR: 2250, 1490, 1450, 1010, 910, and 725 cm^{-1}.[10]

4-Methylphenylmalononitrile (1b): Mp 57—58 °C. ^{1}H NMR: δ=2.39 (s, 3H), 4.93 (s, 1H), and 7.0—7.2 (m, 4H); IR: 2250, 1500, 1005, 805, and 755 cm^{-1}. Found: C, 77.19; H, 5.11; N, 18.22%. Calcd for $C_{10}H_8N_2$: C, 76.90; H, 5.16; N, 17.94%.

4-Nitrophenylmalononitrile (1c): Mp 109—110 °C. ^{1}H NMR: δ=5.21 (s, 1H), 7.76 (d, 2H; J=8 Hz), and 8.40 (d, 2H; *J*=8 Hz); IR: 2255, 1610, 1590, 1525, and 1350 cm^{-1}. Found: C, 57.81; H, 2.45; N, 22.33%. Calcd for $C_9H_5N_3O_2$: C, 57.76; H, 2.69; N, 22.45%.[6]

Reaction of Arylmalononitriles with Nitric Acid. The procedure used in each of the reactions described was identical; therefore, only a typical example of these reactions will be reported in detail. The results are summarized in Table 1.

To a solution of 4-methylphenylmalononitrile (**1b**; 0.156 g) in dichloromethane (1 ml), nitric acid (*d*=1.5; 0.5 ml) was added and the mixture was stirred at room temperature for several hours, during the course of which the initial slightly yellow color gradually deepened to yellowish green, then faded to light yellow after 5 h. Liberation of nitrogen dioxide was observed. The mixture was diluted with water and the resulting turbid solution was extracted with dichloro-

methane. The extract was washed three times with cold water, dried with sodium sulfate, and evaporated under reduced pressure to leave a pale yellow solid. The residue was recrystallized from hexane-chloroform to afford 4-methylbenzoyl cyanide (**2b**) as colorless needles, mp 50—51 °C. Yield, 0.108 g (74%). ^{1}H NMR: δ=2.49 (s, 3H), 7.40 (d, 2H: J=8 Hz), and 8.05 (d, 2H; J=8 Hz); IR: 2215, 1660, 1595, 1260, and 975 cm^{-1}. Found: C, 74.18; H, 4.89; N, 9.66%. Calcd for C_9H_7NO: C, 74.47; H, 4.86; N, 9.65%.

On heating with methanol, **2b** was converted into methyl 4-methylbenzoate, identical with an authentic sample.

4-Nitrobenzoyl Cyanide (2c): Mp 116—117 °C. ^{1}H NMR: δ=8.41 (br. s, 2H) and 8.43 (br. s, 2H); IR: 2215, 1680, 1525, 1345, and 1230 cm^{-1}. Found: C, 54.64; H, 2.29; N, 15.71%. Calcd for $C_8H_4N_2O_3$: C. 54.55, H, 2.29; N, 15.90%.

2,3,5,6-Tetrachloro-4-methylbenzoyl Cyanide (2d): Mp 126—129 °C. ^{1}H NMR: δ=2.63 (s, 3H); IR: 2200, 1700, 1540, 1350, 1340, 1240, 1160, 1055, and 920 cm^{-1}. Found: C, 38.03; H. 1.09; N, 4.71%. Calcd for $C_9H_3NOCl_4$: C, 38.20; H, 1.07; N, 4.95%.

Oxidative Coupling of 4-Nitrophenylmalononitrile to 1,2-Bis(4-nitrophenyl)-1,1,2,2-tetracyanoethane. A solution of dinitrile **1c** in dichloromethane was mixed with nitric acid and the green reaction mixture obtained was quenched with iced water after a few minutes. A pale yellow solid was collected by filtration and fractionally crystallized from tetrahydrofuran-ether. Mp 156—157 °C. Found: C, 58.06; H, 2.03; N, 22.27%. Calcd for $C_{18}H_8N_6O_4$: C, 58.07; H, 2.17; N, 22.57%.

The authors thank Advanced Instrumentation Center for Chemical Analysis, Ehime University, for NMR spectral determinations and elemental analyses.

References

1) The reaction of polysubstituted aromatics. Part LXII; Part LXI: H. Suzuki, H. Abe, N. Ohmasa, and A. Osuka, *Nippon Kagaku Kaishi*, **1982**, 445.

2) J. R. Knowles and R. C. O. Norman, *J. Chem. Soc.*, **1961**, 2938.

3) B. F. Holleman, *Chem. Rev.*, **1**, 187 (1925).

4) B. Flürsheim and E. L. Holmes, *J. Chem. Soc.*, **1928**, 2230.

5) For a review, see H. Suzuki, *Synthesis*, **1977**, 217.

6) H. D. Hartzler, *J. Am. Chem. Soc.*, **86**, 2174 (1964).

7) M. J. Minch, N. Giaccio, and R. Wolff, *J. Am. Chem. Soc.*, **97**, 3766 (1975).

8) E. M. Arnett and E. B. Troughton, *Tetrahedron Lett.*, **24**, 3299 (1983).

9) H. Suzuki, T. Kobayashi, and A. Osuka, *Chem. Lett.*, **1983**, 589.

10) P. B. Russel and G. H. Hitchings, *J. Am. Chem. Soc.*, **74**, 3443 (1952); J. C. Hessler. *Am. Chem. J.*, **32**, 119 (1904).

 © 1988 The Chemical Society of Japan Bull. Chem. Soc. Jpn., 61, 505—512 (1988)

Metal-Catalyzed Organic Photoreactions. Titanium(IV) Chloride-Catalyzed Photoreactions of Aldohexoses

Shuji Ichikawa, Kazuo Takahashi, Masato Tanaka, and Tadashi Sato*
Department of Applied Chemistry, Waseda University, Ookubo 3, Shinjuku-ku, Tokyo 160
(Received September 16, 1987)

Under UV irradiation in the presence of titanium(IV) chloride in methanol, D-glucose, D-mannose, and D-galactose underwent a selective bond cleavage at the C5–C6 position, producing the corresponding pentodialdose derivatives. The reaction was interpreted in terms of the photoinduced electron transfer within a chelate of titanium ion with the carbohydrate molecule. The synthetic utilities of the photoproducts were discussed.

Although carbohydrate molecules are regarded as having either aldehyde or ketone group, the carbonyl groups are in a latent form, and they do not function as an effective chromophor to induce photoreaction. The photochemistry of the parent carbohydrate molecules has been performed either with conventional UV light (>200 nm) in the presence of molecular oxygen or sensitizers, or with shorter wavelength light (185 nm).[1] Under these conditions the reaction has been assumed to be initiated by hydroxyl radical produced from water molecule, and gives product as a mixture of various compouds. Most of the photoreactions of the carbohydrates have been carried out on derivatives having a chromophore at an appropriate position, and therefore they are regarded as the photochemistry of the chromophores, rather than that of carbohydrates themselves. Although these reactions usually proceed with high selectivity at the particular position, several steps are required to introduce the chromophore into the desired position, thus making the carbohydrate photochemistry discouraging in the synthetic chemistry field.

For some time, we have been investigating the effects of metal compounds on the photoreaction of organic molecules, and found that many photoreactions were remarkably affected by the presence of some metal compounds. One of the most unique types of reaction is the titanium(IV) chloride-catalyzed photocoupling reaction of carbonyl compounds with alcohols involving a C–C bond formation, and the reaction was applied successfully to the synthetic purpose.[2] In our previous papers,[3] we reported that D-glucose (**1**) and D-galactose (**3**), when irradiated with UV light in the presence of titanium(IV) chloride in methanol, underwent a selective cleavage of C5–C6 bond, producing pentodialdose derivatives **4** and **6**, respectively. We have schemed the reaction as involving formation of a five-membered titanium chelate with the C5, C6-diol system of the furanose form of the aldohexoses, followed by an electron transfer within the chelate.

In the present study, we irradiated D-mannose (**2**), an another aldohexose, under the same conditions, and obtained the corresponding pentodialdose derivative **5** in 50% yield. The starting carbohydrate was recovered as the corresponding methyl glycoside tetraacetate in 18% yield. Under these conditions, D-galactose was less soluble in the reacting solution, and much amount of the starting material remained unsolved even after 24 h irradiation. Although the reaction proceeded much faster when five-fold excess of titanium(IV) chloride was used, the yield of **6** was 30%, and 46% of the starting material **3** was recovered as methyl glycoside tetraacetate. The amounts of smaller fragments, which might have been derived from the carbohydrate, but of unknown structures, were also larger as compared with the other cases.

In accord with our previous observation that only the primary alcohol function was susceptible to the titanium(IV) chloride-catalyzed photoreaction,[2e] the bond cleavage at the other positions having secondary alcohol function occurred only to a minor extent, giving rise to the high selectivity of the bond cleavage at the C5–C6 position. The reaction is characteristic in that the metal compound imparts the photoreactivity to the carbohydrate molecules, which are otherwise

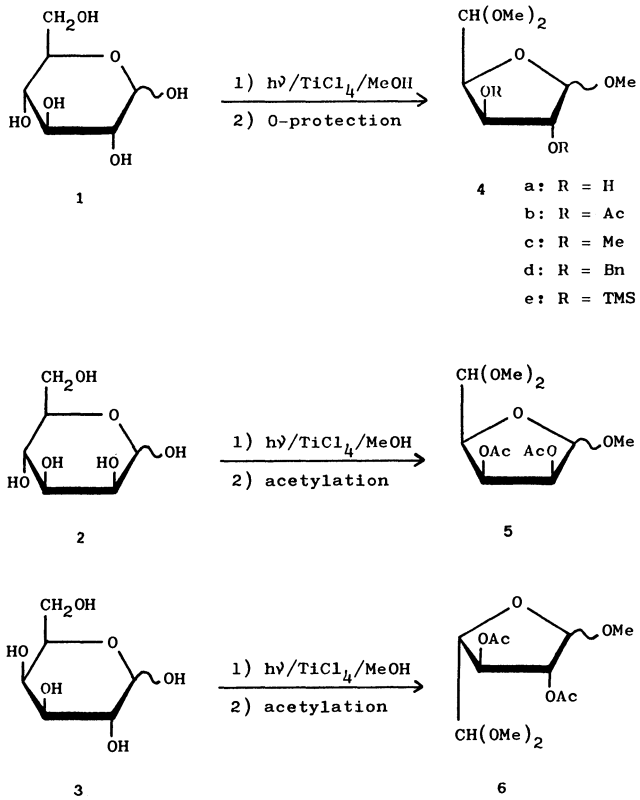

Scheme 1.

inactive towards the UV irradiation, and that the bond cleavage occurs at a specific position even without any prior protection on the carbohydrate molecules.

Since carbohydrate molecules have a series of asymmetric carbons of definite stereochemistry, they have been recognized as potential starting materials for the synthesis of chiral molecules.[4] The drawback in using the carbohydrates for this purpose is that the reactivity of each asymmetric center is quite similar, and hence it is not an easy task to carry out a specific reaction on a specific carbon. D-Glucose has been regarded as the carbohydrate that has the widest potential applicability for the synthetic purpose. It is not only because it is inexpensive, but also because it can be easily converted to some key intermediates, in which only specific positions could be brought into reaction. Therefore, in order to develop a chemisty of carbohydrates as chiral synthons, it is essential to supply with as many key intermediates as possible in which only particular positions could be reacted. We expected that the products of the present photoreaction, pentodialdose derivatives, could serve this purpose, and explored the reaction further into detail.

Since the present reaction proceeds under Lewis acid-methanol system, there might be a possibility of ring opening, and subsequent ring closure at another aldehyde group of the dialdose derivatives, resulting in the establishment of a net equilibrium between I and II (Scheme 2). If this ring scrambling occurred, the product from D-glucose (**1**) should be a racemic mixture,

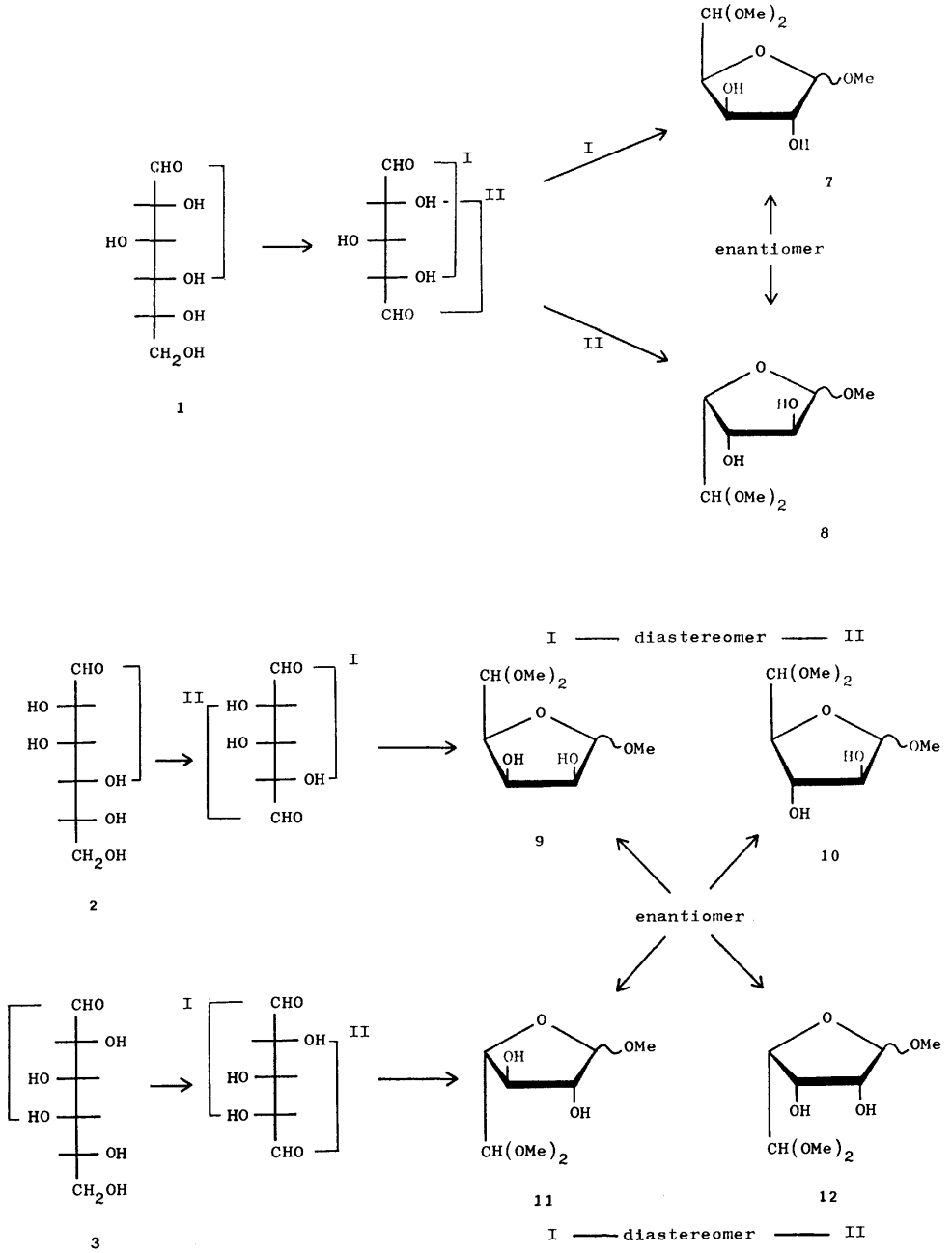

Scheme 2.

7+**8**, while the products from D-mannose (**2**) and D-galactose (**3**) should be diastereomeric mixtures of **9**+**10**, and **11**+**12**, respectively. As evident from the Scheme 2, the mixture of **9**+**10** and that of **11**+**12** should be in the enantiomeric relation of the same set of compounds. Actually, however, it was shown ^{13}C NMR and GLC analyses that the products from **2** and **3** were not identical with each other, and no traces of the enantiomeric isomers were identified. Moreover, the products from D-glucose showed optical activities as shown in the Experimental part. From these observations, we concluded that the equilibrium between I and II does not exist under the present conditions, and only **7**, **9**, and **11** were the actual products from **1**, **2**, and **3**, respectively.

Kitagawa et al.[5] have obtained pentodialdose derivatives by electrolytic oxidation of uronic acids, but, under these conditions, the ring scrambling occurred, and D-mannuronic and D-galacturonic acids gave the corresponding enantiomers of the identical compounds.

In order to evaluate the utilities of these dialdose derivatives as chiral synthons, we investigated the chemoselectivity of the two aldehyde functions and the stereoselectivity in the reactions at C5, intending to apply the photoproducts to the synthesis of polyhydroxy compounds which are furnished with definite stereochemistry and are obtainable only with difficulty by other methods.

With these intentions, we carried out the reaction of **4** with various nucleophiles in the presence of Lewis acids. The results are shown in Table 1. As evident from these results, the reaction occurred predominantly at C5, but under severer conditions, the reaction occurred also at C1. The analysis of ^{13}C NMR signals of the anomeric carbons provided us with much information concerning with the stereochemistry of the products. As shown in Table 2, all these compounds had signals at around δ 100 and 107, characteristic of the anomeric carbons having α and β configurations, respectively.[6] The signal of each region further splitted into two peaks, which we assigned to those of C5 of the corresponding diastereomers, although we could not rule out the possibility of the signal splitting due to the presence of conformers of the furanose ring. Assuming that the intensities of the signals roughly correspond to the amount of each epimers,[7] we concluded that a fair to good diastereoselectivity has been attained in the reaction at C5. Generally, better selectivity has been obtained with acetate than with methyl ethers, but obviously, the selectivity was poor with α glycoside of **17c**.

Table 1. Products and Yields of the Reaction of **4** with Nucleophiles

Substrate	Reagent	Lewis acid	Product (yield/%)
4b	CH_2=CH-CH_2SiMe_3	$TiCl_4$ (1 equiv)	**13b** (98)
4b	CH_2=CH-CH_2SiMe_3	$TiCl_4$ (4 equiv)	**21b** (88)
4b	CH_2=CH-CH_2SiMe_3	TMSOTf	**20b** (60)
4c	CH_2=CH-CH_2SiMe_3	TMSOTf	**13c** (98)
4d	CH_2=CH-CH_2SiMe_3	TMSOTf	**13d** (60)
4b	Me-C($OSiMe_3$)=CH_2	TMSOTf	**14b** (92)
4c	Me-C($OSiMe_3$)=CH_2	TMSOTf	**14c** (90)
4d	Me-C($OSiMe_3$)=CH_2	TMSOTf	**14d** (66)
4d	*n*-BuLi	$TiCl_4$	**15d** (70)
4a	$LiAlH_4$	$AlCl_3$	**16c** (60)[a]
4b	$LiAlH_4$	$AlCl_3$	**16c** (85)[a]
4b	Me_3SiCN	$TiCl_4$	**17b** (89)
4c	Me_3SiCN	TMSOTf	**17c** (94)
4c	CH_2=C(OMe)-$OSiMe_3$	TMSOTf	**18c** (82)

a) After methylation.

Table 2. ^{13}C NMR Signals of Anomeric Carbons[a]

Compound	δ (relative intensity)	
	α anomer	β anomer
13b	100.4 (15), 99.7 (85)	107.1 (83), 106.3 (17)
14b	100.2 (17), 99.9 (83)	107.4 (69), 107.3 (31)
14c	99.4 (30), 99.2 (70)	106.5 (73), 105.9 (27)
β-**14d**		108.3 (83), 107.2 (17)
α-**14d**	100.5 (92), 99.7 (8)	
17b	100.6 (7), 100.4 (93)	107.6 (65), 107.4 (35)
α-**17c**	108.4 (76), 107.8 (24)	
β-**17c**		101.4 (54), 100.7 (46)
19c	100.4 (29), 100.3 (71)	107.8 (72), 107.5 (28)

a) See footnotes 6 and 7.

When the nitrile **17c** was treated with methanol-sulfuric acid, an anomeric mixture of ester **19c** was obtained. Lithium aluminum hydride reduction of **19c**, followed by methylation gave a diastereomeric mixture of permethylated hexofuranoses. The ^{13}C NMR spectrum of the product showed two sets of signals in a relative intensity of 70 : 30, and the minor set of the spectrum was completely identical with that of **24**, prepared from 1,2 : 5,6-di-*O*-isopropylidene-D-glucose by tandem partial deprotection at C5–C6, methylation, deprotection at C1–C2, and methylation. It was concluded, therefore, that the major product was methyl tetra-*O*-methyl-L-idofuranoside **23**.

The stereoselective alkylation of aldehyde **25** to produce 6-deoxyhexose derivatives **26** has been reported, and the reaction proceeds with chelating or non-chelating intermediate depending upon the reaction conditions.[8] However, all attempts at the preparation of hexose derivatives from **25** have been achieved only without any appreciable stereoselectivity.[9] It was found that the diastereoselectivity in the nucleophilic substitution at C5 of **4** stayed around 70 : 30, irrespective of the protective groups in **4** and the reaction conditions. The selectivity was also the same between allylation and acetonylation, since the Wacker oxidation of **13b** gave the same set of the diastereomers as

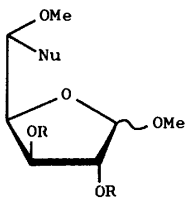

Nu:

13: $CH_2CH=CH_2$
14: CH_2COMe
15: n-Bu
16: H
17: CN
18: CH_2COOMe
19: COOMe

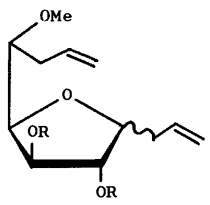

20

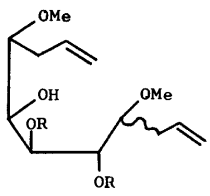

21

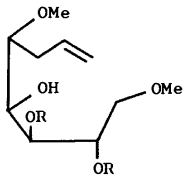

22

a: R = H; b: R = Ac; c: R = Me;
d: R = Bn; e: R = TMS

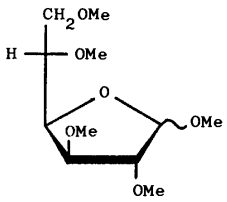

23

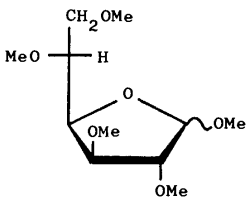

24

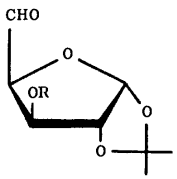

25

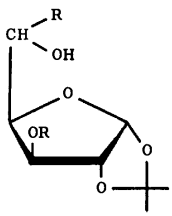

26

that obtained by the direct acetonylation of **4b**. Since we can prepare **4** from D-glucose in only two steps of photoreaction and methylation, the achievement of the higher selectivity could be very useful for setting up the configuration of L-idose system.

When the reduction product **16a** was methylated, it gave permethylated D-xylofuranoside **16c** in 85% yield, which was identical with the compound obtained in minor amount (12%) by the methylation of D-xylose. Since the methylation of D-xylose gave the permethylated product mostly in pyranoside form (85%), the present reaction could be a synthetic method for D-xylofuranoside derivatives. Lithium aluminum hydride reduction of **13c** gave an open chain compound **22c**. The products of the types of **21** and **22** are also promising as chiral synthons, because they have three different types of hydroxyl function of definite stereochemistry: One is unprotected, and the other two have two different protective groups from each other.

Since the preparation of the aldehydes corresponding to **25** from D-mannose and D-galactose in conventional manners are much more difficult as compared with the case from D-glucose, the manipulation of **2** and **3** would lead to an important development of the chemistry from these carbohydrates as chiral synthons.

Experimental

General Procedures and Instrumentation. GLC experiments were carried out on a 2.5 m×3 mm stainless steel column packed with Silicone SE30 or Carbowax 20M on silanized Chromosorb W. Preparative TLC was carried out on silica-gel plates using solvents as indicated. Unless otherwise stated, all the spectroscopic data were determined on a pure sample obtained by either distillation, preparative TLC, or column chromatography. ^1H NMR spectra (60 MHz) were recorded on a Hitachi R-24 or JEOL PMX 60SI spectrometer. ^1H NMR (90 MHz) and ^{13}C NMR spectra were measured on a Hitachi R-90H spectrometer. GC-MS spectra were taken on a Shimadzu QP-1000 mass spectrometer, and high-resolution mass spectra on a JEOL DX-300 mass spectrometer. UV spectra were measured on a Shimadzu UV-240 spectrometer.

All the irradiations were carried out using a high-pressure mercury lamp [Ushio UM 452 (450 W) or Sen HL-1000 (1 kW)] at the temperature of running water.

We tried several methods for the product isolation including column chromatography or HPLC, and found that distillation under the reduced pressure was the most convenient technique without appreciable difference in the product composition. Therefore we used the technique in most of the experiments.

Titanium(IV) Chloride-Catalyzed Photoreaction of D-Glucose (1). D-Glucose (2.0 g, 11.1 mmol) was dissolved in methanol (200 ml) containing $TiCl_4$ (1.5 ml, 13.8 mmol), and the solution was irradiated with a 1 kW lamp in a quartz vessel for 24 h. The solution was neutralized with 4 M NaOHaq (1M=1 mol dm^{-3}), and the precipitates of titanium hydroxide were filtered off. The filtrate was concentrated to dryness, and the residue was vigorously shaken with ethyl acetate several times. The solvent was removed in vacuo from the extract, and the residue was distilled under reduced pressure. After some amount of forerun (0.21 g), the main fraction was obtained as a viscous oil (1.4 g), bp 89—90 °C (0.07 mmHg (1 mmHg=133.322 Pa)). Although the purity

of the distillate could not be analyzed by GLC or TLC, the oil proved to be mainly **4a**, in view of the following results.

Acetylation: The crude **4a** (355 mg) was treated with acetic anhydride (1.4 ml) in pyridine (4.3 ml) for 18 h. Distillation with a Kugelrohr gave a main fraction as a viscous oil (288 mg), bp 150—170 °C (1 mmHg). GLC analysis showed that the fraction contained 85% of **4b**. Further distillation gave a pure sample of **4b**, which was shown to be a mixture of α and β anomers by GLC analysis. β Anomer was isolated in pure state by a preparative GLC, while α anomer was not completely freed from the β anomer. For β-**4b**: GC-MS, m/z (rel intensity) 261 (M^+−OMe, 0.5), 201 (0.3), 159 (4.0), 87 (10.4), 75 (100). ^{1}H NMR (CCl_4), δ=2.14 and 2.16 (6H, s×2, Ac), 3.39, 3.43, and 3.47 (9H, s×3, OMe), 4.21 (1H, dd, $J_{4,3}$=5.8 Hz, $J_{4,5}$=7.6 Hz, H_4), 4.47 (1H, d, $J_{5,4}$=7.6 Hz, H_5), 4.71 (1H, s, H_1), 4.90 (1H, br s, H_2), 5.26 (1H, br, d, $J_{3,4}$=5.8 Hz, H_3). ^{13}C NMR ($CDCl_3$), δ=169.4 (Ac-CO), 107.3 (C_1), 102.1 (C_5), 80.7 (C_4), 78.9 (C_2), 74.4 (C_3), 55.6, 54.5, and 53.0 (OMe), 20.8 and 20.6 (Ac-Me). IR 1738 (AcO), 1221 cm^{-1} (C-O). $[\alpha]_D^{24}$=+2.9 (c 0.05, $CHCl_3$). Found: C, 50.04; H, 6.68%. Calcd for $C_{12}H_{20}O_8$: C, 49.31; H, 6.90%. For α-**4b** (obtained by subtracting the data of β anomer from those of the mixture): GC-MS: same as that of the β anomer. ^{1}H NMR (CCl_4), δ=2.13—2.18 (6H, singlets, Ac), 3.39—3.44 (9H, singlets, OMe), 4.16—4.19 (2H, m, H_4, H_5), 4.79 (1H, br s, H_2), 4.96 (1H, d, $J_{1,2}$=4.5 Hz, H_1), 5.37 (1H, br d, $J_{3,4}$=6.0 Hz, H_3). ^{13}C NMR ($CDCl_3$), δ=169.6 (Ac-CO), 101.4 (C_1), 100.4 (C_5), 77.6 (C_4), 74.5 (C_2), 73.9 (C_3), 55.8, 54.5, and 53.0 (OMe), 20.8 and 20.6 (Ac-Me).

Methylation: Sodium hydride (350 mg, 14.6 mmol) was added to a solution of **4a** (400 mg, 1.9 mmol) in tetrahydrofuran, and the mixture was stirred for 30 min at room temperature. Methyl iodide (1.0 ml, 15 mmol) was added, and the solution was stirred for 20 h. After the addition of methanol, the solution was concentrated to dryness, and ice-water was added. The product was extracted with $CHCl_3$, dried over $MgSO_4$, and the distillation gave **4c** (358 mg), bp 110 °C (0.7 mmHg). GLC analysis showed two peaks corresponding to α and β anomers. Each anomer was separated on a preparative TLC (hexane/ether=1/2). For α-**4c**: GC-MS, m/z (rel intensity) 205 (M^+−OMe, 0.3), 173 (0.4), 161 (1.1), 145 (0.5), 130 (0.8), 75 (100). ^{1}H NMR ($CDCl_3$), δ=3.38, 3.43, 3.44, 3.46, and 3.50 (15H, s×5, OMe), 3.73—4.00 (2H, m, H_2, H_3), 4.20 (1H, t, $J_{4,3}$=$J_{4,5}$=6.3 Hz, H_4), 4.54 (1H, d, $J_{5,4}$=6.3 Hz, H_5), 4.99 (1H, d, $J_{1,2}$=4.5 Hz, H_1). ^{13}C NMR ($CDCl_3$), δ=101.8 (C_1), 101.0 (C_5), 85.7 (C_2), 83.8 (C_3), 77.2 (C_4), 58.5, 58.4, 55.5, 55.2, and 52.8 (OMe). $[\alpha]_D^{24}$=−1.2 (c 0.01, $CHCl_3$). For β-**4c**: GC-MS, same as that of the α anomer. ^{1}H NMR ($CDCl_3$), δ=3.38, 3.40, 3.43, 3.44, 3.47 (15H, s×5, OMe), 3.67—3.75 (2H, br, H_2, H_3), 4.09 (1H, dd, $J_{4,3}$=5.3 Hz, $J_{4,5}$=7.9 Hz, H_4), 4.57 (1H, d, $J_{5,4}$=7.9 Hz, H_5), 4.84 (1H, s, H_1). ^{13}C NMR ($CDCl_3$), δ=108.0 (C_1), 102.9 (C_5), 87.7 (C_2), 83.3 (C_3), 80.1 (C_4), 58.1, 57.3, 55.6, 55.4, and 53.1 (OMe). $[\alpha]_D^{24}$=+5.5 (c 0.013, $CHCl_3$).

Benzylation: The benzylation was carried out in the same way as for the methylation described above. The product **4d** was obtained through preparative TLC as an anomeric mixture (α/β=1/9) in 56% yield. For β-**4d**: ^{1}H NMR (CCl_4), δ=3.27—3.36 (9H, s×3, OMe), 3.88 (1H, br s, H_2), 3.91—4.25 (2H, m, H_3, H_4), 4.57 (1H, d, $J_{5,4}$=7.8 Hz, H_5), 4.79 (1H, s, H_1), 4.40 and 4.45 (4H, s×2, Ar-CH_2), 7.25 (10H, s, Ar). ^{13}C NMR ($CDCl_3$), δ=142.2—127.8 (Ar), 108.3 (C_1), 102.6 (C_5), 86.4 (C_2), 81.3 (C_3), 80.3 (C_4), 72.6 and 72.0 (Ar-CH_2), 55.6, 55.1, and 53.0 (OMe). For α-**4d** (obtained by subtracting the data of β anomer from those of the mixture): ^{13}C NMR ($CDCl_3$), δ=101.8 (C_1), 101.0 (C_5), 83.8 (C_2), 82.4 (C_3), 76.0 (C_4), 59.7, 59.3, and 57.0 (OMe).

Trimethylsilylation: The silylation was carried out using **4a** (620 mg, 3.0 mmol), hexamethyldisilazane (3 ml, 24 mmol), and chlorotrimethylsilane (0.4 ml, 4.4 mmol) in tetrahydrofuran (55 ml) by stirring at room temperature for 43 h. The product **4e** (1.028 g, 98% yield) was obtained in pure state by distillation, bp 190 °C (20 mmHg). For **4e** (as an anomeric mixture): GC-MS, m/z (rel intensity) 321 (M^+−OMe, 0.3), 305 (0.3), 247 (1.1), 231 (1.2), 217 (39.3), 133 (24.9), 75 (100), 73 (41.3). ^{1}H NMR (CCl_4), δ=0.04 (18H, s, TMS), 3.20—3.35 (9H, singlets, OMe), 3.68—4.09 (3H, m, H_2, H_3, H_4), 4.21—4.73 (2H, m, H_1, H_5). ^{13}C NMR ($CDCl_3$), δ=110.7 (β-C_1), 102.5 (α-C_1), 102.7 (β-C_5), 101.9 (α-C_5), 80.3 (β-C_4), 76.8 (α-C_4), 82.1, 78.4, 77.2, and 76.1 (C_2, C_3), 55.5, 54.6, 54.5, 53.0, and 52.6 (OMe), 5.26 (TMS). $[\alpha]_D^{25}$=+0.83 (c 0.380, $CHCl_3$).

Titanium(IV) Chloride-Catalyzed Photoreaction of D-Mannose (2). Under the same conditions as for D-glucose, the product **5** was obtained in 50% yield. For **5** (as an anomeric mixture): GC-MS, m/z (rel intensity) 261 (M^+−OMe, 0.4), 201 (1.6), 169 (3.4), 159 (3.0), 126 (7.1), 115 (3.3), 99 (4.3), 87 (11.0), 75 (100). ^{1}H NMR (CCl_4), δ=2.01—2.16 (6H, singlets, Ac), 3.35—3.41 (9H, singlets, OMe), 3.82—4.61 (3H, m, H_1, H_4, H_5), 4.75—5.19 (2H, m, H_2, H_3). ^{13}C NMR ($CDCl_3$), δ=170.3—169.5 (Ar-CO), 106.9 (α-C_1), 103.4 (β-C_1), 105.1 (α-C_5), 101.5 (β-C_5), 81.5 and 80.9 (C_4), 78.7 and 77.4 (C_2), 76.0 and 75.4 (C_3), 55.7—53.1 (OMe), 23.2 (Ac-Me). $[\alpha]_D^{27}$=+8.6 (c 0.070, $CHCl_3$). HRMS: Found: m/z 261.0984. Calcd for $C_{11}H_{17}O_7$ (M^+−OMe): 261.0974.

Titanium(IV) Chloride-Catalyzed Photoreaction of D-Galactose (3). The photoreaction was carried out using D-galactose (2.0 g, 11.1 mmol) and $TiCl_4$ (6.0 ml, 55.6 mmol) in methanol (200 ml) in the same way as above to produce **6** in 30% yield. For **6** (as an anomeric mixture): GC-MS, m/z (rel intensity) 261 (M^+−OMe, 1.9), 201 (1.6), 169 (3.4), 158 (4.6), 126 (9.8), 115 (3.3), 99 (5.3), 87 (14.0), 75 (100). ^{1}H NMR (CCl_4), δ=1.96—2.11 (6H, singlets, Ac), 3.27—3.41 (9H, singlets, OMe), 3.78—4.39 (3H, m, H_1, H_2, H_5), 4.72—5.14 (2H, m, H_2, H_3). ^{13}C NMR ($CDCl_3$), δ=170.3—168.8 (Ac-CO), 107.2 (α-C_1), 100.8 (β-C_1), 99.8 (α-C_5), 95.9 (β-C_5), 81.3 and 80.3 (C_4), 78.0 and 77.2 (C_2), 76.8 and 75.4 (C_3), 55.1—54.1 (OMe), 20.8 (Ac-Me). HRMS: Found: m/z 261.0985. Calcd for $C_{11}H_{17}O_7$ (M^+−OMe): 261.0974.

Titanium(IV) Chloride-Catalyzed Allylation of 4b. To a solution of **4b** (0.129 g, 0.33 mmol) in CH_2Cl_2 (4.7 ml) was added allyltrimethylsilane (0.16 ml, 1.0 mmol) and then a solution of $TiCl_4$ (0.127 g, 0.67 mmol) in CH_2Cl_2 (0.3 ml) at room temperature. The solution was stirred for 10 min at room temperature, added to cold water, and extracted with ether. The extract was washed with water and dried over Na_2SO_4. Evaporation of the solvent gave an oil, 0.104 g, which proved to be a mixture of **13b** (97%) and **4b** (2.5%) by GLC analysis. Pure sample of **13b** was obtained by a preparative TLC (ether/$CHCl_3$=1/9). For **13b** (as an anomeric mixture): GC-MS, m/z (rel intensity) 271 (M^+−OMe, 0.5), 261 (2.4), 217 (1.3), 201 (2.4), 159 (11.3), 126 (9.9), 115 (17.9), 85 (33.6), 43 (100). ^{1}H NMR (CCl_4), δ=2.02—2.13 (6H, singlets, Ac), 2.20—2.49 (2H, m, -C$\underline{H}_2$CH=CH_2), 3.35—3.53 (6H, singlets, OMe), 3.91—4.27 (2H, m, H_4, H_5), 4.61—5.22 (5H, m, H_1, H_2, H_3, -CH=C$\underline{H}_2$), 5.37—6.18 (1H, m,

-CH=CH_2). ^{13}C NMR ($CDCl_3$), δ=170.2, 170.1, 169.7, and 169.2 (Ac-CO), 134.2 and 134.0 (-CH=CH_2), 117.6 and 117.2 (-CH=CH_2), 107.1 and 106.3 (83:17) (R-C_1), 100.4 and 99.7 (15:85) (S-C_1), 82.9 and 80.0 (C_4), 79.9 and 78.5 (C_5), 76.9 and 76.3 (C_2), 75.1 and 74.4 (C_3), 58.8, 57.9, 55.9, and 55.5 (OMe), 35.3 and 34.8 (-CH_2-CH=CH_2), 20.8, 20.7, and 20.6 (Ac-Me).

When the reaction was carried out with larger amount of the Lewis acid, using **4b** (0.120 g, 0.33 mmol), $TiCl_4$ (0.15 ml, 1.33 mmol), and allyltrimethylsilane (0.21 ml, 1.33 mmol) under the otherwise same conditions as above, the product was **21b**, which was obtained in pure state on a column chromatography. For **21b** (as an anomeric mixture): GC-MS, *m/z* (rel intensity) 303 (M^+−OMe, 0.7), 271 (1.0), 183 (1.0), 169 (1.5), 137 (1.8), 85 (71.6), 55 (21.4), 43 (100). ^{1}H NMR (CCl_4), δ=1.95—2.11 (6H, singlets, Ac), 2.19—2.35 (4H, m, -CH_2-CH=CH_2×2), 3.35 (6H, singlets, OMe), 3.11—3.68 (3H, m, H_1, H_4, H_5), 4.66—5.30 (6H, m, H_2, H_3, CH_2=CH-×2), 5.44—6.13 (2H, m, CH_2=CH-×2). ^{13}C NMR ($CDCl_3$), δ=175.0—172.7 (Ac-CO), 134.0—133.6, 118.1—117.4, and 35.1—33.7 (allyls), 80.0, 79.6, 79.1, and 78.9 (C_1, C_5), 74.1 and 72.8 (C_4), 71.8, 71.7, 76.0, and 69.1 (C_2, C_3), 20.9 (Ac-Me). IR (neat), ν_{max} 3550 (OH), 1740 (acetate), 1650 cm^{-1} (olefin). Found: C, 58.12; H, 7.98%. Calcd for $C_{17}H_{28}O_7$: C, 59.28; H, 8.19%.

Trimethylsilyl Triflate-Catalyzed Allylation of 4b. A mixture of **4b** (0.12 g, 0.41 mmol), allyltrimethylsilane (0.16 ml, 1 mmol), and TMSOTf (22.2 mg, 0.1 mmol) in acetonitrile (2 ml) was stirred for 30 min. The solution was added to Na_2CO_3aq, and extracted with ether. After drying over Na_2SO_4, ether was evaporated to give **13b** (0.125 g, 100% yield) as a single product.

When the reaction time was prolonged to 46 h, or when the solution was refluxed for 1 h, in the above reaction, the crude product remained after the evaporation of ether showed two spots on a TLC. Separation on a preparative TLC gave a diallyl compound **20b** (48 mg, 60% yield) as well as the monoallyl compound **13b** (35 mg, 35% yield). For **20b** (as C_1, C_5-diastereomeric mixture): GC-MS, *m/z* (rel intensity) 281 (M^+−OMe, 0.16), 271 (3.1), 211 (3.0), 169 (8.4), 137 (14.0), 125 (10.3), 109 (10.2), 85 (54.3), 43 (100). ^{1}H NMR (CCl_4), δ=2.02 and 2.05 (6H, s×2, Ac), 2.10—2.40 (4H, m, -CH_2-CH=CH_2×2), 3.28 and 3.32 (6H, s×2, OMe), 3.04—4.32 (3H, m, H_1, H_4, H_5), 4.61—5.22 (6H, m, H_2, H_3, CH_2=CH-×2), 5.31—6.11 (2H, m, CH_2=CH-×2). ^{13}C NMR ($CDCl_3$), δ=169.6 and 169.5 (Ac-CO), 134.2—133.8, 117.4—117.1, and 35.1, 33.9 (allyls), 82.9, 82.2, 80.5, 80.3, 79.5, 79.0, 78.7, 76.7 (C_1—C_5), 58.5 and 58.3 (OMe), 20.9 and 20.8 (Ac-Me).

Acetonylation of 4b, 4c, 4d. 2-(Trimethylsilyloxy)-1-propene (0.16 ml, 1 mmol) was added to a solution of **7b** (0.1 g, 0.34 mmol) in acetonitrile (3 ml), and the solution was cooled to 0 °C. To the solution was added TMSOTf (0.01 ml, 0.05 mmol), and stirred for 20 min at 0 °C. The conventional workup produced crude **14b**, 106 mg. Pure sample was obtained by a preparative TLC. In the same way, methyl (**14c**) and benzyl (**14d**) derivatives were obtained. A preparative TLC of **14d** gave pure sample of (R)-C_1 anomer. For **14b** (as an anomeric mixture): GC-MS, *m/z* (rel intensity) 243 (M^+−Me−AcOH, 0.1), 217 (1.9), 183 (0.3), 158 (1.0), 157 (1.4), 153 (0.9), 115 (13.6), 101 (3.9), 87 (5.0), 43 (100). ^{1}H NMR (CCl_4), δ=1.98—2.13 (9H, singlets, AcO and Ac), 2.31—2.75 (2H, m, $AcCH_2$-), 3.19—3.40 (6H, singlets, OMe), 3.52—4.27 (2H, m, H_4, H_5), 4.65—5.59 (3H, m, H_1, H_2, H_3). ^{13}C NMR ($CDCl_3$), δ=206.6—205.8 (acetonyl-CO), 170.2—169.2 (Ac-CO), 107.4 and 107.3 (69:31, (R)-C_1), 100.2 and 99.9 (17:83, (S)-C_1), 82.7—74.2 (C_2—C_5), 59.3—55.2 (OMe), 46.1—44.3 (acetonyl-CH_2), 31.1—30.9 (acetonyl-Me), 20.7 and 20.6 (Ac-Me). For **14c** (as an anomeric mixture): GC-MS, *m/z* (rel intensity) 231 (M^+−OMe, 13.3), 204 (25.3), 161 (2.5), 101 (100), 88 (17.1), 75 (40.6), 73 (20.8), 45 (20.0), 43 (37.5). ^{1}H NMR (CCl_4), δ=2.12 (3H, s, acetonyl-Me), 2.43—2.61 (2H, m, acetonyl-CH_2), 3.31—3.47 (12H, singlets, OMe), 3.47—4.05 (4H, m, H_2, H_3, H_4, H_5), 4.55—4.82 (1H, m, H_1). ^{13}C NMR ($CDCl_3$), δ=209.2—207.9 (acetonyl-CO), 106.5 and 105.9 (73:27, (R)-C_1), 99.4 and 99.2 (30:70, (S)-C_1), 86.8—80.8 (C_2-C_5), 57.7—53.1 (OMe), 45.1—41.8 (acetonyl-CH_2), 30.5—27.6 (acetonyl-Me). For 1(R)-**14d**: ^{1}H NMR (CCl_4), δ=2.01—2.12 (3H, singlets, acetonyl-Me), 2.41—2.73 (2H, m, acetonyl-CH_2), 3.22—3.39 (6H, singlets, OMe), 3.73—4.17 (4H, m, H_2-H_5), 4.48 (4H, s, benzyl-CH_2×2), 4.87 (1H, d, $J_{1,2}$=7.9 Hz, H_1) 7.25 (10H, s, Ar×2). ^{13}C NMR ($CDCl_3$), δ=207.1 (acetonyl-CO), 108.3 and 107.2 (83:17, C_1), 85.8—75.4 (C_2—C_5), 58.6, 57.6, 55.9, and 54.8 (OMe), 46.8 and 46.2 (acetonyl-CH_2), 30.8 and 28.9 (acetonyl-Me), 72.0, 71.9, 139.7—126.7 (benzyl). For 1(S)-**14d** (obtained by subtracting the data of (R) anomer from those of mixture), ^{1}H NMR (CCl_4), δ=2.01—2.25 (3H, singlets, acetonyl-Me), 2.35—2.92 (2H, m, acetonyl-CH_2), 3.38—3.47 (6H, singlets, OMe), 3.78—4.23 (4H, m, H_2-H_5), 4.51 (4H, m, benzyl-CH_2), 4.81—4.97 (1H, m, H_1), 7.30 (10H, s, Ar). ^{13}C NMR ($CDCl_3$), δ=206.7 (acetonyl-CO), 100.5 and 99.7 (92:8, C_1), 84.9—74.9 (C_2—C_5), 58.1 and 55.0 (OMe), 45.1 and 44.9 (acetonyl-CH_2), 30.4 and 30.3 (acetonyl-Me), 72.0, 71.9, 137.8—127.5 (benzyl).

Methyl D-Xylofuranoside Trimethyl Ether 16c. A suspension of $AlCl_3$ (266 mg, 2 mmol) in ether (1 ml) was stirred at 0 °C for 30 min. To the mixture was added a slurry of LAH (26 mg, 0.67 mmol) in ether (1 ml), and stirred for 30 min. A solution of **4b** (100 mg, 0.34 mmol) in ether (1 ml) was added and stirred for 2 h at room temperature. The reaction mixture was quenched by adding 10% H_2SO_4aq and then neutralized with dil NaOHaq. The solid material was filtered off, and the filtrate was concentrated in vacuo to produce an oil. Upon methylation with MeI and NaH, the oil gave **16c** in 85% yield. This was identical (GC-MS) with the sample prepared by methylation of D-xylose in the same way as above.

Cyanation of 4b and 4c. To a solution of **4c** (80 mg, 0.33 mmol) in acetonitrile (3 ml) was added TMSCN (0.14 ml, 1 mmol) and TMSOTf (0.01 ml, 0.05 mmol), and the solution was stirred for 2.5 h at room temperature. After the reaction, 10% Na_2CO_3aq (10 ml) was added and extracted with ether. The extract was dried over Na_2SO_4, and the solvent was removed to give an oil (78 mg). Pure sample of **17c** (69 mg) was obtained by the bulb-to-bulb distillation. bp 115 °C (0.1 mmHg). A preparative TLC of **17c** gave pure sample of (S)-C_1 anomer. In the same way, the acetate **17b** was obtained from **4b** in 87% yield. Bp 120 °C (0.03 mmHg). The same compound was also obtained from **4b** using $TiCl_4$ as a Lewis acid in CH_2Cl_2 in 89% yield. For 1(S)-**17c**: GC-MS, *m/z* (rel intensity) 200 (M^+−OMe, 0.1), 161 (4.1), 149 (2.0), 140 (1.2), 129 (2.9), 101 (100), 88 (6.8), 75 (70.4). ^{1}H NMR ($CDCl_3$), δ=3.46—3.54 (12H, singlets, OMe), 3.29—4.49 (4H, m, H_2-H_5), [5.05 (1/2H, d, $J_{1,2}$=3.9 Hz) and 5.07 (1/2H, d, $J'_{1,2}$=3.9 Hz), H_1]. ^{13}C NMR ($CDCl_3$), δ=116.3 (CN), 101.4 and 100.7 (1:1, C_1), 85.2 and 85.1 (C_2), 83.0 and 82.2 (C_3), 76.6 and 76.4 (C_4), 70.8 and 69.9 (C_1), 58.8—55.8 (OMe). For

l(R)-**17c** (obtained by subtracting the data of l-(S) anomer from those of mixture): ^{1}H NMR ($CDCl_3$), δ=3.36—3.55 (12H, singlets, OMe), 3.71—4.55 (4H, m, H_2-H_5), 4.85 (1/5H, s, H_1), 4.91 (4/5H, s, H_1). ^{13}C NMR ($CDCl_3$), δ=117.2 and 116.4 (19:81, CN), 108.4 and 107.8 (76:24, C_1), 87.6 and 87.0 (C_2), 84.9 and 83.1 (C_3), 80.7 and 79.4 (C_4), 71.1 and 70.4 (C_5), 59.1—55.5 (OMe). For **17b** (as a diastereomeric mixture): GC-MS, *m/z* (rel intensity) 256 (M^+—OMe, 3.1), 217 (7.0), 157 (30.6), 154 (14.2), 129 (18.5), 115 (100), 87 (43.3). ^{1}H NMR (CCl_4), δ=2.02—2.15 (6H, singlets, Ac), 3.37—3.49 (6H, singlets, OMe), 4.02—4.61 (2H, m, H_4, H_5), 4.72—5.76 (3H, m, H_1, H_2, H_3). ^{13}C NMR ($CDCl_3$), δ=170.0—168.9 (Ac-CO), 116.3—115.4 (CN), 107.6 and 107.4 (65:35, (R)-C_1), 100.6 and 100.4 (7:93, (S)-C_1), 80.5—73.5 (C_2, C_3, C_5), 70.5—69.7 (C_4), 58.5—55.6 (OMe), 20.6—20.3 (Ac-Me).

Methanolysis of the Nitrile 17c. To a solution of **17c** (115 mg, 0.5 mmol) in methanol (5 ml) was added 98% H_2SO_4 (1.5 ml). The solution was kept at room temperature for 24 h, and poured into water. The solution was shaken with $CHCl_3$, and the extract was dried over Na_2SO_4. Evaporation of the solvent gave an oil **19c**, 120 mg. Bulb-to-bulb distillation gave pure sample, 116 mg. Bp 120 °C (0.1 mmHg). For **19c** (as an anomeric mixture): GC-MS, *m/z* (rel intensity) 205 (M^+—COOMe, 48.5), 161 (20.3), 145 (11.2), 129 (10.2), 101 (100), 75 (42.6). ^{1}H NMR ($CDCl_3$), δ=3.18—3.52 (12H, singlets, OMe), 3.76—3.83 (3H, singlets, COOMe), 3.86—4.16 (3H, m, H_2, H_3, H_4), 4.46—4.63 (1H, m, H_5), [4.85 (3/20H, d, δ=0.9 Hz) and 4.89 (7/20H, d, J=0.9 Hz), H_1 of l(R) anomer], 4.97 (1/2H, d, J=3.5 Hz, H_1 of l(S) anomer). ^{13}C NMR ($CDCl_3$), δ=171.4—170.1 (ester-CO), 107.8 and 107.5 (72:28, (R)-C_1), 100.4 and 100.3 (29:71, (S)-C_1), 89.5—76.6 (C_2—C_5), 58.8—54.9 (OMe), 52.6—51.2 (ester-Me). Found: C, 49.99; H, 7.63%. Calcd for $C_{11}H_{20}O_7$: C, 50.45; H, 7.51%.

Methyl L-Idofuranoside Tetramethyl Ether 23. To a solution of **19c** (90 mg, 0.33 mmol) in dry ether (5 ml) was added LAH (39 mg, 1 mmol), and stirred for 2 h at room temperature. Methanol and then 4 M HClaq were added to quench the excess LAH, and the solution was neutralized with 10% NaOHaq. The solid material was filtered off, and the filtrate was concentrated to dryness in vacuo. The remaining material was triturated with dry THF, and washed NaH (50 mg, 2.1 mmol) was added. After the mixture was stirred for 30 min, methyl iodide (1.6 ml, 5 mmol) was added, and the mixture was stirred for 18 h at room temperature. The excess NaH was quenched by addition of methanol, and the solution was concentrated in vacuo. The remaining material was dissolved in water, and extracted with $CHCl_3$. The extract was dried over Na_2SO_4, and the solvent was removed in vacuo. The crude material (84 mg), showing only one peak on a GLC analysis, was distilled to give an oil (77 mg). The ^{13}C NMR of the oil showed two sets of the signals in a ratio of 25:75. The set of the minor signals completely coincided with those of **24**, obtained in a way described below. The data of **23** were obtained by subtracting the data of **24** from those of the mixture oil. For **23**: GC-MS, *m/z* (rel intensity) 205 (M^+—CH_2OMe, 0.4), 173 (1.2), 161 (7.0), 145 (5.0), 101 (100), 75 (58.5), 59 (15.5), 45 (63.4). ^{1}H NMR ($CDCl_3$), δ=3.39—3.57 (15H, singlets, OMe), 3.60—4.36 (6H, m, H_2-H_6), 4.90 (1/2H, d, J=1.1 Hz, H_1 of α anomer (1R)), 4.95 (1/2H, d, J=3.0 Hz, H_1 of β anomer (1S)). ^{13}C NMR ($CDCl_3$), δ=108.1 (C_1 of α anomer), 100.4 (C_1 of β anomer), 87.0 and 85.2 (C_2), 83.3 and 83.0 (C_4), 81.3 and 76.3 (C_3), 79.9 and 77.6 (C_5), 72.2 and 72.0 (C_6), 60.7—55.2 (OMe).

Methyl D-Glucofuranoside Tetramethyl Ether 24. To a solution of 1,2-*O*-isopropylidene-D-glucofuranose (250 mg, 1.14 mmol) in dry THF (20 ml) was added NaH (400 mg, 16.7 mmol), and the mixture was stirred for 30 min. Methyl iodide (1.6 ml, 25 mmol) was added and the mixture was stirred for 18 h at room temperature. Methanol was added to quench the excess NaH, and the solution was concentrated in vacuo. Water was added, and the products were extracted with $CHCl_3$. After dried over Na_2SO_4, the solvent was removed in vacuo to give an oil. The oil (302 mg) was dissolved in methanol (12 ml) and 98% H_2SO_4 was added slowly. The solution was stirred for 20 h at room temperature, poured into water, and extracted with ether. After the extract was dried over Na_2SO_4, the solvent was removed in vacuo to give an oil, 220 mg. The oil was again methylated in the same way as above, and the crude product was distilled to afford a pure sample of **24**, 220 mg, bp 110 °C (0.03 mmHg). For **24**: GC-MS, *m/z* (rel intensity) 205 (M^+—CH_2OMe, 0.8), 173 (2.0), 161 (7.5), 145 (5.8), 101 (100), 75 (65.0), 59 (16.8), 45 (61.3). ^{1}H NMR ($CDCl_3$), δ=3.26—3.48 (15H, singlets, OMe), 3.47—3.91 (5H, m, H_2-H_6), 3.95—4.23 (1H, m, H_4), 4.81 (1/2H, s, H_1 of β anomer (1R)), 4.92 (1/2H, d, J=3.0 Hz, H_1 of α anomer (1S)). ^{13}C NMR ($CDCl_3$), δ=108.1 (C_1 of β anomer), 101.1 (C_1 of α anomer), 87.4 and 86.1 (C_2), 83.8 and 82.7 (C_4), 79.7 and 76.3 (C_3), 78.0 and 77.7 (C_5), 72.6 and 72.4 (C_6), 59.2—55.1 (OMe).

Trimethylsilyl Triflate-Catalyzed Allylation of 4c and 4d To a solution of **4c** (80 mg, 0.33 mmol) in dry acetonitrile (3 ml) was added allyltrimethylsilane (1.6 ml, 1 mmol), and then TMSOTf (0.01 ml, 0.05 mmol) at −30 °C. The mixture was stirred at this temperature for 20 min, and the workup in the same way as for **4b** gave a product **13c** (83 mg, 98% yield). The pure sample was obtained by a preparative TLC. In the same way, benzyl derivative **13d** was obtained from **4d** in 60% yield. For **13c** (as an anomeric mixture): GC-MS, *m/z* (rel intensity) 215 (M^+—OMe, 0.08), 205 (3.5), 173 (3.5), 161 (6.7), 145 (4.3), 101 (99.9), 85 (32.0), 75 (100). ^{1}H NMR (CCl_4), δ=2.09—2.33 (2H, m, -C<u>H</u>$_2$-CH=CH_2), 3.28—3.45 (12H, singlets, OMe), 3.09—4.03 (4H, m, H_2-H_5), 4.65—5.16 (3H, m, H_1, C<u>H</u>$_2$=CH-), 5.28—6.11 (1H, m, CH_2=C<u>H</u>-). For **13d** (as an anomeric mixture): ^{1}H NMR (CCl_4), δ=2.07—2.56 (2H, m, C<u>H</u>$_2$-CH=CH_2), 3.20—3.35 (6H, singlets, OMe), 3.62—4.09 (4H, m, H_2-H_5), 4.43 (4H, s, benzyl-CH_2), 4.72—5.11 (3H, m, H_1, C<u>H</u>$_2$=CH-), 5.42—6.25 (1H, m, CH_2=C<u>H</u>-), 7.25 (10H, s, Ar).

Butylation of 4d. To a solution of **4d** (130 mg, 0.33 mmol) in CH_2Cl_2 (3 ml) was added $TiCl_4$ (0.04 ml, 0.33 mmol) at −78 °C. A hexane solution of 1.4 M *n*-BuLi (0.72 ml, 1 mmol) was added at this temperature, and the mixture was warmed up to room temperature. After stirring for 1 h at room temperature, the mixture was worked up in conventional way to produce **15d** (132 mg, 64% yield) as an oil. Preparative TLC gave a pure sample. For **15d**: ^{1}H NMR (CCl_4), δ=[0.95 (3H, m) and 1.30 (6H, m), *n*-Bu], 3.21—3.37 (6H, singlets, OMe), 3.40—3.61 (1H, m, H_5), 3.73—4.22 (3H, m, H_2, H_3, H_4), 4.40—4.48 (4H, singlets, benzyl-CH_2), 4.55—4.80 (1H, m, H_1), 7.20 (10H, s, Ar).

Wacker Oxidation of 13b to 14b. Oxygen gas was bubbled into a solution of $PdCl_2$ (6.7 mg, 0.038 mmol) and CuCl (40 mg, 0.40 mmol) in a mixture solvent of DMF (1 ml) and water (0.4 ml) for 30 min. To the solution was added **20b** (103 mg, 0.34 mmol), and oxygen gas was bubbled into the

solution for another 6 h. After 3 M HClaq (0.2 ml) was added, the solution was shaken with CH_2Cl_2. The extract was washed with Na_2CO_3aq and then with NaClaq. After dried over Na_2SO_4, the solvent was removed in vacuo. The crude material (120 mg) was purified on a preparative TLC to give an oil which was identical with **14b** obtained from **4b**.

References

1) R. W. Binkley, *Adv. Carbohydr. Chem.*, **38**, 105 (1981), and references cited therein: N. L. Holder, *Chem. Rev.*, **82**, 287 (1982); R. C. Roth and R. W. Binklely, *J. Org. Chem.*, **50**, 690 (1985); S. Hashimoto, I. Kurimoto, Y. Fujii, and R. Noyori, *J. Am. Chem. Soc.*, **107**, 1427 (1985).

2) T. Sato, G. Izumi, and T. Imamura, *J. Chem. Soc., Perkin Trans. 1*, **1976**, 788; T. Sato and S. Yoshiie, *Chem. Lett.*, **1976**, 415; T. Sato, S. Yoshiie, T. Imamura, K. Hasegawa, M. Miyahara, S. Yamamura, and O. Ito, *Bull. Chem. Soc. Jpn.*, **50**, 2714 (1977); T. Sato, S. Yamaguchi, and H. Kaneko, *Tetrahedron Lett.*, **1979**, 1863; T. Sato, H, Kaneko, and S. Yamaguchi, *J. Org. Chem.*, **45**, 3778 (1980). T. Sato, H. Kaneko, and T. Takahashi, *Chem. Lett.*, **1981**, 1469.

3) T. Sato, K. Takahashi, and S. Ichikawa, *Chem. Lett.*, **1983**, 1589; T. Sato, K. Takahashi, and S. Ichikawa, *Nippon Kagaku Kaishi*, **1984**, 119; S. Ichikawa and T. Sato, *Yuki Gosei Kagaku Kyokai Shi*, **44**, 1047 (1986).

4) T. D. Inch, *Tetrahedron*, **40**, 3161 (1984); S. Hanessian, "Total Synthesis of Natural Products: The Chiron Approach," Pergammon Press, New York (1983).

5) I. Kitagawa, M. Yoshikawa, T. Kawaguchi, K. Shirakawa, and Y. Ikeda, *Chem. Pharm. Bull.*, **29**, 2571 (1981).

6) Due to the uncertainty concerning with the newly-created asymmetric center at C5, the anomeric nomenclature of α and β is ambiguous. Throughout the present paper, therefore, we termed α for all compounds having the same anomeric configuration as that of α-D-glucose.

7) The assumption could be generally supported because, with some compounds in which the α and β anomeric protons resonate at separate positions, the estimation from ^{13}C NMR and ^1H NMR spectra coincided.

8) M. T. Reetz, *Angew. Chem., Int. Ed. Engl.*, **23**, 556 (1984).

9) D. Horton and F. O. Swanson, *Carbohydr. Res.*, **14**, 159 (1970).

 © 1988 The Chemical Society of Japan Bull. Chem. Soc. Jpn., 61, 513—520 (1988)

Metal-Catalyzed Organic Photoreactions. Iron(III)-Catalyzed Photoreactions of Aldo- and Ketohexoses[1)]

Shuji Ichikawa, Isao Tomita, Akira Hosaka, and Tadashi Sato*
Department of Applied Chemistry, Waseda University, Ookubo 3, Shinjuku-ku, Tokyo 160
(Received September 16, 1987)

Under UV irradiation in the presence of iron(III) chloride or iron(III) triflate in pyridine, D-glucose, D-mannose, and D-galactose underwent a selective bond cleavage at the C1-C2 position, producing 4-*O*-formyl-D-arabinopyranose and 4-*O*-formyl-D-lyxopyranose. D-Fructose, under the same conditions, gave arabino-γ-lactone. The reaction was interpreted in terms of the photoinduced electron transfer within a chelate of iron ion with the carbohydrate molecule.

In our preceding papers,[2)] we found that the UV irradiation of D-glucose, D-mannose, and D-galactose in methanol in the presence of titanium(IV) chloride induced a selective bond cleaveage of C5-C6 bond of the carbohydrates, producing corresponding pentodialdose derivatives. It was also found that the aldehyde functions in these dialdose derivatives reacted with several nucleophiles with relatively high chemo- and stereoselectivities. In view of our previous observations[3)] that iron(III) chloride, as well as titanium(IV) chloride, exhibited remarkable effects upon the photoreaction of organic molecules, and that the iron(III) chloride-catalyzed photoreaction proceeded most satisfactorily in pyridine, we irradiated several monosaccharides under these reaction conditions, and found now that the iron(III)-catalyzed photoreaction of the carbohydrates in pyridine induced a selective cleavage of C1-C2 bond, in contrast to the C5-C6 bond cleavage by titanium(IV) chloride, and afforded pentose derivatives having formate function only at the C4 position. In view of good selectivity of the reaction and possible utility of the products as chiral synthons, we investigated the reaction in detail.

A pyridine solution of D-glucose (**1**) containing an equivalent amount of iron(III) chloride was irradiated with a high-pressure mercury lamp in a Pyrex tube for 24 h while oxygen gas was bubbled through. After irradiation, the products were isolated as acetates by treating the irradiated solution with acetic anhydride. The major product was an anomeric mixture of an aldopentose derivative **4** (α/β=1/1) in 38% yield, along with the starting material as pentaacetate in 41% yield (Scheme 1). D-Mannose (**2**) gave the same product **4** in 17% yield under the same conditions, along with the starting material as pentaacetate in 74% yield.

The structure **4** was determined in the following way. When the product **4** was treated first with titanium(IV) chloride in methanol, and then with acetic anhydride in pyridine, an oil was obtained which showed two peaks on a gas chromatogram. The oil proved to be an anomeric mixture of methyl D-arabinopyranoside triacetate (**5a**), because the same mixture was obtained by treating D-arabinose (**6**) with titanium(IV) chloride in methanol, followed by acetylation under the same conditions as above. The pyranose ring form for **4** was deduced from the fragmentation pattern of the mass spectrum, in which the M^+-73 peak, typical for the furanose structure (loss of the side chain),[4)] was lacking. The ^{1}H NMR spectrum of **4** indicated the presence of C5 methylene, referring to the data reported for **5b**.[5)] The position of the formate was assigned at C4 in view of the fragmentation peaks at m/z 156 and 128 of the mass spectrum, which could be ascribed to the ions depicted in Scheme 2, referring to the general mass spectrum fragmentation pattern of acylated pyranoses proposed by Biemann and his group.[6)]

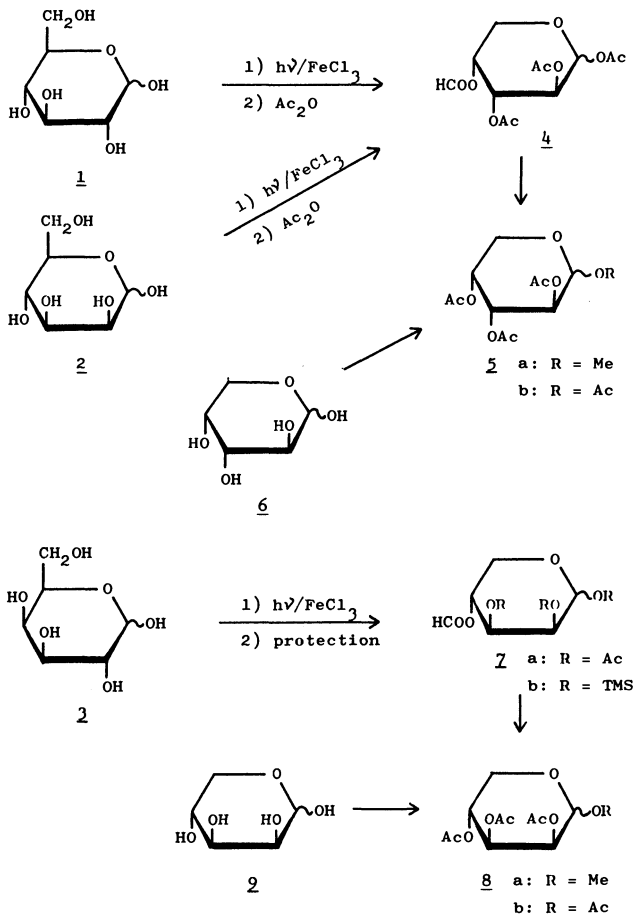

Scheme 1.

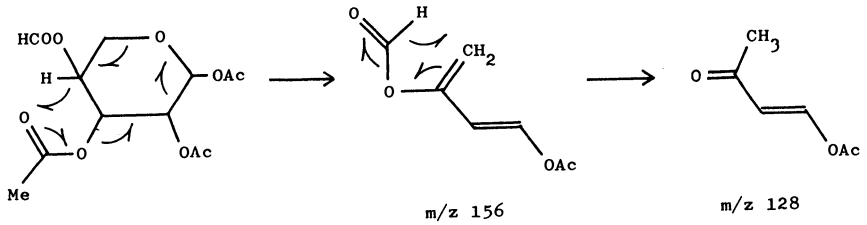

Scheme 2.

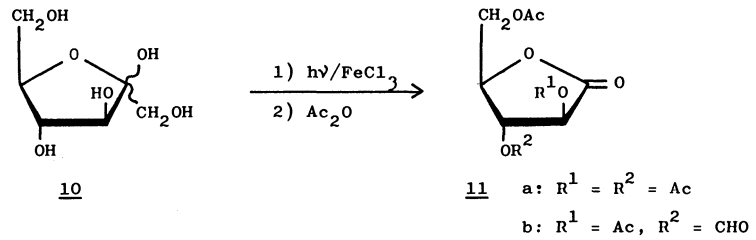

Scheme 3.

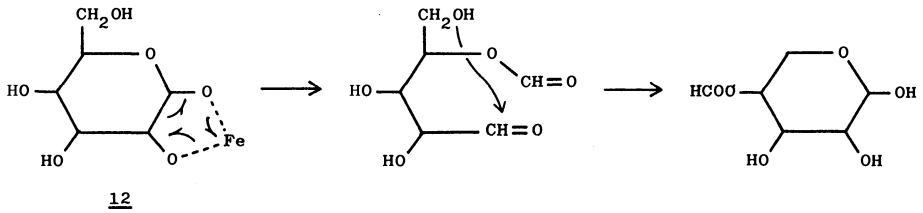

Scheme 4.

D-Galactose (**3**) gave an anomeric mixture **7a** (α/β=7/3) in 35% yield under the same conditions, with the recovery of the starting material in 36% yield. The structure **7a** was confirmed by converting the product into an anomeric mixture of D-lyxoside derivatives **8a**, which was identicai with that obtained from D-lyxose (**9**) in the same way as described for arabinose. When the irradiated solution was treated with trimethylsilyl chloride, a silyl derivative **7b** was isolated. By referring to the ^{13}C NMR spectrum, the product proved to be a single diastereomer. In contrast to the acetate **7a**, the NMR signal of proton on the formate-carrying carbon in **7b** appeared at well separated position from those of the other ring protons, featuring a definite ABMX fine structure. The similar pattern was also observed in **18b** and **18c**. This would be an another indication that the formate function stays at C4 position.

When D-fructose (**10**), a ketohexose, was irradiated under the same conditions, **11a** was obtained in 52% yield after the acetylation (Scheme 3). Evidently the reaction proceeded with selective bond cleavage at C1-C2 position as in the case of aldohexoses. The photoreaction of the ketose was faster than that of the aldohexoses, and no starting material was recovered after the irradiation for 5 h. The structure **11a** was confirmed by comparing the spectroscopic data with those of γ-D-ribonolactone triacetate, synthesized by the reported method.[7]

It has been known that D-glucose does produce D-arabinose under the irradiation in the presence of molecular oxygen in aqueous solution, and the reaction has been believed to be initiated by hydroxyl radical, giving many compounds in small quantities.[8] In view of the facts that the iron(III) chloride-catalyzed photolysis proceeded quite selectively, producing D-arabinose as the main product, and that the reaction proceeded even in the absence of molecular oxygen and water, the possibility of a mechanism involving any species originated from molecular oxygen or water was ruled out. We propose a reaction involving an electron transfer within an iron chelate **12**, followed by the recyclization of the fission product as shown in Scheme 4. In support of this scheme, methyl D-glucopyranoside and 1,2-*O*-isopropylidene-α-D-glucofuranose, lacking the system for the chelate formation, did not undergo the present reaction, and the starting materials were recovered as acetates.

The present reaction proceeded even in the absence of molecular oxygen, although the reaction was much slower under these conditions. Referring to the reaction scheme, iron(III) should have been reduced to iron(II). Presumably, molecular oxygen reoxidized the iron(II) to iron(III), thus resulting in the enhancement of the reaction efficiency. Expectedly, iron(III) chloride behaved as a catalyst in the presence of molecular oxygen, and the reaction proceeded effectively even with 1/100 equivalent of iron(III) to the carbohydrate

molecules, although the amounts of by-products increased to some extent under these conditions.

Although the yields of the present reaction were not necessarily high, the reaction was quite selective and the amounts of the smaller fragments or the products resulted from the bond cleavage at other positions were small. Remarkably, the reaction proceeded only in pyridine in the presence of iron(III) ion. The reaction using other metal salts or solvents gave poor results with little or no amounts of the aldopentoses. Later, we found that iron(III) trifluoromethanesulfonate (triflate) gave even better results than iron(III) chloride. Iron(III) triflate catalyzed the reaction more effectively than the chloride, and hence we could reduce the irradiation time and the amount of the metal compound extensively as shown in Table 1. Even in case of using only 1/100 equivalent of iron(III) triflate, the reaction proceeded quite cleanly, in contrast to the corresponding case using iron(III) chloride.

It has been known that the thermal oxidation of aldohexoses by lead(IV) acetate involves the initial cleavage of C1–C2 bond, followed by a stepwise shortening of the carbon chain.[9] As a comparison with these observations, we examined the thermal reaction of D-glucose and D-fructose under the otherwise same conditions as those of the present photoreaction. As in the case of the photoreaction, the thermal reaction of the ketose was faster than that of the aldose. Upon heating in pyridine at 100 °C in the presence of iron(III) chloride, D-glucose (**1**) gave two compounds **11a** and **11b** as the exclusive product after the acetylation. The triacetate **11a** was the exclusive product of the thermal reaction of D-fructose (**10**), indicating that the reaction pattern of the ketose was the same in the photo and thermal reactions. However, no trace of the photoproduct **4** was identified in the thermal reaction of D-glucose. The structure **11b** was deduced in view of the NMR and mass spectra, which showed that both **11a** and **11b** have identical gross structure. Although we could not distinguish experimentally between two possible structures of 2- and 3-formate for **11b**, the 3-formate structure would be preferable in view of the following reaction scheme (Scheme 5). It has been known that the lead(IV) acetate oxidation of D-glucose proceeds faster from furanose form than from pyranose form.[10] It could be assumed that the iron(III) chloride-initiated oxidation also proceeded from the furanose form of D-glucose **13**, and probably due to the overoxidation of the aldehyde intermediate, the product would be a lactone **14a**. The product suffered a partial hydrolysis of the formate group under the reaction conditions to give **14b**, and afforded the observed products **11a** and **11b** upon acetylation after the reaction. Remarkably, these observations show that the photoreaction proceeds from the pyranose structure, while the thermal reaction proceeds from the furanose structure, both structures being in an equilibrium under the present reaction conditions.

Table 1. Catalytic Activities of Iron(III) Chloride and Iron(III) Triflate in the Photoreaction of **1**

Iron salt	Mol ratio to carbohydrate	Reaction time / h	Relative yield/%	
			Product	Starting material
$FeCl_3$	1	24	45	55
$Fe(OTf)_3$	1	24	64	36
$FeCl_3$	1	2	15	85
$Fe(OTf)_3$	1	2	39	61
$FeCl_3$	1/100	24	19	81
$Fe(OTf)_3$	1/100	24	44	56
$FeCl_3$	1/100	2	7	93
$Fe(OTf)_3$	1/100	2	29	71

Shiraishi and his group reported that the photooxidation of D-glucose and D-mannose in the presence of iron(III) chloride in aqueous solution produced D-erythrose (**15a**) as major product, accompanied in some cases by a minor amount of D-arabinos (**6**).[11] They also found that D-erythrose was the sole product from D-fructose under their conditions. In search for the tetrose derivatives in our reaction, we carefully checked the foreruns obtained in small amounts, and isolated **15b** from **1** and **2** in 3% and 0.7% yields, respectively, and D-threose derivative **16** from **3** in 2.5% yield. We assumed that these compounds were produced by the C1–C2 bond cleavage of the primary products corresponding to **4** and **7**, followed by the ring closure in the similar way as that shown in Scheme 4. When D-arabinose (**6**) was irradiated under the same conditions, **15b** was obtained in 4% yield, while the starting material **6** was recovered as tetraacetate in 63% yield. D-Xylose, an another pentose, was also decomposed only to a minor extent under the same conditions, with the recovery of the starting material in 60% yield.

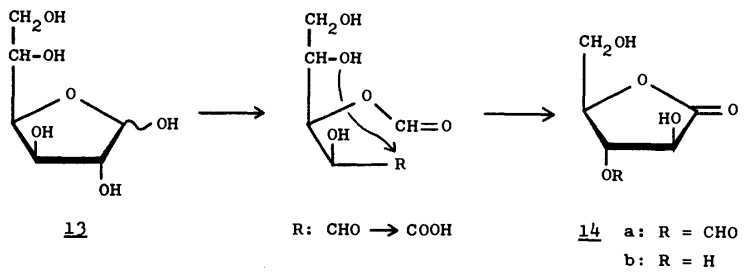

Scheme 5.

These observations indicate that the reaction from the aldopentoses is much slower than that from the aldohexoses. Although we can offer no reasonable explanation for the difference in the reactivity, it should be this difference that makes the present photoreaction fairly selective, terminating the photocleavage at the stage of pentose.

The UV spectroscopic studies also showed that an iron chelate system played an important role in our reaction. We observed that the intensity of the peak at 346 nm in the UV spectrum of iron(III) chloride in pyridine was decreased by the addition of the carbohydrate molecules. Figure 1 shows the change of the UV spectrum of iron(III) chloride in pyridine upon addition of D-galactose up to 100 equivalents. The same trend was observed with other carbohydrates, but the extent of the effect differed from one carbohydrate to another. In Fig. 2 are shown the spectra of iron(III) chloride in pyridine with several carbohydrates added in 100-fold excess. The absorption at 346 nm has been ascribed to the charge transfer from chloride ligand to iron(III) ion.[12] In accord with the assignment, iron(III) triflate did not show any peak in this region, as shown in Fig. 1. We speculated that the addition of the carbohydrate molecules resulted in the expulsion of the chloride ligand from the iron coordination sphere due to the iron chelate formation with the carbohydrate molecule, and we believed that this would be an experimental evidence for the reaction scheme proposed as shown in Scheme 4. myo-Inositol, a carbocyclic polyhydroxy compound, did not undergo the present type of the C–C bond cleavage. Notably, the UV spectrum of iron(III) chloride in pyridine was not affected at all by the addition of myo-inositol or ethylene glycol as the typical 1,2-diol system. Presumably, the presence of 1,2-diol system involving anomeric hydroxyl group was responsible for the chelate formation, and the chelate formation might be requisite for the present reaction to proceed. Although D-fructose, which exhibited the largest effect, actually underwent

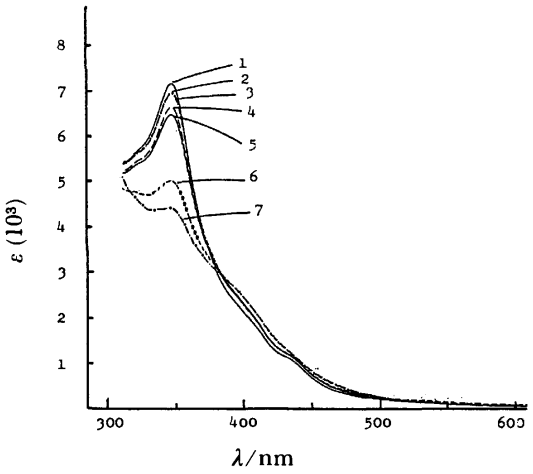

Fig. 1. Change of UV spectrum of iron(III) chloride in pyridine as a function of concentration of D-galactose. $FeCl_3$: 2.25×10^{-4} M. D-Galactose: $n\times 2.25\times10^{-4}$ M; 1: n=0; 2: n=1; 3: n=5; 4: n=10; 5: n=20; 6: n=60; 7: n=100.

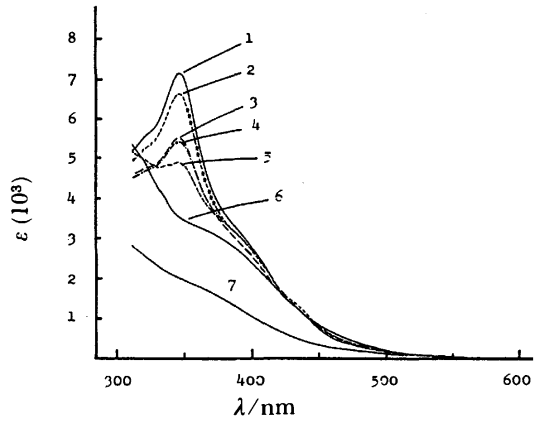

Fig. 2. Change of UV spectrum of iron(III) chloride in pyridine upon addition of carbohydrates (1—6), and UV spectrum of iron(III) triflate in pyridine (7). $FeCl_3$: 2.44×10^{-4} M, $Fe(OTf)_3$: 2.31×10^{-4} M. Carbohydrates: 2.27×10^{-2} M; 1: none; 2: D-glucose; 3: D-galactose; 4: D-mannose; 5: D-fructose; 6: D-arabinose; 7: none.

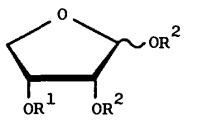

15 a: $R^1 = R^2 = H$
b: R^1 = CHO
R^2 = Ac

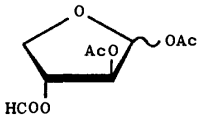

16

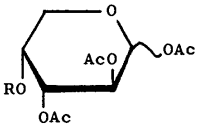

17 a: R = H
b: R = p-tolSO$_2$

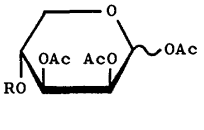

18 a: R = H
b: R = p-tolSO$_2$
c: R = MeSO$_2$

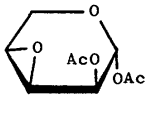

19

the photoreaction most efficiently, there seemed to be no direct correlation between the reactivity and the extent of the influence upon UV spectrum.

The most characteristic point of the present reaction is that the aldohexoses produce the aldopentoses in which only C4 hydroxyl group is protected by formyl group. With a hope to utilize the products as chiral synthons for the synthetic chemistry, the selective manipulation of the formate group was next explored.

When the acetate **4** or **7a** was treated with aluminum chloride in an aqueous methanol, formyl group was removed selectively, producing anomeric mixture of **17a** or **18a** in 84% or 94% yield, respectively. The acetylation of **17a** afforded the corresponding anomeric mixture of tetraacetates **5b**, identical with the authentic samples prepared by the known method.[13] The column chromatography of **7a** afforded pure α anomer, which, upon the selective hydrolysis of the formate and succeeding acetylation, gave pure α anomer of **8b**, identical with the authentic sample.[14] This would be a reasonable indication that no neighboring group participation inducing the possible scrambling of the stereochemistry was involved under these conditions. Tosylation or mesylation of **17a** or **18a** gave the corresponding derivatives **17b**, **18b**, or **18c**. The tosylate **18b**, upon treatment with sodium methoxide, produced L-ribose derivative **19** in 53% yield. We are exploring further applicability of the photoproducts for the synthesis of chiral compounds.

Experimental

The general procedures and instrumentation were the same as those reported in our preceding paper.[2] The NMR spectral assiments were based on the data of structurally similar system.[5,15,16]

Iron(III) Chloride-Catalyzed Photoreaction of D-Glucose (1). A pyridine solution (150 ml) of D-glucose (**1**, 1.50 g, 8.3 mmol) and $FeCl_3 \cdot 6H_2O$ (2.25 g, 8.3 mmol) was irradiated in a Pyrex tube for 24 h while oxygen gas was bubbled through. Acetic anhydride (15 ml, 166 mmol) was added to the solution, and the solution was stirred for 12 h at room temperature. The solution was concentrated in vacuo, washed with dil HClaq, extracted with dichloromethane, and dried over $MgSO_4$. The distillation gave two main fractions. The main product **4** was obtained as the lower boiling fraction, bp 148—150 °C (0.35 mmHg (1 mmHg=133.322 Pa)), 0.958 g, 38% yield, and showed two peaks (1 : 1) on a gas chromatogram which were assigned as α and β anomers, referring to the spectroscopic data and chemical reactions described below. Since the separation of both anomers were unsuccessful, the spectroscopic data were obtained on the mixture sample. For **4**: GC-MS, m/z (for α anomer) 245 (M^+ −OAc, 10.7), 170 (20.2), 156 (60.0), 145 (65.8), 128 (73.1), 103 (78.4), 97 (100): (for β anomer) 245 (M^+ −OAc, 10.4), 170 (20.9), 156 (74.1), 145 (77.4), 128 (93.4), 103 (100), 97 (92.1). ^{1}H NMR ($CDCl_3$) δ=2.01—2.17 (9H, s, Ac), 3.75—4.34 (2H, m, H_5, $H_{5'}$), 5.11—5.53 (3H, m, H_2, H_3, H_4), 5.68 (1/2H, d, J=6.2 Hz, α-H_1), 6.32 (1/2H, d, J=3.7 Hz, β-H_1), 8.14 and 8.17 (1H, s×2, CHO).[5] ^{13}C NMR ($CDCl_3$) δ=20.5 and 20.7 (Ac-Me), 62.4 and 63.6 (C_5), 66.5 and 66.9 (C_4), 68.0 and 68.1 (C_2), 69.7 and 69.8 (C_3), 90.0 and 92.0 (C_1), 159.6—159.8 (CHO), 168.8—170.3 (Ac-CO).[15] HRMS, Found: m/z 245.0686. Calcd for $C_{10}H_{13}O_7$ (M−OAc): 245.0661.

The higher boiling fraction, bp 160 °C (0.35 mmHg), crystallized upon standing, mp 109—115 °C, 1.33g. The compound was identical (GLC, NMR, and MS) with the sample of D-glucose pentaacetate,[17] prepared by the reported method.

The minor amount of the forerun (bp 134—138 °C (0.15 mmHg)) was mostly **15b** (3% yield), identical with the sample obtained by the photoreaction of D-arabinose (see below).

Methyl D-Arabinoside Triacetate (5a). A mixture of **4** (50 mg, 0.16 mmol) and $TiCl_4$ (0.5 ml, 4.6 mmol) in dry methanol (10 ml) was refluxed for 12 h, and the solution was neutralized with dil NaOHaq. The precipitate was removed by the filtration and the filtrate was concentrated to dryness in vacuo. The residue was distilled with a Kugelrohr, bp 100 °C (0.05 mmHg), 38 mg, 80% yield, to afford **5a**. This was completely identical (GLC, NMR, MS) with the sample prepared from D-arabinose under the same conditions. For **5a**: GC-MS, m/z (rel intensity) 259 (M^+ −OMe, 2.2), 199 (1.6), 170 (56.5), 128 (73.8), 69 (100). ^{1}H NMR ($CDCl_3$) δ=2.02—2.14 (9H, s, Ac), 3.41 (3H, s, OMe), 3.63—4.03 (2H, m, H_5, $H_{5'}$), 4.34 (3/5H, m, H_1 of α anomer), 4.91 (2/5H, d, J=3.2 Hz, H_1 of β anomer), 5.07—5.27 (3H, m, H_2, H_3, H_4).

Iron(III) Chloride-Catalyzed Photoreaction of D-Glucose (1) under Anhydrous and Anaerobic Conditions. The reaction solution was prepared from anhydrous reagents and solvent, applying freezing and thawing method. The yield of the product **4** was 13%, and the starting material was recovered in 75% as pentaacetate.

Iron(III) Chloride-Catalyzed Photoreaction of D-Mannose (2). The reaction and the subsequent acetylation were carried out in the same way as described for D-glucose. The product **4**, bp 145—150 °C (0.3 mmHg), was identical with that obtained from D-glucose. The higher boiling fraction, bp 160 °C (0.3 mmHg), was D-mannose pentaacetate, identical with the product prepared from D-mannose. As in the case of D-glucose, **15b** (0.7% yield) was also isolated from the small amount of the forerun, bp 110 °C (0.05 mmHg).

Iron(III) Chloride-Catalyzed Photoreaction of D-Galactose (3). The reaction and the subsequent acetylation were carried out in the same way as described for D-glucose. The crude product gave two fractions as main portion upon distillation. The lower boiling fraction **7a**, bp 156—158 °C (0.2 mmHg), showed two peaks on a gas chromatogram with relative ratio of 7 : 3. The mass spectrum of each component was quite similar to that of **4**. The column chromatography of the crude product gave the major component α-**7a** in pure state, while β-**7b** was not freed from the α anomer. For α-**7a**: GC-MS, m/z (rel intensity) 245 (M^+ −OAc, 3.5), 156 (48.9), 145 (57.5), 114 (47.4), 103 (91.1), 97 (100), 69 (68.4). ^{1}H NMR ($CDCl_3$) δ=2.05, 2.16, and 2.17 (9H, 3s, Ac), 3.73—4.28 (2H, m, H_5, $H_{5'}$), 5.21—5.42 (3H, m, H_2, H_3, H_4), 6.05 (1H, d, J=3.1 Hz, H_1), 8.08 (1H, s, CHO). ^{13}C NMR ($CDCl_3$) δ=20.6 and 20.8 (Ac-Me), 61.6 (C_5), 66.1 (C_2), 68.1 (C_4), 68.2 (C_3), 90.6 (C_1), 159.4 (CHO), 168.3, 169.4 and 169.6 (Ac-CO). HRMS, Found: m/z 245.0690. Calcd for $C_{10}H_{13}O_7$ (M−OAc): 245.0661. For β-**7a**: GC-MS, m/z (rel intensity) 245 (M^+ −OAc, 4.0), 170 (10.4), 156 (44.6), 145 (51.4), 128 (56.9), 114 (63.3), 103 (85.4), 97 (100), 73 (89.5), 69 (93.5). ^{13}C NMR

($CDCl_3$, obtained by subtracting the data of α anomer from those of the mixture) δ=20.6 and 20.8 (Ac-Me), 61.2 (C_5), 66.4 (C_2), 67.1 (C_3), 67.8 (C_4), 89.7 (C_1), 159.4 (CHO), 168.2—170.7 (Ac-CO).

The forerun (bp 135—140 °C (0.2 mmHg)), obtained in only small amount, was mostly **16** (2.5% yield). The pure sample was obtained by a preparative GLC. For **16**: GC-MS, *m/z* (rel intensity) 173 (M^+ −OAc, 14.4), 127 (9.2), 101 (32.3), 85 (100), 73 (61.9). ^{1}H NMR ($CDCl_3$) δ=2.07—2.21 (6H, s, Ac), 3.81—4.75 (2H, m, H_4, $H_{4'}$), 5.25—5.60 (2H, m, H_2, H_3), [6.16 (1/2H, s) and 6.45 (1/2H, d, J=4.8 Hz), H_1], 8.15 (1H, s, CHO).

When the irradiated solution from 200 mg of D-galactose was refluxed for 1 h with chlorotrimethylsilane (5 ml) and hexamethyldisilazane (6 ml) being added, an oil (484 mg) was obtained after the purification on a Florisil column. The oil was further separated into two fractions of R_f's 0.7 and 0.6 on a preparative TLC ($CHCl_3$). The former fraction was identical (NMR, GC-MS) with the authentic pentakis-*O*-trimetylsilyl-D-galactose (298 mg, 50% yield). The latter fraction was **7b**, 151 mg, 34% yield. For **7b**: GC-MS, *m/z* (rel intensity) 394 (M^+, 0.26), 305 (2.4), 231 (11.1), 217 (32.9), 204 (100), 191 (89.1). ^{1}H NMR ($CDCl_3$) δ=0.14—0.17 (27H, s, TMS), 3.61 (1H, dd, $J_{2,1}$=4.6 and $J_{2,3}$=3.1 Hz, H_2), 3.65 (1H, dd, $J_{5',4}$=6.3 and $J_{5',5}$=12.0 Hz, $H_{5'}$), 3.85 (1H, dd, $J_{5,4}$=3.5 and $J_{5,5'}$=12.0 Hz, H_5), 3.98 (1H, dd, $J_{3,2}$=3.1 and $J_{3,4}$=6.4 Hz, H_3), 4.86 (1H, d, $J_{1,2}$=4.6 Hz, H_1), 4.95 (1H, ddd, $J_{4,3}$=6.4, $J_{4,5'}$=6.3, $J_{4,5}$=3.5 Hz, H_4). ^{13}C NMR ($CDCl_3$) δ=0.1, 0.5, and 0.6 (TMS), 61.4 (C_5), 70.5 (C_4), 71.5 (C_2), 73.4 (C_3), 95.4 (C_1), 160.1 (CHO). HRMS, Found: *m/z* 394.1573. Calcd for $C_{15}H_{34}O_6Si_3$ (M): 394.1618.

Methyl D-Lyxoside Triacetate (8a). A mixture of **7a** (51 mg, 0.17 mmol) and 12 M HCl (0.1 ml) (1M=1 mol dm^{-3}) in methanol (8 ml) was refluxed for 12 h. The solution was neutralized with dil NaOH and concentrated in vacuo. To the residue was added dry pyridine (5 ml) and acetic anhydride (2 ml), and the mixture was kept at room temperature for 7 h. Pyridine and acetic anhydride were removed in vacuo, and the residue was passed through a column (silica gel/$CHCl_3$) to produce **8a**, 37 mg, 77% yield, identical with the sample prepared from D-lyxose under the same conditions. For **8a**: GC-MS, *m/z* (rel intensity) 259 (M^+ −Me, 2.0), 199 (2.2), 170 (40.7), 128 (100), 115 (38.5). ^{1}H NMR ($CDCl_3$) δ=2.01—2.12 (9H, s, Ac), 3.38 (1H, s, OMe), 3.58—4.09 (2H, m, H_5, $H_{5'}$), 4.69 (1H, d, J=2.2 Hz, H_1), 4.97—5.29 (3H, m, H_2, H_3, H_4).

Iron(III) Triflate-Catalyzed Photoreaction of D-Glucose (1) and D-Galactose (3). Iron(III) triflate was prepared in the following way. Trifluoromethanesulfonic acid (12.3 g, 81.6 mmol) was gradually added to crystals of $Fe(NO_3)_3 \cdot 9H_2O$ (10.0 g, 24.8 mmol), and the mixture was heated to 250 °C in a porcelain vessel placed on a sand bath until the evolution of nitrogen oxides and water was not noticed. The white crystalline material (12.3 g, 99% yield) was allowed to cool in a desiccator, and used without further purification.

The photolyses of D-glucose (5.56 mmol) and D-galactose (5.56 mmol) were carried out using $Fe(OTf)_3$ (0.056 mmol), under the otherwise same conditions described for the $FeCl_3$-catalyzed photoreactions. The products **4** and **7a** were obtained in 32—40% yield and 29—36% yields, respectively.

1,2,3-Tri-*O*-acetyl-D-lyxopyranose (18a) and 1,2,3,-Tri-*O*-acetyl-D-arabinopyranose (17a). To a solution of **7a** (273 mg, 0.9 mmol, α/β=7/3) in a mixture solvent of methanol (20 ml) and water (1 ml) was added $AlCl_3$ (12 mg, 0.09 mmol) gradually, and the solution was stirred for 13 h at room temperature. The solution was concentrated in vacuo, and water (15 ml) was added. The mixture was shaken with dichloromethane, and, after the extract was dried over $MgSO_4$, the solvent was removed in vacuo. When the remaining oil was passed through a short column of Florisil, **18a** (273 mg, 94% yield) was obtained. Referring to the NMR signals of anomeric protons, the product was a mixture of α and β anomers with a ratio of 7 : 3. Purification on a preparative TLC (silica gel/$CHCl_3$-AcOEt (1 : 1)) gave a pure sample of major component, α-**18a**, 152 mg, 61% yield. For α-**18a**: ^{1}H NMR ($CDCl_3$) δ=2.08, 2.12 and 2.15 (9H, s×3, Ac), 2.96 (1H, br d, OH), 3.54—4.26 (3H, m, H_4, H_5, $H_{5'}$), 5.16 (1H, dd, $J_{3,2}$=3,3 and $J_{3,4}$=9.1 Hz, H_3), 5.22 (1H, dd, $J_{2,1}$=2.6 and $J_{2,3}$=3.3 Hz, H_2), 5.96 (1H, d, $J_{1,2}$=2.6 Hz, H_1). ^{13}C NMR ($CDCl_3$) δ=20.6 and 20.8 (Ac-Me), 64.6 (C_5), 65.0 (C_4), 68.4 (C_3), 71.6 (C_2), 90.9 (C_1), 168.5, 169.5 and 179.5 (Ac-CO). HRMS, Found: *m/z* 276.0845. Calcd for $C_{11}H_{16}O_8$ (M): 276.0891.

The hydrolysis of **4** (1.0 g) was carried out under the same conditions as above to afford the product **17a** (0.763 g, 84% yield). The column chromatography (silica gel/$CHCl_3$) gave β-**17a** in pure state, while α-**17a** was not completely freed from β-**17a**. For β-**17a**: ^{1}H NMR ($CDCl_3$) δ=2.08, 2.12 and 2.15 (9H, s×3, Ac), 2.98 (1H, br s, OH), 3.83 (1H, dd, $J_{5',4}$=2.2 and $J_{5',5}$=12.8 Hz, $H_{5'}$), 4.05 (1H dd, $J_{5,4}$=1.1 and $J_{5,5'}$=12.8 Hz, H5), 4.19 (1H, br, H_4), 5.25 (1H, dd, $J_{2,1}$=3.3 and $J_{2,3}$=9.4 Hz, H_2), 5.45 (1H, dd, $J_{3,2}$=9.4 and $J_{3,4}$=3.0 Hz, H_3), 6.31 (1H, d, $J_{1,2}$=3.3 Hz, H_1). ^{13}C NMR ($CDCl_3$) δ=20.55, 20.64 and 20.8 (Ac-Me), 64.6 (C_5), 66.7 (C_4), 67.3 (C_2), 69.6 (C_3), 90.4 (C_1), 169.1, 169.9 and 170.1 (Ac-CO). For α-**17a** (obtained by subtracting the data of β anomer from those of the mixture): ^{1}H NMR ($CDCl_3$) δ=2.06—2.15 (9H, s, Ac), 3.19 (1H, br, OH), 3.65—4.18 (3H, m, H_4, H_5, $H_{5'}$), 5.12—5.58 (2H, m, H_2, H_3), 5.67 (1H, d, J=6.2 Hz, H_1). ^{13}C NMR ($CDCl_3$) 20.62, 20.67 and 20.8 (Ac-Me), 65.2 (C_5), 65.6 (C_4), 68.3 (C_2), 72.0 (C_3), 91.8 (C_1), 169.0, 169.3 and 170.1 (Ac-CO).

1,2,3-Tri-*O*-acetyl-4-*O*-methylsulfonyl-D-lyxopyranose (18c). To a solution of **18a** (373 mg, 1.35 mmol, α/β=75/25) in dry pyridine (15 ml) was added methanesulfonyl chloride (0.4 ml, 5.2 mmol) dropwise with stirring. The reaction mixture was kept overnight at room temperature, and the solvent was removed in vacuo. The excess of the reagent was decomposed by the cautious addition of cooled water (15 ml), and the product was extracted with dichloromethane. After washed with water and dried over $MgSO_4$, the extract was passed through a Florisil column to give white crystals as an anomeric mixture of **18c**, mp 142—147 °C, 391 mg, 82% yield, α/β=8/2. Column chromatography (silica gel/ether) gave a pure sample of α-**18c**, 301 mg, 63% yield. For α-**18c**; mp 145—146 °C. GC-MS, *m/z* (rel intensity) 354 (M^+, 1.1), 295 (5.9), 206 (61.1), 193 (26.2), 181 (55.0), 139 (79.5), 114 (69.1), 68 (100). ^{1}H NMR ($CDCl_3$) δ=2.07 and 2.16 (9H, s×2, Ac), 3.06 (3H, s, $MeSO_2$), 3.74 (1H, dd, $J_{5',4}$=9.1 and $J_{5',5}$=11.1 Hz, $H_{5'}$), 4.13 (1H, dd, $J_{5',4}$=5.5 and $J_{5,5'}$=11.1 Hz, H_5), 4.98 (1H, ddd, $J_{4',3}$=9.2, $J_{4,5}$=5.5 and $J_{4,5'}$=9.1 Hz, H_4), 5.29 (1H, dd, $J_{2,1}$=2.2 Hz and $J_{2,3}$=3.2 Hz, H_2), 5.40 (1H, dd, $J_{3,2}$=3.2 and $J_{3,4}$=9.4 Hz, H_3), 6.01 (1H, d, $J_{1,2}$=2.2 Hz, H_1). ^{13}C NMR ($CDCl_3$) δ=19.8, 19.9 and 21.2 (Ac-Me), 38.2 ($MeSO_2$), 62.0 (C_5), 67.9 (C_2), 68.4 (C_3), 72.3 (C_4), 90.2 (C_1), 167.9, 168.0 and 169.2 (Ac-CO). HRMS,

Found: m/z 295.0482. Calcd for $C_{10}H_{15}O_8S$ (M-OAc): 295.0476.

1,2,3-Tri-*O*-acetyl-4-*O*-*p*-tolylsulfonyl-α-D-lyxopyranose (18b) and 1,2,3-Tri-*O*-acetyl-4-*O*-*p*-tolylsulfonyl-D-arabinopyranose (17b). A mixture of **18a** (276 mg, 1 mmol, α/β=9/1) and *p*-toluensulfonyl chloride (570 mg, 3 mmol) in dry pyridine (12 ml) was heated at 70 °C under a nitrogen atmosphere with stirring for 17 h. The reaction mixture was cooled, and poured slowly into cold water (20 ml). The solution was extracted with dichloromethane, and the extract was washed with water. After dried over $MgSO_4$, the solvent was evaporated in vacuo, and the product **18b** was isolated through a preparative TLC (silica gel/$CHCl_3$), 259 mg, 60% yield. Referring to ^{13}C NMR, the product was pure α-**18b**. For α-**18b**: GC-MS, m/z (rel intensity) 430 (M^+, 0.13), 371 (6.0), 282 (18.0), 269 (11.0), 215 (37.8), 173 (68.7), 155 (100), 91 (100). ^1H NMR ($CDCl_3$), δ=1.90—2.12 (9H, s, Ac-Me), 3.66—4.09 (2H, m, H_5, $H_{5'}$), 4.79—5.09 (1H, m. H_4), 5.13—5.35 (2H, m, H_2, H_3), 5.93 (1H, d, J=2.3 Hz, H_1), 7.36 and 7.80 (4H, ABq, J=8.3 Hz, Ar), 2.44 (3H, s, Ar-Me). ^{13}C NMR ($CDCl_3$) δ=21.5 (Ar-Me), 61.9 (C_5), 67.6 (C_2), 68.4 (C_3), 72.5 (C_4), 90.2 (C_1), 127.7, 129.8, 133.3, 145.1 (Ar), 169.2 and 169.5 (Ac-CO). HRMS, Found: m/z 430.0956. Calcd for $C_{18}H_{22}O_{16}S$ (M): 430.0934.

In the same way, tosylation of **17a** (172 mg, α/β=1/1) was carried out to give the product **17b** (149 mg, 56% yield) after the chromatograph on a silica gel column (ether). Referring to the NMR signals of anomeric protons, the product was an anomeric mixture (α/β=6/4). For **17b**: GC-MS, m/z (rel intensity) 371 (M^+ −OAc, 5.0), 269 (19.8), 215 (64.7), 172 (47.0), 155 (100), 91 (95.7). ^1H NMR ($CDCl_3$) δ=1.95—2.11 (9H, s, Ac), 2.45 (3H, s, Ar-Me), 3.53—4.11 (2H, m, H_5, $H_{5'}$), 4.90—5.31 (3H, m, H_2, H_3, H_4), 5.62 (3/5H, d, J=6.6 Hz, H_1 of α anomer), 6.31 (2/5H, d, J=3.2 Hz, H_1 of α anomer), 7.35 and 7.80 (4H, ABq, J=8.3 Hz, Ar). ^{13}C NMR ($CDCl_3$) δ=20.3—20.7 (Ac-Me), 62.6 and 63.5 (C_5), 66.2 and 66.7 (C_2), 67.6 and 69.5 (C_3), 73.2 and 75.1 (C_4), 89.9 and 91.7 (C_1) 127.6—145.1 (Ar), 168.6—170.2 (Ac-CO). Found: C, 50.30; H, 5.16%. Calcd for $C_{18}H_{22}O_{16}S$: C, 50.22; H, 5.15%.

1,2-Di-*O*-acetyl-3,4-anhydro-β-L-ribopyranose (19). To a solution of **18b** (α/β=9/1, 101 mg, 0.23 mmol) in methanol (10 ml) was added a methanol solution of NaOMe (0.35 M, 2 ml) dropwise at 0 °C with stirring. After being neutralized with dil HCl, the solution was concentrated to dryness in vacuo. The residue was treated with acetic anhydride (2 ml) and dry pyridine (5 ml), and the solution was concentrated in vacuo. The product was extracted with $CHCl_3$, and the extract was dried over $MgSO_4$. After evaporating the solvent, the product β-**19** was isolated on a preparative TLC (silica gel/ether) in 53% yield 27 mg. For β-**19**: IR (neat) ν_{max} 1740 (acetate), 1240, 895, and 835 (oxirane). GC-MS, m/z (rel intensity) 157 (M^+ −OAc, 12.7), 128 (14.1), 115 (100), 97 (10.2), 89 (39.1), 73 (48.1). ^1H NMR ($CDCl_3$) δ=2.10 and 2.16 (6H, s×2, Ac), 3.31—3.46 (1H, m, H_4), 3.63 (1H, dd, $J_{3,2}$=3.4 and $J_{3,4}$=4.5 Hz, H_3), 4.25 and 4.30 (2H, ABq, H_5, $H_{5'}$),4.97 (1H, dd, $J_{2,1}$=4.5 and $J_{2,3}$=3.4 Hz, H_2), 5.77 (1H, d, $J_{1,2}$=4.5 Hz, H_1). ^{13}C NMR ($CDCl_3$) δ=50.1 and 51.4 (oxirane), 60.7 (C_5), 67.6 (C_2), 89.7 (C_1).

Iron(III) Chloride-Catalyzed Photoreaction of D-Fructose (10). The photoreaction of D-fructose (1.1 g, 6.1 mmol) was carried out under the same conditions as described for D-glucose except shortening the irradiation time to 5 h. After treating with acetic anhydride (15 ml, 159 mmol) the crude sample was distilled to give **11a** as an oil, bp 150—153 °C (0.6 mmHg) 870 mg, 52% yield. The following spectroscopic data were very close to those of γ-ribonolactone triacetate.[7] For **11a**: IR (neat) ν_{max} 1796 (γ-lactone), 1738 cm^{-1} (acetate). GC-MS m/z (rel intensity) 275 (M^+ +1, 13.8), 232 (10.4), 201 (14.0), 172 (23.8), 154 (48.0), 128 (100), 115 (96.0), 100 (80.6), 86 (79.3). ^1H NMR ($CDCl_3$) δ=2.03—2.17 (9H, s×3 Ac), 4.31 (1H, dd, $J_{5',4}$=3.6 and $J_{5',5}$=8.5 Hz, $H_{5'}$), 4.48 (1H, dd, $J_{5,4}$=3.8 and $J_{5,5'}$=8.5 Hz, H_5), 4.60 (1H, ddd, $J_{4,3}$=0.9, $J_{4,5}$=3.8 and $J_{4,5'}$=3.6 Hz, H_4), 5.39 (1H, d, $J_{2,3}$=4.9 Hz, H_2), 5.61 (1H, dd, $J_{3,2}$=4.9 and $J_{3,4}$=0.9 Hz, H_3). ^{13}C NMR ($CDCl_3$) δ=20.3, 20.5 and 20.7 (Ac-Me), 62.2 (C_5), 72.4 and 72.7 (C_2, C_3), 77.5 (C_4) 170.2 (C_1), 168.3, 169.4 and 169.9 (Ac-CO).

Iron(III) Chloride-Catalyzed Thermal Reaction of D-Fructose(10) and D-Glucose (1). A pyridine solution (50 ml) of **10** (500 mg, 2.8 mmol) and $FeCl_3 \cdot 6H_2O$ (750 mg, 2.8 mmol) was stirred for 24 h at room temperature while oxygen gas was bubbled through. The solution was treated with acetic anhydride and worked up in the same way as described for the photoreaction. The product **11a** was obtained through a column chromatography (silica gel/$CHCl_3$) 380 mg, 50% yield.

The thermal reaction of **1** (1.2 g, 6.7 mmol) was performed by refluxing the same pyridine solution as that used for the photoreaction. Treatment with acetic anhydride gave an oil (635 mg), which showed two peaks on a GLC analysis with relative ratio of 6:4. The major component was isolated through a column chromatography (silica gel/hexane-ethyl acetate (1 : 1)), and was shown to be identical (GC-MS, NMR, IR) with **11a** (289 mg, 13% yield). Although the other component was not completely freed from **11a**, it was identified as **11b** from the following spectroscopic data obtained by subtracting the data of **11a** from those of the mixture. For **11b**: IR (neat) ν_{max} 1799 (γ-lactone), 1740 and 1736 cm^{-1} (esters). GC-MS: m/z (rel intensity) 261 (M^+ +1, 9.7), 218 (11.9), 201 (16.3), 128 (100), 99 (57.4), 69 (76.9). ^1H NMR ($CDCl_3$) δ=2.02—2.12 (6H, s, Ac), 4.09—4.44 (3H, m, H_4, H_5), 5.09—5.59 (2H, m, H_2, H_3), 8.10 (1H, s, CHO).

Iron(III) Chloride-Catalyzed Photoreaction of D-Arabinose (6). The photoreaction of D-arabinose (**6**, 1.28 g, 8.5 mmol) and the subsequent acetylation was performed in the same way as described for D-glucose (**1**). The crude product gave two fractions by distillation. The lower boiling fraction, bp 135—140 °C (0.15 mmHg), 98 mg, 5% yield, was **15b**. For **15b**: GC-MS, m/z (rel intensity) 173 (M^+ −OAc, 11.7), 127 (20.9), 101 (29.6), 85 (100). ^1H NMR ($CDCl_3$) δ=1.95—2.20 (6H, s, Ac), 3.81—4.52 (2H, m, H_4, $H_{4'}$), 5.05—5.70 (2H, m, H_2, H_3), 5.72 (1/3H, s, H_1 of β anomer),6.05 (2/3H, d, J=2.1 Hz, H_1 of α anomer), 7.70 and 7.95 (1H, s×2, CHO).

The higher boiling fraction, bp 148—152 °C (0.15 mmHg), was identified as D-arabinose tetraacetate (**5b**, 1.7 g, 63% yield) by comparing the NMR and mass spectra with those of the authentic sample.

References

1) Preliminary report: S. Ichikawa and T. Sato, *Tetrahedron Lett.*, **27**, 45 (1986); S. Ichikawa and T. Sato, *Yuki Gosei Kagaku Kyokai Shi*, **44**, 1047 (1986).

2) Preceding Paper, and references cited therein.

3) E. Murayama and T. Sato, *Tetrahedron Lett.*, **1977**, 4079; E. Murayama, A. Kohda, and T. Sato, *Chem Lett.*, **1978**, 161; E. Murayama and T. Sato, *Bull. Chem. Soc.*

Jpn., **51**, 3022 (1978); E. Murayama, A. Kohda, and T. Sato, *J. Chem. Soc., Perkin Trans. 1*, **1980**, 947; A. Kohda, K. Ueda, and T. Sato, *J. Org. Chem.*, **46**, 509 (1981); A. Kohda, and T. Sato, *J. Chem. Soc., Chem. Commum.*, **1981**, 951; T. Sato, K. Maemoto, and A. Kohda, *J. Chem. Soc., Chem. Commun.*, **1981**, 1116; T. Sato, T. Tonegawa, K. Naoi, and E. Murayama, *Bull. Chem. Soc. Jpn.*, **56**, 285 (1983); A. Kohda, K. Nagayoshi, K. Maemoto, and T. Sato, *J. Org. Chem.*, **48**, 425 (1983); T. Sato, T. Oikawa, K. Kobayashi, *J. Org. Chem.*, **50**, 1646 (1985).

4) D. C. DeJongh and K. Biemann *J. Am. Chem. Soc.*, **85**, 2289 (1963).

5) P. L. Durette and D. Horton, *J. Org. Chem.*, **36**, 2658 (1971).

6) K. Biemann, D. C. DeJongh, and H. K. Schnoes, *J. Am. Chem. Soc.*, **85**, 1763 (1963).

7) G. B. Robbins and F. W. Upson, *J. Am. Chem. Soc.*, **62**, 1074 (1940).

8) G. O. Phillips and G. J. Moody, *J. Chem. Soc.*, **1960**, 3398.

9) A. S. Perlin, *Adv. Carbohydr. Chem.*, **14**, 9 (1959).

10) A. S. Perlin, *Can. J. Chem.*, **42**, 2365 (1964).

11) K. Araki, M. Sakuma, and S. Shiraishi, *Bull. Chem. Soc. Jpn.*, **57**, 997 (1984); K. Araki, and S. Shiraishi, *Bull. Chem. Soc. Jpn.*, **59**, 229 (1986).

12) J. Fajer and H. Linschitz, *J. Inorg. Nucl. Chem.*, **30**, 2263 (1968).

13) C. S. Hudson and J. K. Dale, *J. Am. Chem. Soc.*, **40**, 992 (1918).

14) H. Zinner and H. Brandner, *Chem. Ber.*, **89**, 1507 (1956).

15) E. E. Lee and J. O. Wood, *Carbohydr. Res.*, **89**, 329 (1981).

16) A. S. Perlin, B. Casu, and H. J. Koch, *Can. J. Chem.*, **48**, 2596 (1970).

17) M. L. Wolform and A. Thompson, *Method in Carbohydr. Chem.*, **2**, 211 (1963).

Hydrogen Separation Using $LaNi_5$ Films Deposited on Polymer Membranes

Hiroki SAKAGUCHI, Gin-ya ADACHI,* and Jiro SHIOKAWA
Department of Applied Chemistry, Faculty of Engineering, Osaka University, Yamadaoka, Suita, Osaka 565
(Received July 27, 1987)

Hydrogen separation has been investigated using $LaNi_5$ films deposited by means of a sputtering method on a nickel-coated Teflon or on a nickel-coated polyimide membrane. Separation factors were estimated for an H_2(50 mol%)-Ar(50 mol%) gas mixture. The permeation rate of the Ni/$LaNi_5$ multilayered film was found to be larger than that of the Ni film. Hydrogen was concentrated to as high as 97.6 mol% under the best conditions.

Hydrogen separation has been studied using films of polymers, porous glasses, and metals.[1] A palladium film is known to exhibit excellent properties for hydrogen separation.[2] The film is, however, very expensive and must be operated at an elevated temperature. The use of a cheaper metal or an alloy instead of palladium would be advantageous for the hydrogen industries. $LaNi_5$ is considered to be a good candidate as a hydrogen separation material[3] because it is less expensive than Pd and has an admirable ability to absorb hydrogen at moderate temperatures and pressures. Some $LaNi_5$ films have been prepared by means of a flash evaporation[4-6] and of a sputtering method and have been investigated with respect to the hydrogen content in the films[7] and mechanical properties.[8] One of its most remarkable characteristics is that these films do not pulverize after more than 100 cycles of the hydrogen absorption-desorption process.

This finding led us to explore the possibility of hydrogen separation using the films.[9] We have previously reported the hydrogen-separation characteristics of the films deposited on a porous metal filter.[10]

In the present study, polymer membranes were used as a substrate on which the $LaNi_5$ layer was formed, and the hydrogen-separation capability for the $LaNi_5$-deposited polymer separator was investigated.

Experimental

Preparation of Films. The $LaNi_5$ ingot was supplied by the Santoku Metal Industry Co., Ltd., Kobe. The substrates were two kinds of polymer membranes, Teflon (Toyofuron, 25 μm thick, Toray Co., Ltd.) and polyimide (Kapton, 40 μm thick, Toray-Du Pont Co., Ltd.). These substrates were cleaned in an ultrasonic washing machine filled with acetone.

The metal layers were deposited with an r.f. magnetron sputtering apparatus made by the Daia Vacuum Engineering Co., Ltd., from an Ni or an $LaNi_5$ target. The r.f. generating power applied was 400 W, and the substrate temperature was in the range of 300—373 K. The atmosphere used for the discharge was 99.99%-pure argon at a pressure of 0.395 Pa. The $LaCo_5$ films were prepared by means of a flash evaporating method which has been described in previous papers.[4-6]

Measurement of Properties. A disk membrane 10 mm in diameter was inserted in a separation apparatus as is shown in Fig. 1. The stainless steel filter (Tokyo Seikoh Co., Ltd.) was used as a support for the film against the pressure.

An H_2 (50 mol%)-Ar (50 mol%) gas mixture with a pressure of 1.5×10^5 Pa at 368 K was applied to the $LaNi_5$-deposited side of the membrane. The gas passed through the film was collected in gas samplers at the outlet. The permeation rate was measured from the pressure variation, and the composition of the resulting gas was analyzed using a Hitachi RMU-6E mass spectrometer.

Results and Discussion

Structures of the Films. Figure 2 illustrates the structures of the films used for the experiments. Since the mechanical strength and the durability of the sputtered films were greater than those of the evaporated ones, the metal films were mainly prepared using a sputtering method.

Film b is an $LaNi_5$ film directly deposited on a

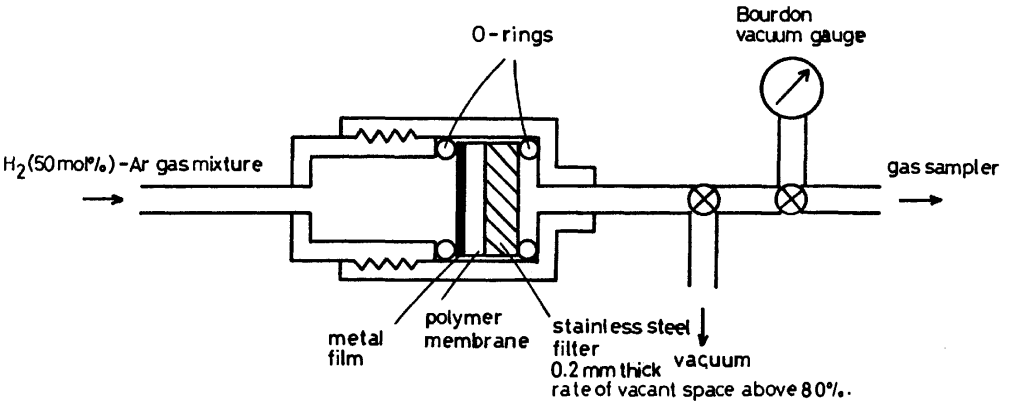

Fig. 1. Apparatus for gas separation.

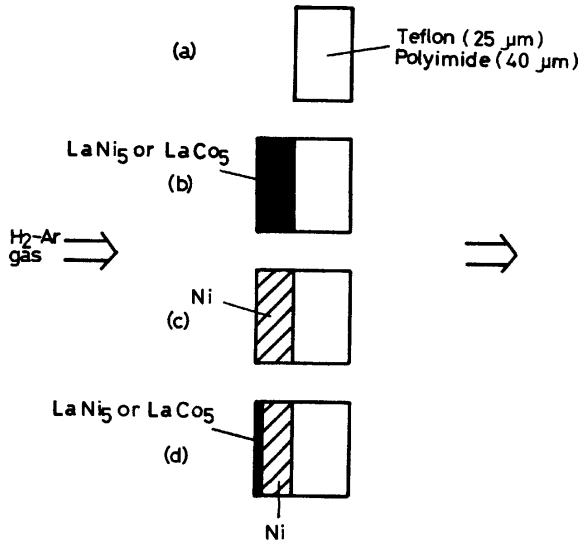

Fig. 2. Structure of films.

Teflon or on a polyimide membrane. The thickness of the metal layer was 0.75 μm. For film d, nickel was first deposited on the substrates (0.73, 1.23, or 1.48 μm thick). The nickel layer was to reinforce the durability of the films. Subsequently, $LaNi_5$ was deposited on the nickel layer. Films a and c were for blank tests.

Performance Characteristics of the Films. Nickel films with various thicknesses deposited on the Teflon membranes were prepared, and the effects of the thickness of the metal layer on the hydrogen separation were studied. As is shown in Fig. 3, for a 0.5 μm-thick film the hydrogen concentration in the permeated gas was slightly larger than that for the Teflon-only membrane. It seems probable that most of the gas mixture passed through pinholes in the nickel film. However, for a 0.75 μm-thick film the hydrogen concentration increased remarkably. It can be considered that, above thickness of 0.75 μm, the Teflon membrane was almost

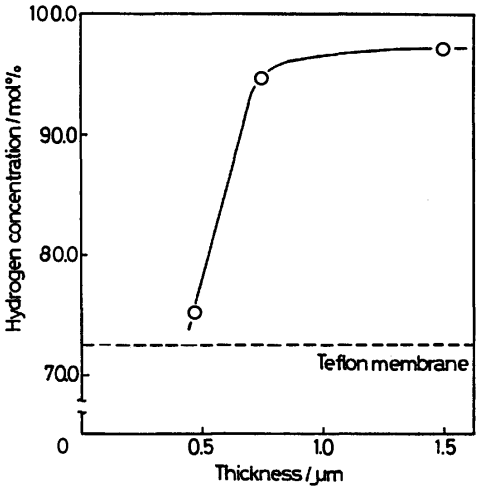

Fig. 3. Effects of thickness of nickel layer on hydrogen concentration in permeated gas.

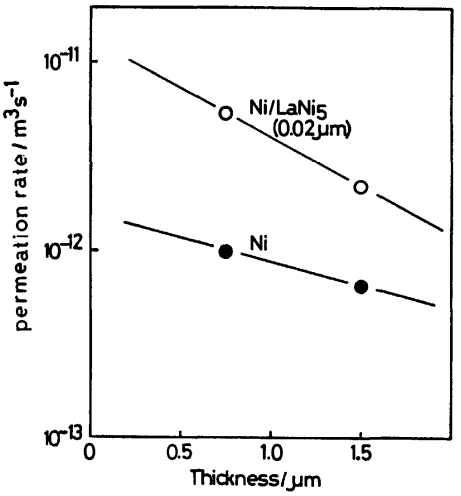

Fig. 4. Relationship between permeation rate and thickness of metal layer.

Table 1. Performance Characteristics of $LaNi_5$ and $LaCo_5$ Films Deposited on the Teflon Membrane

Gas composition / mol%	Film composition	Permeation rate / $m^3s^{-1}\times10^{-12}$	Permeability coefficient / $m^2s^{-1}Pa^{-1/2}\times10^{-16}$ a)	Hydrogen content after treatment / mol%	Separation factor
Ar(50)-H_2(50)	Teflon (T) (25 μm)	43	2400	74.8	2.97
	0.75 μm				
	T/$LaNi_5$	5.3	5.7	89.5	8.52
	T/Ni	0.99	1.1	94.7	17.9
	T/Ni/$LaNi_5$ (0.02 μm)	5.4	6.3	91.9	11.3
	T/$LaCo_5$	<0.5	<0.5	75.2	3.03
	1.50 μm				
	T/Ni	0.55	1.2	97.2	34.7
	T/Ni/$LaNi_5$ (0.02 μm)	2.2	5.1	91.0	10.1
	1.31 μm				
	T/Ni/$LaCo_5$ (0.08 μm)	<0.5	<1.0	83.1	4.92

Primary pressure: 1.5×10^5 Pa; temperature of film, 368 K, a) Units $m^2s^{-1}Pa^{-1/2}$ is derived from (volume of permeated gas (STP))×(thickness of the sample)×(surface area of the sample)$^{-1}$ ×(the time required for permeation)$^{-1}$×(difference in pressure)$^{-1}$.

Table 2. Performance Characteristics of $LaNi_5$ and $LaCo_5$ Films Deposited on the Polyimide Membrane

Gas composition mol%	Film composition	Permeation rate $m^3s^{-1}\times10^{-12}$	Permeability coefficient $m^2s^{-1}Pa^{-1/2}\times10^{-16}$	Hydrogen content after treatment mol%	Separation factor
Ar(50)-H_2(50)	Polyimide (I) (40 μm)	3.1	188	95.2	19.8
	1.25 μm				
	I/Ni	2.1	3.8	96.6	28.4
	I/Ni/$LaNi_5$ (0.02 μm)	2.7	5.0	97.6	40.7
	1.31 μm				
	I/Ni/$LaCo_5$ (0.08 μm)	<0.5	<1.0	95.1	19.4

Primary pressure: 1.5×10^5 Pa; temperature of film, 368 K.

Table 3. Estimation of $LaNi_5$ Films Deposited on the Polymer Membrane for Hydrogen Separation

	Thickness of the metal layer μm	Permeation rate	Hydrogen-separation factor
Pd	100—200	1	Above 66
Metal filter substrate	50	$1/10^2$	2.25—20.6
Polymer substrate	1	$1/10^3$	10—40

completely covered with the nickel film and that the hydrogen applied permeated through the nickel layer.

Table 1 shows the hydrogen-separation ability of the $LaNi_5$ films deposited on the Teflon membrane. A gas of 50 mol% H_2 was found to be concentrated to 74.8 mol% by the use of the Teflon membrane alone. When the metal films were deposited on the Teflon, the hydrogen concentration increased greatly. It was found that the permeation rate of the $LaNi_5$ film was several times as large as that of the Ni film, though the hydrogen concentration for the $LaNi_5$ film was slightly lower than that for the Ni film. There were no differences in characteristics for the permeation rate and the separation factor between the $LaNi_5$ film and the Ni/$LaNi_5$ multilayered film. The nickel film is able to permeate hydrogen easily because the thin $LaNi_5$ film coated on the nickel surface dissociates the hydrogen molecule easily and absorbs much hydrogen. Figure 4 shows the relationship between the permeation rate and the thickness of the metal layer and also the effects of the $LaNi_5$ layer on the hydrogen permeation of the Ni film. The permeation rate decreased with the increase in the thickness of the metal layer. Also, for the 1.5 μm-thick film, the permeation rate for the Ni/$LaNi_5$ multilayered film was larger than that for the Ni film.

Table 2 shows the hydrogen separation characteristics of the $LaNi_5$ film deposited on the polyimide membrane. The polyimide membrane itself exhibited a high hydrogen-separation factor. The highest separation factor was obtained for the Ni/$LaNi_5$ multilayered film. The reason why the separation capability of the Ni/$LaNi_5$ film is excellent seems to be that the adhesion between the polyimide membrane and the metal film was superior to that between the Teflon membrane and the metal film.

An $LaCo_5$ film is not suited for the hydrogen separator because the mass of the permeated gas obtained from the films deposited on both the Teflon and polyimide membranes was extremely small and these separation factors were not so good (Tables 1 and 2). This seems to be caused by the small hydrogen concentration in the $LaCo_5$ film.[1)]

In Table 3, the characteristics of the $LaNi_5$ film using the polymer as a substrate for the hydrogen separation are compared with those of the $LaNi_5$ film deposited on a porous stainless steel filter as well as those of a Pd film.[2,12)] As for the thickness of the metal layer, high-purity hydrogen gas was obtained with a $LaNi_5$ film only 1 μm thick for the polymer-substrate sample. The permeation rate for the $LaNi_5$ film coated on the polymer is very low, but this is not a serious problem, because for the polymer membrane it is easy to increase the area of the gas contact surface. For instance, if a hollow fiber on which the metal layer is formed is bundled, a large surface area can be obtained.

The $LaNi_5$ films deposited on the nickel-coated polymer substrate are relatively cheap and easy to prepare.

References

1) T. Sakai, H. Ishikawa, N. Wakabayashi, K. Oguro, and E. Ishii, *Osaka Kohgyo Shikenjyo Kihoh*, **35**, 60 (1984).

2) Y. Osumi, *Soda to Enso*, **11**, 466 (1984).

3) T. Gamo, Y. Moriwaki, N. Yanagihara, and T. Iwaki, *J. Less-Common Met.*, **89**, 495 (1983).

4) G. Adachi, K. Niki, and J. Shiokawa, *J. Less-Common Met.*, **81**, 345 (1981).

5) G. Adachi, K. Niki, H. Nagai, and J. Shiokawa, *J. Less-Common Met.*, **88**, 213 (1982).

6) G. Adachi, H. Sakaguchi, K. Niki, H. Nagai, and J.

Shiokawa, *J. Less-Common Met.*, **108**, 107 (1985).
7) H. Sakaguchi, N. Taniguchi, G. Adachi, and J. Shiokawa, *J. Phys. Chem.*, **89**, 5550 (1984).
8) H. Sakaguchi, N. Taniguchi, H. Seri, G. Adachi, and J. Shiokawa, *Nippon Kagaku Kaishi*, **1987**, 1875.
9) G. Adachi, H. Nagai, and J. Shiokawa, *J. Less-Common Met.*, **97**, L9 (1984).
10) H. Sakaguchi, H. Nagai, G. Adachi, and J. Shiokawa, *J. Less-Common Met.*, **126**, 83 (1986).
11) H. Sakaguchi, Y. Yagi, N. Taniguchi, G. Adachi, and J. Shiokawa, *J. Less-Common Met.*, **135**, 137 (1987).
12) M. Taguma, M. Tada, and T. C. Huang, *Proc. Fac. Eng. Tokai Univ.*, **1**, 53 (1969).

 © 1988 The Chemical Society of Japan Bull. Chem. Soc. Jpn., 61, 525—531 (1988)

Optical Isomer Effect on the Mechanochemical Interaction of Mandelic Acid with Talc Powder

Akiko IKEKAWA* and Sohachiro HAYAKAWA†

Faculty of Pharmaceutical Sciences, Showa University, Hatanodai, 1-5-8, Shinagawa-ku, Tokyo 142

†Laboratory of Applied Physics, Faculty of Engineering, Chiba University, Yayoi-cho 1-33, Chiba 260

(Received June 20, 1987)

Mandelic acid was ball-milled with talc powder, and the optical isomer effect on the IR spectral change was investigated. The change showed that a complex was formed between talc and the hydroxyl group and the COOH group of mandelic acid. It was also shown that the covalent character in the bond of the C=O group with talc was greater for (*RS*)-mandelic acid than for the R-isomer and the S-isomer. The change in the region of the carbonyl-stretching vibration was affected by the humidity in the ball-milling atmosphere, and the effect on the R-isomer was greater than the effect on the S-isomer. Magnesium mandelate powder was obtained from an ethanolic suspension of the ball-milled mixture with talc. The IR spectra and the elemental analysis showed that the C=O group was covalently bonded to Mg in the complex of the (RS)-compound and that it was ionically bonded in the complex of the R-isomer and the S-isomer. The thermal analysis showed that the decomposition temperature for the complex of the R-isomer was different from the temperature for the complex of the S-isomer. It was suggested that talc powder had a chiral surface when it was mechanically treated.

The optical isomer effect on a chemical reaction is of great interest with regard to the origin of life. Furthermore, it is of practical importance in pharmaceutics. Kwan et al. reported that (S)-(+)-mandelic acid was adsorbed on starch from an aqueous solution of the racemate preferentially over the (R)-(−)-isomer.[1] According to Nagwekar and Kastenbauder, the rate constant for the metabolism of the S-isomer in the human body was approximately twice the rate for the R-isomer.[2]

Previously, the authors reported the optical isomer effect on the racemization of mandelic acid at the surface of talc powder.[3] This paper will deal with the interaction of optically active and racemic mandelic acids with talc powder upon mechanical treatment.

Experimental

The materials used were (*S*)-(+)-mandelic acid [(*S*)-(+)-α-hydroxyphenylacetic acid] and (*R*)-(−)-mandelic acid purchased from the Aldrich Chemical Co, and (*RS*)-mandelic acid (guaranteed-grade), talc, and magnesium oxide (heavy, guaranteed-grade) of Wako Pure Chemicals Industries, Ltd. The ethanol, 2-propanol, 2-butanol, and formic acid were of a guaranteed grade. A 10-g portion of a mixture of mandelic acid with talc or a mixture with MgO was inserted into a stainless-steel mill (10 cm in diameter and with a capacity of 900 cm^3) containing ten stainless-steel balls (with a density of 8.2 $g\,cm^{-3}$ and a diameter of 2.5 cm) and thirty balls 1.9 cm in diameter. The mill was rotated at a velocity of 95 rpm. This procedure will be called "ball-milling" hereafter. The ball-milling was carried out between December and February with a relative humidity of 45—55% or in June and July with a relative humidity of 75—85%. The ball-milled samples were kept in a desiccator containing silica gel.

Various samples were prepared from a mixture of talc containing 10 w/w% of mandelic acid, which had been ball-milled under a relative humidity of 45—55% for 10 h. A suspension of 1.6 g of this mixture in 80 ml of ethanol was stirred at 5 °C for 1 h at a velocity of 380 rpm. It was then centrifuged, and the supernatant, A, was evaporated to dryness at 60 °C under reduced pressure. The powder thus obtained, A′, was weighed, and then 3 ml of ethanol was added to this. This suspension was set aside at 5 °C for 1 h after having been shaken vigorously; a supernatant, B, and a precipitate, C, were obtained by centrifuging. The precipitate C was washed twice with ethanol, dried at 60 °C, and weighed (powder C). Powder C was washed with ethanol eight more times and then dried at 60 °C (powder C′). The supernatant B and the powders, A′, C, and C′, obtained from mixtures of the (RS)-compound and the R-isomer or the S-isomer are, respectively, expressed by B_{RS}, B_R, B_S, A'_{RS}, A'_R, A'_S, C_{RS}, C_R, C_S, C'_{RS}, C'_R, and C'_S. The powders M-Mg and M-Mg′ were prepared as follows. A suspension of MgO in an ethanolic solution of (*RS*)-mandelic acid was set aside for several hours at 60 °C in order to prepare the M-Mg powder and at 5 °C in order to prepare the M-Mg′ powder. These suspensions were then centrifuged, and the precipitates were washed with ethanol several times and dried at 60 °C. These samples were kept in a desiccator containing silica gel.

The IR spectra were measured with a JASCO infrared spectrophotometer (Model 810). The absorption spectra were measured with a Hitachi recording spectrophotometer (Model 340). The optical rotation of the solutions was measured with a JASCO digital polarimeter. The DTA and TG measurements were carried out using a thermal analyser (Model DT-20B and TG-30) of Shimadzu Seisakusho. The supernatant B was developed on a thin layer of silica gel with a solvent system of 2-butanol-2-propanol-formic acid-water (15 : 15 : 4 : 10).[4]

Results and Discussion

IR Spectra. Figures 1 and 2 show the IR spectra of the ball-milled mixtures of mandelic acid and talc. The absorbances around 3400—3420 cm^{-1} and at 1700—1730 cm^{-1} decreased, while new peaks appeared in the 1600—1650 cm^{-1} region, on ball-milling. Under the relative humidity of 75—85%, new peaks appeared at 1610, 1630, and 1650 cm^{-1}, and the absorbance at 1650 cm^{-1} increased remarkably, at the first stage of ball-milling in the case of (*RS*)-mandelic acid. On the ball-milling of the mixture of the R-isomer or

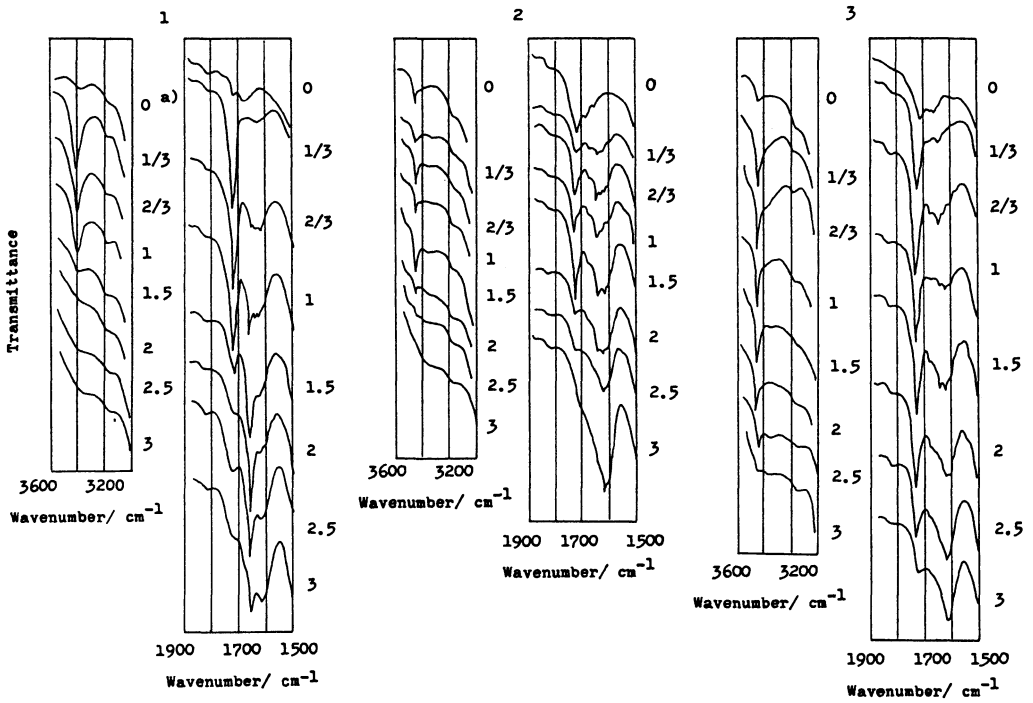

Fig. 1. Change in the IR spectra of mandelic acid upon ball-milling with talc in the atmosphere of high humidity. 1 (*RS*)-mandelic acid, 2 (*R*)-(−)-mandelic acid, 3 (*S*)-(+)-mandelic acid. Ball-milling conditions; the content of mandelic acid 10 w/w%, relative humidity 75—85%. a) Ball-milling time/h.

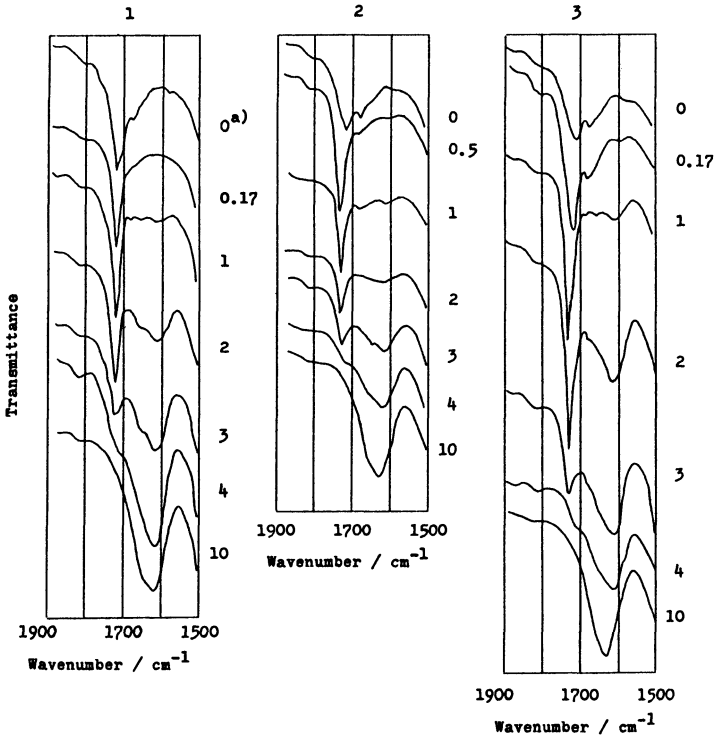

Fig. 2. Change in the IR spectra of mandelic acid upon ball-milling with talc in the atmosphere of low humidity. 1 (*RS*)-mandelic acid, 2 (*R*)-(−)-mandelic acid, 3 (*S*)-(+)-mandelic acid. Ball-milling conditions; the content of mandelic acid 10 w/w%, relative humidity 45—55%. a) Ball-milling time/h.

S-isomer, new peaks appeared at 1600, 1620, and 1640 cm^{-1}. These changes were greater for the R-isomer than those for the S-isomer at the first stage. Under the relative humidity of 45—55%, a new peak also appeared at 1650 cm^{-1} upon the ball-milling of a mixture containing 30 w/w% of the (RS)-compound. However a broad absorption band appeared at 1600—1700 cm^{-1} in the other mixtures, and the optical isomer effect was slight. Figure 3 shows the IR spectra of the ball-milled mixtures in the region between 1200 and 1800 cm^{-1}. In the spectra of the mixtures of the (RS)-compound, the absorbance at 1350 cm^{-1} was high and the absorbance at 1410 cm^{-1} was low when the absorbance at 1650 cm^{-1} was high and the absorbance at 1600—1620 cm^{-1} was low. In the spectra of a mixture of the R-isomer or the S-isomer, the absorbance at 1390 cm^{-1} was high and the absorbance at 1410—1430 cm^{-1} was low when the absorbance at 1640 cm^{-1} was high and the absorbance at 1600—1620 cm^{-1} was low. According to Khadikar et al.,[5] the absorption band of the hydroxyl group is around 3260 cm^{-1} and the COO^- band is around 1600 cm^{-1} in the spectra of the complex of mandelic acid and a bivalent metal ion. It is clear from the above results that a complex is formed between talc and the hydroxyl group and the carboxyl group of mandelic acid. The IR spectra of the complexes of α-hydroxy carboxylic acids, amino acids, or EDTA with such metals as Cu, Ni, and Co have been reported by many workers, and the following facts have been confirmed.[6] When the metal–carboxylato bond is ionic, the asymmetric stretching vibration of the C=O group is in the 1550—1600 cm^{-1} region, and an increase in the frequency occurs with an increase in the covalent character. When the bond is covalent, the band is found at 1650 cm^{-1}. The symmetric stretching vibration of the C=O group for the ionic bond is at 1400—1410 cm^{-1}, and the band shifts to a lower frequency with the increase in the covalent character. It is clear from the above facts that the band at 1640—1650 cm^{-1} is due to the C=O group bonded to talc highly covalently and that the band at 1600—1610 cm^{-1} is due to the C=O group bonded with talc highly ionically. It may also be concluded that the C=O group of the (RS)-compound is more highly covalently bonded with talc than that of the R-isomer or the S-isomer.

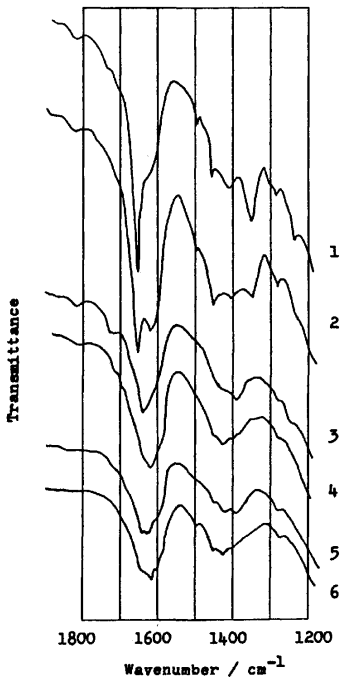

Fig. 3. Change in the symmetric and asymmetric stretching vibrations of the carbonyl group of mandelic acid upon ball-milling with talc.

	The type of mandelic acid	Ball-milling time/h
1	RS	1
2	RS	3
3	R	1
4	R	2.5
5	S	1.5
6	S	2.5

Ball-milling conditions; the content of mandelic acid 10 w/w%, relative humidity 75—85%.

The area surrounded by a straight line, passing through the transmittance at 1780 cm^{-1} and at 1550 cm^{-1}, and the transmittance-wavenumber curve was divided into five parts at the wavenumbers of 1620, 1640, 1660, and 1690 cm^{-1} for the (RS)-compound, and at the wavenumbers of 1610, 1630, 1660, and 1700 cm^{-1} for the R-isomer and the S-isomer. Only the four parts except the part between 1660—w cm^{-1} were discussed, where w is 1690 for the (RS)-compound and 1700 for the R-isomer and the S-isomer. S_Z and S_Z' (Z=I, II, III, or IV) stand for the ratios of the area of each part to the total area for the (RS)-compound and for the R-isomer or the S-isomer respectively, where the wavenumber of part z, ν_z, is in the order of $\nu_I \geqslant \nu_{II} \geqslant \nu_{III} \geqslant \nu_{IV}$. As is

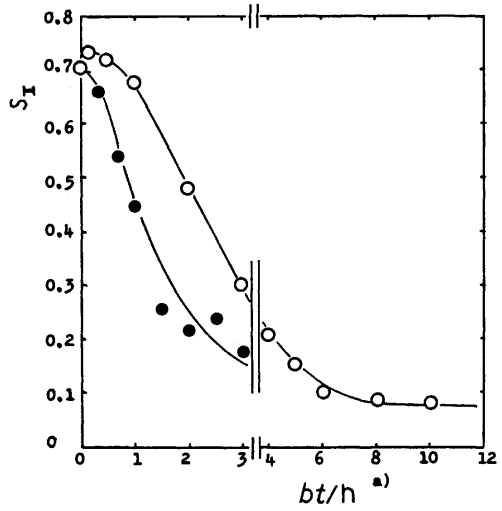

Fig. 4. Variation in S_I with ball-milling. Ball-milling conditions: the content of (*RS*)-mandelic acid 10 w/w%, relative humidity; 45—55% ○, 75—85% ●. a) *bt* is the ball-milling time.

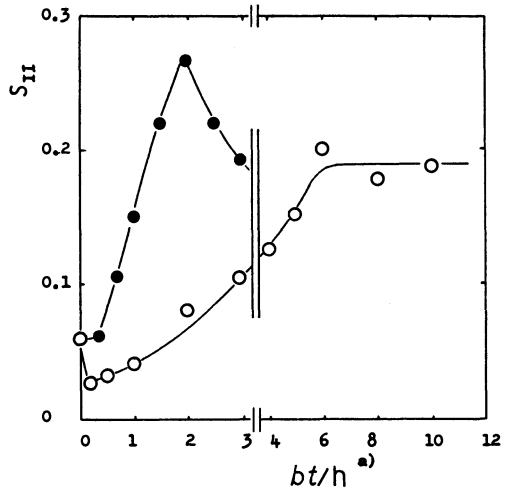

Fig. 5. Variation in S_{II} with ball-milling. Ball-milling conditions: the content of (*RS*)-mandelic acid 10 w/w%, relative humidity; 45—55% ○, 75—85% ●. a) *bt* is the ball-milling time.

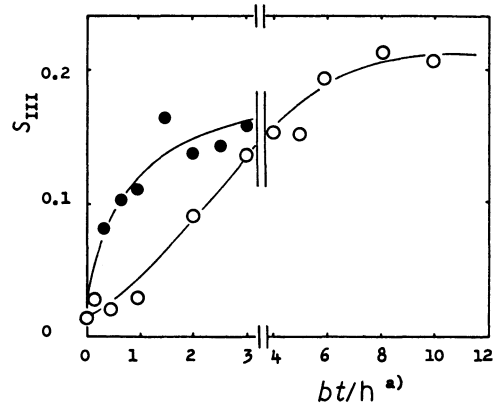

Fig. 6. Variation in S_{III} with ball-milling. Ball-milling conditions: the content of (*RS*)-mandelic acid 10 w/w%, relative humidity; 45—55% ○, 75—85% ● a) *bt* is the ball-milling time.

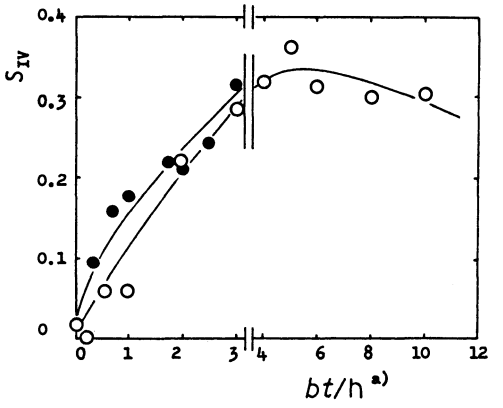

Fig. 7. Variation in S_{IV} with ball-milling. Ball-milling conditions: the content of (*RS*)-mandelic acid 10 w/w%, relative humidity; 45—55% ○, 75—85% ●. a) *bt* is the ball-milling time.

shown in Figs. 4—11, the change in these ratios at the first stage of ball-milling was greater under an atmosphere of high humidity. The effect of the humidity on S_{II} and S_{II}' was greater than the effect on the ratios for lower wavenumbers. The effect of the humidity on the mixture of the R-isomer was greater than the effect on the mixture of the S-isomer.

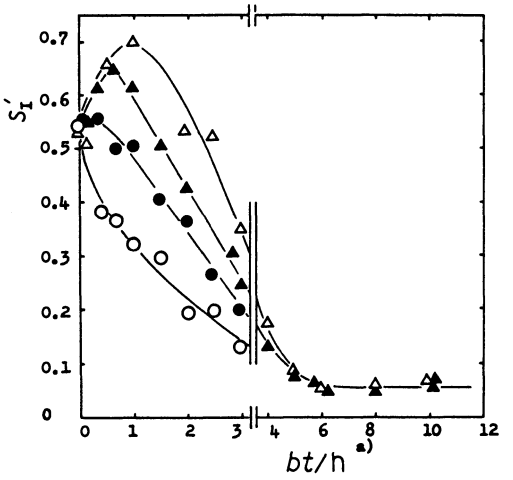

Fig. 8. Variation in S_I' with ball-milling. Ball-milling conditions: the content of mandelic acid 10 w/w%,

The kind of mandelic acid	Relative humidity/%
△ R	45—55
○ R	75—85
▲ S	45—55
● S	75—85

a) *bt* is the ball-milling time.

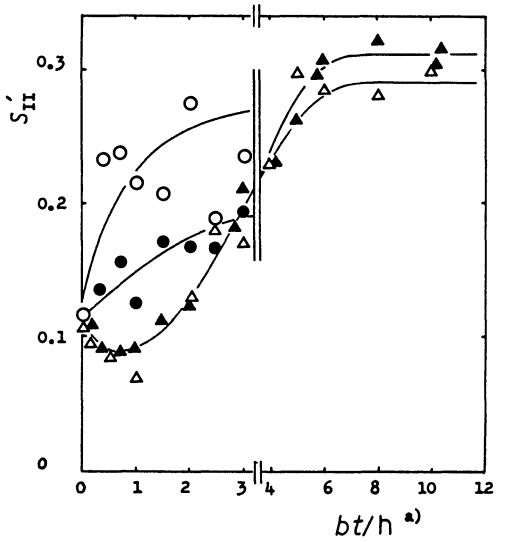

Fig. 9. Variation in S_{II}' with ball-milling. Ball-milling conditions; the content of mandelic acid 10 w/w%,

The kind of mandelic acid	Relative humidity/%
△ R	45—55
○ R	75—85
▲ S	45—55
● S	75—85

a) *bt* is the ball-milling time.

Magnesium Mandelate Powder. It was reported previously that mandelic acid was racemized when its anion was adsorbed very weakly at the surface of talc powder.[3] We have now measured the optical rotation and the absorption spectra for the supernatants of the ethanolic suspensions of the mixtures of mandelic acid with talc at the first stage of the ball-milling. It was clarified, from an analysis of these results, that the mandelic acid in the ball-milled mixture was not racemized, probably because of a strong interaction with talc. Table 1 shows the amounts of the A′ and C powders obtained from an ethanolic suspension of the ball-milled mixture. It is clear that the A'_R and A'_S powders contain more of an ethanol-soluble substance than A'_{RS}. According to many studies concerning the degradation of mandelic acid on γ-irradiation or oxidation, the main products are benzaldehyde, benzoic acid, and phenylglyoxylic acid.[7] By the thin-layer chromatography of B_R and B_S, mandelic acid, benzoic acid, and some substance other than the above three degradation products were detected, but mandelic acid was not detected for B_{RS}. A fine structure due to mandelic acid was observed in the absorption spectra of B_R and B_S, but a fine structure was not observed at all in the spectra of B_{RS}. It is considered that much of the ethanol-soluble substance in A'_R and A'_S powders is mandelic acid. In Table 1 are tabulated the amounts of mandelic acid in Solution A as inferred from the optical rotation of Solutions A and B.

In the IR spectra of C_R and C_S, the antisymmetric stretching vibration of C=O was around 1600 cm^{-1}, while it was at 1655 cm^{-1} in the spectra of C_{RS}. The spectra of C_{RS} were identical with those of M-Mg. In the spectra of M-Mg′ and the ball-milled mixture of mandelic acid with MgO, a broad band, which was a superposition of the bands at 1600 cm^{-1} and at 1655 cm^{-1}, was observed. Probably, powder C is the complex of mandelic acid and Mg, as M-Mg and M-Mg′ are considered to be the complexes of mandelic acid with MgO; this complex is also formed by ball-milling the mixture (Fig. 12).

Table 2 shows the contents of the C and H atoms in various C′ powders, as determined by the elemental

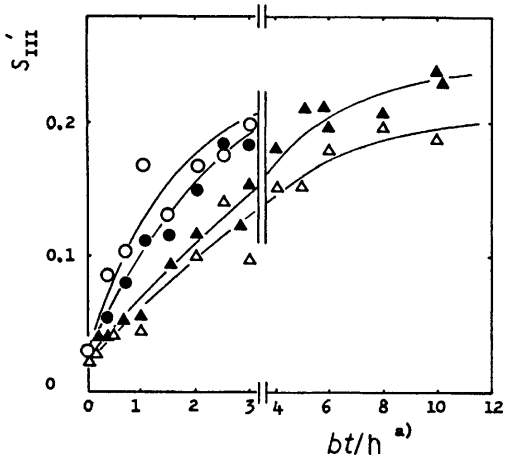

Fig. 10. Variation in S_{III}' with ball-milling. Ball-milling conditions; the content of mandelic acid 10 w/w%,

The kind of mandelic acid	Relative humidity/%
△ R	45—55
○ R	75—85
▲ S	45—55
● S	75—85

a) *bt* is the ball-milling time.

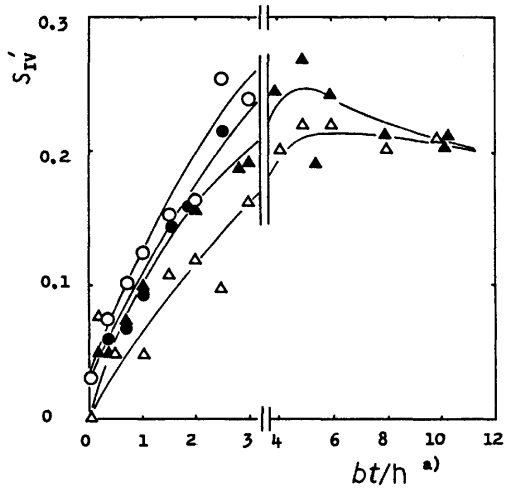

Fig. 11. Variation in S_{IV}' with ball-milling. Ball-milling conditions; the content of mandelic acid 10 w/w%,

The kind of mandelic acid	Relative humidity/%
△ R	45—55
○ R	75—85
▲ S	45—55
● S	75—85

a) *bt* is the ball-milling time.

Table 1. Dissolution of Mandelic Acid from the Ball-Milled Mixture with Talc into Ethanol

Mandelic acid	RS		R		S	
W_A'/mg/80 ml[a)]	29.3	34.6[c)]	30.6	28.5	28.4	29.0
W_C/mg/80 ml[a)]	27.1	30.8	21.9	24.6	20.6	19.8
$W_A'-W_C$/mg/80 ml	2.2	3.8	8.7	3.9	7.8	9.2
W_{MA}/mg/80 ml[b)]	—	—	6.4—7.4	3.4—4.8	4.8—6.0	6.3—7.9

a) W_A' and W_C are the weight amounts of A′ and C in 80 ml of A respectively. b) W_{MA} is the weight amount of mandelic acid in 80 ml of A obtained from the optical rotation of solutions A and B. The large values were obtained assuming that the optical rotation of B was all due to mandelic acid. The small values were obtained assuming that the optical rotation of B from that of A was due to mandelic acid. c) Each measurement was carried out twice.

Table 2. Elemental Analysis of Various C′ Powders

	Calcd/%					Found/%		
	K_A			K_B		C'_{RS}	C'_R	C'_S
x	0	1	2	0	1	—	—	—
C	59.21	56.10	53.29	58.84	55.77	57.84	55.74	55.22
H	3.73	4.12	4.47	4.32	4.68	4.21	4.13	4.22

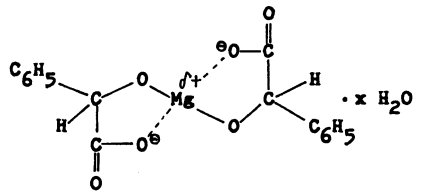

K_A

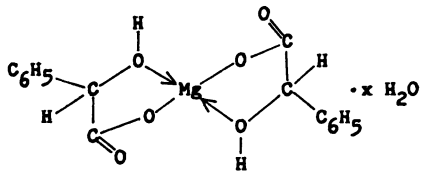

K_B

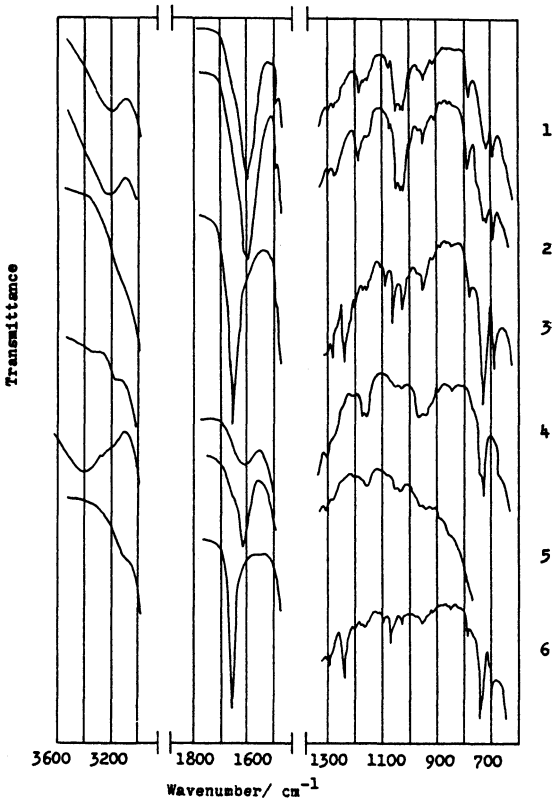

Fig. 12. IR spectra of various powders containing mandelic acid. 1 C_S, 2 C_R, 3 C_{RS}, 4 the ball-milled mixture of (*RS*)-mandelic acid and MgO (One g of mandelic acid and 9 g of MgO were ball-milled for 4 h.), 5 M-Mg′, 6 M-Mg.

analysis, and the values calculated for the substances of the molecular structures of K_A and K_B. A comparison between the found values and the calculated values suggests that the C'_{RS} powder is a substance with the molecular structure of K_B (x=0), mixed with a small amount of a substance with the molecular structure of K_A ($1<x<2$). The results also suggest that the C'_R and C'_S powders are substances with the molecular structure of K_A ($1<x<2$), mixed with only a small amount of a substance with the molecular structure of K_B (x=0).

Large exothermic peaks were observed at 300—400 °C and above 500 °C in the DTA thermograms of the C'_{RS} and C'_R powders. In addition, a small endothermic peak was observed at 280—320 °C in the thermogram of the C'_S powder. In the TG analysis, a mass loss was observed at these temperatures; the mass loss at 280—400 °C was 40—50%. It was determined from these measurements that the decomposition temperatures of the C'_{RS}, C'_R, and C'_S powders were 332, 320, and 282 °C respectively. A mass loss of approximately 4% was observed between room temperature and 100 °C in the case of the C'_S powder, but no mass loss was observed below the decomposition temperature in the cases of the C'_R and C'_{RS} powders. The water in these powders may be structural water, or it may coordinate with Mg, and the hydroxyl group and the COO^- group of mandelic acid may then bind with these coordinating water molecules.

Optical Isomer Effect. It is clear from the above results that the mechanochemical interaction of (*RS*)-mandelic acid with talc is different from the interaction of the R-isomer and the S-isomer. It is also clear that there is some difference between the interaction of the R-isomer and that of the S-isomer. The band of the free hydroxyl group is at 3515 cm^{-1} and this band shifts to a lower frequency upon hydrogen bonding.[8] The band of the hydroxyl group for the (RS)-compound is at 3400 cm^{-1}, while the bands for the R-isomer and the S-isomer are at 3420 cm^{-1}. This shows that intermolecular or intramolecular hydrogen bonds in the (RS)-compound are stronger than the bonds in the R-isomer or the S-isomer. Singurel[8] investigated the IR spectral change in mandelic acid upon interaction with proton acceptors. He pointed out that the C=O vibrations at 1718 cm^{-1} and 1762 cm^{-1} belonged to the dimer and to monomer mandelic acid respectively. When a proton acceptor complexed with the COOH group of mandelic acid, the C=O band

appeared between the monomer band and the dimer band. The C=O band for the optically active mandelic acids at 1715 cm^{-1} shifted to a frequency higher by approximately 10 cm^{-1} at the first stage of ball-milling, but no shift was observed in the C=O band for the (RS)-compound. These facts show that the proton acceptors at the surface of talc powder form hydrogen bonds only with the optically active mandelic acids. Probably this causes the difference between the interactions of (*RS*)-mandelic acid and optically active mandelic acids with talc. The difference between the interaction of the R-isomer and that of the S-isomer also suggests that talc powder has a chiral surface when it is mechanically treated.

The authors wish to express their thanks to the members of the Analytical Center of Showa University for the measurement of the IR spectra and the elemental analysis. The present work was partially supported by a Grant-in-Aid for Scientific Research (No. 61540427) from the Ministry of Education, Science and Culture, to which the authors are grateful.

References

1) M. Ohara, Chau-Yang Chen, and T. Kwan, *Bull. Chem. Soc. Jpn.*, **39**, 137 (1966).

2) J. B. Nagwekar, and H. B. Kostenbauder, *J. Pharm. Sci.*, **59**, 1775 (1970).

3) A. Ikekawa and S. Hayakawa, *Bull. Chem. Soc. Jpn.*, **60**, 19 (1987).

4) A. Verweij, R. de Jong-de Vos, and H. G. J. Teisman, *J. Chromatogr*, **69**, 407 (1972).

5) P. V. Khadikar, R. L. Ameria, M. G. Kekre, and S. D. Chauhan, *J. Inorg. Nucl. Chem.*, **35**, 4301 (1973).

6) D. N. Sen, S. Mizushima, C. Curran, and J. V. Quagliano, *J. Am. Chem. Soc.*, **77**, 211 (1955); M. L. Morris and D. H. Busch, *J. Am. Chem. Soc.*, **78**, 5178 (1956); P. V. Bakore, *Curr. Sci.*, **37**, (3), 193 (1968); K. Nakamoto, Y. Morimoto, and A. E. Martell, *J. Am. Chem. Soc.*, **83**, 4528 (1961).

7) T. J. Kemp and W. A. Walters, *J. Chem Soc.*, **1964**, 1192; S. A. Baker, J. S. Brima Combe, and D. H. Spenee, *J. Chem. Soc. C*, **1966**, 511.

8) Gh. Singurel, *Revue Roumaine do Chimie*, **25**, 1469 (1980).

On the Characterization of Fibonacci Numbers as Maximal Independent Sets of Vertices of Certain Trees

Sherif EL-BASIL†
Chemistry Department, University of Georgia, Athens, Georgia 30602, U.S.A.
(Received November 4, 1986)

Fibonacci numbers are identified for the first time as maximal independent sets of vertices of certain caterpillar trees. Their relation to king patterns of certain classes of polyomino graphs as well as polyhex graphs is illustrated.

More than a decade ago Hosoya[1] defined the concept of nonadjacent numbers in chemistry. Thus for a connected nondirected simple graph, G, the quantity $p(G,k)$ is defined to be the number of ways of choosing k disconnected lines from graph G with $p(G,o)$ being taken to be unity. The Z-counting polynomial, $H(G;x)$ is defined as

$$H(G;x)=\sum_{k=0}^{m} p(G;k)x^k \quad (1)$$

where m is the maximum number of k. The Z-index is the sum of the $p(G,k)$ numbers, i.e.,

$$Z(G)=H(G;1) \quad (2)$$

The above topological index was found to be applicable in many different areas including chemistry, mathematics, dimer statistics, and informatics.[2] The recent revival of interest in graph theory led to a natural extension of the $p(G,k)$ numbers to include other nonadjacent mathematical objects abstracted from molecular graphs. Thus when the concept is applied to benzenoid hydrocarbons[3] $p(G,k)$ becomes $r(B,k)$ i.e. the number of selections of k nonadjacent resonant sextets from the benzenoid graph B. In Clar sextet theory[4] the nonadjacent concept has been extended to sets of nonadjacent vertices $o(G,k)$ chosen from the corresponding Clar graph,[5] C. Further, the latter concept was also recently applied[6] to king polynomials of polyomino graphs.[7] In addition the nonadjacent concept relates to rook theory.[8] Thus, there is a one-to-one correspondence between labelled bipartite graphs with $a+b$ vertices and a chess board, R, with a rows and b columns such that $p(G,k)=\rho(R,k)$ where the latter function counts the number of ways in which one can arrange k non-attacking rooks on R, taking $\rho(R,o)=1$.

Some interesting relations arise for certain types of graphs. Thus the set $\{Z(G_n=L_n)\}$, where L_n is a path on n vertices is the set of Fibonacci numbers,[9] $\{F_n\}$, defined by

$$F_n=\sum_{k=0}^{[n/2]}\binom{n-k}{k} \quad (3)$$

while the set $\{Z(G_n=C_n)\}$, C_n being a cycle on n vertices, generates the Lucas sequence,[9] $\{L_n\}$, where

$$L_n=F_n+F_{n-2};\ n\geqslant 2 \quad (4)$$

The binomial functions of Eq. 3 are coefficients of the Chebyshev polynomials.[10] Because the Fibonacci numbers are well studied any relations to other fields such as chemistry or physics should be interesting. Two classical relations to the Fibonacci numbers are known in chemistry:

(1) The numbers of Kekulé structures, K, of the zigzag nonbranched benzenoid hydrocarbons (phenanthrene, chrysene, picene, fulminene, (benzo[c]picene), ···) are defined by[11]

$$K_n=F_{n+1} \quad (5)$$

n, is the number of rings in the polyhex graph.

The analogous relation in statistical physics is[12]

$$K(2\times n)=F_n \quad (6)$$

where $K(2\times n)$ is the number of perfect matchings in a $(2\times n)$ rectangular lattice.

(2) Let $\gamma_{i(n)}$ be the number of permutation integrals[13] involving i rings in a nonbranched zigzag polyacene containing n rings (observe that $\sum\gamma_i=1/2\sum R_i$, where R_i is a conjugated circuit over i rings,[14]) then[15]

$$\gamma_i(n)=\gamma_{i-1}(n-1) \quad (7)$$

$$\gamma_i(n)=\sum_{k=1}^{\theta} F_{\theta-k}F_{k-1}$$

where $\theta=n+1-i$.

Maximal Independent Sets. The vertices of a graph can be partitioned into a finite number of sets. A set of vertices in which no two vertices are adjacent is called an *independent* set of vertices. An independent set of vertices $\{V(r)\}$ in G is said to be *maximal*[16] if every vertex of G $\epsilon\{V(r)\}$ is adjacent to at least one of the r vertices of $\{V(r)\}$. Figure 1 shows three graphs $\mathcal{C}_1$, $\mathcal{C}_2$, and $\mathcal{C}_3$, arbitrarily labelled as shown. There are seven maximal independent sets of vertices in $\mathcal{C}_1$, viz., {1,4},

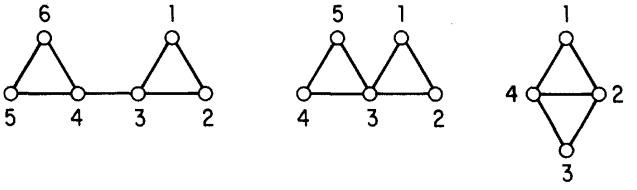

Fig. 1. Three labelled (Clar) graphs.

†Permanent address: Faculty of Pharmacy, Kasr El-Aini Street, Cairo, Egypt.

{1,5}, {1,6}, {2,4}, {2,5}, {2,6}, {3,5}, and {3,6}, while the vertices of $\mathcal{C}_2$, are partitioned into five maximal independent sets: {3}, {1,4}, {1,5}, {2,4}, {2,5}. For $\mathcal{C}_3$ there are only three such sets: {2}, {4}, and {1,4}. Actually $\mathcal{C}_1$ and $\mathcal{C}_2$ are the Clar graphs[5,17] of two nonbranched systems whose ring-annellation[18] sequences are respectively $L^2A^2L^2$ and $L^2A^2L^2$ while $\mathcal{C}_3$ is the Clar graph of pyrene. In fact, quite recently Herndon and Hosoya[17,19,20] identified the number of Clar *structures*[17] of a benzenoid hydrocarbon as the number of maximal independent sets of vertices in the corresponding Clar graphs.

The Comb Tree Graphs

We consider a special type of tree formed by the addition of a single (monovalent) vertex to each of the n vertices of a path, L_n. The resulting caterpillars[21] containing $2n$ vertices are also known as comb trees. The vertices of the original path moiety of such trees will be called *root vertices*. A comb tree will be given the symbol $Tn(1,1,\cdots,1)\equiv T_{n,1}$. An arbitrary labelling of the set of vertices $\{V(r)\}\varepsilon\, T_{n,1}$ is shown below

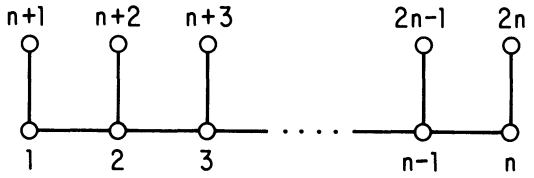

Let us consider the maximal independent sets of vertices of some of the lower members of comb trees.

$V(T_{1,1}) \supset$ {2}; {1}=$V_m(T_{1,1})$

$V(T_{2,1}) \supset$ {3,4}; {1,4}, {2,3}=$V_m(T_{2,1})$

$V(T_{3,1}) \supset$ {4,5,6}; {1,5,6}; {2,4,6}; {3,4,5}; {1,3,5}=$V_m(T_{3,1})$

$V(T_{4,1}) \supset$ {5,6,7,8}; {1,6,7,8}; {2,5,7,8};
{3,5,6,8}; {4,5,6,7}; {1,3,6,8};
{1,4,6,7}; {2,4,5,7}=$V_m(T_{4,1})$

$V(T_{5,1}) \supset$ {6,7,8,9,10}; {1,7,8,9,10}; {2,6,8,9,10};
{3,6,7,9,10}; {4,6,7,8,10}; {5,6,7,8,9,10};
{1,7,3,9,10}; {1,4,7,8,10}; {1,5,7,8,9};
{2,4,6,8,10}; {2,5,6,8,9}; {3,5,6,7,9};
{1,3,5,7,9}=$V_m(T_{5,1})$.

Where $V(T_{n,1})$ is the total set of vertices of $T_{n,1}$ and $V_m(T_{n,1})$ is a subset of it including all the maximum independent sets in $T_{n,1}$. Let $N(V(T_{n,1}))\equiv\zeta_n$ be the number of such sets. We observe the following results:

$\zeta_1=2,\ \zeta_2=3,\ \zeta_3=5,\ \zeta_4=8,\ \zeta_5=13;\ \zeta_3=\zeta_1+\zeta_2;\ \zeta_4=\zeta_3+\zeta_2;\ \zeta_5=\zeta_4+\zeta_3.$

Which reminds us of the Fibonacci numbers F_2, F_3, F_4, F_5, and F_6 respectively. Actually the above set counts recur in the following general way

$$\zeta_n=\zeta_{n-1}+\zeta_{n-2}, \tag{8}$$

where

$$\zeta_n=F_{n+1}. \tag{9}$$

There are two ways of proving (8) and (9).

A. Graph-Theoretical Reasoning

Define the function f such that f: $V_m(T_{n,1})=\overline{V}_m(T_{n,1})$ where

$$\overline{V}_m(T_{n,1})=\{vi/vi\varepsilon\, V_m(T_{n,1});\ i\varepsilon\,(1,2,\cdots,n);\ \notin(n+1,n+2,\cdots,2n)\},$$

where vi is a vertex whose label is i. Therefore the function f maps the set $V_m(T_{n,1})$ into a set of vertices *containing only root type vertices*. The resulting initial sets are:

$\overline{V}_m(T_{1,1})$={∅}; {1}

$\overline{V}_m(T_{2,1})$={∅}; {1}; {2}

$\overline{V}_m(T_{3,1})$={∅}; {1}; {2}; {3}; {1,3}

$\overline{V}_m(T_{4,1})$={∅}; {1}; {2}; {3}; {4}; {1,3}; {1,4}; {2,4}

$\overline{V}_m(T_{5,1})$={∅}; {1}; {2}; {3}; {4}; {5};
{1,3}; {1,4}; {1,5}; {2,4};
{2,5}; {3,5}; {1,3,5}.

In general one can then write:

$\overline{V}_m(T_{n,1})$={∅};
{1}; {2}; ⋯ ; {n};
{1,3}; {1,5}; ⋯ ; {2,4}; {2,5}; ⋯ ; {i, i+2};
{1,3,5}; ⋯ ; {j; j+2; j+4}; ⋯ ,
{k,k+2, k+4, k+6, ⋯ }

The cardinalities of the above sets are nothing else but the independence numbers[5] of paths L_n. Alternatively they are simply the k-matchings of L_{n+1} (observe that L_n is the line graph[22] of L_{n+1}). The latters are indeed the graphical representations of the Fibonacci numbers[9] and since the f function is an injective (i.e. one-to-one) mapping of $V_m(T_{n,1})\rightarrow\overline{V}(T_{n,1})$ relations (8) and (9) become immediate.

The above ideas lead to the more general caterpillar

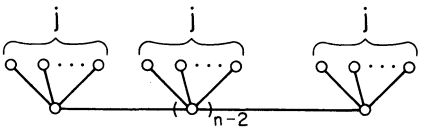

$T_{n,j}$; $j\geq 1$

Obviously,

$$\zeta(T_{n,j})=\zeta(T_{n,1});\ j\geqslant 1 \tag{10}$$

This is because

$$\overline{V}_m(T_{n,j})=\overline{V}_m(T_{n,1});\ j\geqslant 1$$

Note, however, that when j=0 the Fibonacci recursion is lost.[17,20]

B. Coloring Method

Another method of proving the above result (Eqs. 8 and 9) uses a special coloring scheme. Thus the vertices of a $T_{n,j}$, ($j\geqslant 1$); are colored in black and white such that (i) no two black vertices are adjacent and (ii) every white vertex is adjacent to at least one black vertex. The resulting colorings then correspond to maximal independent sets of vertices. For simplicity these indi-

ces are illustrated using $T_{n,2}\equiv T_n$ but the theory can be generalized to $T_{n,j}$.

Lemma 1. $T_{1,2}\equiv T_1$ generates two colorings, viz., α and β:

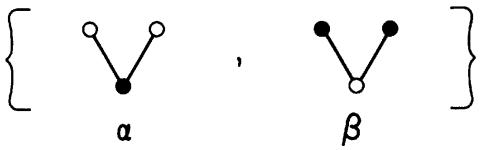

The "allowed" colorings of T_2 can be identified from lemma 1 and rules i and ii as:

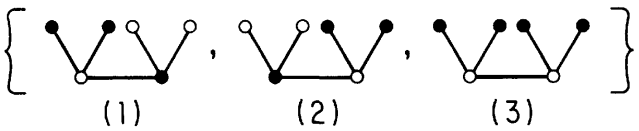

All colorings of T_3 can be obtained by connecting one of the root vertices of (1)—(3) to the root vertices of α and/or β. However, because of (i), the coloring (1α) is not allowed and thus T_3 has $3\times2-1=5$ colorings. Similarly the colorings of T_n can be obtained from those of T_{n-1} and the set $\{\alpha,\beta\}$.

Theorem 1. Let ζ_n be the number of colorings of T_n. Let the number of colorings in a given set which contains a black root vertex at one (arbitrarily the right) end of the tree be β_n.
Then

$$\zeta_n=\beta_{n+2} \tag{11}$$

Proof. The set $\{\beta_{n+2}\}$ is a subset of the set of colorings $\{\zeta_{n+2}\}$ in which all root vertices at the (right) end are black. Now, because of (i), in any member of $\{\beta_{n+2}\}$ the root vertex adjacent to the one at the right end, i.e. the $(n+1)$th vertex is necessarily *white* and therefore the remaining n vertices must generate the set $\{\zeta_n\}$, i.e. $\{\zeta_n\}\varepsilon\{\beta_{n+2}\}$, and Eq. 11 is proved

Theorem 2.

$$\beta_{n+2}=\beta_{n+1}+\beta_n \tag{12}$$

Proof. Let w_n be the number of colorings in $\{A_n\}$ in which the (right) end root vertex is white. Obviously $\beta_n+w_n=\zeta_n$.

Now from rule (i) and lemma 1:

$$\zeta_{n+1}=2\zeta_n-\beta_n$$

and

$$w_n=\beta_{n+1}=\zeta_n-\beta_n$$

$$\text{i.e. } \zeta_n=\beta_n+\beta_{n+1}=\beta_{n+2}$$

Eqs. 11 and 12 lead to Eqs. 8 and 9.

Coloring Polynomial. A counting coloring polynomial, $\xi(T_{n,j};\,x)$ is conveniently defined by

$$\xi(T_{n,j};x)=\sum_{r}^{m}\theta(r)x^r, \tag{13}$$

where $\theta(r)$ is the number of colorings of $T_{n,j}$ containing r black vertices and m is the maximum value of r. Then $\xi(T_{n,j};\,1)=\zeta_n$. Inspection of the first few coloring polynomials of any $T_{n,j}$, $j\geqslant1$, induces Eq. 14, viz.,

$$\xi(T_{n,j};x)=\sum_{k=0}^{[n/2]}\binom{n-k}{k}x^{mn-(m-1)k} \tag{14}$$

As a corollary when $j=1$ the above function becomes simply a monomial in x.

A Special Class of Benzenoid Hydrocarbons. Figure 2 shows a homologous series of benzenoid hydrocarbons denoted as $B(T_{n,1})$'s. The number of Clar structures in which maximum numbers of hexagons are assigned to have resonant sextets of this series conforms to Eqs. 8 and 9. In principle homologation can be extended infinitely, although the polyhex graph

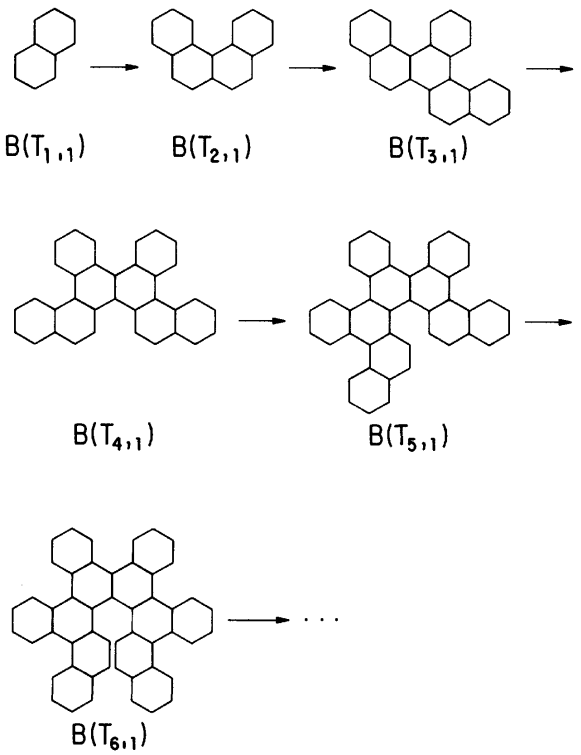

Fig. 2. A homologous series of benzenoid hydrocarbons. The Clar counts, ξ, of the individual members are Fibonacci numbers i.e. $\xi(B(T_{j,1}))=F_{j+1}$.

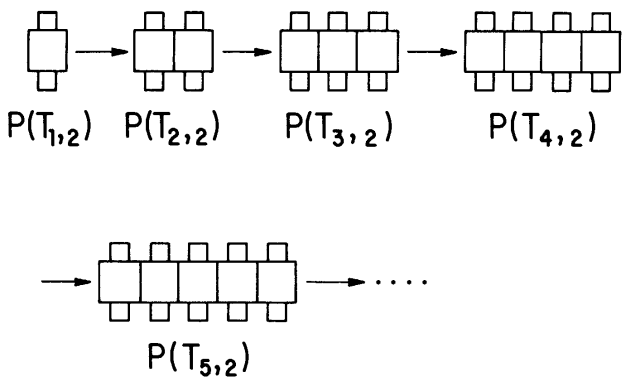

Fig. 3. A homologous series of "bidentate" polyomino graphs. Every graph corresponds to a caterpillar tree $T_{n,2}$, $n=1, 2, 3, 4, 5\cdots$. Relation to other objects is shown in Fig. 4.

above $B(T_{6,1})$ is no long planar. It is interesting to notice that

$$D(B(T_{n,1}))=T_{n,1}$$

where D(G) is the dualist graph[23] of G.

On King Patterns. Motoyama and Hosoya[7] were the first to define king polynomials and king patterns for lattices and polyomino graphs and showed their potential in dimer statistics and the problem of Kekulé count in chemistry. Balasubramanian and Ramaraj[6] demonstrated recently the equivalence between king polynomials and what they called color polynomials[6] of the dualist graphs of the appropriate lattice type. Figure 3 shows a special type of polyomino which corresponds to $T_{n,2}$. But extension to any $T_{n,j}$ is possible. Their king patterns are Fibonacci numbers.

Correspondence with King Pattern,[7] Domino Pattern,[7] and the Matching Pattern.[1,24] A king pattern, {K}, is simply a way of placing kings (circles) on chessboard so that no two kings can take each other. A Kekulé pattern (or dimer pattern), {M}, can be generated by identifying the cells in the chessboard that contain kings as the vertical bonds in the dimer pattern and the empty cells as horizontal bonds (cf. Fig. 4). A "domino pattern," {D}, can also be obtained from the dimer pattern by paving horizontal and vertical rectangles which correspond to horizontal and vertical dimers in the dimer pattern. These relations are depicted in Fig. 4. The set {ζ} is nothing else but the dualist graphs[23] corresponding to the modified polyominos, {P}. Hence one can define two rules of placing kings (circles) in {P} analogous to coloring rules (i), (ii), viz.,

(i′) No two kings are allowed to occupy adjacent cells.

(ii′) Every empty cell is adjacent to at least one occupied cell.

The resulting patterns generate Fibonacci numbers. The last set in Fig. 4, {L}, shows the corresponding matchings in path L_4. The following interesting relation is observed. Let $d\{K_i\}$ be the dualist graph[23] of a member K_i from set {K}, and $L\{L_i\}$ be the line graph[25] of the corresponding member L_i, then

$$d\{K_i\}=L\{L_i\}. \quad (15)$$

The last relation is significant since it is well known that the matching polynomials of the paths may be written as Chebyshev polynomials[26] in $(x/2)$.

Fibonacci numbers have been identified for the first time as maximal independence sets of vertices of certain caterpillar trees. Mappings of such sets to well known topological functions such as perfect matchings of a path as well as certain king patterns are discovered.

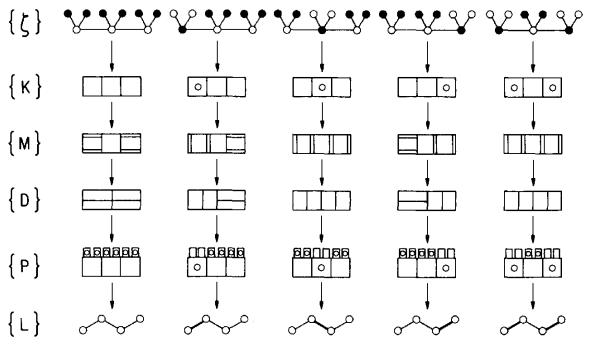

Fig. 4. Fibonacci colorings of $T_{2,2}$ and the corresponding patterns in chemistry and physics. The set {K} is the king pattern, {M} is the dimer pattern, {D} the domino pattern and {P} is a special polyomino pattern. The set {L} is the matchings of L_4.

The author thanks the U.S. Office of Naval Research for partial support of this work. Illuminating remarks of Professor R. B. King are greatly appreciated. Travel assistance from the Fullbright Commission in Cairo is acknowledged.

References

1) H. Hosoya, *Bull. Chem. Soc. Jpn*, **44**, 2332 (1971).
2) H. Hosoya, "Mathematics and Computational Concepts in Chemistry," Ellis Horwood (1986).
3) H. Hosoya and T. Yamaguchi, *Tetrahedron Lett.*, **1975**, 4659.
4) E. Clar, "The Aromatic Sextet," John Wiley, New York (1972). A nice review is found in I. Gutman, *Bull. Soc. Chim. Beograd*, **47**, 453 (1982).
5) I. Gutman, *Z. Naturforsch.*, **37a**, 69 (1982); I. Gutman and S. El-Basil, *ibid.*, **39a**, 276 (1984).
6) K. Balasubramanian and R. Ramaraj, *J. Comput. Chem.*, **6**, 447 (1985).
7) A. Motoyama and H. Hosoya, *J. Math. Phys.*, **18**, 1485 (1977).
8) J. Riordan, "An Introduction to Combinatorial Analysis," Wiley, New York (1958), Chaps. 7 and 8.
9) H. Hosoya, *The Fibonacci Quarterly*, **11**, 255 (1973); **14**, 173 (1974).
10) T. J. Rivlin, "The Chebyshev Polynomials," John Wiley, New York (1974).
11) A. T. Balaban and I. Tomescu, *Croat. Chem. Acta*, **57**, 391 (1984); *Match*, **17**, 91 (1985).
12) H. Hosoya, *Comp. Maths. Appls.*, **12B**, 271 (1986).
13) W. C. Herndon and M. L. Ellzey Jr., *J. Am. Chem. Soc.*, **96**, 6631 (1974).
14) M. Randić, *J. Am. Chem. Soc.*, **99**, 444 (1977); *Tetrahedron*, **33**, 1905 (1977).
15) I. Gutman and S. El-Basil, *Chem. Phys. Lett.*, **115**, 416 (1985).
16) N. Christofides, "Graph Theory, An Algorithmic Approach," Academic Press, New York (1975), Chap. 3.
17) S. El-Basil, *Theor. Chim. Acta*, **70**, 53 (1986).
18) S. El-Basil, *Bull. Chem. Soc. Jpn.*, **56**, 3152 (1983).
19) W. C. Herndon and H. Hosoya, *Tetrahedron*, **40**, 3987 (1984).
20) S. El-Basil, *Disc. Appl. Math.*, (1986) in press.
21) F. Harary and A. J. Schwenk, *Discrete Math.*, **6**, 359 (1973).
22) F. Harary, "Graph Theory," Addison-Wesley, Reading (1969), Chap. 8.

23) C.f., A. T. Balaban and F. Harary, *Tetrahedron*, **24**, 2505 (1968).

24) Actually the first contributions to the theory of matching came from statistical physics: O. J. Heilmann and E. H. Lieb, *Phys. Rev. Lett.*, **24**, 1412 (1970); *Commun. Math. Phys.*, **25**, 190 (1972); H. Kunz, *Phys. Lett.*, **32A**, 311 (1970); C. Gruber and H. Kunz, *Commun. Math. Phys.*, **22**, 133 (1971).

25) Line graphs are defined in: F. Harary, "Graph Theory," Addison-Wesley Publishing Company, Reading, Mass. (1972), p. 71.

26) T. J. Rivilin, "The Chebyshev Polynomials," John Wiley, New York (1974).

 © 1988 The Chemical Society of Japan Bull. Chem. Soc. Jpn., 61, 539—541 (1988)

Activated Nitriles in Heterocyclic Synthesis. Synthesis of Pyrimidine Derivatives

Kamal Usef SADEK,* Mohamed Abdallah EL-MAGHRABY,† Maghraby Ali SELIM,† and Mohamed Hilmy ELNAGDI††
Department of Chemistry, Faculty of Science, Minia University
†Department of Chemistry, Faculty of Science, Aswan University
††Department of Chemistry, Faculty of Science, Cairo University, A.R. Egypt
(Received August 16, 1986)

Synthesis of polyfunctional pyrimidine derivatives via the reaction of acrylonitrile derivatives **1a** and **b** with α,β-unsaturated nitriles **2a—f** has been reported.

Studies on α,β-unsaturated nitriles have revealed that these easily obtained reagents are excellent starting materials for the synthesis of polyfunctionally substituted heterocycles.[1-3] Previously our group reported the use of compounds **1a**, **b**, and **2a—f** for the

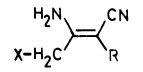

1a. R=X=$CO_2C_2H_5$
b. R=CN; X=$CO_2C_2H_5$
c. R=X=CN

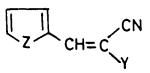

2a. Z=O; Y=CN
b. Z=O; Y=$CO_2C_2H_5$
c. Z=O; Y=COPh
d. Z=S; Y=CN
e. Z=S; Y=$CO_2C_2H_5$
f. Z=S; Y=COPh

synthesis of pyrazoles,[4] pyranopyrazoles,[5] isoxazoles,[6] fused isoxazoles, pyridazines, and pyridine derivatives.[4] In continuation of this work, we report here the results of our investigations on the reactions of **1a** and **b** with **2a—f**. We found that **1a** reacts with **2a** to yield a product of molecular formula $C_{16}H_{12}N_4O_4$ (M^+=324, *m/z*). The ^{1}H NMR spectrum revealed that the reaction product cannot be the dihydropyridine **3**, which would be expected to be formed via a sequence similar to that suggested recently in literature.[7] High resolution ^{1}H NMR spectroscopy revealed signals for an ester function at δ 1.21 (t, 3H, CH_3) and at δ 4.33 (q, 2H, CH_2), as well as signals for furyl protons at δ 8.29, 7.82, and 6.46. In addition, a two-proton signals at δ 4.1 and a one-proton signal at δ 6.17 were observed. The signal at 4.1, overlapping in the 90 MHz ^{1}H NMR spectrum with the methylene signal, was shown to be due to two noncoupled magnetically equivalent protons and did not disappear on D_2O exchange. Hence, it cannot be assigned to the protons a and b in the dihydropyridine form **3**. The ^{13}C NMR spectrum confirms that the product has the pyrimidinone structure **4a** as it revealed C-4 at δ 206. If the product was the dihydropyridine **3**, extra sp^3 carbons should have been observed.

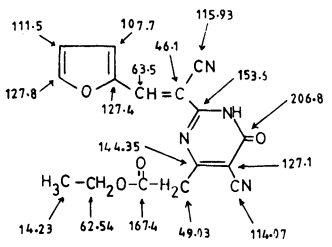

4a

Similarly, compound **1a** reacted with **2b** and **c** to yield the pyrimidinone derivatives **4b** and **c**. The formation of compounds **4a—c** in this reaction is assumed to proceed via addition of the amino function of **1a** to the cyano group in **2a—c** with elimination of ethanol (see Scheme 1). The structure of **4b** and **c** were well-documented by IR and ^{1}H NMR spectroscopy.

In contrast, compound **2d** reacted with **1a** to yield 1:1 adduct. The pyrimidine structure **5a** was formulated for the reaction product based on IR and ^{1}H NMR. Attempts at addition of **2e** and **f** to **1a** under

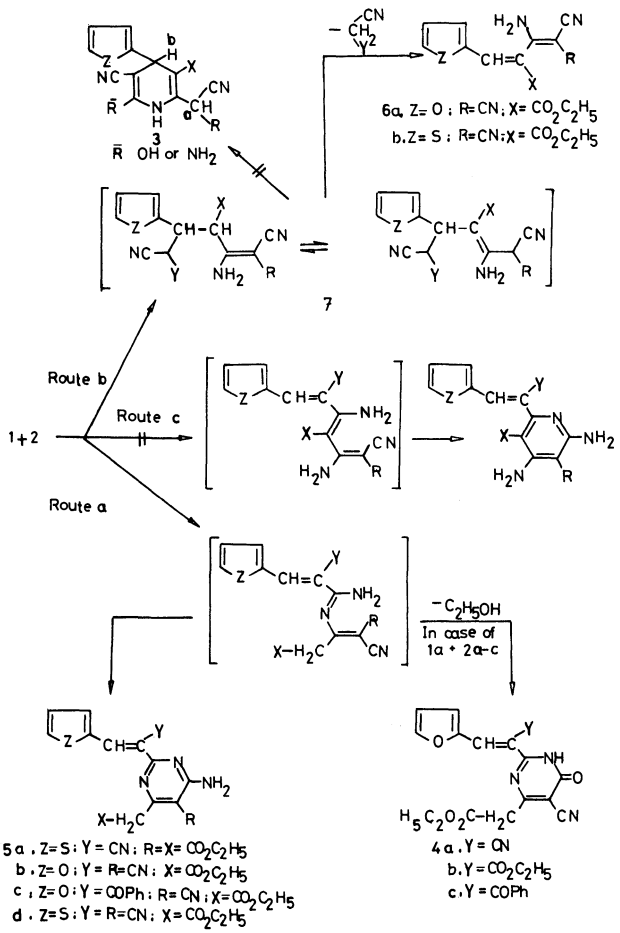

Scheme 1.

the same experimental conditions were unsuccessful. The reactants were recovered almost unchanged after reflux in ethanolic piperidine solution.

Compound **1b** reacted with **2a**, **c**, and **d** to yield 1 : 1 adducts which can be formulated as either the dihydropyridine **3** or as the pyrimidines **5b—d**. The establishment of a pyrimidine structure for the reaction products was based on spectral data which, in each case, revealed the presence of a signal for a CH_2 group. Such a signal cannot be assigned to alternative structures. On the other hand, attempted addition of **1b** to **2b** gave the furfurylidene derivative **6a** which could also be obtained from the reaction of **1b** with furfural. The formation of **6a** is assumed to proceed via the intermediacy of the Michael adduct **7**, which then loses ethyl cyanoacetate to yield the final isolated product. Similar ylidene formation on addition of α,β-unsaturated nitriles to active methylene reagents has been observed by us in several reactions.[8,9] In the same way, compound **1b** reacted with **2f** to yield the thenylidene derivative **6b**. The possible formation of **6** via a retro-aldol reaction of **2** affording an aldehyde which condenses with **1** cannot be completely excluded. In contrast to the observed formation of **6a** and **b** compound **1d** did not react with **2e**. The formation of pyrimidines from the reaction of **1a** and **b** with **2a—f** finds a parallel with the Frankland and Kolbe synthesis of pyrimidines.[10]

The results obtained in our investigation clearly reveal that the reaction of **1** with **2** proceeds via three different routes: i) Addition of the amino function to the cyano group and cyclization to yield pyrimidines

Table 1. Products from the Reactions of Compounds **1a** and **b** with the Nitriles **2a—f**

Compd	Crystallization solvent	Mp θ_m/°C	Yield/%	Mol form (Mol wt)	Analysis/% Found (Calcd)			
					C	H	N	S
4a	Ethanol-water	205	80	$C_{16}H_{12}N_4O_4$ (324)	59.2 (58.7	3.7 4.0	17.3 17.0)	
4b	Methanol-water	112	82	$C_{18}H_{17}N_3O_6$ (371)	58.2 (58.2	4.6 5.0	11.3 11.3)	
4c	Ethanol-water	110	77	$C_{22}H_{17}N_3O_5$ (403)	65.5 (65.8	4.2 4.3	10.4 10.2)	
5a	Ethanol	204	78	$C_{18}H_{18}N_4O_4S$ (386)	56.0 (56.0	4.7 5.0	14.5 14.3	8.2 8.5)
5b	Ethanol-water	230	70	$C_{16}H_{13}N_5O_3$ (323)	59.4 (59.4	4.0 4.0	21.7 21.8)	
5c	Ethanol-water	185	83	$C_{22}H_{18}N_4O_4$ (402)	65.7 (65.8	4.5 4.7	13.9 13.6)	
5d	Ethanol-water	>250	72	$C_{16}H_{13}N_5O_2S$ (339)	56.6 (56.7	3.8 3.5	20.6 20.5	9.4 9.3)
6a	Ethanol-water	90	75	$C_{13}H_{11}N_3O_3$ (257)	60.7 (61.0	4.3 4.5	16.3 16.2)	
6b	Ethanol	>250	76	$C_{13}H_{11}N_3O_2S$ (273)	57.1 (57.0	4.0 4.0	15.4 15.4	11.7 11.8)

Table 2. Selected IR and Complete ^{1}H NMR Data for the Compounds Listed in Table 1

Compd	ν_{max}/cm^{-1}	δ_H
4a	2900, 2970 (CH and CH_3); 2180, 2200 (CN groups); 1715 (CO)	1.2 (t, 3H, CH_3); 3.1 (OH and DOH); 4.1—4.4 (m, 4H, $2CH_2$); 6.7 (s, 1H, ylidene CH); 7.4—8.3 (m, $3H_{furan}$)
4b	2950 (CH and CH_3); 2200 (CN); 1730 (br., CO groups)	1.2, 1.22 (two triplets, 6H, $2CH_3$); 3.3 (OH and DOH); 4.18 (m, 6H, $3CH_2$); 6.3 (s, 1H, ylidene CH); 7.3—8.2 (m, $3H_{furan}$)
4c	2900, 2960 (CH and CH_3); 2200 (CN); 1675, 1730 (CO groups)	1.2 (t, 3H, CH_3); 3.3 (OH and DOH); 4.16 (q, 2H, CH_2); 4.2 (s, 2H, CH_2); 7.0—8.2 (m, 9H, aromatic and ylidene protons)
5a	3200, 3300 (NH_2); 2900 (CH_3); 2200 (CN) and 1630 (CO)	Insoluble in available ^{1}H NMR solvents
5b	3200, 3300 (NH_2); 2900 (CH_3); 2180, 2200 (CN groups) and 1640 (CO)	1.2 (t, 3H, CH_3); 3.3 (br., 2H, NH_2); 4.1 (br, 4H, $2CH_2$); 6.8 (s, 1H, ylidene CH); 7.2—8.2 (m, $3H_{furan}$)
5c	3200, 3350 (NH_2); 2900 (CH_3); 2200 (CN)	Insoluble in available ^{1}H NMR solvents
5d	3050, 3200, 3300 (NH_2); 2150, 2200 (CN groups) and 1640 (CO)	1.3 (t, 3H, CH_3); 3.7 (br., 2H, NH_2); 4.2 (m, 4H, $2CH_2$); 6.7 (s, 1H, ylidene CH); 7.2—8.3 (m, $3H_{furan}$)
6a	3200, 3350 (NH_2); 2900, 2950 (CH and CH_3); 2190, 2200 (CN groups); 1715 (CO)	1.3 (t, 3H, CH_3); 3.6 (br., 2H, NH_2); 4.3 (q, 2H, CH_2); 6.65 (s, 1H, ylidene CH); 7.3—8.2 (m, $3H_{furan}$)
6b	3350, 3450 (NH_2); 2900 (CH); 2180, 2200 (CN groups); 1630 (CO)	Insoluble in available ^{1}H NMR solvents

(route a), ii) Michael addition to the activated double bond of **2** to afford the Michael adducts **7** (route b) (in our hands these adducts usually lose active methylene moiety affording the corresponding ylidene derivatives; cyclization of the Michael adducts into dihydropyridines followed by oxidation into pyridines, as has been reported in the literature,[7] could not be observed), or iii) addition of active methylene to the cyano group and cyclization which may afford the pyridine derivative **8** (route c). This route, which has been recently reported[11] for the reaction of **1a** and **b** with trichloroacetonitrile, did not also take place. The predominance of any of these routes is determined by relative activities of the ylidenic bond, the cyano group and also by the energy of the transition states leading to the end products. In complex systems like those we are dealing with it is very difficult to predect the predominant reaction path. The predominance of route a in our case can be attributed to a decrease in the reactivity of the double bond in **2** being counterbalanced by the effect of the electron-rich heterocycles.

This work shows again that the reaction of α,β-unsaturated nitriles with active methylene reagents do not necessarily follow the simple pattern of Michael addition and cyclization. Alternative structures should always be considered and strong arguments should be introduced when assigning structures to the products of these reactions.

Experimental

All melting points are uncorrected. IR spectrum were recorded (potassium bromide) on a Shimadzu-408 spectrophotometer. ^{1}H NMR were measured in a mixture of chloroform-*d* and methanol-d_4 on a Varian EM-390 spectrophotometer at 90 MHz with TMS as internal reference and chemical shifts are expressed as δ. Microanalytical data (C,H,N,S) were obtained from the Microanalytical Data Unit at Cairo University.

Condensation of Compounds 1a and b with Nitriles 2a—f. General Procedure: A suspension of compound **1a** or **b** (0.01 mol) and the appropriate nitrile **2a—f** (0.01 mol) in ethanol (50 ml) was treated with piperidine (1.0 ml). The reaction mixture was heated under reflux for four hours and then the mixture was evaporated in vacuo. The solid product, so formed, was collected by filtration and recrystallized from the appropriate solvent (see Table 1).

Condensation of 1b with Furfural: Furfural (0.01 mol) was added to a solution of compound **1b** (0.01 mol) in ethanol (50 ml) in the presence of piperidine (1.0 ml). The reaction mixture was heated under reflux for 4h and then evaporated in vacuo. The solid product, so formed, was collected by filtration and recrystallized from an ethanol-water mixture. The product was identical with compound **6a**.

References

1) F. Freeman, *Synthesis*, **1981**, 925.
2) K. U. Sadek, A. E. Mourad, A. E. Abdelhafeez, and M. H. Elnagdi, *Synthesis*, **1983**, 937.
3) M. H. Elnagdi, H. A. Elfahham, and G. E. H. Elgemeie, *Heterocycles*, **20**, 519 (1983).
4) G. E. H. Elgemeie, H. A. Elfahham, S. Elgamal, and M. H. Elnagdi, *Heterocycles*, **23**, 1999, (1985).
5) F. M. Abdelrazek, Z. E. Kandeel, K. M. H. Hilmy, and M. H. Elnagdi, *Synthesis*, **1985**, 432.
6) M. H. Elnagdi, M. R. H. Elmoghayar, E. A. A. Hafez, and H. H. Alnima, *J. Org. Chem.*, **40**, 2604 (1975).
7) S. M. Fahmy, S. O. Abdallah, and R. M. Mohareb, *Synthesis*, **1984**, 976.
8) M. R. H. Elmoghayar, M. K. A. Ibraheim, A. H. Elghandour, and M. H. Elnagdi, *Synthesis*, **1981**, 531.
9) K. U. Sadek, E. A. Hafez, A. E. Mourad, and M. H. Elnagdi, *Z. Naturforsch.*, **39b**, 824 (1984).
10) E. Frankland and H. Kolbe, *Justus Liebigs Ann. Chem.*, **65**, 269 (1848).
11) K. Gewald, M. Hain, and M. Gruner, *Chem. Ber.*, **118**, 2198 (1985).

 © 1988 The Chemical Society of Japan Bull. Chem. Soc. Jpn., 61, 543—547 (1988)

Kinetics of Oxidation of Aliphatic Ketones with Bromamine-T in Acid Medium

Dandinasivara Siddalingaiah MAHADEVAPPA* and Putta SWAMY
Department of Chemistry, University of Mysore, Manasagangothri, Mysore 570006, India
(Received September 26, 1986)

The kinetics of oxidation of 2-propanone, 2-butanone, 2-pentanone, 3-pentanone, and 4-methyl-2-pentanone by sodium salt of *N*-bromo-*p*-toluenesulfonamide or bromamine-T (BAT) in presence of $HClO_4$ was studied at 30 °C. The rate law is:

$$-\frac{d[BAT]}{dt} = k[BAT]^0[ketone]^1[H^+]^1.$$

Variation of ionic strength of medium or addition of reaction product *p*-toluenesulfonamide have no effect on the rate. The dielectric effect is positive. The acid-catalyzed enolization of ketone is assumed to be the rate-limiting step and enolization rate coefficients have been calculated. Proton inventory studies made in H_2O-D_2O mixtures have been employed to calculate the isotopic fractionation factors. Isokinetic temperature is 320 K indicating enthalpy as a controlling factor.

Although the analytical applications and kinetic studies of reactions of the organic chloramines, chloramine-T (CAT) and chloramine-B (CAB) are reviewed,[1] there is scant information in literature about the bromine analogues. As a part of our mechanistic studies of oxidation of substrates by *N*-bromo amides, we report the kinetics of oxidation of aliphatic ketones, 2-propanone, 2-butanone, 2-pentanone, 3-pentanone, and 4-methyl-2-pentanone by bromamine-T (p-$CH_3C_6H_4SO_2NBrNa \cdot 3H_2O$ or BAT) in presence of perchloric acid.

Experimental

Bromamine-T was prepared by the method reported in literature.[2] The authenticity of the product was confirmed by checking iodometrically and then through its mass spectrum and UV, IR, ^1H, and ^{13}C-spectral data. An aqueous solution of BAT was prepared, standardized by the iodometric method and was preserved in brown bottles to prevent its photochemical deterioration.

Analytical grade acetone was used without further purification while other ketones (SDS, India) were redistilled. Aqueous solutions of ketones (≈0.2M) (1 M=1 mol dm^{-3}) were prepared by exact weighing of required quantity of the compound. All other chemicals were of analytical grade. Triply distilled water was used in preparing aqueous solutions.

Regression analysis of experimental data (to get regression coefficient r and standard deviation of the estimate, S) carried out on a TDC-316 (16 bits) computer supplied by Trombay Electronics, India.

Kinetic Measurements. Rate studies were made at 30 °C and details are described in some of the previous communications.[3] The course of reaction was studied for about three half-lives. The pseudo-zero-order rate constants obtained from the plots of $\{[BAT]_0-[BAT]\}$ versus time were converted into standard zero-order constants k_0 through the equation, $k_0=SN/V$ where S is the slope of the plot, N the normality of thiosulfate used for iodometric estimation of unreacted BAT and V is the aliquot of reaction mixture titrated. The pseudo-first-order rate constants k' were calculated by the relation, $k'=k_0/[ketone]$. The rate constants were reproducible to ±3%.

Stoichiometry. Studies on stoichiometry indicated that 2-propanone consumes 3 moles of BAT per mole of ketone corresponding to the formation of HCOOH and CH_3COOH. The ratio was 2 : 1 in the case of other ketones indicating the formation of diketones.

$$\begin{matrix} CH_3 \\ CH_3 \end{matrix}\!\!>\!CO + 3\,RNBrNa + 3\,H_2O \longrightarrow HCOOH + CH_3COOH + 3\,RNH_2 + 3\,Na^+ + 3\,Br^-$$

$$\begin{matrix} C_2H_5 \\ C_2H_5 \end{matrix}\!\!>\!CO + 2\,RNBrNa + H_2O \longrightarrow CH_3COCOC_2H_5 + 2\,RNH_2 + 2\,Na^+ + 2\,Br^-$$

$$\begin{matrix} CH_3 \\ R'CH_2 \end{matrix}\!\!>\!CO + 2\,RNBrNa + H_2O \longrightarrow R'COCOCH_3 + 2\,RNH_2 + 2\,Na^+ + 2\,Br^-$$

where R'=$-CH_3$ for 2-butanone, $-CH_2CH_3$ for 2-pentanone, $-CH(CH_3)CH_3$ for 4-methyl-2-pentanone and R=p-$CH_3C_6H_4SO_2$.

The sulfonamide (reduction product of BAT) was detected by paper chromatography.[3] Formic and acetic acids were identified through TLC followed by conventional spot test analysis and were estimated by titration with standard alkali (Table 1). The reaction mixture was extracted with ether and the diketones present were detected through TLC followed by spot tests. Biacetyl (bp 88—91 °C) formed had a bp of

Table 1. Estimation of the Products of Oxidation of 2-Propanone and 2-Butanone by BAT in Acid Medium

Amount of acid found/10^{-3} mol[a]		Amount of 2,4-DNP hydrazone formed/g[b]	
Theoretical	Found	Theoretical	Found
4.0	3.7	1.50	1.42
6.7	6.5	2.90	2.72
8.0	7.9	5.50	5.10
10.0	8.8	—	—
12.0	11.7	—	—
16.0	15.9	—	—
20.0	19.0	—	—

a) From the reaction of 2-propanone. b) From the reaction of 2-butanone.

90 °C (corrected) and was assayed as its 2,4-DNP derivative (Table 1).

Results

At constant excess ketone concentration (0.05 mol dm^{-3}) and [$HClO_4$]=0.1 mol dm^{-3}, plots of {[BAT]$_0$ −[BAT]} versus time were found to be linear (r>0.9968 S<0.0184) passing through the origin indicating zero-order dependence on [oxidant]. The pseudo-zero-order rate constants are found to be truly constant for different oxidant concentrations indicating that oxidation of substrate is complete (Table 2). The rate increased with [ketone]$_0$ and linear (r>0.9979, S≦0.0120) with unit slope (Table 3). Further, a plot of k_0 versus [ketone]$_0$ is linear (r>0.9988, S≦0.0156) passing through the origin confirming the first-order dependence on [substrate]$_0$ in each case. Increase in [$HClO_4$] increased the rate of reaction and a plot of log k_0 versus log[$HClO_4$] was linear (r>0.9969, S≦0.0208) with a slope of unity (Table 4) showing a first-order dependence on [H^+]. When k_0 versus [$HClO_4$] was plotted, it gave a straight line passing through the origin (r>0.9980, S≦0.0234) indicating that the reaction takes place only through the acid-dependent path. When ionic strength of solution was varied by adding $NaClO_4$, the rate was unaffected (Tables 1 and 2). Addition of reaction product, p-toluenesulfonamide (RNH_2) or Br^- ion had no influence on the rate. The solvent composition was varied by adding methanol to the reaction mixture (0—40% v/v). The rate increased with increase in methanol concentration and a plot of log k_0 versus D^{-1}, where D is the dielectric constant of medium gives a straight line (r>0.9971 S≦0.0126) with a positive slope. Blank experiments showed that

Table 2. Effect of [BAT]$_0$ and Ionic Strength Variation on the Rate of Oxidation of Ketone at 30 °C
[ketone]$_0$=0.05 mol dm^{-3}; [$HClO_4$]=0.10 mol dm^{-3}; μ=0.5 mol dm^{-3}

[BAT]$_0$	k_0/10^{-7} mol dm^{-3} s^{-1}				
10^{-4} mol dm^{-3}	2-Propanone	2-Butanone	2-Pentanone	3-Pentanone	4-Methyl-2-pentanone
6.0	5.08	6.20	5.87	5.80	6.93
7.0	5.07	6.25	5.78	5.67	7.00
8.0	4.80	6.00	5.81	5.83	6.80
9.0	5.00	6.11	5.83	5.75	6.78
10.0	4.75	6.08	5.83	5.67	6.67
11.0	5.00	6.00	5.92	5.81	6.75
9.0[a)]	5.00	6.00	5.80	5.67	6.83
9.0[b)]	4.85	6.08	5.75	5.75	6.93
9.0[c)]	5.00	6.11	5.83	5.75	6.78
9.0[d)]	4.87	6.22	5.92	5.92	6.67

At ionic strength (μ)=0.20, a) 0.30, b) 0.50, c) and 0.80, d) mol dm^{-3}.

Table 3. Variation of [ketone] on the Reaction Rate at 30 °C.
[BAT]$_0$=9.0×10^{-4} mol dm^{-3}; [$HClO_4$]=0.10 mol dm^{-3}; μ=0.5 mol dm^{-3}

[ketone]$_0$	k_0/10^{-7} mol dm^{-3} s^{-1}				
10^{-2} mol dm^{-3}	2-Propanone	2-Butanone	2-Pentanone	3-Pentanone	4-Methyl-2-pentanone
3.0	3.00	3.60	3.44	3.39	4.07
4.0	3.94	4.53	4.80	4.44	5.33
5.0	5.00	6.11	5.83	5.75	6.78
6.0	5.93	7.33	7.00	7.02	8.00
7.0	6.89	8.56	8.50	8.11	9.67
9.0	9.11	10.91	10.33	10.13	12.17

Table 4. Variation of [$HClO_4$] on the Reaction Rate at 30 °C
[BAT]$_0$=9.0×10^{-4} mol dm^{-3}; [ketone]=0.05 mol dm^{-3}; μ=0.5 mol dm^{-3}

[$HClO_4$]$_0$	k_0/10^{-7} mol dm^{-3} s^{-1}				
10^{-2} mol dm^{-3}	2-Propanone	2-Butanone	2-Pentanone	3-Pentanone	4-Methyl-2-pentanone
6.0	2.78	3.83	3.50	3.33	4.17
8.0	4.00	5.00	5.04	4.60	5.42
10.0	5.00	6.11	5.83	5.75	6.78
12.0	5.80	7.67	7.11	6.50	8.40
14.0	6.67	9.17	8.33	8.11	9.83
16.0	8.00	9.83	9.50	9.00	10.83

Table 5. Kinetic and Thermodynamic Parameters for the Oxidation of Ketone by BAT in Perchloric Acid Medium

Ketone	E_a/kJ mol^{-1}	$\Delta H^{\neq}$/kJ mol^{-1}	$\Delta S^{\neq}$/J K^{-1} mol^{-1}	$\Delta G^{\neq}$/kJ mol^{-1}	log A
2-Propanone	77.1	74.6	−94.8	103.3	9.3
2-Butanone	71.3	68.7	−112.3	102.8	8.4
2-Pentanone	74.3	71.7	−102.7	102.9	8.9
3-Pentanone	78.3	75.8	−89.3	102.9	9.6
4-Methyl-2-pentanone	69.6	67.1	−117.2	102.6	8.1

Table 6. Proton Inventory Studies for 2-Propanone in H_2O–D_2O Mixture at 30°C. [BAT]$_0$=9.0×10^{-4} mol dm^{-3}, [ketone]=0.05 mol dm^{-3}; [$HClO_4$]=0.10 mol dm^{-3}; μ=0.5 mol dm^{-3}

Atom fraction of deuterium (n)	k_0^n/10^{-7} mol dm^{-3} s^{-1}
0.00	5.08
0.248	5.75
0.496	6.67
0.744	7.52
0.992	8.57

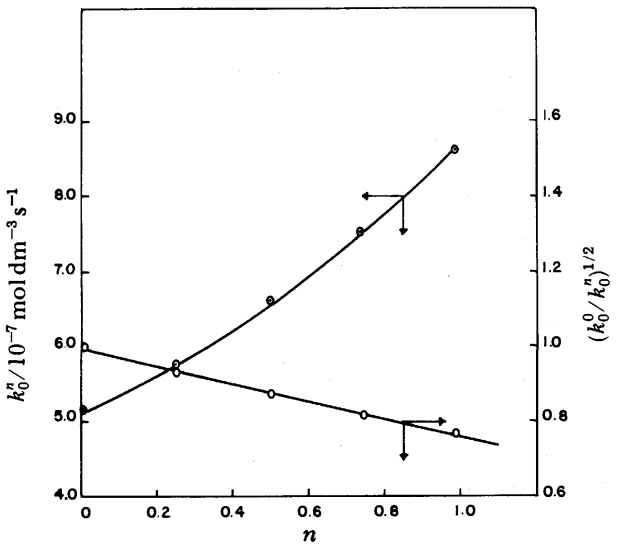

Fig. 1. Proton inventory plot for the oxidation of 2-propanone by BAT in H_2O–D_2O mixtures at 30°C. [BAT]$_0$=9.0×10^{-4} mol dm^{-3}; [ketone]$_0$=0.05 mol dm^{-3}; [$HClO_4$]=0.1 mol dm^{-3}.

methanol is not oxidized by BAT under the present experimental conditions.

Addition of reaction mixture to aqueous acrylamide did not initiate polymerization showing absence of free radicals.

The reaction was studied at different temperatures (293—313 K) and from the Arrhenius plots of log k' versus T^{-1} (r>0.9985, $S\leq$0.037) the kinetic parameters were calculated (Table 5).

Solvent isotope studies were made in D_2O medium. For 2-propanone value of k_0 in D_2O was 8.57×10^{-7} mol dm^{-3} s^{-1} while the corresponding value in H_2O was 5.08×10^{-7} mol dm^{-3} s^{-1} leading to a solvent isotope effect $(k_0)_{H_2O}/(k_0)_{D_2O}$=0.59 with other conditions as in Table 2. Proton inventory studies with 2-propanone as the probe were made in H_2O–D_2O mixtures and these results are shown in Table 6. The corresponding proton inventory plot relating to the rate constant k_0^n in a solvent mixture of deuterium atom fraction n is given in Fig. 1.

Discussion

Bromamine-T is analogous[5] to chloramine-T and chloramine-B and with the assumption of similar equilibria in acidified aqueous solutions of oxidant, the possible oxidizing species in these solutions are RNHBr, $RNBr_2$, and HOBr where R=p-$CH_3C_6H_4SO_2$. But the zero-order dependence on [oxidant] precludes speculation about the identity of kinetically active species. It is likely that the free acid RNHBr which is in higher concentrations[5] compared to the other species would oxidize the ketones in a fast step.

Ketones form oxonium salts on protonation in presence of strong acids leading to enolization:

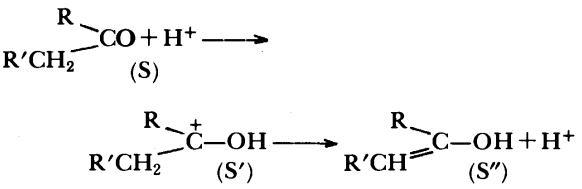

(1)

Here S represents the ketone, S′ its conjugate acid and S″ its enolic form.

The first-order dependence of rate on [ketone] and [H^+] and the zero-order in [BAT]$_0$ shows that the traditional mechanism of Bell and co-workers[6] is followed (Scheme 1):

$$S + H^+ \underset{k_{-1}}{\overset{k_1}{\rightleftharpoons}} S' \text{ (fast)} \quad \text{(i)}$$

$$S' \xrightarrow{k_2} S'' + H^+ \text{ (slow and r.l.s.)} \quad \text{(ii)}$$

$$S'' + n\,RNBrNa \xrightarrow{k_3} n\,RNH_2 + \text{Products (fast)} \quad \text{(iii)}$$

Scheme 1.

Here n=3 for 2-propanone and 2 for other ketones.

Scheme 1 leads to rate law (2) which is in agreement with the observed stoichiometry and kinetic orders:

$$-\frac{d[BAT]}{dt}=\frac{2k_1k_2}{k_{-1}+k_2}[\text{ketone}][H^+] \quad (2)$$

The positive dielectric effect indicates a charge dispersal in transition state pointing towards an ion-dipole reaction and is also in general agreement about its influence[7] on keto-enol equilibria.

The proposed mechanism is also supported by the magnitude of solvent isotope effect. The rate is enhanced in D_2O medium implying preequilibrium fast proton transfer with specific acid catalysis. It is well-known[8] that D_3O^+ is a stronger acid than the hydronium ion and hence a rate enhancement in D_2O should be expected. This is in agreement with the carbonium ion character of the transition state (Eq. 1) and lends support to the participation of enol form in the rate-limiting step. The proton inventory plot (Fig. 1) could throw light on the nature of transition state.[9,10] The dependence of rate constant k_0^n on n, the atom fraction of deuterium in a solvent mixture containing H_2O and D_2O is given by Eq. 3:

$$\frac{k_0^n}{k_0^0}=\frac{\prod_{\text{TS}}(1-n+n\phi_i)}{\prod_{\text{RS}}(1-n+n\phi_j)} \quad (3)$$

Here ϕ_i and ϕ_j are isotopic fractionation factors for isotopically exchangeable hydrogenic sites in the transition state (TS) and reactant site (RS) respectively. If it is assumed that the reaction proceeds through a single transition state, Eq. 3 takes the forms shown by Eqs. 4 and 5:

$$k_0^n=k_0^0(1-n+n\phi_j)^{-2} \quad (4)$$

$$\left(\frac{k_0^0}{k_0^n}\right)^{1/2}=[1+n(\phi_j-1)] \quad (5)$$

Equation 5 indicates a linear relation between $(k_0^0/k_0^n)^{1/2}$ and n and this is shown in Fig. 1 (r=0.9988, S=0.0391). The slope (ϕ_j-1)=−0.24, from which the fractionation factor is found to be 0.76. Kresge and Allred[11] have obtained a value of 0.67 for the fractionation constants of $HClO_4$ in H_2O-D_2O mixtures, while Gold[12] reported a value of 0.69±0.02. Considering the diversity of procedures employed, it may be assumed that there is agreement between the values and the fractionation factor refers to $HClO_4$. Exchange of ketone with D_2O was also checked for a primary isotope effect but this was found to be negligible for the duration of experiment. However, a trial experiment with ordinary acetone equilibrated in 60% D_2O over a period of 48 h showed that k_0=2.51×10^{-7} mol l^{-1} s^{-1} while the corresponding blank value (zero time) was 5.18×10^{-7} mol l^{-1} s^{-1} giving k_H/k_D=2.1. Reitz[13] has shown that acetone-d_6 reacts 7.7 times slower than ordinary acetone under identical conditions. It may therefore be inferred that exchange to an extent of about 27% has occurred in 48 h.

The reaction is characterized by a moderate energy of activation. The large negative ΔS^* values point towards a rigid transition state. Satisfactory structure-reactivity correlations cannot be drawn in the present studies due to the zero-order observed in [oxidant]$_0$. Values of the first-order rate constant $k'=k_0/[\text{ketone}]$ for the different ketones are almost the same indicating the absence of significant effects of structure on the enolization of ketones (Table 7). The enolization coefficients, $k''=k_s/[\text{ketone}][H^+]$ are shown in Table 7. The values for 2-propanone and 3-pentanone are 10.0×10^{-5} and 11.5×10^{-5} dm^3 mol^{-1} s^{-1} at 30 °C which are comparable with those obtained by Toullec and Dubois[14] in H_2SO_4 at 25 °C.

Table 5 shows that the activation parameters ΔH^* and ΔS^* decrease in the order:

4-methyl-2-pentanone<2-butanone
<2-pentanone<2-propanone<3-pentanone

An isokinetic relationship can be envisaged since a plot of ΔH^* versus $-\Delta S^*$ is linear (r=0.9983, S=0.24). From the slope, the value of isokinetic temperature β is 320 K. The relationship was tested through the Exner criterion[15] by plotting log k_{30} versus log k_{20} and was found to be genuine. From this plot, β was found to be 350 K. The value of β is slightly higher than the experimental temperature (303 K) indicating enthalpy as a controlling factor. Current views[16] do not attach much significance to the concept of isokinetic temperature, as the Exner criterion is a necessary follow up factor of the isokinetic relation. The constancy of ΔG^* values however indicates that a similar mechanism is operative in the oxidation of ketones by BAT.

It is noted in the present studies that a zero-order

Table 7. Enolization Coefficients Observed during the Oxidation of Aliphatic Ketones by BAT at Different Temperatures in Presence of 0.1 M $HClO_4$

Ketone	$k'/10^{-6}$ s^{-1}					$k''/10^{-5}$ dm^3 mol^{-2} s^{-1}				
	293	298	303	308	313	293	298	303	308	313
2-Propanone	3.80	5.34	10.00	16.00	28.00	3.80	5.34	10.00	16.00	28.00
2-Butanone	4.66	6.94	12.22	20.26	32.00	4.66	6.94	12.22	20.26	32.00
2-Pentanone	4.38	7.06	11.66	18.00	32.00	4.38	7.06	11.66	18.00	32.00
3-Pentanone	4.26	6.94	11.50	20.00	33.34	4.26	6.94	11.50	20.00	33.34
4-Methyl-2-pentanone	5.34	8.34	13.56	19.66	34.66	5.34	8.34	13.56	19.66	34.66

dependence on $[BAT]_0$ indicates the operation of the traditional mechanism of Bell and co-workers[6] with enolization as rate-limiting step, while with the chlorine analogue, addition of halogen derivative takes place in the rate determining stage. A similar observation is made in the oxidation of dimethyl sulfoxide by the chloramines[17] and bromamines,[18] which probably is a reflection on the relative electrophilicity of the halonium cations, Cl^+ and Br^+ of the compounds, which are involved in the reaction sequence.

One of us (PS) gratefully acknowledges the award of a Post-graduate Research Fellowship to him from the University of Mysore. The authors thank the referees for valuable suggestions.

References

1) M. M. Campbell and G. Johnson, *Chem. Rev.*, **78**, 65 (1978); K. K. Banerji, B. Jayaram, and D. S. Mahadevappa, *J. Sci. Ind. Res.*, in press; B. T. Gowda and D. S. Mahadevappa, *J. Chem. Soc., Perkin Trans 2*, **1983**, 323.

2) C. G. R. Nair, R. Lalithakumari, and P. I. Senan, *Talanta*, **25**, 525 (1978).

3) D. S. Mahadevappa, S. Ananda, M. B. M. Bowda, and K. S. Rangappa, *J. Indian Chem. Soc.*, **61**, 323 (1984); *Indian J. Chem.*, **23A**, 325 (1984); D. S. Mahadevappa and K. Mohan, *Oxidation Comm.*, **8**, 207 (1985/86); *Tetrahedron*, **42**, 4857 (1986).

4) F. Feigl, "Spot Tests in Organic Analysis," Elsevier, Amsterdam (1956), pp. 205, 340.

5) E. Bishop and V. J. Jennings, *Talanta*, **1**, 197 (1958).

6) R. P. Bell and G. Archer, *J. Chem. Soc.*, **1959**, 3228; R. P. Bell and K. Yates, *ibid.*, **1962**, 1927.

7) E. S. Gould, "Mechanism and Structure in Organic Chemistry," Holt, Rinehart and Winston, New York (1964), p. 380.

8) "Isotope Effect in Chemical Reactions," ed by C. J. Collins and N. S. Bowman, Van-Nostrand-Reinhold, New York (1970), p. 267.

9) W. J. Albery and M. H. Davies, *J. Chem. Soc., Faraday Trans.*, **68**, 167 (1972).

10) G. Gopalakrishnan and J. L. Hogg, *J. Org. Chem.*, **50**, 1206 (1985).

11) A. J. Kresge and A. L. Allred, *J. Am. Chem. Soc.*, **85**, 1541 (1963).

12) V. Gold, *Proc. Chem. Soc. (London)*, **1963**, 141.

13) O. Reitz, *Z. Phys. Chem.*, **A179**, 119 (1937).

14) J. Toullec and J. E. Dubois, *Tetrahedron*, **29**, 2851, 2859 (1973).

15) O. Exner, *Collect. Czech. Chem. Commun.*, **29**, 1094 (1964).

16) J. E. Leffler, *J. Org. Chem.*, **31**, 533 (1966).

17) D. S. Mahadevappa, M. B. Jadhav, and H. M. K. Naidu, *Int. J. Chem. Kinet.*, **11**, 261 (1979).

18) D. S. Mahadevappa, S. Ananda, A. S. A. Murthy, and K. S. Rangappa, *Tetrahedron*, **40**, 1673 (1984).

 © 1988 The Chemical Society of Japan Bull. Chem. Soc. Jpn., 61, 549—556 (1988)

Molecular Motion in Some Hydrogen-Bonded Complexes of Trichloroacetic Acid as Studied by ^{35}Cl-NQR

Bolesław NOGAJ
Institute of Physics, A. Mickiewicz University, Grunwaldzka 6, 60-780 Poznań, Poland
(Received September 29, 1986)

The paper presents the results of ^{35}Cl-NQR frequency and spin-lattice relaxation time measurements as a function of the temperature in some solid hydrogen-bonded complexes: Trichloroacetic acid (TCA)-3-cyanopyridine, TCA-4-methylpyridine and $[CCl_3COO\cdots H\cdots OOCCCl_3]^-[K]^+$. The activation energies, E_a, for hindered rotation of CCl_3 group of the TCA molecule were determined. Employing the available E_a data for the other complexes of this type a linear dependence between the activation energy and ^{35}Cl-NQR frequency shift was obtained. This dependence allowed us to find $E_a=f(\Delta pK_a)$ as well as $E_a=f'(P)$ where P is the proton transfer degree. The influence of hydrogen bond on the potential barrier of the rotating CCl_3 groups of TCA in the complexes studied is also discussed.

A series of solid complexes formed by trichloroacetic acid (TCA) with different organic bases ranging from very weak to very strong, was investigated in Refs. 1—5. The purpose of these works was to analyze the proton transfer process in the series investigated via its effect on the chlorine NQR parameters. In the systems studied the hydrogen bond was found to change from the covalent form A–H···B through the symmetric hydrogen bond $A^{\delta-}\cdots H\cdots B^{\delta+}$ to the totally polar form $A^-\cdots H\text{-}B^+$. The more polar the hydrogen bond the lower is the mean NQR frequency of the TCA ^{35}Cl nuclei. The three ^{35}Cl-NQR lines observed for most of the complexes are the indication of crystallographic nonequivalence of the three chlorine atoms of the CCl_3 group in TCA complexed with a base. When the sample temperature is increased the CCl_3 groups would perform hindered rotations across potential barriers the heights of which are likely to depend on the polarity of the hydrogen bonding in the complexes considered. Temperature investigations of ^{35}Cl-NQR spin-lattice relaxation times T_1 allow determination of the activation energies for these hindered rotations. These, in turn should provide helpful data to distinguish between intra- and intermolecular effects in hydrogen-bonded complexes.

In a previous unpublished work, we had measured the ν_Q and T_1 temperature dependences of the ^{35}Cl-NQR in two TCA–B complexes (B=3-cyanopyridine and 4-methylpyridine) both being strongly hydrogen bonded. Moreover we had measured $\nu_Q(T)$ and $T_1(T)$ for complex $[CCl_3COO\cdots H\cdots OOCCCl_3]^-[K]^+$ which has a symmetric hydrogen bond.[6] Later, Fichtner et al.[3] provided further results on TCA complexes including weaker ones and they correlated the ^{35}Cl-NQR frequency shift and the ^{35}Cl-NQR line fading-out temperature for each complex. These facts led us to search for similar correlation between the activation energies and the frequency shifts, the frequency shifts and the $\Delta pK_a=pK_a(\text{base})-pK_a(\text{TCA})$ and consequently the activation energies and the ΔpK_a. In this paper we present the results of this investigation.

Experimental

The complexes with trichloroacetic acid were obtained in a crystalline form by dissolving the anhydrous bases in a small volume of a mixture of chloroform and carbon tetrachloride (1 : 3) and adding the acid.[5] The resulting precipitates were recrystallized from the chloroform-carbon tetrachloride mixture (1 : 3), and analysis results were satisfactory. Melting points were determined with a hot stage microscope and were presented in Ref. 5.

Measurements of ^{35}Cl-NQR frequency, ν_Q, and spin-lattice relaxation time, T_1, were performed on a laboratory built pulse spectrometer. The $\pi/2$-τ-π sequence was used, with typical pulse widths of 15 and 30 μs respectively. The output RF power of the transmitter was of the order of 1 kW. In order to improve the signal to noise ratio and permit signal recording, a two-channel boxcar integrator with a digital memory was used. High stability of the pulse duration, pulse intervals and sequence repetition period was ensured by a programmed digital generator enabling automatization of the measurements. The ^{35}Cl-NQR frequency was measured with an accuracy of ±1 kHz.

The sample was contained in a copper cell in a temperature-controlled cryostat which provided a temperature stability better than 0.1 K and an absolute accuracy of 0.2 K.

Selection of TCA Complexes for Molecular Motion Studies

In Ref. 5 66 complexes are reported among which three were investigated during the end of the experimental period so that they were not taken into account in the calculations we present in this paper. Consequently, only 63 complexes appear in Fig. 1. ^{35}Cl-NQR spectra of all complexes reveal different but always negative shift of the mean ^{35}Cl-NQR frequency with respect to the mean frequency for pure TCA, i.e. $\Delta\bar{\nu}_Q=\bar{\nu}_Q-\bar{\nu}_{TCA}<0$. The relation between $\Delta\bar{\nu}_Q$ and ΔpK_a allows us to draw the curve presented in Fig.1 which illustrates the proton transfer process in the hydrogen bond. The solid line in Fig. 1 has been drawn according to the equation:[5]

$$\Delta\bar{\nu}_Q=\frac{(\bar{\nu}_{HB}-\bar{\nu}_{TCA})+(\bar{\nu}_{PT}-\bar{\nu}_{TCA})\times 10^{\xi\Delta pK_a+C}}{1+10^{\xi\Delta pK_a+C}} \quad (1)$$

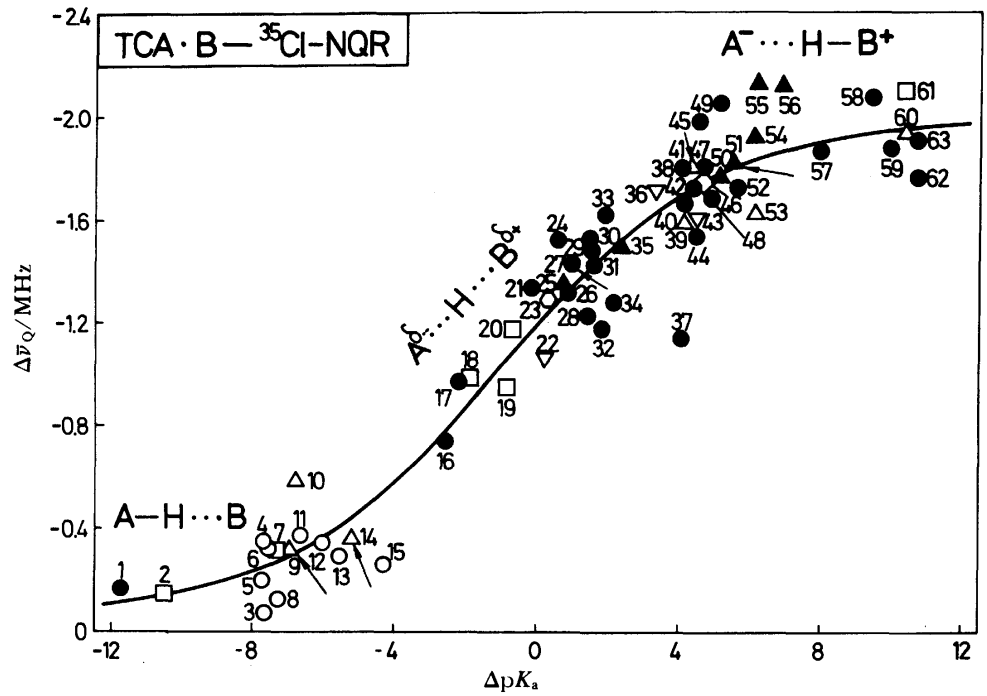

Fig. 1. Shift in mean ^{35}Cl-NQR frequency of the TCA–B complexes versus ΔpK_a. The complexes are labelled according to their base as follows; 1: nitrobenzene, 2: acetonitrile, 3: 2-methylbenzoic acid, 4: acetone, 5: benzoic acid, 6: benzaldehyde, 7: cyclohexanone, 8: phenol, 9: 2-methylbenzaldehyde, 10: 4-methylbenzaldehyde, 11: acetophenone, 12: *p*-anisaldehyde, 13: ethyl acetate, 14: 2,4,6-trimethylbenzaldehyde, 15: *t*-butyl alcohol, 16: triphenylphosphine oxide, 17: 4-nitropyridine *N*-oxide, 18: acetamide, 19: 2-pyrrolidone, 20: *N*,*N*-dimethylacetamide, 21: 4-chloropyridine *N*-oxide, 22: 2-bromopyridine, 23: pyridine *N*-oxide, 24: 3-methylpyridine *N*-oxide, 25: 4-methylpyridine *N*-oxide, 26: 2,6-dimethylpyridine *N*-oxide, 27: 3-cyanopyridine, 28: 4-cyanopyridine, 29: 2,4,6-trimethylpyridine *N*-oxide, 30: 4-benzyloxypyridine *N*-oxide, 31: 4-methoxypyridine *N*-oxide, 32: 4-hydroxypyridine *N*-oxide, 33: 4-methoxy-2-methylpyridine *N*-oxide, 34: 4-phenoxypyridine *N*-oxide, 35: 3-bromopyridine, 36: benzo[*h*]quinoline, 37: cytosine, 38: 8-methylquinoline, 39: aniline, 40: trimethylamine oxide, 41: *N*-methylaniline, 42: 8-quinolinol, 43: quinoline, 44: *N*,*N*-dimethyldodecylamine oxide, 45: 7-methylquinoline, 46: pyridine, 47: 6-methylquinoline, 48: isoquinoline, 49: 3-methylisoquinoline, 50: 4-methylquinoline, 51: 4-methylpyridine, 52: 3,5-dimethylpyridine, 53: *N*,*N*-diethylaniline, 54: 2,4-dimethylpyridine, 55: 2,6-dimethylpyridine, 56: 2,4,6-trimethylpyridine, 57: morpholine, 58: tributylamine, 59: *N*-ethylpiperidine, 60: triethylamine, 61: triethylamine, 62: piperidine, 63: dibutylamine.
Solid line represents the fit with Eq. 1. The complexes studied in this work are denoted by arrows. References: ○;[7] ◇;[8] ;[9] □;[10] ▲;[1] △;[3] ▽;[4] ●.[5]

where (for group of 63 complexes) $\bar{\nu}_{HB}$= 40.066 MHz, $\bar{\nu}_{PT}$=38.123 MHz, $\bar{\nu}_{TCA}$=40.124 MHz, ξ=0.145 and C'= 0.146.

As it has been already mentioned in the introduction the aim of the paper is to find the correlation between the character of the hydrogen bond and the height of the potential barrier for hindered rotation of CCl_3 groups. The investigation was performed on complexes of different degree of proton transfer corresponding to different points on the curve $\Delta\bar{\nu}_Q = f(\Delta pK_a)$ (Fig. 1). The complexes chosen for this investigation are shown by arrows in Fig. 1. They are also listed in Table 1 which gives the ^{35}Cl-NQR frequencies (ν_Q), mean frequencies ($\bar{\nu}_Q$) and corresponding frequency shifts with respect to pure TCA, and the pK_a of the bases. Moreover, Table 1 gives values of proton transfer degree, P, in the hydrogen bond of the complexes TCA-B, determined from the relation used by Chihara and Nakamura in Ref. 8:

$$\bar{\nu}_Q = \bar{\nu}_{HB} + P(\bar{\nu}_{PT} - \bar{\nu}_{HB}). \quad (2)$$

The analysis was performed for the complexes with a weak hydrogen bond (P=0.12; 0.14) as well as for the complexes with almost total proton transfer (P=0.88; 0.90). This table also gives the data for $[A\cdots H\cdots A]^-$-$[Me]^+$ type complexes in which the hydrogen bond remains unchanged while the cation changes. Investigation of this group of compounds will be only used to verify our considerations related to the TCA-B type

Table 1. ^{35}Cl-NQR Frequencies (ν_Q) of Pure TCA and a Series of Complexes of Type TCA-B and $[A\cdots H\cdots A]^-[Me]^+$ (at 77 K) Together with Mean Frequencies ($\bar{\nu}_Q$), Frequency Shifts with Respect to Pure TCA ($\Delta\bar{\nu}_Q$), pK_a Values of the Bases, Values of the Proton Transfer Degree (P) and Calculated Activation Energies for the CCl_3 Group Hindered Rotation (E_a)
^{35}Cl-NQR Frequencies and pK_a Values Were Taken from Refs. 1—3, 5, 6 and This Work

No.	Complex	ν_Q/MHz	$\bar{\nu}_Q$/MHz	$\Delta\bar{\nu}_Q$/MHz	pK_a of base	P	E_a / kJ mol^{-1}
	Trichloroacetic acid (≡TCA)	39.969 40.162 40.242	40.124	0	0.51	—	18.0[a]
1	TCA-2-methylbenzaldehyde	39.651 39.651 40.121	39.808	−0.316	−6.50	0.12	8.3[c]
2	TCA-2,4,6-trimethylbenzaldehyde	39.491 39.624 40.176	39.764	−0.360	−4.70	0.14	10.7[c]
3	TCA-3-cyanopyridine	38.111 38.969 39.023	38.701	−1.423	+1.45	0.69	22.2[b]
4	TCA-*N*-methylaniline	38.086 38.179 38.729	38.331	−1.793	+4.85	0.88	21.9[c]
5	TCA-4-methylpyridine	37.867 38.035 39.002	38.301	−1.823	+6.02	0.90	27.8[b]
6	$(CCl_3COO)_2HRb$	39.121 39.226 40.187	39.511	−0.613	—	—	23.8[c]
7	$(CCl_3COO)_2HK$	39.114 39.146 39.749	39.336	−0.788	—	—	36.7[b]
8	$(CCl_3COO)_2HTl$	39.044 39.099 39.824	39.322	−0.802	—	—	41.6[c]

a) Calculated from $T_1(T)$ dependence (Ref. 13). b) Calculated from $T_1(T)$ dependence (this work). c) Calculated from $\delta\nu_Q$ (T)dependence (Ref. 3).

complexes.

Results of ^{35}Cl-NQR Frequency and Spin-Lattice Relaxation Study and Their Discussion

For compounds **3**, **5**, and **7** presented in Table 1 the temperature measurements of ^{35}Cl-NQR frequencies and spin-lattice relaxation times, were performed. The results of these measurements are shown in Figs. 2—6. For other complexes we employed the data available from Ref. 3. The ^{35}Cl-NQR spectra of all the complexes analyzed (Table 1) are composed of three lines which, in the case of TCA-B complexes, proves crystallographic nonequivalence of the sites of the three Cl atoms of CCl_3 group in TCA molecule. Moreover, only three lines in ^{35}Cl-NQR spectrum of $[A\cdots H\cdots A]^-[Me]^+$ complexes proves that the hydrogen bond in the dimer ion $[CCl_3COO\cdots H\cdots OOCCCl_3]^-$ is symmetrical. Each of the chlorine atoms of CCl_3 group performs torsional vibrations (librations), even at very low temperature. The amplitude of the librations increases with increasing temperature which results in still greater averaging of the electric field gradient evidenced as a decrease in ^{35}Cl-NQR frequency. At higher temperatures the energy of thermal excitations of CCl_3 group is sufficient to overcome the potential barrier separating the equilibrium sites of Cl atoms in the crystal.

The rate of hindered rotation of CCl_3 groups shows an exponential increase with temperature. Introducing the correlation time τ_c, which is a measure of the time a given CCl_3 group spends in the equilibrium position, we can consider the situation where $\tau_c > (2\pi\bar{\nu}_Q)^{-1} \approx 4\times10^{-9}$ s. In such a case the jumps of Cl atoms are not very frequent and the quadrupole transitions

Table 2. Parameters of the Fit of Experimental $\nu_Q(T)$ Values with Bayer Formula —Eq. 3 and Fade-Out Temperatures of the Resonance Lines

Complex	^{35}Cl-NQR line	a/MHz	b/MHz	c/K	$T_{\text{fade-out}}$/K
TCA-3-cyanopyridine	ν_1	38.200	1.912	240.06	145
	ν_2	39.030	3.708	313.05	
	ν_3	39.099	3.170	289.47	
TCA-4-methylpyridine	ν_1	38.031	1.402	173.08	145
	ν_2	38.170	1.270	179.88	
	ν_3	39.099	1.061	189.91	
$(CCl_3COO)_2HK$	ν_1	39.163	1.654	263.04	240
	ν_2	39.179	1.079	266.21	
	ν_3	39.862	1.040	183.75	

can occur if the CCl_3 group is in the stable equilibrium. That is why the slow hindered rotation does not influence the ^{35}Cl-NQR frequency. Thus, librations are mainly responsible for a decrease in NQR frequency with increasing temperature. This was the assumption taken by Bayer[11] who moreover treated a molecule as a quantum harmonic oscillator and obtained the following expression for the temperature dependence of NQR frequency:

$$\nu_Q(T) = a - \frac{b}{\exp(c/T)-1}, \tag{3}$$

$$a = \nu_Q(0);\ b = \frac{6\hbar\nu_Q(0)}{4I\omega_i - 3\hbar};\ c = \frac{\hbar\omega_i}{k}, \tag{4,5,6}$$

$\nu_Q(0)$ is the NQR frequency at 0 K, I is the relevant moment of inertia, ω_i is the librational frequency of the atomic group (here CCl_3). The experimental data of $\nu_Q(T)$ were fit with Eq. 3 (see Figs. 2—4). The appropriate fit parameters are given in Table 2. The data were also fit with other dependences that took into account the unharmonic character of vibrations but using the harmonic approximation of Eq. 3 is quite sufficient in the range of temperature studied which extend from 77 K to the fade-out temperature. At this temperature the lines became so broad and their intensity so small that they reach the sensitivity limit of the spectrometer. This happens when the frequency of the molecular reorientations is of the order of magnitude of the NQR line width. If the temperature is still increased the lines become unobservable. The highest fade-out temperature in this series is 240 K obtained for $(CCl_3COO)_2HK$ (Table 2; Figs. 2—4).

Let us consider now the influence of librations and hindered rotation discussed above on the NQR spin-lattice relaxation. According to Bayer[11] the fluctuations of the electric field gradient caused by librational motions lead to the following relation between T_1 and T:

$$T_1^{-1} = aT^n, \tag{7}$$

where a is a constant, n is usually close to 2. Abrupt changes in electric field gradient due to hindered rotation of molecular groups containing quadrupole nuclei lead to the exponential temperature dependence of relaxation time:[12]

$$T_1^{-1} = b \exp(-E_a/RT), \tag{8}$$

where b is a constant, R the gas constant, and E_a the activation energy of the hindered rotation.

As follows from the dependences $T_1^{-1}(T)$ obtained (Figs. 5—7), both mechanisms of quadrupole spin-lattice relaxation discussed above take place in the complexes studied. Their contribution to the relaxation process add up and this may be expressed as:

$$T_1^{-1} = aT^n + b \exp(-E_a/RT). \tag{9}$$

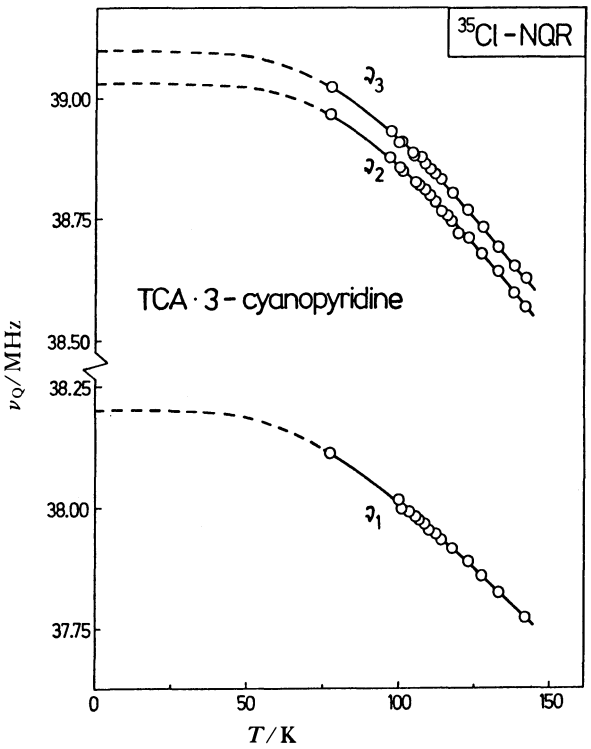

Fig. 2. Temperature dependence of the ^{35}Cl-NQR frequency in TCA-3-cyanopyridine complex. Solid and partly broken line represents the fit with Eq. 3; fitting parameters are given in Table 2.

The appropriate fit parameters between the experimental data of $T_1^{-1}(T)$ and Eq. 9 are given in Table 3. For us, most important are the values of the activation energy for hindered rotation of CCl_3 groups (E_a) in the complexes studied. As follows from Figs. 5—7 the relaxation process may be described at low temperatures by the first term of Eq. 9 only. This term characterizes the influence of librations on the relaxation. For higher temperatures, in the case of TCA-B complexes studied above 110—120 K while for $(CCl_3COO)_2HK$ complex above 170 K, the mechanism of hindered rotation becomes dominating. In these temperature ranges the dependence $T_1^{-1}(T)$ is described by the exponential part of Eq. 9. For the sake of comparison the results of $T_1^{-1}(T)$ for TCA[13] are presented (Table 3). However, this acid cannot be regarded as belonging neither to the TCA-B group nor to the group of $[A\cdots H\cdots A]^-[Me]^+$ complexes. Trichloroacetic acid is a dimer in which two hydrogen bonds of O-H ··· O type occur. It can only be used as a reference standard in investigations of the mean ^{35}Cl-NQR frequency shift in the analyzed complexes. A comparison between $T_1^{-1}(T)$ dependences obtained for the complexes analyzed and the dependence for TCA, taking

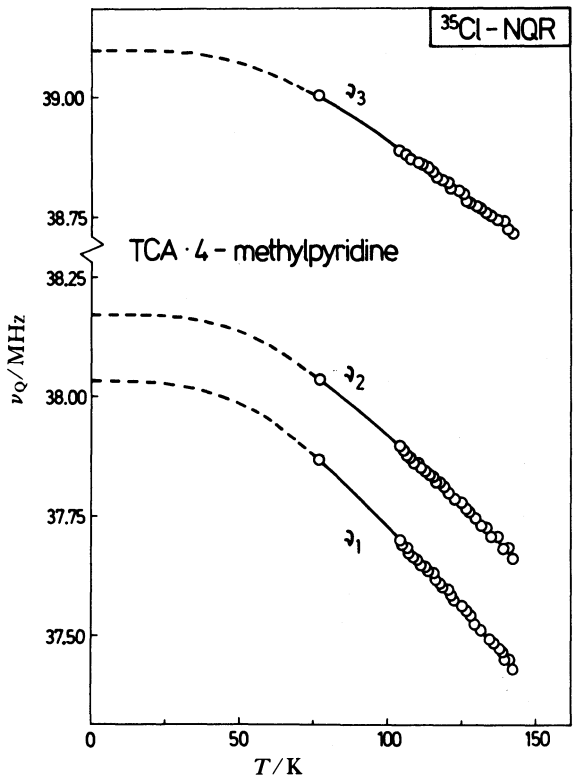

Fig. 3. Temperature dependence of the ^{35}Cl-NQR frequency in TCA-4-methylpyridine complex. Solid and partly broken line represents the fit with Eq. 3; fitting parameters are given in Table 2.

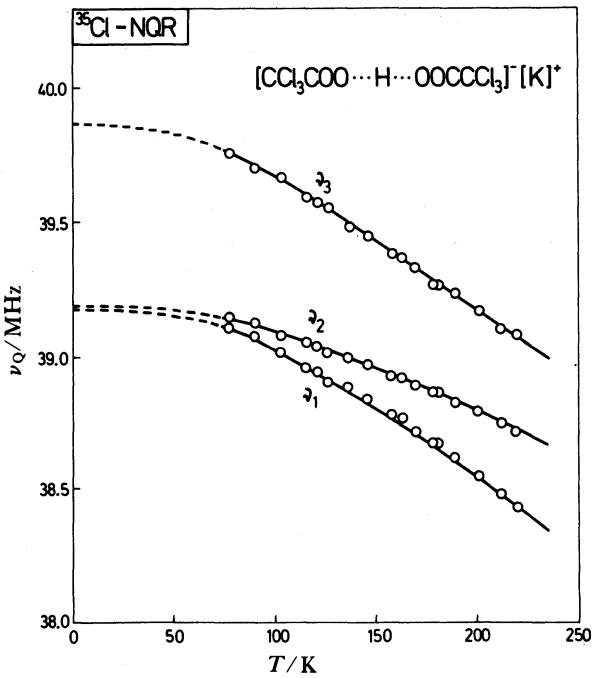

Fig. 4. Temperature dependence of the ^{35}Cl-NQR frequency in $(CCl_3COO)_2HK$. Solid and partly broken line represents the fit with Eq. 3; fitting parameters are given in Table 2.

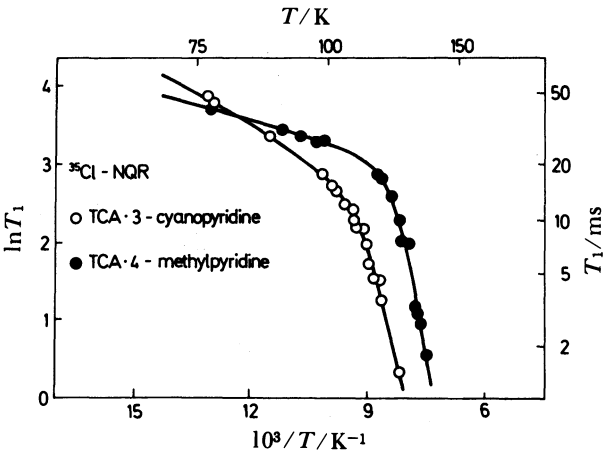

Fig. 5. Temperature dependence of ^{35}Cl-NQR spin-lattice relaxation time in complexes: TCA-3-cyanopyridine and TCA-4-methylpyridine. Solid line is the fit with Eq. 9; fitting parameters are given in Table 3.

Table 3. Parameters of the Fit of Experimental $T_1(T)$ Values with Eq. 9

Complex	$a/s^{-1}K^{-n}$	n	b/s^{-1}	$E_a/kJ\,mol^{-1}$
TCA[a]	6.88×10^{-3}	2	5.2×10^{10}	18.00
TCA-3-cyanopyridine	2.991×10^{-6}	3.64	1.914×10^{12}	22.22
TCA-4-methylpyridine	1.298×10^{-8}	1.74	4.167×10^{13}	27.82
$(CCl_3COO)_2HK$	7.012×10^{-3}	1.90	1.644×10^{13}	36.66

a) Ref. 13.

into account the $T_{\text{fade-out}}$, is given in Fig. 7.

As it has been already mentioned the main aim of the investigation of dynamics of hydrogen-bonded complexes is the determination of the activation energy for the rotation of the CCl_3 group and an attempt to correlate the E_a values with the nature of the hydrogen bond. Table 1 gives the values of E_a for all the complexes analyzed in this paper. An attempt has been made to relate these values with the shift of the mean ^{35}Cl-NQR frequency for TCA-B type complexes (Fig. 8). As a result we have found that with increasing $|\Delta\bar{\nu}_Q|$ i.e. with the hydrogen bond getting more polar the activation energy for CCl_3 group rotation increases. This relation can be described by the following linear expression:

$$E_a = a\Delta\bar{\nu}_Q + b, \qquad (10)$$

where $a=-10.7$ kJ mol^{-1} MHz^{-1} and $b=6.0$ kJ mol^{-1}. This kind of correlation has been supported by the linear dependence between E_a and $\Delta\bar{\nu}_Q$ for the complexes of the type $[CCl_3COO\cdots H\cdots OOCCCl_3]^-$ $[Me]^+$ (Fig. 9). This linear dependence can also be expressed by Eq. 10 but with $a=-85.5$ kJ mol^{-1} MHz^{-1}, $b=-28.8$ kJ mol^{-1}. Despite the fact that for both groups of complexes studied the dependence $E_a(\Delta\bar{\nu}_Q)$ has a linear character we cannot expect an agreement as to the numerical values of E_a, a, and b for the two groups. They are essentially different. In the group of TCA-B complexes the changing nature of hydrogen bond results in an increase in the potential barrier for the rotating CCl_3 groups. In the group of $[CCl_3COO\cdots H\cdots OOCCCl_3]^-$ $[Me]^+$ complexes the hydrogen-bond

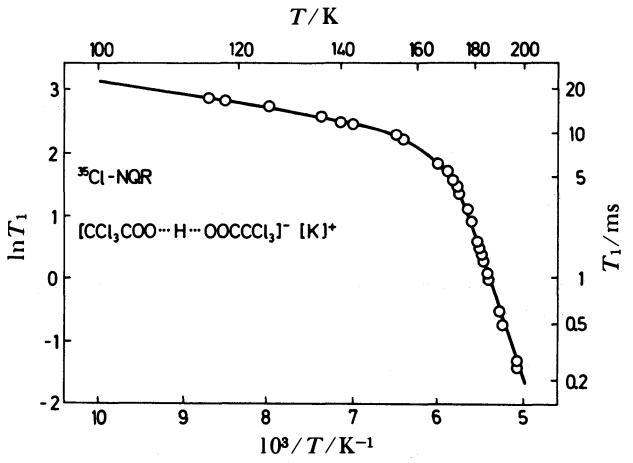

Fig. 6. Temperature dependence of ^{35}Cl-NQR spin-lattice relaxation time in $(CCl_3COO)_2HK$. Solid line is the fit with Eq. 9; fitting parameters are given in Table 3.

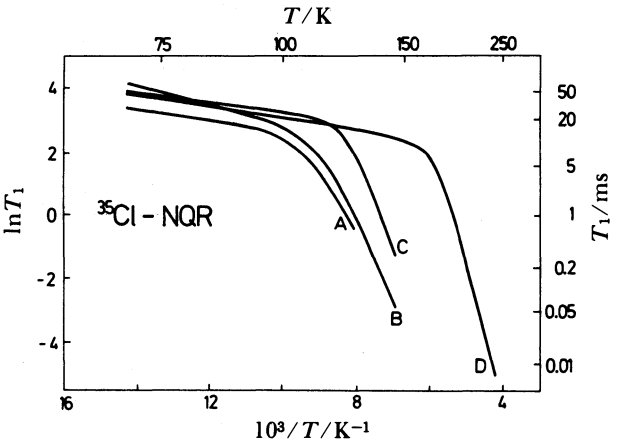

Fig. 7. A comparison of the temperature dependences of ^{35}Cl-NQR spin-lattice relaxation time in; (A): TCA, (B): TCA-3-cyanopyridine, (C): TCA-4-methylpyridine, (D): $(CCl_3COO)_2HK$. The lines were drawn according to Eq. 9 and the appropriate parameters given in Table 3 with $T_{\text{fade-out}}$ taken into account.

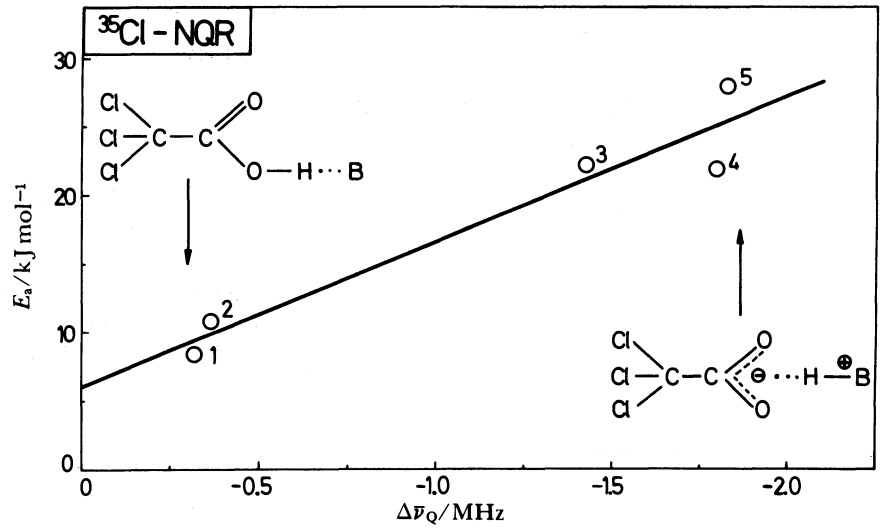

Fig. 8. Activation energy for hindered rotation of CCl_3 group in TCA versus the shift in mean ^{35}Cl-NQR frequency for TCA-B type complexes. Solid line drawn according to Eq. 10; for fitting parameters see text; for notation see Table 1.

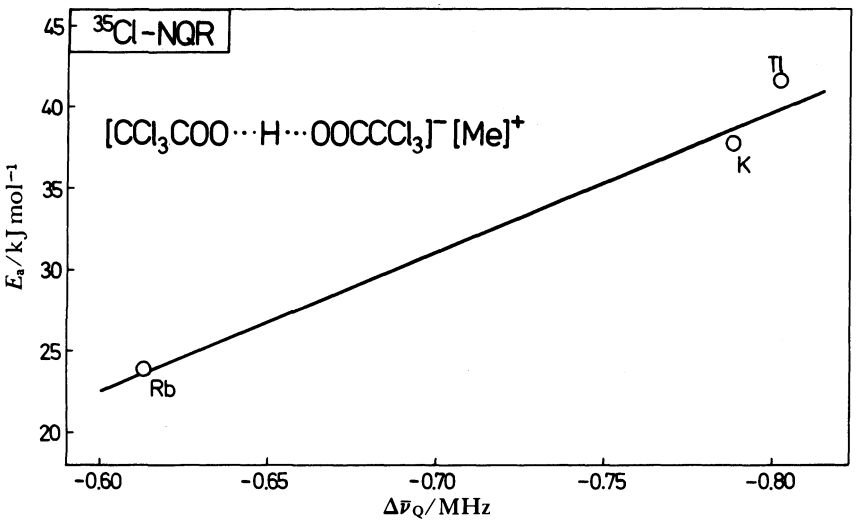

Fig. 9. Activation energy for hindered rotation of CCl_3 group in TCA versus the shift in mean ^{35}Cl-NQR frequency for $[A\cdots H\cdots A]^-[Me]^+$ type complexes. Solid line drawn according to Eq. 10; for fitting parameters see text.

remains the same (symmetrical bond) and the shift in the mean ^{35}Cl-NQR frequency is determined by the influence of $[Me]^+$ cation and in particular by its size as discussed in Refs. 14 and 15.

It is possible to relate the activation energy, E_a, for the rotation of the CCl_3 group in a complex of the series studied, to the parameter, pK_a, describing the strength of the base and acid forming the complex and obtain an expression $E_a=f(\Delta pK_a)$.

Using Eqs. 1 and 10 leads to:

$$E_a=\frac{E_a^{HB}+E_a^{PT}\times 10^{\xi\Delta pK_a+C'}}{1+10^{\xi\Delta pK_a+C'}}, \qquad (11)$$

where $E_a^{HB}=6.6$ kJ mol^{-1} is a constant equal to the activation energy for the rotation of CCl_3 group in a limit-case complex with a purely covalent structure, and $E_a^{PT}=27.3$ kJ mol^{-1} is a similar constant corresponding to the opposite limit case of a completely polar structure of the hydrogen bond. Figure 10 represents the curve corresponding to Eq. 11 for ΔpK_a ranging from -12 to $+12$. As follows from the above considerations the increase in the energy barrier for CCl_3 group rotation in TCA-B complexes is a direct result of the changing character of the hydrogen bond. The degree of proton transfer, P, being a significant parameter to describe the hydrogen bond, it is possible, using Eqs. 2 and 10, to express the activation energy, E_a, in term of this parameter:

$$E_a=20.7\,P+6.6, \qquad (12)$$

with $0\leqslant P\leqslant 1$.

Similarly, considering the series of complexes $[CCl_3COO\cdots H\cdots OOCCCl_3]^-[Me]^+$ it is possible to relate the ^{35}Cl-NQR frequency shift to the ionic radius of the cation (R). Using data available in Ref. 15 for

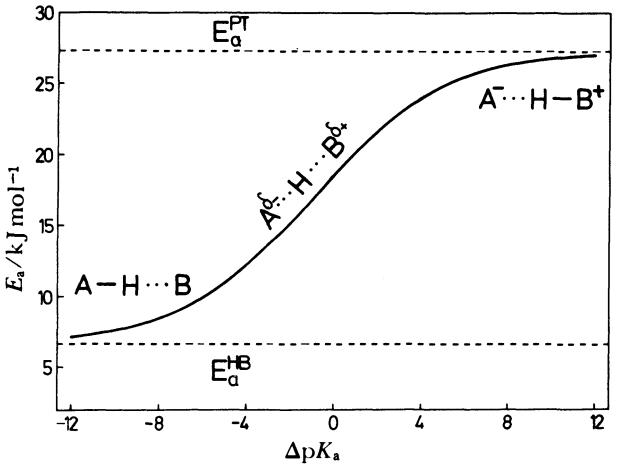

Fig. 10. Activation energy for hindered rotation of CCl_3 group of TCA versus ΔpK_a for TCA-B type complexes. The curve is drawn according to Eq. 11 with the fitting parameters given in the text.

the compounds studied here (Me=Rb, K, Tl) and also for Me=Na and NH_4 one gets the relation:

$$\Delta\bar{\nu}_Q[MHz]=12.3\,R[nm]-2.4. \qquad (13)$$

Then using Eqs. 10 and 13, the corresponding activation energy for the rotation of the CCl_3 group can be written as:

$$E_a=-1054.3\,R+179.9 \qquad (14)$$

However, this relation cannot be applied in a wide range of R values. Both Eqs. 13 and 10 have been derived for a very narrow range of R values: In the case of Eq. 13 R changed between 0.098 nm (Na^+) to 0.149 nm (NH_4) while in the case of Eq. 10 this range was even narrower. Moreover, Eq. 13 cannot be linear as

this is in contradiction to the dependence of the electric field gradient on r^{-3} where r is the distance between the nucleus considered and the charge producing the gradient in question. Despite the above limitations Eq. 14 applied for the appropriately narrow range of R values allows to obtain reasonable values of E_a.

On the other hand Eqs. 11 and 12 derived for TCA-B complexes can be applied on a wider scale. Eq. 1 was derived from the analysis of 63 complexes of ΔpK_a changing in a relatively wide range of values extending from −11.77 to +11.25. The relation between E_a and $\Delta\bar{\nu}_Q$ (Eq. 10) was also obtained for a wide range of ΔpK_a values (from −7.01 to +5.51). It should be however pointed out that the small number of experimental values of E_a which is a consequence of the time-consuming character of $T_1(T)$ measurements may also be a reason for the not very accurate E_a values obtained from Eqs. 11 and 12. In particular E_a^{HB}=6.6 kJ mol^{-1} seems to be too low for a relatively big and heavy CCl_3 group, in spite of the fact that the CCl_3 group in question is in an almost free TCA molecule without any interactions with the base. Nevertheless the relations obtained in this paper and expressed as mathematical formulae allow direct determination of the activation energy for rotation of CCl_3 group of TCA in its different complexes from the values of $\Delta\bar{\nu}_Q$ or from the tabulated pK_a or R values.

Moreover, it was found beyond doubt that the influence of hydrogen bond in TCA-B complexes on the height of the potential barrier of CCl_3 group of TCA forming that complex, is decisive. The hydrogen bond in TCA-B complexes is the main source of the changes in electric field gradient at the Cl nuclei. These changes affect the nuclei studied through induction and polarization effects. The weakening of the O-H covalent bond produced by hydrogen bond formation originates: (1) A charge rearrangement that is relayed to the Cl-C bond through the bonds of the TCA molecule and (2) through two polarization mechanisms consisting of (a) direct effect acting on the Cl atom and (b) an indirect polarization effect acting on the Cl-C bond. As shown in Ref. 14 an increase in the electron density on the nearest O atom in TCA will produce a direct contribution that will increase the Cl frequency while the indirect effect will produce an opposite shift. We can also consider the polarization influence of electric dipole of hydrogen bond which leads only to negative shifts in ^{35}Cl-NQR frequency.[1] In the complexes studied only the negative shifts of NQR frequency were observed. However, without data on the crystal structure of the complexes studied it is difficult to calculate and determine accurately the contribution of individual mechanisms in the eventual shift of ^{35}Cl-NQR frequency. Nevertheless all the mechanisms considered result in a gradual increase in intermolecular interactions with a growing proton transfer degree. This in turn implies an increase in potential barriers for rotating CCl_3 groups. In the case of $[CCl_3COO\cdots H\cdots OOCCCl_3]^-$ $[Me]^+$ type complexes it is also difficult to separate the influence of the cation radius resulting in weakening of intermolecular interactions from the effect of electrostatic interaction of the cation on the electric potential distribution in a dimer ion. However both effects directly influence intermolecular interactions strength and thus, the height of the potential barrier for rotation of CCl_3 groups in these complexes.

Investigation of quadrupole spin-lattice relaxation times T_1 versus temperature performed for a considerable group of complexes should give a more precise correlation between the values of E_a and $\Delta\bar{\nu}_Q$. On the other hand crystallographic studies of the complexes with a hydrogen bond would provide the possibility of more detail analysis of inter- and intramolecular interactions in them.

I would like to thank Professor L. Guibé for his kind reading of the manuscript.

References

1) J. Pietrzak, B. Nogaj, Z. Dega-Szafran, and M. Szafran, *Acta Phys. Pol. A*, **52**, 779 (1977).
2) B. Nogaj, "Nuclear Quadrupole Resonance in Crystalline Complexes with Hydrogen Bond" in "Progress in Applications of Resonance Techniques in Chemistry" (in Polish), ed by L. Sobczyk, Polish Scientific Publisher (PWN), Warsaw (1984), p. 261.
3) W. Fichtner, A. Markworth, N. Weiden, and A. Weiss, *Z. Naturforsch., A*, **41**, 215 (1986).
4) J. Kalenik, L. Sobczyk, and E. Grech, *J. Indian Chem. Soc.*, **62**, 827 (1985).
5) B. Nogaj, B. Brycki, Z. Dega-Szafran, M. Szafran, and M. Maćkowiak, *J. Chem. Soc., Faraday Trans. 1*, **83**, 2541 (1987).
6) J. Pietrzak, B. Nogaj, M. Maćkowiak, and M. Zdanowska, "Nuclear Magnetic Resonance and Its Applications," Proc. VII Seminar, Cracow (1974), p. 222.
7) D. Biedenkapp and A. Weiss, *Ber. Bunsenges. Phys. Chem.*, **70**, 788 (1966).
8) H. Chihara and N. Nakamura, *Bull. Chem. Soc. Jpn.*, **44**, 1980 (1971).
9) H. Chihara and N. Nakamura, *J. Phys. Soc. Jpn.*, **37**, 156 (1974).
10) O. Kh. Poleshchuk, Yu. K. Maksyutin, O. F. Sychev, K. K. Koshelev, and I. G. Orlov, *Izv. Akad. Nauk SSSR, Ser. Khim.*, **6**, 1431 (1975).
11) H. Bayer, *Z. Phys.*, **130**, 227 (1951).
12) S. Alexander and A. Tzalmona, *Phys. Rev.*, **138**, 845 (1965).
13) I. V. Izmestyev and V. S. Grechishkin, *Zh. Strukt. Khim.*, **11**, 927 (1970).
14) R. J. Lynch, T. C. Waddington, J. A. O'Shea, and J. A. Smith, *J. Chem. Soc., Faraday Trans. 2*, **72**, 1980 (1976).
15) J. Murgich and B. Nogaj, *J. Mol. Struct.*, **131**, 291 (1985).

A Conformational Study on Some Thiobenzophenones. Molecular Orbital Calculations

Rafie Hassan Abu-Eittah* and Abdel-Ghany El-Kourashy†
Department of Chemistry, Faculty of Science, King Abdulaziz University, Jeddah, Saudi Arabia
†Department of Chemistry, Faculty of Applied Sciences and Engineering, Umm Al-Qura University, Makkah, Saudi Arabia
(Received December 27, 1986)

MO calculations were performed on the different conformers of thiobenzophenone and on the planar conformer of a number of its derivatives using the INDO-CI procedures. A nonplanar conformer with an angle of 15° between the planes of benzene rings was predicted for thiobenzophenone. Dipole moment and charge density were calculated and correlated to the reactivity of the studied molecules. A Gaussian analysis was performed on the spectra of the studied compounds, results compared satisfactorily with the results of MO calculations.

Relatively, little work has been done on the MO calculations of thiobenzophenone especially in the recent years. However, many spectral studies have been reported on thiones, thiourea and many of their derivatives.

The effect of substitution,[1] solvent,[2] and irradiation[3] on the electronic spectra of thiobenzophenone have been reported. The spectrum of a crystal of thiobenzophenone—doped in a crystal of benzophenone—at 20K indicated that the transition along the C=S direction is intrinsically allowed.[4] Simple molecular orbital calculations (HMO) were performed on some aliphatic and aromatic thiocarbonyl compounds,[5-8] a linear correlation was observed between the wave number of the $n \rightarrow \pi^*$ transition and the Hückel excitation energy.

The crystal structure of thiobenzophenone and thiobenzophenone *S*-oxide were determined, the former is monoclinic whereas the latter is orthorhombic.[9] The photoelectron helium (HeI) spectra of aromatic thiocarbonyls and the corresponding *S*-oxides were determined. For thioketones the ordering of the outermost MO's is: n(S), π_7, π_6, π_5, π_4, π_3, n(S) being the HOMO.

Electron-rich olefins react with n,π^* triplet state of thiobenzophenone yielding 1,4-dithiane or thietane depending on the structure of the olefins whereas electron deficient olefins react with π,π^* singlet states of thiobenzophenone.[11] Photocycloaddition of thiobenzophenone to olefins substituted with electron releasing groups lead to the formation of 1,4-dithianes.[12] However, if the electron-rich olefins are substituted with bulky substituents their photocycloaddition to thiobenzophenone result in thietane and not dithiane derivatives.[13] Photocycloaddition of thiobenzophenone to olefins substituted by electron-withdrawing groups result in the formation of thietane derivatives through a nucleophilic attack on the olefin.[14] It was shown that the π,π^* state plays a role in the reaction which proceeds only on irradiation by 366 nm light.

In this work, INDO-CI molecular orbital calculations were performed on different conformers of thiobenzophenone and the planar conformers of a number of its derivatives. Gausian analysis of the spectra was performed. These results have not been reported before.

Method of Calculations

The all valence-electrons INDO method of calculations was followed. Details and parameterization are found elsewhere.[15] Interaction was considered between nine electronic configurations in which electrons are transferred from the three highest occupied MO's to the three lowest unoccupied MO's. If the wave function of an electronic configuration is ψ_m, the CI wave function ψ_{CI} is given by $\sum_m a_m \psi_m$. The energies of the resulted states are calculated by solving the determinant

$$\det\{H_{mn} - E\delta_{mn}\} = 0. \quad (1)$$

The diagonal elements are the expectation values of the energies of the different configurations whereas the off-diagonal elements of H_{mn} are the expectation values of the Hamiltonian averaged between the two configurations m and n. Calculation of the diagonal and off-diagonal elements of Eq. 1 requires the calculations of the integrals:

$$\varepsilon_{ij} = \langle \psi_i | H_{core} | \psi_j \rangle$$
$$\gamma_{ii} = (\psi_i\psi_i | \psi_i\psi_i)$$
$$\gamma_{ij} = (\psi_i\psi_i | \psi_j\psi_j)$$
$$\delta_{ij} = (\psi_i\psi_j | \psi_j\psi_i)$$
$$\zeta_{ik}^{jl} = (\psi_i\psi_k | \psi_j\psi_l)$$

Substituting the LCAO epression for the molecular orbitals (ψ) one gets[16]

$$\varepsilon_{ij} = \sum_{\mu\nu} C_{i\mu}C_{j\nu} \langle \phi_\mu | H_{core} | \phi_\nu \rangle$$
$$\gamma_{ii} = \sum_{\mu\nu} C_{i\mu}^2 C_{i\nu}^2 (\mu\nu|\nu\nu)$$
$$\gamma_{ij} = \sum_{\mu\nu} C_{i\mu}^2 C_{j\nu}^2 (\mu\nu|\nu\nu)$$
$$\delta_{ij} = \sum_{\mu\nu} C_{i\mu}C_{j\nu}C_{i\nu}C_{j\nu} (\mu\mu|\nu\nu)$$
$$\zeta_{ik}^{jl} = \sum_{\mu\nu} C_{i\mu}C_{k\mu}C_{j\nu}C_{l\nu} (\mu\mu|\nu\nu)$$

The letters i, j, k, and l refer to MO's whereas μ,ν, to AO's. The diagonal and off-diagonal elements of Eq. 1 are calculated as follows[17]

$$\langle\psi_G|\hat{H}|\psi_G\rangle = 2\sum_{i=1}^{n}\varepsilon_i + \sum_{i}^{n}\sum_{i}^{n}(2\gamma_{ij}-\delta_{ij})$$

$$\langle\psi_{k\to s}|\hat{H}|\psi_{k\to s}\rangle = 2\sum_{m}^{n}\varepsilon_m + (\varepsilon_s-\varepsilon_k) + \sum_{m}^{n}\sum_{l}^{n}(2\gamma_{ml}-\delta_{ml}) - \sum_{l=1}^{n}[(2\gamma_{kl}-\delta_{kl})-(2\gamma_{ls}-\delta_{ls})-\gamma_{ks}+2\delta_{ks}]$$

$$\langle\psi_G|\hat{H}|\psi_{k\to s}\rangle = \sqrt{2}\{\varepsilon_{ks} + \sum_{m=1}^{n}[2(mm|ks)-(mk|sm)]\}$$

$$\langle\psi_{k\to s}|\hat{H}|\psi_{l\to r}\rangle = 2(lr|ks)-(lk|sr)$$

$$\langle\psi_{k\to s}|\hat{H}|\psi_{k\to r}\rangle = \varepsilon_{rs} + \sum_{m=1}^{n}[2(mm|rs)-(mr|sm)] + 2(kr|sk)-(kk|rs)$$

$$\langle\psi_{k\to s}|\hat{H}|\psi_{l\to s}\rangle = -\varepsilon_{lk} - \sum_{m=l}^{n}[2(mm|lk)-(ml|km)] + 2(ls|ks)-(lk|ss)$$

The coefficients, c's, used to calculate the above integrals were the self-consistent ones and the two-center electron repulsion integrals were calculated using the Nishimoto-Mataga relation.[18] The computations were performed on IBM-370 computer using INDO-program obtained from QCPE center, to which a CI subroutine was added.

Results and Discussion

Conformational Analysis of Thiobenzophenone. The hexagonal nature of benzene imposes a steric hindrance on the planarity of the molecule. Ortho-ortho-hydrogen interaction will prevent the coplanarity of the two benzene nuclei. The extent of this steric effect is best investigated through the calculations of the total energy of the molecule as a function of angle of rotation of one of the benzene nuclei. The results help one to predict whether the molecule is a "free rotor," rigid or a "quasi-rigid" one. The total energy is calculated by MO calculations using the INDO procedures.

Previous electronic structure calculations were reported on S-containing compounds[19-21] excluding the contribution of the 3d sulfur atomic orbitals. In an ab initio calculation,[22] it has been shown that the 3d's orbitals of sulfur play a very minor role in the population analysis (and hence in bonding) as has been reported before.[23-27]

In this work, MO computations were performed neglecting the 3d sulfur atomic orbital. The configuration adopted (a) for the molecule is shown, bond length and bond angle were taken from the literature.[9] Molecular orbital calculations were performed on the planar conformer as well as nonplanar conformers whereby one of the benzene rings is rotated 15, 30, 45, 60, and 90° around the C_2-C_3 axis. A comparison of the total energy, dipole moment, energy of the lowest electronic transition and the oscillator strength is given in Table 1. The lowest electronic transition is forbidden (f=0.0, HOMO is "n+σ" and LUMO is π^*)

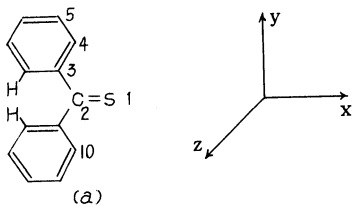

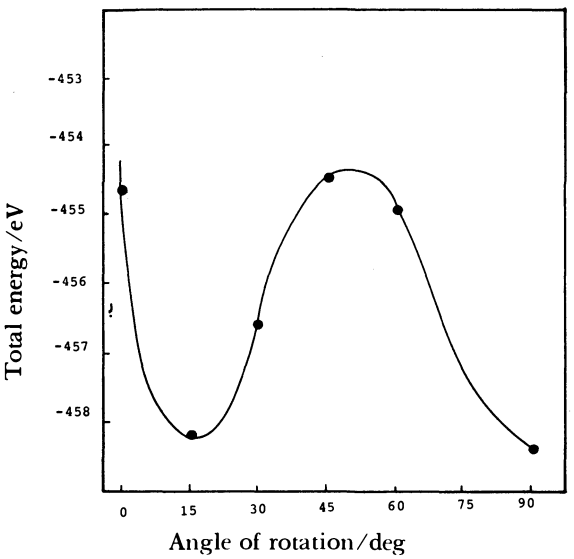

Fig. 1. Variation of INDO-total energy of thiobenzophenone with the angle of rotation of one of the benzene rings.

Table 1. Variation of Total Energy, Dipole Moment, and Transition Energy with Thiobenzophenone Geometry

Angle of rotation/°	Total energy/eV	Dipole moment/D	Lowest transition K/eV	Osc. Str.
0	−454.62	4.08	3.08	0.00
			3.48	0.10
15	−458.20	7.40	3.37	0.16
30	−456.59	7.36	4.02	0.30
45	−454.45	6.92	3.73	0.18
60	−454.92	6.36	4.83	0.27
90	−458.39	5.99	3.25	0.00
			4.29	0.35

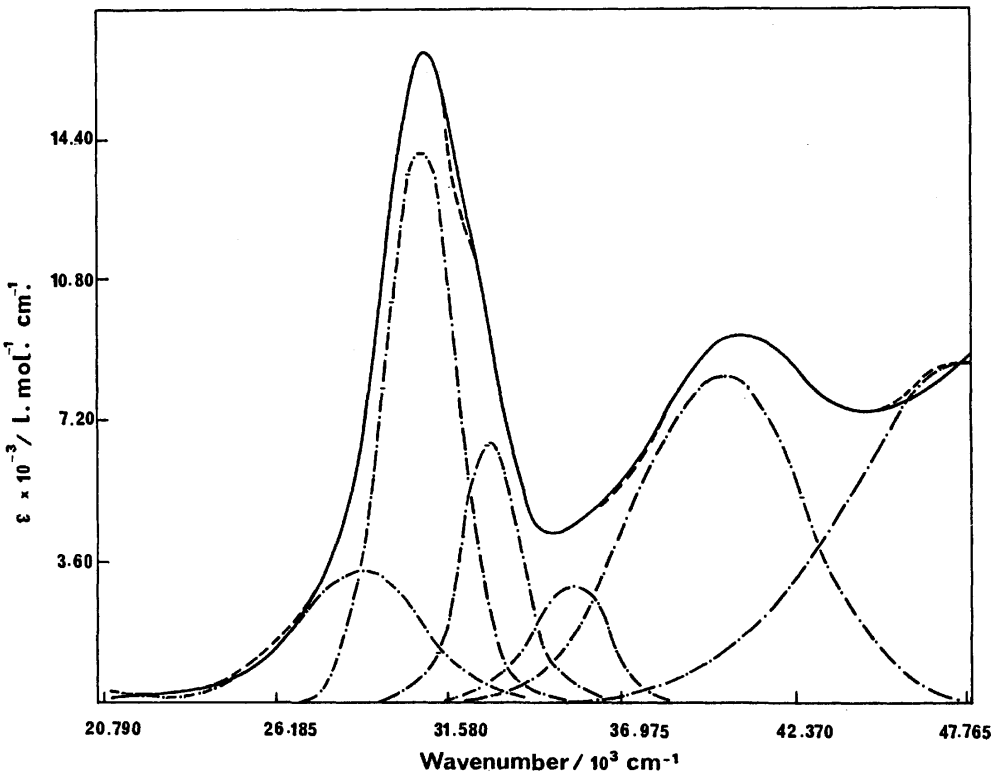

Fig. 2. Electronic absorption spectrum of thiobenzophenone in ethanol.
——: Exp. spectrum, -·---: Gausian component bands, ----: fitted spectrum when not coincident with experimental.

for the planar as well as the perpendicular conformer. For other conformers, mixing of orbitals does not permit the calculation of pure $n(n+\sigma)\rightarrow\pi^*$ transitions. The variation of the total energy of thiobenzophenone with the angle of rotation is shown in Fig. 1. The height of the barrier to internal rotation is of the order of 4 eV indicating that the molecule is not a free rotator. INDO procedures give good results for calculated ground state energy but not as good for the excited states. Generally, calculated energies by the INDO method are slightly higher than those calculated by other more accurate procedures. Results of this work indicate that the most stable conformer of thiobenzophenone has an angle of 15° between the planes of the benzene rings. The lowest $\pi\rightarrow\pi^*$ transition energy (3.37 eV) agrees satisfactory with experiment. Gaussian analysis was performed and the lowest electronic transition was found at 3.56 (in ethanol) and at 3.81 eV (in cyclohexane) Fig. 2.

Dipole moment measurements of a series of thioketones have shown that compounds in which thiocarbonyl group is not subjected to conjugative or resonance effects have smaller dipole moments than the corresponding ketones. This indicates that the polarity of the thiocarbonyl group is considerably smaller and possibly reversed compared with that of C=O group.[28,29] On the other hand, thioketones in which intramolecular perturbation of the C=S group is possible (for example within the aromatic series) have

Table 2. Experimental Values of Dipole Moments of Some Carbonyl and Thiocarbonyl Compounds in Benzene at 20 °C

Compound	C=S	C=O
Thiobenzophenone	3.37	2.95
4,4′-Dimethylthiobenzophenone	3.45	3.45
4,4′-Dimethoxythiobenzophenone	4.44	3.90
4,4′-Bis(dimethylamino)-thiobenzophenone	6.12	5.16

Data are from Refs. 23 and 24.

dipole moments which indicate a higher polarizability for C=S than for the C=O. Table 2 compares some experimental results of dipole moments measured in benzene at 20 °C.[30,31]

Table 1 gives the calculated dipole moment for thiobenzophenone whereas Table 3 gives the dipole moments of substituted thiobenzophenones. The calculated dipole moments are only slightly higher than the experimental ones for thiobenzophenone and 4,4′-dihydroxy derivative but seems to be significantly higher for 4,4′-diaminothiobenzophenone. These effects are direct results of the method of calculation, parameterization, and configurations adopted. The dipole moments lie along the C_{2v} symmetry axis and are strongly dependent upon the orientations of the lone pair of electrons. Consequently, rotating one of the benzene nuclei of thiobenzophenone alters signifi-

Table 3. Comparison of the Calculated Dipole Moments and Total Energies of Some Substituted Thiobenzophenones

Compound	Dipole moment/D	Total energy/eV
Thiobenzophenone	4.08	−454.62
4-Aminothiobenzophenone	4.26	−554.38
4-Hydroxythiobenzophenone	5.59	−676.15
4,4′-Dihydroxythiobenzophenone	4.65	−900.30
4,4′-Diaminothiobenzophenone	10.41	−571.74
4-Amino-4′-hydroxythiobenzophenone	2.85	−778.48

Table 4. Variation of the Net Charge Density on Certain Atoms of Thiobenzophenone as a Function of the Angle of Rotation

Angle of rotation	S_1	C_2	C_4	C_5	C_{10}	C_{11}
0	−0.0349	0.2581	−0.1063	−0.0688	−0.1245	−0.0727
15	−0.1436	0.2116	−0.0189	−0.0382	−0.1499	−0.0852
30	−0.1333	0.1910	−0.0060	−0.0266	−0.1343	−0.0966
45	−0.1404	0.2090	−0.0085	−0.0121	−0.1349	−0.0951
60	−0.1456	0.2302	−0.0190	−0.0124	−0.1351	−0.0949
90	−0.1498	0.2452	−0.0263	−0.0137	−0.1363	−0.0939

cantly the value of calculated dipole moment.

The calculated dipole moments of substituted thiobenzophenones reveal some important results. Generally, substitution by one or two hydroxyl, one or two amino groups increases the dipole moments and increases the polarization of the thiocarbonyl group. However, the calculated dipole moment of 4-hydroxyl-4′-aminothiobenzophenone is significantly smaller than that of the thiobenzophenone. Hence, the -OH and $-NH_2$ groups have acted in opposite directions with a net result of decrcasing the polarizability of the C=S.

The reactivity of a molecule can nicely be correlated with the charge density of the different sites of the molecule whereas the algebraic signs of the coefficients of the AO's constituting the HOMO and LUMO are directly concerned with the pathway of a chemical reaction. In Table 4 one compares the charge densities on the active sites of the molecule (S_1, C_2, C_4, C_5, C_{10}, C_{11}) in the different conformers. We cannot compare the coefficients of the MO's of the different conformers since rotation mixes the different orbitals on the benzene rings. The data in Table 4 indicates some interesting results. The thiocarbonyl group (C=S) has only a slight effect on the reactivity of the benzene rings since no pronounced excess of negative or positive charges is calculated on the different atoms. However, thiobenzophenone is a dipole with calculated moment of 4.08D (planar conformer) compared with the experimental 3.37D. The components of the dipole moment (in Debye) are: u_x=0.58, u_y=4.04, and u=4.08 (0.83

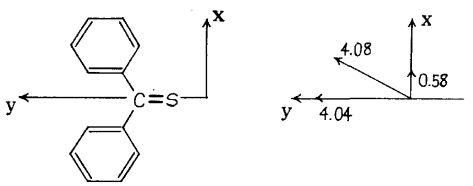

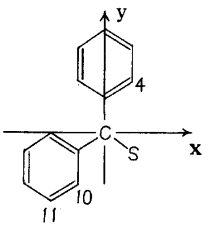

atomic and 3.34 polarization). The dipole moment vector is directed from the C=S to the benzene rings. In other words, there is a net built of negative charge on the benzene rings and one can say that the C=S group activates, though slightly, the molecule. The calculated dipole moment, 7.04D, for the most stable conformer of thiobenzophenoe is remarkably higher than the experimental one. This is probably due to the method of calculations used in this work. INDO procedures lead to relatively higher values of dipole moment, even for the planar conformer. The slight net negative charge on S-atom explains the role of C=S in cycloaddition.

It is interesting to correlate the charge density, on the benzene rings, to the angle of rotation of one of the benzene nuclei aroun the y-axis (b). As the results in Table 4 indicates, the rotation of the benzene ring led to excess of charge density on the S-atom and a lack of the rotating benzene ring from charge density. On the other hand, there has been an increase of charge density on the non-rotating benzene ring (C_{10}).

Rotation of one of the benzene rings is expected to affect the calculated value of the dipole moment. The lowest value of dipole moment, 4.08 D, is computed for the planar conformer whereas the highest value, 7.40 D, is computed for the perpendicular conformer. Rotation of the plane of the benzene ring by 15° almost doubles the dipole moment.

Electronic Structure of Substituted Thiobenzophenones. INDO-molecular orbital calculations were

Table 5. Net Charge Density and Coefficients of the HOMO and LUMO of the Studied Thiobenzophenones (TBP)

Compound	S_1	C_2	C_4	C_5	C_{10}	C_{11}
	−0.0349[a)]	0.2581	−0.1063	−0.0688	−0.1245	−0.0727
TBP	−0.2487[b)]	0.6492	−0.2638	−0.0972	−0.2349	−0.0946
	0.2476[c)]	−0.0081	0.0979	0.1533	−0.4359	0.1533
	−0.0305	0.2512	−0.0887	−0.0911	−0.1037	−0.0944
4-Amino-	−0.0173	0.0297	−0.0898	0.1506	−0.1823	−0.5445
	−0.2454	0.6512	−0.2558	−0.1024	−0.2297	−0.0801
	−0.0366	0.2581	−0.1143	−0.0623	−0.1123	−0.0957
4-Hydroxy-	−0.0083	0.0221	−0.0265	0.1728	−0.2778	−0.5974
	0.2458	−0.6468	0.2642	0.1016	0.2285	0.0752
	−0.0390	0.2449	−0.0894	−0.1170	−0.0987	−0.1051
4,4′-Dihydroxy-	0.0264	−0.0231	−0.1301	0.2361	0.0269	−0.3220
	0.2444	−0.6496	0.2517	0.0725	0.2238	0.0808
	−0.0428	0.2761	−0.1977	−0.2807	−0.1034	−0.1100
4,4′-Diamino-	0.3620	−0.0221	0.0341	0.0323	−0.2425	−0.1757
	−0.3768	0.2452	0.1824	−0.0983	0.0206	−0.1817
	−0.0344	0.2558	−0.1068	−0.1139	−0.1211	−0.0821
4-Hydroxy-4′-amino-	0.0203	−0.0193	−0.1288	0.2291	0.0490	−0.3003
	0.2405	−0.6442	0.2526	0.0739	0.2303	0.0849

a) The values on the first line represent the net charge density. b) The values on the second line represent the coefficients of the HOMO. b) The values on the third line represent the coefficients of the LUMO.

performed on a series of 4,4′-disubstituted thiobenzophenone in order to correlate the reactivity of these compounds to the calculated parameters and to compare the reactivity of the different compounds. Computations were performed on the planar conformers only and Table 5 summarizes some of the calculated parameters for different substituted thiobenzophenone; those of thiobenzophenone are included for comparison. It is noticed that the net negative charge on S-atom is the highest in 4,4′-diamino derivative, it is high in 4-hydroxy- and 4,4′-dihydroxythiobenzophenones than it is in thiobenzophenone. The oxygen and nitrogen atoms of the substituents are σ-acceptor and π-donors[22)] but they did not lead to a decrease of the charge density on S-atom. Substitution by -OH or $-NH_2$ groups has not led to a built up of negative charge density than in the case of thiobenzophenone. The highest charge density (in hydroxy- or amino-thiobenzophenone) is on C_4 and C_{10}.

The numerical values of the coefficients of AO's forming the HOMO and LUMO are dependent on the

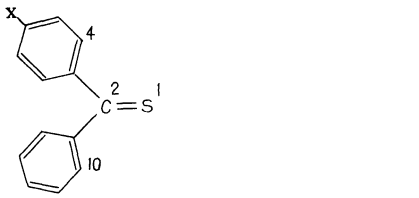

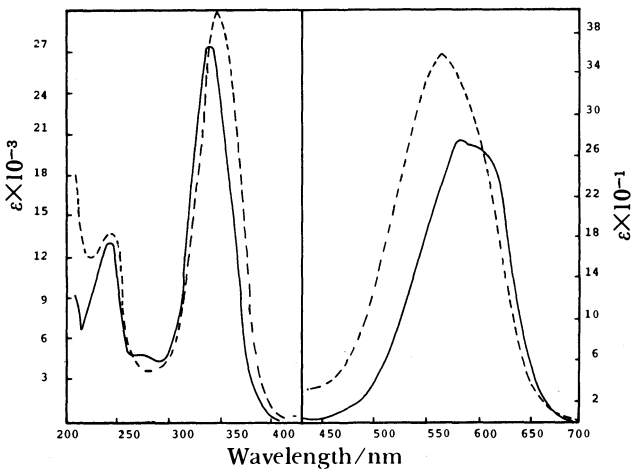

Fig. 3a. Electronic absorption spectra of 4,4′-dimethoxythiobenzophenone.
——: In cyclohexane, ----: in ethanol.

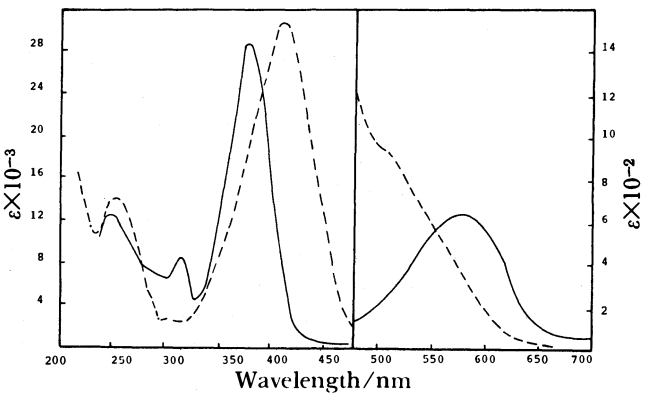

Fig. 3b. Electronic absorption spectra of 4,4′-diaminothiobenzophenone.
——: In carbon tetrachloride, ----: in ethanol.

Table 6. Analysis of the Absorption Spectra of Thiobenzophenone in Different Solvents

Solvent / parameter	Ethanol			Cyclohexane		
	$\bar{\nu}_{max}/cm^{-1}$	ε	f	$\bar{\nu}/cm^{-1}$	ε	f
	30780	13950	0.17	32040	9600	0.10
	39990	8060	0.23	40440	9250	0.39
	47700	8460	0.34	30760	7600	0.12
	32860	6300	0.06	47830	6360	0.14
	28740	3200	0.07	33330	1590	0.01
	35340	2670	0.03	34480	2560	0.03

Table 7. Analysis of the Absorption Spectra of Some Thiobenzophenones in Cyclohexane

Compound	$\bar{\nu}_{max}/cm^{-1}$	ε	f
4-Methoxy-4′-ethoxy-	29500	31190	0.44
	40728	17720	0.48
	47770	18600	0.67
	33118	9890	0.15
	36190	7000	0.08
	26850	3410	
4,4′-Diethoxy-	29210	27410	0.20
	30480	20700	0.16
	40860	20770	0.49
	28040	13430	0.10
	47040	19030	0.42
	32900	8010	0.11
	35890	6810	0.11
	27240	6500	0.11
4,4′-Dimethoxy-	29600	24360	0.29
	41490	8060	0.14
	48530	5620	0.03
	45170	7950	0.23
	31710	6000	0.05
	35160	4710	0.24
	27750	4930	0.05
4,4′-Diamino-[a]	26670	27880	0.41
	40270	11430	0.31
	33360	6250	0.25
	31690	2660	0.01
4,4′-bis(Dimethylamino)-[a]	23990	37970	0.30
	25371	19170	0.16
	38930	18500	0.76
	29330	7220	0.04
	30850	10280	0.12
	27110	10010	0.14
	22710	5830	0.03
	32800	4550	0.05

a) Using carbon tetrachloride as a solvent.

Table 8. Comparison between Calculated and Experimental Transition Energy and Oscillator Strength

Compound	Exp. (G.analysis)		Calcd	
	ΔE/eV	f	ΔE/eV	f
Thiobenzophenone	3.81	0.12	3.48	0.09
	3.97	0.10	3.60	0.00
	4.13	0.01	(a) 4.03	0.27
	4.28	0.03	4.60	0.00
	5.01	0.39	5.61	0.00
	5.93	0.14	6.30	0.30
			3.37	0.35
			(b) 4.11	0.17
			4.46	0.17
			5.68	0.31
			6.01	0.22
4,4′-Dimethoxy-	3.44	0.05	3.26	0.00
	3.67	0.30	(c) 3.49	0.34
	3.93	0.05	3.53	0.15
	4.36	0.24		
	5.14	0.14	5.74	0.50
	6.02	0.03		
4,4′-Diamino-	3.33	0.14	3.11	0.00
	3.92	0.01		
	4.14	0.25	4.17	0.00
			4.77	0.00
	4.98	0.31	4.94	0.17
			5.20	0.41
4-Amino-4-hydroxy-			3.02	0.00
			3.15	0.00
			3.44	0.14
			4.00	0.36
			5.55	0.52
4-Amino-			3.46	0.12
			3.62	0.33
			3.69	0.74
			4.95	0.00
			5.94	0.01
			6.07	0.56
4-Hydroxy-			3.08	0.00
			3.49	0.12
			3.69	0.96
			4.96	0.00
			5.08	0.00
			5.98	0.05
			6.09	0.53

a) Planar conformer. b) An angle of 15° between the planes of benzene rings. c) Data are for 4,4′-dihydroxythiobenzophenone.

type of the substituent (Table 5). In the case of 4-aminothiobenzophenone the coefficient of S-atom is −0.0173 compared to −0.2487 in thiobenzophenone in the highest occupied molecular orbital (HOMO) and is −0.2454 compared to +0.2476 in thiobenzophenone (in the LUMO). Characteristic variations of the coefficients and the net charges are seen for the different atoms in the different MO's as indicated in Table 5.

Spectral Analysis. The electronic absorption spectra of some thiobenzophenones have been reported.[32] The observed bands correspond to highly overlapping transitions (Figs. 3a, b). In order to resolve the individual band parameters a curve analysis has been carried out.[33,34] The electronic absorption spectra were analyzed, using the Gaussian line shape, as shown in Fig. 2 for thiobenzophenone. The resolution of the observed absorption spectrum into its components is used to determine the appropriate values of the

parameters as indicated in Tables 6 and 7. Gaussian analysis shows that there are other transitions taken place underneath the two ultraviolet absorption bands observed experimentally. Such transitions are characterized by low oscillator strength, hence the parameters observed are not quite real due to the overlap of the transitions. Also, it is clear that the band parameters of the experimental curve are affected by both changing the medium and/or the substituent.

Comparison with Experiment. A comparison of the computed transition energy and oscillator strength with those obtained after Gaussian analysis of the spectra of some thiobenzophenones is given in Table 8. Many computed transitions are theoretically forbidden yet they are observed experimentally with weak intensity. From both the experimental and theoretical results it is clear that the spectral band corresponds to a number of overlapping transitions. This overlapping causes inaccuracy in the experimentally calculated oscillator strength and is the reason of the observed discreapancy between the calculated and experimental values. On the other hand, the correspondence between the calculated and experimental transition energies.

Conclusion

The method of calculations used in this work, INDO-CI, proved to be a satisfactory method in explaining and predicting the electronic structure of the studied thiobenzophenones. It has been shown that the most stable conformer of thiobenzophenone is nonplanar with an angle of 15° between the planes of the benzene rings. The height of the barrier to internal rotation is of the order of 4 eV revealing that the molecule is not a free rotator.

Calculations of the charge density and dipole moment led to some important conclusions. Generally, substitution in the benzene rings of thiobenzophenone resulted in an increase in the dipole moment except in the case of 4-hydroxy-4'-aminothiobenzophenone which has a dipole moment lower than the parent compound. This result indicates that the polarization of the C=S group has been diminished or even reversed in this compound. For the studied compounds there has been a net built up of charge density on the benzene rings, hence increasing the activity.

The experimental results of photocycloaddition of thiobenzophenone to substituted olefins[11-14] go along with the theoretical predictions of this work especially for the mechanism of nucleophilic attack of thiobenzophenone on the olefins and the formation of thietane derivatives. The calculated charge densities on C_2 and S_1 as well as their coefficients in the HOMO (Table 5) favors the polar addition of the olefins to the thiocarbonyl group.

No data is available on the reactivities of substituted thiobenzophenones. The results in Table 5 predict that substitution in the thiobenzophenone will affect its reactivity.

References

1) P. Brocklehurst and A. Burawoy, *Tetrahedron*, **10**, 118 (1960).

2) P. Franzosini, *Gazz. Chim. Ital.*, **88**, 1109 (1958); W. A. Lees and A. Burawoy, *Tetrahedron*, **20**, 2229 (1964).

3) G. Oster, L. Citreal, and M. Goodman, *J. Am. Chem. Soc.*, **84**, 703 (1962).

4) S. D. Gupter, M. Chowdhury, and S. C. Bera, *J. Chem. Phys.*, **53**, 1293 (1970).

5) M. J. Jansse and J. Sandstrom, *Tetrahedron*, **20**, 2239 (1964).

6) J. Fabian, A. Mehlhorn, J. Bormann, and R. Mayer, *Wiss. Z. Tech. Univ., Dresden*, **14**, 285 (1965); *Chem. Abstr.*, **64**, 9072c (1966).

7) J. Fabian and A. Mehlhorn, *Z. Chem.*, **7**, 192 (1967).

8) J. Fabian, H. Viola, and R. Mayer, *Tetrahedron*, **23**, 4323 (1967).

9) G. Rindorf and L. Carlsen, *Acta Crystallogr., Sect. B*, **35**, 1179 (1979).

10) F. Bernardi, P. F. Collona, G. Distefano, G. Maccagna, and G. Spunta, *Z. Naturforsch., A*, **33**, 468 (1978).

11) A. Ohno, Y. Ohnoshi, and G. Tsuchihashi, *J. Am. Chem. Soc.*, **91**, 5038 (1969).

12) G. Tsuchihashi, M. Yamauchi, and M. Fukuyama, *Tetrahedron Lett.*, **1967**, 1971.

13) A. Ohno, Y. Ohnishi, and G. Tsuchihashi, *Tetrahedron Lett.*, **1969**, 283.

14) A. Ohno, Y. Ohnishi, and G. Tsuchihashi, *Tetrahedron Lett.*, **1969**, 161.

15) J. A. Pople and D. L. Beveridge, "Approximate Molecular Orbital Theory," McGraw Hill Book Co., New York (1972).

16) R. L. Flurry, Jr., "Molecular Orbital Theories of Bonding in Organic Molecules," Marcel Dekker, New York (1968).

17) S. P. McGlynn, L. G. Vanquickenborne, M. Kinoshita, and D. G. Carroll, "Introduction to Applied Quantum Chemistry," Holt-Rinehart and Winston Inc., New York (1972).

18) I. Fisher-Hjalmars, "Molecular Orbitals in Chemistry, Physics and Biology," ed by P. O. Lowdin, Academic Press, New York (1964), p. 361.

19) R. A. W. Johnstone and F. M. Mellon, *J. Chem. Soc., Faraday Trans. 2*, **1973**, 1155.

20) G. Solmona, R. Faure, and E. J. Vincent, *C. R. Acad. Sci. Ser. C*, **280**, 605 (1975).

21) M. Gelus, P. M. Vay, and G. Berthier, *Theor. Chim. Acta*, **9**, 182 (1967).

22) M. H. Palmer and S. M. F. Kennedy, *J. Mol. Struct.*, **43**, 33 (1978).

23) M. H. Palmer, R. H. Findlay, J. N. Ridyard, A. Barrie, and P. Swift, *J. Mol. Struct.*, **39**, 189 (1977).

24) M. H. Palmer and S. M. F. Kennedy, *J. Chem. Soc., Perkin Trans. 2*, **1978**, 81.

25) M. H. Palmer and S. M. F. Kennedy, *J. Chem. Soc., Perkin Trans. 2*, **1974**, 1893.

26) J. R. Grunwell and W. C. Danison, *Int. J. Sulphur Chem.*, **8**, 379 (1973).

27) M. H. Palmer, R. H. Findlay, and A. J. Gaskell, *J.*

Chem. Soc., Perkin Trans. 2, **1974**, 420.
28) R. Mayer, *Quart. Reports Sulphur Chem.*, **2**, 125 (1970).
29) A. Julg, M. Bonnet, and Y. Ozias, *Theor. Chim. Acta*, **17**, 49 (1970).
30) P. Paquer, *Int. J. Sulphur Chem., (B)*, **7**, 269 (1973).
31) P. Paquer, *Int. J. Sulphur Chem.*, **8**, 173 (1973).
32) R. Abu-Eittah and A. El-Kourashy, *Indian J. Chem.*, **14A**, 6 (1976).
33) B. E. Barker and M. F. Fox, *Chem. Soc. Rev.*, **9**, 143 (1980).
34) A. El-Kourashy and R. Grinter, *J. Chem. Soc., Faraday Trans. 2*, **73**, 1050 (1977).

The Isomerization of 1-Butene to *cis*-2-Butene over CaO by Means of the Pulse-Reaction Method

Kazushi ARATA,* Makoto HINO,† and Sakari KOBAYASHI†
Hokkaido University of Education, Hachiman-cho, Hakodate 040
†Hakodate Technical College, Tokura-cho, Hakodate 042
(Received July 10, 1987)

Synopsis. The title reaction was studied over CaO catalysts which had been prepared by the calcination of $Ca(OH)_2$ in air, followed by heating in a He stream or by thermal decomposition in a He flow. The former catalysts gave high cis/trans ratios (up to 21.6), while the latter ones were higher in activity but showed much lower ratios (ca. 1).

It is well-known that alkaline earth metal oxides, like MgO and CaO, are solid bases which catalyze various kinds of reactions.[1-4] Among a number of reactions over the solid bases, double bond and cis-trans isomerizations of butenes have been studied by many workers to clarify the surface properties. It has been recognized that basic sites convert 1-butene into *cis*-2-butene via π-allyl anion intermediates formed by the abstraction of H^+ from 1-butene;[5,6] the ratio of *cis*-2-butene to *trans*-2-butene is large (8 for CaO and 16 for MgO), compared with 1—2 in the case of the acid catalysts.[7,8]

For the above experiments, the reactions have mostly been carried out in a closed circulating reactor with a fixed-bed catalyst pretreated in vacuo. In this study, the isomerization of 1-butene was performed over CaO under pulse conditions; the results were exceedingly far from those obtained with a recirculation reaction.

Experimental

The calcium oxide was prepared by calcining $Ca(OH)_2$ (Wako Pure Chemical, Ltd.) in air for 3 h. The reactions were carried out in a microcatalytic reactor (3 mm in diameter) of stainless steel with a fixed-bed catalyst [flow rate of He carrier gas: 20 ml/min; pulse size: 0.05 ml (in gas); catalyst: 30 mg (32-60 mesh); height of the catalyst bed: ca. 3 mm]. The reactants were injected into the reactor with a syringe. For analysis, the effluent products were directly introduced into a gas chromatographic column connected to the reactor (VZ-7, 4 m, 25 °C). Since the yields were almost constant with the pulse number, conversions were taken as an average of pulse values from the first to the fifth.

Results and Discussion

The catalytic activity of CaO for the isomerization of 1-butene to 2-butenes and the selectivity to *cis*-2-butene largely depend on the temperatures of calcination in air and of treatment in a He flow in the reactor. $Ca(OH)_2$ was calcined at 300—1000 °C in air, heated in He at various temperatures, and then employed for the reaction of 1-butene. The results are shown in Table 1. The CaO catalysts were also obtained by the thermal decomposition of $Ca(OH)_2$ in a He flow, without calcination in air. High activities were observed with the catalysts heated at 600 or 700 °C in air and then in He; high ratios of *cis*-2-butene to *trans*-2-butene (c/t) were obtained when it was treated at 500 °C in He after 600 or 700 °C in air, the value of 21.4 being exceedingly high. It may be seen that the ratios were lowered with treatment in He at high temperatures, in particular >700 °C. Conversions were high for the catalysts pretreated at higher temperatures, but they lowered with calcination in air at higher temperatures; for instance, the catalysts calcined at 600, 700, 800, 900, and 1000 °C in air, followed by treatment at 600 °C in He, gave conversions of 86, 83, 37, 24, and 0% respectively. The reaction of *cis*-2-butene was performed over the CaO calcined in air at 700 °C; the isomerization of cis- to trans-form was negligible under the conditions shown

Table 1. Isomerizations of 1-Butene and 1-Pentene at 30 °C

Calcination temperature in air/°C	Pretreatment temperature[a] °C	Conversion[c] %	c-2/t-2[c]
300	300	0	
	300[b]	3	
350	350	0	
	400[b]	44	9.4
450	450	19	9.8
500	500	26	13.0
	500[b]	82	6.9
	500[b,d]	60(40)	10.1(5.3)
600	500	18	17.2
600	550	35	14.1
600	600	86	4.5
	600[b]	93	1.0
	600[b,d]	73(73)	7.0(1.6)
700	500	17(8)	21.4(18.8)
700	525	54(36)	15.4(6.2)
700	550	68(50)	11.4(5.5)
700	600	83(85)	5.7(2.3)
700	700	85	1.1
	700[b]	94	0.8
	700[b,d]	85	1.4
800	550	20	17.8
800	600	37	15.8
800	700	75	3.2
800	800	82	1.6
	800[b]	97	0.6
	800[b,d]	83	1.1
900	600	24	15.1
900	700	52	3.0
900	800	55	2.8
900	900	Trace	
	900[b]	88	0.8
	900[b,d]	60	2.7
1000	600	0	

a) In He stream for 1 h. b) $Ca(OH)_2$ was thermally decomposed in He for 1 h. c) Numerals in parentheses show values for the reaction of 1-pentene. d) Catalyst amount: 10 mg.

in Table 1 when the CaO was pretreated at 500—550 °C. The conversion and the c/t ratio were almost steady after a 30-min treatment. The CaO catalysts obtained by calcination in a He stream for 1 h were higher in activity, but much lower in the c/t ratio than those prepared by calcination in air.

The surface areas measured by the BET method using nitrogen gas were 46 and 34 m^2/g for the catalysts calcined at 700 and 900 °C in air respectively. The base strength of the present catalysts was examined by a color-change method using acid indicators; the highest strength was $27.0 \leqq H_- < 33.0$. The CaO prepared by calcination in air and then in He at 600 °C was completely poisoned with butylamine, NH_3, H_2O, and CO_2.

The catalysts heated at 600 and 700 °C, which showed high activities and c/t ratios, were also examined in the isomerization of 1-pentene (Table 1). The reactivity and c/t ratio were lower than those in the case of 1-butene, the highest ratio being 18.8.

High c/t ratios were observed compared with the literature values,[7] and higher values still were obtained from the reaction of 1-butene at 0 °C. That is, the catalyst calcined at 600 °C in air, followed by treatment at 550 °C in He, gave the ratio of 32.6 with a 52% conversion (catalyst amount: 100 mg) and that of 41.6 with a 32% conversion in the case of the catalyst treated at 700 °C in air and 500 °C in He. As for the high ratio given by solid base catalysts, it has been reported that the ratio of 55 was obtained over Na/Na_2CO_3 with only a 5% conversion from 1-butene.[9] O'Grady et al. achieved a reaction at −60 °C over Na/Al_2O_3 in a flow system, where the c/t ratio was observed to be 21.5 with a 54% conversion.[10]

The basic properties of CaO have been studied in detail by Tanabe et al.[1,11,12] The active sites for the isomerization of 1-butene to *cis*-2-butene are strongly basic O^{2-} ions, which occupy a large fraction of the basic sites. The strong basic site, O^{2-}, is easily poisoned with the acidic molecule, CO_2; CO_2 is adsorbed on CaO as a unidentate complex when the pressure of CO_2 is high and as a bidentate complex at low pressure. When CaO is prepared by calcining $Ca(OH)_2$ in air, the basic sites are poisoned with CO_2, and it does not work as a basic catalyst. The CO_2 is removed by evacuation at 300—500 °C, resulting in a high selectivity to *cis*-2-butene; Ca^{2+} ions exposed by evacuation at high temperatures are active as acidic sites for the formation of *trans*-2-butene from 1-butene, the c/t ratio being low. The cis-trans interconversion also occurs on unusually strong basic sites, which appear on evacuation at 700—900 °C.[13]

In view of the above explanation, the high c/t ratios under the pulse conditions may be interpreted by the following scheme. The unidentate CO_2 is removed by

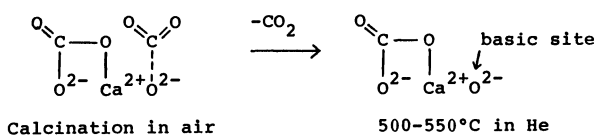

heating at 500—550 °C in a He flow, while the bidentate CO_2 remains at the surface; the exposed basic site, O^{2-}, is effective as the base catalysis for olefines. The following experimental phenomena seem to support this explanation: (1) When the catalyst was pretreated in He over 700 °C, the gas chromatographic peaks, as analyzed by a column connected to the reactor, were broadened; it is considered that the electrons of butenes were adsorbed on the Ca^{2+} created by the elimination of the bidentate CO_2. In this case, the conversion is high, and the c/t ratio is small, because of the acidic effect of Ca^{2+} (Table 1). (2) When CaO was prepared by the thermal decomposition of $Ca(OH)_2$ in a He stream, it is likely that the removal of CO_2 was easier; both acidic, Ca^{2+}, and basic, O^{2-} sites caused high conversions with low c/t ratios (Table 1). (3) The CaO catalyst obtained by calcination in air, followed by pretreatment in He at 450 °C, showed a 69% conversion for the reaction of 1-butene, but it was completely inactive when pretreated in air at 450 °C. (4) The cis to trans interconversion is more suppressed by the short contact time under the present pulse conditions than a closed circulating reaction.

References

1) T. Iizuka, H. Hattori, Y. Ohno, J. Sohma, and K. Tanabe, *J. Catal.*, **22**, 130 (1971).
2) H. Hattori, K. Shimazu, N. Yoshii, and K. Tanabe, *Bull. Chem. Soc. Jpn.*, **49**, 969 (1976).
3) M. Mohri, K. Tanabe, and H. Hattori, *J. Catal.*, **32**, 144 (1974).
4) H. Hattori, K. Maruyama, and K. Tanabe, *J. Catal.*, **44**, 50 (1976).
5) H. Pines and L. A. Schaap, *Adv. Catal.*, **12**, 117 (1960).
6) M. J. Baird and J. H. Lunsford, *J. Catal.*, **26**, 440 (1972).
7) K. Tanabe, N. Yoshii, and H. Hattori, *J. Chem. Soc., Chem. Commun.*, **1971**, 464.
8) H. Hattori, N. Yoshii, and K. Tanabe, Proc. 5th Intern. Congr. Catal., Palm Beach, 10-233 (1973).
9) W. O. Haag and H. Pines, *J. Am. Chem. Soc.*, **82**, 387 (1960).
10) H. Pines and W. M. Stalick, "Base-Catalyzed Reactions of Hydrocarbons and Related Compounds," Academic Press, New York, San Francisco, London (1977), p.32.
11) Y. Fukuda and K. Tanabe, *Bull. Chem. Soc. Jpn.*, **46**, 1616 (1973).
12) K. Tanabe and R. Noyori, "Superacid-Superbase," Kodansha Scientific, Tokyo (1980), p.121.
13) T. Iizuka, Y. Endo, H. Hattori, and K. Tanabe, *Chem. Lett.*, **1976**, 803.

The Crystal and Molecular Structure of 1:2 Molecular Complex of 1,4-Diazabicyclo[3.3.3]octane (DABCO) with *p*-Cresol

Masaaki TAKAMA, Masanori YASUI, Shigeharu HARADA, Nobutami KASAI,* Koichi TANAKA,† and Fumio TODA†
Department of Applied Chemistry, Faculty of Engineering, Osaka University, Yamadaoka, Suita, Osaka 565
†Department of Industrial Chemistry, Faculty of Engineering, Ehime University, Matsuyama 790
(Received July 15, 1987)

Synopsis. X-Ray crystal structure analysis of the title compound is described. $C_6H_{12}N_2$,$2C_7H_8O$, *F. W.* 328.5, monoclinic, space group *C*2/*c*, a=18.494(1), b=9.250(1), c=11.414(1) Å, β=103.67(1)°, V=1897.4(3) Å^3, D_c=1.150 g cm^{-3} for Z=4. The DABCO molecule in the crystal is bound to two *p*-cresol molecules by the strong O-H ··· N hydrogen bonds, and the crystal is composed of *p*-cresol ··· DABCO ··· *p*-cresol complex units.

It has been reported that the optical resolution of tertiary alcohols, especially tertiary acetylenic alcohols, can easily be achieved by complexation with achiral amines, such as 1,4-diazabicyclo[3.3.3]octane (DABCO).[1] Recently, Toda and Tanaka found that DABCO also forms complex with phenols. In order to obtain structural informations on the complexation, the crystal structure of the 1:2 complex of DABCO and *p*-cresol has been determined by means of X-ray diffraction.

Experimental

The crystal used had approximate dimensions of 0.75×0.5×0.25 mm, which was sealed in a thin-walled glass capillary tube in order to prevent sublimation. X-Ray diffraction data were collected on a Rigaku rotating anode four-circle diffractometer using nickel-filltered Cu $K\alpha$ radiation by the θ-2θ scan technique up to 2θ=120°. The scan rate was 4° min^{-1} and the scan width $\Delta\theta$=(1.2+0.15 tan θ)°. Backgrounds were counted for 4 s at both ends of a scan. Three standard reflections measured after every 100 reflections to monitor the stability and orientation of the crystal showed no significant decay through the experiment. Of the 1414 reflections measured, number of reflections observed was 1317 ($|F_o|>2\sigma$ (F_o), where σ is the standard deviation obtained from the counting statistics). Usual Lorentz and polarization corrections were applied but absorption effect was ignored [μ(Cu $K\alpha$)=5.94 cm^{-1}].

Structure Solution and Refinement

The structure was solved by the direct method (*MULTAN* 78),[2] and was refined by the block-diagonal least-squares procedure (*HBLS* V).[3] The nonhydrogen atoms were refined anisotropically. The hydrogen atoms, which located on the difference Fourier map, were refined with isotropic temperature factors. The final R index was 0.073. The weighting scheme used at the final stage of the refinement was $w=[\sigma^2(F_o)+0.1582|F_o|+0.0013|F_o|^2]^{-1}$. Final atomic parameters are given in Tabler 1.†† Atomic scattering factors used were taken from International Tables for X-Ray Crystallography.[5] Computations were done on an ACOS 850S computer at the Crystallographic Research Center, Institute for Protein Research, Osaka University.

Results and Discussion

Molecular structure is shown in Fig. 1.[6] The remarkable feature of the structure is that the DABCO molecule, the center of which lies on a crystallographic two fold axis, is bound to two *p*-cresol molecules at its both ends by the strong O-H ··· N hydrogen bonds [O(1) ··· N(1)=2.713(3), O(1)-H(1)=1.03(4), H(1) ··· N(1)=1.69(4) Å, and O(1)-H(1) ··· N(1)=172(4)°] to form a linear 1:2 molecular complex of *p*-cresol ··· DABCO ··· *p*-cresol. The molecular symmetry of the central DABCO is 2 instead of $\bar{6}m2$ but has a similar structure as that determined by means of neutron diffraction at 298 K, and also as those observed in the 1:2 complex with (−)- and (+)-1-phenyl-1-(*o*-chlorophenyl)-2-propyn-1-ol.[7] The thermal ellipsoids of the C(8), C(9), and C(10) atoms are elongated along the direction approximately perpendicular to the N(1) ··· N(1′) axis of the molecule (equivalent isotropic temperature factors of these atoms are 13.8, 14.4, and

Table 1. Final Atomic Coordinates with Estimated Standard Deviations in Parentheses

a) Nonhydrogen atoms with equivalent isotropic temperature factors[4]

Atom	x	y	z	B_{eq}/Å^2
O(1)	0.4491(2)	0.7146(3)	-0.1068(2)	6.65
N(1)	0.4744(2)	0.7441(3)	0.1361(3)	5.99
C(1)	0.2166(2)	1.0159(4)	-0.4304(3)	6.7
C(2)	0.2787(2)	0.9361(3)	-0.3431(3)	5.28
C(3)	0.3256(2)	0.8412(3)	-0.3840(3)	5.36
C(4)	0.3829(2)	0.7690(3)	-0.3053(3)	5.42
C(5)	0.3937(2)	0.7903(3)	-0.1810(3)	5.17
C(6)	0.3478(2)	0.8862(4)	-0.1383(3)	5.85
C(7)	0.2913(2)	0.9584(4)	-0.2193(3)	5.99
C(8)	0.4242(4)	0.6682(8)	0.1938(4)	13.8
C(9)	0.4541(4)	0.6723(8)	0.3335(5)	14.4
C(10)	0.4824(3)	0.8899(4)	0.1807(4)	8.7

b) Hydrogen atoms with isotropic temperature factors

Atom	x	y	z	B_{eq}/Å^2
H(3)	0.318(2)	0.826(3)	-0.480(3)	3.5(6)
H(4)	0.413(2)	0.693(4)	-0.340(3)	4.4(7)
H(6)	0.357(2)	0.903(4)	-0.045(3)	5.0(8)
H(7)	0.257(2)	1.035(4)	-0.187(3)	5.1(8)
H(81)	0.418(3)	0.552(5)	0.163(5)	9.(2)
H(82)	0.369(3)	0.720(7)	0.173(5)	13.(2)
H(91)	0.459(3)	0.558(6)	0.366(5)	12.(2)
H(92)	0.419(4)	0.724(6)	0.378(6)	11.(2)
H(101)	0.428(3)	0.942(6)	0.163(5)	9.(2)
H(102)	0.516(3)	0.939(6)	0.134(4)	9.(2)
H(1)	0.456(2)	0.734(5)	-0.016(4)	7.(2)
H(11)	0.181(2)	1.061(4)	-0.388(4)	7.(1)
H(12)	0.185(3)	0.954(6)	-0.495(4)	10.(2)
H(13)	0.237(3)	1.098(5)	-0.480(4)	7.(1)

††Tables of anisotropic thermal parameters and observed and calculated structure factors are kept at the Chemical Society of Japan, Document No. 8769.

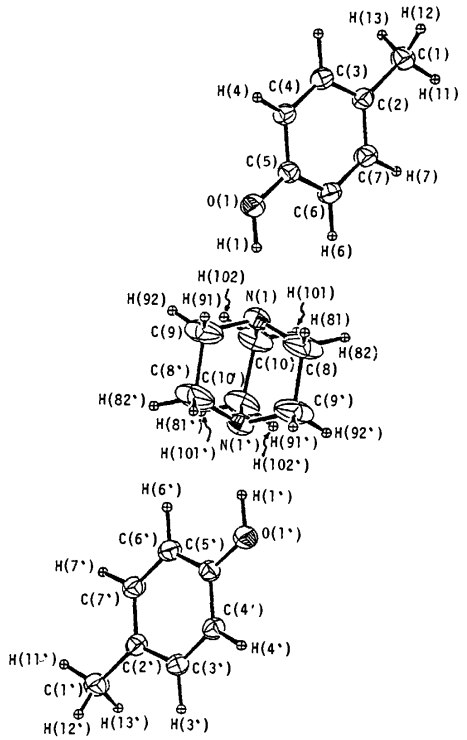

Fig. 1. A perspective view[6] of the 1:2 molecular complex of DABCO with *p*-cresol with the numbering scheme of atoms. Nonhydrogen atoms are drawn as thermal ellipsoids with 20% probability level, and hydrogen atoms with B=1.0 Å^2.

8.7 Å^2, respectively), which suggest a hindered rotation of the DABCO molecule along the N(1)···N(1′) axis. However, three C-N bond lengths [1.437(5), 1.442(7), and 1.447(8) Å] and C-N-C bond angles [108.6(4), 108.6(5), and 109.5(4)°] are respectively equal to the corresponding bond distances and bond angles determined by the neutron diffraction study[8] within the range of error, whereas, the C(8)-C(9′), C(8′)-C(9), and C(10)-C(10′) bond distances [1.56(1), 1.56(1), and 1.561(7) Å, respectively] are slightly smaller than those obtained by the same study. The *p*-cresol molecule attached to the DABCO by the hydrogen bonding has a normal structure.[9] The benzene ring is planar within 0.002 Å. The average C-C bond distance is 1.392 Å and the average C-C-C angle 120°. The C(6)-C(5)-O(1) angle [122.9(3)°] is larger than the C(4)-C(5)-O(1) [117.6(3)°].

As seen in Fig. 2, the crystal structure is composed of

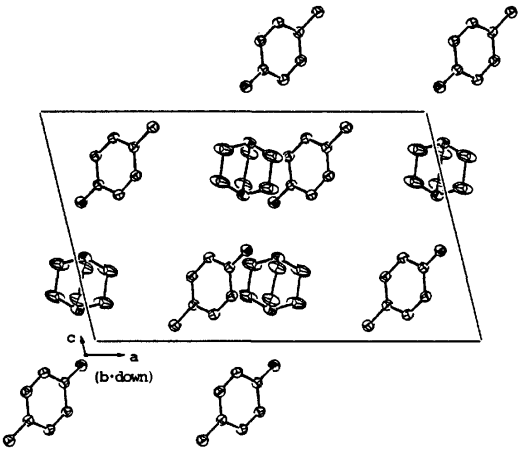

Fig. 2. Crystal structure[6] of the 1:2 molecular complex of DABCO with *p*-cresol projected along the b axis. Nonhydrogen atoms are drawn as thermal ellipsoids with 20% probability level. Hydrogen atoms are omitted for clarity.

a loose packing of the 1:2 complex. The closest intermolecular atomic contact[3.666(5) Å] is observed between the C(5) (x, y, z) and C(1) (0.5−x, −0.5+y, −0.5+z).

The present work was partially supported by a Grant-in-Aid for Scientific Research from the Ministry of Education, Science and Culture.

References

1) F. Toda and K. Tanaka, *Chem. Lett.*, **1986**, 1905.
2) P Main, S. E. Hull, L. Lessinger, G. Germain, J. P. Declerq, and M. M. Woolfson, *MULTAN* 78, "A System Computer Programs for the Automatic Solution of Crystal Structures from X-Ray Diffraction Data," Univs. of York, England and Louvain, Belgium, 1978.
3) T. Ashida, *HBLS* V, "The Universal Crystallographic Computing System-Osaka," The Computation Center, Osaka University, 1979.
4) W. C. Hamiltom, *Acta Crystallogr.*, **12**, 609 (1959).
5) "International Tables for X-Ray Crystallography," Kynoch Press, Birmingham, England (1974), Vol. IV, p. 71.
6) C. K. Jonson, *ORTEP* II, Report ORNL-5138, Oak Ridge National Laboratory, Tennessee, 1976.
7) M. Yasui, T. Yabuki, M. Takama, H. Tezuka, S. Harada, N. Kasai, K. Tanaka, and F. Toda, Unpublished results.
8) J. K. Nimmo and B. W. Lucas, *Acta Crystallogr., Sect. B*, **32**, 348 (1976).
9) C. Bois, *Acta Crystallogr., Sect. B*, **26**, 2086 (1970).

Time-Dependent Metastable Fragmentations. The H_2O Loss from Ethyl Acetate Ions

Ryuichi ARAKAWA
Institute of Chemistry, College of General Education, Osaka University, Toyonaka 560
(Received July 18, 1987)

Synopsis. The metastable transitions for $CH_3COOC_2H_5^+ \rightarrow C_4H_6O^+ + H_2O$ have been measured as a function of the ion lifetime of 0—200 μs by using trapped ion mass spectrometry (TIMS). The experimental data were well explained by tunneling corrections to the prior isomerization rate.

The H_2O loss from ionized ethyl acetate is the lowest energy process, only 0.3 eV higher than the ionization energy. This reaction has a strong metastable peak in a μs time-frame. The reaction mechanism for H_2O loss has been of much interest and has been studied by labeling experiments[1] and by means of the collisional activation spectra[2] for a daughter ion of $C_4H_6O^+$. These results previously reported suggest that all hydrogen atoms and both oxygen atoms participate in the complex reaction mechanism. The photoion-photoelectron coincidence(PIPECO) study by Baer and his co-workers[3] has provided close measurements of the dissociation rate as a function of the photon energy for the rate range of 10^5—10^6 s^{-1}. Moreover, the time-dependent kinetic energy releases have been measured for ion lifetimes up to 20 μs by means of double-focusing mass spectrometry[4] and by means of TIMS.[5] However, there is still an unresolved question as to the ethyl-acetate dissociation near the threshold.

The present paper will report on the slow metastable fragmentations of less than 10^5 s^{-1}, which have not previously been observed for an ethyl acetate system. The metastable intensities for H_2O loss were measured as a function of the ion-source-residence time by means of TIMS. The longest lifetime of 200 μs corresponds to the average rate of ca. 5×10^3 s^{-1}.

Experimental

The ion-trapping technique has been described in detail elsewhere.[6] Briefly, the space charge formed by a continuous 5-eV electron beam was used to trap ions produced when a negative pulse was applied to a filament. At a known delay time after the ionizing pulse, a positive pulse, 4 μs in duration and 5 eV in height, was applied to a repeller electrode in order to remove ions for mass analysis. The delay time was successively varied with a 3.7-μs step. The ionizing pulse was applied to the filament at a 0.5-ms interval. These pulse-sequence and data-acquisition systems were both computer-controlled.

The metastable parent ions, which are selected by the first magnet, decompose in the second-field-free region. The product ions are analyzed by the use of the second magnet. Several hours of data accumulation were statistically needed for the measurement. The temperature of the ion source was 423 K. The ion-accelerating voltage was 1.5 kV. The ion-source pressure was kept at 2×10^{-6} Torr (1 Torr=133.322 Pa). The collision-induced reaction in the field-free region was negligible, because the pressure was less than 1×10^{-6} Torr.

Results and Discussion

Figure 1 shows the metastable-to-main-beam intensity ratio at the electron-impact energy of 40 eV. This metastable decay, of course, reflects the rate constant, and its intensity at the ion-residence time of t is proportional to:[7]

$$m^*(t) \propto \int_0^\infty p(E)\,[\exp(-t_1 k(E)) - \exp(-t_2 k(E))]\,dE.$$

Here, $p(E)$ is the internal energy distribution, t_1 and t_2 are the time windows in the experiment (t_1=6.5+t and t_2=11.7+t μs), and $k(E)$ is the unimolecular rate constant. The photoelectron spectrum for ethyl acetate[8] was assumed to represent $p(E)$.

The PIPECO experimental rates previously reported by Baer and his co-workers[3] are shown in Fig. 2. The RRKM calculation has given a rate 100 times larger than the measured rates. This is mainly because of the low activation energy, that is, the low state density for the reactant. They therefore concluded that the parent ethyl acetate ion rearranges to a more stable structure prior to dissociation. The energy of its isomer, 0.62 eV lower than the ionization energy of ethyl acetate, was determined as a parameter, so that the RRKM rates agreed with the measured rates. Such a prior isomerization mechanism provides a rate-energy curve which is truncated at the threshold (Fig. 2). As may be seen in

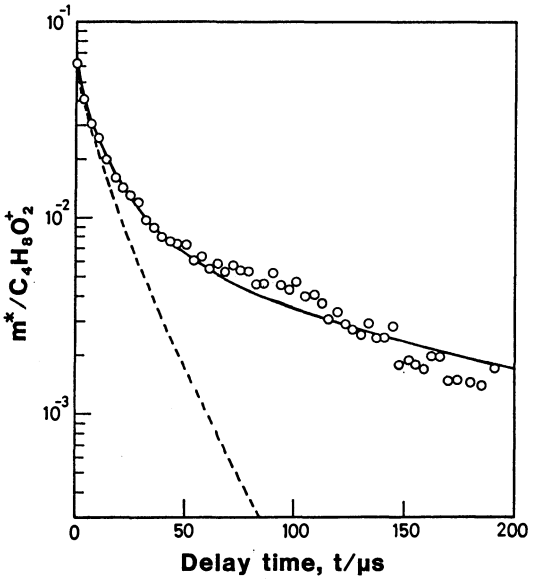

Fig. 1. A plot of the metastable-to-main-beam intensity ratios for $CH_3COOC_2H_5^+ \rightarrow C_4H_6O^+ + H_2O$ against the delay time: experiment(○) and calculated with the prior isomerization rate model, ---- and with the tunneling correction, ——.

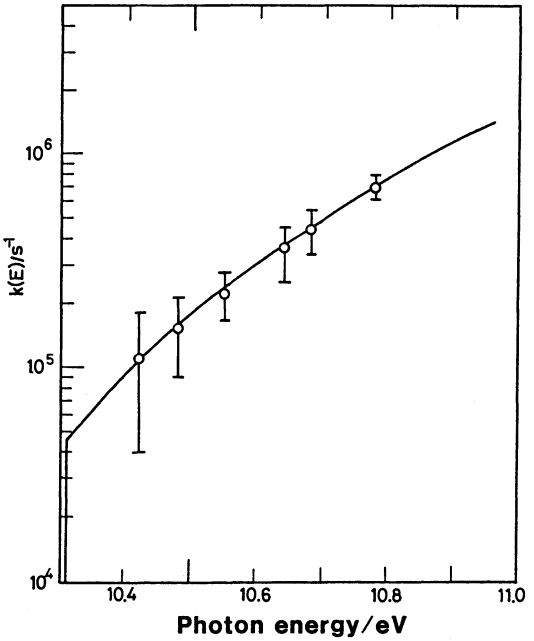

Fig. 2. The dissociation rate $k(E)$ vs. photon energy: the PIPECO experimental rate,[3] (O) and the RRKM rate arising from the prior isomerization mechanism(——).

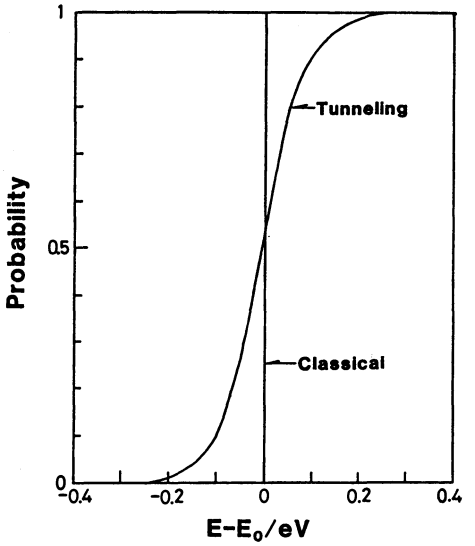

Fig. 3. Tunneling probability near threshold energy, E_0.

Fig. 1, this rate model fails to fit the experimental data. The reason for this failure is probably because the model provides no rate less than 10^4 s^{-1}. From the actual calculation it was found that a decrease in the metastable decay is dependent on the slope of $k(E)$ vs. E, especially in the range of 10^3—10^5 s^{-1}.[7]

In this study, the tunneling effect was examined to explain the slow fragmentations. Tunneling corrections to unimolecular rate constants have previously been investigated for neutral reactions by Miller and his co-workers.[9] Moreover, applications to metastable transitions have been reported for methane,[10] methanol,[11] and phenol[12] cations. These experiments have usually been carried out to observe the temperature dependence on the ratios of the metastable-to-main-beam intensity or on kinetic energy releases. For example, Klots predicted that the metastable intensity, if tunneling through a centrifugal barrier occurs, increases as a square of the temperature.[10]

The probability of tunneling is generally favored for the case of one-step hydrogen-bond cleavage. The H_2O loss of the ethyl acetate cation probably involves a hydrogen migration to a oxygen atom prior to dissociation. On the basis of a Miller modification with the generalized Eckart potential,[8] the tunneling probabilities were calculated, and they are shown in Fig. 3. For the calculation, the activation barrier of 0.92 eV was obtained from the PIPECO results;[3] the reverse barrier was assumed to be 0.5 eV, for the product structure of $C_4H_6O^+$ was not well defined. The probability depends strongly upon an imaginary frequency. Here, the imaginary frequency of 2300 cm^{-1} was taken from Ref. 6. The rate below the threshold was obtained by multiplying the rate at the threshold by the tunneling probability. The tunneling correction to the prior isomerization rate is very satisfactory for the experimental metastable decay in Fig. 1. It may be concluded that the decrease in the metastable intensity with the ion lifetime beyond 20 μs arises from tunneling through a potential barrier. This conclusion is supported by the good agreement between the experimental data and the results of calculation by taking the tunneling effect into account. In other words, this indicates that the hydrogen-atom migration is a rate-determining step for slow fragmentations. However, such consideration has not been definitely confirmed by direct observation. It has been well known that a OH or H_2O loss which involves hydrogen-atom migration is generally a complex mechanism.

References

1) A. N. H. Yeo, *Chem. Commun.*, **1970**, 1154.
2) J. L. Holmes, P. C. Burgers, and J. K. Terlouw, *Can. J. Chem.*, **59**, 1805 (1981).
3) L. F. Monteiro, M. L. F. Monteiro, J. J. Butler, and T. Baer, *J. Phys. Chem.*, **86**, 752 (1982).
4) P. C. Burgers and J. L. Holmes, *Int. J. Mass Spectrom. Ion Processes*, **58**, 15 (1984).
5) V. Aviyente, M. Shaked, A. Feinmesser, S. Gefen, and C. Lifshitz, *Int. J. Mass Spectrom. Ion Processes*, **70**, 67 (1986).
6) A. A. Herod, and A. G. Harrison, *Int. J. Mass Spectrom. Ion Phys.*, **4**, 415 (1970); C. Lifshitz, *Mass Spectrom. Rev.*, **1**, 309 (1982).
7) F. M. Benoit, A. G. Harrison, and F. P. Lossing, *Org. Mass Spectrom.*, **12**, 78 (1977).
8) R. Arakawa and Y. Yoshikawa, *Bull. Chem. Soc. Jpn.*, **60**, 49 (1987).
9) W. H. Miller, *J. Am. Chem. Soc.*, **101**, 6810 (1979); Y. Osamura, H. F. Schaefer, III, S. K. Gray, and W. H. Miller, *J. Am. Chem. Soc.*, **103**, 1904 (1981).
10) B. H. Solka, J. H. Beynon, and R. G. Cooks, *J. Phys. Chem.*, **79**, 859 (1975); C. E. Klots, *J. Phys. Chem.*, **75**, 1526 (1971); L. P. Hills, M. L. Vestal, and J. H. Futrell, *J. Chem. Phys.*, **54**, 3834 (1971).
11) K. C. Smyth and T. W. Shannon, *J. Chem. Phys.*, **51**, 4633 (1969).
12) C. Lifshitz, S. Gefen, and R. Arakawa, *J. Phys. Chem.*, **88**, 4242 (1984).

Stereoselective Alkylation of Lithium Enolates Generated from *t*-Butyl Esters of 4-Alkyl-Substituted 5-Hydroxypentanoic Acids

Yutaka UKAJI and Koichi NARASAKA*
Department of Chemistry, Faculty of Science, The University of Tokyo, Hongo, Bunkyo-ku, Tokyo 113
(Received July 18, 1987)

Synopsis. Alkylation of lithium enolates generated from *t*-butyl esters of 4-alkyl-substituted 5-hydroxypentanoic acid by treatment with lithium pyrrolidinide in THF-HMPA proceeded stereoselectively to afford the corresponding *anti*-α-alkylated esters.

Concerning remote chiral induction directed by a hydroxyl group, we reported that the lithium enolates of *t*-butyl 5-hydroxy carboxylates react with electrophiles such as alkyl halides, ketones and oxaziridines, giving the corresponding 2-substituted products with high diastereoselectivities.[1] In these reactions remote chiral induction (1,4-relationship) is considered to be efficiently controlled by the formation of a lithium chelate, therefore, we successively applied this concept to the stereoselective preparation of 2,4-disubstituted 5-hydroxypentanoates based on the following consideration.

When a 4-alkyl-substituted 5-hydroxypentanoate **1** is treated with lithium amide in tetrahydrofuran (THF) and hexamethylphosphoric triamide (HMPA), it is expected that the (*E*)-enolate would be generated stereoselectively[2] and would form an 8-membered chelate **2**,[1] which would successively react with alkylating reagents in a stereoselective manner.

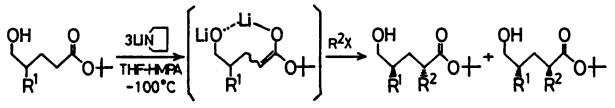

1 **2** **3** **4**

According to the above hypothesis, the enolization of 5-hydroxypentanoates **1A—C**, which have methyl, allyl or benzyl group as a 4-substituent, and the successive reaction with alkylating reagents were examined. The hydroxy ester **1** was treated with 3 molar amounts of lithium pyrrolidinide[3] in THF-HMPA at −100 °C for 1 h, and then the alkylation was performed at the temperature. The diastereoselectivities in these reactions are summarized in Table 1. Generally a good diastereoselectivity is observed and the 4-substituent slightly affects the selectivity. That is, in the case that the substituent is allyl or benzyl group, a higher selectivity is observed as compared with that in reaction of the methyl substituted ester **1A**.

Table 1. Diastereoselectivity in the Alkylation of **1**

R^1	R^2-X	3 : 4	Total yield/%
Me	Me_2SO_4	80 : 20[a)]	78
CH_2=$CHCH_2$	Me_2SO_4	85 : 15[a)]	81
CH_2=$CHCH_2$	$PhCH_2Br$	90 : 10[b)]	96
$PhCH_2$	Me_2SO_4	90 : 10[b)]	80
$PhCH_2$	*n*-BuI[c)]	91 : 9[d)]	76

a) The ratio was determined by GLPC (PEG-HT). b) The ratio was determined by HPLC (Waters RESOLVE). c) After the addition of *n*-BuI, the reaction mixture was stirred for 1 h at −100 °C and gradually warmed to −78 °C.

The alkylated product **3e** was readily converted to the *trans*-2,4-disubstituted 5-pentanolide **5** by treatment with trifluoroacetic acid at room temperature. On the othe hand, an attempt to prepare the *trans*-pentanolide **5** from a cyclic compound such as 4-benzyl-5-pentanolide by the alkylation of the corresponding lithium enolate with butyl iodide failed, resulting in the formation of almost equal amounts of the both isomers (**5** : **6**=59 : 41). Therefore, the present reaction affords a stereoselective method for the preparation of *trans*-2,4-disubstituted pentanolide.

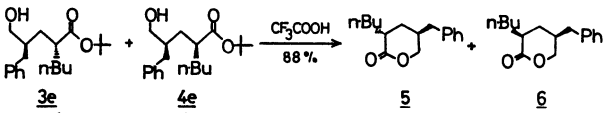

3e (91 : **4e** 9) **5** (91 : **6** 9)

The relative stereochemistry was confirmed by the transformation of **3a** to *dl*-2,4-dimethyl-1,5-pentanediol **7**. The mixture of **3a** and **4a** was reduced with lithium aluminum hydride to the diol **7** and **8** (4 : 1 mixture, respectively). The authentic *meso*-diol **8** was prepared from *meso*-2,4-dimethylglutaric anhydride, and the ^{13}C NMR spectrum of the authentic **8**[4] was identical with that of the minor isomer **8** obtained by the reduction of the mixture of **3a** and **4a**.

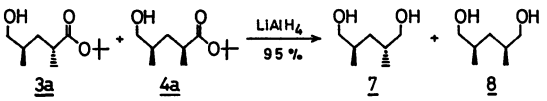

3a (4 : **4a** 1) **7** **8**

In conclusion, *anti*-2,4-disubstituted 5-hydroxy pentanoates **3** are prepared by the stereoselective remote alkylation of the 5-hydroxy esters **1**. The products **3** are considered to be useful synthetic intermediates, because the two different terminal oxygen functions can be effectively used for further transformation.

Experimental

Preparation of *t*-Butyl 5-Hydroxy-4-methylpentanoate (1A). To a THF (90 mL) solution of diisopropylamine (5.27 g, 52 mmol) was added butyllithium (49.6 mL in hexane, 52 mmol) at −78 °C under an argon atmosphere and stirred for 15 min. To the mixture was added a THF (10 mL) solution of ethyl propionate (5.28 g, 52 mmol) and stirred for 1 h at −78 °C. Then a THF (10 mL) solution of *t*-butyl acrylate (5.31 g, 41 mmol) was added to the mixture.[5] After being stirred for 1 h at the temperature, the reaction was quenched with sat. aqueous NH_4Cl and extracted with chloroform. The combined organic extracts were dried over Na_2SO_4, and condensed under reduced pressure. Purification by column chromatography on silica gel (hexane: ethyl acetate=15 : 1, volume ratio) gave the pure Michael

adduct, *t*-butyl 4-ethoxycarbonylpentanoate (6.66 g, 70%). IR (neat) 1730 cm^{-1}. ^1H NMR (CCl_4) δ=1.13 (3H, d, J=6.6 Hz), 1.24 (3H, t, J=7.0 Hz), 1.42 (9H, s), 1.52—1.95 (2H, m), 1.95—2.57 (3H, m), 4.01 (2H, q, J=7.0 Hz).

Next, to a THF (250 mL) solution of lithium aluminum hydride (3.29 g, 87 mmol) was slowly added a THF (20 mL) solution of the above Michael adduct (6.65 g, 29 mmol) at −78 °C under an argon atmosphere, and stirred for 8 h. The mixture was quenched with sat. aqueous Na_2SO_4 (25 mL) and the resulting precipitate was filtered off. The condensed filtrate was purified by column chromatography on silica gel (hexane : ethyl acetate=3 : 1, volume ratio) to give **1A** (2.97 g, 55%), bp 95 °C (bath temp)/2 mmHg (1 mmHg=133.322 Pa). IR (neat) 3430, 1730 cm^{-1}. ^1H NMR (CCl_4) δ=0.90 (3H, d, J=6.0 Hz), 1.20—1.80 (3H, m), 1.43 (9H, s), 2.03—2.53 (3H, m), 3.21—3.53 (2H, m).

4-Alkyl-substituted 5-hydroxy esters **1B** and **1C** were prepared by the method of Yamaguchi.[6] The spectra data are shown below.

***t*-Butyl 4-Benzyl-5-hydroxypentanoate (1C):** Bp 147 °C (bath temp)/2 mmHg. IR (neat) 3430, 1720 cm^{-1}. ^1H NMR (CCl_4) δ=1.20—1.71 (3H, m), 1.27 (9H, s), 1.92—2.28 (2H, m) 2.28—2.57 (3H, m), 3.28 (2H, d, J=4.0 Hz), 7.06 (5H, s).

***t*-Butyl 4-Hydroxymethyl-6-heptenoate (1B):** Bp 120 °C (bath temp)/2 mmHg. IR (neat) 3450, 1725, 1640 cm^{-1}. ^1H NMR δ=1.21—1.80 (3H, m), 1.43 (9H, s), 1.91—2.49 (4H, m), 2.68 (1H, br s), 3.40 (2H, d, J=5.6 Hz), 4.68—5.14 (2H, m), 5.31—6.07 (1H, m).

Stereoselective Alkylation of 1C with Dimethyl Sulfate. To a THF solution of lithium pyrrolidinide (1.67 mmol), which was prepared from pyrrolidine (173 mg, 2.44 mmol) and butyllithium (1.64 M hexane solution (1 M=1 mol dm^{-3}), 1.02 mL) at −78 °C, was added HMPA (0.58 mL, 3.33 mmol) at 0 °C under an argon atmosphere, and cooled to −100 °C. A THF (3 mL) solution of *t*-butyl 4-benzyl-5-hydroxypentanoate (**1C**, 147 mg, 0.56 mmol) was added to the mixture and stirred for 1 h at that temperature. Then a THF (3 mL) solution of dimethyl sulfate (251 mg, 1.99 mmol) was added to the mixture. After being stirred for 1 h at −100 °C, the reaction was quenched with sat. aqueous NH_4Cl and extracted with ether. The combined ether extracts were washed with water and brine, dried over Na_2SO_4, and condensed under reduced pressure. Purification by column chromatography (silica gel, hexane : ethyl acetate=10 : 1, volume ratio) gave *t*-butyl *anti*-4-benzyl-5-hydroxy-2-methylpentanoate (**3d**) and the *syn*-isomer **4d** (total 124 mg, 80%) in the ratio of 90 : 10, respectively.

The preparations of **3a,b,c,e** were carried out by the same procedure. All the alkylated products were isolated as a mixture of the *anti* and *syn* isomers **3** and **4**, which were not able to be separated by column chromatography or TLC. The following spectral data were for a mixture of the *anti* and *syn* isomers (91:9—80:20, respectively).

***t*-Butyl *anti*-5-Hydroxy-2,4-dimethylpentanoate (3a) and the *syn*-Isomer 4a:** IR (neat) 3430, 1720 cm^{-1}. ^1H NMR (CCl_4) δ=0.87 (3H, d, J=6.0 Hz), 0.99 (2.4H, d, J=7.0 Hz, anti), 1.00 (0.6H, d, J=7.4 Hz, syn), 1.20—1.98 (3H, m), 1.42 (9H, s), 2.03—2.60 (1H, m), 3.18—3.41 (3H, m).

***t*-Butyl *anti*-4-Hydroxymethyl-2-methyl-6-heptenoate (3b) and the *syn*-Isomer 4b:** IR (neat) 3430, 1725, 1640 cm^{-1}. ^1H NMR (CCl_4) δ=0.93—2.61 (6H, m), 1.09 (3H, d, J=7.0 Hz), 1.43 (9H, s), 2.97 (1H, br s), 3.27—3.55 (2H, m), 4.70—5.16 (2H, m), 5.35—6.09 (1H, m).

***t*-Butyl *anti*-2-Benzyl-4-hydroxymethyl-6-heptenoate (3c) and the *syn*-Isomer 4c:** IR (neat) 3430, 1720, 1640 cm^{-1}. ^1H NMR (CCl_4) δ=0.77—2.93 (8H, m), 1.26 (9H, s), 2.62 (1H, br s), 3.31—3.55 (2H, m), 4.70—5.13 (2H, m), 5.30—5.93 (1H, m), 7.06 (5H, s).

***t*-Butyl *anti*-4-Benzyl-5-hydroxy-2-methylpentanoate (3d) and the *syn*-Isomer 4d:** IR (neat) 3420, 1725 cm^{-1}. ^1H NMR (CCl_4) δ=1.06 (3H, d, J=6.8 Hz), 1.19—2.92 (6H, m), 1.36 (9H, s), 2.76 (1H, br s), 3.23—3.53 (2H, m), 7.02 (5H, s).

***t*-Butyl *anti*-2-(2-Benzyl-3-hydroxypropyl)hexanoate (3e) and the *syn*-Isomer 4e:** IR (neat) 3450, 1725 cm^{-1}. ^1H NMR (CCl_4) δ=0.63—2.63 (15H, m), 1.23 (8.2H, s, anti), 1.30 (0.8H, s, syn), 2.07 (1H, br s), 3.17—3.43 (2H, m), 7.07 (5H, s).

Transformation of the α-Alkylated Ester 3e to the Lactone 5. A mixture of **3e** and **4e** (total 123 mg, 0.39 mmol) was dissolved in trifluoroacetic acid (2 ml), and stirred for 2 h. After evaporation of the trifluoroacetic acid in vacuo, the residue was purified by preparative TLC on silica gel (hexane : ethyl acetate=3 : 1, volume ratio) to afford *trans*-4-benzyl-2-butyl-5-pentanolide (**5**) and the *cis*-isomer **6** (total 95 mg, 88%) in the ratio of 91 : 9, respectively. The isomeric ratio was determined by HPLC (Waters RESOLVE). *trans*-4-Benzyl-2-butyl-5-pentanolide and the *cis*-isomer: IR (neat) 1735 cm^{-1}. ^1H NMR (CCl_4) δ=0.65—2.73 (15H, m), 3.55—4.27 (2H, m), 6.83—7.10 (5H, m).

2,4-Dimethyl-1,5-pentanediol (7 and 8): Under an argon atmosphere, to a THF (3 mL) solution of lithium aluminum hydride (50 mg, 1.32 mmol) was added a THF (3 mL) solution of *t*-butyl 5-hydroxy-2,4-dimethylpentanoate (**3a** and **4a**, 110 mg, 0.54 mmol, anti : syn=4 : 1) at 0 °C, and the mixture was stirred at room temperature overnight. The mixture was quenched with sat. aqueous Na_2SO_4 (0.4 mL) and the resulting precipitate was filtered off. The condensed filtrate was purified by preparative TLC (ethyl acetate) to furnish the diol (68 mg, 95%). IR (neat) 3300 cm^{-1}. ^1H NMR ($CDCl_3$) δ=0.63—2.06 (4H, m), 0.87 (6H, d, J=6.4 Hz), 2.76—3.93 (2H, m), 3.37 (4H, d, J=6.0 Hz). ^{13}C NMR ($CDCl_3$) δ=16.55 (*dl*), 17.74 (meso), 32.91 (*dl*), 33.21 (meso), 37.03 (*dl*), 37.19 (meso), 67.58 (meso), 68.61 (*dl*).

The ^{13}C NMR spectrum of the minor isomer of diols was agreed with that of the authentic *meso*-diol obtained by the Allinger's method.[4]

References

1) K. Narasaka, Y. Ukaji, and K. Watanabe, *Bull. Chem. Soc. Jpn.*, **60**, 1457 (1987).

2) R. E. Ireland, R. H. Mueller, and A. K. Willard, *J. Am. Chem. Soc.*, **98**, 2868 (1976).

3) The alkylation reaction was examined by using some lithium amides such as lithium diisopropylamide, lithium diethylamide, lithium dimethylamide and lithium pyrrolidinide, and the best anti selectivity was observed when lithium pyrrolidinide was employed as a base.

4) N. L. Allinger, *J. Am. Chem. Soc.*, **81**, 232 (1959).

5) M. Yamaguchi, M. Tsukamoto, and I. Hirao, *Chem. Lett.*, **1984**, 375.

6) M. Yamaguchi, K. Shibato, and I. Hirao, *Tetrahedron Lett.*, **25**, 1159 (1984).

Thermal Cycloaddition Reaction of Tropone to 1,1-Diethoxyethene. Structure Revision of Cantrell's Diels-Alder Adduct

Hitoshi TAKESHITA,* Hisataka NAKASHIMA,† Shigeru SUGIYAMA, and Akira MORI
Institute of Advanced Material Study, 86, Kyushu University, Kasuga-koen, Kasuga, Fukuoka 816
†Graduate School of Engineering Sciences, 39, Kyushu University, Kasuga-koen, Kasuga, Fukuoka 816
(Received July 21, 1987)

Synopsis. A reinvestigation of Cantrell's thermal cycloaddition of tropone to 1,1-diethoxyethene has led to the isolation of three products: [4+2], [6+2], and [8+2] cycloadducts. The structure of the [4+2] cycloadduct was revised on the basis of an NMR analysis of the hydrolyzed diketone, and newly identified was a superficial *anti*-Woodward-Hoffmann [6+2] cycloadduct. These adducts did not cause mutual isomerization by heating under formation conditions.

In connection to our continuing interest on the cycloadditions of tropones, we have recently carried out the reaction of tropone (**1**) with 2-methoxyfuran (**A**) to give 1:1- (**B**) and 2:1-cycloadducts (**C**), for which, the second step of the reaction should fall into a category of the cycloaddition of **1** to a 1,1-dialkoxyethene.[1]

After analyzing the interconversions of these adducts, we noticed a different regioselectivity between the [4+2] cycloadducts found in the C-type products and the Cantrell's [4+2] cycloadduct **2a** prepared from **1** and 1,1-diethoxyethene (**3**).[2] This superficial discrepancy prompted us to reinvestigate the Cantrell's experiment. The findings will be described herein.

When a toluene solution of **1** and **3** was refluxed under a nitrogen atmosphere for 17 h, the formation of two products (**2** and **4**) was recognized as being consistent with Cantrell's result;[2] they seemed to be identical with his [4+2] and [8+2] cycloadducts, respectively. Furthermore, the presence of a third cycloadduct (**5**) was recognized. However, when the reaction was carried out under aerial conditions at 90 °C, the mixture became dark-colored and showed an inferior material balance (Table 1).

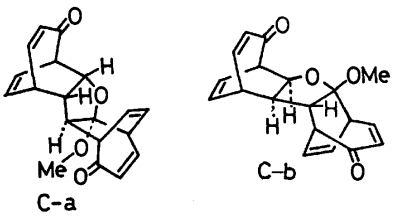

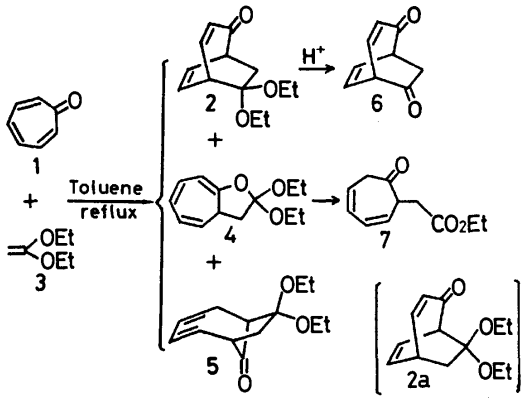

Scheme 1.

Under 3000 bar, the yeilds of **2** and **4** showed considerable improvement (Table 2).

In view of the variable yields depending on the conditions, oxygen-susceptible **5** might be a non-electrocyclic, radical product. On the other hand, an increase in the yields of **2** and **4** by an increase in the pressure shows that **2** and **4** are electrocyclic, concerted reaction products.

The ^{1}H NMR spectrum of **2** disclosed four vinylic protons, as well as two signals due to ethoxyl groups, suggesting that it is the [4+2] cycloadduct. Therefore, the only point to be clarified was the regiochemistry: between two possibilities, Cantrell's proposal, **2a**, and the isomer, **2**. However, we could not discriminate one from the other, since its 100- and 270-MHz ^{1}H NMR spectra showed still overlapped bridge-head protons underneath the methylene signal. A mild hydrolysis of **2** by dil hydrochloric acid yielded a diketone **6**, whose ^{1}H NMR spectrum[3] disclosed, together with four vinyl proton signals, well-separated methylene proton signals with a large vic-coupling (J=19 Hz), and doubly-allylic methine proton signal at δ=3.91. The spin-coupling pattern of this signal had only two large vic-couplings, J=9 and 7 Hz, indicating that the newly-generated carbonyl group is adjacent to the doubly allylic carbon. Thus, **6** is bicyclo[3.2.2]nona-3,8-diene-2,6-dione, and **2** is the corresponding diethyl acetal. The regiochemistry of **2** was in accord to our [4+2]-[4+2] cycloadducts (**C-a** and **C-b**), whose second step of formation could reasonably be explained in terms of a HOMO-LUMO interaction; however, it did

Table 1. The Cycloaddition of **1** to **2**

Condition	Yield/% of product			Recovered
	[8+2]	[6+2]	[4+2]	**1**
90 °C, 48 h/sealed tube	9.2	0.7	1.9	38
110 °C, 17 h, N_2/reflux	47	5.2	15	9.2

Table 2. Change of Product Distributions and Pressure Effect

Condition	Yield/%			Recovery
	[8+2]	[6+2]	[4+2]	**1**
120 °C, 10 h, 1 bar	9.1	3.1	1.1	70
120 °C, 10 h, 3000 bar	17	—	13	84

not follow Cantrell's formula **2a**. Although his structure argument seemed to depend on the ^{1}H NMR criteria, the disclosed evidence alone did not allow any conclusion to be drawn.

The **4** was quantitatively converted to the keto ester **7**, even in chloroform at 50 °C. The ^{1}H NMR spectrum of **4** was identical with the reported figures by Cantrell,[2] and **4** is undoubtedly the [8+2] cycloadduct. The ^{13}C NMR spectrum of **4** disclosed a characteristic signal due to the ortho ester carbon at δ 124.6.

The structure of **5** was again elucidated by the NMR spectroscopy; its ^{1}H NMR revealed AA'BB'-type four vinylic proton signals and its IR showed a peak due to an unconjugated carbonyl stretching frequency at 1750 cm^{-1} and it is the [6+2] cycloadduct. Noteworthy was the occurrence of such a Woodward-Hoffmann-Rule-disallowed process.[4] However, the [6+2] cycloadduct, **5**, might not be a secondary product since its formation could not be explained by symmetry-allowed sigmatropic reactions from **2** or **4**. This was verified when we carried out thermal isomerizations of the adducts; all the cycloadducts were surprisingly stable up to 130 °C, higher than the formation conditions, and recovered the starting materials quantitatively. Therefore, **5** must be formed directly from **1** and **3**.

Experimental

Thermal Cycloaddition of 1 to 3.[2] a) An anhydrous toluene solution (4 cm^3) of **1** (97 mg) and **3** (1.0 g) was refluxed under an N_2 atmosphere for 17 h. After evaporation of the solvent in vacuo, the residue was chromatographed on a silica-gel column to give **4** [a yellow oil, 88 mg; 48%. Found: *m/z* 222.1257 (M^+).[5] Calcd for $C_{13}H_{18}O_3$: M, 222.1255. ^{1}H NMR δ=1.21 (3H, t, *J*=7 Hz), 1.23 (3H, t, *J*=7 Hz), 2.23 (1H, dd, *J*=13, 6 Hz), 2.64 (1H, dd, *J*=13, 10 Hz), 2.8—2.9 (1H, m), 3.67 (2H, q, *J*=7 Hz), 3.68 (2H, q, *J*=7 Hz), 5.00 (1H, dd, *J*=10, 4 Hz), 5.68 (1H, d, *J*=6.5 Hz), 6.07 (1H, ddd, *J*=9.5, 6, 1.5 Hz), 6.22 (1H, dd, *J*=11, 6 Hz), and 6.37 (1H, dd, *J*=11, 6.5 Hz). ^{13}C NMR[6] δ=15.2 (2C, q), 38.5 (d), 39.6 (t), 58.3 (t), 59.0 (t), 97.0 (s), 123.0 (d), 124.3 (d), 124.6 (d), 126.7 (d), 128.6 (d), and 150.7 (s). IR ν: 3000 and 1640 cm^{-1}], **2** [a yellow oil, 28 mg; 15%. Found: *m/z* 222.1256 (M^+). ^{1}H NMR δ=1.16 (6H, t, *J*=7 Hz), 2.16 (2H, overlapped s), 3.3—3.6 (6H, m), 5.79 (1H, dd, *J*=11, 2 Hz), 6.12 (1H, ddd, *J*=8.5, 7.5, 1.5 Hz), 6.44 (1H, ddd, *J*=8.5, 7.5, 1.5 Hz), and 6.88 (1H, dd, *J*=11, 9 Hz). ^{13}C NMR δ=15.2 (2C, q), 33.9 (t), 45.1 (d), 51.4 (d), 56.4 (t), 57.0 (t), 107.8 (s), 126.5 (d), 129.6 (d), 136.2 (d), 149.1 (d), and 197.2 (s). IR ν: 2980 and 1660 cm^{-1}], and **5** [a yellow oil, 10 mg; 5.4%. Found: *m/z* 222.1251 (M^+). ^{1}H NMR δ=1.14 (3H, t, *J*=7 Hz), 1.21 (3H, t, *J*=7 Hz), 2.49 (2H, d, *J*=6.5 Hz), 2.8—2.9 (1H, m), 3.19 (1H, d, *J*=7.5 Hz), 3.4—3.5 (4H, m), 5.37 (1H, dd, *J*=11.5, 7.5 Hz), 5.84 (1H, dd, *J*=10, 7.5 Hz), and 5.9—6.0 (2H, m). ^{13}C NMR δ=15.2 (2C, q), 40.3 (t), 46.4 (d), 56.8 (d), 58.8 (t), 59.6 (t), 112.5 (s), 123.3 (d), 125.5 (d), 125.9 (d), 129.8 (d), and 210.5 (s). IR ν: 3000 and 1750 cm^{-1}]. Recovery of **1** was only 9 mg (9.3%).

Thermal Cycloaddition of 1 to 3 under High-Pressure Conditions. A mixture of **1** (151 mg) and **3** (539 mg) in toluene (2 cm^3) was heated at 120 °C under 3000 bar for 10 h. The product distribution is compiled in Table 2. A careful inspection of every chromatographic fraction assured the absence of **5**.

Attempted Thermal Rearrangement of 2 and 4. Each toluene-d_8 solution (O_2 was carefully removed, 0.4 cm^3) of **2** (25 mg) and **4** (45 mg) was heated in a sealed glass tube at 130 °C for 6 to 7 h. Occasional NMR monitoring of the mixture indicated no occurrence of the reaction.

Hydrolysis of 2. A THF solution (10 cm^3) of **2** (40 mg) and conc HCl (0.5 cm^3) was refluxed for 10 min. The mixture was then diluted with water, and extracted with ether. Silica-gel column chromatography of the extract afforded **6** [a colorless oil, 17 mg; 64%. Found: *m/z* 148.0519 (M^+). Calcd for $C_9H_8O_2$: 148.0524. ^{1}H NMR δ=2.53 (1H, ddd, *J*=19, 5.5, 1.5 Hz), 2.65 (1H, dd, *J*=19, 1.5 Hz), 3.59 (1H, m), 3.91 (1H, ddd, *J*=9, 7, 1 Hz), 6.04 (1H, ddd, *J*=11, 2, 1 Hz), 6.34 (1H, td, *J*=8, 1 Hz), 6.59 (1H, ddd, *J*=8, 7, 1.5 Hz), and 6.91 (1H, dd, *J*=11, 9 Hz). ^{13}C NMR δ=32.1 (t), 50.1 (d), 55.8 (d), 128.6 (d), 132.2 (d), 134.5 (d), 143.9 (d), 193.2 (s), and 202.8 (s). IR ν: 1730 and 1670 cm^{-1}].

References

1) S. Sugiyama, T. Tsuda, A. Mori, H. Takeshita, and M. Kodama, *Bull. Chem. Soc. Jpn.*, **60**, 2695 (1987).

2) T. S. Cantrell, *Tetrahedron Lett.*, **1975**, 907.

3) The NMR spectra were measured in $CDCl_3$ solutions by an FX 100 Model or a GSX 270H Model Spectrometer, JEOL, and the chemical shifts were from the internal Me_4Si in ppm scale.

4) R. B. Woodward and R. Hoffmann, "Conservation of Orbital Symmetry," Verlag Chemie, Weinheim (1975), p. 142.

5) This series of compounds were considerably hygroscopic, and their precise weighing was difficult to obtain acceptable figures from the combustion analyses. However, every new compound described was homogeneous in respect of high-pressure liquid chromatograms (Microporasil column with AcOEt-hexane).

6) Multiplicities of the ^{13}C NMR signals were identified by off-resonance experiments.

Different Acyl Specificity between Mold and Kidney Acylases: Correlation of Hydrolytic Rate to Molecular Size and Electronegative Property of Acyl Group in Acyl-L-phenylalanine Hydrolysis

Shinwon KANG,† Yoshihiro MINEMATSU, Yasuyuki SHIMOHIGASHI,* Michinori WAKI, and Nobuo IZUMIYA†
Laboratory of Biochemistry, Faculty of Science, Kyushu University 33, Fukuoka 812
(Received July 27, 1987)

Synopsis. A series of acyl-L-phenylalanines were hydrolyzed by mold and hog kidney acylases. The formyl was found to be the most susceptible for mold acylase, and the butyryl for kidney acylase, indicating the different preferences of these acylases in molecular size and electronegative property of acyl group of substrates.

A variety of optically active amino acids have been prepared by resolving acyl-DL-amino acids with enzymes. Hog kidney acylase I and mold acylase are the most frequently utilized enzymes in this procedure, and their substrate specificity has been studied focusing mainly on the side chain of acetyl- or chloroacetylamino acids.[1] Recently, mold acylase has become increasingly useful because of its availability in large scale and easy immobilization even in an industrial scale. To obtain a high efficacy of the enzyme in such a system, it seems to be important to find more effective acyl groups other than the acetyl and chloroacetyl, since more susceptible acyl group may preserve or even elicit the hydrolytic efficiency when amino acids having unfavorable side chain for the enzyme should be resolved. However, no systematic studies have been reported for the substrate specificity related to acyl groups. Thus, in this study we measured the acylase-catalyzed hydrolytic rate of a series of synthetic acyl-L-phenylalanine in order to analyze the efficiency of acyl groups on the basis of their molecular size and electronegative property.

Acyl groups to derivatize L-phenylalanine were the formyl (For), acetyl (Ac), propionyl (Prp), butyryl (But), pentanoyl (Pen), hexanoyl (Hex), and chloroacetyl (ClAc). Urethane type acyl groups such as ethoxycarbonyl (Eoc), *t*-butoxycarbonyl (Boc), and benzyloxycarbonyl (Z)[2] were also examined. These derivatives were prepared by the usual methods as described in the literature. For hydrolysis of each acyl-L-phenylalanine, the optimum pH was determined (pH 6.0—7.5 for mold acylase: see Table 1). Although the optimum pH might be above pH 8.5 for kidney acylase, no definite values could be determined because of precipitation of cobalt hydroxide at this pH range. Under the conditions without cobalt ion, acylamino acids have been reported to show a rather broad pH maximum between pH 6.7 and 8.0.[3]

The hydrolytic rates were measured at the optimum pH of each substrate for mold acylase and at pH 7.0 for kidney acylase as reported by others.[3] The relative rates of hydrolysis were shown in Table 1. For mold acylase, the formyl was found to be very susceptible, showing a 3.6-fold larger hydrolytic rate than that of the acetyl. Moreover, the formyl was much more easily hydrolyzed than the chloroacetyl. The order of susceptibility of acyl groups towards the acylase was For > ClAc > Ac > Prp > But > Pen > Hex. A very little hydrolysis was observed for Eoc-derivative, and no hydrolysis for Boc- and Z-derivatives. When the rates were compared among a series of acyl groups, H-$(CH_2)_n$-CO-, it was found that a progressive decrease in the number n of methylene units causes an increase in the rate, and thus the formyl with n=0 became the most labile acyl group to the hydrolysis. This result indicates that mold acylase prefers smaller acyl group in molecular size.

For kidney acylase, the order of susceptibility was But > ClAc > Prp > Pen > Ac > Hex > For (Table 1), indicating that the rate was maximized with n=3 in a series of H-$(CH_2)_n$-CO-. Interestingly, the formyl was quite insusceptible toward kidney acylase in contrast to its high susceptibility toward mold acylase. Similar result was also observed by Fones and Lee.[3] These results show that mold and kidney acylases have different substrate-preferences in molecular size of acyl group.

Shimohigashi et al.[4] reported that electronegative property of acyl group can be estimated by the chemical shift of amide proton of acyl-L-phenylalanine in ^{1}H NMR. The order of the extent of electronegativity was found to be ClAc > For > Ac > Prp ≈ But ≈ Pen ≈ Hex. Although the molecular size of the chloroacetyl is almost equal to that of the propionyl, the susceptibility of these groups were apparently different,

Table 1. Relative Hydrolytic Rate of *N*-Acyl-L-phenylalanines by Acylases[a]

Substrate	Mold acylase[b]		Kidney acylase[b]
Acyl-L-Phe-OH	Optimum pH	Relative hydrolytic rate	Relative hydrolytic rate
For-L-Phe-OH	6.0	3.6	0.19
Ac-L-Phe-OH	7.5	1.0	1.0
ClAc-L-Phe-OH	6.2	1.5	3.3
Prp-L-Phe-OH	7.5	0.46	1.7
But-L-Phe-OH	7.5	0.31	3.7
Pen-L-Phe-OH	7.5	0.24	1.3
Hex-L-Phe-OH	7.5	0.03	0.23
Eoc-L-Phe-OH	7.0	0.004	0.09

a)Substrate conc., 10 mM; Used pH, optimum pH for mold acylase, pH 7.0 for acylase I. b) Enzyme concentrations varied depending on the susceptibility of each acyl derivative.

†Present address: S. K.: Department of Chemistry, College of National Sciences, Pusan National University, Pusan, Korea; and N. I.: Kurume Institute of Technology, Kurume 830.

namely, ClAc>Prp toward both acylases. This means that the electronic state of amide bond in the substrate might be an important rate-determining factor in the hydrolysis and a higher acidity of amide proton seems to be favorable for rapid hydrolysis. However, for kidney acylase, the butyryl was hydrolyzed with almost the same rate as the chloroacetyl. This result clearly indicates that kidney acylase has a much more restricted substrate specificity of molecular size of acyl group than that of its electronegative property. For mold acylase, both factors of molecular size and electronegativity appear equally important, since the formyl, which is fairly electronegative, was hydrolyzed more easily than the chloroacetyl.

The usefulness of the formyl group for resolution was demonstrated by resolving For-DL-Orn(Z)-OH. After complete hydrolysis by mold acylase, H-L-Orn(Z)-OH and For-D-Orn(Z)-OH were separated by extraction in a high yield, and the formyl of For-D-Orn(Z)-OH was selectively removed under the mild condition of treatment with *p*-toluenesulfonic acid without cleaving the Z group. The resolved L- or D-Orn(Z)-OH can be used as an important starting block for constructing bioactive peptides and their analogs containing these optically active nonproteinous amino acid. Owing to a high resolution yield and easy preparation of formyl amino acids, the formyl should be one of the acyl groups which are the candidates for an efficient resolution process using the most common mold acylase.

Experimental

Amino acids were determined with a Hitachi amino acid analyzer KLA-5. Mold acylase and acylase I were purchased from Kyowa Hakko Kogyo Co., Ltd. (Tokyo, Japan) and Tokyo Kasei Kogyo Co., Ltd. (Tokyo, Japan), respectively, and used without further purification.

Synthesis of Compounds. Acylamino acid derivatives of L-Phe were prepared according to the literatures: For,[6] Ac,[7] ClAc,[7] Prp,[8] But,[8] Pen,[9] Hex,[8] Boc,[10] and Z-L-Phe-OH.[11] Eoc-L-Phe-OH was prepared essentially with the same method described for Z-L-Phe-OH[11] using ethoxycarbonyl chloride; yield of DCHA salt, 89%; mp 146—147 °C, $[\alpha]_D^{20}$ +36.5° (*c* 2, EtOH).

Determination of Optimum pH. To a solution of acyl-L-amino acid (0.02 mmol) and 0.1 M NaOH (0.2 ml) (1 M=1 mol dm^{-3}) in a 2-ml flask were added 1/7 M sodium barbital buffer (1 ml) with a specified pH, 1/40 M $CoCl_2$ (0.1 ml), and an aqueous enzyme solution (0.2 ml). The amount of enzymes was varied depending on the susceptibility of the acyl group toward the particular enzyme. The solution was made up to 2.0 ml with water. The reaction mixture was incubated at 38 °C, an aliquot being withdrawn after 1 h. Appearance of L-amino acid was determined with an amino acid analyzer: column, 0.6×10 cm; buffer, standard 0.2 M sodium citrate at pH 4.25. The amount of L-amino acid produced was calculated on the basis of the color value determined for a corresponding authentic amino acid with the analyzer.

Determination of Relative Hydrolytic Rate of Acylamino Acids by Acylases. A mixture of an acyl-L-amino acid (0.02 mmol), 0.1 M NaOH (0.2 ml), 1.7 M sodium barbital buffer (1 ml) with optimum pH of each substrate for mold acylase or with pH 7.0 for acylase I, 1/40 M $CoCl_2$ (0.1 ml) and an aqueous enzyme solution (0.2 ml) was made up to 2.0 ml with water. The rate of hydrolysis at 38 °C was followed by the analyzer under the conditions described above. The hydrolysis of substrates followed zero-order kinetics within experimental error. The relative hydrolytic rate to that of Ac-L-Phe-OH was calculated (Table 1).

Resolution of For-DL-Orn(Z)-OH by Mold Acylase. H-L-Orn(Z)-OH: For-DL-Orn(Z)-OH[12] (0.74 g, 2.5 mmol) was dissolved in aqueous triethylamine, the pH being adjusted to 7.4 (optimum pH). To the solution were added acylase (16 mg), 1/40 M $CoCl_2$ (12.5 ml), and water. After the solution (250 ml) had been left to stand at 38 °C for 7 days, the precipitate formed was collected and washed with water. Combined filtrates were evaporated to a small volume. Aqueous formic acid was added to adjust the pH to 5. Separated oily product was extracted with EtOAc. The extract was used for the preparation of For-D-Orn(Z)-OH. The aqueous layer was loaded on a column (1.7×10 cm) of Dowex 50×8 (H^+ form) to elute with 2 M aqueous ammonia (60 ml). The eluate was evaporated to dryness and the residue was recrystallized from water-EtOH; yield; 0.32 g (97%); mp 244—246 °C (decomp); $[\alpha]_D^{20}$ +19.2° (*c* 2, 5 M HCl). Reported values, mp 246—248 °C (decomp); $[\alpha]_D^{20}$ +18.9° (5 M HCl).[5]

For-D-Orn(Z)-OH: The extract obtained above was dried over Na_2SO_4 and evaporated. The residual solid was recrystallized from EtOAc-ether; yield, 0.33 g (88%); mp 66—70 °C (decomp); $[\alpha]_D^{20}$ −15.6° (*c* 2, EtOH).

H-D-Orn(Z)-OH: To a solution of For-D-Orn(Z)-OH (0.34 mmol) in a mixture of dioxane (9 ml) and water (1 ml) was added TosOH·H_2O (0.37 mmol). After being left at 50 °C for 9 h, aqueous triethylamine was added to adjust the pH to 7. The solution was evaporated to dryness, and the residual solid was recrystallized from water-EtOH; yield, 88%; mp 246—248 °C; $[\alpha]_D^{20}$ −17.7° (*c* 2, 5 M HCl). Reported value of the L-isomer, $[\alpha]_D^{20}$ +18.9° (5 M HCl).[5]

References

1) I. Chibata, K. Toi, and S. Yamada, "Chemistry of Asymmetric Reaction (in Japanese), Kagaku Sosetsu No. 4," The Chemical Society of Japan, Tokyo (1974), p. 245.

2) Abbreviations used: But, butyryl; ClAc, chloroacetyl; Eoc, ethoxycarbonyl; For, formyl; Hex, hexanoyl; Pen, pentanoyl; Prp, propionyl; TosOH, *p*-toluenesulfonic acid.

3) W. S. Fones and M. Lee, *J. Biol. Chem.*, **201**, 847 (1953).

4) Y. Shimohigashi, T. Kato, S. Kang, Y. Minematsu, M. Waki, and N. Izumiya, *Tetrahedron Lett.*, **1979**, 1327.

5) N. Izumiya, H. Uchio, and T. Kamata, *Bull. Chem. Soc. Jpn.*, **33**, 66 (1960).

6) I. Muramatsu, M. Murakami, T. Yoneda, and A. Hagitani, *Bull. Chem. Soc. Jpn.*, **38**, 244 (1965).

7) S.-C. J. Fu, S. M. Birnbaum, and J. P. Greenstein, *J. Am. Chem. Soc.*, **76**, 6054 (1954).

8) T. Tsubone, *Seikagaku*, **35**, 67 (1963).

9) M. Morishita, T. Sowa, F. Sakiyama, and K. Narita, *Bull. Chem. Soc. Jpn.*, **40**, 632 (1967).

10) G. W. Anderson and A. C. McGregor, *J. Am. Chem. Soc.*, **79**, 6180 (1957).

11) W. Grassman and E. Wünsch, *Chem. Ber.*, **91**, 462 (1958).

12) Y. Minematsu, S. Kang, Y. Shimohigashi, M. Waki, and N. Izumiya, *Mem. Fac., Sci., Kyushu Univ., Ser. C*, **11**, 137 (1978).

Strong Solvent and pH Dependence in the Photolysis of Diphenylmethanimine

Angelo G. GIUMANINI,* Giancarlo VERARDO, and Marco POIANA
Department of Chemistry, University of Udine, I-33100 Udine, Italy
(Received December 16, 1986)

Synopsis. Benzophenone imine photolysis shows a strong product solvent and pH dependence: Diphenylmethane is by far the dominating outcome in methanol.

Although a relatively large amount of work has been done on *N*-substituted imines of the general type R′-CH=NR″, the rarity itself of known imines of the type RCH=NH has prevented a wide study of their photochemical behavior. Previous works, nevertheless, have reported the photolytic outcome of diphenylmethanimine (**1**) in isopropyl alcohol.[1]

Experimental

Diphenylmethanimine (**1**) was prepared according to a described procedure.[2] The hydrochloride of **1** (**2**) was obtained by precipitating **1** from an ether solution with dry gaseous hydrogen chloride: The IR spectrum ruled out the presence of ketonic impurities. All other chemicals were obtained from commercial sources and conveniently purified before use.

The yields of diphenylmethane (**3**) were determined by GC with a Carlo Erba HRGC Fractovap 4160 gas chromatograph equipped with an FID using a fused silica capillary column (FFAP, 25 m) by the internal standard (naphtalene) method using a calibration factor. The GC peak for **3** was found homogeneous under the whole area by capillary GC-MS analysis (Finnigan 1020 quadrupole mass spectrometer equipped with gas chromatograph and automatic data retrieval). IR spectrum (recorded with a JASCO DS-702G spectrometer) and ^{1}H NMR spectrum (recorded with a Bruker WP 80 SY spectrometer) of separated **3** were in agreement with those of a pure specimen.

Results and Discussion

We have irradiated **1** with a Hanovia High Pressure lamp (350 W, 48 h) in methanol solution: The outcome was dramatically different, the sole product retaining the benzhydrylidene moiety being diphenylmethane (**3**), separated in 91.6% yield (GC yield:

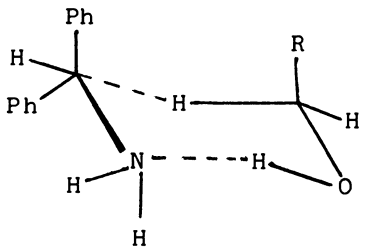

8a R=H; **8b** R=CH_3

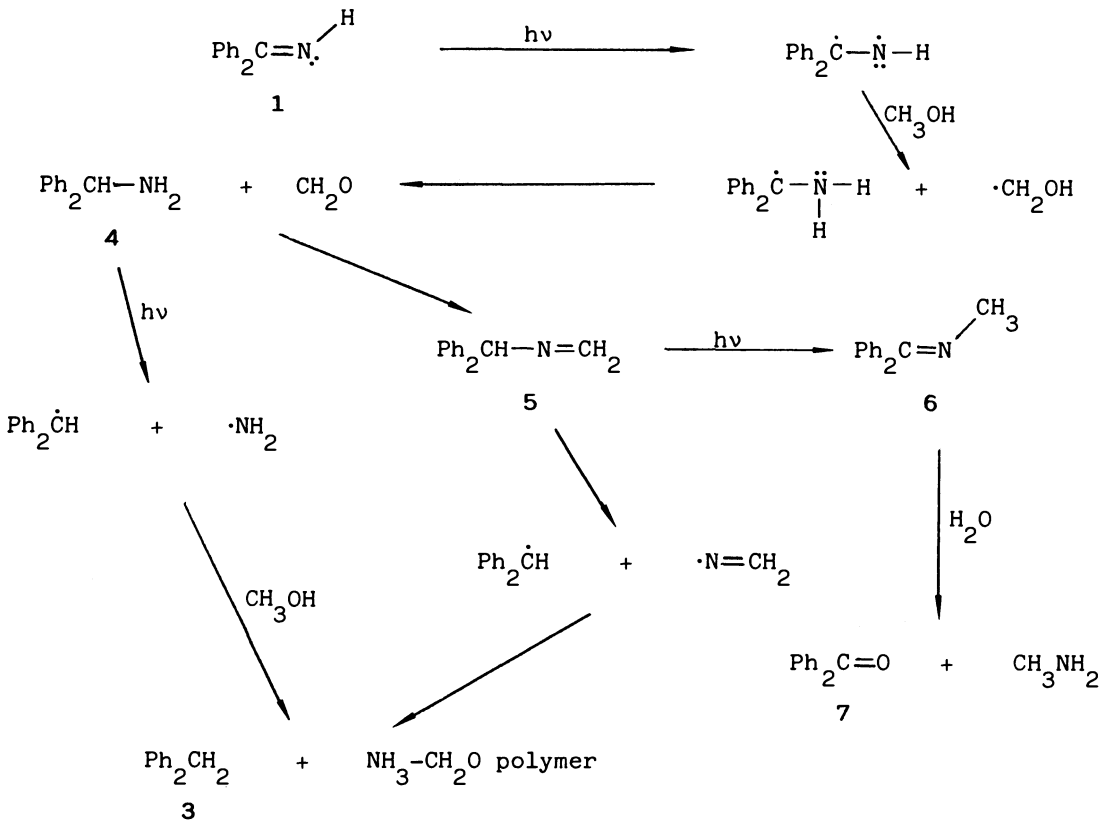

Scheme 1.

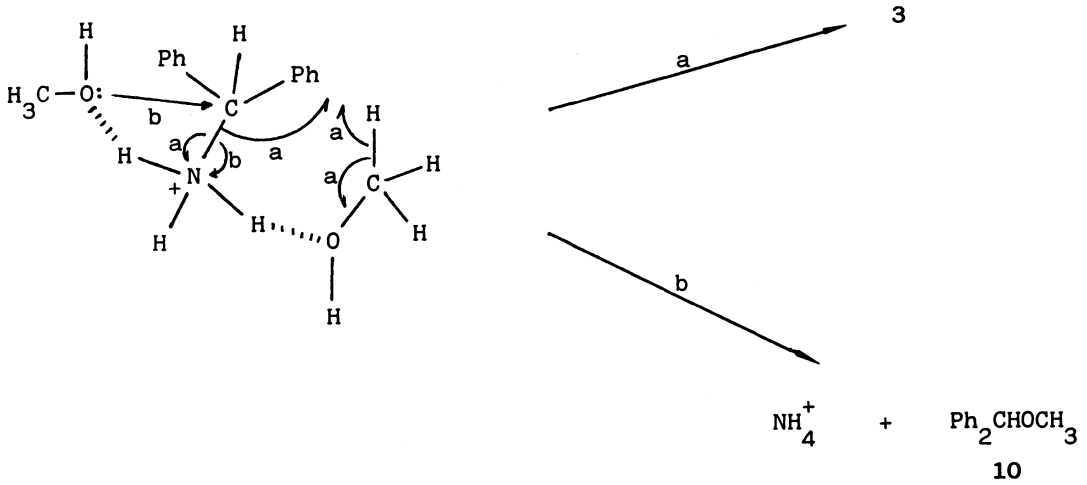

95%). This result indicates a strong solvent effect on product outcome. Since the donor property of hydrogen atoms is considered superior for isopropyl alcohol and the initial abstracting center should be the electronically excited imine's nitrogen atom interacting with the alcohol's tertiary hydrogen, this solvent dependence might be ascribed either to longer reaction times or to a true solvent effect. In fact, shorter reaction times did not change significantly the fate of **1**, only depressing the actual amount transformed.[3] This is an indication that any necessary intermediate in presence of methanol rapidly goes on to **3**. The obvious intermediacy of the reduction product benzhydrylamine[1] (**4**) requires the closer association of the solvent reactive molecule perhaps due to the limited steric hindrance, which allows the prompt capture of the separate fragments before recombination in the solvent cage, as in Scheme 1.

Amine **4** in methanol did photolyze[1b] to hydrocarbon **3**. This ruled out the occurrence of the possible intermediate **5**, as the obligatory passage to **3**: **4** would rather photolyze to isomeric **6**, a minor product eventually reacting with water to yield benzophenone (**7**) also present in traces. The action of light on **4** in methanol can actually be visualized as the interaction of hydrogen bonded tight adduct **8a**. 1,3-Interaction between one of the methyl groups of isopropyl alcohol would make the complex (or transition state) less tight allowing recombination or simply not favoring complete dissociation. In keeping with this rationale, photolysis of **1** in ethanol yielded a good amount (48%, 8 h) of **3**, but photolysis in xylene did not at all. In diethyl ether, capable of a similar but weaker association, adduct **8** again showed poor donor properties toward any eventual (but undetected) **4** (16% **3**, 24 h). Triethylamine, in keeping with this rationale, gave an yield of **3** (20%, 12 h), intermediate between ether and ethanol. When the hydrochloride of **1**, namely **2**, was used in the photolysis in methanol the reactivity pattern as resulting from product composition was deeply affected. The production of **3** was strongly depressed (0.56%, 4 h) and the retention of nitrogen in the molecular structure was favored. Alongside amine **4** (64%), monomethylation products of both the imine **1** and the amine **4** at the nitrogen center were present. They were probably generated by reaction with formed formaldehyde, followed by subsequent reduction induced by some photochemical process. Amine **4** as well as any nitrogen containing species is expected to be largely protonated under the photolysis conditions. Excitation of methanol solvated benzhydrylammonium cation has an additional neutral breakdown alternative, where one charged particle is generated, i.e., the diphenylmethyl cation (**9**) which is immediately captured by a molecule of methanol to eventually produce the observed ether **10**.

The role of apparently dimeric products as well as their precise identification are presently under study in our laboratory.

This work is partially supported by an Italian Ministry of Education Grant for university research in the year 1986.

References

1) a) E. S. Huyser, R. H. S. Wang, and W. T. Short, *J. Org. Chem.*, **33**, 4323 (1968); b) N. Toshima, H. Hirai, and S. Makishima, *Kogyo Kagaku Zasshi*, **72**, 184 (1969); c) H. Hirai and N. Toshima, *J. Fac. Eng. Univ. Tokyo*, **A-8**, 56 (1970).

2) P. L. Pikard and T. L. Tolbert, *J. Org. Chem.*, **26**, 4886 (1961).

3) It was reported[1b] that **1** gives 53% conversion of **1**: Less than 0.5% diphenylmethane (**3**) was produced. At the same time our conversion was about the same, but by far the largest product was **3**.

Crystal Structure and Molecular Structure of Neutral Nickel Bis(5,6-dihydro-1,4-dithiin-2,3-dithiolate), Ni(dddt)$_2$

Hyernjoo KIM,* Akiko KOBAYASHI, Yukiyoshi SASAKI, Reizo KATO,† and Hayao KOBAYASHI†
Department of Chemistry, Faculty of Science, The University of Tokyo, Hongo, Bunkyo-ku, Tokyo 113
†Department of Chemistry, Faculty of Science, Toho University, Funabashi, Chiba 274
(Received June 1, 1987)

Synopsis. Neutral species of multi-sulfur 1,2-dithiolene complex, Ni(dddt)$_2$ (dddt=5,6-dihydro-1,4-dithiin-2,3-dithiolate), was synthesized and the crystal structure has been determined. Crystals are monoclinic, space group $P2_1/c$, with Z=4, a=18.350(10), b=4.672(1), c=20.326(12) Å, β=125.56(3)°, V=1417(1) Å^3. The structure was solved by the Patterson method, and refined by a block-diagonal least-squares method to R=0.081 for 1316 unique reflections. Two independent molecules of Ni(dddt)$_2$ are stacked along the b-axis separately, with interplanar distances of 3.76 Å and 3.74 Å, respectively.

Recent discoveries of the molecular conductors containing metal 1,2-dithiolene complexes have promoted to synthesize new inorganic conductors. In these compounds, the conduction pathways are formed by the overlapping of the ligand-centered π-system (predominantly the sulfur orbitals) and not principally of the metal orbitals.[1] The transverse intermolecular S··S contacts in the metal-dmit complex (dmit=2-thioxo-1,3-dithiole-4,5-dithiolate) suggest the probability of the multi-dimensional molecular conductors.[2]

Recently, we have synthesized M(dddt)$_2$, which is a multi-sulfur 1,2-dithiolene complex as M(dmit)$_2$ and also has ethylene moieties in the outer sides of the ligand as well-known BEDT-TTF (BEDT-TTF=bis-(ethylenedithio)tetrathiafulvalene; In M(dddt)$_2$, the central C=C double bond of BEDT-TTF is replaced by the transition metal). Unlike the case of planar M(dmit)$_2$, steric effect of the ethylene groups of M(dddt)$_2$ will prevent the face-to-face overlapping of the molecules and will enhance the two-dimensional (2-D) molecular contacts to produce the 2-D conductors similar to the BEDT-TTF compounds.

In this paper, we report the molecular and crystal structure of neutral Ni(dddt)$_2$ determined by X-ray analysis.

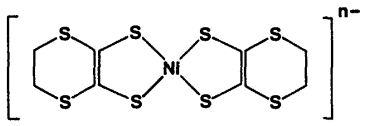

[Ni(dddt)$_2$]$^{n-}$

Experimental

(n-Bu$_4$N)[Ni(dddt)$_2$] was prepared following the method discribed by Kato et al.[3] The black powder of neutral Ni(dddt)$_2$ was prepared by I_2-oxidation of (n-Bu$_4$N)-[Ni(dddt)$_2$]. Black, needle-type single crystal was obtained during the process of recrystallization from benzene.

Crystal data are as follows: Ni(dddt)$_2$, $NiC_8H_8S_8$, F.W.=419.39, monoclinic, $P2_1/c$, a=18.350(10), b=4.672(1), c=20.326(12) Å, β=125.56(3)°, V=1417(1) Å^3, Z=4, d_c=1.97 g cm^{-3}, μ(Mo $K\alpha$)=24.8 cm^{-1}, crystal dimension=0.5 mm×0.08 mm×0.03 mm. X-Ray diffraction data were collected on a Rigaku AFC-6 automated four-circle diffractometer using graphite-monochromated Mo $K\alpha$ radiation (λ=0.71069 Å) and by the 2θ-ω scan technique. The three standard reflections were monitored every 100 reflections, and their intensities showed a good stability. A total of 3713 reflections in the range of 2θ<50° were collected. The intensity data were made for Lorentz and polarization corrections and not for absorption. The 1316 independent reflections with $|F_o|>3\sigma(|F_o|)$ were used for structure analysis. The structure was solved by the heavy atom method and refined by a block-diagonal least-squares method. The hydrogen coordinates were calculated and were included in the final cycles. The weighting scheme $w=(0.001+0.0045|F_o|^2)^{-1}$ for $|F_o|<15.0$ and $(\sigma(|F_o|)^2+0.0045|F_o|^2)^{-1}$ for $|F_o|\geqq 15.0$ was employed. Anisotropic thermal parameters were adopted for Ni, S, and C atoms, and the isotropic temperature factors of H atoms were fixed to 4.0 Å^2. The final R and R_w values are 0.081 and 0.108, respectively. The atomic scattering factors were adopted from International Tables for X-Ray Crystallography.[4] All the calculations were performed on HITAC M-680H computer at the Computer Center of the University of Tokyo, using the program UNICS III.[5]

Results and Discussion

The atomic coordinates are listed in Table 1. The bond distances and angles are shown in Fig. 1. The crystal structure is shown in Fig. 2. The molecules of Ni(dddt)$_2$ are on the center of symmetry. The unit cell contains four Ni(dddt)$_2$ molecules, and the half of

Table 1. Atomic Coordinates (×10^4)

Atom	x	y	z	B_{eq}
Ni1	0	0	0	2.8
Ni2	5000	5000	5000	2.6
S1	1340(3)	1158(12)	482(3)	3.4
S2	−475(3)	2423(12)	−1057(3)	3.0
S3	2319(3)	4461(13)	51(3)	3.7
S4	249(3)	5974(13)	−1726(3)	3.5
S5	6307(3)	6718(12)	4182(3)	3.3
S6	4535(3)	7084(12)	4383(3)	3.0
S7	7251(3)	10297(14)	2759(3)	3.8
S8	5226(3)	10768(11)	2992(3)	3.0
C1	1266(11)	3299(42)	−222(11)	2.9
C2	455(11)	3817(43)	−910(11)	2.9
C3	2056(13)	6696(44)	−768(13)	3.8
C4	1335(11)	5684(54)	−1575(12)	4.0
C5	6230(11)	8760(39)	3521(9)	2.4
C6	5419(10)	8873(38)	3598(9)	2.4
C7	6943(13)	12615(47)	2244(11)	3.6
C8	6367(13)	11132(47)	2057(11)	3.5

$B_{eq}=(4/3)(B_{11}a^2+B_{22}b^2+B_{33}c^2+B_{12}ab\cos\gamma+B_{13}ac\cos\beta+B_{23}bc\cos\alpha)$

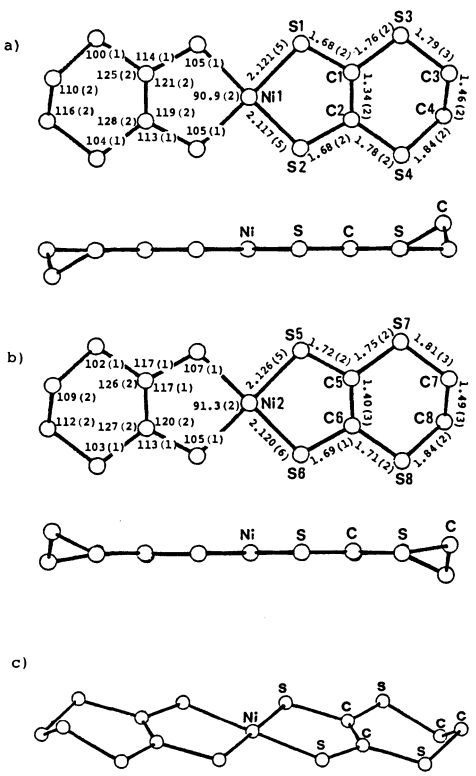

Fig. 1. Molecular structure, bond distances (l/Å) and bond angles (ϕ/°) of Ni(dddt)$_2$; a) molecule-A, b) molecule-B, and c) the conformation of terminal ethylene groups.

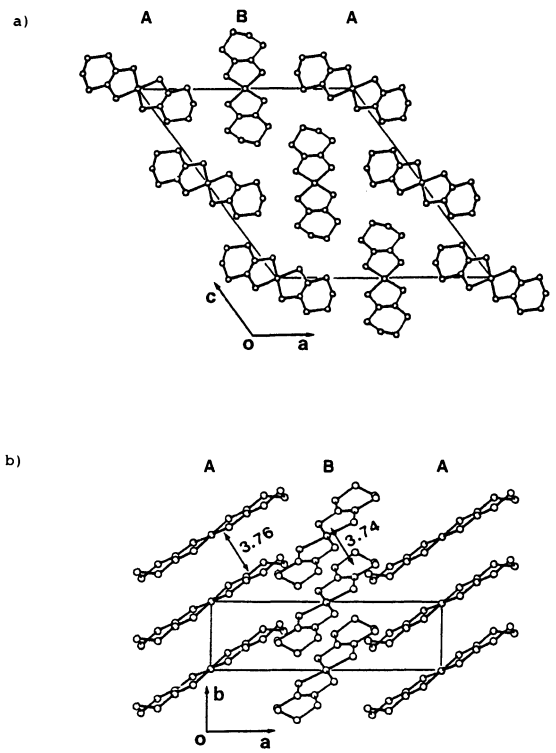

Fig. 2. Crystal structure of Ni(dddt)$_2$; a) projection along the b-axis, b) projection along the c-axis and the interplanar distances (l/Å).

molecule-A and the half of molecule-B are crystallographically independent. The Ni-S bond distance of Ni(dddt)$_2$ is 2.119(5) Å in molecule-A and 2.123(6) Å in molecule-B, which are shorter than 2.148(2) Å in $[Ni(dddt)_2]^{-1}$ anion[6] and are very close to those of other monoanionic nickel dithiolene complexes. Except the terminal ethylene groups, the planarity of molecule-A is better than that of molecule-B. The deviations of atoms from the least-squares planes calculated from all the atoms except the terminal ethylene groups are within 0.01 Å (molecule-A) and 0.04 Å (molecule-B). The equations of the least-squares planes and the deviations of all the atoms are listed in Table 2. Neutral molecule of Ni(dddt)$_2$, as well as $[Ni(dddt)_2]^{-1}$ anion of $(Et_4N)[Ni(dddt)_2]$,[6] has an inversion center, and the conformation of terminal ethylene groups of each side of a molecule is different from that of BEDT-TTF molecules which have pseudo-D_{2h} symmetry. The conformation of terminal ethylene groups of neutral Ni(dddt)$_2$ is shown in Fig. 1.

The molecule-A and molecule-B are arranged separately to form the independent uniform stacks along the b-axis. As for the crystal of neutral BEDT-TTF, we found a dimer structure composed by two neutral BEDT-TTF molecules.[7] But in both cases of neutral Ni(dddt)$_2$ and neutral Ni(dmit)$_2$,[8] they form uniform stacks. Within the stacks of Ni(dddt)$_2$, the Ni-Ni distance is given by the lattice constant of the b-axis, 4.672 Å. The interplanar distances are 3.76 Å in the stacks of molecule-A, and 3.74 Å in those of molecule-B. There is no short intermolecular S··S contact (<3.70 Å) within a stack, and between molecules of adjacent stacks along the c-axis.

Table 2. The Equations of the NiC_2S_4 Least-Squares Planes and the Deviations (l/Å)

Molecule-A $-0.41068X+0.80422Y+0.42961Z+0.0=0$
Molecule-B $-0.11165X-0.80227Y+0.58643Z+8.40681=0$

Molecule-A		Molecule-B	
Ni1	0.0	Ni2	0.0
S1	0.001	S5	0.010
S2	0.005	S6	0.006
S3	−0.010	S7	−0.021
S4	−0.007	S8	−0.004
C1	0.020	C5	0.033
C2	0.002	C6	0.004
C3	0.047	C7	0.215
C4	−0.753	C8	−0.667

The amplitudes of LUMO (lowest unoccupied molecular orbital) were calculated as to $[Ni(dddt)_2]^{-1}$ anion by means of the extended Hückel approximation, with the parameters adopted from Ref. 9, and are shown in Fig. 3. In $[Ni(dmit)_2]^{-1}$, the amplitudes of the "outer sulfur atoms" in the five-membered heteroring are about one-fifth as small as those of the "inner sulfur atoms,"[1] but in $[Ni(dddt)_2]^{-1}$ half as small as those of the "inner sulfur atoms." In M(dmit)$_2$, the side-by-side interactions are not so strong owing to the small amplitude on the "outer sulfur atoms" and the symmetry of LUMO. In BEDT-TTF, the amplitudes of HOMO (highest occupied molecular orbital) on the

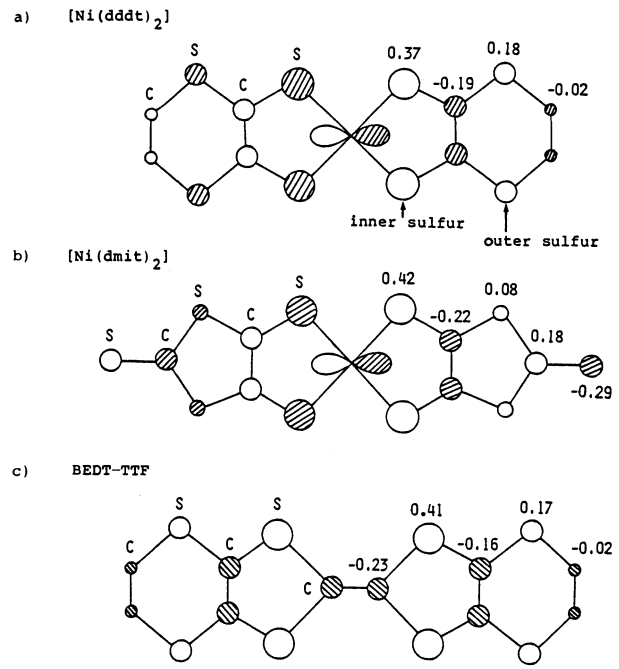

Fig. 3. Schematic drawing of a) LUMO of $Ni(dddt)_2$, b) LUMO of $Ni(dmit)_2$[1] and c) HOMO of BEDT-TTF.[10]

"outer sulfur atoms" are about 40% of those of the "inner sulfur atoms" (Fig. 3). Thus the side-by-side arrangement of $M(dddt)_2$ will be supposed to be sufficient for the realization of the 2-D molecular interaction similar in BEDT-TTF.

Both BEDT-TTF and $M(dddt)_2$ are approximately the same size and both of the molecules seem to have a tendency to form a 2-D layered type structure with close S··S contacts. As mentioned above, however, as for $M(dmit)_2$, we found that the side-by-side interactions by S atoms were weaker than those expected at first, and $M(dmit)_2$ had a tendency to form 1-D system.[1] This discrepancy is originated from the difference in the symmetries of HOMO of BEDT-TTF and LUMO of $M(dmit)_2$, from which the conduction bands are formed. Further, both $M(dddt)_2$ and $M(dmit)_2$ contain tetrathio-substituted ethylene moieties, and have the same type of delocalized π-MO. So that $M(dddt)_2$ is considered to be an intermediate between $M(dmit)_2$ and BEDT-TTF from the electronic and molecular structural points of view. At the same time, it should be recalled that the redox behavior is a very important factor in the systhesis of the molecular conductors. The most prominent difference between $[Ni(dddt)_2]^{-1}$ and $[Ni(dmit)_2]^{-1}$ is their redox behavior. $[Ni(dmit)_2]^{-1}$ is much more easily reduced to the dianion than $[Ni(dddt)_2]^{-1}$.[3] Therefore, further careful works will be required to examine the ability of formation of conducting complex of $[Ni(dddt)_2]$.

The coordinates of the hydrogen atoms, the anisotropic thermal parameters of the Ni, S, and C atoms, and the F_o—F_c tables have been deposited as a Document No. 8783 at the Office of the Editor of Bull. Chem. Soc. Jpn.

References

1) A. Kobayashi, H. Kim, Y. Sasaki, R. Kato, and H. Kobayashi, *Solid State Commun.*, **62**, 57 (1987).

2) M. Bousseau, L. Valade, M.-F. Bruniquel, P. Cassoux, M. Garbauskas, L. V. Interrante, and J. Kasper, *Nouv. J. Chim.*, **8**, 3 (1984); M. Bousseau, L. Valade, J.-P. Legros, P. Cassoux, M. Garbauskas, and L. V. Interrante, *J. Am. Chem. Soc.*, **108**, 1908 (1986); R. Kato, T. Mori, A. Kobayashi, Y. Sasaki, and H. Kobayashi, *Chem. Lett.*, **1984**, 1.

3) R. Kato, H. Kobayashi, A. Kobayashi, and Y. Sasaki, *Bull. Chem. Soc. Jpn.*, **59**, 627 (1986).

4) International Tables for X-Ray Crystallography, Vol. IV. Kynoch Press, Birmingham (1974).

5) T. Sakurai and K. Kobayashi, *Rep. Inst. Phy. Chem. Res.*, **55**, 69 (1979).

6) C. T. Vance, R. D. Bereman, J. Bordner, W. E. Hatfield, and J. H. Helms, *Inorg. Chem.*, **24**, 2905 (1985).

7) H. Kobayashi, A. Kobayashi, Y. Sasaki, G. Saito, and H. Inokuchi, *Bull. Chem. Soc. Jpn.*, **59**, 301 (1986).

8) L. Valade, J.-P. Legros, M. Bousseau, P. Cassoux, M. Garbauskas, and L. V. Interrante, *J. Chem. Soc., Dalton Trans.*, **1985**, 783.

9) A. J. Berlinsky, J. F. Carolan, and L. Weiler, *Solid State Commun.*, **15**, 795 (1974).

10) T. Mori, A. Kobayashi, Y. Sasaki, H. Kobayashi, G. Saito, and H. Inokuchi, *Bull. Chem. Soc. Jpn.*, **57**, 627 (1984).

Counter Ion Effect on the ^{13}C NMR Paramagnetic Relaxation Rate of Water-Methanol or Water-Dimethyl Sulfoxide Mixed Solvent with Ni(II) Solute

Kanya KOBAYASHI, Masatoki YOKOI,* and Eiji KUBOTA
Department of Chemistry, Faculty of Science, Shinshu University, Asahi, Matsumoto 390
(Received June 4, 1987)

Synopsis. The paramagnetic-salt induced ^{13}C spin-lattice relaxation rate of solvents methanol and dimethyl sulfoxide was measured for $Ni(ClO_4)_2$, $NiSO_4$, and NiBDS (BDS: *m*-benzenedisulfonate) solutions in 50 wt.% mixture of each of the solvents and water. Relatively small relaxation rates were found for the solutions containing $NiSO_4$. This fact is ascribed to the exclusion of some solvent molecules from the first coordination shell of Ni^{2+} due to the coordination of SO_4^{2-} to Ni^{2+}.

In our previous paper[1] we have reported the ^{13}C spin-lattice relaxation rate, $1/T_1$, of some alcohol and DMSO molecules in their mixtures with water containing $Ni(ClO_4)_2$. From the data obtained, a conclusion of preferential solvation to Ni^{2+} ion was drawn. In this analysis, ClO_4^- anion was assumed not to coordinate to Ni^{2+} ion directly, and the first coordination sites to be saturated with water and/or solvent molecules. It has been established that in water and DMSO $Ni(ClO_4)_2$ exists as a hexasolvated cation and a non-coordinated ClO_4^- anion.[2,3] An interesting problem arises when an apparent Ni^{2+}-anion interaction exists. If an anion coordinates to Ni^{2+} directly and replaces some solvent molecules in the first coordination shell where the paramagnetic effect is most predominant, then observed $1/T_1$ is expected to decrease. Sulfate anion-cation interaction in solutions has been investigated by NMR,[4-6] Raman spectra,[7] and conductance[8,9] measurements, etc., and solvent-anion mixed ligand complex formation has been considered to explain these results. In this note the anion effect on the coordination of solvent to Ni^{2+} is investigated by measuring the paramagnetic-ion induced spin-lattice relaxation rate of ^{13}C of methanol and DMSO molecules in their mixtures with water containing $NiSO_4$ or NiBDS (BDS: *m*-benzenedisulfonate). These relaxation rates were compared with those of $Ni(ClO_4)_2$ solutions. Since $NiSO_4$ is not sufficiently soluble in neat solvents, its effect was studied in 50 wt.% aqueous mixtures. NiBDS was chosen for comparison with SO_4^{2-} because it has a divalent anion and has enough solubility in both neat solvent and 50 wt.% aqueous mixtures.

Experimental

The preparation of nickel perchlorate is described in Ref. 1. Commercially-available reagent-grade nickel sulfate was recrystallized from water and dried at room temperature. The water content of the salt was determined as 6 moles per mole of the salt by a total cation analysis using a cation-exchange column. The preparation of NiBDS was based closely on that outlined for CuBDS in Ref. 10. The water content of recrystallized NiBDS was 6 moles per mole of the salt. Methanol and DMSO solvents were both reagent grade and were used without further purification. NMR spectra were recorded on a JEOL FX-90Q FT NMR spectrometer by using the standard inversion-recovery technique at 35 °C. The error in the measurement of T_1 was less than 5%.

Results and Discussion

The observed spin-lattice relaxation rate of solvent nuclei in paramagnetic solution will be a sum of two major contributions:

$$\frac{1}{T_1} = \frac{X_M}{T_{1M}} + \frac{(1-X_M)}{T_{1B}} , \quad (1)$$

where the first term is for the electron-nuclear relaxation in the first coordination shell and the second term is the diamagnetic relaxation rate. $1/T_{1M}$ and $1/T_{1B}$ are the relaxation rates of the nuclei of the solvent molecules in the first coordination shell and those in the bulk, respectively. X_M denotes the fraction of the coordinated solvent molecules in the first coordination shell, and is expressed as

$$X_M = n\frac{C_i}{C_s} , \quad (2)$$

where C_i and C_s are the molar concentrations of the ion and the solvent molecule, respectively, and n is the number of coordinated solvent molecules. For the solution of $Ni(ClO_4)_2$ in neat solvent, Ni^{2+} is assumed to be surrounded by six solvent molecules. $1/T_{1M}$ can be obtained as the slope of plots of observed $1/T_1$ against X_M at low concentrations of Ni^{2+} ion. The $1/T_{1M}$ values thus obtained are 230 s^{-1} for methanol and 110 s^{-1} for DMSO. If $1/T_{1M}$ is assumed not to

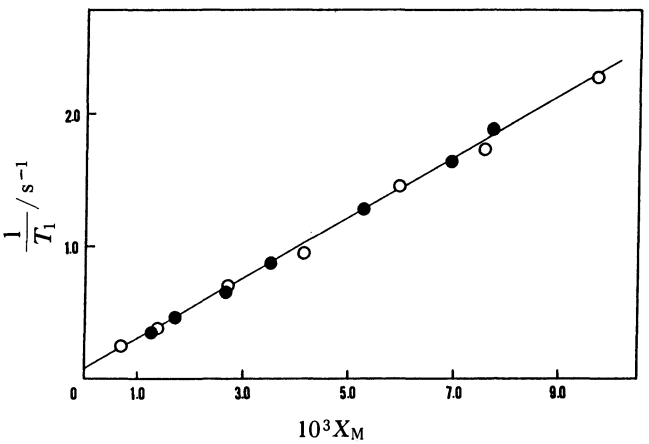

Fig. 1. Plots of ^{13}C spin-lattice relaxation rate as a function of the coordinated solvent fraction, X_M, in methanol. ○: $Ni(ClO_4)_2$,[1] ●: NiBDS.

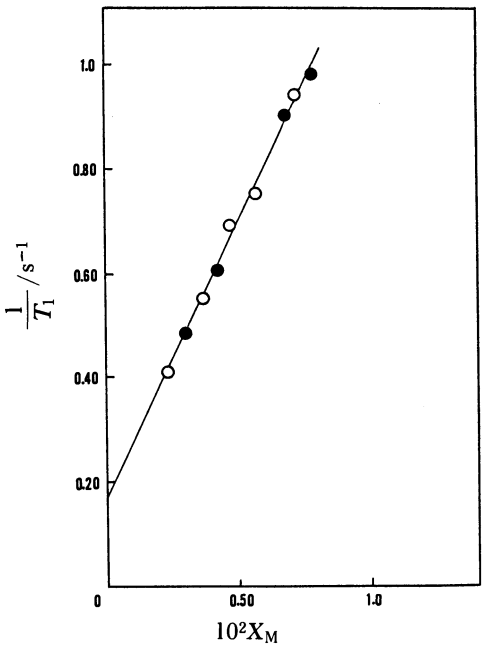

Fig. 2. Plots of ^{13}C spin-lattice relaxation rate as a function of the coordinated solvent fraction, X_M, in DMSO. ○: $Ni(ClO_4)_2$,[1] ●: NiBDS.

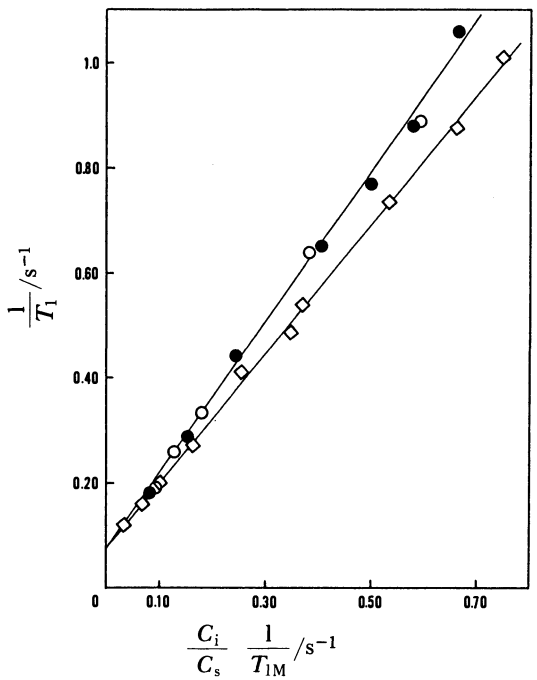

Fig. 3. Plots of ^{13}C spin-lattice relaxation rate versus $C_i/(C_s \cdot T_{1M})$ in water-methanol system. ○: $Ni(ClO_4)_2$, ●: NiBDS, ◇: $NiSO_4$.

change when water or anion occupies several of the six coordinate sites of Ni^{2+}, the number of coordinated solvent molecules is obtained from the slope of plots of $1/T_1$ against $C_i/(C_s \cdot T_{1M})$ at low Ni^{2+} concentrations. In Figs. 1 and 2, the $1/T_1$ values of $Ni(ClO_4)_2$ and NiBDS are plotted as a function of X_M in methanol and DMSO, respectively. In both the figures, the plots appear to fall on a common straight line. The same

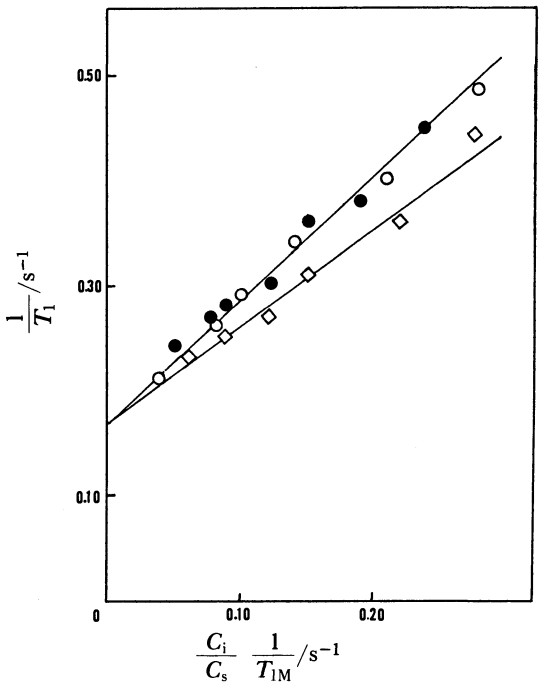

Fig. 4. Plots of ^{13}C spin-lattice relaxation rate versus $C_i/(C_s \cdot T_{1M})$ in water-DMSO system. ○: $Ni(ClO_4)_2$, ●: NiBDS, ◇: $NiSO_4$.

mention can be made for the aqueous methanol and aqueous DMSO systems. In Figs. 3 and 4, the $1/T_1$ values in 50 wt.% aqueous methanol and DMSO, respectively, are plotted versus $C_i/(C_s \cdot T_{1M})$. In both the figures, the plots for $Ni(ClO_4)_2$ and NiBDS appear to fall on their respective common straight lines. Thus for the NiBDS solutions, the possibility that BDS^{2-} replaces the solvent molecules in the first coordination shell may be considered negligible as with ClO_4^- in both neat and aqueous mixtures. The number, n, of the solvent molerules locating in the inner shell of Ni^{2+} is obtained as the slope of the plots shown in Figs. 3 and 4. For 50 wt.% methanol n=1.4 and for 50 wt.% DMSO n=1.1. Since the n values expected from the overall solvent composition are 2.2 and 1.1, respectively, the Ni^{2+} ion is solvated preferentially by water in 50 wt.% methanol, while no preferential solvation is found in 50 wt.% DMSO. On the other hand, in the case of $NiSO_4$, the downward deviation from the plots of $Ni(ClO_4)_2$ is apparent in both the aqueous mixtures. The deviation may be ascribed to the replacement of some solvent molecules by SO_4^{2-} anion in the inner shell of Ni^{2+} ion. The difference in the values between $Ni(ClO_4)_2$ and $NiSO_4$ is 0.3 for water-methanol and 0.2 for water-DMSO, so about 0.3 methanol or 0.2 DMSO molecule is considered to be replaced by SO_4^{2-} in forming the inner shell complex. If SO_4^{2-} anion could replace not only nonaqueous solvent molecules but also water molecules, SO_4^{2-} anion would replace more than 0.3 or 0.2 solvent molecule (nonaqueous or water) in the inner shell. Bechtold et al.[6] studied the Ni(II)-SO_4^{2-} interaction by ^{17}O NMR in aqueous solution. According to their results, $Ni(H_2O)_6^{2+}$ is the most predominant species, which occupies about 90% of the total Ni species at temperatures near 35 °C. The pres-

ent work has given a still higher percentage of the inner-shell complex containing SO_4^{2-}. The addition of nonaqueous solvent may enhance the coordination of SO_4^{2-} anion to Ni^{2+} ion directly. These tendencies are also found in $Al_2(SO_4)_3$-water-nonaqeous solvent systems from ^{27}Al NMR spectra.[4,5] Sulfate anion is a compact divalent anion, while BDS^{2-} is of much larger size and its minus charge is localized to some extent on the functional group. The difference in size and charge distribution would be one of proper explanations for the marked difference in behavior between SO_4^{2-} and BDS^{2-}. Hallada and Atkinson[8] reported a conductance work on MnBDS and $MnSO_4$ in aqueous methanol. The ion association constants evaluated from conductance data of $MnSO_4$ are much larger than those of MnBDS throughout in the solvent composition range studied. Similar results were obtained with systems of $CuSO_4$ and CuBDS in aqueous dioxane.[9] The difference between the ion association constants of the sulfate and the BDS salt may be ascribed to the feasibility of the inner shell coordination of sulfate anion.

The present work was partially supported by a Grant-in-Aid for Science Research No. 62540459 from the Ministry of Education, Science and Culture.

References

1) K. Kobayashi, M. Yokoi, H. Kuroda, and E. Kubota, *Bull. Chem. Soc. Jpn.*, **60**, 2535 (1987).
2) Z. Libuś and T. Sadowska, *J. Phys. Chem.*, **73**, 3229 (1969).
3) W. Libuś and H. Strzelecki, *Electrochim. Acta*, **15**, 703 (1970).
4) M. Yokoi, N. Komatsu, K. Kobayashi, and E. Kubota, 52nd National Meeting of the Chemical Socitey of Japan, Kyoto, April 1986, Abstr., No. 3E38.
5) H. Strehlow and G. Busse, *Ber. Bunsenges. Phys. Chem.*, **88**, 467 (1984).
6) D. B. Bechtold, G. Liu, H. W. Dodgen, and J. P. Hunt, *J. Phys. Chem.*, **82**, 333 (1978).
7) H. Hester and R. A. Plane, *Inorg. Chem.*, **3**, 769 (1964).
8) C. J. Hallada and G. Atkinson, *J. Am. Chem. Soc.*, **83**, 3759 (1961).
9) M. Yokoi and E. Kubota, *Nippon Kagaku Zasshi*, **86**, 894 (1965).
10) E. Kubota, M. Yokoi, and S. Shikata, *Nippon Kagaku Zasshi*, **85**, 89 (1964).

The Solubilization Equilibrium of 7-Ethoxycoumarins in Ionic Micelles

Tetsuo MORIYA
Electrotechnical Laboratory, 1-1-4 Umezono, Tsukuba, Ibaraki 305
(Received June 5, 1987)

Synopsis. The solubilization behavior of 7-ethoxycoumarin (7EC) and 7-ethoxy-4-methylcoumarin (7E4MC) in aqueous micellar solutions of sodium dodecyl sulfate (SDS) and hexadecyltrimethylammonium chloride (HDTC) was studied by fluorescence spectroscopy. The equilibrium constants for the binding of the fluorophores into micelles and their fluorescence yields in the micellar phase were determined.

Several authors[1,2] have studied the characteristics of micelles and vesicles formed of surfactants or phospholipids using hydroxy- and aminocoumarins as the pH indicator, since the absorption spectra of these compounds, when bound to the molecular aggregations, sensitively change reflecting the shift of acid-base equilibria. Recently, it has been revealed that 7-ethoxycoumarins are also solubilized into SDS micelles in aqueous solutions, and their fluorescence is greatly reduced above the critical micelle concentration (cmc) whereas the absorption spectra show little observable change.[3] Since the microenvironment around electronically excited molecules is detectable by means of fluorescence measurements, the fluorescence-probing technique is complementary to the absorption measurement that detects ground-state molecules. The fluorescence method using the coumarin derivatives is advantageous over the absorption method reported, because the latter must use buffer solutions or acids for the control of pH;[1,2] this introduces an inevitable complexity such as the problem of ionic-strength change into the analysis of data. Although several aromatic fluorescent probes have already been proposed,[4,5] heterocyclic compounds such as coumarins are very different from those in regard to interactions with the surroundings, and have interesting solubilization properties for anionic and cationic micelles.

Experimental

High-purity grade reagents of 7-ethoxycoumarin (7EC) and 7-ethoxy-4-methylcoumarin (7E4MC) were obtained from Molecular Probes Inc. and used without further purification. Sodium dodecyl sulfate (SDS, Wako) was of biochemical grade. Hexadecyltrimethylammonium chloride (HDTC, Wako) was treated with charcoal in ethanol, recrystallized, and then washed with ether. Sodium chloride (Kanto) was of special grade. Water was permeated and distilled.

The UV absorption spectra were obtained on a Hitachi 323 spectrophotometer and measurements of the fluorescence spectra and fluorescence yields were made on a Hitachi MPF 4 spectrofluorometer with an S-5 type photomultiplier tube. The temperature of the sample cuvette was thermostated with circulating water from a constant-temperature bath (25±0.1 °C). The wavelengths of excitation light were chosen to be 325 nm for 7EC and 322 nm for 7E4MC, which nearly coincided with their absorption maxima in various solutions; there was no disturbing absorption of surfactants or salts at these wavelengths. The dependence of the absorption spectra on the surfactant concentration was small, while that of the fluorescence spectra was so large that the whole spectrum of the fluorescence was carefully recorded under various conditions. The concentration of 7EC and 7E4MC in the sample solution was $4—5\times10^{-5}$ mol dm^{-3}.

Results

Fluorescence properties of 7-ethoxycoumarin derivatives in simple aqueous solutions have been fully investigated.[6,7] When 7EC or 7E4MC was dissolved in the aqueous SDS solution with a concentration higher than cmc,[8] the absorption spectra were changed slightly from those in the absence of SDS with a peak position red-shifted by ≈1.5 nm and with a peak value of molar extinction coefficient decreased by a few percent. On the other hand, the fluorescence behavior strongly depended on the SDS concentration. When SDS was added to the solution, the fluorescence intensity began to decrease drastically as soon as the cmc of SDS was reached and tended to be constant at higher SDS concentrations than 0.025 mol dm^{-3} for both 7EC and 7E4MC, while the peak position of a fluorescence band blue-shifted by ≈4 nm maintaining the spectral shape.

7-Ethoxycoumarins were also solubilized into cationic micelles such as hexadecyltrimethylammonium chloride (HDTC). The peak shifts of absorption and fluorescence spectra at 0.025 mol dm^{-3} HDTC were similar to those in the SDS solution. The HDTC solution, however, showed an even larger variation in the fluorescence intensity than the SDS solution. Figure 1

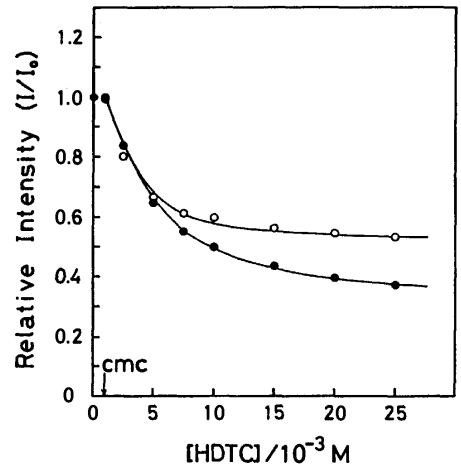

Fig. 1. Plots of the relative fluorescence intensity, I/I_0, vs. the concentration of HDTC at 25 °C. 7EC (●); 7E4MC (○). Solid lines are the theoretical curve predicted by Eq. 3; the aggregation number, n, is assumed to be 80.

presents a plot of the relative fluorescence intensity, I/I_0 vs. [HDTC], where I and I_0 are the fluorescence intensities in the presence and in the absence of HDTC. Since the cmc of HDTC is smaller than the cmc of SDS by about one order of magnitude,[8] a decrease in the fluorescence intensity by the addition of HDTC begins at a lower concentration of the surfactant. The fluorescence intensity tended to be constant for [HDTC]>0.025 mol dm^{-3}.

Since ionic surfactants have their counterions, the fluorescence-quenching phenomena due to various inorganic ions in the solution must be taken into account.[9] The quenching effect for 7EC and 7E4MC due to Na^+ and Cl^-, being the counterions of SDS and HDTC, was negligible in a simple aqueous solution.[6] When NaCl was added to SDS micellar solutions, the fluorescence of 7EC and 7E4MC decreased slightly (≈3% at [NaCl]=0.1 mol dm^{-3}). Considering that micellar parameters such as the aggregation number (n) or the degree of ionization (α) are delicately influenced by the addition of salts, this small change in the fluorescence intensity is, possibly, not due to quenching by Na^+ and Cl^- but due to a micellar parameter change. In either case, the fluorescence quenching by Na^+ and Cl^-, if any, is negligibly small because the employed concentration of SDS and HDTC is not more than 0.025 mol dm^{-3}. This is consistent with the result obtained by phosphorescence measurements of naphthalene in frozen SDS micelles with varying amounts of added NaCl, up to ≈0.2 mol dm^{-3}.[10]

Discussion

To analyze the fluorescence property of 7EC and 7E4MC in aqueous micellar solutions, we may adopt the two-reactive-state model for the light-emitting processes in the aqueous and micellar phases

$$\mathrm{N} \xrightarrow{\varepsilon} \overset{*}{\mathrm{N}} \xrightarrow{\eta} \mathrm{N} + h\nu \qquad (1)$$

$$\mathrm{D}_n\mathrm{N} \xrightarrow{\varepsilon'} \mathrm{D}_n^*\mathrm{N} \xrightarrow{\eta'} \mathrm{D}_n\mathrm{N} + h\nu'$$

and

$$\mathrm{D}_n + \mathrm{N} \underset{}{\overset{K}{\rightleftharpoons}} \mathrm{D}_n\mathrm{N}. \qquad (2)$$

Here, D_n represents the micelle formed of n surfactants. N and D_nN are the fluorescent molecules in the aqueous phase and in the micellar phase, respectively; $\overset{*}{N}$ and D_n^*N are their excited states generated on light illumination. $h\nu$ and $h\nu'$ are the emitted light quanta from the respective molecular species. ε and ε' are the molar extinction coefficients of N and D_nN, respectively. η and η' are the quantum efficiencies for the radiative transition of $\overset{*}{N}$ and D_n^*N to N and D_nN, respectively. Assuming that the fluorophore in an aqueous phase is in equilibrium with the fluorophore in a micelle (Eq. 2), the equilibrium constant is given by $K=[D_nN]/[D_n][N]$. The total concentration of the fluorescent molecule is defined by $C_N=[N]+[D_nN]$, and the total density of the micellar particle is given by $C_M=[D_n]+[D_nN]$. C_N is fixed throughout the measurement. C_M depends on both the added content of a surfactant (C_S) and n as $C_M=(C_S-\mathrm{cmc})/n$ above cmc.

When N and D_nN are excited by the light at a fixed wavelength, the generation rates of $\overset{*}{N}$ and D_n^*N are in proportion to ε and ε' at the wavelength, respectively. Then, the relative fluorescence intensity, I/I_0, is given by

$$\frac{I}{I_0} = \frac{1+(\eta'/\eta)(\varepsilon'/\varepsilon)K[\mathrm{D}_n]}{1+(\varepsilon'/\varepsilon)K[\mathrm{D}_n]}, \qquad (3)$$

where $[D_n]$ is obtained from the definitions of K, C_N, and C_M:

$$[\mathrm{D}_n]=[\{(1+KC_N-KC_M)^2+4KC_M\}^{1/2} - (1+KC_N-KC_M)]/2K. \qquad (4)$$

The detailed derivation of this result appeared in Ref. 3. For usual measurements, C_N was fixed around 4—5×10^{-5} M. If $1+KC_N \ll KC_M$, Eq. 4 predicts $[D_n]\approx C_M-C_N$. In contract, a full expression of Eq. 4 must be employed at small C_M in order to estimate $[D_n]$. Based on Eqs. 3 and 4, the theoretically predicted variation in I/I_0 can be compared with the fluorescence data obtained.

Since almost all fluorophores become solubilized into the micelle at $C_S \gg$ cmc, the ε' values of 7EC and 7E4MC in the micelle can be experimentally determined. ε'/ε for SDS at the excitation wavelength was 0.972 (7EC) and 0.965 (7E4MC); for HDTC, 0.953 (7EC) and 0.960 (7E4MC). The aggregation number of micelles was taken from independent experiments as n=62 (SDS)[11,12] and n=80 (HDTC).[13] Then, unknown parameters to be fixed in Eqs. 3 and 4 are η'/η, K, and cmc, which can be determined by a best-fit analysis for the data points. The theoretical curve derived is plotted with a thin solid line in Fig. 1. The theory explained very well the entire behavior of the data; the determined parameters are cited in Table 1. The inaccuracy in K is brought about by the n value employed; the scattering of n from experiment to experiment was about 10%, so that the same order of uncertainty exists in K, whereas η'/η and cmc are insensitive to such inaccuracy.

For the SDS micelle, K differs by an order of magnitude between 7EC and 7E4MC (Table 1), in spite of the small difference in the molecular structure. A larger K means a stronger binding of the fluorophore to the micelle. The change in the substituent group from hydrogen to methyl at the 4-position is supposed to

Table 1. Ratios of the Quantum Efficiency, η'/η, Equilibrium Constants, K, and Critical Micelle Concentrations, cmc, in Aqueous SDS and HDTC Solutions at 25 °C

Surfactant	Substance	η'/η	K / mol^{-1} dm^3	cmc / mol dm^{-3}
SDS[a]	7EC	0.74	2.8×10^4	6.0×10^{-3}
	7E4MC	0.88	2.6×10^5	
HDTC	7EC	0.30	3.5×10^4	1.0×10^{-3}
	7E4MC	0.51	9.0×10^4	

a) The values for SDS are taken from Ref. 3.

induce such a large influence on the solubilization, probably due to a hydrophobic interaction of the methyl group. This difference in K between 7EC and 7E4MC becomes rather smaller for the HDTC micelle (Table 1). SDS and HDTC form typical anionic and cationic micelles, having different carbon numbers in the alkyl chain (C_{12} and C_{16}, respectively). Although K will be affected by the charge on the micelle, the surfactant length, the solubilization site within the micelle, etc., it seems that the substituent effect would overcome the other factors to induce the higher K value for 7E4MC in both SDS and HDTC solutions.

The fluorescence intensity change in the mixed solvent of water-ethanol was examined as a function of the water content in a previous study.[3] If the quantum efficiency, η', appearing in Eq. 3 is essentially determined by the polarity around the site in the micelle occupied by the fluorophore, this result is conveniently related with η'/η in Table 1. When the fluorescence-yield in the mixed solvent is compared with η'/η=0.74 (7EC) and 0.88 (7E4MC) obtained in the SDS solution, the polarity of the solubilized site is revealed to resemble the polarity in the mixed solvent of 30 wt% aqueous ethanol, having the effective dielectric constant, D_{eff}=62±1 (25 °C).[14] No meaningful difference has been found between the D_{eff} values of 7EC and 7E4MC within an experimental error. Considering that the dielectric constant of a typical aliphatic compound is about 2 and that of water is 78.5, the solubilized fluorophore seems to be located not in the core region of the micelle but near its surface and may be partly exposed to the aqueous atmosphere around the micelle (in the palisade layer). This effective polarity ($D_{eff}\approx$62) is larger than 16—49 obtained for benzene derivatives and naphthalene.[5] Since 7-ethoxycoumarins are heterocyclic compounds with oxygen in the ring and in the substituent, and are insoluble in nonpolar solvents, their affinity to the alkyl chain in micelles is thought to be lower than aromatic compounds. Therefore, it is natural that the solubilized 7EC and 7E4MC is embedded at a shallower site than aromatic molecules.

For the HDTC micelle, D_{eff}=39±1 (25 °C). As is mentioned earlier, the aliphatic chain of HDTC is longer than SDS, so the flexibility of this longer chain may make easier the movement of the fluorophore toward the micelle core. Then, the location of the fluorophore in the HDTC micelle becomes deeper than in the SDS micelle. The interior of n-alkyltrimethylammonium bromide micelles is more polar than sodium n-alkyl sulfate micelles with the same n.[15] If the SDS (n=12) micelle is compared with the HDTC (n=16) micelle as in this work, the interior of the HDTC micelle may be less polar due to the longer alkyl chain of HDTC. By the use of naphthalene as a fluorescent molecule, it has been shown that its solubilized site within n-alkyltrimethylammonium bromide micelles is not close to the polar region of the micelle surface and, also, does not reside in the micelle core.[15] These results are consistent with D_{eff} for the HDTC micelle which is an intermediate value between D of pure water and typical aliphatic solvents. The K value difference between 7EC and 7E4MC may decrease in the HDTC micelle compared with that in the SDS micelle because the hydrophobic interaction of a methyl substituent is supposed to be less effective to distinguish 7EC from 7E4MC at a deeper part in the micelle.

References

1) S. Lukac, *J. Phys. Chem.*, **87**, 5045 (1983).
2) M. S. Fernandez and P. Fromherz, *J. Phys. Chem.*, **81**, 1755 (1977).
3) T. Moriya, *Bull. Electrotech. Lab.*, **50**, 1123, (1986).
4) P. Lianos, M.-L. Viriot, and R. Zana, *J. Phys. Chem.*, **88**, 1098 (1984).
5) P. Mukerjee and J. R. Cardinal, *J. Phys. Chem.*, **82**, 1620 (1978).
6) T. Moriya, *Bull. Chem. Soc. Jpn.*, **57**, 1723 (1984).
7) T. Moriya, *Bull. Chem. Soc. Jpn.*, **59**, 961 (1986).
8) P. Mukerjee and K. J. Mysels. *Nat. Stand. Ref. Data Ser.*, **NBS 36**, 51 (1971); references therein.
9) T. Wolff, *Ber. Bunsenges. Phys. Chem.*, **86**, 1132 (1982).
10) S. Ghosh, M. Petrin, and A. H. Maki, *J. Phys. Chem.*, **90**, 5206 (1986).
11) H. Coll, *J. Phys. Chem.*, **74**, 520 (1970).
12) K. Granath, *Acta Chem. Scand.*, **7**, 297 (1953).
13) S. S. Atik and L. A. Singer, *Chem. Phys. Lett.*, **59**, 519 (1987).
14) Y. Y. Akhadov, "Dielectric Properties of Binary Solutions," Pergamon Press, Oxford (1980).
15) S. Ghosh, A. H. Maki, and M. Petrin, *J. Phys. Chem.*, **90**, 5210 (1986).

The Crystal Structure of a Charge-Transfer Complex of Tetrakis(methylthio)-tetrathiafulvalenium Dibromoiodate, TMT-TTF · IBr_2

Kazumasa HONDA,* Midori GOTO, Masayasu KURAHASHI, Hiroyuki ANZAI,† Madoka TOKUMOTO,† and Takehiko ISHIGURO†

National Chemical Laboratory for Industry, Tsukuba, Ibaraki 305

†Electrotechnical Laboratory, Tsukuba, Ibaraki 305

(Received July 23, 1987)

Synopsis. The crystal structure of the title complex, a semiconductor, has been determined. The space group is $P2_1/n$, with a=8.207(3), b=11.537(4), and c=21.804(12) Å, β=91.88(5)°, and Z=4. The donor cations assume dimer structures with short intermolecular S··· S contacts of 3.43, 3.53, and 3.60 Å.

It has been proposed that two-dimensional electrical properties of a superconductor β-(BEDT-TTF)$_2I_3$ (BEDT-TTF=bis(ethylenedithio)tetrathiafulvalene) and its related compounds derive from the four outer sulfur atoms attached to the tetrathiafulvalene (TTF) skeleton.[1] Tetrakis(alkylthio)-substituted TTFs have also similar sulfur atoms, and the influence of alkyl groups on the dimensionality of the electronic systems has been investigated.[2] Wu and Zheng[3] reported of an X-ray analysis of the title compound, but no precise crystal structure was given. Here the present authors report its crystal structure and electrical properties.

Experimental

Black plates of TMT-TTF · IBr_2 were obtained by electrochemical oxidation[4] (at a constant current of 1 μA under nitrogen stream at 20 °C) from a 60 ml chlorobenzene solution containing 0.13 mmol of TMT-TTF and 0.26 mmol of tetrabutylammonium dibromoiodate. The electrical resistivity of single crystal was measured along the a axis by the four-probe method.

A crystal, with 10 faces, of 0.34×0.50×0.23 mm was mounted on a Rigaku AFC-4 four-circle diffractometer. Intensity data were collected at room temperature by using Mo $K\alpha$ radiation (λ=0.71069 Å, graphite monochromated) in the 2θ-ω scan mode with a scan width of $\Delta\omega$=(1.0+0.5 tan θ)° and a scan speed of 4.0° min^{-1} over the range of 2θ values from 3° up to 55°. Intensities of 5084 reflections were collected and 3147 independent reflections ($|F_o| \geqq 3\sigma(|F_o|)$) were obtained. Three standards measured every 50 reflections showed no significant X-ray damage or crystal decay. Absorption correction following the method of Busing and Levy[5] was applied.

Crystal Data. $C_{10}H_{12}S_8 \cdot IBr_2$: FW=675.43; monoclinic; space group $P2_1/n$; a=8.207(3), b=11.537(4), and c=21.804(12) Å and β=91.88(5)°; U=2063(2) Å^3; D_c=2.17 g cm^{-3} for Z=4; μ(Mo $K\alpha$)=64.4 cm^{-1}.

Structure Analysis and Refinement. The structure was solved by use of the Monte Carlo method.[6] Anisotropic thermal parameters were assumed for all non-hydrogen atoms. Hydrogen atoms were not located. The final full-matrix least-squares refinement for 3147 independent reflections led to the R value of 0.069 and the R_w value of 0.083 in conjunction with the weighting scheme of w=(0.011 $|F_o|^2-|F_o|+20)^{-1}$. The atomic scattering factors were taken from the International Tables for X-Ray Crystallography (1974). All the computations were carried out on a FACOM M-380 computer using the *UNICS* III system.[7]

Results and Discussion

The final atomic parameters of the non-hydrogen atoms are given in Table 1.[8] Wu and Zheng[3] reported that the crystal belongs to the monoclinic space group of $P2_1$ with a=8.21, b=11.56, and c=21.85 Å and β=92.1°. The lattice constants of our result are similar to those reported but the space group is different. Figure 1 shows the projection along the a axis. The

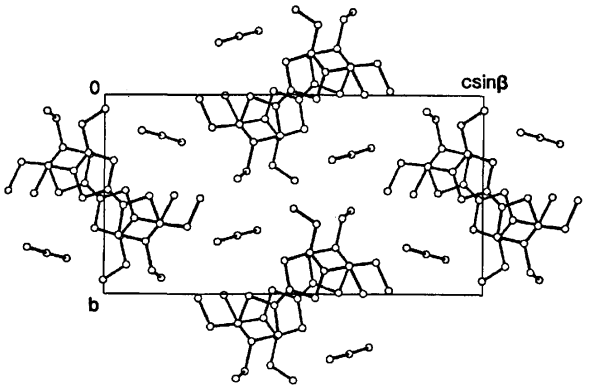

Fig. 1. Crystal structure projected along the a axis.[9]

Table 1. Fractional Atomic Coordinates/×10^4 and Equivalent Isotropic Thermal Parameters, with Estimated Standard Deviations in Parentheses

Atom	x	y	z	B_{eq}/Å^2
I	1040(1)	2040(1)	1497(0.3)	3.91(0.02)
Br(1)	−1860(2)	2358(1)	2019(1)	5.21(0.04)
Br(2)	3974(2)	1778(1)	979(1)	5.48(0.04)
S(1)	1456(3)	2979(2)	−386(1)	3.83(0.06)
S(2)	618(3)	4918(2)	−1188(1)	3.59(0.06)
S(3)	192(4)	1180(2)	−1268(1)	4.52(0.08)
S(4)	−842(4)	3385(3)	−2181(1)	4.80(0.08)
S(5)	3282(3)	4804(2)	569(1)	3.70(0.06)
S(6)	2288(3)	6696(2)	−247(1)	3.60(0.06)
S(7)	5012(4)	6427(3)	1468(1)	4.57(0.07)
S(8)	3730(4)	8530(2)	595(1)	4.51(0.07)
C(1)	552(13)	2648(10)	−1096(5)	4.1(0.3)
C(2)	141(13)	3531(8)	−1466(5)	3.5(0.2)
C(3)	2214(17)	807(10)	−1504(6)	5.3(0.3)
C(4)	−516(18)	4803(11)	−2520(5)	5.8(0.4)
C(5)	3855(12)	6193(9)	798(4)	3.6(0.2)
C(6)	3349(13)	7093(9)	422(5)	3.8(0.2)
C(7)	5019(17)	5037(11)	1839(6)	5.7(0.4)
C(8)	2624(17)	9287(9)	−15(6)	5.3(0.3)
C(9)	1531(12)	4447(9)	−509(4)	3.5(0.2)
C(10)	2292(12)	5227(8)	−106(4)	3.3(0.2)

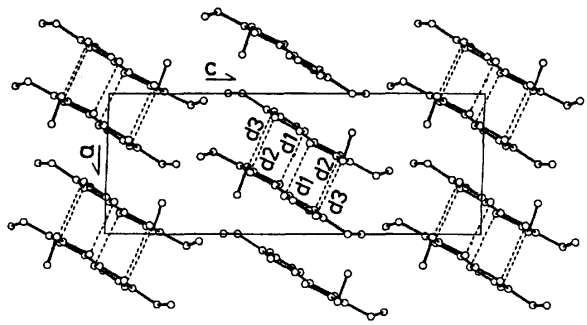

Fig. 2. The packing motif of TMT-TTF molecules projected along the b axis. The S···S contacts of $d1$=3.431(4) (S(1)···S(6)), $d2$=3.529(4) (S(2)···S(5)), and $d3$=3.598(4) (S(3)···S(8)) shorter than the van der Waals distance of 3.7 Å are indicated.

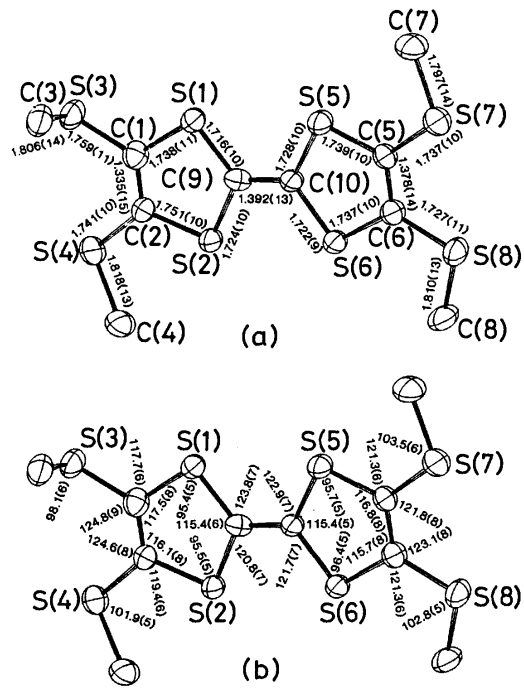

Fig. 3. Molecular structure[12] of TMT-TTF with the numbering system for the non-hydrogen atoms and the bond distances(Å) (a), and the bond angles(°) (b). Thermal ellipsoids are drawn at 40% probability. Bond distances of IBr_2 molecule are 2.698(2) Å and 2.711(2) Å for I-Br(1) and I-Br(2), respectively, and Br(1)-I-Br(2) bond angle is 178.5(1)°.

unit cell contains four TMT-TTF's and four IBr_2's in general positions. They are stacked in segregated columns extending along the a axis. In the case of other TMT-TTF complexes such as (TMT-TTF)-(HCBD)[10] (HCBD=hexacyanobutadiene) and (TMT-TTF)$I_{2.47}$[11] complexes, the stacks of donor TMT-TTF's and those of acceptors form alternate sheets, and the donor TMT-TTF's are aligned almost in the direction of their long axis. In the present complex the crystal does not possess such sheet structures, and the long axis of the TMT-TTF molecule in the position of (x, y, z) is almost perpendicular to those of the molecules in the position of ($1/2-x$, $1/2+y$, $1/2-z$). The extended terminal methyl groups and the anion columns prevent the intermolecular interaction between the donor columns. As shown in Fig. 2, the donor molecules TMT-TTF's face each other to assume a dimeric structure around the inversion center at (0, 1/2, 0) and (1/2, 0, 1/2), with close S···S contacts of $d1$=3.431(4) (S(1)···S(6)), $d2$=3.529(4) (S(2)···S(5)), and $d3$=3.598(4) (S(3)···S(8)), all shorter than the van der Waals distance of 3.7 Å. No close S···S contacts are found between the adjacent dimers. The bond lengths and angles of the TMT-TTF molecule are shown in Fig. 3 along with the molecular structure. It has been demonstrated that central C=C bond lengths of TTF analogues in charge-transfer complexes correlate well to the degree of charge transfer (ρ).[13] Katayama et al.[10] estimated the ρ value of the (TMT-TTF)(HCBD) complex to be 0.4—0.6 since the central C=C bond length of 1.382(6) Å is almost the mean value between 1.348(5) Å of the neutral TMT-TTF molecule ($\rho\equiv0$) and 1.438(12) Å of the (TMT-TTF)(AsF_6) complex ($\rho\equiv1$). In the present complex, however, the corresponding C=C length of 1.392(13) Å (C(9)-C(10)) is shorter than the value for the complete charge transfer (ρ=1) as expected from the chemical stoichiometry of donor TMT-TTF and acceptor IBr_2^-. This discrepancy is a subject for future study. The TMT-TTF molecule moiety without the terminal four methyl groups is nearly planar but slightly folded, possibly due to the dimer formation; the inner S···S contacts are shorter than the outer S···S contacts as mentioned above. The best-fit planes defined by S(1), S(2), S(3), S(4), C(1), and C(2) (plane I), S(5), S(6), S(7), S(8), C(5), and C(6) (plane II), and S(1), S(2), S(5), S(6), C(9), and C(10) (plane III) have dihedral angles of 175.2(1)° for planes I and III and 177.7(1)° for planes II and III. The three methyl groups (C(4), C(7), and C(8)) are not so much displaced from the molecular plane and the other one (C(3)) is almost normal to the plane, which may block the interdimer interactions.

The temperature dependence of the electrical resistivity along the a axis was also measured. The resistivity increases as temperature decreases, which indicates that this crystal is semiconductive ($\rho=1\times10^7$ Ω cm and activation energy E=5.0 eV at room temperature). The observed high resistivity and large activation energy are consistent with the poor interdimer interactions.

The authors thank Dr. Kin-ichi Tsunoda of National Chemical Laboratory for Industry for his elaborating the manuscript.

References

1) G. Saito,T. Enoki, H. Inokuchi, and H. Kobayashi, *J. Phys. (Paris) Colloq.*, **44**, C3-1215 (1983).

2) P. Wu, G. Saito, K. Imaeda, Z. Shi, T. Mori, T. Enoki, and H. Inokuchi, *Chem. Lett.*, **1986**, 411.

3) P. Wu and X. Zheng, 2nd China-Japan Joint Symposium on Conduction and Photo-Conduction in Organic Solids and Related Phenomena, Okazaki, November 18—20, 1986, *Abstr.*, p. 69, and private communication.

4) H. Anzai, M. Tokumoto, and G. Saito, *Mol. Cryst. Liq. Cryst.*, **125**, 385 (1985).

5) W. R. Busing and H. A. Levy, *Acta Crystallogr.*, **10**, 180 (1957).

6) A. Furusaki, *Acta Crystallogr., Sect. A*, **35**, 220 (1979).
7) T. Sakurai and K. Kobayashi, *Rep. Inst. Phys. Chem. Res.*, **55**, 69 (1978).
8) The lists of the observed and calculated structure factors and the anisotropic thermal parameters for the non-hydrogen atoms are deposited at the Chemical Society of Japan as Document No. 8776.
9) A. Takenaka, "A Computer Programme System for the Interactive Graphic Display of Crystal and Molecular Structures," Tokyo Institute of Technology, Yokohama, Japan (1982).
10) C. Katayama, M. Honda, H. Kumagai, J. Tanaka, G. Saito, and H. Inokuchi, *Bull. Chem. Soc. Jpn.*, **58**, 2272 (1985).
11) P. Wu, T. Mori, T. Enoki, K. Imaeda, G. Saito, and H. Inokuchi, *Bull. Chem. Soc. Jpn.*, **59**, 127 (1986).
12) C. K. Johnson. *ORTEP* II, Report ORNL-5138, Oak Ridge National Laboratory, Tennessee, USA (1976).
13) T. J. Kistenmacher, T. E. Phillips, D. O. Cowan. J. P. Ferraris, and A. N. Bloch, *Acta Crystallogr., Sect. B*, **32**, 539 (1976).

A BEDT-TTF Complex Including a Magnetic Anion, $(BEDT\text{-}TTF)_3(MnCl_4)_2$

Takehiko MORI* and Hiroo INOKUCHI
Institute for Molecular Science, Okazaki 444
(Received July 30, 1987)

Synopsis. The title charge-transfer complex is prepared and its crystal structure is determined (BEDT-TTF: bis(ethylenedithio)tetrathiafulvalene). One third of the BEDT-TTF molecules is incorporated in the anion sheet, and holds about 2+ charge. The remaining donors form a conducting sheet with a similar arrangement to β'-$(BEDT\text{-}TTF)_2ICl_2$.

In the past few years, a considerable number of BEDT-TTF complexes have been prepared and their structural and physical properties have been investigated. It has been observed that some of these BEDT-TTF complexes exhibit superconductivity; actually these BEDT-TTF superconductors form a most important family of organic superconductors. On the other hand, though magnetic impurity had been believed to be very harmful to superconductivity, the discoveries of the ternary rhodium borides and the Chevrel series compounds including lanthanoids demonstrated the coexistence of superconductivity and long-range magnetic order.[1] The recent investigations of the high-temperature oxide superconductors show that the substitution of magnetic lanthanides is no more harmful to the Y-Ba-Cu-O series of superconductors.[2] Very little investigation has been, however, done concerning the interrelation of localized spins and conduction electrons in organic systems. Thus it is interesting to explore the BEDT-TTF complexes including magnetic anions. In the present paper, we report the preparation and the crystal structure of $(BEDT\text{-}TTF)_3(MnCl_4)_2$, where the anion has a localized spin on Mn^{2+}.

Experimental

Crystals were obtained by electrochemical crystallization of BEDT-TTF in benzonitrile. The electrolyte $(Me_4N)MnCl_3$ (TMMC), which is well-known as a linear-chain antiferromagnet,[3] was prepared by the reaction of $(Me_4N)Cl$ and $MnCl_4 \cdot 4H_2O$ in hot ethanol, and pale pink crystals were recrystallized from ethanol.

Crystal data: $C_{30}H_{24}S_{24}Mn_2Cl_8$, F.W. 1547.46, triclinic, space group $P\bar{1}$, a=9.714(1), b=20.595(2), c=6.802(1) Å, α=89.70(1), β=101.66(1), γ=93.75(1)°, V=1329.8(3) Å^3, Z=1, and D_x=1.932 g cm^{-1}. Intensity data were measured by the θ-2θ scan technique on a Rigaku automated four-circle diffractometer with monochromatized Mo $K\alpha$ radiation. The structure was solved by the Patterson method and the succeeding Fourier syntheses and refined by the block-diagonal least-squares procedure to an R value of 0.033 by using 3479 independent reflections ($|F_o| > 3\sigma(|F_o|)$). Anisotropic thermal parameters were adopted for all non-hydrogen atoms, and the hydrogen atoms were refined isotropically.

Results and Discussion

For the electrolyte of electrochemical crystal growth of organic conductors, tetrabutylammonium salts are usually used because of their high solubilities in organic solvents. However, many tetrabutylammo-

Table 1. Atomic Parameters (×10^4) of $(BEDT\text{-}TTF)_3(MnCl_4)_2$

Atom	x	y	z	B_{eq}
Mn	6256(1)	3278(1)	−181(1)	2.9
Cl(1)	4077(1)	3071(1)	−2416(2)	3.9
Cl(2)	7970(1)	2488(1)	−51(2)	3.6
Cl(3)	5721(2)	3322(1)	3040(2)	4.3
Cl(4)	7383(1)	4274(1)	−849(2)	4.4
S(1)	219(1)	−911(1)	2180(2)	2.6
S(2)	2613(1)	194(1)	4083(2)	2.7
S(3)	999(1)	−747(1)	−1713(2)	2.7
S(4)	3410(1)	358(1)	197(2)	2.5
S(5)	−1929(1)	−1976(2)	946(2)	2.9
S(6)	4755(1)	1143(1)	6247(2)	3.7
S(7)	−958(1)	−1775(1)	−3767(2)	3.5
S(8)	5616(1)	1403(1)	1488(2)	3.1
SS(1)	13274(1)	4392(1)	3351(2)	3.5
SS(2)	13747(1)	4934(1)	7288(2)	3.9
SS(3)	10390(2)	3878(1)	3201(2)	5.3
SS(4)	10970(2)	4408(1)	8103(2)	4.7
C(1)	1277(4)	−497(2)	753(6)	2.5
C(2)	2310(4)	−31(2)	1598(6)	2.3
C(3)	−678(4)	−1432(2)	272(6)	2.3
C(4)	4011(4)	758(2)	3968(6)	2.4
C(5)	−305(4)	−1348(2)	−1548(6)	2.3
C(6)	4362(4)	847(2)	2151(6)	2.4
C(7)	−2073(7)	−2560(3)	−1058(8)	4.8
C(8)	5868(5)	1799(3)	5501(7)	3.3
C(9)	−2332(7)	−2300(3)	−3054(9)	5.1
C(10)	6674(5)	1607(2)	3942(7)	3.1
CC(1)	14350(5)	4842(2)	5146(7)	2.9
CC(2)	11900(5)	4276(2)	4580(7)	3.1
CC(3)	12146(5)	4519(2)	6485(7)	3.1
CC(4)	9400(7)	3640(4)	5090(11)	6.8
CC(5)	10191(6)	3626(3)	7146(10)	4.9

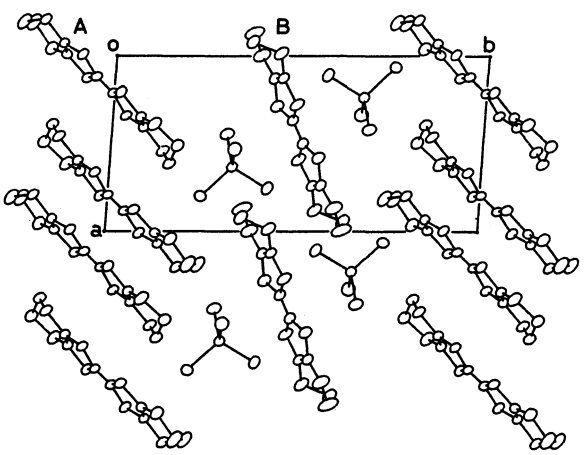

Fig. 1. Crystal structure of $(BEDT\text{-}TTF)_3(MnCl_4)_2$.

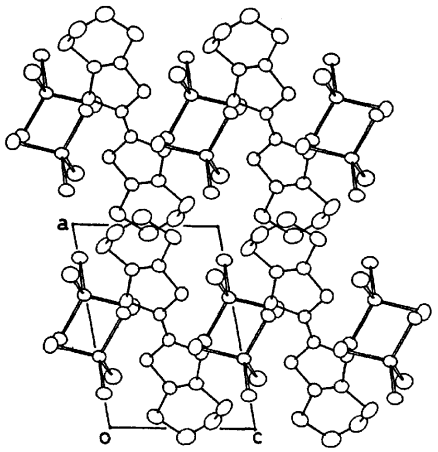

Fig. 2. Structure of the anion and the donors B sheet.

Table 2. Bond Lengths (Å) of the TTF Skeleton of BEDT-TTF, and the Average with the mmm Symmetry

	A	B	D^+
C(1)-C(2)	1.381(6)	1.431(7)	1.38(3)
C(1)-S(1)	1.733(5)	1.677(5)	
C(1)-S(3)	1.720(4)	1.693(5)	
C(2)-S(2)	1.717(4)		
C(2)-S(4)	1.728(5)		
Average	1.725	1.685	1.72(1)
S(1)-C(3)	1.741(4)	1.716(6)	
S(3)-C(5)	1.741(4)	1.713(5)	
S(2)-C(4)	1.743(4)		
S(4)-C(6)	1.741(4)		
Average	1.739	1.715	1.73(1)
C(3)-C(5)	1.365(6)	1.361(7)	
C(4)-C(6)	1.356(6)		
Average	1.361		1.37(2)

D^+: (BEDT-TTF)$ReO_4(THF)_{0.5}$.[6]

nium salts of halogeno transition metals tend to become oily liquid. Tetraethyl- and tetramethylammonium salts are prepared as solids and can be recrystallized easily,[3] while the solubilities of these salts in organic solvents are generally low. Benzonitrile, which shows moderately high polarizability, can fairly dissolve both BEDT-TTF and these ammonium salts. Then we used the combination of the tetramethylammonium salt and benzonitrile. Nitrobenzene is sometimes applicable for the same purpose.

The atomic coordinates are listed in Table 1.[5] The crystal structure is shown in Fig. 1. The anion consists of discrete tetrahedron, $MnCl_4^{2-}$. In a unit cell, 1.5 donor molecules are crystallographically independent. The donors A present on general positions form an ordinary conducting sheet parallel to the (010) plane. On the other hand, the molecules B on inversion centers are incorporated in the anion sheet. Figure 2 shows the structure of the anion and the donors B sheet.

In order to estimate the positive charge present on the donors, the bond lengths of the TTF skeleton are listed in Table 2. In comparison with the reported

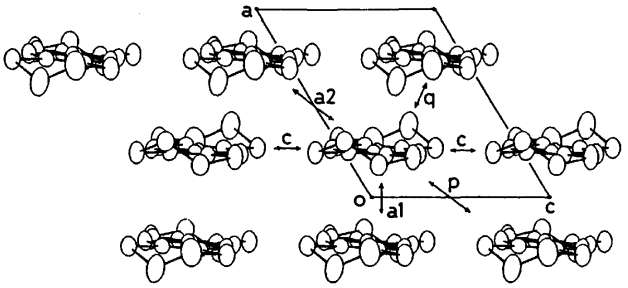

Fig. 3. Arrangement of the donors A in the conducting sheet.

Table 3. Overlap Integrals of the HOMO, the Parameter ϕ: the Angle between the Molecular Plane and the Interaction Direction, and D: the Slip Distance along the Molecular Long Axis[7]

Direction	Overlap/ $\times 10^{-3}$	D/Å	ϕ/°
A a1	27.1	1.8	87
a2	14.0	4.0	36
c	6.1	1.8	5
p	4.9	0.0	24
q	−4.3	5.8	60
B a	−5.7	8.8	85
c	−1.0	2.0	15
a—c	−0.2	10.8	20

data,[6] the charge on the molecule A is estimated to be about 1+. Therefore, from the neutrality of the crystal, the molecule B must hold 2+ charge. This agrees with the change of the bond lengths; in the B molecule, the central C=C distance is anomalously long, and the C-S distances are very short. This systematic change originates in the symmetry of the highest occupied molecular orbital (HOMO), which has nodes on each C-S bond, and bonding nature concerning to every C=C bond. Because even in the 2+ molecule all bond distances change systematically so as to keep the mmm symmetry of the molecule, it can be concluded that in the energy band there is no overlap between the highest occupied band and the next highest band. This observation justifies the energy band calculation which is done by using the HOMO only.[7] The molecule like B, which holds 2+ charge and incorporated in the anion sheet, has also found in (BEDT-TTF)$_5Hg_3Br_{11}$.[8]

The arrangement of the donors A in the conducting sheet is depicted in Fig. 3. The modes of the intermolecular interactions are analyzed according to the method in Ref. 7 (Table 2). Though there are some overlap between the donors B, these molecules contribute very little to the electron transport, because there is no (or little) conduction electrons. The arrangement of the donors A has close resemblance to that of β'-(BEDT-TTF)$_2ICl_2$.[9,10] Along the a axis the 90° interaction (a1) and the 30° interaction (a2) are repeated alternatingly to form a one-dimensional conducting path where the intermolecular overlap integrals are considerably larger than the other interac-

tions. Thus the resulting energy band structure is essentially the same as that of the β'-salt. A very important difference is the band occupancy: 3/4-filled for the β'-salt and 1/2-filled for the present salt. It is interesting that donor sheets with different electron filling exhibit the same structure.

The electrical resistivity is 0.04 Ωcm at room temperature and activated with an activation energy, 0.04 eV in the temperature range between room temperature and (at least down to) 60 K. Though the temperature dependence is semiconducting, it is surprising that the resistivity is lower than that of the β'-salts (>10 Ωcm), because the simple one-electron band model affords a metallic energy band for the β'-salts, and a semiconducting band for the present complex. The semiconducting resistivities of the β'-salts have been attributed to the electron correlation.[9-11] On the other hand, the comparatively low resistivity and the small activation energy of the present salts suggest that the semiconducting transport is not due to the intrinsic one-electron gap in the energy band but due to the electron correlation, where the charge distribution may be a little deviated from $A_2^+B^{2+}$ to result in a metallic one-electron energy band. Since the conduction mechanism of these salts seems to be dominated by the electron correlation, the simple one-electron picture is not helpful to estimate the magnitude of conductivity.

In a preliminary ESR work, there has been observed a rather wide signal whose peak-to-peak linewidth is as large as 360 G at room temperature.

References

1) For a review, see "Superconductivity in Ternary Compounds, Vols. I and II," ed by ϕ. Fischer and M. B. Maple, Springer Verlag, Berlin (1982).

2) For example, see S. Hosoya, S. Shamoto, M. Onoda, and M. Sato, *Jpn. J. Appl. Phys.*, **26**, L456 (1987).

3) R. Dingle, M. E. Lines, and S. L. Holt, *Phys. Rev.*, **187**, 643 (1969).

4) N. S. Grill and F. B. Taylor, *Inorg. Synth.*, **9**, 136 (1967).

5) The parameters of the hydrogen atoms, the anisotropic thermal parameters, and the list of the structure factors are deposited at the office of the Chemical Society of Japan (Document No. 8772).

6) H. Kobayashi, A. Kobayashi, Y. Sasaki, G. Saito, and H. Inokuchi, *Chem. Lett.*, **1984**, 183.

7) T. Mori, A. Kobayashi, Y. Sasaki, H. Kobayashi, G. Saito, and H. Inokuchi, *Bull. Chem. Soc. Jpn.*, **57**, 627 (1984).

8) T. Mori, P. Wang, K. Imaeda, T. Enoki, and H. Inokuchi, *Solid State Commun.*, **64**, 733 (1987).

9) H. Kobayashi, R. Kato, A. Kobayashi, G. Saito, M. Tokumoto, H. Anzai, and T. Ishiguro, *Chem. Lett.*, **1986**, 89.

10) T. J. Emge, H. H. Wang, P. C. W. Leung, P. R. Rust, J. D. Cook, P. L. Jackson, K. D. Carlson, J. M. Williams, M.-H. Whangbo, E. L. Venturini, J. E. Schirber, L. J. Azevedo, and J. R. Ferraro, *J. Am. Chem. Soc.*, **108**, 695 (1986).

11) T. Mori and H. Inokuchi, *Solid State Commun.*, **62**, 525 (1987).

Synthesis and Structure of *cis*(*O*,*O*),*trans*(*N*,*N*)-Chlorobis-(8-quinolinolato-N^1, O^8)nitrosylruthenium

Yukiko KAMATA, Eiichi MIKI, Reiko HIROTA, Kunihiko MIZUMACHI, and Tatsujiro ISHIMORI*
Department of Chemistry, College of Science, Rikkyo University, Nishi-Ikebukuro, Toshima-ku, Tokyo 171
(Received July 28, 1987)

Synopsis. Molecular structure of the title compound has been determined by the X-ray diffraction. The Cl atom is in cis to the NO group, the O atom of one of the two quinolinolato ligands is in trans to the NO group, and the coordinating N and O atoms of two quinolinolato ligands are in cis(O,O) and trans(N,N) configuration.

It is well-known that a coordinating NO^+ possesses weak σ-donor and strong π-acceptor abilities and its property affects synthesis and reactivity of transition metal nitrosyl complexes.[1,2] Recently, we prepared two geometrical isomers of [RuCl(2mqn)$_2$(NO)] (2mqn=2-methyl-8-quinolinolate ion), determined their structures by the X-ray diffraction, and discussed the trans shortening effect of the NO^+ group.[3] In this paper, we have examined the reaction of hydrous nitrosylruthenium(3+) chloride with 8-quinolinol which can coordinate to metal ion by deprotonation without steric hindrance compared with 2-methyl-8-quinolinol, determined the molecular structure of one of two geometrical isomers of [RuCl(qn)$_2$(NO)] (qn= 8-quinolinolate ion) chromatographically separated from the reaction products, and compared the structure of the [RuCl(qn)$_2$(NO)] with that of [RuCl(2mqn)$_2$-(NO)] having the same geometrical configuration.

Experimental

Preparation. A mixture (270 cm^3) of ethyl alcohol solutions of hydrous nitrosylruthenium(3+) chloride (Ru= 30.8%) (3.1 mmol) and 8-quinolinol (30 mmol) was refluxed for 6.5 h. After the solution had been left overnight at room temperature, it was evaporated up. The dried residue was dissolved in dichloromethane and the red filtrate was added on a silica-gel column (Wakogel C-200, ϕ 4 cm×14 cm). Major bands, the first and second red bands, were eluted with dichloromethane. The effluents were separately dried on a rotary evaporator. Terra rosa (**1**) and maroon (**2**) compounds were obtained from the first and second bands, respectively. Yield: 67%, 0.95 g (based on the starting ruthenium compound) for **1**; and 10%, 0.14 g for **2**. Found for **1**: Ru, 22.5; Cl, 8.2; C, 47.5; H, 2.6; N, 9.2%. Found for **2**: Ru, 22.1; Cl, 7.5; C, 47.8; H, 2.9; N, 9.1%. Calcd for [RuCl(qn)$_2$(NO)] ($RuC_{18}ClH_{12}N_3O_3$): Ru, 22.2; Cl, 7.8; C, 47.5; H, 2.6; N, 9.2%. The UV, IR, and conductivity data of **1** and **2** are as follows; **1**: UV (CH_2Cl_2) 31300 cm^{-1} (sh) (log ε 3.7) and 24880 cm^{-1} (log ε 3.85); IR (Nujol) 1838 cm^{-1} (N-O stretching of the NO group) and 338 cm^{-1} (Ru-Cl stretching); Λ_m(CH_2Cl_2, 5.21×10^{-4} mol dm^{-3}, 25 °C) 5.74×10^{-7} S m^2 mol^{-1}.[4] **2**: UV(CH_2Cl_2) 31300 cm^{-1} (sh) (log ε 3.6) and 24750 cm^{-1} (log ε 3.81); IR (Nujol) 1843 cm^{-1} (N-O stretching of the NO group) and 333 cm^{-1} (Ru-Cl stretching).

An X-Ray Crystallographic Analysis of 1. Although the crystals of **2** suitable for an X-ray structural analysis could not be obtained, the crystals of **1** were prepared by concentrating a dilute dichloromethane-acetonitrile solution. Crystallographic data: [RuCl(C_9H_6NO)$_2$(NO)], RuC_{18}-$ClH_{12}N_3O_3$, F. W.=454.9, monoclinic, space group $P2_1/c$, a=14.386(5), b=7.123(1), c=16.315(5) Å, β=95.31(3)°, V= 1664.5(8) Å^3, graphite monochromatized Mo$K\alpha$ radiation (λ=0.71073 Å), D_x=1.815 Mg m^{-3}, D_m=1.81 Mg m^{-3}, Z=4, μ(Mo$K\alpha$)=11.08 cm^{-1}, crystal dimensions 0.25×0.05×0.48 mm. The diffraction data were measured on a Rigaku AFC-4 automated four-circle diffractometer (the X-Ray Analysis Center of the Institute of Physical and Chemical Research). The intensities were collected by the (ω, ω-2θ) scanning technique in $2\theta \leqq 70°$ at a ω scanning speed, 4° min^{-1}. Independent 2614 reflections with $|F_o| > 3\sigma(|F_o|)$ were used for determining the structure. Three standard reflections were measured after every 100 reflections and no decomposition of the crystal was confirmed during the data collection. The ordinary Lorentz and polarization corrections were applied, but no absorption correction was made. The space group was determined with the observed systematic absences, and the lattice parameters were determined by the least-squares refinement using 18 strong reflections. The structure was solved by the heavy atom method and refined by standard Patterson, Fourier, and block-diagonal least-squares procedures. The final refinements were performed using anisotropic temperature factors for non-hydrogen atoms and isotropic ones for hydrogen atoms. The final R value was

Table 1. Atomic and Thermal Parameters of [RuCl(qn)$_2$(NO)] (**1**) (qn=8-Quinolinolate Ion) with Their Estimated Standard Deviations in Parentheses

Atom	x	y	z	B_{eq}/Å^2 [a]
Ru	2360(0)	2551(1)	3919(0)	2.6(0.0)
Cl	1139(1)	3903(3)	4601(1)	4.3(0.0)
O1	1685(3)	−1104(8)	4347(3)	5.3(0.2)
O2	3473(3)	1708(6)	3335(2)	3.2(0.1)
O3	2741(3)	5131(6)	3621(3)	3.3(0.1)
N1	1978(3)	286(7)	4180(3)	2.9(0.1)
N2	3354(3)	2725(8)	4909(3)	3.0(0.1)
N3	1533(3)	2849(7)	2810(3)	3.0(0.1)
Cl	3242(5)	3121(10)	5680(4)	3.7(0.2)
C2	4015(5)	3323(10)	6264(4)	4.2(0.2)
C3	4891(5)	3100(9)	6034(4)	4.0(0.2)
C4	5909(4)	2311(11)	4912(4)	4.0(0.2)
C5	5949(4)	1794(10)	4111(4)	4.1(0.2)
C6	5139(4)	1571(10)	3566(4)	3.6(0.2)
C7	4269(4)	1909(8)	3822(3)	2.7(0.1)
C8	4228(3)	2444(10)	4654(3)	2.8(0.1)
C9	5039(4)	2624(10)	5207(3)	3.1(0.1)
C11	912(4)	1680(10)	2449(4)	3.7(0.2)
C12	420(4)	2120(11)	1685(4)	4.3(0.2)
C13	571(5)	3807(12)	1323(4)	4.4(0.2)
C14	1395(5)	6907(11)	1399(4)	4.3(0.2)
C15	2034(5)	8026(10)	1830(4)	4.6(0.2)
C16	2503(4)	7492(11)	2590(4)	3.9(0.1)
C17	2329(4)	5757(9)	2908(3)	2.9(0.1)
C18	1687(4)	4566(8)	2465(3)	2.8(0.1)
C19	1197(4)	5117(10)	1699(3)	3.5(0.2)

Atomic parameters are multiplied by 10^4. a) B_{eq}= $4/3(B_{11}a^2+B_{22}b^2+B_{33}c^2+B_{13}ac\cos\beta)$.

0.0408. The calculations were performed on a FACOM M-200 computer using the UNICS-III Program System.[5] The atomic and thermal parameters are given in Table 1. Tables of anisotropic thermal parameters, coordinates of hydrogen atoms, and the complete F_o-F_c data are deposited as Document No. 8780 at the Office of the Editor of Bull. Chem. Soc. Jpn.

Results and Discussion

The molecular structure of **1** is shown in Fig. 1. The coordination geometry was similar to that of **1** of [RuCl(2mqn)$_2$(NO)] (2mqn=2-methyl-8-quinolinolate ion) (named hereafter **A**) reported previously;[3] the Cl is in cis to the NO, the O atom of one of the two quinolinolato ligands is in trans to the NO, and the N and O atoms of the two quinolinolato ligands are in trans (N,N) and cis (O,O) configuration.

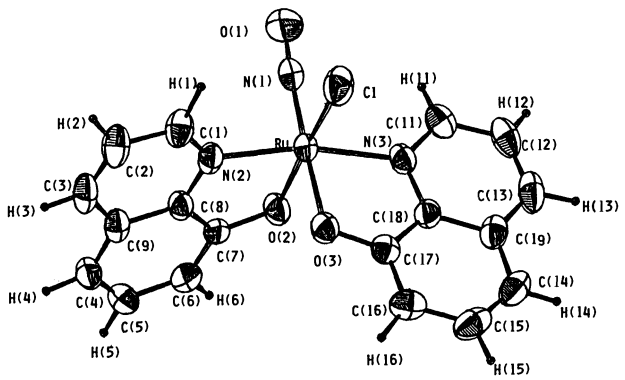

Fig. 1. ORTEP drawing of [RuCl(qn)$_2$(NO)] (**1**) (qn=8-quinolinolate ion) (Thermal ellipsoids are drawn at 50% probability).

Table 2. Interatomic Distances (l/Å) and Bond Angles (ϕ/°) of the Coordination Sphere for [RuCl(qn)$_2$(NO)] (**1**) (qn=8-Quinolinolate Ion) (Their Estimated Standard Deviations in Parentheses)

Distance (l/Å)	
Ru-Cl	2.369(2)
Ru-N(1)	1.769(5)
N(1)-O(1)	1.120(8)
Ru-N(2)	2.059(4)
Ru-N(3)	2.082(4)
Ru-O(2)	2.029(4)
Ru-O(3)	1.991(4)
Angle (ϕ/°)	
Ru-N(1)-O(1)	175.9(5)
N(2)-Ru-O(2)	82.2(2)
N(3)-Ru-O(3)	80.9(2)
Cl-Ru-N(1)	89.9(2)
Cl-Ru-N(2)	95.7(1)
Cl-Ru-N(3)	88.7(1)
Cl-Ru-O(2)	173.1(1)
Cl-Ru-O(3)	88.4(1)
N(3)-Ru-O(2)	92.0(2)
N(1)-Ru-N(3)	97.9(2)
N(2)-Ru-N(3)	167.1(2)
N(2)-Ru-O(3)	87.1(2)
O(2)-Ru-O(3)	84.9(2)

The bond distances and angles in the coordination sphere are given in Table 2. The RuNO angle, ca. 176°, shows that the NO is formally bound as NO$^+$.[6] The Ru-N(1) and the N(1)-O(1) bond distances were comparable to those in other six-coordinate nitrosylruthenium(3+) complexes.[3,6] The Ru-O(3) bond distance trans to the NO was shorter than the Ru-O(2) bond distance trans to the Cl by 0.038 Å due to the trans shortening effect of the NO$^+$ as was discussed in Refs. 2 and 3. Furthermore, the Ru-O(2) and the Ru-O(3) bond distances of **1** were longer than those of **A** by 0.024 and 0.020 Å, respectively.[3] The phenolic oxygen atom of 2-methyl-8-quinolinolate ion seems to be slightly stronger as a π-donor than that of 8-quinolinolate ion due to electron-donating power of the methyl group. As the NO$^+$ group is a strong π-acceptor, the π-electron densities of the O(3) of **A** more favorably flow into the NO$^+$ through the Ru as compared with those of the O(3) of **1**; the Ru-O(3) bond distance of **1** is expected to be longer than that of **A**. As a chloride ion is considered to be weaker as a π-donor than the phenolic oxygen of the quinolinolate ion, the Ru-O(2) bond distance of **1** is also expected to be longer than that of **A**. The Ru-N(2) and Ru-N(3) bond distances of **1** were shorter than those of **A** by 0.053 and 0.018 Å, respectively because of exclusion of the steric hindrance of the methyl groups. This influence was also found to the bond angles; the Cl-Ru-N(2) and N(1)-Ru-N(3) bond angles of **1** were smaller than those of **A** by ca. 8° and 5°, respectively, while the N(3)-Ru-O(2), N(2)-Ru-N(3), and N(2)-Ru-O(3) bond angles of **1** being larger than those of **A** by 3—6°. The coordination geometry of **1** is close to regular octahedral compared with that of **A**.

The chemical composition of **2** was equal to that of **1**. The IR, visible spectra, and the chromatographic behavior suggest that **2** is geometrically isomeric with **1** as observed for two of the 2-methyl-8-quinolinolato complexes;[3] **2** is in cis(O,O) and cis(N,N) configuration with respect to the two quinolinolato ligands.

The more geometrical isomers of the formula [RuCl(qn)$_2$(NO)] were expected to be isolated because 8-quinolinolate ion can coordinate as bidentate ligand to nitrosylruthenium(3+) group without steric hindrance compared with 2-methyl-8-quinolinolate ion. However, the two geometrical isomers were isolated similarly to the 2-methyl-8-quinolinolato complexes.

The authors wish to express their thanks to Professor Makoto Shima (present: Yokohama National University), Professor Toshio Sakurai (present: Shinshu University), and Miss Kimiko Kobayashi of the Institute of Physical and Chemical Research for providing the X-ray facilities and for assisting the calculations of the structural analysis. The present work was partially supported by a Grant-in-Aid for Scientific Research No. 58470038 from the Ministry of Education, Science and Culture.

References

1) J. H. Enemark and R. D. Feltham, *Coord. Chem. Rev.*, **13**, 339 (1974).

2) F. Bottomley, *Coord. Chem. Rev.*, **26**, 7 (1978).
3) Y. Kamata, T. Kimura, R. Hirota, E. Miki, K. Mizumachi, and T. Ishimori, *Bull. Chem. Soc. Jpn.*, **60**, 1343 (1987).
4) W. L. Geary, *Coord. Chem. Rev.*, **7**, 81 (1971). The molar conductivity in dichloromethane corresponded to that of a nonelectrolyte.
5) T. Sakurai and K. Kobayashi, *Rikagaku Kenkyusho Hokoku*, **55**, 69 (1979).
6) R. D. Feltham and J. H. Enemark, "Structures of Metal Nitrosyls," in "Topics in Stereochemistry," ed by G. L. Geoffroy, John Wiley & Sons, New York (1981), Vol. 12, pp. 155—215.

Halogenation Using Quaternary Ammonium Polyhalides. VI.[1] Bromination of Aromatic Amines by Use of Benzyltrimethylammonium Tribromide

Shoji KAJIGAESHI,* Takaaki KAKINAMI,† Kazuhisa INOUE,† Manabu KONDO,† Hiroko NAKAMURA,† Masahiro FUJIKAWA,† and Tsuyoshi OKAMOTO†

Department of Industrial Chemistry, Faculty of Engineering, Yamaguchi University, Tokiwadai, Ube 755
†Department of Industrial Chemistry, Ube Technical College, Tokiwadai, Ube 755

(Received July 11, 1987)

Synopsis. The reaction of aromatic amines with benzyltrimethylammonium tribromide in dichloromethane-methanol containing calcium carbonate powder for 0.5 h at room temperature gave bromo-substituted aromatic amines in good yields.

It has recently been shown in our laboratories that quaternary ammonium polyhalides such as benzyltrimethylammonium tribromide (BTMA Br_3) or tetrabutylammonium tribromide (TBA Br_3) are useful brominating agents.[2] In the present paper, we wish to report on a facile synthetic method of bromo-substituted aromatic amines **1** by the use of BTMA Br_3.

Results and Discussion

The reaction of aromatic amines **2** with BTMA Br_3 in dichloromethane-methanol containing calcium carbonate powder for 0.5 h at room temperature gave **1** in good yields. In these cases, the calcium carbonate powder was used in order to neutralize a generating hydrogen bromide; the reaction was remarkably promoted by the presence of methanol, as shown in previous our reports.[2b]

The reagent BTMA Br_3 (stable orange crystals, mp 100—101 °C)[2c] has one merit in that it can be quantitatively treated, compared with liquid bromine, because

Table 1. Bromination of Aromatic Amines **2** using Benzyltrimethylammonium Tribromide (BTMA Br_3)

	Substrate **2**	Product **1**	Molar ratio (BTMA Br_3/**2**)	Yield[a] %	Mp θ_m/°C Found	Mp θ_m/°C Reported
1		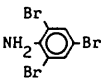	3.1	93	121—123	119—120[4]
2		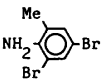	2.1	94	44—45	45—46[5]
3		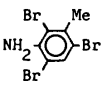	3.1	91	101—102	100—101.6[6]
4	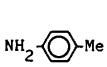	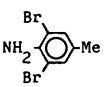	2.1	94	75—76	79[7]
5		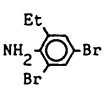	2.1	92	18—20	—
6		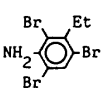	3.1	94	68—70	—
7	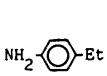	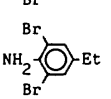	2.1	95	80—82	85[8]
8		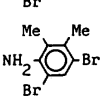	2.1	93	56—57	56[9]
9	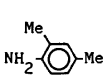	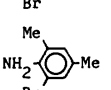	1.1	91	46—47	47—48[10]
10	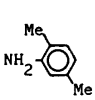	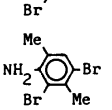	2.1	92	64.5—66	65[11]

Table 1. (Continued)

	Substrate **2**	Product **1**	Molar ratio (BTMA Br_3/**2**)	Yield[a] %	Mp θ_m/°C Found	Mp θ_m/°C Reported
11		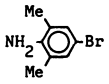	1.1	83	47—48	49—50[12]
12	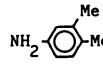	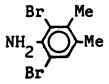	2.1	95	58—59	63[9]
13	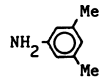	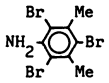	3.1	91	196—197	195[9]
14		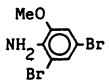	2.1	68[b]	25—26	27[13]
15		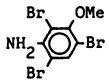	3.1	95	83—84	—
16		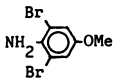	2.1	78[b]	79—80	81[14]
17		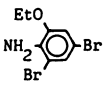	2.1	71[b]	53.5—54.5	52.5[15]
18	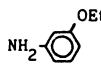	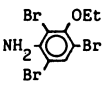	3.1	93	93—94	—
19	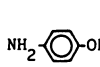	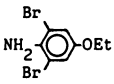	2.1	78[b]	72—73	80[16]
20		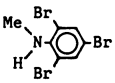	3.1	93	37—39	39[17]
21		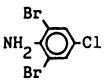	2.1	95	93—94	94[18]
22		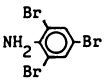	2.1	91	121—123	119—120[4]
23	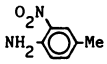	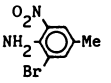	1.1	93	65.5—66.5	64.5[19]
24	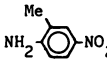	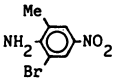	1.1	91	183	180.3—181.3[20]
25	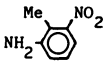	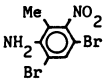	2.1	95	103—104	105[21]
26		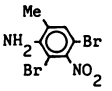	2.1	95	105.5	104[22]
27	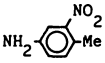	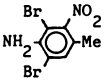	2.1	80[b]	81—82	82[23]
28		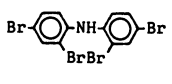	4.1	90	189—190	182[24]
29		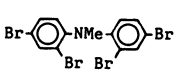	4.1	95	142	142[24]

a) Yield of isolated product. b) Product was isolated by column chromatography on alumina.

of its solid character. Furthermore, the end point of a reaction can be easily confirmed by a decolorization of the orange-colored solution. The results are summarized in Table 1.

Recently, Berthelot et al. reported that TBA Br_3 is a useful para-selective monobrominating agent for aromatic amines.[3] However, the reaction of aromatic amines with BTMA Br_3 gave polybromo-substituted aromatic amines since BTMA Br_3 is a stronger brominating agent than TBA Br_3.[25] Syntheses of bromomethoxyanilines and bromomethylnitroanilines are usually difficult. Our method easily gave these compounds in good yields.

We believe that the procedure for the bromination of aromatic amines using BTMA Br_3 is a highly useful method owing to its ease, simplicity, mildness of conditions, and good product yields.

Experimental

2,4,6-Tribromoaniline (1-*1*); General procedure: To a solution of aniline (**2-*1***) (0.50 g, 5.37 mmol) in dichloromethane (50 ml)-methanol (20 ml) was added BTMA Br_3 (6.49 g, 16.64 mmol) and calcium carbonate powder (2 g) at room temperature. The mixture was stirred for 30 min until a fading of the orange color took place. The solid calcium carbonate was filtered off, the filtrate was concentrated and to the obtained residue was added water (20 ml). The mixture was extracted with ether (40 ml×4). The ether layer was then dried with magnesium sulfate and evaporated in vacuo to give a residue which was recrystallized from methanol-water (1 : 3) affording **1-*1*** as colorless crystals; yield 1.65 g (93%); Mp 121—123 °C (lit,[4] Mp 119—120 °C).

2,4-Dibromo-6-ethylaniline (1-*5*): Mp 18—20 °C (1 : 3 methanol-water); ^{1}H NMR ($CDCl_3$) δ=1.15 (3H, t, J=7Hz, CH_3), 2.38 (2H, q, J=7Hz, CH_2), 4.10 (2H, s, NH_2), 6.98 (1H, d, J=2Hz, 3-H), and 7.33 (1H, d, J=2Hz, 5-H). Found: C, 34.17; H, 3.09; N, 4.58; Br, 56.97%. Calcd for $C_8H_9NBr_2$: C, 34.44; H, 3.25; N, 5.02; Br, 57.28%.

2,4,6-Tribromo-3-ethylaniline (1-*6*): Mp 68—70 °C (1 : 3 methanol-water); ^{1}H NMR ($CDCl_3$) δ=1.12 (3H, t, J=7 Hz, CH_3), 4.00 (2H, q, J=7 Hz, CH_2), 4.50 (2H, br. s, NH_2), and 7.50 (1H, s, 5-H). Found: C, 26.75; H, 2.45; N, 4.16; Br, 67.09%. Calcd for $C_8H_8NBr_3$: C, 26.85; H, 2.25; N, 3.91; Br, 66.96%.

2,4,6-Tribromo-3-methoxyaniline (1-*15*): Mp 83—84 °C (1 : 3 methanol-water); ^{1}H NMR ($CDCl_3$) δ=3.83 (3H, s, OCH_3), 4.63 (2H, br. s, NH_2), and 7.52 (1H, s, 5-H). Found: C, 23.37; H, 1.99; N, 4.15: Br, 66.46%. Calcd for $C_7H_6NOBr_3$: C, 23.37; H, 1.68; N, 3.89; Br, 66.61%.

2,4,6-Tribromo-3-ethoxyaniline (1-*18*): Mp 93—94 °C (1 : 3 methanol-water), ^{1}H NMR ($CDCl_3$) δ=1.44 (3H, t, J=7 Hz, CH_3), 4.00 (2H, q, J=7 Hz, CH_2), 4.50 (2H, s, NH_2), and 7.50 (1H, s, 5-H). Found: C, 25.64; H, 2.36; N, 3.97; Br, 64.25%. Calcd for $C_8H_8NOBr_3$: C, 25.70; H, 2.16; N, 3.75; Br, 64.12%.

We wish to thank Dr. Mamoru Nakai and Mr. Katsumasa Harada, Ube Laboratory, Ube Industries, Ltd., for the elemental analysis.

References

1) Part V, S. Kajigaeshi, T. Kakinami, H. Yamasaki, S. Fujisaki, M. Kondo, and T. Okamoto, *Chem. Lett.*, **1987**, 2109.

2) a) S. Kajigaeshi, T. Kakinami, T. Okamoto, and S. Fujisaki, *Bull. Chem. Soc. Jpn.*, **60**, 1159 (1987). b) S. Kajigaeshi, T. Kakinami, H. Tokiyama, T. Hirakawa, and T. Okamoto, *Chem. Lett.*, **1987**, 627. c) S. Kajigaeshi, T. Kakinami, H. Tokiyama, T. Hirakawa, and T. Okamoto, *Bull. Chem. Soc. Jpn.*, **60**, 2667 (1987).

3) J. Berthelot, C. Guette, M. Essayegh, P. L. Desbene, and J. J. Basselier, *Synth. Commun.*, **16**, 1641 (1986).

4) R. Fittig and E. Büchner, *Justus Liebigs Ann. Chem.*, **188**, 26 (1877).

5) R. Nevile and A. Winther, *Ber.*, **13**, 966 (1880).

6) R. Nevile and A. Winther, *Ber.*, **13**, 975 (1880).

7) R. Nevile and A. Winther, *Ber.*, **13**, 1948 (1880).

8) E. L. Cline and E. E. Reid, *J. Am. Chem. Soc.*, **49**, 3155 (1927).

9) F. Jaeger and J. Blanksma, *Rec. Trav. Chim. Pays-Bas*, **25**, 253 (1906).

10) E. Noelting, A. Braun, and G. Thesmar, *Ber.*, **34**, 2256 (1901).

11) F. Jaeger and J. Blanksma, *Rec. Trav. Chim. Pays-Bas*, **25**, 362 (1906).

12) E. Fisher and A. Windaus, *Ber.*, **33**, 1974 (1900).

13) W. Fuchs, *Monatsh. Chem.*, **38**, 136 (1917).

14) H. Wieland, *Ber.*, **43**, 718 (1910).

15) E. Bamberger and E. Kraus, *Ber.*, **39**, 4251 (1906).

16) W. Fuchs, *Monatsh. Chem.*, **38**, 337 (1917).

17) K. Fries, *Justus Liebigs Ann. Chem.*, **346**, 175 (1906).

18) W. Reed and K. Orton, *J. Chem. Soc.*, **91**, 1552 (1907).

19) R. Nevile and A. Winther, *Ber.*, **13**, 964 (1880).

20) R. Nevile and A. Winther, *Ber.*, **13**, 968 (1880).

21) J. Blanksma, *Chem. Zentralbl.*, **I**, 971 (1914).

22) G. T. Morgan and A. Clayton, *J. Chem. Soc.*, **87**, 951 (1905).

23) J. Blanksma, *Chem. Zentralbl.*, **II**, 1219 (1909).

24) K. Fries, *Justus Liebigs Ann. Chem.*, **346**, 213 (1906).

25) For instance, the reaction of 4-methyl-2-nitroaniline (**2-*23***) with an equimolecular amount of BTMA Br_3 in dichloromethane-methanol for 0.5 h at room temperature gave 2-bromo-4-methyl-6-nitroaniline (**1-*23***) in 93% yield. However, the treatment of **2-*23*** with TBA Br_3 under the same conditions described above gave a mixture of **1-*23*** and **2-*23*** (7 : 3 on its ^{1}H NMR spectrum).

Halogenation Using Quaternary Ammonium Polyhalides. VII.[1] Iodination of Aromatic Amines by Use of Benzyltrimethylammonium Dichloroiodate(1−)

Shoji KAJIGAESHI,* Takaaki KAKINAMI,† Hiromichi YAMASAKI, Shizuo FUJISAKI, and Tsuyoshi OKAMOTO†
Department of Industrial Chemistry, Faculty of Engineering, Yamaguchi University, Tokiwadai, Ube 755
†Department of Industrial Chemistry, Ube Technical College, Tokiwadai, Ube 755
(Received July 11, 1987)

Synopsis. The reaction of aromatic amines with benzyltrimethylammonium dichloroiodate(1−) in dichloromethane-methanol in the presence of calcium carbonate powder for several hours at room temperature gave selectively iodo-substituted aromatic amines in good yields.

Recent work in this series has shown that a new reagent, benzyltrimethylammonium dichloroiodate (1−) (BTMA ICl_2), is an excellent iodinating agent to phenols.[2] In the present paper we wish to also report on a selective iodination of aromatic amines **1** by the use of BTMA ICl_2.

Results and Discussion

The reaction of **1** with BTMA ICl_2 in dichloromethane-methanol in the presence of calcium carbonate powder for several hours at room temperature gave iodo-substituted aromatic amines **2** in good yields.

Usually, the reaction of aniline, toluidines and xylidines with calculated amounts of BTMA ICl_2 gave the desirable mono- and diiodo-substituted corresponding aromatic amines. For instance, the reaction of aniline (**1a**) with 1.0 equiv of BTMA ICl_2 gave 4-iodoaniline (**2a**) in 94% yield, and with 2.1 equiv of BTMA ICl_2 gave 2,4-diiodoaniline (**2b**) in 75% yield, respectively. That is, the iodination of these compounds first occurred at the para-position of the amino group and subsequent iodination at the ortho-position.

However, as a limitation of this new iodination method by use of BTMA ICl_2, the reaction was unsuccessfully carried out with less reactive nitroanilines. The results are summarized in Table 1.

We noticed that the presence of methanol markedly facilitated the iodination of **1**. In this case, the main active species which generates I^+ is probably methyl hypoiodite produced from a reaction of BTMA ICl_2 with methanol. The reaction of **1** with the active intermediate methyl hypoiodite must give **2** and methanol, which can be empolyed repeatedly. The generated hydrogen chloride should be neutralized by additional calcium carbonate.

$$PhCH_2(CH_3)_3N^+ICl_2^- + CH_3OH \rightarrow PhCH_2(CH_3)_3N^+Cl^- + CH_3OI + HCl$$
$$\mathbf{1} + CH_3OI \rightarrow \mathbf{2} + CH_3OH$$

Experimental

Benzyltrimethylammonium Dichloroiodate(1−) (BTMA ICl_2): To a black solution of ICl (16.20 g, 0.1 mol) in dichloromethane (200 ml) was added dropwise a solution of benzyltrimethylammonium chloride (18.60 g, 0.1 mol) in water (100 ml) under stirring at room temperature. After the mixture was stirred for 30 min, the dichloromethane layer was separated and dried with magnesium sulfate, and then evaporated in vacuo to give a residue which was recrystallized from dichloromethane-ether (3 : 1) affording BTMA ICl_2 as stable brilliant yellow needles; yield 30.0 g (86%); Mp 125—125 °C. Found: C, 34.51; H, 4.67; N, 4.11%. Calcd for $C_{10}H_{16}NCl_2I$: C, 34.50; H, 4.63; N, 4.03%.

4-Iodoaniline (2a). Typical Procedure: To a solution of aniline (0.50 g, 5.37 mmol) in dichloromethane (50 ml)-methanol (20 ml) was added BTMA ICl_2 (1.87 g, 5.37 mmol) and calcium carbonate (0.7 g). The mixture was stirred for 30 min at room temperature, during which the color of the solution gradually changed from yellow to light brown. Excess calcium carbonate was filtered and filtrate was concentrated; then, to the obtained residue was added a $NaHSO_3$ solution (5%, 20 ml). The mixture was extracted with ether (40 ml×4). The ether layer was dried with $MgSO_4$ and evaporated in vacuo to give **2a** as colorless crystals (from 1 : 3 methanol-water); yield 1.13 g (96%); Mp 66 °C (lit,[3] Mp 67—68 °C).

4,6-Diiodo-2-methylaniline (2d): Mp 80—81 °C (1 : 3 methanol-water); ^1H NMR ($CDCl_3$) δ= 2.20 (3H, s, CH_3), 4.10 (2H, br. s, NH_2), 7.30 (1H, d, J=3 Hz, 3-H), and 7.80 (1H, d, J=3 Hz, 5-H). Found: C, 23.40; H, 1.87; N, 3.69%. Calcd for $C_7H_7NI_2$: C, 23.42; H, 1.97; N, 3.90%.

4-Iodo-2,3-dimethylaniline (2i): Mp 56 °C (1 : 3 methanol-water); ^1H NMR ($CDCl_3$) δ=2.15 (3H, s, 2-CH_3), 3.33 (3H, s, 3-CH_3), 3.59 (2H, s, NH_2), 6.33 (1H, d, J=8 Hz, 6-H), and 7.50 (1H, d, J=8 Hz, 5-H). Found: C, 38.90; H, 3.96; N, 5.59%. Calcd for $C_8H_{10}NI$: C, 38.89; H, 4.08; N, 5.67%.

4,6-Diiodo-2,3-dimethylaniline (2j): Mp 89—90 °C (1 : 3 methanol-water); ^1H NMR ($CDCl_3$) δ= 2.23 (3H, s, 2-CH_3), 2.41 (3H, s, 3-CH_3), 3.94 (2H, br. s, NH_2), and 7.95 (1H, s, 5-H). Found: C, 25.83; H, 2.48; N, 3.85%. Calcd for $C_8H_9NI_2$: C, 25.76; H, 2.43; N, 3.76%.

4-Iodo-2,5-dimethylaniline (2k): Mp 69 °C (1 : 3 methanol-water); ^1H NMR ($CDCl_3$) δ=2.06 (3H, s, 2-CH_3), 2.29 (3H, s, 5-CH_3), 3.55 (2H, s, NH_2), 6.69 (1H, s, 6-H), and 7.44 (1H, s, 3-H). Found: C, 38.96; H, 4.09; N, 5.64%. Calcd for $C_8H_{10}NI$: C, 38.89; H, 4.08; N, 5.67%.

4,6-Diiodo-2,5-dimethylaniline (2l): Mp 105—106 °C (1 : 3 methanol-water); ^1H NMR ($CDCl_3$) δ= 2.25 (3H, s, 2-CH_3), 2.83 (3H, s, 5-CH_3), 4.25 (2H, br. s, NH_2), and 7.52 (1H, s, 3-H). Found: C, 25.82; H, 2.45; N, 3.87%. Calcd for $C_8H_9NI_2$: C, 25.76; H, 2.43; N, 3.76%.

4-Iodo-3,5-dimethylaniline (2m): Mp 112—113 °C (1 : 3 methanol-water); ^1H NMR ($CDCl_3$) δ=2.36 (6H, s, 3 and 5-CH_3), 3.53 (2H, br. s, NH_2), and 6.44 (2H, s, 2 and 6-H). Found: C, 38.99; H, 4.10; N, 5.53%. Calcd for $C_8H_{10}NI$: C, 38.89; H, 4.08; N, 5.67%.

2,4-Diiodo-3,5-dimethylaniline (2n): Mp 95—96 °C (1 : 3 methanol-water); ^1H NMR ($CDCl_3$) δ=2.35 (3H, s, 5-CH_3), 2.80 (3H, s, 3-CH_3), 4.02 (2H, s, NH_2), and 6.50 (1H, s, 6-H). Found: C, 25.83; H, 2.45; N, 3.87%. Calcd for $C_8H_9NI_2$: C,

Table 1. Iodo Aromatic Amines **2** from Aromatic Amines **1**

	Substrate **1**	Product **2**	Molar ratio (BTMA ICl_2/**1**)	Reaction time/h	Yield[a] %	Mp θ_m/°C Found	Mp θ_m/°C Reported
a	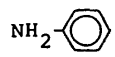	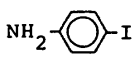	1.0	0.5	94	66	67—68[3]
b		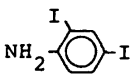	2.1	2.0	75	94—94.5	95—95.5[4]
c	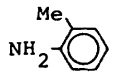	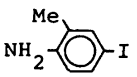	1.0	2.0	92	88.5—89.5	86—88[5]
d		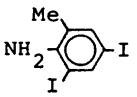	2.1	4.0	89	80—81	—
e	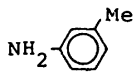	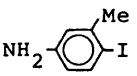	1.0	1.0	81	46.5—47	46[6]
f		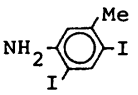	2.1	8.0	96	68—71	73—74[7]
g	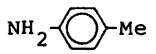	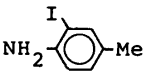	1.0	2.5	77	37—39	40[8]
h		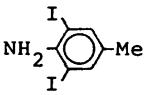	2.1	4.0	73	123.5—125	124.5[4]
i	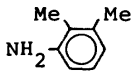	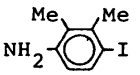	1.0	0.5	75	56	—
j		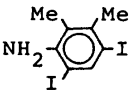	2.1	8.0	94	89—90	—
k	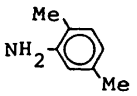	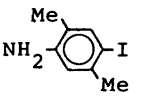	1.0	0.5	87	69	—
l		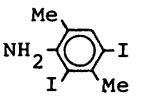	2.1	8.0	95	105—106	—
m	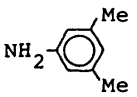	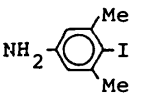	1.0	0.5	96	112—113	—
n		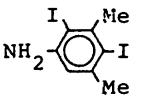	2.1	1.0	86	95—96	—
o	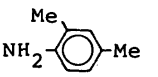	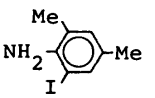	1.1	1.0	82	64.5—65.5	65[9]
p	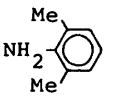	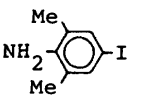	1.1	1.0	96	56	52—53[9]

Table 1. (Continued)

	Substrate 1	Product 2	Molar ratio (BTMA ICl_2/1)	Reaction time/h	Yield[a] %	Mp θ_m/°C Found	Mp θ_m/°C Reported
q	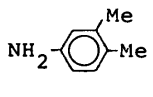	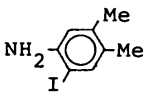	1.1	0.5	87	51—52.5	—
r	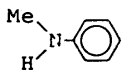	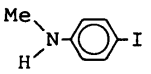	1.0	0.5	88	31.5	—
s	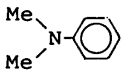	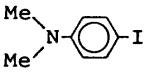	1.0	1.0	85	73—74	78—79[8]
t	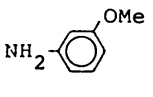	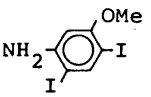	2.1	8.0	92	120—121	—
u	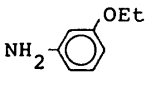	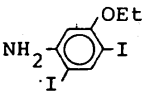	2.1	8.0	96	70.5—71.5	—
v	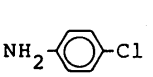	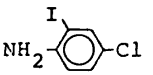	1.1	8.0	86	39.5—40.5	46[10]
w	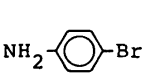	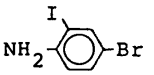	1.1	8.0	89	71	71[10]
x	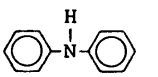	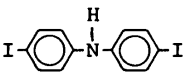	2.1	4.0	96	123—124	—
y	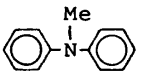	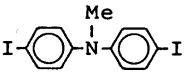	2.1	4.0	96	122—123	—

a) Yield of isolated product.

25.76; H, 2.43; N, 3.76%.

6-Iodo-3,4-dimethylaniline (2o): Mp 51—52.5 °C (1 : 3 methanol-water); ^{1}H NMR ($CDCl_3$) δ=2.12 (6H, s, 3 and 4-CH_3), 3.73 (2H, s, NH_2), 6.58 (1H, s, 2-H), and 7.42 (1H, s, 5-H). Found: C, 38.79; H, 4.17; N, 5.57%. Calcd for $C_8H_{10}NI$: C, 38.89; H, 4.08: N, 5.67%.

4-Iodo-*N*-methylaniline (2r): Mp 31.5 °C (1 : 3 methanol-water); ^{1}H NMR ($CDCl_3$) δ=2.79 (3H, s, CH_3), 3.73 (1H, br. s, NH), 6.36 (2H, d, J=8 Hz, 2 and 6-H), and 7.41 (2H, d, J=8 Hz, 3 and 5-H). Found: C, 35.90; H, 3.61; N, 5.78%. Calcd for C_7H_8NI: C, 36.08; H, 3.46; N, 6.01%.

4,6-Diiodo-3-methoxyaniline (2t): Mp 120—121 °C (1 : 3 methanol-water); ^{1}H NMR ($CDCl_3$) δ=3.37 (3H, s, OCH_3), 3.98 (2H, br. s, NH_2), 6.23 (1H, s, 2-H), and 7.83 (1H, s, 5-H). Found: C, 22.44; H, 1.84; N, 3.70%. Calcd for $C_7H_7NOI_2$: C, 22.42; H, 1.88; N, 3.74%.

4,6-Diiodo-3-ethoxyaniline (2u): Mp 70.5—71.5 °C (1 : 3 methanol-water); ^{1}H NMR ($CDCl_3$) δ=1.38 (3H, t, J=11 Hz, CH_3), 3.87 (2H, q, J=11 Hz, CH_2), 4.20 (2H, br. s, NH_2), 6.18 (1H, s, 2-H), and 7.80 (1H, s, 5-H). Found: C, 24.82; H, 2.08; N, 3.75%. Calcd for $C_8H_9NOI_2$: C, 24.70; H, 2.33; N, 3.60%.

4,4′-Diiododiphenylamine (2x): Mp 123—124 °C (1 : 3 methanol-water); ^{1}H NMR ($CDCl_3$) δ=4.72 (1H, br. s, NH), 6.83 (4H, d, J=15Hz, 2,2′,6,6′-H), and 7.53 (4H, d, J=15 Hz, 3,3′,5,5′-H). Found: C, 34.44; H, 2.00; N, 3.35%. Calcd for $C_{12}H_9NI_2$: C, 34.23; H, 2.15; N, 3.33%.

4,4′-Diiodo-*N*-methyldiphenylamine (2y): Mp 122—123 °C (1 : 3 methanol-water); ^{1}H NMR ($CDCl_3$) δ=3.37 (3H, s, CH_3), 6.90 (4H, d, J=15 Hz, 2,2′,6,6′-H), and 7.63 (4H, d, J=15 Hz, 3,3′5,5′-H). Found: C, 35.88; H, 2.39; N, 3.06%. Calcd for $C_{13}H_{11}NI_2$: C, 35.89; H, 2.55; N, 3.22%.

We wish to thank Dr. Mamoru Nakai and Mr. Katsumasa Harada, Ube Laboratory, Ube Industries, Ltd., for elemental analysis.

References

1) Part VI, S. Kajigaeshi, T. Kakinami, K. Inoue, M. Kondo, H. Nakamura, M. Fujikawa, and T. Okamoto, *Bull. Chem. Soc. Jpn.*, **61**, 597 (1988).

2) S. Kajigaeshi, T. Kakinami, H. Yamasaki, S. Fujisaki, M. Kondo, and T. Okamoto, *Chem. Lett.*, **1987**, 2109.

3) A. Baeyer, *Ber.*, **38**, 2762 (1905).

4) A. Michael and L. M. Norton, *Ber.*, **11**, 109 (1878).

5) W. Militzer, E. Smith, and E. Evans, *J. Am. Chem. Soc.*, **63**, 436 (1941).

6) P. Artmann, *Monatsh. Chem.*, **26**, 1099 (1905).

7) H. L. Weeler, *Am. Chem. J.*, **44**, 129 (1910).

8) K. T. Potts, *J. Am. Chem. Soc.*, **75**, 3711 (1953).

9) H. Suzuki, K. Maruyama, and R. Goto, *Bull. Chem. Soc. Jpn.*, **38**, 1954 (1965).

10) F. B. Dains, T. H. Vaughan, and W. H. Janney, *J. Am. Chem. Soc.*, **40**, 931 (1918).

Catalytic Asymmetric Cyclization of Some Bromohydrins with Chiral Cobalt Complex

Tsutomu TAKEICHI,*,† Teruo TAKAKURA, Michihiro ISHIMORI, and Teiji TSURUTA††
Department of Synthetic Chemistry, Faculty of Engineering, University of Tokyo, Bunkyo-ku, Tokyo 113
†School of Materials Science, Toyohashi University of Technology, Tempaku-cho, Toyohashi 440
(Received July 13, 1987)

Synopsis. Asymmetric cyclization of a variety of bromohydrins with base was examined in the presence of an optically active cobalt(salen) type complex. Optically active oxiranes of modest optical purities were obtanied. *erythro*-3-Bromo-2-butanol and *threo*-3-bromo-2-butanol were cyclized similarly, and only *trans*-2,3-dimethyloxirane and *cis*-2,3-dimethyloxirane were obtained, respectively, indicating that the cyclization of bromohydrin proceeds by complete S_N2 type reaction.

An optically active cobalt (salen) type complex, (1*R*,2*R*)-*N*,*N*′-disalicylidene-1,2-cyclohexanediaminatocobalt(II), Co*, whose structure is well-defined as square-planar tetradentate Schiff base complex,[1] has been used as a catalyst for several kinds of asymmetric reaction, such as the kinetic resolution of oxiranes,[1] one-step synthesis of optically active oxiranes from racemic chlorohydrins,[2] asymmetric fixation of carbon dioxide,[3] and others.[4] In the course of our studies on the asymmetric synthesis of optically active oxiranes, we report here our attempts to evaluate the effect of alkyl substituents of bromohydrins on the asymmetric induction, and also to explore the mechanistic feature of the reaction.

Experimental

Measurements. The NMR spectra were taken on a JEOL JNM-PS-100 spectrometer. Optical rotations were determined by means of a Perkin-Elmer model 241 polarimeter. The GLC analyses were carried out with a Hitachi model K-53 or Yanagimoto model G80 Gas Chromatograph equipped with a column containing PEG. IR spectra were measured using a Hitachi model EPI-G3 spectrometer.

Materials. 2-Bromo-1-propanol was prepared from 2-bromopropanoic acid by treating with $SOCl_2$ and then with $LiAlH_4$; bp 58—59 °C/20 mmHg (1 mmHg=133.322 Pa), yield 50%. 1-Bromo-2-propanol was prepared by the $LiAlH_4$ reduction of bromoacetone; bp 50 °C/16 mmHg, yield 15%. 2-Bromo-1-butanol was prepared by the $LiAlH_4$ reduction of 2-bromobutanoyl bromide; bp 65—66 °C/15 mmHg, yield 50%. 1-Bromo-3,3-dimethyl-2-butanol was prepared according to the procedure of Jackman et al.[5] *erythro*-3-Bromo-2-butanol and *threo*-3-bromo-2-butanol were prepared by the method of Bigley et al.[6]

Asymmetric Reaction of Bromohydrins. Catalytic amount of Co* and K_2CO_3 (base) were added into a flask, and dried at 130—150 °C for 3 h in vacuo. To the flask were added the solvent and the substrate under a dry nitrogen atmosphere with stirring. After an appropriate reaction time, the mixture was analyzed by gas chromatography. The oxirane formed and the unreacted bromohydrin were seperated by fractional distillation and the optical activity was measured. The structure of the oxirane was confirmed by GC, IR, and NMR.

The optical purities (e.e.) of oxiranes were evaluated from the following values; $[\alpha]_D$=+12.53° (neat) for optically pure (*R*)(+)-methyloxirane;[7,9] $[\alpha]_D^{16}$=+12.4° for (*R*)-ethyloxirane;[8] $[\alpha]_D^{25}$=−20.4° (neat) and $[\alpha]_D^{25}$=−18.1° (*c* 1.83 benzene) for (*R*)-*t*-butyloxirane;[9] $[\alpha]_D^{25}$=+59.0° for (2*R*,3*R*)-2,3-dimethyloxirane.[11] The expected optical purities (e.e.$_{calcd}$)[2a] of methyloxirane were evaluated from the optical purities of the unreacted substrate by assuming the reaction to proceed by kinetic resolution mechanism : e.e.$_{calcd}$(%)($[\alpha]_D/[\alpha_o]_D$)×{(100−conv.)/conv.}×100; $[\alpha_o]_D$=−14.4° (neat) for (*R*)-(−)-2-bromo-1-propanol.[10]

Results and Discussion

Asymmetric Cyclization of Propylene Bromohydrins. The asymmetric cyclization of 2-bromo-1-propanol and 1-bromo-2-propanol were carried out with K_2CO_3 in the presence of Co*. The results are summarized in Table 1.

Optically active methyloxirane was formed selectively from 2-bromo-1-propanol and 1-bromo-2-propanol. The configuration of methyloxirane, both from the two substrates, was S, which was also the case with the corresponding chlorohydrins.[2a] The optical activity of methyloxirane formed and unreacted substrate show that (*R*)-(−)-2-bromo-1-propanol reacted preferentially to form (*S*)-(−)-methyloxirane by the inversion of asymmetric carbon. In the reaction of 1-bromo-2-propanol, the unreacted substrate could not be recovered and thus the optical rotation was not

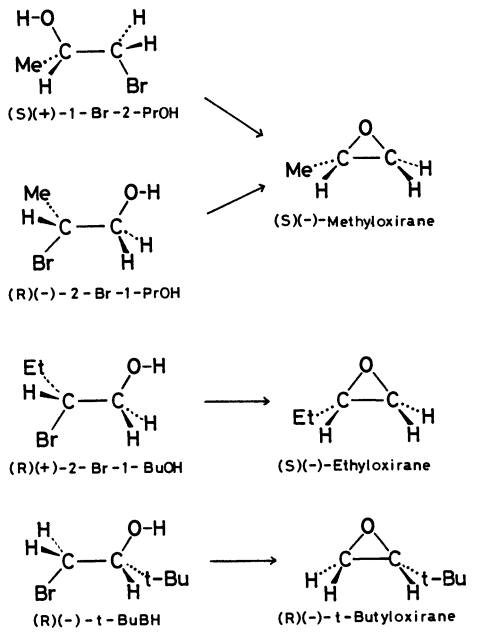

Scheme 1.

††Present address: Department of Chemistry, Faculty of Engineering, Science University of Tokyo, Kagurazaka, Shinjuku-ku, Tokyo 162.

Table 1. Synthesis of Optically Active Methyloxirane (MO) by the Cyclization of Propylene Bromohydrin (2-Br-1-PrOH or 1-Br-2-PrOH)

Substrate	Co* mmol	K_2CO_3[a] PBH	Solv[b]	Temp °C	Time day	conv[c] %	MO[d] PBH %	MO $[\alpha]_D$[e] °	MO e.e.[f] %	PBH $[\alpha]_D$[g] °	PBH e.e.$_{calcd}$[h] %
2-Br-1-PrOH	0.5	1/2	Diox	25	5	14	72	—	—	+ 1.70	72
	0.5	2/3	Diox	25	5	37	89	−3.40	27.1	+ 2.93	34
	0.5	3/2	Diox	25	5	59	78	−1.83	14.6	+ 5.10	19
	0.5	2/1	Diox	25	5	84	70	−1.30	10.4	+10.58	14
	0	1/2	Diox	25	5	10	91	0	0	0	0
	0.5	1/2	Diox	40	2	63	34	−2.65	21.1	—	—
	0.5	1/2	Diox	5—10	7	39	70	−3.17	25.2	+ 2.93	34
	0.5	1/2	PrOH	25	5	58	73	−0.09	0.7	+ 0.13	0.7
	0	1/2	PrOH	25	5	47	76	0	0	0	0
	0.5	1/2	DCE	25	5	67	57	−0.10	0.7	+ 0.16	0.5
	0	1/2	DCE	25	5	45	71	0	0	0	0
1-Br-2-PrOH	0.5	1/2	Diox	25	5	51	47	−1.20	9.6	—	—
	0	1/2	Diox	25	5	29	53	0	0	0	0

a) Molar ratio of K_2CO_3 to PBH; 1/2=60/120 (mmol/mmol), 2/3=80/120 (mmol/mmol), 3/2=120/80 (mmol/mmol), 2/1=80/40 (mmol/mmol). b) 40 cm^3, Diox: dioxane, PrOH: 1-propanol, DCE: 1,2-dichloroethane. c) Conversion of PBH. d) MO formed/ PBH converted (mol/mol)×100. e) Specific rotation of MO formed. f) Optical purity of MO. g) Specific rotation of unreacted PBH recovered. h) Optical purity of MO evaluated from the optical purity of unreacted PBH.

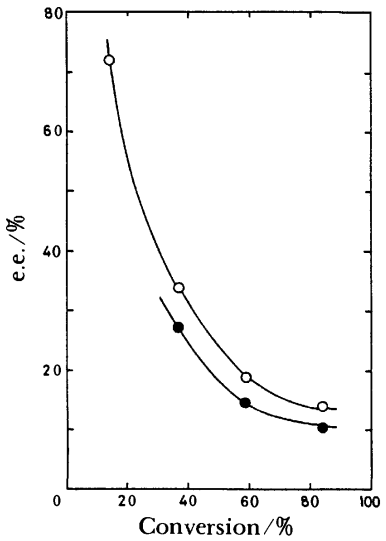

Fig. 1. The relation between e.e. (observed and calculated) of methyloxirane and conversion of 2-bromo-1-propanol. —○— e.e. of methyloxirane calculated from recovered 2-bromo-1-propanol, —●— e.e. of methyloxirane.

measured. However, the formation of (*S*)-(−)-methyloxirane (Table 1) indicates that (*S*)-(+)-1-bromo-2-propanol is preferentially cyclized because the asymmetric center is not involved in this cyclization reaction.

As the conversion increased, the optical purity of methyloxirane decreased, as shown in Fig. 1, showing that this asymmetric cyclization proceeds by the kinetic resolution. The highest optical yield of isolated methyloxirane was 27.1%, achieved in the reaction of 2-bromo-1-propanol with K_2CO_3 in dioxane at 37% of conversion. Much higher enantioselectivity is expected at the initial stage of this reaction. As the solvent for this asymmetric reaction, dioxane was found to be the best among the solvents examined; 1-propanol and 1,2-dichloroethane were found poor as the solvent, probably because the reaction proceeds significantly even without the asymmetric catalyst in these solvents.

Optical purity of methyloxirane did not vary significantly as reaction temperature was changed (at 40 °C, 21% e.e.; 25 °C, 24%; 5—10 °C, 21—25%); the high enantioselectivity was not observed even at lower temperature.

The observed e.e. values of methyloxirane are lower than the e.e.$_{calcd}$ values. The following explanation might be possible for the above differences between e.e. and e.e.$_{calcd}$; (1) the racemization of the prefered enantiomer of the substrate may occur in the cyclization by the catalysis of cobalt complex, (2) a side reaction with high enantioselectivity may take place in parallel with the above kinetic resolution. As by-products for the reaction, a small amount of propylene carbonate and polyether were confirmed by GC, IR, and NMR.

Asymmetric Cyclization of Some Bromohydrins. The interaction of chiral catalyst and the substrate is crucial for asymmetric induction in the catalytic asymmetric reaction. To evaluate the effect of substituent, a variety of bromohydrins were synthesized and the asymmetric cyclization were carried out with K_2CO_3 (Eq. 1).

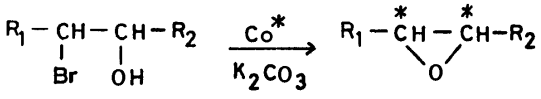

(1)

The results are summarized in Table 2. Corresponding oxiranes were formed selectively in every cases. From 2-bromo-1-butanol, (*S*)-(−)-ethyloxirane was formed in 8.9% e.e., which was much lower than that for methyloxirane. The configuration of oxirane formed was S, which was the same as that of methyl-

Table 2. Synthesis of Optically Active Oxiranes by the Asymmetric Cyclization of Bromohydrins[a]

Substrate[b]	Co* / mmol	K_2CO_3[c] / Sub	Solv[d]	Conv[e] / %	Oxir[f] / Sub %	Oxirane $[\alpha]_D$[g] / °	Oxirane Config	Oxirane e.e.[h] / %	Sub $[\alpha]_D$[i] / °
BBH	0.5	50/137	Diox	33	76	−0.46	S	3.7	—
2-Br-1-BuOH	0.1	50/132	Diox	28	93	−1.11	S	8.9	−1.78
2-Br-1-BuOH	0	50/132	Diox	Trace	—	0	—	0	0
t-BuBH	0.5	50/100	CH_2Cl_2	33	97	−0.72[j]	R	4.0	+1.42
t-BuBH	0	50/100	CH_2Cl_2	20	94	0	—	0	0
erythro-3-Br-2-BuOH	0.1	40/ 80	Diox	18	94	+5.97	R,R	10	−0.47
threo-3-Br-2-BuOH	0.1	40/ 80	Diox	37	86	0	—	0	+0.26

a) Solvent 40 cm^3, 25 °C, 5 days. b) BBH: commercial butylene bromohydrin (1-bromo-2-butanol/2-bromo-1-butanol=4/1), 2-Br-1-BuOH: 2-bromo-1-butanol, *t*-BuBH: 1-bromo-3,3-dimethyl-2-butanol, *erythro*-3-Br-2-BuOH: *erythro*-3-bromo-2-butanol, *threo*-3-Br-2-BuOH: *threo*-3-bromo-2-butanol. c) Molar ratio of K_2CO_3 to substrate (mmol/mmol). d) Diox: dioxane. e) Conversion of substrate. f) Oxirane formed/substrate converted (mmol/mmol). g) Specific rotation of oxirane formed. h) Optical purity of oxirane formed. i) Specific rotation of unreacted substrate recovered. j) Measured in benzene (*c* 13.0).

oxirane. The absolute configuration of 2-bromo-1-butanol is not known but based on the similarity of the reaction with 2-bromo-1-propanol, the absolute configuration of (+)-2-bromo-1-butanol is considered to be R. From 1-bromo-3,3-dimethyl-2-butanol(*t*-BuBH), (*R*)-(−)-*t*-butyloxirane was obtained. The optical purity of *t*-butyloxirane (4.0% e.e.) is also much lower than that of methyloxirane. The configuration of (−)-*t*-BuBH, which is preferentially cyclized in this reaction, is considered to be R, since the asymmetric carbon of the substrate does not participate in the cyclization as described for 1-bromo-2-propanol. Judging from the above two cases, the bulky groups do not necessarily induce high asymmetric induction. It is also interesting to note that methyl- and ethyloxirane were obtained in *S* configuration while *t*-butyloxirane in R configuration.

3-Bromo-2-butanol has two isomers, *erythro*-3-bromo-2-butanol and *threo*-3-bromo-2-butanol, which would be helpful in examining the mechanistic feature of this asymmetric cyclization. When the reaction proceeds by the complete S_N2 type cyclization, only *trans*-2,3-dimethyloxirane will be formed from *erythro*-3-bromo-2-butanol, and only *cis*-2,3-dimethyloxirane will be formed from *threo*-3-bromo-2-butanol. As was expected, the NMR and GC analyses of the products showed that only trans-oxirane was formed from erythro-isomer and only cis-oxirane from threo-isomer. The above results indicate that the reaction proceeds exclusively via the S_N2 mechanism in the presence of cobalt(salen) type complex. This results

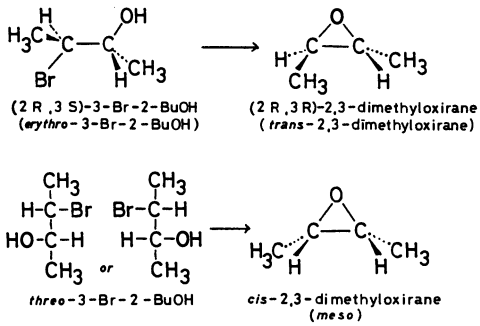

Scheme 2.

lead to the conclusion that racemization of the selected substrate, mentioned before, is not likely to occur.

The optical activities of the substrate and product show that (2*R*,3*S*)-3-bromo-2-butanol[12] reacted preferentially to form (2*R*,3*R*)-dimethyloxirane by the inversion of the carbon at 3-position having bromide function. The results with 1-bromo-2-propanol and 2-bromo-1-propanol suggest that the S configuration is favored at the carbon bearing OH group, while R configuration at the carbon bearing Br atom. The result for (2*R*,3*S*)-3-bromo-2-butanol was, however, contrary to the prediction. It indicates that the enantioselection at the asymmetric moiety of the chiral cobalt complex is vulnerable to various factors. The idea of "Template"[13] may explain the results.

References

1) H. Aoi, M. Ishimori, S. Yoshikawa, and T. Tsuruta, *J. Organomet. Chem.*, **85**, 241 (1975); H. Aoi, M. Ishimori, and T. Tsuruta, *Bull. Chem. Soc. Jpn.*, **48**, 1897 (1975).

2) a) T. Takeichi, M. Ishimori, and T. Tsuruta, *Bull. Chem. Soc. Jpn*, **52**, 2614 (1979); b) T. Takeichi, M. Arihara, M. Ishimori, and T. Tsuruta, *Tetrahedron*, **36**, 3391 (1980).

3) T. Takeichi, Y. Ozaki, and Y. Takayama, *Chem. Lett.*, **1987**, 1137.

4) M. Ishimori, H. Aoi, Y. Tezuka, and T. Tsuruta, *Bull. Chem. Soc. Jpn.*, **50**, 769 (1977); T. Takeichi and Y. Takayama, *Polymer Preprints, Japan*, **32**, 1495 (1983).

5) M. Jackman, M. Klenk, B. Fishburn, B. F. Tullar, and S. Archer, *J. Am. Chem. Soc.*, **70**, 2884 (1948).

6) D. B. Bigley, C. Brown, and R. H. Weatherhead, *J. Chem. Soc., Perkin Trans. 2*, **1976**, 701.

7) Y. Kumata, J. Furukawa, and T. Fueno, *Bull. Chem. Soc. Jpn.*, **43**, 3920 (1970); B. T. Golding, D. R. Hall, and S. Sakrikar, *J. Chem. Soc., Perkin Trans. 1*, **1973**, 1214.

8) J. L. Coke and R. S. Shue, *J. Org. Chem.*, **38**, 2210 (1973).

9) N. Spassky, P. Dumas, N. Sepulchre, and P. Sigwalt, *J. Polym. Sci., Symposium*, **52**, 327 (1975).

10) B. Franzus and J. H. Surridge, *J. Org. Chem.*, **31**, 4286 (1966).

11) H. J. Lucas and H. K. Garner, *J. Am. Chem. Soc.*, **70**, 990 (1948).

12) H. J. Lucas and H. K. Garner, *J. Am. Chem. Soc.*, **72**, 2145 (1950).

13) M. Ishimori, *Shokubai*, **19**, 419 (1977).

An Improvement of the Anderson Test by the Use of High Performance Liquid Chromatography

Toshifumi MIYAZAWA,* Takashi YAMADA, and Shigeru KUWATA
Department of Chemistry, Faculty of Science, Konan University, Higashinada-ku, Kobe 658
(Received July 25, 1987)

Synopsis. The replacement of the *N*-benzyloxycarbonyl (Z) group in the Anderson peptide (Z-Gly-L/D-Phe-Gly-OEt) by Z-L-Ala and the subsequent separation of the diastereomers of the resulting tetrapeptide by reversed-phase HPLC offer a more convenient version with higher accuracy to the original Anderson test for studying racemization in peptide synthesis.

There have been known a variety of tests[1] devised for the estimation of the racemization extent during peptide bond formation. Among them the model coupling of Z-Gly-L-Phe-OH[2] with H-Gly-OEt proposed by Anderson et al.[3] has widely been used for investigating coupling methods and conditions in peptide synthesis, through which extensive data have been accumulated.[4] Since this test measures the weight of racemate isolated by fractional crystallization, the limit of detection has been shown to be ca. 1—2% racemate.[1a] Moreover, in some cases the presence of by-products of the reaction is prone to make it difficult to separate the pure racemate. Kemp et al.[5] applied to the original the multiple isotope dilution procedure, which extended the sensitivity of the test by several orders of magnitude.[1a] However, this procedure still necessitates the isolation of a small amount of pure racemate by crystallization. Therefore, both the original and the improved procedures are not free from a troublesome manipulation of the separation. Thus, an improvement of the Anderson test is very desirable, which would omit the isolation of racemate and allow the analysis to be accomplished more conveniently and with higher accuracy.

Recently, we have found that the diastereomeric pairs of a series of protected tripeptides, Z-L/D-AA-Gly-L-Phe-OMe (where AA denotes various amino acid residues), can well be separated by reversed-phase high-performance liquid chromatography (RP-HPLC).[6] Moreover, the kinetic resolution was found to be almost negligible in the coupling of Z-L/D-AA-OH with H-Gly-L-Phe-OMe, probably because achiral Gly occupies the coupling site in the amino component. Thus, it is reasonable to anticipate that the replacement of the Z group in the Anderson peptide (**1**) by an appropriate Z-L-AA will make it possible to separate the diastereomers of the resulting tetrapeptide (**2**) by RP-HPLC for the quantitation of the epimer in **1** (Scheme 1). As shown in Table 1, this was the case with the tetrapeptides **2** for AA=Ala, Val, Leu, and Pro. When the *N*-hydroxysuccinimide ester of Z-L-AA-OH (Z-L-AA-OSu) (for AA=Ala, Val, and Leu) was reacted with H-Gly-DL-Phe-Gly-OEt,[7] the diastereomer ratio of the resulting tetrapeptide was close to 50 : 50.[8]

Z-Gly-L/D-Phe-Gly-OEt → H-Gly-L/D-Phe-Gly-OEt
1
→ Z-L-AA-Gly-L/D-Phe-Gly-OEt
2

Scheme 1.

Based on the above results, we chose the simplest Z-L-Ala and decided on our version for the Anderson test as follows. The crude product obtained through the coupling of Z-Gly-L-Phe-OH with H-Gly-OEt by the method under consideration is hydrogenated over Pd-carbon in ethanol in the presence of 1 equiv. of concd hydrochloric acid. The debenzyloxycarbonylated product is then reacted with 2 equiv. of Z-L-Ala-OSu in DMF in the presence of 1 equiv. of triethylamine for 24 h. The resulting tetrapeptide, after suitable washings, is submitted to a separation of the diastereomers by RP-HPLC. The limit of detection

Table 1. HPLC Separation of Diastereomers of Z-AA-Gly-Phe-Gly-OEt (**2**)[a]

AA	Mobile phase[b]	k'[c]		α[d]
		L-L	L-D	
Ala	A	9.49	11.17	1.18
Val	B	8.79	10.45	1.19
Leu	C	7.82	8.99	1.15
Pro	B	6.61	8.59	1.30
Phe	B	8.76	8.76	1.00

a) Conditions: column, Cosmosil $5C_{18}$ (4.6 mm I.D.×150 mm); flow rate, 1.0 ml min^{-1}; column temperature, 30 °C; detection, 254 nm. b) A, 55% MeOH aq; B, 60% MeOH aq; C, 65% MeOH aq. c) Capacity factor, $k'=(t_R-t_0)/t_0$, where t_0 denotes the void time (ca. 1.5 min). d) Separation factor, $\alpha=k'_{L\text{-}D}/k'_{L\text{-}L}$.

Table 2. Racemization Extent during the Coupling of Z-Gly-L-Phe-OH with H-Gly-OEt by the DCC Method plus Additive[a]

Additive	D %[b]
None	5.3
HOBt	<0.1[c]
HOSu	<0.1[c]
HONB	<0.1[c]
Stearic acid	1.2
Oleic acid	2.8
Palmitic acid	2.8
Lauric acid	3.6
$CuCl_2$	<0.1[c]

a) Reaction conditions: Z-Gly-L-Phe-OH/H-Gly-OEt/additive/DCC, 1 : 1 : 1 : 1 equiv.; solvent, THF (reactant concentration, 0.083 mol dm^{-3}); duration and temperature, 24 h at 5 °C. b) Obtained as L-D % of the tetrapeptide **2** for AA=Ala. c) Sensitivity range, 0.01 a.u.f.s.

was estimated as ca. 0.1% epimer.

Table 2 shows the results obtained by our improved procedure on the racemization suppressing effect of several additives in the dicyclohexylcarbodiimide (DCC) mediated couplings affording the Anderson peptide. By the use of copper(II) chloride[9] as well as the common *N*-hydroxy compounds such as 1-hydroxybenzotriazole (HOBt), *N*-hydroxysuccinimide (HOSu), and *N*-hydroxy-5-norbornene-*endo*-2,3-dicarboximide (HONB),[10] practically no racemization could be detected. On the other hand, the effect of the long-chain fatty acids, regarded as factors ordering the reaction medium, whose usefulness as a new type of additives had been demonstrated using the conventional Anderson test,[4g] proved to be considerable but not complete. Probably this discrepancy is partly due to the fact that the reaction conditions in both cases were not identical; primarily, though, it is due to the difference in the procedure for the quantitation of the epimer in the Anderson peptide.

A combination of the present improvement utilizing the HPLC separation of the diastereomers of the tetrapeptide derived from the Anderson peptide, and the multiple dilution procedure as applied by Kemp et al.[5] would increase the limit of detection in the Anderson test with greater precision.

Experimental

All melting points are uncorrected. Optical rotations were measured with a JASCO DIP-4 polarimeter. TLC and preparative TLC were performed on Merck Kieselgel 60 F_{254} and Kieselgel GF_{254} (Type 60), respectively. The liquid chromatograph employed was a Shimadzu LC-3A instrument, equipped with a Shimadzu SPD-2A variable wavelength UV monitor and a Shimadzu Chromatopac C-R1A data processor. A prepacked ODS column (Cosmosil $5C_{18}$) was consisted of a stainless steel tube, 4.6 mm I.D. and 150 mm long.

Z-Gly-DL-Phe-Gly-OEt. This was prepared by the reaction of Z-Gly-OSu with H-DL-Phe-Gly-OEt·HBr[11] in CH_2Cl_2; yield, 85%; mp 132—133 °C (acetone aq). [lit,[12] mp 132—133 °C].

Z-Gly-L-Phe-Gly-OEt. This compound has previously been prepared through the coupling of Z-Gly-L-Phe-OH with H-Gly-OEt by various methods (Anderson test), while its preparation by the stepwise elongation procedure has not been reported so far, to our knowledge. The reaction of Z-Gly-OSu with H-L-Phe-Gly-OEt·HCl[11] (prepared through the debenzyloxycarbonylation of Z-L-Phe-Gly-OEt[13] by hydrogenation in the presence of 5% Pd-C and concd HCl) in CH_2Cl_2 afforded white crystals; yield, 87%; mp 118—119 °C (EtOAc-hexane); $[\alpha]_D^{25}$ −12.5° (*c* 1.0, EtOH).

HPLC Separation of the Diastereomers of Z-AA-Gly-Phe-Gly-OEt. Z-L-AA-OSu (for AA=Ala, Val, Leu, Pro, and Phe) (0.125 mmol) and H-Gly-DL-Phe-Gly-OEt·HCl (prepared through the debenzyloxycarbonylation of Z-Gly-DL-Phe-Gly-OEt by hydrogenation in the presence of 5% Pd-C and concd HCl) (0.125 mmol) were stirred in DMF (1.5 ml) in the presence of TEA (0.125 mmol) at room temperature overnight. The neutral fraction was separated from the reaction mixture as usual. This fraction was submitted to separation of diastereomers by RP-HPLC under the conditions described in Table 1.

On the other hand, Z-L-AA-Gly-L-Phe-Gly-OEt (for AA=the same residues) was prepared from Z-L-AA-OSu and H-Gly-L-Phe-Gly-OEt·HCl[11] in a manner similar to that described above, and submitted to HPLC analysis.

Z-L-Ala-Gly-L-Phe-Gly-OEt. Z-L-Ala-OSu (298 mg) and H-Gly-L-Phe-Gly-OEt·HCl (prepared through the debenzyloxycarbonylation of Z-Gly-L-Phe-Gly-OEt by hydrogenation in the presence of 5% Pd-C and concd HCl) (310 mg) were stirred in the presence of TEA (91 mg) at room temperature for 3 d. To the reaction mixture was EtOAc added, and the resulting suspension was washed successively with 5% HCl, water, sat. $NaHCO_3$, and water, and dried over Na_2SO_4. Removal of the solvent afforded crystals, which were recrystallized from MeOH; yield, 304 mg (66%); mp 189—190 °C; $[\alpha]_D^{25}$ −9.6° (*c* 1.0, DMF). Found: C, 60.66; H, 6.08; N, 10.97. Calcd for $C_{26}H_{32}N_4O_7$: C, 60.93; H, 6.29; N, 10.93.

Z-D-Phe-Gly-OEt. This was prepared from Z-D-Phe-OH and H-Gly-OEt·HCl[11] by the DCC method in CH_2Cl_2; yield, 90%; mp 110—111 °C (EtOAc-petroleum ether); $[\alpha]_D^{25}$ +17.3° (*c* 2.0, EtOH). Cf. lit[13] for the L isomer, mp 110—110.5 °C, $[\alpha]_D^{25}$ −17.1° (*c* 2, EtOH).

Z-Gly-D-Phe-Gly-OEt. This was obtained by the coupling of Z-Gly-OSu with H-D-Phe-Gly-OEt·HCl[11] as described for the corresponding L isomer; yield, 90%; mp 118—119 °C (EtOAc-hexane); $[\alpha]_D^{25}$ +12.4° (*c* 1.0, EtOH). Found: C, 62.76; H, 6.18; N, 9.47. Calcd for $C_{22}H_{27}N_3O_6$: C, 62.57; H, 6.16; N, 9.52.

Z-L-Ala-Gly-D-Phe-Gly-OEt. This was prepared from Z-L-Ala-OSu and H-Gly-D-Phe-Gly-OEt·HCl[11] as described for the corresponding L-L isomer. The final purification was conducted by preparative TLC with $CHCl_3$-MeOH (9:1) to afford the desired compound as a syrup; yield, 77%; $[\alpha]_D^{25}$ +1.6° (*c* 1.0, DMF). Found: C, 60.71; H, 6.42; N, 10.88.

Z-Gly-L-Phe-OH. A solution of Z-Gly-OSu (12.25 g) in acetonitrile (70 ml) was added to a solution of H-L-Phe-OH (9.91 g) and $NaHCO_3$ (10.08 g) in water (180 ml) with stirring at room temperature. After 6 h of stirring, the reaction mixture was concentrated to ca. 120 ml and acidified with concd HCl to pH 2. The separated oil was extracted with EtOAc, washed with water, and dried over Na_2SO_4. Evaporation of the solvent in vacuo afforded crystals, which were recrystallized from EtOAc-petroleum ether; yield, 11.86 g (83%); mp, 128.5—129.5 °C; $[\alpha]_D^{25}$ +38.7° (*c* 1.0, EtOH). [lit,[14] mp 127—128 °C, $[\alpha]_D^{25}$ +36.6°±0.5° (*c* 5, EtOH)].

A part of the sample was esterified with diazomethane in ether, hydrogenated in the presence of 5% Pd-C and concd HCl, and then coupled[11] with Z-L-Ala-OH using 1-ethyl-3-(3-dimethylaminopropyl)carbodiimide hydrochloride in the presence of HOBt in THF according to a previous report.[6] The HPLC analysis of the resulting product showed no presence of the D-L isomer, under the following conditions: mobile phase, 60% MeOH aq; flow rate, 1.0 ml min^{-1}; column temperature, 30 °C; detection, 254 nm; sensitivity range, 0.02 absorbance units full scale (a.u.f.s.). The L-L isomer of Z-Ala-Gly-Phe-OMe had t_R=11.10 min and the D-L isomer t_R=12.72 min.

Determination of Racemization in the Anderson Test. a) General Procedure: Z-Gly-L-Phe-OH (0.125 mmol) was coupled with H-Gly-OEt (0.125 mmol) by a certain coupling method. After suitable washes, the crude product obtained was dissolved in EtOH (5 ml), and hydrogenated in the presence of 5% Pd-C (15 mg) and concd HCl (0.011 ml). After filtration of the catalyst and a successive removal of the solvent, the residue was dried by the addition of MeOH followed by evaporation in vacuo and then dissolved in DMF (1 ml). To this solution Z-L-Ala-OSu (0.25 mmol) was added, followed by TEA (0.125 mmol). After the mixture had been stirred at 23 °C for 24 h, 1-(2-aminoethyl)piperazine (16 mg) was added and stirring was continued for 20 min. The mixture was distributed between EtOAc and 5% HCl, and the organic layer was further washed with 5% HCl, water, sat. $NaHCO_3$, and water, and dried over Na_2SO_4. After evapora-

tion of the solvent, the residue was dissolved in MeOH (3 ml). This solution (5 μl) was injected through a microsyringe into the HPLC apparatus under the following conditions: mobile phase, 55% MeOH aq; flow rate, 1.0 ml min^{-1}; column temperature, 30 °C; detection, 254 nm; sensitivity range, 0.02 a.u.f.s. The L-L isomer of Z-Ala-Gly-Phe-Gly-OEt had t_R=16.37 min and the L-D isomer t_R=18.99 min, while the void time was t_0=1.56 min.

Thus, the percentage of D isomer in the original Anderson peptide was determined by the percentage of L-D isomer of the tetrapeptide. The limit of detection was estimated as ca. 0.1% epimer.

b) Racemization during the Coupling by the DCC Method plus Additive: Reactions were run by dissolving Z-Gly-L-Phe-OH, H-Gly-OEt, and additive where pertinent (1 : 1 : 1 equiv.) in THF (reactant concentration, 0.018 mol dm^{-3}) and adding 1 equiv. of DCC. After the mixture had been stirred at 5 °C for 24 h, it was diluted with EtOAc and treated as usual. The crude product was hydrogenated, and then reacted with Z-L-Ala-OSu as described above. The results are summarized in Table 2.

References

1) a) D. S. Kemp, "The Peptides," ed by E. Gross and J. Meienhofer, Academic Press, New York, Vol. 1 (1979), Chap. 7, p. 366. b) N. L. Benoiton, *ibid.*, Vol. 5 (1983), Chap. 4, p. 227.

2) Abbreviations given by the IUPAC-IUB Joint Commission (*Eur. J. Biochem.*, **138**, 9 (1984)) are used throughout. Additional abbreviations: Z, benzyloxycarbonyl; DMF, *N*,*N*-dimethylformamide; TEA, triethylamine; THF, tetrahydrofuran.

3) G. W. Anderson and R. W. Young, *J. Am. Chem. Soc.*, **74**, 5307 (1952); G. W. Anderson, J. Blodinger, and A. D. Welcher, *ibid.*, **74**, 5309 (1952); G. W. Anderson and F. M. Callahan, *ibid.*, **80**, 2902 (1958).

4) For recent investigations using this test, see, a) J. Przybylski, H. Jeschkeit, and G. Kupryszewski, *Rocz. Chem.*, **51**, 939 (1977). b) J. Przybylski and H. Miecznikowska, *Pol. J. Chem.*, **52**, 1179 (1978). c) H.-D. Jakubke, Ch. Klessen, E. Berger, and K. Neubert, *Tetrahedron Lett.*, **1978**, 1497. d) J. Przybylski, *Pol. J. Chem.*, **53**, 2627 (1979). e) J. Przybylski, H. Miecznikowska, G. Kupryszewski, and H. Jeschkeit, "Peptides, Structure and Biological Function," ed by E. Gross and J. Meienhofer, Pierce Chem. Co., Rockford (1979), p. 393; H. Jeschkeit, M. Strube, J. Przybylski, H. Miecznikowska, and G. Kupryszewski, *J. Prakt. Chem.*, **326**, 638 (1984). f) C. Birr, I. Krück, R. Pipkorn, and C. Voss, "Peptides 1982," ed by K. Bláha and P. Maloň, Walter de Gruyter, Berlin (1983), p. 145. g) J. Przybylski, H. Miecznikowska, G. Kupryszewski, H. Jeschkeit, and M. Strube, *ibid.*, p. 149. h) S. Minchev and H. Nedev, "Peptides 1984," ed by U. Ragnarsson, Almqvist & Wiksell International, Stockholm (1984), p. 109. i) J. Przybylski, H. Miecznikowska, and G. Kupryszewski, *ibid.*, p. 117.

5) D. S. Kemp, S. W. Wang, G. Busby, III, and G. Hugel, *J. Am. Chem. Soc.*, **92**, 1043 (1970).

6) T. Yamada, M. Shimamura, T. Miyazawa, and S. Kuwata, "Peptide Chemistry 1983," ed by E. Munekata, Protein Research Foundation, Osaka (1984), p. 31.

7) This was used in the form of hydrochloride in the presence of an equimolar amount of TEA.

8) The diastereomer ratios (L-L% vs. L-D%) were as follows: AA=Ala, 49.9: 50.1; Val, 50.3: 49.7; Leu, 49.7: 50.3; Pro, 48.7: 51.3.

9) a) T. Miyazawa, T. Otomatsu, T. Yamada, and S. Kuwata, *Tetrahedron Lett.*, **25**, 771 (1984). b) T. Miyazawa, T. Otomatsu, Y. Fukui, T. Yamada, and S. Kuwata, "Peptide Chemistry 1984," ed by N. Izumiya, Protein Research Foundation, Osaka (1985), p. 265.

10) M. Fujino, S. Kobayashi, M. Obayashi, T. Fukuda, S. Shinagawa, and O. Nishimura, *Chem. Pharm. Bull.*, **22**, 1857 (1974).

11) Used in the presence of an equimolar amount of TEA.

12) R. B. Woodward, R. A. Olofson, and H. Mayer, *Tetrahedron*, Suppl. 8, Part I, 321 (1966).

13) R. Matsueda, H. Maruyama, M. Ueki, and T. Mukaiyama, *Bull. Chem. Soc. Jpn.*, **44**, 1373 (1971).

14) G. W. Anderson and F. M. Callahan, *J. Am. Chem. Soc.*, **82**, 3359 (1960).

Formation of *N,N'*-Disubstituted Methanediamine Derivatives from Hexamethyldisilazane and Aldehydes via Stepwise Reactions

Kozaburo NISHIYAMA,* Masaki SAITO, and Makoto OBA
Department of Chemistry, Tokyo Metropolitan University, 2-1-1, Fukasawa, Setagaya, Tokyo 158
(Received July 31, 1987)

Synopsis. The $ZnCl_2$-catalyzed reaction of aldehydes with hexamethyldisilazane (HMDS) resulted in the formation of *N,N'*-disubstituted methanediamines, which were found to be formed stepwisely via 1:1- and 1:2-adducts of HMDS and aldehydes.

Although alkali metal salts of hexamethyldisilazane (HMDS) are well-known to be hindered bases for organic synthesis, only a few reports concerning the synthetic utility of disilazane itself can be found in the literature. Recently, two groups[1] reported the introduction of an amino moiety into organic molecules by using HMDS; the conversion of acyl halides into amides. On the other hand, we have been interested in the reactivity of a variety of Si-N bond of organosilicon compounds, e.g. silyl azide,[2] silyl isocyanate,[3] and silyl isothiocyanate.[4] As a continuation of our work in this area, the $ZnCl_2$-catalyzed reaction of aldehydes (**1**) with hexamethyldisilazane (HMDS), having two reactive Si-N bonds in a molecule, was investigated and we now report our results in this paper.

Results and Discussion

Treatment of benzaldehyde (**1a**) with 2 equiv of HMDS and a catalytic amount of $ZnCl_2$ in dichloromethane at room temperature for 24 h resulted in the formation of colorless needles (hexane), mp 100—101 °C, which were identified as *N,N'*-dibenzylidenephenylmethanediamine (**4a**). Without zinc chloride or in hexane, the reaction between benzaldehyde and HMDS did not proceed at all and starting materials were quantitatively recovered. When the reaction was interrupted in 1 h, the sole product was **4a** in a low yield (16%). Analogously, four *N,N'*-bis(arylmethylene)arylmethanediamines (**4b—e**) were obtained from the corresponding aromatic aldehydes (Eq. 1 and Table 1). On the other hand, Duffaut and

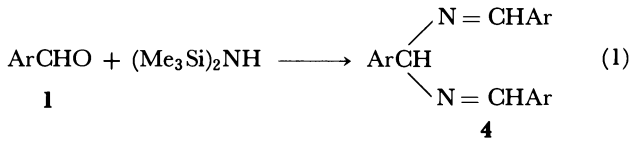

(1)

a, Ar=Ph, **b**, Ar=*p*-$MeOC_6H_4$, **c**, Ar=*p*-MeC_6H_4, **d**, Ar=*p*-CNC_6H_5, **e**, Ar=*p*-$NO_2C_6H_4$

Dupin reported that the treatment of ketones and benzaldehyde with silazanes [$(Me_3Si)_2NR$; R=H and Me] and silyl amines ($Me_3SiNHPh$ and Ph_3SiNH_2) in the presence of Zn/Cd at 165 °C for 40 h gave the corresponding imines (>C=NR; R=H, Me, and Ph) in yields of 30—95%.[5]

With *p*-cyanobenzaldehyde (**1d**), a trace amount of *N*-(*p*-cyanobenzylidene)-1-(*p*-cyanophenyl)-1-(trimethylsiloxy)methanamine (**3d**) with **4d** (46%) was isolated by fractional recrystallization from benzene and hexane. Since compound **3d** could be a precursor of **4d**, the reaction of **1d** with HMDS was again carried out for 10 h at room temperature. Consequently, compounds **3d** and **4d** were obtained in 23 and 32% yields, respectively. Similarly, the treatment of **1e** with HMDS for 24 h afforded a mixture of **3e**, which was too unstable to be fully characterized, and **4e** (30%). An attempt to separate the mixture by column chromatography on alumina (eluent; $CHCl_3$) gave *p*-nitrobenzylideneamino-*p*-nitrophenylmethanol (**3e'**).

Table 1. $ZnCl_2$-Induced Reaction of Carbonyl Compound with HMDS

Carbonyl compd	Product	(Yield/%)	Mp θ_m (bp θ_b)/°C
1a		(0)[a]	
1a	**4a**	(16)[b]	100—101
1a	**4a**	(79)	
1b	**4b**	(66)	128—129
1c	**4c**	(73)	93—94
1d[c]	**3d**	(23)	117
	4d	(32)	122—124
1d	**4d**	(46)	
1e	**4e**	(30)	140 (decomp)
t-BuCHO (**1f**)	**4f**	(42)	(173/2 mmHg)
cyclo-$C_6H_{10}O$ (**1g**)	**4g**	(53)	(163/2 mmHg)
Cl_3CCHO (**1h**)	**2h**	(70)	(80—82/4 mmHg)

a) Without $ZnCl_2$. b) Stirred for 1 h. c) Stirred for 10 h.

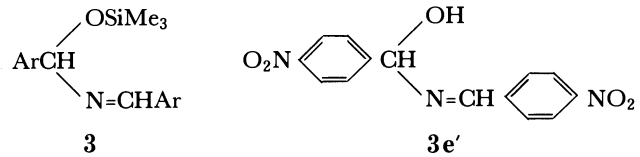

From these findings, it is clear that the formation of **4** involves stepwise reactions which must proceed via **3** and that an electron-withdrawing group of the aldehyde would retard either step(s) of the successive reactions. More remarkably, in cases of aliphatic aldehydes, the product was dependent upon an electronic rather than a steric effect of the alkyl group. With 2,2-dimethylpropanal (**1f**) and cyclohexanone (**1g**), *N,N'*-bis(2,2-dimethylpropylidene)-2,2-dimethyl-1,1-propanediamine (**4f**) and *N,N'*-dicyclohexylidene-1,1-cyclohexanediamine (**4g**) were produced in 42% and 53% yields,[6] respectively, as a sole product, whereas only a 1:1-adduct of trichloroethanal (**1h**) and HMDS, *N*-trimethylsilyl-1-trimethylsiloxy-2,2,2-trichloroethanamine (**2h**), was obtained in a 70% yield. The treatment of **2h** with benzaldehyde under similar conditions gave *N*-benzylidene-1-trimethylsiloxy-2,2,2-trichloroethanamine (**3h'**) in a 53% yield. As to this

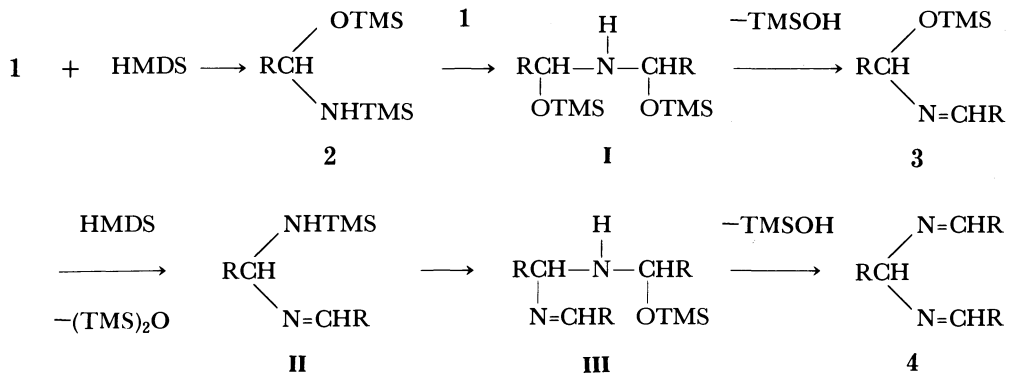

Scheme

reaction course, it was postulated that the addition of the remaining Si-N bond in **2h** to benzaldehyde followed by the elimination of trimethylsilanol occurred to give **3h'** (Eq. 2).

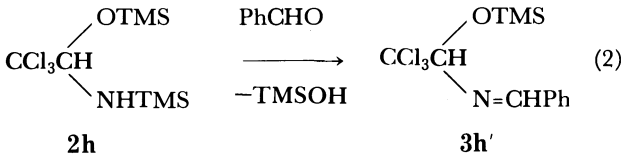

(2)

On the basis of the above results, we suggest the reaction pathway shown in the Scheme to account for the formation of the *N,N'*-bis(arylmethylene)arylmethanediamines **4** from aldehyde with HMDS. The first and second steps are $ZnCl_2$-induced addition reactions of Si-N bonds to the carbonyl group of the aldehyde, giving the 1:1-adduct **2** and 1:2-adduct **I**, respectively. Furthermore, the latter undergoes the elimination of trimethylsilanol to produce *N*-benzylidenephenylmethane derivative **3**. Condensation of **3** with HMDS gives hexamethyldisiloxane and the diamino intermediate **II**; **II** adds to another aldehyde to give the adduct **III**, which would be subjected to the further elimination of trimethylsilanol, giving the final product **4**. The conversion step of **3** into **II** finds analogy in another study of ours; in which *gem*-diazides were found to be isolated via α-siloxy azides from the similar reaction of aldehydes[2] and ketones[7] with silyl azide. For these reactions, an electron-withdrawing group of aldehydes retards the addition process and compounds **4** having an electron-donationg group were obtained in higher yields under the conditions employed.

Compound **4** is important as an intermediate for trisubstituted imidazole derivatives; the dehydrogenation of *N,N'*-dibenzylidenephenylmethanediamine gives 2,4,5-triphenyl-1*H*-imidazole.[8]

Experimental

Melting points are uncorrected. Infrared spectra were measured on a Hitachi 260-10 infrared spectrometer. ^1H NMR spectra were determined with a Hitachi R-600 using tetramethylsilane as an internal standard. Mass spectra (MS) were obtained using a JEOL DX-300 spectrometer.

Hexamethyldisilazane (HMDS) and aldehydes were commercial products and were purified by distillation or recrystallization if necessary.

$ZnCl_2$-Induced Reaction between Aldehyde (1a—1f) and HMDS. General Procedure. A suspension of aldehyde (30 mmol), HMDS (60 mmol), and $ZnCl_2$ (6 mmol) in CH_2Cl_2 (30 cm^3) was stirred for 24 h at room temperature. The reaction mixture was poured into water (30 cm^3) and dichloromethane (30 cm^3). Extraction with three 30 cm^3 portions of dichloromethane followed by washing with water completed the work-up. The extract was dried over anhydrous $MgSO_4$ and concentrated in vacuo. The resulting mixture was triturated with hexane (for **4a—4d**) or benzene (for **4e**) and the precipitated solid was collected by filtration. The solid was recrystallized from an appropriate solvent (hexane, a mixture of hexane and benzene, or acetonitrile). When the product was liquid (**4f** and **4g**), it was directly distilled under reduced pressure. The yields of products are listed in Table 1. Spectral and physical data are as follows.

4a: colorless needles (hexane); mp 100—101 °C (lit,[9] 100 °C). IR (KBr) ν 1625 (C=N) cm^{-1}. MS *m/z* 194 (M^+ −N=CHPh). ^1H NMR ($CDCl_3$) δ=5.93 (s, 1H), 7.20—7.89 (m, 15H), and 8.51 (s, 2H). **4b:** colorless needles (hexane); mp 128—129 °C IR (KBr) ν 1620 (C=N) cm^{-1}. MS *m/z* 254 (M^+−N=$CHC_6H_4OCH_3$-*p*). ^1H NMR ($CDCl_3$) δ=3.75 (s, 3H), 3.81 (s, 6H), 5.80 (s, 1H), 6.84, 7.38 (ABq, 4H), 6.86, 7.74 (ABq, 8H), and 8.40 (s, 2H). Found: C, 74.15; H, 6.30; N, 7.20%. Calcd for $C_{24}H_{24}N_2O_3$: C, 74.21; H, 6.23; N, 7.21%. **4c:** colorless powder (hexane); mp 93—94 °C. IR (KBr) ν 1620 (C=N) cm^{-1}. MS *m/z* 222 (M^+−N=$CHC_6H_4CH_3$-*p*). ^1H NMR ($CDCl_3$) δ=2.32 (s, 3H), 2.40 (s, 6H), 5.87 (s, 1H), 7.13, 7.35 (ABq, 4H), 7.16, 7.68 (ABq, 8H), and 8.45 (s, 2H). Found: C, 84.96; H, 7.43; N, 8.01%. Calcd for $C_{24}H_{24}N_2$: C, 84.67; H, 7.11; N, 8.23%. **4d**: pale yellow powder (1:1 mixture of benzene and hexane), mp 122—124 °C. IR (KBr) ν 2210 (C≡N) and 1625 (C=N) cm^{-1}. MS *m/z* 244 (M^+−N=CHC_6H_4CN-*p*). ^1H NMR ($CDCl_3$) δ=6.06 (s, 1H), 7.62 (s, 8H), 7.67, 7.92 (ABq, 4H), and 8.53 (s, 2H). Found: C, 77.43; H, 4.24: N, 18.96%. Calcd for $C_{24}H_{15}N_5$: C, 77.20; H, 4.05; N, 18.75%. The mother liquor of **4d** was concentrated in vacuo and the residual solid was recrystallized from hexane, giving colorless needles, **3d**, mp 116—117 °C. IR (KBr) ν 2200 (C≡N), 1630 (C=N), and 1060 (Si-O-C) cm^{-1}. MS *m/z* 204 (M^+ −N=CHC_6H_4CN-*p*). ^1H NMR ($CDCl_3$) δ=0.20 (s, 9H), 6.30 (s, 1H), 7.57 (s, 4H), 7.66, 7.83 (ABq, 4H), and 8.50 (s, 1H). Found: C, 68.50; H, 5.85; N, 12.53%. Calcd for $C_{19}H_{19}N_3OSi$: C, 68.44; H, 5.74; N, 12.60%. **4e**: pale yellow plates (acetonitrile), mp 140 °C (decomp). IR (KBr) ν 1625 (C=N) and 1505, 1340 (NO_2) cm^{-1}. MS *m/z* 283 (M^+ −N=$CHC_6H_4NO_2$-*p*). Found: C, 58.23; H, 3.44; N, 15.98%. Calcd for $C_{21}H_{15}N_5O_6$: C, 58.20; H, 3.49; N, 16.16%. The ^1H NMR spectrum of **4e** could not be determined because the isolated **4e** did not disolve in $CDCl_3$ and CD_3CN and decomposed in DMSO-d_6. **3e'**: pale yellow powder ($CHCl_3$), mp 203—204 °C. IR (KBr) ν 3275 (OH), 1635 (C=N), and 1500,

1340 (NO_2) cm^{-1}. MS m/z 301 (M^+). Found: C, 55.40; H, 3.62; N, 14.00%. Calcd for $C_{14}H_{11}N_3O_5$: C, 55.82%; H, 3.68; N, 13.95%. **4f**: colorless liquid, bp 173 °C/2 mmHg (1 mmHg=133.322 Pa.). IR (neat) ν 1660 (C=N) cm^{-1}. MS m/z 154 (M^+ −N=CHBu-*t*). ^1H NMR ($CDCl_3$) δ=0.89 (s, 9H), 1.09 (s, 18H), 3.83 (s, 1H), and 7.49 (s, 2H). **4g**: colorless liquid, bp 155—163 °C/2 mmHg. IR (neat) ν 1660 (C=N) cm^{-1}. MS m/z 274 (M^+). ^1H NMR ($CDCl_3$) δ=1.00—2.40 (m).

Reaction of Trichloroethanal (1h) with HMDS. A mixture of **1h** (4.42 g, 30 mmol), HMDS (9.69 g, 60 mmol), and $ZnCl_2$ (0.82 g, 6 mmol) in CH_2Cl_2 (30 cm^3) was stirred for 75 h at room temperature. Direct distillation of the reaction mixture gave a colorless oil, which boiled at 80—82 °C/4 mmHg and was assigned to **2h**, yield, 6.48 g (70%). IR (neat) ν 3380 (NH) and 1250 (C-$SiMe_3$) cm^{-1}. MS m/z 190 (M^+ −CCl_3). ^1H NMR ($CDCl_3$) δ=0.20 (s, 9H), 0.25 (s, 9H), 4.63 (s, 1H), and 4.85 (s, 1H). Found: C, 30.81; H, 6.59; N, 4.55%. Calcd for $C_8H_{20}Cl_3OSi_2$: C, 31.12; H, 6.53; N, 4.54%.

When the reaction between **1h** (11.08 g, 75 mmol) and HMDS (12.13 g, 75 mmol) in the presence of $ZnCl_2$ (2.05 g, 15 mmol) in CH_2Cl_2 (75 cm^3) was carried out for 24 h at room temperature, repeated distillation afforded a detrimethylsilylated compound **2h'** (1-trimethylsiloxy-2,2,2-trichloroethanamine) instead of **2h**, yield 6.12 g (35%). Bp 49—50 °C/4 mmHg. IR (neat) ν 3400 and 3300 (NH_2) and 1250 (C-$SiMe_3$) cm^{-1}. MS m/z 118 (M^+ −CCl_3). ^1H NMR ($CDCl_3$) δ=0.18 (s, 9H), 2.00 (s, 2H), and 4.60 (s, 1H). Found: C, 25.55; H, 5.15; N, 6.08%. Calcd for $C_5H_{12}Cl_3NOSi$: C, 25.38; H, 5.11; N, 5.92%.

Reaction of 2h with Benzaldehyde. A mixture of **2h** (5.26 g, 17 mmol), benzaldehyde (**1a**, 1.81 g, 17 mmol), and $ZnCl_2$ (0.46 g, 3.4 mmol) in CH_2Cl_2 (17 cm^3) was stirred for 24 h at room temperature. After usual work-up, direct distillation (bp 108 °C/2 mmHg) of the dried mixture gave a pale yellow liquid which was characterized to *N*-benzylidene-1-trimethylsiloxy-2,2,2-trichloroethanamine (**3h'**), yield 2.1 g (38%). IR (neat) ν 1635 (C=N) and 1250 (C-$SiMe_3$) cm^{-1}. MS m/z 206 (M^+ −CCl_3). ^1H NMR ($CDCl_3$) δ=0.35 (s, 9H), 5.61 (s, 1H), 7.40—7.96 (m, 5H), and 8.53 (s, 1H). Found: C, 44.49; H, 5.26; N, 4.35%. Calcd for $C_{12}H_{16}Cl_3NOSi$: C, 44.39; H, 4.97; N, 4.31%.

References

1) J. R. Bowser, P. J. Williams, and K. Kurz, *J. Org. Chem.*, **48**, 4111 (1983); R. Pellegata, A. Italia, and M. Villa, *Synthesis*, **1985**, 517.

2) K. Nishiyama, M. Oba, and A. Watanabe, *Tetrahedron*, **43**, 693 (1987).

3) K. Nishiyama and M. Sai, unpublished results.

4) K. Nishiyama and M. Oba, *Bull. Chem. Soc. Jpn.*, **60**, 2289 (1987); **60**, 2692 (1987).

5) N. Duffaut and J. P. Dupin, *Bull. Soc. Chim. Fr.*, **1966**, 3205.

6) These compounds were only spectroscopically confirmed as they were too unstable to be satisfied by microanalysis.

7) K. Nishiyama and A. Watanabe, *Chem. Lett.*, **1984**, 455; K. Nishiyama and T. Yamaguchi, *Synthesis*, in press.

8) E. S. Schipper and A. R. Day, "Heterocyclic Compounds," ed by R. C. Elderfield, John Wiley & Sons, New York (1957), Vol. 5, Chap. 4, pp. 194—297 and references cited therein.

9) S. Capuano and L. Giammanco, *Gazz. Chim. Ital.*, **86**, 109 (1956); *Chem. Abstr.*, **51**, 1206e (1957).

Electroreduction of Phenylhydrazones in Methanol-Water Mixtures

Vepa KAMESWARA RAO, Chitoor Sivaramakrishnan VENKATACHALAM, and Chatty KALIDAS*
Department of Chemistry, Indian Institute of Technology, Madras 600036, India
(Received December 22, 1986)

Synopsis. The electroreduction of a few substituted phenylhydrazones on mercury cathode has been studied in methanol-water mixtures using polarography, cyclic voltammetry, micro- and macrocontrolled-potential electrolysis. These compounds are reduced in a single four-electron step to yield the corresponding amino products. A linear relationship between the half-wave potentials ($E_{1/2}$) and Hammett substituent constants (σ) has been observed.

The electrochemical reduction of various phenylhydrazones received the attention of several authors in recent years[1-5] in view of thier biological activity. In our earlier communications,[6,7] the electroreduction of some substituted phenylhydrazones in amphiprotic media has been reported. In continuation of this work, we present here the results of the electrochemical behavior of 2,2-dimethyl-1,3-dioxane-4,5,6-trione 5-(phenylhydrazone) (**1**) and 2,2-dimethyl-1,3-dioxane-4,5,6-trione 5-(4-acetylphenylhydrazone) (**2**) in methanol-water mixtures of varying composition and pH. The effect of substituents on the mechanism of the electrode reaction (Hammett correlation) is also discussed.

Experimental

The phenylhydrazones used in the present work, (**1** and **2**) were prepared by coupling the appropriate diazotized aromatic amine with Meldrum's acid (cyclic isopropylidene malonate). The yellow amber colored compounds were recrystallized from aqueous methanol or benzene-hexane mixture and their purity checked by TLC. The mp of **1** is 171—172 °C (reported[8] value 171—172 °C) and that of **2** is 182 °C. Analysis for compound **2**. Found: C, 57.59; H, 4.87; N, 9.61%. Calcd for $C_{14}H_{14}N_2O_5$: C, 57.69; H, 4.83; N, 9.61%.

Methanol (Reechem) was purified by standard procedure. Potassium chloride (AR) was used as the supporting electrolyte without further purification. Britton-Robinson[9] (BR) and Clark-Cubs (CL) buffers were used to control the pH of the experimental solutions. The dme had the following capillary characteristics: m=0.7933 mg s^{-1} and t=6 s at 53 cm height (uncorrected for back pressure) of the mercury column under open-circuit conditions. A Metrohm EA 290 hanging mercury drop electrode (hmde) having an area of 0.01296±0.006 cm^2 was used for cyclic voltammetric experiments. The polarographic measurements were carried out with a Metrohm E 506 polarecord, saturated calomel as the reference electrode and a platinum foil as the counter electrode. Cyclic voltammograms were recorded employing PAR 175 Universal programmer and PAR 173 potentiostat in conjunction with an x-y recorder (Digital Electronics, Bombay). Electrolysis products were analyzed by HPLC. The details of microcoulometric measurements for determining the number of electrons (n_{app}) transferred in the electrode process have been described previously.[10] Polarograms and cyclic voltammograms were recorded for solutions containing the depolarizer (1.0×10^{-3} M, (1M=1 mol dm^{-3})), the maximum suppressor (0.002% Triton-X-100), supporting electrolyte (KCl) and required amount of buffers (BR and CL) in methanol-water mixtures of various compositions.

All measurements were caried out at 30 °C.

Results and Discussion

The electrochemical reduction of **1** and **2** was carried out in 60—80% (v/v) methanol-water mixtures in the pH range 1.00—7.00. These compounds are found to be unstable in alkaline solutions as indicated by the decrease in polarographic currents with time. This might probably due to the hydrolysis of Meldrum's acid moiety in buffered alkaline media.[11] Both the compounds give a single well-defined dc polarogram and a single ac peak corresponding to the dc step at all pH values in different compositions of methanol-water mixtures. The polarographic data are presented in Tables 1 and 2. Analysis of the polarographic data revealed the diffusion-controlled nature of the electrode process. The half-wave potentials of the depolarizers are shifted cathodically with increase in pH values and with increase in composition of methanol. At a given pH and composition, the summit potentials (E_s) are more negative than the corresponding dc $E_{1/2}$ values thereby indicating the irreversible nature of the

Table 1. Polarographic Data of Compound (**1**) (1.0×10^{-3} M) in 60% (v/v) Methanol-Water Mixture at Various pH Values Containing 0.002% Triton-X-100 as Maximum Suppressor and 0.2 M KCl as Supporting Electrolyte

No.	pH	Wave height / μA	Half-wave potential, $-E_{1/2}$/V vs. SCE	$-(E_{3/4}-E_{1/4})$ / V	$-dE/d\log(\frac{i_d-i}{i})$	Summit potential, $-E_s$/V vs. SCE
1	1.24[a]	9.05	0.380	0.100	0.111	0.44
2	3.37	9.30	0.650	0.120	0.127	0.75
3	4.51	9.70	0.700	0.110	0.111	0.80
4	5.25	9.20	0.745	0.075	0.100	0.83
5	6.40	9.70	0.795	0.115	0.100	0.91
6	6.91	9.90	0.885	0.150	0.123	0.94

a) 0.1 M HCl (unbuffered).

Table 2. Polarographic Data of Compound **2** (1.0×10^{-3} M) in 60% (v/v) Methanol-Water Mixture at Various pH Values Containing 0.002% Triton-X-100 as Maximum Suppressor and 0.2 M KCl as Supporting Electrolyte

No.	pH	Wave height / μA	Half-wave potential, $-E_{1/2}$/V vs. SCE	$-(E_{3/4}-E_{1/4})$ / V	$-dE/d\log(\frac{i_d-i}{i})$	Summit potential, $-E_s$/V vs. SCE
1	1.31[a)]	8.5	0.255	0.060	0.063	0.35
2	3.54	8.4	0.465	0.120	0.115	0.58
3	4.25	8.4	0.540	0.110	0.119	0.62
4	5.35	8.7	0.595	0.070	0.098	0.66
5	6.79	8.3	0.710	0.115	0.106	0.80

a) 0.1 M HCl (unbuffered).

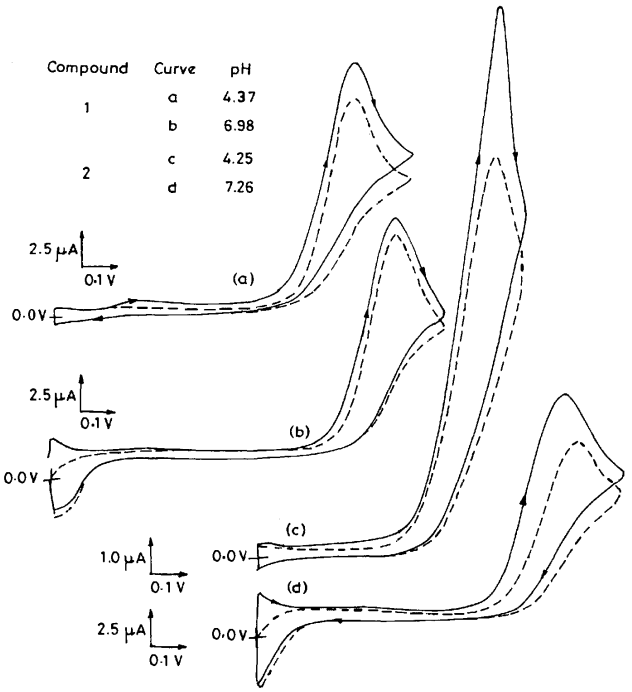

Fig. 1. Cyclic voltammograms of **1** and **2** in buffered 60% (v/v) methanol-water mixture containing 0.002/Triton-X-100 as maximum suppressor and 0.2 M KCl as supporting electrolyte; sweep rate, 0.100 V s^{-1}. Solid lines represent firstsweep and broken lines represent repeated cycle.

electrode process. The $(E_{3/4}-E_{1/4})$ and the slope values of $-E$ vs. $\log(i_d-i)/i$ plots also confirm the irreversible behavior.

The cyclic voltammetric data of phenylhydrazones indicate the diffusion-controlled and irreversible nature of the electrode processes. Figure 1 shows typical cyclic voltammograms of the compounds **1** and **2** obtained in 60% (v/v) methanol in acidic and neutral media. Both the compounds give a single cathodic peak in the forward scan and no anodic peak in the reverse direction indicating the irreversible behavior of the electrode process. The diffusion-controlled nature of the electrode process was indicated by the linear relationship between the cathodic peak current values ($i_{p,c}$) and the square root of the scan rate ($v^{1/2}$). In all the cases, however, an anodic peak (close to 0.0 V) is observed in the reverse scan in neutral buffered methanol-water mixtures. The peak separation of the redox couple (ΔE_p) around 0.070 V suggests a quasi-reversible single electron-transfer step in the oxidation of the product formed at the electrode surface in neutral media.

The microcoulometric experiments carried out at the limiting region of the polarographic waves of **1** and **2** showed a transfer of four electrons ($n_{app}=4$) in the reduction step. The controlled-potential electrolysis of **1** and **2** yielded aniline (retention time 3.3 min) and *p*-aminoacetophenone (retention time 3.14 min), respectively, as the final products. The retention times of the electrolysis products were found to be in good agreement with those of the authentic samples. The other expected product, namely, amino-substituted Meldrum's acid could not be identified possibly due to its hydrolysis during working up procedure in basic medium.

Based on the results obtained, the following stoichiometry is suggested for the reduction of the phenylhydrazones in buffered methanolic solutions under acidic and neutral conditions:

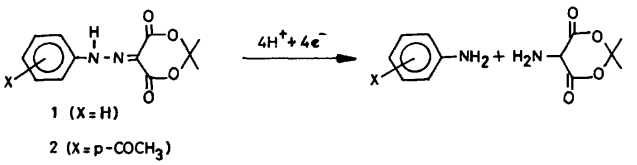

It may be pointed out that the deliberate addition of pure aniline or *p*-aminoacetophenone in the reduction of **1** and **2** did not increase the peak height of the anodic wave observed very close to 0.0 V in the reverse scan in cyclic voltammetric experiments. This positively suggests that the observation of the anodic peak during the reverse scan may be due to the oxidation of amino-substituted Meldrum's acid formed at the electrode surface during the cathodic reduction of phenylhydrazones.

An attempt has been made in the present investigation to correlate the half-wave potentials of phenylhydrazones with Hammett substituent constants (σ). Such a correlation was possible due to a similar behavior of these compounds at the electrode-electrolyte interface. The Hammett equation when applied to reversible as well as irreversible electrode processes, $dE_{1/2}=\rho\sigma$ belongs to the family of linear free energy relationships (LFER)-equations.[12] Figure 2 shows

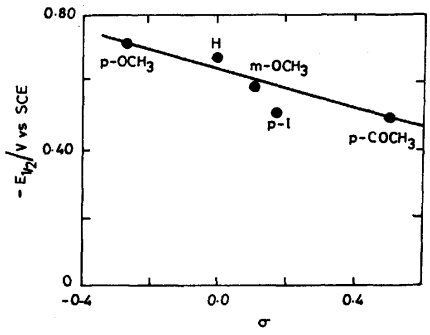

Fig. 2. Hammett correlation for various substituted phenylhydrazones in 60% (v/v) methanol-water mixtures at pH=4.00.

such a Hammett correlation for various substituted phenylhydrazones in 60% (v/v) methanol-water mixture at a constant pH. The linear plot has a ρ-value of 0.308 with a correlation coefficient 0.895. It may be noted from the correlation that the ease of reduction of these phenylhydrazones decreases in the order p-$COCH_3$<p-I<m-OCH_3<p-OCH_3 with decreasing order of the electron withdrawing nature of the substituents studied.

References

1) W. U. Malik, R. N. Goyal, and P. N. Dua, *Indian J. Chem.*, **21A**, 114 (1982).
2) R. N. Goyal, R. Bhusan, and A. Agarwal, *J. Electroanal. Chem.*, **171**, 281 (1984).
3) H. Lund, "Electrochemistry of the Carbon-Nitrogen Double Bond," in "Chemistry of Carbon-Nitrogen Double Bond," ed by S. Patai, Interscience Publishers, London (1970), Chap. 11, pp. 505—564.
4) W. U. Malik, V. K. Mahesh, and M. Gupta, *Electrochim. Acta*, **26**, 1857 (1981).
5) H. M. Fahmy and M. H. Elnagidi, *Electrochim. Acta*, **23**, 255 (1978).
6) V. Kameswara Rao, S. R. Ramadas, C. S. Venkatachalam, and C. Kalidas, *Trans. SAEST*, **19**, 287 (1984).
7) V. Kameswara Rao, C. S. Venkatachalam, and C. Kalidas, *Indian J. Chem.*, under publication.
8) B. Vickery, and G. R. Willey, *J. Chem. Soc., Perkin Trans. 2*, **1981**, 1454.
9) H. T. S. Britton, "Hydrogen Ions," Van Nostrand, New York (1956), Vol. 1, Chap. 17, pp. 352—376.
10) V. Varkey, C. S. Venkatachalam, and C. Kalidas, *Trans. SAEST*, **9**, 162 (1974).
11) Kaleviphlaya and Mattiseilo, *Acta. Chem. Scand.*, **23**, 3003 (1969).
12) P. Zuman, "The Elucidation of Organic Electrode Process," Academic Press, New York and London (1969), Chap. 4, pp. 112—152.

 © 1988 The Chemical Society of Japan Bull. Chem. Soc. Jpn., 61, 615—620 (1988)

Atomization Enthalpies of Aliphatic Compounds with Alternately Adjacent Carbonyl Groups and Nitrogen Atoms†

Minoru SAKIYAMA,* Nobuhiro KURIYAMA, Akira IMAMURA, and Shigeo MURATA
Chemical Thermodynamics Laboratory, Faculty of Science, Osaka University, Toyonaka 560
(Received February 23, 1987)

Hückel MO calculations were made for the title compounds using Hess-Schaad heteroatom parameters. The bond-contribution values were determined for the total π-bonding energies of the acyclic compounds. No resonance stabilization is present for molecules with six-, eight-, and ten-membered rings composed of CO-N linkages. Graph-theoretical calculations gave a similar result. Atomization enthalpies were calculated from the available thermochemical data and analyzed within the framework of the Hess-Schaad theory. The destabilization energies of normal alkanamides and *N*,*N*-dimethylformamide are close to zero. Diacetamide is not destabilized, while *N*-butyldiacetamide and triacetamide showed small destabilization energies. Trimethyl isocyanurate is not significantly strained. The total strengths of the CO-N bonds are in this order: amide>(urea and diacetamide)>internal bond of acetylurea.

It is well-known that the π-electrons of a carbonyl group in an amide molecule interact with the conjugated lone-pair electrons on the adjacent nitrogen atom to provide the interconnecting C-N bond, which has a significant double bond character. This bond is an important one, since it occurs not only in amides and ureas, but also in proteins, DNA bases, and synthetic polyamides. In another paper,[1] the standard enthalpies of formation, in the gaseous state, of acetylurea and trimethyl isocyanurate [1,3,5-trimethyl-1,3,5-triazine-2,4,6(2*H*,4*H*,6*H*)-trione] were reported, and the estimated stabilization energies of acetamide and urea as well as of these compounds were empirically analyzed in order to study the effect of the elongation and cyclization of an alternating CO-N chain on the stabilization energy. The present study aims at the theoretical interpretation of the extensive thermochemical data for aliphatic compounds containing CO-N linkages, within the framework of the Hess-Schaad theory based on the Hückel MO method.

According to Hess and Schaad,[2,3] the atomization enthalpy of a conjugated alkene is expressed as a sum of the σ-bond contribution terms minus the π-bonding energy, B_π:

$$\Delta_a H = \sum E'(\dot{C}\text{-H}) + \sum E'(\dot{C}\text{-}\dot{C}) - B_\pi, \qquad (1)$$

where $E'(\dot{C}\text{-H})$ and $E'(\dot{C}\text{-}\dot{C})$ are the C-H and C-C σ-bond-contribution terms respectively. In this paper, a 2p electron that takes part in the formation of a π-bond or a lone-pair orbital of a nitrogen atom is denoted by a dot above the atomic symbol. In Method A of Ref. 3, the bond-compression terms were explicitly given, but in Method B they were included in B_π, as is shown in Eq. 1, by treating the resonance integral, β, as a parameter. This treatment was subsequently extended to conjugated amines,[4] ethers,[4] ketones,[5] thiols,[6] thioethers,[6] imines,[7] and fluorides.[8] In addition, Hess and Schaad showed that the difference between a properly calculated π-bonding energy and the corresponding estimated value based on the bond additivity of a cyclic compound is a reasonable measure for the Dewar resonance energy.[2-8]

† Contribution No. 117 from Chemical Thermodynamics Laboratory, Faculty of Science, Osaka University.

Calculation

Hückel molecular orbital calculations were carried out for forty cyclic and acyclic molecules with alternating CO-N skeleton, and with or without branching, using the Hess-Schaad heteroatom parameter set.[4,5] The π-electron energy of a single localized carbonyl group was $(2\alpha+2.212\beta)$, while that of a nitrogen atom was $(2\alpha+3\beta)$, where α and β are the Coulomb and resonance integrals of carbon atoms respectively. Dewar-type resonance energies were calculated also by means of Aihara's graph-theoretical method.[9]

Results and Discussion

π-Bond Order and π-Bonding Energy. The calculated π-bond orders are summarized in Table 1, while the classification of bonds is illustrated in Fig. 1. The bond order of a C-N bond that involves a branching nitrogen atom is systematically lower than the value for a C-N bond that does not involve a branching nitrogen atom.

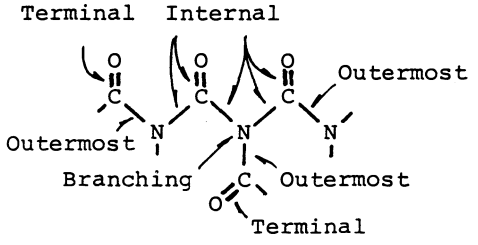

Fig. 1. Classification of bonds and atoms. Hydrogen atoms or alkyl groups bonded to terminal carbon or nitrogen atoms are not shown.

Table 1. C-N and C=O π-Bond Orders. Upper and Lower Bounds Are Shown. Parenthesized Values Are Those for C-N Bonds That Involve a Branching Nitrogen Atom. For Classification of Bonds, See Fig. 1

Bond	Position		π-Bond order
C-N	Open chain	amide	0.400
		outermost	0.392±0.003(0.374±0.001)
		internal	0.372±0.003(0.356±0.001)
	Ring	m=2	0.356(0.338)
	$+CO-N+_m$	m=3, 4, or 5	0.374(0.356)
C=O	Open chain	amide	0.899
		terminal	0.900±0.010
		internal	0.820±0.015
	Ring	m=2	0.837±0.006
	$+CO-N+_m$	m=3, 4, or 5	0.825±0.006

Table 2. Bond-Contribution Values B_π(C-N) and B_π(C=O) to Total π-Bonding Energy B_π of Acyclic Molecules. Parenthesized Values Are Those for C-N Bonds Involving a Branching Nitrogen Atom. For Classification of Bonds, See Fig. 1

Bond	B_π(bond)/β	Position	B_π(C=O)/β
C-N, amide	0.374	Amide	1.992
C-N, out[a]	0.367(0.360)	Terminal	1.992
C-N, int[b]	0.360(0.352)	Internal	1.992

a) Outermost C-N bond. b) Internal C-N bond.

The calculated π-bonding energies of acyclic molecules were empirically analyzed; the bond-contribution values thus derived are shown in Table 2. The bond contribution values were uniquely determined except for amide. It is notable that the value of B_π(C=O), which is the bond-contribution term from a carbonyl group to the π-bonding energy, of acyclic molecules other than amide is constant and equal to the π-bonding energy of a ketone or aldehyde molecule with an isolated carbonyl group. This implies that the delocalization energy of one of the molecules under study is given by the sum of the bond contribution terms of C-N bonds to the π-bonding energy. It was found that the delocalization energy, E_d, of a linear molecule is expressed by this equation:

$$E_d/\beta = 0.360(n_b - 1) + 0.374, \quad (2)$$

where n_b is the number of C-N bonds in the molecule. It follows that the bond-contribution term from the C-N bond of an amide molecule B_π(C-N,amide) is related to those of the outermost and internal C-N bonds, B_π(C-N,out) and B_π(C-N,int) respectively of other linear molecules by the equation:

$$B_\pi(\text{C-N,amide}) = 2B_\pi(\text{C-N,out}) - B_\pi(\text{C-N,int}). \quad (3)$$

Thus, the values of B_π(C-N,amide) and B_π(C=O) for amide were determined to be as is shown in Table 2. The latter value is equal to the value of B_π(C=O), which is common to the other acyclic molecules. By using the bond-contribution values given in Table 2, the π-bonding energy of acyclic molecules may be reproduced with deviations less than 0.004β.

Hess-Schaad Resonance Energies. π-bonding energies based on the additivity were calculated for the cyclic molecules without branching by using the bond-contribution values of the internal C-N bonds and that of a C=O bond of acyclic molecules; they were then compared with properly calculated values. As is shown in Table 3, no resonance stabilization was found for six-, eight-, and ten-membered ring molecules, while the four-membered ring molecule is, though quite slightly, destabilized.

Graph-Theoretical Resonance Energies. The total π-electron energies of real cyclic systems are compared with those of the corresponding hypothetical reference molecules in Table 3. The conclusion to be derived from the comparison is the same as that from the Hess-Schaad method.

σ-Bond Contribution Terms. CODATA key values for thermodynamics[10] were used to calculate the atomization enthalpies of the compounds given in Table 4 from the standard enthalpies of formation in the gaseous state.[11] The uncertainties for the atomization enthalpies were calculated by combining the related uncertainties by means of the error propagation equation.

The value of β employed in this paper is −128.0 kJ mol^{-1}, which is the mean among the values given by Hess and Schaad for conjugated alkenes (−128.4 kJ mol^{-1}),[3] imines (−127.1 kJ mol^{-1}),[4] amines (−128.1 kJ mol^{-1}),[5] ketones (−130.4 kJ mol^{-1}),[5] and ethers

Table 3. Resonace Energies E_R of Cyclic Molecules, $\left[\text{CO-N}\right]_n$. B_π Is the Calculated π-Bonding Energy, and B_π(est) Is The Estimated Value Based on the Bond Additivity. E_π and E_π(ref) Are the Toral Total π-Electron Energies of a Real Molecule and the Corresponding Hypothetical Reference Molecule Respectively

(a) Hess-Schaad method

n	2	3	4	5
B_π/β	5.392	8.132	10.846	13.552
B_π(est)/β	5.424	8.136	10.848	13.560
E_R/β	0.032	0.004	0.002	0.008

(b) Aihara's method

n	2	3	4	5
E_π	$8\alpha+11.832\beta$	$12\alpha+17.792\beta$	$16\alpha+23.726\beta$	$20\alpha+29.656\beta$
E_π(ref)	$8\alpha+11.862\beta$	$12\alpha+17.794\beta$	$16\alpha+23.725\beta$	$20\alpha+29.656\beta$
E_R/β	0.030	0.002	−0.001	0.000

Table 4. Atomization Enthalpies and Its Components According to Eq. 4. B_π: π-Bonding Energy, E(bond): σ-Bond-Contribution Term, and E_{destab}: Destabilization Energy

Compound	$\Delta_a H$(exp)	$-B_\pi$	$\sum E$(bond)	E_{destab}
	kJ mol^{-1}	kJ mol^{-1}	kJ mol^{-1}	kJ mol^{-1}
CH_3NH_2	2302.3±0.8	0	2302	0
$(CH_3)_2NH$	3450.6±1.3	0	3460	9
$(CH_3)_3N$	4608.4±1.6	0	4619	11
$(CH_3)_2CO$	3924.5±1.5	254.9	3671	1
CH_3CHO	2720.6±1.0	254.9	2465	−1
H_2CO	1510.4±0.7	254.9	1258	3
CH_3CONH_2	3483.5±1.3	302.8	3181	0
NH_2CONH_2	3029.0±2.3	349.1	2679	−1
$CH_3CONHCONH_2$[a]	5329 ±3	650.0	4680	1
$CH_3CH_2CONH_2$	4656.7±1.5	302.8	4354	0
$CH_3(CH_2)_2CONH_2$	5828.7±2.1	302.8	5528	2
$CH_3(CH_2)_3CONH_2$	6993.7±2.5	302.8	6701	10
$CH_3(CH_2)_4CONH_2$	8180.6±3.2	302.8	7875	−3
$CH_3(CH_2)_6CONH_2$	10523.9±4.7	302.8	10222	0
$HCON(CH_3)_2$	4589.5±2.4	302.8	4291	4
$CH_3CONH(CH_2)_3CH_3$	8160.9±3.4	302.8	7860	2
$(CH_3CO)_2NH$	5787.9±2.2[b]	604.0	5182	−2
$(CH_3CO)_2N(CH_2)_3CH_3$	10448.8±4.0	604.0	9861	16
$(CH_3CO)_3N$	8032.3±2.9	903.2	7146	17
$\left[\text{CO-N(CH}_3\text{)}\right]_3$	9017.2±3.3	1040.9	7975	−1
$\left[\text{CO-NH}\right]_3$[c]	5630.0±2.8	1040.9	4497	90
$\left[\text{CO-NH(CH}_2\text{)}_5\right]$	7666.0±3.0	302.8	7382	19

a) Trans-trans conformer. b) Recalculated value.[12] c) Crystalline state.

(-125.9 kJ mol^{-1}).[6]

The atomization enthalpies were analyzed according to the following equation:

$$\Delta_a H = \sum E(\text{bond}) - B_\pi - E_{\text{destab}}, \quad (4)$$

where E(bond) is the σ-bond contribution term of a bond; the summation extends over all the σ-bonds in the molecule, and $E_{\text{destab}}(>0)$ is the destabilization energy.

As was described in the previous paper, the atomization enthalpy of normal alkanes may be expressed by the simplest bond-additivity scheme:

$$\Delta_a H(C_kH_{2k+2}) = (2k+2)E(\text{C-H}) + (k-1)E(\text{C-C}), \quad (5)$$

where E(C-H)=412.9 kJ mol^{-1} and E(C-C)=347.7 kJ mol^{-1}. These σ-bond-contribution values were transferred to the normal alkyl chains of the present compounds.

For σ-bond-contribution terms of the C-N and N-H bonds, $E(\text{C-}\ddot{\text{N}})$ and $E(\ddot{\text{N}}\text{-H})$, the values which were found to reproduce the atomization enthalpies of methyl-substituted amines[1] [$E(\text{C-}\ddot{\text{N}})$=297.0 kJ mol^{-1} and $E(\ddot{\text{N}}\text{-H})$=383.0 kJ mol^{-1}] were transferred to the present compounds. However, these values led to a significantly negative destabilization energy (-22 kJ mol^{-1}) for trimethyl isocyanurate, for which the energetic stabilization should have been fully accounted for by the π-bonding energy. Consequently, only the atomization enthalpy of methylamine was used to define the magnitude of [$E(\text{C-}\ddot{\text{N}})+2E(\ddot{\text{N}}\text{-H})$]. Likewise, initially we attempted to determine $E(\dot{\text{C}}\text{-C})$, $E(\dot{\text{C}}\text{-H})$, and $E(\dot{\text{C}}\text{-}\dot{\text{O}})$ from the atomization enthalpies of acetone, acetaldehyde, and formaldehyde. However, these terms were not uniquely determined, since the atomization enthalpy of acetaldehyde is expressed as the arithmetic mean of those of acetone and formaldehyde, in terms of the present bond-energy scheme. Cosequently, $E(\dot{\text{C}}\text{-C})$ was chosen as a parameter.

By analogy with the π-bonding energy, the following three assumptions were made to derive CO-N and C-O σ-bond contribution terms from the atomization enthalpies of the open chain compounds: (1) The CO-N bonds of the linear molecules are classified into three kinds by their position in a molecule. $E(\dot{\text{C}}\text{-}\ddot{\text{N}}\text{,amide})$, $E(\dot{\text{C}}\text{-}\ddot{\text{N}}\text{,out})$, and $E(\dot{\text{C}}\text{-}\ddot{\text{N}}\text{,int})$ are the terms for an amidic C-N bond, an outermost C-N bond, and an internal C-N bond respectively. (2) The following equation holds:

$$E(\dot{\text{C}}\text{-}\ddot{\text{N}}\text{, out}) = [E(\dot{\text{C}}\text{-}\ddot{\text{N}}\text{, amide}) + E(\dot{\text{C}}\text{-}\ddot{\text{N}}\text{, int})]/2. \quad (6)$$

(3) The bond-contribution term of a carbonyl group which is conjugated with lone-pair electrons of an adjacent nitrogen atom, $E(\dot{\text{C}}\text{-}\dot{\text{O}}\text{,conj})$, is a constant, independent of the position of the bond in the molecule.

If the value of $E(\dot{\text{C}}\text{-C})$ can once be tentatively assigned, the terms to be determined are $E(\ddot{\text{N}}\text{-H})$, $E(\text{C-}\ddot{\text{N}})$, $E(\dot{\text{C}}\text{-}\ddot{\text{N}}\text{,amide})$, $E(\dot{\text{C}}\text{-}\ddot{\text{N}}\text{,out})$, $E(\dot{\text{C}}\text{-}\ddot{\text{N}}\text{,int})$, and $E(\dot{\text{C}}\text{-}\dot{\text{O}}\text{,conj})$. It seems, at a glance, that these six terms can be determined from the atomization enthalpies of methylamine, acetamide, urea, acetylurea, and diacetamide, together with Eq. 6. However, the atomization enthalpy of diacetamide is equal to the sum of the atomization enthalpies of acetamide and acetylurea, minus that of urea, in the present scheme. Hence, these terms are not uniquely determined. Consequently, the atomization enthalpy of *N*-butylacetamide was used in place of that of diacetamide in the above method.

The derived bond-contribution values are presented in Table 5, and the experimental atomization enthalpies are decomposed into components according to Eq. 4 in Table 4. The values of $E(\text{C-}\ddot{\text{N}})$ and $E(\ddot{\text{N}}\text{-H})$ are slightly different from those given above; the present values lead to small destabilization energies for dimethylamine and trimethylamine. The values of $E(\dot{\text{C}}\text{-H})$ and $E(\dot{\text{C}}\text{-}\dot{\text{O}})$ given in Table 5 were derived by assuming that $E(\dot{\text{C}}\text{-C})$=347.0 kJ mol^{-1}. A change x in the value of $E(\dot{\text{C}}\text{-C})$ leads to other changes x and $-2x$ in the values of $E(\dot{\text{C}}\text{-H})$ and $E(\dot{\text{C}}\text{-}\dot{\text{O}})$ respectively. $E(\dot{\text{C}}\text{-}\ddot{\text{N}}\text{,amide})$, $E(\dot{\text{C}}\text{-}\ddot{\text{N}}\text{,out})$, $E(\dot{\text{C}}\text{-}\ddot{\text{N}}\text{,int})$, and $E(\dot{\text{C}}\text{-}\dot{\text{O}}\text{,conj})$ also depend on the value of $E(\dot{\text{C}}\text{-C})$. The values of these terms given in Table 5 are based on the assumption that $E(\dot{\text{C}}\text{-C})$=347.0 kJ mol^{-1}. By a change x in the value of $E(\dot{\text{C}}\text{-C})$, each of the values of the former three terms changes by x, while that of the latter one changes by $-2x$. It is notable that the sum of the σ-bond-contribution terms for a molecule being studied is not influenced by a change in the value of $E(\dot{\text{C}}\text{-C})$, because a carbonyl C-O σ-bond is always accompanied by two $\dot{\text{C}}$-C bonds, two CO-N bonds, or a $\dot{\text{C}}$-C bond and a CO-N bond, which are adjacent to the C-O σ-bond, in the molecules.

The value of $E(\dot{\text{C}}\text{-}\dot{\text{O}}\text{,conj})$ is lower by 29 kJ mol^{-1} than $E(\dot{\text{C}}\text{-}\dot{\text{O}})$, the difference being independent of x. This shows a weakening of a C-O σ-bond triggered by the π-electron interaction with an adjacent nitrogen atom. Correspondingly, $E(\dot{\text{C}}\text{-}\ddot{\text{N}}\text{,amide})$, $E(\dot{\text{C}}\text{-}\ddot{\text{N}}\text{,out})$,

Table 5. σ-Bond-Contribution Terms. For Classification of the Bonds, See Fig. 1 and the Text

Bond	E(bond) / kJ mol^{-1}	Bond	E(bond) / kJ mol^{-1}
$\text{C-}\ddot{\text{N}}$	301.0	$\dot{\text{C}}\text{-}\ddot{\text{N}}$, amide	358.7
$\ddot{\text{N}}\text{-H}$	381.0	$\dot{\text{C}}\text{-}\ddot{\text{N}}$, out	340.5
$\dot{\text{C}}\text{-C}$	347.0[a]	$\dot{\text{C}}\text{-}\ddot{\text{N}}$, out	322.2
$\dot{\text{C}}\text{-H}$	379.0	C-O, conj	474.1
$\dot{\text{C}}\text{-}\dot{\text{O}}$	500.0		

a) Tentatively assigned.

and $E(\dot{C}\text{–}\ddot{N},\text{int})$ can be expected to be higher than $E(\text{C–}\ddot{N})$, which is the case for the values given in Table 5.

The magnitudes of the σ-bond-contribution terms for CO–N bonds are in this order: $E(\dot{C}\text{–}\ddot{N},\text{amide}) > E(\dot{C}\text{–}\ddot{N},\text{out}) > E(\dot{C}\text{–}\ddot{N},\text{int})$, which is in accord with the trend of the π-bond contribution terms, the increment being larger in the former. This means that the total strength of a CO–N bond is highest for amide, in the second place for urea and diacetylimide, and in the third place for the internal bond of acetylurea, which, in turn, would be stronger than the C–N bond of methylamine.

Destabilization Energies. For normal alkanamides and *N,N*-dimethylformamide, the destabilization energies are close to zero, with the exception of pentanamide.

The destabilization energy of diacetamide with the CO–N–CO skeleton is nearly zero. The agreement between the calculated and experimental atomization enthalpies for diacetamide shows that the present treatment is a reasonable one. The small destabilization energy of *N*-butyldiacetamide is probably due to repulsion between the three groups bonded to the nitrogen atom.[12]

A triacetamide molecule contains three outermost CO–N bonds that involve a common branching nitrogen atom. For this kind of bond, the σ-bond-contribution value has not been determined. Consequently, the σ-bond-contribution value was assumed to be equal to that of the internal CO–N bond which does not involve a branching nitrogen atom, judging from the similarity in the value of π-bond order. The destabilization energy is attributable to repulsion between the three acetyl groups.[12]

Trimethyl isocyanurate is not significantly destabilized by ring strain. The experimental value for isocyanuric acid is not the atomization enthalpy, but the enthalpy difference between the atomic gases and the crystalline state. The value given in the column of destabilization energy seems to be of a reasonable magnitude as a sublimation enthalpy.

The negative of the destabilization energy (due to the ring strain) of 6-hexanlactam corresponds to standard enthalpy change for the following hypothetical gas-phase ring-opening polymerization reaction:

$$\boxed{\text{–CO–NH–(CH}_2\text{)}_5\text{–}} = (1/n)\{\text{–CO–NH–(CH}_2\text{)}_5\text{–}\}_n. \quad (7)$$

Thermochemical Stabilization Energies. In Ref. 1, the stabilization energies were evaluated for acetamide, urea, acetylurea(*trans–trans*), and trimethyl isocyanurate as standard enthalpy changes of the following gas-phase isodesmic reactions:

$$CH_3CONH_2 + C_2H_6 = CH_3COCH_3 + CH_3NH_2, \quad (8)$$

$$NH_2CONH_2 + 2C_2H_6 = CH_3COCH_3 + 2CH_3NH_2, \quad (9)$$

$$CH_3CONHCONH_2 + 3C_2H_6 = 2CH_3COCH_3 + CH_3NH_2 + (CH_3)_2NH, \quad (10)$$

$$\boxed{\{\text{CO–N(CH}_3\text{)}\}_3} + 6C_2H_6 = 3CH_3COCH_3 + 3(CH_3)_3N. \quad (11)$$

Enthalpy changes were decomposed into components according to Eq. 4; the results are shown in Table 6. As expected, in every reaction the contribution from π-bonding energies is more dominant than that related to the σ-bonding energies. It is notable that the contribution from the π-bonding energy is underestimated in the present treatment, because the destabilizing effect of bond compression has been included in this energy.[3]

Thus, the atomization enthalpies of the present compounds have been reasonably interpreted within the framework of the Hess–Schaad theory, and new findings have been obtained on the strength of the CO–N bonds of various molecules.

The authors are grateful to Dr. Junichi Aihara of Shizuoka University, who kindly supplied a BASIC program for the calculation of the graph-theoretical resonance energy prior to publication.

References

1) A. Imamura, S. Murata, and M. Sakiyama, *J. Chem. Thermodyn.*, **20**, 389 (1988).
2) B. A. Hess, Jr., and L. J. Schaad, *J. Am. Chem. Soc.*, **93**, 305 (1971).
3) B. A. Hess, Jr., and L. J. Schaad, *J. Am. Chem. Soc.*, **94**, 3068 (1972).
4) B. A. Hess, Jr., L. J. Schaad, and C. W. Holyoke, Jr., *Tetrahedron*, **28**, 3657 (1972).

Table 6. Decomposition of Reaction Enthalpies into Components

Reaction	$\Delta_f H°$ / kJ mol^{-1}	Contribution/kJ mol^{-1}				
		π-Bonding energy	σ-Bonding energy			Destabilization energy
			Total	$\dot{C}$–C and $\dot{C}$–$\ddot{N}$	$\dot{C}$–$\dot{O}$	
(8)	81.8	47.9	33	59	−26	1
(9)	150.1	94.2	55	81	−26	1
(10)	202	140.2	50	102	−52	12
(11)	369.5	276.2	53	131	−78	40

5) B. A. Hess, Jr., L. J. Schaad, and C. W. Holyoke, Jr., *Tetrahedron*, **28**, 5299 (1972).
6) B. A. Hess, Jr., and L. J. Schaad, *J. Am. Chem. Soc.*, **95**, 3907 (1973).
7) B. A. Hess, Jr., L. J. Schaad, and C. W. Holyoke, Jr., *Tetrahedron*, **31**, 295 (1975).
8) B. A. Hess, Jr., and L. J. Schaad, *Israel J. Chem.*, **17**, 155 (1978).
9) J. Aihara, *Pure Appl. Chem.*, **54**, 1115 (1982) and the references cited therein.
10) CODATA Committee on Key Values of Thermodynamics, *J. Chem. Thermodyn.*, **10**, 903 (1978).
11) J. B. Pedley, R. D. Naylor, and S. P. Kirby, "Thermochemical Data of Organic Compounds," 2nd ed., Chapman and Hall, London (1986).
12) I. Wadsö, *Acta Chem. Scand.*, **19**, 1079 (1965).

 © 1988 The Chemical Society of Japan Bull. Chem. Soc. Jpn., 61, 621—626 (1988)

Catalytic Properties of Perovskite-Type Mixed Oxides (ABO_3) Consisting of Rare Earth and 3d Transition Metals. The Roles of the A- and B-Site Ions

Taihei NITADORI,†,* Tatsumi ICHIKI,†† and Makoto MISONO
Department of Synthetic Chemistry, Faculty of Engineering, The University of Tokyo, Hongo, Bunkyo-ku, Tokyo 113
†Central Research Institute, Japan Tobacco, Inc., Umegaoka, Midori-ku, Yokohama, Kanagawa 227
(Received April 1, 1987)

The catalytic activities of perovskite-type mixed oxides ($LnBO_3$ and $Ln_{0.8}Sr_{0.2}CoO_3$, Ln=rare-earth (lanthanoid) elements, B=3d transition metals) for the oxidation of propane and methanol have been studied comparatively. It has been found that the catalytic activities of $LnBO_3$ were principally determined by the B-site elements and were similar to those of the corresponding oxides of the B-site elements. The roles of the rare-earth ions of the A-site were secondary as long as they were trivalent. Upon the partial replacement of Ln^{3+} by Sr^{2+}, the catalytic activities of $LnCoO_3$ increased several times, the magnitude of the increase being similar among all the rare-earth ions. These results demonstrate that the kind and the valence of a B-site metal are of primary importance for the control of the catalytic activity for oxidation, almost regardless of the kind of trivalent rare-earth elements at the A-site.

Perovskite-type mixed oxides (ABO_3) are typical mixed oxides and many are known with various A- and B-site ions.[1] Because of this nature and the stability of the perovskite structure, the compositions and oxygen vacancies as well as the oxidation state of metal ions can be varied in a regular way. These oxides are, therefore, suitable model compounds for the study of the relationships between the solid state chemistry and the catalytic action of mixed metal oxides. Moreover, the perovskite-type mixed oxides with Co or Mn ions on the B-site have possible applications as fuel cell electrodes[2] and oxidation catalysts.[3,4]

We previously reported some remarkable effects of the valence control of the B-site ions and reasonably explained those effects in terms of the redox properties of the catalysts. For example, the Sr substitution for La of $LaCoO_3$ changed the catalytic activity greatly; paticularly, $La_{0.8}Sr_{0.2}CoO_3$ was the most active, and its activity for oxidation was higher than a Pt catalyst.[4] We further investigated the effects of the Sr, Ce, and Hf substitutions of $LaBO_3$ (B=Co, Fe, and Mn).[5–9] These studies confirmed that the valence of the B-site ions and the oxygen or metal vacancy in the bulk phase are the most important factors controlling the catalytic properties. It was revealed at the same time that the effects of those factors significantly changed with the kind of constituent element.

Therefore, in the present work, in order to elucidate more generally the roles of the constituent elements, we investigated comparatively the effects of rare-earth ions at the A-site and of 3d transition metal ions at the B-site. The effects on the valence control were examined in the case of the Sr substitution for $LnCoO_3$, which previously showed a remarkable positive effect. Although several works on those effects have been reported,[4,10–16] there have been very few studies in which both A- and B-site ions were varied simultaneously and extensively, and no studies about the effect of the A-site ion in valence control.

Experimental

Catalysts. The perovskite-type mixed oxides used as catalysts are summarized in Table 1. They were prepared from mixtures of metal nitrates of each component in the same manner as has been described in the previous paper.[4] The precipitates which had been obtained from mixed nitrate solutions by adding butylamine were filtered, decomposed in air at 300 °C for 3 h, and calcined in air, usually at 850 °C for 5—10 h. Some were calcined at 1100 °C for 10 h. Powder X-ray diffraction patterns were recorded on a powder X-ray diffractometer (Rigaku Denki, Rotaflex, RU-200) using Cu $K\alpha$ radiation. The surface areas of the samples were measured by means of the BET method (N_2 adsorption).

Component single oxides (rare earth=La, Ce, Pr, Nd, Sm, Eu, and Gd; 3d transition metal=Mn, Fe, and Co) were obtained by the calcination of metal acetates or nitrates of a reagent grade at 850 °C for 5 h in air. XPS measurements were carried out for $La_{1-x}Sr_xCoO_3$ with the Mg $K\alpha$ (1253.6 eV) source by the use of ESCA 750 (Shimadzu). The binding energies were calibrated with reference to a C1s electron line (285.0 eV).

Apparatus. Conventional flow, pulse, and closed circulation systems as described before[4–6] were used.

Procedure. Catalytic Oxidation of Propane and Methanol: The oxidation reactions of propane and methanol were carried out with the flow system following the procedure described previously.[4,9] Prior to the reaction, the catalysts (300 mg) were usually pretreated in an O_2 stream for 1 h at 300 °C. A gas mixture of propane (0.83%), O_2 (33.3%), and N_2 (balance) was used for the propane oxidation, and a mixture of methanol (6.0%), O_2 (9.0%), and N_2 (balance) for the methanol oxidation.

Reduction of Catalysts by CO: The reduction of catalysts by CO was carried out with the circulation system. Before the reduction, the catalysts (300 mg) were treated in

†† Present address: Tonen Sekiyukagaku K. K., Ohimachi, Saitama.

O_2 at 300 °C for 1 h, and then they were evacuated for 1 h at the reduction temperature. The initial CO pressure was about 20 Torr (1 Torr=133.3 Pa). The rates of the reduction were measured by the pressure decrease of CO, while the CO_2 produced was condensed in a trap kept at the temperature of liquid nitrogen.

Temperature-Programmed Desorption (TPD) of Oxygen: The TPD of oxygen was carried out using helium as a carrier gas (25 cm^3 min^{-1}) as has been described previously.[9] Prior to each run, the sample (1 g) was pretreated in an O_2 stream at 300 °C for 1 h (except for the $LnMnO_3$'s, which were pretreated at 800 °C). The rate of the temperature rise was 20 deg min^{-1}. In the first run for each sample, CO_2 and H_2O envolved in addition to O_2. In the subsequent runs, however, neither CO_2 nor H_2O was detected above the background level, and the TPD curves were reproducible. The data of the second runs were, therefore, adopted as in the previous papers.[5,9]

Results

Structures and Surface Areas of Perovskite Catalysts. The surface areas and the crystal structures of the catalysts used in the present study are summarized in Table 1. Perovskite-type structures of the samples were confirmed by reference to ASTM cards. The XRD patterns of these samples showed only the perovskite structure. The diffraction peaks of $LaFeO_3$ and $GdFeO_3$ calcined at 1100 °C became narrower, and the surface areas smaller, indicating the increased crystallinity. According to XRD, all of the rare-earth oxides were sesqui-oxides except for CeO_2 and Pr_6O_{11}; the oxides of the component 3d transition metals prepared were Mn_2O_3, Fe_2O_3, and Co_3O_4.

Table 1. Surface Area and Structure of Catalysts

Catalyst	Calcination		Surface area/m^2g^{-1}	Structure[a]
	Temp/°C	Time/h		
$LaCoO_3$	850	10	1.8	P(R)
$PrCoO_3$	850	10	2.1	P(C)
$NdCoO_3$	850	10	2.2	P(C)
$SmCoO_3$	850	10	2.4	P(O)
$EuCoO_3$	850	10	1.0	P(O)
$GdCoO_3$	850	10	2.0	P(O)
$LaFeO_3$	850	5	6.8	P(O)
	1100	10	0.4	P(O)
$SmFeO_3$	850	5	4.9	P(O)
$GdFeO_3$	850	5	5.2	P(O)
	1100	10	0.4	P(O)
$LaMnO_3$	850	10	8.3	P(O)
$SmMnO_3$	850	10	7.3	P(O)
$GdMnO_3$	850	10	6.8	P(O)
$La_{0.8}Sr_{0.2}CoO_3$	850	10	3.0	P(C)
$Pr_{0.8}Sr_{0.2}CoO_3$	850	10	2.2	P(C)
$Nd_{0.8}Sr_{0.2}CoO_3$	850	10	2.9	P(C)
$Sm_{0.8}Sr_{0.2}CoO_3$	850	10	4.6	P(O)
$Eu_{0.8}Sr_{0.2}CoO_3$	850	10	3.6	P(O)
$Gd_{0.9}Sr_{0.1}CoO_3$	850	10	3.8	P(O)
$Gd_{0.8}Sr_{0.2}CoO_3$	850	10	5.5	P(O)
$Gd_{0.6}Sr_{0.4}CoO_3$	850	10	3.4	P(O)

a) P: perovskite structure, R: rhombohedral, C: cubic O: orthorhombic (judged from the splitting of the main peaks).

The surface composition of $La_{1-x}Sr_xCoO_3$, as estimated by XPS, is shown in Table 2. It was calculated from Eq. 1.[17]

$$\frac{N_a}{N_b} = \frac{n_a \cdot \lambda_a \cdot \sigma_a \cdot s_a}{n_b \cdot \lambda_b \cdot \sigma_b \cdot s_b} \quad (1)$$

where N: peak intensity, n: atoms per unit volume, λ: mean free path of electron, σ: ionization cross-section, and s: instrumental factor. The peak areas of La4d, Co2p (the average of 2p3/2 and 2p1/2) and Sr3d, including the satellite peak, were used for N, while the values of σ were taken from the literature.[18] "$\lambda \cdot s$" was assumed in this study to be constant, as has been suggested by the manufacturer. This assumption is not very accurate (though the errors are estimated to be no more than 15%), but it may be sufficient to compare the relative change in the surface composition for a series of catalysts. Therefore, the data in Table 2 may be considered as semi-quantitative values reflecting the trends of the surface segregation compared with the bulk composition. Thus, it may be stated, on the basis of the data in Table 2, that La was richer on the surface than in the bulk and that the Co content increased monotonically with an increase in the Sr content. The binding energies (780.3—780.9 and 795.5—796.1 eV), the spin-orbit splitting (15.2 eV), and the satellite splitting (9.8—10.0 eV) for Co2p were consistent with those of Co^{3+}.[19] Therefore, most of the Co in the surface may be Co^{3+}, although the possibility of the presence of Co^{4+} can not be excluded, since no data were reported for Co^{4+}.

Comparison of the Catalytic Activity for Oxidation. The catalytic activities of the perovskites and the rare-earth oxides for propane oxidation are shown in Fig. 1A, where are given the rates normalized to the unit surface area. CO_2 and H_2O were the only products in these experiments. It is notable that the Ln ions at A-site had a much smaller effect on the activity than did the transition metal ions at B-site, the order of the activity being always $LnCoO_3 > LnMnO_3 \gg LnFeO_3$. The activities of the component rare-earth oxides were very low. The activation energies obtained from the data at low conversion levels in these

Table 2. The Surface Compositions of $La_{1-x}Sr_xCoO_3$

	$x=0$		$x=0.2$			$x=0.6$		
	La	Co	La	Sr	Co	La	Sr	Co
Surface	0.68	0.32	0.48	0.14	0.38	0.26	0.23	0.51
Bulk[a]	0.50	0.50	0.40	0.10	0.50	0.20	0.30	0.50

a) Calculated from the starting materials.

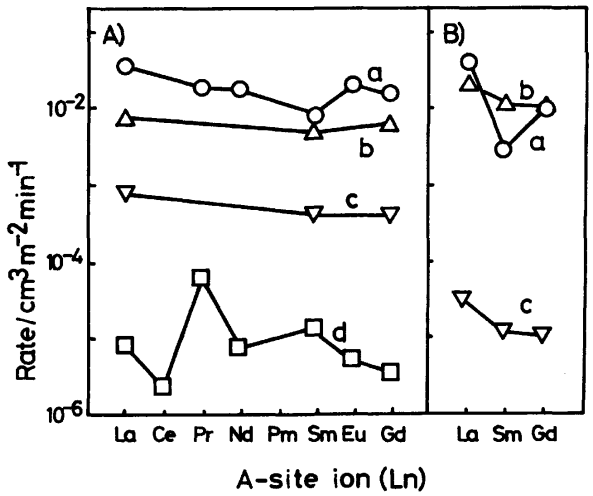

Fig. 1. Catalytic activities of perovskites and rare-earth oxides for propane oxidation at 227 °C and methanol oxidation 200 °C.
a: $LnCoO_3$, b: $LnMnO_3$, c: $LnFeO_3$, d: Ln oxide.
A) Propane, B) methanol.

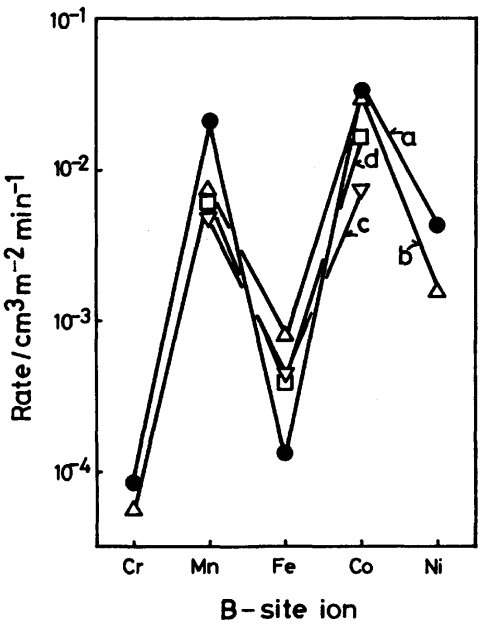

Fig. 2. Catalytic activities of perovskite and B-site oxide for propane oxidation at 227 °C.
a: Oxides of B-site metals, b: $LaBO_3$, c: $SmBO_3$, d: $GdBO_3$.

experiments were 18.2—20.9 kcal mol^{-1} ($LnCoO_3$), 19.5—21.6 ($LnMnO_3$), and 24.0—25.8 ($LnFeO_3$), respectively. The greater effect of B-site ions than of Ln ions was also observed for methanol oxidation, as is shown in Fig. 1B (Co, Mn≫Fe). Complete oxidation was again the only reaction observed. The activation energies were 47—55 kcal mol^{-1}. The methanol oxidation was also measured over $LaFeO_3$ and $GdFeO_3$, which had been calcined at 1100 °C. In this case also, the difference in Ln had only a small effect.

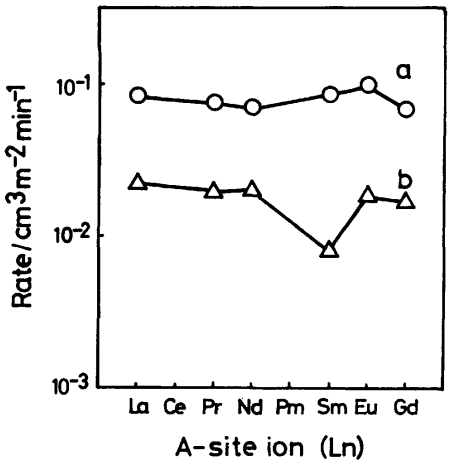

Fig. 3. Catalytic activities of $Ln_{0.8}Sr_{0.2}CoO_3$ for propane oxidation at 227 °C.
a: $Ln_{0.8}Sr_{0.2}CoO_3$, b: $LnCoO_3$.

The activity patterns of the perovskites and metal oxides containing the same 3d metals are compared in Fig. 2, including those of Cr[20] and Ni.[4] The differences in the activities among the catalysts on the whole were more than two orders of magnitude, whereas the differences between the perovskites and the corresponding B-site oxide were less than one order; also both the perovskites and B-site oxides showed very similar activity patterns, with twin peaks at Mn and Co. A similar pattern has been reported for $LaBO_3$ by Tascon et al.[21] This pattern resembles the trend reported for the oxidation of CH_4 and H_2[22] and may, therefore, be considered to reflect the ability of metal oxide to activate O_2. This pattern is different from the so called "Dowden pattern."[23] The Dowden pattern, which was often observed for hydrogenation reactions and which reflects the ability to activate H_2, has twin peaks at Cr and Co.

The Effect of Sr Substitution at A-Site for the Catalytic Activity. The effect of Sr substitution was examined for several rare-earth ions in the case of $LnCoO_3$, since a marked increase in the catalytic activity was previously found for $LaCoO_3$.[5,6] As shown in Fig. 3, the substitution by Sr for 20% of the A-site ions of $LnCoO_3$ increased 5—10 times the catalytic activity for propane oxidation; the magnitude of the increase was similar among the rare-earth ions. The surface areas tended to increase upon the Sr substitution, so the increases in the catalytic activity per catalyst weight were still greater. Figure 4 shows the effect of the extent of Sr substitution for $GdCoO_3$, together with the previous results for $LaCoO_3$.[4-6] The oxidation activity varied similarly for both systems, showing maxima at x=0.1—0.2. A similar effect was also found for methanol oxidation.

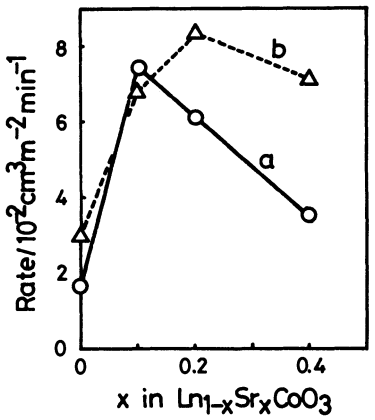

Fig. 4. Effect of Sr substitution on the catalytic activities of $LnCoO_3$ for oxidation of propane at 227 °C.
a: $Gd_{1-x}Sr_xCoO_3$, b: $La_{1-x}Sr_xCoO_3$.

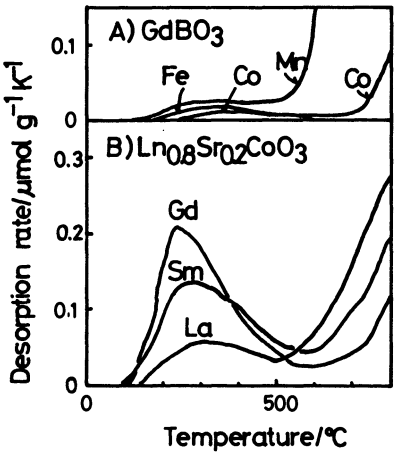

Fig. 5. TPD profiles of oxygen from perovskites.
A) $GdBO_3$, B) $Ln_{0.8}Sr_{0.2}CoO_3$.

TPD of Oxygen. Figure 5A shows the TPD of oxygen from $GdBO_3$ (B=Co, Fe, and Mn). Each TPD curve resembles that we previously reported for $LaBO_3$, with the same B-site element.[5,7,9] Broad and low peaks appeared at 150—500 °C for all three samples. The amounts of oxygen desorbed below 500 °C, which were previously indicated to be related to the catalytic function, were small, the order being Mn>Fe>Co. Even for $GdMnO_3$ the amount was only 0.12 cm^3 g^{-1}, which corresponded to 0.3 times the surface monolayer of oxygen. The large peak for Mn above 500 °C is likely to be due to the removal of excess oxygen, as has been discussed previously for $LaMnO_3$.[9]

The TPD profiles of $Ln_{0.8}Sr_{0.2}CoO_3$ (Ln=La, Sm, and Gd) are shown in Fig. 5B. The amounts of oxygen desorbed increased remarkably upon the Sr substitution, as has previously been reported for the $LaCoO_3$ system.[5,24] The amounts of oxygen desorbed

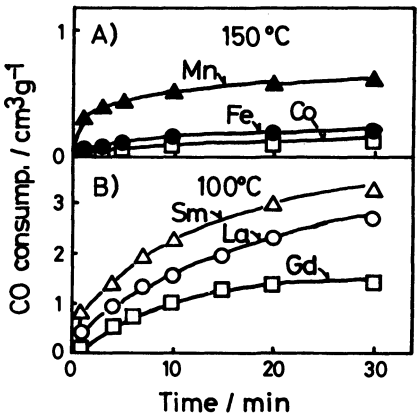

Fig. 6. Reduction of perovskite by CO.
A) $GdBO_3$, B) $Ln_{0.8}Sr_{0.2}CoO_3$.

below 500 °C were 0.34 (La)<0.82 (Sm)<1.00 (Gd) cm^3 g^{-1}. These values corresponded to about 0.6 (La) and 1.0 (Sm, Gd) surface monolayer. The amounts desorbed up to 800 °C were 1.17 (La), 1.40 (Sm), and 1.31 (Gd) cm^3 g^{-1}, which corresponded to 1.3—2.2 surface monolayers. Since the adsorbed oxygen is usually scarce, significant parts of the desorbed oxygen are from the catalyst bulk.

Reduction of the Catalyst by CO. Figure 6A shows the rate of the CO consumption of $GdBO_3$ (B=Co, Fe, and Mn) as measured in the circulation system at 150 °C. The amounts of CO consumed in 30 min were 0.1 (Co), 0.21 (Fe), and 0.63 (Mn) cm^3 g^{-1}, respectively, values which corresponded to 0.1—0.4 surface monolayer of oxygen. This tendency agreed with that of the amount of oxygen desorbed below 500 °C in the TPD described above (Fig. 5A). Figure 6B shows the results of the reduction for $Ln_{0.8}Sr_{0.2}CoO_3$ at 100 °C. $Ln_{0.8}Sr_{0.2}CoO_3$ was appreciably more easily reduced by CO than by $LnBO_3$ in spite of the lower reduction temperature. The amounts of CO consumed in 30 min were 2.27 (La), 3.35 (Sm), and 1.42 (Gd) cm^3 g^{-1}, corresponding to 2.6, 2.0, and 0.7 surface monolayers, respectively.

Discussion

Roles of A- and B-Site Ions. We have previously reported that the catalytic activities of $LaBO_3$ (B=Fe, Co, and Mn) for the oxidations of hydrocarbons and CO were approximately on the same level at those of the oxides of the B-site metals and that the catalytic properties reflected mainly the nature of the B-site metals.[4] This has also been pointed out by other investigators.[10-14] To explain this, the electronic state of the d electron of the B-site ion,[11] the binding energy of the B–O bond,[12] and the stabilization energy of the crystal field[13] have been proposed as the controlling factors of the catalytic activity. Although these factors are different, all of these explanations are based on the

nature of the B-site ions.

In this study, the rare-earth ion (Ln) at the A-site was changed variously. It was thus found that the effect of Ln was relatively small (Fig. 1) and that the activity patterns of the peroviske catalysts were the same as that of the oxides of the B-site transition metals (Fig. 2). By contrast, the order of the catalytic activities observed for the rare-earth oxides was quite different from that of the corresponding perovskites, and the activities were much lower. Among them, Pr_6O_{11} was the most active, and CeO_2, the least. This tendency is in agreement with the result reported for butane oxidation by Hattori et al.,[25] while it is different from the trend for $LnCoO_3$.

The physical properties of the rare-earth ions, such as the ionic radius, the charge density, and the magnetic moment, change significantly from La to Gd. The structures of the perovskites containing these elements also vary, for example, from $LaCoO_3$ (rhombohedral) to $GdCoO_3$ (orthorhombic). These changes would influence the electronic state of the B-site ion, but the effect seems less important than the B-site element itself. Thus, the effect of the A-site ion is presumed to be secondary as long as it is trivalent.

Nevertheless, several examples in which this secondary effect is significant have been reported. Parkash et al.[15] observed the highest activities for CO oxidation for Nd and Ho among $LnCoO_3$ (Ln=La, Pr, Nd, Gd, and Ho) and discussed this result based on the relative ratio of low- to high-spin Co^{3+}. Arakawa et al. reported that the catalytic activity of $LnFeO_3$ (calcined at 1200 °C) for methanol oxidation increased remarkably from La to Gd; they concluded that this was a result of the decrease in the covalency of the Fe–O bond.[16] In the present study, the catalytic activity for methanol oxidation over $LnFeO_3$ did not change much (Fig. 1B). Though the reason for this difference is not clear at present, the alteration of the composition on the surface and/or in the bulk of the catalyst might have occurred because of the different calcination conditions.

The Effects of Ln for the Valance Control of $LnCoO_3$. The catalytic activity increased several times upon the Sr substitution for Ln of $LnCoO_3$ regardless of the kind of trivalent rare-earth ion (Fig. 3). As for the extent of the substitution, a maximum was observed at x=0.1 for $Gd_{1-x}Sr_xCoO_3$ (Fig. 4). These results generally agree with our previous results for $La_{1-x}Sr_xCoO_3$.[6] The catalytic activity of $La_{1-x}Sr_x$-CoO_3 increased initially with an increase in x and showed a maximum at x=0.2. This variation in activity was semi-quantitatively explained as follows based on the change in the oxidation–reduction properties of the catalyst.[5,6]

Upon the Sr substitution, a part of the Co^{3+} is oxidized to Co^{4+} (Eq. 2). Since the Co^{4+} is unstable, however, the oxide ions tend to be removed and the Co^{4+} returns to Co^{3+} (Eq. 3):[5,6,24,26]

$$Ln^{3+}Co^{3+}O_3 \xrightarrow{Sr} Ln^{3+}_{1-x}Sr^{2+}_xCo^{3+}_{1-x}Co^{4+}_xO_3 \quad (2)$$

$$Ln_{1-x}Sr_xCo^{3+}_{1-x}Co^{4+}_xO_3 \longrightarrow Ln_{1-x}Sr_xCo^{3+}_{1-x+2\delta}Co^{4+}_{x-2\delta}O_{3-\delta} + (\delta/2)O_2 \quad (3)$$

This is in agreement with the present results that the oxygen desorbed in TPD increased remarkably and that the reduction by CO became much easier upon the Sr substitution (Figs. 5 and 6). This means that the oxidation power of $LnCoO_3$ is increased by the valence control. Since the increase in the oxidation power promotes the catalytic activity of the oxide catalysts for oxidation, the initial increase in the activity by the Sr substitution is understandable. The decrease in the catalytic activity at higher extents of substitution may be explained by the slower re-oxidation step in the redox cycle of the catalysts, as has been demonstrated previously,[6] or by the lower reactivity of the surface oxygen.[27] Therefore, the mechanism of the Sr substitution for $LnCoO_3$ in the valence control and the catalytic activity may be similar to that for $LaCoO_3$. The possibility that an unknown La- or Sr-rich phase segregated on the surface of the perovskites having high Sr contents and lowered the activity may not be excluded. However, this is not likely to be the main reason for the decrease in activity, since the surface compositions estimated by XPS indicated monotonous changes in the Co and Sr contents when x was increased (Table 2).

There were relatively small, but definite, differences between $LnCoO_3$'s, and the trends among the Ln ions observed for the TPD, the reducibility and the catalytic activity did not agree well with one another. For example, the amount of oxygen desorbed in TPD for $Ln_{0.8}Sr_{0.2}CoO_3$ (Fig. 6B; Gd>Sm>La for 25—500 °C) did not parallel the catalytic activity (Fig. 3; La>Gd>Sm) and the reducibility of $Ln_{0.8}Sr_{0.2}CoO_3$ (Fig. 6B; Sm>La>Gd). The reason for the disagreement observed for the secondary effects is not clear at present. Part of these discrepancies may, however, be related to the difference in the compositions between the surface and bulk or to the differences in the relative rates of the chemical processes on the surface to those in the bulk. A possible example of the chemical processes is the supply of oxygen species to surface sites. It can be from the gas phase through adsorption or from the bulk through diffusion.

The effect of Sr substitution on the Mn systems was examined only for $La_{1-x}Sr_xMnO_3$,[9] but the effects may be similar for other Ln ions, because it was reported by Raj et al.[28] that $LnMnO_3$ (Ln: La—Gd) calcined in air 950 °C has a similar oxidative nonstoichiometry. As the Sr content increases, the composition changes from oxygen-excess to oxygen-deficient and the catalytic activity changes moderately, showing maxima at about x=0.6.[9]

Conclusion

The following conclusions may be deduced for the roles of the A- and B-site ions of $LnBO_3$ for oxidation catalysis: (i) the kind and valence of the 3d transition metal ion at the B-site are of primary importance, (ii) the role of the rare-earth ion at the A-site is secondary as long as it is trivalent, (iii) the substitution of the A-site ion by ions with a different valence is very influential; this is caused by the change in the oxidation state of the B-site ion and the formation of an anion vacancy.[4-9]

References

1) R. J. H. Voorhoeve, "Advanced Materials in Catalysis," ed by J. J. Burton and R. L. Garten, Academic Press, New York (1977), p. 129.
2) D. B. Meadowcroft, *Nature (London)*, **226**, 847 (1970).
3) W. F. Libby, *Science*, **171**, 499 (1971).
4) T. Nakamura, M. Misono, T. Uchijima, and Y. Yoneda, *Nippon Kagaku Kaishi*, **1980**, 1679.
5) T. Nakamura, M. Misono, and Y. Yoneda, *Bull. Chem. Soc. Jpn.*, **55**, 394 (1982); *Chem. Lett.*, **1981**, 1585.
6) T. Nakamura, M. Misono, and Y. Yoneda, *J. Catal.*, **83**, 151 (1983).
7) T. Nitadori and M. Misono, *J. Catal.*, **93**, 459 (1985).
8) M. Misono and T. Nitadori, "Adsorption and Catalysis on Oxide Surface," Elsevier, Amsterdam (1985), p. 409.
9) T. Nitadori, S. Kurihara, and M. Misono, *J. Catal.*, **98**, 221 (1986).
10) N. Yamazoe and Y. Teraoka, *Shokubai*, **25**, 196 (1983).
11) R. J. H. Voorhoeve, J. P. Remeika, and L. E. Trimble, *Ann. N. Y. Acad. Sci.*, **272**, 3 (1976).
12) T. Shimizu, *Chem. Lett.*, **1980**, 1.
13) J. M. D. Tascon and L. G. Tejuca, *React. Kinet. Catal. Lett.*, **15**, 185 (1980).
14) W. B. Li, H. Yoneyama, and H. Tamura, *Nippon Kagaku Kaishi*, **1982**, 761.
15) O. Parkash, P. Ganguly, G. R. Rao, C. N. R. Rao, D. S. Rajoria, and V. G. Hide, *Mater. Res. Bull.*, **9**, 1173 (1974).
16) T. Arakawa, S. Tsuchiya, and J. Shiokawa, *J. Catal.*, **74**, 317 (1982).
17) K. Hirokawa, *Hyomen Kagaku*, **7**, 237 (1986).
18) J. H. Scofield, *J. Electr. Spectr. Relat. Phenom.*, **8**, 129 (1976).
19) J. Okamoto, H. Nakano, T. Imanaka, and S. Teranishi, *Bull. Chem. Soc. Jpn.*, **48**, 1163 (1975).
20) T. Nitadori and M. Misono, unpublished data.
21) G. Kremenic, J. M. L. Nieto, J. M. D. Tascon, and L. G. Tejuca, *J. Chem. Soc., Faraday Trans. 1*, **81**, 939 (1985).
22) G. K. Boreskov, *Kinet. Katal.*, **14**, 2 (1973).
23) D. A. Dowden, *Catal. Rev. Sci. Eng.*, **5**, 1 (1972).
24) N. Yamazoe, Y. Teraoka, and T. Seiyama, *Chem. Lett.*, **1981**, 1767.
25) T. Hattori, J. Inoko, and Y. Murakami, *J. Catal.*, **42**, 60 (1976).
26) H. Obayashi, T. Kudo, and T. Gejo, *Jpn. J. Appl. Phys.*, **13**, 1 (1974).
27) Y. Teraoka, M. Yoshimatsu, N. Yamazoe, and T. Seiyama, *Shokubai*, **26**, 106 (1984).
28) S. Louis Raj and V. Srinivasan, *J. Catal.*, **65**, 121 (1980).

 © 1988 The Chemical Society of Japan Bull. Chem. Soc. Jpn., 61, 627—632 (1988)

A Conductance Study of 1:1 Complexes of 15-Crown-5, 16-Crown-5, and Benzo-15-crown-5 with Alkali Metal Ions in Nonaqueous Solvents

Yasuyuki TAKEDA,* Koji KATSUTA, Yoshihisa INOUE,† and Tadao HAKUSHI††
Department of Chemistry, Faculty of Science, Chiba University, Yayoi-cho, Chiba 260
†Basic Research Laboratory, Himeji Institute of Technology, 2167 Shosha, Himeji, Hyogo 671-22
††Department of Applied Chemistry, Himeji Institute of Technology, 2167 Shosha, Himeji, Hyogo 671-22
(Received June 18, 1987)

Conductivities of alkali metal salts in the presence of 15-crown-5 (15C5), 16-crown-5 (16C5), and benzo-15-crown-5 (B15C5) were measured at 25 °C in acetonitrile, propylene carbonate, and methanol. Formation constants (K_{ML^+}) of 1:1 complexes of 15C5 and 16C5 with alkali metal ions and conductance parameters (λ^0 and $\mathring{a}$) of the Na^+ complexes of 15C5, 16C5, and B15C5 were determined, λ^0 and $\mathring{a}$ being limiting ionic molar conductivity and distance of closest approach of ions, respectively. In general, selectivities of 15C5 and 16C5 for alkali metal ions show the size-fit correlation. In contrast to 15C5, 16C5 forms much the most stable complex with Na^+ in every solvent. Generally, K_{ML^+}-value sequences of a given crown ether complex for the solvents are the reverse of donor-number sequences of the solvents. Value of $\mathring{a}$ increases with an increase in the cationic size ($Na^+ \rightarrow Na(15C5)^+ \rightarrow Na(16C5)^+ \rightarrow Na(B15C5)^+$). Mobility of the Na^+-crown ether complex decreases with an increase in the size of the crown ether. From λ^0 values and Walden products of these Na(crown ether)$^+$ complexes and a tetrapropylammonium ion, it seems likely that $Na(15C5)^+$ and $Na(16C5)^+$ act as structure breakers in hydrogen-bonding solvents, whereas $Na(B15C5)^+$ as a structure maker.

Conductance measurements of a solution of alkali metal salt in the presence of crown ether provide two valuable information; that is, (1) stability of the crown ether–alkali metal ion complex, and (2) transport phenomena of the crown ether–alkali metal salt complex in the solution.[1] Many data have been reported on stabilities of 15-crown-5 (15C5)- and benzo-15-crown-5 (B15C5)–alkali metal ion complexes in solutions, but a few data on solvation behavior of the crown ether complexes in solutions.[2] It has recently been presented that 16-crown-5 (16C5), possessing the same number of donor oxygen atoms but reduced symmetry, exhibits much higher selectivity for Na^+ among alkali metal ions than 15C5.[3,20] In the present study, in order to obtain systematic and detailed information on stabilities and solvation behavior of 15C5–, 16C5–, and B15C5–alkali metal ion complexes, conductivities of alkali metal salts in the presence of these three crown ethers were measured at 25 °C in acetonitrile, propylene carbonate, and methanol.

Experimental

Materials. 15-Crown-5 (Nisso Co., Ltd.) was purified twice by distillation under vacuum (bp 128.5—129.5 °C, 2.5 mmHg (1 mmHg≈133.322 Pa)). The preparation of 16C5 was just the same as that described in the previous paper.[3] Benzo-15-crown-5 (Merck Japan Ltd.) was dissolved in heptane, and filtered while hot. Then it was recrystallized from heptane three times and, prior to use, dried at 40 °C in vacuo for 50 h.

Extremely pure $LiCl \cdot H_2O$, NaCl, KCl, RbCl, and CsCl were purchased from Merck Japan Ltd., and were used without further purification. Rubidium and caesium perchlorates were prepared by adding a little excess of perchloric acid to aqueous solutions of the RbCl and CsCl, respectively. Lithium, sodium, and potassium perchlorates were obtained from Merck Japan Ltd. All the perchlorates were recrystallized four times from distilled water and, prior to use, dried at 150 °C in a vacuum oven.

The method of purification of acetonitrile,[4] propylene carbonate,[5] and methanol[6] was previously described. Middle 70% of distillate of the solvents was used. Conductivities of the purified acetonitrile, propylene carbonate, and methanol were less than 3×10^{-7}, 6×10^{-8}, and 2×10^{-7} Ω^{-1} cm^{-1}, respectively.

Alkali metal chlorides were employed for the methanol system and alkali metal perchlorates for the other solvent systems.

Apparatus and Procedure. The conductance measurements were made on a Fuso conductivity apparatus, model 362A, in a water bath thermostated at 25±0.005 °C.

The experimental procedure to obtain formation constants of crown ether complexes with alkali metal ions was almost the same as that described in a previous paper.[5]

The experimental procedure to obtain molar conductivities (Λ) of the crown ether–sodium salt complexes was as follows. A solution of crown ether (6×10^{-3} mol dm^{-3}, 200 cm^3) was placed in the cell and the resistance of the solution was measured. Then a step-by-step increase in the sodium salt concentration was effected by a rapid transfer from a solution of the sodium salt (1×10^{-2} mol dm^{-3}) to the cell with a pipet, until the total concentration of the crown ether was about five times as large as that of the sodium salt. The resistance of the solution in the cell was remeasured after each transfer.

Results

The molar conductivity vs. $[L]_t/[M]_t$ plots of the $16C5/LiClO_4$/propylene carbonate system show an increase in Λ with an increase in the 16C5 concentration, $[L]_t$ and $[M]_t$ denoting total concentrations of the crown ether and the alkali metal, respectively. This indicates that a 16C5–Li^+ complex is more

mobile in propylene carbonate than a free Li^+ ion. For 15C5 and 16C5/LiCl/CH_3OH and 15C5/NaCl/CH_3OH systems, there is a negligible change in Λ in spite of an increase in the crown ether concentration. Consequently, the complex-formation constants could not be determined. When the complex is unstable or mobilities of the complex and the corresponding alkali metal ion are equal, conductometric determination of the complex-formation constant is impossible. For all the other systems, Λ vs. $[L]_t/[M]_t$ plots show a decrease in Λ with an increase in the crown ether concentration. This reveals that the crown ether complex is less mobile than the corresponding free alkali metal ion. By way of example, Λ vs. $[L]_t/[M]_t$ plots for 15C5/ and 16C5/acetonitrile systems at 25 °C are given in Figs. 1 and 2, respectively.

From Figs. 1 and 2, in the cases of 15C5/ and 16C5/$NaClO_4$ systems, the slope of each curve changes sharply at $[L]_t/[M]_t=1$. The same tendency was

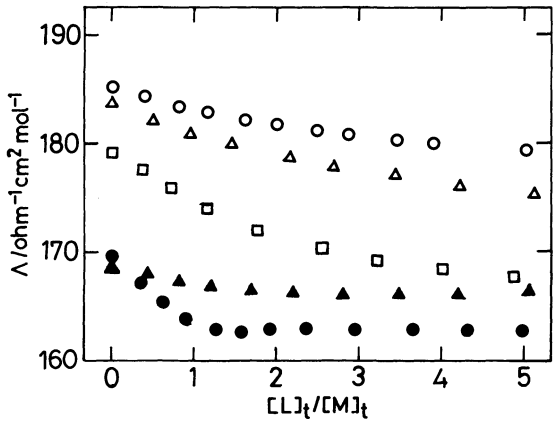

Fig. 1. Λ vs. $[L]_t/[M]_t$ curves for 15C5-alkali metal perchlorate systems in acetonitrile at 25 °C
▲ Li, ● Na, □ K, △ Rb, ○ Cs, $[M]_t=6\times10^{-4}$ M.

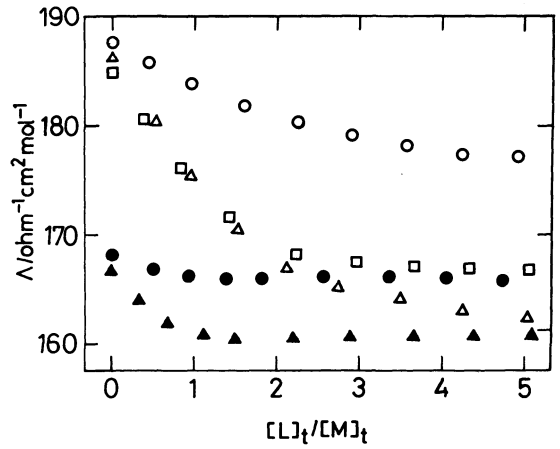

Fig. 2. Λ vs. $[L]_t/[M]_t$ curves for 16C5-alkali metal perchlorate systems in acetonitrile at 25 °C
● Li, ▲ Na, △ K, □ Rb, ○ Cs, $[M]_t=6\times10^{-4}$ M.

observed for 16C5/$NaClO_4$/propylene carbonate system. It follows from this that the crown ethers form 1:1 complexes with Na^+. For the other systems, no such clear breaking point was observed.

When a crown ether forms a 1:1 complex with an alkali metal ion, the equilibrium equation is written as

$$\underset{\alpha[M]_t}{M^+} + \underset{[L]_t-(1-\alpha)[M]_t}{L} \rightleftarrows \underset{(1-\alpha)[M]_t,}{ML^+} \quad (1)$$

where M^+, L, and α are the alkali metal ion, crown ether, and the fraction of free alkali metal ions. Thus, the complex-formation constant, K_{ML^+}, is defined by

$$K_{ML^+} = [ML^+]/[M^+][L] = (1-\alpha)/\alpha[L]. \quad (2)$$

The observed conductivity, κ, is given by

$$\kappa = \kappa_{MA} + \kappa_{MLA}, \quad (3)$$

where A^- denotes an anion, and κ_{MA} and κ_{MLA} refer to conductivities of alkali metal salt and alkali metal crown ether salt, respectively. The molar conductivities are as follows.

$$\Lambda_{MA} = \kappa_{MA}/[M^+] = \kappa_{MA}/\alpha[M]_t, \quad (4)$$

$$\Lambda_{MLA} = \kappa_{MLA}/[ML^+] = \kappa_{MLA}/(1-\alpha)[M]_t, \quad (5)$$

Λ_{MA} and Λ_{MLA} designating molar conductivities of alkali metal salt and alkali metal crown ether salt, respectively. As a consequence of Eqs. 4 and 5, Eq. 3 can be transformed into

$$\Lambda = \kappa/[M]_t = \alpha\Lambda_{MA} + (1-\alpha)\Lambda_{MLA}. \quad (6)$$

In this study, corrections for viscosity changes were neglected. As a consequence of Eq. 6, Eq. 2 can be transformed into

$$K_{ML^+} = (\Lambda_{MA}-\Lambda)/(\Lambda-\Lambda_{MLA})[L], \quad (7)$$

where $[L]=[L]_t-[M]_t(\Lambda_{MA}-\Lambda)/(\Lambda_{MA}-\Lambda_{MLA})$. The K_{ML^+} value can be obtained by the following procedure. The Λ_{MLA} value is estimated from the Λ values at the points of large $[L]_t$ to $[M]_t$ ratios. Using this Λ_{MLA} value, the K_{ML^+} value in Eq. 7 is calculated. The actual K_{ML^+} and Λ_{MLA} values are calculated by a successive approximation method. The actual Λ_{MLA} values at nearly equal $[M]_t$ values are listed in Table 1. The log K_{ML^+} values are summarized in Table 2.

Conductance data of crown ether–sodium salt complexes (NaLA) were analyzed by the Fuoss–Onsager equations:[21]

$$\Lambda = \Lambda_0 - SC^{1/2} + EC\log C + JC \quad (8)$$

for unassociated electrolytes, and

$$\Lambda = \Lambda_0 - S(C\gamma)^{1/2} + EC\gamma \log C\gamma + JC\gamma - K_A\Lambda_0 f^2 C\gamma \quad (9)$$

for associated electrolytes, where K_A is ion-pair association constant and the other symbols have their usual meaning. In order to obtain the parameters of Eqs. 8 and 9, values of dielectric constants and viscosities listed in Table 6 were employed. It was found that every crown ether–sodium salt complex (NaLA) completely dissociates into cation and anion in the solvents. Limiting molar conductivities (Λ_0) and ion-size parameters (å) obtained in this work are summarized in Table 3.

Table 1. Λ_{MLA} Values at 25 °C

L	Solvent	MA	$\Lambda_{MLA}/\Omega^{-1}$ cm^2 mol^{-1}	$[M]_t \times 10^4$/mol dm^{-3}
15C5	AN[a]	$LiClO_4$	163.67	3.9866
		$NaClO_4$	163.64	3.8645
		$KClO_4$	159.38	4.0249
		$CsClO_4$	161.13	4.0809
	CH_3OH	NaCl	89.18	8.5552
		CsCl	89.39	8.0501
16C5	AN[a]	$LiClO_4$	160.52	5.8525
		$NaClO_4$	160.11	3.8457
			159.41	5.6345
		$KClO_4$	159.24	4.8213
		$RbClO_4$	164.04	4.0587
		$CsClO_4$	162.52	4.8808
	PC[b]	$NaClO_4$	26.55	4.7872
		$KClO_4$	27.17	4.7476
		$RbClO_4$	27.04	4.8989
		$CsClO_4$	28.30	4.6545

a) Acetonitrile. b) Propylene carbonate.

Table 2. Log (K_{ML^+}/mol^{-1} dm^3) Values at 25 °C

	CH_3CN		Propylene carbonate		CH_3OH	
	15C5	16C5	15C5	16C5	15C5	16C5
Li^+	5.3_4	4.4_8	4.2_6[5]	3.2_5	1.23[b,8]	—
	3.60[a,7]		>4[b,8]			
	>4[b,8]					
Na^+	5.3_8	5.3_9	3.7[5]	5.7	3.48[11]	4.10
	4.9[9]				3.30[12,15]	3.51[20]
	5.28[c,7]				3.14[13]	
	>4[10]				3.25[14]	
					3.24[16]	
					3.27[17]	
					3.31[18]	
K^+	3.9_8	3.5_7	3.4_1[5]	3.3_4	3.3	2.9_2
	2.9_8[d,7]				3.77[11]	2.63[20]
					3.35[12]	
					3.1[19]	
					3.61[13]	
					3.34[15,18]	
					3.43[16]	
Rb^+	3.4_2	2.9_4	3.0_4[5]	2.5_9	2.7_2	2.4_6
Cs^+	3.1_4	2.3_8	2.6_9[5]	2.1_7	2.6_6	2.0_9
					2.62[12]	
					2.18[11]	

a) LiI. b) At 27±1 °C, $LiClO_4$. c) $NaBPh_4$. d) $KBPh_4$.

Table 3. Values of Λ_0, K_A, and $\mathring{a}$ at 25 °C in Nonaqueous Solvents

Salt	Solvent	Λ_0/Ω^{-1} cm^2 mol^{-1}	K_A/mol^{-1} dm^3	$\mathring{a}$/Å
$NaClO_4$[22]	AN[a]	180.63	11	3.7
$Na(15C5)ClO_4$	AN[a]	170.43±0.36		4.12±0.08
$Na(16C5)ClO_4$	AN[a]	165.84±0.04		5.5±0.3
$Na(B15C5)ClO_4$	AN[a]	164.59±0.12		6.5±0.5
Bu_4NClO_4[23]	AN[a]	165.06±0.01		3.57
$NaClO_4$	PC[b]	27.98±0.01		2.9±0.1
$NaClO_4$[24]	PC[b]	27.89±0.01	−1.1	
		27.89±0.002	−1.3	
$Na(15C5)ClO_4$	PC[b]	28.32±0.02		4.3±0.2
$Na(16C5)ClO_4$	PC[b]	27.17±0.03		5.1±0.2
$Na(B15C5)ClO_4$	PC[b]	26.64±0.02		5.7±0.1
NaCl[25]	CH_3OH	97.53		3.73
Na(15C5)Cl	CH_3OH	96.48±0.05		4.97±0.36
Na(16C5)Cl	CH_3OH	93.50±0.04		5.5±0.2
Na(B15C5)Cl	CH_3OH	90.06±0.01		6.2±0.2
Bu_4NCl[26]	CH_3OH	91.38	0.0	3.9

a) Acetonitrile. b) Propylene carbonate.

Table 4. Crystal Ionic Radii of Alkali Metals and Cavity Radius of Crown Ethers (Å)

Cation	Crystal ionic radius[27]	Crown ether	Cavity radius[a]
Li^+	0.60	15C5	0.85
Na^+	0.95	16C5	0.9
K^+	1.33		
Rb^+	1.48		
Cs^+	1.69		

a) Estimated by CPK space-filling molecular models.

Discussion

Stability of Crown Ether Complexes. As can be seen from Tables 2 and 4, selectivity of 15C5 for alkali metal ions shows the size-fit correlation except for the cases of Li^+ in acetonitrile and propylene carbonate and Na^+ in CH_3OH. In comparison with the case of 16C5, Li^+–15C5 complex is very stable among alkali metal ion–15C5 complexes in acetonitrile and propylene carbonate. It is interesting that, in contrast to 15C5, 16C5 forms much the most stable complex with Na^+ of all the alkali metal ions in every solvent. In particular, selectivity of 16C5 for Na^+ in propylene carbonate is the most striking of all the systems. Moreover, the 16C5–Na^+ complex in propylene carbonate is the most stable among all the 15C5 and 16C5 complexes. Thus, a remarkable enhancement of selectivity for Na^+ is caused by an extra methylene group in the 16C5 ring. The more closely an alkali metal ion fits into the 16C5 cavity, the more stable is the 16C5–alkali metal ion complex. This tendency can be explained by the size-fit concept.

Log K_{ML^+}-value sequences of a given crown ether–alkali metal ion complex for the solvents are acetonitrile>propylene carbonate>CH_3OH only except for those of 16C5–Na^+ complex for propylene carbonate and acetonitrile (Table 2). The log K_{ML^+}-value sequences are completely the reverse of donor-number sequences of the solvents (acetonitrile<propylene carbonate<CH_3OH, from Table 6). Donor number of the solvent seems to be a dominant factor governing the stability of the crown ether–alkali metal ion complex.[1] From Table 6, ε_r values of the solvents increase in the order CH_3OH<acetonitrile<propylene carbonate. This indicates that there is no relationship between stability of the crown ether–alkali metal ion complex and dielectric constant of the solvent.

A 15C5–alkali metal ion complex is more stable than the corresponding 16C5 complex except for the case of Na^+. In propylene carbonate and CH_3OH, the reverse is true of 15C5- and 16C5–Na^+ complexes. In acetonitrile, log K_{ML^+} values of 15C5- and 16C5–Na^+ complexes are almost the same. This tendency may be explained in terms of examination of CPK molecular models, that is, Na^+ has a more suitable size for the cavity of 16C5 than that of 15C5, and the donor oxygen atoms of 16C5 arrange more nicely around Na^+ compared to 15C5. However, lower symmetry of 16C5 causes more unfavorable orientation of the donor oxygen atoms for the less size-fitted cations, Li^+, K^+, Rb^+, and Cs^+.

Behavior of Crown Ether Complexes in Solutions. From Table 3, a slight association to ion-pairs is found for $NaClO_4$ in acetonitrile, but all the crown ether–sodium salt complexes completely dissociate into ions. Since mobilities of these three crown ether–Na^+ complexes are much smaller than that of a Na^+ ion in acetonitrile (Table 5), an apparent cationic size is much larger for the crown ether–Na^+ complexes

Table 5. Limiting Ionic Molar Conductivities (λ^0) in Various Solvents at 25 °C

	λ^0/Ω^{-1} cm^2 mol^{-1}		
	AN[a]	PC[b]	CH_3OH
Na^+	76.9[29]	9.7_0	45.17[25]
		9.45[24]	
$Na(15C5)^+$	66.7_3	10.0_4	44.12
	65.5[30]		
$Na(16C5)^+$	62.1_4	8.8_9	41.14
$Na(B15C5)^+$	60.8_9	8.3_6	37.70
Pr_4N^+	70.3[29]	11.0_0[31]	46.08[26]
Cl^-	—	—	52.36[32]
ClO_4^-	103.7[29]	18.2_8[31]	—

a) Acetonitrile. b) Propylene carbonate.

Table 6. Walden Products at 25 °C

	AN[d]	PC[e]	CH_3OH
η_0/mP[a] (at 25 °C)	3.39[37]	25.3[38]	5.42[39]
DN[b,36]	14.1	15.1	19
ε_r[c] (at 25 °C)	35.95[29]	64.4[38]	32.6[39]
$Na(15C5)^+$	0.226	0.254	0.239
$Na(16C5)^+$	0.211	0.22_5	0.223
$Na(B15C5)^+$	0.206	0.21_2	0.204
Pr_4N^+	0.238	0.278	0.250

a) η_0 denotes viscosity and 1P=0.1 Pa s. b) DN denotes donor number. c) ε_r denotes dielectric constant. d) Acetonitrile. e) Propylene carbonate.

than for the Na^+ ion. This is responsible for a complete dissociation of crown ether-$NaClO_4$ complexes into ions and a slight association of $NaClO_4$ to ion-pairs in acetonitrile.

Table 3 shows that $\mathring{a}$ value increases with an increase in the cationic size ($Na^+ \rightarrow Na(15C5)^+ \rightarrow Na(16C5)^+ \rightarrow Na(B15C5)^+$) regardless of a variety of anions and solvents. It follows from this finding that the anion does not always approach the sodium ion trapped in the cavity in a direction perpendicular to the plane of the crown ether ring.

By using ionic radii of $Na(15C5)^+$ (4.6 Å[5]), ClO_4^- (2.26 Å[28]), and Cl^- (1.81 Å[27]), center-to-center distance of the cation and the anion is calculated to be 6.86 Å for $Na(15C5)ClO_4$ and 6.41 Å for Na(15C5)Cl, which are greater than the largest $\mathring{a}$ values of B15C5-sodium salt complexes.

For 15C5 and 16C5, $\mathring{a}$ values of the crown ether-$NaClO_4$ complex in acetonitrile and propylene carbonate are much the same. Although ionic radius of Cl^- is 0.45 Å smaller than that of ClO_4^-, $\mathring{a}$ value of the crown ether-sodium salt complex in CH_3OH is larger than or nearly equal to those in aprotic solvents. The same behavior is observed for both sodium and tetrabutyl ammonium salts (Table 3). This may be attributed to much stronger solvation of Cl^- in CH_3OH compared to ClO_4^-.

It can be seen from Table 5 that the mobility of Na^+-crown ether complex decreases with an increase in the size of crown ether, indicating that the mobility of the complexed sodium ion is governed completely by the size of the complex. It is of interest to note that only an additional methylene group causes the lower mobility of $Na(16C5)^+$ compared to $Na(15C5)^+$. Mobilities of Na^+ in acetonitrile and CH_3OH show the same tendency as stated above, but that in propylene carbonate the opposite trend. It has been reported that the degree of solvation of large ions is determined predominantly by the dipole moment of solvent molecules, whereas that of small ions by the acid-base properties of solvent molecules.[22] Although propylene carbonate has a slightly larger and smaller donor number than acetonitrile and CH_3OH, respectively (Table 6), and has a larger dipole moment (4.94 D[33]) than acetonitrile (3.37 D[33]) and CH_3OH (1.73 D[33]), $Na(15C5)^+$ is more mobile than Na^+ in propylene carbonate, and the reverse is true of acetonitrile and CH_3OH. The lower mobility (the larger moving entity) of Na^+ in propylene carbonate may be attributed to the larger size of the propylene carbonate molecule (molecular radii of propylene carbonate, acetonitrile, and CH_3OH are 3.23, 2.75, and 2.52 Å, respectively[31]).

Although the ionic radius of $Na(15C5)^+$ is nearly equal to that of tetrapropylammonium ion (Pr_4N^+) (4.52 Å[34]), $Na(15C5)^+$ is less mobile than Pr_4N^+. For $Na(15C5)^+$, there exists a possible interaction of the central Na^+ with solvent molecules on two axial sides of the 15C5 plane, whereas, for Pr_4N^+, the charge of the nitrogen atom is effectively screened by four propyl groups. Consequently, the interaction of $Na(15C5)^+$ with solvent dipole seems to be stronger than that of Pr_4N^+. This may be responsible for the lower mobility of $Na(15C5)^+$ compared to Pr_4N^+.

In the cases of L=15C5 and 16C5, sequences of $|\lambda^0(Pr_4N^+)/\lambda^0(NaL^+)-1|$ value for the solvents are $CH_3OH < CH_3CN <$ propylene carbonate. This shows that a difference in mobility in CH_3OH between NaL^+ and Pr_4N^+ is the smallest of all the solvents. The same behavior was observed for the case of $K(18C6^{**})^+$ complex and tetrabutylammonium ion (Bu_4N^+).[4] In the previous papers,[4,35] it was reported that $K(18C6)^+$ acts as a structure breaker in hydrogen-bonding solvents. From Walden products of Pr_4N^+ in Table 6, Pr_4N^+ is more mobile in CH_3OH than in acetonitrile. It thus appears that hydrogen-bonded structure of CH_3OH scarcely decreases the mobility of Pr_4N^+. Although hydrogen bonds of ether oxygen atoms of 15C5 and 16C5 with methanol molecules would decrease mobilities of $Na(15C5)^+$ and $Na(16C5)^+$ complexes, the mobility of NaL^+(L=15C5 and 16C5) approaches that of Pr_4N^+ most closely in CH_3OH of

**18C6=18-crown-6.

all the solvents. Therefore, it can be considered that $Na(15C5)^+$ and $Na(16C5)^+$ in CH_3OH are more mobile than expected. This is supported by the data in Table 6; namely, Walden products of $Na(15C5)^+$ and $Na(16C5)^+$ in CH_3OH are larger than those in acetonitrile. Consequently, from the data of $K(18C6)^+$ [4,35] and the above discussion, it seems likely that $Na(15C5)^+$ and $Na(16C5)^+$ act as structure breakers in hydrogen-bonding solvents.

For $Na(B15C5)^+$, sequences of $\lambda^0(Pr_4N^+)/\lambda^0(Na(B15C5)^+)$ value for the solvents are $CH_3CN<CH_3OH<$propylene carbonate. The order of CH_3CN and CH_3OH for $Na(B15C5)^+$ is in the reverse of that for $Na(15C5)^+$ and $Na(16C5)^+$. This indicates that the mobility of $Na(B15C5)^+$ in CH_3OH is lower than expected on the basis of those of $Na(15C5)^+$ and $Na(16C5)^+$. Enforcement of a hydrogen-bonded structure of CH_3OH for the benzo group may decrease the mobility of $Na(B15C5)^+$. This is supported by the data of Walden products of $Na(B15C5)^+$ in Table 6; the $\lambda^0\eta_0$ value of CH_3OH of $Na(B15C5)^+$ is the smallest of all the solvents. This suggests that, on account of the benzo group, $Na(B15C5)^+$ acts as a structure maker in hydrogen-bonding solvents.

For these three Na(crown ether)$^+$ complexes as well as Pr_4N^+, Walden products in propylene carbonate, which has the greatest ε_r value, are the largest.

References

1) Y. Takeda, *IONICS*, **11**, 49 (1985).
2) R. M. Izatt, J. S. Bradshaw, S. A. Nielsen, J. D. Lamb, J. J. Christensen, and D. Sen, *Chem. Rev.*, **85**, 271 (1985).
3) M. Ouchi, Y. Inoue, H. Sakamoto, A. Yamahira, M. Yoshinaga, and T. Hakushi, *J. Org. Chem.*, **48**, 3168 (1983); M. Ouchi, Y. Inoue, T. Kanzaki, and T. Hakushi, *ibid.*, **49**, 1408 (1984); Y. Inoue, M. Ouchi, and T. Hakushi, *Bull. Chem. Soc. Jpn.*, **58**, 525 (1985).
4) Y. Takeda, *Bull. Chem. Soc. Jpn.*, **56**, 866 (1983).
5) Y. Takeda, H. Yano, M. Ishibashi, and H. Isozumi, *Bull. Chem. Soc. Jpn.*, **53**, 72 (1980).
6) Y. Takeda and H. Yano, *Bull. Chem. Soc. Jpn.*, **53**, 1720 (1980).
7) H. P. Hopkins, Jr. and A. B. Norman, *J. Phys. Chem.*, **84**, 309 (1980).
8) A. J. Smetana and A. I. Popov, *J. Solution Chem.*, **9**, 183 (1980).
9) T. Nakamura, Y. Yumoto, and K. Izutsu, *Bull. Chem. Soc. Jpn.*, **55**, 1850 (1982).
10) J. D. Lin and A. I. Popov, *J. Am. Chem. Soc.*, **103**, 3773 (1981).
11) J. D. Lamb, R. M. Izatt, C. S. Swain, and J. J. Christensen, *J. Am. Chem. Soc.*, **102**, 475 (1980).
12) R. B. Davidson, R. M. Izatt, J. J. Christensen, R. A. Schultz, D. M. Dishong, and G. W. Gokel, *J. Org. Chem.*, **49**, 5080 (1984).
13) G. Michaux and J. Reise, *J. Am. Chem. Soc.*, **104**, 6895 (1982).
14) D. M. Dishong and G. W. Gokel, *J. Org. Chem.*, **47**, 147 (1982).
15) T. Miyazaki, S. Yanagida, A. Itoh, and M. Okahara, *Bull. Chem. Soc. Jpn.*, **55**, 2005 (1982).
16) G. W. Gokel, D. M. Goli, C. Minganti, and L. Echegoyen, *J. Am. Chem. Soc.*, **105**, 6786 (1983).
17) Y. Nakatsuji, T. Nakamura, and M. Okahara, *Chem. Lett.*, **1982**, 1207.
18) I. Ikeda, H. Emura, S. Yamamura, and M. Okahara, *J. Org. Chem.*, **47**, 5150 (1982).
19) D. G. Parsons, M. R. Truter, and J. N. Wingfield, *Inorg. Chim. Acta*, **47**, 81 (1980).
20) Y. Nakatsuji, M. Yonetani, and M. Okahara, *Chem. Lett.*, **1984**, 2143.
21) R. M. Fuoss and F. Accascina, "Electrolytic Conductances," Interscience Publishers, New York, N. Y. (1959).
22) R. L. Kay, B. J. Hales, and G. P. Cunningham, *J. Phys. Chem.*, **71**, 3925 (1967).
23) J. F. Coetzee and G. P. Cunningham, *J. Am. Chem. Soc.*, **87**, 2529 (1965).
24) M. L. Jansen and H. L. Yeager, *J. Phys. Chem.*, **77**, 3089 (1973).
25) R. L. Kay, *J. Am. Chem. Soc.*, **82**, 2099 (1960).
26) R. L. Kay, C. Zawoyski, and D. F. Evans, *J. Phys. Chem.*, **69**, 4208 (1965).
27) L. Pauling, "The Nature of the Chemical Bond," 3rd ed, Cornell Univ. Press (1960).
28) H. D. B. Jenkins and K. P. Thakur, *J. Chem. Educ.*, **56**, 576 (1979).
29) C. H. Springer, J. F. Coetzee, and R. L. Kay, *J. Phys. Chem.*, **73**, 471 (1969).
30) M. D. Monica, A. Ceglie, and A. Agostiano, *Electrochim. Acta*, **28**, 529 (1983).
31) N. Matsuura, K. Umemoto, and Y. Takeda, *Bull. Chem. Soc. Jpn.*, **48**, 2253 (1975).
32) R. L. Kay and D. F. Evans, *J. Phys. Chem.*, **70**, 2325 (1966).
33) A. L. McClellan, "Tables of Experimental Dipole Moments," W. H. Freeman Co., San Francisco, Calif. (1963).
34) R. A. Robinson and R. H. Stokes, "Electrolyte Solutions," Butterworths, London (1959).
35) Y. Takeda and Y. Matsumoto, *Bull. Chem. Soc. Jpn.*, **60**, 2313 (1987).
36) V. Gutmann, "Coordination Chemistry in Nonaqueous Solutions," Springer-Verlag, Berlin (1968).
37) J. P. Karnes, *Diss. Abs.*, **26**, 1367 (1965).
38) H. F. Bauman, *Proc. Ann. Power Sources Conf.*, **18**, 89 (1964).
39) P. G. Sears, R. R. Holmes, and L. R. Dawson, *J. Electrochem. Soc.*, **102**, 145 (1955).

 © 1988 The Chemical Society of Japan Bull. Chem. Soc. Jpn., 61, 633—642 (1988)

The Volumes of Hydrated Glucose, Sucrose and Raffinose Molecules, and the Osmotic Pressures of These Aqueous Saccharide Solutions as Measured by the Freezing-Point-Depression Method

Keitaro KIYOSAWA
Department of Biophysical Engineering, Faculty of Engineering Science, Osaka University, Toyonaka, Osaka 560
(Received April 21, 1987)

The osmotic pressures of aqueous saccharide solutions were calculated from the data obtained by means of the freezing-point-depression method. Thus, the water activity and the osmotic pressure of D-glucose, sucrose, and raffinose solutions were measured by the freezing-point-depression method. For dilute aqueous saccharide solutions, the freezing-point depression was proportional to their molal concentrations. However, the higher the molal concentration, the larger the freezing-point depression observed became than those to be expected from the molal concentration dependent on the size of the saccharide molecules. The osmotic pressures calculated from the data of the freezing-point-depression method were compared with those measured with semi-permeable membranes by Morse and his colleagues. To obtain the apparent volumes of hydrated D-glucose, sucrose, and raffinose molecules, their partial molal volumes were measured, together with the partial molal volumes of the water of their solutions. The partial molal volumes of the water were verified to be equal to the molar volumes of pure water up to the highest concentrations examined. The apparent volumes of the hydrated D-glucose, sucrose, and raffinose molecules were calculated to be 0.1865, 0.3525, and 0.5105 nm^3 respectively.

To physiologists who study water relations in plant and animal cells, and membrane phenomena, it has become common knowledge that the osmotic pressure inside and outside a cell[1-5] and the ionic component[6-8] both have important effects on its activities. Thus, various aqueous electrolyte solutions, such as KCl, NaCl, CsCl, RbCl, $RbNO_3$, RbF, $CaCl_2$, $Ca(NO_3)_2$, and $MgSO_4$,[7,9-12] have been used to control the ionic condition and the osmotic pressure inside and outside cells. Various saccharides, such as glucose, sucrose,[13,14] and raffinose, and their derivatives, such as mannitol,[2,15,16] and sorbitol,[17] have also been used.

Although we have very detailed data about the freezing-point depression of simple aqueous electrolyte solutions,[18] we have only a few data about the osmotic pressure of saccharide and its derivative solutions.[18-20]

In this paper, the water activity, the osmotic pressure, the activity coefficient of the water, and the osmotic coefficients of aqueous D-glucose, sucrose and raffinose solutions, as calculated from the freezing-point-depression data and the partial molal volume of the water as well as the partial molal volumes of these saccharides, are reported as functions of their concentration. The values of the partial molal volume thus obtained were then used to calculate the volume of a hydrated saccharide molecule.

Materials and Methods

The D-glucose, sucrose, and raffinose used were of a reagent grade from Nakarai Chemicals, Ltd., and Wako Pure Chemical Industries, Ltd. The raffinose, a hydrate, had been kept in a petri dish for a few months so as to make it in equilibrium with the water in the air. These saccharides were not further purified by the method of recrystalization from their hot concentrated aqueous solutions by adding alcohol because our preliminary test using the atomic-absorption method had shown that the saccharides were fairly free from contaminating electrolytes, such as K^+, Na^+, Ca^{2+}, and Mg^{2+}. On the other hand, ethyl alcohol which had been stored in a glass bottle for a long period contained a small amount of Na^+.

The water used had been distilled from a deionized supply. The air dissolved in the distilled water was not completely removed except when the effect of the dissolved air was examined. The air dissolved in the aqueous solutions was not a serious problem in measuring their density with the mechanically oscillating densimeter except in winter. The effect of the dissolved air in the solutions will be discussed later from the biological point of view.

The freezing-point depression was measured with an osmometer (Advanced Instruments, Inc.; Type 3W) which had been calibrated with standard aqueous NaCl solutions whose freezing-point depressions are listed in "Handbook of Physics and Chemistry".[21] The osmometer was equipped with a thermister to detect the freezing point of the aqueous solution to be examined and a cooling bath in which a glass tube containing the aqueous solution was designed so as to be cooled gently.

Calculation of osmotic pressure from the data measured with the osmometer: The osmometer expresses the freezing-point depression $\theta(=T°-T)$ in terms of mosmol, where $T°$ and T are the freezing points of pure water and the aqueous solution to be tested respectively. 1.0000 mosmol is defined as the molal concentration of an ideal aqueous solution, whose freezing-point depression θ is 1.86×10^{-3} °C.

The equation used to express precisely the freezing-point depression is as follows (cf. Appendix):

$$\Delta_{fus}Hm_{(1)}(T^\circ)\left(\frac{1}{T}-\frac{1}{T^\circ}\right) - \frac{1}{T}\int_T^{T^\circ}\{Cp,m_{(1)}^{l}(T'')-Cp,m_{(1)}^{s}(T'')\}dT'' + \int_T^{T^\circ}\frac{Cp,m_{(1)}^{l}(T'')-Cp,m_{(1)}^{s}(T'')}{T''}dT'' = -R\ln x_1 f_1 \quad (1)$$

$$= -\phi R\ln x_1 \quad (2)$$

where $Cp,m_{(1)}^{l}(T)$, $Cp,m_{(1)}^{s}(T)$, x_1, f_1, and ϕ are the molar heat capacities at a constant pressure of liquid and solid water as functions of the temperature; the mole fraction of water; the activity coefficient of water, and the osmotic coefficient of the solution respectively.

Actually, however, we are at present forced to adopt the following equation to calculate the water activity because of the lack of precise values of $Cp,m_{(1)}^{l}(T)$ and $Cp,m_{(1)}^{s}(T)$ in Eqs. 1 and 2 of the aqueous solutions to be examined (cf. Dorsey[22]). That is :

$$\Delta_{fus}Hm_{(1)}(T^\circ)\left(\frac{1}{T}-\frac{1}{T^\circ}\right) = -R\ln x_1 f_1 \quad (3)$$

$$= -\phi R\ln x_1. \quad (4)$$

It will be shown in the Discussion section that Eq. 3 or 4 gives values of the water activity of, at least, sucrose solutions fairly consistent with those obtained with semi-permeable membranes. Thus, from Eqs. 3 and 4, $\ln x_1 f_1$, f_1, and ϕ are calculated after T has been calculated from both T° and θ.

The osmotic pressure π which should be generated between an aqueous solution of the mole fraction x_1 and pure water $x_1=1$ across a semi-permeable membrane is defined as the osmotic pressure of the solution and is expressed by this equation:[23,24]

$$\Pi = -\frac{RT\ln x_1 f_1}{Vm_{(1)}(T,0)\left\{1-\frac{1}{2}\kappa_1(P'+P'')\right\}} \quad (5)$$

or by:

$$\Pi = -\frac{\phi RT\ln x_1}{Vm_{(1)}(T,0)\left\{1-\frac{1}{2}\kappa_1(P'+P'')\right\}} \quad (6)$$

where $Vm_{(1)}(T,0)$ is the molar volume of water extrapolated to zero pressure at the temperature T K; κ_1, the compressibility of water (4.6×10^{-5} atm^{-1} or 4.5×10^{-10} Pa^{-1} at 298.15K[22]); and P' and P'', the pressures of the pure-water phase and the aqueous-solution phase respectively.

Since, in ordinary solutions used in physiology, $1\gg1/2\kappa_1(P'+P'')$ and T=17—25 °C, we obtain:

$$\Pi = -\frac{TR}{Vm_{(1)}(298.15,0)}\ln x_1 f_1 \quad (7)$$

where $Vm_{(1)}$ (298.15,0) is the molar volume of water extrapolated to zero pressure at 25 °C: approximately 1.8075×10^{-2} dm^3 mol^{-1}. Therefore, in order to relate the results obtained from the freezing-point-depression method to the osmotic pressure, it is essential to calculate the value of $\ln x_1 f_1$ or $\phi\ln x_1$ from θ, T°, and T.

Partial molal volume of the water: In order to estimate the effect of saccharides on the water structures in their aqueous solutions, the partial molal volume of the water of the aqueous saccharide solutions were determined as functions of their concentrations. The partial molal volume of the water $Vm_{(1)}$ of an aqueous solution was determined as an intersect of the linear curve obtained by plotting the mean molar volume $V_{1,2}$ against the mole fraction of saccharide x_2 with the $V_{1,2}$-axis. $V_{1,2}$ was expressed by the mole fraction of the water x_1 and the solute x_2, the partial molal volume of water $Vm_{(1)}$ and a saccharide $Vm_{(2)}$ as :[24,25]

$$V_{1,2} = Vm_{(1)}x_1 + Vm_{(2)}x_2 \quad (8)$$

In this study, $V_{1,2}$ was calculated from the density ρ of the solution by means of this equation:

$$V_{1,2} = \frac{1}{\rho}\frac{1.0000+M_2m}{55.5093+m} \quad (9)$$

where M_2 and m are the molecular weight of the solute and the molal concentration of its aqueous solution and where 55.5093 moles is the mole number of 1.0000 kg of water respectively. In the calculation of the molal concentration of each aqueous solution, the buoyancy due to air was corrected.

The density of the saccharide solutions was measured with a mechanically oscillating densimeter (Shibayama SS-D-200) at 25.00±0.01 °C. The effects of the viscosity of the solution on the density measurement with the densimeter[26] was negligibly small up to the highest concentrations of the solutions tested in this study.

Results

Table 1 shows the freezing-point depression of D-glucose, sucrose, and raffinose solutions and the osmotic pressure calculated from the data of the freezing-point depression. They are averages of 4—9 measurements and are expressed in terms of mosmol; atm and Pa are, respectively, functions of the molal and molar concentrations. The activity coefficient f_1 and the osmotic coefficient ϕ, which were determined by means of Eqs. 3 and 4, are also shown in Table 1.

At higher concentration than about 420 mmol kg^{-1}, raffinose was precipitated when ice was formed by agitation in its supercooled aqueous solution. In concentrated D-glucose and sucrose solutions, the formation of ice seemed to occur more slowly by the same agitation in supercooled states.

Table 1. Freezing-Point Depression, Water Activity in Terms of $-\ln x_1 f_1$, Osmotic Pressure Π, Activity Coefficient of Water f_1, and Osmotic Coefficient ϕ of Aqueous Saccharide Solutions

Concentration		Freezing-point depression		$-\ln x_1 f_1$	Π		f_1	ϕ
m/mol kg^{-1}	c/mol dm^{-3}	mosmol	θ/°C		$\times 10^5$Pa	atm		
				D-Glucose				
0.04984	0.04942	49.8	0.0926	8.9749×10^{-4}	1.231	1.215	1.000	0.9997
0.05077	0.05034	50.7	0.0943	9.1397	1.253	1.237	1.000	0.9992
0.10021	0.09881	101.0	0.1879	1.8218×10^{-3}	2.499	2.466	1.000	1.010
0.10078	0.09937	101.4	0.1879	1.8218	2.499	2.466	1.000	1.004
0.14994	0.14702	151.1	0.2810	2.7254	3.738	3.690	1.000	1.009
0.15149	0.14852	152.2	0.2831	2.7457	3.766	3.717	1.000	1.007
0.19955	0.19462	200.9	0.3737	3.6257	4.973	4.909	1.000	1.010
0.19992	0.19502	201.5	0.3748	3.6364	4.987	4.923	1.000	1.011
0.25077	0.24320	251.9	0.4685	4.5470	6.236	6.156	1.000	1.008
0.25110	0.24350	253.3	0.4711	4.5723	6.271	6.190	0.9999	1.013
0.29816	0.28766	301.1	0.5600	5.4369	7.457	7.361	0.9999	1.015
0.30039	0.28976	303.5	0.5645	5.4807	7.517	7.420	0.9999	1.015
0.39874	0.38059	404.2	0.7518	7.3041	10.017	9.889	0.9999	1.020
0.39919	0.38098	404.6	0.7526	7.3119	10.028	9.899	0.9999	1.020
0.59871	0.55939	612.7	1.1396	1.10876×10^{-2}	15.206	15.011	0.9996	1.033
0.59939	0.55997	614.1	1.1422	1.11130	15.241	15.045	0.9996	1.034
0.79965	0.73166	824.7	1.5339	1.49456	20.497	20.234	0.9994	1.045
0.80065	0.73246	825.0	1.5345	1.49514	20.505	20.242	0.9994	1.044
0.99847	0.89515	1036.3	1.9275	1.88079	25.794	25.463	0.9990	1.055
1.00029	0.89661	1040.4	1.9351	1.88825	25.897	25.564	0.9990	1.057
1.19751	1.05235	1251.8	2.3283	2.27523	31.205	30.804	0.9986	1.066
1.19822	1.05286	1254.4	2.3332	2.28006	31.271	30.870	0.9986	1.067
1.39665	1.20343	1474.6	2.7428	2.68440	36.817	36.344	0.9980	1.080
1.39818	1.20459	1475.6	2.7446	2.68617	36.841	36.368	0.9980	1.079
1.59715	1.34972	1697.7	3.1577	3.09521	42.451	41.906	0.9974	1.091
1.59734	1.34985	1692.0	3.1471	3.08470	42.307	41.764	0.9975	1.087
1.79670	1.48987	1910.8	3.5541	3.48889	47.850	47.236	0.9970	1.095
1.79870	1.49098	1907.7	3.5483	3.48312	47.771	47.158	0.9971	1.092
				Sucrose				
0.03001	—	30.5	0.0567	5.4908×10^{-4}	0.753	0.743	1.000	1.016
0.03007	—	30.5	0.0568	5.5083	0.755	0.746	1.000	1.017
0.05000	0.04912	50.6	0.0941	9.1222	1.251	1.235	1.000	1.013
0.05008	—	50.8	0.0944	9.1494	1.255	1.239	1.000	1.014
0.09982	0.09688	101.1	0.1880	1.82323×10^{-3}	2.501	2.468	1.000	1.014
0.10000	0.09732	100.7	0.1873	1.81557	2.490	2.458	1.000	1.008
0.14985	0.14507	151.7	0.2822	2.73720	3.754	3.706	1.000	1.015
0.15003	0.14527	151.7	0.2821	2.73574	3.752	3.704	1.000	1.013
0.19997	0.19093	202.9	0.3774	3.66151	5.022	4.957	0.9999	1.018
0.20002	0.19102	203.7	0.3789	3.67599	5.042	4.977	0.9999	1.022
0.24983	0.23644	255.5	0.4752	4.61243	6.326	6.245	0.9999	1.027
0.25001	0.23688	255.4	0.4750	4.60970	6.322	6.241	0.9999	1.025
0.29971	0.28154	307.8	0.5725	5.55858	7.624	7.526	0.9998	1.032
0.30008	0.28166	308.1	0.5730	5.56344	7.630	7.532	0.9998	1.031
0.35009	0.32499	360.9	0.6713	6.52040	8.943	8.828	0.9998	1.037
0.35021	0.32512	358.8	0.6673	6.48145	8.889	8.775	0.9998	1.030
0.39551	0.36391	410.9	0.7643	7.42563	10.184	10.053	0.9997	1.045
0.40050	0.36814	416.0	0.7737	7.51790	10.311	10.178	0.9997	1.045
0.44952	0.40958	467.8	0.8701	8.45666	11.598	11.449	0.9996	1.048
0.45012	0.41008	469.7	0.8736	8.49167	11.646	11.497	0.9996	1.050
0.49661	0.45061	521.6	0.9703	9.43405	12.939	12.773	0.9995	1.059
0.49773	0.45085	522.3	0.9714	9.44518	12.954	12.773	0.9995	1.058

Table 1. (Continued)

Concentration		Freezing-point depression		$-\ln x_1 f_1$	Π		f_1	ϕ
m/mol kg^{-1}	c/mol dm^{-3}	mosmol	θ/°C		$\times 10^5$Pa	atm		
0.54993	0.49115	582.7	1.0839	1.05431×10^{-2}	14.460	14.274	0.9993	1.069
0.55039	0.49150	583.0	1.0844	1.05480	14.467	14.281	0.9993	1.069
0.59637	0.52796	634.3	1.1797	1.14796	15.744	15.542	0.9992	1.074
0.59671	0.52821	635.5	1.1820	1.15024	15.776	15.573	0.9992	1.075
0.64803	0.56814	694.7	1.2921	1.25783	17.251	17.030	0.9990	1.083
0.64903	0.56891	694.6	1.2910	1.25773	17.250	17.028	0.9991	1.081
0.70095	0.60857	754.3	1.4031	1.36642	18.740	18.500	0.9989	1.088
0.70099	0.60854	755.3	1.4049	1.36818	18.765	18.524	0.9989	1.090
0.74781	0.64375	809.1	1.5050	1.46622	20.109	19.851	0.9987	1.095
0.74817	0.64394	811.7	1.5097	1.47088	20.173	19.914	0.9987	1.098
0.79922	0.68144	872.5	1.6229	1.58176	21.694	21.415	0.9985	1.106
0.79931	0.68156	871.9	1.6216	1.58056	21.677	21.399	0.9985	1.105
0.84769	0.71643	931.9	1.7333	1.69004	23.179	22.881	0.9983	1.115
0.84869	0.71721	932.6	1.7346	1.69136	23.197	22.899	0.9983	1.114
0.89920	0.75302	990.4	1.8422	1.79701	24.646	24.330	0.9981	1.118
0.89937	0.75313	991.8	1.8447	1.79941	24.679	24.362	0.9981	1.119
0.94906	0.78769	1052.3	1.9573	1.91010	26.197	25.861	0.9979	1.126
0.94915	0.78774	1051.7	1.9561	1.90890	26.181	25.845	0.9979	1.125
0.99965	0.82239	1114.4	2.0727	2.02358	27.753	27.397	0.9976	1.133
1.00005	0.82263	1116.3	2.0762	2.02702	27.801	27.444	0.9976	1.135
1.19662	0.95164	1374.0	2.5555	2.49940	34.279	33.839	0.9964	1.171
1.19743	0.95179	1367.1	2.5427	2.48673	34.106	33.668	0.9965	1.165
				Raffinose				
0.03000	—	30.2	0.0562	5.4433×10^{-4}	0.747	0.737	1.000	1.007
0.03002	—	30.3	0.0564	5.4617	0.749	0.739	1.000	1.010
0.04990	—	50.8	0.0945	9.1581	1.256	1.240	1.000	1.019
0.04997	—	50.6	0.0941	9.1222	1.251	1.235	1.000	1.013
0.10004	—	102.4	0.1905	1.84661×10^{-1}	2.533	2.500	1.000	1.025
0.10007	—	102.0	0.1897	1.83944	2.523	2.490	1.000	1.021
0.14990	—	154.2	0.2868	2.78176	3.815	3.766	0.9999	1.031
0.14990	—	153.6	0.2857	2.77099	3.800	3.750	0.9999	1.027
0.19989	—	208.0	0.3869	3.75372	5.148	5.082	0.9998	1.044
0.20003	—	207.7	0.3863	3.74827	5.141	5.075	0.9999	1.042
0.24973	—	260.7	0.4849	4.70645	6.455	6.372	0.9998	1.048
0.24983	—	262.0	0.4873	4.72997	6.487	6.404	0.9998	1.053
0.29994	—	318.1	0.5917	5.74502	7.879	7.778	0.9996	1.066
0.29997	—	318.5	0.5924	5.75220	7.889	7.788	0.9996	1.067
0.34989	—	375.4	0.6982	6.78243	9.302	9.183	0.9995	1.079
0.35000	—	375.4	0.6982	6.78243	9.302	9.183	0.9995	1.079
0.39986	—	436.5	0.8119	7.88968	10.821	10.682	0.9993	1.099
0.39992	—	436.1	0.8112	7.88246	10.811	10.672	0.9993	1.098

The molal concentrations at which the osmolality of the solutions became larger than their molal concentration by 3% were about 800 mmol kg^{-1} for D-glucose, about 350 mmol kg^{-1} for sucrose, and about 150 mmol kg^{-1} for raffinose. In the dilute ideal aqueous solutions, plotting the osmolality against its molal concentration gives a linear curve. Actually, however, the degree of the deviation of the osmolality from the molal concentration depended on the molecular weight or the molecular volume. That is, the larger the molecular weight or the molecular volume, the larger the deviation became at the same concentration.

Table 2 shows the mean molar volumes $V_{1,2}$ of D-glucose, sucrose, and raffinose solutions at 25 °C. In order to obtain the partial molal volumes of water of the saccharide solutions, their $V_{1,2}$ values were plotted against the mole fraction of the saccharide x_2. All of them gave linear curves up to the highest concentrations examined, and all of the curves intersected with the $V_{1,2}$-axis at 0.01807 dm^3 mol^{-1}. Figure 1 shows plots of $V_{1,2}$ of the aqueous sucrose solution against x_2

Table 2. Mean Molar Volumes $V_{1,2}$ of Glucose, Sucrose, and Raffinose Aqueous Solutions as Functions of the Molal Concentrations m and Mole Fractions of Saccharides x_2

Concentration		Mean molar volume
m/mol kg^{-1}	x_2	$V_{1,2}$/dm^3 mol^{-1}
	D-Glucose	
0.05077	9.1433×10^{-4}	0.01815
0.10021	18.029	0.01824
0.14994	26.950	0.01832
0.19955	35.835	0.01840
0.25077	44.991	0.01849
0.30039	53.846	0.01857
0.39919	71.429	0.01874
0.59871	106.75	0.01907
0.80065	142.24	0.01941
0.99847	176.77	0.01974
1.19751	211.26	0.02007
1.39665	245.53	0.02039
1.59734	279.79	0.02072
1.79870	313.99	0.02105
	Sucrose	
0.04978	8.9635×10^{-4}	0.01824
0.09899	17.809	0.01841
0.15032	27.020	0.01859
0.19965	35.854	0.01876
0.24964	44.791	0.01894
0.30028	53.830	0.01911
0.35021	62.724	0.01928
0.39551	70.779	0.01944
0.44987	80.428	0.01963
0.49999	89.310	0.01980
0.55039	98.224	0.01998
0.59671	106.40	0.02013
0.64803	115.45	0.02031
0.70099	124.77	0.02049
0.74817	133.05	0.02065
0.79931	142.02	0.02083
0.84868	150.65	0.02100
0.89921	159.48	0.02117
0.94906	168.17	0.02134
1.00004	177.05	0.02151
1.19743	211.26	0.02219
	Raffinose	
0.049899	8.9854×10^{-4}	0.01833
0.099881	17.970	0.01859
0.15043	27.039	0.01885
0.20010	35.935	0.01911
0.24984	44.829	0.01937
0.29989	53.760	0.01963
0.35004	62.693	0.01988
0.40033	71.637	0.02014

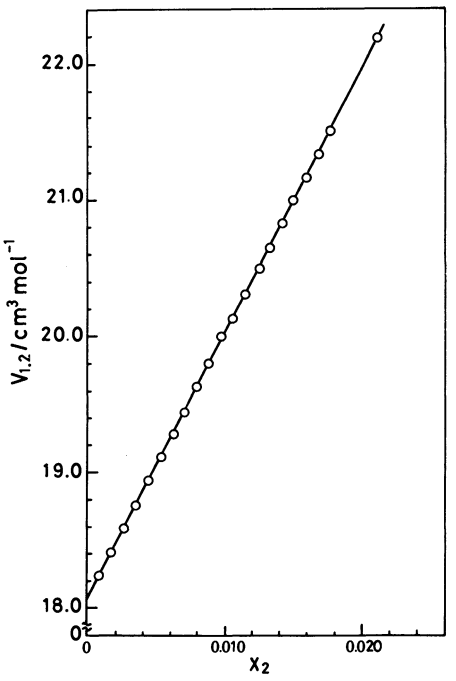

Fig. 1. Mean molar volume of aqueous sucrose solution $V_{1,2}$ as a function of sucrose mole fraction x_2.

as an example. The value of 0.01807 dm^3 mol^{-1} is almost equal to the molar volume of pure water, 0.0180685 dm^3 mol^{-1}, at 25 °C. This fact suggests that the aqueous saccharide solutions consist of a water phase which has the same property as bulky pure water and that of hydrated saccharide molecules scattered in the water phase, at least up to the highest concentrations examined in this study.

The partial molal volume $Vm_{(2)}$ of the 2 solute was calculated from the density ρ and the molar concentration c of the solution as follows. Assuming that the aqueous saccharide solution is composed of pure water and hydrated saccharide molecules, its density ρ is expressed by this equation:

$$\rho = \frac{M_2c+\rho_1(1.0000-Vm_{(2)}c)}{1.0000}\text{kg dm}^{-3} \qquad (10)$$

where M_2 and ρ_1 are the molecular weight of saccharide and the density of pure water respectively. By re-arranging Eq. 10, we obtain:

$$\rho = (M_2-\rho_1Vm_{(2)})c + \rho_1. \qquad (11)$$

Thus, if $Vm_{(2)}$ is constant, plots of the density ρ against c should give a linear curve whose slope is $(M_2-\rho_1Vm_{(2)})$ and $Vm_{(2)}$ can be calculated from the slope of this linear curve. After a linear relationship between ρ and c has been ascertained, the partial molal volume of a saccharide $Vm_{(2)}$ at each concentration c can also be calculated from the values of ρ, ρ_1, c, and M_2.

Table 3 shows the densities ρ of the D-glucose,

Table 3. Densities of Aqueous Saccharide Solutions ρ, Partial Molal Volumes of Saccharides $Vm_{(2)}$, Apparent Hydrated Volumes v_2^0 and Equivalent Radii r_2 of a Hydrated Saccharide Molecule at 25.00±0.01 °C

Concentration		Density	Partial molal volume	Apparent hydrated volume	Equivalent radius
m/mol kg^{-1}	c/mol dm^{-3}	ρ/kg dm^{-3}	$Vm_{(2)}$/dm^3 mol^{-1}	v_2^0/nm^3	r_2/nm
			D-Glucose		
0.04984	0.04942	1.0005	0.1111	0.1845	0.353
0.05077	0.05034	1.0005	0.1123	0.1865	0.354
0.10021	0.09881	1.0038	0.1124	0.1866	0.354
0.10078	0.09937	1.0039	0.1118	0.1856	0.354
0.14994	0.14702	1.0071	0.1123	0.1865	0.354
0.15149	0.14852	1.0072	0.1123	0.1865	0.354
0.19955	0.19462	1.0104	0.1120	0.1860	0.354
0.19992	0.19502	1.0104	0.1121	0.1861	0.354
0.25077	0.24320	1.0137	0.1121	0.1861	0.354
0.25110	0.24350	1.0137	0.1122	0.1863	0.354
0.29816	0.28766	1.0167	0.1122	0.1863	0.354
0.30039	0.28976	1.0167	0.1120	0.1860	0.354
0.39874	0.38059	1.0231	0.1121	0.1861	0.354
0.39919	0.38098	1.0231	0.1122	0.1863	0.354
0.59871	0.55939	1.0352	0.1123	0.1865	0.354
0.59939	0.55997	1.0352	0.1124	0.1866	0.354
0.79965	0.73166	1.0469	0.1124	0.1866	0.354
0.80065	0.73246	1.0469	0.1125	0.1868	0.355
0.99847	0.89515	1.0579	0.1125	0.1868	0.355
1.00029	0.89661	1.0580	0.1125	0.1868	0.355
1.19751	1.05235	1.0685	0.1126	0.1870	0.355
1.19822	1.05286	1.0685	0.1127	0.1871	0.355
1.39665	1.20343	1.0786	0.1127	0.1871	0.355
1.39818	1.20459	1.0787	0.1127	0.1871	0.355
1.59715	1.34972	1.0884	0.1128	0.1873	0.355
1.59734	1.34985	1.0884	0.1128	0.1873	0.355
1.79670	1.48987	1.0977	0.1130	0.1876	0.355
1.79870	1.49098	1.0978	0.1129	0.1875	0.355
			Sucrose		
0.05000	0.04912	1.0035	0.2120	0.3520	0.438
0.09982	0.09668	1.0098	0.2113	0.3508	0.438
0.10000	0.09732	1.0099	0.2111	0.3505	0.437
0.14985	0.14507	1.0161	0.2117	0.3515	0.438
0.15003	0.14527	1.0162	0.2112	0.3507	0.437
0.19997	0.19093	1.0221	0.2118	0.3517	0.438
0.20002	0.19102	1.0222	0.2114	0.3510	0.438
0.24983	0.23644	1.0281	0.2117	0.3515	0.438
0.25001	0.23688	1.0282	0.2115	0.3512	0.438
0.29971	0.28154	1.0340	0.2118	0.3517	0.438
0.30008	0.28166	1.0340	0.2118	0.3517	0.438
0.35009	0.32499	1.0391	0.2121	0.3522	0.438
0.35021	0.32512	1.0397	0.2118	0.3517	0.438
0.39551	0.36391	1.0447	0.2120	0.3520	0.438
0.40050	0.36814	1.0453	0.2119	0.3518	0.438
0.44952	0.40958	1.0507	0.2120	0.3520	0.438
0.45012	0.41008	1.0508	0.2119	0.3518	0.438
0.49661	0.45061	1.0561	0.2119	0.3518	0.438
0.49773	0.45085	1.0561	0.2120	0.3520	0.438
0.54993	0.49115	1.0613	0.2122	0.3523	0.438
0.55039	0.49150	1.0613	0.2122	0.3523	0.438
0.59637	0.52796	1.0661	0.2122	0.3523	0.438
0.59671	0.52821	1.0661	0.2122	0.3523	0.438

Table 3. (Continued)

Concentration		Density	Partial molal volume	Apparent hydrated volume	Equivalent radius
m/mol kg^{-1}	c/mol dm^{-1}	ρ/kg dm^{-3}	$Vm_{(2)}$/dm^3 mol^{-1}	v_2°/nm^3	r_2/nm^3
0.64803	0.56814	1.0713	0.2123	0.3525	0.438
0.64903	0.56891	1.0714	0.2123	0.3525	0.438
0.70095	0.60857	1.0766	0.2122	0.3523	0.438
0.70099	0.60854	1.0765	0.2124	0.3527	0.438
0.74781	0.64375	1.0813	0.2121	0.3522	0.438
0.74817	0.64394	1.0812	0.2123	0.3525	0.438
0.79922	0.68144	1.0860	0.2124	0.3527	0.438
0.79931	0.68156	1.0861	0.2123	0.3525	0.438
0.84769	0.71643	1.0905	0.2125	0.3528	0.438
0.84869	0.71721	1.0907	0.2124	0.3527	0.438
0.89920	0.75302	1.0953	0.2125	0.3528	0.438
0.89937	0.75313	1.0953	0.2125	0.3528	0.438
0.94906	0.78769	1.0997	0.2126	0.3530	0.438
0.94915	0.78774	1.0997	0.2126	0.3530	0.438
0.99965	0.82239	1.1043	0.2125	0.3528	0.438
1.00005	0.82263	1.1043	0.2126	0.3530	0.438
1.19662	0.95164	1.1208	0.2129	0.3535	0.439
1.19743	0.95179	1.1208	0.2129	0.3535	0.439
		Raffinose			
0.049899	0.049004	1.0068	0.3068	0.5094	0.495
0.099881	0.096629	1.0162	0.3074	0.5104	0.496
0.15043	0.14337	1.0255	0.3070	0.5098	0.496
0.20010	0.18797	1.0343	0.3074	0.5104	0.496
0.24984	0.23136	1.0428	0.3077	0.5109	0.496
0.29989	0.27381	1.0512	0.3076	0.5107	0.496
0.35004	0.31515	1.0594	0.3076	0.5107	0.496
0.40033	0.35545	1.0673	0.3078	0.5111	0.496

sucrose, and raffinose solutions as functions of the molal m and molar c concentrations. When the ρ values are plotted against c, they give straight curves in all the concentrations up to the highest in the freezing-point-depression experiments. The partial molal volumes of D-glucose, sucrose, and raffinose, as calculated from their slopes, were almost constant from diluted up to concentrated concentrations; they were 0.1123, 0.2123, and 0.3075 dm^3 mol^{-1} respectively. The values of the density ρ and the molal volume $Vm_{(2)}$ of the saccharides examined were almost coincident with those reported by Shahidi et al.[27]

Since the partial molal volume of the saccharide is constant up to an infinitely diluted concentration where the partial molal volume of the water is equal to the molar volume of pure water and where solute–solute interactions can be disregarded, it is safe to say that the partial molal volume of the saccharide is equal to the volume of the apparent volume of a hydrated saccharide molecule multiplied by the Avogadro number. Thus, the apparent volume of a hydrated saccharide molecule v_2° was obtained by dividing $Vm_{(2)}$ by the Avogadro number N_A, i.e.,

$$v_2^\circ = Vm_{(2)}/N_A. \tag{12}$$

The equivalent radius of a hydrated saccharide molecule r_2 was calculated as follows. Assuming that the hydrated saccharide molecule is spherical,

$$v_2^\circ = \frac{4}{3}\pi r_2^3. \tag{13}$$

Thus,

$$r_2 = \sqrt[3]{\frac{3}{4\pi}v_2^\circ}. \tag{14}$$

The calculated results are also shown in Table 3.

The apparent volume of one hydrated D-glucose, sucrose, or raffinose molecule was obtained as 0.1865, 0.3525, or 0.5105 nm^3 respectively. These values indicate that the apparent volume of the hydrated saccharide molecule is approximately proportional to the molecular weight.

Discussion

The present studies have made it clear that (1) the osmolality and the freezing-point depression of aqueous saccharide solutions are proportional to the molal concentration at dilute concentrations, although they become larger than the values of the molal concentration at higher concentrations; (2) the degree of the deviation depends on the molecular weight or the molecular volume of the solute; (3) the

activity coefficients of the water of aqueous saccharide solutions at the freezing point are almost unity up to 1.0 mol kg^{-1} for D-glucose, up to 0.65 mol kg^{-1} for sucrose, and up to 0.4 mol kg^{-1} for raffinose, while the osmotic coefficients of aqueous saccharide solutions tend to increase with an increase in the saccharide concentration; (4) the addition of saccharide molecules to the aqueous saccharide solution has little effect on the partial molal volume of the water, which is almost equal to the molar volume of pure water, at least up to the highest concentrations examined, and (5) the volume of a hydrated saccharide molecule is proportional to the molecular weight.

The fact that the addition of saccharide molecules to water or to its aqueous solution has little effect on the partial molal volume of the water suggests that their addition induces insignificant changes in the water structure, except in the vicinity of the solute molecules of the aqueous solution. Further, this suggests that we may ignore the effects of the saccharide molecules on the structure of the water phase surrounding the cell membrane, especially in the neighborhood of the inlet or outlet of the water-filled pores[28] and ion pores.

Miyajima et al.,[29] measuring the excess partial molar entropy, one of the thermodynamic quantities, of water for D-glucose, D-mannose, and D-galactose, reported that the ordering of water molecules occurred by the dissolution of these monosaccharides. Judging from the present results, their results may reflect an ordering of the water structure in the vicinity of the solute molecule as a result of hydration. However, this discrepancy between the present results and Miyajima et al.'s cannot be explained until an analysis of water structure is done by some other methods, such as X-ray diffraction or neutron scattering, that will enable us to detect some actual changes in the water structure.

Since the $R\ln x_1$ term is derived from the entropy of mixing $\Delta S_{1,2}$ on the basis of statistical mechanics,[25,30] the type of its expression should be different depending on the model adopted to evaluate the entropy of mixing. From primary statistical mechanics, the second term of the chemical potential equation, expressed as $R\ln x_1$, is derived based on the well-known lattice model under the assumptions that the solvent and the solute are nearly equal in size and that the distance between the lattice is constant, though arbitrary.

Based on the lattice model, some modified equations have been proposed to explain the entropy change of the mixing of solutions composed of solute and solvent molecules of different sizes.[31-35] However, since the present author thought of those models as less actual, he omitted the analysis of the molecular-weight or molecular-size dependence of $R\ln x_1$ as a function of the concentration.

Beginning in 1902[36] Morse and his colleagues extensively studied the osmotic pressure of rather dilute sucrose solutions using an apparatus of their own design, equipped with a semi-permeable membrane formed from both potassium ferocyanide and copper sulphate solutions. Since no one else has ever measured the osmotic pressure of dilute aqueous saccharide solutions using semi-permeable membranes, the present author has shown their results[37] in Table 4 to compare them with his own values calculated from the freezing-point-depression method. The osmotic pressure calculated coincides well with those directly measured by Morse et al. at 20 °C in the range of lower concentrations, while at higher concentrations the present results coincide well with those measured previously at 25 °C. However, the present results give values a little higher than Morse et al.'s at 0 °C. These small differences between the present results and Morse et al.'s might come from the difference between Eq. 1 and Eq. 3, used to calculate the water activity using the freezing-point-depression method. This problem should be checked when the molar-heat capacities of water and ice are precisely measured.

The equivalent radii of the hydrated saccharide molecules obtained by the present author are smaller

Table 4. The Osmotic Pressure of Sucrose Solutions as Functions of the Temperature (Morse et al.[37])

Concentration m	Osmotic pressure/atm					
	Temperature/°C					
	0	5	10	15	20	25
0.1	2.462	2.452	2.498	2.541	2.590	2.634
0.2	4.722	4.818	4.893	4.985	5.064	5.148
0.3	7.085	7.198	7.334	7.476	7.605	7.729
0.4	9.442	9.608	9.790	9.949	10.137	10.296
0.5	11.895	12.100	12.297	12.549	12.748	12.943
0.6	14.381	14.605	14.855	15.144	15.388	15.624
0.7	16.886	17.206	17.503	17.815	18.128	18.434
0.8	19.476	19.822	20.161	20.535	20.905	21.254
0.9	22.118	22.478	22.884	23.305	23.717	24.126
1.0	24.825	25.283	25.693	26.189	26.638	27.053

than those adopted by Durbin[38] to estimate the equivalent pore radius of the cellulose membrane. Hereafter, however, the equivalent radii of the hydrated saccharide molecules obtained by the present author will be used to estimate the equivalent pore radius of the membrane through which water and solute molecules pass, for the present author's procedure to obtain them seems to be more reasonable.

In studies of water and solute flows across such permeable membranes as the cell wall[39] and water and permeable-solute flows across the cell membrane,[40-42] not only the equivalent radius but also the properties of the surfaces of the saccharide molecules[43] and the permeable molecules are important, for solute–solute, solute–solvent, and solvent–solvent interactions at the inlet of the water-filled pores, those in the water-filled pores and/or ion pores, and solute-solvent-surface molecules of the water-filled pore and/or ion pore interactions at the inlet, and those in the water-filled pores and/or ion pores may have much to do with the membrane phenomena.[28,44]

The freezing point of the water containing dissolved air was lower than that of the air-free water by 0.36 mosmol, or 0.0007 °C on the average. However, under physiological conditions, the solutions inside (cytoplasm and vacuolar sap) and outside a cell can be considered to contain nearly equal amounts of such gases as N_2, O_2, and CO_2. Therefore, the effect of the dissolved air on the difference in the osmotic pressure between inside and outside the cell is not only practically, but also theoretically, insignificant.

Appendix

A Precise Equation of Freezing-Point Depression. The actual phenomena occurring in freezing-point depression in an aqueous solution consist of an unstable state caused by the creation of a chemical potential difference between the liquid water and the ice of the aqueous solution by supercooling up to a certain temperature T' K below the freezing point of the aqueous solution to be tested, T K, and pure water, T° K, a non-equilibrium process, which is followed by an equilibrium state. During the non-equilibrium process, ice grows and the temperature of the aqueous mixture containing the ice rises to T K from T' K, which is dependent on the water activity of the aqueous solution: this nullifies the difference in the chemical potential. The difference in temperature between T° and T is the freezing-point depression.

Thus, the difference in the chemical potential between the ice and the liquid water at T' K shouls be calculated as a function of the temperature. To do this, chemical potentials of both the ice and the water must be obtained as functions of the temperature and the water concentration. The chemical potentials of ice $\mu_1^{\circ s}(T)$ and of liquid water $\mu_1^{\circ l}(T)$ are formulated as, respectively:

$$\mu_1^{\circ s}(T) = \overset{s}{Hm}_{(1)}(T) - T\overset{s}{Sm}_{(1)}(T) \tag{1}$$

$$\mu_1^{\circ l}(T) = \overset{l}{Hm}_{(1)}(T) - T\overset{l}{Sm}_{(1)}(T) \tag{2}$$

where $Hm_{(1)}(T)$ and $Sm_{(1)}(T)$ are the partial molar enthalpy and the partial molar entropy of water respectively, and where the suffixes s, l, and 1 repesrent solid(ice) and liquid states, and water, respectively. For an ideal aqueous solution where the mole fraction of water is x_1:

$$\mu_1^l(T) = \overset{l}{Hm}_{(1)}(T) - T\overset{l}{Sm}_{(1)}(T) + TR\ln x_1. \tag{3}$$

Here,

$$\overset{s}{Hm}_{(1)}(T) = \int_0^T \overset{s}{Cp,m_{(1)}}(T'')\mathrm{d}T'' \tag{4}$$

$$\overset{l}{Hm}_{(1)}(T) = \int_0^{T^\circ} \overset{s}{Cp,m_{(1)}}(T'')\mathrm{d}T'' + \Delta_{fus}Hm_{(1)}(T^\circ) - \int_T^{T^\circ} \overset{l}{Cp,m_{(1)}}(T'')\mathrm{d}T'', \tag{5}$$

$$\overset{s}{Sm}_{(1)}(T) = \int_0^T \overset{s}{Cp,m_{(1)}}(T'')\frac{\mathrm{d}T''}{T''}, \tag{6}$$

$$\overset{l}{Sm}_{(1)}(T) = \int_0^{T^\circ} \overset{s}{Cp,m_{(1)}}(T'')\frac{\mathrm{d}T''}{T''} + \frac{\Delta_{fus}Hm_{(1)}(T^\circ)}{T^\circ} - \int_T^{T^\circ} \overset{l}{Cp,m_{(1)}}(T'')\frac{\mathrm{d}T''}{T''} \tag{7}$$

where $\overset{s}{Cp,m_{(1)}}(T)$, $\overset{l}{Cp,m_{(1)}}(T)$, and $\Delta_{fus}Hm_{(1)}(T)$ are the molar heat capacity of ice(solid) and liquid water as functions of the temperature at a constant pressure, and the molar heat of the fusion of ice at temperature T K, respectively.

In the equilibrium state,

$$\mu_1^l(T) = \mu_1^{\circ s}(T). \tag{8}$$

From Eqs. 1 and 3, Eq. 8 becomes:

$$\overset{l}{Hm}_{(1)}(T) - \overset{s}{Hm}_{(1)}(T) = T\{\overset{l}{Sm}_{(1)}(T) - \overset{s}{Sm}_{(1)}(T) - R\ln x_1\}. \tag{9}$$

Since

$$\overset{l}{Hm}_{(1)}(T) - \overset{s}{Hm}_{(1)}(T) = \Delta_{fus}Hm_{(1)}(T), \tag{10}$$

Eq. 9 becomes:

$$\frac{\Delta_{fus}Hm_{(1)}(T)}{T} = \overset{l}{Sm}_{(1)}(T) - \overset{s}{Sm}_{(1)}(T) - R\ln x_1. \tag{11}$$

For pure water, we have the same equation as Eq. 11, i.e.;

$$\frac{\Delta_{fus}Hm_{(1)}(T^\circ)}{T^\circ} = \overset{l}{Sm}_{(1)}(T^\circ) - \overset{s}{Sm}_{(1)}(T^\circ). \tag{12}$$

Thus, from Eqs. 11 and 12, we obtain this equation:

$$\frac{\Delta_{fus}Hm_{(1)}(T)}{T} - \frac{\Delta_{fus}Hm_{(1)}(T^\circ)}{T^\circ} + \overset{l}{Sm}_{(1)}(T^\circ) - \overset{l}{Sm}_{(1)}(T) - \overset{s}{Sm}_{(1)}(T^\circ) + \overset{s}{Sm}_{(1)}(T) = -R\ln x_1. \tag{13}$$

Since the molar heat of the fusion of ice at T' K, $\Delta_{fus}Hm_{(1)}(T')$, is expressed with the molar heat of the fusion of ice at T° K, $\Delta_{fus}Hm_{(1)}(T^\circ)$, by this equation:

$$\Delta_{fus}Hm_{(1)}(T') = \Delta_{fus}Hm_{(1)}(T^\circ) - \int_{T'}^{T^\circ} \{\overset{l}{Cp,m_{(1)}}(T'') - \overset{s}{Cp,m_{(1)}}(T'')\}\mathrm{d}T'', \tag{14}$$

introducing Eqs. 4, 5, 6, 7, and 14 into Eq. 13 and then rearranging it gives:

$$\Delta_{fus}Hm_{(1)}(T^\circ)\left(\frac{1}{T}-\frac{1}{T^\circ}\right) - \frac{1}{T}\int_T^{T^\circ}\{\overset{1}{Cp},m_{(1)}(T'')-\overset{s}{Cp},m_{(1)}(T'')\}dT'' + \int_T^{T^\circ}\frac{\overset{1}{Cp},m_{(1)}(T'')-\overset{s}{Cp},m_{(1)}(T'')}{T''}dT'' = -R\ln x_1. \quad (15)$$

This equation is a theoretically precise expression of the freezing-point depression in ideal aqueous solutions.

The author should like to thank Prof. Takashi Katayama, Dr. Tomoshige Nitta, and Dr. Manabu Yamaguchi, Department of Chemical Engineering, Faculty of Engineering Science, Osaka University, for permitting him to use the densimeter. He also wishes to thank Miss Atsuko Ookawa for typewriting this manuscript.

References

1) M. Tazawa and N. Kamiya, *Aust. J. Biol. Sci.*, **19**, 399 (1966).
2) K. Kiyosawa and M. Tazawa, *Protoplasma*, **74**, 257 (1972).
3) K. Kiyosawa and M. Tazawa, *Protoplasma*, **78**, 203 (1973).
4) J. Gutknecht and M. A. Bisson, "Water Relations in Membrane Transport in Plants and Animals," ed by A. M. Jungreis, T. K. Hodges, A. Kleinzeller, and S. G. Schultz, Academic Press, New York (1977).
5) K. Raschke, "Water Relations in Membrane Transport in Plants and Animals," ed by A. M. Jungreis, T. K. Hodges, A. Kleinzeller, and S. G. Schultz, Academic Press, New York (1977).
6) I. Tasaki, I. Singer, and T. Takenaka, *J. Gen. Physiol.*, **48**, 1095 (1965).
7) I. Tasaki, "Nerve Excitation," Charles C. Thomas Publisher, Springfield, Illionis (1968).
8) M. Tazawa and T. Shimmen, *Seitai No Kagaku*, **28**, 193 (1977).
9) E. J. Hewitt and T. A. Smith, "Plant Mineral Nutrition," The English University Press, Ltd., London (1974).
10) U. Lüttge and N. Higinbotham, "Transport in Plants," Springer-Verlag, New York (1979).
11) J. A. Raven, "Transport in Plants, IIA," ed by U. Lüttge and M. G. Pitman, Springer-Verlag, Berlin (1976).
12) D. H. Junnings, "Transport in Plants, IIA," ed by U. Lüttge and M. G. Pitman, Springer-Verlag, Berlin (1976).
13) N. Kamiya and M. Tazawa, *Protoplasma*, **46**, 394 (1956).
14) M. Tazawa and N. Kamiya, *Ann. Rep. Biol. Works, Fac. Sci., Osaka Univ.*, **13**, 123 (1965).
15) M. Tazawa and K. Kiyosawa, *Ann. Rep. Biol. Works, Fac. Sci., Osaka Univ.*, **18**, 57 (1970).
16) S. Nakagawa, H. Kataoka, and M. Tazawa, *Plant Cell Physiol.*, **15**, 457 (1974).
17) T. Shimmen and M. Tazawa, *J. Membr. Biol.*, **37**, 167 (1977).
18) K. Schäfer and E. Lax, "Landolt-Börnstein: Zahlenwerte und Funktionen aus Physik, Chemie, Astronomie, Geophysik und Technik IIa: Gleichgewichte Dampf-Kondensat und Osmotische Phänomene," Springer-Verlag (1960).
19) I. Hatakeyama, "Seibutsu Butsuri Handobukku," Yoshioka Shoten, Kyoto (1970).
20) I. Honjo, W. Oosawa, T. Kira, Y. Koshida, and M. Tazawa, "Kiso Seibutsu Handobukku," Iwanami Shoten, Tokyo (1980).
21) "Handbook of Chemistry and Physics," ed by R. C. Weast, CRC Press, Cleveland, Ohio (1974).
22) N. E. Dorsey, "Properties of Ordinary Water-Substance," Hafner Publishing Co., New York (1968).
23) F. G. Donnan and E. A. Guggenheim, *Z. Phys. Chem.*, **A162**, 346 (1932).
24) I. Prigogine and R. Defay, "Thermodynamique Chimique," Editions Desoer, Liege (1944).
25) R. Fujishiro and T. Kuroiwa, "Yoeki No Seishitsu," Tokyo-Kagaku-Dojin, Tokyo (1966).
26) J. Bernhardt and H. Pauly, *J. Phys. Chem.*, **84**, 158 (1980).
27) F. Shahidi, P. G. Farrell, and J. T. Edward, *J. Solution Chem.*, **5**, 807 (1976).
28) K. Kiyosawa and K. Ogata, *Plant Cell Physiol.*, **28**, 1013 (1987).
29) K. Miyajima, M. Sawada, and M. Nakagaki, *Bull. Chem. Soc. Jpn.*, **56**, 1620 (1983).
30) D. A. T. Dick, "Cell Water," Butterworths, London (1966).
31) R. H. Fowler and G. S. Rushbrooke, *Trans. Faraday Soc.*, **33**, 1272 (1937).
32) F. Oosawa, *Busseiron Kenkyu*, **8**, 40 (1947).
33) E. A. Guggenheim, "Mixtures: The Theory of the Equilibrium Properties of Some Simple Classes of Mixtures, Solutions and Alloys," Oxford University Press, London (1952).
34) I. Prigogine, N. Trappeniers, and V. Mathot, *Discuss. Faraday Soc.*, **No. 15**, 93 (1953).
35) B. E. Conway and R. E. Verrall, *J. Phys. Chem.*, **70**, 1473 (1966).
36) H. N. Morse and J. C. W. Frazer, *Am. Chem. J.*, **28**, 1 (1902).
37) H. N. Morse, W. W. Holland, E. G. Zies, C. N. Nyers, W. M. Clark, and E. E. Gill, *Am. Chem. J.*, **45**, 554 (1911).
38) R. P. Durbin, *J. Gen. Physiol.*, **44**, 315 (1960).
39) K. Kiyosawa, *Bot. Mag. Tokyo*, **88**, 47 (1975).
40) O. Kedem and A. Katchalsky, *J. Gen. Physiol.*, **45**, 143 (1961).
41) J. Dainty and B. Z. Ginzburg, *J. Theor. Biol.*, **5**, 256 (1963).
42) E. Steudle and S. D. Tyerman, *J. Membrane Biol.*, **75**, 85 (1983).
43) K. Miyajima, K. Machida, and M. Nakagaki, *Bull. Chem. Soc. Jpn.*, **58**, 2595 (1985).
44) K. Kiyosawa and K. Okihara, *Plant Cell Physiol.*, **29**, 9 (1988).

Kinetics of the Interaction between DNA and Acridine Orange

Naohisa KURE, Takayuki SANO,* Shoji HARADA, and Tatsuya YASUNAGA
Department of Materials Science, Faculty of Science, Hiroshima University, Hiroshima 730
(Received July 14, 1987)

Both static and kinetic investigations have been performed on the interaction of calf thymus DNA with Acridine Orange (AO). The binding isotherm obtained spectrophotometrically was analyzed by a site exclusion theory and revealed the presence of two binding modes of dye molecule corresponding to intercalation and dimerization on DNA. In the kinetic experiments focusing on the intercalation mode by the temperature-jump technique, three relaxations were observed. From the analyses of both the relaxation time and amplitude, the two fast relaxations were ascribed to parallel binding reactions including a bimolecular pathway for direct transfer of dye molecule on the polymer and the slow relaxation was attributable to a conformational change of DNA molecules. The binding parameters kinetically obtained suggest that 80% of bound AO is in intercalated form and the remainder is in partially intercalated one as an external bound form.

The interaction of acridine dyes with deoxyribonucleic acid (DNA) has been extensively studied because of their wide biological activities.[1-5] Acridine dyes have two binding modes on DNA with different affinities. Most experiments have been focused on the strong binding mode which has been related to the biological activity of the dyes, and elucidated that this binding mode structurally corresponds to an intercalation of dye between two adjacent base pairs of DNA.[6-12]

The stoichiometry of the binding of acridine dyes to DNA has been investigated by equilibrium dialysis[13-19] and/or visible spectroscopy.[13,20-22] The affinity of the intercalation mode has been found firstly to be independent of the base composition of DNA.[13,20,21] For this reason, various static and kinetic models have been proposed on the assumption of homogeneous DNA sites for the binding of acridine dyes.[16,23-27] However, the heterogeneity of the binding site has been pointed out from the fluorescence studies on several acridine dye-DNA complexes.[28-36] Given these circumstances, the investigation on more fundamental nature of the binding through the reexamination of the proposed binding models are desirable. For this purpose, Acridine Orange (AO) would be most favorable since this dye is known to form the intercalative complex independent of the base specificity of DNA.[32,33,35,37]

In this paper, thus the interaction between AO and calf thymus DNA focusing on the intercalative binding mode was studied by visible spectrophotometry and temperature-jump spectroscopy. A basic nature of the binding mechanism of acridine dyes with double stranded DNA was also discussed.

Experimental

Calf thymus DNA (sodium salt, type I) was purchased from Sigma Chemical Company and purified twice by phenol extraction. The hyperchromicity on thermal denaturation at 260 nm was 37—38% at pH 6.5 in the 1 mM† phosphate buffer. The concentration of DNA was determined using $\varepsilon_{260}=6600\ M^{-1}\ cm^{-1}$ per nucleotide. Acridine Orange (AO) was purchased from Eastman Kodak Company and was recrystallized twice as the base from a solution of Acridine Orange hydrochloride in a 1:1 water–ethanol mixture. The concentration of AO was determined spectrophotometrically at 492 nm by using the molar extinction coefficient proposed by Stone and Bradley.[38] Other chemicals used were reagent grade. All sample solutions were prepared in lmM phosphate buffer containing 0.2 M sodium chloride at pH 6.5.

Absorption spectra were measured with a Union Giken SM 401 spectrophotometer. Kinetic measurements were performed using the joule heating temperature-jump apparatus of which detail has been described elsewhere.[39] The light source was a halogen lamp (250 W) and the path length of the cell was 10 mm. The rise time and magnitude of the temperature-jump were about 10 μs and 7 °C, respectively. The orientational effect of DNA was canceled out by placing the polarizer between the cell and the monochromator.

All the static and kinetic measurements were performed at 25.0±0.2 °C. The data were analyzed on the basis of the neighbor exclusion model established by McGhee and von Hippel.[40]

Results

Binding Isotherm. The visible absorption spectra of AO–DNA complexes at various P/D (the ratio of DNA phosphate to dye) values in 0.2 M NaCl solution displayed an isosbestic point at 496 nm, in agreement with the results reported by Fredericq and Houssier.[17] They tried to obtain a binding isotherm from spectral shifts using the absorbance at 465 nm, but failed to obtain the consistent results with the equilibrium dialysis ones. This discrepancy in the binding data seems to come from the fact that molar extinction coefficient at 465 nm of bound AO varies significantly depending on the binding ratio r (bound AO/DNA phosphate).

In the present study, the binding isotherm was determined spectrophotometrically using the absorbance at 492 nm since the molar extinction coefficient on bound AO at this wavelength was reported to be

† 1 M=1 mol dm^{-3}.

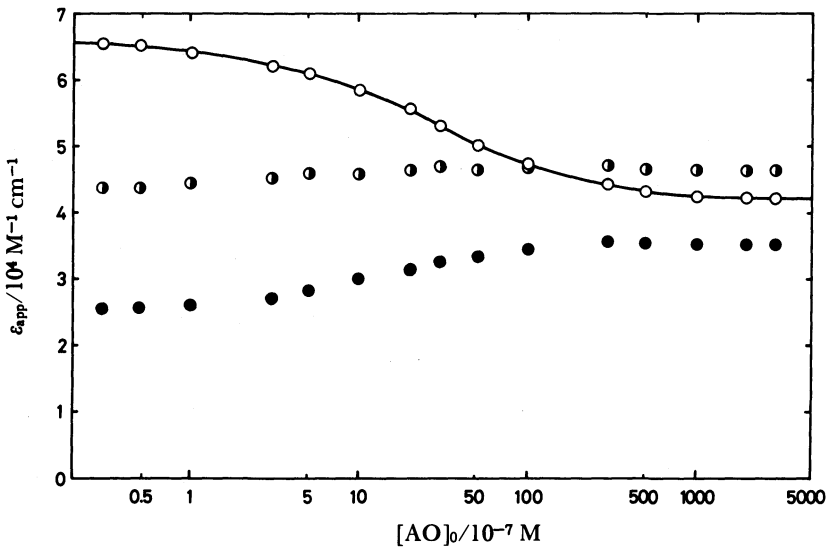

Fig. 1. Change in apparent molar extinction coefficient (ε_{app}) of AO–DNA solution with increasing AO concentration at a fixed P/D of 10 and 25 °C: (O), at 492 nm; (O), at 504 nm; (●), at 510 nm.

invariant for r below 0.2.[16] The apparent molar extinction coefficient (ε_{app}) of AO–DNA solutions were measured at various AO concentrations from 3×10^{-8} M to 3×10^{-4} M by holding P/D equal to 10, and represented in Fig. 1. In the solution of AO alone, generally, the dimerization equilibrium of the dye must exist. But in the system involving DNA under the present experimental condition of $r<0.2$, the contribution of dimeric species to the free AO molecule is less than 5%. Consequently, in the present analyses, the free AO molecule was regarded as all monomeric species. From the lower and higher limits of concentration in this figure, the extinction coefficients at 492 nm were obtained to be $\varepsilon_f=66000$ $M^{-1}cm^{-1}$ for free AO and $\varepsilon_b=42000\ M^{-1}cm^{-1}$ for bound AO, respectively. The concentration of free dye, A, and the binding ratio, r, were determined from the next equations:

$$A=\frac{\varepsilon_{app}-\varepsilon_b}{\varepsilon_f-\varepsilon_b}A_0 \tag{1}$$

$$r=\frac{A_0-A}{P_0} \tag{2}$$

where A_0 and P_0 are the total concentrations of AO and DNA (in phosphate unit), respectively. In Fig. 2, a Scatchard plot using these equations was illustrated together with those obtained from equilibrium dialysis experiments by Armstrong et al.,[16] and Fredericq et al.[17] A good agreement between these isotherms suggests the validity of the spectrophotometrical method employed in this study.

The obtained binding isotherm was analyzed by considering a dimeric species formed by an additional

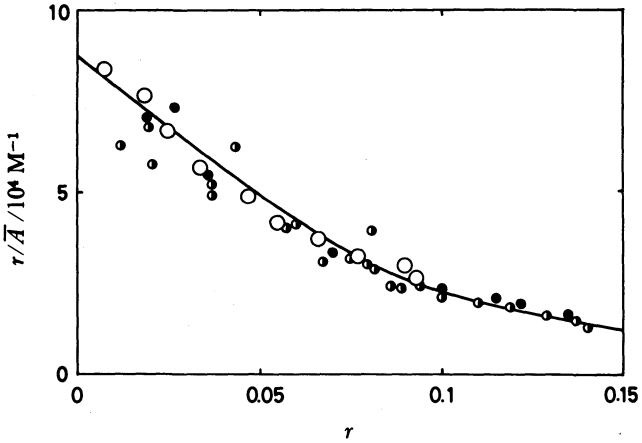

Fig. 2. Scatchard plots of binding of AO to DNA at 25 °C: (O), obtained from the present spectrophotometrical method in 0.2 M NaCl solution; (●), by Armstrong et al.,[16] in 0.2 M NaCl solution; (◑), by Fredericq and Houssier[17] in 0.1 M NaCl solution. The solid line shows the theoretical curve calculated using $n=3$, $K_I=1.8\times10^5\ M^{-1}$, and $K_D=3\times10^4\ M^{-1}$.

binding of free dye to bound dye on DNA reported by Armstrong et al.[16] The Scatchard equation, based on the site exclusion theory including such dimerization mode was reported to be[19]

$$\frac{r}{\bar{A}}=\frac{K_I}{2}\frac{\{(1-2nr)+2K_D\bar{A}(1-nr)\}^n}{\{[1-2(n-1)r]+2K_D\bar{A}[1-(n-1)r]\}^{n-1}} \tag{3}$$

where K_I, K_D, n, and the overbar refer to the binding constant for intercalation, that of dimerization on the polymer, the number of sites blocked by one bound

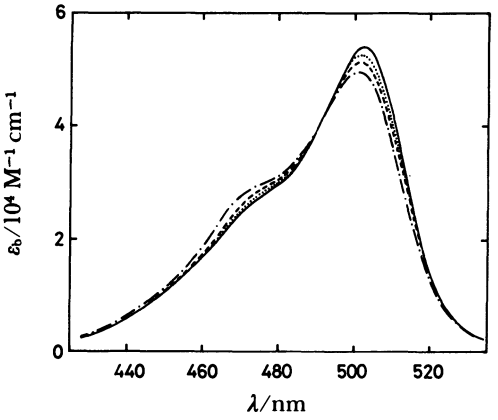

Fig. 3. Absorption spectra of AO-DNA complexes in 0.2 M NaCl solution at various values of binding ratio r: (——), r=0.01; (·····), r=0.032; (---), r=0.045; (—·—), r=0.076. The total dye concentration is 10^{-5} M.

dye, and the equilibrium concentration, respectively. The analysis of the binding isotherm using this equation yields the following binding parameters: K_I=1.8×10^5 M^{-1}, K_D=3×10^4 M^{-1}, and n=3. As can be seen in Fig. 2, all observed data fall on the theoretical curve calculated using these values within an experimental uncertainty. These results are consistent with the assignment of the binding isotherm to the intercalation and dimerization modes.

Spectral Properties of Intercalated AO. In order to examine the spectral properties of intercalative species, the absorption spectra of AO-DNA complex were measured for P/D values above 10 at constant DNA concentration, where the contribution of bound dimer species is negligibly small (estimated from the values of K_I and K_D). Figure 3 illustrates the spectra of bound dye molecules obtained by a substraction of the contribution of free dye. As judged from the figure, an absorption peak at longer wavelength is progressively depressed and a shoulder at shorter one increases gradually with binding. This kind of spectral behavior has been reported as characteristics of AO-AO interactions on polymers.[41] Since the bound dimer species is negligible under the present experimental condition of r<0.1, the observed spectral variation would be attributable to the interaction between monomeric intercalated AO molecules. This assignment is supported by other optical properties of bound AO observed in the corresponding range of r, e.g., fluorescence depolarization[17,35] and exciton splitting in circular dichroism.[17,42,43]

As an additional remark, it should be noted that the constant absorbance at 492 nm of bound AO in Fig. 3, led us to using of this wavelength to obtain the binding isotherm in the preceding section.

Characteristics of Relaxation. Since our primary attention is the intercalation mechanism, the temperature-jump measurements were performed in the range of r below 0.1. An instantaneous and small absorbance change, beyond the resolution time of the apparatus, was followed by three distinguishable relaxation processes as shown in Figs. 4a and 4b. These three processes are named fast, middle and slow processes in order of the time region fast to slow. The relaxation amplitudes of these relaxations are represented in Fig. 5. As shown in Fig. 5a, the spectra of relaxation amplitudes of the fast and middle processes are well correlated to the difference spectrum between free AO and intercalated AO (the difference spectrum was illustrated using the extinction coefficients in Fig. 1). On the other hand, as shown in Fig. 5b, the spectrum of relaxation amplitude of the slow process is quite similar to the difference spectra between intercalated AO at different binding ratios (the difference spectra were obtained from the spectra in Fig. 3).

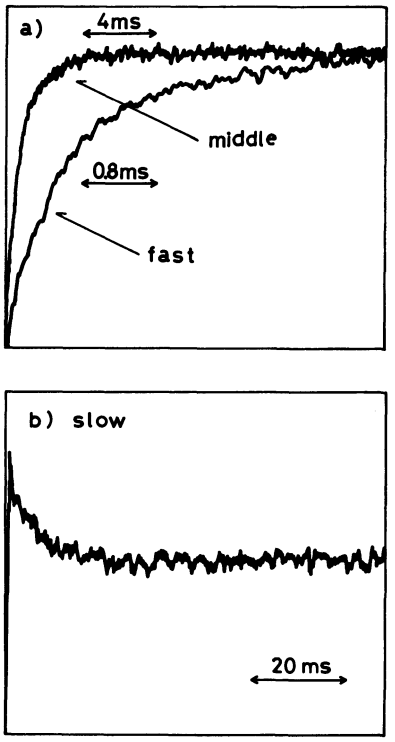

Fig. 4. Typical relaxation curves observed for AO-DNA system in 0.2 M NaCl solution at 480 nm (absorbance increasing upward): (a), fast and middle process, [AO]=1.0×10^{-5} M and [DNA]-phosphate=1.0×10^{-5} M; (b), slow process observed by averaging 4 repetitions, [AO]=3.0×10^{-5} M and [DNA]phosphate=9×10^{-4} M. The final temperature is 25 °C.

To see the reaction mechanism in more detail two kinds of concentration dependence of the reciprocal relaxation times were measured for each process: Figure 6 shows their concentration dependences at

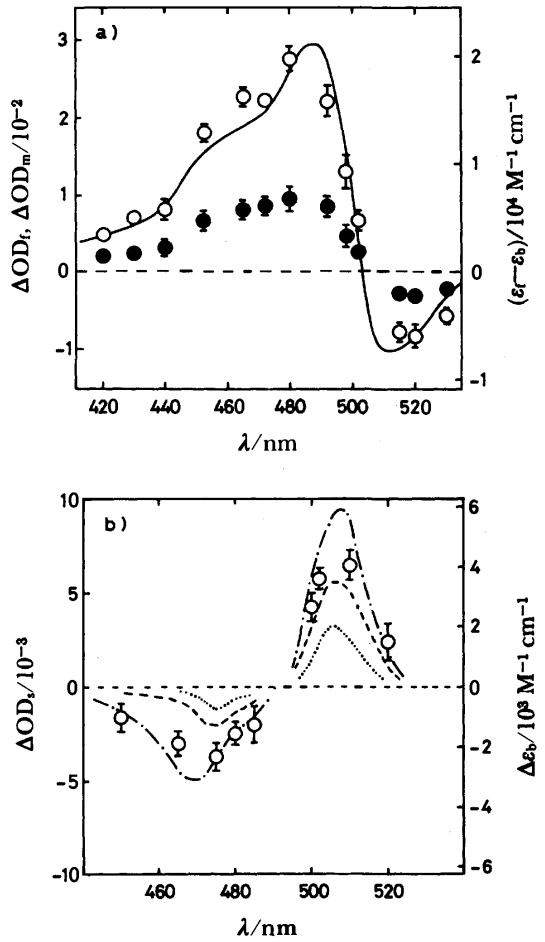

Fig. 5. Wavelength depedence of relaxation amplitude of each process. (a) , (○) and (●) represent the experimental values of ΔOD_f and ΔOD_m, respectively, at [AO]=1.0×10^{-5} M and [DNA]phosphate=1.0×10^{-4} M. The solid curve shows the difference spectrum between free and intercalated AO ($\varepsilon_f-\varepsilon_b$). (b), (○) represents the experimental values of ΔOD_s at [AO]=5×10^{-3} M and [DNA]phosphate=1.5×10^{-3} M. The curves show the difference spectra between intercalated AO at different values of r: (—·—), $\varepsilon_b^{0.01}-\varepsilon_b^{0.076}$; (---), $\varepsilon_b^{0.01}-\varepsilon_b^{0.045}$, (·····), $\varepsilon_b^{0.01}-\varepsilon_b^{0.032}$, where superscripts refer to binding ratio.

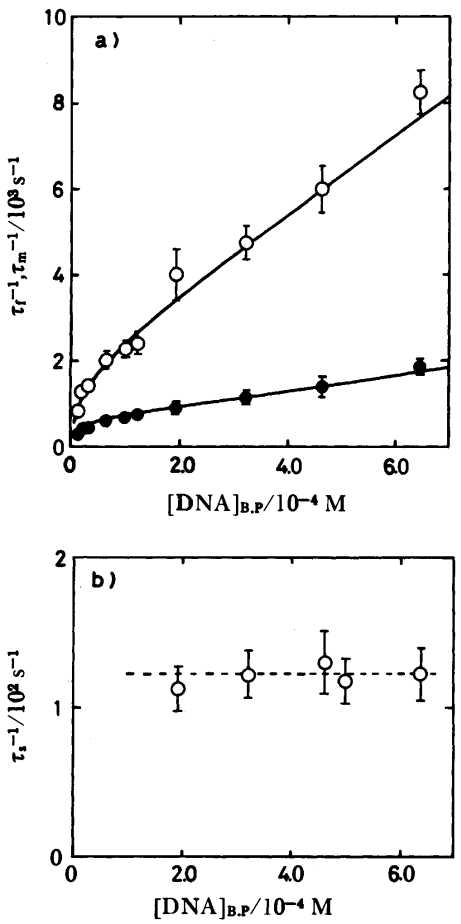

Fig. 6. Dependence of the reciprocal relaxation time of each process on total DNA concentration (base pairs unit) at P/D=10: (a), fast (○) and middle (●) processes, solid lines show the theoretical curves calculated from Eqs. 4 and 5 with constants listed in Table 1; (b), slow processes.

constant P/D=10; Fig. 7 shows the AO concentration dependences at 5×10^{-5} M of DNA (in base pairs unit) in the range of P/D≧10. As judged from Figs. 6a and 7a, the relaxation times of the fast and middle processes τ_f and τ_m are close to each other and both the relaxation times show similar dependences against DNA and AO concentration, respectively. While, the slow processes and the reciprocal relaxation time τ_s^{-1} displays no dependence on either DNA and AO concentrations (Figs. 6b and 7b).

Reaction Mechanism. The following three kinetic models have been proposed for the binding of several acridine and/or phenanthridine dyes to DNA on the assumption of homogeneity of intercalation sites:

$$A + S \underset{}{\overset{K_1}{\rightleftharpoons}} C, \qquad \text{(I)}$$

$$A + S \overset{K_1}{\rightleftharpoons} C_1 \overset{K_2}{\rightleftharpoons} C_2, \qquad \text{(II)}$$

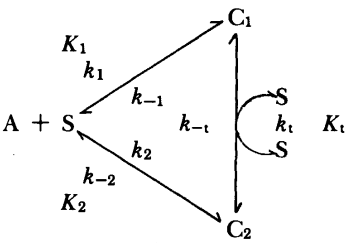

(III)

where A, S, and C_i denote free dye molecule, free site, and bound species, respectively; K_i, k_i, and k_{-i} (i=1, 2, and t) are the equilibrium constant, forward and backward rate constants in each process, respectively. Model I represents a simple bimolecular binding which has been proposed for ethidium-poly[d(A-T)] system.[44] Model II is a two-step binding model which

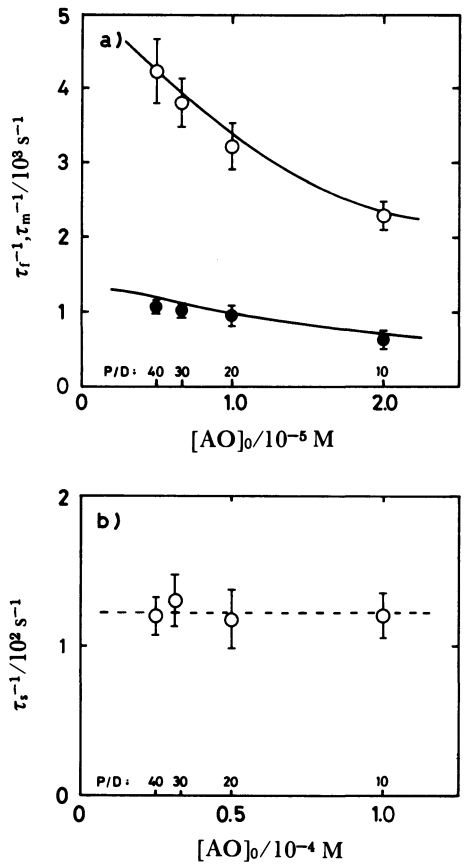

Fig. 7. Dependence of the reciprocal relaxation time of each process on total AO concentration at a constant DNA concentration: (a), fast (O) and middle (●) processes, solid lines show the theoretical curves calculated from Eqs. 4 and 5 with constants listed in Table 1; (b), slow process.

has been proposed for proflavine–DNA[23] and poly(A)–poly(U)[45] systems. The binding of AO to DNA has been interpreted by this model for the earlier studies using stopped-flow technique.[24,25] While Model III was originally proposed for ethidium–DNA system[26] and subsequently reported for several phenanthridine dyes and 10-methyl-9-aminoacridine.[27] The present kinetic data obtained for AO–DNA system were examined in detail for these three kinetic models.

(i) Fast and Middle Processes. At first, the fast and middle processes are analyzed since these are closely coupled and sufficiently faster than slow one. Among the kinetic models above, Model I of a single step reaction process can firstly be excluded from possible one. Secondarily, the concentration dependences of relaxation times calculated for Model II were quite different from the present observation. This fact also eliminated the Model II. Finally, Model III is examined. By an application of site exclusion theory, the kinetic analyses for this cyclic model give two relaxation times corresponding to the fast and middle processes (see Appendix A):

$$\tau_f^{-1} = \frac{1}{2}\{a_{11} + a_{22} + \sqrt{(a_{11} - a_{22})^2 + 4a_{12}a_{21}}\} \tag{4}$$

$$\tau_m^{-1} = \frac{1}{2}\{a_{11} + a_{22} - \sqrt{(a_{11} - a_{22})^2 + 4a_{12}a_{21}}\} \tag{5}$$

with

$$a_{11} = k_1(S_0 f(r) - \bar{A} f'(r)) + k_{-1} + k_t(S_0 f(r) + \bar{C}_1 f'(r)) - k_{-t}\bar{C}_2 f'(r), \tag{6}$$

$$a_{12} = k_1(S_0 f(r) - \bar{A} f'(r)) + k_t \bar{C}_1 f'(r) - k_{-t}(S_0 f(r) + \bar{C}_2 f'(r)), \tag{7}$$

$$a_{21} = k_2(S_0 f(r) - \bar{A} f'(r)) - k_t(S_0 f(r) + \bar{C}_1 f'(r)) + k_{-t}\bar{C}_2 f'(r), \tag{8}$$

and

$$a_{22} = k_2(S_0 f(r) - \bar{A} f'(r)) + k_{-2} - k_t \bar{C}_1 f'(r) + k_{-t}(S_0 f(r) + \bar{C}_2 f'(r)), \tag{9}$$

where S_0 and r denote the total concentration of binding site and the ratio of the bound dye to the total number of binding site, i.e., $r=(\bar{C}_1+\bar{C}_2)/S_0$, respectively; $f(r)$ and its derivative $f'(r)$ are the correction functions due to site exclusion and have the following general forms[44]

$$f(r) = \frac{(1-nr)^n}{\{1-(n-1)r\}^{n-1}} \tag{10}$$

$$f'(r) = \frac{\{(n-1)nr - 2n + 1\}(1-nr)^{n-1}}{\{1-(n-1)r\}^n} \tag{11}$$

The cyclic reaction of this model gives a relationship between six rate constants:

$$\frac{k_2}{k_{-2}} = \frac{k_1}{k_{-1}} \cdot \frac{k_t}{k_{-t}} \tag{12}$$

Seven unknown parameters (six rate constants and n) are involved in these equations. The analyses of τ_f^{-1} and τ_m^{-1} by a successive approximation method yield both $n=3$ and various sets of values for six rate constants which give the theoretical curves interpreting nicely all experimental data. However, a unique value for each rate constant could not be determined from this analysis. Accordingly, in order to determine unique values of six rate constants, the relaxation amplitudes of the fast and middle processes, ΔOD_f and ΔOD_m, were also examined on the basis of Model III. The relaxation amplitudes of ΔOD_f, ΔOD_m, and their ratio of $\Delta OD_f/\Delta OD_m$ are given by

$$\Delta OD_f = \frac{(\varepsilon_1 - \varepsilon_f) - (\varepsilon_2 - \varepsilon_f)\beta_m}{\beta_f - \beta_m} y_f^0, \tag{13}$$

$$\Delta OD_m = -\frac{(\varepsilon_1-\varepsilon_f)-(\varepsilon_2-\varepsilon_f)\beta_f}{\beta_f-\beta_m}y_m^0, \quad (14)$$

$$\frac{\Delta OD_f}{\Delta OD_m} = -\frac{(\varepsilon_1-\varepsilon_f)-(\varepsilon_2-\varepsilon_f)\beta_m y_f^0}{(\varepsilon_1-\varepsilon_f)-(\varepsilon_2-\varepsilon_f)\beta_f y_m^0}, \quad (15)$$

with

$$y_{f,m}^0 = \bar{A}\bar{S}\{\beta_{f,m}+\alpha K_1K_2+(1+\beta_{f,m})(1-\alpha)K_2(\bar{S}-\bar{A}f'(r))\}\delta K_1/\{1+(K_1+K_2)(\bar{S}-\bar{A}f'(r))\} \quad (16)$$

$$\beta_{f,m} = (\tau^{-1}{}_{f,m}-a_{22})/a_{12} \quad (17)$$

$$\alpha = \Delta H_2/\Delta H_1 = (\delta K_2/\delta K_1)(K_1/K_2), \quad (18)$$

where ε_f, ε_i, ΔH_i, and δK_i (i=1,2) denote the molar extinction coefficient of free AO, that of complex C_i, the standard enthalpies, and equilibrium shifts by the temperature-jump in process i, respectively. The derivation of these equations are shown in Appendix B. As can be seen from Fig. 5a, the wavelength dependences of ΔOD_f and ΔOD_m are not only quite similar each other, but both are well correlated with the difference spectrum between free and bound AO. Further, the value of $\Delta OD_f/\Delta OD_m$ calculated using the data in Fig. 5a is constant against wavelength within an experimental uncertainty as shown in Fig. 8. These experimental results require that both ΔOD_f and ΔOD_m in Eqs. 13 and 14 should be proportional to $(\varepsilon_b-\varepsilon_f)$, and that the representation of Eq. 15 for $\Delta OD_f/\Delta OD_m$ should be independent of wavelength. To satisfy these requirements, any one of the following three relationships among ε_1, ε_2, ε_f, and ε_b must be hold at every wavelengths: (a) $\varepsilon_1=\varepsilon_2=\varepsilon_b$, (b) $\varepsilon_1=\varepsilon_f$ and $\varepsilon_2=\varepsilon_b$, and (c) $\varepsilon_1=\varepsilon_b$ and $\varepsilon_2=\varepsilon_f$. Thus, the concentration dependences of $\Delta OD_f/\Delta OD_m$ was analyzed in detail using Eq. 15 for the cases (a), (b), and (c), respectively. In the cases of (a), (b), however, calculated values of $\Delta OD_f/\Delta OD_m$ were quite different from the experimental data. In the case of (c), Eq. 15 can be simplified as

$$\left(\frac{\Delta OD_f}{\Delta OD_m}\right)_c = -\frac{y_f^0}{y_m^0}, \quad (19)$$

where subscript c refer to the case (c). The analysis using this equation for the various values for α and rate constants obtained above yields α=0.9±0.1, n=3, and unique set of rate constants listed in Table 1, which fully satisfy all the experimental data. As shown in Fig. 9, a plot of $\Delta OD_f/\Delta OD_m$ measured versus $(\Delta OD_f/\Delta OD_m)_c$ calculated using the obtained parameters showed an excellent fitting. The all observed data of τ_f^{-1} and τ_m^{-1} fall on the theoretical curves calculated, for the same parameters, using Eqs. 4 and 5 as can be seen from Figs. 6a and 7a. These agreements confirm the plausibility of Model III as well as the equivalence in spectral behaviors of species C_1 with the bound AO and C_2 with the free AO.

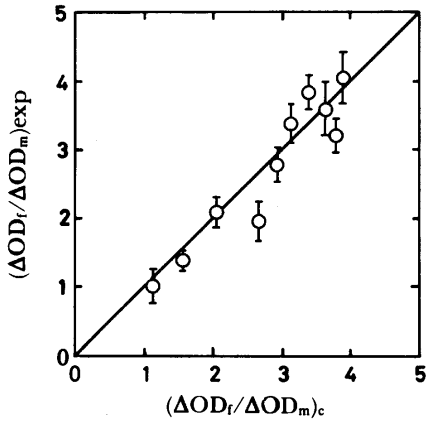

Fig. 9. A plot of $\Delta OD_f/\Delta OD_m$ obtained experimentally at various concentrations vs. $(\Delta OD_f/\Delta OD_m)_c$ calculated from Eq. 19 using parameters listed in Table 1.

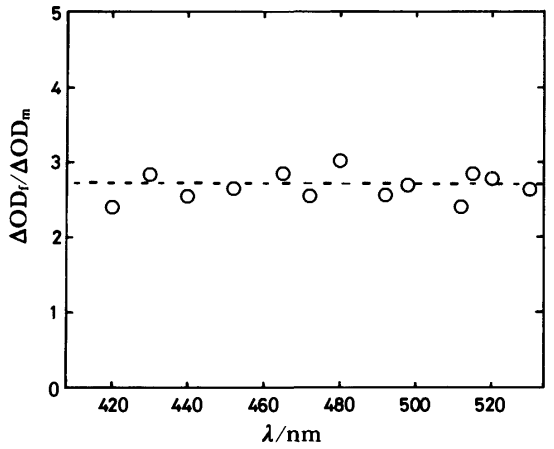

Fig. 8. Wavelength dependence of the experimental values of the relative amplitude $\Delta OD_f/\Delta OD_m$, obtained using the data in Fig. 5a.

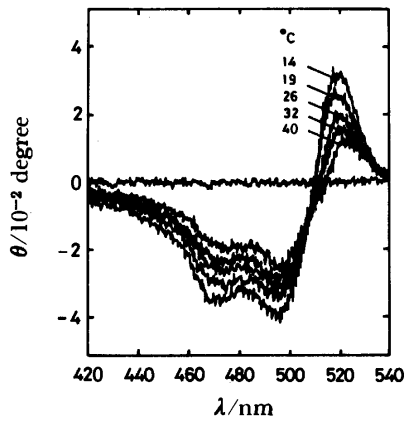

Fig. 10. CD spectra of AO in the presence of DNA in 0.2 M NaCl solution at various temperature in the premelt range. [AO]=3.3×10^{-5} M, [DNA]-phosphate=6.6×10^{-4} M (P/D=20).

Furthermore, the value of $n=3$ determined kinetically is identical with the value obtained from the analysis of the binding isoterm. The overall binding constant, $K_1+K_2=(1.6\pm0.3)\times10^5\ M^{-1}$, calculated from the obtained rate constants is nicely consistent with the binding constant for intercalation mode, $K_I=1.8\times10^5\ M^{-1}$, determined statically. These facts give further confidence for the present assignment.

(ii) Slow Process. As can be seen from Fig. 5b, the spectrum of the relaxation amplitude of the slow process is well associated with the spectral variations resulting from the interaction between intercalated AO molecules. To see this point further, the CD spectra of AO-DNA complex, which is sensitive to dye-dye interactions, were measured at P/D=20 as a function of temperature in the premelt range. As shown in Fig. 10, the exciton splitting due to intercalated AO-AO interaction[17,44] was observed, and decreased with elevation of temperature. Since the amount of bound dye can be regarded as approximately constant in this temperature range,[15,18] this CD shift clearly demonstrates that the interaction between intercalated dyes depends considerably on temperature. Furthermore, the direction of CD shift indicates that this interaction successively weaken with temperature increase. This is compatible with the direction of the relaxation observed by temperature-jump measurements. The slow relaxation process is thus attributable to intercalated AO-AO interaction which depends on temperature.

By the way, the strength of interaction between the intercalated dye molecules depends strongly on both the distance and angle between the interacting dye molecules.[46] In the case of intercalating dyes, these stereochemical parameters would be determined by the double helical structure of DNA. Therefore, the present relaxation seems to result from a thermally induced configurational alternation of DNA molecule itself, which brings about the changes on the steteochemical relationship between intercalated AO molecules. In the case that this configurational alternation arises from an equilibrium shift between two states of DNA structure, the reaction scheme for this process may be represented by the following simple form independent of the fast two relaxations:

$$[\mathrm{DNA}]_X \underset{k_{-3}}{\overset{k_3}{\rightleftharpoons}} [\mathrm{DNA}]_Y, \qquad \text{(IV)}$$

where $[DNA]_X$, $[DNA]_Y$, k_3, and k_{-3} denote the two states of DNA structure named X and Y, the forward and backward rare constants, respectively. The equation of the reciprocal relaxation time, τ_3^{-1}, is given by

$$\tau_3^{-1} = k_3 + k_{-3}, \qquad (20)$$

where the relaxation time is essentially independent of DNA and AO concentrations, which is consistent with the experimental results as seen in Figs. 6b and 7b. By averaging the experimental values of τ_3^{-1}, k_3+k_{-3} was obtained to be $120\pm10\ s^{-1}$. The states X and Y introduced above can not be identified in the present study. However, these may be associated with the thermally induced premelt transition of DNA which has been demonstrated by CD spectroscopies[47,48] and NMR studies.[49]

When the whole results are reviewed, it should be noted that the only faster two of three relaxations were assigned to the actual interactions between AO and DNA molecules. This is consistent with the fact that the overall association constant K_1+K_2 determined kinetically for the two fast relaxations agrees well with the binding constant K_I estimated statically.

Discussion

Intercalating Species. The present kinetic results elucidated the presence of two types of bound dye species (C_1 and C_2) in the range of $r<0.1$. The values of binding constants for these species, K_1 and K_2, listed in Table 1 indicate that more than 80% of bound AO is in complex form C_1. In addition, the absorption spectrum of C_1 determined from the analyses of the relaxation amplitude is approximately identical with that of statically observed intercalated AO. These results strongly suggest that the species C_1 is attributable to the intercalative species.

The values of rate constants for the formation of complex C_1 can be compared to those reported for other intercalating dyes, and for a nonintercalating dye. The present results of $k_1=(3.4\pm0.2)\times10^7\ M^{-1}\ s^{-1}$

Table 1. Kinetic and Stoichiometric Constants for Binding of Acridine Orange to Calf Thymus DNA (25 °C, 0.2 M NaCl)

k_1	k_{-1}	k_2	k_{-2}	k_t	k_{-t}
$10^7\ M^{-1}\ s^{-1}$	$10^2\ s^{-1}$	$10^7\ M^{-1}\ s^{-1}$	$10^2\ s^{-1}$	$10^6\ M^{-1}\ s^{-1}$	$10^6\ M^{-1}\ s^{-1}$
3.4±0.2	2.35±0.15	1.55±0.15	5.55±0.15	1.2±0.2	8.0±0.5
n	K_1	K_2	K_t	K_I[a]	K_D[a]
	$10^5\ M^{-1}$	$10^4\ M^{-1}$		$10^5\ M^{-1}$	$10^4\ M^{-1}$
3	1.45±0.2	2.8±0.3	0.25±0.04	1.8	3.0

a) Obtained from the binding isotherm.

and $k_{-1}=235\pm15\ s^{-1}$ at 0.2 M NaCl are similar to those obtained for the intercalating dyes; $k_f \fallingdotseq 10^6\ M^{-1}\ s^{-1}$ and $k_b=50—7000\ s^{-1}$ for 10-methyl-9-aminoacridine, ethidium, and several phenanthridine dyes-DNA systems at 1.0 M NaCl,[26,27] $k_f=1.7\times10^7\ M^{-1}\ s^{-1}$ and $k_b=30\ s^{-1}$ for ethidium bromide-poly[d(A-T)] at 0.1 M KCl,[44] and $k_{1f}=2.2\times10^7\ M^{-1}\ s^{-1}$ and $k_{1b}=200\ s^{-1}$ for (A-T) like site[50] and $k_{2f}=3.4\times10^7\ M^{-1}\ s^{-1}$ and $k_{2b}=120\ s^{-1}$ for (G-C) like site[51] for a typical base-specific acridine dye of proflavine at 0.1 M NaCl, but not to those for the nonintercalating dye; $k_{1f}=1.5\times10^8\ M^{-1}\ s^{-1}$, $k_{1b}=5\times10^4\ s^{-1}$ and $k_{2f}=1.4\times10^8\ M^{-1}\ s^{-1}$, $k_{2b}=4\times10^3\ s^{-1}$ for di-*t*-butylproflavine-DNA system at 0.2 M NaCl.[52] Especially, the values of forward rate constants of intercalation obtained at quite similar ionic strength of 0.1 and 0.2 are quite similar each other. This may indicate that differences in the structure of dye and the base specificity are not dominant factors determining the rate of intercalation, but some specific conformational alternation of DNA helix resulting from the intercalation of dye molecule may be the rate-determining step for the intercalation process.

Externally Bound Species. The analyses of the relaxation amplitude revealed that the absorption spectrum of complex C_2 is approximately same with that of free AO molecules. Similar results were reported for the monomeric AO-polyphosphate complex.[41] Consequently, the species C_2 is reasonably attributable to an externally bound species fixed on the surface of DNA. The value of binding constant $K_2=3\times10^4\ M^{-1}$ is fairly large compared with that of electrostatic binding of acridines to the negatively charged residues of synthetic polymers ($K \fallingdotseq 10^2\ M^{-1}$).[53-55] This fact indicates that bound species C_2 is different from a simple electrostatic binding between AO and phosphate residue of DNA. Meanwhile, the rate constants $k_2=(1.55\pm0.15)\times10^7\ M^{-1}\ s^{-1}$ and $k_{-2}=(5.55\pm0.15)\times10^2\ s^{-1}$ are similar to those of other intercalating dyes rather than that of the nonintercalating dye. Accordingly, as a possible mechanism for the formation of complex C_2, we propose the partially intercalationg model adopted for the binding some acridine dyes to DNA.[56] In the present case, either one of twe dimethylamino residues of AO molecule is partially intercalating between base pairs holding the electrostatic binding of the phosphate residue of DNA ribose and the acridine ring of AO molecule is remained in the outside of DNA helix; a heavily hydrated environment around DNA helix[57] may give the absorption spectrum of AO similar to that of free AO.

As for the dimerization of AO molecule on the DNA, which is expected to occur under the condition of $r>0.1$ beyond the present experimental condition, Armstrong et al.[16] assumed that an intercalated AO molecule affords an additional binding site for free AO to form a dimerized species on DNA helix. However, this model appears suspicious from a consideration of X-ray crystallographic studies of AO-iodo CpG crystals by Reddy et al.[57] They revealed that the acridine ring of intercalated AO as well as other acridine is almost fully sandwiched between upper and lower sides of base pairs. With regard to this point, the present results would afford a better interpretation that the dimerization of AO molecules on DNA helix most likely results from a binding of free AO to an external bound species C_2, but not to an intercalative species C_1.

Magnitude of Site Exclusion Effect. Among all studies on the binding of various acridine dyes to DNA reported so far, the present study is the first study in which the value of n, a parameter indicating the magnitude of site exclusion effect, was determined kinetically.

In earlier equilibrium dialysis studies by Armstrong et al.,[16] and by Fredericq and Houssier,[17] the binding isotherm of AO-DNA system has been analyzed with $n=2$. Fornaslero and Kurucsev,[19] however, have reanalyzed the data by Armstrong et al. and pointed out that the binding isotherm in 0.1 M NaCl solution could be satisfactorily interpreted with rather $n=3$ than 2. The present result of $n=3$ in 0.2 M NaCl solution supports further the results given by Fornaslero and Kurucsev. This value ($n=3$) indicates that the three consecutive intercalation sites are blocked by one bound AO molecule. The molecular basis of this effect may be afforded by γ-kinked B DNA structure proposed by Sobell et al.[58] in their X-ray crystallographic studies of intercalating dyes-dinucleoside monophosphate crystalline complexes.

Transfer of Bound Dye between Binding Sites. One of the most important feature of the kinetic mechanism (Model III) is to involve a bimolecular pathway for direct transfer of dye molecule from one site to another. Besides the present AO-DNA system, this kind of direct transfer process has kinetically been recognized for the binding of ethidium,[26] carboxy dimidium, ethyl phenidium, desphenyl dimidium and 10-methyl-9-aminoacridine to DNA.[27] Quite recent observations by Kubota and Fujisaki suggested that proflavine and acriflavine, typical base-specific acridines, also bind to DNA via the direct transfer pathway.[59] Moreover, such transfer reactions have been demonstrated in the protein-DNA system.[60] These facts indicate that the direct transfer reaction is one of the fundamental dynamic features of DNA interaction with various ligands, and this reaction may play an important role in translocation of ligands seeking specific binding sites on DNA. Since the kinetic studies are of great advantage for elucidation of such dynamic features, extensive studies of kinetics of DNA with various kind of ligands would be required.

Finally, we should refer to kinetic models proposed for AO-DNA system by other workers. Geacintov et

al.[61] proposed by using flash photolysis technique that the intercalation takes place bimolecularly, which is consistent with the present result. However, the process of direct transfer of dye molecules was not observed in their study. This is probably because that the flash photolysis technique is insensitive to the transfer of dyes. While, Sakoda et al.[24,25] observed a single reaction step by the absorption and fluorescence stopped-flow experiments in the concentration range below 5×10^{-5} M of DNA (base pairs unit), and proposed a two-step mechanism (Model II) on the basis of the independence of the relaxation time on concentration. The values of the reciprocal relaxation times (300 s^{-1}) reported by them are in good agreement with those of the present τ_m^{-1} in the corresponding concentration range. As can be seen from Fig. 6a, however, the dependence of τ_m^{-1} on the concentration becomes remarkable at higher concentration. This facts may suggest that the stopped-flow experiments by Sakoda et al. have been done under unfavorable concentration conditions for the unambiguous elucidation of the binding mechanism.

Appendix

[A]. The cyclic reaction presented by mechanism III affords two independent rate equations. In the case that the perturbation give to the system is small, these equations can be linearized as

$$-\frac{d}{dt}\delta C_1(t) = -k_1(\bar{A}\delta S(t) + \bar{S}\delta A(t)) + k_{-1}\delta C_1(t) + k_t(\bar{S}\delta C_1(t) + \bar{C}_1\delta S(t)) - k_{-t}(\bar{S}\delta C_2(t) + \bar{C}_2\delta S(t)), \quad (A1)$$

$$-\frac{d}{dt}\delta C_2(t) = -k_2(\bar{A}\delta S(t) + \bar{S}\delta A(t)) + k_{-2}\delta C_2(t) - k_t(\bar{S}\delta C_1(t) + \bar{C}_1\delta S(t)) + k_{-t}(\bar{S}\delta C_2(t) + \bar{C}_2\delta S(t)), \quad (A2)$$

where $\delta S(t)$, $\delta A(t)$, and $\delta C_i(t)$ are the time-dependent small deviations of each reaction species from the equilibrium states after the perturbation given at $t=0$.

According to the site exclusion theory proposed by McGhee and von Hippel,[40] a function $f(r)$ represented by Eq. 10 in the text denotes the fraction of free binding site, thus

$$\bar{S}/S_0 = f(r). \quad (A3)$$

The differential of Eq. A3 affords the small deviation for S:[44]

$$\delta S(t) = f'(r)S_0\delta r(t) = f'(r)(\delta C_1(t) + \delta C_2(t)), \quad (A4)$$

where the function $f'(r)$ is the derivative of $f(r)$ (see Eq. 11 in the text). While, mass balance condition for dye requires

$$\delta A(t) = -(\delta C_1(t) + \delta C_2(t)). \quad (A5)$$

Introducing Eqs. A3, A4, and A5 into Eqs. A1 and A2, we obtain

$$-\frac{d}{dt}\delta C_1(t) = a_{11}\delta C_1(t) + a_{12}\delta C_2(t), \quad (A6)$$

$$-\frac{d}{dt}\delta C_2(t) = a_{21}\delta C_1(t) + a_{22}\delta C_2(t), \quad (A7)$$

where the coefficients a_{ij} (i, j=1 or 2) are given by Eqs. 6—9 in the text. The reciprocal relaxation times (Eqs. 4 and 5 in the text) are obtained by solving characteristic equation for the matrix $[a_{ij}]$.

[B]. The total absorbance of the solution is given by the concentration of AO in its different states and the corresponding extinction coefficients:

$$OD = \varepsilon_f\bar{A} + \varepsilon_1\bar{C_1} + \varepsilon_2\bar{C_2}. \quad (B1)$$

The time variation of the absorbance after a temperature-jump is

$$\Delta OD(t) = \varepsilon_f\delta A(t) + \varepsilon_1\delta C_1(t) + \varepsilon_2\delta C_2(t). \quad (B2)$$

A substitution of $\delta A(t)$ from Eq. A5 into Eq. B2 leads to

$$\Delta OD(t) = (\varepsilon_1 - \varepsilon_f)\delta C_1(t) + (\varepsilon_2 - \varepsilon_f)\delta C_2(t). \quad (B3)$$

The normal concentration deviations are written by linear combinations of $\delta C_1(t)$ and $\delta C_2(t)$:

$$y_i(t) = y_i^0\exp(-t/\tau_i) = \beta_i\delta C_1(t) + \delta C_2(t) \quad (B4)$$

with

$$\beta_i = (\tau_i^{-1} - a_{22})/a_{12}. \quad (B5)$$

Where the subscript i (=f, m) refers to the normal modes corresponding to the fast and middle processes, and the superscript 0 represents the value for time $t=0$. From Eq. B4, it follows

$$\delta C_1(t) = \frac{-y_f^0\exp(-t/\tau_f) + y_m^0\exp(-t/\tau_m)}{\beta_m - \beta_f}, \quad (B6)$$

$$\delta C_2(t) = \frac{\beta_m y_f^0\exp(-t/\tau_f) - \beta_f y_m^0\exp(-t/\tau_m)}{\beta_m - \beta_f}. \quad (B7)$$

Inserting Eqs. B6 and B7 into B3 yields

$$\Delta OD(t) = \Delta OD_f\exp(-t/\tau_f) + \Delta OD_m\exp(-t/\tau_m), \quad (B8)$$

with

$$\Delta OD_f = \frac{(\varepsilon_1 - \varepsilon_f) - (\varepsilon_2 - \varepsilon_f)\beta_m}{\beta_f - \beta_m}y_f^0, \quad (B9)$$

$$\Delta OD_f = \frac{(\varepsilon_1 - \varepsilon_f) - (\varepsilon_2 - \varepsilon_f)\beta_f}{\beta_f - \beta_m}y_m^0. \quad (B10)$$

As judged from Eq. B8, ΔOD_f and ΔOD_m are the amplitudes corresponding to τ_f^{-1} and τ_m^{-1}, respectively. The normal concentration, y_i^0 in Eqs. B9 and B10 can be written using the equilibrium concentrations of the actually existing reactants ans the equilitrium shifts, δK_1 and δK_2 caused by a temperature rise. From Eq. B4, the following relation is

obtained for $t=0$:

$$y_i^0 = \beta_i \delta C_1^0 + \delta C_2^0 \tag{B11}$$

According to the general procedure for the derivation of the net concentration shifts of the reacting species, we have

$$\delta C_1^0 = -\frac{f'(r)\bar{A}\bar{S}\{1 + K_2(\bar{S} - f'(r)\bar{A})\}}{1 + (K_1 + K_2)(\bar{S} + f'(r)\bar{A})}\delta K_1 + \frac{K_1 f'(r)\bar{A}\bar{S}(\bar{S} - f'(r)\bar{A})}{1 + (K_1 + K_2)(\bar{S} - f'(r)\bar{A})}\delta K_2 \tag{B12}$$

$$\delta C_2^0 = \frac{K_2 f'(r)\bar{A}\bar{S}(\bar{S} - f'(r)\bar{A})}{1 + (K_1 + K_2)(\bar{S} - f'(r)\bar{A})}\delta K_1 - \frac{f'(r)\bar{A}\bar{S}\{1 + K_1(\bar{S} - f'(r)\bar{A})\}}{1 + (K_1 + K_2)(\bar{S} - f'(r)\bar{A})}\delta K_2 \tag{B13}$$

By defining α as $\Delta H_1/\Delta H_2$ (where ΔH_1 and ΔH_2 denote the standard enthalpies in each process), δK_1 and δK_2 are connected by the relation

$$\alpha = (\delta K_1/\delta K_2)(K_1/K_2), \tag{B14}$$

If Eq. B11 is rearranged using Eqs. B12, B13, and B14, the values of y_i^0 (i=f, m) are given by the forms represented by Eq. 16 in the text.

References

1) F. H. C. Crick, L. Barnett, S. Brenner, and R. J. Watts-Tobin, *Nature (London)*, **192**, 1227 (1961).

2) S. Brenner, L. Barnett, F. H. C. Crick, and A. Orgel, *J. Mol. Biol.*, **3**, 121 (1961).

3) N. Yamamoto, *J. Bacteriol.*, **75**, 443 (1958).

4) A. Albert, "Selective Toxicity," 2nd ed, Champman & Hall, London (1973).

5) J. Ciak and F. E. Hahn, *Science*, **156**, 655 (1967).

6) A. Blake and A. R. Peacocke, *Biopolymers*, **6**, 1225 (1968).

7) E. F. Gale, E. Cundliffe, P. E. Reynolds, M. H. Richmond, and M. J. Waring, "The Molecular Basis of Antibiotic Action," Wiley, New York (1972).

8) N. C. Seeman, R. O. Day, and A. Rich, *Fed. Proc., Fed. Am. Soc. Exp. Biol.*, **33**, 1537 (1974).

9) C. Tsai, S. C. Jain, and H. M. Sobell, *J. Mol. Biol.*, **114**, 301 (1977).

10) S. C. Jain, C. Tsai, and H. M. Sobell, *J. Mol. Biol.*, **114**, 317 (1977).

11) H. M. Sobell, C. Tsai, S. C. Jain, and S. G. Gilbert, *J. Mol. Biol.*, **114**, 333 (1977).

12) S. Neidle, A. Achari, G. L. Taylor, H. M. Berman, H. L. Carrell, J. P. Glusker, and W. C. Stalling, *Nature (London)*, **269**, 304 (1977).

13) A. R. Peacocke and J. N. H. Skerrett, *Trans. Faraday Soc.*, **52**, 261 (1956).

14) J. Chambron, M. Daune, and C. H. Sadron, *Biochim. Biophys. Acta*, **123**, 306 (1966).

15) S. Ichimura, M. Zama, H. Fujita, and T. Ito, *Biochim. Biophys. Acta*, **190**, 116 (1970).

16) R. W. Armstrong, T. Kurucsev, and U. P. Strauss, *J. Am. Chem. Soc.*, **92**, 3174 (1970).

17) E. Fredericq and C. Houssier, *Biopolymers*, **11**, 2281 (1972).

18) Y. Kubota, Y. Eguchi, K. Hashimoto, M. Wakita, Y. Honda, and Y. Fujisaki, *Bull. Chem. Soc. Jpn.*, **49**, 2424 (1976).

19) D. Fornaslero and T. Kurucsev, *J. Phys. Chem.*, **85**, 613 (1981).

20) M. J. Waring, *J. Mol. Biol.*, **13**, 269 (1965).

21) L. M. Chan and Q. Van Winkle, *J. Mol. Biol.*, **40**, 491 (1969).

22) S. Tanaka, Y. Baba, A. Kagemoto, and R. Fujishiro, *Makromol. Chem.*, **181**, 2175 (1980).

23) H. J. Li and D. M. Crothers, *J. Mol. Biol.*, **39**, 461 (1969).

24) M. Sakoda, K. Hiromi, and K. Akasaka, *Biopolymers*, **10**, 1003 (1971).

25) M. Sakoda, K. Hiromi, and K. Akasaka, *J. Biochem.*, **71**, 891 (1972).

26) J. L. Breslofe and D. M. Crothers, *J. Mol. Biol.*, **95**, 103 (1975).

27) L. P. G. Wakelin and M. J. Waring, *J. Mol. Biol.*, **144**, 183 (1980).

28) R. K. Tubbs, W. E. Ditmars Jr., and Q. Van Winkle, *J. Mol. Biol.*, **9**, 545 (1964).

29) J. C. Thomes, G. Weill, and M. Daune, *Biopolymers*, **8**, 647 (1969).

30) N. F. Ellerton and I. Isenberg, *Biopolymers*, **8**, 767 (1969).

31) B. Weisblum and P. L. de Haseth, *Proc. Natl. Acad. Sci. U. S. A.*, **69**, 629 (1972).

32) Y. Kubota, *Chem. Lett.*, **1973**, 299.

33) J. P. Shreiber and M. P. Daune, *J. Mol. Biol.*, **38**, 487 (1974).

34) S. A. Latt, S. Brodie, and S. H. Munroe, *Chromosoma*, **49**, 17 (1974).

35) Y. Kubota and R. F. Steiner, *Biophys. Chem.*, **6**, 279 (1977).

36) S. Georghion, *Photochem. Photobiol.*, **22**, 103 (1975).

37) G. Weill and M. Calvin, *Biopolymers*, **1**, 401 (1963).

38) A. L. Stone and D. F. Bradley, *J. Am. Chem. Soc.*, **83**, 3627 (1961).

39) S. Inoue, Y. Toyoshima, and T. Yasunaga, *J. Phys. Chem.*, **85**, 1401 (1981).

40) J. D. McGhee and P. H. von Hippel, *J. Mol. Biol.*, **86**, 469 (1974).

41) D. F. Bradley and M. K. Wolf, *Proc. Natl. Acad. Sci. U. S. A.*, **45**, 944 (1959).

42) B. J. Gardner and S. F. Mason, *Biopolymers*, **5**, 79 (1967).

43) M. Zama and S. Ichimura, *Biopolymers*, **9**, 53 (1970).

44) T. M. Jovin and G. Striker, *Mol. Biol. Biochem. Biophys.*, **24**, 245 (1978).

45) D. E. V. Schmechel and D. M. Crothers, *Biopolymers*, **10**, 465 (1971).

46) N. Harada and K. Nakanishi, *Acc. Chem. Res.*, **5**, 257 (1972).

47) R. B. Gennis and C. R. Cantor, *J. Mol. Biol.*, **65**, 381 (1972).

48) A. Chan, R. Kilkuskie, and S. Hanlon, *Biochemistry*, **18**, 84 (1979).

49) D. J. Patel, S. A. Kozlowski, J. W. Suggs, and S. D.

Cox, *Proc, Natl. Acad. Sci. U. S. A.*, **78**, 4063 (1981).

50) The binding of proflavine to (A–T) sites was analyzed according to a two-step mechanism, and the first-order forward rate constant ($3.3\times10^3\ s^{-1}$) was given in the literature.[51] In order to facilitate the comparison with other systems, the product of this value and the equilibrium constant for the preequilibrium ($6.6\times10^3\ M^{-1}$), which provides the apparent second-order rate constant for the intercalation, was cited in this paper.

51) J. Ramstein, M. Ehrenverg, and R. Riyler, *Biochemistry*, **19**, 3938 (1980).

52) W. Muller, D. M. Crothers, and M. J. Waring, *Eur. J. Biochem.*, **39**, 223 (1973).

53) G. Schwarz, S. Klose, and W. Balthasar, *Eur. J. Biochem.*, **12**, 454 (1972).

54) G. Schwarz and W. Balthasar, *Eur. J. Biochem.*, **12**, 461 (1972).

55) G. Schwarz and S. Klose, *Eur. J. Biochem.*, **29**, 249 (1972).

56) P. S. Drummond, V. F. W. Simpson, and A. R. Peacocke, *Biopolymers*, **3**, 135 (1965); H. Ushio, *J. Sci. Hiroshima Univ., Ser. A*, **41**, 209 (1977).

57) B. S. Reddy, T. P. Seshadri, T. D. Sakore, and H. M. Sobell, *J. Mol. Biol.*, **135**, 787 (1979).

58) H. M. Sobell, C. Tsai, S. G. Jain, and S. G. Gilbert, *J. Mol. Biol.*, **114**, 333 (1977).

59) Y. Kubota and Y. Fujisaki, unpublished results.

60) D. M. Crothers and M. Fried, *Cold Spring Habor Symp. Quantum Biol.*, **47**, 263 (1983).

61) N. E. Geacintov, J. Waldmeyer, V. A. Kuzmin, and T. Kolubayev, *J. Phys. Chem.*, **85**, 3608 (1981).

Stabilities and Transfer Activity Coefficients of Benzo-15-crown-5-Alkali Metal Ion Complexes in Various Solvents

Yasuyuki TAKEDA* and Toshihiro KUMAZAWA
Department of Chemistry, Faculty of Science, Chiba University, Yayoi-cho, Chiba 260
(Received July 15, 1987)

Stability constants in acetonitrile and methanol of 1:1 benzo-15-crown-5 (B15C5)–alkali metal ion complexes and the solubility of B15C5 in acetonitrile, propylene carbonate, methanol, and water were determined at 25 °C by conductometry and spectrophotometry, respectively. In general, selectivity tendency of B15C5 for the alkali metal ions except for Li^+ can be interpreted in terms of size-relationship. Stability sequences of the B15C5–alkali metal ion complex among the solvents, except for Rb^+ and Cs^+ complexes, are the reverse of solvation-ability sequences of the solvents to the corresponding alkali metal ion. By using the stability constants of the B15C5–alkali metal ion complexes, transfer activity coefficients (γ) of the B15C5 complexes were then calculated from γ values of B15C5 (obtained from solubilities of B15C5) and those of alkali metal ions. The γ value of the B15C5 complex from methanol to acetonitrile and propylene carbonate generally varies with a variety of alkali metal ions. From γ values of the B15C5 complexes, it is concluded that there exists a possible specific interaction between the alkali metal ion held in the B15C5 cavity and solvent molecules when the alkali metal ion is much smaller or larger than the B15C5 cavity.

In the previous study,[1] molar conductivities of alkali metal perchlorates were measured in propylene carbonate in the presence of benzo-15-crown-5 (B15C5), and stabilities and solvation properties of the 1:1 complexes of B15C5 with alkali metal ions were discussed from the standpoint of thermodynamics and transport phenomena, respectively. Stability sequences of the B15C5–alkali metal ion complexes in propylene carbonate are in the order $Na^+>Li^+>K^+>Rb^+>Cs^+$, which is consistent with the size-fit concept; namely, correlation between relative sizes of cation and crown ether cavity. In the cases of Na^+, K^+, Rb^+, and Cs^+, the size of the moving entity in propylene carbonate is larger for the B15C5 complex than for the corresponding alkali metal ion, whereas, in the case of Li^+, that is completely the reverse.

In the present study, in order to further investigate complexing-power tendency of B15C5 for alkali metal ions and medium effects on stabilities of the 1:1 B15C5–alkali metal ion complexes, formation constants of the B15C5 complexes in acetonitrile and methanol were conductometrically determined at 25 °C. In addition, by using the formation constants of the B15C5 complexes, transfer activity coefficients (γ) of the B15C5 complexes were then calculated from γ values of B15C5 (obtained from solubilities of B15C5) and those of alkali metal ions. From the γ values of the B15C5 complexes, properties of solute–solvent interaction of the B15C5 complexes were discussed in detail.

Experimental

Materials. The method of purification of B15C5 (Merck Japan Ltd.) was the same as that described previously.[1] Extremely pure alkali metal (Li, Na, K, Rb, Cs) chlorides were purchased from Merck Japan Ltd., and were used without further purification. Rubidium and caesium perchlorates were prepared by adding a little excess of $HClO_4$ to aqueous solutions of RbCl and CsCl, respectively. Lithium, sodium, and potassium perchlorates were commercially obtained from Merck Japan Ltd. All the perchlorates were recrystallized four times from distilled water and, prior to use, dried at 150 °C in vacuo. The method of purification of acetonitrile,[2] propylene carbonate,[3] and methanol[4] was previously reported. The conductivities of acetonitrile, propylene carbonate, methanol, and water thus purified were less than 3×10^{-7}, 5×10^{-8}, 2×10^{-7}, and 6×10^{-7} Ω^{-1} cm^{-1}, respectively. For conductometric titrations, alkali metal chlorides and perchlorates were used for methanol and acetonitrile systems, respectively.

Apparatus and Procedure. The conductance measurements were made on a Fuso conductivity apparatus, model 362 A, in a water bath thermostated at 25±0.01 °C. Two cells were used, cell constants of which were 0.059701 and 0.097765 cm^{-1}. Experimental procedures to obtain formation constants of B15C5–alkali metal ion complexes were the same as those described in a preceding paper.[3]

Solubilities of B15C5. A B15C5 suspension in a given solvent was stirred at 25±0.02 °C for 3 days, and then the solution saturated with B15C5 was filtered under nitrogen. The B15C5 concentration of the solution was determined spectrophotometrically (at 226, 222, 220, and 200 nm in acetonitrile, propylene carbonate, methanol, and water, respectively). Solubilities of B15C5 at 25 °C are 1.9, 1.2, 4.0×10^{-1}, and 1.1×10^{-1} M (1 M=1 mol dm^{-3}) in acetonitrile, propylene carbonate, methanol, and water, respectively.

Results and Discussion

The method for obtaining formation constants (K_{ML^+}) of B15C5–alkali metal ion complexes was the same as that described in a previous paper,[3] where $K_{ML^+}=[ML^+]/[M^+][L]$. M^+ and L denote an alkali metal ion and a crown ether, respectively. In this work, it is assumed that the association between a cation and an anion is negligible and that B15C5 forms a 1:1 complex with an alkali metal ion. The $\log K_{ML^+}$ values are summarized in Table 1.

Molar conductivity (Λ) vs. $[L]_t/[M]_t$ plots for

Table 1. Log(K_{ML^+}/mol^{-1} dm^3) Values of B15C5 at 25 °C and Crystal Ionic Radii of Alkali Metals (Å)

	Li^+	Na^+	K^+	Rb^+	Cs^+
Crystal ionic radius[5]	0.60	0.95	1.33	1.48	1.69
AN[a]	4.46±0.02	4.25±0.01	2.49±0.01	2.72±0.03	2.39±0.03
PC[b]	3.77±0.03[1]	4.35±0.01[1]	2.78±0.01[1]	2.38±0.03[1]	2.03±0.04[1]
H_2O	—	—	0.38[6]	—	—
CH_3OH	2.31±0.03	2.99±0.02	2.71±0.01	2.40±0.02	2.15±0.04

a) Acetonitrile. b) Propylene carbonate.

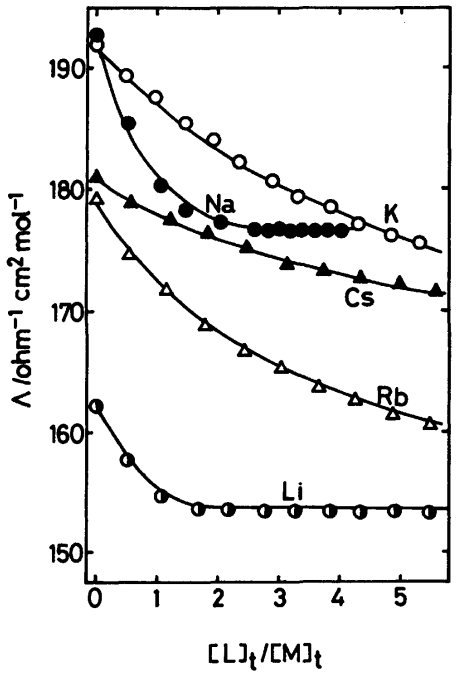

Fig. 1. Λ vs. $[L]_t/[M]_t$ curves for B15C5-alkali metal perchlorate systems in acetonitrile at 25 °C.
—— calculated curve by using K_{ML^+} value. $[M]_t$= (5.0—6.0)×10^{-4} M.

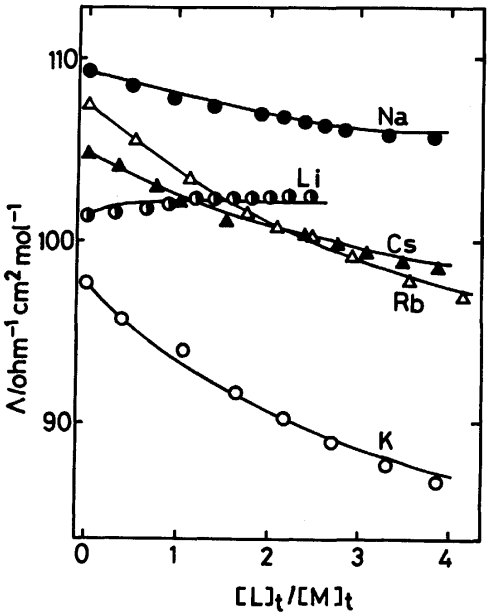

Fig. 2. Λ vs. $[L]_t/[M]_t$ curves for B15C5-alkali metal chloride systems in methanol at 25 °C.
—— calculated curve by using K_{ML^+} value. $[M]_t$= (6.0—8.0)×10^{-4} M.

acetonitrile and methanol are given in Figs. 1 and 2, $[L]_t$ and $[M]_t$ denoting total concentrations of B15C5 and the alkali metal ion, respectively. Every Λ vs. $[L]_t/[M]_t$ plot, except for the LiCl-CH_3OH system, shows a decrease in Λ with an increase in $[L]_t$, indicating that the mobility of the B15C5-alkali metal ion complex is smaller than that of the corresponding uncomplexed alkali metal ion. This can be expected on the basis of much larger size of the B15C5-alkali metal ion complex compared to the corresponding alkali metal ion. The Λ vs. $[L]_t/[M]_t$ plot of the LiCl-CH_3OH system, on the other hand, shows that moving entity of Li^+ is larger than that of the B15C5-Li^+ complex. Generally, such a phenomenon can be observed for the combination of smaller alkali metal ions (e.g., Li^+ and Na^+) and the smaller crown ethers compared to 18-crown-6 in a solvent of lower donicity (e.g., acetonitrile and propylene carbonate).[1,3] A possible explanation is as follows. In a solvent of lower donicity, a stable complex is formed even between a small alkali metal ion and a small crown ether which has a poor binding ability. On account of strong solvation of the small alkali metal ion and less solvation of its complex with the small crown ether, moving entity of the alkali metal ion is larger than that of its crown ether complex.

From Figs. 1 and 2, it is evident that a clear breaking point at $[L]_t/[M]_t=1$ is observed only in the case of the Li-acetonitrile system. It is responsible for the clear breaking point that B15C5 forms a very stable 1:1 complex with Li^+ and the complex has a lower mobility than a Li^+ ion.

Stability Constants. From Table 1, selectivity sequences of B15C5 for the alkali metal ions in acetonitrile, propylene carbonate, and methanol are as follows:

AN: $Li^+ > Na^+ \gg Rb^+ > K^+ > Cs^+$,
PC: $Na^+ > Li^+ > K^+ > Rb^+ > Cs^+$,
CH_3OH: $Na^+ > K^+ > Rb^+ > Li^+ > Cs^+$.

Table 2. Transfer Activity Coefficients at 25 °C

		s=AN[a]		s=PC[b]		s=H_2O	
log $^{CH_3OH}\gamma^s(M^+)$							
	Li^+[8]	4.4_7		3.1_5		—	
	Na^+[9]	0.9		1.5_4		—	
	K^+[9]	−0.4		-0.1_6		−1.7	
	Rb^+[9]	−0.6		-0.4_8		—	
	Cs^+[9]	−0.8		-0.6_6		—	
log $^{CH_3OH}\gamma^s(L)$		B15C5	B18C6[10]	B15C5	B18C6[10]	B15C5	B18C6
		−0.68	1.0	−0.48	0.082	0.56	—
log $^{CH_3OH}\gamma^s(ML^+)$							
	Li^+	1.6_4	—	1.2_1	—	—	—
	Na^+	−1.0	1.5	-0.2_9	0.8	—	—
	K^+	−0.9	1.0	-0.7_0	0.2	1.1_9	—
	Rb^+	−1.6	1.1	-0.9_3	0.2	—	—
	Cs^+	−1.7	0.5	-1.0_1	−0.08	—	—

a) Acetonitrile. b) Propylene carbonate.

Selectivity tendency of B15C5 for the alkali metal ions except for Li^+ is roughly consistent with size-relationship regardless of a variety of solvents; that is, the more closely the alkali metal ion fits into the B15C5 cavity (cavity radius 0.85 Å[7]), the more stable is the B15C5–alkali metal ion complex. For Li^+ ion, however, log K_{ML^+} value is the greatest in acetonitrile, the second largest in propylene carbonate, and the second smallest in CH_3OH among alkali metal ions. Stability of the B15C5–Li^+ complex seems to be governed largely not only by the size-relationship but also by the strength of solvation of the solvent for the free Li^+ ion. Li^+ probably undergoes the strongest solvation of all the alkali metal ions. Solvation-ability (i.e., relative solubility) sequences of the solvents for Li^+ derived from the data[8] on transfer activity coefficients are acetonitrile≪propylene carbonate≪CH_3OH, and the difference in solvation-ability of solvent[8] between Li^+ and the other alkali metal ion increases in the order acetonitrile<propylene carbonate<CH_3OH. This is responsible for the above-mentioned results of the Li^+ complex.

Stability sequences of the respective B15C5–alkali metal ion complexes for the solvents are as follows:

Li^+: AN > PC > CH_3OH,
Na^+: PC > AN > CH_3OH,
K^+: PC ≥ CH_3OH > AN ≫ H_2O,
Rb^+: AN > CH_3OH ≥ PC,
Cs^+: AN > CH_3OH > PC.

Solvation-ability sequences[8,9] of the solvents for the alkali metal ion are as follows:

Li^+: AN ≪ PC ≪ CH_3OH,
Na^+: PC < AN < CH_3OH,
K^+: CH_3OH ≤ PC < AN ≪ H_2O,
Rb^+: CH_3OH < PC ≤ AN,
Cs^+: CH_3OH < PC ≤ AN.

Stability sequences of the respective B15C5–alkali metal ion complexes in the solvents, except for the cases of Rb^+ and Cs^+ complexes in acetonitrile, are the reverse of solvation-ability sequences of the solvents for the corresponding alkali metal ion. This indicates that the B15C5–alkali metal ion complex is stable in a solvent with poor solvation-ability to the free alkali metal ion and the reverse is true. The author cannot explain the exceptional behavior of Rb^+ and Cs^+ complexes in acetonitrile at the present time.

Transfer Activity Coefficient. Logarithm of transfer activity coefficient (log $^{s_1}\gamma^{s_2}(ML^+)^\dagger$) of a B15C5–alkali metal ion complex between solvent s_1 and solvent s_2 is calculated by Eq. 1.

$$\log {}^{s_1}\gamma^{s_2}(ML^+) = (\log K_{ML^+})_{s_1} - (\log K_{ML^+})_{s_2} + \log {}^{s_1}\gamma^{s_2}(L) + \log {}^{s_1}\gamma^{s_2}(M^+), \quad (1)$$

where log $^{s_1}\gamma^{s_2}(L)^\dagger$ and log $^{s_1}\gamma^{s_2}(M^+)^\dagger$ refer to logarithm of transfer activity coefficients of B15C5 itself and a free alkali metal ion between solvent s_1 and solvent s_2, respectively, and $(\log K_{ML^+})_s$ designates log K_{ML^+} value in solvent s. By way of example, a positive log $^{s_1}\gamma^{s_2}(ML^+)$ value means that the complex, ML^+, undergoes stronger solvation in s_1 than in s_2. Transfer activity coefficient values of ML^+, M^+, and L when s_1=CH_3OH are summarized in Table 2.

From the solubility data of B15C5 determined in this study, solubility sequences of B15C5 for the solvents are in the order acetonitrile>propylene carbonate>methanol>water although there exist hydrogen bonds between ether oxygen atoms and protic solvents such as water and methanol, and, moreover, the hydrogen bonding is much stronger in water than in methanol.[11] This may be attributed to superiority of lipophilic effects of the benzo and ethylene groups over hydrogen-bonding effects of ether oxygen atoms. Benzo-18-crown-6 (B18C6) is larger in size than B15C5

† $^{s_1}\gamma^{s_2}(X)=[X]_{s_1}/[X]_{s_2}$, X denoting ML^+, L, or M^+.

by an ether oxygen atom and an ethylene group. When s=AN and PC, the log $^{CH_3OH}\gamma^{s}$(L) value changes from negative to positive in going from B15C5 to B18C6. This may be due to the additional hydrogen bonding between the added ether oxygen atom of B18C6 and methanol.

It can be seen from Table 2 that, in general, the log $^{CH_3OH}\gamma^{s}$(ML^+) value of B15C5 varies with a variety of alkali metal ions when s=AN and PC. Positive log $^{CH_3OH}\gamma^{s}$(ML^+) values of B15C5 are found only for the case of Li^+. They are much larger compared to those of other alkali metal ions. From Eq. 1 and Tables 1 and 2, this is attributed completely to very large and positive log $^{CH_3OH}\gamma^{s}$(Li^+) values; namely, the fact that the B15C5-Li^+ complex undergoes much stronger solvation in methanol than in acetonitrile and propylene carbonate is due entirely to much stronger solvation of the central Li^+ in methanol than in acetonitrile and propylene carbonate.

For B15C5, the log $^{CH_3OH}\gamma^{s}$ value decreases on moving from M^+ to ML^+ when s=AN and PC, and the contrary holds for B18C6 except for the case of M^+=Na^+ and s=PC. This is owing largely to the fact that B15C5 is less solvated in methanol than in AN and PC, while B18C6 is more solvated in methanol than in AN and PC. The higher solvation of B15C5 in methanol than in H_2O is mostly responsible for the fact that the log $^{CH_3OH}\gamma^{H_2O}$ value increases in going from K^+ to B15C5-K^+ complex (Table 2).

In the cases of s=AN and PC, the log $^{CH_3OH}\gamma^{s}$(ML^+) value increases from B15C5 to B18C6. This shows that the B18C6-alkali metal ion complex is more solvated in methanol than in AN and PC in comparison with the B15C5 complex. In each case of s=AN and PC, the difference in log $^{CH_3OH}\gamma^{s}$(ML^+) values between B15C5 and B18C6 is roughly constant regardless of the alkali metal ions except for the system of M^+=K^+ and s=AN. As mentioned above for free B15C5 and B18C6, this may be caused primarily by the effect of the additional hydrogen bonding between the increased ether oxygen atom of B18C6 and methanol.

When L=B15C5, s=AN and PC, and M^+=Na^+ and K^+, log $^{CH_3OH}\gamma^{s}$ values for ML^+ and L are nearly the same. Log $^{PC}\gamma^{AN}$ values for B15C5-K^+ and B15C5 at 25 °C are identical (−0.2). This indicates that, generally, property of solute-solvent interaction of the B15C5-alkali metal ion complex mostly reflects that of the free B15C5 unless the alkali metal ion in the B15C5 complex is much smaller or larger than the B15C5 cavity; when log $^{s_1}\gamma^{s_2}$ values for B15C5-M^+ and B15C5 are fairly different from each other, it seems that there exists a specific interaction between the alkali metal ion in the B15C5 cavity and the solvents, where, in most cases, the alkali metal ion in the B15C5 cavity has a much smaller or larger size than that of the B15C5 cavity. A similar tendency is observed for B18C6 and its alkali metal ion complexes (Table 2 and log $^{PC}\gamma^{AN}$(B18C6)=0.92, log $^{PC}\gamma^{AN}$(M^+-B18C6)=0.7 (Na^+), 0.8 (K^+), 0.9 (Rb^+), and 0.58 (Cs^+) at 25 °C[10]).

Solvation-ability sequences of the solvents for the B15C5-alkali metal ion complex obtained from log $^{CH_3OH}\gamma^{s}$(ML^+) values in Table 2 are as follows:

Li^+-B15C5: $AN < PC \ll CH_3OH$,

Na^+-B15C5: $CH_3OH < PC < AN$,

K^+-B15C5: $H_2O < CH_3OH < PC < AN$,

Rb^+-B15C5: $CH_3OH < PC < AN$,

Cs^+-B15C5: $CH_3OH < PC < AN$.

From the solubility data of B15C5 in this study, solvation-ability sequences of the solvents for B15C5 are $H_2O<CH_3OH<PC<AN$; they agree completely with those for the B15C5-alkali metal ion complex except for B15C5-Li^+ complex. Solvation-ability sequences of the solvents for the B15C5-alkali metal ion complex are consistent with those for the corresponding alkali metal ion except for the cases of CH_3OH for B15C5-Na^+ complex and H_2O for B15C5-K^+ complex. Property of solute-solvent interaction of the B15C5-alkali metal ion complex is characterized by that of the corresponding free alkali metal ion and/or by that of the B15C5 itself. Whereas, property of solute-solvent interaction in AN, PC, and CH_3OH of the B18C6-alkali metal ion complex, whose ligand is larger than B15C5, is characterized by that of the B18C6 itself (solvation-ability sequences of the solvents for B18C6: $AN<PC\leq CH_3OH$).

References

1) Y. Takeda, *Bull. Chem. Soc. Jpn.*, **55**, 2040 (1982).
2) Y. Takeda, *Bull. Chem. Soc. Jpn.*, **56**, 866 (1983).
3) Y. Takeda, H. Yano, M. Ishibashi, and H. Isozumi, *Bull. Chem. Soc. Jpn.*, **53**, 72 (1980).
4) Y. Takeda and H. Yano, *Bull. Chem. Soc. Jpn.*, **53**, 1720 (1980).
5) L. Pauling, "The Nature of the Chemical Bond," 3rd ed, Cornell Univ. Press (1960).
6) R. M. Izatt, R. E. Terry, D. P. Nelson, Y. Chan, D. J. Eatough, J. S. Bradshaw, L. D. Hansen, and J. J. Christensen, *J. Am. Chem. Soc.*, **98**, 7626 (1976).
7) "Progress in Macrocyclic Chemistry," ed by R. M. Izatt and J. J. Christensen, John Wiley and Sons, New York (1981), Vol. 2.
8) B. G. Cox, "Electrolyte Solutions in Dipolar Aprotic Solvents," Physical Chemistry Part 1, The Chemical Society, London (1973), p. 256.
9) I. M. Kolthoff and M. K. Chantooni, Jr., *Anal. Chem.*, **52**, 1039 (1980).
10) Y. Takeda, Y. Ohyagi, and S. Akabori, *Bull. Chem. Soc. Jpn.*, **57**, 3381 (1984).
11) M. K. Chantooni, Jr. and I. M. Kolthoff, *Proc. Natl. Acad. Sci. U.S.A.*, **78**, 7245 (1981).

 © 1988 The Chemical Society of Japan Bull. Chem. Soc. Jpn., 61, 659—666 (1988)

Roles of Kinetic and Potential Energies in Conjugation. I. A Study of Prototypes

Hiroshi Ichikawa,* Yukiko Ebisawa, and Keiichiro Sameshima
Hoshi College of Pharmacy, Shinagawa, Tokyo 142
(Received August 3, 1987)

The analysis of the potential and kinetic energy changes between conjugative and nonconjugative structure in vinylamine and nitroethene led to the conclusion that there were two different types of conjugations: the conjugative stability caused by a decrease in the kinetic energy and that given by a decrease in the potential energy. Those two types could be termed conjugations of *kinetic energy origin* and *potential energy origin* respectively. The cojugative stability in vinylamine is produced by an excess decrease in the kinetic energy over the increase in the potential energy (*kinetic energy origin*), which was attributed to a release of the kinetic energy pressure of the lone pair of electrons on nitrogen. On the other hand, the conjugation of nitroethene causes an overwhelming decrease in the potential energy, especially in that belonging to the nitro group (*potential energy origin*).

Conjugation between a substituent and the π system (e.g., the phenyl group) produces a stabilization energy which is referred to as 'conjugation energy.' Conjugation also affects the electron density in a π system to determine the resultant appearance. According to the electronic effect, functional groups have been classified by organic chemists into two groups, i.e., the electron-donating and electron-withdrawing groups. Such an effect of a substituent on the π system is symbolized by using 'arrows' in organic electron theory. This arrow expression has been so widely used that it has come to be one of the basic concepts in organic chemistry. However, one cannot extract any physical meaning from such arrows.

A large number of MO theoretical calculations have been carried out on substituted benzenes,[1] and the conjugation between a substituent and the phenyl group seems to be thoroughly understood. Indeed, an MO calculation reveals the electron density in the system, and the conjugation is usually interpreted in terms of the interaction between the π system and its substituent.[2] However, fundamental questions remain as to why they must interact, why such a conjugation stability is produced, and why a lone pair of electrons delocalizes into the π system. There may be various theoretical approaches. However, as far as organic chemistry is concerned, a theoretical study must contribute to the establishment of a bridge between the basic concepts of organic chemistry and those of physics.

The total energy of any molecular system consists of two fundamental components, the kinetic and potential energies, which are defined according to distinctly different concepts of energy in nature. The interpretation of chemical phenomena through such energy terms is most fundamental and decisive. Recently, we ourselves have shown that the kinetic energy of π electrons plays the decisive role in the stability or instability of an aromatic or antiaromatic system.[3] The physical meaning of aromaticity has been given as the relaxation of the kinetic-energy pressure of π electrons in isolated double-bonds.[4] The kinetic-energy pressure is a different expression of the most fundamental phenomenon and/or concept in modern physics,[5] i.e., Heisenberg's uncertainty principle.[6] Therefore, aromaticity/antiaromaticity, which is also one of the most fundamental concepts in organic chemistry, has been interpreted in terms of the basic principles of nature.

If wave functions are to provide an understanding of the behavior of electrons in a molecule, we must try somehow to extract information on the physically essential features of electronic energies. One of the methods along this line is energy partitioning. The Hamiltonian of a molecular system is composed of operators related to the kinetic energy, the potential energy for an electron in the field of a nuclear charge, and the repulsion energy between electrons. Thus, the electronic energy (E^{el}) is composed of the kinetic energy of electrons (E^T) and the electronic potential energies. The latter is further partitioned into the attractive one-electron potential (E^{V}) and the repulsive two-electron potential energies (E^J).[7] Our strategy in solving the present problems is to identify the roles of these partitioned energies in conjugation.

This paper will discuss the cases of vinylamine and nitroethene as prototypes of conjugation between a π system and an electron-donating or an electron-withdrawing substituent. These systems are appropriate for the present study in that the conjugation between the substituent and the ethenyl group can be terminated by making the conformation of the substituent orthogonal to the plane of the ethenyl group. As a sophisticated MO method, we used the 6-311 G** method[8] throughout this work.

It has been indicated that the components of the total energy are very sensitive to the scale factor of the wave function.[9] Since the scale factor applies to the electronic coordinates as well as the nuclear coordinates, the condition or threshold of geometry optimization is considered to affect seriously the

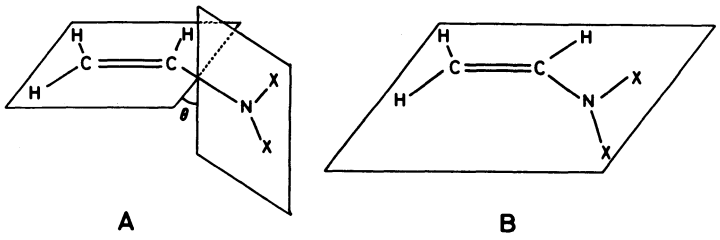

Scheme 1.

components of the total energy. Therefore, the threshold of geometry optimization was set at 0.00003 (maximum) as well as 0.00002 (rms) Hartree/Bohr or radian, which is one tenth of the standard geometry optimization.[10]

Driving Force Which Leads to Conjugation. Vinylamine and nitroethene have near-planar geometries.[11,12] Such a planarity may be maintained by conjugation. If there were no conjugation, the orthogonal structure might be considered to be the most stable geometry because it has the least interatomic repulsions (steric effect), just as ethane favors the staggered conformation. Therefore, we may expect that there are some driving forces that lead to conjugation.

Let us consider how conjugation takes place starting from an orthogonal structure. We suppose that the system follows the minimum-energy path. The orthogonal structure (θ=90° in Scheme 1) and the planar structure (θ=0°) have the maximum-energy and minimum-energy cols; therefore, the torsional forces, $\partial E/\partial\theta$, are zero. Except for these cols, the differential has a positive value. Take any geometry with $0<\theta<90°$, where a certain torsional force is imposed on the C–N bond to lead θ to $\theta-\Delta\theta$. Change in θ is followed by change in all geometrical parameters such as, $R_j \rightarrow R_j+\Delta R_j$ and $\phi_k \rightarrow \phi_k+\Delta\phi_k$, where R_j and ϕ_k are the bond lengths and the bond angles. The cause of the torsion that is put on the C–N bond may be interpreted as the cause of the conjugation.

The total energy is composed of the potential energy (V) and the kinetic energy of electrons (T):

$$E = T + V \tag{1}$$

$$T = E^T \tag{2}$$

$$V = E^V + E^J + E^N \tag{3}$$

where E^N is the nuclear repusion energy.

The differentiation of E with respect to θ gives:

$$\partial E/\partial\theta = \partial T/\partial\theta + \partial V/\partial\theta \tag{4}$$

where $\partial T/\partial\theta$ and $\partial V/\partial\theta$ are the forces due to the kinetic and potential energies, respectively. The

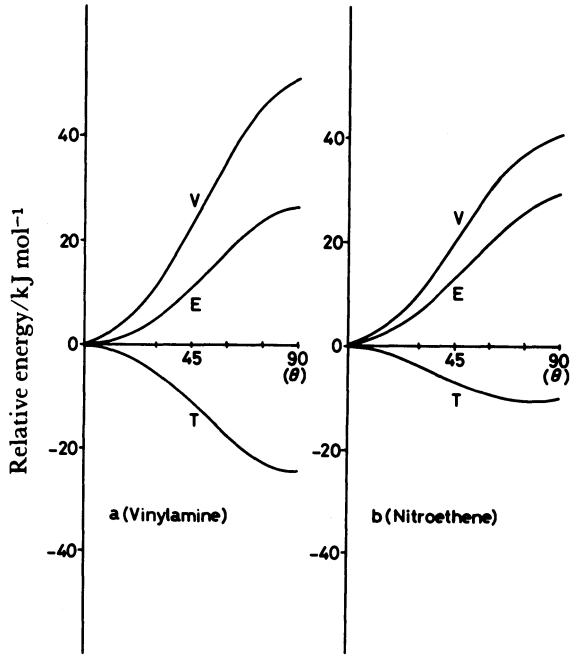

Fig. 1. Plots of the total (E), kinetic (T), and potential (V) energies (kJ mol^{-1}) vs. θ as the conformation changes from A to B through the minimum energy path in vinylamine (a) and nitroethene (b).

positive and negative values represent the increase and the decrease in the corresponding energies as θ increases. At θ=0 or 90°, $\partial E/\partial\theta$ is zero, with $|\partial T/\partial\theta| = |\partial V/\partial\theta|$. When $0°<\theta<90°$, these forces are not balanced. Before an analysis of these forces, let us look at the energy changes in the minimum energy path.

Figure 1 shows the changes in the total, kinetic, and potential energies as functions of θ, where all the geometrical parameters except θ were optimized with respect to the total energy. It is important to note here that these curves are not pure functions of θ, since geometry optimization is carried out at every θ.

Both total energies increase as θ increases. The difference in total energy between 0 and 90° may correspond to the conjugation energy. It is calculated as 26 and 30 kJ mol^{-1} respectively for vinylamine and nitroethene.[13] Nelander has shown that, if all bond lengths are optimized with respect to the total energy,

the virial theorem ($T=-V/2$) should hold, where angular coordinates have no contribution to the virial ratio.[14,15] The energy profiles of the components in Fig. 1 satisfy this requirement reasonably in vinylamine, but qualitatively in nitroethene. These results imply that the potential energy is always responsible for leading to conjugation, since the sign of the gradient of the potential energy is the same as that of the total energy. This is not true, however, since, as has been mentioned, geometry optimization does not take place at the same time as the change in θ, but *as a result of the change in* θ.

We estimated $\partial E/\partial\theta$, $\partial T/\partial\theta$, and $\partial V/\partial\theta$ by means of the divided differences, $\Delta E/\Delta\theta$, $\Delta T/\Delta\theta$, and $\Delta V/\Delta\theta$, which were obtained as follows. First, the energies were calculated at a θ value with full geometry optimization (except only for θ) to give $E(\theta)$, $T(\theta)$, and $V(\theta)$. Then, θ was increased by $\Delta\theta$ and, *without optimization*, those energies are obtained as $E(\theta+\Delta\theta)$, $T(\theta+\Delta\theta)$, and $V(\theta+\Delta\theta)$. The divided differences were $(E(\theta+\Delta\theta)-E(\theta))/\Delta\theta$, etc. We fixed $\Delta\theta$ at 1°.

The gradients of the curves in Fig. 1 correspond to the divided differences when the geometries at both θ and $\theta+\Delta\theta$ are optimized. In fact, the values at $\theta=45°$, for example in vinylamine, were calculated to be 0.51, −0.73, and 1.24 kJ mol^{-1} deg^{-1} for the total, kinetic, and potential energies respectively; these values correspond to the gradients at 45° in Fig. 1-a.

Table 1 shows the divided differences at $\theta=30$, 45, and 60°. In both vinylamine and nitroethene, $\Delta E/\Delta\theta$ is positive, showing that the systems resist the rotation of the substituent planes; i.e., both systems resist breaking conjugation. The divided differences of the energy components of vinylamine appear to be prominently different from those of nitroethene.

In vinylamine, $\Delta T/\Delta\theta$ is positive, while $\Delta V/\Delta\theta$ is negative, with the former being larger than the latter in quantity. This confirms that the force due to the kinetic energy resists breaking conjugation. The divided difference, $\Delta X/\Delta(-\theta)$ (where $X=E$, T, or V), means the force when the orthogonal conformation becomes the conjugative planar structure. Therefore, it may be deduced that the driving force that leads to conjugation in vinylamine is that by the kinetic energy of electrons.

Nitroethene gave the opposite results: $\Delta V/\Delta\theta$ is positive, while $\Delta T/\Delta\theta$ is negavive. This time, the force due to the potential energy is against the rotation of the functional group, while that due to the kinetic energy helps such a rotation. Since the former exceeds the latter, the planarity is maintained; therefore, it may be concluded that the potential energy is the cause of conjugation in nitroethene.

What Happens to Energy Components by Conjugation. This section will discuss the effect of conjugation on the energy components of the total energy. As has already been stated, if there were no conjugation, the orthogonal structure would be the most stable conformation in both vinylamine and nitroethene. Table 2 shows the geometrical parameters of the optimized orthogonal and planar structures. Considerable differences as to the C–C and C–N bonds can be seen between them. Such geometrical changes are considered to be brought forth by the introduction of conjugation.

Here let us make the point of the problem clear: it is conjugation that changes the molecular geometries; i.e., a change of geometry occurs following a presentation of conjugation. Thus, we regarded the orthogonal structure (A in Scheme 2) as the reactant structure for conjugation. With a retention of the bond lengths and the bond angles, the substituent was rotated to a planar structure (the intermediate structure: B′), and all the bond lengths and bond angles were optimized with respect to the total energy (the product structure: B). We investigated the energy changes between A, B′, and B: the energy change between A and B′ includes the effect of conjugation, while that between B′and B corresponds to the effect of the geometrical change after conjugation.

There is another way of considering this question. The optimized structure in conjugation (B) may appear to be near-planar. The rotation of the amino or nitro group in B involves an energy barrier which

Table 1. Divided Differences of Total, Kinetic, and Potential Energies with Respect to the Twist Angle θ[a]

	$\Delta E/\Delta\theta$[b]	$\Delta T/\Delta\theta$[b]	$\Delta V/\Delta\theta$[b]
Vinylamine			
30°	0.37	3.59	−3.21
45°	0.51	3.63	−3.12
60°	0.47	3.49	−3.02
Nitroethene			
30°	1.98	−5.78	7.76
45°	2.20	−5.37	7.57
60°	1.81	−3.63	5.45

a) $\Delta\theta$ is set at 1°. b) In kJ mol^{-1} deg^{-1}.

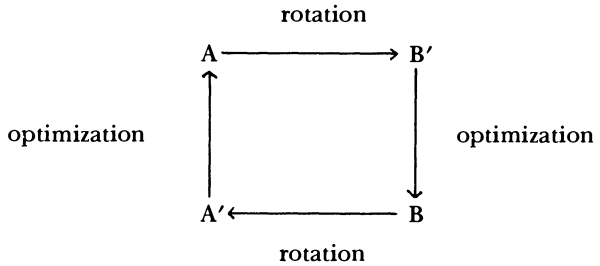

A: geometry-optimized orthogonal structure

B: geometry-optimized planar structure

Scheme 2.

Table 2. Optimized Geometries of A and B Conformations

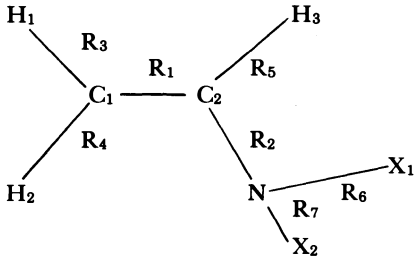

	Vinylamine (X=H)		Nitroethene (X=O)	
	A	B	A	B
Bond length[a]				
R_1	1.3167	1.3218	1.3057	1.3102
R_2	1.4323	1.3906	1.4665	1.4589
R_3	1.0757	1.0734	1.0740	1.0740
R_4	1.0778	1.0773	1.0748	1.0729
R_5	1.0781	1.0776	1.0720	1.0696
R_6	0.9998	0.9963	1.1843	1.1864
R_7		0.9954		1.1862
Bond angle[b]				
$<C_1C_2N$	125.96	126.76	120.99	120.88
$<H_1C_1C_2$	120.82	120.34	119.98	119.71
$<H_2C_1C_2$	121.89	122.06	121.98	121.32
$<H_3C_2C_1$	119.73	119.75	126.87	127.23
$<X_1NC_2$	111.02	114.56	116.96	118.86
$<X_2NC_2$		114.31		115.56
Twist angle[c]				
$<X_1NC_2C_1$	66.1	16.2	−89.1	0.0
$<X_2NC_2C_1$	−66.1	146.7	89.1	180.0

a) In terms of A. b) In terms of degree. c) Counterclockwise twist angle around the C-N bond to the molecular plane in terms of deg.

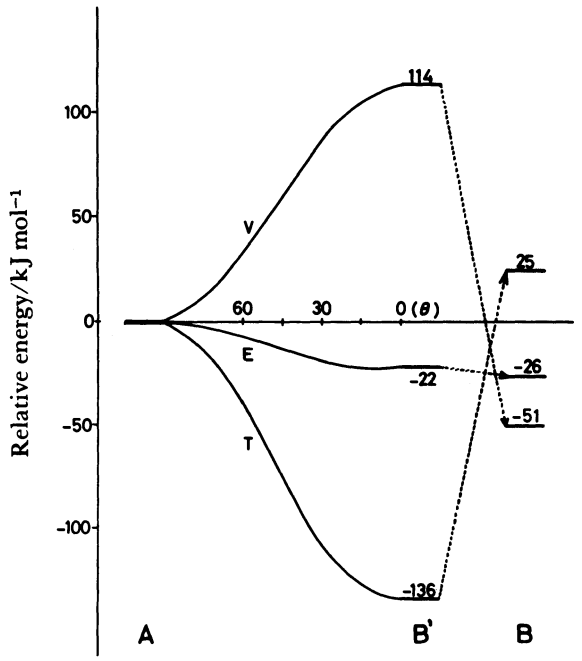

Fig. 2. Plots of the total (E), kinetic (T), and potential (V) energies (kJ mol^{-1}) vs. θ as the conformation changes from A to B′ in vinylamine.

may be caused by a broken conjugation. We also examined the energy change when the substituent at B was rotated to an orthogonal structure (A′), with bond lengths and bond angles being kept at those of B.

Vinylamine. Figure 2 shows the change in the total, kinetic, and potential energies of vinylamine as functions of θ. All the bond lengths and bond angles except for θ were kept the same as those in A. The geometries at θ=90 and 0° are equal to A and B′ respectively. As θ decreases, the total energy decreases by ca. 20 kJ mol^{-1} (at B′). Such a stabilization is produced by conjugation and is a driving energy toward a planar conjugative structure. It is important to note that the potential energy increases, while the kinetic energy decreases, as the geometry is varied from the orthogonal to the planar forms, and that the change in the kinetic energy is larger than that in the potential energy. This simply means that the decrease in kinetic energy is the original conjugation stability.

If all the bond lengths are optimized with respect to the total energy, the virial theorem ($T=-V/2$) should hold where angular coordinates make no contribution.[14-16] Therefore, the energy change between A and B may be supposed to satisfy this relationship:

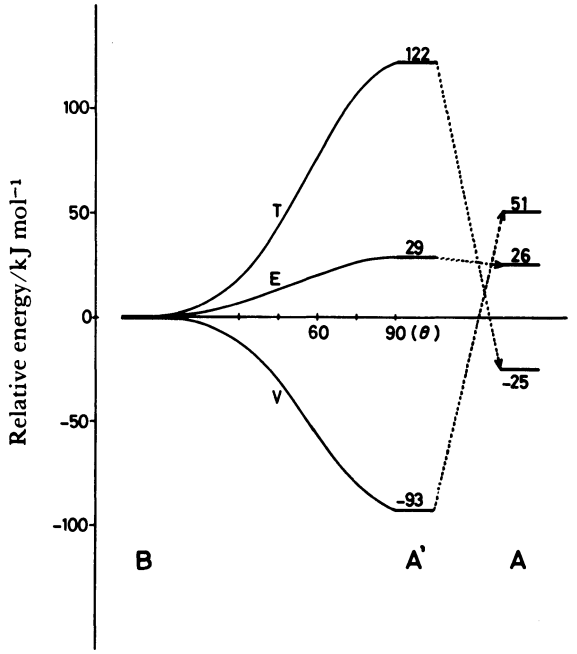

Fig. 3. Plots of the total (E) kinetic (T), and potebtial (V) energies (kJ mol^{-1}) vs. θ as the conformation changes from B to A′ in vinylamine.

$\Delta T=-\Delta V/2$. A comparison between B′ and B shows that the optimization of all geometrical parameters does not produce a large change in the total energy, but does in the potential and kinetic energies. The virial relationship can be seen with a reasonable accuracy.

Figure 3 shows the case when the conjugation between the ethenyl and amino groups is forced to terminate, i.e., the plots of the energy change vs. θ when θ is varied from 0° (B) to 90° (A′) with all the geometrical parameters at B except for θ. The total and kinetic energies increase monotonously as θ increases. At A′, the difference in total energy is around 29 kJ mol^{-1}, and we see that the kinetic energy is the main source of the increase in the total energy. Again, the optimization of all bond lengths and bond angles causes a large change in the potential and kinetic energies to meet the virial theorem, although the lowering of the total energy is less than 5 kJ mol^{-1}. From the results thus obtained, we may conclude that the kinetic energy is the factor in leading to conjugation in vinylamine.

Nitroethene. The nitro group is a representative substituent that withdraws the π electrons of the conjugated π system. Figure 4 shows the changes in the total, potential, and kinetic energies of nitroethene as functions of θ. Again, all the geometrical parameters but θ are kept the same as those in A. Although geometry optimization on B′ does not lower the total energy more than 2 kJ mol^{-1}, its components encounter a considerable change (more than 24 kJ mol^{-1}), much as in the case of vinylamine.

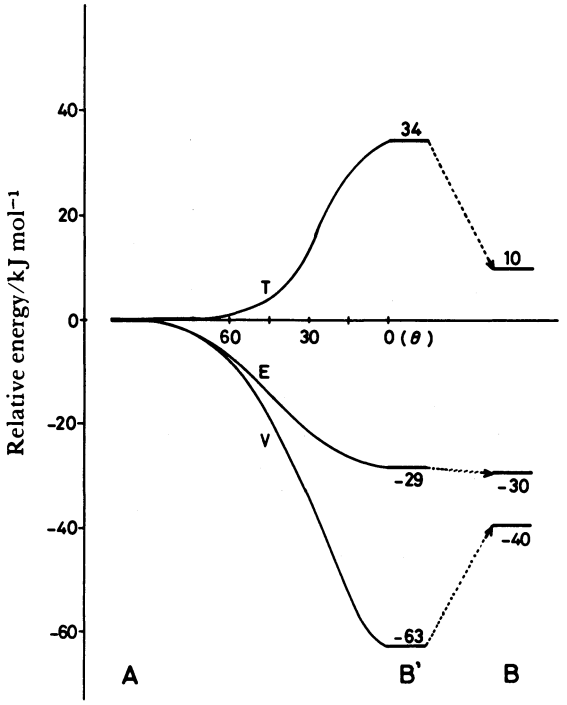

Fig. 4. Plots of the total (E), kinetic (T), and potential (V) energies (kJ mol^{-1}) vs. θ as the conformation changes from A to B′ in nitroethene.

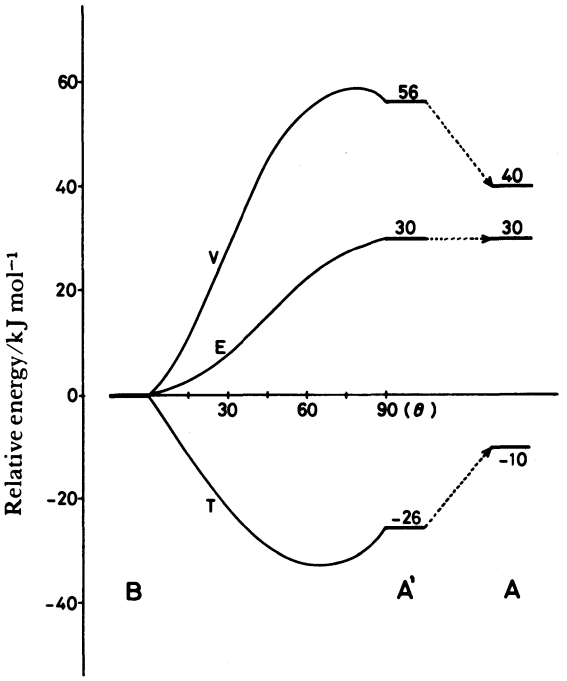

Fig. 5. Plots of the total (E), kinetic (T), and potential (V) energies (kJ mol^{-1}) vs. θ as the conformation changes from B to A′ in nitroethene.

The energy profile in Fig. 4 also seems similar to that in Fig. 2. However, the contents are the exact opposite of those of vinylamine in that as θ decreases, the kinetic energy increases, while the potential

energy decreases, and in that the amount of the decrease is larger than that of the increase. Therefore, it may be said that the conjugation stability is given by a decrease in the potential energy.

The energy profile in Fig. 5 is different from that in Fig. 3: the total and potential energies increase, while the kinetic energy decreases, as θ increases, leading to the conclusion that, contrary to the case of vinylamine, here the increase in the potential energy is the cause of the resistance against the rotation of NO_2. The conclusion in nitroethene is that the potential energy is the factor which leads to conjugation.

Concerning the Virial Theorem. We observed drastic changes in the partitioned energies between Structures A′ and A or between Structures B′ and B. Here we will give the reason.

The large change in the partitioned energies may be explained in terms of the scaling error. The virial relationship (i.e., $V=-2T$) may be supposed to hold at an equilibrium geometry. The scaling factor of the wave function for this geometry is unity. At a non-equilibrium geometry, however, the scaling factor must be adjusted in order to satisfy the virial relationship.[17]

If the molecular geometry is expressed by a set of internuclear distances R_j and angular coordinates ϕ_k, the virial theorem for a polyatomic molecule may be written as:[14,16]

$$2T+V+\sum R_j(\partial E/\partial R_j)=0 \tag{5}$$

Suppose that the total energy, geometry, and wave function at a non-equilibrium geometry are expressed by E, $G(R_j,\phi_k)$, and $\psi(\mu_i;R_j,\phi_k)$, where μ_i are the electronic coordinates. Here, we introduce a scaling factor η:

$G(R_j,\phi_k)$	$G(\eta R_j,\phi_k)$
$\psi(\mu_i;R_j,\phi_k)$	$\eta^{(3N/2)}\psi(\eta\mu_i;\eta R_j,\phi_k)$
E	E'
Unscaled system	Scaled system

where N is the number of electrons and E' is the total energy of the scaled wave function.

We can now obtain the normal virial relationship between the scaled potential and kinetic energies, i.e., $V'=-2T'$. Thus, each geometry has its own scaling factor that satisfies the virial relationship. If we consider the scaled wave function, a geometrical change from the one to the other gives rise to a scaling error for the wave function.

Pedersen and Morokuma[9] considered the effect of the scaling of the wave function on the total energy and its components. Introducing a scaling error $\gamma(=\eta-1)$ and expanding the differences between the scaled and unscaled energies in a power series or γ, they obtained these differences in energy:

$$\begin{aligned}\Delta E &= E(\gamma^2+\cdots\cdots)\\ \Delta T &= E(-2\gamma+3\gamma^2+\cdots)\\ \Delta V &= E(2\gamma-2\gamma^2+\cdots)\end{aligned} \tag{6}$$

These expressions clearly show that the kinetic and potential energies change in the first order of γ, while the total energy changes only in the second order. The present problem is a case of just this, since the geometries at A′ and B′ are non-equilibrium.

Here we must make another possibly confusing point clear. E' is always lower than E.[18] A question is, then: "Should we consider the scaled energies (T' and V') instead of the unscaled energies (T and V) at A′ and B′?" The answer is "No!" for the geometry for the scaled wave function is no longer the same as that for the unscaled wave function (namely, the R_j values are multiplied by η in G for the scaled wave function). What we need is the unscaled energy at A′ or B′ where the third term of Eq. 5 is surely far from null.

What Happens to the Substituent upon Conjugation. So far, we have discussed the changes in the partitioned energies in the whole system. In order to see the details of conjugation, this section will now deal with the changes in those energies for atoms in ethenyl and amino or nitro groups as the θ value changes.

Since, in the LCAO MO theory, each MO is expanded by a linear combination of atomic orbitals (AO's), and since, via the Fock matrix, the three- and four-center terms are reduced to two-center terms, the Hartree–Fock equation is formally expressed by the sum of monocentric (E_A) and bicentric (E_{AB}) terms:

$$E=E_A+\sum_{A>B}E_{AB} \tag{7}$$

These terms can be further partitioned as:

$$E_A=E_A{}^T+E_A{}^V+E_A{}^J \tag{8}$$

$$E_{AB}=E_{AB}{}^T+E_{AB}{}^V+E_{AB}{}^J+E_{AB}{}^N \tag{9}$$

where $E_{AB}{}^N$ is the nuclear repulsion energy between atoms A and B; it is, of course, one of the potential energies in the given system. The details of the calculation method have been given elsewhere.[3,7]

Following the method presented in the definition of Mulliken population analysis,[19] the kinetic and potential energies concerning the electrons belonging to a specified atom, X, $T(X)$, and $V(X)$, are defined as;

$$T(X)=E_X{}^T+1/2\sum_{A\neq X}E_{XA}{}^T \tag{10}$$

$$V(X)=E_X{}^V+E_X{}^J+1/2\sum_{A\neq X}(E_{XA}{}^V+E_{XA}{}^J+E_{XA}{}^N) \tag{11}$$

The electronic effect of enamine may be expressed in organic chemistry as follows.[20]

$$\overset{\curvearrowleft}{C_1}=C_2-\overset{\curvearrowleft}{\dot{N}} \longleftrightarrow C_1^- - C_2=N^+$$

1 2

Table 3. Electron Density, Kinetic Energy, and Potential Energy on an Atom in Orthogonal Conformation and Their Differences from the Planar Conformation(B′)

	Electron density		Kinetic energy		Potential energy	
	A	Difference[a]	A	Difference[b]	A	Difference[b]
Vinylamine						
C_1	6.2105	68.0	37.802446	97.2	−76.170861	−488.9
C_2	6.0045	−46.1	37.767568	−77.9	−75.488585	523.1
N	7.5127	−44.0	54.410705	−97.2	−110.686940	402.3
Nitroethene						
C_1	6.1460	−29.6	37.768174	70.9	−76.146852	169.0
C_2	5.9815	44.9	37.839717	4.8	−75.275044	−730.0
N	6.5987	43.7	54.303856	−73.8	−106.642428	964.4
O_1	8.3624	31.5	74.968693	43.8	−151.656224	−696.8
O_2	8.3624	5.9	74.968693	−5.4	−151.656224	33.2

a) $D(B')-D(A)$ in 10^{-3} electron units. b) $X(B')-X(A)$ in kJ mol^{-1}, where X is the kinetic or potential energy.

These expressions indicate that some of the lone-pair electrons on the nitrogen atom flow to the π system and are localized on the β carbon atom.

Table 3 shows the differences, between A and B′, of $T(X)$ and $V(X)$, as well as the total atomic charges of the carbon, nitrogen, and oxygen atoms. Agreeing with the cannonical structure **2**, the conformation change from A to B′, i.e., the introduction of conjugation in vinylamine, reduces the electron densities of N as well as of C_2 and enriches that of C_1.[21] Since the potential energy and kinetic energy of electrons on an atom are essentially proportional to its electron density,[22] a change in electron density involves proportional changes in the kinetic and potential energies, which are agreeingly reproduced, as may be seen in Table 3.

The substituent effect of the nitrogen group on a π system may be symbolized as follows:

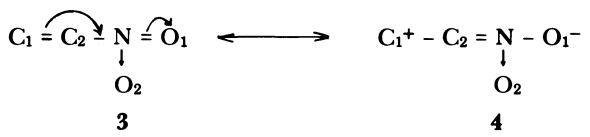

3 **4**

which indicates that conjugation makes the electron density of the β carbon atoms low and only one of the oxygen atoms high. The results in Table 3 coincide well with the above symbols. That is, on a conjugative structure, the electron density at the β carbon atom is reduced, while that of O_1 is increased. An increase in the electron density at C_2 is observed. This may be interpreted as C_2 being at the allylic position to O_1 and O_2, which have three or two lone pairs of electrons respectively.

An electron migration takes place because such a migration produces a stabilization energy; the degree of migration is determined by the lowest total energy, which is given by including all the interactions in the system. However, the only structural difference between vinylamine and nitroethene is in the substituent. Therefore, the differences in conjugation thus far discussed should be totally attributed to the nature of the substituent. That is, the sources of conjugation in vinylamine and nitroethene are the kinetic energy of electrons and the potential energy, which are given by the electronic effects of the amino and nitro groups respectively.

Concluding Remarks. In an orthogonal conformation, the movement of mobile electrons in both the ethenyl and substituent groups is restricted by the orthogonalized overlap of the p AO's, while in a planar structure those electrons are allowed to move. This produces two situations: (1) The electrons on the substituent move to the π system or (2) the electrons in the π system are withdrawn by the substituent.

The kinetic energy of an electron reflects the degree of the restriction of electron movement. An orthogonal conformation of vinylamine restricts the movement of the lone pair of electrons within the nitrogen atom, resulting in a high kinetic energy of the electrons, equivocally a high kinetic-energy pressure of the electrons. A planar structure allows the electrons to move. Such a less-restricted movement generally causes a decrease in the kinetic energy, i.e., a relaxation of the kinetic-energy pressure. This concept may be extended to any electron-donating substituent.

In nitroethene, the allowed movement of π electrons causes a localization of the π electrons on one of the oxygen atoms; this is a result of the strong electrostatic potentials of the hetero atom, which produces an increase in the kinetic energy, but also an overwhelming decrease in the potential energy. In this way, the cause of conjugation can be of either *kinetic-energy origin or potential-energy origin.*

References

1) Eg. W. J. Hehre, L. Radom, and J. A. Pople, *J. Am. Chem. Soc.*, **94**, 1496 (1972).

2) For a recent review, see A. Pross and L. Radom in "Progress in Physical Organic Chemistry," ed by R. W. Taft, John Wiley & Sons, New York (1981), Chap. 1.

3) H. Ichikawa and Y. Ebisawa, *J. Am. Chem. Soc.*, **107**, 1161 (1985).

4) H. Ichikawa, *J. Am. Chem. Soc.*, **105**, 7457 (1983); **106**, 6249 (1984).

5) M. J. Feinber and K. J. Ruedenberg, *J. Chem. Phys.*, **54**, 1495 (1971).

6) W. Heisenberg, *Z. Physik.*, **43**, 172 (1927).

7) H. Kollmar, *Theoret. Chim. Acta*, **50**, 235 (1978). See also, a) E. Clemeti and W. von Niessen, *J. Chem. Phys.*, **54**, 521 (1971), b) C. W. Wilson, Jr., and W. A. Goddard, III, *Theoret. Chim. Acta*, **26**, 195 (1972); **26**, 211 (1972), and Ref. 3.

8) R. Krishnan, J. S. Binkley, R. Seeger, and J. A. Pople, *J. Chem. Phys.*, **72**, 650 (1980).

9) L. Pedersen and K. Morokuma, *J. Chem. Phys.*, **46**, 3941 (1967).

10) We have used the GAUSSIAN 80H program (a Hitac version of GAUSSIAN 80 (QCPE 437, 1982)) at the Computer Center of the University of Tokyo.

11) R. A. Eads, D. A. Weil, M. R. Ellenberger, W. E. Farneth, D. A. Dixon, and C. H. Douglass, Jr., *J. Am. Chem. Soc.*, **103**, 5372 (1981).

12) a) P. Nosberger, A. Bauder, and Hs. H. Gunthard, *Chem. Phys.*, **8**, 245 (1975); b) G. H. Penner, *J. Mol. Str. (Theochem.)*, **137**, 121 (1986).

13) The experimental value for nitroethene was found to be 20.22 kJ mol^{-1} (R. Meyer, A. Gammeter, M. P. Smith, H. Kune, P. Nosberger, and Hs. H. Gunthard, *J. Mol. Spectrosc.*, **46**, 399 (1973)). Since vinylamine favors the imino form, the experimental rotational barrier may not be obtained. However, it has been calculated to be 26 or 32 kJ mol^{-1} (Ref. 11).

14) B. J. Nelander, *J. Chem. Phys.*, **51**, 469 (1969).

15) B. J. Nelander, *J. Chem. Phys.*, **55**, 2949 (1971).

16) S. Srebrenik and R. Messer, *J. Chem. Phys.*, **63**, 276 (1975).

17) P. -O. Löwdin, *J. Mol. Spectrosc.*, **3**, 46 (1959).

18) It can easily be seen that E' is always lower than E since E' is obtained by the variation principle.

19) R. S. Mulliken, *J. Chem. Soc.*, **23**, 1833 (1955); **23**, 1841 (1955); **23**, 2338 (1955); **23**, 2343 (1955).

20) Eg., A. G. Cook, "Enamines, Synthesis, Structure and Reactions," Marcel Dekker, New York (1969).

21) The electron density of C_2 is reduced because it is adjacent to the positively charged nitrogen atom.

22) H. Ichikawa, K. Sameshima, and Y. Ebisawa, *Bull. Chem. Soc. Jpn.*, **59**, 2729 (1986).

 © 1988 The Chemical Society of Japan Bull. Chem. Soc. Jpn., 61, 667—671 (1988)

The CO-H_2 Reaction over ZrO_2 to Form Isobutene Selectively

Ken-ichi MARUYA,* Tatsuichi MAEHASHI, Takashi HARAOKA, Shinichiro NARUI, Yukihiko ASAKAWA, Kazunari DOMEN, and Takaharu ONISHI*

Research Laboratory of Resources Utilization, Tokyo Institute of Technology, 4259 Nagatsuta, Midori-ku, Yokohama 227

(Received August 3, 1987)

The CO-H_2 reaction over ZrO_2 was studied in detail. Methanol and isobutene were selectively formed at 473—523 and 623—673 K, respectively. The activation energies for C_2, C_3, and linear C_4 hydrocarbon formation are 79, 84, and 96 kJ mol^{-1} (523—723 K), while that for branched-chain C_4 hydrocarbons is about 210 kJ mol^{-1} (523—623 K). At 673 K the rate of C_4 hydrocarbon formation is as follows: $r=kP_{H_2}\cdot P_{CO}^2$, while those of C_1, C_2, and C_3 are written by the functions having the maximum values regarding CO pressure. C_4 hydrocarbons consist mostly of isobutene at the temperature. From these results it was concluded that isobutene is formed via different path from those of C_1, C_2, C_3, and linear C_4 hydrocarbons. The addition of high electronegative oxides such as SiO_2 and Nb_2O_5 resulted in the decrease of isobutene and the increase of methane. The selective formation of isobutene proceeds over pure ZrO_2 and ZrO_2 modified with 3a Group and basic metal oxides. The nature of active site for isobutene formation was discussed.

There have been vast researches on the hydrogenation of CO over transition metal catalysts and the products obtained are mostly comprised of hundreds of hydrocarbons and oxgenated products. In those cases the carbon chains of the products are usually linear and the distributions of hydrocarbons are described by the Schulz-Flory rule. Therefore, there have been only few studies on the selective formation of special hydrocarbons,[1-5] and even in the cases with high selectivity the catalysts are not so stable for the long time reaction and the high temperature treatment, because of the delicate method of catalyst preparation.[2,4,5]

On the other hand, difficultly reducible metal oxides have been used as catalyst supports and only few have been studied as catalysts. One of the features of metal oxide catalysts is to form branched-chain hydrocarbon products directly from CO and H_2. Thus, ThO_2,[6] La_2O_3,[7] and Dy_2O_3[7] produce branched-chain, saturated, and aliphatic hydrocarbons such as isobutane under very severe conditions, and ZrO_2 selectively forms isobutene under mild conditions such as at 69 kPa and 623 K.[8] These catalysts are stable for the reaction at 723 K[6,8] and the pretreatment at 973 K.[8] The selective formation of isobutene is found out also in the other oxide catalysts such as CeO_2 and La_2O_3 under the mild conditions.[9] In this paper we describe in detail the CO-H_2 reaction over ZrO_2 to form isobutene selectively.

Experimental

Materials. Zirconium hydroxide was precipitated by hydrolysis of $ZrO(NO_3)_2$ with about 5% aqueous ammonia solution, washed with deionized water until no ammonia was detected with Nesler's test, dried overnight at 393 K, and calcined at 773 K for 3 h. Mixed oxides of ZrO_2 with oxides of Ca, Sc, Y, Nd, and Sm were prepared from the mixed solution of $ZrO(NO_3)_2$ and each of the nitrates in similar manners to the ZrO_2 case. The impregnated ZrO_2 catalysts with Al_2O_3 and SiO_2 were prepared using the nitrate and the ethoxide solution, respectively, and were calcined around 673 K for several hours in order to remove the nitrate and the ethoxide ions and then at 773 K for 3 h. A mixed hydroxide of ZrO_2 and Nb_2O_5 was precipitated from aqueous HCl solutions of $NbCl_5$ and $ZrOCl_2$ with aqueous ammonia solution, and treated similarly to the ZrO_2 case. Zirconium sponge was purchased from Mitsuwa Pure Chemicals.

Procedure. Reactions were carried out in a glass vacuum reaction system with a gas-circulating pump and also a flow system under the atmospheric pressure. In the reaction with the vacuum system a mixture of CO and H_2 (1:3) was purified by gas circulation through a trap at liquid nitrogen temperature for 1 h before contacting with the catalyst (1.5 g), which was preevacuated at 973 K for 3 h. The initial pressure was 69 kPa and the gas flow rate was about 35 ml(STP) min^{-1}.

The reaction was also carried out in the flow system with a quartz reactor of 12 mm of outside diameter, to investigate the pressure dependence of the reaction rate. The reaction temperature was measured by a thermocouple inserted in the catalyst bed (5.0 g). The catalyst was heated at 873 K for 3 h under a nitrogen stream at about 100 ml(STP) min^{-1}, and then H_2 and CO were introduced after cooling the catalyst to a given reaction temperature. The total flow rate was kept constant by changing that of nitrogen.

Analyses. Products except for methane were collected at the liquid nitrogen temperature. GC, IR, and MS were used for analyses of products and CO. Quantitative analyses were conducted by GC equipped with a Porapak Q column for CO_2, H_2O, methanol, dimethyl ether, and hydrocarbons including CH_4, VZ-7 and VZ-10 columns (Gasukuro Kogyo Inc.) for isomer of C_4 and C_5 hydrocarbons, and a molecular sieve 5A column (Nishio Industry Co.) for CO.

Results and Discussion

Temperature Dependence of Hydrocarbon Formation. Table 1 shows the yield of products formed from the CO-H_2 reaction over ZrO_2 using the gas-circulating glass reaction system at the temperature from 473 to 723 K for the initial 25 h. Yields of methanol and dimethyl ether reaches the maximum values around 523 and 573 K, respectively, and that of

Table 1. Product Yield from $CO-H_2$ Reaction over ZrO_2[a]

T/K	Yield/C-base μmol				
	Hydrocarbon	MeOH	Me_2O	CO_2	H_2
473	0.17	11	3.6	0.6	4.5
523	0.86	43	22	11	37
573	8.8	16	84	60	38
623	145	2.7	9.2	240	47
673	282	0.0	0.28	350	160
723	308	0.0	0.0	430	200

a) ZrO_2 (1.5 g) was evacuated at 973 K for 3 h before reaction. Initial pressure ($H_2/CO=3$) was 69 kPa. Products were collected for the initial 25 h.

Table 2. Product Distributions in C_4 Hydrocarbons

T/K	Selectivity/mol%						$C_4/\sum C_i$
	n-C_4H_{10}	i-C_4H_{10}	1-C_4H_8	t-2-C_4H_8	c-2-C_4H_8	i-C_4H_8	C-base %
523	3.0	0.4	63	3.3	1.3	29	27
573	0.3	0.0	0.5	7.7	0.5	91	60
623	0.0	1.1	0.2	1.0	0.7	97	89
673	0.3	4.2	1.7	3.4	2.4	88	78
723	10	11	3.0	8.0	11	57	49

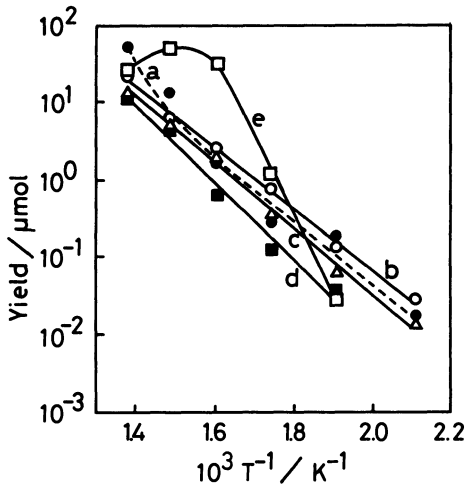

Fig. 1. Arrhenius plots of hydrocarbon yields formed from $CO-H_2$ reaction over ZrO_2 at 60 kPa ($H_2/CO=3$). a(●): C_1, b(○): C_2, c(△): C_3, d(■): linear C_4, and e(□): branched-chain C_4.

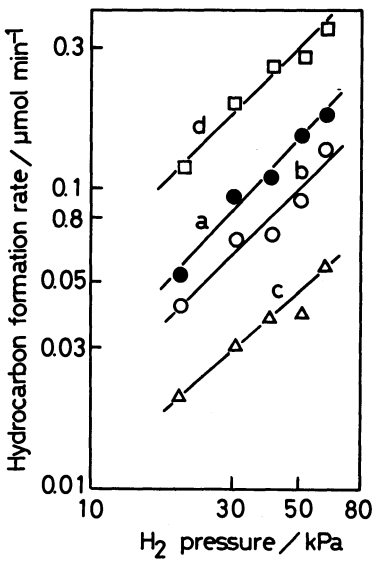

Fig. 2. H_2 pressure dependence of hydrocarbon formation rate at 673 K and 40 kPa of CO pressure. a: C_1, b: C_2, c: C_3, and d: C_4.

hydrocarbons increases rapidly with an increase in the reaction temperature. The temperature dependences of the yields of C_1 to C_4 hydrocarbons are shown in Fig. 1. The plots for C_2 and C_3 hydrocarbons are almost linear in the wide temperature range between 523 and 723 K and their apparent activation energies are 79 and 84 kJ mol^{-1}, respectively. Methane yields are close to those of C_2 and C_3 hydrocarbons, although they are rather scattered. The yields of linear C_4 hydrocarbons evaluated from the isomer distribution shown in Table 2 are plotted rather linearly in the temperature range and the activation energy is about 96 kJ mol^{-1}. On the other hand, the yield of branched-chain C_4 hydrocarbons has maximum value around 673 K. The activation energy evaluated in the narrow range between 523 and 623 K is about 210 kJ mol^{-1}. The isomer distributions in Table 2 show that at 523 K 1-butene is mainly formed but above 573 K the main product is isobutene and no or little skeletal isomerization takes place at 623 K. These results indicate that the branched-chain hydrocarbons are probably formed by the different path from the linear ones.

Pressure Dependence of Hydrocarbon Formation. Figure 2 shows the H_2 pressure dependences of the formation rates of hydrocarbons from C_1 to C_4. The rates are proportional to the pressure. For the rate of

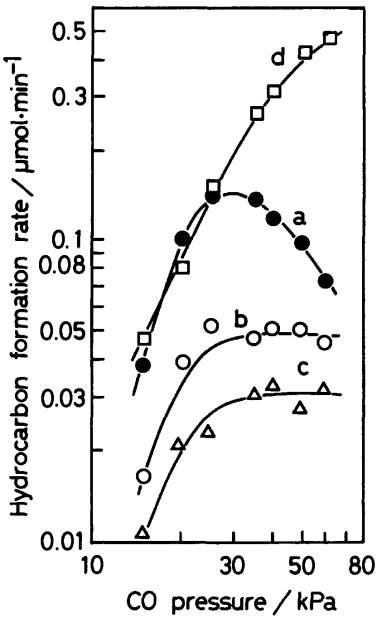

Fig. 3. CO pressure dependence of hydrocarbon formation rate at 673 K and 40 kPa of H_2.

methanation over metal catalysts it is reported that the exponents of the H_2 pressure vary between 0.7 and 1.6.[10,11] For the Fischer-Tropsch reaction various values between 0 and 2 are reported, although the exponent value under usual conditions is reported to be about 1.[12,13] Thus, oxide catalysts such as ZrO_2 show the same dependence on the H_2 pressure as the metal catalysts.

Figure 3 shows the CO pressure dependence of the rates. Differing from the H_2 pressure dependence, the plots are not linear for all hydrocarbons. The rates of C_1, C_2, and C_3 hydrocarbon formation increase with an increase in the pressure range of about 30 kPa. The rate of C_1 hydrocarbon formation reaches the maximum value around 30 kPa, while those of C_2 and C_3 become nearly constant above that value. On the other hand, the rate of C_4 hydrocarbon formation is almost proportional to the square of the pressure. Since C_4 hydrocarbons consist mostly of isobutene at the temperature shown in Table 2, the difference of the CO pressure dependence means that the mechanism of isobutene formation is probably different from those of linear hydrocarbons.

The formation of branched-chain, aliphatic, and saturated hydrocarbons in the isosynthesis reaction has been explained by the mechanism of the conversion of methanol which is produced as a primary product.[6,7] Since ZrO_2 is one of the isosynthesis catalysts[6] and methoxide species is observed on the ZrO_2 surface under the reaction conditions,[14] the surface methoxide species is one of the possible precursor for the hydrocarbon formations. The formation of linear hydrocarbons such as C_{1-3} and linear C_4 hydrocarbons might take place in a similar mechanism to isosynthesis reactions, because the Arrhenius plots are almost linear from the low temperature, at which methanol is selectively formed, to the high temperature and methoxide species are observed in the temperature range under the reaction conditions.[14] On the other hand, the formation of isobutene begins to take place above 623 K, at which the amounts of methanol and dimethyl ether decrease and the rate of the formation depends on the CO pressure in the second order. These results suggest that the formation of isobutene proceeds probably via some species in addition to the methoxide. That is, the formation path of isobutene from the CO-H_2 reaction over ZrO_2 may be different from the methanol conversion suggested in the isosynthesis. Recently, the mechanisms of aldol condensation type have been proposed for the formation of branched-chain olefins over ZrO_2[15] and CeO[16] catalysts. However, the lack of experimental evidence in the former case and the low selectivity of C_4 hydrocarbons in the latter case make obscure the agreement with the highly selective CO-H_2 reaction over ZrO_2 in the present study. Reaction mechanisms for the isobutene formation are under investigation.

Effect of Metal Oxide Additives over ZrO_2. It has been shown that the preparation methods of the ZrO_2 catalyst affect the product selectivity, i.e., ZrO_2 prepared from zirconium oxynitrate with aqueous ammonia solution produces isobutene selectively from CO and H_2, while ZrO_2 from the alkoxide with water produces methane.[17] Therefore, the modification of ZrO_2 by the addition of the second oxide component may lead to the change of product selectivity and the hydrocarbon formation activity. Table 3 shows the hydrocarbon yields and selectivities with some modified ZrO_2 catalysts. When the CO-H_2 reaction over Zr sponges proceeds, a large amount of H_2 was absorbed and small amounts of widely dispersed hydrocarbons were formed. Zirconium sponges pretreated with H_2 gives methane as a main product. Therefore, isobutene formation over the ZrO_2 catalyst hardly participates in low valent zirconium.

Among the mixed oxide catalysts, SiO_2- and Nb_2O_5-added catalysts are not C_4-selective but rather methane-selective. In the reaction using these catalysts the large amounts of hydrocarbons are produced than those of CO_2. On the other hand, in the case of the other mixed oxide catalysts the amounts of hydrocarbons formed are less than that of CO_2, indicating the presence of unrecovered carbon species. Since methoxide species and formate ions are formed on the ZrO_2 surface under the reaction conditions,[14] the time course of the reaction showed the large amount of CO-H_2 gas absorption in the initial few hours of the reaction, and no coke formation was

Table 3. Effect of Metal Oxide Addition to ZrO_2 on Hydrocarbon Formation Activity and Selectivity[a]

No.	Catal.[b]	Area	Yield (C-base μmol)			Selectivity (C-base%)					
		$m^2 \cdot g^{-1}$	H.C.	MeOH & Me_2O	CO_2	C_1	C_2	C_3	C_4	C_5	C_6
1	Zr[c]	ca. 3	7	+	3	18	29	24	9	4	16
2	Zr(H)[d]	ca. 3	20	0	11	64	19	8	7	1	1
3	ZrO_2	59	364	6	370	4	6	7	77	5	1
4	NaOH(13)[e]	33	93	6	106	3	1	3	85	6	2
5	CaO(10)	25	257	5	320	15	11	9	59	6	1
6	Al_2O_3(10)	—[f]	31	13	72	33	27	2	28	5	5
7	SiO_2(10)	—[f]	67	0	6	90	5	2	3	1	+
8	Sc_2O_3(1)	75	227	3	260	15	8	6	66	4	1
9	Y_2O_3(1)	61	356	6	426	4	5	6	77	7	1
10	CeO_2(10)	69	381	3	434	5	4	5	73	12	2
11	Nd_2O_3(1)	67	366	3	371	4	6	6	77	7	+
12	Nd_2O_3(5)	55	246	4	386	5	5	4	77	8	1
13	Sm_2O_3(1)	54	356	7	497	6	6	6	74	7	1
14	Nb_2O_5(10)[g]	67	287	+	84	65	4	3	13	12	2

a) Catalyst: 1.5 g, initial pressure: 67(Nos. 6, 7), 71(Nos. 1, 2, 4), and 84 kPa(the others), reaction temperature: 623(Nos. 6, 7) and 673 K(the others), reaction time: initial 24(Nos. 1, 2, 4) and 25 h(Nos. 6, 7), and 5—24 h(the others). b) ZrO_2 used as the catalyst (No. 3) and mixed oxide catalysts (Nos. 4—13) were prepared from $ZrO(NO_3)_2$ and numbers in parentheses mean the atomic ratio of added metal to 100 of Zr. c) Preevacuation temperature: 673 K. d) Pretreatment with H_2: 873 K, 91 kPa, and 3 h. e) The catalyst was prepared by the addition of aqueous NaOH solution to $ZrO(NO_3)_2$ solution and XPS spectra showed that the ratio of Na to Zr on the surface was about 0.13. f) Not determined. g) The catalyst was prepared from hydrochloric solution of $NbCl_5$ and $ZrOCl_2$ (1:10) by the coprecipitation method using aqueous ammonia solution.

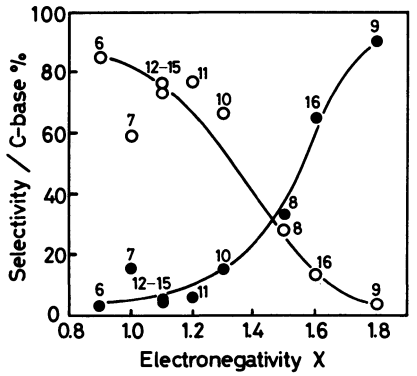

Fig. 4. Relation of C_1 (—●—) and C_4 (—○—) hydrocarbon selectivity to electronegativity. Numbers correspond to the Run No. in Table 3.

observed for 24 h reaction, most of the unrecovered carbon could be the surface-adsorbed species and a part of the carbon might be unrecovered higher hydrocarbons.

The presence of NaOH on ZrO_2 causes a little increase in the isobutene selectivity (85%) compared with that (77%) over the unmodified ZrO_2 catalyst, although the activity is lowered to about one forth. The addition of Al_2O_3 results in the lower selectivity for C_4 hydrocarbons. The SiO_2-added catalyst is rather methane-selective. These results indicate that there are two types of active sites on ZrO_2, one of which is effective for C_4 hydrocarbon formation and the other is for methane formation. Then, oxides of Sc, Y, some La Group elements, and Nb were used as difficulty reducible transition metal oxides. The addition of elements of lanthanum group, Sc, and Y oxides causes the selectivity and the activity to change only little, while that of Nb_2O_5 leads to the decrease of C_4 hydrocarbon and the increase of methane. Since the mixed oxide of SiO_2 or Al_2O_3 with ZrO_2 exhibits the solid acidity, which is not found on both oxides,[18] this selectivity change may relate to the electronegativity[19] of the additives. Figure 4 shows the relation of the electronegativity to the selectivity of C_1 and C_4 hydrocarbons. The addition of higher electronegative oxide results in the lower selectivity for C_4 hydrocarbons and the higher selectivity for methane. This may indicate that the increase in the acidity on ZrO_2 promotes the formation of methane and retards the formation of C_4 hydrocarbons. In the presence of NaOH with the much lower electronegativity than ZrO_2, the selectivity of C_4 hydrocarbons has the highest value. Thus, the pure ZrO_2 catalyst, ZrO_2 with 3a group and also basic metal oxides such as NaOH are the effective catalysts for selective formation of C_4 hydrocarbons, especially isobutene. This suggests the importance of basic character of active site for isobutene formation.

References

1) Y. Iwasawa and N. Ito, *J. Catal.*, **96**, 613 (1985); T. Tatsumi, H. Odajima, and H. Tominaga, *J. Chem. Soc., Chem. Commun.*, **1985**, 207.

2) D. Fraenkel and B. G. Gates, *J. Am. Chem. Soc.*, **102**, 2478 (1980).

3) M. van der Reit, G. J. Hutchings, and R. G. Copperthwaite, *J. Chem. Soc., Chem. Commun.*, **1986**, 798.
4) F. Hugues, P. Bussiere, and J. M. Basset, Proc. 7th Int. Congr. Catal. A, ed. by T. Seiyama and K. Tanabe, Kodansha Ltd., Tokyo (1980), p. 418.
5) L. F. Nazar, G. A. Ozin, F. Hugues, J. Godber, and D. Rancourt, *Angew. Chem.*, **95**, 645 (1983).
6) H. Pichler and K. H. Ziesecke, *Brennst. Chem.*, **30**, 13, 60, 81, 333 (1949).
7) R. Kieffer, J. Varela, and A. Deluzarche, *J. Chem. Soc., Chem. Commun.*, **1983**, 763.
8) T. Maehashi, K. Maruya, K. Domen, K. Aika, and T. Onishi, *Chem. Lett.*, **1984**, 747.
9) K. Maruya, A. Inabe, T. Maehashi, K. Domen, and T. Onishi, *J. Chem. Soc., Chem. Commun.*, **1985**, 487.
10) P. Biloen and W. M. H. Sachtler, *Adv. Catal.*, **30**, 165 (1981).
11) F. Solimosi, I. Tombacz, and M. Kocsis, *J. Catal.*, **75**, 78 (1982).
12) M. A. Vannice, *Catal. Rev.*, **14**, 153 (1976).
13) M. E. Dry, "Catalysis-Science and Technology," ed. by J. R. Anderson and M. Boudart, Springer-Verlag, New York (1981), Vol. 1, p. 159.
14) H. Abe, K. Maruya, K. Domen, and T. Onishi, *Chem. Lett.*, **1984**, 1875.
15) T. J. Mazanec, *J. Catal.*, **98**, 115 (1986).
16) R. Kieffer, G. Cherry, and R. El Bacha, *C_1 Mol. Chem.*, **2**, 11 (1987).
17) K. Maruya, T. Maehashi, H. Haraoka, S. Narui, K. Domen, and T. Onishi, *J. Chem. Soc., Chem. Commun.*, **1985**, 1494.
18) K. Tanabe, "Catalysis-Science and Technology," ed. by J. R. Anderson and M. Boudart, Springer-Verlag, New York (1981), Vol. 2, p. 231.
19) H. O. Pritcheard and H. A. Skinner, *Chem. Rev.*, **55**, 745 (1955).

 © 1988 The Chemical Society of Japan Bull. Chem. Soc. Jpn., 61, 673—677 (1988)

Solvation of Alkylbenzenes Studied by Photoelectron Emission Spectroscopy of Organic Solutions

To-oru NAKAYAMA, Iwao WATANABE,* and Shigero IKEDA
Department of Chemistry, Faculty of Science, Osaka University, Toyonaka, Osaka 560
(Received August 29, 1987)

The external ionization potentials for alkylbenzenes in acetonitrile and nitrobenzene have been measured by photoelectron emission spectroscopy to determine electronic polarization energies and reorganization energies. The polarization energy is used to discuss the solvation structure of alkylbenzene. The solvation behavior of alkylbenzene is found to be different from that of butylamine, previously reported. We have obtained the evidence of the approach of solvent molecules to the plane of benzene ring.

The radii of solvation sphere for butylamines in acetonitrile have been determined by using photoelectron emission (PEE) technique.[1] Though their molecular shapes are not spherical, their radii correlate excellently with the molecular sizes estimated from their densities. In the present study, PEE spectra are obtained for acetonitrile and nitrobenzene solutions of several alkylbenzenes including highly symmetrical hexamethylbenzene and *o*-, *m*-, and *p*-xylene to investigate the effect of solute–solvent interaction on the size of solvation sphere.

The linear correlation has been reported by Kochi et al.[2] between ionization potential in vacuum (I_p) and oxidation potential in solution (E_{ox}) for alkylbenzene. External ionization potential (E_t) determined from PEE spectra can be combined with I_p and E_{ox} to discuss solvation structure and mechanism. The E_t value is related to I_p or the standard oxidation potential (E°_{ox}) as follows,[1,3]

$$P_+ = I_p - E_t, \tag{1}$$

$$\Delta G_r = E_t - E^\circ_{ox} - \Delta G_H, \tag{2}$$

where P_+ is the polarization energy of the solvent molecules, ΔG_r is the reorganization energy, and ΔG_H is the potential of vacuum level referred to NHE, which is estimated to be 4.5 eV.[4,5]

The polarization of solvent molecule is induced by the positive charge of photoionized solute molecule and it depends on the number of solvating molecules and their geometrical arrangement. The P_+ is related to an effective solvation radius[1] (r_{P_+}) through Born type equation,

$$P_+ = e^2(1 - 1/\varepsilon_{op})/2r_{P_+}, \tag{3}$$

where e is the charge of an electron, and ε_{op} is the optical dielectric constant of the solvent. Thus the PEE technique is expected to provide us a new parameter, the effective solvation radius, which should be used to investigate solute–solvent interaction.

The ΔG_r contains the energy caused by the change in orientation of surrounding solvent molecules (R_{out}) which is closely related to the solvation radius, and the relaxation energy of the produced cation molecule (R_{in}).

Experimental

Materials. The alkylbenzenes were purified by distillation or recrystallization. Purities of the samples were certified to be >98% by HPLC. Acetonitrile of spectra-grade was fractionated from P_2O_5 after stirring overnight. Nitrobenzene was of reagent-grade and was dried over $CaCl_2$, decanted, and distilled under reduced pressure. Tetrabutylammonium perchlorate was of special-grade (Nakarai Chemicals Co.) and used as purchased.

Photoelectron Emission Spectra. The external ionization potentials for alkylbenzenes were measured as photoionization threshold energy (E_t) by PEE technique which has been reported.[1] Sample solutions were prepared just before measurement. PEE spectra were taken at −30 °C with 0.1 mol dm^{-3} concentration for benzene, toluene, *o*-, *m*-, and *p*-xylene, mesitylene and ethylbenzene in acetonitrile. The conditions for other samples were; +1 °C, 0.025 mol dm^{-3} for hexamethylbenzene and hexaethylbenzene in acetonitrile; room temperature, 0.1 mol dm^{-3} for all samples in nitrobenzene. PEE spectra in acetonitrile were also obtained at −15 °C and +1 °C. No dependence of E_t value on temperature was detected.

Water contents in acetonitrile and nitrobenzene used in this study were measured by Karl Fischer titration analysis and the contents were $3—15\times10^{-3}$ mol dm^{-3}. It was found, however, that water in the solvents does not affect PEE spectra at all.

Cyclic Voltammetry. Cyclic voltammograms (CV) were obtained for 5×10^{-3} mol dm^{-3} of *o*-, *m*-, and *p*-xylene, mesitylene, hexamethylbenzene, and hexaethylbenzene in nitrobenzene containing 0.1 mol dm^{-3} tetrabutylammonium perchlorate at room temperature in air-tight cell under nitrogen atmosphere. The scan rate was 8.42 V s^{-1} for all the samples. The working electrode was a 0.1 mm-diameter platinum disk electrode embedded in glass. The counter electrode was a platinum spiral wire. The reference electrode was Ag/$AgNO_3$ (0.1 mol dm^{-3}) in acetonitrile, separated from sample solution by a cracked glass. The electrode was calibrated relative to ferrocene/ferrocenium standard after every measurement and the potential was converted into NHE value by adding 0.400 V.[6]

Table 1. Photoionization Energies of Substituted Benzenes in the Gas Phase (I_p) and in the Solvents (E_t) (NB=Nitrobenzene, AN=Acetonitrile), the Oxidation Potential (E^p_{ox}), the Polarization Energies (P_+), the Reorganization Energies (ΔG_r), the Effective Solvation Radii (r_{P_+}), and the Radii of the Solute Molecules (r_d)

Solute	I_p/eV	E_t/eV		E^p_{ox}/V		P_+/eV		ΔG_r/eV		r_{P_+}/Å		r_d/Å
		NB	AN	NB	AN	NB	AN	NB	AN	NB	AN	
Benzene	9.24		8.02		2.86		1.22		0.66		2.78	2.64
Toluene	8.82	7.77	7.87		2.49	1.05	0.95		0.88	4.02	3.57	2.80
o-Xylene	8.56	7.67	7.70	2.07	2.40	0.89	0.86	1.10	0.80	4.75	3.94	2.93
m-Xylene	8.56	7.69	7.67	2.13	2.35	0.87	0.89	1.06	0.82	4.86	3.81	2.94
p-Xylene	8.44	7.64	7.56	2.07		0.80	0.88	1.07		5.28	3.85	2.95
Mesitylene	8.42	7.60	7.60	2.06	2.26	0.82	0.82	1.06	0.84	5.15	4.13	3.07
Hexamethylbenzene	7.85	7.13	7.12	1.60	1.82	0.72	0.73	1.03	0.80	5.87	4.53	3.16
Ethylbenzene	8.77	7.70	7.81		2.51	1.07	0.96		0.80	3.95	3.53	2.94
Hexaethylbenzene	7.71	7.02	7.00	1.73	1.95	0.69	0.71	0.79	0.55	6.12	4.66	3.95

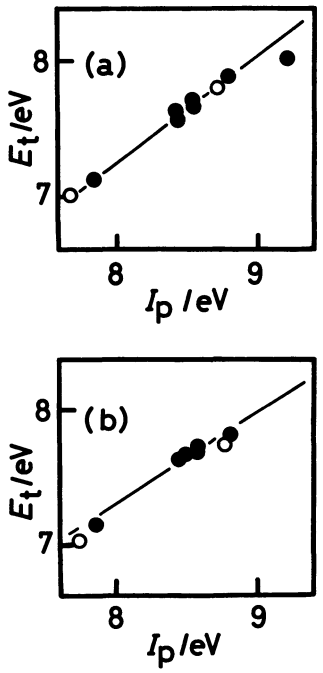

Fig. 1. The relationship between the ionization potentials in gas phase (I_p) and the external ionization potentials (E_t) in acetonitrile (a) and nitrobenzene (b). Closed circles are for methyl-substituted and open circles for ethyl-substituted benzenes.

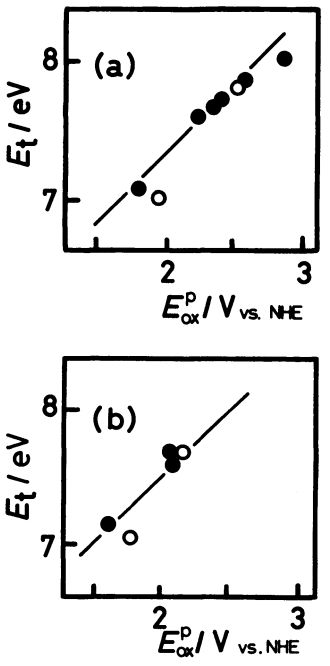

Fig. 2. The relationship between the anodic peak potentials (E^p_{ox}) and the external ionization potentials (E_t) in acetonitrile (a) and nitrobenzene (b). Closed circles represent methyl-substituted and open circles ethyl-substituted benzenes.

Results and Discussion

Correlations between E_t vs. I_p and E_t vs. E_{ox}. The E_t values obtained for alkylbenzenes are collected in Table 1, which includes I_p and anodic peak potentials of CV (E^p_{ox}). The values of I_p and E^p_{ox} in acetonitrile are taken from the work done by Kochi et al.[2] Figure 1 shows the correlation between E_t and I_p both in acetonitrile and nitrobenzene. The plot of E_t vs. I_p (except for benzene in acetonitrile) gives linear correlation as follows,

$$E_t = 0.78 \times I_p + 1.01 \text{ eV (in acetonitrile)}, \quad (4)$$

$$E_t = 0.69 \times I_p + 1.74 \text{ eV (in nitrobenzene)}. \quad (5)$$

The smaller values of the slopes than unity indicate that the polarization energy is smaller for alkylbenzene having smaller I_p value or for larger benzene in size. The linear correlation also exists between E_t and E^p_{ox} as shown in Fig. 2 and the slopes are almost unity.

$$E_t = 0.89 \times E^p_{ox} + 5.56 \text{ eV (in acetonitrile)}, \quad (6)$$

$$E_t = 1.04 \times E^p_{ox} + 5.17 \text{ eV (in nitrobenzene)}. \quad (7)$$

Polarization Energy, P_+. The polarization energy P_+ determined from the difference ($I_p - E_t$) gives us the

information about the size of solvation sphere around the photoionized cation radical molecule. The solvation structure of the cation molecule is exactly the same as that of the original neutral molecule, because the photoionization process is subjected to the Franck–Condon transition.

Figures 3 and 4 show the correlation between P_+ and the number n of alkyl groups introduced to a benzene molecule. Both in acetonitrile and nitrobenzene, P_+ decreases with n, which should be the effect of the alkyl groups working as insulator locating between the positive charge on benzene ring and solvent molecules.

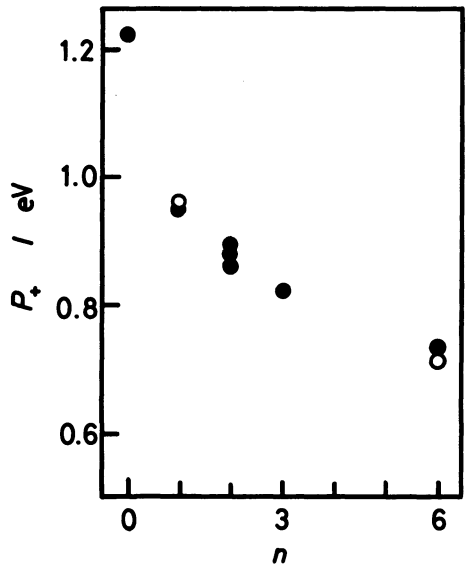

Fig. 3. The relationship between the polarization energies (P_+) and the number n of substituents introduced to benzene in acetonitrile.

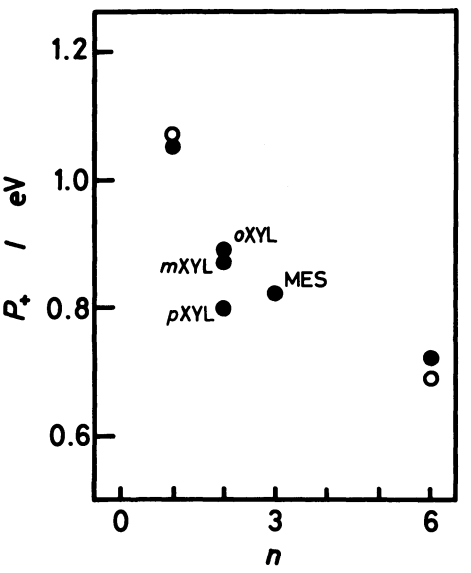

Fig. 4. The correlation of polarization energies (P_+) and the number n of substituents introduced to benzene in nitrobenzene. Closed circles are for methyl-substituted and open circles for ethyl-substituted benzenes. (*o*, *m*, *p*XYL: *o*-, *m*-, *p*-xylene, MES: mesitylene).

Symmetry of the sample molecule is distinguished by nitrobenzene solvent. Among the three dimethylbenzenes, *p*-xylene has the smallest P_+ value, and the value is even smaller than that for mesitylene. This is not the case in acetonitrile. This peculiar effect of the solvent should be related to the size, shape or dipole moment of the solvent molecule.

The change in substituent, methyl or ethyl group, causes no change in P_+ in both solvents. This will be discussed in the next section considering the effective solvation radius.

The Effective Solvation Radius, r_{P_+}. The effective solvation radius (r_{P_+}) calculated from P_+ value using Eq. 3 is compared with the radius (r_d) evaluated from the density (d) of pure substance,

$$r_d = 0.5 \times (M/dN_A)^{1/3}, \quad (8)$$

where M is the molecular weight and N_A Avogadro's constant, and the result is shown in Fig. 5. The solid line in the figure indicates the position where both of r

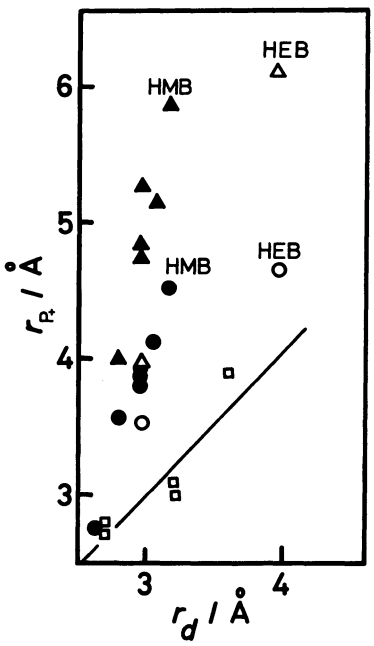

Fig. 5. The relationship between the radii calculated from the densities of the pure solutes (r_d) and the effective solvation radii calculated from the polarization energies (r_{P_+}). Closed circles are for methyl-, open circles for ethyl-substituted benzenes in acetonitrile, closed triangles are for methyl-, open triangles for ethyl-substituted benzenes in nitrobenzene. The data for butylamines are also included in this figure as open tetragons (Ref. 7). The solid line indicates the position of $r_{P_+}=r_d$.

values are the same. This figure includes the results for butylamines in acetonitrile which is previously reported.[7] While the points for amines come to the solid line excellently, the values of r_{P_+} for aromatic hydrocarbons are larger than r_d for all the samples except for benzene in acetonitrile. The experimental fact pointed out in the previous section that the substitution of methyl groups on the benzene molecule with ethyl groups does not affect the P_+ energy contradicts the prediction derived from Eq. 3. Though the value of r_d for hexaethylbenzene is significantly larger than that for hexamethylbenzene, their values of r_{P_+} are almost the same. Since the r_{P_+} is considered to be the distance of the nearest solvent molecules from the charge of the cation which locates at benzene ring,[8] the solvation structure for hexaethylbenzene can be considered to be the same as that for hexamethylbenzene. It means that the solvent molecules around hexaethylbenzene and hexamethylbenzene must locate above and beneath the benzene-ring plane of the sample molecule. If the nearest solvent molecules were in the benzene-ring plane beyond the alkyl groups, the change in length of the alkyl group should affect r_{P_+} and these two samples should have quite different r_{P_+} values.

The same trend is observed for the cases of toluene, ethylbenzene in both solvents.

Reorganization Energy, ΔG_r. The difference between E_t and the standard oxidation potential referred to the vacuum level is the reorganization energy (ΔG_r) after one-electron oxidation reaction (Eq. 2). The values of $E°_{ox}$ for alkylbenzenes used in the present work are not available because of their irreversible nature in CV both in acetonitrile[2] and nitrobenzene except for hexaethylbenzene. Therefore, the ΔG_r values can not be evaluated for most of the samples of this work. It is interesting, however, to point out that, according to the work by Kochi et al.,[2] the alkylbenzenes give reversible CV waves in trifluoroacetic acid. Therefore we have made great efforts to obtain PEE spectra of trifluoroacetic acid solutions, and yet could not obtain the spectra because of their high vapor pressure of the solvent. Kochi et al. also reported that the equilibrium oxidation potentials in trifluoroacetic acid $E°_{ox}$(TFA) correspond perfectly to the peak potentials E^p_{ox} measured in acetonitrile (at sweep rate of 100 mV s^{-1}) as $E°_{ox}(\mathrm{TFA}) = 1.01 \times E^p_{ox} - 0.001$. We may presume that real equilibrium potentials of alkylbenzenes in acetonitrile must not be very different from the standard oxidation potentials in trifluoroacetic acid, nor from the peak potentials in acetonitrile reported by them. Under such an assumption, the peak potentials will be used instead of the standard potentials to extract the alkyl substitution effect on the reorganization energy.

Figures 6 and 7 show the correlation between ΔG_r so determined and n. The ΔG_r has no relation with n,

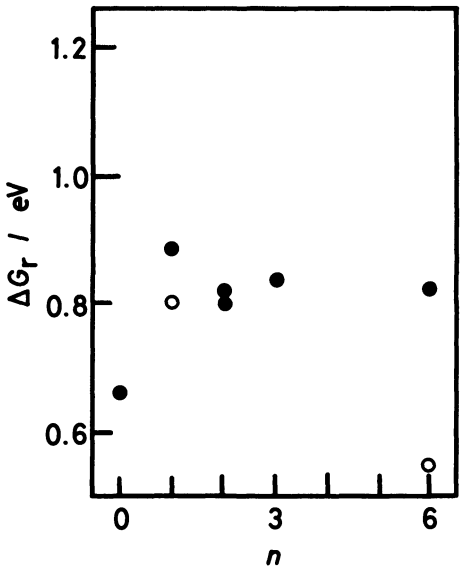

Fig. 6. The correlation of ΔG_r in acetonitrile and the number n of substituents introduced to benzene.

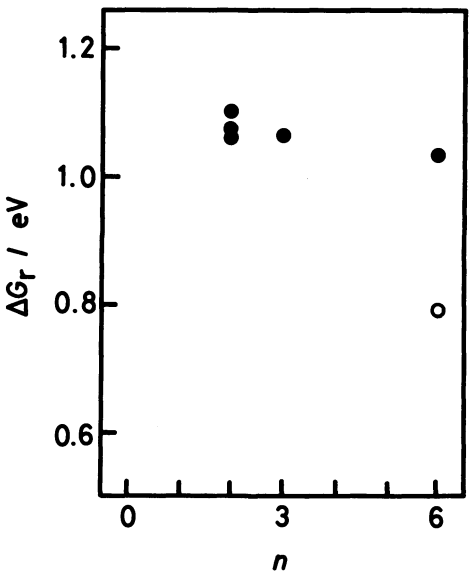

Fig. 7. The correlation of ΔG_r in nitrobenzene and the number n of substituents introduced to benzene.

but different alkyl group causes different ΔG_r value such as hexamethylbenzene/hexaethylbenzene or toluene/ethylbenzene.

It is noted that hexaethylbenzene has the smallest ΔG_r value, and displays totally reversible CV waves in both solvents. This fact may indicate that the reversibility of oxidation reaction of alkylbenzene depends on the degree of reorganization of the molecule.

This work was supported by Grant-in-Aid for Scientific Research Nos. 58540285 and 62540356, and for Special Project Research No. 60129031 from the Ministry of Education, Science and Culture.

References

1) I. Watanabe, K. Maya, Y. Yabuhara, and S. Ikeda, *Bull. Chem. Soc. Jpn.*, **59**, 907 (1986).

2) J. O. Howell, J. M. Goncalves, C. Amatore, L. Klansinc, R. M. Wightman, and J. K. Kochi, *J. Am. Chem. Soc.*, **106**, 3968 (1984).

3) P. Delahay, "Electron Spectroscopy: Theory, Techniques and Applications," ed by C. R. Brundle and A. D. Baker, Academic Press, London (1984), Vol. 5, pp. 124—196.

4) H. Reiss and A. Heller, *J. Phys. Chem.*, **89**, 4207 (1985).

5) R. M. Noyes, *J. Am. Chem. Soc.*, **84**, 513 (1962).

6) R. R. Gagné, C. A. Koval, and G. C. Lisensky, *Inorg. Chem.*, **19**, 2854 (1980).

7) The r_{P_+} values for butylamines in this paper are revised from Ref. 1, because we have found an error (about 10%) in the previous calculations.

8) Distribution of the charge on the radical cation is studied by ESR and reported to be spreading over the benzene ring. See for toluene a) T. Komatsu, A. Lund, and P.-O. Kinell, *J. Phys. Chem.*, **76**, 1721 (1972), for xylenes b) M. C. R. Symons, and L. Harris, *J. Chem. Res. (S)*, **1982**, 268, for hexamethylbenzene c) C. J. Schlesener, C. Amatore, and J. K. Kochi, *J. Am. Chem. Soc.*, **106**, 3567 (1984), for hexaethylbenzene d) I. H. Elson and J. K. Kochi, *J. Am. Chem. Soc.*, **95**, 5060 (1973).

Incommensurate Phase Transitions and Anomalous Lattice Heat Capacities of Biphenyl†

Kazuya SAITO,†† Tooru ATAKE,††† and Hideaki CHIHARA*
Department of Chemistry and Chemical Thermodynamics Laboratory, Faculty of Science, Osaka University, Toyonaka, Osaka 560
(Received September 9, 1987)

Heat capacities of crystalline biphenyl were measured between 3 and 300 K by adiabatic calorimetry and some thermodynamic functions including the calorimetric standard entropy were tabulated. Thermodynamic properties of the successive phase transitions were determined; for the twist transition at (40.4±0.2) K, $\Delta_{trs}H$=(5.02±0.08) J·mol^{-1} and $\Delta_{trs}S$=(0.129±0.003) J·K^{-1}·mol^{-1}, and for the lock-in transition at (16.8±0.1) K, $\Delta_{trs}H$=(0.15±0.02) J·mol^{-1} and $\Delta_{trs}S$=(0.009±0.001) J·K^{-1}·mol^{-1}. Anomalously large heat capacities at low temperatures were analyzed based on lattice dynamics calculation, and the crossover of the low temperature heat capacities of biphenyl and *p*-terphenyl was attributed to the greater activity of the twisting mode in biphenyl. The relation of the bond flexibility to the incommensurability is discussed through the comparison of the low temperature heat capacities of biphenyl, *p*-terphenyl, and 4,4′-difluorobiphenyl.

Biphenyl is an interesting molecule which changes its conformation according as the state of aggregation changes. While molecules are twisted by about 40° about its central C–C bond in the gaseous state[1,2] and about 30° in the liquid state,[2–6] they crystallize in the structure of the space group $P2_1/a$ with the planar conformation at room temperature.[7–14] On cooling, however, they resume the twisted conformation below the phase transition temperature at about 40 K;[15–17] a similar phase transition, "twist transition," has also been found in *p*-terphenyl[18–21] and in *p*-quaterphenyl.[22,23]

The soft-modes have been found by optical[24–26] and neutron scattering[27] experiments. The softening occurs at the general point (x^*, y^*, z^*) near the B (0, 1/2, 0) point in the reciprocal space and the new phase is of two dimensionally incommensurate structure[28,29] classified to the five dimensional Bravais lattice of $P^{P2/m}_{cmm}$.[30] The modulation wave which characterizes this phase is expressed as $q^*=\pm(\delta_a a^*-\delta_c c^*)\pm 1/2\times(1-\delta_b)b^*$. The mean approximate structure was obtained neglecting satellite reflections in the diffraction diagram and was classified to Pa.[15] Dworkin and Cailleau[31] reported the results of their heat capacity measurements on biphenyl, in which they could not detect any anomaly in the heat capacity curve. On the other hand, Cullick and Gerkin[32] found the temperature halt at 42 K in the cooling curves, which strongly suggested that the transition is of the first-order. However, other authors[24–27,33–38] reported by making use of several experimental techniques that the transition is of higher-order.

On further cooling, the incommensurate-commensurate transition (so-called lock-in transition) in the one direction takes place at about 17 K,[28,29,34] i.e. δ_a and δ_c equal 0 below the lock-in transition. Below this transition, however, the crystal still remains incommensurate along the b^* axis. The structure was determined to be of the super-space group $P^{P2_1/a}_{1\bar{1}}$ by using neutron diffraction technique.[16] The essential aspect of the incommensurate modulation was a torsion about the central C–C bond with an amplitude of 5.5° for each phenyl ring, the maximum twisting angle being 11°. The lock-in transition has been revealed to be of the first-order by using optical[34] and neutron diffraction[28,38] techniques. More direct evidence of the first-order nature is the co-existence of the two phases observed in neutron experiments. On the other hand, no abrupt change was observed in Brillouin scattering experiments[36] and in electronic spectra of molecules.[35]

The lock-in transition in the direction of the b^* axis has not been observed so far down to 1.4 K.[38]

Dynamics in the incommensurate phases have been investigated by using some experimental techniques. The dispersion of the phason and the amplitudon branches were determined by neutron[27,40] and Brillouin[36] scattering experiments. The damping of the phason branch near the zone center was rather small. NMR results by Liu and Conradi[41] showed the existence of the slow process ($\tau\simeq 10^3$ s at 4.2 K) in the incommensurate phases. They proposed the term, "incommensurate glass," in biphenyl in the lowest temperature region. Recently, Benkert and Heine[42] interpreted the slow process as the shifting of the modulation boundaries.

It must be noted that the pressure dependence of the transition temperatures are negative.[37,43] This clearly shows that the transitions are connected with a subtle balance between intra- and intermolecular interactions.

Since Hochstrasser et al.[44] discovered the phase

† Contribution No. 130 from Chemical Thermodynamics Laboratory, Faculty of Science, Osaka University.

†† Present address: Department of Chemistry, Faculty of Science, Tokyo Metropolitan University, Fukazawa, Setagaya-ku, Tokyo 158.

††† Present address: Research Laboratory of Engineering Materials, Tokyo Institute of Technology, 4259 Nagatsuta-cho, Midori-ku, Yokohama 227.

transition in biphenyl crystal, many interesting features have been revealed by making use of several experimental techniques as briefly summarized above. Theoretical treatments[39,42,45-50] have also been presented based on these experimental results. However, accurate thermodynamic properties have been lacking although they should give an important clue to the nature of the transition and provide a critical test of theory. These situations led us to begin a series of thermodynamic studies on the successive phase transitions in crystalline biphenyl and related substances, parts of which were published elsewhere.[51-59] This paper provides the full description of precision heat capacity measurements. The anomalous lattice heat capacity at low temperatures will be analyzed by using the method of lattice dynamics.

Experimental

Commercially available biphenyl (Nakarai Chemicals, Ltd.) was purified by fractional sublimation in vacuum at room temperature. In order to avoid possible formation of metastable phases and/or poor crystallinity, the sublimed specimen was melted under a helium atmosphere (10^5 Pa) and cooled gradually down to room temperature for recrystallization. The purity of the specimen was better than 99.9 moles per cent as confirmed by gas chromatography.

The powdered specimen was loaded into the calorimeter vessel and sealed off with some helium gas for heat exchange (3 kPa at room temperature). The contribution of the helium gas to the total heat capacity was negligibly small. The mass of the sample used for calorimetry was 17.950 g (0.11640 mol). The contribution of the sample to the total heat capacity including that of the calorimeter vessel was larger than 70 per cent below 20 K. It decreased to 46 per cent at 100 K as temperature increased; however, it increased again to 59 per cent at 300 K.

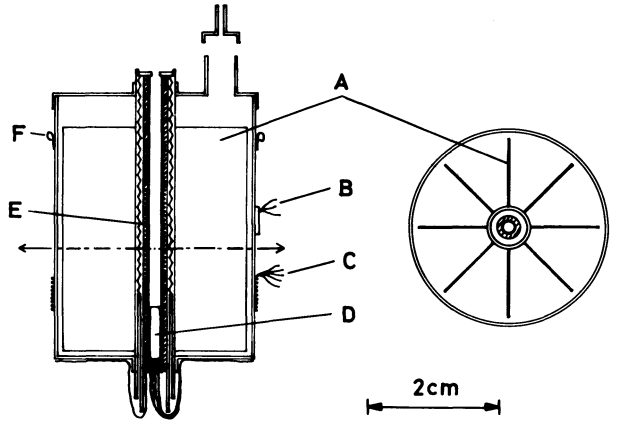

Fig. 1. Sectional plan of the new calorimeter vessel. A eight vanes to assist in thermal uniformity; B Au+0.07%Fe vs. Chromel-P thermocouples for adiabatic control (diameter 0.1 mm); C lead wires (diameter 0.1 mm); D germanium thermometer (model N2D, SI Inc.); E heater (KARMA, total 190 Ω); F hooks for hanging the vessel.

The apparatus for calorimetry has been described elsewhere.[59] A platinum resistance thermometer (model 8164, Leeds & Northrup Co.) and a germanium resistance thermometer (model CR-1000, CryoCal Inc.) were used. Their temperature scales are based on IPTS-68, helium gas thermometry, and the 1958 ^{4}He vapor pressure scale.[60,61]

The measurements using the ordinary calorimeter vessel failed to detect the lock-in transition at 16.8 K. To improve the sensitivity, a new calorimeter vessel was constructed with the following considerations; (1) use of a single, sensitive thermometer and one smooth temperature scale between 3 and 20 K, (2) amount of the sample that can be loaded and its packing in the vessel, and (3) attainment of better adiabatic conditions.

The sectional plan of the new calorimeter vessel (gold-plated copper) is shown in Fig. 1. In order to load a sufficient amount of the sample and to discard the use of helium gas for heat exchange in the vessel, the purified specimen was loaded and melted under a helium atmosphere (10^5 Pa) in the vessel before installation of the KARMA heater, the thermometer and thermocouples. The vessel was then evacuated and sealed off without addition of helium gas. The sample thus loaded weighed 24.957 g (0.16184 mol) in vacuum.

A germanium resistance thermometer (model N2D, SI Inc.) with commercial calibration was used. The calibration was based on the 1962 ^{3}He vapor pressure scale below 3.2 K and on the 1965 Provisional Helium Acoustic Scale between 2 and 20 K. The accuracy of the calibration was stated to be better than ±0.005 K below 5 K and better than ±0.01 K between 5 and 20 K. The 35 calibration points were fitted to the equation,

$$\ln(R/\Omega) = \sum_{i=1}^{9} A_i \{\ln(T/\mathrm{K})\}^{i-2}.$$

Since the main purpose of the measurements using this vessel was a search for the lock-in transition, an emphasis was placed on the smoothness of the temperature scale.

The Au+0.07%Fe vs. Chromel-P thermocouple (0.1 mm in diameter) was used for detecting the temperature difference between the vessel and the walls of adiabatic shield in order to improve the adiabatic conditions. The sensitivity of this thermocouple in the temperature region between 3 and 20 K is ten times as large as that of Chromel-P vs. Constantan thermocouple which has been attached to the ordinary vessel.

The new vessel thus constructed has an empty mass of 39.72 g with inside capacity of 25.06 cm^3. Other components of cryostat/calorimeter assembly were the same as used previously.[59] The sample contributed more than 85 per cent to the total heat capacity over the region studied (3—20 K) and the desired precision was attained.

Results and Discussion

Heat Capacities and Thermodynamic Functions.

The molar heat capacities measured with the ordinary (old) vessel are tabulated in Table 1 in the chronological order of measurement. The data obtained with the new vessel are shown as series 26 through 34 in Table 1. These were consistent with data obtained using the old vessel except for the lock-in

Table 1. Measured Molar Heat Capacities of Biphenyl

T	$C_{p,m}$	T	$C_{p,m}$	T	$C_{p,m}$	T	$C_{p,m}$	T	$C_{p,m}$
K	J K^{-1} mol^{-1}	K	J K^{-1} mol^{-1}	K	J K^{-1} mol^{-1}	K	J K^{-1} mol^{-1}	K	J K^{-1} mol^{-1}
Series 1		92.570	71.807	295.734	196.43	6.556	1.154	7.789	1.709
22.893	18.498	94.766	72.905	299.152	198.94	7.005	1.323	8.229	1.981
24.316	20.354	96.977	74.063	Series 15		7.477	1.570	8.712	2.302
25.736	22.177	99.242	75.199	14.181	7.506	8.013	1.899	9.238	2.678
27.178	24.002	101.587	76.333	14.921	8.365	8.621	2.295	9.805	3.118
28.647	25.811	103.975	77.585	15.769	9.351	Series 24		10.401	3.622
30.247	27.775	106.377	79.00	Series 16		5.591	0.723	11.021	4.149
31.954	29.863	108.758	80.24	18.738	12.984	5.940	0.851	11.642	4.665
33.668	31.832	Series 8		19.828	14.495	6.311	1.005	12.274	5.367
35.376	33.756	109.158	80.23	20.927	15.903	6.709	1.183	Series 31	
37.060	35.623	111.493	81.49	22.009	17.314	7.137	1.396	10.725	3.896
38.805	37.448	113.761	82.67	23.106	18.750	7.610	1.658	11.136	4.277
40.600	39.223	116.069	83.81	Series 17		8.154	1.992	11.581	4.696
42.342	40.689	118.417	85.02	14.089	7.394	8.781	2.414	12.056	5.154
44.038	41.926	120.787	86.27	14.847	8.290	9.479	2.935	12.571	5.672
45.727	43.163	123.163	87.46	15.635	9.197	10.256	3.582	13.164	6.292
47.417	44.462	125.545	88.57	16.467	10.202	11.114	4.319	13.807	6.999
49.116	45.762	Series 9		17.331	11.308	12.057	5.234	14.479	7.757
Series 2		125.967	88.83	18.232	12.452	13.030	6.186	15.210	8.628
22.785	18.352	128.403	90.10	19.183	13.661	13.963	7.228	15.964	9.569
24.241	20.261	130.793	91.31	20.109	14.847	Series 25		16.713	10.584
25.688	22.112	133.193	92.61	20.975	15.890	15.546	9.121	17.429	11.493
27.155	23.970	135.581	93.89	21.823	16.994	16.272	9.995	18.123	12.424
28.656	25.823	137.956	95.12	22.662	18.114	17.008	10.912	18.828	13.485
30.218	27.742	140.338	96.38	23.496	19.233	17.765	11.850	19.536	14.654
31.859	29.728	142.722	97.65	Series 18		18.551	12.850	20.250	18.386
33.493	31.639	145.104	98.95	4.051	0.300	19.372	13.893	Series 32	
35.048	33.404	Series 10		4.487	0.403	20.239	15.012	11.708	4.800
36.532	35.041	145.258	98.98	4.969	0.530	21.130	16.142	12.060	5.156
37.987	36.602	147.664	100.27	5.491	0.703	22.019	17.289	12.397	5.485
39.447	38.091	150.066	101.53	6.045	0.907	22.906	18.441	12.729	5.831
40.897	39.493	152.484	102.87	6.592	1.148	23.783	19.592	13.063	6.174
42.337	40.691	154.930	104.28	7.122	1.388	Seres 26		13.395	6.531
43.774	41.726	157.365	105.64	Series 19		6.543	1.057	13.722	6.895
45.209	42.796	159.778	106.99	3.855	0.243	6.928	1.234	14.049	7.258
46.657	43.873	162.177	108.36	4.224	0.332	7.403	1.487	14.377	7.633
48.132	45.001	Series 11		4.605	0.422	7.930	1.787	14.708	8.020
49.761	46.248	164.585	109.71	5.004	0.538	8.492	2.152	15.043	8.415
51.634	47.623	167.013	111.11	5.447	0.678	9.104	2.585	15.382	8.826
53.566	49.046	169.462	112.48	5.935	0.857	9.783	3.099	15.726	9.264
55.431	50.339	171.923	113.92	6.461	1.078	10.544	3.727	16.077	9.702
57.249	51.595	Series 12		7.003	1.334	11.394	4.499	16.431	10.180
59.027	52.793	172.821	114.52	Series 20		Series 27		16.784	10.688
60.796	53.955	175.305	116.04	4.443	0.382	4.105	0.288	17.139	11.117
Series 3		177.802	117.47	4.884	0.503	4.388	0.350	17.496	11.560
53.638	49.090	180.351	119.03	5.331	0.640	4.767	0.440	17.854	12.038
55.451	50.339	182.902	120.59	5.788	0.801	5.202	0.562	18.212	12.532
57.233	51.572	185.448	122.04	6.263	0.984	5.658	0.709	18.569	13.060
58.994	52.774	187.977	123.48	6.737	1.199	6.121	0.883	18.923	13.627
Series 4		190.505	125.01	7.243	1.453	6.591	1.083	19.273	14.174
32.858	30.907	193.048	126.59	7.805	1.775	7.063	1.309	19.629	14.794
34.022	32.239	195.582	128.11	8.434	2.174	7.541	1.567	19.978	15.454
35.130	33.482	198.157	129.76	9.146	2.676	8.043	1.871	Series 33	
36.186	34.659	Series 13		9.952	3.318	8.578	2.215	13.648	6.819
37.201	35.775	200.711	131.29	10.817	4.063	9.152	2.618	13.961	7.214
38.188	36.823	203.324	132.93	11.679	4.866	9.776	3.092	Series 34	
39.152	37.800	205.969	134.57	12.517	5.664	Series 28		14.244	7.472

Table 1. (Continued)

T	$C_{p,m}$	T	$C_{p,m}$	T	$C_{p,m}$	T	$C_{p,m}$	T	$C_{p,m}$
K	J K^{-1} mol^{-1}	K	J K^{-1} mol^{-1}	K	J K^{-1} mol^{-1}	K	J K^{-1} mol^{-1}	K	J K^{-1} mol^{-1}
40.094	38.742	208.606	136.40	13.353	6.568	10.453	3.656	14.459	7.727
41.031	39.619	211.190	137.97	Series 21		11.171	4.302	14.679	7.965
41.958	40.392	213.768	139.64	9.882	3.267	11.944	5.042	14.904	8.231
42.883	41.110	216.395	141.29	10.642	3.917	12.701	5.811	15.132	8.500
43.819	41.768	219.046	143.00	11.384	4.585	13.445	6.597	15.361	8.785
Series 5		221.726	144.89	12.110	5.269	14.171	7.401	15.591	9.066
60.493	53.726	224.437	146.63	12.836	6.012	14.890	8.244	15.822	9.351
62.242	54.872	227.180	148.49	13.576	6.779	15.606	9.101	16.053	9.661
63.980	55.960	229.946	150.29	Series 22		16.334	10.036	16.279	9.938
65.786	57.054	232.738	152.46	14.132	7.486	17.085	11.026	16.503	10.252
67.659	58.173	235.561	154.13	14.838	8.318	17.852	12.029	16.727	10.576
69.539	59.296	238.415	156.46	15.648	9.264	18.617	13.169	16.949	10.856
71.436	60.404	Series 14		16.532	10.340	19.357	14.279	17.169	11.137
73.337	61.494	241.166	157.68	17.451	11.490	20.057	15.732	17.390	11.391
75.222	62.533	244.021	159.79	18.406	12.691	Series 29		17.610	11.678
77.095	63.584	246.985	161.76	19.370	13.942	3.668	0.206	17.830	11.979
79.014	64.643	250.014	163.80	20.302	15.111	3.847	0.239	18.050	12.260
81.032	65.744	253.076	165.93	21.189	16.245	4.085	0.284	18.268	12.585
Series 6		256.170	168.01	22.041	17.365	4.389	0.348	18.487	12.899
81.058	65.822	259.302	170.31	22.865	18.432	4.740	0.434	18.706	13.233
83.133	66.814	262.477	172.48	23.667	19.481	5.126	0.540	18.924	13.559
85.160	67.875	265.702	174.70	Series 23		Series 30		19.142	13.955
87.174	68.926	268.951	177.13	3.594	0.222	3.686	0.207	19.359	14.299
89.175	70.030	272.209	179.02	3.907	0.288	3.878	0.244	19.576	14.684
91.166	71.037	275.491	181.90	4.164	0.327	4.128	0.293	19.793	15.058
Series 7		278.789	184.12	4.520	0.401	4.449	0.363	20.009	15.530
90.405	70.652	282.116	186.40	4.909	0.503	4.835	0.458		
		285.481	188.86	5.312	0.631	5.258	0.579		
		288.879	191.59	5.719	0.774	5.694	0.723		
		292.304	193.93	6.131	0.938	6.129	0.887		
						6.556	1.067		
						6.969	1.263		
						7.375	1.475		

The ordinary calorimeter vessel was used in series 1 through 25, and the new vessel in series 26 through 34.

transition region. The temperature increment of each measurement may be deduced from the adjacent mean temperatures and it is sufficiently small to ignore the curvature correction in comparison with the experimental precision. After each energy input was over, thermal equilibrium within calorimeter vessel was attained in 1 min below 10 K, in 5 min at 50 K, and 15 min above 100 K in the measurements using the old calorimeter vessel as well as the new vessel. There was nothing anomalous concerning thermal equilibration in the transition regions contrary to the observation of Dworkin and Cailleau,[31] and in the lowest temperature region either, where the possibility of the "incommensurate glass" was suggested by Liu and Conradi.[41] Although our results are systematically larger by 0.4 per cent than the data reported by Huffman et al.,[62] the two sets of data are in satisfactory agreement within combined experimental uncertainties where comparison can be made.

Some molar thermodynamic functions derived from the measured data are tabulated in Table 2, where small contribution below 4 K was estimated by smooth extrapolation from the higher temperature side. The calorimetric standard entropy of biphenyl in the standard ideal gas state was calculated using the vapor pressure[63] and sublimation[64] data as summarized in Table 3.

Twist Transition. Generally, a small anomaly in a heat capacity curve can be made more prominent by plotting the equivalent Debye characteristic temperatures corresponding to the heat capacity values. It is shown in Fig. 2, where it is arbitrarily assumed that there are 9 degrees of freedom per molecule. A small, broad minimum is seen at about 40 K in Fig. 2. The normal portion of the heat capacity was evaluated by drawing a smooth interpolating curve as the lower and the higher temperature sides guide the eyes as shown by the solid curve in Fig. 2. This graph was used to separate the excess heat capacities that are shown in Fig. 3. The anomaly is very broad extending from 30 K to 47 K with a maximum at (40.4±0.2) K. The enthalpy and the entropy of transition were determined as (5.02±0.08) J·mol^{-1} and (0.129±0.003) J·K^{-1}·mol^{-1}, respectively, by graphical integration of the excess heat capacities.

Biphenyl is known to show the twist transition of

Table 2. Molar Thermodynamic Functions of Biphenyl

T	$C_{p,m}$	$[H^\circ_m(T)-H^\circ_m(0)]/T$	$S^\circ_m(T)-S^\circ_m(0)$	$-[G^\circ_m(T)-H^\circ_m(0)]/T$
K	J K^{-1} mol^{-1}	J K^{-1} mol^{-1}	J K^{-1} mol^{-1}	J K^{-1} mol^{-1}
5	0.504	0.133	0.173	0.040
10	3.26	0.90	1.21	0.32
20	14.68	4.75	6.71	1.96
30	27.46	10.21	15.11	4.89
40	38.63	15.97	24.59	8.62
50	46.42	21.30	34.07	12.77
60	53.43	26.08	43.17	17.08
70	59.57	30.44	51.87	21.44
80	65.19	34.44	60.20	25.76
90	70.44	38.14	68.18	30.04
100	75.57	41.63	75.87	34.24
110	80.72	44.95	83.31	38.36
120	85.83	48.14	90.56	42.41
130	90.89	51.24	97.63	46.39
140	96.23	54.26	104.56	50.30
150	101.53	57.23	111.38	54.14
160	107.11	60.18	118.11	57.93
170	112.85	63.11	124.77	61.67
180	118.82	66.03	131.39	65.36
190	124.75	68.97	137.97	69.00
200	130.90	71.91	144.53	72.62
210	137.21	74.87	151.07	76.20
220	143.68	77.85	157.60	79.75
230	150.49	80.86	164.13	83.28
240	157.19	83.90	170.68	86.78
250	163.77	86.96	177.23	90.27
260	170.73	90.05	183.79	93.74
270	177.90	93.17	190.37	97.20
280	185.10	96.33	196.97	100.64
290	192.30	99.51	203.59	104.08
300	199.50	102.72	210.23	107.50
298.15	198.17	102.13	209.00	106.87

Table 3. Calorimetric Entropy of Biphenyl

	S°_m/J K^{-1} mol^{-1}
0 to 4 K (smooth extrapolation)	0.089
4 to 298.15 K (graphical)	208.9
Sublimation[a]	274.2
Entropy of real gas at 298.15 K	483.2
Compression[b] and correction to ideal gas[c]	−93.7
S°_m(biphenyl, 298.15 K, g, p=100000 Pa)	389.5

a) $\Delta_{vap}H$=81760 J · mol^{-1} at 298.15 K.[64] b) p=1.30 Pa at 298.15 K.[63] c) Using Berthelot's equation of state.

Table 4. Properties of the Successive Phase Transitions of Biphenyl

	Lock-in transition	Twist transition
T_{trs}/K	16.8±0.1	40.4±0.2
Region/K	15.3−18.3	30−47
$\Delta_{trs}H$/J mol^{-1}	0.15±0.02	5.02±0.08
$\Delta_{trs}S$/J K^{-1} mol^{-1}	0.009±0.001	0.129±0.003

the displacive type associated with some soft-modes.[24-27] The properties of the twist transition in biphenyl are summarized in Table 4. The shape of the anomaly and the smallness of the entropy of transition are consistent with the higher-order, displacive nature of the twist transition. On the other hand, *p*-terphenyl and *p*-quaterphenyl crystals undergo the twist transition of the order-disorder type[21,65] at much higher temperatures (193.5 K[66] and 233.0 K,[55] respectively) compared with biphenyl. The heat capacity anomalies of biphenyl and *p*-quaterphenyl are both very broad but that of *p*-terphenyl is

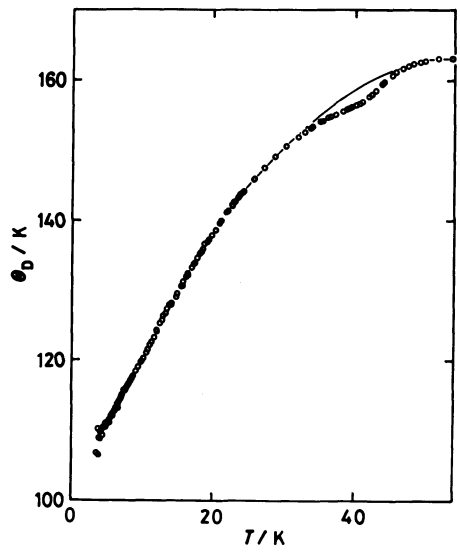

Fig. 2. Debye characteristic temperatures corresponding to the measured heat capacities of biphenyl assuming 9 degrees of freedom per molecule.

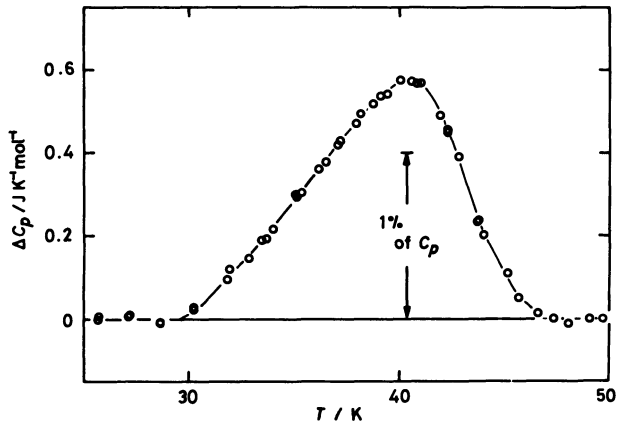

Fig. 3. Excess heat capacities due to the twist transition of biphenyl.

sharp.[66-68] The behavior of the three substances has been discussed[55] in terms of the molecular symmetry and the potentials for the intramolecular twisting modes.

Lock-in Transitions. No anomaly corresponding to the lock-in transition can be discerned in Fig. 2, which are the results obtained by using the old calorimeter vessel; the slight distortion at about 11 K is probably due to a failure in the germanium temperature scale.[51,52] The results of measurements using the new vessel are shown in Fig. 4 in the form of θ_D plot, where the data obtained in series 34 of measurements are shown. In this series, the temperature increment of each measurement was about 0.2 K. A broad anomaly is now clearly seen. The excess heat capacities were then separated by drawing the normal portion as shown by the solid

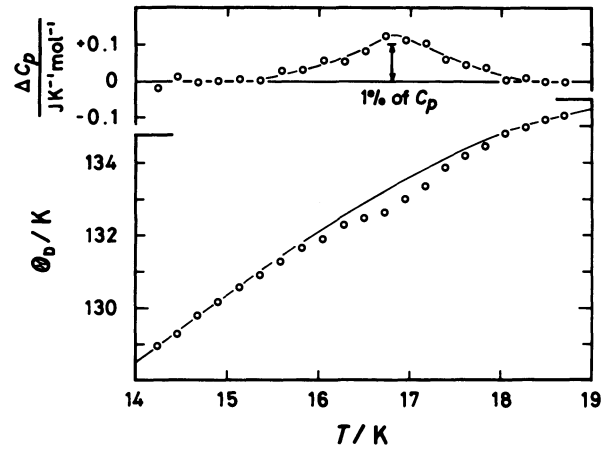

Fig. 4. Shape of the anomaly due to the lock-in transition of biphenyl (data of a typical run).

curve. The anomaly is broad extending from 15.3 K to 18.3 K with a maximum at (16.8±0.1) K, showing a large tail on the high temperature side. The enthalpy and the entropy of transition were determined as (0.15±0.02) J·mol^{-1} and (0.009±0.001) J·K^{-1}·mol^{-1}, respectively. This transition obviously corresponds to the reported lock-in transition by which the lattice becomes commensurate except for the b^* direction. The properties of the lock-in transition are also summarized in Table 4.

The shape of the anomaly and the smallness of the entropy of transition suggest that the lock-in transition is a higher-order transition. However, some evidences that the lock-in transition is of the first-order have been reported,[28,34,38] and the Landau's phenomenology[45,48] also predicts that it must be so. The present heat capacity results are smooth to within ±0.1 per cent at the top of the anomaly, 16.8 K, and there was no indication of latent heat. Similar discrepancy was reported in the case of K_2SeO_4.[69] There are two possible explanations of such a discrepancy on the notion that the transition is in fact of the first order. One is that the latent heat is so small that its effect is not reflected in the heat capacity runs. As one sees from the upper portion of Fig. 4, the anomalous part is smooth to within about 0.1 per cent; therefore the latent heat, if any, must be smaller than about 0.01 J·mol^{-1}. The other possibility, which is more likely, is that crystallites have a different lock-in transition temperature, i.e. the overall heat effects are smeared.

The large tail on the higher temperature side at the lock-in transition has been observed also in other substances,[69-71] and it may be accompanied with discommensuration mechanism proposed by McMillan.[72]

No further anomaly was found at lower temperatures in spite of a search for the other lock-in transition in the direction of the b^* axis. Any

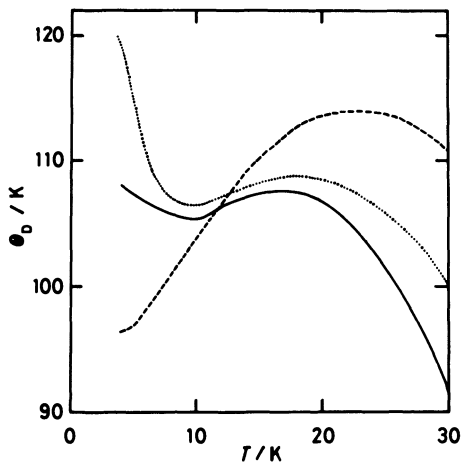

Fig. 5. Debye characteristic temperatures corresponding to the measured heat capacities of biphenyl (broken curve), *p*-terphenyl (solid curve) and 4,4′-difluorobiphenyl (dotted curve) assuming 6 degrees of freedom per molecule.

indication of freezing of some motional degrees of freedom was not observed either.[41] A simple interpretation of this fact is that the lock-in transition in the b^* direction could exist below 3 K, the lowest temperature reached in the present experiments. The other, more tempting interpretation is that the incommensurate phase could be stable down to the absolute zero. If the latter is the case, the crystal would represent a new type of thermodynamic stability. Determination of the spectroscopic entropy in the gas phase will give us a clue to this problem. It must be emphasized, however, the "residual entropy," if present, is expected to be very small taking the smallness of the entropy of lock-in transitions into account.

Crossover of Low Temperature Heat Capacities. The comparison of the low temperature heat capacities of biphenyl and *p*-terphenyl[53,66] is shown in Fig. 5 in terms of corresponding Debye characteristic temperatures assuming 6 degrees of freedom per molecule. Below about 20 K, the heat capacity of biphenyl decreases less steeply than that of *p*-terphenyl as the temperature decreases, and they cross each other at about 12 K. The crossover between biphenyl and *p*-quaterphenyl was also observed at about 6 K.[55]

Since biphenyl and *p*-terphenyl have similar crystal structures and their intermolecular interactions are also similar, one would expect that the relative magnitude of their heat capacities is determined primarily by the relative molecular mass, i.e. the heavier molecule should show a larger heat capacity at a low temperature, where only low-lying lattice modes are excited. Therefore, there must be some motional mode or modes in biphenyl for which the force constant is much smaller than for the corresponding mode(s) in *p*-terphenyl. The twisting mode about the central C–C bond in biphenyl seems to be the candidate of such a mode because (1) it is the only conceivable intramolecular mode that is susceptible to the crystal field, (2) the coupling of the twisting motion with the lattice vibration has been pointed out in many experimental[73–75] and theoretical[46,73,74,76,77] studies on the lattice vibrations of biphenyl crystal, and (3) the twisted conformation in *p*-terphenyl has been substantiated[20,23] below the order-disorder transition[21,65] in contrast with biphenyl. Thus, an attempt will be made to interpret the observed crossover by a simple model calculation of lattice vibration spectra for biphenyl and *p*-terphenyl crystals.

For biphenyl the average crystal structure at 22 K[15] was used, ignoring the incommensurability which will play an important role only in the very low temperature region where the contribution of phason becomes dominant.[78] The structure of *p*-terphenyl at 113 K[20] was corrected for thermal expansion down to 22 K by a linear extrapolation from the room temperature data.[21]

The intermolecular interaction was expressed by the sum of atom–atom pair potentials of Buckingham type, in which the parameters were taken from the literature.[79] The interactions were summed over molecules within a radius of 1 nm. Phenyl rings were assumed to be rigid.

The Lagrangian L of the system was written in terms of translational (superscript; t), rotational (r), and twisting (τ) coordinates in the harmonic approximation as follows:[80]

$$L = K - \Phi,$$

$$K = \frac{1}{2}\sum_{l}\sum_{\kappa}\sum_{\alpha} m\,[\dot{u}^{t}_{\alpha}(l\kappa)]^2 + \frac{1}{2}\sum_{l}\sum_{k}\sum_{\alpha,\beta} I_{\alpha\beta}(\kappa)\,\dot{u}^{r}_{\alpha}(l\kappa)\,\dot{u}^{r}_{\beta}(l\kappa) + \frac{1}{2}\sum_{l}\sum_{\kappa} I_{\tau}\,[\dot{u}^{\tau}(l\kappa)]^2,$$

$$\Phi = \Phi_0 + \frac{1}{2}\sum_{l,l'}\sum_{\kappa,\kappa'}\sum_{\alpha,\beta} \phi^{tt}_{\alpha\beta}(l\kappa; l'\kappa')\,u^{t}_{\alpha}(l\kappa)\,u^{t}_{\beta}(l'\kappa') + \frac{1}{2}\sum_{l,l'}\sum_{\kappa,\kappa'}\sum_{\alpha,\beta} \phi^{tr}_{\alpha\beta}(l\kappa; l'\kappa')\,u^{t}_{\alpha}(l\kappa)\,u^{r}_{\beta}(l'\kappa') + \frac{1}{2}\sum_{l,l'}\sum_{\kappa,\kappa'}\sum_{\alpha,\beta} \phi^{rt}_{\alpha\beta}(l\kappa; l'\kappa')\,u^{r}_{\alpha}(l\kappa)\,u^{t}_{\beta}(l'\kappa') + \frac{1}{2}\sum_{l,l'}\sum_{\kappa,\kappa'}\sum_{\alpha,\beta} \phi^{rr}_{\alpha\beta}(l\kappa; l'\kappa')\,u^{r}_{\alpha}(l\kappa)\,u^{r}_{\beta}(l'\kappa')$$

$$+\frac{1}{2}\sum_{l,l'}\sum_{\kappa,\kappa'}\sum_{\alpha}\phi_{\alpha}^{rr}(l\kappa;l'\kappa')u_{\alpha}^{r}(l\kappa)u^{\tau}(l'\kappa')$$

$$+\frac{1}{2}\sum_{l,l'}\sum_{\kappa,\kappa'}\sum_{\alpha}\phi_{\alpha}^{\tau r}(l\kappa;l'\kappa')u^{\tau}(l\kappa)u_{\alpha}^{r}(l'\kappa')$$

$$+\frac{1}{2}\sum_{l,l'}\sum_{\kappa,\kappa'}\sum_{\alpha}\phi_{\alpha}^{r\tau}(l\kappa;l'\kappa')u_{\alpha}^{r}(l\kappa)u^{\tau}(l'\kappa')$$

$$+\frac{1}{2}\sum_{l,l'}\sum_{\kappa,\kappa'}\sum_{\alpha}\phi_{\alpha}^{\tau r}(l\kappa;l'\kappa')u^{\tau}(l\kappa)u_{\alpha}^{r}(l'\kappa')$$

$$+\frac{1}{2}\sum_{l,l'}\sum_{\kappa,\kappa'}\phi^{\tau\tau}(l\kappa;l'\kappa')u^{\tau}(l\kappa)u^{\tau}(l'\kappa')$$

$$\phi_{\alpha\beta}^{ab}(l\kappa;l'\kappa')=\frac{\partial^2\Phi}{\partial u_{\alpha}^{a}(l\kappa)\,\partial u_{\beta}^{b}(l'\kappa')},$$

where u is the displacement from an equilibrium position and α and β mean x, y, or z permutatively. Thus, $u_{\alpha}(l\kappa)$ denotes the displacement of the κ-th molecule in the l-th cell in the direction α. The equations of motion derived from the Lagrangian were numerically solved for 512 points picked up uniformly in the first Brillouin zone.

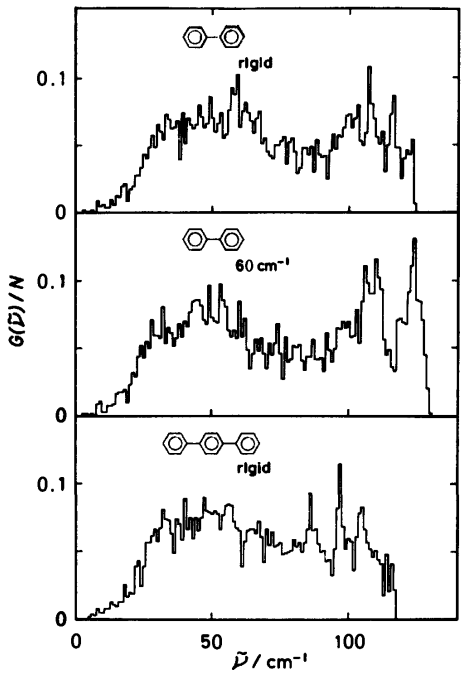

Fig. 6. Calculated density of states for rigid biphenyl, flexible biphenyl and rigid p-terphenyl.

The results of calculation are shown in Figs. 6 and 7. On the assumption of the rigid body, where there are no terms involving the twisting coordinates in the Lagrangian, p-terphenyl shows larger heat capacities than biphenyl at all the temperatures, as expected from the relative molecular mass. However, when one introduces flexibility into the biphenyl molecule with regard to the twisting of phenyl rings (a force constant corresponding to 60 cm^{-1} as the intramolecular contribution), biphenyl comes to show higher density of states in the low frequency region. On the other hand, p-terphenyl has higher density between 25 and 45 cm^{-1} due to its larger mass. Figure 7 shows the Debye temperature curve calculated from the spectra of Fig. 6 and the twisting flexibility is reflected in the crossover in the heat capacities at about 12 K. Now, we conclude qualitatively that the crossover can be attributed to the low-frequency twisting mode contribution of phenyl rings in biphenyl.

The same interpretation applies to the comparison between biphenyl and 4,4′-difluorobiphenyl which also has an analogous crystal structure at room temperature.[54,81–83]

The behavior of the Debye temperature of 4,4′-difluorobiphenyl[56] assuming 6 degrees of freedom per molecule is also shown in Fig. 5. The heat capacity of biphenyl is larger than that of 4,4′-difluorobiphenyl below about 13 K in spite of the smaller mass of the former molecule.[56] Thus, it is clear that the heat capacities of biphenyl crystal are much larger at low temperatures than those of the homologous molecules and derivatives. Therefore, the central C–C bond of biphenyl is extremely soft with regard to the internal rotation: The competing effect of the intra- and intermolecular interactions is very subtle and it plays

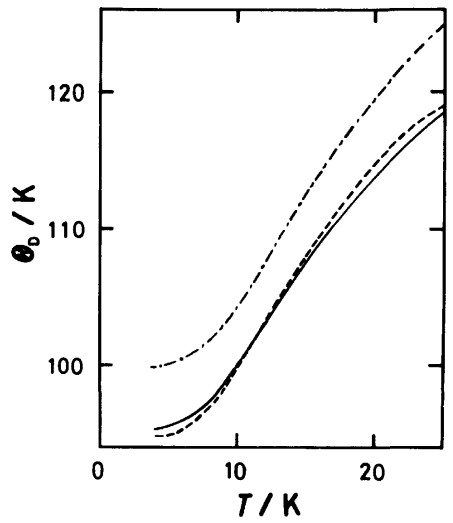

Fig. 7. Calculated Debye characteristic temperatures of rigid p-terphenyl(solid curve), flexible biphenyl (broken curve) and rigid biphenyl (dot-dash curve), assuming 6 degrees of freedom per molecule.

a critical role in the incommensurate structure of the crystal in such a way that the twisting mode in strongly coupled to the lattice vibration to such as extent that is not realized in similar other molecules.

References

1) O. Bastiansen, *Acta Chem. Scand.*, **3**, 408 (1949).
2) H. Suzuki, *Bull. Chem. Soc. Jpn.*, **32**, 1340 (1959).
3) J. Dale, *Acta Chem. Scand.*, **11**, 640 (1957); **11**, 650 (1957).
4) V. J. Eaton and D. Steele, *J. Chem. Soc., Faraday Trans. 2*, **69**, 1601 (1973).
5) A. J. Grumadas, D. P. Poshkus, and A. V. Kiselev, *J. Chem. Soc., Faraday Trans. 2*, **75**, 1398 (1979).
6) A. J. Grumadas, D. P. Poshkus, and A. V. Kiselev, *J. Chem. Soc., Faraday Trans. 2*, **78**, 2013 (1982).
7) G. L. Clark and L. W. Pickett, *J. Am. Chem. Soc.*, **53**, 167 (1931).
8) J. Dhar, *Indian J. Phys.*, **7**, 43 (1932).
9) J. Trotter, *Acta Crystallogr.*, **14**, 1135 (1961).
10) G. B. Robertson, *Nature (London)*, **191**, 593 (1961).
11) A. Hargreaves and S. H. Rizvi, *Acta Crystallogr.*, **15**, 365 (1962).
12) V. M. Kozhin and K. V. Mirskaya, *Sov. Phys. Crystallogr.*, **14**, 938 (1970).
13) G. P. Charboneau and Y. Delugeard, *Acta Crystallogr., Sect. B*, **32**, 1420 (1976).
14) G. P. Charboneau and Y. Delugeard, *Acta Crystallogr., Sect. B*, **33**, 1586 (1977).
15) H. Cailleau, J. L. Baudour, and C. M. E. Zeyen, *Acta Crystallogr., Sect. B*, **35**, 426 (1979).
16) J. L. Baudour and M. Sanquer, *Acta Crystallogr., Sect. B*, **39**, 75 (1983).
17) V. Petricek, P. Coppens, and P. Becker, *Acta Crystallogr., Sect. A*, **41**, 478 (1985).
18) H. M. Rietveld, E. N. Maslen, and C. J. B. Clews, *Acta Crystallogr., Sect. B*, **26**, 693 (1970).
19) J. L. Baudour, *Acta Crystallogr., Sect. B*, **28**, 1649 (1972).
20) J. L. Baudour, Y. Delugeard, and H. Cailleau, *Acta Crystallogr., Sect. B*, **32**, 150 (1976).
21) J. L. Baudour, H. Cailleau, and W. B. Yelon, *Acta Crystallogr., Sect. B*, **33**, 1773 (1977).
22) Y. Delugeard, J. Desuche, and J. L. Baudour, *Acta Crystallogr., Sect. B*, **32**, 702 (1976).
23) J. L. Baudour, Y. Delugeard, and P. Rivet, *Acta Crystallogr., Sect. B*, **34**, 625 (1978).
24) P. S. Friedman, P. Kopelman, and P. N. Prasad, *Chem. Phys. Lett.*, **24**, 15 (1974).
25) A. Bree and M. Edelson, *Chem. Phys. Lett.*, **46**, 500 (1977).
26) M. Wada, A. Sawada, and Y. Ishibashi, *J. Phys. Soc. Jpn.*; **50**, 737 (1980).
27) H. Cailleau, A. Girard, F. Moussa, and C. M. E. Zeyen, *Solid State Commun.*, **29**, 259 (1979).
28) H. Cailleau, F. Moussa, and J. Mons, *Solid State Commun.*, **31**, 521 (1979).
29) H. Cailleau, J. C. Messager, F. Moussa, F. Bugaut, C. M. E. Zeyen, and C. Vettier, *Ferroelectrics*, **67**, 3 (1986).
30) A. Janner, T. Janssen, and P. M. de Wolff, *Acta Crystallogr., Sect. A*, **39**, 671 (1983).
31) A. Dworkin and H. Cailleau, *J. Phys. (Paris) Lett.*, **41**, L-83 (1980).
32) A. S. Cullick and R. E. Gerkin, *Chem. Phys.*, **23**, 217 (1977).
33) A. S. Cullick and R. E. Gerkin, *Chem. Phys. Lett.*, **42**, 589 (1976).
34) A. Bree and M. Edelson, *Chem. Phys. Lett.*, **55**, 319 (1978).
35) N. I. Wakayama, *Chem. Phys. Lett.*, **83**, 413 (1981).
36) C. Ecolivet, M. Sanquer, J. Pellegrin, and J. DeWitte, *J. Chem. Phys.*, **78**, 6317 (1983).
37) D. Kirin, S. L. Chaplot, G. A. Mackenzie, and G. S. Pawley, *Chem. Phys. Lett.*, **102**, 105 (1983).
38) J. L. Baudour, L. Toupet, Y. Delugeard, and S. Ghemid, *Acta Crystallogr., Sect. C*, **42**, 1211 (1986).
39) V. Heine and S. L. Price, *J. Phys. C*, **18**, 5259 (1985).
40) H. Cailleau, F. Moussa, C. M. E. Zeyen, and J. Bouillot, *Solid State Commun.*, **33**, 407 (1980).
41) S. B. Liu and M. S. Conradi, *Phys. Rev. Lett.*, **54**, 1287 (1985).
42) C. Benkert and V. Heine, *Phys. Rev. Lett.*, **58**, 2232 (1987).
43) H. Cailleau, A. Girard, J. C. Messager, Y. Delugeard, and C. Vettier, *Ferroelectrics*, **54**, 257 (1984).
44) R. M. Hochstrasser, R. D. McAlpine, and J. D. Whiteman, *J. Chem. Phys.*, **58**, 5078 (1973).
45) Y. Ishibashi, *J. Phys. Soc. Jpn.*, **50**, 1255 (1981).
46) N. M. Plakida, A. V. Belushkin, I. Natkaniec, and T. Wasiutyński, *Phys. Status Solidi B*, **118**, 129 (1983).
47) W. R. Busing, *Acta Crystallogr., Sect. A*, **39**, 340 (1983).
48) P. Toledano and M. Guilluy, *Ferroelectrics*, **53**, 311 (1984).
49) J. C. Raich and E. R. Bernstein, *Mol. Phys.*, **53**, 597 (1984).
50) T. Janssen, *Jpn. J. Appl. Phys.*, **24**, Suppl. 24-2, 747 (1985).
51) T. Atake and H. Chihara, *Solid State Commun.*, **35**, 131 (1980).
52) T. Atake, K. Saito, and H. Chihara, *Chem. Lett.*, **1983**, 493.
53) K. Saito, T. Atake, and H. Chihara, *Chem. Lett.*, **1984**, 521.
54) K. Saito, H. Chihara, T. Atake, and Y. Saito, *Jpn. J. Appl. Phys.*, **24**, Suppl. 24-2, 838 (1985).
55) K. Saito, T. Atake, and H. Chihara, *J. Chem. Thermodyn.*, **17**, 539 (1985).
56) K. Saito, T. Atake, and H. Chihara, *J. Chem. Thermodyn.*, **18**, 407 (1986).
57) K. Saito, T. Atake, and H. Chihara, *Thermochim. Acta*, **109**, 45 (1986).
58) K. Saito, T. Atake, and H. Chihara, *J. Chem. Thermodyn.*, **19**, 9 (1987).
59) K. Saito, T. Atake, and H. Chihara, *J. Chem. Thermodyn.*, **19**, 633 (1987).
60) T. Atake and H. Chihara, *Bull. Chem. Soc. Jpn.*, **47**, 2126 (1974).
61) T. Atake and H. Chihara, (unpublished).
62) H. G. Huffman, G. S. Parks, A. C. Daniels, *J. Am. Chem. Soc.*, **52**, 1547 (1930).
63) R. S. Bradley and T. G. Cleasby, *J. Chem. Soc.*, **1953**, 1690.
64) E. Morawetz, *J. Chem. Thermodyn.*, **4**, 455 (1972).

65) B. A. Bolton and P. N. Prasad, *Chem. Phys.*, **35**, 331 (1978).
66) K. Saito, T. Atake, and H. Chihara, (unpublished).
67) H. Cailleau and A. Dworkin, *Mol. Cryst. Liq. Cryst.*, **50**, 217 (1979).
68) S. S. Chang, *J. Chem. Phys.*, **79**, 6229 (1983).
69) K. Nomoto, T. Atake, B. K. Chaudhuri, and H. Chihara, *J. Phys. Soc. Jpn.*, **52**, 3475 (1983).
70) T. Atake, K. Nomoto, B. K. Chaudhuri, and H. Chihara, *J. Chem. Thermodyn.*, **15**, 339 (1983).
71) T. Atake, K. Nomoto, B. K. Chaudhuri, and H. Chihara, *J. Chem. Thermodyn.*, **15**, 383 (1983).
72) W. L. McMillan, *Phys. Rev. B*, **14**, 1496 (1976).
73) I. Natkaniec, A. V. Belushkin, and T. Wasiutyński, *Phys. Status Solidi B*, **105**, 413 (1981).
74) H. Takeuchi, S. Suzuki, A. J. Dianoux, and G. Allen, *Chem. Phys.*, **55**, 153 (1981).
75) A. V. Belushkin, I. Natkaniec, J. Wasicki, and T. Zaleski, *Phys. Status Solidi B*, **123**, K115 (1984).
76) E. Burgos, H. Bonadeo, and E. D'Alessio, *J. Chem. Phys.*, **65**, 2460 (1976).
77) H. Bonadeo and E. Burgos, *Acta Crystallogr., Sect. A*, **38**, 29 (1982).
78) M. L. Boriack and A. W. Overhauser, *Phys. Rev. B*, **18**, 6454 (1978).
79) D. E. Williams, *J. Chem. Phys.*, **47**, 4680 (1967).
80) G. Venkataraman and V. C. Sahni, *Rev. Mod. Phys.*, **42**, 409 (1970).
81) T. K. Halstead, H. W. Spiess, and U. Haeberlen, *Mol. Phys.*, **31**, 1569 (1976).
82) T. K. Halstead, J. Tagenfeldt, and U. Haeberlen, *J. Chem. Soc., Faraday Trans. 2*, **77**, 1817 (1981).
83) K. Saito, T. Atake, and H. Chihara, *Acta Crystallogr., Sect. B*, **43**, 383 (1987).

 © 1988 The Chemical Society of Japan Bull. Chem. Soc. Jpn., 61, 689—692 (1988)

Spectrophotometric Study of Complexation Equilibria between Lanthanoids(III) and 2-(5-Bromo-2-pyridylazo)-5-(*N*-propyl-3-sulfopropylamino)phenol

Emiko Ohyoshi
Yatsushiro National College of Technology, Hirayamashinmachi 2627, Yatsushiro, 866
(Received May 6, 1987)

Complex formation (1:1) between lanthanoids(III) and 2-(5-bromo-2-pyridylazo)-5-(*N*-propyl-3-sulfopropylamino)phenol (5-Br-PAPS, HL) has been studied by spectrophotometry at 25 °C and at I=0.1 ($NaNO_3$). The protonated complex MHL is found to exist in equilibrium with the normal complex ML at pH 5—6. The formation constants K_{ML} and K_{MHL} are obtained by a graphical analysis. The K_{ML} values uniformly increase with increasing atomic number except for those in the Gd-Ho region where a distinct decrease is observed. However, there is little variation in the K_{MHL} values with atomic number. A linear relation holds well between log K_{ML} values of 5-Br-PAPS and 4-(2-pyridylazo)resorcinol (PAR) complexes for the elements up to Eu(III), the intercept of which reflects the difference in the basicity of the oxygen atom ortho to the azo group between the two ligands. This is not the case for log K_{MHL} of the two systems.

Recently, a highly sensitive reagent 2-(5-bromo-2-pyridylazo)-5-(*N*-propyl-3-sulfopropylamino)phenol (5-Br-PAPS, HL) has been developed and shown to be useful for spectrophotometric determination of some transition metals.[1-3] It has the same reacting group as 4-(2-pyridylazo)resorcinol (PAR) but has a different substituent in the para position to the azo group. Shibata et al.[4] suggested that the dialkylamino group which is a strongly electron-donating group existing in the para position to the azo group may play an important role in the high molar absorptivity and stability of the metal complex. However, very few studies on the stability of the metal complex with this type of reagent have been reported.

In this paper, the complexation of 5-Br-PAPS with lanthanoids(III) is studied spectrophotometrically and the results are compared with those of the PAR complexes.[5]

Experimental

Materials. All chemicals used were of G. R. grade. 5-Br-PAPS was obtained from Dojindo Chemical Co., and its purity was checked spectrophotometrically by using the standard solution of Zn(II). The molar absorptivity of ZnL_2 (L=5-Br-PAPS) at 553 nm is 1.28×10^5 M^{-1} cm^{-1} (1 M=1 mol dm^{-3}) which agreed with the reported value of 1.3×10^5 M^{-1} cm^{-1}.[1] A weighed quantity of 5-Br-PAPS was dissolved in distilled water to prepare the stock solution of 1.0×10^{-2} M. The lanthanoid(III) nitrate solutions were prepared by dissolving the oxides or nitrates in nitric acid and were standardized by EDTA titration. 2-Morpholinoethanesulfonic acid (MES, Good's buffer reagent) and sodium nitrate were used to maintain the pH at 4.8—6.1 and the ionic strength at 0.1, respectively.

Procedure. The metal solution was added in small aliquots, 50 μl each, using a microliter pipet to a 10 ml of the buffered solution of 5-Br-PAPS ($1.5—2.0\times10^{-5}$ M), to give concentrations of 10^{-4}—3×10^{-3} M. Before and after the addition of the metal for each 50 μl, the absorbance at the peak of 5-Br-PAPS (446 nm) was measured by using a Shimadzu UV-260 spectrophotometer. No precipitation occurred under these experimental conditions.

Results and Discussion

Absorption Spectra of the Reagent (HL^-) and the Complexes. The absorption spectra of the reagent were studied at various pH adjusted with a dilute nitric acid or sodium hydroxide solution. Three species of the reagent, H_2L (λ_{max}=466 nm, pH<2.5), HL^- (λ_{max}=446 nm, pH 4—9), and L^{2-} (λ_{max}=512 nm, pH>11) are involved in its acid-base equilibria. The protonation constants of HL^- and L^{2-}, $K^H_{H_2L}=[H_2L]/([HL^-][H^+])$ and $K^H_{HL}=[HL^-]/([L^{2-}][H^+])$, were determined by the method of Schwarzenbach.[6] The values of 2.78±0.05 and 10.56±0.03 were obtained for log $K^H_{H_2L}$ and log K^H_{HL}, respectively at 25 °C and I=0.1. According to these values and the known acidity constants of analogous azo dyes,[4] $K^H_{H_2L}$ and K^H_{HL} refer to the protonation of the amino group and of the phenolic oxygen, respectively.

Under the conditions where the metal is in large excess over the ligand, the absorption spectra of the complexes had two maxima at 533 and 566 nm for all the lanthanoids(III). Their apparent molar absorptivities which were different for different lanthanoids(III) at constant pH increased with increasing pH and reached the limiting values of $4.6—5.0\times10^4$ M^{-1} cm^{-1} at 533 nm and of $5.5—6.0\times10^4$ M^{-1} cm^{-1} at 566 nm. The reagent 5-Br-PAPS is shown to be almost twice as sensitive as PAR[5] for the determination of lanthanoids(III).

Determination of the Complex Formation Constant. The formation of the 1:1 complex, ML, has been studied by measuring the absorbance of the ligand, L, in the absence (A_o) and the presence (A) of the metal, M, under conditions where $C_M \gg C_L$ (C_M and C_L are the total concentrations of M and L) and pH=constant.[7] The complex formation constant so obtained may be regarded as the conditional

formation constant, $K_{ML'}$, as defined by Eq. 1, by considering any side reactions.

$$K_{ML'} = [ML']/([M'][L']) \quad (1)$$

where [ML'], [M'], and [L'] represent all forms of the metal complexes, the uncomplexed metal and the uncomplexed ligand, respectively. The expressions for C_L and A are then given as follows:

$$C_L = [ML'] + [L'] \quad (2)$$

$$A = \varepsilon_{ML'}[ML'] + \varepsilon_{L'}[L'] \quad (3)$$

where $\varepsilon_{ML'}$ and $\varepsilon_{L'}$ are the apparent molar absorptivity of ML' and L', respectively. Combining Eqs. 1, 2, and 3, and substituting A_o for $\varepsilon_{L'}C_L$ and C_M for [M] (since $C_M \gg C_L$) in the resulting equation, we obtain

$$K_{ML'} - \frac{\varepsilon_{ML'}K_{ML'}}{\varepsilon_{L'}}\frac{A_o}{A} = (A_o/A - 1)/C_M. \quad (4)$$

From Eq. 4, a linear relation between $(A_o/A-1)/C_M$ and A_o/A should be obtained at a constant pH, the intercept of which yields the $K_{ML'}$ value. This value can be related to the formation constant K_{ML} by means of the side reaction coefficient, α, viz.

$$K_{ML'} = K_{ML}\alpha_{ML}/(\alpha_M\alpha_L) \quad (5)$$

where α_{ML}=[ML']/[ML], α_M=[M']/[M], and α_L=[L']/[L].

From the measured absorbance decreases at the peak of 5-Br-PAPS (446 nm) with increasing metal concentrations at a constant pH, we plotted the relation expressed by Eq. 4. Figure 1 shows the plots obtained at pH 5.51 for different lanthanoids(III). This linear relation was shown to be independent of C_L. The experimental data showed no detectable difference in the plots for Yb(III) and Lu(III) (line 1), and for Tb(III) through Ho(III) (line 6), respectively. Similar plots were obtained at different pH values as exemplified for the Eu(III)-5-Br-PAPS system in Fig. 2. As seen in Figs. 1 and 2, the $K_{ML'}$ values given as the intercept increase with either increasing atomic number (though a discontinuity is shown in the Gd–Ho region) or pH. From the pH dependency of $K_{ML'}$, the side reactions are considered to be the protonation of L and the formation of the MHL complex. The α coefficients for these reactions, α_L and α_{ML} are given by

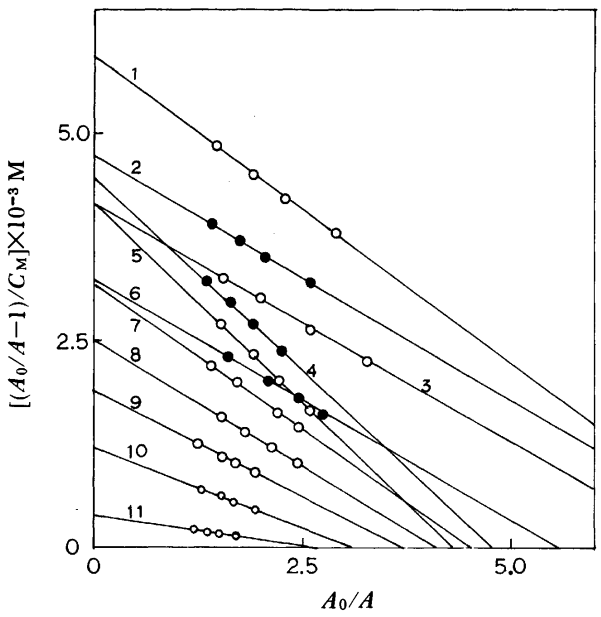

Fig. 1. Plots according to Eq. 4 at a constant pH of 5.51 for the system of 5-Br-PAPS and lanthanoids-(III). 1) Lu, Tb; 2) Tm; 3) Er; 4) Eu; 5) Sm; 6) Ho, Dy, Tb; 7) Gd; 8) Nd; 9) Pr; 10) Ce; and 11) La.

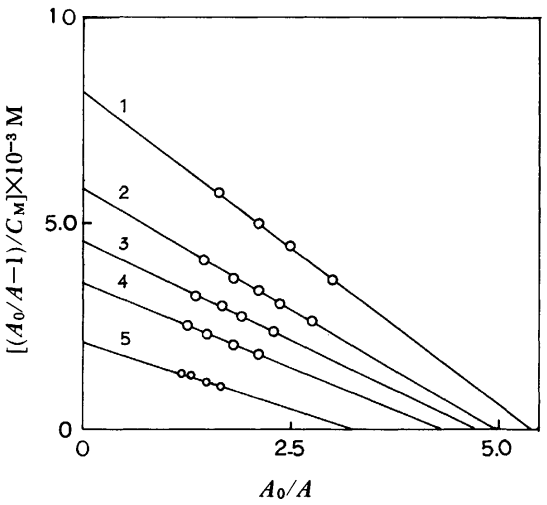

Fig. 2. Plots according to Eq. 4 at different pH values for the Eu(III)-5-Br-PAPS system. pH: 1) 5.81, 2) 5.65, 3) 5.51, 4) 5.40, and 5) 5.12.

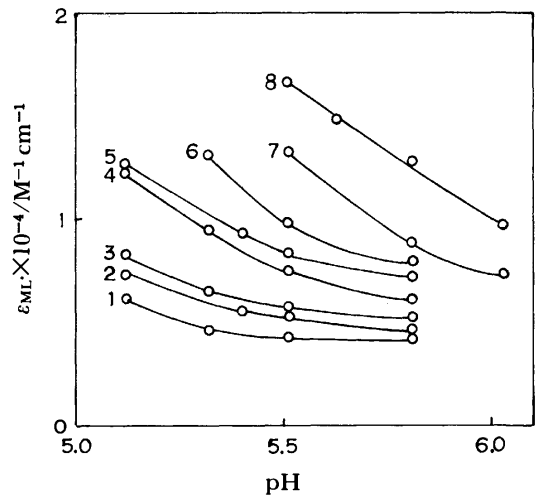

Fig. 3. Plots of the apparent molar absorptivity of ML', $\varepsilon_{ML'}$, at 446 nm vs. pH for the system of 5-Br-PAPS and lanthanoids(III). 1) Yb, 2) Tm, 3) Er, 4) Ho, 5) Eu, 6) Pr, 7) Ce, and 8) La.

$$\alpha_L = [L']/[L] = ([L] + [HL])/[L] = 1 + K^H_{HL}[H] \quad (6)$$

$$\alpha_{ML'} = [ML']/[ML] = ([ML] + [MHL])/[ML] = 1 + K^H_{MLH}[H] \quad (7)$$

where K^H_{HL}=[HL]/([H][L]) and K^H_{MLH}=[MHL]/([ML][H]). The relation between $K_{ML'}$ and α_L (Eqs. 5 and 6) coincides with the observed dependence of $K_{ML'}$ on pH, confirming that the former side reaction occurs. However, no such confirmation is given for the latter. This was found to occur by studying the dependence of the apparent molar absorptivity of ML', $\varepsilon_{ML'}$ on pH (Fig. 3). To calculate the $\varepsilon_{ML'}$ values we used the intercept of the A_0/A axis of the plot of Eq. 4 which equals $\varepsilon_{L'}/\varepsilon_{ML'}$. With increasing pH the $\varepsilon_{ML'}$ values for different lanthanoids initially decrease showing the presence of MHL and ML, and tend to reach the limiting values (ε_{ML}) different for different lanthanoids where only one component, ML exists. In the acidic media used in this study there are no hydroxo complexes.[8] No complexes with buffer ions were also found by studying the effect of buffer concentrations on the $K_{ML'}$ values. Thus,

$$\alpha_M \simeq 1. \quad (8)$$

Substituting Eqs. 6, 7, and 8 into Eq. 5, we obtain

$$K_{ML'}(1 + K^H_{HL}[H]) = K_{ML}(1 + K^H_{MLH}[H]) \quad (9)$$

With the formation constant of MHL, K_{MHL}=[MHL]/[M][HL])=$K_{ML}K^H_{MLH}/K^H_{HL}$, Eq. 9 is rewritten in the form

$$K_{ML'}(1 + K^H_{HL}[H]) = K_{ML} + K_{MHL}K^H_{HL}[H] \quad (10)$$

According to Eq. 10, a plot of the left-hand side of Eq. 10 against [H] by using values of $K_{ML'}$ obtained at constant pH yields K_{ML} as the intercept and K_{MHL} as the slope/K^H_{HL} ratio.

The results of the plots of Eq. 10 are linear with intercepts (Fig. 4), indicating the presence of both MHL and ML complexes in this pH range for all the lanthanoids(III). The formation constants K_{MHL} and K_{ML} calculated from the slope and the intercept of the plots in Fig. 4 by applying the least squares method are listed in Table 1 together with the corresponding values of the PAR complexes for comparison. It is noted that the difference in K_{ML} is greater than that in K_{MHL} for different elements. Comparison of the 5-Br-PAPS and PAR systems shows both the MHL and the ML complexes of 5-Br-PAPS to be less stable than those of PAR.

For the ML complexes, 5-Br-PAPS and PAR show a similar coordination trend to the lanthanoids(III) except for several elements heavier than Gd(III). It is seen from Fig. 5 that for the elements up to Eu(III) the

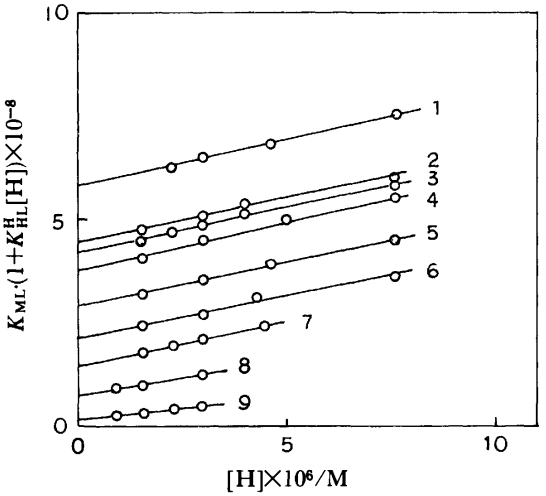

Fig. 4. Plots according to Eq. 10 for the system of 5-Br-PAPS and lanthanoids(III). 1) Lu, Yb; 2) Tm; 3) Eu; 4) Er, Sm; 5) Ho, Dy, Tb, Gd; 6) Nd; 7) Pr; 8) Ce; and 9) La.

Table 1. Formation Constants, K_{MHL} and K_{ML}, for 5-Br-PAPS and PAR Complexes of Lanthanoids(III) I=0.1 ($NaNO_3$), 25 °C

Element	5-Br-PAPS		PAR[5,7]	
	log K_{MHL}	log K_{ML}	log K_{MHL}	log K_{ML}
La	2.38	7.22	3.18	8.91
Ce	2.60	7.90	3.78	9.61
Pr	2.77	8.16	3.95	9.78
Nd	2.74	8.33	4.07	10.02
Sm	2.80	8.58	4.28	10.25
Eu	2.76	8.63	4.28	10.25
Gd	2.79	8.46	4.28	10.25
Tb	2.79	8.46	4.28	10.25
Dy	2.79	8.46	4.29	10.36
Ho	2.79	8.46	4.29	10.47
Er	2.80	8.58	4.31	10.52
Tm	2.76	8.65	4.34	10.57
Yb	2.79	8.77	4.39	10.70
Lu	2.79	8.77	4.39	10.70

The relative errors of K_{MHL} and K_{ML} are 8—12% and 4—8%, respectively.

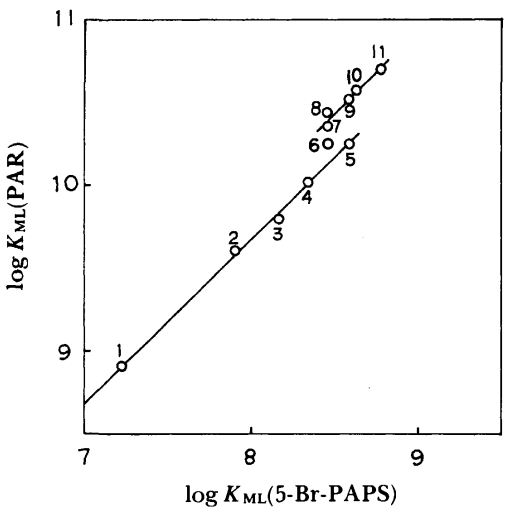

Fig. 5. Relationship between log K_{ML} values of 5-Br-PAPS and PAR complexes with lanthanoids(III). 1) La; 2) Ce; 3) Pr; 4) Nd; 5) Sm, Eu; 6) Gd, Tb; 7) Dy; 8) Ho; 9) Er; 10) Tm; and 11) Yb, Lu.

linear relationship holds well between log K_{ML} values of 5-Br-PAPS and PAR complexes with the slope of unity and the intercept of 1.7 which reflects the difference in the basicity of the ortho-oxygen atom to the azo group between the two ligands (log K^{H}_{HL}=12.30 for PAR[9] and log K^{H}_{HL}=10.56 for 5-Br-PAPS). This is not the case for log K_{MHL} of the two systems. A recent study,[10] showed that such a linear relation has been obtained between log K_{MHL} as well as log K_{ML} for the lanthanoid(III) complexes with a pair of ligands, PAR and 4-(2-thiazolylazo)resorcinol (TAR), both of which have a *p*- and an *o*-hydroxyl group. These facts suggest that the effect of the difference in character between 5-Br-PAPS and PAR on the formation of MHL is much larger than that on the formation of ML. These two ligands have a different functional group in the para position to the azo group, the dipropylamino group (5-Br-PAPS) or the hydroxyl group (PAR), and thus have one dissociable proton (5-Br-PAPS) or two (PAR), respectively.

When the complexation of PAR occurs at pH values lower than either values of log $K^{H}_{H_2L}$=5.50 (para) or log K^{H}_{HL}=12.30 (ortho),[9] it is assumed that protons are released preferentially from the *o*-hydroxyl group. This means that PAR reacts in the thermodynamically unfavored form, *HL$^-$ where *H denotes the para proton for which the dissociation constant is not known. Corcini et al.[11] proposed to use $1/K^{H}_{HL}$ (ortho) as an approximation. On the other hand, 5-Br-PAPS used in this study has only the proton (ortho) dissociable, existing as HL in the pH range studied. The lanthanoid ion thus reacts with HL to form the MHL complex in which the ortho proton does not dissociate. This type of coordination has been reported for the complexes of Be(II),[12] Cu(II),[13] and lanthanoids(III)[14] with 5-sulfosalicylic acid. Hence, the phenolic oxygen would weakly bond either to the proton or to the metal ion. This is consistent with the observation that the absorption bands due to the MHL complex overlap each of the peaks assigned to the HL (proton–ortho-oxygen bond) species and the ML (metal–ortho-oxygen bond) species. This was found by studying changes in the apparent molar absorptivity, $\varepsilon_{ML'}$ at each peak with pH, i.e., $\varepsilon_{ML'}$ at 446 nm (HL) decreased (Fig. 3) but those at 533 and 566 nm (ML) increased with increasing pH. Similarly, the absorption spectra of the PAR complexes of this type (MHL) showed the two maxima at 410 and 495 nm each of which is very close to that of HL at 415 nm and to that of ML at 505 nm.[5] From these facts, the structure of the MHL complexes of the PAR system might be similar to that of the 5-Br-PAPS system, i.e., PAR normally ionizes the para proton first on complexation. It may be reasonable to infer that the para phenolate ion O$^-$ enhances the negative charge on the azo nitrogen; this would make the stability of MHL for the PAR complexes larger and more different from metal to metal than that for the 5-Br-PAPS complexes.

This work was supported by a Grant-in-Aid for Scientific Research from the Ministry of Education (No. 60540383).

References

1) T. Makino, M. Saito, D. Horiguchi and K. Kina, *Clin. Chim. Acta*, **120**, 127 (1982).
2) Y. Shijo and K. Sakai, *Bunseki Kagaku*, **33**, E 435 (1984).
3) Y. Shijo and K. Sakai, *Bull. Chem. Soc. Jpn.*, **59**, 1455 (1986).
4) S. Shibata, M. Furukawa, and K. Toei, *Anal. Chim. Acta*, **66**, 397 (1973).
5) E. Ohyoshi, *Talanta*, **31**, 1129 (1984).
6) G. Schwarzenbach and W. Biedermann, *Helv. Chim. Acta*, **31**, 678 (1948).
7) E. Ohyoshi, *Anal. Chem.*, **55**, 2404 (1983).
8) L. G. Sillen and A. E. Martell, "Stability Constants of Metal-Ion Complexes, and Supplement No. 1," The Chemical Society, London (1971).
9) W. J. Geary, G. Nickless, and F. H. Pollard, *Anal. Chim. Acta*, **27**, 71 (1962).
10) E. Ohyoshi, *Polyhedron*, **5**, 1165 (1986).
11) A. Corsini, I. Mai-Ling Yih, Q. Fernando, and H. Freiser, *Anal. Chem.*, **34**, 1090 (1962).
12) J. Schubert and A. Lindenbaum, *J. Biol. Chem.*, **208**, 359 (1954).
13) S. E. Turner and R. C. Anderson, *J. Am. Chem. Soc.*, **71**, 912 (1949).
14) N. V. Thakur, S. M. Jogdeo, and C. R. Kanekar, *J. Inorg. Nucl. Chem.*, **28**, 2297 (1966); C. R. Karekar, N. V. Thakur, and S. M. Jogdeo, *Bull. Chem. Soc. Jpn.*, **41**, 759 (1968).

A Quantitative Scale of the Spectrochemical Series for the Mixed Ligand Complexes of d^6 Metals

(the late) Yoichi SHIMURA
Department of Chemistry, Faculty of Science, Osaka University, Toyonaka, Osaka 560
(Received June 25, 1987)

Quantitative scale of a new parameter d has been proposed for the spectrochemical series of ligands in the mixed ligand complexes of d^6 metals, which enables us to predict the positions of low energy d-d absorption bands of a d^6 complex. Introduction of a new reduction parameter α has improved the prediction of the d-d bands of mixed cyano complexes of cobalt(III), mixed halogeno complexes of rhodium(III), iridium-(III), and platinum(IV), and also several mixed carbonyl complexes of low-valent d^6 metals.

Some quantitative scales were presented for the spectrochemical series of ligands,[1] i.e., ligand field splitting energy Δ(=10 Dq) of a given metal ion, or in an exact sense f(ligand) value of Jørgensen's formula $\Delta = f(\text{ligand}) \cdot g(\text{central ion})$,[2] but these are limited for non-mixed ligand complexes only. On the other hand, to predict the position of d-d absorption band of a mixed complex, Yamatera's δ parameters[3] have frequently been used, but they are also unsatisfactory because it has been reported that the Yamatera rule was not exactly fit for the mixed cyano complexes of cobalt(III)[4] and the mixed halogeno complexes of rhodium(III) or iridium(III).[5] In the present paper, a new quantitative scale will be proposed for the spectrochemical series of ligands in the mixed complexes of d^6 metals, which enables us to predict the energy values of long wavelength d-d absorption bands of almost all the d^6 complexes.

Results and Discussion

Spectrochemical Series of Ligands. The energies of three components of the first spin-allowed d-d absorption band of an octahedral complex $[ML_{(1)}L_{(2)}L_{(3)}L_{(4)}L_{(5)}L_{(6)}]$ (Fig. 1) may be written:

$$\begin{aligned} \sigma_{xy} &= \alpha(d_2 + d_3 + d_4 + d_5)/4, \\ \sigma_{yz} &= \alpha(d_1 + d_2 + d_4 + d_6)/4, \\ \sigma_{zx} &= \alpha(d_1 + d_3 + d_5 + d_6)/4, \end{aligned} \quad (1)$$

where d_n (n=1,2,...6) is a parameter of the ligand $L_{(n)}$ previously defined[6] as δ and α a reduction parameter. Then it becomes,

$$\begin{aligned} \sigma &= (\sigma_{xy} + \sigma_{yz} + \sigma_{zx})/3 \\ &= \alpha(d_1 + d_2 + d_3 + d_4 + d_5 + d_6)/6, \end{aligned} \quad (2)$$

where σ is a mean energy of the first d-d absorption band. When α=1.00, Eqs. 1 and 2 reduce to the

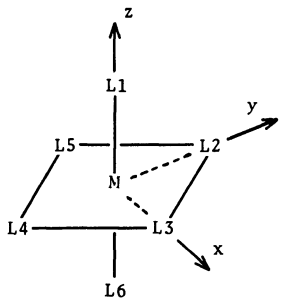

Fig. 1. An octahedral complex $[ML_{(1)}L_{(2)}L_{(3)}L_{(4)}L_{(5)}L_{(6)}]$.

Table 1. Empirical α Values for the Mixed Complexes [M $a_x b_{6-x}$] of Holohedrized D_{4h} Symmetry[a,b]

a[c]	b[c]	M=Fe(II)	Co(III)	Rh(III)	Ir(III)	Pd(IV)	Pt(IV)
CN^-	P,As	—	0.98[0.96]	—	—	—	—
CN^-	N	0.90	0.955[0.91]	0.97	0.83	—	—
CN^-	O	—	0.94[0.88]	0.965	0.81	—	—
CN^-	Cl^-	—	0.935	0.95	0.80	—	0.67[0.64?]
CN^-	Br^-	—	0.93	0.92	0.77	—	—
CN^-	I^-	—	0.92	0.87	0.74	—	—
P,As	O		0.97[0.94]	—	—	—	—
P,As	Cl^-	0.90[0.80]	0.95[0.90]	0.94[0.88]	0.92[0.84]	—	—
N	Cl^-	—	0.98[0.96]	0.97[0.94]	0.96[0.92]	0.93[0.86]	0.92[0.84]
N	Br^-	—	0.965[0.93]	0.95[0.90]	0.93[0.86]	0.92[0.84]	0.81[0.79?]
N	I^-	—	0.96[0.92]	0.92[0.91?]	0.86[0.84?]	—	0.77
O	Cl^-	—	—	0.98[0.96]	0.98[0.96]	—	0.95[0.90]
O	Br^-	—	—	0.95[0.90]	—	—	—

a) The value in sequare brackets is for the complexes of *trans*-[M a_4b_2] and -[M a_2b_4] types. b) As to the carbonyl complexes $[M(CO)_xX_{6-x}]$(X=N, O, Cl^-, Br^-, or I^-), α=0.86 for M=V(−I), 0.87 Cr(0), 0.94 Mo(0), 0.90 W(0), 0.95 Mn(I), 0.91 Re(I), 0.93 Ru(II), and 0.90 Os(II). c) An element symbol underlined shows a ligating atom.

Yamatera rule[3,6] and the rule of average environment,[7] respectively. Most of the N,O-mixed[6] and all of the non-mixed complexes of low-spin d^6 type obey Eqs. 1 and 2 with α=1.00, but the other mixed complexes, for example the mixed cyano complexes seem to have α values smaller than 1.00 as shown in Table 1, where α values are estimated empirically from a compilation of absorption data of a variety of d^6 complexes.

It has been found that only three different α values are sufficient for prediction of the first d-d band energies of a series of mixed complexes [M a_xb_{6-x}] (x=1—5) except for *mer*-[M a_3b_3]: one is for [M a_5b], *cis*-[M a_4b_2], *cis*-[M a_2b_4], and [M ab_5], amounting to 1.00−β ($0 \leqq \beta \leqq 0.4$), and the second is for *trans*-[M a_4b_2] and -[M a_2b_4], amounting to 1.00−2β, and the third is for *fac*-[M a_3b_3], remaining to be 1.00. This fact means that the reduction parameter α is related to the order of lowering (from O_h to D_{4h}) of the holohedrized symmetry[8] of a given complex. It is remarkable that all tris-chelate complexes have α=1.00 regardless of the ligating atoms.

The d value (in 10^3 cm^{-1}) of each ligand for different complexes of a given metal can be evaluated from the observed data of mean σ or its components σ_{xy}, σ_{yz}, or σ_{zx} using Eqs. 1 and 2. Of course the position of the first d-d band of a [M a_6]-type is equal to the d value of the ligand a for that metal, because α=1.00 in this case. For a bidentate ligand A~B, the d value can be defined as,

$$d\langle \mathrm{A}\sim\mathrm{B}\rangle^n = (d\langle -\mathrm{A}\rangle^n + d\langle -\mathrm{B}\rangle^n)/2, \quad (3)$$

where n means chelate ring size, for example n=7 for $d\langle NH_2CH_2CH_2CH_2CH_2NH_2\rangle^7 = d\langle -CH_2NH_2\rangle^7$, and n=6 for $d\langle\beta\text{-ala}\rangle^6 = d\langle NH_2CH_2CH_2CO_2^-\rangle^6 = (d\langle -CH_2NH_2\rangle^6 + d\langle -CO_2^-\rangle^6)/2$. Besides the d values for different unidentate ligands, those of such chelate ends are also arranged in Table 2.

Table 2 gives d_{Co} values obtained for 100 ligands (or chelate ends) of cobalt(III) complexes, ranging from the highest value 35.0 for CO to the lowest value 7.0 for $\langle -CH_2Se^-\rangle^5$, which is selenolato end of a bidentate ligand forming 5-membered chelate ring. In Table 3, σ_{obs} of the typical mixed cobalt(III) complexes are compared to σ_{calc} obtained from the d values in Table 2 by applying Eq. 1 or 2. The deviation Δ is generally within ±2%.

Spectrochemical Series of Metals. For the metals (M) other than cobalt(III), a series of d_M can be obtained from the existing data. A plot of d_M versus d_{Co} makes a straight line passing the origin (Fig. 2):

$$d_M = m d_{Co}, \quad (4)$$

where m is the spectrochemical parameter for the metal M. The m values obtained from Eq. 4 are tabulated in Table 4. The m value can be correlated to the Jørgensen's g (central ion) value[9] (Fig. 3), while d_{Co} (and d_M also) to the Jørgensen's f (ligand) value[9] (Fig. 4).

Table 2. Spectrochemical Series of Ligands:[a,b] d_{Co} Values in 10^3 cm^{-1}

CO	35.0	$\langle NH_2C_6H_4NH_2\rangle^5$	20.9	$\langle -CH_2OH\rangle^5$	16.4	F^-	14.8
CN^-	32.1	$\langle$bgH$\rangle^5$	20.9	$\langle NO_3^-\rangle^4$	16.4	$\langle R_2NCSe_2^-\rangle^4$	14.4
$P(OMe)_3$	29.4	py	20.8	NCS^-	16.3	$\langle -CH_2O^-\rangle^5$	14.4
$\langle -CH_2SO_2^-\rangle^5$	27.6	NH_2CHO	20.7	$OCOCF_3^-$	16.3	$OP(OR)_3$	14.2
$\langle Me_2PC_6H_4PMe_2\rangle^5$	27.6	$\langle -CH_2NH_2\rangle^6$, tn	20.4	CH_3OH	16.2	$OSMe_2$	14.0
$\langle -CH_2PMe_2\rangle^5$	26.0	$\langle -CH_2SO^-\rangle^5$	20.2	$\langle EtOCS_2^-\rangle^4$	16.2	$OCMe_2$	14.0
$\langle Ph_2PC_6H_4PPh_2\rangle^5$	25.6	$NCNH_2$	20.2	$OCOCHRNH_3$	16.1	$CH_3SO_3^-$	14.0
PMe_3	25.6	$\langle -CH_2NHMe\rangle^5$	20.0	$\langle CS_3^{2-}\rangle^4$	16.0	N_3^-	13.9
SO_3^{2-}	25.6	NH_2Me	20.0	$OCOCCl_3^-$	16.0	$\langle PO_4^{3-}\rangle^4$	13.9
NO_2^-	25.3	$\langle -CH_2NH_2\rangle^7$	19.9	$\langle -CH_2SeMe\rangle^5$	15.8	$P_2O_7^{4-}$	13.8
$\langle -CH_2PMe_2\rangle^6$	25.3	$\langle -C_6H_4NH_2\rangle^7$	19.3	NCO^-	15.8	$OSeO_2^{2-}$	13.8
$PhSO_2^-$	24.1	ONO^-	18.2	$\langle P_2O_7^{4-}\rangle^6$	15.7	$\langle (RO)_2PS_2^-\rangle^4$	13.55
$\langle Me_2AsC_6H_4AsMe_2\rangle^5$	23.6	$\langle -CH_2SH\rangle^5$	17.9	$\langle R_2NCS_2^-\rangle^4$	15.6	$CF_3SO_3^-$	13.5
NCMe	23.5	$\langle -CH_2SMe\rangle^5$	17.7	O_2^-	15.6	PO_4^{3-}	13.2
PPh_3	23.2	$\langle -CH_2SeO^-\rangle^5$	17.6	$\langle CO_3^{2-}\rangle^4$	15.5	ReO_4^-	13.2
$\langle =CHPPh_2\rangle^5$	23.0	$\langle -CH_2NHPh\rangle^5$	17.6	$OCOMe^-$	15.5	SCN^-	13.0
$\langle -CH_2AsMe_2\rangle^5$	23.0	$\langle O_2^{2-}\rangle^3$	17.0	OH^-	15.4	$\langle Me_2PS_2^-\rangle^4$	12.75
NH_2OH	22.8	$\langle RCS_2^-\rangle^4$	16.95	OCO_2^{2-}	15.4	Cl^-	12.5
$\langle =CHAsMe_2\rangle^5$	22.7	$\langle$acac$^-\rangle^6$	16.9	$OCOCO_2^{2-}$	15.4	SSO_3^{2-}	12.0
$\langle -CH_2AsMe_2\rangle^6$	22.4	$\langle -CH_2NMe_2\rangle^5$	16.8	$OCONH_2^-$	15.4	$SeCN^-$	11.8
$\langle$bpy$\rangle^5$	22.2	$NCSe^-$	16.8	$OCHNMe_2$	15.3	Br^-	11.7
$\langle$phen$\rangle^5$	22.0	$\langle -CO_2^-\rangle^5$, ox	16.6	NO_3^-	15.2	CrO_4^{2-}	11.1
$\langle -CH_2NH_2\rangle^5$, en	21.4	H_2O	16.5	$OC(NH_2)_2$	15.15	I^-	9.0
imH	21.2	$\langle TeO_6H_4^{2-}\rangle^4$	16.5	$\langle SO_4^{2-}\rangle^4$	15.0	$\langle -CH_2S^-\rangle^5$	9.3—7.5[c]
NH_3	21.0	$\langle -CO_2^-\rangle^6$, mal	16.45	SO_4^{2-}	15.0	$\langle -CH_2Se^-\rangle^5$	7.0

a) Abbreviations of ligands: acac, acetylacetonate $CH_3COCHCOCH_3^-$; bgH, biguanide $NHC(NH_2)NHC(NH_2)NH$; bpy, 2,2′-bipyridine $C_{10}H_8N_2$; en, ethylenediamine $NH_2CH_2CH_2NH_2$; imH, imidazole $C_3H_4N_2$; mal, malonate $CH_2(CO_2)_2^{2-}$; ox, oxalate $C_2O_4^{2-}$; phen, 1,10-phenanthroline $C_{12}H_8N_2$; py, pyridine C_5H_5N; tn, trimethylenediamine $NH_2CH_2CH_2CH_2NH_2$. For some frequently appearing ligands such as en, tn, ox, mal etc., the angle bracket with chelate ring size, $\langle\ \rangle^n$, are omitted for convenience. b) An element symbol underlined shows a ligating atom. c) The d value of thiolato chelate end $\langle -CH_2S^-\rangle^5$ is subject to some variation from complex to another (see Table 6).

Table 3. Observed and Calculated First d-d Band Positions ($10^3\,cm^{-1}$) of the Typical Cobalt(III) Complexes

No.	Complex	σ_{obs}	σ_{calc}[a]	Eq.	α	Δ/%[b]	d[c]	Ref.
1	$[Co(CO)(CN)_5]^{2-}$	32.6	32.58	(2)	1.00	−0.1	CO 35.0; CN^- 32.1	10)
2	$[Co(CN)(NH_3)_5]^{2+}$	22.7	22.71	(1)	0.955	+0.0	CN^- 32.1; NH_3 21.0	11)
3	*fac*-$[Co(NH_2CH_2CH_2PMe_2)_3]^{3+}$	23.70	23.70	(2)	1.00	0.0	$<-CH_2PMe_2>^5$ 26.0[d]	12)
4	*fac*-$[Co(NH_2CH_2CH_2CO_2)_3]$	18.7	18.43	(2)	1.00	−1.4	tn 20.4; mal 16.45	13)
5	$[Co(en)_2(CO_3)]^+$	19.5	19.43	(2)	1.00	−0.4	$<CO_3^{2-}>^4$ 15.5	14)
6	$[CoCl(NH_3)_5]^{2+}$	18.65	18.50	(1)	0.98	−0.8	Cl^- 12.5; NH_3 21.0	15)
7	*trans*-$[CoCl_2(en)_2]^+$	16.3	16.27	(1)	0.96	−0.2	Cl^- 12.5	16)
8	*cis*-$[CoCl_2(en)_2]^+$	18.7	18.79	(1)	0.98	+0.5	Cl^- 12.5	17)
9	$[CoBr(CN)_5]^{3-}$	25.2	25.11	(1)	0.93	−0.4	Br^- 11.7; CN^- 32.1	18)
10	*trans*-$[CoI_2(en)_2]^+$	14.0	13.98	(1)	0.92	−0.1	I^- 9.0	19)

a) The position from Eq. 1 refers to the doubly degenerate component. b) $\Delta=100(\sigma_{calc}-\sigma_{obs})/\sigma_{obs}$. c) $d<en>^5=d<-CH_2NH_2>^5=21.4$. d) $d<NH_2CH_2CH_2PMe_2>^5=(d<-CH_2NH_2>^5+d<-CH_2PMe_2>^5)/2=(21.4+26.0)/2=23.7$.

Table 4. Spectrochemical Series of Central Metals: Values of m Obtained from Eq. 4

V(−I)	0.715	Cr(0)	0.890	Mn(I)	0.945	Fe(II)	0.965	Co(III)	1.00	Ni(IV)	1.28
Nb(−I)	0.695	Mo(0)	0.875	Tc(I)	—	Ru(II)	1.22	Rh(III)	1.56	Pd(IV)	1.70
Ta(−I)	0.705	W(0)	0.910	Re(I)	1.16	Os(II)	1.43	Ir(III)	1.90	Pt(IV)	2.10

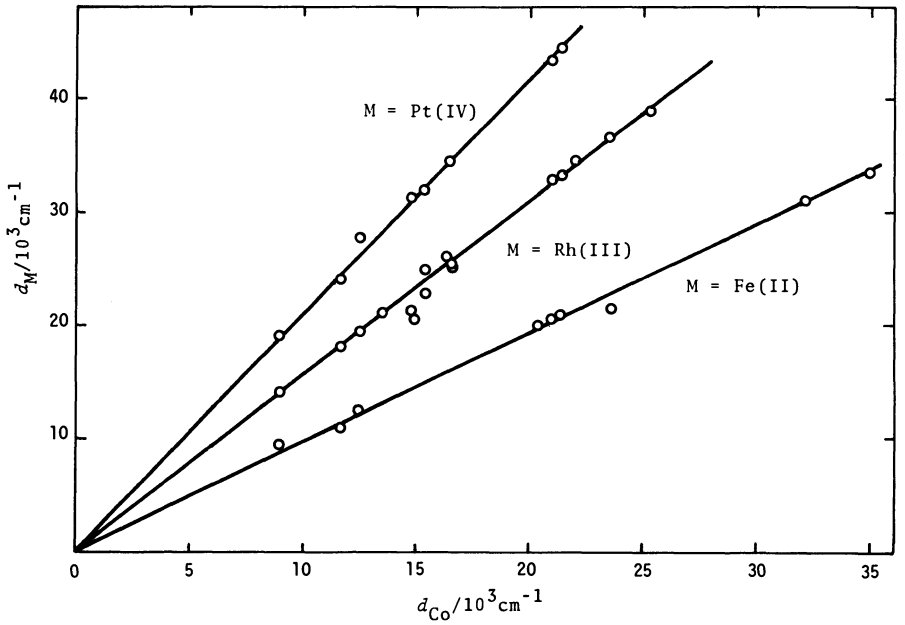

Fig. 2. Plots of d_M versus d_{Co}: $d_M=md_{Co}$ for M=Fe(II), Rh(III), and Pt(IV).

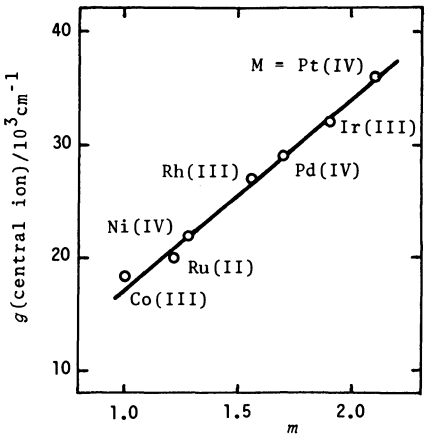

Fig. 3. A plot of m versus g (central ion).

In Table 5, σ_{obs} of the typical d^6 complexes are compared with σ_{calc} obtained from the d_{Co} and m values. The deviation Δ is generally within ±3%.

S- or Se-Ligands. As is seen in Table 2, the sulfur-donor (or selenium-donor) ligands distribute widely along the spectrochemical series, where the thiolato (or selenolato) ligands being on the weakest end. Houlding et al.[34] pointed out a striking characteristic of such thiolato (or selenolato) complexes of cobalt(III), i.e., that these have an extra shoulder band on the low-energy side of the first d-d absorption band. In Table 6, the splitting of the first d-d band of the thiolato (or selenolato), and the related S- (or Se-) ligands such as SCN^- and SSO_3^{2-} is interpreted by an assumption of anisotropy of the antibonding contribu-

Table 5. Observed and Calculated First d-d Band Positions (10^3 cm^{-1}) of the d^6 Metals except for Cobalt(III)

No.	Complex	σ_{obs}[a]	σ_{calc}[b]	Eq.	α	Δ/%[c]	d_M from Eq. 4	Ref.
11	$[V(CO)_5(NH_3)]^-$	19.5	19.35	(1)	0.86	−0.8	CO 25.0; NH_3 15.0	20)
12	$[Cr(CO)_4(en)]$	23.6	23.61	(2)	0.87	+0.0	CO 31.2; en 19.0	21)
13	$[Cr(CO)_5F]^-$	23.0	23.23	(1)	0.87	+0.8	CO 31.2; F^- 13.2	22)
14	$[Mo(CO)_5(NH_3)]$	25.6	25.90	(1)	0.94	+1.0	CO 30.6; NH_3 18.4	23)
15	$[W(CO)_5(OH)]^-$	24.0	24.68	(1)	0.90	+2.7	CO 31.9; OH^- 14.0	22)
16	$[Mn(CO)_5Cl]$	26.5	26.39	(1)	0.95	−0.5	CO 33.1; Cl^- 11.8	23)
17	$[Re(CO)_5Cl]$	31.1	30.85	(1)	0.91	−0.7	CO 40.4; Cl^- 14.4	23)
18	$[Fe(CO)(CN)_5]^{3-}$	31.4	31.47	(2)	1.00	+0.2	CO 33.8; CN^- 31.0	24)
19	$[Fe(CN)_4(en)]^{2-}$	25.6	25.58	(1)	0.90	−0.1	CN^- 31.0; en 20.7	25)
20	$[Ru(NH_3)_5(H_2O)]^{2+}$	24.1	24.23	(1)	1.00	+0.5	NH_3 25.6; H_2O 20.1	26)
21	$[Os(CO)(NH_3)_5]^{2+}$	31.6	31.52	(1)	0.90	−0.3	CO 50.1; NH_3 30.0	27)
22	*trans*-$[Rh(N_3)_2(en)_2]^+$	26.7	27.45	(1)	1.00	+2.8	en 33.3; N_3^- 21.6	28)
23	*trans*-$[RhCl_2(en)_2]^+$	24.6	24.77	(1)	0.94	+0.7	en 33.3; Cl^- 19.4	5)
24	*cis*-$[RhCl_2(en)_2]^+$	28.4	28.93	(1)	0.97	+1.9	en 33.3; Cl^- 19.4	5)
25	*trans*-$[IrCl_2(ox)_2]^{3-}$	27.2sh	26.50	(1)	0.96	−2.8	ox^{2-} 31.5; Cl^- 23.7	29)
26	*cis*-$[IrCl_2(ox)_2]^{3-}$	27.8sh	28.32	(2)	0.98	+1.9	ox^{2-} 31.5; Cl^- 23.7	29)
27	$[IrCl_5(H_2O)]^{2-}$	24.7	24.47	(2)	0.98	−0.9	H_2O 31.3; Cl^- 23.7	29)
28	*trans*-$[PdCl_2(en)_2]^{2+}$	24.6sh	24.81	(1)	0.86	+0.9	en 36.4; Cl^- 21.3	30)
29	$[PtCl(NH_3)_5]^{3+}$	35.4	36.48	(1)	0.92	+3.1	NH_3 44.1; Cl^- 26.3	31)
30	*trans*-$[PtCl_2(NH_3)_4]^{2+}$	29.9	29.57	(1)	0.84	−1.1	NH_3 44.1; Cl^- 26.3	31)
31	*trans*-$[PtCl_4(NH_3)_2]$	29.4	29.57	(1)	0.84	+0.6	NH_3 44.1; Cl^- 26.3	32)
32	$[PtCl_5(NH_3)]^-$	29.1	28.29	(1)	0.92	−2.8	NH_3 44.1; Cl^- 26.3	33)

a) sh=shoulder band. b) The position from Eq. 1 refers to the doubly degenerate component. c) $\Delta=100(\sigma_{calc}-\sigma_{obs})/\sigma_{obs}$.

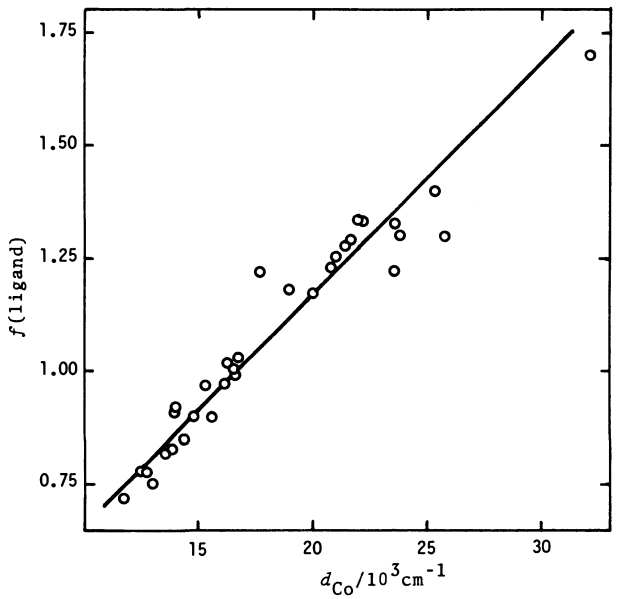

Fig. 4. A plot of d_{Co} versus f (ligand).

tion of S (or Se) donor atoms, and then the $d_{(S)}$ parameter is written as:

$$d_{(S)} = (d_{(S)//} + d_{(S)\perp})/2. \quad (5)$$

Thus, in a CoN_5S-type complex containing the thiolato-like S atom, the three σ components are expressed by $\alpha d_{(N)}$, $\alpha(3d_{(N)}+d_{(S)//})/4$, and $\alpha(3d_{(N)}+d_{(S)\perp})/4$. If the S atom is no more anisotropic, the latter two components combine to give a degenerate one $\alpha(3d_{(N)}+d_{(S)})/4$. In the case of complexes Nos. 35—37, the component at longer wavelength is observed as a shoulder, and the next peak observed is an overlap of the two components at shorter wavelength.

Mixed Cyano Complexes. An empirical rule of Shimura,[39,40] which states that, for the first d-d bands of cis and trans isomers of [M a_4b_2] of a d^6 metal M, $\Delta\sigma=\sigma(cis)-\sigma(trans)<0$ if b is ahead of a in the spectrochemical series, while $\Delta\sigma>0$ if b is behind a, suffers from a few exceptions. An example is the isomers of $[Co(CN)_2(NH_3)_4]^+$ which show $\Delta\sigma_{obs}=+1.4$. By the present introduction of reduction parameter α, however, most of the exceptions can be explained reasonably because the different α values are assigned to the geometrical isomers (Table 7).

The introduction of the parameter α has also improved the predicted values of σ for a variety of mixed cyano complexes, which were heretofore regarded as serious exception of the Yamatera rule[4] (see complexes Nos. 2, 9, 19, and 38—43 in Tables 3, 5, and 7). Fujinami et al.[41] proposed an angular overlap treatment taking into account of (i) mixing of 3d orbitals with 4s and 4p by the lowering of symmetry in the mixed complexes and (ii) a configuration interaction between excited states, these factors being probably in line with the present introduction of empirical parameter α.

Mixed Halogeno Complexes. Ogino and Bailar[5] pointed out that there were big discrepancies between the predicted and the observed σ values of mixed halogeno complexes of rhodium(III) and iridium(III), when the predicted value was calculated from the d values obtained from the observed σ value of non-mixed halogeno complexes. Such discrepancies,

Table 6. Anisotropic *d* Parameters of the Thiolato-Like S- or Se-Ligands

No.	Complex	σ_{obs}[a]	σ_{calc}	Eq.	α	Δ/%[b]	*d*(S or Se)		Ref.
33	$[Co(SCN)(NH_3)_5]^{2+}$	17.8sh	17.76[c]	(1)	0.98	−0.2	9.5	SCN^+ 13.0	35)
		19.5	19.48[d]	(1)	0.98	−0.1	16.5		
34	$[Co(SSO_3)(NH_3)_5]^+$	17sh	17.03[c]	(1)	0.98	+0.2	6.5	SSO_3^{2-} 12.0	36)
		19.6	19.72[d]	(1)	0.98	+0.6	17.5		
35	$[Co(SCH_2CH_2NH_2)(en)_2]^{2+}$	16.7sh	16.70[c]	(1)	1.00	0.0	2.6	<-CH_2S->[5] 9.3	37)
		20.72	20.73[d]	(1)	1.00	+0.0	16.0		
36	$[Co(SCH_2CO_2)(en)_2]^+$	16.2sh	16.20[c]	(1)	1.00	0.0	5.4	<-CH_2S->[5] 7.5	37)
		19.3	19.33[d]	(1)	1.00	0.0	9.6		
37	$[Co(SeCH_2CH_2NH_2)(en)_2]^{2+}$	16.5sh	16.45[c]	(1)	1.00	−0.3	1.6	<-CH_2Se->[5] 7.0	38)
		20.4	20.28[d]	(1)	1.00	−0.3	12.4		

a) sh=shoulder band. b) $\Delta=100(\sigma_{calc}-\sigma_{obs})/\sigma_{obs}$. c) The non-degenerate component. d) A mean of the two shorter wavelength components.

Table 7. Geometrical Isomers of the Mixed Cyano Complexes

No.	Complex	σ_{obs}	σ_{calc}	Eq.	α	Δ/%[a]	$\Delta\sigma_{obs}$[b]	$\Delta\sigma_{calc}$[b]	Ref.
38	*cis*-$[Co(CN)_4(NH_3)_2]^-$	28.0	28.01	(1)	0.955	+0.0	+3.8	+3.85	11)
39	*trans*-$[Co(CN)_4(NH_3)_2]^-$	24.2	24.16	(1)	0.91	−0.2			
40	*cis*-$[Co(CN)_2(NH_3)_4]^+$	25.3	25.36[c]	(1)	0.955	+0.2	+1.4	+1.2	4)
41	*trans*-$[Co(CN)_2(NH_3)_4]^+$	23.9	24.16	(1)	0.91	+1.1			
42	*cis*-$[Co(CN)_2(en)_2]^+$	24.7	25.55[c]	(1)	0.955	+3.4	+0.3	+1.2	4)
43	*trans*-$[Co(CN)_2(en)_2]^+$	24.4	24.34	(1)	0.91	−0.2			

a) $\Delta=100(\sigma_{calc}-\sigma_{obs})/\sigma_{obs}$. b) $\Delta\sigma=\sigma$(cis)$-\sigma$(trans). c) The shorter wavelength non-degenerate component.

however, have disappeared in the present treatment with α, as is seen in complexes Nos. 23—27 in Table 5.

For the halogeno rhodium(III), iridium(III), and platinum(IV) complexes of the trans type, some irregularities were found in the empirical α values in Table 1. The α value for the trans isomer (in bracket in Table 1) is nearly equal to or only a little smaller than that for the cis isomer in the case of $[Rh(\underline{N})_xI_{6-x}]$-, $[Ir(\underline{N})_xI_{6-x}]$-, $[Pt(CN)_xCl_{6-x}]$-, and $[Pt(\underline{N})_xBr_{6-x}]$-type of complexes. The reason may be found in the strong spin-orbit coupling in such complexes.

References

1) R. Tsuchida, *Bull. Chem. Soc. Jpn.*, **13**, 388 (1938); Y. Shimura and R. Tsuchida, *ibid.*, **29**, 311 (1956).

2) C. K. Jørgensen, *Discuss. Faraday Soc.*, **26**, 110 (1958).

3) H. Yamatera, *Bull. Chem. Soc. Jpn.*, **31**, 95 (1958).

4) K. Konya, H. Nishikawa, and M. Shibata, *Inorg. Chem.*, **7**, 1165 (1968).

5) H. Ogino and J. C. Bailar, Jr., *Inorg. Chem.*, **17**, 1118 (1978).

6) N. Matsuoka, J. Hidaka, and Y. Shimura, *Bull. Chem. Soc. Jpn.*, **40**, 1868 (1967).

7) O. Bostrup and C. K. Jørgensen, *Acta Chem. Scand.*, **11**, 1223 (1957).

8) C. E. Schäffer and C. K. Jørgensen, K. Dan. Vidensk., Mat.-Fys. Medd., **34**, No. 13 (1965).

9) C. K. Jørgensen, "Modern Aspects of Ligand Field Theory," North-Holland (1971), pp. 347—348.

10) R. Palmans, L. Viaene, and J. D'olieslager, *Inorg. Chem.*, **23**, 1792 (1984).

11) M. Shibata, "Modern Syntheses of Cobalt(III) Complexes," Springer-Verlag (1983), p. 22.

12) I. Kinoshita, K. Kashiwabara, J. Fujita, K. Matsumoto, and S. Ooi, *Bull. Chem. Soc. Jpn.*, **54**, 2683 (1981).

13) H. Yoneda and T. Yoshizawa, *Chem. Lett.*, **1976**, 707.

14) Y. Shimura and R. Tsuchida, *Bull. Chem. Soc. Jpn.*, **29**, 311 (1956).

15) L. F. Book, K. Y. Hui, O. W. Lau, and W.-K. Li, *Z. Anorg. Chem.*, **426**, 227 (1976).

16) Y. Shimura and R. Tsuchida, *Bull. Chem. Soc. Jpn.*, **28**, 572 (1955).

17) Y. Yamamoto and Y. Shimura, *Bull. Chem. Soc. Jpn.*, **54**, 3351 (1981).

18) J. Fujita and Y. Shimura, *Bull. Chem. Soc. Jpn.*, **36**, 1281 (1963).

19) M. Nakahara and M. Mitsuya, *Bull. Chem. Soc. Jpn.*, **45**, 2209 (1972).

20) D. Rehder, *J. Organomet. Chem.*, **37**, 303 (1972).

21) H. Saito, J. Fujita, and K. Saito, *Bull. Chem. Soc. Jpn.*, **41**, 359 (1968).

22) J. L. Cihonski and R. A. Lewenson, *Inorg. Chem.*, **14**,

1717 (1975).
23) M. S. Wrighton, D. L. Morse, H. B. Gray, and D. K. Ottesen, *J. Am. Chem. Soc.*, **98**, 1111 (1976).
24) F. A. Cotton, D. R. Monchamp, R. J. M. Henry, and R. C. Young, *J. Inorg. Nucl. Chem.*, **10**, 28 (1959).
25) M. Goto, H. Nakayabu, H. Ito, H. Tsubamoto, K. Nakabayashi, Y. Kuroda, and T. Sakai, *Inorg. Chem.*, **25**, 1684 (1986).
26) T. Matsubara and P. C. Ford, *Inorg. Chem.*, **17**, 1747 (1978).
27) A. D. Allen and J. R. Stevens, *Can. J. Chem.*, **50**, 3093 (1972).
28) S. A. Johnson and F. Basolo, *Inorg. Chem.*, **1**, 925 (1962).
29) C. K. Jørgensen, *Acta Chem. Scand.*, **11**, 151 (1957).
30) W. R. Mason, *Inorg. Chem.*, **12**, 20 (1973).
31) W. D. Blanchard and W. R. Mason, *Inorg. Chim. Acta*, **28**, 159 (1978).
32) L. E. Cox and D. G. Peters, *Inorg. Chem.*, **9**, 1927 (1970).
33) P. E. Fanwick and D. S. Martin, Jr., *Inorg. Chem.*, **12**, 24 (1973).
34) V. A. Houlding, H. Mäcke, and A. W. Adamson, *Inorg. Chem.*, **20**, 4279 (1981).
35) D. A. Buckingham, I. I. Creaser, and A. M. Sargeson, *Inorg. Chem.*, **9**, 655 (1970).
36) J. Hidaka, J. Fujita, and Y. Shimura, *Bull. Chem. Soc. Jpn.*, **32**, 1317 (1959).
37) K. Yamanari and Y. Shimura, *Bull. Chem. Soc. Jpn.*, **57**, 1596 (1984).
38) T. Konno, K. Okamoto, and J. Hidaka, *Bull. Chem. Soc. Jpn.*, **57**, 3104 (1984).
39) Y. Shimura, *Bull. Chem. Soc. Jpn.*, **25**, 49 (1952); "Coordination Stereochemistry," 2nd revised edition, Baifukan (1981), p. 129.
40) R. G. Wilkins and M. J. G. Williams, "Modern Coordination Chemistry," ed by J. Lewis and R. G. Wilkins, Interscience Pub. Ltd. (1960), p. 190.
41) S. Fujinami and H. Yamatera, the 32nd National Meeting of the Chemical Society of Japan, Tokyo, April 1975, Abstr., No. 3M47; S. Fujinami, Y. Nakata, and M. Shibata, the 28th Symposium on the Coordination Chemistry, Matsuyama, Oct. 1978, Abstr., No. 3A07.

 © 1988 The Chemical Society of Japan Bull. Chem. Soc. Jpn., 61, 699—705 (1988)

Dynamic NMR as a Nondestructive Method for the Determination of Rates of Dissociation. XII. Dissociation of the Olefin in *trans*-Dichloro(4-methyl-1-pentene)(4-substituted pyridine 1-oxide)platinum(II) Complexes[1)]

Shinji Toyota and Michinori Ōki*
Department of Chemistry, Faculty of Science, The University of Tokyo, Bunkyo-ku, Tokyo 113
(Received June 30, 1987)

The rates of dissociation of the olefin in the title compounds were determined by the dynamic NMR technique by taking advantage of the line shape change due to the isopropyl-methyl protons. The rates of dissociation were independent of concentration in bromoform-*d* solutions. The free energy of activation was between 17.0 and 19.1 kcal mol^{-1} at 353 K for the compounds, of which line shapes were fully analyzed, depending upon the substituent in the pyridine ring and electron-withdrawing substituents giving low activation energy. The solvent effect was noticed on the dissociation rates: Aromatic hydrocarbons give higher rates of dissociation than halogenated hydrocarbons. Although solvents of strong affinity toward platinum(II) tend to decompose the complex, tetrahydrofuran-d_8 was found to give definitely higher rates of dissociation of the olefin in *trans*-dichloro(4-methoxycarbonylpyridine 1-oxide)(3-methyl-1-butene)platinum-(II) than bromoform-*d*, when it was used as a solvent. The mechanism of dissociation was discussed from the available data.

The dynamic NMR technique has been proved useful in investigation of bond breaking-and-forming processes as well as intramolecular dynamics.[2,3)] The bond breaking-and-forming processes are of particular interest because by the investigation of the kinetics the process provides fundamental knowledge for the understanding of dissociation reactions in a sense that the phenomenon could be observed in the absence of any foreign materials in the dynamic NMR technique.

The technique requires some molecular features. The molecule to be studied should possess a pair of diastereotopic nuclei of which magnetic sites are exchanged by dissociation-and-combination and the time scale must fall within the range suitable for the technique, 10^0—10^3 s^{-1}, although the rates are adjustable to some extent by changing temperatures of observation. If a molecule meets the requirements, it is possible to observe various dissociation processes. We have reported the dissociation of an organic halide,[4)] an organic carboxylate,[5)] ammonium salts,[6,7)] and amine ligands from organometallic compounds.[8)] The olefin–metal complex also falls in the category that can be investigated by this technique because chirality is found according to the face of the olefin to which a metal is bonded,[9)] and racemization takes place when the olefin dissociates and reforming of the bond from the other face of the olefin after rotation takes place. The point is how to find a suitable compound for the investigation by the dynamic NMR technique.

Platinum(II)–olefin complexes are well-known and the racemization of their optically active members has been studied by the classical methods. They are usually stable enough to be isolated as chemical entities to mean that the complexes should be in general destabilized for the investigation by the dynamic NMR technique because the time scale of NMR spectroscopy is much faster than the classical laboratory time scale.

Platinum(II)–olefin complexes are known to exchange the olefin in the presence of the excess of an olefin. Potassium trichloro(ethylene)platinate(II) is known to undergo the olefin exchange in the presence of ethylene faster than the NMR time scale even at low temperatures.[10)] The ethylene ligand can also be exchanged by other olefins if the olefin is present.[11)] There is wealth of information on the exchange of olefins in the platinum(II)–olefin complexes.[12–17)]

In the absence of the excess of olefin, the dissociation of the olefin in platinum(II)–olefin complexes seems to be very slow. There are only a few reports that have dealt with the dissociation of the complexes in the absence of an olefin. Frits and Sellmann reported that the coupling of the olefin protons with ^{195}Pt disappeared on dissolution of dichloro(ethylene)(4-substituted pyridine)platinum(II) complexes in acetone, if the 4-substituent in the pyridine ring was electron-withdrawing.[18)] Kaplan et al. generalized the loss of coupling of olefinic protons with the platinum nucleus in *trans*-dichloro(olefin)-(substituted pyridine)platinum(II) complexes in acetone at ambient temperature for the compounds that carry an electron-withdrawing substituent.[19)] The latter authors suggested the role of pyridine base which was present in a minute amount in the system in the olefin exchange.[20)] However, they did not report the kinetic data for the exchange.

There are two strategies to facilitate racemization of the platinum(II)–olefin complexes, as judged from the literatures. One is to use a less basic base to the trans position of an olefin: The strong base stabilizes the olefin complex by the trans influence.[21)] And the other is to use a solvent of strong affinity towards the

platinum(II) ion. On the basis of NMR point of view, it is also important to render the chemical shift difference of the two exchanging protons small in order that we observe the exchange process at low temperatures.

We started from *trans*-dichloro(olefin)(pyridine)-platinum(II) where the olefin was 3-methyl-1-butene that possesses the potential diastereotopic protons. It was not possible to observe the change in line shapes of the signals due to the diastereotopic protons in the olefin in nonpolar solvents and the complex decomposed in polar solvents. In order to facilitate the racemization, pyridine 1-oxide was introduced to the trans position of 3-methyl-1-butene. Although this compound showed a sign of racemization, namely line-broadening of the signals due to the isopropyl-methyl protons, it was not stable enough to survive the measurements at 100 °C or higher temperatures that were needed for the line shape analyses: The situation was improved relative to the pyridine case but was still not good enough for the dynamic NMR work. Finally we introduced 4-methyl-1-pentene as an olefin and 4-methoxycarbonylpyridine 1-oxide as a base in the trans position to the olefin to find that the complex was suitable for the NMR work. This paper reports the results of such investigations and discusses the substituent effects in the pyridine ring and the solvent effects on the rates of racemization as well as the mechanism of dissociation.

Results

The syntheses of the complexes used in this study were carried out in the following way. Potassium trichloro(ethylene)platinate(II)[22] was dimerized by acidification[23] and the dimer **1** was treated with 4-methyl-1-pentene to replace the ethylene ligand. The resulted olefin complex **2** was then treated with 4-substituted pyridine 1-oxide to give the desired compound **3**.[24]

The kinetic parameters obtained as the results of the line shape analysis are given in Tables 1—3. The feature of the data is that the electron-donating substituent in the 4-position of the pyridine ring reduces the rates of racemization considerably and we found that only line broadening to a small extent for the methyl and unsubstituted compounds. The plot of the free energy of activation for racemization at 353 K against pK_a values of the pyridine 1-oxide[25] gave a straight line, the correlation coefficient being

Table 1. The Effect of Concentration on the Kinetic Parameters for Dissociation of the Olefin in *trans*-Dichloro(4-methyl-1-pentene)(4-methoxycarbonyl-pyridine 1-oxide)platinum(II) in Bromoform-*d*

Concentration / 10^{-2} mol L^{-1}	$\Delta H^{\ddagger}$/kcal mol^{-1} [a]	$\Delta S^{\ddagger}$/cal mol^{-1} K^{-1} [a]	$\Delta G^{\ddagger}_{353}$/kcal mol^{-1} [a]	r [b]
1.8	17.4±0.6	−3.2±1.9	18.5	0.9996
3.4	17.6±0.5	−2.7±1.3	18.5	0.9998
5.0	17.2±0.4	−3.6±1.1	18.5	0.9998

a) 1 cal=4.184 J. b) Correlation coefficient.

Table 2. Substituent Effects on the Kinetic Parameters for Dissociation of the Olefin Ligand in *trans*-Dichloro(4-methyl-1-pentene)(4-substituted pyridine 1-oxide)platinum(II) in Bromoform-*d* at ca. 40 mmol L^{-1}

Substituent	$\Delta H^{\ddagger}$/kcal mol^{-1}	$\Delta S^{\ddagger}$/cal mol^{-1} K^{-1}	$\Delta G^{\ddagger}_{353}$/kcal mol^{-1}	r [b]
CH_3			20.4[b]	
H			19.6	
Cl	18.1±0.6	−2.8±1.9	19.1	0.9996
CH_3OCO	17.6±0.5	−2.7±1.3	18.5	0.9998
NO_2	13.8±0.7	−9.0±2.1	17.0	0.9994[c]

a) Correlation coefficient. b) At 363 K. c) 14 mmol L^{-1} in chloroform-*d*.

Table 3. Solvent Effects on the Kinetic Parameters for Dissociation of the Olefin Ligand in *trans*-Dichloro(4-methyl-1-pentene)(4-methoxycarbonylpyridine 1-oxide)platinum(II)

Solvent	$\Delta H^{\ddagger}$/kcal mol^{-1}	$\Delta S^{\ddagger}$/cal mol^{-1} K^{-1}	$\Delta G^{\ddagger}_{323}$/kcal mol^{-1}	r [a]
$CDBr_3$	17.6±0.5	−2.7±1.3	18.4	0.9998
$C_2D_2Cl_4$[b]	19.0±0.9	2.7±2.7	18.2	0.9994
C_6D_6	16.3±0.5	−3.8±1.4	17.5	0.9998
$C_6D_5CD_3$	16.7±0.3	−3.1±1.7	17.7	0.9997

a) Correlation coefficient. b) 1,1,2,2-Tetrachloroethane-d_2.

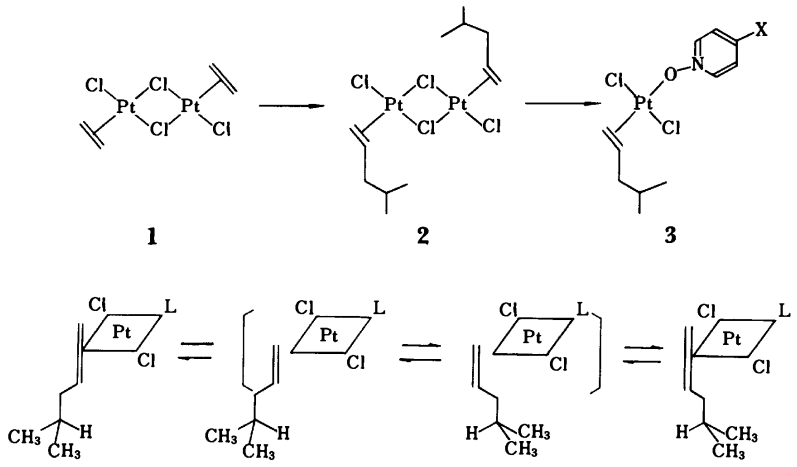

L=pyridine 1-oxide

Scheme 1.

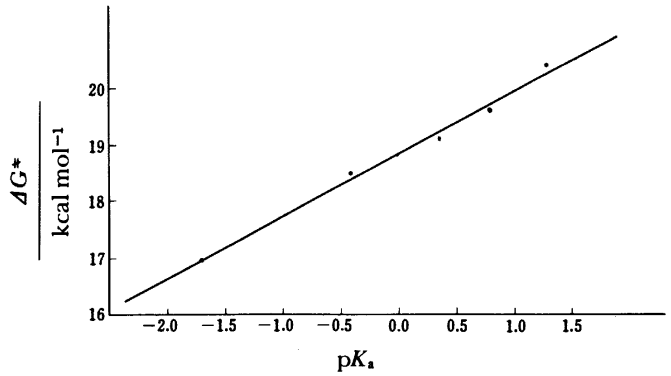

Fig. 1. Relationship between pK_a's of 4-substituted pyridine 1-oxide and free energies of activation for the dissociation of the olefin in *trans*-dichloro(4-methyl-1-pentene)(4-substituted pyridine 1-oxide)-platinum(II) at 353 K.

0.995, when ΔG^* for the methyl compound at 363 K is included (Fig. 1). We believe the inclusion of the latter data is permissible because the entropy of activation is small for other compounds in the series examined, rendering the change in the free energy of activation from 353 K to 363 K small.

Discussion

The results in Table 1 clearly indicate that the rates of racemization are not affected by the concentration of the substrate. This will exclude the mechanisms that involve the catalytic action of the free pyridine oxide that is present in a minute amount, though this mechanism was suggested by Kaplan et al.[20] Then we can assume the process be unimolecular, although solvent assistance in the dissociation is not ruled out. Then over simplified mechanism of the racemization can be written as in Scheme 1, where the species shown in the brackets are the intermediates that are not observed. The results in Table 2 together with the fact that the complex that contains pyridine to the trans position of the olefin ligand shows much slower rates of racemization than those listed in Table 2 are examples of typical trans effects.[26]

Since the role of solvent molecules is important in racemization of the olefin complexes, it will be of interest to see the solvent effect on the rates of racemization. Table 3 clearly indicates that, whereas halogenated hydrocarbons, $CDBr_3$ and $C_2D_2Cl_4$, give about the same free energy of activation, the aromatic solvents do again about the same free energy of activation, the aromatic solvents giving definitely larger rates of dissociation of the olefin. It is interesting to note that the rates of dissociation are not dependent on the polarity of the solvent molecules. Rather they seem to indicate that the affinity of the solvent molecule towards platinum(II) is important.

For further understanding we have changed solvents to see the effects on the rates of dissociation. However, the complexes tend to decompose in solvents such as dimethyl-d_6 sulfoxide, nitromethane-d_3, acetonitrile-d_3, methanol-d_4, and *N*,*N*-dimethylformamide-d_7. In tetrahydrofuran-d_8, the complex also decomposed at high temperatures. However, *trans*-dichloro(4-methoxycarbonylpyridine 1-oxide)(3-methyl-1-butene)platinum(II) was found to survive to afford kinetic data for dissociation at one point of temperature: 16.4 kcal mol^{-1} at 300 K.[27] Comparing the results with the fact that dissociation of the olefin was not detectable in the same complex in bromoform-*d* at 330 K, we conclude that solvent molecules coordinate to the platinum ion before ligand dissociation.

The entropy of activation should reflect the mechanism, dissociative or associative. Although it is known that the entropy of activation is large negative if a solvent molecule participate in an associative reaction,[17] the entropy of activation shown in Tables 1—3 are all close to zero except one case which is still closer to zero than -10 cal mol^{-1} K^{-1}. Recently, the

entropy of activation of dissociative reactions in platinum complexes has been reported to be small positive.[28,29] This quantity of entropy of activation agrees with those obtained for extrusion of a particle from an organic compound.[30] Thus interpretation of these results is difficult in a straightforward manner. It is also true that the entropy of activation should be discussed with care because some dissociative reactions are known to give negative entropy of activation[31] and associative reactions give positive entropy of activation.[16] It might even be the quality of kinetic data that give confusing results in entropy of activation or the randomly dispersing data of the entropy of activation might reflect factors that have not been considered. Therefore, we should like to defer further discussion on the quantity of entropy of activation except mentioning on one point. The participation of the solvent molecule in dissociation of the olefin ligand is apparent from the data given above. It is possible that in these cases of square planar complexes, to which a solvent molecule loosely associates even at the ground state, the entropy of activation could be near zero even in associative reactions, because acquiring freedom of motion by the olefin ligand in the transition state could be important. Further study on this point is awaited.

Admitting the participation of the solvent molecule in the dissociation of the olefin ligand, we can write two mechanisms. One is the process which proceeds via substitution of the solvent for the pyridine oxide ligand followed by the dissociation of the olefin ligand (Eq. 1). The other is the process in which the solvent assists directly the dissociation of the olefin without affecting the pyridine oxide ligand (Eq. 2).

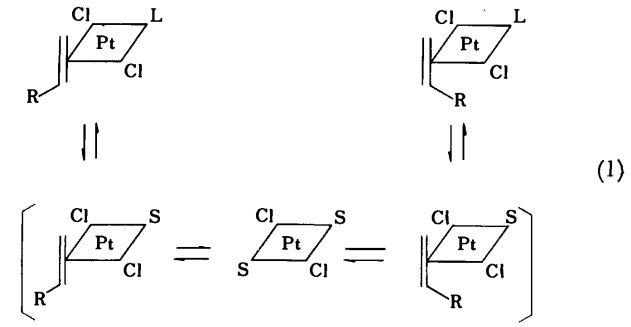

(1)

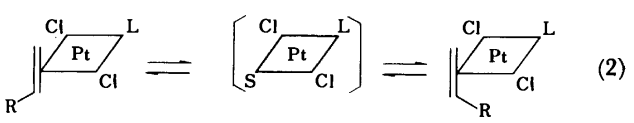

(2)

If the first possibility is the case that we observe, the rate-determining step must be the dissociation of the pyridine oxide ligand, because, if the dissociation of the olefin were rate-determining, we could not explain the substituent effects seen in the dissociation of the olefin. If the second case is the one we observe, we may have to assume that, although the pyridine oxide ligand dissociates faster than the olefin ligand, there are species that permit dissociation of the olefin ligand, without affecting the pyridine oxide ligand.

It is difficult to determine which is the real case at present but we are inclined to conclude that the second is more likely to be the case for the following reasons. Firstly, although it is still to be confirmed, less basic ligands in the platinum complexes will dissociate more easily than the more basic. Since pyridine 1-oxides are weaker bases than pyridines and the dissociation of the pyridine base from platinum(II) complexes are known,[18-20] it is natural to assume that pyridine 1-oxides will dissociate much more easily than monosubstituted olefins. Therefore, that the rate-determining step in the dissociation of the olefin is the dissociation of the pyridine oxide ligand is less likely. Secondly, although more of the molecules are in the process of dissociation of the pyridine oxide ligand than those in the process of the dissociation of the olefin, we do not observe the dissociated or solvent-ligated molecules to mean that the concentration of the complex is practically the same during the process observed by the dynamic NMR spectroscopy. Therefore, the slow dissociation of the olefin and the fast dissociation of the pyridine oxide ligand do not hamper the Eq. 2 for being the true mechanism of the reaction.

Finally we should like to mention on another possibility of the racemization mechanism which had been proposed in a literature.[32] That is, a platinum-olefin complex would racemize via a sigma-complex. In this mechanism, the process has to pass a transition state or an intermediate which has charge separation. Should this situation take place, it is expected that solvents that stabilize ionic species should enhance the reaction rates. In spite of this expectation, aromatic hydrocarbons show lower barrier to the transformation than halogenated hydrocarbons, although every solvent parameter suggests that the latters should more stabilize ionic species than the formers.[33] Thus the possibility of intervention of a sigma-bonded intermediate (or transition state) is less likely. We favor the solvent assisted mechanism over the sigma-complex mechanism.

Experimental

Dynamic NMR Measurements and Analyses of the Data. The ^{1}H NMR spectra were obtained on a JEOL GX-270 spectrometer which operates at 270 MHz. Samples were dissolved to make up ca. 50 mmol L^{-1} solutions in appropriate solvents except for the determination of the effects of concentration (Table 1) on the rates and for 4-nitropyridine 1-oxide complex which was sparingly soluble in $CDCl_3$. In the latter case, the concentration was

14 mmol L^{-1}. Temperature was measured directly by a thermometer. The chemical shift differences of the signals due to isopropyl-methyl protons drifted when temperature was varied. The drift was measured at several points in the slow exchange limit and the linear relation between the temperature and the chemical shift difference was obtained as shown in Table 4. The chemical shift difference at the temperature of simulation was obtained by extrapolation with the use of the equations. The coupling constants between the methyl protons and the methine proton were independent of temperature (6.6—6.8 Hz), though small differences were noted from condition to condition. T_2's were determined by considering the line shapes in the slow exchange limit and were used throughout the temperature range examined. They were 0.08—0.17 s. The spectra were analyzed as the exchange $A_3B_3X \rightleftharpoons B_3A_3X$ with the use of DNMR 3 program.[34] The rate constants thus obtained were doubled to obtain rates of dissociation in order to accommodate the fact that the rates of racemization is twice of those of dissociation. The rate constants of dissociation are summarized in Table 5.

For the calculation of the line shapes of the complexes with 4-methyl and unsubstituted pyridine 1-oxide, the observed chemical shift difference, 10.7 and 11.1 Hz, respectively, were directly used. T_2's were 0.12 and 0.14 s, respectively, for the former and the latter. For the complex with 3-methyl-1-butene, the chemical shift difference, T_2, and rate constant at 300 K were 104.1 Hz, 0.10 s, and 6.7 s^{-1}, respectively.

Syntheses. Pyridine 1-oxide, 4-nitropyridine 1-oxide, 3-methyl-1-butene, and 4-methyl-1-pentene were available from Tokyo Kasei, Co. 4-Methoxycarbonylpyridine 1-oxide[35] and 4-chloropyridine 1-oxide[36] were prepared as were reported in literatures. The following is the typical method of synthesis of the complexes. The yields were 65—88%.

***trans*-Dichloro(4-methyl-1-pentene)(pyridine 1-oxide)platinum(II).** To a solution of 0.10 g (0.17 mmol) of tetrachlorobis(ethylene)diplatinum(II)[23] in 5 mL of dichloromethane was added 1 mL of 4-methyl-1-pentene and the whole was stirred for several minutes at room temperature. The volatile materials were evaporated and the residue was recrystallized from hexane to give 0.11 g of tetrachlorobis(4-methyl-1-pentene)diplatinum(II) as orange crystals. The crystals were dissolved in 5 mL of dichloromethane and stirred with 30 mg (0.32 mmol) of pyridine 1-oxide for 10 min. Evaporation of the solvent followed by recrystallization of the residue from dichloromethane–hexane afforded 89 mg (65%) of pale yellow crystals.

The melting point of this compound and analytical data are given in Table 6 together with those for other *trans*-dichloro(4-methyl-1-pentene)(4-substituted pyridine 1-oxide)-platinum(II) complexes. ^1H NMR data are given in Table 7.

trans-Dichloro(4-methoxycarbonylpyridine 1-oxide)(3-methyl-1-butene)platinum(II), mp 121—122 °C (decomp), was similarly prepared as described for the preparation of the 4-methyl-1-pentene complexes. Found: C, 29.36; H, 3.49; N, 2.73%. Calcd for $C_{12}H_{17}Cl_2NO_3Pt$: C, 29.46; H, 3.50;

Table 4. Temperature Dependence of the Chemical Shift Differences between the Diastereotopic Pairs of Methyls in *trans*-Dichloro(4-methyl-1-pentene)(4-substituted pyridine 1-oxide)platinum(II)

Substituent	Solvent	Correlation[a]	r[b]
Cl	$CDBr_3$	$-0.05956t+16.15$	0.9929
CH_3OCO[c]	$CDBr_3$	$-0.06413t+16.35$	0.9968
CH_3OCO[d]	$CDBr_3$	$-0.07172t+16.69$	0.9995
CH_3OCO[e]	$CDBr_3$	$-0.06245t+16.24$	0.9982
CH_3OCO	$C_2D_2Cl_4$[f]	$-0.07468t+16.38$	0.9969
CH_3OCO	C_6D_6	$-0.05901t+10.11$	0.9994
CH_3OCO	$C_6D_5CD_3$	$-0.05832t+9.33$	0.9972
NO_2	$CDCl_3$	$-0.07857t+14.98$	0.9930

a) The correlation is given by $\Delta\nu = At + B$, where t is temperature in °C. b) Correlation coefficient. c) Concentration 34 mmol L^{-1}. d) Concentration 18 mmol L^{-1}. e) Concentration 50 mmol L^{-1}. f) 1,1,2,2-Tetrachloroethane-d_2.

Table 5. The Rates of Dissociation of the Olefin Ligand in *trans*-Dichloro(4-methyl-1-pentene)(4-substituted pyridine 1-oxide)platinum(II)

Substituent	Solvent	k/s^{-1}(temperature/°C)
CH_3	$CDBr_3$	4.2 (90.4)
H	$CDBr_3$	5.8 (80.4)
Cl	$CDBr_3$	4.0 (67.4), 5.4 (71.0), 7.0 (74.7), 9.6 (78.4), 13.0 (82.3), 17.0 (86.2)
CH_3OCO[a]	$CDBr_3$	6.6 (62.6), 8.6 (65.7), 10.8 (68.6), 13.6 (71.6), 17.0 (74.5), 21.2 (77.6)
CH_3OCO[b]	$CDBr_3$	6.4 (62.4), 8.6 (65.5), 10.6 (68.5), 13.4 (71.5), 16.8 (74.5), 20.6 (77.5)
CH_3OCO[c]	$CDBr_3$	7.0 (62.5), 8.8 (65.4), 11.2 (68.5), 13.8 (71.4), 17.4 (74.5), 22.0 (77.4)
CH_3OCO	$C_2D_2Cl_4$[d]	6.2 (56.5), 8.6 (59.7), 11.0 (62.7), 14.4 (65.6), 18.2 (68.4), 23.2 (71.6)
CH_3OCO	C_6D_6	6.4 (45.0), 8.2 (48.0), 10.6 (50.9), 14.0 (54.6), 17.2 (57.3), 22.4 (60.5)
CH_3OCO	$C_6D_5CD_3$	6.3 (48.9), 8.6 (52.5), 11.2 (55.5), 13.8 (58.3), 17.6 (61.5), 22.0 (64.4)
NO_2	$CDCl_3$	6.4 (28.1), 8.8 (32.3), 12.0 (36.0), 14.8 (38.6), 18.2 (41.8), 22.0 (44.5)

a) Concentration 34 mmol L^{-1}. b) Concentration 18 mmol L^{-1}. c) Concentration 50 mmol L^{-1}. d) 1,1,2,2-Tetrachloroethane-d_2.

Table 6. Melting Points and Analytical Data of *trans*-Dichloro(4-methyl-1-pentene)(4-substituted pyridine 1-oxide)platinum(II)

Substituent	Found/%			Calcd/%			Mp[a]
	C	H	N	C	H	N	θ_m/°C
CH_3	31.18	4.16	3.05	31.38	4.17	3.05	131—135
H	29.43	4.00	3.13	29.67	3.85	3.15	119—123
Cl	27.27	3.14	2.90	27.54	3.36	2.92	146—148
CH_3OCO	30.78	3.77	2.81	31.02	3.81	2.78	128—129
NO_2	26.84	3.20	5.56	26.95	3.29	5.71	153—154

a) With decomposition.

Table 7. ^{1}H NMR data (δ) of *trans*-Dichloro(4-methyl-1-pentene)(4-substituted pyridine 1-oxide)platinum(II) in $CDCl_3$ at 270 MHz at 22 °C

Substituent	Signal due to olefin					Signal due to pyridine		
	methyl[a]	methine	methylene	terminal CH_2[b]	α-H[b]	3,5-H	2,6-H	others
CH_3	0.96 (d) 1.01 (d)	1.95 (m)	1.52 (m) 2.19 (m)	4.18—4.29 (m)	5.00 (m)	7.47 (d) (J=6.7 Hz)	8.46 (d)	2.67 (s) (3H)
H	0.98 (d) 1.03 (d)	1.99 (m)	1.55 (m) 2.24 (m)	4.27—4.36 (m)	5.14 (m)	7.66 (t) (J=6.9 Hz)	8.59 (d)	7.89 (t) (1H)
Cl	0.97 (d) 1.03 (d)	1.97 (m)	1.52 (m) 2.19 (m)	4.26—4.38 (m)	5.07 (m)	7.71 (d) (J=7.0 Hz)	8.60 (d)	
CH_3OCO	0.99 (d) 1.04 (d)	2.00 (m)	1.53 (m) 2.22 (m)	4.33—4.44 (m)	5.21 (m)	8.17 (d) (J=7.0 Hz)	8.64 (d)	4.02 (s) (3H)
NO_2	1.01 (d) 1.07 (d)	2.07 (m)	1.47 (m) 2.22 (m)	4.40—4.68 (m)	5.41 (m)	8.23 (d) (J=7.5 Hz)	8.50 (d)	

a) The coupling constants were all 6.6 Hz except for the methyl compound (6.5 Hz). b) The coupling with ^{195}Pt was observed.

N, 2.86%. ^{1}H NMR ($CDCl_3$) δ=1.13 (3H, d, J=6.8 Hz), 1.55 (3H, d, J=6.4 Hz), 2.18 (1H, m), 4.02 (3H, s), 4.28—4.35 (2H, m), 5.01 (1H, m), 8.17 and 8.63 (4H, ABq, J=7.0 Hz).

This work was supported by a Grant-in-Aid for Fundamental Scientific Research (No. 61134043) of the Ministry of Education, Science and Culture.

References

1) For Part XI of this series, see the preliminary note of this work, S. Toyota and M. Ōki, *Chem. Lett.*, **1987**, 199.
2) "Dynamic Nuclear Magnetic Resonance Spectroscopy," ed by L. M. Jackman and F. A. Cotton, Academic Press, New York (1975).
3) M. Ōki, "Applications of Dynamic NMR Spectroscopy to Organic Chemistry," VCH Publishers, Deerfield Beach (1985).
4) A. Shimizu, Y. Sakamaki, K. Azuma, H. Kihara, N. Nakamura, and M. Ōki, *Bull. Chem. Soc. Jpn.*, **54**, 2774 (1981).
5) M. Ōki and S. Ito, *Chem. Lett.*, **1984**, 985.
6) M. Ōki, M. Ohira, Y. Yoshioka, T. Morita, H. Kihara, and N. Nakamura, *Bull. Chem. Soc. Jpn.*, **57**, 2224 (1984).
7) T. Morita and M. Ōki, *Bull. Chem. Soc. Jpn.*, **59**, 3605 (1986).
8) M. Ōki and M. Ohira, *Bull. Chem. Soc. Jpn.*, **57**, 3117 (1984).
9) G. Paiaro, *Organomet. Chem. Rev.*, **A6**, 319 (1970).
10) R. Cramer, *Inorg. Chem.*, **4**, 445 (1965).
11) J. S. Anderson, *J. Chem. Soc.*, **1936**, 1042.
12) J. R. Joy and M. Orchin, *J. Am. Chem. Soc.*, **81**, 305 (1959).
13) G. Paiaro and A. Panunzi, *Ric. Sci.*, **34**, 601 (1964).
14) S. Hupp and G. Dahlgren, *Inorg. Chem.*, **15**, 2349 (1976).
15) G. Guillot-Edelheit and J. C. Chottard, *J. Chem. Soc., Dalton Trans.*, **1984**, 169.
16) S. Miya, K. Kashiwabara, and K. Saito, *Inorg. Chem.*, **19**, 98 (1980).
17) K. Konya, J. Fujita, H. Kida, and K. Saito, *Bull. Chem. Soc. Jpn.*, **45**, 2161 (1972).
18) H. P. Fritz and D. Sellmann, *Z. Naturforsch.*, **22b**, 610 (1967).
19) P. D. Kaplan, P. Schmidt, and M. Orchin, *J. Am. Chem. Soc.*, **89**, 4537 (1967).
20) P. D. Kaplan, P. Schmidt, A. Brause, and M. Orchin, *J. Am. Chem. Soc.*, **91**, 85 (1969).
21) A. Pidcock, R. E. Richards, and I. M. Venanzi, *J. Chem. Soc. A*, **1966**, 1707: T. G. Appleton, H. C. Clark, and L. E. Manzer, *Coord. Chem. Rev.*, **10**, 335 (1973).
22) P. B. Chock, J. Halpern, and F. E. Paulik, *Inorg. Synth.*, **14**, 90 (1973).
23) J. Chatt and M. L. Searle, *Inorg. Synth.*, **5**, 210 (1957).
24) P. Schmidt and M. Orchin, *Inorg. Chem.*, **6**, 1260 (1967).

25) S. I. Shupack and M. Orchin, *J. Am. Chem. Soc.*, **85**, 902 (1963).
26) F. R. Hartley, *Chem. Soc. Rev.*, **2**, 163 (1973).
27) The line shape change at various temperatures was observed at the temperature range of 20—46 °C. However the rate constants thus obtained gave a line with a slight curvature in the Eyring plot, probably because of decomposition at high temperatures. Thus we report the free energy of activation at 300 K only.
28) S. Lanza, D. Minniti, P. Moore, J. Sachinidis, R. Romeo, and M. L. Tobe, *Inorg. Chem.*, **23**, 4428 (1984).
29) G. Alibrandi, G. Bruno, S. Lanza, D. Minniti, R. Romeo, and M. L. Tobe, *Inorg. Chem.*, **26**, 185 (1987).
30) R. A. Y. Jones, "Physical and Mechanistic Organic Chemistry," 2nd ed, Cambridge University Press, Cambridge (1984), p. 249.
31) R. Romeo, D. Minniti, and M. Trozzi, *Inorg. Chem.*, **15**, 1134 (1976).
32) P. D. Kaplan, P. Schmidt, and M. Orchin, *J. Am. Chem. Soc.*, **90**, 4175 (1968).
33) C. Reichardt, "Solvent Effects in Organic Chemistry," Verlag Chemie, Weinheim (1979).
34) G. Binsch, *Top. Stereochem.*, **3**, 97 (1968).
35) A. R. Katritsky, *J. Chem. Soc.*, **1956**, 2404.
36) E. Ochiai, *J. Org. Chem.*, **18**, 534 (1953).

Sulfur Inversion in and Molecular Structure of *meso*-3,4-Diethyl-3,4-dimethyl-1-phenylthiolanium Tetrafluoroborate

Michinori ŌKI,* Yasuhisa YAMADA, and Shigeru MURATA†
Department of Chemistry, Faculty of Science, The University of Tokyo, Bunkyo-ku, Tokyo 113
†Institute for Molecular Science, Myodaiji, Okazaki 444
(Received June 30, 1987)

Kinetics of sulfur inversion in the title compound was studied by the classical method to afford the following kinetic parameters for the process (1*r*,3*R*,4*S*)→(1*s*,3*R*,4*S*): $\Delta H^{\ddagger}$ 25.7±0.3 kcal mol^{-1}, $\Delta S^{\ddagger}$ −2.2± 0.8 cal mol^{-1} K^{-1}. X-Ray crystallography of one isomer (1*r*,3*R*,4*S*) in which the methyl groups are cis to the phenyl group shows some abnormal bond lengths and conformations due to the steric congestion in the 3,4-region of the thiolane ring. The anomalies in the structure are pointed out by comparing the structure with those closely related and the correlation of them with the barrier height to inversion is discussed.

Although racemization of optically active sulfonium ions attracted interests of many investigators[1] since the discovery of fairly facile racemization of this class of compounds by Darwish et al.[2] through sulfur inversion, the reports have mainly concerned with racemization at one point of temperature and the literatures which report enthalpy and entropy of activation are very few.[3] During the course of work on dissociation of molecular species by the dynamic NMR technique, we have come across an idea that entropies of activation can be used as decisive information in diagnosing the mechanism of topomerization,[4] and have felt the necessity of providing the kinetic data of sulfur inversion at various temperatures.

Our first aim of the investigation was to design a molecule that suits to both classical and NMR study of the kinetics of sulfur inversion. In principle, any barrier to a transformation may be reduced by either stabilization of the transition state for the transformation or the destabilization of the ground state. Since normal sulfonium salts racemize with a barrier of ca. 26—35 kcal mol^{-1},[1] it is necessary to design a molecule that possesses a lower barrier to sulfur inversion than usual, if we wish to investigate the inversion by the dynamic NMR technique. For the stabilization of the transition state for inversion, it seemed that we could do little: Although introduction of a phenyl group into the sulfonium moiety is known to cause reduction in the inversion barrier,[5] this may not be ascribed to the stabilization of the transition state, because the substituent constant (σ) of a methylthio group is close to zero,[6] and this is believed to be caused by poor 2p–3p conjugation relative to the 2p–2p case.[7] Thus we decided to work on destabilization of the ground state by introducing the steric effects. This paper reports the results of such investigations: Although the barrier was not reduced large enough to be amenable to the dynamic NMR investigation, it was indeed reduced by destabilizing the ground state by steric congestion, that is discussed from the molecular structure obtained by X-ray crystallography, even for a cyclic compound.

We decided to use a sulfonium salt which could be derived from a cyclic sulfide for two reasons. The first is the difficulty of selecting suitable alkyl groups in the open chains. The mechanism of racemization of sulfonium compounds is known to be three fold:[8] Simple sulfur inversion, sulfur inversion after dissociation when a stable carbocation is formed, and sulfur inversion with intermediates of a thioether and a product which is derived by the attak of the nucleophile on one of the alkyl groups attached to the sulfonium-sulfur. Since we are concerned in the entropy of activation of pure sulfur-inversion, any possibility of the dissociation mechanism must be avoided. There is a report that claims that even *t*-butylethylmethylsulfonium ion racemizes by a dissociation mechanism from a study of volume of activation.[9] We preferred therefore to use primary alkyl groups or aryl groups where possible in the sulfonium salt that gives large rates of inversion. This type of molecular design is not possible in the noncyclic compounds, because the bulky groups which are not directly bonded to the sulfonium-sulfur will avoid each other by taking a suitable conformation. The second is to use this restriction of the freedom of taking conformations in the cyclic compounds. Even though a sulfur atom may be bonded to two primary alkyl groups in a cyclic sulfide, it is possible to give large steric congestion by introducing substituents to the beta or farther positions relative to the sulfur.

A literature reports that compounds **1** and **2** change their optical activity with rate constants, 1.08×10^{-4} and 0.81×10^{-4} s^{-1}, respectively at 100 °C in acetic acid.[10] If we could add another pair of *gem*-dimethyl groups in another beta-position relative to the sulfur, there could be a low barrier to inversion of sulfur. Because of the ease of syntheses, we selected the five-membered sulfide as a target molecule, though the 5-membered ring system could give higher barrier to inversion due to the small bond angle in the planar structure than the 6-membered.

1 2

2,2,3,3-Tetramethyl-1,4-butanediol (**3a**) had been known.[11] This compound was treated with *p*-toluenesulfonyl chloride in the presence of pyridine to afford the desired product, 3,3,4,4-tetramethylthiolane (**4a**). The thiolane was converted to 1,3,3,4,4-pentamethylthiolanium salts (**5a**): The iodide decomposed very easily because of the nucleophilic attack of the iodide ion, the tosylate also decomposed at above 100 °C, and the trifluoromethanesulfonate survived heating at above 150 °C. However, these compounds did not show evidence that the sulfur-inversion was taking place on the NMR time scale under the conditions of heating mentioned above. Although we introduced a phenyl group to the sulfur atom of the thiolane in a hope that **6a** should further lower the barrier to inversion, that trial did not work as expected. No change in the NMR line shapes was observed at 200 °C at 60 MHz.

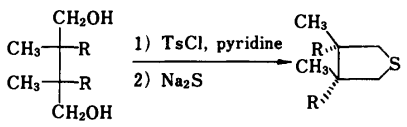

3 a : R=CH_3 b : R=C_2H_5 4

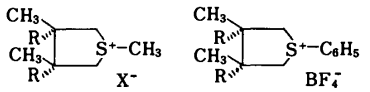

5 6

At this point we turned our attention to the synthesis of other compounds that might fit to the classical equilibration and decided to synthesize derivatives of *meso*-3,4-diethyl-3,4-dimethylthiolane (**4b**). The syntheses could be carried out analogously with the tetramethyl compound, although the corresponding diol **3b** was unknown. Methylation of the thiolane **4b** with methyl trifluoromethanesulfonate afforded a mixture of stereoisomers of **5b** (X=CF_3SO_3) which could not be separated, whereas phenylation of **4b** with diphenyliodonium tetrafluoroborate in the presence of copper(II) benzoate afforded a mixture of stereoisomers of **6b** which could give one pure isomer by recrystallization from ethanol. The stereochemistry of the recrystallized isomer was expected to be (1*r*,3*R*,4*S*)-**6b** from the kinetic consideration, because this isomer was the major product as well as because this form was the preferred of the two at equilibrium. However, it was not possible to determine the stereochemistry unambiguously by the chemical means. That the stereochemistry of this product is really 1*r*,3*R*,4*S* was established by X-ray crystallography.

The isomerization of **6b** in chloroform-*d* solutions was followed by ^{1}H NMR technique, using the signals due to 2,5-methylene protons, which show completely separated AB signals at 270 MHz for the two isomers. The rate constants thus obtained at 5 temperatures are listed in Table 1. From these results, the following activation parameters were obtained: $\Delta H^{\ddagger}$ 25.7±0.3 kcal mol^{-1} (1 cal=4.184 J), $\Delta S^{\ddagger}$ −2.2±0.8 cal mol^{-1} K^{-1}. The feature of the kinetic parameters is the near-zero entropy of activation and confirms that, if pure sulfur-inversion takes place, the entropy of activation is close to zero as is described in the literature.[3] This result is reasonable in that during the inversion of sulfur net charge does not change nor a new particle is formed.

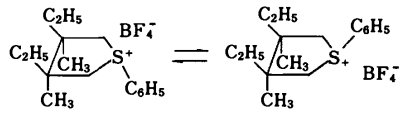

(1*r*,3*R*,4*S*)-**6b** (1*s*,3*R*,4*S*)-**6b**

That we do not observe other reactions but real inversion of sulfur was proved by enriching the other isomer: the solution obtained by the equilibration of **6b**, that contained the product and the starting material in ca. 3:4 ratio was concentrated and fractionally recrystallized from ethanol. It was possible to enrich the product to 6:1 purity. Satisfactory elementary analyses of the enriched product and expected ^{1}H NMR spectra support the structure of the isomer. Furthermore, the product, when heated in chloroform-*d*, afforded the identical mixture of the isomers of **6b**, which was obtained by heating the original isomer.

Table 1. Rate Constants of Sulfur-Inversion in *meso*-3,4-Diethyl-3,4-dimethylthiolanium Tetrafluoroborate in Chloroform-*d*

Temp/°C	$k/10^{-5}$ s^{-1} (1*r*,3*R*,4*S*)→(1*s*,3*R*,4*S*)	*K* (1*s*,3*R*,4*S*)/(1*r*,3*R*,4*S*)
60.3	3.42±0.03	0.76
65.3	6.14±0.06	0.74
70.3	10.8 ±0.1	0.74
75.3	18.8 ±0.1	0.75
80.3	32.6 ±0.1	0.77

Table 2. Atomic Positional Parameters ($\times 10^4$) with Estimated Deviations in Parentheses and Equivalent Isotropic Thermal Parameters of (1*r*,3*R*,4*S*)-3,4-Diethyl-3,4-dimethyl-1-phenylthiolanium Tetrafluoroborate

Atom	*x*	*y*	*z*	B_{eq}[a]	Atom	*x*	*y*	*z*	B_{eq}[a]
S	−2847(1)	629(1)	−3469(1)	3.6	$C_{3'}$	−207(6)	4134(5)	−2326(6)	5.2
C_2	−3571(4)	−380(5)	−1635(5)	3.7	$C_{4'}$	1005(5)	4511(5)	−3093(6)	5.2
C_3	−3156(4)	−1783(5)	−1036(5)	3.4	$C_{5'}$	1029(5)	3670(5)	−3934(6)	5.1
C_4	−3096(4)	−2214(5)	−2455(5)	3.4	$C_{6'}$	−91(5)	2486(5)	−4009(5)	4.7
C_5	−2174(4)	−794(5)	−3523(5)	3.9	B	−2108(6)	1388(7)	−7793(7)	4.9
C_{3a}	−1674(5)	−1422(6)	−243(6)	4.9	F_1*	−2908(5)	1135(6)	−8981(5)	9.9
C_{3b}	−4232(5)	−2958(5)	49(5)	4.5	F_2*	−1288(5)	505(6)	−7309(6)	10.4
$C_{3b'}$	−4404(6)	2606(6)	1411(6)	6.1	F_3*	−2896(6)	1293(9)	−6812(5)	14.7
C_{4a}	−2344(5)	−3363(5)	−2100(6)	5.1	F_4*	−1389(9)	2844(7)	−8462(10)	18.4
C_{4b}	−4588(5)	−2759(5)	−3147(5)	4.2	$F_{1'}$*	−3333(14)	277(14)	−7079(19)	3.6
$C_{4b'}$	−4710(6)	−2995(7)	−4651(6)	6.4	$F_{2'}$*	−1823(28)	2178(21)	−7006(24)	8.6
$C_{1'}$	−1292(5)	2094(4)	−3227(5)	3.5	$F_{3'}$*	−1014(22)	1535(46)	−6928(25)	16.2
$C_{2'}$	−1351(5)	2941(5)	−2393(5)	4.4	$F_{4'}$*	−1692(40)	1253(49)	−8867(32)	18.4

* Occupancies for the disordered atoms are 0.85 for F_1—F_4 and 0.15 for $F_{1'}$—$F_{4'}$.
a) Equivalent isotropic temperature factor defined by Hamilton.[12]

Table 3. Selected Bond Distances in (1*r*,3*R*,4*S*)-3,4-Diethyl-3,4-dimethyl-1-phenylthiolanium Tetrafluoroborate

Atom(1)–Atom(2)	Distance/Å	Atom (1)–Atom(2)	Distance/Å
S–C_2	1.825(4)	C_3–C_{3b}	1.512(6)
S–C_5	1.831(6)	C_4–C_5	1.537(5)
S–$C_{1'}$	1.793(4)	C_4–C_{4a}	1.531(8)
C_2–C_3	1.535(7)	C_4–C_{4b}	1.527(6)
C_3–C_4	1.586(7)	C_{3b}–$C_{3b'}$	1.521(9)
C_3–C_{3a}	1.558(7)	C_{4b}–$C_{4b'}$	1.524(9)

The observed barrier to sulfur-inversion is indeed lower than that in **1** by ca. 2 kcal mol^{-1} and represents the lowest barrier known so far for purely aliphatic cyclic sulfonium salts, yet it is higher than that in 1-adamantylethylmethylsulfonium perchlorate.[3] We were thus interested in the investigation of the cause for the relatively high barrier to sulfur-inversion in compound **6b**, irrespective to the fact that the molecular models of the compound suggested that the high degree of congestion was possible in the molecule. Thus X-ray crystallography of the starting material **6b** was carried out. This as well provides unambiguous assignment of the stereochemistry of the isomers involved.

Atomic coordinates, bond lengths, bond angles, and some selected dihedral angles are given in Tables 2, 3, 4, and 5, respectively. The ORTEP diagram is given in Fig. 1 for the enantiomer of the molecule that is defined by the atomic coordinates in Table 2, for the convenience of the comparison with the molecule of **8**. It is clear that the prediction of stereochemistry given by considering both kinetic and thermodynamic preference is correct. The originally preferred compound is (1*r*,3*R*,4*S*)-3,4-diethyl-3,4-dimethyl-1-phenylthiolanium tetrafluoroborate. Thus the product by equilibration must be (1*s*,3*R*,4*S*)-3,4-diethyl-3,4-dimethyl-1-phenylthiolanium tetrafluoroborate.

The compound **6b** has some interesting structural features that follow. These must be caused by the presence of neighboring two pairs of *gem*-ethyl-and-methyl groups which interact strongly with each other. The methyls of the ethyl groups are directing outward relative to the five-membered ring to avoid the interaction with other groups. The C_3–C_4 bond is

Table 4. Selected Bond Angles in (1*r*,3*R*,4*S*)-3,4-Diethyl-3,4-dimethyl-1-phenylthiolanium Tetrafluoroborate

Atom(1)–Atom(2)–Atom(3)	Angle/°
C_2–S–C_5	94.5(2)
C_2–S–$C_{1'}$	106.4(2)
C_5–S–$C_{1'}$	105.3(2)
S–C_2–C_3	107.8(4)
C_2–C_3–C_4	105.4(3)
C_2–C_3–C_{3a}	108.3(4)
C_2–C_3–C_{3b}	110.0(4)
C_4–C_3–C_{3a}	109.9(4)
C_4–C_3–C_{3b}	113.0(4)
C_{3a}–C_3–C_{3b}	110.0(3)
C_3–C_4–C_5	104.5(4)
C_3–C_4–C_{4a}	112.0(4)
C_3–C_4–C_{4b}	111.2(4)
C_5–C_4–C_{4a}	107.7(4)
C_5–C_4–C_{4b}	111.3(3)
C_{4a}–C_4–C_{4b}	110.0(4)
S–C_5–C_4	104.7(4)
C_3–C_{3b}–$C_{3b'}$	116.4(4)
C_4–C_{4b}–$C_{4b'}$	117.9(5)

very long as an sp^3–sp^3 carbon bond and is even longer than the C–C bond in tetramethylsuccinonitrile.[13] This is probably caused by the fact that the steric size of a cyano group is smaller than a methylene group.

Another interesting feature is that the C_4 occupies the tip of the envelope conformation of the thiolane ring in contrast to the fact that the sulfur atom occupies the tip position in 1-methylthiolanium iodide.[14] The cause was again considered to be the steric effects at the 3 and 4 positions, because, if the sulfur atom occupies the tip, the methyl and the ethyl groups at 3,4-positions must take near-eclipsing conformations

Table 5. Selected Torsion Angles in (1*r*,3*R*,4*S*)-3,4-Diethyl-3,4-dimethyl-1-phenylthiolanium Tetrafluoroborate

Atom(1)–Atom(2)–Atom(3)–Atom(4)	Angle/°
C_5–S–C_2–C_3	4.6(3)
$C_{1'}$–S–C_2–C_3	−102.8(3)
C_2–S–C_5–C_4	24.0(3)
$C_{1'}$–S–C_5–C_4	132.4(3)
C_2–S–$C_{1'}$–$C_{2'}$	−46.3(4)
C_2–S–$C_{1'}$–$C_{6'}$	141.1(4)
C_5–S–$C_{1'}$–$C_{2'}$	−145.8(4)
C_5–S–$C_{1'}$–$C_{6'}$	41.6(4)
S–C_2–C_3–C_4	−31.2(4)
S–C_2–C_3–C_{3a}	86.4(4)
S–C_2–C_3–C_{3b}	−153.3(3)
C_2–C_3–C_4–C_5	49.5(4)
C_2–C_3–C_4–C_{4a}	165.8(4)
C_2–C_3–C_4–C_{4b}	−70.6(4)
C_{3a}–C_3–C_4–C_5	−67.0(4)
C_{3a}–C_3–C_4–C_{4a}	49.3(5)
C_{3a}–C_3–C_4–C_{4b}	172.9(4)
C_{3b}–C_3–C_4–C_5	169.7(4)
C_{3b}–C_3–C_4–C_{4a}	−74.0(5)
C_{3b}–C_3–C_4–C_{4b}	49.6(5)
C_3–C_4–C_5–S	−45.0(4)
C_{4a}–C_4–C_5–S	−164.3(3)
C_{4b}–C_4–C_5–S	75.0(4)

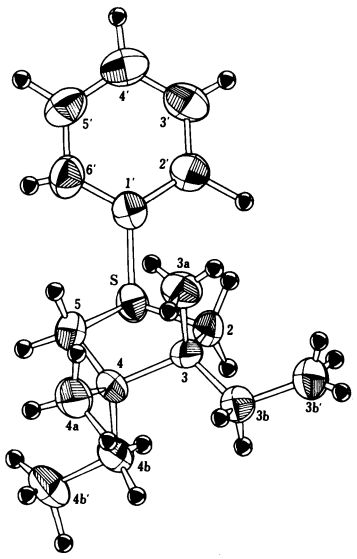

Fig. 1. An ORTEP diagram of (1*r*,3*R*,4*S*)-3,4-diethyl-3,4-dimethyl-1-phenylthiolanium ion. Number of atoms corresponds with that in Tables 2—5.

Table 6. Atomic Positional Parameters (×10⁴) with Estimated Standard Deviations in Parentheses and Equivalent Isotropic Thermal Parameters of 1-Phenylthiolanium Perchlorate

	Molecule 1					Molecule 2			
Atom	*x*	*y*	*z*	B_{eq}[a]	Atom	*x*	*y*	*z*	B_{eq}[a]
S	6675(2)	9141(2)	1494(3)	4.4	S	2918(2)	4061(2)	3444(3)	4.9
C_2	6754(8)	9178(8)	3254(12)	5.7	C_2	2943(9)	4225(8)	1727(13)	6.3
C_3	6108(10)	8468(9)	3689(14)	7.9	C_3	3556(11)	4269(11)	1170(16)	10.7
C_4	5312(8)	8462(9)	2757(13)	6.7	C_4	4146(10)	3627(9)	1764(17)	9.5
C_5	5609(8)	8554(8)	1386(12)	5.4	C_5	4069(8)	3648(8)	3279(16)	7.2
$C_{1'}$	7525(7)	8395(7)	1082(12)	4.0	$C_{1'}$	2246(7)	3163(7)	3844(12)	4.1
$C_{2'}$	7507(9)	7568(7)	1513(12)	5.2	$C_{2'}$	2289(9)	2406(7)	3169(13)	5.4
$C_{3'}$	8251(9)	7046(8)	1189(13)	6.4	$C_{3'}$	1755(8)	1746(7)	3600(14)	6.1
$C_{4'}$	8888(8)	7334(9)	459(14)	6.6	$C_{4'}$	1217(8)	1839(8)	4622(12)	5.6
$C_{5'}$	8888(8)	8139(10)	8(12)	6.8	$C_{5'}$	1174(8)	2572(9)	5274(14)	6.5
$C_{6'}$	8209(8)	8683(8)	334(12)	5.3	$C_{6'}$	1691(8)	3257(8)	4904(12)	5.6
Cl	5590(2)	9223(2)	7783(3)	5.4	Cl	4103(2)	4302(2)	7264(3)	5.7
O_1*	5479(12)	9533(11)	6420(15)	11.1	O_1*	4354(12)	3565(9)	8003(18)	9.4
O_2*	4738(9)	9378(8)	8320(14)	7.6	O_2*	3378(15)	4134(14)	6586(22)	14.4
O_3*	5704(10)	8378(10)	8003(16)	9.2	O_3*	4624(10)	4657(10)	6314(15)	8.0
O_4*	6140(9)	9788(9)	8501(13)	7.5	O_4*	4067(12)	5044(11)	8092(18)	10.4
$O_{1'}$*	5440(27)	8444(28)	6928(40)	16.3	$O_{1'}$*	3210(15)	4554(17)	7439(27)	11.4
$O_{2'}$*	6074(17)	8566(19)	8652(19)	9.2	$O_{2'}$*	4039(18)	3462(21)	6411(38)	15.1
$O_{3'}$*	5887(16)	9294(18)	6596(28)	8.6	$O_{3'}$*	4990(17)	4479(17)	6994(38)	13.6
$O_{4'}$*	4450(15)	3943(15)	8325(20)	5.9	$O_{4'}$*	4672(17)	9414(19)	7670(39)	13.9

* Occupancies for the disordered atoms are 0.65 for O_1—O_4 and 0.35 for $O_{1'}$—$O_{4'}$, in molecule 1, and 0.60 for O_1—O_4 and 0.40 for $O_{1'}$—$O_{4'}$ in molecule 2, respectively.

a) Equivalent isotropic temperature factor defined by Hamilton.[12]

that are of very high energy.

Another interesting point in the structure of **6b** is that the 1-phenyl group takes a conformation that is nearly perpendicular to the lone-pair orbital of the sulfur atom. This makes an interesting contrast to the structure of dimethylphenylsulfonium ion in which the phenyl group nearly bisects the CH_3-S-CH_3 angle.[15] To get further insight into the implication of the structure, we have carried out the X-ray crystallography of 1-phenylthiolanium perchlorate (**8**) which was easily prepared by treating (4-bromobutylthio)benzene (**7**) with silver perchlorate. The results are shown in Tables 6, 7, 8, and 9.

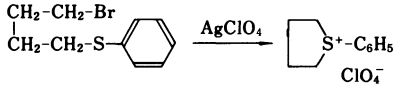

7 8

The diffraction data were best interpreted by assuming that there were two kinds of molecules in the crystals in addition to their enantiomers. The two independent molecules are those which differ in the positions of the carbon-3 of the thiolane ring. Thus they are diastereomers. However, their structures are similar except that the position of C_3 which is up or down relative to the plane made by others, C_2-S-C_5-C_4: the torsion angle $C_{1'}$-S-C_2-C_3 in molecule 2 is much larger than that in molecule 1, reflecting the relative positions of C_3. The ORTEP diagrams of these molecules are shown in Fig. 2. Thus only one form (molecule 2) will be used for comparison of the structures of **6b** and **8** that follows. It is interesting that in these molecules C_3 occupies the tip of the envelope. However, the cause for the difference between **8** and 1-methylthiolanium ion[14] is not well understood at present.

Table 7. Selected Bond Distances (Å) in 1-Phenylthiolanium Perchlorate

Atom(1)-Atom(2)	Molecule 1	Molecule 2
S-C_2	1.808(12)	1.803(13)
S-C_5	1.826(12)	1.842(12)
S-$C_{1'}$	1.801(12)	1.806(11)
C_2-C_3	1.565(19)	1.515(22)
C_3-C_4	1.462(19)	1.442(22)
C_4-C_5	1.515(19)	1.572(25)

Table 8. Selected Bond Angles (°) in 1-Phenylthiolanium Perchlorate

Atom(1)-Atom(2)-Atom(3)	Molecule 1	Molecule 2
C_2-S-C_5	94.1(6)	96.0(7)
C_2-S-$C_{1'}$	105.1(6)	104.5(6)
C_5-S-$C_{1'}$	105.2(5)	105.3(5)
S-C_2-C_3	105.4(9)	103.4(9)
C_2-C_3-C_4	107.1(11)	109.2(14)
C_3-C_4-C_5	109.7(11)	108.8(13)
S-C_5-C_4	107.4(8)	103.5(9)

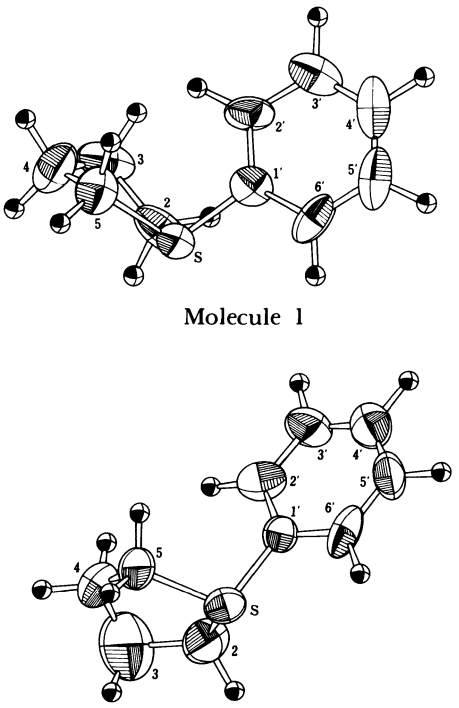

Molecule 1

Molecule 2

Fig. 2. ORTEP diagrams of two forms of 1-phenylthiolanium ion. Number of atoms corresponds with that in Tables 6—9.

Table 9. Selected Torsion Angles (°) in 1-Phenylthiolanium Perchlorate

Atom(1)-Atom(2)-Atom(3)-Atom(4)	Molecule 1	Molecule 2
C_5-S-C_2-C_3	18.6(9)	−21.2(10)
$C_{1'}$-S-C_2-C_3	−88.2(9)	−128.6(9)
C_2-S-C_5-C_4	4.1(9)	−2.7(10)
$C_{1'}$-S-C_5-C_4	111.1(9)	104.1(9)
C_2-S-$C_{1'}$-$C_{2'}$	59.1(11)	54.4(11)
C_2-S-$C_{1'}$-$C_{6'}$	−119.8(9)	−127.4(9)
C_5-S-$C_{1'}$-$C_{2'}$	−39.4(11)	−46.1(11)
C_5-S-$C_{1'}$-$C_{6'}$	141.6(9)	132.1(9)
S-C_2-C_3-C_4	−37.9(12)	42.4(14)
C_2-C_3-C_4-C_5	42.9(14)	−46.9(16)
C_3-C_4-C_5-S	−28.1(13)	28.0(14)

The feature of the structure of **8** is that the phenyl group nearly bisects the angle C_2–S–C_5 although it is tilted a little toward C_4. It seems that in normal dialkylphenylsulfonium ions the phenyl group nearly bisects the C–S–C angle. The tilting of the phenyl group to a small degree in **8** must be caused by avoiding the van der Waals repulsion between the groups concerned. Since, if the phenyl group takes the similar conformation as in **8**, severe steric interactions between the 3-methyl group and the phenyl group are unavoidable in **6b**, the phenyl group seems to take the conformation that is observed by the X-ray crystallography. Indeed, the distance between $C_{2'}$ and the methyl group at C_3 and that between $C_{6'}$ and the same methyl group in **6b** are 4.16 and 4.37 Å, respectively. That is, the ortho carbons of the phenyl group are at about the same distance from the methyl group and are in close contact at about the sum of the van der Waals radii.

The sulfur pyramid in **6b** is not significantly different from that in the 1-phenylthiolanium perchlorate (**8**). However, the five-membered ring is a little more distorted in **6b** than in **8**. This is because, due to the steric effects in the 3,4-positions, the conformation about the C_3–C_4 bond is very close to the perfectly staggered. The carbon atom that occupies the tip of the envelope is 0.68 and 0.58 Å out of the average plane that is made by the other four atoms of the ring in **6b** and **8**, respectively.

We summarize from the structural features of the thiolanium ion discussed above that **6b** has an unusual structure about the C_3–C_4 region because of the steric effects of the two methyl and two ethyl groups. However, this abnormality may not affect the structure of the sulfur pyramid except that the phenyl conformation is unusual in **6b**. Although there is no evidence that the structure of the molecule in the solid state is taken in solution, it is tempting to consider that the lowering of the sulfur-inversion barrier in **6b** to a small extent relative to **1** is ascribable to the fact that the sulfur pyramid is not unusual except that the phenyl group takes a conformation that is perpendicular to the direction of the lone pair orbital of the sulfur atom. Namely the steric effect of the four alkyl groups in 3 and 4 positions appears only at the unusual conformations about the S–$C_{1'}$ bond as far as the barrier to sulfur-inversion concerns.

Experimental

Determination of Rates of Sulfur-Inversion. **6b** was dissolved in chloroform-*d* to make up ca. 0.1 mol L^{-1} solutions. The solution was heated in a thermostatted bath at a given temperature. The starting material and the product were analyzed with the use of ^1H NMR spectra of the methylene protons at 270 MHz. The spectrometer was a JEOL GX-270. The integration method and the weight method afforded agreeable data within the error limit. The data were treated by assuming the reversible first order reaction and the rate constants were put into the Eyring equation to afford kinetic parameters.

X-Ray Crystallography. Crystals suitable for the crystallography were grown from dichloromethane–hexane and acetone–hexane, respectively, for **6b** and **8**.

Colorless crystals (0.5×0.3×0.3 mm) were mounted on a Rigaku AFC-5 automated four-circle diffractometer and the intensity data were collected using Mo $K\alpha$ radiation (λ=0.71073 Å). The ω–2θ scan technique was employed at a scan rate of 3° min^{-1} in ω, and the scan range was calculated by $1.1°+0.5°\tan\theta$. For **6b**, 4218 independent reflections within the range $2\theta<55°$ were measured, and 1851 reflections with $|F_o|>3\sigma|F_o|$ were judged as observed and were used for the structure determination and refinement. For **8**, the total number of measured reflections and the observed reflections were 4644 ($2\theta<50°$) and 1299, respectively. The crystal data and the methods of structure determination were as follows.

6b: $C_{16}H_{25}BF_4S$, F.W.=336.24, triclinic, space group $P\bar{1}$, a=10.025(2), b=10.268(2), c=9.599(1) Å, α=69.91(1)°, β=99.42(2)°, γ=110.68(1)°, V=867.2 Å^3, Z=2, D_c=1.29 g cm^{-3}, μ=2.21 cm^{-1}. The structure was solved by direct methods (MULTAN 78) and refined by the block-diagonal least-squares technique with anisotropic thermal parameters for non-hydrogen atoms and isotropic for hydrogens. All the hydrogen atoms were located on a difference map but their positional parameters were not refined. The atomic scattering factors were taken from International Tables for X-Ray Crystallography.[16] Difference syntheses revealed the disorder of the tetrafluoroborate anion, and their positional and anisotropic thermal parameters were refined. The weighting scheme $w=[\sigma_c^2+(0.02|F_o|^2)]^{-1}$ was employed. The final R and R_w values were 6.13 and 8.44%, respectively.

8: $C_{10}H_{13}ClO_4S$, F.W.=264.72, monoclinic, space group $P2_1/n$, a=14.760(1), b=15.928(2), c=10.294(1) Å, β=94.18(1)°, V=2413.6 Å^3, Z=8, D_c=1.46 g cm^{-3}, μ=4.81 cm^{-1}. The structure was solved by direct methods (MULTAN 78), assuming the temperature factor of 2.30, to reveal the positions of four heavy atoms. Two kinds of independent molecules were found in a unit cell. Calculation of structure factors based on the four atoms gave an R value of 55.8%. The Fourier syntheses and successive difference syntheses indicated all the non-hydrogen atoms in addition to the disorder of the perchlorate anion, the positional and anisotropic thermal parameters of which were refined by the block-diagonal least-squares technique. The positions of all hydrogens were obtained by calculation. The positional and isotropic thermal parameters (assumed to be 10.5) of hydrogens were not refined, but were included in the calculation of structure factors. The final R and R_w values were 5.99 and 7.82%, respectively.

All the calculations were carried out on a HITAC M-200H computer with crystallographic computation program system, MULTAN and UNICS III, filed at the Computer Center of the Institute for Molecular Science. The complete F_o-F_c data are deposited as Document No. 8771 at the Office of the Editor of the Bulletin of the Chemical Society of Japan.

3,3,4,4-Tetramethylthiolane (4a). To a mixture of 5.4 g (37 mmol) of 2,2,3,3-tetramethyl-1,4-butanediol[11] and 17 mL of dry pyridine, was added 16.8 g (88 mmol) of *p*-

toluenesulfonyl chloride in portions with ice-cooling and stirring. After several hours of stirring, the mixture was allowed to stand in a refrigerator and then poured into 100 mL of water. The precipitates were collected by filtration to give the crude ditosylate, mp 98—107 °C, in 80% yield. ^{1}H NMR ($CDCl_3$) δ=0.83 (12H, s), 2.44 (6H, s), 3.79 (4H, s), 7.36 and 7.69 (8H, ABq, J=8.4 Hz). This crude ditosylate was directly used for the next reaction.

To a solution of 3.0 g (6.6 mmol) of the crude ditosylate in 100 mL of *N,N*-dimethylformamide, was added 3.0 g (13 mmol) of sodium sulfide nonahydrate. The whole was heated under reflux for 2 h and steam-distilled to give 0.7 g (74%) of the desired compound. The pure sample was obtained by sublimation, mp 151—152 °C (sealed tube). High resolution MS: M^+ 144.0973. Calcd for $C_8H_{16}S$: M^+ 144.0973. ^{1}H NMR ($CDCl_3$) δ=0.98 (12H, s), 2.69 (4H, s).

1,3,3,4,4-Pentamethylthiolanium Trifluoromethanesulfonate (5a: X=CF_3SO_3). To a solution of 0.1 g (0.7 mmol) of the thiolane in 2 mL of carefully dried (distilled from CaH_2) dichloromethane, was added 0.1 mL (0.15 g or 0.9 mmol) of methyl trifluoromethanesulfonate and stirred for 1.5 h at room temperature. Addition of ether to the mixture afforded 0.17 g (80%) of the desired compound, mp 120.5—122.0 °C. Recrystallization from ethanol afforded the pure sample, mp 123.5—124.5 °C. Found: C, 38.69; H, 6.16; S, 20.99%. Calcd for $C_{10}H_{19}F_3S_2O_3$: C, 38.95; H, 6.12; S, 20.79%. ^{1}H NMR ($CDCl_3$) δ=1.10 (6H, s), 1.23 (6H, s), 3.22 (3H, s), 3.44 and 3.68 (4H, ABq, J=13.5 Hz).

3,3,4,4-Tetramethyl-1-phenylthiolanium Tetrafluoroborate (6a). A solution of 0.12 g (0.83 mmol) of the thiolane, 0.31 g (0.84 mmol) of diphenyliodonium tetrafluoroborate,[17] and 10 mg of copper(II) benzoate in 3 mL of *N,N*-dimethylformamide was heated in an oil bath at 120—125 °C for 4 h. After the mixture was cooled, ether was added to the mixture and the precipitates were collected by filtration. Recrystallization from ethanol afforded 0.16 g (63%) of the desired product, mp 241.0—245.5 °C. Found: C, 54.51; H, 6.57; S, 10.87%. Calcd for $C_{14}H_{21}BF_4S$: C, 54.56; H, 6.87; S, 10.40%. ^{1}H NMR (DMSO-d_6) δ=1.06 (6H, s), 1.12 (6H, s), 3.97 and 4.07 (4H, ABq, J=13.5 Hz), 7.6—7.8 (3H, m), 7.9—8.1 (2H, m).

***meso*-2,3-Diethyl-2,3-dimethyl-1,4-butanediol (3b).** A solution of 14.0 g of *meso*-2,3-diethyl-2,3-dimethylsuccinic acid[18] in 50 mL of methanol was heated with 5 mL of sulfuric acid for 12 h and poured into water. The mixture was extracted with ether and the ether extracts were dried over magnesium sulfate. Evaporation of the solvent afforded 14.7 g of the crude half-ester of the succinic acid derivative. ^{1}H NMR ($CDCl_3$) δ=0.82 (3H, t, J=7.5 Hz), 0.87 (3H, t, J=7.5 Hz), 1.17 (3H, s), 1.20 (3H, s), 1.5—2.4 (4H, m), 3.68 (3H, s), 10.7 (1H, br s). A solution of the crude monomethyl ester (11.9 g or 55 mmol) in 50 mL of ether was added to 4.0 g (0.1 mol) of lithium tetrahydridoaluminate in 200 mL of ether with ice-cooling and the mixture was heated for 14 h. The mixture was treated with water and then with dilute sulfuric acid with ice-cooling and the ether layer was separated. The aqueous layer was extracted several times with ether. The combined ether extracts were washed with water and dried over sodium sulfate. Evaporation of the solvent afforded 9.4 g (78% based on the succinic acid) of the desired diol, which was purified by recrystallization from dichloromethane-pentane, mp 33.0—34.5 °C. Found: C, 68.67; H, 12.96%. Calcd for $C_{10}H_{22}O_2$: C, 68.92; H, 12.72%. ^{1}H NMR ($CDCl_3$) δ=0.77 (6H, s), 0.83 (6H, t, J=7.5 Hz), 1.1—1.7 (4H, m), 3.46 (4H, s), 4.55 (2H, br s).

***meso*-3,4-Diethyl-3,4-dimethylthiolane (4b).** This compound was obtained in a similar manner as described for the tetramethyl compound **4a**, starting from **3b**; tosylation of the diol followed by treatment with sodium sulfide. The yield was 66%. It was obtained as an oil. High resolution MS: M^+ 172.1308. Calcd for $C_{10}H_{20}S$: M^+ 172.1286. ^{1}H NMR ($CDCl_3$) δ=0.77 (6H, t, J=7.5 Hz), 0.93 (6H, s), 1.17 (4H, q, J=7.5 Hz), 2.58 and 2.73 (4H, ABq, J=10.5 Hz).

Methylation of 4b with Methyl Trifluoromethanesulfonate. To a solution of 0.1 g (0.6 mmol) of the thiolane (**4b**) in 2 mL of dry dichloromethane was added 0.1 mL (0.15 g or 0.9 mmol) of methyl trifluoromethanesulfonate. The product was a ca. 1:1.3 mixture of two isomers which were not assigned. Attempted separation of the stereoisomers failed. The following ^{1}H NMR ($CDCl_3$, δ) were collected. One isomer: 0.98 (6H, t, J=7.5 Hz), 1.05 (6H, s), 1.3—1.5 (4H, m), 3.12 (3H, s), 3.44 and 3.60 (4H, ABq, J=13.7 Hz). Other isomer: 1.01 (6H, t, J=7.5 Hz), 1.16 (6H, s), 1.54 (4H, q, J=7.5 Hz), 3.17 (3H, s), 3.30 and 3.80 (4H, ABq, J=13.6 Hz). The assignment of the peaks at δ 0.98 and 1.01 for the methyl protons may be reversed because their intensities were equal.

(1*r*,3*R*,4*S*)-3,4-Diethyl-3,4-dimethyl-1-phenylthiolanium Tetrafluoroborate (6b). The thiolane (0.60 g or 3.5 mmol) and 1.30 g (3.53 mmol) of diphenyliodonium tetrafluoroborate were treated similarly as described for the synthesis of **4a**. The precipitate (0.75 g) obtained by adding ether to the reaction mixture was recrystallized from ethanol to give 0.32 g (27%) of the desired material, mp 156.5—157.5 °C. Found: C, 57.00; H, 7.37; S, 9.39%. Calcd for $C_{16}H_{25}BF_4S$: C, 57.15; H, 7.49; S, 9.53%. ^{1}H NMR ($CDCl_3$) δ=0.99 (6H, t, J=7.4 Hz), 1.07 (6H, s), 1.49 (4H, q, J=7.4 Hz), 3.58 and 4.20 (4H, ABq, J=13.4 Hz), 7.56—7.61 (3H, m), 7.82—7.86 (2H, m). The crude product contained some stereoisomer of **6b** which was apparently removed by recrystallization.

After equilibration of **6b** by heating, the chloroform solution was concentrated to produce crystals that contained mainly (1*r*,3*R*,4*S*)-**6b**. The repetition of the procedure finally gave a 1:6 mixture of (1*r*,3*R*,4*S*)-**6b** and (1*s*,3*R*,4*S*)-**6b**. Recrystallization of the mixture from ethanol or dichloromethane-hexane did not improve the purity. Found: C, 56.98; H, 7.60%. Calcd for $C_{16}H_{25}BF_4S$: C, 57.15; H, 7.49%. The following ^{1}H NMR data ($CDCl_3$, δ) of (1*s*,3*R*,4*S*)-**6b** were obtained by subtracting the signals due to (1*r*,3*R*,4*S*)-**6b**: 0.89 (6H, t, J=7.3 Hz), 1.11 (6H, s), 1.39 and 1.49 (4H, AB part of ABX_3, J_{AB}=14.1 Hz, J_{AX}=J_{BX}=7.3 Hz), 3.74 and 4.06 (4H, ABq, J=13.2 Hz), 7.61—7.63 (3H, m), 7.78—7.81 (2H, m).

1-Phenylthiolanium Perchlorate (8). To a solution of 0.24 g (0.98 mmol) of (4-bromobutylthio)benzene (**7**)[19] in 20 mL of dichloromethane was added 0.20 g (0.96 mmol) of silver perchlorate and the whole was stirred overnight at room temperature. The precipitate was removed by filtration and the filtrate was concentrated in vacuo. The crystals thus obtained were recrystallized from ethanol to afford 0.20 g (77%) of the desired product, mp 90.0—91.5 °C. Found: C, 45.12; H, 4.96%. Calcd for $C_{10}H_{13}ClO_4S$: C, 45.37; H, 4.95%. ^{1}H NMR ($CDCl_3$) δ=2.55—2.61 (4H, m), 3.66—3.76 (2H, m), 4.17—4.26 (2H, m), 7.61—7.73 (3H, m), 7.80—7.82 (2H, m).

This work was supported by a Grant-in-Aid for Fundamental Scientific Research (No. 61134043) of the Ministry of Education, Science and Culture.

References

1) P. H. Laur, "Sulphur in Organic and Inorganic Chemistry," ed by A. Senning, Mercel-Dekker, New York (1972), Vol. 3, p. 91; M. Mikolajczyk and J. Drabowicz, *Top. Stereochem.*, **13**, 333 (1982).

2) D. Darwish and G. Tourigny, *J. Am. Chem. Soc.*, **88**, 4303 (1966).

3) R. Scartazzini and K. Mislow, *Tetrahedron Lett.*, **1967**, 2719.

4) T. Morita and M. Ōki, *Bull. Chem. Soc. Jpn.*, **59**, 3603 (1986) and papers cited therein.

5) D. Darwish and C. E. Scott, *Can. J. Chem.*, **51**, 3647 (1973).

6) H. H. Jaffé, *Chem. Rev.*, **53**, 191 (1953).

7) F. G. Bordwell and G. D. Cooper, *J. Am. Chem. Soc.*, **74**, 1058 (1952).

8) D. Darwish, S. H. Hui, and R. Tomilson, *J. Am. Chem. Soc.*, **90**, 5631 (1968); see also Ref. 2.

9) K. R. Brower and T.-L. Wu, *J. Am. Chem. Soc.*, **92**, 5303 (1970).

10) A. Garbesi, N. Corsi, and A. Fava, *Helv. Chim. Acta*, **53**, 1499 (1970).

11) M. F. Ansell, W. J. Hickinbottom, and P. G. Holton, *J. Chem. Soc.*, **1955**, 349.

12) W. C. Hamilton, *Acta Crystallogr.*, **12**, 609 (1959).

13) W. B. Gleason and D. Britton, *Cryst. Struct. Commun.*, **11**, 1159 (1982).

14) F. Miyoshi, K. Tokuno, T. Watanabe, M. Matsui, and T. Ohashi, *Yakugaku Zasshi*, **99**, 924 (1979).

15) A. Lopez-Castro and M. R. Truter, *Acta Crsystallogr.*, **17**, 465 (1964).

16) International Tables for X-Ray Crystallography (1974), Vol. IV, Kynoch Press, Birmingham.

17) J. V. Crivello and J. W. Lam, *J. Org. Chem.*, **43**, 3055 (1978).

18) L. Eberson, *Acta Chem. Scand.*, **14**, 641 (1960).

19) S. Torii, Y. Matsuyama, K. Kawasaki, and K. Uneyama, *Bull. Chem. Soc. Jpn.*, **46**, 2912 (1971).

 © 1988 The Chemical Society of Japan Bull. Chem. Soc. Jpn., 61, 715—722 (1988)

An X-Ray Diffraction Study on the Structures of Monochloropentakis(*N,N*-dimethylformamide)copper(II), Trichloromono(*N,N*-dimethylformamide)- and Tetrachlorocuprate(II) Complexes in *N,N*-Dimethylformamide

Kazuhiko Ozutsumi, Shin-ichi Ishiguro,* and Hitoshi Ohtaki†
Coordination Chemistry Laboratories, Institute for Molecular Science, Myodaiji, Okazaki 444
†Department of Electronic Chemistry, Tokyo Institute of Technology, Nagatsuta-cho 4259, Midori-ku, Yokohama 227
(Received August 17, 1987)

The structure of the monochlorocopper(II), trichloro- and tetrachlorocuprate(II) complexes in *N,N*-dimethylformamide (DMF) has been studied by the X-ray diffraction method at 25 °C. The radial distribution curve obtained for a solution containing the monochlorocopper(II) complex as the predominant species reveals the presence of an axially elongated octahedral $[CuCl(dmf)_5]^+$ complex, three Cu–O(eq) and two Cu–O(ax) bond lengths being 199(1) and 239(4) pm, respectively. The chloride ion binds to the copper(II) ion at the equatorial site and the Cu–Cl distance is 220(2) pm. The Cu–O(eq) bond length within the $[CuCl(dmf)_5]^+$ complex is practically the same as that within the $[Cu(dmf)_6]^{2+}$ (203 pm). The X-ray scattering data of solutions containing the tri- and tetrachlorocuprate(II) complexes as the main species are well explained in terms of the existence of the distorted tetrahedral $[CuCl_3(dmf)]^-$ and $[CuCl_4]^{2-}$ complexes, respectively, in the solutions. The Cu–Cl and Cu–O bond lengths within the $[CuCl_3(dmf)]^-$ complex are 219(1) and 230(13) pm, respectively. The Cu–O distance within the complex is longer than that of the equatorial Cu–O bond within the $[Cu(dmf)_6]^{2+}$ and $[CuCl(dmf)_5]^+$ ions. The Cu–Cl bond length within the $[CuCl_4]^{2-}$ complex is 226(1) pm and is longer than that within the $[CuCl_3(dmf)]^{2-}$ complex. The nonbonding Cl···Cl distances within the $[CuCl_4]^{2-}$ complex are 346(3) and 412(6) pm.

The structure of complexes between copper(II) and chloride ions in aqueous $CuCl_2$ solutions with varying concentrations has been investigated by X-ray,[1,2] neutron diffraction,[3] and EXAFS methods,[4] and the data are interpreted in terms of the formation of various monomeric and/or polymeric chloro complexes. X-Ray scattering measurements have also been carried out for methanolic solutions of $CuCl_2$ and the presence of monomeric complexes with various numbers of chloride ions was proposed in the solutions.[5] However, the data analysis of the solutions so far examined was performed for the average structure of some complexes coexisting and no structural information has been given for individual complex species in solution with adjusting the concentration ratios of copper(II) to chloride ions on the basis of the stability constants of copper(II)–chloro complexes.

The structure of the $[CuCl_3]^-$ and $[CuCl_4]^{2-}$ complexes in crystal has been investigated from magnetic and thermochromic points of view. The former complex has been concluded to have a dimeric structure with a square-planar coordination geometry around a copper(II) ion,[6–8] and the latter has either a square-planar or a distorted tetrahedral structure.[9–18] The structure of the complexes in solution, however, has never been studied.

A series of mononuclear copper(II)–chloro complexes are formed and formation of the complexes is enhanced in aprotic solvents such as *N,N*-dimethylformamide (DMF), dimethyl sulfoxide, and acetonitrile and the formation constants of each complex have been determined.[19–22] In DMF the mono-, tri-, and tetrachloro complexes of copper(II) ion are formed as the main species at suitable concentration ratios of chloride to copper(II) ions.[19] Therefore, in the present study we determined the structure of the monochlorocopper(II), trichloro- and tetrachlorocuprate(II) complexes in DMF by the X-ray diffraction method. The structure of the dichlorocopper(II) complex was not determinable because the formation of the complex is suppressed in DMF.

Experimental

Preparation of Sample Solutions. All chemicals used were of reagent grade. *Copper(II) perchlorate DMF solvate* was prepared by the method described in a previous paper.[19] *Copper(II) chloride* was prepared by dissolving copper(II) oxide in hydrochloric acid and then recrystallized from aqueous dilute hydrochloric acid and dried in a vacuum oven at 100 °C. *Lithium chloride* was recrystallized from water and dried in vacuum at 200 °C. *N,N*-Dimethylformamide was purified as described elsewhere.[19]

Sample solutions A to D were prepared as listed in Table 1. Solution A was prepared by dissolving anhydrous

Table 1. The Composition (mol dm^{-3}), Stoichiometric Volumes V per Copper Atom and Densities ρ of the Sample Solutions

	A	B	C	D
Cu^{2+}	1.189	1.380	1.358	1.081
Cl^-	1.202	4.178	5.351	4.685
Li^+	—	1.418	2.635	2.523
ClO_4^-	1.176	—	—	—
DMF	12.28	12.06	11.87	12.10
$V/10^9$ pm^3	1.397	1.203	1.223	1.536
ρ/g cm^{-3}	1.133	1.127	1.162	1.137
C_{Cl}/C_{Cu}	1.011	3.027	3.940	4.334

copper(II) chloride and copper(II) perchlorate DMF solvate in DMF and solutions B to D by dissolving anhydrous copper(II) and lithium chlorides. Mole ratios C_{Cl}/C_{Cu}, where C_i represents the total concentration of species i, were so chosen that solutions A, B, and C contained the mono-, tri-, and tetrachloro complexes, respectively, as the main species according to the formation constants in the literature.[19] Since the solubility of LiCl in DMF is not sufficiently large, the tetrachlorocuprate(II) complex is not fully yielded in DMF. The yield of the complex in solution C was about 70 mol% of the total copper(II) ions, and therefore, in order to check the reproducibility of the structural analysis, solution D with the slightly higher C_{Cl}/C_{Cu} mole ratio than that of solution C was also examined. Solution A thus prepared is green, solution B orange and solutions C and D yellow. Concentrations of copper(II) ions in the sample solutions were determined by electrogravimetry. Concentrations of chloride ions were gravimetrically determined as AgCl. Concentrations of perchlorate ions in solution A and lithium ions in solutions B to D were evaluated by the material balance of ions in the solutions. Densities of the test solutions were measured pycnometrically.

X-Ray Scattering Measurements. X-Ray scattering measurements were performed on a θ-θ type diffractometer (JEOL DX-GO-Y) by using Mo $K\alpha$ radiation (λ=71.07 pm). The method of measurements and data treatments are described elsewhere.[23] The accessible range of scattering angle (2θ) was 2—140°, which corresponds to the scattering vector ($s=4\pi\lambda^{-1}\sin\theta$) range of 0.3×10^{-2}—16.6×10^{-2} pm^{-1}. Times required to accumulate 160000 counts were recorded at each angle of 2θ.

The reduced intensities $i(s)$ were extracted from the measured intensities $I(s)$, which had been scaled to the absolute ones after corrections for absorption, polarization and double scatterings of X-rays, according to Eq. 1:

$$i(s) = I(s) - \sum_i n_i[\{f_i(s) + \Delta f_i'\}^2 + (\Delta f_i'')^2], \quad (1)$$

where n_i is the number of atom i in a stoichiometric volume V per copper atom and $f_i(s)$ denotes the atomic scattering factors at s of atom i. $\Delta f_i'$ and $\Delta f_i''$ represent the real and imaginary parts of anomalous dispersion, respectively. The reduced intensities multiplied by s of the sample solutions are depicted in Fig. 1. The $s\cdot i(s)$ values were converted by the Fourier transform into the radial distribution function $D(r)$ as

$$D(r) = 4\pi r^2\rho_o + \frac{2r}{\pi}\int_0^{s_{max}} s\cdot i(s)\cdot M(s)\cdot\sin(rs)ds, \quad (2)$$

where ρ_o is the average scattering density in a stoichiometric volume of the solution and s_{max} denotes the maximum s-value attained in the measurement. $M(s)$ is the modification function defined as

$$M(s) = \frac{\sum_i n_i\{(f_i(0) + \Delta f_i')^2 + (\Delta f_i'')^2\}}{\sum_i n_i\{(f_i(s) + \Delta f_i')^2 + (\Delta f_i'')^2\}}\cdot\exp(-ks^2) \quad (3)$$

The damping factor k was chosen as 100 pm^2 in the present study. The differential radial distribution curves, $D(r)-4\pi r^2\rho_o$, for solutions A to D are shown in Fig. 2.

All calculations were performed by using programs KURVLR[24] and NLPLSQ.[25]

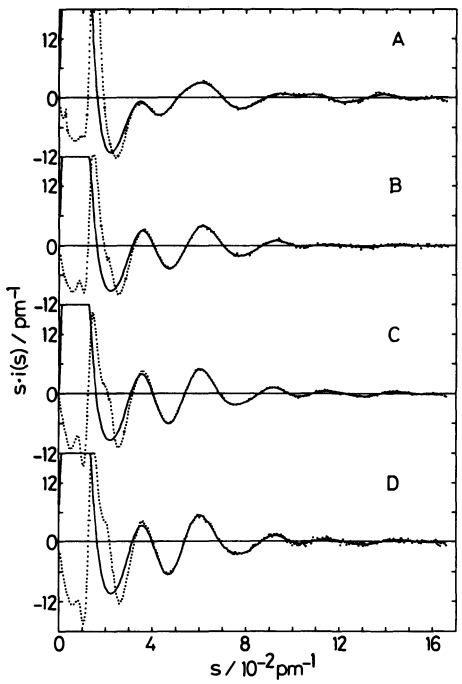

Fig. 1. The reduced intensities multiplied by s for solutions A, B, C, and D. The observed $s\cdot i(s)$ values are shown by the dotted lines and calulated ones by the solid lines.

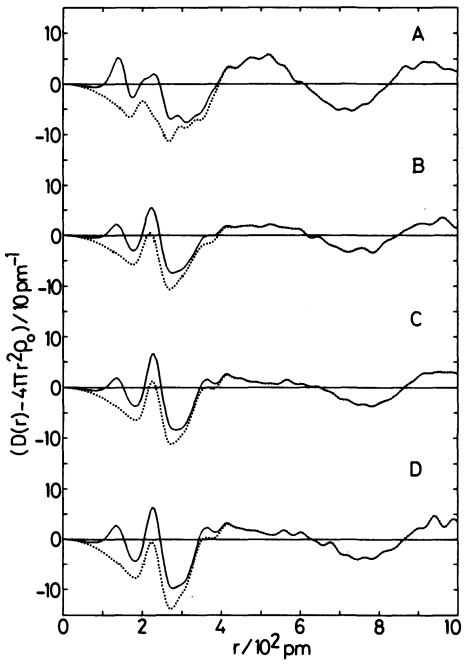

Fig. 2. The differential radial distribution curve, $(D(r)-4\pi r^2\rho_o)$, for solutions A, B, C, and D (solid lines). The dotted lines represent the residual curves after subtracting peaks due to the intramolecular interactions of DMF molecules for solutions A to D and perchlorate ions for solution A.

Results and Discussion

Structure of the $[CuCl]^+$ Complex. According to the stability constants for the copper(II)-chloro complexes in DMF,[19] the $[CuCl]^+$ complex is expected to be formed as the predominant species in solution A. Figure 3 depicts the $(D(r)-4\pi r^2\rho_o)$ curve of solution A as well as the calculated peak shapes for atom pairs in the solution which will be discussed later. In the curve four peaks appear around 130, 230, 290, and 410 pm, and a shoulder and a small hump are also observed at about 200 and 320 pm, respectively.

From the X-ray analysis of liquid DMF[26] it was shown that two peaks originating from the intramolecular interactions within DMF molecule appeared at 130 and 230 pm in the radial distribution function and no appreciable intermolecular interactions are observed because of its disordered liquid structure. Accordingly, the first peak at 130 pm should be due to the C-H, C=O, and C-N bonds within DMF molecules. The Cl-O bonds within perchlorate ions are also contained in the peak. The second peak at about 230 pm with a shoulder at 200 pm may be ascribable to interactions between

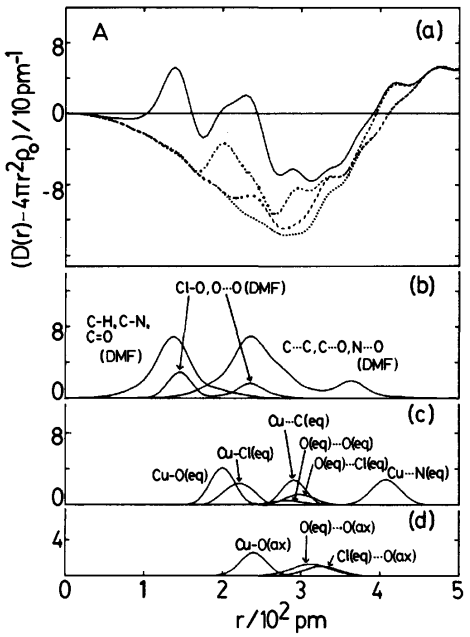

Fig. 3. (a) The $(D(r)-4\pi r^2\rho_o)$ curve for solution A. (b) The theoretical peaks for intramolecular interactions within DMF molecule and perchlorate ion. (c) The theoretical peak shapes due to the Cu-O(eq), Cu-Cl(eq), Cl···Cl, Cl···O, Cu···C(eq), and Cu···N(eq) interactions within the monochloropentakis(*N*,*N*-dimethylformamide)copper(II) complex. (d) The calculated peaks for Cu-O(ax), Cl···Cl, and Cl···O interactions within the mono-complex. The chain, dashed and dotted lines represent the residual curves after subtraction of the theoretical peaks in (b), (c), and (d), respectively.

copper(II) ion and ligand atoms within the monochlorocopper(II) complex. The nonbonding N···O, C···C, and C···O interactions within DMF molecules and the O···O contacts within perchlorate ions also contribute to the peak. The third peak and a small hump at 290 and 320 pm, respectively, may be due to the Cu···C interactions and the nonbonding interligand interactions within the monochlorocopper(II) complex. The Cu···N(DMF) nonbonding interactions should be involved in the peak at 410 pm as have been seen in the solvated copper(II) ion.[27]

At the first step of analysis of the radial distribution curve, the theoretical peak shapes due to the intramolecular interactions within DMF molecules and perchlorate ions were subtracted from the original curve. The structural parameter values were assumed to be the same as those obtained in liquid DMF and are quoted from the literature.[26] The residual curve drawn by the chain line (Fig. 3a) shows a large peak at 200 pm with a shoulder at 230 pm and three peaks around 290, 320, and 400 pm, which are all ascribable to the intramolecular interactions within the $[CuCl]^+$ complex. The peak at 200—230 pm should be due to the bonds between copper(II) ion and ligand atoms within the complex and the peak shape suggests that it consists of at least two interactions. However, the peak shape could not be analyzed by any assumption of only two kind Cu-O (ca. 200 pm) and Cu-Cl (ca. 230 pm) bonds with the values of the temperature factor of 20 and 70 pm^2,[3,5] respectively, and was possible to be explained by the introduction of a distorted octahedral model of the monochlorocopper(II) complex with three kinds of bonds: i.e., the equatorial Cu-O bond (ca. 200 pm) with the frequency factor 3, an equatorial Cu-Cl (ca. 220 pm) and two axial Cu-O bonds (ca. 240 pm). Moreover, the small peak observed at 320 pm was also explainable from the distorted octahedral model to be nonbonding interligand Cl(eq)···O(ax) interactions. The radial distribution curve and reduced intensities calculated on the basis of other structure models such as a square-planar four-coordination, a trigonal bipyramidal or a square pyramidal five-coordination structure did not fit the experimental values. Therefore, the monochlorocopper(II) complex was concluded to have a distorted octahedral structure.

The structure parameters of the $[CuCl(dmf)_5]^+$ complex were refined by a least-squares calculation for the $s\cdot i(s)$ curve over the region $s>4\times10^{-2}$ pm^{-1}, where the intramolecular interactions within the complex and those of DMF molecules and perchlorate ions mainly contribute to the $s\cdot i(s)$ values. In order to avoid errors introduced by neglecting long-range intermolecular interactions, the lower limit of the s-values was varied from 4×10^{-2} to 7×10^{-2} pm^{-1}. In the course of the calculation, the parameter values for the intramolecular interactions of DMF and perchlorate ion were fixed at the literature values.[26,28]

Table 2. Results of the Least-Squares Refinements of Solution A. Standard Deviations Are Given in Parentheses

Interaction	Parameter	A-I ($s>4\times10^{-2}$ pm^{-1})	A-II ($s>5\times10^{-2}$ pm^{-1})
Cu-O(eq)	r/pm	199(1)	199(1)
	b/10 pm^2	1(1)	1(1)
	n	3[a]	3[a]
Cu-Cl(eq)	r/pm	220(2)	221(3)
	b/10 pm^2	12(4)	14(5)
	n	1[a]	1[a]
Cu-O(ax)	r/pm	239(4)	240(4)
	b/10 pm^2	4(1)	3(1)
	n	2[a]	2[a]
O(eq)···O(eq)	r[b]/pm	281	281
	b/10 pm^2	6[a]	6[a]
	n	2[a]	2[a]
Cl(eq)···O(eq)	r[c]/pm	297	297
	b/10 pm^2	6[a]	6[a]
	n	2[a]	2[a]
O(eq)···O(ax)	r[d]/pm	311	312
	b/10 pm^2	12[a]	12[a]
	n	6[a]	6[a]
Cl(eq)···O(ax)	r[e]/pm	325	326
	b/10 pm^2	12[a]	12[a]
	n	2[a]	2[a]
Cu···C(eq)	r/pm	288(2)	288(1)
	b/10 pm^2	7(2)	5(3)
	n	3[a]	3[a]
Cu···N(eq)	r/pm	404(3)	412(2)
	b/10 pm^2	10(4)	7(3)
	n	3[a]	3[a]

a) The values were kept constant during the calculation. b) $r_{O(eq)\cdots O(eq)}=\sqrt{2}\,r_{Cu-O(eq)}$. c) $r_{Cl(eq)\cdots O(eq)}=\sqrt{r_{Cu-O(eq)}^2+r_{Cu-Cl(eq)}^2}$. d) $r_{O(eq)\cdots O(ax)}=\sqrt{r_{Cu-O(eq)}^2+r_{Cu-O(ax)}^2}$. e) $r_{Cl(eq)\cdots O(ax)}=\sqrt{r_{Cu-Cl(eq)}^2+r_{Cu-O(ax)}^2}$.

Some constraints were set for the distances of nonbonding interligand interactions as indicated at the footnote in Table 2 and the frequency factors of all interactions in the table were kept constant at the given values estimated from the distorted octahedral model of the complex in the course of the calculation. The Cu-O(eq), Cu-Cl(eq), and Cu-O(ax) bond distances were finally determined to be 199, 220, and 239 pm, respectively.

Structure of the $[CuCl_3]^-$ Complex. Solution B contains the trichlorocuprate(II) complex as the main species. Figure 4a shows the $(D(r)-4\pi r^2\rho_o)$ curve (solid line) of the solution, in which four peaks are observed around 130, 225, 360, and 410 pm. The first peak at 130 pm is due to the C-H, C=O, and C-N bonds within DMF molecules. The large peak at 225 pm is expected to be due to the Cu-Cl bonds from the sum of their ionic radii and partly to the Cu-O bonds within the $[CuCl_3]^-$ complex if some solvent molecules coordinate to copper(II) ion. The peak might also contain peaks due to intramolecular nonbonding N···O, C···C, and C···O interactions of DMF. The Li-O contacts within the solvated lithium ions also contribute, in part, to the peak as have been shown by a study of solution X-ray diffraction of solvated lithium ions.[29] However, because of the low concentration of lithium ions in solution B and the

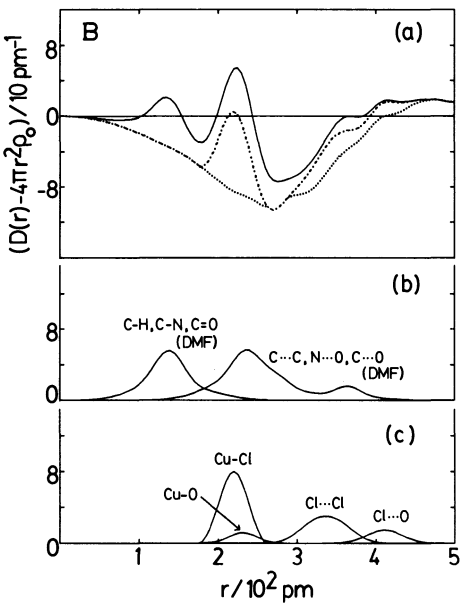

Fig. 4. (a) The $(D(r)-4\pi r^2\rho_o)$ curve for solution B, (b) The theoretical peaks for intramolecular interactions within DMF molecule. (c) The theoretical peak shapes due to the Cu-Cl, Cu-O, Cl···Cl, and Cl···O interactions within the trichloromono(*N*,*N*-dimethylformamide)cuprate(II) complex. The chain and dotted lines represent the residual curves after subtraction of the theoretical peaks in (b) and (c), respectively.

weak scattering power of lithium atom, the contribution of the solvated lithium ions to the scattered intensities is not significant, and it was neglected in the course of the data analysis. The third and fourth peaks around 360 and 410 pm, respectively, could be ascribed to the interligand interactions within the $[CuCl_3]^-$ complex.

After subtracting the theoretical peak shapes due to the intramolecular interactions within DMF molecules from the original curve, the residual curve expressed by the chain line (Fig. 4a) shows the predominant peak centered at 220 pm which can be attributed to the bonds between copper and ligand atoms in the trichlorocuprate(II) complex. The structure parameters of the complex were evaluated from the shape of the peak at 220 pm by a trial-and-error method. From the analysis a possibility of a dimeric structure ($[Cu_2Cl_6]^{2-}$) of the complex found in crystals[6-8] was ruled out since the peak area is appreciably smaller than that corresponding to four Cu-Cl bonds. The peak is well-reproduced by assuming three Cu-Cl bonds and one Cu-O bond with the lengths of 220 and 230 pm, respectively, as seen in Fig. 4a (dotted line). The Cu-O distance is also reasonably expected from the interligand interactions as discussed in the following section. The calculated $s \cdot i(s)$ values based on the structural model of $[CuCl_3(dmf)]^-$ give a better fit to the experimental ones than those of the trianglar or pyramidal $[CuCl_3]^-$ structure without a DMF molecule and of the $[Cu_2Cl_6]^{2-}$ dimer structure over $s>6\times10^{-2}$ pm^{-1}, where the intramolecular interactions within the complex and those of DMF molecules mainly contribute to the $s \cdot i(s)$ curve.

In the residual curve (chain line in Fig. 4a) two peaks, besides the peak at 220 pm, appear at about 350 and 410 pm which may be attributable to various combinations of nonbonding Cl···Cl and Cl···O interactions within the $[CuCl_3(dmf)]^-$ complex. These peaks could not be originated from a square-planar structure with the Cu-Cl bond length of 220 pm. The two peaks at 350 and 410 pm are only explainable when the complex has a distorted tetrahedral structure with the Cu-Cl and Cu-O bond distance of 220 and 230 pm, respectively.

A least-squares method was applied to the high-angle region ($s>4\times10^{-2}$ pm^{-1}) of the $s \cdot i(s)$ curve in order to refine the structural parameters obtained for the $[CuCl_3(dmf)]^-$ complex by a trial-and-error method. The initial structure parameter values inserted were those estimated from the analysis of the radial distribution curve as mentioned previously. In the course of the calculation the frequency factors of each interatomic interaction were kept at the same values as those obtained from the distorted tetrahedral model of the complex. The results are summarized in Table 3. The Cu-Cl and Cu-O lengths are finally evaluated to be 219 and 230 pm, respectively.

Structure of the $[CuCl_4]^{2-}$ Complex. The radial distribution curves for solutions C and D illustrated in Figs. 5 and 6, respectively, were analyzed by essentially the same procedure as that employed for solution B. Since the analysis of the intensity data by assuming the sole $[CuCl_4]^{2-}$ complex as the predominant species gave slightly different results between solutions C and D for the structure parameters of the complex, we can not neglect the $[CuCl_3(dmf)]^-$ complex coexisting in the solutions. The concentrations of the $[CuCl_3(dmf)]^-$ complex in solutions C and D are estimated to be 30 and 20 mol%, respectively, from the stability constants reported for the 1 mol dm^{-3} $LiClO_4$ DMF solution.[19]

Subtraction of theoretical peaks due to the C-H, C=O, C-N, N···O, C···C, and C···O interactions within DMF molecules and the Cu-Cl, Cu-O, Cl···Cl, and Cl···O pairs within the $[CuCl_3(dmf)]^-$ complex (Figs. 5b and 6b) from the radial distribution curve experimentally obtained leads to a residual curve

Table 3. Results of the Least-Squares Refinements of Solution B. Standard Deviations Are Given in Parentheses

Interaction	Parameter	B-I ($s>4\times10^{-2}$ pm^{-1})	B-II ($s>5\times10^{-2}$ pm^{-1})
Cu-Cl	r/pm	218(1)	219(1)
	b/10 pm^2	8(1)	8(1)
	n	3[b]	3[b]
Cu-O	r/pm	230(12)	230(13)
	b[a]/10 pm^2	4[b]	4[b]
	n	1[b]	1[b]
Cl···Cl[c]	r/pm	340(3)	346(2)
Cl···O[c]	b/10 pm^2	17(2)	18(3)
	n	2[b]	2[b]
Cl···Cl[c]	r/pm	410(3)	409(4)
Cl···O[c]	b/10 pm^2	30(4)	30(4)
	n	1[b]	1[b]

a) The values of the temperature factor were changed from 3 to 7, but practically the same results were obtained. b) The values were kept constant during the calculation. c) Assumed that $r_{Cl\cdots Cl}=r_{Cl\cdots O}$ and $b_{Cl\cdots Cl}=b_{Cl\cdots O}$.

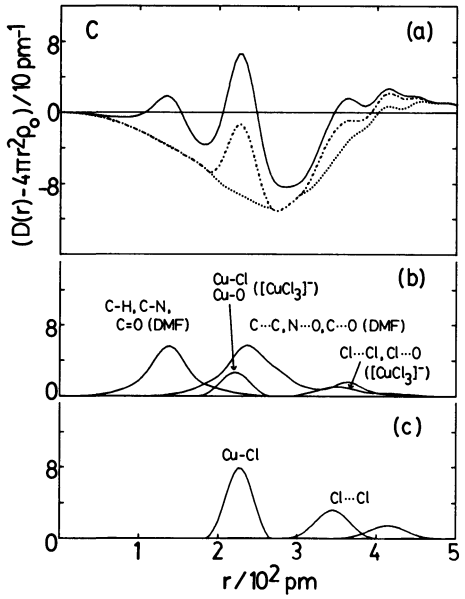

Fig. 5. (a) The $(D(r)-4\pi r^2\rho_o)$ curve for solution C. (b) The theoretical peaks for intramolecular interactions within DMF molecule and Cu-Cl, Cu-O, Cl···Cl, and Cl···O pairs within the trichloromono-(*N*,*N*-dimethylformamide)cuprate(II) complex. (c) The theoretical peak shapes calculated for the Cu-Cl and Cl···Cl interactions within the tetrachlorocuprate(II) complex. The chain and dotted lines indicate the residual curves after subtracting the theoretical peaks in (b) and (c), respectively.

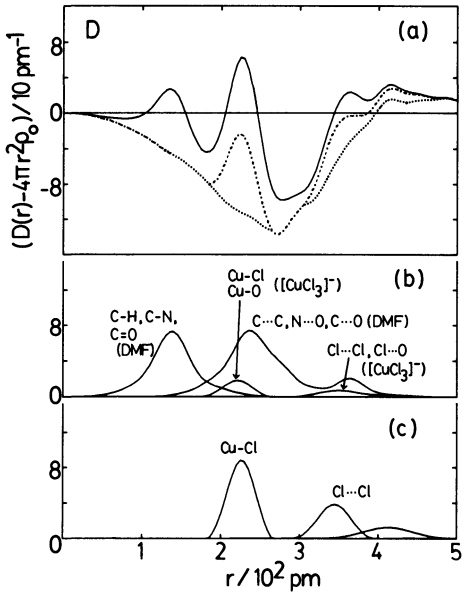

Fig. 6. (a) The $(D(r)-4\pi r^2\rho_o)$ curve for solution D. (b) The theoretical peaks for intramolecular interactions within DMF molecule and Cu-Cl, Cu-O, Cl···Cl, and Cl···O pairs within the trichloromono-(*N*,*N*-dimethylformamide)cuprate(II) complex. (c) The theoretical peak shapes calculated for the Cu-Cl and Cl···Cl interactions within the tetrachlorocuprate(II) complex. The chain and dotted lines indicate the residual curves after subtracting the theoretical peaks in (b) and (c), respeactively.

Table 4. Crystal Data of the $[CuCl_4]^{2-}$ Complex Ion with Various Cations[a)]

Complex	Distance(r/pm) r_{Cu-Cl}	$r_{Cl\cdots Cl}$	Angle(degree) ∠Cl-Cu-Cl	Ref.
Square planar (D_{4h})				
$(NH_4)_2[CuCl_4]$	232	328	90	9
		463	180	
$(C_2H_5NH_3)_2[CuCl_4]$	228	323	90	10
		456	180	
$(C_3H_7NH_3)_2[CuCl_4]$	229	324	90	11
		458	180	
$[(NH_3CH_2CH_2)_2NH_2]Cl[CuCl_4]$	227	321	90	12
		456	180	
$[(C_6H_5)CH_2CH_2NH_2(CH_3)]_2[CuCl_4]$ (low temp phase)	226	320	90	13
		453	180	
Distorted tetrahedral (D_{2d})				
$Cs_2[CuCl_4]$	220	343	103	14
		389	124	
$[C_6H_5CH_2N(CH_3)_3]_2[CuCl_4]$	226	344	99	15
		413	133	
$(CH_3NC_5H_4C_5H_4NCH_3)[CuCl_4]$	225	346	101	16
		406	129	
$(C_{13}H_{19}N_2OS)_2[CuCl_4]$	224	332	96	17
		425	143	
$[(CH_3)_3NH]_2[CuCl_4]$	224	339	98	18
		414	135	
$[(C_6H_5)CH_2CH_2NH_2(CH_3)]_2[CuCl_4]$ (high temp phase)	221	338	100	13
		400	131	

a) The interatomic distances and bond angles are averaged values.

(chain line in Figs. 5a and 6a), in which a major peak and two humps appear at 225, 350, and 410 pm. The peak at 225 pm is ascribable to the Cu-Cl bonds within the $[CuCl_4]^{2-}$ complex. The peak area corresponds to four Cu-Cl interactions and was found no evidence that any solvent molecule coordinated to copper(II) ion. The two humps at 350 and 410 pm, which are attributable to the nonbonding Cl···Cl interactions within the $[CuCl_4]^{2-}$ complex suggest that the complex has not a regular tetrahedral structure which should give only one peak originating from six Cl···Cl pairs at about 370 ($=225\times\sqrt{8/3}$) pm.

The structure of the $[CuCl_4]^{2-}$ complexes with various cations in crystal[9-18] can be classified into two groups; complexes in the first group are those having a square-planar structure (D_{4h} symmetry) and the others have a flattened tetrahedral structure (D_{2d} symmetry). Crystallographic data of these complexes are summarized in Table 4. In the square-planar complexes the Cu-Cl bond length is 226—232 pm, which is slightly longer than the Cu-Cl bond within the distorted tetrahedral complexes (r_{Cu-Cl}=220—226 pm). The nonbonding Cl···Cl distances within the square-planar complexes are in the range of 320—330 pm for four Cl···Cl interactions and 450—460 pm for the other two Cl···Cl interactions, while the distorted tetrahedral complexes have slightly longer Cl···Cl interactions for four Cl···Cl pairs (330—350 pm) but shorter Cl···Cl ones for the other two (400—420 pm). Since two humps are observed at 350 and 410 pm for solutions C and D (Figs. 5a and 6a, respectively), we conclude that the $[CuCl_4]^{2-}$ complex has a distorted tetrahedral structure with D_{2d} symmetry.

The structure parameters for the $[CuCl_4]^{2-}$ complex were finally determined by a least-squares calculation for the $s\cdot i(s)$ values over the range $s>4\times10^{-2}$ pm^{-1}. The refinement was carried out by floating the values of interatomic distances and temperature factors of the complex as independent variables, while the frequency factors of the interactions were kept unchanged. The results obtained for solutions C and D are summarized in Table 5. Essentially the same results were obtained for both solutions. The Cu-Cl bond length thus determined is 226 pm and the nonbonding Cl···Cl distances are 346 and 412 pm. The Cl-Cu-Cl bond angles are 100° and 131° in the complex.

The structure of the $[CuCl(dmf)_5]^+$ complex is distorted octahedral as the $[Cu(dmf)_6]^{2+}$ ion is. The Cu-O(eq) bond length (199(1) pm) within the $[CuCl(dmf)_5]^+$ is practically the same as that within the $[Cu(dmf)_6]^{2+}$ (203(3) pm).[27]

Both $[CuCl_3(dmf)]^-$ and $[CuCl_4]^{2-}$ complexes have a distorted tetrahedral structure. The Cu-O bond length (230(13) pm) within the $[CuCl_3(dmf)]^-$ complex is significantly longer than that of the equatorial Cu-O bonds in the $[Cu(dmf)_6]^{2+}$(203(3) pm)[27] and the $[CuCl(dmf)_5]^+$(199(1) pm). The DMF molecule within the trichlorocuprate(II) complex much more weekly solvates the central metal ion than the DMF molecules within the $[Cu(dmf)_6]^{2+}$ and $[CuCl(dmf)_5]^+$ complexes. On the other hand, the Cu-Cl distance of 225(1) pm within the $[CuCl_4]^{2-}$ complex is longer than that (219(1) pm) in $[CuCl_3(dmf)]^-$. The lengthening of the coordination bond with an increase in the number of chloride ions bound to the copper(II) ion may be caused by an increase in the electron donation of the chloride ions coordinated to the central metal ion and in the electrorepulsive force among the ligands.

The work has been financially supported by the Grant-in-Aid for Special Project Research No. 61134043 from the Ministry of Education, Science and Culture. Computer calculations were performed at the computer center of the Institute for Molecular Science in Okazaki.

References

1) J. R. Bell, J. L. Tyvoll, and D. L. Wertz, *J. Am. Chem. Soc.*, **95**, 1456 (1973).
2) M. Magini, *J. Chem. Phys.*, **74**, 2523 (1981).
3) G. W. Neilson, *J. Phys. C*, **15**, L233 (1982).
4) P. Lagarde, A. Fontaine, D. Raoux, A. Sadoc, and P. Migliardo, *J. Chem. Phys.*, **72**, 3061 (1980).
5) M. Ichihashi, H. Wakita and I. Masuda, *Bull. Chem.*

Table 5. Results of the Least-Squares Calculation for the Structural Parameters of the Distorted Tetrahedral $[CuCl_4]^{2-}$ Ion. The Values in Parentheses Represent Standard Deviations

Interaction	Parameter	Solution C	Solution D
Cu-Cl	r/pm	226.1(4)	225.1(2)
	b/10 pm^2	5.9(3)	7.6(5)
	n	4[a]	4[a]
Cl···Cl	r/pm	346(2)	345(2)
	b/10 pm^2	14(1)	14(3)
	n	4[a]	4[a]
Cl···Cl	r/pm	414(5)	411(5)
	b/10 pm^2	28(10)	23(7)
	n	2[a]	2[a]

a) The values were kept constant during the calculation.

Soc. Jpn., **56**, 3761 (1983).
6) S. C. Abrahams and H. J. Williams, *J. Chem. Phys.*, **39**, 2923 (1963).
7) R. D. Willett, C. Dwiggins, Jr., R. F. Kruh, and R. E. Rundle, *J. Chem. Phys.*, **38**, 2429 (1963).
8) A. W. Schlueter, R. A. Jacobson, and R. E. Rundle, *Inorg. Chem.*, **5**, 277 (1966).
9) R. D. Willett, *J. Chem. Phys.*, **41**, 2243 (1964).
10) J. P. Steadman and R. D. Willett, *Inorg. Chem.*, **4**, 367 (1970).
11) F. Barendregt and H. Schenk, *Physica*, **49**, 465 (1970).
12) G. L. Ferguson and B. Zaslow, *Acta Crystallogr., Sect. B*, **27**, 849 (1971).
13) R. L. Harlow, W. J. Wells, III, G. W. Watt, and S. H. Simonsen, *Inorg. Chem.*, **13**, 2106 (1974).
14) B. Morosin and E. C. Lingafelter, *J. Phys. Chem.*, **65**, 50 (1961).
15) M. Bonamico, G. Dessy, and V. Vaciago, *Theor. Chim. Acta*, **7**, 367 (1967).
16) J. H. Russell and S. C. Wallwork, *Acta Crystallogr., Sect. B*, **25**, 1691 (1969).
17) A. C. Bonamartini, M. Nardelli, C. Palmieri, and C. Pelizzi, *Acta Crystallogr., Sect. B*, **27**, 1775 (1971).
18) Par J. Lamotte-Brasseur, L. Dupont, and O. Dideberg, *Acta Crystallogr., Sect. B*, **29**, 241 (1973).
19) S. Ishiguro, B. G. Jeliazkova, and H. Ohtaki, *Bull. Chem. Soc. Jpn.*, **58**, 1143 (1985).
20) S. Ishiguro, B. G. Jeliazkova, and H. Ohtaki, *Bull. Chem. Soc. Jpn.*, **58**, 1749 (1985).
21) S. Ishiguro, H. Suzuki, B. G. Jeliazkova, and H. Ohtaki, *Bull. Chem. Soc. Jpn.*, **59**, 2407 (1986).
22) M. A. Khan and M. J. Schwing-Weill, *Inorg. Chem.*, **15**, 2202 (1976).
23) H. Ohtaki, *Rev. Inorg. Chem.*, **4**, 103 (1982).
24) G. Johansson and M. Sandström, *Chem. Scr.*, **4**, 195 (1973).
25) T. Yamaguchi, Doctor Thesis, Tokyo Institute of Technology, March (1978).
26) H. Ohtaki, S. Itoh, T. Yamaguchi, S. Ishiguro, and B. M. Rode, *Bull. Chem. Soc. Jpn.*, **56**, 3406 (1983).
27) K. Ozutsumi, S. Ishiguro, and H. Ohtaki, *Bull. Chem. Soc. Jpn.*, in press.
28) H. Ohtaki, T. Yamaguchi and M. Maeda, *Bull. Chem. Soc. Jpn.*, **49**, 701 (1976).
29) H. Ohtaki and H. Wada, *J. Solution Chem.*, **14**, 209 (1985).

 © 1988 The Chemical Society of Japan Bull. Chem. Soc. Jpn., 61, 723—727 (1988)

The Conversion of (+)-Dehydroabietic Acid into Steroidal Hormones

Takashi MATSUMOTO,* Sachihiko IMAI, Yasuhiro SUNAOKA, and Takashi YOSHINARI
Department of Chemistry, Faculty of Science, Hiroshima University,
Higashisenda-machi, Naka-ku, Hiroshima 730
(Received April 24, 1987)

A resin acid, (+)-dehydroabietic acid, was converted into 3,4,4a,9,10,10a-hexahydro-7-methoxy-10aβ-methyl-4aαH-phenanthren-1(2H)-one (**2**) by the introduction of oxygen functions at the C-4 and C-13 positions, and a rearrangement of the angular methyl group to the C-5 position. The hydrophenanthrene derivative **2** was further transformed into 2,3,3a,4,5,9b-hexahydro-7-methoxy-3aβ-methyl-9bαH-1H-benz[e]inden-3β-ol (**3**). Since the conversion of **3** into steroidal hormones has already been reported, the present synthesis can be regarded as the synthesis of steroidal hormones from (+)-dehydroabietic acid.

The conversion of (+)-dehydroabietic acid (**1**) into steroidal compounds has been attempted by several groups.[1-4] Jeger et al. have reported the transformation of **1** into 3-oxo-17β-acetoxy-14α-methyl-Δ^4-8α,9β,10α,13α-esterene. However, other groups have carried out only partial modifications of **1**, and have not reported the synthesis of natural steroids. We have also investigated the utilization of **1** as a starting material for the syntheses of optically active steroids. In this paper, we describe the transformation of **1** into 2,3,3a,4,5,9b-hexahydro-7-methoxy-3aβ-methyl-9bαH-1H-benz[e]inden-3β-ol (**3**), a useful intermediate for the syntheses of steroidal hormones, which has already been converted into estradiol (**4**), adrenosterone, and so on.[5] Our basic strategy for the synthesis of steroidal hormones is the modification of the A, B, and C rings in the diterpene skeleton to the D, C, and B rings of the steroidal skeleton, as shown in Scheme 1. Namely, (+)-dehydroabietic acid (**1**) was converted into 3,4,4a,9,10,10a-hexahydro-7-methoxy-10aβ-methyl-4aαH-phenanthren-1(2H)-one (**2**) by the introduction of oxygen functions at the C-4 and C-13 positions, and a rearrangement of the angular methyl group at the C-10 position to the C-5 position. Ring contraction of the cyclohexanone moiety in **2** gave the corresponding cyclopentanol derivative **3**.

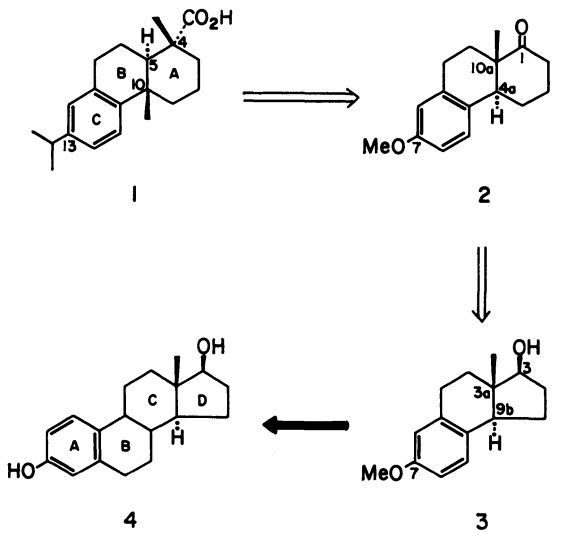

Scheme 1.

The oxidation of (+)-dehydroabietic acid (**1**) with chromium trioxide and acetic anhydride in acetic acid, followed by alkaline hydrolysis in refluxing diethylene glycol, afforded 13-acetyl-7-oxo-8,11,13-podocarpatrien-18-oic acid[6] (**5**: 8%) and 15-hydroxy-7-oxo-8,11,13-abietatrien-18-oic acid (**6**: 26%). The acid **6** was treated with diazomethane in ether and the resulting ester **7** (97%) was oxidized with t-butyl hydroperoxide in acetic acid containing concentrated sulfuric acid to give methyl 13-hydroxy-7-oxo-8,11,13-podocarpatrien-18-oate[6] (**8**: 76%). This compound **8** was also obtained in 32% yield from **5** by a series of reactions: esterification with diazomethane, Baeyer–Villiger oxidation with m-chloroperbenzoic acid, and alkaline hydrolysis. The methylation of **8** with methyl iodide and anhydrous potassium carbonate in refluxing ethyl methyl ketone gave a methyl ether **9** (97%), which was converted into methyl 13-methoxy-8,11,13-podocarpatrien-18-oate[7-9] (**10**: 87%) by acidic hydrogenolysis using Pd–C and perchloric acid in ethyl acetate. The Grignard reaction of **10** with phenylmagnesium bromide afforded a diphenylmethanol derivative **11** in 81% yield, which was then treated with lead tetraacetate and calcium carbonate in refluxing benzene to give a mixture of Δ^3, Δ^4, and $\Delta^{4(18)}$-19-nor compounds **12** in 70% yield. Ozonolysis of **12** in dichloromethane afforded 3,4,4a,9,10,10a-hexahydro-7-methoxy-4aβ-methyl-10aαH-phenanthren-1(2H)-one (**13**) in 60% yield. This ketone **13** was transformed into a tetraene compound **15** (93%) via a mesylate **14** by a series of reactions: lithium aluminium hydride reduction, mesylation, and refluxing with 2,4-lutidine. Subsequently, a rearrangement of the angular methyl group at the C-4a position to the C-10a position was carried out as follows. Epoxidation of **15** with m-chloroperbenzoic acid, followed by treatment with boron trifluoride etherate in dichloromethane, afforded a rearranged alcohol (**16**)[10] in 52% yield. This was then hydrogenated over Pd–C in ethanol to give 1,2,3,4,4a,9,10,10a-octahydro-7-methoxy-10aβ-methyl-4aαH-phenanthren-1β-ol (**17**: 99%) which gave an acetate **18** (96%). The β-configuration of the hydroxyl group in **17** was

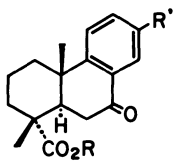

5 R=H, R'=Ac
8 R=Me, R'=OH
9 R=Me, R'=OMe

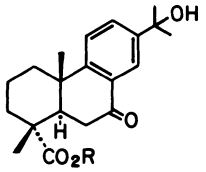

6 R=H
7 R=Me

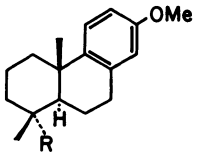

10 R=CO_2Me
11 R=C(OH)Ph_2

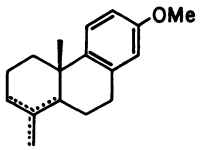

12

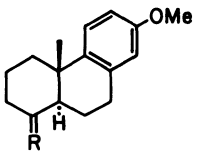

13 R=O
14 R=β-OMs, α-H

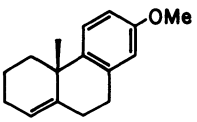

15

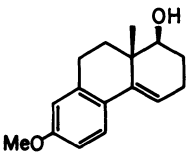

16

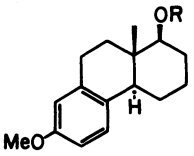

17 R=H
18 R=Ac

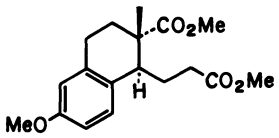

19

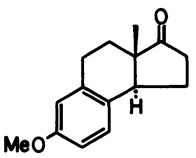

20

supported from its ^1H NMR spectrum, which showed a broad signal due to the C-1 proton at δ 3.1—3.5, suggesting the presence of an axial α proton. Oxidation of **17** with pyridinium chlorochromate in dichloromethane afforded the desired ketone **2** in 89% yield.

According to the method of Rao and Banerjee,[11] the ketone **2** was submitted to oxidative cleavage with potassium hypoiodite and subsequent esterification with diazomethane to afford a dimethyl ester **19** in 49% yield. Dieckmann cyclization of **19** with potassium *t*-butoxide in refluxing benzene, followed by hydrolysis and subsequent decarboxylation, produced 3a,4,5,9b-tetrahydro-7-methoxy-3aβ-methyl-9bαH-1H-benz-[*e*]inden-3(2H)-one (**20**) in 78% yield. This was reduced with lithium aluminium hydride in ether to give the desired alcohol **3** in 91% yield.

Since the syntheses of steroidal hormones from **3** have already been reported, the present synthesis of **3** can be regarded as the synthesis of steroidal hormones from a resin acid, (+)-dehydroabietic acid (**1**).

Experimental

All melting points are uncorrected. The IR spectra and optical rotations were measured in chloroform, and the ^1H NMR spectra in carbon tetrachloride at 60 MHz, with tetramethylsilane as an internal standard, unless otherwise stated; s: singlet, bs: broad singlet, d: doublet, bd: broad doublet, dd: double doublet, t: triplet, m: multiplet. The column chromatography was performed using Merck silica gel (0.063 mm).

Oxidation of (+)-Dehydroabietic Acid (1) with Chromium Trioxide. Chromium trioxide (43.0 g) was added to a stirred solution of (+)-dehydroabietic acid (**1**) (30.0 g) and acetic anhydride (200 ml) in acetic acid (150 ml) with cooling in a water bath at 15—25 °C over a period of 2 h. After stirring at room temperature for 1 h, methanol (75 ml) was added dropwise to the stirred mixture with cooling in an ice-water bath at 10—15 °C over a period of 1 h. The mixture was concentrated in vacuo, diluted with water, and extracted with benzene. The benzene extract was washed with brine, dried over sodium sulfate, and evaporated in vacuo. The residue was chromatographed on silica gel (Mallinckrodt CC-4, 150 g) using ether-benzene (1:9 and then 3:7) as eluents, to give a mixture (25.1 g) of 15-acetoxy-7-oxo-8,11,13-abietatrien-18-oic acid and 13-acetyl-7-oxo-8,11,13-podocarpatrien-18-oic acid (**5**).[6]

The above mixture (25.1 g) was refluxed with aqueous potassium hydroxide (25%, 30 ml) in diethylene glycol (100 ml) for 2 h. The mixture was cooled, acidified with dilute hydrochloric acid, and extracted with ether. The ether extract was washed with brine, dried, and evaporated in vacuo. The residue was chromatographed on silica gel (Mallinckrodt CC-4, 300 g), using ether-benzene (15:85) as the eluent, to give **5** (2.6 g:8.3%). This was recrystallized from a mixture of acetone and hexane, mp 192—193.5 °C, $[\alpha]_D$ +29.7° (*c* 3.61), IR 3600—2300 and 1686 cm^{-1}, ^1H NMR ($CDCl_3$) δ=1.30 (3H, s) and 1.38 (3H, s) (C_4-CH_3 and C_{10}-CH_3), 2.63 (3H, s, -$COCH_3$), 7.48 (1H, d, J=8 Hz, C_{11}-H), 8.13 (1H, dd, J=8 and 2 Hz, C_{12}-H), 8.52 (1H, d, J=2 Hz, C_{14}-H), 9.5 (1H, bs, -CO_2H). Found: C, 72.41; H, 7.35%. Calcd for $C_{19}H_{22}O_4$:C, 72.59; H, 7.05%. Further elution with ether-benzene (35:65) gave 15-hydroxy-7-oxo-8,11,13-abietatrien-18-oic acid (**6**) (8.4 g:25.5%). This was recrystallized from benzene, mp 118—120 °C, $[\alpha]_D$ +10.4° (*c* 5.21), IR 3600—2300, 1698, and 1682 cm^{-1}, ^1H NMR ($CDCl_3$) δ=1.27 (3H, s) and 1.35 (3H, s) (C_4-CH_3 and C_{10}-CH_3), 1.58 (6H, s, -$C(CH_3)_2OH$), 7.34 (1H, d, J=9 Hz, C_{11}-H), 7.74 (1H, dd, J=9 and 2 Hz, C_{12}-H), 8.06 (1H, d,

J=2 Hz, C_{14}-H). Found: C, 72.40; H, 7.99%. Calcd for $C_{20}H_{26}O_4$: C, 72.70; H, 7.93%.

Methyl 15-Hydroxy-7-oxo-8,11,13-abietatrien-18-oate (7). The acid **6** (3.325 g) was treated with an ethereal diazomethane solution at room temperature for 30 min. After the usual work-up, the crude product was chromatographed on silica gel (0.063—0.200 mm, 120 g), using ether-benzene (3:7) as the eluent, to give an oily **7** (3.355 g:96.8%), $[\alpha]_D$ +15.0° (*c* 6.00), IR 3594, 1720, and 1678 cm^{-1}; ^1H NMR δ=1.23 (3H, s) and 1.30 (3H, s) (C_4-CH_3 and C_{10}-CH_3), 1.51 (6H, s, -C(CH_3)$_2$OH), 3.63 (3H, s, -CO_2CH_3), 7.21 (1H, d, J=8 Hz, C_{11}-H), 7.62 (1H, dd, J=8 and 2 Hz, C_{12}-H), 7.87 (1H, d, J=2 Hz, C_{14}-H). Found: C, 73.43; H, 8.11%. Calcd for $C_{21}H_{28}O_4$: C, 73.22; H, 8.19%.

Methyl 13-Hydroxy-7-oxo-8,11,13-podocarpatrien-18-oate (8). *a*): A stirred mixture of **7** (5.973 g), *t*-butyl hydroperoxide (70%, 5.0 ml), and concentrated sulfuric acid (1.2 ml) in acetic acid (59 ml) was heated at 50 °C for 3 h. The mixture was cooled, poured into aqueous sodium hydrogencarbonate, and extracted with ether. The ether extract was washed with brine, dried, and evaporated in vacuo. The residue was chromatographed on silica gel (0.063—0.200 mm, 60 g), using ether-benzene (1:9) as the eluent, to give **8** (3.966 g:75.6%). This was recrystallized from benzene, mp 197—198.5 °C, $[\alpha]_D$ −11.4° (*c* 7.47), IR 3325, 1720, and 1675 cm^{-1}; ^1H NMR ($CDCl_3$) δ=1.22 (3H, s) and 1.33 (3H, s) (C_4-CH_3 and C_{10}-CH_3), 3.65 (3H, s, -CO_2CH_3), 7.02 (1H, dd, J=9 and 2.5 Hz, C_{12}-H), 7.22 (1H, d, J=9 Hz, C_{11}-H), 7.54 (1H, d, J=2.5 Hz, C_{14}-H), 7.83 (1H, bs, -OH). Found: C, 71.78; H, 7.49%. Calcd for $C_{18}H_{22}O_4$: C, 71.50; H, 7.33%.

b): The acid **5** (1.920 g) was treated with an ethereal diazomethane solution at room temperature for 30 min to give a crude ester (2.003 g), IR 1722 and 1685 cm^{-1}.

The above ester (2.003 g) was refluxed with *m*-chloroperbenzoic acid (85%, 1.218 g) and *p*-toluenesulfonic acid (18 mg) in 1,2-dichloroethane (18 ml) for 4 h. The mixture was cooled, diluted with ether, and washed successively with aqueous potassium iodide, aqueous sodium thiosulfate, aqueous sodium hydrogencarbonate, and brine. After removal of the solvent in vacuo, the residue was refluxed with sodium hydrogencarbonate (1.40 g) and water (10 ml) in methanol (40 ml) for 2 h. The mixture was concentrated in vacuo, diluted with water, and extracted with ether. The ether extract was washed with aqueous sodium hydroxide and water, dried, and evaporated in vacuo. The residue was chromatographed on silica gel (0.063—0.200 mm, 30 g), using ether-benzene (1:9) as the eluent, to give the recovered methyl 13-acetyl-7-oxo-8,11,13-podocarpatrien-18-oate (582 mg).

The alkaline washing was acidified with dilute hydrochloric acid and extracted with ether. The ether extract was washed with brine, dried, and evaporated in vacuo. The residue was chromatographed on silica gel (0.063—0.200 mm, 30 g), using ether-benzene (1:9) as the eluent, to give **8** (581 mg:31.6%), whose IR and ^1H NMR spectra were identical with those of the authentic sample.

Methyl 13-Methoxy-7-oxo-8,11,13-podocarpatrien-18-oate (9). A stirred mixture of **8** (8.778 g), methyl iodide (6.2 ml), and anhydrous potassium carbonate (25.0 g) in ethyl methyl ketone (90 ml) was refluxed for 8 h. The mixture was cooled, diluted with ether, and washed successively with water, aqueous sodium thiosulfate, and brine. The dried solution was evaporated in vacuo. The residue was chromatographed on silica gel (0.063—0.200 mm, 200 g), using ether-benzene (3:97) as the eluent, to give an oily **9** (8.917 g: 97.2%), $[\alpha]_D$ +11.4° (*c* 3.78), IR 1725 and 1676 cm^{-1}, ^1H NMR δ=1.21 (3H, s) and 1.30 (3H, s) (C_4-CH_3 and C_{10}-CH_3), 3.63 (3H, s, -CO_2CH_3), 3.79 (3H, s, -OCH_3), 6.92 (1H, dd, J=9 and 3 Hz, C_{12}-H), 7.19 (1H, d, J=9 Hz, C_{11}-H), 7.33 (1H, d, J=3 Hz, C_{14}-H). Found: C, 72.34; H, 7.69%. Calcd for $C_{19}H_{24}O_4$: C, 72.12; H, 7.65%.

Methyl 13-Methoxy-8,11,13-podocarpatrien-18-oate (10). A mixture of **9** (21.268 g), Pd-C (10%, 4.0 g), and perchloric acid (60%, 4.0 ml) in ethyl acetate (100 ml) was hydrogenated at room temperature under an atmosphere of hydrogen for 9 h. After the usual work-up, the crude product was recrystallized from methanol to give **10** (13.328 g:65.6%), mp 79.5—80 °C, $[\alpha]_D$ +60.7° (*c* 1.52), IR 1720 cm^{-1}, ^1H NMR δ=1.14 (3H, s) and 1.21 (3H, s)(C_4-CH_3 and C_{10}-CH_3), 3.60 (3H, s) and 3.67 (3H, s) (-CO_2CH_3 and -OCH_3), 6.40 (1H, bs, C_{14}-H), 6.50 (1H, dd, J=8 and 2 Hz, C_{12}-H), 6.99 (1H, d, J=8 Hz, C_{11}-H). Found: C, 75.41; H, 8.54%. Calcd for $C_{19}H_{26}O_3$: C, 75.46; H, 8.67%. The mother liquor of recrystallization was evaporated in vacuo. The residue was chromatographed on silica gel (150 g), using ether-benzene (1:99) as the eluent, to give an additional **10** (4.378 g:21.5%).

Grignard Reaction of 10 with Phenylmagnesium Bromide. A solution of **10** (3.975 g) in dry ether (25 ml) was added to a stirred ether solution of phenylmagnesium bromide prepared from magnesium turnings (1.60 g) and bromobenzene (6.9 ml) in dry ether (15 ml). The mixture was refluxed for 30 min and the ether was removed. The viscous residue was heated at 90—100 °C for 5.5 h. After cooling, the mass was hydrolyzed with a mixture of dilute hydrochloric acid and ice, and then extracted with ether. The ether extract was washed succesively with aqueous sodium thiosulfate and brine, dried, and evaporated in vacuo. The residue was chromatographed on silica gel (150 g), using hexane-benzene (1:4) as the eluent, to give a diphenylmethanol derivative **11** (4.555 g:81.2%). This was recrystallized from acetone-hexane, mp 178.5—182 °C, $[\alpha]_D$ +65.8° (*c* 3.71), IR 3580 cm^{-1}, ^1H NMR δ=1.17 (3H, s, C_{10}-CH_3), 1.32 (3H, s, C_4-CH_3), 3.58 (3H, s, -OCH_3), 6.18 (1H, d, J=2.5 Hz, C_{14}-H), 6.43 (1H, dd, J=9 and 2.5 Hz, C_{12}-H), 6.94 (1H, d, J=9 Hz, C_{11}-H), 7.0—7.9 (10H, m, 2-C_6H_5). Found: C, 84.22; H, 8.01%. Calcd for $C_{30}H_{34}O_2$: C, 84.46; H, 8.03%.

Oxidation of 11 with Lead Tetraacetate. A stirred mixture of **11** (8.316 g), lead tetraacetate (91.4%, 12.30 g), and calcium carbonate (10.60 g) in dry benzene (110 ml) was refluxed for 5 h. The mixture was cooled, diluted with ether and water, and then filtered. The filtrate was extracted with ether. The ether extract was washed successively with aqueous potassium iodide, aqueous sodium thiosulfate, aqueous sodium hydrogencarbonate, and brine. The dried solution was evaporated in vacuo. The crude product was chromatographed on silica gel (200 g), using hexane-benzene (9:1) as the eluent, to give 13-methoxy-19-norpodocarpa-4(18),8,11,13-tetraene (**12**) 3.307 g:70.0%) containing small amounts of Δ^3- and Δ^4-isomers. ^1H NMR δ=0.96 (3H, s, C_{10}-CH_3), 3.78 (3H, s, -OCH_3), 4.64 (1H, bs) and 4.79 (1H, bs) (-$\overset{|}{C}$=CH_2), 6.48 (1H, bs, C_{14}-H), 6.55 (1H, dd, J=9 and 3 Hz, C_{12}-H), 7.07 (1H, d, J=9 Hz, C_{11}-H). Found: C, 84.50; H, 9.08%. Calcd for $C_{17}H_{22}O$: C, 84.25; H, 9.15%.

3,4,4a,9,10,10a-Hexahydro-7-methoxy-4aβ-methyl-10aα*H*-phenanthren-1(2*H*)-one (13). A solution of **12** (1.937 g) in dichloromethane (20 ml) was ozonized at −65 °C for 1 h. The solution was evaporated in vacuo. The residue was heated with zinc powder (1.37 g) in aqueous acetic acid (50%, 46 ml) at 80 °C for 1 h and then filtered. The filtrate was concentrated in vacuo and extracted with ether. The ether extract was washed with aqueous sodium hydrogencarbonate and brine, dried, and evaporated in vacuo. The residue was chromatographed on silica gel (50 g), using ether–benzene (2:98) as the eluent, to give **13** (1.172 g:60.0%). This was recrystallized from hexane, mp 70.5—71 °C, $[\alpha]_D$ +189° (*c* 3.93), IR 1707 cm^{-1}, ^1H NMR δ=0.99 (3H, s, C_{4a}-CH_3), 3.70 (3H, s, -OCH_3), 6.47 (1H, bs, C_8-H), 6.55 (1H, dd, *J*=8 and 2.5 Hz, C_6-H), 7.07 (1H, d, *J*=8 Hz, C_5-H). Found: C, 78.49; H, 8.19%. Calcd for $C_{16}H_{20}O_2$: C, 78.65; H, 8.25%.

2,3,4,4a,9,10-Hexahydro-7-methoxy-4aβ-methylphenanthrene (15). A solution of **13** (940 mg) in dry ether (10 ml) was reduced with lithium aluminium hydride (73 mg) at room temperature for 1 h. The mixture was poured into dilute hydrochloric acid and extracted with ether. The ether extract was washed with brine, dried, and evaporated in vacuo. The residue was dissolved in pyridine (4.5 ml) and mesylated with methanesulfonyl chloride (0.45 ml) at room temperature for 19 h. The mixture was poured into dilute hydrochloric acid and extracted with ether; the extract was washed successively with aqueous sodium hydrogencarbonate and brine. The dried solution was evaporated in vacuo to give a crude mesylate **14** (1.210 g), IR 1340 and 1175 cm^{-1}, ^1H NMR δ=1.21 (3H, s, C_{4a}-CH_3), 2.92 (3H, s, -OSO_2CH_3), 3.70 (3H, s, -OCH_3), 4.85 (1H, $W_{1/2}$=6 Hz, C_1-H), 6.46 (1H, bs, C_8-H), 6.54 (1H, dd, *J*=9 and 3 Hz, C_6-H), 7.02 (1H, d, *J*=9 Hz, C_5-H).

A solution of the crude mesylate **14** (1.210 g) in 2,4-lutidine (4.0 ml) was refluxed for 2.5 h under a stream of nitrogen. The solution was cooled, poured into dilute hydrochloric acid, and extracted with ether. The ether extract was washed with brine, dried, and evaporated in vacuo. The crude product was chromatographed on silica gel (25 g), using hexane–benzene (1:1) as the eluent, to give **15** (815 mg:92.8% from **13**). This was recrystallized from hexane, mp 69—69.5 °C, $[\alpha]_D$ +233° (*c* 3.41), ^1H NMR δ=1.34 (3H, s, C_{4a}-CH_3), 3.70 (3H, s, -OCH_3), 5.39 (1H, br, C_1-H), 6.40 (1H, d, *J*=3 Hz, C_8-H), 6.60 (1H, dd, *J*=9 and 3 Hz, C_6-H), 7.06 (1H, d, *J*=9 Hz, C_5-H). Found: C, 83.95; H, 9.08%. Calcd for $C_{16}H_{20}O$: C, 84.16; H, 8.83%.

1,2,3,9,10,10a-Hexahydro-7-methoxy-10aβ-methyl-1β-phenanthrenol (16). A mixture of **15** (303 mg) and *m*-chloroperbenzoic acid (80%, 315 mg) in dichloromethane (10 ml) was stirred at room temperature for 2 h. The mixture was diluted with ether and washed successively with aqueous potassium iodide, aqueous sodium thiosulfate, aqueous sodium hydrogencarbonate, and water. The dried solution was evaporated in vacuo. The residual oil was dissolved in dichloromethane (4.0 ml) and boron trifluoride etherate (0.49 ml) was added at 2—8 °C. After stirring at 2—3 °C for 40 min, the mixture was diluted with ether, poured into dilute hydrochloric acid, and extracted with ether. The ether extract was washed with water, dried, and evaporated in vacuo. The crude product was chromatographed on silica gel (15 g), using ether–benzene (1:9) as the eluent, to give **16** (168 mg:51.8%). This was recrystallized from acetone–hexane, mp 133.5—135.5 °C, IR 3610 and 3435 cm^{-1}, ^1H NMR ($CDCl_3$) δ=1.01 (3H, s, C_{10a}-CH_3), 3.80 (3H, s, -OCH_3), 5.99 (1H, t, *J*=3.5 Hz, C_4-H), 6.62 (1H, s, C_8-H), 6.71 (1H, dd, *J*=9 and 2 Hz, C_6-H), 7.47 (1H, d, *J*=9 Hz, C_5-H). Found: C, 78.40; H, 8.35%. Calcd for $C_{16}H_{20}O_2$: C, 78.65; H, 8.25%.

1,2,3,4 4a,9,10,10a-Octahydro-7-methoxy-10aβ-methyl-4aα*H*-phenanthren-1β-ol (17) and Its Acetate (18). *a*): A mixture of **16** (69.3 mg) and Pd-C (5%, 30 mg) in ethanol (15 ml) was hydrogenated at room temperature under an atmosphere of hydrogen for 3 h. After the usual work-up, the product **17** (69.0 mg:98.8%) was recrystallized from hexane, mp 100—101.5 °C, IR 3610 and 3450 cm^{-1}, ^1H NMR δ=0.69 (3H, s, C_{10a}-CH_3), 3.1—3.5 (1H, m, C_1-H), 3.73 (3H, s, -OCH_3), 6.35—6.65 (2H, m, C_6-H and C_8-H), 6.99 (1H, d, *J*=9 Hz, C_5-H). Found: C, 78.04; H, 9.27%. Calcd for $C_{16}H_{22}O_2$: C, 78.01; H, 9.00%.

b): A solution of **17** (39.0 mg) and acetic anhydride (0.5 ml) in pyridine (0.5 ml) was heated at 75—80 °C for 2 h. After the usual work-up, the crude product was chromatographed on silica gel (5.0 g), using benzene as the eluent, to give an acetate **18** (44.5 mg:96.2%). This was recrystallized from hexane, mp 141.5—142 °C, IR 1720 cm^{-1}, ^1H NMR (90 MHz) δ=0.75 (3H, s, C_{10a}-CH_3), 1.97 (3H, s, -$OCOCH_3$), 3.69 (3H, s, -OCH_3), 4.45—4.7 (1H, m, C_1-H), 6.49 (1H, s, C_8-H), 6.54 (1H, dd, *J*=9 and 3 Hz, C_6-H), 6.99 (1H, d, *J*=9 Hz, C_5-H). Found: C, 74.81; H, 8.61%. Calcd for $C_{18}H_{24}O_3$: C, 74.97; H, 8.39%.

Oxidation of 17 into 3,4,4a,9,10,10a-Hexahydro-7-methoxy-10aβ-methyl-4aα*H*-phenanthren-1(2*H*)-one (2). A mixture of **17** (38.0 mg) and pyridinium chlorochromate (56.5 mg) in dichloromethane (3.0 ml) was stirred at 0—5 °C for 5 min and at room temperature for 3 h. After the addition of aqueous sodium hydrogencarbonate, the mixture was extracted with ether. The ether extract was washed with water, dried, and evaporated in vacuo. The crude product was chromatographed on silica gel (5.0 g), using benzene as the eluent, to give **2** (34.1 mg:89.3%). This was recrystallized from hexane, mp 91—92 °C, IR 1701 cm^{-1}, ^1H NMR δ=0.94 (3H, s, C_{10a}-CH_3), 3.73 (3H, s, -OCH_3), 6.51 (1H, s, C_8-H), 6.58 (1H, dd, *J*=9 and 2 Hz, C_6-H), 7.05 (1H, d, *J*=9 Hz, C_5-H). Found: C, 78.48; H, 8.46%. Calcd for $C_{16}H_{20}O_2$: C, 78.65; H, 8.25%.

Methyl 1,2,3,4-Tetrahydro-6-methoxy-2α-methoxycarbonyl-2β-methyl-1α*H*-naphthalene-1-propionate (19). A solution of **2** (164.7 mg) in methanol (14 ml) was treated alternately with three drops of a solution of iodine (494.1 mg) in methanol (8.2 ml) and one drop of a solution of potassium hydroxide (889.4 mg) in water (1.8 ml) and methanol (4.9 ml) with vigorous stirring at room temperature under a stream of nitrogen over a period of 1 h. The mixture was allowed to stand at room temperature for 23 h and the methanol was removed in vacuo. The residue was acidified with dilute hydrochloric acid and extracted with ether. The ether extract was washed successively with water, aqueous sodium thiosulfate, and water. The dried solution was evaporated in vacuo and the residue was treated with ethereal diazomethane solution at room temperature for 30 min. After the usual work-up, the crude product was chromatographed on silica gel (10 g), using ether–benzene (1:99) as the eluent, to give an oily **19** (104.7 mg:48.5%), IR 1728 cm^{-1}, ^1H NMR δ=1.22 (3H, s, C_2-CH_3), 3.45 (3H, s) and 3.58 (3H, s) (2-CO_2CH_3), 3.69 (3H, s, -OCH_3), 6.43 (1H, bs),

6.51 (1H , dd, J=9 and 3 Hz), and 6.82 (1H, d, J=9 Hz) (aromatic protons). Found: C, 67.65; H, 7.79%. Calcd for $C_{18}H_{24}O_5$: C, 67.48; H, 7.55%.

3a,4,5,9b-Tetrahydro-7-methoxy-3aβ-methyl-9bα*H*-1*H*-benz[*e*]inden-3(2*H*)-one (20). A stirred mixture of **19** (63.0 mg) and potassium *t*-butoxide (220.6 mg) in dry benzene (4.5 ml) was refluxed for 5 h under a stream of nitrogen. The mixture was cooled, poured into dilute hydrochloric acid, and extracted with ether. The ether extract was washed with water, dried, and evaporated in vacuo to give an oil (60 mg).

A mixture of the above oil (60 mg), concentrated hydrochloric acid (1.5 ml), and water (0.4 ml) in acetic acid (3.0 ml) was refluxed for 1.5 h under a stream of nitrogen. The mixture was evaporated in vacuo. The residue was dissolved in methanol (5.5 ml) and aqueous sodium hydroxide (5%, 4.0 ml), and then refluxed for 1 h under a stream of nitrogen. After removal of the methanol in vacuo, the residue was extracted with ether. The ether extract was washed with water, dried, and evaporated in vacuo. The crude product was chromatographed on silica gel (10 g), using ether-benzene (2:98) as the eluent, to give **20** (35.2 mg:77.7%). This was recrystallized from hexane, mp 115.5—116.5 °C, $[\alpha]_D$ +5° (c 1.2), IR 1734 cm^{-1}, ^1H NMR δ=0.68 (3H, s, C_{3a}-CH_3), 3.73 (3H, s, -OCH_3), 6.4—6.7 (2H, m) and 6.90 (1H, d, J=9 Hz) (aromatic protons). Found:C, 78.19; H, 7.92%. Calcd for $C_{15}H_{18}O_2$: C, 78.23; H, 7.88%.

2,3,3a,4,5,9b-Hexahydro-7-methoxy-3aβ-methyl-9bα*H*-1*H*-benz[*e*]inden-3β-ol (3). A mixture of **20** (24.0 mg) and lithium aluminium hydride (10.0 mg) in dry ether (2.0 ml) was stirred at room temperature for 1 h. The mixture was poured into dilute hydrochloric acid and extracted with ether. The ether extract was washed with brine, dried, and evaporated in vacuo. The residue was chromatographed on silica gel (6.0 g), using ether-benzene (5:95) as the eluent, to give **3** (22.1 mg:91.3%). This was recrystallized from hexane, mp 72.5—73 °C[12] (lit,[5] mp 69 °C), IR 3610 and 3430 cm^{-1}, ^1H NMR δ=0.61 (3H, s, C_{3a}-CH_3), 3.72 (3H, s, -OCH_3), 6.4—6.9 (3H, m, aromatic protons). ^1H NMR (C_5D_5N) δ=0.89 (3H, s, C_{3a}-CH_3), 3.69 (3H, s, -OCH_3), 6.7—7.3 (3H, m, aromatic protons). Found: C, 77.56; H, 8.74%. Calcd for $C_{15}H_{20}O_2$: C, 77.55; H, 8.68%.

This work was supported by a Grant-in-Aid for Scientific Research No. 60540353 from the Ministry of Education, Science and Culture.

References

1) Y. Harigaya, M. Onda, and A. Tahara, *Chem. Lett.*, **1974**, 919.

2) A. Tahara, M. Shimagaki, M. Itoh, Y. Harigaya, and M. Onda, *Chem. Lett.*, **1974**, 651.

3) T. Wirthlin, H. Wehrli, and O. Jeger, *Helv. Chim. Acta*, **57**, 351, 368 (1974), and references cited therein.

4) J. W. Huffman, *J. Org. Chem.*, **35**, 478 (1970), and references cited therein.

5) L. Velluz, G. Nonine, and J. Mathieu, *Angew. Chem.*, **72**, 725 (1960).

6) P. F. Ritchie, T. F. Sanderson, and L. F. McBurney, *J. Am. Chem. Soc.*, **76**, 723 (1954).

7) E. Wenkert, R. W. J. Carney, and C. Kaneko, *J. Am. Chem. Soc.*, **83**, 4440 (1961).

8) A. W. Burgstahler and L. R. Worden, *J. Am. Chem. Soc.*, **86**, 96 (1964).

9) R. C. Cambie and R. A. Franich, *Aust. J. Chem.*, **24**, 117 (1971).

10) Presumably, rearrangement of the epoxide into the alcohol **16** would proceed via the C-10a carbonium ion intermediate.

11) C. S. Rao and D. K. Banerjee, *Tetrahedron*, **19**, 1611 (1963).

12) Optical rotation could not be measured accurately, because of insufficient material and low rotation value.

Friedel-Crafts Acetylations of Methoxy-4*H*-cyclopenta[*def*]-phenanthrenes and the 4-Ketones

Masahiro MINABE,* Masaaki YOSHIDA, Yutaka TAKABAYASHI, and Masatoshi MASUDA
Department of Industrial Chemistry, Faculty of Engineering, Utsunomiya University, Ishiicho, Utsunomiya 321
(Received June 27, 1987)

Acetylations of 2- and 3-methoxy-4*H*-cyclopenta[*def*]phenanthrene gave predominantly the 1- and 8-acetyl derivatives, respectively. The acetylation of the 1-methoxy compound afforded the 2-, 3-, 5-, 7-, and 8-yl ketones and the reaction of the 8-methoxy derivative yielded the 1- and 3-acetyl derivatives. Similar reactions of 1-, 2-, 3-, and 8-methoxy-4*H*-cyclopenta[*def*]phenanthren-4-one occurred mainly at the 2-, 1-, 8-, and 9-positions, respectively.

The hydrocarbon, 4*H*-cyclopenta[*def*]phenanthrene is one of the interesting polycyclic aromatic hydrocarbons[1] because of the combination of their ring moieties and for carcinogenic screening tests. Our previous papers concerned the electrophilic substitution of electron-attractive acetyl-, bromo-, and nitro-4*H*-cyclopenta[*def*]phenanthrenes[2] and the bromination of cyclopentaphenanthrenamine derivatives having an electron-donating property.[3]

The present paper deals with the Friedel–Crafts acetylations of 1- (**1a**), 2- (**2a**), 3- (**3a**), 8-methoxy- (**4a**), and 8,9-dihydro-2-methoxy-4*H*-cyclopenta[*def*]-phenanthrene(**5a**) in order to obtain further information regarding the reactivities of the parent hydrocarbon with electrophiles. It also concerns the acylation of the methoxy ketones, **6a—10a** (Scheme 1).

Acetylations of **1a—4a** were carried out according to the modified Perrier procedure[4] by means of the addition of a substrate into the resulting mixture of acetic anhydride and aluminium chloride. The reaction mixture was analyzed by means of gas chromatographic technique (Table 1). The reaction of **1a** afforded 2- (**1b**), 3- (**1c**), 5- (**1d**), 7- (**1e**), and 8-acetyl compound (**1f**). The reactions of **2a** and **3a** gave predominantly 2-methoxy-1-acetyl compound **2b** and 3-methoxy-8-acetyl derivative **3b**, respectively. The acetylation of **4a** yielded two isomers, **4b** and **4c**. Similar trends were observed in the case of acetyl chloride as the acylating agent.[5]

The orientations on these reactions can be explained by the combination of reactivities of methoxynaphthalene[6] and of parent 4*H*-cyclopenta[*def*]phenanthrene;[7] electrophile attacks mainly the 1- and 3-positions of the latter accompanied by a substitution at the 2- and 8-positions. The formations of **1c**, **1d**, and **1e** from **1a** are due to the original reactivity of the parent hydrocarbon. Also, the production of **1b** and **1f** (and a part of **1c**) are due to the 1-methoxy group

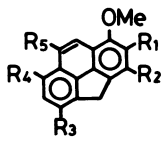

1a (all of R=H)
1b (R_1=Ac, other R=H)
1c (R_2=Ac, other R=H)
1d (R_3=Ac, other R=H)
1e (R_4=Ac, other R=H)
1f (R_5=Ac, other R=H)

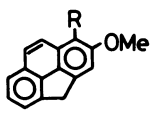

2a (R=H)
2b (R=Ac)

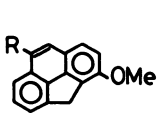

3a (R=H)
3b (R=Ac)

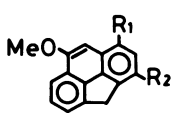

4a (R_1=R_2=H)
4b (R_1=Ac, R_2=H)
4c (R_1=H, R_2=Ac)

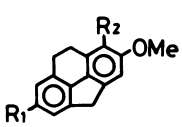

5a (R_1=R_2=H)
5b (R_1=Ac, R_2=H)
5c (R_1=R_2=Ac)

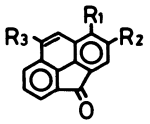

6a (R_1=OMe, R_2=R_3=H)
6b (R_1=OH, R_2=Ac, R_3=H)
6c (R_1=OMe, R_2=H, R_3=Ac)

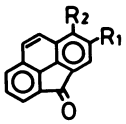

7a (R_1=OMe, R_2=H)
7b (R_1=OMe, R_2=Ac)
7c (R_1=OH, R_2=Ac)

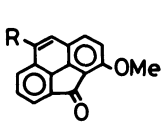

8a (R=H)
8b (R=Ac)

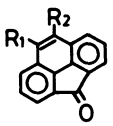

9a (R_1=OMe, R_2=H)
9b (R_1=OH, R_2=Ac)

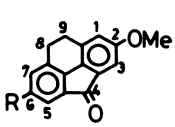

10a (R=H)
10b (R=Ac)

Scheme 1.

Table 1. The Friedel-Crafts Acetylation of **1a—4a**

Reactant	[$AlCl_3$]	Solvent	Temp	Yield	Isomer distribution/%						Recovd.
	[Reactant]	ml	°C	%	1-	2-	3-	5-	7-	8-	%
						(**1b**)	(**1c**)	(**1d**)	(**1e**)	(**1f**)	
1a	2.2	60	20	11		30	12	2	16	40	89
1a	2.2	60	75	19		14	23	7	14	42	78
1a	3.3	60	20	42		66	4	1	7	24	55
					(**2b**)						
2a	2.2	60	20	80	100						14
										(**3b**)	
3a	2.2	180	20	92						100	5
					(**4b**)		(**4c**)				
4a	2.2	90	20	8	37		63				88
4a	2.2	90	75	40	31		69				60
4a	3.3	90	20	86	67		33				13

which may accelerate the 2- and 8-positions by a resonance effect, as is 1-methoxynaphthalene. The reactions of **2a**, **3a**, and **4a** are postulated to be those of 2-methoxynaphthalene derivatives in which the 1-, 6-, and 8-positions are accelerated.

The methoxyl group on **2a** and **3a** enhances the acylation more than the case of **1a** and **4a**. Experiments at different temperatures show that the formation of **1b** is kinetically controlled and that the formations of **1c** and **1d** are thermodynamically controlled. Also **4b** and **4c** are formed from **4a** under kinetic and thermodynamic controls under these conditions. The molar ratio of aluminium chloride against the substrate influences not only the reaction rate but also the regioselectivities.[6] An increase in the ratio causes an acceleration of the reaction and gives kinetically-controlled products, such as **1b** and **4b**.

The acetylation of **5a** afforded predominantly **5b**. The second attack of the reagent occurred at the 1-position, giving 1,6-diacetyl compound **5c**. The reactivity at the 6-position of **5a** is accelerated by the methoxy group more than that of the 7-position of 2-methoxyfluorene.[8]

4*H*-Cyclopenta[*def*]phenanthren-4-one is less reactive to electrophile than the parent hydrocarbon and the reaction of the ketone occurs mainly at the 8-position accompanied by the minor 2-isomer.[9] The next interesting point concerns the Friedel-Crafts acetylations of 4-oxo derivatives of **1a—5a**. The reaction of **6a** afforded **6b** as the main product and **6c** as the minor product. The acetylation of **7a** occurred giving 1-acetyl-2-methoxy compound **7b** and the acetyl phenol **7c**. The isomeric **8a** gave the corresponding **8b**, and the another isomer, **9a** yielded **9b**. Also, the substitution of **10a** produced **10b**.

Because of the low reactivity due to the 4-carbonyl, the reaction required a long time in the presence of a large amount of acylating complex. A substitution adjacent to the methoxyl group causes a fission of the methyl group followed by the formation of a chelate ring, such as **6b**, **7c**, or **9b**, under these conditions.

The reactive position of **6a**, **7a**, **8a**, and **10a** are similar to that of **1a**, **2a**, **3a**, and **5a**, respectively. On the other hand, the excited position of **9a** to the electrophile is the 9-position, differing from the case of **4a**, but the same as that of *N*-acetyl-4*H*-cyclopenta[*def*]phenanthren-8-amine.[3] This should be simply interpreted as indicating that the 8-methoxy group is not an effective electron-donating group compared to the amino and acetylamino groups, and affects only on the adjacent 9-position of the deactivated ketone.

Experimental

All the melting points are uncorrected. The ^1H NMR spectra were measured using a Jeol JNM C-60 HL or a Varian VXR-300 spectrometer in $CDCl_3$ using TMS as an internal reference. The IR (KBr-pellet), UV data (cyclohexane), and mass spectra were recorded on a Jasco IR-G, a Shimadzu UV-180, and a Hitachi M-80 spectrometer, respectively.

1-Methoxy-4*H*-cyclopenta[*def*]phenanthrene (1a).[10] To a mixture of 4*H*-cyclopenta[*def*]phenanthren-1-ol[11] (434 mg, 2.1 mmol) in acetone (5 ml) was added aq KOH (1.12 g, 20 mmol) in H_2O (1 ml), and Me_2SO_4 (0.66 ml, 7 mmol) was added dropwise at room temperature giving 434 mg (90%) of **1a**: mp 99—100 °C (lit,[10] mp 96—98 °C); IR, 1241 cm^{-1}; ^1H NMR, δ=4.06 (3H, s), 4.29 (2H, s), 7.01 (1H, d, J=7.6 Hz), 7.58—7.66 (3H, m), 7.78—7.82 (2H, m), and 8.02 (1H, d, J=9.0 Hz); UV, λ_{max} 352 (log ε 3.62), 345 (3.16), 335 (3.45), 328 (3.16), 311 (4.13), 298 (4.08), 270 (4.36), 261 (4.44), and 252 nm (4.42); MS, m/z 220 (M^+) and 205. Found: C, 87.08; H, 5.69%. Calcd for $C_{16}H_{12}O$: C, 87.24; H, 5.49%.

2a; yield 95%; mp 86—87 °C; IR, 1192 cm^{-1}; ^1H NMR, δ=3.99 (3H, s), 4.31 (2H, s), 7.28 (1H, s), 7.36 (1H, s), 7.54—7.66 (2H, m), and 7.75—7.84 (3H, m); UV, λ_{max} 357 (log ε 3.53), 350 (3.17), 339 (3.33), 333 (3.08), 324 (3.03), 301 (3.99), 289 (4.00), 280 (4.12), and 257 nm (4.87); MS, m/z 220 (M^+), 205, and 177. Found: C, 87.22; H, 5.76%.

3a; yield 87%; mp 47—48 °C; IR, 1242 cm^{-1}; ^1H NMR, δ=4.01 (3H, s), 4.24 (2H, s), 7.06 (1H, d, J=8.4 Hz), and 7.39—7.72 (6H, m); UV, λ_{max} 349 (log ε 3.37), 342 (2.99), 333 (3.26), 312 (4.14), 300 (4.16), 277 (4.11), and 250 nm (4.70); MS, m/z 220 (M^+) and 205. Found: C, 87.43; H, 5.36%.

4a; yield 88%; mp 129—130 °C; IR, 1148 cm^{-1}; ^1H NMR, δ=4.12 (3H, s), 4.33 (2H, s), 7.04 (1H, s), 7.56—7.73 (5H, m), and 8.00 (1H, dd, J=7.9, 0.7 Hz); UV, λ_{max} 346 (log ε 3.29), 339 (2.92), 330 (3.19), 309 (3.92), 297 (4.08), and 248 nm (4.74); MS, m/z 220 (M^+), 205, and 177. Found: C, 87.06; H, 5.29%.

5a; yield 87%; mp 67—68 °C; IR, 1134 cm^{-1}; ^1H NMR, δ=3.11 (4H, s), 3.85 (5H, s), 6.71 (1H, d, J=1.6 Hz), 6.93 (1H, d, J=1.6 Hz), 7.07—7.15 (2H, m), and 7.30 (1H, d, J=6.9 Hz); UV, λ_{max} 281 nm (log ε 4.39); MS, m/z 222 (M^+), 207, and 178. Found: C, 86.70; H, 6.64%. Calcd for $C_{16}H_{14}O$: C, 86.45; H, 6.35%.

1-Methoxy-4*H*-cyclopenta[*def*]phenanthren-4-one (6a). To a mixture of **1a** (770 mg, 3.5 mmol) in pyridine (50 ml) was bubbled oxygen in the presence of Triton B (40% in MeOH, 0.35 ml) for 5 h at room temperature to give **6a** (663 mg, 81%); mp 186.5—187.5 °C; IR, 1706, 1626, and 1240 cm^{-1}; ^1H NMR, δ=4.08 (3H, s), 6.85 (1H, d, J=7.8 Hz), 7.54—7.79 (4H, m), 8.87 (1H, d, J=8.1 Hz), and 7.92 (1H, d, J=9.1 Hz); UV, λ_{max} 390 (log ε 3.05), 371 (3.13), 315 (4.21), 302 (4.14), and 243 nm (4.87). Found: C, 82.03; H, 4.32%. Calcd for $C_{16}H_{10}O_2$: C, 82.04; H, 4.30%.

7a; yield 75%; mp 140—141 °C; IR, 1712, 1628, and 1268 cm^{-1}; ^1H NMR δ=3.95 (3H, s), 7.24 (1H, d, J=1.7 Hz), 7.43 (1H, d, J=1.7 Hz), 7.44—7.49 (1H, m), 7.63—7.73 (3H, m), and 7.83 (1H, d, J=8.1 Hz); UV, λ_{max} 404 (log ε 2.84), 380 (2.85), 360 (2.87), 326 (3.84), 311 (3.72), 295 (3.74), and 242 nm (5.09). Found: C, 82.08; H, 4.19%.

8a; yield 56%; mp 123—124 °C; IR, 1704, 1624, and 1268 cm^{-1}; ^1H NMR, δ=4.14 (3H, s), 7.02 (1H, d, J=8.4 Hz), and 7.30—7.82 (6H, m); UV, λ_{max} 415 (log ε 3.14), 392 (3.22), 311 (3.73), 296 (4.22), and 231 nm (4.79). Found: C, 82.02; H, 4.21%.

9a; yield 89%; mp 201.5—202.5 °C; IR, 1704, 1626, and 1268 cm^{-1}; ^1H NMR, δ=4.04 (3H, s), 6.81 (1H, s), and 7.35—8.08 (6H, m); UV, λ_{max} 428 (log ε 2.81), 418 (2.79), 404 (2.95), 381 (2.95), 321 (3.67), 286 (4.02), 260 (4.10), and 236 nm (4.98). Found: C, 81.84; H, 4.05%.

10a; yield 90%; mp 116.5—117.5 °C; IR, 1702 and 1592 cm^{-1}; ^1H NMR, δ=3.00 (4H, s), 3.81 (3H, s), 6.75 (1H, d, J=1.8 Hz), 6.94 (1H, d, J=1.8 Hz), 7.05 (1H, t, J=7.4 Hz), 7.15 (1H, d, J=7.4 Hz), and 7.30 (1H, d, J=7.4 Hz); UV, λ_{max} 453 (log ε 2.96), 311 (3.58), 300 (3.85), 276 (4.75), and 266 nm (4.61). Found: C, 81.30; H, 5.32%. Calcd for $C_{16}H_{12}O_2$: C, 81.34; H, 5.12%.

Friedel-Crafts Acetylation of 1a—4a. General Procedure. To aluminium chloride (2.2—3.3 mmol) in 1,2-dichloroethane (60—180 ml), acetic anhydride (1.1 mmol) was added at 20 °C (or 75 °C) and the mixture was stirred until it became a homogeneous solution (30 min). All of the finely-powdered methoxy compound (1.0 mmol) was added and stirred for 5 min.

Upon the usual treatment of the reaction mixture, a part of the organic layer was submitted to GC (Shimadzu 6AMFP apparatus attached a column containing Dexsil 300 GC (5%), at 250 °C) after the addition of 2-acetyl-8,9-dihydro-4*H*-cyclopenta[*def*]phenanthrene as an internal standard.

Acetylation of 1a. To a mixture of Ac_2O (0.07 ml, 0.7 mmol) and $AlCl_3$ (150 mg, 1.1 mmol) in $PhNO_2$ (30 ml), **1a** (107 mg, 0.49 mmol) was added at room temperature, followed by stirring for 30 min. Upon the usual treatment, the organic layer was distilled with steam and the residue was chromatographed on silica gel with benzene. The first colorless band afforded 42 mg (39%) of **1a**, mp 98—100 °C.

The second light yellow band gave a trace amount of **1d**: mp 149—150 °C (EtOH); IR, 1664 and 1270 cm^{-1}; ^1H NMR, δ=2.61 (3H, s), 4.08 (3H, s), 4.46 (2H, s), 6.85 (1H, d, J=7.8 Hz), 7.39—7.91 (4H, m), and 7.84 (1H, d, J=7.8 Hz); UV, λ_{max} 377 (log ε 3.67), 360 (3.71), 329 (4.06), and 243 nm (4.53); MS, m/z 262 (M^+), 247, and 204. Found: C, 82.40; H, 5.43%. Calcd for $C_{18}H_{14}O_2$: C, 82.42; H, 5.38%.

The next yellow band was collected and gave the following three compounds: **1f** (24 mg, 19%); mp 154—155 °C (EtOH); IR, 1656 and 1274 cm^{-1}; ^1H NMR, δ=2.86 (3H, s), 4.07 (3H, s), 4.24 (2H, s), 6.98 (1H, d, J=7.8 Hz), 7.43—7.81 (3H, m), and 8.64—8.95 (2H, m); UV, λ_{max} 377 (log ε 3.67), 360 (3.71), 329 (4.06), and 243 nm (4.53); MS, m/z 262 (M^+) and 149. Found: C, 82.31; H, 5.55%.

1e (trace); mp 155—156 °C (EtOH); IR, 1664 and 1246 cm^{-1}; ^1H NMR, δ=2.82 (3H, s), 4.07 (3H, s), 4.32 (2H, s), 7.06 (1H, d, J=7.8 Hz), 7.63 (1H, d, J=7.8 Hz), 7.71 (1H, d, J=7.5 Hz), 8.21 (1H, d, J=9.2 Hz), 8.23 (1H, d, J=7.5 Hz), and 8.86 (1H, d, J=9.2 Hz); UV, λ_{max} 360 (log ε 3.30), 316 (4.06), 300 (4.15), and 250 nm (4.80); MS, m/z 262 (M^+) and 149. Found: C, 82.20; H, 5.25%.

1c (35 mg, 27%); mp 138—139 °C (EtOH); IR, 1668 and 1234 cm^{-1}; ^1H NMR, δ=2.77 (3H, s), 4.09 (3H, s), 4.48 (2H, s), 7.43 (1H, s), and 7.56—8.16 (5H, m); UV, λ_{max} 364 (log ε 3.36), 347 (3.34), 300 (3.90), and 260 nm (4.51); MS, m/z 262 (M^+), 247, and 149. Found: C, 82.21; H, 5.45%.

The next yellow band yielded a trace amount of **1b**; mp 78—79 °C; IR, 1672 and 1380 cm^{-1}: ^1H NMR, δ=2.81 (3H, s), 4.12 (3H, s), 4.30 (2H, s), 7.46—7.98 (5H, m), and 8.02 (1H, d, J=9.0 Hz); UV, λ_{max} 364 (log ε 3.02), 346 (3.12), 301 (4.19), 274 (4.70), and 266 nm (4.72); MS, m/z 262 (M^+), 247, and 149. Found: C, 82.35; H, 5.51%.

The Reaction of 2a. A mixture of Ac_2O (0.09 ml, 0.9 mmol) and $AlCl_3$ (190 mg, 1.4 mmol) in $PhNO_2$ (40 ml) was stirred with **2a** (140 mg, 0.64 mmol) at 20 °C for 30 min. Upon the treatment as described above, **2a** (17 mg, 12%, mp 82—84 °C) and **2b** (139 mg, 83%) were isolated by means of silica-gel column chromatography. **2b**; mp 128—129 °C; IR, 1656 and 1386 cm^{-1}; ^1H NMR, δ=2.72 (3H, s), 4.06 (3H, s), 4.34 (2H, s), 7.47 (1H, s), 7.57—7.68 (2H, m), 7.80 (1H, d, J=7.8 Hz), 7.88 (1H, d, J=9.1 Hz), and 8.06 (1H, d, J=9.1 Hz); UV, λ_{max} 364 (log ε 3.46), 347 (3.43), 299 (4.02), and 257 nm (4.67); MS, m/z 262 (M^+), 247, 232, 189, 176, and 149. Found: C, 82.65; H, 5.62%. Calcd for $C_{18}H_{14}O_2$: C, 82.42; H, 5.38%.

Acetylation of 3a. A solution of **3a** (220 mg, 1 mmol) was added into a mixture of Ac_2O (0.11 ml, 1.2 mmol) and $AlCl_3$ (290 mg, 2.2 mmol) in $PhNO_2$ (120 ml), and the resulting mixture was stirred at 20 °C for 30 min giving **3b** (240 mg, 92%); mp 156—157 °C; IR, 1650, 1258, and 1234 cm^{-1}; ^1H NMR, δ=2.84 (3H, s), 4.13 (3H, s), 4.37 (2H, s), 7.31 (1H, d, J=8.6 Hz), 7.71—7.73 (2H, m), 7.91 (1H, d, J=8.6 Hz), 8.48 (1H, s), and 8.81—8.84 (1H, m); UV, λ_{max} 332 (log ε 4.28), 286 (4.16), and 252 nm (4.62); MS, m/z 262 (M^+), 247, 223, 176, and 149. Found: C, 82.25; H, 5.39%. Calcd for $C_{18}H_{14}O_2$: C, 82.42; H, 5.38%.

Acetylation of 4a. A mixture of **4a** (116 mg, 0.53 mmol) was mixed with a mixture of Ac_2O (0.07 ml, 0.7 mmol) and $AlCl_3$ (150 mg, 1.1 mmol) in $C_2H_4Cl_2$ (30 ml) and stirred at 20 °C for 30 min. Upon the usual treatment, the resulting

residue was chromatographed on a silica-gel column. The first colorless eluate afforded 14 mg (12%) of **4a**, mp 129—130 C. The first fraction of yellow band gave 77 mg (56%) of **4b**; mp 160—161 °C; IR, 1654, 1246, and 1151 cm^{-1}; ^1H NMR, δ=2.81 (3H, s), 4.18 (3H, s), 4.37 (2H, s), 7.57—7.75 (3H, m), 8.05 (1H, d, J=7.8 Hz), 8.22 (1H, d, J=7.6 Hz), and 8.33 (1H, s); UV, λ_{max} 373 (log ε 3.93), 356 (3.83), 328 (4.12), 314 (4.04), 284 (4.13), 273 (4.15), and 258 nm (4.66); MS, m/z 262 (M^+), 247, 219, 176, and 149. Found: C, 82.50; H, 5.56%. Calcd for $C_{18}H_{14}O_2$: C, 82.42; H, 5.38%.

The second fraction yielded 32 mg (23%) of **4c**; mp 151—153 °C; IR, 1666, 1270, and 1149 cm^{-1}; ^1H NMR, δ=2.76 (3H, s), 4.14 (3H, s), 4.65 (2H, s), 7.04 (1H, s), 7.65—7.80 (3H, m), 8.02 (1H, d, J=7.7 Hz), and 8.10 (1H, d, J=8.4 Hz); UV, λ_{max} 336 (log ε 4.28), 323 (4.33), 280 (4.23), and 260 nm (4.58); MS, m/z 262 (M^+), 247, 204, 176, and 149. Found: C, 82.40; H, 5.63%.

Friedel-Crafts Reaction of 5a. A 1,2-dichloroethane (30 ml) solution of **5a** (111 mg, 0.5 mmol), Ac_2O (0.07 ml, 0.7 mmol), and $AlCl_3$ (150 mg, 1.1 mmol) was stirred at room temperature. Upon column chromatography (SiO_2), 54 mg (41%) of **5b** and a trace amount of **5c** were isolated. **5b**; mp 109—110 °C; IR, 1660 and 1286 cm^{-1}; ^1H NMR, δ=2.62 (3H, s), 3.13 (4H, s), 3.85 (3H, s), 3.90 (2H, s), 6.74 (1H, s), 6.96 (1H, s), 7.77 (1H, s), and 7.95 (1H, s); UV, λ_{max} 341 (log ε 4.47) and 326 nm (4.49); MS, m/z 264 (M^+), 249, and 221. Found: C, 81.57; H, 5.89%. Calcd for $C_{18}H_{16}O_2$: C, 81.79; H, 6.10%.

5c; mp 167—168 °C; IR, 1668, 1642, and 1286 cm^{-1}; ^1H NMR, δ=2.62 (3H, s), 2.63 (3H, s), 3.16 (4H, s), 3.95 (3H, s), 4.14 (2H, s), 6.83 (1H, s), 7.77 (1H, s), and 7.95 (1H, s); MS, m/z 306 (M^+), 291, 279, 247, 206, and 167. Found: C, 78.59; H, 5.80%. Calcd for $C_{20}H_{18}O_3$: C, 78.41; H, 5.92%.

In an another experiment with a long reaction time (1h), a small amount of 1,6-diacetyl-8,9-dihydro-4*H*-cyclopenta-[*def*]phenanthren-2-ol was obtained in addition to **5b** and **5c**: mp 228—230 °C; IR, 1666, 1631, and 1220 cm^{-1}; ^1H NMR, δ=2.62 (3H, s), 2.73 (3H, s), 3.12 (4H, s), 4.08 (2H, s), 6.76 (1H, s), 7.73 (1H, s), 7.94 (1H, s), and 13.13 (1H, s); MS, m/z 292 (M^+), 277, 249, 206, and 176. Found: C, 77.81; H, 5.68%. Calcd for $C_{19}H_{16}O_3$: C, 78.06; H, 5.52%.

The Friedel-Crafts Acetylation of 6a. Ketone **6a** (117 mg, 0.5 mmol) was added into a mixture of Ac_2O (0.32 ml, 3 mmol) and $AlCl_3$ (800 mg, 6 mmol) in $C_2H_4Cl_2$ (7.5 ml) and stirred at room temperature for 72 h. Upon the usual treatment, the residue was chromatographed on silica gel and the light yellow band afforded 89 mg (68%) of **6b**: mp 270.5—272.0 °C (from benzene); IR, 2600, 1706, 1630, and 1230 cm^{-1}; ^1H NMR, δ=2.79 (3H, s), 7.70—7.75 (1H, m), 7.82 (1H, d, J=9.0 Hz), 7.88 (1H, d, J=7.9 Hz), 7.98 (1H, d, J=8.0 Hz), 8.10 (1H, d, J=9.0 Hz), 8.21 (1H, s), and 14.85 (1H, s). Found: C, 78.06; H, 3.85%. Calcd for $C_{17}H_{10}O_3$: C, 77.85; H, 3.84%.

The next yellow band yielded 21 mg (15%) of **6c**: mp 229—230 °C (from cyclohexane); IR, 1694, 1668, and 1272 cm^{-1}; ^1H NMR, δ=2.79 (3H, s), 4.07 (3H, s), 6.76 (1H, d, J=7.8 Hz), 7.43—7.80 (3H, m), 8.42 (1H, s), and 8.73—8.89 (1H, m). Found: C, 78.68; H, 4.35%. Calcd for $C_{18}H_{12}O_3$: C, 78.25; H, 4.38%.

Reaction of 7a. A mixture of **7a** (117 mg, 0.5 mmol), Ac_2O (0.16 ml, 1.7 mmol), and $AlCl_3$ (400 mg, 3 mmol) in $C_2H_4Cl_2$ (7.5 ml) was stirred at room temperature for 10 h giving **7b** (71 mg, 51%) and **7c** (37 mg, 28%), respectively.

7b: mp 176.5—177.5 °C (from benzene-hexane) which was confirmed by oxidation of **2b** with oxygen in the presence of Triton B (40%) in pyridine; IR, 1718, 1668, and 1272 cm^{-1}; ^1H NMR, δ=2.69 (3H, s), 4.04 (3H, s), 7.51—7.54 (1H, m), 7.57 (1H, s), and 7.74—7.87 (4H, m); UV, λ_{max} 400 (log ε 2.98), 331 (3.82), 317 (3.75), 296 (4.00), and 244 nm (4.98). Found: C, 78.23; H, 4.43%. Calcd for $C_{18}H_{12}O_3$: C, 78.25; H, 4.38%.

7c: mp 213.0—213.5°C (from benzene); IR, 2630, 1706, 1624, and 1200 cm^{-1}; ^1H NMR, δ=3.91 (3H, s), 7.24 (1H, s), 7.32—8.04 (5H, m), and 14.14 (1H, s); UV, λ_{max} 440 (log ε 3.06), 392 (3.13), 346 (3.94), 330 (3.80), 313 (3.83), 300 (3.95), 270 (4.33), and 249 nm (4.74). Found: C, 77.82; H, 3.53%. Calcd for $C_{17}H_{10}O_3$: C, 77.85; H, 3.84%.

Reaction of 8a. A mixture of **8a** (234 mg, 1 mmol), Ac_2O (0.32 ml, 3.4 mmol), and $AlCl_3$ (800 mg, 6 mmol) in $C_2H_4Cl_2$ (15 ml) was stirred at room temperature for 10 h. The usual procedure afforded 14 mg (6%) of **8a** and 254 mg (92%) of **8b**. **8b**: mp 166.0—166.5 °C (from benzene-hexane); IR, 1702, 1662, and 1258 cm^{-1}; ^1H NMR, δ=2.80 (3H, s), 4.26 (3H, s), 7.18 (1H, d, J=8.8 Hz), 7.65—7.67 (1H, m), 7.82 (1H, d, J=7.0 Hz), 7.91 (1H, d, J=8.8 Hz), 8.32 (1H, s), and 8.92 (1H, d, J=8.4 Hz); UV, λ_{max} 383 (log ε 3.20), 334 (4.14), 303 (4.25), and 252 nm (4.67). Found: C, 78.28; H, 4.12%. Calcd for $C_{18}H_{12}O_3$: C, 78.25; H, 4.38%.

Reaction of 9a. Ketone **9a** (58.5 mg, 0.25 mmol) was treated with Ac_2O (0.16 ml, 1.7 mmol) and $AlCl_3$ (400 mg, 3 mmol) in $C_2H_4Cl_2$ (7.5 ml) at room temperature for 10 h to yield 34 mg (52%) of **9b** and 16 mg (27%) of **9a**. **9b**: mp 210.0—210.5 °C (from benzene-hexane); IR, 2650, 1708, 1664, and 1384 cm^{-1}; ^1H NMR, δ=2.97 (3H, s), 7.60—7.70 (3H, m), 7.91 (1H, d, J=6.7 Hz), 8.12 (1H, dd, J=8.0, 4.3 Hz), 8.27 (1H, d, J=8.0 Hz), and 16.61 (1H, s); UV, λ_{max} 359 (log ε 3.87), 325 (3.88), and 231 nm (4.75). Found: C, 78.02; H, 3.89%. Calcd for $C_{17}H_{10}O_3$: C, 77.85; H, 3.84%.

Reaction of 10a. A mixture of **10a** (321 mg, 1.36 mmol), Ac_2O (0.32 ml, 3.4 mmol), and $AlCl_3$ (800 mg, 6 mmol) in $C_2H_4Cl_2$ (30 ml) was stirred at room temperature for 34 h to give 25 mg (8%) of **10a** and 256 mg (68%) of **10b**, respectively. **10b**: mp 220—221 °C (red needles from benzene-hexane); IR, 1704, 1668, and 1264 cm^{-1}; ^1H NMR, δ=2.58 (3H, s), 3.06 (4H, s), 3.84 (3H, s), 6.80 (1H, s), 6.99 (1H, s), 7.89 (1H, s), and 7.91 (1H, s); UV, λ_{max} 452 (log ε 3.25), 340 (4.07), 326 (4.09), 291 (4.59), and 254 nm (4.26). Found: C, 77.47; H, 5.27%. Calcd for $C_{18}H_{14}O_3$: C, 77.68; H, 5.07%.

Friedel-Crafts Acetylation of 4*H*-Cyclopenta[*def*]phenanthren-4-one. A mixture of the ketone (404 mg, 2 mmol), Ac_2O (4.4 ml, 47 mmol), and $AlCl_3$ (10.6 g, 79 mmol) in $C_2H_4Cl_2$ (15 ml) was stirred at room temperature for 20 d to give the recovered ketone (195 mg, 48%) and 8-acetyl-4*H*-cyclopenta[*def*]phenanthren-4-one (45 mg, 9%); mp 171.5—173.0 °C (from cyclohexane); IR, 1706 and 1664 cm^{-1}; ^1H NMR, δ=2.84 (3H, s), 7.61—7.67 (2H, m), 7.83—7.90 (2H, m), 7.99 (1H, d, J=8.0 Hz) 8.43 (1H, s), and 8.89 (1H, d, J=8.4 Hz); UV, λ_{max} 340 (log ε 3.17), 307 (4.13), and 240 nm (4.82). Found: C, 83.04; H, 3.88%. Calcd for $C_{17}H_{10}O_2$: C, 82.91; H, 4.09%.

The authors wish to thank Emeritus Professor Kazuo Suzuki and Professor Takashi Toda Utsunomiya University for their valuable discussion.

References

1) M. Minabe and K. Suzuki, *Yuki Gosei Kagaku Kyokai Shi*, **44**, 421 (1986).
2) M. Yoshida, H. Hirota, M. Minabe, and K. Suzuki, *J. Chem. Eng. Data*, **26**, 220 (1981).
3) M. Yoshida, M. Minabe, W. Ookawa, and K. Suzuki, *Bull. Chem. Soc. Jpn.*, **56**, 1259 (1983).
4) G. Perrier, *Ber.*, **33**, 815 (1900).
5) I. Hashimoto, *Nippon Kagaku Kaishi*, **1982**, 1179.
6) R. B. Girdler, P. H. Gore, and J. A. Hoskins, *J. Chem. Soc. C*, **1966**, 181; C. Eaborn, P. Golborn, R. E. Spillett, and R. Taylor, *J. Chem. Soc. B*, **1968**, 1112.
7) M. Yoshida, K. Hishida, M. Minabe, and K. Suzuki, *J. Org. Chem.*, **45**, 1783 (1980).
8) G. W. Gray, J. B. Hartley, and A. Ibbotson, *J. Chem. Soc.*, **1955**, 1686.
9) M. Yoshida, M. Kobayashi, M. Minabe, and K. Suzuki, *Bull. Chem. Soc. Jpn.*, **54**, 1159 (1981).
10) A. Sieglitz and W. Schidlo, *Chem. Ber.*, **96**, 1098 (1963).
11) M. Minabe, M. Yoshida, T. Amimoto, T. Nagata, and M. Kobori, *Bull. Chem. Soc. Jpn.*, **61**, 879 (1988).

 © 1988 The Chemical Society of Japan Bull. Chem. Soc. Jpn., 61, 735—740 (1988)

A New Method of α-Functionalization for Tertiary Amines by Nucleophilic Substitution of α-Siloxy Amines

Norihiro Tokitoh† and Renji Okazaki*
Department of Chemistry, Faculty of Science, The University of Tokyo,
Hongo, Bunkyo-ku, Tokyo 113
(Received July 7, 1987)

α-Siloxy amines, which were easily prepared by "silicon Polonovski reaction" of tertiary amine *N*-oxides with trialkylsilyl trifluoromethanesulfonate, were treated with various nucleophiles to give the corresponding α-functionalized tertiary amines in moderate to good yields. This new method has the advantage that it enables the α-substitution of amines not only by alkyl groups but also by alkenyl and aryl groups with sp^2 carbon as a reaction center, since the introduction of such groups is difficult in electrophilic substitution of dipole-stabilized α-lithio amines. Besides the organometallics such as Grignard and organoaluminum reagents, trimethylsilyl cyanide and silyl enol ether could also be employed as nucleophiles in the presence of an appropriate Lewis acid.

The carbon–carbon bond formation at the α-position of amines is one of the most important problems in the syntheses of nitrogen-containing natural products such as alkaloids. Although the electrophilic α-substitution methods have been developed extensively in recent years using dipole-stabilized α-lithio amines[1] as shown in Eq. 1, all of them are only applicable to secondary amine

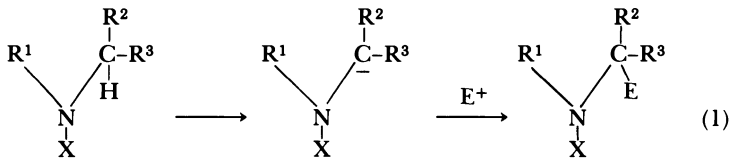

(1)

X=NO, COR, CH=N-Bu^t, etc.

derivatives and there are very few reports on the direct generation of α-carbanion of tertiary amines.[2] On the other hand, the conventional Mannich type of nucleophilic introduction of α-substituents into primary and secondary amines[3] have been studied widely but direct α-functionalization of tertiary amines has not been fully investigated. We have recently reported a facile formation of α-siloxy amines **3** ("silicon Polonovski reaction") by the base-promoted rearrangement of siloxyammonium salts **2** obtained by treatment of tertiary amine *N*-oxides **1** with trialkylsilyl trifluoromethanesulfonate and their reactions with some electrophiles (Eq. 2).[4]

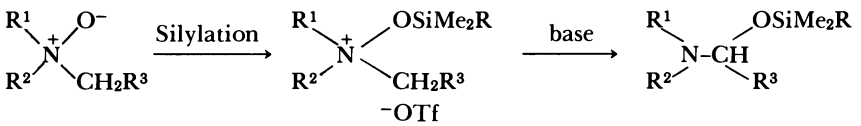

1 **2** **3**

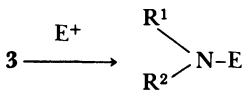

(2)

As an extension of the above reactions we have examined nucleophilic substitutions of the siloxyl group of **3** in the hope of the development of a new and general nucleophilic α-functionalization method for tertiary amines (Eq. 3).[5]

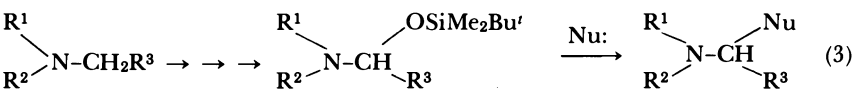

3

(3)

† Present address; Department of Chemistry, University of Tsukuba, Tsukuba, Ibaraki 305.

Results and Discussion

Nucleophilic Substitution with Organometallics.

a) Reactions with Grignard Reagents. The reactions of α-siloxy amines **3** with Grignard reagents as nucleophiles were examined. In the case of *N*-methylpiperidine *N*-oxide (**1a**), treatment of the corresponding α-siloxy amine **3a** obtained in situ from **1a** with several Grignard reagents afforded the expected α-substituted products **4a** in moderate to good yields when the solvent was replaced by toluene before the reaction with the Grignard reagents. These results are given in Table 1.

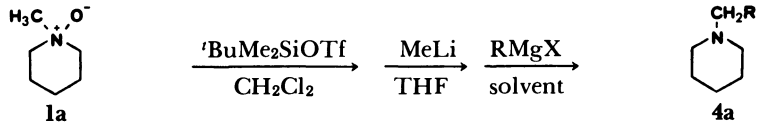

1a **4a**

When the Grignard reagent was added without the solvent exchange into toluene, the yield of **4a** was somewhat diminished (Entry 1).

This α-substitution reaction was applied to the introduction of substituents into the 1-position of tetrahydroisoquinoline skeleton which is important in the alkaloid synthesis using *N*-methyl-1,2,3,4-tetrahydroisoquinoline *N*-oxide (**1b**) as a substrate. In this case the addition of Lewis acid before that of the Grignard reagent was necessary in contrast to the reaction of **1a**. The results listed in Table 2 show that the substitution proceeded most effectively when α-siloxy amine **3b** was treated with trimethylsilyl trifluoromethanesulfonate (TMSOTf).

1b **4b**

When this reaction was carried out in the absence of Lewis acid, the yield and reproducibility in the formation of **4b** became poorer.

b) Reactions with Trialkylaluminums. Substitution of the siloxyl group in **3** with trialkylaluminums was next examined.[6] The results obtained from the reactions of several amine *N*-oxides are given in Table 3 and in all cases the expected α-substitution products

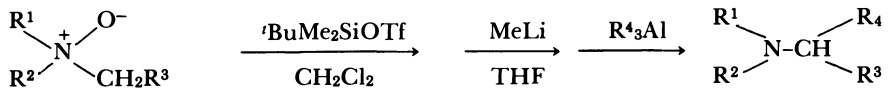

1 **4**

4 were obtained in moderate to good yields. In contrast to the substitution reaction by Grignard reagents mentioned above, organoaluminum reagents gave the α-substitution products **4** in good yields without the solvent exchange into toluene before the addition of the orgnometallics except in the case of **1b**, where the α-substitution product **4b** was obtained only in 20% yield using dichloromethane as a solvent in the last step.[7]

Table 1. α-Substitution of **1a** with Grignard Reagents

Entry	Grignard reagent	Solvent	Yield of **4a**/%
1	PhMgBr	THF	58
2	PhMgBr	Toluene	74(80)[a]
3	CH_2=CHMgBr	Toluene	51
4	$PhCH_2MgBr$	Toluene	52(71)[a]
5	CH_3CH_2MgBr	Toluene	47

a) Values in parentheses denote NMR yields.

Table 2. α-Substitution of **1b** with Grignard Reagents

Entry	Lewis acid	RMgX	Solvent	Yield/%
1	$TiCl_4$	PhMgBr/THF	Toluene	27
2	$BF_3 \cdot Et_2O$	PhMgBr/THF	Toluene	17
3	Me_3SiOTf	PhMgBr/THF	Toluene	56
4	Me_3SiOTf	CH_3CH_2MgBr/THF	Toluene	41
5	Me_3SiOTf	CH_2=CHMgBr/THF	Toluene	54
6	Me_3SiOTf	$PhCH_2MgBr$/THF	Toluene	11
7	Me_3SiOTf	CH_3MgI/Et_2O	THF-Et_2O (1:2)	29

Reactions with Other Nucleophiles. Lewis Acid-Promoted Nucleophilic Substitution of α-Siloxy Amines. Since the Lewis acidity of the organometallics seemed to play an important role in the above-mentioned nucleophilic substitution of α-siloxy amines **3** with organometallics, some attempts were made to extend this substitution to some other nucleophiles by use of an appropriate Lewis acid.

a) Reactions with Trimethylsilyl Cyanide; a New Synthesis of α-Cyano Amines.[8] When the α-siloxy amines **3** obtained in situ from the corresponding amine *N*-oxides **1** were treated with titanium tetrachloride and trimethylsilyl cyanide after replacement of the solvent into dichloromethane, the α-cyanated products **5** were obtained in good yields. As a Lewis acid titanium tetrachloride was most effective; trimethylsilyl trifluoromethanesulfonate (TMSOTf) and tin(IV) chloride could also be used but the yields of **5** were somewhat diminished. Results obtained from the reactions of several amine *N*-oxides are summarized in Table 4. The results suggest that, as in the dealkylation of tertiary amines via α-siloxy amines **3**,[4] the regioselectivity of this cyanation is controlled by the acidity of the α-hydrogen of substituents on the ammonium salt **2** which is deprotonated by the base. Thus, **1a** and *N,N*-dimethylcyclohexylamine oxide (**1d**) were cyanated at the methyl group and **1b** at the benzyl group exclusively, while *N,N*-dimethylbenzylamine oxide (**1e**) gave two regioisomers (**5e** and **5e'**). It appears that the deprotonation of the methyl group in

Table 3. α-Substitution by Organoaluminum Reagents

Entry	*N*-Oxide **1**		R_3Al	Yield of **4**	
1	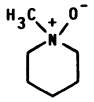	**1a**	*i*-Bu_3Al	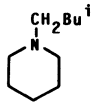	45
2	**1a**		Et_3Al	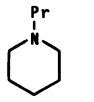	69(91)[a]
3	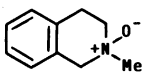	**1b**	Me_3Al	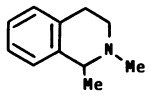	20
4	$(PhCH_2)_3N^+-O^-$	**1c**	Et_3Al	$(PhCH_2)_2NCH(Et)Ph$	75

a) Values in parentheses denote NMR yields.

Table 4. α-Cyanation of Tertiary Amines via α-Siloxy Amines

Entry	*N*-Oxide **1**		Lewis acid	Product **5**		Yield/%
1	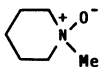	**1a**	$TiCl_4$	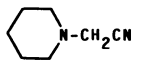	**5a**	61
2	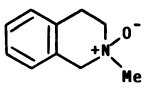	**1b**	$TiCl_4$	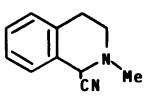	**5b**	63
3	**1b**		Me_3SiOTf	**5b**		24
4	**1b**		$SnCl_4$	**5b**		17
5	$(PhCH_2)_3N^+-O^-$	**1c**	$TiCl_4$	$(PhCH_2)_2NCH(CN)Ph$	**5c**	78
6	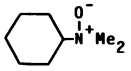	**1d**	$TiCl_4$	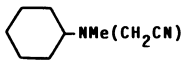	**5d**	71
7	$PhCH_2(Me)_2N^+-O^-$	**1e**	$TiCl_4$	$PhCH(CN)NMe_2$ $PhCH_2NMe(CH_2CN)$	**5e** **5e'**	22 40

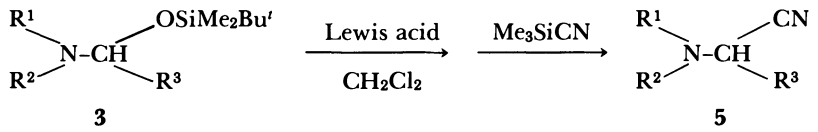

3 5

the reactions with **1a** and **1d** predominates over that of the methylene and methine groups but the preference between methyl and benzyl groups in the deprotonation depends on the structure of the *N*-oxides (**1e** vs. **1b**). In the absence of Lewis acids this cyanation did not proceed in contrast to the reactions with Grignard and organoaluminum reagents.

b) Reactions with Silyl Enol Ether. As another application of this Lewis acid promoted substitution reaction of α-siloxy amines, reactions with a silyl enol ether were examined. Thus, **1a** was converted into the corresponding α-siloxy amine **3a** and then after replacement of the solvent into dichloromethane **3a** was treated with α-trimethylsiloxystyrene in the presence of some kinds of Lewis acids. The results are given in Table 5. As a Lewis acid TMSOTf was most effective; with other Lewis acids the yiels of **6a** were much lower and the reaction became complicated. In this sustitution the addition of fluoride ion resulted in improvement of the yield (Run 4).

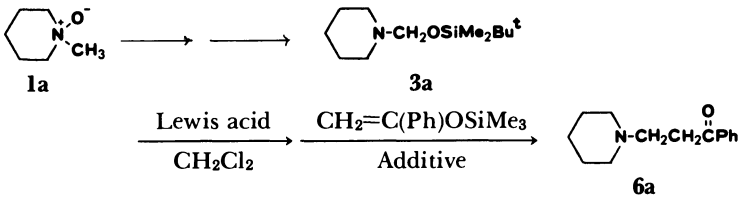

1a **3a** **6a**

In summary we have established a new and convenient α-substitution method for teriary amines not only by simple alkyl groups but also by alkenyl, aryl, cyano, and β-oxoalkyl groups using α-siloxy amines. In view of ready availability of amine *N*-oxides and nucleophiles and a wide variety of the synthetic application of this α-functionalization method described here, we believe that this type of transformation reaction of tertiary amines will provide a new methodology in organic synthesis, especially in the syntheses of nitrogen-containing natural products.

Experimental

All the melting points and boiling points were not corrected. ^{1}H NMR spectra were measured with Hitachi R-24B, Hitachi R-20B (60 MHz), and JEOL JNM-FX90Q (90 MHz) spectrometers using tetramethylsilane as an internal standard. ^{13}C NMR spectra were measured with a JEOL JNM-FX90Q (90 MHz) spectrometer. The NMR spectra were measured in deuteriochloroform at room temperature unless otherwise noted. MS spectra were measured with a JEOL JMS-D300 mass spectrometer. All the experiments were carried out in argon or nitrogen atmosphere. Chromatographic separation was carried out with hexane–ether as solvent. Isolated products were homogeneous in thin layer chromatography and their NMR spectra did not show the presence of impurity.

Table 5. Reactions of **3a** with α-Trimethylsiloxystyrene

Run	Lewis acid	Additive	Yield of **6a**/%
1	$TiCl_4$	—	13
2	$Ti(O\text{-}i\text{-}Pr)_4$	—	6
3	Me_3SiOTf	—	39
4	Me_3SiOTf	KF	47

Materials. Amine *N*-oxides were prepared by oxidation of the corresponding amines by either 30% hydrogen peroxide or m-chloroperbenzoic acid. *N*-Methyl-1,2,3,4-tetrahydroisoquinoline[9] and *N*-benzylpiperidine[10] were prepared by the reported method. The other amines used were commercial products.

Reactions with Grignard Reagents. Reaction of *N*-Methylpiperidine *N*-Oxide (1a). The procedure with phenylmagnesium bromide is typical.

General Procedure. Transformation of 1a into *N*-Benzylpiperidine (4a). To a solution of **1a** (120.7 mg, 1.05 mmol) in 10 ml of dichloromethane was added TBDMSOTf (291 mg, 1.05 equiv), the solvent was carefully removed with a vacuum pump and then THF (10 ml) and MeLi (1.2 mmol, 1.1 equiv) were added at 0 °C. After further replacement of the solvent by toluene (10 ml) in a similar way, phenylmagnesium bromide (1.58 mmol, 1.5 equiv) was added at 0 °C and the mixture was stirred overnight at room temperature. After evaporation of the solvent the mixture was shaken with 50 ml of 5% aq NaOH solution and 50 ml of dichloromethane and the aqueous layer was extracted with dichloromethane (30 ml×3). The extracts and the organic layer were combined, dried over $MgSO_4$, and concentrated. The ^{1}H NMR spectrum of the resulting crude oil showed the exclusive formation of the expected *N*-benzylpiperidine (**4a**; R=Ph) and *t*-butyldimethylsilanol and the NMR yield of **4a** (R=Ph) was estimated 80%. Chromatography of the crude oil on alumina afforded **4a** (R=Ph) in 74% yield (136.4 mg) as a colorless oil.

Other reactions of **1a** listed in Table 1 were carried out in a similar way to the above-mentioned reaction with phenylmagnesium bromide to give the corresponding α-substituted products (**4a**; R=CH=CH_2, CH_2Ph, and CH_2CH_3) in 51, 52,

and 47% yields, respectively.

4a, R=CH=CH$_2$: ^{1}H NMR δ=1.2—2.1 (m, 6H), 2.3—2.7 (m, 4H), 2.9—3.1 (m, 2H), and 4.9—6.7 (m, 3H); MS, *m/z* 125 (M$^+$, 5%), 124 (8), 108 (6), 98 (15), 88 (52), and 75 (100); pale yellow oil.[11]

4a, R=CH$_2$Ph: ^{1}H NMR δ=1.0—2.0 (m, 6H), 2.0—2.7 (m, 4H), 2.2—3.1 (m, 4H), and 7.31 (s, 5H); MS, *m/z* 190 (2%), 189 (M$^+$, 6), 188 (3), 149 (3), 105 (23), 99 (38), 98 (100), 91 (9), and 77 (15); pale yellow oil.[12]

4a, R=CH$_2$CH$_3$: ^{1}H NMR δ=0.8—1.7 (m, 11H), and 2.0-2.5 (m, 6H); ^{13}C NMR δ=61.68, 54.74, 26.14, 24.65, 20.15, and 12.11; colorless oil.[13]

Reactions with *N*-Methyl-1,2,3,4-tetrahydroisoquinoline *N*-Oxide (1b). As a typical example of the reactions of **1b**, the procedure with phenylmagnesium bromide and trimethylsilyl trifluoromethanesulfonate is described.

Transformation of 1b to 4b. To a solution of *N*-oxide **1b** (130 mg, 0.8 mmol) in 10 ml of dichloromethane was added TBDMSOTf (232 mg, 1.1 equiv) and after the solvent exchange into THF (10 ml) was added MeLi (0.96 mmol, 1.2 equiv) at 0 °C. After replacement of the solvent into toluene (10 ml) was added MeLi (0.96 mmol, 1.2 equiv) at 0 °C. After the solvent was exchanged into toluene (10 ml) was added trimethylsilyl trifluoromethanesulfonate (TMSOTf) (213 mg, 1.2 equiv) at −78 °C and the mixture was warmed to room temperature with stirring. Phenylmagnesium bromide (1.2 mmol, 1.5 equiv) was then added to this mixture at 0 °C and the mixture was warmed to 70 °C with stirring for 24 h. It was then shaken with 50 ml of 5% aq NaOH solution and 50 ml of ether, and the aqueous layer was extracted with dichloromethane (30 ml×3). The extracts and organic layer were combined, dried over MgSO$_4$, and concentrated. Chromatography of the residual oil on alumina gave the α-phenylated product (**4b**, R=Ph) (100.2 mg, 56%) as a pale yellow solid.

4b, R=Ph: ^{1}H NMR δ=2.21 (s, 3H), 2.3—3.8 (m, 4H), 4.24 (brs, 1H), 6.5—7.5 (m, 4H), and 7.27 (s, 5H); MS, *m/z* 223 (M$^+$, 19%), 222 (15), 179 (17), 178 (10), 165 (6), 147 (22), 146 (100), 131 (6), 118 (2), 103 (2), 91 (5), and 77 (5); high-MS, *m/z* Found 223.1381, Calcd for C$_{16}$H$_{17}$N: 223.1361; mp 69—70 °C (lit,[14] 72 °C).

The other reaction of **1b** listed in Table 2 were carried out similarly to give the corresponding α-substitution products. In the case of the reaction with methylmagnesium iodide (Entry 7) the yield of **4b** (R=Me) decreased to 15% when toluene was used as a solvent instead of a mixed solvent (THF-ether=1:2).

4b, R=CH$_2$CH$_3$: ^{1}H NMR δ=0.84 (t, *J*=7 Hz, 3H), 1.5—2.1 (m, 2H), 2.33 (s, 3H), 2.4—3.6 (m, 5H), and 7.09 (s, 4H), MS, *m/z* 175 (M$^+$, 2%), 174 (28), 147 (9), 146 (100), 131 (4), 115 (2), 91 (2), and 77 (2); high-MS, *m/z* Found 175.1354, Calcd for C$_{12}$H$_{17}$N: 175.1360; pale yellow oil.

4b, R=CH=CH$_2$: ^{1}H NMR δ=2.1—3.4 (m, 4H), 2.39 (s, 3H), 3.70 (d, *J*=7.5 Hz, 1H), 4.9—6.1 (m, 3H), and 7.09 (s, 4H); MS, *m/z* 173 (M$^+$, 6%), 172 (7), 146 (55), 119 (13), 118 (100), 91 (20), 90 (46), 77 (13), 71 (39), and 57 (45); high-MS, *m/z* found 173.1205, Calcd for C$_{12}$H$_{15}$N: 173.1205; yellow oil.

4b, R=CH$_2$Ph: ^{1}H NMR δ=2.46 (s, 3H), 2.7—3.6 (m, 6H), 3.84 (t, *J*=6 Hz, 1H), and 7.0—7.5 (m, 9H); MS, *m/z* 237 (M$^+$, 8%), 236 (26), 234 (29), 160 (7), 147 (7), 146 (100), 145 (16), 144 (58), 131 (19), 105 (18), 91 (36), and 77 (15); high-MS, *m/z* Found 237.1467, Calcd for C$_{17}$H$_{19}$N: 237.1517; yellow oil.

4b, R=CH$_3$: ^{1}H NMR δ=1.39 (d, *J*=7 Hz, 3H), 2.48 (s, 3H), 2.4—3.7 (m, 5H), and 7.0-7.3 (m, 4H); MS, *m/z* 161 (M$^+$, 7%), 160 (5), 146 (20), 147 (100), 144 (7), 131 (8), 118 (12), 114 (17), 91 (6), and 77 (7); yellow oil.[15]

Reactions with Trialkylaluminums; α-Substitution of 1a by Triisobutylaluminum. To a solution of **1a** (165.6 mg, 1.44 mmol) in 10 ml of dichloromethane was added TBDMSOTf (424 mg, 1.1 equiv) and after the solvent exchange into THF (10 ml) was added MeLi (1.73 mmol, 1.2 equiv) at 0 °C. To this solution was added triisobutylaluminum (1.73 mmol, 1.2 equiv in 15% hexane solution) at −78 °C and then the mixture was warmed to room temperature with stirring. After stirring for 14 h, the solvent was evaporated and the resulting oil was subjected to chromatography (alumina, hexane-ether=5:2) to give *N*-isopentylpiperidine (**4a**; R=*i*-Bu)(100 mg, 45%) as a colorless oil.[16]

4a, R=*i*-Bu: ^{1}H NMR δ=0.7—1.1 (m, 6H), 1.1—2.0 (m, 9H), and 2.0—2.6 (m, 6H); MS, *m/z* 155 (M$^+$, 8%), 154 (1), 110 (4), 99 (9), 98 (100), 85 (4), 84 (4), 71 (5), and 57 (8).

Reactions of Other *N*-Oxides with Trialkylaluminums. Reactions of **1a** and **1c** with triethylaluminum were carried out similarly to the above-mentioned α-isobutylation to afford the corresponding α-ethylated products (**4a**, R=CH$_2$CH$_3$) and (**4c**, R=CH$_2$CH$_3$) in 69 and 75% yields, respectively. α-Methylation of **1b** with trimethylaluminum was carried out in dichloromethane instead of THF to give the α-methylated product (**4b**, R=CH$_3$) in 20% yield.

4c, R=CH$_2$CH$_3$: ^{1}H NMR δ=0.9 (t, *J*=8 Hz, 3H), 1.5—2.3 (m, 2H), 3.48 (ABq, δ_{AB}=0.42, J_{AB}=14 Hz, 4H), 3.59 (t, *J*=8 Hz, 1H), and 7.0—7.6 (m, 15H); ^{13}C NMR δ=140.44, 139.17, 128.96, 128.74, 127.88, 126.68, 64.01, 53.82, 24.30, and 11.67; MS, *m/z* 315 (M$^+$, 1%), 287 (13), 286 (46), 210 (3), 194 (8), 181 (5), 118 (4), 92 (9), 91 (100), and 65 (8); high-MS, *m/z* Found 315.1962, Calcd for C$_{23}$N$_{25}$N: 315.1987; yellow oil.

α-Cyanation. As a typical example of α-cyanations, the procedure with **1b** is described. Transformation of **1b** into **5b**. To a solution of **1b** (156 mg, 0.96 mmol) in 10 ml of dichloromethane was added TBDMSOTf (279 mg, 1.1 equiv) and after replacement of the solvent by THF (10 ml) was added MeLi (1.15 mmol, 1.2equiv) at 0 °C. After the solvent was again exchanged into dichloromethane (10 ml), titanium tetrachloride (237 mg, 1.3 equiv) was added at −78 °C and the mixture was stirred for 1 h at this temperature. To the greenish-brown suspension was then added trimethylsilyl cyanide (0.19 ml, 1.5 equiv) at −78 °C. After stirring overnight at room temperature, the mixture was shaken with 50 ml of 5% aq NaOH solution and 50 ml of dichloromethane, and the aqueous layer was extracted with dichloromethan (30 ml×3). The extracts and organic layer were combined, dried over MgSO$_4$, and concentrated. Chromatography of the residual oil gave 1-cyano-*N*-methyl-1,2,3,4-tetrahydroisoquinoline (**5b**) (103.9 mg, 63%) as a pale yellow solid.

5b: ^{1}H NMR δ=2.5—3.3 (m, 4H), 2.58 (s, 3H), 4.70 (s, 1H), and 6.9—7.3 (m, 4H); ^{13}C NMR δ=133.94, 129.72, 129.39, 128.50, 127.14, 126.49, 116.53, 56.96, 48.46, and 28.44; MS, *m/z* 172 (M$^+$, 45%), 171 (43), 149 (43), 146 (31), 145 (38), 144 (100), 129 (99), and 57 (27); high-MS, *m/z* Found 172.0999, Calcd for C$_{11}$H$_{12}$N$_2$: 172.0999; mp 75—77 °C (lit,[17] 76—78 °C).

The other reactions listed in Table 4 were carried out similarly to the above procedure to give the corresponding

α-cyano amines.

5a: ^{1}H NMR δ=1.0—2.0 (m, 6H), 2.2—2.7 (m, 4H), and 3.5 (s, 2H); ^{13}C NMR δ=114.87, 53.12, 46.89, 25.71, and 23.32; MS, *m/z* 124 (M^+, 40%), 123 (100), 98 (6), 96 (12), 83 (27), and 57 (22); high-MS, *m/z* Found 124.0973, Calcd for $C_7H_{12}N_2$: 124.0999; colorless oil.

5c: ^{1}H NMR δ=3.64 (ABq, δ_{AB}=0.5, J_{AB}=13.5 Hz,4H), 4.9 (s, 1H), and 7.0—7.7 (m, 15H); ^{13}C NMR δ=139.58, 137.71, 133.97, 128.74, 128.58, 128.17, 127.63, 126.82, 115.31, 57.32, and 54.99; MS, *m/z* 312 (M^+, 0.3%), 287 (4), 239 (2), 210 (4), 165 (12), 125 (10), 123 (28), 105 (14), 93 (33), 91 (100), and 55 (52); high-MS, *m/z* Found 312.1624, Calcd for $C_{22}H_{20}N_2$: 312.1624; white solid, mp 103—104 °C (lit,[18] 103—104 °C).

5d: ^{1}H NMR δ=0.8—2.5 (m, 11H), 2.37 (s, 3H), and 3.57 (s, 2H); ^{13}C NMR δ=115.99, 61.30, 42.44, 38.98, 29.96, 25.89, and 25.14; MS, *m/z* 152 (M^+, 10%), 110 (7), 109 (100), 96 (9), and 83 (8), high-MS, *m/z* Found 152.1304, Calcd for $C_9H_{16}N_2$: 152.1312; colorless oil.

5e: ^{1}H NMR δ=2.31 (s, 6H), 4.9 (s, 1H), and 7.1—8.0 (m, 5H); MS, *m/z* 160 (M^+, 50%), 159 (16), 116 (29), 92 (29), 91 (100), and 83 (95); high-MS, *m/z* Found 116.1007, Calcd for $C_{10}H_{12}N_2$: 160.1001; colorless oil.

5e′: ^{1}H NMR δ=2.35 (s, 3H), 3.38 (s, 2H), 3.55 (s, 2H), and 7.38 (s, 5H); ^{13}C NMR δ=137.09, 128.96, 128.58, 127.78, 114.52, 60.16, 44.18, and 42.23; MS, *m/z* 160 (M^+, 39), 159 (13), 118 (3), 92 (34), 91 (100), and 83 (44); high-MS, *m/z* Found 160.1000, Calcd for $C_{10}H_{12}N_2$: 160.1001; pale yellow oil.

Reactions with a Silyl Enol Ether. Transforation of 1a into 6a. As a typical example the procedure with **1a** in the presence of TMSOTf and potassium fluoride is described. To a solution of **1a** (134 mg, 1.17 mmol) in 10 ml of dichloromethane was added TBDMSOTf (324 mg, 1.05 equiv) and after the solvent exchange into THF (15 ml) was added MeLi (1.29 mmol, 1.1 equiv). After replacement of the solvent by dichloromethane (10 ml) TMSOTf (312 mg, 1.2 equiv) was added at 0 °C. The mixture was stirred for 2 h at room temperature and then to the mixture was added α-trimethylsiloxystyrene (270 mg, 1.2 equiv) at this temperature. After stirring for 1 h at room temperature potassium fluoride (75 mg, 1.1 equiv; dried by heating at about 100 °C in vacuo just before use) was added in one portion and the mixture was refluxed for 16 h. Then the mixture was shaken with 50 ml of 5% aq NaOH solution and 50 ml of dichloromethane, and the aqueous layer was extracted with dichloromethane (30 ml×3). The extracts were combined with the organic layer, dried over $MgSO_4$, and concentrated. Chromatography of the residual oil (alumina, ether-hexane=2:1) afforded the expected α-substituted product **6a** (120 mg, 47%) as a pale yellow oil.[19]

6a: ^{1}H NMR δ=1.2—1.7 (m, 6H), 2.4—2.6 (m, 4H), 2.6—3.3 (m, 4H), 7.3—7.7 (m, 3H), and 7.8—8.2 (m, 2H); ^{13}C NMR δ=199.36, 137.17, 132.94, 128.58, 128.07, 54.63, 54.01, 34.46, 26.03, and 24.32; MS, *m/z* 217 (M^+, 6%), 132 (7), 105 (30), 99 (8), 98 (100), 97 (33), 86 (10), 84 (16), and 77 (23).

The authors are grateful to Shin-etsu Chemical Co. Ltd. for the generous gift of chlorosilanes.

References

1) P. Beak and D.B. Reitz, *Chem. Rev.*, **78**, 275 (1978); A. I. Meyers and L. M. Fuentus, *J. Am. Chem. Soc.*, **105**, 117 (1983) and previous papers of this series; D. Seebach, J. J. Lohman, M. D. Syfrig, and M. Yoshifuji, *Tetrahedron*, **39**, 1963 (1983) and references cited therein; P. Beak and W. J. Zaidel, *J. Am. Chem. Soc.*, **106**, 1010 (1984) and references cited therein.

2) H. Ahlbrecht and H. Dollinger, *Tetrahedron Lett.*, **25**, 1353 (1984).

3) F. F. Blicke, "Organic Reactions," Wiley, New York (1942) Vol. 1, p. 303; M. Tramontini, *Synthesis*, **1973**, 703 and references cited therein.

4) R. Okazaki and N. Tokitoh, *J. Chem. Soc., Chem. Commun.*, **1984**, 192; N. Tokitoh and R. Okazaki, *Chem. Lett.*, **1984**, 1937; *idem, Bull. Chem. Soc. Jpn.*, in press.

5) Part of this work has been reported as preliminary communications: N. Tokitoh and R. Okazaki, *Tetrahedron Lett.*, **25**, 4677 (1984); *idem, Chem. Lett.*, **1985**, 241.

6) Although the reactions of **3** with alkyllithiums were also examined, desired substitution reactions did not occur perhaps due to the rather lower affinity of lithium reagents toward an oxygen atom of the siloxy group compared with magnesium and aluminum reagents.

7) When **3b** prepared in situ from **1b** was treated with trimethylaluminum in THF, only a tarry complex mixture was obtained.

8) a) Recently, different approaches to α-cyano amines have been reported: K. Mai and G. Patil, Tetrahedron Lett., 25, 4583 (1984); H. Yamanaka, S. Nishimura, S. Kaneda, and T. Sakamoto, *Synthesis*, **1984**, 681. b) The α-cyano amines can also be a useful intermediate for the synthesis of α-alkyl-substituted amines via an alkylation-decyanation procedure; G. Stork, R. M. Jacobson, and R. Levitz, *Tetrahedron Lett.*, **1979**, 771, M. Bonin, J. R. Romeo, D. S. Grieson, and H.-P. Husson, *J. Org. Chem.*, **49**, 2392 (1984).

9) N. J. Leonard and G. W. Leubner, *J. Am. Chem. Soc.*, **71**, 3408 (1949).

10) H. B. Ponahoe, S. J. Trotz, and K. K. Kimura, *J. Org. Chem.*, **25**, 1059 (1960).

11) C. Glacet and R. Coupe, *Bull. Soc. Chim. Fr.*, **1963**, 2464; T, Turiddu and D. Leonesi, *Ann. Chim. (Rome)*, **53**, 1113 (1963).

12) B. William and J. R. Wright, *J. Org. Chem.*, **27**, 1042 (1962); H. Sekiya and Y. Terao, *Chem. Pharm. Bull.*, **1970**, 947.

13) S. Landa, Z. Kafka, V. Galik, and M. Safar, *Collect. Czech. Chem. Commun.*, **1969**, 34 (3588).

14) P. R. Brrok and P. Karrer, *Helv. Chim. Acta*, **40**, 260 (1957).

15) S. Yamada and S. Ikegami, *Chem. Pharm. Bull.*, **1966**, 14, 1382.

16) V. Galik, Z. Kafka, S. Landa, and M. Sfar, *Collect. Czech. Chem. Commun.*, **1968**, 33, 609.

17) B. Jaques and R. G. Wallace, *Tetrahedron*, **33**, 581 (1977).

18) P. A. S. Smith and R. N. Leopplely, *J. Am. Chem. Soc.*, **89**, 1147 (1967).

19) R. Andrisano, A. S. Angeloni, and S. Marzocchi, *Tetrahedron*, **29**, 913 (1973).

 © 1988 The Chemical Society of Japan Bull. Chem. Soc. Jpn., 61, 741—743 (1988)

New Series of Organic Metal. Radical Salts of Unsymmetrical Donors Containing Pyrazino Group

Koichi KIKUCHI,* Hiroyuki KAMIO, Kazuya SAITO, Stelios Y. YIANNOPOULOS,†
George C. PAPAVASSILIOU,† Keiji KOBAYASHI,†† and Isao IKEMOTO
Department of Chemistry, Faculty of Science, Tokyo Metropolitan University,
Fukazawa, Setagaya-ku, Tokyo 158
†Theoretical and Physical Chemistry Institute, The National Hellenic Research Foundation,
48, Vass. Constantinou Ave., Athens 116/35, GREECE
††Department of Chemistry, College of Arts and Sciences, The University of Tokyo,
Komaba, Meguro-ku, Tokyo 153
(Received July 14, 1987)

The I_3, ClO_4, and PF_6 salts of unsymmetrical donors containing fused pyrazino groups (DMPDSDTF and DM(DMP)DSDTF) were prepared electrochemically and their electrical conductivities were measured. The I_3 salt of DM(DMP)DSDTF exhibited a metallic behavior down to about 120 K. The radical salts of unsymmetrical donors showed much larger conductivities than those of the corresponding symmetrical donors containing pyrazino groups.

In the past decade, much attention has been concentrated on the construction of organic superconductors. It has been recognized in such studies that higher dimensionality is preferred because low dimensional systems of electrons intrinsically possess the instability against to a lattice distortion with a period of $1/2k_F$. Indeed, at low temperature many organic conductors undergo a CDW (Peierls), SDW or spin-Peierls transition, below which they behave as insulators.

One way to increase dimensionality of the system is compression of a sample under high pressure. The first organic superconductor $(TMTSF)_2PF_6$[1] has been obtained through application of high pressure of 0.65 GPa. Besides physical compression, there exists another strategy to increase dimensionality, i.e. chemical decoration of a molecule. TMTSF[1] and BEDT-TTF,[2] of which radical salts have been discovered so far to undergo a superconducting transition, are in fact analogues of one of the most famous donor, TTF.

From the second point of view, the donors containing nitrogen atoms are interesting because the lone pair electrons will possibly enhance the dimensionality of electronic systems in crystals. However, only a few reports have been published so far about the salts of such donors.[3-7]

Very recently, the superconductivity in $(DMET)_2Au(CN)_2$[8] (DMET: dimethyl(ethylenedithio)diselenadithiafulvalene) and $(DMET)_2AuBr_2$[9] has been discovered, which indicates that a symmetrical donor is not necessary to organic superconductors. These situation prompted us to start the studies on the unsymmetrical donors containing a pyrazino group. The donors we have chosen are DMPDSDTF (dimethyl(pyrazino)diselenadithiafulvalene) and DM-(DMP)DSDTF (dimethyl(dimethylpyrazino)diselenadithiafulvalene) (Fig. 1), which have a partial structure of TMTSF. If any properties of the partial structures of the donor contribute additively to the properties of crystals, enhanced dimensionality and high electrical conductivity will be realized. In order to clarify this point, some radical salts of the unsymmetrical donors were prepared and the electrical conductivities were compared with those of the corresponding symmetrical donors, BPTTF (bispyrazinotetrathiafulvalene) and BDMPTTF (bis(dimethylpyrazino)tetrathiafulvalene) (see Fig. 1).

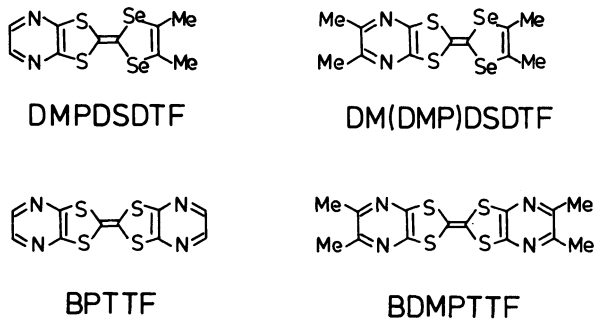

Fig. 1. Molecular structures of the donors.

Experimental

The unsymmetrical and symmetrical donors were synthesized according to the methods described previously.[10] The radical salts of the donors were grown at room temperature by the electrochemical method with constant current of 2 μA in dichloromethane. The supporting electrolytes used were $(n\text{-}Bu)_4N\cdot I_3$, $(n\text{-}Bu)_4N\cdot ClO_4$, and $(n\text{-}Bu)_4N\cdot PF_6$, which cover a variety of counter anions of linear, tetrahedral, and octahedral structures. The single crystals of ClO_4 salts of the unsymmetrical donors and of the PF_6 salt of BDMPTTF were needle-like, and others were plate-like.

The electrical conductivities were measured along the growth axis of the crystal by standard four probe AC (20 Hz) and DC methods at constant current (1—10 μA) between liquid nitrogen and room temperatures. As both methods of conductivity measurements gave consistent results, we will not mention about the methods in the following. The size of the samples used for conductivity measurements was typically $2\times0.3\times0.03$ mm^3.

Results and Discussion

The room temperature conductivities of radical salts are tabulated in Table 1. While all of the radical salts of DMPDSDTF, BPTTF and BDMPTTF

Table 1. Electrical Properties of Radical Salts. Room Temperature Conductivities in $S\,cm^{-1}$ and Band Gap Energies in eV (in Parenthesis)

	PF_6	ClO_4	I_3
Unsymmetrical			
DMPDSDTF	Semiconductor 4.0(0.12)	Semiconductor 1.5(0.56)	Semiconductor 1.6(0.10)
DM(DMP)DSDTF	Semiconductor 3.2(0.25)	Metal[a] 44	Metal[b] 92
Symmetrical			
BPTTF	Semiconductor 0.68(0.38)	—[c]	—[c]
BDMPTTF	Semiconductor 0.060(0.20)	—[c]	—[c]

a) Below about 250 K, semiconductor with the band gap energy 0.09 eV. b) Below about 120 K, semiconductor with the band gap energy 0.04 eV. c) Single crystals could not be prepared.

exhibited semiconducting behaviors at room temperature, two radical salts of DM(DMP)DSDTF behaved as metallic. The band gap energies were deduced from Arrhenius plots of conductivities in semiconducting region and are also given in Table 1.

It is interesting to compare the properties of the single crystals of radical salts of symmetrical and unsymmetrical donors. Only a series of PF_6 salts is available for this purpose, as radical salts of other anions with symmetrical donors could not be prepared. The room temperature conductivity of the DMPDSDTF salt is larger than that of the BPTTF salt by an order of magnitude. Similarly, that of the DM(DMP)DSDTF salt is larger than that of the BDMPTTF salt by a factor 50. Moreover, ClO_4 and I_3 salts of DM(DMP)DSDTF showed metallic properties. Thus, introduction of a partial structure of TMTSF increases an electrical conductivity. It is noteworthy that in the case of I_3 salt of DM(DMP)DSDTF the conductivity perpendicular to the crystal growth axis was smaller than that along the axis by only a factor 5, which suggests that the salts have high dimensionality. Similar effects were observed also in salts of the unsymmetrical donor,[7] PEDTTTF, which has a partial structure of BEDT-TTF. Hence, we conclude that partial structures of a donor contribute additively to the electrical property of radical salts.

In addition to improvement of room temperature conductivity, there is another remarkable finding: Although all of three radical salts of DMPDSDTF were semiconducting, the radical salts of DM(DMP)-DSDTF showed a variety of temperature dependences of conductivity. The results of the conductivity measurements on a series of the salts of DM(DMP)-DSDTF are shown in Fig. 2. It is interesting that the higher is the symmetry of an anion, the lower is an electrical conductivity of the corresponding radical salt (Table 1). The PF_6 salt exhibits a semiconducting behavior in the temperature range studied. In contrast to the PF_6 salt, the I_3 salt behaves as metallic down to about 120 K, below which the salt is a semiconductor. It is emphasized that this is the second observation that an organic conductor consisting of an donor containing pyrazino group(s) shows a metallic behavior down to such a low temperature.[7] The ClO_4 salt is also metallic at room temperature though it is

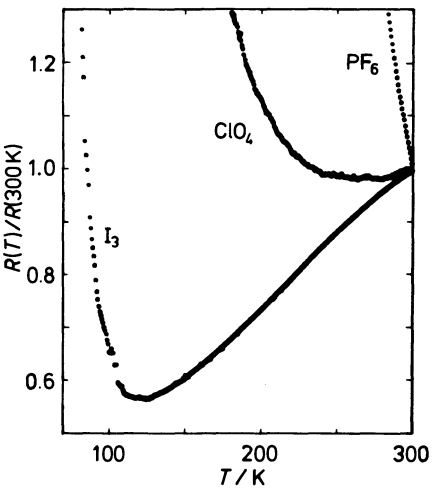

Fig. 2. Electrical resistivities of a series of radical salts of DM(DMP)DSDTF. Counter anions are indicated in the figure. For the values of R(300 K), see Table 1.

hardly recognized in Fig. 2. As the temperature dependence of the conductivity is very weak, it is hard to locate unambiguously the metal-insulator transition point on the basis of the present data.

Structural and high pressure studies are interesting and in progress in this laboratory. These will be published shortly.

This study was supported by the Grant-in-Aid for Scientific Research No. 6143003 from the Ministry of Education, Science and Culture.

References

1) D. Jerome, A. Mazaud, M. Ribault, and K. Bechgaard, *J. Phys. (Paris) Lett.*, **41**, L95 (1980).

2) S. S. P. Parkin, E. M. Englar, R. R. Schumaker, R. Ligaier, V. Y. Lee, J. Voiron, K. Carneiro, J. C. Scott, and R. L. Greene, *Phys. Rev. Lett.*, **50**, 270 (1982).

3) G. C. Papavassiliou, S. Y. Yiannopoulos, and J. S. Zambounis, *Mol. Cryst. Liq. Cryst.*, **120**, 333 (1986).

4) G. C. Papavassiliou, S. Y. Yiannopoulos, and J. S. Zambounis, *Physica*, **143B**, 310 (1986).

5) A. Terzis, A. Hountas, and G. C. Papavassiliou, *Acta Crystallogr., Sect. C*, **42**, 1584 (1986).

6) A. E. Underhill, B. Kaye, G. C. Papavassiliou, and S. Y. Yiannopoulos, *Mol. Cryst. Liq. Cryst.*, **134**, 59 (1986).
7) G. C. Papavassiliou, A. Terzis, A. E. Underhill, H. P. Geserich, B. Kaye, A. Hountas, and S. Y. Yiannopoulos, *Synth. Metals*, **19**, 703 (1987).
8) K. Kikuchi, M. Kikuchi, T. Namiki, K. Saito, I. Ikemoto, K. Murata, I. Ishiguro, and K. Kobayashi, *Chem. Lett.*, **1983**, 931.
9) K. Kikuchi, K. Murata, Y. Honda, T. Namiki, K. Saito, K. Kobayashi, I. Ishiguro, and I. Ikemoto, *J. Phys. Soc. Jpn.*, **56**, 2627 (1987).
10) G. C. Papavassiliou, S. Y. Yinnopoulos, J. S. Zambounis, K. Kobayashi, and K. Umemoto, *Chem. Lett.*, **1987**, 1279.

 © 1988 The Chemical Society of Japan Bull. Chem. Soc. Jpn., 61, 745—751 (1988)

Interference Effects of Helium on Motion of Xenon in Micropores of 5A Zeolites

Yusuke YASUDA* and Satoshi SHINBO
Faculty of Science, Toyama University, Toyama 930
(Received June 22, 1987)

Striking interference effects of He molecules on the motion of Xe in micropores of 5A zeolites have been found by the frequency response method. Results of the systems reveal that the absorbed Xe molecules may be divided into two abspecies, c_1' and c_2', in the presence of He molecules which were inert in a single component system: (i) at 273 K, c_1' diffuses faster and c_2' slower than pure Xe; (ii) at 255 K, c_1' diffuses faster than pure Xe, while the motion of c_2' is regarded as not diffusion but adsorption. The interference effects at 273 K have been explained quantitatively by decoupling a more general form of Fick's law containing cross terms.

Since zeolites have a molecular-sieve action, the binary or multicomponent diffusion of gases in the micropores of zeolites has been of considerable interest after the discovery of zeolite crystals in the late 1950s. However, conclusions seem controversial: (i) the diffusion of one component is enhanced in a mixture,[1] (ii) both diffusion coefficients of a binary gas mixture are considerably smaller than those of pure components,[2] and (iii) each component of a mixture (using He as a carrier gas) diffuses independently with the same intrinsic mobility as for single-component diffusion.[3]

In the first application of the frequency response (FR) method to a system of a binary gas mixture, CH_4+He or CH_4+Kr over Linde 5A at 195 K, striking mutual interference effects have been observed in the diffusion process.[4] The aim of the present article is to confirm that the interference occurs in micropores rather than on the exposed surface of a zeolite. The dependence of the effects on the crystal size of a zeolite was investigated using simpler gas systems of Xe+He over two kinds of 5A zeolites, Ca-A2 and Ca-A6, of which the mean crystal sizes were 2 and 6 μm, respectively.

Experimental

Zeolite Preparation and Materials. Synthetic 5A zeolites supplied by Toyo Soda Manufacturing Co., Ca-A2 and Ca-A6, were used; their properties are summarized in Table 1. SEM photographs of the samples are shown in Fig. 1. Crystal-size distributions of the two samples were determined by measuring the size of ca. 700 crystals; that of Ca-A2 was practically normal on a weight or volume fraction basis, but that of Ca-A6 was distorted.

Table 1. Cation Exchange and Size Distribution of 5A Zeolite Crystals

Zeolite	%Ca[a]	N[b]	$(2a_m/\mu m)$[c]	(σ/a_m)[d]
Ca-A2	96	660	1.7	0.28
Ca-A6	94	800	5.5	0.4

a) Expressed as % of original Na^+ ions replaced by Ca^{++}. b) Number of particles measured. c) Mean cube side. d) Relative standard deviation.

Powders were first pelleted under a pressure of ca. 1×10^3 kg cm^{-2}, crushed, and dehydrated at 383 K for 10 h. The temperature was then raised to 623 K and the system evacuated at that level for at least 20 h. Practically the same FR results were obtained for samples both with and without compression.

No impurities were detected in the Xe or He by mass spectrometer analysis.

Apparatus and Procedure. The FR apparatus was described in a previous paper.[4] The gas space V of the system was varied sinusoidally as

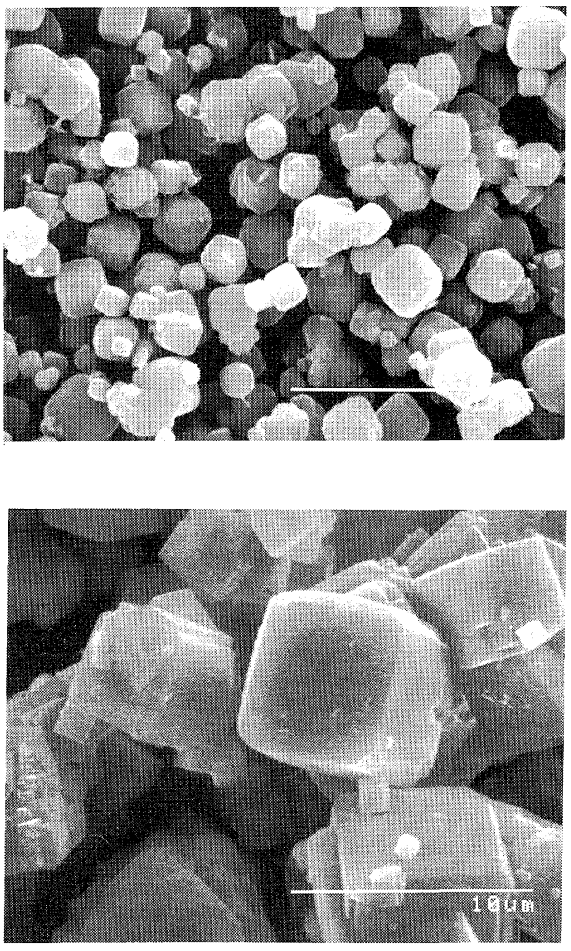

Fig. 1. SEM photographs of (a) Ca-A2 and (b) Ca-A6 zeolites.

$$V(t) = V_e(1 - ve^{i\omega t}), \quad (1)$$

where V_e is the equilibrium or the mean volume of the oscillation, v the relative amplitude and ω the angular velocity. The induced pressure variation can be well expressed by

$$P(t) = P_e\{1 + pe^{i(\omega t+\varphi)}\}. \quad (2)$$

In order to remove any apparent change in the p or φ characteristic of the apparatus due to a delay of the pressure-gauge reading, blank experiments were carried out without zeolites.

Actual values of v and φ were determined by

$$v = p_B \text{ and } \varphi = \varphi' - \varphi_B, \quad (3)$$

where p_B and φ_B denote the results obtained in a blank experiment carried out under almost the same conditions for P_e, T_e, and further at the same ω. φ' is the value of raw data obtained in a system with zeolites.

The various conditions for the pure Xe and Xe+He systems should be regarded as identical, since after each run of ω's for a pure Xe system was completed, small amounts of He were introduced into the system while repeating the scanning of ω. The (total) equilibrium pressure, P_e, was measured using a conventional mercury manometer.

Results

Dependence of p/v and φ on ω. In preliminary experiments for pure He systems, various results agreed with those of the blank experiments. It is concluded, therefore, that

$$p/v = 1 \text{ and } \varphi = 0 \quad (4)$$

with respect to the pure He system.

The results of p/v and φ obtained from single and binary gas systems of Ca-A2 at 273 K are shown in Figs. 2(a) and 2(b), for which the experimental conditions are given in Table 2.

If both Xe and He molecules behave independently in the mixture, the values of p/v and φ corresponding to ΔP_T in Fig. 3 are expected to be intermediate of those corresponding to ΔP_{Xe} and ΔP_{He} (as illustrated in Fig. 3). Calculated results from the triangle are represented by the dashed curves in Figs. 2(a) and 2(b). The discrepancy between the two dashed curves, one

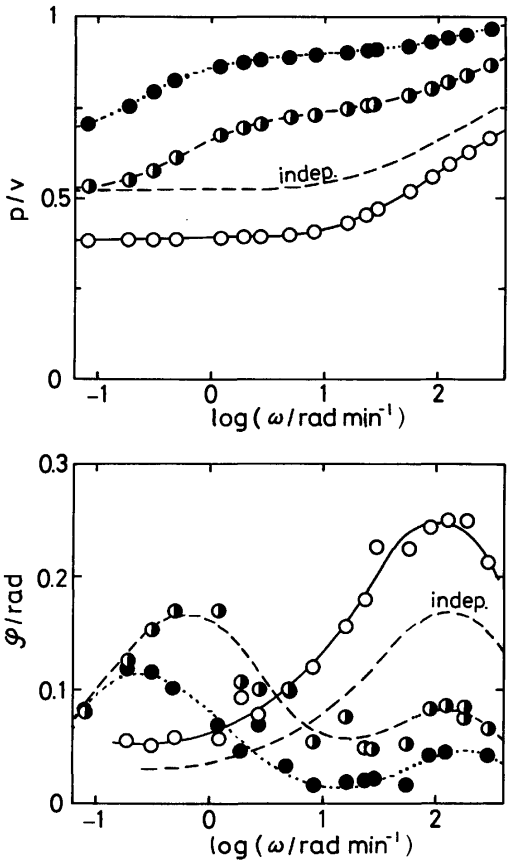

Fig. 2. Raw data of Xe and Xe+He mixtures over Ca-A2 at 273 K; (a) p/v and (b) φ versus ω. ○, pure Xe(Exp. No. 1); ◑, Xe:He=4:1(Exp. No. 2); ●, Xe:He=4:3(Exp. No. 3). The dashed curves indicated by "indep." represent calculated results under the assumption that each component of Xe:He=4:1 behaves independently.

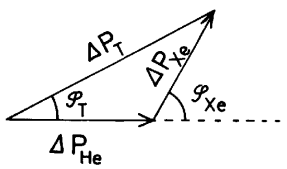

Fig. 3. Relations among total and partial pressure variation; $P_T(t)=P_T^{(e)}+\Delta P_T\cos(\omega t+\varphi_T)$, $P_{He}(t)=P_{He}^{(e)}+\Delta P_{He}\cos(\omega t+0)$, and $P_{Xe}(t)=P_{Xe}^{(e)}+\Delta P_{Xe}\cos(\omega t+\varphi_{Xe})$. An equality of $P_T(t)=P_{He}(t)+P_{Xe}(t)$ leads to the triangle.

Table 2. Summary of Experimental Conditions

Exp. No.	T_e/K	Absorbent	P_{Xe}[a]/Torr	P_{He}[a]/Torr	Xe molecule per cavity	K_T[b]
1	273	Ca-A2[d]	3.6	0	0.9×10^{-1}	(1.93)[c]
2			3.6	1.0		1.05
3			3.6	3.1		0.55
4		Ca-A6[e]	3.1	0	1.2×10^{-1}	(2.90)
5			3.1	1.1		1.23
6	255	Ca-A2	4.1	0	2.2×10^{-1}	(4.75)
7			4.1	1.2		1.77
8		Ca-A6	3.6	0	3.3×10^{-1}	(8.05)
9			3.6	0.9		2.39

a) Partial pressure of each component (1 Torr=133.322 Pa). b) Calculated from the gradient of absorption isotherm according to Eq. 9. c) $=K_2^{(0)}$. d) 7.84 g in a dehydrated state. e) 7.85 g in a dehydrated state.

experimental and the other calculated, suggests considerable interference effects between Xe and He. It should be noted that the *single* peak in φ's of the pure Xe system seems to split into *two* peaks in the presence of "inert" (see Eq. 4) molecules of He.

Frequency Response of the Systems. Results at 273 K: The in-phase and out-of-phase components of the FR, $(v/p)\cos\varphi$-1 and $(v/p)\sin\varphi$, respectively, which were calculated from the data in Figs. 2(a) and 2(b), are shown in Figs. 4(a) and 4(b). In order to demonstrate the effects of He, they are divided by a constant K_T (Table 2).

The value of K_T for a single-component system was determined by the gradient of the absorption isotherm:[5]

$$K_T = \frac{RT_0}{V_e}\left(\frac{dB^{(0)}}{dP}\right)_e, \tag{5}$$

where B denotes the amount of abspecies and the superscript, (0), indicates the value in a pure gas system.

The value of K_T of a multicomponent system may be given by (Appendix 1)

$$K_T = \frac{\sum_m x_m K_m/(K_m+1)}{\sum_n x_n/(K_n+1)}, \tag{6}$$

where x_m denotes the mole fraction of the m-component in the *gas* phase. K_m is defined as

$$K_m = \frac{RT_0}{V_e}\left(\frac{dB_m}{dP_m}\right)_e, \tag{7}$$

where B_m denotes the amount of the m-molecules absorbed; P_m is the partial pressure of the component.

In the present work, the absorption isotherm of pure Xe was practically unaltered by the addition of He. Therefore, the values of K_1 and K_2 (the subscript 1 and 2 refer to He and Xe, respectively) can be determined by those obtained in the single-component system:

$$K_1 = K_1^{(0)} (= 0)$$

and

$$K_2 = K_2^{(0)}\left(= \frac{RT_0}{V_e}\left(\frac{dB_2^{(0)}}{dP}\right)_e\right). \tag{8}$$

The amount of Xe molecules, $B_2^{(0)}$, was proportional to the equilibrium pressure. The constants of $K_2^{(0)}$ are given in Table 2. Consequently, K_T of the binary gas mixture can be evaluated by

$$K_T = \frac{x_2 K_2^{(0)}}{1 + x_1 K_2^{(0)}}. \tag{9}$$

The values of K_T, thus obtained, are given in Table 2; K_T is expected to be the upper limit of the in-phase components.[5]

Results of Ca-A6 are plotted in Figs. 5(a) and 5(b) together with those of Ca-A2 which were obtained

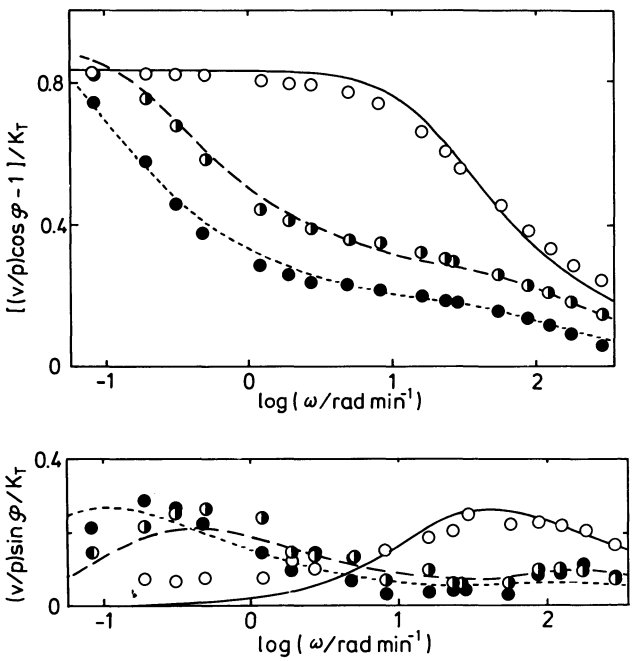

Fig. 4. Frequency response of Xe and Xe+He mixtures over Ca-A2 at 273 K; (a) in-phase and (b) out-of-phase components normalized by K_T versus ω. Notation is that of Fig. 2. Various curves represent calculated results according to Eqs. 10 and 11 with the parameters given in Table 3.

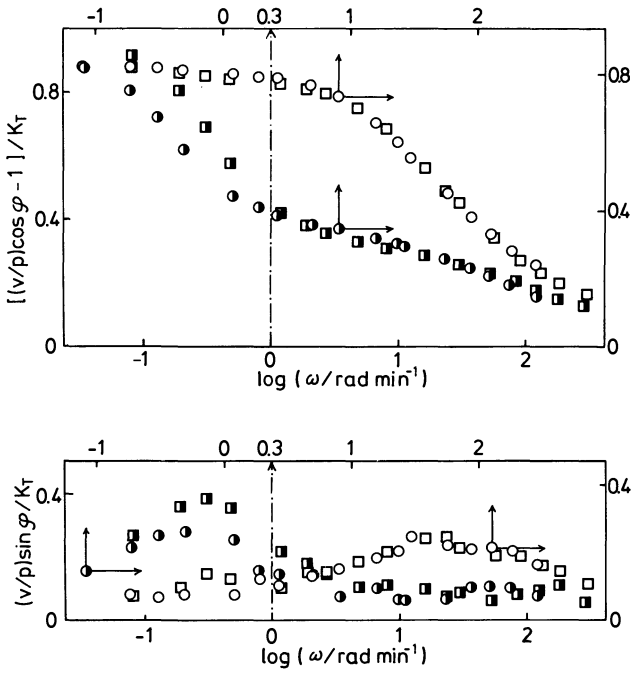

Fig. 5. Dependence of crystal size on FR of the systems; (a) in-phase and (b) out-of-phase components normalized by K_T versus ω. Squares are the results obtained from Ca-A6 systems; □, pure Xe (Exp. No. 4); ◨, Xe:He=3:1(Exp. No. 5). Circles correspond to those in Fig. 4.

under similar conditions; they were almost superimposable by being moved parallel to the abscissa of 0.30.

Results at 255 K: Similar experiments were carried out at 255 K. Their experimental conditions are summarized in Table 2. The values of FR of the various systems are shown together in Fig. 6. It is worthwhile noting that the results obtained in the lower ω region seem to be independent of the crystal size, whereas those in the higher ω region depend on it.

FR Data Analysis

FR at 273 K. On the basis of the experimental results, it is assumed that *two* diffusion processes are involved in the binary gas systems, so that the FR may be described by[4]

$$\{(v/p)\cos\varphi - 1\}/K_T = \tilde{K}_1\bar{\delta}_{3c}(2\omega a_m^2/D_1') + \tilde{K}_2\bar{\delta}_{3c}(2\omega a_m^2/D_2') \quad (10)$$

and

$$(v/p)\sin\varphi/K_T = \tilde{K}_1\bar{\delta}_{3s}(2\omega a_m^2/D_1') + \tilde{K}_2\bar{\delta}_{3s}(2\omega a_m^2/D_2'), \quad (11)$$

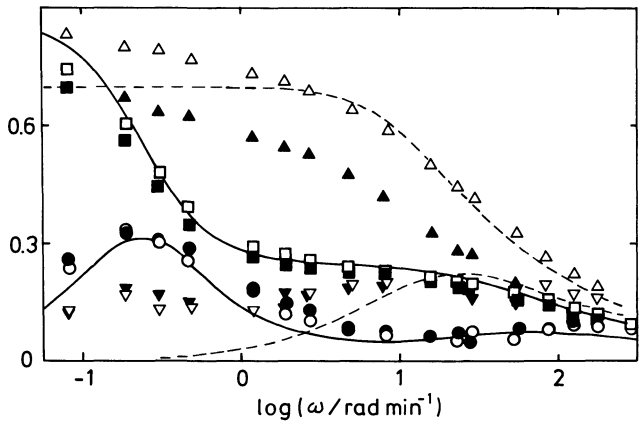

Fig. 6 Frequency response of Xe and Xe+He mixtures over Ca-A2 (open symbols) and Ca-A6(solid symbols) at 255 K. △(Exp. No. 6) and ▲(Exp. No. 8), in-phase(normalized) components of pure Xe systems; ▽ and ▼, out-of-phase(normalized) components of the same systems. □(Exp. No. 7) and ■(Exp. No. 9), the in-phase components of Xe:He=4:1 systems; ○ and ●, the out-of-phase components of the same systems. The solid curves represent calculated results according to Eqs. 13 14 with the parameters of $\tilde{K}_1$=0.25, D_1'/a_m^2=6.2 min^{-1}, $\tilde{K}_2$=0.63, and κ_{-2}=0.24 min^{-1}.

where $\tilde{K}_i$ is a constant giving the fraction of the i-th term; D_i' is the Fickian diffusivity.

The characteristic functions of $2\omega a_m^2/D_i'$ for the diffusion process, $\bar{\delta}_{3c}$ and $\bar{\delta}_{3s}$, were computed using

$$\bar{\delta}_{3j}(2\omega a_m^2/D_i') = \frac{1}{\sqrt{2\pi}\sigma}\int_0^\infty [\delta_{3j}(2\omega a^2/D_i') \exp\{-\frac{(a-a_m)^2}{2\sigma^2}\}]\,da, \quad (12)$$

(j = c or s)

where the values of a_m and σ in Table 1 were inserted. Two analytical functions of x, $\delta_{3c}(x)$, and $\delta_{3s}(x)$, were given explicitly in a previous paper.[5]

The theoretical results, thus calculated, are represented by various curves in Figs. 4(a) and 4(b), of which the parameters determined on a trial and error basis ($\tilde{K}_1$, D_1'/a_m^2, $\tilde{K}_2$, and D_2'/a_m^2) are summarized in Table 3.

FR at 255 K. Results obtained at 255 K could not be reproduced by the two-diffusion model of Eqs. 10 and 11. However, they seem to be described by

$$\{(v/p)\cos\varphi - 1\}/K_T = \tilde{K}_1\bar{\delta}_{3c}(2\omega a_m^2/D_1') + \tilde{K}_2\frac{1}{1+(\omega/\kappa_{-2})^2} \quad (13)$$

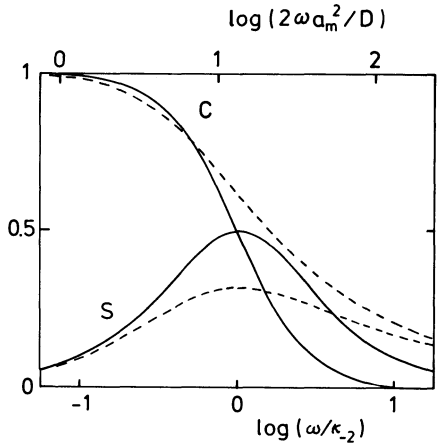

Fig. 7. Comparison of two kinds of characteristic functions: solid curves represent $1/\{1+(\omega/\kappa_{-2})^2\}$ (C) and $(\omega/\kappa_{-2})/\{1+(\omega/\kappa_{-2})^2\}$ (S) applicable to an adsorption-desorption process; dashed curves are $\bar{\delta}_{3c}$ (C) and $\bar{\delta}_{3c}$ (S) applicable to the diffusion process in Ca-A2(σ=0.28).

Table 3. Parameters for $\tilde{K}_i$ and D_i'/a_m^2 in Eqs. 10 and 11

Exp. No.	$\tilde{K}_1$	(D_1'/a_m^2)/min^{-1}	$\tilde{K}_2$	(D_2'/a_m^2)/min^{-1}
1	(0.83	3.05)		
2	0.23	18.1	0.67	3.0×10^{-2}
3	0.15	11.9	0.85	8.0×10^{-3}

and

$$(v/p)\sin\varphi/K_T = \tilde{K}_1\bar{\delta}_{3s}(2\omega a_m^2/D_1') + \tilde{K}_2\frac{(\omega/\kappa_{-2})}{1+(\omega/\kappa_{-2})^2}. \quad (14)$$

Each second term on the right hand side is a characteristic function for the adsorption-desorption process,[6] which is compared with $\bar{\delta}_{3c}$ or $\bar{\delta}_{3s}$ in Fig. 7; evidently they are very different.

The theoretical results for the systems of Ca-A2 are represented by the solid curves in Fig. 6.

Discussion

Pure Xe Systems. Almost all abspecies of Xe (more than 80%, see Fig. 4(a)) may be regarded as identical; the out-of-phase components could be reproduced by the solid curve stemming from a single term in Eq. 10 (see Table 3). The moved distance (0.30) in Figs. 5(a) and 5(b), on the other hand, leads to

$$\frac{D_2^{(0)}/a_m^2 \text{ of Ca-A2}}{D_2^{(0)}/a_m^2 \text{ of Ca-A6}} = 2.0, \quad (15)$$

where $D_2^{(0)}$ denotes the Fickian diffusivity of a pure Xe system. Substitution of the values of a_m's leads to

$$\begin{aligned} D_2^{(0)}/10^{-14}\,\mathrm{m^2\,s^{-1}} &= 3.7 \quad \text{for Ca-A2} \\ &= 19 \quad \text{for Ca-A6} \\ (&= 15 \quad \text{for Linde-5A})^{7} \end{aligned} \quad (16)$$

Contrary to our expectation, the difference in this diffusivity was considerable. It is noted, however, that the absorption isotherm of these two kinds of zeolites were considerably different (see $K_2^{(0)}$'s in Table 2). The diffusivities for small commercial zeolite crystals were found to be substantially smaller than for large laboratory synthesized crystals.[8] The reproducibility of the theoretical curves at 255 K was not so good (see dashed curves in Fig. 6).

Binary Gas Systems. Since the FR of mixture was affected by the change in the crystal size, the interference effects due to He would be attributed to processes occurring not on exposed surfaces, but within micropores.

The experimental results can be summarized as follows: (i) there is only one diffusion process in the pure Xe system, (ii) no FR of He was observed in a pure He system since the absorption of He was negligible and, thus, $K_1^{(0)}=0$ and (iii) (only) two diffusion processes were needed to theoretically reproduce FR data on a binary gas system. On the basis of these results, a more general form of Fick's law,

$$\frac{\partial c_m}{\partial t} = \sum_{n=1}^{2} D_{mn}\nabla^2 c_n, \qquad m = 1 \text{ or } 2 \quad (17)$$

is assumed. Here, c_m denotes the concentration of the m-component and D_{mn} is the Fickian diffusivity ($D_{11}>D_{22}$). Every D_{mn} would depend on both c_1 and c_2. However, since the perturbation of the FR method was very small (e.g. $v\sim10^{-2}$) and, therefore, $c_m\fallingdotseq c_m^{(e)}$, D_{mn} can be regarded as a constant.

The coupled equations may be decoupled by the transformations:

$$c_1' = \{1+(D_-/D_+)\}c_1 + (D_-/D_+)c_2 \quad (18)$$

and

$$c_2' = -(D_-/D_+)c_1 + \{1-(D_-/D_+)\}c_2. \quad (19)$$

In these equations the short notations

$$D_+ \equiv D_{21} + D_{12} \quad (20)$$

and

$$D_- \equiv D_{21} - D_{12} \quad (21)$$

are introduced.

Substitution of c_m' for c_m in Eq. 17 leads to

$$\frac{\partial c_m'}{\partial t} = D_m'\nabla^2 c_m' \qquad m = 1 \text{ or } 2, \quad (22)$$

where

$$D_1' = D_{11} + \frac{1}{2}D_-, \quad (23)$$

and

$$D_2' = D_{22} + \frac{1}{2}D_-. \quad (24)$$

The values of D_i' in Table 3 are expected to correspond to these eigenvalues.

In the present work, c_1 is sufficiently small. A comparison of Eqs. 18 and 19 with Eqs. 10 and 11 would lead to

$$\frac{\tilde{K}_1}{\tilde{K}_2} = \frac{(D_-/D_+)}{1-(D_-/D_+)}. \quad (25)$$

When the value of D_-/D_+ is found from the $\tilde{K}_i$'s (Table 3) all four coefficients, D_{mn}, can be evaluated successively (Appendix 2). The derived values are given in Table 4 and are plotted in Fig. 8.

Since the values of (D_{mn}/a_m^2)'s were determined after many steps of calculation from the raw data on $K_2^{(0)}$, P_e, ΔP, and φ, their absolute values are not very reliable; the ambiguity estimated is indicated by the vertical lines in Fig. 8 (most of the ambiguity would arise from errors in P_e's in the present work). However, the conclusions that

$$D_{12} \fallingdotseq D_{21} \fallingdotseq (D_{11}D_{22})^{1/2} \quad (26)$$

Table 4. Values of D_{mn}/a_m^2 Derived (in $\mathrm{min^{-1}}$ Units)

Exp. No.	D_{11}/a_m^2	D_{12}/a_m^2	D_{21}/a_m^2	D_{22}/a_m^2
2	16.9	3.44	5.80	1.21
3	11.6	1.51	2.05	0.28

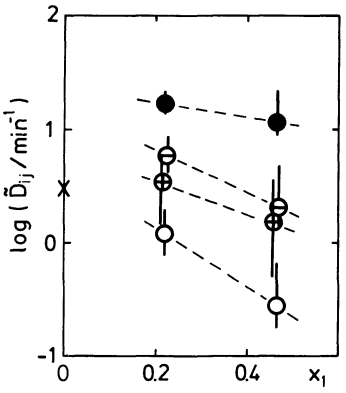

Fig. 8. Diffusional time constant $\tilde{D}_{ij}$'s of Xe+He/Ca-A2 systems at 273 K versus the mole fraction of He in gas phase, x_1. ●, $\tilde{D}_{11}$; ⊕, $\tilde{D}_{12}$; ⊖, $\tilde{D}_{21}$; ○, $\tilde{D}_{22}$, where $\tilde{D}_{ij}=D_{ij}/a_m^2$. × indicates the value of pure Xe.

and

$$D_{12} < D_{21} \tag{27}$$

should be reliable, since they are governed by the values of D_1'/a_m^2 and the *ratio* of $\tilde{K}_1/\tilde{K}_2$.

Four constants of D_{mn}'s with respect to a heptane+benzene over NaX system have been determined empirically by a sorption method.[9] The results lead to

$$D_{12} > D_{21} \tag{28}$$

in contrast to the result of Eq. 27, though the method is based on the supposition that all D_{mn}'s do not depend on the concentrations.

The cross-terms, D_{12} and D_{21}, have been determined by a random-walk approach.[10] The application of the method to a simultaneous sorption of two sorbates in an initially empty pore system shows very significant multicomponent effects due to the contribution of the cross terms.

In summary, Xe molecules in micropores may be divided into two species in a Xe+He mixture; the division into c_1' and c_2' species depends on the ratio of D_-/D_+; one of the two species becomes an adspecies with decreasing temperature.

Appendix 1

Since the vapor may be regarded as ideal,

$$p_T = x_1p_1 + x_2p_2, \tag{A1}$$

where the subscript T indicates the value of the total pressure. On the other hand, in consideration of a case at $\omega \fallingdotseq 0$, one finds

$$v - p_{0T} = K_1x_1p_{01} + K_2x_2p_{02}, \tag{A2}$$

where the subscript 0 indicates the value in the quasistatic state.

The asymptotic value of the in-phase component, K_T, is given by

$$K_T = (v/p_{0T}) - 1 \tag{A3}$$

since φ tends to zero as $\omega \to 0$. In the same way,

$$K_i = (v/p_{0i}) - 1. \tag{A4}$$

Eliminating p_{0T}, p_{01}, and p_{02}, one finds

$$K_T = \frac{\sum_{m=1}^{2} x_mK_m/(K_m + 1)}{\sum_{n=1}^{2} x_n/(K_n + 1)} = \frac{K_1K_2 + x_1K_1 + x_2K_2}{1 + x_1K_2 + x_2K_1}. \tag{A5}$$

Appendix 2

Other parameters, D' and d, are introduced:

$$D_{21} = D' + d \tag{A6}$$

and

$$D_{12} = D' - d \tag{A7}$$

or

$$D_+ = 2D' \tag{A8}$$

and

$$D_- = 2d. \tag{A9}$$

The ratio D_-/D_+ or d/D' is replaced by δ for simplicity:

$$D_-/D_+ = d/D' = \delta. \tag{A10}$$

Equations 23 and 24 lead to

$$D_1' - D_2' = D_{11} - D_{22} + D_-. \tag{A11}$$

In the transformation of Eqs. 18 and 19, the relation

$$c_1' + c_2' = c_1 + c_2 \tag{A12}$$

is always satisfied. This necessary condition requires a relation among the D_{mn}'s:

$$D_+^2 = 2D_-(D_{11} - D_{22} + D_-). \tag{A13}$$

Substitution of Eq. A10 into Eq. A13 leads to

$$D' = \delta(D_1' - D_2'). \tag{A14}$$

When δ is determined, Eq. A14 gives D' and Eq. A10 gives the value of d. Consequently, the four coefficients may be determined as

$$D_{11} = D_1' - d, \tag{A15}$$

$$D_{12} = D' - d, \tag{A16}$$

$$D_{21} = D' + d, \tag{A17}$$

and

$$D_{22} = D_2' + d. \tag{A18}$$

Notation

a : radius of an isotropic sphere (cubic crystals are approximated by the sphere).

a_m : mean radius of the sphere.

$B^{(0)}$: amount of molecules absorbed in a single component system.
B_m : amount of abspecies of m-component in a mixture.
c_m : concentration of abspecies of m-component in micropores.
$c_m^{(e)}$: c_m at an equilibrium.
c_i' : concentration of a mixed abspecies of c_1 and c_2 derived mathematically by decoupling coupled equations.
$D_2^{(0)}$: Fickian diffusivity of a pure Xe system.
D_i' : Fickian diffusivity of c_i'.
D_{mn} : Fickian diffusivity in a more general form.
$K_m^{(0)}$: coefficient calculated from the gradient of absorption isotherm of a pure gas system.
K_m : coefficient correlated to the gradient of absorption isotherm of m-component in a multicomponent system.
K_T : asymptotic value of the in-phase component at $\omega \rightarrow 0$ of a single or multicomponent system.
$\widetilde{K}_i$: coefficient indicating contribution of i-th characteristic function to FR data.
P : gas pressure.
P_e : P at an equilibrium.
P_m : partial pressure of m-component in a mixture.
p : relative amplitude of pressure variation.
T_e : equilibrium temperature of absorbent.
T_0 : (RT_0/V_e) is a conversion factor; T_0 is usually room temperature.
V : volume of gas space of a system.
V_e : V at an equilibrium.
v : relative amplitude of volume variation.
x_m : mole fraction of m-component in gas phase.

Greek Letters
δ_{3j} : characteristic function of diffusion for FR.
$\bar{\delta}_{3j}$: δ_{3j} modified by the crystal size distribution.
φ : phase lag between volume and pressure variation.
κ_{-2} : parameter characteristic of an adsorption-desorption process.
σ : standard deviation of a normal distribution.
ω : angular velocity of sinusoidal oscillation.

The SEM photographs were supplied by Toyo Soda Manufacturing Co.

References

1) H. W. Habgood, *Can. J. Chem.*, **36**, 1384 (1958).
2) Y. H. Ma and T. Y. Lee, *Ind. Eng. Chem., Fundam.*, **16**, 44 (1977).
3) R. Kumer, R. C. Duncan and D. M. Ruthven, *Can. J. Chem. Eng.*, **60**, 493 (1982).
4) Y. Yasuda, Y. Yamada, and I. Matsuura, Proc. 7th Int. Zeolite Conf., Tokyo, 1986. ed by Y. Murakami, A. Iijima, and J. W. Ward (Kodansha-Elsevier, Tokyo, 1986), p. 587.
5) Y. Yasuda, *J. Phys. Chem.*, **86**, 1913 (1982).
6) Y. Yasuda, *J. Phys. Chem.*, **80**, 1867 (1976).
7) Y. Yasuda and G. Sugasawa, *J. Catal.*, **88**, 530 (1984).
8) D. M. Ruthven, Principles of Adsorption and Adsorption Processes (John Wiley, New York, 1984) p. 150.
9) R. M. Marutovsky and M. Bülow, *Z. phys. Chem., Leipzing*, **263**, 849 (1982).
10) M. G. Palekar and R. A. Rajadhyaksha, *Chem. Eng. Sci.* **41**, 463 (1986).

Excited-State Reactions of Coumarins in Aqueous Solutions. VI. Fluorescence Quenching of 7-Hydroxycoumarins by Chloride Ions in Acidic Solutions

Tetsuo MORIYA
Electrotechnical Laboratory, Umezono, Tsukuba, Ibaraki 305
(Received June 29, 1987)

The fluorescence behavior of 7-hydroxycoumarin and 7-hydroxy-4-methylcoumarin has been studied in acidic aqueous solutions by changing the concentration of chloride ions as a fluorescence quencher. The intensity decrease and lifetime change in fluorescence from neutral and tautomeric forms of photo-excited states are explained by an interaction between protonated molecules generated in excited state and chloride ions. The magnitude of quenching-rate constant is estimated under steady-state conditions and the result is compared with the analysis using time-dependent response.

Complex fluorescent behavior of coumarin derivatives with 7-hydroxyl substituent has been studied in various organic solvents, and in neutral, acidic, and basic aqueous solutions.[1-4] It has been revealed that four fluorescent species typically exist in the photo-excited state according to solvent conditions; they have been identified as neutral, anionic, tautomeric, and protonated species of the excited molecule.

In the acidic region where $[H^+] \approx 0.5$ mol dm^{-3}, a very interesting situation occurs in the fluorescence of aqueous 7-hydroxycoumarin (7HC) and 7-hydroxy-4-methylcoumarin (7H4MC) solutions. The fluorescence bands from neutral form ($\overset{*}{N}$) and tautomeric form ($\overset{*}{T}$) in their excited states are observable, but those from anionic form ($\overset{*}{A}^-$) and cationic form ($\overset{*}{C}^+$) are not detected.[4] This means that generated $\overset{*}{A}^-$ and $\overset{*}{C}^+$, if any, are instantaneously converted to $\overset{*}{N}$ or $\overset{*}{T}$ before they are deactivated radiatively to the ground state. Two fluorescence bands of $\overset{*}{N}$ and $\overset{*}{T}$ are separated in wavelength so enough that the measurement of each band is easily performed. Moreover, with the addition of chloride ions to the solution, these fluorescence bands are effectively quenched; this enables us to confirm detailed mechanisms of acid-base, phototautomerization, and fluorescence-quenching reactions.

The main purpose of this work is to analyze quantitatively the reaction kinetics of the photo-excited 7-hydroxycoumarins in acidic aqueous solutions. The theoretical consideration using rate-equation formulation will be useful to understand the feature of excited-state reactions. The fluorescence data under steady-state conditions and the fluorescence-lifetime measurements will be consistently explained by means of a unified model.

Experimental

Materials. The commercial grade reagents of 7-hydroxycoumarin (7HC) from Wako Pure Chemical Ind. and 7-hydroxy-4-methylcoumarin (7H4MC) from Tokyo Kasei were purified by recrystallization from ethanol and by washing with diethyl ether; 7HC, mp 234 °C; 7H4MC, mp 186 °C. Hydrochloric acid and perchloric acid were of pure quality from Wako Pure Chemical Ind. Water was permeated and distilled.

Methods. UV absorption and fluorescence spectra of the aqueous 7HC and 7H4MC solutions of $\approx 6 \times 10^{-5}$ mol dm^{-3} were measured at 20 °C. The pH of the solution was controlled with HCl and $HClO_4$, the chloride ion concentration being adjusted by changing their ratio. Fluorescence-lifetime measurements were performed by means of a time-correlated single-photon-counting fluorometer similar to that described in Ref. 5. Since the lifetime of fluorescers was close to the decay time of a repetitive short-pulsed light at 337 nm from an air-flash lamp, the data were deconvoluted to know the true decay character unaffected by a response function of the measurement system; the typical accuracy of this procedure was ± 0.05 ns.

Results

In a previous paper,[4] the complex pH dependence of absorption and fluorescence spectra of 7HC and 7H4MC in aqueous solutions has been fully investigated. Since the present interest is concentrated on the pH range with $[H^+]$ of ≈ 0.5 mol dm^{-3}, the spectral behavior of these fluorophores is summarized as follows. In the electronic ground state, there exists only a neutral molecular species (N), the absorption maxima of which are 324 nm (7HC) and 321 nm (7H4MC). If this neutral species is optically excited at the absorption-peak wavelength, two molecular species formed in the excited state are observable. One is usual neutral molecule ($\overset{*}{N}$), and the other is tautomeric molecule ($\overset{*}{T}$) in which a hydrogen of the 7-hydroxyl group is transferred to the carbonyl group at 2-position. As will be mentioned later, cationic form ($\overset{*}{C}^+$) protonated at the carbonyl group and anionic form ($\overset{*}{A}^-$) deprotonated at the hydroxyl group can exist in principle, but they are not spectroscopically detected around $[H^+]$ of 0.5 mol dm^{-3}. The fluorescence maxima of $\overset{*}{N}$ and $\overset{*}{T}$ are at 397 and 478 nm for 7HC, and at 390 and 475 nm for 7H4MC,

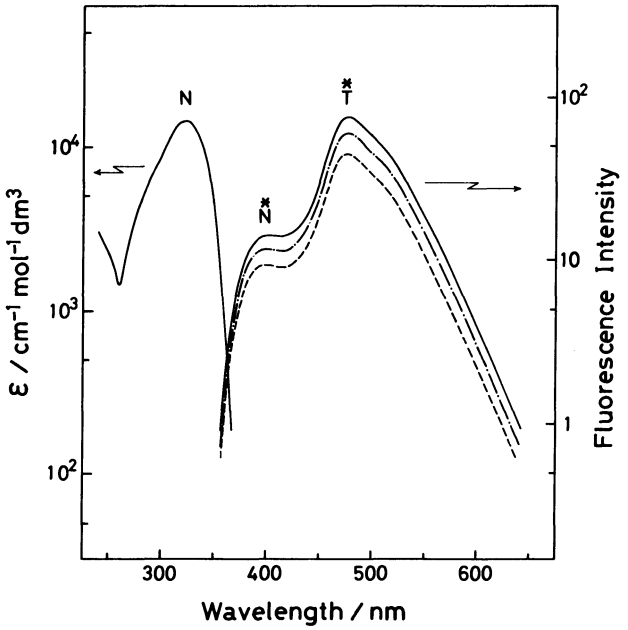

Fig. 1. Absorption and fluorescence spectra of 7HC in the acidic aqueous solution at 20 °C. $[HClO_4]+[HCl]=0.5$ mol dm^{-3}. (——), $[HCl]=0$; (—·—), $[HCl]=0.2$ mol dm^{-3}; (---), $[HCl]=0.5$ mol dm^{-3}. N describes the neutral ground state, and $\overset{*}{N}$ and $\overset{*}{T}$ describe the neutral and tautomeric excited state, respectively.

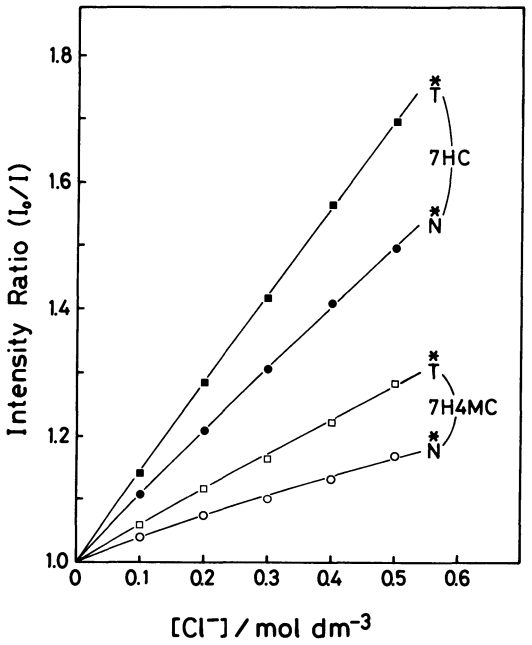

Fig. 2. Dependence of the fluorescence intensity ratio, I_0/I, on $[Cl^-]$ in the acidic aqueous solution ($[H^+]=0.5$ mol dm^{-3}) at 20 °C. 7HC (●), (■); 7H4MC (○), (□). $\overset{*}{N}$ and $\overset{*}{T}$ describe the excited states of neutral and phototautomeric molecular forms, respectively.

respectively. In Fig. 1, the absorption and fluorescence spectra of an aqueous 7HC solution with 0.5 mol dm^{-3} $HClO_4$ are shown by the solid lines.

When $[Cl^-]$ is changed by the amount of an added HCl component with holding pH of the solution as $[HClO_4]+[HCl]=0.5$ mol dm^{-3} ($H_0\approx0.20$),[6] the fluorescence intensity from $\overset{*}{N}$ and $\overset{*}{T}$ has been quenched depending on $[Cl^-]$ as shown by the dashed curves in Fig. 1. Since the fluorescence bands of $\overset{*}{N}$ and $\overset{*}{T}$ are separated far enough to each other, the respective fluorescence yields can be monitored at 397 and 478 nm (7HC), and at 390 and 475 nm (7H4MC), respectively. Figure 2 describes plots of I_0/I for $\overset{*}{N}$ and $\overset{*}{T}$ vs. $[Cl^-]$ where I_0 and I are the fluorescence intensity for each excited species in the absence and in the presence of chloride ions. Slight deviation from the usual Stern-Volmer linear relationship is observed for both I_0^N/I^N and I_0^T/I^T.

Under the pulsed light excitation at 337 nm which generates $\overset{*}{N}$ at the moment of light absorption, the decay characteristic of fluorescence from neutral and tautomeric fluorescers has been measured at the peak wavelength of each fluorescence band with keeping $[H^+]$ at 0.5 mol dm^{-3} but with different $[Cl^-]$. The time-dependent light intensity, $i^N(t)$ and $i^T(t)$, of $\overset{*}{N}$ and $\overset{*}{T}$ was fitted satisfactorily for the double-exponential decay character:

$$i^N(t) \propto \exp(-t/\tau_+) + C\cdot\exp(-t/\tau_-) \quad (1)$$

and

$$i^T(t) \propto \exp(-t/\tau_+) - \exp(-t/\tau_-). \quad (2)$$

The best-fitted values for τ_+, τ_-, and C are given in Table 1.

Table 1. Values for the Fluorescence Lifetime Parameters, τ_+, τ_-, and C, of 7HC and 7H4MC in Acidic Aqueous Solutions ($[H^+]=0.5$ mol dm^{-3}) at 20 °C

Substance	$[Cl^-]$ / mol dm^{-3}	τ_+ / ns	τ_- / ns	C
7HC	0	4.5_0	0.2_0	2.5
	0.1	3.9_5	0.2_{25}	2.5
	0.2	3.5_5	0.2_5	2.0
	0.3	3.2_0	0.3_0	2.0
	0.4	2.9_0	0.3_{25}	2.0
	0.5	2.6_0	0.3_5	1.5
7H4MC	0	5.0_5	0.1_{25}	13
	0.1	4.7_5	0.1_5	12
	0.2	4.5_0	0.1_5	11
	0.3	4.2_0	0.1_{75}	10
	0.4	4.0_5	0.1_{75}	10
	0.5	3.8_0	0.2_0	8.5

Discussion

Fluorescence Quenching by Chloride Ions in Acidic Solutions. Based on the generalized scheme for excited-state reactions of coumarins in aqueous solutions confirmed in Ref. 4, we may adopt the following scheme if only the neutral molecule exists in the ground state at $[H^+]$ of ≈ 0.5 mol dm^{-3}:

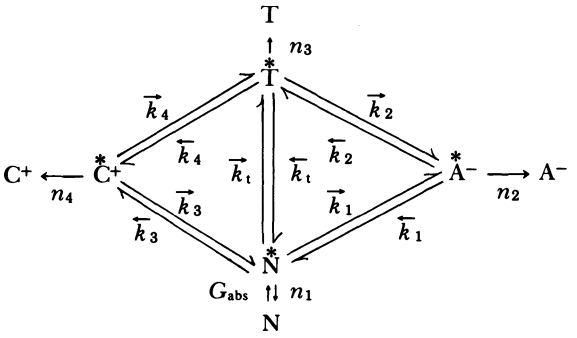

Scheme 1.

Here, G_{abs} is the generation rate of $\overset{*}{N}$ and n_j's are the transition rates of the excited species to their ground states. $\vec{k}_j$'s and $\overleftarrow{k}_j$'s are the protonation and deprotonation rate constants between acids and bases in the excited state. $\vec{k}_t$ and $\overleftarrow{k}_t$ represent the reaction pathway of tautomerization that does not involve stepwise protonation or deprotonation processes, i.e., the "nondissociative" reaction pathway.[4,7] Because the fluorescence of $\overset{*}{A}^-$ and $\overset{*}{C}^+$, which should appear in the wavelength region between $\overset{*}{N}$ and $\overset{*}{T}$ bands, is not detected at $[H^+]$ of 0.5 mol dm^{-3}, the following conditions will be satisfied:

$$\vec{k}_1 \ll \overleftarrow{k}_1[H^+],\ \vec{k}_2 \ll \overleftarrow{k}_2[H^+] \text{ and } \overleftarrow{k}_3[H^+] \ll \vec{k}_3,\ \overleftarrow{k}_4[H^+] \ll \vec{k}_4. \tag{3}$$

If all decay rates of the excited species, n_j's are of the same order, the ratio of fluorescence intensity of $\overset{*}{T}$ to that of $\overset{*}{N}$ in the absence of Cl^- is obtained by means of the rate equation analysis as carried out in Ref. 4 under the conditions of Eq. 3 (cf. Appendix):

$$\frac{I_0^T}{I_0^N} = \frac{n_3^r}{n_1^r} \frac{\vec{k}_t + \beta\overleftarrow{k}_3[H^+]}{n_3 + \overleftarrow{k}_t + \alpha\overleftarrow{k}_4[H^+]}, \tag{4}$$

where I_0's represent the fluorescence intensity at $[Cl^-]=0$, n_1^r and n_3^r are the radiative transition probabilities of $\overset{*}{N}$ and $\overset{*}{T}$ to their ground states, respectively, and

$$\vec{k}_t = \vec{k}_t + \vec{k}_1 \frac{\overleftarrow{k}_2[H^+]}{n_2 + \overleftarrow{k}_1[H^+] + \overleftarrow{k}_2[H^+]},$$

$$\overleftarrow{k}_t = \overleftarrow{k}_t + \vec{k}_2 \frac{\overleftarrow{k}_1[H^+]}{n_2 + \overleftarrow{k}_1[H^+] + \overleftarrow{k}_2[H^+]},$$

$$\alpha = \frac{\vec{k}_3}{n_4 + \vec{k}_3 + \vec{k}_4}, \text{ and } \beta = \frac{\vec{k}_4}{n_4 + \vec{k}_3 + \vec{k}_4}. \tag{5}$$

When 0.3 mol dm^{-3} NaCl is added to the acidic solution with 0.5 mol dm^{-3} $HClO_4$, the fluorescence of $\overset{*}{N}$ and $\overset{*}{T}$ is decreased, while the addition of 0.3 mol dm^{-3} $NaClO_4$ induces no fluorescence change. This fact shows that Cl^- affects the fluorescence-quenching phenomenon contrary to other inorganic ions such as Na^+ and ClO_4^-. It is observed in general that halide ions have the quenching ability in order of $Cl^- < Br^- < I^-$.[8] Further, the fluorescence of $\overset{*}{N}$, $\overset{*}{T}$, and $\overset{*}{A}^-$ does not depend on Cl^- quencher over the pH range where $\overset{*}{C}^+$ is not formed in the excited state (pH≧2).[4] All these results lead to the conclusion that $\overset{*}{N}$ and $\overset{*}{T}$ fluorescers are quenched only through an interaction of the protonated excited state, $\overset{*}{C}^+$, with Cl^-, and that the quenching mechanism will be essentially the same as proposed in Ref. 9:

$$W: \overset{*}{C}^+ + Cl^- \xrightarrow{k_q} C^+ + Cl^-. \tag{6}$$

Here, the fraction W of $\overset{*}{C}^+$ in Scheme 1 additionally obeys a collisional quenching process where the encounter complex, $(\overset{*}{C}^+ \cdot Cl^-)$, decays nonradiatively to C^+ and Cl^- with a rate of k_q; the remaining fraction $1-W$ of $\overset{*}{C}^+$ obeys the instantaneous or "static" deactivation process. The additional factor W (a function of the quencher concentration $[Cl^-]$) can be approximated by $\exp(-V[Cl^-])$, where V is the static quenching constant. If the model of Frank and Vavilov[10] is applied to the static quenching process, an instantaneous quenching results when the quencher is within the "sphere of action" having a volume of V/N', where N' is the Avogadro number per millimole.[11]

Since illuminating light is absorbed solely by neutral molecules under the experimental conditions and the fraction $1-W$ of $\overset{*}{C}^+$ is immediately quenched without emitting any light quantum, the effective generation rate of $\overset{*}{N}$, $\tilde{G}([Cl^-])$, must be somewhat reduced from G_{abs}.[9] However, this alteration does not appear explicitly in the ratio of fluorescence intensity of $\overset{*}{N}$ to that of $\overset{*}{T}$, I^T/I^N. In the presence of Cl^-, straightforward rate-equation analysis as before gives the relation:

$$\frac{I^T}{I^N} = \frac{n_3^r}{n_1^r} \frac{\vec{k}_t + \overleftarrow{k}_3[H^+] \dfrac{\beta}{1+\gamma[Cl^-]}}{n_3 + \overleftarrow{k}_t + \overleftarrow{k}_4[H^+] \dfrac{\alpha + \gamma[Cl^-]}{1+\gamma[Cl^-]}}, \tag{7}$$

where

$$\gamma = \frac{k_q}{n_4 + \vec{k}_3 + \vec{k}_4}. \tag{8}$$

From Eqs. 4 and 7, we have

$$\frac{I_0^T/I^T}{I_0^N/I^N} = \frac{1 + \{(n_3 + \overleftarrow{k'_t} + \overleftarrow{k}_4[H^+])/(n_3 + \overleftarrow{k'_t} + \alpha\overleftarrow{k}_4[H^+])\}\cdot\gamma[Cl^-]}{1 + \{\overrightarrow{k'_t}/(\overrightarrow{k'_t} + \beta\overleftarrow{k}_3[H^+])\}\cdot\gamma[Cl^-]} \quad (9)$$

and finally

$$\frac{1}{\{(I_0^T/I^T)/(I_0^N/I^N)\}-1} = \{\frac{n_3 + \overleftarrow{k'_t} + \overleftarrow{k}_4[H^+]}{n_3 + \overleftarrow{k'_t} + \alpha\overleftarrow{k}_4[H^+]} - \frac{\overrightarrow{k'_t}}{\overrightarrow{k'_t} + \beta\overleftarrow{k}_3[H^+]}\}^{-1} \times\{\frac{\overrightarrow{k'_t}}{\overrightarrow{k'_t} + \beta\overleftarrow{k}_3[H^+]} + \frac{1}{\gamma[Cl^-]}\}. \quad (10)$$

Since α, $\beta<1$, the first term on the right-hand side of Eq. 10 which is contained in curly brackets is positive. Therefore, the plot of $1/\{(I_0^T/I^T)/(I_0^N/I^N)-1\}$ vs. $1/[Cl^-]$ becomes linear and its slope is positive from the theoretical prediction.

The experimental result shown in Fig. 2 is replotted in Fig. 3 in accordance with Eq. 10. It is seen that the data follow very well the predicted linear dependence. By using the intercept and slope of this plot, $\{\overrightarrow{k'_t}/(\overrightarrow{k'_t}+\beta\overleftarrow{k}_3[H^+])\}\cdot\gamma$ and $\{(n_3+\overleftarrow{k'_t}+\overleftarrow{k}_4[H^+])/(n_3+\overleftarrow{k'_t}+\alpha\overleftarrow{k}_4[H^+])\}\cdot\gamma$ are given as 0.406 and 0.729 for 7HC, and 0.120 and 0.324 for 7H4MC, respectively. Although the exact value or γ is not obtained only from this information, its region becomes restricted by the relation:

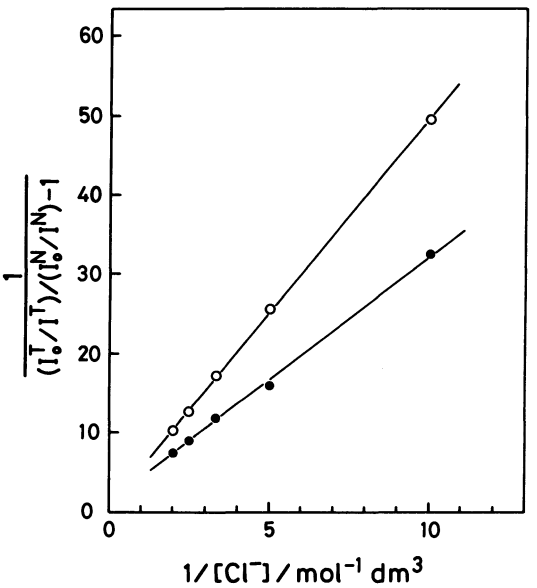

Fig. 3. Plots of $1/\{(I_0^T/I^T)/(I_0^N/I^N)-1\}$ vs. $1/[Cl^-]$ for 7HC (●) and 7H4MC (○) in the acidic solution ($[H^+]$=0.5 mol dm^{-3}) at 20 °C.

$$0.406<\gamma<0.729 \text{ for 7HC and } 0.120<\gamma<0.324 \text{ for 7H4MC.} \quad (11)$$

because $\alpha,\beta<1$. Considering the definition of γ (Eq. 8), these results mean that the quenching rate constant k_q is less than the decay rate of $\overset{*}{C}^+$ in the absence of quenchers, $n_4+\overrightarrow{k}_3+\overrightarrow{k}_4$, but has the same order of magnitude. From Eq. 11, it is seen that the quenching efficiency of 7H4MC due to Cl^- ions is lower than that of 7HC. Possibly, 4-methyl substituent acts protectively on the quenching process, which is conceivable from the general tendency observed in 7-ethoxycoumarins under various conditions.[8,9,12]

Fluorescence Lifetimes in Acidic Solutions. As described in Scheme 1, the real reactions in the excited state are complicatedly correlated with each other. However, the fundamental aspect of the transient response to a pulsed-light excitation will be approximated by the following simple scheme, if the rate equations are examined in detail under the same situation as discussed in the case of steady-state conditions (cf. Eq. 7):

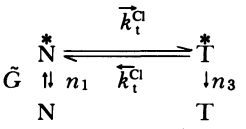

Scheme 2.

where

$$\overrightarrow{k}_t^{Cl} = \overrightarrow{k'_t} + \frac{\beta\overleftarrow{k}_3[H^+]}{1+\gamma[Cl^-]} \text{ and}$$

$$\overleftarrow{k}_t^{Cl} = \overleftarrow{k'_t} + \frac{(\alpha+\gamma[Cl^-])\overleftarrow{k}_4[H^+]}{1+\gamma[Cl^-]} \quad (12)$$

Then, in accordance with Eqs. 1 and 2, the lifetimes $\tau_\pm$ of $i^N(t)$ and $i^T(t)$ for a light pulse of ideal δ-function are written as[13]

$$\tau_\pm^{-1} = \tfrac{1}{2}(n_1 + \overrightarrow{k}_t^{Cl} + n_3 + \overleftarrow{k}_t^{Cl}) \mp \tfrac{1}{2}[(n_1 + \overrightarrow{k}_t^{Cl} + n_3 + \overleftarrow{k}_t^{Cl})^2 - 4\{(n_1 + \overrightarrow{k}_t^{Cl})(n_3 + \overleftarrow{k}_t^{Cl}) - \overrightarrow{k}_t^{Cl}\overleftarrow{k}_t^{Cl}\}]^{1/2}. \quad (13)$$

From Table 1, the condition, $\tau_+ \gg \tau_-$, is satisfied for both 7HC and 7H4MC, which is equivalent to the case that the second term in the root of Eq. 13 contained in the curly brackets is much smaller than the first term. Then, we have approximate equations:

$$\frac{1}{\tau_+} \approx \frac{n_1n_3 + n_3\overrightarrow{k}_t^{Cl} + n_1\overleftarrow{k}_t^{Cl}}{n_1 + \overrightarrow{k}_t^{Cl} + n_3 + \overleftarrow{k}_t^{Cl}} \text{ and}$$

$$\frac{1}{\tau_-} \approx n_1 + \overrightarrow{k}_t^{Cl} + n_3 + \overleftarrow{k}_t^{Cl} \quad (14)$$

Further, letting the value of τ_+ at $[Cl^-]=0$ be τ_+^0, the following relation is obtained:

$$\frac{1}{(\tau_+^0/\tau_+)-1} = \left\{ \frac{n_1+\vec{k}_t'+(n_1/n_3)\overleftarrow{k}_t'+(n_1/n_3)\overleftarrow{k}_4[H^+]}{n_1+\vec{k}_t'+(n_1/n_3)\overleftarrow{k}_t'+\beta\overleftarrow{k}_3[H^+]+(n_1/n_3)\alpha\overleftarrow{k}_4[H^+]} - \frac{n_1+\vec{k}_t'+n_3+\overleftarrow{k}_t'+\overleftarrow{k}_4[H^+]}{n_1+\vec{k}_t'+n_3+\overleftarrow{k}_t'+\beta\overleftarrow{k}_3[H^+]+\alpha\overleftarrow{k}_4[H^+]} \right\}^{-1} \times \left\{ \frac{n_1+\vec{k}_t'+n_3+\overleftarrow{k}_t'+\overleftarrow{k}_4[H^+]}{n_1+\vec{k}_t'+n_3+\overleftarrow{k}_t'+\beta\overleftarrow{k}_3[H^+]+\alpha\overleftarrow{k}_4[H^+]} + \frac{1}{\gamma[Cl^-]} \right\}. \quad (15)$$

Equation 15 predicts the linear relationship for the plot of $1/\{(\tau_+^0/\tau_+)-1\}$ vs. $1/[Cl^-]$. Figure 4 shows the plot where the data in Table 1 are employed. It is seen from the result that the linear relationship is well applicable in the region where $\tau_+ \gg \tau_-$. By using the intercept and slope of the plot, the ratio of complicated combination of various rate constants is again obtained as in the case of steady-state analysis; $\{(n_1+\vec{k}_t'+n_3+\overleftarrow{k}_t'+\overleftarrow{k}_4[H^+])/(n_1+\vec{k}_t'+n_3+\overleftarrow{k}_t'+\beta\overleftarrow{k}_3[H^+]+\alpha\overleftarrow{k}_4[H^+]\}\cdot\gamma$ and $[\{n_1+\vec{k}_t'+(n_1/n_3)\overleftarrow{k}_t'+(n_1/n_3)\overleftarrow{k}_4[H^+]\}/\{n_1+\vec{k}_t'+(n_1/n_3)\overleftarrow{k}_t'+\beta\overleftarrow{k}_3[H^+]+(n_1/n_3)\alpha\overleftarrow{k}_4[H^+]\}]\cdot\gamma$ are 0.065 and 1.45 for 7HC, and 0.020 and 0.685 for 7H4MC, respectively. Although each rate constant cannot be estimated, the γ values restricted by Eq. 11 are consistent with this result if $n_1 > n_3$. Because of relatively low accuracy of deconvolution for the fast decay component (τ_- and C), the analysis is less fruitful than the consideration on τ_+, whereas the qualitative tendency is predictable according to the same assumption.

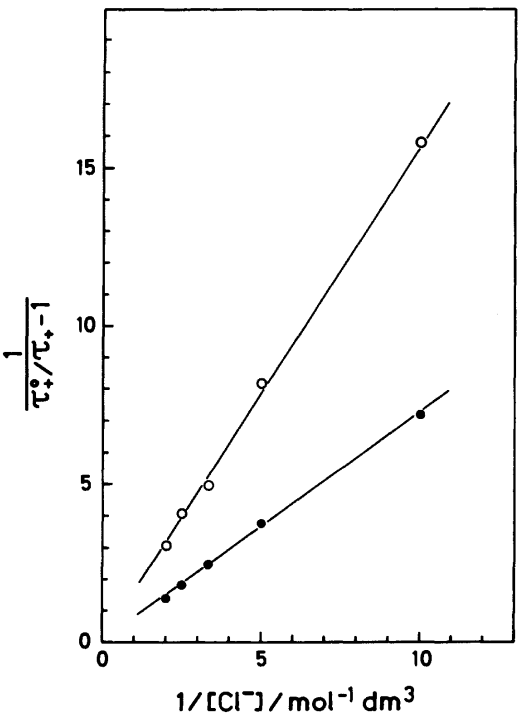

Fig. 4. Plots of $1/\{(\tau_+^0/\tau_+)-1\}$ vs. $1/[Cl^-]$ for 7HC (●) and 7H4MC (○) in the acidic solution ($[H^+]$= 0.5 mol dm^{-3}) at 20 °C.

The lifetime analysis based on the fluorescence components from $\overset{*}{N}$ and $\overset{*}{T}$ of 7HC and 7H4MC is analogous with the lifetime measurement on monomer and exciplex forms in aromatic compound-quencher systems where an exciplex is generated to result in fluorescence quenching.[13] It should be mentioned here that the excited-state reaction of coumarin derivatives is classified essentially into an acid-base reaction and has time constants of nanosecond order due to high mobility of participating species such as H^+ and Cl^-, whereas the exciplex-formation reaction is a usually slower phenomenon by one or more orders.

The Relationship between Fluorescence Yield and Fluorescence Lifetime Measurements. At the early stage of theoretical analysis on the fluorescence yield, we have assumed that the natural lifetimes, n_j^{-1}, of four molecular species generated in the excited state are of the same order. This is readily conceivable from the experimental result that the ground-state molecules, N, C^+, and A^-, have the similar values of molar extinction coefficients which are closely related to radiative transition probabilities.[14] The absorption spectrum of T cannot be observed in any pH range, because its ground state is energetically unstable in contrast to the other three species. However, theoretical calculations of the energy level and the transition moment of N and T have shown that optical characteristics of these two species are similar, whereas the molecular structure and the energy separation between the highest occupied and the lowest unoccupied orbital are very different.[15] It is thus expected for natural lifetimes of $\overset{*}{N}$, $\overset{*}{T}$, $\overset{*}{C}^+$, and $\overset{*}{A}^-$ to be in the range of 1.5—6 ns; it is supported by lifetime measurements over wide pH ranges in aqueous solutions.[4]

Generally, the analysis using fluorescence lifetimes is more tractable than the steady-state analysis in that the instantaneous or "static" quenching process does not appear explicitly. A clear example is presented by Efftink and Ghiron[11] who showed experimentally in an indole-quencher system that τ^0/τ is independent of the factor, $W=\exp(-V[Q])$, in contrast to I_0/I. In the present case, the fraction W of the excited state $\overset{*}{C}^+$ generated by light illumination is actually quenched by the collisional mechanism corresponding to the rate constant k_q. The remaining fraction $1-W$ is

deactivated almost instantaneously after being formed because the quencher Cl^- is accidentally positioned in the proximity of excited molecule and interacts strongly with the latter. Only when such a static quenching mechanism is appropriately included, the fluorescence-yield decrease of 7-hydroxycoumarins as well as of 7-ethoxycoumarins[9] in each fluorescence band under steady-state conditions is reasonably understood. It has been already shown that the static quenching effect is easily taken into account in the framework of rate-equation analysis, if the generation rate G_{abs} is replaced formally by $\tilde{G}(Q)=G_{abs}\cdot\{(n_1+\vec{k}_t'+W(Q)\overleftarrow{k}_3[H^+])/(n_1+\vec{k}_t'+\overleftarrow{k}_3[H^+])\}$.[9] Because both I^N and I^T contain $\tilde{G}(Q)$ as a common multiple factor, it has been an ingenious way for us to examine the ratio of I^T to I^N in order to avoid the appearance of W in the analytical formulation.

In the case of pulsed excitation, the rate equations for time-variations of $[\overset{*}{N}]$ and $[\overset{*}{T}]$ need not include the fraction of excited species that never give fluorescence over an observing interval typically of 50 ns. Namely, the generation rate G_{abs} of $\overset{*}{N}$ has only to be reduced formally in the first approximation to $\tilde{G}(Q)$ with maintaining the same equational form as $W=1$. Since $\tilde{G}(Q)$ is included only in the intensity amplitude of $i^N(t)$ and $i^T(t)$, the appropriately normalized intensity of them is in principle given by Eqs. 1 and 2 even if $W\neq1$, while the fluorescence yield integrated over a time range is not correctly derived without considering the quencher dependency of W. More rigorous treatment of such transient phenomena has appeared in the serial works of Ware et al.[13] who formulated it by introducing a time-dependent rate constant, instead of W, in the rate equation. However, two different ways of analysis give essentially the same result as pointed out by Effink and Ghiron.[11]

Reaction Pathways for the Phototautomerization. It has been shown in Ref. 4 that the tautomerization of $\overset{*}{N}$ to $\overset{*}{T}$ can be promoted by dissociative and nondissociative processes. The dissociative mechanism has two possible pathways: one generates the intermediate protonated species as $\overset{*}{N}\rightarrow\overset{*}{C}^+\rightarrow\overset{*}{T}$, and the other generates the intermediate deprotonated species as $\overset{*}{N}\rightarrow\overset{*}{A}^-\rightarrow\overset{*}{T}$. In aqueous solutions, there occurs another possibility that $\overset{*}{N}$ is directly converted to $\overset{*}{T}$ by means of concerted transfer of hydrogen from hydroxyl site to carbonyl site with the aid of hydrogen bonding of water molecules:

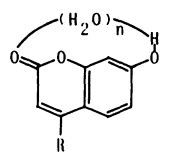

R = H, 7HC; R = CH_3, 7H4MC

Scheme 3.

Since the fluorescence of $\overset{*}{N}$, $\overset{*}{T}$, and $\overset{*}{A}^-$ are unaffected by the addition of Cl^-, the reaction pathways $\overset{*}{N}\rightarrow\overset{*}{A}^-\rightarrow\overset{*}{T}$ and $\overset{*}{N}\rightarrow\overset{*}{T}$ are not disturbed by Cl^- if the ionic strength does not vary largely. On the other hand, the reaction pathway $\overset{*}{N}\rightarrow\overset{*}{C}^+\rightarrow\overset{*}{T}$ is extremely disturbed by Cl^- due to the attractive interaction between $\overset{*}{C}^+$ and Cl^-. Probably, the electron transfer from Cl^- to $\overset{*}{C}^+$ within an encounter complex will result in the effective deactivation of $\overset{*}{C}^+$. The same discussion is applicable to three reversed reaction pathways from $\overset{*}{T}$ to $\overset{*}{N}$. In the pH region except for $[H^+]$ of ≈0.5 mol dm^{-3}, the fluorescence band of $\overset{*}{A}^-$ or $\overset{*}{C}^+$ is observable at a wavelength between the fluorescence bands of $\overset{*}{N}$ and $\overset{*}{T}$. It is only accidental for 7HC and 7H4MC that the fluorescence from both $\overset{*}{A}^-$ and $\overset{*}{C}^+$ is negligible at $[H^+]$ of 0.5 mol dm^{-3}, and this situation enables us to attain clear-cut understanding of the tautomerization reaction and of the quenching reaction by Cl^-.

Rapid Equilibration Limit. Consideration for the limiting case of rapid equilibration will help understanding the optically induced tautomeric reaction, although the limit is somewhat different from the real case of the present problem, i.e., $\tau_+\gg\tau_-$. If the transformation between $\overset{*}{N}$ and $\overset{*}{T}$ is rapid, a quasiequilibrium is realized in the excited state. Such a condition is described by $\vec{k}_t^{Cl}$, $\overleftarrow{k}_t^{Cl}\gg n_1$, n_3. Then, slow and fast decay components of lifetimes corresponding to Eq. 14 become as follows:

$$\frac{1}{\tau_+}\approx\frac{n_3\vec{k}_t^{Cl}+n_1\overleftarrow{k}_t^{Cl}}{\vec{k}_t^{Cl}+\overleftarrow{k}_t^{Cl}}\quad\text{and}\quad\frac{1}{\tau_-}\approx\vec{k}_t^{Cl}+\overleftarrow{k}_t^{Cl}. \tag{16}$$

Equation 16 clearly states that the excited-state equilibration is attained in a short time of τ_- and the total concentration of excited species will decrease rather slowly with the time constant of τ_+ which is the reciprocal of weighted average of decay rates, n_1 and n_3. Although the case of $\tau_+\gg\tau_-$ dose not completely coincide with the case of rapid equilibration, the similar situation will be realized in the present case of 7HC and 7H4MC based on rough order estimation of n_j's and k_t^{Cl}'s using meansured τ_+ and τ_-. From experimental data, $1/\tau_-$ is $\approx5\times10^9\,s^{-1}$, and n_1 and n_3 are supposed to be in the region of $0.2—0.5\times10^9\,s^{-1}$; therefore, $\vec{k}_t^{Cl}$ and $\overleftarrow{k}_t^{Cl}$ are estimated to be $\approx4\times10^9\,s^{-1}$ by using Eq. 14. Such conditions correspond nearly to the rapid equilibration limit.

Appendix

Derivation of Eqs. 4 and 5. Letting $I_0^N=n_1^r[\overset{*}{N}]$ and $I_0^T=n_3^r[\overset{*}{T}]$, $I_0^T/I_0^N=(n_3^r/n_1^r)\cdot([\overset{*}{T}]/[\overset{*}{N}])$. The ratio, $[\overset{*}{T}]/[\overset{*}{N}]$, can be obtained by using Eqs. 2—5 in Ref. 4 under steady-state conditions. Thus, we have

$$\frac{I_0^{\mathrm{I}}}{I_0^{\mathrm{N}}} = \frac{n_3^{\mathrm{I}}}{n_1^{\mathrm{I}}} \cdot \frac{\vec{k}_t' + \beta\overleftarrow{k}_3[\mathrm{H}^+]}{n_3 + \overleftarrow{k}_t'' + \alpha'\overleftarrow{k}_4[\mathrm{H}^+]}, \tag{4a}$$

where $\vec{k}_t'$ and β are given in Eq. 5, and $\overleftarrow{k}_t''$ and α' are given by

$$\overleftarrow{k}_t'' = \overleftarrow{k}_t + \vec{k}_2 \cdot \frac{n_2 + \overleftarrow{k}_1[\mathrm{H}^+]}{n_2 + \overleftarrow{k}_1[\mathrm{H}^+] + \overleftarrow{k}_2[\mathrm{H}^+]}$$

$$\text{and } \alpha' = \frac{n_4 + \vec{k}_3}{n_4 + \vec{k}_3 + \vec{k}_4} \cdot \tag{5a}$$

From Eq. 3, the relations

$$\frac{\vec{k}_1}{n_2 + \overleftarrow{k}_1[\mathrm{H}^+] + \overleftarrow{k}_2[\mathrm{H}^+]},$$

$$\frac{\vec{k}_2}{n_2 + \overleftarrow{k}_1[\mathrm{H}^+] + \overleftarrow{k}_2[\mathrm{H}^+]} \ll 1 \tag{17}$$

and

$$\frac{\overleftarrow{k}_3[\mathrm{H}^+]}{n_4 + \vec{k}_3 + \vec{k}_4}, \quad \frac{\overleftarrow{k}_4[\mathrm{H}^+]}{n_4 + \vec{k}_3 + \vec{k}_4} \ll 1 \tag{18}$$

are automatically satisfied. Since the n_1—n_4 are assumed to be of the same order, we obtain the inequalities:

$$n_3 \gg n_2 \cdot \frac{\vec{k}_2}{n_2 + \overleftarrow{k}_1[\mathrm{H}^+] + \overleftarrow{k}_2[\mathrm{H}^+]}$$

$$\text{and } n_3 \gg n_4 \cdot \frac{\overleftarrow{k}_4[\mathrm{H}^+]}{n_4 + \vec{k}_3 + \vec{k}_4} \cdot \tag{19}$$

The application of Eq. 19 to Eqs. 4a and 5a results in Eqs. 4 and 5. It is noted that, under the conditions of Eqs. 17 and 18, the fluorescence intensity from $\overset{*}{\mathrm{C}}{}^+$ and $\overset{*}{\mathrm{A}}{}^-$ (I_0^{C} and I_0^{A}) is negligibly small. If relations $n_2 \ll \overleftarrow{k}_1[\mathrm{H}^+]$ and $n_4 \ll \vec{k}_3$ are additionally satisfied, which have been assumed in Ref. 4 around pH≈0, $\vec{k}_t'$, $\overleftarrow{k}_t'$, α, and β in Eq. 5 are simplified as $\vec{k}_t' = \vec{k}_t + \vec{k}_1 \cdot \vec{k}_2/(\vec{k}_1 + \vec{k}_2)$, $\overleftarrow{k}_t' = \overleftarrow{k}_t + \vec{k}_2 \cdot \overleftarrow{k}_1/(\overleftarrow{k}_1 + \vec{k}_2)$, $\alpha = \vec{k}_3/(\vec{k}_3 + \vec{k}_4)$, and $\beta = \vec{k}_4/(\vec{k}_3 + \vec{k}_4)$.

The author gratefully acknowledges financial support by the special research program on "Molecular Electronics" of the Ministry of International Trade and Industry, Agency of Industrial Science and Technology.

References

1) M. R. Groves, S. C. Haydon, and O. M. Williams, *Opt. Commun.*, **9**, 42 (1973).
2) A. Diens, C. V. Shank, and R. L. Kohn, *IEEE J. Quantum Electron.*, **QE-9**, 833 (1973).
3) A. Bergman and J. Jortner, *J. Lumin.*, **6**, 390 (1973).
4) T. Moriya, *Bull. Chem. Soc. Jpn.*, **56**, 6 (1983).
5) C. Lewis, W. R. Ware, L. J. Doemeny, and T. L. Nemzek, *Rev. Sci. Instrum.*, **44**, 107 (1973).
6) M. A. Paul and F. A. Long, *Chem. Rev.*, **57**, 1 (1957).
7) O. Bensaude, M. Dreyfus, G. Dodin, and J. E. Dubois, *J. Am. Chem. Soc.*, **99**, 4438 (1977).
8) T. Moriya, *Bull. Chem. Soc. Jpn.*, **57**, 1723 (1984).
9) T. Moriya, *Bull. Chem. Soc. Jpn.*, **59**, 962 (1986).
10) J. M. Frank and S. J. Vavilov, *Z. Phys.*, **69**, 100 (1931).
11) M. R. Efftink and C. A. Ghiron, *J. Phys. Chem.*, **80**, 486 (1976).
12) T. Moriya, *Bull. Chem. Soc. Jpn.*, **60**, 3855 (1987).
13) D. V. O' Connor and R. W. Ware, *J. Am. Chem. Soc.*, **101**, 121 (1979) and the references cited therein.
14) N. J. Turro, "Modern Molecular Photochemistry," Benjamin, Menlo Park (1978), Chap. 5.
15) J. Grzywacz, S. Taszner, and J. Kruszewski, *Z. Naturforsch.*, **33a**, 1307 (1978).

Surface States of Titania(Rutile and Anatase)-Supported Vanadium Oxide Catalysts as Prepared by a Column-Exchange Adsorption Method and Their Catalytic Features

Yoshiya KERA,* Takashi INOUE, and Yoshihiro MATSUKAZE
Department of Applied Chemistry, Faculty of Science and Engineering, Kinki University, Higashiosaka, Osaka 577
(Received July 6, 1987)

Monolayer or less monolayer vanadium oxide catalysts supported on TiO_2(rutile and anatase), V_2O_5/R- and A-TiO_2, were prepared by a "column-exchange adsorption" method such as passing an oxovanadium ion solution, the pH of which was adjusted at 2, 4, and 7, through a column packed with titania (TiO_2) for impregnation. V_2O_5/R-TiO_2 pretreated at 450 °C showed an ESR spectrum with an unresoluved hfs for V(IV) ions at 77 K without depending upon the pH upon impregnation. V_2O_5/A-TiO_2 pretreated at room temperature showed quite small ESR signals due to Ti(III) and V(IV) ions. These signals tended to be intensive with increasing pH upon impregnation. After a heat treatment at 400 °C a huge and quite broad spectrum, which was ascribed to some reduced vanadia species($V_2O_{5-\delta}$), appeared in addition to the spectra for the Ti(III) and V(IV) ions, while such a change was never found in V_2O_5/R-TiO_2. Based on a theoretical treatment for the g-values, V(IV) ions on V_2O_5/R-TiO_2 have been confirmed to be replaced just into Ti ion sites on rutile(almost D_{2h} symmetry). With V_2O_5/A-TiO_2, V(IV) ions were shown to be placed so as to be partially subject to an anatase surface field(almost D_{2d} symmetry); that is, to be placed only near the vacant Ti ion site on anatase. From a comparison of the hf-coupling constant the vanadia species on rutile was clearly shown to interact more strongly with the surface than that on anatase. The 2-propanol decomposition rates over the catalysts were measured in the temperature range 270—350 °C as a test reaction. The activity of V_2O_5/R-TiO_2 was generally higher than that of V_2O_5/A-TiO_2. The lowest activation energy was obtained upon the impregnation at pH=2 for V_2O_5/R-TiO_2 and at pH=7 for V_2O_5/A-TiO_2. The best catalyst was not necessarily prepared through conditions with pH=4, which had been suggested as giving an effective monolayer-vanadia species.

Supported vanadium oxide catalysts have been widely used for the selective oxidation of hydrocarbons. They are usually prepared by the impregnation of oxovanadium ions on carriers; e.g., from aqueous solutions of NH_4VO_3,[1-3] oxalic acid solutions of NH_4VO_3[4] and V_2O_5,[5] and $VOSO_4$ aqueous solutions.[6] Their deposited states have been favorably investigated by analyzing ESR spectra for the V(IV) ion as a probe.[1-4,7,8] Roozeboom et al.[9-11] suggested that the so-called monolayer vanadium oxide catalyst could be favorably prepared by the impregnation of oxovanadium ions at a controlled pH of 4, since the oxovanadium ion has been known to be in such a polymerized state as decavanadate ion at pH=3—4 in aqueous solution.[12] Such a trial has already been reported by Sonnemans and Mars for the preparation of an alumina-supported MoO_3 catalyst[13] They showed that a vanadium oxide monolayer catalyst supported on titania(a mixture of rutile and anatase) is significantly active for methanol oxidation to formaldehyde.[11] Recently, many investigators have reported that "monolayered" vanadia deposited on titania, especially on anatase, has an excellent selectivity for the oxidation of hydrocarbons. They have discussed variously its deposited or interacting states according to ESR data, laser Raman spectroscopy, XPS, and TPD.[14-16] We have been interested in why such a supperior selectivity arises from the vanadia-titania system, especially from such monolayer vanadia on anatase. With respect to a rutile supported vanadia catalyst, which was prepared according to Roozeboom et al.,[9] we analyzed the deposited state of the vanadia species by ESR spectrometry and confirmed that the vanadia species dispersed quite homogeneously over the surface and that vanadium ions replaced mainly the surface Ti ion sites.[17]

In the present study, in order to make clear whether or not such pH-control upon impregnation is really effective, we prepared titania(rutile and anatase)-supported vanadium oxide catalysts by impregnation at different pH(=2, 4, and 7) and investigated their deposited states by ESR and their catalytic activitis for 2-propanol decomposition as a test reaction. In this paper we also discuss how the difference in the morphorogy of the carriers, rutile and anatase, affects the deposited state and catalytic features.

Experimental

1) Materials and Preparation Procedures. Anatase(A-TiO_2 Kanto Chem. Co. Ltd., guaranteed grade) were pulverised with an agate mortar and sieved between 100 and 170 meshes. Rutile(R-TiO_2), which was prepared from the anatase by heat treatment at 100 °C for 3 h, was pulverized and sieved between 100 and 170 meshes. V_2O_5 powder was prepared by the thermal decomposition of NH_4VO_3(Wako Pure Chem. Co. Ltd., guaranteed grade) in an air stream at 600 °C for 3 h for use as a reference catalyst.

7.9 grams of Sample R-TiO_2 was packed into a glass column (O.D.=15 mm), the length of which was about

75 mm. About 0.5 wt% of NH_4VO_3(Kanto Chem. Co. Ltd., guaranteed grade) aqueous solutions, the pH of which were exactly adjusted to 2, 4, and 7 by adding HNO_3 and NH_4OH, were poured into the column in order to cause the oxovanadium ion to be adsorbed. Each 3 ml of the effluent solution was collected in order to trace any changes in the pH and the concentration of vanadium ion while passing through the column. The effluent speed was about 0.1 ml min^{-1}. In the case of Sample A-TiO_2, 7.2 g were packed into the column; the NH_4VO_3 solution was also poured until both the pH and the vanadium ion concentration had recovered just to the original values. The values were determined by the use of a pH meter, TOA(model HM-7B), and by the usual Mohr salt method, respectively. The R- and A-TiO_2 adsorbing oxovanadium ion were dried at 110 °C for 8 h, and then calcined at 400 °C for 2 h in order to prepare titania supported vanadium oxide catalysts, V_2O_5/R-TiO_2 and V_2O_5/A-TiO_2, respectively.

2) Measurements and Computer Simulation. The surface areas of V_2O_5/R-TiO_2 and A-TiO_2 were determined by the usual BET method; N_2 gas adsorption at 77 K is shown in the 2nd column of Table 1. The surface area of V_2O_5 powder was similarily determined to be 8.5 $m^2 g^{-1}$. Those TiO_2 were identified by comparing their X-ray powder diffraction patterns with ASTM cards. The X-ray diffractometer used was a Rigagu Denki Model GF-Rad-γA; Cu *K*α- radiation(40 kV and 120 mA) and a nickel filter were also used. The deposited states of vanadium oxides were examined by ESR spectrometry. The ESR spectrometer used was a Nippon Denshi Model JES-PE(X-band 9.3 GHz and 100 kHz modulation). Computer simulation of the ESR spectrum was performed using an IBM 4381 system (described in detail later). The catalytic activities for 2-propanol decomposition, as a test reaction, were measured by the use of a closed circulation system(ca. 0.5 dm^3) connected directly to a gas chromatgraphy system with a Porapac-Q column(1 m). 20 mg of the catalysts were widely spread on the bottom of the vessel and preheated at the reaction temperature in air for 1 h before the reaction. The vessel containing 2-propanol was cooled by an ice-water bath during the reaction in order to maintain the vapor pressure constant at 8.4 mmHg (1 mmHg=133.322 Pa). The amount of the main product, which was confirmed to be propylene, was measured at intervals of 2 min. The decomposition rates were determined from the amount produced during the initial 20 min. The reaction temperature was controlled within±0.5 °C in the range 270—350 °C.

Results

1) The Amounts of Vanadium Oxide Deposited on Rutile and Anatase. When about 0.5 wt% of an ammonium metavanadate solution was poured into a glass column packed with rutile(R-TiO_2), the pH and vanadium ion (V-ion) concentration of the effluent solution varied as shown in Fig. 1. The pH initially increased from 2 to 5.5 in a run of pH=2, and from 4 to about 6 in a run of pH=4; it decreased from 7 to near 6 for pH=7. Eventually, they all returned to their original values. The amounts of oxovanadium ion adsorbed on R-TiO_2 were evaluated according to the

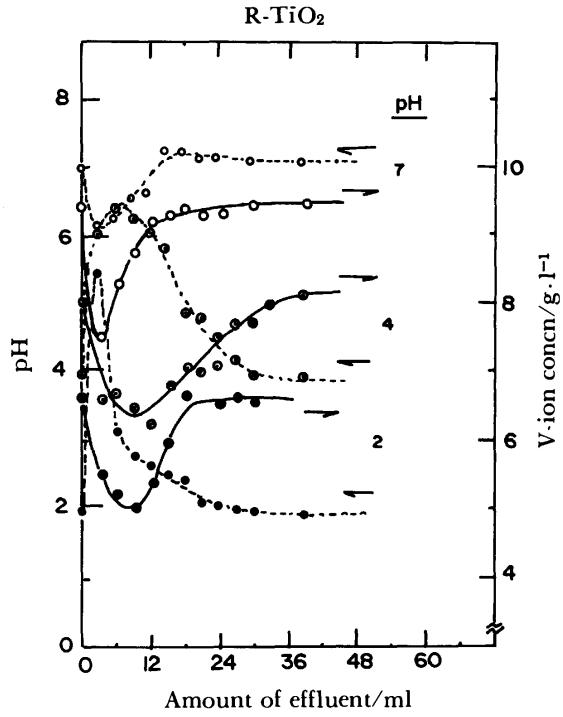

Fig. 1. The variations in the pH and the vanadium ion concentration of ammonium metavanadate solution during passing through the rutile-packed column. ----: pH changes and ——: V-ion concentration changes in the original solutions of pH=2, 4, and 7.

V-ion concentration vs. time-curve. The adsorbed amounts of oxovanadium ion, which was estimated under the assumption that it was deposited in the form of V_2O_5, are given in the 3rd and 4th column of Table 1 (in units of mg(V_2O_5)/g-carrier and mg-(V_2O_5)/m^2, respectively). The surface coverages are given in the 5th column of Table 1. They had been estimated under the assumptions that the V-O-V network of V_2O_5 extends two-dimensionally on the surface and that the V-O bond length is 2.0 Å.

For A-TiO_2, the changes in the pH and the V-ion concentrations of the effluent solutions are shown in Fig. 2. The pH value initially increased in all cases and then gradually returned to the original values. The pH initially increased up to 7.5, even in the run for pH=7; this suggests that the A-TiO_2 has a weak basisity. The vanadium ion concentrations initially decreased and then recovered to the original values accompanied by pH changes. We similarly estimated the amount of vanadium oxide deposited (given in the 3rd and 4th columns of Table 1; the surface coverage is given in the 5th column).

2) ESR Spectra of V(IV) and Ti(III) Ions on R- and A-TiO_2-Supported Vanadium Oxide Catalysts. The spectrum for an R-TiO_2-supported vanadium oxide catalyst (V_2O_5/R-TiO_2) impregnated at pH=2 is illustrated in Fig. 3. This is the most clear spectrum among the catalysts impregnated at pH=2, 4, and 7,

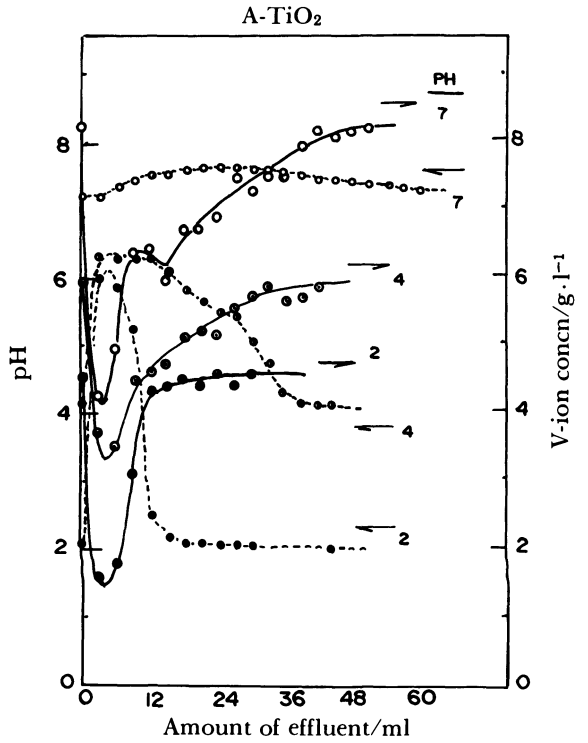

Fig. 2. The variations in the pH and the vanadium ion concentration of ammonium metavanadate solution during passing through the anatase-packed column. ----; pH changes and ——: V-ion concentration changes in the original solutions of pH=2, 4, and 7.

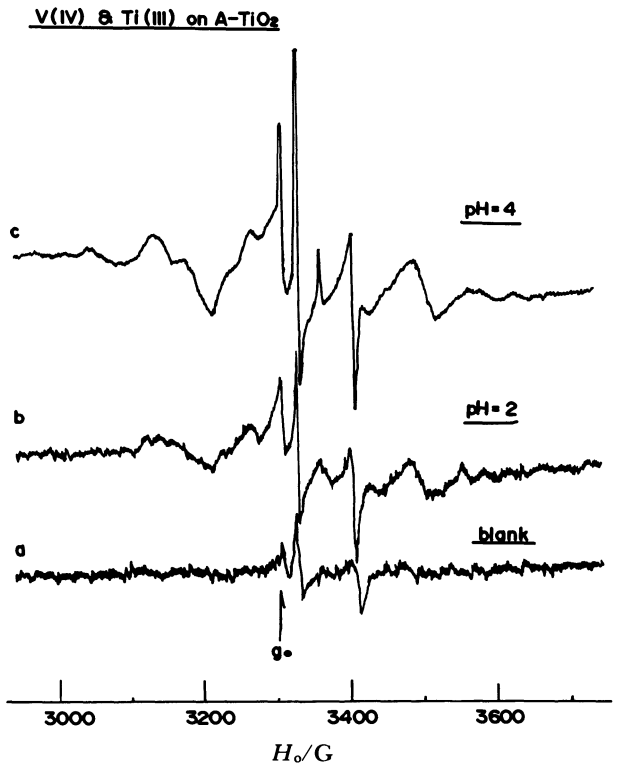

Fig. 4. The ESR spectra of anatase-carrier and V_2O_5/A-TiO_2 impregnated at pH=2 and 4, which were measured at 77 K after an evacuation at room temperature.

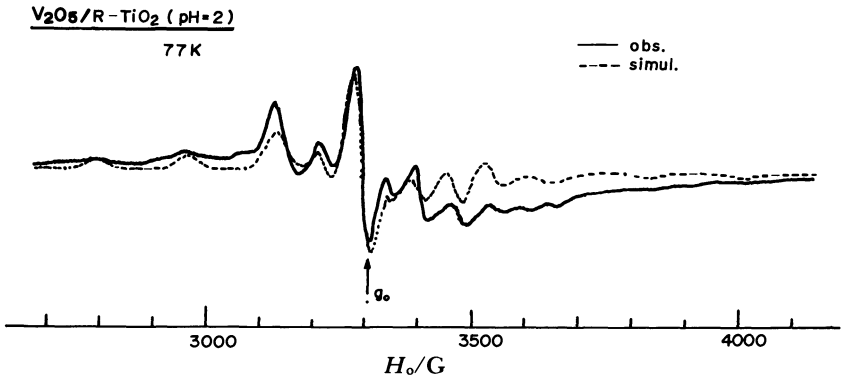

Fig. 3. The ESR spectrum for V_2O_5/R-TiO_2 and the best-fit spectrum previously simulated.[17] ——: observed and ----: simulated.

Table 1. Surface Areas of V_2O_5/R- and A-TiO_2 Catalysts, the Deposited Amounts of Vanadium Oxide (Reduced to V_2O_5), and the Surface Coverages

Catalyst	Surface area/$m^2 \cdot g^{-1}$	Deposited amount (V_2O_5) mg/g-carrier	Deposited amount (V_2O_5) $mg \cdot m^{-2}$	Surface coverage θ
R-TiO_2-carrier	2	—	—	—
V_2O_5/R-TiO_2 (pH=2)	2	2.66	1.30	0.66
V_2O_5/R-TiO_2 (pH=4)	2	4.88	2.44	1.2
V_2O_5/R-TiO_2 (pH=7)	2	1.81	0.90	0.47
A-TiO_2-carrier	8.5	—	—	—
V_2O_5/A-TiO_2 (pH=2)	6.7	3.2	0.48	0.25
V_2O_5/A-TiO_2 (pH=4)	6.4	6.6	1.03	0.53
V_2O_5/A-TiO_2 (pH=7)	6.5	10.2	1.57	0.82
V_2O_5-powder	8.5	—	—	—

which have been observed at 77 K after evacuation at 470 °C for 1 h. The spectrum had been regarded as containing poorly resolved hfs of vanadium(^{51}V) nucleus(I=7/2).[17] The result of a computer simulation is given along with a broken line in Fig. 3; the best-fit parameters used are given in Table 2. The spectrum was assigned to the V(IV) ion substituting the titanium ion site on the rutile surface.[17] V_2O_5/R-TiO_2 prepared at the other pH(=4 and 7) gave a similar spectrum, although the intensity was relatively low; thus, the spectrum could not be clearly observed.

An A-TiO_2 carrier, itself, gives a very weak signal due to Ti(III) ions. The intensity, however, became intensive along with the deposition of vanadium oxide. The ESR spectra for an A-TiO_2-supported vanadium oxide catalyst(V_2O_5/A-TiO_2) prepared at 2, 4, and 7 are illustrated in Figs. 4-b, c and 5-C. They

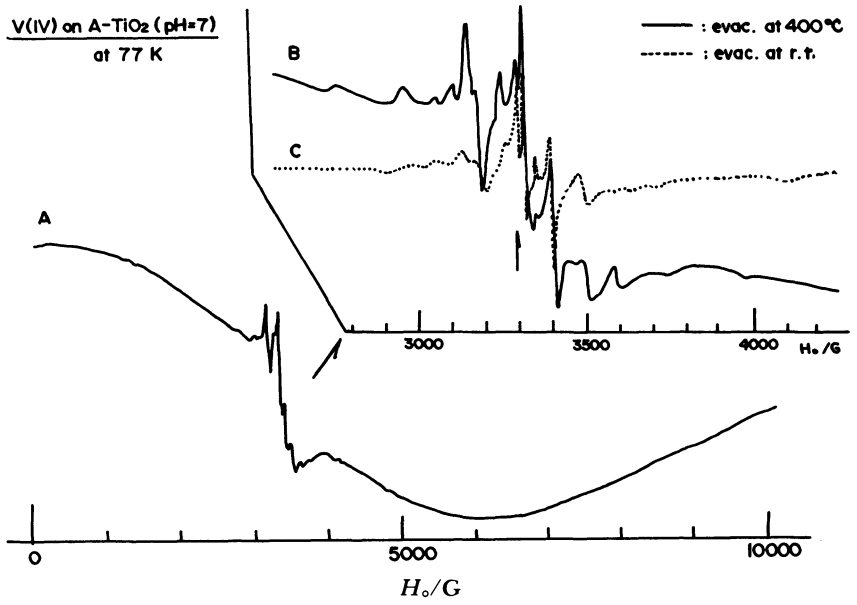

Fig. 5. The ESR spectrum of V_2O_5/A-TiO_2 impregnated at pH=7: Spectrum A indicates the wide range spectrum from zero to 10000 G, measured at 77 K after the evacuation at 400 °C: Spectrum B is the spectrum A that was recorded in the field between 2600 and 4200 G in order to show clearly the signal corresponding to the V(IV) and Ti(III) ions: Spectrum C the spectrum that was recorded in the field between 2600 and 4200 G at 77 K after the evacuation at room temperature.

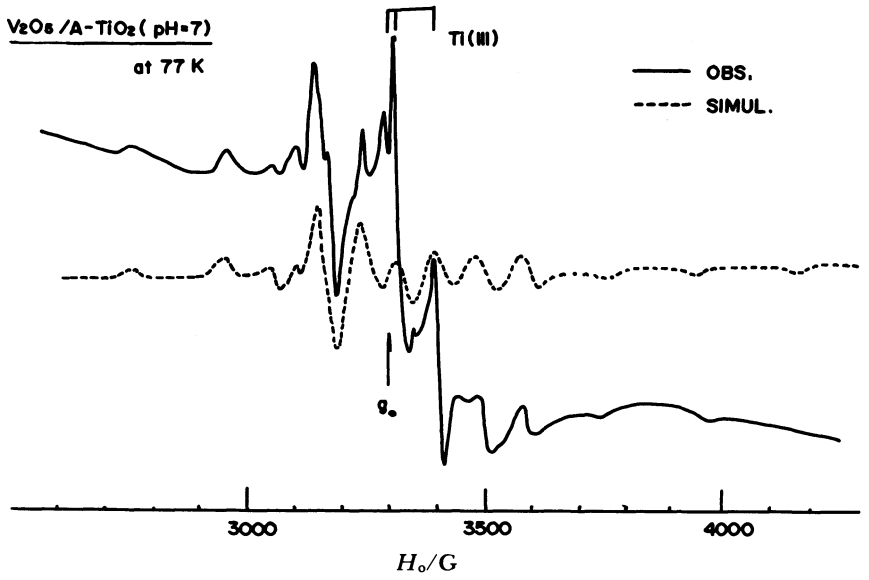

Fig. 6. The observed spectrum for V(IV) ion on V_2O_5/A-TiO_2(pH=7) and the best-fit spectrum simulated. ——: observed and ----: simulated.

were measured at 77 K after evacuation at room temperature for 1 h. The signal intensities for Ti(III) and V(IV) ions tends to increase simulteneously as the pH upon impregnation becomes high (pH=2→7). This change corresponds well to the surface coverage of the vanadia species (Table 1). When V_2O_5/A-TiO_2 was pretreated at 400 °C for 1 h, the spectrum varied greatly: A very large, broad signal appeared and the unresolved hf-lines ascribed to the V(IV) ion became more clear, while the intensity of the signal corresponding to Ti(III) ion almost didn't change

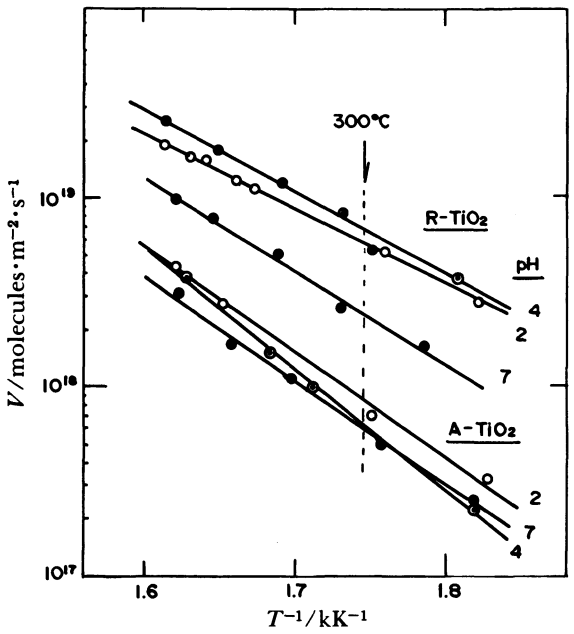

Fig. 7. Arrhenius plots of the 2-propanol decomposition rates over V_2O_5/R- and A-TiO_2 impregnated at various pH.

(Figs. 5-A and B). We applied a computer simulation to the component of the V(IV) ion in Fig. 5-B. The first derivative curve was calculated according to the usual simulation method[18,19] at intervals of 10 G (1G=10^{-4} T) in a magnetic field of 2500—4300 G (as described previously[17]). The intensity of the microwave absorption at each resonance field was obtained by numerical integrations at intervals of 1.5° to θ and ϕ for all directions under the assumption of a Gaussian shape function and 35 G of the half width. The best-fit parameters are given in Table 2 and the simulated spectrum for the V(IV) component is indicated by the broken line in Fig. 6. The g-tensor for the Ti(III) ion(Fig. 6) was estimated as $g_{//}$=1.94 and $g_{\perp}$=2.00 and 1.99 (Table 2).

3) Decomposition Rates of 2-Propanol over V_2O_5/R-TiO_2 and A-TiO_2. The rates of 2-propanol decomposition over titania-supported vanadium oxide catalysts were determined from changes in the GC-peak intensity for the produced propylene in the temperature range 270—350 °C. Arrhenius plots for the initial mean rates, thus obtained, are summarized in Fig. 7. Arrhenius parameters, log V_o and E_a, estimated from those plots, are given in Table 3. The minimum activation energy was obtained as 18.1 kcal mol^{-1} (1cal=4.184 J) for V_2O_5/R-TiO_2 prepared at pH=2, while the maximum as 29.6 kcal mol^{-1} for V_2O_5/A-TiO_2 prepared at pH=4. With respect to V_2O_5/R-TiO_2 the higher the pH upon impregnation, the larger the E_a. With V_2O_5/A-TiO_2, the catalyst prepared at pH=7 gives a minimum activation energy and that at pH=4 a maximum. The decomposition rate at 300 °C estimated with units of molecules/m^2s and molecules/mg(V_2O_5)s, are summarized in Figs. 8 and 9, respectively. The reaction rates over a V_2O_5 powder and the carrier, themselves(Blank), were added

Table 2. The Best Fitting Parameters Used for the Simulation of ESR Spectra of V(IV) Ion in V_2O_5/R- and A-TiO_2 Catalysts Evacuated at 400 °C

Catalyst	Species	g-value		A-value	
		$g_{//}$	$g_{\perp}$	$A_{//}$	$A_{\perp}$
V_2O_5/R-TiO_2	V(IV)	1.950	1.983	173.1	55
V_2O_5/A-TiO_2	V(IV)	1.912	1.981	200	75
V_2O_5/A-TiO_2	Ti(III)	1.94	1.99 2.00	—	—

Table 3. Arrhenius Parameters of 2-Propanol Decomposition over V_2O_5/R- and A-TiO_2 Catalysts Impregnated at pH=2, 4, and 7

Catalyst	log V_o/molecules·m^{-2}·s^{-1}	E_a/kcal mol^{-1}
V_2O_5/R-TiO_2 (pH=2)	25.6	18.1
V_2O_5/R-TiO_2 (pH=4)	26.5	20.3
V_2O_5/R-TiO_2 (pH=7)	27.1	23.0
V_2O_5/A-TiO_2 (pH=2)	27.8	26.0
V_2O_5/A-TiO_2 (pH=4)	29.0	29.6
V_2O_5/A-TiO_2 (pH=7)	27.3	25.1

in Figs. 8 and 9 for a comparison. The activity of V_2O_5/R-TiO_2, per m^2s, is 3—10 times higher than that of the carrier itself; also, the activity of V_2O_5/A-TiO_2 is about 3—4 times higher than that of the carrier itself. In both V_2O_5/R-TiO_2 and A-TiO_2 catalysts the activity, per mg(V_2O_5)s, became maximum upon impregnation at pH=2; further, those values are 50—130 times higher than that of V_2O_5 powder. Thus, it is evident that vanadium oxide is very effectively dispersed on the titania, especially on rutile impregnated at pH=2.

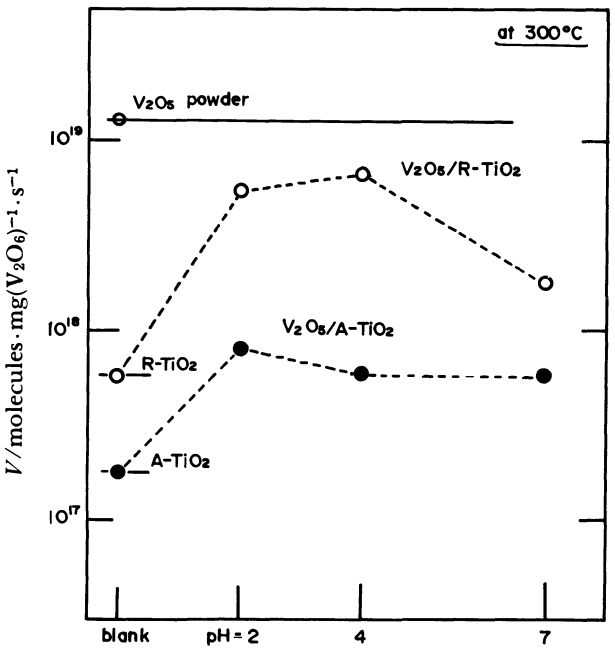

Fig. 8. Comparison of the activity(molecules/m^2 s) for 2-propanol decomposition among V_2O_5 powder, the carrier themselves, and the supported vanadium oxide catalysts at 300 °C.

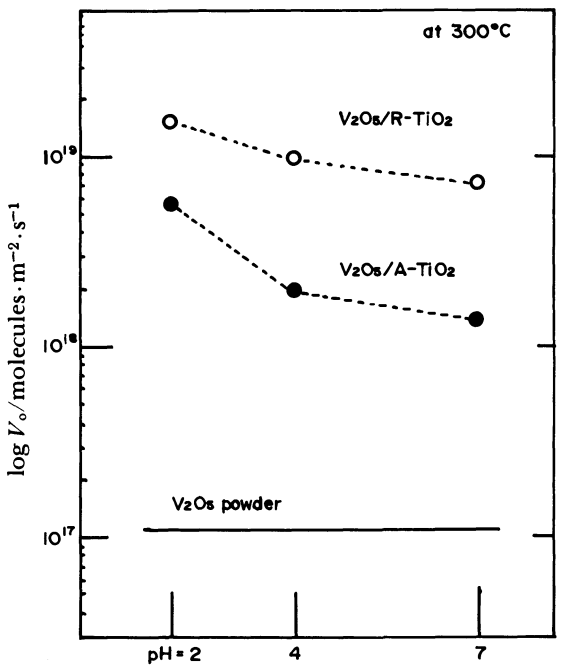

Fig. 9. Comparison of the activity(molecules/mg(V_2O_5)s) among the V_2O_5 powder and the supported catalysts at 300 °C.

Discussion

Deposited States of Vanadium Oxide on TiO_2-(Rutile and Anatase). Shimizu[20] has strictly investigated the relationship between the *g*-tensor and the crystal field splitting of the d-orbital for V(IV) ions doped in a TiO_2(rutile) single crystal subject to a D_{2h} symmetry field. We successfully applied the theory to an analysis of V(IV) ions placed into a V_2O_5 single crystal and subjected to the field of a distorted square pyramid.[21] Furthermore, the field symmetry around the V(IV) ions on rutile(V_2O_5/R-TiO_2) was clearly shown to be quite similar with that around V(IV) in the V_2O_5 single crystal.[17]

The anatase structure belong to the tetragonal symmetry of the space group $I4_1/amd$ and the Ti ion is in a distorted oxygen octahedra of the symmetry group D_{2d}:[22] Qualitatively oxygen ions placed on square corners of an octahedra deviate a little (althernatively up and down from the plane[23] accompanied by a transition of rutile to anatase) as the coordination model in Figs. 10-(a) and (b) shows. The relationship between the *g*-tensor and the crystal field splitting for d^1-metal placed in a tetragonal field (D_{4h} symmetry) and in a slightly distorted tetragonal field, e.g., rohmbic and trigonal distortions,[24,25] is given approximately as

$$g_{//} = g_0 - 8\lambda/\Delta \text{ and } g_{\perp} = g_0 - 2\lambda/\delta, \quad (1)$$

where Δ and δ are the crystal field splitting constants

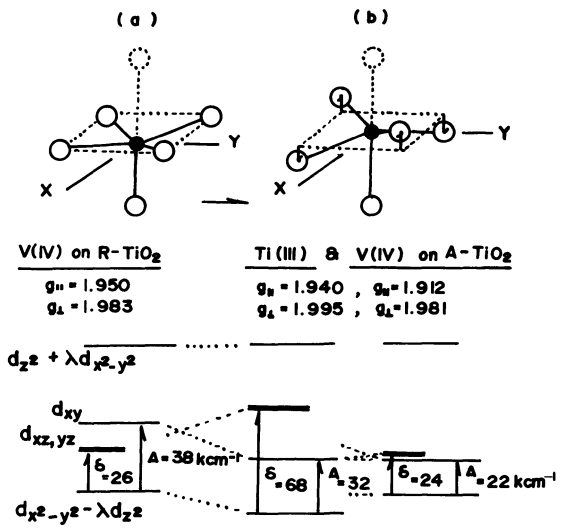

Fig. 10 Coordination model and crystal field splitting for the surface V(IV) ion in V_2O_5/R-TiO_2 and V_2O_5/A-TiO_2.

and λ the spin-orbit coupling constant (reasonably assumed to be 250 cm^{-1}[26]). If such a symmetry change as $D_{2h} \rightarrow D_{2d}$ accompanied by the transition, rutile→anatase, is not too large for the application of the theory to the present system, we can similarly estimate the field splitting around V(IV) ion on V_2O_5/A-TiO_2. Such a deviation of the oxygen ions should directly cause the d_{xy}-level to be lower and the $d_{x^2-y^2}$ to be lower to some extnet; however, the d_{xz} and d_{yz} increase to some extent. The field splitting around the Ti(III) ion, which was estimated by appling Eq. 1 to the g-value in Table 2, agrees well with the expected value, as shown in Fig. 10-(b). With the V(IV) ion the d_{xy}-level decreased considerably, but the degree of the increase in the d_{xz}- and d_{yz}-levels and the decrease in the $d_{x^2-y^2}$ are not as large as expected (Fig. 10-(b)). The energy diagram suggests that the V(IV) ion is partially subjected to a symmetry field of the anatase surface; therefore, it may be placed only near a vacant Ti site on the anatase surface. Since both λ/Δ and λ/δ were less than 0.1 in the present estimation,[26] this theory could reasonably well be applied to this system.

Wacks et al.[16] suggested that two types of vanadia species were present on anatase deposited with V_2O_5: A surface vanadia species coordinated to the anatase and the crystallites of V_2O_5. In V_2O_5/TiO_2(anatase) with 2% or less V_2O_5, a monolayer of surface vanadia species was formed without any crystallite V_2O_5. Inomata et al.[27] observed the same ESR spectrum with unresolved hfs for a multilayered vanadium oxide deposited on rutile and anatase. They indicated that the g-value, $\langle g \rangle$=1.971, was close to that in the V_2O_5 matrix. The present g-value corresponds well to that reported by Akimoto et al.[28] The present samples show almost the same extent of deposition with the monolayer or the less monolayer catalysts of Wacks et al.;[16] therefore, the deposited state is comparable with them. According to an FT-IR study by Miyata et al.,[29] the V=0 stretching band for the vanadia species on a less monolayer V_2O_5/anatase catalyst was found at 983 cm^{-1}. Kozlowski et al.[30] found by EXAFS and XANES measurements that a vanadium monolayer supported on anatase did not have the structural characteristics of crystalline V_2O_5 and suggested that the basic unit was a species with two terminal and two bridging bonds. The V(IV) ion placed near the site (expected by the coordination model in Fig. 10-(b)) may correspond to all these vanadia species. It was clearly mentioned in the discussion that the vanadia species were strongly affected by the surface field symmetry of the carrier; it was further suggested that V(IV) ions were placed just in and near the titanium ion vacant sites on rutile and anatase surfaces (cf. Figs. 10-(a) and (b), respectively. However, such models express only one of the possible deposited states and, of course, the possibility of a topochemical deposition of vanadium oxide just on the titania surfaces would not be ruled out.

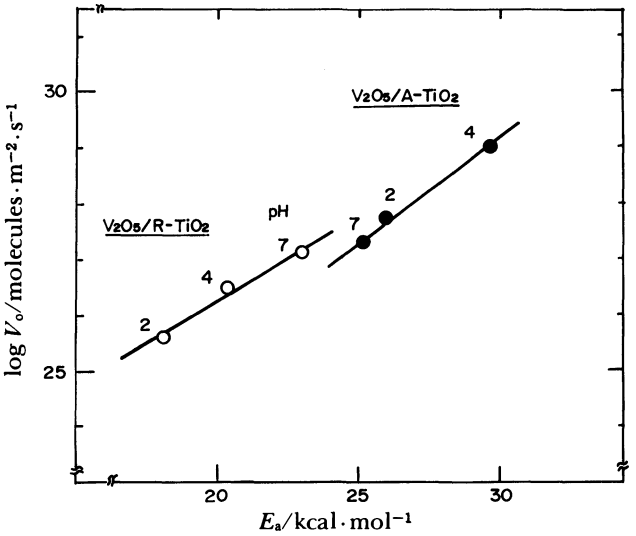

Fig. 11. Relationship between the pre-exponential factor(log V_o) and the activation energy(E_a) for 2-propanol decomposition over the titania supported vanadium oxide catalysts.

A huge ESR signal that appeared in V_2O_5/A-TiO_2 upon evacuation at 400 °C(Fig. 5) might have been due to a kind of dipole-dipole interaction between the V(IV) ions or to a triplet state of the V(III) ion. Reduced vanadia species were easily formed on an anatase supported vanadia catalyst, as also indicated by other authors.[15,16] Thus, the huge and broad ESR signal might be ascribed to some kind of reduced vanadia species that were placed in a micropore and were inhomogeneously dispersed on the anatase surface.

V_2O_5/R-TiO_2 showed a sharp ESR signal, which was assigned to the V(IV) ion, weakly interacting with the remaining oxygen molecules, upon evacuation at room temperature. No reduced type of spectrum was formed upon evacuation at 470 °C; only a simple spectrum with broad hfs for V(IV) ions has already been reported.[17] The hf-coupling constants($A_{//}$ and $A_{\perp}$) are considerably larger in V_2O_5/A-TiO_2 than V_2O_5/R-TiO_2, as shown in Table 2. This suggests that the unpaired electron is located to a much greater extent on V_2O_5/A-TiO_2 than V_2O_5/R-TiO_2; thus, the vanadia species interacts more weakly with anatase than the rutile surface. This may correspond to the suggestion by Kozlowski et al.[30] that differences occur in the structure of the active phase when supported on different materials.

Catalytic Properties of V_2O_5/R-TiO_2 and A-TiO_2. Previously, we found a kinetic compensation effect for alcohol decomposition over alkali-modified vanadium oxide catalysts for successfully analyzing its activated states.[31] In the activated state of an alcohol molecule the internal frictional rotation of the alkyl group, especially the methyl group, has been insisted

as being an important parameter. A compensation relation holds well between log V_o and E_a for catalysts impregnated at different pH(=2, 4, and 7) in Table 3, as shown in Fig. 11. A desired catalyst should be located(relatively) on the left-hand side and on the upperpart of log V_o vs. E_a-plots. From this point of view V_2O_5/R-TiO_2 is more desirable than V_2O_5/A-TiO_2, as can be clearly seen by comparing Figs. 8 and 9. Furthermore, with V_2O_5/R-TiO_2 the lowest activation energy was obtained upon impregnation at pH=2 and with V_2O_5/A-TiO_2 upon that at pH=7 instead of pH=4. Therefore, we could not find any special ability in catalysts prepared by impregnation at pH=4 (reported by Roozeboom et al. for preparation of a monolayer catalyst[9]). Through kinetic consideration, however, not only the kind of carrier but also the pH upon impregnation could be clearly demonstrated to delicately affect the deposit state of vanadia species, although ESR measurements have never detected such difference with the pH.

Many investigators have shown that monolayer vanadia species supported on TiO_2, especially on anatase, are superior catalysts for oxidation of *o*-xylene.[14-16] V_2O_5/A-TiO_2 seems to be considerably reduced during 2-propanol decomposition, while being kept in an oxidative state during the oxidation reaction. This means that the catalytic feature for 2-propanol decomposition can not be compared simply with that for oxidation. We will not discuss further their abilities as oxidation catalysts in the present paper.

References

1) L. L. Van Reijen and P. Cossee, *Disc. Faraday Soc.*, **41**, 277 (1966).

2) V. A. Shvets, V. M. Vortyntsev, and V. B. Kazansky, *Kinet. Katal.*, **10**, 356 (1969); V. A. Shvets and V. B. Kazansky, *J. Catal.*, **25**, 123 (1972).

3) S. Yoshida, T. Iguchi, S. Ishida, and K. Tarama, *Bull. Chem. Soc. Jpn.*, **45**, 376 (1972).

4) H. Takahashi, M. Shiotani, H. Kobayashi, and J. Sohoma, *J. Catal.*, **14**, 134 (1969).

5) Y. Murakami, M. Inomata, A. Miyamoto, and K. Mori, 7th Intern. Cong. Catal., Tokyo, 1980, B-49.

6) K. Tarama, S. Teranishi, S. Yoshida, N, Tamura, and S. Ishida, *Kogyo Kagaku Zasshi*, **68**, 1499 (1965).

7) J. C. W. Chien, *J. Am. Chem. Soc.*, **93**, 4675 (1971).

8) K. C. Kulbe, R. S. Mann, and A. Manoogian, *J. Chem. Phys.*, **60**, 4810 (1974).

9) F. Roozeboom, T. Fransen, P. Mars, and P. J. Gellings, *Z. Anorg. Allg. Chem.*, **449**, 25 (1979).

10) F. Roozeboom, J. Medema, and P. J. Gellings, *Z. Phys. Chem., NF*, **111**, 215 (1978).

11) F. Roozeboom, P. D. Cordingley, and P. J. Gellings, *J. Catal.*, **68**, 464 (1981).

12) For instance, D. L. Kepert, "Comprehensive Inorganic Chem. IV", p. 607.

13) J. Sonnemans and P. Mars, *J. Catal.*, **31**, 209, 220 (1973).

14) G. C. Bond and K. Brukman, *Faraday Discuss. Chem. Soc.*, **72**, 235 (1981); G. C. Bond and P. Konig, *J. Catal.*, **77**, 309 (1982).

15) M. Rusiecka, B. Grzybowska, and M. Gasior, *Appl. Catal.*, **10**, 101 (1984).

16) I. E. Wachs, R. Y. Saleh, S. Chan, and C. C. Chersich, *Appl. Catal.*, **15**, 339 (1985); R. Y. Saleh, I. E. Wachs, S. S. Chan, and C. C. Chersich, *J. Catal.*, **98**, 102 (1986).

17) Y. Kera and Y. Matsukaze, *J. Phys. Chem.*, **90**, 5752 (1986).

18) B. Bleaney, *Philos. Mag.*, **42**, 441 (1951); A. Rockenbauer, P. Simon, *J. Mag. Reson.*, **11**, 217 (1973); S. Ishida, Y. Magatani, Y. Kobayashi, and S. Yoshida, Annu. Meeting Catal. Soc. Jpn., Fukuoka, 1979, 4R01.

19) R. H. Sand, *Phys. Rev.*, **99**, 1222 (1955); R. Lefebvre, J. Maruani, *J. Chem. Phys.*, **42**, 1480 (1965).

20) T. Shimizu, *J. Phys. Soc. Jpn.*, **23**, 848 (1967).

21) Y. Kera and K. Kuwata, *Bull. Chem. Soc. Jpn.*, **52**, 1268 (1979).

22) V. S. Grunin, V. A. Ioffe, I. V. Patrina, and G. D. Davtyan, *Sov. Phys. Solid State*, **17**, 2012 (1976).

23) W. Huckel, "Structural Chemistry of Inorganic Compounds(II)," Elsevior Sci., New York (1951), pp. 675—678.

24) B. N. Misra and R. Kripal, *Indian J. Phys.*, **55A**, 74 (1981).

25) B. A. Goodman and J. B. Baynor, *Advan. Inorg. Chem. Radiochem.*, **13**, 135 (1970).

26) G. C. Pake, "*Paramagnetic Resonace*," W. A. Benjamin, New York New York (1962).

27) M. Inomata, K. Mori, A. Miyamoto, T. Ui, and Y. Murakami, *J. Phys. Chem.*, **87**, 754 (1983).

28) M. Akimoto, M. Usami, and E. Echigoya, *Bull. Chem. Soc. Jpn.*, **51**, 2195 (1978).

29) H. Miyata, K. Fujii, T. Ono, Y. Kubokawa, T. Ohon, and F. Hatayama, *J. Chem. Soc., Faraday Trans. 1*, **83**, 675 (1987).

30) R. Kozlowski, R. F. Pettlfer, and J. M. Thomas, *J. Phys. Chem.*, **87**, 5172, 5176 (1983).

31) Y. Kera and M. Negoro, *J. Catal.*, **99**, 198 (1986).

 © 1988 The Chemical Society of Japan Bull. Chem. Soc. Jpn., 61, 769—774 (1988)

The Temperature Dependence of the Quenching Rate of the 307.6 nm Zinc Resonance Line by Some Alkane Hydrocarbons

Shunzo YAMAMOTO
Department of Chemistry, Faculty of Science, Okayama University,
3-1-1, Tsushima-naka, Okayama
(Received July 15, 1987)

The intensities of the 307.6 nm resonance line of zinc were measured as a function of the alkane pressure at various temperatures between 556 and 696 K, and the quenching rate was determined on the basis of the Stern-Volmer plots. Assuming that the quenching rate constant, k_Q, of a certain alkane is equal to the sum of the quenching-rate constant, k_i, for each C-H bond, the ratios of k_s/k_p and k_t/k_p (k_p, k_s, and k_t are the quenching-rate constants for primary, secondary, and tertiary C-H bonds) were estimated from the ratios of the quenching rates of butane, isobutane, and neopentane. The differences in the activation energies for the quenching for primary, secondary, and tertiary C-H bonds were obtained from the temperature dependence of the ratios of k_s/k_p and k_t/k_p and were interpreted in terms of the modified bond-energy-bond-order (BEBO) method.

In a previous paper,[1] a remarkable dependence of the quenching of the cross section of the 307.6 nm zinc resonance line by alkane hydrocarbons on the C-H bond strength was reported. It was pointed out that the quenching cross-section of a certain alkane can be estimated as the sum of the quenching cross-section for each individual quenching site (C-H bond). The above findings show that the excited zinc atoms attack not only the weakest C-H bond, but all kinds of C-H bonds, with efficiencies which depend on the bond strength, and it was concluded that hydrogen-atom abstraction from hydrocarbons by means of excited zinc atoms plays an important role in the quenching of $Zn(^3P_J)$.

In this study, relative quenching-rate constants for butane, isobutane, and neopentane were determined over the temperature range of 556—696 K, and from these values the ratios of k_s/k_p and k_t/k_p (k_p, k_s, and k_t are quenching-rate constants for primary, secondary, and tertiary C-H bonds) were estimated at various temperatures.

Experimental

The apparatus and the procedure were the same as those described previously.[1,2]

The zinc metal used was high-purity zinc (99.9999%) manufactured by the Osaka Asahi Metal Co. The ethane, butane, isobutane, and neopentane (Tokyo Kasei Kogyo Co., Ltd.; G.R. grade) were freeze-pumped several times and repeatedly subjected to trap-to-trap distillation. Pure-grade argon (Daido Sanso Co.; 99.999%) was used without further purification.

When a cell containing zinc vapor was illuminated by the exciting lamp, a resonance line was observed at 307.6 nm. Upon the addition of argon, the intensity of the line increased with the increase in the argon pressure. This was attributed to the increase in the light intensity absorbed by zinc atoms as a result of the pressure broadening of the absorption line.[1,2] In order to minimize this effect of the pressure broadening of the absorption line, quenchers were diluted with a large amount of argon (total pressures: 1333—2666 Pa).

Results and Discussion

In a previous paper, the following reaction scheme was proposed for the quenching of $Zn(^3P_J)$[1,2]

$Zn(^1S_0) + h\nu(307.6\,nm) \longrightarrow Zn(^3P_1)$	I_a
$Zn(^3P_1) \longrightarrow Zn(^1S_0) + h\nu(307.6\,nm)$	k_0
$Zn(^3P_1) + M \rightleftharpoons Zn(^3P_0) + M$	k_1, k_{-1}
$Zn(^3P_1) + M \rightleftharpoons Zn(^3P_2) + M$	k_2, k_{-2}
$Zn(^3P_0) + Q \longrightarrow$ quenching	k_3
$Zn(^3P_1) + Q \longrightarrow$ quenching	k_4
$Zn(^3P_2) + Q \longrightarrow$ quenching	k_5.

Here, M denotes Ar and quenchers, and Q represents quenchers. By assuming the steady state for $Zn(^3P_{0,1,2})$, the following equation can be derived:

$$\frac{I^\circ}{I} = 1 + \frac{1}{k_0}\left(\frac{k_1}{k_{-1}}k_3 + k_4 + \frac{k_2}{k_{-2}}k_5\right)[Q]. \quad (1)$$

where I° and I are the intensities of the resonance line in the absence and in the presence of quenchers respectively. Stern-Volmer plots for the quenching by butane at various temperatures are shown in Fig. 1.

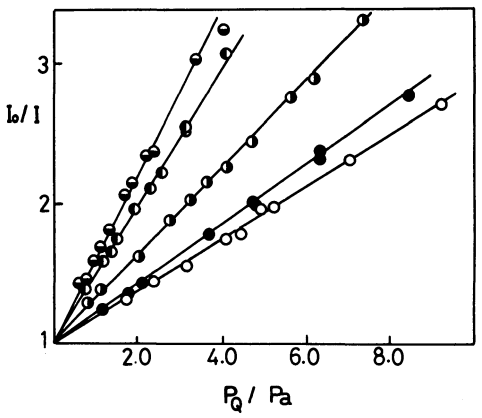

Fig. 1. Stern-Volmer plots for the quenching of $Zn(^3P_J)$ by butane at various temperatures.
556 (○), 605 (●), 636 (◑), 666 (◐), and 696 K (◒).

Table 1. $k_Q\tau$ Values in the Quenching of $Zn(^3P_J)$ Atoms by Butane, Isobutane, and Neopentane at Various Temperatures

T/K	$k_Q\tau$/Pa^{-1} Butane	Isobutane	Neopentane
556	0.188±0.003	0.127±0.003	0.105±0.002
578	0.194±0.003	0.133±0.003	0.112±0.003
605	0.208±0.003	0.144±0.003	0.125±0.003
636	0.317±0.005	0.219±0.004	0.195±0.003
666	0.500±0.008	0.350±0.006	0.320±0.006
696	0.798±0.013	0.559±0.009	0.518±0.009

Table 2. Quenching Rate Constants of Neopentane and Ethane

T/K	$k_Q\tau$/Pa^{-1}	k_Q'/10^{-12} cm^3 molecule^{-1} s^{-1}	k_Q''/10^{-12} cm^3 molecule^{-1} s^{-1}
Neopentane			
548	0.095±0.002	3.00±0.08	2.97
556	0.105±0.002	3.36±0.08	3.33
567	0.107±0.002	3.50±0.08	3.43
578	0.112±0.003	3.74±0.12	3.60
588	0.119±0.003	4.03±0.12	3.80
596	0.124±0.003	4.27±0.13	3.92
605	0.125±0.003	4.35±0.13	3.85
636	0.195±0.003	7.14±0.13	4.64
666	0.320±0.006	12.3 ±0.2	4.22
696	0.518±0.009	20.8 ±0.3	3.37
Ethane			
553	0.063±0.001	4.02±0.04	3.98
563	0.065±0.001	4.18±0.04	4.14
568	0.068±0.002	4.45±0.08	4.36
573	0.073±0.002	4.80±0.08	4.62
588	0.076±0.002	5.13±0.08	4.84
599	0.081±0.002	5.57±0.08	5.11
613	0.094±0.003	6.62±0.13	5.76

Similar plots were obtained for other quenchers. From the slope of the straight lines, the values of $k_Q\tau$ ($k_Q=(k_1/k_{-1})k_3+k_4+(k_2/k_{-2})k_5$ and $\tau=1/k_0$) were estimated; they are listed in Tables 1 and 2.

As has been mentioned above, k_Q is the composite rate constant for the quenching of $Zn(^3P_0)$, $Zn(^3P_1)$, and $Zn(^3P_2)$. Since the three triplet states are in equilibrium, $k_1/k_{-1}=(1/3)\exp(2.30\ \text{kJ mol}^{-1}/RT)$ and $k_2/k_{-2}=(5/3)\exp(-4.70\ \text{kJ mol}^{-1}/RT)$,[2] k_1/k_{-1} and k_2/k_{-2} are temperature-dependent. As these equations show, k_1/k_{-1} decreases slightly, and k_2/k_{-2} increases with an increase in the temperature, but their changes are small.

The quenching rate constant, k_Q, can be rewritten as follow:

$$k_Q = k_4\left(\frac{k_1}{k_{-1}}\frac{k_3}{k_4} + 1 + \frac{k_2}{k_{-2}}\frac{k_5}{k_4}\right) \quad (2)$$

Since the excitation energy increases in this order: $Zn(^3P_0)$, $Zn(^3P_1)$, and $Zn(^3P_2)$, the activation energies for k_3, k_4, and k_5 decrease in that order. Therefore, k_3/k_4 increases, and k_5/k_4 decreases, with the temperature. Since the changes in k_1/k_{-1} and k_2/k_{-2} are compensated for by the changes in k_3/k_4 and k_5/k_4, the temperature-dependence of the value in parentheses in Eq. 2 seems to be very small. It can be said that k_Q is approximately proportional to k_4.

In Fig. 1, the Stern-Volmer plots at various temperatures for butane are shown. The slope of the line increases with the temperature. A similar temperature-dependence was observed for the quenching by isobutane and neopentane.

As has been mentioned above, the value of $k_Q\tau$ can be obtained from the slope of the Stern-Volmer plots. These values for butane, isobutane, and neopentane are shown in Fig. 2 as a function of the temperature. As is shown in Fig. 2, the value of $k_Q\tau$ slightly increases with the temperature below about 606 K, while the $k_Q\tau$ value increases more rapidly at temperatures higher than 606 K. This indicates that the effective lifetime (τ) of $Zn(^3P_1)$ may be hardly lengthened at all by the radiation imprisonment below 606 K. However, the effect of imprisonment can not be neglected at temperatures higher than 606 K.

Therefore, the quenching rate constant, k_Q, can be calculated from the slope by using the natural lifetime (2.0×10^{-5} s)[3] as τ below 606 K, but not at higher temperatures. Only the relative rate constant can be estimated from the slope at higher temperatures.

The ratios of the imprisonment lifetime to the natural lifetime at various temperatures were calculated by the use of the following equation, given by Milne for infinite slab geometry:[4]

$$\tau/\tau_0 = 1 + (kl/\lambda)^2, \quad (3)$$

where k is the absorption coefficient at the line center, l is the thickness of the slab, and λ is the root between 0 and $\pi/2$ of the equation:

$$\tan y = kl/y. \quad (4)$$

Samson[5] has modified Milne's theory so that an equivalent opacity $\bar{k}\,l$ is used in Eqs. 3 and 4 instead of kl, the opacity at the line center. The equivalent opacity for the Doppler line-shape is defined by :

$$\exp(-\bar{k}l) = \frac{\int_{-\infty}^{\infty}\exp(-\omega^2)\exp[-kl\exp(-\omega^2)]d\omega}{\int_{-\infty}^{\infty}\exp(-\omega^2)d\omega}, \quad (5)$$

where $\omega=[2(\nu-\nu_0)/\Delta\nu_D](\ln 2)^{1/2}$ ($\Delta\nu_D$ is the Doppler breadth). k can be estimated by means of this equation:

$$k = (2/\Delta\nu_D)(\ln 2/\pi)^{1/2}(\lambda_0^2/8)(g_2/g_1)([Zn]/\tau_0) \quad (6)$$

where g_2 and g_1 are the degeneracies of the upper and lower states respectively, λ_0 is the wavelength at the center of the atomic line, and τ_0 is the natural lifetime of an excited atom. The values of $\bar{k}\,l$ for the Doppler case were obtained by the interpolation of the values given by Zemansky[6] and Blickensderfer et al.[7]

The values of τ/τ_0 calculted by Samson's method are shown in Table 3. As Table 3 shows, the imprisonment effect can be nearly neglected below 605 K, but it becomes significant at higher temperatures. This finding is in agreement with the tendency observed above.

In Fig. 3, the ratios of k_Q(butane)/k_Q(neopentane) and k_Q(isobutane)/k_Q(neopentane) are shown as a function of $1/T$. These plots give curves. This can be explained by considering that butane and isobutane have two types of reaction sites (the former has primary and secondary C-H bonds, while the latter

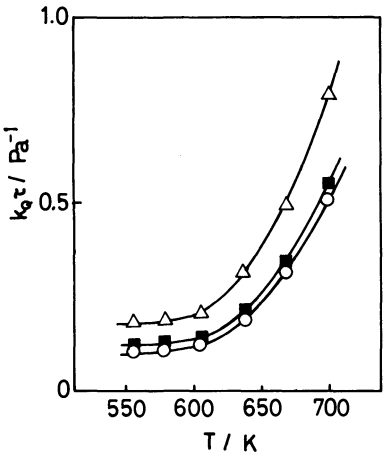

Fig. 2. Temperature dependence of $k_Q\tau$.
Butane (△), isobutane (■), and neopentane (○).

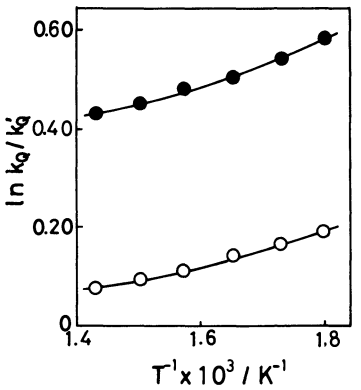

Fig. 3. Temperature dependence of rate constant ratio.
k_Q(butane)/k_Q(neopentane) (●) and k_Q(isobutane)/k_Q(neopentane) (○).

Table 3. $k_Q\tau$ Values in the Quenching of Zn(^3P_J) Atoms by Neopentane and the Imprisonment Lifetime at Various Temperatures

T	P_{Zn}[a]	k[b]	$k_Q\tau$	τ
K	Pa	cm^{-1}	Pa^{-1}	τ_0
548	0.045	0.016	0.095±0.002	1.01
556	0.070	0.024	0.105±0.002	1.01
567	0.124	0.041	0.107±0.002	1.02
578	0.217	0.069	0.112±0.003	1.04
588	0.353	0.110	0.119±0.003	1.06
596	0.515	0.157	0.124±0.003	1.09
605	0.779	0.233	0.125±0.003	1.13
636	2.96	0.822	0.195±0.003	1.54
666	9.57	2.48	0.320±0.006	2.91
696	27.99	6.79	0.518±0.009	6.15

a) $\log(133.33P_{Zn}/\text{Pa}) = -7198/T + 9.664$: J. D. McKinley and J. E. Vance, *J. Chem. Phys.*, **22**, 1120 (1954). b) The absorption coefficient at the center of the Doppler-broadened line.

has primary and tertiary C-H bonds) and that the activation energies for the rates of quenching by these C-H bonds are not equal to each other.

In a previous paper,[1] we reported that the quenching cross section for any C_1—C_5 alkanes can be calculated by the following equation:

$$\sigma_Q = \sum n_i \sigma_i \tag{7}$$

where n_i is the number of the C-H bond of Type i (CH_3-H, primary C-H, secondary C-H, and tertiary C-H) and where σ_i is the cross section for each C-H bond of Type i. If a similar additivity can be applied for the quenching rates by butane, isobutane, and neopentane at every temperature examined, the following equations must hold:

$$\frac{k_Q(\text{butane})}{k_Q(\text{neopentane})} = \frac{6k_p + 4k_s}{12k_p} = \frac{1}{2} + \frac{1}{3}\frac{k_s}{k_p} \tag{8}$$

$$\frac{k_Q(\text{isobutane})}{k_Q(\text{neopentane})} = \frac{9k_p + k_s}{12k_p} = \frac{3}{4} + \frac{1}{12}\frac{k_t}{k_p} \tag{9}$$

Therefore, the following equations can be obtained:

$$\frac{k_s}{k_p} = \left\{ \frac{k_Q(\text{butane})}{k_Q(\text{neopentane})} - \frac{1}{2} \right\} \times 3 \tag{10}$$

$$\frac{k_t}{k_p} = \left\{ \frac{k_Q(\text{isobutane})}{k_Q(\text{neopentane})} - \frac{3}{4} \right\} \times 12 \tag{11}$$

From the experimental values for k_Q(butane)/k_Q(neopentane) and k_Q(isobutane)/k_Q(neopentane) shown in Fig. 3, the ratios of k_s/k_p and k_t/k_p at various temperatures can be calculated. In Fig. 4, the Arrhenius plots for k_s/k_p and k_t/k_p are shown. These Arrhenius plots give straight lines. The differences in the activation energies for k_s and k_p and for k_t and k_p were found to be 4.6±0.4 and 7.5±0.5 kJ mol^{-1} respectively.

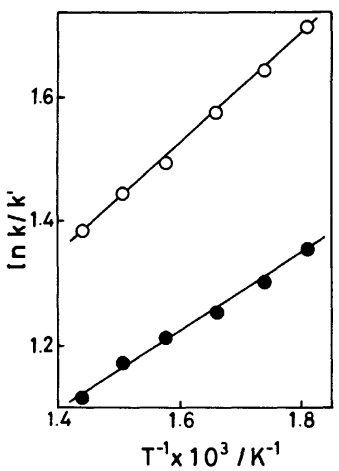

Fig. 4. Arrhenius plots for k_s/k_p (●) and k_t/k_p (○).

Since the imprisonment effect is nearly neglected below 606 K, as has been mentioned above, the quenching-rate constant, k_Q, can be calculated from the $k_Q\tau$ value using the natural lifetime as τ. In Table 2, the quenching-rate constants(k_Q') per C-H bond for neopentane and ethane, which have only primary C-H bonds, are shown. The optimized expressions for the rate constants(k_Q'), in the units cm^{3}molecule^{-1}s^{-1}, are:

$$k_Q'(\text{neopentane}) = (1.9 \pm 0.3) \times 10^{-10} \times \exp\{(-18.7 \pm 1.6)\text{kJ mol}^{-1}/RT\} \tag{12}$$

$$k_Q'(\text{ethane}) = (2.5 \pm 0.3) \times 10^{-10} \times \exp\{(-19.0 \pm 2.0)\text{kJ mol}^{-1}/RT\} \tag{13}$$

The activation energies for neopentane and ethane are in good agreement with each other. The activation energy for a primary C-H bond is determined to be 18.9±1.8 kJ mol^{-1}. The ratio (1.32) of the frequency factors of k'_Q for ethane and neopentane is approximately equal to the ratio (1.29) of the relative velocities for Zn*+ethane and Zn*+neopentane. This is in agreement with the prediction from the simple collision theory. Equations 12 and 13 show that the quenching cross-sections per C-H bond for neopentane and ethane are in agreement with each other at every temperature.

As has been mentioned above, the imprisonment effect below 605 K is very small and was neglected in the above treatment. If the imprisonment effect is taken into account, that is, if the effective lifetime of the excited zinc atoms shown in Table 3 is used, somewhat smaller quenching rate constants (k_Q'') are obtained from the $k_Q\tau$ values (Table 2). The activation energies calculated from these rate constants below 636 K are a little smaller (13.1±1.8 kJ mol^{-1} for neopentane and 14.8±1.8 kJ mol^{-1} for ethane) than those obtained using the natural lifetime.

Since the rate constant for neopentane calculated using the effective lifetime shown above decreases with the temperature above 636 K, and since the difference in the activation energies obtained from k_Q'' for ethane and neopentane is larger than that obtained from k_Q', and since the ratio of the frequency factors (1.8) of k_Q'' for ethane and neopentane is considerably larger than that predicted from the simple collision theory, the imprisonment lifetime shown in Table 3 does not seem to be precise (it may be too large at higher temperatures). The above estimation of the imprisonment lifetime may include some uncertainty because of the effect of collision broadening, the presence of the isotopes of the zinc atom, and the difference in the experimental conditions from the ideal conditions of infinite slub and uniform external excitation. Therefore, the activation energies calculated from k_Q'' seem to be lower limits, whereas those estimated from k_Q' (by neglecting the imprisonment effect) are upper limits. The activation energy for the

Table 4. Potential Energies of Activation as Calculated by the BEBO Method

Parameter	V_a/kJ mol^{-1}		
	Primary	Secondary	Tertiary
Old	7.5	4.9	3.7
Old modified[a)]	18.4	14.6	12.0
Gilliom's	6.4	3.9	2.3
Gilliom's modified[a)]	15.0	11.1	8.9
Experimental	16.5±2.5	11.9±2.5	9.0±2.5

a) The correction for zero-point energy is made using the calculated frequencies of the transition state and the stretching frequency of the reactant (Ref. 12).

primary C–H bond was concluded to be 16.5±2.5 kJ mol^{-1}. From this value and the values of the differences in the activation energies for k_p, k_s, and k_t shown above, the activation energies for secondary and tertiary C–H bonds were calculated; they are listed in Table 4.

Strausz et al.[8] calculated the potential energies of activation for the mercury-photosensitized decomposition of alkanes by the BEBO method by assuming the following model:

$$RH + Hg^* \longrightarrow R\text{--}H\text{--}Hg \longrightarrow R + HHg.$$

Since the repulsive triplet term was neglected, they pointed out that their calculation was somewhat oversimplified and that only the relative values were significant.

We have also applied the BEBO method to the quenching of excited zinc atoms by alkane by assuming the following model:

$$RH + Zn^* \longrightarrow R\text{--}H\text{--}Zn \longrightarrow R + HZn.$$

We could thus qualitatively interpret the relative decrease in the quenching cross section with an increase in the C–H bond strength.[1]

In the BEBO formulation, the value of the potential energy of activation, V_a, is obtained by finding the value of n, the bond order of the breaking C–H bond, that causes V to reach its maximum value, subject to the constraint that the sum of the bond orders of the forming Zn–H bond and of the breaking C–H bond is unity.[9]

$$V = D_{DH}(1-n^p) - D_{ZnH}(1-n)^q + C_1 D_{ZnC} B(n-n^2)^\gamma\{1+B(n-n^2)^\gamma\} \quad (14)$$

where:

$$B = C_2 \exp\{-\beta(R_{CH} + R_{ZnH} - R_{ZnC})\} \quad (15)$$

$$\gamma = C_3\beta \quad (16)$$

The BEBO parameters p and q are given by:

$$p = C_3 \ln(D_{HC}/D_{HeNe})(R_{HeNe} - R_{HC}) \quad (17)$$

$$q = C_3 \ln(D_{ZnH}/D_{KrHe})/(R_{KrHe} - R_{ZnH}) \quad (18)$$

In these expressions, C_1 is the factor of the anti-Morse function (the old, C_1=1, old-modified, C_1=2, as suggested by Mayer and Schieler,[10] Gilliom's, C_1=1 and Gilliom's modified parameters, C_1=2,[11] were used) C_2 is 0.5 for the old BEBO method and is 0.45 for the Gilliom's method, C_3 is the Pauling constant (Gilliom recommended C_3=0.28 rather than the older value of 0.26), β is the Morse-function parameter for ZnC, and D and R are the normal single-bond energy (corrected for zero-point energy) and the distance for the indicated molecule respectively.

Table 4 gives the potential energies of activation as calculated by the BEBO method using the parameters shown above. Table 4 shows that the old modified and Gilliom's modified methods, which are generally used for the hydrogen-atom abstraction by such triplet species as O(^{3}P), give activation energies which are almost within the limits of experimental error.

Gilliom[11] compared the activation energies calculated by the BEBO method with the experimental values for about 100 reactions and pointed out that the BEBO method in its original form gives an average error of 6.4 kJ mol^{-1}, while his method affords an average error of 5.4 kJ mol^{-1}. Thus, the agreement between experimental and calculated activation energies for the present study seems to be good considering the experimental error and the empiricism of the BEBO method.

As has been mentioned above, the experimental activation energies for the quenching of Zn(^3P_J) by alkanes are in good agreement with those calculated by the BEBO method by assuming this model: RH+Zn*→R--H--Zn→R+H-Zn. This strongly suggests that, in the initial stage of zinc-photosensitized reaction of alkanes, the hydrogen-atom abstraction by excited zinc atoms from alkane molecules occurs. In order to make sure of this point, further studies are in progress of the isotope effect on the quenching rate and of the zinc-photosensitized decomposition of ethane and propane based on product analysis.

References

1) S. Yamamoto and N. Nishimura, *Bull. Chem. Soc. Jpn.*, **55**, 1395 (1982).

2) S. Yamamoto, T. Takei, N. Nishimura, and S. Hasegawa, *Bull. Chem. Soc. Jpn.*, **53**, 860 (1980).

3) F. W. Byron, M. N. McDermott, R. Novick, B. W. Perry, and E. Saloman, *Phys. Rev. A*, **134**, 47 (1964).
4) E. Milne, *J. Londin. Math. Soc.*, **1**, 1 (1926).
5) E. W. Samson, *Phys. Rev.*, **40**, 940 (1932).
6) A. C. G. Mitchell and M. W. Zemansky, "Resonance Radiation and Excited Atoms," Cambridge University Press, London (1971), Chap. 3.
7) R. P. Blickensderfer, W. H. Breckenridge, and J. Simons, *J. Phys. Chem.*, **80**, 653 (1976).
8) H. Guning, J. Campbell, H. Sandhu, and O. P. Strausz, *J. Am. Chem. Soc.*, **95**, 746 (1973).
9) H. S. Johnston and C. Parr, *J. Am. Chem. Soc.*, **85**, 2544 (1963).
10) S. W. Mayer and L. Schieler, *J. Phys. Chem.*, **72**, 2628 (1968).
11) R. D. Gilliom, *J. Am. Chem. Soc.*, **99**, 8399 (1977).

 © 1988 The Chemical Society of Japan Bull. Chem. Soc. Jpn., 61, 775—781 (1988)

Synthetic, Spectroscopic and X-Ray Crystallographic Studies of Bivalent Metal Complexes with Amino Acids Having a Thiazolidine Ring. I. Properties of Bivalent Metal Complexes with (*S*)-4-Thiazolidinecarboxylic Acid and the Structure of Chloro((*S*)-4-thiazolidinecarboxylato)((*S*)-thiazolidinium-4-carboxylate)zinc(II)

Makoto NAGASE, Yasuhiko YUKAWA,† Yoshie INOMATA,* and Toshio TAKEUCHI
Department of Natural Sciences, Faculty of Science and Technology, Sophia University, 7-1, Kioi-cho, Chiyoda-ku, Tokyo 102
(Received July 22, 1987)

Complexes of five bivalent metals with (*S*)-4-thiazolidinecarboxylic acid($\overline{CH_2\text{-}S\text{-}CH_2\text{-}NH\text{-}CH}$-COOH) have been prepared by three methods and characterized by means of infrared absorption, reflection spectra, magnetic susceptibility, thermal analysis, powder X-ray patterns, and single crystal X-ray diffraction. Two types of complexes were found. The first type[A] included $ML_2 \cdot nH_2O$ (M=Co(II), Ni(II), Cu(II), Zn(II), Cd(II); L=(*S*)-4-thiazolidinecarboxylate anion) and ZnClL(HL) was the second type[B]. In A-type complexes, the ligand coordinates to the metal with a nitrogen atom and an oxygen atom. From the results of single-crystal X-ray diffraction studies, the second type-B ZnClL(HL) was found to be orthorhombic, with the space group $P2_12_12_1$; a=9.719(2), b=22.194(4), c=5.8537(5) Å, U=1262.6(4) Å^3, Z=4, D_m=1.91 Mg m^{-3}, D_x=1.93 Mg m^{-3}, and μ(Mo $K\alpha$)=25.3 cm^{-1}. Block-diagonal least-squares refinements have led to a final R value of 0.045. The zinc atom is penta-coordinated, being ligated with one carboxylate oxygen atom of (*S*)-thiazolidinium-4-carboxylate, which has a zwitter ion structure, two carboxylato oxygen atoms and one nitrogen atom of (*S*)-4-thiazolidinecarboxylate anion, and a chloride atom. The structure comprises one-dimensional polymers by the carboxylate oxygen atom of this anion-type ligand. The plane extends in the direction of c-axis. In neither the A- nor the B-type complexes does the ligand coordinate to a metal with a sulfur atom.

In our laboratory, we have been investigating the syntheses, spectral properties[1] and crystal structures[2,3] of the metal complexes of various amino acids and their derivatives. This study is one part of that program. (*S*)-4-Thiazolidinecarboxylic acid is a very interesting ligand, since it has four coordination atoms. They are the sulfur and nitrogen atoms of the thiazolidine ring and two oxygen atoms of the carboxyl group.

Recently, this amino acid has been reported to be a new type of anticancer agent which can induce a reverse transformation.[4–7] Thus, many studies have been reported about the stability constants,[8–11] ESR[12] and NMR spectra[13,14] for metal complexes with this ligand in aqueous solution.

The crystal structures of copper(II),[15] zinc(II),[13] and cobalt(III) complexes[16] in the solid state have been reported and their IR spectra discussed.[8]

In the present work, we prepared bivalent metal complexes of (*S*)-4-thiazolidinecarboxylic acid (HL) and systematically investigated their spectral and thermal properties as well as magnetic susceptibilities in the solid state. We then determined the structure of ZnClL(HL) by the single-crystal X-ray diffraction method.

Experimental

Preparation of Compounds. Cobalt(II)-A complex was prepared by adding 0.01 mol cobalt(II) hydroxide to an aqueous solution containing 0.02 mol (*S*)-4-thiazolidinecarboxylic acid. The mixed solution was stirred and concentrated to a small volume in a water bath under 60 °C. The pink precipitate which formed was filtered and washed with water.

Nickel(II)-A, cadmium(II)-A, and zinc(II)-A complexes were prepared by the same method as used for the cobalt(II)-A complex. Zinc(II)-A complex was recrystallized from water.

Copper(II)-A complex was prepared by adding 0.01 mol copper(II) hydroxide to an ethanol solution containing 0.02 mol of this ligand in suspension. This solution was evaporated at room temperature. The resulting complex was recrystallized from methanol.

Zinc(II)-B complex was prepared by adding 0.01 mol of zinc(II) chloride to an aqueous solution containing 0.02 mol of the ligand. The mixed solution was stirred in a water bath, then concentrated to a small volume below 60 °C and filtered. The obtained crude crystals were recrystallized by water under 60 °C. All complexes were dried in vacuo.

Deuterated complexes were obtained by recrystallization in D_2O.

Reflection Spectra. Reflection spectra from 800 to 2000 nm were obtained with a Japan Spectroscopic Co. UVIDEC-590 spectrophotometer. The spectra from 370 to 800 nm were obtained with a Hitachi 624 digital spectrophotometer. Both spectrophotometers were equipped with a standard reflection attachment and a magnesium oxide standard.

† Present address: Division of Chemistry, General Education Department, Niigata University, 8050, Ikarashi, Nino-cho, Niigata 950-21.

Magnetic Studies. The magnetic moments of these complexes were obtained for the solid samples by the Gouy method, using $Hg[Co(SCN)_4]$ as the calibration standard at 23.5 °C. However, copper(II)-A type complex was measured by the Faraday method.

Infrared and Far Infrared Absorption Spectra. Infrared absorption spectra from 4000 to 400 cm^{-1} were measured using a Hitachi spectrophotometer, type EPI-G_2. Far-infrared absorption spectra from 700 to 200 cm^{-1} were measured using a Hitachi spectrophotometer, type EPI-L. Samples were prepared as KBr disks and Nujol mulls. The spectra were calibrated with polystyrene and atmospheric water vapor.

Thermal Analysis. Simultaneous TG-DTA measurements were carried out with a Rigaku Denki M8075, using a sample weight of about 9 mg in each operation. The heating rate was 10 °C min^{-1}, under static air, using α-alumina as a reference.

Powder X-Ray Diffraction. Powder X-ray diffraction patterns were obtained with a Rigaku RAD IIA powder X-ray diffractometer, using Cu $K\alpha$ radiation over a 2θ range from 50° to 5°.

Single-Crystal X-Ray Analysis. The reflection intensities were collected by the θ-2θ scan technique ($2\theta<70°$) on a Rigaku AFC-6A automated four-circule diffractometer. The intensities were corrected for Lorenz and polarization factors; however, no corrections were made for absorption and extinction $\mu r(=0.51)$. Independent reflections (2378) with $|F_o|>3\sigma(|F_o|)$ were used for a structure determination. All calculations were carried out on a HITAC M-680H computer at the Computer Center of the University of Tokyo, using a local version of UNICS.[17] The scattering factors were taken from Ref. 18.

The structure was solved by the heavy-atom method and refined by a block-diagonal least-squares method. The positions of the zinc and chlorine atoms were obtained from a three-dimensional Patterson map, while the positions of all the other non-hydrogen atoms were successively located by Fourier syntheses. Since the positions of hydrogen atoms were obtained by difference-Fourier syntheses, all of the positions were calculated and fixed. Their isotropic temperature factors were all assumed to be 3.0 $Å^2$. The weighting scheme was $W=1/[\{\sigma(|F_o|)\}^2+(0.02\times|F_o|)^2]$. In the last cycle of the refinement with anisotropic temperature factors for all non-hydrogen atoms, all the parameter shifts were less than one-third of the corresponding standard deviations. The final R values ($R=\sum||F_o|-|F_c||/\sum|F_o|$) was 0.045.

Results and Discussion

The results of elemental analyses and infrared spectra suggest that there are two types of complexes: A and B types. A type is $ML_2\cdot nH_2O$ (M=Co(II), Ni(II), Cu(II), Zn(II), Cd(II)); HL=(*S*)-4-thiazolidinecarboxylic acid; n=0, 2). B type is ZnClL(HL).

Reflection Spectra and Magnetic Moments. The results obtained from elemental analyses, reflection spectra and magnetic moment calculations are listed in Table 1. Each peak of these reflection spectra is due to a d-d transition. The magnetic moment of the cobalt(II)-A complex is within the range expected for high-spin complexes (4.1—5.2 B M for cobalt(II).[19] For nickel(II)-A and copper(II)-A complexes the magnetic moments are within the ranges expected for two unpaired electrons (2.8—4.0 B M for nickel(II)[19]) and for one unpaired electron (1.7—2.2 B M for copper(II)[19]), respectively.

Infrared Absorption Spectra. The infrared spectra data are listed in Table 2. The assignments of observed spectra have been made by referring to L-proline,[20] 4-hydroxy-L-proline[1] and their metal complexes,[1,20] and zinc(II) complex with (*S*)-4-thiazolidinecarboxylic acid.[8]

(*S*)-4-Thiazolidinecarboxylic Acid: X-Ray analyses showed that this amino acid has a zwitter ion structure.[21,22] Therefore, some absorption bands which shift to low-frequency regions on deuteration were assigned to NH_2^+ stretching and bending vibrations. The antisymmetric and symmetric stretching vibrations of the carboxyl group appear at 1625 and 1387 cm^{-1}, respectively.

A Type Complexes: According to the X-ray

Table 1. Analytical Data and Physical Properties

Complex	Found (Calcd)/% H	C	N	M	Cl	Magnetic moment μ_{eff}/BM	Reflection spectra λ/nm
CoL_2	3.70 (3.74)	29.19 (29.72)	8.58 (8.67)	17.6 (18.23)	— (0)	4.59	1555, 1160, 543, 500, 467
$NiL_2\cdot 2H_2O$	4.43 (4.49)	26.13 (26.76)	7.63 (7.80)	16.7 (16.35)	— (0)	3.14	1730, 1010, 752, 640, 478, 389
(A) CuL_2	3.66 (3.69)	28.92 (29.30)	8.47 (8.55)	19.2 (19.38)	— (0)	1.76	1725, 1560, 655
$ZnL_2\cdot 2H_2O$	4.35 (4.41)	25.90 (26.27)	7.53 (7.66)	18.0 (17.88)	— (0)	dia	—
CdL_2	3.19 (3.21)	25.30 (25.50)	7.44 (7.44)	29.7 (29.84)	— (0)	dia	—
(B) ZnClL(HL)	3.51 (3.58)	26.09 (26.24)	7.60 (7.65)	18.0 (17.86)	9.96 (9.68)	dia	—

HL=(*S*)-4-thiazolidinecarboxylic acid.

Table 2. Assignments of Infrared Absorption Spectra Related with Metal-Ligand Bonds (cm^{-1})[a]

Ligand	Co(II)-A	Ni(II)-A	Cu(II)-A	Zn(II)-A	Cd(II)-A	Zn(II)-B	Assignment
	3225 s	3195 s	3250 s 3197 sh	3190 s	3265 s	3228 m	NH str.
3040 m						3085 m 3025 m 1683 sh 1635 sh	NH_2^+ str.
1625 vs	1609 vs	1599 vs	1637 vs	1603 vs	1592 vs	1624 vs	COO^- asym. str.
1547 w						1583 sh	NH_2^+ scissors
1463 w						1457 w	NH_2^+ wagging
1387 s	1404 w	1405 s	1362 s	1402 s	1407 s	1403 s	COO^- sym. str.
862 s						867 m	NH_2^+ rocking
751 m		736 w	748 w	732 w		749 w	COO^- scissors
623 s	638 w 628 w	635 w		627 s	626 w	634 s	C-S str.
592 w	583 sh				593 vw	604 w	COO^- wagging
462 m		445 b	440 w	445 w	421 w	460 w	COO^- rocking
	320 m	325 vwb	320 m		324 s	328 m	M-O str.

a) Abbreviations: s=strong; m=medium; w=weak; v=very; sh=shoulder; b=broad.

analysis of Tatarowski et al. diaquabis((*S*)-4-thiazolidinecarboxylato)zinc(II) has an octahedral configuration with the two water molecules occupying cis positions and with nitrogen and oxygen atoms in the ligands.[13]

Zinc(II)-A complex has a few absorption bands which shift to lower-frequency regions on deuteration. These were assigned to NH stretching and bending vibrations. The antisymmetric stretching vibration of the carboxyl group shifts to a lower-frequency region compared with that of the ligand, and the symmetric stretching vibration shifts to a higher-frequency region. The C-S stretching vibration was observed at the same position as that of the free ligand. Therefore, in this complex, the zinc atom is not coordinated through a sulfur atom, but is coordinated through an oxygen atom of the carboxyl group and a nitrogen atom of the thiazolidine ring; this agrees with Tatarowski's result.[13]

Bigoli et al. have investigated the structure of *trans*-diaqua((*S*)-4-thiazolidinecarboxylato)((*S*)-4,5-dihydro-4-thiazolecarboxylato)copper(II) by a single-crystal X-ray analysis.[15] They reported that part of the thiazolidine ligand was oxidized during the reaction. Two different ligands were involved in the complex and the coordination polyhedron around copper(II) atom was a distorted tetragonal bipyramid with the apices of the elongated axis occupied unsymmetrically by water molecules. Since the results of the elemental analyses of copper(II)-A complex show that this complex has two molecules of (*S*)-4-thiazolidinecarboxylate ion for one copper atom, its structure must be different from that of the copper(II) complex which was determined by Bigoli et al.

The absorption bands due to the vibration of the carboxyl and the amino groups for cobalt(II)-A, nickel(II)-A, copper(II)-A, and cadmium(II)-A complexes appear in the same region as those of the zinc(II)-A complex (as shown in Table 2). Therefore, the metal is coordinated through one oxygen and one nitrogen atom for A-type complexes.

From 500 to 200 cm^{-1}, absorption bands which cannot be observed in the ligand appear in cobalt(II)-A, copper(II)-A, cadmium(II)-A, and zinc(II)-B complexes. These are assigned to the M-O stretching vibrations by comparing these spectra with those of metal complexes with L-proline[20] and 4-hydroxy-L-proline.[1] For nickel(II)-A and zinc(II)-A complexes, the corresponding bands could not be clearly observed due to water molecules.

The powder X-ray diffraction pattern of the cobalt(II)-A complex is similar to zinc(II)-A in crystal structure.

B Type Complex ZnClL(HL): The infrared absorption spectra of zinc(II)-B complex is different from that of zinc(II)-A complex. In zinc(II)-B complex, some absorption bands due to NH_2^+ vibrations could be observed in the same region as in the free ligand.

The bands which split at about 1600 cm^{-1} were assigned to the COO^- antisymmetric stretching vibrations of (*S*)-4-thiazolidinecarboxylate anion and of (*S*)-thiazolidinium-4-carboxylate, which has a zwitter ion structure, by making a comparison with the spectra of the free ligand and of zinc(II)-A.

The results of elemental analyses suggest that zinc(II)-B complex has two types of this ligand: the first is (*S*)-4-thiazolidinecarboxylate anion and the second is (*S*)-thiazolidinium-4-carboxylate, which has a zwitter ion structure.

Structure of ZnClL(HL). Crystal data are given in Table 3. The final atomic parameters are listed in Table 4.[23] The bond lengths and bond angles are shown in Tables 5 and 6, respectively. A perspective

drawing of the complex, together with the numbering scheme of the non-hydrogen atoms, is shown in Fig. 1. The projection of the unit cell along the c-axis is shown in Fig. 2.

As expected from the infrared absorption spectra and the elemental analysis, the complex has two types of ligands: one is (*S*)-thiazolidinium-4-carboxylate, which assumes a zwitter ion structure, and the other is (*S*)-4-thiazolidinecarboxylate anion.

The structure of the complex consists of a one-dimensional polymer chain bridged by the carboxylate group of the anionic ligand. One carboxylate

Table 3. Crystal Data

$ZnCl(C_4H_6NO_2S)(C_4H_7NO_2S)$	
F. W.	366.18
Orthorhombic	
space group	$P2_12_12_1$
a/Å	9.719(2)
b/Å	22.194(4)
c/Å	5.8537(5)
U/Å^3	1262.6(4)
Z	4
D_m/Mg m^{-3}	1.91
D_x/Mg m^{-3}	1.93
μ(Mo $K\alpha$)/cm^{-1}	25.3

Table 5. Interatomic Distances of ZnClL(HL) with the Estimated Standard Deviations in Parentheses

Interatomic distance	l/Å	Interatomic distance	l/Å
Zn-Cl	2.369(1)	S (2)-C(5)	1.821(5)
Zn-O(1)	2.017(3)	S (2)-C(7)	1.818(5)
Zn-O(3)	2.218(3)	N(1)-C(1)	1.506(6)
Zn-N(2)	2.071(4)	N(1)-C(2)	1.496(6)
Zn-O(4)^{I}	1.968(3)	N(2)-C(5)	1.453(7)
O(1)-C(4)	1.261(5)	N(2)-C(6)	1.471(5)
O(2)-C(4)	1.225(5)	C(2)-C(3)	1.534(6)
O(3)-C(8)	1.239(5)	C(2)-C(4)	1.534(6)
O(4)-C(8)	1.259(5)	C(6)-C(7)	1.522(6)
S (1)-C(1)	1.788(6)	C(6)-C(8)	1.536(5)
S (1)-C(3)	1.800(5)	O(1)···N(1)	2.658(5)

Key to symmetry operation: I. 0.5−x, −y, −0.5+z.

Table 4. Final Positional Parameters (×10^4 for Non-Hydrogen Atoms; ×10^3 for Hydrogen Atoms) and Equivalent Isotropic Temperature Factors (B_{eq}/Å^2)[a] for ZnClL(HL) with the Estimated Standard Deviations

Atom	x	y	z	B_{eq}/Å^2
Zn	1205.9(5)	−849.1(2)	1551.0(8)	1.48
Cl	−475.1(11)	−1404.7(5)	−487.7(20)	2.08
S(1)	1853.5(16)	−3122.1(6)	5813.0(28)	3.22
S(2)	−1264.2(14)	289.9(6)	6391.7(24)	2.81
O(1)	1723 (3)	−1458 (1)	3960 (5)	2.00
O(2)	3405 (4)	−1897 (2)	1969 (6)	2.52
O(3)	2400 (3)	−167 (1)	3485 (6)	1.89
O(4)	2360 (3)	819 (1)	4180 (5)	1.99
N(1)	2230 (4)	−2068 (2)	7775 (6)	1.67
N(2)	−252 (4)	−232 (2)	2641 (7)	1.72
C(1)	1602 (5)	−2673 (2)	8313 (10)	2.57
C(2)	3265 (4)	−2113 (2)	5890 (7)	1.66
C(3)	3529 (5)	−2786 (2)	5495 (9)	2.54
C(4)	2749 (4)	−1799 (2)	3718 (7)	1.55
C(5)	−648 (5)	−387 (2)	4961 (9)	2.39
C(6)	332 (4)	379 (2)	2688 (7)	1.55
C(7)	−570 (5)	778 (2)	4179 (10)	2.55
C(8)	1827 (4)	332 (2)	3520 (7)	1.45
H(31)[b]	386 (6)	−285 (3)	393 (10)	
H(32)	416 (6)	−298 (2)	663 (10)	
H(11)	68 (6)	−262 (2)	864 (10)	
H(12)	199 (6)	−287 (2)	970 (10)	
H(21)	412 (6)	−189 (2)	642 (10)	
H(N11)	274 (6)	−195 (2)	908 (9)	
H(N12)	152 (6)	−182 (2)	750 (11)	
H(N21)	−97 (6)	−23 (2)	179 (11)	
H(71)	−142 (6)	93 (2)	356 (9)	
H(72)	9 (6)	115 (2)	478 (10)	
H(51)	14 (6)	−54 (2)	591 (10)	
H(52)	−148 (6)	−65 (3)	475 (10)	
H(61)	35 (6)	53 (2)	126 (10)	

a) The equivalent isotropic temperature factors for non-hydrogen atoms were computed using the following expression: $B_{eq}=4/3(B_{11}a^2+B_{22}b^2+B_{33}c^2+B_{12}ab\cos\gamma+B_{13}ac\cos\beta+B_{23}bc\cos\alpha)$. The B_{ij}'s are defined by: $\exp[-(h^2B_{11}+k^2B_{22}+l^2B_{33}+2klB_{23}+2hlB_{13}+2hkB_{12})]$. b) The numbering scheme of hydrogen atoms is based on the number of the atom attached to the hydrogen atom.

Table 6. Bond Angles of ZnClL(HL) with the Estimated Standard Deviations in Parenthese

Bond angle	ϕ/°	Bond angle	ϕ/°
Cl-Zn-O(1)	100.09(9)	C(5)-N(2)-C(6)	107.6(4)
Cl-Zn-O(3)	166.64(9)	S (1)-C(1)-N(1)	105.7(3)
Cl-Zn-N(2)	91.6(1)	N(1)-C(2)-C(3)	106.7(3)
O(1)-Zn-O(3)	88.3(1)	N(1)-C(2)-C(4)	111.2(3)
O(1)-Zn-N(2)	113.5(1)	C(3)-C(2)-C(4)	111.8(3)
O(3)-Zn-N(2)	75.5(1)	S (1)-C(3)-C(2)	103.7(3)
$O(4)^I$-Zn-Cl	98.7(1)	O(1)-C(4)-O(2)	127.7(4)
$O(4)^I$-Zn-N(2)	132.8(1)	O(1)-C(4)-C(2)	116.0(4)
$O(4)^I$-Zn-O(3)	88.1(1)	O(2)-C(4)-C(2)	116.3(4)
$O(4)^I$-Zn-O(1)	109.8(1)	S (2)-C(5)-N(2)	108.8(3)
C(1)-S(1)-C(3)	88.7(3)	N(2)-C(6)-C(7)	109.0(3)
C(5)-S(2)-C(7)	92.4(2)	N(2)-C(6)-C(8)	108.0(3)
Zn-O(1)-C(4)	121.4(3)	C(7)-C(6)-C(8)	113.8(4)
Zn-O(3)-C(8)	112.6(3)	S (2)-C(7)-C(6)	106.0(3)
C(1)-N(1)-C(2)	111.6(3)	O(3)-C(8)-O(4)	126.0(4)
Zn-N(2)-C(5)	108.3(3)	O(3)-C(8)-C(6)	118.7(3)
Zn-N(2)-C(6)	110.6(2)	O(4)-C(8)-C(6)	115.4(3)

Key to symmetry operation: I. 0.5−x, −y, −0.5+z.

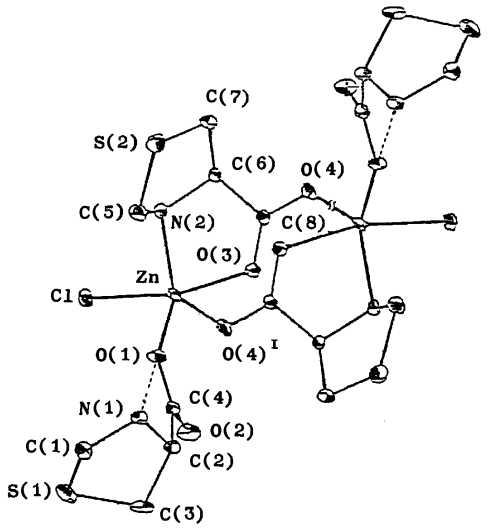

Fig. 1. The perspective drawing of ZnClL(HL) (zinc(II)-B) and the numbering scheme of non-hydrogen atoms.
-----: Hydrogen bonding.

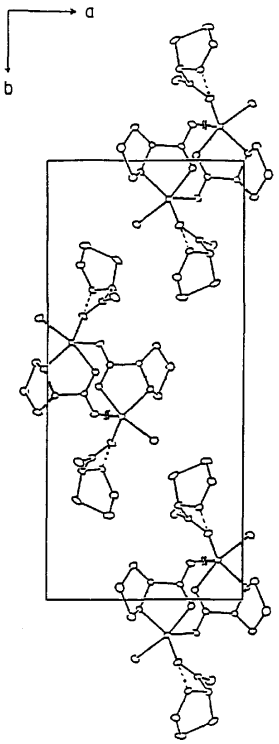

Fig. 2. The molecuar packing of ZnClL(HL) (zinc-(II)-B) along the c axis. -----: Hydrogen bonding.

oxygen atom of the anionic ligand is coordinated to the zinc atom and the other is coordinated to the neighboring zinc atom to form a Zn-O-C-O-Zn bridge. This polymer chain extends in the direction of the c-axis.

The zinc atom is surrounded by five atoms: one carboxylate oxygen atom O(1) of the non-charged ligand, one carboxylate oxygen atom O(3) and one nitrogen atom N(2) of the anionic ligand, one carboxylate oxygen atom $O(4)^I$ of the anionic ligand in the neighboring molecule, and one chlorine atom. It is novel that the same amino acid ligands have two types in one complex molecule.

This complex is in a distorted penta-coordinated trigonal bipyramidal geometry, which has a triangular plane formed by O(1), N(2), and $O(4)^I$. The angle of Cl-Zn-O(3) is 166.64(9)°. This angle is smaller than ideal bond angle 180°.

In this geometry, the plane formed by Zn, Cl, N(2), and O(3) is a fairly flat plane, as shown in Table 7. All other least-squares planes are listed in Table 7.

The bond length of Zn-O(3), 2.218(3) Å is longest among the three Zn-O bonds; Zn-O(3), Zn-O(1) and $Zn-O(4)^I$. The bond lengths of Zn-O(1) and $Zn-O(4)^I$ are shorter than Tatarowski's results[13] (Zn-O: 2.137(8)

and 2.172(8) Å).

The bond length of Zn–N(2), 2.071(4) Å and the bond angle of O(3)–Zn–N(2) 75.5(1)° are smaller than Tatarowski's results:[13] Zn–N: 2.149(12) Å and 2.134(12) Å, O–Zn–N: 78.1(4)°.

There are some differences in the bond lengths of the non-charged ligand and the anionic ligand, as shown in Table 5.

Let's compare the bond lengths of this complex with that of the free ligand determined by Chacko:[22] C(2)–C(4), C(6)–C(8), C(3)–S(1), and C(5)–N(2) are shorter than the corresponding bond lengths of the free ligand, while S(2)–C(5) is longer than that of the free ligand.

Table 7. Least-Squares Planes and the Deviations of Atoms (l/Å) in ZnClL(HL)

Plane(1) [O(4)^{I}, Zn, N(2), O(1)]
$-0.6442X-0.5692Y-0.5109Z+0.3362=0$
O(4)^{I}, −0.0369; Zn, 0.1896; N(2), −0.0023; O(1), −0.0854

Plane(2) [O(4)^{I}, Zn, Cl, O(3)]
$-0.3915X+0.7936Y-0.4657Z+2.2329=0$
O(4)^{I}, 0.0095; Zn, −0.1446; Cl, 0.0721; O(3) 0.0760

Plane(3) [O(1), Zn, Cl, O(3)]
$-0.7577X+0.2703Y+0.5940Z+0.7447=0$
O(1), −0.0227; Zn, −0.1139; Cl, 0.0816; O(3), 0.0887

Plane(4) [N(2), Zn, Cl, O(3)]
$0.1381X+0.5548Y-0.8205Z+1.5836=0$
N(2), −0.0048; Zn, −0.0448 Cl, 0.0247; O(3), 0.0269

Plane(5) [N(1), C(1), C(2), C(3), S(1)]
$-0.6063X+0.3747Y-0.7014Z+6.3362=0$
N(1), 0.1087; C(1), −0.2448; C(2), 0.2359; C(3), −0.3173; S(1), 0.2595

Plane(6) [C(5), C(6), C(7), S(2)]
$-0.8269X+0.0211Y-0.5619Z+1.0038=0$
C(5), −0.1256; C(6), −0.1296; C(7), 0.1242; S(2), −0.0689; N(2), 0.3264

Thermal Analysis and Powder X-Ray Diffraction. The reaction temperature range and the mass loss obtained from TG and DTA curves of complexes are summarized in Table 8. Nickel(II)-A and zinc(II)-A complexes give endothermic reactions below about 180 °C. In these reactions, the percentages of the mass loss for both complexes agree with the values which were calculated by assuming that two molecules of water are released in these steps. Copper(II)-A and zinc(II)-B complexes give two steps of exothermic reactions with a mass loss, as shown in Table 8.

The powder X-ray patterns of the residual materials yielded by the final exothermic reactions are very similar to those of the corresponding metal oxide, except for cadmium (II)-A complex among the A-type complexes. Cadmium(II)-A complex seems to become cadmium(II) sulfide through an exo thermic reaction.

For the zinc(II)-B complex the data suggest that in the first exothermic reaction at 206 °C this complex becomes $ZnCl_2$ and ZnO, while in the second at 465 °C only $ZnCl_2$ sublimates.

$$2ZnClL(HL) \xrightarrow[\text{ca. } 206\,^{\circ}C]{\text{heat}} ZnCl_2 + ZnO \xrightarrow[\text{ca. } 465\,^{\circ}C]{\text{heat}} ZnO$$

The percentage of the mass loss calculated from this assumption is in good agreement with the experimental value, as shown in Table 8.

The authors wish to express their thanks to Professor Akira Ouchi of The University of Tokyo and Associate Professor Mamoru Shimoi of Tohoku University for X-ray diffractometer measurements. They would also like to thank Dr. F. S. Howell and Mr. H. Yamaguchi of Sophia University for their helpful advice and for correcting the manuscript.

Table 8. Temperature Range of Decomposition and Mass Loss

Complex	Temperature range/°C	Thermal reaction	Mass loss/%	
			Obsd	Calcd
Co(II)-A	270—297	exo		
	423—558	exo	74.3	77.0*
Ni(II)-A	116—180	endo	9.1	10.0
	246—582	exo	72.0	79.2*
Cu(II)-A	150—285	exo		
	357—459	exo	75.0	75.8*
Zn(II)-A	90—150	endo	8.8	9.8
	236—621	exo	74.1	77.5*
Cd(II)-A	200—520	exo		
	520—555	exo	57.4	61.7**
Zn(II)-B	206—228	exo		
	465—600	exo	87.8	88.9*

*as metal oxide. **as metal sulfide.

References

1) Y. Inomata, T. Takeuchi, and T. Moriwaki, *Inorg. Chim. Acta,* **68**, 187 (1983).
2) Y. Yukawa, Y. Inomata, T. Takeuchi, M. Shimoi, and A. Ouchi, *Bull. Chem. Soc. Jpn.*, **55**, 3135 (1982).
3) S. Itoh, Y. Yukawa, Y. Inomata, and T. Takeuchi, *Bull. Chem. Soc. Jpn.*, **60**, 899 (1987).
4) T. Puck, *Proc. Natl. Acad. Sci. U.S.A.*, **74**, 4491 (1977).
5) M. Gosalves, C. Vivero and I. Alvarez, *Biochem. Soc. Trans.*, **7**, 191 (1979).
6) M. Gosalves, *Abstract, Proc. AACR San Diego,* **528**, 132 (1980).
7) M. Gosalves, *Proc. Am. Assoc. Cancer Res.*, **20**, 17 (1979).
8) Z. X. Huang, P. M. May, and D. R. Williams, *Inorg. Chim. Acta,* **56**, 41 (1981).
9) Z. X. Huang, P. M. May, and D. R. Williams, *Eur. J. Cancer Clin. Oncol.*, **17**, 1151 (1981).
10) P. Ramesh, B. V. Kumar and M. G. Reddy, *Indian J. Chem.*, **22A**, 822 (1983).
11) Z. X. Huang, H. S. Al-Falahi, A. Cole, J. R. Duffield, C. Furnival, D. C. Jones, P. M. May, G. L. Smith, and D. R. Williams, *Polyhedron,* **1**, 153 (1982).
12) J. R. Pilbrow, T. D. Smith, and A. D. Toy, *Aust. J. Chem.*, **23**, 2287 (1970).
13) T. Tatarowski, M. Kubiak, J. P. Morawiec, and H. Kozlowski, *Inorg. Chim. Acta,* **93**, L3 (1984).
14) B. Radomska, T. Tatarowski, J. P. Morawiec and H. Kozlowski, *Inorg. Chim. Acta,* **106**, L29 (1985).
15) F. Bigoli, M. Lanfranchi, E. Leporati, and M. A. Pellinghelli, *Cryst. Struct. Commum.*, **9**, 1255 (1980).
16) G. J. Gainsford, W. G. Jackson, A. M. Sargeon, and A. Watson, *Aust. J. Chem.*, **33**, 1213 (1980).
17) "The Universal Crystallographic Computation Program System (UNICS)," ed by T. Sakurai, Crystallographic Society of Japan, Tokyo (1967).
18) "International Tables for X-Ray Crystallography," Kynoch Press, Birmingham, U. K. (1974), Vol. IV.
19) F. A. Cotton and G. Wilkinson, "Advanced Inorganic Chemistry," 4th ed., John Wiley & Sons, New York (1980), pp. 689—821.
20) A. W. Herlinger and T. V. Long, II, *J. Am. Chem. Soc.*, **92**, 6481 (1970).
21) J. Loscalzo, R. G. Kallen, and D. Voet, *Arch. Biochem. Biophys.*, **157**, 426 (1973).
22) K. K. Chacko, *Cryst. Struct. Commun.*, **3**, 561 (1974).
23) The final thermal parameters and the final F_o-F_c table are deposited as Document No. 8781 at the office of the Editor of the Bulletin of the Chemical Society of Japan.

 © 1988 The Chemical Society of Japan Bull. Chem. Soc. Jpn., 61, 783—786 (1988)

Nematic Fumaric Ester Derivatives and Their Electro-Optical Properties

Kohei SHIRAISHI, Kazuo SUGIYAMA,* Akihiko SAKAMOTO, and Takayuki OTSU†
Department of Industrial Chemistry, Faculty of Engineering, Kinki University, Hiro, Kure 737-01
†Department of Applied Chemistry, Faculty of Engineering, Osaka City University, Sugimoto, Sumiyoshi-ku, Osaka 558
(Received July 24, 1987)

Senven enantiotropically nematic fumaric ester derivatives, 1-[[(*E*)-3-alkoxycarbonyl)acryloyl]oxy]-4-(4-methoxyphenylazo)benzene (**1**), were prepared. The **1** compounds which have unbranched ester alkyl groups showed decreased phase-transition temperatures and narrowed nematic states with the increase in the length of the alkyl chain, while the **1** compounds with terminal branched alkyl groups decrease drastically in nematic thermal stability. From the electro-optical effect originating in the dynamical scattering at the nematic state of the **1** compounds with unbranched ester groups, it was found that both the threshold voltage (E_{thres}) of deformation and the electro-optial response time (τ_r) decrease with the decrease in the chain lengh of alkyl groups. In addition, τ_r is scarcely influenced over the wide temperature range above 12 eV·cm^{-1} of the electric field.

During the last years, interest has been increasingly devoted to liquid crystalline side-chain polymers.[1-5] This interest has been justified by the creation of novel functional materials which bind the properties of low molecular liquid crystals to macromolecules.[6,7] In these polymers, the mesogenic groups become flexible polysiloxianes[1,3] or types of vinyl backbone, such as polyacrylates[4,7] and polymethacrylates.[2] On the other hand, it has been found that dialkyl fumarates can polymerize radically to produce nonflexible rodlike polymers with a high molecular weight.[8,9] In the course of an investigation of fumaric ester derivatives with properties of liquid crystals,[10,11] a series of polymerizable fumarates, 1-[[(*E*)-3-(alkoxycarbonyl)acryloyl]oxy]-4-(4-methoxyphenylazo)benzene, **1**, were prepared in an attempt to obtain a new type of liquid crystal side-chain polymers. In this paper, we would like to report the thermal and the electro-optical properties of **1**.

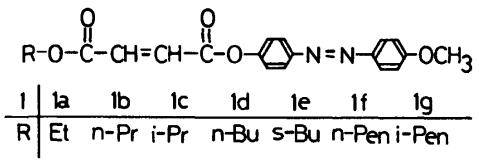

Scheme 1.

Results and Discussion

Thermal Properties. The **1** compounds were synthesized by a direct esterification of 4-(4-hydroxyphenylazo)anisole with (*E*)-3-(chloroformyl)acrylic acid alkyl esters. Alkyl groups were either ethyl(**1a**), propyl(**1b**), isopropyl(**1c**), butyl(**1d**), *s*-butyl(**1e**), pentyl(**1f**), or isopentyl(**1g**) as is shown in Scheme 1. A DSC study showed that all of the **1** compounds turned into enantiotropic liquid crystals, for showes two endothermic peaks and two exothermic peaks on heating and cooling cycles respectively. As a typical instance, the DSC curve of **1a** is shown in Fig. 1. The mesophase of **1** showed a schlieren texture and was

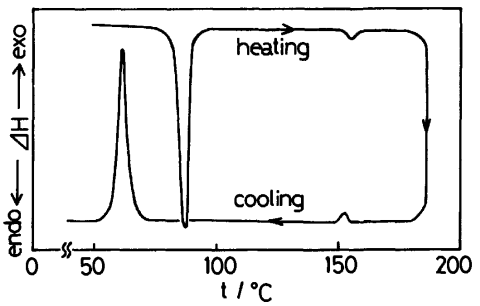

Fig. 1. DSC curve of **1a**.

Table 1. Phase Transition Temperatures and Electro-Optical Properties of **1** Compounds

Compound	R	Phase transition temperature[a]/°C	ΔT_N / °C	E_{thres}[b] / kV·cm^{-1}	Int[c] / %	τ_r[c] / ms
1a	Et	K 53.0 N 160.6 I	107.6	0.18	63	0.9
1b	*n*-Pr	K 50.0 N 153.1 I	103.1	0.28	45	1.0
1c	*i*-Pr	K 39.6 N 67.8 I	28.2	—	—	—
1d	*n*-Bu	K 27.0 N 114.4 I	87.4	0.26	80	5.7
1e	*s*-Bu	K 26.0 N 38.6 I	12.6	—	—	—
1f	*n*-Pen	K 34.0 N 118.3 I	84.3	0.40	50	4.5
1g	*i*-Pen	K 31.5 N 92.2 I	60.7	0.84	—	—

a) K, N, and I represent the crystalline, and nematic phases, and the isotropic melt respectively. b) E_{thres} was measured at T*°C(T_{N-I}−10 °C). c) Int represents the transmission intensity of the He-Ne laser. d) τ_r was measured on 16 kV·cm^{-1} of an electric field at T*°C(T_{N-I}−10 °C).

identified as a nematic phase by observation and a polarization microscopy of thin samples. The phase-transition temperature of **1** determined by DSC is compatible with the temperature obtained from the polarization microscopic and electro-optical measuremens to be described below. The results are tabulated in Table 1.

From the phase-transition temperature of **1**, the following conclusions can be drawn. Every fumarate exhibits an enantiotropically nematic phase independent of the ester alkyl groups. The phase-transition temperature is, however, strongly influenced by the structures of alkyl groups. In the case of unbranched alkyl groups (**1a**, **1b**, **1d**, **1f**), with an increase in the length of the alkyl chain the nematic-isotropic melt transition point loweres and the nematic state is narrowed. Comparing the unbranched type (**1b**, **1d**, **1f**), with the branched type (**1c**, **1e**, **1g**), the latter samples show lower transition temperatures. This suggests that the bulkiness of an alkyl group decreases the attractive interaction between the molecules; that is, a branching of a terminal alkyl group decreases the nematic thermal stability.[12,13] Especially, **1c** and **1e** with a methyl group at the α-position in the alkyl group are found to exhibit an extremely low nematic-isotropic melt transition. This explains the destruction of the molecular order by the methyl group at the α-position.[14]

Electro-Optical Properties. In order to obtain basic data for such practical uses as optical switching and display devices, electro-optical measurements were carried out for **1a**, **1b**, **1d**, and **1f** as follows. The sample cell was set in the optical path of a He-Ne laser(632.8 nm), and the change in the transmission with the application of an electric field was monitored by means of a photodiode.[15] As a typical example, the transmission intensity of the He-Ne laser through the **1a** cell on cooling cycles is shown in Fig. 2. The lines in Fig. 2 alternately indicate, the presence or absence of the dependence of the transmission intensities of the He-Ne laser through the cell on the applied voltage. When no voltage is applied, the transmission intensity decreases abruptly because of characteristic nematic light scattering just after the phase transition from the isotropic melt to the nematic phase at 160.6 °C, and then it gradually increases up to 63% of the original intensity by forming a stable nematic phase. On the other hand, upon the application of a voltage, the transmission intensity is zero over the nematic range of **1a** because of dynamical scattering caused by the d.c. current. The extent of these changes in the transmission intensity upon the application of an electric field is evaluated as a contrast in liquid-crystal displays. The threshold voltage of the observed deformation was measured at a definite temperature, T^* °C(T^*= T_{N-I}−10 °C), the results are listed in Table 1. Liquid crystals with a long alkyl group show a considerably higher threshold voltage of dynamical scattering. This is believed to be due to the higher viscosity of the nematic phase of **1** with the longer alkyl groups. The electro-optical response time (τ_r) of the decrease in the transmission caused by the voltage application was

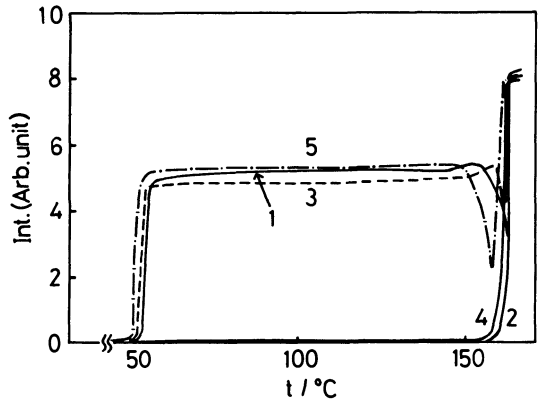

Fig. 2. Transmission intensities of a He-Ne laser for **1a** cell thickness; 50 μm, 1; (OFF), 2; 20 V(ON), 3; (OFF), 4; 40 V(ON), 5; (OFF).

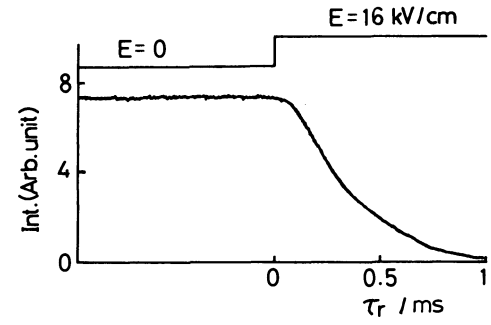

Fig. 3. Electro-optical response time(τ_r) in the nematic phase of **1a** at 16 kV·cm^{-1}.

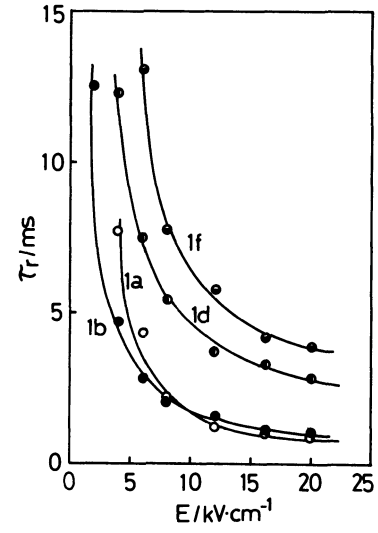

Fig. 4. Effect of electric field (E) on electro-optical response time (τ_r) for **1** at T^*° C(T^*=T_{N-I}−10 °C).

then measured over the voltage range from 5V (electric field, E=1 kV·cm^{-1}) to 100 V (E=20 kV·cm^{-1}) at T^* °C. In the case of **1a**, τ_r at 150.6 °C with E=16 kV·cm^{-1} is shown in Fig. 3. τ_r is the time taken to reach the stage of a transmission intensity decrease of 10%. τ_r for **1a** is, then, found to be 0.9 ms.

τ_r was also measured for other samples in a similar manner, by changing the applied voltage. The relation of τ_r and, the electric field applied at T^* °C is shown in Fig. 4. This figure shows that an increase in the applied voltage results in a faster optical response time, while an increase in the length of alkyl chain in **1** results in a slower response time. In order to clarify the effect of the electric field on the optical response time, τ_r was plotted on log-log graph paper as a function of the electric field, as is shown in Fig. 5.

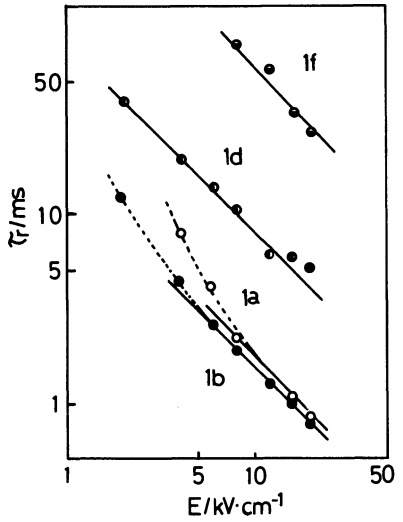

Fig. 5. Log-log plots of electro-optical response time (τ_r) and electric field (E) for **1** at T^*°C(T^*= T_{N-I}−10 °C).

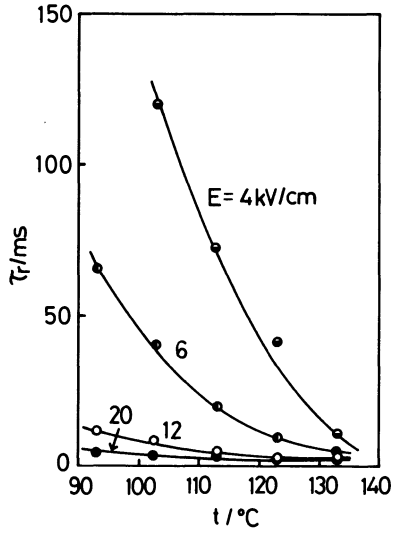

Fig. 6. Effect of temperature on electro-optical response time (τ_r) at various electric fields (E).

Since the slope of the lines is approximately −1, the τ_r of these liquid crystals is found to be proportional to the reciprocal of the electric field applied.[16] In the cases of **1a** and **1b** the plots deviate from the lines at somewhat lower electric fields. The reason for this phenomenon is now under consideration.

The effect of the temperature on τ_r was also studied by changing the applied voltage. As a typical example, the relationship between τ_r and the temperature for **1b** is shown in Fig. 6. It is found that τ_r is scarcely influenced over the wide temperature range above E=12 eV·cm^{-1} of the electric field. The transmission intensities of a He-Ne laser, τ_r, for **1a**, **1b**, **1d**, and **1f** are summarized in Table 1. Both a short response time and a clear contrast attributable to the change of transmission are realized with these liquid crystals. In general, the most desirable properties of a liquid crystal to be used as a material for display devices are as follows: i) the phase-transition temperature is low, and the temperature range of its mesophase is wide; ii) the optical response can occur at a low electric field and is accompanied by a high contrast; iii) the response times of rise and decay show an approximately exponential decrease with the temperature, and iv) the threshold voltage for the electric-field effect is proportional to the reciprocal of dielectric anisotropy. The liquid crystals obtained in this work can, therefore, be applied practically as display devices. The polymerization of **1** is now under investigation.

Experimental

Preparation of 1. 4-(4-Hydroxyphenylazo)anisole was obtained from the diazotization of *p*-anisidine and coupling with phenol according to the method used in the preparation of 4-(4-hydroxyphenylazo)benzonitrile.[17] 4-(4-Hydroxyphenylazo)anisole was dissolved in 300 mL of freshly distilled chloroform and 130 mmol of triethylamine. Then a trace of 1,4-benzoquinone was stirred in, the solution was cooled at 0 °C, and a 80-mmol portion of (*E*)-3-(chloroformyl)acrylic acid alkyl esters was dropped into the solution. After stirring for 2 h at 60 °C, ca. 200 mL of water was added to the reaction mixture. The chloroform layer was then washed with water and evaporated to dryness, and the residue was recrystallized from ethanol. **1** was chracterized by IR, ^{1}H NMR, and elemental analysis as follows:

1a (R=CH_3CH_2-): 65.6% yield; ^{1}H NMR ($CDCl_3$) δ= 1.26—1.66 (t, 3H, $C\underline{H}_3CH_2$-), 4.00 (s, 3H, $C\underline{H}_3O$-), 4.30—4.82 (q, 2H, $CH_3C\underline{H}_2$-), 7.34 (s, 2H, -C<u>H</u>=C<u>H</u>-), 7.88—8.62 (q, 8H, Aromatic): $C_{19}H_{18}O_5N_2$ (354.36); Found C, 64.3; H, 5.1; N, 7.7%. Calcd for C, 64.40; H, 5.12; N, 7.91%.

1b (R=$CH_3CH_2CH_2$-): 67.2% yield; ^{1}H NMR ($CDCl_3$) δ=0.90—1.40 (t, 3H, $C\underline{H}_3CH_2CH_2$-), 1.62—2.12 (sex, 2H, $CH_3C\underline{H}_2CH_2$-), 4.04 (s, 3H, $C\underline{H}_3O$-), 4.30—4.68 (t, 2H, $CH_3CH_2C\underline{H}_2$-), 7.36 (s, 2H, -C<u>H</u>=C<u>H</u>-), 7.54—8.56 (q, 8H, Aromatic): $C_{20}H_{20}O_5N_2$ (368.39); Found C, 65.3; H, 5.4; N, 7.4%. Calcd for C, 65.21; H, 5.47; N, 7.64%.

1c (R=$(CH_3)_2CH$-): ^{1}H NMR ($CDCl_3$) δ=1.34, 1.40 (s, s,

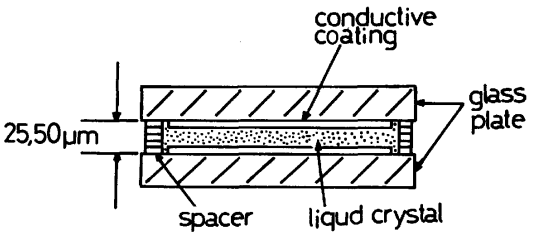

Fig. 7. Schematic representation of sandwiched cell for electro-optical measurement.

6H, $(CH_3)_2CH$-), 4.04 (s, 3H, CH_3O-), 5.16—5.52 (pent, 1H, $(CH_3)_2CH$-), 7.34 (s, 2H, -CH=CH-), 7.50—8.68 (q, 8H, Aromatic): $C_{20}H_{20}O_5N_2$ (368.39): Found C, 65.3; H, 5.4; N, 7.4 Calcd for C, 65.21; H, 5.47; N, 7.64%.

1d (R=$CH_3CH_2CH_2CH_2$-): 57.1% yield; ^1H NMR ($CDCl_3$) δ=0.92—1.06 (t, 3H, $CH_3CH_2CH_2CH_2$-), 1.32—2.06 (m, 4H, $CH_3CH_2CH_2CH_2$-), 3.98 (s, 3H, CH_3O-), 4.32—4.80 (t, 2H, $CH_3CH_2CH_2CH_2$-), 7.34 (s, 2H, -CH=CH-), 7.50—8.78 (q, 8H, Aromatic): $C_{21}H_{22}O_5N_2$ (382.42); Found C, 65.9; H, 5.8; N, 7.7%. Calcd for C, 65.96; H, 5.80; N, 7.33%.

1e (R=$CH_3CH_2(CH_3)CH$-): 74.5% yield; ^1H NMR ($CDCl_3$) δ=0.92-1.04 (m, 3H, CH_3-), 1.32-1.36 (d, 3H, CH_3-), 1.54-2.02 (m, 2H, $-CH_2$-), 4.10 (s, 3H, CH_3O-), 5.02-5.48 (m, 1H, -CH-), 7.34 (s, 2H, -CH=CH-), 7.50-8.80 (q, 8H, Aromatic): $C_{21}H_{22}O_5N_2$ (382.42): Found C, 66.0; H, 5.8; N, 7.1%. Calcd for C, 65.96; H, 5.80; N, 7.33%.

1f (R=$CH_3(CH_2)_3CH_2$-): 70.7% yield; ^1H NMR ($CDCl_3$) δ=0.86-1.20 (t, 3H, CH_3-), 1.32—2.12 (m, 6H, CH_3-$(CH_2)_3CH_2$-), 4.04 (s, 3H, CH_3O-), 4.34—4.66 (t, 2H, $CH_3(CH_2)_3CH_2$-), 7.36 (s, 2H, -CH=CH-), 7.54—8.56 (q, 8H, Aromatic): $C_{22}H_{24}O_5N_2$ (395.42): Found C, 66.4; H, 6.1; N, 7.2%. Calcd for C, 66.65; H, 6.10; N, 7.70%.

1g (R=$(CH_3)_2CHCH_2CH_2$-): 75.2% yield; ^1H NMR ($CDCl_3$) δ=0.98, 1.04 (s, s, 6H, $(CH_3)_2CHCH_2CH_2$-), 1.54—2.14 (m, 3H, $(CH_3)_2CHCH_2CH_2$-), 4.06 (s, 3H, CH_3O-), 7.36 (s, 2H, -CH=CH-), 7.54-8.64 (q, 8H, Aromatic): $C_{22}H_{24}O_5N_2$ (396.42): Found C, 66.4; H, 6.1; N, 7.1%. Calcd for C, 66.64; H, 6.10; N, 7.07%.

Measurements. The ^1H NMR measurements were carried out with a 100-MHz Jeol JNM-MH100 spectrometer. The phase-transition temperature were determined by means of differential scanning calorimetry, using a Rigaku Thermoflex apparatus DSC-8230B, with almost the same heating and cooling rates (10 K·min^{-1}). The sample sizes varied from 5 to 10 mg.

Microscopic investigations were performed by means of an Olympus microscope, with the temperature of the sample controlled by the heating stage. The thin samples were sandwiched between two glass slides whose surfaces had been unidirectionally rubbed with cotton wool to obtain a homogeneous alignment.[18-20] The spacing between top and bottom glass plates was 25 μm, with a stretched polyester film used as the spacer material. The samples were studied at both decreasing and increasing temperatures.

The sandwiched cell used in electro-opotical measurements is schematically illustrated in Fig. 7. The surfaces of the glass plates were coated with a transparent conductive material(InO_2); the surface resistance was about 100 ohms·square^{-1}. The spacings between top and bottom glass plates was 50 μm. A He-Ne laser(wavelength; 632.8 nm, output power; 1 mW) was used as the light source for the measurements of the transmission intensity. The incident light was performed with both an attenuator and a slit. The transmission lights were measured using a photomultiplier and were calculated using a microcomputer (NEC-9801).

References

1) H. Pranoto, F-J. Bormuth, and W. Haase, *Makromol. Chem.*, **187**, 2453 (1986).

2) C. Boeffel, H. W. Spiess, B. Hisgen, H. Ringsdorf, H. Ohm, and R. G. Kirste, *Makromol. Chem. Rapid Commun.*, **7**, 777 (1986).

3) G. W. Gray, D. Lacey, G. Nestor, and M. S. White, *Makromol. Chem. Rapid Commun.*, **7**, 71 (1986).

4) P. Keller, *Macromolecules*, **20**, 462 (1987).

5) M. Eich, J. H. Wendorff, B. Reck, and H. Ringsdorf, *Makromol. Chem., Rapid Commun.*, **8**, 59 (1987).

6) H. J. Coles and R. Simon, *Polymer*, **26**, 1801 (1985).

7) G. R. Mitchell, F. J. Davis, and A. Ashman, *Polymer*, **28**, 639 (1987).

8) T. Otsu and K. Shiraishi, *Macromolecules*, **18**, 1795 (1985).

9) T. Otsu, A. Tatsumi, and A. Matsumoto, *J. Polym. Sci., Polym. Lett. Ed.*, **24**, 113 (1986).

10) K. Sugiyama, A. Sakamoto, Y. Murata, K. Shiraishi, and T. Otsu, *Nippon Kagaku Kaishi*, **1987**, 1064.

11) K. Shiraishi, A. Sakamoto, and K. Sugiyama, *Chem. Express* **2**, 475 (1987).

12) G. W. Gray and K. J. Harrison, *Symp. Faraday Soc.*, **5**, 54 (1971).

13) G. W. Gray and K. J. Harrison, *Mol. Cryst. Liq. Cryst.*, **13**, 37 (1971).

14) Y. Matsunaga and N. Miyajima, *Bull. Chem. Soc. Jpn.*, **57**, 1413 (1984).

15) S. Kishio, M. Ozaki, K. Yoshino, and A. Sakamoto, *Mol. Cryst. Liq. Cryst.* in press.

16) E. Jakeman and E. P. Raynes, *Phys. Lett., A*, **39**, 69 (1972).

17) H. Ringsdorf and H.-W. Schmidt, *Makromol. Chem.*, **185**, 1327 (1984).

18) F. J. Kahn, G. N. Taylor, and H. Schonborn, *Proc. IEEE.*, **61**, 823 (1976).

19) R. W. Gurtler and J. W. Casey, *Mol. Cryst. Liq. Cryst.*, **35**, 275 (1976).

20) K. Kuroda and I. Tsunoda, 8th International Liq. Cryst. Conf. J-4p (1980).

Electrochemical Studies of Poly(mercaptohydroquinone) and Poly(mercapto-*p*-benzoquinone) Films Prepared by Electropolymerization. II. Fixation of Heavy Metals and Their Electrochemical Properties

Gorou Arai,* Takayuki Ishii, Sumi Yamamoto, and Iwao Yasumori
Department of Applied Chemistry, Faculty of Engineering, Kanagawa University, Kanagawa-ku, Yokohama 221
(Received July 30, 1987)

Heavy metal ions, Ag^+, Hg^{2+}, Cd^{2+}, Cu^{2+}, Pb^{2+}, Pd^{2+}, Fe^{3+}, and Pt^{4+}, were each fixed on a conductive redox film of poly(mercapto-*p*-benzoquinone) or poly(mercaptohydroquinone) by mercaptide formation. Of these mercaptide-modified electrodes, the Pt(IV)-, Pd(II)-, and Ag(I)-modified electrodes possess some catalytic properties for electrochemical hydrogen evolution. These mercaptide-modified electrodes display a nearly Nernstian response to their respective heavy metal ions in aqueous solution and exhibit good durability when stored under appropriate conditions. Especially, the Hg(II)-modified electrode displays an excellent function as an Hg^{2+} ion sensor. The effect of miniaturization of substrates upon response ability was investigated by using two different-sized Pt wires (0.5 mm and 0.03 mm in diameter).

Electrode surface modification using various electrocatalytic materials has been investigated in the field of electrocatalysis. Catalytic electrodes modified at the monolayer level have not successfully been utilized because they lack stability and conductivity.[1] Polymer-modified electrodes have recently been used for immobilization of metal ions and metal complex ions.[2] Many investigations have thus far been undertaken to devise more active and stabler catalyst systems for the electrochemical evolution of hydrogen,[3] the electrochemical reduction of oxygen,[4] and other inorganic and organic reactions.[5] Some basic applications[6] of catalytic electrodes have been reported. We prepared poly(mercapto-*p*-benzoquinone) (SQE_{Ox}) and poly(mercaptohydroquinone) (SQE_{Red}) films,[7] and reported their electrochemical properties.[8] Many heavy metal ions were fixed on the redox polymers (SQE, standing for SQE_{Red} and/or SQE_{Ox}) in the form of mercaptides. This fixation is easy and can be carried out under mild conditions as described below. Mercaptide-modified electrodes (ME-M's) are stable and possess a characteristic structure in which heavy metal atoms or particles are connected with a substrate electrode via a conductive polymer of SQE. As described in our previous paper,[7] the thickness of SQE can be controlled by the duration of electrolysis of mercaptohydroquinone. We report here on the method of fixing heavy metal ions on SQE and on some items of basic electrochemical behavior of various ME-M's.

Experimental

Mercaptohydroquinone was synthesized and purified according to the method described in our previous paper.[7] The chemicals used for the synthesis of mercaptohydroquinone were of reagent grade. The other inorganic reagents were of reagent grade and used without further purification. Deionized water was used for the preparation of solutions, final washing of electrode surface, and rinsing SQE. The substrate electrodes used were two different-sized platinum wires ($Pt_{0.5}$ and $Pt_{0.03}$), 0.5 and 0.03 mm in diameter, respectively, and both ca. 5 mm in effective length,[9] and a Yanagimoto GC-P2 glassy carbon electrode (GCE) 3 mm in diameter. The apparatus used for the preparation of SQE on these electrodes was the same as that used in the previous paper.[7] The reference electrode used was a saturated calomel electrode (SCE). Voltammetric measurements were carried out with a three-electrode system consisting of an ME-M working electrode, a Pt plate counter electrode, and an SCE reference electrode having an agar salt bridge of saturated KNO_3. Purified nitrogen gas was bubbled for 30 min to remove dissolved oxygen. Current-potential curves were recorded on a Yanagimoto P-8 polarograph. Potentiometric measurements were carried out in the conventional manner. An ME-M was set in a glass beaker containing a test solution. An SCE was set in another beaker containing an aqueous solution saturated with KCl. The two glass beakers were connected with each other by an agar salt bridge of saturated KNO_3. Potentials of ME-M's were measured with a Toho Chemical Research EM-02 electrometer. Each test solution contained 0.1 M (1 M=1 mol dm^{-3}) KNO_3 to provide a constant ionic strength (μ=0.1) and was brought to pH 5.0±0.1 by addition of an appropriate quantity of dilute nitric acid. The test solution was prepared just before potentiometric measurement to avoid the dissolution of atmospheric carbon dioxide. All potentiometric measurements were carried out at 25±0.1 °C.

Results and Discussion

Fixation of Heavy Metal Ions on SQE. SQE_{Ox} was prepared on $Pt_{0.03}$, $Pt_{0.5}$, and GCE by an electrochemical oxidation of 0.4 mM mercaptohydroquinone at a constant potential of +0.3 V for 30 min in a Britton-Robinson buffer solution of pH 5.0 containing 20 vol% ethanol. When 0.3 mC cm^{-2} was passed during the electropolymerization under the conditions described above, the surface density of quinone units in the SQE_{Ox} thus prepared was found to be ca. 8×10^{14} cm^{-2} on each electrode surface by measurement

of the charge associated with the reduction of the SQE_{ox}. After finishing the electropolymerization, the SQE_{ox}-modified electrodes were thoroughly rinsed with water and then immersed in a Britton-Robinson buffer solution containing 1 mM NaHS for 1 h at room temperature under a nitrogen atmosphere for the conversion to **1** by the reaction

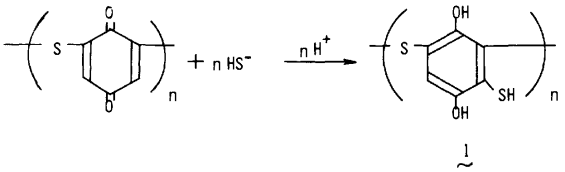

1

In order to confirm the above-described addition to have proceeded effectively, spectrophotometric measurements were carried out by using a pH 5.0 Britton-Robinson buffer solution containing 1 mM NaHS and 0.4 mM *p*-benzoquinone under a nitrogen atmosphere. The absorption spectrum with λ_{max}=246 nm due to *p*-benzoquinone rapidly decreased with lapse of time, while a new absorption spectrum with λ_{max}=298 nm increased. This absorption maximum is in fair agreement with that of 0.4 mM mercaptohydroquinone in wavelength and absorbance. On the basis of this spectrophotometric measurement, it is clear that the addition of HS^- ions to the majority of the quinone rings in SQE_{ox} has occurred to give **1**. After thorough rinsing with water, the **1**-modified electrodes were immersed in an aqueous solution containing 1 mM heavy metal ion for more than 1 h under a nitrogen atmosphere in order to fix the heavy metal ion on **1** by allowing its mercaptide to be formed which is insoluble or sparingly soluble in aqueous solution. Thus far Ag^+ or Hg^{2+} has been used for the titration of mercapto groups in various proteins.[11] After rinsing with a large amount of water to remove unreacted heavy metal ion, the **2**-modified electrodes were kept for 10 min at +0.3 V in 0.1 M KNO_3 solution in order to reduce **2** into **3** because the latter is superior to the former in durability:

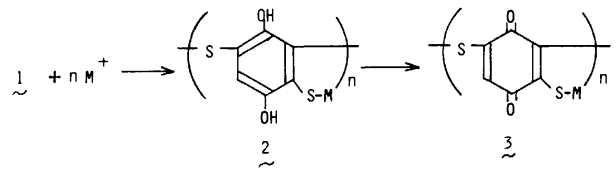

2 **3**

where M^+ indicates a univalent heavy metal ion. The **3**-modified electrodes thus prepared were kept in an aqueous solution containing the same heavy metal ion (1 mM) and were rinsed with water just before use for measurement. In order to confirm the mercaptide formation described above, the reaction between mercaptohydroquinone and Ag^+ was followed spectrophotometrically in aqueous solution. Figure 1 shows that mercaptohydroquinone and Ag^+ rapidly undergo an equimolar reaction to give an insoluble Ag-mercaptide. The mercaptide formation was confirmed for the other heavy metal ions, Hg^{2+}, Pd^{2+}, Cd^{2+}, Pb^{2+}, Cu^{2+}, Fe^{3+}, and Pt^{4+}. Hence it has been established that these heavy metal ions can be fixed on SQE via the formation of mercaptide **2** or **3**.

Voltammetric Behavior in Aqueous Solution. Voltammetric measurements were performed with a GCE as the substrate electrode because of its higher hydrogen overvoltage than that of Pt. Each ME-M gave a cathodic voltammogram characteristic of the metal ion species fixed on SQE. Their cathodic voltammograms were reproducible except those obtained during initial two or three potential scannings. As shown in Fig. 2, hydrogen evolution potentials become more positive in the order: Pt≈Pd>Ag>Cu≈Cd>Hg. The order observed here is inversely proportional to the magnitude of their hydrogen overvoltages. Of the SQE's having no mercapto groups, only those which had been immersed in Pt^{4+} or Pd^{2+} solution in the same manner, were observed to show small positive shifts in hydrogen evolution potential even after repeated rinsings with a large quantity of water. However, these small positive shifts decreased quickly with repeated potential scannings between 0 V and the hydrogen evolution potential. This salient difference in voltammetric behavior between SQE having mercapto group and SQE alone which were each

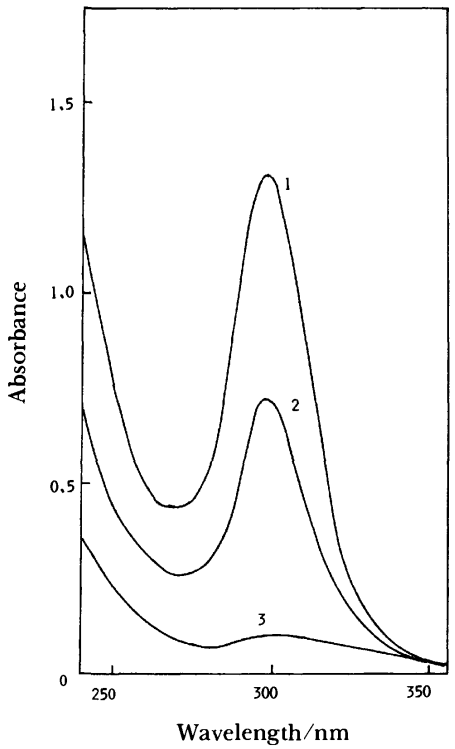

Fig. 1. Absorption spectra of mercaptohydroquinone (0.4 mM) in aqueous solution in the presence of Ag^+ in N_2 atmosphere. Concentration of $AgNO_3$: 1, 0 M; 2, 0.2 mM; 2, 0.4 mM.

immersed in the metal ion solution, strongly supports the above-mentioned judgment that the addition of HS^- ion to SQE_{Ox} gives **1**. Figure 3 shows that the hydrogen evolution potential of ME-Ag shifts negatively with an increase in the pH of buffer solution. This negative shift in hydrogen evolution potential was observed also with the other ME-M's. These results indicate that the electroactive sites where the hydrogen evolution occurs are solely the metals fixed on SQE and are neither the surface of GCE nor the SQE itself. Moreover, the above information strongly suggests that many metals which can form mercaptides may be electrochemically nucleated and grown on the electroactive sites, i.e., the metals fixed on SQE by means of the electroreduction of these metal ions in aqueous solution. The metal nucleation on the heavy metals fixed on SQE will be reported elsewhere.

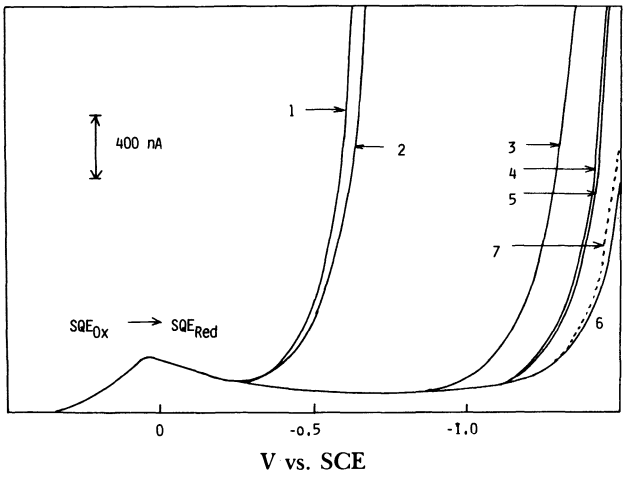

Fig. 2. Current-potential curves of ME-M's in the Britton-Robinson buffer solution having pH 5.0 in N_2 atmosphere. The potential was scanned at 3.3 mV s^{-1}.
1, ME-Pt(IV); 2, ME-Pd(II); 3, ME-Ag(I); 4, ME-Cu(II); 5, ME-Cd(II); 6, ME-Hg(II); 7, SQE alone.

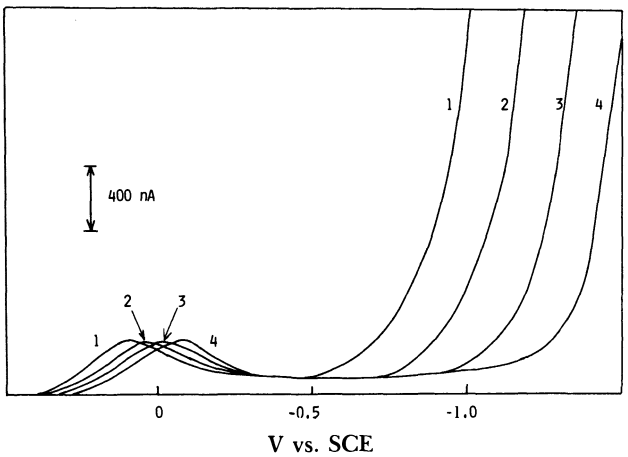

Fig. 3. Effect of pH on the current-potential curves of ME-Ag(I) using the Britton-Robinson buffer solution in N_2 atmosphere. The potential was scanned at 3.3 mV s^{-1}.
1, pH 3.0; 2, pH 4.0; 3, pH 5.0; 4, pH 6.0.

Potentiometric Behavior in Metal Ion Solution. We reported that Pt electrodes modified with a few species of mercaptides show a nearly Nernstian response to the same heavy metal ion as that of the mercaptide in 0.1 M KNO_3 aqueous solution.[12] In this work, potentiometric measurements were carried out by using two different-sized Pt electrodes, $Pt_{0.5}$ and $Pt_{0.03}$, modified with **3** in order to investigate on the deterioration in durability caused by the miniaturization of the substrate electrode. As a result of this investigation, no marked difference in the response characteristics such as response time and response concentration range was found to exist between the two electrodes. However, $Pt_{0.03}$ modified with **3** was occasionally dislodged or bent on insertion of the electrode into a test solution containing heavy metal ions. These defects encountered are obviously attributed to the fine flexible body of $Pt_{0.03}$ itself and need, therefore, to be overcome by fixation of $Pt_{0.03}$ on some hard substrate. As shown in Fig. 4, ME-Ag(I) displays a good Nernstian response to Ag^+ and has good durability. The response characteristics of various mercaptide-modified $Pt_{0.5}$'s are summarized in Table 1. The ME-M's show an almost Nernstian

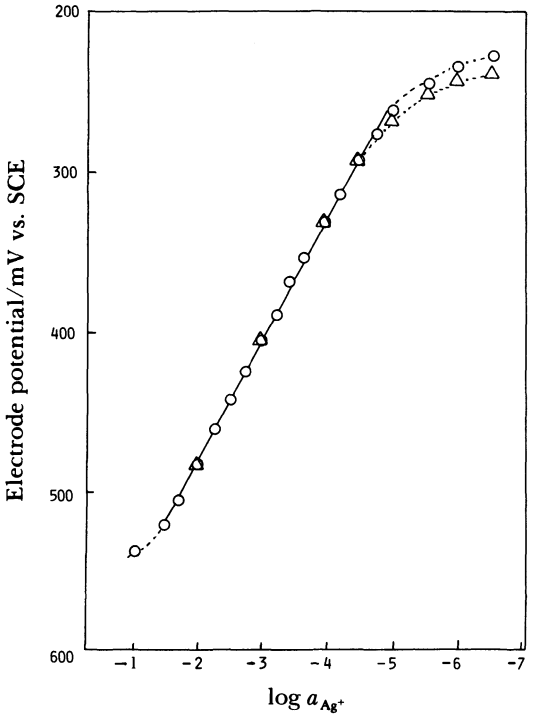

Fig. 4. Relationship between potential of ME-Ag(I) ($Pt_{0.5}$) and log a_{Ag^+} in 0.1 M KNO_3.
O: By Me-Ag(I) prepared just before the measurement, Δ: by ME-Ag(I) permitted to stand for one month.

Table 1. Response Characteristics of ME-M's ($Pt_{0.5}$)

Electrode	Test ion	Slope[a] mV/−log a	Range of linear response/M
ME-Ag(I)	Ag^+	60—61	$10^{-1.5}$—10^{-5}
ME-Hg(II)	Hg^{2+}	90—91	10^{-3}—10^{-5}
ME-Cu(II)	Cu^{2+}	27—28	5×10^{-3}—10^{-5}
ME-Pb(II)	Pb^{2+}	26—27	5×10^{-3}—10^{-5}
ME-Cd(II)	Cd^{2+}	30—31	5×10^{-3}—10^{-5}
ME-Fe(III)	Fe^{3+}	54—55	10^{-2}—10^{-5}

a) Each value range was obtained as the average from five or six measurements.

Table 2. Selectivity Coefficients (K_{Sel}'s) of ME-M's and Standard Redox Potentials (E^0's) of Mercaptide-Forming Heavy Metals

Electrode	K_{Sel}[a]	E^0[b] V vs. SHE
ME-Hg(II)	Ag^+, Cu^{2+}, Pb^{2+}, Cd^{2+}, Fe^{3+} ($<10^{-2}$)	+0.920($2Hg^{2+}/Hg_2^{2+}$)
ME-Ag(I)	$Hg^{2+}(10^2)$, $Fe^{3+}(1)$, Cu^{2+}, Pb^{2+}, $Cd^{2+}(10^{-2})$	+0.799(Ag^+/Ag)
ME-Fe(III)	$Hg^{2+}(10^2)$, $Ag^+(1)$, Cu^{2+}, Pb^{2+}, $Cd^{2+}(10^{-2})$	+0.771(Fe^{3+}/Fe^{2+})
ME-Cu(II)	$Hg^{2+}(10^3)$, Ag^+, $Fe^{3+}(10^2)$, Pb^{2+}, $Cd^{2+}(10^{-2})$	+0.337(Cu^{2+}/Cu)
ME-Pb(II)	$Hg^{2+}(10^3)$, Ag^+, Cu^{2+}, $Fe^{3+}(10^2)$, $Cd^{2+}(1)$	−0.126(Pb^{2+}/Pb)
ME-Cd(II)	Ag^+, Hg^{2+}, $Fe^{3+}(10^3)$, $Cu^{2+}(10^2)$, $Pb^{2+}(1)$	−0.403(Cd^{2+}/Cd)

a) K_{Sel}=[A]/[B] where [A] is the concentration of mercaptide-forming metal ion and [B] is that of interfering metal ion.
b) Ref. 15.

response to the heavy metal ions except ME-Hg(II) and ME-Fe(III). All of them respond within 10 s and usually have long service lives when stored in 1 mM nitrate solution weakly acidified with nitric acid. Especially, in the case of ME-Ag(I), its response behavior shown in Table 1 is fairly reproducible for at least one month when stored in a weakly acidic 1 mM $AgNO_3$ solution in a dark place. As we expected, the response characteristics, such as response range and response slope, of ME-Ag(I) were observed to be in good agreement with those of a naked Ag wire 0.5 mm in diameter, though the naked wire could respond more quickly. Similar agreement in response characteristics was also observed between ME-Cu (II) and a naked Cu wire. The potentiometric characteristics observed of ME-M's support the idea that some degree of interaction between heavy metals fixed on SQE and heavy metal ions in aqueous solution should cause the change in electrode potential of ME-M's, and suggest that the interaction between them is fundamentally equal to the reversible reduction-oxidation reaction between any naked metals and their ions in aqueous medium. The divalent and trivalent heavy metals fixed on SQE in the form of mercaptide should have more complicate bond structures than that given by -S-M in **2** or **3**. Especially, in the case of ME-Hg(II) and ME-Fe(III), large deviations in response slope from the Nernstian response expected for Hg^{2+} and Fe^{3+} were observed with the two electrodes, though their response characteristics were reproducible in five different measurements with five ME-Hg(II)'s or five ME-Fe(III)'s each prepared separately. Stricks et al.[13] have reported that the mercapto group in cystein (RSH) reacts with Hg^{2+} to give mercaptides such as $(RS)_2Hg$, $(RS)_2Hg_2^{2+}$, and $(RS)_2Hg_3^{4+}$ depending upon reaction conditions. However, from the fair reproducibility in response behavior observed of the two electrodes, it can be presumed that the two electrodes have certain definite bond structures under the preparation conditions used in this work. The selectivity coefficients (K_{Sel}'s) of the ME-M's and the standard redox potentials (E^0's) of the mercaptide-forming heavy metals are presented in Table 2. The K_{Sel}'s were determined by the mixed solution method described by Rechnitz et al.[14] These data show that ME-Hg(II) has an excellent selectivity to Hg^{2+} and that the electrode is subjected to negligible interference from the other heavy metal ions used here. Hence ME-Hg(II) possesses a useful function as a selective Hg^{2+} sensor. In addition, Table 2 shows that K_{Sel}'s are correlated closely to E^0's that is, the potential of any mercaptide-modified electrodes is very sensitive to interfering ions having more positive E^0's but is insensitive to those having more negative ones. This correlation between K_{Sel} and E^0 strongly suggests that certain redox reaction should occur in aqueous solution between any one species of heavy metal fixed on SQE and any one other species of heavy metal ion having more positive E^0, and supports the idea that the function of ME-M's as heavy metal ion sensors results from a redox interaction between the fixed heavy metal and its ion. Judging from their voltammetric and potentiometric characteristics observed in this work, it may be concluded that ME-M's

are applicable to many catalytic or selective electrochemical reactions and to the preparation of new types of metal ion sensors.

References

1) A. Bettelheim, R. Parash, and D. Ozet, *J. Electrochem. Soc.*, **129**, 2247 (1982); D. A. Butty and F. C. Anson, *J. Am. Chem. Soc.*, **106**, 59 (1984).

2) N. Oyama and F. C. Anson, *J. Am. Chem. Soc.*, **101**, 3450 (1979); R. N. Dominey, N. S. Lewis, J. A. Bruce, D. C. Bookbinder, and M. S. Wrighton, *J. Am. Chem. Soc.*, **104**, 467 (1982); P. C. Pickup and R. W. Murray, *J. Electrochem. Soc.*, **130**, 2205 (1983).

3) G. Tourillon and F. Garnier, *J. Phys. Chem.*, **88**, 5281 (1984); R. A. Simon, T. E. Mallouk, and M. S. Wrighton, *Inorg. Chem.*, **24**, 3119 (1985); D. E. Bartak, B. Kazee, K. Shimazu, and T. Kuwana, *Anal. Chem.*, **58**, 2756 (1986).

4) O. Ikeda, K. Okabayashi, N. Yoshida, and H. Tamura, *J. Electroanal. Chem.*, **191**, 157 (1985); T. Osaka, K. Naoi, T. Hirabayashi, and S. Nakamura, *Bull. Chem. Soc. Jpn.*, **59**, 2717 (1986).

5) C. J. Stalder, S. Chao, and M. S. Wrighton, *J. Am. Chem. Soc.*, **106**, 3673 (1984); A. K. Aramata and R. Ohnishi, *J. Am. Chem. Soc.*, **105**, 658 (1983).

6) J. W. Thackeray, H. S. White, and M. S. Wrighton, *J. Phys. Chem.*, **89**, 5133 (1985); J. W. Thackeray and M. S. Wrighton, *J. Phys. Chem.*, **90**, 6674 (1986).

7) G. Arai and M. Furui, *Nippon Kagaku Kaishi*, **1984**, 673.

8) G. Arai, K. Akiba, K. Yanagisawa, and I. Yasumori, *Nippon Kagaku Kaishi*, **1984**. 1867; G. Arai, T. Koike, and I. Yasumori, *Chem. Lett.*, **1986**, 867.

9) The effective length means the length of Pt wire immersed in a sample solution.

10) G. Arai, T. Koike, and I. Yasumori, *Bull. Chem. Soc. Jpn.*, **60**, 806 (1987).

11) R. Cecil and J. R. McFhee, *Ad. Protein Chem.*, **14**, 255 (1959); I. M. Kolthoff, W. Stricks, and L. Morren, *Anal. Chem.*, **26**, 366 (1954).

12) G. Arai, A. Fujii, and I. Yasumori, *Chem. Lett.*, **1985**, 1091.

13) W. Stricks, I. M. Kolthoff, and N. Tanaka, *Anal. Chem.*, **26**, 299 (1954).

14) G. A. Rechnitz, M. R. Kresz, and S. B. Zamochnick, *Anal. Chem.*, **38**, 973 (1966).

15) A. J. Bard and L. R. Faulkner, "Electrochemical Methods," John Wiley & Sons, New York (1980), pp. 699—701.

 © 1988 The Chemical Society of Japan Bull. Chem. Soc. Jpn., 61, 793—797 (1988)

A Behavior of Donnan Salt within Membrane

Akira YAMAUCHI,* Masashi DATE, Yukiko YAMAMOTO, Yutaka HIRATA, and Hideo KIMIZUKA

Department of Chemistry, Faculty of Science, Kyushu University 33, Hakozaki, Higashi-ku, Fukuoka 812

(Received September 11, 1987)

In an amphoteric ion exchange membrane-electrolyte system, three independent experiments were carried out, that is, the membrane potential, membrane conductance and concentration of ions within membrane were measured, respectively. The electrolytes adopted in the systems were NaCl, $CaCl_2$, $LaCl_3$. From the analysis of the results, the specific conductance attributed to Donnan salt within membrane was separated. As a result, it was pointed out that the dynamic state of Donnan salt is obviously different from that of salt in aqueous solution. Furthermore, the comparison between the ions constituting Donnan salt and the counterions which interact with the ion-exchange sites suggested us the existance of two different dynamic states on the ions within membrane.

Up to the present, a number of investigations concerning ion transport phenomena in membrane-electrolyte solution system have been reported.[1-3] We have also studied the membrane phenomena in systems using an ion-exchange membrane or an amphoteric ion-exchange membrane.[4-10] There may be several factors controlling the membrane phenomena, such as ion flux through the membrane, distribution coefficient at the interface between the membrane and electrolyte solution, the ionic concentration within membrane and etc. Of these, the ions within membrane may play an important role in the transport phenomena. The ions may exist in two different states, that is, due to ion exchange with sites and due to Donnan adsorption. It would be interesting to separate the two states experimentally, and in particular, to compare the behavior of Donnan salt with that of free ion in solution. Moreover, it is predicted that in the amphoteric membrane having the cationic and anionic exchange sites, the ions within membrane behave differently from usual monotonic ion-exchange membrane.[6,11]

Unfortunately, the detailed investigation has not been done concerning the mobilities of Donnan salt within membrane. Therefore, in this work, first, it was tried to separate the two states, and second, the behavior of Donnan salt was discussed. In order to satisfy a story mentioned above, the measurements of membrane potential and membrane conductance, and the determination of ionic concentration within membrane were carried out.

Experimental

Materials. An amphoteric membrane used in this study was supplied by Tokuyama Soda Co. Ltd., of which the characterestics were described already elsewhere.[7-10] The electrolytes (NaCl, $CaCl_2$, $LaCl_3$) of extra pure reagents were used without further purification.

Apparatus. The cell for membrane potential and conductance was made of glass, and consisted of 20 cm^3 compartments. Two 1.57 cm^2 platinum black electrodes were equipped in the glass cells for membrane conductance. The membrane was placed between two compartments and the available areas of membrane were 3.14 cm^2. The details for the measurements were described elsewhere.[7-10]

The Determination of Ionic Concentration within Membrane. After the membrane (5×5 cm^2) was equilibrated with the sample solutions from 10^{-3} to 10^{0} mol dm^{-3} for 72 h, the membranes were transferred into the distilled water and stood for 72 h in order to remove the electrolytes due to Donnan adsorption. Then, the ions within membrane due to ion exchange with sites were eluted by 1.0 mol dm^{-3} HNO_3. The two different concentrations $\bar{C}^E$ and $\bar{C}^D$, were determined by the atomic absorption spectroscopy (Hitachi Co., Ltd., Model 180-50). In the case of La ion, the calorimetric method with arsenaso III reagent was employed because the sensitivity of the atomic absorption was insufficient.

During the course of this experiment, the solution phases were sufficiently stirred by the magnetic stirrers and temperature was kept at 25 °C.

Theoretical

The consideration[12] based on the nonequilibrium thermodynamics gives us the equation concerning the specific conductance of membrane, $\bar{\kappa}$,

$$\begin{aligned}\bar{\kappa} &= \nu_1 Z_1 \bar{C} F(\bar{U}_1 + \bar{U}_2) \\ &= \nu_1 Z_1 \bar{C} F(\bar{U}_{11} + 2\bar{U}_{12} + \bar{U}_{22}),\end{aligned} \tag{1}$$

where

$$\bar{U}_1 = \frac{Z_1^2 l_{11}}{\nu_1 Z_1 \bar{C}} F + \frac{Z_1 Z_2 l_{12}}{\nu_1 Z_1 \bar{C}} F \equiv \bar{U}_{11} + \bar{U}_{12}, \tag{2}$$

and

$$\bar{U}_2 = \frac{Z_1 Z_2 l_{21}}{\nu_1 Z_1 \bar{C}} F + \frac{Z_2^2 l_{22}}{\nu_1 Z_1 \bar{C}} F \equiv \bar{U}_{12} + \bar{U}_{22}, \tag{3}$$

where the subscripts 1 and 2 refer to cation and anion; ν, Z, $\bar{C}$, and F, the stoichiometric number, the ionic charge, the concentration of electrolyte within membrane, and Faraday constant, respectively; $\bar{U}_1$ and $\bar{U}_2$ are the ionic mobilities within membrane defined by Eqs. 2 and 3; l's are the phenomenological

coefficients involving the interactions between ions and it is assumed that Onsager's reciprocal relation is held among l's. Accordingly, the mobilities, $\bar{U}_1$ and $\bar{U}_2$, are also the quantities involving the effect of interactions between different ionic species, $\bar{U}_{12}$.

On the other hand, the concentration of electrolyte whthin membrane may be shared into two terms due to ion exchange with site and Donnan adsorption as

$$\bar{C} = \bar{C}^{E} + \bar{C}^{D}. \tag{4}$$

Corresponding to two kinds of concentrations in Eq. 4, there may be presumably two different transport processes which are characterized by the mobilities, $\bar{U}^{E}$ and $\bar{U}^{D}$. Each process may be described by means of Eq. 1. Provided the additivity between the processes can be assumed, the total specific conductance, $\bar{\kappa}^{T}$, is given as sum of the two processes. Therefore, one can write the following equation,

$$\begin{aligned}\bar{\kappa}^{T} &= \bar{\kappa}^{E} + \bar{\kappa}^{D} \\ &= \nu_1 Z_1 F \bar{C}^{E}(\bar{U}_1^{E} + \bar{U}_2^{E}) + \nu_1 Z_1 F \bar{C}^{D}(\bar{U}_1^{D} + \bar{U}_2^{D}),\end{aligned} \tag{5}$$

where $\bar{\kappa}^{E}$ and $\bar{\kappa}^{D}$ represent the contributions due to ion exchange and Donnan adsorption, and $\bar{U}^{E}$ and $\bar{U}^{D}$ also express the mobilities in the corresponding states, respectively. Under the experimental conditions that the concentrations of Donnan salt are nearly equal to zero, Eq. 5 is reduced to Eq. 6,

$$\bar{\kappa}^{T}_{\bar{C}^{D}\to 0} \simeq \bar{\kappa}^{E}. \tag{6}$$

Assuming that $\bar{\kappa}^{E}$ ($=\bar{\kappa}^{T}_{\bar{C}^{D}\to 0}$) can be separated into cationic and anionic contributions, the transport numbers, t_1 and t_2 may be defined as

$$t_1 = \bar{\kappa}_1^{E}/\bar{\kappa}^{E}, \tag{7a}$$

and

$$t_2 = \bar{\kappa}_2^{E}/\bar{\kappa}^{E}, \tag{7b}$$

where $\bar{\kappa}_1^{E}$ and $\bar{\kappa}_2^{E}$ denote respectively the specific conductances of cation and anion, which can not be directly obtained from the experiments. However, $\bar{\kappa}_1^{E}$ and $\bar{\kappa}_2^{E}$ may be easily separated by means of Eq. 7 provided t_1 and t_2 can be measured experimentally.

Moreover, when $\bar{C}^{D}$ is not zero but the finite value, $\bar{\kappa}^{D}$ in Eq. 5 is evaluated as the difference between the total specific conductance and that due to ion exchange. If the additivity for $\bar{\kappa}^{T}$ is assumed in the same manner as Eq. 7, the transport numbers, t_1' and t_2' may be described as

$$t_1' = (\bar{\kappa}_1^{E} + \bar{\kappa}_1^{D})/\bar{\kappa}^{T}, \tag{8a}$$

and

$$t_2' = (\bar{\kappa}_2^{E} + \bar{\kappa}_2^{D})/\bar{\kappa}^{T}. \tag{8b}$$

Generally, the apparent transport number, which can be obtained by the membrane potential, is approximately independent of the concentration of outer electrolyte solution.[4,10] Then, t_1' and t_2' may be equal to t_1 and t_2, respectively.

Thus, one can finally get to the following equations,

$$\bar{\kappa}_1^{D} = t_1'\bar{\kappa}^{T} - \bar{\kappa}_1^{E} = t_1(\bar{\kappa}^{T} - \bar{\kappa}^{E}), \tag{9a}$$

and

$$\bar{\kappa}_2^{D} = t_2'\bar{\kappa}^{T} - \bar{\kappa}_2^{E} = t_2(\bar{\kappa}^{T} - \bar{\kappa}^{E}). \tag{9b}$$

The specific conductance of Donnan salt, $\bar{\kappa}^{D}$, can be obtained from Eq. 9 as

$$\bar{\kappa}^{D} = \bar{\kappa}_1^{D} + \bar{\kappa}_2^{D} = \bar{\kappa}^{T} - \bar{\kappa}^{E}, \tag{10}$$

which is obviously the same as Eq. 5.

Results and Discussion

In Fig. 1, logarithms of the specific conductance of membrane, $\bar{\kappa}^{T}$ were given against logarithm of outer aqueous electrolyte solutions in the case of NaCl, $CaCl_2$, and $LaCl_3$, respectively. $\bar{\kappa}^{T}$ values increased with the concentrations of outer electrolyte solution which were equilibrated with the membrane. The order was $\bar{\kappa}^{T}(NaCl) > \bar{\kappa}^{T}(CaCl_2) > \bar{\kappa}^{T}(LaCl_3)$ in all the range of concentration examined in this study.

$\bar{C}^{E}$ and $\bar{C}^{D}$ obtained separately were given as the functions of the concentrations of outer electrolyte solution in Fig. 2 in which $\bar{C}^{E}$'s were constant within experimental errors, and $\bar{C}^{D}$'s increased with the concentration of outer electrolyte solution in the same manner as $\bar{\kappa}^{T}$. The difference of $\bar{C}^{E}$ between cation and anion may be neglected in this study. Taking allowance for Eq. 5, the increase of $\bar{\kappa}^{T}$ may be attributed to the Donnan salt, $\bar{C}^{D}$ as indicated later. Accordingly, $\bar{\kappa}^{E}$ can be determined from the values of

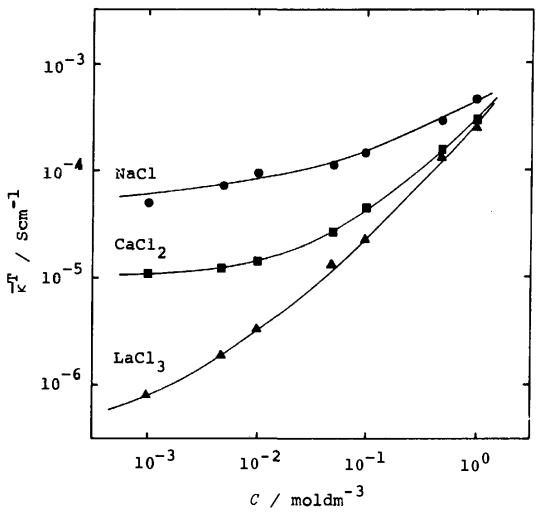

Fig. 1. Specific membrane conductance against the concentration of outer electrolyte solution equilibrated with membrane. ●: NaCl, ■: $CaCl_2$, ▲: $LaCl_3$.

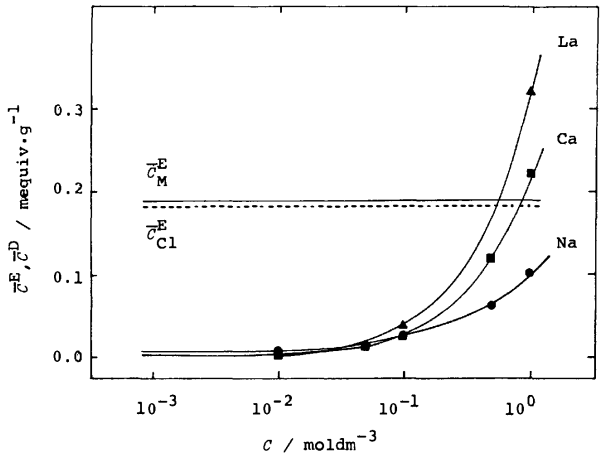

Fig. 2. Concentration of ion within membrane. Horizontal lines (solid and broken) denote the concentration due to ion exchange with sites, $\bar{C}^E$. Curved lines denote the concentration of Donnan salt, $\bar{C}^D$. ●: NaCl, ■: $CaCl_2$ ▲: $LaCl_3$. The abscissa is the same as in Fig. 1.

Table 1. Apparent Transport Numbers Evaluated from Membrane Potentials

Salt	t_M	t_{Cl}
NaCl	0.95	0.05
$CaCl_2$	0.91	0.09
$LaCl_3$	0.13	0.87

$\bar{\kappa}^T$ at $\bar{C}^D=0$ (Eq. 6). In general, $\bar{\kappa}^E$ should be constant independent of the concentration of outer electrolyte solution because it interacts strongly with ion-exchange sites having constant exchange capacity. The values were estimated as 5.37×10^{-5} (NaCl), 1.14×10^{-5} ($CaCl_2$), and 3.39×10^{-6} S cm^{-1} ($LaCl_3$) in this study, respectively. Inserting $\bar{\kappa}^E$ values into Eq. 5 or 10, $\bar{\kappa}^D$ can be obtained. The results as to 3 couples of electrolytes were given in Fig. 3.

On the other hand, the transport numbers in the system of NaCl, $CaCl_2$, and $LaCl_3$ were evaluated from the membrane potential measurements, and summarized in Table 1. As discussed in theoretical section, the experimental facts show that t's are approximately constant independent of the concentration of outer electrolyte solution.[9,10] Therefore, using the values in Table 1 and Eqs. 7 and 9, the cationic and anionic conductances of $\bar{\kappa}^E$ and $\bar{\kappa}^D$ were separately calculated. The results were given in Fig. 4 in which the broken lines indicate the constant $\bar{\kappa}^E$ originated from ion-exchange capacity, and the solid lines indicate $\bar{\kappa}^D$ due to Donnan adsorption.

Here, taking into account the electroneutrality for Donnan salt, and that the cationic and anionic exchange capacities are nearly equal, we can obtain the next relations,

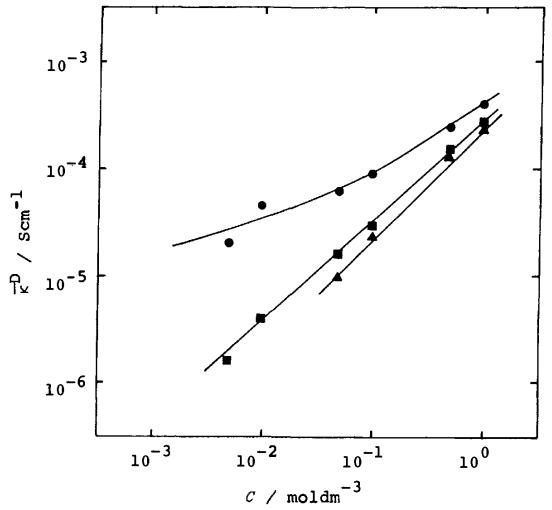

Fig. 3. Specific conductance originated from Donnan salt, $\bar{\kappa}^D$. Symbols and the abscissa are the same as in Fig. 2.

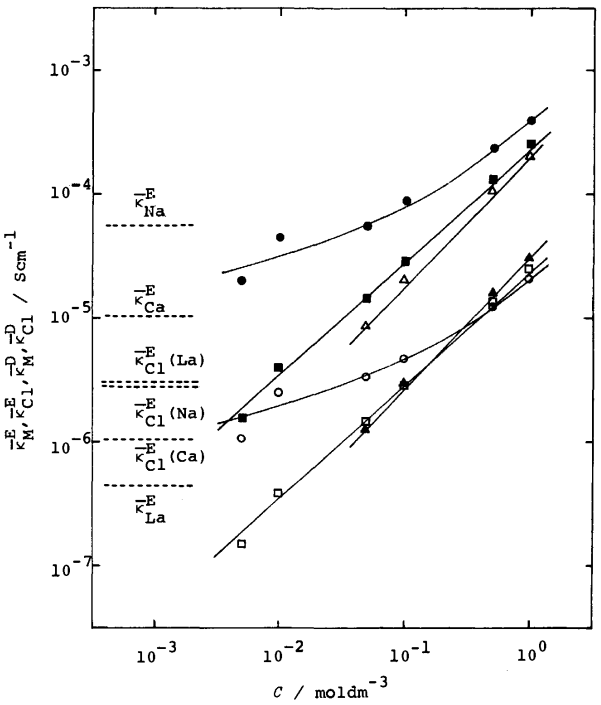

Fig. 4. Specific conductances of the respective ions. The broken lines are $\bar{\kappa}^E$ and indicate constant values in range of concentration examined though not seen in Fig. The solid lines are $\bar{\kappa}^D$. ●:Na, ■: Ca, ▲: La, ○: Cl(Na), □: Cl(Ca), △: Cl(La). The abscissa is the same as in Fig. 2.

$$\bar{C}^E = Z_1\bar{C}^E_1 \simeq Z_2\bar{C}^E_2, \tag{11}$$

and

$$\bar{C}^D = Z_1\bar{C}^D_1 \simeq Z_2\bar{C}^D_2. \tag{12}$$

On the other hand, rearranging Eqs. 6 and 10, we obtain,

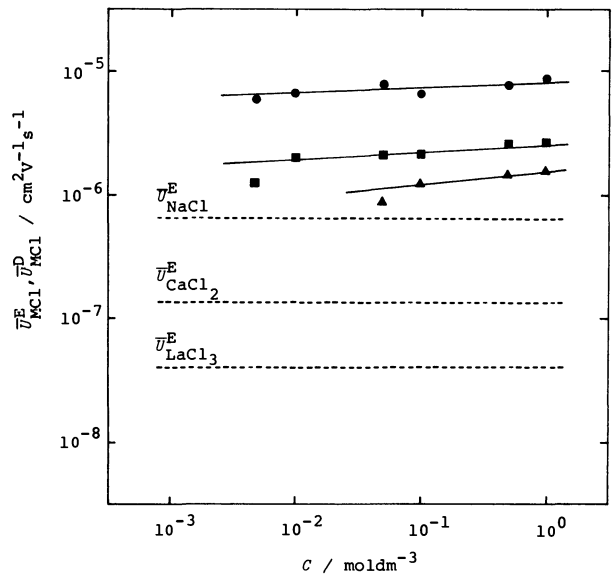

Fig. 5. Mobilities of salt within membrane. The broken lines denote $\bar{U}^{E}_{MCl}$. The solid lines denote $\bar{U}^{D}_{MCl}$. Note the difference between $\bar{U}^{E}_{MCl}$ and $\bar{U}^{D}_{MCl}$ depending upon ionic charges.

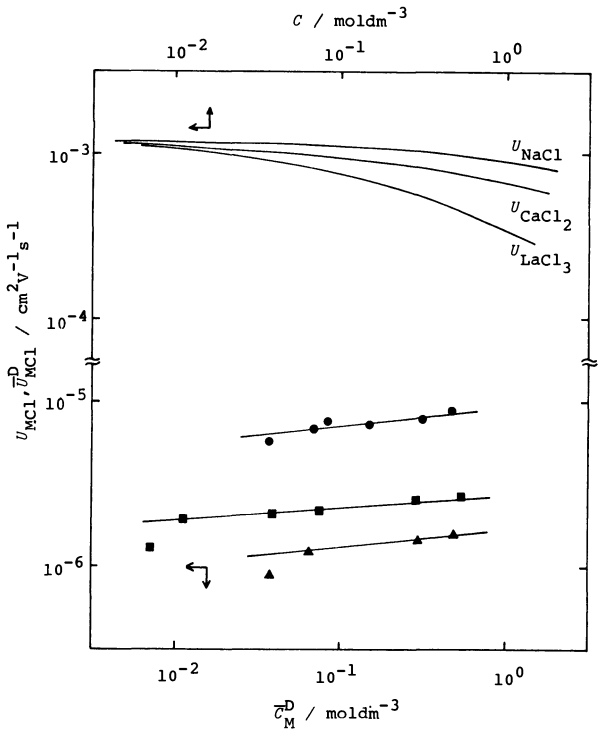

Fig. 6. A comparison between the mobility of Donnan salt and that of salt in solution. Lower abscissa indicates the concentration of Donnan salt. Symbols are the same as in Fig. 1.

$$\bar{U}^{E}_{MCl} = \bar{U}^{E}_{M} + \bar{U}^{E}_{Cl} = \bar{\kappa}^{E}/F|Z_M|\bar{C}^{E}_{M}, \quad (13)$$

and

$$\bar{U}^{D}_{MCl} = \bar{U}^{D}_{M} + \bar{U}^{D}_{Cl} = \bar{\kappa}^{D}/F|Z_M|\bar{C}^{D}_{M}, \quad (14)$$

where the subscript, MCl refers to the electrolyte, and M and Cl correspond to 1 and 2 mentioned before, respectively. According to the relations, Eqs. 11, 12, 13, and 14, we can calculate the mobility of the salt at each state. A comparison of $\bar{U}^{D}_{MCl}$ with $\bar{U}^{E}_{MCl}$ was given in Fig. 5, in which the difference of mobilities is evident. In contrast to $\bar{\kappa}^{D}$, the values of $\bar{U}^{D}_{MCl}$ indicated approximately constant independent of the concentration of outer electrolyte solution. The facts take out the following important conclusion: the increase of the specific conductance, $\bar{\kappa}^{T}$ is attributed to the increase of Donnan salt within membrane. The $\bar{U}^{D}_{MCl}$ increased slightly in concentrated range of outer electrolyte solution, but it is not clear at present whether the cause comes from the experimental errors or the variation of the water content within membrane. As for $\bar{U}^{E}_{MCl}$, the values are constant and obviously were less than $\bar{U}^{D}_{MCl}$. It can be therefore pointed out that there exist two different ionic states in the membrane from the results in Fig. 5.

For the comparison, the mobilities of salts in solution were calculated by means of the molar conductances, Λ_{MCl} in literature[13] as follow,

$$U_{MCl} = \Lambda_{MCl}/|Z_M|F. \quad (15)$$

In Fig. 6, $\bar{U}^{D}_{MCl}$ and U_{MCl} were plotted against the concentrations of Donnan salt and solution, $\bar{C}^{D}$ and C, respectively. It is shown in Fig. 6 that $\bar{U}^{D}_{MCl}$ which is about 10^{-6}cm^2 v^{-1} s^{-1}, reduces by three orders than U_{MCl} in solution. A comparison between the electrolytes examined in this study shows that the order of mobility of Donnan salts is $\bar{U}^{D}$(NaCl)>$\bar{U}^{D}$(CaCl$_2$)>$\bar{U}^{D}$(LaCl$_3$) corresponding to that in concentrated electrolyte solution. Contrary to our prediction, the experimental facts indicated that Donnan salt within membrane and salt in solution are in different states distinctly. One of the reasons is that Donnan salt is affected by the pore size in membrane matrix and is partly attributed to electric field around the exchange sites. Consequently, it is considered that the domains of membrane pores have an influence owing to the strong electric field produced by cation- and anion-exchange sites.[6]

Though the mobilities of salts have been discussed, so far, ionic mobility can be also estimated from the results in Fig. 4. The results were essentially the same as the case of salt. Therefore, the discussion as to the ionic form was excluded in this paper.

References

1) N. Lakshminarayanaiah, "Transport Phenomena in Membranes," Academic Press, New York, NY (1969).

2) O. Kedem and A. Katchalsky, *Trans. Faraday Soc.*, **59**, 1918, 1931, 1941 (1963).

3) C. R. Gardner, J. N. Weinstein, and S. R. Caplan, *Desalination*, **12**, 19 (1973).

4) A. Yamauchi and H. Kimizuka, *J. Theor. Biol.*, **30**, 285 (1971).
5) A. Yamauchi, S. Tsuruyama, H. Masumori, Y. Nagata, K. Kaibara, and H. Kimizuka, *Bull. Chem. Soc. Jpn.*, **55**, 3297 (1982).
6) Y. Nagata, K. Kohara, W. K. Yang, A. Yamauchi, and H. Kimizuka, *Bull. Chem. Soc. Jpn.*, **59**, 2689 (1986).
7) M. Shinoda, Y. Hirata, A. Yamauchi, and H. Kimizuka, *Mem. Fac. Sci., Kyushu Univ., Ser. C*, **15**, 195 (1986).
8) A. Yamauchi, H. Shinohara, M. Shinoda, M. Date, Y. Hirata, and H. Kimizuka, *Bull. Chem. Soc. Jpn.*, **60**, 1645 (1987).
9) Y. Hirata, M. Date, Y. Yamamoto, A. Yamauchi, and H. Kimizuka, *Bull. Chem. Soc. Jpn.*, **60**, 2215 (1987).
10) A. Yamauchi, Y. Okazaki, R. Kurosaki, Y. Hirata, and H. Kimizuka, *J. Membr. Sci.*, **32**, 281 (1987).
11) M. J. Hach, J. A. Dillon, and H. B. Smith, *Ind. Eng. Chem.*, **49**, 1812 (1957).
12) A. Katchalsky and P. F. Curran, "Nonequilibrium Thermodynamics in Biophysics," Harvard Univ. Press, Cambridge, Massachusetts (1965).
13) "Kagaku Binran," ed by Chemical Society of Japan, (1966), p. 1034.

Application of Hydrogen Ion Sensitive Field Effect Transistor to the Kinetic Study of Fast Reaction in Solution

Thoru NAKATSUKA, Michihiro NAKAMURA,† and Takayuki SANO*
Department of Materials Science, Faculty of Science, Hiroshima University, Higashisenda-machi, Hiroshima 730
†Central Research Laboratories, Kuraray Co., Ltd., Kurashiki, Okayama 710
(Received September 19, 1987)

The ion sensitive field effect transistor(ISFET) developed for pH measurement was incorporated with the stopped flow apparatus for direct detection of the fast change in the hydrogen ion concentration. By the experiments on the dehydration reaction of carbonic acid, it was proved that the pH sensor has a fast response time (<2 ms) beyond the resolution time of stopped flow apparatus, and the constructed apparatus can be satisfactorily applied to the fast reaction kinetics with the sensitivity for the pH change more than 0.01 pH unit.

The stopped flow method is one of most useful methods for study of fast reaction in solution.[1,2] The modes of detection for monitoring the time course of reaction are classified as follows: optical[3,4] (absorption, fluorescence, ORD, CD, etc.), electrochemical[5] (conductivity, electrode detection), thermal,[6] and magnetic resonance[7,8] (ESR, NMR) detections. The choice of the detection mode depends on the information necessary for elucidation of reaction mechanism and on the detectable probe in the reaction system.

Hydrogen ion plays important roles in various kinds of reactions such as not only simple protolysis reactions but also biologically interesting reactions; e.g., proton pump by H^+-ATPases in mitochondria, chloroplasts and bacteria in which ATP is synthesized at the expense of a transmembrane proton gradient.[9-11]

On the other hand, the kinetic experiments on the reaction associated with the hydrogen ion have been widely performed using a pH indicator so far.[12] However, an addition of the indicator to reaction system makes its mechanism complicated, and, in some cases, the added indicator inhibits the intended reactions through its direct interaction with reaction species. Hence, the apparatus for direct detection of hydrogen ion with high resolution in both the sensitivity and response time is necessary for the study of the fast reaction in these interesting systems.

A glass electrode can detect directly hydrogen ion concentration. Some applications of the glass electrode to detection of fast reactions have been reported.[13-15] Sirs has applied the glass electrode to the stopped flow apparatus and attained maximum sensitivity of 0.004±0.0005 pH unit using 0.5 ml of solution for each run, but its time resolution is up to half-lives of 0.05 s. Meanwhile, the combination of the glass electrode with the continuous flow method has been tried by Rossi-Bernardi and Berger, and Nakamura, because this method dose not require the fast response of a detector. Rossi-Bernardi and Berger have constructed the apparatus having high resolution in both the reaction rate and sensitivity; the dead time of 3 ms and precision of ±0.005 pH unit, which are superior to those by Nakamura. However, the continuous flow method has disadvantage of requirement of a large quantity of sample solution. Thus, the continuous flow method is not suitable for invaluable samples. Consequently, the pH detector with fast response time was desired to combine with the stopped flow method which requires rather small amount of sample solution.

Recently, a new kind of pH sensor, i.e., ion sensitive field effect transistor (pH-ISFET),[16,17] has been commercially available. The sensor has the characteristics of its small dimensions and faster response time than 0.1 s.[18] In spite of these striking properties of the pH sensor, the application of the sensor to the kinetic study of the fast reaction have not been succeeded in yet. Accordingly, we examined the possibility of a sensor responsive much faster than 0.1 s and constructed a stopped flow apparatus incorporated with that pH sensor.

The present paper describes the applicability of the stopped flow apparatus equipped with a pH-ISFET (ISFET-stopped flow apparatus) to the kinetic study of fast reaction.

Experimental

The pH sensor (PH-2135, Kuraray Co., Ltd.) used in the present study, which is commercially obtainable as a part of the pH meter (KR-500), is developed for the medical use such as pH monitoring in a blood vessel and stomach. The sensor (diameter, 1.0 mm, 350 mm long) consists of the ISFET (0.15 mm thick, 0.40 mm wide, and 5.5 mm long) integrated with a temperature sensor, reference electrode, and a guard electrode for preventing induced noise, which are packed all together in a catheter. The reference electrode is made of silver-silver chloride. Physiological saline solution retained in the porous hollow fiber is used as a inner solution of the reference electrode.

The stopped flow apparatus (RA-401, Union Giken Co., Ltd.) used is the gas pressure-driven type. The dead time of this apparatus is determined to be 3 ms by test measurement

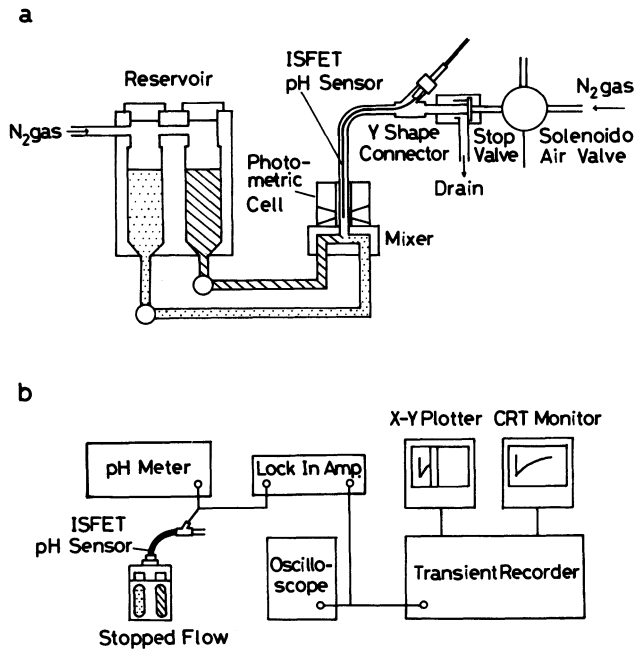

Fig. 1. (a) Combination of the ISFET pH sensor with the stopped flow apparatus. (b) Block diagram of the whole apparatus.

using optical detection. The solution of 0.2 ml is necessary for each run.

The sensor is inserted into the observation cell through the drain tube using the Y shape connector, as shown in Fig. 1(a). Figure 1(b) represents a block diagram of whole apparatus. For the rapid measurement of pH, the signal from the sensor is directly led to a lock-in amplifier and recorded with a transient recorder. A remarkably improved signal to noise ratio was obtained by shielding the equipment and by using a voltage regulator. The maximum sensitivity of the pH sensor was 0.0018 pH unit. For the optical detection experiments, Bromophenol Blue was used as a pH indicator. All experiments were carried out at 25±1 °C.

Results and Discussion

The response time of the pH sensor combined with stopped flow was examined by detecting pH change after mixing of $NaHCO_3$ and HCl solutions in which the pH change comes from the replacement of the mixed solution in equilibrium with new one prior to the slow reaction. The same measurement was performed with a pH indicator Bromophenol Blue. The rapid pH change detected in these ways is shown in Fig. 2 where the time constants were estimated to be 2 ms for both experiments. As a result, the response time of the sensor was proved to be so faster than 2 ms beyond the dead time of stopped flow apparatus.

Next, the experiments on the dehydration reaction of carbonic acid were carried out to check the validity of the ISFET-stopped flow apparatus. Figure 3 shows the reaction curves observed by two detecting ways:

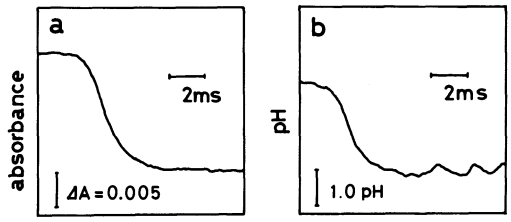

Fig. 2. Measurement of the response time of the pH sensor. A rapid pH change was caused by mixing 2.5×10^{-3} M HCl (1 M=1 mol dm^{-3}) and 5.0×10^{-3} M $NaHCO_3$ solution containing Bromophenol Blue (the concentrations are those after mixing) at 25 °C. (a) The rapid pH change detected spectrophotometrically at 435 nm and (b) that by using the pH sensor. The magnitude of absorbance change ΔA and that of pH change are indicated by the bar in the lower left-hand corner.

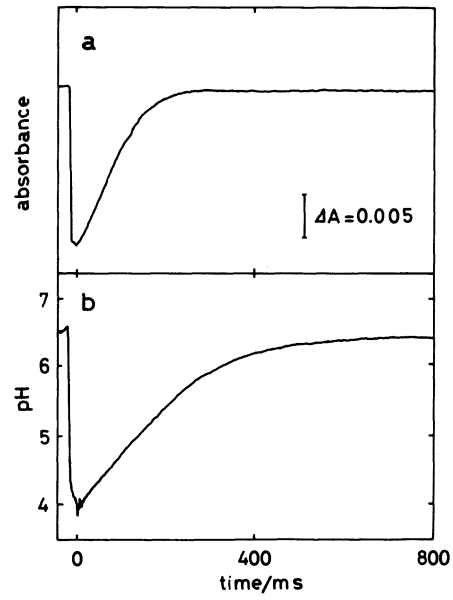

Fig. 3. Reaction curve of dehydration of carbonic acid; (a) by pH indicator and (b) by the pH sensor. The experimental conditions are the same as in Fig. 2.

one is to use the sensor and the other to use Bromophenol Blue as a pH indicator. As can be seen in Fig. 3, their time courses are apparently different. This is because the ordinates of the two curves are different, i.e., the scale for the sensor is pH, while that for the indicator is absorbance. In case of the optical detection, the relaxation time was obtained from the slope of the semilogarithmic plot of the absorbance change against time, as shown in Fig. 4(a). On the other hand, for the case of the pH sensor, the output signal should be converted to hydrogen ion concentration which was plotted in Fig. 4(b). The relaxation times estimated are 17.5±0.5 s^{-1} and 17.0±1.3 s^{-1} for the sensor and indicator, respectively. This good

agreement suggests the pH sensor incorporated with the ISFET-stopped flow apparatus is working correctly. In order to confirm this utility, kinetic experiments were continued under various concentrations.

The dehydration reaction of carbonic acid is represented by next reaction scheme

$$HCO_3^- + H^+ \underset{}{\overset{K_1}{\longleftrightarrow}} H_2CO_3 \underset{k_{-2}}{\overset{k_2}{\longleftrightarrow}} CO_2 + H_2O, \quad (1)$$

where K_1 and K_2 denote the equilibrium constants of the first and the second steps, and k_2 and k_{-2} forward and backward rate constants of the second step, respectively. Since the first step in the above reaction is faster than the second one, the relaxation time τ^{-1} for the second process can be represented by

$$\tau^{-1} = k_2 \left(\frac{[H^+] + [HCO_3^-]}{K_1 + [H^+] + [HCO_3^-]} + \frac{1}{K_2} \right). \quad (2)$$

According to this equation, the relaxation time obtained was plotted against concentration term which can be calculated by using K_1 and K_2. By using the values of 1.72×10^{-4} M^{-1} reported for K_1[19] and 4.7×10^2 assumed for K_2, a best straight line passing the origin was obtained as can be seen in Fig. 5. The slope of the straight line gives the value of (18±1) s^{-1} for k_2 and the value of k_{-2} was calculated to be $(4.0\pm0.2)\times10^{-2}$ M^{-1} s^{-1} from K_2 and k_2. As for the dehydration reaction, the values of (13.7—27.9) s^{-1} for k_2 and $(3.6—4.3)\times10^{-2}$ M^{-1} s^{-1} for k_{-2} have been reported.[14,20-23] The values estimated in the present work are in good accordance with these reported so far. Consequently, the ISFET-stopped flow apparatus constructed was proved to be nicely working.

As for the comparison of the two data obtained by pH sensor and pH indicator, it should be emphasized that pH indicator has some disadvantages; the change in absorbance of pH indicator can correctly reflect that in the hydrogen ion only for the small change in the concentration. In practice, obvious deviation from the straight line in Fig. 4(a) was recognized. Further, a single pH indicator can be used only at limited pH

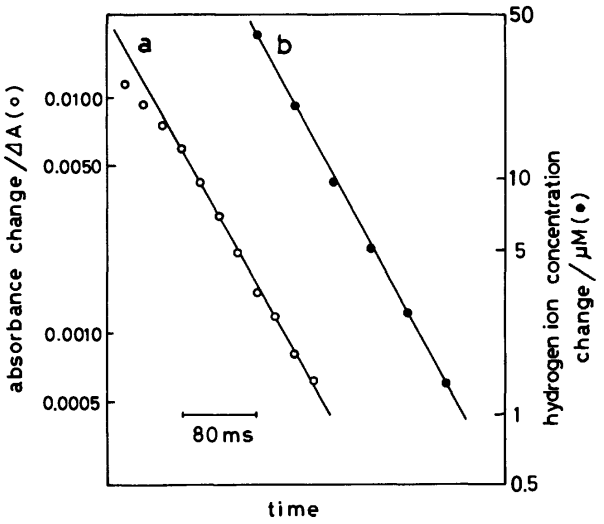

Fig. 4. Semilogarithmic plots of the observed reaction curve against time; (a) absorbance change detected by pH indicator and (b) hydrogen ion concentration change by the pH sensor.

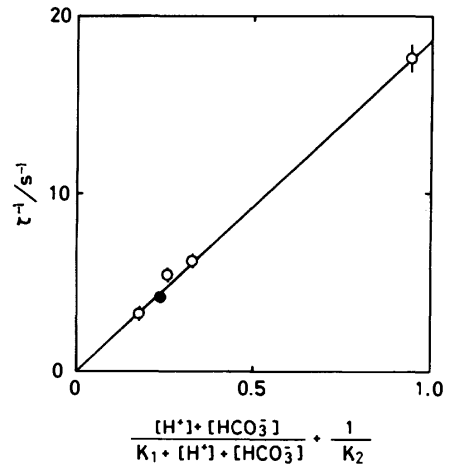

Fig. 5. A plot of τ^{-1} vs. the concentration term in Eq. 2. (●) denotes the data at ionic strength of 0.1 M.

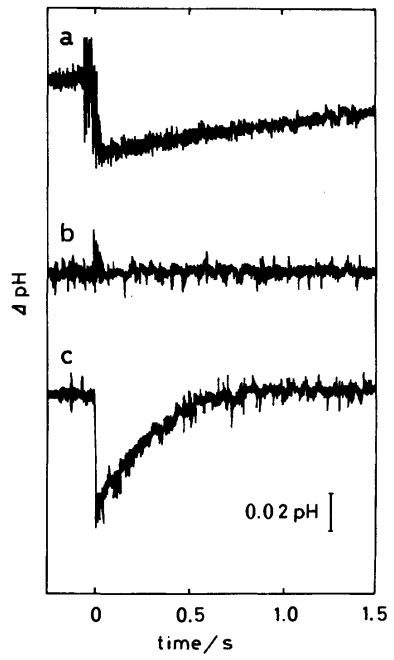

Fig. 6. Measurement of small pH change. (a) The artifact arisen from the flow of the 10^{-4} M NaCl solution. (b) Elimination of the artifact by the flow of 0.1 M NaCl solution. (c) Reaction curve of dehydration of carbonic acid at ionic strength of 0.1 NaCl; 1×10^{-4} M HCl and 5×10^{-5} M $NaHCO_3$ solution were mixed.

range. Meanwhile, the single pH sensor can be satisfactorily used for the kinetic study in solution over wide range of pH value 1—13.

In general, the pH measurement using an electrode is affected by the ionic strength of solution. This effect comes from the distortion and restoration of the ionic atmosphere around the tip of the reference electrode, and brings about the slowing down of its response time and the instability of the pH value. In the case of the pH sensor, such effect was observed as an artifact in the stopped flow experiments as shown in Fig. 6(a). However, as shown in Fig. 6(b), the artifact can be eliminated by holding the ionic strength at 0.1 M, and then the reaction curve could be nicely detected even for small change of 0.04 in pH unit as in Fig. 6(c); the relaxation time obtained from this data is also reasonably on the line in Fig. 5. In addition, most kinetic studies, especially for biological system, have been carried out at relatively high ionic strength around 0.1 M, therefore, the artifact must be not so serious problem.

In the present work, the pH-ISFET was, for the first time, combined with the stopped flow apparatus, and proved to be useful for the kinetic studies of the fast reaction up to 3 ms associated with the large change as well as small change in pH. Further, the present results may suggest the similar applicability of the ISFET developed for other ion to the kinetic investigation of fast reactions associated with biologically interesting ions such as Ca^{2+}, Mg^{2+}, K^{+}, and Na^{+}.

The authors are indebted to Drs. Kojiro Takahashi and Takao Kodama of Okayama University Dental School for giving a motivation to start the present work. This study was supported in part by a Grant-in-Aid for Scientific Research No. 61470165 from the Ministry of Education, Science and Culture.

References

1) K. Hiromi, "Kinetics of Enzyme Reactions. Theory and Practice," Kodansha, Tokyo and John Wiley & Sons, New York (1979).

2) B. Chance, "Investigation of Rates and Mechanisms of Reactions," in "Technique of Chemistry," 3rd ed, ed by G. G. Hammes, Wiley-Interscience, New York (1974), Vol. VI, Part 2, Chap. II.

3) K. Hiromi, S. Ono, S. Itoh, and T. Nagamura, *J. Biochem.*, **64**, 897 (1968).

4) P. M. Bayley, *Prog. Biophys. Mol. Biol.*, **37**, 149 (1981).

5) T. Okubo, *Makromol. Chem. Suppl.*, **14**, 161 (1985).

6) R. L. Berger and L. C. Stoddart, *Rev, Sci. Instrum.*, **36**, 78 (1965).

7) I. Yamazaki and L. H. Piette, *Biochem. Biophys. Acta*, **50**, 62 (1961).

8) J. J. Grimaldi and B. D. Sykes, *J. Biol. Chem.*, **250**, 1618 (1975).

9) P. Mitchell and J. Moyle, *Eur. J. Biochem.*, **4**, 530 (1968).

10) P. Mitchell, *Biochem. Soc. Trans.*, **4**, 399 (1976).

11) N. Sone, M. Yoshida, H. Hirata, and Y. Kagawa, *J. Biol. Chem.*, **252**, 2956 (1977).

12) A. F. Yatel, Jr., and R. Lumry, *Methods Biochem. Anal.*, **20**, 169 (1971).

13) J. A. Sirs, *Trans. Faraday Soc.*, **54**, 207 (1958).

14) L. Rossi-Bernardi and R. L. Berger, *J. Biol. Chem.*, **243**, 1297 (1968).

15) T. Nakamura, *J. Biochem.*, **70**, 961 (1971).

16) P. Bergveld, *IEEE Trans. on BME*, **17**, 70 (1970).

17) T. Matsuo and K. D. Wise, *IEEE Trans. on BME*, **21**, 485 (1974).

18) M. Esashi and T. Matsuo, *IEEE Trans. on BME*, **25**, 184 (1978).

19) K. F. Wissbrun, D. M. French, and A. Patterson, *J. Phys. Chem.*, **58**, 693 (1954).

20) M. Eigen, K. Kustin, and G. Maass, *Z. Phys. Chem.* (N. F.), **30**, 130 (1961).

21) C. Ho and J. M. Sturtevant, *J. Biol. Chem.*, **238**, 3499 (1963).

22) B. H. Gibbons and J. T. Edsall, *J. Biol. Chem.*, **238**, 3502 (1963).

23) R. G. Pearson, R. E. Meeker, and F. Basolo, *J. Am. Chem. Soc.*, **78**, 709 (1958).

 © 1988 The Chemical Society of Japan Bull. Chem. Soc. Jpn., 61, 803—807 (1988)

The Solvent Extraction of Palladium(II) from Aqueous Chloride Media with 7-Tridecanone Oxime

Katsutoshi INOUE,* Yoshinari BABA, Kazuharu YOSHIZUKA, and Tetsuji OKA
Department of Applied Chemistry, Faculty of Science and Engineering, Saga University, Honjo-machi, Saga 840
(Received May 14, 1987)

The extraction behavior of palladium(II) from the aqueous ammonium chloride solutions with the title extractant in toluene was investigated in terms of the equilibrium and the kinetics, while the aqueous solubility and the interfacial adsorption equilibrium of the extractant were estimated. The extraction rate of the 1:2 palladium(II)–extractant complex was explained by the interfacial reaction model, in which the rate-determining steps were assumed to be the elementary reactions between the aquatrichloro- and tetrachloropalladate(II) in the aqueous phase and the extractant molecule adsorbed at the interface.

Great attention has been paid to developing solvent extraction or chelating ion exchange techniques in order to replace the conventional precipitation techniques for the recovery and purification of precious metals on commercial scale. Various extracting agents and chelating resins with high loading capacities and excellent selectivities to precious metals have become commercially available as novel techniques have been developed. The precious metals are extracted or adsorbed from aqueous chloride media rather than from nitrate, sulfate, cyanide, or thiocyanide media in the currently applied techniques.

Recently we have investigated the solvent extraction of palladium(II) from aqueous chloride media with various extracting agents, such as sulfur-containing extractants[1–4] and a hydroxy oxime.[5] In these works, the kinetics of the solvent extraction has been found to be significantly affected by the interfacial activities of the extracting agents as well as by their aqueous solubilities. In the extraction with dihexyl sulfide (DHS), triisobutylphosphine sulfide (TIBPS), and 2′-hydroxy-5′-nonylacetophenone oxime, all of which have low aqueous solubilities and high interfacial activities, the rate-determining complex formation reaction takes place at the interface between the aqueous and organic phases, while it takes place in the aqueous phase in the extraction with 1,2-bis(*tert*-hexylthio)ethane (*t*-BHTE), which has a very low interfacial activity and a relatively high aqueous solubility. The kinetic data of the former extraction systems were reasonably interpreted in terms of the heterogeneous interfacial reaction model, while those of the latter extraction system were interpreted in terms of the classical homogeneous heterophase reaction model of complex formation.

Holland et al.[6,7] investigated extensively the solvent extraction of metals with various kinds of dialkyl ketone oximes with relatively short alkyl chains, either symmetric or unsymmetric, and found that the so-called soft metals, such as palladium(II), silver(I), mercury(II), and gold(III), are effectively extracted into chloroform. However, their studies aimed at the analytical use of these oximes as extractants and were rather qualitative; the extraction mechanisms have remained unclarified.

This paper will report in detail on the extraction behavior of palladium(II) from aqueous chloride media with 7-tridecanone oxime, one of the symmetric dialkyl ketone oximes. The extraction equilibrium and kinetics, including the interfacial adsorption equilibrium of the extractant, were investigated quantitatively; the aqueous solubility of the extractant was also determined.

Experimental

Reagents. The 7-tridecanone oxime, abbreviated as 7-TDO and denoted by HR hereafter, was synthesized from 7-tridecanone in ethanol and an aqueous mixture of hydroxylamine hydrochloride and sodium acetate by a conventional method according to the following reaction:

$$(C_6H_{13})_2CO + NH_2OH\cdot HCl + CH_3COONa \longrightarrow (C_6H_{13})_2C{=}NOH + CH_3COOH + NaCl + H_2O$$

After washing with water and phase separation, the product was purified by means of vacuum distillation (bp 109—110 °C/0.1 mmHg (1 mmHg=133.322 Pa)). The purified viscous, pale yellow liquid product was identified by means of IR and NMR spectroscopies; the purity was confirmed by means of elemental analysis. Found: C, 73.11; H, 12.76; N, 6.63%. Calcd for $C_{13}H_{27}NO$: C, 73.18; H, 12.75; N, 6.56%. The organic phase was prepared on a gravimetric basis by diluting the purified reagent with toluene of an analytical grade. The aqueous phase was prepared by dissolving palladium(II) chloride in aqueous ammonium chloride solutions containing a small amount of hydrochloric acid (about 0.01 mol dm^{-3}).

Determination of the Stoichiometry of the Extracted Species. Under an excess concentration of 7-TDO over the palladium(II) concentration in the aqueous phase, the palladium(II) was almost completely extracted over the whole concentration region of chloride ions in the present experiment (0.01—6 mol dm^{-3}). The remaining amount of palladium(II) was too small for a precise quantitative analysis to be made. Therefore, only a loading test was carried out to determine the molar ratio of palladium(II) extracted into the organic phase to 7-TDO by varying the

concentration ratio of 7-TDO in the organic phase to that of palladium(II) in the aqueous phase under the conditions of a large excess of the palladium(II) concentrations, as in the extraction with DHS, TIBPS, and *t*-BHTE.[1,3,4]

Equal volumes (0.02 dm^3) of two phases of known concentrations were vigorously shaken for 2 h in a separatory funnel using an Iwaki V-DV-type mechanical shaker in a thermostated air bath maintained at 303 K. It had been confirmed by a preliminary experiment that the equilibrium was attained within 2 h. After the separation of the two phases, the palladium(II) concentration in the aqueous phase was determined by means of atomic absorption spectroscopy using a Nippon Jarrell-Ash model AA 782 spectrophotometer. The palladium(II) concentration in the organic phase was calculated from the mass balance of the aqueous palladium(II) concentrations before and after the equilibration.

Measurement of Aqueous Solubility of the Extractant. The distribution of 7-TDO between the organic and aqueous phases was measured spectrophotometrically at 303 K by a method similar to that described in previous papers.[1,4]

A toluene solution of 7-TDO of a known concentration and a 0.1 mol dm^{-3} aqueous ammonium choride solution with a volume ratio of the aqueous phase to the organic phase of 10:1 were shaken vigorously for 24 h using the mechanical shaker. After phase-separation, a portion of the aqueous phase (0.19 dm^3) was transferred into a separatory funnel. In order to convert completely any 7-TDO dissolved in the aqueous phase to its palladium(II) complex, 5×10^{-2} dm^3 of a 2 mmol dm^{-3} aqueous palladium(II) chloride solution containing 10 mmol dm^{-3} of hydrochloric acid and 1×10^{-2} dm^3 of toluene were added to the separatory funnel, after which the mixture was shaken for 24 h using a mechanical shaker. The absorbance of the palladium(II) complex in toluene was measured at 284 nm against a toluene blank using a Shimadzu UV 140 spectrophotometer.

Measurement of Interfacial Adsorption Equilibrium. The interfacial tension between the organic solution and the 0.1 mol dm^{-3} aqueous ammonium chloride solution was measured at 303 K by means of the pendant-drop method in order to examine the interfacial adsorption equilibrium of 7-TDO.

Measurement of Extraction Rate. The extraction rate of palladium(II) was measured using a batch-type glass stirred cell with an inner diameter of 0.1 m and a depth of 0.15 m; it was fitted with four baffles made of poly(tetrafluoroethylene), each of which was 0.01 m wide and 0.15 m long. It was the same as that used for the measurement of the extraction rate of palladium(II) with *t*-BHTE and TIBPS in the previous works.[1,4]

Stirring was carried out at a constant stirring speed of 1500 min^{-1} using a turbine impeller with six flat blades connected to a speed controller. Equal volumes (0.3 dm^3) of the organic and aqueous phases were introduced into the cell placed in a water bath maintained at 303 K. After the initiation of stirring, small amount of samples were taken out at definite time intervals in order to measure the variation in the palladium(II) concentration in the aqueous phase with time; the concentration was determined by means of atomic absorption spectrophotometry.

The initial palladium(II) concentration was 0.5 mmol dm^{-3} in all kinetic runs, while the concentrations of the extractant and chloride ion were varied over the ranges of 2—150 mmol dm^{-3} and 5×10^{-3}—5 mol dm^{-3} respectively.

Results

Selectivity of 7-TDO to Various Metals. Figure 1 shows the results of the solvent extraction of various metals from hydrochloric acid solutions with 7-TDO. Palladium(II) is completely extracted over the whole concentration region of hydrochloric acid, while relatively small amounts of mercury(II) and platinum(IV) are extracted, especially in the low-concentration region of hydrochloric acid. The base metals, such as copper(II), zinc(II), nickel(II), cobalt(II), and aluminum(III), are not practically extracted, not even in the high-concentration region of hydrochloric acid, though considerable amounts of copper(II) and nickel(II) were extracted in such high-concentration regions as above 0.1 and 2 mol dm^{-3} respectively in the extraction with 2-ethylhexanal oxime in a previous work[8]. Palladium(II) extracted by 7-TDO can be

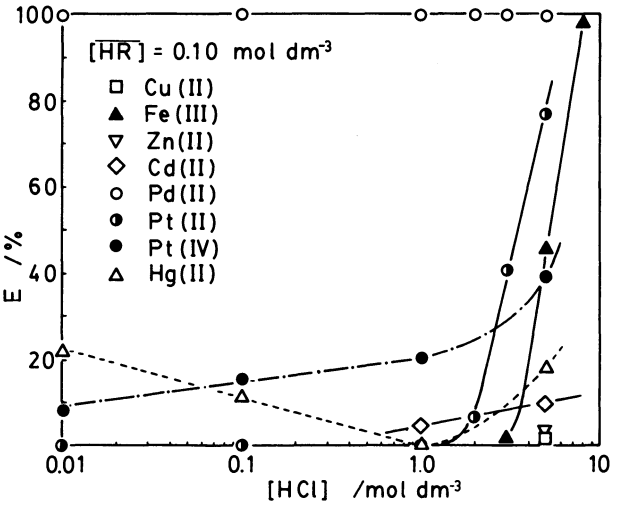

Fig. 1. Percentage extraction of various metals from hydrochloric acid with 0.1 mol dm^{-3} 7-tridecanone oxime in toluene. Initial metal concentration=100 ppm for Pd(II) and Pt(II and IV) or 0.01 mol dm^{-3} for other metals.

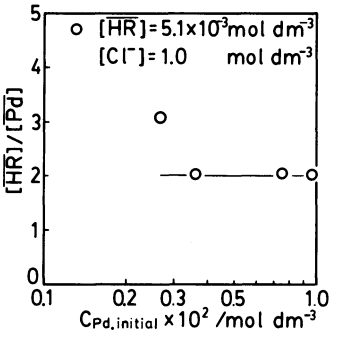

Fig. 2. Experimental results of the loading test.

easily and completely stripped by aqueous thiourea or ammonium thiocyanate solutions; however, only a partial stripping can be accomplished by aqueous ammonia and sodium or ammonium thiosulfate solutions. Thus, 7-TDO is an excellent extracting reagent, suitable for the separation of palladium(II) from platinum(II and IV) and base metals in the low-concentration region of hydrochloric acid in particular.

Stoichiometry of the Extracted Species. Figure 2 shows the result of the loading test. The mole ratio of 7-TDO to palladium(II) in the organic phase asymptotically approaches 2 with an increase in the aqueous palladium(II) concentration. This suggests that palladium(II) is extracted as a 1:2 metal:reagent complex into the organic phase.

Taking account of the results of the previous work,[8] the stoichiometry is expressed in manner similar to that used for copper(II) with 2-ethylhexanal oxime:

$$PdCl_i^{(i-2)-} + 2\overline{HR} \rightleftharpoons \overline{PdCl_2 \cdot 2HR} + (i-2)Cl^- \quad (1)$$

where the overline denotes the species existing in the organic phase.

Aqueous Solubility of 7-TDO. Assuming that free 7-TDO is monomeric, the distribution of 7-TDO between the organic and aqueous phases is expressed as follows:

$$\overline{HR} \rightleftharpoons HR \quad (2)$$

$$K_D = [HR]/[\overline{HR}] \quad (3)$$

where K_D is the partition coefficient of 7-TDO. From Eq. 3, we obtain:

$$\log[HR] = \log[\overline{HR}] + \log K_D \quad (4)$$

The partition coefficient is so small that the concentration of 7-TDO in the organic phase, $[\overline{HR}]$, is nearly equal to its initial concentration, C_{B0}.

As may be expected from Eq. 4, the plot of the logarithm of the concentration of 7-TDO in the aqueous phase against that in the organic phase gives a linear relationship, as is shown in Fig. 3. From the intercept of the straight line with the ordinate in Fig. 3, the partition coefficient was evaluated as $K_D = 7.0\times10^{-6}$ according to Eq. 4. This value is very close to that of TIBPS ($=5.4\times10^{-6}$).[4]

This result supports the idea that 7-TDO is monomeric in toluene, as has been confirmed by the measurement of the molecular weight by means of vapor-phase osmometry.

Interfacial Tension. Figure 4 shows the plot of the interfacial tension, γ, between an organic solution containing 7-TDO and a 0.1 mol dm^{-3} aqueous ammonium chloride solution against the concentration of 7-TDO in the organic phase. The interfacial tension decreases with an increase in the concentration of 7-TDO in its high-concentration region, which indicates that 7-TDO is interfacially active.

The adsorption equilibrium of 7-TDO at the interface is described as follows:

$$\overline{HR} \rightleftharpoons HR_{ad} \quad ; K_{ad} \quad (5)$$

where the subscript "ad" denotes the adsorbed species at the interface. The relationship between the interfacial tension, γ, and the concentration of 7-TDO in the organic phase, $[\overline{HR}]$, is given in Eq. 6, which has been obtained by combining the Gibbs adsorption isotherm with Langmuir's monolayer adsorption model applied to the above-mentioned adsorption equilibrium similarly as to the adsorption equilibrium of TIBPS:[4]

$$\gamma = \gamma_0 - (RT/S_{HR})\ln(1 + K_{ad}[\overline{HR}]) \quad (6)$$

where γ_0 denotes the interfacial tension between the pure diluent and the 0.1 mol dm^{-3} aqueous ammonium chloride solution and where S_{HR} denotes the interfacial area occupied by a unit mole of 7-TDO. From the results shown in Fig. 4, the values of K_{ad} and S_{HR} were evaluated by the nonlinear, least-squares

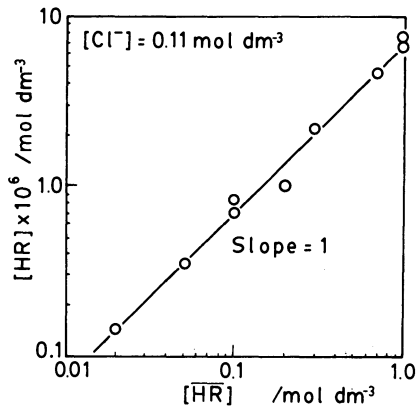

Fig. 3. Aqueous solubility of 7-TDO to aqueous ammonium chloride solution.

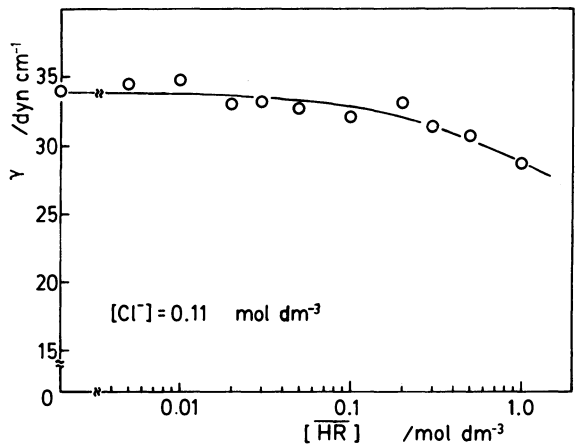

Fig. 4. Relation between interfacial tension and 7-TDO concentration in the organic phase.

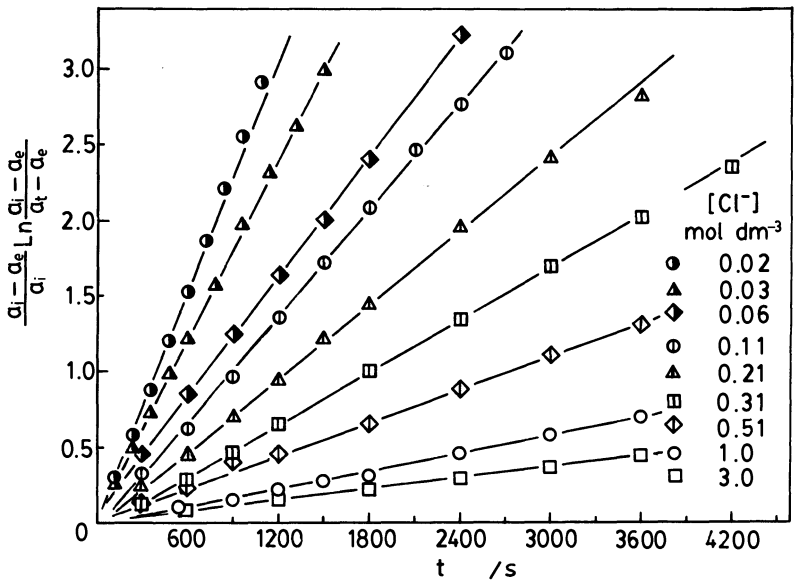

Fig. 5. A typical plot of the experimental results of extraction rate based on the pseudo-first-order rate expression ([$\overline{HR}$]=0.01 mol dm^{-3}).

method based on Eq. 6: K_{ad}=6.3 dm^3 mol^{-1}, S_{HR}= 9.6×10^5 m^2 mol^{-1}. These values are very close to those of TIBPS (K_{ad}=4.4 dm^{3}mol^{-1}, S_S=6.3×10^5 m^2 mol^{-1})[4]. The curve in Fig. 4 is calculated from Eq. 6 using these values. The calculated curve is in good agreement with the experimental results.

Extraction Kinetics. The variation in the palladium(II) concentration in the aqueous phase with time was rearranged and plotted according to Eq. 7 on the assumption that the forward and reverse reactions are pseudo-first-order with respect to the palladium(II) concentration in the aqueous and organic phases respectively:

$$\frac{a_i - a_e}{a_i} \ln \frac{a_i - a_e}{a_t - a_e} = k_f t \qquad (7)$$

where k_f represents the observed reaction rate-constant for the forward reaction and where the quantities with the subscripts "t", "i", and "e" denote the concentration after time t, at t=0, and at equilibrium respectively.

Figure 5 shows a typical set of the experimental results plotted according to Eq. 7. The plots in this figure give straight lines, as is to be expected from Eq. 7, suggesting that the forward reaction rate of palladium(II) extraction is first-order with respect to the palladium(II) concentration in the aqueous phase. The apparent reaction-rate constants were obtained from the slopes of these straight lines. Since the apparent reaction-rate constant was found in the preliminary experiment to be independent of the stirring speed over the range greater than 1300 min^{-1}, subsequent experiments were carried out at a constant stirring speed of 1500 min^{-1}, as will be discussed earlier.

Figure 6 shows the effect of the chloride-ion

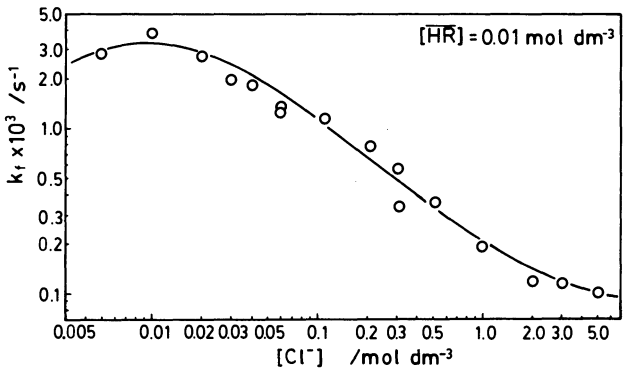

Fig. 6. Effect of chloride ion concentration on the observed extraction rate constant.

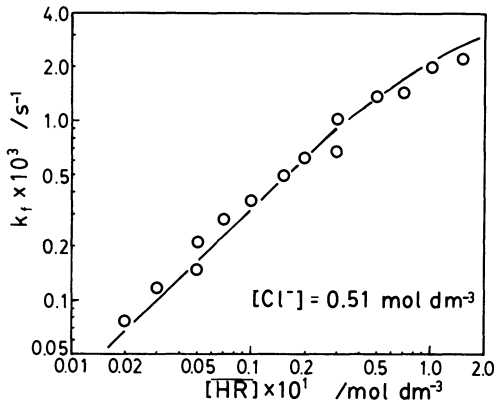

Fig. 7. Effect of 7-TDO concentration on the observed extraction rate constant.

concentration on the observed reaction-rate constant. The plots in this figure appear to approach a constant value with decrease or increase of the chloride-ion concentration in its low- and high-concentration regions respectively. Figure 7 shows the effect of the

7-TDO concentration on the observed reaction rate constant. The plots in this figure lie on a straight line with a slope of 1 and tend to approach a constant value in the high-concentration region.

These tendencies of the concentration dependencies of the reactant species on the extraction rate of palladium(II) are partly similar to those observed in the extraction with TIBPS.[4] Therefore, the experimental results of the extraction kinetics were analyzed on the basis of the heterogeneous interfacial reaction model applied to the analysis of the extraction kinetics by TIBPS[4], as will be described in the following section.

Discussion

The following results obtained in the present work suggest that a certain elementary process taking place at the interface plays an important role in the reaction mechanism of the present extraction system: (1) The aqueous solubility of 7-TDO is too low to assume that homogeneous reactions take place to any considerable extent in the aqueous phase; (2) 7-TDO has interfacial activity, and (3) the reaction order with respect to the extractant is less than unity in its high-concentration region.

Consequently, in a manner similar to that employed in the analysis of the extraction kinetics with TIBPS,[4] palladium(II) is considered to be extracted by 7-TDO from aqueous chloride media according to the following reaction scheme:

$$[PdCl_3(H_2O)]^- + HR_{ad} \xrightarrow{k_1} [PdCl_3 \cdot HR]^-_{ad} + H_2O \quad (8)$$

$$[PdCl_4]^{2-} + HR_{ad} \xrightarrow{k_2} [PdCl_3 \cdot HR]^-_{ad} + Cl^- \quad (9)$$

$$[PdCl_3 \cdot HR]^-_{ad} + HR \rightleftharpoons \overline{[PdCl_2 \cdot 2HR]} + Cl^- \quad (10)$$

Assuming that the parallel elementary reactions to form the intermediate complex at the interface, $[PdCl_3 \cdot HR]^-_{ad}$, as described by Eqs. 8 and 9, are rate-determining, and taking account of the fact that the aquatrichloro complex, $[PdCl_3(H_2O)]^-$, and the tetrachloro complex, $[PdCl_4]^{2-}$, are predominant under the present experimental conditions, the rate of the present extraction reaction can be approximately described as follows:

$$-\frac{da_t}{dt} = \frac{K_{ad}[\overline{HR}]}{1 + K_{ad}[\overline{HR}]} \left(\frac{k_1\beta_3 + k_2\beta_4[Cl^-]}{\beta_3 + \beta_4[Cl^-]}\right) a_t \quad (11)$$

where β_3 and β_4 denote the stability constants of aquatrichloro- and tetrachloropalladate(II). The effects of varying the concentrations of each reactant species on the extraction rates shown in Figs. 6 and 7 can be qualitatively interpreted by Eq. 11, derived from the proposed interfacial reaction scheme.

The optimum values of the rate constants, k_1 and k_2, of the rate-determining steps described by Eqs. 8 and 9 were calculated by the nonlinear, least-squares method from the data in Figs. 6 and 7, using the value of K_{ad} obtained in the preceding section and the stability constants of the palladium(II) chloro complexes in the literature[10] ($\beta_3=2.00\times10^{10}$, $\beta_4=7.94\times10^{11}$): $k_1=9.7\times10^{-2}$ s^{-1}, $k_1=1.3\times10^{-3}$ s^{-1}. The magnitudes of the orders of these values are very close to those observed in the extraction with TIBPS from hydrochloric acid ($k_1=6.1\times10^{-1}$ s^{-1}, $k_2=1.7\times10^{-3}$ s^{-1}). The solid lines shown in Figs. 6 and 7 are the curves calculated from Eq. 11 using these values. These lines are in fairly good agreement with the experimental results.

Conclusion

The partition coefficient of 7-TDO to the aqueous solution and its adsorption equilibrium parameters, the interfacial area occupied by a unit mole of the extractant, and the interfacial adsorption equiibrium constant are very close to those of triisobutylphosphine sulfide (TIBPS) as reported in a previous work.[4] Palladium(II) is extracted as a mononuclear complex by the use of 7-TDO, while it is extracted as a binuclear complex when TIBPS is used.

The experimental results of the extraction kinetics were quantitatively explained by the interfacial reaction model proposed for the kinetics of extraction with TIBPS, in which the ligand substitution between the extractant molecule adsorbed at the interface and aquatrichloro- and tetrachloropalladate(II) in the aqueous phase are rate-determining. The extraction rate was satisfactorily expressed by Eq. 11, which was derived from the interfacial reaction model presented above. The values of the reaction-rate constants in Eq. 11 were found to be close to those observed in the extraction with TIBPS.

References

1) Y. Baba, T. Eguchi, and K. Inoue, *Bull. Chem. Soc. Jpn.*, **59**, 1321 (1986).

2) Y. Baba, A. Goto, and K. Inoue, *Solvent Extr. Ion Exch.*, **4**, 255 (1986).

3) Y. Baba, T. Eguchi, and K. Inoue, *J. Chem. Eng. Jpn.*, **19**, 361 (1986)

4) Y. Baba, M. Ohshima, and K. Inoue, *Bull. Chem. Soc. Jpn.*, **59**, 3829 (1986).

5) K. Inoue and T. Maruuchi, *Hydrometallurgy*, **16**, 93 (1986).

6) W. J. Holland, R. D. Dimenna, and R. J. Walker, *Mikrochim. Acta*, 1972, 183.

7) P. W. Beaupre and W. J. Holland, *Mikrochim. Acta III*, 1983, 341.

8) K. Inoue, Y. Baba, and T. Oka, *Solvent Extr. Ion Exch.*, **4**, 237 (1986).

9) K. Inoue, Y. Kawano, F. Nakashio, and W. Sakai, *Kagaku Kogaku*, **38**, 41 (1974).

10) M. I. Gelfman and N. V. Kiseleva, *Zh. Neorg. Khim.*, **14**, 502 (1969).

 © 1988 The Chemical Society of Japan Bull. Chem. Soc. Jpn., 61, 809—814 (1988)

The Wetting of Alumina Substrate by Liquid Gold†

Masumi USHIO* and Yoshihiro SUMIYOSHI
Department of Applied Chemistry, Faculty of Engineering, Gunma University,
Tenjin-cho, Kiryu-shi 376
(Received June 17, 1987)

The wetting of an Al_2O_3 substrate by liquid gold was investigated by means of the sessile-drop method in an atmosphere of argon. An empirical relation was estabilished between the contact angle and the temperature or surface tension of the liquid drop by the use of the diameter and the height of the sessile drop. The contact angle was constant with time, but decreased linearly with an increase in temperature. The variation in the contact angle with temperature is correlated with the surface tension of the sessile drop. The surface tension of liquid gold was obtained as 933 dyn cm^{-1} at 1080 °C and 917 dyn cm^{-1} at 1100 °C and the temperature coefficient of the surface tension of liquid could be estimated to be −0.80 dyn cm^{-1} $°C^{-1}$. The critical surface tension (γ_c) and the surface tension of liquid gold at 0 K of Al_2O_3 (γ°_{Lv}) were 20 and 2015 dyn cm^{-1}, respectively.

As was reported in the first part,[1] the wetting of an Al_2O_3 substrate by liquid Ag was investigated by the sessile drop technique under an atmosphere of argon. An empirical relation was established between the contact angle and the temperature or surface tension of the liquid drop, by use of Rhee's equation. The contact angle was constant with increasing time and decreased linearly with increasing temperature. The variation of the contact angle with temperature could be correlated with the surface tension of the sessile drop. The critical surface tension (γ_c) of Al_2O_3 is 923 dyn cm^{-1}, and the surface tension of liquid Ag at 0 K was 1130 dyn cm^{-1}.

In the present paper, the wettability of a sintered alumina substrate with a surface that was polished to be flat and smooth by liquid Au was investigated by the sessile drop techniques in an atmosphere of argon in much the same way as was reported in the first part.

This was done in order to obtain values of the surface tension of liquid Au, the temperature coefficient of the surface tension of liquid Au, the critical surface tension (γ_c), and the surface tension of liquid Au at 0 K. Since sufficient results were obtained, details are reported here.

Experimental

The sintered alumina (99.5%, Kyocera Co.) was used as a substrate with dimensions 20×20×3 mm^3, its surface was polished to a mirror-like finish. The high-purity gold (99.99%, Ishifuku Co.) was cut into a disk. The dimensions of the gold disk were 4 mm in diameter and 3 mm in thickness; its purity was 99.99%.

The sessile-drop apparatus used to measure the contact angle was the same as that mensioned in a previous paper.[1] A Pt-Pt13%Rh thermocouple was used for temperature measurements. The furnace was operated in an atmosphere of argon at a rate of about 0.9 L min^{-1}. The gold disk and substrate were cleaned with acetone and then dried in a vaccum. The gold disk after being placed on an alumina substrate was put queitly into the furnace.

After adjusting the horizontal position, argon gas was flowed. The furnace temperature was increased to a specified value and then maintained for 30 min.

The shadow of a sessile drop of gold was then photographed from the back by using light produced by a mercury lamp. The contact angle of the drop was bilaterally measured and its mean value was taken as the measured value.

In the case of a constant temperature of 1080 °C, the contact angle was measured at 5-minute intervals for a period of 60 min. On the other hand, for various temperatures from 1070 to 1100 °C, the contact angle of a gold drop was also measured at intervals of 5 °C. From many photographs, the diameters and heights of the sessile drops of gold were also measured. These diameters were used to calculate the surface tension of liquid gold as well as the critical surface tension for spreading (γ_c) for the Au/Al_2O_3 system.

The human error was found to be about ±1° by measuring the contact angle from ten photographs. The temperature deviation was ±2 °C. The regions of the gold drop/alumina substrate were using an optical microscope and a scanning electron microscope.

Results

In the case of a constant temperature of 1080 °C, the photographs used in measuring the contact angles of the gold drops are shown in Fig. 1, while the measured values of contact angles are shown in Table 1 and Figs. 2 and 3. These experimental results showed that a contact angle of the liquid gold sessile drop resting on an alumina substrate was about 127°. However there were some differences in the wettability, depending on the test pieces of alumina substrates. Each straight line in Figs. 2 and 3 represents the results of two independent runs.

In the case of different temperature between 1070 and 1100 °C, with the contact angle measured at intervals of 5 °C, the photographs used in measuring the contact angle of a liquid gold sessile drop resting on an alumina substrate are shown in Fig. 4. The effect of the temperature on the contact angle is shown

† Study on Preparation and Characteristic of Functional Inorganic Materials. II.

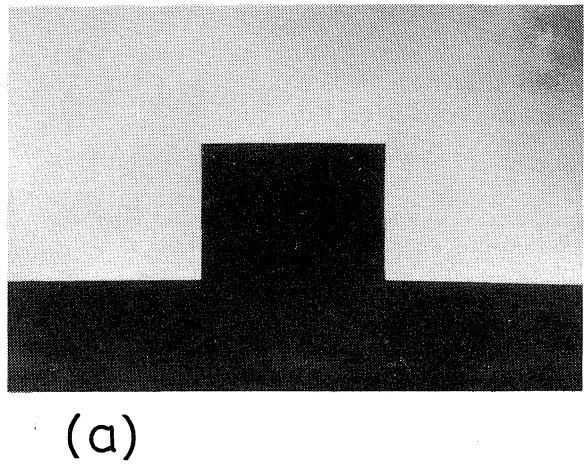

(a)

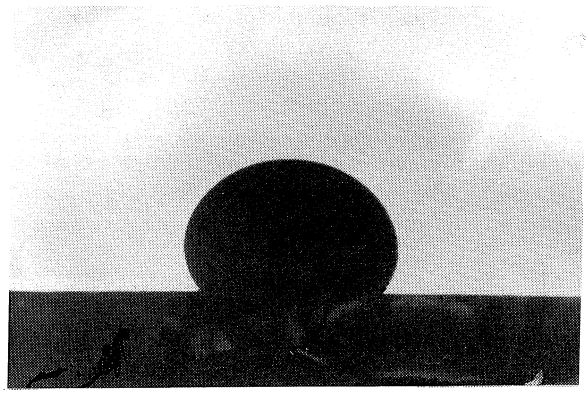

(b)

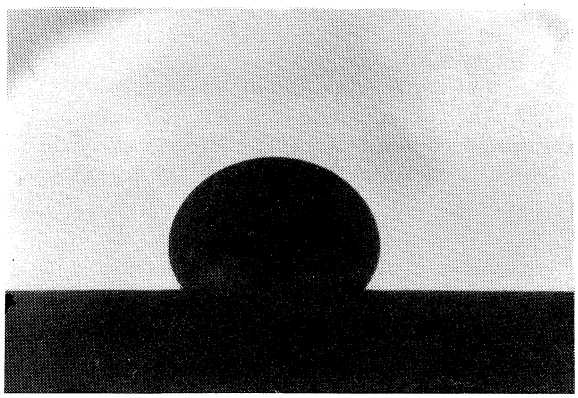

(c)

Fig. 1. Sessile drops of liquid gold on alumina at 1080 °C for Run No. (T-1).
(a) T=0 min (Au metal disk), (b) T=30 min, (c) T= 60 min.

in Table 2 and Figs. 5 and 6. Each straight line in Figs. 5 and 6 also represents the results of two independent runs.

Table 2 shows that the contact angles of liquid gold on the alumina substrate decrease linearly with an increase in the temperature. That is, liquid gold is

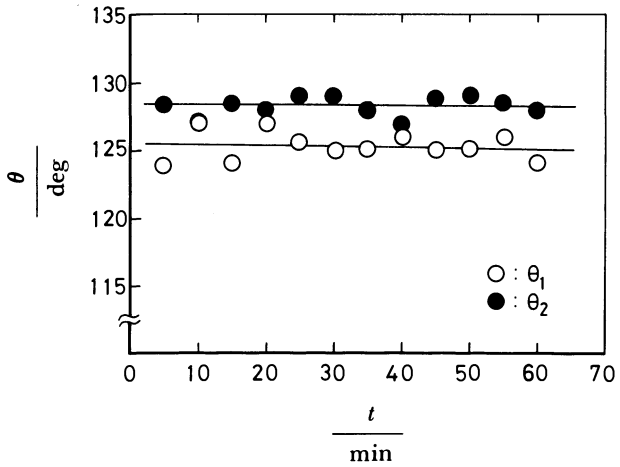

Fig. 2. Change in contact angle with time for a system Au/Al_2O_3 of Run No. (T-1).

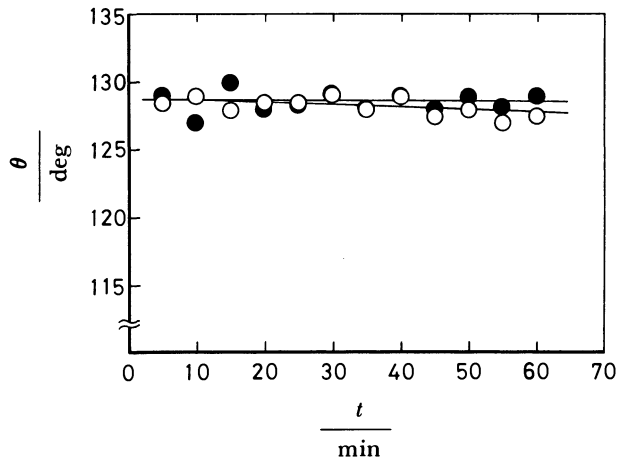

Fig. 3. Change in contact angle with time for a system Au/Al_2O_5 of Run No. (T-2).

Table 1. Experimental Results of the Contact Angles of Liquid Gold Sessile Drops for Each Substrate at 1080°C

Run No. / t min	T-1 θ_1 °	T-1 θ_2 °	T-2 θ_1 °	T-2 θ_2 °	$\theta_{ave.}$ °
5	124.0	128.0	128.5	129.0	127.0
10	127.0	127.0	129.0	127.0	127.5
15	124.0	128.5	128.0	130.0	127.6
20	127.0	128.0	128.5	128.0	127.9
25	125.5	129.0	128.5	128.5	127.9
30	125.0	129.0	129.0	129.0	128.0
35	125.0	128.0	128.0	128.0	127.3
40	126.0	127.0	129.0	129.0	127.8
45	125.0	129.0	127.5	128.0	127.4
50	125.0	129.0	128.0	129.0	127.8
55	126.0	129.5	127.0	128.0	127.4
60	124.0	128.0	127.5	129.0	127.1
Ave.	125.3	128.3	128.2	128.5	127.6

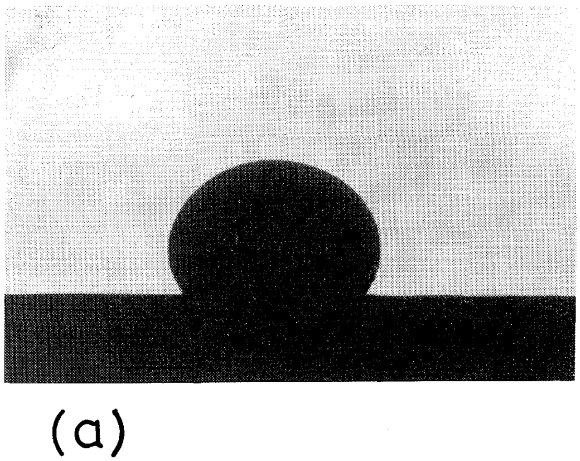

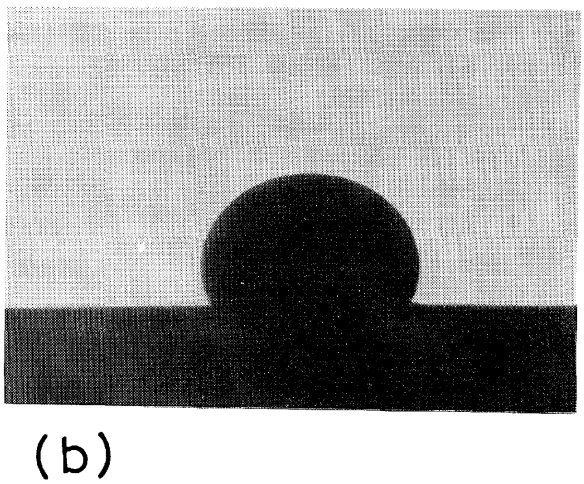

Fig. 4. Sessile drops of liquid gold on alumina for Run No. (T-3).
(a) At 1070 °C, (b) at 1100 °C.

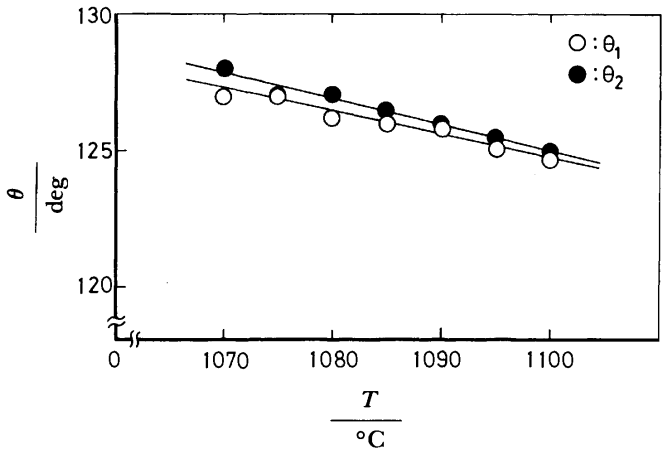

Fig. 5. Change in contact angle with temperature for a system Au/Al_2O_5 for Run No. (T-3).

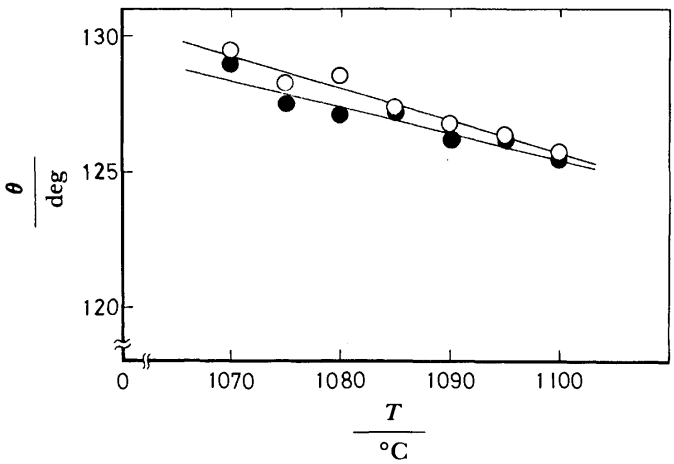

Fig. 6. Change in contact angle with temperature for a system Au/Al_2O_3 for Run No. (T-4).

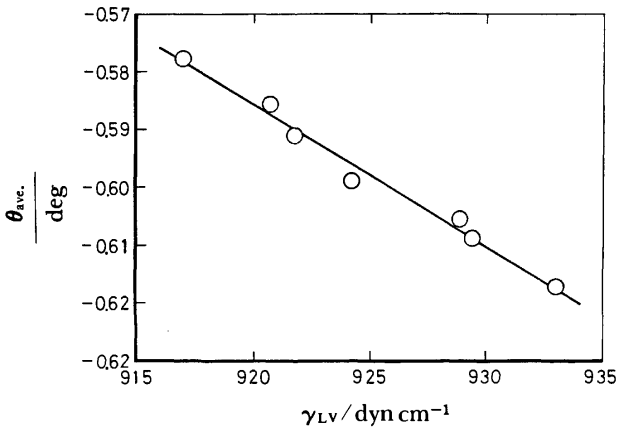

Fig. 7. Cosine of contact angle vs. surface tension of liquid gold for Au/Al_2O_3.

Table 2. Experimental Results of the Effects of Different Temperatures on the Contact Angles of Liquid Gold for Each Substrate at Intervals of 5 °C

t / °C \ Run No.	T-3		T-4		θave. / °
	θ1 / °	θ2 / °	θ1 / °	θ2 / °	
1070	127.0	128.0	129.5	128.0	128.1
1075	127.0	127.0	128.3	127.5	127.5
1080	126.2	127.1	128.6	127.1	127.3
1085	126.0	126.5	127.4	127.2	126.8
1090	125.8	126.0	126.8	126.2	126.2
1095	125.1	125.5	126.4	126.3	125.8
1100	124.7	125.0	125.8	125.5	125.3

liable to wet an alumina substrate.

The state of the surface of an alumina substrate directly under liquid gold was investigated before and after thermal treatment. Before the thermal treatment, it was smooth and flat; however, it was revealed that

the flatness of the surface had been destroyed after the treatment. It seems that a reaction between an alumina substrate and liquid gold took place. A comparison with the case of liquid silver, showed that it had been destroyed less than for liquid gold.[1]

Discussion

The effect of time on the contact angle of a liquid gold sessile drop resting on an alumima substrate was examined at a contact temperature of 1080 °C for runs of (T-1) and (T-2). Each straight line in Fig. 2 can be fitted by means of the following equations:

Run (T-1)

$$\theta_1 = -0.0073x + 125.5$$
$$\theta_2 = 0.0105x + 127.9$$

Run (T-2)

$$\theta_1 = -0.023x + 129.0$$
$$\theta_2 = 0.017x + 128.5$$

In the above x is the time in minutes and θ is the contact angle.

The slopes of these equations were within the absolute value of $|0.0105—0.023|$; they were very small and near zero. Therefore, it can be assumed that the contact angle of liquid gold on an alumina substrate is scarcely changed at a constant temperature of 1080 °C. This result is the same as that observed for a system Ag/Al_2O_3.[1]

The effect of the temperature on the contact angle of liquid gold on an alumina substrate was also investigated for runs of (T-3) and (T-4). The values of the slopes of all the straight lines are negative, as is obvious from Fig. 5. This figure indicates that the contact angle decreases linearly with an increase in temperature and that liquid gold is apt to wet an alumina substrate better. The reason for this may be considered to be that the contact angle becomes small as the forces between molecules of gold decreases with an increase in temperature causing a decrease in the surface tension of gold. However, the contact angle of liquid gold on an alumina substrate was larger than that of liquid silver. That is, using liquid gold it was rather more difficult to wet an alumina substrate than using liquid silver.

The amounts of scatter in the measured values of the contact angle (θ_1 and θ_2) are shown in Tables 1 and 2. It may be assumed that this scatter was due to human measurements errors of ±2°, etc. That is, since sintered alumina was used as a substrate, the effect of binder agents, the difficulty in producing homogeneous finished goods, atmospheric effects, etc. must be considerd.

The alumina substrate was chemically inert to liquid gold in the temperature range investigated, judging from the optical-microscopy and scanning-electron microscope studies. However, the surface of an alumina substrate became fairly rough, judged from surface observations after thermal treatments.

If the surface of an alumina substrate was worn by a thermal treatment, the contact angle of the liquid gold was fairly influenced.

It is necessary to increase the reproducibility in order to produce homogeneous finished goods, to clean the surface of the alumina substrate, to standarize the roughness of the work surface, and to decrease the temperature fluctuation, etc.

Various values of the surface tension of liquid gold have been reported. Values of the surface tension ranged between 580 and 1000 dyn cm^{-1} at 1070 °C in air[2] and 1410 dyn cm^{-1} at 1027 °C.[3] On the other hand, the values of the surface tension of liquid gold by the creep method were 1100 dyn cm^{-1} at 1130 °C in air and 1400 dyn cm^{-1} at 1030 °C in helium.[4]

The surface tension at 1200 °C in hydrogen gas was 1120 dyn cm^{-1}. Another report concerning the surface tension of liquid gold at 1120 °C in hydrogen gas was 1128 dyn cm^{-1} and 1120 dyn cm^{-1} at 1200 °C and 1110 dyn cm^{-1} at 1300 °C.[6] In turn, the surface tension of the solid, that is, gold foil, was 1205 dyn cm^{-1} at 700 °C.[7]

The liquid-solid interface energy, γ_{LS}, is 133 dyn cm^{-1} for gold.[8] It has also been reported that for metal, $\gamma_{LS}=(0.12\pm0.03)\ T_m$, where T_m is the melting point (K).[9] From this equation, we can now estimate it to be between 121 and 201 dyn cm^{-1}, while Southin et al. and Zettlemoyer reported that $\gamma_{LS}=130$ dyn cm^{-1} of the mean value.[10]

Another emprical relation is

$$\gamma_{LS} = \frac{K\Delta H_m}{N_o^{1/3} V_m^{2/3}}$$

where ΔH_m is the latent heat of fusion per mole, V_m the molar volume, N_o Avogadro's number and $K=0.45$ for metals.[9] From this empirical equation, we estimate γ_{LS} to be 126 and 123 dyn cm^{-1}, using $K=0.45$, $N_o=6.02\times10^{23}$ mol^{-1}, $V_m=10.2_2$ cm^3, $\Delta H_m=12.7$ kJ mol^{-1},[11] and 2.955 kcal mol^{-1} (about 12.4 kJ mol^{-1})[12] respectively.

The temperature coefficient of the surface tension of liquid gold has not yet been reported.

From Dorsey's empirical formula,[13] based on Bashforth and Adams table, we can estimate the surface tension of liquid gold to be 933 dyn cm^{-1} at 1080 °C and 917 dyn cm^{-1} at 1100 °C, by using the present experimental results of the maximum diameter, the θ-value of the sessile drop and the distance from the sessile drop and the distance from the apex of the drop to be a 45° tangent: 0.468 cm, 127.6° (at 1080 °C), and 0.109 cm, respectively, and 0.478 cm, 125.5° (at 1100 °C), and 0.112 cm, respectively.

The temperature coefficient of the surface tension of liquid gold could be estimated to be −0.80 dyn cm^{-1} °C^{-1} from the present experiment results shown

in Table 2.

It is found that the calculated values of the surface tension of liquid gold by using other formulas[14] were about 15 to 25% smaller than the values predicted by the Dorsey formula.

We also attempted to calculate the critical surface tension and the surface tension at 0 K for the Au/Al_2O_3 system and, therefore, adopted the values obtained by using the Dorsey formula. The critical surface tension and the surface tension at 0 K were discussed by Rhee.[1,15]

As described above, the cosine of the contact angle increases linearly with an increase in temperature in the Au/Al_2O_3 system. The variation of the cosine of the contact angle with a decrease in the surface tension of liquid gold is shown in Fig. 7 for the Au/Al_2O_3 system. The extrapolation of the straight line to $\cos\theta=+1$ produces the critical surface tension for spreading ($\gamma_c=20$ dyn cm^{-1}) for the Au/Al_2O_3 system, with the surface tension ($\gamma_{LV}^{0}=2015$ dyn cm^{-1}) of liquid gold at 0 K.

For liquid gold, γ_c for Al_2O_3 system, with the surface tension ($\gamma_c=361$ dyn cm^{-1}),[1] but $\gamma_{LV}^{0}=$ for Al_2O_3 is larger that for liquid silver ($\gamma_{LV}^{0}=790$ dyn cm^{-1}).

The melting point and the boiling point for Au are 1063 °C and 2707 °C, respectively. For gold, the values of the vapor pressures follow the Antoine equation:

$$\log_{10} P = -\frac{52.23\,B}{T} + C,$$

where P is the vapor pressure of gold in mm of mercury and T is the absolute temperature. Values for constants B and C are 385 and 9.853, respectively.[16] For the temperature range 2315 to 2500 °C, vapor pressures of 121 values to 399 mmHg (1 mmHg= 133.322 Pa) can be obtained. Other vapor-pressure values are 20 mmHg at 2256 °C and 100 mmHg at 2521 °C, obtained from the Harlacher-Braun equation.[17]

When measuring values of the critical surface tension, etc, the gold vapor near the melting point may be ignored and assumed not being absorbed on the Al_2O_3 substrate.

Conclusion

1) The surface tension of liquid gold in argon was obtained as 933 dyn cm^{-1} at 1080 °C and 917 dyn cm^{-1} at 1100 °C, and expressed in the temperature range 1070 to 1100 °C by γ_{LV} (dyn cm^{-1})=1797−0.80 T(°C). On the other hand, for liquid silver, the surface tension was 650 dyn cm^{-1} (960 °C) and 610 dyn cm^{-1} (1000 °C), the surface tension was 650 dyn cm^{-1} (960 °C) and 610 dyn cm^{-1} (1000 °C), expressed in the temperature range 960 to 1000 °C by γ_{LV} (dyn cm^{-1})= 1610−1.0 T (°C).[1]

2) In a liquid gold/alumina system, a linear relation exists between the cosine of the contact angle and the surface tension of a gold sessile drop when the temperature of the system is varied. This result with a system Au/Al_2O_3 is the same as that with a system Ag/Al_2O_3.[1]

The temperature coefficient of the surface tension of liquid gold in argon was obtained to be −0.80 dyn cm^{-1} °C^{-1}, compared with −1.00 dyn cm^{-1} °C^{-1} of a liquid silver.[1]

3) The liquid-solid interface energy, γ_{LS} was obtained to be 123—126 dyn cm^{-1} in comparison with 115 dyn cm^{-1} of a liquid silver.

4) The critical surface tension, γ_c of a liquid gold was obtained 20 dyn cm^{-1}, against 361 dyn cm^{-1} of a liquid silver.[1]

5) The obtained surface tension at 0 K (γ_{LV}^{0}) for the Au/Al_2O_3 system was to be 2015 dyn cm^{-1} compared with 790 dyn cm^{-1} for liquid silver.[1]

6) According to the Antoine equation, the gold vapor near the melting point can be ignored and thought of as not being absorbed on the Al_2O_3 substrate same as for silver vapor.[1]

The difference between liquid gold and liquid silver of these measured values were attributed to the difference in the electronegativities or electric charges of the atomic nucleus for each metal, although a d-orbital (4s or 5d-orbital) and an s-orbital (5s or 6s-orbital) were similarly used to form the bond.

The authers wish to thank Mr. Hiroshi Watanuki for his assistance during the experimental work.

References

1) M. Ushio and Y. Sumiyoshi, *Bull. Chem. Soc. Jpn.*, **60**, 2041 (1987).

2) Landolt-Börnstein, "Physikalischen-Chemische Tabellen," 5th ed., **1**, 198 (1923); International Critical Tables, **1**, 103 (1926), *ibid*, **4**, 435 (1928).

3) J. M. Blakey and P. S. Maiya, "Surface and Interfaces," ed by T. T. Burke, N. L. Read, and V. Weiss, Syracuse University Press, (1967), p. 325; G. Ehrlich, "Surface Phenomena of Metals," Sociely of Chemical Industry, Monograph, No. 28, 1968, p. 13.

4) M. Maeda, "Hyoumen-busseikougaku-nyumon," Asakura Co., (1970), pp. 32—40.

5) International Critical Tables, **4**, 436 (1928); I. Lauermann, *Z. phys. Chem.*, **68**, 216 (1961).

6) J. Dans and E. Lax, "Taschenbuch für Chemiker und Physiker," (1949), p. 231.

7) S. Majima, M. Ishii, and S. Sakui, *Rikengohou*, **10**, 1061 (1931); G. Tammann and W. Boehme, *Ann. Physik*, **12**, 824 (1932).

8) J. C. Brice, "The Growth of Crystals from Liquids," North-Holland, London (1973), p. 92.

9) J. C. Brice, "The Growth of Crystals from Liquids," North-Holland, London (1973), p. 93.

10) R. J. Southin and G. A. Chadwick, *Sci. Prog.*, **57**, 353

(1969); A. C. Zettlemoyer, "Nucleation," ed by Dekker, New York (1949), p. 91.

11) F. D. Rossini, "Selected Values of Chemical Thermodynamic Properties," U. S. Goverment Printing Office, 1952, p. 145; Landolt-Börnstein Tabellen, 6 Aufl., II, Band, 1951, p. 232.

12) Lange's Handbook of Chemistry, Eleventh ed., ed by J. E. Dean, McGraw-Hill, New York (1973), pp. 4—135.

13) N. E. Dorsey, *J. Wash. Acad. Sci.*, **18**, 606 (1928).

14) G. Quinche, *Ann. Physik.*, **105**, 1 (1985); H. V. Tartar, V. Siverts and R. E. Reitweier, *J. Am. Chem. Soc.*, **63**, 84 (1941); A. W. Porter, *Phil. Mag.*, **15**, 163 (1933); R. S. Bradley, *J. Phys. Chem.*, **33**, 232 (1934); V. K. Semenchenko, "Surface Phenomena in Metals and Alloys," Pergamon Press, New York (1962), p. 236; V. K. Semenchenko and L. P. Shikhobalova, *J. Phys. Chem. (USSR).*, **21**, 613, 707 (1970).

15) S. K. Rhee, *J. Am. Chem. Soc.*, **53**, 639 (1970).

16) Lange's Handbook of Chemistry, Eleventh ed., ed by J. A. Dean, McGraw-Hill, New York (1973), pp. 10—37.

17) Kagakubinran-Kisohen 11, ed by the Chemical Society of Japan, Maruzen Co., Tokyo (1985), pp. 11—112.

Preparation and Properties of Iron(II) Hydroxide-(Sodium Fluoride Tetrasilicic Mica) Intercalation Complexes

Kunio OHTSUKA,* Mitsuru SUDA, and Mikiya ONO
Research & Development Center, Ceramics, Mitsubishi Mining & Cement Co., Ltd.,
2270 Yokoze, Chichibu-gun, Saitama 368
(Received July 7, 1987)

Iron(II) hydroxide-(sodium fluoride tetrasilicic mica) intercalation complexes, which have a chlorite-like structure, were prepared by titrating iron(II) sulfate solutions in the presence of mica with sodium hydroxide under oxygen-free conditions. The formation of iron(II) hydroxide sheets between the silicate layers was evaluated by chemical analysis, XRD, DTA-TGA, and surface-area measurement. The presence of water is essential for the oxidizing of these complexes to occur at room temperature by air, because the O_2 attack on the surface of these iron(II) hydroxide sheets is hindered by the silicate layers. Fine highly dispersed iron metal particles (α-Fe) were formed on the external surface of the silicate by the H_2 reduction of the complexes.

We previously reported that ultra-fine, highly dispersed metal (Ni, Co) particles can be prepared on the external surface of silicates by the reduction of metal (Ni, Co) hydroxide-layer silicate complexes.[1,2] This method of preparation, providing isolated metal atoms on the carrier, leads to many applications for catalysts, magnetic materials, electronics, etc. Therefore, it is desired that this technique is applicable to the iron element as well as to the nickel and cobalt elements; the iron element is essential for those applications.

Besides, iron(II) hydroxide-layer silicate complexes, if possible. should be novel reducing agents which are easy to handle, for iron(II) hydroxide has a strong reducing power and this iron(II) hydroxide sheet would be sandwiched between the silicate layers.

Although many attempts have been made to prepare these iron hydroxide-layer silicate complexes,[3-7] no clear evidence for the formation of these complexes has yet been obtained. These attempts to study clay minerals have been connected with the transformation of expansible layer silicate (2:1 layer silicate) to metal hydroxide-layer silicate, which has a chlorite-like structure. Chlorites have a 2:1 layer structure with a metal hydroxide interlayer, and iron(II, III) is considered to exist in both the hydroxide sheet and the 2:1 layer of chlorites.[8-12]

In this work, the preparation and properties of iron hydroxide-layer silicate (sodium fluoride tetrasilicic mica) complexes were investigated. We have attempted to prepare these complexes with the iron(II) ion, not with the iron(III) ion, because we consider that there is an essential difficulty in forming an iron hydroxide interlayer with the iron(III) ion; the iron(III) ion in the metal hydroxide interlayer of chlorites must be introduced by the oxidation of the iron(II) ion or by coprecipitation as a minor constituent with a major constituent (Al, Mg etc.). One of the reasons why the preparation of iron hydroxide-layer silicate complexes has rarely been carried out with the iron(II) ion is evidently that iron(II)-ion solutions are easily oxidized by air. The problems of what kind of cations can give these hydroxide interlayers and of the mechanism of these transformations will be explained in detail in our next paper.

Experimental

Starting Materials. A 10 wt% sol of sodium fluoride tetrasilicic mica ($NaMg_{2.5}Si_4O_{10}F_2$), obtained from Topy Ind., Co., under the name of Na-TSM, was used. Since this mica sol contains a little α-cristobalite and magnesium fluoride richiterite ($Na_2Mg_6F_2(Si_4O_{11})_2$) as impurities, the sol was diluted with distilled water, and then most of the impurities were separated by centrifugation. Finally sodium fluoride tetrasilicic mica was dried in air at 100 °C.

The characteristics of this mica were described in detail in our previous work.[1] Sodium fluoride tetrasilicic mica is an expansible 2:1 layer silicate. Na^+ ions are located between the silicate layers to balance the negative layer charge of the −1 derived from the vacancies in the silicate layers. These Na^+ ions are exchangeable in water, the theoretical cation-exchange capacity being 254 meq/100 g·mica.

Preparation of Iron(II) Hydroxide-Mica Complexes. Iron(II) hydroxide-(sodium fluoride tetrasilicic mica) complexes were prepared by the titration method: iron(II) sulfate solutions in the presence of mica were titrated with sodium hydroxide under oxygen-free conditions.

The iron(II) ion is thermodynamically unstable with respect to atmospheric oxidation and, especially in alkaline solutions, is rapidly oxidized by the oxygen in the air.[13,14] Hence, great care was taken to prevent it from touching with O_2 during the preparation. The preparation procedures were operated under a N_2 gas atmosphere; N_2 gas was passed through a disoxidation agent in advance. All the solutions were prepared using distilled water free of O_2; dissolved oxygen was expelled by keeping N_2 gas bubbling through the boiling water.

Figure 1 shows the process of preparing the complexes, while Fig. 2 shows the scheme of the preparation system. Oxygen-free water was added to the mica powder, and then this suspension was refluxed in a N_2 flow to expel the oxygen absorbed on the surface of mica. As the iron(II) sulfate reagent has a few iron(III) ions, iron(II) sulfate solutions were aged for 1 day and then passed through glass filters by means of N_2-gas pressure to remove any iron(III) hydroxide. These iron(II) sulfate solutions, thus filtered and

transported to the reaction flask, were then mixed with the mica sol to give a 1 mol Fe/100 g·mica, where the concentration of Fe in these mixed suspensions was 0.1 M (1 M=1 mol dm^{-3}). These mixed suspensions were stirred for 1 day to promote ion-exchange between the iron(II) ion and the sodium ion within the mica. Subsequently, in order for the hydrolysis between the silicate layers to proceed, these suspensions were titrated with 0.1 M sodium hydroxide solutions at the rate of 20 ml h^{-1} to yield OH/Fe molar ratios of 0, 0.2, 0.4, 0.6, 0.8, and 1.0 respectively under vigorous stirring. After these additions, stirring was continued for 2 days. The resulting products were washed in oxygen-free water to remove electrolytes, the supernatant being taken out by means of N_2-gas pressure. Finally, these products were centrifuged, dried at 50 °C in a vacuum oven, and stored under nitrogen in a tightly closed desiccator.

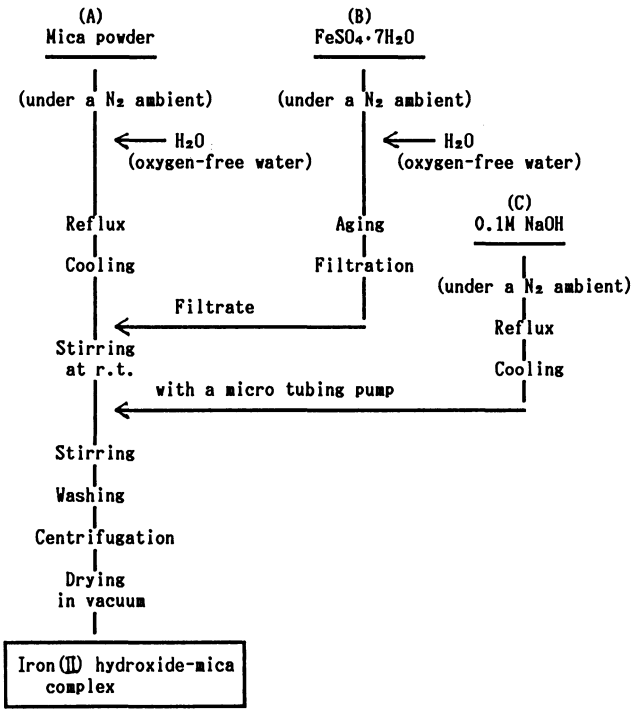

Fig. 1. Process of preparing iron(II) hydroxide-(sodium fluoride tetrasilicic mica).

Techniques of Characterizing the Complexes. Chemical analyses of the complexes were carried out by atomic-absorption analysis. The X-ray diffraction (XRD) patterns were obtained with a Rigaku diffractometer RU-200, using Cu $K\alpha$ radiation, from specimens basally oriented on glass slides. The surface areas were measured by the nitrogen-adsorption method at the temperature of liquid nitrogen with a Carlo Elba Sorptomatic, Series 1800. The samples were evacuated at 50 °C overnight prior to the measurements. Differential thermal analysis and thermogravimetric analysis (DTA-TGA) were made with a Rigaku Thermoanalyzer M8076 in a N_2 flow at a heating rate of 10 °C min^{-1}. Transmission electron microscopy (TEM) was performed with a JEOL, Model JEM-1200EX. The thermal stability of the complexes in an inert gas and their reduction behavior with H_2 were investigated in a range of 100—700 °C at a heating rate of 10 °C min^{-1}, because this mica is stable below 800 °C.

Measurement of the Room-Temperature Oxidation of the Complexes in Air. In our preliminary experiment, it was found that these complexes were not oxidized only by oxygen, but that the presence of water appeared to be essential for oxidizing to occur at room temperature by air. Therefore, the room-temperature oxidation of these complexes by air was investigated in an air flow with water vapor, the weight change during exposure to air being measured by means of the gravimetric McBain-Bakr balance technique. Samples of about 0.2 g were hung with a quartz spring and evacuated. Subsequently, N_2 gas with a saturated water-vapor pressure (at 30 °C) was passed over the sample (at 31 °C) at a flow rate of 100 ml min^{-1}, the relative humidity being 94%. After a constant weight was achieved, the flow was then switched to air with a saturated water-

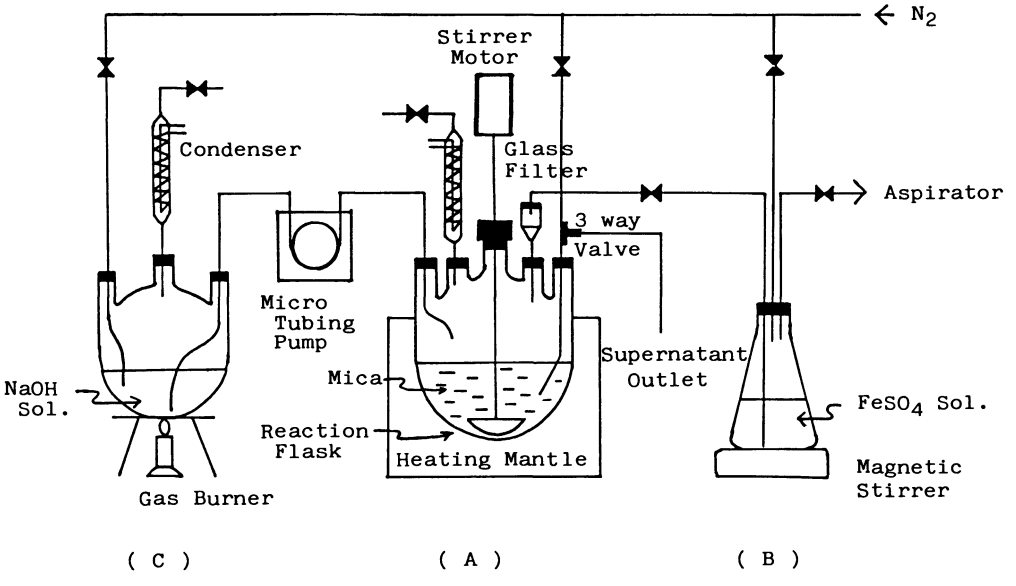

Fig. 2. Schematic of apparatus for preparing iron(II) hydroxide-(sodium fluoride tetrasilicic mica).

vapor pressure (at 30 °C) until the weight gain by oxidation was equilibrated.

Results and Discussion

Chemical Analyses. The results of the chemical analyses of the mica and its intercalation complexes are listed in Table 1. The iron content increased with an increase in the OH/Fe ratio, and the extent of the ion-exchange ratio in the resulting products was almost constant (81—82%). At an OH/Fe ratio of 1.0, the iron content of the complexes was 2.4 mol per formula unit of the mica 82% ion-exchanged, corresponding to 2.9 mol per formula unit of the mica 100% ion-exchanged. The ideal composition of the iron (II) hydroxide-mica complexes, which have a chlorite-like structure, is $[Fe_3(OH)_5(H_2O)](Mg_{2.5}Si_4O_{10}F_2)$;[1,2] the maximum iron content of the complexes is 3 mol per formula unit of the mica 100% ion-exchanged. Therefore, at an OH/Fe ratio of 1.0, the iron(II) hydroxide interlayers in the complex must be well-developed.

XRD Measurement and Specific Surface Area. The X-ray powder diffraction patterns of these complexes are shown in Fig. 3. The basal spacings of these complexes expanded to about 14.3—14.7 Å from the 9.6 Å basal spacing of the mica (Table 2); these basal spacings were almost independent of the iron content. Moreover, with an increase in the OH/Fe

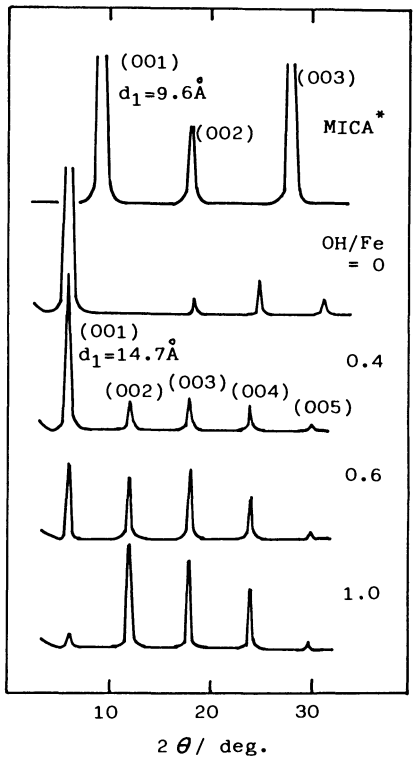

Fig. 3. X-Ray powder diffraction patterns of iron(II) hydroxide-(sodium fluoride tetrasilicic mica). MICA*: anhydrous form.

Table 1. Conditions of Preparation and Chemical Analyses of Sodium Fluoride Tetrasilicic Mica and Iron(II) Hydroxide-(Sodium Fluoride Tetrasilicic Mica)

No.	Condition of preparation	Chemical analysis/wt%			Molar ratio (SiO_2=4)			Ion exchange ratio/%[b]
	OH/Fe	SiO_2	Na	Fe	SiO_2	Na	Fe	
MICA[a]		57.34	4.36	—	4.00	0.80	—	—
1	0.0	53.51	0.96	3.29	4.00	0.19	0.26	81
2	0.2	50.43	0.89	8.10	4.00	0.18	0.69	82
3	0.4	47.38	0.82	12.40	4.00	0.18	1.13	82
4	0.6	44.55	0.77	15.98	4.00	0.18	1.54	82
5	0.8	41.94	0.71	19.72	4.00	0.18	2.02	82
6	1.0	39.36	0.67	21.95	4.00	0.18	2.40	82

a) Sodium fluoride tetrasilicic mica ($NaMg_{2.5}Si_4O_{10}F_2$). Interlayer charge is +1 per formula unit. Initial interlayer cations are Na^+; part of these Na^+ ions are displaced by H^+ ions when the silicate sol is diluted in distilled water to eliminate impurities. b) Ion-exchange ratio is calculated by means of: (1−Na molar ratio)×100.

Table 2. Basal Spacings (Å) of Iron(II) Hydroxide-(Sodium Fluoride Tetrasilicic Mica) After Heat Treatment

No.	OH/Fe	Basal spacing/Å			
		50 °C[a] in a vacuum	200 °C[b] in Ar	300 °C[b] in Ar	500 °C[b] in Ar
Initial mica		9.6	9.6	9.6	9.6
1	0.0	14.3	9.7	9.6	9.6
2	0.2	14.7	9.7	9.6	9.6
3	0.4	14.7	ML[c]	ML	9.6
4	0.6	14.7	14.6	ML	9.6
5	0.8	14.7	14.7	14.6	9.6
6	1.0	14.7	14.7	14.6	9.6

a) Drying in a vacuum for 24 h. b) Heat-treatment in Ar for 2 h. c) ML=mixed layer (mixtures of 14.7 Å and 9.6 Å layers).

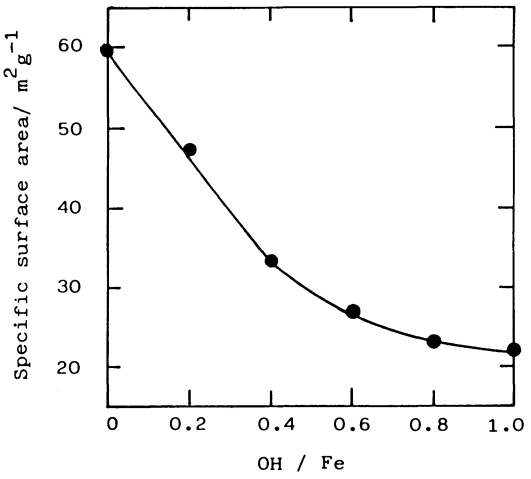

Fig. 4. Specific surface areas of iron(II) hydroxide-(sodium fluoride tetrasilicic mica).

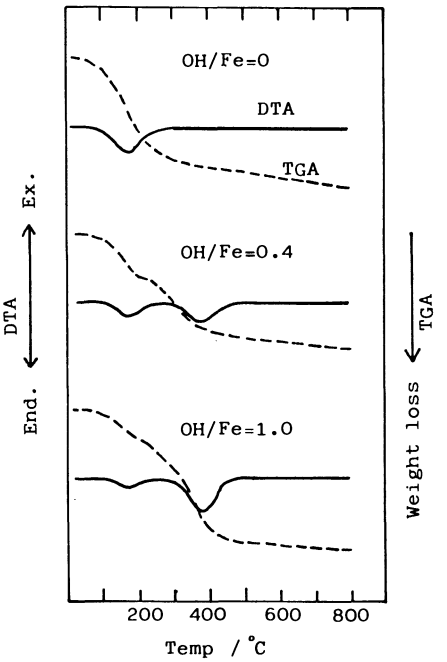

Fig. 5. DTA-TGA curves, obtained using a nitrogen atmosphere, for iron(II) hydroxide-(sodium fluoride tetrasilicic mica).

ratio, the (001) first-order reflection decreased in intensity; on the contrary, the (002)—(004) higher-order reflections increased in intensities. These changes in the relative intensities were the same as those observed in the formation reactions of nickel(II) or cobalt(II) hydroxide-mica complexes, indicating that an iron-(II) hydroxide-forming reaction took place between the silicate layers. The XRD patterns of the complexes with OH/Fe ratios of 0.8 and 1.0 showed the essential X-ray characteristics of chlorites. Moreover, XRD analysis revealed the absence of any iron oxide in these heat-treated samples.

The specific surface areas of the complexes are shown in Fig. 4. With an increase in the OH/Fe ratio, the specific surface areas decreased because the development of iron(II) hydroxide between the silicate layers begins at the cation-exchange sites, which are apart from each other, and finally the internal spaces are completely stacked with this iron(II) hydroxide interlayer. These changes are the same as those observed in nickel(II) or cobalt(II) hydroxide-mica complexes.

Thermal Analysis. The DTA-TGA curves for the complexes are shown in Fig. 5. Complexes with an OH/Fe ratio of 0.0 showed a single endothermic peak at about 170 °C. This dehydration is due to the hydration water associated with the iron(II) ions introduced by ion-exchange between the silicate layers. The composition of these iron(II) ions appears to be $[Fe(OH)_\delta(H_2O)_{6-\delta}]^{2-\delta}$, because the hydration water of the cation in expansible layer silicates is much more dissociated than in liquid water.[15] However, as the OH/Fe ratio increased, another peak appeared at about 375 °C, while the peak at about 170 °C was diminished. These findings indicate that iron(II) hydroxide $[Fe_x(OH)_y(H_2O)_m]^{2x-y}$ developed between the silicate layers with the progressive hydrolysis and olation of iron(II) cations by the addition of alkali. Therefore, the second peak corresponds to the loss of the hydroxyl group.

Table 2 shows the changes in the basal spacings after heat treatment in an Ar flow. Complexes with OH/Fe ratios of 0.8 and 1.0, which have a well developed iron(II) hydroxide interlayer, did not collapse even upon heat treatment at 300 °C. As iron(II) hydroxide decomposes to FeO at about 200 °C,[16] well-developed iron(II) hydroxide between the silicate layers has a higher thermal stability than iron(II) hydroxide in the bulk state and is strongly fixed to the silicate layers.

Reduction Behavior with H_2. The complexes were heated in a H_2 flow at 400—700 °C for 2 h. The XRD patterns of the reduced complexes with an OH/Fe ratio of 1.0 are shown in Fig. 6. These complexes collapsed to a basal spacing of 9.6 Å, and metallic iron (α-Fe) was detected above 500 °C. As the reducing temperature rose, the reflection intensity of iron increased and the (001) mica basal reflection peak became sharper: reduced iron atoms gradually migrated from the interlayer of the silicate to its external surface.

A TEM photograph of the H_2-reduced complexes with an OH/Fe ratio of 1.0 at 700 °C is shown in Fig. 7. Metallic iron particles with a clear cubic crystal habit are distributed on the external surface of the mica. The grain diameter of these metallic iron particles increased with an increase in the reducing temperature.

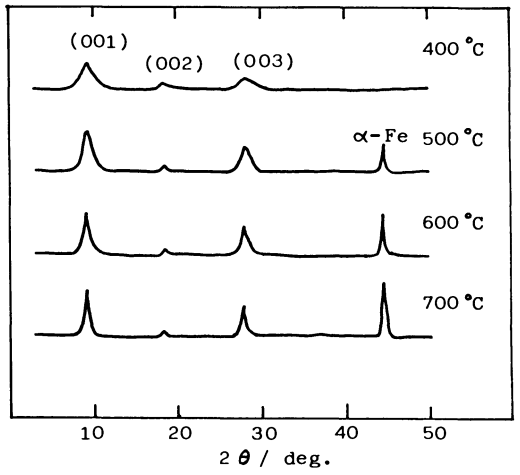

Fig. 6. X-Ray powder diffraction patterns of H_2 reduced iron(II) hydroxide-(sodium fluoride tetrasilicic mica) with a OH/Fe ratio of 1.0 at various temperatures.

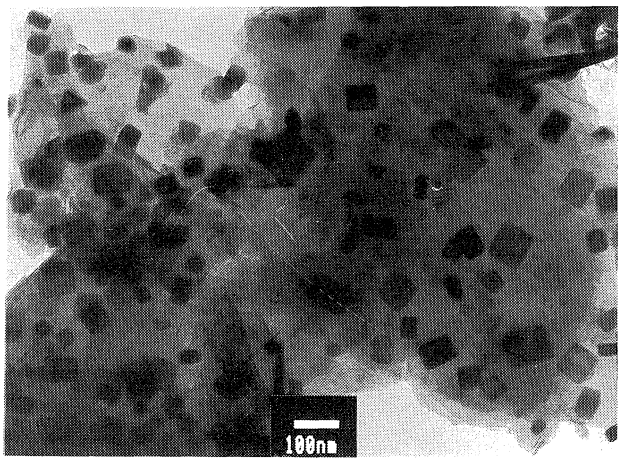

Fig. 7. Transmission electron micrograph of H_2 reduced iron(II) hydroxide-(sodium fluoride tetrasilicic mica) with a OH/Fe ratio of 1.0 at 700 °C.

Room-Temperature Oxidation of the Complexes in Air. Figure 8 shows the room-temperature oxidation of the complexes with time in air with water vapor (P_{H_2O}=4.24 kPa); temp=31 °C, R.H.=94%, air flow rate=100 ml min^{-1}. The weight-gain values are plotted against the time in the logarithmic scale. Oxidation occured gradually, and weight change by oxidation was large in the complexes with high OH/Fe ratios. The final weight-gain of the complexes with an OH/Fe ratio 1.0 was about 5 wt%. With the progress of oxidation, the color of the complexes changed from blue-green to yellow-orange and the chlorite-like structure was destroyed (Fig. 9). The oxidation rate was largely governed by the relative humidity and the reaction temperature, being controlled by the partial isomorphous substitution of

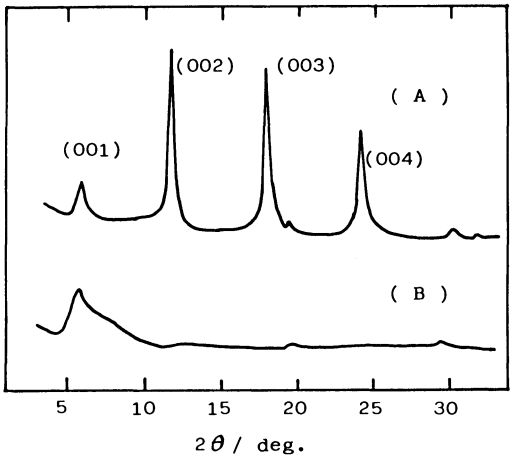

Fig. 9. X-Ray powder diffraction patterns of iron-(II) hydroxide-(sodium fluoride tetrasilicic mica) after oxidation in air.
(A): original iron(II) hydroxide-(sodium fluoride tetrasilicic mica) complex with a OH/Fe ratio of 1.0; (B): oxidized complex in air with water vapor (P_{H_2O}=4.24 kPa; R.H.=94%) at 31 °C for 2 d.

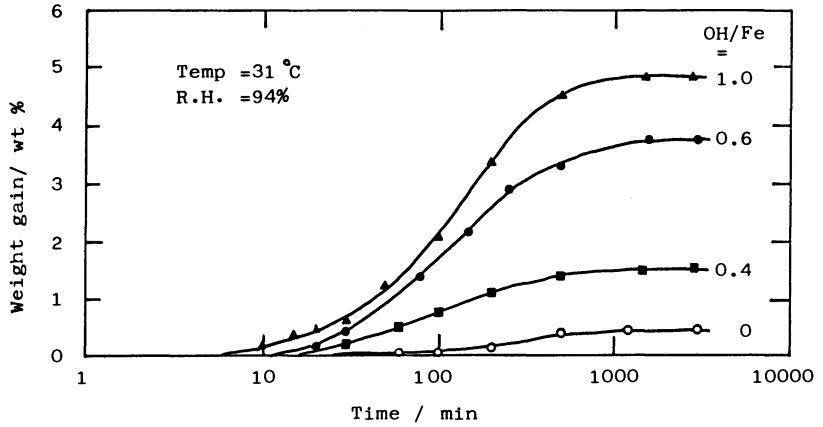

Fig. 8. Weight gain for iron(II) hydroxide-(sodium fluoride tetrasilicic mica) with time in air with water vapor (P_{H_2O}=4.24 kPa; R.H.=94%) at 31 °C. R.H.= relative humidity.

iron(II) ions. The details of this will be given in our next paper.

In contrast, iron(II) hydroxide in the bulk state is rapidly oxidized and ignites spontaneously on exposure to air because of its strong reducing power.

Mechanism of the Room-Temperature Oxidation of the Iron(II) Hydroxide Interlayer in Air. The oxidation of iron(II) hydroxide in air seems to be similar to that in aqueous solutions; the latter has been studied extensively. The oxidation processes in aqueous solutions can be classified into two types.

One consists of solid-phase reactions (surface reactions) which take place rapidly on the surface of iron(II) hydroxide with oxygen. This process is accepted as a topotactic reaction and follows this equation:[16,17]

$$\underset{\text{(hcp)}}{Fe(OH)_2} + 1/4\,O_2 \rightarrow \underset{\text{(hcp)}}{\delta\text{-FeOOH}} + 1/2\,H_2O. \quad (1)$$

This reaction process can be observed in strong alkaline solutions with a rapid oxidizing agent, because in strong alkaline solutions the concentration of iron(II) ions is extremely small.

The other type consists of liquid-phase reactions (dissolution-precipitation reactions) which take place gradually in the liquid phase.[18,19] When slow oxidation occurs by oxygen dissolved in the solution, iron(II) ions are oxidized in the solution and precipitated as α-FeOOH, γ-FeOOH, Fe_3O_4, or a mixture of them, according to the pH, the reaction temperature, and the kind of anion present.

Therefore, the oxidation process of iron(II) hydroxide in air can be considered to proceed as follows: on exposure to air, rapid oxidation on the surface of iron(II) hydroxide occurs (Eq. 1). However, since this reaction takes place with an evolution of heat, the oxidation and dehydration proceed simultaneously, and result in the formation of γ-Fe_2O_3:

$$Fe(OH)_2 + 1/4\,O_2 \xrightarrow[\text{rapid oxidation}]{\text{in air}} 1/2\ \gamma\text{-}Fe_2O_3 + H_2O. \quad (2)$$

In the case of the oxidation of iron(II) hydroxide–mica complexes in air, the solid-phase reaction on the surface of iron(II) hydroxide interlayers does not proceed, bacause these iron(II) hydroxide sheets are sandwiched between the silicate layers; the O_2 attack on the surface of iron(II) hydroxide sheets is hindered by the silicate layers. In fact, iron(II) hydroxide interlayers were not oxidized only by oxygen; the presence of water was indispensable to their oxidation by air at room temperature, as has been mentioned above. Hence, the oxidation of iron(II) hydroxide interlayers occurs in air with water vapor according to the liquid phase reaction: water is absorbed on the edge of the iron(II) hydroxide sheets, and then the dissolved Fe^{2+} ions are oxidized. Consequently, the oxidation rate is slow and depends on the water-vapor pressure. This oxidation process is different from that of iron(II) which is present in the 2:1 silicate layer of clay minerals.[20–23]

References

1) K. Ohtsuka, M. Suda, M. Ono, M. Takahashi, M. Sato, and S. Ishio, *Bull. Chem. Soc. Jpn.*, **60**, 871 (1987).

2) K. Ohtsuka, J. Koga, M. Suda, M. Ono, and M. Takahashi, *Bull. Chem. Soc. Jpn.*, **60**, 2843 (1987).

3) D. D. Carstea, *Clays Clay Miner.*, **16**, 231 (1968).

4) D. D. Carstea, M. E. Harward, and E. G. Knox, *Soil Sci. Soc. Am. Proc.*, **34**, 517 (1970).

5) D. D. Carstea, M. E. Harward, and E. G. Knox, *Soil Sci. Soc. Am. Proc.*, **34**, 522 (1970).

6) S. Caillere and S. Henin, *Mineral. Mag.*, **28**, 612 (1949).

7) R. Herrera and M. Peech, *Soil Sci. Soc. Am. Proc.*, **34**, 740 (1970).

8) G. J. Ross and H. Kodama, *Clays Clay Miner.*, **24**, 183 (1976).

9) L. Makumbi and A. J. Herbillon, *Bull. Groupe Fr. Argiles*, **24**, 153 (1972).

10) G. J. Ross, *Nature (London)*, **225**, 133 (1975).

11) G. J. Ross and H. Kodama, *Clays Clay Miner.*, **22**, 205 (1974).

12) B. A. Goodman and D. C. Bain, "Proc. Int. Clay Conference, Oxford, 1978," ed by M. M. Mortland and V. C. Farmer, Elsevier, Amsterdam (1979), p. 65.

13) M. Pourbaix, "Atlas of Electrochemical Equilibria in Aqueous Solutions," Pergamon Press, Oxford (1966), p. 307.

14) D. Nicholls, "Comprehensive Inorganic Chemistry," ed by J. C. Bailar, H. J. Emeleus, Sir Ronald Nyholm, and A. F. Trotman-Dickenson, Pergamon Press, Oxford (1973), Vol. 3, p. 1005.

15) D. M. C. MacEvan and M. J. Wilson, "Crystal Structures of Clay Minerals and Their X-ray Identification," ed by G. W. Brindley and G. Brown, Mineralogical Society, London (1980), p. 219.

16) J. D. Bernal, D. R. Dasgupta, and A. L. Mackay, *Clay Min. Bull.*, **4**, 15 (1959).

17) W. Feitknecht, *Z. Elektrochem.*, **63**, 34 (1959).

18) M. Kiyama, *Bull. Chem. Soc. Jpn.*, **47**, 1646 (1974).

19) T. Sato, S. Okamoto, and K. Hashimoto, *Yogyo Kyokai Shi*, **94**, 1201 (1986).

20) O. K. Borggaard, H. B. Lindgreen, and S. Morup, *Clays Clay Miner.*, **30**, 353 (1982).

21) N. Kohyama, S. Simoda and T. Sudo, *Clays Clay Miner.*, **21**, 229 (1973).

22) C. C. Addison, W. E. Addison, G. H. Neal, and J. H. Sharp, *J. Chem. Soc., Pt. II*, **1962**, 1468.

23) G. W. Brindley and R. F. Youell, *Miner. Mag.*, **30**, 57 (1953).

 © 1988 The Chemical Society of Japan Bull. Chem. Soc. Jpn., 61, 821—826 (1988)

The Crystal and Molecular Structure of Aquachloro (*meso*-tetraphenylporphyrinato)cobalt(III)

Yasuhiro IIMURA,* Tosio SAKURAI,† and Kiyoko YAMAMOTO
The Institute of Physical and Chemical Research (Riken), Wako-shi, Saitama 351-01
†Faculty of Education, Shinshu University, Nishinagano, Nagano 380
(Received August 17, 1987)

The crystal and molecular structure of the title compounds, [Co^{III}Cl(tpp)(H$_2$O)], has been determined by means of X-ray diffraction techniques. The compound crystallizes in the monoclinic system; space group $P2_1/c$. The unit cell has a=13.542(2), b=25.760(2), c=10.423(1) Å, β=99.33(2)°, and Z=4. The cobalt atom is coordinated by four porphyrinato nitrogen atoms, one chlorine atom, and one oxygen atom of water, and is displaced by 0.039(2) Å from the mean plane defined by the four porphyrinato nitrogen atoms towards the axial chlorine atom. The average Co–N(tpp) distance is 1.955(2) Å. The Co–Cl distance is 2.216(1), and the Co–O(water) distance, 1.979(3) Å. The porphyrinato core is significantly ruffled and has an approximate $\bar{4}$ symmetry. The [Co^{III}Cl(tpp)(H$_2$O)] molecules are stacked along the c axis by O–H···Cl hydrogen bonds.

In our investigation of chloro (*meso*-tetraphenylporphyrinato)cobalt(III), [Co^{III}Cl(tpp)], its characteristic phenomena, behavior, or properties have been found by the use of optical absorption, NMR, and ESR spectral techniques.[1] The crystallization of the complex from common solvents gives crystals of various external forms: obelisk, pyramid, prism, and/or bulky shapes from a dichloromethane or chloroform solution, and only obelisks from a methanol solution. A previous X-ray diffraction study[2] of the obelisk crystals isolated from a dichloromethane or chloroform solution demonstrated that the complex can be represented as a five-coordinate cobalt complex of tpp having square-pyramid structure with a chlorine atom at the apex. However, a subsequent X-ray diffraction study[3] of the pyramid crystals obtained from a dichloromethane or chloroform solution suggested that there is an unidentified atom in the sixth axial position. The possibility of the partial coordination of water at the sixth ligand position was considered, because it has been well known that the cobalt(III) complex is stable in the case of six-coordination.[4] Presumably, water in the atmosphere contaminated the solution being crystallized. However, an IR examination of the crystals did not find any OH stretchings. In order to elucidate the coordination of a water molecule as the sixth ligand, crystals of species with one water molecule, [Co^{III}Cl(tpp)(H$_2$O)], were prepared from a solution of dichloromethane saturated with water and then analyzed by means of X-ray diffraction. The result shows that when the water molecule coordinates at the sixth axial position, the crystal and molecular structure is completely different from that of [Co^{III}Cl(tpp)]. The present paper will deal with the structure of [Co^{III}Cl(tpp)(H$_2$O)].

Experimental

Materials. The chloro(*meso*-tetraphenylporphyrinato)-cobalt(III), [Co^{III}Cl(tpp)], was prepared by the method previously reported.[2] The complex was dissolved in a solution of dichloromethane saturated with water and evaporated spontaneously; metallic lustrous reddish-purple prismatic crystals were thus obtained.

Found: C, 72.71; H, 4.07; Cl, 4.90; Co, 8.37; N, 7.75; O, 2.40%. Calcd for $C_{44}H_{30}ClCoN_4O$ ([Co^{III}Cl(tpp)(H$_2$O)]): C, 72.88; H, 4.17; Cl, 4.89; Co, 8.13; N, 7.73; O, 2.21%.

X-Ray Measurements. The crystal used was 0.25×0.31×0.75 mm in size. The preliminary Weissenberg photographs showed that the crystal belongs to the monoclinic system. The systematic absences ($h0l$ for l odd and $0k0$ for k odd) led to the space group $P2_1/c$. The least-squares refinement of the setting angles of 24 reflections, measured on a Rigaku AFC-4 four-circle diffractometer with graphite-monochromated Mo $K\alpha$ radiation (λ=0.71073 Å), gave the following cell constants: a=13.542(2), b=25.760(2), c=10.423(1) Å, and β=99.33(2)°. The calculated density (1.342 g cm^{-3}) agreed with the observed value (1.345 g cm^{-3}) obtained by the floatation method in a tetrachloromethane–methylcyclohexane mixture. Intensity data within the range ($\sin\theta/\lambda$<0.75598 Å^{-1}) were collected by the use of the ω scan (2θ<30°) and ω–2θ scan methods (2θ≧30°), with a scan speed of 4° min^{-1} in ω. The three standard reflections ($\bar{2}$ 2 1, 0 2 5, and 6 10 0), measured every 100 reflections, showed no significant deterioration. The ordinary Lorentz and polarization corrections and absorption correction were applied. The absorption coefficient for Mo$K\alpha$ radiation was 5.899 cm^{-1}. The minimum and maximum transmission coefficients were 0.83 and 0.87 respectively. 13597 reflections were measured, and 5873 unique reflections obtained with $F_o \geqq 3.0\,\sigma(F_o)$. 7114 reflections were unobserved with the criterion of $F_o < 3.0\,\sigma(F_o)$.

Structure Analysis

The structure was solved by the heavy-atom method and refined by the block-diagonal least-squares method. Difference Fourier syntheses gave the positions of all the hydrogen atoms. In the final stage, the structure was refined by the full-matrix least-squares method, based on $|F_o|$, with isotropic and anisotropic temperature factors for hydrogen and non-hydrogen atoms respectively. The function minimized was $\sum w(|F_o|-|F_c|)^2$, where w=1.0. The final R and R_w values were 0.055 and 0.054 respectively. In

the final cycle of refinement, the largest shift/error was 0.931 for B_{33} of the C(9C) atom. The maximum and minimum heights in the final difference synthesis were 0.57 and −0.61 e Å^{-3} respectively. Calculations were carried out on the FACOM M-380 computer of this Institute using the UNICS III program system[5] and the best-plane calculation with the BP70 program.[6] The atomic-scattering factors, including anomalous scattering corrections, were taken from the International Tables for X-Ray Crystallography.[7]

Results and Discussion

The atomic coordinates except hydrogen atoms are listed in Table 1.[8] The molecular structure of [Co^{III}Cl(tpp)(H_2O)] is shown in Fig. 1, along with the atomic numbering and the thermal ellipsoids. The intramolecular bond distances(Å) are listed in Table 2, while the crystal structure projected along the a axis is shown in Fig. 2.

The coordination around the cobalt atom is

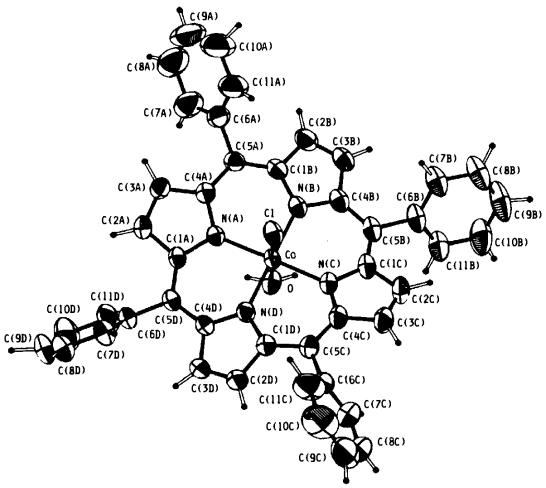

Fig. 1. The molecular structure.
The thermal ellipsoids are at 50% probabillity for non-hydrogen atoms (hydrogen atoms are arbitrarily scaled).

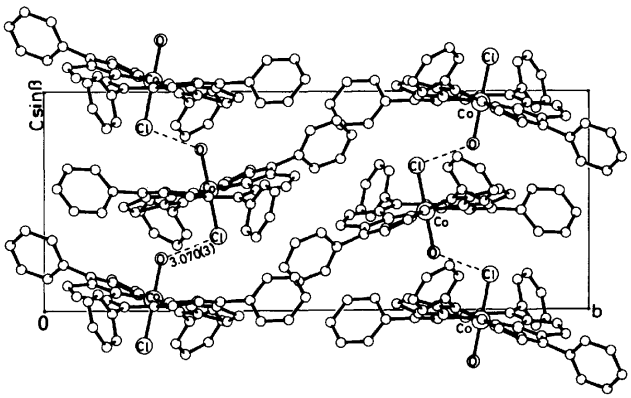

Fig. 2. The crystal structure projected along the a axis.
Hydrogen atoms are omitted for clarity. Broken lines show the O-H···Cl hydrogen bonds (distances in Å).

Table 1. Atomic Coordinates with Estimated Standard Deviations in Parentheses. Positional Parameters Are Multiplied by 10^4. B_{eq} Values Are Equivalent Isotropic Temperature Factors

$$B_{eq} = \frac{4}{3}\sum_i\sum_j B_{ij}\boldsymbol{a}_i\cdot\boldsymbol{a}_j$$

Atom	x	y	z	B_{eq}/Å^2	Atom	x	y	z	B_{eq}/Å^2
CO	1661.8(4)	1992.3(2)	513.4(5)	2.7	C(9B)	48(6)	−621(2)	3019(7)	8.1
Cl	1321.3(8)	1821.6(4)	−1596.1(9)	3.7	C(10B)	825(6)	−346(2)	3677(6)	7.4
O	1984(2)	2135(1)	2400(3)	3.6	C(11B)	1081(5)	137(2)	3228(5)	5.4
N(A)	1090(2)	2686(1)	238(3)	2.8	C(1C)	1799(3)	869(1)	1247(4)	3.8
N(B)	358(2)	1721(1)	764(3)	3.1	C(2C)	2429(4)	424(2)	1150(5)	4.9
N(C)	2254(2)	1302(1)	841(3)	3.3	C(3C)	3227(4)	583(2)	671(5)	4.8
N(D)	2978(2)	2277(1)	357(3)	3.1	C(4C)	3147(3)	1137(1)	507(4)	3.7
C(1A)	1595(3)	3145(1)	194(3)	2.9	C(5C)	3886(3)	1457(2)	182(4)	3.9
C(2A)	898(3)	3551(1)	−256(4)	3.5	C(6C)	4835(3)	1235(2)	−136(6)	5.1
C(3A)	−16(3)	3337(2)	−501(4)	3.5	C(7C)	5506(5)	976(2)	757(9)	7.6
C(4A)	87(3)	2802(1)	−143(3)	3.1	C(8C)	6406(6)	793(3)	434(15)	11.1
C(5A)	−696(3)	2466(2)	−49(4)	3.4	C(9C)	6634(7)	881(3)	−737(15)	11.3
C(6A)	−1740(3)	2651(2)	−489(5)	4.7	C(10C)	5988(7)	1135(4)	−1650(11)	10.1
C(7A)	−2132(4)	3071(3)	53(7)	6.5	C(11C)	5077(5)	1314(3)	−1359(7)	7.2
C(8A)	−3107(6)	3246(3)	−446(10)	8.4	C(1D)	3817(3)	1999(2)	211(4)	3.6
C(9A)	−3634(5)	2997(5)	−1451(11)	9.9	C(2D)	4653(3)	2341(2)	225(5)	4.5
C(10A)	−3271(6)	2573(4)	−2004(9)	9.5	C(3D)	4323(3)	2822(2)	404(5)	4.2
C(11A)	−2330(4)	2403(3)	−1514(6)	6.8	C(4D)	3270(3)	2789(1)	445(4)	3.2
C(1B)	−547(3)	1971(2)	483(4)	3.6	C(5D)	2625(3)	3209(1)	404(4)	3.2
C(2B)	−1312(4)	1659(2)	905(5)	4.4	C(6D)	3025(3)	3750(1)	462(4)	3.9
C(3B)	−876(4)	1231(2)	1428(4)	4.4	C(7D)	3496(4)	3950(2)	−506(6)	5.3
C(4B)	162(3)	1249(1)	1307(4)	3.5	C(8D)	3834(5)	4460(2)	−440(8)	7.1
C(5B)	842(3)	845(1)	1571(4)	3.8	C(9D)	3708(5)	4770(2)	581(9)	8.2
C(6B)	528(4)	345(2)	2113(4)	4.4	C(10D)	3231(6)	4577(2)	1516(9)	8.1
C(7B)	−280(4)	63(2)	1486(5)	5.3	C(11D)	2881(4)	4069(2)	1476(6)	5.7
C(8B)	−516(6)	−419(2)	1924(6)	6.8					

illustrated in Fig. 3. The cobalt atom is coordinated by four porphyrinato nitrogen atoms, one chlorine atom, and one oxygen atom of water. The axial Co–Cl distance of 2.216(1) Å is shorter than those of $[Co^{III}Cl(tpp)(py)]$ (2.251(3) Å)[9] and $[Co^{III}Cl(NH_3)_5]Cl_2$ (2.286(2) Å),[10] and it is close to the sum of the covalent radii[11] of Co(III)(1.22 Å) and Cl(0.99 Å). Another axial Co–O distance of 1.979(3) Å is longer than those

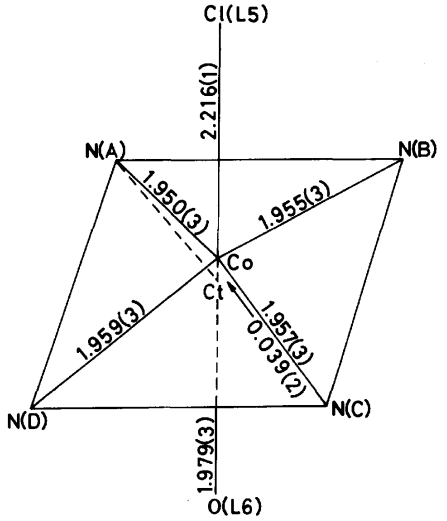

Fig. 3. Perspective diagram of the six-coordination around the cobalt(III) atom.
Ct represents the center of four porphyrinato nitrogen atoms.

of $[Co^{III}(tpp)(H_2O)_2]ClO_4$ (1.936(5) Å),[12] $[Co^{III}(CH_3O)(tpp)(py)]$(1.92 Å),[13] and $[Co^{III}(H_2O)(NH_3)_5]_2(S_2O_6)_3 \cdot 2H_2O$ (1.954(1) Å);[14] furthermore, it is longer than the sum of the covalent radii of Co(III) and O(0.66 Å) and comparable with that of the ionic radii of Co(+3) (0.63 Å) and O(−2)(1.40 Å).

The cobalt atom is displaced by 0.039(2) Å from the mean plane defined by four porphyrinato nitrogen atoms (4N plane) towards the axial chlorine atom, as is shown in Fig. 3. The displacement of the cobalt atom is common in five-coordinate complexes,[2,15,16] but is observed only for the present complex among the six-coordinate complexes.[9,13,17–19] A small displacement (0.013(2) Å) of the cobalt atom is observed for $[Co^{III}(NO_2)(tpp)(lut)]$,[20] but it is buried in the mean 4N plane(±0.04(2) Å). The displacement of the metal atom has been well-known in iron porphyrin complexes, depending on its oxidation state and spin state.[21] In the present complex, the Co–Cl distance is short, while that of Co–O is long; hence a rather strong coordination of the chloride ligand to the cobalt atom and a weak coordination of the water ligand. Therefore, the displacement of cobalt in the present complex may result from a compromise between (1) the necessity for the best σ-overlapping of the chlorine and oxygen atoms of axial ligands with the cobalt atom and (2) the planarity for the optimum π-bonding of the porphyrinato ligand.

The average distance between cobalt and the porphyrinato nitrogen atom (Co–N(tpp)) is 1.955(2)

Table 2. Intramolecular Bond Distances with e.s.d.'s in Parentheses

Type	*l*/Å	Type	*l*/Å	Type	*l*/Å
Co-Cl	2.216(1)	(Cβ-Cβ')		C(10A)-C(11A)	1.367(10)
Co-O	1.979(3)	C(2A)-C(3A)	1.340(6)	C(11A)-C(6A)	1.383(8)
		C(2B)-C(3B)	1.327(7)		
Co-N(A)	1.950(3)	C(2C)-C(3C)	1.326(8)	C(6B)-C(7B)	1.387(7)
Co-N(B)	1.955(3)	C(2D)-C(3D)	1.341(6)	C(7B)-C(8B)	1.378(8)
Co-N(C)	1.957(3)			C(8B)-C(9B)	1.368(9)
Co-N(D)	1.959(3)	(Cα-Cm)		C(9B)-C(10B)	1.358(10)
		C(4A)-C(5A)	1.386(6)	C(10B)-C(11B)	1.394(8)
(N-Cα)		C(5A)-C(1B)	1.391(6)	C(11B)-C(6B)	1.384(7)
N(A)-C(1A)	1.371(5)	C(4B)-C(5B)	1.387(6)		
N(A)-C(4A)	1.385(5)	C(5B)-C(1C)	1.392(7)	C(6C)-C(7C)	1.366(9)
N(B)-C(1B)	1.375(5)	C(4C)-C(5C)	1.381(6)	C(7C)-C(8C)	1.397(12)
N(B)-C(4B)	1.386(5)	C(5C)-C(1D)	1.400(6)	C(8C)-C(9C)	1.326(22)
N(C)-C(1C)	1.374(5)	C(4D)-C(5D)	1.388(5)	C(9C)-C(10C)	1.353(15)
N(C)-C(4C)	1.379(6)	C(5D)-C(1A)	1.386(6)	C(10C)-C(11C)	1.396(12)
N(D)-C(1D)	1.372(5)			C(11C)-C(6C)	1.382(10)
N(D)-C(4D)	1.375(5)	(Cm-Cp)			
		C(5A)-C(6A)	1.491(6)	C(6D)-C(7D)	1.377(8)
(Cα-Cβ)		C(5B)-C(6B)	1.495(6)	C(7D)-C(8D)	1.391(8)
C(1A)-C(2A)	1.436(5)	C(5C)-C(6C)	1.492(7)	C(8D)-C(9D)	1.361(12)
C(3A)-C(4A)	1.429(5)	C(5D)-C(6D)	1.492(5)	C(9D)-C(10D)	1.349(13)
C(1B)-C(2B)	1.436(7)			C(10D)-C(11D)	1.388(8)
C(3B)-C(4B)	1.432(7)	(Phenyl group)		C(11D)-C(6D)	1.378(7)
C(1C)-C(2C)	1.442(6)	C(6A)-C(7A)	1.368(9)		
C(3C)-C(4C)	1.440(6)	C(7A)-C(8A)	1.412(10)		
C(1D)-C(2D)	1.432(6)	C(8A)-C(9A)	1.332(14)		
C(3D)-C(4D)	1.436(6)	C(9A)-C(10A)	1.362(15)		

Å. This distance is located near the lower end of the range of distances (1.948—1.985 Å) of the reported Co^{III}(tpp) complexes.[2,9,12,13,15-20] It is shorter than the Co-NH_3 distances of $[Co^{III}(NH_3)_6][Co^{III}(CN)_6]$ (1.972(1) Å),[22] $[Co^{III}Cl(NH_3)_5]Cl_2$ (1.976 Å), and $[Co^{III}(H_2O)(NH_3)_5]_2(S_2O_6)_3 \cdot 2H_2O$ (1.961 Å).

The average distances of other chemically analogous types are: N-Cα=1.377(6), Cα-Cβ=1.435(4), Cβ-Cβ'=1.334(8), Cα-Cm=1.389(6), and Cm-Cp=1.492(2) Å, where Cα and Cβ (Cβ') denote α and β carbon atoms in pyrrole rings; Cm, methine carbon atoms; and Cp, phenyl carbon atoms. The figure in parentheses is the standard deviation. Except for Cm-Cp, these distances are very similar to those of the reported Co^{III}(tpp) complexes.

The intramolecular bond angles are listed in Table 3. The average value of four N-Co-N angles is 90.0(2)° (max. —min.: 90.3(1)—89.4(1)°); the cobalt atom is surrounded by a square-planar array of pyrrole nitrogen atoms. The average angles of the other chemically analogous types are: Co-N-Cα=126.8(2), Cα-N-Cα=106.0(2), N-Cα-Cβ=109.5(2), N-Cα-Cm=125.5(2), Cm-Cα-Cβ=124.8(3), Cα-Cβ-Cβ'=107.5(2), Cα-Cm-Cα=122.1(2), and Cα-Cm-Cp=118.7(5)°. These angles are comparable to those of $[Co^{III}(NO_2)(tpp)(lut)]$ and $[Co^{III}(tpp)(H_2O)_2]^+$ in that the porphyrinato cores are ruffled, but differ somewhat from those of $[Co^{III}Cl(tpp)]$ in that the core is planar.

The deviations of 24 atoms from the least-squares plane of the porphyrinato core are shown in Fig. 4. The porphyrinato core is considerably ruffled. The ruffled core has an approximate $\bar{4}$ symmetry. As is usual, a local flatness (within 0.02 Å) is maintained in

Table 3. Intramolecular Bond Angles with e.s.d.'s in Parentheses

Type	ϕ/°	Type	ϕ/°	Type	ϕ/°
Cl-Co-O	179.0(1)	N(D)-C(4D)-C(3D)	109.3(3)	C(4C)-C(5C)-C(6C)	120.7(4)
Cl-Co-N(A)	91.24(9)			C(1D)-C(5C)-C(6C)	116.7(4)
Cl-Co-N(B)	90.84(9)	(N-Cα-Cm)		C(4D)-C(5D)-C(6D)	120.3(4)
Cl-Co-N(C)	90.4(1)	N(A)-C(1A)-C(5D)	126.3(3)	C(1A)-C(5D)-C(6D)	117.9(3)
Cl-Co-N(D)	92.2(1)	N(A)-C(4A)-C(5A)	124.8(3)		
		N(B)-C(1B)-C(5A)	125.6(4)	(Cm-Cp-Cp')	
O-Co-N(A)	89.7(1)	N(B)-C(4B)-C(5B)	125.0(4)	C(5A)-C(6A)-C(7A)	122.6(4)
O-Co-N(B)	89.5(1)	N(C)-C(1C)-C(5B)	126.3(4)	C(5A)-C(6A)-C(11A)	119.3(5)
O-Co-N(C)	88.7(1)	N(C)-C(4C)-C(5C)	125.3(4)	C(5B)-C(6B)-C(7B)	121.7(4)
O-Co-N(D)	87.5(1)	N(D)-C(1D)-C(5C)	125.5(4)	C(5B)-C(6B)-C(11B)	120.2(4)
		N(D)-C(4D)-C(5D)	125.0(4)	C(5C)-C(6C)-C(7C)	122.6(6)
N(A)-Co-N(B)	90.1(1)			C(5C)-C(6C)-C(11C)	119.4(5)
N(B)-Co-N(C)	90.3(1)	(Cm-Cα-Cβ)		C(5D)-C(6D)-C(7D)	121.8(4)
N(C)-Co-N(D)	90.1(1)	C(5D)-C(1A)-C(2A)	123.8(3)	C(5D)-C(6D)-C(11D)	119.5(4)
N(D)-Co-N(A)	89.4(1)	C(5A)-C(4A)-C(3A)	125.4(4)		
		C(5A)-C(1B)-C(2B)	124.8(4)	(Phenyl group)	
N(A)-Co-N(C)	178.3(1)	C(5B)-C(4B)-C(3B)	126.0(4)	C(6A)-C(7A)-C(8A)	120.2(6)
N(B)-Co-N(D)	177.0(1)	C(5B)-C(1C)-C(2C)	124.5(4)	C(7A)-C(8A)-C(9A)	119.1(8)
		C(5C)-C(4C)-C(3C)	125.3(4)	C(8A)-C(9A)-C(10A)	122.3(8)
(Co-N-Cα)		C(5C)-C(1D)-C(2D)	123.9(4)	C(9A)-C(10A)-C(11A)	118.6(8)
Co-N(A)-C(1A)	127.4(3)	C(5D)-C(4D)-C(3D)	125.1(4)	C(10A)-C(11A)-C(6A)	121.8(7)
Co-N(A)-C(4A)	126.1(2)			C(11A)-C(6A)-C(7A)	118.1(5)
Co-N(B)-C(1B)	126.7(3)	(Cα-Cβ-Cβ')			
Co-N(B)-C(4B)	127.3(3)	C(1A)-C(2A)-C(3A)	107.5(3)	C(6B)-C(7B)-C(8B)	121.6(5)
Co-N(C)-C(1C)	126.9(3)	C(4A)-C(3A)-C(2A)	107.4(4)	C(7B)-C(8B)-C(9B)	119.4(6)
Co-N(C)-C(4C)	126.0(3)	C(1B)-C(2B)-C(3B)	107.3(4)	C(8B)-C(9B)-C(10B)	120.3(6)
Co-N(D)-C(1D)	126.6(3)	C(4B)-C(3B)-C(2B)	108.3(4)	C(9B)-C(10B)-C(11B)	120.7(6)
Co-N(D)-C(4D)	127.5(3)	C(1C)-C(2C)-C(3C)	108.0(4)	C(10B)-C(11B)-C(6B)	119.9(5)
		C(4C)-C(3C)-C(2C)	107.4(4)	C(11B)-C(6B)-C(7B)	118.1(4)
(Cα-N-Cα)		C(1D)-C(2D)-C(3D)	106.8(4)		
C(1A)-N(A)-C(4A)	106.0(3)	C(4D)-C(3D)-C(2D)	107.7(4)	C(6C)-C(7C)-C(8C)	120.8(9)
C(1B)-N(B)-C(4B)	106.0(3)			C(7C)-C(8C)-C(9C)	120.4(9)
C(1C)-N(C)-C(4C)	106.4(3)	(Cα-Cm-Cα)		C(8C)-C(9C)-C(10C)	120.7(10)
C(1D)-N(D)-C(4D)	105.8(3)	C(4A)-C(5A)-C(1B)	122.5(4)	C(9C)-C(10C)-C(11C)	120.0(11)
		C(4B)-C(5B)-C(1C)	122.2(4)	V(10C)-C(11C)-C(6C)	120.2(7)
(N-Cα-Cβ)		C(4C)-C(5C)-C(1D)	122.5(4)	C(11C)-C(6C)-C(7C)	118.0(6)
N(A)-C(1A)-C(2A)	109.5(3)	C(4D)-C(5D)-C(1A)	121.6(3)		
N(A)-C(4A)-C(3A)	109.5(3)			C(6D)-C(7D)-C(8D)	120.3(6)
N(B)-C(1B)-C(2B)	109.6(4)	(Cα-Cm-Cp)		C(7D)-C(8D)-C(9D)	120.7(7)
N(B)-C(4B)-C(3B)	108.7(4)	C(4A)-C(5A)-C(6A)	118.4(4)	C(8D)-C(9D)-C(10D)	119.0(6)
N(C)-C(1C)-C(2C)	108.9(4)	C(1B)-C(5A)-C(6A)	119.0(4)	C(9D)-C(10D)-C(11D)	121.7(8)
N(C)-C(4C)-C(3C)	109.2(4)	C(4B)-C(5B)-C(6B)	120.0(4)	C(10D)-C(11D)-C(6D)	119.7(6)
N(D)-C(1D)-C(2D)	110.3(3)	C(1C)-C(5B)-C(6B)	117.6(4)	C(11D)-C(6D)-C(7D)	118.6(4)

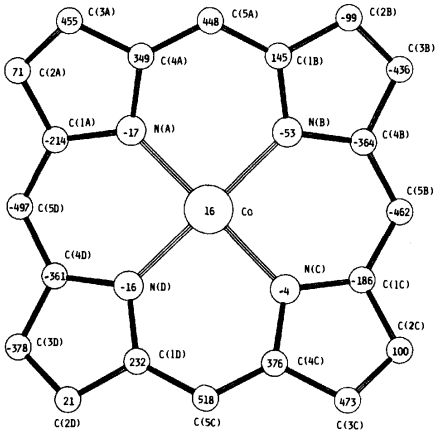

Fig. 4. A diagram of the porphyrinato core showing displacement of atoms, in units of 0.001 Å, from the mean plane at the 24 atom core.

the pyrrole rings. The four pyrrole rings are swiveled about the Co–N(tpp) bond; the dihedral angles between the pyrrole rings and the porphyrinato mean plane are 17.0, 14.9, 17.0, and 16.6°. Similar conformations have been observed for [$Co^{III}Cl$(tpp)(py)], [$Co^{III}(CH_3O)$(tpp)(py)], [$Co^{III}(NO_2)$(tpp)(lut)], and [Co^{III}(tpp)$(H_2O)_2]^+$. Recently, by comparing various Co^{III}(tpp) complexes, we found[23] a linear relationship between the ruffling of the porphyrinato core and the Co–N(tpp) distance; the porphyrinato core is ruffled as the Co–N(tpp) distance decreases.

The two oppisite phenyl groups are above, and the two other phenyl groups are below, the porphyrinato core, as is shown in Fig. 2. The dihedral angles between the mean plane of the porphyrinato core and the plane of the four phenyl groups are 59.9(2), 52.5(2), 61.5(2), and 62.2(2)°, their average value being 59°. In general, the angles smaller than 60° are precluded by steric interactions between the pyrrole hydrogen and phenyl hydrogen atoms.[9] The dihedral angle of 52.5° obtained from the present study is the smallest among those of Co^{III}(tpp) complexes thus far reported. Masuda et al.[12] have pointed out a linear relationship between the dihedral angles and the Cm–Cp distance. The average Cm–Cp distance of the present complex is 1.492(3) Å. This distance is the shortest among those reported of the Co^{III}(tpp) complexes; also it is close to that observed for the central C–C bond of the planar biphenyl molecule.[24] Through the short distance of Cm–Cp, the π-conjugate system of the porphyrinato core may be slightly delocalized over the phenyl rings, although the π-conjugate system might be weakened because of its ruffled conformation.[12]

The short C···C intermolecular van der Waal's contacts are shown in Table 4. Two less than 3.55 Å are observed between phenyl-carbon and pyrrole-carbon atoms. The shortest phenyl carbon–phenyl carbon distance (3.322(8) Å) is between C(7B) and $C(7B)^V$ atoms; the shortest pyrrole carbon–pyrrole carbon distance (3.411(6) Å) is between C(3A) and $C(3B)^{IV}$ atoms.

Table 4. The Short Intermolecular van der Waal's Contacts

Symmetry Code:

I	$1+x, y, z$	II	$-1+x, y, z$
III	$1+x, y, 1+z$	IV	$x, -y+1/2, z-1/2$
V	$-x, -y, -z$	VI	$1-x, -y, -z$
VII	$-x, y+1/2, -z+1/2$		

Type		l/Å
Pyrrole carbon ··· phenyl carbon		
C(2A) ···	$C(9B)^{VII}$	3.550(9)
C(2D) ···	$C(9A)^{I}$	3.549(12)
C(3A) ···	$C(9B)^{VII}$	3.732(8)
C(3D) ···	$C(9A)^{I}$	3.650(11)
C(2D) ···	$C(10A)^{III}$	3.696(9)
C(2B) ···	$C(9C)^{II}$	3.626(11)
C(1C) ···	$C(8B)^{V}$	3.665(7)
C(2C) ···	$C(9C)^{VI}$	3.643(10)
Pyrrole carbon ··· pyrrole carbon		
C(3A) ···	$C(3B)^{IV}$	3.411(6)
C(3A) ···	$C(4B)^{IV}$	3.539(6)
Phenyl carbon ··· phenyl carbon		
C(7B) ···	$C(7B)^{V}$	3.322(8)
C(11C)···	$C(11D)^{IV}$	3.568(8)

The porphyrinato core is almost vertical to the bc plane, as seen from the crystal structure shown in Fig. 2. The Co–Cl bond makes an angle of 16.6° from the c axis. The porphyrin molecule is transferred by the c glide operation and is stacked along the c axis. The hydrogen bond between an axial water molecule of a [$Co^{III}Cl$(tpp)(H_2O)] molecule and an axial chlorine atom of the neighbor [$Co^{III}Cl$(tpp)(H_2O)] molecule is zigzagged along the c axis direction. The hydrogen-bond distance, O–H···Cl, is 3.070(3) Å.

The authors are grateful to Dr. Haruo Honma of this Institute for his helpful advice on crystallization and on the elementary analyses of this complex.

References

1) K. Yamamoto, *Sci. Papers Inst. Phys. Chem. Res*, **71**, 111 (1977); K. Yamamoto, J. Uzawa, and T. Chijimatsu, *Chem. Lett.*, **1979**, 89; K. Yamamoto, M, Kohno, and H. Ohya-Nishiguchi, *Chem. Lett.*, **1981**, 255; M. Kohno, H. Ohya-Nishiguchi, K. Yamamoto, and T. Sakurai, *Bull. Chem. Soc. Jpn.*, **56**, 822 (1983); M. Kohno, H. Ohya-Nishiguchi, K. Yamamoto, and T. Sakurai, *Bull. Chem. Soc. Jpn.*, **57**, 932 (1984); K. Yamamoto, M. Hoshino, M. Kohno, and H. Ohya-Nishiguchi, *Bull. Chem. Soc. Jpn.*, **59**, 351 (1986).

2) T. Sakurai, K. Yamamoto, H. Naito, and N. Nakamoto, *Bull. Chem. Soc. Jpn.*, **49**, 3042 (1976).

3) T. Sakurai and K. Yamamoto, Proceedings of the 30th Annual Meeting of Coordination Chemistry (1980), p. 106.

4) L. E. Orgel, "An Introduction to Transition-Metal

Chemistry," Methuen, London (1960), p. 41.
5) T. Sakurai and K. Kobayashi, *Rikagaku Kenkyusho Hokoku*, **55**, 69 (1979).
6) T. Ito, *Acta Crystallogr., Sect. A*, **38**, 869 (1982).
7) "International Tables for X-Ray Crystallography," ed by J. A. Ibers and W. C. Hamilton, Kynoch Press, Birmingham, England (1974), Vol. IV, pp. 71, 148.
8) The anisotropic temperature factors for the non-hydrogen atoms, the atomic coordinates for the hydrogen atoms, and the lists of structure factors are deposited as Document No. 8778 at the Office of the Editor of the Bull. Chem. Soc. Jpn.
9) T. Sakurai, K. Yamamoto, N. Seino, and M. Katsuta, *Acta Crystallogr., Sect. B*, **31**, 2514 (1975).
10) G. G. Messmer and E. L. Amma, *Acta Crystallogr., Sect. B*, **24**, 417 (1968).
11) L. Pauling, "The Nature of the Chemical Bond," 3rd ed., Cornell University Press (1960), (Japanese translation by M. Koizumi), Kyoritsu Shuppan, Tokyo (1962), pp. 204, 226, 469, 470.
12) H. Masuda, T. Taga, K. Osaki, H. Sugimoto, and M. Mori, *Bull. Chem. Soc. Jpn.*, **55**, 4 (1982).
13) C. Riche and A. Chiaroni, M. Perree-Fauvet, and A. Gaudemer, *Acta Crystallogr., Sect. B*, **34**, 1868 (1978).
14) X. Solans, C. Miravitlles, G. Germain, and J. P. Declerco, *Acta Crystallogr., Sect. B*, **35**, 2181 (1979).
15) M. E. Kastner and W. R. Scheidt, *J. Organomet. Chem.*, **157**, 109 (1978).
16) H. Masuda, T. Taga, H. Sugimoto, and M. Mori, *J. Organomet. Chem.*, **273**, 385 (1984).
17) J. W. Lauher and J. A. Ibers, *J. Am. Chem. Soc.*, **96**, 4447 (1974).
18) W. R. Scheidt, J. A. Cunningham, and J. L. Hoard, *J. Am. Chem. Soc.*, **95**, 8289 (1973).
19) C. Riche, A. Chiaroni, M. Gouedard, and A. Gaudemer, *J. Chem. Res. (S)*, **32**, (*M*) 534 (1978).
20) J. A. Kaduk and W. R. Scheidt, *Inorg. Chem.*, **13**, 1875 (1974).
21) E. B. Fleischer, *Acc. Chem, Res.*, **3**, 105 (1969); W. R. Scheidt, *ibid.*, **10**, 339 (1977); J. L. Hoard, "Porphyrins and Metalloporphyrins," ed by K. M. Smith, Elsevier, Amsterdam (1975), p. 317; J. L. Hoard, *Ann. N. Y. Acad. Sci.*, **206**, 18 (1973); R. G. Little and J. A. Ibers, *J. Am. Chem. Soc.*, **96**, 4440 (1974).
22) M. Iwata and Y. Saito, *Acta Crystallogr., Sect. B*, **29**, 822 (1973).
23) Y. Iimura, T. Sakurai, and K. Yamamoto, Proceedings of the 36th Annual Meeting of Coordination Chemistry (1986), p. 425.
24) G. P. Charbonneau and Y. Delugeard, *Acta Crystallogr., Sect. B*, **33**, 1586 (1977).

^{57}Fe-Moessbauer and ^{13}C-CP-MAS NMR Spectroscopic Studies of the Reaction Products of Ruthenocene Derivatives with Lewis Acids

Masanobu WATANABE, Yuichi MASUDA, Izumi MOTOYAMA, and Hirotoshi SANO*
Department of Chemistry, Faculty of Science, Tokyo Metropolitan University, Fukasawa, Setagaya-ku, Tokyo 158
(Received August 18, 1987)

Adducts of ruthenocene with Lewis acids, such as $HgCl_2$, $SnCl_4$, and I_2, are studied mainly by means of high resolution solid state ^{13}C NMR spectroscopy and ^{57}Fe-Moessbauer spectroscopy. The large low-field shifts found in the ^{13}C-CP-MAS NMR spectroscopy suggest the presence of a direct chemical bond between the ruthenium and the Lewis acids. Ferrocenylruthenocene and biruthenocene give stable adducts with $HgCl_2$ and I_2. ^{57}Fe-Moessbauer and ^{13}C-CP-MAS NMR spectroscopic studies suggest the presence of a chemical bond, such as Ru-Hg, Ru-I, in the adducts.

The basicity of the nonbonding e_{2g} electrons around the iron and ruthenium atoms in ferrocene and ruthenocene derivatives respectively has been studied in the reaction of ferrocene and ruthenocene derivatives with protons in a solution, such as $CHCl_3$, CX_3COOH (X=Cl, F), and H_2SO_4.[1,2] Especially, [2]ferrocenophanes react with an appropriate Lewis acid species, such as $HgCl_2$, $SnCl_4$, and I_2, to give diamagnetic stable adducts with a direct chemical bond between the iron atom and the Lewis acids.[3-5] Ruthenocene also reacts with the Lewis acids and it gives much more stable adducts than ferrocene because ruthenocene has less steric hindrance in donating e_{2g} electrons than does ferrocene. Although [2]ferrocenophane and ruthenocene are well-soluble in most organic solvents, the adducts are less soluble in the solvents. Thus far, all attempts to obtain a single crystal of [2]ferrocenophane-3$HgCl_2$ and -1.5$SnCl_4$ have been unsuccessful, while a few adducts, such as ruthenocene-3$HgCl_2$ and -1.8$HgBr_2$, [2]ferrocenophane-2I_2, were obtained as single crystals in which direct metal-metal chemical bonds (Ru-Hg and Fe-I respectively) have been found on the basis of the results of X-ray diffraction studies.[5,6]

Recently, improvements in sensitivity, in the resolution in cross-polarization (CP), in dipolar decoupling, and in magic-angle-spinning (MAS) techniques have made it possible to obtain a high-resolution ^{13}C NMR spectrum, even in the solid state.[7-10] The present studies were undertaken to clarify the structure of some ruthenocene derivative-Lewis acid adducts, such as $HgCl_2$, $SnCl_4$, and I_2, by means of ^{57}Fe-Moessbauer and high-resolution ^{13}C-CP-MAS NMR spectroscopy.

Experimental

Materials: The ferrocenylruthenocene was prepared by the Ullmann coupling of bromoruthenocene and bromoferrocene, instead of iodoruthenocene and iodoferrocene, at 120 °C for 12 h.[11] Biruthenocene was prepared by the same method using bromoruthenocene. ^{1}H NMR ($CDCl_3$); δ=4.79(t)($H_{2,5}$), 4.54(t)($H_{3,4}$), 4.44(s)(π-C_5H_5) for the ruthenocene group, δ=4.23(t)($H_{2,5}$), 4.09(t)($H_{3,4}$), 4.05(s)(π-C_5H_5) for the ferrocene group in ferrocenylruthenocene, δ=4.69(t)($H_{2,5}$), 4.47(t)($H_{3,4}$) and 4.50(s)(π-C_5H_5) for biruthenocene. Ferrocenyl ruthenocenyl ketone was prepared by following the previously reported method.[12] The purity of the metallocenes was confirmed by elemental analysis. Adducts of ruthenocene with $HgCl_2$, $SnCl_4$, and I_2 were prepared by following the methods in the previous reports.[6,13,14] Adducts of ferrocenylruthenocene, biruthenocene, and ferrocenyl ruthenocenyl ketone with $HgCl_2$ were prepared in diethyl ether by a method similar to that used in the case of the ruthenocene-3$HgCl_2$ adduct. Found: C, 14.17; H, 1.27%. Calcd for ferrocenylruthenocene-5$HgCl_2$, $C_{20}H_{18}FeRu$-5$HgCl_2$: C, 13.55; H, 1.07%. Found: C, 17.02; H, 1.48%. Calcd for biruthenocene-3.5$HgCl_2$, $C_{20}H_{18}Ru_2$-3.5$HgCl_2$: C, 17.02; H, 1.29%. Found: C, 18.01; H, 1.50%. Calcd for ferrocenyl ruthenocenyl ketone-3.5$HgCl_2$, $C_{21}H_{18}OFeRu$-3.5$HgCl_2$: C, 18.10; H, 1.30%, respectively. Adducts of ferrocenylruthenocene and biruthenocene with I_2 were prepared by mixing I_2 with the metallocenes in a dry benzene-hexane mixture. Found: C, 26.00; H, 1.91%. Calcd for ferrocenylruthenocene-2I_2, $C_{20}H_{18}FeRu$-2I_2: C, 26.03; H, 1.97%. Found: C, 24.88; H, 1.98%. Calcd for biruthenocene-2I_2, $C_{20}H_{18}Ru_2$-2I_2: C, 24.81; H, 1.87%.

Measurements: The ^{13}C-CP-MAS NMR spectra were obtained at the frequency of 50.18 MHz using a JEOL FX-200 Fourier Transform NMR Spectrometer. Four thousands datum points at a sweep width setting of 20 kHz were collected by following a spin-locking cross-polarization sequence. Both the ^{1}H- and ^{13}C-rf field strengths were 50 kHz. Magic angle sample spinning rates of 3 to 3.5 kHz were achieved by using Kel-F rotors. The chemical shifts were measured with respect to external adamantane and then converted to the shifts from TMS. The ^{1}H and ^{13}C NMR spectra in solution were measured with the same spectrometer at 199.56 and 50.18 MHz respectively, using TMS as a standard. The assignment of the ^{13}C signals of the metallocenes was carried out by selective proton-decoupling experiments.

The ^{57}Fe-Moessbauer spectroscopic measurements were carried out by using a ^{57}Co(Rh) source moving in a constant acceleration mode. All the isomer-shift (I. S.) values for the ^{57}Fe-Moessbauer spectra are given relative to metallic iron; the experimental errors of the I. S. and quadrupole-splitting (Q. S.) values are estimated to be within $\pm$0.02 mm s^{-1}.

Results and Discussion

Figure 1 shows the ^{13}C-CP-MAS NMR spectra of the ruthenocene (a) and its $-3HgCl_2$(b), $-1.5SnCl_4$(c), and $-2I_2$(d) adducts; the ^{13}C chemical-shift (δ) values of the adduct and related compounds are listed in Table 1. The π-C_5H_5 ring carbon signal in the ruthenocene appears at δ=73.2, and its adducts, at δ=81.2, 89.1, and 93.4 for the $-3HgCl_2$, $-1.5SnCl_4$, and $-2I_2$ adducts, respectively. These large low-field shifts ($\Delta\delta$=8.0, 15.9, and 20.2 for the $-3HgCl_2$, $-1.5SnCl_4$, and $-2I_2$ adducts respectively) can be attributed to the Ru–Hg, Ru–Sn, and Ru–I bond formation in the adducts as has already been verified by means of X-ray-diffraction[6,13] and ^{119}Sn-Moessbauer spectroscopic studies.[4] The increasing values of the low-field shift in the Lewis acid adducts suggest that the interaction between the ruthenocene and the Lewis acids increases in the order of $HgCl_2<SnCl_4<I_2$. As has previously been mentioned, [2]ferrocenophane–Lewis acid adducts give large Q. S. values (3.29, 3.49, and 3.65 mm s^{-1}, for the $-3HgCl_2$, $-1.5SnCl_4$, and $-2I_2$ adducts, respectively) in their ^{57}Fe-Moessbauer spectra.[3-5] The fact that the order of the increase in

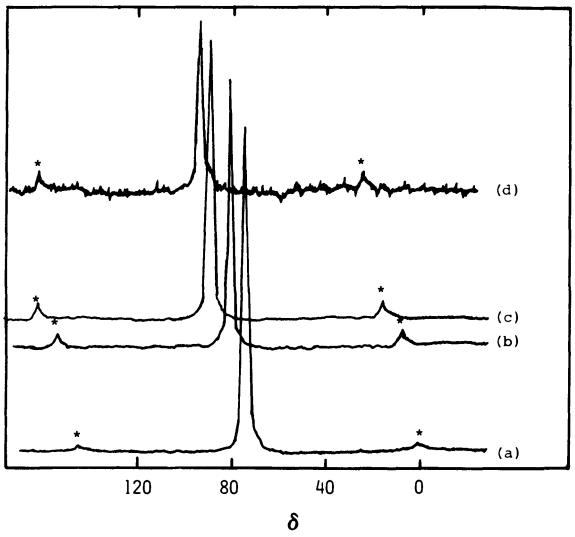

Fig. 1. ^{13}C-CP-MAS NMR spectra of the ruthenocene (a) and its $-3HgCl_2$(b), $-1.5SnCl_4$(c), and $-2I_2$ (d) adducts.
The sample spinning side band (SSB) is represented by * in the Figure.

Table 1. ^{13}C Chemical-Shifts of Ruthenocene and Related Compounds in the Solid State and in a Chloroform Solution

Compound	Ruthenocene δ	Ferrocene δ	
Ruthenocene	73.2		
Ruthenocene-$3HgCl_2$	81.2		
Ruthenocene-$1.5SnCl_4$	89.1		
Ruthenocene-$2I_2$	93.4		
Ferrocenylruthenocene	88.5(C_1)	84.6(C_1)	
	72.9(π-C_5H_5)	71.3(π-C_5H_5)	
		67.9($C_{2,5}$)	
Ferrocenylruthenocene-$3HgCl_2$	81.4(π-C_5H_5)	79.1(π-C_5H_5)	
Ferrocenylruthenocene-$2I_2$	93.6(π-C_5H_5)	76.5(π-C_5H_5)	
Biruthenocene	87.5(C_1)		
	72.3(π-C_5H_5)		
	69.1($C_{3,4}$)		
Biruthenocene-$3.5HgCl_2$	81.2(π-C_5H_5)		
Biruthenocene-$2I_2$	92.9(π-C_5H_5)		
	77.4(π-C_5H_5)		
Ferroceny ruthenocenyl	86.0(C_1)	80.7(C_1)	197.9(CO)
Ketone	72.7(π-C_5H_5)	71.3(π-C_5H_5)	
Ferrocenyl ruthenocenyl	81.0(π-C_5H_5)	72.6(π-C_5H_5)	195.2(CO)
Ketone-$3.5HgCl_2$			
Ferrocenylruthenocene*	87.9(C_1)	83.5(C_1)	
	71.0(π-C_5H_5)	69.2(π-C_5H_5)	
	69.9($C_{2,5}$)	67.4($C_{3,4}$)	
	69.6($C_{3,4}$)	67.2($C_{2,5}$)	
Biferrocene*		83.9(C_1)	
		69.2(π-C_5H_5)	
		67.6($C_{3,4}$)	
		66.4($C_{2,5}$)	
Biruthenocene*	87.5(C_1)		
	70.9(π-C_5H_5)		
	71.3($C_{2,5}$)		
	69.6($C_{3,4}$)		

*: Stands for a CD_3Cl solution.

the low-field shifts of the ruthenocene-Lewis acids adducts is similar to that of the Q. S. values of the [2]-ferrocenophane-Lewis acid adducts suggests that the effect of Lewis acids on the ruthenium atoms in ruthenocene is similar to that on the iron atoms in [2]ferrocenophane.

Similar large low-field shifts are also observed for the ^{1}H NMR spectra of the ruthenocene-Lewis acid adducts in CD_3CN. The ^{1}H NMR spectra of the adducts are shown in Fig. 2, while their chemical shift values are summarized in Table 2. The fact that the decreasing shift ($\Delta\delta$=1.50) for the ruthenocene-$2I_2$ adduct is much larger than that of the -$3HgCl_2$ adduct ($\Delta\delta$=0.84), as in the case of the ^{13}C-CP-MAS NMR spectra, shows that the ruthenium atom interacts with the iodine atom more strongly than with the mercury atom in the solution.

Table 2. ^{1}H NMR Chemical-Shifts of Ruthenocene and Related Compounds in Acetonitrile

Compound	Chemical shift δ
Ruthenocene	5.37
Ruthenocene-$3HgCl_2$	6.21
Ruthenocene-$1.5SnCl_4$	5.35
Ruthenocene-$2I_2$	6.87
Biruthenocene	5.53($H_{2,5}$)
	5.30($H_{3,4}$)
	5.32(π-C_5H_5)
Biruthenocene-$2I_2$	6.90($H_{2,5}$)
	6.54($H_{3,4}$)
	6.65(π-C_5H_5)

Although the ruthenocene-$2I_2$ and $3HgCl_2$ adducts are stable in acetonitrile, the -$1.5SnCl_4$ adduct is unstable in the solution; i.e., the yellow solution of the -$1.5SnCl_4$ adduct dissociates in acetonitrile, becoming colorless in a few minutes after the dissolution, while the electronic spectrum becomes the same as that of ruthenocene itself. The ^{1}H chemical-shift observed in the ruthenocene-$1.5SnCl_4$ adduct (δ=5.35) in the solution corresponds well to that of the ruthenocene (δ=5.37), also indicating the dissociation of the -$1.5SnCl_4$ adduct in acetonitrile. It seems very reasonable to conclude that the structure of the -$1.5SnCl_4$ adduct can be expressed as $[(C_5H_5)_2Ru\text{-}SnCl_2\text{-}Ru(C_5H_5)_2]^{2+}(SnCl_5^-)_2$, on the basis of the ^{13}C-CP-MAS NMR data, as has already been proposed by Mann et al. based on their infrared spectroscopic study[14] and by us based on our ^{119}Sn-Moessbauer spectroscopic study.[4]

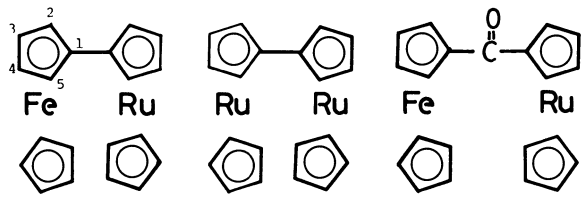

Ferrocenylruthenocene Biruthenocene Ferrocenyl ruthenocenyl ketone

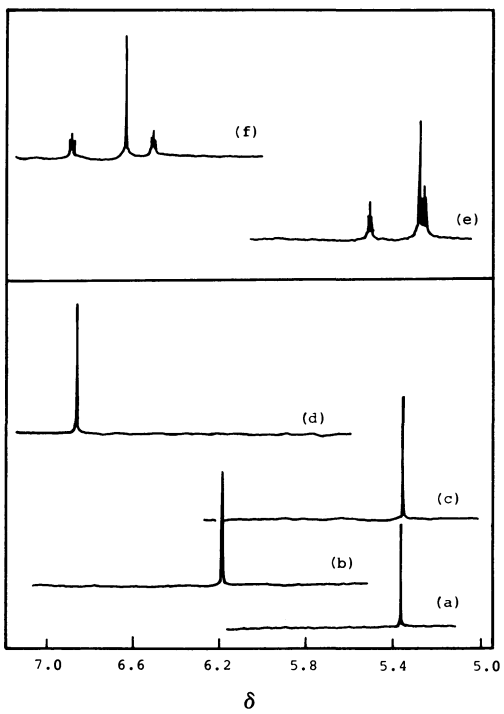

Fig. 2. ^{1}H NMR spectra of the ruthenocene(a), ruthenocene-$3HgCl_2$(b), ruthenocene-$1.5SbCl_4$(c), ruthenocene-$2I_2$(d), biruthenocene(e), biruthenocene-$2I_2$(e) compounds in the acetonitrile solution.

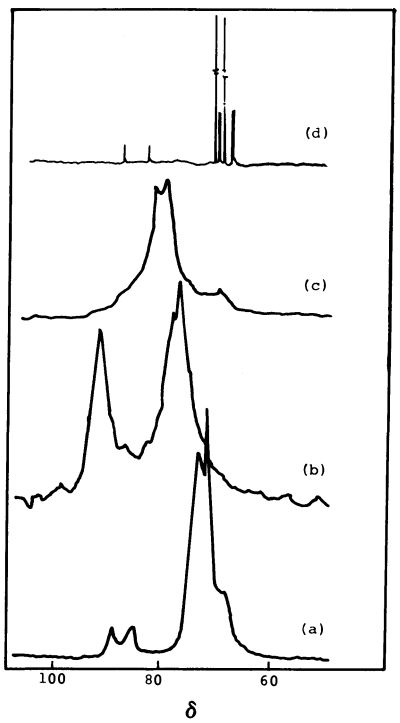

Fig. 3. ^{13}C-CP-NAS NMR spectra of ferrocenylruthenocene(a), and its -$2I_2$(b), -$5HgCl_2$(c) adducts and ^{13}C NMR spectrum of ferrocenylruthenocene(d) in chloroform solution.

Ferrocenylruthenocene was first synthesized by the reaction of the Ullmann coupling of iodoruthenocene with a large excess of iodoferrocene by Neuse in 1981.[11] In the present study, ferrocenylruthenocene is found to react with I_2 and $HgCl_2$ to give stable diamagnetic precipitates, which have been analyzed as ferrocenylruthenocene-$2I_2$ and ferrocenylruthenocene-$5HgCl_2$ adducts.[15] Figure 3 shows the ^{13}C-CP-MAS NMR spectra of the original metallocene(a) and its -$2I_2$(b), -$5HgCl_2$(c) adducts, together with the higher-resolution ^{13}C NMR spectrum of the metallocene in the $CDCl_3$ solution(d).

As is shown in Fig. 3(d), the two groups of resonances for the ferrocene and ruthenocene moieties are separately observed; i.e., the ferrocene signals appear at a higher field than do the ruthenocene signals, and these signals are in good agreement with the ^{13}C NMR spectra of biferrocene and biruthenocene in the same solution, as is shown in Table 1. The carbon signals were assigned by using selective proton decoupling experiments based on the results of previous reports.[11,16]

The broad ^{13}C-CP-MAS NMR spectra of ferrocenylruthenocene(a) cannot, however, be resolved into individual carbon signals. The ^{13}C chemical-shift values of the metallocene in the solid state are shown in Table 1. The signals of $C_{3,4}$ and $C_{2,5}$ for the ruthenocene moiety and of $C_{3,4}$ for the ferrocene moiety are not well resolved, being superimposed on by large and broad π-C_5H_5 signals in the ^{13}C-CP-MAS NMR spectra. Therefore, only the low-field shift values of π-C_5H_5 will be discussed. As is shown in Fig. 3-c, the two broad π-C_5H_5 ring signals (δ=81.4 for the ruthenocene moiety and δ=79.1 for the ferrocene moiety) are found in the ferrocenylruthenocene-$5HgCl_2$ adduct. The former value agrees with the value of the ruthenocene-$3HgCl_2$ adduct (δ=81.2). The observed low-field shifts ($\Delta\delta$=7.8 and 8.5 for the ferrocene and ruthenocene moieties respectively) are similar to that of ruthenocene-$3HgCl_2$ adduct ($\Delta\delta$=8.0). This fact shows the presence of two kinds of direct chemical bondings, Fe-Hg and Ru-Hg, in the -$5HgCl_2$ adduct.

On the other hand, broader signals (δ=93.6 for the ruthenocene moiety and δ=76.5 for the ferrocene moiety) are found for the ferrocenylruthenocene-$2I_2$ adduct (3-b). Although a small low-field shift in the ferrocene moiety ($\Delta\delta$=5.2) is found, a relatively large shift ($\Delta\delta$=20.7) is found for the ruthenocene moiety. The latter value is quite similar to that of the ruthenocene-$2I_2$ adduct ($\Delta\delta$=20.2). These facts indicate that only the ruthenium atom is bound with the iodine atom in the ferrocenylruthenocene-$2I_2$ adduct.

Figure 4 shows the ^{57}Fe-Moessbauer spectra of ferrocenylruthenocene(a) and its -$5HgCl_2$(b), -$2I_2$(c) adducts. An anomalously large Q. S. value (2.99 mm s^{-1} at 78 K) is found in the -$5HgCl_2$ adduct, showing direct chemical Fe-Hg bond formation, while a slightly smaller Q. S. value (2.16 mm s^{-1}) than that of the original metallocene (2.36 mm s^{-1}) is found in the -$2I_2$ adduct. The smaller Q. S. value may be caused by the decreased e_{2g} electrons of the iron atom in the -$2I_2$ adduct containing the Ru-I bond. The absence of a large Q. S. line, as in the case of the -$5HgCl_2$ adduct, shows that the iron atom is not bound to the iodine atom in the ferrocenylruthenocene-$2I_2$ adduct. The ^{57}Fe-Moessbauer results are in

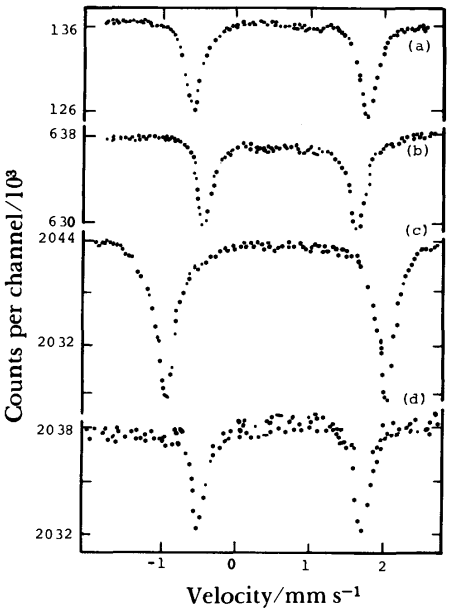

Fig. 4. ^{57}Fe-Moessbauer spectra of ferrocenylruthenocene(a) and its -$2I_2$(b), -$5HCl_2$(c) adducts and ferrocenyl ruthenocenyl ketone-$3.5HgCl_2$ adduct(d), all at 78 K.

Table 3. ^{57}Fe-Moessbauer Parameters of Ferrocenylruthenocene and Related Compounds

Compound	Temperature/K	Q. S./mm s^{-1}	I. S./mm s^{-1}
Ferrocenylruthenocene	78	2.36	0.53
	300	2.29	0.46
Ferrocenylruthenocene-$5HgCl_2$	78	2.99	0.57
Ferrocenylruthenocene-$2I_2$	78	2.16	0.52
	300	2.16	0.43
Ferrocenyl ruthenocenyl ketone	78	2.29	0.54
Ferrocenyl ruthenocenyl ketone-$3.5HgCl_2$	78	2.29	0.54

accordance with those of the ^{13}C-CP-MAS NMR spectroscopic studies of the ferrocenylruthenocene-$2I_2$ and -$5HgCl_2$ adducts. All the results obtained in the present studies indicate that the -$2I_2$ adduct may be expressed as $[(C_5H_5)(C_5H_4)Fe(C_5H_4)(C_5H_5)Ru\text{-}I]^+I_3^-$ in the solid state,[15] which is in accord with the elemental analysis datum.

The -$2I_2$ adduct is found to be unstable; that is, when the adduct is dissolved in acetonitrile, it turns green and an electronic absorption peak characteristic of a ferrocenium (λ_{max}=640 nm) increases rapidly, suggesting that the ferrocene moiety is rapidly oxidized in acetonitrile, giving ferrocenium-type cations. The fact that there is no evidence for Ru-I bond formation in the ferrocenylruthenocene-$2I_2$ adduct in acetonitrile in the studies done by means of ^{1}H and ^{13}C NMR agrees with the magnetic data, which show paramagnetism for the acetonitrile solution of the ferrocenylruthenocene-$2I_2$ adduct.

It is found that the ferrocenylruthenocene-$5HgCl_2$ adduct has two kinds of chemical bonds (Ru-Hg and Fe-Hg), while the ferrocenylruthenocene-$2I_2$ adduct has only a Ru-I bond in the solid state. These results can be explained on the basis of the fact that the van der Waals radius of iodine is much larger than that of the mercury atom. It is known that the Cp-rings are separated by 3.32 Å in ferrocene[17] and by 3.68 Å in ruthenocene.[18] The longer separation between the Cp-rings in the ruthenocene moiety may explain why only the ruthenocene moiety in ferrocenylruthenocene reacts with iodine, giving a stable Ru-I bond, while a ferrocene moiety does not give such a stable bond with an iodine atom bacause of van der Waals repulsion between Cp and the iodine atom.

Biruthenocene reacts with $HgCl_2$ and I_2, giving two stable adducts, analyzed as biruthenocene-$3.5HgCl_2$ and -$2I_2$ respectively. The ^{13}C-CP-MAS NMR spectra of the metallocene(a) and its -$3.5HgCl_2$(b), -$2I_2$(c) adducts are shown in Fig. 5, while the ^{13}C-chemical-shift values are shown in Table 1. A broad signal is found for the -$3.5HgCl_2$ adduct with the chemical-shift value of π-C_5H_5 ring (δ=81.2). This value corresponds to that of the ruthenocene-$3HgCl_2$ adduct (δ=81.2), and the relatively large low-field shift ($\Delta\delta$=8.9) shows the chemical-bond formation between the ruthenium and mercury atoms. These facts indicate that the two ruthenium atoms in the biruthenocene-$3.5HgCl_2$ adduct are bound equivalently to the mercury atoms.

On the other hand, two kinds of broad signals (δ= 92.9 and 77.4) are found for the -$2I_2$ adduct, as is shown in Fig. 5-c. The former value corresponds to that of the ruthenocene-$2I_2$ adduct(δ=93.4), and the latter to that of original biruthenocene itself (δ=72.3). The fact that two kinds of low-field shift values ($\Delta\delta$=20.6 and 5.1) are found indicates that only one of the ruthenium atoms in a biruthenocene molecule is

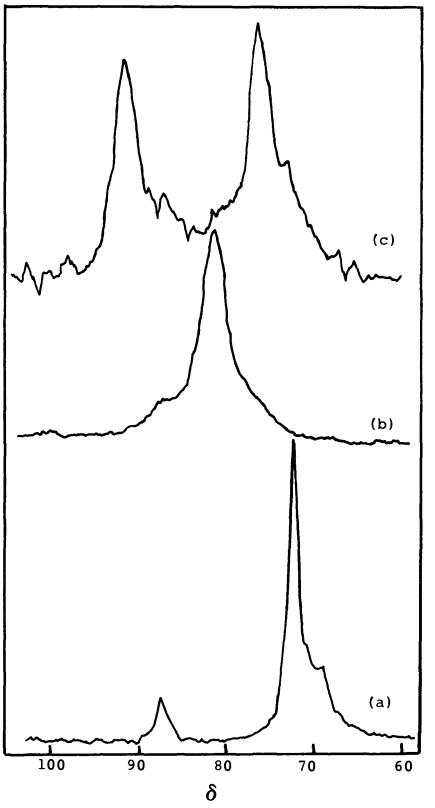

Fig. 5. ^{13}C-CP-MAS NMR spectra of biruthenocene (a) and its -$2I_2$(b), -$3.5HgCl_2$(c) adducts.

bound with the iodine atom; the adduct may be expressed as $[(C_5H_5)(C_5H_4)Ru(C_5H_4)(C_5H_5)Ru\text{-}I]^+I_3^-$ in the solid state, which is in good agreement with the elemental analysis data.

Although biruthenocene-$3.5HgCl_2$ is hardly soluble in acetonitrile, the -$2I_2$ adduct is well-soluble in acetonitrile. The ^{1}H NMR spectrum of the adduct is shown in Fig. 2(f), while the ^{1}H chemical-shift values of ruthenocene and biruthenocene in an acetonitrile solution are shown in Table 2. As in the case of the ^{13}C-CP-MAS NMR spectrum, large low-field shifts are found in the ^{1}H NMR spectra of the iodine adducts of the metallocenes in the acetonitrile. The smaller low-field shift of the Cp ring's ^{1}H chemical-shift of the biruthenocene-$2I_2$ adduct ($\Delta\delta$=1.33) compared to that of ruthenocene-$2I_2$ ($\Delta\delta$=1.50) was observed. The fact that the chemical states of the two ruthenocene moieties of the -$2I_2$ adduct are equivalent in the solution, while the chemical states are different in the solid state, suggests the possibility of a rapid exchange of the iodine between the two ruthenium atoms, $[Ru(C_5H_5)(C_5H_4)(C_5H_4)(C_5H_5)Ru\text{-}I]^+I_3^- \rightleftharpoons [I\text{-}Ru(C_5H_5)(C_5H_4)\text{-}(C_5H_4)(C_5H_5)]Ru]^+I_3^-$, in acetonitrile.

Ferrocenyl ruthenocenyl ketone was first prepared by Rausch et al. by means of the reaction of ferrocenyl chloride with ruthenocene in the presence of aluminum chloride.[12] Ferrocenyl ruthenocenyl

ketone is one of the most suitable compounds for the present studies. Recently, Clemance et al. have reported that diacetylferrocene reacts with a Lewis acid species, such as $AlCl_3$, $SnCl_4$, or $TiCl_4$, to give adducts. All the adducts show smaller Q. S. values (2.10—2.05 mm s^{-1} at 78 K) than the value of the original diacetylferrocene (2.14 mm s^{-1} at 78 K).[19] The results of the ^{57}Fe-Moessbauer spectroscopic studies indicate the absence of chemical bonding between the iron atom and the central metal atom of the Lewis acids, and it has been proposed that the central metal atoms of the Lewis acids are bound to the carbonyl oxygen atoms in the adducts.[19]

Ferrocenyl ruthenocenyl ketone reacts with $HgCl_2$ under the same conditions as those used in the preparation of the ferrocenylruthenocene-5$HgCl_2$ adduct, giving a stable diamagnetic adduct, expressed as ferrocenyl ruthenocenyl ketone-3.5$HgCl_2$ on the basis of the elemental analysis. The color of the adduct is purple, although most $HgCl_2$ adducts with ruthenocene or ferrocene derivatives are yellow or orange respectively. The ^{57}Fe-Moessbauer parameters of the adduct (I. S.=0.54 mm s^{-1}, Q. S.=2.29 mm s^{-1} at 78 K) are the same as those of the original ferrocenyl ruthenocenyl ketone, as is shown in Table 3 and Fig. 4(d). These facts suggest that there is no direct interaction between the mercury and iron atoms in the adduct.

The ^{13}C-CP-MAS NMR spectra of the metallocene(a) and its -3.5$HgCl_2$(b) adduct are shown in Fig. 6, while and the ^{13}C chemical-shift values of the metallocene and its adducts are shown in Table 1. The signals of $C_{2,5}$ and $C_{3,4}$ are overlapped with the

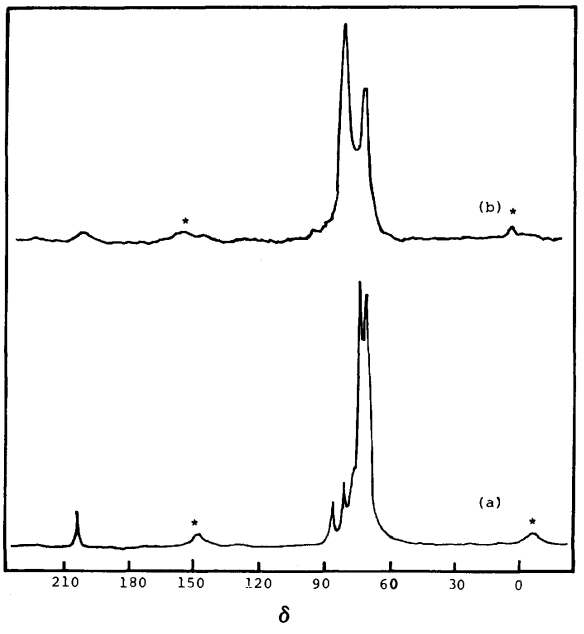

Fig. 6. ^{13}C-CP-MAS NMR spectra of ferrocenyl ruthenocenyl ketone(a) and its -3.5$HgCl_2$ adduct(b).

π-C_5H_5 ring main peaks. Two kinds of broad signals (δ=81.0 for ruthenocene and δ=72.6 for ferrocene) are found for the -3.5$HgCl_2$ adduct. The latter value is very similar to that of the original compound ($\Delta\delta$=0.9), whereas a relatively large low-field shift is observed for the former ($\Delta\delta$=8.3), its value corresponding to that of ruthenocene-3$HgCl_2$ ($\Delta\delta$=8.0). The carbonyl carbon signal appears at δ=195.2. This value is almost the same as that of the original metallocene (δ=197.9). The infrared spectrum for the original metallocene shows a strong band at 1610 cm^{-1} which can be assigned to a C=O stretching mode; this band is almost the same in position and intensity as that of the -3.5$HgCl_2$ adduct (1600 cm^{-1}). These facts indicate that there is only one kind of chemical bonding between the ruthenium and mercury atoms in the -3.5$HgCl_2$ adduct.

The absence of the chemical bonding between the iron and mercury atoms in the $HgCl_2$ adduct can be explained as follows; the steric hindrance in the ferrocene moiety makes it impossible to form a chemical bond between the iron and mercury atoms in the -3.5$HgCl_2$ adduct, whereas the ruthenocene moiety can form a chemical bond between the ruthenium and mercury atoms because it has less steric hindrance.

This work is partly supported by a Grant-in-Aid from the Ministry of Education (No. 60430014).

References

1) C. W. Fung and R. M. G. Roberts, *Tetrahedron*, **36**, 3289 (1980).
2) G. Cerichelli, G. Illuminati, G. Ortaggi, and A. M. Giuliani, *J. Organomet. Chem.*, **127**, 357 (1977).
3) M. Watanabe, H. Ichikawa, I. Motoyama, and H. Sano, *Bull. Chem. Soc. Jpn.*, **56**, 3291 (1983).
4) M. Watanabe, I. Motoyama, and H. Sano, *Bull. Chem. Soc. Jpn.*, **59**, 2109 (1986).
5) M. Watanabe, K. Sato, I. Motoyama, and H. Sano, *Chem. Lett.*, **1983**, 1775.
6) W. H. Morrison, Jr., and D. N. Hendrickson, *Inorg. Chem.*, **11**, 2912 (1972).
7) S. R. Hartman and E. L. Hahn, *Phys. Rev.*, **128**, 2042 (1962).
8) A. Pines, M. G. Gibby, and J. S. Waugh, *J. Chem. Phys.*, **59**, 569 (1973).
9) J. Schaefer, S. H. Chin, and S. I. Weissman, *Macromolecules*, **5**, 798 (1972).
10) J. Schaefer, E. O. Stejskal, and R. Buckdahl, *Macromolecules*, **10**, 384 (1977).
11) E. W. Neuse and M. S. Loonat, *Transition Met. Chem.*, **6**, 260 (1981).
12) N. D. Rausch, E. O. Fischer, and H. Grubert, *J. Am. Chem. Soc.*, **82**, 76 (1960).
13) Y. S. Sohn, A. W. Schlueter, D. N. Hendrickson, and H. B. Gray, *Inorg. Chem.*, **13**, 301 (1974).
14) K. R. Mann, W. H. Morrison, Jr., and D. N. Hendrickson, *Inorg. Chem.*, **13**, 1180 (1974).

15) M. Watanabe, I. Motoyama, and H. Sano, *Chem. Lett.*, **1987**, 309.
16) F. H. Kohler and G. E. Matubayashi, *J. Organomet. Chem.*, **96**, 391 (1975); R. W. Crecely, K. M. Crecely, and J. H. Goldstien, *Inorg. Chem.*, **8**, 252 (1969).
17) J. D. Dunitz, L. E. Orgel, and A. Rich, *Acta Crystallogr.*, **9**, 373 (1956).
18) G. L. Herdgrove and D. H. Templeton, *Acta Crystallogr.*, **12**, 28 (1959).
19) M. C. Clemance, R. M. G. Roberts, and J. Silver, *J. Organomet. Chem.*, **247**, 219 (1983); G. Neshvad, R. M. G. Roberts, and J. Silver, *J. Organomet. Chem.*, **236**, 349 (1982).

 © 1988 The Chemical Society of Japan Bull. Chem. Soc. Jpn., 61, 835—839 (1988)

Effects of Methyl Substituent on Solvent Extraction of Copper(II) with *o*-, *m*-, and *p*-Methylbenzoic Acids

Hiromichi YAMADA,* Shiho HORIKAWA, Yukio FUJII, and Masateru MIZUTA
Faculty of Engineering, Gifu University, 1-1 Yanagido, Gifu 501-11
(Received August 27, 1987)

The extraction of copper(II) with *o*-, *m*-, and *p*-methylbenzoic acids in 1-octanol was carried out at 25 °C and aqueous ionic strength of 0.1 mol dm^{-3} ($NaClO_4$). In contrast to the extraction with benzoic acid, in which only the monomeric copper(II) benzoate is extracted, the dimeric copper(II) species is also responsible for the extraction of copper(II) with *o*- and *m*-methylbenzoic acids in 1-octanol together with the monomeric one. On the other hand, *p*-methylbenzoic acid has a poorer extracting capability than *o*- and *m*-methylbenzoic acids and only the monomeric copper(II) species is responsible for the extraction.

Compared with aliphatic carboxylic acids, aromatic carboxylic acids have been scarcely employed as extracting agents owing to their poor extracting capability. In the previous investigations on the extraction of copper(II) with benzoic,[1] and decanoic[2,3] acids, it has been shown that there was a remarkable difference in the extraction equilibrium between aromatic and aliphatic carboxylic acids. For example, copper(II) benzoate cannot be extracted in benzene, but can be easily extracted in 1-octanol as a monomeric species CuA_2 (A: carboxylate anion).[1] In the copper(II) decanoate extraction systems, the dimeric species $Cu_2A_4(HA)_2$ can be extracted in nonsolvating solvents such as benzene, while not only the dimeric copper(II) decanoates but also the monomeric ones are responsible for the extraction in solvating solvents[3-5] such as 1-octanol. These results suggest that the formation of the dimeric copper(II) carboxylate is essential for the extraction of copper(II) carboxylates into nonsolvating solvents such as benzene, and in solvating solvents the solvation of the monomeric copper(II) species by some solvent molecules makes possible the extraction of copper(II) without any detectable formation of the dimeric copper(II) species.

The present paper deals with the extraction of copper(II) with *o*-, *m*-, and *p*-methylbenzoic acids in 1-octanol. It was found that with *p*-methylbenzoic acid, the copper(II) ion is extracted through a mechanism different from the extraction with *o*- and *m*-methylbenzoic acids, in which the monomeric and dimeric copper(II) species are responsible for the extraction.

Experimental

Reagents. *o*-, *m*-, and *p*-Methylbenzoic Acids: Commercial methylbenzoic acids (purity: over 99%) were dissolved in 1-octanol. **Copper(II) perchlorate, sodium perchlorate, and 1-octanol** were the same as employed previously.[3] All other reagents were reagent grade and used without further purification.

Procedure. Partition was performed at a total copper concentration of 5×10^{-3} mol dm^{-3} and methylbenzoic acids concentration of 0.3—1.6 mol dm^{-3} in a bath thermostated at 25.0±0.2 °C. Ionic strength of the aqueous phase was adjusted to 0.1 mol dm^{-3} with sodium perchlorate. Shaking for about 1 h was sufficient for complete equilibration. The concentrations of copper(II) and hydrogen ions in the aqueous phase were determined by the same manner as employed previously.[1] The dissociation constants of methylbenzoic acids were potentiometrically estimated. In the determination of the partition constants of *o*-, *m*-, and *p*-methylbenzoic acids between water and 1-octanol, the absorption maxima at 279, 281, and 241 nm of the respective acids were used for the determination of the concentration of the respective acids in the aqueous phase.

Apparatus. For mechanical shaking in a thermostat, centrifugation, pH measurements, and spectrophotometric determinations, the apparatus were the same as employed previously.[1]

Results and Discussion

Partition of Methylbenzoic Acids. In the extraction of metals with carboxylic acids, it is indispensable to have information about the partition of the carboxylic acids. The following equilibria on the carboxylic acid HA should be considered: (a) The dissociation of HA in the aqueous phase ($K_a=[H^+][A^-]/[HA]$), (b) the partition of HA into the organic phase ($K_{D,HA}=[HA]_o/[HA]$), and (c) the dimerization of HA in the organic phase ($K_{2,HA}=[(HA)_2]_o/[HA]_o^2$). The dissociation constant of *o*-, *m*-, and *p*-methylbenzoic acids were potentiometrically determined at the ionic strength of 0.1 mol dm^{-3} ($NaClO_4$). The values obtained are summarized in Table 1. These values are in agreement with those already presented[6] with making activity coefficient corrections.

The partition of the respective methylbenzoic acids was carried out between 1-octanol and 0.1 mol dm^{-3} perchloric acid, in which the dissociation of the methylbenzoic acids can be neglected. The distribution ratio of methylbenzoic acids was observed to be constant, irrespective of the concentration of the acids. Then it was recognized that the dimerization of the respective acids in 1-octanol does not occur to any appreciable extent and that the distribution ratio of each acid is equal to its partition constant $K_{D,HA}$. The respective partition constants are shown in Table 1.

The partition constant obtained increases in the following order: *m*-methylbenzoic>*p*-methylbenzoic> *o*-methylbenzoic>benzoic acids. Replacement of a hydrogen atom on the aromatic ring in benzoic acid with methyl moiety results in an increase in the partition constant of the acids, as expected. From the information about three kinds of methylbenzoic acids, the concentration of monomeric methylbenzoic acids in 1-octanol can be regarded as the total concentration of the respective acids under the present experimental conditions, that is, $[HA]_o=C_{HA}$.

Extraction of Copper(II) with Methylbenzoic Acids. If a *j*-merized copper(II) methylbenzoate, $Cu_jA_{2j}(HA)_a$ is extracted, the extraction equilibrium can be represented as:

$$jCu^{2+} + (2j + a)(HA)_o \overset{K_{ex(ja)}}{\rightleftharpoons} (Cu_jA_{2j}(HA)_a)_o + 2jH^+$$

with the extraction constant:

$$K_{ex(ja)} = [Cu_jA_{2j}(HA)_a]_o[H^+]^{2j}[Cu^{2+}]^{-j}[HA]_o^{-(2j+a)} \quad (1)$$

where the subscript o refers to the organic phase.

Total concentration of copper(II) in the organic phase, $C_{Cu,o}$ is written as follows:

$$C_{Cu,o} = \sum_j \sum_a jK_{ex(ja)}[Cu^{2+}]^j[HA]_o^{(2j+a)}[H^+]^{-2j}. \quad (2)$$

Suppose that only $Cu_jA_{2j}(HA)_a$ is responsible for the extraction, the following expression can be obtained:

$$\log C_{Cu,o} = j(\log[Cu^{2+}] - 2\log[H^+]) + (2j + a)\log[HA]_o + \log j + \log K_{ex(ja)}. \quad (3)$$

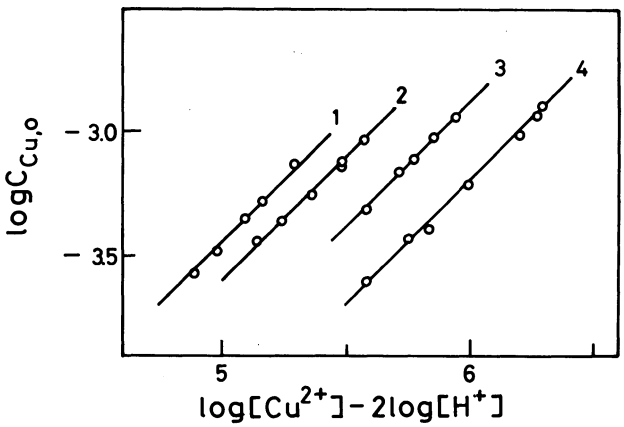

Fig. 2. Determination of the degree of polymerization of the copper(II) *p*-methylbenzoate.
Solid lines are the straight lines with a slope of 1.0.
C_{HA}; 1: 0.5, 2: 0.4, 3:0.3, 4: 0.2 mol dm^{-3}.

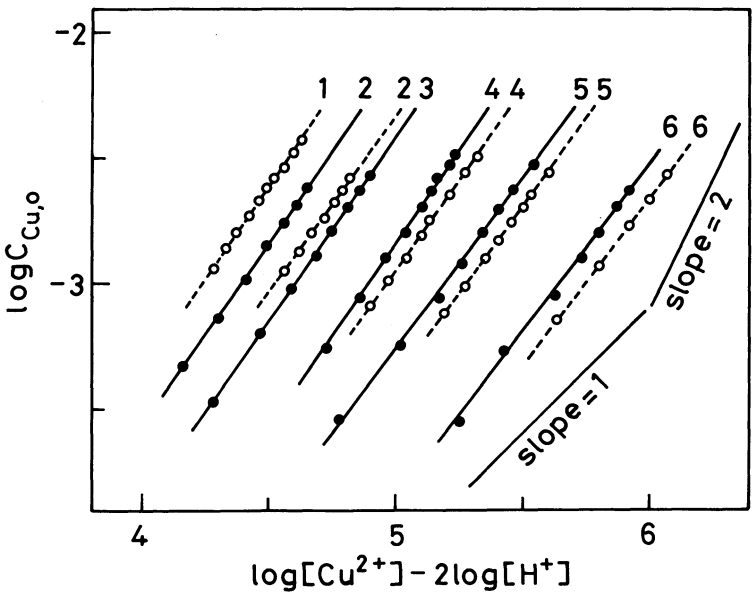

Fig. 1. Determination of the degree of polymerization of the extracted species.
Closed and open symbols refer to *o*- and *m*-methylbenzoic acids, respectively.
C_{HA}; 1: 1.6, 2: 1.2, 3: 1.0, 4: 0.7, 5: 0.5, 6: 0.3 mol dm^{-3}.

Table 1. Various Constants (at 25 °C and Aqueous Ionic Strength of 0.1 mol dm^{-3})

Acid	pK_a	log $K_{D,HA}$	log $K_{ex(10)}$	log $K_{ex(20)}$	log K_{2,CuA_2}
o-Methylbenzoic	3.73	2.21	−7.84	−12.84	2.84
m-Methylbenzoic	4.09	2.41	−7.84	−13.15	2.53
p-Methylbenzoic	4.21	2.33	−7.84		
Benzoic[a)]	4.04	1.88	−7.70		

Solvent: 1-Octanol. a) Ref. 1.

According to Eq. 3, the degree of polymerization of the extracted species can be found from the slope of the plot of $\log C_{Cu,o}$ against $(\log[Cu^{2+}]-2\log[H^+])$ at constant $[HA]_o$.

The results are shown in Figs. 1 and 2. As shown in Fig. 1, the slope of the plots lies from 1.3 to 1.5 and tends to be steeper with increasing copper concentration in the organic phase. Therefore, it is expected that the monomeric and dimeric copper(II) methylbenzoates are responsible for the extraction with *o*- and *m*-methylbenzoic acids. On the other hand, the plots in Fig. 2 fall on a straight lines with a slope of 1.0. This suggests that only the monomeric copper(II) species is responsible for the extraction with *p*-methylbenzoic acid.

In the extraction of copper(II) with *o*- and *m*-methylbenzoic acids, the following relation can be derived from Eq. 2:

$$\log C_{Cu,o} - \log[Cu^{2+}] + 2\log[H^+] = \log K_{ex(1a)} + (2+a)\log[HA]_o + \log\left(1 + \frac{2K_{ex(2b)}}{K_{ex(1a)}}[HA]_o^{(2+b-a)}[Cu^{2+}][H^+]^{-2}\right) \quad (4)$$

where $K_{ex(1a)}$ and $K_{ex(2b)}$ represent the extraction constants of the monomer $CuA_2(HA)_a$ and the dimer $Cu_2A_4(HA)_b$, respectively. According to Eq. 4, by comparing the plot of $(\log C_{Cu,o}-\log[Cu^{2+}]+2\log[H^+])$ against $(\log[Cu^{2+}]-2\log[H^+])$ at constant $[HA]_o$ with the normalized curve, $\log(1+X)$ vs. $\log X$, the degree of polymerization of the extracted species can be identified. As shown in Fig. 3, the plots fit well with the normalized curve. It was proved that the monomeric and dimeric copper(II) species are responsible for the extraction with *o*- and *m*-methylbenzoic acids in 1-octanol.

In the region where the monomer prevails, that is, the whole region in Fig. 2 and the region on the straight line asymptotes with a slope of zero in Fig. 3, the following expression can be derived from Eq. 2:

$$\log C_{Cu,o} - \log[Cu^{2+}] + 2\log[H^+] = \log \sum_a (K_{ex(1a)}[HA]_o^{(2+a)}). \quad (5)$$

According to Eq. 5, the number of methylbenzoic acid molecules involved in the monomeric copper(II) methylbenzoates can be determined from the slope of the plot of $(\log C_{Cu,o}-\log[Cu^{2+}]+2\log[H^+])$ against $\log[HA]_o$. The results are illustrated in Fig. 4 for *o*-, *m*-, and *p*-methylbenzoates. The plots fall on the same straight line with a slope of 2.0 in each acid: $2+a=2$, that is, $a=0$. Then, the composition of the monomer is CuA_2, irrespective of the position of the methyl substituent. The extraction constant of CuA_2 for each acid can be obtained from the intercept of the straight line with a slope of two. The values are listed in Table 1 together with other constants. Though

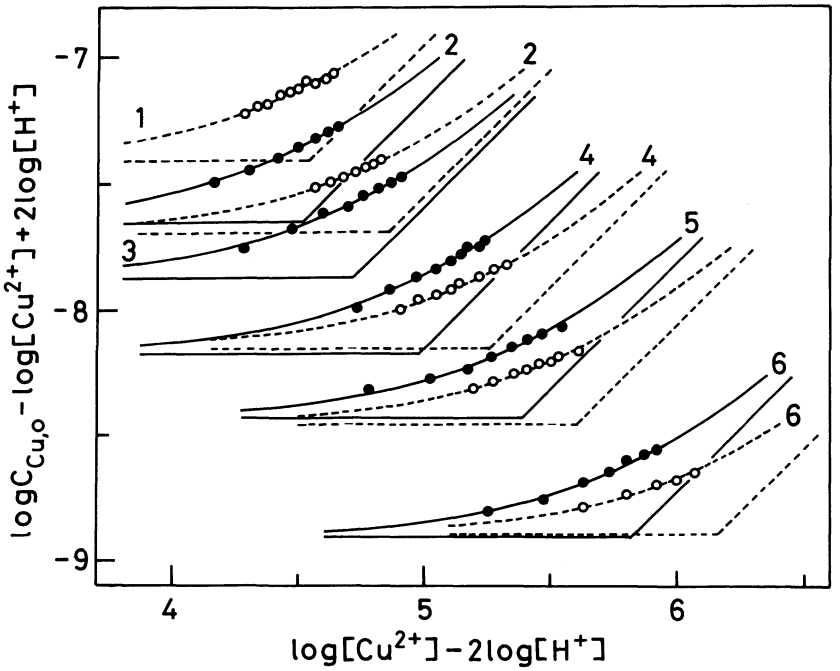

Fig. 3. The identification of the degree of polymerization of the copper(II) *o*- and *m*-methylbenzoates.
Symbols and numbers are the same as in Fig. 1. Curves are the normalized curve, $\log(1+X)$ vs. $\log X$. Straight lines are the asymptotes of the respective normalized curves.

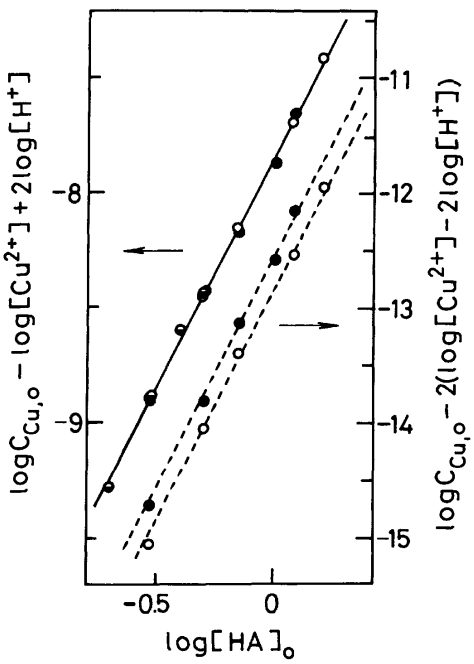

Fig. 4. Determination of the number of *o*-, *m*-, and *p*-methylbenzoic acid molecules involved in the monomeric and dimeric copper(II) species, respectively.
Solid and dotted lines are the straight lines with a slope of 2.0 and 4.0, respectively. Closed, open, and half-closed symbols refer to *o*-, *m*-, and *p*-methylbenzoic acids, respectively.

each of the three kinds of acids has a clear individuality, the same value for $K_{ex(10)}$ was obtained for each acid.

On the other hand, in the region where the predominant extracted species is the dimer, that is, the plots in Fig. 3 fit by extrapolation with the straight line asymptotes with a slope of unity, the following expression is derived from Eq. 2:

$$\log C_{Cu,o} - 2(\log[Cu^{2+}] - 2\log[H^+]) = \log 2\sum_b (K_{ex(2b)}[HA]_o^{(4+b)}). \quad (6)$$

According to Eq. 6, the number of the acid molecules involved in the dimeric copper(II) species was found to be four, as the plots of $\{\log C_{Cu,o} - 2(\log[Cu^{2+}] - 2\log[H^+])\}$ against $\log[HA]_o$ shown in Fig. 4 fell on the straight lines with a slope of 4.0 in both *o*- and *m*-methylbenzoates. The extraction constant of Cu_2A_4 can be determined from the intercept of the respective straight lines in Fig. 4. The values obtained are listed in Table 1 together with other constants.

Consequently, we conclude that the extraction equilibria for the present extraction systems are expressed as follows:

o- and *m*-methylbenzoic acids:

$$Cu^{2+} + 2(HA)_o \overset{K_{ex(10)}}{\rightleftharpoons} (CuA_2)_o + 2H^+$$

$$2Cu^{2+} + 4(HA)_o \overset{K_{ex(20)}}{\rightleftharpoons} (Cu_2A_4)_o + 4H^+,$$

p-methylbenzoic acid:

$$Cu^{2+} + 2(HA)_o \overset{K_{ex(10)}}{\rightleftharpoons} (CuA_2)_o + 2H^+.$$

Irrespective of the *o*- and *p*-orientations of the methyl group, the extraction equilibrium for copper(II) ortho-substituted benzoate coincides not with that for para-substituted one but for meta-substituted one.

In the extraction systems for *o*- and *m*-methylbenzoic acids the dimerization reaction of copper(II) species in the 1-octanol phase can be expressed as follows:

$$2(CuA_2)_o \overset{K_{2,CuA_2}}{\rightleftharpoons} (Cu_2A_4)_o,$$

where K_{2,CuA_2} refers to the dimerization constant of copper(II) *o*- and *m*-methylbenzoates, which can be calculated from the respective extraction constants. The values are summarized in Table 1. As the dimerization of copper(II) carboxylate in the organic phase in the extraction of copper(II) with a carboxylic acid results in an effect similar to the synergistic effect, substituting a hydrogen atom at the ortho- and meta-positions in benzoic acid by the methyl group can enhance the extractability of copper(II). It was found that the formation of the dimeric copper(II) species was not sterically hindered by the methyl group at the *o*-position.

The introduction of methyl substituent at the *p*-position in benzoic acid results in the decrease in the solubility of the acid in both water and 1-octanol. In this extraction system, the emulsion was observed in the region where the percent extraction of copper(II) exceeds 30%, and only the monomeric copper(II) species was responsible for the extraction under the conditions where the emulsion does not appear.

By preliminary experiments, it has been revealed that substituting a hydrogen atom at the *o*-, *m*-, and *p*-positions in benzoic acid by the methyl moiety has partially enabled the extraction of copper(II) using benzene as solvent, which was impossible in the unsubstituted benzoic acid–benzene extraction system. This is attributable to an increase in the affinity of copper(II) methylbenzoates for benzene by the introduction of the methyl substituent.

Judging from the present results, it seems reasonable to assume that the mesomeric effect of the methyl group on the conjugated system in benzoic acid has enabled the formation of the dimeric copper(II) species which was not perceived in the extraction of copper(II) with unsubstituted benzoic acid,[1] and some special function only for *p*-methylbenzoic acid will result in the fact that for *p*-methylbenzoic acid the dimerization of copper(II) species cannot be detected to any appreciable extent. This problem will be elucidated by the more detail investigations from different points of view.

The present work was partially supported by a Grant-in-Aid for Scientific Research No. 62540432 from the Ministry of Education, Science and Culture.

References

1) H. Yamada, K. Adachi, Y. Fujii, and M. Mizuta, *Solvent Extr. Ion Exch.*, **4**, 1109 (1986).

2) H. Yamada and M. Tanaka, *J. Inorg. Nucl. Chem.*, **38**, 1501 (1976).

3) H. Yamada, S. Suzuki, and M. Tanaka, *J. Inorg. Nucl. Chem.*, **43**, 1873 (1981).

4) H. Yamada, R. Kitazaki, and I. Kakimi, *Bull. Chem. Soc. Jpn.*, **56**, 3302 (1983).

5) H. Yamada, K. Takahashi, Y. Fujii, and M. Mizuta, *Bull. Chem. Soc. Jpn.*, **57**, 2847 (1984).

6) "CRC Handbook of Chemistry and Physics," 67th ed, 1986—1987, ed by C. W. Robert, CRC Press Inc. (1986), p. D-162.

 © 1988 The Chemical Society of Japan Bull. Chem. Soc. Jpn., 61, 841—848 (1988)

Raman Spectral Characteristics of Bis(terdentate)cobalt(III) Complexes with N and O Donor Atoms

Tatsuya KAWAMOTO,* Takaji YASUI,† Hisahiko EINAGA,†† and Jinsai HIDAKA
Department of Chemistry, University of Tsukuba, Tsukuba, Ibaraki 305
†Department of Chemistry, Faculty of Science, Kochi University, Akebono-cho, Kochi 780
††Institute of Materials Science, University of Tsukuba, Tsukuba, Ibaraki 305
(Received September 1, 1987)

The Raman spectra were measured for the bis and mixed type cobalt(III) complexes with ethylenediamine-*N*-acetate (edma) in an aqueous solution in the skeletal vibration region. The Raman bands could be classified into five vibration modes; a totally symmetric stretching vibration mode in the 510—650 cm^{-1} region, a stretching vibration mode excluding the totally symmetric one in the 410—540 cm^{-1} region, a skeletal breathing vibration mode in the 370—490 cm^{-1} region, a skeletal bending deformation mode in the 270—420 cm^{-1} region, and a chelate ring deformation mode in the 220—270 cm^{-1} region. Differences in the skeletal vibrations were observed between the fac and mer isomers for the chelate ring arrangement. Further, differences for the chelate ring arrangement between the Raman spectra of sym-fac and unsym-fac isomers were observed in the skeletal bending deformation mode. The cobalt(III) complexes with the terdentate ligands containing N-methyl group exhibited Raman bands shifted to a lower frequency than those of the corresponding cobalt(III) complexes containing no N-methyl group in the totally symmetric stretching vibration mode region.

The Raman spectral criteria in the skeletal vibration region have recently been established for differentiating the geometrical isomers of several cobalt(III) complexes.[1] Further, the nitro-ammine series of cobalt(III) complexes have also been studied in order to establish the assignments of the Raman bands.[2] In previous works, the Raman spectra of $[Co(gly)_x(ox)_y(en)_z]$-type complexes[3] (gly, glycinate; ox, oxalate; and en, 1,2-ethanediamine), of tris(bidentate)cobalt(III) complexes containing six-membered chelate rings,[4] and of cobalt(III) complexes with the quadridentate ligands[5] have been investigated in order to ascertain the relation between their Raman spectra in the skeletal vibration region and the structures of these complexes. Furthermore, the $[Co(ida)_n(dien)_{2-n}]$-type complexes (ida, iminodiacetate and dien, 3-azapentane-1,5-diamine) have been established to possess clearly different Raman spectral features between the fac and mer isomers.[6]

In this work, the Raman spectra of bis and mixed type cobalt(III) complexes with an asymmetrical linear terdentate ligand, ethylenediamine-*N*-acetate (edma), are measured in order to extend the investigation of the $[Co(ida)_n(dien)_{2-n}]$-type complexes and to find more general information on the relation between the stereochemical properties and the Raman spectra of the bis(terdentate)cobalt(III) complexes. The abbreviations used for the ligands are as follows: edma, ethylenediamine-*N*-acetate ($NH_2CH_2CH_2NHCH_2COO^-$); dien, 3-azapentane-1,5-diamine ($NH_2CH_2CH_2NHCH_2CH_2NH_2$); ida, iminodiacetate ($^-OOCCH_2NHCH_2COO^-$); mdien, 3-methyl-3-azapentane-1,5-diamine ($NH_2CH_2CH_2N(CH_3)CH_2CH_2NH_2$), and mida, *N*-methyliminodiacetate ($^-OOCCH_2N(CH_3)CH_2COO^-$). The prefixes sym-fac, unsym-fac, and mer represent the chelate ring arrangements, and the fac(N_t), mer(N_t), trans(N_t), cis(N_t), cis(N_t)trans(O), cis(N_t)cis(O), fac(N), and mer(N) abbreviations represent the coordinated atom arrangements. The N_t and N_c symbols stand for the terminal and central nitrogen atoms respectively of the linear terdentate ligands.

Experimental

Complexes. The complexes were prepared and characterized according to the literature procedures: *sym-fac*-[Co(edma)(dien)]Cl_2,[7] *unsym-fac-fac*(N_t)-[Co(edma)(dien)]Cl_2,[7] *unsym-fac-mer*(N_t)-[Co(edma)(dien)]Cl_2,[7] *mer*-[Co(edma)(dien)]Cl_2,[7] *sym-fac-trans*(N_t)-[Co(edma)$_2$]Cl,[8,9] *sym-fac-cis*(N_t)-[Co(edma)$_2$]Br,[8,9] *unsym-fac-cis*(N_t)*trans*(*O*)-[Co(edma)$_2$]Cl,[8,9] *unsym-fac-cis*(N_t)*cis*(*O*)-[Co(edma)$_2$]Cl,[8,9] *unsym-fac-trans*(N_t)-[Co(edma)$_2$]Cl,[8,9] *mer*-[Co(edma)$_2$]Br,[8,9] *sym-fac*-[Co(ida)(edma)],[10] *unsym-fac-mer*(*N*)-[Co(ida)(edma)],[10] *sym-fac*-[Co(edma)(mdien)]SO_4,[7] *unsym-fac-fac*(N_t)-[Co(edma)(mdien)]Br_2,[7] *unsym-fac-mer*(N_t)-[Co(edma)(mdien)]SO_4,[7] *mer*-[Co(edma)(mdien)]SO_4,[7] *sym-fac*-[Co(ida)(mdien)]Cl,[11] *unsym-fac*-[Co(ida)(mdien)]Cl,[11] *mer*-[Co(ida)(mdien)]Cl,[11] *sym-fac*-[Co(mida)(edma)],[12] and *unsym-fac-fac*(*N*)-[Co(mida)(edma)].[12]

Measurements. The Raman spectra were recorded on a JASCO Laser Raman spectrometer, which was constructed specially with a double monochromator, model CT-25, a He-Ne laser, model NEC GLG-8500, and a data processor, model DP-500, as the main components. The sample solution was excited at 632.8 nm and the Raman spectra were calibrated with indene.

Results and Discussion

General Assignments of the Raman Spectra of [Co(edma)(dien)]$^{2+}$, [Co(edma)$_2$]$^+$, and [Co(ida)(edma)]. The possible geometrical isomers of [Co(edma)(dien)]$^{2+}$, [Co(edma)$_2$]$^+$, and [Co(ida)(edma)] are four, six, and four respectively, as is depicted in Figs. 1, 2, and 3.[7-10] The Raman spectral data in the skeletal vibration region of the isomers are summarized in

Table 1. Raman Spectral Data of Bis(terdetate)cobalt(III) Complexes with N and O Donor Atoms

No.	Complex	Raman frequency/cm^{-1}[a]				
1	*sym-fac*-[Co(edma)(dien)]$^{2+}$	641 w(p) 553 s(p)	509 w(dp) 456 w(dp)	401 m(p)		235 w(p)
2	*unsym-fac-fac*(N_t)-[Co(edma)(dien)]$^{2+}$	642 w(p) 558 s(p)	506 w(—) 473 vw(—) 447 vw(—)	421 m(p)	307 vw(—)	
3	*unsym-fac-mer*(N_t)-[Co(edma)(dien)]$^{2+}$	635 w(p) 547 s(p)	514 w(—) 453 m(dp)	411 m(p)	306 vw(—)	247 w(—)
4	*mer*-[Co(edma)(dien)]$^{2+}$	577 vw(—) 538 w(p) 518 vw(—)		481 vw(—) 445 m(p)	414 w(dp)	
5	*sym-fac-trans*(N_t)-[Co(edma)$_2$]$^{+}$	635 m(p) 549 s(p) 523 s(p)	459 w(dp)	407 m(p) 381 sh(—)		233 m(p)
6	*sym-fac-cis*(N_t)-[Co(edma)$_2$]$^{+}$	639 m(p) 577 s(p) 529 m(p)	486 w(dp)	394 s(p)		240 vw(p)
7	*unsym-fac-cis*(N_t)*trans*(O)-[Co(edma)$_2$]$^{+}$	649 m(p) 570 s(p) 522 s(p)	467 w(dp)	417 m(p)	305 w(—)	261 vw(—)
8	*unsym-fac-cis*(N_t)*cis*(O)-[Co(edma)$_2$]$^{+}$	645 m(p) 569 s(p) 526 s(p)	485 w(dp)	419 m(p) 400 sh(—)	299 vw(—)	243 w(p)
9	*unsym-fac-trans*(N_t)-[Co(edma)$_2$]$^{+}$	638 m(p) 552 s(p) 526 s(p)	470 w(dp)	415 m(p)	294 vw(—)	245 w(p)
10	*mer*-[Co(edma)$_2$]$^{+}$	634 w(p) 544 m(p) 510 w(p)	470 vw(—)[b] 461 vw(—)[b]	421 s(p)	379 w(dp)	
11	*sym-fac*-[Co(ida)(edma)]	618 w(—) 573 m(p)	533 w(—) 497 vw(—)	390 m(p)		229 vw(—)
12	*unsym-fac-mer*(N)-[Co(ida)(edma)]	645 w(—) 565 m(p)	529 w(—)	409 m(p) 401 m(p)	290 vw(—)	
13	*sym-fac*-[Co(edma)(mdien)]$^{2+}$	643 w(p) 554 sh(—) 529 s(p)	466 sh(—) 443 m(dp)	401 m(p)		235 s(p)
14	*unsym-fac-fac*(N_t)-[Co(edma)(mdien)]$^{2+}$	637 vw(—) 555 m(—) 527 s(p)	450 m(dp)	403 w(—)	346 m(—) 289 vw(—)	249 w(—)
15	*unsym-fac-mer*(N_t)-[Co(edma)(mdien)]$^{2+}$	636 w(p) 585 vw(—) 529 s(p)	450 w(dp) 417 vw(dp)	378 vw(—)		237 vw(—)
16	*mer*-[Co(edma)(mdien)]$^{2+}$	631 vw(—) 533 s(p)	503 sh(—)	442 s(p) 417 m(—)	373 vw(—) 326 vw(—) 279 sh(—)	
17	*sym-fac*-[Co(ida)(mdien)]$^{+}$	614 w(p) 529 s(p)	518 w(dp) 471 vw(—) 442 w(—)	390 m(p)		225 vw(p)
18	*unsym-fac*-[Co(ida)(mdien)]$^{+}$	617 w(p) 533 s(p)	517 w(dp) 450 w(—)	403 w(—)		237 vw(p)

Table 1. (Continued)

No.	Complex	Raman frequency/cm^{-1}[a]				
19	*mer*-[Co(ida)(mdien)]$^+$	538 m(p)	499 vw(—)	442 m(p) 386 m(p)		
20	*sym-fac*-[Co(mida)(edma)]	644 w(p) 569 sh(p) 537 s(p)	498 m(—) 458 vw(—)	406 m(p) 378 m(p)		
21	*unsym-fac-fac(N)*-[Co(mida)(edma)]	642 vw(—) 534 m(p)	498 vw(—)	413 w(—)		
22	[Co(gly)(en)$_2$]$^{2+}$[c]	584 w(p) 521 s(p)	471 vw(dp) 447 w(dp)		374 w(dp)	279 s(p)
23	*trans(O)*-[Co(gly)$_2$(en)]$^+$[c]	596 m(p) 523 m(p)	504 sh(dp) 458 w(dp)		368 w(dp)	275 s(p)
24	*sym-fac*-[Co(dien)$_2$]$^{3+}$[d]	549 s(p)	478 m(dp) 448 vw(—) 437 m(dp)	401 m(p)		260 vw(—) 230 vw(—)
25	*unsym-fac*-[Co(dien)$_2$]$^{3+}$[d]	546 s(p)	485 m(dp) 444 m(dp) 434 m(dp)	409 w(p)	321 m(dp)	255 vw(—)
26	*sym-fac*-[Co(ida)(dien)]$^+$[d]	609 m(p) 546 s(p)	510 w(dp) 472 w(dp) 461 sh(dp)	418 w(—) 387 s(p)		235 s(p)
27	*unsym-fac*-[Co(ida)(dien)]$^+$[d]	610 m(p) 546 s(p)	504 m(dp) 470 vw(dp) 453 vw(dp)	410 m(p) 401 m(p)	301 w(dp)	235 w(p)
28	*sym-fac*-[Co(ida)$_2$]$^-$[d]	610 s(p) 569 m(p)	522 vw(dp)	394 w(—) 372 m(p)		229 m(p)
29	*unsym-fac*-[Co(ida)$_2$]$^-$[d]	621 s(p) 562 m(p)	446 vw(—)	398 m(p) 382 vw(—)	291 w(—)	
	Assignment[a]	ν_{ts}(Co-L)	ν(Co-L)	ν_{br}	δ_{sbd}(L-Co-L)	δ_{crd}(Co$\langle^{L}_{L}$)

a) The following abbrevations are used: s, strong; m, medium; w, weak; vw, very weak; sh, shoulder; p, polarized; dp, depolarized; ν_{ts}, totally symmetric stretching vibration mode; ν, stretching vibration mode excluding the totally symmetric stretching character; ν_{br}, skeletal breathing vibration mode; δ_{sbd}, skeletal bending deformation mode; δ_{crd}, chelate ring deformation mode. The Raman band intensities (s, m, w, vw, and sh) are classified by a comparison of all the Raman bands among all the complexes. b) Consult the text. c) Ref. 3. d) Ref. 6.

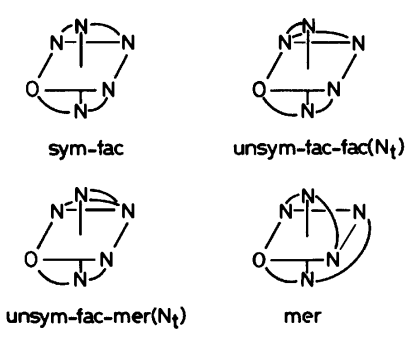

Fig. 1. Four geometrical isomers of [Co(edma)-(dien)]$^{2+}$.

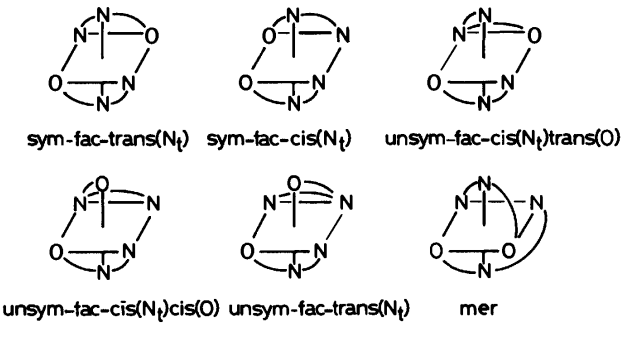

Fig. 2. Six geometrical isomers of [Co(edma)$_2$]$^+$.

Table 1, together with those of the related complexes of primary concern.

Figure 4 shows the Raman spectra of *unsym-fac-mer*(N_t)-[Co(edma)(dien)]$^{2+}$, [Co(gly)(en)$_2$]$^{2+}$, *unsym-fac-cis*(N_t)*trans*(O)-[Co(edma)$_2$]$^+$, and *trans*(O)-[Co(gly)$_2$(en)]$^+$, chosen as representative for a general spectral consideration. In a previous paper,[6] the Raman bands of *unsym-fac*-[Co(dien)$_2$]$^{3+}$ and *unsym-fac*-[Co(ida)(dien)]$^+$ have all been correlated to those of [Co(en)$_3$]$^{3+}$ and C_2-*cis*(O)-[Co(gly)$_2$(en)]$^+$ respectively except for one, which was assigned to the skeletal breathing vibration mode. The Raman bands at 547—635, 453—514, 306, and 247 cm^{-1} of *unsym-fac-mer*(N_t)-[Co(edma)(dien)]$^{2+}$ correspond to those at 521—584, 447—471, 374, and 279 cm^{-1} of [Co(gly)(en)$_2$]$^{2+}$ respectively, and the Raman bands at 570—649, 467—522, 305, and 261 cm^{-1} of *unsym-fac-cis*(N_t)*trans*(O)-[Co(edma)$_2$]$^+$ correspond to those at 523—596, 458—504, 368, and 275 cm^{-1} of *trans*(O)-[Co(gly)$_2$(en)]$^+$ respectively. Thus, a comparison of these spectra demonstrates that the cobalt(III) complexes with the edma ligand give the same spectral patterns as the tris(bidentate)cobalt(III) complexes[3] with the same donor atom arrangement, except for the Raman bands at ca. 400 cm^{-1}; this is characteristic of [Co(ida)$_n$-(dien)$_{2-n}$]-type complexes.[6] In addition, as is shown in Fig. 5, the Raman spectral patterns of *cis*(O)-[Co(edma)$_2$]$^+$ and *cis*(O)-[Co(ida)(dien)]$^+$ are similar to each other throughout the spectral regions except for the somewhat high frequency shift in the Raman bands of [Co(edma)$_2$]$^+$ in comparison with those of [Co(ida)(dien)]$^+$ and the difference in degree of the depolarization ratios of the Raman bands at ca. 500—530 cm^{-1}. On the basis of these observations and the Raman spectral characteristics summarized in Table 1, the Raman spectra of the present edma complexes can be classified into five vibration modes as in the case of the [Co(ida)$_n$(dien)$_{2-n}$]-type complexes;[6] that is, the polarized bands in the 510—650 cm^{-1} region, depolarized ones in the 410—540 cm^{-1} region, polar-

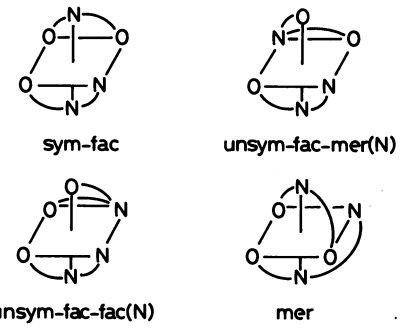

Fig. 3. Four geometical isomers of [Co(ida)(edma)].

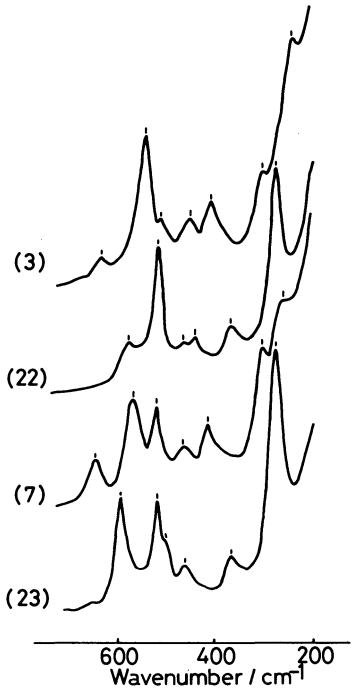

Fig. 4. Raman spectra of *unsym-fac-mer*(N_t)-[Co(edma)(dien)]$^{2+}$, [Co(gly)(en)$_2$]$^{2+}$, *unsym-fac-cis*(N_t)*trans*(O)-[Co(edma)$_2$]$^+$, and *trans*(O)-[Co(gly)$_2$(en)]$^+$. Numbers in parentheses correspond to those in Table 1.

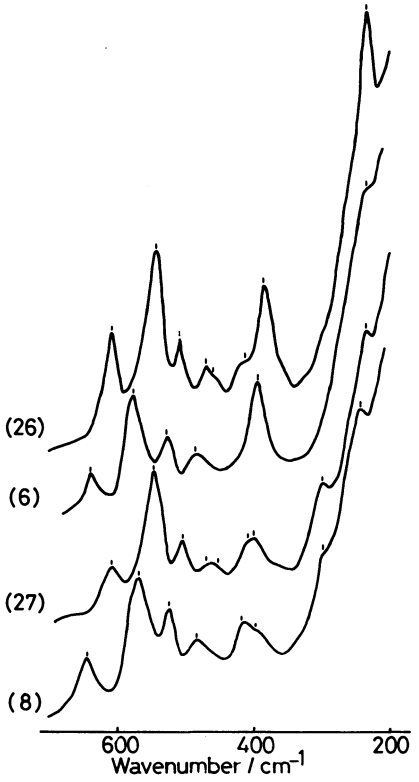

Fig. 5. Raman spectra of *sym-fac*-[Co(ida)(dien)]$^+$, *sym-fac-cis*(N_t)-[Co(edma)$_2$]$^+$, *unsym-fac*-[Co(ida)-(dien)]$^+$, and *unsym-fac-cis*(N_t)*cis*(O)-[Co(edma)$_2$]$^+$. Numbers in parentheses correspond to those in Table 1.

ized ones in the 370—490 cm^{-1} region, depolarized ones in the 270—420 cm^{-1} region, and polarized ones in the 220—270 cm^{-1} region can be assigned to the totally symmetric stretching vibration, the stretching vibration excluding the totally symmetric stretching character, the skeletal breathing vibration, the skeletal bending deformation, and the chelate ring deformation modes respectively. Furthermore, the skeletal breathing vibration mode can be regarded as the key bands for the bis(terdentate)cobalt(III) complexes with linear terdentate ligands.

Raman Spectral Characteristics of the Geometrical Isomers of [Co(edma)(dien)]$^{2+}$, [Co(edma)$_2$]$^+$, and [Co(ida)(edma)]. The *fac*- and *mer*-[Co(edma)(dien)]$^{2+}$ isomers exhibit a striking difference in the chelate ring arrangements on their Raman spectra (Fig. 6). Similar spectral behavior has also been substantiated for the *fac*- and *mer*-[Co(edma)$_2$]$^+$ isomers (Fig. 7). This spectral behavior corresponds well to that of the [Co(ida)$_n$(dien)$_{2-n}$]-type complexes.[6] That is, in the skeletal breathing vibration mode, the mer isomers exhibit sharp Raman bands at higher frequencies than the fac isomers; the Raman bands caused by the skeletal bending deformation of the mer isomers also appear at higher frequencies. Furthermore, the mer isomers have no bands in the chelate ring deformation mode region, as in the case of [Co(ida)(dien)].[6] These features can be ascribed to the difference in strain energy in the vibrational motion between the ligand of the meridional arrangement and that of the facial one. It has been reported in the previous paper[6] that the mer isomers of [Co(ida)(dien)]$^+$ and [Co(dien)$_2$]$^{3+}$ exhibit the polarized character in the stretching vibration region, while the fac isomers give depolarized Raman bands. A close inspection of the Raman frequencies, intensities, and depolarization ratios of *mer*-[Co(edma)(dien)]$^{2+}$ reveals a retention of the polarized character of the mer isomers of [Co(ida)(dien)]$^+$ and [Co(dien)$_2$]$^{3+}$. This polarized character, however, was found to be obscured in *mer*-[Co(edma)$_2$]$^+$; (an attempt at a reliable estimation of the Raman bands at 470 and 461 cm^{-1} relative to the polarized Raman bands was unsuccessful because they were too weak for their depolarization ratios to be measured precisely; rather, they were tentatively classified as depolarized ones based on the profiles of the polarized and depolarized Raman spectra in this region). The obscurity of the polarized character in *mer*-[Co(edma)$_2$]$^+$ may, in part, be attributed to the disturbance of the overall harmonic stretching vibrational motion by different terminal donor atoms and force constants.

The difference in the chelate ring arrangement between the sym-fac and unsym-fac isomers is noticeable in the skeletal bending deformation mode (Figs. 6 and 7). Each unsym-fac isomer has a

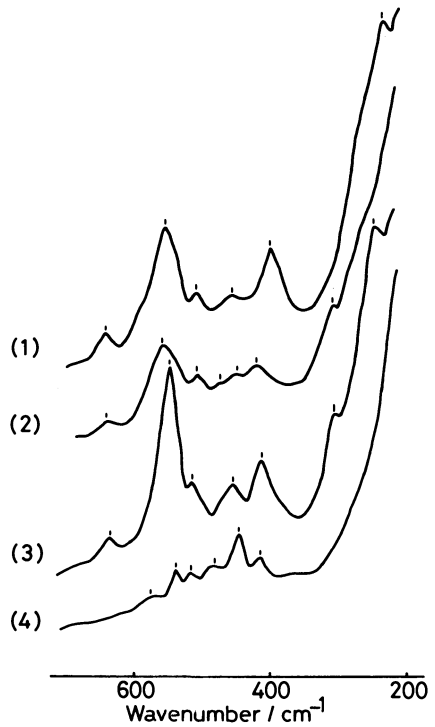

Fig. 6. Raman spectra of four geometrical isomers of [Co(edma)(dien)]$^{2+}$. Numbers in parentheses correspond to those in Table 1.

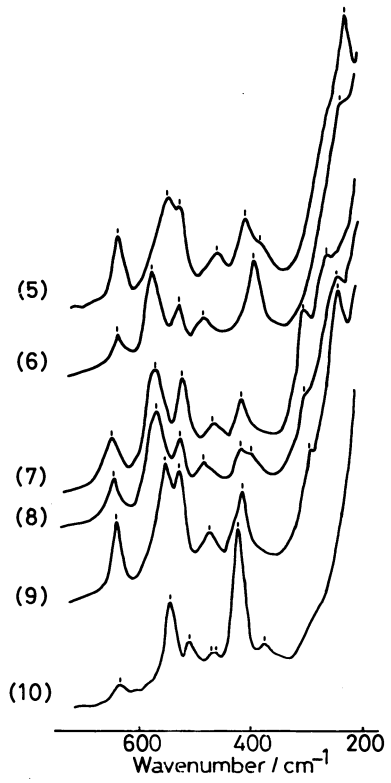

Fig. 7. Raman spectra of six geometrical isomers of [Co(edma)$_2$]$^+$. Numbers in parentheses correspond to those in Table 1.

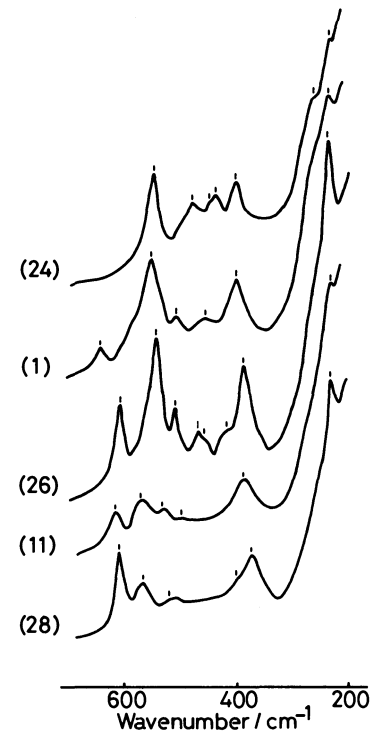

Fig. 8. Raman spectra of sym-fac isomers for chelate ring arrangement of $[Co(dien)_2]^{3+}$, $[Co(edma)(dien)]^{2+}$, $[Co(ida)(dien)]^{+}$, $[Co(ida)(edma)]$, $[Co(ida)_2]^{-}$. Numbers in parentheses correspond to those in Table 1.

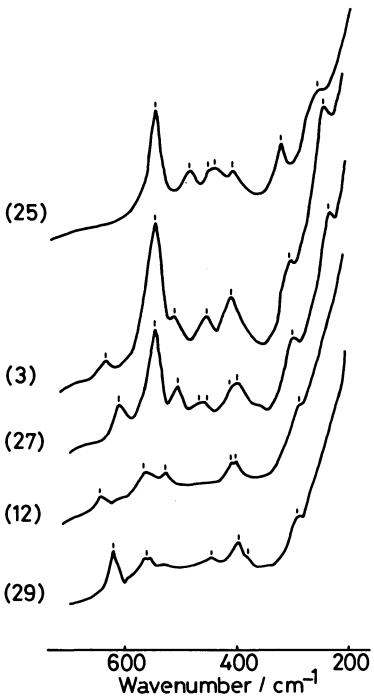

Fig. 9. Raman spectra of unsym-fac isomers for chelate ring arrangement of $[Co(dien)_2]^{3+}$, $[Co(edma)(dien)]^{2+}$, $[Co(ida)(dien)]^{+}$, $[Co(ida)(edma)]$, $[Co(ida)_2]^{-}$. Numbers in parentheses correspond to those in Table 1.

depolarized band, while the sym-fac isomers have none. This spectral feature has also been found in the $[Co(ida)_n(dien)_{2-n}]$-type complexes.[6] Furthermore, the *sym-fac-trans*(N_t)- and *unsym-fac-cis*(N_t)*cis*(O)-$[Co(edma)_2]^{+}$ with lower symmetries, C_i and C_1 respectively, give a doublet in the skeletal breathing mode, whereas *sym-fac-cis*(N_t)-, *unsym-fac-cis*(N_t)*trans*-(O)-, and *unsym-fac-trans*(N_t)-$[Co(edma)_2]^{+}$, having a higher symmetry, C_2, give only one Raman band in this region. By contrast, the Raman spectral difference between the trans(O) and cis(O) isomers of $[Co(edma)_2]^{+}$ is of no intrinsic importance. Accordingly, these findings suggest that, so far as the bis(terdentate)cobalt(III) complexes with equal numbers of coordinated nitrogen and oxygen atoms are concerned, the Raman spectral characteristics depend mainly on the arrangement of the chelate ring around the central metal atom.

Role of Coordinated Atoms on Raman Spectral Characteristics. Figures 8 and 9 show the Raman spectra of the sym-fac and unsym-fac isomers with different numbers of coordinated nitrogen and oxygen atoms. The Raman bands above 600 cm^{-1} of the sym-fac and unsym-fac isomers are intensified with an increase in the number of coordinated oxygen atoms, whereas those at ca. 460 and 550 cm^{-1} become weaker with a decrease in the number of coordinated nitrogen atoms. Accordingly, the former bands may have a largely Co–O stretching character, and the latter ones, a Co–N stretching character. Furthermore, it is observed that the number of Raman bands in the skeletal breathing mode increases with an increase in the number of coordinated oxygen atoms.

The Raman spectra of the isomers of $[Co(ida)(dien)]^{+}$ can be regarded as a superposition of those of $[Co(dien)_2]^{3+}$ and $[Co(ida)_2]^{-}$.[6] Moreover, as is shown in Fig. 5, the Raman spectra of the isomers of $[Co(edma)_2]^{+}$ can also be correlated to those of $[Co(ida)(dien)]^{+}$. It is not surprising that $[Co(edma)_2]^{+}$ can be considered to have both of the spectral features of the corresponding isomers of $[Co(dien)_2]^{3+}$ and $[Co(ida)_2]^{-}$, because the Raman spectral characteristics of the bis(terdentate)cobalt(III) complexes with equal numbers of coordinated nitrogen and oxygen atoms depend mainly on the arrangement of the chelate ring around the central metal atom.

In conclusion, the empirical rule derived from bis(terdentate)cobalt(III) complexes with symmetrical linear terdentate ligands holds also for those with asymmetrical linear terdentate ligands.

Raman Spectra of $[Co(edma)(mdien)]^{2+}$, $[Co(ida)(mdien)]^{+}$, and $[Co(mida)(edma)]$. The Raman spectra of $[Co(edma)(mdien)]^{2+}$ and $[Co(ida)(mdien)]^{+}$ are shown in Figs. 10 and 11 respectively. The Raman bands in the skeletal bending deformation mode region, which were observed on the unsym-fac isomers

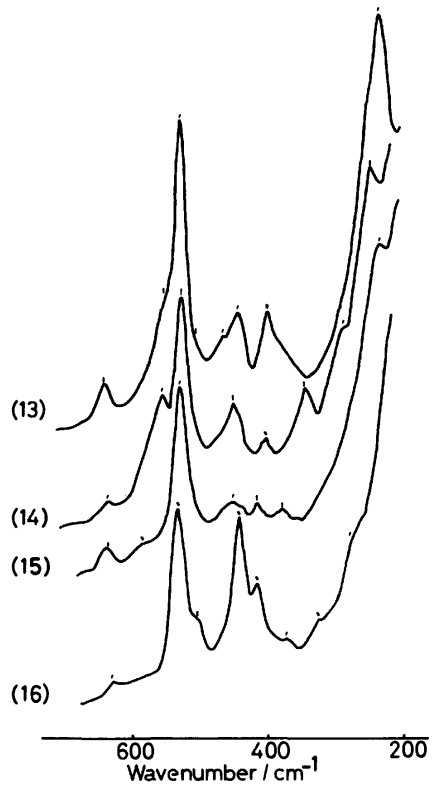

Fig. 10. Raman spectra of four geometrical isomers of [Co(edma)(mdien)]$^{2+}$. Numbers in parentheses correspond to those in Table 1.

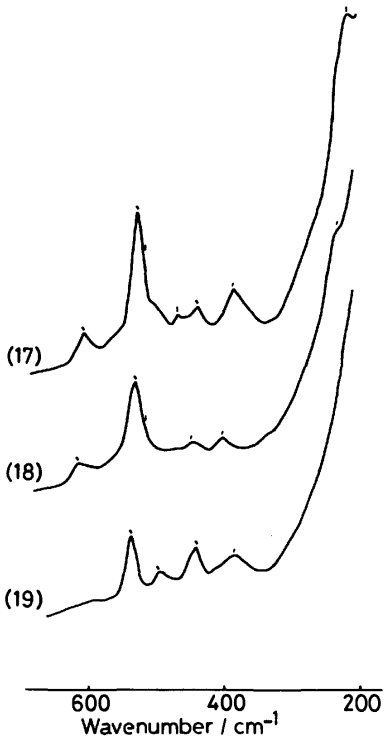

Fig. 11. Raman spectra of three geometrical isomers of [Co(ida)(mdien)]$^{+}$. Numbers in parentheses correspond to those in Table 1.

of [Co(edma)(dien)]$^{2+}$, [Co(ida)(dien)]$^{+}$, and [Co(ida)-(edma)] (Figs. 6 and 9 and Ref. 6), are no longer present in the Raman spectra of *unsym-fac-mer*(N_t)-[Co(edma)(mdien)]$^{2+}$, *unsym-fac*-[Co(ida)(mdien)]$^{+}$, and *unsym-fac-fac*(N)-[Co(mida)(edma)] (Table 1). By contrast, two Raman bands are observed in the skeletal bending deformation mode region for the unsym-fac-fac(N_t) isomer of [Co(edma)(mdien)]$^{2+}$. This may be related to the change in the O–Co–N_c angles caused by the steric interaction between the methyl group of the mdien ligand and the methylene group of the edma ligand.[7] With all these differences, the cobalt(III) complexes with the terdentate ligands, mdien and mida, exhibit Raman spectral features corresponding to those of the cobalt(III) complexes with terdentate ligands, dien, edma, and ida. Accordingly, the Raman bands of the cobalt(III) complexes containing an N-methyl group can also be classified into the five vibrational modes. Especially, the Raman bands above 600 cm^{-1}, those appearing at ca. 615 cm^{-1} for the ida complexes and at ca. 640 cm^{-1} for the edma complexes, can be used as vibrational criterion for differentiating complexes containing either ida or edma, except for [Co(ida)(edma)], which shows the Raman bands at 618 cm^{-1} characteristic of the sym-fac isomer and at 645 cm^{-1} characteristic of the unsym-fac-mer(N) isomer because of the intensification of the one at the sacrifice of the other.

The cobalt(III) complexes containing an N-methyl group also show some characteristic Raman spectral behavior. First, the strongest Raman bands attributable to the totally symmetric stretching vibration of the cobalt(III) complexes containing an N-methyl group, except for *mer*-[Co(ida)(mdien)]$^{+}$, appear at a lower frequency region compared with the Raman spectra of the corresponding cobalt(III) complexes containing no N-methyl group. This fact suggests the existence of a mass effect in the totally symmetric stretching vibration mode as a result of the replacement of a hydrogen atom on the imino nitrogen by a methyl group, similar to the isotope shifts, and/or the difference in the central metal–donor atom bond strength, which can be related to the ligand field strength. In fact, the first and the second absorption maxima shift to the lower energy side when the methyl group is introduced on the central donor atom of the terdentate ligands. However, the shift to the lower frequency region in the Raman bands of the cobalt(III) complexes containing an N-methyl group could not be found in other vibrational modes. The replacement of a hydrogen atom on the imino nitrogen by a methyl group is responsible for concomitant changes in the spectra depending on the geometrical structure of the complexes. Second, the cobalt(III) complexes with the mida ligand ([Co-(mida)(mdien)]$^{+}$,[6] [Co(mida)(edma)], and [Co(ida)-(mida)]$^{-}$[6]) exhibit several Raman bands in the

skeletal breathing vibration mode region. This feature may be correlated with the increase in the number of coordinated oxygen atoms, as in the case of the cobalt(III) complexes containing no N-methyl group. Third, the mer isomers of the cobalt(III) complexes containing an N-methyl group also exhibit spectral features appreciably different from those of the fac isomers. That is, the mer isomers have sharp Raman bands in a higher frequency region in the skeletal breathing vibration mode and have no Raman bands in the chelate ring deformation mode, except for *mer*-$[Co(mida)_2]^-$ and *mer*-[Co(mida)(mdien)]$^+$, which have two terdentate ligands containing an N-methyl group.[6] The fact that *mer*-$[Co(mida)_2]^-$ and *mer*-[Co(mida)(mdien)]$^+$ have Raman bands in the chelate ring deformation mode may be related to the high stability of these complexes; for example, *mer*-$[Co(mida)_2]^-$ has been found more stable than *mer*-[Co(ida)(mida)]$^-$ even in a weakly basic aqueous solution.[13] However, these features are in line with the general characteristics of the Raman spectra of the cobalt(III) complexes containing no N-methyl group.

References

1) a) K. Kanamori and K. Kawai, *Bull. Chem. Soc. Jpn.*, **53**, 2520 (1980); b) K. Kanamori and K. Kawai, *Bull. Chem. Soc. Jpn.*, **55**, 764 (1982); c) K. Kanamori, I. Ichinose, and K. Kawai, *Bull. Chem. Soc. Jpn.*, **55**, 1315 (1982); d) K. Kanamori, Y. Nunomura, M. Takashima, K. Nagata, K. Kawai, and J. Hidaka, *Bull. Chem. Soc. Jpn.*, **58**, 92 (1985); e) K. Kanamori, I. Bansho, K. Kawai, K. Akamatsu, and Y. Shimura, *Bull. Chem. Soc. Jpn.*, **58**, 943 (1985); f) K. Kanamori and K. Kawai, *Inorg. Chem.*, **25**, 3711 (1986).

2) K. Kanamori, T. Morikawa, and K. Kawai, *Bull. Chem. Soc. Jpn.*, **53**, 2787 (1980).

3) T. F. Maruyama, K. Okamoto, J. Hidaka, and H. Einaga, *Bull. Chem. Soc. Jpn.*, **56**, 2610 (1983).

4) T. Kawamoto, H. Einaga, and J. Hidaka, *Bull. Chem. Soc. Jpn.*, **60**, 919 (1987).

5) T. Kawamoto, J. Hidaka, and H. Einaga, *Bull. Chem. Soc. Jpn.*, **61**, 229 (1988).

6) T. Kawamoto, T. F. Maruyama, T. Yasui, K. Okamoto, J. Hidaka, and H. Einaga, *Bull. Chem. Soc. Jpn.*, **59**, 2393 (1986).

7) T. Yasui, T. Shikiji, N. Koine, T. Ama, and H. Kawaguchi, *Bull. Chem. Soc. Jpn.*, **60**, 595 (1987). The prefixes mer(N_t)trans(N_c), fac(N_t)cis(N_c), mer(N_t)cis(N_c), and mer(ch) in this literature correspond to sym-fac, unsym-fac-fac(N_t), unsym-fac-mer(N_t), and mer respectively in the present paper.

8) T. Yasui, H. Kawaguchi, and T. Ama, *Chem. Lett.*, **1983**, 1277.

9) T. Ama, H. Kawaguchi, T. Yasui, K. Matsumoto, and S. Ooi, *Bull. Chem. Soc. Jpn.*, **58**, 2561 (1985). The prefixes C_i-trans(O), cis(O)trans(NH), C_2-trans(O), C_1-cis(O), and cis(O)trans(NH_2) in this literature correspond to sym-fac-trans(N_t), sym-fac-cis(N_t), unsym-fac-cis(N_t)trans(O), unsym-fac-cis(N_t)cis(O), and unsym-fac-trans(N_t) respectively in the present paper.

10) T. Ama, H. Kawaguchi, and T. Yasui, *Bull. Chem. Soc. Jpn.*, **59**, 1471 (1986). The prefixes mer(O)trans(NH), mer(O)cis(NH), fac(O), and mer(O)mer(ch) in this literature correspond to sym-fac, unsym-fac-mer(N), unsym-fac-fac(N), and mer respectively in the present paper.

11) Presented at the Symposium by the Chemical Society of Japan, Kochi, 1984, Abstract, p. 91.

12) T. Ama, R. Niiyama, H. Kawaguchi, and T. Yasui, *Bull. Chem. Soc. Jpn.*, **60**, 119 (1987). The prefixes mer(O)trans(N_c), mer(O)cis(N_c), fac(O), and mer(O)mer(ch) in this literature correspond to sym-fac, unsym-fac-mer(N), unsym-fac-fac(N), and mer respectively in the present paper.

13) a) T. Ama, H. Kawaguchi, and T. Yasui, *Chem. Lett.*, **1981**, 323; b) T. Yasui, H. Kawaguchi, N. Koine, and T. Ama, *Bull. Chem. Soc. Jpn.*, **56**, 127 (1983); c) H. Kawaguchi, T. Ama, and T. Yasui, *Bull. Chem. Soc. Jpn.*, **57**, 2422 (1984).

 © 1988 The Chemical Society of Japan Bull. Chem. Soc. Jpn., 61, 849—856 (1988)

Reactions of Coordination Compounds in the Solid State. II. The Interconversion of the Isomers of Dichloro(triethylenetetramine)-cobalt(III) Chloride, $[Co(trien)Cl_2]Cl$, upon Heating in the Solid State

Terufumi FUJIWARA and John C. BAILAR, Jr.*
School of Chemical Sciences, University of Illinois, Urbana, Illinois 61801, U.S.A.
(Received July 30, 1987)

The three isomers of the ion $[Co(trien)Cl_2]^+$, where trien=triethylenetetramine, have been synthesized and their interconversion upon heating in the solid state has been studied. The trans isomer changes to the β-cis isomer, which in turn is converted to the α-cis isomer. The changes have been followed by proton NMR spectroscopy. The first change cannot be explained by a twist mechanism. Experiments with the trans monohydrate or hydrochloride in sealed tubes or in an atmosphere of HCl show that the presence of H_2O accelerates the conversion of the trans isomer to the cis-β isomer, and the presence of HCl accelerates the conversion of cis-β to cis-α, suggesting that the former conversion takes place through an aquation, followed by anation and for the latter conversion nucleophilic attack of a chloride ion on the cis-β isomer is important.

Octahedral complexes of the type $[M(trien)X_2]^+$ exist in three isomeric forms which are called trans, cis-α, and cis-β.

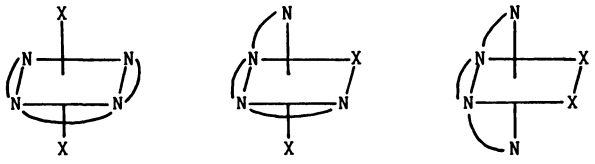

trans cis-β cis-α

Several investigators have studied the interconversion of the isomers of the cobalt(III) and chromium(III) compounds in which X represents Cl, but nearly all of their work has been concerned with the compounds in solution. Most notable is the work of Buckingham, Marzilli and Sargeson,[1] who made a thorough study of the cobalt(III) compounds. Even they has little to say about the behavior of these compounds in the solid, crystalline state. We have therefore made an extensive study of these isomers and their interconversion. In any case in which isomerization takes place, the trans isomer is converted to the cis-β form, which then goes more slowly to the cis-α form. The changes are not reversible, in which the cobalt(III) compounds seem to differ from their chromium(III) analogues.[2]

It has been pointed out[3] that the nature of X in $[Co(trien)X_2]^+$ makes a great difference in the relative stabilities of the isomers. Thus, if X=Cl, the order of stability in methanol is β-cis<trans<α-cis, but if X is H_2O, the order in aqueous solution is trans<α-cis<β-cis.

In addition, Asperger,[4] who studied the cobalt(III) complex of the analogous ligand, *N,N'*-bis[(*S*)-2-amino-3-phenylpropyl]-(1*R*,2*R*)-1,2-cyclohexanediamine, reported that the L-cis-β compound isomerizes to the trans compound in the solid state when heated to 110 °C. In that case, the conformation of the ring may exert an important influence.

Experimental

Preparation of Compounds. The triethylenetetramine (trien) compound, *trans*-$[Co(trien)Cl_2]Cl \cdot H_2O$, was prepared according to the published method.[1] The product was recrystallized by evaporating a saturated methanolic solution of the complex quickly in a steam of dry air to less than half of its volume. The hydrochloride of the trans form, *trans*-$[Co(trien)Cl_2]Cl \cdot 0.5HCl \cdot 2H_2O$, was prepared by recrystallizing the product from concentrated HCl, washing it with ethanol and acetone, and drying in air. The cis-isomers, *cis*-α- and *cis*-β-$[Co(trien)Cl_2]Cl$, was prepared and recrystallized as described in the literature.[3,5]

The 60—100 mesh sample of hydrochloride of the trans isomer was prepared by gently breaking larger crystals with a pestle, passing these through a 60 mesh screen, and catching the suitably sized particles on a 100 mesh screen. Samples of the finely powdered complex compounds were also prepared by grinding with a mortar and pestle. Elemental analyses of the chloride salts of the isomers are given in Table 1.

Physical Measurements. Proton magnetic resonance spectra were taken with a Varian XL-200 200-MHz FT-NMR Spectrometer fitted with a computer at the normal temperature of the probe (ca. 20 °C) and 100 transients (scanning times) were employed. Tetramethylsilane (TMS) was used as a reference standard. ^1H NMR spectra were observed in dimethyl-d_6 sulfoxide (DMSO-d_6). Although the complexes used here, especially the cis-α isomer, are sparingly soluble in DMSO, 4—5 mg of complex was dissolved in ca. 0.7 mL of solvent in the nmr tube by vigorous shaking[6] and the spectrum was recorded as soon as possible after dissolution.

Thermogravimetric analysis (TGA) was carried out with a Perkin-Elmer TGA 7 thermogravimetric analyzer. Samples weighing 4 to 6 mg, heated in a flow of He (ca. 20 mL min^{-1}) at a rate of 10° C min^{-1}, were employed.

X-Ray powder patterns were obtained using a 114.6-mm diameter camera and nickel-filtered Cu $K\alpha$ radiation. The samples used were contained in 0.7 mm glass capillaries, and exposure times ranged from 18 to 25 h.

Infrared spectra were obtained using a Perkin-Elmer 599B

Table 1. Analytical Data

Compound	Calcd/%				Found/%			
	C	H	N	Cl	C	H	N	Cl
cis-α-[Co(trien)Cl_2]Cl·1.5H_2O	21.29	6.25	16.55	31.42	21.36	6.11	16.57	31.24
cis-β-[Co(trien)Cl_2]Cl·H_2O	21.87	6.12	17.00	32.27	21.83	6.17	16.92	31.81
trans-[Co(trien)Cl_2]Cl·H_2O					22.00	6.11	16.54	32.48
trans-[Co(trien)Cl_2]Cl·0.5HCl·2H_2O	19.70	6.20	15.32	33.92	19.62	6.33	15.27	33.99

Infrared Spectrophotometer. The KBr-disk method was employed for all spectral runs (1 mg of sample in 100 mg of KBr) with air in the reference beam.

Rate Studies. Kinetic studies in static air were conducted by heating solid samples of the complexes in the same way as described in our previous study,[9] using an Abderhalden drying apparatus and uncapped aluminum boats. Further, some samples were contained in glass tubes (ca. 3.5 mm in diameter, ca. 4 cm in length) which were sealed off with a torch. Water (bp 100 °C) and *N,N'*-dimethylformamide (bp 152 °C) were used in the boiler as liquids of appropriate boiling points. Kinetic runs in an atmosphere of HCl were also conducted by passing HCl gas at 100 °C into the Abderhalden apparatus, in which samples were mounted in uncapped platinum boats (11 mm in length, 4 mm in width) in place of the aluminum boats. The stream of HCl was preheated to 100 °C in another Abderhalden apparatus connected to the apparatus containing the sample. The stream of HCl was very slow, so the reaction took place in an almost static atmosphere of HCl. The 60—100 mesh and the finely powdered samples were all heated in static air. Samples of the powdered material were also heated in a sealed tube and in an HCl atmosphere. Generally, two to four of the samples (8—11 mg) were heated simultaneously. As soon as possible after taking each sample out of the heating apparatus but before the ^1H NMR measurement, the mass loss accompanying the heating was measured.

Results

NMR Studies. For *cis*-α-[Co(trien)Cl_2]Cl in DMSO-d_6, there are three peaks for the NH protons at δ 5.68, 5.76, and 6.15 with the intensity ratio 2:2:2 but the first two peaks are not separated clearly and the first absorption shows some fine structure (Fig. 1).

The cis-β isomer has six clearly separated NH absorptions of equal intensity (Fig. 2). Four of them show some fine structure with centers at δ 3.86, 4.96, 5.28, and 5.64, respectively, and the other two peaks are broad singlets at δ 7.36 and 7.77, respectively.

The trans isomer shows three NH bands (two quintets with centers at δ 5.13 and 5.58, respectively, and one singlet at δ 6.87) with the intensity ratio 2:2:2 (Fig. 3). The spectrum arising from the NH and NH_2 groups for the hydrochloride are almost identical to that for the monohydrate.

All CH_2 absorptions in these isomers appear at higher field than the NH absorptions and some fine structure, which is probably the superposition of two or more multiplets, is observed. The results in the CH region are even more complex than in the NH region;

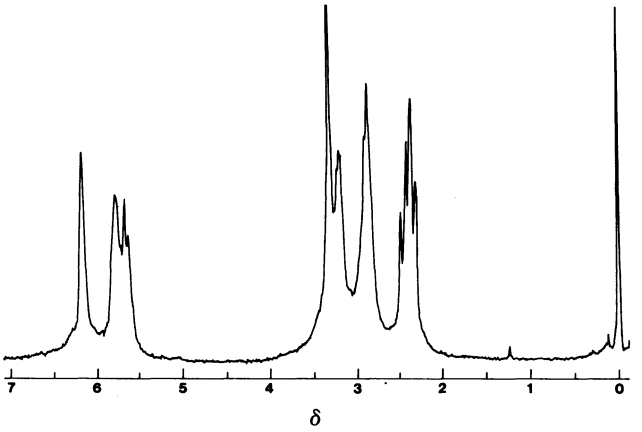

Fig. 1. ^1H NMR spectrum of *cis*-α-[Co(trien)Cl_2]Cl·1.5H_2O in DMSO-d_6.

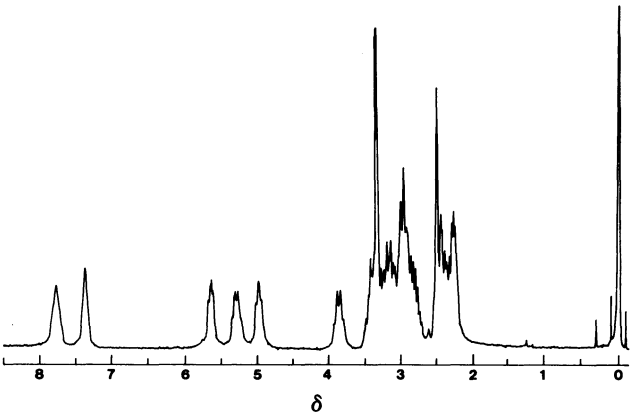

Fig. 2. ^1H NMR spectrum of *cis*-β-[Co(trien)Cl_2]Cl·H_2O in DMSO-d_6.

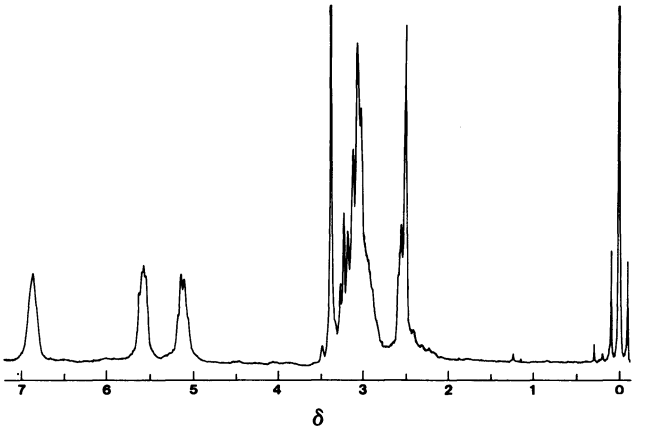

Fig. 3. ^1H NMR spectrum of *trans*-[Co(trien)Cl_2]Cl·H_2O in DMSO-d_6.

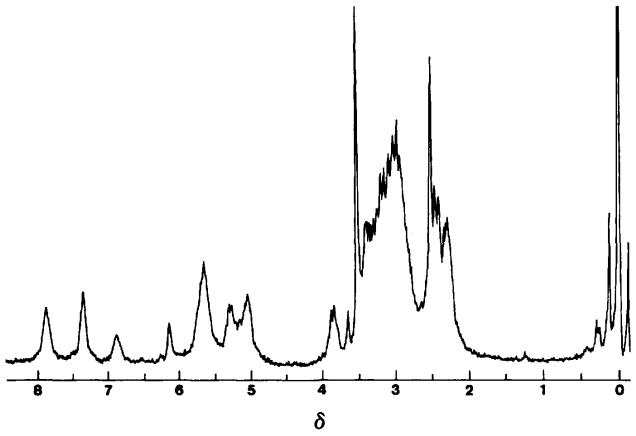

Fig. 4. ^{1}H NMR spectrum of a 60—100 mesh sample of *trans*-[Co(trien)Cl_2]Cl·0.5HCl·2H_2O in DMSO-d_6 after heating at 100 °C for 20.4 h in static air.

the spectrum of the cis-α isomer is less complex than that of the cis-β isomer, as is described in the literature[3] and the CH region in the trans isomer is more symmetrical than that in the cis-α isomer. Furthermore, the signal due to H_2O in the DMSO-d_6 solutions of the isomers and the solvent signal absorb at δ ca. 3.3[10] and 2.50, respectively, and overlap the spectra arising from the CH_2 groups for the cis isomers.

In a mixture of these isomers, overlapping of some NH signals is observed while one NH absorption at δ 6.15 for the cis-α isomer, the three at δ 3.86, 7.36, and 7.77 for the cis-β isomer, and the one at δ 6.87 for the trans isomer separate clearly from each other (for example, Fig. 4). These signals can be used to estimate the relative amounts of the cis-α, cis-β, and trans isomers if no other isomer or complex is present. However, the position of the NH resonance at the lowest field (δ 7.77) is strongly dependent upon the HCl concentration; this is due to the presence of the hydrochloride of the trans isomer. Furthermore, the H_2O peak moves downfield with increase of the HCl concentration and the shift results in overlapping of the H_2O signal with the NH signal at δ 3.86 in the spectrum of the cis-β isomer. For these reasons, only the NH absorption at δ 7.36 (one proton) in the cis-β isomer is used with the NH absorptions (two protons each) in the cis-α and trans isomers for the estimation of their relative amounts by calculating from the peak areas (or intensity ratios) of the NH protons. To check the method, samples of known composition were made and estimated by ^{1}H NMR with the calculated values to within ±3%.[11] In addition, the monohydrate of the trans isomer and the hydrochloride prepared here show the NH absorptions for the cis-β isomer with very small intensities indicating that the cis isomer is present in very small amounts (less than 4%).

TGA Studies. TGA runs on the hydrated chlorides of the cis-α, cis-β, and trans isomers show that dehydration starts soon after heating is begun (at about 30—35 °C). Anhydrous weight levels are attained at 110—120 °C for the cis-α isomer and at 130—140 °C for the cis-β and trans isomers. As the temperature is raised further, no loss of weight is observed until there is a slow loss due to decomposition at 215—230 °C for all of the isomers. The TGA curve for the hydrochloride of the trans isomer shows that the loss of HCl and H_2O takes place at the same time at 90—100 °C. This mass loss is complete at 150—160 °C, and a subsequent slow loss of weight resulting from the decomposition of the complex occurs at 220—230 °C. Similar single-step loss of HCl and H_2O has been reported for the hydrochloride salts of the chloride complexes, *trans*-[Co(en)$_2Cl_2$]Cl·HCl·2H_2O and *trans*-[Co(pn)Cl_2]Cl·HCl·2H_2O, which contain the $H_5O_2^+$ ion.[13]

Rate Studies. Heating *trans*-[Co(trien)Cl_2]Cl·0.5HCl·2H_2O to 100 °C yields a mixture of the cis-α, cis-β, and trans isomers as evidenced by comparisons of infrared[14] and ^{1}H NMR spectra; for example, Fig. 4 shows an ^{1}H NMR spectrum of the 60—100 mesh sample of the trans isomer which was heated at 100 °C for 20.4 h in static air (the product is 16% cis-α, 68% cis-β, and 16% trans). The data for the relative amounts of the isomers formed as a function of time, together with the data for % weight of the remaining material are shown in Fig. 5 for the isomerization of the 60—100 mesh and the finely powdered samples of the trans isomer by heating at 100 °C in static air. A rapid initial rate of isomerization of the trans isomer, mainly to the cis-β is observed. Similar behavior has been observed for the solid state racemization of several tris chelated complexes:[15-17] $K_3[Cr(C_2O_4)_3]$, $[Co(en)_3]X_3 \cdot nH_2O$, $[M(phen)_3]X_2$ (M=Fe, Ni), $[Co(phen)_3]X_3$, and $[Co(phen)_2en]X_3$. During this initial period, a very rapid loss of weight also occurs. Subsequently, the trans isomer isomerizes more slowly to a mixture of the cis-α and β isomers; the mass loss is also very slow. Nearly complete isomerization is observed after about 45 h, at which time dehydration-dehydrochlorination of the samples is almost complete. However, there is still slow conversion of the cis-β isomer to the cis-α isomer. The 60—100 mesh sample, after heating at 100 °C for 5.32 h, does not pass through the 100 mesh screen, indicating that no change in particle size of the sample occurs during the dehydration-dehydrochlorination.

Figure 5 shows that the 60—100 mesh and the finely powdered samples isomerize at considerably different rates. The initial isomerization of the powdered samples is slower than that of the 60—100 mesh samples. After this initial period, the powdered samples show only a slightly lower rate of isomerization. This behavior is contrary to the observation that the rate of isomerization of *trans*-[Co(pn)$_2Cl_2$](H_5O_2)-

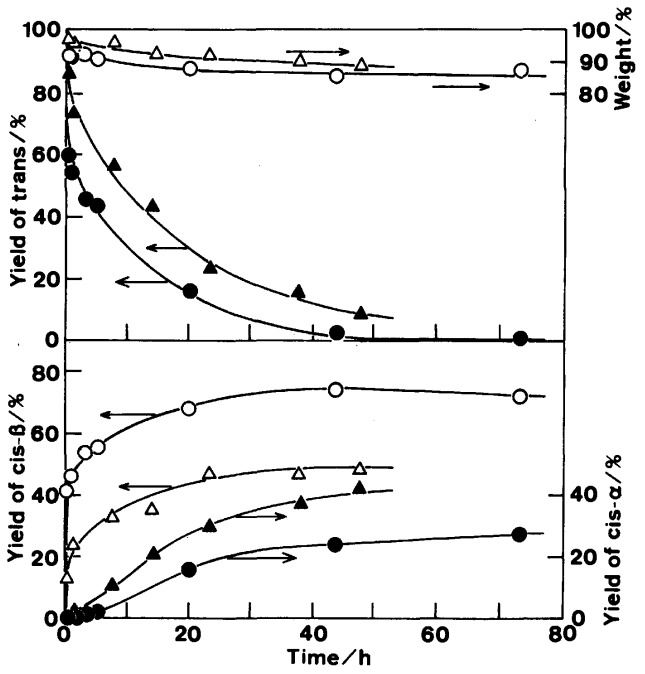

Fig. 5. Isomerization at 100 °C of 60—100 mesh (○, ●) and powdered (△, ▲) samples of *trans*-[Co(trien)-Cl_2]Cl·0.5HCl·2H_2O in static air, with about 10% weight of material remaining.

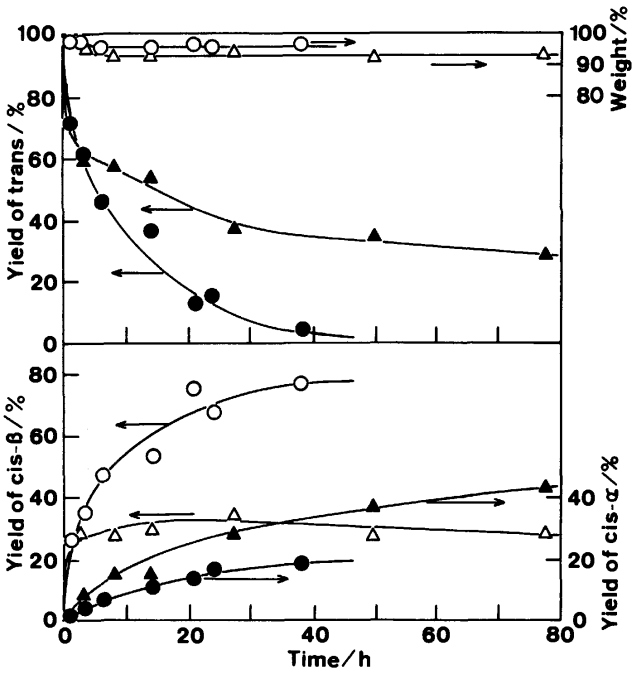

Fig. 6. Isomerization at 100 °C of powdered samples of *trans*-[Co(trien)Cl_2]Cl·H_2O in static air (○, ●) and *trans*-[Co(trien)Cl_2]Cl·0.5HCl·2H_2O in an atmosphere of HCl (△, ▲), with about 6% weight of material remaining.

Cl_2 increases as particle size is reduced.[18] On the other hand, for the solid-state racemization of [Co(en)$_3$]X_3, it was reported that there is little difference between the 20—40 and 200—325 mesh samples.[16] However, a higher rate of conversion to the cis-α isomer is observed for the powdered samples and apparent cessation of conversion to the cis-β isomer occurs (after about 25 h) prior to complete isomerization of the trans isomer; the extent of loss in weight for the powdered samples is smaller than that for the 60—100 mesh samples.

Heating the powdered samples of the trans isomer at 152 °C results in almost complete isomerization and dehydration-dehydrochlorination during the initial period; the product is a mixture of 42% cis-α, 57% cis-β, and 1% trans isomers. Thereafter, there is only slight conversion of the cis-β isomer into the cis-α isomer (less than 4% after about one day).

Although the trans hydrochloride undergoes no isomerization on standing at room temperature, even after one year, powdered samples of the trans monohydrate, *trans*-[Co(trien)Cl_2]Cl·H_2O,[19] (no hydrogen chloride of "crystallization") give 88% cis-β (12% trans) after three months and 95% cis-β (5% trans) after five months; neither product contains the cis-α isomer. This is similar to the reported conversion of the solid monohydrate into pure *cis*-β-[Co(trien)Cl_2]-Cl by heating at 90 °C.[1] However, Fig. 6 shows that heating powdered samples of the monohydrate at 100 °C results in isomerization to a mixture of the cis-α and β isomers, although the product is mainly the cis-β isomer; for example, 77% cis-β, 18% cis-α, and 5% trans after 38.2 h. The powdered monohydrate samples show a higher rate of isomerization than those containing HCl but the rate of conversion to the cis-α isomer is lower, and during this reaction the dehydration is not complete.

Table 2. Isomerization of *trans*- and *cis*-β-Dichlorotriethylenetetramine Complexes in Sealed Tubes at 100 °C

Time of heating/h	% trans	% cis-β	% cis-α
	trans-[Co(trien)Cl_2]Cl·0.5HCl·2H_2O		
0.50	0	97	3
0.80	0	98	2
2.43	0	88	12
66.5	0	53	47
97.8	0	53	47
	95% *cis*-β-[Co(trien)Cl_2]Cl·H_2O[a]		
43.7	0	73	27
70.4	0	64	36
	cis-β-[Co(trien)Cl_2]Cl·H_2O[b]		
2.43	0	100	0
26.3	0	100	0
43.7	0	93	7
70.4	0	89	11

a) Obtained by allowing the trans monohydrate to stand at room temperature for five months. b) Obtained by crystallizing from solution.

Table 3. The Prominent Lines of the X-Ray Powder Patterns of Several [Co(trien)Cl_2]Cl Complexes

cis-α-[Co(trien)Cl_2]Cl·1.5H_2O	*cis*-β-[Co(trien)Cl_2]Cl·H_2O	*trans*-[Co(trien)Cl_2]Cl·H_2O
d/Å	*d*/Å	*d*/Å
7.33(w)[a]	6.67(s)	9.29(w)
6.61(s)	6.23(s)	8.02(vw)
5.68(m)	5.45(w)	7.17(s)
5.19(vw)		5.98(s)
4.76(w)		5.39(w)
4.12(vw)		4.93(m)
3.70(vw)	3.66(w)	4.22(m)
3.45(m)	3.42(m)	3.98(vw)
3.14(vw)	3.12(vw)	3.83(vw)
2.91(w)	2.89(w)	3.18(w)
2.76(vw)	2.54(w)	2.94(w)
2.56(vw)	2.43(vw)	2.87(vw)
2.39(w)	2.28(w)	2.67(vw)
	2.16(w)	2.47(w)
		2.36(w)
		2.27(vw)
		2.17(w)
		2.02(m)
		1.93(vw)
		1.85(w)

trans-[Co(trien)Cl_2]Cl·0.5HCl·2H_2O

100°C in open boat, 44.03 h → 74% *cis*-β-[Co(trien)Cl_2]Cl[b]

100°C in sealed tube, 0.50 h → 97% *cis*-β-[Co(trien)Cl_2]Cl[c]

d/Å	*d*/Å	*d*/Å
9.31(m)	8.87(vw)	6.69(s)
8.06(w)	6.82(s)	
7.14(s)	6.28(m)	6.25(s)
5.40(m)	5.88(s)	
4.94(s)	5.50(w)	5.48(vw)
4.20(m)	3.70(m)	3.68(w)
3.99(vw)	3.46(m)	3.44(m)
3.83(w)	3.14(vw)	3.14(vw)
3.19(m)	3.01(vw)	3.00(vw)
3.04(w)	2.91(w)	2.90(w)
2.95(vw)	2.81(vw)	
2.88(m)	2.69(vw)	2.68(vw)
2.79(w)	2.56(w)	2.55(w)
2.48(m)	2.45(vw)	2.45(vw)
2.29(vw)	2.29(m)	2.29(w)
2.19(w)	2.17(m)	2.16(w)
2.13(vw)	2.11(vw)	2.11(vw)
2.03(m)		
1.95(vw)		
1.88(vw)		
1.71(vw)		
1.69(vw)		
1.63(w)		
1.56(vw)		
1.53(w)		

trans-[Co(trien)Cl_2]Cl·H_2O

room temp, 5 months → 95% *cis*-β-[Co(trien)Cl_2]Cl·H_2O[d]

d/Å
7.17(w)
6.67(s)
6.23(s)

Table 3. (Continued)

	5.77(vw)
	5.46(w)
	3.68(w)
	3.42(m)
	3.12(vw)
	2.98(vw)
	2.88(w)
	2.67(vw)
	2.54(w)
	2.43(vw)
	2.27(w)
	2.16(w)
	2.11(vw)

a) Intensities estimated visually: s=strong, m=medium, w=weak, vw=very weak. b) Sample 98% isomerized (contains 24% cis-α isomer). c) Sample 100% isomerized (contains 3% cis-α isomer). d) Sample 95% isomerized (contains no cis-α isomer).

When powdered samples of trans hydrochloride are heated at 100° in an atmosphere of HCl, they isomerize more slowly than when heated in air (Fig. 6). After the initial period, conversion to the cis-β isomer seems to stop while the rate of conversion to the cis-α isomer is almost the same as that in air. Thus, there is a larger amount of the cis-α isomer than of the cis-β isomer in the reaction mixtures after about 30 h. Cessation of mass loss is also observed prior to complete dehydration-dehydrochlorination after the initial mass loss.

When the chlorides of the cis-α and β are heated to 100 °C in air or in HCl, there is no observable isomerization. When kept at 152 °C for 30 h, no significant isomerization occurs, other than a very small (less than 4%) conversion of the β chloride to its α isomer. This is rather surprising in view of the report that the trans chloride is prepared by heating the moist cis isomer to 180 °C.[20] When the chlorides are heated to 152 °C for a long time they develop a greenish cast. This appears after about 30 h. This may be due to some reduction of the cobalt to the +2 state,[1] for the ^{1}H NMR and infrared spectra do not show the presence of any of the green trans isomer. These results for the *cis*-dichloro cobalt(III) complexes are very different from those reported for the dichloro chromium(III) complex, which shows a reversible cis-$\beta \rightleftarrows$cis-α isomerization on heating to 70—285 °C.[2]

Runs in sealed glass tubes show that the powdered hydrochloride samples of the trans isomer isomerize completely to the cis-β isomer on heating within 30 min at 100 °C (Table 2). After the initial rapid conversion to the cis-β isomer, subsequent conversion to the cis-α isomer occurs at a lower rate and then, apparently, the reaction stops, when the mixture is 47% cis-α and 53% cis-β.

On the other hand, under similar conditions, two samples of the cis-β isomer containing no HCl, one of which had been made by rearrangement of the trans isomer at room temperature (5 months) and the other by crystallizing from solution, were converted more slowly to cis-α form than samples which contained HCl. The sample prepared by crystallization isomerized more slowly than the one prepared from the trans isomer. Heating the samples of the cis-β isomer at 152 °C in sealed tubes for 1.10 h gives a mixture of 2% cis-α and 98% cis-β isomers, but heating the cis-α isomer for 2.02 h gives no observable conversion.

X-Ray Studies. The main reflections from the X-ray powder photographs of samples of a series of the $[Co(trien)Cl_2]Cl$ complexes are given in Table 3. As samples of the hydrochloride of the trans isomer are isomerized along with dehydration–dehydrochlorination, great changes occur in the X-ray powder patterns, indicating that the crystal structure undergoes a change during the reaction. Similar behavior has been reported for the solid-state racemization of *l-cis*-$[Cr(en)_2Cl_2]Cl \cdot H_2O$, which occurs only during dehydration;[21] this is in contrast to the observation that the powder patterns taken before and after dehydration for (+)-$[Co(en)_3]X_3 \cdot H_2O$ (X=I^- and Br^-) are different, while heating the anhydrous complexes caused partial racemization but no changes in the powder patterns.[16] When the trans monohydrate isomerized at room temperature without dehydration, changes were evident in the powder patterns, suggesting that in this case, the crystal change seems to parallel isomerization. The products which form when the trans monohydrate is allowed to stand at room temperature for five months (almost pure cis-β isomer) and by heating the trans hydrochloride in a sealed tube at 100 °C for 0.5 h have almost the same crystal structure as a sample of the cis-β isomer crystallized from solution, as shown in Table 3. However, they isomerize at different rates.

Discussion

One can imagine several ways in which the

$[Co(trien)Cl_2]^+$ ion can isomerize, chief of which are (1) a twist mechanism, (2) a dissociation mechanism, in which the metal momentarily has a coordination number of five, and (3) an associative mechanism, in which the coordination number is seven. Twist mechanisms have been discussed for the isomerization of the complex of a tetradentate ligand.[22] The tetragonal (Rây-Dutt) twist[23] is not applicable to rearrangements of compounds of this type. The trigonal (Bailar) twist[24] and the rhombic (Springer-Sievers) twist[25] do not allow the trans isomer to isomerize to the cis-β isomer but lead to the α-isomer. Therefore, these twist mechanisms can be ruled out for the conversion of the trans isomer to the cis-β isomer. On the other hand, the cis-β isomer can be formed by a dissociation mechanism, with one of the primary nitrogen atoms moving to a position originally occupied by a chloro group in the trans isomer. In the solid state, such a dissociation mechanism seems to be a particularly unfavorable one since there is no possibility of solvation, either of the complex or of the freed amino group which would moderate the large energy required for the charge separation in the transition state caused by the bond breaking. In this study, the presence of water and/or HCl is found to be important to the conversion of the trans isomer to the cis-β isomer. This occurs during dehydration, is accelerated in sealed tubes, and is retarded in an atmosphere of HCl; these observations parallel dehydration and/or dehydrochlorination behavior. This behavior of the trans isomer can be explained by an aquation-anation pathway as proposed for the solid-state racemization of *l-cis*-$[Cr(en)_2Cl_2]Cl \cdot H_2O$[21] and the solid-state isomerization of *trans*-$[Co(pn)_2Cl_2](H_5O_2)Cl_2$.[18] It has been reported that in aqueous solution the trans isomer aquates stereospecifically to the cis-β-$[Co(trien)ClOH_2]^{2+}$ ion.[8] Assuming that the cis-β-chloroaqua complex is formed as an intermediate, it is also supposed that the rate-determining step is the first reaction in the following scheme:

$$\textit{trans}\text{-}[Co(trien)Cl_2]^+ \underset{-Cl^-}{\overset{+H_2O}{\longrightarrow}} \textit{cis}\text{-}\beta\text{-}[Co(trien)ClOH_2]^{2+}$$

$$\underset{-H_2O}{\overset{+Cl^-}{\longrightarrow}} \textit{cis}\text{-}\beta\text{-}[Co(trien)Cl_2]^+$$

in which in the presence of HCl the activity of H_2O is diminished by protonation and the dissociation of the Co–Cl bond is unfavorable.

Conversion of the trans isomer to the cis-α isomer by a twist (Bailar or Springer-Sievers) mechanism is unlikely, for heating the trans isomer in a sealed tube causes the immediate formation of the pure cis-β isomer; the subsequent conversion of the cis-β isomer to the cis-α isomer occurs slowly.

Runs in an atmosphere of HCl or in sealed tubes show that the conversion of the cis-β isomer to the cis-α isomer is accelerated by the presence of HCl, in direct contradiction to the conversion of the trans isomer into the cis-β isomer, and heating the hydrochloride in open boats yields larger amounts of the cis-α isomer compared with the monohydrate. However, there is little influence of a water molecule on the reaction. The effect of HCl cannot be understood on the basis of a twist mechanism. For the isomerization of *cis*-$[Co(trien)X_2]^+$, a pathway involving a "back-side attack" on the cis isomers by an incoming group has been postulated.[12] The isomerization pathway may explain the conversion behavior of the cis-β isomer if it is assumed that the chloride ion plays the role of a base as an incoming group,[26] although the "back-side attack" on the cis-β isomer will give equal amounts of the trans and cis-α isomers, and so the following reaction scheme may be assumed:

$$\textit{trans}\text{-}[Co(trien)Cl_2]Cl \underset{k_{-1}}{\overset{k_1}{\rightleftharpoons}} \textit{cis}\text{-}\beta\text{-}[Co(trien)Cl_2]Cl$$

$$\xrightarrow{k_2} \textit{cis}\text{-}\alpha\text{-}[Co(trien)Cl_2]Cl$$

where $k_1 > k_2 \simeq k_{-1}$.

It is found that as particle size is reduced, the rate of isomerization of the trans hydrochloride decreases and the rate of dehydration-dehydrochlorination also decreases while the conversion of the resultant cis-β isomer to the cis-α isomer increases (Fig. 5). An explanation of this by the process proposed here is reasonable if it is assumed that the rate of dehydrochlorination decreases more than that of dehydration as particle size is reduced. This follows from the fact that the presence of HCl causes a decrease in k_1 (conversion of the trans isomer) but an increase in k_2 (conversion of the cis-β isomer). Moreover, it has been reported that the *cis*-α-$[Co(trien)Cl(H_2O)]Cl_2 \cdot H_2O$ complex in the solid state dehydrates completely to the *cis*-α-$[Co(trien)Cl_2]Cl$ complex with retention of configuration,[27] suggesting that the cis-α form is the stable one.

The importance of lattice defects in determining the rate of racemization of some tris complexes in the solid state has been discussed;[16,17] the complex ions near a defect experience enhanced reactivity.[28] We found that the two substances, one of which is the almost pure cis-β isomer formed when the trans monohydrate is allowed to stand at room temperature for five months, and another, which is the cis-β monohydrate crystallized from solution, have almost the same lattices as evidenced by the X-ray powder patterns but isomerize at different rates in sealed tubes. This result may be explained by a difference in number of defects in the solid.

The work described in this paper was done under the sponsorship of the Petroleum Research Fund, administered by the American Chemical Society, for which the authors express their gratitude.

References

1) D. A. Buckingham, P. A. Marzilli, and A. M. Sargeson, *Inorg. Chem.*, **6**, 1032 (1967).
2) R. Tsuchiya, A. Uehara, K. Noji, and H. Yamamura, *Bull. Chem. Soc. Jpn.*, **51**, 2942 (1978).
3) A. M. Sargeson and G. H. Searle, *Inorg. Chem.*, **6**, 787 (1967).
4) R. G. Asperger, *Inorg. Chem.*, **8**, 2127 (1969).
5) E. Kyuno, L. J. Boucher, and J. C. Bailar, Jr., *J. Am. Chem. Soc.*, **87**, 4458 (1965).
6) The dichloro complexes used here are more soluble in DMSO than in 1.8 mol dm^{-3} D_2SO_4 solutions, in which ^1H NMR spectra for the corresponding diaqua complexes were observed in Ref. 3. The DMSO solutions show essentially identical spectra after 30 min, while the complexes aquate rapidly in aqueous solution as reported in Refs. 7 and 8.
7) A. M. Sargeson and G. H. Searle, *Inorg. Chem.*, **4**, 45 (1965).
8) A. M. Sargeson and G. H. Searle, *Inorg. Chem.*, **6**, 2172 (1967).
9) T. Fujiwara and J. C. Bailar, Jr., *Inorg. Chem.*, **25**, 1806 (1986).
10) The H_2O peak in the spectrum of the hydrochloride of the trans isomer appears at δ ca. 4.
11) The amounts of the cis-α and β isomers in a mixture of the isomers is difficult to determine spectrophotometrically owing to the similarity of their visible spectra; data on the spectra and the absorption maxima of the isomers are available from Refs. 3 and 12, respectively.
12) E. Kyuno and J. C. Bailar, Jr., *J. Am. Chem. Soc.*, **88**, 1120 (1966).
13) H. E. LeMay, Jr., *Inorg. Chem.*, **7**, 2531 (1968).
14) D. A. Buckingham and D. Jones, *Inorg. Chem.*, **4**, 1387 (1965).
15) D. M. Chowdhury and G. M. Harris, *J. Phys. Chem.*, **73**, 3366 (1969).
16) C. Kutal and J. C. Bailar, Jr., *J. Phys. Chem.*, **76**, 119 (1972).
17) T. Fujiwara and Y. Yamamoto, *Inorg. Chem.*, **19**, 1903 (1980); T. Fujiwara, *Bull. Chem. Soc. Jpn.*, **56**, 122 (1983).
18) H. E.LeMay, Jr., *Inorg. Chem.*, **10**, 1990 (1971).
19) The monohydrate of the trans isomer is obtained as a fine powder by the method described here.
20) R. D. Gillard and G. Wilkinson, *J. Chem. Soc.*, **1963**, 3193 .
21) H. E. LeMay, Jr. and J. C. Bailar, Jr., *J. Am. Chem. Soc.*, **90**, 1729 (1968).
22) A. Sault, F. Fry, and J. C. Bailar, Jr., *J. Inorg. Nucl. Chem.*, **42**, 201 (1980).
23) P. Rây and N. K. Dutt, *J. Indian Chem. Soc.*, **20**, 81 (1943).
24) J. C. Bailar, Jr., *J. Inorg. Nucl. Chem.*, **8**, 165 (1958).
25) C. S. Springer and R. E. Sievers, *Inorg. Chem.*, **6**, 852 (1967).
26) For complexes of the type $[Co(trien)X_2]^{n+}$, it is assumed that when X=Cl, Br, or I, it is bound less strongly than triethylenetetramine and dissociation of the Co-X bond occurs by attack of an incoming group, while when it is bound more strongly, X=NH_3 or OH, isomerization takes place by opening the chelate ring and then protonation at the nitrogen atom of the ring may be important as described for complexes of the type $[Co(en)_2XOH]^{n+}$ in the literature: F. Basolo and R. G. Pearson, "Mechanisms of Inorganic Reactions," 2nd ed, John Wiley & Sons, New York (1967), pp. 282—283.
27) R. Tsuchiya, M. Omote, A. Uehara, and E. Kyuno, *Bull. Chem. Soc. Jpn.*, **49**, 1027 (1976).
28) J. M. Thomas, *Chem. Britain*, **6**, 60 (1970).

 © 1988 The Chemical Society of Japan Bull. Chem. Soc. Jpn., 61, 857—860 (1988)

Reactions of Coordination Compounds in the Solid State. III. The Behavior of the Isomers of Dichloro(triethylenetetramine)cobalt(III) Bromide and Iodide, [Co(trien)Cl_2]X

Terufumi FUJIWARA and John C. BAILAR, Jr.*
School of Chemical Sciences, University of Illinois, Urbana, Illinois 61801, U.S.A.
(Received July 30, 1987)

The rearrangement of the isomers of dichloro(triethylenetetramine)cobalt(III) bromide and iodide upon heating in the solid state has been studied in relation to the corresponding isomers of the chloride. The behavior of the bromide and iodide has been found to be different from that of the chloride, supporting the existence of anion effects in the solid-state reactions. With respect to the nature of the anions, several factors which are responsible for the differences are discussed in relation to mechanism.

In the second paper of this series, the rearrangement of the geometrical isomers of dichloro(triethylenetetramine)cobalt(III) chloride was considered.[1] It has been found that the anion plays an important role in these isomerizations, and that the dichloro bromide and dichloro iodide do not behave in the same way as the chloride. These differences are described here. It is not yet clear whether these differences arise from differences in the crystal lattices, from charge transfer effects, from differences in hydrogen bonding of the hydrates or from some other cause. We hope to clarify this point in later communications. Here we record only the observed differences in behavior, with preliminary comments on possible causes.

Experimental

Preparation of Compounds. The bromide salts of the triethylenetetramine (trien) compound, *trans*-[Co(trien)Cl_2]Br·0.5HBr·2H_2O, *cis*-α-[Co(trien)Cl_2]Br, and *cis*-β-[Co(trien)Cl_2]Br·H_2O, were prepared by grinding a slurry of the solids of the corresponding chloride salts[1] in a mortar with concentrated HBr (twice) followed by filtration, washing with ethanol and acetone, and drying in air. The crystalline bromide salt of the trans isomer was identified as the dihydrate by a coulometric determination of lattice water with a Hiranuma AQ-3 Aquacounter and a Karl Fischer reagent in which the bromide salt was dissolved.

The cis-β complex was resolved by the method given by Sargeson and Searle.[2] The optically active salt, (−)$_D$-sodium bis(oxalato)(ethylenediamine)cobaltate, prepared following the improved procedure of Worrell,[3] was used as the resolving agent for the cis-β isomer and the optically active product was obtained as the iodide. A DMSO solution of (+)$_D$-*cis*-β-[Co(trien)Cl_2]I·0.5H_2O (3.02 mg in 25 ml) gave α_D +0.046, whence $[\alpha]_D$=+190. The optically active cis-β isomer has a CD curve similar to the curve for the corresponding cis isomer.[4] Elemental analyses of the bromide and iodide salts of the isomers are given in Table 1.

Physical Measurements. Proton magnetic resonance measurements were made as before[1] on a Varian XL-200 200-MHz FT-NMR Spectrometer operating at the normal temperature of the probe (ca. 20 °C). All spectra were run in dimethyl-d_6 sulfoxide (DMSO-d_6) solutions (ca. 0.5—0.6 wt% complex),[5] as described previously,[1] as soon as possible after dissolution and chemical shifts were measured relative to tetramethylsilane as a reference standard.

Optical rotations were measured in a 2-dm tube with a Rudolph Research Autopol III Automatic Polarimeter using a sodium lamp. CD curves were measured on a JASCO Model J-40/J-41 Automatic Recording Spectropolarimeter in a 1-cm cell. DMSO was used as solvent for the polarimetric measurements.[6] Thermogravimetric analysis (TGA) was obtained as before[1] but by using a Sinku-Riko Model TGD-3000-RH thermogravimetric analyzer and a flow of N_2 (ca. 40 ml min^{-1}).

Rate Studies. Powdered samples (8—11 mg) of the

Table 1. Analytical Data

Compound	Calcd/%						
	C	H	N	Cl	Br	I	Co
cis-α-[Co(trien)Cl_2]Br	20.24	5.10	15.74	19.92	22.45	—	—
cis-β-[Co(trien)Cl_2]Br·H_2O	19.27	5.39	14.98	18.96	21.37	—	—
trans-[Co(trien)Cl_2]Br·0.5HBr·2H_2O	16.66	5.24	12.96	16.40	27.72	—	—
(+)$_D$-*cis*-β-[Co(trien)Cl_2]I·0.5H_2O	17.49	4.65	13.60	17.21	—	30.80	14.30
Compound	Found/%						
	C	H	N	Cl	Br	I	Co
cis-α-[Co(trien)Cl_2]Br	20.03	5.06	15.59	19.74	22.66	—	—
cis-β-[Co(trien)Cl_2]Br·H_2O	19.13	5.45	15.14	19.01	21.38		
trans-[Co(trien)Cl_2]Br·0.5HBr·2H_2O	16.80	5.28	12.77	16.40	27.78		
(+)$_D$-*cis*-β-[Co(trien)Cl_2]I·0.5H_2O	17.68	4.59	13.66	17.04	—	32.10	14.46

complex salts used here were mounted in uncapped aluminum boats and were heated in an Abderhalden apparatus containing water (bp 100 °C) or *N,N*-dimethylformamide (bp 152 °C) as a liquid of appropriate boiling point in the same way as described in our previous studies.[1,7] Also samples of the optically active iodide were heated at 100 °C in glass tubes (ca. 3.5 mm in diameter, ca. 4 cm in length) which were sealed off with a torch.

Before the ^{1}H NMR and/or polarimetric measurements, the mass loss accompanying the heating was measured as soon as possible after removing the samples from the heating apparatus at fixed times. For the CD measurements, samples of the optically active cis isomer were weighed (4—5 mg) into a 5 mL volumetric flask, dissolved in DMSO by vigorous shaking, and diluted to volume.

Results and Discussion

The ^{1}H NMR spectra of the bromide and iodide of the cis-α isomer are similar to that of the chloride, for which there are three peaks for the NH protons with the intensity ratio 2:2:2 (Figs. 1 and 2). One of the NH absorptions, which shows fine structure, appears slightly downfield (a triplet at δ 5.70 for the bromide and a quintet with center at δ 5.75 for the iodide) while the other two peaks shift upfield (at δ 5.58 and 5.94 for the bromide and at δ 5.53 and 5.89 for the iodide, respectively). In the bromide and iodide of the cis-β isomer, four of the six NH absorptions of equal intensity appear at positions similar to those of the corresponding NH absorptions in the chloride (Figs. 3 and 4); three quintets with centers at δ 3.94, 5.32, and 5.60, respectively, and one singlet at δ 7.40 for the bromide, and the three quintets with centers at δ 3.95, 5.32, and 5.58, respectively, and one singlet at δ 7.43 for the iodide). On the other hand, the other two absorptions shift upfield; one quintet with the center at δ 4.34 and one singlet at δ 6.75, for the bromide and the quintet centered at δ 4.08 and the singlet at δ 6.26 for the iodide. An ^{1}H NMR spectrum arising from the NH and NH_2 groups for the hydrobromide of the trans bromide is almost identical to that for the corresponding chloride monohydrate, which shows three NH bands (two quintets with centers at δ 5.13 and 5.58, respectively, and one singlet at δ 6.87) with the intensity ratio 2:2:2 (Fig. 5).

All CH_2 absorptions in these isomers appear at higher field than the NH absorptions and show some fine structure, which is probably the superposition of two or more multiplets, as well as those for the

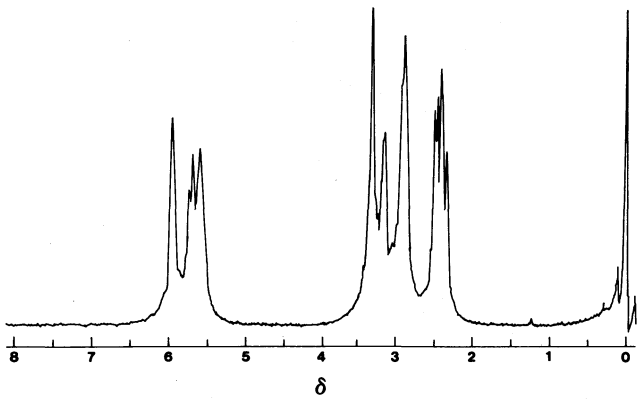

Fig. 1. ^{1}H NMR spectrum of *cis*-α-[Co(trien)Cl_2]Br in DMSO-d_6.

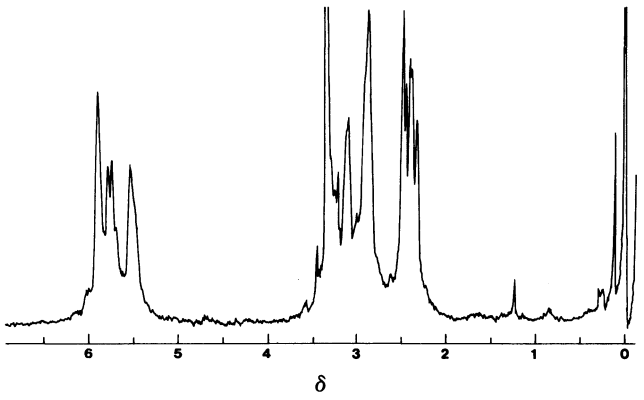

Fig. 2. ^{1}H NMR spectrum of *cis*-α-[Co(trien)Cl_2]I in DMSO-d_6.

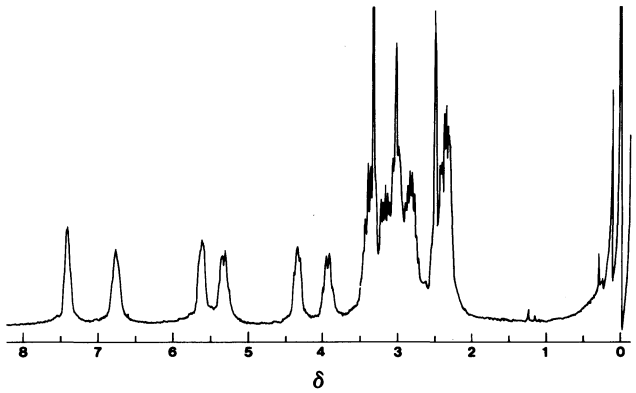

Fig. 3. ^{1}H NMR spectrum of *cis*-β-[Co(trien)Cl_2]Br·H_2O in DMSO-d_6.

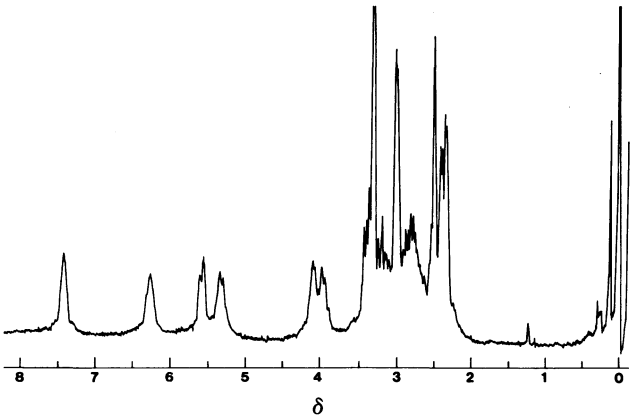

Fig. 4. ^{1}H NMR spectrum of *cis*-β-[Co(trien)Cl_2]I·$0.5H_2O$ in DMSO-d_6.

corresponding cis-α, cis-β, and trans chlorides.[1] Furthermore, the signal due to H_2O (mainly as an impurity) in the DMSO-d_6 solutions of the isomers and the solvent signal overlap the spectra arising from the CH_2 groups for the cis isomers as observed for DMSO-d_6 solutions of the chlorides.[1] For the estimation of the relative amounts of the cis-α, cis-β, and trans isomers for a mixture of them (or a product) by calculation of the peak areas (or intensity ratios) of the NH protons, the NH absorptions at δ 7.40, 5.94, and 6.87 for the bromides of the cis-β, cis-α, and trans isomers, respectively, can be used.[1]

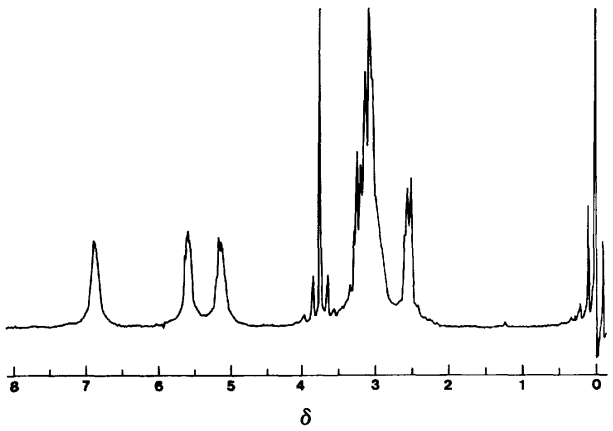

Fig. 5. ^{1}H NMR spectrum of *trans*-[Co(trien)Cl_2]Br·0.5HBr·2H_2O in DMSO-d_6.

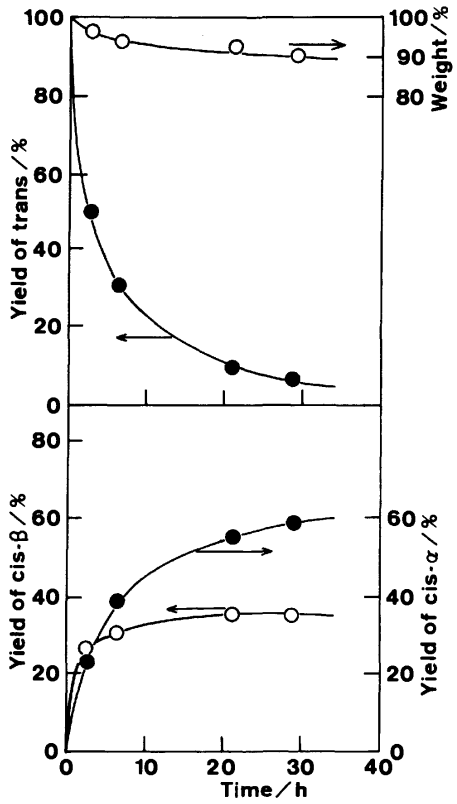

Fig. 6. Isomerization at 100 °C of powdered samples of *trans*-[Co(trien)Cl_2]Br·0.5HBr·2H_2O in static air, with %weight of material remaining.

In a previous study,[1] we found that heating the green chloride salt, *trans*-[Co(trien)Cl_2]Cl·0.5HCl·2H_2O, to 100 °C yields a mixture of the cis-α, cis-β, and trans isomers. In any case in which isomerization takes place, the trans isomer is converted to the cis-β form, which then goes more slowly to the cis-α form. Similarly, finely powdered samples of the trans hydrobromide, *trans*-[Co(trien)Cl_2]Br·0.5HBr·2H_2O, are isomerized to a mixture of the cis-α and -β isomers when heated at 100 °C in air (Fig. 6). Also, a TGA curve for the trans hydrobromide is similar to the curve for the trans hydrochloride.[1] There is a single-step loss of HBr and H_2O at 85—95 °C and the mass loss is complete at 150—160 °C. A subsequent slow loss of weight due to decomposition occurs at 230—240 °C.

The conversion of the trans isomer to the cis-β isomer cannot be expected by the Rây-Dutt,[10] Bailar,[11] or Springer-Sievers[12] twists, as discussed in previous papers.[1,13] Moreover, the green crystals of the dibromo bromide, *trans*-[Co(trien)Br_2]Br·HCl, show no isomerization during drying overnight at 90 °C or dehydrochlorination at 110 °C for two days.[14] The difference between the dichloro and dibromo complexes indicates that the rate of isomerization may be affected strongly by the Co–X bond strength. In the reaction mixtures, two new NH absorptions for the cis-α isomer appear at δ 5.88 and 6.08 in addition to the NH absorption at δ 5.98 which is similar to that of the bromide, *cis*-α-[Co(trien)Cl_2]Br. When the bromide of the cis-α isomer is prepared by the method described above, the ^{1}H NMR spectrum of the product has similar NH absorptions if the chlorobromo complex, *cis*-α-[Co(trien)ClBr]Br, is present as a byproduct. These indicate that the *cis*-α-[Co(trien)ClBr]$^+$ ion is formed as one of the products when the *trans*-[Co(trien)Cl_2]Br·0.5HBr·2H_2O is heated; such a ligand substitution cannot be expected by a twist mechanism. The conversion behavior of the trans bromide to the cis-β and the subsequent conversion of the cis-β bromide to the cis-α, as well as those of the corresponding trans and cis-β chlorides,[1] respectively, can be explained by an aquation-anation pathway[15] and a pathway involving a "back-side attack" on the cis isomer by an incoming group,[16] respectively.

The nature of the counterion and/or the HX is also important, as shown by the fact that the rate of isomerization for the hydrobromide is higher than for the hydrochloride but the rate of mass loss caused by dehydration-dehydrobromination is lower (dehydration-dehydrobromination is not complete, which was confirmed by a TGA run on the trans hydrobromide at a constant temperature of 100 °C). For example, a powder sample of *trans*-[Co(trien)Cl_2]Cl·0.5HCl·2H_2O,

on heating to 100°C, yields 49% cis-β and 42% cis-α in 48 h, whereas the corresponding bromide, *trans*-[Co(trien)Cl_2]Br·0.5HBr·$2H_2O$, upon heating for only 29.4 h, yields 35% cis-β and 58% cis-α (after about 3 h, there is more cis-α isomer in the mixture than cis-β). Similar effects appear in reactions of the solid-state racemization of $(+)_D$-[Co(en)$_3$]$X_3 \cdot nH_2O$[17] and thermal decomposition of [Co(NH_3)$_6$]X_3 in the solid state.[18] In the case of $(+)_D$-[Co(en)$_3$]X_3, the iodide was found to racemize the most readily, the bromide somewhat less so, and the chloride, hardly at all and it was presumed that hydrogen bonding of the type N-H···X is responsible for the rate differences in the series. In the case of [Co(NH_3)$_6$]X_3, the rate of decomposition decreases in the order of anions $I^- > Br^- > Cl^-$ and it was considered that electron transfer from an outer-sphere anion to the central cobalt(III) ion plays a role in forming the thermally less stable cobalt(II) complex. It may be that both factors are responsible for the above difference in the rate of conversion between the chloride and bromide of the trans or cis-β isomer of the trien complex studied here but it is not clear whether the rate differences arise from charge transfer effects or from differences in hydrogen bonding. The anion effects on the conversion of the trans and cis-β isomers may also be explainable in terms of a defect-diffusion mechanism proposed for solid-state reactions of coordination compounds by House.[19] For the conversion, the process involving anation would require that the anion leave a lattice site and migrate to the complex ion to form a transition state, which would involve the vacating of an anion site with the formation of a Schottky type defect (Fig. 2 of Ref. 19), and the activation energy required by the process would be expected to increase with increasing lattice energy. Since for a given cation the lattice energy would increase as the size of the anion decreases, it is reasonable that the chloride should have a higher lattice energy and so a higher activation energy than the bromide.

On the other hand, when the bromides of the cis-α and β are heated to 100 °C in air there is no observable isomerization. When the α or β bromides are kept at 152 °C for 30 h, no significant isomerization occurs, while a very small (less than 4%) conversion of the β chloride to its α isomer is observed in a previous study.[1] The optically active iodide $(+)_D$-*cis*-β-[Co(trien)Cl_2]I·0.5H_2O does not undergo significant racemization or isomerization upon heating in an open boat at 152 °C for 22.8 h or even in a sealed tube at 100 °C for 237 h whereas the cis-β chloride in a sealed tube at 100 °C is converted to cis-α form (11% after 70.4 h in Table 2 of Ref. 1), although TGA runs on the iodide and chloride of the cis-β isomer show that the iodide decomposes at a lower temperature (190—200 °C) than the chloride (215—230 °C[1]). A similar trend in anion effects on the conversion of the cis-β isomer to the cis-α isomer is observed for the solid-state racemization of [M(phen)$_3$]X_2 (M=Fe, Ni) and [Co(phen)$_3$]X_3,[20] where the rate differences would be attributed to a nucleophilic interaction of the counterions with the central metal: the donor ability of the chloride ion is larger than that of the bromide or iodide ion. On the other hand, these effects "opposite" to the above ones observed for the hydrobromide and hydrochloride salts of the trans isomer suggest that the rearrangements depend to a large extent on the packing of ions in the crystal, rather than upon any specific chemical property.

The work described in this paper was done under the sponsorship of the Petroleum Research Fund, administered by the American Chemical Society, for which the authors express their gratitude.

References

1) T. Fujiwara and J. C. Bailar, Jr., the part II, *Bull. Chem. Soc. Jpn.*, **61**, 849 (1988).
2) A. M. Sargeson and G. H. Searle, *Inorg. Chem.*, **6**, 787 (1967).
3) J. H. Worrell, *Inorg. Chem.*, **10**, 870 (1971).
4) A. M. Sargeson and G. H. Searle, *Inorg. Chem.*, **4**, 45 (1965).
5) The complex bromides and iodides used here are more soluble in DMSO than the chlorides reported already in Ref. 1.
6) The DMSO solutions show no rotational change in two days.
7) T. Fujiwara and J. C. Bailar, Jr., *Inorg. Chem.*, **25**, 1806 (1986).
8) The iodide of the cis-α isomer was also prepared but for it no kinetic study was conducted.
9) An H_2O peak at δ ca. 4 is observed for the hydrobromide of the trans isomer and moves upfield with decrease of the HBr concentration in the DMSO solution. The shift results in overlapping of the H_2O signal with the NH signal at δ 3.94 in the cis-β isomer.
10) P. Rây and N. K. Dutt, *J. Indian Chem.*, **20**, 81 (1943).
11) J. C. Bailar, Jr., *J. Inorg. Nucl. Chem.*, **8**, 165 (1958).
12) C. S. Springer and R. E. Sievers, *Inorg. Chem.*, **6**, 852 (1967).
13) A. Sault, F. Fry and J. C. Bailar, Jr., *J. Inorg. Nucl. Chem.*, **42**, 201 (1980).
14) J. Selbin and J. C. Bailar, Jr., *J. Am. Chem. Soc.*, **82**, 1524 (1960).
15) H. E. LeMay, Jr. and J. C. Bailar, Jr., *J. Am. Chem. Soc.*, **90**, 1729 (1968).
16) E. Kyuno and J. C. Bailar, Jr., *J. Am. Chem. Soc.*, **88**, 1120 (1966).
17) C. Kutal and J. C. Bailar, Jr., *J. Phys. Chem.*, **76**, 119 (1972).
18) N. Tanaka and K. Nagase, *Bull. Chem. Soc. Jpn.*, **40**, 546 (1967).
19) J. E. House, Jr., *Thermochim. Acta*, **38**, 59 (1980).
20) T. Fujiwara and Y. Yamamoto, *Inorg. Chem.*, **19**, 1903 (1980); T. Fujiwara, *Bull. Chem. Soc. Jpn.*, **56**, 122 (1983).

Synthesis and Reactions of Selenoketones

Akihiko Ishii, Renji Okazaki,* and Naoki Inamoto
Department of Chemistry, Faculty of Science, The University of Tokyo,
Hongo, Tokyo 113
(Received June 23, 1987)

A new, convenient method for the synthesis of selenoketones has been reported. The reaction of dimagnesium salts of ketone hydrazones with diselenium dichloride affords an intermediate tentatively assigned as tetraselenides, which are converted into selenoketones by heating in the presence of tributylamine. A comparative study on the reactions of 1,1,3,3-tetramethyl-2-indanselone and the corresponding thioketone with Grignard and organolithium reagents have been carried out. Analysis of the reaction products has revealed that the heterophilic attack of the organometallic reagents is much more significant in the reaction with the selone than with the thione.

Organoselenium chemistry is of current interest[1] and considerable attention has been paid to the chemistry of selenoketones in recent years. They have been used as synthetic intermediates for hindered olefins[2] and their physical properties have been studied rather extensively.[3] Until our preliminary communication in 1983,[4] however, there had been known only two synthetic routes to these compounds, i.e., 1) the reaction of triphenylphosphoranylidenehydrazones with selenium metal above their melting points developed by Barton and his co-workers[2a] and 2) the reaction of ketones with bis(tricyclohexyltin) selenide in the presence of boron trichloride.[5] At almost the same time as with our communication, Guziec, Jr. and Moustakis reported the synthesis of selenoketones by the reaction of hydrazones with diselenium dibromide.[6] As for the reactions of selenoketones, some interesting examples have been reported,[2a,7] but the reactions with Grignard and organolithium reagents have not been reported. This is in contrast with thioketones because considerable attention has been paid in recent years to their reactions with organometallics which show unique heterophilic nature.[8] The purpose of this paper is to describe a full account of the synthesis of selenoketones and their reactions with organometallics.[9]

Results and Discussion

Synthesis of Selenoketones. 1) Method A. We previously reported the method for preparation of thioketones from the corresponding hydrazones and disulfur dichloride (Eq. 1).[10]

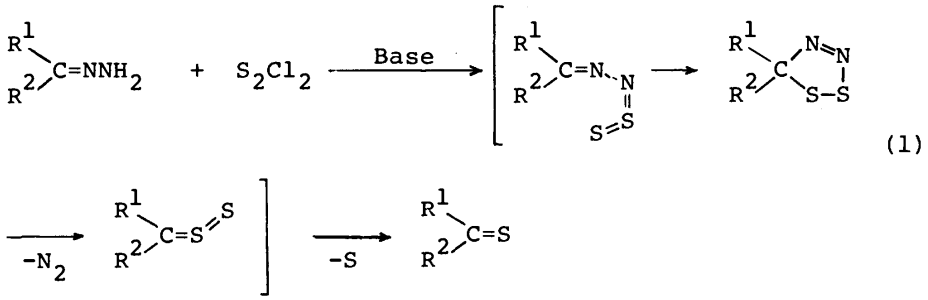

(1)

We became interested in whether this method would be applicable to selenoketone synthesis by using diselenium dichloride (Se_2Cl_2) instead of disulfur dichloride.

Optimization of the reaction conditions were carried out by using the reaction of di-*t*-butyl ketone hydrazone (**1**) with diselenium dichloride and the results are shown in Table 1. The maximum yield of di-*t*-butyl selenoketone (**2**) (28%) was obtained in benzene at 60 °C in the presence of 4-dimethylaminopyridine as tertiary base (Run 6).

Table 1. Reaction Conditions and Yields for Method A[a]

Run	Base(equiv)	Temp °C	Yield of 2 %
1	Et_3N(3.6)	5	7
2	DABCO[b](5.0)	5	11
3	*n*-Bu_3N(5.0)	5	17
4	DMAP[c](5.0)	5	21
5	DMAP(5.0)	r.t.	24
6	DMAP(5.0)	60	28
7	DMAP(5.0)	refl.	0

a) All reactions were carried out in benzene. b) 1,4-Diazabicyclo[2.2.2]octane. c) 4-Dimethylaminopyridine.

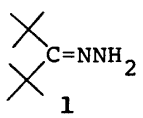

1

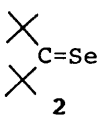

2

Table 2. Yields of Selenoketones by Methods A and B

Run	Selenoketone	Yield/%	
		Method A	Method B
1	$(t\text{-Bu})_2C{=}Se$ (**2**)	28	51(58)[a]
2	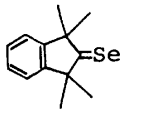 (**3**)	31	82
3	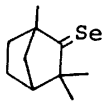	7	24
4	$(1\text{-Ad})_2C{=}Se$	24	53
5	$(1\text{-Ad})(t\text{-Bu})C{=}Se$		43
6	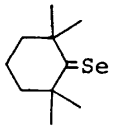	3	35
7	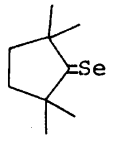	14	18

a) A yield obtained by the simultaneous addition method. b) 1-Ad denotes 1-adamantyl.

Under these optimized conditions some other selenoketones were synthesized and the results are summarized in Table 2. The yields of selenoketones by this method (Method A) are uniformly rather poor with a maximum (31%) for 1,1,3,3-tetramethyl-2-indanselone (**3**).

2) Method B. Since the yields by Method A were not satisfactory, we next attempted activation of hydrazones. Hydrazone **1** was converted to dimagnesium salt **4** by the reaction with 2 equiv of ethylmagnesium bromide in THF at 60 °C. After exchanging the solvent from THF to benzene, **4** was

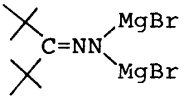

4

reacted with Se_2Cl_2 at room temperature in the presence of n-Bu_3N and the reaction solution was allowed to warm to 60 °C. Under these conditions selenoketone **2** was obtained in a 51% yield. The yields of other selenoketones were also increased (Table 2). If the reaction proceeds via a similar mechanism depicted in Eq. 1 for thioketones, a tertiary amine, tributylamine in this case, should be unnecessary. In the absence of tributylamine, however, only an orange material was obtained without formation of any selenoketone. This orange material, though stable during aqueous workup, was thermally not very stable and could not survive the chromatographic purification on silica gel, alumina, or Florisil undergoing decomposition with deposition of selenium. Although the instability did not permit further purification of this compound, its elemental analysis suggested the composition of $C_9H_{18}ClSe_2$. The ^1H NMR spectrum showed only one peak due to the t-butyl group at δ 1.4 and ^{77}Se NMR spectrum showed two peaks at 702 and 785 with almost comparable intensity along with some small peaks. On the basis of these data, the structure of the orange material is tentatively assigned as tetraselenide **5**, which would be converted into selenoketone **2** by treatment with tributylamine. Indeed, **2** was formed when a benzene solution of **5** was treated with tributylamine at 60 °C (60% yield based on **5**) or heated in vacuo (63% yield based on **5**). In contrast to this result it is interesting that Guziec, Jr. and Moustakis reported that 4*H*-1,2,3-selenadiazete **6** was an intermediate in the reaction of a

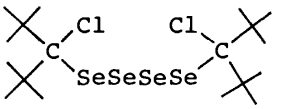

5

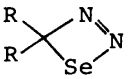

6

hydrazone and diselenium dibromide.[6] The formation mechanism of **5** is not clear at present. The formation of **5** was similarly observed in other selenoketone syntheses. Although the reactions of tributylamine with the tetraselenide were sometimes incomplete, selenoketones could be obtained by pyrolysis of the tetraselenide in vacuo in such cases.

The present method has some interesting features: (1) It provides selenoketones in a one-pot reaction unlike the Barton's method which requires isolation of the phosphoranylidenehydrazones. (2) Since the reaction is conducted under homogeneous conditions, there are none of the problems in a small scale synthesis encountered in the Barton's method where the reaction is conducted under heterogeneous conditions.[2a] (3) When two benzene solutions of dimagnesium salts of hydrazones and diselenium dichloride are added simultaneously and dropwise to a benzene solution of tributylamine, the yield is somewhat improved (Table 2, Run 1).

Reactions of 1,1,3,3-Tetramethyl-2-indanelone (3) with Grignard and Organolithium Reagents. Selenoketone **3** was selected for this investigation because **3** was obtained in a high yield and easily crystallized.

The reactions were carried out in ether at room temperature and four types of products **7**—**10** were isolated (Eq. 2). As **7** and **10** were easily oxidized to the corresponding diselenides in the air, their yields were determined after the conversion to diselenides **11** and **12**, respectively.

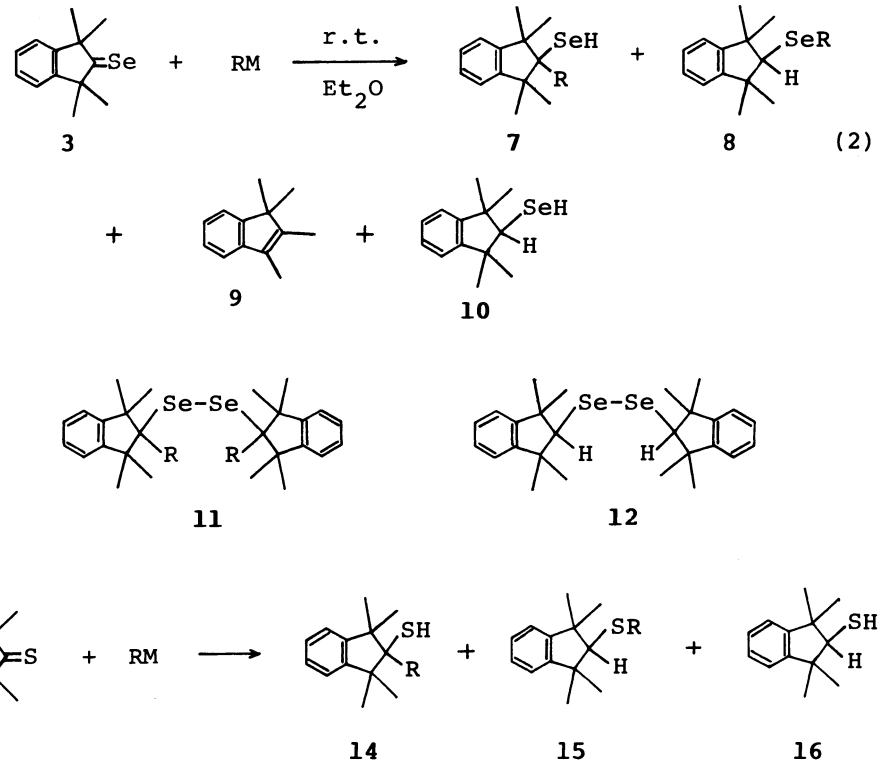

3 7 8 (2)

9 10

11 12

13 14 15 16 (3)

In order to compare the reactivity of the seleno- and thioketones, the reactions of the corresponding thioketone **13** with some organolithium reagents were also carried out under similar conditions (Eq. 3) to afford **14**—**16**. The results of these reactions are also shown in Table 3.

The products are classified as follows: (A) carbophilic addition products, **7** and **14**; (B) heterophilic addition products, **8**, **15**, and **9**; (C) reduction products, **10** and **16**. The results shown in Table 3 indicate that the reactions of organometallic reagents with selenoketone **3** are very unique in that the heterophilic nature is much more significant than those with thioketone **13**. Thus both selenophilic and carbophilic products were formed in the reaction of methyllithium with **3** whereas only the carbophilic product was formed for **13** (Run 1). The reaction of

Table 3. Reactions of **3** or **13** with Grignard or Organolithium Reagents

Run	RM	Yield/%						
		7[a]	**8**	**9**	**10**[a]	**14**	**15**	**16**
1	MeLi	73	10			91		
2	MeMgI	69						
3	*t*-BuLi		9		66			57
4	*t*-BuMgCl		15	22	44			
5	$PhCH_2Li$	86				95		
6	PhLi		47			56	24	
7	PhMgBr		3	14				

a) The yield was determined after the conversion to the corresponding diselenide.

t-butyllithium with **3** (Run 3) gave some selenophilic product **8**, while **13** did not afford any thiophilic product. In the reaction with phenyllithium (Run 6) the preference of the heterophilic attack is even more obvious; the selenophilic product **8** was the sole product from **3** whereas the carbophilic product **14** was a main product from **13**. At the present time we do not have a definite answer to the question why the heterophilic nature is larger in the reaction of the selenoketone than in that of the thioketone. One possible explanation, however, is that the spin density in an intermediary anion radical (see below) is larger on selenium than on carbon.

Other interesting features are the formation of the reduction product **10** and 1,1,2,3-tetramethyl-1*H*-indene (**9**). It has been reported[8] that the reaction between thioketones and organometallic reagents bearing a β-hydrogen gave the reduction product. This has been explained in terms of the hydrogen abstraction of the anion radical formed by single electron transfer (SET) from the organometallic reagent to the thioketone. In the present reactions the reduction product **10** is obtained only in the reactions with *t*-BuLi and *t*-BuMgCl. This suggests that these reactions begin with a SET process giving anion radical I, which would abstract a hydrogen from a

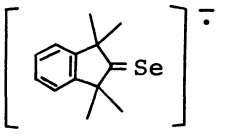

I

t-butyl radical to yield **10** (after protonation) and 2-methylpropene. Reactions with other Grignard and organolithium reagents also probably proceed via a SET process.

The formation of 1,1,2,3-tetramethyl-1*H*-indene (**9**) can be accounted for as shown in Scheme 1. Thus RSeM is eliminated from initially formed selenophilic adduct **17** to give carbene **18**, which then rearranges to **9**. There are some precedents of such carbene-forming reactions for sulfur-stabilized carbanions.[11] This type of elimination is known to occur when both a thioketone and an organometallic reagent are bulky and hence the cleavage of the intermediate is sterically accelerated and when the intermediate has a good leaving group. The present reactions of **3** with *t*-BuMgCl and PhMgBr meet these conditions: **3** is sterically crowded and the leaving group is either bulky (i.e., *t*-BuSe$^-$) or easily cleaved (i.e., PhSe$^-$). This type of carbene-forming reaction is, to our knowledge, the first example for selenoketones, although we recently reported a similar reaction between *O*-alkyl selenoformates and 2,4,6-tri-*t*-butylphenyllithium.[12]

The whole mechanistic scheme is shown in Scheme 2.

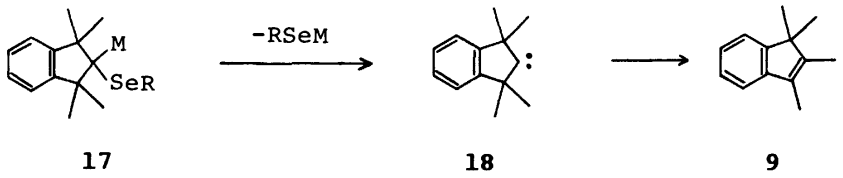

Scheme 1.

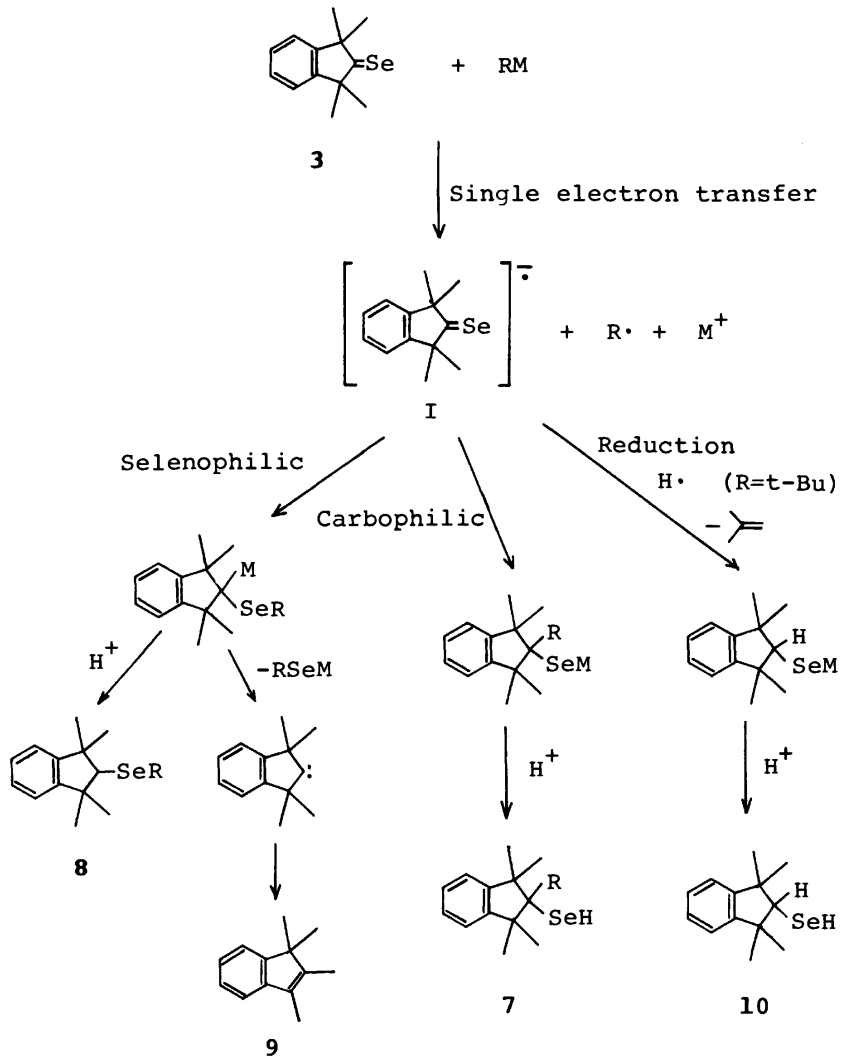

Scheme 2.

Experimental

Melting points are uncorrected. ^1H(89.60 MHz) and ^{13}C(22.53 MHz) NMR spectra were measured in $CDCl_3$ with a JEOL FX-90Q spectrometer using tetramethylsilane as an internal standard. ^{77}Se NMR spectra were recorded at 17.09 MHz with a JEOL FX-90Q spectrometer, whose chemical shifts were measured in $CDCl_3$ with dimethyl selenide as an external standard. Infrared spectra were recorded on a Hitachi 260-30 infrared spectrometer. Ultraviolet and visible spectra were taken on a Hitachi 343 recording spectrophotometer. Mass and high-resolution mass spectra were obtained with a JEOL D-300 mass spectrometer. All reactions were carried out under an argon atmosphere.

Materials. Diselenium dichloride (Se_2Cl_2),[13] di-*t*-butyl ketone,[14] di-1-adamantyl ketone,[14] and 1-adamantyl *t*-butyl ketone hydrazones[14] were prepared by the reported method. The hydrazones of 1,1,3,3-tetramethyl-2-indanone, fenchone, 2,2,6,6-tetramethylcyclohexanone, and 2,2,5,5-tetramethylcyclopentanone were prepared from the corresponding ketones by the method of Barton.[15]

Syntheses of Selenoketones. General Procedure. 1) Method A. To 4-dimethylaminopyridine (5 mmol) in benzene (7 ml), preheated at 60 °C, were added simultaneously a hydrazone (1 mmol) in benzene (7 ml) and Se_2Cl_2 (1.5 mmol) in benzene (7 ml) at about the same rate by using two dropping funnels during 25 min. After stirring for 4 h at this temperature were added water and ether. Red-brown precipitates were removed by filtration and the yellow-green filtrate was washed with water and dried over anhydrous $MgSO_4$. The solvent was removed under reduced pressure. Selenoketones in the residue were purified by silica-gel chromatography (hexane).

2) Method B. A THF (5 ml) solution of hydrazone (1 mmol) was added dropwise to ethylmagnesium bromide (2 mmol) in THF (5 ml) at 60 °C. The reaction occurred with evolution of ethane. After stirring for 1 h at this temperature, THF was removed under reduced pressure and benzene (80 ml) and tributylamine (1 mmol) were added. To this solution was added Se_2Cl_2 (1.2 mmol) in benzene (20 ml) at 5 °C during 20 min. Then the mixture was stirred at 60 °C for 3 h. After addition of water, the green-blue solution was washed with 2M HCl (1M=1 mol dm^{-3}) and water and dried over anhydrous $MgSO_4$. The residue obtained after the removal of the solvent under reduced pressure was heated at ca. 130 °C in vacuo (0.05 mmHg) (1 mmHg=133.322 Pa) in an apparatus with a cold trap. Crude selenoketones were purified by silica-gel chromatography (hexane). The yields of selenoketones by Methods A and B are listed in Table 1.

Di-*t*-butyl selenoketone,[3b,16] 1,1,3,3-tetramethyl-2-indanselone,[3b,7c] selenofenchone,[3b,16] and 2,2,5,5-tetramethylcyclopentaneselone[6] were identified by comparison of the chemical shifts of their ^1H and ^{13}C NMR spectra with their reported values.

Di-1-adamantyl Selenoketone: Blue crystals: mp 161—162 °C (hexane). ^1H NMR δ=1.61—1.81 (m, 12H), 1.92—2.21 (m, 6H), 2.21—2.42 (m, 12H); ^{13}C NMR δ=29.3, 36.6, 43.6, 63.7, 293.9 (C=Se, $^1J_{^{13}C-^{77}Se}$=209.0 Hz); ^{77}Se NMR δ=2134. IR(KBr) 2910, 2855, 1640, 1540, 1452, 1366, 1345, 1308, 1264, 1189, 1125, 1105, 1092, 1025, 1005, 982, 920, 825, 810, 736, 706, 670, 626 cm^{-1}. UV-VIS (cyclohexane) λ_{max} 712 nm (ε=23.7), 279 (6830), 239 (3990). Found: *m/z* 362.1511. Calcd for $C_{21}H_{30}{}^{80}Se$: M, 362.1513.

1-Adamantyl *t*-Butyl Selenoketone: Blue crystals; mp 39—41 °C (hexane). ^1H NMR δ=1.53 (s, 9H), 1.61—1.78 (m, 6H), 1.95—2.19 (m, 3H), 2.19—2.35 (m, 6H); ^{13}C NMR δ=29.2, 32.6, 36.6, 43.7, 60.4, 63.1, 292.9 (C=Se, $^1J_{^{13}C-^{77}Se}$=210.9 Hz); ^{77}Se NMR δ=2120. IR(KBr) 2900, 2845, 1636, 1535, 1472, 1444, 1392, 1358, 1342, 1308, 1258, 1216, 1180, 1118, 1096, 1046, 1028, 998, 946, 925, 818, 778, 715, 656, 634 cm^{-1}. UV-VIS (cyclohexane) λ_{max} 708 nm (ε=23.7), 274 (6920), 234 (3200). MS *m/z* 284(M^+), 227, 135 (base). Found: *m/z* 284.1064. Calcd for $C_{15}H_{24}{}^{80}Se$: M, 284.1043.

2,2,6,6-Tetramethylcyclohexaneselone: Blue liquid. ^1H NMR δ=1.41 (s, 12H), 1.81 (s, 6H);[6] ^{13}C NMR δ=18.3, 33.5, 38.4, 58.8, 294.4 (C=Se)[3d]; ^{77}Se NMR δ=2026 (lit,[3d] δ=2034); IR (neat) 3000, 2975, 2945, 2875, 1468, 1388, 1368, 1180, 1140, 1102, 1070, 1038, 1012, 990, 980, 952, 940, 882, 862, 778, 740, 668 cm^{-1}.[6] UV-VIS (cyclohexane) λ_{max} 686 nm (ε=24.3), 273 (6230), 227 (2300).[3d] Found: *m/z* 218.0582. Calcd for $C_{10}H_{18}{}^{80}Se$: M, 218.0572.

Reaction of Di-*t*-butyl Ketone Hydrazone (1) with Se_2Cl_2 in the Absence of Tributylamine. (a) Hydrazone **1** (63.0 mg, 0.403 mmol) was converted to bis(bromomagnesio)hydrazone **4** by Method B. This salt dissolved in benzene (6 ml) and Se_2Cl_2 (110 mg, 0.48 mmol) in benzene (6 ml) were simultaneously added to benzene (30 ml) at room temperature. The mixture was stirred at room temperature for 1 h. Water was added and the organic layer was washed with water and dried over anhydrous $MgSO_4$. The evaporation of the solvent gave an orange oil (88 mg), whose ^1H NMR spectrum showed a peak at δ 1.4 and the absense of di-*t*-butyl selenoketone. This orange oil was dissolved in benzene (40 ml) and tributylamine (0.12 g, 0.63 mmol) was added. After the resulting solution was stirred at 60 °C for 5 h, water was added. The organic layer was washed with 2M HCl and water and dried over anhydrous $MgSO_4$. From the residue obtained after the removal of the solvent, di-*t*-butyl selenoketone (24.8 mg, 30% based on the hydrazone) was collected in a cold trap in vacuo. (b) Hydrazone **1** (148 mg, 0.948 mmol) was converted to bis(bromomagnesio)hydrazone as described in Method B. This salt in benzene (5 ml) and Se_2Cl_2 (260 mg, 1.14 mmol) in benzene (5 ml) was simultaneously added to benzene (10 ml) at room temperature. The mixture was stirred for 1 h at room temperature and for 1 h at 60 °C. The organic layer was washed with water and dried over anhydrous $MgSO_4$ and the solvent was removed under reduced pressure. The resulting orange oil (272 mg), whose ^1H NMR spectrum showed a peak at δ 1.4, was pyrolyzed (ca. 100—200 °C) in vacuo and di-*t*-butyl selenoketone (79 mg, 38% based on hydrazone used) was collected in a cold trap. (c) Hydrazone **1** (316 mg, 2.02 mmol) in benzene (10 ml) and Se_2Cl_2(555 mg, 2.42 mmol) in benzene (10 ml) was simultaneously added to triethylamine (489 mg, 4.84 mmol) in benzene (20 ml) at room temperature. After water was added, the organic layer was washed with water and dried over anhydrous $MgSO_4$. The solvent was removed under reduced pressure and then volatile materials were removed completely in vacuo. ^{77}Se NMR spectrum of the residual orange oil showed mainly two comparable peaks at δ 702 and 785. Its elemental analysis was as follows: C, 34.59; H, 6.01; Cl, 9.55; N, 1.09%. These data suggested the composition

$C_9H_{18}ClSe_2$. Calcd for $C_9H_{18}ClSe_2$; C, 33.93; H, 5.69; Cl, 11.13%.

Reactions of 1,1,3,3-Tetramethyl-2-indanselone (3) with Methyllithium. To methyllithium (1.82 mmol) in ether (6 ml) was added the selone **3** (152 mg, 0.606 mmol) in ether (10 ml) at room temperature. The green solution became colorless after 80 min. After stirring for additional 30 min was added aqueous ammonium chloride. The organic layer was separated, washed with water, and dried over anhydrous $MgSO_4$. Removal of the solvent gave an almost colorless oil with characteristic smell of selenol, whose ^1H NMR spectrum showed a peak at δ −0.45 due to a selenol proton. To convert the selenol to the corresponding diselenide the mixture was dissolved in KOH (0.3 g)-MeOH (10 ml) and the solution was stirred at room temperature overnight. Methanol was removed and the residue was extracted with ether. The ethereal layer was washed with water and dried over anhydrous $MgSO_4$ and ether was evaporated. The products were separated by preparative thin-layer chromatography (silica gel, hexane) to give 1,1,3,3-tetramethyl-2-(methylseleno)indan (**8**, R=CH_3) (16 mg, 10%) and bis-(1,1,2,3,3-pentamethyl-2-indanyl) diselenide (**11**, R=CH_3) (118 mg, 73%). **8** (R=CH_3): colorless crystals, mp 54.5—55.0 °C. ^1H NMR δ=1.25 (s, 6H), 1.40 (s, 6H), 2.11 (s, 3H, $SeCH_3$), 3.30 (s, 1H), 7.18 (s, 4H); MS *m/z* (rel intensity) 268 (M^+, 32), 173 (60), 131 (100), 57 (68). Found: *m/z* 268.0722. Calcd for $C_{14}H_{20}{}^{80}Se$: M, 268.0728. **11** (R=CH_3): yellow crystals, mp 143.0—143.5 °C. ^1H NMR δ=1.37 (s, 12H), 1.52 (s, 18H), 7.1—7.2 (m, 8H); ^{13}C NMR δ=25.7, 28.3, 32.6, 50.6, 122.3, 127.0, 148.7; ^{77}Se NMR δ=628; MS *m/z* (rel intensity) 534 (M^+, 0.8), 506 (0.7), 348 (1), 268 (3), 187 (100), 171 (56), 145 (51), 131 (27), 57 (40). Found: C, 62.90; H, 7.11%. Calcd for $C_{28}H_{38}Se_2$: C, 63.15; H, 7.19%.

In a similar manner the following reactions were carried out.

With MeMgI. **3** (72.2 mg, 0.287 mmol) and MeMgI (3.4 equiv) were reacted overnight. **11** (R=CH_3): 53 mg (69%).

With *t*-BuLi. In the case of the reaction of **3** (154 mg, 0.612 mmol) with *t*-BuLi (3 equiv), **3** was not completely consumed even after 3 d. Therefore additional *t*-BuLi (1.5 equiv) was added. *t*-Butyl 1,1,3,3-tetramethyl-2-indanyl selenide (**8**, R=*t*-Bu; 9%): colorless crystals, mp 84.0—84.5 °C. ^1H NMR δ=1.21 (s, 6H), 1.38 (s, 6H), 1.50 (s, 9H, *t*-Bu), 3.04 (s, 1H), 7.19 (s, 4H); ^{13}C NMR δ=28.5, 28.7, 33.7, 38.3, 45.9, 62.8, 122.7, 126.7, 149.70; ^{77}Se NMR δ=325; MS *m/z* (rel intensity) 310 (M^+, 13), 254 (14), 239 (7), 173 (58), 157 (27), 131 (23), 119 (23), 86 (50), 84 (78), 57 (100). Found: *m/z* 310.1214. Calcd for $C_{17}H_{26}{}^{80}Se$: M, 310.1999. Bis(1,1,3,3-tetrametyl-2-indanyl) diselenide (**12**, 66%): yellow crystals, mp 140.5—141.0 °C. ^1H NMR δ=1.25 (s, 12H), 1.48 (s, 12H), 3.69 (s, 2H), 7.19 (s, 8H); ^{13}C NMR δ=28.2, 29.1, 46.9, 74.7, 122.5, 127.0, 149.0; ^{77}Se NMR δ=278; MS *m/z* (rel intensity) 506 (M^+, 0.8), 310 (4), 254 (5), 173 (26), 157 (11), 131 (14), 119 (9), 57 (100). Found: *m/z* 506.1032. Calcd for $C_{26}H_{34}{}^{80}Se_2$: M, 506.0990.

With *t*-BuMgCl. **3** (155 mg, 0.616 mmol) were reacted with *t*-BuMgCl (3 equiv) for 1.25 h. **8** (R=*t*-Bu) (28 mg, 15%), **12** (69 mg, 44%), and 1,1,2,3-tetramethyl-1*H*-indene (**9**) (21 mg, 22%)[17] were obtained.

With $PhCH_2Li$. **3** (107 mg, 0.427 mmol) and $PhCH_2Li$ (3.5 equiv) were reacted for 2 h. 2-Benzyl-1,1,3,3-tetramethyl-2-indanselenol (**7**, R=CH_2Ph; 86%): ^1H NMR δ=−0.5 (s, 1H), 1.5 (s, 6H), 1.6 (s, 6H), 3.3 (s, 2H), 7.0—7.6 (m, 9H); MS *m/z* (rel intensity) 344 (M^+, 2), 263 (20), 247 (12), 171 (8), 157 (8), 91 (65), 74 (64), 59 (100).

With PhLi. **3** (156 mg, 0.620 mmol) was reacted with PhLi (3 equiv) for 30 min. 1,1,3,3-Tetramethyl-2-indanyl phenyl selenide (**8**, R=Ph; 47%): mp 77.0—78.0 °C. ^1H NMR δ=1.31 (s, 6H), 1.32 (s, 6H), 3.49 (s, 1H), 7.1—7.8 (m, 9H); ^{13}C NMR δ=28.5, 28.7, 46.5, 70.9, 122.6, 126.9, 127.1, 129.0, 131.3, 134.2, 149.2; ^{77}Se NMR δ=234; MS *m/z* (rel intensity) 330 (M^+, 24), 173 (100), 158 (11), 131 (75), 99 (8), 91 (29), 85 (14), 71 (17), 57 (61). Found: *m/z* 330.0842. Calcd for $C_{19}H_{22}{}^{80}Se$: M, 330.0884.

With PhMgBr. The reaction of **3** (64 mg, 0.26 mmol) with PhMgBr (2 equiv) was so slow that 1 and 2 equiv. of PhMgBr were added after 7 and 18 h, respectively, and the mixture was warmed at 35 °C for 2 h. **8** (R=Ph) (2.4 mg, 3%) and **9** (6.3 mg, 14%) were obtained.

Preparation of 1,1,3,3-Tetramethyl-2-indanthione (13). **13** was prepared by the reaction of 1,1,3,3-tetramethyl-2-indanone hydrazone (1.04 g, 5.13 mmol) with disulfur dichloride (0.726 g, 5.38 mmol) in benzene.[10] Yield: 0.87 g (83%). Orange crystals; mp 38—43 °C (lit,[7c] 42 °C); ^1H NMR δ=1.47 (s, 12H), 7.31 (s, 4H);[7c] IR (KBr) 1100 cm^{-1}(C=S).

Reactions of 13 with Organolithium Reagents. The reactions were carried out in a similar manner to that described in the reactions of **3** with organometallic reagents.

With MeLi. **13** (102 mg, 0.498 mmol) was reacted with MeLi (3 equiv) for 30 min. 1,1,2,3,3-Pentamethyl-2-indanthiol (**14**, R=CH_3) (100 mg, 91%) was obtained: colorless oil, ^1H NMR δ=1.22 (s, 3H), 1.28 (s, 6H), 1.39 (s, 6H), 7.12—7.20 (br s, 4H); IR (neat) 2585 cm^{-1} (S-H).

With *t*-BuLi. **13** (124 mg, 0.606 mmol) and *t*-BuLi (3 equiv) were reacted for 12 h to give 1,1,3,3-tetramethyl-2-indanethiol (**16**) (40%, 57% based on the consumed thione) and recovered **13** (30%). **16**: mp 33.0—34.5 °C. MS *m/z* (rel intensity) 206 (M^+, 20), 173 (100), 157 (48). Found: *m/z* 206.1136. Calcd for $C_{13}H_{18}S$: M, 206.1129.

With $PhCH_2Li$. **13** (125 mg, 0.610 mmol) and $PhCH_2Li$ (3 equiv) were reacted for 3 h. 2-Benzyl-1,1,3,3-tetramethyl-2-indanethiol (**14**, R=CH_2Ph) (172 mg, 95%): mp 99.0—100.5 °C; ^1H NMR δ=1.1 (s, 1H), 1.4 (s, 6H), 1.6 (s, 6H), 3.1 (s, 2H), 6.9—7.5 (m, 9H); MS *m/z* (rel intensity) 296 (M^+, 2), 262 (45), 247 (52), 232 (8), 204 (23), 171 (67), 157 (21), 91 (100). Found: *m/z* 296.1603. Calcd for $C_{20}H_{24}S$: M, 296.1598.

With PhLi. **13** (165 mg, 0.809 mmol) was reacted with PhLi (3 equiv) for 4 h. 1,1,3,3-Tetramethyl-2-phenyl-2-indanethiol (**14**, R=Ph) (56%) and 1,1,3,3-tetramethyl-2-indanyl phenyl sulfide (**15**, R=Ph) (24%) were obtained. **14** (R=Ph): mp 87.8—89.2 °C; ^1H NMR δ=0.96 (s, 6H), 1.55 (s, 6H), 1.64 (s, 1H), 6.95—7.66 (m, 9H); MS *m/z* (rel intensity) 282 (M^+, 8), 267 (4), 249 (100), 233 (75), 218 (31), 202 (15), 159 (24), 105 (54), 91 (19). Found: *m/z* 282.1437. Calcd for $C_{19}H_{22}S$: M, 282.1442. **15** (R=Ph): ^1H NMR ($CDCl_3$) δ=1.31 (s, 12H), 3.46 (s, 1H), 6.95—7.66 (m, 9H); (C_6D_6) δ=1.27 (s, 6H), 1.36 (s, 6H), 3.49 (s, 1H), 6.87—7.63 (m, 9H).

References

1) D. L. J. Clive, *Tetrahedron*, **34**, 1049 (1978); H. J. Reich, *Acc. Chem. Res.*, **12**, 22 (1979); D. Liotta, *Acc. Chem. Res.*, **17**, 28 (1984); "The Chemistry of Organic Selenium and

Tellurium Compounds," ed by S. Patai and Z. Rapport, John Wiley & Sons, New York (1986), Vol. 1; C. Paulmier, "Selenium Reagents and Intermediates in Organic Synthesis," Pergamon Press, Oxford (1986).

2) a) T. G. Back, D. H. R. Barton, M. R. Britten-Kelly, and F. S. Guziec, Jr., *J. Chem. Soc., Perkin Trans. 1*, **1976**, 2079; b) F. S. Guziec, Jr. and C. J. Murphy, *J. Org. Chem.*, **45**, 2890 (1980); c) A. Krebs, W. Rüger, and W.-U. Nickel, *Tetrahedron Lett.*, **22**, 4937 (1981); d) E. R. Cullen, F. S. Guziec, Jr., and C. J. Murphy, *J. Org. Chem.*, **47**, 3563 (1982).

3) a) E. R. Cullen, F. S. Guziec, Jr., C. J. Murphy, T. C. Wong, and K. K. Andersen, *J. Am. Chem. Soc.*, **103**, 7055 (1981); b) *J. Chem. Soc., Perkin Trans. 2*, **1982**, 473; c) K. K. Andersen, D. M. Gash, and J. D. Robertson, *Tetrahedron Lett.*, **23**, 911 (1982); d) T. C. Wong, F. S. Guziec, Jr., and C. A. Moustakis, *J. Chem. Soc., Perkin Trans. 2*, **1983**, 1471.

4) R. Okazaki, A. Ishii, and N. Inamoto, *J. Chem. Soc., Chem. Commun.*, **1983**, 1429.

5) K. Steliou and M. Mrani, *J. Am. Chem. Soc.*, **104**, 3104 (1982).

6) F. S. Guziec, Jr. and C. A. Moustakis, *J. Org. Chem.*, **49**, 189 (1984).

7) a) J. C. Scaiano and K. U. Ingold, *J. Phys. Chem.*, **80**, 1901 (1976); *J. Am. Chem. Soc.*, **99**, 2079 (1977); b) B. J. Mckinnon, P. de Mayo, N. C. Payne, and B. Ruge, *Nouv. J. Chem.*, **2**, 91 (1978); N. Y. M. Fung, P. de Mayo, B. Ruge, A. C. Weedon, and S. K. Wong, *Can. J. Chem.*, **58**, 6 (1980); c) C.-P. Klages and J. Voβ, *Chem. Ber.*, **113**, 2255 (1980); d) F. S. Guziec, Jr. and C. A. Moustakis, *J. Chem. Soc., Chem. Commun.*, **1984**, 63.

8) a) Specialist Periodical Reports, "Organic Compounds of Sulfur, Selenium, and Tellurium," Vols. 1—6. The Chemical Society (1970—1981); b) F. Duus, "Comprehensive Organic Chemistry," ed by D. H. R. Barton and W. D. Ollis, Pergamon Press, New York (1978), Vol. 3, p. 373; c) K. Nakamura and A. Ohno, *Kagaku No Ryoiki*, **32**, 74 (1978).

9) A preliminary communication, R. Okazaki, A. Ishii, and N. Inamoto, *Tetrahedron Lett.*, **25**, 5147 (1984). See also Ref. 4.

10) R. Okazaki, K. Inoue, and N. Inamoto, *Bull. Chem. Soc. Jpn.*, **54**, 3541 (1981).

11) A. Ohno, K. Nakamura, Y. Shizume, and S. Oka, *Bull. Chem. Soc. Jpn.*, **50**, 1003 (1977); P. Beak and J. W. Worley, *J. Am. Chem. Soc.*, **94**, 597 (1972).

12) A. Ishii, R. Okazaki, and N. Inamoto, *Bull. Chem. Soc. Jpn.*, **59**, 2529 (1986).

13) "Handbook of Preparative Inorganic Chemistry," 2nd ed, ed by G. Brauer, Academic Press, New York, London (1963), Vol. 1, p. 422.

14) J. H. Wieringa, H. Wynberg, and J. Strating, *Tetrahedron*, **30**, 3053 (1974).

15) D. H. R. Barton, F. S. Guziec, Jr., and I. Shahak, *J. Chem. Soc., Perkin Trans. 1*, **1974**, 1794.

16) T. G. Back, D. H. R. Barton, M. R. Britten-Kelly, and F. S. Guziec, Jr., *J. Chem. Soc., Chem. Commun.*, **1975**, 539.

17) J. Buddrus, *Chem. Ber.*, **101**, 4152 (1968).

 © 1988 The Chemical Society of Japan Bull. Chem. Soc. Jpn., 61, 869—878 (1988)

Enantioselectivity in the Biotransformation of Mono- and Bicyclic Monoterpenoids with the Cultured Cells of *Nicotiana tabacum*

Hiroki HAMADA
Department of Fundamental Natural Science, Okayama University of Science, Ridai-cho, Okayama 700
(Received June 29, 1987)

The biotransformation of the enantiomeric pairs of *p*-menthane and bicyclo[2.2.1] and [3.1.1]heptane derivatives with the cultured cells of *Nicotiana tabacum* was investigated. It was found that (i) the cultured cells discriminate the enantiomers of *p*-menthan-2-ol and bicyclo[2.2.1]heptan-2-ol and bicyclo[3.1.1]heptan-3-ol derivatives, and enantioselectively convert these alcohols to the corresponding ketones, (ii) the cells reduce the carbonyl group of *p*-menthan-2-one derivatives to a high extent, but not that of *p*-menthan-3-ones, and (iii) the cells discriminate the enantiomers of bicyclo[3.1.1]hept-2-en-4-one (verbenone) and enantioselectively reduce the C-C double bond of the (1*S*,5*S*)-enantiomer.

The ability of cultured plant cells to metabolize foreign substrates and/or to convert these substrates to more useful substances is of considerable interest because of the specificity of the transformation which may be effected by such cells.[1-4] In such a status, many investigations on the biotransformation of the monoterpenoids[5-13] with the cultured cells of *Nicotiana tabacum* "Bright Yellow" are performed, and the cultured cells were found to not only reduce stereoselectively the C-C double bond adjacent to the carbonyl group of carvone and then the carbonyl group,[8,9] but also discriminate the enantiomers of monoterpene acetates and enantioselectively hydrolize one of the enantiomers.[6,12] The author has now investigated the enantioselectivity in the oxidative and reductive transformations of the enantiomeric pairs of mono- and bicyclic monoterpenoids, such as *p*-menthane and bicyclo[2.2.1] and bicyclo[3.1.1]heptane derivatives, with the cultured cells of *N. tabacum*.[14]

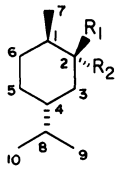

1a: R_1=H, R_2=OH
2a: R_1=OH, R_2=H
13a: R_1,R_2=O

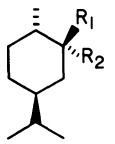

1b: R_1=OH, R_2=H
2b: R_1=H, R_2=OH
13b: R_1,R_2=O

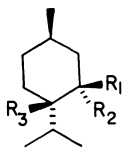

3a: R_1=OH, R_2,R_3=H
4a: R_1,R_3=H, R_2=OH
14a: R_1,R_2=O, R_3=H
23a: R_1,R_2=O, R_3=OH

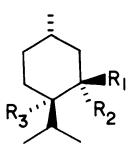

3b: R_1,R_3=H, R_2=OH
4b: R_1=OH, R_2,R_3=H
14b: R_1,R_2=O, R_3=H
23b: R_1,R_2=O, R_3=OH

5a: R_1=H, R_2=OH
6a: R_1=OH, R_2=H
15a: R_1,R_2=O

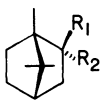

5b: R_1=H, R_2=OH
6b: R_1=OH, R_2=H
15b: R_1,R_2=O

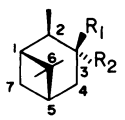

7a: R_1=H, R_2=OH
8a: R_1=OH, R_2=H
16a: R_1,R_2=O

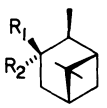

7b: R_1=H, R_2=OH
8b: R_1=OH, R_2=H
16b: R_1,R_2=O

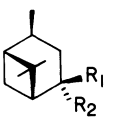

9a: R_1=OH, R_2=H
17a: R_1,R_2=O

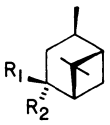

9b: R_1=OH, R_2=H
17b: R_1,R_2=O

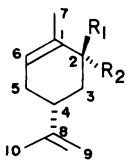

10a: R_1=H, R_2=OH
11a: R_1=OH, R_2=H
22a: R_1,R_2=O

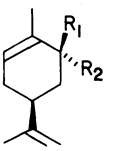

10b: R_1=OH, R_2=H
11b: R_1=H, R_2=OH
22b: R_1,R_2=O

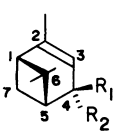

12a: R_1=OH, R_2=H
18a: R_1,R_2=O

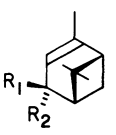

12b: R_1=OH, R_2=H
18b: R_1,R_2=O

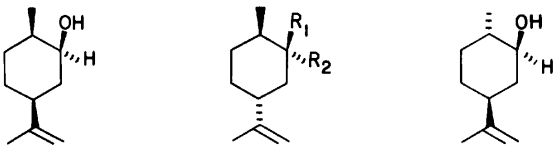

19 20: R_1=OH, R_2=H 25
21: R_1,R_2=O

24a 24b

Results and Discussion

The same tobacco callus tissues induced from the stem of *N. tabacum* "Bright Yellow" as those used in our previous works were also used in this investigation. The callus tissues, just prior to use, were transplanted to the freshly prepared Murashige and Skoog's medium[18] containing 2 ppm of 2,4-dichlorophenoxyacetic acid as auxin and 3% of sucrose and then were grown with continuous shaking for 2—3 weeks at 25 °C in the dark. To these cultured cells, the filter-sterilized monoterpenoid was administered, and then the cultures were incubated at 25 °C for 7—10 d in a shaker. At a regular time interval, a part of the incubation mixture (suspension of cells and medium) was withdrawn with a pipette under sterile conditions and extracted with ether. Each ether extract, after removal of the solvent, was subjected to the GLC analysis to study the time-courses in the biotransformation of the enantiomeric pairs of the monoterpenoids.

Enantioselectivity in the Oxidation of the Secondary Alcohols. Enantioselectivity in the oxidation of monoterpenoids having a secondary hydroxyl group was examined with the enantiomeric pairs of 2- and 3-hydroxylated *p*-menthane derivatives, 2-hydroxylated bicyclo[2.2.1]heptane derivatives, and 3- and 4-hydroxylated bicyclo[3.1.1]heptane derivatives, such as (1*R*,2*R*,4*R*)-(−)- and (1*S*,2*S*,4*S*)-(+)-carvomenthols (**1a** and **1b**), (1*R*,2*S*,4*R*)-(+)- and (1*S*,2*R*,4*S*)-(−)-neocarvomenthols (**2a** and **2b**), (1*R*,3*R*,4*S*)-(−)- and (1*S*,3*S*,4*R*)-(+)-menthols (**3a** and **3b**), (1*R*,3*S*,4*S*)-(+)- and (1*S*,3*R*,4*R*)-(−)-neomenthols (**4a** and **4b**), (1*R*,2*S*,4*R*)-(+)- and (1*S*,2*R*,4*S*)-(−)-borneols (**5a** and **5b**), (1*R*,2*R*,4*R*)-(−)- and (1*S*,2*S*,4*S*)-(+)-isoborneols (**6a** and **6b**), (1*R*,2*R*,3*R*,5*S*)-(−)- and (1*S*,2*S*,3*S*,5*R*)-(+)-

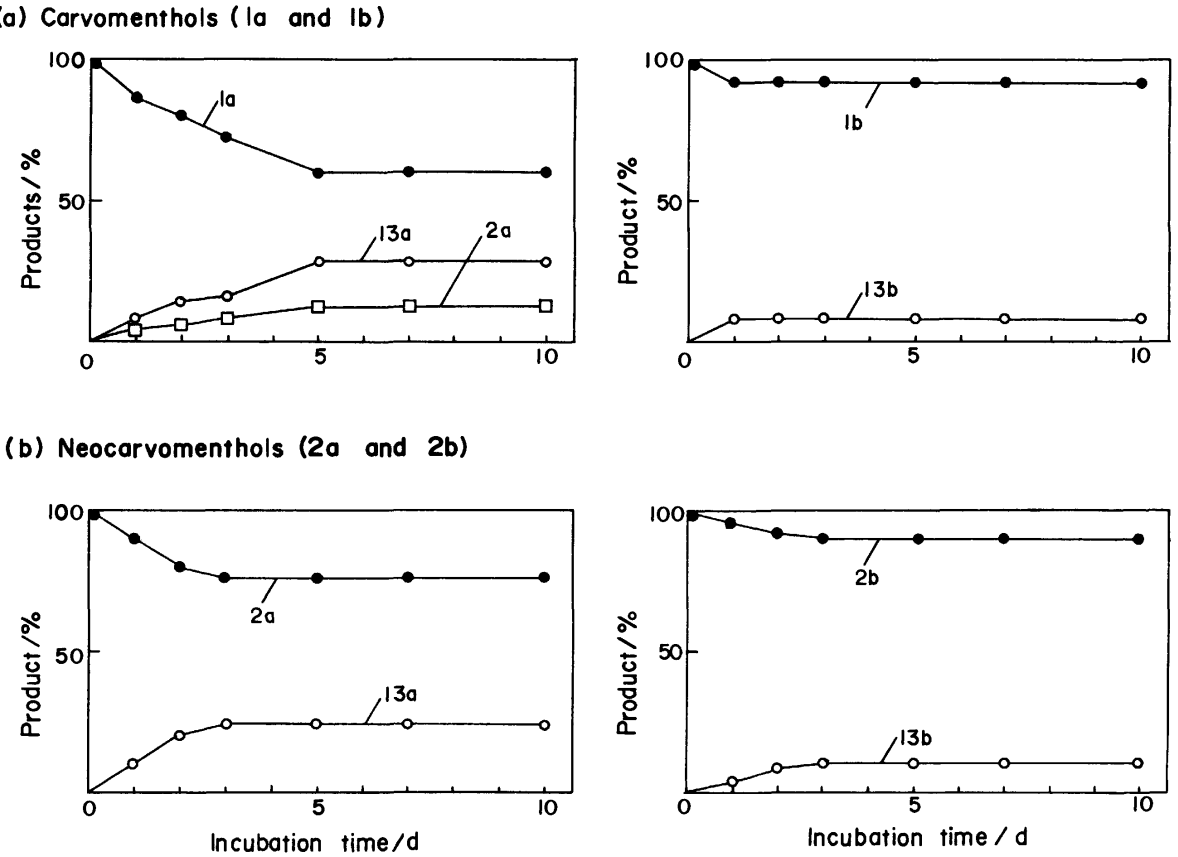

Fig. 1. The time-courses in the biotransformation of the enantiomeric pairs of (a) carvomenthols (**1a** and **1b**) and (b) neocarvomenthols (**2a** and **2b**).

isopinocampheols (**7a** and **7b**), (1*R*,2*R*,3*S*,5*S*)-(+)- and (1*S*,2*S*,3*R*,5*R*)-(−)-neoisopinocampheols (**8a** and **8b**) and (1*R*,2*S*,4*R*,5*R*)-(+)- and (1*S*,2*R*,4*S*,5*S*)-(−)-neoisoverbanols (**9a** and **9b**).

As shown in Fig. 1, the *p*-menthan-2-ols, **1a** and **2a**, were converted to (1*R*,4*R*)-(+)-carvomenthone (**13a**), whereas their enantiomers, **1b** and **2b**, were scarcely converted to the corresponding ketone **13b**. The biotransformation of **1a** gave, in addition to **13a**, (+)-neocarvomenthol (**2a**) as a minor product; the formation of **2a** may be caused by further reductive conversion of (+)-carvomenthone (**13a**). In the biotransformation of enantiomeric pairs of the *p*-menthan-3-ols, on the other hand, not only (1*R*,3*R*,4*S*)-(−)-menthol (**3a**) and (1*R*,3*S*,4*S*)-(+)-neomenthol (**4a**), but also their enantiomers, **3b** and **4b**, were scarcely converted to their corresponding ketones, **14a** and **14b**.

Figure 2 shows the time-courses in the biotransformation of the bicyclo[2.2.1]heptan-2-ols, such as borneols (**5a** and **5b**) and isoborneols (**6a** and **6b**). (1*R*,2*S*,4*R*)-(+)-Borneol (**5a**) and (1*R*,2*R*,4*R*)-(−)-isoborneol (**6a**) were quantitatively converted to (1*R*,4*R*)-(+)-camphor (**15a**), whereas the conversion of their enantiomers, **5b** and **6b**, to (1*S*,4*R*)-(−)-camphor (**15b**) occurred to a slight extent. Such an enantioselective transformation was further confirmed by feeding experiments of the racemic substrates of borneol (**5**) and isoborneol (**6**). After incubation of the racemic substrates with the cultured cells, the product and the unchanged substrate in the incubation mixture were separated from each other and then their optical

Table 1. Enantioselective Transformation of (±)-Borneol (**5**) and (±)-Isoborneol (**6**) into (+)-Camphor (**15a**) with the Cultured Cells of *N. tabacum*

Substrate used	**15a**			**5b** and **6b** recovered		
	$[\alpha]_D^{25}$/°	(*c*, solv.)	O.p.[a]	$[\alpha]_D^{25}$/°	(*c*, solv.)	O.p.[a]
(±)-Borneol (**5**)	+40.7	(1.4, EtOH)	92.1	−36.4	(0.6, EtOH)	95.5
(±)-Isoborneol (**6**)	+40.1	(1.0, EtOH)	90.7	+32.5	(2.0, EtOH)	94.8

a) O.p. denotes the optical purity (e. e. %), which was calculated on the basis of the specific rotation cited in the literature.[28]

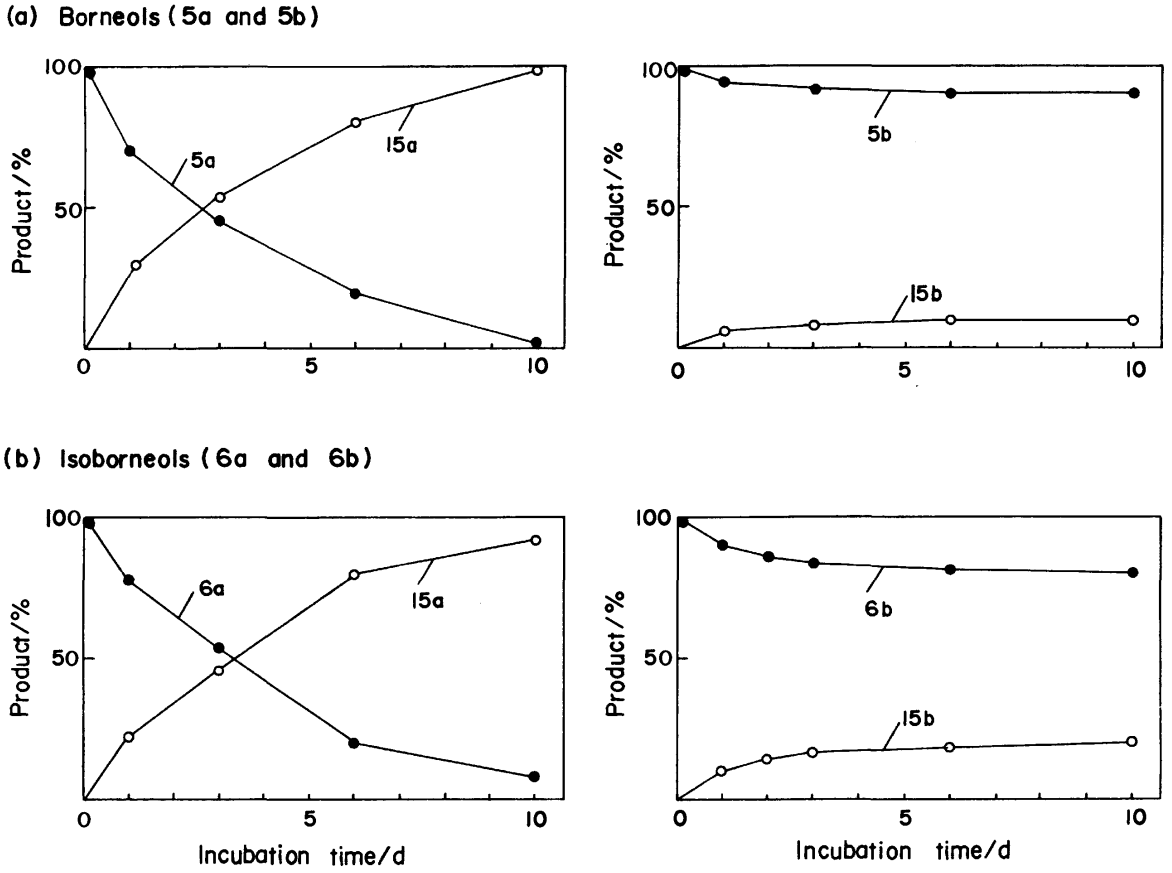

Fig. 2. The time-courses in the biotransformation of the enantiomeric pairs of (a) borneols (**5a** and **5b**) and (b) isoborneols (**6a** and **6b**).

purities were determined. The data given in Table 1 indicates that one enantiomer in the racemate was selectively susceptible to the oxidation with the cultured cells; (+)-borneol (**5a**) and (−)-isoborneol (**6a**) quantitatively transformed into (+)-camphor (**15a**), but their enantiomers remain unchanged.

The time-courses in the biotransformation of bicyclo[3.1.1]heptan-3-ols and -4-ols are shown in Figs. 3 and 4. (1*S*,2*S*,3*S*,5*R*)-(+)-isopinocampheol (**7b**) and (1*S*,2*S*,3*R*,5*R*)-(−)-neoisopinocampheol (**8b**) were quantitatively converted to (1*S*,2*S*,5*R*)-(−)-isopinocamphone (**16b**). However, their enantiomer, **7a** and **8a**, was hardly converted to their corresponding ketone. On the other hand, both enantiomers, **9a** and **9b**, of neoisoverbanol were quantitatively converted to their corresponding ketones **17a** and **17b**, respectively (Fig. 4).

Enantioselectivity in the Oxidation of the Allylic Alcohols. Enantioselectivity in the oxidation of monoterpenoids having an allylic hydroxyl group was

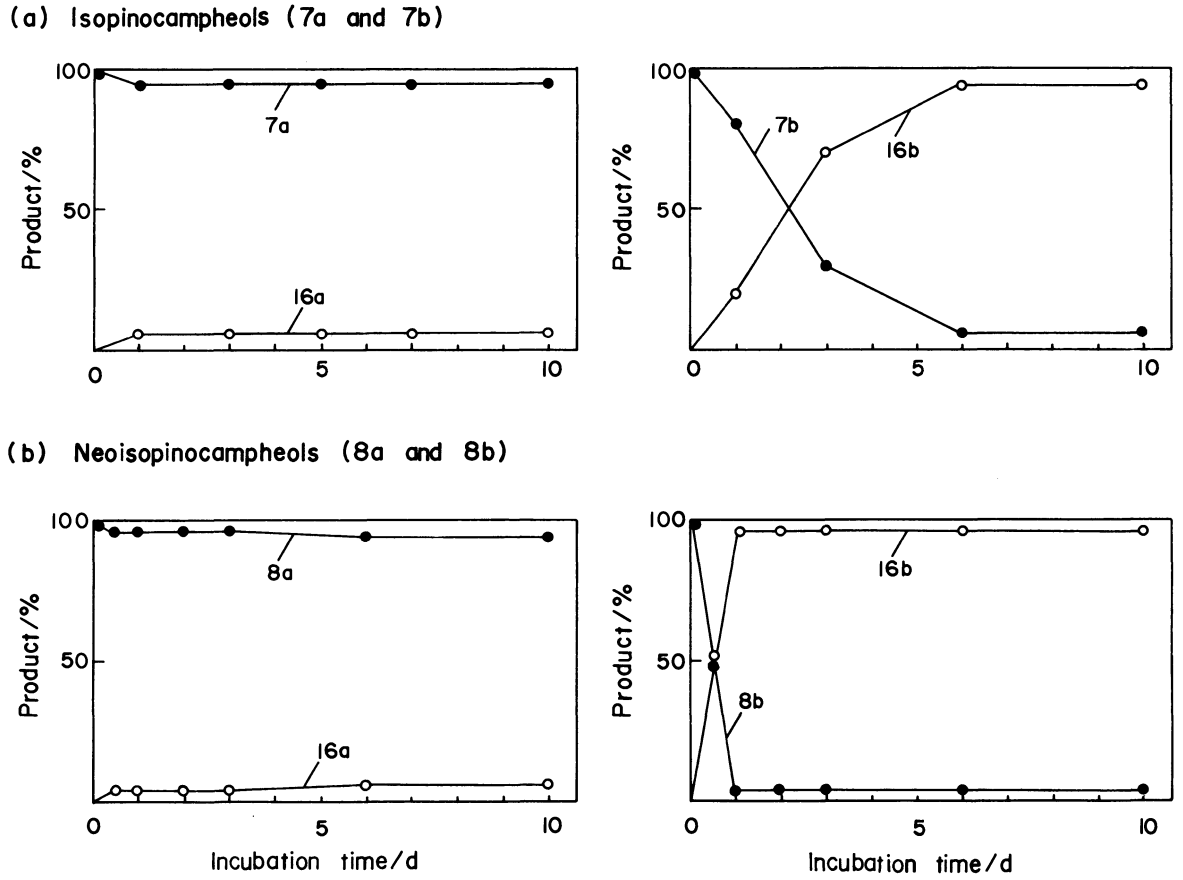

Fig. 3. The time-courses in the biotransformation of the enantiomeric pairs of (a) isopinocampheols (**7a** and **7b**) and (b) neoisopinocampheols (**8a** and **8b**).

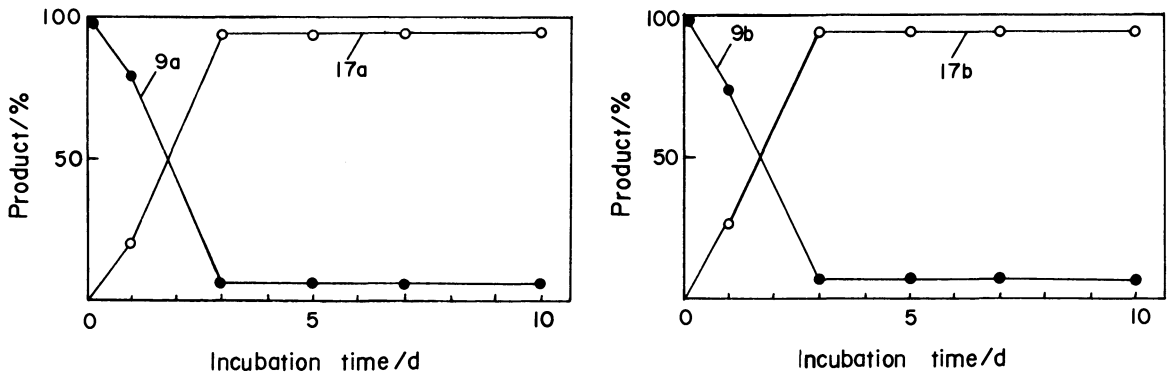

Fig. 4. The time-courses in the biotransformation of the enantiomeric pairs of neoisoverbanols (**9a** and **9b**).

examined with the enantiomeric pairs of 2-hydroxylated *p*-menthene derivatives and 4-hydroxylated bicyclo[3.1.1]heptene derivatives, such as (2*R*,4*R*)-(−)- and (2*S*,4*S*)-(+)-*cis*-carveols (**10a** and **10b**), (2*S*,4*R*)-(−)- and (2*R*,4*S*)-(+)-*trans*-carveols (**11a** and **11b**), and (1*R*,4*R*,5*R*)-(+)- and (1*S*,4*S*,5*S*)-(−)-*cis*-verbenols (**12a** and **12b**). Figure 5 shows the time-courses in the biotransformation of enantiomeric pairs of *cis*-carveol (**10a** and **10b**) and *trans*-carveol (**11a** and **11b**). The (2*S*,4*S*)-*cis*- and (2*S*,4*R*)-*trans*-carveols (**10b** and **11a**) were converted to the corresponding ketones **22b** and **22a** to a large extent, respectively, whereas the conversion of their enantiomers **10a** and **11b** to their corresponding ketones **22a** and **22b** occurred to a slight extent. These facts indicate that the cultured cells preferentially oxidize the allylic alcohols having the chirality of *S* at C-2 and this oxidation is independent of the chirality at C-4. In the biotransformation of *cis*-carveol (**10b**) a remarkable increase in the formation of neoisodihydrocarveol (**19**) after 3 d incubation was observed. However, it is not clear whether this formation was caused by the

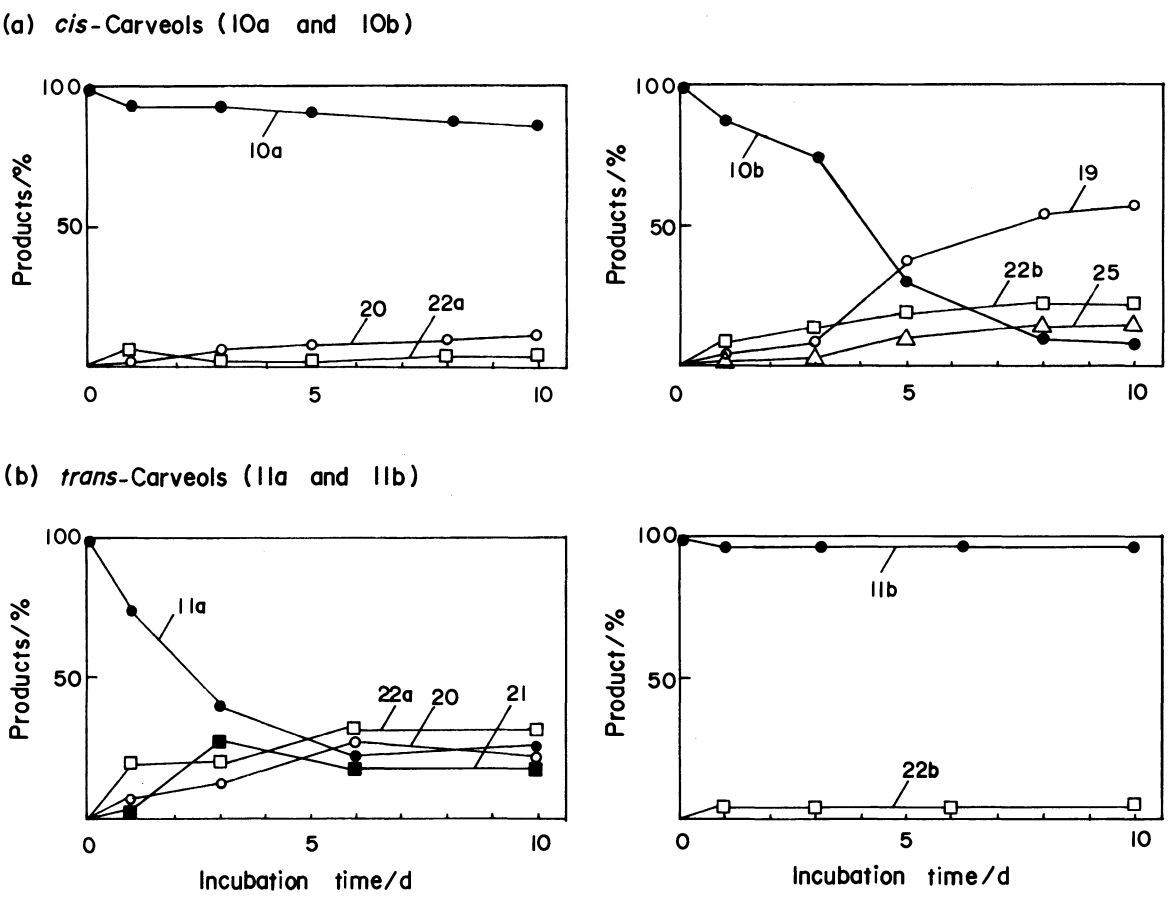

Fig. 5. The time-courses in the biotransformation of the enantiomeric pairs of (a) *cis*-carveols (**10a** and **10b**) and (b) *trans*-carveols (**11a** and **11b**).

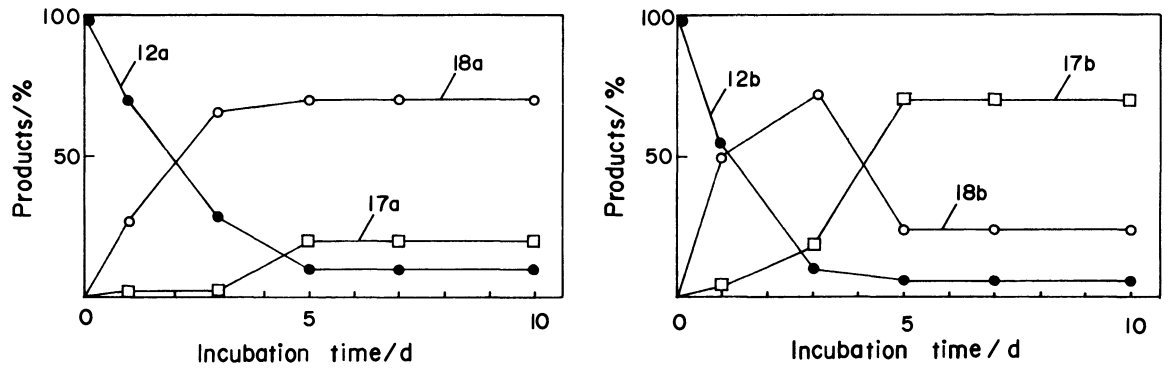

Fig. 6. The time-courses in the biotransformation of the enantiomeric pairs of *cis*-verbenols (**12a** and **12b**).

reduction of carvone (**22b**) produced or by the direct reduction of the C–C double bond of *cis*-carveol (**10b**). The time-courses in the biotransformation of enantiomeric pairs of *cis*-verbenol (**12a** and **12b**) are shown in Fig. 6. Both enantiomers were quantitatively transformed to their corresponding ketones **18a** and **18b** respectively, after 3 day's incubation. In the biotransformation of **12b**, the product **18b** was formed in high yield in the early stage of the incubation, but **18b** decreased after 3 d with a gradual increase in the formation of (1*S*,2*R*,5*S*)-*cis*-verbanone (**17b**). Such further transformation occurred to a small extent in the case of **12a**. Accordingly, in the biotransformation of the monoterpenoids having an allylic hydroxyl group, this hydroxyl group is enantioselectively oxidized to the carbonyl group and then the C–C double bond adjacent to the carbonyl group of α,β-unsaturated carbonyl compounds produced is stereoselectively hydrogenated to a saturated carbonyl compounds. However, the C–C double bond in the 1-methylethenyl group is not at all hydrogenated.

Enantioselectivity in the Reduction of the Carbonyl Compounds. Enantioselectivity in the reduction of monoterpenoids having a carbonyl group was examined with the enantiomeric pairs of *p*-menthan-2-one and -3-one derivatives and bicyclo[2.2.1]heptan-2-one and bicyclo[3.1.1]heptan-3-one and -4-one derivatives, such as (1*R*,4*R*)-(+)- and (1*S*,4*S*)-(−)-carvomenthones (**13a** and **13b**), (1*R*,4*S*)-(−)- and (1*S*,4*R*)-(+)-menthones (**14a** and **14b**), (1*R*,4*R*)-(+)- and (1*S*,4*S*)-(−)-camphors (**15a** and **15b**), (1*R*,2*R*,5*S*)-(+)- and (1*S*,2*S*,5*R*)-isopinocamphones (**16a** and **16b**), and (1*R*,2*S*,5*R*)-(+)- and (1*S*,2*R*,5*S*)-(−)-*cis*-verbanones (**17a** and **17b**). The time-courses in the biotransformation of carvomenthones (**13a** and **13b**) and menthones (**14a** and **14b**) are shown in Figs. 7 and 8. (1*R*,4*R*)-(+)-Carvomenthone (**13a**) was quantitatively converted to (1*R*,2*S*,4*R*)-(+)-neocarvomenthol (**2a**), whereas its (1*S*,4*S*)-(−)-enantiomer **13b** was converted to (1*S*,2*S*,4*S*)-(+)-carvomenthol (**1b**) and (1*S*,2*R*,4*S*)-(−)-neocarvomenthol (**2b**) in a ratio of 2:1. The preferential formation of (+)-neocarvomenthol (**2a**) and (+)-carvomenthol (**1b**) indicates that the carvomenthones (**13a** and **13b**) are stereospecifically reduced to the hydroxy compounds with the chirarity of *S* at the C-2. The extent of the stereoselectivity in the reduction of the enantiomers was different each other; the selectivity was very high for the reduction of (1*R*,4*R*)-carvomenthone (**13a**), but low for that of the enantiomer **13b**. On the other hand, the biotransformation of (1*R*,4*S*)-(−)- and (1*S*,4*R*)-(+)-menthones (**14a** and **14b**) gave (1*R*,4*R*)- and (1*S*,4*S*)-4-hydroxy-*p*-menthan-3-ones (**23a** and **23b**), respectively,[19] in addition to isomenthones (**24a** and **24b**) and menthols (**3b**, **4a**, and **4b**) (Fig. 8). The time-course experiments show that the reduction of the carbonyl group of

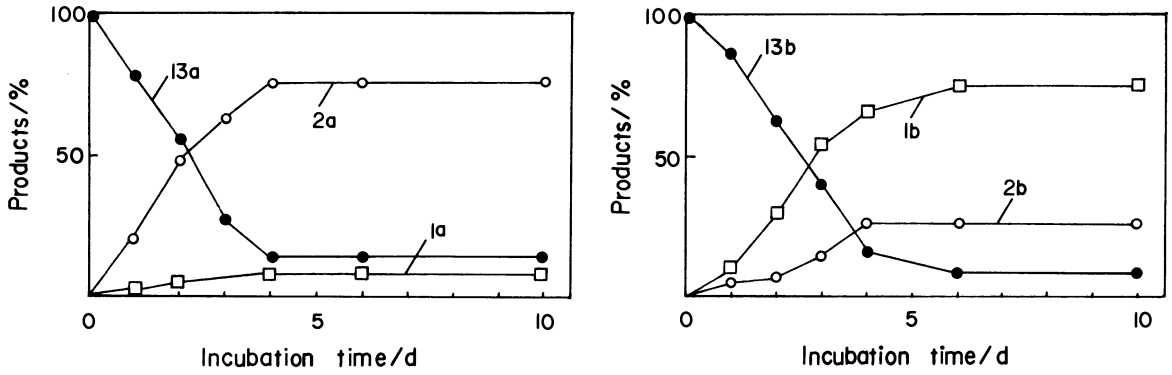

Fig. 7. The time-courses in the biotransformation of the enantiomeric pairs of carvomenthones (**13a** and **13b**).

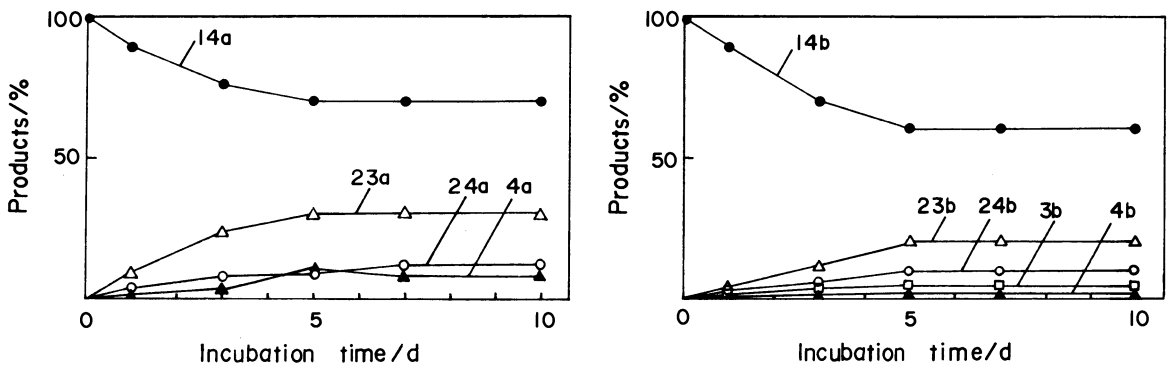

Fig. 8. The time-courses in the biotransformation of the enantiomeric pairs of menthones (**14a** and **14b**).

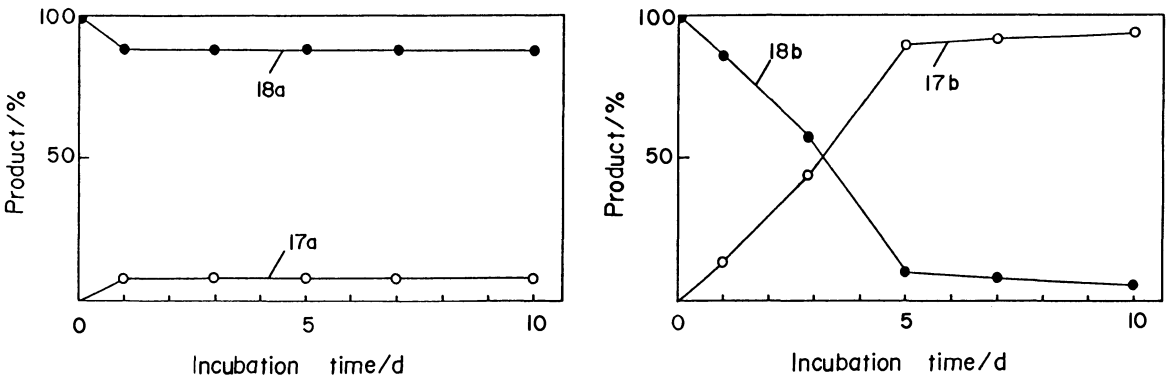

Fig. 9. The time-courses in the biotransformation of the enantiomeric pairs of verbenones (**18a** and **18b**).

menthones (**14a** and **14b**) occurred to a slight extent. This low conversion, as compared with the case of *p*-menthan-2-ones, **1a** and **1b**, may be caused by the steric hindrance owing to the 1-methyl ethyl group adjacent to the carbonyl group. On the other hand, (1*R*,4*R*)-(+)- and (1*S*,4*S*)-(−)-camphors (**15a** and **15b**), (1*R*,2*R*,5*S*)-(+)- and (1*S*,2*S*,5*R*)-(−)-isopinocamphones (**16a** and **16b**), and (1*R*,2*S*,5*R*)-(+)- and (1*S*,2*R*,5*S*)-(−)-*cis*-verbanones (**17a** and **17b**) were scarcely converted to their corresponding alcohols. These results may be explained by assuming that the balance of the equilibrium between the ketones and the corresponding alcohols in the oxidoreduction in the cultured cells is predicted to lie toward the side of the ketones.[10]

Enantioselectivity in the Reduction of the C–C Double Bond of α,β-Unsaturated Carbonyl Compounds. Enantioselectivity in the reduction of the C–C double bond of monoterpenoids having an α,β-unsaturated carbonyl group was examined with the enantiomeric pairs of bicyclo[3.1.1]hept-2-en-4-ones, such as (1*R*,5*R*)-(+)- and (1*S*,5*S*)-(−)-verbenones (**18a** and **18b**). Figure 9 shows the time-courses in the biotransformation of (1*R*,5*R*)-(+)-verbenone (**18a**) and its enantiomer **18b**. The (1*S*,5*S*)-enantiomer **18b** was quantitatively converted to (1*S*,2*R*,5*S*)-(−)-*cis*-verbanone (**17b**) after 10 d incubation, whereas the conversion of (1*R*,5*R*)-enantiomer **18a** to the corresponding ketone **17a** scarecely occurred. These facts indicate that the cultured cells discriminate the enantiomers and reduce the C–C double bond of the (1*S*,5*S*)-enantiomer **18b**. In addition, the hydrogenation of **18b** with the cultured cells gave only *cis*-verbanone (**17b**), but not its trans-isomer. This indicates that the hydrogen attack to the C–C double bond of **18b** stereospecifically occurs from the *re*-face at C-2 of **18b**. No further conversion of the *cis*-verbanone (**17b**) into neoisoverbanol (**9b**) was observed. This may be explained by assuming that the balance of the equilibrium between **17b** and its corresponding alcohol **9b** in the oxidoreduction in the cultured cells is predicted to lie toward the side of the *cis*-verbanone (**17b**), because the equilibrium constant in the oxidoreduction of **9b**⇄**17b** is estimated to be about 1.4 on the basis of the ^{13}C NMR chemical shift (δ 214.1) of the carbonyl carbon of **17b**.[10]

Concluding Remarks. The enantioselectivity in the oxidative and reductive transformation of the enantiomeric pairs of *p*-menthane and bicyclo[2.2.1] and bicyclo[3.1.1]heptane derivatives with the cultured cells of *N. tabacum* was established as follows. (i) The cultured cells discriminated the enantiomers of *p*-menthan-2-ols, bicyclo[2.2.1]heptan-2-ols, and bicyclo[3.1.1]heptan-3-ols, and enantioselectively oxidized these secondary alcohols, but this was not the case for the *p*-menthan-3-ols and bicyclo[3.1.1]heptan-4-ols. (ii) In the case of allylic alcohols, also, the cultured cells discriminated the enantiomers of 6-*p*-menthen-2-ols, and enantioselectively oxidized these allylic alcohols, but this was not the case for the bicyclo[3.1.1]hept-2-en-4-ol. (iii) The cultured cells discriminated the enantiomers of *p*-menthan-2-ones in their reductive conversion to the corresponding hydroxy compounds, but this was not the case for the *p*-menthan-3-ones. The hydrogen attack in the reduction took place preferentially from the *re*-face of the carbonyl group to give the alcohols with the chirality of *S* at the position bearing the hydroxyl group. (iv) The cultured cells discriminated the enantiomers of bicyclo[3.1.1]hept-2-en-4-one, and enantioselectively reduced its C–C double bond. The hydrogen attack in the hydrogenation took place stereospecifically from the *re*-face of the C–C double bond.

Thus, the main finding in the oxidative and reductive transformation is that the enantioselective transformation takes place for the only substrate having the methyl group on the vicinal position of the functional group.

Experimental

Analytical and preparative TLC were carried out on 0.25-mm and 0.5-mm thick silica-gel plates (Merck silica gel 60,

GF_{254}), respectively. GLC analyses were performed on an instrument equipped with FID and a glass column (3 mm×2 m) packed with 15% DEGS, 5% PEG-20M, and 2% OV-17 on Chromosorb W (AW-DMCS; 80—100 mesh) at 100, 120, and 90—200 °C (3 °C min^{-1}), respectively. ^1H NMR spectra were obtained at 60 and 90 MHz in $CDCl_3$ with TMS as an internal standared. GC-MS spectra were recorded on a mass spectrometer equipped with a gas chromatograph with 15% DEGS column (3 mm×2 m) by EI mode at 70 ev. The areas of the peaks on the gas liquid chromatogram were determined by using a Shimadzu C-R1B Chromatopac recording data processor for chromatography.

Substrates. (i) Monoterpene Alcohols. (1*R*,2*R*,4*R*)-(−)-Carvomenthol (**1a**) was prepared from (−)-dihydrocarveols[20] by hydrogenation in the presence of 10% Pd-C. The hydrogenation of (+)-neodihydrocarveol[20] in the presence of 10% Pd-C gave (1*R*,2*S*,4*R*)-(+)-neocarvomenthol (**2a**). (1*R*,3*R*,4*S*)-(−)-Menthol (**3a**) and its enantiomer **3b** were commercial materials of Aldrich Chem. Company. (1*R*,3*S*,4*S*)-(+)-Neomenthol (**4a**) was prepared from (−)-menthone[33] by reduction with $NaBH_4$. The reduction of (+)-camphor[28] with $LiAlH_4$ gave (1*R*,2*S*,4*R*)-(+)-borneol (**5a**) and (1*R*,2*R*,4*R*)-(−)-isoborneol (**6a**). (1*R*,2*R*,3*R*,5*S*)-(−)-Isopinocampheol (**7a**) was prepared by the hydroboration-oxidation of (+)-α-pinene.[21] The isopinocampheol (**7a**) was oxidized by pyridinium dichromate[23] to yield (+)-isopinocamphone,[21] which was reduced by $NaBH_4$ to give (1*R*,2*R*,3*S*,5*S*)-(+)-neoisopinocampheol (**8a**). (1*R*,2*S*,4*R*,5*R*)-(+)-Neoisoverbanol (**9a**) was prepared from (+)-*cis*-verbanone[34] by reduction with $LiAlH_4$. (2*R*,4*R*)-(−)-*cis*-Carveol (**10a**) and (2*S*,4*R*)-(−)-*trans*-carveol (**11a**) were prepared by the Meerwein-Pondorf reduction of (−)-carvone.[22] The reduction of (−)-verbenone[31] with $NaBH_4$ in MeOH at 0 °C gave (1*R*,4*R*,5*R*)-(−)-*cis*-verbenol (**12a**). On the other hand, the enantiomers of the alcohols described above were prepared from the corresponding compounds in the same manner as above.

(ii) Monoterpene Ketones. (1*R*,4*R*)-(+)-Carvomenthone (**13a**) was prepared from (+)-dihydrocarvone[20] by hydrogenation in the presence of 10% Pd-C. (1*R*,4*S*)-(−)-Menthone (**14a**) was prepared from (−)-menthol[26] by oxidation with pyridinium dichromate.[23] (1*R*,4*R*)-(+)-Camphor (**15a**) was prepared from (+)-borneol[28] by pyridinium dichromate oxidation.[23] Oxidation of (+)-neoisopinocampheol[21] with $Na_2Cr_2O_7$ gave (1*R*,2*R*,5*S*)-(+)-isopinocamphone (**16a**). (1*R*,2*S*,5*R*)-(+)-*cis*-Verbanone (**17a**) was prepared from (+)-verbenone[31] by hydrogenation in the presence of 10% Pd-C. (1*R*,5*R*)-(+)-Verbenone (**18a**) was prepared from (−)-α-pinene by oxidation with *t*-butyl chromate.[24] The enantiomers of the ketones described

Table 2. Physical Properties of the Substrates

Compound	Mp θ_m/°C	n_D^{25}	$[\alpha]_D^{25}$/°
1a		1.4628	−21.0 (*c* 1.0, MeOH) (lit,[25] −22.0)
1b		1.4624	+21.7 (*c* 1.8, MeOH)
2a		1.4647	+40.3 (*c* 1.5, MeOH) (lit,[25] +43.7)
2b		1.4643	−40.6 (*c* 2.0, MeOH)
3a			−49.3 (*c* 2.0, EtOH) (lit.,[26] −49.6)
3b			+48.7 (*c* 1.5, EtOH)
4a		1.4601	+20.1 (*c* 1.0, EtOH) (lit,[27] +19.6)
4b		1.4600	−20.7 (*c* 2.3, EtOH)
5a	201—202		+37.6 (*c* 1.0, EtOH) (lit,[28] +37.9)
5b			−37.1 (*c* 1.0, EtOH)
6a	210—211		−33.6 (*c* 1.0, EtOH) (lit,[28] −34.3)
6b			+34.1 (*c* 2.0, EtOH)
7a	55—57		−31.7 (*c* 0.8, C_6H_6) (lit,[21] −32.8)
7b			+30.1 (*c* 1.6, C_6H_6)
8a	45—47		+34.5 (*c* 1.3, C_6H_6) (lit,[21] +36.0)
8b			−33.8 (*c* 2.0, C_6H_6)
9a			+5.2 (*c* 1.3, C_6H_6) (lit,[29] +5.3)
9b			−5.0 (*c* 1.5, C_6H_6)
10a		1.4925	−21.5 (*c* 0.75, $CHCl_3$)
10b		1.4932	+22.1 (*c* 1.9, $CHCl_3$) (lit,[30] +23.9)
11a		1.4930	−207.0 (*c* 1.0, $CHCl_3$)
11b		1.4938	+210.2 (*c* 2.0, $CHCl_3$) (lit,[30] +213.1)
12a			+8.7 (*c* 1.0, $CHCl_3$) (lit,[31] +9.3)
12b			−8.3 (*c* 2.1, $CHCl_3$)
13a		1.4546	+5.9 (*c* 1.0, EtOH)
13b		1.4542	−5.3 (*c* 2.3, EtOH) (lit,[32] −6.0)
14a		1.4503	−27.3 (*c* 1.0, EtOH) (lit,[33] −29.9)
14b		1.4505	+28.0 (*c* 1.5, EtOH)
15a	174—175		+42.9 (*c* 1.1, EtOH) (lit,[28] +44.2)
15b			−42.6 (*c* 1.5, EtOH)
16a		1.4741	+11.2 (*c* 1.5, EtOH) (lit,[21] +10.5)
16b		1.4747	−10.0 (*c* 2.0, EtOH)
17a		1.4773	+55.3 (*c* 1.7, $CHCl_3$) (lit,[34] +52.5)
17b		1.4775	−53.3 (*c* 2.0, $CHCl_3$)
18a		1.4966	+210.5 (*c* 1.5, $CHCl_3$)
18b		1.4968	−209.3 (*c* 2.3, $CHCl_3$) (lit,[31] −208)

Table 3. Physical and Spectral Data of the Products

Compound	$[\alpha]_D^{25}$/°	^{1}H NMR in $CDCl_3$	m/z (rel intensity)
13	+6.4 (*c* 0.5, EtOH)	0.87 (3H, d, *J*=6.0 Hz, 1-Me) 0.97 (6H, 9,10-Me)	154 (M^+, 21), 111 ($M^+-CH(Me)_2$, 100), 83 (27), 69 (24)
15	+44.4 (*c* 1.1, EtOH)	0.86 (s, 8-Me), 0.92 (s, 9-Me) 0.98 (s, 10-Me)	152 (M^+, 40), 137 (M^+-Me, 7), 109 (30), 95 (100)
16	−9.9 (*c* 2.0, EtOH)	0.88 (s, 9-Me), 1.20 (d, *J*=6.0 Hz, 10-Me), 1.31 (s, 8-Me)	152 (M^+, 15), 110 ($M^+-C(Me)_2$, 13), 95 (30), 83 (78), 69 (90)
17	+53.2 (*c* 0.8, $CHCl_3$)	1.07 (3H, d, *J*=6.0 Hz, 7-Me), 1.23 (3H, s, 8-Me) 1.35 (3H, s, 9-Me)	152 (M^+, 10), 137 (M^+-Me, 10), 109 (27), 95 (48), 83 (100)

above were prepared from the corresponding alcohols in the same manner as above. All the samples were >99% pure by GLC, and these physical data are given in Table 2.

Feeding of the Monoterpenes to the Tobacco Cultured Cells. The callus tissues used in this study were induced from the stem of *N. tabacum* "Bright Yellow" and have been maintained for about 15 years.[5] Just prior to use for this work, a part of the callus tissuse as transplanted to freshly prepared Murashige and Skoog's medium[18] (100 cm^3 in a 300 cm^3-conical flask) containing 2 ppm of 2,4-dichlorophenoxyacetic acid and 3% sucrose and grown with continuous shaking for 2—3 weeks at 25 °C in the dark. The substrate (10 mg/flask) was added to the suspension cultures (about 50—70 g cells/flask) and the cultures were incubated at 25 °C for 7—10 d on a rotary shaker (70 rpm) in the dark.

Isolation and Identification of the Products. The incubation mixture was filtered and the mass obtained was triturated with MeOH. The MeOH extract was concentrated and extracted with ether. The culture medium filtered was extracted with ether. The two ether extracts were bulked, since they exhibited the same behavior on TLC and GLC. Transformation products were isolated from the extract by prep. TLC on silica gel (EtOAc–hexane, 1:4) and identified by direct comparison of physical constants, TLC, GLC, and spectral data with those of authentic samples. The physical constants and spectral data of the products are given in Table 3. The minor products were identified by direct comparison of TLC, GLC and/or GC-MS with those of authentic samples.

Time-Course Experiments in the Biotransformation of the Substrates. The substrate (10 mg) was incubated at 25 °C for 10 d with shaking (70 rpm) in the dark. At a regular time interval, a part (10 cm^3) of the incubation mixture was pipetted out under sterile conditions and then extracted with ether. The yields of the products were determined on the basis of the peak area from GLC and are expressed as a relative percentage to the total amount of the whole reaction products extracted. These results are shown in Figs. 1—9 in the text.

The details of the time-course experiments are described below in the case of **1a** as an example. A part of the callus tissues was transplanted to 100 cm^3 of Murashige and Skoog's medium[18] in a 300 cm^3-conical flask and grown with continuous shaking for 2—3 weeks at 25 °C in the dark. The substrate **1a** (10 mg) was administered to the precultured cells (about 70 g) in a 300 cm^3-conical flask and the cultures were incubated at 25 °C in a rotary shaker (70 rpm) in the dark. At a regular time interval, a part of the incubation mixture (10 cm^3) was pipetted out under sterile conditions and extracted with ether. The ether extract was made up to 0.2 cm^3 and 0.002 cm^3 of the ether solution was subjected to GLC with a 15% DEGS column at 120 °C by use of a microsyringe. The yields of the products were determined on the basis of the peak area from the GLC and are expressed as a relative percentage to the total amount of the whole reaction products extracted. Identification of the products were performed by comparison (co-GLC and GC-MS) with authentic samples.[25,32] Thus, the time-course in the biotransformation of **1a** as shown in Fig. 1 was obtained.

The author wishes to express his heartfelt gratitude to Professor Takayuki Suga of Hiroshima University for his encouragement and guidance in the course of this work and his critical reading of the manuscript and to Dr. Toshifumi Hirata for his valuable suggestions.

References

1) E. Reinhard and A. W. Alfermann, *Adv. Biochem. Eng.*, **16**, 49 (1980); A. W. Alfermann and E. Reinhard, *Bull. Soc. Chim. Fr.*, **1980**, II-35.

2) T. Suga and T. Hirata, *Nippon Kagaku Kaishi*, **1983**, 1352.

3) K. H. Neumann, W. Barz, and E. Reinhard, "Primary and Secondary Metabolism of Plant Cell Cultures," Springer-Verlag Heidelberg New York Tokyo (1985), p. 316.

4) R. A. Dixon, "Plant Cell Culture a practical approach," IRL PRESS Oxford Washington DC (1985), p. 127.

5) T. Hirata, T. Aoki, Y. Hirano, T. Ito, and T. Suga, *Bull. Chem. Soc. Jpn.*, **54**, 3527 (1981).

6) T. Suga, T. Hirata, and Y. S. Lee, *Chem. Lett.*, **1982**, 1595.

7) Y. S. Lee, T. Hirata, and T. Suga, *J. Chem. Soc., Perkin Trans. 1*, **1983**, 2475.

8) T. Hirata, H. Hamada, T. Aoki, and T. Suga, *Phytochemistry*, **21**, 2209 (1982).

9) T. Suga, T. Hirata, and H. Hamada, *Bull. Chem. Soc. Jpn.*, **59**, 2865 (1986).

10) T. Suga, S. Izumi, and T. Hirata, *Chem. Lett.*, **1986**, 2053.

11) T. Suga, H. Hamada, and T. Hirata, *Plant Cell Rep.*,

2, 66 (1983).
12) T. Suga, T. Hirata, and S. Izumi, *Phytochemistry*, **25**, 2791 (1986).
13) T. Suga, S. Izumi, T. Hirata, and H. Hamada, *Chem. Lett.*, **1987**, 425.
14) The results have been partly outlined in the preliminary communications.[15-17]
15) T. Suga, T. Hirata, H. Hamada, and M. Futatsugi, *Plant Cell Rep.*, **2**, 186 (1983).
16) T. Suga, H. Hamada, and T. Hirata, *Chem. Lett.*, **1987**, 471.
17) T. Suga, H. Hamada, T. Hirata, and S. Izumi, *Chem. Lett.*, **1987**, 903.
18) T. Murashige and F. Skoog, *Physoil. Plant*, **15**, 473 (1962).
19) A detail for the formation of the 4-hydroxylated products **23a** and **23b** will be reported elsewhere in the near future.
20) Y. Noma and C. Tatsumi, *Nippon Nogeikagaku Kaishi*, **47**, 705 (1973).
21) G. Zweifel and H. C. Brown, *J. Am. Chem. Soc.*, **86**, 393 (1964).
22) R. G. Johnston and J. Read, *J. Chem. Soc.*, **1934**, 233.
23) E. J. Corey and G. Schmidt, *Tettrahedron Lett.*, **1979**, 399.
24) T. Matsuura and K. Fujita, *J. Sci. Hiroshima Univ., Ser. A*, **16**, 173 (1952).
25) S. H. Schroeter and E. L. Eliel, *J. Org. Chem.*, **30**, 1 (1965).
26) J. Read and W. J. Grubb, *J. Chem. Soc.*, **1934**, 1779.
27) S. Dev, A. P. S. Narula, J. S. Yadav, "CRC Handbook of Terpenoids," CRC Press, Boca Raton, Florida (1982), Vol. II, p. 205.
28) E. Guenther, "The Essential Oils," Vol. II, D. Van Nostrand Comp., Inc. (1949), pp. 242, 245, 433.
29) L. Shulz and W. Doll, Ber. Schimmel & Co. Akt.-Ges., 1942-3, 50; *Chem. Abst.* **41**, 739a (1947).
30) R. G. Johnston and J. Read, *J. Chem. Soc.*, **1934**, 233.
31) K. Mori, N. Mizumachi, and M. Matsui, *Agric. Biol. Chem.*, **40**, 1611 (1976).
32) R. G. Johnston and J. Read, *J. Chem. Soc.*, **1935**, 1138.
33) H. C. Brown and C. P. Garg, *J. Am. Chem. Soc.*, **83**, 2952 (1961).
34) J. S. Glasby, "Encyclopaedia of the Terpenoids," John Willey and Sons (1982), p. 2440.

The Fries Rearrangement of 4*H*-Cyclopenta[*def*]phenanthrenyl Acetate

Masahiro MINABE,* Masaaki YOSHIDA, Tsukasa AMIMOTO, Toshihiro NAGATA, and Masamichi KOBORI

Department of Industrial Chemistry, Faculty of Engineering, Utsunomiya University, Ishiicho, Utsunomiya 321

(Received July 4, 1987)

A Fries rearrangement of 4*H*-cyclopenta[*def*]phenanthren-1-yl acetate gave 2- and 7-acetyl derivatives. The reaction of isomeric 2-acetoxy compound afforded 1- and 7-acetyl derivatives. The acetyl group of the 3- and 8-acetoxy compounds rearranged into the 2- and 9-positions, respectively. In addition, 1-, 2-, 3-, 4-isopropyl compounds were derived from the corresponding acetyl derivatives.

The Fries rearrangement is one of the important synthetic methods for obtaining acyl-substituted phenols from the corresponding acyloxy compounds. This reaction has been investigated widely, but has scarcely been applied to polycyclic aromatic hydrocarbons (PAH).[1,2]

4*H*-Cyclopenta[*def*]phenanthrene (CPP) is one of the interesting PAH; some reactions involving CPP derivatives have been reported.[3] Recently, we have reported Friedel–Crafts acetylations of methoxy-4*H*-cyclopenta[*def*]phenanthrenes.[4] The effect of the methoxyl group was different from that of the amino group on CPP.[5]

The present paper deals with a Fries rearrangement of acetoxy derivatives of CPP, **1a—5a**. This is expected to yield valuable informations concerning both the reactivities of the electrophilic substitution of substituted CPP, and the mechanism of the Fries rearrangement (Scheme 1). The reactants, **1a—5a**, were synthesized by a rearrangement of the corresponding acetyl derivatives, **6a—10a**,[6,7] with *m*-chloroperbenzoic acid (MCPB) in moderate yields. Also, **6a—10a** were converted into isopropyl compounds: **6d—10d** via **6b—10b** and **6c—10c** (Scheme 2).

The acetyl group of 4*H*-cyclopenta[*def*]phenanthren-1- (**1a**), 2- (**2a**), 3- (**3a**), and 8-yl acetate (**4a**) migrated upon stirring with aluminium chloride in nitrobenzene, giving 2-acetyl-1-hydroxy- (**1b**), 1-acetyl-2-hydroxy- (**2b**), 2-acetyl-3-hydroxy- (**3b**), 9-acetyl-8-hydroxy-4*H*-cyclopenta[*def*]phenanthrene (**4b**), respectively, in moderate yields (summarized in Table 1). The phenolic compounds, **1e—4e**, were isolated as by-products of the reactions.

The reaction of **2a** afforded 7-acetyl-2-acetoxy compound, **2d**, accompanied by a trace amount of 7-acetyl-2-hydroxy derivative, **2c**, through a treatment in

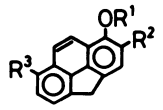

1a (R^1=Ac, R^2=R^3=H)
1b (R^1=R^3=H, R^2=Ac)
1c (R^1=R^2=H, R^3=Ac)
1d (R^1=R^3=Ac, R^2=H)
1e (R^1=R^2=R^3=H)

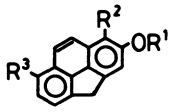

2a (R^1=Ac, R^2=R^3=H)
2b (R^1=R^3=H, R^2=Ac)
2c (R^1=R^2=H, R^3=Ac)
2d (R^1=R^3=Ac, R^2=H)
2e (R^1=R^2=R^3=H)

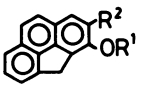

3a (R^1=Ac, R^2=H)
3b (R^1=H, R^2=Ac)
3e (R^1=R^2=H)

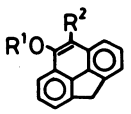

4a (R^1=Ac, R^2=H)
4b (R^1=H, R^2=Ac)
4e (R^1=R^2=H)

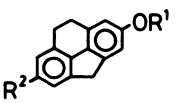

5a (R^1=Ac, R^2=H)
5c (R^1=H, R^2=Ac)
5d (R^1=R^2=Ac)
5e (R^1=R^2=H)

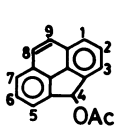

11

Scheme 1.

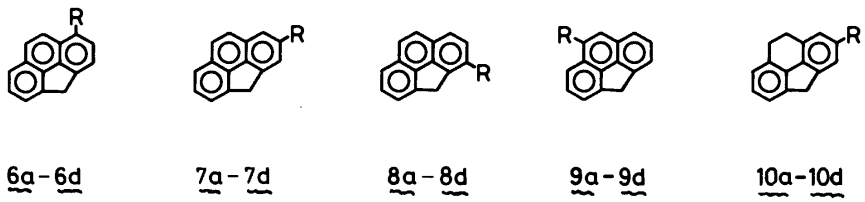

6a-6d 7a-7d 8a-8d 9a-9d 10a-10d

a: R=Ac b: R= -CMe2 (OH) c: R= -C(Me)=CH2 d: R=Pr-i

Scheme 2.

Table 1. The Fries Rearrangements of **1a—5a**

Reactant	Solv.	Temp °C	Time h	Product/%		Recovd/%	
1a	$PhNO_2$	r.t.	2	**1b**(85)			
2a	$C_2H_4Cl_2$	r.t.	3	**2c**(trace)	**2d**(34)	**2a**(2)	**2e**(18)
2a	$C_2H_4Cl_2$	refl.	1	**2b**(33)			
2a	$PhNO_2$	40	2	**2b**(65)		**2a**(10)	**2e**(9)
3a	$PhNO_2$	40	2	**3b**(62)		**3a**(20)	**3e**(3)
4a[a]	$PhNO_2$	r.t.	3	**4b**(51)			**4e**(trace)
5a[a]	PhCl	refl.	1	**5c**(8)		**5a**(10)	

a) Isolated yield.

1,2-dichloroethane at room temperature. On the other hand, **2b** was the main product under reflux conditions, similar to the case in nitrobenzene. Similar trends were observed in a reaction of **1a** in 1,2-dichloroethane.

A Fries rearrangement of the 8,9-dihydro-2-acetoxy derivative **5a** yielded 6-acetyl-2-hydroxy compound, **5c**, as the solely isolated product. A reaction of 4-acetoxy compound, **11**, gave no identified products.

These results fairly differ from reactions of the amino[5] and methoxy derivatives[4] of CPP. One of the remarkable results of Fries rearrangements in nitrobenzene is that the acetyl group is introduced into the adjacent position to the original acetoxyl group of **1a—4a**. This is similar to the cases of 1-, 2-, and 8-amines[5] and 1- and 2-ethers.[4] On the other hand, **2a** gives diacetyl derivative **2d** under relatively mild conditions using 1,2-dichloroethane; position 7 in the parent CPP is the most reactive position to electrophile.[3,8] These can be explained by the fact that the formations of **1d** and **2d** are kinetically controlled and those of **1b** and **2b** are thermodynamically controlled. The driving force of thermodynamic stabilities of the compounds would be caused by the formation of a chelating ring between the vicinal acetyl and the hydroxyl groups.

From the predominant formations of **1b—4b** by reactions in nitrobenzene it is postulated that the solvent prefers the formation of thermodynamically-controlled products, in spite of the fact that the attack of the electrophile on the ortho position of substituent requires more energy and may attack the other positions.[9] The solvated acetyl chloride-aluminium chloride complex is the attacking species in the Friedel-Crafts acetylation using nitrobenzene as a solvent.[10] Also, in this case, the solvated reactant-aluminium chloride complex furnishs the rearrangement by moving the acetyl group from the oxygen atom to the adjacent carbon in the solvated state under the reaction conditions.

The following mechanisms have been proposed for the Fries rearrangement:[1] (i) an intramolecular reaction, (ii) a Friedel-Crafts acetylation by acyl chloride to the aryl-$OAlCl_2$ formed from the original acyloxy compound with aluminium chloride, or (iii) a disproportionation reaction of two acyloxy derivatives (these would operate simultaneously). A brief experiment involving a cross-Fries rearrangement between **1e** and **2a** in the presence of aluminium chloride in nitrobenzene afforded a mixture of **1b** and **2b** in a ratio of ca 4:1; this supports the idea that the reaction proceeds via an intermolecular mechanism. The disproportionation mechanism (iii) would be one of the reasonable mechanisms, since fair amounts of **1e** and **2e** were obtained as by-products during the formations of **1d** and **2d**. The production of **1b—4b** in nitrobenzene has been explained by the intramolecular mechanism (i), since the yields of **1b—4b** are moderately high, in spite of the adjacent attack being restricted due to the steric factor.[9]

The acetates, **1a—5a**, were synthesized by Baeyer-Villiger rearrangements of 1- (**6a**),[6] 2- (**7a**),[6] 3- (**8a**),[6,7] 8- (**9a**),[6] and 8,9-dihydro-2-acetyl-4*H*-cyclopenta[*def*]-phenanthrene (**10a**)[6] with MCPB. The alkaline hydrolyses of **1a—5a** afforded phenols **1e—5e**. Reactions of **6a—10a** with methylmagnesium iodide gave the corresponding 2-substituted 2-propanol isomers, **6b—10b**. The alcohols were converted into propylene derivatives **6c—10c** by treatments with acetic anhydride. The olefins gave isopropyl compounds, **6d—10d**, by hydrogenation with Raney nickel.

Experimental

All of the melting points are uncorrected. The ^{1}H NMR spectra were obtained with a Jeol C-60 HL or a Varian VXR-300 spectrometers in $CDCl_3$ from TMS. The IR (KBr-pellet) and mass spectra were recorded on a Jasco IR-G and a Hitachi M-80 apparatus.

Acetyl compounds **6a—10a** were obtained according to the method described elsewhere.[6] Oxime of **6a**: mp 206.0—207.5 °C; yield 74%; IR, 3200 cm^{-1}; ^{1}H NMR (C_6D_6), δ=2.33 (3H, s), 3.88 (2H, s), 7.30—7.66 (5H, m), 7.82 (1H, d, J=9.0 Hz), 8.22 (1H, bs), and 8.58 (1H, d, J=9.0 Hz); MS, m/z 247 (M$^+$), 230, and 189. Found: C, 82.86; H, 5.40%. Calcd for $C_{17}H_{13}NO$: C, 82.57; H, 5.30%.

Oxime of **7a**: mp 193—194 °C; yield 95%; IR, 3250 cm^{-1}; ^{1}H NMR, δ=2.51 (3H, s), 4.39 (2H, s), 7.66—7.75 (2H, m), 7.86 (1H, d, J=8.7 Hz), 7.87 (2H, s), 7.98 (1H, bs), and 8.08 (2H, s); MS, m/z 247 (M$^+$), 231, and 189. Found: C, 82.60; H, 5.53; N, 5.92%. Calcd for $C_{17}H_{13}NO$: N, 5.66%.

Oxime of **8a**:[7] yield 77%; mp 151.5—152.0 °C; IR, 3300 cm^{-1}; ^{1}H NMR (C_6D_6), δ=2.24 (3H, s), 4.23 (2H, s), 7.36—7.89 (7H, m), and 8.52 (1H, bs); MS, m/z 247 (M$^+$), 231, 214, and 189. Found: C, 82.87; H, 5.60%.

Oxime of **10a**: mp 181.0—181.5 °C; yield 88%; IR, 3250 cm^{-1}; ^{1}H NMR, δ=2.34 (3H, s), 3.16 (4H, s), 3.91 (2H, s), 7.12 (1H, d, J=7.2 Hz), 7.21 (1H, t, J=7.2 Hz), 7.35 (1H, d, J=7.2 Hz), 7.41 (1H, s), 7.62 (1H, s), and 8.20 (1H, bs); MS, m/z 249 (M$^+$), 232, 217, and 191. Found: C, 82.15; H, 6.37%. Calcd for $C_{17}H_{15}NO$: C, 81.90; H, 5.30%.

3-Acetoxy-4*H*-cyclopenta[*def*]phenanthrene (3a) by the Baeyer-Villiger Rearrangement of the Corresponding Ketone. Typical Procedure. A mixture of **8a**[6,7] (1.392 g, 6 mmol) in $CHCl_3$ (100 ml, percolated through alumina before use) was cooled in a refrigerator; MCPB (690 mg, 4 mmol) was added and stirred. Additional MCPB (690 mg) was added after 8 and 16 h (total 2.07 g, 12 mmol). The stirring was continued for 3 d below 5 °C. After treatment with aqueous sodium hydrogencarbonate, the organic layer was evaporated. The residue was chromatographed on SiO_2 with benzene and the first colorless eluate gave **3a** (1.027 g, 69%); mp 109—110 °C (EtOH); IR, 1753 and 1193 cm^{-1}; ^{1}H NMR, δ=2.42 (3H, s), 4.23 (2H, s), 7.26 (1H, d, J=8.4 Hz), and 7.51—7.84 (6H, m); MS, m/z 248 (M$^+$), 206, 205, 189, and 177. Found: C, 82.43; H, 4.82%. Calcd for $C_{17}H_{12}O_2$: C, 82.24; H, 4.87%.

1a; yield 67%; mp 130—131 °C; IR, 1752 and 1205 cm^{-1}; ^{1}H NMR, δ=2.50 (3H, s), 4.35 (2H, s), 7.36 (1H, d, J=7.6 Hz), 7.64—7.74 (4H, m), and 7.83—7.88 (2H, m); MS, m/z 248 (M$^+$), 206, 205, 177, and 176. Found: C, 82.40; H, 4.92%.

2a; yield 67%; mp 111.5—112.5 °C; IR, 1751, 1219, and 1206 cm^{-1}; ^{1}H NMR, δ=2.41 (3H, s), 4.37 (2H, s), 7.44 (1H, s), 7.54 (1H, s), 7.62—7.77 (2H, m), and 7.78—7.89 (3H, m); MS, m/z 248 (M$^+$), 206, 205, 177, and 176. Found: C, 82.50; H, 5.00%.

5a; yield 74%; mp 124.5—125.0 °C; IR, 1751 and 1203 cm^{-1}; ^{1}H NMR, δ=2.25 (3H, s), 3.13 (4H, s), 3.83 (2H, s), 6.72 (1H, s), 6.94 (1H, s), and 6.98—7.31 (3H, m); MS, m/z 250 (M$^+$), 208, 207, 191, and 189. Found: C, 81.85; H, 5.71%. Calcd for $C_{17}H_{14}O_2$: C, 81.58; H, 5.64%.

11; obtained by acetylation of the corresponding alcohol[11] in 85% yield; mp 93—94 °C; IR, 1723 and 1223 cm^{-1}; ^{1}H NMR, δ=2.22 (3H, s), 6.93 (1H, s), and 7.30—7.65 (8H, m); MS, m/z 248 (M$^+$), 206, and 189. Found: C, 82.52; H, 4.78%. Calcd for $C_{17}H_{12}O_2$: C, 82.24; H, 4.87%.

4a;[12] yield 81%; mp 97—98 °C. Hydrolysis of **4a** gave **4e**,[12] in 68% yield; mp 167—168 °C.

4*H*-Cyclopenta[*def*]phenanthren-1-ol (1e). The acetate **1a** (620 mg, 2.5 mmol) was dissolved in EtOH (10 ml) and a solution of KOH (2.5 g) in H_2O (10 ml) was added in a small portion into a warmed (60—70 °C) solution of **1a**. After 5 min, the resulting mixture was allowed to stand at room temperature and acidified by HCl to give **1e**; 489 mg (95%); mp 148—149 °C (cyclohexane); IR, 3340 cm^{-1}; ^{1}H NMR, δ=4.22 (2H, s), 5.23 (1H, s), 6.93 (1H, d, J=7.8 Hz), and 7.39—7.84 (7H, m); MS, m/z 206 (M$^+$) and 189. Found: C, 87.46; H, 4.90%. Calcd for $C_{15}H_{10}O$: C, 87.35; H, 4.89%.

2e; yield 95%; mp 169—170 °C; IR, 3320 cm^{-1}; ^{1}H NMR, δ=4.23 (2H, s), 5.02 (1H, s), 7.14 (1H, s), 7.18 (1H, s), and 7.44—7.70 (5H, m); MS, m/z 206, 189, and 176. Found: C, 87.53; H, 4.66%.

3e;[7] yield 93%; mp 165—166 °C; IR, 3350 and 3250 cm^{-1}; ^{1}H NMR, δ=4.29 (2H, s), 5.05 (1H, s), 7.15 (1H, d, J=7.8 Hz), and 7.59—7.92 (6H, m); MS, m/z 206, 189, and 176. Found: C, 87.09; H, 4.64%.

5e; yield 96%; mp 155—156 °C; IR, 3200 cm^{-1}; ^{1}H NMR, δ=3.01 (4H, s), 3.83 (2H, s), 4.76 (1H, s), 6.62 (1H, s), 6.83 (1H, s), and 7.05—7.36 (3H, m); MS, m/z 208 (M$^+$), 191, and 189. Found: C, 86.34; H, 6.04%. Calcd for $C_{15}H_{12}O$: 86.51; H, 5.81%.

Fries Rearrangements of 1a—5a and 7. Typical Procedure. Into a mixture of powdered $AlCl_3$ (64 mg, 0.48 mmol) in $PhNO_2$ (5 ml) was added a solution of **1a** (50 mg, 0.2 mmol) in $PhNO_2$ (5 ml) and stirred for 2 h at room temperature. Upon stirring with aq. HCl for 3 h, the reaction mixture was analyzed with a suitable hydrocarbon as an internal standard by means of gas chromatography (Shimadzu 6AMFP apparatus attached a column containing Silicone SE-30).

A pure specimen of **1b** was obtained by the reaction of **1e** (41 mg, 0.2 mmol) in $C_2H_4Cl_2$ (10 ml) with Ac_2O (0.023 ml, 0.24 mmol) and $AlCl_3$ (64 mg, 0.48 mmol) at room temperature for 30 min, yield 40 mg (80%); mp 178—179 °C; IR, 3450, 2690, 1639, and 1385 cm^{-1}; ^{1}H NMR, δ=2.66 (3H, s), 4.03 (2H, s), 7.48—7.70 (5H, m), 7.94 (1H, d, J=9.0 Hz), and 13.76 (1H, s); MS, m/z 248 (M$^+$), 233, 205, and 176. Found: C, 82.21; H, 5.04%. Calcd for $C_{17}H_{12}O_2$: C, 82.24; H, 4.87%.

Compound **1d** was isolated from the reaction of **1a** (248 mg, 1 mmol) with Ac_2O-$AlCl_3$ in $CHCl_3$; yield 221 mg (76%); mp 155—156 °C; IR, 1751, 1660, and 1195 cm^{-1}; ^{1}H NMR, δ=2.39 (3H, s), 2.78 (3H, s), 4.27 (2H, s), 7.35 (1H, d, J=7.8 Hz), 7.58—7.70 (2H, m), 7.81 (1H, d, J=9.0 Hz), 8.15

(1H, d, J=7.8 Hz), and 8.91 (1H, d, J=9.0 Hz). Found: C, 78.40; H, 4.99%. Calcd for $C_{19}H_{14}O_3$: C, 78.60; H, 4.85%.

Diketone **1d** was hydrolyzed with aqueous KOH in EtOH to give **1c**; yield 38%; mp 183—185 °C; IR, 3250, 1645, and 1254 cm^{-1}; ^{1}H NMR (DMSO-d_6), δ=2.76 (3H, s), 4.32 (2H, s), 7.09 (1H, d, J=7.5 Hz), 7.59 (1H, d, J=7.5 Hz), 7.80 (1H, d, J=7.5 Hz), 8.10 (1H, d, J=9.6 Hz), 8.86 (1H, d, J=7.5 Hz), 8.70 (1H, d, J=9.6 Hz), and 9.90 (1H, s); MS, m/z 248 (M$^+$), 233, 217, 205, and 189. Found: C, 82.55; H, 5.06%. Calcd for $C_{17}H_{12}O_2$: C, 82.24; H, 4.87%.

Fries Rearrangement of 2a. Acetate **2a** (50 mg, 0.2 mmol) was treated with $AlCl_3$ (64 mg, 0.48 mmol) in $C_2H_4Cl_2$ (10 ml) at room temperature for 3 h. The composition of the reaction mixture was submitted to GC. The main portion was chromatographed on SiO_2 with benzene to give **2d**; yield 12 mg (20%); mp 196—197 °C; IR, 1758, 1659, and 1201 cm^{-1}; ^{1}H NMR, δ=2.40 (3H, s), 2.79 (3H, s), 4.27 (2H, s), 7.38 (1H, s), 7.52 (1H, s), 7.62 (1H, d, J=7.8 Hz), 7.88 (1H, d, J=9.0 Hz), 8.09 (1H, d, J=7.8 Hz), and 8.34 (1H, d, J=9.0 Hz); MS, m/z 290 (M$^+$), 248, 233, 205, and 176. Found: C, 78.86; H, 5.16%. Calcd for $C_{19}H_{14}O_3$: 78.60; H, 4.85%.

The diketone **2d** was hydrolyzed to give **2c**; yield 80%; mp 129—130 °C; IR, 3260, 1637, and 1217 cm^{-1}; ^{1}H NMR, δ=3.00 (3H, s), 4.27 (2H, s), 5.25 (1H, s), and 7.10—8.10 (6H, m). Found: C, 82.52; H, 4.96%. Calcd for $C_{17}H_{12}O_2$: C, 82.24; H, 4.87%.

The isomeric **2b** was obtained by the reaction of **2e** (103 mg, 0.5 mmol) with Ac_2O (0.057 ml, 0.6 mmol) and $AlCl_3$ (200 mg, 1.5 mmol) in $C_2H_4Cl_2$ (40 ml) at room temperature for 30 min; yield 87 mg (70%); mp 153.5—154.5 °C; IR, 3450, 2580, 1607, and 1210 cm^{-1}; ^{1}H NMR, δ=2.95 (3H, s), 4.17 (2H, s), 7.20 (1H, s), 7.45—7.84 (3H, m), 7.88 (1H, d, J=9.0 Hz), 8.02 (1H, d, J=9.0 Hz), and 14.27 (1H, s); MS, m/z 248 (M$^+$), 233, and 176. Found: C, 82.48; H, 4.71%.

Fries Rearrangement of 3a. A reaction of **3a** (50 mg, 0.2 mmol) was carried out similar as described above. The reaction mixture yielded **3b**; yield 12 mg (24%); mp 176—177 °C; IR, 3400, 3200, 1640, and 1300 cm^{-1}; ^{1}H NMR, δ=2.84 (3H, s), 4.33 (2H, s), 7.61—7.77 (5H, m), 8.33 (1H, s), and 12.59 (1H, s); MS, m/z 248 (M$^+$), 233, 205, and 176. Found: C, 82.04; H, 4.98%. Calcd for $C_{17}H_{12}O_2$: C, 82.24; H, 4.87%.

Fries Rearrangement of 4a. Compound **4a** (50 mg, 0.2 mmol) was treated in a manner similar to that described above, giving 25.5 mg (51%) of **4b**; mp 152.5—153.5 °C; IR, 3400, 2650, 1639, 1447, and 1380 cm^{-1}; ^{1}H NMR, δ=2.99 (3H, s), 4.27 (2H, s), 7.58—7.68 (3H, m), 7.83 (1H, d, J=7.2 Hz), 8.00 (1H, d, J=8.0 Hz), 8.22 (1H, d, J=8.0 Hz), and 16.62 (1H, s); MS, m/z 248 (M$^+$), 233, and 176. Found: C, 82.02; H, 4.79%. Calcd for $C_{17}H_{12}O_2$: C, 82.24; H, 4.87%.

The Reaction of 5a. Compound **5a** (125 mg, 0.5 mmol) was treated with $AlCl_3$ (160 mg, 1.2 mmol) in PhCl (10 ml) with refluxing for 1 h to give 10 mg (8%) of **5c** and 12 mg (10%) of **5a**. **5c**; mp 186—187 °C; IR, 3300, 1650, 1575, 1368, and 1288 cm^{-1}; ^{1}H NMR, δ=2.62 (3H, s), 3.12 (4H, s), 3.85 (2H, s), 5.45 (1H, s), 6.64 (1H, s), 6.83 (1H, s), 7.72 (1H, s), and 7.90 (1H, s); MS, m/z 250 (M$^+$), 235, 207, and 189.

Diketone **5d** was obtained by a treatment of **5c** with Ac_2O in benzene; mp 116.0—116.5 °C; IR, 3550, 1757, 1665, and 1200 cm^{-1}; ^{1}H NMR, δ=2.34 (3H, s), 2.65 (3H, s), 3.19 (4H, s), 3.93 (2H, s), 6.90 (1H, s), 7.11 (1H, s), 7.80 (1H, s), and 7.98 (1H, s); MS, m/z 292 (M$^+$), 250, 235, and 207. Found: C, 77.84; H, 5.40%. Calcd for $C_{19}H_{16}O_3$: C, 78.06; H, 5.52%.

Reaction of 11. Compound **11** (248 mg, 1.0 mmol) in PhCl (30 ml) was refluxed with $AlCl_3$ (170 mg, 1.3 mmol) for 1 h; only **11** (120 mg, 48%) was isolated from the reaction mixture.

2-(4*H*-Cyclopenta[*def*]phenanthren-1-yl)-2-propanol (6b). A mixture of **6a** (1.872 g, 8 mmol) in PhH (30 ml) was added dropwise into MeMgI (prepared from 2.0 g (12 mmol) of CH_3I and 290 mg (12 mg atom) of Mg in ether); the mixture was refluxed for 4 h. Upon the usual treatment, the residue was chromatographed on SiO_2 with PhH giving 1.517 g (76%) of **6b**, 263 mg (14%) of **6c** (mp 50—51 °C), and 56 mg (3%) of **6a**. **6b**; mp 113.0—114.5 °C; IR, 3270 and 1148 cm^{-1}; ^{1}H NMR, δ=1.83 (6H, s), 2.09 (1H, bs), 4.20 (2H, s), 7.52—7.86 (5H, m), 7.76 (1H, d, J=9.0 Hz), and 8.47 (1H, d, J=9.0 Hz); MS, m/z 248 (M$^+$), 233, 230, 215, and 189. Found: C, 87.29; H, 6.73%. Calcd for $C_{18}H_{16}O$: C, 87.06; H, 6.50%.

7b; yield 38%; mp 88—89 °C; IR, 3370 and 1168 cm^{-1}; ^{1}H NMR, δ=1.62 (6H, s), 2.43 (1H, s), 4.05 (2H, s), and 7.35—7.75 (7H, m); MS, m/z 248 (M$^+$), 233, 230, 215, and 189. Found: C, 87.20; H, 6.79%.

8b; yield 81% (crude); IR, 3420 and 1170 cm^{-1}; ^{1}H NMR, δ=1.79 (6H, s), 2.01 (1H, s), 4.54 (2H, s), and 7.57—7.80 (7H, m); MS, m/z 248 (M$^+$), 230, 215, 202, and 189. Found: C, 86.99; H, 6.46%.

9b; yield 86%; mp 108—109 °C; IR, 3320 and 1150 cm^{-1}; ^{1}H NMR, δ=1.93 (6H, m), 2.07 (1H, s), 4.33 (2H, s), 7.58—7.80 (5H, m), 7.84 (1H, s), and 8.40 (1H, m); MS, m/z 248 (M$^+$), 233, 230, 215, and 189. Found: C, 87.01; H, 6.63%.

1-Isopropenyl-4*H*-cyclopenta[*def*]phenanthrene (6c). A mixture of **6b** (248 mg, 1 mmol) in Ac_2O (4 ml) was refluxed for 5 h giving 209 mg (91%) of **6c** by column chromatography; mp 50.5—51.0 °C; IR, 1622 cm^{-1}; ^{1}H NMR, δ=2.32 (3H, s), 4.34 (2H, s), 5.23—5.24 (1H, m), 5.45—5.46 (1H, m), 7.53 (1H, d, J=7.3 Hz), 7.61—7.71 (3H, m), 7.82 (1H, d, J=7.7 Hz), 7.83 (1H, d, J=9.1 Hz), and 8.05 (1H, d, J=9.1 Hz); MS, m/z 230 (M$^+$), 215, and 189. Found: C, 93.87; H, 5.93%. Calcd for $C_{18}H_{14}$: C, 93.87; H, 6.13%.

7c; yield 68%; mp 65—66 °C; IR, 1612 cm^{-1}; ^{1}H NMR, δ=2.32 (3H, s), 4.27 (2H, s), 5.14 (1H, m), 5.42 (1H, m), and 7.50—7.90 (7H, m); MS, m/z 230 (M$^+$), 215, and 189. Found: C, 93.88; H, 5.86%.

8c; yield 26% from crude **8b**; mp 29.5—30.0 °C; IR, 1620 cm^{-1}; ^{1}H NMR, δ=2.32 (3H, s), 4.26 (2H, s), 5.20 (1H, s), 5.36 (1H, s), and 7.34—7.68 (7H, m); MS, m/z 230 (M$^+$), 215, and 189. Found: C, 93.64; H, 6.17%.

9c; yield 63%; mp 31.0—31.5 °C; IR, 1632 and 1624 cm^{-1}; ^{1}H NMR, δ=2.33 (3H, s), 4.30 (2H, s), 5.25 (1H, m), 5.40 (1H, m), and 7.47—8.00 (7H, m); MS, m/z 230 (M$^+$), 215, 213, and 189. Found: C, 93.58; H, 6.05%.

10c; yield 84% from **1e**; mp 55—56 °C; IR, 1614 cm^{-1}; ^{1}H NMR, δ=2.16 (3H, s), 3.08 (4H, s), 3.76 (2H, s), 4.92 (1H, s), 5.20 (1H, s), 6.87—7.13 (4H, m), and 7.33 (1H, s); MS, m/z 232 (M$^+$), 217, and 191. Found: C, 92.86; H, 7.14%. Calcd for $C_{18}H_{16}$: C, 93.06; H, 6.94%.

1-Isopropyl-4*H*-cyclopenta[*def*]phenanthrene (6d). A solution of **6c** (115 mg, 0.5 mmol) in EtOH (60 ml) was shaken with Raney nickel (W-7, 0.15 g) under an atmosphere of hydrogen for 15 min at room temperature to give **6d** (60 mg, 52%); mp 70—71 °C; ^{1}H NMR, δ=1.45 (6H, d, J=6.6 Hz), 3.73 (1H, sep, J=6.6 Hz), 4.21 (2H, s), 7.14—7.73 (6H, m),

and 7.90 (1H, d, J=9.0 Hz); MS, m/z 232 (M^+), 217, 215, 202, and 189. Found: C, 93.27; H, 7.21%. Calcd for $C_{18}H_{16}$: C, 93.06; H, 6.94%.

7d; yield 47%; mp 75—76 °C; ^{1}H NMR, δ=1.35 (6H, d, J=7.0 Hz), 3.00 (1H, sep, J=7.0 Hz), 4.14 (2H, s), and 7.30—7.75 (7H, m); MS, m/z 232 (M^+), 217, 202, and 189. Found: C, 93.27; H, 7.21%.

8d; yield 52%; mp 45.5—46.0 °C; ^{1}H NMR, δ=1.44 (6H, d, J=7.0 Hz), 3.37 (1H, sep, J=7.0 Hz), 4.34 (2H, s), and 7.54—7.82 (7H, m); MS, m/z 232 (M^+), 217, 202, and 189. Found: C, 93.02; H, 7.27%.

9d; yield 32%; mp 33.5—34.0 C; ^{1}H NMR, δ=1.50 (6H, d, J=6.6 Hz), 3.71 (1H, sep, J=6.6 Hz), 4.24 (2H, s), and 7.30—7.92 (7H, m); MS, m/z 232 (M^+), 217, 202, and 189. Found: C, 93.12; H, 6.68%.

10d; yield 60%; mp 97.5—98.0 °C; ^{1}H NMR, δ=1.30 (6H, d, J=6.9 Hz), 2.96 (1H, sep, J=6.9 Hz), 3.13 (4H, s), 3.86 (2H, s), 7.00 (1H, s), 7.07—7.18 (2H, m), 7.23 (1H, s), and 7.31 (1H, d, J=7.3 Hz); MS, m/z 234 (M^+), 219, 202, 191, and 189. Found: C, 92.26; H, 7.88%. Calcd for $C_{18}H_{18}$: C, 92.26; H, 7.74%.

We greatly thank Professor Takashi Toda and Emeritus Professor Kazuo Suzuki, Utsunomiya University for their continuing interest and encouragement.

References

1) A. H. Blatt, *Org. Reactions*, **1**, 342 (1942).
2) H. Kwart and K. Sing, "Chemistry of Carboxylic Acids and Esters," ed by S. Patai, Interscience, N. Y. (1969), p. 341.
3) M. Minabe and K. Suzuki, *Yuki Gosei Kagaku Kyokai Shi*, **44**, 421 (1986).
4) M. Minabe, M. Yoshida, Y. Takabayashi, and M. Masuda, *Bull. Chem. Soc. Jpn.*, **61**, 729 (1988).
5) M. Yoshida, M. Minabe, W. Ookawa, and K. Suzuki, *Bull. Chem. Soc. Jpn.*, **56**, 1259 (1983).
6) M. Yoshida, K. Hishida, M. Minabe, and K. Suzuki, *J. Org.Chem.*, **45**, 1783 (1980).
7) A. Sieglitz and W. Schidlo, *Chem. Ber.*, **96**, 1098 (1963).
8) M. Yoshida, M. Minabe, and K. Suzuki, *J. Org. Chem.*, **44**, 3029 (1979).
9) L. I. Kruse and J. K. Cha, *J. Chem. Soc., Chem. Commun.*, **1982**, 1333.
10) P. H. Gore and M. Jehangir, *J. Chem. Soc., Perkin Trans. 1*, **1979**, 3007; R. B. Girdler, P. H. Gore, and C. K. Thadani, *J. Chem. Soc. C*, **1967**, 2619.
11) T. Kimura, M. Minabe, and K. Suzuki, *J. Org. Chem.*, **43**, 1247 (1978).
12) M. Yoshida, M. Minabe, and K. Suzuki, *Bull. Chem. Soc. Jpn.*, **56**, 2179 (1983).

 © 1988 The Chemical Society of Japan Bull. Chem. Soc. Jpn., 61, 885—891 (1988)

Dehydrooligopeptides. VIII. Convenient Syntheses of Various Dehydrotyrosine Derivatives Protected with Useful N, O-Protecting Groups via *N*-Carboxy Dehydrotyrosine Anhydrides[1)]

Chung-gi SHIN,* Yasuchika YONEZAWA, Takumi OBARA, and Hiroaki NISHIO
Laboratory of Organic Chemistry, Faculty of Technology, Kanagawa University, Rokkakubashi, Kanagawa-ku, Yokohama 221
(Received July 22, 1987)

Various *N*-benzyloxycarbonyl (Cbz) O-protected dehydrotyrosine (*Δ*Tyr) esters have been successfully synthesized mainly via two routes, in which reactions of (diethoxyphosphinyl)glycine ester with *p*-substituted benzaldehyde were included. Subsequent hydrolyses of the esters under various alkaline conditions were carried out in order to produce corresponding Cbz-*Δ*Tyr-OH derivatives, which were further converted with thionyl chloride to give *N*-carboxy dehydrotyrosine anhydrides [*Δ*Tyr·NCA]. In addition to these topics, the transformation of *Δ*Tyr·NCA to various kinds of *Δ*Tyr derivatives and a discussion on the configurational determination of all the new compounds are presented.

In the course of our work on the syntheses of various α-dehydroamino acids (DHA), which seem to be important residues in naturally occurring[2-5)] and synthetic dehydropeptides (DHP),[6)] we reported on several versatile synthetic methods for DHA and DHP.[1,7-9)] Recently, such DHA and DHP derivatives have been utilized for studies on both structure-biological activity correlation[10)] and asymmetric hydrogenation.[11)] So far, the syntheses and reactions of various kinds of neutral aliphatic, aromatic, and acidic DHA and their DHP derivatives have been reported.[12,13)] In addition, we already reported that *N*-carboxy α-dehydroamino acid anhydrides (*Δ* NCA), derived from benzyloxycarbonyl (Cbz)-DHA and thionyl chloride, were very useful for syntheses of DHP and for transformations to other DHA derivatives.[8)] Consequently, the *Δ* NCAs and their derivatives became a very important synthon as the building block of DHP. However, the syntheses and properties of DHA and its *Δ* NCA derivatives, which have another functional group in their side chains, such as a hydroxyl group, have never been investigated in detail, except for our brief report.[12,14)] In particular, in the case of DHA as well as an α-amino acid ester possessing two functional groups, e.g., amino and hydroxyl, it is usually necessary to protect them with different protecting groups for peptide synthesis. Therefore, we thoroughly examined the syntheses of several dehydrotyrosine (*Δ* Tyr) and its *Δ* NCA derivatives (*Δ* Tyr·NCA) mainly concerning two routes; we also tried to protect their functional groups by various combinations of useful N,O-protecting groups.[12)]

Results and Discussion

Synthesis of Dehydrotyrosine Derivatives. Since it was found that the methoxymethyl (MOM) group is effective for the protection of the phenolic hydroxyl group,[15)] the starting *p*-methoxymethoxybenzaldehyde (**1b**), derived from *p*-hydroxybenzaldehyde and methoxymethyl chloride by the usual method, was used in the following type condensation. According to the Hemetsberger method,[16)] the condensation of ethyl 2-azidoacetate with **1b** in the presence of sodium ethoxide was performed in order to produce (*Z*)-2-azido-(*p*-MOM)oxycinnamate (**2**) in a 57% yield. Although the yield of **2** was slightly low, compound **2** was subsequently subjected to a reduction. The selective hydrogenolysis of the azido group of **2** with aluminum-amalgam (Al-Hg) was smoothly carried out to give (*O*-MOM)dehydrotyrosine ethyl ester [*Δ*Tyr(MOM)-OEt] (**3**) in an almost quantitative yield. Unfortunately, however, it was found that a subsequent acylation of **3** with Cbz-Cl in the presence of a base such as triethylamine (TEA) or sodium hydride in CH_2Cl_2 or tetrahydrofuran (THF), did not take place, whereas a similar treatment of aliphatic DHA with Cbz-Cl proceeded.[7)]

Furthermore, in the presence of pyridine, the analogous acylation of **3** took place to give Cbz-(*O*-MOM)dehydrotyrosine ester [Cbz-*Δ*Tyr(MOM)-OY] (**4b**; Y=Et) in only a 33% yield. In order to increase the yield of **4b**, phase-transfer catalyst, such as $[CH_3(CH_2)_3]_4NBr$ (TBAB), was added to a heterogeneous solution of **3** and Cbz-Cl in the presence of powdered NaOH in CH_2Cl_2 at room temperature. As a result, the yield of **4b** ultimately increased to a 63%.

On the other hand, recently, Schmidt and coworkers have reported an interesting and convenient synthetic method for DHA by using an *N*-acyl-2-(dialkoxyphosphinyl)glycine ester as a Wittig-Horner reagent to an arbitrary aldehyde.[17)] Using the above-mentioned method, *N*-Cbz-2-(diethoxyphosphinyl)-glycinemethyl ester was prepared and then reacted with several *p*-substituted benzaldehydes (**1**) in the presence of potassium *t*-butoxide in CH_2Cl_2 at room temperature to give the expected Cbz-*Δ*Tyr(R)-OMe [**4**: **a**; R=CH_3 (Me), **b**; R=CH_3OCH_2 (MOM), **c**; R=CH_3CO (Ac)] in ca. a 50% yield (summarized in

Table 1. Dehydrotyrosine Ester Derivatives **4**

Compound No.	Y	Yield %	Mp θ_m/°C	Formula	Found (Calcd)/% C	H	N
4a	Me	42	syrup	$C_{19}H_{19}NO_5$	66.72 (66.85	5.45 5.61	4.25 4.10)
4b	Me	38	64—65[a]	$C_{20}H_{21}NO_6$	64.61 (64.68	5.77 5.70	3.70 3.77)
4b	Et	63	syrup	$C_{21}H_{23}NO_6$	65.64 (65.44	6.21 6.02	3.60 3.63)
4c	Me	69	126—128[b]	$C_{20}H_{19}NO_6$	65.21 (65.03	5.24 5.19	3.72 3.79)
4d	Me	85	156—158[c]	$C_{18}H_{17}NO_5$	66.18 (66.05	5.39 5.24	4.32 4.28)

a) Colorless needles from diisopropyl ether. b) Colorless prisms from ethyl acetate. c) Colorless needles from hexane–ethyl acetate.

Table 2. Properties of Dehydrotyrosine Ester Derivatives **4**

Compound No.	IR, ν/cm^{-1} in KBr NH	COO	C=C	^{1}H NMR, δ in $CDCl_3$ -CH=	-NH- (-OH)
4a	3300	1720	1640	7.32s	6.34bs
4b (Y=Me)	3310	1720	1640	7.16s	6.24bs
4b (Y=Et)	3310	1720	1640	7.28s	6.56bs
4c	3250	1762 1718	1640	7.30s	6.47s
4d	3270	1685	1632	7.20s	8.85bs[a] (9.90bs)

a) Measured in DMSO-d_6.

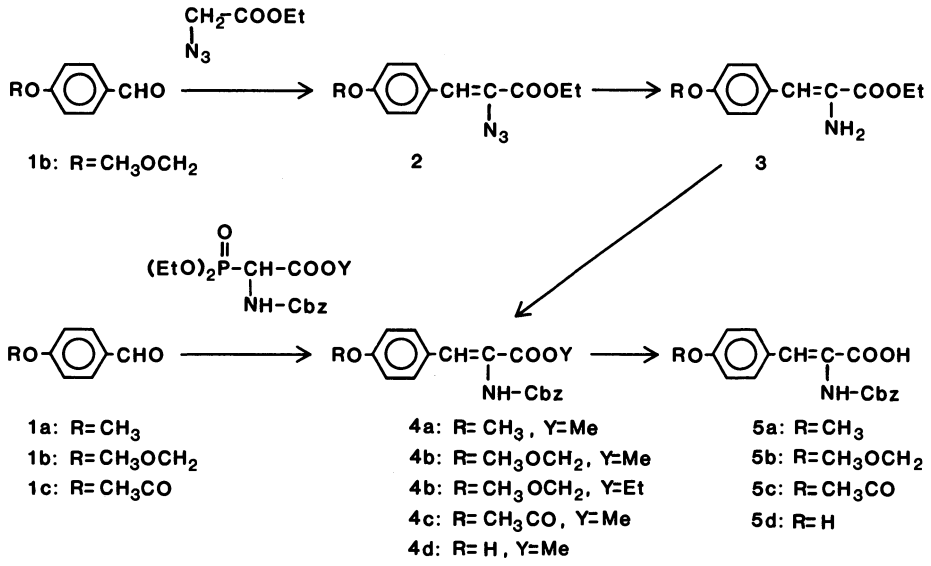

Scheme 1.

Tables 1 and 2). From the results, in the case of *p*-acetoxybenzaldehyde (**1c**), the obtained yield of Cbz-⊿Tyr(Ac)-OMe (**4c**) was a 69%. Moreover, Cbz-⊿Tyr-(R)-OMe (**4d**; R=H) was independently derived by the hydrolysis of **4c** with K_2CO_3 (as mentioned later).

Furthermore, in order to synthesize for the first time various kinds of useful ⊿Tyr·NCA derivatives, compounds **4a—c** had to be submitted to ester hydrolysis under mild conditions. The conventional hydrolysis of **4a** with 2-M† NaOH (1.0 equiv mol) at room temperature, even for more than 24 h, proceeded to give Cbz-⊿Tyr(Me)-OH (**5a**) in an only 10% yield. On the other hand, as shown in Tables 3 and 4, when 1-M LiOH instead of NaOH was used in the

† 1 M=1 mol dm^{-3}.

Table 3. Hydrolysis of **4** with a Few Bases

Compound No.	Reaction condition			Yield/%			
	Base (equiv)		Time/h	**5a**	**5b**	**5d**	**4d**
4a	2 M NaOH	1.0	24	10			
4a	1 M LiOH	1.0	3.5	75			
4b (Y=Me)	1 M LiOH	1.2	4		92		
4b (Y=Et)	1 M LiOH	1.2	4		89		
4c	1 M K_2CO_3	2.0	4			0	85
4c	1 M NaOH	3.3	22			24	0
4c	1 M $Ba(OH)_2$	3.3	22			47	25
4c	1 M LiOH	3.3	22			59	20
4c	2 M LiOH	5.0	22			71	5

Table 4. Dehydrotyrosine Derivatives **5**

Compound No.	Mp θ_m/°C	Formula	Found (Calcd)/%			IR, ν/cm^{-1} in KBr			^{1}H NMR, δ in DMSO-d_6	
			C	H	N	NH	COOH	C=C	-CH=	-NH= (-OH)
5a	179—180[a]	$C_{18}H_{17}NO_5$	66.10 (66.05	5.19 5.24	4.30 4.28)	3250	1685	1630	7.36s	8.78bs
5b	148—149[a]	$C_{19}H_{19}NO_6$	63.92 (63.86	5.30 5.36	3.82 3.92)	3250	1700	1640	7.34s	9.84bs
5c	167—168[a]	$C_{19}H_{17}NO_6$	64.52 (64.22	4.82 4.82	4.12 3.94)	3275	1690	1645	7.40s	9.10bs
5d	168—170[b]	$C_{17}H_{15}NO_5$	64.97 (65.17	4.91 4.82	4.32 4.47)	3275	1685	1630	7.26s	8.72bs (9.90bs)

a) Colorless needles from benzene. b) Colorless prisms from ethyl acetate.

hydrolysis, the desired **5a** could be obtained within a short time of 3.5 h in ca. a 75% yield. In a similar manner, the hydrolysis of **4b** (Y=Me and Et) was also worked up to give Cbz-⊿Tyr(MOM)-OH (**5b**) almost quantitatively. However, when 1-M of LiOH or 1-M $Ba(OH)_2$ was used in the analogous hydrolysis of **4c**, two products, **4d** and Cbz-⊿Tyr-OH (**5d**), instead of expected Cbz-⊿Tyr(Ac)-OH (**5c**), were obtained in ca. a 76% overall yield (in about a 1:2 ratio) accompanying an elimination of the acetyl group.

In addition, in the case of 2-M LiOH (5.0 equiv mol) for 22 h, the ester hydrolysis and the elimination of the acetyl group of **4c** occurred simultaneously to give **5d** as the main product (71%). Consequently, a high-yield synthesis of **5c** was accomplished by the acetylation of **5d** with acetyl chloride by the usual method. On the other hand, when 1-M K_2CO_3 was used as a weak base, only a deacetylation of **4c** was found to take place to give **4d** in an 85% yield.

Eventually, in almost all the cases mentioned above, it was proved that the acetyl group as the O-protecting group of ⊿Tyr derivatives was always labile under alkaline conditions, while the ester was gradually hydrolyzed upon increasing the concentration of the base.

The yields, melting points, and spectral data (IR and ^{1}H NMR) of **4** and **5** are summarized in Tables 1, 2, and 4.

In the IR spectra of **4** and **5**, the characteristic absorption bands of NH, acid carbonyl, and carbon–carbon double bond functions appear at 3250—3310, 1685—1720, and 1632—1645 cm^{-1} regions, respectively. Furthermore, in the ^{1}H NMR spectra, all the olefin protons of **4** and **5** shift at the δ 7.40—7.16 region as a singlet. In particular based on the ^{1}H NMR spectral data, the configurations of **4** and **5** could be tentatively determined to be in the (*Z*)-geometry, since the chemical shifts and the spectral patterns of (*Z*)-configurational DHA derivatives, the olefin protons of which shifted at comparatively higher magnetic fields than those of (*E*)-isomer,[18] were quite similar to those of the ⊿Tyr derivatives. Accordingly, the configuration of **2** and **3** could be also confirmed to be (*Z*)-geometry.

Synthesis and Conversion of ⊿Try·NCA to Various ⊿Tyr Derivatives. In order to synthesize *N*-carboxy dehydrotyrosine anhydride derivatives (⊿Tyr·NCA) (**6**), compounds **5a—d** (mentioned above) were subjected to cyclization of **5a** and **5c** with $SOCl_2$ in CH_2Cl_2 proceeded smoothly to give *N*-carboxy (*O*-Me)dehydrotyrosine anhydride [⊿Tyr(Me)·NCA] (**6a**) and *N*-carboxy (*O*-Ac)dehydrotyrosine anhydride [⊿Tyr(Ac)·NCA] (**6c**) in high yields, respectively, according to our previously reported technique.[12] On the other hand, the cyclization of **5b** also took place, but the O-protecting MOM group was found to behave interestingly under certain reaction conditions. In particular, when acetyl chloride or CH_2Cl_2 was used as the solvent, the cyclization and partial deprotection of **5b** readily proceeded to give only *N*-

Table 5. Conversion of **5** to *N*-Carboxy Dehydrotyrosine Anhydrides **6a—d**

Substrate[a] No.	Reaction condition Solvent-$SOCl_2$ (ml)		Time/h	Yield/% 6a	6b	6c	6d
5a	AcCl	1:1	1.0	76			
5b	AcCl	1:1	1.5				70
	CH_2Cl_2	1:1	1.5				93
	Et_2O	1:1	1.5		79		17
	Et_2O	2:1	1.5		98		
5c	CH_2Cl_2	1:1	1.5			93	
5d	CH_2Cl_2	1:1	1.5				86

a) 100 mg of **5** was used.

Table 6. *N*-Carboxy Dehydrotyrosine Anhydride Derivatives **6**

Compound No.	Yield %	Mp θ_m/°C	Formula	Found (Calcd)/% C	H	N	IR, $\tilde{\nu}$/cm^{-1} in KBr CO-O-CO	C=C	^{1}H NMR (δ, DMSO-d_6) -NH- (-OH)	-CH=
6a	76	197—198[a]	$C_{11}H_9NO_4$	60.19	4.18	6.33	1840	1670	11.39	6.66
				(60.27	4.14	6.39)	1770			
6b	98	148—149[b]	$C_{12}H_{11}NO_5$	57.77	4.51	5.58	1838	1670	11.30	6.68
				(57.85	4.45	5.62)	1780			
6c	93	192[c,e]	$C_{12}H_9NO_5$	58.41	3.55	5.47	1830	1680	7.40	6.76
				(58.30	3.69	5.67)	1780			
6d	86	196[d,e]	$C_{10}H_7NO_4$	58.15	3.49	6.78	1830	1662	10.05	6.70
				(58.54	3.44	6.83)	1770		(11.30)	

a) Colorless needles from ethyl acetate. b) Colorless needles from benzene. c) Colorless needles from chloroform. d) Colorless prisms from dioxane. e) Decomposition.

carboxy *O*-free-dehydrotyrosine anhydride [ΔTyr·NCA] (**6d**) almost quantitatively, instead of the desired *N*-carboxy (*O*-MOM)dehydrotyrosine anhydride [ΔTyr-(MOM)·NCA] (**6b**). However, interestingly, when diethyl ether was used as the solvent, a similar treatment of **5b** yielded another crystalline product in addition to a small amount of **6d** (17%). From the spectroscopic data and satisfactory elemental analytical results, the structure of the main isolated product was determined to be **6b**. As a result, the MOM protecting group was found to remain unchanged. Additionally, as shown in Tables 5 and 6, when the quantity of diethyl ether was doubled, only **6b** was obtained in an almost quantitative yield.

From the above results, it was found that diethyl ether used as the solvent behaved as a scavanger of the HCl gas that evolved during the reaction of **5b** with $SOCl_2$. Accordingly, in the former case in the absence of ether, it was clarified that the cyclization of **5b** initially formed **6b** as an intermediate, the MOM group of which was immediately eliminated with HCl to give **6d** in high yield. Consequently, it was clearly demonstrated that either compound **6b** or **6d** could be selectively prepared, according to the reaction conditions listed in Table 5. These results provide useful information for the dehydropeptide synthesis regarding the protection of side chain functional groups.

Furthermore, to be utilized in a wide variety of peptide syntheses, both the hydroxyl and amino groups of the ΔTyr derivatives must be easily and selectively protected with such groups as Cbz and *t*-butoxycarbonyl (Boc). In addition, we are interested in not only the protection but also the reactivity of the newly formed ΔNCA ring, itself. Thus, compound **6d** was chosen and directly applied for transformations to other DHA derivatives under various reaction conditions.

Compound **6d** was treated with di-*t*-butyl carbonate [$((CH_3)_3COCO)_2O$; $(Boc)_2O$] in the presence of a few drops of pyridine in THF; then, methanol was added. The resulting solution was made basic to pH 9 with *N*-methylmorpholine (NMM) in order to give *N*-free (*O*-Boc)dehydrotyrosine methyl ester [ΔTyr(Boc)-OMe] (**7a**) in an 80% yield. On the other hand, in the case of using Cbz-Cl instead of $(Boc)_2O$, a similar reaction was carried out to give the (*O*-Cbz)dehydrotyrosine methyl ester [ΔTyr(Cbz)-OMe] (**7b**) in an 84% yield (Scheme 2.)

From the above results and by a comparison with the reactivity of two reaction points of **6d**, the phenolic hydroxyl group was found to be acylated more easily than the imino group of the ΔNCA ring.

Furthermore, for one-pot syntheses of the ΔTyr

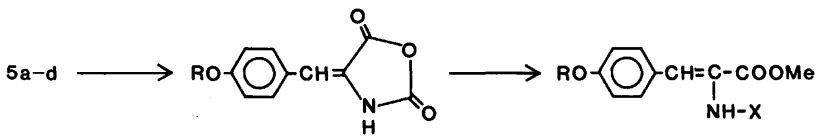

6a: R=CH_3
6b: R=CH_3OCH_2
6c: R=CH_3CO
6d: R=H

7a: R=Boc, X=H
7b: R=Cbz, X=H
7c: R=Boc, X=Cbz
7d: R=Cbz, X=Boc

Scheme 2.

Table 7. O-Protected Dehydrotyrosine Methyl Ester Derivatives **7**

Compound No.	Yield %	Mp θ_m/°C	Formula	Found (Calcd)/% C	H	N	IR, $\tilde{\nu}$/cm^{-1} in KBr $-NH_2$ (-NH-)	C=C	^{1}H NMR (δ, $CDCl_3$) -NH	-CH=
7a	80	113—115[a]	$C_{15}H_{19}NO_5$	61.82 (61.42	6.26 6.53	4.34 4.78)	3455 3380	1630	4.24bs	6.50s
7b	84	93—95[a]	$C_{18}H_{17}NO_5$	66.23 (66.05	5.19 5.24	4.22 4.28)	3480 3400	1630	4.24bs	6.48s
7c	46	97—98[b]	$C_{23}H_{25}NO_7$	64.38 (64.62	5.98 5.90	3.22 3.28)	(3325)	1645	6.48bs	7.12—7.52m (Ph+H)
7d	52	78—80[b]	$C_{23}H_{25}NO_7$	64.44 (64.62	5.95 5.90	3.19 3.28)	(3350)	1650	6.20bs	7.32s

a) Colorless prisms from hexane. b) Colorless needles from diisopropyl ether.

derivatives N,O-protected with different groups, a similar treatment of **6d** with $(Boc)_2O$ in THF was worked up, followed by consecutive treatments with TEA and Cbz-Cl. Finally, the reaction solution was treated further with MeOH to give the expected *N*-Cbz-(*O*-Boc)dehydrotyrosine methyl ester [Cbz-ΔTyr-(Boc)-OMe] (**7c**) in ca. a 46% yield. Contrary to the above successive reactions, similar treatments of **6d** with Cbz-Cl, $(Boc)_2O$, and then MeOH were also performed to give *N*-Boc-(*O*-Cbz)dehydrotyrosine methyl ester [Boc-ΔTyr(Cbz)-OMe] (**7d**) in ca. a 52% yield (Table 7).

In conclusion, facile syntheses of various kinds of ΔTyr and ΔTyr·NCA derivatives were accomplished in high yield; detailed knowledge concerning their protection and deprotection mechanisms were obtained. These results should be very useful regarding dehydropeptide synthesis.

Experimental

General. Melting points were determined with a Yamato (Model Mp-21) micro melting-point apparatus, and were not corrected. IR spectra were recorded with a Hitachi EPI-G2 spectrometer. ^{1}H NMR spectra were measured with a JEOL LMN PS-100 spectrometer in a $CDCl_3$ or DMSO-d_6 solution with tetramethylsilane as the internal standard.

Ethyl (*Z*)-2-Azido-(*p*-MOM)oxycinnamate (2). Into a solution of ethyl 2-azidoacetate (5.12 g, 40 mmol) and **1b** (6.64 g, 40 mmol) in dry benzene (120 ml) was added sodium ethoxide (made from Na 0.9 g, 40 mmol) in dry ethanol (24 ml) drop by drop, with stirring, at 5—8 °C. After allowing the solution to stand at room temperature for 2 h, the reaction solution was diluted with benzene (100 ml) and washed with a saturated aqueous ammonium chloride solution and then with chilled water. The organic layer was dried over anhydrous sodium sulfate. After removing the solvent under reduced pressure, the residual syrup was purified on a silica-gel column using benzene as the eluent to give **2** as a colorless viscous syrup. Yield 57%. IR ν_{max}^{KBr} (cm^{-1}) 2153 (N_3), 1650 (C=C); ^{1}H NMR ($CDCl_3$) δ=6.86 (s, 1H, -CH=). Found: C, 56.48; H, 5.32; N, 15.33%. Calcd for $C_{13}H_{15}N_3O_4$: C, 56.31; H, 5.45; N, 15.16%.

(*Z*)-ΔTyr(MOM)-OEt (3). A solution of **2** (6.0 g, 22 mmol) in ether (70 ml) was added to a suspension of Al–Hg (made from 9.94 g of Al and 9.94 g of $HgCl_2$) in ether (200 ml) with vigorous stirring at room temperature. After a few minutes, the ether began to reflux; this was maintained by the addition of a few drops of water at about 20 min intervals. After completing the addition of the solution, stirring was continued for 3 h. After removing on insoluble substance, the filtrate was washed several times with ice-water. The organic layer was dried over anhydrous sodium sulfate and then evaporated under reduced pressure. The residual syrup was purified on a silica-gel column using a mixture of benzene and ethyl acetate (10:1 v/v) as the eluent to give **3** as colorless viscous syrup. Yield 97%. IR ν_{max}^{KBr} (cm^{-1}) 3360, 3350 (NH_2), 1640 (C=C); ^{1}H NMR ($CDCl_3$) δ=6.48 (s, 1 H, -CH=), 4.16 (bs, 2H, $-NH_2$). Found: C, 61.87; H, 7.03; N, 5.81%. Calcd for $C_{13}H_{17}NO_4$: C, 62.14; H, 6.82; N, 5.57%.

(*Z*)-Cbz-ΔTyr(MOM)-OY (4b; Y=Me and Et). a) Method A. Into a solution of **3** (5.0 g, 20 mmol) in pyridine (40 ml) was added slowly Cbz-Cl (6.4 g, 40 mmol), with stirring, at 5—8 °C. The resultant solution was allowed to stand at room temperature and then stirred continuously for 2 h.

After removing the solvent under reduced pressure, the residual syrup was dissolved in ethyl acetate (200 ml) and washed twice, successively, with a 10% citric acid solution and with water; it was then dried over anhydrous sodium sulfate. Evaporation of the solvent under reduced pressure gave a viscous syrup, which was then purified on a silica-gel column using a mixture of hexane and ethyl acetate (20:1 v/v) as the eluent to give **4b** (Y=Et) as a colorless syrup. Yield 33%.

b) Method B. Into a suspension of **3** (5.0 g, 20 mmol) and powdered NaOH (2.0 g, 50 mmol) in the presence of TBAB (0.66 g, 2 mmol) in dry CH_2Cl_2 (50 ml) was added a solution of Cbz-Cl (4.8 g, 30 mmol) in CH_2Cl_2 (10 ml), with stirring, at 5—8 °C. The stirring was continued at room temperature for 8 h. An insoluble substance was filtered off and the filtrate was diluted with $CHCl_3$ (50 ml). The resultant solution was washed twice, successively, with a 10% citric acid solution and with water and then dried over anhydrous sodium sulfate. By removing the solvent under reduced pressure a crude syrup was obtained which could be similarly purified on a silica-gel column to give **4b** (Y=Et). Yield 63%.

c) Method C. Into a solution of potassium *t*-butoxide (3.1 g, 28 mmol) in dry CH_2Cl_2 (40 ml) was added a solution of *N*-Cbz-2-(diethoxyphosphinyl)glycine methyl ester (10 g, 28 mmol), with stirring, at −60 °C. After stirring for 15 min, the resulting solution was further stirred with an appropriate aldehyde (**1a—c**; 28 mmol) below −60 °C. After allowing this solution to stand at room temperature for 12 h, the reaction solution was concentrated under reduced pressure to give a residual syrup, which was dissolved in ethyl acetate (150 ml). The resultant solution was washed, successively, with a saturated aqueous ammonium chloride solution and water and finally dried over anhydrous sodium sulfate. The evaporation of the solvent under reduced pressure gave a viscous syrup, which was similarly worked up to give **4a—c** as a colorless syrup or crystals. (See Tables 1 and 2).

(*Z*)-Cbz-⊿Tyr(Me)-OH (5a). a) Method A. A solution of **4a** (1.71 g, 5 mmol) in dioxane (4 ml) and 2-M NaOH (2.5 ml) was stirred at room temperature for 24 h. After removing the solvent under reduced pressure, the residue was dissolved in water (20 ml). The resultant solution was washed twice with ethyl acetate and then the aqueous layer was made acidic to pH 2 with 3-M HCl. The acidic solution was extracted three times with ethyl acetate; the combined extracts were then washed with saturated aqueous NaCl solution and dried over anhydrous sodium sulfate. The concentration of the solution under reduced pressure gave crude crystals, which were recrystallized from a mixture of ethyl acetate and hexane to give **5a** as colorless prisms. Yield 10%.

b) Method B. In a similar manner, the treatment of **4a** (5 mmol) in dioxane (4 ml) with a 1-M LiOH solution (5 ml) was worked up at room temperature for 3.5 h to give **5a**. Yield 75%

(*Z*)-Cbz-⊿Tyr(MOM)-OH (5b). Treatment of **4b** (Y=Me; 4.5 g, 12 mmol) in dioxane (9 ml) with 1-M LiOH solution (14 ml) was similarly worked up for 4.5 h to give a crystalline substance. The residue was dissolved in water (40 ml) and then washed twice with ethyl acetate. The aqueous layer was made acidic to pH 2 with 3-M HCl. The acidic solution was extracted three times with ethyl acetate; the combined extracts were washed with a saturated aqueous NaCl solution and then dried over anhydrous sodium sulfate. Removing the solvent under reduced pressure gave crude crystals, which were recrystallized from a mixture of ethyl acetate and hexane or benzene alone to give **5b** as colorless prisms. Yield 92%.

In a similar manner, the treatment of **4b** (Y=Et) with 1-M LiOH was worked up to give **5b** in an 89% yield.

(*Z*)-Cbz-⊿Tyr-OH (5d) and (*Z*)-Cbz-⊿Tyr-OMe (4d). Into a solution of **4c** (1.85 g, 5 mmol) in dioxane (5 ml) was added a 2-M LiOH solution (12.5 ml), with stirring, at room temperature. The resulting solution was stirred continuously for 22 h. After removing dioxane under reduced pressure, water (30 ml) was added to the residual substance; the aqueous solution, thus obtained, was washed twice with ethyl acetate. The aqueous layer was made acidic to pH 2 with 3-M HCl and then extracted twice with ethyl acetate. The combined extracts were washed with a saturated aqueous NaCl solution and finally dried over anhydrous sodium sulfate. After removing the solvent under reduced pressure, a crystalline product was obtained as a mixture of **5d** and a small amount of **4d**. The mixture was washed well with benzene; the remaining crystals were then collected. Recrystallization from ethyl acetate gave only **5d** as colorless prisms.

In a similar manner, the treatment of **4c** (1.85 g, 5 mmol) in dioxane (5 ml) with a 1-M K_2CO_3 solution (10 ml) was worked up at room temperature for 4 h and then made acidic to pH 3 with 3-M HCl to give crude crystals. Recrystallization from CCl_4 gave only **4d** as colorless prisms.

Furthermore, the treatment of **4c** with 1-M NaOH, 1-M LiOH, or 1-M $Ba(OH)_2$ was similarly worked up to give a mixture of **4d** and **5d**, except for the case of 1-M NaOH (Table 3).

(*Z*)-Cbz-⊿Tyr(Ac)-OH (5). Into a suspension of **5d** (1.57 g, 5 mmol) and acetyl chloride (0.47 g, 6 mmol) in dry CH_2Cl_2 (10 ml) was added pyridine (0.47 g, 6 mmol), with stirring, at room temperature. After stirring for 2 h, chloroform (30 ml) was added to the reaction solution. The resulting solution was washed, successively, with 1-M HCl and three times with a saturated aqueous NaCl solution and then dried over anhydrous sodium sulfate. After removing the solvent, the residual syrup was crystallized with cyclohexane; the crystals collected were then recrystallized from benzene to give **5c** as colorless needles.

⊿Tyr(Me)·NCA (6a). Into a suspension of **5a** (0.63 g, 2 mmol) in dry CH_2Cl_2 (6 ml) was added $SOCl_2$ (6 ml), with stirring, below 0 °C. The resulting solution was then stirred continuously at room temperature for 2 h. After removing the solvent and excess $SOCl_2$ under reduced pressure, the residual syrup was dissolved in CCl_4 (10 ml) and then concentrated under reduced pressure. This procedure was repeated three times; then, the crystals collected were recrystallized from ethyl acetate to give **6a** as colorless needles.

⊿Tyr(MOM)·NCA (6b) and ⊿Tyr·NCA (6d). A solution of **5b** (0.2 g, 0.56 mmol) and $SOCl_2$ (2 ml) in dry ethyl ehter (2 ml) was stirred below 0 °C for 1.5 h. The reaction solution was concentrated under reduced pressure and the residure, thus obtained, was dissolved in CCl_4 (6 ml) and again concentrated. This procedure was repeated three

times. Finally, the crude crystals collected were washed with warm chloroform and then recrystallized from dioxane to give **6d** as colorless prisms in a 17% yield. On the other hand, a chloroform filtrate was concentrated to give crude crystals, which were recrystallized from benzene to give **6b** as colorless needles in a 79% yield.

In a similar manner, the treatment of **5b** with $SOCl_2$ in dry ethyl ether (4 ml) was worked up to give only **6b** quantitatively. See Table 5.

⊿Tyr(Ac)·NCA (6c). Similarly, the treatment of **5c** with $SOCl_2$ in CH_2Cl_2 was worked up to give **6c** as colorless needles.

⊿Tyr·NCA (6d). In a similar manner, the treatment of **5d** with $SOCl_2$ was worked up to give crude crystals, which were recrystallized from dioxane to give **6d** as colorless prisms.

(*Z*)-⊿Tyr(Boc)-OMe (7a). To a solution of **6d** (0.2 g, 0.97 mmol) and $(Boc)_2O$ (0.23 g, 1.05 mmol) in THF (2 ml) was added pyridine (30 μl); the resulting solution was stirred continuously at room temperature for 12 h. After adding methanol (5 ml), the reaction solution was made basic to pH 9 with NMM and then stirred for 1 h. After removing the solvent under reduced pressure, the residue was dissolved in ethyl acetate (15 ml); the resultant solution was then washed with water and dried over anhydrous sodium sulfate. After concentrating the solution under reduced pressure, thus obtained, the residue was purified on a silica-gel column using a mixture of hexane and ethyl acetate (20:1 v/v) as the eluent. The fraction eluted was concentrated under reduced pressure to give residual crystals, which were recrystallized from hexane to give **7a** as colorless prisms.

(*Z*)-⊿Tyr(Cbz)-OMe (7b). To a solution of **6d** (0.2 g, 0.97 mmol) and pyridine (94 μl, 1.16 mmol) in THF (2 ml) was added, drop by drop, a solution of Cbz-Cl (0.17 ml, 1.06 mmol) in THF (1 ml) at room temperature. The reaction solution was similarly worked up to give **7b**.

(*Z*)-Boc-⊿Tyr(Cbz)-OMe (7c). A solution of **6d** (0.2 g, 0.97 mmol) and $(Boc)_2O$ (0.23 g, 1.05 mmol) in the presence of pyridine (30 μl) in THF (2 ml) was stirred at room temperature for 12 h. After first adding triethylamine (0.22 ml) and then a solution of Cbz-Cl (0.25 ml, 1.46 mmol) in THF (1 ml), the resulting solution was stirred for 4 h. Methanol (20 ml) was further added to the reaction solution, which was then made basic to pH 9—10 with NMM; stirring continued at room temperature for 3 h. After evaporating the solvent under reduced pressure, the residue was dissolved in ethyl acetate (20 ml); the resultant solution was then washed three times with water and finally dried over anhydrous sodium sulfate. After concentrating under reduced pressure, the residue, thus obtained, was purified on a silica-gel column using a mixture of hexane and ethyl acetate (20:1 v/v) as the eluent. The fraction eluted was concentrated to give residual crystals, which were recrystallized from diisopropyl ether to give **7c** as colorless needles.

(*Z*)-Cbz-⊿Tyr(Boc)-OMe (7d). To a solution of **6d** (0.2 g, 0.97 mmol) and pyridine (94 μl, 1.16 mmol) in THF (2 ml) was added, drop by drop, a solution of Cbz-Cl (0.17 ml, 1.06 mmol) in THF (1 ml) at room temperature. After stirring for 1.5 h, triethylamine (0.17 ml) and then $(Boc)_2O$ (0.27 g, 1.23 mmol) were added to the resulting solution. The reaction solution was similarly worked up at room temperature for 18 h to give **7d** as colorless needles.

References

1) Part VII. C. Shin, Y. Yonezawa, and M. Ikeda, *Bull. Chem. Soc. Jpn.*, **59**, 3573 (1986).

2) N. Shimada, K. Morimoto, H. Naganawa, T. Takita, M. Hamada, K. Maeda, T. Takeuchi, and H. Umezawa, *J. Antibiot.*, **34**, 1613 (1981).

3) T. Shiroza, N. Ebisawa, K. Furihata, T. Endo, H. Seto, and N. Otake, *Agric. Biol. Chem.*, **46**, 865 (1982).

4) T. Komori, M. Ezaki, E. Kino, M. Kohsaka, H. Aoki, and H. Imanaka, *J. Antibiot.*, **38**, 691 (1985).

5) C. C. Culvenor, P. A. Cockrum, J. A. Edgar, J. L. Frahn, C. P. Gorst-Allman, A. J. Johones, W. F. O. Marasas, K. E. Murray, L. W. Smith, P. S. Steyn, R. Vleggaar, and P. L. Wesseis, *J. Chem. Soc., Chem. Commun.*, **1983**, 1259.

6) For example, Y. Shimohigashi, H. Chen, and C. H. Stammer, *Peptides*, **3**, 985 (1982).

7) Y. Yonezawa, C. Shin, Y. Ono, and J. Yoshimura, *Bull. Chem. Soc. Jpn.*, **53**, 2905 (1980).

8) C. Shin, Y. Yonezawa, and T. Yamada, *Chem. Pharm. Bull.*, **32**, 3934 (1984).

9) C. Shin and Y. Yonezawa, *Chem. Lett.*, **1985**, 519.

10) For example, Y. Shimohigashi and C. H. Stammer, *J. Chem. Soc., Perkin Trans. 1*, **1983**, 803.

11) For examples, a) I. Ojima and N. Noda, *Tetrahedron Lett.*, **23**, 2175 (1982); b) M. Takasaki and K. Harada, *J. Chem. Soc., Chem. Commun.*, **1987**, 571.

12) C. Shin, Y. Yonezawa, and T. Obara, *Heterocycles*, **27**, 1561 (1986).

13) C. Shin, Y. Yonezawa, and E. Watanabe, *Tetrahedron Lett.*, **26**, 85 (1985).

14) C. Shin, T. Obara, S. Segami, and Y. Yonezawa, *Tetrahedron Lett.*, **28**, 3827 (1987).

15) C. Shin, Y. Nakajima, T. Haga, and Y. Sato, *Bull. Chem. Soc. Jpn.*, **59**, 3917 (1986).

16) H. Hemetsberger, D. Knittel, and H. Weidmann, *Monatsh. Chem.*, **100**, 1599 (1969).

17) a) U. Schmidt, A. Lieberknecht, and J. Wild, *Synthesis*, **1984**, 53. b) U. Schmidt, A. Lieberknecht, U. Schanbacher, T. Beuttler, and J. Wild, *Angew. Chem., Int. Ed. Engl.*, **21**, 776 (1982).

18) C. Shin, M. Hayakawa, T. Suzuki, A. Ohtsuka, and J. Yoshimura, *Bull. Chem. Soc. Jpn.*, **51**, 550 (1978).

Photochemical Reactions of Phthalazine in 2-Propanol

Hiroyasu INOUE,* Tadamitsu SAKURAI, Koichi TOMIYAMA, Ryo SANO, Masahiro OSHIO, Toshihiko HOSHI,† and Jun OKUBO†

Department of Applied Chemistry, Faculty of Technology, Kanagawa University, Kanagawa-ku, Yokohama 221

†Department of Chemistry, College of Science and Engineering, Aoyama Gakuin University, Setagaya-ku, Tokyo 157

(Received July 27, 1987)

Phthalazine undergoes dual photoreactions to simultaneously give two photoproducts, 1,2-dihydrophthalazine (**1**) and 1,1′,2,2′-tetrahydro-1,1′-biphthalazine (**2**), upon ultraviolet light irradiation in 2-propanol under nitrogen. There occurs neither photochemical nor thermal interconversion between **1** and **2**; these compounds are formed independently from a common intermediate through different reaction pathways. The results of quenching and sensitization experiments for both the reactions and the phosphorescence emission show that the lowest excited singlet and triplet states of phthalazine participate in the formation of **1** and **2**, respectively. The observed photochemical behaviors under various conditions lead us to propose a reaction mechanism: Phthalazine is photoreduced in the S_1 state to form 1,2-dihydro-1-phthalazinyl radical. The resulting radical in a solvent cage undergoes a subsequent hydrogen abstraction to form **1**. On the other hand, the same radical produced in the T_1 state escapes from the solvent cage to cause a dimerization which affords **2**.

The photochemical behavior of a variety of nitrogen heterocyclic compounds have been studied.[1,2] Especially, the photoreductions of acridine and phenazine have been extensively studied.[3–6] However, little is known concerning the photochemical behavior of ortho-diazines. Chen et al.[7] studied the photoreaction of 4-methylcinnoline in ethers, and showed that a 1,4-addition of the ethers occurred. Davis and Cohen[8] reported that benzo[*c*]cinnoline underwent a photoreduction to give 5,6-dihydrobenzo[*c*]cinnoline in a benzene solution containing triethylamine. In previous papers[9] we reported that the photoirradiation of benzo[*c*]cinnoline in acidified alcoholic solutions leads to the formation of 2,2′-diaminobiphenyl or carbazole as the final product, depending on the experimental conditions. It was found that 5,6-dihydrobenzo[*c*]cinnoline is formed through the lowest triplet state at the initial stage in both of these reactions.

As for phthalazine, there have not been many descriptions concerning its photochemical behavior. Previously, Wake et al.[10] reported that phthalazine undergoes photoalkylation in acidified alcohols. They also noted that a reductive dimerization product was obtained upon irradiation in 2-propanol without added acid. However, the mechanism of this reaction has not yet been ascertained.

In this paper, we describe photochemical reactions of phthalazine in 2-propanol. Analyses of the photoproducts are given, showing that two products were formed. The reactive excited states for each product which were determined are discussed along with the reaction mechanism in terms of the observed cage effects.

Experimental

Materials. Phthalazine was obtained from Aldrich Chem. Co. and was recrystallized from a mixture of benzene and hexane. 2,4-Hexadien-1-ol (Tokyo Kasei Kogyo) was purified by fractional crystallization, and 4,4′-bis(dimethylamino)benzophenone (Michler's ketone) was recrystallized from ethanol. Hexadecyltrimethylammonium chloride and bromide were obtained from Wako Pure Chemical Ind. and were recrystallized from a mixture of acetone and methanol.

Measurements. UV absorption spectra were measured with a Shimadzu UV-210A spectrophotometer. Phosphorescence spectra were recorded on a Shimadzu RF-500 spectrofluorimeter equipped with a cylindrical rotating sector at 77 K. IR spectra were obtained with a Hitachi EPI-G3 infrared spectrometer in a KBr disk. Proton NMR spectra were taken with a JEOL PS-100 100 MHz spectrometer in deuterated chloroform.

Light Source and Irradiation. In the preparative experiments, two light sources were employed using no filter: (I) a 400 W high-pressure mercury lamp (Rikagaku Sangyo UVL-400 HA) and (II) a 160 W low-pressure mercury lamp (Rikagaku Sangyo UVL-160 LA). For the 254-nm light irradiation, a 70 W low-pressure mercury lamp (Ushio UL1-7SQ) and a solution filter ($NiSO_4$ 500 g dm^{-3}) were used. For the 313-nm light irradiation, a 450 W high-pressure mercury lamp (Ushio UM-452) and a set of filters comprising a solution (1% K_2CO_3 containing 10^{-2} mol dm^{-3} K_2CrO_4) and a Corning glass (CS-7-54) were used. For the 366-nm light irradiation, a 450W high-pressure mercury lamp and Corning glass filters (CS-7-54 and CS-0-52) were used.

Unless otherwise noted, all irradiations were carried out in a 5×10^{-2} dm^3 quartz cylindrical vessel at room temperature. Solutions of phthalazine were flushed with nitrogen passed through a pyrogallol solution before and during irradiation.

Actinometry and Analysis of Products. For a determination of the quantum yields for photoreactions, the light intensities were measured using a potassium trioxalatoferrate(III) solution as an actinometer.[11] The amounts of photoproducts were spectrophotometrically determined using the molar extinction coefficients of the UV absorption bands of the products described in the text.

Isolation and Identification of the Photoproducts. A 3×10^{-3}mol dm^{-3} solution of phthalazine in 0.5 dm^3 of 2-propanol was irradiated for 5 h using light-source (I) under nitrogen. The irradiated solution was evaporated to dryness and the residue was subjected to TLC (silica gel, chloroform–methanol 30:1). The compound, thus obtained, showed the following properties: IR(KBr) 3250 (NH) and 1440 cm^{-1} (CH_2); ^{1}H NMR($CDCl_3$) δ=4.2(2H, s, CH_2), 5.3 (1H, m, NH) and 6.8—7.6(5H, m, aromatic H); mp 62.5—64.0 °C (decomp). The product **1** was identified as 1,2-dihydrophthalazine. Further supporting evidence for the identification of **1** was obtained from the benzoyl derivative of the isolated product. A treatment of the product with *p*-methylbenzoyl chloride gave a benzoyl derivative which was characterized by IR and elemental analyses.

A 1.5×10^{-2} mol dm^{-3} solution of phthalazine in 0.5 dm^3 of 2-propanol was irradiated for 8 h using light-source (II) under nitrogen. The irradiated solution was concentrated under reduced pressure. The precipitated crystals were collected by filtration and recrystallized twice from methanol. The physical properties of the crystals were identical with those of the dimerization product reported by Wake et al.[10] Product **2** was identified as 1,1′,2,2′-tetrahydro-1,1′-biphthalazine.

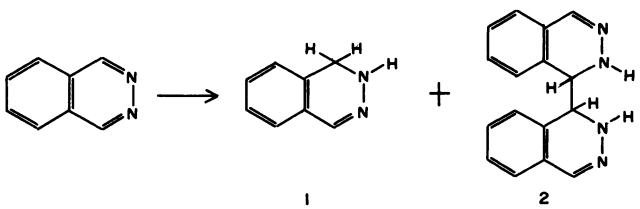

1 2

Results and Discussion

Reaction Products. The absorption spectral change caused by the irradiation of a 2-propanol solution of phthalazine is shown in Fig. 1. During the initial stage of the reaction, an absorption band appeared around 335 nm. With successive irradiation the absorption maximum shifted progressively to shorter wavelengths accompanying an increase in intensity. These spectral features indicate that there are at least two main photoproducts. From the preparative experiments mentioned above, two photoproducts

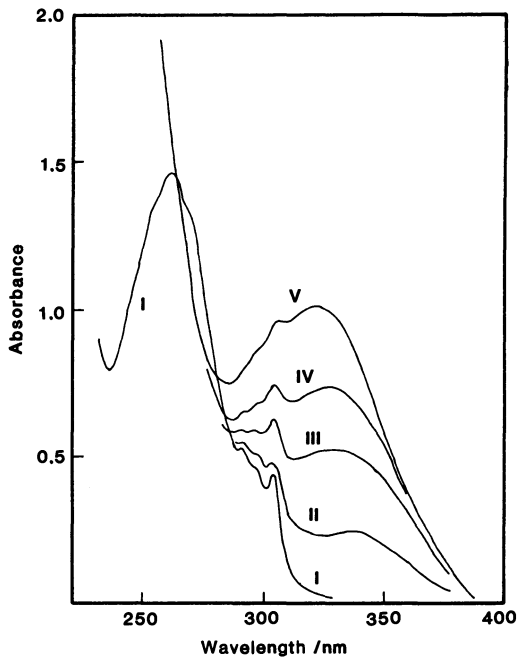

Fig. 1. Spectral change caused by the 254 nm light irradiation upon a 2-propanol solution of phthalazine (4.0×10^{-4} mol dm^{-3}).
Irradiation time (min); I: 0, II: 10, III: 40, IV: 80, V: 160.

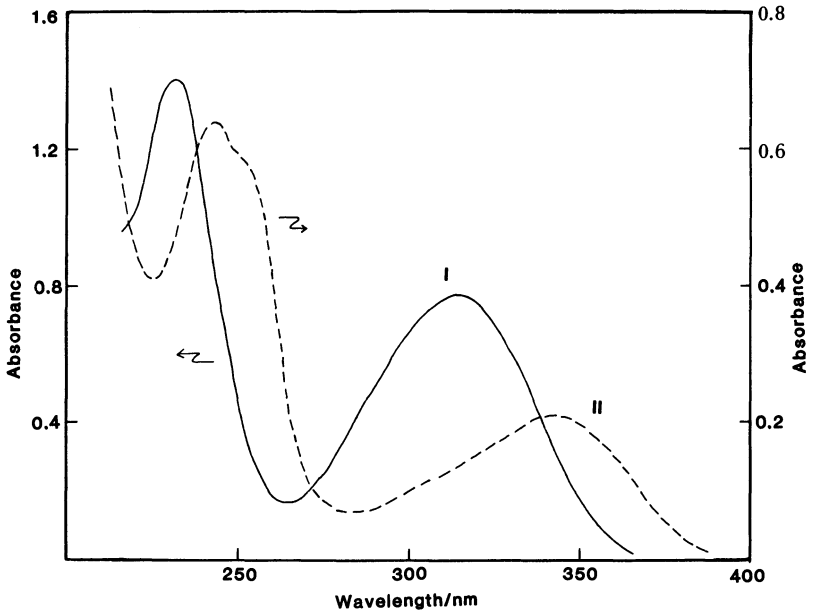

Fig. 2. Absorption spectra of the photoproducts in 2-propanol.
I: **1** (1.4×10^{-4} mol dm^{-3}), II: **2** (2.3×10^{-5} mol dm^{-3}).

were obtained: 1,2-dihydrophthalazine (**1**) and 1,1′,2,2′-tetrahydro-1,1′-biphthalazine (**2**). The absorption spectra of these compounds are presented in Fig. 2.

Changes in the concentrations of **1** and **2** during the course of the reactions were determined using the molar absorption coefficients of **1** and **2** (Fig. 3). It can be seen that the amount of **1** gradually increased with the irradiation time (37% yield based on the starting material at 140 min irradiation), whereas the amount of **2** reached a constant value after irradiation for an appropriate period (40% yield). However, **2** formed more rapidly than **1** during the initial stage of the reaction. These results could plausibly be interpreted as indicating that **2** was formed first, and then decomposed to give **1**. However, this is not the case (as indicated below).

In order to examine the possibilities of an interconversion between **1** and **2**, the photochemical behavior of **1** and **2** were studied using these compounds isolated in preparative experiments. Irradiation of 366-nm light for 50 min on a 2-propanol solution of **2** (3.6×10^{-5} mol dm^{-3}) resulted in the photodecomposition yielding phthalazine almost quantitatively.[12] Therefore, the saturation of the amount of **2** produced in the course of the photoreaction of phthalazine (curve II in Fig. 3) can be attributed to this backward photoreaction; the photostationary state could be established between phthalazine and **2** under the irradiation of light which could be absorbed by both compounds. On the other hand, the irradiation of 313-nm light on a solution of **1** did not cause a pronounced photoreaction. Consequently, it can be said that phthalazine undergoes photoreactions through two distinct pathways to afford **1** and **2** independently. A similar photochemical behavior has been found for acridine, which gives 9,10-dihydroacridine together with 9,9′,10,10′-tetrahydro-9,9′-biacridine.[13–16] Kira and Koizumi[17] reported that the photoproduct of 9,9′,10,10′-tetrahydro-9,9′-biacridine is acridine. This reaction is quite similar to the photoreaction of **2** (described above).

Quenching and Sensitization. In order to elucidate the reactive excited states for the observed photoreactions, triplet quenching experiments were conducted employing 2,4-hexadien-1-ol having a lower triplet energy (E_T=249 kJ mol^{-1})[19] than that of phthalazine (E_T=256 kJ mol^{-1}). Quenching data are presented in Fig. 4. The value of ϕ_0 (quantum yield without quencher) for **1** and **2** are 0.013 and 0.041, respectively. As can be seen from Fig. 4, the formation of **2** is apparently quenched, while that of **1** is not influenced by the addition of the quencher (up to 1.0×10^{-3}mol dm^{-3}). In addition, quenching for the phosphorescence emission of phthalazine in a mixture of ethanol and methanol (1:1 v/v) at 77 K has also been observed in the presence of the same quencher (Fig. 5).

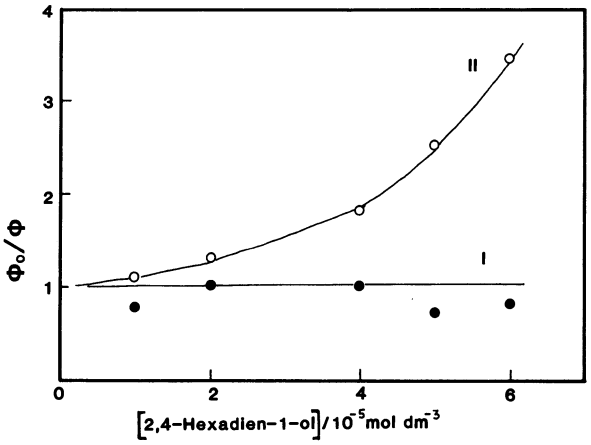

Fig. 4. Stern-Volmer quenching plots for the quantum yields of the formation of **1** (I) and **2** (II). [phthalazine]=2.0×10^{-4} mol dm^{-3}, excitation wavelength=313 nm.

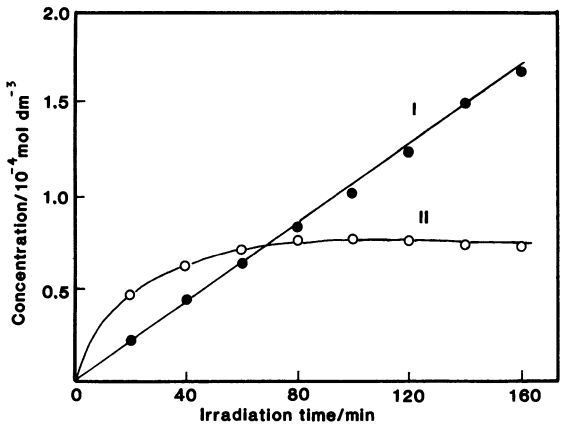

Fig. 3. Change in the concentrations of the products **1** (I) and **2** (II) with the 254 nm light irradiation of phthalazine (4.0×10^{-4} mol dm^{-3}) in 2-propanol.

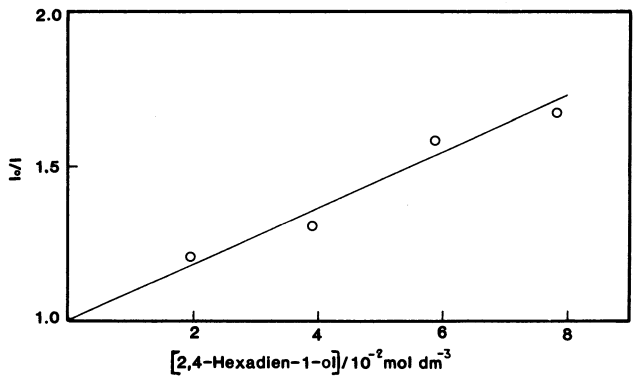

Fig. 5. Stern-Volmer quenching plots for the phosphorescence of phthalazine (480 nm) at 77 K. [phthalazine]=1.0×10^{-3} mol dm^{-3}, excitation wavelength=313 nm.

The feature of the reaction quenching plot (curve II in Fig. 4) differs from that of the phosphorescence. The observed upward curvature for the quenching plot at higher temperatures could be tentatively attributed to the quenching of two excited states, T_1 and T_2,[20] which are known to be located very close to each other;[21,22] thus, both states are in equilibrium at higher temperatures. However, further detailed studies need to be conducted before this subject can be solved.

Since the shapes of the absorption and the phosphorescence spectra of phthalazine have been confirmed to remain unaltered by the quencher, it may be considered that there are no specific interactions such as the ground-state complexing or an exciplex formation between the reactant and the quencher. In the present quenching system, a singlet-singlet energy transfer from the reactant to the quencher can evidently be ruled out as the quenching mechanism in view of the S_1 state energies of the compounds concerned.[23] Consequently, the quenching observed for the formation of **2** can be interpreted in terms of a triplet-triplet energy transfer. The obtained results suggest that the reactive excited states for the formations of **1** and **2** are the lowest excited singlet state and the lowest triplet state, respectively.

Supporting evidence for this suggestion has been provided by triplet sensitization studies. 4,4'-Bis(dimethylamino)benzophenone (Michler's ketone) was used as the triplet sensitizer under excitation with 366-nm light which was absorbed by only the sensitizer. This compound is photostable and has a triplet energy, E_T=259 kJ mol^{-1}.[24,25] A Stern-Volmer sensitization plot is shown in Fig. 6, in which a linear relationship is established between the reciprocal of the quantum yield and the reciprocal of the phthalazine concentration at a fixed concentration of the sensitizer (2.0×10^{-5} mol dm^{-3}). It can clearly be seen from Fig. 6 that the formation of **2** can be efficiently sensitized by Michler's ketone donor, while no sensitization is noted for the formation of **1**. In this connection, the occurrence of a triplet-triplet energy transfer from the ketone to the phthalazine acceptor can readily be recognized from the phosphorescence emission behavior illustrated in Fig. 7. A lack of the sensitization in the formation of **1** indicates that the S_1 mechanism is operative in the formation of **1** with a direct excitation of the substrate.

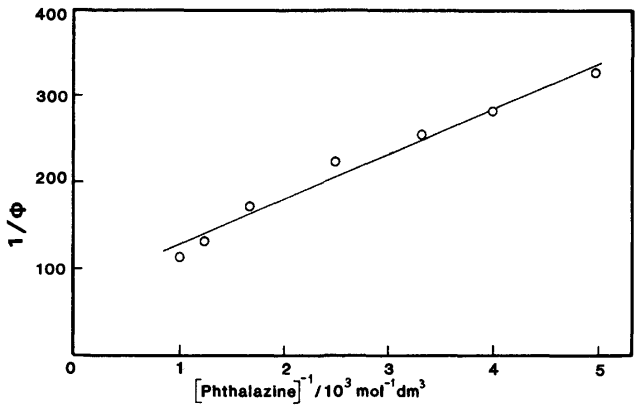

Fig. 6. Sensitization plots for the formation of **2**.
[4,4'-bis(dimethylamino)benzophenone]=2.0×10^{-5} mol dm^{-3}, excitation wavelength=366 nm.

According to the present reaction mechanism, an S_1-T_1 intersystem crossing is required to take place appreciably in order to account for the formation of **2**. In this connection, the triplet quantum yield of phthalazine was recently reported to be 0.43 at room temperature[22] and 0.49 at 77 K.[26]

Effects of Surfactants. In view of the type of both reactions described above, it may be probable that during the primary step phthalazine (P), both in the S_1 and T_1 excited states, similarly undergoes hydrogen atom abstraction from 2-propanol (RH) to afford an 1,2-dihydro-1-phthalazinyl radical (PH·) and an alcohol radical (**R**·). In fact, Kanamaru et al.[27]

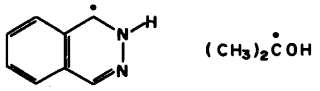

PH· R·

reported the transient absorption spectrum of 1,2-dihydro-1-phthalazinyl radical generated in an alcoholic solution by flash photolysis method at room temperature. Castellano et al.[28] also obtained the same radical by UV irradiation at 115 K. It seems quite reasonable, therefore, that the production of **2** can be ascribed to the combination of 1,2-dihydro-1-

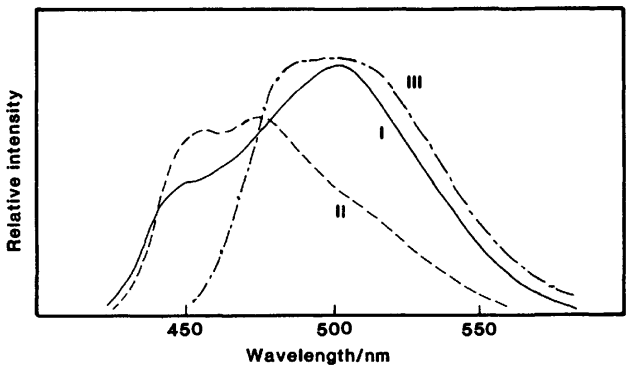

Fig. 7. Sensitization of the phosphorescence of phthalazine by 4,4'-bis(dimethylamino)benzophenone in a methylcyclohexane matrix.
I: [phthalazine]=6.0×10^{-4} mol dm^{-3}, [4,4'-bis(dimethylamino)benzophenone]=2.0×10^{-5} mol dm^{-3}, excitation wavelength=366 nm; II: [4,4'-bis(dimethylamino)benzophenone]=2.0×10^{-5} mol dm^{-3}, excitation wavelength=366 nm; III: [phthalazine]=6.0×10^{-4} mol dm^{-3}, excitation wavelength=305 nm.

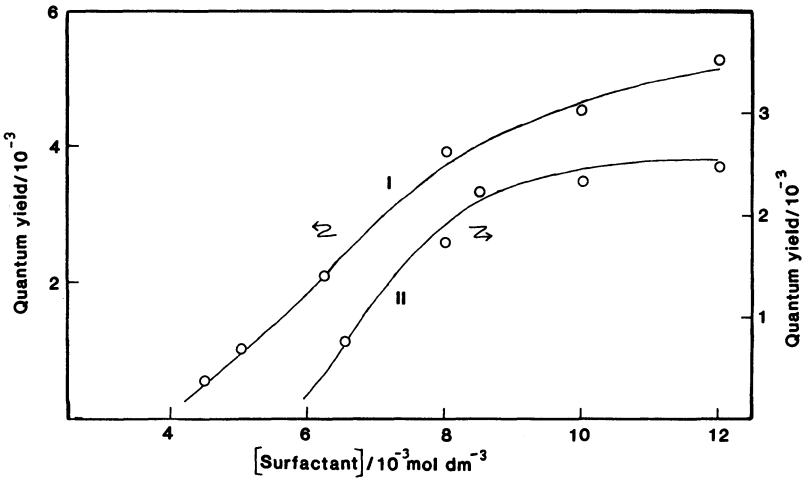

Fig. 8. Effects of the surfactants on the quantum yield of the formation of **1** in aqueous 2-propanol (0.3 mol dm^{-3}).
I: hexadecyltrimethylammonium chloride; II: hexadecyltrimethylammonium bromide, [phthalazine]=4.0×10^{-3} mol dm^{-3}, excitation wavelength=254 nm.

phthalazinyl radicals produced from the triplet precursor. A similar photoreductive dimerization was reported earlier for acridine.[13–16] Thus, the formation of 9,9′,10,10′-tetrahydro-9,9′-biacridine has been ascertained in the photoreduction of acridine in hydrogen-donating solvents; also, a semiquinone radical with an unpaired electron on 9-carbon atom is regarded as an intermediate in the dimerization.[17]

To obtain suggestive information concerning the mechanism for the formation of **1** as well as the origin of the different behavior between the 1,2-dihydro-1-phthalazinyl radical formed from the S_1 and that from the T_1 states of phthalazine, cage effects on the reactions were examined using surface-active agents. Micelles are known to become a good means for causing an efficient cage reaction of radical pair produced photochemically or thermally.[29–31] Figure 8 shows the results of the micellar effects on the photoreactions. The quantum yield for the production of **1** is significantly affected by the addition of the surfactants. The production of **1** is apparently observed above the cmc of surfactants.[32] On the other hand, **2** is formed to a very small extent, even at high concentrations of the surfactants. These results strongly indicate that **1** can be produced in micelles, but **2** cannot. Therefore, it is conceivable that for the photoreaction system in a 2-propanol solution, the 1,2-dihydro-1-phthalazinyl radical formed through the S_1 state and the alcohol radical are trapped as a radical pair in a solvent cage. This results in a further hydrogen abstraction, leading to product **1** and acetone. Although we cannot rule out the possibility of the participation of an alcohol molecule in the second hydrogen abstraction, at this time the hydrogen atom can be considered as coming from the alcohol radical, since the triplet sensitization reaction does not give product **1**. In any case, 2-propanol may be expected to give acetone; in fact, acetone has been detected in irradiated solutions by gas chromatography.

Here, it is particularly noteworthy that generally radical pairs produced from S_1 states undergo more effective cage reactions or micellar reactions than radical pairs from T_1 states.[30,33–35] Recently we have reported that some hydroxylamines undergo photorearrangements through a singlet-derived radical pair in a solvent cage as well as photofragmentation through a triplet-derived radical pair after escaping from a solvent cage.[36]

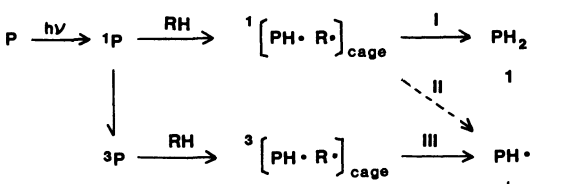

P: Phthalazine
^{1}P: P in the S_1 state
^{3}P: P in the T_1 state
RH: 2-Propanol
PH·: 1,2-Dihydro-1-phthalazinyl radical
R·: 1-Hydroxy-1-methylethyl radical
^{1}[ ]: Singlet state radical pair in solvent cage
^{3}[ ]: Triplet state radical pair in solvent cage

In conclusion, we propose a reaction mechanism for the dual photochemical reactions of phthalazine, as illustrated in the scheme. The pathway, denoted I, refers to the reaction of the 1,2-dihydro-1-phthalazinyl radical in the S_1 cage. Process II is a plausible escape route for radicals from the S_1 cage, taking place in

competition with I. Although the extent of the contribution of this process to the formation of a free PH·radical is not clear, it cannot be ruled out only from the experimental results obtained here. Process III can be considered to result in a very efficient diffusion of the radical pair from the T_1 cage into solution. In a triplet cage, neither an intersystem crossing to the singlet radical pair nor a second hydrogen abstraction can take place sufficiently.

Accordingly, the results mentioned here are examples of photochemical reactions in which an excited molecule in the S_1 state abstracts hydrogen with an efficiency which is comparable to that of an intersystem crossing to the T_1 state. In this connection, the rate of the S_1–T_1 intersystem crossing (k_{ISC}) at room temperature has been reported to be about 1.5 ns^{-1}.[21,22]

References

1) N. J. Turro, "Energy Transfer and Organic Photochemistry," Wiley, New York (1969), p. 275.

2) M. Mousseron-Canet and J. C. Mani, "Photochemistry and Molecular Reactions," Translated by J. Schmorak, Israel Program for Scientific Translations Ltd. (1972), p. 83.

3) D. G. Whitten and Y. J. Lee, *J. Am. Chem. Soc.*, **93**, 961 (1971).

4) G. A. Davis, J. D. Gresser, and P. A. Carapellucci, *J. Am. Chem. Soc.*, **93**, 2179 (1971).

5) D. N. Bailey, D. K. Roe, and D. M. Hercules, *J. Am. Chem.Soc.*, **90**, 6291 (1968).

6) K. Kikuchi, K. Kasama, A. Kanemoto, K. Uji-ie, and H. Kokubun, *J. Phys. Chem.*, **89**, 868 (1985).

7) T. T. Chen, W. Dörscheln, H. Göth, M. Hesse, and H. Schmid, *Helv. Chim. Acta*, **51**, 632 (1968).

8) G. A. Davis and S. G. Cohen, *J. Chem. Soc., Chem. Commun.*, **1971**, 675.

9) H. Inoue, T. Sakurai, and F. Tanaka, *Bull. Chem. Soc. Jpn.*, **48**, 924 (1975); H. Inoue, Y. Hiroshima, and N. Makita, *ibid.*, **52**, 351 (1979); H. Inoue, Y. Hiroshima, K. Miyazaki, *ibid.*, **52**, 664 (1979); H. Inoue, Y. Hiroshima, T. Sakai, T. Sakurai, and N. Fukuda, *ibid.*, **54**, 2829 (1981).

10) S. Wake, Y. Takayama, Y. Otsuji, and E. Imoto, *Bull. Chem. Soc. Jpn.*, **47**, 1257 (1974).

11) C. G. Hatchard and C. A. Parker, *Proc. R. Soc. London, Ser. A*, **235**, 518 (1956).

12) Because **2** has the absorption band at longer wavelengths than that of phthalazine, the selective excitation of **2** can be performed with 366 nm light irradiation without the excitation of phthalazine produced from **2**.

13) F. Mader and V. Zanker, *Chem. Ber.*, **97**, 2418 (1964).

14) M. Giurgea, G. Mihai, V. Topa, and M. Musa, *J. Chim. Phys.*, **61**, 619 (1964).

15) A. Kellman, *J. Chim. Phys.*, **63**, 936 (1966).

16) H. Göth, P. Cerutti, and H. Schmid, *Helv. Chim. Acta*, **48**, 1395 (1965).

17) A. Kira and M. Koizumi, *Bull. Chem. Soc. Jpn.*, **42**, 625 (1969).

18) S. L. Murov, "Handbook of Photochemistry," Marcel Dekker Inc., New York (1973), p. 4.

19) H. Rau, *Ber. Bunsenges. Phys. Chem.*, **72**, 408 (1968).

20) P. J. Wagner, "Creation and Detection of the Excited State, ed by A. A. Lamola, vol. 1, Part A, Marcel Dekker, Inc., New York (1971), p. 173.

21) R. W. Anderson and W. Knox, *J. Lumin.*, **24/25**, 647 (1981).

22) D. W. Boldridge, G. W. Scott, and T. A. Spiglanin, *J. Phys. Chem.* **86**, 1976 (1982).

23) Although the energy of the lowest excited singlet state of 2,4-hexadien-1-ol is not known, it is evident from the absorption spectra that it is higher than that of phthalazine.

24) E. V. Donckt and G. Porter, *J. Chem. Phys.*, **46**, 1173 (1967).

25) G. Porter and P. Suppan, *Trans. Faraday Soc.*, **61**, 1664 (1965).

26) T. Takemura, K. Yamamoto, I. Yamazaki, and H. Baba, *Bull. Chem. Soc. Jpn.*, **45**, 1639 (1972).

27) N. Kanamaru, S. Nagakura, and K. Kimura, *Bull. Chem. Soc. Jpn.*, **47**, 745 (1974).

28) A. Castellano, J. P. Catteau, A. Lablache-Combier, and B. Tinland, *J. Chem. Res. (S)*, **1979**, 70; A. Castellano, J. P. Catteau, and A. Lablache-Combier, *Tetrahedron*, **31**, 2255 (1975); A. Castellano, J. P. Catteau, A. Lablache-Combier, and B. Planckaert, *Tetrahedron Lett.*, **1973** 4185.

29) N. J. Turro, B. Kraeuter, and D. R. Anderson, *J. Am. Chem. Soc.*, **101**, 7435 (1979).

30) N. J. Turro and G. C. Weed, *J. Am. Chem. Soc.*, **105**, 1861 (1983).

31) P. Herve, F. Nome, and J. H. Fendler, *J. Am. Chem. Soc.*, **106**, 8291 (1984).

32) S. S. Atik and A. Singer, *Chem. Phys. Lett.* **59**, 519 (1978).

33) G. S. Hammond and J. R. Fox, *J. Am. Chem. Soc.*, **86**, 1918 (1964).

34) J. R. Fox and G. S. Hammond, *J. Am. Chem. Soc.*, **86**, 4031 (1964).

35) P. D. Bartlett and N. A. Porter, *J. Am. Chem. Soc.*, **90**, 5317 (1968).

36) a) T. Sakurai, H. Yamamoto, S. Yamada, and H. Inoue, *Bull. Chem. Soc. Jpn.*, **58**, 1174 (1985). b) T. Sakurai, H. Sukegawa, and H. Inoue, *ibid.*, **58**, 2875 (1985).

 © 1988 The Chemical Society of Japan Bull. Chem. Soc. Jpn., 61, 899—903 (1988)

Racemic Structure and Optical Resolution by Preferential Crystallization of (±)-Organic Ammonium Hydrogen Malates

Tadashi SHIRAIWA,* Yujin SADO, Mitsuo INOUE, Keiji SAKAMOTO, Hideya MIYAZAKI, and Hidemoto KUROKAWA
Faculty of Engineering, Kansai University, Yamate-cho, Suita, Osaka 564
(Received July 29, 1987)

Gibbs energies of formation of racemate, binary melting point diagrams, and ternary solubility diagrams indicate that (±)-propylammonium ((±)-PA salt) and (±)-1,1,3,3-tetramethylbutylammonium ((±)-TMB salt) hydrogen malates are conglomerates at room temperature, whereas (±)-TMB salt forms a racemic compound at its melting point. Free energies of critical nucleation in supersaturated solutions were examined to resolve (±)-PA and -TMB salts efficiently by preferential crystallization. Successive preferential crystallization of (±)-PA salt in methanol at 10 °C and that of (±)-TMB salt in water give (+)- and (−)-PA and -TMB salts with about 90% optical purity. Optically pure (+)- and (−)-malic acids are obtained from purified (−)- and (+)-salts.

Optically active malic acid (abbreviated as MAL) is a useful material for food additives and medicines and a resolving agent for racemic organic amines. (±)-MAL has been optically resolved by preferential crystallization in the form of (±)-ammonium[1] and (±)-α-methylbenzylammonium[2] hydrogen malates and by the diastereomeric procedure using (+)-tartaric acid[3] as a resolving agent. This paper describes an attempt to resolve optically (±)-organic ammonium hydrogen malates by preferential crystallization. The examined (±)-salts were methylammonium ((±)-MA salt), ethylammonium ((±)-EA salt), propylammonium ((±)-PA salt), isopropylammonium ((±)-IPA salt), butylammonium ((±)-BA salt), isobutylammonium ((±)-IBA salt), *t*-butylammonium ((±)-TBA salt), pentylammonium ((±)-PTA salt), hexylammonium ((±)-HA salt), octylammonium ((±)-OA salt), 1,1,3,3-tetramethylbutylammonium ((±)-TMB salt), anilinium ((±)-AN salt), diisobutylammonium ((±)-DIB salt), dicyclohexylammonium ((±)-DCH salt), dibenzylammonium ((±)-DBZ salt), and cyclohexylmethylammonium ((±)-CMA salt) salts.

The racemic structure of the (±)-salts was determined by thermodynamic analysis.[4,5] (±)-PA and -TMB salts which seemed to be conglomerates were subjected to a resolution by preferential crystallization. The free energy of critical nucleation in supersaturated solutions of the (+)- and (−)-salts was examined to find the appropriate conditions for the optical resolution.[6-8]

Experimental

Materials. (±)-Malic acid and amines were purchased from Wako Pure Chemicals Ind. and Kanto Chemical Co., Ltd., and (+)- and (−)-MAL were donated from Fuso Chemical Co., Ltd.; (+)-MAL $[\alpha]_D^{20}$+2.90° (*c* 30.0, methanol); (−)-MAL $[\alpha]_D^{20}$−2.92° (*c* 30.0, methanol) (lit,[9] $[\alpha]_D$−2.92° (*c* 30%, methanol)).

Preparation of Organic Ammonium Salt. A solution of 0.01 mol of (±)-, (+)-, or (−)-MAL and equimolar amine in acetone was allowed to stand overnight at 5 °C. The salt formed was filtered and recrystallized from an appropriate solvent; the PA salt was recrystallized from 1-propanol and the TMB salt from ethanol. The (+)-salts were formed from (−)-MAL and amines, and the (−)-salts from (+)-MAL and amines.

(±)-PA salt: Found C, 43.33; H, 7.78; N, 7.13% (calcd for $C_7H_{15}NO_5$: C, 43.52; H, 7.83; N, 7.25%); solubility 11.593 g/(100 cm³ methanol) at 10 °C. (+)-PA salt: Found C, 43.45; H, 7.82; N, 7.29%; $[\alpha]_{436}^{25}$+11.6° (*c* 1.00, methanol); solubility 5.135 g/(100 cm³ methanol) at 10 °C.

(±)-TMB salt: Found C, 54.53; H, 9.47; N, 5.35% (calcd for $C_{12}H_{25}NO_5$: C, 54.73; H, 9.57; N, 5.32%); solubility 8.640 g/(100 cm³ water) and 5.644 g/(100 cm³ methanol) at 10 °C. (+)-TMB salt: Found C, 54.56; H, 9.49; N, 5.34%; $[\alpha]_{436}^{25}$+11.9° (*c* 1.00, methanol); solubility 5.959 g/(100 cm³ water) and 3.320 g/(100 cm³ methanol) at 10 °C.

Optical Resolution. Preferential Crystallization: (±)-PA or -TMB salt was dissolved in 50 cm³ of methanol or water, respectively, at 40 °C to give racemic solutions with different degrees of supersaturation of 120—200%. The solution was slowly cooled to 10 °C and seeded with 0.050 g of the (+)-salt. After stirring the mixture at 10 °C, the precipitated salt was collected by filtration, washed with a small amount of diethyl ether, and dried.

Successive Preferential Crystallization: A methanol solution of (±)-PA salt with 180% supersaturation was seeded with 0.050 g of the (+)-salt at 10 °C. After stirring the mixture for 30 min at 10 °C, the precipitated salt was filtered. (±)-PA salt (0.918 g) was dissolved in the filtrate at 40 °C; the amount was equal to that of the crystallized salt. After seeding the solution with 0.050 g of the (−)-salt at 10 °C, the mixture was treated similarly to above.

An optical resolution of (±)-TMB salt was performed on an aqueous solution with 155% supersaturation, similarly to (±)-PA salt.

The degree of resolution of the (+)- and (−)-salts was calculated by

$$\text{Degree of resolution}/\% = [\text{YOPM}\times 100/\text{g}]/[(\text{Operation amount of the (+)- or (−)-salt/g}) - \text{M/g}],$$

where M is 2.898 g for the PA salt and 2.160 g for the TMB salt, and YOPM is the yield of optically pure modification.[10]

Preparation of Optically Active Malic Acid. The purified (+)- or (−)-PA salt (1.93 g) or -TMB salt (2.63 g) with 100% optical purity was treated as aqueous solutions through a 1.3×17.8 cm column of Amberlite IR-120 of H^+ form by eluting with water. The eluent was evaporated to dryness under reduced pressure at 40 °C; optically pure (+)-MAL was obtained in 1.12 g yield from the (−)-PA salt and in 1.29 g yield from the (−)-TMB salt, and optically pure (−)-MAL was obtained in 1.20 g yield from the (+)-PA salt and in 1.31 g yield from the (+)-TMB salt.

Measurements. Specific rotation was measured by a Union Giken PM-101 digital polarimeter with a quartz cell of 1.0 dm path length. Infrared spectra were obtained in the range 4000—400 cm^{-1} with a JASCO A-102 infrared spectrophotometer by the KBr disk method. Enthalpies of fusion and melting points were determined with a Rigaku Denki differential scanning calorimeter DSC-8230.

Saturated solutions of (±)- and (+)-PA and -TMB salts were prepared at 10 °C; methanol was employed as a solvent for PA salt and water for TMB salt. Refractive index was measured with a Shimadzu refractometer Abbe 3L. Solubility was determined by using the refractive index from calibration curves.

Results and Discussion

Racemic Structure. Racemic Structure at Melting Point: The Gibbs energy of formation of racemate (ΔG_T^F/kJ mol^{-1}) is calculated from enthalpies of fusion (ΔH^f/kJ mol^{-1}) and melting points.[4,5] These values are listed in Table 1; the ΔG_T^F value of (±)-TBA salt could not be calculated because (+)-TBA salt decomposed on heating.

All the (±)-salts give negative values of ΔG_{mp}^F at their melting points except (±)-PA salt. Eutectic temperatures and compositions calculated on the basis of ΔH^f and melting point[11] are listed in Table 1, together with observed melting points of mixtures with eutectic compositions. The melting points agree well with the calculated eutectic temperatures. Only PA salt shows a composition of 0.5 and the other salts those of 0.60—0.93; the binary melting point diagrams of PA and TMB salts are shown in Figs. 1 and 2, respectively. These results have led us to infer that only (±)-PA salt is a conglomerate at the melting point and that the other (±)-salts form racemic compounds.

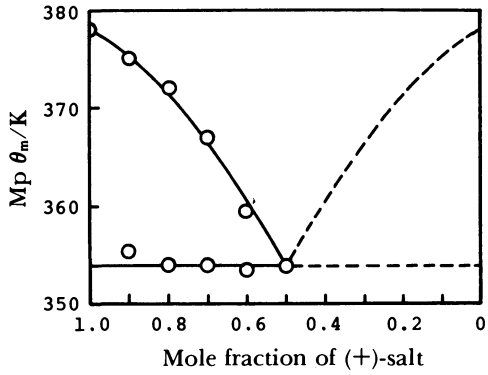

Fig. 1. Binary melting point diagram of propylammonium hydrogen malate.

Table 1. Thermodynamic Data of Organic Ammonium Hydrogen Malate

Salt	Mp θ_m/K		ΔH^f[a]/kJ mol^{-1}		ΔG_T^F[b]/kJ mol^{-1}		Eutectic point		
	(±)	(+)	(±)	(+)	ΔG_{mp}^F	ΔG_{283}^F	Mole fraction[c]	Temperature/K	
								Calcd[c]	Found
MA[e]	349	361	29.7	31.1	−0.98	−0.59	0.66	347	346
EA[f]	398	410	36.0	35.8	−1.25	−0.80	0.68	395	397
PA[g]	354	378	33.2	36.1	+0.44	+0.44	0.50	356	354
IPA[h]	402	402	40.2	38.8	−2.32	−1.49	0.80	394	393
BA[i]	338	334	20.8	23.4	−2.17	−1.25	0.82	326	328
IBA[j]	371	351	32.8	28.7	−3.79	−3.19	0.93	348	349
TBA[k]	440	450[d]	29.2	—	—	—	—	—	—
PTA[l]	350	346	21.2	20.2	−2.24	−1.75	0.83	337	336
HA[m]	346	343	35.7	36.0	−2.29	−1.61	0.84	338	336
OA[n]	350	349	36.0	35.9	−2.11	−1.52	0.81	343	344
TMB[o]	438	457	33.0	41.8	−0.79	+2.73	0.60	437	436
AN[p]	416	411	40.2	40.5	−2.85	−1.08	0.84	405	405
DIB[q]	414	413	33.9	33.7	−2.46	−1.07	0.80	404	405
DCH[r]	437	441	24.2	23.9	−2.30	−0.89	0.78	425	427
DBZ[s]	435	444	45.4	42.3	−1.65	−1.66	0.71	431	433
CMA[t]	364	377	35.5	33.9	−0.93	−1.12	0.64	362	363

a) ΔH^f: Enthalpy of fusion. b) ΔG_T^F: Gibbs energy of formation of racemate. c) These values were calculated from the Schröder-Van Laar and Prigogine-Defay equations. d) Decomposition. e) MA: Methylammonium salt. f) EA: Ethylammonium salt. g) PA: Propylammonium salt. h) IPA: Isopropylammonium salt. i) BA: Butylammonium salt. j) IBA: Isobuytlammonium salt. k) TBA: *t*-Butylammonium salt. l) PTA: Pentylammonium salt. m) HA: Hexylammonium salt. n) OA: Octylammonium salt. o) TMB: 1,1,3,3-Tetramethylbutylammonium salt. p) AN: Anilinium salt. q) DIB: Diisobutylammonium salt. r) DCH: Dicyclohexylammonium salt. s) DBZ: Dibenzylammonium salt. t) CMA: Cyclohexylmethylammonium salt.

Racemic Structure at Room Temperature: (±)-PA and -TMB salts give positive values of ΔG^{F}_{283} at 283 K, whereas the values of the other (±)-salts are negative. (±)-PA and -TMB salts show infrared spectra indentical with those of the corresponding (+)-salts and are more soluble than the (+)-salts as described in the experimental section. The ternary solubility diagram of TMB salt, shown in Fig. 3, illustrates the pattern of a conglomerate.[12] These results indicate that (±)-PA and -TMB salts are conglomerates at room temperature, though (±)-TMB salt forms a racemic compound at its melting point.

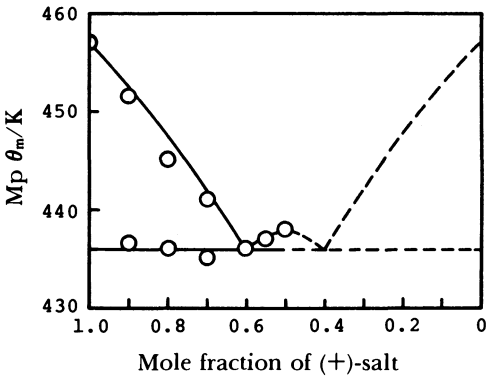

Fig. 2. Binary melting point diagram of 1,1,3,3-tetramethylbutylammonium hydrogen malate.

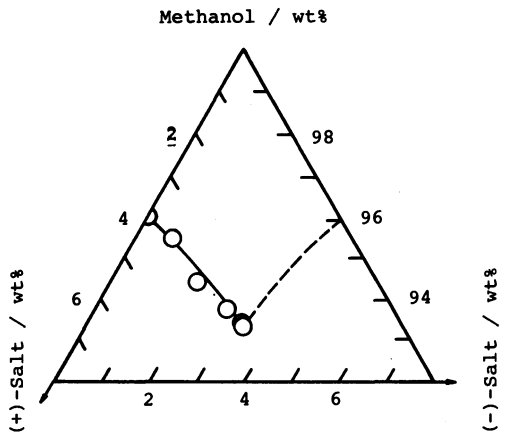

Fig. 3. Ternary solubility diagram of 1,1,3,3-tetramethylbutylammonium hydrogen malate. Solvent: Methanol. Temperature: 10 °C.

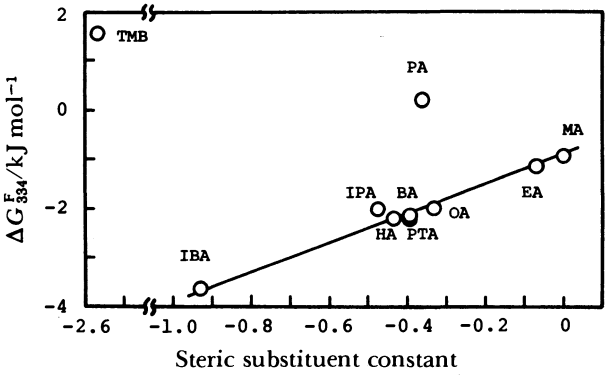

Fig. 4. Relationship between Gibbs energy of formation of racemate and steric substituent constant. ΔG^{F}_{334}: Gibbs energy of formation of racemate at 334 K. E_s: Steric substituent constant; see Ref. 13.

Since the infrared spectra of the other (±)-salts and (±)-TBA salt, of which the corresponding (+)-salt decomposes on heating, are different from those of the corresponding (+)-salts, these (±)-salts may be concluded to form racemic compounds at room temperature.

Substituent Effect on the Gibbs Energy of Formation of Racemic Compound: The formation of racemic compounds of the salts of (±)-MAL with primary amines having an alkyl side chain was examined from the relationship between steric substituent constant (E_S)[13] and ΔG^{F}_{334} value, shown in Fig. 4; the ΔG^{F}_{334} values at 334 K were calculated for comparison at the same temperature.[4,5]

(±)-PA and -TMB salts show positive ΔG^{F}_{334} values, whereas the ΔG^{F}_{334} values of the other (±)-salts are negative. The absolute value of ΔG^{F}_{334} tends to increase with an increase in the absolute value of E_S. Since (±)-PA and -TMB salts and (±)-salts with aromatic amines or secondary amines are out of this relationship, it is impossible to draw any conclusion on conglomerate formation from this relationship. However, Fig. 4 suggests that racemic compounds with smaller alkyl side chains become less stable. This may be related to the fact that the (±)-ammonium hydrogen malate with "the smallest side chain" has been optically resolved by preferential crystallization.[1]

Appropriate Conditions for Preferential Crystallization. (±)-PA salt was optically resolved by preferential crystallization in 50 cm^3 of methanol at 10 °C with 0.050 g of the (+)-salt as seed crystals, and (±)-TMB salt in 50 cm^3 of water. The amount of crystallization of the (+)- and (−)-salts calculated from results of optical resolution[10] and the relationship between the amount and resolution time are shown in Figs. 5 and 6, respectively. (±)-PA and -TMB salts have been confirmed from these results to be conglomerates at 10 °C.

Appropriate conditions for the optical resolution of (±)-PA and -TMB salts were estimated from the free energy of critical nucleation[6-8,14] (Δg_{max}/J nucleus^{-1}), the speed of crystallization of the (+)-salt ($R_{(+)}$/g min^{-1}), and the retardation time of crystallization of the (−)-salt ($\theta_{(-)}$/min);[8] the value of $R_{(+)}$ was calculated from the linear plots of Figs. 5 and 6, with $\theta_{(-)}$ defined as the resolution time before the (−)-salt begins to crystallize rapidly. The value of Δg_{max} and other related factors for crystallization are listed in Table 2.

Table 2. Free Energy of Critical Nucleation and Factors for Crystallization[a]

Salt	Degree of supersaturation / %	Δg_{max}[b] / 10^{-18} J nucleus^{-1}	$R_{(+)}$[c] / 10^{-2} g min^{-1}	$\theta_{(-)}$[d] / min	$W_{(-5)}$[e]/g Found	$W_{(-5)}$[e]/g Calcd[f]
PA[g]	160	2.88	1.25	75	0.879	0.837
	170	2.14	2.03	45	0.851	0.866
	180	1.66	3.00[i]	34[j]	0.897	0.878
	190	1.32	4.41	25	0.871	0.871
	200	1.08	5.72	20	0.852	0.845
TMB[h]	120	59.3	0.116	345	0.380	0.361
	140	15.8	0.501	75	0.336	0.435
	150	10.4	1.17	45	0.434	0.449
	155	8.73	1.36[k]	38[l]	0.447	0.451
	180	4.39	3.53	18	0.415	0.419

a) Conditions of crystallization: 50 cm^3 of solvent (methanol for PA salt; water for TMB salt); seed crystals 0.050 g of (+)-salt; temperature 10 °C. b) Δg_{max}: Free energy of critical nucleation at 10 °C. c) $R_{(+)}$: Speed of crystallization of (+)-salt. d) $\theta_{(-)}$: Retardation time for crystallization of (−)-salt. e) $W_{(-5)}$: Amount of crystallization of (+)-salt at $\theta_{(-)}-5$ min. f) The values were calculated from Eq. 5 or 6. g) PA: Propylammonium salt. h) TMB: 1,1,3,3-Tetramethylbutylammonium salt. i) The value was calculated from Eq. 1. j) The value was calculated from Eq. 2. k) The value was calculated from Eq. 3. l) The value was calculated from Eq. 4.

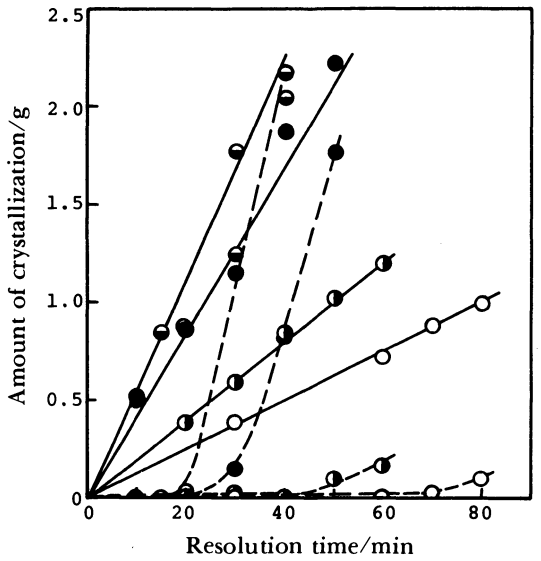

Fig. 5. Relationship between amount of crystallization and resolution time for propylammonium hydrogen malate.
Conditions: Solvent 50 cm^3 of methanol; temperature 10 °C; seed crystals 0.050 g of (+)-salt. Degree of supersaturation: ○ 160%; ◑ 170%; ● 190%; ◒ 200%, ——: (+)-Salt. ——: (−)-Salt.

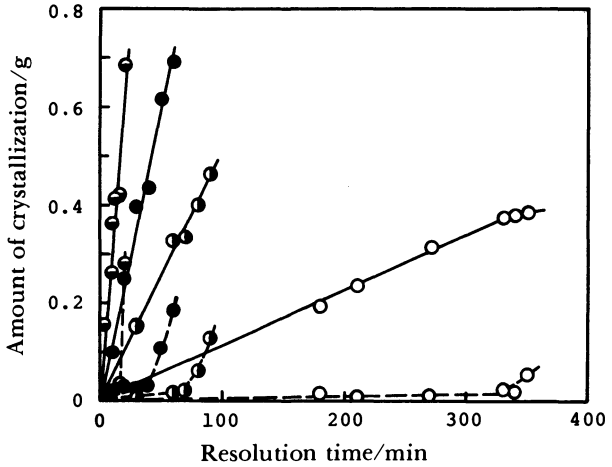

Fig. 6. Relationship between amount of crystallization and resolution time for 1,1,3,3-tetramethylbutylammonium hydrogen malate.
Conditions: Solvent 50 cm^3 of water; temperature 10 °C; seed crystals 0.050 g of (+)-salt. Degree of supersaturation: ○120%; ◑140%; ●150%; ◒180%. ——: (+)-Salt. ——: (−)-Salt.

For PA salt, the relationship between $R_{(+)}$ and Δg_{max} for different degrees of supersaturation of 160, 170, 190, and 200% and that between $\theta_{(-)}$ and Δg_{max} were obtained from the following equations:[8]

$$\ln R_{(+)} = -1.572 \ln \Delta g_{max} - 67.87, \quad (1)$$

$$\ln \theta_{(-)} = 1.332 \ln \Delta g_{max} + 58.08, \quad (2)$$

where the correlation coefficients for Eqs. 1 and 2 are 0.999 and 0.996, respectively. For TMB salt, the following equations were obtained for different degrees of supersaturation of 120, 140, 150, and 180%:

$$\ln R_{(+)} = -1.321 \ln \Delta g_{max} - 56.18, \quad (3)$$

$$\ln \theta_{(-)} = -1.140 \ln \Delta g_{max} + 48.43, \quad (4)$$

where the correlation coefficients for Eqs. 3 and 4 are 0.995 and 0.999, respectively.

The optical resolution at $\theta_{(-)}-5$ min seems to be a better criterion for evaluating results of optical resolution than that at $\theta_{(-)}$ min because the unseeded (−)-salt begins to crystallize rapidly after $\theta_{(-)}$ min. The amounts of crystallization of (+)-PA and -TMB

Table 3. Successive Preferential Crystallization of (±)-Propylammonium and (±)-1,1,3,3-Tetramethylbutylammonium Hydrogen Malate[a]

(±)-Salt	Run	Added amount of (±)-salt	Operation amount[b]/g		Resolution time	Salt obtained				
							Yield	Optical purity	YOPM[c]	Degree of resolution
		g	(+)	(−)	min		g	%	g	%
PA[d]	1	10.434	5.217	5.217	30	(+)	0.968	95.6	0.875	37.7
	2	0.918	4.779	5.654	30	(−)	1.634	94.6	1.496	54.3
	3	1.584	5.527	4.906	30	(+)	1.491	93.9	1.350	51.3
	4	1.441	4.852	5.581	30	(−)	1.907	90.1	1.668	62.2
TMB[e]	1	6.696	3.348	3.348	33	(+)	0.521	90.6	0.422	35.5
	2	0.471	3.137	3.559	40	(−)	0.734	91.7	0.623	44.5
	3	0.684	3.448	3.247	35	(+)	0.606	91.6	0.505	39.2
	4	0.556	3.195	3.499	35	(−)	0.696	88.6	0.567	42.3

a) Solvent: 50 cm^3 of methanol for PA salt; 50 cm^3 of water for TMB salt. Seed crystals: 0.050 g of (+)- or (−)-salt. Temperature: 10 °C. b) The operation amounts of (+)- and (−)-salts were calculated on the basis of analyses of the salt obtained in Runs 1—3. c) YOPM: Yield of optically pure modification. d) PA: Propylammonium salt. e) TMB: 1,1,3,3-Tetramethylbutylammonium salt.

salts ($W_{(-5)}/g=R_{(+)}(\theta_{(-)}-5)$) are given by the following equations, as derived from Eqs. 1—4:

$$W_{(-5)}^{PA} = 5.609 \times 10^{-5}\Delta g_{max}^{-0.2398} - 1.676 \times 10^{-29}\Delta g_{max}^{-1.572}, \quad (5)$$

$$W_{(-5)}^{TMB} = 4.268 \times 10^{-4}\Delta g_{max}^{-0.1807} - 1.992 \times 10^{-24}\Delta g_{max}^{-1.321}. \quad (6)$$

The value of Δg_{max} that gives the maximum $W_{(-5)}$ is calculated from Eqs. 5 and 6 to be 1.60×10^{-18} J nucleus^{-1} for (±)-PA salt and 8.38×10^{-10} J nucleus^{-1} for (±)-TMB salt. This Δg_{max} value for (±)-PA salt is approximately equal to the value for 180% supersaturation, and that for (±)-TMB salt to the value for 155% supersaturation.

The optical resolution of (±)-PA salt for 180% supersaturation and that of (±)-TMB salt for 155% supersaturation were carried out at $\theta_{(-)}-5$ min as calculated from Eqs. 2 and 4, respectively. The amounts of crystallization of the (+)-salts derived from their experimental results agree well with the $W_{(-5)}$ values calculated from Eqs. 5 and 6, as shown in Table 2.

Successive Preferential Crystallization of (±)-Propylammonium and 1,1,3,3-Tetramethylbutylammonium Salts. Based on the above results, the successive preferential crystallization of (±)-PA salt was carried out in 50 cm^3 of methanol at 10 °C by using a solution with 180% initial supersaturation, and that of the (±)-TMB salt by using an aqueous solution with 155% initial supersaturation, details being as listed in Table 3. (+)- and (−)-PA and -TMB salts with optical purity of 88—96% were obtained at degree of resolution of 37—62%. The purified (+)- and (−)-salts gave optically pure (−)- and (+)-MAL, respectively.

The authors are grateful to Fuso Chemical Co., Ltd. for the gift of (+)- and (−)-MAL.

References

1) K. Harada, M. Matsuyama, Y. Kataoka, and K. Mizumoto, Japan Patent 156433 (1982); *Chem. Abstr.*, **98**, 142963 p (1983).
2) T. Shiraiwa, M. Morita, K. Iwafuji, and H. Kurokawa, *Nippon Kagaku Kaishi*, **1983**, 1743.
3) V. C. Arsenijevic, *C. R. Acad. Sci.*, **245**, 317 (1957).
4) M. Leclercq, A. Collet, and J. Jacques, *Tetrahedron*, **32**, 821 (1976).
5) T. Shiraiwa, H. Miyazaki, A. Uramoto, M. Sunami, and H. Kurokawa, *Bull. Chem. Soc. Jpn.*, **60**, 1465 (1987).
6) T. Nakai, *Bull. Chem. Soc. Jpn.*, **42**, 2143 (1969).
7) T. Nakai, "Shoseki Kogaku," Baifukan, Tokyo (1986), Section 2.
8) T. Shiraiwa, H. Miyazaki, T. Imai, M. Sunami, and H. Kurokawa, *Bull. Chem. Soc. Jpn.*, **60**, 661 (1987).
9) "Kagaku Daijiten," ed by Kagaku Daijiten Henshu Iinkai, Kyoritsu Shuppan, Tokyo (1971), Vol. 9, p. 790.
10) T. Shiraiwa, Y. Sado, M. Komure, and H. Kurokawa, *Bull. Chem. Soc. Jpn.*, **60**, 3277 (1987).
11) S. H. Wilen, A. Collet, and J. Jacques, *Tetrahedron*, **33**, 2725 (1977).
12) A. Collet, M. J. Brienne, *Chem. Rev.*, **80**, 215 (1980).
13) S. H. Unger and C. Hansch, *Prog. Phys. Org. Chem.*, **12**, 91 (1976).
14) In order to calculate the Δg_{max} of PA salt, the value of molecular volume (V_0) was measured at 10 °C in methanol to be 2.21×10^{-28} m^3; the molecular radius (r_0) was calculated to be 3.75×10^{-10} m on the assumption of spherical molecule. The values of the radius (r_{sa} 4.83×10^{-10} m) and interfacial energy (σ_{sa} 1.01×10^{-2} J m^{-2}) of the embryo in the saturated methanol solution at 10 °C were calculated on the basis of the solubility of (±)-PA salt according to the procedure described in Refs. 6—8; the average number (j_{sa}) of PA salt molecules forming the embryo in the saturated solution is 2.13. (±)-TMB salt in water at 10 °C: V_0 3.70×10^{-28} m^3; r_0 4.45×10^{-10} m; r_{sa} 5.67×10^{-10} m; σ_{sa} 9.25×10^{-3} J m^{-2}; j_{sa} 2.06.

Phase-Transfer-Catalyzed Azo Coupling Reactions in Two-Phase Systems

Yoji HASHIDA,* Kazuhiro KUBOTA, and Shizen SEKIGUCHI
Department of Chemistry, Faculty of Engineering, Gunma University, Kiryu, Gunma 376
(Received July 30, 1987)

The azo coupling reaction of *p*-methoxybenzenediazonium tetrafluoroborate with *N,N*-dimethylaniline has been investigated in a water–1,2-dichloroethane system. It has been found that, among the several additives examined, the phenolate ion, generated from picric acid or 2,4-dinitro-1-naphthol, acted as an effective phase-transfer catalyst. Further, the reaction of *p*-diethylaminobenzenediazonium tetrafluoroborate with dimedone, an active methylene compound, has also been investigated in the same two-phase system; a remarkable acceleration in the rate was observed in the presence of tetraalkyl onium salts, and even in their absence.

Today, phase-transfer catalysis is a well-established technique in preparative chemistry.[1] However, it has been confined almost exclusively to nucleophilic or base-mediated reactions. On the other hand, azo coupling reactions under phase-transfer-catalyzed conditions have been intensively studied in recent years as a model for electrophilic substitution reactions. In such chlorinated hydrocarbons as chloroform and dichloromethane, pyrroles, arylamines, and phenol can easily react with diazonium salts in the presence of crown ether,[2] tetramethylammonium chloride,[3] tetraarylborate ion,[4] and/or silica gel,[5] showing their function as liquid-solid phase-transfer catalysts (PTC). It has also been claimed that tetraarylborate[4] and dodecylbenzenesulfonate[6] ions act as a PTC for the azo coupling reactions of arylamines in a water–dichloromethane two-phase system, although the effect of the latter might complicate the reaction by micelle formation.[7,8]

Here we wish to report that picrate and 2,4-dinitronaphtholate ions, as well as perchlorate and periodate ions, act as efficient anionic PTCs for an azo coupling reaction with an arylamine in a liquid-liquid two-phase system. Reactions with an active methylene compound in two-phase systems are also described in which a remarkable acceleration in the rate was observed in the presence of tetraalkyl onium salts, and even their absence.

Results and Discussion

Reaction with *N,N*-Dimethylaniline. The reaction of *N,N*-dimethylaniline (**1**), a neutral substrate, with *p*-methoxybenzenediazonium tetrafluoroborate (**2**) in the water–1,2-dichloroethane system was examined.

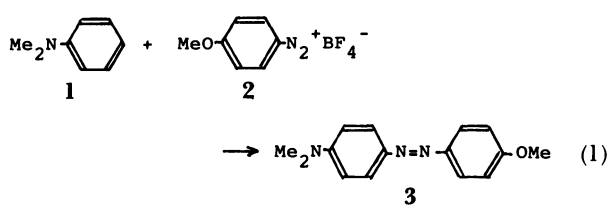

1 2 3 (1)

The rate measurements were performed by monitoring the absorbance at 410 nm due to **3**, in the presence of a 50-fold excess of **1** compared to **2**. Under these conditions, an excellent pseudo-first-order kinetic plot with respect to **2** was obtained with a correlation coefficient (r) greater than 0.99 in the range from 10 to 70% reaction in each run (Eq. 2):

$$\text{Rate} = k' [\text{Ar} - \text{N}_2^+]. \quad (2)$$

The influence of the stirring speed on the reaction rate was checked in the two-phase system (Fig. 1). Stirring at rates higher than about 600 rpm had essentially no effect on the reaction rate, suggesting that a transfer of the diazonium ion from the aqueous to the organic phase is fairly fast and that the rate is determined by the reaction in the organic phase.

The rates in the presence of several additives at 700 rpm are summarized in Table 1, including those in homogeneous solutions (Runs 1 and 2). The effects of arenesulfonate ions as PTCs were small (Runs 10 and 11). On the other hand, it is noteworthy that picric acid and 2,4-dinitro-1-naphthol exhibited considerable acceleration in the rate: the rate was proportional to the catalyst concentration, as has been observed in other phase-transfer-catalyzed azo coupling reactions.[4] In general, a phenol blocked by a substituent at the 2-, 4-, and 6-positions reacts with a diazonium ion to form covalently-bonded diazoether

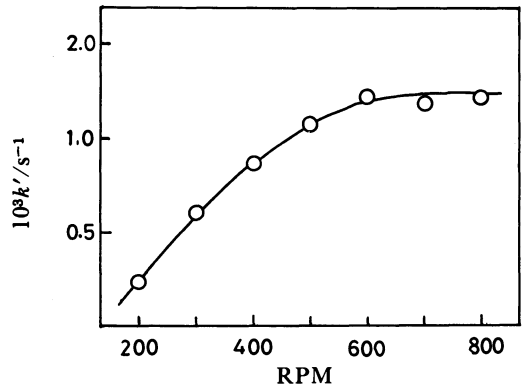

Fig. 1. Effect of stirring speed (RPM) on the reaction rate in the water/1,2-dichloroethane at 15 °C: $ArN_2^+NF_4^-$ 1.0×10^{-4} mol dm^{-3}; $PhNMe_2$ 5.0×10^{-3} mol dm^{-3}; picric acid 1.0×10^{-5} mol dm^{-3}.

Table 1. Pseudo-First-Order Rate Constants for the Reaction of *p*-Methoxybenzenediazonium Tetrafluoroborate with *N,N*-Dimethylaniline in Water–1,2-Dichloroethane System at 15 °C[a]

Run	Additive/mol dm^{-3}	k'/s^{-1}
1[b]	—	2.1×10^{-4}
2[c]	—	3.3×10^{-3}
3	—	3.6×10^{-5}
4	Picric acid (3.6×10^{-5})	1.0×10^{-3}
5	Picric acid (6.0×10^{-5})	1.4×10^{-3}
6	Picric acid (3.0×10^{-4})	4.0×10^{-3}
7	Picric acid (6.0×10^{-4})	6.2×10^{-3}
8	Picric acid (3.0×10^{-3})	3.1×10^{-2}
9	2,4-Dinitro-1-naphthol (3.0×10^{-3})	1.2×10^{-2}
10	2,4,6-Trinitrobenzenesulfonic acid (3.0×10^{-3})	3.6×10^{-3}
11	Sodium 1-naphthalenesulfonate (3.0×10^{-2})	1.7×10^{-4}
12	Sodium perchlorate (6.0×10^{-5})	2.4×10^{-4}
13	Sodium perchlorate (1.2×10^{-3})	3.4×10^{-4}
14	Sodium perchlorate (1.2×10^{-2})	6.1×10^{-4}
15	Sodium perchlorate (6.0×10^{-2})	1.3×10^{-3}
16	Sodium periodate (3.0×10^{-2})	5.2×10^{-4}
17	Sodium chlorate (3.0×10^{-2})	7.6×10^{-5}

a) Reaction conditions: at 700 rpm; $ArN_2^+BF_4^-$ 1.0×10^{-4} mol dm^{-3}; $PhNMe_2$ 5.0×10^{-3} mol dm^{-3}. b) In aqueous methanol (1 : 1, v/v). c) In 1,2-dichloroethane.

(**4**).[9] Indeed, no catalytic effect was observed for 2,4,6-

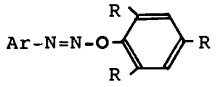

4

trichlorophenol; however, it immediately gave a compound with an absorption maximum at 357 nm, presumably due to its diazoether. On the other hand, it seems likely that a diazonium ion forms an ion pair with a picrate or dinitronaphtholate ion of low nucleophilicity, which migrates into the organic phase. The reactivity of the diazonium ion is thereby increased by a minimization of solvent interactions. The phenolate ion liberated in the organic phase is used in the next PTC cycle, i.e., it forms an ion pair with a protonated arylamine formed by proton abstraction from a σ-complex. It then reverts to the aqueous phase. It is also noteworthy that the rates (Runs 6—8) in the presence of picrate ion in a two-phase system exceed that of the diazonium tetrafluoroborate in dichloroethane (Run 2), suggesting that the reactivity of the diazonium ion with the picrate ion as a counter ion is higher than that with the tetrafluoroborate ion. The higher reactivity of the diazonium ion with the picrate ion may be ascribed to its weak ion-pairing; this is because a strong ion-pairing would be expected to cause a decrease in the electrophilicity of the diazonium ion.[10,11]

Table 2. Pseudo-First-Order Rate Constants for the Reaction of Potassium 5,5-Dimethyl-1,3-cyclohexanedionide with *p*-Diethylaminobenzenediazonium Tetrafluorobrate at 25 °C[a]

Run	Solvent	18-Crown-6 / mol dm^{-3}	k' / s^{-1}
1	H_2O	None	3.7×10^{-6}
2	MeOH	None	2.5×10^{-6}
3	MeCN	None	9.3×10^{1}
4	MeCN	2.0×10^{-3}	2.3×10^{2}
5	CH_2Cl_2	3.0×10^{-3}	3.5×10^{2}
6	$CHCl_3$	2.8×10^{-3}	1.2×10^{2}
7	THF	3.3×10^{-3}	6.5×10^{1}
8	$ClCH_2CH_2Cl$	2.9×10^{-3}	1.4×10^{2}
9	$ClCH_2CH_2Cl$	7.9×10^{-3}	3.0×10^{2}
10	$ClCH_2CH_2Cl$	2.3×10^{-2}	2.9×10^{1}
11	$ClCH_2CH_2Cl$	5.8×10^{-2}	6.8

a) Reaction conditions: $ArN_2^+BF_4^-$ 5.0×10^{-5} mol dm^{-3}; Substrate 2.5×10^{-3} mol dm^{-3}.

The addition of such inorganic ions as perchlorate (Runs 12—15) and periodate (Run 16), which are of high extraction capability toward common onium cations into chlorinated hydrocarbon,[12] also accelerated the two-phase reaction. A similar acceleration by iodide ion to that by the perchlorate ion was observed. However, the iodide ion seems to be of no practical significance, since it catalyzed the homolytic decomposition[13] of the diazonium ion giving an impure azo compound.

Reaction with Dimedone. Secondary, the reaction of 5,5-dimethyl-1,3-cyclohexanedione (dimedone **5**, pK_a=5.2[14]), an active methylene compound, with *p*-diethylaminobenzenediazonium tetrafluoroborate (**6**) was selected, since the rate could be measured directly in all the solvent systems investigated.

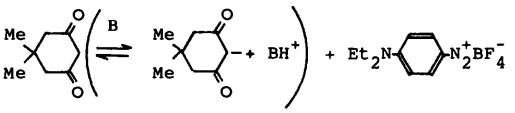

5 **5′** **6**

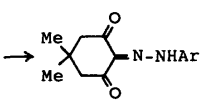

(3)

7

Prior to the study in the two-phase system, the solvent effects on the reactivity of the carbanion (**5′**) were investigated in homogeneous solutions. The potassium salt of **5′** was completely solubilized into a solvent by adding 18-crown-6 (hereafter called crown), except for water and methanol. After a solution of **6** in the same organic solvent was added into this solution, the absorbance at 490 nm due to product **7** was followed under the pseudo-first-order kinetic conditions (Table 2). In contrast to the azo coupling reaction with *N,N*-dimethylaniline, in which no

significant solvent effects have been observed,[15] it can be seen that there are large differences in the rates between water and organic solvents; e.g., reactions in chlorinated hydrocarbons proceed faster than in water by ca. an order of magnitude of 8. Under these conditions, in which nearly an equivalent of the crown to the substrate was present, the crown probably tended to complex with the potassium salt of **5′** rather than **6**, giving a "naked carbanion" of high reactivity. The addition of a large excess of the crown, however, retarded the reaction (Runs 10 and 11), due to a partial conversion of the diazonium ion into its unreactive complex with the crown.[16]

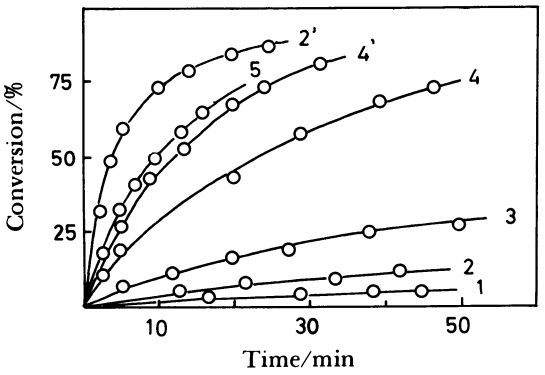

Fig. 2. Reaction of dimedone with *p*-diethylaminobenzenediazonium tetrafluoroborate in the water/1,2-dichloroethane at 15 °C: $ArN_2^+BF_4^-$ 1.0×10^{-4} mol dm^{-3}; substrate 6.0×10^{-3} mol dm^{-3}.
1) In water; 2) 300 rpm; 3) 400 rpm; 4) 500 rpm; 5) 700 rpm; 2′) 300 rpm; $Bu_4N^+Br^-$ 8.0×10^{-3} mol dm^{-3}; 4′) 500 rpm; $Bu_4N^+Br^-$ 6.5×10^{-4} mol dm^{-3}.

From these results, it was expected that the same reaction would be accelerated under appropriate conditions in synthetically more useful liquid-liquid systems. Figure 2 shows a typical rate profile for the reaction of **5** with **6** in the water–1,2-dichloroethane system. It can be seen that the reaction is remarkably accelerated in the two-phase system, even in the absence of a catalyst. Also, the stirring speed is quite important. These results may be understandable by postulating that when a part of both reactants, **5′** and **6**, transfer into an organic phase, the reaction immediately takes place. In contrast, when benzene or cyclohexane was employed as an organic phase, no appreciable acceleration in rate was observed, presumably because both reactants were essentially insoluble in the organic phase. The addition of quaternary onium salts,[17] which are common PTCs for reactions involving carbanion, accelerated the reaction (as illustrated in the case of tetrabutylammonium bromide). It has been expected that the combined use of PTCs for both reactants, i.e., diazonium ion and carbanion, might be effective in the present system. However, no pronounced catalysis was observed; e.g., the addition of tetrabutylammonium bromide and sodium 1-naphthalenesulfonate showed only a slight acceleration compared to a reaction when the former was employed alone. This result may be understandable since the catalytic activities of both PTCs should be decreased owing to a mutual interaction.

Synthesis of Azo Compounds. The usefulness of the present two-phase system was examined in the preparative scale by using various substrates, including particularly unreactive coupling components in

Table 3. Preparation of Azo-compounds

Run	Substrate	Substituent in $Ar-N_2^+$	Solvent	Condition		Yield[a]/%
				PTC/mol%	Time/h	
1	Dimedone	*p*-NEt_2	H_2O	—	5	5
2			H_2O	—	120	40
3			H_2O-DCE[b]	TBAB[c] (1)	0.7	72
4			H_2O-DCE	TBAB (10)	0.5	90
5	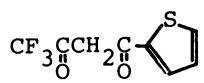	*p*-NEt_2	H_2O	—	27	22
6			H_2O-$CHCl_3$	TBAB (5)	3	64
7	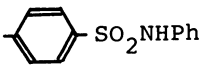	*p*-Cl	H_2O	—	2	—[d]
8			H_2O-DCE	TBAB (10)	1	40
9	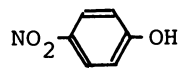	*p*-OMe	H_2O	—	10	—[d]
10			H_2O-$CHCl_3$	TBAB (10)	10	43
11	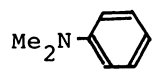	*p*-OMe	H_2O-DCE	$NaClO_4$ (10)	2	70
12			H_2O-DCE	Picric acid (5)	0.7	76

a) Isolated yield of azo compound. b) 1,2-Dichloroethane. c) Tetrabutylammonium bromide. d) Not isolated.

the conventional aqueous system (Table 3). In the case of *p*-toluenesulfonanilide (Run 7), its reactive form is considered to be an anion resulting from the ionization of the N-H bond.[18] The reaction was conducted by using an equimolar amount of a substrate. After the consumption of a diazonium ion was confirmed (except Run 1) through a test with 4-amino-5-hydroxy-2,7-naphthalenedisulfonic acid, resulting azo compounds were isolated by the usual work-up procedure. In contrast to the reaction in an aqueous solution in which the decomposition of the diazonium ion was the major reaction, it can be seen that the present PTC system is very useful for preparing azo compounds.

Experimental

Materials Arenediazonium tetrafluoroborates were prepared by using a general procedure.[19] The crude salt was washed with diethyl ether, dissolved in a minimum amount of acetonitrile, precipitated by adding diethyl ether, and then dried over diphosphorus pentaoxide in vacuo: **2** mp 143—144 °C (decomp); **6** mp 112—113 °C (decomp). Potassium 5,5-dimethyl-1,3-cyclohexanedionide was prepared by adding an equivalent of potassium hydroxide into a methanolic solution of **5**; the solvent was removed and the resulting residue was dried over silica gel. The other materials were obtained from commercial sources, and standardized before use.

Rate Measurements in Homogeneous Systems. The rates in homogeneous solution were measured by using a previously described procedure.[14] The solution (ca. 1×10^{-4} mol dm^{-3}) of a diazonium salt in chlorinated hydrocarbons was prepared as follows: a suspension of diazonium salt (6—7 mg) in a solvent (25 ml) was shaken vigorously for 10 min; then, the residual salt (if present) was filtered off. The fast reactions (Runs 3—11, Table 2) were followed by a stopped-flow technique on a Union Giken RA-1300 instrument.

Rate Measurements in Two-Phase Systems. A mixture of water (25 ml), buffered with sodium carbonate and sodium borate (1×10^{-2} mol dm^{-3} each) at ca. pH 9.5, and 1,2-dichloroethane (30 ml) containing a substrate and a PTC was stirred in a vessel thermostated at the prescribed temperature. After an aqueous solution (5 ml 6×10^{-3} mol dm^{-3}) of the diazonium salt was further added, the mixture was stirred with a flat-bladed mechanical stirrer rotating at a constant speed. At a definite time stirring was stopped and a portion was taken out from the organic phase and diluted with the same solvent to a definite volume. The absorbance due to any azo compound formed was then measured with a Hitachi Model 200-10 spectrometer.

Preparation of Azo Compounds. Into a flask with a mechanical stirrer was added water (100 ml), 1,2-dichloroethane (100 ml), dimedone (2.00 g, 14.3 mmol), sodium carbonate (2.32 g, 21.8 mmol), tetrabutylammonium bromide (0.46 g, 1.4 mmol), and finally *p*-diethylaminobenzenediazonium tetrafluoroborate (3.76 g, 14.3 mmol). The mixture was stirred vigorously for 30 min at 0—5 °C. The organic layer was separated, washed with water, dried over $MgSO_4$, and then evaporated. The residue was recrystallized from benzene–ligroin (1:1) to give 2-(4-diethylaminophenylhydrazono)-5,5-dimethyl-1,3-cyclohexanedione (**7**): mp 128—129 °C; MS, *m/z* 315 (M^+); UV ($ClCH_2CH_2Cl$) 490 nm (ε 22100). Anal. ($C_{18}H_{25}N_3O_2$) C, H, N.

The other azo compounds listed in Table 3 were obtained in a similar manner except that, in the cases of Runs 5, 8, and 10, the crude products were purified on a silica-gel column with benzene.

2-(4-Diethylaminophenylhydrazono)-4,4,4-trifluoro-1-(2-thienyl)-1,3-butanedione: Mp 161—162 °C; MS *m/z* 397 (M^+). Anal. ($C_{18}H_{18}O_2N_3SF_3$) C,H,N.

N-[4-(4-Chlorophenylazo)phenyl]-*p*-toluenesulfonamide: Mp 185—186 °C; MS, *m/z* 385 (M^+). Anal. ($C_{19}H_{16}N_3O_2SCl$) C, H, N.

2-(4-Methoxyphenylazo)-4-nitrophenol: Mp 188—189 °C; MS, *m/z* 241 (M^+). Anal. ($C_{13}H_{11}N_3O_2$) C, H, N.

4-(4-Methoxyphenylazo)-*N*,*N*-dimethylaniline: Mp 159—160 °C (lit,[20] 161—163 °C); UV ($ClCH_2CH_2Cl$) 410 nm (ε 31400).

The present work was partially supported by a Grant-in-Aid for Scientific Research (No. 60550600) from the Ministry of Education, Science and Culture.

References

1) a) C. M. Starks and C. Liotta, "Phase Transfer Catalysis," Academic Press, New York (1978); b) E. V. Demlow and S. S. Demlow, "Phase Transfer Catalysis," Verlag Chemie, Weinheim (1980); C) W. P. Weber and G. W. Gokel, "Phase Transfer Catalysis in Organic Synthesis," Springer Verlag, Berlin (1977); d) F. Montanari, D. Landini, and F. Rolla, "Phase-transfer Catalyzed Reactions," in "Topics in Current Chemistry," ed by F. L. Boschke, Springer Verlag (1981), Vol. 101, p. 147.

2) A. R. Butler and P. T. Shepherd, *J. Chem. Res. (S)*, **1978**, 339.

3) S. H. Korzeniowski and G. W. Gokel, *Tetrahedron Lett.*, **1977**, 1637.

4) H. Iwamoto, M. Yoshimura, T. Sonoda, and H. Kobayashi, *Bull. Chem. Soc. Jpn.*, **56**, 796 (1983).

5) S. Tamagaki, K. Suzuki, and W. Tagaki, *Chem. Lett.*, **1982**, 1237.

6) M. Ellwood, J. Griffiths, and P. Gregory, *J. Chem. Soc., Chem. Commun.*, **1980**, 181.

7) M. Poindexter and B. McKay, *J. Org. Chem.*, **37**, 1674 (1972).

8) I. Szele and H. Zollinger, "Azo-coupling Reaction, Structures and Mechanism," in "Topics in Current Chemistry," ed by F. L. Boschke, Springer Verlag (1983), Vol. 112, p. 1.

9) O. Dimroth, H. Leichtlin, and O. Friedmann, *Chem. Ber.*, **50**, 1534 (1917).

10) P. N. Juri and R. A. Bartsch, *J. Org. Chem.*, **45**, 2028 (1980).

11) B. Gloor and H. Zollinger, *Helv. Chim. Acta*, **54**, 553 (1971).

12) Ref. 1a, p. 16, 1b, p. 13, and references cited therein.

13) P. R. Singh and R. Kumer, *Aust. J. Chem.*, **25**, 2133 (1972).

14) Y. Hashida, M. Kobayashi, and K. Matsui, *Bull. Chem. Soc. Jpn.*, **44**, 2506 (1971).

15) J. R. Penton and H. Zollinger, *Helv. Chim. Acta*, **54**, 573 (1971).
16) W. A. Sheppard, G. W. Gokel, D. W. Webster, K. Betterton, and J. W. Timberlake, *J. Org. Chem.*, **44**, 1717 (1979); R. A. Bartsch, H. Chen, N. F. Haddock, and P. N. Juri, *J. Am. Chem. Soc.*, **98**, 6753 (1976).
17) The catalytic activities of tetraalkyl onium salts examined were in the following order: $(C_4H_9)_4N^+Br^- \approx (C_4H_9)_4P^+Cl^- > (C_8H_{17})_3N^+C_4H_9Br^- > (CH_3)_4N^+Br^- > (C_8H_{17})_4N^+Br^-$.
18) Ref. 8, p. 32.
19) R. A. Cox and J. Kumamoto, *J. Org. Chem.*, **30**, 4254 (1965).
20) D. Vorländer and E. Wolferts, *Chem. Ber.*, **56**, 1237 (1923).

 © 1988 The Chemical Society of Japan Bull. Chem. Soc. Jpn., 61, 911—919 (1988)

The Oxidation of Some Naphthols with Benzoyl Peroxide

Takashi MATSUMOTO,* Sachihiko IMAI,* and Naoya YAMAMOTO
Department of Chemistry, Faculty of Science, Hiroshima University,
Higashisenda-machi, Naka-ku, Hiroshima 730
(Received August 3, 1987)

The reactions of four naphthols (1-naphthol (**1**), 2-naphthol (**2**), 4-isopropyl-1-naphthol (**18**), and 3-isopropyl-2-naphthol (**19**)) with benzoyl peroxide were examined under two reaction conditions (A and B). Each of the naphthols **1**, **2**, **18**, and **19** was oxidized with 0.95 equivalent moles of benzoyl peroxide at room temperature for 24 h (condition A) to give mainly the corresponding ortho-benzoyloxylated product which was isolated in moderate yield as an equilibrium mixture, resulting from its trans-benzoylation. The naphthols **18** and **19** were also oxidized with 2.25 equivalent moles of benzoyl peroxide at room temperature for 48 h (condition B) to give mainly 2,2-bis(benzoyloxy)-4-isopropyl-1(2*H*)-naphthalenone and 2,2-bis(benzoyloxy)-3-isopropyl-1(2*H*)-naphthalenone in good yields. The oxidations of **1** and **2** under condition B produced the same product, 2,2-bis(benzoyloxy)-1(2*H*)-naphthalenone, in low yields.

Although the oxidation of various phenols with benzoyl peroxide has been considerably investigated,[1,2] comparatively little research has been performed on the oxidation of naphthol compounds. In 1963, Edward and Samad[3] reported that both 1-naphthol (**1**) and 2-naphthol (**2**) yielded the same product, 2-(4-nitrobenzoyloxy)-1-naphthol (**3**), through oxidation with bis(4-nitrobenzoyl) peroxide in refluxing chloroform. However, when benzoyl peroxide was used, the corresponding benzoyloxy derivative could not be obtained. Bhatia and Mathur[1,4] also reported the oxidation of **2** with benzoyl peroxide in refluxing chloroform; they obtained a trace of 1-benzoyloxy-2-naphthol (**4**) and a small amount (1% yield) of 1,1-bis(benzoyloxy)-2(1*H*)-naphthalenone (**5**), the revised structure of which is described later. A similar oxidation[5] of **1** produced 4,4′-dihydroxy-1,1′-binaphthyl (**6**: 45%) and 1,4-naphthoquinone (**7**: 16%). However, 1-bromo-2-naphthol (**8**)[5] yielded only 1,2-naphthoquinone (**9**) in 25% yield. Mathur et al. further demonstrated the oxidations of two more bromonaphthols in refluxing chloroform. That is, 4-bromo-1-naphthol (**10**)[6] produced three compounds: 2-benzoyloxy-4-bromo-1-naphthol (**11**: 6%), 1,2-bis(benzoyloxy)-4-bromonaphthalene (**12**: 2%), and 2-benzoyloxy-1,4-naphthoquinone (**13**). On the other hand, 6-bromo-2-naphthol (**14**)[7] afforded two compounds: 1-benzoyloxy-6-bromo-2-naphthol (**15**: 13%) and 1,1-bis(benzoyloxy)-6-bromo-2(1*H*)-naphthalenone (**16**: 4%).

In connection with our synthetic study[8] of the natural coleon A (**17**),[9-11] we have also investigated the oxidations of various naphthol compounds with benzoyl peroxide in order to obtain further information on the introduction of oxygen functions in the naphthol skeleton. This paper describes the reactions of 1-naphthol (**1**), 2-naphthol (**2**), 4-isopropyl-1-naphthol (**18**), and 3-isopropyl-2-naphthol (**19**) with benzoyl peroxide.

Each of the naphthols was oxidized under two reaction conditions (A and B); the results are

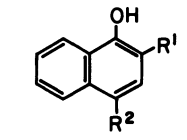

1 $R^1=R^2=H$
3 $R^1=OCOC_6H_4NO_2(p)$, $R^2=H$
10 $R^1=H$, $R^2=Br$
11 $R^1=OBz$, $R^2=Br$

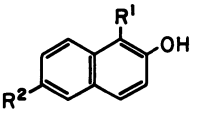

2 $R^1=R^2=H$
4 $R^1=OBz$, $R^2=H$
8 $R^1=Br$, $R^2=H$
14 $R^1=H$, $R^2=Br$
15 $R^1=OBz$, $R^2=Br$

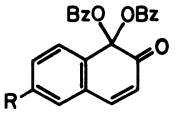

5 R=H
16 R=Br

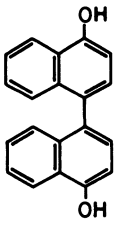

6

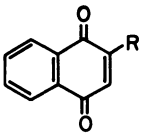

7 R=H
13 R=OBz

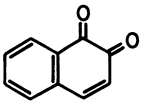

9

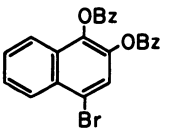

12

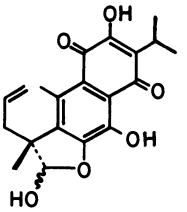

17

summarized in Table 1.

The oxidation of 1-naphthol (**1**) with 0.95 equivalent moles of benzoyl peroxide in dichloromethane at room temperature for 24 h (condition A) afforded a ca. 1:1 mixture (25%) of 1-benzoyloxy-2-naphthol (**4**) and 2-benzoyloxy-1-naphthol (**20**), together with 2,2-bis(benzoyloxy)-1(2*H*)-naphthalenone (**21**: 4%), 4-benzoyloxy-1-naphthol (**22**: 3%), and the starting **1** (16%). However, the oxidation of **1** with 2.25 equivalent moles of benzoyl peroxide in dichloromethane at room temperature for 48 h (condition B) afforded a complicated mixture, from which **21** and 2-benzoyloxy-1,4-naphthoquinone (**13**) were isolated in low yields of 6 and 5%, respectively.

Similarly, 2-naphthol (**2**) was oxidized under condition A to give a ca. 1:1 mixture (52%) of **4** and **20**, **21** (8%), 1,1-bis(benzoyloxy)-2(1*H*)-naphthalenone (**5**: 3%), and the starting **2** (28%). Under condition B, **2** produced **21** and **5** in 26 and 6% yields, respectively.

The oxidation of 4-isopropyl-1-naphthol (**18**) under condition A afforded a ca. 2:3 mixture (42%) of 2-benzoyloxy-4-isopropyl-1-naphthol (**23**) and 1-benzoyloxy-4-isopropyl-2-naphthol (**24**), along with 2,2-bis(benzoyloxy)-4-isopropyl-1(2*H*)-naphthalenone (**25**: 14%), 4,4′-diisopropyl-2,2′-bi-1-naphthol (**26**: 7%), and a trace of 1,1′,2,2′-tetrahydro-4,4′-diisopropyl-1,1′-dioxo-2,2′-binaphthylidene (**27**: 1%). However, when **18** was oxidized under condition B, it gave a ca. 2:3 mixture (4%) of **23** and **24**, **25** (65%), **27** (3%), and 1,1-bis(benzoyloxy)-4-isopropyl-2(1*H*)-naphthalenone (**28**: 4%).

3-Isopropyl-2-naphthol (**19**) was also oxidized

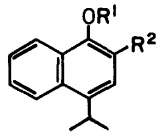

18 R^1=R^2=H
23 R^1=H, R^2=OBz
24 R^1=Bz, R^2=OH
38 R^1=Bz, R^2=OAc

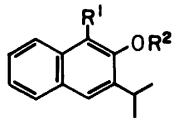

19 R^1=R^2=H
29 R^1=OH, R^2=Bz
30 R^1=OBz, R^2=H
39 R^1=OAc, R^2=Bz

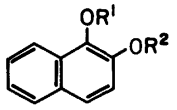

20 R^1=H, R^2=Bz
33 R^1=Ac, R^2=Bz
34 R^1=Bz, R^2=Ac

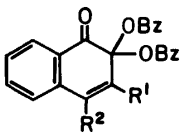

21 R^1=R^2=H
25 R^1=H, R^2=i-Pr
31 R^1=i-Pr, R^2=H

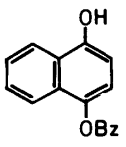

22

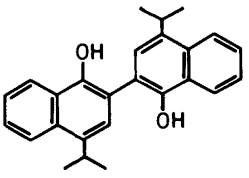

26

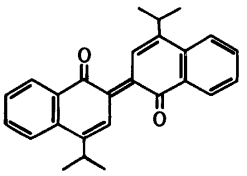

27

28 R^1=H, R^2=i-Pr
32 R^1=i-Pr, R^2=H

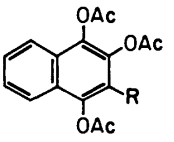

35 R=H
41 R=i-Pr

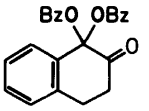

36

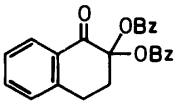

37

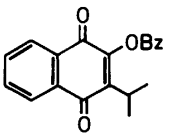

40

Table 1. Oxidations of Naphthols with Benzoyl Peroxide in Dichloromethane at Room Temperature

Substrate	Condition[a]	Product (Yield/%)			
1	A	**4**+**20** (25)	**21** (4)	**22** (3)	—
	B	—	**21** (6)	—	**13** (5)
2	A	**4**+**20** (52)	**21** (8)	**5** (3)	—
	B	—	**21** (26)	**5** (6)	—
18	A	**23**+**24** (42)	**25** (14)	**26** (7)	**27** (1)
	B	**23**+**24** (4)	**25** (65)	**28** (4)	**27** (3)
19	A	**29**+**30** (66)	**31** (9)	—	—
	B	**29**+**30** (5)	**31** (65)	**32** (14)	—

a) A: 0.95 equivalent moles of benzoyl peroxide for 24 h. B: 2.25 equivalent moles of benzoyl peroxide for 48 h.

under condition A to give a ca. 1:1 mixture (66%) of 2-benzoyloxy-3-isopropyl-1-naphthol (**29**) and 1-benzoyloxy-3-isopropyl-2-naphthol (**30**), 2,2-bis(benzoyloxy)-3-isopropyl-1(2*H*)-naphthalenone (**31**: 9%), and the starting **19** (16%). The oxidation of **19** under condition B produced a ca. 1:1 mixture (5%) of **29** and **30**, **31** (65%), and 1,1-bis(benzoyloxy)-3-isopropyl-2(1*H*)-naphthalenone (**32**: 14%). The structures of the oxidation products were determined by the following chemical and spectroscopic studies.

Phenolic compounds, **4** and **20**, were obtained as a mixture (ca. 1:1), whose IR spectrum indicated the presence of hydroxyl (3575 and 3280 cm^{-1}) and benzoyloxyl (1745 cm^{-1}) groups. The ^1H NMR spectrum of the mixture showed doublet signals due to C-3 and C-4 protons at δ 7.22 and 7.65 for **4** and at δ 7.30 and 7.46 for **20**. The difference in these chemical shifts of the C-4 protons is obviously attributable to the C-1 substituent (hydroxyl or benzoyloxyl group): the presence of a hydroxyl group at the C-1 position causes an upfield shift of the C-4 proton. Therefore, the structures of **4** and **20** were assigned to be 1-benzoyloxy-2-naphthol and 2-benzoyloxy-1-naphthol, respectively. Acetylation of the mixture (ca. 1:1) with isopropenyl acetate and *p*-toluenesulfonic acid in refluxing toluene afforded two separable acetates,[12] **33** and **34**, in 28 and 71% yields. The ^1H NMR spectrum of **33** indicated signals due to an acetoxy methyl at δ 2.30 (singlet) and a C-3 aromatic proton at δ 7.43 (doublet, J=9 Hz), while that of **34** indicated the corresponding signals at δ 2.16 (singlet) and 7.35 (doublet, J=9 Hz). Since the acetoxy methyl and the C-3 proton in **33** were more deshielded than those in **34** by the effect of aromatic rings, the structures of **33** and **34** were assigned to be 1-acetoxy-2-benzoyloxynaphthalene and 2-acetoxy-1-benzoyloxynaphthalene, respectively.

Compound **21** (mp 195—196 °C) showed absorption bands at 1732 and 1709 cm^{-1} in its IR spectrum, indicating the presence of benzoyloxyl groups and a conjugated carbonyl group. The ^1H NMR spectrum of **21** showed two doublet signals due to C-3 and C-4 olefinic protons at δ 6.33 and 6.98.

Compound **5** (mp 239—240 °C) also showed similar spectral data: IR 1736 and 1695 cm^{-1}, ^1H NMR δ 6.56 and 7.50 (each 1 H and doublet). Comparisons of these spectral data with those of **21** suggested that the carbonyl group in **5** is conjugated with the C-3 and C-4 double bond. To obtain a further confirmation on the structures of **5** and **21**, the following reactions were carried out. Compounds **5** and **21** were each treated with acetic anhydride containing concentrated sulfuric acid to give the same product, 1,2,4-triacetoxynaphthalene (**35**),[4] in 90 and 73% yields, respectively. The catalytic hydrogenation of **5** over 5% Rh–Al_2O_3 in 1,4-dioxane afforded the corresponding tetrahydro ketone (**36**: 32%), along with a mixture of the phenolic compounds (**4** and **20**: 66%). This ketone **36** showed the presence of a nonconjugated carbonyl group (1727 cm^{-1}) in its IR spectrum. A similar catalytic hydrogenation of **21** also afforded the tetrahydro compound (**37**: 60%) and a mixture of **4** and **20** (38%). The IR spectrum of **37** showed absorption bands at 1735 and 1710 cm^{-1}, indicating the presence of benzoyloxyl groups and a conjugated carbonyl group. Thus, the structures of **5** and **21** were assigned to be 1,1-bis(benzoyloxy)-2(1*H*)-naphthalenone and 2,2-bis(benzoyloxy)-1(2*H*)-naphthalenone, respectively.

Bhatia and Mathur[4] prepared the bis(benzoyloxy)-naphthalenone derivative (mp 186—187 °C) and proposed its structure as being **5**. However, the reported melting point is quite different from that of **5**, but similar to that of **21**. For a direct comparison with the product of Bhatia and Mathur, 2-naphthol (**2**) was also oxidized under their reaction condition using one equivalent mole of benzoyl peroxide in refluxing chloroform[4] to give 2,2-bis(benzoyloxy)-1(2*H*)-naphthalenone (**21**: mp 195—196 °C) in 7.5% yield. Therefore, the proposed structure **5** must be revised to **21**.

Compound **22** showed the presence of a hydroxyl group (3580 and 3320 cm^{-1}) and a benzoyloxyl group (1730 cm^{-1}) in its IR spectrum. The ^1H NMR spectrum of **22** showed signals due to a pair of ortho-coupling aromatic protons at δ 6.61 and 7.07 (each 1H, doublet, and J=8 Hz). Thus, the structure of **22** was assigned to be 4-benzoyloxy-1-naphthol.

Compound **13** showed the presence of a benzoyloxyl group (IR 1749 cm^{-1}) and a *p*-quinone moiety [IR 1667 cm^{-1}, ^1H NMR δ 6.93 (1H, singlet, C-3 proton)]. This compound was also obtained by the oxidation of a phenolic mixture (**4** and **20**) with Jones reagent in 14% yield or by the oxidation of the naphthalenone compound **21** with *m*-chloroperbenzoic acid in 22% yield. Thus, the structure of **13** was assigned to be 2-benzoyloxy-1,4-naphthoquinone.

Phenolic compounds, **23** and **24**, were obtained as a mixture (ca. 2:3), the IR spectrum of which indicated the presence of hydroxyl (3570 and 3320 cm^{-1}) and benzoyloxyl (1740 cm^{-1}) groups. The ^1H NMR spectrum of the mixture showed signals due to hydroxyl, C-3, and C-8 protons at δ 6.10 (broad), 7.19 (singlet), and 8.31 (multiplet) for the minor phenol **23**, and at δ 5.85 (broad), 7.19 (singlet), and 7.84 (multiplet) for the major phenol **24**. The appearance of the C-8 proton signal of **23** in a very low field (δ 8.31) suggested the presence of a hydroxyl group at the C-1 position. Thus, the structures of **23** and **24** were assigned to be 2-benzoyloxy-4-isopropyl-1-naphthol and 1-benzoyloxy-4-isopropyl 2-naphthol, respectively. Acetylation of the mixture (**23** and **24**) with isopropenyl acetate and *p*-toluenesulfonic acid in refluxing toluene afforded an acetate (64%), the

structure of which was assigned to be 2-acetoxy-1-benzoyloxy-4-isopropylnaphthalene (**38**) by comparisons of its ^{1}H NMR spectrum with those of **33** and **34**. The hydrolysis of **38** with dilute hydrochloric acid in refluxing methanol produced **24** containing a small amount of **23**. This was dissolved in deuteriochloroform and then allowed to stand at room temperature for 24 h to give an equilibrium mixture of **23** and **24** (ca. 2:3).[13]

Compound **25** indicated the presence of benzoyloxyl groups (1727 cm^{-1}) and a conjugated carbonyl group (1703 cm^{-1}) in its IR spectrum. The ^{1}H NMR spectrum of **25** showed a singlet signal due to a C-3 olefinic proton at δ 6.18. Thus, the structure of **25** was assigned to be 2,2-bis(benzoyloxy)-4-isopropyl-1(2*H*)-naphthalenone. This structure was further supported by its UV spectrum (Fig. 1).

Compound **26** was identified as 4,4′-diisopropyl-2,2′-bi-1-naphthol by the following spectral data; MS *m/z* 370 (M$^+$), IR 3535 and 3270 cm^{-1}, and ^{1}H NMR δ 5.56 (singlet, hydroxyls) and 7.32 (singlet, C-3 and C-3′ protons).

Compound **27**, IR 1629 cm^{-1} (conjugated carbonyls) and ^{1}H NMR δ 8.29 (singlet, C-3 and C-3′ protons), was also obtained by the oxidation of **26** with potassium hexacyanoferrate(III) in an alkaline solution in 81% yield. Thus, the structure of **27** was assigned to be 1,1′,2,2′-tetrahydro-4,4′-diisopropyl-1,1′-dioxo-2,2′-binaphthylidene.

Compound **28** showed the presence of benzoyloxyl groups (1737 cm^{-1}) and a conjugated carbonyl group (1680 cm^{-1}) in the IR spectrum. Its ^{1}H NMR spectrum showed a singlet signal due to a C-3 olefinic proton at δ 6.51. Thus, the structure of **28** was assigned to be 1,1-bis(benzoyloxy)-4-isopropyl-2(1*H*)-naphthalenone. This structure was further supported by its UV spectrum (Fig. 2).

Phenolic compounds, **29** and **30**, were obtained as a mixture (ca. 1:1), the IR spectrum of which indicated the presence of hydroxyl (3575 and 3320 cm^{-1}) and benzoyloxyl (1737 cm^{-1}) groups. Recrystallization of the mixture afforded pure crystalline **30**. The ^{1}H NMR spectrum of **30** showed a singlet signal due to a C-4 aromatic proton at δ 7.60, while that of **29** showed a corresponding signal at δ 7.38. The appearance of the C-4 proton signal of **29** in a high field suggested the presence of a hydroxyl group at the C-1 position. Thus, the structures of **29** and **30** were assigned to be 2-benzoyloxy-3-isopropyl-1-naphthol and 1-benzoyloxy-3-isopropyl-2-naphthol, respectively. Acetylation of the mixture (ca. 1:1) of **29** and **30** with isopropenyl acetate and *p*-toluenesulfonic acid in refluxing toluene afforded 1-acetoxy-2-benzoyloxy-3-isopropylnaphthalene (**39**: 76%),[12] which was hy-

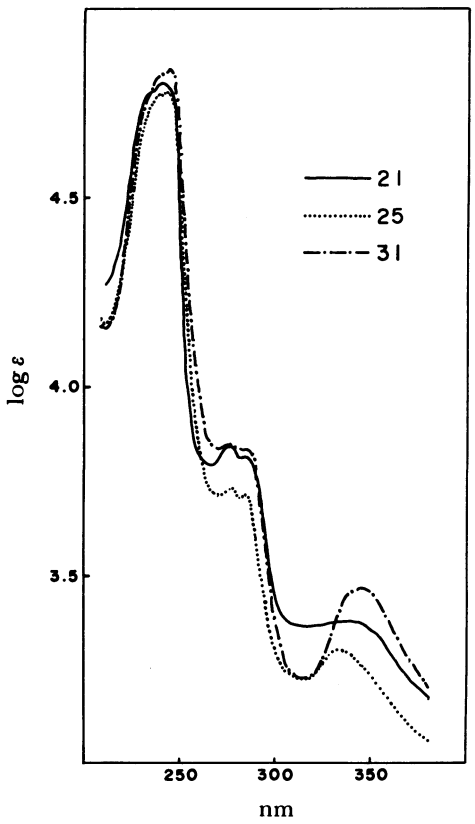

Fig. 1. The UV spectra of 2,2-bis(benzoyloxy)-1(2*H*)-naphthalenone derivatives **21**, **25**, and **31** in ethanol.

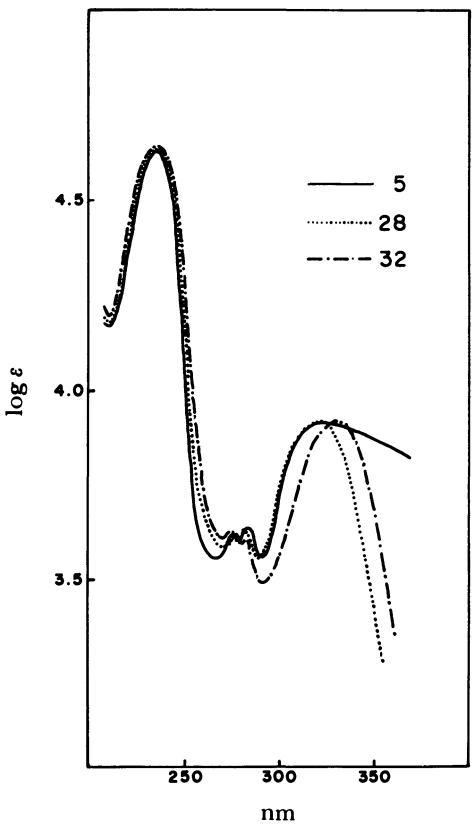

Fig. 2. The UV spectra of 1,1-bis(benzoyloxy)-2(1*H*)-naphthalenone derivatives **5**, **28**, and **32** in ethanol.

drolyzed with dilute hydrochloric acid in refluxing methanol to give **29** containing a small amount of **30**. This was dissolved in deuteriochloroform and then allowed to stand at room temperature for 24 h to give an equilibrium mixture of **29** and **30** (ca. 1:1).[13] Compound **30** was oxidized with Jones reagent to afford 2-benzoyloxy-3-isopropyl-1,4-naphthoquinone (**40**) in 32% yield.

Compound **31** indicated the presence of benzoyloxyl groups (1729 cm^{-1}) and a conjugated carbonyl group (1703 cm^{-1}) in the IR spectrum. Its ^1H NMR spectrum showed a singlet signal due to a C-4 olefinic proton at δ 6.88. Thus, the structure of **31** was assigned to be 2,2-bis(benzoyloxy)-3-isopropyl-1(2*H*)-naphthalenone. This structure was further supported by its UV spectrum (Fig. 1). The oxidation of **31** with *m*-chloroperbenzoic acid afforded the quinone **40** in 36% yield. Compound **31** was also treated with acetic anhydride containing concentrated sulfuric acid to give 1,2,4-triacetoxy-3-isopropylnaphthalene (**41**) in 86% yield.

Compound **32** was identified as 1,1-bis(benzoyloxy)-3-isopropyl-2(1*H*)-naphthalenone by the following spectral data: IR 1731 and 1683 cm^{-1}, ^1H NMR δ 7.23 (singlet, C-4 proton), and UV (Fig. 2). The treatment of **32** with acetic anhydride containing concentrated sulfuric acid produced the triacetate **41** in 83% yield.

As shown in Table 1, the naphthols **1**, **2**, **18**, and **19** were oxidized under condition A to give mainly the corresponding ortho-benzoyloxylated product which was isolated as an equilibrium mixture (**4**+**20**, **23**+**24**, and **29**+**30**), resulting from its trans-benzoylation. On the other hand, oxidations of these naphthols under condition B produced mainly the corresponding bis(benzoyloxy)naphthalenone derivatives **5**, **21**, **25**, **28**, **31**, and **32**, although in the case of **1** the yield was very low.

From the present study, it is clear that the benzoyl peroxide oxidation is effective for the introduction of oxygen functions to the naphthol skeleton, in contrast to the results of Edward and Samad,[3] and Mathur et al.[4-7]

Experimental

All melting points are uncorrected. The IR spectrum were measured in chloroform and the ^1H NMR spectra in deuteriochloroform at 90 MHz with tetramethylsilane as an internal standard unless otherwise stated; s: singlet, bs: broad singlet, d: doublet, dd: double doublet, m: multiplet. The column chromatography was performed using Merck silica gel (0.063—0.200 mm).

4-Isopropyl-1-naphthol (18). A solution of 4-acetyl-1-naphthol[14] (1.862 g) in dry tetrahydrofuran (20 ml) was added dropwise to a stirred ether solution of methylmagnesium iodide prepared from magnesium turnings (961 mg) and methyl iodide (2.49 ml) in dry ether (24 ml). The mixture was refluxed for 2 h, poured into a mixture of ice and aqueous ammonium chloride, and extracted with ether. The ether extract was washed with brine, dried over sodium sulfate, and evaporated in vacuo to give a crude 4-(1-hydroxy-1-methylethyl)-1-naphthol, IR 3600 and 3220 cm^{-1}.

The above crude product was refluxed with acetic anhydride (15 ml) and sodium acetate (3.0 g) for 7 h. After evaporation of the acetic anhydride in vacuo, the residue was diluted with water and extracted with ether. The ether extract was washed with aqueous sodium hydrogencarbonate and brine, dried, and evaporated in vacuo. The residue was chromatographed on silica gel (200 g), using benzene as an eluent, to give 1-acetoxy-4-isopropenylnaphthalene (2.163 g: 95.6%), IR 1765 cm^{-1}, ^1H NMR (60 MHz) δ=2.18 (3H, m, $C\underline{H}_3C(=CH_2)$), 2.44 (3H, s, $-OCOCH_3$), 5.03 (1H, m) and 5.37 (1H, m) ($-C(=CH_2)$), 7.17 and 7.29 (each 1H, d, and J=8.5 Hz, C_2-H and C_3-H), 7.30—7.65 (2H, m, C_6-H and C_7-H), 7.70—8.20 (2H, m, C_5-H and C_8-H).

A mixture of the above acetate (2.163 g), 5% Pd-C (540 mg), and concentrated hydrochloric acid (0.2 ml) in methanol (40 ml) was hydrogenated at room temperature under an atmosphere of hydrogen for 19 h. After the usual work-up, the crude product was chromatographed on silica gel (200 g), using benzene as an eluent, to give **18**[15] (1.430 g: 79.8%). This was recrystallized from hexane-cyclohexane, mp 65—66 °C, IR 3600 and 3325br cm^{-1}, ^1H NMR δ=1.35 (6H, d, J=7 Hz, $-CH(C\underline{H}_3)_2$), 3.64 (1H, m, $-C\underline{H}(CH_3)_2$), 5.17 (1H, bs, $-OH$), 6.74 (1H, d, J=8 Hz, C_2-H), 7.18 (1H, d, J=8 Hz, C_3-H), 7.33—7.52 (2H, m, C_6-H and C_7-H), and 7.96—8.28 (2H, m, C_5-H and C_8-H). Found: C, 83.75; H, 7.92%. Calcd for $C_{13}H_{14}O$: C, 83.83; H, 7.58%.

3-Isopropyl-2-naphthol (19). A solution of methyl 2-hydroxy-3-naphthoate (10.110 g) in dry ether (300 ml) was added dropwise to a stirred ether solution of methylmagnesium iodide prepared from magnesium turnings (7.292 g) and methyl iodide (18.7 ml) in dry ether (200 ml). The mixture was refluxed for 1.5 h, poured into a mixture of ice and aqueous ammonium chloride, and extracted with ether. The ether extract was washed with brine, dried, and evaporated in vacuo. The residue was refluxed with acetic anhydride (50 ml) and sodium acetate (15.0 g) for 7 h. After the work-up (as described above) the crude product was chromatographed on silica gel (250 g), using benzene as an eluent, to give 2-acetoxy-3-isopropenylnaphthalene (10.860 g: 96.0%), IR 1755 cm^{-1}, ^1H NMR (60 MHz) δ=2.12 (3H, bs, $C\underline{H}_3C(=CH_2)$), 2.28 (3H, s, $-OCOCH_3$), 5.11 (1H, m) and 5.21 (1H, m) ($-C(=CH_2)$), 7.30—7.58 (2H, m, C_6-H and C_7-H), 7.48 (1H, s, C_1-H), 7.58-7.90 (2H, m, C_5-H and C_8-H), and 7.72 (1H, s, C_4-H).

A mixture of the above acetate (10.860 g) and 5% Pd-C (2.80 g) in methanol (160 ml) was hydrogenated at room temperature under an atmosphere of hydrogen for 17 h to give 2-acetoxy-3-isopropylnaphthalene (10.366 g), IR 1750 cm^{-1}, ^1H MMR (60 MHz) δ=1.34 (6H, d, J=7 Hz, $-CH(C\underline{H}_3)_2$), 2.36 (3H, s, $-OCOCH_3$), 3.12 (1H, m, $-C\underline{H}(CH_3)_2$), 7.25—7.58 (2H, m, C_6-H and C_7-H), 7.48 (1H, s, C_1-H), 7.58—7.93 (2H, m, C_5-H and C_8-H), and 7.72 (1H, s, C_4-H).

The above crude acetate (10.366 g) was treated with lithium aluminium hydride (2.584 g) in dry ether (200 ml) at room temperature for 2 h. The mixture was poured into ice-aqueous ammonium chloride and extracted with ether. The ether extract was washed with brine, dried, and

evaporated in vacuo. The residue was chromatographed on silica gel (250 g), using benzene as an eluent, to give **19**[16] (7.562 g: 84.6%). This was recrystallized from hexane, mp 81—82 °C, IR 3590 and 3290 cm^{-1}, ^1H NMR δ=1.33 (6H, d, J=7 Hz, -CH(C$\underline{H}_3$)$_2$), 3.33 (1H, m, -C$\underline{H}$(CH$_3$)$_2$), 4.96 (1H, s, -OH), 6.98 (1H, s, C_1-H), 7.59 (1H, s, C_4-H), 7.14—7.45 (2H, m, C_6-H and C_7-H), and 7.45—7.80 (2H, m, C_5-H and C_8-H). Found: C, 83.97; H, 7.83%. Calcd for $C_{13}H_{14}O$: C, 83.83; H, 7.58%.

Oxidation of 1-Naphthol (1) with Benzoyl Peroxide. *a*): **The Condition A.** A solution of **1** (288.0 mg) and benzoyl peroxide (460.0 mg) in dichloromethane (6.0 ml) was protected from light and stirred at room temperature for 24 h. After the addition of ether (20 ml), acetic acid (0.2 ml), and aqueous potassium iodide (20%, 5.0 ml), the mixture was further stirred at room temperature for 3 h. The mixture was washed successively with water, aqueous sodium thiosulfate, and brine. The dried solution was evaporated in vacuo and the residue was chromatographed on silica gel (50 g), using hexane-benzene (1:1) as an eluent, to give the starting **1** (46.5 mg: 16.1%). Further elution with benzene and ether-benzene (1:99) afforded four compounds **4**, **20**, **21**, and **22**.

1-Benzoyloxy-2-naphthol (**4**) and 2-benzoyloxy-1-naphthol (**20**) in a ratio of ca. 1:1 (133.2 mg: 25.2%), mp 173—176 °C (ca. 1:1 mixture from chloroform), IR 3575, 3280br, and 1745 cm^{-1}. ^1H NMR of **4** δ=5.91 (1H, bs, C_2-OH), 7.22 (1H, d, J=8.5 Hz, C_3-H), 7.32—7.88 (7H, m, C_5-H, C_6-H, C_7-H, C_8-H, and C_3-H, C_4-H, C_5-H of benzoyloxyl group), 7.65 (1H, d, J=8.5 Hz, C_4-H), and 8.33 (2H, dd, J=8 and 2 Hz, C_2-H and C_6-H of benzoyloxyl group). ^1H NMR of **20** δ=6.18 (1H, bs, C_1-OH), 7.30 (1H, d, J=9 Hz, C_3-H), 7.32—7.88 (6H, m, C_5-H, C_6-H, C_7-H, and C_3-H, C_4-H, C_5-H of benzoyloxyl group), 7.46 (1H, d, J=9 Hz, C_4-H), 8.24 (2H, dd, J=8 and 2 Hz, C_2-H and C_6-H of benzoyloxyl group), and ca. 8.25 (1H, m, C_8-H). Found: C, 77.41; H, 4.43%. Calcd for $C_{17}H_{12}O_3$: C, 77.26; H, 4.58%.

2,2-Bis(benzoyloxy)-1(2*H*)-naphthalenone (**21**) (27.9 mg: 3.6%), mp 195—196 °C decomp (from acetone), IR 1732 and 1709 cm^{-1}, ^1H NMR δ=6.33 (1H, d, J=10 Hz, C_3-H), 6.98 (1H, d, J=10 Hz, C_4-H), 7.27—7.75 (9H, m, C_5-H, C_6-H, C_7-H, and C_3-H, C_4-H, C_5-H of benzoyloxyl groups), 8.08 (4H, dd, J=8 and 2 Hz, C_2-H and C_6-H of benzoyloxyl groups), and 8.18 (1H, bd, J=7.5 Hz, C_8-H). Found: C, 75.00; H, 4.08%. Calcd for $C_{24}H_{16}O_5$: C, 74.99; H, 4.20%.

4-Benzoyloxy-1-naphthol (**22**) (13.3 mg: 2.5%), IR 3580, 3320br, and 1730 cm^{-1}. ^1H NMR δ=6.61 (1H, d, J=8 Hz, C_2-H), 7.07 (1H, d, J=8 Hz, C_3-H), 7.30—7.70 (5H, m, C_6-H, C_7-H, and C_3-H, C_4-H, C_5-H of benzoyloxyl group), ca. 7.81 (1H, m, C_5-H), ca. 8.10 (1H, m, C_8-H), and 8.30 (2H, dd, J=8 and 2 Hz, C_2-H and C_6-H of benzoyloxyl group). Found: C, 77.50; H, 4.40%. Calcd for $C_{17}H_{12}O_3$: C, 77.26; H, 4.58%.

b): **The Condition B.** A solution of **1** (288.0 mg) and benzoyl peroxide (1090.0 mg) in dichloromethane (10 ml) was protected from light and stirred at room temperature for 48 h. After the work-up (as described in *a*)) the crude product was purified by column chromatography on silica gel to give **21** (45.8 mg: 6.0%) and 2-benzoyloxy-1,4-naphthoquinone (**13**) (29.9 mg: 5.3%), mp 118—119 °C (from acetone-hexane), IR 1749 and 1667 cm^{-1}, ^1H NMR δ=6.93 (1H, s, C_3-H), 7.38—7.93 (5H, m, C_6-H, C_7-H, and C_3-H, C_4-H, C_5-H of benzoyloxyl group), ca. 8.11 (2H, m, C_5-H and C_8-H), and 8.18 (2H, dd, J=8 and 2 Hz, C_2-H and C_6-H of benzoyloxyl group). Found: C, 73.59; H, 3.50%. Calcd for $C_{17}H_{10}O_4$: C, 73.38; H, 3.62%.

Oxidation of 2-Naphthol (2) with Benzoyl Peroxide. *a*): A solution of **2** (288.0 mg) and benzoyl peroxide (460.0 mg) in dichloromethane (6.0 ml) was treated under condition A (room temp, 24 h). The crude product was purified by column chromatography on silica gel to give the starting **2** (80.6 mg: 28.0%), a mixture (ca. 1:1) of **4** and **20** (274.0 mg: 51.9%), **21** (57.6 mg: 7.5%), and 1,1-bis(benzoyloxy)-2(1*H*)-naphthalenone (**5**) (21.4 mg: 2.8%), mp 239—240 °C (from acetone), IR 1736 and 1695 cm^{-1}, ^1H NMR δ=6.56 (1H, d, J=10 Hz, C_3-H), 7.26—7.62 (8H, m, C_6-H, C_7-H, and C_3-H, C_4-H, C_5-H of benzoyloxyl groups), 7.50 (1H, d, J=10 Hz, C_4-H), ca. 7.73 (2H, m, C_5-H and C_8-H), and 8.06 (4H, dd, J=8 and 2 Hz, C_2-H and C_6-H of benzoyloxyl groups). Found: C, 75.16; H, 3.97%. Calcd for $C_{24}H_{16}O_5$: C, 74.99; H, 4.20%.

b): A solution of **2** (288.0 mg) and benzoyl peroxide (1090.0 mg) in dichloromethane (10 ml) was treated under condition B (room temp., 48 h). The crude product was purified by column chromatography on silica gel to give **5** (49.1 mg: 6.4%) and **21** (202.6 mg: 26.4%).

c): **The condition of Bhatia and Mathur.**[4] A solution of **2** (1.440 g: 10.0 mmol) and benzoyl peroxide (2.495 g: 10.3 mmol) in chloroform (12.5 ml) was refluxed for 6 h and then treated by the following our method.[17] The reaction mixture was diluted with ether (15 ml), acetic acid (0.5 ml), and aqueous potassium iodide (20%, 20 ml). After stirring at room temperature for 3 h, the mixture was extracted with ether and the ether extract was washed successively with water, aqueous sodium thiosulfate, aqueous sodium hydrogencarbonate, and brine. The dried solution was evaporated in vacuo. The residue was purified by column chromatography on silica gel to give the starting **2** (341 mg: 23.7%), a mixture (ca. 1:1, mp 173—176 °C from chloroform) of **4** and **20** (653 mg: 24.7%), **21** (mp 195—196 °C decomp. from acetone, 287 mg: 7.5%), and **5** (mp 239—240 °C from acetone, 92 mg: 2.4%).

Oxidation of 4-Isopropyl-1-naphthol (18) with Benzoyl Peroxide. *a*): A solution of **18** (372.5 mg) and benzoyl peroxide (460.0 mg) in dichloromethane (6.0 ml) was treated under the condition A (room temp, 24 h). The crude product was chromatographed on silica gel to give five compounds **23**, **24**, **25**, **26**, and **27**.

2-Benzoyloxy-4-isopropyl-1-naphthol (**23**) and 1-benzoyloxy-4-isopropyl-2-naphthol (**24**) in a ratio of ca. 2:3 (258.9 mg: 42.3%), mp 138—142 °C (ca. 2:3 mixture from carbon tetrachloride), IR 3570, 3320br, and 1740 cm^{-1}. Found: C, 78.11; H, 6.01%. Calcd for $C_{20}H_{18}O_3$: C, 78.41; H, 5.92%. ^1H NMR of **23** δ=1.38 (6H, d, J=7 Hz, -CH(C$\underline{H}_3$)$_2$), 3.70 (1H, m, -C$\underline{H}$(CH$_3$)$_2$), 6.10 (1H, br, C_1-OH), 7.19 (1H, s, C_3-H), 7.33—7.73 (5H, m, C_6-H, C_7-H, and C_3-H, C_4-H, C_5-H of benzoyloxyl group), ca. 8.06 (1H, m, C_5-H), 8.26 (2H, dd, J=8 and 2 Hz, C_2-H and C_6-H of benzoyloxyl group), and 8.31 (1H, m, C_8-H). ^1H NMR of **24** δ=1.38 (6H, d, J=7 Hz -CH(C$\underline{H}_3$)$_2$), 3.70 (1H, m, -C$\underline{H}$(CH$_3$)$_2$), 5.85 (1H, br, C_2-OH), 7.19 (1H, s, C_3-H), 7.33—7.73 (5H, m, C_6-H, C_7-H and C_3-H, C_4-H C_5-H of benzoyloxyl group), 7.84 (1H, m, C_8-H), ca. 8.06 (1H, m, C_5-H), and 8.34 (2H, dd, J=8 and 2 Hz, C_2-H and C_6-H of benzoyloxyl group).

2,2-Bis(benzoyloxy)-4-isopropyl-1(2*H*)-naphthalenone (**25**) (121.1 mg: 14.2%), mp 195—197 °C (from benzene), IR 1727 and 1703 cm^{-1}, ^1H NMR δ=1.23 (6H, d, J=7 Hz, -CH($C\underline{H}_3$)$_2$), 3.17 (1H, m, -$C\underline{H}$(CH_3)$_2$), 6.18 (1H, bs, C_3-H), 7.30-7.70 (9H, m, C_5-H, C_6-H, C_7-H, and C_3-H, C_4-H, C_5-H of benzoyloxyl groups), 8.06 (4H, dd, J= 8 and 2 Hz, C_2-H and C_6-H of benzoyloxyl groups), and 8.23 (1H, bd, J=8 Hz, C_8-H). Found: C, 75.86; H, 5.43%. Calcd for $C_{27}H_{22}O_5$: C, 76.04; H, 5.20%.

4,4'-Diisopropyl-2,2'-bi-1-naphthol (**26**) (72.0 mg: 6.5%), mp 210—212 °C (from hexane-acetone), MS m/z 370 (M^+), IR 3535 and 3270br cm^{-1}, ^1H NMR δ=1.41 (12H, d, J=7 Hz, 2-CH($C\underline{H}_3$)$_2$), 3.72 (2H, m, 2-$C\underline{H}$(CH_3)$_2$), 5.56 (2H, bs, 2-OH), 7.32 (2H, bs, C_3-H and $C_{3'}$-H), 7.40—7.73 (4H, bm, C_6-H, $C_{6'}$-H, C_7-H, and $C_{7'}$-H), 7.98—8.27 (2H, bm, C_5-H and $C_{5'}$-H), and 8.27—8.53 (2H, bm, C_8-H and $C_{8'}$-H). Found: C, 84.54; H, 7.31%. Calcd for $C_{26}H_{26}O_2$: C, 84.29; H, 7.07%. Compound **26** (18.5 mg) was acetylated with acetic anhydride (1.0 ml) in pyridine (1.0 ml) at room temperature for 15 h to give the corresponding diacetate (20.8 mg: 91.5%), mp 166—167 °C (from methanol), IR 1760 cm^{-1}, ^1H NMR δ=1.41 (12H, d, J=7 Hz, 2-CH($C\underline{H}_3$)$_2$), 2.10 (6H, s, 2-$OCOCH_3$), 3.77 (2H, m, 2-$C\underline{H}$(CH_3)$_2$), 7.43 (2H, s, C_3-H and $C_{3'}$-H), 7.47—7.68 (4H, m, C_6-H, $C_{6'}$-H, C_7-H, and $C_{7'}$-H), 7.72—7.93 (2H, m, C_8-H and $C_{8'}$-H), and 8.05—8.28 (2H, m, C_5-H and $C_{5'}$-H). Found: C, 78.98; H, 6.71%. Calcd for $C_{30}H_{30}O_4$: C, 79.29; H, 6.65%.

1,1',2,2'-Tetrahydro-4,4'-diisopropyl-1,1'-dioxo-2,2'-binaphthylidene (**27**) (9.8 mg: 1.3%), mp 167—168 °C (from benzene), IR 1629 cm^{-1}, ^1H NMR δ=1.36 (12H, d, J=7 Hz, 2-CH($C\underline{H}_3$)$_2$), 3.26 (2H, m, 2-$C\underline{H}$(CH_3)$_2$), 7.27—7.63 (6H, m, C_5-H, $C_{5'}$-H, C_6-H, $C_{6'}$-H, C_7-H, and $C_{7'}$-H), 8.14 (2H, bd, J=8 Hz, C_8-H and $C_{8'}$-H), and 8.29 (2H, bs, C_3-H and $C_{3'}$-H). Found: C, 84.83; H, 6.49%. Calcd for $C_{26}H_{24}O_2$: C, 84.75; H, 6.57%.

b): A solution of **18** (372.5 mg) and benzoyl peroxide (1090.0 mg) in dichloromethane (10 ml) was treated under condition B (room temp, 48 h). The crude product was chromatographed on silica gel to give a mixture (ca. 2:3) of **23** and **24** (27.0 mg: 4.4%), **25** (557.8 mg: 65.4%), **27** (32.8 mg: 3.1%), and 1,1-bis(benzoyloxy)-4-isopropyl-2(1*H*)-naphthalenone (**28**) (35.8 mg: 4.2%), mp 204—205 °C (from methanol-acetone), IR 1737 and 1680 cm^{-1}, ^1H NMR δ=1.41 (6H, d, J=7 Hz, -CH($C\underline{H}_3$)$_2$), 3.35 (1H, m, -$C\underline{H}$(CH_3)$_2$), 6.51 (1H, bs, C_3-H), 7.30—7.87 (10H, m, C_5-H, C_6-H, C_7-H, C_8-H, and C_3-H, C_4-H, C_5-H of benzoyloxyl groups), and 8.06 (4H, dd, J=8 and 2 Hz, C_2-H and C_6-H of benzoyloxyl groups). Found: C, 75.82; H, 5.00%. Calcd for $C_{27}H_{22}O_5$: C, 76.04 H, 5.20%.

Oxidation of 3-Isopropyl-2-naphthol (19) with Benzoyl Peroxide. *a*): A solution of **19** (372.5 mg) and benzoyl peroxide (460.0 mg) in dichloromethane (6.0 ml) was treated under condition A (room temp, 24 h). The crude product was chromatographed on silica gel to give the starting **19** (59.5 mg: 16.0%) and three other compounds **29**, **30**, and **31**.

2-Benzoyloxy-3-isopropyl-1-naphthol (**29**) and 1-benzoyloxy-3-isopropyl-2-naphthol (**30**) in a ratio of ca. 1:1 (405.7 mg: 66.2%), IR 3575, 3320br, and 1737 cm^{-1}. The mixture was recrystallized from carbon tetrachloride to give pure **30**, mp 137—138 °C, ^1H NMR δ=1.36 (6H, d, J=7 Hz, -CH($C\underline{H}_3$)$_2$), 3.47 (1H, m, -$C\underline{H}$(CH_3)$_2$), 5.76 (1H, bs, C_2-OH), 7.27—7.87 (7H, m, C_5-H, C_6-H, C_7-H, C_8-H, and C_3-H, C_4-H, C_5-H of benzoyloxyl group), 7.60 (1H, s, C_4-H), and 8.34 (2H, dd, J=8 and 2 Hz, C_2-H and C_6-H of benzoyloxyl group). Found: C, 78.29; H, 5.89%. Calcd for $C_{20}H_{18}O_3$: C, 78.41; H, 5.92%. ^1H NMR of **29** δ=1.32 (6H, d, J=7 Hz, -CH($C\underline{H}_3$)$_2$), 3.18 (1H, m, -$C\underline{H}$(CH_3)$_2$), 5.85 (1H, br, C_1-OH), 7.29—7.89 (6H, m, C_5-H, C_6-H, C_7-H, and C_3-H, C_4-H, C_5-H of benzoyloxyl group), 7.38 (1H, s, C_4-H), ca. 8.20 (1H, m, C_8-H), and 8.26 (2H, dd, J=8 and 2 Hz, C_2-H and C_6-H of benzoyloxyl group).

2,2-Bis(benzoyloxy)-3-isopropyl-1(2*H*)-naphthalenone (**31**) (72.1 mg: 8.5%), mp 219—220 °C (from acetone), IR 1729 and 1703 cm^{-1}, ^1H NMR δ=1.11 (6H, d, J=7 Hz, -CH($C\underline{H}_3$)$_2$), 2.95 (1H, m, -$C\underline{H}$(CH_3)$_2$), 6.88 (1H, bs, C_4-H), 7.25—7.73 (9H, m, C_5-H, C_6-H, C_7-H, and C_3-H, C_4-H, C_5-H of benzoyloxyl groups), ca. 8.10 (1H, m, C_8-H), and 8.10 (4H, dd, J=8 and 2 Hz, C_2-H and C_6-H of benzoyloxyl groups). Found: C, 76.20; H, 5.13%. Calcd for $C_{27}H_{22}O_5$: C, 76.04; H, 5.20%.

b): A solution of **19** (372.5 mg) and benzoyl peroxide (1090.0 mg) in dichloromethane (10 ml) was treated under condition B (room temp., 48 h). The crude product was chromatographed on silica gel to give a mixture (ca. 1:1) of **29** and **30** (30.6 mg: 5.0%), **31** (554.4 mg: 65.0%), and 1,1-bis(benzoyloxy)-3-isopropyl-2(1*H*)-naphthalenone (**32**) (122.9 mg: 14.4%), mp 198—199 °C (from acetone), IR 1731 and 1683 cm^{-1}, ^1H NMR δ=1.27 (6H, d, J=7 Hz, -CH($C\underline{H}_3$)$_2$), 3.17 (1H, m, -$C\underline{H}$(CH_3)$_2$), 7.18—7.62 (9H, m, C_5-H, C_6-H, C_7-H, and C_3-H, C_4-H, C_5-H of benzoyloxyl groups), 7.23 (1H, bs, C_4-H), ca. 7.70 (1H, m, C_8-H), and 8.06 (4H, dd, J=8 and 2 Hz, C_2-H and C_6-H of benzoyloxyl groups). Found: C, 76.06; H, 5.24%. Calcd for $C_{27}H_{22}O_5$: C, 76.04; H, 5.20%.

2-Benzoyloxy-1,4-naphthoquinone (13). *a*): A mixture (ca. 1:1) of **4** and **20** (52.8 mg) was oxidized with Jones reagent (2.5 mol dm^{-3}: 0.24 ml) in acetone (2.0 ml) at 0—5 °C for 15 min. The mixture was diluted with water and extracted with ether. The ether extract was washed with brine, dried, and evaporated in vacuo. The residue was chromatographed on silica gel (5.0 g), using benzene as an eluent, to give a quinone (7.6 mg: 13.7%), the IR and ^1H NMR spectra of which were identical with those of **13**.

b): A solution of **21** (38.4 mg), *m*-chloroperbenzoic acid (80%, 25.8 mg), and *p*-toluenesulfonic acid monohydrate (4.0 mg) in dichloromethane (1.0 ml) was refluxed for 2 h. The solution was cooled, diluted with ether, and then washed successively with aqueous potassium iodide, aqueous sodium thiosulfate, aqueous sodium hydrogencarbonate, and brine. The dried solution was evaporated in vacuo. The residue was chromatographed on silica gel (5.0 g), using hexane-benzene (1:1) as an eluent, to give the recovered **21** (14.3 mg) and a quinone (6.0 mg: 21.6%), whose IR and ^1H NMR spectra were identical with those of **13**.

Oxidation of 26 with Potassium Hexacyanoferrate(III). A solution of potassium hexacyanoferrate(III) (150.0 mg) in aqueous potassium hydroxide (0.2 mol dm^{-3}, 15.0 ml) was added dropwise to a stirred solution of **26** (24.6 mg) in methanol (5.0 ml) with cooling in an ice-water bath. The mixture was further stirred at room temperature for 15 min. The precipitated product was collected and washed with water. The dried product was recrystallized from benzene to give **27** (20.0 mg: 80.7%), mp 167—168 °C, the IR and ^1H NMR spectra of which were identical with those of the

authentic sample.

1-Acetoxy-2-benzoyloxynaphthalene (33) and 2-Acetoxy-1-benzoyloxynaphthalene (34). A mixture (ca. 1:1) of **4** and **20** (63.0 mg) was refluxed with isopropenyl acetate (0.27 ml) and *p*-toluenesulfonic acid monohydrate (3.2 mg) in toluene (0.7 ml) for 3 h. The mixture was cooled, diluted with ether, and washed with aqueous sodium hydrogencarbonate and brine. The dried solution was evaporated in vacuo. The residue was chromatographed on silica gel (10 g), using benzene as an eluent, to give **33** (20.6 mg: 28.0%), mp 144—145 °C (from methanol), IR 1763 and 1740 cm^{-1}, ^1H NMR δ=2.30 (3H, s, $-OCOCH_3$), 7.40—7.95 (7H, m, C_5-H, C_6-H, C_7-H, C_8-H, and C_3-H, C_4-H, C_5-H of benzoyloxyl group), 7.43 (1H, d, J=9 Hz, C_3-H), 7.78 (1H, d, J=9 Hz, C_4-H), and 8.20 (2H, dd, J=8 and 2 Hz, C_2-H and C_6-H of benzoyloxyl group). Found: C, 74.56; H, 4.67%. Calcd for $C_{19}H_{14}O_4$: C, 74.45; H, 4.60%.

Further elution with ether-benzene (1:99) afforded **34** (51.8 mg: 70.5%), mp 99—103 °C (from methanol), IR 1763 and 1740 cm^{-1}, ^1H NMR δ=2.16 (3H, s, $-OCOCH_3$), 7.35 (1H, d, J=9 Hz, C_3-H), 7.40—7.98 (7H, m, C_5-H, C_6-H, C_7-H, C_8-H, and C_3-H, C_4-H, C_5-H of benzoyloxyl group), 7.78 (1H, d, J=9 Hz, C_4-H), and 8.29 (2H, dd, J=8 and 2 Hz, C_2-H and C_6-H of benzoyloxyl group). Found: C, 74.62; H, 4.58%. Calcd for $C_{19}H_{14}O_4$: C, 74.45; H, 4.60%.

1,2,4-Triacetoxynaphthalene (35). *a*): A solution of **21** (76.9 mg) in acetic anhydride (1.0 ml) containing concentrated sulfuric acid (30 mg) was stirred at 50 °C for 2 h. The solution was poured into ice-water and extracted with ether. The ether extract was washed successively with brine, aqueous sodium hydrogencarbonate, and brine. The dried solution was evaporated in vacuo. The residue was chromatographed on silica gel (10 g), using ether-benzene (5:95) as an eluent, to give **35** (44.3 mg: 73.3%), mp 137—138 °C (from methanol), IR 1775 cm^{-1}, ^1H NMR δ=2.31 (3H, s, $-OCOCH_3$), 2.43 (6H, s, 2-$OCOCH_3$), 7.28 (1H, s, C_3-H), 7.43—7.67 (2H, m, C_6-H and C_7-H), and 7.76—7.98 (2H, m, C_5-H and C_8-H). Found: C, 63.63; H, 4.65%. Calcd for $C_{16}H_{14}O_6$: C, 63.57; H, 4.67%.

b): A solution of **5** (19.2 mg) in acetic anhydride (0.25 ml) containing concentrated sulfuric acid (7.5 mg) was stirred at 50 °C for 2 h. After the work-up (as described in *a*)) the crude product was purified by column chromatography on silica gel (5.0 g) to give **35** (13.6 mg: 90.0%), whose IR and ^1H NMR spectra were identical with those of the authentic sample.

Catalytic Hydrogenation of 5 and 21. *a*): A mixture of **5** (76.9 mg) and 5% Rh-Al_2O_3 (23.1 mg) in 1,4-dioxane (1.5 ml) was hydrogenated at room temperature under an atmosphere of hydrogen for 3 h. After the usual work-up, the crude product was chromatographed on silica gel (10 g), using hexane-benzene (1:1) as an eluent, to give an oily 1,1-bis(benzoyloxy)-3,4-dihydro-2(1*H*)-naphthalenone (**36**) (24.6 mg: 31.8%) IR 1727 cm^{-1}, ^1H NMR δ=3.10—3.58 (4H, m, $-CH_2CH_2-$), 7.20—7.62 (9H, m, C_5-H, C_6-H, C_7-H, and C_3-H, C_4-H, C_5-H of benzoyloxyl groups), ca. 7.70 (1H, m, C_8-H), and 8.07 (4H, dd, J=8 and 2 Hz, C_2-H and C_6-H of benzoyloxyl groups), MS m/z 386 (M^+). Further elution with benzene afforded a mixture of **4** and **20** (34.6 mg: 65.5%), the IR and ^1H NMR spectra of which were identical with those of the authentic mixture.

b): A mixture of **21** (76.9 mg) and 5% Rh-Al_2O_3 (23.1 mg) in 1,4-dioxane (1.5 ml) was hydrogenated as described in *a*). The crude product was chromatographed on silica gel (10 g), using benzene as an eluent, to give an oily 2,2-bis(benzoyloxy)-3,4-dihydro-1(2*H*)-naphthalenone (**37**) (46.3 mg: 60.0%), IR 1735 and 1710 cm^{-1}, ^1H NMR δ=3.00—3.44 (4H, m, $-CH_2CH_2-$), 7.18—7.86 (9H, m, C_5-H, C_6-H, C_7-H, and C_3-H, C_4-H, C_5-H of benzoyloxyl groups), 8.06 (4H, dd, J=8 and 2 Hz, C_2-H and C_6-H of benzoyloxyl groups), and ca. 8.17 (1H, m, C_8-H), MS m/z 386 (M^+). Further elution with benzene afforded a mixture of **4** and **20** (20.1 mg: 38.0%), the IR and ^1H NMR spectra of which were identical with those of the authentic mixture.

2-Acetoxy-1-benzoyloxy-4-isopropylnaphthalene (38). A mixture (ca. 2:3) of **23** and **24** (66.8 mg) was refluxed with isopropenyl acetate (0.24 ml) and *p*-toluenesulfonic acid monohydrate (3.4 mg) in toluene (1.3 ml) for 5 h. After the work-up (as described above) the crude product was chromatographed on silica gel (10 g), using ether-benzene (1:99) as an eluent, to give **38** (49.2 mg: 64.2%), mp 142—143 °C (from methanol), IR 1769 and 1744 cm^{-1}, ^1H NMR δ=1.41 (6H, d, J=7 Hz, $-CH(C\underline{H}_3)_2$), 2.17 (3H, s, $-OCOCH_3$), 3.75 (1H, m, $-C\underline{H}(CH_3)_2$), 7.25 (1H, s, C_3-H), 7.30—7.71 (5H, m, C_6-H, C_7-H, and C_3-H, C_4-H, C_5-H of benzoyloxyl group), ca. 7.90 (1H, m, C_8-H), ca. 8.12 (1H, m, C_5-H), and 8.28 (2H, dd, J=8 and 2 Hz, C_2-H and C_6-H of benzoyloxyl group). Found: C, 76.13; H, 6.04%. Calcd for $C_{22}H_{20}O_4$: C, 75.84; H, 5.79%.

The acetate **38** (10.2 mg) was refluxed with dilute hydrochloric acid (15%, 0.1 ml) in methanol (0.9 ml) for 1 h. The mixture was diluted with brine and extracted with ether. The ether extract was washed with brine, dried, and evaporated in vacuo to give **24** (8.7 mg) containing a small amount of **23** (by ^1H NMR analysis). This was dissolved in deuteriochloroform and then allowed to stand at room temperature for 24 h to give an equilibrium mixture of **23** and **24** (ca 2:3).[13]

1-Acetoxy-2-benzoyloxy-3-isopropylnaphthalene (39) and 2-Benzoyloxy-3-isopropyl-1,4-naphthoquinone (40). *a*): A mixture (ca. 1:1) of **29** and **30** (91.2 mg) was refluxed with isopropenyl acetate (0.33 ml) and *p*-toluenesulfonic acid monohydrate (4.6 mg) in toluene (0.9 ml) for 5 h. After the work-up (as described above) the crude product was chromatographed on silica gel (0.040—0.063 mm, 15 g), using hexane-benzene (6:4) as an eluent, to give **40** (20.6 mg: 21.6%), mp 123—125 °C (from hexane), IR 1743 and 1672 cm^{-1}, ^1H NMR δ=1.32 (6H, d, J=7 Hz, $-CH(C\underline{H}_3)_2$), 3.43 (1H, m, $-C\underline{H}(CH_3)_2$), 7.42—7.87 (5H, m, C_6-H, C_7-H, and C_3-H, C_4-H, C_5-H of benzoyloxyl group), ca. 8.12 (2H, m, C_5-H and C_8-H), and 8.20 (2H, dd, J=8 and 2 Hz, C_2-H and C_6-H of benzoyloxyl group). Found: C, 75.01; H, 5.13%. Calcd for $C_{20}H_{16}O_4$: C, 74.99; H, 5.03%.

Further elution with hexane-benzene (25:75) afforded **39** (78.7 mg: 75.9%), mp 161—164 °C (from methanol), IR 1773 and 1741 cm^{-1}, ^1H NMR δ=1.32 (6H, d, J=7 Hz, $-CH(C\underline{H}_3)_2$), 2.18 (3H, s, $-OCOCH_3$), 3.19 (1H, m, $-C\underline{H}(CH_3)_2$), 7.32-7.90 (7H, m, C_5-H, C_6-H, C_7-H, C_8-H, and C_3-H, C_4-H, C_5-H of benzoyloxyl group), 7.71 (1H, s, C_4-H), and 8.25 (2H, dd, J=8 and 2 Hz, C_2-H and C_6-H of benzoyloxyl group). Found: 75.70; H, 5.88%. Calcd for $C_{22}H_{20}O_4$: C, 75.84; H, 5.79%.

The acetate **39** (10.5 mg) was refluxed with dilute hydrochloric acid (15%, 0.1 ml) in methanol (0.9 ml) for 1 h.

The mixture was diluted with brine and extracted with ether. The ether extract was washed with brine, dried, and evaporated in vacuo to give **29** (8.5 mg) containing a small amount of **30** (by ^{1}H NMR analysis). This was dissolved in deuteriochloroform and then allowed to stand at room temperature for 24 h to afford an equilibrium mixture of **29** and **30** (ca. 1:1).[13]

b): A solution of **30** (31.6 mg) in acetone (1.0 ml) was oxidized with Jones reagent (2.5 mol dm^{-3}: 0.12 ml) at 0—5 °C for 20 min. After the work-up (as described above) the crude product was chromatographed on silica gel (5.0 g), using hexane–benzene (1:1) as an eluent, to give **40** (10.4 mg: 31.5%), mp 123—125 °C, whose IR and ^{1}H NMR spectra were identical with those of the authentic sample.

c): A solution of **31** (21.3 mg), *m*-chloroperbenzoic acid (80%, 12.9 mg), and *p*-toluenesulfonic acid monohydrate (3.0 mg) in dichloromethane (0.5 ml) was refluxed for 8 h. After the work-up (as described above) the crude product was chromatographed on silica gel (5.0 g), using benzene as an eluent, to give **40** (5.7 mg: 35.6%), mp 123—125 °C, the IR and ^{1}H NMR spectra of which were identical with those of the authentic sample.

1,2,4-Triacetoxy-3-isopropylnaphthalene (41). *a*): A solution of **31** (85.2 mg) and concentrated sulfuric acid (30 mg) in acetic anhydride (1.0 ml) was stirred at 50 °C for 2 h. After the work-up (as described above) the crude product was chromatographed on silica gel (15 g), using ether–benzene (1:99 and then 3:97) as eluents, to give **41** (59.2 mg: 86.0%), mp 152—153 °C (from methanol), IR 1772 cm^{-1}, ^{1}H NMR δ=1.30 (6H, d, J=7 Hz, -CH(C$\underline{H}_3$)$_2$), 2.34 (3H, s), 2.39 (3H, s), and 2.46 (3H, s) (3-OCOCH_3), 3.24 (1H, m, -C$\underline{H}$(CH$_3$)$_2$), and 7.36—7.80 (4H, m, C$_5$-H, C$_6$-H, C$_7$-H, and C$_8$-H). Found: C, 66.29; H, 6.05%. Calcd for $C_{19}H_{20}O_6$: C, 66.27; H, 5.85%.

b): A solution of **32** (42.5 mg) and concentrated sulfuric acid (15 mg) in acetic anhydride (0.5 ml) was treated as described in *a*). The crude product was chromatographed on silica gel (5.0 g) to give **41** (28.4 mg: 82.8%), mp 152—153 °C, the IR and ^{1}H NMR spectra of which were identical with those of the authentic sample.

References

1) D. J. Rawlinson and G. Sosnovsky, *Synthesis*, **1972**, 1, and references cited therein.

2) T. Matsumoto, Y. Ohsuga, S. Harada, and K. Fukui, *Bull. Chem. Soc. Jpn.*, **50**, 266 (1977); T. Matsumoto, H. Kawashima, and K. Iyo, *ibid.*, **55**, 1168 (1982).

3) J. T. Edward and S. A. Samad, *Can. J. Chem.*, **41**, 1027 (1963).

4) V. P. Bhatia and K. B. L. Mathur, *Tetrahedron Lett.*, **1966**, 4057.

5) Y. S. Chauhan and K. B. L. Mathur, *Indian J. Chem.*, **13**, 38 (1975).

6) K. N. Sawhney and K. B. L. Mathur, *Indian J. Chem.*, **16B**, 863 (1978).

7) M. A. Ansari, K. B. L. Mathur, and V. K. Ahluwalia, *Indian J. Chem.*, **19B**, 587 (1980).

8) T. Matsumoto, S. Imai, T. Hirata, Y. Fukuda, T. Yamaguchi, and K. Inoue, *Bull. Chem. Soc. Jpn.*, **56**, 3471 (1983).

9) C. H. Eugster, H. P. Küng, H. Kühnis, and P. Karrer, *Helv. Chim. Acta*, **46**, 530 (1963).

10) D. Karanatsios and C. H. Eugster, *Helv. Chim. Acta*, **48**, 471 (1965).

11) C. H. Eugster, *Ber. Deutsch. Bot. Ges.*, **88**, 141, (1975).

12) During the reaction, trans-benzoylation occurred.

13) The ratio was estimated by its ^{1}H NMR spectrum.

14) K. Matsui and M. Motoi, *Bull. Chem. Soc. Jpn.*, **46**, 565 (1973).

15) H. Meyer and K. Bernhauser, *Monatsh. Chem.*, **53** and **54**, 721 (1929); *Chem. Abstr.*, **24**, 346 (1930).

16) S. K. Sengupta, R. N. Biswas, and B. K. Bhattacharyya, *J. Indian. Chem. Soc.*, **36**, 659 (1959); *Chem. Abstr.*, **54**, 17347f (1960).

17) Bhatia and Mathur treated the reaction mixture by a different method.[4]

 © 1988 The Chemical Society of Japan Bull. Chem. Soc. Jpn., 61, 921—925 (1988)

The Reaction of Oxiranes with Carbon Disulfide under High Pressure

Yoichi TAGUCHI,* Koshin YANAGIYA, Isao SHIBUYA, and Yasuo SUHARA
National Chemical Laboratory for Industry, Higashi, Tsukuba, Ibaraki 305
(Received August 4, 1987)

The reaction of 2,2-dimetyloxirane with carbon disulfide in the presence of triethylamine was accelerated under high pressure to give 5,5-dimethyl-1,3-oxathiolane-2-thione in a high yield, while 2-hexyloxirane under the same reaction condition formeds 4-hexyl-1,3-dithiolane-2-thione (**2b**) as the main product and 5-hexyl-1,3-oxathiolane-2-thione (**1b**) as a minor product. A feasible mechanism for this formation is that **1b** and 2-hexylthiirane (**4b**) are produced in the first stage of reaction, and that **2b** is then formed by the reaction of **1b** or **4b** with carbon disulfide. In reactions of a variety of oxiranes with carbon disulfide, 1,3-dithiolane-2-thiones were obtained in high yields under 800 MPa at 100 °C within 20 h. Concerning the effect of substituents in oxiranes, the selectivity for product **2b** is in the decreasing order; 2-phenyl->2-methyl->2-ethyl->2-hexyl->2,3-tetramethylene->2,2-dimethyl->2-(chloromethyl)-. Tertiary amines, such as *N,N*-dimethylethylamine, pyridine, and *N*-methylmorpholine, serve as good catalysts for the reaction.

There have been many reports[1-8] that oxiranes react with carbon disulfide to form various products such as thiiranes, 1,3-dithiolane-2-thiones, and 1,3-oxathiolane-2-thiones, but these products except thiiranes have not been obtained in good yield. Many organic reactions, when conducted under high pressure, show product selectivities different from those they show under ordinary pressure,[9] and we found that the reaction of thiiranes with carbon disulfide was accelerated under high pressure to give 1,3-dithiolane-2-thiones with high selectivity and yield:[10]

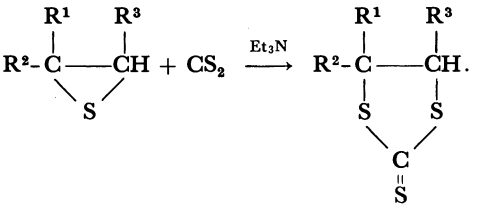

Therefore, it is expected that acceleration by compression may be observed also with the reaction of oxiranes, and that the formation of thiiranes, which are often main products under ordinary pressure, may be suppressed by compression.

In this paper, we report that the reaction of oxiranes with carbon disulfide is also accelerated by compression to give 1,3-dithiolane-2-thiones, 1,3-oxathiolane-2-thiones, 1,3-oxathiolan-2-ones, and thiiranes, and that the proportion of these products is dependent on pressure, temperature, the amount and kind of catalyst, and substituents in oxiranes. Furthermore, formation mechanisms for these products are discussed, and the reactivity of oxiranes is compared with that of thiiranes.

Results and Discussion

A reaction of 2,2-dimethyloxirane with carbon disulfide in a sealed tube at 100 °C for 20 h gave only 4% of 4,4-dimethyl-1,3-oxathiolane-2-thione (**1a**), but, when conducted under 800 MPa, gave 68% of **1a** and 8% of 5,5-dimethyl-1,3-dithiolane-2-thione (**2a**), which verifies that this reaction is to be accelerated remarkably by compression.

The structure of **1a** was assigned based on IR, ^{1}H NMR, and CI-MS spectra, and the spectral data of **2a** agreed with the known data.[10] The isomer of **1a**, 4,4-dimethyl-1,3-oxathiolane-2-thione, was not detected. Table 1 shows effects of pressure, temperature, and the kind of catalysts on the reaction. *N,N*-Dimethylethylamine, triethylamine, *N*-methylmorpholine, pyridine, and tetraethylammonium bromide are good catalysts under high pressure, and the ratio of **2a** to total yield decreases in the above-listed order (Runs 2 and 6—9). This order agrees with that of their catalytic activities for the reaction of 2,2-dimethylthiirane with carbon disulfide.[10] Table 1 also shows that the ratio of **2a** to total yield increases at higher temperatures or in the presence of strong catalyst (Runs 2 and 6).

Table 2 shows the effect of reaction conditions on the reaction of 2-hexyloxirane with carbon disulfide:

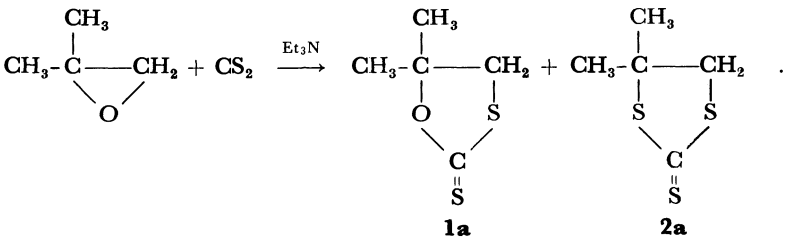

Table 1. Reaction of 2,2-Dimethyloxirane with CS_2[a]

Run No.	Catalyst	Press.	Temp	Yield/%		
		MPa	°C	**1a**	**2a**	Total
1	Et_3N	0.1[b]	100	4	—	4
2	Et_3N	800	100	68	8	76
3	Et_3N	800	70	82	2	84
4	Et_3N	800	40	54	3	57
5	Et_3N	300	40	Trace	—	Trace
6	*N,N*-Dimethylethylamine	800	100	67	18	85
7	*N*-Methylmorpholine	800	100	89	5	94
8	Pyridine	800	100	88	4	92
9	Et_4NBr	800	100	62	2	64

a) 2,2-Dimethyloxirane 5 mmol; CS_2 25 mmol; reaction time 20 h; catalyst 0.5 mmol. b) In a sealed glass tube.

Table 2. Reaction of 2-Hexyloxirane with CS_2[a]

Run No.	Press.	Temp	Time	Conv.	Yield/%				
	MPa	°C	h	%	**1b**	**2b**	**3b**	**4b**	Total
1	0.1[b]	100	20	52	17	1	—	7	25
2	200	100	20	94	57	27	—	—	84
3	500	100	20	100	17	59	7	—	83
4	800	100	20	100	5	71	12	1	89
5	500	40	20	47	4	10	4	22	40
6	500	70	20	100	18	26	5	3	52
7	800	40	20	100	4	10	—	24	38
8	800	70	20	100	17	53	9	6	85
9	800	100	7	100	15	63	15	—	93

a) 2-Hexyloxirane 5 mmol; CS_2 25 mmol; Et_3N 0.5 mmol. b) In a sealed glass tube.

Table 3. Effect of Various Catalysts on the Reaction of 2-Hexyloxirane with CS_2[a]

Run No.	Catalyst	Conv.	Yield/%				
		%	**1b**	**2b**	**3b**	**4b**	Total
1	*N,N*-Dimethylethylamine	100	5	67	13	—	85
2	Et_3N	100	5	71	12	1	89
3	*N*-Methylmorpholine	100	30	46	13	—	89
4	Pyridine	100	20	43	8	1	72
5	Et_4NBr	64	13	9	11	3	36
6	LiCl	41	9	Trace	4	1	14

a) 2-Hexyloxirane 5 mmol; CS_2 25 mmol; catalyst 0.5 mmol; pressure 800 MPa; reaction temperature 100 °C; reaction time 20 h.

This reaction under 800 MPa at 100 °C for 20 h gave 4-hexyl-1,3-dithiolane-2-thione (**2b**) as the main product, and the yield of 5-hexyl-1,3-oxathiolane-2-thione (**1b**) was only 5%, in contrast to that for the reaction of 2,2-dimethyloxirane with carbon disulfide. 5-Hexyl-1,3-oxathiolan-2-one (**3b**) and 2-hexylthiirane (**4b**) were also produced as minor products. The structures of **1b** and **3b** were assigned based on their IR, ^1H NMR, and CI-MS spectra taken after purification by column chromatography, and the spectral data

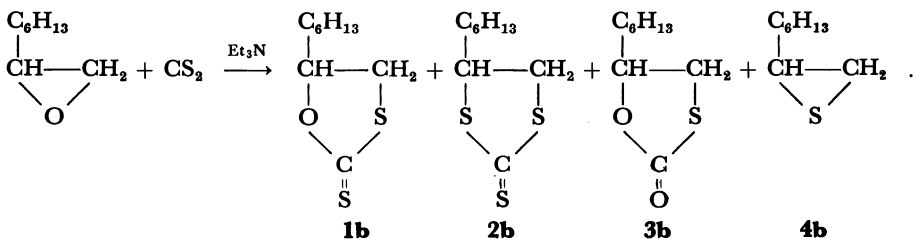

of **2b** and **4b** agreed with the known data.[10] The isomer of **1b**, 4-hexyl-1,3-oxathiolane-2-thione, was not detected. For this reaction, at 100 °C the yield of **2b** increased as pressure or reaction time was increased (Runs 1—4 and 7), and at 40 °C **4b** was obtained as the main product though its yield was not high (Runs 5 and 7).

Table 3 shows the effect of various catalysts on the reaction. Lithium chloride has no catalytic activity for the reaction of thiiranes with carbon disulfide,[10] but it has a little catalytic activity for the reaction of 2-hexyloxirane (Run 6). A dependence similar to that indicated by the results in Table 1 was observed with respect to the ratio of **2b** to total yield, that is, the ratio decreased in the order; triethylamine≥*N*,*N*-dimethylethylamine>pyridine≥*N*-methylmorpholine>tetraethylammonium bromide>lithium chloride. As a result, it is suggested that **1b** is formed as the main product in the first stage and then converted into **2b** as reaction proceeds.

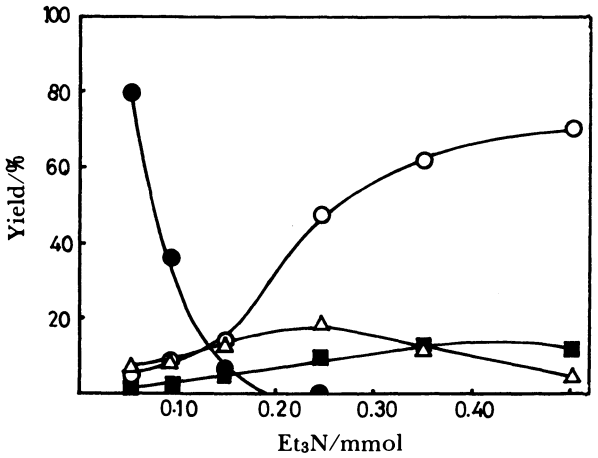

Fig. 1. Effect of amount of Et_3N on the reaction of 2-hexyloxirane with CS_2; reaction temperature: 100 °C, reaction time: 20 h, pressure: 800 MPa, 2-hexyloxirane: 5 mmol. CS_2: 25 mmol.
—△—: **1b**. —○—:**2b**, —■—: **3b**, —●—: 2-hexyloxirane.

Figure 1 shows the relation between products and the amount of triethylamine used as a catalyst for the reaction. As the rate of the reaction of thiiranes with carbon disulfide is proportional to the amount of triethylamine catalyst,[10] it is considered that the rate of the reaction of 2-hexyloxirane is proportional to the amount of triethylamine in the range 0.05—0.50 mmol. In the first stage **1b** was formed as the main product but its yield was not so much increased as reaction proceeded. On the other hand, the yield of **2b** increased as reaction proceeded even after 2-hexyloxirane was consumed completely. This fact also supports the suggestion that **2b** is formed as a result of the conversion of **1b**.

Table 4 shows products and yields for the reaction of various oxiranes with carbon disulfide. Two kinds of reaction conditions were used for comparison of reactivities of oxiranes. The conditions of Method A (catalyst *N*-methylmorpholine, 800 MPa, 70 °C, 20 h) is milder than that of Method B (catalyst triethylamine, 800 MPa, 100 °C, 20 h). 2-Phenyloxirane reacted with carbon disulfide to give 4-phenyl-1,3-dithiolane-2-thione with high selectivity even by

Table 4. Reaction of Various Oxiranes with CS_2[a]

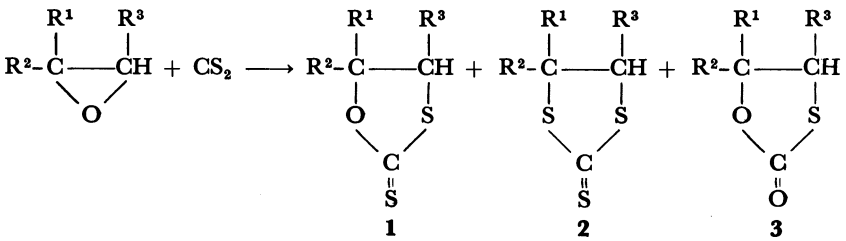

Run No.	Epoxide			Method	Yield/%			
	R^1	R^2	R^3		**1**	**2**	**3**	Total
1	CH_3	H	H	A[b]	9	41	9	59
2	CH_3	H	H	B[c]	—	83	7	90
3	C_2H_5	H	H	A	20	37	9	66
4	C_2H_5	H	H	B	5	68	17	90
5	C_6H_{13}	H	H	B	28	27	12	67
6	C_6H_5	H	H	A	—	86	—	86
7	C_6H_5	H	H	B	—	93	—	93
8	H	$(CH_2)_4$		A	54	36	6	96
9	H	$(CH_2)_4$		B	6	76	5	87
10	CH_3	CH_3	H	B	82	2	—	84
11	$ClCH_2$	H	H	B	35	—	16	51

a) Epoxide 5 mmol; CS_2 25 mmol; pressure 800 MPa; reaction time 20 h. b) *N*-Methylmorpholine 0.5 mmol; reaction temperature 70 °C. c) Et_3N 0.5 mmol; reaction temperature 100 °C.

Method A. 2-(Chloromethyl)oxirane reacted with carbon disulfide to give **1** and **3** with low yields. This might be due to lowered catalytic activity caused by an interaction between chlorine atom and triethylamine. A similar low reactivity has been observed with the reaction of thiiranes with carbon disulfide.[10] For the series of these oxiranes, the ratio of **2** to total yield is in the decreasing sequence: 2-phenyl->2-methyl->2-ethyl->2-hexyl->2,3-tetramethylene->2,2-dimethyl->2-(chloromethyl)-.

The reaction of 2-hexyloxirane with carbon disulfide in the presence of triethylamine seems to proceed as follows:

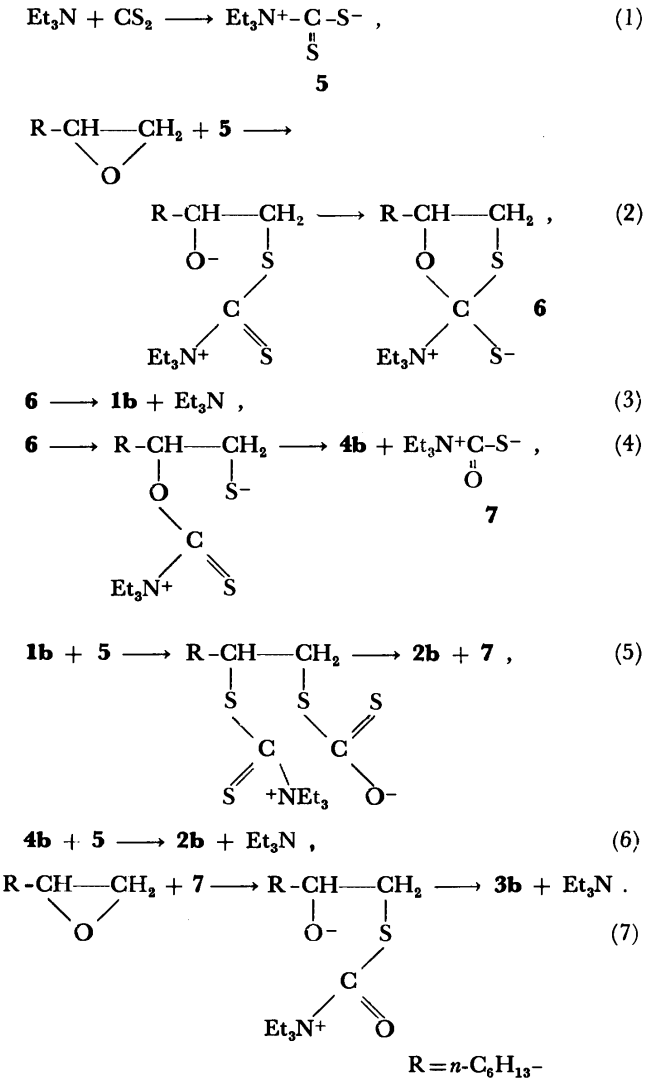

Reaction 1, the first step of adduct **5** formation from carbon disulfide and triethylamine, is followed by Reaction 2, consisting successively of the addition of **5** to 2-hexyloxirane and the ring closure yielding **6**. Reaction 3 is the elimination of triethylamine from **6** to give **1b**. The two carbon atoms of the oxirane ring can be attacked by **5**, but in practice, only product **1b** was formed selectively, which product may be considered to have been produced by an selective attack of **5** at the less-hindered carbon atom of the oxirane ring. It is well-known that nucleophilic attack in the presence of base will occur at sterically less-hindered sites.[11] Thus, the formation of **1b** conforms to this rule on. In addition, part of **6** also is converted to **4b** and adduct **7** (Reaction 4). This conversion is similar in mechanism to the reaction of oxiranes with thiourea to produce thiiranes.[12] At such a low temperature as 40 °C a considerable amount of **4b** was formed (Runs 5 and 7, Table 2), which phenomenon suggests that the formation of **4b** proceeds faster than that of **1b**.

It was confirmed that the reaction of **1b** with carbon disulfide in the presence of triethylamine under 800 MPa gave 71% of **2b**. There are two possible mechanisms for the formation of **2b** from **1b**. One involves initial thermal dissociation of **1b** into **4b** and carbonyl sulfide; it has been reported that the reaction of oxiranes with carbon disulfide followed by pyrolysis will produce thiiranes.[7,8] However, it is questionable that the reaction in which one molecule (**1b**) decomposes into two molecules (**4b** and carbonyl sulfide) should be accelerated by compression, considering that **1b** can be stably distilled in vacuo above 100 °C. The other mechanism involves the attack of **5** at the 5-position carbon of **1b** followed by the elimination of **7** (Reaction 5). The 5-position of **1a** is expected to be hindered sterically, and consequently, **1a** is obtained as a main product even by Method B (Run 10, Table 4). This phenomenon supports the latter mechanism, so that Reaction 5 is more likely for the formation of **2b**. It is known that a carbon atom adjacent to a phenyl group is liable to be attacked by nucleophilic reagents,[13] and this liability can be responsible for the reaction in which phenyloxirane affords 4-phenyl-1,3-dithiolane-2-thione dominantly (Runs 6 and 7, Table 4). It has been reported that Reaction 6 is accelerated by compression,[10] and **3b** is considered to be derived via the reaction of 2-hexyloxirane with **7**, Reaction **7**, similar to Reaction 6.

Of Reactions 1—7, the compression is considered to have an accelerating effect on Reactions 1, 2, and 5—7, and the reason why **2b** is obtained as the main product under high pressure is considered to be connected with the acceleration of Reaction 5 by compression. Similarly, in the reaction of a variety of oxiranes with carbon disulfide under high pressure, 1,3-dithiolane-2-thiones can be obtained in high yields.

Experimental

Apparatus. The apparatus used for the reaction under high pressure was the same as that described previously.[13]

Measurement. GLC was carried out by a JEOL 20KF chromatograph with 20% SE-30 columns. ^{1}H NMR spectra were measured with a Hitachi R-40 spectrometer. Mass spectra were measured with a JEOL D-300 GC-MS

spectrometer by the CI (chemical ion) method with isobutane. IR spectra were obtained with a JASCO A-302 spectrophotometer.

Reaction of Oxiranes with Carbon Disulfide. The typical procedure is as follows: A homogeneous mixture of 2-hexyloxirane (5 mmol), carbon disulfide (25 mmol), and *N*-methylmorpholine (0.5 mmol) in a sealed Teflon tube was compressed to 800 MPa, heated at 70 °C, and maintained for 20 h in a high-pressure equipment. The resulting mixture was subjected to evaporation and the residue was distilled with a Kugelrohr. The distillate, a mixture of **1b—3b** was separated by column chromatography on silica gel using a mixture of hexane and chloroform (7:3 v/v) as an eluent. The spectral data of **2b** and **4b** agreed with the known data.[10] **1b**: IR 1189 and 1048 cm^{-1}; ^1H NMR δ=0.89 (t, 3H, CH_3), 1.32 (s, 8H, C_4H_8), 1.73—2.30 (m, 2H, CH_2), 3.35—3.80 (m, 2H, CH_2), and 4.95—5.35(m, 1H, CH); QM^+ 205. **3b**: IR 1736 cm^{-1}; ^1H NMR δ=0.89 (t, 3H, CH_3), 1.33 (s, 8H, C_4H_8), 1.65—2.25 (m, 2H, CH_2), 3.13—3.68 (m, 2H, CH_2), and 4.55—4.85 (m, 1H, CH); QM^+ 189.

2-Methyloxirane, 2-ethyloxirane, 2,2-dimethyloxirane, 2,3-tetramethyleneoxirane, 2-phenyloxirane, and 2-chloromethyloxirane were treated with carbon disulfide similarly to 2-hexyloxirane. The spectral data of 1,3-dithiolane-2-thione derivatives and 5-methyl-1,3-oxathiolane-2-thione from these reactions agreed with the known data.[10,15] The spectral data of the other products of these reactions are as follows:

5-Methyl-1,3-oxathiolan-2-one: IR 1729 cm^{-1}; ^1H NMR δ=1.53 (d, 3H,CH_3), 3.10—3.73 (m, 2H, CH_2), and 4.63—5.05 (m, 1H, CH); QM^+ 119.

5-Methyl-1,3-oxathiolane-2-thione: IR 1188 cm^{-1}; ^1H NMR δ=1.09 (t, 3H, CH_3), 1.53—2.20 (m, 2H, CH_2), 3.50—3.74 (m, 2H, CH_2), and 4.90—5.28 (m, 1H, CH); QM^+ 149.

5-Ethyl-1,3-oxathiolan-2-one: IR 1718 cm^{-1}; ^1H NMR δ=1.09 (t, 3H, CH_3), 1.28—2.12 (m, 2H, CH_2), 3.08—3.60 (m, 2H, CH_2), and 4.40—4.76 (m, 1H, CH); QM^+: 133.

1a: IR 1252, 1127, 1198, and 1086 cm^{-1}; ^1H NMR δ=1.67 (s, 6H, $2CH_3$), and 3.48 (s, 2H, CH_2); QM^+ 149. Found: C, 40.66; H, 5.43%. Calcd for $C_5H_8OS_2$: C, 40.51; H, 5.44%.

4,5-Tetramethylene-1,3-oxathiolane-2-thione: IR 1179 and 1041 cm^{-1}, ^1H NMR δ=1.00—2.65 (m, CH_2, C_4H_8), 3.54—4.00 (m, 1H, CH), and 4.13—4.65 (m, 1H, CH); QM^+ 175.

4,5-Tetramethylene-1,3-oxathiolan-2-one: IR: 1736 cm^{-1}; ^1H NMR δ=1.16—2.56 (m, 8H, C_4H_8) and 3.46—3.85 (m, 1H, CH); QM^+ 158.

5-Chloromethyl-1,3-oxathiolane-2-thione: IR: 1175 and 1035 cm^{-1}; ^1H NMR δ=3.62—4.08 (m, 4H, $2CH_2$) and 5.16—5.32 (m, 1H, CH); QM^+ 169.

5-Chloromethyl-1,3-oxathiolane-2-one: IR 1739 cm^{-1}; ^1H NMR δ=3.24—4.04 (m, 4H, $2CH_2$) and 4.72—5.10 (m, 1H, CH); QM^+ 153.

Reaction of 1b with Carbon Disulfide. A homogeneous mixture of **1b** (43.3 mg), carbon disulfide (200 mg), triethylamine (3.8 mg), and tetradecane (5.9 mg) in a sealed Teflon tube was compressed to 800 MPa, heated at 100 °C, and maintained for 20 h in a high pressure equipment. The GLC analysis using tetradecane as a standard showed that 71% of **2b** was obtained.

References

1) Ethylene-Plastique S. A., Brit. Patent 1135800 (1968); *Chem. Abstr.*, **70**, 47278g (1969). Ethylene-Plastique S. A., Fr. Patent 1505715 (1967); *Chem. Abstr.*, **70**, 19908u (1969).

2) Thiokol Chemical Corp., Brit. Patent 1092610 (1967); *Chem. Abstr.*, **68**, 21823q (1968).

3) J. A. Durden. Jr., H. A. Stansbury. Jr., and W. H. Catlette, *J. Am. Chem. Soc.*, **82**, 3082 (1960).

4) V. S. Etlis, L. N. Grobov, and G. A. Razuvaev, *Dokl. Akad. Nauk SSSR*, **140**, 623 (1961); *Chem. Abstr.*, **56**, 11528d (1962).

5) Ethylene-Plastique S. A., Fr. Patent 1515077 (1968); *Chem. Abstr.*, **70**, 96782a (1969).

6) G. A. Razuvaev and V. S. Etlis, *Zh. Obshch. Khim.*, **33**, 1366 (1963); *Chem. Abstr.*, **59**, 9827b (1963).

7) Rohm and Haas Co., U. S. Patent 3409635 (1968); *Chem. Abstr.*, **70**, 20047u (1969).

8) Esso Research and Engineering Co., U. S. Patent 3687976 (1972); *Chem. Abstr.*, **77**, 152831z (1972).

9) K. Matsumoto and A. Sera, *Synthesis*, **1985**, 999.

10) Y. Taguchi, K. Yanagiya, I. Shibuya, and Y. Suhara, *Bull. Chem. Soc. Jpn.*, **60**, 727 (1987).

11) J. G. Smith, *Synthesis*, **1984**, 630.

12) M. Sander, *Chem. Revs.*, **66**, 297 (1966).

13) Y. Taguchi and Y. Suhara, *Bull. Chem. Soc. Jpn.*, **59**, 2321 (1986).

14) M. Kurabayashi, K. Yanagiya, and M. Yasumoto, *Bull. Chem. Soc. Jpn.*, **44**, 3413 (1971).

15) N. Adachi, Y. Kido, and K. Shibata, *J. Polym. Sci., Polym. Chem. Ed.*, **15**, 937 (1977).

 © 1988 The Chemical Society of Japan Bull. Chem. Soc. Jpn., 61, 927—930 (1988)

Studies on Chitin. 14. *N*-Acetylation Behavior of Chitosan with Acetyl Chloride and Acetic Anhydride in a Highly Swelled State

Keisuke KURITA,* Satoyuki CHIKAOKA, Mami KAMIYA, and Yoshiyuki KOYAMA
Department of Industrial Chemistry, Faculty of Engineering, Seikei University, Musashino-shi, Tokyo
(Received August 8, 1987)

N-Acetylation on chitosan has been studied in a highly swelled state with acetyl chloride in comparison with that with acetic anhydride under various conditions to establish the general possibility and scope of the acylation reactions on chitosan and other polysaccharides. A highly swelled chitosan precipitate prepared by pouring a chitosan solution in aqueous acetic acid/methanol into pyridine is quite suitable for efficient modifications, and the reaction with either acylating reagent proceeded smoothly and reproducibly under mild conditions. Although acetic anhydride is generally more appropriate in protic solvens, acetyl chloride is effective and advantageous especially in pyridine containing only small amounts of protic solvents.

Although chitin is structurally similar to cellulose and quite abundant in nature, it has been discarded and thus attracting much attention recently as an unutilized resource. It is considered of interest as a raw material of high potentials for developing new functional materials from the viewpoint of chemical modifications owing to the presence of the reactive amino groups in addition to hydroxyl groups.[1] Various types of reactions have been reported thus far for utilization of this amino polysaccharide, but severe conditions are generally necessary on account of the strong intermolecular hydrogen bonding which limits the solubility in ordinary organic solvents.[2,3] Among the modification reactions, acetylation is one of the most fundamental and important reactions to not only chitin but also many kinds of other polysaccharides to afford derivatives of a wide variety of attractive properties.

We have already reported the efficient acylation with acetic and some cyclic aromatic acid anhydrides in a highly swelled state by making use of the advantage of water-soluble nature of the 50% deacetylated chitin samples prepared under homogeneous hydrolysis conditions.[4,5]

Although acid anhydrides have been by far most commonly used for acylation, it is useful to establish the controlled acylation with more easily available and more reactive but less stable acyl chlorides under mild conditions. Several papers have dealt with the acylation of chitin, i.e., esterification at the hydroxyl groups, with a large excess of acyl chlorides,[6-10] but not much information has been obtained regarding the reaction on chitosan. Fujii and co-workers reported the acylation on chitosan where long-chain fatty acid chlorides were subjected to the reaction in a mixture of pyridine and chloroform under reflux to give polyacylated derivatives with degrees of substitution of up to 4.[11] These reactions have, however, been normally carried out under rather severe conditions, and thus difficulties are sometimes encountered in controlling the reactions. No attempt has been made to elucidate the conditions and course of the reaction on chitosan with varying amounts of acyl chlorides and also acid anhydrides for practical acylation. We have thus examined the progress of *N*-acetylation on chitosan with both acetyl chloride and acetic anhydride under mild conditions to provide a versatile modification for this naturally abundant amino polysaccharide.

Experimental

Chitosan with a degree of deacetylation of 88% was prepared by heating pulverized chitin in a 50% aqueous sodium hydroxide solution at 135 °C for 3.5 h under a nitrogen stream.[12] The degree of acetylation of the acetylated products obtained in this study was determined by IR spectroscopy.[13]

Acetylation of Chitosan with Acetyl Chloride in a Mixture of Aqueous Acetic Acid, Methanol, and Pyridine: Chitosan, 0.3 g, was dissolved in 8 ml of 10% aqueous acetic acid,

Table 1. Acetylation of Chitosan with Acetyl Chloride in a Mixture of Aqueous Acetic Acid, Methanol, and Pyridine

Chitosan/g	Acetyl chloride/ml	-COCl/-NH_2[a)]	Yield/g	Degree of acetylation/%
0.304	5.0	44	0.263	16
0.304	16.8	147	0.240	25
0.301	35.0	307	0.258	34

a) Molar ratio.

Table 2. Acetylation of Chitosan with Acetyl Chloride after Repeated Replacement of the Solvent by Pyridine

Chitosan/g	Acetyl chloride/ml	$-COCl/-NH_2$[a)]	Yield/g	Degree of acetylation/%
0.100	0.19	5.0	0.075	41
0.100	0.38	10	0.074	78
0.101	1.95	25	0.093	84

a) Molar ratio.

Table 3. Acetylation of Chitosan with Acetic Anhydride

Chitosan/g	Acetic anhydride/ml	$Ac_2O/-NH_2$[a)]	Yield/g	Degree of acetylation/%
0.900	3.85	8.5	0.825	31
0.300	1.85	12	0.221	38
0.299	2.46	16	0.225	42
0.300	3.08	20	0.223	50
0.301	3.85	25	0.289	53
0.301	4.62	31	0.220	62

a) Molar ratio.

and the solution was diluted with 8 ml of methanol. The solution was poured into 100 ml of pyridine with stirring to afford a highly swelled precipitate of chitosan. The mixture was cooled at 0 °C in an ice bath, and a given amount of acetyl chloride was added dropwise with stirring. It was allowed to warm to room temperature, stirred for 16 h 40 min, and poured into 500 ml of a mixture of acetone and water (7:1) to coagulate the acetylated derivative. The product was isolated by filtration and washed with acetone and then with methanol. Without drying, it was treated with 100 ml of 1 M potassium hydroxide (1 M=1 mol dm^{-3}) in methanol at room temperature for 4 h. Filtration, washing with methanol and acetone, and drying in vacuo gave an acetylated product as a slightly yellow solid. The results are summarized in Table 1.

The reaction appeared to be fairly rapid and complete within 1 h, judging from the values of the degree of acetylation of the resulting products obtained after various periods of reaction. The reaction time was thus fixed at 3 h in the subsequent reactions.

Acetylation of Chitosan with Acetyl Chloride after Repeated Replacement of the Solvent by Pyridine: A solution of 0.1 g of chitosan in a mixture of 2.6 ml of 10% aqueous acetic acid and 2.6 ml of methanol was poured into 33 ml of pyridine. The mixture was centrifuged, and 25.5 ml of the supernatant was replaced by the same amount of fresh pyridine. After repeating this solvent replacement five times, acetyl chloride diluted with tetrahydrofuran to 5 ml was added dropwise at 0 °C with stirring. The mixture was allowed to warm to room temperature, and after 3 h the product was isolated in the same manner as described above. The results are listed in Table 2.

Acetylation of Chitosan with Acetic Anhydride: To 100 ml of pyridine was added a solution of 0.3 g of chitosan in a mixture of 8 ml of 10% aqueous acetic acid and 8 ml of methanol. Acetic anhydride was added, and the mixture was stirred at room temperature for 5 h. The product was isolated in the same manner. Table 3 shows the results.

Results and Discussion

Acetylations of chitosan with varying amounts of acetyl chloride and acetic anhydride were examined in order to make clear the general possibility and scope of the acetylation methods. The reactions were carried out in a highly swelled state brought about by pouring a solution of chitosan in a mixture of aqueous acetic acid and methanol into pyridine to enable efficient acetylation under mild reaction conditions. In the absence of methanol, the precipitate became rather sticky, and methanol helps disperse the swelled precipitate to realize an almost homogeneous mixture. Furthermore, methanol is effective to prevent phase separation of the reaction mixture on addition of hydrophobic organic reagents.

The resulting products with both acetyl chloride and acetic anhydride showed weak peaks in the IR spectra due to ester linkages formed by acetylation at the hydroxyl groups. The ester peaks were also observed even in the absence of pyridine with acetic anhydride. This indicates the reaction selectivity to the amino groups against the hydroxyl groups to be not sufficient. After the reaction, the products were thus treated with methanolic potassium hydroxide to ensure the removal of the ester groups and also to regenerate the amino groups lost by the salt formation with acetic acid. The treatment with 1 M methanolic potassium hydroxide for 4 h at room temperature was confirmed to be satisfactory for the purpose and not to harm the acetamide groups.

The resulting products showed medium to strong amide bands at 1650 and 1550 cm^{-1} and no distinct ester band at 1730 cm^{-1}.

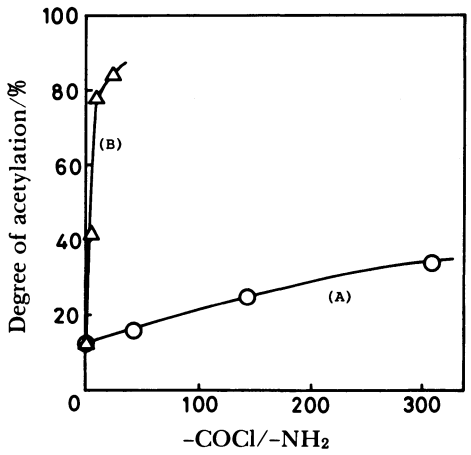

Fig. 1. Progresses of acetylation with acetyl chloride; (A) acetylation in a mixture of aqueous acetic acid, methanol, and pyridine, (B) acetylation after repeated solvent replacement by pyridine.

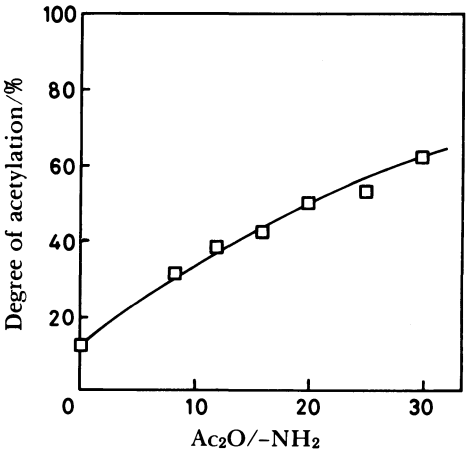

Fig. 2. Progress of acetylation with acetic anhydride in a mixture of aqueous acetic acid, methanol, and pyridine.

When acetyl chloride was added to a swelled precipitate of chitosan in aqueous acetic acid/methanol/pyridine, acetylation required a large excess of acetyl chloride as shown by the results in Fig. 1. With 307-fold excess acetyl chloride, an acetylated product with a degree of acetylation of 34% was obtained, indicating the acetyl chloride to have been consumed largely by some side reactions with the protic solvent components such as water and methanol during the expected reaction with the amino groups. Triethylamine was then added to the reaction mixture to regenerate the amino groups from the salt form for the facilitated reaction, but no improvement in the acetylation was observed. This is due to the high reactivity of acetyl chloride and suggested to decrease the contents of protic solvents for increased reaction efficiency.

The mixture containing a highly swelled chitosan precipitate was thus centrifuged, and the supernatant was replaced by fresh pyridine. After repeating this replacement procedure five times, the contents of protic solvents should have been reduced markedly, and noteworthily chitosan still remained highly swelled in the solvent yet. The reaction after this solvent replacement proceeded quite smoothly as expected, and in this way, a degree of acetylation of 78% was attained with only 10-fold excess acetyl chloride under these mild reaction conditions at 0 °C. The difference in the progress of the acetylation reaction under these different conditions is evident in Fig. 1.

The acetylation of chitosan was then examined with acetic anhydride in the same swelled state. Although the reaction was conducted in a mixture of aqueous acetic acid, methanol, and pyridine as in the first case of the reaction with acetyl chloride, acetylation proceeded fairly efficiently. As shown in Fig. 2, a 31-fold excess of acetic anhydride resulted in the formation of a derivative with a degree of acetylation of 62%. Qualitative solubility was examined in aqueous acetic acid, and the derivatives with degrees of acetylation below around 60% were soluble.

Consequently, these results indicate that 1) controlled acetylation on chitosan can be achieved effectively and reproducibly with either acetyl chloride or acetic anhydride under mild conditions in a highly swelled state, 2) a mixture containing highly swelled chitosan obtained by replacing the aqueous solvent by pyridine is especially suitable for efficient modifications of chitosan, and 3) acetyl chloride was found to be quite advantageous under these conditions, although acetic anhydride is generally more appropriate in the acetylation of chitosan in protic solvents.

The present work was partly supported by the Science Research Promotion Fund, Japan Private School Promotion Foundation, and by the Grant-in-Aid for Scientific Research on Priority Areas, New Functionality Materials —Design, Preparations, and Control—, the Ministry of Education, Science and Culture, No. 62604600.

References

1) K. Kurita, *Yuki Gosei Kagaku Kyokai Shi*, **42**, 567 (1984); *Kobunshi*, **36**, 406 (1987).

2) R. A. A. Muzzarelli, "Chitin," Pergamon, Oxford (1977).

3) K. Kurita, "Chemical Modifications of Chitin and Chitosan" in "Chitin in Nature and Technology" ed by R. A. A. Muzzarelli, C. Jeuniaux, and G. W. Gooday, Plenum, New York (1986), p. 287.

4) K. Kurita, T. Sannan, and Y. Iwakura, *Makromol. Chem.*, **178**, 2595 (1977).

5) K. Kurita, H. Ichikawa, S. Ishizeki, H. Fujisaki, and Y. Iwakura, *Makromol. Chem.*, **183**, 1161 (1982).

6) K. Akagane and G. G. Allan, *Shikizai Kyokaishi*, **46**, 379 (1973).
7) S. Hirano and Y. Koide, *Carbohydr. Res.*, **65**, 166 (1978).
8) O. Somorin, N. Nishi, S. Tokura, and J. Noguchi, *Polym. J.*, **11**, 391 (1979).
9) C. L. McCormick and D. K. Lichatowich, *J. Polym. Sci., Polym. Lett. Ed.*, **17**, 479 (1979).
10) K. Kaifu, N. Nishi, and T. Komai, *J. Polym. Sci., Polym. Chem. Ed.*, **19**, 2361 (1981).
11) S. Fujii, H. Kumagai, and M. Noda, *Carbohydr. Res.*, **83**, 389 (1980).
12) K. Kurita, T. Sannan, and Y. Iwakura, *Makromol. Chem.*, **178**, 3197 (1977).
13) T. Sannan, K. Kurita, K. Ogura, and Y. Iwakura, *Polymer*, **19**, 458 (1978).

 © 1988 The Chemical Society of Japan Bull. Chem. Soc. Jpn., 61, 931—938 (1988)

Nitrene-Transfer Reaction between Azide and Unsaturated Ether in the Presence of Pd(II) Catalyst

Toshihiko MIGITA,* Kazuya HONGOH, Hiroyuki NAKA, Setsuko NAKAIDO, and Masanori KOSUGI
Department of Chemistry, Faculty of Technology, Gunma University, Kiryu, Gunma 376
(Received September 7, 1987)

Azidoformate reacted with allylic ethers to give 1-alkoxy-1-(alkoxycarbonylimino)alkane under catalysis by $PdCl_2(PhCN)_2$. The same imines were formed almost quantitatively by noncatalyzed reaction of the azide with the corresponding vinylic ethers. The rate of the catalyzed reaction was found to be first order each in the allylic ether and in the azide. Easiness of the imine formation from the allylic ethers depended on the nature of azide, decreasing in the order of $N_3SO_2Me > N_3CO_2Me > N_3Ph$. Based on these results the most probable mechanism for the catalyzed reaction is proposed.

Photoreaction of azidoformate with allylic ethers has been known to give aziridines (nitrene adducts) **2** and rearranged insertion products **1**, while the thermal reaction at 80 °C in benzene gives only aziridines (30%).[1] In the presence of palladium catalysts, however, the thermal reaction has been found to give quite different products, 1-alkoxy-1-(alkoxycarbonylimino)alkanes **3**,[2] and dichlorobis(benzonitrile)palladium $PdCl_2(PhCN)_2$ has been reported to be the most effective catalyst for the imine formation.[3]

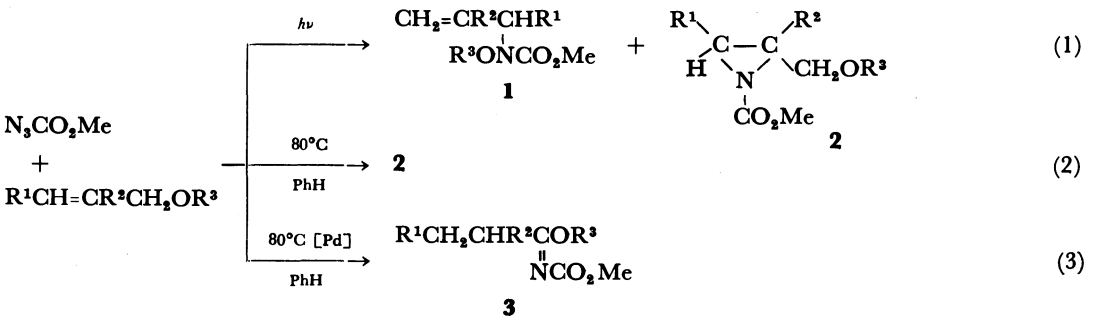

Furthermore, not only allylic but also other unsaturated ethers such as 3-butenyl or 4-pentenyl ethyl ether were found to react similarly giving the corresponding 1-alkoxy-1-(alkoxycarbonylimino)alkanes, **3**, (see Tabe 1).[4]

To elucidate the mechanism of the apparently peculiar nitrene-transfer reaction and to survey its scope and limitation, some kinetic and analytical studies were performed. Since vinylic ether reacts with azidoformate smoothly without any catalyst to give the corresponding **3**,[5,6] and olefinic compounds have been known to undergo double bond migration under Pd(II)-catalysis,[7,8] the most attractive mechanism might involve the Pd(II)-catalyzed isomerization of unsaturated ethers to the corresponding vinylic ether, which then reacts with azide to give **3**, as shown in Scheme 1.

The results shown below, however, suggest that the mechanism has more profound aspects involving ligand exchange in Pd(II) complex and isomerization of the ethers followed by interaction with azide in the Pd(II) coordinate sphere.

Results

Products of Pd(II)-Catalyzed Reaction of Unsaturated Ethers with Azidoformate. The reaction was carried out by heating a degassed solution of unsaturated ethers and azidoformate containing $PdCl_2(PhCN)_2$ (1 mol%) in a sealed tube at 80 °C for 24 h. The products detected in the reaction mixtures were listed in Table 1.

Imines **3** formed in good yields, and the corresponding aziridines were produced in only trivial amounts.

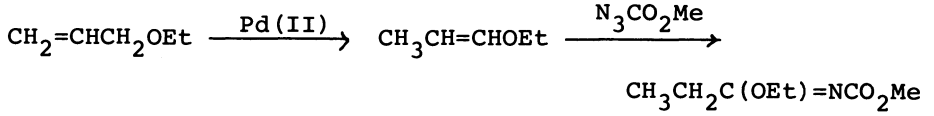

Scheme 1.

Table 1. Pd(II)-Catalyzed Reaction of Methyl Azidoformate with Unsaturated Ethers

Run	Ether	Product	Yield/%
1	CH_2=$CHCH_2OEt$	$CH_3CH_2C(OEt)$=NCO_2Me	67
2	CH_2=$CHCH_2CH_2OEt$	$CH_3CH_2CH_2C(OEt)$=NCO_2Me	72
3	CH_2=$CH(CH_2)_3OEt$	$CH_3(CH_2)_3C(OEt)$=NCO_2Me	72
4	CH_2=$CMeCH_2OEt$	$Me_2CHC(OEt)$=NCO_2Me	95
5	CH_2=$CHCHMeOEt$	$Me_2CHC(OEt)$=NCO_2Me	44[a]
6	CH_3CH=$CHOEt$	$CH_3CH_2C(OEt)$=NCO_2Me	100[b]

a) $CH_3CH_2C(OEt)$=NCO_2Me also formed, 8%. b) Without the catalyst.

The essentially same results were obtained when benzene was used as a solvent.

It is interesting that 1-methyl-2-propenyl ether reacted under these conditions to give the imine **3** identical to that obtained from 2-methyl-2-propenyl ether, indicating that the methyl group as well as the hydrogen atom on the allylic α-position of the substrate migrated to the adjacent carbon atom, and the C=N bond formed always at the α-position (Runs 4 and 5).

3-Butenyl and 4-pentenyl ethers (Runs 2 and 3) also afforded good yields of the corresponding imines **3**, in which C=N bonds were introduced again at the α-position of the ethers.

Pd(II)-Catalyzed Isomerization of Unsaturated Ether. Golborn et al. showed that allylic alkenyl phenyl ethers were able to isomerize to vinylic alkenyl phenyl ethers by the aid of $PdCl_2(PhCN)_2$, and the capability of the isomerization depended on the structure of the allylic alkenyl group.[8] But isomerization of alkenyl alkyl ether has not been studied. After 3-butenyl or 4-pentenyl ethyl ether was kept at 80 °C in the presence of 1 mol% of $PdCl_2(PhCN)_2$, the GLC analysis of the mixture showed that the double bond migration occurred considerably. It is noteworthy that the mixture contained allylic ether as shown in the following scheme, but not vinylic ether.

$$CH_2{=}CHCH_2CH_2OEt \xrightarrow[80°C,\ 1\,h]{PdCl_2(PhCN)_2} CH_3CH{=}CHCH_2OEt\ 30\% \quad (4)$$

$$CH_2{=}CHCH_2CH_2CH_2OEt \xrightarrow[80°C,\ 12\,h]{PdCl_2(PhCN)_2} CH_3CH_2CH{=}CHCH_2OEt\ 10\% + CH_3CH{=}CHCH_2CH_2OEt\ 36\% \quad (5)$$

This implies difficulty of isomerization of allylic to vinylic ethers in the presence of $PdCl_2(PhCN)_2$. In fact 2-methyl-2-propenyl ethyl ether which afforded **3** in 95% yield through the Pd(II)-catalyzed reaction with azidoformate (80 °C, 20 h) isomerized quite sluggishly in the presence of the Pd(II)-catalyst alone: after 72h at 80 °C only several % of 2-methyl-1-propenyl ethyl ether was detected.

$$CH_2{=}CMeCH_2OEt \xrightarrow[80°C,\ 72\,h]{PdCl_2(PhCN)_2} Me_2C{=}CHOEt\ \ 5\text{—}6\% \quad (6)$$

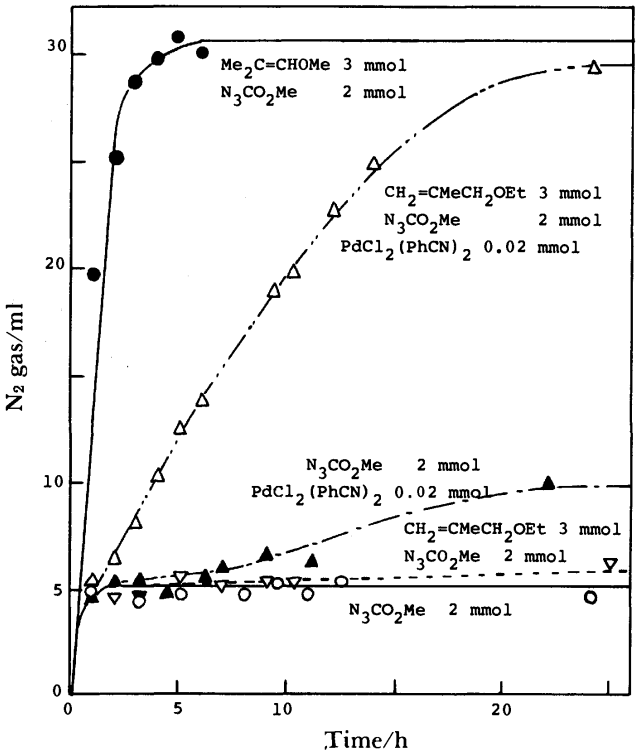

Fig. 1. Evolution of nitrogen.
Solvent=PhH 1 ml, Temp=80 °C.

Kinetic Observation. Rates of nitrogen evolution were followed under various conditions using 2-methyl-2-propenyl ethyl ether which was the best substrate for the Pd(II)-catalyzed reaction with azidoformate. Figure 1 shows amount of gas evolved vs. reaction time. As seen in Fig 1, spontaneous decomposition of azidoformate did not occur in any appreciable extent. The presence of the allylic ether did not promote the decomposition of the azide, although a binary system of the azide and the vinylic ether evolved nitrogen and the reaction was almost completed after several hours at 80 °C. Addition of 1 mol% of $PdCl_2(PhCN)_2$ in an azide solution at 80 °C slightly accelerated the decomposition of the azide, the yield of evolved nitrogen was only 25% based on the azide after 24 h. These facts suggest that some interaction arises between the azide and Pd(II), but the presence of allylic ether much accelerated the Pd(II)-catalyzed decomposition of the azide.

Table 2. The Reaction of Vinylic Ether with Methyl Azidoformate

Vinylic ether	Product	Yield/%
$CH_3CH=CHOEt$	$CH_3CH_2C(OEt)=NCO_2Me$	98
$CH_3CH_2CH=CHOMe$	$CH_3CH_2CH_2C(OMe)=NCO_2Me$	95
$Me_2C=CHOMe$	$Me_2CHC(OMe)=NCO_2Me$	98
$Me_2C=CHOEt$	$Me_2CHC(OEt)=NCO_2Me$	98
$CH_3CH=CMeOMe$	$Me_2CHC(OMe)=NCO_2Me$	72
	$CH_3CH_2C(OMe)=NCO_2Me$	5

Table 3. Pd(II)-Catalyzed Reaction of Allylic Ethers with Azides

Azide	Allylic ether	Pd(II)-catalyzed aziridine/%	Pd(II)-catalyzed imine/%	Uncatalyzed aziridine/%
$N_3SO_2CH_3$	$CH_2=CHCH_2OMe$	0	100	33
	$CH_2=CHCH_2OEt$	0	100	51
	$CH_2=CMeCH_2OMe$	0	100	36
	$CH_2=CMeCH_2OEt$	0	100	45
$N_3CO_2CH_3$	$CH_2=CHCH_2OMe$	8	53	46
	$CH_2=CHCH_2OEt$	Trace	67	42
	$CH_2=CMeCH_2Me$	Trace	95	45
	$CH_2=CMeCH_2OEt$	Trace	95	16
N_3Ph	$CH_2=CHCH_2OMe$	67	5	62
	$CH_2=CHCH_2OEt$	55	6	68
	$CH_2=CMeCH_2OMe$	15	61	26
	$CH_2=CMeCH_2OEt$	15	74	26

The profile of amount of nitrogen evolved vs. reaction time for the system of azide–ether–Pd(II) showed a sigmoid curve, suggesting the consecutive nature of the reaction. Accurate kinetic treatment of the catalyzed reaction was difficult probably due to that the concentration of the species of the real catalysts could not be controlled easily. Semiquantitative survey using a benzene solution of azidoformate and 2-methyl-2-propenyl ethyl ether (molar ratio of 1: 2—8) containing 1 mol% of $PdCl_2(PhCN)_2$ and using a solution of the azide and 1 mol% of the catalyst in a large excess of the ether showed the first-order dependence of the catalyzed reaction rate on both the azide and the allylic ether. These observations show that the mechanism of the catalyzed reaction is not so simple as shown in Scheme 1, which involves a very slow isomerization of allylic ether followed by a relatively rapid bimolecular reaction.

Comparison with the Reation of Vinylic Ethers. In order to check the similarity in products between the Pd(II)-catalyzed reaction of an allylic ether and the reaction of the corresponding vinylic ether, various vinylic ethers were allowed to react with azidoformate, and the products were compared with those obtained from the corresponding allylic ether. The results were summarized in Table 2.

All vinylic ethers bearing no substituent on its α-position reacted with azidoformate to give the corresponding imines **3** almost quantitatively. As shown in Table 1, the Pd(II)-catalyzed reaction of 1-methyl-2-propenyl ethyl ether gave the methyl-migrated product and the demethylated imine in 44% and 8%, respectively. It is noteworthy that the α-substituted vinylic ether, 1-methyl-1-propyl methyl ether reacted with the azide without the catalyst gave the methyl migrated and the demethylated imines in 72 and 5%, respectively. Under the same conditions (in the presence of 1 mol% of the catalyst, in benzene at 80 °C for 24 h) both 1-methyl-2-propenyl methyl ether and 1-methyl-1-propyl methyl ether gave the same products in similar yields.

$$\begin{array}{l} CH_2=CHCHMeOMe + N_3CO_2Me \\ \quad 4\ mmol \quad\quad 2\ mmol \\ \qquad\qquad\quad \downarrow\ 0.02\ mmol\ PdCl_2(PhCN)_2,\ in\ PhH,\ 80°C,\ 24\ h \\ \quad 24\% \qquad\qquad\quad trace \\ Me_2CHC(OMe)=NCO_2Me,\quad EtC(OMe)=NCO_2Me \\ \quad 31\% \qquad\qquad\quad trace \\ \qquad\qquad\quad \uparrow\ 0.02\ mmol\ PdCl_2(PhCN)_2,\ in\ PhH,\ 80°C,\ 24\ h \\ MeCH=CMeOMe + N_3CO_2Me \\ \quad 4\ mmol \quad\quad 2\ mmol \end{array} \qquad (7)$$

Such similarity strongly supports the occurrence of the isomerization of allylic to vinylic substrates in the Pd(II)-catalyzed reaction of allylic ether.

Reaction of Other Azides. Table 3 shows the products of the reaction of methanesulfonyl and

Table 4. Reaction of Methyl Azidoformate with Allylic Sulfides in the Presence of $PdCl_2(PhCN)_2$

Sulfide	Product	Yield/%
CH_2=$CMeCH_2SMe$	CH_2=$CMeCH_2N(SMe)CO_2Me$	70
CH_3CH=$CHCH_2SMe$	CH_2=$CHCHMeN(SMe)CO_2Me$	65[a]
Me_2C=$CHCH_2SMe$	CH_2=$CHCMe_2N(SMe)CO_2Me$	60
CH_2=$CHCHMeSMe$	CH_3CH=$CHCH_2N(SMe)CO_2Me$	56
PhCH=$CHCH_2SMe$	CH_2=$CHCHPhN(SMe)CO_2Me$	54

a) Cf. 26% (in photoreaction) and 27% (without the catalyst).

phenyl azides with allylic ethers in the presence of $PdCl_2(PhCN)_2$ catalyst, containing also the results on azidoformate for comparison. Without the catalyst, only aziridines (nitrene adduct to the double bond of the allylic ether) were produced in rather low yield. The presence of $PdCl_2(PhCN)_2$, however, lead the reaction to production of the corresponding α-imino ethers. And tendency toward α-imino ether formation decreases in the following order: N_3SO_2Me>N_3CO_2Me>N_3Ph.

$$R^1CH{=}CR^2CH_2OR^3 + N_3R \longrightarrow R^1CH_2CHR^2C(OR^3){=}NR + \underset{\text{aziridine}}{\text{(aziridine)}} \quad (8)$$

α-imino ether

Thus the catalyzed reaction of sulfonyl azide gave the α-imino ethers almost quantitatively. Phenyl azide gave the α-imino ethers as well as aziridines, and the distribution of the products seriously depended on the allylic structure.

On the other hand, these all azides gave the α-imino ethers almost quantitatively through the noncatalyzed reaction with vinylic ethers. These facts again imply that imine production from allylic ethers may be related to the Pd(II)-assisted isomerization of allylic to vinylic ether.

Reaction of Allylic Sulfides. The reaction of allylic sulfides, sulfur analogues of allylic ethers, with azidoformate did not give the imino compounds corresponding to **3**, but the [1·5] rearranged C–S nitrene insertion products even in the presence of $PdCl_2(PhCN)_2$ as shown in Table 4. Photo- and thermal reactions of allylic sulfides have been known to react with azidoformate to give the [1·5] rearranged C–S nitrene insertion products which is considered to form via the ylide formation between nitrene and the sulfur atom, and enamines which have been considered to be derived from adducts between the azide and the sulfides, in total yield of about 30%.[1] Comparing these facts with the present results, the presence of $PdCl_2(PhCN)_2$ is thought to enhance the formation of the nitrene-ylide.

Discussion

The results which allow us to discuss the mechanism of the Pd(II)-catalyzed reaction of azides with unsaturated ethers are summarized as follows.

(1) In the presence of $PdCl_2(PhCN)_2$ alone, isomerization of allylic to vinylic ether is extremely slow, although the more remotely functionated substrates isomerize to allylic ether (Eqs. 4 and 5).

(2) The catalyzed reaction is first order in the allylic ether as well as in the azide. Since the reaction of azidoformate with allylic ether without the Pd(II) catalyst does not give imine, the Pd(II)-catalyzed imine-formation is not, at least, zeroth-order in Pd(II). The overall kinetic observation shows that the transition state of the rate determining step should be composed of three species, Pd(II), allylic ether, and azide.

(3) Products of the catalyzed reaction of any kind of allylic ethers are the same as those of the reaction of the corresponding vinylic ethers, showing an important role of the Pd(II)-catalyed isomerization of allylic to vinylic ether.

(4) Easiness of formation of the imino products by the catalyzed reaction depends on the nature of the azide: the more electron-withdrawing group the azide has, the better yield of the imine is observed.

Based on these features, the mechanism shown in Scheme 2 is proposed to be most probable for the Pd(II)-catalyzed reaction of azides with allylic ethers. The mechanism involves the Pd(II)-catalyzed isomerization of allylic to vinylic ether as the rate-determining step. But the real catalyst is thought to be $PdCl_2(PhCN)(N_3R)$ which may be formed by the ligand exchange between $PdCl_2(PhCN)_2$ and the azide. Unfortunately preparative or spectroscopic evidences for the ligand exchange could not be obtained, perhaps due to that the complex thus formed is rather labile and the azide ligand is apt to decompose as seen in the gradual evolution of nitrogen from the system of the azide–$PdCl_2(PhCN)_2$(Fig. 1). Since the Pd(II)-catalyzed isomerization is essentially the hydride transfer between Pd(II) and the ether, the rate would be influenced by the nature of the ligand coordinated to Pd(II). The more electron demanding the ligand is, the faster the hydride abstraction from the allyic ether

would be. The tendency is thought to be reflected on the yields of the imino-ethers from the reaction of a series of azides: the electron-withdrawing group on azide promotes the formation of the imino ether (Table 3).

Table 3 also clearly shows that 2-methyl-2-propenyl ether is a better substrate for the imino-ether formation than 2-propenyl ether. This result is quite interesting and probably due to the steric or electronic effects on the reaction in the Pd(II) coordinate sphere, although the real reason is not yet clear.

The vinylic ether thus formed reacts with the azide to give the imino-ether, via 1,3-dipolar addition followed by heterolysis of the triazoline as proposed by Huisgen et al. for the thermal reaction of enol ether with aryl azide.[5] Since appreciable amounts of vinylic ethers were not detected in the reaction mixtures during and after the reaction carried out in the large excess of allylic ethers, the interaction between the vinylic ether and the azide is considered to take place in the Pd(II) coordinate sphere, that is, the coordinated azide molecule is brought into the interaction with vinylic ether derived in the Pd(II) coordinate sphere.

On the heterolysis of the triazoline and evolution of nitrogen, a hydrogen atom or a methyl group located on the α-position of the ether can be migrated to the electron deficient β-carbon via 1,2-shift. Thus the α-methylated allylic or vinylic ethers afford the rearranged imino products (Tables 1 and 2). These ethers also gave the demethylated imino products as shown in Tables 1 and 2. Although their yields are quite low, the results may be interesting, suggesting new aspects of decomposition of the triazolines. Because the carbonium ion formed after nitrogen evolution is hardly thought to degradate with a C–C bond rupture. To elucidate its mechanism, however, further surveys are required.

The Pd(II)-catalyzed reaction of allylic sulfides did not lead to formation of the imino products but [1·5] rearranged insertion products. This may be due to the greater nucleophilic reactivity of a sulfur atom compared with an oxygen atom. Much higher yields of the rearranged products in the catalyzed reaction compared with those in the ordinary thermal reaction (Table 4) and accelerated nitrogen evolution in the presence of $PdCl_2(PhCN)_2$ suggest that the production

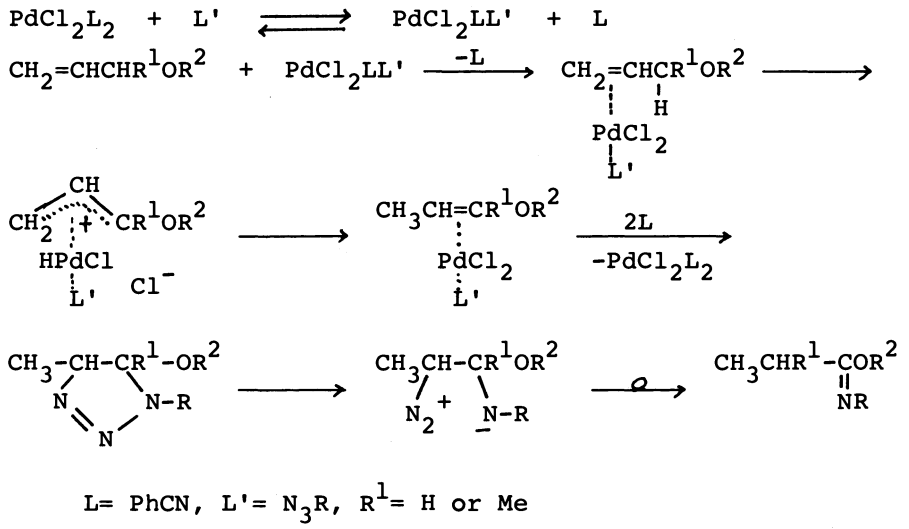

Scheme 2.

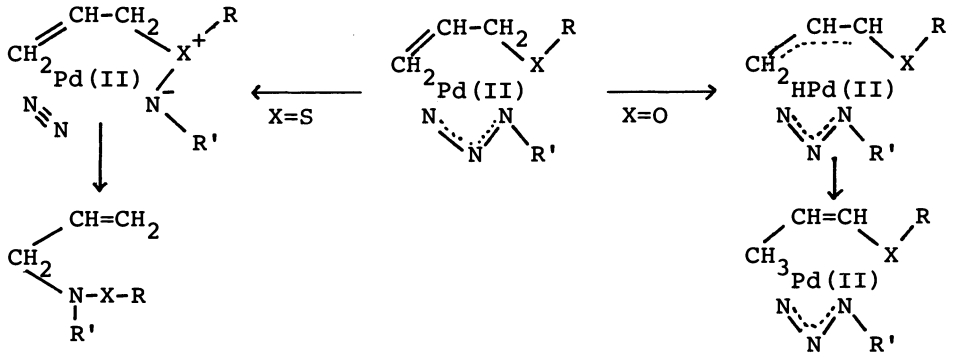

Scheme 3.

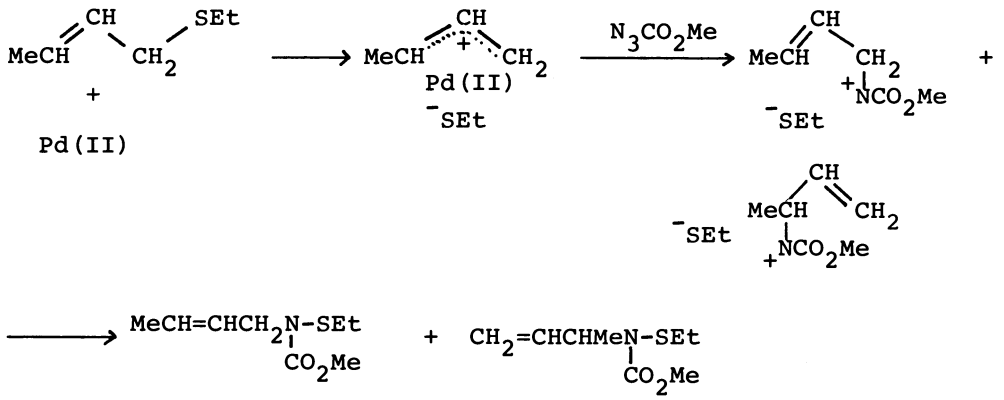

Scheme 4.

of the insertion products are also controlled by the Pd(II) coordinate sphere.

The coordinated azide molecule has an enhanced electrophilicity and easily interacts with a nucleophilic sulfur atom of the sulfide, to produce the nitrene-ylide, which undergoes [1·5] rearrangement through the cyclic transition state as well documented.[1] In the case of sulfides, therefore, the ylide formation seems much faster than the hydride transfer between Pd(II) and the substrate sulfide. Summarized scheme involving allylic sulfide and ether are shown in Scheme 3.

The route shown in Scheme 4 in which a π-allyl complex is formed from allylic sulfide and Pd(II) and reacts with nitrene from the azide to give the insertion product is unlikely. If this were the true mechanism, unsymetrically substituted π-allyl complexes should give both rearranged and unrearranged insertion products, and the products through the attack of nitrene on the less sterically hindered site of the π-allyl complex would be the major. The results (Table 4) is not the case, showing the formation of the C–N bond exclusively at a γ-carbon atom of allylic sulfide, even though the site is more hindered.

Experimental

Materials. Methyl azidoformate (bp 36—37 °C/58 mmHg (1 mmHg=133.322 Pa)),[9] phenylazide (bp 41 °C/5 mmHg),[10] methanesulfonyl azide (bp 44—45 °C/1 mmHg)[11] were prepared by the known methods. 2-Methyl-2-propenyl alkyl ethers, and 3-butenyl and 4-pentenyl ethyl ethers were prepared by Williamson method[12] from the corresponding chloride, and 1-methyl-2-propenyl methyl ether (bp 55.5 °C)[13] was synthesized by the reaction of acrylaldehyde with methylmagnesium iodide. 1-Methyl- and 1-ethyl-2-methylpropene[14] were prepared from the corresponding acetals of 2-methylpropanal by the *p*-toluenesulfonic acid catalyzed elimination of alcohols. Dichlorobis(benzonitrile)palladium(II)[15] was obtained by treatment of palladium(II) chloride with benzonitrile.

Products of the Reactions. The reaction was carried out according to the procedure already described.[2] The structural determination of aziridines derived from allylic ethers[1] or [1·5] rearranged insertion products from allylic sulfides[1] has been described elsewhere. Analytical data of some unknown α-imino ethers are presented in Table 5.

Kinetic Measurement. i) Three stock solutions were prepared by dissolving a weighed amount of azidoformate (20 mmol) in 5 ml of benzene, $PdCl_2(PhCN)_2$ (0.2 mmol) in 25 ml of benzene, and acetophenone (the internal standard, 1 mmol) in 5 ml of benzene. To a 10 ml volumetric flask, 1 ml, 5 ml, and 0.5 ml of the stock solution of the azide, Pd(II), and the internal standard, respectively, were taken, and a weighed amount of 2-methyl-2-propenyl ethyl ether (8, 16, or 32 mmol) was added, and the solution was diluted to 10 ml. One ml of the solution was put into a reaction tube and degassed. The tube was sealed and immersed in a thermostatt kept at 80 °C. After an appropriate reaction time, the mixture was analyzed for the imine product by GLC. The amounts of the imine formed were accomodated approximately to the second-order rate law (first-order each in azide and in ether), and the apparent second-order rate constants obtained for the solution containing the ether at the concentration of 0.8, 1.6, and 3.2 mol·l^{-1} were almost constant, being 1.4, 1.5, and 1.4×10^{-6} s^{-1}·mol^{-1}·l, respectively.

ii) An amount (0.2 mmol) of $PdCl_2(PhCN)_2$ was dissolved in 25 ml of 2-methyl-2-propenyl ethyl ether. To a 10 ml volumetric flask, 1 ml of the above solution and weighed amounts of azidoformate (2 or 4 mmol) and acetophenone (the internal standard, 0.2 or 0.4 mmol) were taken and diluted by 2-methyl-2-propenyl ethyl ether to 10 ml. One ml of the solution was degassed and kept at 80 °C in a sealed tube. The amounts of the imine formed were determined by GLC. The rate obeyed to the psudo-first-order rate law, giving the rate constants 4.3 and 4.8 s^{-1} for the 0.2 and 0.4 mol dm^{-3} solution of the azide, respectively.

The present work was partially supported by a Grant-in-Aid for Scientific Research No. 59470015 from the Ministry of Education, Science and Culture.

Table 5. Analytical Data for the Imines

$CH_3CH_2C(=NCO_2CH_3)CH_3$	IR (CCl_4): 1719 (C=O), 1673 (C=N), 1230 (CO_2CH_3) cm^{-1}.
	^1H NMR (CCl_4): δ=1.15 (3H, t, J=7Hz), 2.36 (2H, q, J=7Hz), 3.70 (3H, s), 3.73 (3H, s).
	Found: C, 50.30; H, 7.60; N, 9.76%. Calcd for $C_6H_{11}NO_3$: C, 49.65; H, 7.64; N, 9.65%.
$CH_3CH_2C(=NCO_2CH_3)CH_2CH_3$	IR (CCl_4): 1728 (C=O), 1678 (C=N), 1234 (CO_2CH_3) cm^{-1}.
	^1H NMR (CCl_4): δ=1.19 (3H, t, J=7Hz), 1.33 (3H, t, J=6Hz), 2.37 (2H, q, J=7Hz), 3.73 (3H, s), 4.17 (2H, q, J=6Hz).
	Found: C, 52.45; H, 8.10; N, 8.98%. Calcd for $C_7H_{13}NO_3$: C, 52.81; H, 8.23; N, 8.80%.
$(CH_3)_2CHC(=NCO_2CH_3)CH_2CH_3$	IR (CCl_4): 1720 (C=O), 1668 (C=N), 1240 (CO_2CH_3) cm^{-1}.
	^1H NMR (CCl_4): δ=1.18 (6H, d, J=7Hz), 1.30 (3H, t, J=6Hz), 2.73 (1H, m), 3.72 (3H, s), 4.18 (2H, q, J=7Hz).
	Found: C, 56.13; H, 8.61; N, 8.42%. Calcd for $C_8H_{15}NO_3$: C, 55.47; H, 8.73; N, 8.09%.
$CH_3(CH_2)_2C(=NCO_2CH_3)CH_3$	IR (CCl_4): 1728 (C=O), 1680 (C=N), 1249 (CO_2CH_3) cm^{-1}.
	^1H NMR (CCl_4): δ=0.89 (3H, t, J=7Hz), 1.16 (2H, m), 2.30 (2H, t, J=7Hz), 3.70 (3H, s), 3.72 (3H, s).
	Found: C, 52.45; H, 8.02; N, 9.21%. Calcd for $C_7H_{13}NO_3$: C, 52.81; H, 8.23; N, 8.80%.
$CH_3(CH_2)_3C(=NCO_2CH_3)CH_2CH_3$	IR (CCl_4): 1720 (C=O), 1670 (C=N) cm^{-1}.
	^1H NMR (CCl_4): δ=0.75—1.90 (10H, m), 2.31 (2H, t, J=7Hz), 3.68 (3H, s), 4.14 (2H, q, J=7Hz).
	Found: C, 57.53; H, 8.83; N, 7.19%. Calcd for $C_9H_{17}NO_3$: C, 57.73; H, 9.15; N, 7.48.
$CH_3CH_2C(=NSO_2CH_3)CH_3$	IR (CCl_4): 1670 (C=N) cm^{-1}.
	^1H NMR (CCl_4): δ=1.16 (3H, t, J=8Hz), 2.75 (2H, q, J=8Hz), 2.93 (3H, s), 4.18 (3H, s).
$CH_3CH_2C(=NSO_2CH_3)CH_2CH_3$	IR (CCl_4): 1670 (C=O) cm^{-1}.
	^1H NMR (CCl_4): δ=1.16 (3H, t, J=8HZ), 1.29 (3H, t, J=6Hz), 2.80 (2H, q, J=8Hz), 2.90 (3H, s), 4.20 (2H, q, J=6Hz).
	Found: C, 40.50; H, 7.28; N, 7.58%. Calcd for $C_6H_{13}NO_3S$: C, 40.21; H, 7.31; N, 7.81%.
$(CH_3)_2CHC(=NSO_2CH_3)CH_3$	IR (CCl_4): 1670 (C=N) cm^{-1}.
	^1H NMR (CCl_4): δ=1.25 (6H, d, J=8Hz), 2.98 (3H, s), 3.54 (1H, m), 3.80 (3H, s).
	Found: C, 40.00; H, 7.03; N, 7.41%. Calcd for $C_6H_{13}NO_3S$: C, 40.21; H, 7.31; N, 7.81%.
$(CH_3)_2CHC(=NSO_2CH_3)CH_2CH_3$	IR (CCl_4): 1670 (C=N) cm^{-1}.
	^1H NMR (CCl_4): δ=1.0—1.45 (9H, m), 2.94 (3H, s), 3.50 (1H, m), 4.16 (2H, q, J=7Hz).
	Found: C, 43.12; H, 7.46; N, 7.36%. Calcd for $C_7H_{15}NO_3S$; C, 43.50; H, 7.82; N, 7.25%.
$CH_3CH_2C(=NPh)CH_3$	IR (CCl_4): 1670 (C=N) cm^{-1}.
	^1H NMR (CCl_4): δ=1.16 (3H, t, J=7Hz), 2.37 (2H, q, J=7Hz), 3.71 (3H, s), 7.00 (5H, Ph).
$CH_3CH_2C(=NPh)CH_2CH_3$	IR (CCl_4): 1670 (C=N) cm^{-1}.
	^1H NMR (CCl_4): δ=1.16 (3H, t, J=7Hz), 1.29 (3H, t, J=6Hz), 2.20 (2H, q, J=7Hz), 4.16 (2H, q, J=6Hz), 7.00 (5H, Ph).
	Found: m/z 177.1220. Calcd for $C_{11}H_{15}ON$: M, 177.1154.
$(CH_3)_2CHC(=NPh)CH_3$	IR (CCl_4): 1670 (C=N) cm^{-1}.
	^1H NMR (CCl_4): δ=1.07 (6H, d, J=7Hz), 2.65 (1H, m), 3.73 (3H, s), 7.06 (5H, Ph).
	Found: m/z 177.1129; Calcd for $C_{11}H_{15}NO$: M, 177.1154.
$(CH_3)_2CHC(=NPh)CH_2CH_3$	IR (CCl_4): 1670 (C=N) cm^{-1}.
	^1H NMR (CCl_4): δ=1.17 (6H, d, J=Hz), 1.29 (3H, t, J=6Hz), 2.76 (1H, m), 4.14 (2H, q, J=6Hz), 7.06 (5H, Ph).
	MS (70 eV) m/z (rel intensity) 191 (M^+, 90), 120 (45), 104 (25), 93 (100), 77 (25).

References

1) W. Ando, H. Fujii, I. Nakamura, N. Ogino, and T. Migita, *Int. J. Sulfur Chem.*, **8**, 13 (1973).
2) T. Migita, M. Chiba, M. Kosugi, and S. Nakaido, *Chem. Lett.*, **1978**, 1403.
3) T. Migita, M. Chiba, K. Takahashi, N. Saitoh, S. Nakaido, and M. Kosugi, *Bull. Chem. Soc. Jpn.*, **55**, 3943 (1982).
4) T. Migita, N. Saitoh, H. Iizuka, C. Ogyu, M. Kosugi, and S. Nakaido, *Chem. Lett.*, **1982**, 1015.
5) R. Huisgen, L. Möbius, and G. Szeimies, *Chem. Ber.*, **98**, 1138 (1965).
6) P. Scheiner, *J. Org. Chem.*, **32**, 2022 (1967).
7) R. Hüttel and H. Christ, *Chem. Ber.*, **97**, 1439 (1964).
8) P. Golborn and F. Scheimann, *J. Chem. Soc., Perkin Trans. 1*, **1973**, 2870.
9) W. Lwowski and T. W. Mattingly Jr., *J. Am. Chem. Soc.*, **87**, 1947 (1965).
10) R. O. Lindsay and C. F. H. Allen, *Org. Synth.*, Coll. Vol. III, 710 (1955).
11) D. S. Breslow, M. F. Sloan, N. R. Newburg, and W. B. Renfrow, *J. Am. Chem. Soc.*, **91**, 2273 (1969).
12) W. T. Olson, H. F. Hipsher, C. M. Buess, I. A. Goodman, I. Hart, J. H. Lamneck Jr., and L. C. Gibbons, *J. Am. Chem. Soc.*, **69**, 2451 (1947).
13) E. A. Braude, E. R. H. Jones, and E. S. Stern, *J. Chem. Soc.*, **1949**, 396.
14) J. C. Martin, V. W. Goodlett, and R. D. Burpitt, *J. Org. Chem.*, **30**, 4309 (1965).
15) M. S. Kharasch, R. C. Seyler, and F. R. Mayo, *J. Am. Chem. Soc.*, **60**, 882 (1938).

 © 1988 The Chemical Society of Japan Bull. Chem. Soc. Jpn., 61, 939—943 (1988)

Crystal and Molecular Structure of (*E*)-1,1′-Bitetralinylidene

Keiichiro Ogawa,* Hiroshi Suzuki,§ Motoko Futakami, Shin Yoshimura, Tosio Sakurai,† Kimiko Kobayashi,†† and Akira Kira††

Department of Chemistry, The College of Arts and Sciences, The University of Tokyo, Komaba, Meguro, Tokyo 153
†Department of Science, Faculty of Education, Shinsyu University, Nishinagano, Nagano 380
††The Institute of Physical and Chemical Research, Wako, Saitama 351

(Received September 8, 1987)

The crystal structure of the title compound was determined by X-ray diffraction. The crystals have monoclinic symmetry with a=13.481(5), b=8.285(5), c=13.092(3) Å. β=96.24(3)°, and space group $P2_1/n$ with Z=4. The final R-factor was 0.065 for 2191 independent reflections. The torsion angles of the C–Ph bonds are 47.4(4) and 44.4(4)°. The cyclohexene rings have approximate twist-boat conformations. The molecular structure in the crystal is compared with that in the solution phase, that of (*E*)-stilbenes, and the results of the molecular mechanics calculations. It is also discussed in relation to the molecular packing.

In connection with our continuing studies of the geometry of stilbene systems,[1,2] the molecular structure of the title compound (*E*)-1,1′-bitetralinylidene (**1**) is of interest, because **1** has the (*E*)-stilbene skeleton that is geometrically fixed by two methylene chains. Electronic absorption spectroscopic study of **1** has revealed that the torsion angle of the C–Ph bonds substantially deviates from 0° in the fluid and the glassy solution.[2] Molecular mechanics study using MMP1[3] has shown that the torsion angle of the C–Ph bonds is 54° and that the cyclohexene rings have approximate twist-boat conformations in the isolated molecule.[4] The purpose of the present study is to investigate the geometry of this molecule in the crystalline state and to compare it with that in the solution phase, with the geometry of (*E*)-stilbenes, and with the results of the molecular mechanics calculations.

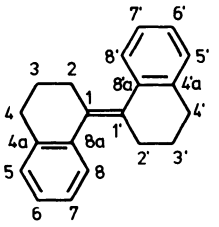

1

Experimental

The sample of **1** was prepared by the method described in literature.[4] Single crystals were recrystallized from isopropyl alcohol.

Crystal Data. $C_{20}H_{20}$, M=260.36. Monoclinic, a=13.481 (5), b=8.285 (5), c=13.092 (3) Å, β=96.24 (3)°, V=1454 (1) Å^3 (by least-squares refinement on 20 reflections with $18 \leq 2\theta \leq 20°$, λ=0.71073 Å), space group $P2_1/n$, Z=4, D_x=1.190 g cm^{-3}, D_m not determined. The crystal used was a colourless plate. Approximate dimensions 0.8×0.4×0.2 mm, μ(Mo $K\alpha$)=0.0622 mm^{-1}. F(000)=560. T=296 K.

Data Collection and Processing. The integrated intensities were collected on a Rigaku AFC-4 automated four-circle diffractometer using graphite-monochromatized Mo $K\alpha$ radiation. The ω–2θ scan technique was employed at an ω rate of 4.0° min^{-1}. $2\theta_{max}$=55°, collection range h=−17 to 17, k=0 to 10, l=0 to 16. Three standard reflections $\bar{1}21$, 710, and 264 were measured every 100 reflections, intensity variation≤2.1%. 2419 reflections with $|F_o| > 3\sigma(F_o)$ were obtained. The intensities were corrected for Lorentz and polarization effects but not for absorption. 2191 reflections were unique and were used for refinement. 1298 reflections were unobserved.

Structure Analysis and Refinement. Structure was solved by direct methods with MULTAN78[5] and was refined by full-matrix least squares minimizing $\Sigma w(|F_o|^2 - |F_c|)^2$, $w=(0.00462|F_o|^2 - 0.06153|F_o| + 0.68041)^{-1}$. 16 H atoms were obtained by the difference Fourier synthesis and 4 H atoms were located by standard bond lengths and angles. Isotropic temperature factors were assigned to all of the H atoms. 261 parameters consisting of 120 positional parameters, 120 anisotropic temperature factors, 20 isotropic temperature factors, and a scale factor were refined. In the final least squares refinement, R=0.072, wR=0.083, S=1.1696, and $(\Delta/\sigma)_{max}$=0.790. The maximum and the minimum height in the final difference Fourier synthesis were +0.441 and −0.658 e Å^{-3}, respectively. For the structure at this stage (structure **A**), it was found that the temperature factors of C3 and C4 were exceptionally large (B_{eq}=9.9 Å^2 for C3 and B_{eq}=7.0 Å^2 for C4).

Therefore, further refinement was carried out on the basis of a disorder model constructed as follows. New atoms C3+ and C3− were located on the normal to the plane through C2, C3, and C4, which passes through C3, 0.25 Å above and below the plane, respectively. In a similar way, new atoms C4+ and C4− were located above and below the plane through C3, C4, and C4a. Then C3, C4, and hydrogen atoms attached to these atoms were deleted. Hydrogen atoms attached to the new carbon atoms were located by molecular mechanics calculations. Multiplicities of all of the new atoms were fixed to 0.5. For this model, 295 parameters consisting of 138 positional parameters, 132 anisotropic temperature factors, 24 isotropic temperature factors, and a scale factor were refined by full-matrix least squares minimizing $\Sigma w(|F_o| - |F_o|)^2$, $w=(0.00314\ |F_o|^2 - 0.04503\ |F_o| + 0.55851)^{-1}$. In the final least squares refinement, R=0.065, wR=0.063, S=0.9538, and $(\Delta/\sigma)_{max}$=0.007. The maximum and the minimum height in final difference Fourier synthesis were +0.342 and −0.249 e Å^{-3},

§ Present address: Department of Chemistry, School of Medicine, Juntendo University, Inba-mura, Inba-gun, Chiba 270-16.

respectively.

Atomic scattering factors were taken from the International Tables for X-Ray Crystallography.[6] Crystallographic calculations were performed on FACOM M-380 and M-780 computers at the Institute and on FACOM M-360 at the University of Tokyo using UNICSIII program system.[7] The molecular mechanics calculations were performed using the MMP2 program[8] on a HITAC M-682H computer of the Computer Centre of the University of Tokyo.

Results and Discussion

The final atomic parameters are listed in Table 1[†††] and the geometrical parameters in Table 2. A perspective view of the molecule is shown in Fig. 1.

Table 2 and Fig. 1 show that the observed structure is asymmetric. However, in a rough approximation, it has a C_2 axis perpendicular to the ethylenic plane, in sharp contrast with (*E*)-stilbene (ES) and (*E*)-α,β-dimethylstilbene (EαβDMS), which have an inversion center (see Table 3).

The (*E*)-2-butene skeleton C8a-C1-C1′-C8′a holds the planar geometry. The double bond C1-C1′ has a normal length 1.347 Å. It is nearly equal to the length of the ethylenic double bond of EαβDMS and is a little longer than that of ES. Absolute values of the torsion angles of the C-Ph bonds of **1** are much larger than those of ES, but are significantly smaller than those of EαβDMS, in accordance with the results of our UV study.[2]

Another (*E*)-2-butene skeleton C2-C1-C1′-C2′ deviates from the planarity as shown by its torsion angle, and C2 and C2′ atoms, as well as other sp^3 carbon atoms, are placed on a same side of the ethylenic plane (C8a-C1-C1′-C8′a). The two cyclohexene rings have approximate twist-boat conformations as shown in Fig. 2.

These results are essentially consistent also with the results of molecular mechanics calculations using MMP2. The most stable molecular structure obtained by the calculations is nearly C_2 symmetric and has the following geometrical parameters (cf. Table 2): Bond length C1-C1′, 1.361 Å; torsion angles C1′-C1-C8a-C8, −49.3°; C1-C1′-C8′a-C8′, −49.4°; C2-C1-C1′-C2′, 157.1°; C2-C1-C1′-C8′a, −10.4°; C2′-C1′-C1-C8a, −10.5°.

One of the most interesting features of the X-ray structure is that there is a disorder in C3 and C4 but not in C3′ and C4′. This may be explained in terms of the intermolecular nonbonding interactions in the crystal as follows.

The crystal structure is shown in Fig. 3. In a unit cell, there are 28 intermolecular nonbonding atom pairs whose distances (2.64—2.87 Å for C···H and 2.12—2.39 Å for H···H) are slightly shorter than the sum of the relevant van der Waals radii (2.90 Å for

Table 1. Final Atomic Coordinates (×10⁴) and Equivalent Isotropic Thermal Parameters[a] for (*E*)-1,1′-Bitetralinylidene, with Estimated Standard Deviations in Parentheses

Atom	*x*	*y*	*z*	B_{eq}/Å²
C1	3484(1)	1442(2)	1122(2)	2.9
C2	2990(2)	3101(3)	1163(2)	3.9
C3+	1870(5)	3101(8)	1264(5)	3.3
C3−	2078(6)	2923(13)	1773(9)	6.4
C4+	1388(6)	1590(1)	1557(6)	4.0
C4−	1670(5)	1536(9)	1910(5)	3.1
C4a	1818(2)	153(3)	1099(2)	4.1
C5	1142(2)	−1068(4)	800(3)	5.3
C6	1403(2)	−2318(4)	181(2)	5.3
C7	2344(2)	−2348(3)	−164(2)	4.6
C8	3022(2)	−1134(3)	132(2)	3.7
C8a	2782(2)	124(2)	780(2)	3.0
C1′	4452(1)	1186(2)	1454(1)	2.8
C2′	4907(2)	−506(3)	1590(2)	3.5
C3′	5733(2)	−656(3)	2480(2)	5.1
C4′	5716(2)	705(3)	3254(2)	4.7
C4′a	5789(2)	2303(3)	2708(2)	3.4
C5′	6442(2)	3531(3)	3061(2)	4.2
C6′	6488(2)	4946(3)	2509(2)	4.4
C7′	5888(2)	5151(3)	1591(2)	4.3
C8′	5231(2)	3937(3)	1230(2)	3.7
C8′a	5155(1)	2506(2)	1794(2)	2.9

a) $B_{eq}=\frac{4}{3}(a^2\beta_{11}+b^2\beta_{22}+c^2\beta_{33}+2ab\beta_{12}\cos\gamma+2ac\beta_{13}\cos\beta+2bc\beta_{23}\cos\alpha)$.

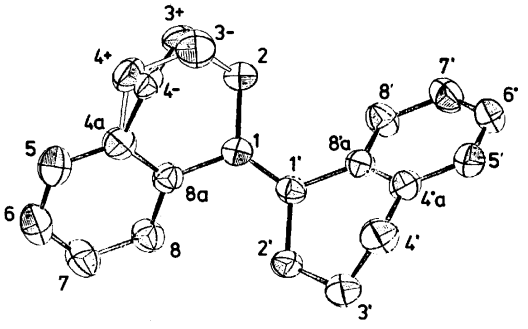

Fig. 1. Prespective view of (*E*)-1,1′-bitetralinylidene, drawn by ORTEP.[9]

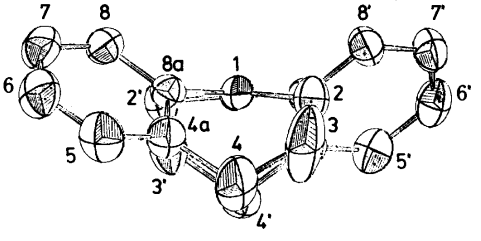

Fig. 2. End view of (*E*)-1,1′-bitetralinylidene. For the clarity, structure A is drawn.

††† List of H-atom coordinates, anisotropic temperature factors, and observed and calculated structure factors are deposited as Document No. 8784 at the Office of the Editor of Bull. Chem. Soc. Jpn.

Table 2. Geometrical Parameters for (*E*)-1,1′-Bitetralinylidene

Bond length/Å[a]			
C1-C2	1.530(3)	C1′-C2′	1.533(3)
		C2′-C3′	1.527(4)
		C3′-C4′	1.518(4)
		C4′-C4′a	1.513(4)
C4a-C5	1.389(4)	C4′a-C5′	1.391(3)
C5-C6	1.384(4)	C5′-C6′	1.383(4)
C6-C7	1.393(4)	C6′-C7′	1.384(4)
C7-C8	1.385(4)	C7′-C8′	1.388(3)
C8-C8a	1.404(3)	C8′-C8′a	1.406(3)
C4a-C8a	1.408(3)	C4′a-C8′a	1.404(3)
C1-C8a	1.482(3)	C1′-C8′a	1.483(3)
C1-C1′	1.347(3)		
Bond angle/°[a]			
		C1′-C2′-C3′	114.4(2)
		C2′-C3′-C4′	112.7(2)
		C3′-C4′-C4′a	109.2(2)
		C4′-C4′a-C5′	123.7(2)
		C4′-C4′a-C8′a	116.3(2)
C4a-C5-C6	120.6(3)	C4′a-C5′-C6′	120.6(2)
C5-C6-C7	120.2(3)	C5′-C6′-C7′	120.2(2)
C6-C7-C8	119.5(3)	C6′-C7′-C8′	119.5(2)
C7-C8-C8a	121.3(2)	C7′-C8′-C8′a	120.8(2)
C8-C8a-C4a	118.2(2)	C8′-C8′a-C4′a	118.5(2)
C1-C8a-C8	123.3(2)	C1′-C8′a-C8′	123.0(2)
C1-C8a-C4a	118.5(2)	C1′-C8′a-C4′a	118.5(2)
C8a-C1-C1′	123.1(2)	C8′a-C1′-C1	123.1(2)
Torsion angle/°			
C1-C2-C3+-C4−	31.7(5)	C1′-C2′-C3′-C4′	18.7(3)
C1-C2-C3−-C4+	−46.1(9)		
C2-C3+-C4−-C4a	−71.0(5)	C2′-C3′-C4′-C4′a	−56.6(3)
C2-C3−-C4+-C4a	24.9(11)		
C3+-C4−-C4a-C8a	61.0(5)	C3′-C4′-C4′a-C8′a	47.3(3)
C3−-C4+-C4a-C8a	−7.2(9)		
C4−-C4a-C8a-C1	−6.9(4)	C4′-C4′a-C8′a-C1′	1.9(3)
C4+-C4a-C8a-C1	14.1(5)		
C4a-C8a-C1-C2	−37.3(3)	C4′a-C8′a-C1′-C2′	−41.6(3)
C8a-C1-C2-C3+	22.8(4)	C8′a-C1′-C2′-C3′	29.5(3)
C8a-C1-C2-C3−	50.3(5)		
C8a-C1-C1′-C8′a	179.8(2)		
C1′-C1-C8a-C8	−44.4(3)	C1-C1′-C8′a-C8′	−47.4(3)
C2-C1-C1′-C2′	169.1(2)		
C2-C1-C1′-C8′a	−6.2(3)	C2′-C1′-C1-C8a	−4.9(3)

a) The bond lengths and angles related to the disordered atoms, C3± and C4±, are not listed in this table, because they are not reliable. They will be approximately equal to the corresponding ones in which C3′ and/or C4′ are involved.

C···H and 2.40 Å for H···H) as shown in Table 4,[12] where parts of the molecule are designated as follows. A half of the molecule that has the atom numbers without primes in Fig. 1 is designated as *n*. Another half that has atom numbers with primes in Fig. 1 is designated as *n*′. An atom of the methylene groups and an atom of the benzene ring in the half *n*(or *n*′) are designated as *M* (or M′) and *B* (or *B*′), respectively.

The fact that all of the 28 van der Waals contact atom pairs involve the half of the molecule *n*′ shows that it is sterically more crowded than the another half *n*. The fact that 4 van der Waals contact atom pairs involve atoms *M* while 16 van der Waals contact pairs involve atoms *M*′ shows that the methylene groups of the cyclohexene ring for which the disorder was observed are sterically much less crowded than those of the cyclohexene ring for which the disorder was not observed. The fact that there are 25 van der Waals contact atom pairs in which atoms of the benzene rings are involved shows that the benzene rings are sterically more crowded than the cyclohexene rings. Thus, the difference between the packing of the two halves of the molecule results in the asymmetrical molecular structure in the crystal.

References

1) H. Suzuki, "Electronic Absorption Spectra and Geometry of Organic Molecules," Academic Press Inc., New York (1967), Chap. 14; T. Kobayashi, H. Suzuki, and K. Ogawa, *Bull. Chem. Soc. Jpn.*, **55**, 1734 (1982); H. Suzuki, K.

Table 3. Comparison of Geometrical Parameters for (*E*)-1,1′-Bitetralinylidene and (*E*)-Stilbenes

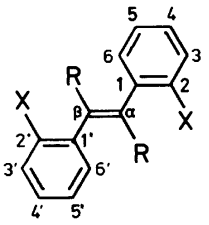

Compound	ES[a] R=X=H	**1**[b] R=X=$(CH_2)_3$	E$\alpha\beta$DMS[c] R=CH_3, X=H
Bond length/Å			
α-β	1.326(2)	1.347(3)	1.341(19)
α-1	1.471(2)	1.482(3)	1.549(8)
β-1′	1.471(2)	1.483(3)	1.549(8)
Bond angle/°			
1-α-β	126.4(1)	123.1(2)	114.7(9)
1′-β-α	126.4(1)	123.1(2)	114.7(9)
Torsion angle/°			
1-α-β-1′	180.0	179.8(2)	180.0
6-1-α-β	5.3(2)	−44.4(3)	66.2
6′-1′-β-α	−5.3(2)	−47.4(3)	−66.2

a) Ref. 10. b) Data for structure **B** in this work. c) Ref. 11.

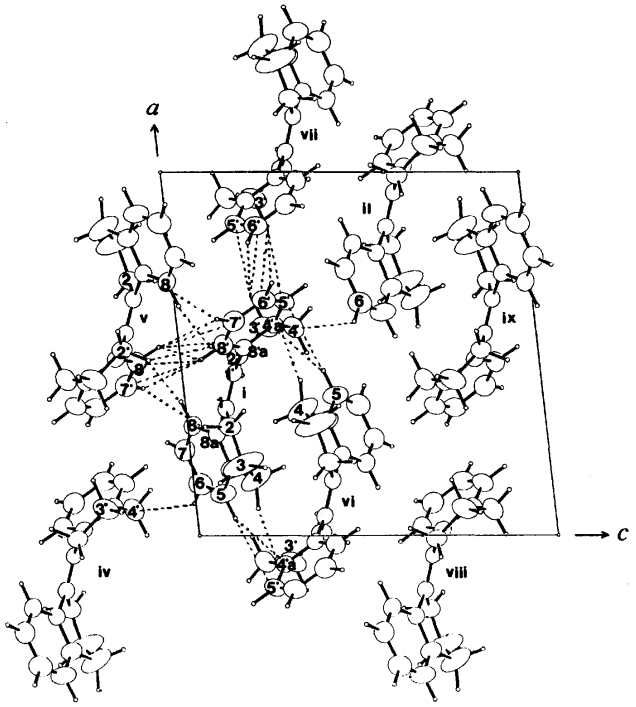

Fig. 3. The crystal structure of (*E*)-1,1′-bitetralinylidene viewed along the *b* axis. Dotted lines indicate van der Waals contact atom pairs. Molecules (structure **A**) generated by the following symmetry operations are drawn: (i) x, y, z; (ii) $x, \bar{y}+0.5, z+0.5$; (iii) $x+0.5, \bar{y}-0.5, z+0.5$; (iv) $x-0.5, \bar{y}+0.5, z-0.5$; (v) $\bar{x}+1, \bar{y}+1, \bar{z}$; (vi) $\bar{x}+0.5, y+0.5, \bar{z}+0.5$; (vii) $\bar{x}+1.5, y+0.5, \bar{z}+0.5$; (viii) $x-0.5, \bar{y}+0.5, z+0.5$; (ix) $\bar{x}+1, \bar{y}+1, \bar{z}+1$. Molecule iii is hidden by molecule ii.

Table 4. Van der Waals Contact[a] Atom Pairs in a Unit Cell

Class n,n	0 pairs		
Class n,n'	14 pairs		
Subclass	Atom 1[b]	Atom 2[b]	Distance/Å
M,M'	H(C4−)1[i]	H(C3′)2[vi]	2.32(6)
M,M'	H(C3′)2[i]	H(C4−)1[vi]	2.32(6)
M,B'	H(C2)2[i]	H(C7′)[v]	2.22(5)
M,B'	H(C7′)[i]	H(C2)2[v]	2.22(5)
B,M'	C4′[i]	H(C6)[iii]	2.86(4)
B,M'	C4′a[i]	H(C5)[vi]	2.70(3)
B,M'	H(C6)[i]	C4′[iv]	2.86(4)
B,M'	H(C6)[i]	H(C3′)[iv]	2.12(6)
B,M'	H(C8)[i]	H(C2′)2[v]	2.34(4)
B,M'	H(C2′)2[i]	H(C8)[v]	2.34(4)
B,M'	H(C3′)2[i]	H(C6)[ii]	2.12(6)
B,B'	C5′[i]	H(C5)[vi]	2.85(3)
B,B'	H(C5)[i]	C4′a[vi]	2.70(3)
B,B'	H(C5)[i]	C5′[vi]	2.85(3)
Class n',n'	14 pairs		
Subclass	Atom 1[b]	Atom 2[b]	Distance/Å
M',M'	H(C2′)2[i]	H(C2′)2[v]	2.39(5)
M',B'	C5′[i]	H(C3′)1[vii]	2.85(4)
M',B'	C6′[i]	H(C3′)1[vii]	2.64(4)
M',B'	H(C3′)1[i]	C5′[vii]	2.85(4)
M',B'	H(C3′)1[i]	C6′[vii]	2.64(4)
M',B'	H(C3′)1[i]	H(C6′)[vii]	2.25(5)
M',B'	H(C6′)[i]	H(C3′)1[vii]	2.25(5)
B',B'	C7′[i]	H(C8′)[v]	2.87(3)
B',B'	C8′[i]	H(C8′)[v]	2.82(3)
B',B'	H(C7′)[i]	H(C8′)[v]	2.15(4)
B',B'	H(C8′)[i]	C7′[v]	2.87(3)
B',B'	H(C8′)[i]	C8′[v]	2.82(3)
B',B'	H(C8′)[i]	H(C7′)[v]	2.15(4)
B',B'	H(C8′)[i]	H(C8′)[v]	2.18(4)

a) Following van der Walls radii were used: H, 1.20; C, 1.70 Å.[13] b) Symmetry codes are given in the caption of Fig. 3.

Koyano, T. Shida, and A. Kira, *ibid.*, **55**, 3690 (1982); H. Suzuki, K. Ogawa, T. Shida, and A. Kira, *ibid.*, **56**, 66 (1983); J. Higuchi, K. Ishizu, F. Nemoto, K. Tajima, H. Suzuki, and K. Ogawa, *J. Am. Chem. Soc.*, **106**, 5403 (1984).

2) K. Ogawa, H. Suzuki, and M. Futakami, *J. Chem. Soc., Perkin Trans. 2*, **1988**, 39.

3) N. L. Allinger and Y. Yuh, *Quantum Chemistry Program Exchange*, Indiana University, Program No. 318 (1975).

4) P. Lemmen and D. Lenoir, *Chem. Ber.*, **117**, 2300 (1984).

5) P. Main, S. E. Hull, L. Lessinger, G. Germain, J.-P. Declercq, and M. M. Woolfson, MULTAN78, A System of Computer Programs for the Automatic Solution of Crystal Structures from X-Ray Diffraction Data, Univs. York, England and Louvain, Belgium (1978).

6) "International Tables for X-Ray Crystallography," Vol. IV. Kynoch Press, Birmingham (1974).

7) T. Sakurai and K. Kobayashi, *Rikagaku Kenkyusho Houkoku*, **55**, 69 (1979).

8) N. L. Allinger, "Quantum Chemistry Program Exchange," Indiana University, Program MMP2 (1982); N.

L. Allinger and H. L. Flanagan, *J. Comput. Chem.*, **4**, 399 (1983).

9) C. K. Johnson, ORTEP. Report ORNL3794, Oak Ridge National Laboratory, Oak Ridge, Tennessee (1965).

10) J. A. Boustra, A. Schouten, and J. Kroon, *Acta Crystallogr., Sect. C*, **40**, 428 (1984).

11) G. Valle, V. Busetti, and G. Galiazzo, *Cryst. Struct. Commun.*, **10**, 867 (1981).

12) The data given in Table 4 are based on the crystal structure of the disorder model. The crystal structure shown in Fig. 3 is, however, based on molecular structure **A** for the clarity, because a figure of the crystal structure of the disorder model is too much complicated for the indication of the van der Waals contact atom pairs.

13) A. Bondi, *J. Phys. Chem.*, **68**, 441 (1964).

 © 1988 The Chemical Society of Japan Bull. Chem. Soc. Jpn., 61, 945—951 (1988)

Solvation Structure of Copper(II) Ion in *N,N*-Dimethylformamide and *N,N*-Dimethylformamide–Acetonitrile Mixtures Determined by the X-Ray Diffraction Method

Kazuhiko Ozutsumi, Shin-ichi Ishiguro,* and Hitoshi Ohtaki†
Coordination Chemistry Laboratories, Institute for Molecular Science, Myodaiji, Okazaki 444
†Department of Electronic Chemistry, Tokyo Institute of Technology at Nagatsuta, Nagatsuta-cho 4259, Midori-ku, Yokohama 227
(Received September 14, 1987)

The solvation structure of copper(II) ion in *N,N*-dimethylformamide (DMF) and *N,N*-dimethylformamide–acetonitrile (AN) mixtures has been investigated by means of X-ray diffraction at 25 °C. The X-ray scattering data for the copper(II) perchlorate DMF solution were well-interpreted in terms of the presence of the axially elongated octahedral $[Cu(dmf)_6]^{2+}$ ion in DMF. Among the six DMF molecules, four of them are at the distance of 203(3) pm at the equatorial position and the other two are at 243(5) pm at the axial one. On the other hand, in copper(II) perchlorate DMF–AN solutions with the C_{dmf}/C_{Cu} mole ratios of 5.308 and 7.435, where C_i denotes the total concentrations of species i, the copper(II) ion is coordinated with four DMF molecules within the square-plane and with no solvent molecule along the axis of the plane. The equatorial Cu–O bond length is 200(1) pm and practically the same as that within the $[Cu(dmf)_6]^{2+}$ ion in DMF. In copper(II) nitrate DMF solutions (1.086 and 1.500 mol dm^{-3}), a nitrate ion binds to copper(II) ion at the equatoral position and the distorted octahedral $[CuNO_3(dmf)_5]^+$ complex is formed.

Complex formation reactions between copper(II) and chloride ions in *N,N*-dimethylformamide (DMF) and in acetonitrile (AN) have been investigated[1,2] and it was found that the formation of copper(II)–chloro complexes ($[CuCl_n]^{(2-n)+}$, n=1—4) is more favorable in AN than in DMF. The more enhanced formation of the complexes in AN than in DMF is mainly ascribed to the difference in the donor property between the two solvents, i.e. copper(II) ion is more strongly solvated with DMF than with AN. Accordingly, copper(II) ion is preferentially solvated with DMF molecules in DMF–AN mixtures[3] and complex formation between copper(II) and chloride ions in the mixtures depends on the solvent composition.[4]

According to the X-ray diffraction study, copper(II) ion in aqueous solution is coordinated with six water molecules and the $[Cu(H_2O)_6]^{2+}$ ion has an axially elongated octahedral structure.[5] However, structural information on solvated copper(II) ion in other solvents has never been given by the diffraction method. In the present study we aimed at determining the solvation structure of copper(II) ion in DMF and in DMF–AN mixtures by the X-ray diffraction method. It was difficult to determine the solvation structure of copper(II) ion in AN because of a low solubility of copper(II) perchlorate in AN.

Experimental

Preparation of Sample Solutions. All chemicals used were of reagent grade. *Copper(II) perchlorate DMF solvate* was prepared by dissolving copper(II) perchlorate hydrate crystals in DMF and by repeated evaporation of DMF to remove water, and was finally isolated by adding ether. Crude crystals thus obtained were recrystallized from a DMF–acetone mixture. *Copper(II) nitrate DMF solvate* was obtained by a similar way to that used for copper(II) pechlorate DMF solvate and then recrystallized from DMF. Crystals thus obtained were dried at 40 °C in a vaccum oven for several days and stored in a vaccum desiccator over P_2O_5. From the electrogravimetric analysis of copper, the composition of the solvate crystals prepared was found to be $Cu(ClO_4)_2(dmf)_4$ and $Cu(NO_3)_2(dmf)_2$. *N,N*-Dimethyformamide and acetonitrile were purified by similar ways to those described in previous papers.[1,2]

Five test solutions A to E were prepared for X-ray diffraction measurements as shown in Table 1. Solution A was prepared by dissolving the copper(II) perchlorate DMF solv-

Table 1. The Composition (mol dm^{-3}), Stoichiometric Volumes V per Copper Atom and Densities ρ of the Sample Solutions

	A	B	C	D	E
Cu^{2+}	0.5513	1.086	1.500	0.9388	0.8856
ClO_4^-	1.103	—	—	1.878	1.771
NO_3^-	—	2.172	3.000	—	—
DMF	12.54	12.28	11.99	4.983	6.584
AN	—	—	—	10.83	8.510
$V/10^9$ pm^3	3.012	1.592	1.107	1.769	1.875
ρ/g cm^{-3}	1.061	1.101	1.158	1.055	1.063
$C_{dmf}/C_{Cu^{2+}}$	22.75	11.31	7.993	5.308	7.435

ate in DMF and was an almost saturated one at room temperature. Solutions B and C are copper(II) nitrate DMF solution in which the concentration of copper(II) ions is higher than that in solution A. Solutions D and E are copper(II) perchlorate solutions in DMF–AN mixtures of different molar ratios. Concentrations of copper(II) ions in the test solutions were determined by electrogravimetry. Concentrations of perchlorate and nitrate ions in the solutions were estimated from the stoichiometry of the copper(II) salts used. Densities of the sample solutions were measured by using a pycnometer.

X-Ray Scattering Measurements. X-Ray scattering measurements were carried out with a θ–θ type diffractometer (JEOL DX-GO-Y) by using an Mo X-ray tube (λ=71.07 pm). Scattered X-rays were monochromatized by a Johansson-type graphite monochromator and a pulse-height analyzer. The observed range of the scattering angle 2θ was from 2° to 140° and times required to collect 240000 counts at each angle were recorded. Corrections for the scattered intensities were made by the same manner as that described elsewhere.[6]

The reduced intensities $i(s)$ were obtained by subtracting independent coherent scatterings from the measured intensities $I(s)$ as follows:

$$i(s) = K \cdot I(s) - \sum_i n_i[\{f_i(s) + \Delta f_i\}^2 + (\Delta f_i'')^2], \quad (1)$$

where K stands for a normalization factor of the measured intensities to the absolute ones. n_i is the number of atom i in a stoichiometric volume V per copper atom of the test solutions. $f_i(s)$ represents the atomic scattering factors at s, and $\Delta f_i'$ and $\Delta f_i''$ denote the real and imaginary parts of anomolous dispersion, respectively, of atom i. The reduced intensities multiplied by s ($=4\pi\lambda^{-1}\sin\theta$) for the sample solutions are shown in Fig. 1.

The radial distribution function $D(r)$ was calculated by the Fourier transform of the reduced intensities according to Eq. 2:

$$D(r) = 4\pi r^2\rho_0 + \frac{2r}{\pi}\int_0^{s_{max}} s \cdot i(s) \cdot M(s) \cdot \sin(rs)ds, \quad (2)$$

where ρ_0 ($=\{\sum n_i \cdot f_i(0)\}^2/V$) is the average scattering density in a stoichiometric volume of the sample solution and s_{max} represents the maximum s-value attained in the measurement (s_{max}=16.6×10^{-2} pm^{-1}). The modification function $M(s)$ is given as

$$M(s) = \frac{\sum_i n_i\{(f_i(0) + \Delta f_i)^2 + (\Delta f_i'')^2\}}{\sum_i n_i\{(f_i(s) + \Delta f_i)^2 + (\Delta f_i'')^2\}} \cdot \exp(-ks^2). \quad (3)$$

The damping factor k was chosen as 100 pm^2 in the present case. The differential radial distribution curves, $D(r)-4\pi r^2\rho_0$, for the test solutions are depicted in Fig. 2.

A least-squares calculation for the refinement of the structure parameters was applied to the reduced intensities so as to minimize the error-square sum U,

$$U = \sum_{s_{max}}^{s_{max}} s^2\{i(s)_{obsd} - i(s)_{calcd}\}^2. \quad (4)$$

The theoretical intensities $i(s)_{calcd}$ arising from the inter-

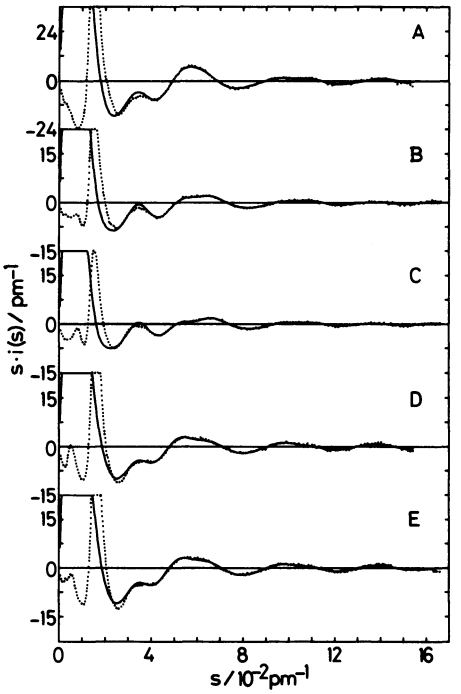

Fig. 1. The reduced intensities multiplied by s for solutions A to E. The observed $s \cdot i(s)$ values are shown by the dotted lines and calculated ones by the solid lines.

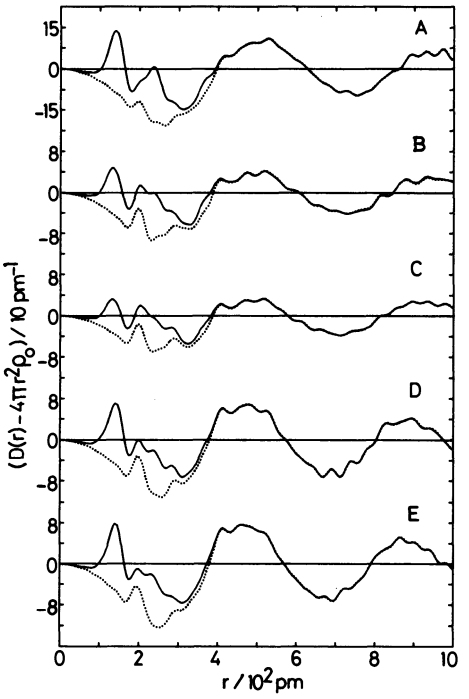

Fig. 2. The differential radial distribution curves, $(D(r)-4\pi r^2\rho_0)$, for solutions A to E. The dotted lines indicate the residual curves after subtraction of peaks due to intramolecular interactions of solvent molecules and anions.

atomic interactions in the solutions are obtained as follows:

$$i(s)_{calcd}=\sum_{i}\sum_{j\neq i} n_{ij}[\{f_i(s)+\Delta f_i\}\{f_j(s)+\Delta f_j\}+(\Delta f_i'')(\Delta f_j'')] \cdot \frac{\sin(r_{ij}s)}{r_{ij}s}\cdot\exp(-b_{ij}s^2), \quad (5)$$

where r_{ij}, b_{ij}, and n_{ij} represent the distance, the temperature factor, and the frequency factor of the atom-pair i-j, respectively.

All calculations were performed by using programs KURVLR[7] and NLPLSQ.[8]

Results and Discussion

The observed $(D(r)-4\pi r^2\rho_o)$ curves for solutions A to E drawn by the solid lines in Fig. 2 show five peaks around 140, 200, 240, 290, and 400 pm in the range of $r \leqslant 400$ pm. Two large peaks are observed around 400—600 and 800—1000 pm, which are due to ion-ion, ion-solvent, and solvent-solvent long range intermolecular interactions, and they, except for the small peak at 400 pm, are not analyzed in the present study. Diffraction studies on the structure of liquid DMF[9] and AN[10,11] showed that the peaks resulting from the intramolecular interactions within solvent molecules appeared at 130 and 230 pm for DMF and 130 and 260 pm for AN. The first peak at 140 pm, therefore, consists of peaks due to C-H, C=O, and C-N bonds within DMF molecules in solutions A to E and due to C-H, C-C, and C≡N bonds within AN molecules in solutions D and E. The Cl-O bonds within perchlorate ions in solutions A, D and E, and the N-O bonds within nitrate ions in solutions B and C also contribute to the peak. The third peak appearing at 240 pm is due to the nonbonding N···O, C···C, and C···O interactions within DMF molecules and the C···N interactions within AN molecules. The O···O contacts within perchlorate and nitrate ions are partly contained in the peak.

In order to extract peaks due to the sole intramolecular interactions within solvated copper(II) ion, the calculated peak shapes due to the intramolecular interactions of solvent molecules and anions must be subtracted from the observed radial distribution functions. For the calculation the structural parameters of each solvent molecule were assumed to be the same as those reported in the liquid state.[9-11] The parameter values of perchlorate and nitrate ions were also taken from the literature.[5,12]

The dotted lines in Fig. 2 represent the residual radial distribution curves after subtracting the theoretical peak shapes due to the intramolecular interactions of solvent molecules and anions, and the curve shows the peaks originating from the intramolecular interactions within the solvated copper(II) ion over the region $r<400$ pm. The structure parameters of the solvated copper(II) ions in DMF and in DMF-AN mixtures, details of which will be discussed in the following sections, were evaluated by analyzing the residual curves.

Copper(II) Perchlorate DMF Solution. Figure 3a depicts the $(D(r)-4\pi r^2\rho_o)$ curve of solution A. Subtraction of the calculated peak shapes due to the intramolecular structure of DMF molecule and perchlorate ion from the original curve (solid line) gives the residual curve (chain line), which shows three peaks at 200, 290, and 400 pm and a small hump at 240 pm. The peak centered at 200 pm is ascribable to the Cu-O(dmf) bonds similar to the Cu-O(H_2O) within the hexaaquacopper(II) ion.[5] The area under the peak gives the frequency factor of four for the Cu-O bond. The peak at 290 pm is attributable to the nonbonding Cu···C interactions when the DMF molecules at the equatorial position direct lone-pair electrons of the oxygen atom to the central copper(II) ion as found in $SbCl_5$·DMF solvate crystal.[13] The nonbonding interligand O(eq)···O(eq) interactions might also be contained in the peak. If the structure of DMF molecules within the metal solvate is the same as that in the liquid state,[9] it is expected that the nonbonding Cu···N(eq) distance should

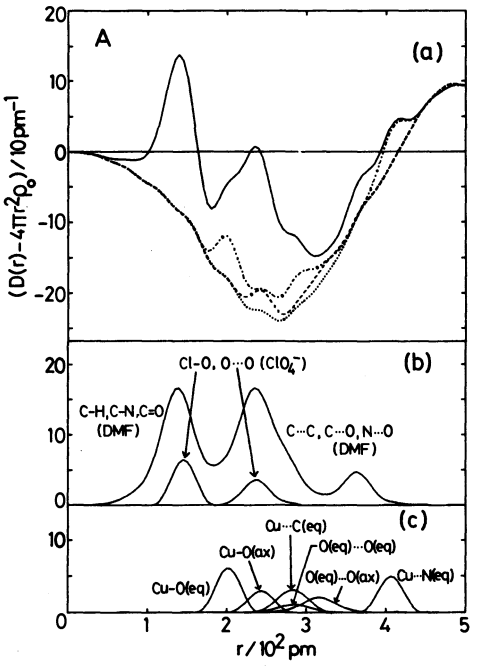

Fig. 3. (a); The $(D(r)-4\pi r^2\rho_o)$ curve for solution A. The chain line represents the residual curve after subtracting the theoretical peaks shown in (b). The dashed line indicates the residual curve after subtraction of the peak shapes due to the Cu-O(eq), Cu···C(eq), O(eq)···O(eq), and Cu···N(eq) interactions. The dotted line is finally obtained by subtraction of the caluclated peaks due to the Cu-O(ax) and O(eq)···O(ax) interactions. (b) and (c); The theoretical peak shapes of each atom-pair.

appear at about 400 pm, and the corresponding peak is in fact observed in the residual differential radial distribution curve.

Subtraction of peaks for the Cu–O(eq), Cu···C(eq), O(eq)···O(eq), and Cu···N(eq) interactions in the equatorial plane gives the residual curve (dashed line in Fig. 3a), in which a peak and a shoulder remain at 240 and 320 pm, respectively. The peak at 240 pm is thus ascribable to the Cu–O(ax) bonds within the distorted octahedral copper(II) ion. When the hexasolvated copper(II) ion has such a distorted octahedral structure, the interligand O(eq)···O(ax) interactions should cause a peak at about 320 pm. Since the areas under the peak at 240 pm and the shoulder at 320 pm correspond to two Cu–O bonds and approximately eight O(eq)···O(ax) interactions, respectively, we concluded that the solvated copper(II) ion in DMF has a distorted octahedral structure with six DMF molecules. Subtraction of the peaks due to the Cu–O(ax) and O(eq)···O(ax) interactions led to a smooth background curve (dotted line) having no appreciable peak remaining over the range $r<400$ pm.

The structural parameters for the $[Cu(dmf)_6]^{2+}$ ion were refined by the least-squares method for the $s\cdot i(s)$ values over the range $s\geqslant 4\times10^{-2}$ pm^{-1} (Table 2). Structure parameters of atom-pairs within DMF molecules and perchlorate ions were quoted from the literature[5,9] and were fixed at the given values in the course of the calculation. The interatomic distances and temperature factors of interactions between copper(II) ion and atoms within DMF molecule were refined as independent variables as seen in the table (Column A). Lengths of interligand O(eq)···O(eq) and O(eq)···O(ax) interactions between DMF molecules coordinating to copper(II) ion were determined by the optimized Cu–O(eq) and Cu–O(ax) distances. Frequency factors of all interactions were kept constant during the calculation at the given values listed in the table which were evaluated on the basis of the distorted octahedral $[Cu(dmf)_6]^{2+}$ structure model. The Cu–O(eq) and Cu–O(ax) distances within the $[Cu(dmf)_6]^{2+}$ in DMF were finally determined to be 203 (3) and 243 (5) pm, respectively.

Table 2. Results of the Least-Squares Refinements of Solutions A to C. Standard Deviations Are Given in Parentheses

Interaction	Parameter	A	B	C
Cu–O(eq)	r/pm	203(3)	201(1)	201(1)
	b/10 pm^2	2(1)	1(1)	1(1)
	n	4[a]	4[a]	4[a]
Cu–O(ax)	r/pm	243(5)	246(4)	246(2)
	b/10 pm^2	3(1)	3(1)	4(1)
	n	2[a]	2[a]	2[a]
O(eq)···O(eq)	r[b]/pm	287	284	284
	b/10 pm^2	6[a]	6[a]	6[a]
	n	4[a]	4[a]	4[a]
O(eq)···O(ax)	r[c]/pm	317	318	317
	b/10 pm^2	12[a]	12[a]	12[a]
	n	8[a]	8[a]	8[a]
Cu···C(eq)	r/pm	289(5)	287(1)	287(1)
	b/10 pm^2	5(2)	5(1)	4(1)
	n	4[a]	4[a]	4[a]
Cu···O(eq) (NO_3^-)	r/pm	—	370(5)	367(2)
	b/10 pm^2	—	12(4)	14(5)
	n	—	2[a]	2[a]
Cu···N(eq)	r/pm	404(9)	402(3)	402(2)
	b/10 pm^2	11(10)	10(4)	9(3)
	n	4[a]	3[a]	3[a]

a) The values were kept constant during the calculation. b) $r_{O(eq)\cdots O(eq)}=\sqrt{2}\,r_{Cu-O(eq)}$. c) $r_{O(eq)\cdots O(ax)}=\sqrt{r_{Cu-O(eq)}^2+r_{Cu-O(ax)}^2}$.

Copper(II) Nitrate DMF Solutions. Since concentrations of copper(II) ions in solutions B and C are much higher than the concentration in solution A, the structure analysis for the copper(II) ion in solutions B and C may give more reliable results than those obtained in solution A. However, a possibility of formation of contact ion pairs between copper(II) and nitrate ions should be taken into consideration in such concentrated solutions.

The $(D(r)-4\pi r^2\rho_o)$ curve of solution B depicted in Fig. 4a was analyzed by the similar way to that employed for solution A. We first assumed that the copper(II) ion in solution B has the same structure as that in solution A. Subtraction of theoretical peaks originating from the intramolecular interactions of DMF molecules and nitrate ions gave the chain line in Fig. 4a. Further subtraction of peaks arising from the Cu–dmf(eq) interactions, i.e., the Cu–O(eq), Cu···C(eq), O(eq)···O(eq), and Cu···N(eq), led to the residual curve expressed by the dashed line. In the curve we see a distinct peak at 245 pm and very broad humps around 320 and 370 pm. The peak at 245 pm is easily attributable to the Cu–O(ax) bond. Therefore, the first hump around 320 pm may be ascribable to the O(eq)···O(ax) interaction as also found in solution A. The broad hump around 370 pm has not been observed in solution A and thus it might be the one characteristic of metal nitrate DMF solutions. Such a broad peak has been observed in the radial distribution curve of nickel(II) nitrate DMF solution,[16] but not in DMF solutions of the perchlorate.[17] Accordingly, the peak is expected to be due to interactions between copper(II) ion and atoms within nitrate ion.[18]

Nitrate ion can coordinate to copper(II) ion as

The Cu–O(eq) bond length within the $[Cu(dmf)_6]^{2+}$ complex in DMF is longer than that within the $[Cu(H_2O)_6]^{2+}$ in aqueous solution (194—197 pm)[5,14] and that within the $[CuCl_n(CH_3OH)_{6-n}]^{(2-n)+}$ (n=1—3) in methanolic solution (192.6—195.0 pm).[15] On the other hand, the Cu–O(ax) distance within the $[Cu(dmf)_6]^{2+}$ ion is practically the same as that within the $[Cu(H_2O)_6]^{2+}$.[5]

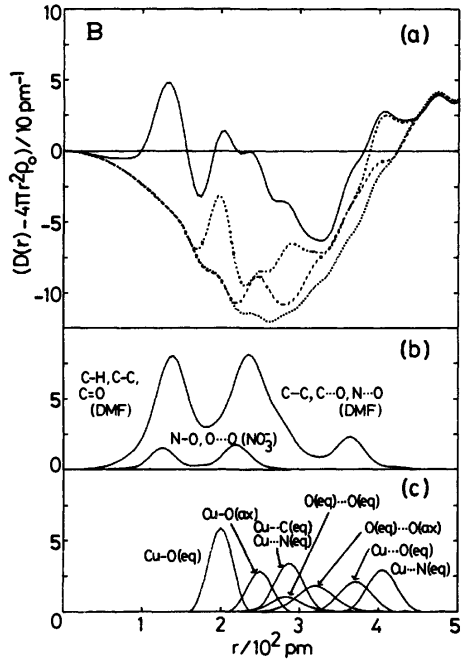

Fig. 4. (a); The $(D(r)-4\pi r^2\rho_o)$ curve for solution B. The chain line represents the residual curve after subtracting the theoretical peaks shown in (b). The dashed line indicates the residual curve after subtraction of the peak shapes due to the Cu-O(eq), Cu···C(eq), O(eq)···O(eq), and Cu···N(eq) interactions. The dotted line is finally obtained by subtraction of the calculated peaks due to the Cu-O(ax), O(eq)···O(ax), and Cu···O(eq) interactions. (b) and (c); The theoretical peak shapes of each atom pair.

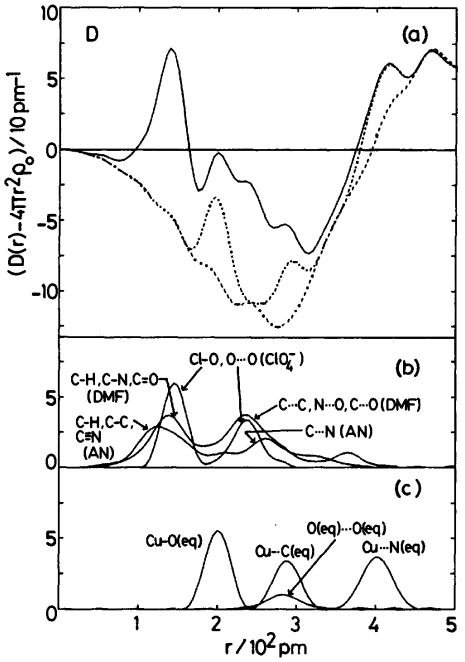

Fig. 5. (a); The $(D(r)-4\pi r^2\rho_o)$ curve for solution D. The chain line represents the residual curve after subtracting the theoretical peaks shown in (b). The dashed line indicates the residual curve after subtraction of the peak shapes due to the Cu-O(eq), Cu···C(eq), O(eq)···O(eq), and Cu···N(eq) interactions shown in (c). (b) and (c); The theoretical peak shapes of each atom pair.

either mono- or bidentate ligand. However, the broad peak at 370 pm observed could not be reproduced by a model that two oxygen atoms of a nitrate ion bind to copper(II) ion at the distance of 200 pm as a bidentate ligand. Therefore, it is suggested that a nitrate ion binds to copper(II) ion at the equatorial position to form $[CuNO_3(dmf)_5]^+$. In order to reproduce the peak at 370 pm, we examined various configurations of nitrate ion within the $[CuNO_3(dmf)_5]^+$ complex. The most plausible binding mode of a nitrate ion to the copper(II) ion is that a nitrate ion directs one oxygen atom toward the copper(II) ion with the Cu-O-N angle of ca. 120° in the equatorial plane of the copper(II) ion and the triangular plane of the nitrate ion is perpendicular to the square-plane within the complex. According to the model, the broad peak at 370 pm is due to two nonbonding $Cu\cdots O(NO_3^-)$ interactions. In fact, the area under the hump corresponds to two Cu···O interactions.

The $(D(r)-4\pi r^2\rho_o)$ curve for solution C was also well explained in terms of the formation of the $[CuNO_3(dmf)_5]^+$ complex having the distorted octahedral structure as has been seen in solution B.

The structure parameters for the $[CuNO_3(dmf)_5]^+$ in solutions B and C were optimized by least-squares calculations by using the data in the high-angle region of $s\cdot i(s)$ ($s \geqslant 4\times10^{-2}$ pm^{-1}) and the results are summarized in Table 2 (Columns B and C). Very similar results are obtained for both solutions. In the course of the calculation the $Cu\cdots N(NO_3^-)$ interaction was regarded as one of the four Cu···C(eq) interactions, since nitrogen atom is practically indistinguishable from carbon atom by the X-ray diffraction method and no significant error could be introduced by this simplification. Other assumptions adopted for the refinements are the same as those for solution A. The Cu-O(eq) and Cu-O(ax) bond lengths thus optimized are 201 (1) and 246 (4) pm, respectively.

Copper(II) Perchlorate DMF-AN Solutions. From the stability constants reported for copper(II)-dmf complexes in AN,[3] both $[Cu(dmf)_4]^{2+}$ and $[Cu(dmf)_6]^{2+}$ ions are expected to exist in solutions D and E.

The solid and chain lines in Fig. 5a represent the observed $(D(r)-4\pi r^2\rho_o)$ curve for solution D and the residual curve after subtraction of peaks due to the atom pairs within DMF, AN and perchlorate indicated in Fig. 5b from the original one, respectively. In

the residual curve three peaks appear around 200, 290, and 400 pm as seen in solutions A to C, which can be assigned to the Cu–O, Cu···C, and Cu···N interactions, respectively, in the equatorial plane, because the shape analysis of the peak at 200 pm gave the coordination number of four for the Cu–O bonds. On the other hand, no clear indication was obtained for the Cu–X(ax) bonds, where X denotes either oxygen atom within DMF or nitrogen atom within AN, over the region $r<300$ pm in contrast to the case of solutions A to C. Subtraction of peaks due to the Cu–O(eq), Cu···C(eq), O(eq)···O(eq), and Cu···N(eq) interactions led to the residual curve (dashed line in Fig. 5a), in which a small peak appearing at about 250 pm suggests that a part of copper(II) ions might have some interactions with the solvent molecules along the axis of copper(II) ion, but it is obvious that this peak is too small to conclude that all of copper(II) ions have the six-coordination structure as have been seen in solutions A to C.

The average scattering density ρ_o in a stoichiometric volume of solution D (1.993×10^{-4} pm^{-3}) is very close to the ρ_o value of solution B (1.934×10^{-4} pm^{-3}), and hence the background curves for both solutions should have the same feature. Therefore, the residual curve drawn by the dashed line in Fig. 5a, in which the Cu–X(ax) bonds were not taken into account, should overlap the one represented by the dotted line in Fig. 4a, which was obtained by taking the Cu–O(ax) bonds into consideration, in the region of $r<300$ pm. The two curves sufficiently fit each other and thus copper(II) ion in solution D is practically not solvated at the axial position within 300 pm.

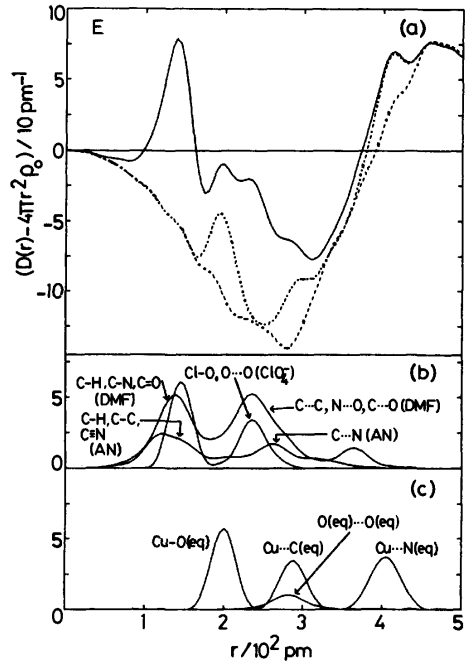

Fig. 6. (a); The $(D(r)-4\pi r^2\rho_o)$ curve for solution E. The chain line represents the residual curve after subtracting the theoretical peaks shown in (b). The dashed line indicates the residual curve after subtraction of the peak shapes due to the Cu–O(eq), Cu···C(eq), O(eq)···O(eq), and Cu···N(eq) interactions shown in (c). (b) and (c); The theoretical peak shapes of each atom pair.

Analysis of the $(D(r)-4\pi r^2\rho_o)$ curve shown in Fig. 6a for solution E, in which the concentration of DMF is higher than that in solution D, gave the similar result to that obtained for solution D. In the residual curve (dashed line) after subtraction of the peak shapes due to the intramolecular structure of DMF, AN and perchlorate and due to the Cu–O(eq), Cu···C(eq), O(eq)···O(eq), and Cu···N(eq) interactions, no distinct peak to be assignable to the Cu–X(ax) bonds was observed over the range $r<300$ pm. The X-ray scattering data for solution E colud be well reproduced by the same structural model as that for solution D and, therefore, we concluded that most of the solvated copper(II) ion in solutions D and E has the square-planar structure and solvent molecules do practically not coordinate to the copper(II) ion along the axis through the square-plane.

The structure parameters for the $[Cu(dmf)_4]^{2+}$ ion in DMF–AN mixtures were finally determined by least-squares calculations. The least-squares method was applied to the $s\cdot i(s)$ curve over the range $s\geqslant4\times10^{-2}$ pm^{-1} by using similar assumptions to those adopted for solutions A to C. The results obtained are listed in Table 3. The Cu–O(eq) distance is 200 (1) pm and practically the same as that within the $[Cu(dmf)_6]^{2+}$ ion in DMF.

In a previous calorimetric investigation of dilute solution of copper(II) ions in DMF–AN mixtures, formation of the $[Cu(dmf)_6]^{2+}$ complex is proposed in AN containing a large excess of DMF (ca. 1 mol dm^{-3}) compared with copper(II) ions.[3] In

Table 3. Results of the Least-Squares Refinements of Solutions D and E. Standard Deviations Are Given in Parentheses

Interaction	Parameter	D	E
Cu–O(eq)	r/pm	200(1)	199(1)
	b/10 pm^2	2(1)	1(1)
	n	4[a]	4[a]
O(eq)···O(eq)	r[b]/pm	282	282
	b/10 pm^2	6[a]	6[a]
	n	4[a]	4[a]
Cu···C(eq)	r/pm	285(2)	288(1)
	b/10 pm^2	5(2)	5(1)
	n	4[a]	4[a]
Cu···N(eq)	r/pm	399(3)	402(2)
	b/10 pm^2	15(5)	13(3)
	n	4[a]	4[a]

a) The values were kept constant during the calculation. b) $r_{O(eq)\cdots O(eq)}=\sqrt{2}\,r_{Cu-O(eq)}$.

DMF-AN mixtures of concentrated copper(II) perchlorate solutions which have relatively low C_{dmf}/C_{Cu} values of 5—7 examined in this study, the concentration of free DMF may not be sufficiently high to establish the equilibrium completely to the right-hand side

$$[Cu(dmf)_4]^{2+} + 2dmf \rightleftharpoons [Cu(dmf)_6]^{2+}$$

by forming the weak Cu-O(ax) bonds. Interactions between DMF and AN[19,20] may lower the activity of free DMF in the bulk of the mixture so as to prevent establishment of the equilibrium. Acetonitrile solvates copper(II) ion much more weakly than DMF does, and thus copper(II) ions in solutions D and E mainly exist as the square-planar $[Cu(dmf)_4]^{2+}$ species.

The work has been financially supported by the Grant-in-Aid for Special Project Research No. 61134043 from the Ministry of Education, Science and Calture. Computer calculations were carried out at the computer center of the Institute for Molecular Science in Okazaki.

References

1) S. Ishiguro, B. G. Jeliazkova, and H. Ohtaki, *Bull. Chem. Soc. Jpn.*, **58**, 1143 (1985).
2) S. Ishiguro, B. G. Jeliazkova, and H. Ohtaki, *Bull. Chem. Soc. Jpn.*, **58**, 1749 (1985).
3) S. Ishiguro, B. G. Jeliazkova, and H. Ohtaki, *J. Solution Chem.*, **16**, 1 (1987).
4) S. Ishiguro, B. G. Jeliazkova, and H. Ohtaki, *Bull. Chem. Soc. Jpn.*, **59**, 1073 (1986).
5) H. Ohtaki and M. Maeda, *Bull. Chem. Soc. Jpn.*, **47**, 2197 (1974).
6) H. Ohtaki, *Rev. Inorg. Chem.*, **4**, 103 (1982).
7) G. Johansson and M. Sandström, *Chem. Scr.*, **4**, 195 (1973).
8) T. Yamaguchi, Doctor Thesis, Tokyo Institute of Technology, 1978.
9) H. Ohtaki, S. Itoh, T. Yamaguchi, S. Ishiguro, and B. M. Rode, *Bull. Chem. Soc. Jpn.*, **56**, 3406 (1983).
10) A. Kratochwill, J. U. Weidner, and H. Zimmermann, *Ber. Bunsenges. Phys. Chem.*, **77**, 408 (1973).
11) H. Bertagnolli, P. Chieux, and M. D. Zeidler, *Mol. Phys.*, **32**, 759, 1731 (1976).
12) R. Caminiti, G. Licheri, G. Piccaluga, and G. Pinna, *J. Chem. Phys.*, **68**, 1967 (1978).
13) L. B. Brun and C.-I. Brändén, *Acta Crystallogr.*, **20**, 749 (1966).
14) M. Magini, *Inorg. Chem.*, **21**, 1535 (1982).
15) M. Ichihashi, H. Wakita, and I. Masuda, *Bull. Chem. Soc. Jpn.*, **56**, 3761 (1983).
16) K. Ozutsumi, S. Ishiguro, and H. Ohtaki, unpublished data.
17) K. Ozutsumi, T. Takamuku, S. Ishiguro, and H. Ohtaki, to be published.
18) An electronic spectrum for solution B shows a larger absorption maxima (ε=600 $dm^2 mol^{-1}$ at λ=797 nm) than that for solution A (ε=260 $dm^2 mol^{-1}$ at λ=790 nm), suggesting the coordination of nitrate ion to copper(II) ion.
19) I. Katime and L. C. Cesteros, *J. Chem. Soc., Faraday Trans. 2*, **80**, 1215 (1984).
20) A. K. Sharman, D. R. Sharman, and D. S. Gill, *J. Phys. D*, **18**, 1199 (1985).

Syntheses and Properties of 2,2′-Binaphtho[1,8-*de*]-1,3-dithiinylidene and Its Selenium Analog, 2-(1,3-Dithiol-2-ylidene)naphtho[1,8-*de*]-1,3-dithiin, and 2-(4*H*-Thiopyran-4-ylidene)naphtho[1,8-*de*]-1,3-dithiin

Koji Yui, Yoshio Aso, Tetsuo Otsubo, and Fumio Ogura*
Department of Applied Chemistry, Faculty of Engineering, Hiroshima University, Saijo, Higashi-Hiroshima 724
(Received October 3, 1987)

In order to discover new electron donors for conducting charge-transfer complexes, the four title compouds **1**—**4** composed of two heterocycles have been prepared via 1,8-dichalcogen-bridged naphthalene. The cyclic voltammetery indicates that symmetrical **1** and **2** are poor donors, but unsymmetrical **3** and **4** possess considerable donor abilities. The latter compounds are thus capable of forming some crystalline charge-transfer complexes with strong acceptors such as TCNQ, $TCNQF_4$, and DDQ, which are, however, semi-conducting.

The discovery of tetrathiafulvalene (TTF) and tetraselenafulvalene (TSF), forming highly conducting charge-transfer salts, has stirred considerable interest in searching novel electron donors which have similar behavior.[1] 2,2′-Binaphtho[1,8-*de*]-1,3-dithiinylidene (**1**) and its selenium analog (**2**) involve not only six-membered heterocyclic fragments fused with a naphtho ring, but also the same tetrachalcogenaethylene skeleton as do TTF and TSF. From another viewpoint, they may be regarded as an extended type with ethylene conjugation of 1,8-dichalcogen-bridged naphthalenes, which have been noticeable as a novel class of donor.[2] These unique structural features have prompted us to examine the syntheses and properties of hitherto unknown **1** and **2**. In addition to the symmetrical series, we have studied two unsymmetrical compounds **3** and **4**, into which a structural fragment of TTF or bithiopyranylidene[3] is introduced as the counter heterocycle. They are also

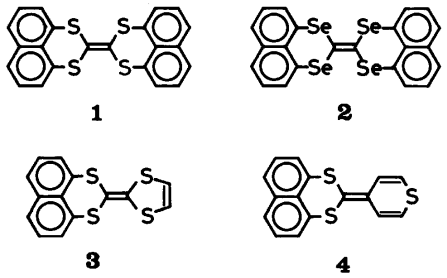

interesting, since unsymmetrical donors often make better conductors than symmetrical ones.[4]

Results and Discussion

Syntheses: The synthetic route of the target molecule **1** is shown in Scheme 1. Nakayama et al. already reported a key intermediate **9**, which was, however, formed as a minor product on photolysis of

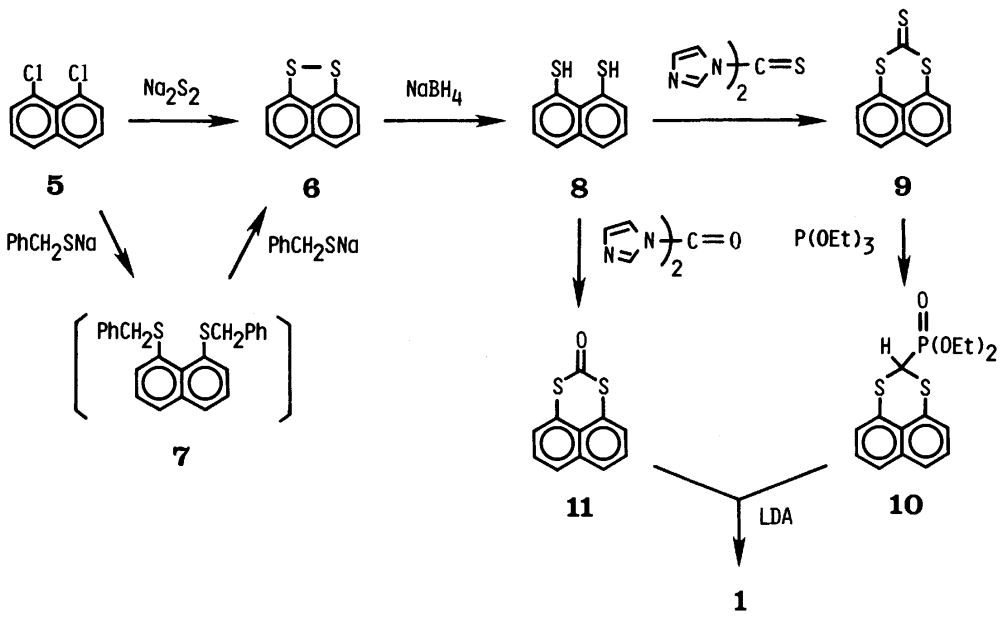

Scheme 1.

naphtho[1,8-*de*]-1,2,3-thiadiazine in carbon disulfide.[5] We have developed an alternative route to thione **9** via naphtho[1,8-*cd*]-1,2-dithiole (**6**), which is of choice on large-scale preparation. There have been known some methods in which the intermediate **6** may be formed, i.e., a direct thermal reaction of naphthalene and sulfur,[6] multistage reactions starting with diazotization of 8-aminonaphthalene-1-sulfonic acid,[7] and a reaction of 1,8-dilithionaphthalene with sulfur.[2] We have found that a nucleophilic substitution reaction of 1,8-dichloronaphthalene (**5**)[8] with sodium disulfide in hexamethylphosphoric triamide (HMPA) provide a convenient method of obtaining **6** (46% yield). However, it has later turned out that treatment of **5** with excess sodium α-toluenethiolate in HMPA gives a higher yield (78%) of **6** rather than 1,8-bis(benzylthio)naphthalene (**7**) as an expected product. This reaction is supposed to involve the initial substitution reactions to provide **7**, followed by reductive fission of the benzyl-S bond with excess sodium α-toluenethiolate and finally air-oxidation of the resulting 1,8-naththalenedithiolate forming S–S bond. Reduction of **6** with sodium borohydride in tetrahydrofuran-ethanol at RT gave almost quantitatively 1,8-naphthalenedithiol (**8**), which was subsequently treated with *N,N'*-thiocarbonyldiimidazole to afford **9** in 94% yield. Symmetrical TTF derivatives are generally prepared by desulfurizing coupling of two identical 1,3-dithiole-2-thiones using a phosphorus reagent.[9] However, all such conventional attempts to convert **9** into the target molecule **1** were unsuccessful. Treatment of **9** with triethyl phosphite at 110 °C gave diethyl [naphtho[1,8-*de*]-1,3-dithiin-2-yl]phosphonate (**10**) in 92% yield, though the other phosphorus reagents such as trimethyl phosphite and triphenylphosphine led to unidentified products. A plausible mechanism for the formation of **10** is shown in Scheme 2. However, **10** is available for another approach to **1** using a Wittig modification developed by Wadsworth and Emmons.[10] In this connection, naphtho[1,8-*de*]-1,3-dithiin-2-one (**11**) as a counterpart was prepared in 97% yield from a reaction of dithiol **8** and *N,N'*-carbonyldiimidazole. Thus, **10** was treated with lithium diisopropylamide at −78 °C to generate the corresponding phosphonate carbanion, which was then allowed to react with **11**, giving the desired product **1** in 92% yield.

The synthesis of the selenium analog **2** was carried out in a similar, but shorter route as shown in Scheme 3. Thus, a reaction of **5** with sodium diselenide in HMPA at 100 °C gave naphtho[1,8-*cd*]-1,2-diselenole (**12**) in 69% yield. The reduction of **12** with lithium aluminium hydride at RT in THF, followed by treatment with thiophosgene produced naphtho[1,8-*de*]-1,3-diselenin-2-thione (**13**) in 45% yield. In contrast to the above sulfur case, a reaction of **13** with trimethyl phosphite in toluene under reflux directly gave the desired product **2** in 66% yield.

The synthetic route of unsymmetrical compound **3**

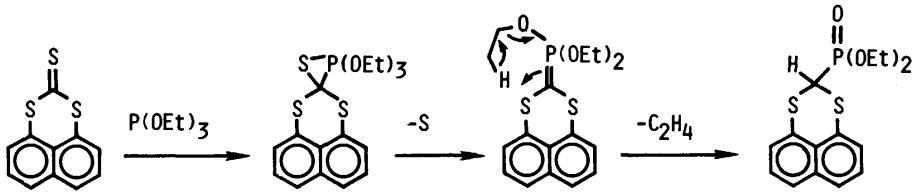

Scheme 2.

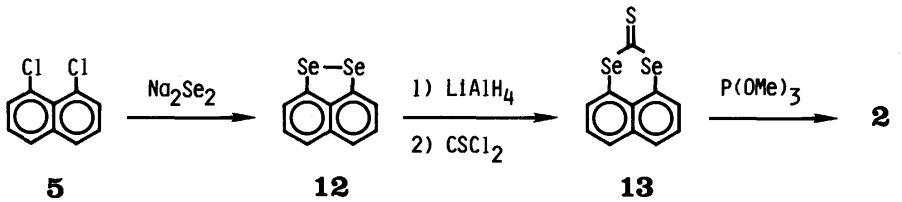

Scheme 3.

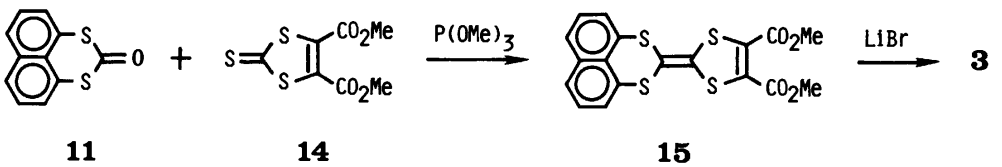

Scheme 4.

is shown in Scheme 4. A cross coupling reaction between **11** and dimethyl 2-thioxo-1,3-dithiole-4,5-dicarboxylate (**14**)[11] in benzene containing trimethyl phosphite at reflux smoothly proceeded to afford diester **15** in 45% yield. Hydrolysis/decarboxylation of **15** occurred on treatment with lithium bromide in HMPA at 150 °C, giving the desired compound **3** in 70% yield.

The synthetic route of another unsymmetrical compound **4** is shown in Scheme 5. The phosphonate carbanion from **10** was treated with 4*H*-thiopyran-4-one (**16**) to give tetrahydro derivative **17** in a quantitative yield. Direct conversion of **17** to **4** using chloranil or DDQ as a dehydrogenating agent failed. We then adopted a stepwise route via the conversion of sulfoxide to vinyl sulfide according to the procedure of Miller and Mckean.[12] Thus, sulfide **17** was oxidized with *m*-chloroperbenzoic acid in dichloromethane at RT to sulfoxide **18** in 63% yield, which was subsequently treated with *N,N′*-diisopropylethylamine and iodotrimethylsilane in dichloromethane at 0 °C to give dihydro derivative **19** in 86% yield. The same reactions were repeated for **19**, giving the desired product **4** in 43% overall yield.

In addition, three reference compounds **21**—**23** were prepared for spectroscopic comparison. Thus, **21** was accessible in 95% yield from a reaction between the phosphonate anion of **10** and acetone. Compounds **22** and **23** were obtained from treatment of diiodomethane with 1,8-naphthalenedithiolate in 26% yield and with the diselenolate in 32% yield, respectively.

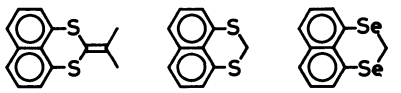

21 **22** **23**

Properties: Table 1 summarizes the UV data as well as oxidation potentials of **1**—**4** together with reference compounds **21**—**23**. All the compounds **1**—**4** have two strong absorptions around 240 and 350 nm in the electronic spectra. The longer wavelength absorptions extend to visible regions, resulting in yellow or orange coloration. These absorptions very closely resemble the corresponding ones of reference compounds **21**—**23** in wavelength except in intensity. This evidently indicates that the principal chromophor is 1,8-dichalcogenonaphthalene and an extended

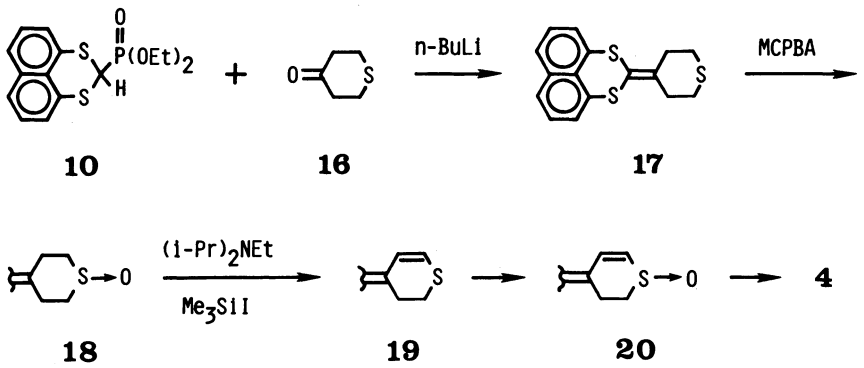

10 **16** **17**

18 **19** **20** **4**

Scheme 5.

Table 1. UV Data and Oxidation Potentials of **1**—**4** and Reference Compounds **22**—**24**

Compound	Absorption maximum/nm (Intensity/ε)[a]	Oxidation peak/V[b]
1	239(56600), 352(30700)	1.19(1.14)[c]
2	244(47500), 352(25800)	1.17
3	243(33100), 326(21400), 339sh(13800)	0.87(0.79)[c], 1.22
4	244(31500), 354(38800)	0.66(0.76)[c], 1.08
21	246(36300), 268sh(6100), 337sh(10500), 350(11600)	1.28
22	246(26400), 274(2190), 339sh(9890), 348(10800)	1.36
23	255(14200), 354(9250)	1.21

a) Measured in tetrahydrofuran. b) Measured at 100 mV s^{-1} scan rate in benzonitrile solution (10^{-3}—10^{-4} mol dm^{-3} with added tetrabutylammonium perchlorate (0.1 mol dm^{-3}) using a Ag/AgCl reference electrode and platinum working and counter electrodes. c) Values in parentheses indicate half-wave oxidation potentials.

Table 2. Charge-Transfer Complexes of **3** and **4**

Complex	Appearance	DP[a]/°C	Found (Calcd)[c]/%			Conductivity[d]/S cm^{-1}
			C	H	N	
3·DDQ	Dark brown powder from chloroform	220	49.10 (49.72	1.45 1.52	5.20 5.27)	2.3×10^{-7}
3·$TCNQF_4$	Dark green powder from chloroform	187—188[b]	53.78 (53.79	1.33 1.39	9.48 9.65)	4.4×10^{-3}
4·DDQ	Black powder from acetonitrile	130	54.35 (54.86	1.88 1.92	5.95 5.33)	6.5×10^{-5}
4·TCNQ	Black needles from acetonitrile	179—184[b]	66.87 (66.91	2.94 2.81	10.39 11.15)	6.8×10^{-8}
4·$TCNQF_4$	Deep green powder from acetonitrile	225	58.76 (58.53	1.68 1.75	9.67 9.75)	1.8×10^{-7}

a) Decomposition temperature. b) With melt. c) Calculated as 1:1 stoichiometry of donor and acceptor. d) Measured on compressed pellets with a two-probe method at room temperature.

conjugation through the central olefin between the two chromophors is not significant. A structural consideration of **1** and **2** on a molecular model favors nonplanar conformers which are somewhat bent at the sulfur or selenium atoms. This nonplanarity is certainly responsible for reduction in extended conjugation.

The cyclic voltammetry of **21—23** demonstrates irreversible oxidation at 1.21—1.36 V vs. Ag/AgCl reference electrode in benzonitrile. On the other hand, **1** undergoes oxidation at a somewhat lower potential (1.19 V) and keeps a reversible redox cycle with a half-wave potential at 1.14 V, which is, however, still too high as an electron donor. The somewhat easier oxidation of **1** and the higher stability of the resulting radical cation, contrary to the above spectroscopic discussion, suggest the existence of some conjugation through the central olefin. The selenium analog **2** unlike **1** shows an irreversible oxidation, whose peak potential (1.17 V) is the almost same as that of **1** or a reference compound **23**. Thus, the substitution of selenium for sulfur in **1** does not serve to enhance its donor character, but rather leads to ready decomposition of the radical cation owing to introduction of labile C–Se bond relative to C–S bond. On the other hand, unsymmetrical compounds **3** and **4** have two oxidation steps, the first of which is reversible and the second is irreversible. The first oxidation potentials (0.87 V for **3** and 0.66 V for **4**) are drastically lower than those of **1** and **2**. Since the counter heterocyclic fragments can take aromatization in the oxidation state, i.e., 1,3-dithiolylium and thiopyranylium cations, they certainly make a significant contribution to the ready oxidations.

Owing to their poor donor strength, **1** and **2** could not form any charge-transfer complexes even with strong electron acceptors such as 7,7,8,8-tetracyanoquinodimethane (TCNQ), 2,3,5,6-tetrafluoro-7,7,8,8-tetracyanoquinodimethane ($TCNQF_4$), and 2,3-dichloro-5,6-dicyano-*p*-benzoquinone (DDQ). On the other hand, **3** and **4** bearing improved donor abilities formed deeply colored 1:1 charge-transfer complexes with such acceptors. As summarized in Table 2, the electrical conductivities measured on compressed pellets with a two probe method are 10^{-3}—10^{-8} S·cm^{-1}. This semi-conducting behavior suggests a mixed stacking mode of alternate donor and acceptor in the crystal structures.[13]

Experimental

General. Melting points are uncorrected. All solvents are of reagent grades. NMR measurements were made on a JEOL PMX-60 (60 MHz) or a Bruker-WM 360 spectrometer (360 MHz) using TMS as an internal standard. IR spectra were taken on a Hitachi 260-30 spectrophotometer, and MS spectra on a JEOL JMS-DX 300 spectrometer at 70 eV using a direct insertion technique. Electronic spectra were recorded on a JASCO UVIDEC-610A spectrophotometer. Cyclic voltammetry was performed on a Hokuto Denko HA-301 potentiostat and a Hokuto Denko HB-104 function generator.

Naphtho[1,8-*cd*]-1,2-dithiol (6). A) With Sodium α-Toluenethiolate. Into a stirred solution of sodium α-toluenethiolate, which was in situ prepared from α-toluenethiol (42.3 cm^3, 0.36 mol) and sodium hydride (60% oily, 15.8 g, 0.40 mol) in HMPA (400 cm^3), was added a solution of 1,8-dichloronaphthalene (**5**)[7] (11.8 g, 60 mmol) in HMPA (50 cm^3) under argon. The mixture was heated at 160—165 °C for 17 h and cooled to RT. After water (500 cm^3) was added, it was vigorously stirred with bubbling air for 20 h, poured into water, and extracted with benzene. The extract was thoroughly washed with water, dried ($MgSO_4$), and concentrated in vacuo. The resulting solid was purified by column chromatography on silica gel with hexane and then recrystallization from hexane to give **6** as

reddish brown plates (8.95 g, 78%): 123 °C (lit,[6] 116 °C); ^{1}H NMR (60 MHz, CCl_4) δ=7.1—7.7 (ABC m).

B) With Sodium Disulfide. A mixture of sulfur (48 mg, 1.5 mmol) and sodium (38 mg, 1.65 mmol) was heated at 110 °C in dry HMPA (3 cm^3) for 2.5 h under argon. Into the resulting blue solution of sodium disulfide was added a solution of **5** (99 mg, 0.5 mmol) in dry HMPA (2 cm^3). The mixture was heated at 150 °C for 27 h, poured into water, and extracted with benzene. In the same way as described in Method A, compound **6** was obtained from the extract (44 mg, 46%).

1,8-Naphthalenedithiol (8). A solution of **6** (9.51 g, 500 mmol) in dry THF (100 cm^3) was added into an ice-cooled suspension of sodium borohydride (5.00 g, 132 mmol) in ethanol (90 cm^3) under argon. The mixture was stirred for 30 min, quenched with 10% HCl, and extracted with chloroform. The extract was washed with water, dried ($MgSO_4$), and concentrated in vacuo to give **8** (9.45 g, 98%). Recrystallization from THF-hexane in an argon atmosphere afforded colorless leaflets: mp 122 °C (lit,[5b] 115 °C); IR(KBr) 2450, 2520 cm^{-1} (S-H); ^{1}H NMR (60 MHz, CCl_4) δ=3.97 (s, 2H), 6.95—7.65 (ABC m, 6H).

Naphtho[1,8-*de*]-1,3-dithiin-2-thione (9). A solution of *N,N′*-thiocarbonyldiimidazole (1.39 g, 7.04 mmol) in dry THF (30 cm^3) was slowly added into a stirred solution of **8** (1.22 g, 6.40 mmol) in dry THF (30 cm^3) at −15—−20 °C under argon. The mixture was gradually warmed to RT and allowed to stand overnight. After concentration in vacuo, the resulting solid was dissolved in chloroform, washed with water, and dried ($MgSO_4$). The solvent was evaporated, and column chromatography of the residue on silica gel with benzene gave **9** (1.40 g, 94%): orange needles from benzene-hexane, mp 201—202 °C (lit,[4] 199—201 °C); IR(KBr) 1040 cm^{-1} (C=S); ^{1}H NMR (60 MHz, $CDCl_3$) δ=7.1—7.7 (ABC m).

Diethyl [Naphtho[1,8-*de*]-1,3-dithiin-2-yl]phosphonate (10). Thione **9** (113 mg, 0.482 mmol) was heated at 110 °C in triethyl phosphite (6 cm^3) for 2 h under argon. After concentration in vacuo, the residue was filtered through a short column of silica gel with chloroform and then recrystallized from benzene-hexane to give **10** as colorless columns (150 mg, 92%): mp 120 °C; IR (KBr) 1243 (P=O), 1030, 1010, 970, 950 cm^{-1} (P-O-C); ^{1}H NMR (60 MHz, CCl_4) δ=1.20 (t, J_{CH-CH}=7.4 Hz, 6H), 4.02 (d, J_{CH-P}=17 Hz, 1H), 7.2—7.7 (m, 6H); Anal. ($C_{15}H_{17}O_3S_2P$) C, H.

Naphtho[1,8-*de*]-1,3-dithiin-2-one (11). A solution of *N,N′*-carbonyldiimidazole (357 mg, 2.2 mmol) in dry THF (15 cm^3) was slowly added into a stirred solution of **8** (385 mg, 2.0 mmol) in dry THF (30 cm^3) at −15 °C under argon. The mixture was warmed to RT and allowed to stand for several hours. After concentration in vacuo, the resulting solid was filtered through a short column of silica gel with hexane-benzene (1:1) and recrystallized from benzene-hexane to give **11** as colorless needles (391 mg, 97%): mp 140 °C; IR (KBr) 1630 cm^1 (C=O); ^{1}H NMR (60 MHz, CCl_4) δ=7.1—7.7 (ABC m); Anal. ($C_{11}H_6OS_2$) C, H.

2,2′-Binaphtho[1,8-*de*]-1,3-dithiinylidene (1). A solution of LDA (1 mol m^{-3}, 1.05 cm^3) in THF-hexane (1:2.7) was dropwise added into a stirred solution of **10** (340 mg, 1.0 mmol) in dry THF (10 cm^3) at −78 °C during 10 min under argon. A solution of **11** (240 mg, 1.1 mmol) in dry THF (6 cm^3) was successively added, and then the mixture was gradually warmed to 0 °C. The resulting precipitate was collected by filtration, washed with water, and dried. Recrystallization from carbon disulfide gave pale yellow fine prisms of **1** (372 mg, 92%): mp 297 °C; ^{1}H NMR (360 MHz, CS_2) δ=7.22—7.28 (m, 8H), 7.486 (dd, J=7.37 and 1.92 Hz, 4H); MS *m/z* 404 (M$^+$); Anal. ($C_{22}H_{12}S_4$) C, H.

Naphtho[1,8-*cd*]-1,2-diselenole (12). A mixture of selenium powder (4.03 g, 51 mmol) and sodium (1.17 g, 51 mmol) was heated at 120 °C in dry HMPA (35 cm^3) for 4 h under argon. Into the resulting reddish brown solution of sodium diselenide was added a solution of **5** (2.95 g, 15 mmol) in dry HMPA (15 cm^3). The mixture was heated at the same temperature for additional 19 h, poured into water (450 cm^3), and extracted with benzene. The extract was thoroughly washed with water, dried ($MgSO_4$), and concentrated in vacuo. The residual solid was purified by column chromatography on silica gel with benzene and then gel-permeation liquid chromatography with chloroform to give **12** (2.95 g, 69%): deep violet needles from hexane, mp 124 °C (lit,[2] 127—129 °C); ^{1}H NMR (60 MHz, CCl_4) δ=7.1—7.7 (ABC m).

Naphtho[1,8-*de*]-1,3-diselenin-2-thione (13). Compound **12** (142 mg, 0.50 mmol) was treated with LAH (10.4 mg, 0.275 mmol) in dry THF (7 cm^3) for 40 min at RT. Into the mixture at −30—−40 °C was slowly added a solution of thiophosgene (46 mm^3, 0.60 mmol) in dry THF (7 cm^3). The mixture was gradually warmed to RT and stirred further 1.5 h. After concentration, the residue was poured into aq. satd. ammonium chloride and extracted with chloroform. The extract was washed with water, dried ($MgSO_4$), and evaporated. The resulting solid was purified by column chromatography on silica gel with hexane and then gel-permeation liquid chromatography to give **13** (74 mg, 45%): orange needles from hexane, mp 153—154 °C; IR (KBr) 1021 cm^{-1} (C=S); ^{1}H NMR (60 MHz, $CDCl_3$) δ=7.2—7.9 (ABC m); Anal. ($C_{11}H_6SSe_2$) C, H.

2,2′-Binaphtho[1,8-*de*]-1,3-diseleninylidene (2). A mixture of **13** (73 mg, 0.22 mmol), trimethyl phosphite (0.10 cm^3, 0.88 mmol), and toluene (3 cm^3) was heated at reflux for 4 h. The resulting precipitate was collected by filtration, washed with cold acetone, and recrystallized from toluene to give pale yellow fine crystals of **2** (43 mg, 66%): mp 287—287.5 °C; ^{1}H NMR (360 MHz, CS_2) δ=7.286 (t, J=7.7 Hz, 4H), 7.476 (bd, J=7.3 Hz, 4H), 7.610 (bd, J=8.1 Hz, 4H); MS *m/z* 594 (M$^+$); Anal. ($C_{22}H_{12}Se_4$) C, H.

2-[4,5-Bis(methoxycarbonyl)-1,3-dithiol-2-ylidene]naphtho[1,8-*de*]-1,3-dithiin (15). A mixture of **11** (1.53 g, 7 mmol) and dimethyl 2-thioxo-1,3-dithiol-4,5-dicarboxylate (**14**)[10] (3.50 g, 14 mmol) was refluxed in dry benzene (50 cm^3) containing trimethyl phosphite (21 cm^3) for 1.5 h under argon. After concentration in vacuo, the residue was chromatographed on silica gel with benzene to give **15** (1.31 g, 45%): orange fine needles from hexane-benzene, mp 217—218 °C; IR (KBr) 1730, 1710 cm^{-1} (C=O); ^{1}H NMR (60 MHz, $CDCl_3$) δ=3.80 (s, 6H), 7.2—7.8 (m, 6H); Anal. ($C_{18}H_{12}O_4S_4$) C, H.

2-(1,3-Dithiol-2-ylidene)naphtho[1,8-*de*]-1,3-dithiin (3). A solution of diester **15** (1.31 g, 3.12 mmol) and lithium bromide monohydrate (3.27 g, 31.2 mmol) in HMPA (50 cm^3) was heated at 100 °C for one h and then at 150 °C for another h. The mixture was cooled to RT, poured into

water, and extracted with benzene. The extract was washed with water, dried ($MgSO_4$), and concentrated in vacuo. The residue was chromatographed on silica gel with hexane–benzene (1:1) to give **3** (0.66 g, 70%): lemon yellow prisms from benzene–hexane, mp 173.5—175 °C; ^{1}H NMR (60 MHz, $CDCl_3$) δ=6.33 (s, 2H), 7.2—7.8 (m, 6H); MS *m/z* 304 (M^+); Anal. ($C_{14}H_8S_4$) C, H.

2-(Tetrahydro-4*H*-thiopyran-4-ylidene)naphtho[1,8-*de*]-1,3-dithiin (17). A hexane solution of butyllithium (1.6 mol dm^{-3}, 9.4 cm^3, 15 mmol) was dropwise added into a stirred solution of **10** (5.11 g, 15 mmol) in dry THF (200 cm^3) at −78 °C under argon. A solution of 4*H*-thiopyran-4-one (**16**) (1.92 g, 16.5 mmol) in dry THF (30 cm^3) was subsequently added. The mixture was warmed to RT over a period of 3 h. After the solvent was evaporated, the residue was dissolved in chloroform, washed with brine, and dried ($MgSO_4$). After concentration, the residue was chromatographed on silica gel with benzene to give **17** (4.49 g, 99%): colorless plates from hexane, mp 142—143 °C; ^{1}H NMR (60 MHz, CCl_4) δ=2.85 (A_2B_2 m, 8H), 7.1—7.6 (ABC m, 6H); Anal. ($C_{16}H_{14}S_3$) C, H.

4-[Naphtho[1,8-*de*]-1,3-dithiin-2-ylidene]tetrahydro-4*H*-thiopyran *S*-Oxide (18). A solution of MCPBA (4.0 g, 23.2 mmol) in dichloromethane (20 cm^3) was dropwise added into a solution of **17** (4.54 g, 15 mmol) in dichloromethane (100 cm^3) at −15—−20 °C. The mixture was stirred at 0 °C for 2 h and then at RT for 30 min. It was successively washed with aq. satd. $NaHSO_3$, aq. 5% $NaHCO_3$, and water. The solution was dried ($MgSO_4$) and concentrated in vacuo. The residue was chromatographed on silica gel with chloroform to give **18** (3.0 g, 63%): colorless leaflets from benzene–hexane, mp 203—206 °C; ^{1}H NMR (60 MHz, $CDCl_3$) δ=2.95 (A_2B_2 m, 8H), 7.2—7.8 (ABC m, 6H); Anal. ($C_{16}H_{14}OS_3$) C, H.

2-(2,3-Dihydro-4*H*-thiopyran-4-ylidene)naphtho[1,8-*de*]-1,3-dithiin (19). Iodotrimethylsilane (3.58 cm^3, 25.2 mmol) was dropwise added into a stirred solution of **18** (4.0 g, 12.6 mmol) and *N*,*N*-diisopropylethylamine (4.81 cm^3, 27.6 mmol) in dry dichloromethane (100 cm^3) at 0 °C under argon. The mixture was stirred at 0 °C for 4 h and then at RT for 2 h, diluted with ether (100 cm^3), and poured into 10% sulfuric acid. The organic layer was separated, succesively washed with aq. 5% $NaHCO_3$ and with water, and dried ($MgSO_4$). After concentration in vacuo, the residual solid was chromatographed on silica gel with chloroform to give **19** (3.25 g, 86%): pale yellow leaflets from benzene–hexane, mp 117—118 °C; ^{1}H NMR (60 MHz, $CDCl_3$) δ=2.97 (A_2B_2 m, 4H), 6.35 (d, J=10 Hz, 1H), 6.99 (d, J=10 Hz, 1H), 7.1—7.8 (ABC m, 6H); Anal. ($C_{16}H_{12}S_3$) C, H.

4-[Naphtho[1,8-*de*]-1,3-dithiin-2-ylidene]-2,3-dihydro-4*H*-thiopyran *S*-Oxide (20). Compound **20** was obtained in 63% yield by oxidation of **19** with MCPBA in a similar manner as described for the synthesis of **18**: pale yellow crystals from acetone–dichloromethane, mp 158—160 °C; ^{1}H NMR (60 MHz, $CDCl_3$) δ=3.0 (A_2B_2 m, 4H), 6.42 (d, J=10 Hz, 1H), 7.0—7.8 (m, 7H); Anal. ($C_{16}H_{12}OS_3$) C, H.

2-(4*H*-Thiopyran-4-ylidene)naphtho[1,8-*de*]-1,3-dithiin (4). Compound **4** was obtained in 68% yield from **20** by the same method as described for the conversion of **18** into **19**: orange needles from benzene–hexane, mp 155—157 °C; ^{1}H NMR (60 MHz, $CDCl_3$) δ=6.37 (d, J=10 Hz, 2H), 7.0—7.8 (m, 8H); Anal. ($C_{16}H_{10}S_3$) C, H.

2-Isopropylidenenaphtho[1,8-*de*]-1,3-dithiin (21). Into a solution of **10** (42 mg, 0.12 mmol) in dry THF (2 cm^3) at −78 °C under argon were dropwise added a solution of LDA (1 mol m^{-3}, 0.13 cm^3) in THF–hexane (1:2.7) and subsequently a solution of acetone (9:6 mm^3, 0.13 mmol) in dry THF (0.5 cm^3). The mixture was gradually warmed to RT, poured into aq. satd. ammonium chloride, and extracted with chloroform. The extract was washed with water, dried ($MgSO_4$), and concentrated in vacuo. The residue was chromatographed on silica gel with hexane to give **21** (28 mg, 95%): colorless prisms from hexane, mp 106 °C; ^{1}H NMR (60 MHz, CCl_4) δ=2.06 (s, 6H), 7.1—7.6 (ABC m, 6H); Anal. ($C_{14}H_{12}S_2$) C, H.

Naphtho[1,8-*de*]-1,3-dithiin (22). A solution of **8** (1.05 g, 5.26 mmol) and diiodomethane (1.41 g, 5.26 mmol) in dry THF (300 cm^3) was dropwise added into a stirred suspension of sodium hydride (60% oily, 505 mg, 12.6 mmol) in dry THF (100 cm^3) at RT under argon. The addition took 40 h. After the addition, stirring was continued further 6 h. The reaction mixture was concentrated in vacuo, poured into water, and extracted with chloroform. The extract was washed with water, dried ($MgSO_4$), and concentrated. The residue was chromatographed on silica gel with hexane–benzene to give colorless plates of **22** (280 mg, 26%): mp 124—125 °C; ^{1}H NMR (60 MHz, CCl_4) δ=4.01 (s, 2H), 6.95—7.70 (ABC m, 6H); Anal. ($C_{11}H_8S_2$) C, H.

Naphtho[1,8-*de*]-1,3-diselenin (23). A solution of **12** (568 mg, 2.0 mmol) in dry THF (25 cm^3) was slowly added into a stirred suspension of sodium borohydride (267 mg, 7.06 mmol) in ethanol (8 cm^3) at RT under argon. It was then transferred into a dropping funnel. A solution of diiodomethane (836 mg, 3.2 mmol) in dry THF (25 cm^3) was placed in another dropping funnel. Both solutions were simultaneously added into a stirred THF solution (10 cm^3) at RT over a period of 3 h. The mixture was concentrated, dissolved in chloroform, and washed with water. After it was dried ($MgSO_4$) and again concentrated, the residue was purified by column chromatography on silica gel with hexane–chloroform (1:1) and then gel-permeation liquid chromatography with chloroform to give **23** (190 mg, 32%): pale orange leaflets from hexane, mp 128.5 °C; ^{1}H NMR (60 MHz, CCl_4) δ=3.91 (s and t, J_{Se-C-H}=7 Hz, 2H), 7.0—7.7 (ABC m, 6H); Anal. ($C_{11}H_8Se_2$) C, H.

Preparation of Charge-Transfer Complexes. All CT complexes described in this paper were prepared by mixing the two hot saturated solutions of donor and acceptor in chloroform or acetonitrile. The deeply colored complexes precipitated out immediately or on cooling in a refrigerator, which were collected by filtration.

This work was partially supported by a Grant-in-Aid of Scientific Research No. 62550635 from the Ministry of Education, Science and Culture, Japan and Mazda Foundation's Research Grant.

References

1) For recent reviews on organic metals, see F. Wudl, *Acc. Chem. Res.*, **17**, 227 (1984); M. R. Bryce and L. C. Murphy, *Nature (London)*, **309**, 119 (1984); J. M. Williams, M. A. Beno, H. H. Wang, P. C. W. Leung, T. J. Emge, U. Geiser, and K. D. Carlson, *Acc. Chem. Res.*, **18**, 261 (1985).

2) J. Meinwald, D. Dauplaise, F. Wudl, and J. J. Hauser, *J. Am. Chem. Soc.*, **99**, 255 (1977); J. Meinwald, D. Dauplaise, and J. Clardy, *ibid.*, **99**, 7743 (1977); D. Dauplaise, J. Meinwald, J. C. Scott, H. Temkin, and J. Clardy, *Ann. N. Y. Acad. Sci.*, **313**, 382 (1978).

3) S. Hünig, B. J. Garner, G. Ruider, and W. Schenk, *Justus Liebigs Ann. Chem.*, **1973**, 1036.

4) J. M. Fabre, L. Giral, E. Dupart, C. Coulon, and P. Delhaes, *J. Chem. Soc., Chem. Commun.*, **1983**, 426; J. M. Fabre, L. Giral, E. Dupart, C. Coulon, J. P. Manceau, and P. Delhaes, *ibid.*, **1983**, 1477; H. Tatemitsu, E. Nishikawa, Y. Sakata, and S. Misumi, *ibid.*, **1985**, 106.

5) J. Nakayama, T. Fukushima, E. Seki, and M. Hoshino, *J. Am. Chem. Soc.*, **101**, 7684 (1979); J. Nakayama, S. Dan, and M. Hoshino, *J. Chem. Soc., Perkin Trans. 1*, **1981**, 413.

6) M. Lanfrey, *C. R. Acad. Sci.*, **152**, 92 (1911); H. S. Desai and B. D. Tilak, *J. Sci. Ind. Res. (India)*, **19**, 390 (1960).

7) W. B. Price and S. Smiles, *J. Chem. Soc.*, **1928**, 2372; A. Zweig and A. K. Hoffmann, *J. Org. Chem.*, **30**, 3997 (1965).

8) G. C. Hampson and A. Weissberger, *J. Chem. Soc.*, **1936**, 393.

9) M. Narita and C. U. Pittman, Jr., *Synthesis*, **1976**, 489; M. R. Bryce, *Aldrichimica Acta*, **18**, 73 (1985); A. Krief, *Tetrahedron*, **42**, 1209 (1986).

10) W. S. Wadsworth, Jr., *Org. React.*, **25**, 77 (1977).

11) L. R. Melby, H. D. Hartzler, and W. A. Sheppard, *J. Org. Chem.*, **39**, 2456 (1974).

12) R. D. Miller and D. R. Mckean, *Tetrahedron Lett.*, **24**, 2619 (1983).

13) A. F. Garito and A. J. Heeger, *Acc. Chem. Res.*, **7**, 232 (1974).

Liquid-Phase Dehydrogenation of 2-Propanol by Suspended Nickel Fine-Particle Catalyst

Michio NODA, Sumio SHINODA,† and Yasukazu SAITO*
Institute of Industrial Science, University of Tokyo, 22-1 Roppongi 7 Chome, Minato-ku, Tokyo 106
(Received June 26, 1987)

Nickel fine particles that were prepared by a gas evaporation method were used to catalyze the liquid-phase dehydrogenation of 2-propanol efficiently in the suspended state. Rate retardation due to the product acetone without catalytic-site deactivation was confirmed kinetically. High reaction rates were attained under the boiling conditions and a reasonable activation energy as well as adsorption heat of acetone was obtained. A useful application of the present catalytic process is proposed.

Dehydrogenation of 2-propanol in gas phase

$$(CH_3)_2CHOH \longrightarrow (CH_3)_2CO + H_2 \quad (1)$$

is unfavored thermodynamically below 202 °C, at which $\Delta G°$(gas) becomes zero.[1] Reactions over zinc oxide or other heterogeneous catalysts that yielded acetone and hydrogen required a rather high temperature (e.g., 350 °C for ZnO).[2]

When homogeneous[3–7] or heterogeneous[8–14] catalysts were used in the liquid phase, however, Reaction 1 proceeded at a moderate temperature (e.g., 82.4 °C for Raney Ni),[8,10] since hydrogen dissolved slightly in the solvent[15] and was easily separated as a gaseous substance.

Among solid catalysts active in the suspended state, nickel fine particles prepared by a gas evaporation method[16,17] have attracted our attention[14] on account of the following characteristics:[18,19]

1) Highly-crystallized spherical particles.
2) Sharp particle-size distribution.
3) Large specific surface area without pores.
4) High chemical purity except for surface oxide.
5) Stability of the suspended state in some polar solvents.

In the present study, the dehydrogenation of 2-propanol with a suspended nickel fine-particle catalyst was investigated from a kinetical viewpoint in order to explore useful applications.

Experimental

Catalyst. Fine particles of nickel were obtained as a soot-like product by evaporating molten nickel metal (99.99% pure) in an argon atmosphere.[16] They were slowly oxidized with nitrogen-diluted air to form thin surface oxide layers. These layers prevent the particles from deep oxidation at room temperature in air. According to electron micrographic measurements, nonporous highly-crystallized spherical particles with a sharp size distribution (average diameter: 19.7 nm) were prepared.[16] The surface-oxidized particles (oxygen content: 10 wt%) gave a BET specific surface area of 43.8 $m^2 g^{-1}$.[20]

Apparatus. Prior to the reaction, a heating treatment under a hydrogen atmosphere was required in order to disclose active sites by reducing the surface oxide.[21] A closed system consisting of a round-bottom three-neck flask (300 ml) and a gas buret (500 ml) was adopted for measuring hydrogen consumption. A flask containing the reduced catalyst and the reactant 2-propanol inside was connected to another set of gas burets (500 ml and 1 l) through a water-cooled condenser. In this closed system the gaseous product was pursued volumetrically.

An open-ended system was used for a long-period run, in which a round-bottom three-neck flask was connected to a gas-flow meter (STEC Inc., SEF series) and a gas sampler (Gasukuro Kogyo Inc., GS-5000 A). A data processor (Eto Denki Co., Thermodac 32) recorded time-sequentially such reaction data as the flow rate of the gaseous product and the temperature, either inside or outside the flask. The gaseous components were monitored by a gas chromatograph (Shimadzu Co., GC-8APT) with a peak integrator (Shimadzu Co., CR-2A) assisted.

Procedure. A prescribed amount (200 mg) of the nickel fine particles in the flask was heated under hydrogen up to 160 °C in 15 min, held at 160 °C for 1 min and rapidly cooled.[22]

After reduction and evacuation of the nickel fine particles, the flask was filled with the degassed 2-propanol reactant (200 ml) under an argon or nitrogen atmosphere and treated for dispersion with an ultrasonic vibration cleaner (Sharp Co., UTB-152) at room temperature for 1 min.

The reaction proceeded by heating the suspension under boiling conditions. The rate of hydrogen evolution was determined from the volumetric accumulation of hydrogen in the closed apparatus or pursued with a flow meter in the open-ended system. The temperature dependence of the reaction rate was examined by the addition of hexane to 2-propanol in order to decrease the boiling point.[11]

Products were analyzed by gas chromatography using active carbon (gas phase) and PEG 1000 (liquid phase) columns.

Results and Discussion

1. Dispersion Stability of the Nickel Fine Particles in 2-Propanol. The nickel fine particles were easily suspended in 2-propanol through an ultrasonic treatment. The suspension was sufficiently stable.

As shown in Fig. 1a, sedimentation of the nickel

† Present address: Department of Industrial Chemistry, Faculty of Engineering, Seikei University, 3-1 Kichijyoji-Kitamachi 3 Chome, Musashino-Shi, Tokyo 180.

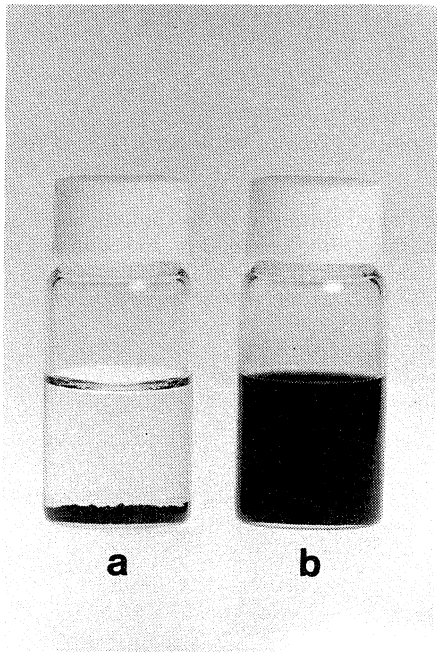

Fig. 1. Effect of the ultrasonic treatment on dispersion of nickel fine particles in 2-propanol.
(a) Effect of vigorous hand-shaking on the nickel fine particles (5 mg) in 2-propanol (5 ml). (b) Effect of the ultrasonic treatment on the same materials.

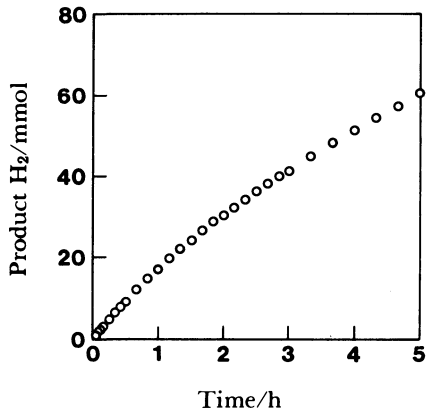

Fig. 2. Time course of H_2 evolution by liquid-phase dehydrogenation of 2-propanol with the nickel fine-particle catalyst under boiling conditions.
Nickel fine-particle catalyst (200 mg) suspended in 2-propanol (200 ml).

fine particles took place rapidly, when both materials (nickel 5 mg/2-propanol 5 ml) were hand-shaked vigorously. On the other hand, an ultrasonic treatment at a room temperature for 1 min resulted in a well-dispersed state (Fig. 1b). Without stirring, partial sedimentation was observed after 24 h. Continuous stirring with a conventional magnetic stirrer (1500 rpm) was sufficient for retaining the suspended state for a long period. The adopted stirring conditions were ascertained to sufficiently agitate the suspension, since the total time courses of hydrogen evolution were well-reproduced at different stirring rates.[23]

The ultrasonic treatment gave a stable suspension that could be maintained for 24 h or more by using the following solvents: dimethyl sulfoxide, *N*,*N*-dimethylformamide, bis(2-methoxyethyl) ether, methanol and cyclohexanol. On the contrary, sedimentation started within 1 h in suspensions of hexane, cyclohexane, toluene, ethylbenzene, triethylamine, diethyl ether, ethyl acetate, chloroform, carbon tetrachloride, nitromethane, tetrahydrofuran, acetone, and ethanol. Ethylene glycol, acetonitrile, 2-butanone, cyclohexanone, acetic acid, formic acid, and water gave an intermediately-stable suspension.

Since a well-dispersed state is important in liquid-phase reactions, nickel fine particles suspended in 2-propanol are of interest as a catalyst for Reaction 1.

2. Effect of Acetone on the Rate of 2-Propanol Dehydrogenation. The dehydrogenation of 2-propanol with suspended nickel fine particles gave no other reaction product than hydrogen and acetone gas-chromatographically.[14] Since only hydrogen passed the condenser, acetone gradually accumulated during the reaction. The concentration of 2-propanol remained almost constant, since it was used both as the solvent and as the reactant.

The time course of hydrogen evolution is shown in Fig. 2. A gradual decrease of the reaction rate observed regarding the nickel catalysts was similarly ascribed to a product retardation. The reaction rates were well-expressed by

$$v = k/(1 + K[\text{acetone}]), \quad (2)$$

where k was a rate constant and K was an equilibrium constant of acetone adsorption.[8-11] A linear correlation of the inverse rate with the product acetone can be derived from Eq. 2:[11]

$$1/v = 1/k + (K/k)[\text{acetone}],$$

which was verified to hold for a nickel fine-particle catalyst. The time course of Fig. 2 was converted into Fig. 3 as a function of the acetone. The retardation effect of acetone was ascertained by the following experimental approaches.

In the first place, the effect of acetone on a fresh catalyst was examined. In a reference experiment (Fig. 4a) the reaction started with neat 2-propanol and the product acetone accumulated up to 5.0% after 6 h. The 2-propanol/acetone premixed solvent prepared to be 5.0% of acetone was then used for the reaction (Fig. 4b). The initial rate of the latter was almost the same as the final rate of the former. Acetone was thus responsible for the rate decrease.

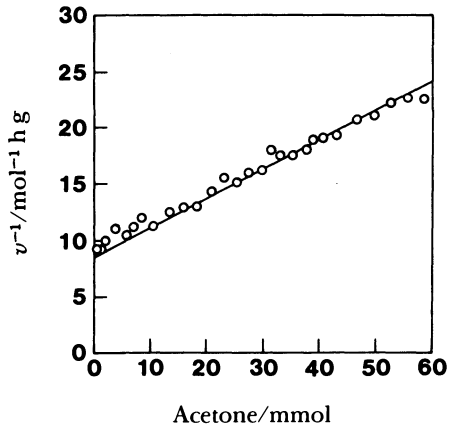

Fig. 3. Rate analysis of Fig. 2 on the postulate of acetone retardation.

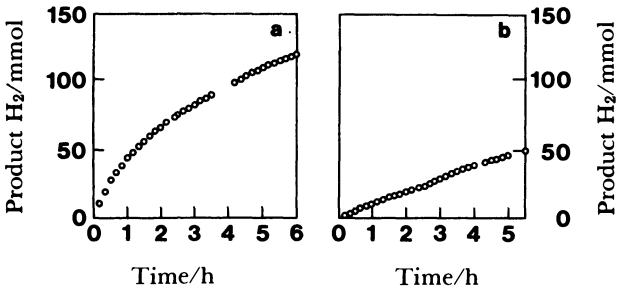

Fig. 4. Effect of initial addition of acetone on the liquid-phase dehydrogenation of 2-propanol with the nickel fine-particle catalyst.
Nickel fine particle catalyst (1.00 g) reduced on the severe conditions and suspended in (a) 2-propanol (200 ml) or (b) 2-propanol containing acetone (200 ml in total) prepared by initial addition of acetone upto the same concentration (5.0%) as in suspension a after the 6-h reaction.

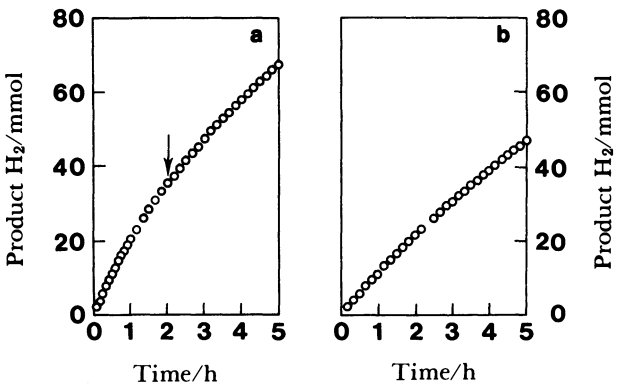

Fig. 5. Effect of partial removal of acetone on the liquid-phase dehydrogenation of 2-propanol with the nickel fine-particle catalyst.
(a) Nickel fine-particle catalyst (200 mg) suspended in 2-propanol (200 ml). (b) Partial solvent removal from suspension a after the 5-h reaction and the replenishment with neat 2-propanol to the same acetone concentration as the arrow-indicated level (1.2%).

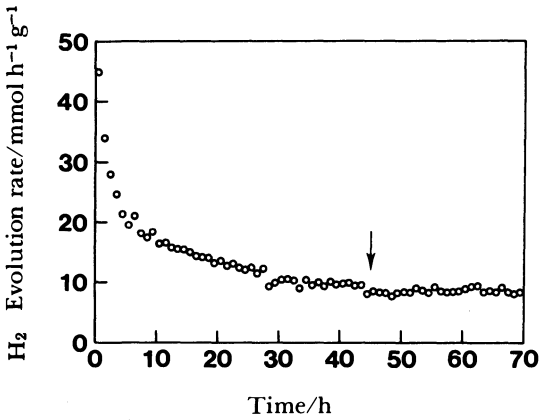

Fig. 6. Effect of accumulation and succeeding stationary removal of acetone on the liquid-phase dehydrogenation of 2-propanol with the nickel fine-particle catalyst.
Nickel fine-particle catalyst (200 mg) suspended in 2-propanol (300 ml) was used in the open-ended apparatus under partial distillation conditions.

The second approach was tried in order to reveal the equilibrium adsorption of acetone. After a 5-h reaction the suspension was rapidly cooled (Fig. 5a), followed by a partial removal of the solvent from the reactor under vacuum. Neat 2-propanol was added to the residual suspension until the liquid was supplemented in amount. Not only the amount of acetone left in the solvent after this transfer procedure but also the initial rate in the 2-propanol/acetone solvent thus prepared (Fig. 5b) was the same as that marked by an arrow. The rate-time correlation was obtained in a duplicated manner thereafter. The catalytically-active sites were occupied with acetone by a reversible adsorption from the bulk solvent.

The third experiment produced a state in which the concentration of acetone in the solvent was constant under partial distillation conditions.[10] Two kinds of condensers were set in series in the open-ended apparatus. The product acetone in excess and a small amount of 2-propanol were evaporated from the reactor and passed through the first condenser (57 °C). They were trapped with the second condenser (−10 °C). As shown in Fig. 6, a gradual rate decrease was observed in the initial reaction stage (0—45 h); then, the rate became constant and did not change thereafter (45—70 h). Except for the initial reaction stage, newly formed acetone was removed stationarily under the adopted distillation conditions.

Therefore, it is concluded that active sites of the nickel fine-particle catalyst are occupied by the product acetone without irreversible deactivation.

The rate constant of Eq. 2 of the nickel fine-particle catalyst (116 mmol h^{-1} g^{-1}) was larger than the values reported previously concerning Raney nickel (55

mmol h^{-1} g^{-1})[8] and nickel boride (60 mmol h^{-1} g^{-1})[11] catalysts. It has been pointed out that the equilibrium constant of acetone adsorption was sensitive to the conditions of acetone diffusion, which was regulated by the stirring rate. Sufficient stirring conditions resulted in an adsorption constant of 8.6 l mol^{-1} to the nickel boride catalyst. However, values as large as 10—16 l mol^{-1} were obtained for the Raney nickel catalyst under diffusion-controlling conditions.[11] A rather small adsorption constant (6.0 l mol^{-1}) was obtained for the well dispersed nickel fine particles (Fig. 3), suggesting that this catalyst was not affected by diffusion-controlling conditions.

3. Effect of Temperature on the Reaction Rate. An efficient removal of the product acetone from the catalyst surface was important to Reaction 1. The temperature effect on the reaction rates was examined with and without adopting the boiling conditions. In one series, an inert and soluble substance, i.e., hexane was added to 2-propanol little by little in order to maintain the boiling conditions at various temperatures.[24] In the other, the suspension was heated without boiling in the temperature region below 82.4 °C.[6]

As shown in Fig. 7, the reaction rates on the boiling conditions in the 2-propanol/hexane solvent prepared by the successive addition of hexane were higher than those in the neat 2-propanol without boiling. The rate difference was large in the low-temperature region. One possible interpretation is as follows: The retardation effect owing to acetone adsorption on the catalyst is large at low temperatures without boiling. Bubbles made under boiling conditions favor the desorption of acetone and result in a relatively high reaction rate.

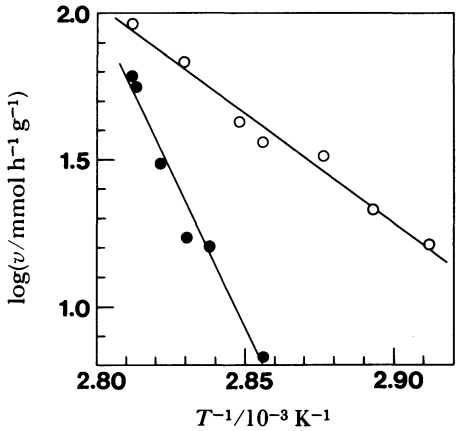

Fig. 7. Temperature dependence of the rate of 2-propanol dehydrogenation with the nickel fine-particle catalyst on boiling or non-boiling conditions. Reaction temperatures were controlled by adding hexane with the boiling conditions kept (○) or by varying the extent of heat supply without boiling (●).

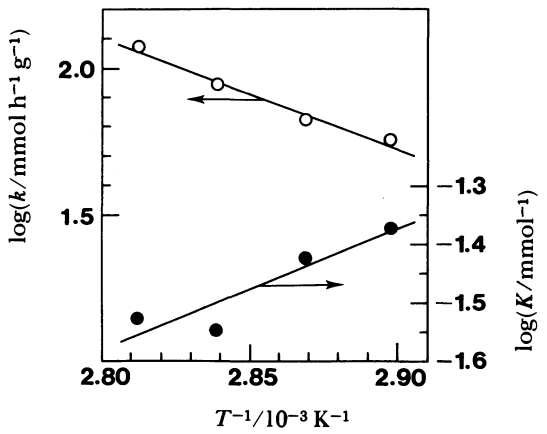

Fig. 8. Temperature dependence of the rate constant of 2-propanol dehydrogenation and the equilibrium constant of acetone adsorption of the nickel fine-particle catalyst under boiling conditions. Reaction temperatures were controlled by changing the amount of hexane added to the suspension.

An accurate temperature dependence of the kinetical parameters k and K in Eq. 2 was examined by the use of a series of 2-propanol (200 ml)/hexane solvents with 0, 8, 21, and 38 ml of hexane, which exhibited boiling temperatures of 82.4, 79.1, 75.4, and 72.0 °C, respectively. An Arrhenius plot and a similar plot of the constant K are shown in Fig. 8.

During each experiment the boiling point of the solvent was slightly lowered by the accumulated acetone. The frequency factor and the exponential coefficient of k and K were determined by a least-square optimization to all of the experimental values, during which slight changes in the boiling point were taken into account. The activation energy of the nickel fine-particle catalyst (71.4 kJ mol^{-1}), surpassing slightly the enthalpy change of this endothermic reaction (69.9 kJ mol^{-1}), was similar in magnitude to those of the heterogeneous nickel boride (85.8 kJ mol^{-1})[11] and Raney nickel (73.2 kJ mol^{-1})[8] catalysts or of the homogeneous tin(II)-coordinated rhodium(III) complexes (117 kJ mol^{-1}).[6] The adsorption heat of acetone of this catalyst (−33.3 kJ mol^{-1}) was a little larger than that of the nickel boride catalyst (−20.9 kJ mol^{-1}).[11]

4. Application of 2-Propanol Dehydrogenation by Suspended Nickel Fine-Particle Catalyst. The reverse of Reaction 1 is favored below 202 °C.

$$(CH_3)_2CO + H_2 \longrightarrow (CH_3)_2CHOH \qquad (3)$$

An endothermic low-temperature Reaction 1 in the liquid phase can be coupled to exothermic high-temperature Reaction 3 in the gas phase, as long as acetone (bp 56.3 °C) and 2-propanol (bp 82.4 °C) are separated by cooling through distillation. Since these reactions proceed at different temperatures, simul-

taneously and stationarily, a new heat-pump system will be constituted, with which low-quality heat at 80 °C can be partially upgraded to 200 °C by heat expense at 30 °C.[25] A heat supply is required for both the dehydrogenation reaction and the evaporation of organic compounds.

Appropriate catalysts are indispensable for this chemical heat-pump system. In order to efficiently convert the thermal energy of low-quality heat into chemical energy, 2-propanol dehydrogenation should be catalyzed with high activity and selectivity under boiling conditions.

The nickel fine-particle catalyst is advantageous for this purpose, since it is well-suspended through conventional stirring with an attainable high space-time yield. However, the development of a catalyst that is active in much acetone is desired, since both the low boiling point of the solvent and the large vapor pressure of acetone are favorable for this chemical heat-pump system.

References

1) D. R. Stull, E. F. Westrum, Jr., and G. C. Sinke, "The Chemical Thermodynamics of Organic Compounds," John Wiley & Sons, New York (1969), pp. 649—651.

2) A. J. Papa, "Kirk-Othmer Encyclopedia of Chemical Technology," 3rd ed, John Wiley & Sons, New York (1982), Vol. 19, pp. 198—220.

3) H. B. Charman, *J. Chem. Soc. B*, **1970**, 584.

4) A. Dobson and S. D. Robinson, *J. Organomet. Chem.*, **87**, C52 (1975); *idem, Inorg. Chem.*, **16**, 137 (1977).

5) C. W. Jung and P. E. Garrou, *Organometallics*, **1**, 658 (1982).

6) H. Moriyama, T. Aoki, S. Shinoda, and Y. Saito, *J. Chem. Soc., Perkin Trans. 2*, **1982**, 369.

7) S. Shinoda, T. Kojima, and Y. Saito, *J. Mol. Catal.*, **18**, 99 (1983).

8) F. Claes and J. C. Jungers, *Bull. Soc. Chim. Fr., Ser. 5*, **25**, 1167 (1958).

9) F. Velasco, *Chim. Ind. (Milan)*, **81**, 521 (1959).

10) S. L. Kiperman, N. V. Nikolaeva, and I. R. Davydova, *Kinetika i Kataliz*, **4**, 723 (1963).

11) D. E. Mears and M. Boudart, *AIChE J.*, **12**, 313 (1966).

12) W. K. Rybak and J. J. Ziólkowski, *J. Mol. Catal.*, **11**, 367 (1981).

13) S. Shinoda, Y. Tokushige, T. Kojima, and Y. Saito, *J. Mol. Catal.*, **17**, 81 (1982).

14) M. Noda, S. Shinoda, and Y. Saito, *Nippon Kagaku Kaishi*, **1984**, 1017.

15) A. Seidell, "Solubilities of Inorganic and Metal Organic Compounds," 3rd ed, D. Van Norstrand, New York (1953), Vol. 1, pp. 564—567.

16) S. Kashu, M. Nagase, C. Hayashi, R. Uyeda, N. Wada, and A. Tasaki, *Jpn. J. Appl. Phys.*, Suppl. 2, Pt. 1, 491 (1974).

17) M. Hida, N. Wada, H. Maeda, H. Terauchi, Y. Tsu, and N. Kamijo, *Jpn. J. Appl. Phys.*, **24**, L3 (1985).

18) T. Hayashi and Y. Saito, *Kagaku*, **39**, 667 (1984).

19) Y. Saito, Kagaku Sosetsu, No. 48, "Chobiryushi—Kagaku To Oyo," ed by Chem. Soc. Jpn., Gakkai Shuppan Center, Tokyo (1985), pp. 193—196.

20) The nickel fine particles are commercially available from Vacuum Metallurgical Co. Ltd., Chiba Pref., Japan.

21) T. Hayashi and T. Nagayama, *Nippon Kagaku Kaishi*, **1984**, 1050.

22) When rather severe reducing conditions were adopted, the retardation effect of acetone increased extremely.

23) M. Yamashita and Y. Saito, unpublished results.

24) The decrease of the boiling point down to 62 °C by addition of hexane (48 vol%) to 2-propanol was reported previously. In the solvent the rate equation of pseudo-zeroth order with respect to 2-propanol was ascertained to the reaction with a suspended nickel boride catalyst.[11]

25) Y. Saito, H. Kameyama, and K. Yoshida, *Energy Research*, **11**, 549 (1987).

The Liquid-Phase Oxidation of *p*-Methoxytoluene to *p*-Anisaldehyde with $Co(OAc)_2/Ce(OAc)_3/Cr(OAc)_3$ Catalyst

Nobumasa KITAJIMA,* Shigeru SUNAGA, Yoshihiko MORO-OKA,* Tadatsugu YOSHIKUNI,† Mitsuo AKADA,† Yoshihisa TOMOTAKI,† and Masatoshi TANIGUCHI†
Research Laboratory of Resources Utilization, Tokyo Institute of Technology, Nagatsuta, Midori-ku, Yokohama 227
†Tokushima Research Laboratory, Otsuka Chemical Co., Ltd., 463 Kagasuno, Kawauchi-cho, Tokushima 771-01
(Received August 10, 1987)

The liquid-phase oxidation of *p*-methoxytoluene to *p*-anisaldehyde in the presence of Co based catalysts has been studied. With $Co(OAc)_2$ alone in acetic acid as a solvent, only a trace amount of *p*-anisaldehyde could be obtained; however, upon the addition of a second metal salt (e.g., $Mn(OAc)_2$ or $Ce(OAc)_3$) a considerable improvement in the yield (up to 60%) was observed. The synergism of Co and the second component as well as the optimization of the reaction conditions were investigated. $Co(OAc)_2$–$Ce(OAc)_3$–$Cr(OAc)_3$ (3:1:2) was finally found to be the most effective catalytic system, which gave a 76% yield of *p*-anisaldehyde under 3 atm O_2 at 110° for 3 h.

The liquid-phase oxidation of substituted toluenes to the corresponding aldehydes has been receiving increasing attention from an industrial point of view[1] owing to a growing demand for these aldehydes as manufactural key intermediates for the production of medicines, perfumes, agricultural chemicals and so on. The current processes for the production of these aldehydes, based mainly on the stoichiometric chemical oxidations, have several disadvantages regarding waste treatment, small manufactural scale as well as high costs.

Although the liquid-phase oxidation of hydrocarbons has been the subject of numerous studies for many years,[2] the feature of the reaction mechanism is not simple and there is still no unified view in terms of the control of the catalytic activity and selectivity to oxidize specific substrates. In general, the aldehydes are more reactive toward oxidation than the starting substances and, thus, the selective synthesis of the aldehyde with the liquid-phase oxidation has been regarded as not being easily achieved.

p-Anisaldehyde is an useful chemical as an additive for metal plating brighteners or perfumes, as well as a source material for medicines. Recently, several attempts to produce *p*-anisaldehyde from *p*-methoxytoluene through liquid-phase oxidation have been reported. Okada and Kamiya[3] reported that only less than 10% yield of *p*-anisaldehyde can be obtained by the liquid-phase oxidation of *p*-methoxytoluene with a Co–Cu–Br catalytic system. A relatively good yield (60%) was reported by Imamura et al.[4] using a Co based catalyst under optimized reaction conditions.

In the present study, a catalytic survey for a highly selective liquid-phase oxidation of *p*-methoxytoluene to *p*-anisaldehyde was performed; multicomponent metal systems, including the most efficient system Co–Ce–Cr, have been found to give a higher yield.

Experimental

p-Methoxytoluene (purchased from Tokyo Kasei), $Co(OAc)_2 \cdot 4H_2O$ (Wako), $Ce(OAc)_3 \cdot H_2O$ (Wako), $Cr(OAc)_3 \cdot H_2O$ (Wako) and the other reagents were used without further purification. A 50 ml stainless autoclave (SUS-316) was used for the reaction. Into the autoclave, were added the substrate, a solvent (AcOH), and metal salts with a magnetic bar. The autoclave was heated in a prewarmed oil bath with vigorous magnetic stirring at 110 °C under 3 atm of O_2. The products were isolated by TLC and the structures were assigned based on their IR, NMR, and mass spectra. Through routine procedures, these products were quantitatively analyzed by GC on SE-30 supported on Chromosorb W.

Results and Discussion

Oxidation with $Co(OAc)_2$–$Mn(OAc)_2$ Catalytic System. When 2 mmol of *p*-methoxytoluene was allowed in 10 ml of AcOH in the presence of 0.75 mmol of $Co(OAc)_2$ (generally known to be effective for a wide variety of liquid-phase oxidations of hydrocarbons) at 110 °C for 3 h under 3 atm O_2, an only trace amount of *p*-anisaldehyde was formed (although the conversion was close to 100%). As by-products, *p*-methoxybenzoic acid and *p*-anisyl acetate were formed, implying that the oxidizing capability of $Co(OAc)_2$, itself, is too high to give *p*-anisaldehyde in good yield.

The mixture of $Co(OAc)_2$ and $Mn(OAc)_2$ (known as an active catalytic system in several liquid-phase oxidation reactions[5–7]) was found to be effective for the present reaction. In Fig. 1, the yield of *p*-anisaldehyde is plotted against the Mn content per Co+Mn catalyst. The reaction was carried out at 110 °C for 3 h in the presence of 0.75 mmol of the total catalyst. The yield of *p*-anisaldehyde depended strongly on the Co–Mn ratio. $Mn(OAc)_2$, itself, showed only a limited activity toward the oxidation compared with $Co(OAc)_2$, whereas the selectivity to

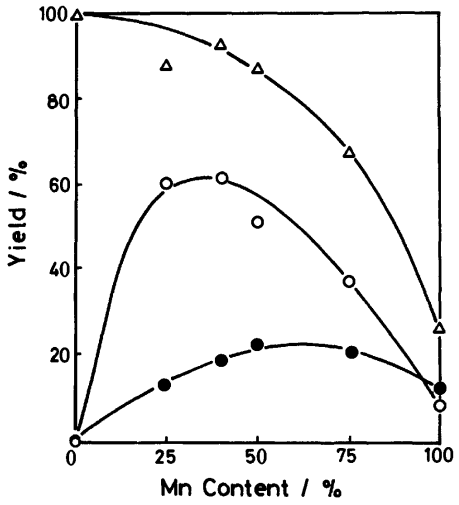

Fig. 1. The dependence of the product yield on Mn content in the oxidation of *p*-methoxytoluene with $Co(OAc)_2$-$Mn(OAc)_2$.
Total catalyst amount, 0.75 mmol; *p*-methoxytoluene, 2.0 mmol; AcOH, 10 ml; O_2, 3 atm; at 110 °C for 3 h. (△) Conversion, (○) *p*-anisaldehyde, (●) *p*-anisyl acetate.

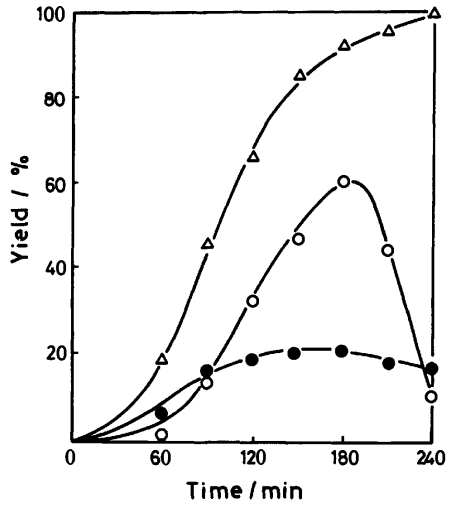

Fig. 2. The time course of *p*-methoxytoluene oxidation with $Co(OAc)_2$-$Mn(OAc)_2$ catalyst.
$Co(OAc)_2 \cdot 4H_2O$-$Mn(OAc)_2 \cdot 4H_2O$ (3:2), 0.75 mmol; O_2, 3 atm; *p*-methoxytoluene, 2.0 mmol; AcOH, 10 ml; at 110 °C.
(△) Conversion, (○) *p*-anisaldehyde, (●) *p*-anisyl acetate.

p-anisaldehyde was higher. A mixture of the two metal salts in any composition gives a higher yield of the aldehyde. A synergism is therefore evident. The highest yield (61%) was obtained when the ratio of Co: Mn was 3:2.

In Fig. 2, the change in the liquid-phase composition with the reaction time is shown. 0.75 mmol of the Co-Mn (3:2) catalyst was used for these experiments. In the initial ca. 0.5 h, the induction period was observed. The following yield of *p*-anisaldehyde increased with the reaction time and reached the highest value after 3 h. The longer reaction time resulted in a lower yield, presumably because of a subsequent oxidation of the aldehyde into undetermined polymeric by-products. Neither the increase of the catalyst concentration nor the O_2 pressure significantly affects the yield.

In order to clarify the reaction pathways for producing *p*-anisaldehyde, *p*-anisyl alcohol, *p*-anisyl acetate, and *p*-anisaldehyde were oxidized, respectively, in the presence of $Co(OAc)_2$-$Mn(OAc)_2$ (3:2) at 110 °C. The amount of the substance used was 2.0 mmol each; the other reaction conditions were the same as employed for *p*-methoxytoluene oxidation. As summarized in Scheme 1, *p*-anisaldehyde was found to be reasonably stable under the reaction conditions. The oxidation of the acetate to the aldehyde is desirable in order to obtain a higher yield of *p*-anisaldehyde. *p*-Anisyl acetate, however, was found to be stable with regard to further oxidation, giving only a trace amount of the aldehyde. *p*-Anisyl

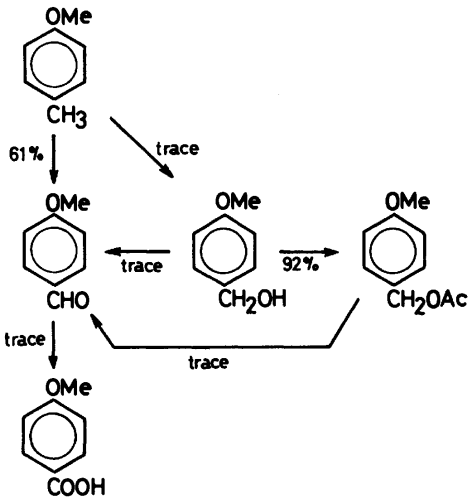

Scheme 1.

alcohol was not oxidized to *p*-anisaldehyde either, but was mainly converted to the acetate; this implies that *p*-anisaldehyde is formed directly from *p*-methoxytoluene, but not via the *p*-anisyl alcohol. Therefore, following factors seem to be the key factors for developing a more selective catalytic system: 1) the formation of alcohol should be suppressed and 2) the reaction conditions for retarding esterification is preferable. Based on these criteria, the medium oxidizing capability between $Co(OAc)_2$ and $Co(OAc)_2$-$Mn(OAc)_2$ may be suitable for the selective formation of *p*-anisaldehyde.

The Effect of Water or Anhydrous Acetic Acid. The additive effects of water[8] and anhydrous acetic

Table 1. Liquid-Phase Oxidations of *p*-Methoxytoluene with $Co(OAc)_2$–$Mn(OAc)_2$ (3:2) in the Presence of an Additive[a)]

Additive	Conv.	Ph'CHO	Ph'CH_2OAc	Ph'CH_2OH	Ph'COOH
mmol	%	%	%	%	%
H_2O, 27.8	19.4	3.4	0	0	0
H_2O, 27.8[b)]	56.1	23.6	0	0	0
Ac_2O, 17.5	100.0	49.4	0	0	0
NaBr, 0.75	100.0	19.1	0	0	0

a) Ph' denotes *p*-methoxyphenyl; O_2, 3atm; solvent (AcOH), 10 ml; *p*-methoxytoluene (Ph'CH_3), 2.0 mmol; temp, 110°C; $Co(OAc)_2 \cdot 4H_2O$–$Mn(OAc)_2 \cdot 4H_2O$ (3:2), 0.75 mmol; reaction time, 3 h. b) Reaction time, 6 h.

Table 2. Liquid-Phase Oxidations of *p*-Methoxytoluene with $Co(OAc)_2$ in the Presence of the Second Metal Salt[a)]

Metal salt	Conv.	Ph'CHO	Ph'CH_2OAc	Ph'CH_2OH	Ph'COOH
	%	%	%	%	%
$Ni(OAc)_2 \cdot 4H_2O$	100.0	0	0	Trace	Trace
$Cu(OAc)_2 \cdot H_2O$	3.0	0	0	0	0
$Cr(OAc)_3 \cdot H_2O$	100.0	1.6	0	3.6	Trace
$Ce(OAc)_3 \cdot H_2O$	100.0	67.9	21.7	0	0

a) $Co(OAc)_2 \cdot 4H_2O$, 0.56 mmol; metal salt, 0.19 mmol; O_2, 3 atm, temp, 110°C; solvent (AcOH), 10 ml; *p*-methoxytoluene (Ph'CH_3), 2.0 mmol, reaction time, 3 h.

acid were examined (as summarized in Table 1). When 0.5 ml of H_2O was added to the Co–Mn catalytic system, the only obtained product was a 19.4% conversion to *p*-methoxytoluene for 3 h. When a longer reaction time was employed, a higher conversion was obtained; however, the yield of *p*-anisaldehyde was not high. Therefore, the addition of H_2O retards both the catalytic activity and the selectivity. The addition of anhydrous acetic acid or NaBr was also attempted. The addition accelerates the consumed rate of the reaction. When 0.5 ml of anhydrous acetic acid or 0.75 mmol of NaBr was added into the system, a 100% conversion of *p*-methoxytoluene was obtained in both cases. However, the yields of *p*-anisaldehyde were not very high. Anhydrous acetic acid and NaBr are known to be effective additives which can enhance the catalytic activity of the Co salt in several hydrocarbon oxidations.[2,9)] However, the use of these additives for the present reaction causes a further oxidation of the target product, *p*-anisaldehyde, and unfavorably lowers the selectivity.

The Effect of $Ce(OAc)_3$ Addition. It is generally believed that the enhancement of the catalytic activity upon the addition of the second metal component is due to the reoxidation of Co^{2+} to the catalytically active Co^{3+}. For example,[2)] the additive effect of the Mn^{2+} salt combining with the Co salt can be explained in terms of an electron transfer from the Mn^{3+} generated by the oxidation of Mn^{2+} with $RO_2\cdot$, as follows:

$$Mn^{2+} + RO_2\cdot \longrightarrow Mn^{3+} + RO_2^-$$

$$Mn^{3+} + Co^{2+} \longrightarrow Mn^{2+} + Co^{3+}$$

However, the addition of Mn in the present reaction rather lowers the oxidizing capability of the Co^{3+} species and enhances the selectivity for the production of *p*-anisaldehyde. Since the medium oxidizing capability between $Co(OAc)_2$ and $Co(OAc)_2$–$Mn(OAc)_2$ (as described above) was expected to be effective for the selective production of *p*-anisaldehyde, the other metal salt, which by itself slightly retards the oxidizing capability of the $Co(OAc)_2$ less than $Mn(OAc)_2$, seemed to be suitable as an additive for the present reaction. For these reasons the additive effects of several other metal salts, instead of $Mn(OAc)_2$, combined with $Co(OAc)_2$ were examined. The results are summarized in Table 2. In these experiments, the molar ratio of a metal salt to $Co(OAc)_2$ was fixed at 1:3. With $Co(OAc)_2$–$Ce(OAc)_3$, a considerable improvement in *p*-anisaldehyde yield was obtained, whereas the addition of $Cu(OAc)_2$ resulted in an apparent retardation of the catalytic activity. The addition of $Cr(OAc)_3$ and $Ni(OAc)_2$ also caused a further oxidation, yielding only a small amount of *p*-anisaldehyde.

The dependence of the *p*-anisaldehyde yield on the mixing ratio of $Ce(OAc)_3$ to $Co(OAc)_2$ is shown in Fig. 3. As in the Co–Mn system, a synergistic effect was evident. The highest yield (67.9%) of *p*-anisaldehyde was obtained when the molar ratio of Co:Ce was 3:1. With a smaller amount of Ce, the yield was low, although almost a complete consumption of *p*-methoxytoluene was observed. The addition of a greater amount of Ce caused a decrease in the catalytic activity, while the yield of *p*-anisyl acetate increased. The time course of the reaction in the presence of a $Co(OAc)_2$–$Ce(OAc)_3$ (3:1) catalyst is shown in Fig. 4.

The yield of *p*-anisaldehyde, as well as *p*-anisyl acetate, increased with time and reached a maximum value at 3 h. Any further reaction, however, tended to lower the yield of the aldehyde.

Oxidation with Three Components Catalysts. The additive effect of several metal salts into the effective catalytic system, $Co(OAc)_3$–$Mn(OAc)_2$ (3:2) and $Co(OAc)_2$–$Ce(OAc)_3$ (3:1), were examined (see Table 3). A slight improvement of the *p*-anisaldehyde yield was found upon the addition of $Cr(OAc)_3$ in both systems. The highest yield of *p*-anisaldehyde was obtained with a three-component catalytic system, $Co(OAc)_2$–$Ce(OAc)_3$–$Cr(OAc)_3$.

The effect of the added amount of $Cr(OAc)_3$ into a fixed amount (0.75 mmol) of $Co(OAc)_2$–$Cr(OAc)_3$ (3:1) was examined. The highest yield (72.7%) was obtained when the molar ratio of the components was 3:1:2 for Co:Mn:Cr. The change in the liquid-phase composition as a function of the reaction time

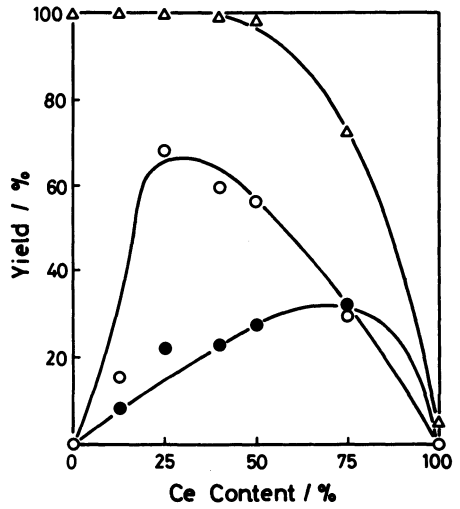

Fig. 3. The dependence of the product yield on Ce content in the oxidation of *p*-methoxytoluene with $Co(OAc)_2$–$Ce(OAc)_3$.
Total catalyst amount, 0.75 mmol; *p*-methoxytoluene, 2.0 mmol; AcOH, 10 ml; O_2, 3 atm; at 110 °C for 3 h.
(△) Conversion, (○) *p*-anisaldehyde, (●) *p*-anisyl acetate.

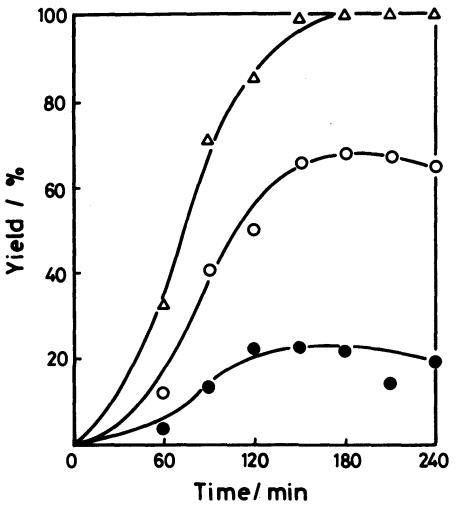

Fig. 4. The time course of *p*-methoxytoluene oxidation with $Co(OAc)_2$–$Ce(OAc)_3$ catalyst.
$Co(OAc)_2 \cdot 4H_2O$–$Ce(OAc)_3 \cdot H_2O$ (3:1), 0.75 mmol; O_2, 3 atm; *p*-methoxytoluene, 2.0 mmol; AcOH, 10 ml; at 110 °C.
(△) Conversion, (○)*p*-anisaldehyde, (●) *p*-anisyl acetate.

Table 3. Liquid-Phase Oxidations of *p*-Methoxytoluene with Three Component Metal Mixtures

Catalyst (molar ratio)	Conv. %	Ph'CHO %	Ph'CH_2OAc %	Ph'CH_2OH %	Ph'COOH %
$Co(OAc)_2$–$Mn(OAc)_2$–$Ni(OAc)_2$ (3) (2) (1)	93.0	53.0	0	Trace	0
$Co(OAc)_2$–$Mn(OAc)_2$–$Ce(OAc)_3$ (3) (2) (1)	98.2	63.5	0	Trace	0
$Co(OAc)_2$–$Mn(OAc)_2$–$Cr(OAc)_3$ (3) (2) (1)	98.2	64.6	0	Trace	0
$Co(OAc)_2$–$Mn(OAc)_2$–$Cu(OAc)_2$ (3) (2) (1)	99.2	63.4	0	Trace	0
$Co(OAc)_2$–$Ce(OAc)_3$–$Cu(OAc)_2$ (3) (1) (1)	99.1	62.9	0	Trace	Trace
$Co(OAc)_2$–$Ce(OAc)_3$–$Cr(OAc)_3$ (3) (1) (1)	98.5	68.7	14.4	Trace	Trace
$Co(OAc)_2$–$Ce(OAc)_3$–$Cr(OAc)_3$ (3) (1) (2)	99.9	72.7	14.1	0	0
$Co(OAc)_2$–$Ce(OAc)_3$–$Cr(OAc)_3$[a] (3) (1) (2)	100.0	75.9	12.8	0	0

The catalyst amount of $Co(OAc)_2$–$Mn(OAc)_2$ (3:2) or $Co(OAc)_2$–$Ce(OAc)_3$ (3:1) was fixed, 0.75 mmol except the case, a) when the total catalyst amount was 1.75 mmol. O_2, 3 atm; 110 °C; *p*-methoxytoluene (Ph'CH_3), 2.0 mmol; solvent (AcOH), 10 ml; the reaction time, 3 h.

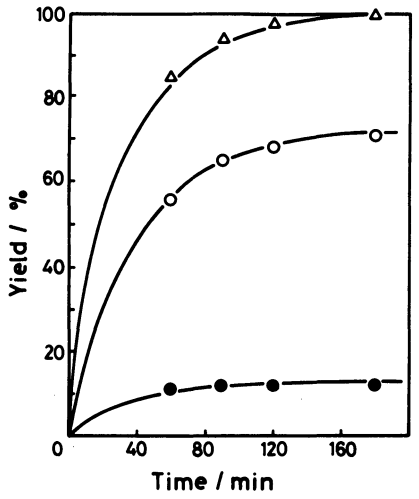

Fig. 5. The time course of *p*-methoxytoluene oxidation with $Co(OAc)_2$–$Ce(OAc)_3$–$Cr(OAc)_3$ catalyst. $Co(OAc)_2 \cdot 4H_2O$–$Ce(OAc)_3 \cdot H_2O$–$Cr(OAc)_3 \cdot H_2O$ (3:1:2), 0.75 mmol, *p*methoxytoluene, 2.0 mmol; AcOH, 10 ml; O_2, 3 atm; at 110 °C.
(△) Conversion, (○) *p*-anisaldehyde, (●) *p*-anisyl acetate.

catalyzed by this effective system is shown in Fig. 5. A similar feature of the reaction obtained in $Co(OAc)_2$–$Mn(OAc)_2$ and $Co(OAc)_2$–$Ce(OAc)_3$ systems was noted; the best reaction time for obtaining *p*-anisaldehyde was 3 h.

Finally, the dependence of the *p*-anisaldehyde yield on the catalyst concentration was examined. Reactions were performed at 110° for 3 h with $Co(OAc)_2$–$Mn(OAc)_2$–$Cr(OAc)_3$ (3:1:2). The yield slightly depended on the concentration in the range of the total amount of the catalyst, 0.5 to 2.0 mmol; the highest yield (75.9%) was obtained when 1.75 mmol of the total amount of the catalyst was used.

Okada and Kamiya reported that only a limited yield (2.7%) of *p*-anisaldehyde was obtained in the presence of $Co(OAc)_2$–$Cu(OAc)_2$–NaBr under 40 atm of air at 150 °C for 1 h.[3] Under their experimental conditions, the molar ratio of *p*-methoxytoluene: AcOH:Co was 4.2:100:0.33. Imamura et al. made a detailed investigation of suitable reaction conditions for the selective formation of *p*-anisaldehyde with a cobalt based catalytic system. They found that the highest yield (70%) of *p*-anisaldehyde was obtained with $Co(OAc)_2$ alone under 60 atm of O_2 at 120—124 °C. The molar ratio in this case was 10:100:2 for *p*-methoxytoluene:AcOH:Co. The yield was, however, significantly lower (<20%) under an ambient pressure of O_2. They examined the additive effect of several bromide additives (e.g., NaBr, HBr, $CoBr_2$) although no apparent improvement in the *p*-anisaldehyde yield was obtained. Compared with these systems, the present catalytic system is evidently more effective; a higher yield (76%) of *p*-anisaldehyde was obtainable under milder reaction conditions (at 110 °C and 3 atm of O_2, *p*-methoxytoluene:AcOH:Co was 1.1:100:0.45).

From an industrial point of view, the deactivation of the catalyst should be notable. Repeated oxidations of *p*-methoxytoluene were, thus, attempted using $Co(OAc)_2$–$Ce(OAc)_3$–$Cr(OAc)_3$. After the first reaction carried out under the same reaction conditions (described above), the catalyst was extracted with water and used for a subsequent experiment. Three repetitions of similar oxidations did not result in any deactivation, although the further repetitions caused a slight deactivation of the catalyst with a loss of the total amount of the catalyst in the extraction procedure.

References

1) J. Imamura, *J. Synth. Org. Chem. Jpn.*, **37**, 667 (1979).
2) Y. Kamiya, "Yuki Sanka Hannou," Gihōdō (1973).
3) T. Okada and Y. Kamiya, *Bull. Chem. Soc. Jpn.*, **54**, 2724 (1981).
4) K. Shimizu, K. Kizawa, T. Yoshimoto, and J. Imamura, *J. Jpn. Petrol. Inst.*, **75**, 7 (1982).
5) Y. Kamiya, "Oxidation of Organic Compounds, 2," p. 193 (1968), Am. Chem. Soc.
6) T. Taguchi, A. Naito, S. Futamura, and Y. Kamiya, Pre-prints, 19th Ann. Symp. Oxi. React., p. 7 (1985).
7) N. Kitajima, K. Takemura, Y. Moro-oka, T. Yoshikuni, M. Akada, Y. Tomotaki, and M. Taniguchi, *Bull. Chem. Soc. Jpn.*, **61**, 1035 (1988).
8) T. Taguchi, N. Naito, S. Futamura, and Y. Kamiya, Pre-prints, 20th Ann. Symp. Oxi. React., p. 7 (1986).
9) Y. Kamiya, T. Nakajima, and K. Sakota, *Bull. Chem. Soc. Jpn.*, **39**, 2211 (1966).

 © 1988 The Chemical Society of Japan Bull. Chem. Soc. Jpn., 61, 973—981 (1988)

Alumina-Anchored Cobalt Porphine Catalysts for the Conversion of Quadricyclane to Norbornadiene

Sadao Miki, Yoshinobu Asako, Masayoshi Morimoto, Toshinobu Ohno, Zen-ichi Yoshida,* Toshiro Maruyama,† Masahiro Fukuoka,† and Tomoaki Takada†

Department of Synthetic Chemistry, Kyoto University, Yoshida, Kyoto 606
†Department of Chemical Engineering, Kyoto University, Yoshida, Kyoto 606
(Received August 27, 1987)

Methods are described for the preparation of cobalt(II) deuteroporphyrin and cobalt(II) tetrakis(*p*-sulfonatophenyl)porphine anchored on alumina beads coated with polyaminesulfone-A. Wavelength dispersive X-ray microanalysis showed that the cobalt(II) porphine distributes within the catalyst outer surface layer of ca. 100 μm depth. The catalysts are highly active for the cycloreversion of quadricyclane to norbornadiene. A detailed kinetics of the isomerization using an isothermal recycle reactor gave a rate expression of Langmuir-Hinshelwood type. The catalysts gradually lose their activity, which can be regenerated completely by heating the catalysts at 200 °C in vacuo.

Heterogeneous catalysts have merit to eliminate disadvantages of homogeneous catalysts, the difficulties in separation of catalyst from product as well as the loss of expensive catalyst by entrainment. Solar energy storage system based on photochemical formation of highly strained molecules coupled with catalyzed reversion of the photoproduct is the case.[1-8] In the connection with the recent importance of solar chemical latent energy system, several heterogeneous catalysts have been developed for the conversion of quadricyclane (Q) to norbornadiene (NBD),[9-12] and the criteria for an ideal catalyst have been pointed out by King and Sweet.[9] A serious problem for the catalysts reported so far seems to be loss of catalyst activity upon repeated use and its regeneration.

This paper describes our new method for preparation of heterogeneous catalyst by immobilizing cobalt(II) porphine derivatives on alumina beads.

In evaluating the catalysis system, it is essential to know the kinetic profiles over a wide range of substrate concentration. Most of kinetic studies reported so far have been carried out at low quadricyclane concentrations (e.g., 0.1 mol·L^{-1})[9]. Here, we have examined kinetics of our heterogeneous catalysis system over a range of the substrate concentration of 0.1—1.0 mol·L^{-1} using an isothermal recycle reactor. Furthermore, energy releasing process (Q→NBD) has been run on an adiabatic fixed bed reactor and the temperature profiles of the system are discussed based on the kinetic studies.

Results and Discussion

Preparation of the Catalysts, Co(II)TPPS/PAS/Alumina (1) and Co(II)DPIX/PAS/Alumina (2). By soaking activated alumina beads (mean diameter of 3 mm) in aqueous solution of polyaminesulfone-A (PAS, **3**, MW=2×10^5), **3** was adsorbed on the alumina beads, and the alumina beads were modified to have the anion binding ability. Thus, upon contact with a solution of cobalt(II) sodium tetrakis(*p*-sulfonatophenyl)porphine (Co(II)TPP(*p*-$SO_3Na)_4$, **4**) in methanol the alumina beads coated with PAS adsorbed the porphynato cobalt(II) to afford the catalyst Co(II)-TPPS/PAS/Alumina (**1**). The adsorption was effective, and in typical run using 9.1 g of **4**, the complete disappearance of the color of **4** in the liquid phase was observed by the PAS/Alumina (190 g). For cobalt(II) deuteroporphyrin (Co(II)DPIX, **5**), pyridine was used as solvent. In this case, by the rapid adsorption of **5** by PAS/Alumina Co(II)DPIX/PAS/Alumina (**2**) was obtained. Four kinds of heterogeneous catalysts, A—D of **2** were prepared, which incorporated 19 mmol, 39 mmol, 72 mmol, and 139 mmol of **5** per 1 kg of the resulting catalyst, respectively. In each case adsorption of cobalt(II) porphines was carried out under unaerobic conditions. These cobalt contained catalysts are, however, stable to air in dry state. The conditions for the preparation of each catalysts are shown in Table 1.

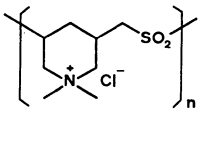

PAS, 3

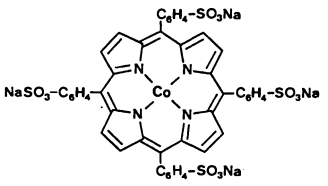

Co(II)TPP(p-$SO_3Na)_4$, 4

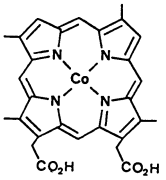

Co(II)DPIX, 5

Table 1. Preparation of the Modified Alumina-Anchored Cobalt(II) Porphine Catalysts

Catalyst (batch)	Co(II) porphine	PAS/alumina	Solvent	Catalyst obtained	Co(II) porphine[a] incorporation
		g		g	mmol·kg^{-1}
1	9.12 g Co(II)TPP(p-SO_3Na)$_4$	190	2000 mL Methanol	194	43
2(A)	0.75 g Co(II)DPIX	69	160 mL Pyridine	70	19
2(B)	2.6 g Co(II)DPIX	114	500 mL Pyridine	116	39
2(C)	0.2 g Co(II)DPIX	4.67	40 mL Pyridine	4.9	72
2(D)	0.4 g Co(II)DPIX	4.60	80 mL Pyridine	5.0	139

a) Evaluated based on the weight of catalyst obtained and the amount of Co(II) Porphine used, because almost complete adsorption of the metal porphine was observed in each case.

Table 2. Activities of Cobalt(II) Porphines Anchored on Alumina Beads Modified by PAS for the Conversion of Q to NBD[a]

Catalyst[b]	Mol of Co(II) Porphine	$k_w \times 10^5$	k_p
	mol·g^{-1}	L·s^{-1}·g^{-1}	L·s^{-1}·mol^{-1}
1	0.043	2.45	0.57
2-A	0.019	2.95	1.6
2-B	0.039	6.00	1.5
2-C	0.072	7.93	1.1
2-D	0.14	10.8	0.77

a) Kinetic studies were carried out using pentane solution of Q, initially 0.02 mol·L^{-1} and ca. 70 mg of the catalysts at 21±1°C. b) A—D refer to the batch numbers in Table 1.

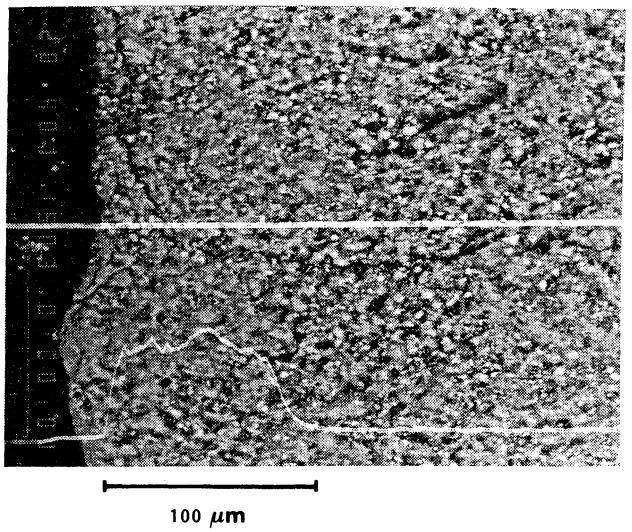

Fig. 1. SEM photograph as well as distribution of Co atoms for the cross section of the bead of Co(II)-TPPS/PAS/Alumina. The waved line shows the distribution of Co atoms along the corresponding white straight line.

Scanning Electron Microscopy (SEM) and Wavelength Dispersive X-Ray Microanalysis on Cross Section of Beads of Co(II)TPPS/PAS/Alumina (1). Figure 1 depicts SEM photograph of the cross section of the beads of **1**. The white waved line refers to distribution of Co atoms along the diameter on the cross section of the bead corresponding to the white straight line. As depicted by the waved line in Fig. 1, the distribution of Co atoms was found to be within a catalyst surface layer of 100 μm depth.

Activities of Co(II)TPPS/PAS/Alumina and Co(II)DPIX/PAS/Alumina as Catalysts. The catalysts **1** and **2** showed remarkably large catalytic activities for the reversion of Q to NBD. As one exmple, when a solution of 4 ml of Q in 6 ml of benzene was treated with 1 g of **2**-A, the exothermic reaction occurred immediately within 5 s, and the solution began to boil vigorously. After 1 min, more than 99% conversion of Q was observed by a GC analysis.

The conversion of Q to NBD catalyzed by these catalysts was followed kinetically in an isothermal batch reactor. The disappearance of Q (initial concentration=0.02 mol·L^{-1}), in pentane and the concomitant formation of NBD at 21±1 °C were monitored by GC. At such a low concentration of Q, a first order kinetic plots gave a straight line, whereas the reaction at higher concentration of Q could not be expressed by pseudo-first-order kinetic treatment. As the catalytic activities we use the values k_w L·s^{-1}·g^{-1} which are the first order kinetic constants normalized to 1 g of catalyst in 1 L of solution. The values were obtained from runs with ca. 70 mg of catalyst in 5 mL of solution (Table 2). In Table 2, k_p is the activity based on cobalt(II) porphine content. Table 2 shows the variation of the activity of **2** when the amount of Co(II)DPIX adsorbed was changed. At the low content of the cobalt(II) porphine below 39 mmol·g^{-1}, catalytic activity is proportional to the amount of Co(II)DPIX adsorbed. On the contrary, at higher content no correlation is observed, where k_w varies

Table 3. Pseudo-First-Order Kinetic Constants of Catalyzed Reversion of Q to NBD at Various Temperatures[a)]

Catalyst	Temperature °C	$k_{obsd} \times 10^4$ s^{-1}
1	19	3.27
1	24	3.65
1	29	4.10
1	34	4.65
2-A	16	3.88
2-A	21	4.46
2-A	25	4.69
2-A	30	5.65

a) First order kinetic constants were measured in an isothermal batch reactor using 5 mL of pentane solution of Q, initially 0.02 mol·L^{-1}, with 70 mg of the catalysts.

only from 6.00 to 10.8 L·s^{-1}·g^{-1} while the amount of Co(II)DPIX adsorbed varies from 39 to 140 mmol·g^{-1}. Although the reason of the lack of the correlation at higher amount of Co(II)DPIX is not apparent, it seems likely that the distribution of the catalyst monomer to deeper layer of the catalyst particle and the correspondingly occurring inner mass diffusion limitation might reduce the apparent activity of the catalyst monomer at its high content.

Temperature dependence of the pseudo-first-order kinetic constant is shown in Table 3. An Arrhenius plots corresponding to Table 3 gave energy of activation of the reaction of 16.9 and 18.8 kJ mol^{-1} for 1 and 2-A, respectively, indicating that the active species for each catalyst is fairly effective for the cycloreversion of Q to NBD.

Kinetic Study at High Quadricyclane Concentration by an Isothermal Recycle Reactor. A more detailed analysis was undertaken of the kinetics of the conversion of Q to NBD catalyzed by 1 and 2, i.e., kinetic profiles with respect to Q concentration and the retention of catalytic activities. These subjects are difficult to be examined by an usual batch type reactor. Here, the reaction rate was measured by an isothermal recycle reactor (batch of solid and flow of fluid, Fig. 2)[13] which eliminates the external mass transfer resistance. Isooctane was used as a solvent in this case.

In Fig. 2 C_{Bi} and C_B are concentrations of Q for inlet and outlet of the reactor, respectively. The solution was fed by steady rate of v m^3·s^{-1}. Catalyst of the weight of W kg was used. The value γ is recycle ratio, which was set large enough to treat the reactor as an ideal CSTR (continuous stirred tank reactor). Thus, we can set up Eq. 1 for the material balance

$$vC_{Bi} - vC_B - rW = 0 \quad (1)$$

where r denotes the reaction rate over catalyst (mol·s^{-1}·kg^{-1}). Thus the reaction rate normalized to

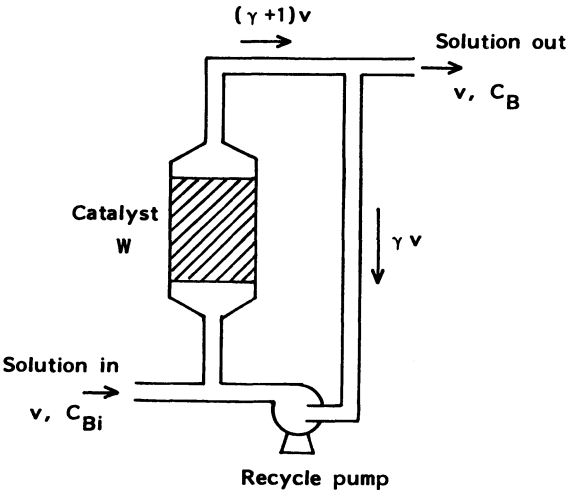

Fig. 2. Recycle reactor.

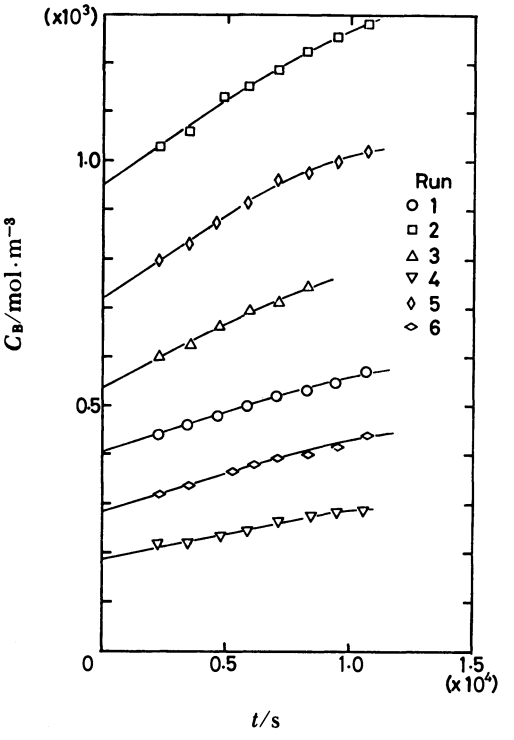

Fig. 3. Concentration of Q as a function of time. Run numbers refer to the experimental run given in Table 4.

1 kg of catalyst is given by Eq. 2.

$$-r = v(C_{Bi} - C_B)/W \quad (2)$$

A description of the experimental conditions for Co(II)TPPS/PAS/Alumina 1 is given in Table 4.

After the reaction system reached to pseudo-steady state, Q concentration (C_B) was monitored at appropriate time intervals. Figure 3 shows the C_B as a function of time for Runs 1—6 for example, and the corresponding reaction rates ($-r$) are plotted vs. time

Table 4. Experimental Conditions for the Kinetic Study of the Reversion of Q Catalyzed by 1[a)]

Run	$C_{Bi}\times10^{-3}$ mol·m^{-3}	$W\times10^{3}$ kg	$v\times10^{7}$ m^3·s^{-1}	T °C	Catalyst
1	0.76	1.02	1.64	11.0	Fresh
2	1.53	1.05	1.65	11.0	Fresh
3	0.97	0.99	1.71	11.0	Fresh
4	0.44	1.00	1.61	11.0	Fresh
5	1.23	1.02	1.63	11.0	Fresh
6	0.59	1.01	1.68	11.0	Fresh
7	0.34	1.03	2.89	42.0	Fresh
10	1.64	1.03	2.68	42.0	Fresh
11	1.03	0.99	2.74	42.0	Fresh
12	1.36	0.78	2.46	42.0	Fresh
13	0.73	0.79	2.44	42.0	Fresh
14	0.45	0.74	2.35	42.0	Fresh
15	1.61	0.75	1.75	25.0	Fresh
16	1.12	0.78	1.78	25.0	Fresh
17	0.39	0.78	1.73	25.0	Fresh
18	1.24	0.74	1.79	25.0	Fresh
19	0.78	0.75	1.80	25.0	Fresh
20	0.54	0.83	1.73	25.0	Fresh
21	1.24	0.74	2.09	25.0	Reactivated (Used in Run 18)
22	0.55	0.73	1.81	25.0	Reactivated (Used in Run 20)
23	1.26	0.73	1.80	25.0	Reactivated (Used in Run 21)

a) Values C_{Bi}, W, and v refer to symbols in Fig. 2, (see text).

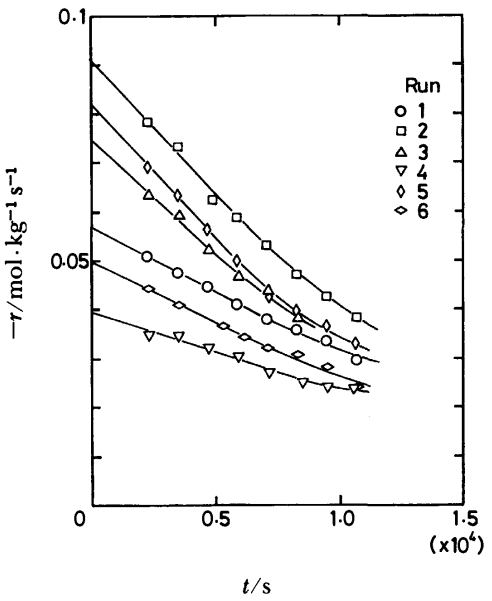

Fig. 4. Reaction rate as a function of time. Run numbers refer to the experimental run given in Table 4.

in Fig. 4. The decrease in the reaction rate arises from the partial loss of activity of the catalyst. The value r_0 estimated by extrapolation at t=0 was adopted as a reaction rate for the corresponding Q concentration C_{B0}. Plots of $-r_0$ vs. C_{B0} are shown in Fig. 5 for three different temperatures. If the reaction were first order with respect to Q the plots should be linear. The plots shown in Fig. 5 can be expressed by equations indicated in the same figure for each temperature. The equations can be correlated to Langmuir-Hinshelwood type rate expression

$$-r = kKC_B/(1 + KC_B) \quad (3)$$

Kinetic constant k mol·kg^{-1} s^{-1} and absorption constant K m^3·mol^{-1} were obtained from experimental correlation shown in Fig. 5 and are summarized in Table 5. Figure 6 shows Arrhenius Plots for k and K which gave temperature dependences of these values as indicated in the same figure. Thus, reaction rate of the reversion of Q to NBD catalyzed by **1** can be written as following.

$$-r = \frac{0.406\exp(-2062/T)C_B}{1 + 1.01 \times 10^{-3}\exp(213/T)C_B} \quad (4)$$

In the case of Co(II)DPIX/PAS/Alumina (**2**-B), the similar experiments gave qualitatively the same results as the case of **1**. The kinetic profiles for **2**-B are shown in Table 5, and the rate expression is

$$-r = \frac{0.539\exp(-1832/T)C_B}{1 + 1.58 \times 10^{-4}\exp(593/T)C_B} \quad (5)$$

The retension of the catalytic activity of **2**-B after

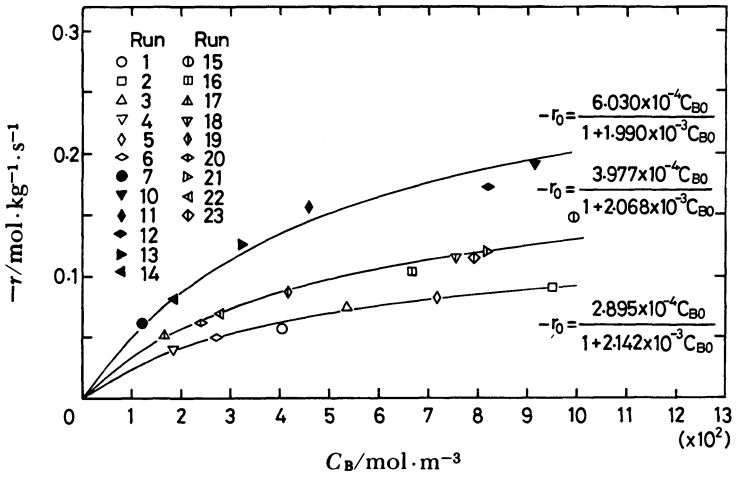

Fig. 5. Plots of reaction rates vs. Q concentration at t=0. Run numbers correspond to the experimental conditions given in Table 4. Upper curve is for 42.0 °C (Runs 7—14), middle curve for 25.0 °C (Runs 15—23) and bottom curve for 11.0 °C (Run 1—6).

Table 5. Kinetic Parameters for the Reversion of Q to NBD Catalyzed by Co(II)TPPS/PAS/Alumina (**1**) and Co(II)DPIX/PAS/Alumina (**2-B**)[a)]

Catalyst	Temp	k	10^3K	E_a	ΔH
	°C	$\mathrm{mol\cdot kg^{-1}\cdot s^{-1}}$	$\mathrm{m^3\cdot mol^{-1}}$	$\mathrm{kJ\cdot mol^{-1}}$	$\mathrm{kJ\cdot mol^{-1}}$
	11.0	0.135	2.14		
1	25.0	0.192	2.07	18.9	−1.77
	42.0	0.303	1.99		
	11.0	0.714	1.24		
2-B	20.0	0.833	1.20	20.2	−4.93
	40.0	1.51	1.04		

a) k and K refer to the symbols in Eq. 3. E_a is energy of activation obtained based on an Arrhenius plots for k and ΔH heat of adsorption for K.

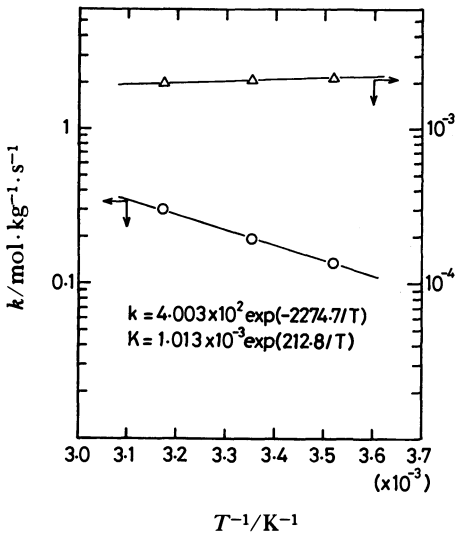

Fig. 6. Arrhenius plots for the kinetic constant k and adsorption constant K given in Table 5 for the Co(II)TPPS/PAS/Alumina catalyzed reversion of Q.

repeated use was examined by an isothermal (30±1 °C) batch reactor according to the method described by King and Sweet.[9)] A 0.17 g charge of catalyst **2-B** (6.6×10^{-4} mol·L^{-1} Co) was examined for loss of activity upon repeated recycling using 10 mL of 0.1 mol·L^{-1} Q in pentane. After five times batch of repeated use, ca. 40% loss of activity was observed while they reported ca. 50% loss of activity when 0.107 g of their polystyrene-anchored Co(II)TPP (8.1×10^{-4} mol·L^{-1} Co) was used. The deactivation of catalytic activity was examined quantitatively based on the kinetic studies by the use of the isothermal recycle reactor. For this purpose, fractional activity (a) is defined as

$$a = -r(C_B,t)/-r(C_B,0) \quad (6)$$

where $-r(C_B,0)$ is the initial rate expressed by Eq. 4 or Eq. 5 corresponding to the fresh catalyst, and $-r(C_B,t)$ denotes the reaction rate corresponding to catalyst which has worked for t s being exposed in Q solution of the concentration C_B. Numerical treatments

Table 6. Values, α and β, in Eq. 7 Characterizing the Retension of Activities of Catalysts **1** and **2-B**

Catalyst	Temperature °C	$10^3\alpha$	$10^6\beta$
1	11	31	2.9
1	20	31	3.3
2-B	11	3.7	0.27
2-B	20	3.7	0.27
2-B	40	16	1.1

afforded the expression of the fractional activity as a function of C_B and t

$$a = \exp[(-\beta C_B/1 + \alpha C_B)t] \quad (7)$$

where the values, α and β, for **1** and **2-B** at various temperatures are reported in Table 6.

Although the mechanism of the loss of activity is not clear, Eq. 7 indicates that Q molecule should be included in the mechanism. King and Sweet reported[9] that the loss in catalytic activity of their polystyrene-anchored Co(II)TPP arised from partial oxidation of the cobalt metal, and they demonstrated that the loss could be partially regenerated by the treatment with a strong reducing agent. In our case of cobalt(II) porphine anchored on PAS/Alumina, the decrease in the activity could be regenerated by heating the used catalyst at 200 °C in vacuo. In the Runs 21 and 22 seen in Table 4, used catalysts reactivated by this method were employed. As shown in Fig. 5 the plots for these runs is on the line obtained for the runs with fresh catalysts, which indicates the complete recovery of the catalytic activity. Even in the case of Run 23 in which the catalyst used has experienced two times reactivations, an almost complete regeneration of the catalytic activity was observed. The same reactivation procedure was effective for Co(II)DPIX/PAS/Alumina. These results indicate that the loss of catalytic activity of **1** and **2** should be due to fouling which arises from a kind of reaction of Q molecule and which can be eliminated by heating in vacuo.

A Bench-Scale Examination of Energy-Releasing Process, Q→NBD, Catalyzed by Co(II)DPIX/PAS/Alumina, 2-B. The feature of the heat-releasing process based on the reversion of Q catalyzed by **2-B** was examined by using a bench scale fixed bed reactor. A schematic of the flow system is shown in Fig. 7. The reactor was made of Pyrex glass, 2 cm in inner diameter and 70 cm in length, and packed with solid catalyst **2-B** of ca. 200 cm^3 in volume. Measurement of the axial temperature distribution in the reactor was made by the twenty thermocouples fixed at the axis of the reactor. Isooctane solution of Q at room temperature was introduced into the reactor by means of a roller pump. Table 7 lists the experimental conditions and the physical properties of the solution.

Table 7. Experimental Conditions and Physical Properties of Isooctane Solution of Q

Flow rate	$0.157\,cm\cdot s^{-1}$ a)
Solution	
Q concentration	$1.09\,mol\cdot L^{-1}$ b)
Mean value of heat capacity at constant pressure	$2.28\,J\cdot g^{-1}\cdot K^{-1}$ c)
Density	$0.793\,g\cdot cm^{-3}$
Heat of reversion of Q	$96.2\,kJ\cdot mol^{-1}$ d)

a) Superficial velocity. b) Initial concentration. c) Heat capacity of isooctane at 55 °C was employed. d) Determined by a microcalorimetry of the isomerization catalyzed by $Rh_2Cl_2(NBD)_2$.

At the experimental conditions, both conversions and temperature rise were close to equilibrium. That is, Q in the inlet solution was isomerized to NBD during the flow through the catalyst bed with a concomitant evolution of heat and with no detectable by-products. Conversion at the exit of the reactor was unity, and maximum temperature rise was 58.5 °C which agrees well with the adiabatic temperature rise calculated based on the values in Table 7.

Figure 8 shows the axial temperature profiles along the reactor. With increasing distance Z, the temperature T rapidly increases and reaches a constant value. This system could conceivably have external mass transport resistance with Damköhler number being 11.5 at 40 °C. Therefore one-dimensional heterogeneous model accounting for interfacial gradient was used to predict the longitudinal distribution of temperature in the adiabatic fixed bed.[14] Here, the rate expression, Eq. 5, includes the internal mass transfer resistance. Although measurements show a little larger rate of the catalyst deactivation, they are well represented by the solid lines.

Conclusion

Polyaminesulfone modified alumina beads adsorbed cobalt(II) porphine derivatives possessing acidic group through ionic linkages, which provides an very easy method to immobilize cobalt(II) porphines on solid support. Using cobalt(II) tetrakis(*p*-sulfonatophenyl)porphine and cobalt(II) deuteroporphyrin, the method provides active catalysts for the valence isomerization of Q to NBD. The catalysts reveal prominent properties; high activity, small deactivation rate and moreover ability of regeneration of activity by heating the catalyst at 200 °C in vacuo. Furthermore, the distribution of the active species in the catalyst particle is restricted to a thin layer on the surface of the support. The catalyst showed strong resistivity against temperature (250 °C).

The reaction rate of the catalyzed isomerization of Q

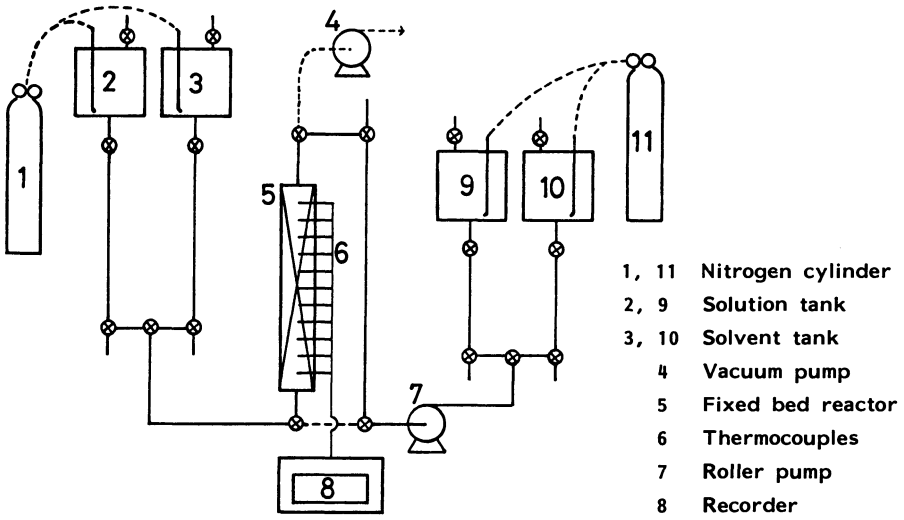

Fig. 7. Schematic of flow system.

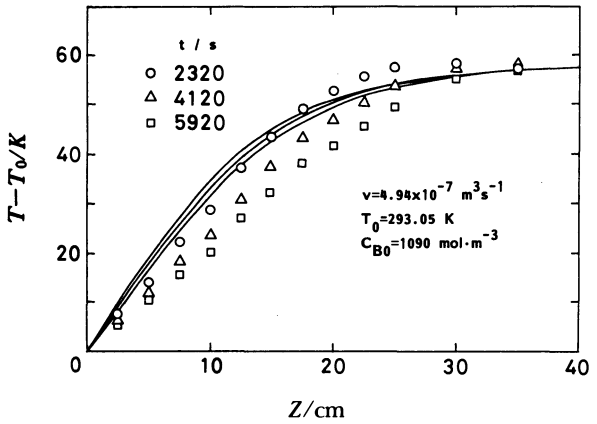

Fig. 8. Temperature profiles along the axis of the fixed bed reactor (**5**, Fig. 7) for the energy releasing process catalyzed by Co(II)DPIX/PAS/Alumina.

obeys Langmuir-Hinshelwood type rate expression. In a bench scale test, the catalysts revealed efficient activities to evolve heat rapidly upon contact with Q. The relatively large particle size of the catalyst and correspondingly the small pressure drop when packed in a column is presumably a preferable property in practical process. Furthermore, the catalysts did not swell up upon contact with any solvent.

Experimental

Materials. Polyaminesulfone-A (PAS) and activated alumina beads (Sumitomo Alumi NKH-1) were offered by Nittobo Co. Ltd. and Sumitomo Aluminium Smelting Co. Ltd., respectively. Deuteroporphyrin IX was prepared from protohemin according to the method of Fischer.[15] Incorporation of cobalt(II) was performed by the method of Yamamoto.[16] Pyridine was distilled over KOH under argon. Quadricyclane was prepared by a modification of King's method.[9] Pentane and isooctane used in kinetic studies were guaranteed grade commercially available and were used without further purification.

Analytical Method. Gas chromatographic analyses were carried out on a GC system composed of a Shimadzu GC-7A with TCD detector and a Shimadzu Chromatopac C-E1B. A Pyrex glass column, 5 mm in inner diameter and 1 m in length, was packed with Silicone DC-550. Helium was used as a carrier with flow rate of 50 mL·min^{-1}. Treatment of the packed column with five times injections of 50 μL triethylamine followed by baking out for 3 h at 150 °C eliminated the isomerization of Q in the column. Samples were analyzed using an injector temperature of 120 °C and a column temperature of 70 °C.

Sodium Tetrakis(*p*-sulfonatophenyl)porphinatocobalt(II) Complex (Co(II)TPPS, 4). A solution of 9.95 g (8 mmol) of sodium tetrakis(*p*-sulfonatophenyl)porphine and 1.99 g (8 mmol) of cobalt acetate in 100 mL of DMF was refluxed for 5 min. After cooling the reaction mixture, addition of benzene afforded 10 g (98%) of **4**.

PAS Modified Alumina Beads. To a 1 L solution of polyaminesulfone-A (PAS, **3**) (mean MW=2×10^5, Nittobo Co. LTD.) in water (10 wt%) was added 200 g of activated alumina beads (mean diameter of 3 mm, Sumitomo Aluminium Smelting Co. Ltd., NKH-1). The mixture was stood for 12 h with occasional swirling. Separation of the beads by filtration with a stainless steel net, air-drying at 100 °C for 2 days and drying at 80 °C in vacuo for 3 h afforded 245 g of the PAS modified alumina beads, PAS/Alumina.

Co(II)TPPS/PAS/Alumina (1). A two-necked round-bottomed flask equipped with a septum rubber stopper and three way valve was charged with a 190 g of PAS/Alumina, air in the flask was replaced with argon by means of a pump and argon balloon. To this was added a solution of 9.12 g (7.2 mmol) of **4** in a 2 L of degassed methanol by means of a canalation by positive argon pressure using a teflon tubing with 3 mm in inner diameter. The mixture was stood for 2 days under positive argon pressure with occasional swirling. After 2 days the color of the cobalt(II) porphine of the supernant was disappeared almost completely. The catalyst beads were filtered under nitrogen atmosphere and dried for

6 h at 120 °C in vacuo to give 174 g of the title catalyst. The catalyst was stocked under positive argon pressure.

Co(II)DPIX/PAS/Alumina (2). A solution of 0.75 g (1.3 mmol) of cobalt(II) deuteroporphyrin (Co(II)DPIXCo, **5**) in 160 ml of dry pyridine degassed by freeze and pumping was introduced onto a 69 g of PAS/Alumina beads under argon atmosphere. After the color of the cobalt(II) porphyrin was disappeared from the supernant, the beads were separated by filtration under argon and dried for 5 h at 150 °C in vacuo to give 70 g of **2** of batch-A. Batch-B, C, and D of **2** were prepared by similar manner. The specific quantities of materials and the solvent employed in the preparation of each batch are shown in Table 1.

Scanning Electron Microscopy and Wavelength Dispersive X-Ray Microanalysis. Scanning electron microscopy and the wavelength dispersive X-ray microanalysis on catalyst **1** were simultaneously carried out by the use of a JXA-733 of JOEL Co. Ltd. The specimen for the analysis of the cross section of the bead was prepared by dividing a bead into two hemispheres.

Measurements of Catalytic Activities and Studies on the Recycling Catalytic Run. A reaction cell of 20 mL in volume mantled with a jacket was equipped with a magnetic stirring bar and a septum rubber stopper. Thermostated water was circulated through the jacket in order to regulate the temperature of the reaction cell. The cell was charged with a weighed catalyst (ca. 70 mg) under argon atmosphere and was added a Q solution in pentane being set at reaction temperature by a syringe and the timing begun. Samples of the reaction solution (10 μL) were withdrawn for GC analyses. The initial sample was withdrawn at 30 s with subsequent samples at 120 s intervals, and more than 15 samples were analyzed.

The recycling study was carried out in a similar manner. At the end of the reaction period (more than 90% conversion), the reaction solution was decanted. The employed catalyst was washed two times with 5 mL of pentane and was dried up for 5 min under reduced pressure before using it for the next catalytic run.

Kinetic Studies Using an Isothermal Recycle Reactor. A schematic illustration of a recycle reactor is shown in Fig. 2. As shown in Table 4, around 1 g of catalyst was charged in the batch of the reactor. The whole system was immersed in a water bath thermostated at desired temperature. Solution of Q in isooctane was introduced into the reactor with precise control of the flow rate. In the experimental runs, recycling ratio γ was set above 67 so that the reactor could be treated as an ideal CSTR.[13] The superficial velocity in the catalyst fixed bed reactor above 4.2 $cm \cdot s^{-1}$ was employed in order to eliminate external diffusion resistance.[17] Samples of the reaction solution were withdrawn at the exit of the reactor and were analyzed on a GC system. After the reaction system reached to pseudo-steady state samplings were carried out at such time intervals indicated in Fig. 4.

Bench Scale Examination of the Catalytic Energy-Releasing Process on Co(II)DPIX/PAS/Alumina 2-B. A schematic of the flow system is shown in Fig. 7. The apparatus was made of teflon except a glass reactor and a rubber (Biton) tubing in pump. Each tank was 5 L in volume and the pipeline which connects a reactor with tanks was 6 mm in diameter. Feed was introduced into the reactor by means of a roller pump which provides very precise control of flow rate over the range of 120—1200 $mL \cdot h^{-1}$. A cylindrical reactor was used, which is made of Pyrex glass, 2 cm in inner diameter and 70 cm in length. The reactor was packed with **2-B** of 200 cm^3 in volume. The active catalytic portion was contained between inert fore and aft sections of glass beads. The reactor was thermally insulated from its surroundings with asbestos. The twenty copper-constantan thermocouples were fixed at the axis of the reactor to measure the axial temperature distribution in the reactor. A hybrid recorder was used to record the outputs of the thermocouples. The concentrations of both Q and NBD were measured with a GC. Isooctane was used as a solvent.

In operation, feed at room temperature (20.1 °C) was introduced into the reactor by means of a roller pump at a constant flow rate. The solvent feed was initially passed through the reactor, establishing a steady flow. Once steady flow was achieved a three way valve was switched, sending the solution stream through the reactor. Temporal changes in temperature were measured by the thermocouples and samplings of the solution were made at the exit of the reactor. Their compositions were analyzed with the GC. During the experiments, the solution and solvent in tank has been bubbling by nitrogen gas from a cylinder to prevent a polymerization of NBD by dissolved oxygen. Reaction periods of about 1—2 h were employed. Table 7 lists the experimental conditions and the physical properties of the solutions.

References

1) T. Laird, *Chem. Ind.*, **1978**, 186.
2) "Solar Energy: Chemical Conversion and Storage," ed by R. R. Hautala, R. B. King, and C. Kutal, Humana Press, Clifton, NJ (1979).
3) Z. Yoshida, *J. Photochem.*, **29**, 27 (1985).
4) K. Maruyama, T. Terada, and Y. Yamamoto, *J. Org. Chem.*, **46**, 5294 (1981).
5) K. Maruyama, H. Tamiaki, and S. Kawabata, *J. Org. Chem.*, **50**, 4742 (1985).
6) T. Toda, E. Hasegawa, T. Mukai, H. Tsuruta, T. Hagiwara, and T. Yoshida, *Chem. Lett.*, **1982**, 1551.
7) K. Hirao, A. Ando, T. Hamada, and O. Yonemitsu, *J. Chem. Soc., Chem. Commun.*, **1984**, 300.
8) H. Ikezawa, C. Kutal, K. Yasufuku, and H. Yamazaki, *J. Am. Chem. Soc.*, **108**, 1589 (1986).
9) R. B. King and E. M. Sweet, *J. Org. Chem.*, **44**, 385 (1979).
10) R. B. King and R. M. Hanes, *J. Org. Chem.*, **44**, 1092 (1979).
11) R. J. Card and D. C. Neckers, *J. Org. Chem.*, **43**, 2958 (1978).
12) M. E. Landies, D. Gremaud, and T. B. Patrick, *Tetrahedron Lett.*, **23**, 375 (1982).
13) S. Wedel and J. Villadson, *Chem. Eng. Sci.*, **38**, 1346 (1983).
14) The steady state equations are:
Fluid
$$-u \cdot dC_B/dZ = \rho_b \cdot k_c \cdot a_s \cdot (C_B - C_{BW})$$
$$u \cdot \rho \cdot C_{pm} \cdot dT/dZ = \rho_b \cdot h \cdot a_s \cdot (T_W - T)$$
Solid
$$-r = k_c \cdot a_s \cdot (C_B - C_{BW})$$
$$(-\Delta H) \cdot (-r) = h \cdot a_s \cdot (T_W - T)$$

where u: superficial velocity
C_B: molar concentration of quadricyclane
C_{Bw}: molar concentration of quadricyclane at catalyst pellet surface
Z: axial distance coordinate in fixed bed reactor
ρ_b: bulk catalyst density
k_c: liquid-solid mass transfer coefficient
a_s: external surface area of catalyst particle per unit mass
ρ: liquid density
C_{pm}: specific heat capacity of liquid
T: bulk liquid temperature
T_w: liquid temperature at catalyst pellet surface
h: liquid-solid heat transfer coefficient
$-r$: reaction rate
$-\Delta H$: heat of reaction

The model is extended to the pseudo-steady state by introducing the fractional activity of catalyst, a.

15) H. Fischer and H. Orth, "Die Chemie des Pyrroles, Vol. II," Academische Verlag, Leipzig (1937), p. 44.
16) T. Yonetani, H. Yamamoto, and G. V. Woodrow III, *J. Biol. Chem.*, **249**, 682 (1974).
17) J. J. Carberry, "Chemical and Catalytic Reaction Engineering," McGraw-Hill, New York (1976), p. 205.

Synthesis, Reactions, Spectral (IR and Visible) and Magnetic Studies of Bimetallic Alkoxides Containing Co(μ-OR)$_3$M (M=Nb or Ta) Bridging Units

Raj Kumar Dubey, Anirudh Singh, and Ram Charan Mehrotra*
Department of Chemistry, University of Rajasthan, Jaipur 302004, India
(Received December 15, 1986)

Interactions of $CoCl_2$ with K{M(OPr^i)$_6$} in 1:2 molar ratio in Pr^{i}OH and C_6H_6 result in products with the composition [Co{M(OPr^i)$_6$}$_2$] (M=Nb or Ta) in quantitative yields. Interchange reactions of these isopropoxide derivatives with alcohols of varying steric bulk (e.g., MeOH, EtOH, Pr^{n}OH, Bu^{n}OH, and Bu^{t}OH, or Am^{t}OH) yield derivatives of composition, [Co{M(OR)$_6$}$_2$] (R=Me, Et, Pr^n, and Bu^s); [Co{M(OPr^i)$_3$(OBu^s)$_3$}$_2$]; [Co{M(OPr^i)$_5$(OBu^t)}$_2$] and [Co{M(OPr^i)$_2$(OR)$_4$}$_2$] (R=Bu^t or Am^t). All these novel compounds have been characterized by elemental analyses and molecular weight determinations as well as by infrared, visible spectral and magnetic studies.

In contrast to the well-known chemistry of alkoxy derivatives of earlier transition metals,[1,2] alkoxides of later transition metals have received only scanty attention possibly due to their insolubility and polymeric nature. One of the fascinating developments in the alkoxide chemistry of later '3d' metals (including cobalt) has been the synthesis[3] of soluble, monomeric, volatile, bimetallic alkoxides, [M{Al(OR)$_4$}$_n$] (where n=3, when M=Cr(III), Fe(III) and n=2, when M=Co(II), Ni(II), Cu(II)) in our laboratories. The {Al(OR)$_4$}$^-$ has proved to be an excellent ligand and depicts an interesting variation in its ligating behavior; e.g., it acts as a bidentate ligand towards Cr(III),[4] and Fe(III),[5] but it exhibits a tridentate ligating behavior with Co(II)[6] and Cu(II);[7] and with Ni(II),[8] an ambidentate (both bi- and tri-) behavior has been observed. By contrast, bimetallic alkoxide derivatives containing both early and later d-block elements bridged by alkoxy groups have been much less studied. These bimetallic alkoxides could be expected to find useful applications (i) as homogeneous catalysts,[9] (ii) in ceramic industry[10] and (iii) in organic syntheses. In view of the above, we report herein some aspects of bimetallic alkoxide derivatives of cobalt(II) containing Co(μ-OR)$_3$M (M=Nb or Ta) bridging units.

Experimental

General. Stringent precautions were taken to exclude atmospheric moisture from the glasswares, solvents and the reagents were purified by literature methods prior to use.

Anhydrous $CoCl_2$ was prepared by heating the hydrated $CoCl_2 \cdot 6H_2O$ in a current of dry HCl gas and analyzed. Analysis for $CoCl_2$: Found: Co, 45.41; Cl, 54.59; Calcd: Co, 45.39; Cl, 54.61%.

Niobium and tantalum isopropoxides were prepared[11] by passing dry NH_3 gas in a solution of their pentachlorides (Fluka) in isopropyl alcohol.

Cobalt in bimetallic derivatives was estimated gravimetrically[12] as [Co(C$_5$H$_5$N)$_4$](NCS)$_2$ and niobium (tantalum) was estimated as oxide. From the solution of the bimetallic alkoxides in hydrochloric acid, hydrated niobium (tantalum) oxide is first precipitated with only slight excess of aqueous ammonia and cobalt is then precipitated as [Co(C$_5$H$_5$N)$_4$](NCS)$_2$ by addition of NH_4SCN followed by pyridine to the filtrate. Blank determinations with known solutions showed that niobium (tantalum) tends to be about 2% higher and cobalt about 1—2% lower under these conditions.

Alcohols were determined by an oxidimetric method.[13]

The infrared spectra were recorded in the range 4000—400 cm^{-1} on a Perkin-Elmer 557 spectrometer using Nujol mull. The visible spectra have been recorded on a Pye-Unicam SP8-100 spectrophotometer. The magnetic susceptibilities were measured on a Gouy balance using Hg[Co(NCS)$_4$] as standard. The magnetic moments, μ_{eff}, were calculated by the expression: $\mu_{eff}=2.84\sqrt{\chi_M^{Corr} \cdot T}$ (where χ_M^{Corr} is the molar susceptibility corrected for the diamagnetism of the constituent atoms by the use of Pascal's constants). Helium gas compressor was used for low temperature susceptibility measurements. Molecular weights were determined cryoscopically.

Syntheses and Reactions. Methods of synthesis of [Co{M(OPr^i)$_6$}$_2$] derivatives and some of their typical reactions are described briefly below. The amount of chemicals used in each reaction, the yield of the product, the elemental analyses and other details are given in Table 1.

A. Preparation of [Co{M(OPr^i)$_6$}$_2$] (M=Nb or Ta). A weighed amount of K{M(OPr^i)$_6$} in benzene (40 cm^3) was added to a suspension of $CoCl_2$ in Pr^{i}OH (30 cm^3). The reaction mixture was refluxed for≈5 h and precipitated KCl was removed by filtration. The excess of solvent was distilled out and the concentrate kept at room temperature; purple-red crystalline solid [Co{M(OPr^i)$_6$}$_2$] crystallized out. The product was further recrystallized unchanged either from Pr^{i}OH-PhH or hexane.

B. Reactions of [Co{M(OPr^i)$_6$}$_2$]. (i) With Excess of MeOH (at Room Temperature). To a benzene solution of [Co{M(OPr^i)$_6$}$_2$], an excess of MeOH was added. The reaction mixture was stirred for≈6 h, during which the color changed from purple-red to violet. After removal of the volatiles under reduced pressure a violet colored solid product of composition, [Co{M(OMe)$_6$}$_2$] was isolated, which could be recrystallized unchanged from hexane.

(ii) With Excess of EtOH (at Room Temperature). EtOH was added to a benzene solution of [Co{Ta(OPr^i)$_6$}$_2$] and stirred for≈6 h at room temperature. The solvent was removed under reduced pressure to yield a violet red solid

Table 1. Synthesis and Alcohol Interchange Reactions of $[Co\{M(OPr^i)_6\}_2]$ (M=Nb or Ta)

Reaction Number	Reactant/g	Product/g[e]	Physical state	Analysis Found (Calcd) Co	M	OR	Pr^iOH/g Liberated Found (Calcd)
1	$CoCl_2$+K{Nb(OPr^i)$_6$} 0.86 6.47	$[Co\{Nb(OPr^i)_6\}_2]$[a] 5.68 (6.31)	Purple red crystalline solid	5.87 (6.18)	19.55 (19.48)	73.60 (74.34)	
2	$[Co\{Nb(OPr^i)_6\}_2]$+MeOH 1.15 ≈35 cm^3	$[Co\{Nb(OMe)_6\}_2]$[b] 0.65 (0.74)	Violet solid	9.54 (9.55)	30.73 (30.11)	—	
3	$[Co\{Nb(OPr^i)_6\}_2]$+EtOH 1.68 ≈40 cm^3	$[Co\{Nb(OEt)_6\}_2]$[c] 1.30 (1.38)	Violet solid	7.38 (7.50)	23.60 (23.65)	68.90 (68.84)	
4	$[Co\{Nb(OPr^i)_6\}_2]$+Pr^{n}OH 1.54 ≈40 cm^3	$[Co\{Nb(OPr^n)_6\}_2]$[c] 1.50 (1.54)	Violet crystalline solid	5.91 (6.18)	19.65 (19.48)		
5	$[Co\{Nb(OPr^i)_6\}_2]$+Bu^{n}OH 1.02 ≈45 cm^3	$[Co\{Nb(OBu^n)_6\}_2]$[c] 1.10 (1.17)	Violet crystalline solid	5.26 (5.25)	16.62 (16.56)	—	
6	$[Co\{Nb(OPr^i)_6\}_2]$+Bu^{s}OH 1.60 ≈40 cm^3	$[Co\{Nb(OBu^s)_6\}_2]$[d] 1.85 (1.87)	Violet red solid	5.19 (5.25)	17.50 (16.56)	—	0.81 (0.80)
7	$[Co\{Nb(OPr^i)_6\}_2]$+Bu^{t}OH 1.54 ≈25 cm^3	$[Co\{Nb(OPr^i)_5(OBu^t)\}_2]$[c] 1.57 (1.58)	Violet red solid	5.96 (6.00)	18.98 (18.92)	60.16 (60.18)	—
8	$[Co\{Nb(OPr^i)_6\}_2]$+Bu^{t}OH 1.61 ≈45 cm^3	$[Co\{Nb(OPr^i)_2(OBu^t)_4\}_2]$[d] 1.71 (1.79)	Violet red solid	5.50 (5.53)	17.60 (17.43)	22.10 (22.17)	0.81 (0.81)
9	$CoCl_2$+K{Ta(OPr^i)$_6$} 0.49 4.37	$[Co\{Ta(OPr^i)_6\}_2]$[a] 3.85 (4.26)	Purple red crystalline solid	5.16 (5.22)	32.30 (32.03)	62.54 (62.75)	
10	$[Co\{Ta(OPr^i)_6\}_2]$+MeOH 1.41 ≈45 cm^3	$[Co\{Ta(OMe)_6\}_2]$[b] 0.95 (0.98)	Violet solid	7.32 (7.43)	46.39 (46.62)	—	
11	$[Co\{Ta(OPr^i)_6\}_2]$+EtOH 1.18 ≈40 cm^3	$[Co\{Ta(OEt)_6\}_2]$[c] 1.50 (1.53)	Violet solid	6.17 (6.13)	37.55 (37.64)	56.04 (56.24)	
12	$[Co\{Ta(OPr^i)_6\}_2]$+EtOH 1.24 ≈25 cm^3	$[Co\{Ta(OPr^i)_2(OEt)_4\}_2]$[b] 1.05 (1.11)	Violet red solid	5.48 (5.79)	36.24 (35.56)	—	
13	$[Co\{Ta(OPr^i)_6\}_2]$+Pr^{n}OH 1.20 ≈35 cm^3	$[Co\{Ta(OPr^n)_6\}_2]$[c] 1.18 (1.20)	Violet crystalline solid	5.22 (5.22)	32.12 (32.03)	—	—
14	$[Co\{Ta(OPr^i)_6\}_2]$+Bu^{n}OH 1.45 ≈40 cm^3	$[Co\{Ta(OBu^n)_6\}_2]$[c] 1.54 (1.66)	Violet crystalline solid	4.49 (4.54)	27.79 (27.87)	—	—
15	$[Co\{Ta(OPr^i)_6\}_2]$+Bu^{s}OH 1.10 ≈25 cm^3	$[Co\{Ta(OPr^i)_3(OBu^s)_3\}_2]$[b] 1.17 (1.18)	Violet red solid	4.83 (4.85)	30.67 (29.81)	29.17 (29.20)	—
16	$[Co\{Ta(OPr^i)_6\}_2]$+Bu^{s}OH 1.41 ≈25 cm^3	$[Co\{Ta(OPr^i)_2(OBu^s)_4\}_2]$[c] 1.49 (1.54)	Violet red solid	4.80 (4.74)	30.05 (29.13)	18.82 (19.03)	—
17	$[Co\{Ta(OPr^i)_6\}_2]$+Am^{t}OH 1.58 ≈50 cm^3	$[Co\{Ta(OPr^i)_2(OAm^t)_4\}_2]$[d] 1.85 (1.90)	Violet red solid	4.38 (4.35)	26.78 (26.72)	17.40 (17.45)	0.65 (0.66)

a) Yield of the crystallized product and molecular weight of $[Co\{Nb(OPr^i)_6\}_2]$, Found: 901; Calcd (954) and for $[Co\{Ta(OPr^i)_6\}_2]$ Found: 1015; Calcd (1130). b) Reaction was carried out at room temperature. c) Reaction was carried out in refluxing C_6H_6 (without azeotropic removal of Pr^iOH). d) Reaction was carried out in refluxing C_6H_6 with azeotropic removal of Pr^iOH. e) Stoichiometric yield in parenthesis.

product of composition $[Co\{Ta(OPr^i)_2(OEt)_4\}_2]$.

(iii) With EtOH, Pr^{n}OH, and Bu^{n}OH in Refluxing Benzene. Interaction of a benzene solution of $[Co\{M(OPr^i)_6\}_2]$ with excess of EtOH followed by refluxing for≈6 h, resulted the change in color from purple red to violet. Removal of the solvent under reduced pressure afforded a solid of composition $[Co\{M(OEt)_6\}_2]$ which could be purified unchanged by recrystallization from hexane.

Derivatives of *n*-propyl and butyl alcohols were prepared similarly.

(iv) With Excess of Bu^{s}OH at Room Temperature. An excess of *s*-butyl alcohol was added to a benzene solution of $[Co\{Ta(OPr^i)_6\}_2]$ and the resulting reaction mixture was stirred for≈6 h. The removal of the solvent produced a violet solid of composition $[Co\{Ta(OPr^i)_3(OBu^s)_3\}_2]$.

(v) Reaction with Bu^{s}OH in Refluxing Benzene. To a benzene solution of $[Co\{Ta(OPr^i)_6\}_2]$ *s*-butyl alcohol was added and the reaction mixture was refluxed for ≈6 h. The removal of the solvent under reduced pressure afforded a violet red solid product of composition, $[Co\{Ta(OPr^i)_2(OBu^s)_4\}_2]$.

(vi) With Excess of Bu^{s}OH (Azeotropically). To a solution of $[Co\{Nb(OPr^i)_6\}_2]$ in benzene an excess of *s*-butyl alcohol was added and reaction mixture was refluxed for ≈6 h during which the liberated isopropyl alcohol was collected and estimated. After complete removal of the isopropyl alcohol, the solvent was stripped off under reduced pressure to afford a violet red solid $[Co\{Nb(OBu^s)_6\}_2]$.

(vii) With Excess of Bu^{t}OH (in Refluxing Benzene). To a benzene solution of $[Co\{Nb(OPr^i)_6\}_2]$ *t*-butyl alcohol

was added and refluxed for ≈6 h. After removal of the solvent under reduced pressure and drying a violet red solid product of composition, $[Co\{Nb(OPr^i)_5(OBu^t)\}_2]$ was obtained.

(viii) With Excess of Bu^tOH/Am^tOH (Azeotropically). $[Co\{Nb(OPr^i)_6\}_2]$ was dissolved in benzene and excess of *t*-butyl alcohol was then added. The reaction mixture was continued to reflux for ≈25 h, with continuous removal of the liberated isopropyl alcohol. When the liberation of isopropyl alcohol ceased off, the volatiles were removed and the product was dried under reduced pressure to afford violet red solid of composition, $[Co\{Nb(OPr^i)_2(OBu^i)_4\}_2]$.

A similar procedure was employed for the preparation of $[Co\{Ta(OPr^i)_2(OAm^t)_4\}_2]$.

Results and Discussion

Bis(hexaisopropoxy) derivatives $[Co\{M(OPr^i)_6\}_2]$ (M=Nb or Ta) have been synthesized by the reactions of anhydrous cobalt(II) chloride with $K\{M(OPr^i)_6\}$ in 1 : 2 molar ratio in Pr^iOH and C_6H_6:

$$CoCl_2 + 2K\{M(OPr^i)_6\} \xrightarrow[\text{reflux}]{Pr^iOH\text{-}PhH} [Co\{M(OPr^i)_6\}_2] + 2\ KCl\downarrow$$

Products from the above reactions have been isolated in quantitative yields and purified by recrystallization either from Pr^iOH–PhH or hexane. These bimetallic isopropoxides are purple red crystalline solids and depict monomeric behavior (cryoscopically) in benzene. On heating even under reduced pressure, these appear to disproportionate into the corresponding volatile isopropoxide, $M(OPr^i)_5$ and non-volatile, $\{Co(OPr^i)_2\}_n$.

Alcoholysis reactions of these bimetallic isopropoxides $[Co\{M(OPr^i)_6\}_2]$ with different alcohols have shown interesting results. The extent of substitution reactions vary with experimental conditions and the bulk of the reacting alcohol; these are indicated by the following equations:

$$[Co\{M(OPr^i)_6\}_2] + 12\ \underset{\text{(excess)}}{MeOH} \xrightarrow{rt} [Co\{M(OMe)_6\}_2] + 12\ Pr^iOH\uparrow \quad (1)$$

$$[Co\{Ta(OPr^i)_6\}_2] + 8\ \underset{\text{(excess)}}{EtOH} \xrightarrow{rt} [Co\{Ta(OPr^i)_2(OEt)_4\}_2] + 8\ Pr^iOH\uparrow \quad (2)$$

$$[Co\{M(OPr^i)_6\}_2] + 12\ \underset{\text{(excess)}}{ROH} \xrightarrow[\text{reflux}]{PhH} [Co\{M(OR)_6\}_2] + 12\ Pr^iOH\uparrow \quad (3)$$

$$[Co\{Ta(OPr^i)_6\}_2] + 6\ \underset{\text{(excess)}}{Bu^sOH} \xrightarrow[\text{stirred at rt}]{PhH} [Co\{Ta(OPr^i)_3(OBu^s)_3\}_2] + 6\ Pr^iOH\uparrow \quad (4)$$

$$[Co\{Ta(OPr^i)_6\}_2] + 8\ Bu^sOH \xrightarrow[\text{reflux}]{PhH} [Co\{Ta(OPr^i)_2(OBu^s)_4\}_2] + 8\ Pr^iOH\uparrow \quad (5)$$

However, Reaction 5 also could be pushed to completion if the liberated isopropyl alcohol is removed azeotropically with benzene:

$$[Co\{Nb(OPr^i)_6\}_2] + 12\ \underset{\text{(excess)}}{Bu^sOH} \xrightarrow[\text{reflux}]{PhH} [Co\{Nb(OBu^s)_6\}_2] + 12\ Pr^iOH\uparrow \quad (6)$$

Reactions of $[Co\{Ta(OPr^i)_6\}_2]$ with an excess of *t*-butyl alcohol in benzene at room temperature showed no evidence of reaction. However, when the reactions were carried out in refluxing benzene without azeotropic removal of isopropyl alcohol, two moles of isopropyl alcohol could be replaced and the analyses of the product corresponded to the formulae $[Co\{Nb(OPr^i)_5(OBu^t)\}_2]$:

$$[Co\{Nb(OPr^i)_6\}_2] + 2\ Bu^tOH \xrightarrow[\text{reflux}]{PhH} [Co\{Nb(OPr^i)_5(OBu^t)\}_2] + 2\ Pr^iOH\uparrow \quad (7)$$

Further, the reactions of $[Co\{Nb(OPr^i)_6\}_2]$ with an excess of *t*-butyl alcohol in benzene under azeotropic conditions gave only mixed derivative of composition $[Co\{Nb(OPr^i)_2(OBu^t)_4\}_2]$ even after ≈25 h of fractionation:

$$[Co\{Nb(OPr^i)_6\}_2] + 8\ \underset{\text{(excess)}}{Bu^tOH} \xrightarrow[\text{reflux}]{PhH} [Co\{Nb(OPr^i)_2(OBu^t)_4\}_2] + 8\ Pr^iOH\uparrow \quad (8)$$

The reactions with Am^tOH were slower in comparison to Bu^tOH and required ≈30 h of fractionation to yield product of the composition $[Co\{Ta(OPr^i)_2(OAm^t)_4\}_2]$.

The above alcoholysis experiments indicate that the ease of replacement of isopropoxy groups in $[Co\{M(OPr^i)_6\}_2]$ decreases with the size and ramification of the alkyl group. The extent of replacement increases under refluxing conditions. However, even when attempt is made to shift the equilibrium by continuous removal of Pr^iOH, the reactions can not be pushed to completion with tertiary alcohols.

These alcoholysis results as well as physico-chem-

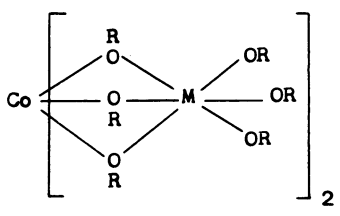

Fig. 1. Proposed structure for $[Co\{M(OR)_6\}_2]$ (M=Nb or Ta).

Table 2. Room Temperature Magnetic Moments and Some Characteristic IR Absorption Frequencies (cm^{-1}) for $[Co\{M(OR)_6\}_2]$ (M=Nb or Ta)

S. No.	Compound	μ_{eff}/BM	$\nu_{(C-O)M}$	$\nu_{(M-O)}$	$\nu_{(Co-O)}$
1	$[Co\{Nb(OMe)_6\}_2]$	4.85	1120 mw, 1130 mw, 1050 s	595 wbr, 530 wbr	460 wbr
2	$[Co\{Ta(OMe)_6\}_2]$	4.90	1165 mbr, 1065 s, 1150 mbr	595 wbr, 510 wbr	465 wbr
3	$[Co\{Nb(OEt)_6\}_2]$	4.90	1165 s, 1030 s, 900 w, 1070 m, 1050 m	610 mbr, 580 wbr, 550 wbr	420 wbr
4	$[Co\{Ta(OEt)_6\}_2]$	5.06	1160 s, 1120 s, 1090 wbr, 1050 w	610 wbr, 590 wbr	480 wbr
5	$[Co\{Nb(OPr^n)_6\}_2]$	5.12	1130 m, 1080 mbr, 1000 wbr	610 wbr, 580 mbr	470 wbr, 450 w
6	$[Co\{Ta(OPr^n)_6\}_2]$	5.11	1155 s, 1115 s, 995 m, 935m	585 m, 565 w	455 w, 410 wbr
7	$[Co\{Nb(OBu^n)_6\}_2]$	5.11	1110 wm, 960 m, 1020 wm	570 wbr, 510 wbr	430 w
8	$[Co\{Ta(OBu^n)_6\}_2]$	5.07	1150 m, 1110 s, 1050s, 970 w	610 m, 560 w	480 wbr
9	$[Co\{Nb(OPr^i)_6\}_2]$	5.08	1170 s, 1140 s, 1030 m, 990 s	595 s, 540 w	475 wbr
10	$[Co\{Ta(OPr^i)_6\}_2]$	5.07	1150 m, 1120 s, 1020 w, 900 s, 935 m	580 mbr, 600 w	450 w
11	$[Co\{Nb(OBu^s)_6\}_2]$	5.01	1160 s, 1120 s, 1020 s, 995 s, 940 m	590 s, 560 m	465 m, 410 w
12	$[Co\{Ta(OPr^i)_2(OBu^t)_4\}_2]$	4.94	1175 w, 1135 s, 1110 s, 1065 s, 965 s	565 m, 550 mbr	425 wbr

ical (magnetic and spectroscopic) properties described later can be explained on the basis of the plausible structure (Fig. 1) for these bimetallic species.

On making actual models of the above structures, it becomes apparent that out of the three bridging alkoxy groups per niobium (tantalum) atom, one would be in a rather strained state; this is reflected in the alcoholysis results, where four of the six isopropoxy groups per niobium (tantalum) atom tend to behave differently from the remaining two. Further steric crowding around niobium (tantalum) atoms in derivatives like $[Co\{(OPr^i)_2(OBu^t)Nb(OBu^t)_3\}_2]$ appears to hinder any further alcoholysis with excess tertiary alcohol, but in the corresponding less crowded structures as in $[Co\{(OPr^i)_2(OBu^n)Nb(OBu^n)_3\}_2]$, further replacement with excess Bu^nOH could be expected and is actually observed.

All these new bimetallic cobalt(II) alkoxides are colored (purple-red/violet) solids which are highly soluble in organic solvents such as benzene, carbon tetrachloride and hexane, but these exhibit lower solubility in parent alcohols except the methoxide derivatives which are highly soluble in methanol also. It may be pertinent to note that whereas the methoxides of most of the metals (e.g., Al, Ga, Ti, and Zr) are insoluble in organic solvents, methoxides of niobium and tantalum are quite readily soluble possibly due to their monomeric nature.

Infrared Spectral Studies. The infrared spectra (in the range 4000—400 cm^{-1}) of these new bimetallic alkoxides exhibited structurally significant absorption bands[1,14-16] (Table 2) at 1180—900 cm^{-1} for $\nu_{(C-O)M}$ and at 610—510 cm^{-1} for $\nu_{(M-O)}$ (M=Nb or Ta) and at 480—410 cm^{-1} for $\nu_{(Co-O)}$.

Table 3. Visible Spectral[a] Data of Bimetallic Alkoxide of Cobalt(II) with Nb(V) or Ta(V)

S. No.	Compound	$^4T_{1g}(F) \xrightarrow{\nu_3} {}^4T_{1g}(P)$ $10^{-3}\nu_{max}/cm^{-1}$
1	$[Co\{Nb(OPr^i)_6\}_2]$[b]	18.0, 19.3 (sh)
2	$[Co\{Ta(OPr^i)_6\}_2]$	(i) 18.0, 19.8 (sh) (ii) 18.5 (Pyridine)
3	$[Co\{Nb(OBu^s)_6\}_2]$	18.1, 19.5 (sh)
4	$[Co\{Ta(OEt)_6\}_2]$	18.1, 19.7 (sh)
5	$[Co\{Nb(OBu^n)_6\}_2]$	18.1, 19.6 (sh)
6	$[Co\{Nb(OMe)_6\}_2]$	17.5, 19.6 (sh)
7	$[Co\{Ta(OMe)_6\}_2]$	17.5, 19.6 (sh)
8	$[Co\{Ta(OPr^n)_6\}_2]$	17.4, 19.7 (sh)
9	$[Co\{Ta(OPr^i)_2(OBu^t)_4\}_2]$	17.8, 19.7 (sh)

a) All spectra recorded in benzene unless otherwise indicated. b) Only in the case of $[Co\{Nb(OPr^i)_6\}_2]$ (see the text), an additional band was observed at $14.9\times10^3 cm^{-1}$, which can be ascribed to $^4T_{1g}(F) \xrightarrow{\nu_2} {}^4A_{2g}(F)$.

Visible Spectral Studies. The visible spectra of cobalt(II) bimetallic derivatives studied herein showed a multiple band (asymmetric) (Table 3) in the region 17.8×10^3 cm^{-1} which may assigned[17,18,20] as $^4T_{1g}(F) \xrightarrow{\nu_3} {}^4T_{1g}(P)$ transition and the shoulder on the higher frequency side in the region 19.5×10^3 cm^{-1} being assigned to spin forbidden transitions to doublet states derived from the free ion ^2G and ^2H terms, which are characteristic of octahedral geometry.[17,19] The $^4A_{2g}(F) \xleftarrow{\nu_2} {}^4T_{1g}(F)$ transition is not normally

observed in most of the cobalt(II) derivatives, being formally a two electron transition. However, only the spectrum of $[Co\{Nb(OPr^i)_6\}_2]$ in visible region did show a very weak band at 14.9×10^3 cm^{-1} (sh) possibly due to the ν_2 transition.

The value of Dq for $[Co\{Nb(OPr^i)_6\}_2]$ has been calculated to be 795 cm^{-1} by using Underhill and Billing equation[21] and the ligand $\{Nb(OPr^i)_6\}^-$ can be placed in the following spectrochemical order:

$$\underset{(649)}{Br^-} < \underset{(764)}{Cl^-} < \underset{(795)}{\{Nb(OPr^i)_6\}^-} < \underset{(920)}{H_2O} < \underset{(1020)}{NH_3}$$

The nephelauxetic ratio (β) is 0.71 for $[Co\{Nb(OPr^i)_6\}_2]$ which is less than that (0.85) for $\{Co(H_2O)_6\}^{2+}$ ion, indicating a more covalent nature of the bimetallic derivative.

Magnetic Studies. For high spin octahedral cobalt(II) derivatives, magnetic moment values are expected to lie in the range of 4.7—5.3 BM, depending upon the extent of orbital contribution.[22] The room temperature magnetic moment values for new cobalt(II) bimetallic derivatives are in the range 5.01 ± 0.11 BM (Table 2), which are in agreement with the values reported for cobalt(II) in octahedral geometry.

The variable temperature data for $[Co\{Ta(OPr^i)_6\}_2]$ have been measured in the temperature range 14.4—295 K; the calculated values of χ_M (including correction of 545×10^{-6} CGS) are 200340 (16.4), 180490 (17.8), 152700 (21.0), 132860 (25.2), 113670 (28.8), 75960 (43.6), 36930 (86.6), 23700 (134), 10930 (295), with temperatures in parenthesis. The plot of $1/\chi_M^{Corr}$ versus T is a straight line obeying the Curie-Weiss law. The magnetic moment values increase slightly (from 5.07 to 5.28 BM) with decrease of temperature (from 295 to 16.4 K) resulting in a positive value of θ and showing the presence of weak cooperative phenomenon.

We wish to thank Prof. S. Mitra, Tata Institute of Fundamental Research, Bombay (India) for providing facilities for magnetic susceptibility measurements. The authors are grateful to Department of Science and Technology (Govt. of India), New Delhi for financial assistance in the form of a research project.

References

1) D. C. Bradley, D. P. Gaur, and R. C. Mehrotra, "Metal Alkoxides," Academic Press, London (1978).
2) R. C. Mehrotra, *Adv. Inorg. Radiochem.*, **26**, 269 (1983).
3) R. C. Mehrotra, *Coord. Chem.* (IUPAC), **21**, 113 (1981).
4) R. C. Mehrotra and J. V. Singh, *Inorg. Chem.*, **23**, 1046 (1984).
5) J. V. Singh, Ph. D. Thesis, Univ. of Delhi, India, 1980.
6) R. C. Mehrotra and J. V. Singh, *J. Coord. Chem.*, **13**, 273 (1984).
7) R. C. Mehrotra and J. V. Singh, *Z. Anorg. Allg. Chem.*, **512**, 221 (1984).
8) R. C. Mehrotra and J. V. Singh, *Can. J. Chem.*, **62**, 1003 (1984).
9) M. Osgan, J. J. Pasero, and P. Teyssie, *Polym. Lett.*, **88**, 219 (1970).
10) J. D. Mackenzie, *J. Non-Cryst. Solids*, **1**, 48 (1962); K. Jones, T. J. Davies, H. G. Emblem, and P. Parkes, *Mat. Res. Soc. Symp.*, **73**, 111 (1986).
11) D. C. Bradley, B. N. Chakravarti, A. K. Chatterjee, W. Wardlaw, and A. Whitley, *J. Chem. Soc.*, **1958**, 99.
12) A. I. Vogel, "A Text Book of Quantitative Inorganic Analysis," Longman Group Limited (1978).
13) R. C. Mehrotra, *J. Indian Chem. Soc.*, **30**, 585 (1953).
14) K. Nakamoto, "The Infra-red Spectra of Inorganic and Coordination Compounds," Wiley Interscience, London (1970).
15) V. A. Sipachev and A. I. Grigorev, *Russ. J. Inorg. Chem.*, **17**, 176 (1972).
16) C. J. Barraclough, D. C. Bradley, J. Lewis, and J. M. Thomas, *J. Chem. Soc.*, **1961**, 2601.
17) A. B. P. Lever, "Inorganic Electronic Spectroscopy," Elsevier Amsterdam, 2nd ed. (1984).
18) B. N. Figgis, "Introduction to Ligand Fields," Wiley Eastern Limited, Delhi (1976).
19) J. Reeclijk, J. M. Mulder, and J. A. Smit, *Inorg. Chim. Acta*, **13**, 219 (1975).
20) R. W. Adams, E. Bishop, R. L. Martin, and G. Winter, *Aust. J. Chem.*, **19**, 207 (1966).
21) A. E. Underhill and D. E. Billing, *Nature (London)*, **210**, 834 (1966).
22) B. N. Figgis and J. Lewis, *Prog. Inorg. Chem.*, **6**, 37 (1964).

Adsorption of Xenon in the Zeolitic Pore in the Henry's Law Region of the Isotherms

Toshihisa YOSHIDA*, Jun-ichi KOIZUMI, and Yoshio AKAI†
Faculty of Education, Saitama University, Urawa 338
†The Central Research Laboratory, Idemitsu Kosan Co. Ltd., Sodegaura-machi, Chiba 292-01
(Received July 9, 1987)

Synopsis. The isotherms and the ^{129}Xe NMR spectra of Xe adsorbed on HY and USY zeolites of faujasite structure were measured. There were two kinds of Xe species, which could be distinguished as one trapped on the internal surface of the supercage and the other freely mobile in the supercage.

Zeolites with their specific and rather well-defined structure show some interesting properties related to the adsorption of gases in the intense potential fields, which exist in cavities of molecular dimensions; this causes an increased intermolecular solid-gas interaction, even in the case of nonpolar gases such as xenon.

In recent years, much effort has been devoted to investigations of adsorption in restricted geometries, such as zeolite structure. It has been proposed that the adsorption of various gasses on activated charcoals and zeolites (5A and 13X) is a superimposed two-site Langmuir adsorption.[1] In the following studies of the adsorption of xenon, the experimental results in zeolitic pore (H-ferrierite) have been fully analyzed by statistical thermodynamics.[2] The ^{129}Xe NMR study of xenon adsorbed on Y zeolites has also revealed characteristic properties of a faujasite structure.[3]

We have now observed the interesting behavior of xenon adsorbed on zeolites (faujasite) in the Henry's law region of the adsorption isotherms. This note is therefore, devoted to the elucidating of the behavior of xenon adsorbed on Y zeolites. The isotherms and the ^{129}Xe NMR spectra of xenon adsorbed on HY and USY zeolites were measured and compared.

Experimental

Commercial synthetic NaY zeolites (Union Showa, Japan) were used. HY zeolite was prepared from NaY type. USY zeolite (Si/Al_2=22.7) was prepared from HY type by dealuminations, steaming and leaching with acid. Before the xenon was adsorbed on the zeolites, these were pretreated for 4 h at 400 °C under vacuum (10^{-5} Torr[4]). The adsorption isotherms of xenon (99.5%) were measured on a volumetric apparatus at −78 °C. NMR absorptions of ^{129}Xe adsorbed on the samples were observed by using FX-90Q (FT-NMR; JEOL, Japan) at a frequency of 24.785 MHz and a magnetic field of 21.1 kG (1G=10^{-4}T) with D lock. The radio frequency field pulse was repeated every second, which was sufficiently long compared to the relaxation time. The reference signal, 24.7850 MHz of ^{129}Xe was taken as that of Xe gas at 5 atm in the presence of about 5% of oxygen as a paramagnetic impurity.[3] All resonance signals of ^{129}Xe adsorbed on zeolites were obtained after 2000 accumulations and shifted to higher frequency relative to the reference.

After the xenon had been adsorbed on each zeolite and the NMR tubes had been sealed at −78 °C, the ^{129}Xe NMR spectra were observed at −78 °C (for HY zeolite, 31.5 Torr of xenon and for USY one, 37.3 Torr of xenon at each adsorption equilibrium) and by cooling to −100 °C (for HY one and for USY one), respectively.

Results and Discussion

The adsorption isotherms of xenon adsorbed on HY (empty circles) and USY (crosses) zeolites at −78 °C are shown in Fig. 1. The amounts of xenon adsorption are proportional to the pressure in the Henry's law region of the isotherms, but these change to a different linear dependence at higher adsorption pressure. These isotherms are at first convex towards the pressure axis at these adsorption equilibria and have an inflection point. The interesting and strange results obtained here are similar to those observed by Aristov, et al.[5] They considered that localized and non-localized xenon adsorptions often co-exist on crystals of zeolites LiX and NaX. These features of the

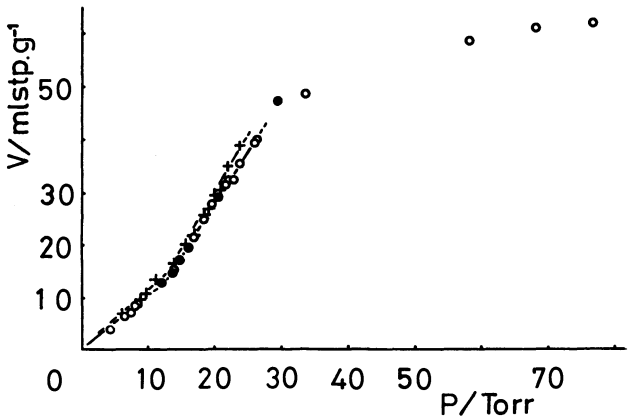

Fig. 1. The amounts for xenon adsorbed vs. pressures of the adsorption equilibrium at −78 °C on HY (circles; ○ for the adsorption, ● for the desorption) and USY zeolites (crosses).

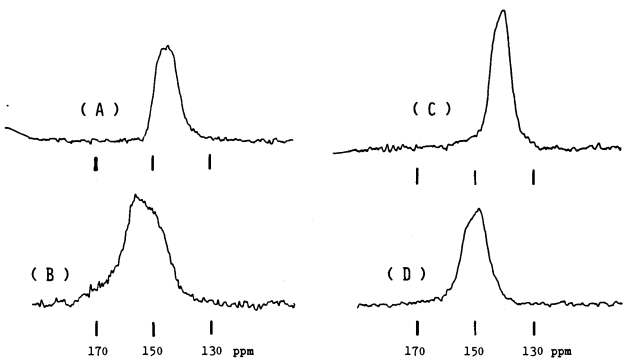

Fig. 2. ^{129}Xe NMR spectra of xenon adsorbed, on HY zeolite at −78 °C under 31.5 Torr of xenon at the adsorption equilibrium (A) and then cooled to −100 °C (B), and on USY zeolite at −78 °C under 37.3 Torr of xenon (C) and also cooled to −100 °C (D), respectively.

isotherms can also be interpreted by a superimposed two-site Langmuir model.[1] The data obtained were highly reproducible. No hystereses of these isotherms were observed, that is, the amount adsorbed for xenon in the adsorptive process equals strictly that in the desorptive one at the same equilibrium pressure, shown by full circles in Fig. 1. From this, it follows that the xenon adsorption occurs in intense potential fields, not by pore filling.[6] The isosteric differential heat of adsorption, q_{iso} of xenon was 16—18 kJ mol^{-1} in the Henry's law region of the isotherms on HY and USY zeolites, different from the heat of vaporization of xenon 12.6 kJ mol^{-1}.[7]

Figure 2 shows the ^{129}Xe NMR spectra of xenon adsorbed at −78 °C and −100 °C, on HY and USY zeolites. Each ^{129}Xe line shape is characteristic in width and suggests it consists of two signals. The NMR signal of ^{129}Xe adsorbed on zeolite shifts increasingly with increasing the xenon pressure at the adsorption equilibrium. When the ^{129}Xe NMR spectra were observed by cooling the NMR tubes to −100 °C, the two NMR signals in Fig. 2 (B) or (D) could be clearly separated into one peak, 146 or 148 ppm and another, 152 or 158 ppm shifted to the reference, respectively.

The distinguishable differences between the two NMR signals and between two heats of xenon adsorption corresponded to each NMR signals are extremely small. The relaxation time for the higher field signal and for the other were approximately 10 and 70 ms, respectively. Comparatively speaking, the xenon species adsorbed and corresponding to the higher field signal is considered to be strongly trapped on the internal surface of the supercage and the other to be freely mobile in the supercage of the faujasite structure. We deduce therefore, that the higher field signal for our NMR spectra appeared at lower xenon densities (within 7—9 xenon atoms/unit cell) must be due to the interactions between a xenon atom and the internal surface of the supercage. Another lower field signal appeared at higher xenon densities is also deduced to be caused by mutual interactions between xenon atoms in the supercage.[3] This conclusion agrees perfectly with that of the superimposed two-site Langmuir model.[1]

The superimposed two-site Langmuir model was not based on spectroscopical evidence. Here we propose this supporting evidence based on the NMR signals of ^{129}Xe adsorbed on zeolites. We infer the adsorption states of Xe adsorbed on HY zeolite are comparatively similar to those on USY one.

References

1) J. Koresh and A. Soffer, *J. Colloid Interface Sci.*, **92**, 517 (1983).

2) Tetsuya Takaishi, Proceedings of the 7th International Zeolite Conference, (AD-5-1), 511-520 (1986) & a private communication.

3) T. Ito, *J. Chem. Phys.*, **76**, 5225 (1982).

4) 1 Torr=133.322 Pa.

5) B. G. Aristov, V. Bosacek, and A. V. Kiselev, *Trans. Faraday Soc. I*, **63**, 2057 (1967).

6) N. Hara and H. Takahashi, "Zeolite-the bases and applications," Kohdansha Scientifics, Tokyo (1975) p. 92.

7) "The handbook of Chemistry, 2nd ed.," ed by the Chem. Soc. of Japan, Maruzen, Tokyo (1975), p. 914.

The Crystal Structure of the Gold(III) Complex, Tribromo(dibenzyl sulfide)gold(III)

Kazuhiro TAKAHASHI* and Katsuo KATO†
Electrotechnical Laboratory, 1-1-4 Umezono, Tsukuba, Ibaraki 305
†National Institute for Research in Inorganic Materials, 1-1 Namiki, Tsukuba, Ibaraki 305
(Received April 30, 1987)

Synopsis. The crystal structure of tribromo(dibenzyl sulfide) gold(III) has been determined. The crystal belongs to the triclinic system, with a=7.002(1), b=7.949(1), c=17.244(2) Å, α=88.83(1), β=79.52(1), and γ=66.35(1)°, with the space group $P\bar{1}$ and with Z=2. The complex has a square-planar coordination geometry with 3BrlS donor atoms. The bond lengths of the three Au-Br coordinations are in the range of 2.41—2.43 Å.

Since the gold complexes of dibenzyl sulfide (DBS) were first reported by Herrmann,[1] more than ten species of gold(I), gold(III), and mixed-valence gold(I)-gold(III) complexes have been synthesized and characterized.[2]

We have begun to study the structures and electronic states of a series of halogen-gold-DBS ternaly complexes, taking special interest in the coordination mode of the alkyl sulfide and the correlation between the structure and the valence of the gold ion.[3] However, the molecular structures of most of the gold-DBS complexes have not yet been revealed. Though detailed structural studies of the above compounds are much to be desired, the crystal structure determinations of only two DBS-gold(I) complexes have thus far been reported.[4]

In order to obtain details of the molecular structure and the coordination mode of DBS, we have in this study prepared good single crystals of the gold(III) compound, [$AuBr_3$(DBS)], and determined its molecular structure by the use of the X-ray diffraction method.

Experimental

The [$AuBr_3$(DBS)] was prepared by Brain's method.[2] The deep brown prismatic crystals were obtained by recrystallization from a 1,2-dibromoethane/diethyl ether solution (Found: C, 25.62; H, 2.10%) at ca. 5 °C. The intensity data were collected at room temperature with a Rigaku AFC-3 four-circle diffractometer using graphite monochromated Mo $K\alpha$ radiation (λ=0.71073 Å). The unit cell parameters were determined from 47 reflections with $15<2\theta<30°$.

Crystal Data: $C_{14}H_{14}SBr_3Au$, M=651.0; triclinic; space group $P\bar{1}$; a=7.002(1), b=7.949(1), c=17.244(2) Å, α=88.83(1), β=79.52(1), γ=66.35(1)°, V=863.0(2) Å^3; D_m=2.47 (by floatation), D_c=2.51 g cm^{-3}; Z=2; μ=130 cm^{-1}; crystal size 0.1×0.2×0.2 mm^3. A total of 5039 reflections were collected by the ω scan ($2\theta\leqq30°$) and ω-2θ scan techniques ($30\leqq2\theta\leqq60°$), with a 2θ scan rate for 4° min^{-1}, and by monitoring 5 check reflections after each 50 measurements. The check reflections showed a max. 14.2% (on F_o) intensity drop during the course of the data collection. The intensity data were corrected for Lorents-polarization effects, decay, and absorption using 10 crystal faces.[5] 3866 independent reflections with $|F_o|\geqq3\sigma(|F_o|)$ were used for the structure analysis. The structure was solved by the direct method, and was then refined by the full-matrix least-squares procedure. Anisotropic thermal parameters were adopted for the non-hydrogen atoms. Fourteen hydrogens were placed at the calculated positions and were included in the last cycle of the final refinements with B_{eq}=8.0 Å^2 (fix). The final $R_1(=\sum||F_o|-|F_c||/\sum|F_o|)$ and $R_2(=\{\sum||F_o|-|F_c||^2/\sum|F_o|^2\}^{1/2})$ values are 0.041 and 0.043, respectively. All the calculations were carried out on a FACOM M-340S computer at the NIRIM, using UNICS III computing systems.[6] The final atomic positional and isotropic thermal parameters of the non-hydrogen atoms are given in Table 1.††

Results and Discussion

An ORTEP drawing of the complex molecule is shown in Fig. 1. Table 1 lists the final atomic coordinates of the non-hydrogen atoms.

As is shown in Fig. 1, the Au atom is four-coordinated, with the square-planar coordination geometry normally observed in mononuclear Au(III) complexes. The square plane consists of three bromine atoms and the sulfur atom of DBS. The

Table 1. Atomic Positional(×10^4) and Isotropic Thermal Parameters for Non-Hydrogen Atoms, with Their Estimated Standard Deviations in Parentheses

Atom	x	y	z	B_{eq}/Å$^{2a)}$
Au	−1222(1)	1470.7(5)	7517.0(2)	2.30
Br(1)	1981(2)	−1326(1)	7352(1)	4.10
Br(2)	−4390(2)	4285(2)	7578(1)	4.77
Br(3)	−3368(2)	−302(2)	7692(1)	4.40
S	985(4)	3068(3)	7448(1)	2.97
C(1)	360(19)	4676(14)	6657(6)	3.91
C(2)	1414(18)	3629(14)	5876(6)	3.77
C(3)	3458(21)	3495(19)	5531(8)	5.36
C(4)	4421(26)	2526(24)	4785(9)	6.84
C(5)	3376(31)	1755(23)	4399(9)	7.09
C(6)	1354(29)	1909(19)	4738(8)	6.05
C(7)	310(23)	2880(17)	5493(7)	5.05
C(8)	−211(18)	4712(13)	8329(6)	3.65
C(9)	−104(19)	3656(13)	9062(6)	3.68
C(10)	−1997(23)	3600(18)	9490(7)	5.21
C(11)	−1922(33)	2663(22)	10217(8)	7.05
C(12)	−27(36)	1854(19)	10471(9)	7.10
C(13)	1874(31)	1905(19)	10039(9)	6.79
C(14)	1786(22)	2821(16)	9321(7)	4.87

a) $B_{eq}=4/3\sum_i\sum_j\beta_{ij}\boldsymbol{a}_i\boldsymbol{a}_j$.

†† Lists of structure factors, the anisotropic thermal parameters, the coordinates of the hydrogen atoms, the bond distances and angles, and the results of the least-squares plane calculations are deposited at the office of the Chemical Society of Japan as Document No. 8775.

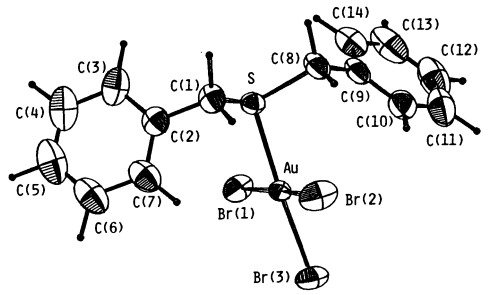

Fig. 1. ORTEP drawing of the molecule with atom numbering scheme for non-hydrogen atoms(thermal ellipsoids are drawn at 50% probability level). Hydrogen atoms are drawn at an arbitraty small size. Selected interatomic distances(l/Å) and angles(ϕ/°) around the coordination sphere of Au are: Au-Br(1) 2.418(1), Au-Br(2) 2.425(1), Au-Br(3) 2.419(2), Au-S 2.349(3), Br(1)-Au-Br(2) 175.78(5), Br(1)-Au-Br(3) 90.54(4), Br-(1)-Au-S 86.88(6), Br(2)-Au-Br(3) 90.21(5), Br(2)-Au-S 92.70(6), Br(3)-Au-S 174.78(7).

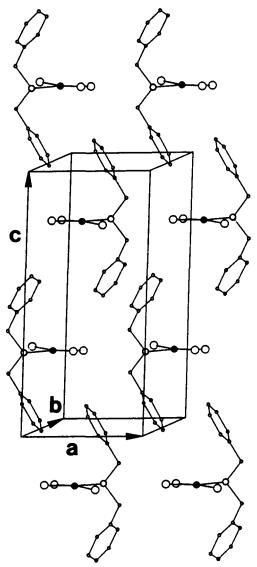

Fig. 2. Perspective view of the crystal structure.

deviations of the Au and donor atoms from the least-squares plane (through Br(1), Br(2), Br(3), and S) are less than 0.1 Å. The bond lengths of the three Au-Br coordinations are in the range from 2.418 to 2.425 Å, and Au-S is 2.349(3) Å. The values of the Au-Br bonds fall within the range observed for the previously reported gold(III) tribromide complexes (2.40—2.47 Å).[7] The Au-S bond length could not be compared with those of other sulfide-coordinated gold(III) complexes because of the lack of any structural study of similar complexes. The dihedral angles of coordination bonds across the Au atom are in the 86—93° range, deviating slightly from the ideal angle, 90°. These results indicate that the first coordination sphere of Au is little affected sterically by the bulky benzyl groups of DBS.

In the case of trihalogeno(phosphine)gold(III) complexes, which possess a coordination structure similar to that of [$AuBr_3$(DBS)], the Au–halogen bond trans to the Au–P bond is appreciably longer than the other two Au–halogen bonds (ca. 0.05 Å). This is due to the strong trans influence of the coordinated phosphine.[7] In the present complex, however, no such strong effect of the trans ligand DBS is observed on the Au–Br(3) bond. The above remarkable difference in the effect from the trans donor species, phosphine and sulfide, seems to reflect the order of the electronegativities of coorddinated sulfur and phosphorus atoms in each ligand (Phosphine<Au^{3+} (2.7)[8]<DBS).

The crystal structure of [$AuBr_3$(DBS)] is shown in Fig. 2. The significant intermolecular distances less than 3.5 Å are: Br(1)-Br(2)(symmetry code: $x+1$, $y-1$,z; 3.460(2) Å), C(11)-C(12)($-x$,$-y$,$2-z$; 3.44(2) Å) and C(12)-C(12)($-x$,$-y$,$2-z$; 3.38(3) Å). In the crystal structure of the two-coordinated gold(I)-DBS complex, [AuBr(DBS)], the short intermolecular distance of Au^+–Au^+ (3.30 Å) is observed.[4] No such adjacency of gold atoms is observed in the crystal structure of [$AuBr_3$(DBS)](the shortest distance of Au^{3+}–Au^{3+} (x,y,$z+1$); 7.002(1) Å).

One of the present authors(KT) wishes to express his thanks to Dr. Hiroshi Tanino, Dr. Takafumi Yao, and Dr. Takehiko Ishiguro(ETL) for their continuous interest and encouragement.

References

1) F. Herrmann, *Ber.*, **38**, 2813 (1905).
2) F. H. Brain, C. S. Gibson, J. A. J. Jarvis, R. F. Phillips, H. M. Powell, and A. Tyabji, *J. Chem. Soc.*, **1952**, 3686; P. C. Ray and D. C. Sen, *J. Indian Chem. Soc.*, **7**, 67 (1930); G. M. Smith, *J. Am. Chem. Soc.*, **44**, 1769 (1922); L. V. Interrante and F. P. Bundy, *J. Inorg. Nucl. Chem.*, **39**, 1333 (1977); H. N. Adams, W. Hiller, and J. Strähle, *Z. Anorg. Allg. Chem.*, **485**, 81 (1982).
3) K. Takahashi and H. Tanino, *Photon Factory Activity Report*, **4**, 176 (1987).
4) J. Strähle, W. Hiller, and W. Conzelmann, *Z. Naturfosch., B*, **39**, 538 (1984).
5) W. R. Busing and H. A. Levy, *Acta Crystallogr.*, **10**, 180 (1957).
6) T. Sakurai and K. Kobayashi, *Rep. Inst. Phys. Chem. Res.*, **55**, 69 (1978).
7) D. S. Eggleston, D. F. Chodosh, D. T. Hill, and G. R. Girard, *Acta Crystallogr., Sect. C*, **40**, 1357 (1984).
8) F. W. Lytle, P. S. P. Wei, and R. B. Greegor, *J. Chem. Phys.*, **70**, 4849 (1979); J. E. Huheey, "Inorganic Chemistry," 3rd ed, Harper & Row, New York (1983), Chap. 3.

An Improved Synthesis of Methyl 7-(2-Hydroxy-5-oxo-1-cyclopentenyl)heptanoate

Hirokazu NAORA,* Takashi OHNUKI, and Asao NAKAMURA
Applied Research Dept., Central Laboratories, Ajinomoto Co., Inc.,
1-1, Suzuki-cho, Kawasaki, Kanagawa 210
(Received May 13, 1987)

Synopsis. Methyl 7-(2-hydroxy-5-oxo-1-cyclopentenyl)-heptanoate, which is a valuable synthon for prostanoids, was prepared in a good yield from dibenzyl malonate via three steps.

A polymeric prostaglandin, PGB_X, with biochemical and physiological properties very different from those of any other prostaglandin derivatives, was first synthesised by Polis et al.[1] PGB_X has such biological properties as restoring the oxidative phosphorylation of isolated degraded rat liver mitochondria in vitro and increasing in survival after otherwise lethal episodes of myocardial ischemia in monkeys and hypocia in dogs in vivo.[2] PGB_X is an oligomeric mixture (4—6 monomer units) of the 15-dehydro-PGB_1 methyl ester. The total syntheses of PGB_1 or its equivalents have already been known,[3] and methyl 7-(2-hydroxy-5-oxo-1-cyclopentenyl)heptanoate (**4**) is a key intermediate in all cases. **4** is a valuable synthon not only for PGB_1 but also for other prostanoids, for other synthetic intermediates for primary prostaglandins can easily be derived from **4**.[4] We thought that a simple method of preparing a large quantity of **4** would be of significant synthetic and pharmaceutical interest and so started to investigate it.

We modified Bowmann's general method of ketone synthesis[5] and obtained **4** from dibenzyl malonate in a short time and in a good yield. In our method, **4** was prepared in only three steps because the tetraester **2**, which is difficult to prepare by Bowmann's method, was obtained in a single step.

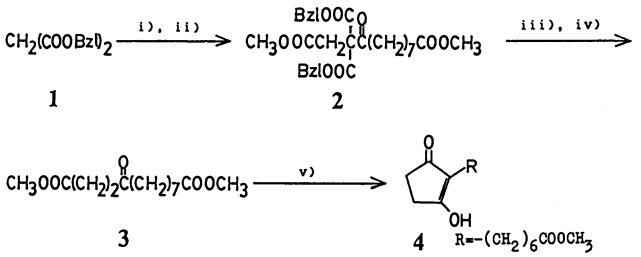

1 2 3 4

i) NaH, $BrCH_2CO_2CH_3$ ii) NaH, $CH_3O_2C(CH_2)_7COCl$ iii) H_2, Pd/C iv) Δ v) $NaOCH_3$

Tetraester **2** was prepared from dibenzyl malonate (**1**) in one pot by base-promoted alkylation with methyl bromoacetate, followed by acylation with methyl 8-chloroformyloctanoate. The crude yield of this one pot reaction was 92% from dibenzyl malonate (**1**). Although the tetraester **2** was used in the next step without further purification, it can be purified by silica-gel column chromatography if necessary. The structure of **2** was elucidated by means of the spectroscopic data.

Thermal decarboxylation after the removal of the benzyl groups of the tetraester **2** gave the keto diester[3] **3** in a 58% yield. This step was achieved by hydrogenolysis in mixture of 10% palladium on charcoal and by subsequent thermal decomposition under reflux in ethyl alcohol. All the spectroscopic data of **3** support its structure.

The keto diester **3** was cyclized with sodium methoxide to give methyl 7-(2-hydroxy-5-oxo-1-cyclopentenyl)heptanoate[3,4] (**4**) in a 94% yield. The IR and NMR spectra of **4** were identical with those of an authentic sample.[3]

Experimental

Dimethyl 3-Bis(benzyloxycarbonyl)-4-oxo-1,12-dodecanedioate (2). A solution of 40 g of dibenzyl malonate (**1**: Aldrich No. 16040-7) in 100 ml of benzene was added to a suspension of 3.36 g (0.14 mol) of sodium hydride in 400 ml of benzene dropwisely. Benzene (200 ml) was then added to the reaction mixture, after which it was gently heated to reflux. After 15 min, a solution of 21.6 g (0.14 mol) of methyl bromoacetate in 100 ml of benzene was added at 50 °C, and then the reaction mixture was heated under reflux for 90 min.

The resultant mixture was added dropwise to a suspension of 3.36 g (0.14 mol) of sodium hydride in 400 ml of benzene with stirring at room temperature. The reaction mixture was kept at 50 °C for 30 min during the evolution of hydrogen gas and then heated under reflux for 15 additional min.

At 50 °C, to the stirred mixture was added a solution of 30.8 g (0.14 mol) of methyl 8-chloroformyloctanoate in 100 ml of benzene dropwisely. The mixture was then cooled to room temperature after refluxing for 2 h. The organic materials were extracted with 1000 ml of ether, and the ethereal layer was washed with 500 ml of water, 300 ml of aq. sat. $NaHCO_3$, 500 ml of water (three times), and brine, and then dried over $MgSO_4$. The removal of the solvents and volatile components under 0.4 mmHg (1 mmHg=133.322 Pa) at 160 °C for 2 h gave 70 g of crude **2** in a 92% yield. Crude **2** can be used for the next step without further purification. Column chromatography (LiCroprep Si 60; hexane–ethyl acetate=3:1) gave pure **2**: ^1H NMR (90 MHz, chloroform-d_1, TMS) δ=7.29 (br., 10H), 5.16 (s, 4H), 3.66 (s, 3H), 3.58 (s, 3H), 3.13 (s, 2H), 2.55 (t, J=7.5 Hz, 2H), 2.27 (t, J=7.5 Hz, 2H), 1.4—1.8 (br., 4H), and 1.0—1.4 (br., 6H); IR (film) 2940, 2850, 1735, 1455, and 1440 cm^{-1}; MS (LREI) 540 (M^+), 509 (M−MeO), 508 (M−MeOH), 477 (M−MeO−MeOH), and 449 (M−Bzl); (HREI) Found: m/z 540.2347. Calcd for $C_{30}H_{36}O_9$: M, 540.2336.

Dimethyl 4-Oxo-1,12-dodecanedioate[3] (3). The hydrogenolysis of 25.5 g (0.047 mol) of **2** was carried out in 150 ml of 95% ethyl alcohol with hydrogen gas at atmospheric pressure over 2 g of 10% palladium on charcoal for 24 h. After the removal of the catalyst by filtration, the reaction mixture was heated under reflux for 2 h. The resultant

product was distilled at 159—160 °C (0.7 mmHg) to give 7.47 g of **3** in a 58% yield: ^{1}H NMR (100 MHz, chloroform-d_1, TMS) δ=3.63 (s, 6H), 2.80—2.08 (m, 8H), and 1.80—1.05 (m, 10H); IR (KBr) 2940, 2850, 1740, 1710, and 1440 cm^{-1}.

Methyl 7-(2-Hydroxy-5-oxo-1-cyclopentenyl)heptanoate[3,4] (4). Dimethyl 4-oxo-1,12-dodecanedioate (**3**: 2.72 g; 10 mmol) in 20 ml of dry toluene was added dropwise to a suspension of 20 mmol of sodium methoxide in 50 ml of dry toluene under reflux. The reaction mixture was then heated under reflux for 30 min, followed by the azeotropic removal of the generating methyl alcohol for 2 h. After it had then been cooled to room temperature, the resultant mixture was diluted with 20 ml of water and acidified with 1 M HCl (1 M=1 mol dm^{-3}) between pH 1 and pH 2. The organic materials were extracted with 20 ml of ethyl acetate twice. The organic layer was washed successively with equal volumes of 1 M HCl, water, and brine. The subsequent removal of the solvents gave 2.26 g (94% yield) of **4**: ^{1}H NMR (90 MHz, chloroform-d_1, TMS) δ=4.75—4.0 (br., 1H), 3.66 (s, 3H), 2.66 (br., 4H), 2.75—1.95 (m, 4H), and 1.9—1.0 (m, 8H); IR (KBr) 2910, 2860, and 1740 cm^{-1}.

References

1) B. D. Polis, R. P. Miller, and A. M. Grandizio, *Physiol. Chem. Phys.*, **6**, 287 (1974).

2) B. D. Polis, E. Polis, and S. Kwong, *Proc. Natl. Acad. Sci. U.S.A.*, **76**, 1598 (1979); E. T. Angelakos, R. L. Riley, and B. D. Polis, *Physiol. Chem. Phys.*, **12**, 81 (1980); B. D. Polis and E. Polis, *ibid.*, **8**, 429 (1976); B. D. Polis and E. Polis, *ibid.*, **11**, 3 (1979); B. D. Polis, S. Kwong, E. Polis, and G. L. Nelson, *ibid.*, **12**, 167 (1980); H. W. Shmuckler, S. F. Kwong, E. Polis, M. G. Zawryt, and E. Soffer, *ibid.*, **12**, 551 (1980).

3) P. W. Collins, C. J. Jung, and R. Pappo, *Isr. J. Chem.*, **6**, 839 (1968); J. Katsube and M. Matsui, *Agric. Biol. Chem.*, **33**, 1078 (1969); Y. Yura and J. Ide, *Chem. Pharm. Bull.*, **17**, 408 (1969); B. D. Polis, S. Kwong, E. Polis, G. Nelson, and H. W. Shmukler, *Physiol. Chem. Phys.*, **11**, 109 (1979).

4) L. Novák, G. Baán, J. Marosfalvi, and C. Szántay, *Chem. Ber.*, **113**, 2939 (1980).

5) R. E. Bowman, *J. Chem. Soc.*, **1950**, 325.

A Facile Synthesis of 4*H*-Cyclopenta[*def*]phenanthrene

Masahiro MINABE,* Masaaki YOSHIDA, and Tokuei TAKAYANAGI
Department of Industrial Chemistry, Faculty of Engineering, Utsunomiya University, Ishiicho, Utsunomiya 321
(Received July 15, 1987)

Synopsis. A facile and cheap method for synthesis of 4*H*-cyclopenta[*def*]phenanthrene was achieved from fluorene as the starting material via di-*t*-butylfluorene.

In order to learn how to facilely obtain 4*H*-cyclopenta[*def*]phenanthrene (**1**) is one of the important reasons for studing the chemistry of **1**.[1] About ten procedures have been proposed for the synthesis of **1**; usually pyrene[2] and diphenic acid[3] are used as the starting materials in more facile methods. The preparation from tetralin is cheap but needs a long sequence.[4]

We wish to report here on a convenient, cheap method to make **1** from fluorene (**2**).

Hydrocarbon **2** is known to react with electrophile, mainly at the 2,7-positions, accompanied by a minor amount of the 2,5-positional isomer. For the preparation of the 4-substituted fluorene, it is necessary to block the 2,7-positions by the positional protecting group. The *t*-butyl group is convenient for the protection;[5] the synthesis of 4-bromofluorene by this method has been reported by Kajigaeshi et al.[6]

The sequence of the preparation of **1** from **2** is summarized in Scheme 1. We first planned to make 4-iodofluorene via **4e**;[6] however, trans-*t*-butylations of **4e** and **7** were difficult. The second plan, to convert **4e** into **4f**, was not effective due to the low yield. The final design was a route through **4a**.[6] The chloromethylation of **3** using chloromethyl methyl ether in the presence of titanium tetrachloride gave **4a** in a good yield accompanied by the formation of dimeric **8**. The conversion of **4a** to **4c**[6] was furnished by a treatment of potassium cyanide in DMF to give **4b**[6] followed by acidic hydrolysis to form **4c** in good yields, respectively.

The ring closure of the acid chloride **4d** gave the phenol **5** which was so unstable as to change into reddish materials containing the quinone. Crude **5** was submitted to a reduction using hydriodic acid-red phosphorus in acetic acid, giving a mixture of **1**, **6a**, and maybe **6b**. The mixture was directly treated with aluminium chloride in toluene, yielding expected hydrocarbon **1**.

This procedure can give **1** from **2** via 8-steps in a total yield of 12—13%, and be facile comparable to the method from diphenic acid[3] (40—50% yield through 10-steps). However, the available diphenic acid is more costly (more than three times) than commercial fluorene. The preparation is the most facile and cheap way to obtain **1** within the established procedures.

Experimental

All the melting points are uncorrected. The ^{1}H NMR spectra were measured using Varian VXR-300 or Jeol JNM C-60 HL spectrometers in $CDCl_3$ using TMS. The IR (KBr-pellet), UV data (cyclohexane), and MS spectra were recorded on Jasco IR-G, Shimadzu UV-180 and Hitachi M-80 spectrometers, respectively.

Compounds **3** and **4e** were synthesized according to a method similar to that given in the literature.[6] ^{1}H NMR of **4e**, δ=1.35 (9H, s) 1.38 (9H, s), 3.87 (2H, s), 7.47—7.56 (3H, m), 7.80 (1H, s), and 8.66 (1H, d, J=8.5 Hz).

Trans-*t*-butylation of 4e. A mixture of **4e** (808 mg, 2 mmol) and $AlCl_3$ (200 mg, 1.5 mmol) in toluene (20 ml) was stirred at 50 °C for 6 h; only **2** was isolated from the resulting mixture: 73.2 mg (22%); mp 112—114 °C.

2,7-Di-*t*-butyl-4-iodo-9-fluorenone (7). A mixture of **4e** (2.02 g, 5 mmol) and $KMnO_4$ (4.42 g, 28 mmol) in acetone (100 ml) was stirred at room temperature for 10 h. After decomposition with aqueous $NaHSO_3$, the resulting mixture was extracted with benzene and chromatographed on a SiO_2 column. The yellow eluate was evaporated to give 1.85 g (89%) of **7**: mp 140.5—141.5 °C (hexane); IR, 1710 cm^{-1}; ^{1}H NMR, δ=1.32 (9H, s), 1.34 (9H, s), 7.58 (1H, dd, J=8.1, 2.0 Hz), 7.69 (1H, d, J=1.7 Hz), 7.73 (1H, d, J=2.0 Hz), 7.82 (1H, d, J=1.7 Hz), and 8.41 (1H, d, J=8.1 Hz); UV, λ_{max} 410 (log ε 3.01), 336 (3.00), 305 (3.62), 274 (4.74), 264 (4.68), and 240 (4.40); MS, m/z 418 (M^+) and

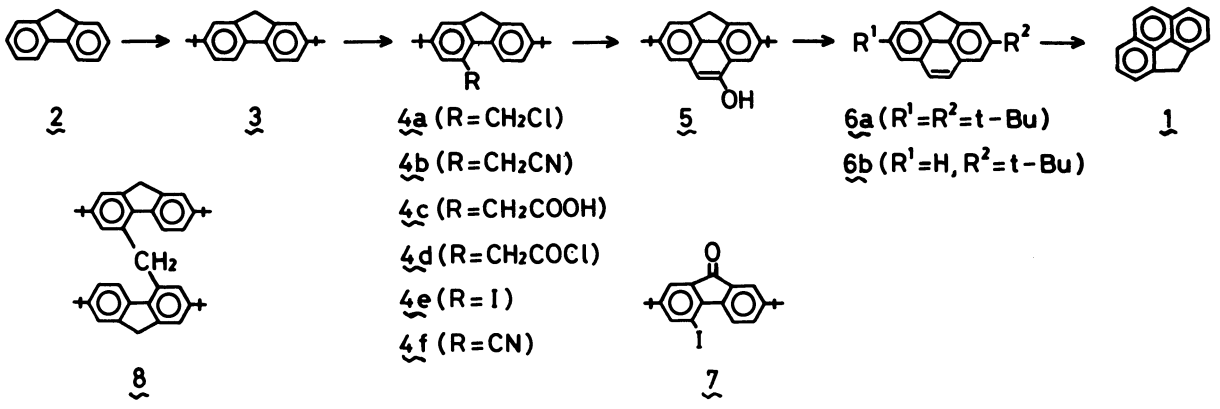

Scheme 1.

403. Found: C, 60.11; H, 5.29%. Calcd for $C_{21}H_{23}OI$: C, 60.29; H, 5.06%.

A mixture of **7** (418.5 mg, 1 mmol) and $AlCl_3$ (540 mg, 4 mmol) in toluene (10 ml) was stirred at 70 °C for 40 h, but no specific material was obtained except **7** (262 mg, 62%, mp 139.5—141.5 °C).

4-Cyano-2,7-di-*t*-butylfluorene (4f). A mixture of **4e** (809 mg, 2 mmol), KCN (263 mg, 4 mmol), and CuCN (361 mg, 4 mmol) in DMF (10 ml) was refluxed for 17 h. The mixture was extracted with benzene, washed with dil. HCl, successively with water, dried, and chromatographed on SiO_2 giving **4f** (110 mg, 20%); mp 192—193 °C (hexane); IR, 2250 cm^{-1}; ^1H NMR, δ=1.37 (9H, s), 1.38 (9H, s), 3.88 (2H, s), 7.49 (1H, dd, J=8.1, 1.8 Hz), 7.60—7.61 (2H, m), 7.74 (1H, s), and 8.29 (1H, d, J=8.1 Hz); UV, λ_{max} 329 (log ε 4.24), 316 (4.15), 273 (4.37), and 241 (4.27); MS, m/z 303 (M^+) and 270. Found: C, 86.92; H, 8.09; N, 4.43%. Calcd for $C_{22}H_{25}N$: C, 87.14; H, 8.24; N, 4.62%.

4-Chloromethyl-2,7-di-*t*-butylfluorene (4a).[6] To a mixture of **3** (2.78 g, 10 mmol) in CS_2 (100 ml), there was added chloromethyl methyl ether (2.30 ml, 30 mmol), and successively added $TiCl_4$ (1.30 ml, 11.6 mmol) for 5 min with ice-cooling. Upon stirring for 2 h at the temperature, the reaction was quenched by pouring into ice-water, and the organic layer was evaporated and purified by sublimation in vacuo to yield **4a** (2.84 g, 87%); mp 98.5—99.5 °C (lit,[6] mp 90—93 °C); UV, λ_{max} 310 (log ε 4.05) and 273 (4.34); ^1H NMR,[6] δ=1.38 (9H, s), 1.39 (9H, s), 3.89 (2H, s), 5.00 (2H, s), 7.31 (1H, s), 7.46 (1H, d, J=8.3 Hz), 7.54 (1H, s), 7.59 (1H, s), and 7.90 (1H, d, J=8.3 Hz).

The residue of sublimation afforded **8**: mp 230—231 °C; IR, 1260 cm^{-1}; ^1H NMR, δ=1.18 (18H, s), 1.34 (18H, s), 3.95 (4H, s), 4.87 (2H, s), 7.00 (2H, s), 7.23—7.26 (2H, m), 7.46 (2H, s), 7.59 (2H, s), and 7.64 (2H, d, J=8.0 Hz); MS, m/z 568 (M^+), 553, and 269. Found: C, 90.83; H, 9.37%. Calcd for $C_{43}H_{52}$: C, 90.79; H, 9.21%.

4-Cyanomethyl-2,7-di-*t*-butylfluorene (4b).[6] A solution of **4a** (655 mg, 2 mmol) in DMF (20 ml) was stirred at room temperature with KCN (260 mg, 4.0 mmol) in H_2O (0.35 ml) for 24 h. Upon decomposition with dil. HCl, the residue was extracted with benzene and chromatographed on SiO_2 to give 530 mg (84%) of **4b**: mp 187—188 °C (lit,[6] mp 186—187 °C); UV, λ_{max} 304 (log ε 4.07), 292 (4.11), 285 (4.29), and 274 (4.44).

2,7-Di-*t*-butyl-9*H*-fluorene-4-acetic acid (4c).[6] A solution of **4b** (318 mg, 1 mmol) in AcOH (10 ml) was refluxed with conc. H_2SO_4 (0.8 ml) and H_2O (0.8 ml) for 3.5 h. Upon dilution with H_2O, the precipitate was recrystallized from benzene–cyclohexane to give **4c** (298 mg, 89%): mp 178—179 °C (lit,[6] mp 177—178 °C); UV, λ_{max} 335 (log ε 2.66), 305 (4.01), 293 (4.05), 285 (4.30), and 273 (4.45).

2,6-Di-*t*-butyl-4*H*-cyclopenta[*def*]phenanthren-8-ol (5) through Acid Chloride 4d. A mixture of **4c** (170 mg, 0.5 mmol) in $SOCl_2$ (5 ml) was refluxed for 30 min giving oily **4d**: IR, 1792 cm^{-1}; ^1H NMR, δ=1.39 (18H, s), 3.87 (2H, s), 4.55 (2H, s), and 7.13—7.54 (5H, m).

The above oil was added dropwise into a mixture of $AlCl_3$ (100 mg, 8 mmol) in $C_2H_4Cl_2$ (10 ml) at −8 °C, and the resulting mixture was stirred for 2 h giving 119 mg (75%) of **5**: mp>200 °C; IR, 3420 cm^{-1}; ^1H NMR, δ=1.45 (18H, s), 4.19 (2H, s), 6.94 (1H, s), 7.36 (1H, s), 7.50 (1H, s), 7.69 (1H, s), and 7.96 (1H, s).

The alcohol **5** was easily decomposed into red by standing for a few hour, and was failed to measure of the elemental analysis: the main portion may be 2,6-di-*t*-butyl-4*H*-cyclopenta[*def*]phenanthrene-8,9-dione (IR, 1671 cm^{-1}; MS, m/z 332, 318).

Reduction of 5. Carboxylic acid **4c** (340 mg, 1.0 mmol) was converted into **5** by a method similar to above; the resulting crude **5** was dissolved in AcOH (50 ml) and refluxed with HI (57%, 10 ml) and red phosphorus (1.0 g) for 90 h. Upon the usual treatment, a part of the resulting mixture was submitted GLPC (5% Dexsil 300 GC on Chromosorb, 1.0 Kg cm^{-2}, 230 °C): **1** (retention time 2.4 min, 8%) and **6a** (14.2 min, 31%) were confirmed by comparison with the authentic specimens. The major peak (6.3 min, 56%) might correspond to the monoalkylated compound **6b**.

The separation of the residual part of the mixture gave small amount of 2,6-di-*t*-butyl-4*H*-cyclopenta[*def*]phenanthrene (**6a**): mp 224—225 °C; IR, 1342 and 1210 cm^{-1}; ^1H NMR, δ=1.51 (18H, s), 4.31 (2H, s), 7.76 (2H, s), and ca. 7.8 (4H, s); MS, m/z 302 (M^+), 288, and 287. (Found: C, 91.80; H, 8.29%. Calcd for $C_{23}H_{26}$: C, 91.33; H, 8.67%.)

4*H*-Cyclopenta[*def*]phenanthrene (1). Acid **4c** (672 mg, 2 mmol) was treated in a way similar to the above, yielding a mixture of **6a**, **6b**, and **1**. The reaction mixture was dried, dissolved in toluene (40 ml), and stirred with $AlCl_3$ (36 mg, 0.3 mmol) at room temperature for 1.5 h giving 104 mg (27% based on **4c**) of **1**, mp 114—115 °C. This is identical in all respects with the authentic specimen.

We are grateful to Professor Takashi Toda, Utsunomiya University for his encouragement.

References

1) M. Minabe and K. Suzuki, *Yuki Gosei Kagaku Kyokai Shi*, **44**, 421 (1986).
2) H. Medenwald, *Chem. Ber.*, **86**, 287 (1953).
3) M. Yoshida, M. Minabe, and K. Suzuki, *Bull. Chem. Soc. Jpn.*, **56**, 2179 (1983).
4) K. G. Rutherford and M. S. Newman, *J. Am. Chem. Soc.*, **79**, 213 (1957).
5) M. Tashiro and T. Yamato, *Synthesis*, **1978**, 435; M. Tashiro, T. Yamato, and G. Fukata, *J. Org. Chem.*, **43**, 1413 (1978).
6) S. Kajigaeshi, T. Kadowaki, A. Nishida, S. Fujisaki, and M. Noguchi, *Synthesis*, **1984**, 335; S. Kajigaeshi, T. Kadowaki, A. Nishida, and S. Fujisaki, *Bull. Chem. Soc. Jpn.*, **59**, 97 (1986).

Active and Selective Transports of Alkali Metal Ions through Hydrophobic Membrane

Takashi HAYASHITA,* Kiyotaka TEDO, Takeo YAMABE, and Manabu IGAWA
Department of Applied Chemistry, Faculty of Engineering, Kanagawa University, Rokkakubashi, Kanagawa-ku, Yokohama 221
(Received August 1, 1987)

Synopsis. The active and selective transport of alkali metal ions coupled with proton permeation, were observed through a dense hydrophobic membrane. The flux of alkali metal ions increased with the decrease in the degree of hydration. The behavior can be comprehended in terms of the asymmetrical permeabilities of ions through the hydrophobic membrane.

Active and selective transport phenomena have been intensively studied as models of biological membranes and with a view to the practical application in industry.[1,2] Active transport has been observed through a liquid membrane containing ionophore[3–5] and an artificial membrane with containing ion-exchange groups.[6–8] We wish to report herein the findings that a dense hydrophobic membrane are also revealed active and selective transport for alkali metal ions. Such specific transport, depending on the hydrophobic environment, is considered to play an important role in artificial and biological membranes.

Experimental

A thin and dense hydrophobic membrane was prepared by coating a fluorocarbon polymer (FEP-120 dispersion, purchased from the Dupont Co.) on a "fluoropore", porous support membrane (FP-010, obtained from the Sumitomo Electric Co., Ltd.; pore size, 0.1 μm), followed by melting at 300 °C.[9,10] The SEM studies indicated that the thickness of the polymer layer on the membrane surface was about 6 to 8 μm. A homogeneous and dense layer was formed on the support membrane.[9] The coating density of the membrane used in this experiment was 0.79 mg cm^{-2}.

The dialysis experiments were carried out with a cell in which 100 mL of an aqueous solution containing 1 mmol dm^{-3} of alkali metal salts (L-side) and 100 mL of an aqueous solution containing equimolar amounts of alkali metal salts in addition to 0.1 mol dm^{-3} additive salts for producing active transport (R-side) were circulated separately into two chambers divided by the hydrophobic membrane.[11] The change in the concentration of the metal ions with time in both chambers was measured by means of an atomic-absorption spectrophotometer (Shimadzu AA-630-02).

The transport number was determined with two glass cells separated by a membrane and equipped with calomel electrodes. A metal sulfate solution of a different concentration (0.01—0.001 mol dm^{-3}) was circulated in each cell.[12]

Results and Discussion

Figure 1 shows the change in the concentration of the alkali metal ions and the pH changes on the L-side and the R-side through the hydrophobic membrane. The concentration of potassium ions on the R-side increased with the decrease in the pH on the L-side. The permeation flux of sodium ions was low

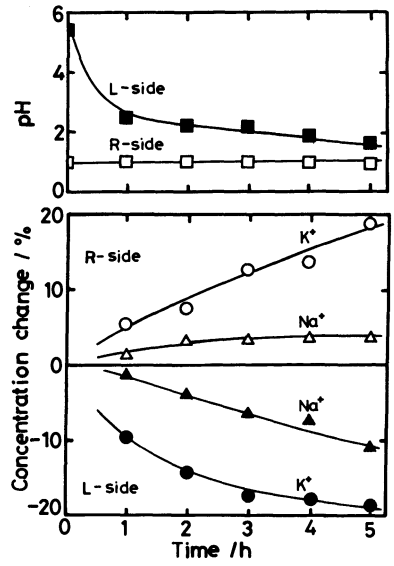

Fig. 1. Time-transport curves of Na^+, K^+ and pH through the hydrophobic membrane. L-side soln.: $[Na_2SO_4]=[K_2SO_4]=1$ mmol dm^{-3} (closed symbols). R-side soln.: $[Na_2SO_4]=[K_2SO_4]=1$ mmol dm^{-3}, $[H_2SO_4]=0.1$ mol dm^{-3} (open symbols).

compared with that of potassium ions. These results indicate that the selective and active transport of the alkali metal ions occurred coupled with the proton permeation. The behavior can be explained as a consequence of the asymmetrical permeabilities of the cations and the anion through the membrane, because the hydrophobic membrane repels the penetration of highly hydrated ions. It should be noted that some permeation lags were observed in this system. That is, the increment of alkali metal ions in the R-side solution were somewhat low compared with the decreasing degree of the L-side solution. This suggests that the rate of ion-exchange migration in the membrane was slower than that of distribution into the membrane.

These selectivities were only observed through a dense hydrophobic membrane. When the support membrane before coating was used as a barrier, an osmotic flow of water occurred and stable measurements could not be attained. To prevent such an osmotic flow, a coating density of at least 0.5 mg cm^{-2} was needed. The measurements are also considered to be difficult in the case of excess coating because of the low diffusibility of ions in the dense hydrophobic region of the membrane. Therefore, an appropriate amount of coating density (0.5—1.0 mg cm^{-2}) was required in these measurements.

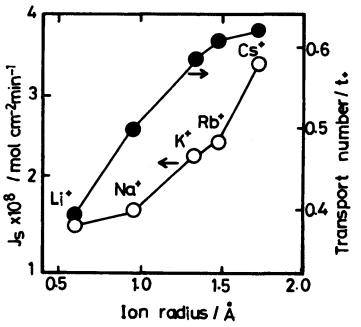

Fig. 2. Effect of ion radius on ion flux and transport number of permeate cations. ○: Ion flux (which were measured in the single component systems). L-side soln.: $[M_2SO_4]$=1 mmol dm^{-3}. R-side soln.: $[M_2SO_4]$=1 mmol dm^{-3}, $[H_2SO_4]$=0.1 mol dm^{-3}. ●: Transport number through the hydrophobic membrane.

Table 1. Effects of Additive Species on the Ion Flux[a)]

Additive	$J\times10^8$/mol cm^{-2} min^{-1} K$^+$	Na$^+$	J_{K^+}/J_{Na^+}
H_2SO_4	2.38	0.69	3.4
HCl	1.39	0.79	1.8
NH_4Cl	0.20	0.27	0.7
LiCl	−0.55	−0.26	2.1

a) Measurements were carried out in the Na$^+$, K$^+$ binary system. L-side soln.: $[Na_mX]=[K_mX]$=1 mmol dm^{-3}. R-side soln.: $[Na_mX]=[K_mX]$=1 mmol dm^{-3}, [Additive]=0.1 mol dm^{-3} (X=Cl$^-$ or SO_4^{2-}, m=1 or 2).

The effect of the ion radius of alkali metal ions on the ion flux, as calculated from the initial change in the concentration on the R-side, is shown in Fig. 2. The measurements were carried out in a single-component system. The hydration degree of an ion is known to decrease with the increase in the ion radius.[13)] From the figure, the flux of metal ions is seen to increase with the decrease in the hydration degree. In a hydrophobic environment, a low-hydrated ion is considered to be more permeable. These differences in permeability depending on the hydration degree are also proved by the values of the transport numbers for the cations. As may be seen from the figure, the transport number of cations increased with the decrease of hydration degree, similarly with the propensity of the ion flux (Fig. 2).

The effect of additive species in producing the active transports is shown in Table 1. As the proton has a high permeability because of the different permeation mechanism (the transport number of protons through the membrane (t_{H^+}) was 0.69 for H_2SO_4), which is known as a proton-jump mechanism coupled with water molecules,[14)] the metal ions were effectively transported couples with proton permeation. However, when a cation with a low membrane permeability, such as the lithium ion, was used as the additive, the flux depending on the antiport mechanism decreased significantly, while, on the contrary, the symport permeation of alkali metal ions, coupled with the permeation of chloride anions, was found to occur. These results also indicate that asymmetrical permeabilities of ions through the hydrophobic membrane are the cause of these specific permeations.

In conclusion, the selective and active transport of alkali metal ions was found to be attained through a dense hydrophobic membrane prepared by coating a fluorocarbon polymer on a support membrane. We consider that the hydrophobic membrane is a useful model for studing an ion channel consisting of a hydrophobic environment. Further studies of these specific permeations for other ionic solutes are in progress.

References

1) M. Takagi and K. Ueno, *Membrane*, **4**, 348 (1979); T. Shimizu, *Kobunshi*, **32**, 78 (1983).

2) T. Hayashita, "Kagaku-kogyo," **37**, 809 (1986); T. Hayashita, K. Kojima, M. Igawa, and M. Takagi, *Chem. Lett.*, **1986**, 1603.

3) J. H. Moore and R. S. Schechter, *Nature (London)*, **222**, 476 (1969).

4) F. Caracciolo, E. L. Cussler, and D. F. Evans, *AIChE J.*, **21**, 160 (1975).

5) W. J. Molnar, C. P. Wang, D. F. Evans, and E. L. Cussler, *J. Memb. Sci.*, **4**, 129 (1978).

6) R. M. Wallace, *Ind. Eng. Chem., Process Des. Dev.*, **3**, 423 (1967).

7) Y. Kikuchi and N. Kubota, *J. Appl. Polym. Sci.*, **30**, 2565 (1985).

8) M. Yoshikawa, Y. Yatsuzuka, K. Sanui, and N. Ogata, *Macromolecules*, **19**, 995 (1986).

9) M. Igawa, K. Torii, M. Tanaka, and M. Senō, *J. Appl. Polym. Sci.*, **29**, 117 (1984).

10) M. Igawa, T. Tachibana, K. Yoshida, M. Tanaka, and M. Senō, *Chem. Lett.*, **1984**, 1527.

11) M. Igawa, K. Saitou, F. Monoe, K. Nishida, M. Tanaka, and T. Yamabe, *Nippon Kagaku Kaishi*, **1985**, 826.

12) The transport number of the cation (t_+) was determined using the following equation:

$$E = \left(\left(\frac{1}{z_+} - \frac{1}{z_-}\right)t_+ + \frac{1}{z_-}\right)\frac{RT}{F}\ln\frac{a_R}{a_L}$$

Here, E is the membrane potential; z represents the ionic charge; R, T, and F are the gas constant, the absolute temperature, and the faraday constant respectively and a_R and a_L are the salt activities of the R-side and L-side solutions respectively.

13) F. Basolo and R. Johnson, "Coordination Chemistry," Benjamin, New York (1964), p. 122.

14) J. B. Bernal and R. H. Fowler, *J. Chem. Phys.*, **1**, 515 (1933).

Heats of Solution and Viscosity *B* Coefficients for Some Cyclic Mono- and Bis(quaternary ammonium) Salts

Kunio TAMAKI,* Takeshi KITAZAWA, and Misako ASADA
Department of Chemistry, Yokohama City University, Kanazawa-ku, Yokohama 236
(Received May 27, 1987)

Synopsis. Heats of solution and viscosity *B* coefficients, for cyclic mono(quaternary ammonium) salts, $(CH_3)_2N(CH_2)_nBr$ (n=4—6) and cyclic bis(quaternary ammonium) salts, 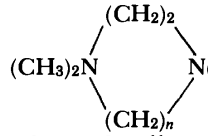 (n=1—3) in water were measured, and the effect of structural changes in the solvent water upon the dissolution of both series of electrolytes is discussed.

In previous papers,[1,2] the balance of ionic hydration and hydrophobic hydration in aqueous solutions of *N,N'*-polymethylenebis(trimethylammonium) dibromides and alkyltrimethylammonium bromides was discussed on the basis of the change in the heat capacity upon dissolution in water and the temperature dependence of the viscosity *B* coefficients in aqueous solutions.

Noguchi and Rembaum[3-5] reported that, in the course of the synthetic studies of polyelectrolytes by the Menschutkin reaction between *N,N,N',N'*-tetramethyl-α,ω-alkanediamines $(CH_3)_2N(CH_2)_xN(CH_3)_2$ (I) and α,ω-dibromoalkanes $Br(CH_2)_yBr$ (II), syntheses of polyelectrolytes were unsuccessful when the reaction systems with small values of x's and/or y's were carried out, and various linear and cyclic mono- and diammonium salts of low molecular weights were isolated. It seems that it would be of interest to study the solution properties of these low molecular weight compounds in water. We selected some cyclic mono(quaternary ammonium) salts $(CH_3)_2N(CH_2)_nBr$ (n=4—6; which will be abbreviated as NC_n[6]) and cyclic bis(quaternary ammonium) salts 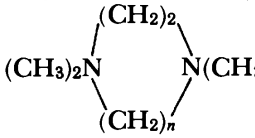 (n=1—3; which will be abbreviated as NC_nC_2N[7]) from the products reported by Noguchi and Rembaum.[3-5] The experimental results will be reported on the heats of solution and the viscosity *B* coefficients of aqueous solutions of these five-, six-, and seven-membered cyclic mono- and bis(quaternary ammonium) salts in this paper.

Experimental

All the salts were prepared by the reaction of ditertiary amines (I) with dibromides (II) in acetonitrile at room temperature according to the procedure described by Noguchi and Rembaum.[3-5] After the solvent had been removed, the salts were purified several times by recrystallization from suitable solvents. The reaction system and the solvents for recrystallization are summarized in Table 1. As NC_1C_2N was obtained in poor yield by the method of Noguchi and Rembaum,[4] the iodide salt of NC_1C_2N was prepared by the reaction of *N*-methylpyrrolidine with methyl iodide in ethanol,[8] the product was then converted to the bromide salt using the anion-exchange resin. All the salts were dried in vacuo at room temperature for several days, and then analyzed for bromide ion by argentometric titration. The salts were found to have a purity greater than 99.3%. Water was triply distilled. The solutions were made by weight.

Table 1. Reaction System and the Solvents for Recrystallization

Compound	x-y Reaction	Solvent
NC_4	2-1	EtOH–water (12:1)
NC_5	1-2	EtOH–water (5:1)
NC_6	2-3	EtOH–water (7:1)
NC_1C_2N	1-4	EtOAc–EtOH (1:1)
NC_2C_2N	1-5	EtOAc–EtOH (1:1)
NC_3C_2N	1-6	EtOAc–EtOH (2:1)

The heats of solution were measured at 15, 25, and 35 °C using a twin isoperibol calorimeter, TIC-2C, of the Tokyo Riko Co., Ltd., by a method similar to that described in a previous paper.[9]

The viscosities were measured at 25 and 35 °C using an automatic viscometer of the Shibayama Scientific Co., Ltd. The densities were measured using a vibrating-tube densimeter, twin-type SS-D-200, of the Shibayama Scientific Co., Ltd. The details of the procedure were described in a previous paper.[9] The electric conductivities were measured with an LCR meter, AG-4301B, of the Ando Electric Co., Ltd., using a frequency of 1000 Hz.

Results and Discussion

Heats of Solution. Heat-of-solution measurements were carried out in the concentration range of $(1.5—2.8)\times10^{-3}$ mol dm^{-3}. In this concentration range, any dependence of the heat of solution on the concentration is within the limit of experimental error, so the average of three or more measurements has been taken as the heat of solution at infinite dilution, ΔH_s^0. The ΔH_s^0 values of NC_n and NC_nC_2N in water are listed in Table 2. The ΔH_s^0 values were all endothermic, and the results from the ΔH_s^0 values were used to calculate the change in the heat capacity for dissolution at infinite dilution, ΔC_p^0:

$$\Delta C_p^0 = d\Delta H_s^0/dT, \quad (1)$$

where T is the temperature. The ΔC_p^0 values obtained at 25 °C are also listed in Table 2.

The sign and magnitude of ΔC_p^0 can be taken as a relative measure of the structural effect upon the solvent water.[10,11] The ΔC_p^0 values of common salts

Table 2. Heats of Solution and Heat-Capacity Changes

n		ΔH_s^0/kJ mol^{-1}		ΔC_p^0/J K^{-1} mol^{-1}
	T/°C 15	25	35	25
		NC_n		
4	17.79±0.08	17.61±0.04	17.73±0.08	−3±6
5	18.80±0.09	19.03±0.03	19.20±0.10	20±7
6	14.92±0.10	15.47±0.05	16.18±0.07	63±6
		NC_nC_2N		
1	32.60±0.15	29.19±0.07	26.52±0.08	−304±9
2	52.42±0.21	49.52±0.25	47.10±0.28	−266±18
3	37.04±0.07	34.86±0.11	32.41±0.10	−231±6

indicate negative values, whereas the ΔC_p^0 values of hydrophobic solutes indicate positive values.

As may be seen in Table 2, the values of ΔH_s^0 of NC_4 are insensitive to the temperature, this means that ionic and hydrophobic hydration balance each other. In the case of NC_5 and NC_6, the ΔC_p^0 values become positive, and they are hydrophobic structure-makers. With the NC_nC_2N series, three salts showed the negative ΔC_p^0 values, though the magnitude of ΔC_p^0 become less negative as the number of carbon atoms in the methylene groups increases; they are water-structure-breakers. On comparing of the ΔC_p^0 values of NC_n and NC_nC_2N in Table 2 with those of alkyltrimethylammonium bromides and *N,N'*-polymethylenebis(trimethylammonium) dibromides reported in a previous paper,[1] it is found that, for the same number of carbon atoms, the hydrophobicity of the cyclic mono- and bis(quaternary ammonium) salts is weaker than that of the linear mono- and bis(quaternary ammonium) salts respectively.

The Viscosity *B* Coefficients. The viscosity of an aqueous solution of an electrolyte, η, for concentrations up to about 0.1 mol dm^{-3} can be represented by the Jones-Dole equation:[12]

$$\eta/\eta_0 = 1 + Ac^{1/2} + Bc, \quad (2)$$

where η_0 is the viscosity of water, and A and B, the characteristic constants of the solutes. The A coefficient was interpreted theoretically by Falkenhagen and Vernon;[13] it can be calculated using the data of the limiting equivalent conductivities of the salt, the cation, and the anion. The B coefficient is related to the ion-solvent interaction and to the size and shape of the ion, and it is highly specific for the electrolyte and the temperature. Equation 2 may be converted to:

$$\eta/\eta_0 - 1 - Ac^{1/2} = Bc. \quad (3)$$

When the left-hand side of Eq. 3, using the calculated values of A, is plotted against c, the viscosity B coefficient is obtained as the slope of a straight line. Figures 1 and 2 show the results of plotting Eq. 3. The values of A and B are listed in Table 3. It is noted that the B values of cyclic mono- and bis(quaternary ammonium) salts studied in this work are smaller than those of respective mono- and bis(quaternary ammonium) salts with the same number of carbon atoms reported in a previous paper.[2] Previous experimental results of viscosity B coefficients at 25 °C

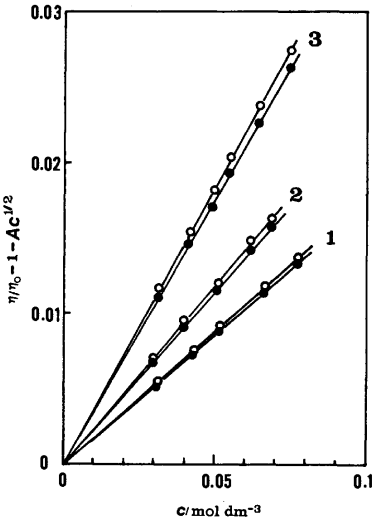

Fig. 1. Plots of $\eta/\eta_0-1-Ac^{1/2}$ against c for NC_n. 1, NC_4, 2, NC_5; 3, NC_6. O, 25 °C; ●, 35 °C.

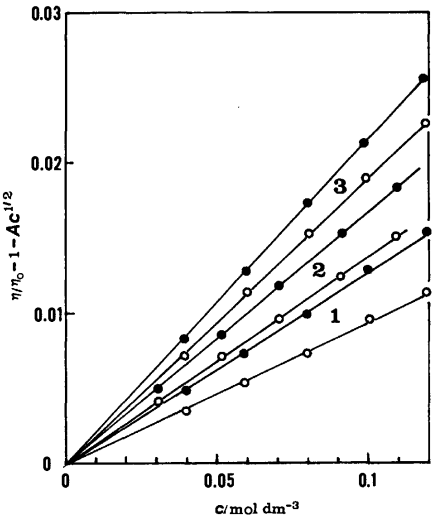

Fig. 2. Plots of $\eta/\eta_0-1-Ac^{1/2}$ against c for NC_nC_2N. 1, NC_1C_2N; 2, NC_2C_2N; 3, NC_3C_2N. O, 25 °C; ●, 35 °C

are available for iodide salts of NC_4 (0.142 dm^3 mol^{-1})[14] and NC_5 (0.208 dm^3 mol^{-1}).[14]

The temperature dependence of the B values may be regarded as an index of the solute-solvent interaction;

Table 3. The Values of A, B, and B_{ion}

n	T/°C	A/dm$^{3/2}$ mol$^{-1/2}$ 25	35	B/dm^3 mol^{-1} 25	35	B_{ion}/dm^3 mol^{-1} 25	35
				NC_n			
4		0.0066	0.0068	0.177	0.175	0.217	0.201
5		0.0067	0.0070	0.238	0.230	0.278	0.256
6		0.0069	0.0071	0.368	0.354	0.408	0.380
				NC_nC_2N			
1		0.0131	0.0136	0.094	0.128	0.174	0.180
2		0.0132	0.0137	0.137	0.168	0.217	0.220
3		0.0135	0.0140	0.189	0.216	0.269	0.268

the B values increase with the temperature for a solvent-structure-breaking salt, while they decrease with temperature for a solvent-structure-making solute.[15] For the NC_n series, it may be seen in Table 3 that the B values decrease as the temperature is raised from 25 to 35 °C; these salts may be considered to behave as structure-making salts in the water phase. However, as the difference in the B values of NC_4 between 25 and 35 °C is small, NC_4 may therefore be considered to behave as a borderline salt. For all the salts of NC_nC_2N used, the B values increase as the temperature is raised from 25 to 35 °C; these salts may be classified as structure-breaking salts in the water phase.

The B values of electrolytes are determined by adding the individual contributions of the ions. Out and Los[16] reported the ionic B values, B_{ion}, of the Br^- ion as a function of temperature according to the convention of Gurney[17] that the B_{ion} values for K^+ and Cl^- ion are equal. The B_{ion} values of Br^- ion[16] are -0.040 and -0.026 dm^3 mol^{-1} at 25 and 35 °C, respectively. The B_{ion} values of organic ions obtained are included in Table 3. With the NC_n^+ series, the B_{ion} values decrease with the temperature, so they are classified as structure-making ions. With the $NC_nC_2N^{2+}$ series, the B_{ion} values vary little with temperature. In this case the ionic hydration due to the two charge-bearing $>N(CH_3)_2^+$-groups may interfere with the interaction of hydrophobic-$(CH_2)_n$-groups with water. For both series of NC_n^+ and $NC_nC_2N^{2+}$ ions, the changes in the B_{ion} values, which occur as the temperature is raised from 25 to 35 °C, decrease with n; this indicates that hydrophobic hydration gradually increases with the number of methylene groups.

References

1) K. Tamaki and R. Furuya, *Bull. Chem. Soc. Jpn.*, **57**, 3325 (1984).
2) K. Tamaki and A. Fujiwara, *Bull. Chem. Soc. Jpn.*, **58**, 3367 (1985).
3) H. Noguchi and A. Rembaum, *J. Polym. Sci., Polym. Lett. Ed.*, **7**, 383 (1969).
4) H. Noguchi and A. Rembaum, *Macromolecules*, **5**, 253 (1972).
5) A. Rembaum and H. Noguchi, *Macromolecules*, **5**, 261 (1972).
6) n=4: 1,1-dimethylpyrrolidinium bromide. n=5: 1,1-dimethylpiperidinium bromode. n=6: 1,1-dimethylhexahydroazepinium bromide.
7) n=1: tetrahydro-1,1,3,3-tetramethylimidazolium dibromide. n=2: 1,1,4,4-tetramethylpiperazinium dibromide. n=3: hexahydro-1,1,4,4-tetramethyl-1,4-diazepinium dibromide.
8) D. R. Smith, J. W. Curry, and R. L. Eifert, *J. Am. Chem. Soc.*, **72**, 2969 (1950).
9) K. Tamaki, Y. Ōhara, M. Inabe, T. Mori, and F. Numata, *Bull. Chem. Soc, Jpn.*, **56**, 1930 (1983).
10) E. M. Arnett and J. J. Campion, *J. Am. Chem. Soc.*, **92**, 7097 (1970).
11) T. S. Sarma and J. C. Ahluwalia, *Chem. Soc. Rev.*, **2**, 203 (1973).
12) G. Jones and M. Dole, *J. Am. Chem. Soc.*, **51**, 2950 (1929).
13) H. Falkenhagen and E. L. Vernon, *Z. Physik.*, **33**, 140 (1932).
14) B. M. Lowe and H. M. Rendall, *Trans. Faraday Soc.*, **67**, 2318 (1971).
15) R. L. Kay, T. Vituccio, C. Zawoyski, and D. F. Evans, *J. Phys. Chem.*, **70**, 2336 (1966).
16) D. J. P. Out and L. M. Los, *J. Solution Chem.*, **9**, 19 (1980).
17) R. W. Gurney, "Ionic Processes in Solution," McGraw-Hill, New York (1953), p. 159.

^{27}Al NMR Study on the Interaction between Aluminate and Silicate Ions in Alkaline Solution

Takushi YOKOYAMA,* Setsuko KINOSHITA,† Hisanobu WAKITA,† and Toshikazu TARUTANI
Department of Chemistry, Faculty of Science, Kyushu University,
Hakozaki, Higashiku, Fukuoka 812
†Department of Chemistry, Faculty of Science, Fukuoka University,
Nanakuma, Jonanku, Fukuoka 814-01
(Received May 16, 1987)

Synopsis. An interaction between aluminate and silicate ions in highly alkaline solution was investigated by a high-resolution ^{27}Al NMR study. The interaction greatly varied with alkali concentration, and did not occur at 1.0 mol dm^{-3} NaOH. At 0.10 mol dm^{-3} NaOH, the formation of a monomeric species with an ≡Al-O-Si≡ bond (Si/Al=1) was suggested and the formation constant was estimated to be 22.8 dm^3 mol^{-1}. At 0.015 mol dm^{-3} NaOH, polynuclear species with ≡Al-O-Si≡ bond was expected to be formed.

An important advantage of ^{27}Al is its 100% isotopic abundance, which makes ^{27}Al NMR a very sensitive probe. Much work has been reported on the environment of Al atoms in solid aluminosilicates, while little has been published on the characterization of solutions containing aluminosilicates or aluminate and silicate ions by the ^{27}Al NMR technique. Mueller et al.[1] observed four resonance lines of ^{27}Al NMR for tetramethylammonium aluminosilicate solutions of different molar ratios of Si and Al and assigned their lines to four kinds of monomeric AlO_4 tetrahedrons bonded to zero, one, two, and three silicon atoms, respectively. Glasser and Harvey[2] reported that for a given alkali-silicate-aluminate composition, the distribution of aluminium between uncomplexed aluminate and aluminosilicate complexes may vary with the cation present.

In this work an interaction between aluminate and silicate ions in strongly alkaline solutions was studied by a high-resolution ^{27}Al NMR.

Experimental

Sample and Reagents. All the reagents used were of analytical reagent grade. The sodium silicate solution (10^{-2} mol dm^{-3} Si) was prepared by dissolving silica gel in sodium hydroxide solution. The silicon concentration in the solution was determined spectrophotometrically. The sodium aluminate solution (10^{-2} mol dm^{-3} Al) was prepared by dissolving $AlCl_3 \cdot 6H_2O$ in sodium hydroxide solution. The aluminium concentration was standardized by EDTA titration.

Sample solutions with various molar ratios of Si and Al (Si/Al) up to 5 were prepared by mixing aluminate and silicate solutions. The aluminium concentration was fixed at 10^{-3} mol dm^{-3} and the sodium hydroxide concentration was adjusted to (a) 1.0, (b) 0.10, and (c) 0.015 mol dm^{-3}, respectively.

^{27}Al NMR Measurement. The ^{27}Al NMR spectra were recorded at 52 MHz on a JEOL FX-200 spectrometer. The sample solution was placed in a glass tube of 15 mm diameter. An aqueous $AlCl_3$ solution enclosed in a glass tube of 1 mm diameter was used as an external standard. The $AlCl_3$ solution (10^{-1} mol dm^{-3} Al) was prepared by dissolving $AlCl_3 \cdot 6H_2O$ in 1 mol dm^{-3} hydrochloric acid. The D_2O concentration in the standard and sample solutions was ca. 40% to operate the field frequency lock. NMR measurements were carried out at room temperature after allowing the sample solution to stand more than 24 h.

Results and Discussion

System (a) (1.0 mol dm^{-3} NaOH). The ^{27}Al NMR allows a clear distinction between AlO_6 octahedral and AlO_4 tetrahedral sites in aluminium-oxygen compounds. An ^{27}Al NMR spectrum of the sample solution (Si/Al=0) is shown in Fig. 1. The peak on the right is due to standard $[Al(H_2O)_6]^{3+}$ (Octahedral) and peak on the left (denotes as peak X) is due to the sample solution. The chemical shift (ppm) and the intensity of peak X were determined relative to the peak of standard $[Al(H_2O)_6]^{3+}$. The positive sign of the chemical shift denotes a downfield shift. The chemical shift of the peak X is 80.2 ppm and the signal is typical of monomeric $[Al(OH)_4]^-$ anions.[3]

In the spectra of the sample solutions of different Si/Al ratios, the peak X always appeared at 80.2 ppm. Moreover, the relative intensity of peak X, defined as follows, was unity independent of the Si/Al ratio:

$$RI = (A_X/A_s)/(A_0/A_s)$$

where A_x is the area of peak X, A_0 is the peak area for $[Al(OH)_4]^-$ (Si/Al=0), and A_s is the peak area for $[Al(H_2O)_6]^{3+}$. These facts indicate that no interaction between aluminate and silicate ions occurs, because of the high alkali concentration.

System (b) (0.10 mol dm^{-3} NaOH). The ^{27}Al NMR spectra did not change for several days after preparation of the sample solutions, indicating that an equilibrium was rapidly achieved in the system (b). Peak X of the sample solution (Si/Al>0) shifted

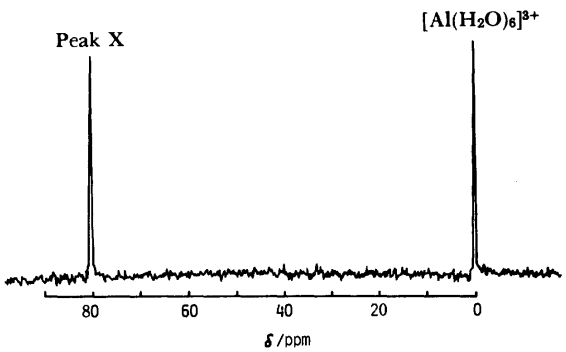

Fig. 1. ^{27}Al NMR spectra of sample solution (peak X) and external standard solution ($[Al(H_2O)_6]^{3+}$). NaOH concentration: 0.10 mol dm^{-3}. Si/Al=0.

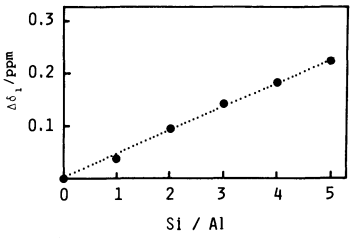

Fig. 2. Variation of chemical shift ($\Delta\delta_1$) with Si/Al ratio.
NaOH concentration: 0.10 mol dm^{-3}.

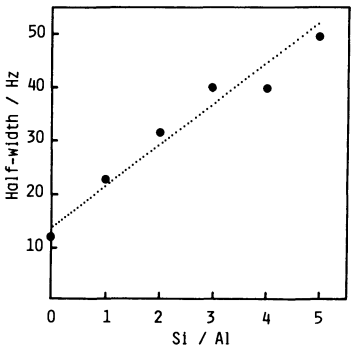

Fig. 3. Variation of half-width of peak X with Si/Al ratio.
NaOH concentration: 0.1 mol dm^{-3}.

slightly toward higher field from the peak of $[Al(OH)_4]^-$. The chemical shift difference between the peak X and the peak of $[Al(OH)_4]^-$, $\Delta\delta_1$, increased with increasing Si/Al ratio. Figure 2 shows the variation of $\Delta\delta_1$ with the Si/Al ratio. The half-width for peak X also increased with increasing Si/Al ratio, as shown in Fig. 3.

The electron donating property of the substituent to aluminium is a major factor in determining the chemical shift. The ^{27}Al upfield shift is due to the increased overall electron density of aluminium. The increase in the half-width of the peak X with increasing Si/Al ratio resulted from an increment of tetrahedrally coordinated aluminium atoms with low symmetry compared with the $[Al(OH)_4]^-$ tetrahedron. Consequently, the formation of species with an ≡Al–O–Si≡ bond was suggested. The relative intensity of peak X was unity regardless of the difference in the Si/Al ratio, indicating that all the aluminium was detected.

It seems reasonable that the species formed is assumed to be a 1:1 complex of aluminium and silicate (Si/Al=1) since the alkali concentration is high, the Al and Si concentrations are relatively low, and the $\Delta\delta_1$ values are small. Considering only a 1:1 complex formation, the reaction can be written as follows:

$$A + L \rightleftarrows AL \quad (1)$$

where A is aluminate ion, L is silicate ion, and AL is a 1:1 complex. The formation constant of AL, K, is

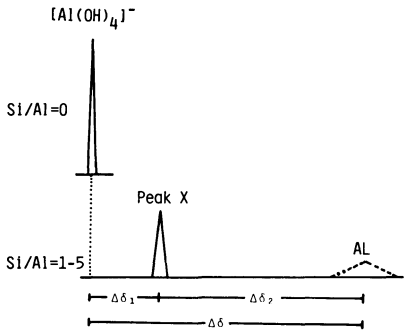

Fig. 4. Chemical shift profile in the system (b).
Peak A and Peak X can be observed, while peak AL is hypothetical one.

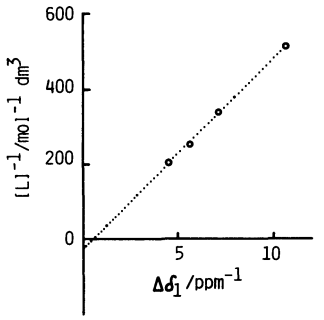

Fig. 5. Plot of $1/[L]$ against $1/\Delta\delta_1$.

represented by Eq. 2.

$$K = [AL]/[A]\cdot[L] \quad (2)$$

When an exchange rate between A and AL is rapid on the NMR time scale, the following relations can be valid.

$$\Delta\delta_1 : \Delta\delta_2 = [AL] : [A] \quad (3)$$

$$\Delta\delta = \Delta\delta_1 + \Delta\delta_2 \quad (4)$$

$\Delta\delta_2$ and $\Delta\delta$ are the chemical shift difference between peak X and peak AL and between peak A and peak AL, respectively (Fig. 4). From these equations, a following equation can be derived.

$$1/[L] = K\cdot\Delta\delta/\Delta\delta_1 - K \quad (5)$$

Since $\Delta\delta_1$ values were small, it can be considered that K is small and $[L]\simeq[L^*]$, ([L]: the concentration of free Si at equilibrium, [L*]: total concentration of Si). K and $\Delta\delta$ values were determined by a succesive approximation method. A plot of $1/[L]$ against $1/\Delta\delta_1$ is shown in Fig. 5. The plot gave a straight line and the correlation coefficient was 0.999. From the intersection and the slope of this line, K and $\Delta\delta$ values were calculated to be 22.8 (dm^3 mol^{-1}) and 2.2 (ppm), respectively.

On the other hand, the half-width for peak X, W_X, can be represented by Eq. 6, where W_A and W_{AL} denote the half-width for peak A and peak AL, respectively.

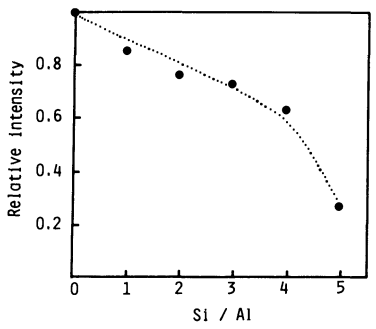

Fig. 6. Variation of the relative intensity for peak X with Si/Al ratio.
NaOH concentration: 0.015 mol dm^{-3}.

$$W_X = W_A \cdot [A]/([A] + [AL]) + W_{AL} \cdot [AL]/([A] + [AL]) \quad (6)$$

From Eqs. 2 and 6

$$W_{AL} = (W_X - W_A)/(K[L]) + W_X \quad (7)$$

The half-width of peak AL was calculated to be about 400 Hz, putting W_A, K, W_X, and [L] values in Eq. 7.

When the sample solution of Si/Al=4 was heated at 42 °C and 55 °C, the $\Delta\delta_1$ value and the half-width were found to approach those of the Si/Al=0 solution with increasing temperature, though the relative intensities were almost constant. The interaction between aluminate and silicate ions may not be allowed at higher temperature.

System (c) (0.015 mol dm^{-3} NaOH). Peak X appeared at 80.2 ppm independent of Si/Al ratio, while the relative intensity of peak X decreased with increasing Si/Al ratio (Fig. 6), indicating that the $[Al(OH)_4]^-$ species left in the solution decreases with increasing Si/Al ratio. Part of the aluminate ions in the solution is supposed to be irreversibly changed to a polynuclear species with an ≡Al–O–Si≡ bond. The relative intensity of the peak X decreased gradually over several days. The ^{27}Al NMR signal of the polynuclear species is considered to be too broad to be observed because of its lower symmetry.

The interaction between aluminate and silicate ions is greatly influenced by the alkali concentration.

References

1) D. Mueller, D. Hoebbel, and W. Gessner, *Chem. Phys. Lett.*, **84**, 25 (1981).
2) J. W. Akitt and W. Gessner, *J. Chem. Soc., Dalton Trans.*, **1984**, 147.
3) L. S. D. Glasser and G. Harvey, *J. Chem. Soc., Chem. Commun.*, **1984**, 1250.

Solvent- and Wavelength-Dependence of the Photocleavage of the Cyclobutane Ring in *N,N'*-Dibutyl-*c*-3,*c*-4-bis-(2-hydroxyphenyl)-*r*-1,*c*-2-cyclobutanedicarboxamide

Noriyuki YONEZAWA,† Masataka KUBO,†† Kazuhiko SAIGO, and Masaki HASEGAWA*
Department of Synthetic Chemistry, Faculty of Engineering, The University of Tokyo, Hongo, Bunkyo-ku, Tokyo 113
(Received March 31, 1987)

Synopsis. The ratio between two photocleavage directions of the cyclobutane ring in the title compound varies with the solvent polarity and the irradiation wavelength, and the effect of the solvent polarity appears much larger in protic solvents than aprotic ones.

Head-to-head type cyclobutane compounds have two possible cleavage modes, namely, symmetric and asymmetric cleavages.[1] Most of the lactone-opened derivatives of head-to-head coumarin dimers have only one photocleavage direction, but the derivatives, of which all the substituents are situated in the cis positions to each other on the cyclobutane ring such as *N,N'*-dibutyl-*c*-3,*c*-4-bis(2-hydroxyphenyl)-*r*-1,*c*-2-cyclobutanedicarboxamide (**1**), were confirmed to undergo symmetric and asymmetric photocleavages competitively.[2-4] To clarify the factors which govern the photocleavage mode of these compounds, the photoscission reaction of **1** was investigated under various conditions by comparing with those of *N,N'*-dibutyl-*t*-3,*c*-4-bis(2-hydroxyphenyl)-*r*-1,*t*-2-cyclobutanedicarboxamide (**5**) and syn and anti head-to-head coumarin dimers **6** and **7**.

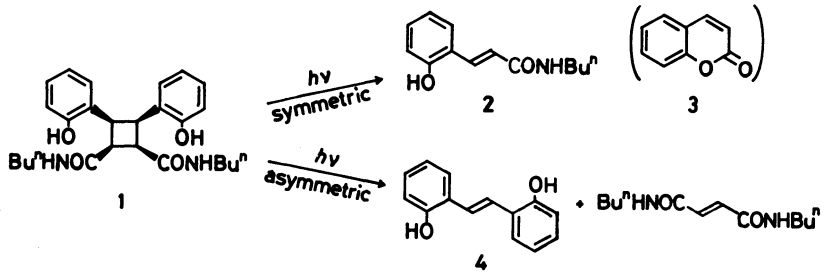

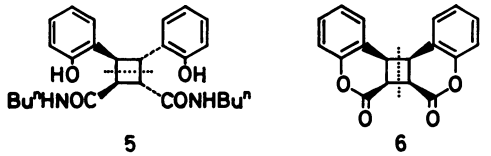

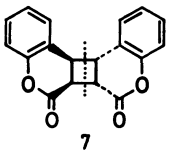

Results and Discussion

Irradiation of **1** was carried out in alcohols (protic) and MeCN (ε 37.5)/dioxane (ε 2.2) mixed solvents (aprotic). The products of photolysis were confirmed by comparing their retention times of HPLC analysis with those of the authentic samples. The conversions and the ratios between photocleavage modes were estimated by the area of elution bands and the molar absorptivities of the starting material, the products, and the standard sample as shown in the Eqs. 1 and 2, respectively:

conversion

$$= [S_h/\varepsilon_h + (S_c/\varepsilon_c + S_{cis}/\varepsilon_{cis} + S_{trans}/\varepsilon_{trans})/2]/(aS_s/\varepsilon_s) \quad (1)$$

symmetric fission/asymmetric fission

$$= (S_c/\varepsilon_c + S_{cis}/\varepsilon_{cis} + S_{trans}/\varepsilon_{trans})/(2S_h/\varepsilon_h) \quad (2)$$

where S is the area of the elution band recorded by the UV detector at 320 nm and ε is the molar absorptivity at 320 nm; h, c, cis, trans, s, and a denote **4**, **3**, *cis-N*-butylcoumaramide, **2**, standard meterial, and the ratio of the starting material to the standard material, respectively.

The molar absorptivity of *cis-N*-butylcoumaramide was determined by HPLC analysis of the solution of **2** after irradiation using Eq. 1. The isolation of *cis-N*-butylcoumaramide was unsuccessful because of its spontaneous relactonization to coumarin at room temperature, and the isomerization of **4** was not observed in our experiments.

The ratio between the two photocleavage modes of **1** varied with the solvent polarity and the wavelength of light as shown in Fig. 1. Though the symmetric cleavage mode was predominant in every case, asymmetric one gradually increased with shortening the wavelength, and protic solvents were favorable for asymmetric cleavage as compared to aprotic solvents.

† Present address: Nippon Kokan K. K., Kawasaki-ku, Kawasaki 210.

†† Present address: Mie University, Tsu, Mie 514.

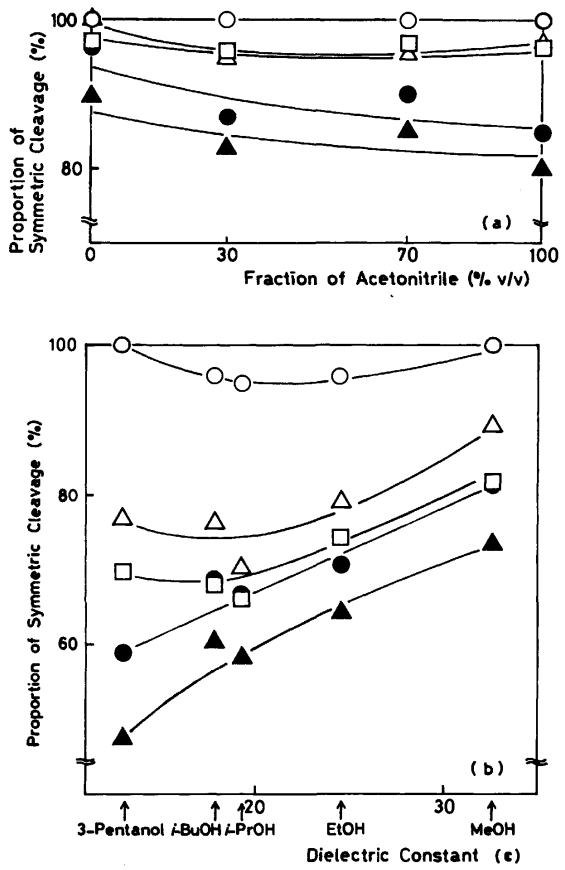

Fig. 1. The ratio between symmetric and asymmetric modes of the cyclocleavage reaction of **1** in (a) MeCN–dioxane and (b) alcohols (○: 330 nm, △: 304 nm, □: 277 nm, ●: 251 nm, and ▲: 224 nm).

The effects of solvent polarity appeared more remarkably at the range of shorter wavelength in both protic and aprotic solvents.

In protic solvents symmetric cleavage became more advantageous as the polarity of the solvent increased. In addition, the quantum yields for the formation of olefins in MeOH, calculated on the basis of Eq. 1, had also distinct dependence on the irradiation wavelength, i.e., $\phi_{224}=0.27$, $\phi_{251}=0.06$, $\phi_{277}=0.33$, and $\phi_{304}=0.05$. These results indicate that there exist at least two routes for this cyclocleavage reaction. On the other hand, the proportion of asymmetric photocleavage was almost constant in aprotic solvents.

In contrast, the exclusively asymmetric cleavage of the cyclobutane ring in **5** did not change by the wavelength nor by the solvent (dioxane, MeCN, or MeOH). And the irradiation of **6** or **7** in MeCN or dioxane solution always gave coumarin (**3**) as a sole product of the exclusively symmetric cleavage.

When the irradiation was carried out with the light of 251±10 nm wavelength using benzene as a sensitizer, the photocleavage reaction of **5**—**7** was accelerated by 3.2—3.5 times. But, the photocleavage reaction of **1** was sensitized by only 1.4 times. From the phosphorescence spectra of **1** and **5**, the triplet excited energies in MeOH were estimated to be 70 and 66 kcal mol^{-1}, respectively. Furthermore, the photocleavage reaction of **1** was not quenched by biacetyl and hardly sensitized by acetone or acetophenone. These results suggest that the cyclocleavage reaction of **1** proceeds predominantly via singlet excited state although the sensitization of the reaction with benzene indicates the existence of the reaction route via triplet excited state.

The dependence of the quantum yields on the irradiation wavelength and the different wavelength dependence between aprotic and protic solvents are considered to be attributed to the abilities of the solvents to stabilize **1** in both ground state and/or excitation process and the intermediates in the cyclocleavage reaction, presumably through hydrogen bonding interaction. In the ground state and the early stage of excitation, 2-hydroxyphenyl chromophore should interact with butylcarbamoyl group in several manners causing at least two excitation states in the ratio determined in accordance with the property of the medium. Moreover, one possible intermediate in the photocleavage reaction of **1** is an intramolecular excimer as observed in the cycloaddition of coumarin in ethanol to yield **6**.[5] But the evidence for the formation of the intramolecular excimer could not be obtained by the emission spectra. These phenomena show that in both protic and aprotic solvents at least two intermediates should exist and indicates that particularly in protic solvents the minor reaction routes was probably accelerated. The competitive photocleavage of **1** is distinctly different from exclusively one-directioned photocleavages of other lactone-opened derivatives of **6** and **7**.[2,4] This characteristic photochemical behavior of **1** was clearly brought in by the largely hindered cis-syn-cis configuration on the cyclobutane ring of **1**, which might make **1** to have peculiar conformations enabling the formation of intramolecular excimer and highly reactive intermediate by interaction of 2-hydroxyphenyl and carbamoyl groups, reflecting the hydrogen bonding and electrostatic effects of solvents.

Experimental

Irradiation was carried out with a JASCO CRM-FA spectroirradiator at room temperature. UV spectra were recorded on a Hitachi Model 100-60 spectrophotometer. Emission and phosphorescence spectra were recorded on a Hitachi MPF-4 fluorescence spectrophotometer. HPLC analysis was performed on a steel column (4 mm×250 mm) packed with LiChrosorb SI60 (5 μm, Merck and Co.) and the absorbance at 320 nm was monitored on a TOYO SODA UV8 Model II spectrophotometer at a flow rate of 0.4 ml min^{-1} using benzene–ethyl acetate (70:30 v/v) as an eluent.

Spectrograde solvents were used for reaction and UV measurement without further purification. **1** and **5**—**7** were prepared according to the literatures.[6,7] Standard and authentic samples for HPLC analysis, 4-ethoxycarbonyl-, and 4-phenoxycarbonylchalcones,[8] *trans*-*N*-butylcoumaramide (**2**),[9,10] and 2,2′-dihydroxystilbene (**4**),[2] were prepared according to the methods in the literatures. Other reagents were purified by the ordinary methods.[11]

Photolysis of 1 and 5—7. Through a solution of **1**, **5—7** (ca. 5×10^{-5} mol dm^{-3}) in a quartz cell, anhydrous nitrogen was bubbled for ca. 1 min. The photocleavage reaction was monitored by the UV spectrophotometer during the irradiation. Before the new absorption reached a maximum, the irradiation was stopped, and the solution was concentrated under reduced pressure. Then the residue was dissolved in benzene–ethyl acetate (70:30 v/v) containing a constant amount of a standard material (4-ethoxycarbonylchalcone, or 4-phenoxycarbonylchalcone) and analyzed by HPLC.

Quantum Yield. The quantity of the light absorbed was measured by the chemical actinometry.[12] The quantum yields for the formation of olefins in the photocleavage of MeOH solution **1** was determined as follows: Two quartz cells were set in series along the line of the irradiation light, where the former cell was for the photoreaction or blank, and the second for chemical actinometry. The photoirradiation of MeOH solution of **1** and MeOH alone performed under exactly same conditions. The quantum of the light absorbed by **1** was calculated on the basis of the difference of the quantities of the light absorbed by the solution in the second cell. The amount of total olefins calculated by Eq. 1 and the quantity of light absorbed by **1** afforded the quantum yield.

The relative rates of the photocleavage were determined as follows: Two quartz cells were set in the same manner as the quantum yield measurement described above. First, only the solvent was placed in the former cell and the solution of the cyclobutane compounds containing sensitizer or quencher in the second cell, then the photoirradiation was undertaken. Then, solvent containing same amount of sensitizer or quencher was placed in the former cell and the solution of substrate in the second cell, and photoirradiation was undertaken under the exactly same conditions. Relative rate was calculated by the ratio of conversion between above two photoirradiation.

References

1) E. Schaumann and R. Ketcham, *Angew. Chem., Int. Ed. Engl.*, **21**, 225 (1982).
2) N. Yonezawa, T. Yoshida, and M. Hasegawa, *J. Chem. Soc., Perkin Trans. 1*, **1983**, 1083.
3) M. Hasegawa, K. Saigo, H. Katsuki, N. Yonezawa, and T. Kanoe, *J. Polym. Sci., Polym. Chem. Ed.*, **21**, 2345 (1983).
4) N. Yonezawa, T. Yamashita, T. Kanoe, K. Saigo, and M. Hasegawa, *Ind. Eng. Chem., Prod. Res. Dev.*, **24**, 593 (1985).
5) G. S. Hammond, C. A. Stout, and A. A. Lamola, *J. Am. Chem. Soc.*, **86**, 3103 (1964).
6) C. H. Krauch, S. Farid, and G. O. Schenck, *Chem. Ber.*, **99**, 625 (1966).
7) N. Yonezawa and M. Hasegawa, *Bull. Chem. Soc. Jpn.*, **56**, 367 (1983).
8) M. Hasegawa, H. Arioka, H. Harashina, M. Nohara, M. Kubo, and T. Nishikubo, *Isr. J. Chem.*, **25**, 302 (1985).
9) W. Schultz, *J. Pharm. Sci.*, **52**, 503 (1963).
10) V. A. Zagorevskii and V. L. Sarel'ev, *J. Gen. Chem. USSR (Engl. Transl.)*, **34**, 2302 (1964).
11) D. D. Perrin, W. L. F. Armarego, D. R. Perrin, "Purification of Laboratory Chemicals," 2nd ed, Pergamon Press, Oxford (1980).
12) C. G. Hatchard and C. A. Parker, *Proc. R. Soc. London, Ser. A*, **235**, 518 (1956).

Aldol Condensation Reaction between Formaldehyde and Acetone over Heat-Treated Synthetic Hydrotalcite and Hydrotalcite-Like Compounds

Eiichi Suzuki* and Yoshio Ono
Department of Chemical Engineering, Tokyo Institute of Technology, Ookayama, Meguro-ku, Tokyo 152
(Received July 30, 1987)

Synopsis. Synthetic hydrotalcite, $Mg_6Al_2(OH)_{16}CO_3 \cdot 4H_2O$, and its analogues were synthesized, heat-treated at 773 K, and used as catalysts for the title reaction to form methyl vinyl ketone (MVK) at 673 K. MVK was formed over all the catalysts examined, the highest MVK yield (20% on acetone basis) being found over the heat-treated hydrotalcite.

Hydrotalcite is one of the naturally occurring anionic clay minerals and is represented by the formula: $Mg_6Al_2(OH)_{16}CO_3 \cdot 4H_2O$.[1,2] Thus, magnesium-aluminium hydroxide octahedra form positively-charged layers, which are stacked on top of each other. Carbonate ions are located between the layers as interlayer anions. Hydrotalcite-like minerals, i.e. cation-substituted and/or anion-exchanged hydrotalcites, can be obtained by isomorphous substitution of the cations in the layer and/or of the anions in the interlayer of hydrotalcite.[3-7] It has been reported that these minerals can be synthesized[8] and have basicity upon heat treatment.[9] Several base-catalyzed reactions have been demonstrated: polymerizations of β-propiolactone[10] and of propylene oxide,[11] and self-aldol condensation of acetone.[12,13]

The present work was concerned with testing heat-treated hydrotalcite and hydrotalcite-like compounds as catalysts for a cross-aldol condensation reaction which is known to be catalyzed by acids or bases.[14] Here, a reaction between formaldehyde and acetone is examined, where methyl vinyl ketone (MVK) is the condensation product.

Experimental

Synthesis of Hydrotalcite and Hydrotalcite-Like Compounds. Hydrotalcite was synthesized by the procedures described by Reichle,[13] using $Mg(NO_3)_2 \cdot 6H_2O$, $Al(NO_3)_3 \cdot 9H_2O$, NaOH, and Na_2CO_3. According to the method reported by Miyata et al.,[6,8] was prepared isomorphous-substituted hydrotalcite with NO_3^{2-}, SO_4^{2-}, or CrO_4^{2-} anions. Isomorphous-substituted hydrotalcite, containing Co^{2+}-Al^{3+},[13] Ni^{2+}-Al^{3+},[13] Zn^{2+}-Cr^{3+},[13] or Li^{+}-Al^{3+} [15,16] ions in place of Mg^{2+}-Al^{3+} ions in hydrotalcite, was also prepared. The X-ray diffraction (XRD) patterns of the materials, thus synthesized, were identical to those previously reported.[3,6,16,17]

Cross-Aldol Condensation Reactions. The reactions were performed with a continuous-flow reactor operating at atmospheric pressure. The synthetic minerals were heated under a helium stream at a given temperature for 2 h before starting the reactions. A mixture of acetone and formalin, containing 36.8wt% of HCHO and 6.6wt% of methanol with a given HCHO/acetone molar ratio, was delivered to the reactor. The products from the outlet of the reactor were periodically analyzed by gas chromatograph.

Results and Discussion

Reactions over Anion-Exchanged Hydrotalcites. In Table 1, are summarized the results of reactions at 623 K with W/F of 7.9 g h mol^{-1} over the anion-exchanged hydrotalcites treated at 623 K, where W and F stand for the weight (g) of the catalyst used and the flow rate (mol h^{-1}) of the feed (formaldehyde+acetone +nitrogen+water), respectively. The heating of hydrotalcite samples at 623 K to obtain catalysts gave rise to changes in the XRD patterns of the samples:

Table 1. Reactions between Formaldehyde and Acetone over Anion-Exchanged Hydrotalcites, Containing Mg^{2+}-Al^{3+}-X^{n-} Ions[a]

Interlayer anion (X^{n-})	Acetone conversion/%	Selectivity to MVK[b]/%
CO_3^{2-}	20	93
NO_3^{-}	12	97
SO_4^{2-}	6.0	98
CrO_4^{2-}	3.7	100

a) Reaction conditions: pretreatment temperature= 623 K, reaction temperature=623 K, HCHO=10.1 kPa, Acetone=9.1 kPa and W/F=7.9 g h mol^{-1}. b) On acetone basis.

Table 2. Reactions between Formaldehyde and Acetone over Heated Cation-Substituted Hydrotalcites, Containing M_1^{2+}- or M_1^{+}-M_2^{3+}-CO_3^{2-} Ions[a]

Cations in layer M_1^{2+}- or M_1^{+}-M_2^{3+}	Acetone conversion/%	Selectivity to MVK/%	
		(Acetone)[b]	(HCHO)[c]
Mg^{2+}-Al^{3+}	21	96	64
Li^{+}-Al^{3+}	12	100	37
Co^{2+}-Al^{3+}	9.5	98	28
Ni^{2+}-Al^{3+}	11	69	21
Zn^{2+}-Cr^{3+}	2.7	73	5.4

a) Reaction conditions: pretreatment temperature=773 K, reaction temperature=673 K, HCHO=3.0 kPa, acetone=9.1 kPa and W/F=2.7 g h mol^{-1}. b) On acetone basis. c) On formaldehyde basis.

The pattern consisted of diffractions for both hydrotalcite and MgO for CO_3^{2-}- or NO_3^--exchanged hydrotalcite,[18,19] whereas the only pattern observed was that of hydrotalcite for SO_4^{2-}- or CrO_4^{2-}-exchanged one. The formation of MVK was observed for all the catalyst samples examined: Acetone conversion ranged from 3.7 to 20% and the selectivity to MVK on an acetone basis fell within the range 93—100%. The highest yield of MVK (19%) was obtained with heat-treated hydrotalcite containing CO_3^{2-} anions, with which further experiments were conducted.

Reactions over Cation-Substituted Hydrotalcites. In Table 2, are summarized the results of reactions over cation-substituted hydrotalcites. The heat-treated (at 773 K) hydrotalcite containing Li^+-Al^{3+} cations showed a diffuse XRD pattern for hydrotalcite, together with broad and indefinable diffractions. For all the other heated (at 773 K) hydrotalcites examined, no XRD pattern for hydrotalcite could be observed; the MgO phase for a hydrotalcite containing Mg^{2+}-Al^{3+} cations, a Co_3O_4 phase for Co^{2+}-Al^{3+}, a NiO phase for Ni^{2+}-Al^{3+}, and a ZnO phase for Zn^{2+}-Cr^{3+} were observed. Acetone conversion fell within the range 2.7—21%, the selectivity to MVK on an acetone basis being in the range of 69—100%. The selectivity to MVK on a formaldehyde basis decreased to 37% upon substituting Li^+ for Mg^{2+}, the major product being CH_3OH. The substitution of transition metal cations for Mg^{2+} or Al^{3+} also resulted in a decrease in the selectivity to MVK on a formaldehyde basis: Carbon dioxide was detected as the major product, together with CO and CH_3OH. Hydrotalcite, containing Mg^{2+}-Al^{3+}-CO_3^{2-} ions, was found to be the most effective precursor for a catalyst among the hydrotalcites examined.

Effect of Reaction Temperature. With an increasing reaction temperature, acetone conversion increased and reached 21—22% at 673—723 K over heat-treated hydrotalcite containing Mg^{2+}-Al^{3+}-CO_3^{2-} ions (Fig. 1). The selectivity to MVK on an acetone basis was constant (95%) throughout the whole reaction temperature range examined. The selectivity to MVK on a formaldehyde basis slightly depended on the reaction temperature (Fig. 1) and was 25% at 673—723 K.

Effect of Partial Pressure of Formaldehyde. The formation of CH_3OH can be attributed to a bimolecular reaction of formaldehyde, through a Cannizzaro reaction.[14] The Cannizzaro reaction may be suppressed by lowering the partial pressure of formaldehyde. In Fig. 2 the selectivities to MVK are shown both on an acetone and on a formaldehyde basis as a function of the partial pressure of formaldehyde. The selectivity to MVK on an acetone basis is in the range of 94—99%, while that on a formaldehyde basis is 25% at 10 kPa and 87% at 1.2 kPa. The acetone conversion is also given in Fig. 2 and is almost constant (20%) above 3.0 kPa of formaldehyde pressure; it decreases to 5% at 1.2 kPa. Thus, as expected, a higher selectivity to MVK on a formaldehyde basis was obtained at a low formaldehyde pressure, though the acetone conversion decreased drastically.

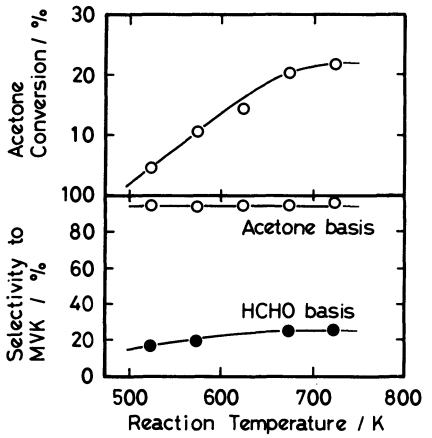

Fig. 1. Temperature dependence of acetone conversion and of selectivity to MVK.
Reaction conditions: pretreatment temperature=773 K, acetone=9.1 kPa, HCHO=10 kPa, and W/F=2.7 g h mol^{-1}.

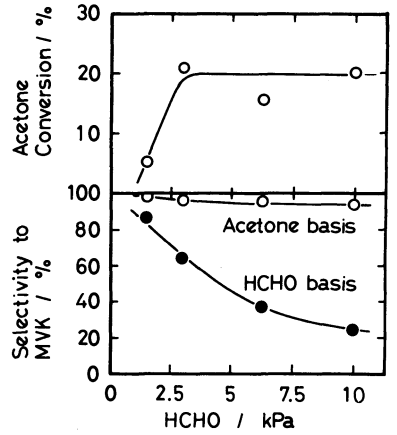

Fig. 2. Dependence of acetone conversion and of selectivity to MVK on partial pressure of formaldehyde.
Reaction conditions: pretreatment temperature=773 K, reaction temperature=673 K, acetone=9.1 kPa, and W/F=2.7 g h mol^{-1}.

Comparison of Results with Literature Data. Several catalytic cross-aldol condensation reactions between formaldehyde and acetone on solid catalysts have been reported. Malinowski et al.[20] obtained a 1% acetone conversion over a Na/SiO_2 catalyst. Tanaka et al.[21] examined the reaction at 573 K, W/F=27 g h mol^{-1} and acetone/HCHO molar ratio=1 over calcium hydroxyapatite ($Ca_5(OH)(PO_4)_3$) calcined at 773 K and obtained a 24% yield of MVK together with mesityl oxide of 2%. Igarashi et al.[22] examined the reaction over a ZrO_2-SiO_2 catalyst at an acetone/HCHO molar ratio ranging from 1 to 4 and obtained an 18—13% MVK yield on an acetone basis and 18—54% on a formaldehyde basis at 573 K and W/F=5 g h mol^{-1}. In the present work, over heat-treated

hydrotalcite, a 20% MVK yield on an acetone basis and a 62% on a formaldehyde basis were obtained at W/F=5 g h mol^{-1}. It therefore follows that the MVK yield on an acetone basis obtained in this study falls in the range of those reported earlier. The most predominant effect of using heat-treated hydrotalcite as a catalyst can be found in a slightly enhanced MVK yield on a formaldehyde basis.

In conclusion, heat-treated hydrotalcite and hydrotalcite-like minerals can catalyze the cross-aldol condensation reaction between formaldehyde and acetone. Among these, heat-treated hydrotalcite gave the highest MVK yield.

References

1) C. Frondel, *Am. Mineral.*, **26**, 295 (1941).
2) R. Allmann, *Chimia*, **24**, 99 (1970).
3) D. Bish, *Bull. Mineral*, **103**, 170 (1980).
4) S. Miyata and T. Kumura, *Chem. Lett.*, **1973**, 843.
5) H.-P. Boehm, J. Steinle, and C. Vieweger, *Angew. Chem., Int. Ed. Engl.*, **16**, 265 (1977).
6) S. Miyata and K. Okada, *Clay Clay Miner.*, **25**, 14 (1977).
7) M. J. Hernandez-Moreno, M. A. Ulibarri, J. L. Rendon, and C. J. Serna, *Phys. Chem. Minerals*, **12**, 34 (1985).
8) S. Miyata, *Clay Clay Miner.*, **23**, 369 (1975).
9) S. Miyata, T. Kumura, H. Hattori, and K. Tanabe, *Nippon Kagaku Zasshi*, **92**, 514 (1971).
10) T. Nakatsuka, H. Kawasaki, S. Yamashita, and S. Kohjiya, *Bull. Chem. Soc. Jpn.*, **52**, 2449 (1979).
11) S. Kohjiya, T. Sato, T. Nakayama, and S. Yamashita, *Makromol. Chem., Rapid Commun.*, **2**, 231 (1981).
12) W. T. Reichle, United States Patent, 4458026 (1984).
13) W. T. Reichle, *J. Catal.*, **94**, 547 (1985).
14) T. A. Geissman, "Organic Reactions," Vol. 2., ed by W. E. Bachmann, J. R. Johnson, L. F. Fieser, and H. R. Snyder, Robert E. Krieger Publishing Company, Florida (1981), pp. 94—113.
15) C. J. Serna, J. L. White, and S. L. Hem, *Clay Clay Miner.*, **25**, 384 (1977).
16) C. J. Serna, J. L. Rendon, and J. E. Iglesias, *Clay Clay Miner.*, **30**, 180 (1982).
17) W. T. Reichle, S. Y. Kang, and D. S. Everhardt, *J. Catal.*, **101**, 352 (1986).
18) W. T. Reichle, *Chemtech*, **1986**, 58.
19) S. Miyata, *Clay Clay Miner.*, **28**, 50 (1980).
20) S. Malinowski, S. Basinski, S. Szczepanska, and W. Kiewlics, "Proc. Third Intern. Congr. Catal.," ed by W. M. H. Sachtler, G. C. A. Schuit, and P. Zwietering, North-Holland Publishing Co., Amsterdam (1965), pp. 441—449.
21) Y. Tanaka, K. Urabe, and Y. Izumi, 41st National Meeting of the Chemical Society of Japan, Osaka, April 1980, Abstr., No. 3T29.
22) T. Igarashi and M. Suzuki, *Kanagawa Daigaku Kogakubu Kenkyu Hokoku*, **19**, 64 (1981).

The ^{127}I Nuclear Quadrupole Resonance of an Iodine Complex with 1,3-Dithiane, $C_4H_8S_2 \cdot 2I_2$

Hiromitsu TERAO* and Hiroshi SAKAI†
Faculty of Integrated Arts and Sciences, Tokushima University,
Minamijosanjima-cho, Tokushima 770
†Research Reactor Institute, Kyoto University, Kumatori-cho, Sennan-gun, Osaka 590-04
(Received August 29, 1987)

Synopsis. The ^{127}I nuclear quadrupole resonance spectrum of 1,3-dithiane-$2I_2$ is reported. Two distinct S···I-I arrangements are present in the crystal. The charge on each iodine atom is obtained; the bonding in the complex is discussed in connection with analogous thioether-iodine complexes. The resonance lines for terminal iodine atoms indicate positive temperature coefficients.

It is well-known that halogen (or interhalogen) molecules act as electron acceptors toward electron-pair donor molecules (such as amines, ethers, and thioeters) and form n-σ-type charge-transfer (CT) complexes with them. In addition, the empirical results obtained from structural investigations show that if CT-bonds in the complexes are comparatively strong, isolated units of complex molecules involving almost linear arrangements of donor atom···halogen-halogen are found in the solid state. In this case, the CT-interaction between donor and acceptor appears to be simple and archetypal. It is, therefore, of great interest to evaluate the charge distributions on the halogen atoms in such complex molecules in order to clarify the nature of the CT-interation.

Many amine-halogen complexes belonging to this class have been investigated for this purpose by means of the halogen[1-3] (and also the nitrogen[4,5]) nuclear quadrupole resonance (NQR) and the ^{129}I Mössbauer effect.[6-8] However, complete results have been obtained for only a small number of complexes, since the NQR signals of the terminal halogen atoms were not detected in many cases and since the ^{129}I Mössbauer effect has been applied to only a few iodine complexes of this class.

Recently we ourselves have applied the ^{127}I NQR[9] and the ^{129}I Mössbauer effect[10] to a series of thioether-iodine complexes (involving a S···I_A-I_B arrangement), such as tetrahydrothiopyran (thiane)-iodine (1:1), 1,4-dithiane-iodine (1:2), and 1,4-thioxane-iodine (1:1), and have estimated the charges on both bridging iodine (I_A) and terminal iodine (I_B) atoms. In the present communication, we with to report the ^{127}I NQR results of 1,3-dithiane-$2I_2$, which has been selected in order to confirm the conclusion deduced in a previous investigation[9] of thioether-iodine complexes.

Experimental

Stoichiometric amounts of iodine and 1,3-dithiane were treated in a carbon tetrachloride solution at room temperature, because the complex had a tendency to decompose in a hot solution. After concentrating the solution under reduced pressure, we filtered the resulting purplish-black crystalline product. The product was extracted in a Soxhlet extractor with dichloromethane to obtain a well-crystallized sample suitable for the NQR measurements. Found: C, 7.72; H, 1.30; I, 81.06%. Calcd for $C_4H_8S_2$-$2I_2$: C, 7.65; H, 1.28; I, 80.85%.

The NQR measurements were carried out using an externally quenched super-regenerative Lecher-line oscillator, as has been described previously.[9]

Results and Discussion

Four resonance lines of the $m=\pm1/2\leftrightarrow\pm3/2$ transitions by the ^{127}I nuclei were observed for the 1,3-dithiane-$2I_2$ complex between 77 K and room temperature; the frequency values at 77 and 298 K are listed in Table 1, together with the corresponding frequencies for 1,4-dithiane-$2I_2$.[9] The assignment of the resonance lines to the $m=\pm1/2\leftrightarrow\pm3/2$ transitions was done on the basis of the ^{127}I NQR spectra[9] and the ^{129}I Mössbauer spectra[10] of analogous thioether-iodine complexes.

In the crystal structure of 1,4-dithiane-$2I_2$,[11] each sulfur atom is linked to one iodine moiety, and all the

Table 1. $^{127}I(m=\pm1/2\leftrightarrow\pm3/2)$ NQR Frequencies in 1,3-Dithiane-$2I_2$[a]

Compound	Frequency/MHz		$(d\nu/dT)_{T=273K}$	Assignment[b]
	77 K	298 K	kHz/K	
1,3-Dithiane-$2I_2$	377.34(7)[c]	372.24(2.5)	−28.9	$I_A(1)$
	371.56(13)	367.20(4.5)	−23.9	$I_A(2)$
	247.07(4.5)	252.04(2)	26.1	$I_B(1)$
	243.95(8)	248.67(3.5)	25.0	$I_B(2)$
1,4-Dithiane-$2I_2$[d]	377.81(6)	374.83(3)	−16.5	I_A
	233.37(2.5)	238.02(2)	25.4	I_B

a) The accuracy of the measurements was estimated to be within ±0.01 MHz in frequency and ±1 K in temperature. b) I_A and I_B denote the bridging and the terminal iodine atoms respectively. c) The numbers in parentheses are the signal-to-noise ratios as measured on an oscilloscope. d) Ref. 9.

S···I_A–I_B arrangements are identical. In accordance with this, only two resonance lines, corresponding to the bridging iodine (I_A) and the terminal iodine (I_B) atoms, have been observed. However, the observation of four resonance lines, though no crystallographic data is known, indicates that two distinct S···I_A–I_B arrangements are present in the 1,3-dithiane–$2I_2$ crystal. Presumably the respective S atoms at the 1- and 3-positions of the C_4S_2 ring are linked to one iodine moiety in such a way that these atoms are no longer equivalent to each other in the crystal.

The assignment of the resonance lines to the I_A or the I_B atoms can be done unambiguously, since it is well-established that the lines for the I_B atoms have lower frequency values than those for the I_A atoms and that the frequency difference between them is very large. Further, considering that the signal-to-noise ratios of each two lines for the I_A and the I_B atoms are evidently different (ca. 1:1.8), we have tentatively made pairs of the weaker I_A line and the weaker I_B line and of the stronger I_A line and the stronger I_B line (Table 1).

A simple three-center four-electron bonding theory,[1,3,10] using only the valence p-orbitals of halogens, has been successfully applied to the donor atom···halogen–halogen systems. The charges on the halogen atoms can be well-explained with the theory.[12] By considering only the p-orbitals for the bondings of iodine atoms, therefore, we estimate the charges on both I_A and I_B atoms according to the Townes-Dailey approximation (in the previous paper[9] we reported this equation incorrectly):

$$\rho = (e^2q_{zz}Q/h)/(e^2q_{at}Q/h) - 1, \qquad (1)$$

where ρ is the charge on the iodine atom, where $e^2q_{zz}Q/h$ is the observed quadrupole coupling constant, and where $e^2q_{at}Q/h$ is the atomic quadrupole coupling constant (2292.7 MHz for ^{127}I).

As the arrangement of S···I_A–I_B is considered to be almost linear, the asymmetry parameters (η) are expected to be small for both I_A and I_B atoms. In fact, practically zero values of η were observed from the ^{127}I NQR measurements for the I_A atoms of several amine–I_2 complexes[3] and for the I_B atom of the thiane–I_2 complex.[9] By neglecting the expected small η value, the relation between the $e^2q_{zz}Q/h$ and the frequency (ν) are simplified to $e^2q_{zz}Q/h=20/3\cdot\nu$ for the ^{127}I ($m=\pm1/2\leftrightarrow\pm3/2$) transitions. Then, the ρ on the iodine atoms (and also the charges on the donors) are obtained from Eq. 1, by using the ν values at 77 K, as follows:

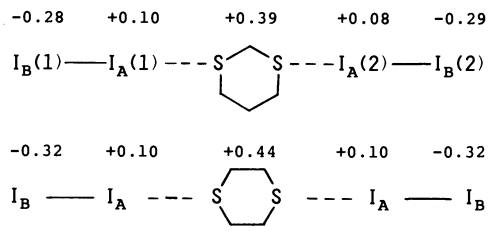

The charge transferred from the donor to the iodine moiety is slightly less in 1,3-dithiane–$2I_2$ than in 1,4-dithiane–$2I_2$. This is consistent with the observation that the former complex is more labile than the latter.

For comparison, in Fig. 1 the present data for the charge distributions in 1,3-dithiane–$2I_2$ are added to a previous figure[9] representing the relation of the charges on the I_A and the I_B atoms to the charges (per donor atom) on the donors. In the figure, the average values were used as the respective charges on the I_A

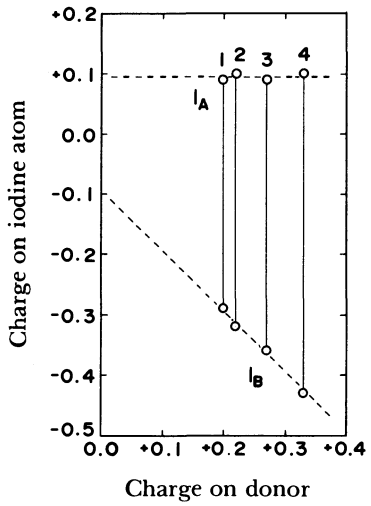

Fig. 1. Plot of the charges on I atoms vs. the charges on donors. (1) 1,3-Dithiane–$2I_2$, (2) 1,4-dithiane–$2I_2$,[9] (3) 1,4-thioxane–I_2,[9] (4) thiane–I_2.[9]

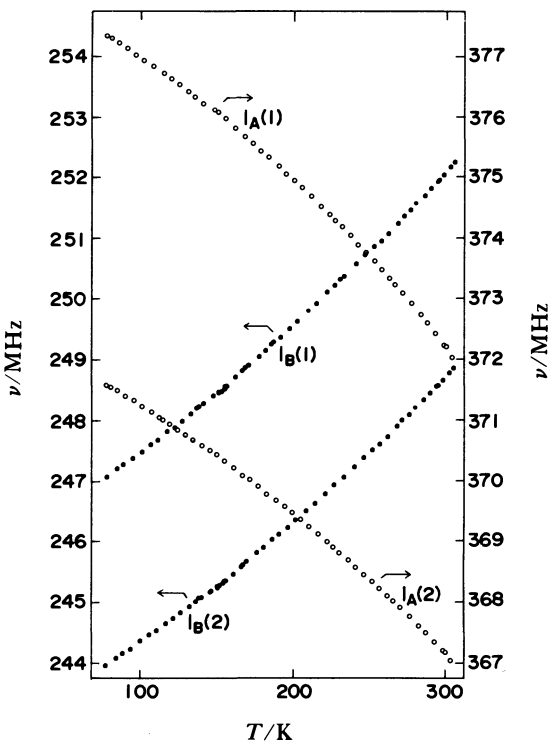

Fig. 2. Temperature dependence of the ^{127}I ($m=\pm1/2\leftrightarrow\pm3/2$) NQR frequencies in 1,3-dithiane–$2I_2$.

and the I_B atoms in 1,3-dithiane-$2I_2$.

Obviously, our previous finding is confirmed in Fig. 1:[9] The charges on the I_A atoms are almost independent of the charges on the donors, and hence the negative charges on the I_B atoms increase linearly with the increase in the charges on the donors. This observation suggests that the formation of the complex is followed by two effects: One is the polarization[2] of the iodine moiety by the donor, $I^{\delta+}$ $I^{\delta-}$ (represented as a no-bond ionic structure[1,9] in the valence-bond expression), and the other is the CT from the donor to the iodine moiety. Further, Fig. 1 shows that (1) the polarization effects are maintained at an almost constant value for the same donor atom[9] (ca. ± 0.1 *e* charges are polarized on the respective I_A and I_B atoms of an iodine moiety in the case of the S donors) and (2) the charges (ca. 0.2—0.3 *e*) transferred from the donors to the iodine moieties are mostly piled up on the I_B atoms.

The temperature dependence of the resonance frequencies measured between 77 K and room temperature is shown in Fig. 2. In accordance with the previous observations[1,2,4,9] the resonance lines of terminal iodine atoms have positive temperature coefficients (Table 1). This trend is qualitatively realized by considering the weakening of the CT-bond with the increasing temperature.[9]

References

1) G. A. Bowmaker and S. Hacobian, *Aust. J. Chem.*, **22**, 2047 (1969).
2) H. C. Fleming and M. W. Hanna, *J. Am. Chem. Soc.*, **93**, 5030 (1971).
3) R. Brüggemann, F. Reiter, and J. Voitländer, *Z. Naturforsch., A*, **27**, 1525 (1972).
4) G. A. Bowmaker, *J. Chem. Soc., Faraday Trans. 2*, **72**, 1964 (1976).
5) G. V. Rubenacker and T. L. Brown, *Inorg. Chem.*, **19**, 392 (1980); **19**, 398 (1980).
6) S. Bukshpan, C. Goldstein, T. Sonnino, L. May, and M. Pasternak, *J. Chem. Phys.*, **62**, 2606 (1975).
7) S. Ichiba, H. Sakai, H. Negita, and Y. Maeda, *J. Chem. Phys.*, **54**, 1627 (1971).
8) H. Sakai, Y. Maeda, S. Ichiba, and H. Negita, *J. Chem. Phys.*, **72**, 6192 (1980).
9) H. Terao, H. Sakai, and H. Negita, *Bull. Chem. Soc. Jpn.*, **58**, 2318 (1985).
10) H. Sakai. T. Matsuyama, and Y. Maeda, *Bull. Chem. Soc. Jpn.*, **59**, 981 (1986).
11) G. Y. Chao and J. D. McCullough, *Acta Crystallogr.*, **13**, 727 (1960).
12) Recently, Sakai et al.[8,10] found, in their ^{129}I Mössbauer investigations, that the quadrupole coupling constants ($e^2q_{zz}Q/h$) obtained from the quadrupole splittings are always smaller than the values to be expected from the isomer shifts (δ) in the case of the I_A atoms, whereas the two values were in fair agreement in the case of the I_B atoms. Those facts may indicate that the model using only the valence p-orbitals is oversimplified for the I_A atoms apart from the I_B atoms.

Ab Initio Calculation for Interaction Potential of He-He

Akira ICHIHARA, Kohtoku SASAGANE, Tohru IZAKI,* Tomoo MIYAZAKI, and Reikichi ITOH
Department of Chemistry, Faculty of Science and Engineering, Waseda University, 3-4-1 Ohkubo, Shinjuku-ku, Tokyo 160
(Received September 19, 1987)

Synopsis. Using the help of an ab initio calculation with a configuration interaction (CI) treatment, the potential energy of a He dimer system could be calculated in due consideration of a correction for the basis set superposition error. In evaluating CI matrix elements, the graphical unitary group approach was adopted.

There have been several reports in which the interaction potential of a He dimer system was calculated by the use of an ab initio MO method with a limited CI treatment.[1-6] In this paper, our results concerning SD and full CI calculations for the potential energy of the He dimer, comprising a small basis set, are compared with the results of calculations for the same system with a large basis set by Dacre[5] and Tatewaki.[6]

In an LCAO-MO-SCF-CI calculation, the introduction of a large basis set in order to increase the level of the approximation results in a rapid increase of CI matrix elements and computer time. Consequently, a limited CI treatment is generally adopted. It appears to be of interest to investigate the description of the interaction potential for a system with a small basis set. On the other hand, it is possible to adopt a treatment in which many electron excited configurations are introduced instead of employing a large basis set. It is, therefore, possible to further investigate the effect of many excited electron configurations on the CI treatment of the interaction potential for a system with a small basis set.

By using a graphical unitary group approach (GUGA)[7-11] to evaluate the CI matrix elements, it can be expected to facilitate a CI calculation while considering many electron excited configurations. As a first step, we provided our own computer program for the application of GUGA to the many electron excited correlation problem according to a treatment introduced by Shavitt.[10]

In this CI calculation, three different Gaussian basis sets [4S1P], [4S4P], and [4S1P1D] for a He atom were employed. These Gaussian basis sets comprised Schmidt (16s) primitive functions[12] augmented by Wells (4p) primitives.[13-14] The [4S] contraction was performed so that the atomic energy with the contracted set came close to that with an uncontracted set. In practice, the Schmidt (16s) primitives were contracted to the (6;5;4;1). The [1P] contraction was performed in the He dimer system at an internuclear distance of 5.6 Bohr after an SCF calculation with an uncontracted (4p) set placed on the [4S] contracted set. The [4S1P1D] basis set comprised the [4S1P] set augmented with an optimized single Gaussian d-type function.

It has already been pointed out that the result of CI calculations for the interaction energy of the supermolecule system must be corrected in order to eliminate the type error called a "basis set superposition error".[15-17] Boys first introduced the function counterpoise method[15] in order to overcome this error. In this method, the He dimer interaction energy (E_{int}) is calculated using the difference between the CI energy of the He dimer (E_{He_2}) and an appropriate reference energy (E_{ref}):

$$E_{int}(R) = E_{He_2}(R) - E_{ref}(R), \quad (1)$$

where R is the internuclear distance of the He dimer. The reference energy E_{ref} is defined as twice the CI energy of the He atom, with "ghost" orbitals at the expected location of the other He atom. The term "ghost" represents an atom with a nuclear charge zero and without any electrons. We employed this method in the case of a full CI calculation. Also, the counterpoise method introduced by Price[16] was used in for a SD CI calculation. Here, E_{ref} in Eq. 1 is defined as

$$E_{ref}(R) = \{2E_{ref}^{T}(R) - 2(1 - a_0^2)[E_{ref}^{CORR}(R) + (1 - a_0^2)E_{ref}^{SCF}(R)]\}/[a_0^2(2 - a_0^2)] + \varepsilon, \quad (2)$$

where E_{ref}^{SCF}, E_{ref}^{CORR}, E_{ref}^{T}, and a_0 represent the SCF, SD CI correlation, total (SCF and SD CI correlation) energy and the SCF ground-state coefficient of the He atom with ghost orbitals at an internuclear distance R. The constant ε was determined so that the interaction energy becomes zero at $R=\infty$.

In the present work, the spatial symmetry considered in the calculation of the He dimer system is $D_{\infty h}$. The MO calculation was performed by using the Gaussian 82 program provided by Pople and HITAC M680H system of the Computer Center of the University of Tokyo.

Results and Discussion

Tables 1 and 2 indicate the interaction potentials for the [4S1P] and [4S4P] basis sets by the SD CI calculation. It can be seen from Tables 1 and 2 that the SCF energy contributes to the repulsion between the He atoms, and that the correlation energy contributes to the attraction.[1-6] Each interaction potential predicts a minimum of 7.0 K at 5.8—6.0 Bohr. Reliable experimental values are 10.57—11.01 K at 5.6—5.63 Bohr.[5,18-21] From these results, it can be seen that the SD CI treatment for the [4S1P] and [4S4P] basis set is insufficient for describing a reliable interaction potential of the He dimer. On the other hand, it is obvious that the interaction potential curve is little affected by the [1P] contraction of Wells (4p)

Table 1. The He Dimer Interaction Potential (E_{int}) for the [4S1P] Basis by the SD CI Calculation

R/Bohr[c]	E_{He_2}/a.u.[a]		E_{ref}		E_{int}/K[b]
	SCF	correlation	E_{ref}[d]/a.u.	$E_{ref}(R)-E_{He_2}(\infty)$/K	
5.0	−5.7232327	−0.0390468	−5.7623344	−261.1	17.3
5.5	−5.7233216	−0.0387617	−5.7620716	−178.1	−3.7
6.0	−5.7233481	−0.0385461	−5.7618722	−115.1	−7.0
7.0	−5.7233581	−0.0382936	−5.7616385	−41.3	−4.2
8.0	−5.7233590	−0.0381944	−5.7615474	−12.6	−1.9
10.0	−5.7233591	−0.0381527	−5.7615103	−0.9	−0.4
∞	−5.7233591	−0.0381485	−5.7615076	0.0	0.0

a) 1 a.u.=4.359814×10^{-18} J. b) 1 K=1.380662×10^{-23} J. c) 1 Bohr=0.529177×10^{-10} m. d) ε in E_{ref} is −0.56 K.

Table 2. The He Dimer Interaction Potential (E_{int}) for the [4S4P] Basis by the SD CI Calculation

R/Bohr[c]	E_{He_2}/a.u.[a]		E_{ref}		E_{int}/K[b]
	SCF	correlation	E_{ref}[d]/a.u.	$E_{ref}(R)-E_{He_2}(\infty)$/K	
5.0	−5.7232330	−0.0564875	−5.7797617	−326.2	13.1
5.5	−5.7233216	−0.0562450	−5.7795513	−259.7	−4.8
6.0	−5.7233481	−0.0560454	−5.7793713	−202.9	−6.9
7.0	−5.7233581	−0.0557695	−5.7791151	−122.0	−3.9
8.0	−5.7233590	−0.0556127	−5.7789660	−75.0	−1.8
10.0	−5.7233591	−0.0554235	−5.7787811	−16.6	−0.5
∞	−5.7233591	−0.0553696	−5.7787287	0.0	0.0

a) 1 a.u.=4.359814×10^{-18} J. b) 1 K=1.380662×10^{-23} J. c) 1 Bohr=0.529177×10^{-10} m. d) ε in E_{ref} is −0.98 K.

Table 3. The He Dimer Interaction Potential (E_{int}) for the [4S1P] Basis by the Full CI Calculation

R/Bohr[c]	E_{int}/a.u.[a]	E_{ref}		E_{int}/K[b]			
	correlation	E_{ref}/a.u.	$E_{ref}(R)-2E_{He}$[d]/K	This work	Dacre[e]	Tatewaki[f]	Experimental[g]
5.0	−0.0392868	−5.7625707	−263.7	16.2	7.3	0.5	0.2
5.5	−0.0389979	−5.7623053	−179.9	−4.5	−7.0	(−9.6)[h]	(−10.4)[i]
6.0	−0.0387794	−5.7621039	−116.3	−7.5	−7.7	−8.6	−9.6
7.0	−0.0385236	−5.7618679	−41.7	−4.4	−4.0	−4.0	−4.6
8.0	−0.0384230	−5.7617759	−12.7	−1.9	−1.8	−1.8	−2.1
10.0	−0.0383808	−5.7617385	−0.9	−0.5	−0.5	—	−0.5
∞	-0.0383765_2	-5.7617355_5	0.0	0.0	—	—	—

a) 1 a.u.=4.359814×10^{-18} J. b) 1 K=1.380662×10^{-23} J. c) 1 Bohr=0.529177×10^{-10} m. d) The SCF and correlation energies of the He atom without ghost orbitals are −2.86167953 and −0.01918825 a.u., respectively. e) From Ref. 5. f) From Ref. 6. g) From Ref. 21. h) Estimated from a graphical plot. i) Estimated from a graphical plot.

primitive functions. We then investigated the effect of triple and higher excitation configurations on the CI treatment for the [4S1P] basis set.

Table 3 indicates the interaction potential for the [4S1P] basis set through a full CI calculation. There are 857 configurations which can contribute to the full CI calculation. The results of the limited CI calculation by Dacre[5] and Tatewaki[6] are also indicated in Table 3. In Dacre's work, a large Gaussian-type basis set including polarization functions was employed. He removed the triple and higher excitation effect from the reference energy. On the other hand, a Slater-type basis set was employed in Tatewaki's calculation. He performed first-order CI in which the triple and higher excitation configurations were effectively included. The basis set superposition error was considered to be almost negligible for his interaction potential.

The interaction potential given in Table 3 predicts a minimum of 7.8 K at 5.9 Bohr. These data are in good agreement with those results (8.4 K at 5.7 Bohr) by Dacre. In comparison with the results of our SD CI calculation, the full CI calculation lowers the potential depth by about 0.8 K. However, these calculated potential well depths are shallower than the experimental results. Tatewaki's results (9.8 K at 5.61 Bohr) reproduce the experimental values well.

Table 4 indicates the results of the interaction potential for the [4S1P1D] basis set by the SD CI calculation. This [4S1P1D] basis set for the He atom is composed of the [4S1P] basis and the single Gaussian d function. The exponent of the d function was optimized in order to describe the reliable interaction potential in the range 5 to 10 Bohr. The

Table 4. The He Dimer Interaction Potential (E_{int}) for the [4S1P1D] Basis by the SD CI Calculation

R/Bohr[c]	E_{He_2}/a.u.[a]		E_{ref}		E_{int}/K[b]
	SCF	correlation	E_{ref}[d]/a.u.	$E_{ref}(R)-E_{He_2}(\infty)$/K	
5.0	−5.7232328	−0.0396326	−5.7628827	−427.9	5.5
5.5	−5.7233216	−0.0391572	−5.7624473	−290.4	−9.9
5.71	−5.7233366	−0.0389983	−5.7623007	−244.2	−10.8
6.0	−5.7233481	−0.0388111	−5.7621271	−189.3	−10.1
7.0	−5.7233581	−0.0383993	−5.7617415	−67.6	−5.1
8.0	−5.7233590	−0.0382362	−5.7615884	−19.2	−2.2
10.0	−5.7233591	−0.0381735	−5.7615312	−1.2	−0.4
∞	−5.7233591	−0.0381684	−5.7615275	0.0	0.0

a) 1 a.u. = 4.359814×10^{-18} J. b) 1 K = 1.380662×10^{-23} J. c) 1 Bohr = 0.529177×10^{-10} m. d) ε in E_{ref} is −0.61 K.

Table 5. The He Dimer Interaction Potential (E_{int}) for the [4S1P1D] Basis by the Full CI Calculation

R/Bohr[c]	E_{He_2}/a.u.[a]	E_{ref}		E_{int}/K[b]
	correlation	E_{ref}/a.u.	$E_{ref}(R)-2E_{He}$[d]/K	
5.0	−0.0398799	−5.7631227	−431.8	3.1
5.5	−0.0393981	−5.7626837	−293.1	−11.4
5.71	−0.0392371	−5.7625359	−246.5	−11.9
6.0	−0.0390475	−5.7623607	−191.2	−11.0
7.0	−0.0386303	−5.7619713	−68.2	−5.4
8.0	−0.0384650	−5.7618167	−19.4	−2.3
10.0	−0.0384016	−5.7617591	−1.2	−0.5

a) 1 a.u. = 4.359814×10^{-18} J. b) 1 K = 1.380662×10^{-23} J. c) 1 Bohr = 0.529177×10^{-10} m. d) The SCF and correlation energies of the He atom without ghost orbitals are −2.86167953 and −0.01919811 a.u., respectively.

optimum exponent was found to be 0.20. The potential minimum of this calculation is 10.8 K at 5.71 Bohr; this potential is in good agreement with the experimental results[21] of this range. From these results, it is obvious that the d-type function makes an important contribution to the interaction potential of the He dimer.

Finally, we investigated the interaction potential for the [4S1P1D] basis set by a full CI calculation in order to confirm the effect of triple and higher excitation configurations. There are 5944 configurations which can contribute to a full CI calculation. The new interaction potential appeared lower than the experimental results. This result may have been caused by using a d function which is not optimum for a full CI calculation.

It may be concluded from the results of this investigation that a small basis set [4S1P1D] can give the interaction potential of the He dimer by the aid of the CI calculation and the function counterpoise method.

We would like to thank Dr. Kazunari Suzuki for suggesting this problem and for stimulating our interest in it.

References

1) D. R. McLaughlin and H. F. Schaefer III, *Chem. Phys. Lett.*, **12**, 244 (1971).
2) B. Liu and A. D. McLean, *J. Chem. Phys.*, **59**, 4557 (1973).
3) P. E. S. Wormer, T. van Berkel, and A. van der Avoird, *Mol. Phys.*, **29**, 1181 (1975).
4) P. D. Dacre, *Chem. Phys. Lett.*, **50**, 147 (1977).
5) P. D. Dacre, *Mol. Phys.*, **37**, 1529 (1979).
6) H. Tatewaki, K. Tanaka, Y. Ohno, and T. Nakamura, *Mol. Phys.*, **53**, 233 (1984).
7) I. Shavitt, *Int. J. Quantum. Chem., Symp.*, **12**, 5 (1978).
8) I. Shavitt, *Chem. Phys. Lett.*, **63**, 421 (1979).
9) J. Paldus, "Lecture Notes in Chemistry 22," Springer Berlin (1981), pp. 1—50.
10) I. Shavitt, "Lecture Notes in Chemistry 22," Springer Berlin (1981), pp. 51—99.
11) F. A. Matsen and R. Pauncz, "The Unitary Group in Quantum Chemistry," Elsevier Amsterdam (1986), **44**, pp. 1—223.
12) M. W. Schmidt and K. Ruedenberg, *J. Chem. Phys.*, **71**, 3951 (1979).
13) B. H. Wells, *Chem. Phys. Lett.*, **101**, 429 (1983).
14) B. H. Wells, *Mol. Phys.*, **55**, 199 (1985).
15) S. F. Boys and F. Bernardi, *Mol. Phys.*, **19**, 553 (1970).
16) S. L. Price and A. J. Stone, *Chem. Phys. Lett.*, **65**, 127 (1979).
17) J. R. Collins and G. A. Gallup, *Chem. Phys. Lett.*, **123**, 56 (1986).
18) P. E. Siska, J. M. Parson, T. P. Schafer, and Y. T. Lee, *J. Chem. Phys.*, **55**, 5762 (1971).
19) A. L. J. Burgmans, J. M. Farrar, and Y. T. Lee, *J. Chem. Phys.*, **64**, 1345 (1976).
20) J. M. Farrar and Y. T. Lee, *J. Chem. Phys.*, **56**, 5801 (1972).
21) R. Feltgen, H. Krist, K. A. Kohler, and H. Pauly, *J. Chem. Phys.*, **76**, 2360 (1982).

Photoacoustic in Situ Measurement of Quantum Efficiencies for Photoanodic Reactions at n-Type Semiconductor Electrodes

Sachio YOSHIHARA,* Ayyasamy ARUCHAMY, and Akira FUJISHIMA
Department of Synthetic Chemistry, Faculty of Engineering, The University of Tokyo, Hongo, Bunkyo-ku, Tokyo 113
(Received September 19, 1987)

Synopsis. The time required for the in situ measurement of quantum efficiencies during photoelectrochemical reactions is qreatly reduced by the photoacoustic spectroscopy (PAS) employing a piezoelectric transducer (PZT). PAS has been successfully applied for several reactions at TiO_2, ZnO, and CdS photoelectrodes and compared with previous studies by the photothermal spectroscopy (PTS).

In recent papers, we have reported on the measurement of quantum efficiencies during photoelectrochemical reactions by the photothermal spectroscopy (PTS).[1-4] In PTS, the heat produced during the relaxation of the excited carriers is detected as the change in the temperature of the semiconductor electrode. The advantage of this method is that the quantum efficiency determination does not require the calibration of the light source. But, PTS requires a longer measurement time because the time constant of the thermistor used as the sensor is quite large (ca. ls). So, we had to measure the PT signal for various potentials fixing the electrode potential at each value. The slope of the straight line plot of PT signal vs. electrode potential gave the quantum efficiency. Therefore, it is of interest to utilize sensors having faster response.

In the present work, we have been able to measure quantum efficiencies within a very short time by the photoacoustic spectroscopy (PAS) employing a piezoelectric transducer (PZT). Since the time constant of the PZT employed is very small (approximately 0.1 μs), we considered that the experiment time may be significantly reduced. This method may also be developed for the investigation of certain relaxation processes during the photoelectrochemical reactions.

Experimental

Instrumental. The complete setup for this experiment is shown in Fig. 1. Either He-Cd laser (325 nm; CDR 80 SG. Kimmon Electric Company Limited) or Ar-ion laser (488 nm; Spectra Physics 164) was employed as the light source. The laser beam was chopped by a light chopper (8—800 Hz; CH-353. NF Circuit Design Block).

The cell was equipped with a platinum counter electrode and a saturated calomel reference electrode (SCE). The laser beam was transmitted into the cell through an optically flat window of the cell. A nitrogen bubbler was employed for deoxygenating the solutions.

The working electrodes were cadmium sulfide single crystal [(001) surface, Teikoku Tsushin Company Limited] which had dimensions 10×10×1 mm^3 and a carrier density of 4.8×10^{16} cm^{-3}, titanium dioxide prepared by firing Ti plate, and zinc oxide polycrystals [ZnO powder, ca. lg (Wako Pure Chemical Industries) pressed at 150 kg cm^{-2} and sintered at 1300 °C for 3 h] which had dimensions 15φ×1.5 mm^3. The ohmic contact was made by In-Ga alloy on one side of each crystal and then a copper wire was attached to the contact with silver paste. A piezoelectric transducer (NEPEC NPM, N 21 or N 6; 10φ×1 mm^3, Tohoku Metal Industries) was attached to the same side where the contact has been given after interposing thin epoxy resin layer. Finally, the whole of the electrode except the front surface was covered with epoxy resin. The structure of the semiconductor electrode (with a PZT in place) is shown in Fig. 2. The semiconductor surface was etched just before use in concentrated hydrochloric acid for 10 s.

The signal from the piezoelectric transducer was detected by a lock-in amplifier (LI-574, NF Circuit Design Block) and the current-potential curve was measured under potentiostatic conditions using a potentiostat (HF 301, Hokuto Denko Company Limited) and a potential programmer (NPS-2, Nikko Keisoku Company Limited). The cyclic voltammogram was displayed on an X-Y recorder (Type 3033, Yokogawa Electric Works).

All chemicals were of reagent grade and were used without further purification.

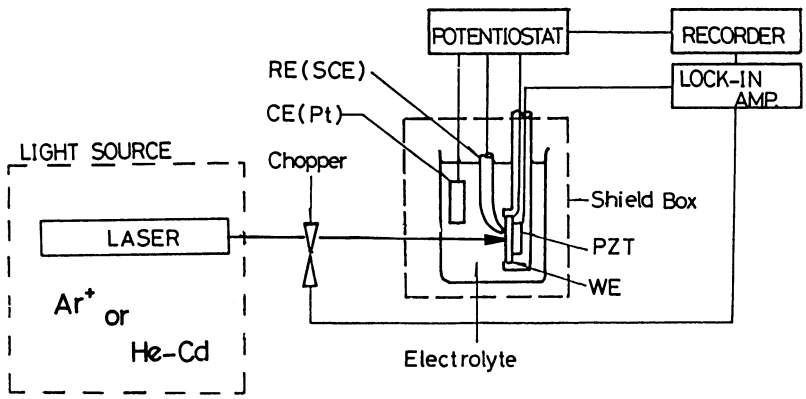

Fig. 1. Schematic diagram of the experimental setup for PAS.

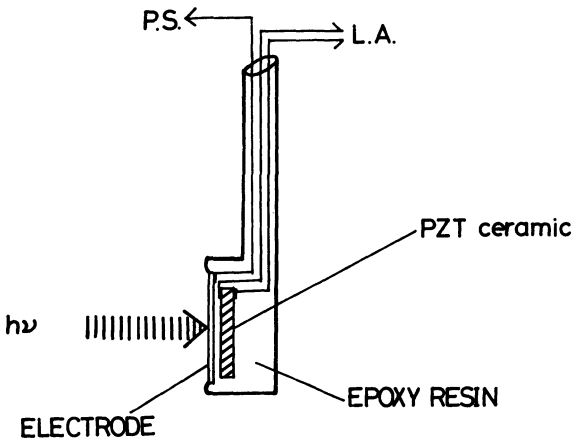

Fig. 2. Structure of the photoelectrode for PAS measurement.

Results and Discussion

The equation developed for the PTS[1] can be applied to the PAS also, since both mothods involve essentially the measurement of heat signals and the theoretical considerations are the same. For PAS the equation becomes

$$E(\Delta P/\Delta P_o) = (Q_{sc} + T\Delta S)/(It) + e\eta_q(V - V_{fb})$$

where E is the energy of the incident monochromatic light (eV/photon), I is the average absorbed intensity of light (photons/s), t is the illumination time (s), Q_{sc} is the heat evolved in the semiconductor via recombination and other radiationless processes, $T\Delta S$ is the heat evolved in term of an entropy change for the whole cell reaction (Electrochemical Peltier heat), e is elementary electric charge. η_q is the quantum efficiency of the photooxidation, ΔP and ΔP_0 are the PA signal amplitudes from the PZT at applied potential V and in the open circuit respectively, V_{fb} is the flatband potential.

Therefore, under constant illumination conditions (i.e. EIt held constant), a plot of $E(\Delta P/\Delta P_0)$ against $(V-V_{fb})$ yields the quantum efficiency, η_q, from the slope of the straight line.

The following semiconductor/electrolyte systems were investigated.

(1) n-TiO_2/Na_2SO_4, aq. ($4OH^- \rightarrow O_2+2H_2O+4e^-$)

(2) n-CdS/Na_2SO_4, Na_2SO_3aq. ($2SO_3^{2-}+2p^+ \rightarrow S_2O_6^{2-}$)[5-7]

(3) n-ZnO/Na_2SO_4 aq. ($2ZnO+4p^+ \rightarrow 2Zn^{2+}+O_2$)[8]

(4) n-TiO_2/Na_2SO_4, HCOONa aq. ($p^++HCOO^- \rightarrow CO_2+H^++e^-$; Current doubling)[9,10]

(5) n-CdS/Na_2SO_4, HCOONa aq. ($p^++HCOO^- \rightarrow CO_2+H^++e^-$; Current doubling)[11]

(6) n-ZnO/Na_2SO_4, HCOOH aq. ($ZnO+2p^++2HCOO^- \rightarrow Zn^{2+}+H_2O+2CO_2+2e^-$; Current doubling)[12-14]

Figure 3 shows the dependence of the photocurrent and the relative change in the PA signal ($\Delta P/\Delta P_0$) multiplied by the photon energy (E) on the electrode potential (V) for the CdS/Na_2SO_4, Na_2SO_3 aq. system. It is seen that the PA signal amplitude is proportional

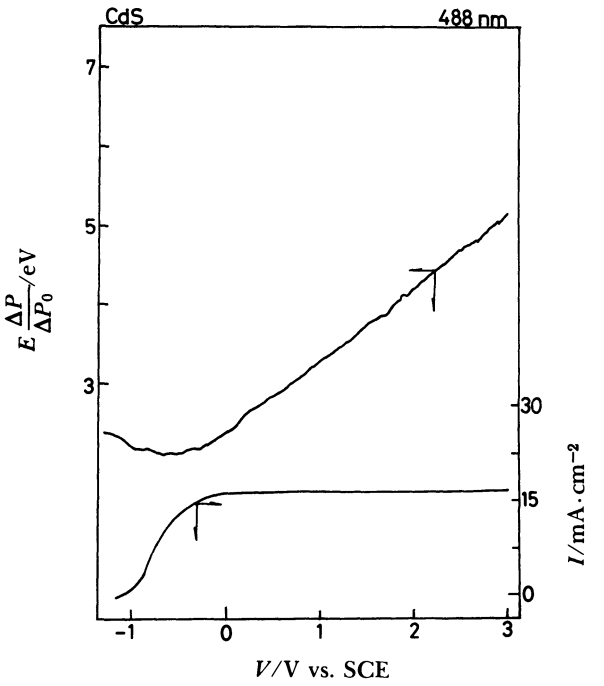

Fig. 3. Dependence of I (Photocurrent) and $E(\Delta P/\Delta P_0)$ on V (Applied potential) n-CdS Photoelectrode in 0.2 mol dm^{-3} Na_2SO_4, 1 mol dm^{-3} Na_2SO_3 aq. (Chopping frequency: 10 Hz).

to the electrode potential in the saturated photocurrent region. Taking the slope equal to the quantum efficiency, we found that the η values measured by PAS in this study are in good agreement with those obtained by PTS.[1-4] (See Tables 1 and 2) We have already reported that the quantum efficiency obtained by PTS coincides with the one obtained by actinometry. The apparently large difference in the η values of TiO_2 in Tables 1 and 2 is due to the fact that a single crystal was used for the earlier PTS study whereas we used a polycrystalline TiO_2 prepared by thermal oxidation of Ti in the present study. It is also known that the thermally formed TiO_2 gives a higher quantum efficiency.[15,16]

The dependence of ΔP_0 and the quantum efficiency on the chopping frequency have also been measured in order to find out the optimum conditions for measurement. Since the signal is detected by the lock-in method, the magnitude of the PAS signal is expected to decrease exponentially and Fig. 4 shows such behavior. On the other hand, the quantum efficiency is almost independent of the frequency. However, η shows a larger scatter at high frequencies while the value appears to be precise at lower frequencies. This is because the quantum efficiency is determined from ΔP_0 and ΔP and the precision is greater when ΔP and ΔP_0 become larger. The signals are large in the lower frequency region. However at too low frequencies (<1 Hz), sensitivity of the PZT used decreases. Therefore, a moderate chopping frequency must be chosen for this experiment.

Table 1. Measured Quantum Efficiencies for n-TiO_2, n-CdS, and n-ZnO by Photoacoustic Spectroscopy, ( ) Stands for the Value in the Case of Current Doubling Reaction

	Saturation current[a]	Quantum efficiency
	mA cm^{-2}	η
n-TiO_2[b]	5.44 (6.24)	0.8±0.05 (1.0±0.05)
n-CdS	16.4 (28.0)	0.9±0.01 (1.5±0.01)
n-ZnO	2.72 (5.36)	0.8±0.1 (1.5±0.1)

a) For TiO_2 and ZnO relatively low powder He-Cd laser (325 nm) and for CdS high power Ar-ion laser (488 nm) were used. b) TiO_2 electrode was prepared by thermal oxidation of Ti metal plate.

Table 2. Measured Quantum Efficiencies for n-TiO_2, n-CdS, and n-ZnO by Photothermal Spectroscopy,[1-4] ( ) Stands for the Value in the Case of Current Doubling Reaction

	Saturation current	Quantum efficiency
	mA cm^{-2}	η
n-TiO_2[a]	1.63 (2.15)	0.6 (0.7)
n-CdS	0.85 (1.43)	1.0 (1.7)
n-ZnO	1.23 (2.25)	0.9 (1.8)

a) Single crystal TiO_2.

Conclusion

In the PAS technique the Joule heat or the heat generated by the recombination of the excited carriers is detected as the distortion of the material or the acoustic wave from the material. This method requires much shorter time than the PTS for evaluating the quantum efficiency because of the very short time constant of the PZT. The efficiency values determined by PAS are in good agreement with PTS measurements. In future PAS utilizing PZT may be developed to obtain information concerning the recombination rates of photogenerated carriers by measuring the dependence of PA signal on the chopping frequency or the phase difference between PA signal and the reference signal. The recombination rates between CB and VB, the trapping rates of the photogenerated minority carriers at the surface recombination centers and the tunneling rates of electrons are some of the most important parameters in the semiconductor/electrolyte system. Work in this laboratory is under way to estimate above factors in the case of p-InP photoelectrodes.

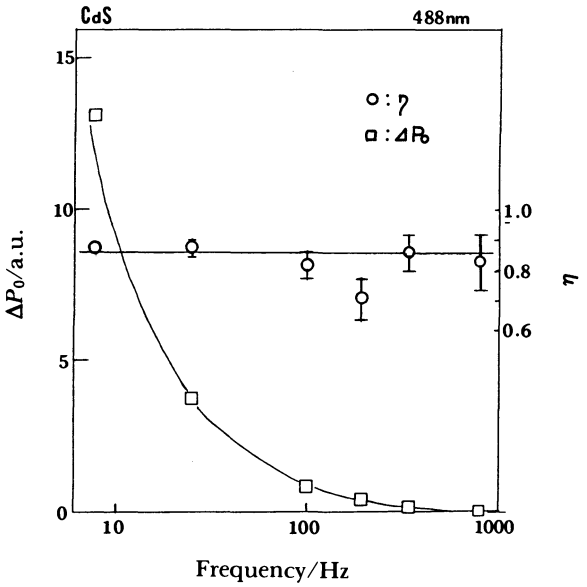

Fig. 4. Dependences of η (Quantum efficiency) and ΔP_0 (Photoacoustic signal amplitude at open circuit) on Chopping frequency, n-CdS Photoelectrode on 0.2 mol dm^{-3} Na_2SO_4, 1 mol dm^{-3} Na_2SO_3 aq.

We wish to thank Hisao Nakajima for his technical assistance and appreciate financial support from Ministry of Education, Science and Culture, Grant-in-Aid.

References

1) A. Fujishima, Y. Maeda, G. H. Brilmyer, and A. J. Bard, *J. Electrochem. Soc.*, **127**, 840 (1980).
2) Y. Maeda, A. Fujishima, and K. Honda, *Chem. Lett.*, **1980**, 271.
3) A. Fujishima, Y. Maeda, and K. Honda, *Bull. Chem. Soc. Jpn.*, **53**, 2735 (1980).
4) Y. Maeda, A. Fujishima, and K. Honda, *J. Electrochem. Soc.*, **128**, 1731 (1981).
5) T. Inoue, T. Watanabe, A. Fujishima, K. Honda, and K. Kohayakawa, *J. Electrochem. Soc.*, **124**, 719 (1977).
6) H. Gerischer and J. Gobrecht, *Ber. Bunsenges. Phys. Chem.*, **80**, 327 (1976).
7) H. Minoura and M. Tsuiki, *Electrochim. Acta.*, **23**, 1377 (1978).
8) H. Gerischer, *J. Electrochem. Soc.*, **113**, 1174 (1966).
9) V. A. Benderskii, Ya. M. Zolotovitskii, Ya. L. Kogan, M. L. Khidekel, and B. M. Shub, *Dokl. Akad. Nauk. SSSR*, **222**, 606 (1975).
10) M. Miyake, H. Yoneyama, and H. Tamura, *Chem. Lett.*, **1976**, 635.
11) H. Gerischer, *Surf. Sci.*, **18**, 97 (1969).
12) M. Morrison and T. Freund, *J. Chem. Phys.*, **47**, 1543 (1967).
13) S. R. Morrison and T. Freund, *Electrochim. Acta*, **13**, 1343 (1968).
14) W. P. Gomes, T. Freund, and S. R. Morrison, *J. Electrochem. Soc.*, **115**, 818 (1968).
15) E. C. Dutoit, F. Cardon, F. Vanderkerchove, and W. P. Gomes, *J. Appl. Electrochem.*, **8**, 247 (1978).
16) A. Aruchamy, Ph. D. Thesis, Indian Institute of Technology, Madras, India (1981).

The Complexing of the Magnesium and Barium Ions in Acetonitrile with Other Solvents. Investigation by the Use of a Polyacrylamide-Tetraethylene Glycol Monododecyl Ether Membrane Ion-Selective Electrode

Toshio NAKAMURA,* Hisakazu HIGUCHI, and Kosuke IZUTSU
Department of Chemistry, Faculty of Science, Shinshu University, Asahi, Matsumoto 390
(Received July 1, 1987)

Synopsis. The complexations of magnesium and barium ions in acetonitrile with DMF, DMSO, and HMPA were studied potentiometrically by the use of an organic polymer membrane electrode. The formation constants for 1:1 complexes of magnesium and barium ions, respectively, were 2.1×10^2 and 19 with DMF, 4.5×10^2 and 41 with DMSO, and (5.5×10^3) and 1.6×10^3 with HMPA. The roles of the basicity of the complexing solvent, crystallographic radius, and charge of the cations are discussed briefly.

Some types of ion-selective electrodes have been successfully used in physicochemical as well as in analytical studies of nonaqueous solutions.[1] Univalent cation-sensitive glass electrodes have been used in the studies of the complex formations of alkali metal ions in acetonitrile(AN)[2] and propylene carbonate[3] with other donor solvents and macrocyclic polyethers as well as in solvation studies of alkali metal ions in mixed nonaqueous solvents. The solid state copper sulfide electrode for copper(II)[4] and lanthanum fluoride electrode for fluoride ion[5] have also been used in solvation studies.

Recently, we have developed alkaline earth metal ion-sensitive electrodes for use in dipolar aprotic solvents. One was constructed by coating a platinum disk with polyacrylamide(PAA) coupled to a crown ether[6] and the other with PAA polymer coupled to acyclic polyether neutral carriers.[7] In the present report, the latter was used for a study of the complexing of magnesium and barium ions in AN with such solvent molecules as *N,N*-dimethylformamide(DMF), dimethyl sulfoxide(DMSO), and hexamethylphosphoric triamide(HMPA).

The emf of the following cell was measured: Ag/0.01 M $AgNO_3$+0.01 M Et_4NClO_4(AN)//0.05 M Et_4NClO_4(AN)//10^{-4} M $M^{2+}(ClO_4^-)_2$+0.01 M Et_4NClO_4 (AN+D)/PAA-POE4/Pt···Cell I where D denotes DMF, DMSO, or HMPA, M^{2+} the magnesium or barium ion to be investigated, and M is in mol dm^{-3}. POE4 is an abbreviation for tetraethylene glycol monododecyl ether. From the emf measurements of Cell I, the complex formation constants for the reaction of Eq. 1 were obtained by using Eqs. 2 to 4.

$$M_s^{2+} + xD = M_{xD}^{2+} \quad (1)$$

$$\beta_x = a(M_{xD}^{2+})/a(M_s^{2+})[D]^x \quad (2)$$

$$R_1 \equiv \{10^{(E_{AN}-E_{AN-D})/29.6} - 1\}/[D] = \sum_{i=1} \beta_i[D]^{i-1} \quad (3)$$

$$R_j \equiv (R_{j-1} - \beta_{j-1})/[D] = \sum_{i=j} \beta_i[D]^{i-j}, \quad (4)$$

where M_s^{2+} is M^{2+} solvated only by AN and M_{xD}^{2+} is M^{2+} cosolvated by x molecules of D; $a(M_s^{2+})$ and $a(M_{xD}^{2+})$ represent the activities of the respective species. [D] is the molar concentration of D. E_{AN} and E_{AN-D} represent the emfs of Cell I(in mV) in pure AN and AN-D, respectively.

Experimental

Apparatus. The construction of the electrodes, the cell assembly, and the potentiometric measurements were the same as those in a previous report.[7] A complexing solvent D was added to the cell with a microburette(Gilmont instruments, Inc. S1100A or S1200A), 5 μl in each step until its volume percent became 1%. In each step, the steady state potential was digitally read to ±0.1 mV. Analyses of the potentiometric data were carried out with a personal computer, NEC PC-9801 or Hewlett-Packard 86.

Reagents. Reagent grade magnesium and barium perchlorates were obtained from Wako Pure Chemical Industries, Ltd. Barium metal was the product of Kanto Chemical Co., Inc. Other reagents and solvents used in this experiment were the same as those in the previous report.[7]

Results

As shown by the typical potential-time curves in Fig. 1, a steady potential was quickly established after each addition of D to Cell I. Figure 2 shows an example of the relation between R_1, defined by Eq. 3, and [D] for the case in which D and M^{2+} were DMF and the magnesium ion, respectively. From the intercept and the slope of the straight line, $\beta_1=1.9\times10^2$ and $\beta_2=2.2\times10^3$ were obtained. For Mg^{2+}–DMSO and Ba^{2+}–DMF the formation constants, β_1 and β_2, were obtained in the same way. For Ba^{2+}–DMSO and Ba^{2+}–HMPA the relations between R_1 and [D] were not linear and a R_2–[D] relation defined by Eq. 4 was also used to determine the formation constants, β_2 and

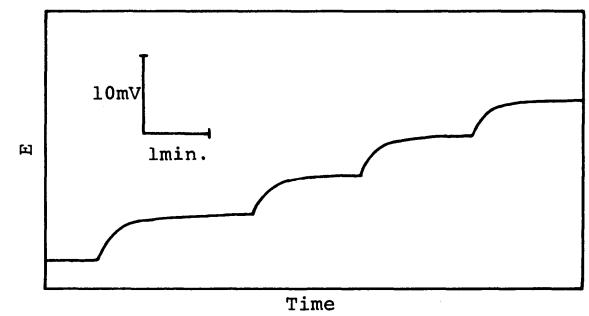

Fig. 1. Typical time vs. potential curve for titration of the barium ion(1×10^{-4}) M) in AN with DMSO. Ten μl DMSO was added to 10 ml of 0.01 M Et_4NClO_4–AN solution at each step.

Table 1. Complex Formation Constants of M^+ and M^{2+} in Acetonitrile with Other Solvent Molecules (at 25 °C)

Ion / Solvent	$Li^+(r_c:0.60)$[a]		$Mg^{2+}(r_c:0.65)$		$K^+(r_c:1.33)$[a]		$Ba^{2+}(r_c:1.35)$	
	β_1	β_2	β_1	β_2	β_1	β_2	β_1	β_2
DMF	16	1.1×10^2	2.1×10^2	2.2×10^3	1.5	1.1	19	57
DMSO	49	9.8×10^2	4.5×10^2	5.3×10^3	2.9	2.3	41	3.2×10^2
HMPA	2.1×10^3	3.2×10^5	(5.5×10^3)	(2.2×10^6)[b]	6.9	10	1.6×10^3	3.1×10^4

r_c: crystallographic ionic radius (Å). a) See Ref. 2. b) See text.

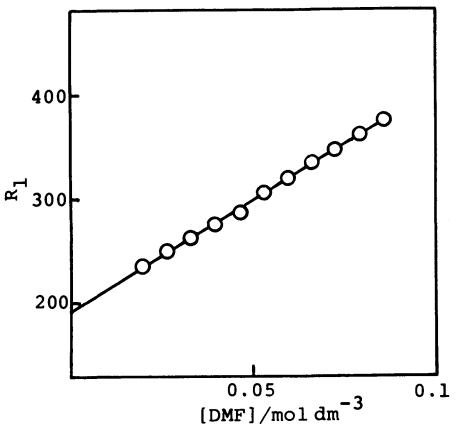

Fig. 2. The relation between R_1 vs. [DMF] for the magnesium ion in AN.

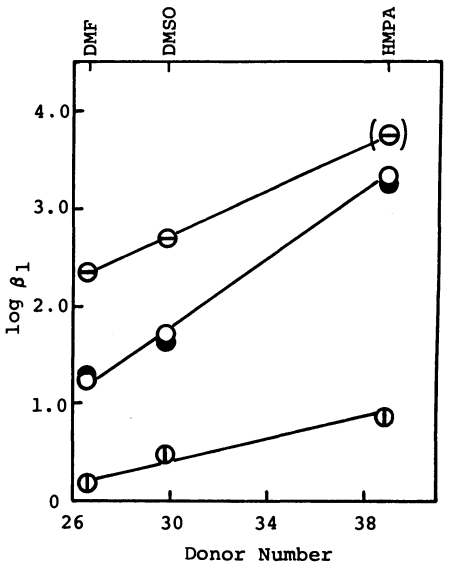

Fig. 3. The relation between log β_1 and donor numbers of solvents: (⊖) Mg^{2+}, (●) Ba^{2+}, (○) Li^+, (Φ) K^+.

β_3. In Table 1, however, only β_1 and β_2 are listed, since the reliability of β_3 was not sufficient in this experiment. A small amount of D was added to the solution in order to suppress any change of the organic membrane phase by the solvent effect. For D of DMF, DMSO, and HMPA, the maximum molar fraction of D added to Cell I was about 0.005, except if otherwise mentioned. The results are summarized in Table 1. The value of β_1 for the Ba^{2+}–DMF complex was also obtained by using a barium amalgam electrode instead of the PAA-POE4 electrode in Cell I. The barium metal was dissolved in mercury in order to construct the electrode; its concentration was about 0.33M for 1×10^{-3} M of the barium ion in Cell I. The experiment was carried out under oxygen-free conditions. The obtained β_1-value agreed with the value in Table 1 within the reliability of the experiment. The formation constants for the Mg^{2+}–HMPA complex in Table 1 were obtained in a somewhat different way since the potential after the addition of HMPA to the Mg^{2+}–AN solution gradually became ill-defined. The interaction of the magnesium ion with HMPA was so strong that the magnesium ion trapped by POE4 in the organic membrane phase seemed to become unstable; the electrode potential may be irreproducible. The method was as follows: To a 1×10^{-3} M solution of magnesium ion in Cell I was added twice equivalent of HMPA to the magnesium ion (the potentials before and after the addition were measured). The values of β_1 and β_2 were obtained from the potential jump by assuming that K_1/K_2(ratio of the stepwise formation constants) was the same as that for the Li^+–HMPA complexes in AN(i.e., $K_1:K_2=14:1$).

Discussion

From Table 1 the stabilities of the complexes of both the magnesium and barium ions in AN with DMF, DMSO, and HMPA increase in the order: DMF(26.6)<DMSO(29.8)≪HMPA(38.8). The figures in the parentheses show the Gutmann's donor number.[8] These orders are the same as those for the lithium and potassium ions. When the formation constants for the magnesium ion with DMF and DMSO are compared with those for the lithium ion, which has a crystallographic ionic radius very close to the magnesium ion, the former has β_1 and β_2 that are about one order larger than those of the latter. The situation is approximately the same for the case in which the ions are potassium and barium ions, although the stability of the HMPA complex with the barium ion is much larger than expected. These results may be attributed to the difference in the ionic charge. On the other hand, the larger complex formation abilities of the magnesium ion compared with those of the barium ion may be reasonably explained if we considered that the crystallographic radius of the magnesium ion is smaller than that of

the barium ion. Except for the complex of Mg^{2+}–HMPA, the values of β_1 in Table 1 seem to be reliable within ±10%, while those of β_2 within ±20%. The relations between the donor numbers of the complexing solvents and log β_1 are plotted in Fig. 3. It is interesting that in each case a linear relation was obtained. Complex formations of the barium ion occur with almost the same stability as those of the lithium ion.

Recently, we have plenty of thermodynamic and kinetic data concerning cation-macrocyclic ligand interactions in nonaqueous solvents.[9] However data concerning relatively weaker metal–ligand interactions, such as ion-solvent molecule interactions in the present study, are very scarce. The information obtained using the present electrode may effectively be used for a comparison of the relative strength of the solvation phenomena and specific interactions[8] between metal cations and dipolar aprotic solvent molecules.

This work was partially supported by a Grant-in-Aid for Scientific Research from the Ministry of Education, Science and Culture.

References

1) E. Pungor, K. Toth, P. G. Klatsmanyi, and K. Izutsu, *Pure Appl. Chem.*, **55**, 2029 (1983).

2) K. Izutsu, T. Nakamura, and K. Iwata, *Anal. Chim. Acta*, **117**, 329 (1980); T. Nakamura, Y. Yumoto, and K. Izutsu, *Bull. Chem. Soc. Jpn.*, **55**, 1850 (1982).

3) B. G. Cox, W. E. Waghorne, and C. K. Pigott, *J. Chem. Soc., Faraday Trans. 1*, **75**, 227 (1979).

4) L. F. Heerman and G. A. Rechnitz, *Anal. Chem.* **44**, 1655 (1972).

5) J. F. Coetzee and W. K. Martin, *Anal.Chem.*, **52**, 2412 (1980).

6) T. Nakamura and G. A. Rechnitz, *Anal. Chem.*, **57**, 393 (1985).

7) T. Nakamura, K. Ogiwara, K. Izutsu, and G. A. Rechnitz, *Bull. Chem. Soc. Jpn.*, **58**, 3409 (1985).

8) V. Gutmann; "The Donor-Acceptor Approach to Molecular Interactions," Plenum Press, New York (1978).

9) R. M. Izatt, J. S. Bradshaw, S. A. Nielsen, J. D. Lamb, J. J. Christensen, and D. Sen, *Chem. Rev.*, **85**, 271 (1985).

Electrochemical Studies on Metal-Metal Interactions in Bismacrocyclic Ni(II) Complexes

Katsura MOCHIZUKI
Department of Chemistry, Yokohama City University, Yokohama 236
(Received July 15, 1987)

Synopsis. Studies on five Ni(II) complexes, i.e., 7,7′-*polymethylene*bis[2,12-dimethyl-3,7,11,17-tetraazabicyclo-[11.3.1]heptadeca-1(17),2,11,13,15-pentaene]dinickel(II) perchlorates with *polymethylene* bridges of 2—6-C length, by cyclic voltammetry and differential pulse polarography, have revealed that the half-wave potentials of the $[Ni^{II}Ni^{II}]/[Ni^{II}Ni^{III}]$ and $[Ni^{II}Ni^{III}]/[Ni^{III}Ni^{III}]$ couples are not changed among the hexa- to tetramethylene derivatives but shifted toward the positive side in the following order: tetramethylene<trimethylene<ethylene derivative. These results are explainable in terms of the electrostatic repulsion due to these two metal ions.

Binuclear metal complexes with bis(tetraazamacrocycle) linked by a polymethylene or a carbon-carbon bridge have been used for studies on metal-metal interactions.[1-10] For example, Murase et al.[4] investigated bismacrocyclic Cu(II) complexes with **2**—**6**[11] by ESR spectroscopy and found effects of polymethylene length on antiferromagnetic interaction. Metal-metal interactions of Ni(II) complexes with ligands bis(cyclam)[1,10] and bis(isocyclam)[8] were studied by electrochemical methods and attributed to an electrostatic repulsion between two cations located close to each other. A limited number of Ni(II) complexes bridged by a carbon-carbon bond,[1,10] ethylene,[8] or *p*-xylylene[8], have been investigated. Ligands **2**—**6** seem to have the following advantages: 1) the length of the polymethylene bridge can be varied without causing any structural change in the tetraaza moieties; 2) observed metal-metal interactions are free from the delocalization of the two macrocycles. The author, therefore, has performed electrochemical studies on the series of Ni(II) complexes with **1a**, **1b**, and **2**—**6**.

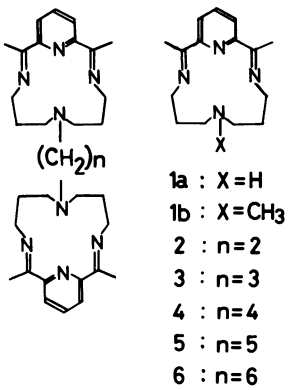

The oxidation of the Ni(II) complexes with **1a**, **1b**, and **2**—**6** in acetonitrile was studied. Figure 1 shows cyclic voltammograms (CVs) and differential pulse polarograms (DPs). Both the electrochemical measurements apparently reveal that the facility of the oxidation is affected by the bridge length of ligand. All the Ni(II) complexes with **4**, **5**, and **6** show CVs in which one anodic and one cathodic peak appear with a ratio i_{pa}/i_{pc} of almost unity. Their respective DPs show one nearly symmetrical peak. Similar results were obtained in the case of monomacrocyclic Ni(II) complexes with **1a** and **1b**. The Ni(II) complexes with **2** and **3** give quite different CVs and DPs. The CV of $[Ni^{II}_2(\mathbf{3})]^{4+}$ has two shoulders each near the anodic and near the cathodic peak. The CV of $[Ni^{II}_2(\mathbf{2})]^{4+}$ has two anodic peaks at 1.25 and 1.35 V and two cathodic ones at 1.22 and 1.32 V. In the DP of $[Ni^{II}_2(\mathbf{3})]^{4+}$ one broad peak is observed; its half-width is larger than those of the Ni(II) complexes with **1a**, **1b**, and **4**—**6** (See Table 1). The DP of $[Ni^{II}_2(\mathbf{2})]^{4+}$ has two distinct peaks (1.30_0 and 1.23_5 V) with nearly equal intensities. These results indicate that the Ni(II) complexes having short bridges are oxidized stepwise at distinctly different potentials according to the consecutive reaction

$$[Ni^{II}Ni^{II}]^{4+} \overset{-e}{\rightleftharpoons} [Ni^{II}Ni^{III}]^{5+} \overset{-e}{\rightleftharpoons} [Ni^{III}Ni^{III}]^{6+}. \quad (1)$$

Table 1 lists electrochemical data evaluated from the DPs. The values of $E_{1/2}{}^{1}$ ($[Ni^{II}Ni^{II}]/[Ni^{II}Ni^{III}]$) of

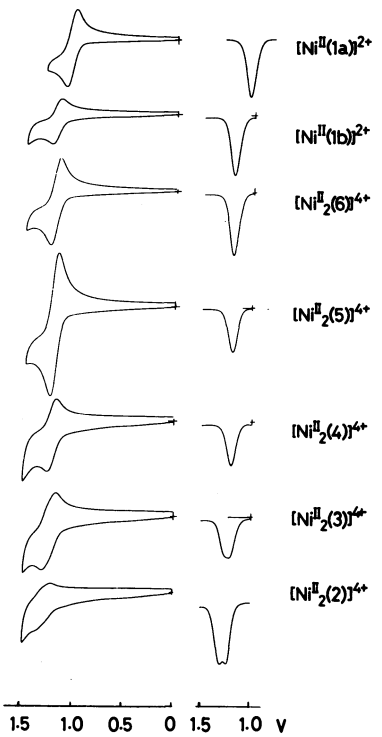

Fig. 1. Cyclic voltammograms (scan rate: 100 mV s^{-1}) and the respective differential pulse polarograms (scan rate: 1 mV s^{-1}; pulse amplitude: 10 mV) in acetonitrile. V vs. $Ag-Ag^+$ (0.01 mol dm^{-3} $AgNO_3$). Glassy carbon electrode.[18] T=25 °C.

Table 1. Data of Differential Pulse Polarography[a]

Complex	E_p/V	Half-width/mV	$E_{1/2}$/mV[b]	$E_{1/2}{}^1$ or $E_{1/2}{}^2$/V[b]
$[Ni^{II}(\mathbf{1a})]^{2+}$	1.03_8	10_5		1.04_3
$[Ni^{II}(\mathbf{1b})]^{2+}$	1.19_0	10_6		1.19_5
$[Ni^{II}{}_2(\mathbf{6})]^{4+}$	1.20_2	10_7	4_9	1.18_3
				1.23_2
$[Ni^{II}{}_2(\mathbf{5})]^{4+}$	1.20_5	10_7	4_9	1.18_5
				1.23_4
$[Ni^{II}{}_2(\mathbf{4})]^{4+}$	1.20_5	10_7	4_9	1.18_5
				1.23_4
$[Ni^{II}{}_2(\mathbf{3})]^{4+}$	1.23_7	15_1	7_5	1.21_5
				1.28_0
$[Ni^{II}{}_2(\mathbf{2})]^{4+}$	1.23_5	17_2	$8_9(8_7)$	1.22_9
	1.30_0			1.31_7

a) In acetonitrile, vs. $Ag\text{-}Ag^+$ (0.01 mol dm^{-3} $AgNO_3$), T=25 °C, and I=0.1 (Et_4NClO_4). b) Evaluated from half-width data by the method of Ref. 14. The value in parentheses was evaluated from E_p data.

the Ni(II) complexes with **4**—**6**, independent of bridge length, are very close to that of $[Ni^{II}(\mathbf{1b})]^{2+}$.[12] The $E_{1/2}{}^1$ values shift toward the positive side in the sequence of ligands: **2**>**3**>**4**. A similar but more pronounced trend is observed with the second oxidation step, $E_{1/2}{}^2$ ($[Ni^{II}Ni^{III}]/[Ni^{III}Ni^{III}]$). On a theoretical ground, consecutive oxidation of two equivalent and independent metal centers involves a potential separation, $\Delta E_{1/2}=E_{1/2}{}^2-E_{1/2}{}^1$, of 36 mV.[13,14] Thus, the larger value (49 mV) is observed with the Ni(II) complexes with **4**—**6**. More remarkable differences are found with $[Ni^{II}{}_2(\mathbf{2})]^{4+}$ (89 mV) and $[Ni^{II}{}_2(\mathbf{3})]^{4+}$ (75 mV). These results are reasonable because the electrostatic repulsion due to two metal ions undoubtedly increases with decrease in their distance.[15] Furthermore, the more pronounced effects observed for the second oxidation step as well as $\Delta E_{1/2}$ are acceptable, since the electrostatic repulsion due to two Ni(III) ions should be larger than that due to Ni(II) and Ni(III), which is in turn larger than that due to two Ni(II) ions.

Thus, all the data obtained show that the metal-metal interaction of the bismacrocyclic Ni(II) complexes is affected by the bridge length; the interaction is increased in the following sequence of ligands **2**>**3**>**4**=**5**=**6**. The crucial bridge length for the interaction lies between tri- and tetramethylene; to our best knowledge, such a finding is unprecedented in the literature.

Experimental

Materials. Monomacrocyclic Ni(II) complexes **1a** and **1b** were prepared according to the method described by Karn and Busch.[16] Bismacrocyclic Ni(II) complexes were synthesized by a method similar to that reported by Murase et al.[4]

Physical data of new compounds are given below together with some comments.

$[Ni^{II}{}_2(\mathbf{2})](ClO_4)_4$: A crude product was purified by column chromatography with ion-exchange resin (SP-Sephadex C-25) and 0.6 mol dm^{-3} NaCl as the eluant. The counter ion of the complex thus purified was replaced with perchlorate by the conventional method. Found: C, 36.28; H, 4.30; N, 10.27; Ni, 10.44%. Calcd for $C_{32}H_{46}N_8Ni_2Cl_4O_{16}$: C, 36.33; H, 4.38; N, 10.59; Ni, 11.09%. IR (Nujol): 1630 (C=N) and 1580 cm^{-1} (py); ^{13}C NMR (CF_3COOD, TMS) δ=17.8 (q), 25.2 (t), 41.9 (t), 51.7 (t), 55.6 (t), 127.8 (d), 145.1 (d), 156.7 (s), and 181.0 (s).

$[Ni^{II}{}_2(\mathbf{2})]Cl_4$: MS (FAB) m/z 764 ($[M-Cl+H]^+$), 729 ($[M-2Cl+H]^+$) and 693 ($[M-3Cl+H]^+$).

$[Ni^{II}{}_2(\mathbf{5})](ClO_4)_4\cdot 2H_2O$: Found: C, 36.86; H, 4.60; N, 9.68%. Calcd for $C_{35}H_{52}N_8Ni_2Cl_4O_{16}\cdot 2H_2O$: C, 37.00; H, 4.97; N, 9.86%. IR (Nujol): 1628 (C=N) and 1583 cm^{-1} (py); ^{13}C NMR (CF_3COOD, TMS) δ=17.5 (q), 20.1 (t), 24.2 (t), 25.8 (t), 51.6 (t), 52.3 (t), 55.2 (t), 127.7 (d), 146.1 (d), 156.2 (s), and 181.2 (s).

$[Ni^{II}{}_2(\mathbf{6})](ClO_4)_4\cdot H_2O$: Found: C, 38.04; H, 4.83; N, 9.94%. Calcd for $C_{36}H_{54}N_8Ni_2Cl_4O_{16}\cdot H_2O$: C, 38.19; H, 4.99; N, 9.90%. IR (Nujol): 1635 (C=N) and 1580 cm^{-1} (py); ^{13}C NMR (CF_3COOD, TMS) δ=17.3 (q), 19.7 (t), 24.0 (t), 27.6 (t), 51.3 (2t), 54.9 (t), 127.8 (d), 145.8 (d), 156.4 (s), and 181.2 (s).

The isolation of the Ni(II) complex perchlorates with **3** and **4** was also confirmed by elemental analysis, IR, and ^{13}C NMR.

Measurements: Electrochemical measurements were performed according to the same method as described in our previous paper.[17] The concentration of the Ni(II) complexes was ca. 1×10^{-3} mol dm^{-3}. Tetraethylammonium perchlorate (0.1 mol dm^{-3}) was used as the supporting electrolyte.

The author wishes to thank Dr. Eiji Nakamura of Institute for Life Science of Mitsubishi Kasei for the measurement of FAB-mass spectra.

References

1) E. K. Barefield, D. Chueng, D. G. Van Derveer, and F. J. Wagner, *J. Chem. Soc., Chem. Commun.*, **1981**, 302.
2) N. Tanaka, Y. Kobayashi, and S. Takamoto, *Chem. Lett.*, **1977**, 107.
3) I. Murase, K. Hamada, and S. Kida, *Inorg. Chim. Acta*, **54**, L171 (1981).
4) I. Murase, K. Hamada, S. Ueno, and S. Kida, *Synth. React. Inorg. Met.-Org. Chem.*, **13**, 191 (1983).
5) I. Murase, S. Ueno, and S. Kida, *Inorg. Chim. Acta*, **111**, 57 (1986).
6) M. Ciampolini, M. Micheloni, N. Nardi, F. Vizza, A. Buttafava, L. Fabbrizzi, and A. Perotti, *J. Chem. Soc., Chem. Commun.*, **1984**, 998.
7) K. Wieghardt, I. Tolksdorf, and W. Herrmann, *Inorg. Chem.*, **24**, 1230 (1985).
8) R. Schneider, A. Riesen, and T. A. Kadan, *Helv. Chim. Acta*, **68**, 53 (1985).
9) E. Garcia-España, M. Micheloni, P. Paoletti, and A.

Bianchi, *Gazz. Chim. Ital.*, **115**, 115 (1985).
10) L. Fabbrizzi, L. Montagna, T. A. Kadan, and L. C. Siegfried, *Inorg. Chem.*, **25**, 2672 (1986).
11) Ligand abbreviations: 2,12-dimethyl-3,7,11,17-tetraazabicyclo[11.3.1]heptadeca-1(17),2,11,13,15-pentaene (**1a**), 2,7,12-trimethyl-3,7,11,17-tetraazabicyclo[11.3.1]heptadeca-1(17), 2,11,13,15-pentaene (**1b**), and 7,7′-*polymethylene*bis[2,12-dimethyl-3,7,11,17-tetraazabicyclo[11.3.1]heptadeca-1(17),2,11, 13,15-pentaene], where *polymethylene* is ethylene (**2**), trimethylene (**3**), tetramethylene (**4**), pentamethylene (**5**), or hexamethylene (**6**).
12) The $E_{1/2}$[1] values of $[Ni^{II}(\mathbf{1b})]^{2+}$ and the bismacrocyclic Ni(II) complexes are more positive than that of $[Ni^{II}(\mathbf{1a})]^{2+}$, which indicates that the Ni(II) complex with one tertially nitrogen atom is more resistant to oxidation than that with one secondary nitrogen atom.
13) R. R. Gagńe and C. L. Spiro, *J. Am. Chem. Soc.*, **102**, 1443 (1980).
14) D. E. Richardson and H. Taube, *Inorg. Chem.*, **20**, 1278 (1981).
15) The molecular model suggests that the approximate distance between the two Ni(II) ions in $[Ni^{II}_2(\mathbf{n})]^{4+}$ is 7.1 (**n**=**2**), 8.1 (**3**), 9.3 (**4**), 10.5 (**5**), or 12.0 Å (**6**), if the two rings are positioned as far as possible.
16) J. L. Karn and D. H. Busch, *Inorg. Chem.*, **8**, 1149 (1969).
17) K. Mochizuki and M. Fujimoto, *Bull. Chem. Soc. Jpn.*, **58**, 1520 (1985).
18) Similar results were obtained with Pt-electrode.

The Crystal Structure of Phenanthrene:Picric Acid Molecular Complex

Shin-ichi YAMAGUCHI,† Motoaki GOTO, Hiroaki TAKAYANAGI, and Haruo OGURA*
School of Parmaceutical Sciences, Kitasato University, Shirokane, Minato-ku, Tokyo 108
†Pharmaceutical Development Laboratories, Meiji Seika Kaisha, Ltd.,
580, Horikawa-cho, Saiwai-ku, Kawasaki, Kanagawa 210
(Received June 24, 1987)

Synopsis. The crystal structure of phenanthrene:picric acid molecular complex was determined by X-ray crystal analysis. Phenanthrene and picric acid molecules are stacked alternately along the c-axis, making their molecular planes parallel to each other. The intramolecular hydrogen bonding exists in a picric acid.

Phenanthrene:picric acid is one of the π-molecular complexes. Three polymorphs at least have been known.[1] Herbstein and Kaftory reported cell dimensions,[2] but crystal structures have not been described. We have tried to elucidate the crystal structure and will report here the results obtained.

Experimental

The components in equimolar ratio were solved in an excess of methanol. Yellow needles were precipitated by evaporation of the solution at room temperature. The diffraction intensities were measured on a Rigaku AFC-5 four-circle diffractometer with graphite-monochromated Cu $K\alpha$ radiation at 23 °C. Crystallographic and other information is summarized in Table 1.

The ω–2θ scan mode with a scan rate of 8° min^{-1} was employed with the ω scan range $(1.1+0.5\tan\theta)°$. A total of 2807 reflections with $|F_o|>3\sigma(|F_o|)$ was collected up to 2θ of 140°. No absorption correction was applied [μ(Cu $K\alpha$)= 10.99 cm^{-1}]. The structure was solved by a direct method using the program MULTAN[3] and refined by the block-diagonal least-squares method using initially B_{iso} and finally B_{ij} for non-hydrogen atoms. The difference Fourier synthesis showed two H atoms of phenanthrene and picric acid, and H atom of picric acid OH. The positions of other ten H atoms were calculated and refined. Final R was 0.076 (R_w= 0.083, S=1.045). The function minimized was $\Sigma w(|F_o|-|F_c|)^2$, where w of 1.0 was used. Atomic scattering factors were quoted from International Tables for X-Ray Crystallography (1974).[4]

Table 1. Crystallographic and Other Information for Phenanthrene:Picric Acid Complex

Molecular formula	$C_{14}H_{10}:C_6H_3N_3O_7$
Formula weight	407.33
Crystal dimensions/mm^3	0.3×0.2×0.1
Crystal system	Triclinic
Space group	$P\bar{1}$
Cell dimensions a /Å	8.812(2)
Cell dimensions b /Å	14.546(2)
Cell dimensions c /Å	7.052(1)
Cell dimensions α/°	95.18(2)
Cell dimensions β/°	92.07(2)
Cell dimensions γ/°	97.34(1)
Melting point/°C	146
Density D_m/g cm^{-3}	1.50
Density D_x/g cm^{-3}	1.517
Z	2
μ(Cu $K\alpha$)/cm^{-1}	10.99

Results and Discussion

Cell dimensions are significantly different from those reported by Herbstein and Kaftory (a=8.99, b=14.81, c=7.12 Å, α=101.5, β=99.2, and γ=102.1°). The crystal used in this study is different from that used by Herbstein in morphology. The final atomic

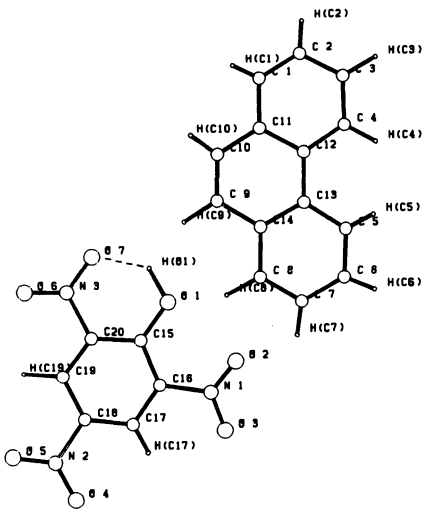

Fig. 1. Atomic numbering and a hydrogen bonding (dashed line).

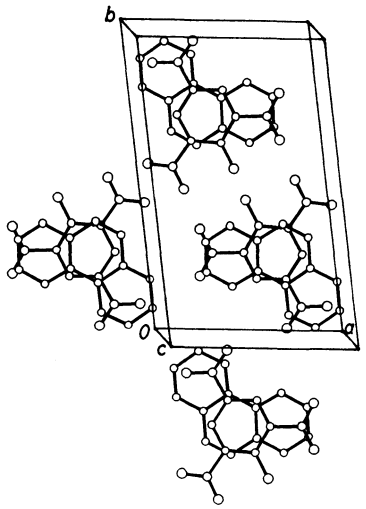

Fig. 2. Arrangement of molecules in the unit cell (some molecules along the edges have been removed for clarity).

Table 2. Atomic Coordinates ($\times 10^4$) and Equivalent Isotropic Temperature Factors (/Å^2) of Phenanthrene:Picric Acid Complex Standard Deviations are in Parentheses

Atom	x	y	z	B_{eq}[a]	Atom	x	y	z	B_{eq}[a]
O 1	5518(4)	4270(2)	1017(5)	4.4	C 6	2710(5)	2169(3)	5098(7)	3.8
O 2	8216(5)	5018(3)	2216(12)	10.9	C 7	2820(5)	3140(4)	5110(7)	4.3
O 3	9995(4)	4219(3)	2336(11)	9.9	C 8	4176(6)	3688(3)	5635(7)	3.8
O 4	9138(4)	977(3)	2647(6)	5.5	C 9	6941(5)	3838(3)	6668(6)	3.3
O 5	6898(5)	201(2)	1938(6)	5.7	C10	8173(5)	3448(3)	7155(7)	3.3
O 6	2702(4)	1777(3)	352(6)	5.8	C11	8118(4)	2467(3)	7208(6)	2.6
O 7	2969(4)	3273(3)	182(6)	5.4	C12	6721(4)	1874(3)	6725(6)	2.3
N 1	8676(4)	4296(3)	2150(7)	4.2	C13	5382(4)	2283(3)	6161(6)	2.3
N 2	7785(5)	922(2)	2177(6)	3.9	C14	5503(5)	3270(3)	6158(6)	2.8
N 3	3462(4)	2533(3)	471(6)	4.0	C15	6040(5)	3463(3)	1285(6)	2.9
C 1	9427(5)	2067(3)	7775(7)	3.6	C16	7581(4)	3435(3)	1843(6)	2.7
C 2	9379(5)	1131(4)	7828(7)	4.1	C17	8146(4)	2624(3)	2131(6)	2.9
C 3	8011(6)	541(3)	7358(7)	4.0	C18	7164(5)	1799(3)	1858(6)	2.8
C 4	6701(5)	914(3)	6829(7)	3.1	C19	5643(5)	1765(3)	1312(6)	2.9
C 5	3958(4)	1748(3)	5624(6)	3.0	C20	5119(4)	2591(3)	1032(6)	2.8

a)The equivalent isotropic temperature factors were computed using the following equation:
$B_{eq}=4/3(B_{11}a^2+B_{22}b^2+B_{33}c^2+B_{12}ab\cos\gamma+B_{13}ac\cos\beta+B_{23}bc\cos\alpha)$.

Table 3. Bond Lengths(/Å) and Bond Angles(/°) of Phenanthrene:Picric Acid Complex Standard Deviations are in Parentheses

O1-C15	1.340(5)	C11-C12	1.421(4)	O2-N1-O3	123.0(4)	C4-C12-C13	122.8(3)
O2-N1	1.170(5)	C12-C13	1.446(5)	O2-N1-C16	119.4(3)	C11-C12-C13	118.9(3)
O3-N1	1.186(5)	C13-C14	1.425(5)	O3-N1-C16	117.6(3)	C5-C13-C12	122.8(3)
O4-N2	1.216(5)	C15-C16	1.407(5)	O4-N2-O5	125.2(4)	C5-C13-C14	118.5(3)
O5-N2	1.220(4)	C15-C20	1.409(5)	O4-N2-C18	117.6(3)	C12-C13-C14	118.7(3)
O6-N3	1.206(5)	C16-C17	1.367(6)	O5-N2-C18	117.3(3)	C8-C14-C9	120.4(3)
O7-N3	1.242(6)	C17-C18	1.381(5)	O6-N3-O7	125.1(3)	C8-C14-C13	119.4(3)
N1-C16	1.474(4)	C18-C19	1.374(5)	O6-N3-C20	117.9(4)	C9-C14-C13	120.2(3)
N2-C18	1.483(5)	C19-C20	1.370(6)	O7-N3-C20	117.0(3)	O1-C15-C16	121.3(3)
N3-C20	1.488(5)			C2-C1-C11	121.4(3)	O1-C15-C20	123.6(3)
C1-C2	1.362(7)			C1-C2-C3	120.1(4)	C16-C15-C20	115.1(3)
C1-C11	1.417(6)			C2-C3-C4	119.8(4)	N1-C16-C15	120.8(3)
C2-C3	1.398(6)			C3-C4-C12	121.4(3)	N1-C16-C17	116.5(3)
C3-C4	1.390(6)			C6-C5-C13	120.7(3)	C15-C16-C17	122.7(3)
C4-C12	1.404(5)			C5-C6-C7	120.9(3)	C16-C17-C18	118.6(3)
C5-C6	1.381(6)			C6-C7-C8	120.4(4)	N2-C18-C17	118.2(3)
C5-C13	1.410(5)			C7-C8-C14	120.0(4)	N2-C18-C19	119.3(3)
C6-C7	1.402(7)			C10-C9-C14	120.4(3)	C17-C18-C19	122.5(3)
C7-C8	1.369(6)			C9-C10-C11	122.0(3)	C18-C19-C20	117.3(3)
C8-C14	1.437(6)			C1-C11-C10	121.2(3)	N3-C20-C15	120.1(3)
C9-C10	1.336(6)			C1-C11-C12	118.9(3)	N3-C20-C19	116.0(3)
C9-C14	1.437(5)			C10-C11-C12	119.8(3)	C15-C20-C19	123.9(3)
C10-C11	1.426(6)			C4-C12-C11	118.3(3)		

parameters are listed in Table 2.[††]

Bond lengths and interbond angles are given in Table 3. The atomic numbering is shown in Fig. 1.[5]

The arrangement of the molecules in a unit cell is shown in Fig. 2. Phenanthrene and picric acid molecules are stacked along the c-axis, making their molecular planes parallel to each other. The distance between them is 3.4 Å. Those in opposite directions in a stack are also 3.4 Å. Thus there is no indication of 'pairing' of molecules within a stack.

The nitro group O2–N1–O3 (dihedral angle 11.8° to a plane of benzene ring) protrudes from the stacked column. Other two nitro groups are sandwiched in between two phenanthrene molecules (dihedral angles 0.53° for the nitro group O4–N2–O5 and 2.55° for O6–N3–O7).

In the crystal of picric acid the possibility of an intermolecular hydrogen bonding have been envisaged by Srikrishnan et al.[6] In the crystal of phenanthrene:picric acid complex, however, a difference Fourier map showed no clear evidence of an intermolecular hydrogen bonding. The H atom (H(O1)) of phenol OH is located at a reasonable position for intramolecular hydrogen bonding bet-

[††] The complete tables of observed and calculated structure factors, isotropic thermal parameters and the atomic coordinates of hydrogen atoms, and anisotropic thermal parameters of non-hydrogen atoms are kept as Document No. 8779 at the Office of the Editor of the Bulletin of the Chemical Society of Japan.

ween O(1) and O(7), the distances from which are 1.13 and 1.67 Å respectively. Such an intramolecular hydrogen bonding may cause the difference between the two N–O distances of the nitro group O6–N3–O7.

References

1) Y. Matsunaga, *Bull. Chem. Soc. Jpn.*, **44**, 2868 (1971).
2) F. H. Herbstein and M. Kaftory, *Acta Crystallogr., Sect. B*, **31**, 60 (1975).
3) P. Main, S. E. Hull, L. L. Lessinger, G. German, J. P. Declercq, and M. M. Woolfson, *MULTAN78*, "A system of computer programs for the automatic solution of crystal structures for X-ray diffraction data," University of York, England, and University of Louvain, Belgium (1978).
4) "International Tables for X-Ray Crystallography," Kynoch Press, Birmingham (1974), Vol. IV, pp. 72—149.
5) C. K. Johnson, "ORTEP," Oak Ridge National Laboratory Report ORNL-3794 (1965).
6) T. Srikrishnan, M. Soriano-Garcia, and R. Parthasarathy, *Z. Kristallogr.*, **151**, 317 (1980).

The Cyclic Voltammetry of *p*-Tropoquinone Acetals

Akira MORI,* Shun-ichi HIRAYAMA,† Yasutomo GOTO,† and Hitoshi TAKESHITA*
Institute of Advanced Material Study, 86, Kyushu University, Kasuga-koen, Kasuga, Fukuoka 816
†Graduate School of Engineering Sciences, 39, Kyushu University, Kasuga-koen, Kasuga, Fukuoka 816
(Received August 5, 1987)

Synopsis. The cyclic voltammetry of *p*-tropoquinone mono- and bisacetals was analyzed. Monoacetals showed an irreversible redox couple and an oxidation wave around +0.16 to −0.1 V vs. Ag/AgCl, the latter of which was due to a dianion species.

Recently, we have shown that, according to a cyclic voltammetry (CV) analysis, the redox process of tropoquinones generally occurs via two one-electron paths; however, the intensity of the second oxidation wave was sometimes diminished by subsequent chemical reactions of the anion radical species.[1,2] Here, we show the electrochemical behaviors of *p*-tropoquinone acetals, masked tropoquinone derivatives, which are suitable for CV studies when tropoquinones are unstable under the experimental conditions.

p-Tropoquinone acetals **1**—**3** were prepared as previously described,[3] except for 5-cyano-3-methyl-7,7-dimethoxy-2,5-cycloheptadiene-1,4-dione (**4**), which was prepared as shown in Scheme 1; 2,5-dimethoxy-4,6-bis(morpholinomethyl)tropone (**5**)[4] was treated with ethyl chloroformate[5] to give bis(chloromethyl) derivative (**6**) in 78% yield.

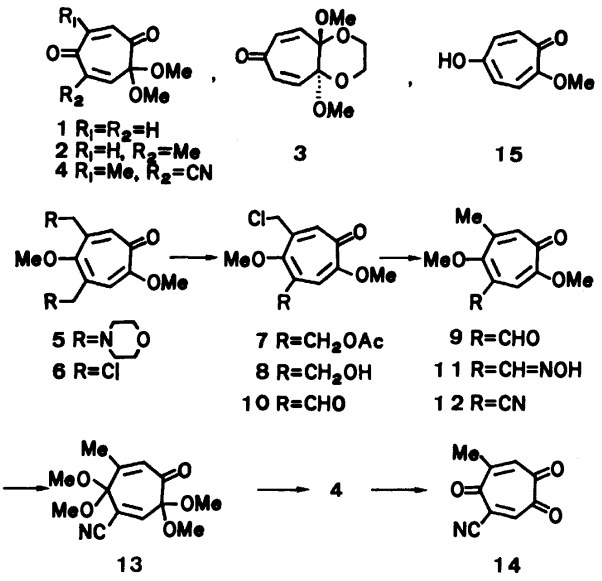

Next, an acetic acid solution of **6** with silver acetate at 80 °C quantitatively gave 4-acetoxymethyl-6-chloromethyl-2,5-dimethoxytropone (**7**), the saponification of which afforded air-sensitive 6-chloromethyl-4-hydroxymethyl-2,5-dimethoxytropone (**8**). The manganese(IV) oxide oxidation of **8** gave aldehydes **9** and **10**.

An oxime **11**, prepared from **9**, was a syn/anti-mixture (2:3) and dehydrated to a cyano derivative **12** in 28% yield. A subsequent cerium(IV) ammonium nitrate (CAN)-oxidation[6] of **12** gave a bisacetal **13** in 31% yield; upon an acid hydrolysis at 40 °C for 1.5 h, **13** gave a monoacetal **4** in 94% yield; however, the same treatment at 50 °C for 4.5 h gave 4-cyano-6-methyl-*p*-tropoquinone (**14**) in 1% yield.

The redox potentials of acetals, determined by CV, are summarized in Table 1. Among them, the second redox couple of **4** was hardly recognizable and the peak height of the second oxidation peak of **1** and **2** decreased.

The first and second reduction peak potentials ($E_{pr}1$ and $E_{pr}2$) of **1** were ca. 0.6 V more negative than those

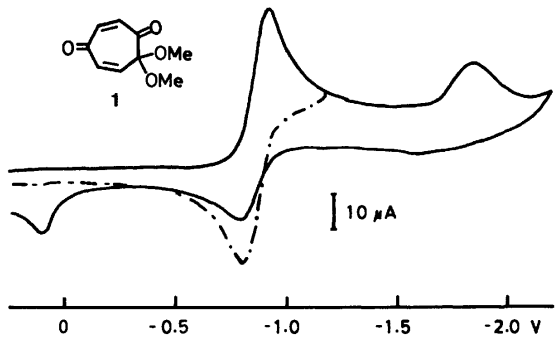

Fig. 1. The CV curves of **1**.

Table 1. Reduction and Oxidation Peak Potentials of Acetals and the Related Compounds[a]

	$E_{pr}1/E_{po}1$	$E_{pr}2/E_{po}2$
1[b]	−0.87/−0.74 (−0.81)[c]	−1.68/−1.46 (−1.65)
2[b]	−0.93/−0.77 (−0.85)	−1.88/— (−1.70)
3	−1.54/−1.38 (−1.48)	
4[b]	−0.56/−0.48 (−0.49)	−1.43/—
p-Tropoquinone	(−0.21)	(−1.10)
4-Methyl-*p*-tropoquinone	(−0.28)	(−1.15)

a) The CV were measured in anhydrous DMF with 0.1 M TBAF using Pyrex-glass sealed Pt wire as working and counter electrodes and standard Ag/AgCl as a reference electrode at 22—23 °C under N_2 atmosphere with a scan rate of 100 mV/s. b) Additional oxidation peaks were observed at +0.16, +0.09, and −0.11 V for **1**, **2**, and **4**, respectively. c) The values in parentheses showed the half-wave potentials.

of *p*-tropoquinone. The substituent effect (0.04 V) of a methyl group in *p*-tropoquinone acetal series was nearly the same as that (0.07 V) of the *p*-tropoquinone series.[1] In the case of **4**, the first reduction peak potential became more positive (by 0.36 V) due to a cyano group, a strong electron-attractive group. In the CV of monoacetals **1** and **2**, an oxidation wave was observed around +0.16 to −0.1 V vs. Ag/AgCl. These waves in **1** and **2** disappeared and their CV showed a reversible redox couple when the scanning was returned around −1.2 V. While the CV of 5-hydroxy-2-methoxytropone (**15**) showed an oxidation peak at +0.16 V, together with E_{pr}=−1.34 and E_{po}=−0.57 V, it is conceivable that the anion **C** was formed by the eliminations of a methoxide anion from dianion **B** and/or the methoxide radical from **A**, and that **C** was oxidized to the radical **D** at +0.16 V. Furthermore, since it has been established[6] that the one-electron oxidation of **15** gave dimers together with **1**, the irreversible redox couples of monoacetals must be due to a formation of dimeric products under CV conditions. The low intensity of the second peak could, thus, be explained by the involvement of alternative routes to **D** via eliminations of a methoxide ion and/or radical. In the case of **4**, routes **A** to **D** might become easier since the cyano group at C-5 should stabilize the radical intermediate **D**. Therefore, the process from **A** to **B** might be diminished.

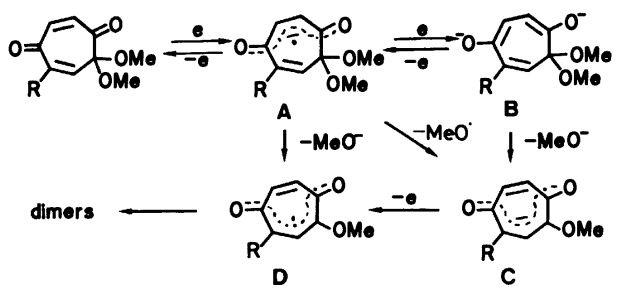

Furthermore, the CV of **3** showed a quasi-reversible couple at E_{pr}=−1.54 and E_{po}=−1.38 V, and the substituents varied with the electrochemical behaviors of tropoquinone acetals.

Since an introduction of each cyano group was estimated to enhance the redox potentials by 0.36 V, the enhanced redox potentials of the fully substituted *p*-tropoquinones, such as dicyanodihalogeno-*p*-tropoquinones, could be estimated as +0.65 V vs. Ag/AgCl,[1] which may overcome the potential of 2,3-dichloro-5,6-dicyano-*p*-benzoquinone (DDQ), the strongest oxidizing aromatic quinone presently available.

Experimental

Preparation of 6. To an anhydrous benzene solution (10 cm³) of ethyl chloroformate (1 g) was added an anhydrous benzene solution (20 cm³) of **5**[4] (814 mg) at 0—5 °C. After stirring at 40 °C for 10 h, the precipitates were filtered off and the filtrate was chromatographed on a silica-gel column to give **6** [yellow needles, mp 71—73 °C, 460 mg; 78%. Found: C, 50.35; H, 4.65%; *m/z*, 262.0180, 264.0147, 266.0137 (M⁺).[7] Calcd for $C_{11}H_{12}O_3Cl_2$: C, 50.21; H, 4.60%; *m/z*, 262.0164, 264.0135, 266.0104. ^{1}H NMR δ[8]=3.87 (3H, s), 3.94 (3H, s), 4.50 (2H, s), 4.63 (2H, s), 6.68 (1H, s), and 7.40 (1H, s). ^{13}C NMR δ=44.4, 45.0, 56.4, 63.5, 114.0, 132.5, 138.4, 143.2, 154.9, 161.7, and 178.5. IR *ν*: 1620, 1595, and 1570 cm⁻¹].

Reaction of 6 with AgOAc. An AcOH solution (10 cm³) of **6** (55 mg) and AgOAc (370 mg) was heated at 80 °C for 2 h. The resultant precipitates were filtered off, and the filtrate was chromatographed on a silica-gel column to give **7** [yellow needles, mp 96—98 °C (decomp), 60 mg; 100%. Found: *m/z*, 286.0580, 288.0564 (M⁺). Calcd for $C_{13}H_{15}O_5Cl$: 286.0605, 288.0576. ^{1}H NMR δ=2.14 (3H, s), 3.83 (3H, s), 3.90 (3H, s), 4.52 (2H, s), 5.16 (2H, s), 6.77 (1H, s), and 7.42 (1H, s). ^{13}C NMR δ=20.6, 44.8, 55.9, 63.2, 63.5, 113.2, 131.4, 138.3, 143.3, 155.4, 161.7, 170.5, and 178.4. IR *ν*: 1750, 1625, and 1600 cm⁻¹].

Saponification of 7 to 8 and Subsequent MnO_2-Oxidation to 9 and 10. To an MeOH solution (10 cm³) of **7** (555 mg) was added aqueous NaOH (1 M, 2 cm³ (1 M=1 mol dm⁻³)). After stirring for 5 min, the resultant brown solution was heated in vacuo in order to remove the solvent; the residue was diluted with water, acidified with dil HCl, and extracted with $CHCl_3$. The organic layer was dried over $MgSO_4$ and evaporated in vacuo to give **8** [a brown oil, 468 mg; 99%. ^{1}H NMR δ=3.78 (3H, s), 3.90 (3H, s), 4.50 (2H, s), 4.76 (2H, s), 7.21 (1H, s), and 7.35 (1H, s). ^{13}C NMR δ=45.1, 58.4, 61.9, 62.9, 113.5, 137.5, 138.3, 144.1, 154.4, 162.5, and 178.7]. Subsequently, to an anhydrous benzene solution (10 cm³) of **8** (474 mg) was added MnO_2 (113 mg). After refluxing for 4 h, the mixture was passed through a Celite column. The combined eluent was evaporated in vacuo and the residue was chromatographed on a silica-gel column to give **9** [pale yellow needles, mp 121—122 °C, 396 mg; 98%. Found: *m/z*, 208.0732 (M⁺). Calcd for $C_{11}H_{12}O_4$: 208.0733. ^{1}H NMR δ=2.38 (3H, d, *J*=1 Hz), 3.84 (3H, s), 3.94 (3H, s) 7.16 (1H, s), 7.38 (1H, q, *J*=1 Hz), and 10.36 (1H, s). ^{13}C NMR δ=21.6, 56.4, 64.5, 106.6, 128.2, 141.5, 145.5, 161.2, 165.4, 179.1, and 190.7. IR *ν*: 1680, 1620, 1600, and 1575 cm⁻¹] and **10** [yellow needles, mp 158—159 °C, 1.6 mg; 0.3%. Found: *m/z*, 242.0308, 244.0297 (M⁺). Calcd for $C_{11}H_{11}O_4Cl$: 242.0343, 244.0304. ^{1}H NMR δ=3.97 (3H, s), 4.00 (3H, s), 4.55 (2H, s), 7.21 (1H, s), 7.54 (1H, s), and 10.34 (1H, s)].

Preparation of 11. An MeOH solution (10 cm³) of **9** (396 mg) and NH_2OH (100 mg) was refluxed for 1.5 h. After evaporating the solvent, the residue was diluted with water, and extracted with $CHCl_3$. The organic layer was dried over $MgSO_4$ and evaporated in vacuo, leaving **11** [pale yellow crystals, mp 171—172 °C, 386 mg; 91%. Found: *m/z*, 223.0841 (M⁺). Calcd for $C_{11}H_{13}O_4N$: 223.0842. ^{1}H NMR δ=2.33 (3H, d, *J*=1 Hz), 3.67 (3H, s), 3.90 (3H, s), 7.18 (1H, q, *J*=1 Hz), 7.36 (1H, s), and 8.44 (1H, s) for a major anti-isomer; 2.58 (3H, s), 3.47 (3H, s), 3.92 (3H, s), 6.78 (1H, s), 7.2 (1H, overlapped with solvent signal) and 8.55 (1H, s) for a minor syn-isomer. ^{13}C NMR δ=22.8, 56.7, 62.8, 111.1, 129.9, 137.8, 147.7, 148.9, 159.1, 162.0, and 180.7 for anti-isomer; 20.2, 57.0, 62.8, 106.1, 129.9, 137.0, 147.7, 148.9, 161.2, 163.1, and 180.7 for syn-isomer. IR *ν*: 3140, 3010, 2860, 1740, 1615, 1590, and 1545 cm⁻¹].

Preparation of 12. An Ac_2O solution (5 cm³) of **11** (29.3 mg) was heated at 120 °C for 4 h. After removing the solvent, the residue was chromatographed on a silica-gel column to give **12** [pale yellow crystals, mp 157—158 °C, 4.8 mg; 28%. Found: *m/z*, 205.0721 (M⁺). Calcd for $C_{11}H_{11}O_3N$: 205.0737. ^{1}H NMR δ=2.33 (3H, d, *J*=1 Hz), 3.90 (3H, s), 3.95 (3H, s), 6.48 (1H, s), and 7.30 (1H, q, *J*=1 Hz). ^{13}C NMR δ=22.1, 56.7, 62.3, 107.5, 109.8, 117.7, 140.7, 143.9, 161.6, 164.2, and 178.5. IR *ν*: 2220, 1620, 1595, and 1575 cm⁻¹] and **11** (10.9 mg).

The CAN-Oxidation of 12. A mixture of **12** (72.7 mg) and CAN (798 mg) was stirred at room temperature for 4 h.

The resultant mixture was extracted with $CHCl_3$ and the organic layer was washed with aq $NaHCO_3$ and dried over $MgSO_4$. The solvent was evaporated in vacuo and the residue was chromatographed on a silica-gel column to give **13** [a pale yellow oil, 29.3 mg; 31%. Found: *m/z*, 267.1104 (M^+). Calcd for $C_{13}H_{17}O_5N$: 267.1104. ^1H NMR δ=1.93 (3H, d, J=1.3 Hz), 3.24 (6H, s), 3.29 (6H, s), 5.80 (1H, q, J=1.3 Hz), and 6.61 (1H, s). ^{13}C NMR δ=18.8, 50.7 (4C), 97.3, 100.7, 115.9, 124.2, 125.3, 147.6, 152.8, and 190.7. IR ν: 2230, 1745, 1710, and 1605 cm^{-1}].

Hydrolysis of 13 to 4. A mixture of acetone (5 cm^3), $HClO_4$ (2 M, 5 cm^3), and **13** (27 mg) was stirred at 40 °C for 1.5 h. The mixture was then diluted with water and extracted with $CHCl_3$. The extract was dried on $MgSO_4$ and evaporated in vacuo, leaving **4** [a yellow oil, 21 mg; 94%. Found: *m/z*, 221.0700 (M^+). Calcd for $C_{11}H_{11}O_4N$: 221.0689. ^1H NMR δ=2.10 (3H, d, J=1.3 Hz), 3.31 (6H, s), 6.06 (1H, q, J=1.3 Hz), and 6.78 (1H, s)].

Preparation of 14. To an acetone solution (1 cm^3) of **4** (12.9 mg) was added aq $HClO_4$ (1 M, 1 cm^3) and heated at 50 °C for 4.5 h. The mixture was diluted with water and extracted with $CHCl_3$. The extract was dried on $MgSO_4$ and evaporated in vacuo. The residue was chromatographed on a silica-gel column to give **14** [1 mg; 1%. Found: *m/z*, 175.0289 (M^+). Calcd for $C_9H_5O_3N$: 175.0269. ^1H NMR δ=2.44 (3H, d, J=1 Hz), 7.17 (1H, s), and 7.47 (1H, q, J=1 Hz)].

The authors wish to thank The Ministry of Education, Science, and Culture for a financial assistance to A. M. through a Grant-in-Aid for Scientific Research (No. 60470025).

References

1) A. Mori, T. Kusaba, Y. Isayama, and H. Takeshita, *Chem. Lett.*, **1986**, 155.

2) H. Takeshita, A. Mori, Y. Goto, and T. Nagao, *Bull. Chem. Soc. Jpn.*, **60**, 1747 (1987).

3) H. Takeshita, A. Mori, and Y. Isayama, *Bull. Chem. Soc. Jpn.*, **58**, 1678 (1985).

4) A. Mori, Y. Isayama, T. Kusaba, and H. Takeshita, *Kyushu Daigaku Sogo Rikogaku Kenkyuka Hokoku*, **6**, 185 (1985).

5) R. Mornet and L. Gouin, *Synthesis*, **1977**, 786.

6) A. Mori, Y. Isayama, and H. Takeshita, *Bull. Chem. Soc. Jpn.*, **59**, 511 (1986).

7) Three separated peaks, due to $^{35}Cl_2$-, $^{35}Cl^{37}Cl$-, and $^{37}Cl_2$-isotope compositions, revealed a reasonable relative ratio of intensities, 9:3:1. Mass-spectral behaviors of other chloro derivatives were similar.

8) All the NMR spectra were measured in $CDCl_3$ solutions.

Convenient Optical Resolution of Axially Chiral 1,1'-Binaphthyl-2,2'-dicarboxylic Acid

Shigeyoshi KANOH, Yukihiko HONGOH, Masatoshi MOTOI, and Hiroshi SUDA*
Department of Chemistry and Chemical Engineering, Faculty of Technology, Kanazawa University, 2-40-20 Kodatsuno, Kanazawa 920
(Received September 8, 1987)

Synopsis. Axially chiral 1,1'-binaphthyl-2,2'-dicarboxylic acid was conveniently resolved through its brucine salts in satisfactory yields. The resolved diacids were confirmed to be optically pure from high-performance liquid chromatographic analyses of the dimethyl esters derived from them on an optically active poly(diphenyl-2-pyridylmethyl methacrylate) column.

In the last decade, much attention has been drawn to a variety of asymmetric reactions assisted by chirally hinged biaryl compounds.[1] For example, 2,2'-dihydroxy-1,1'-binaphthyl (**1**) has been well-known to bring about great success in complexation with chiral crown ethers[2] and asymmetric reductions of carbonyl compounds.[3] Besides the diol **1**, 1,1'-binaphthyl-2,2'-dicarboxylic acid (**2**) has been successfully utilized to the construction of chirality-recognizing units, as well.[4] Concerning the design of such chiral auxiliaries, the carboxylic substituents are advantageous for easy transformations into various functionalities.[5]

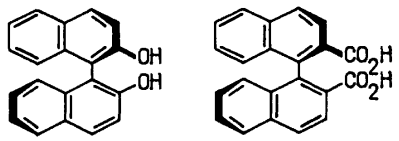

(R)-1 (R)-2

Regardless of the above excellent results, the enantiomers of **2** have been prepared by means of a conventional resolution through its quinine salt.[5b] The procedure seemed to be quite tedious, and the efficiency of resolution was rather low. As pointed out by Hall and Turner,[5b] the salt, which gave a higher optical rotation, was not always composed of optically pure **2**.[6] Moreover, the chiroptical property of the resolved salt was complicated by the fact that the salt formed clathrates with solvents used for recrystallization.[5b]

On the other hand, there is a direct synthetic route to homochiral **2** by Miyano et al.[7] via an intramolecular Ullmann coupling of the bis(bromonaphthoic) ester derived from optically active **1**. However, this route required a stoichiometric amount of axially chiral **1**, and the yield of the cyclic diester was not so high.[7]

Herein we wish to describe the improved optical resolution of (*RS*)-**2**. We found that brucine formed a nicely crystallizable salt with an equimolar amount of **2**. In order to effectively separate a mixture of the diastereomeric salts by recrystallization, solvents and the requisite quantities of solvent were screened. Consequently, it was found that a dextrorotatory salt with a relatively high optical purity was obtained under rather high dilution conditions in acetone. Recrystallization of the less soluble salt from acetone/methanol and work-up of the mother liquor led to pure (+)-brucine salt of (*R*)-**2** in a total 41% yield based on racemic **2**. This salt was identified as an acetone clathrate in a 1:1:1 (**2**:brucine:acetone) stoichiometry. In contrast to the case of the previous quinine salt, both the stoichiometric composition of the clathrate and its stability toward vacuum drying under ambient temperature facilitated the unambiguous estimation of the optical purity of each crop. Decomposition of the (+)-salt with diluted hydrochloric acid gave (*R*)-**2** in a 40% yield; the absolute configuration of the diacid was known.[8]

Similar decomposition of the salt in the mother liquor after removal of the (+)-salt gave (*S*)-enriched **2**. A small amount of the opposite (*R*)-**2** could be removed by a simple filtration, because the minor enantiomer formed a *racemic compound* which was sparingly soluble in diethyl ether. Thus, optically active (*S*)-**2** was obtained in a 45% yield. Any recrystallization process of the more soluble (−)-salt[9] was not needed for the acquisition of optically pure (*S*)-**2**; this is another merit of our method.

The diacids resolved thus may be recrystallized from diethyl ether. The rotation values of the purified enantiomers compare favorably with the earlier records.[5b,8] Of course, most of the resolving agent was reusable.

The optical purity of the resolved **2** was determined

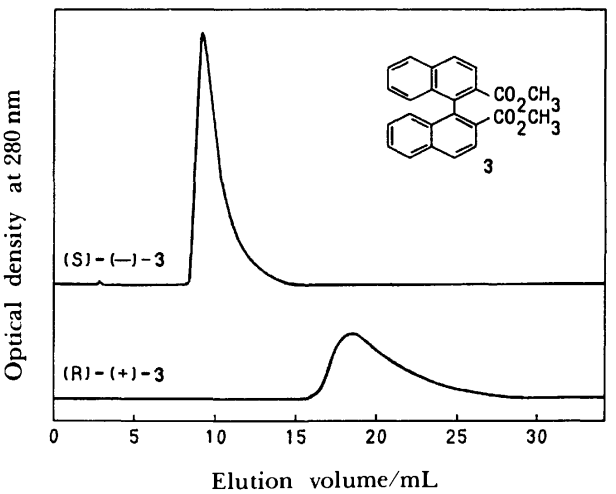

Fig. 1. Chromatograms of the dimethyl ester (**3**) derived from optically resolved **2**. Column: (−)-poly(D2PyMA), 25×0.46 (i.d.) cm; eluent: methanol; flow rate: 1.0 cm^3 min^{-1}; temperature, 25 °C.

from an HPLC analysis of the dimethyl ester (**3**) derived from the diacid. The packing material used for the optically active column was (−)-poly(diphenyl-2-pyridylmethyl methacrylate) [poly(D2PyMA)][10] coated on macroporous silica gel.[11] Base-line resolved separation was accomplished for racemic **3** on this column, using methanol as an eluent.[12] Figure 1 shows chromatograms of (+)- and (−)-**3** under the same conditions as those operated for the racemic material. The enantiomers were eluted at a different retention time to each other, which was in near agreement with that of either of two peaks observed for racemic **3**, and both chromatograms showed the absence of the opposite enantiomer. These results indicate that the diacids resolved in the present method are almost optically pure.

Although the present resolution method relies on a classical recrystallization of the diastereomeric salts, the operational simplicity and high efficiency will help chemists wishing to use the optically pure diacid **2**.

Experimental

General. Melting points are uncorrected. A thermal analysis was carried out with a DAINI SEIKOSHA differential scanning calorimeter SSC/560S, at a heating rate of 5 °C min^{-1}, using an aluminum open sample pan. IR and ^{1}H NMR spectra were recorded on a JASCO A-202 and a JEOL JNM-FX-100S (100 MHz) spectrometer, respectively. Optical rotations were determined on a JASCO DIP-360 digital polarimeter. High-performance liquid chromatograms (HPLC) were run on a 25×0.46 (i.d.)-cm stainless column of (−)-poly(D2PyMA), using a JASCO 880-PU pump equipped with a JASCO UVIDEC-100-II UV detector at 280 nm. Resolution was carried out with methanol at a flow rate of 1.0 cm^3 min^{-1} at 25 °C.

(*RS*)-1,1′-Binaphthyl-2,2′-dicarboxylic Acid (2). The titled compound was prepared by the method reported in the literature.[5b] The racemic diacid (**2**) was recrystallized from acetone to give a 2:1 stoichiometric clathrate of acetone to **2** as transparent prisms, the de-solvation of which converted them gradually into a nontransparent material during storage in an open vessel under ordinary conditions. The clathrate released the acetone molecules at 68 °C, and then melted at 276 °C under atmospheric pressure (from a differential scanning calorimetric analysis). Acetone clathrate of **2**; IR (KBr) 3500—2500, 1725, 1690, 1615, 1595, 1240, 1210, 1195, 1150, 1140 cm^{-1}; ^{1}H NMR (DMSO-d_6) δ=2.09 (s, acetone, 12H), 6.8—8.2 (m, ArH, 12H), 12.2 (br s, -COOH). Found: C, 73.34; H, 5.46%. Calcd for $C_{22}H_{14}O_4 \cdot 2C_3H_6O$: C, 73.35; H, 5.72%. A sample was dried at 90 °C under vacuum to give the de-solvated diacid; mp 272—274 °C (lit,[5b] mp 272—274 °C); IR (KBr) 3500—2500, 1680, 1615, 1595, 1280, 1250, 1165, 1140 cm^{-1}; ^{1}H NMR (DMSO-d_6) δ=3.3 (br s, -COOH, 2H), 6.8—8.2 (m, ArH, 12H).

Optical Resolution of (*RS*)-1,1′-Binaphthyl-2,2′-dicarboxylic Acid (2). All yields were based on (*RS*)-**2** used. A solution of 30.0 g (87.6 mmol) of de-solvated (*RS*)-**2** in 450 cm^3 of acetone was added to a refluxing solution of 34.6 g (87.7 mmol) of anhydrous brucine (*caution: highly poisonous*[13]) in 1.0 dm^3 of acetone. Colorless needles soon began to deposit from the resulting solution and the mixture was cooled in a refrigerator overnight. The separated crystals were filtered and washed with acetone to give 38.7 g of the less soluble salt after air-drying: $[\alpha]_D^{25}$ +125° (*c* 0.5, chloroform). The crude (+)-salt was dissolved in 1 dm^3 of methanol under refluxing, and then the hot solution was diluted with 500 cm^3 of hot acetone. Cooling the solution gave colorless needles, drying of which for 3 h at room temperature under vacuum gave 24.9 g (36%) of brucine salt of (*R*)-**2** as a 1:1 stoichiometric acetone clathrate: mp 211—214 °C; $[\alpha]_D^{25}$ +200° (*c* 0.5, chloroform). The filtrate was concentrated to about 150 cm^3 to give an additional (+)-salt. This work-up was repeated until (−)-brucine salt crystallized, and a small amount of a nearly inactive salt was discarded. The total yield of the pure (+)-salt was 41% (28.8 g). Found: C, 72.48; H, 5.71; N, 3.62%. Calcd for $C_{45}H_{40}N_2O_8 \cdot C_3H_6O$: C, 72.53; H, 5.83; N, 3.52%.

The (+)-salt was shaken with diethyl ether (200 cm^3) and 6 mol dm^{-3} hydrochloric acid, and the aqueous layer was extracted with ether (50 cm^3×2). The combined ethereal extracts were washed with 1 mol dm^{-3} hydrochloric acid and then brine, dried over Na_2SO_4, and evaporated to dryness. Drying of the amorphous powder at 90 °C under vacuum over P_2O_5 gave 12.1 g (40%) of (*R*)-**2**: $[\alpha]_{546}^{25}$ +123° (*c* 1.0, 0.1 mol dm^{-3} NaOH). An analytical sample was recrystallized from ether to give colorless platelets, that were dried under the same conditions as above: mp 197—199 °C (decomp), reported[5b] decomposition at ca. 120 °C for a 0.5 hydrate; $[\alpha]_{546}^{25}$ +127° (*c* 1.0, 0.1 mol dm^{-3} NaOH) (lit[5b] $[\alpha]_{546}^{20}$ +124.2° (*c* 1.115)). Found: C, 76.90, H, 3.95%. Calcd for $C_{22}H_{14}O_4$: C, 77.18, H, 4.12%.

The mother liquor from the initial salt formation was combined with the (−)-salt and the final filtrate, which were obtained in the above purification of the (+)-salt. The mixture was evaporated to dryness. The residual salt was similarly converted into **2**. The solids of (−)-enriched **2** were mixed with 100 cm^3 of ether, and the suspension was warmed to boiling and then cooled. Insoluble materials were filtered off, and the filtrate was reworked. The final filtrate was evaporated under reduced pressure, and the residue was dried at 90 °C under vacuum over P_2O_5 to give 13.5 g (45%) of (*S*)-**2** as an amorphous powder: $[\alpha]_{546}^{25}$ −125° (*c* 1.0, 0.1 mol dm^{-3} NaOH). Pure (*S*)-**2** was obtained by recrystallization from ether as colorless platelets: mp 199—200 °C (decomp), reported[5b] decomposition at ca. 120 °C for a 0.5 hydrate; $[\alpha]_{546}^{25}$ −127° (*c* 1.0, 0.1 mol dm^{-3} NaOH) (lit,[5b] $[\alpha]_{546}^{22}$ −125.2° (*c* 1.023)). Found: C, 77.17, H. 3.85%. Calcd for $C_{22}H_{14}O_4$: C, 77.18, H, 4.12%.

The acidic layers from the decomposition of the salts were combined, and basified by the addition of aqueous ammonia, and the precipitate was collected. Most of the used brucine was recovered by recrystallization from ethanol.

(*S*)-Methyl 1,1′-Binaphthyl-2,2′-dicarboxylate, (*S*)-3, and (*R*)-3. The resolved diacid (*S*)-**2** was treated with diazomethane, and the evaporated residue was chromatographed with benzene on silica gel to give the diester **3** (96%) as a white powder, which gave $[\alpha]_D^{25}$ −20.5° (*c* 1.0, methanol). A part of the solid was used as an HPLC sample without further purification. The remainder was recrystallized from methanol to give crystalline (*S*)-**3**:[14] mp 157—158 °C (lit,[8] mp 154—155 °C); $[\alpha]_D^{25}$ −21.7° (*c* 1.0, methanol), reported[8] ($[\alpha]_D^{25}$ −18° (*c* 1.2); IR (KBr) 1730, 1240, 1135, 765 cm^{-1}; ^{1}H NMR ($CDCl_3$) δ=3.49 (*s*, -OCH_3, 6H), 7.0—8.2 (m, ArH, 12H).

Similarly (*R*)-**2** was converted into (*R*)-**3**; mp 156.5—157.5 °C; $[\alpha]_D^{25}$ +22.4° (*c* 1.0, methanol).

The authors are indebted to Dr. Akito Ichida of Daicel Chemical Industries, Ltd. for packing the

poly(D2PyMA) column for HPLC. This work was supported in part by a Grant-in-Aid for Scientific Research No. 61470105 from the Ministry of Education, Science and Culture.

References

1) Recent and most comprehensive presentation of this topic: S. Miyano and H. Hashimoto, *Yuki Gosei Kagaku Kyokai Shi*, **44**, 714 (1986).

2) For example, D. J. Cram and J. M. Cram, *Acc. Chem. Res.*, **11**, 8 (1978).

3) R. Noyori, I. Tomino, Y. Tanimoto, and M. Nishizawa, *J. Am. Chem. Soc.*, **106**, 6709 (1984).

4) a) J.-P. Mazaleyrat and D. J. Cram, *J. Am. Chem. Soc.*, **103**, 4585 (1981); b) N. Maigrot, J.-P. Mazaleyrat, and Z. Welvart, *J. Org. Chem.*, **50**, 3916 (1985); c) S. Kanoh, N. Kawaguchi, T. Sumino, Y. Hongoh, and H. Suda, *J. Polym. Sci., Part A, Polym. Chem.*, **25**, 1603 (1987); d) J.-P. Mazaleyrat, *Tetrahedron Lett.*, **24**, 1243 (1983).

5) a) S. Miyano, S. Okada, T. Suzuki, S. Handa, and H. Hashimoto, *Bull. Chem. Soc. Jpn.*, **59**, 2044 (1986); b) D. M. Hall and E. E. Turner, *J. Chem. Soc.*, **1955**, 1242; c) F. Cottineau, N. Maigrot, and J.-P. Mazaleyrat, *Tetrahedron Lett.*, **26**, 421 (1985); d) E. Weber, I. Csöregh, B. Stensland, and M. Czugler, *J. Am. Chem. Soc.*, **106**, 3297 (1984).

6) In our trial, optically pure (−)-**2** was obtained not only from the (−)-salt but also, surprisingly, from the (+)-salt, the $[\alpha]_{546}^{25}$ of which were −109°[5b] and +225°, respectively, (*c* 1.0, acetone).

7) S. Miyano, M. Tobita, M. Nawa, S. Sato, and H. Hashimoto, *J. Chem. Soc., Chem. Commun.*, **1980**, 1233.

8) D. D. Fitts, M. Siegel, and K. Mislow, *J. Am. Chem. Soc.*, **80**, 480 (1958).

9) Brucine salt of (*S*)-**2**: colorless needles; mp 190—210 °C with previous softening; $[\alpha]_D^{25}$ −154° (*c* 0.5, chloroform).

10) (−)-Poly(D2PyMA) of $[\alpha]_D^{25}$ −314° (*c* 1.0, $CHCl_3$–10%CF_3CH_2OH) was prepared by the asymmetric polymerization of the achiral monomer with a chiral benzyllithium complex in toluene at −78 °C.[4c]

11) Y. Okamoto, H. Mohri, I. Ishikura, K. Hatada, and H. Yuki, *J. Polym. Sci., Polym. Symp.*, **74**, 125 (1986).

12) Results of the chromatographic resolution of (*RS*)-**3**: capacity factors, k_1' (to less retained (*R*)-**3**)=2.61 and k_2'=6.05; separation factor, α=2.32; resolution factor, R_S=2.52; void volume, V_0=2.52 ml (water in methanol).

13) Toxicity of brucine: LD_{50} orally in rats, 1 mg kg^{-1}; "Registry of Toxic Effects of Chemical Substances," ed by R. J. Lewis and R. L. Tatken, Vol. 1, (1979), p. 324.

14) In a preparative scale, **2** was esterified with methanol containing concd H_2SO_4 under refluxing: yield, more than 90%.

The Selective Liquid-Phase Oxidation of 3,4,5-Trimethoxytoluene to 3,4,5-Trimethoxybenzaldehyde

Nobumasa KITAJIMA,* Kazuya TAKEMURA, Yoshihiko MORO-OKA,* Tadatsugu YOSHIKUNI,† Mitsuo AKADA,† Yoshihisa TOMOTAKI,† and Masatoshi TANIGUCHI†

Research Laboratory of Resources Utilization, Tokyo Institute of Technology, 4259 Nagatsuta, Midori-ku, Yokohama 227

†Tokushima Research Laboratory, Otsuka Chemical Co., Ltd. 463 Kagasuno, Kawauchi-cho, Tokushima 771-01

(Received August 10, 1987)

Synopsis. The selective liquid-phase oxidation of 3,4,5-trimethoxytoluene to 3,4,5-trimethoxybenzaldehyde, an important chemical intermediate for medicine production, was developed; when 2.0 mmol of the reactant was heated at 110 °C for 2 h in an autoclave under 3 atm O_2 with 10 ml of acetic acid in the presence of 0.75 mmol of $Co(OAc)_2$–$Mn(OAc)_2$ (3:1 mole ratio), a 92% yield of the aldehyde was obtained.

3,4,5-Trimethoxybenzaldehyde, an important chemical intermediate for medicine production, is produced by a stoichiometric synthesis from vanillin or an electrochemical oxidation of 3,4,5-trimethoxytoluene in the current manufacturing processes.[1] These procedures, however, still have several disadvantages which need to be improved. For example, a recent improvement in the electrochemical process has resulted in excessive electricity consumption. The liquid-phase oxidation of 3,4,5-trimethoxytoluene to 3,4,5-trimethoxybenzaldehyde is another attractive procedure from an industrial point of view. In a previous paper,[2] we demonstrated the potential effectiveness of the liquid-phase oxidation of substituted toluenes to the corresponding aldehydes; *p*-anisaldehyde could be obtained in a relatively high yield from *p*-methoxytoluene using multi-component metal salts. Through continuous efforts, we have developed a very selective method for the liquid-phase oxidation of 3,4,5-trimethoxytoluene to the aldehyde using a $Co(OAc)_2$–$Mn(OAc)_2$ mixture as the catalyst.

Experimental

Materials. The acetic acid, $Co(OAc)_2 \cdot 4H_2O$ (purchased from Wako), $Mn(OAc)_2 \cdot 4H_2O$ and all other reagents were used without further purification. 3,4,5-Trimethoxytoluene was obtained from Otsuka Chem. Co Ltd. 3,4,5-Trimethoxybenzyl alcohol and 3,4,5-trimethoxybenzyl acetate used as authentic standards for GC analysis were synthesized by an LAH reduction of 3,4,5-trimethoxybenzaldehyde and an esterification of 3,4,5-trimethoxybenzyl alcohol with acetic acid.

Procedure and Analysis. In a 50-ml autoclave, the substrate, catalysts, acetic acid, and the additives were mixed with a magnetic stirring bar. The autoclave was pressurized under 3.0 atm of O_2 and placed in an oil bath pre-warmed to the reaction temperature. After vigorous stirring for the prescribed time, the reaction was quenched by immersing the autoclave in an ice bath. After the reaction, naphthalene was added into the reaction mixture as an internal standard; the products were analyzed by GC on a Thermon 3000 on Chromosorb W.

Results and Discussion

Oxidation with $Co(OAc)_2$. The catalytic activities of various metal salts for the liquid-phase oxidation of 3,4,5-trimethoxytoluene were investigated. The results are summarized in Table 1. The reaction was carried out at 110 °C under 3 atm of O_2 in AcOH. With most of the metal salts, the reaction did not proceed. However, several cobalt salts, CoO, $Co(OAc)_2 \cdot 4H_2O$, and $Co_3(PO_4)_2 \cdot 8H_2O$, were found to be effective for the production of 3,4,5-trimethoxybenzaldehyde. The other products include 3,4,5-trimethoxybenzyl acetate and 3,4,5-trimethoxybenzyl alcohol. No detectable amount of 3,4,5-trimethoxybenzoic acid was yielded. The time course of the reaction of the oxidation of 3,4,5-trimethoxytoluene

Table 1. Liquid-Phase Oxidations of 3,4,5-Trimethoxytoluene with Various Metal Salts

Metal salt	Conv.	Ph'CHO	Ph'CH_2OAc	Ph'CH_2OH	Ph'COOH
	%	%	%	%	%
NiO	17.0	4.6	3.0	0	0
MnO_2	42.9	8.1	3.9	0	0
$Pd(NO_3)_2 \cdot 2H_2O$	64.7	0.6	12.5	0	0
$Ce(NO_3) \cdot 6H_2O$	84.9	6.4	36.1	0	0
CuCl	33.7	0	0	0	0
$FeCl_2 \cdot 4H_2O$	38.0	0	0	0	0
CoO	100.0	72.9	1.2	21.4	0
$CoF_2 \cdot 3H_2O$	31.4	5.6	6.8	0	0
$CoCl_2 \cdot 6H_2O$	16.0	0	0	0	0
$CoBr_2 \cdot 6H_2O$	19.8	0	0	0	0
$Co(OAc)_2 \cdot 4H_2O$	100.0	73.6	2.4	0	0
$Co_3(PO_4)_2 \cdot 8H_2O$	100.0	63.7	1.3	0	0

Ph' denotes 3,4,5-trimethoxyphenyl; O_2, 3 atm; temp, 110 °C; time, 2 h; Ph'CH_3, 2.0 mmol; cat. amount, 0.5 mmol.

Table 2. Liquid-Phase Oxidations of 3,4,5-Trimethoxytoluene with $Co(OAc)_2 \cdot 4H_2O$ in the Presence of an Additive

$Co(OAc)_2 \cdot 4H_2O$	Additive	Conv.	Ph'CHO	$Ph'CH_2OAc$	$Ph'CH_2OH$	Ph'COOH
mmol	mmol	%	%	%	%	%
0.50	NaBr, 1.0	4.6	3.4	Trace	0	Trace
0.50	$MgBr_2$, 1.0	11.3	4.7	0	0	0
0.50	H_2O, 27.8	80.5	29.5	19.0	4.3	3.6
0.50	Ac_2O, 52.6	100.0	49.5	0	0	0
0.56	$Ni(OAc)_2 \cdot 4H_2O$, 0.19	100.0	76.4	2.2	0	0
0.56	$Cr(OAc)_3 \cdot H_2O$, 0.19	100.0	76.8	0	0	0
0.56	$Cu(OAc)_2 \cdot H_2O$, 0.19	65.2	45.1	22.6	0	0
0.56	$Ce(OAc)_3 \cdot H_2O$, 0.19	100.0	80.2	7.9	0	0
0.56	$Mn(OAc)_2 \cdot 4H_2O$, 0.19	100.0	91.2	4.2	0	0

O_2, 3 atm; temp, 110 °C; time, 2 h; $Ph'CH_3$, 2.0 mmol.

catalyzed by $Co(OAc)_2 \cdot 4H_2O$ was examined under the same reaction conditions employed for the experiments outlined in Table 1. The conversion of 3,4,5-trimethoxytoluene initially increased with the reaction time and reached 100% at 1.5 h, when a 70% yield of 3,4,5-trimethoxybenzaldehyde was obtained. A further reaction did not increase the yield of 3,4,5-trimethoxybenzaldehyde (the yields were almost constant). The by-products, mainly 3,4,5-trimethoxybenzyl acetate, were formed during the initial 1.5 h; however, they were only detectable in trace amounts for longer reaction times. The total material balance decreased significantly, implying the formation of undetermined polymeric products. The effects of the reaction temperature and O_2 pressure were investigated in order to optimize the reaction conditions to obtain higher yields of the aldehyde; however, with $Co(OAc)_2 \cdot 4H_2O$, the maximum yield did not exceed 70%.

Synergism of $Co(OAc)_2$ and $Mn(OAc)_2$. The effects of several additives for the present reaction were examined (summarized in Table 2). The addition of metal bromides[3] critically lowered the catalytic activity; the yield of 3,4,5-trimethoxybenzaldehyde was very low. The addition of water[4] also retarded the catalytic activity. Ac_2O addition evidently enhances the activity; however, it causes an unpreferable further oxidation of the aldehyde.

The addition of several metal acetate salts were also attempted. Neither $Cr(OAc)_3$, $Ni(OAc)_2$ nor $Cu(OAc)_2$ resulted in a favorable improvement of the 3,4,5-trimethoxybenzaldehyde yield. However, upon the addition of $Ce(OAc)_3$ or $Mn(OAc)_2$ a considerable improvement was found. Especially, a $Co(OAc)_2$–$Mn(OAc)_2$ (3:1) mixture gave a very high yield of the aldehyde (91%). The synergistic effect of $Co(OAc)_2$ and $Mn(OAc)_2$ is evident from Fig. 1, in which the yield of 3,4,5-trimethoxybenzaldehyde is plotted against the ratio of $Mn(OAc)_2$ to $Mn(OA)_2$+$Co(OAc)_2$. $Mn(OAc)_2$, itself, shows only a low activity regarding oxidation. However, when it was combined with $Co(OAc)_2$, the mixture showed a higher activity for the production of 3,4,5-trimethoxybenzaldehyde than $Co(OAc)_2$ alone. The yield of the aldehyde strongly depends on the mixing ratio; the highest yield was obtained for a Co:Mn ratio of 3:1. The yield of the aldehyde also depended upon the total amount of the catalyst. In the range of the catalyst amount up to 0.75 mmol (with the fixed Co:Mn ratio, 3:1), the yield was almost proportional to the amount of catalyst, and reached the highest yield. The use of more catalyst, however, did not affect the yield very much.

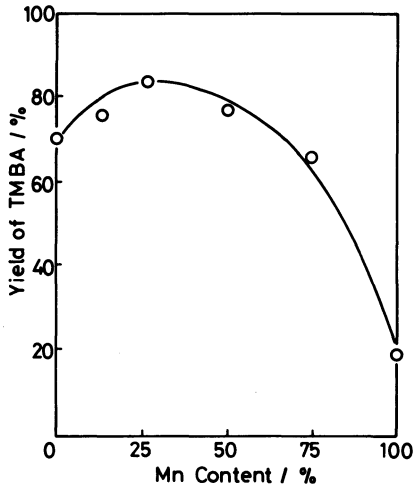

Fig. 1. The dependence of 3,4,5-trimethoxybenzaldehyde (TMBA) yield on Mn content in the oxidation of 3,4,5-trimethoxytoluene with $Co(OAc)_2$–$Mn(OAc)_2$ catalyst. O_2, 3 atm; 3,4,5-trimethoxytoluene, 2.0 mmol; solvent(AcOH), 10 ml; $Co(OAc)_2 \cdot 4H_2O$+$Mn(OAc)_2 \cdot 4H_2O$ 0.5 mmol; at 110 °C for 2 h.

Since a relatively high concentration of the catalyst was required to obtain a high yield of 3,4,5-trimethoxybenzaldehyde, recycling uses of the catalyst are desirable for industrial applications. Hence, the repeated oxidations of 3,4,5-trimethoxytoluene with the recovered catalyst from the resulting reaction mixture by extraction were attempted. Almost no decline in the catalytic activity and selectivity was observed, even after repeating 25 times. These results indicate the high utility of the present catalytic system for industrial use.

References

1) T. Hirashima and I. Nishiguchi, *J. Synth. Org. Chem.*

Jpn., **43**, 634 (1985); K. Shimizu, K. Kizawa, T. Yoshimoto, and J. Imamura, *J. Japan Petrol. Inst.*, **25**, 7 (1982).

2) N. Kitajima, S. Sunaga, Y. Moro-oka, T. Yoshikuni, M. Akada, Y. Tomotaki, and M. Taniguchi, *Bull. Chem. Soc. Jpn.*, **61**, 967 (1988).

3) C. E. H. Bawn and T. K. Wright, *Discuss. Faraday Soc.*, **46**, 164, (1969).

4) Y. Kamiya, "Yuki Sanka Hannou," Gihōdō (1973); T. Taguchi, N. Okabayashi, S. Futamura, and Y. Kamiya, Preprints, 20th Ann. Symp. Oxi. React., p. 7 (1986).

 © 1988 The Chemical Society of Japan Bull. Chem. Soc. Jpn., 61, 1039—1044 (1988)

Infrared Spectra of Nitrogen Adsorbed on Ion-Exchanged ZSM-5 Zeolite

Tatsuya YAMAZAKI,* Isao WATANUKI, Sentaro OZAWA, and Yoshisada OGINO
Department of Chemical Engineering, Faculty of Engineering, Tohoku University, Aramaki-Aoba, Sendai 980
(Received August 11, 1987)

Amounts of nitrogen adsorbed by ion-exchanged ZSM-5 zeolites (H^+, Li^+, Na^+, K^+, Rb^+, and Cs^+) and silicalite have been measured under various conditions; pressure=6.7×10^2—6.7×10^4 Pa, temperature=196—273 K. IR spectra of adsorbed nitrogen have also been measured at 226 K under various nitrogen pressures (1.3×10^2—4.0×10^4 Pa). The adsorption capacity, the specific surface area, and the heat of adsorption have been evaluated from the adsorption data. These quantities coupled with the IR peak shifts observed have revealed that the nitrogen molecule adsorbed on a small and strong cationic site (Li^+, Na^+) has an orientation in which the longer molecular axis lies in parallel with the direction of the electric field of the cation site. It has also been revealed that the nitrogen molecule adsorbed on a large (K^+, Rb^+, Cs^+) or weak (H^+) cationic site takes on no special orientation. The electric field evaluated by analyzing the IR intensity is consistent with the adsorption model obtained.

ZSM-5 type zeolites have been studied extensively[1] as molecular shape selective catalysts and catalyst carriers. The adsorptive properties of the zeolites have also been studied by many researchers.[2-5] Nevertheless details of the molecular behavior of adsorbates in the zeolite pore still remain to be discovered. The present authors[6-8] have attempted to clarify the nature of the adsorption site over the ZSM-5 zeolite surface using an infrared spectroscopic technique developed by Cohen de Lara et al.[9-12] As reported in earlier papers,[6-8] this technique has yielded valuable information about the behavior of methane adsorbed on ZSM-5 zeolites. Nitrogen adsorption has been studied by the same technique in the present work, in order to accumulate further information about the adsorptive properties of the zeolites. Interesting results concerning interaction between the nitrogen molecule and the cationic adsorption site have been obtained. The purpose of this paper is to describe the experimental results and discuss the adsorption model.

Experimental

Materials. The zeolites used as adsorbents are listed in Table 1, which also summarizes adsorptive properties of these zeolites. The zeolites other than silicalite and NaZSM-5 were prepared by a conventional ion exchange method using 0.3—1.0 mol dm^{-3} solution containing a desired cation. A chemical analysis of the sample prepared proved that the ion exchange had been completed.

Commercial high purity nitrogen was used as an adsorbate gas after passage through a cold trap immersed in liquid nitrogen.

Methods. Details of the experimental methods have already been reported[6] and only important points are described below.

The amount of adsorption was measured using a conventional constant pressure type adsorption apparatus. The adsorbent was degassed at 573 K for 12 h at 1.3×10^{-3} Pa. The temperature range of the adsorption measurement was 196—273 K and the pressure range was 6.7×10^2—6.7×10^4 Pa. Part of the adsorption data was obtained at 77 K and used for the surface area (A_s) calculation; a finite layer BET theory (1.2—1.6 layers depending on the sample) was applied.

A cell reported in the previous paper[6] was used in the infrared (IR) spectroscopic study. A sample disk with a thickness of ca. 100 μm was degassed in the cell at 573 K for 12 h at 1.3×10^{-3} Pa. The IR spectra were recorded on a JEOL-JIR-100 FTIR spectrometer at a resolution of 2 cm^{-1} by averaging 200 scans. The temperature of the IR

Table 1. Adsorptive Properties of Ion-Exchanged ZSM-5 Zeolites and Silicalite

Zeolite	Ionic radius[a] of cation, r_0	Surface[b] area, A_s	Adsorption capacity, V_m	Heat of adsorption, q°_{st}	Number of cationic sites, b_c
	Å	$m^2\ g^{-1}$	10^{-6} m^3-NTP/g	kJ mol^{-1}	10^{-3} mol g^{-1}
HZSM-5	−0.04[c]	442 (1.58)	44.3	16.6	1.32
LiZSM-5	0.60	439 (1.41)	45.9	36.3	0.94
NaZSM-5[d]	0.95	414 (1.23)	48.8	27.9	1.28
KZSM-5	1.33	390 (1.29)	44.9	23.7	1.25
RbZSM-5	1.48	359 (1.29)	38.7	21.6	1.18
CsZSM-5	1.69	310 (1.24)	29.6	20.8	1.12
Silicalite[e]	—	337 (1.55)	42.0	16.2	0.02

a) Except for the value of H^+, the values reported by L. Pauling in "The Nature of The Chemical Bond," 3rd ed, p. 518, Cornell University Press (1960) are shown. b) Values in parenthesis are the number of layers. c) The value reported by R. D. Shannon and C. T. Prewitt, *Acta Crystallogr., Sect. B*, **25**, 925 (1969). d) Original zeolite kindly provided by Mr. K. Igawa, Chem. Res. Lab., Toyo Soda Manufacturing, Co. Ltd.. SiO_2/Al_2O_3=23.3 in molar ratio. e) Kindly provided by Prof. T. Yashima, Tokyo Inst. Techn. SiO_2/Al_2O_3=2000 in molar ratio.

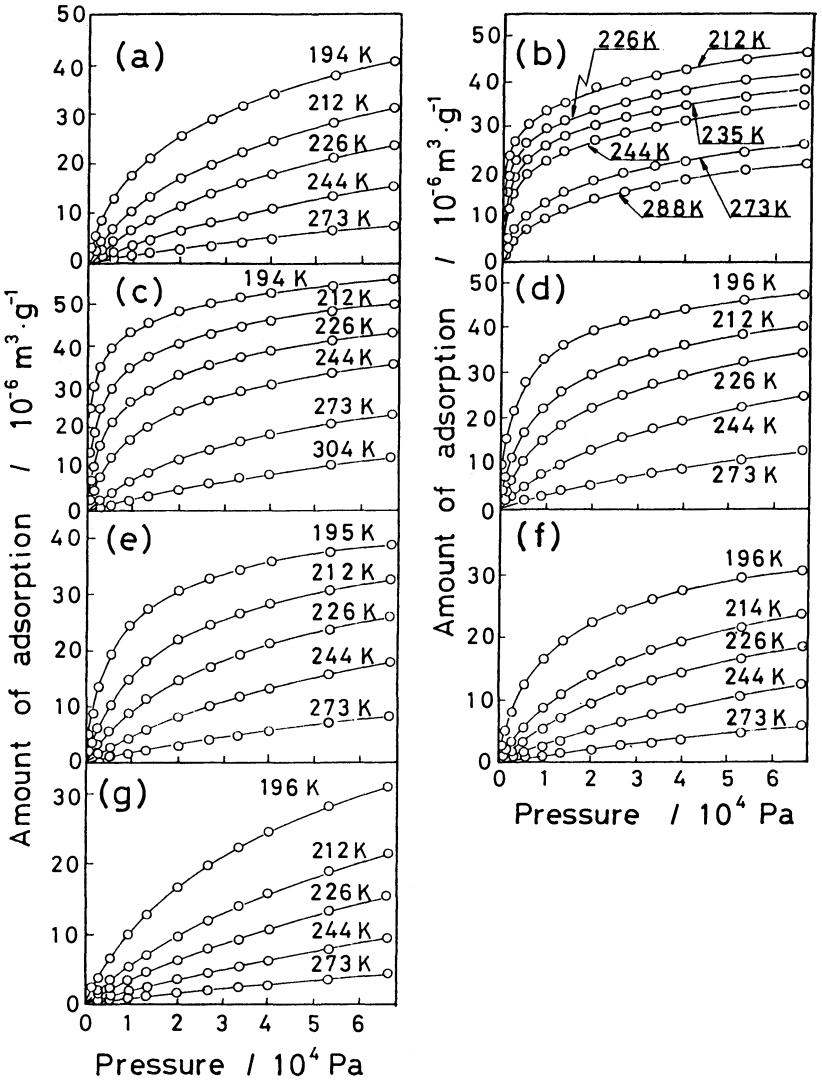

Fig. 1. Isotherms for nitrogen adsorption on ion-exchanged ZSM-5 zeolites and silicalite. a: HZSM-5, b: LiZSM-5, c: NaZSM-5, d: KZSM-5, e: RbZSM-5, f: CsZSM-5, g: silicalite.

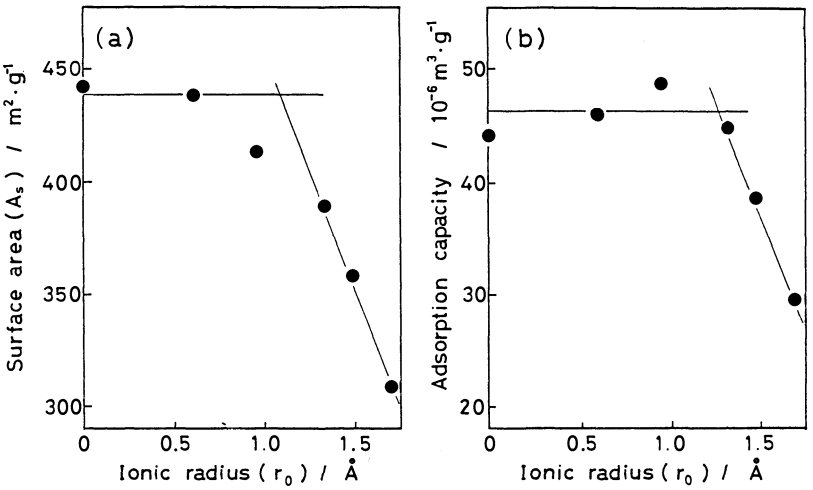

Fig. 2. Surface area and adsorption capacity of ion-exchanged ZSM-5 zeolites as a function of ionic radius of cation incorporated.
a: surface area, b: adsorption capacity.

measurement was 226 K and the pressure range was 1.3×10^{2}—4.0×10^{4} Pa.

Results and Discussion

Amount of Adsorption. Adsorption isotherms obtained are shown in Fig. 1 (a—g). The shapes of all the isotherms are analogous. It must be pointed out, however, that even silicalite, which contains few cationic adsorption sites, adsorbs a significant amount of nitrogen. This suggests that the pore wall itself provides nitrogen with adsorption sites and the ZSM-5 zeolite would have two kinds of adsorption sites, i.e. cationic sites and silicalite-like sites.

Although the full range of the adsorption isotherm could not be expressed by a Langmuir adsorption equation, part of the isotherm ranging from 1.3×10^{4} to 6.7×10^{4} Pa could be approximated by this adsorption equation and enabled us to estimate the maximum adsorption capacity V_m of the adsorbent. The V_m values thus obtained and the specific surface area A_s are shown in Fig. 2(a,b) as a function of the ionic radius (r_0)[13] of the cation incorporated into the zeolite. It is interesting that, both for RbZSM-5 and for CsZSM-5, the V_m value as well as the A_s value are remarkably small compared with the values for other zeolites.

The above mentioned relationships between V_m (or A_s) and r_0 have led the authors to draw the adsorption model illustrated in Fig. 3(a,b). The model assumes that pentagonal oxide ion rings[14] constitute the pore wall and the oxide ion has an ionic radius of 1.4 Å.[13] As shown in Fig. 3a, the void surrounded by five oxide ions can accept the whole body of a cation with a small radius; H^+, Li^+, and Na^+. On the other hand, as shown in Fig. 3b, the void can accept only part of the body of a large cation and a considerable part of the pore space over the pentagonal site is occupied by the cation itself; Rb^+ and Cs^+. The situation of K^+ is somewhat similar to that shown in Fig. 3b, though the extent of occupation of the pore space by the cation is small. It is thus obvious that an incorporation of such a small cation as H^+, Li^+, or Na^+ has little effect on the adsorption capacity as well as the specific surface area of the zeolite. The same situation is expected for K^+. On the other hand, the incorporation of Rb^+ or Cs^+ is expected to reduce V_m and A_s.

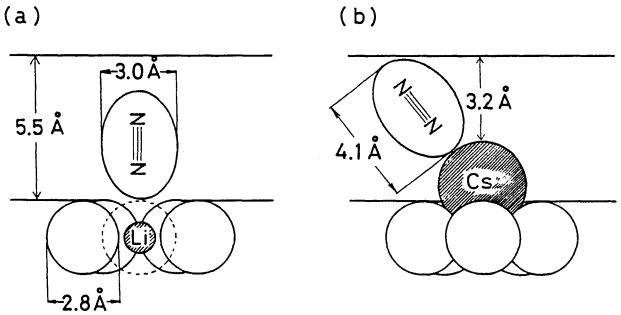

Fig. 3. Model for nitrogen adsorption on the cationic site. a: N_2 on Li^+ site, b: N_2 on Cs^+ site. (molecular size of nitrogen was taken from Ref. 15; pore size was taken from Ref. 14; O^{2-} size was taken from Ref. 13).

The model shown in Fig. 3 induces a discussion on the orientation of the nitrogen molecule adsorbed on the cationic site. As shown in Fig. 3a, the nitrogen molecule adsorbed on a small cationic site can take an orientation wherein the longer molecular axis is parallel with the direction of the electric field of the cation (perpendicular to the pore surface). On the other hand, as shown in Fig. 3b, the nitrogen molecule adsorbed on a large cation would find it difficult to assume such an orientation. Here, the discussion is rather speculative but its importance becomes clear in the later section of this discussion.

Heat of Adsorption. The adsorption isotherms shown in Fig. 1 enabled us to evaluated the isosteric heat of adsorption q_{st} using the Clausius-Clapeyron equation. An extrapolation of the q_{st} values obtained at different coverages to zero-coverage was carried out, in order to evaluate the heat of adsorption q°_{st} at zero coverage. The q°_{st} values thus obtained are also listed in Table 1. The decreasing order of the q°_{st} value is $Li^+ > Na^+ > K^+ > Rb^+ > Cs^+ > H^+ >$ silicalite. The larger q°_{st} value for ion-exchanged zeolites than that for silicalite strongly suggests that the adsorptive forces of all the cations are stronger than that of the pore wall (silicalite-like site). The adsorptive force of a cation consists of a dispersion force, an attractive force exerted upon the induced dipole on the adsorbed nitrogen, and an attractive force exerted upon the quadrupole of the adsorbed nitrogen molecule,[15] except for the repulsive force. The attractive forces mostly increase when the ionic radius of the cation becomes small. Thus the above sequence of q°_{st} values is reasonable, except for the small q°_{st} value for HZSM-5. Since the size of H^+ is very small (−0.04 Å),[16] oxide ions surrounding it would hinder the adsorbed nitrogen molecule from contacting with H^+. Namely, the steric hindrance of the oxide ions would separete the admolecule far from H^+, resulting in a weak adsorptive force and hence a small q°_{st}. A small ionic character[17] of H^+ might also be the cause of the small q°_{st} value of the HZSM-5 zeolite.

IR Spectra of Adsorbed Nitrogen. IR spectra of nitrogen-ion-exchanged zeolite adsorption systems are shown in Fig. 4(a—f). The observed spectra (dotted line) were found to be well simulated by a Lorentzian function as shown in the figure (solid line). According to the literature,[18] the IR band observed is assigned to the nitrogen stretching vibration $\nu_{N\text{-}N}$ which is usually IR inactive. An electric field of the cationic site probably has induced an IR active state of the adsorbed nitrogen.[18] This view has been supported by the fact that no absorption band has been observed for the silicalite-N_2 system. It is thus expected that the IR spectra shown in Fig. 4 would contain much informa-

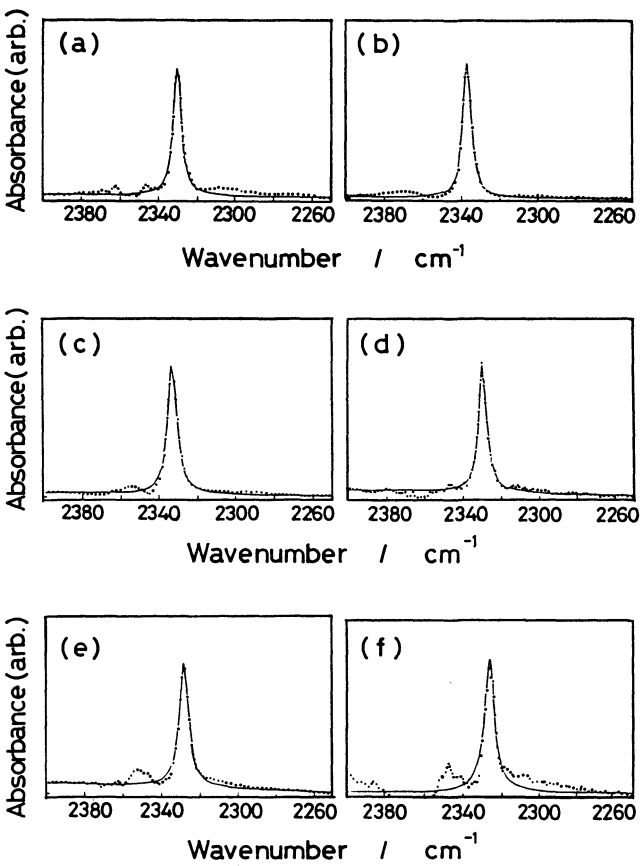

Fig. 4. IR absorption spectra for N_2- ion-exchanged ZSM-5 adsorption systems. a: HZSM-5, b: LiZSM-5, c: NaZSM-5, d: KZSM-5, e: RbZSM-5, f: CsZSM-5. (·····) observed, (-----) simulated.

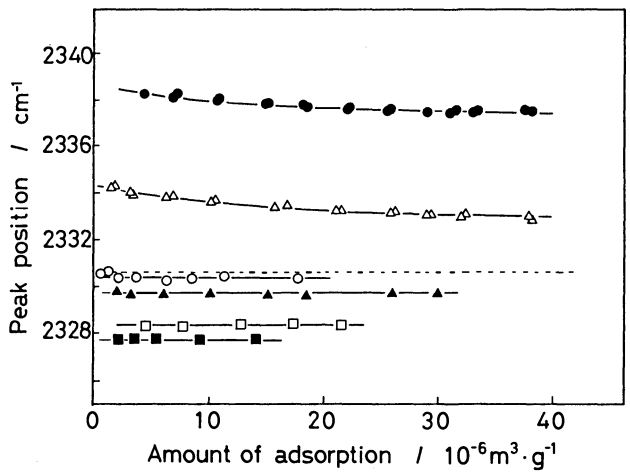

Fig. 5. Peak positions of IR bands for nitrogen adsorbed on ion-exchanged ZSM-5 zeolites. ●: N_2-LiZSM-5, △: N_2-NaZSM-5, ○: N_2-HZSM-5, ▲: N_2-KZSM-5, □: N_2-RbZSM-5, ■: N_2-CsZSM-5, ----: N_2-gas.

tion about the interaction between the adsorbed nitrogen molecule and the cationic site. On account of the IR data, the adsorption characteristics suggested by the preceding discussion are expected to be further clarified.

IR Peak Position. IR peak positions for all the ZSM-5-N_2 adsorption systems are shown in Fig. 5 as a function of the amount of adsorption. The peak position varied little with the change in the amount of adsorption. The peak for the LiZSM-5-N_2 system was found at the highest wavenumber position and was followed by those for the other adsorption systems. The descending order of the peak position was $Li^+ > Na^+ > K^+ \simeq H^+ > Rb^+ \simeq Cs^+$. It must be pointed out, in addition, that the peak positions both for the LiZSM-5-N_2 system and for the NaZSM-5-N_2 system are located at considerably higher wavenumber than the gaseous nitrogen peak expressed by a dotted line (2330.7 cm^{-1}; Raman spectral value).[19]

The high frequency shifts observed (LiZSM-5-N_2, NaZSM-5-N_2) suggest that the adsorbed nitrogen molecule takes on an orientation as exemplified in Fig. 3a. According to the theoretical calculation of Cohen de Lara et al.,[10] a high frequency shift of the nitrogen IR band results from the orientation of the nitrogen molecule toward the direction of the electric field of the cationic site. The ionic radii of Li^+ and Na^+ are small and hence there are little geometrical restriction for the molecule to take such an orientation as mentioned above and illustrated in Fig. 3a. In addition, the strong attractive forces of these cations would be favorable to maintaining this orientation. On the other hand, a weak adsorptive force at the H^+ site probable can not maintain the orientation, though there is little geometrical restriction. The adsorptive force of the K^+ site is not so strong and, in addition, a small geometrical restriction due to the somewhat large ionic radius of this cation may exist. Thus the molecular orientation mentioned above would not persist on the K^+ site, though it might momentarily be induced. Both for the Rb^+-N_2 system and for the Cs^+-N_2 system, the adsorptive forces are weak and the Li^+-N_2 like orientation of adsorbed nitrogen is geometrically hindered as shown in Fig. 3b. Approximately speaking, therefore, nitrogen molecules on H^+, K^+, Rb^+, Cs^+ cationic sites would be in a random orientation state. This view is supported by the experimental observation that the IR peak positions for these systems are located close to that of the gaseous nitrogen (Fig. 5).

IR Peak Intensity. The integral molar extinction coefficient A needed to discribe the intensity of IR spectra of an adsorbed species is defined by[9]

$$A = (1/n \cdot l) \int \log (I_0/I)\, d\tilde{\nu}, \quad (1)$$

where I_0 is the intensity of incident light, I is the intensity of transmitted light, $\tilde{\nu}$ is the wavenumber, n is the number of moles of the vibrator in unit volume of the sample, and l is the thickness of the sample.

If we express the sample weight, the total amount of admolecules on the cationic sites of the sample, and the cross-sectional area of the sample by W (g), m_c (mol), and a (cm^2), respectively, Eq. 1 can be rewritten

as follows;

$$A=[1/(m_c/W)(W/a)]\int \log(I_0/I)\,d\tilde{\nu}, \quad (2)$$

or more concisely

$$AM_c=S, \quad (3)$$

where $M_c=m_c/W$, and $S=[1/(W/a)]\int \log(I_0/I)d\tilde{\nu}$. Since the right hand side of Eq. 3 can be evaluated from the experimental data, the molar extinction coefficient A is obtainable if we know the value of M_c. It must be pointed out here that the experimentally measured amount of adsorption M involves the amount of adsorption onto the pore wall (silicalite-like adsorption; M_s). Thus we can not use the adsorption isotherms shown in Fig. 1 to obtain the M_c value.

The evaluation of A can, however, be carried out in the following manner. Namely, if we assume that a Langmuir type adsorption equation is applicable to the nitrogen adsorption onto the cationic sites, the following relation should hold;

$$S=AM_c=AK_cb_cP/(1+K_cP), \quad (4)$$

where K_c, b_c, and P denote the adsorption equilibrium constant, the number of moles of the cation sites in unit weight of the zeolite sample, and the equilibrium nitrogen pressure, respectively. This equation (Eq. 4) enables us to evaluate A from the IR peak areas obtained under varying pressures.

According to Eq. 4, plots of P/S against P should be linear because

$$P/S=1/(AK_cb_c)+P/Ab_c. \quad (5)$$

Indeed, as we can see in Fig. 6, the straight line relationship between P/S and P has been found for all the adsorption systems. Since the value of b_c is known (Table 1), we can obtain A from the slope of the straight line. Values of A obtained in the present study are listed in Table 2. The decreasing order of the A value is $A_{Li^+}>A_{Na^+}>A_{K^+}>A_{Rb^+}>A_{Cs^+}>A_{H^+}$. This is parallel with the decreasing order of the heat of adsorption q°_{st} and very reasonable.

Electric Field of the Cationic Site. The electric field E of the cationic site in the ZSM-5 zeolite has already been determined[8] using methane as a probing molecule. Since the average size of the nitrogen molecule is almost the same as that of methane, the electric field determined by nitrogen should be identical with that obtained by methane. Thus we can examine the validity of the preceding discussion by comparing the E value obtained for nitrogen with that obtained for methane.

The relation between the electric field E and the IR extinction coefficient A varies, depending on the orientation of the probe molecule at the adsorption site. According to the preceding discussion, nitrogen molecules adsorbed on any of H^+, K^+, Rb^+, and Cs^+ site are considered to be almost randomly oriented. Thus the following relation[9] would be applicable;

$$A=(\pi/3c^2)E^2[(\partial\bar{\alpha}/\partial q)^2+(2/9)(\partial\gamma/\partial q)^2], \quad (6)$$

where c is the velocity of light, $\bar{\alpha}$ is the average polarizability defined from the polarizability ($\alpha_{||}$) along the direction of the electric field and that ($\alpha_\perp$) perpendicular to the direction of the electric field by $(1/3)(\alpha_{||}+2\alpha_\perp)$, γ is defined by $(\alpha_{||}-\alpha_\perp)$ to express an anisotropy in the polarizability, and q is the normal coordinate of vibration.

On the other hand, the following relation[9] would be applicable in evaluating the electric fields of the Li^+ site and the Na^+ site, because the nitrogen molecules on these sites are expected to take an orientation such

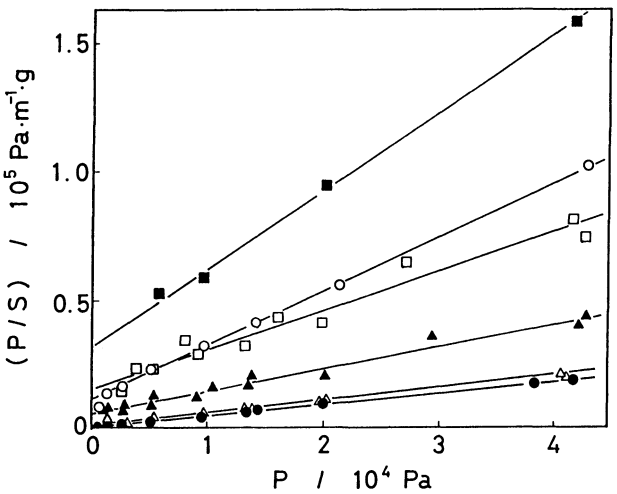

Fig. 6. Plots showing linear relationships between P/S and P. ●: N_2–LiZSM-5, △: N_2–NaZSM-5, ▲: N_2–KZSM-5, □: N_2–RbZSM-5, ○: N_2–HZSM-5, ■: N_2–CsZSM-5.

Table 2. IR Spectroscopic Data for Nitrogen Adsorbed on Ion-Exchanged ZSM-5 Zeolites

Zeolite	Peak position[a]	Extinction coefficient, A	Electric field of cation, E[b,c]
	cm^{-1}	m mol^{-1}	10^5 esu
HZSM-5	2330	351	1.19 (0.80)
LiZSM-5	2338	2457	2.00 (1.58)
NaZSM-5	2334	1602	1.62 (1.55)
KZSM-5	2330	897	1.91 (1.47)
RbZSM-5	2328	552	1.50 (1.36)
CsZSM-5	2328	297	1.10 (1.21)

a) Values at $M=10\times10^{-6}$ m^3-NTP/g are listed; M denotes the amount of adsorption. b) Values in parenthesis are the electric fields measured with methane. c) 1 esu=3×10^4 V m^{-1}.

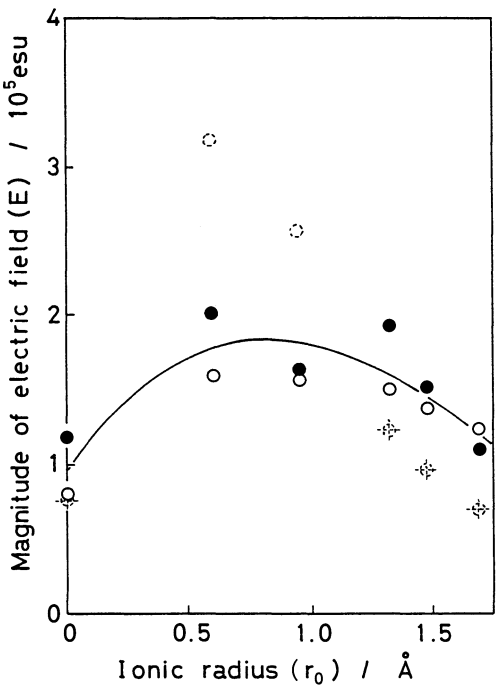

Fig. 7. Electric fields of cationic sites. ●: obtained from nitrogen IR data, O: obtained from methane IR data, ◌: values for random orientation (N_2–Li^+, and N_2–Na^+), ⊕: values with orientation (N_2–H^+, N_2–K^+, N_2–Rb^+, and N_2–Cs^+).

as is exemplified in Fig. 3a;

$$A=(\pi/3c^2)E^2[(\partial\bar{\alpha}/\partial q)+(2/3)(\partial\gamma/\partial q)]^2. \quad (7)$$

The results of the calculation are shown in Fig. 7. A close agreement between the E values obtained from the nitrogen IR data and those obtained from the methane IR data (Table 2) proves the validity of the adsorption model hitherto discussed. It must finally be noted that the following literature values[9] have been used in the above mentioned calculation of E;

$$|\partial\bar{\alpha}/\partial q| = 0.66\, N^{1/2}\, 10^{-16}\ \mathrm{cm^2\, g^{-1/2}},$$
$$|\partial\bar{\gamma}/\partial q| = 0.82\, N^{1/2}\, 10^{-16}\ \mathrm{cm^2\, g^{-1/2}},$$

where N is the Avogadro number.

Both derivatives have been assumed to be positive, in the present study. It is reported in the literature[9] that the positive value for $\partial\bar{\alpha}/\partial q$ appears pertinent. The use of negative value for $\partial\gamma/\partial q$ with positive value of $\partial\bar{\alpha}/\partial q$ in the calculation of Eq. 7 results in anomalously large values of E for every cation examined in the present study.

References

1) For instance; P. B. Weitze, "Proc. of the 7th Intern. Congr. on Catal.," ed by T. Seiyama and K. Tanabe, Kodansha Tokyo (1981), p. 3.

2) P. A. Jacobs, H. K. Beyer, and J. Valyon, *Zeolites*, **1**, 161 (1981).

3) S. Furuyama, M. Miyazaki, and H. Inoue, *J. Phys. Chem.*, **88**, 1741 (1984).

4) P. Wu and Y. H. Ma, "Proc. of the 6th Intern. Zeolite Coference," ed by D. Olsen and A. Bisio, Butterworths Guildford (1984), p. 251

5) R. E. Richards and L. V. C. Rees, *Langmuire*, **3**, 335 (1987).

6) T. Yamazaki, I. Watanuki, S. Ozawa, and Y. Ogino, *Nippon Kagaku Kaishi*, **1987**, 1535.

7) T. Yamazaki, Y. Abe, I. Watanuki, T. F. Ding, S. Ozawa, and Y. Ogino, *Chem. Lett.*, **1987**, 1457.

8) T. Yamazaki, I. Watanuki, S. Ozawa, and Y. Ogino, *Langmuire*, submitted.

9) E. Cohen de Lara and Y. Delaval, *J. Chem. Soc., Faraday Trans. 2*, **74**, 790 (1978).

10) E. Cohen de Lara, *J. Chem. Soc., Faraday Trans. 2*, **77**, 355 (1981).

11) E. Cohen de Lara, R. Kahn, and R. Seloudoux, *J. Chem. Phys.*, **83**, 2646 (1985).

12) B. Barrachin and E. Cohen de Lara, *J. Chem. Soc., Faraday Trans. 2*, **82**, 1953 (1986).

13) L. Pauling, "The Nature of The Chemical Bond," 3rd ed., Cornell University Press, Ithaca, New York (1960), p. 514.

14) G. T. Kokotailo, S. L. Lawton, D. H. Olsen, and W. M. Meier, *Nature (London)*, **272**, 437 (1978).

15) R. M. Barrer and W. I. Stuart, *Proc. R. Soc. London, Ser. A*, **237**, 439 (1959).

16) R. D. Shannon and C. T. Prewitt, *Acta Crystallogr. Sect. B*, **25**, 925 (1969).

17) L. Pauling, "The Nature of The Chemical Bond," 3rd ed., Cornell University Press, Ithaca, New York (1960), p. 97.

18) H. Föster and M. Schuldt, *J. Chem. Phys.*, **66**, 5237 (1977).

19) F. Rasetti, *Phys. Rev.*, **34**, 367 (1929).

Micellar Catalytic Effect on the Base Dissociation of Methylamine Studied by the Ultrasonic Absorption Method

Shoji HARADA,* Takayuki SANO, Teruyo YAMASHITA,† Hiroshige YANO,† Tadaomi INOUE,†† and Tatsuya YASUNAGA††

Faculty of Science, Hiroshima University, Higashisenda-machi, 1-1-89, Nakaku, Hiroshima 730
†Daiichi College of Pharmaceutical Science, Tamagawa-cho, 22-1, Minami-ku, Fukuoka 815
††Faculty of Engineering, Kinki University, Hiro-machi, Kure 737-01

(Received August 21, 1987)

Micellar catalytic effects on the base dissociation of methylamine have been studied by ultrasonic absorption method. The dissociation constant, the rate constants, and the volume change of the reaction were obtained in the absence and in the presence of SDS. The micellar catalytic effects observed for methylamine was smaller than those for amines of long alkyl chain, which was ascribed to the facts that the former is incorporated into the micellar ionic atmosphere in the concentrated micellar solution while the latters are solubilized into micelles.

In a series of investigations by the ultrasonic absorption method, we have studied the micellar catalytic effects on the acid dissociation of aromatic carboxylic acids[1,2] and the base dissociation of amines.[3-6] In most of these micellar catalyzed reactions, the reactants have been solubilized in the micelles.[1-9] If the solubilization is a prerequisite for the micellar catalysis, one cannot expect micellar catalytic effects for carboxylic acids and alkylamines of short alkyl chain. The present work was intended to examine this problem. Static and kinetic studies were carried out for the base dissociation of methylamine, which has the shortest alkyl group of the alkylamines, in the presence of the SDS micelles. Comparing the results with those for the homologous alkylamines, the dependence of the micellar catalytic effects on the alkyl-chain length of the amines is discussed.

Experimental

Methylamine (MA), in the form of 30% aqueous solution, and propylamine were purchased from Tokyo Kasei and used without further purification. The concentration of MA was determined by pH titration. SDS purchased from Pierce was recrystallized twice in methanol. The critical micelle concentration (cmc) determined by conductivity measurements was found to be 8.0×10^{-3} M§ at 30 °C. All other chemicals were of reagent grade.

pH measurements were carried out with a pH meter (HM-20) using an electrode (GS-135C) of TOA Electronics Ltd. Ultrasonic absorption measurements were carried out by the pulse method in the frequency range of 7.5 to 95 MHz. Details of the apparatus have been described elsewhere.[10] All the absorption data fitted the single relaxation equation[11,12]

$$\frac{\alpha}{f^2} = \frac{A}{1+(f/f_r)^2} + B, \qquad (1)$$

where α is the absorption coefficient, f the frequency, f_r the relaxation frequency, and A and B are the relaxation and non-relaxation absorptions, respectively. The three parameters, f_r, A, and B, were determined by computer simulation. Experimental errors were within 8%, 5%, and 5% of the corresponding values, respectively. The velocity of sound was measured by the sing-around method at 1.92 MHz.[13] All the measurements were performed under nitrogen atmosphere and thermostated conditions. In the case of MA aqueous solution, the ionic strength, μ, was kept constant at 0.3 by the addition of NaCl.

§ 1 M=1 mol dm^{-3}.

Results and Discussion

Static and Kinetic Studies of the Base Dissociation of MA in Aqueous Solution. The base dissociation of MA in the absence of SDS was studied first in order to obtain referential data for the MA-SDS system.

For the reaction;

$$CH_3NH_3^+ + OH^- \underset{k_b}{\overset{k_f}{\longleftrightarrow}} CH_3NH_2 + H_2O\ , \qquad (2)$$

the base dissociation constant, K_b^0, is defined as,

$$K_b^0 = \frac{k_b}{k_f} = \frac{\gamma^2[CH_3NH_3^+][OH^-]}{[CH_3NH_2]} = \frac{\gamma^2\sigma^2C_0}{1-\sigma}\ , \qquad (3)$$

where γ is the mean activity coefficient, σ the degree of ionization, and C_0 the total concentration of MA. From the pH values in Table 1 and the activity coefficients calculated by the Davies equation,[14] pK_b^0 was obtained to be 3.44 (±0.02). This is in agreement with the literature value.[15]

Ultrasonic relaxation absorption was observed in the aqueous solution of MA in the MHz frequency range as shown in Fig. 1. The experimental condi-

Table 1. pH and Ultrasonic Absorption Parameters for the Methylamine Aqueous Solution at μ=0.3 and 30 °C

C_0 / M	pH	f_r / MHz	A (10^{-17})	B (10^{-17})
0.01	11.04	24.5	52	18
0.02	11.23	35.0	57	18
0.03	11.32	40.0	65	18
0.04	11.40	49.3	65	18
0.05	11.44	54.7	67	18

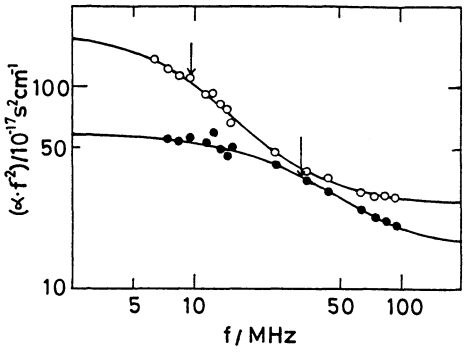

Fig. 1. Representative ultrasonic absorption spectra at 30°C: ●, MA(0.01 M) aqueous solution at μ=0.3; ○, MA(0.01 M)-SDS(0.30 M) system. The arrows indicate the relaxation frequency.

tions and the relaxation parameters obtained are listed in Table 1. As has been clarified by previous studies on a series of alkylamines,[16,17] the dependence of the relaxation parameters for the concentration and the pH indicates that the relaxation absorption is due to the base dissociation of MA. For Reaction 2, the relaxation parameters are related to the kinetic parameters by the following equations:[11,12]

$$(2\pi f_r)^2 = 4\gamma^2 k_f k_b C_0 + k_b^2, \quad (4)$$

$$(\alpha'\lambda)_{max} = \frac{\rho u^2 \pi}{2RT} \cdot (\Delta V)^2 \cdot \Gamma^{-1} \quad (5a)$$

with

$$\Gamma = [CH_3NH_3^+]^{-1} + [OH^-]^{-1} + [CH_3NH_2]^{-1}, \quad (5b)$$

where α' is the excess absorption coefficient, λ the wavelength, ρ the density, u the sound velocity, ΔV the volume change of the reaction, and the subscript max indicates maximum value. Plots of $(2\pi f_r)^2$ and $(\alpha'\lambda)_{max}$ against the concentration terms are shown in Figs. 2a and 2b, respectively. The kinetic parameters were obtained to be $\gamma^2 k_f$=2.7 (±0.4)×10^{10} M^{-1}s^{-1}, k_b=2.2 (±0.4)×10^7 s^{-1}, and ΔV=25.8 (±0.8) cm^3 mol^{-1}. The apparent base dissociation constant, K_b ($=k_b/\gamma^2 k_f$), was obtained from the pH data as pK_b=3.09 (±0.02).

Base Dissociation of MA in Micellar Solutions of SDS. The addition of SDS to a MA solution induces an increase of pH as shown in Fig. 3. As seen in this figure, pH changes very little in the region below the cmc, but increases rapidly above the cmc. This result implies that the base dissociation of MA is accerelated by its incorporation into the SDS micelles, and at rather high SDS concentration, the micellar effect, i.e., the incorporation saturates. Similar experiments were carried out also on propylamine. As shown in Fig. 3, the value of pH saturates at a somewhat lower concentration of SDS compared to that in the case of the MA-SDS system, and the change of pH induced by the addition of SDS is larger. These differences in the micellar effects on the two amines are discussed later.

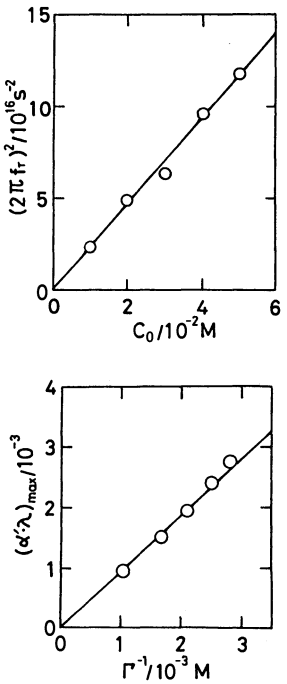

Fig. 2. Plots of (a) $(2\pi f_r)^2$ vs. MA concentration and (b) $(\alpha'\lambda)_{max}$ vs. Γ^{-1} for MA aqueous solution at μ= 0.3 and 30°C.

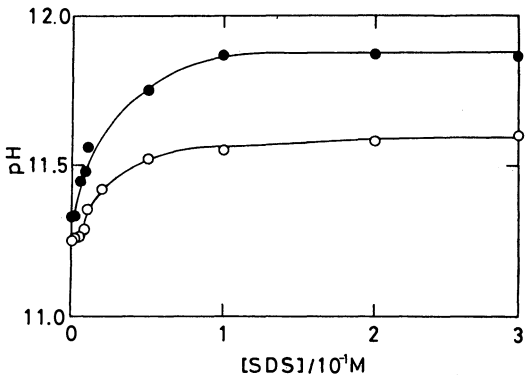

Fig. 3. pH of the alkylamine(0.01 M)-SDS systems at 30°C: ○, MA; ●, propylamine.

Table 2. pH and Ultrasonic Absorption Parameters for the Methylamine-SDS (0.30 M) System at 30 °C

[MA] / M	pH	f_r / MHz	A (10^{-17})	B (10^{-17})
0.01	11.41	9.9	159	26
0.02	11.60	12.9	237	27
0.03	11.70	16.3	254	27
0.04	11.78	18.4	240	26
0.05	11.83	20.3	272	27

Quantitative measurements of pH and ultrasonic absorption were performed on solutions of various concentrations of MA containing a constant concentration (0.30 M) of SDS. The experimental conditions and the obtained data are summarized in Table 2.

Taking into account small hydrophobicity of MA, it is probable that the base dissociation of MA occurs both in bulk and on the micellar surface, and the following coupled reaction mechanism is proposed:

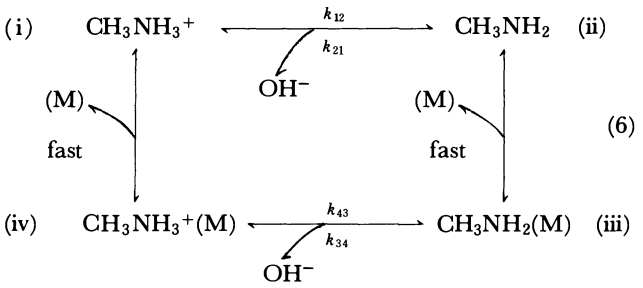

where (M) indicates an adsorption site on the micelle and (i)—(iv) mean different states of MA. The apparent dissociation constant of MA in the 0.30 M SDS micellar solution, $\bar{K}_b$ (M), defined as,

$$\bar{K}_b(M) = \frac{\{[CH_3NH_3^+(M)] + [CH_3NH_3^+]\} \cdot [OH^-]}{\{[CH_3NH_2(M)] + [CH_3NH_2]\}}, \quad (7)$$

was obtained from the pH data as $p\bar{K}_b$ (M)=2.18 (±0.01).

Ultrasonic relaxation absorption of the MA-SDS system takes place in a lower frequency range and the relaxation amplitude is larger than those of the pure MA in aqueous solution (Fig. 1). Since the association and dissociation of MA to and from the micelles are very fast,[18] the relaxation time, τ, for the slowest process in Reaction 6 is given by the following equation:[19]

$$\tau^{-1} (= 2\pi f_r) =$$
$$\gamma^2 k_{12}\left\{2[CH_3NH_3^+] + \frac{[CH_3NH_2]}{[CH_3NH_2(M)]+[CH_3NH_2]} \cdot K_{12}\right\} +$$
$$\gamma^2 k_{43}\left\{2[CH_3NH_3^+(M)] + \frac{[CH_3NH_2(M)]}{[CH_3NH_2(M)]+[CH_3NH_2]} \cdot K_{43}\right\}, \quad (8)$$

with

$$K_{12} = \frac{k_{21}}{\gamma^2 k_{12}} = \frac{[CH_3NH_3^+] \cdot [OH^-]}{[CH_3NH_2]} = K_b(W), \quad (9)$$

$$K_{43} = \frac{k_{34}}{\gamma^2 k_{43}} = \frac{[CH_3NH_3^+(M)] \cdot [OH^-]}{[CH_3NH_2(M)]} = K_b(M), \quad (10)$$

where K_b (W) and K_b (M) are the apparent base dissociation constants of MA in the bulk and on the micelle, respectively. If the value of K_b (M) is given, we can calculate the concentrations of MA of the different states with use of Eqs. 7,9, and 10. Then the first term of the right hand side of Eq. 8 was calculated by introducing the kinetic value obtained above for the base dissociation of MA in aqueous solution, and τ^{-1} ($=2\pi f_r$) was plotted against the value in the parenthesis of the second term. When K_b (M) is properly assumed, this plot gives a straight line. Then the plot was examined by changing the K_b (M) values in the range of K_b (W) to $\bar{K}_b$ (M). A good linear relationship was obtained only for the K_b (M) values very close to $\bar{K}_b$ (M). The result indicates that Reaction 6 can be approximated by the equilibrium (iv)$\rightleftarrows$(iii), or in other words, all the MA is incorporated into the SDS micelles. The same result was suggested also from the pH saturation behavior at concentrated SDS solution as mentioned above. Consequently, the base dissociation of MA in the 0.30 M SDS solution can be approximated by the reaction,

$$CH_3NH_3^+(M) + OH^- \underset{k_b}{\overset{k_f}{\rightleftarrows}} CH_3NH_2(M) + H_2O. \quad (11)$$

Since this reaction is quite similar to Reaction 2, we can apply Eqs. 4 and 5 for the analysis of the relaxation parameters. Each plot of the relaxation parameters is shown in Figs. 4a and 4b. From these plots, the kinetic parameters for Reaction 11 were obtained to be: $\gamma^2 k_f$=3.5 (±0.6)×10^9 M^{-1}s^{-1}, k_b=2.3 (±0.4)×10^7 s^{-1}, and ΔV=22.4 (±0.7) cm^3 mol^{-1} at 30 °C.

Ultrasonic absorption was measured also in the MA-SDS system with changing pH. Experimental conditions and the results are listed in Table 3. For Reaction 11, f_r is related to the rate constants as follows:[11,12,19]

$$2\pi f_r = \gamma^2 k_f\{[CH_3NH_3^+(M)] + [OH^-]\} + k_b. \quad (12)$$

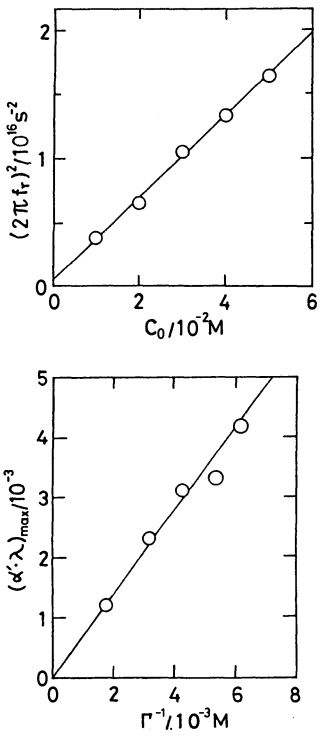

Fig. 4. Plots of (a) $(2\pi f_r)^2$ vs. MA concentration and (b) $(\alpha' \lambda)_{max}$ vs. Γ^{-1} for MA-SDS(0.30 M) system at 30 °C.

Table 3. Ultrasonic Absorption Parameters for the Methylamine (0.03 M)-SDS (0.30 M) System at Various pH and 30 °C

pH	f_r	A	B
	MHz	(10^{-17})	
10.80	18.0	36	30
11.14	16.8	88	28
11.43	13.4	152	30
11.73	16.5	195	28
12.18	26.2	98	26

The concentrations of the MA cation and OH^- were calculated from the pH, C_0, and K_b (M). Then, the value of $(2\pi f_r)$ was plotted against the concentration term of Eq. 12, and the rate constants were obtained to be; $\gamma\,{}^2k_f=3.6\,(\pm0.6)\times10^9\,M^{-1}s^{-1}$ and $k_b=2.4\,(\pm0.4)\times10^7\,s^{-1}$. For the relaxation absorption amplitude analysis, Eq. 5 can be applied. From the plot of $(\alpha'\lambda)_{max}$ vs. the concentration term, the value of ΔV was given to be 20.0 ($\pm$0.6) $cm^3\,mol^{-1}$. The fact that the absorption parameters can be satisfactorily analyzed by Eqs. 12 and 5 supports the assignment of the relaxation absorption to Reaction 11. Furthermore, the kinetic values were in reasonable agreement with the corresponding value obtained in the above experiments of MA concentration change.

Dependence of the Micellar Catalytic Effects on the Alkyl-Chain Length of the Amines. Magnitude of the micellar catalytic effects on the base dissociation of amines depends on their alkyl-chain length, e.g., as seen above, the pH change induced by the addition of SDS is larger for propylamine than for MA. Further examinations are performed in the following way.

Comparison of the values of pK_b^0 and pK_b (M) obtained above shows that the dissociation of MA is promoted by 1.26 pK_b unit in the micellar solution. Since the micellar effect has been about 1.5 pK_b unit for a series of amines of long alkyl chain in a 0.30 M detergent solution,[3-6] the micellar effect is smaller for MA.

Ultrasonic relaxation absorption spectrum reflects the difference of the alkyl-chain length of the amines in micellar solution. As shown in Fig. 5, f_r shifts to the lower frequency region and the absorption amplitude increases with increase of the alkyl-chain length of the amine. However, these dependences on the alkyl-chain length saturate rapidly and the absorption spectra for the systems of amines of C_{4-10}-SDS are almost indistinguishable from each other.[3-6]

For the base dissociation of alkylamines in a micellar solution, we have found that $\gamma\,{}^2k_f$ and k_b are both dependent on the base dissociation constant.[1-6] These situations are shown in Fig. 6 where the rate constants for MA obtained in this work are also plotted. Looking into this figure, we can discover the following features. (i) The rate constants for MA in an aqueous solution fall on the line expected from the corresponding literature values for the homologous amines.[16,17] (ii) The rate constants for MA in the micellar solution are much smaller than the corresponding values in aqueous solution at the same pK_b but larger than those for the amines of long alkyl chain in the micellar solution.[3,4] These results indicate that the base dissociation of MA is catalyzed by the SDS micelles but the catalytic effects are smaller than those for the amines of long alkyl chain.

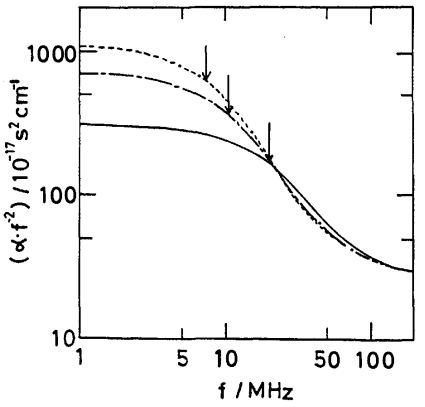

Fig. 5. Representative ultrasonic absorption spectra of the alkylamine(0.05 M)-SDS(0.30 M) solutions at 30°C: (——), MA; (-·-·-), propylamine; (----), amines of alkyl chain of C_{4-10}.

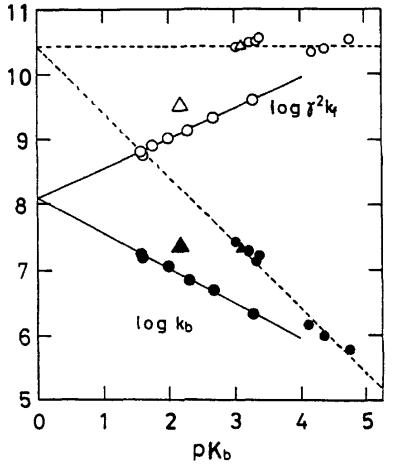

Fig. 6. pK_b dependencies of the rate constants for the base dissociation of the amines in the presence of 0.30 M SDS (large signs, data from Refs. 3—6) and in the absence of the micelles (small signs, data from Refs. 16 and 17): triangle indicates MA. The amines cited for the two conditions are not corresponding to each other.

Taking into consideration the fact that the pK_b values of alkylamines are almost the same in aqueous solution,[15] dependence of the micellar catalytic effects on the alkyl-chain length of amines should be ascribed to the position of the amino group in the micellar atmosphere. Judging from the behavior of saturation of the effects with the alkyl-chain length, the amino group of the amines of alkyl chains longer than C_4 is

in the Stern layer due to the solubilization of the alkyl chain into the micellar core. For the amines of alkyl chain shorter than C_4, the solubilization is inadequate, and the amino group may be outside of the Stern layer. Especially in the case of MA, ordinary solubilization is not conceivable. Then, the smaller micellar catalytic effects for MA are interpreted as follows.

The MA cation can be incorporated into the micellar atmosphere as a counter ion because of its small predominance in the hydrophobicity compared to Na^+.[20] On the other hand, undissociated MA may not be solubilized preferentially into the micelle. In a rather concentrated detergent solution, however, the micelle-micelle interaction becomes predominant because of the high cocentration of micellar aggregates,[21,22] and the free bulk will essentially disappear. Therefore, both dissociated and undissociated MA, which were in the bulk at lower detergent concentration are now incorporated into the micellar ionic atmosphere, i.e., Gouy-Chapman double layer. In fact, in recent investigations, we have found that noncharged amphiphilic molecules of short alkyl chain, e.g., methyl or ethyl group, can be incorporated into micelles at high detergent concentration.[23] As a consequence, we conclude that, in a concentrated SDS solution as in the present case, all the MA are incorporated into the micellar ionic atmosphere and the base dissociation is catalyzed moderately.

The authors wish to thank Professor Z. A. Schelly of University of Texas at Arlington and Mr. S. Nishioka of Hiroshima University for helps in this experiment.

References

1) S. Harada, T. Yamashita, H. Yano, N. Higa, and T. Yasunaga, *J. Phys. Chem.*, **88**, 5406 (1984).

2) S. Harada, H. Yano, T. Yamashita, S. Nishioka, and T. Yasunaga, *J. Colloid Interface Sci.*, **110**, 272 (1986).

3) T. Yamashita, H. Yano, S. Harada, and T. Yasunaga, *J. Phys. Chem.*, **87**, 5482 (1983).

4) T. Yamashita, H. Yano, S. Harada, and T. Yasunage, *J. Phys. Chem.*, **88**, 2671 (1984).

5) T. Yamashita, M. Sumino, H. Yano, S. Harada, and T. Yasunaga, *Bull. Chem. Soc. Jpn.*, **57**, 2352 (1984).

6) T. Yamashita, *J. Sci, Hiroshima Univ. Ser. A.*, **48**, 87 (1984).

7) J. Fendler and E. Fendler, "Catalysis in Micellar and Macromolecular Systems," Academic Press, New York (1975).

8) "Micellization, Solubilization, and Microemulsions," ed by K. L. Mittal, Plenum Press, New York (1977).

9) "Reaction Kinetics in Micelles," ed by E. H. Cordes, Plenum Press, New York (1973).

10) N. Tatsumoto, *J. Chem. Phys.*, **47**, 4561 (1967).

11) M. J. Blandamer, "Introduction to Chemical Ultrasonics," Academic Press, New York (1973).

12) C. F. Bernasconi, "Relaxation Kinetics," Academic Press, New York (1976).

13) T. Yasunage, N. Tatsumoto, and M. Miura, *Bull. Chem. Soc. Jpn.*, **37**, 1655 (1964).

14) C. W. Davies, "Ion Association," Butterworths, London (1962).

15) "CRC Handbook of Chemistry and Physics," ed by R. C. Weast, CRC Press, Cleveland (1987).

16) M. Eigen, G. Mass, and G. Schwarz, *Z. Phys. Chem.*, **74**, 319 (1971).

17) S. Nishikawa, T. Yasunaga, and K. Takahashi, *Bull. Chem. Soc. Jpn.*, **46**, 2992 (1973).

18) H. Hoffman, H. Nusslein, and W. Ulbricht, in Ref 2, p. 263.

19) G. H. Czerlinski, "Chemical Relaxation," Marcel Dekker, New York (1966).

20) S. Harada, unpublished data. Counter ion exchange between Na^+ and MA cation was observed using a sodium ion electrode.

21) D. Stigter and K. J. Mysels, *J. Phys. Chem.*, **59**, 45 (1955).

22) P. Ekwall, L. Mandell, and P. Solyom, *J. Colloid Interface Sci.*, **35**, 519 (1971).

23) S. Harada, unpublished data.

 © 1988 The Chemical Society of Japan Bull. Chem. Soc. Jpn., 61, 1051—1055 (1988)

Shape Selectivity of ZSM-5 Type Zeolite for Alkylation of Ethylbenzene with Ethanol

Jong-Ho KIM, Seitaro NAMBA,* and Tatsuaki YASHIMA
Department of Chemistry, Tokyo Institute of Technology, Ookayama, Meguro-ku, Tokyo 152
(Received August 22, 1987)

The alkylation of ethylbenzene with ethanol on ZSM-5 zeolites was studied at 673 K. The primary product in this alkylation on HZSM-5 catalyst was only *p*-diethylbenzene because of the transition-state selectivity. Therefore, the isomerization of *p*-diethylbenzene has to be restrained for the selective formation of *p*-diethylbenzene. The modified HZSM-5 catalysts with oxide of magnesium, phosphorus or boron showed much higher para-selectivity than the parent HZSM-5. The modification reduced not only the effective pore dimension of HZSM-5 but also the amount of strong acid sites. We claim that the absence of strong acid sites is necessary rather than the narrowness of pores for the suppression of the isomerization of *p*-diethylbenzene produced as a primary product.

The main channel of ZSM-5 type zeolite is cylindrical and its window is composed of a 10-membered oxygen ring, whose dimension is smaller than that of Y type zeolite.[1] In fact, *p*-xylene can be adsorbed selectively in the pores of HZSM-5 in the liquid phase competitive adsorption of the three xylene isomers at a low temperture as 273 K.[2] Therefore, it was expected that *p*-xylene could be selectively produced in the alkylation of toluene with methanol on HZSM-5 type zeolite catalysts. However, Yashima et al.[3] and Kaeding et al.[4] have reported that the equilibrium composition of xylene isomers is obtained in the alkylation of toluene with methanol on HZSM-5 at a high yield of xylene. When oxide of magnesium,[3,4] phosphorus,[4] or boron[4] is incorporated into HZSM-5 catalyst, a dramatic increase in para-selectivity is observed. That is, the fraction of the para-isomer in xylenes produced is above 90%. It has been also reported that in the ethylation of toluene[5] and ethylbenzene[6] on modified ZSM-5 zeolites a high para-selectivity is observed.

Many researchers suggest that the high para-selectivity for the alkylations mentioned above is caused by the shape selectivity of the modified ZSM-5 zeolites.[3-6] Kaeding et al. have proposed that the high para-selectivity of modified ZSM-5 zeolites is due to product selectivity (a kind of shape selectivity), namely the much higher intracrystalline diffusivity of the para-isomer in relation to the other two isomers.[4,6] Wei has presented a theoretical explanation for the experimental data, assuming product selectivity, and has concluded that the enhancement of para-selectivity happens under decreasing in conversion of alkylation and under increasing in catalytic activity for isomerization.[7]

On the other hand, Yashima et al. have reported the results of the alkylation of toluene with methanol on HY and HZSM-5 catalysts.[3] In the case of HY, *o*- and *p*-xylenes are primary products, while on HZSM-5, only *p*-xylene is a primary product. This is because of transition-state selectivity (a kind of shape selectivity) of HZSM-5. Accordingly, the alkylation to form any xylene other than the para-isomer is prevented as the transition state necessary for the alkylation to proceed is not reached due to steric and space restriction. When HZSM-5 is modified with oxide of magnesium, an enhancement in para-selectivity is observed. They suggested that the amount of strong acid sites must be reduced for the suppression of the isomerization of *p*-xylene produced preferentially in order to produce *p*-xylene selectively.

In this paper, we aim to clarify a role of oxide compounds, whose incorporation results in the improvement of para-selectivity of ZSM-5 zeolites. We choose the alkylation of ethylbenzene with ethanol as a para-selective reaction, because the larger alkyl groups in diethylbenzene are expected to provide clearer results compared with the case of the alkylation of toluene with methanol.

Experimental

Materials. ZSM-5 type zeolite was synthesized by a similar method to that described in Mobil's patent[8] using tetrapropylammonium bromide, sodium silicate, aluminium sulfate, sulfuric acid and sodium chloride. The synthesized zeolite was calcined at 773 K for 3 h in air. Its sodium cation was exchanged for a proton by using 1 mol dm^{-3} hydrochloric acid at 333 K. The HZSM-5 (Si/Al=96) modified with magnesium oxide, designated as Mg-HZSM-5, was prepared by impregnation of HZSM-5 with aqueous magnesium acetate solution followed by drying at 373 K and calcined at 823 K for 18 h in an air stream. P-HZSM-5, B-HZSM-5 were prepared by impregnation of HZSM-5 with aqueous phosphoric acid solution and aqueous boric acid solution, respectively, followed by a method similar to that for Mg-HZSM-5. The weighed catalyst was set in a quartz reactor and dehydrated at 823 K for 1 h in a helium stream before use.

Apparatus and Procedure. The reaction was carried out in a fixed bed type apparatus with a continuous flow system at atmospheric pressure. The reactant (ethylbenzene/ethanol=1/1 mol/mol) was fed with a microfeeder. Helium was used as a carrier gas. The conditions of the alkylation of ethylbenzene with ethanol on HZSM-5 were: activation

temperature=823 K; reaction temperature=673 K; (carrier gas)/(reactants)=(3 mol)/(2 mol); W/F=7.14 g h mol^{-1}. The effluent gas was cooled with an ice trap, and samples for analysis were collected periodically and were analyzed by gas chromatography.

The measurements of temperature programmed ammonia desorption (NH_3-TPD) from the catalysts were carried out as follows. After the catalyst was evacuated at 823 K for 1 h and exposed 80 Pa of ammonia gas at room temperature for 15 min, the catalyst was evacuated at room temperature for 15 min and then the temperature was brought to 773 K at a constant rate of 10 K min^{-1} under evacuation through the capillary. The relative amount of ammonia desorbed from the catalyst was determined by measuring the pressure in the system.

The competitive adsorption of three cresol isomers was carried out at 313 K using 1,3,5-triisopropylbenzene as solvent the molecular dimension of which was too large to enter the pores of the adsorbents. The competitive adsorption was initiated by adding 2 ml of 2 wt% adsorbate solution to 0.5 g of adsorbent. The amount of each isomer adsorbed was obtained from the change of concentration of each isomer in liquid phase. The concentration was determined by gas chromatographic analysis.

Results and Discussion

In the alkylation of ethylbenzene with ethanol on the HZSM-5 zeolite, *p*- and *m*-diethylbenzenes, benzene, ethylmethylbenzenes, and xylenes were observed as aromatic products and unreacted ethanol was not observed. Figure 1 shows the results of the alkylation. The activity and the selectivity for the catalyst did not change with process time. The conversion of ethylbenzene was 44% and the yield of diethylbenzene was 26%. The main product was diethylbenzene. The fraction of para-isomer in the diethylbenzenes produced was 39% and little *o*-diethylbenzene was produced. Therefore, it seems that HZSM-5 zeolites do not exhibit the para-selectivity.

In order to clarify the primary product in the alkylation of ethylbenzene with ethanol on HY or HZSM-5, the change in the distribution of diethylbenzene isomers with decreasing W/F was determined. The results on HY (Toyo Soda Ind. Co., Lot Y-30) at 548 K in the diethylbenzenes yield range of 41 to about 4% are shown in Fig. 2. The fraction of *m*-diethylbenzene decreased but those of *p*- and *o*-diethylbenzenes increased with decreasing W/F. In the case of HY catalyst, the primary product is not clear, but may be *p*- and *o*-diethylbenzenes. HY is not thought to exhibit the shape selectivity for this alkylation and the para/ortho orientation for this alkylation generally predominates.

The results on HZSM-5 at 673 K in the diethylben-

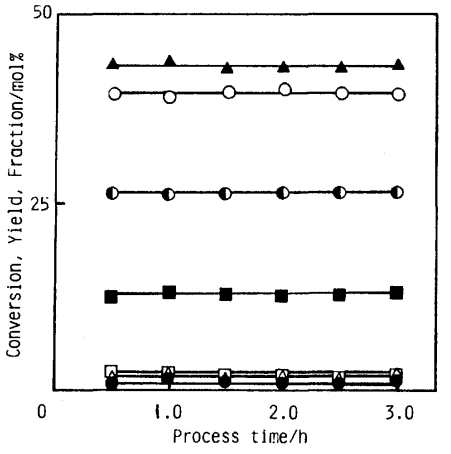

Fig. 1. Alkylation of ethylbenzene with ethanol on HZSM-5 at 673 K and W/F=7.14 g h mol^{-1}. Conversion of ethylbenzene (▲), fraction of para-isomer in diethylbenzene produced (○) and yields of diethylbenzene (◐), benzene (■), ethyltoluene (□), toluene (△), and xylene (●), as a function of process time.

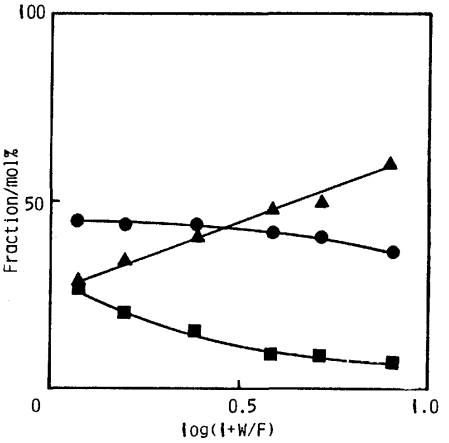

Fig. 2. Change in fraction of each diethylbenzene isomer with W/F in alkylation of ethylbenzene with ethanol on HY at 548 K. Fractions of para-isomer (●), meta-isomer (▲) and ortho-isomer (■) in diethylbenzene produced.

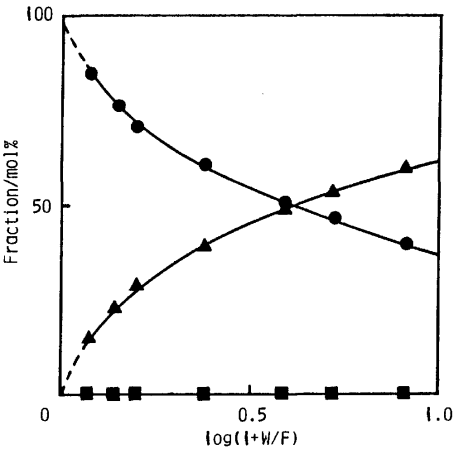

Fig. 3. Change in fraction of each diethylbenzene isomer with W/F in alkylation of ethylbenzene with ethanol on HZSM-5 at 673 K. Fraction of para-isomer (●), meta-isomer (▲), and ortho-isomer (■) in diethylbenzene produced.

zene yield range of 26 to about 3% are shown in Fig. 3. Although the molecular dimension of *o*-diethylbenzene was almost the same as that of *m*-diethylbenzene, little *o*-diethylbenzene was observed in these experiments. This indicates that HZSM-5 catalysts do not exhibit the product selectivity due to configurational diffusion effects. Instead they exhibit transition-state selectivity due to transition state restrictions. The formation of *o*-diethylbenzene through the alkylation of ethylbenzene with ethanol and through the isomerization of diethylbenzene produced is accordingly suppressed. The fraction of *p*-diethylbenzene increased to 100%, and the fraction of *m*-diethylbenzene decreased to 0% with decreasing W/F to 0. These results clearly indicate that the primary product of this alkylation on HZSM-5 catalyst is only *p*-diethylbenzene. The primary product on HZSM-5 is different from that of HY because of the transition-state selectivity of HZSM-5.

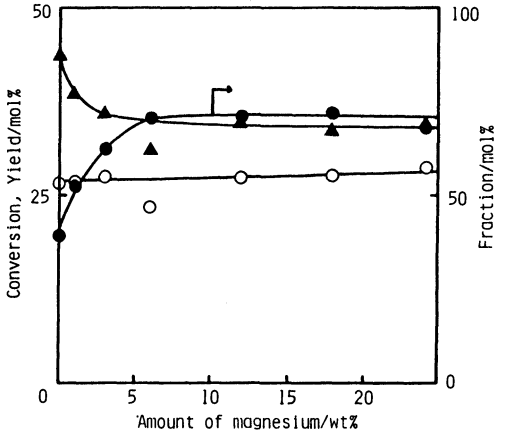

Fig. 4. Effect of amount of magnesium added to HZSM-5 on conversion of ethylbenzene (▲), yield of diethylbenzene (○), and fraction of para-isomer in diethylbenzene produced (●) at 673 K and W/F=7.14 g h mol^{-1}.

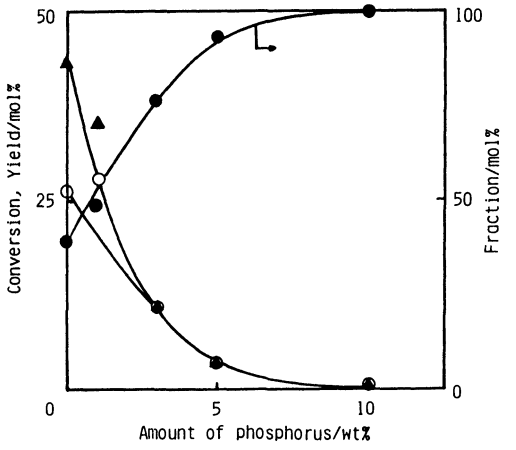

Fig. 5. Effect of amount of phosphorus added to HZSM-5 on conversion of ethylbenzene (▲), yield of diethylbenzene (○), and fraction of para-isomer in diethylbenzene produced (●) at 673 K and W/F=7.14 g h mol^{-1}.

Therefore, we believe that for the selective formation of *p*-diethylbenzene, the isomerization of *p*-diethylbenzene produced as a primary product must be suppressed.

The HZSM-5 loaded with oxide of magnesium, phosphorus or boron showed much higher selectivity for *p*-diethylbenzene formation than the parent HZSM-5 catalyst as observed in the alkylation of toluene with methanol.[3,4] Figures 4, 5, and 6 show the effect of the amount of magnesium, phosphorus or boron added to HZSM-5 zeolite on the fraction of *p*-diethylbenzene in diethylbenzenes produced, on the conversion of ethylbenzene and on the yield of diethylbenzenes. On the Mg-HZSM-5 (Fig. 4), the fraction of *p*-diethylbenzene increased and the conversion of ethylbenzene decreased with increasing amounts of magnesium added. It reached a maximum around 6 wt% of magnesium. In this case, the fraction of para-isomer in diethylbenzenes produced was 73%, and the conversion of ethylbenzene was 34%. The yield of diethylbenzene increased slightly with increasing amounts of magnesium (26—28%).

On the P-HZSM-5 (Fig. 5), the fraction of *p*-diethylbenzene increased to 100% with increasing amounts of phosphorus up to 10 wt%. However, the conversion of ethylbenzene and the yield of diethylbenzene decreased notably with increasing amounts of phosphorus, suggesting that the zeolite channels were rigorously blocked with phosphorus oxide and/or that the acid sites on the zeolite disappeared on the addition of phosphorus oxide.

On the B-HZSM-5 (Fig. 6), the fraction of *p*-diethylbenzene increased with increasing amounts of boron added, as well as magnesium and phosphorus. However, on B(10)HZSM-5 (Number in parentheses indicates the amount of boron added in wt%) the fraction of *p*-diethylbenzene was 100% at a conversion of ethylbenzene and a yield of diethylbenzene of 17, 14%,

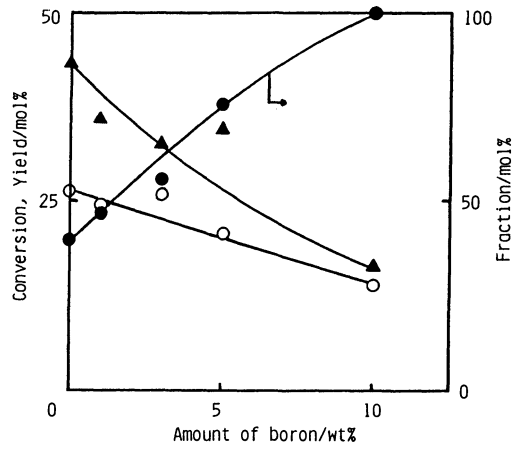

Fig. 6. Effect of amount of boron added to HZSM-5 on conversion of ethylbenzene (▲), yield of diethylbenzene (○), and fraction of para-isomer in diethylbenzene produced (●) at 673 K and W/F=7.14 g h mol^{-1}.

respectively. Although the B(10)HZSM-5 catalyst exhibited a relatively high activity, it showed an extremely high para-selectivity compared with P-HZSM-5 and Mg-HZSM-5 catalysts. The activity and the para-selectivity of Mg-HZSM-5 or P-HZSM-5 catalyst did not change with process time. However, in the case of B-HZSM-5, the conversion of ethylbenzene and the yield of diethylbenzene increased with process time, while the fraction of para-isomer in the diethylbenzene produced slightly decreased. This suggests that boron emerged from the catalyst system during the process time. The modified HZSM-5 type catalysts showed much higher selectivity for *p*-diethylbenzene formation than the parent HZSM-5.

As suggested before, modified HZSM-5 zeolites with the higher para-selectivity must exhibit the lower catalytic activity for the isomerization of *p*-diethylbenzene. In order to clarify the isomerization activity of the modified HZSM-5 catalysts, the reaction of *p*-diethylbenzene on HZSM-5, Mg(18)HZSM-5, P(5)HZSM-5, and B(10)HZSM-5 was carried out at 673 K. The results are shown in Table 1. In the reaction of *p*-diethylbenzene, the isomerization of *p*-diethylbenzene occurred simultaneously with the dealkylation, which was the reverse reaction of the alkylation. In the isomerization of *p*-diethylbenzene, *m*-diethylbenzene was produced, but *o*-diethylbenzene was not. This indicates the transition-state selectivity of HZSM-5. The order of the activities of the various catalysts examined here for the dealkylation of *p*-diethylbenzene agrees with that for the alkylation of ethylbenzene with ethanol. Namely, the order is HZSM-5 > Mg(18)-HZSM-5 > P(5)HZSM-5 > B(10)HZSM-5.

The order of the activities for isomerization of *p*-diethylbenzene is HZSM-5 > Mg(18)HZSM-5 > P(5)-HZSM-5 > B(10)HZSM-5. This order is exactly in reverse order of para-selectivities. From these results, it is concluded that the isomerization of *p*-diethylbenzene, which is the primary product in the alkylation of ethylbenzene with ethanol on the HZSM-5 catalyst, has to be suppressed for the selective formation of *p*-diethylbenzene.

In order to clarify that the modified catalyst, which shows the higher para-selectivity, exhibits the lower activity for *p*-diethylbenzene isomerization than the parent HZSM-5, the competitive adsorption of three cresol isomers and NH_3-TPD were examined. The results of the competitive adsorption and of NH_3-TPD give us the informations on the effective pore dimension of ZSM-5 zeolites[2] and on the acidic properties of the catalysts, respectively. The results of competitive adsorption of three cresol isomers are summarized in Table 2. The adsorption equilibrium was attained within 24 h. Therefore, the total amount of cresol isomers adsorbed and the para-selectivity were determined from the results at 24 h of adsorption time. The total amount of cresol isomers adsorbed decreased by the modification, suggesting that the oxide of magnesium, phosphorus or boron added reduces the effective pore dimension of HZSM-5 and/or blocks the zeolite channels. On the other hand, the para-selectivity for the competitive adsorption (see fraction of *p*-isomer in Table 2.) increased by the modification. This indicates that the effective pore dimension is reduced by the modification. The order of para-selectivities for the competitive adsorption of three cresol isomers are B(10)HZSM-5 > Mg(18)HZSM-5 > P(5)HZSM-5 > HZSM-5. This order is thought to correspond to that of the effective pore dimensions.[2] However it disagrees with that of para-selectivity for the alkylation of ethylbenzene with ethanol, that is, B(10)HZSM-5 > P(5)HZSM-5 > Mg(18)HZSM-5 > HZSM-5. This disagreement may suggest that the narrowness of the effective pore dimension is not so important to improve the para-selectivity in this alkylation on ZSM-5 zeolites.

Figure 7 shows the profiles of NH_3-TPD for HZSM-5 and modified HZSM-5 catalyts. The desorbed gas was only ammonia through the run. The HZSM-5 catalyst exhibited two peaks. One at 373 K corresponds to weak acid sites and the other at 603 K corresponds to strong acid sites. The amount of strong acid sites was remarkably reduced by the modification of HZSM-5 with oxide of magnesium, phosphorus or boron. The Mg(18)HZSM-5 catalyst still has a small amount of strong acid sites, while the P(5)HZSM-5 and B(10)HZSM-5 catalysts have few strong acid sites. The order of the amounts of the strong acid sites are HZSM-5 > Mg(18)HZSM-5 > P(5)HZSM-5 > B(10)HZSM-5. This order exactly coincides not only with the order of para-selectivities but also with that of activities for *p*-diethylbenzene isomerization shown in Table 1. These

Table 1. Reaction of *p*-Diethylbenzene on HZSM-5 and Modified HZSM-5 Catalysts at 673 K and W/F=7.14 g h mol^{-1}

	Conversion for isomerization	Conversion for dealkylation
	mol%	mol%
HZSM-5	19	54
Mg(18)HZSM-5	8.2	49
P(5)HZSM-5	0.29	1.6
B(10)HZSM-5	0.27	32

Table 2. Competitive Adsorption of Three Cresol Isomers on HZSM-5 and Modified HZSM-5 Zeolites at 313 K

	Fraction of each cresol isomer adsorbed/%			Total amount adsorbed /mg g^{-1}
	o-	*m*-	*p*-	
HZSM-5	25.7	43.2	31.1	114.3
Mg(18)HZSM-5	22.2	38.5	39.3	104.5
P(5)HZSM-5	25.1	39.6	35.5	78.0
B(10)HZSM-5	21.8	36.8	41.4	89.5

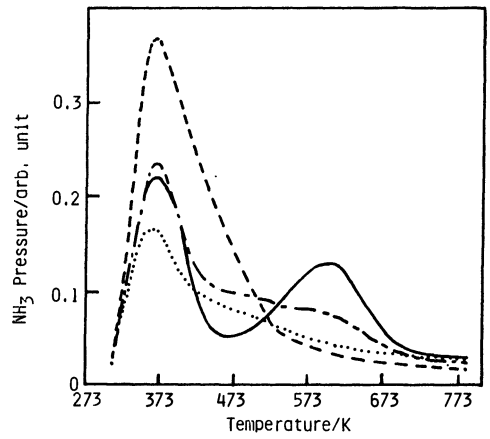

Fig. 7. Profiles of NH_3-TPD for HZSM-5 (——), Mg(18)HZSM-5 (-·-·-), P(5)HZSM-5 (·····), and B(10)HZSM-5 (----).

facts suggest that the isomerization of *p*-diethylbenzene is more accelerated by the strong acid sites than the alkylation. Moreover, the intrinsic alkylation activities of the catalyst examined here except P-HZSM-5 are high enough, because ethanol is completely converted under our reaction conditions. Therefore, it is concluded that the strong acid sites on the catalyst have to be reduced for the selective formation of *p*-diethylbenzene by the alkylation of ethylbenzene with ethanol.

There is a large difference in yield of ethylbenzene in the alkylation of ethylbenzene with ethanol between P(5)HZSM-5 and B(10)HZSM-5. The difference in the acid properties between P(5)HZSM-5 and B(10)HZSM-5 is in the amount and strength of the weak acid sites. The B(10)HZSM-5 catalyst has more weak acid sites and exhibits a wider distribution in the weak acid site region (up to about 523 K in NH_3-TPD profile) compared with the P(5)HZSM-5 catalyst. Therefore, it is suggested that the activity for the alkylation of ethylbenzene with ethanol is related not only to the strong acid sites but also to the weak acid sites. However, the activity for the isomerization of diethylbenzene is related solely to the strong acid sites.

From these results, we conclude as follows. The isomerization of *p*-diethylbenzene, which is the primary poduct in the alkylation of ethylbenzene with ethanol on the HZSM-5 catalyst, has to be suppressed for the selective formation of *p*-diethylbenzene. The suppression of the isomerization of *p*-diethylbenzene is achieved by reducing the amount of strong acid sites rather than by reducing the effective pore dimension of the HZSM-5 zeolites.

References

1) G. T. Kokotailo, S. L. Lawton, D. H. Olson, and W. M. Meier, *Nature (London)*, **272**, 437 (1978).

2) S. Namba, Y. Kanai, H. Shoji, and T. Yashima, *Zeolites*, **4**, 77 (1984).

3) T. Yashima, Y. Sakaguchi, and S. Namba, *Stud. Surf. Sci. Catal.* (Proc. Seventh Int. Congr. Catal., Tokyo 1980), **7**, p. 739. (1981).

4) W. W. Kaeding, C. Chu, L.B. Young, B. Weinstein, and S. A. Butter, *J. Catal.*, **67**, 159 (1981).

5) K. H. Chandavar, S. G. Hegde, S. B. Kulkarni, P. Ratnassamy, G. Chitlangia, A. Singh, and A. V. Deo, "Proc. 6th Int. Zeolite Conf.," ed by D. Olson and A. Bisio, Butterworths Guildford, U.K. (1983), p. 325.

6) Warren W. Kaeding, *J. Catal.*, **95**, 512 (1985).

7) J. Wei, *J. Catal.*, **76**, 433 (1982).

8) Brit. Patent 1402981.

 © 1988 The Chemical Society of Japan Bull. Chem. Soc. Jpn., 61, 1057—1062 (1988)

Photooxidation of the Evaporated Films of Polycyclic Aromatic Hydrocarbons Studied by X-Ray Photoelectron Spectroscopy

Masamichi YAMADA,† Isao IKEMOTO,†† and Haruo KURODA*
Department of Chemistry, Faculty of Science, The University of Tokyo, Hongo, Bunkyo-ku, Tokyo 113
(Received August 29, 1987)

Photooxidations of the evaporated films of rubrene, naphthacene, and pentacene were investigated by means of X-ray photoelectron spectroscopy. A rubrene film was found to be photooxidized far more easily than a naphthacene film although the molecules of rubrene and naphthacene in solution are known to be almost equally reactive for photooxidation. Although pentacene is photooxidized very easily in solution, the oxidation rate of a pentacene film was little enhanced by the light irradiation. Discussion is given on these behaviors of the evaporated films by considering the molecular packing in the solid state and the mechanism of photooxidation.

Photoconductivities of polycyclic aromatic hydrocarbons are known to be influenced more or less by the presence of oxygen in the ambient atmosphere.[1] Frankevich and his collaborators investigated the magnetic field effect on the photoconductive behaviors of evaporated films of rubrene (5,6,11,12-tetraphenylnaphthacene)[2] and naphthacene[3] in the oxygen atmosphere.

On the other hand, the photochemical reactions of polycyclic aromatic hydrocarbons with oxygen in solution have been extensively studied.[4,5] Polyacenes such as naphthacene and pentacene are rapidly converted to their transannular peroxides when their aerated solutions are irradiated with light.[4-6] Therefore one could expect that photooxidation will take place more or less when the photoconduction experiments are done on the solids of these hydrocarbons in the atmosphere containing oxygen.

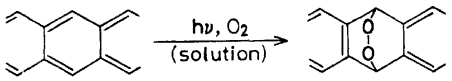

However, little is known so far about the solid-state photooxidation of above-mentioned hydrocarbons except for rubrene.[7] This lack of information is largely due to the situation that, even if the photooxidation occurs in the solid state, it proceeds very slowly from the surface to the bulk in most organic solids, hence it is hard to follow the progress of oxidation by means of conventional experimental methods.

A variety of surface-sensitive techniques such as electron spectroscopies have developed since 1970's. However, they have scarcely been utilized in the studies of the reactions at the surfaces of organic molecular solids. Harada, Ohno and their collaborators examined the photooxidation of evaporated films of rubrene and naphthacene by ultraviolet photoelectron spectroscopy (UPS) and by Penning ionization electron spectroscopy (PIES).[8,9] They observed spectral changes due to photooxidation, and reported that a rubrene film is more easily photooxidized than a naphthacene film.

X-Ray photoelectron spectroscopy (XPS) is one of the most suitable techniques in such studies, because it can reveal non-destructively the elemental composition near the surface of molecular solids. We have previously studied the oxidation which proceeds in the dark, on the surfaces of the evaporated films of polycyclic aromatic hydrocarbons, by means of XPS.[10] In the present paper, we will report the results obtained on the photooxidation of the evaporated films of rubrene (**1**), naphthacene (**2**), and pentacene (**3**).

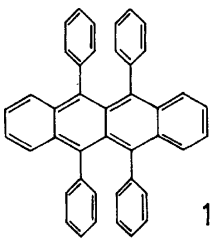
1

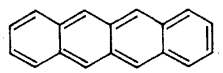
2

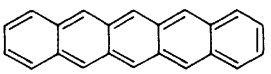
3

Experimental

Rubrene and naphthacene were commercially obtained and purified by sublimation in vacuo. Pentacene which had already been purified, was kindly supplied by Professor H. Inokuchi, Institute for Molecular Science.

X-Ray photoelectron spectra were measured with a McPherson ESCA 36 photoelectron spectrometer by using Mg $K\alpha$ (1253.6 eV) as the stimulating radiation. The sample chamber of the spectrometer was a little modified for the purpose of the present study. The layout of the modified sample chamber is illustrated in Fig. 1(a).

On each hydrocarbon, we carried out experiments with the following sequence. With the setup shown in Fig. 1(a), the

† Present address: Optoelectronics Technology Research Corporation, 5-5, Tohkodai, Toyosato, Tsukuba-gun, Ibaraki 300-26.

†† Present address: Department of Chemistry, Faculty of Science, Tokyo Metropolitan University, Fukazawa, Setagaya-ku, Tokyo 158.

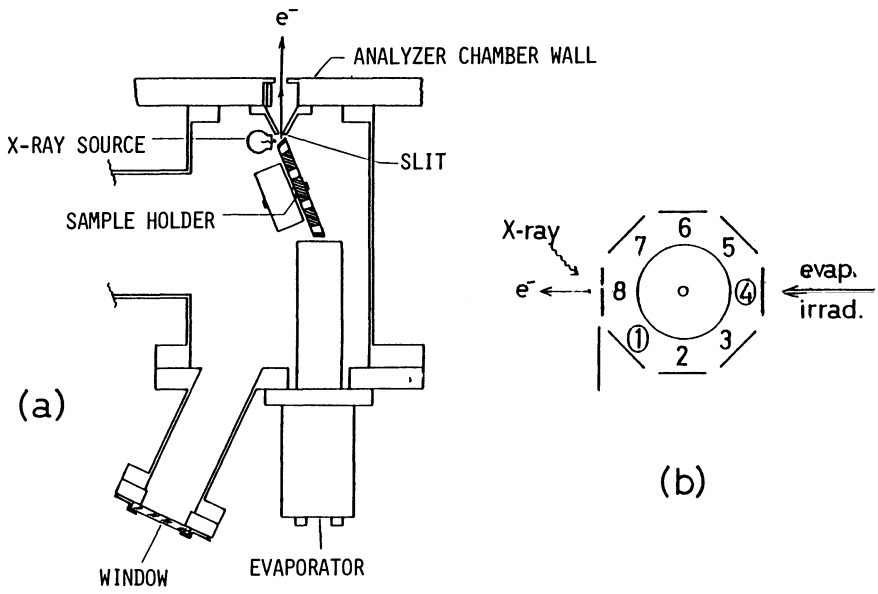

Fig. 1. (a) Layout of the sample chamber arranged for a photooxidation experiment, and (b) the side view of the 8-position sample holder. Sample films are prepared at the positions No. 1 and No. 4.

sample was deposited by sublimation in vacuo onto the substrates (aluminum or quartz plates) at the two different positions (No. 1 and No. 4 in Fig. 1(b)) of the 8-position rotatable sample holder, successively, and the first XPS measurement was done immediately. Then, the sample evaporator was quickly replaced with a Pyrex glass window while purging the sample chamber continuously with nitrogen. Since the oxidation of the sample film proceeds very slowly in the dark,[10] the above-mentioned procedure is allowable for the purpose of the present study even though we cannot completely avoid the contact of the sample film with oxygen. After the replacement of the evaporator with the window, the sample chamber was evacuated and the second XPS measurement was carried out. Next, we introduced oxygen to a desired pressure into the sample chamber, and one of the two sample films was irradiated with the light from a 500 W incandescent lamp through the window. During this procedure, the other sample film was sheltered from the light behind the sample holder. After the sample films were kept under the above-mentioned conditios for an appropriate period, the sample chamber was evacuated to carry out XPS measurement. Thereafter a similar procedure was repeated with different oxygen pressure and with different light irradiation time. The light irradiation was given to the two sample films alternately.

For each film, the binding energies, E_B's, were referenced to the Cls line (284.3 eV).[11]

Results

In the XPS spectra which were measured immediately after the preparation of the sample films under a high vacuum, all three hydrocarbons exhibited only a strong and sharp Cls peak, with the FWHM (full width at half maximum) of 1.5—1.7 eV.

Figure 2 illustrates the growth of the Ols peak in the spectrum of rubrene films at successive experimental stages. After the replacement of the evaporator with the window, both of rubrene films gave a weak Ols peak (see Fig. 2(b)). Figure 2(c) shows the Ols peaks measured after the films were kept in the oxygen of 1.5 kPa for 17 min, during which one film (at position

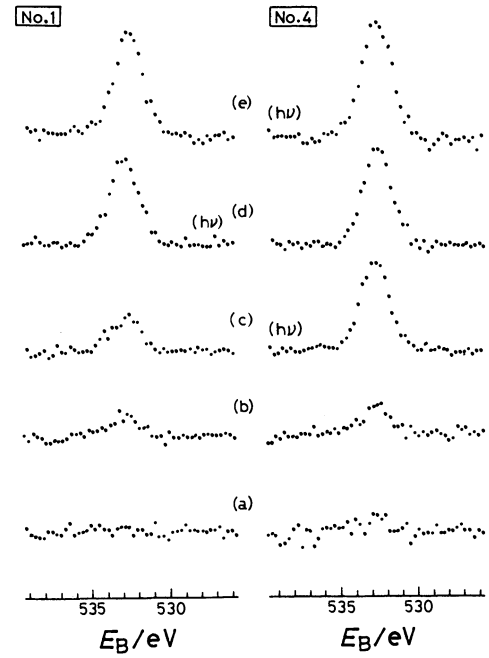

Fig. 2. Growth of the Ols peaks from two evaporated films of rubrene. "$(h\nu)$" indicates the irradiated film at each stage. (a) Freshly evaporated films. (b) After replacement of the evaporator with the window. (c) After exposure to 1.5 kPa oxygen for 17 min, No. 4 irradiated for 10 min. (d) After exposure to 1.6 kPa oxygen for 19 min, No. 1 irradiated for 11 min. (e) After exposure to 5.7 kPa oxygen for 69 min, No. 4 irradiated for 60 min.

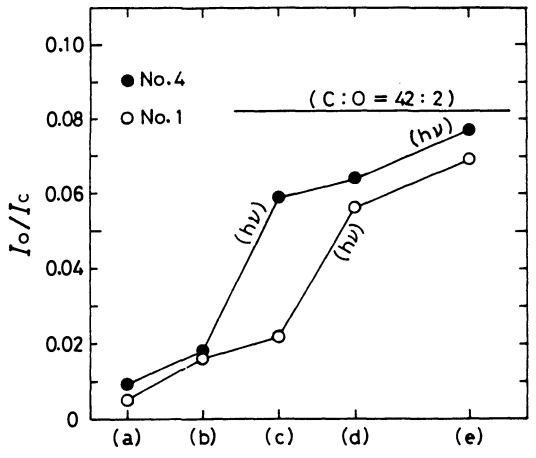

Fig. 3. Variation of the intensity ratios, Io/Ic, for two evaporated films of rubrene. "$(h\nu)$" indicates the irradiated film at each stage. The line designated by "C:O=42:2" indicates the ratio expected for the transannular peroxide of rubrene. Note that the ordinate is expanded twice as compared to those in Figs. 4 and 5. (a)—(e) on the abscissa correspond to (a)—(e) in Fig. 2.

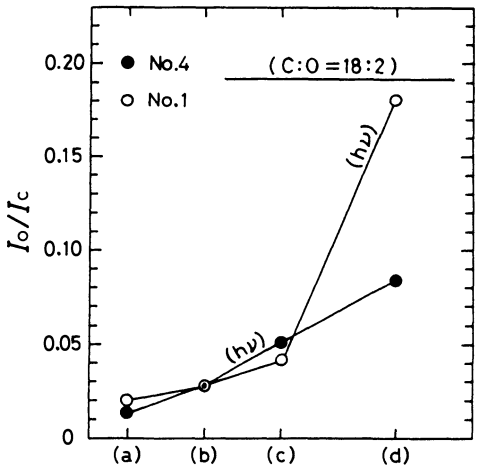

Fig. 4. Variation of the intensity ratios, Io/Ic, for two evaporated films of naphthacene. (a) Freshly evaporated films. (b) After replacement of the evaporator with the window. (c) After exposure to 5.1 kPa oxygen for 67 min, No. 4 irradiated for 61 min. (d) After exposure to 12.9 kPa oxygen for 620 min, No. 1 irradiated for 605 min.

No. 4 of the sample holder) was irradiated with light for 10 min. Note that a pronounced intensity increase occurred in the case of the irradiated film, while the Ols peak of the nonirradiated film increased little. In the next stage, the films were kept in the oxygen of 1.6 kPa for 19 min, and the film (at position No. 1) which had not been irradiated in the previous oxygen exposure, was irradiated with light for 11 min. Then the Ols peak of the irradiated film appreciably increased its intensity, and the intensity of Ols peak became almost equal between the two sample films as shown in Fig. 2(d). These results clearly demonstrate that the oxidation of a rubrene film is markedly enhanced by the light irradiation. Figure 2(e) shows the spectra measured after an exposure to the oxygen of 5.7 kPa for 69 min, during which one film (at position No. 4) was irradiated with light for 60 min. As compared with Fig. 2(d), the change of Ols spectrum is very little both with and without the light irradiation. Seemingly the intensity of Ols peak had nearly saturated already in the preceding stage.

The ratio of the integrated intensity of the Ols peak to that of the Cls peak, Io/Ic, was determined from the spectrum measured at each experimental stage. The results are plotted in Fig. 3, where the horizontal line designated by "C:O=42:2" represents the value expected for the transannular peroxide of rubrene under the assumption that the relative sensitivity of detection for carbon and oxygen is 0.58 : 1.00.[12] Note that the ratio obtained in the final stage is close to the value mentioned above.

The corresponding data for naphthacene and pentacene films are shown in Figs. 4 and 5, respectively.

In the case of a naphthacene film, the Io/Ic ratio was far below the value for the transannular peroxide even after the 61 min light irradiation in the oxygen of 5.1 kPa. It approached to the latter ratio when a film was irradiated for about 10 hours in the oxygen of 12.9 kPa. Thus markedly severer conditions seem to be necessary to photooxidize a naphthacene film as compared with a rubrene film.

The behavior of a pentacene film is very different from those of naphthacene and rubrene films. As can be seen from Fig. 5, the oxidation of a pentacene film is enhanced only little by the light irradiation, and the Io/Ic ratio was still about half of the value expected for the transannular peroxide even if the film had been irradiated with light for 9 hours in the oxygen of 14.4 kPa. It is hard to make a quantitative comparison of

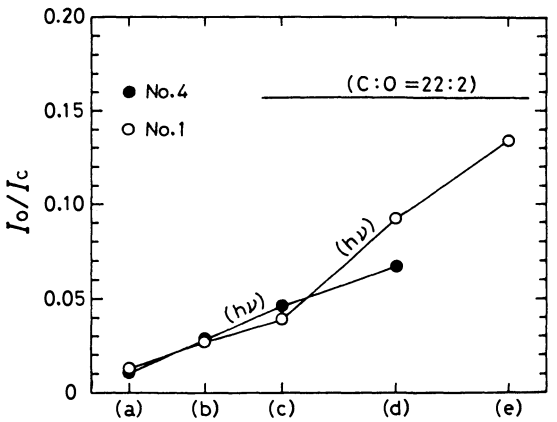

Fig. 5. Variation of the intensity ratios, Io/Ic, for two evaporated films of pentacene. (a) Freshly evaporated films. (b) After replacement of the evaporator with the window. (c) After exposure to 4.4 kPa oxygen for 146 min, No. 4 irradiated for 135 min. (d) After exposure to 14.4 kPa oxygen for 555 min, No. 1 irradiated for 540 min. (e) After kept in the air (dark) for 12 days.

photooxidation activities of three hydrocarbons from the results of the present study. But we may safely conclude that a pentacene film is far less reactive for photooxidation than rubrene and naphthacene films.

For the three hydrocarbons studied here, the binding energies of their Cls peaks are expected to be almost the same.[11] Furthermore, they will change little under our experimental conditions since, as seen in Figs. 3—5, less than two atoms among 18—42 carbon atoms in a molecule may be directly bound to oxygen atom in their oxidation products. Therefore, we utilized the Cls peak (284.3 eV) as the reference for the binding energy scale.

The observed binding energies, E_B's, and FWHM's of Ols peaks from oxidized hydrocarbon films are summarized in Table 1 together with the corresponding values of polycyclic carbonyl compounds. Note that the Ols binding energy is 532.5—532.7 eV in the case of the photooxidation products while it is 530.6—530.9 eV in the case of carbonyl compounds. This fact shows that carbonyl compounds are not the predominant products of photooxidation. In effect, the photooxidation product of rubrene in the solid state is considered to be the transannular peroxide[2,7-9] as is the case with photooxidation in solution.

The main photooxidation product is likely to be the transannular peroxide also in the case of a naphthacene film since the observed Ols binding energy is equal to the one observed of a rubrene film. But it is conceivable that some other oxidized species coexist in the case of a naphthacene film because the observed Ols peak is appreciably broader than that of a rubrene film. Probably, a part of the transannular peroxide is further transformed to more stable species. The Ols peak from an oxidized pentacene film is similar in position and width to that from a photooxidized naphthacene film. Some oxygen-containing species (including the transannular peroxide) may coexist on the surface of a pentacene film.

Table 1. Binding Energies and FWHM's of the Ols Peaks from Photooxidized Hydrocarbons and Polycyclic Carbonyl Compounds[a]

Compound	E_B/eV	FWHM/eV
Rubrene	532.7	2.3
Naphthacene	532.6	2.7
Pentacene	532.5	2.7
Anthraquinone	530.9[b]	1.7
Anthrone	530.9[b]	1.8
Mesonaphthodianthrone[c]	530.6[b]	1.7

a) Mg$K\alpha$ spectra of carbonyl compounds were obtained from the films freshly deposited in the sample chamber. b) The binding energy was referenced to the main Cls line, whose binding energy was assumed to be 284.3 eV. c) Phenanthro[1,10,9,8-*opqra*]-perylene-7,14-dione.

Discussion

As we have already mentioned, the three hydrocarbons studied here form the transannular peroxides by the photooxidation in solution. The following scheme has been proposed for the self-sensitized photoperoxidation of aromatic hydrocarbons.[13,14]

$$M(S_0) + h\nu \rightarrow M^*(S_1) \quad (1)$$
$$M^*(S_1) \rightarrow M^*(T_1) \quad (2)$$
$$M^*(S_1) + O_2(^3\Sigma) \rightarrow M^*(T_1) + O_2(^3\Sigma) \quad (3)$$
$$M^*(T_1) + O_2(^3\Sigma) \rightarrow M(S_0) + O_2^*(^1\Delta) \quad (4)$$
$$M(S_0) + O_2^*(^1\Delta) \rightarrow MO_2[\text{peroxide}] \quad (5)$$

where $M(S_0)$, $M^*(S_1)$, and $M^*(T_1)$ are the hydrocarbon molecules in the ground, singlet excited and triplet excited state, respectively, and $O_2(^3\Sigma)$ and $O_2^*(^1\Delta)$ are the oxygen molecules in the ground and singlet excited state (0.98 eV above the ground state),[15] respectively. Recently, it was established that $O_2^*(^1\Delta)$ can be generated also by the following process.[16]

$$M^*(S_1) + O_2(^3\Sigma) \rightarrow M^*(T_1) + O_2^*(^1\Delta) \quad (6)$$

In an aerated solution, $M^*(S_1)$ is quenched by oxygen via the process (3) or (6) with a diffusion controlled rate,[13] the rate constant being of the order of 10^{10} dm^3 mol^{-1} s^{-1}. The process (4) which produces the singlet oxygen $O_2^*(^1\Delta)$ by the energy transfer from $M^*(T_1)$, is also known to proceed rapidly with a rate constant of about one-ninth of the diffusion controlled value provided that the triplet state of the hydrocarbon, $M^*(T_1)$, has an energy in the range of 1.2—1.9 eV (e.g., naphthacene and anthracene).[13,17] Thus once $M^*(T_1)$ is formed, $O_2^*(^1\Delta)$ is produced with a yield of about unity via the process (4) in an air-saturated solution. On the other hand, the rate constant of the process (5) which gives the transannular peroxide by the reaction between $M(S_0)$ and $O_2^*(^1\Delta)$ is significantly lower than the diffusion controlled value except for extremely reactive hydrocarbons such as pentacene: It has been reported to be 4.2×10^7, 1.2×10^7, and 4.2×10^9 dm^3 mol^{-1} s^{-1} for rubrene, naphthacene and pentacene, respectively.[18] Therefore, the overall photooxidation rate will be primarily determined by the rate constant of the process (5), and consequently, pentacene will be the most reactive, and the reaction rate will be comparable between naphthacene and rubrene.

However, the results described in the preceding section, show that the situation is quite different in the solid state: the photooxidation takes place most easily in a rubrene film, and least in a pentacene film.

If we take an analogy to the above-mentioned scheme of the photooxidation in solution, we can consider that the solid-state photooxidation proceeds by the interaction of a hydrocarbon molecule with a singlet oxygen, $O_2^*(^1\Delta)$, which is formed by the energy transfer to an oxygen molecule either from a triplet exciton or from a singlet exciton of the hydrocarbon solid.

It is known that triplet excitons are produced with high efficiency in a naphthacene crystal via the fission

of a singlet exciton into two triplet excitons.[19] The same process takes place also in a rubrene crystal.[20] In the case of a naphthacene crystal, the interaction of a triplet exciton with oxygen[21] will occur only on the crystal surface, because naphthacene molecules are closely packed in the crystal,[22] so that it is difficult for oxygen molecules to diffuse into the bulk. It is well known that a transannular peroxide has a folded configuration whereas its parent hydrocarbon is planar. Close packing of molecules will hinder such large change of molecular shape, and consequently, retard the photooxidation. Therefore the oxidation will proceed only very slowly from the surface to the bulk. On the other hand, rubrene molecules are loosely packed in the crystal because of the four bulky, noncoplanar, substituents.[23] Thus oxygen molecules can easily diffuse into the bulk, and the formation of $O_2^*(^1\Delta)$[21] as well as that of the peroxide can occur not only on the crystal surface but also in the bulk. Furthermore, the distortion of the crystal lattice accompanying the formation of the transannular peroxide will easily take place in the bulk. Seemingly, these differences arising from the molecular packing in the crystal, are the origin of the significant difference in photooxidation reactivity between a naphthacene film and a rubrene film.

The fission of a singlet exciton to two triplet excitons can also take place in a pentacene crystal.[24] But, the energy of the triplet exciton[24] is lower than 0.98 eV and insufficient to produce a singlet oxygen by the energy transfer. Under this situation, a singlet oxygen $O_2^*(^1\Delta)$ is probably formed via the energy transfer from a singlet exciton to oxygen. This will primarily occur on the crystal surface since pentacene molecules are closely packed in the crystal to prevent the diffusion of oxygen into the bulk.[25] However, there will not be much probability that a singlet exciton reaches the crystal surface since the fission of the singlet exciton efficiently takes place in the bulk. Seemingly this explains why the oxidation of a pentacene film is little enhanced by the light irradiation though, in solution,[26] pentacene is photooxidized rapidly.

The authors wish to express their thanks to Professor Yoshiya Harada, the University of Tokyo, for helpful discussions, and to Professor Hirochika Sakuragi, the University of Tsukuba, for helpful information on singlet oxygen chemistry. We also would like to thank Professor Hiroo Inokuchi, Institute for Molecular Science, for kindly supplying pentacene.

References

1) Some examples are listed below with the compound in parentheses: A. G. Chynoweth, *J. Chem. Phys.*, **22**, 1029 (1954) (anthracene); A. Bree and L. E. Lyons, *J. Chem. Soc.*, **1960**, 5179 (anthracene); H. Kuroda and E. A. Flood, *Can. J. Chem.*, **39**, 1981 (1961) (pentacene); Y. Kamura, H. Inokuchi, J. Aoki, and S. Fujisawa, *Chem. Phys. Lett.*, **46**, 356 (1977) (tetrabenzo[*a, cd, j, lm*]perylene).

2) E. L. Frankevich, M. M. Tribel, and I. A. Sokolik, *Phys. Status Solidi B*, **77**, 265 (1976).

3) E. L. Frankevich and I. A. Sokolik, *Khim. Vys. Energ.*, **6**, 433 (1972) [*High Energy Chem. (USSR)*, **6**, 382 (1972)]; E. L. Frankevich and I. A. Sokolik, *Pis'ma Zh. Eksp. Teor. Fiz.*, **14**, 577 (1971) [*JETP Letters*, **14**, 401 (1971)].

4) K. Gollnick and G. O. Schenck, "1,4-Cycloaddition Reactions," ed by J. Hamer, Academic Press, New York (1967), Chap. 10.

5) R. W. Denny and A. Nickon, *Org. React.*, **20**, 133 (1973).

6) E. Clar, "Polycyclic Hydrocarbons," Academic Press, London (1964), pp. 55—56, 397—399.

7) R. M. Hochstrasser and M. Ritchie, *Trans. Faraday Soc.*, **52**, 1363 (1956); R. M. Hochstrasser, *Can. J. Chem.*, **37**, 1123 (1959).

8) Y. Harada, T. Takahashi, S. Fujisawa, and T. Kajiwara, *Chem. Phys. Lett.*, **62**, 283 (1979).

9) K. Ohno, H. Mutoh, and Y. Harada, *Surf. Sci.*, **115**, L128 (1982).

10) M. Yamada, I. Ikemoto, and H. Kuroda, *Bull. Chem. Soc. Jpn.*, **50**, 2262 (1977).

11) In our preceding work (Ref. 10), we determined the binding energies of core peaks from polycyclic aromatic hydrocarbons by reference to $Au4f_{7/2}$ line (84.0 eV) from gold deposited on samples. The Cls binding energies thus obtained for four hydrocarbons were 284.3—284.6 eV (the average: 284.5 eV). However, according to Johansson et al. (G. Johansson, J. Hedman, A. Berndtsson, M. Klasson, and R. Nilsson, *J. Electron Spectrosc. Relat. Phenom.*, **2**, 295 (1973)), the binding energy of $Au4f_{7/2}$ line should be set at 83.8 eV (i.e., smaller by 0.2 eV than the previous value). Therefore, we adopted the value 284.3 eV for the Cls line in the present study.

12) The sensitivity ratio between Cls and Ols peaks used in this study (0.58 : 1.00) was derived from Mg $K\alpha$ spectra of the three carbonyl compounds listed in Table 1.

13) J. B. Birks, "Photophysics of Aromatic Molecules," Wiley-Interscience, London (1970), Chap. 10.

14) B. Stevens, *Acc. Chem. Res.*, **6**, 90 (1973).

15) Literature on singlet oxygen: (review) D. R. Kearns, *Chem. Rev.*, **71**, 395 (1971); (book) "Singlet Oxygen," ed by H. H. Wasserman and R. W. Murray, Academic Press, New York (1979).

16) For example: H.-D. Brauer, A. Acs, W. Drews, R. Gabriel, S. Ghaeni, and R. Schmidt, *J. Photochem.*, **25**, 475 (1984); A. P. Darmanyan, *Chem. Phys. Lett.*, **86**, 405 (1982); G. P. Gurinovich and K. I. Salokhiddinov, *Chem. Phys. Lett.*, **85**, 9 (1982).

17) O. L. J. Gijzeman, F. Kaufman, and G. Porter, *J. Chem. Soc., Faraday Trans. 2*, **69**, 708 (1973).

18) B. Stevens, S. R. Perez, and J. A. Ors, *J. Am. Chem. Soc.*, **96**, 6846 (1974). For compiled rate data, see F. Wilkinson and J. G. Brummer, *J. Phys. Chem. Ref. Data*, **10**, 809 (1981).

19) For example, R. P. Groff, P. Avakian, and R. E. Merrifield, *Phys. Rev. B*, **1**, 815 (1970).

20) B. M. Rumyantsev, V. I. Lesin, and E. L. Frankevich, *Opt. Spektrosk.*, **38**, 89 (1975) [*Opt. Spectrosc.*, **38**, 49 (1975)].

21) Triplet energy of naphthacene in the solid state is 1.25 eV (Y. Tomkiewicz, R. P. Groff, and P. Avakian, *J. Chem. Phys.*, **54**, 4504 (1971)), and that of rubrene is 1.21 eV (E. L.

Frankevich, B. M. Rumyantsev, and V. I. Lesin, *J. Lumin.*, **11**, 91 (1975)). Both exceed the excitation energy (0.98 eV) of a singlet oxygen, $O_2^*(^1\Delta)$.

22) J. M. Robertson, V. C. Sinclair, and J. Trotter, *Acta Crystallogr.*, **14**, 697 (1961). See also, R. B. Campbell and J. M. Robertson, *ibid.*, **15**, 289 (1962).

23) I. Bulgarovskaya, V. Vozzhennikov, S. Aleksandrov, and V. Belskii, *Latv. PSR Zinat. Akad. Vestis, Fiz. Teh. Zinat. Ser.*, **1983**, (4), 53.

24) S_1 and T_1 states of pentacene in the solid state are located at 1.88 eV (E. A. Silinsh, A. I. Belkind, D. R. Balode, A. J. Biseniece, V. V. Grechov, L. F. Taure, M. V. Kurik, J. I. Vertzymacha, and I. Bok, *Phys. Status Solidi A*, **25**, 339 (1974)), and at 0.86 eV (J. Burgos, M. Pope, Ch. E. Swenberg, and R. R. Alfano, *Phys. Status Solidi B*, **83**, 249 (1977)), respectively. The S_1 energy is higher than double the T_1 energy.

25) R. B. Campbell, J. M. Robertson, and J. Trotter, *Acta Crystallogr.*, **14**, 705 (1961). See also, R. B. Campbell and J. M. Robertson, *ibid.*, **15**, 289 (1962).

26) See Ref. 18, p. 6847.

 © 1988 The Chemical Society of Japan Bull. Chem. Soc. Jpn., 61, 1063—1070 (1988)

A Through Space/Bond Interaction Analysis of the Shape of the Band Structure of Polyacetylene

Yuriko Aoki, Akira Imamura,* and Takae Sasaki
Department of Chemistry, Faculty of Science, Hiroshima University, Higashisenda-machi, Hiroshima 730
(Received September 14, 1987)

The band structure of all-*trans*-polyacetylene is examined by using through space/bond interaction analysis. It is found that the cross-term in the perturbation expansion between two kinds of interactions governs the band shape near the gap: One kind is the interaction within the backbone, and the other is that between the backbone and the side chain. The relationship between the band structure and the symmetry of the interacting orbitals is also discussed.

The relationship between the structure of a polymer and its electronic states has attracted considerable attention from the theoretical point of view. All-*trans*-polyacetylene is a simple linear conjugated π system and is an insulator with a degenerate ground state because of the alternation of the C-C bond length. The electronic properties of pure polyacetylene have been investigated by using the Hartree-Fock tight-binding approximation both within one-electron pictures[1-9] and including electron-correlation effects.[10,11] There are other methods, for example, using the X_α approach[12,13] and the GKS potential,[14] which give better agreements with the experimental data than do the RHF results. Many theoretical studies show that the conductivity of such a system is intimately related to the distortion of the symmetry attributable to the bond alternation, which gives rise to the formation of a gap between the HOMO π band and the LUMO π^* band.[15-19] This polymer has recently been the focus of enormous interest because of the discovery that the conductivity can be controlled by doping with electron donors and acceptors.[20-27]. Brédas et al. showed, at the level of the ab initio method, that there is a relationship between the structural change in the bond alternation and the magnitude of the charge-transfer interaction between the polyacetylene and dopants.[28,29] Kertész carried out three-dimensional energy band calculations on highly doped donor and acceptor compounds of polyacetylene based on the rigid-band model[30] and discussed the interaction of the polymer π orbital with the orbitals of the dopants.[31] These facts imply that the conductivity of a Peierls-distorted[32] linear chain is strongly dependent on the environment of polymers in connection with the gap between the top of the filled π-electron valence band and the bottom of the unfilled π^*-electron conduction band.

On the other hand, there have been few studies of the energy band of σ electron orbitals, which are considered to be hardly responsible at all for the conductivity. Hoffmann's group has developed a chemical and theoretical approach to the electronic structures of solids, which mainly have two-dimensional layers, at the level of the extended Hückel method. In their studies, the band structures including σ orbitals of many inorganic crystals have been predicted and interpreted successfully in terms of the symmetry of the crystal orbitals. In order to obtain some insight into the behavior of the σ orbitals near the gap, we ourselves have extended the concept of the interaction of orbitals through-space and through-bonds, a concept that has been presented by Hoffmann et al.,[33] to a polymer system. In our previous paper,[34] this method was applied to the lone-pair orbitals of polynitrilomethylidyne, and it was found that the relationship between the energy band and the interaction of atomic orbitals can be interpreted in terms of the symmetry of the crystal orbitals. In the present article, we use this method for characterizing the electronic properties of polyacetylene on the presumption that the band structure with a high conductivity must be reflected in the interaction between orbitals near the gap. We expect that this analysis will provide information useful for the prediction of various properties of the polymers.

Calculation of Band Structure

The crystal orbital method has been described in the literature.[8,35] The necessary equations will, therefore, merely be listed below in explanation of the through space/bond interaction analysis. The ab initio crystal orbital method used in this study is based on the general SCF tight-binding LCAO formalism,[36] which corresponds essentially to Roothaan's Hartree-Fock equation for molecules.[37] A delocalized wave function of a single electron in the periodic potential of a one-dimensional crystal is represented as a linear combination of Bloch basis orbitals, which are symmetry-adapted combinations of atomic orbitals, χ_r, in this form:

$$\phi_i^k(r_1) = (2N+1)^{-1/2} \sum_{m=-N}^{+N} \sum_{r}^{n_r} \exp(ikR_m) C_{ir}(k) \chi_r(r_1 - R_m) \quad (1)$$

where k denotes a wavenumber vector in the first Brillouin zone, and i, an energy band. The $\chi_r(r_1-R_m)$ term stands for an atomic orbital localized in the m-th cell at $R_m(m=0, 1, 2, \cdots, N)$, while $2N+1$ is the number of elementary cells. For a given atomic basis and in the restricted HF-Roothaan scheme, the optimal set of one-electron wave functions, $\phi_i^k(r_1)$, is obtained by

solving the following equations:

$$\sum_S C_{is}(k)[F_{rs}(k) - S_{rs}(k)E_i(k)] = 0 \qquad (2)$$
$$r = 1, 2, \cdots\cdots, n_r$$

where,

$$F_{rs}(k) = \sum_{m=-M}^{+M} \exp(ikR_m)F_{rs}^{Qm}(R_m), \qquad (3)$$

$$S_{rs}(k) = \sum_{m=-M}^{+M} \exp(ikR_m)S_{rs}^{Qm}(R_m), \qquad (4)$$

whose solutions at various k points in BZ provide the band structure of $E_i(k)$. F_{rs}^{Qm} is the Fock matrix element between the r-th atomic orbital χ_r in the central cell and the s-th atomic orbital χ_s^m in the m-th cell. S_{rs}^{Qm} is the overlap integral between these orbitals.

Based on this scheme, the polymer Gaussian 74 program has been extensively developed by Suhai et al.[8] Previous to the through space/bond interaction analysis, ab initio calculations were performed on all-*trans*-polyacetylene by using this program, with an STO-3G basis set. Ten k-points in half the Brillouin zone were used, and the convergence criterion of 10^{-6} for the difference in density-matrix elements was adopted. Twice the magnitude of the lattice vector was taken as a translational vector corresponding to the unit cell of polyacetylene shown in Fig. 1.

The truncation of lattice sums in the Fock matrix given by Eq. 3 is a serious problem in obtaining the convergent energy values. Delhalle et al. have previously reported in considerable detail on the convergence properties of the long-range Coulombic contributions, using the Fourier representation technique, etc;[38-41] they have recently reported also on the behavior of exchange-energy contributions, which is important in the metallic system.[42-44] Recent data for *trans*-polyacetylene show that the difference in the band gap is less than 3kcal/cell in the region of included neighbors 4-50 C2H2- units at the HF/STO-3G level.[45] We made sure in the previous work on polynitrilometylidyne[38] that the absolute values of orbital energies are changed by a cut-off after a finite interaction range, but that the shapes of the band structures are retained, even when up to 16 CHN units are included. Therefore, in employing the through space/bond interaction analysis we used the Fock matrix elements by taking into account the contribution up to the third neighbor interaction (6 units) in the core-resonance integrals and the two-electron integrals.

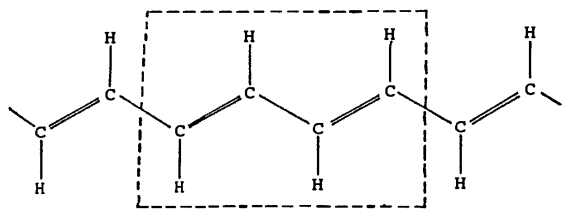

Fig. 1. Structure of all-trans polyacetylene. The unit cell is sorrounded with broken lines.

The geometries used here (Table 1) are the same as those described in Ref. 8. The band structures and the density of the states calculated indicate that the system is an insulator with a band gap of 8.12 eV, as is shown in Fig. 2. This value is, however, too large compared with the experimental value of ca. 2 eV.[46] Suhai has reported that the smaller bond alternation when correlation effects are included leads to a smaller gap (ΔE_g(HF/STO-3G)$\simeq$8.9 eV, ΔE_g (HF/6-31G**)$\simeq$5.1 eV, ΔE_g(HF+MP2/6-31G**)$\simeq$4.4 eV) at their optimal geometries) which should cover 70—75% of the valence-shell correlation energy.[11] This indicates that the correlation effects are essential for obtaining a good agreement with the experimental value in calculation including correlation effects. However, the purpose of our study is to obtain information with respect to the relationship between the orbital-energy dependence on the wavenumber vectors and the interactions of the crystal orbitals. If the nature of the material properties can be explained qualitatively from the point of view of orbital symmetry, without carrying out accurate calculations directly, it must be possible to provide easily a fundamental aspect for experimental investigation. As the first step in roughly predicting the electronic properties of polymers affected from the structural change or substitution effects, we have applied the through space/bond interaction analysis at the HF/STO-3G level to *trans*-polyacetylene.

Through Space/Bond Interaction Analysis

Method. For the analysis based on the through space/bond concept, all the Fock matrix elements and overlap integrals, which had been converged by ab initio SCF calculations, were classified into two kinds of interaction patterns. One type included those terms relating to the through-bond interactions, and the other type, the through-space interactions. The former type included the Fock matrices given by Eq. 3 and the overlap integrals given by Eq. 4 for diagonal elements and as well as off-diagonal elements between orbitals belonging to the same atom and between valence orbitals belonging only to the nearest neighboring atoms. For *trans*-polyacetylene, the valence orbitals indicate the 2s, $2p_x$, $2p_y$, and $2p_z$ orbitals on the C atom and the 1s orbitals on the H atoms. These elements were included for all cases of analyses. The latter type includes all the terms except those for the through-bond interaction, that is, those between particular valence orbitals belonging to remote atoms, between which there are no bonds. By investigating the influence of these through-space interactions on

Table 1. Geometries of $\{CH=CH\}_n$

r(C=C)	1.35Å	Angle (C=C-C)	120°
r(C-H)	1.09Å	Angle (C=C-H)	120°
r(C-C)	1.46Å		

the former through-bond interactions, the important through-space interaction for determining the band structure can be found. The technical details of the through space/bond method have been extensively described in a previous paper.[34] In this work, first, conspicuous through-space interactions governing the band shape are found by variational analysis, and next the concrete terms that contribute to the through-space interaction are analyzed by the perturbation method.

Variational Analysis. For performing the through-space/bond interaction variational analysis of the matrix elements, converged by the ab initio SCF calculations for Eq. 2, only the through-bond and some particular through-space components are reserved, the others are completely neglected. The eigenvalue problem for this new secular equation is solved only once, without further iterations for each wavenumber vector. By using the eigenvalue thus obtained, the effect of various through-space interactions on the band structure of the pure through-bond interaction can be investigated. The energy bands obtained by increasing the through-space components approach quantitatively to the results with full interaction, that is, the solution for Eq. 2 with full matrix elements. In this process, the most significant through-space interaction is found by comparing the changes in the band shapes. Furthermore, the relationship between band shapes and crystal orbitals for each through-space interaction can be investigated.

First, we calculated the energy bands of the pure through-bond interaction. The energy-band structure thus obtained is shown in Fig. 3. By comparing this band structure with the full interaction shown in Fig. 2, it is found that there is little difference in π and π^* bands between these two kinds of interactions. This is likely because the nature of the band structures for π-electron orbitals can be derived by a Hückel-type Hamiltonian, analogous to the pure through-bond interaction. On the other hand, it is noted that the LUMO σ^* band is greatly lowered by 0.7 au at $k=0°$, so that the gap between the valence and the conduction bands is extinguished. It is noteworthy that this band structure, calculated by including only the pure through-bond interactions, indicates a nearly metallic state. Therefore, we focused on this LUMO σ band and searched for the through-space interaction that elevates the LUMO σ^* energy to the insulator level.

We adopted the three kinds of through-space interactions shown in Fig 4., which exert significant effects on the band shapes of the pure through-bond interactions. The results of the analysis by various through-space interactions are shown in Figs. 5—7. Upon interaction between valence orbitals on the nonbonding C atoms (C-C interaction), no significant change in the LUMO σ^* band shape can be observed (Figs. 3 and 5). When the interaction between valence orbitals on C and the 1s orbital of H (C-H interaction) is added to the through-bond interaction, although the energy of the MO is unchanged at $k=0°$, it is raised by 0.5 au at $k=180°$ (Figs. 3 and 6). Moreover, by adding the C-C and C-H interactions, the LUMO σ^* energy level at $k=0°$ is raised and an energy gap between π and π^* bands appears (Figs. 3 and 7). The major part of the energetic destabilization at $k=0°$ originates from the coupling of the interaction within the backbone (C-C) with the interaction between the backbone and the side chain (C-H). This concurrent effect seems to be strong enough to give rise to the appearance of the

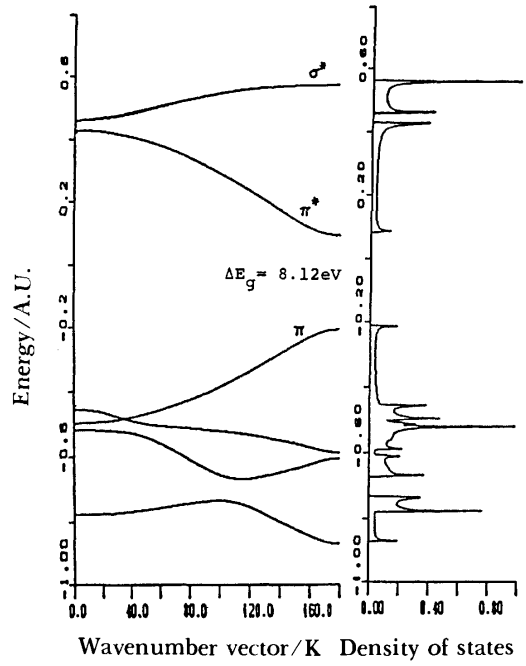

Fig. 2. Band structure and desity of states of all-*trans*-polyacetylene.

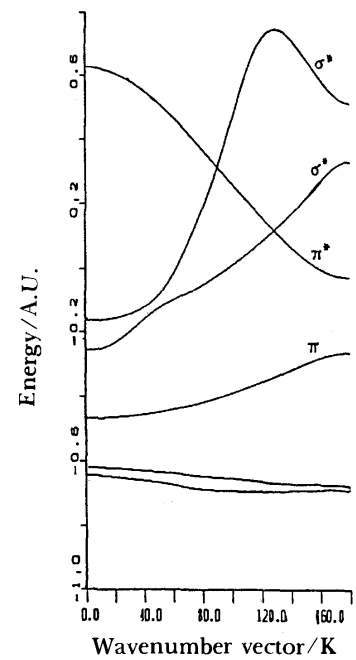

Fig. 3. Band structure for pure through bond interaction of all-*trans*-polyacetylene.

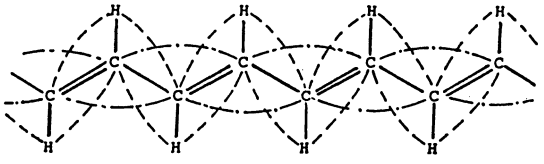

Fig. 4. The through space interactions used in this analysis. -·-·- C-C interaction, ----- C-H interaction.

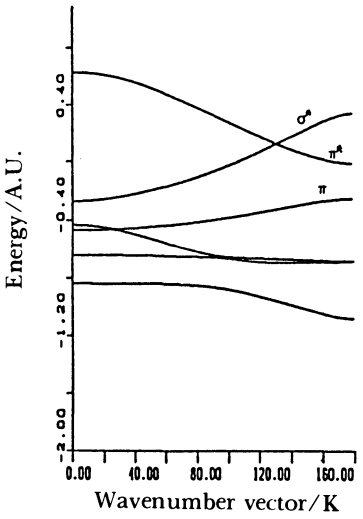

Fig. 5. The band structure for the pure through bond+C-C interaction.

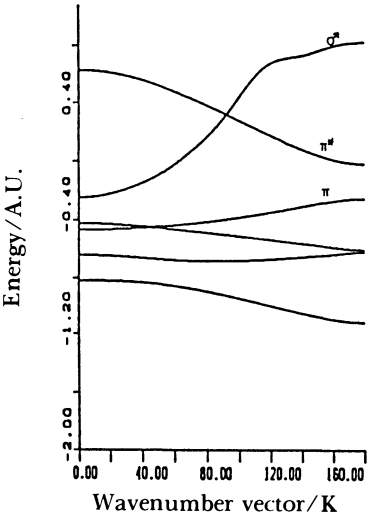

Fig. 6. The band structure for the pure through bond+C-H interaction.

gap, although each interaction (C-C) or (C-H) makes no apparent contribution. This behavior near k=0° turns out to be especially different from that at k=180° which satisfies the additivity rule for individual through-space interactions.

Perturbational Analysis. In order to account for the anomalous behavior at k=0° indicated by the variational analysis, we investigated the band structure in more detail by means of a perturbative treatment. By using formula from the general perturbation theory

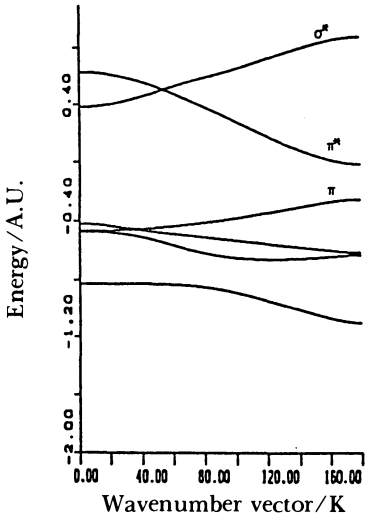

Fig. 7. The band structure for the pure through bond+(C-C+C-H) interaction.

for the extended Hückel method, which has been reported previously,[47] the first- and the second-order terms in the energy and coefficient are given as follows:

$$C_{ti}^{(1)} = -\sum_{\substack{j \\ (j\neq i)}}{}' C_{tj}^{(0)}/(E_j^{(0)} - E_i^{(0)}) \sum_r \sum_s (F_{rs}^{(1)} - S_{rs}^{(1)} E_i^{(0)}) C_{si}^{(0)} C_{rj}^{(0)*} - \frac{1}{2} C_{ti}^{(0)} \sum_r \sum_s C_{ri}^{(0)*} C_{si}^{(0)} S_{rs}^{(1)} \quad (5)$$

$$E_i^{(1)} = \sum_r \sum_s (F_{rs}^{(1)} - S_{rs}^{(1)} E_i^{(0)}) C_{ri}^{(0)*} C_{si}^{(0)} \quad (6)$$

$$C_{ti}^{(2)} = -\sum_{\substack{j \\ (j\neq i)}} C_{tj}^{(0)}/(E_j^{(0)} - E_i^{(0)}) [-\sum_r \sum_s S_{rs}^{(1)} E_i^{(1)} C_{si}^{(0)} C_{rj}^{(0)*} + \sum_r \sum_s \{F_{rs}^{(1)} - (S_{rs}^{(0)} E_i^{(1)} + S_{rs}^{(1)} E_i^{(0)})\} C_{si}^{(1)} C_{rj}^{(0)*}] - \frac{1}{2} C_{ti}^{(0)} \sum_r \sum_s [C_{ri}^{(1)*} C_{si}^{(1)} S_{rs}^{(0)} + (C_{ri}^{(1)*} C_{si}^{(0)} + C_{ri}^{(0)*} C_{si}^{(1)}) S_{rs}^{(1)} \quad (7)$$

$$E_i^{(2)} = -\sum_r \sum_s S_{rs}^{(1)} E_i^{(1)} C_{ri}^{(0)} C_{si}^{(0)*} + \sum_r \sum_s \{F_{rs}^{(1)} - (S_{rs}^{(0)} E_i^{(1)} + S_{rs}^{(1)} E_i^{(0)})\} C_{ri}^{(1)} C_{si}^{(0)*} \quad (8)$$

where i and j denote molecular orbitals, and r and s, atomic orbitals, and where $\sum_j'$ means that the summation covers all levels except i. In this study, the zero-order matrix elements $F_{rs}^{(0)}$ and $S_{rs}^{(0)}$ and the coresponding crystal orbital $C_{ti}^{(0)}$ and energy $E_i^{(0)}$ values, are the terms for the pure through-bond interaction. The first-order terms $F_{rs}^{(1)}$ and $S_{rs}^{(1)}$ are matrix elements for a selected pair of through-space components.

Equations 5 and 6 are calculated by taking a through-space interaction as a perturbation; then the concrete contribution included in the energy change obtained by solving Eq. 2 can be found. Figure 8 shows the energy bands of the LUMO σ^* orbital obtained by the first-order perturbation that is, $E^{(0)}(k)+E^{(1)}(k)$, for three kinds of through-space inter-

actions compared with the results obtained by the variation method. By C-C interaction the energy is raised at k=0° by 0.4 au; likewise C-H interaction raises it at k=180° by 0.5 au. The first-order energies by both C-C and C-H interactions, that is, the sum of the true interactions, change the energy band in the direction of the variational result.

The change in the band structure by the first-order perturbation should be predictable from the crystal orbitals for the pure through-bond interaction, the zero-th order wave function, and the perturbed matrix elements. The crystal orbitals at k=0° and 180° are shown schematically in Fig. 9. The crystal orbitals on C atoms at k=0° are directed to the z axis, which are out-of-phase between $2p_z$ orbitals on the C1 and C3. On the other hand, those at k=180° are directed to the hydrogen atoms, which are out-of-phase between C1 and H2 or C2 and H1. The positive overlap implies bonding, and the negative one, antibonding. Therefore, C-C interaction destabilizes the MO at k=0°, as does C-H interaction at k=180°. In this manner, this behavior can reasonably be interpreted in terms of the symmetry or the phase of crystal orbitals.

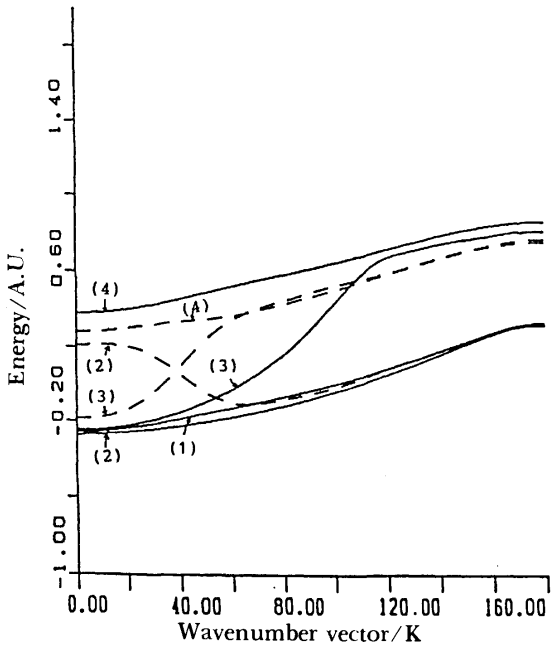

Fig. 8. The energy band of LUMO σ^* orbital by through space/bond interaction analysis. —— Variative analysis, ---- perturbative analysis (1) pure through bond interaction (2) C-C interaction (3) C-H interaction (4) (C-C+C-H) interaction.

It is noteworthy that the perturbation by the C-C interaction does not change the energy when the variational treatment is used, but it is raised at k=0° by the first-order perturbational treatment. This suggests that the terms more than first-order contribute greatly to the change in the energy band. It seems profitable to calculate the second-order energies in order to examine the concrete terms which elevate the LUMO σ band to the insulator level. The leading interaction term with the other levels in the second-order energy can be derived because, as can be seen from Eq. 8, the $E_i^{(2)}$ includes the term $C_{ii}^{(1)}$ that is given by the sum of the interactions with all the levels except i. Table 2 shows the first-order energies obtained by the three kinds of through-space interactions in comparison with the energy changes obtained by the variational treatment at k=0° and 180°.

At k=180°, the second-order energy obtained by the (C-C+C-H) interaction is almost equal to the sum of those obtained by both the C-C and C-H interactions; that is, the additivity rule holds for these interactions. The sum of the first-and the second-order energies gives values which are nearly equal to the energy changes obtained by the variational treatment. This shows that the substantial effect on the energy band of the through-space interactions may reasonably be interpreted by only the first-order term in the perturba-

Table 2. Gained Energies by Through-Space Interactions for the LUMO σ^* Orbitals (a.u.)

k=0°	Through space	C-C	C-H	C-C+C-H
	Perturbation			
	$E^{(1)}$	0.463	0.070	0.534
	$E^{(2)}$	−0.328	−0.402	0.205
	Variation	−0.015	0.008	0.635
k=180°	Through space	C-C	C-H	C-C+C-H
	Perturbation			
	$E^{(1)}$	−0.017	0.435	0.419
	$E^{(2)}$	−0.003	0.091	0.087
	Variation	−0.008	0.479	0.525

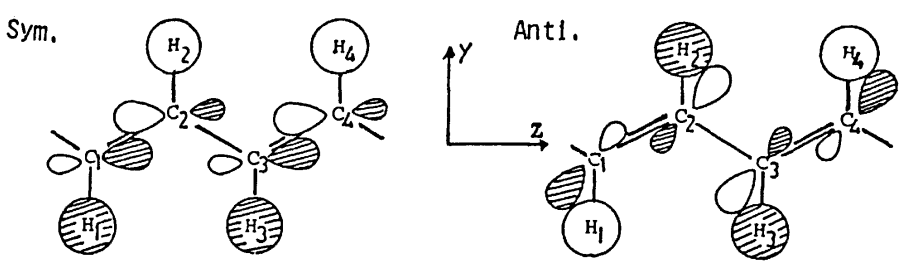

Fig. 9. Schematic representation of the magnitude of the coefficients of atomic orbitals in the crystal orbitals for the pure through bond interaction of all-*trans*-polyacetylene. Shaded areas represent positive lobes; unshaded negative. Sym. corresponds to k=0° and Anti. to k=180°.

tion expansion.

At k=0°, on the other hand, the second-order energy by the (C-C+C-H) interaction (0.205) is greatly different from the sum of those by both C-C and C-H interactions (−0.328, −0.402), even in sign. This behavior implies that the cross-terms included in the (C-C+C-H) interaction contribute positively to the second-order energy.

The cross-term is given by the following equation:

$$\begin{aligned} E_i^{(2)}(\text{cross}) &= -\sum_r\sum_s \{S^{(1)}_{rs(\text{C-C})} E^{(1)}_{i(\text{C-H})} + S^{(1)}_{rs(\text{C-H})} E^{(1)}_{i(\text{C-C})}\} C^{(0)}_{ri} C^{(0)*}_{si} \\ &+ \sum_r\sum_s (F^{(1)}_{rs(\text{C-C})} - S^{(1)}_{rs(\text{C-C})} E^{(0)}_i) C^{(1)}_{ri(\text{C-H})} C^{(0)*}_{si} \\ &+ \sum_r\sum_s (F^{(1)}_{rs(\text{C-H})} - S^{(1)}_{rs(\text{C-H})} E^{(0)}_i) C^{(1)}_{ri(\text{C-C})} C^{(0)*}_{si} \end{aligned} \quad (9)$$

where $S^{(1)}_{rs(\text{C-C})}$ and $F^{(1)}_{rs(\text{C-C})}$ represent the matrix elements for the through-space C-C interaction, and $S^{(1)}_{rs(\text{C-H})}$ and $F^{(1)}_{rs(\text{C-H})}$, those for the C-H interaction $E^{(1)}_{i(\text{C-H})}$ and $C^{(1)}_{rs(\text{C-H})}$ are the first-order perturbation energy and the corresponding coefficient obtained by only the C-H through-space interaction. $E^{(1)}_{i(\text{C-C})}$ and $C^{(1)}_{ri(\text{C-C})}$ have the same meaning. The cross-terms given by Eq. 9, which corresponds to the difference between $E^{(2)}_{i(\text{C-C+C-H})}$ and $E^{(2)}_{i(\text{C-C})}+E^{(2)}_{i(\text{C-H})}$, are 0.934 for k=0° and 0.001 for k=180°. The value of the cross-term is positive enough to elevate the LUMO σ^* band to the insulator level, in spite of the negative values caused by the C-C interaction (−0.328) and the C-H interaction (−0.402). Furthermore, the $C^{(1)}_{ri(\text{C-C})}$ and $C^{(1)}_{ri(\text{C-H})}$ terms, that include interaction with the other levels, result in a dominant factor in Eq. 9. From these results it seems reasonable to assume that the conspicuous results obtained by the variational treatment can essentially be interpreted by examining the second-order term. Therefore, the cross-term included in the second-order will be analyzed in order to investigate its explicit contribution.

We attempt to represent the second-order energy explicitly by the zero-order crystal orbitals instead of the first-order crystal orbitals. We define:

$$T^{(1)}_{rs,i} = F^{(1)}_{rs} - S^{(1)}_{rs} E^{(0)}_i , \quad (10)$$

and substitute Eqs. 5, 6, and 10 into Eq. 8; then the second-order energy is expressed as follows:

$$\begin{aligned} E_i^{(2)} &= -\sum_r\sum_s S^{(1)}_{rs} \sum_p\sum_q T^{(1)}_{pq,i} C^{(0)}_{pi} C^{(0)*}_{qi} C^{(0)}_{ri} C^{(0)*}_{si} \\ &- \sum_r\sum_s (T^{(1)}_{rs,i} - S^{(0)}_{rs} \sum_p\sum_q T^{(1)}_{pq,i} C^{(0)}_{pi} C^{(0)*}_{qi}) \\ &\times \{ \sum'_{j(\neq i)} C^{(0)}_{rj} \sum_t\sum_u T^{(1)}_{tu,i} C^{(0)}_{ti} C^{(0)*}_{uj} / (E^{(0)}_j - E^{(0)}_i) \\ &+ \frac{1}{2} C^{(0)}_{ri} \sum_t\sum_u C^{(0)}_{ti} C^{(0)*}_{ui} S^{(1)}_{tu} \} C^{(0)*}_{si} \end{aligned} \quad (11)$$

Neglecting the term $S^{(0)}_{rs} E^{(1)}_i$, that is, $S^{(0)}_{rs} \sum_p\sum_q T^{(1)}_{pq,i} C^{(0)}_{pi} C^{(0)*}_{qi}$ because of its small value, Eq. 11 becomes approximately:

$$\begin{aligned} E_i^{(2)} &= -\frac{3}{2} \sum_r\sum_s T^{(1)}_{rs,i} C^{(0)}_{ri} C^{(0)*}_{si} \sum_t\sum_u S^{(1)}_{tu} C^{(0)}_{ti} C^{(0)*}_{ui} \\ &- \sum_r\sum_s T^{(1)}_{rs,i} \sum'_{j(\neq i)} C^{(0)}_{rj} \sum_t\sum_u T^{(1)}_{tu,i} C^{(0)}_{ti} C^{(0)*}_{uj} C^{(0)*}_{si} / (E^{(0)}_j - E^{(0)}_i) . \end{aligned} \quad (12)$$

The first term relates only to the i-th crystal orbital, and the second term, to the other crystal orbitals belonging to all levels except i. The behavior of the energy band near k=0° suggests a great contribution of the second-order term in Eq. 12. Suppose that the focused i-th crystal orbital interacts strongly with the k-th crystal orbital and weakly with the other crystal orbitals: then Eq. 12 becomes approximately:

$$E^{(2)'}_{i(k)} = -\sum_r\sum_s T^{(1)}_{rs,i} C^{(0)*}_{si} C^{(0)}_{rk} \sum_t\sum_u T^{(1)}_{tu,i} C^{(0)}_{ti} C^{(0)*}_{uk} / (E^{(0)}_k - E^{(0)}_i) \quad (13)$$

where the interactions with all levels except k are completely neglected. We write:

$$\sum_r\sum_s T^{(1)}_{rs,i} C^{(0)*}_{si} C^{(0)}_{rk} = H^{(1)}_{ik} \quad (14)$$

and using the fact that $T^{(1)}_{rs,i}$ is Hermitian, Eq. 13 is reduced to:

$$E^{(2)'}_{i(k)} = -|H^{(1)}_{ik}|^2 / (E^{(0)}_k - E^{(0)}_i) \quad (15)$$

When the $H^{(1)}_{ik}$ includes two kinds of interactions, $H^{(1)}_{\text{A}}$ and $H^{(1)}_{\text{B}}$, Eq. 15 becomes:

$$E^{(2)'}_{i(k)} = -|H^{(1)}_{\text{A}} + H^{(1)}_{\text{B}}|^2 / (E^{(0)}_k - E^{(0)}_i) \quad (16)$$

where,

$$H^{(1)}_{\text{A}} = \sum_r\sum_s (F^{(1)}_{rs}(\text{A}) - S^{(1)}_{rs}(\text{A}) E^{(0)}_i) C^{(0)*}_{ri} C^{(0)}_{sk} \quad (17)$$

$$H^{(1)}_{\text{B}} = \sum_r\sum_s (F^{(1)}_{rs}(\text{B}) - S^{(1)}_{rs}(\text{B}) E^{(0)}_i) C^{(0)*}_{ri} C^{(0)}_{sk} \quad (18)$$

This means that the i-th orbital is stabilized in the second-order energy by the interaction with the upper levels of crystal orbitals, while it is destabilized with the lower ones. We have here evidence for the well-known conclusion that the energy levels with like symmetry crystal orbitals repel each other. As is implied by Eq. 16, $E^{(2)}_{i(k)}$ is destabilized only by the interaction with the energy levels in the proximity of the i-th level. The cross-term between the A and B interactions is expressed approximately as:

$$E^{(2)'}_i(\text{cross}) = -2Re(H^{(1)}_{\text{A}} H^{(1)*}_{\text{B}}) / (E^{(0)}_k - E^{(0)}_i), \quad (19)$$

provided that only the pair of the i-th and k-th crystal orbitals interacts strongly with each other. The terms relating only to the $H^{(1)}_{\text{A}}$ or $H^{(1)}_{\text{B}}$, that is $-|H^{(1)}_{\text{A}}|^2/(E^{(0)}_k - E^{(0)}_i)$ or $-|H^{(1)}_{\text{B}}|^2/(E^{(0)}_k - E^{(0)}_i)$, usually give negative values. The cross-term $E^{(2)'}_i$ (cross) given by Eq. 19 is a negative values if $H^{(1)}_{\text{A}}$ and $H^{(1)}_{\text{B}}$ have the same signs and a positive value if $H^{(1)}_{\text{A}}$ and $H^{(1)}_{\text{B}}$ have different signs. By means of the formulae thus described, we can proceed to an analysis of specific cases of energy-band structures.

As can be seen from the band structure for the pure through-bond interaction, shown in Fig. 3, the LUMO σ^* band and the upper σ^* band approach each other closely at $k=0°$. This shows that the LUMO σ^* band is referred especially to the influence of the upper σ^* band so as to avoid the crossing with it. Therefore, it seems reasonable to apply the above-mentioned approximation given by Eq. 16 to the case at $k=0°$. In the present case, the value of $H_A^{(1)}$ corresponding to the C-C interaction and that of $H_B^{(1)}$ corresponding to the C-H interaction are -0.185 and 0.171, respectively. The different signs of the two terms support the idea that the cross- term between these two kinds of interactions should be positive so as to destabilize the second-order energy of the LUMO σ^*.

Next, we will attempt to predict readily the contribution of the cross-term to the second-order energy in terms of the phase of the zero-order crystal orbitals without calculating the term $E_{i(k)}^{(2)}$ (cross). Equations 17 and 18 imply that whether or not the signs of the $H_{C\text{-}C}^{(1)}$ and the $H_{C\text{-}H}^{(1)}$ are the same can be elucidated by means of the i-th and the k-th zero-order crystal orbitals. The crystal orbitals for the pure through-bond interaction are shown schematically in Fig. 10 for the i-th LUMO σ^* orbital and the upper k-th σ^* orbital. The 2p orbital on Cl of the i-th orbital and that on C3 of the k-th orbital, for example, are in-phase along the direction of the z-axis, as are the 2p orbital on Cl of the k-th orbital and that on C3 of the i-th orbital, so that the $H_{C\text{-}C}^{(1)}$ become negative. The ls orbital on Hl of the i-th orbital and the 2p orbital on C2 of the k-th orbital are out-of-phase along the direction of the y-axis, as

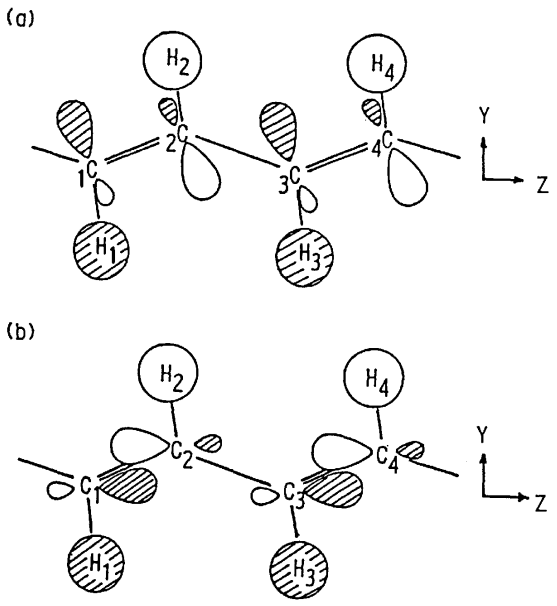

Fig. 10. Schematic representation of the magnitude of the coefficients of atomic orbitals in the crystal orbitals at $k=0°$ for the pure through bond interaction of all-*trans*-polyacetylene. Shaded areas represent positive lobes; unshaded negative. (a) k-th and (b) i-th levels in Eqs. 13—18.

are the 1s orbital on H1 of the k-th orbital and the 2p orbital on C2 of the i-th orbital, so that the $H_{C\text{-}H}^{(1)}$ is positive. This explication is consistent with the results obtained by calculating the $H_{C\text{-}C}^{(1)}$ and $H_{C\text{-}H}^{(1)}$ terms. This shows that the effect of the cross-term on the band shape should be predictable from the phase of the crystal orbitals with only the pure through-bond interaction. As a result of the perturbative analysis, it was found that the large positive cross term (0.934) between the $H_{C\text{-}C}^{(1)}$ and the $H_{C\text{-}H}^{(1)}$ terms governs the LUMO σ^*-band shape near $k=0°$ for the full interaction and is responsible for the appearance of the gap between the π and π^* bands. This method seems useful for investigating the relationship between the structural problem of a polymer and its band structure, which plays an important role in the conducting mechanism. Henceforth, we intend to apply this approach to the estimation of the structures of various polymers which are favorable for a high conductivity.

Conclusion

In this article we discuss the features of the band structure of all-*trans* polyacetylene as obtained by the use of through space/bond interaction analysis. The band structure for the pure through-bond interaction shows that the LUMO σ^* orbital is greatly lowered at $k=0°$ and extinguishes the gap between the π and π^* bands. The results obtained by the variational analysis for the LUMO σ^* orbital at $k=0°$ are different from those obtained at $k=180°$ with regard to the dependences of the band structure on through-space interactions. The most interesting feature is that there is a large coupling between two interactions; one is the interaction between C atoms belonging to the neighboring cells, and the other is that between the C atom and the H atom bonded to the neighboring C atom. It is this coupling term that is responsible for the band shape near $k=0°$. This fact suggests an important rule of the cross term between these two kinds of interactions. With the aid of the perturbation method, a simple formula for the cross-term is derived when two particular energy levels interact very strongly so as to avoid crossing. This formula enabled us to predict, though in a somewhat rough way, the behavior of the σ orbital near the gap in the band structure of all-*trans*-polyacetylene.

This work was supported by a Grant-in-Aid for Scientific Research from the Ministry of Education for which we express our gratitude. The computations were carried out on HITAC M-200H computers at the Information Processing Center of Hiroshima University and HITAC M-680H computers at the Institute for Molecular Science.

References

1) B. Kirtman, W. B. Nilsson, and W. E. Palke, *Solid*

State Commun., **45**, 791 (1983).
2) T. Yamabe, K. Tanaka, H. Teramae, K. Fukui, and A. Imamura, *J. Phys. C. Solid State Phys.*, **12**, 1257 (1979).
3) J. L. Brédas, R. R. Chance, R. Silbey, G. Nicolas, and Ph. Durand, *J. Chem. Phys.*, **75**, 255 (1981).
4) J. L. Brédas, R. R. Chance, R. H. Baughman, and R. Silbey, *J. Chem. Phys.*, **76**, 3673 (1982).
5) M. Kertész, *Int. Rev. Phys. Chem.*, **4**, 125 (1985).
6) H. Teramae, T. Yamabe, and A. Imamura, *J. Chem. Phys.*, **81**, 3564 (1984).
7) T. Yamabe, T. Tanaka, H. Teramae, K. Fukui, A. Imamura, H. Shirakawa, and S. Ikeda, *Solid State Commun.*, **29**, 329 (1979).
8) S. Suhai, *J. Chem. Phys.*, **73**, 3843 (1980).
9) P. M. Grant and I. P. Betra, *Solid State Commun.*, **29**, 225 (1979).
10) S. Suhai, *Int. J. Quantum Chem.*, **23**, 1239 (1980).
11) S. Suhai, *Chem. Phys. Lett.*, **96**, 619 (1983).
12) J. W. Mintmire and C. T. White, *Phys. Rev. Lett.*, **50**, 101 (1983).
13) J. W. Mintmire and C. T. White, *Phys. Rev. B*, **28**, 3283 (1983).
14) J. von Boehm, P. Kuivalainen, and J.-L. Calais, *Solid State Commun.*, **48**, 1085 (1983).
15) A. Karpfen and J. Petkov, *Theor. Chim. Acta (Berl.)*, **53**, 65 (1979).
16) A. Karpfen and J. Petkov, *Solid State Commun.*, **19**, 251 (1979).
17) A. Karpfen and H. Holler, *Solid State Commun.*, **37**, 179 (1981).
18) M. Kertész, J. Koller, and A. Azman, *Int. J. Quantum Chem.*, **18**, 645 (1980).
19) M. Kertész, J. Koller, and A. Azman, *Phys. Rev. B*, **29**, 2034 (1979).
20) K. Tanaka, K. Yoshizawa, K. Ohzeki, and T. Yamabe, *Solid State Commun.*, **45**, 391 (1983).
21) K. Tanaka, T. Koike, K. Yoshizawa, K. Ohzeki, and T. Yamabe, *Solid State Commun.*, **49**, 165 (1984).
22) C. K. Chiang, C. R. Fincher, Jr., Y. W. Park, A. J. Heeger, H. Shirakawa, E. J. Louis, S. C. Gau, and A. G. MacDiarmid, *Phys. Rev. Lett.*, **39**, 1098 (1977).
23) C. R. Fincher, Jr., M. Ozaki, A. J. Heeger, and A. G. MacDiarmid, *Phys. Rev. B*, **19**, 4140 (1978).
24) H. Shirakawa, T. Sasaki, and S. Ikeda, *Chem. Lett.*, **1978**, 1113.
25) I. Harada, M. Tasumi, and H. Shirakawa, *Chem. Lett.*, **1978**, 1411.
26) C. K. Chiang, M. A. Druy, S. G. Gau, A. J. Heeger, E. J. Louis, A. G. MacDiarmid, Y. W. Park, and H. Shirakawa, *J. Am. Chem. Soc.*, **100**, 1013 (1978).
27) H. Shirakawa, E. J. Louis, A. G. MacDiamid, C. K. Chiang, and A. J. Heeger, *Chem. Commun.*, **1977**, 578.
28) J. L. Brédas, R. R. Chance, and R. Silbey, *J. Phys. Chem.*, **85**, 756 (1981).
29) M. Kertész, *Mol. Cryst. Liq. Cryst.*, **126**, 103 (1985).
30) M. Kertész, *Int. J. Quantum Chem.*, **29**, 1165 (1986).
31) M. Kertész, F. Vonderviszt, and S. Pekker, *Chem. Phys. Lett.*, **90**, 430 (1982).
32) R. Peierls, "Quantum Theory of Solids," Clarendon Press, Oxford (1955), p. 108.
33) R. Hoffmann, A. Imamura, and W. J. Hehre, *J. Am. Chem. Soc.*, **90**, 1499 (1968).
34) Y. Aoki, A. Imamura, and H. Teramae, *Bull. Chem. Soc. Jpn.*, **58**, 2737 (1985).
35) J. M. Andre, *J. Chem. Phys.*, **50**, 1536 (1969).
36) G. Del Re, J. Ladik, and G. Biczo, *Phys. Rev.*, **155**, 997 (1967).
37) C. C. J. Roothaan, *Rev. Mod. Phys.*, **23**, 69 (1951).
38) J. Delhalle, J. M. Andre, Ch. Demanet, and J. L. Brédas, *Chem. Phys. Lett.*, **54**, 186 (1978).
39) L. Piela and J. Delhalle, *Int. J. Quantum Chem.*, **13**, 605 (1978).
40) J. Delhalle, L. Piela, J. L. Brédas, and J. M. Andre, *Phys. Rev. B*, **22**, 6254 (1980).
41) J. Delhalle, J. G. Fripiat, and L. Piela, *Int. J. Quantum Chem.*, **S14**, 431 (1980).
42) L. Piela, J. M. Andre, J. G. Fripiat, and J. Delhalle, *Chem. Phys. Lett.*, **77**, 143 (1981).
43) H. Monkhorst and M. Kertész. *Phys. Rev. B*, **24**, 3025 (1981).
44) J. Delhalle and J. L. Calais, *J. Chem. Phys.*, **85**, 5286 (1986).
45) H. Teramae, *J. Chem. Phys.*, **85**, 990 (1986).
46) S. Etemad, A. J. Heeger, L. Lanchlan, T.-C. Chung, and A. G. MacDiarmid, *Mol. Cryst. Liq. Cryst.*, **77**, 43 (1981).
47) A. Imamura, *Mol. Phys.*, **15**, 225 (1968).

 © 1988 The Chemical Society of Japan Bull. Chem. Soc. Jpn., 61, 1071—1075 (1988)

Studies of the Rate of the Formation of Talc under Hydrothermal Conditions at 400—460 °C

Haruto MURAISHI
Department of Chemistry, Fukuoka University of Education, Akama, Munakata, Fukuoka 811-41
(Received September 16, 1987)

The rate of the formation of talc from brucite powders with soluble silica under hydrothermal conditions was investigated in the temperature range of 400—460 °C, a range including the equilibrium temperature for the reaction: brucite+serpentine⇄2 forsterite+3H_2O. Serpentine appeared as an intermediate phase below 415 °C, while above 430 °C forsterite appeared in addition to serpentine. The apparent reaction can be represented as:

(below 415° C) brucite → serpentine → talc

(above 430° C) brucite → serpentine, brucite → forsterite, serpentine → talc, forsterite → talc

The reaction was apparently expressed as a pseudo-first-order reaction. The overall rate of the reaction did not increase with the increase in the temperature. Arrhenius plots of the rate constants for the overall reaction showed a curve with a maximum at about 415 °C and a minimum at about 445 °C which was caused by the alteration of the reaction by the appearance of forsterite at 430 °C.

The mechanism of the formation of silicates under hydrothermal conditions has been investigated from the standpoints of synthesis[1-3] and metamorphic reactions.[4-7] In spite of the many investigations into the synthesis of zeolite which have been done, however, the mechanism for the formation of zeolite has not yet been completely revealed. For the metamorphic reaction, though, the rates of hydration and dehydration (or forward and backward reactions) have been well investigated near the equilibrium temperature, and an effective rate constant has been obtained.

The kinetic study of solid-state reactions is generally attended with several problems. One of the problems with the reaction is that the observed overall rate of the reaction is usually controlled by the diffusion step (e.g., lattice diffusion) and is then influenced by the size and the shape of the starting materials. A physical process, such as diffusion, will not give useful information on surface reactions, nucleation, and intermediate formation. In order to obtain some information on these reactions of hydrothermal synthesis, it is necessary to simplify the reaction system and to set up a suitable reaction situation. From these points of view, we have now studied the hydrothermal synthesis of the MgO-SiO_2-H_2O system.

It has been found that the reaction of brucite ($Mg(OH)_2$) with SiO_2 involved the dissolution process of SiO_2 and that the dissolved silica was adsorbed on the surface of brucite in the initial step of the reaction. The adsorption was chemisorption, and the surface of the silica-adsorbed brucite consisted of an amorphous silicate layer at atmospheric pressure.[8,9] When the resulting amorphous silicate on the brucite was treated hydrothermally, it crystallized as serpentine ($Mg_3Si_2O_5(OH)_4$) at temperatures below 400 °C and was further transformed into forsterite (Mg_2SiO_4) above 420 °C.[10] In addition, it was found from the kinetic study that the difference in the particle size of brucite powder influenced not only the overall reaction rate but also the rate-determining step.[11]

In this study, the formation of talc ($Mg_3Si_4O_{10}(OH)_2$) was followed as a function of the time at various temperatures (400—460 °C) including the equilibrium temperature for the reaction: brucite+serpentine⇄2 forsterite+3 H_2O. The reaction was carried out under such conditions that the silica could react with the solid brucite in the state of soluble silica in an autoclave; the concentration was kept almost constant during the reaction by the use of a large excess of silica. This simplified reaction system led to a kinetic analysis of the formation of talc through intermediate products. The most reasonable process of the formation of talc around the equilibrium temperature will be discussed based on these results.

Experimental

Two-tenths of a gram of $Mg(OH)_2$ powder, packed naturally into a basket mounted on a holder, was placed above 2.0 g of silica gel powder situated at the bottom of a modified Mory-type autoclave with a capacity of about 30 cm^3. The filling ratio of water in the autoclave was 35%; this ratio corresponds to a pressure of about 300—500 bars at 400—460 °C. A solution in an autoclave was kept saturated with soluble silica at a concentration of 700—900 ppm throughout the reactions in the temperature range of 400—460 °C, since a large excess of silica was used as the silica source.

After a definite time of heating, the autoclave was rapidly quenched with water and the materials were taken out. The reactant and products were identified by the use of X-ray diffractometry and DTA. Their quantities could be determined with a gravimetric technique (TGA) and by means of their X-ray diffraction patterns. These methods have been fully described in a previous paper.[11,12]

Results and Discussion

Analysis of Experimental Conversion Curves. Figure

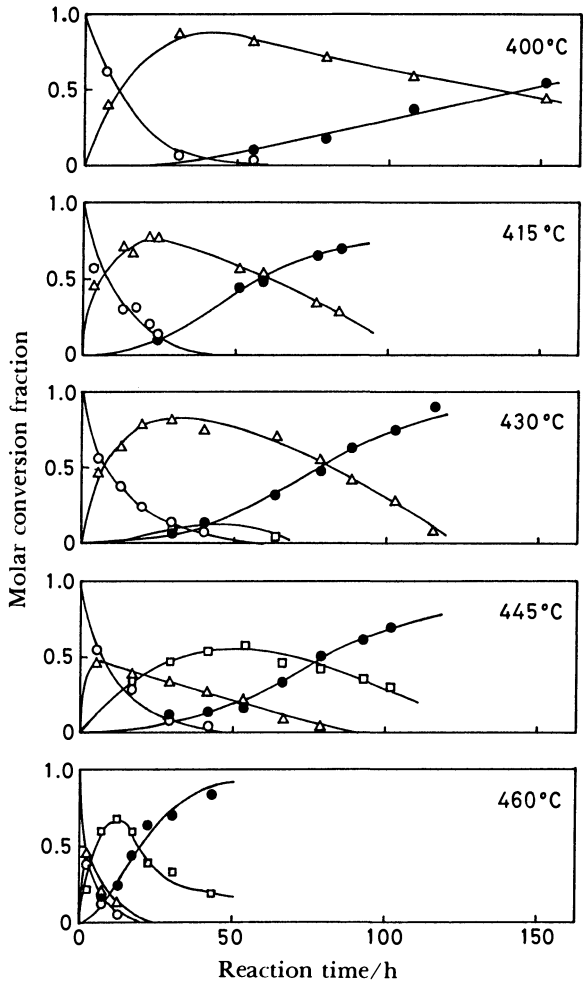

Fig. 1. Experimental conversion curves for the reaction of brucite with soluble silica at 400—460°C.
○: brucite, △: serpentine, □: forsterite, ●: talc.

1 shows the molar conversion curves for the reaction of solid brucite with soluble silica at 400—460 °C. Talc was formed through serpentine at 415 °C or below and through serpentine and forsterite as intermediates above 430 °C. It was noted that the temperature where forsterite appeared in the present kinetic study was higher than that in the equilibrium data obtained previously by Bowen and Tuttle.[13] When serpentine alone appeared as an intermediate substance, the reaction represented, as has been described previously,[11] a first-order consecutive irreversible reaction:

$$\text{brucite} \rightarrow (\text{serpentine}) \rightarrow \text{talc} \qquad (1)$$

When forsterite appeared in addition to serpentine, its overall reaction, brucite→(serpentine, forsterite)→talc, may be summarized in the following apparent process including Reaction 1:

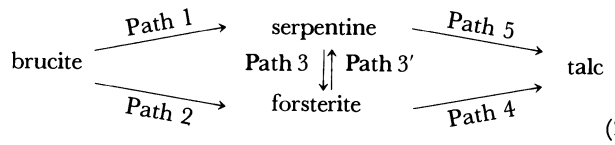

(2)

Each reaction pathway can be expressed by the following reactions, which proceed in the direction of the most stable form under the present experimental conditions:

$$\text{Path 1} \quad 3Mg(OH)_2 + 2SiO_2 \rightarrow Mg_3Si_2O_5(OH)_4 + H_2O \qquad (3)$$

$$\text{Path 2} \quad 2Mg(OH)_2 + SiO_2 \rightarrow Mg_2SiO_4 + 2H_2O \qquad (4)$$

$$\text{Path 3} \quad 2Mg_3Si_2O_5(OH)_4 \rightarrow 3Mg_2SiO_4 + SiO_2 + 4H_2O \qquad (5)$$

$$\text{Path 3'} \quad 3Mg_2SiO_4 + SiO_2 + 4H_2O \rightarrow 2Mg_3Si_2O_5(OH)_4 \qquad (6)$$

$$\text{Path 4} \quad 3Mg_2SiO_4 + 5SiO_2 + 2H_2O \rightarrow 2Mg_3Si_4O_{10}(OH)_2 \qquad (7)$$

$$\text{Path 5} \quad Mg_3Si_2O_5(OH)_4 + 2SiO_2 \rightarrow Mg_3Si_4O_{10}(OH)_2 + H_2O \qquad (8)$$

These equations are all similar in form to the reactions of magnesium compounds with silica. When the plural reactants except silica take part in magnesium silicate formation, the reaction are summarized in the following equations.

$$\text{Path 2+3} \quad Mg(OH)_2 + Mg_3Si_2O_5(OH)_4 \rightarrow 2Mg_2SiO_4 + 3H_2O \qquad (9)$$

$$\text{Path 2+3'} \quad 4Mg(OH)_2 + Mg_2SiO_4 + 3SiO_2 \rightarrow 2Mg_3Si_2O_5(OH)_4 \qquad (10)$$

Unfortunately, Reactions 9 and 10 may be actually indistinguishable from the sums of Reactions 4 and 5, and Reactions 4 and 6, respectively.

In order to quantitatively determine some experimental observations on the formation of talc, we tried to analyze the experimental conversion curves. Some preliminary discussion will, however, be useful before an analysis of the rate of solid-state reaction is attempted.

(a) The fraction reacted in a solid-state reaction is represented by a quantity of the reacting species, α_i, instead of the concentration, C_i, in a homogeneous reaction, since the concept of concentration in the reactivity of a solid is meaningless:

$$\text{Rate} = kf(\alpha_i)$$

(b) The silica concentration in hydrothermal solutions was almost constant during the reaction times, as has been described above. The silica concentration (C_{SiO_2}) can, therefore, be considered to be a constant factor of the rate constant, k:

$$k = k'C_{SiO_2}$$

We can picture a generalized reaction scheme based on the apparent reaction process 2 as follows:

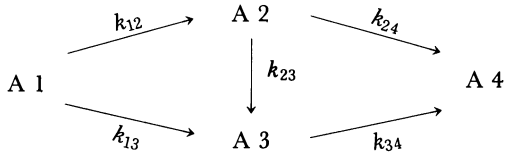

where Al and A4 are brucite as a starting material and

talc as a final product respectively and where A2 and A3 are arbitrarily assigned to serpentine and forsterite as intermediate species in the reaction system. k_{12}, k_{13}, k_{23}, k_{24}, and K_{34} are the rate constants for the reaction paths. If the reaction is a first-order reaction similar to Reaction 1, described previously, the differential rate equations will be expressed as follows:

$$\frac{d\alpha_1}{dt} = -(k_{12} + k_{13})\alpha_1 \tag{11}$$

$$\frac{d\alpha_2}{dt} = k_{12}\alpha_1 - (k_{23} + k_{24})\alpha_2 \tag{12}$$

$$\frac{d\alpha_3}{dt} = k_{13}\alpha_1 + k_{23}\alpha_2 + k_{34}\alpha_3 \tag{13}$$

$$\frac{d\alpha_4}{dt} = k_{24}\alpha_2 + k_{34}\alpha_3 \tag{14}$$

where α_1, α_2, α_3, and α_4 indicate the numbers of moles of A1, A2, A3, and A4 respectively to one mole of the starting material, A1.

$$t = 0 \quad \begin{cases} \alpha_1 = 1 \\ \alpha_2 = \alpha_3 = \alpha_4 = 0 \end{cases}$$

$$t = \infty \quad \begin{cases} \alpha_1 = \alpha_2 = \alpha_3 = 0 \\ \alpha_4 = 1 \end{cases}$$

The solutions of Eqs. 11, 12, 13, and 14 are given as:

$$\alpha_1 = \exp\{-(k_{12} + k_{13})t\} \tag{15}$$

$$\alpha_2 = \frac{k_{12}}{k_{23}+k_{24}+k_{12}-k_{13}}[\exp\{-(k_{12}+k_{13})t\} - \exp\{-(k_{23}+k_{24})t\}] \tag{16}$$

$$\alpha_3 = \frac{1}{k_{34}-k_{12}-k_{13}}\left(k_{13} + \frac{k_{12}k_{23}}{k_{23}+k_{24}-k_{12}-k_{13}}\right) \times \exp\{-(k_{12}+k_{13})t\} - \frac{k_{12}k_{23}}{(k_{23}+k_{24}-k_{12}-k_{13})(k_{34}-k_{23}-k_{24})}\exp\{-(k_{23}+k_{24})t\} - \left\{\frac{1}{k_{34}-k_{12}-k_{13}}\left(k_{13} + \frac{k_{12}k_{23}}{k_{23}+k_{24}-k_{12}-k_{13}}\right) + \frac{k_{12}k_{23}}{(k_{23}+k_{24}-k_{12}-k_{13})(k_{34}-k_{23}-k_{24})}\right\}\exp(-k_{34}t) \tag{17}$$

$$\alpha_4 = 1 - \alpha_1 - \alpha_2 - \alpha_3 \tag{18}$$

These equations can be applied in any type of reaction which begins at A1 and terminates at A4 (e.g., A1→A2→A4, A1→A3→A4, A1→A2→A3→A4).

The experimental conversion curves shown in Fig. 1 were analyzed by a procedure which obtained a model curve fitted to the experimental data using a computer. These model curves are shown in Fig. 2 in comparison with the experimental data. It may be seen from this figure that the experimental observations are successfully represented by the theoretical equations except for the latter half-term of the formation of talc.

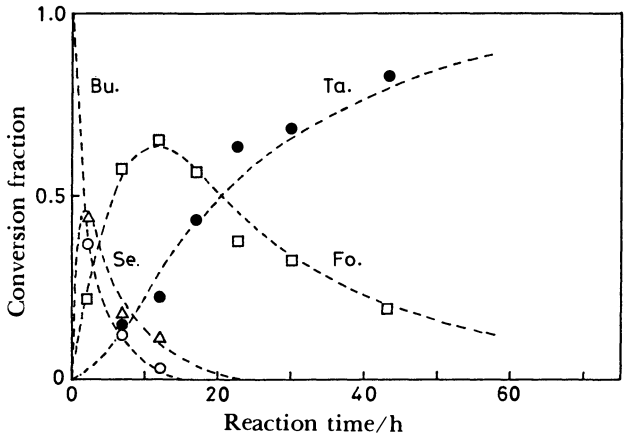

Fig. 2. Calculated conversion curves as compared to experimental conversion data at 460°C.
Bu.: brucite, Se.: serpentine, Fo.: forsterite, Ta.: talc.

The reason why the experimental rate data are represented by a first-order equation is as follows:

(a) In the present study, the concentration of silica was not a variable in the rate equation, but one of the constant factors that were contained in the rate-constant term, since the silica concentration was almost constant throughout the reaction, as has been described previously. The reaction may, therefore, be simplified to a pseudo-first-order reaction.

(b) The brucite used as a starting material was found, by electron microscopy and X-ray diffractometry, to consist of smaller disk like grains (or crystallites) a few hundred angstromes in size. Moreover, it has been observed that the amount of brucite was reduced with the reaction time, while the crystallite size of the residual brucite was changed very little by the reaction. The crystallinity of the intermediate product was also small in size (such as brucite) and did not grow during the reaction term. These results suggest that crystallites are units of the reaction and that the conversion process is controlled by a surface reaction and/or nuclei formation rather than by mass transfer. This reaction may be expressed by this equation:

$$\alpha = 1 - \exp(-kt^n) \tag{19}$$

which is universally applicable to nuclei formation and crystal growth.[14] When the rate-determining step is nuclei formation or a surface reaction, the value of n is 1. The rate of the reaction, therefore, is expressed by this equation:

$$\ln(1-\alpha) = kt \tag{20}$$

which is equal to the first-order reactions in homogeneous reactions.

The rate constants obtained are shown in Table 1.

Effect of the Equilibrium Temperature on the Overall Rate of the Reaction. Figure 3 shows the plot of log $(1/t_{0.5})$ vs. $1/T$, where $t_{0.5}$ is the time for a 50%

Table 1. Rate Constants for the Reaction of Brucite with Soluble Silica

Reaction temp	Rate constants $10^2k/h^{-1}$				
°C	k_{12}	k_{13}	k_{23}	k_{34}	k_{24}
400	6.8	—	—	—	0.63
415	11.0	—	—	—	1.4
430	8.5	0.22	0.05	0.11	1.1
445	8.0	2.7	3.5	1.3	0.42
460	28.0	8.1	19.0	4.0	3.1

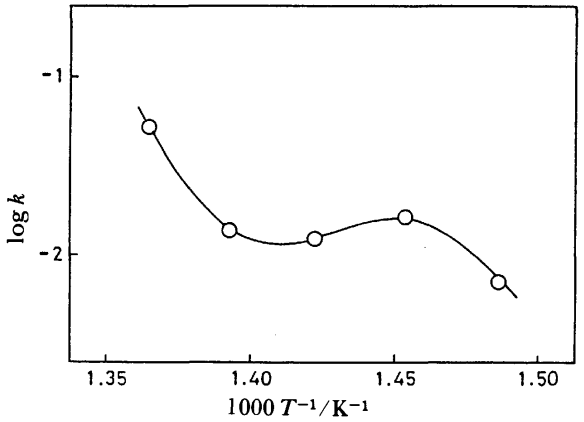

Fig. 3. Arrhenius plot of rate constant ($k=t_{0.5}^{-1}$) for the overall rate of talc formation.

formation of talc as the final product. The unit of the rate constant, $k=t_{0.5}^{-1}$, involves the h^{-1} unit. The characteristic plot obtained has a double hump; this plot is given by a lowering of the reaction rate to near the temperature at which forsterite appeared. The plots for the rate constants below 415 °C and above 445 °C may reflect the apparent activation energies for Reactions 1 and 2 respectively. In the temperature range of 415—445 °C, a plot with a slightly positive slope with a negative activation energy was obtained. This region may reflect intermediate values, behaving as a weighted means of two kinds of apparent activation energies of Reactions 1 and 2. If the rate-controlling step (or the reaction path) in such reactions as A→B→C and $A \begin{matrix} \nearrow B \\ \searrow C \end{matrix}$ changes at a particular temperature, typical plots in which two straight lines cross each other at that temperature will be obtained. In the present study, however, other factors further complicated the situation.

Arrhenius plots for the five rate constants given in Table 1 are shown in Fig. 4. The plots for k_{13}, k_{23}, and k_{34} are found to have a steep slope. These rate constants for the formation of forsterite are essentially zero at the equilibrium temperature for the brucite+serpentine⇆2 forsterite+3 H_2O reaction. Since the direction of departure from the equilibrium temperature is also equal to the direction of the rise in the temperature, the slopes of the plots for these rate constants are larger

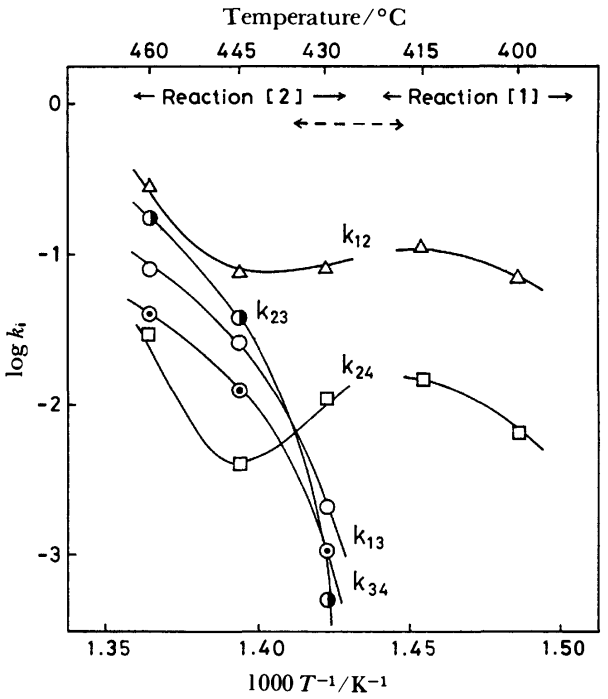

Fig. 4. Arrhenius plots of rate constants k_{12}, k_{13}, k_{23}, k_{24}, and k_{34} for each reaction path.

than the others. The plots for k_{12} and k_{24} are similar to that for the overall reaction shown in Fig. 3. These plots may be divided into three regions as has been described above. The rate of Reaction 1, which is represented by k_{12} and k_{24} at the temperature of 415 °C and below, may essentially tend to increase with an increase in the temperature, even at the temperature of 430 °C, since there are no other factors that influence the kinetics of Reaction 1 except for the appearance of forsterite. However, a part of the serpentine produced at 430 °C is transformed into forsterite, and then the apparent rate of the formation of serpentine may be lowered. The rate of talc formation may also be lowered as a result of some distortion of the nucleation. Above 445 °C, forsterite is directly formed on brucite (Path 2) rather than through serpentine (Paths 1 and 3); that is, the main path of the formation of talc consists of Paths 2 and 4. It may, then, be said that the reaction path for forsterite becomes the most important factors controlling the overall reaction with an increase in the temperature.

Some Considerations on the Formation of Intermediates. The intermediates in talc formation appeared in the order of serpentine→frosterite, as may be seen in the experimental conversion curves above 445 °C (see Fig. 1). It has also been observed that silica-adsorbed brucite, when treated hydrothermally above 420 °C, was transformed into forsterite through serpentine-like silicate,[10] although, at higher temperatures, serpentine was no longer detectable. On the other hand, the equilibrium data on the stable phases of magnesium silicate in hydrothermal solutions containing sil-

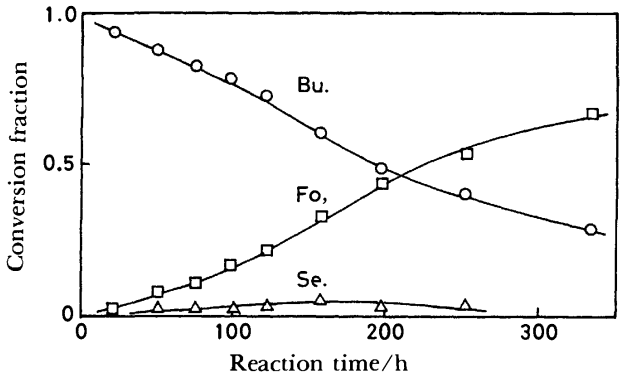

Fig. 5. Experimental conversion curve for the reaction of brucite with a low concentration solution of silica at 445°C.

ica reported by Hemley et al.[15] are different. They reported that magnesium silicates were transformed from brucite into forsterite→serpentine→talc with increases in the concentrations of silica and that the SiO_2/MgO ratios increase in that same order.

The reason why the kinetics of the formation of serpentine is much faster than that of forsterite is as follows: It may be presumed that the brucite surface is an excellent substrate for the nucleation of serpentine, since both brucite and serpentine are made of the same layered structure consisting of a Mg-O framework. The crystal nuclei of serpentine may, therefore, be generated with ease. In addition, since the formation of forsterite in accompanied by the severance of the Mg-O framework of brucite, it may require a large activation energy in the reconstructive reaction.

In order to obtain further information on the formation of serpentine and forsterite, a qualitative kinetic study was attempted under various conditions.

(a) Brucite was allowed to react under a low concentration of silica. A piece of quartz or serpentine, as a silica source, and same brucite were placed apart from each other in the same way. The reaction was very slow, and it produced a mere trace amount of serpentine. The conversion curves for the reaction of the brucite with the silica liberated from the serpentine are shown in Fig. 5.

(b) On the other hand, we employed a lod-like briquette consisting of the brucite powder as a starting material, with a smaller surface area, and examined it in the same manner as in the reaction of brucite with soluble silica. Its briquette was prepared by compressing the powder at a pressure of 50 $kg\,cm^{-2}$ by using a piston anvil. The reaction was very slow, similar to a diffusion-controlled bulk reaction in a solid. The reacted briquette was scrapped, step by step, from its surface and then evaluated. Talc, forsterite, and brucite were found to have been formed, in this order, from the surface toward the inner part. Only a small amount of serpentine was detected throughout the reaction.

In addition to the reaction rate, the differences in the reaction conditions influenced the appearance of intermediates. It can be seen from these results that the surface of the brucite powders contribute much to the nucleation of serpentine; when its surface is in contact with a higher concentration of silica solutions, they contribute still more. On the other hand, forsterite as a intermediate mainly appears when larger grains of brucite are used, when there is lower concentrated solution of silica, and at a temperature higher than the equilibrium temperature. Thus, in addition to the temperature, both the apparent (or net) grain size of the reactant and the silica concentration contribute to the appearance of an intermediate.

The author wishes to express his thanks to Dr. Shigeto Kitahara for his kind guidance and continuous encouragement throughout this work. The author also would like to thank Mr. Hideo Nagata for his assistance in the preparation of the silicate and in obtaining the X-ray diffraction data.

References

1) G. T. Kerr, *J. Phys. Chem.*, **70**, 1047 (1966).
2) J. Ciric, *J. Colloid Interface Sci.*, **28**. 315 (1968).
3) R. A. Cournoyer, W. L. Kranich, and L. B. Sand, *J. Phys. Chem.*, **79**, 1578 (1975).
4) H. Kacirek and H. Lechert, *J. Phys. Chem.*, **80**, 1291 (1976).
5) B. Martine and W. S. Fife, *Chem. Geol.*, **6**, 185 (1970).
6) W. W. Wegner and W. G. Ernst, *Am. J. Sci.*, **283-A**, 151 (1983).
7) A. B. Thompson, *Am. J. Sci.*, **268**, 454 (1970): **271**, 79 (1971).
8) S. Kitahara and H. Muraishi, *Nippon Kagaku Kaishi*, **1978**, 555.
9) H. Muraishi and S. Kitahara, *Nippon Kagaku Kaishi*, **1978**, 1457.
10) H. Muraishi, *Bull. Chem. Soc. Jpn.*, **54**, 1610 (1981).
11) H. Muraishi, *Bull. Chem. Soc. Jpn.*, **54**, 878 (1981).
12) H. Muraishi and S. Kitahara, Proc. First Internat. Sympo. Hydrothermal Reac., ed by S. Somiya, Gakujutsu Bunken Fukyu-kai, Tokyo (1982), p. 377.
13) N. L. Bowen and O. F. Tattle, *Bull. Geol. Soc. Am.*, **60**, 439 (1949).
14) J. W. Christian, "The Theory of Transformations in Metals and Alloys," Pergamon Press, London (1965), p. 973.
15) J. J. Hemley, J. W. Montary, C. L. Christ, and P. B. Hostetler, *Am. J. Sci.*, **227**, 322 (1977).

The Effects of the Sol-Gel Transition of Alginates on Effective Charge Densities

Masakatsu YONESE,* Kazuhiko BABA, and Hiroshi KISHIMOTO
Faculty of Pharmaceutical Sciences, Nagoya City University, Tanabe-dori, Mizuho-ku, Nagoya 467
(Received September 28, 1987)

The counterion binding properties of alginate (Alg) sol and gel were studied by using the membrane potential method, in which membranes were constructed of an Alg layer sandwiched between supporting films. The concentrations of Alg W_{Alg} ranged from 0.0025 to 0.0063 g cm^{-3}, and the membrane potentials were measured in NaCl, $MgCl_2$, and $CaCl_2$ solutions. The effective charge densities of Alg (θ^{*2}) were obtained by curve fittings with the theoretical values of the multimembrane potentials. The ratios of θ^{*2} to the concentration of uronate units θ_0 were found not to depend on W_{Alg}; their mean values were 0.45, 0.28, and 0.12 for Na-, Mg-, and CaAlg. The results of Na- and MgAlg in the sol state were bigger than Manning's theoretical values. The much smaller values of CaAlg in the gel state than MgAlg in the sol state showed that the Ca ion binding was enhanced by the gellation not only in the junction, but also in the networks.

Alginate (Alg) is a major structural polysaccharide found in intercelluar substances of brown algae, such as Laminaria hyperbória and Laminaria digitata, and is a linear block copolymer of β-D-mannuronate (M) and its C-5 epimer, α-L-guluronate (G). They link together in an alternative way (MG block) or in consecutive homopolymeric ways (G and M block). The ratio of M and G and the block compositions vary with the sources of brown algaes, and even with the same source, they vary by part and by age.[1] Alginates are gelled by the addition of divalent metal ions M^{++}, except for Mg^{++} ions. The crosslinks are formed by the stackings of the G blocks of alginate chains mediated by M^{++}.[2-4] Differing from thermotropic gels, such as carrageenan, Alg shows a sol-gel transition without any alteration in the temperature.[5] Therefore, it is a very valuable polysaccharide for basic studies of gel and for applications in the pharmaceutical field.[6,7]

The counterion-binding properties of Alg have been studied primarily by means of a dialysis-equilibrium method, and the divalent metal ions inducing its gellation have been reported to bind spcifically.[8-10] To elucidate the counterion-binding properties of Alg in sol and gel states, the membrane potential method[11] was used; in the method, membranes are constructed of an Alg sol and gel layer sandwiched between supporting films. The effective charge densities of Alg are studied. This method makes it possible to study the charge densities of both the sol and the gel, i.e., the effects of the sol-gel transition of Alg on counterion-bindings.

Experimental

Materials. Purified sodium alginate (NaAlg) was prepared from commercial NaAlg (Tokyo Kasei Kogyo Co., Ltd.) by dialyzing it against distilled water for 3 days, followed by filtration to remove any insoluble substances. The NaAlg thus purifed was stored under refrigeration after freeze-drying. The weight average molar mass of NaAlg was determined to be $M_w=1.32\cdot10^5$ g mol^{-1} by using a light scattering photometer LS-8 (Toyo Soda Manufacturing Co., Ltd., Japan). The compositions of NaAlg were analyzed by means of circular dichroism, CD,[12] and ^{1}H NMR.[13] The guluronate fraction F_G was found to be 0.33 or 0.37 by the two methods, while the fraction of the consecutive guluronate block F_{GG} and that of the alternative block composed of guluronate and mannuronate F_{MG} were determined to be 0.28 and 0.18 by ^{1}H NMR. All the other reagents were special grade. Distilled and deionized water was used for the preparation of aqueous solutions.

Measurement of Membrane Potential. In order to estimate the effective charge densities of polyelectrolyte solutions, the membrane potentials were studied by using the multimembrane, shown in Fig. 1 (a), constructed of a poly-

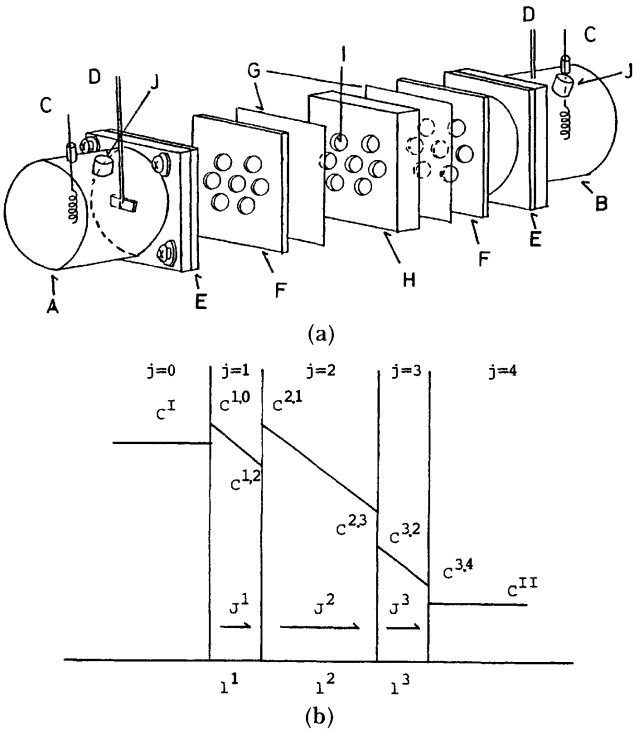

Fig. 1. Schemes of multimembrane. (a) Membrane potential measurement cell. A; compartment I, B; compartment II, C; Ag/AgCl electrode, D; stirring bar, E; silicone rubber, F; perforated stainless steel plate, G; support film (first and third layer), H; perforated polyacrylic resin plate, I; sample injection hole (second layer), J; inlet for solution injection. (b) Notations of concentrations for multimembrane system. $C^{0,1}$ and $C^{4,3}$ denote C^I and C^{II}.

electrolyte solution layer (I) sandwiched between supporting films (G): Solution I |Film| Polyelectrolyte solution layer |Film| Solution II. Dialysis membranes, C.M., (0.0033 cm in thickness, Seamless Cellulose Tubing, Union Carbide Corp.) was used as supporting films. NaAlg solutions were put into holes (I) (0.25 cm in radius) in a perforated polyacrylic resin plate (H) (0.3 cm thick, with 7 holes in it), and the supporting films on both sides were fixed by means of perforated stainless steel plates (F). The concentrations of Alg W_{Alg} were in the range from 0.0025 to 0.00626 g cm^{-3}. The concentration ratios of electrolyte solutions in the Compartments I (A) and II (B), R ($=C^{I}/C^{II}$) were 10 and 2. Both solutions were stirred at 500 rpm by means of stirring bars (D) so as to attain a constant thickness of the stagnant layer (=40 μm), a value which was obtained by measuring the permeability coefficients of NaCl through the single and double dialysis membranes.[14] The membrane potentials E between Solution I and Solution II were measured by means of Ag/AgCl electrodes (C), whose electrode potentials had been obtained by using Kieland's individual activil coefficients.[15] To obtain the effective charge density of the supporting films, C.M., the membrane potentials were measured in the following systems: Solution I |Supporting film| Solution II. All the membrane potentials were measured at 25 °C.

Theory and Method

Membrane Potential of Supporting Film. When a charged membrane separates electrolyte solution I and II whose concentration ratio C^{I}/C^{II} is R, the membrane potentials E are obtained by the summation of the diffusion potential in the membrane phase E^* and the Donnan potentials E_B at both interfaces;[16-18] they are expressed by the following equation:

$$E=E^{II}-E^{I}=(RT/F)((1/z_A)\ln R+(1/z_A)\ln(C^{II}/C^{I}) +((1/z_M-1/z_A)T_A^*-1/z_M)\times \ln((\bar{C}^{I}-(1/z_A)(1-T_A^*)\theta^*)/(\bar{C}^{II}-(1/z_A)(1-T_A^*)\theta^*)) \quad (1)$$

where θ^* and T_A^* are effective charge density of the membrane and the transference number of the anion in it. $\bar{C}_A^{I}$ and $\bar{C}_A^{II}$ are the interfacial concentration of the anion, and z_A and z_M are algebraic valences of the anion and the cation. The interfacial concentrations can be obtained by using the Donnan equilibrium between ions in the membrane phase and in bulk solutions, expressed by Eq. 2, and the electro-neutrality condition expressed by Eq. 3:

$$(\bar{C}_A/C_A)^{1/z_A}=(\bar{C}_M/C_M)^{1/z_M} \quad (2)$$

$$z_M\bar{C}_M+z_A\bar{C}_A+\theta^*=0 \quad (3)$$

Membrane Potentials of Multimembranes. The multimembrane, consisting of the polyelectrolyte solution sandwiched between supporting films, is shown in Fig. 1. The membrane potential E is the summation of the interfacial potentials generated at each interface of the multimembrane and the diffusion potential in each layer. According to the notations in Fig. 1 (b), E is expressed by the following equation:

$$E=\sum_{j=0}^{3}E_B^{j,j+1}+\sum_{j=1}^{3}E^{*j} \quad (4)$$

where $E_B^{j,j+1}$ and E^{*j} are the donnan potential at each interface and the diffusion potential in each layer respectively; the superscripts j and $(j,j+1)$ denote the jth layer and the interface between j and the $(j+1)$th layer respectively. The superscripts 0 and 4 denote Solution I and II, the first and third layers are supporting films, and the second one is the polyelectrolyte-solution layer. Denoting the concentration of the jth layer at the interface j and $(j+1)$th one by $\bar{C}^{j,j+1}$, and the effective charge density of the jth layer by θ^{*j}, E can be expressed by:

$$E=\frac{RT}{F}\left[\sum_{j=0}^{3}\ln\frac{\bar{C}_A^{j+1,j}}{\bar{C}_A^{j,j+1}}+\left\{\left(\frac{1}{z_M}+\frac{1}{z_A}\right)T_A^{*j}-\frac{1}{z_M}\right\}\times \sum_{j=1}^{3}\frac{\bar{C}_A^{j,j-1}+\frac{1}{z_A}(1-T_A^{*j})\theta^{*j}}{\bar{C}_A^{j,j+1}+\frac{1}{z_A}(1-T_A^{*j})\theta^{*j}}\right] \quad (5)$$

where T_A^{*j} is the transference number of the anion A in the jth layer. The Donnan equilibrium and the electro-neutrality conditions at each interface are expressed by the following equations:

$$(\bar{C}_A^{j+1,j}/\bar{C}_A^{j,j+1})^{1/z_A}=(\bar{C}_M^{j+1,j}/\bar{C}_M^{j,j+1})^{1/z_M} \quad (6)$$

$$z_M\bar{C}_M^{j,j+1}+z_A\bar{C}_A^{j,j+1}+\theta^{*j}=0 \quad (7)$$

$$z_M\bar{C}_M^{j+1,j}+z_A\bar{C}_A^{j+1,j}+\theta^{*j+1}=0 \quad (8)$$

j=0, 1, 2, and 3

where θ^{*0} and θ^{*4}, denoting the values of Solution I and II, are equal to 0. When θ^{*1} and θ^{*3} are known, $\bar{C}_A^{1,0}$ $\bar{C}_M^{1,0}$, $\bar{C}_A^{3,4}$, and $\bar{C}_M^{3,4}$ can be obtained by means of Eqs. 6—8 and as functions of C^{I} or C^{II}. Under steady state conditions, the fluxes of the ions J_i^j are equal in each layer, according to the continuity law:

$$J_i^1=J_i^2=J_i^3 \quad (9)$$

Approximating that concentrations of ions in each layer vary linearly,[19-21] the fluxes of the anion A are expressed by:

$$J_A^j=-P_A^j\frac{\bar{C}_A^{j,j+1}-\bar{C}_A^{j,j-1}}{l^j}(1+X) \quad (10)$$

$$X=\frac{\frac{z_M}{z_M-z_A}\theta^{*j}(\frac{1}{z_M}-\frac{1}{z_A})T_A^{*j}}{\bar{C}_A^{j,j+1}-\bar{C}_A^{j,j-1}}\times \ln\frac{\frac{z_M-z_A}{z_M}\bar{C}_A^{j,j+1}-(\frac{1}{z_M}-\frac{1}{z_A})(1-T_A^{*j})\theta^{*j}}{\frac{z_M-z_A}{z_M}\bar{C}_A^{j,j-1}-(\frac{1}{z_M}-\frac{1}{z_A})(1-T_A^{*j})\theta^{*j}} \quad (11)$$

j=1, 2, and 3

where P_A^j is the permeabiity coefficient of the anion in the j layer and where l^j is the thickness of the j layer. So as to satisfy Eq. 9, $\bar{C}_A^{1,2}$, $\bar{C}_A^{2,1}$, $\bar{C}_A^{2,3}$, and $\bar{C}_A^{3,2}$ can be obtained from Eq. 10 by numerical analysis. Then, the

membrane potentials E can be obtained from Eq. 5.

The effects of the supporting films on the membrane potential of the multimembrane can be discussed theoretically. Figures 2 and 3 show some of the calculated membrane potentials. The effects of the effective charge densities of the supporting films ($\theta^{*1}=\theta^{*3}$) on the membrane potentials are shown in Fig. 2. The effective charge density of the second layer is $\theta^{*2}=-0.01$ mol dm^{-3}, while those of the supporting films (θ^{*1} and θ^{*3}) vary from 0 to -0.1. The effects of θ^{*2} on E are shown in Fig. 3. The effective charge densities of the supporting films are $\theta^{*1}=\theta^{*3}=-0.01$ mol dm^{-3}, while that of the second layer varies from 0 to -0.1. In the calculations, Solution I and II are assumed to be NaCl solutions, and their ratio R to be 10. The P^{*1} ($=P^{*3}$) value is $1.92\cdot10^{-6}$ cm^2 s^{-1} which was obtained experimentally, and P^{*2} is $1.60\cdot10^{-5}$ cm^2 s^{-1}, which is approximated to be equal to the diffusion coefficient in an aqueous solution. The transference numbers of ions in membranes have been reported to be almost equal to those in their solutions.[16-18] Then, as the T_A^* value, the transference number of Cl^- in an NaCl solution was cited from the literature.[22] The thickness of the supporting films and the second layer are 0.0033 cm ($=l^1=l^3$) and 0.3 cm respectively, which are the same dimensions as those in the cell shown in Fig. 1 (a). It should be noted that the membrane potentials are affected not only by the effective charge densities of these layers but also by the diffusivities of ions through them. As the effective charge density of a supporting film θ^{*1} ($=\theta^{*3}$) drcreases under a constant θ^{*2}, as is shown in Fig. 2, the membrane potentials E are found to decrease abruptly in the lower-concentration region. When the θ^{*1} values are smaller than -0.001, the E values are almost the same; i.e., if θ^{*1} is at least smaller than one tenth of θ^{*2}, E is almost equal to those of $\theta^{*1}=0$. As is shown in Fig. 3, even when the θ^{*2} values are smaller than θ^{*1} ($=-0.01$), such as $\theta^{*2}=-0.001$ and -0.005, the differences between their membrane potentials are found to be clear, and even in these cases the θ^{*2} values can be obtained by the curve-fitting method.

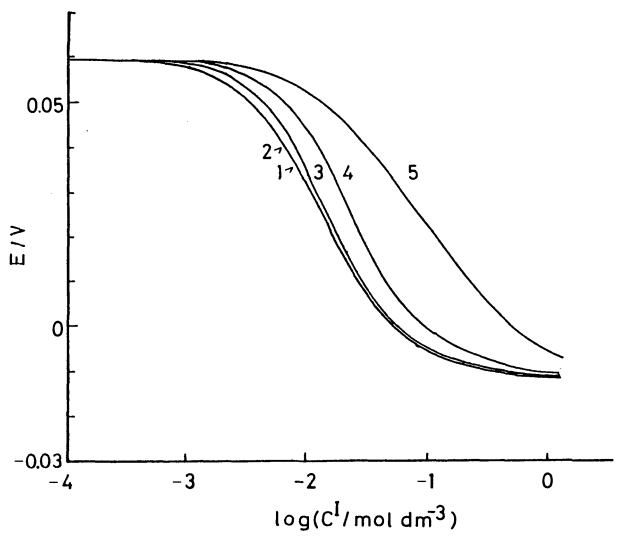

Fig. 2. Effects of effective charge densities of support film on membrane potentials E of multimembrane for NaCl solution at $R(=C^{I}/C^{II})=10$.
Effective charge densities of support films ($\theta^{*1}=\theta^{*2}$): 1; 0, 2; -0.0001, 3; -0.001, 4; -0.01, 5; -0.1. Effective charge density of second layer θ^{*2}: -0.01. Other data used in the calculations are as follows. $l^1=l^3=0.003$ cm, $l^2=0.3$ cm, $D^{*1}=D^{*3}=1.92\cdot10^{-6}$ cm^{2}s^{-1}, $D^{*2}=1.60\cdot10^{-5}$cm^{2}s^{-1}, $T_A{}^{*1}=T_A{}^{*2}=T_A{}^{*3}=0.601$.

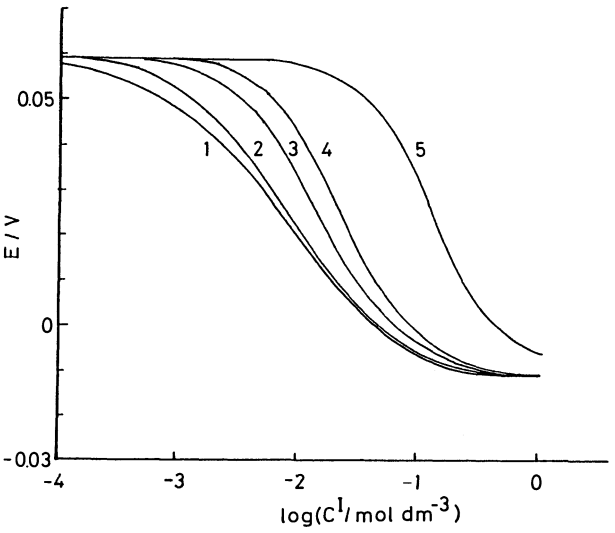

Fig. 3. Effects of effective charge densities of second layer on membrane potentials E of multimembrane for NaCl solution at $R=10$.
Effective charge densities of second layer θ^{*2}: 1; 0, 2; -0.001, 3; -0.005, 4; -0.01, 5; -0.1. Effective charge densities of support films $\theta^{*1}=\theta^{*3}$: -0.01. Other data used in the calculations are the same as in Fig. 2.

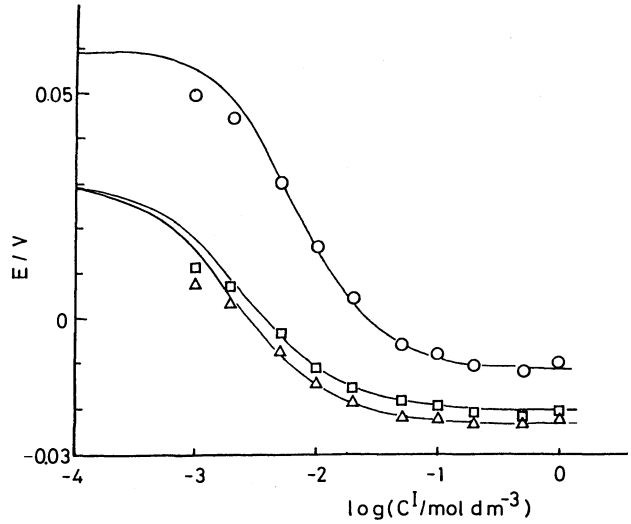

Fig. 4. Membrane potentials of support films for various electrolyte solutions at $R=10$.
○: NaCl, △: $MgCl_2$, □: $CaCl_2$. Solid curves show theoretical values obtained from Eq. 1 by selecting the most suitable effective charge densities.

Results

Effective Charge Density of Support Film. The membrane potentials of the supporting films C.M. were measured for NaCl, $MgCl_2$, and $CaCl_2$ solutions; the results are shown as functions of log C^I in Fig. 4. Their concentration ratios R ($=C^I/C^{II}$) were 10. The E values showed a shift from Donnan potentials to diffusion potentials with the increase in C^I. By the curve-fitting method, the effective charge densities of the film C.M., θ^*, were determined. The solid curves show the theoretical values obtained from Eq. 1 by selecting their most suitable values θ^* so as to agree with the experimental results in the high-concentration regions. In the calculations of the theoretical values, as the T_A^* values the transference numbers of the anion in the solutions were cited from the literature.[22] The θ^* values of the supporting film were found to be -0.0028, -0.0025, and -0.0026 mol dm^{-3} for NaCl, $MgCl_2$ and $CaCl_2$ solutions.

Effective Charge Densities of Alginates. The membrane potentials of the multimembranes (|Film C.M. |Alg Solution|Film C.M.|) were measured for the NaCl and $MgCl_2$ solutions, whose concentration ratio R was 10. The Alg solutions in the membrane ranged from W_{Alg}=0.00250 to 0.00262 g cm^{-3}. As is shown in Fig. 5, the E values showed abrupt decreases in the higher-concentration regions with the increase of W_{Alg}. The solid curves show the theoretical values obtained by selecting the most suitable values for the effective charge densities of alginate solutions, θ^{*2}, so as to agree with the experimental results. The θ^{*2} values are shown in Table 1, in which the effective

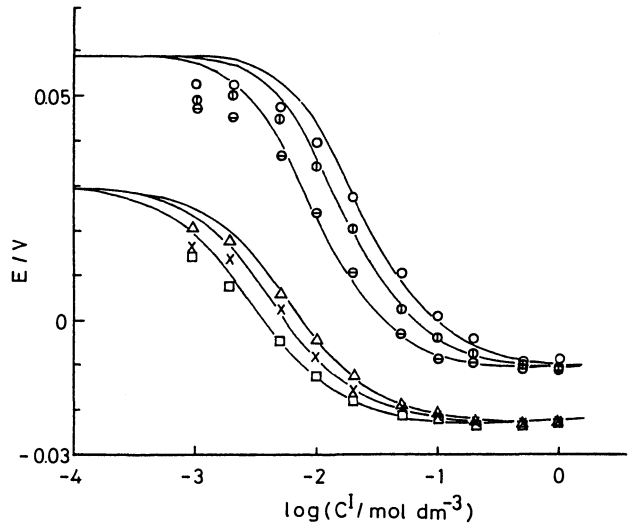

Fig. 5. Effects of concentration of Alg W_{Alg} on membrane potentials of multimembranes for NaCl and $MgCl_2$ solutions at R=10.
W_{Alg} (for NaCl solution): ○; 0.00626, ⊕; 0.00420, ⊖; 0.00250. W_{Alg} (for $MgCl_2$ solution): △; 0.00626, ×; 0.00420, □; 0.00250. Solid curves show theoretical values obtained by selecting the most suitable effective charge densities.

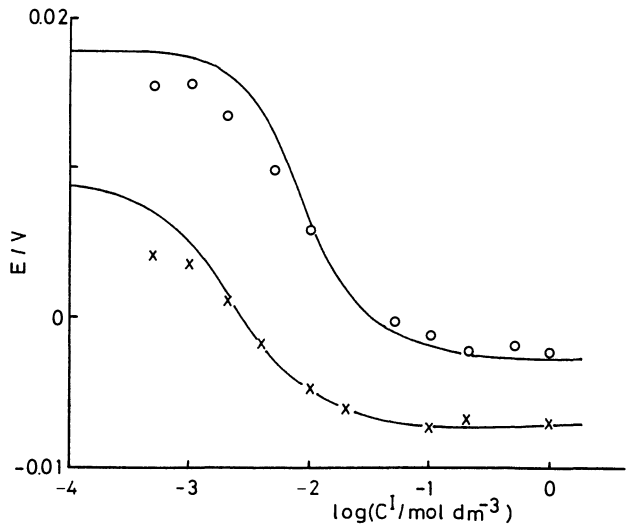

Fig. 6. Membrane potentials of multimembranes composed of alginate sol layer for NaCl and $MgCl_2$ solutions at R=2.
○; NaCl (W_{Alg}=0.00420), ×; $MgCl_2$ (W_{Alg}=0.00420). Solid curves show theoretical values obtained by selecting the most suitable effective charge densities.

Table 1. Characteristic Values of Alginate Sol and Gel

Solute	$-\theta^{*1}$/mol dm^{-3}	R	W_{Alg}/g cm^{-3}	$T_A^{*b)}$	$-\theta^{2*}$/mol dm^{-3}	θ^{2*}/θ_0
NaCl	0.0028	10	0.00626	0.601	0.014	0.44
NaCl	0.0028	10	0.00420	0.601	0.010	0.47
NaCl	0.0028	2	0.00420	0.601	0.010	0.47
NaCl	0.0028	10	0.00250	0.601	0.0050	0.40
$MgCl_2$	0.0025	10	0.00626	0.605	0.0080	0.25
$MgCl_2$	0.0025	10	0.00420	0.605	0.0065	0.31
$MgCl_2$	0.0025	2	0.00420	0.605	0.0060	0.28
$MgCl_2$	0.0025	10	0.00250	0.605	0.0035	0.28
$CaCl_2$[a)]	0.0026	10	0.00626	0.562	0.0035	0.11
$CaCl_2$[a)]	0.0026	10	0.00420	0.562	0.0025	0.12
$CaCl_2$[a)]	0.0026	10	0.00250	0.562	0.0015	0.12
NaCl[a)]	0.0028	10	0.00626	0.601	0.0070	0.22
NaCl[a)]	0.0028	2	0.00420	0.601	0.0060	0.28

a) CaAlg gelled by 1.0 mol dm^{-3}. b): $T_A^*=T_A^{*1}=T_A^{*2}=T_A^{*3}$. θ^{*1}: charge density of supporting film C.M.($=\theta^{*3}$). θ^{*2}: charge density of Alg. θ_0: concentration of Alg on the basis of uronate units.

charge densities of the supporting films C.M. θ^{*1} ($=\theta^{*3}$) and the transference numbers of the anion T_A^{*i} used in calculations are also shown. The absolute values θ^{*2} for the NaCl solution were bigger than those for $MgCl_2$, and they increased with the increase in W_{Alg}. Figure 6 shows the membrane potentials for the NaCl and $MgCl_2$ solutions, whose concentration ratio R was 2. The most suitable θ^{*2} values of Alg are shown in Table 1, also. They were in good agreement with the θ^{*2} values obtained when R=10.

In the cases of the NaCl and $MgCl_2$ solutions, the Alg were in sol states, but in the case of the $CaCl_2$ solutions they were in the gel state. The membrane potentials of the Alg in the gel state were measured as follows. The Alg sols (NaAlg) in the second layer were transited to gel by putting $CaCl_2$ solutions (1.0 mol dm^{-3}) into both compartments, I and II, and before the measurements of E, the free ions in the CaAlg gel layer were removed by dialysis against distilled water. Figure 7 shows the membrane potentials of the multimembranes containing CaAlg gels for NaCl and $CaCl_2$ solutions (R=10) and also the theoretical curves obtained by using the most suitable effective charge densities θ^{2*}, which are shown in Table 1. The absolute values of the effective charge density of CaAlg were found to be less than those of MgAlg. This is attributable to the capture of the Ca ion in the junctions. The absolute values of θ^{*2} of CaAlg for NaCl-solution systems were bigger than those for $CaCl_2$ solutions. This is considered to result from the partial ion-exchange of Ca with Na ions.

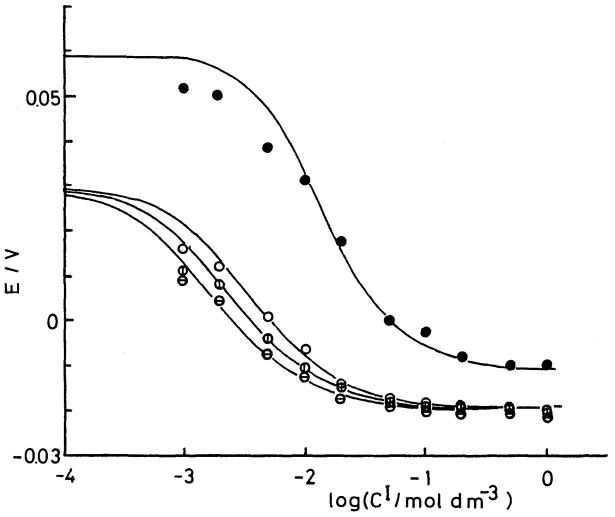

Fig. 7. Membrane potentials of multimembranes composed of alginate gel layer for NaCl and $CaCl_2$ solutions at R=10.
W_{Alg} (for $CaCl_2$ solution): ○; 0.00626, ⊕; 0.00420, ⊖; 0.00250. W_{Alg} (for NaCl solution): ●; 0.00626.

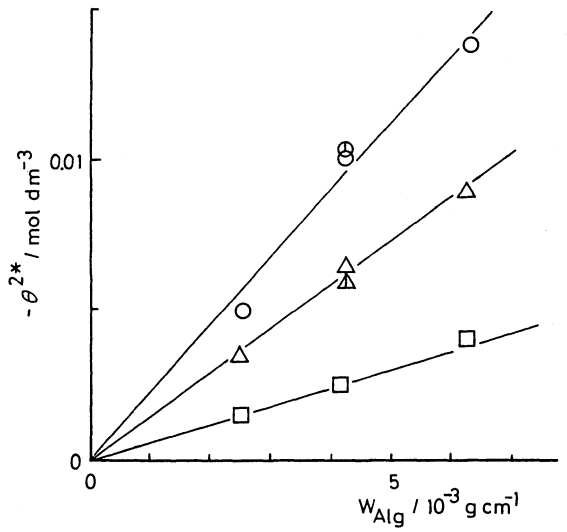

Fig. 8. Effective charge densities vs. concentrations of alginates. NaAlg: ○ (R=10), ⊕ (R=2). MgAlg: △ (R=10), ▲ (R=2). CaAlg: □ (R=10).

Figure 8 shows the effective charge densities of alginates as a function of the concentration of alginates W_{Alg}. As W_{Alg} increases, the absolute values increase almost linearly; their magnitudes were as follows; Na- > Mg- > Ca-Alg.

Discussion

Counterion-Binding Characteristics of Alginates. The concentration of Alg based on the uronate units, which corresponds to the concentration of carboxyl groups C_{car} mol dm^{-3}, is obtained by the use of Eq. 12. If all the carboxyl groups work as charged groups, the absolute value of the charge density of Alg is equal to C_{car}:

$$C_{car}=|\theta_0|=10^3\, W_{Alg}/M_u, \qquad (12)$$

where M_u is the molar mass of the uronates. The ratios of the effective charge density of Alg to θ_0, θ^{*2}/θ_0, show the fractions of the ionized carboxyl groups. The W_{Alg} in the second layer might decrease because of osmotic pressures. However, by the help of the perforated support plates (F) shown in Fig. 1 (a), we estimate that the decrease in W_{Alg} could be neglected. As is shown in Table 1, the θ^{*2}/θ_0 values were found not to depend remarkably on W_{Alg} in the experimental region. The mean θ^{*2}/θ_0 values for Na-, Mg-, and CaAlg were 0.45, 0.28, and 0.12 respectively. Na- and MgAlg were in sol states. The interactions of Na^+ and Mg^{2+} with Alg were dominantly electrostatical. Therefore, the differences in their values θ^{*2}/θ_0 can be surmised to result from their valence effects. Ca ions mediate the stackings of Alg molecules to form the junctions.[2-4] Then, the much smaller value of CaAlg than MgAlg results from the constraints of Ca ions in the junctions and in the networks.

Alg can be considered to behave as a rod like polyelectrolyte in diluted solutions, because of the electrostatical repulsive force between the charged groups and the rigidity of their saccharide structure. Manning's theory[23,24] is appropriate for discussing the thermodynamic quantities of rod like polyelectrolytes in diluted solutions.[25-30] By comparing our results with the

theoretical results, the effects of the polymer-polymer interactions and the network formations on counterion bindings can be discussed. In theory, the interaction of polyelectrolytes with counterions are considered to be of two modes: the Debye-Hückel ion atmosphere and the condensation on charged groups. The key parameter, ξ, for the counterion condensation in Manning's theory is defined by Eq. 13 and is proportional to the line charge density,[23,24] i.e., the reciprocal of the distance between the neighbouring charged groups b:

$$\xi = e^2/(4\pi\varepsilon kTb) \quad (13)$$

where e is the protonic charge and where ε is the permitivity of the solvent. The b value of NaAlg has been reported to be 0.497 nm, and the ξ value, 1.43.[31] The osmotic coefficients ϕ_M of salt-free polyelectrolytes are expressed by:

$$\phi_M = 1/(2z_i\xi) \quad (14)$$

The theoretical ϕ_M values of Alg with monovalent and divalent counterions are 0.35 and 0.17. The ϕ_M value can be considered approximately to be the degree of ionization of the charged groups in polymers.[32] By comparing the experimental θ^{*2}/θ_0 values shown in Table 1 with the ϕ_M values, we can see that both results for Na- and MgAlg were much larger than the ϕ_M values. Kobatake et al.[11] discussed precisely the thermodynamical and hydrodynamical effective charge densities of Poly (styrenesulfonate) (PSS) solutions by using the membrane-potential and Donnan-potential methods. Their θ^{*2}/θ_0 values of potassium salt of PSS (KPSS) obtained from the membrane potential were reported to be 0.4. As the theoretical value ϕ_M of KPSS is 0.18,[24] the effective charge density was also much greater than the ϕ_M value. It is a significant problem that the effective charge densities of polyelectrolyte solutions are much greater than the ϕ_M values. This might be the effect of the hydrodynamical effects described by Kobatake et al.[11]

Effects of Gellation on Ca-Ion Bindings. The electrostatical interactions of Mg and Ca ions with Alg are assumed to be equal. Then, the difference in θ^{*2}/θ_0 between Mg- and CaAlg, $|(\theta^{*2}(\text{MgAlg})-\theta^{*2}(\text{CaAlg}))/\theta_0|=0.16$, shows the ratio of the enhanced Ca-ion bindings due to the gellation of Alg. Whether this increase results primarily from the entrapping of Ca ions in the junctions should be discussed. When the fraction of the junctions in a Alg molecule is F_j, on the basis of the concentration of the uronate units, and when the Ca-ion binding ratio in the junctions and in the Alg chains between the junctions are $(\sigma_j)_{Ca}$ and $(\sigma_i)_{Ca}$, the fraction of ionized carboxyl groups in CaAlg gels $(\theta^{*2}/\theta_0)_{Ca}$ can be expressed by the following equation:

$$(\theta^{*2}/\theta_0)_{Ca} = F_j(1-(\sigma_j)_{Ca}) + (1-F_j)(1-(\sigma_i)_{Ca}). \quad (15)$$

The Ca ions entrapped in the junctions can be assumed to bind completely to Alg,[33] i.e., $(\sigma_j)_{Ca}=1$, and all GG blocks are assumed to contribute to the formation of the junctions, i.e., $F_j=F_{GG}=0.28$. Under these assumptions, the value $(\sigma_i)_{Ca}$ of CaAlg is calculated from the result $(\theta^{*2}/\theta_0)_{Ca}$ (=0.12); it is 0.83, which is bigger than the Mg-ion-binding ratio σ_{Mg} (=$(1-(\theta^{*2}/\theta_0)_{Mg}$=0.72). Actually, F_j is considered to be smaller than F_{GG}. Therefore, $(\sigma_i)_{Ca}$ should be bigger than 0.83. From these considerations, it can be concluded that the Ca-ion bindings are enhanced by the gellation not only in the junction, but even in the regions between the junctions, i.e., in the networks.

References

1) A.Haug, B. Larsen, and O. Smidsrod, *Carbohydr. Res.*, **32**, 217 (1974).
2) D. A. Rees, *Biochem. J.*, **126(2)**, 257 (1972).
3) E. R. Morris, D. A. Rees, and D. Thom, *Carbohydr. Res.*, **66**, 143 (1978).
4) T. A. Bryce, A. A. McKinnon, E. R. Morris, D. A. Rees, and D. Thom, *Faraday Discuss. Chem. Soc.*, **57**, 221 (1974).
5) A. Suggett, "Water," ed by F. Franks, Vol. 4, Plenum Press, New York (1975), p. 519.
6) Y. F. Leung, G. M. O'Shea, M. F. A. Coosen, and A. M. Sun, *Artif. Organs*, **7(2)**, 208 (1983).
7) H. Tanaka, M. Matsumura, and I. A. Veliky, *Biotechnol. Bioeng.*, **26**, 53 (1984).
8) R. Kohn, I. Furda, A. Haug, and O. Smidsrod, *Acta Chem. Scand.*, **22**, 3098 (1968).
9) O. Smidsrod, and A. Haug. *Acta Chem. Scand.*, **22**, 1989 (1968).
10) A. Haug, and O. Smidsrod, *Acta Chem. Scand.*, **24**, 843 (1970).
11) M. Yuasa, Y. Kobatake, and H. Fujita, *J. Phys. Chem.*, **72(8)**, 2871 (1968).
12) E. R. Morris, D. A. Rees, and D. Thom, *Carbohydr. Res.*, **81**, 305 (1980).
13) H. Grasdalen, B. Larsen, and O. Smidsrod, *Carbohydr. Res.*, **68**, 23 (1979).
14) M. Yonese, *Hyoumen*, **18**, 692 (1980).
15) J. Kielland, *J. Am. Chem. Soc.*, **59**, 1675 (1937).
16) N. Takeguchi and M. Nakagaki, *Biochim. Biophys., Acta*, **219**, 405 (1970).
17) M. Nakagaki and K. Miyata, *Yakugaku Zasshi*, **93**, 1105 (1973).
18) M. Yonese and M. Nakagaki, *Yakugaku Zasshi*, **96**, 299 (1976).
19) P. Henderson, *Z. Physik. Chem.*, **59**, 118 (1907).
20) M. Nakagaki and M. Kobayashi, *Yakugaku Zasshi*, **93**, 964 (1973).
21) M. Nakagaki and R. Takagi, *Membranes*, **4**, 183 (1979).
22) R. Parsons, "Handbook of Electrochemical Constants," Butterworths Scientific Publications, London (1959), p. 87.
23) G. S. Manning, *Annu. Rev. Phys. Chem.*, **23**, 117 (1972).
24) G. S. Manning, "Charged and Reactive Polymers I, Polyelectrolytes," ed by E. Selegny, D. Reidel Publishing Co., Boston (1972), p. 9.
25) M. Yonese, H. Tsuge, and H, Kishimoto, *Nippon Kagaku Kaishi*, **1978**, 108.

26) H. Tsuge, M. Yonese, and H. Kishimoto, *Bull. Chem. Soc. Jpn.*, **52**, 2846 (1979).
27) M. Yonese, H. Tsuge, and H. Kishimoto, *Bull. Chem. Soc. Jpn.*, **54**, 20 (1981).
28) H. Tsuge, M. Yonese, and H. Kishimoto, *Nippon Kagaku Kaishi*, **1978**, 609.
29) H. Tsuge, M. Yonese, and H. Kishimoto, *Nippon Kagaku Kaishi*, **1982**, 1583.
30) M. Yonese, H. Tsuge, and H. Kishimoto, *J. Phys. Chem.*, **91**, 1971 (1987).
31) T. J. Podlas and P. Ander, *Macromolecules*, **3**, 154 (1970).
32) M. Nakagaki, S, Shimabayashi, E. Hayakawa, and T. Kotsuki, *Yakugaku Zasshi*, **99**, 618 (1979).
33) A. Katchalsky, R. E. Cooper, J. Upadhyay, and A. Wassermann, *J. Chem. Soc.*, **1961**, 5198.
34) R. Kohn and B. Larsen, *Acta Chem. Scand.*, **26**, 2455 (1972).

 © 1988 The Chemical Society of Japan Bull. Chem. Soc. Jpn., 61, 1085—1090 (1988)

The Crystal and Molecular Structures of *N*-Phenyl-4-nitrobenzylamine, *N*-Phenyl-4-nitrophenethylamine, and *N*-Methyl-*N*-*p*-tolyl-4-nitrophenethylamine

Fujiko IWASAKI,* Yoshiaki MASUKO, Sachiko MONMA, Toshiya WATANABE, and Kiyoshi MUTAI†
Department of Materials Science, The University of Electro-Communications, Chofu-shi, Tokyo 182
†Department of Chemistry, College of General Education, University of Tokyo, Komaba, Meguro, Tokyo 153
(Received October 2, 1987)

The crystal and molecular structures of *N*-phenyl-4-nitrobenzylamine (**1**), *N*-phenyl-4-nitrophenethylamine (**2**), and *N*-methyl-*N*-*p*-tolyl-4-nitrophenethylamine (**3**) have been determined by the X-ray method. The crystals of **1** are monoclinic, $P2_1/n$, a=16.924(1), b=8.792(1), c=7.642(1) Å, β=91.59(1)°, V=1136.8(1) Å^3, Z=4, D_x=1.334 Mg m^{-3}. **2** is triclinic, $P\bar{1}$, a=15.106(1), b=9.573(1), c=9.427(1) Å, α=113.22(1), β=91.27(1), γ=83.61(1)°, V=1244.7(2) Å^3, Z=4, D_x=1.293 Mg m^{-3}. **3** is trigonal, $P3_1$, a=b=8.435(1), c=17.758(1) Å, α=β=90°, γ=120°, V=1094.2 Å^3, Z=3, D_x=1.231 Mg m^{-3}. The final R values are 0.064, 0.059, and 0.045 for 1625, 3606, and 1131 observed reflections of **1**, **2**, and **3**, respectively. About the amino-methylene N–C bond the phenyl group is trans to C for the molecules of **1** and **2**, while in **3** the phenyl group is gauche to C about the N–C bond. The nitrophenyl plane of **3** is stacked on the *p*-toluidino plane of the neighbouring molecule alternately with the mean distance of 3.40 Å. The presence of the intermolecular CT interaction of **3** has been confirmed by the electronic absorption spectra of these compounds in the solid state.

Intramolecular interactions, especially a charge-transfer interaction, are extensively studied for *N*-[ω-(4-nitrophenyl)alkyl]anilines in which electron donor (anilino) and acceptor (4-nitrophenyl) moieties are bound together by a polymethylene chain.[1] The study with UV-VIS spectroscopy revealed that the solutions of the lower homologs show the presence of an intramolecular charge-transfer interaction, which is also detectable by the pale yellow color of the dilute solutions (ca. 10^{-4} mol dm^{-3}). Since the color persists in solid, even in the higher homologs, we suspected the presence of another type of intramolecular donor-acceptor interaction in the solid state. The crystal structure analysis of *N*-phenyl-4-nitrobenzylamine (**1**), *N*-phenyl-4-nitrophenethylamine (**2**), and *N*-methyl-*N*-*p*-tolyl-4-nitrophenethylamine (**3**) was carried out by the X-ray method in order to determine their molecular conformations and intra- and/or intermo-

Table 1. Crystal Data and Experimental Conditions

	1	**2**	**3**
	$C_{13}H_{12}N_2O_2$	$C_{14}H_{14}N_2O_2$	$C_{16}H_{18}N_2O_2$
Color	Pale-brown	Pale-brown	Orange-red
Mw	228.25	242.28	270.33
Crystal system	Monoclinic	Triclinic	Trigonal
Space group	$P2_1/n$	$P\bar{1}$	$P3_1$
a/Å	16.924(1)	15.106(1)	8.435(1)
b/Å	8.792(1)	9.573(1)	8.435(1)
c/Å	7.642(1)	9.427(1)	17.758(2)
α/°	90.0	113.22(1)	90.0
β/°	91.59(1)	91.27(1)	90.0
γ/°	90.0	83.61(1)	120.0
V/Å^3	1136.8(1)	1244.7(2)	1094.2(1)
Z	4	4	3
D_x/Mg m^{-3}	1.334	1.293	1.231
Radiation	Cu $K\alpha_1$	Cu $K\alpha_1$	Cu $K\alpha_1$
μ/mm^{-1} (Cu $K\alpha$)	0.711	0.677	0.624
Crystal size/mm	0.40×0.35×0.05	0.40×0.40×0.30	0.30×0.35×0.20
Scan range/°	$2<2\theta<130$	$2<2\theta<130$	$2<2\theta<130$
Scan width/°	$1.2+0.5\tan\theta$	$1.2+0.5\tan\theta$	$1.2+0.5\tan\theta$
Max. h, k, l	±19, 10, 9	±17, 11, ±11	9, ±9, 20
No. of Reflections			
measured	2187	4775	2423
unique	1923	4472	1699
observed	1625	3606	1131
refinement	1620	3595	1130
R (refinement)	0.060	0.051	0.041
R_w (refinement)	0.074	0.051	0.043
R (observed)	0.064	0.059	0.045
S	1.003	0.612	0.721

lecular interactions. The compounds **1** and **2** were chosen because they are the first two members of the homologous series of the most basic group studied so far. The compound **3** was chosen on account of its remarkable orange-red color in the crystals, while the other derivatives studied are all pale brown or yellow in the solid state.

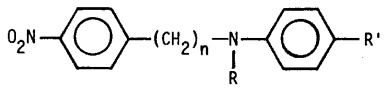

(**1**) n=1 R=H R′=H
(**2**) n=2 R=H R′=H
(**3**) n=2 R=CH_3 R′=CH_3

Experimental

X-Ray Crystal Structure Determination. Crystal data and some experimental conditions are listed in Table 1. Intensities were collected on a Rigaku automatic diffractometer with graphite-monochromated Cu $K\alpha_1$ (λ=1.54051 Å) radiation, using the ω-2θ scan technique with a scanning rate of 4° min^{-1} in 2θ. At both ends of the scan range 10s background counts were taken for each reflection. Three reflections were monitored after every 50 reflections. Variations of intensities of the monitored reflections were within 1, 1.5, and 2% for **1**, **2**, and **3**, respectively. Reflections with $|F_o| \geqslant 3\sigma(F_o)$ were used for structure determination.

The structures were solved by the direct method with the program MULTAN 78.[2] All non-hydrogen atoms were refined by the block-diagonal least-squares with anisotropic temperature factors. Difference maps showed all the hydrogen atoms. During the final stage of the refinement 5, 11, and 1 strong reflections which were seriously affected by extinction were omitted from the reflection data of **1**, **2**, and **3**, respectively. Least-squares refinements with anisotropic temperature factors for the non-hydrogen atoms and iso-

Table 2. Atomic Coordinates (×10^4) and Equivalent Isotropic Temperature Factors for Non-H Atoms

Atom	x	y	z	B_{eq}/Å^2	Atom	x	y	z	B_{eq}/Å^2
(a) **1**									
O(1)	6260(2)	363(3)	3806(4)	7.7	C(6)	2653(2)	2945(3)	−4748(3)	4.0
O(2)	5611(2)	1424(3)	5830(3)	7.2	C(7)	3807(2)	4264(3)	−864(4)	4.3
N(1)	3595(1)	3342(3)	−2366(3)	4.1	C(9)	4307(2)	3416(3)	470(3)	3.6
N(2)	5733(1)	1189(3)	4300(3)	4.8	C(10)	4883(2)	2389(3)	−17(4)	4.0
C(1)	3080(1)	3943(3)	−3655(3)	3.4	C(11)	5352(2)	1648(3)	1226(4)	4.0
C(2)	2998(2)	5489(3)	−3936(3)	4.0	C(12)	5234(1)	1963(3)	2961(3)	3.7
C(3)	2508(2)	6029(4)	−5278(4)	4.6	C(13)	4670(2)	2965(4)	3499(4)	4.4
C(4)	2084(2)	5041(4)	−6345(4)	4.8	C(14)	4208(2)	3698(4)	2236(4)	4.3
C(5)	2158(2)	3502(4)	−6060(4)	4.5					
(b) **2**									
O(1A)	10831(1)	6407(3)	7832(3)	10.0	O(1B)	5773(1)	3739(2)	7225(3)	7.5
O(2A)	10645(1)	8865(3)	8598(3)	9.8	O(2B)	5951(1)	1289(2)	6376(2)	7.0
N(1A)	5310(1)	7104(2)	6287(2)	4.8	N(1B)	423(1)	2932(3)	8689(2)	6.0
N(2A)	10382(1)	7622(3)	8004(3)	6.9	N(2B)	5508(1)	2519(2)	7028(2)	5.1
C(1A)	4572(1)	7332(2)	7234(2)	3.9	C(1B)	−313(2)	2686(3)	7746(3)	4.5
C(2A)	4593(2)	8006(3)	8830(3)	4.5	C(2B)	−244(2)	2029(3)	6148(3)	5.2
C(3A)	3823(2)	8312(3)	9720(3)	4.9	C(3B)	−1000(2)	1739(3)	5276(3)	5.6
C(4A)	3017(2)	7935(3)	9041(3)	4.9	C(4B)	−1839(2)	2100(3)	5956(3)	5.4
C(5A)	2993(2)	7233(3)	7459(3)	4.7	C(5B)	−1911(2)	2772(3)	7534(3)	5.2
C(6A)	3755(2)	6934(3)	6557(3)	4.4	C(6B)	−1167(2)	3064(3)	8423(3)	5.0
C(7A)	6208(2)	7253(3)	6886(3)	4.7	C(7B)	1325(2)	2663(3)	8058(3)	5.6
C(8A)	6847(2)	7235(3)	5670(3)	5.1	C(8B)	1995(2)	2649(3)	9268(3)	5.6
C(9A)	7782(1)	7340(3)	6244(3)	4.1	C(9B)	2928(2)	2596(3)	8705(3)	4.5
C(10A)	8335(2)	6043(3)	6097(3)	5.2	C(10B)	3287(2)	3938(3)	8937(3)	5.2
C(11A)	9182(2)	6123(3)	6675(3)	5.5	C(11B)	4125(2)	3922(3)	8397(3)	4.9
C(12A)	9471(1)	7535(3)	7399(3)	4.7	C(12B)	4608(1)	2537(3)	7608(2)	4.0
C(13A)	8950(2)	8850(3)	7561(3)	5.3	C(13B)	4282(2)	1176(3)	7344(3)	4.6
C(14A)	8100(2)	8744(3)	6971(3)	4.9	C(14B)	3440(2)	1221(3)	7899(3)	4.9
(c) **3**									
O(1)	14888(4)	4718(4)	589(2)	8.9	C(7)	5406(5)	427(5)	1079(2)	5.8
O(2)	14224(4)	2714(4)	−280(1)	8.0	C(8)	6413(5)	−559(4)	1320(2)	5.4
N(1)	3433(4)	−599(5)	1190(2)	6.6	C(9)	8368(4)	417(4)	1058(2)	4.8
N(2)	13811(4)	3317(4)	262(2)	6.2	C(10)	9666(5)	2040(5)	1403(2)	5.5
C(1)	2337(4)	−2029(5)	712(2)	5.5	C(11)	11442(4)	2990(5)	1143(2)	5.6
C(2)	3006(5)	−2355(5)	44(2)	6.0	C(12)	11910(4)	2311(4)	536(2)	4.8
C(3)	1870(5)	−3728(5)	−447(2)	6.1	C(13)	10681(4)	718(5)	179(2)	5.5
C(4)	25(5)	−4874(5)	−307(2)	6.0	C(14)	8914(4)	−209(5)	445(2)	5.4
C(5)	−626(5)	−4555(5)	357(2)	6.4	C(15)	−1182(6)	−6377(6)	−831(3)	8.2
C(6)	467(5)	−3207(5)	853(2)	5.9	C(16)	2766(6)	−487(6)	1924(2)	6.9

$B_{eq}=4/3\sum_i\sum_j \beta_{ij}\boldsymbol{a}_i\cdot\boldsymbol{a}_j$.
The e.s.d.'s in parentheses refer to the last digits.

tropic ones for H gave the final R values of 0.060, 0.051, and 0.041 for 1620, 3595, and 1130 reflections of **1**, **2**, and **3**, respectively. The quantity minimized was $\sum w(|F_o|-k^{-1}|F_c|)^2$. For **1**, $w=1/(0.41515-0.0188|F_o|+0.0016|F_o|^2)$, for **2**, $w=1$ for all reflections, and for **3**, $w=1/(0.1936+0.0157|F_o|+0.0014|F_o|^2)$. The R values for 1625, 3606, and 1131 observed reflections of **1**, **2**, and **3** were 0.064, 0.059, and 0.045, respectively. Atomic scattering factors were taken from International Tables for X-Ray Crystallography.[3] All computations were performed on a HITAC M180 Computer of the Data Processing Center of the University of Electro-Communications with the programs UNICS III,[4] MULTAN 78,[2] and ORTEP II.[5] The final atomic parameters are given in Table 2.[6]

Electronic Spectra. A small amount of crystals of **1**—**3** was melted on a quartz plate (22×13×1 mm^3), covered with another quartz plate of nearly the same size, and left to crystallize. No attempt was made to control the thickness of the solid. The absorption spectrum of the plate was recorded on a Hitachi UV-3200 spectrophotometer.

Discussion

Molecular Structures. The molecular structures with the atomic numbering are shown in Fig. 1. Bond distances and angles are listed in Table 3. Some torsion angles are listed in Table 4. For **2**, there are two crystallographically independent molecules, **A** and **B**, in an asymmetric unit. These two molecules, however, have the same structures within the experimental errors. For **1** the phenyl group is trans to the 4-nitrophenyl group about the N(1)-C(7) bond. The

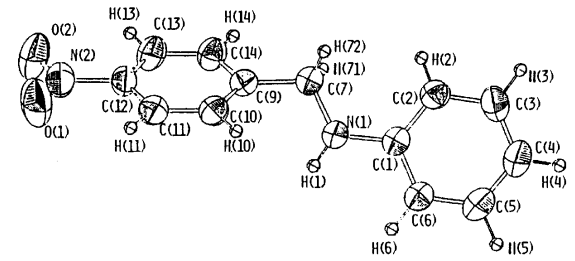

(a)

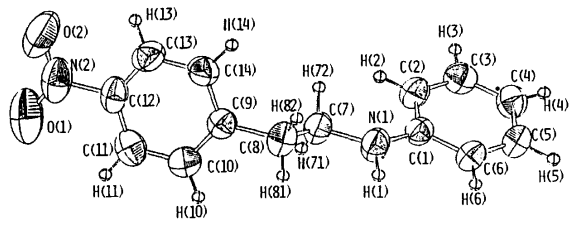

(b)

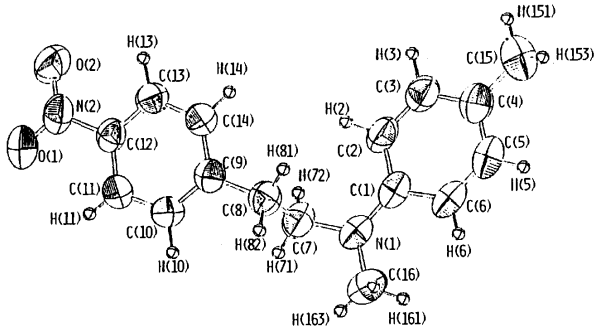

(c)

Fig. 1. Atomic numbering of the molecules. (a) **1**, (b) **2A**, and (c) **3**. The thermal ellipsoids for non-H atoms are drawn at 50% probability.

Table 3. Bond Lengths (l) and Angles (θ)

Distance	**1** l/Å	**2A** l/Å	**2B** l/Å	**3** l/Å
O(1)-N(2)	1.218(4)	1.233(5)	1.221(3)	1.218(5)
O(2)-N(2)	1.211(4)	1.207(4)	1.218(3)	1.219(5)
N(1)-C(1)	1.400(4)	1.387(3)	1.390(4)	1.384(6)
N(1)-C(7)	1.443(4)	1.458(4)	1.455(4)	1.455(6)
N(1)-C(16)				1.441(6)
N(2)-C(12)	1.474(4)	1.477(4)	1.471(3)	1.472(5)
C(1)-C(2)	1.383(4)	1.385(4)	1.386(4)	1.399(6)
C(1)-C(6)	1.399(4)	1.399(3)	1.397(4)	1.404(6)
C(2)-C(3)	1.386(4)	1.385(4)	1.381(4)	1.382(6)
C(3)-C(4)	1.378(5)	1.379(4)	1.378(4)	1.383(6)
C(4)-C(5)	1.376(5)	1.375(4)	1.370(4)	1.382(6)
C(4)-C(15)				1.490(7)
C(5)-C(6)	1.378(4)	1.381(4)	1.373(4)	1.368(6)
C(7)-C(8)		1.509(4)	1.511(4)	1.518(6)
C(8)-C(9)	1.505(4)[a]	1.500(4)	1.506(4)	1.503(5)
C(9)-C(10)	1.386(4)	1.378(4)	1.386(4)	1.396(5)
C(9)-C(14)	1.387(4)	1.382(4)	1.385(4)	1.384(5)
C(10)-C(11)	1.385(4)	1.377(4)	1.371(4)	1.378(6)
C(11)-C(12)	1.375(4)	1.368(4)	1.370(4)	1.369(5)
C(12)-C(13)	1.370(4)	1.364(4)	1.373(4)	1.375(6)
C(13)-C(14)	1.384(5)	1.386(4)	1.376(4)	1.375(6)

Angle	**1** θ/°	**2A** θ/°	**2B** θ/°	**3** θ/°
C(1)-N(1)-C(7)	119.0(2)	122.0(2)	121.7(2)	120.1(4)
C(1)-N(1)-C(16)				119.9(4)
C(7)-N(1)-C(16)				116.9(4)
O(1)-N(2)-O(2)	123.1(3)	124.5(3)	123.2(3)	123.4(4)
O(1)-N(2)-C(12)	118.0(3)	117.3(3)	118.3(2)	118.1(4)
O(2)-N(2)-C(12)	118.8(3)	118.2(3)	118.5(2)	118.4(4)
N(1)-C(1)-C(2)	122.5(2)	123.1(2)	123.0(2)	122.2(4)
N(1)-C(1)-C(6)	119.0(2)	118.9(2)	119.2(2)	122.1(4)
C(2)-C(1)-C(6)	118.4(3)	117.9(2)	117.8(2)	115.7(4)
C(1)-C(2)-C(3)	120.4(3)	120.8(2)	120.3(3)	121.4(4)
C(2)-C(3)-C(4)	120.9(3)	120.9(3)	121.5(3)	122.6(4)
C(3)-C(4)-C(5)	118.8(3)	118.7(3)	118.4(3)	115.8(4)
C(3)-C(4)-C(15)				122.3(4)
C(5)-C(4)-C(15)				121.9(4)
C(4)-C(5)-C(6)	121.0(3)	121.0(2)	121.1(3)	122.9(4)
C(1)-C(6)-C(5)	120.3(3)	120.6(2)	121.0(3)	121.7(4)
N(1)-C(7)-C(8)	112.6(2)[b]	110.3(2)	110.4(3)	115.0(3)
C(7)-C(8)-C(9)		111.3(2)	110.8(2)	111.9(3)
C(8)-C(9)-C(10)	121.8(2)[c]	120.8(2)	120.4(2)	120.6(3)
C(8)-C(9)-C(14)	119.3(2)[d]	120.8(2)	121.6(2)	121.2(3)
C(10)-C(9)-C(14)	118.9(3)	118.4(2)	118.0(2)	118.1(3)
C(9)-C(10)-C(11)	121.1(3)	121.6(3)	121.6(3)	121.0(4)
C(10)-C(11)-C(12)	118.1(3)	118.3(3)	118.4(3)	118.5(4)
N(2)-C(12)-C(11)	118.7(2)	118.4(3)	118.4(2)	118.6(3)
N(2)-C(12)-C(13)	118.6(3)	119.4(3)	119.3(2)	118.9(3)
C(11)-C(12)-C(13)	122.7(3)	122.2(3)	122.3(2)	122.5(4)
C(12)-C(13)-C(14)	118.3(3)	118.5(3)	118.3(2)	118.1(4)
C(9)-C(14)-C(13)	120.9(3)	121.0(3)	121.4(3)	121.8(4)

For **1**, a) C(7)-C(9) b) N(1)-C(7)-C(9) c) C(7)-C(9)-C(10) d) C(7)-C(9)-C(14).

Table 4. Some Torsion Angles (τ) and Dihedral Angles (ω)

Torsion angle	**1** τ/°	**2A** τ/°	**2B** τ/°	**3** τ/°
C(7)-N(1)-C(1)-C(2)	−25.2(3)	13.4(3)	6.6(3)	−10.8(5)
C(7)-N(1)-C(1)-C(6)	157.3(2)	−169.8(2)	−175.6(2)	171.5(3)
C(8)-C(7)-N(1)-C(1)	175.2(2)[a]	−169.5(2)	−166.4(2)	−74.9(4)
C(8)-C(7)-N(1)-C(16)	36.8(20)[b]	38.2(17)[c]	34.8(22)[c]	85.3(4)
C(9)-C(8)-C(7)-N(1)		−178.3(2)	−171.9(2)	169.2(3)
C(7)-C(8)-C(9)-C(10)	37.3(3)[d]	87.5(3)	88.4(3)	73.7(4)
C(7)-C(8)-C(9)-C(14)	−144.2(2)[e]	−90.7(2)	−89.3(3)	−103.0(3)

a) C(9)-C(7)-N(1)-C(1) b) C(9)-C(7)-N(1)-H(1)
c) C(8)-C(7)-N(1)-H(1) d) N(1)-C(7)-C(9)-C(10)
e) N(1)-C(7)-C(9)-C(14)

Plane (1) C(1)—C(6) Plane (2) C(9)—C(14)
Plane (3) N(1)-C(7)-C(8) (for **1**, N(1)-C(7)-C(9))

Dihedral angle	**1** ω/°	**2A** ω/°	**2B** ω/°	**3** ω/°
(1) (2)	58.6	71.3	69.1	10.4
(1) (3)	21.9	21.5	19.1	82.2
(2) (3)	36.8	91.0	92.2	72.0

Table 5. Intermolecular Contacts Less than 3.6 Å with Their Estimated Standard Deviations

a) **1**

superscript								
	(none)	x	y	z	(iv)	x+1/2	−y+1/2	z+3/2
	(i)	x	y	z+1	(v)	x−1/2	−y+1/2	z−1/2
	(ii)	−x+1	−y	−z	(vi)	−x+1/2	y−1/2	−z−1/2
	(iii)	−x+1	−y	−z+1				

Distance	l/Å	Distance	l/Å
O(1)···O(2^{iii})	3.552(4)	O(2)···C(5^{iv})	3.487(5)
O(1)···N(1^{ii})	3.449(4)	O(2)···C(10^{i})	3.539(4)
O(1)···C(6^{ii})	3.506(4)	O(2)···C(12^{iii})	3.441(4)
O(2)···O(2^{iii})	3.466(4)	N(1)···C(3^{vi})	3.451(4)
O(2)···N(2^{iii})	3.232(4)	N(2)···N(2^{iii})	3.437(5)
O(2)···C(4^{iv})	3.498(5)	C(5)···C(11^{v})	3.565(4)

b) **2**

superscript								
	(none)	x	y	z	(iii)	−x+1	−y+1	−z+1
	(i)	x+1	y	z	(iv)	−x+1	−y+1	−z+2
	(ii)	−x+1	−y	−z+1	(v)	−x+2	−y+2	−z+2

Distance	l/Å	Distance	l/Å
O(1)···C(5^{i})	3.503(4)	N(2)···C(3B^{iii})	3.543(4)
O(1)···C(6B^{iv})	3.398(4)	C(3)···O(2B^{iv})	3.560(4)
O(2)···O(2^{v})	3.203(6)	C(3)···N(2B^{iv})	3.558(4)
O(2)···C(13^{v})	3.496(4)	C(6)···O(1B^{iii})	3.441(3)
O(2)···C(3B^{iii})	3.509(4)	O(1B)···C(5B^{i})	3.554(4)
N(1)···N(2B^{iii})	3.471(3)	O(2B)···C(4B^{i})	3.577(4)
N(1)···O(1B^{iii})	3.499(3)	O(2B)···C(13B^{ii})	3.405(3)

c) **3**

superscript								
	(none)	x	y	z	(iii)	x+2	y+1	z
	(i)	x−1	y	z	(iv)	−y+1	x−y	z+1/3
	(ii)	x+1	y+1	z	(v)	−y+1	x−y−1	z+1/3

Distance	l/Å	Distance	l/Å
O(1)···C(5^{iii})	3.542(5)	C(6)···C(14^{i})	3.457(6)
O(1)···C(15^{iv})	3.575(6)	C(7)···O(2^{i})	3.531(6)
N(1)···N(2^{i})	3.560(5)	C(8)···O(2^{v})	3.431(5)
N(1)···C(12^{i})	3.490(5)	C(10)···O(2^{v})	3.452(5)
N(1)···C(13^{i})	3.525(6)	C(10)···C(5^{ii})	3.531(6)
C(1)···C(13^{i})	3.384(6)	C(11)···C(5^{ii})	3.591(6)
C(6)···C(13^{i})	3.439(6)		

torsion angle of C(1)-N(1)-C(7)-C(9) is 175.2(2)°, while the corresponding angle of *N*-(2-bromophenyl)-2-bromobenzylamine is 88.5° because of the existence of large ortho substituents.[7] For **2** the phenyl group is trans to C(8) about the N(1)-C(7) bond and N(1) is trans to the 4-nitrophenyl group about the C(7)-C(8) bond. On the other hand in the case of **3** the phenyl group is gauche to C(8) about the N(1)-C(7) bond and N(1) is trans to 4-nitrophenyl group about the C(7)-C(8) bond. To analyze the planarity of molecular moieties, each molecule has been devided into three fragments: (1) C(1)—C(6) plane of the phenyl or *p*-tolyl groups; (2) C(9)—C(14) of the nitrophenyl groups; and (3) the central chain N(1)-C(7)-C(9) of **1** or N(1)-C(7)-C(8) of **2** and **3**. The dihedral angles of these planes are also listed in Table 4. The phenyl group of **1** and **2** is roughly parallel to the central chain and the 4-nitrophenyl group of **2** is perpendicular to the plane (3). For **3** both six membered rings are almost perpendicular to the central chain, and they are approximately parallel to each other. The nitro group of each compound is nearly coplanar to the phenyl ring. The dihedral angles beween the plane (2) and the nitro group are 3.6, 2.7, 2.6, and 0.4°, for **1**, **2A**, **2B**, and **3**, respectively.

Significant differences are observed about the dimensions of the amino groups between **1** and the other compounds, **2** and **3**. The N(1)-C(1) bond of **1** is longer than those of **2** and **3**, while the N(1)-C(7) bond of **1** is shorter than those of **2** and **3**. The bond angle of C(1)-N(1)-C(7) of **1** is slightly smaller than the corresponding angles of **2** and **3**. The N(1)-C(1) bonds of **2** and **3** show a larger double-bonded character compared with those of anilines. The corresponding length of *N*-benzylideneaniline is 1.460 Å.[8] These features correspond to the difference of the planarity of the amino plane C(1)-N(1)R-C(7) (R=H(1) or C(16)) between the benzyl and phenethyl compounds. The deviations of N(1) from the plane defined by C(1), C(7) and H(1)/C(16) are 0.259, 0.167, 0.125, and 0.145 Å for **1**, **2A**, **2B**, and **3**, respectively.

Crystal Stuctures and Interactions. Crystal structures are shown in Fig. 2 and some intermolecular contacts are listed in Table 5. The packing mode of the molecules in the crystal **2** is approximately $P2_1/c$. There are no special contacts suggesting an intermolecular CT interaction nor an NH ··· O hydrogen bond for **1** and **2**, in spite of the possibility of these interactions. On the other hand in the case of **3** the nitrophenyl plane is stacked on the *p*-tolyl plane of the neighbouring molecule alternately, as shown in Fig. 3.

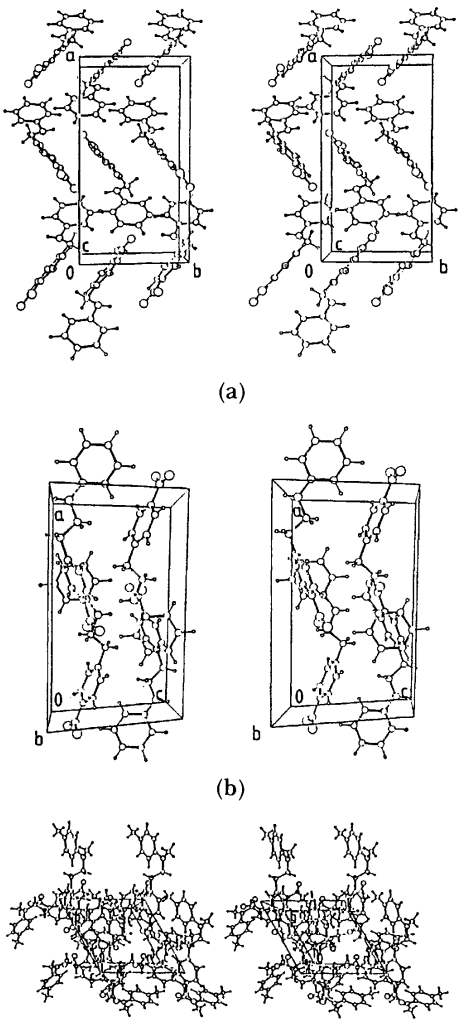

Fig. 2. Stereoscopic view of the crystal structures. (a) **1**, (b) **2**, and (c) **3**.

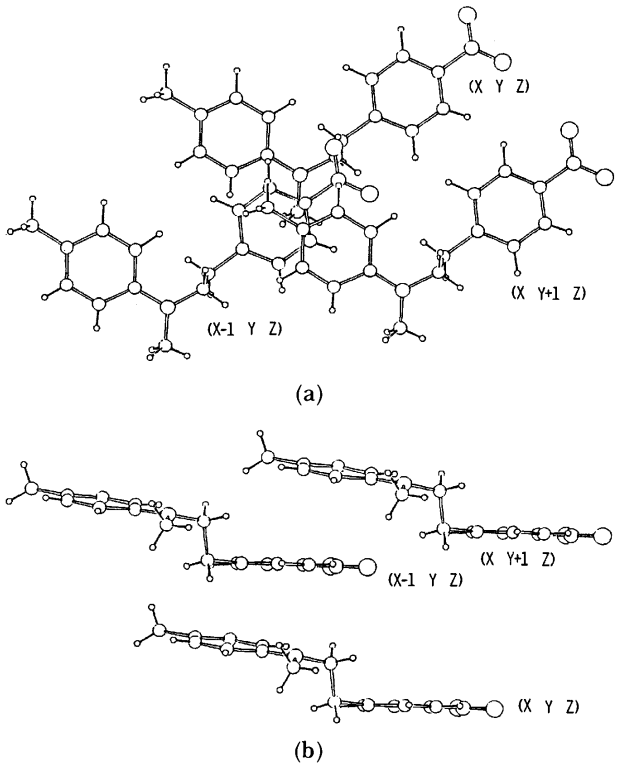

Fig. 3. Molecular stacking of **3**. (a) Projection to the nitrophenyl plane. (b) Side view of the stacking

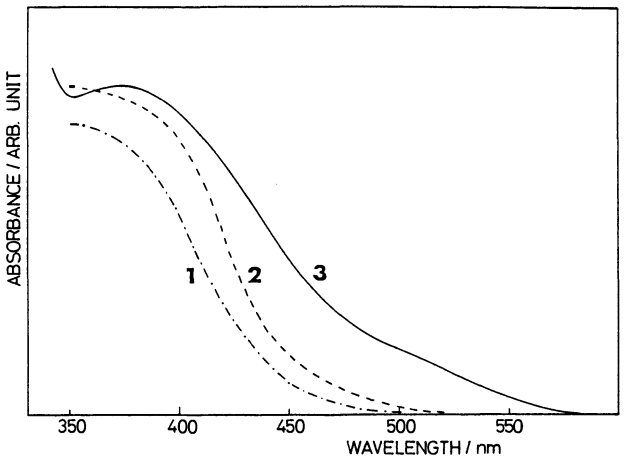

Fig. 4. Electronic spectra of **1**, **2**, and **3** in the solid state. Absorbance is in an arbitrary unit.

The mean distance between these planes is 3.40 Å, which is short enough for π-π overlap or CT interaction and this may relate to the orange-red color of the crystals of **3** compared to pale-brown of **1** and **2**. In order to confirm the presence of the interaction, the electronic absorption spectra of these compounds in the solid state were measured. As illustrated in Fig. 4, **1** and **2** show almost a similar spectral curve. On the other hand **3** has an extra absorption at 400—600 nm region, which is undoubtedly responsible for its orange-red color. Taking into account the molecular arrangement of **3** in the crystals, it is reasonable to conclude that there is an intermolecular CT interaction between 4-nitrophenyl and *p*-toluidino moieties.

This work was supported in part by a Grand-in-Aid for Scientific Research from the Ministry of Education, Science and Culture.

References

1) M. Oki and K. Mutai, *Tetrahedron*, **26**, 1181 (1970); K. Mutai, *Bull. Chem. Soc. Jpn.*, **45**, 2635 (1972).

2) P. Main, S. E. Hull, L. Lessinger, G. Germain, J. P. Declercq, and M. M. Woolfson, MULTAN78. A System of Computer Programs for the Automatic Solution of Crystal Structures from X-Ray Diffraction Data. Univs. of York, England and Louvain-la-Nerve, Belgium (1978).

3) International Tables for X-Ray Crystallography, Vol. IV, Kynoch Press, Birmingham (1974).

4) T. Sakurai and K. Kobayashi, *Rikagaku Kenkyusho Hokoku*, **55**, 69 (1979).

5) C. K. Johnson. ORTEP II, Report ORNL-5138, Oak Ridge National Laboratory, Tennessee (1976).

6) The tables for the anisotropic temperature factors for non-hydrogen atoms, the tables for the atomic parameters for the hydrogen atoms and the Fo-Fc list are deposited as Document No. 8789 at the Office of the Editor of the Bulletin of the Chemical Society of Japan.

7) A. F. Berndt and E. O. Schlemper, *Acta Crystallogr., Sect. B*, **38**, 2493 (1982).

8) H. B. Bürgi and J. D. Dunitz, *Helv. Chim. Acta*, **53**, 1747 (1970).

 © 1988 The Chemical Society of Japan Bull. Chem. Soc. Jpn., 61, 1091—1094 (1988)

Solution Structure and Preferred Orientation of 3,7-Dichloro-10*H*-phenothiazine Dissolved in Nematic Liquid Crystal†

Hideaki FUJIWARA,* Masayuki WATANABE, and Yoshio SASAKI
Faculty of Pharmaceutical Sciences, Osaka University, 1-6 Yamadaoka, Suita, Osaka 565
(Received October 3, 1987)

^{1}H NMR spectrum of the title compound was measured in a nematic liquid crystal ZLI1167 and analyzed utilizing modified versions of the LAOCN program. Direct couplings obtained were interpreted on the basis of a folded structure of tricyclic framework. The results show that the dihedral angle between the two benzene rings is 153.1±2.0° and the angle of S ··· N-H is 170.9±6.7°. Hence a "H-intra" conformation is dominant in a mobile state dissolved in the nematic liquid crystal. The preferred orientation of this molecule in ZLI1167 is discussed by comparing the results with those of the dibromo analogue reported previously and by comparing the principal axes of the order tensor with those of the moment of inertia. The chlorine and bromine atoms are supposed to exert a special steric effect on the ordering of these molecules.

We have studied the solution structure and orientation of 3,7-dibromo-10*H*-phenothiazine dissolved in a thermotropic liquid crystal in a previous report of this series.[1] In that work the "H-intra" conformation was

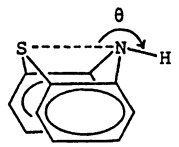

"H-intra" form

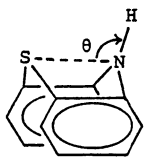

"H-extra" form

evidenced in a mobile state in conformity with a theoretical prediction[2] and crystal data[3] for 10*H*-phenothiazine. The dihedral angle between two benzene rings was observed to be smaller by ca. 10° than that reported for crystal of the unsubstituted compound. With regard to the orientation of solute in liquid crystal, bromine atoms were suggested to exert a steric effect in 3,7-dibromo-10*H*-phenothiazine.

Hitherto, several factors have been reported to be responsible for the orientation of molecules in liquid crystal, i.e., the dispersion force,[4-7] the electric dipole-dipole interaction,[4,5] and the Lewis acid-base interaction[8] between solute and solvent molecules, and further the molecular shape and the moment of inertia of solute.[9] The steric effect of substituent is also pointed out as one of these factors.[10] To investigate further the effect of substituent on the solution structure as well as on the preferred orientation, 3,7-dichloro-10*H*-phenothiazine is synthesized and analyzed in the present study. The results are discussed by comparison with those for the dibromo derivative.

Experimental

3,7-Dichloro-10*H*-phenothiazine was synthesized by the chlorination of 10*H*-phenothiazine.[11] The raw product was recrystallized from benzene after decolorizing by sodium dithionite $Na_2S_2O_4$. The final pale-green product melts at 227—229°C (lit., 227 °C[11]).

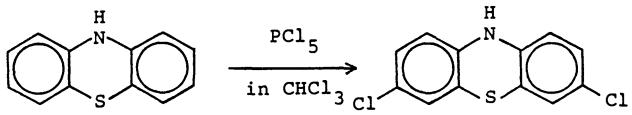

The liquid crystal ZLI1167 from Merck was used without further purification. The solute was dissolved in this solvent at a concentration of 6.7 wt%. ^{1}H NMR spectrum was measured on a Varian XL-200 NMR spectrometer operating at 200 MHz, and the prove temperature was 34.1 °C. 5000 fids were accumulated using a 40° pulse (4 μs). The acquisition time was 0.4 s over a spectral width of 8000 Hz. The data were Fourier transformed to obtain a convolution difference spectrum for 16k data points (CD=0.05 and CCD=1.0). The resulting line width was ca. 10 Hz in the center and ca. 20 Hz in the edges of the spectrum. A small amount of 1,10-phenanthlorine was added to suppress the extraordinary line broadening observed in preliminary measurements. Such broadening was probably induced by a trace amount of paramagnetic impurity. The normal spectrum in isotropic solution was measured on a Hitachi R-22 NMR spectrometer in the CW mode at 90 MHz and at 34.1 °C. Solvent used was a mixture of dimethyl sulfoxide and carbon tetrachloride (20/80 vol%), in which a better separation in chemical shift was obtained.

Analysis of the NMR spectrum observed in ZLI1167 was made by the use of programs LAO3D9 and LAO3D9D which are versions of LAOCN3 modified by the authors.[1] A program SHAPE[12] was used to calculate structural and order parameters from the experimental direct couplings. Only the diagonal terms (variances) were input for the error analysis in this program. The principal axes of moment of inertia were determined by utilizing a program XYZ.[13]

All the above calculations were done on NEAC S-1000 and SX-1 computers at the Computation Center in Osaka University.

Results and Discussion

The indirect couplings of 3,7-dichloro-10*H*-phenothiazine measured in the isotropic medium were J_{12}= 8.25 and J_{23}=2.25 Hz, other couplings being very small. The spectrum in ZLI1167 was simulated using direct couplings obtained previously for the dibromo deriv-

† NMR Study of Molecules in Anisotropic Systems. VII.

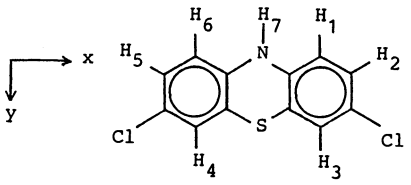

ative as an initial set of parameters.[1] Although the spectrum in the present case resembles to that in the previous report, simulation could not be accomplished straightforwardly. Therefore, some difference in orientation or in solution structure was expected between the two derivatives. NMR parameters reached at the completion of spectral analysis are given in Table 1. Sixty-one lines were assigned and the final rms error was 1.47 Hz in the LAOCN calculation. The

Table 1. NMR Parameters of 3,7-Dichloro-10*H*-phenothiazine Dissolved in Nematic Phase ZLI1167

Direct coupling/Hz:			
D_{12}	733.81±0.18	D_{34}	84.90±0.33
D_{13}	74.64±0.32	D_{37}	60.97±0.33
D_{14}	32.52±0.34		
D_{15}	40.88±0.22	Chemical shift/Hz:[a]	
D_{16}	137.07±0.56	1	105.73±0.40
D_{17}	882.98±0.20	2	180.40±0.37
D_{23}	116.91±0.30	3	180.06±0.58
D_{24}	22.95±0.32	7	466.81±0.65
D_{25}	19.82±0.38		
D_{27}	117.16±0.31		

a) Given in Hz at 200 MHz. Positive toward the low field side.

experimental and the simulated spectra are depicted in Fig. 1. We analyzed the experimental direct couplings to derive the solution structure and preferred orientation of solute in liquid crystal. The inversion rate of tricyclic framework was assumed to be slower than the rate of whole molecular reorientaion. In the previous study[1] we did not find any significant difference in the structural and ordering parameters for the two limiting models of a fast inversion and a slow one. The results of the present analysis are listed in Table 2. The weighted rms error between experimental and recalculated direct couplings was 0.202 Hz. This is a little larger than the error usually encountered in the NMR study using liquid crystal solvents. But such an error would be inevitable in the present case because experimental direct couplings contain larger errors coming from the line broadening in NMR spectrum observed especially in the edges. Such broadening may be due to a residual trace amount of paramagnetic impurity as stated above. In Table 2 structural parameters are also listed for the dibromo derivative[1] together with the crystal data of 10*H*-phenothiazine.[3] Dihedral angle (ϕ_0) and angle of S ··· N-H (θ) are both smaller in the dihalogeno derivatives as compared to those in unsubstituted 10*H*-phenothiazine. For further quantitative discussion of these angles, systematic work by the NMR spectroscopy would be necessary for other derivatives including 10*H*-phenothiazine itself.

The order parameters of S_{zz} and S_{yz} are larger for the dichloro derivative as compared to those for the

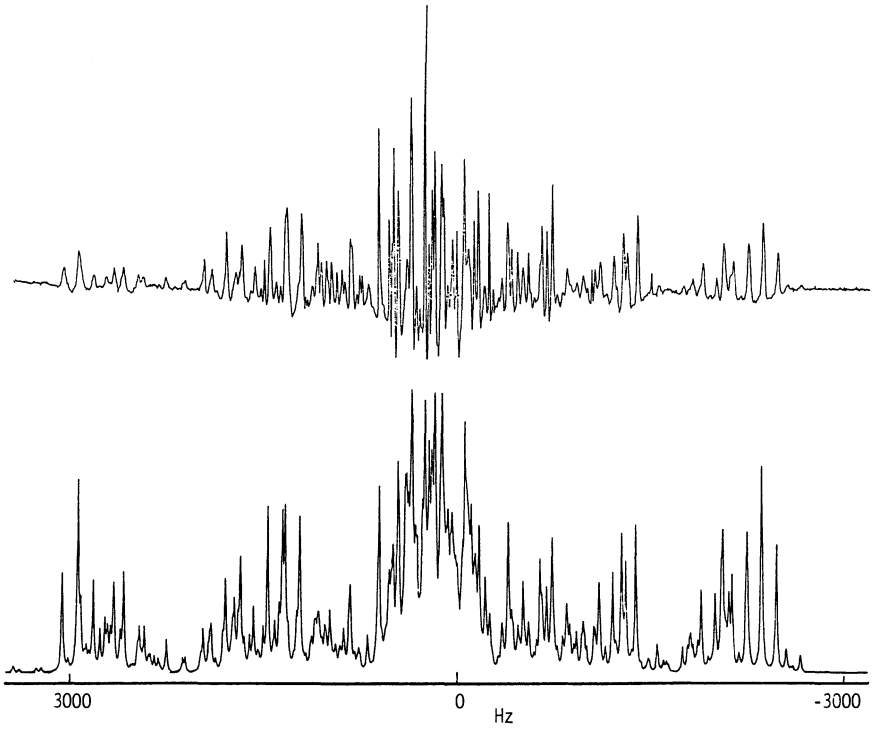

Fig. 1. Experimental (upper) and simulated (lower) ^{1}H NMR spectra of 3,7-dichloro-10*H*-phenothiazine dissolved in a nematic liquid crystal ZLI1167.

Table 2. The Structural and Order Parameters of 3,7-Dihalogeno-10*H*-Phenothiazine Dissolved in ZLI1167

	Dichloro[a]	Dibromo[b]	10*H*-Phenothiazine[c]
	Distance ratios		
r_{13}/r_{12}	2.109±0.048	2.092±0.013	1.979
r_{14}/r_{12}	3.010±0.029	2.958±0.013	2.860
r_{15}/r_{12}	2.923±0.027	2.854±0.025	2.835
r_{16}/r_{12}	1.983±0.022	1.904±0.018	1.902
r_{17}/r_{12}	1.037±0.014	1.003±0.013	0.969
r_{23}/r_{12}	1.946±0.031	1.952±0.045	1.750
r_{24}/r_{12}	3.554±0.035	3.525±0.055	3.368
r_{25}/r_{12}	3.805±0.040	3.753±0.036	3.697
r_{27}/r_{12}	1.963±0.020	1.929±0.020	1.858
r_{34}/r_{12}	2.325±0.025	2.296±0.041	2.240
r_{37}/r_{12}	2.225±0.049	2.175±0.027	2.248
	Angles/degree		
ϕ_0[d]	153.1±2.0	149.1±2.5	158.5
θ[e]	169.6±6.7	169.3±3.4	181.9
	Order parameters[f]		
S_{xx}	−0.1162±0.0007	−0.1223±0.0009	
S_{zz}	0.1922±0.0070	0.1834±0.0013	
S_{yz}	0.0692±0.0158	0.0659±0.0234	

a) 3,7-Dichloro-10*H*-phenothiazine(this work). b) 3,7-Dibromo-10*H*-phenothiazine.[1] c) Crystal data.[3] d) The dihedral angle. e) The angle of S---N-H. f) r_{12}=2.356 Å assumed.

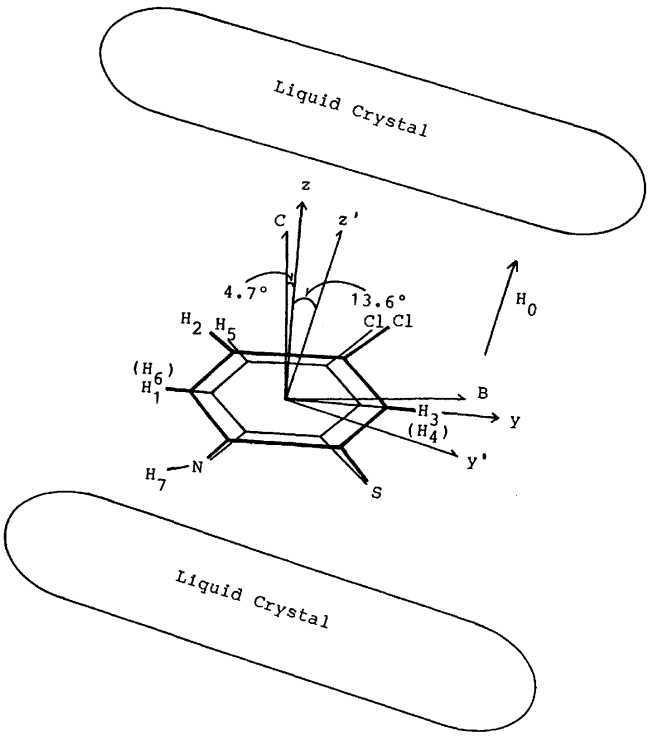

Fig. 2. Principal axis systems for the order tensor (x', y', z') and for the moment of inertia (A, B, C) in 3,7-dichloro-10*H*-phenothiazine (side view). The x' and A axes coincide with the x axis from the C_s symmetry, but these three axes are abbreviated for simplicity in the Figure. The x, y, and z axes are defined so as to place protons of H_1, H_3, H_4, and H_6 on the xy plane. The angles of rotation are −13.6° for y' and z' and 4.7° for B and C with respect to the y and z axes. H_0 denotes the direction of external magnetic field.

dibromo analogue. The absolute value of S_{xx} is, however, smaller for the dichloro derivative. This is a reason why the NMR spectrum of the dichloro derivative is not simply similar to that of the dibromo derivative. Such a decrease in S_{xx} means lowering of orientational order along x axis. This is in accordance with a shortening in diameter along the x direction for the chlorine derivative as compared to the bromine derivative. The positive large values of S_{zz} for both the dichloro and dibromo derivatives indicate that the molecule is most liable to orient with its z axis parallel to the external magnetic field. This leads to the most preferred orientaion of tricyclic plane perpendicular to the long axis of solvent which also orients perpendicular to the external magnetic field.[14] Such orientational behavior is better understood by considering the principal values of the order parameter. The principal axes of the order parameter(x', y', and z') can be obtained by rotating y and z axes anticlockwise around the x axis by an angle of ω which satisfies a relation: $\mathrm{TAN}(2\omega)=2S_{yz}/(S_{yy}-S_{zz})$.[1] From this equation $\omega=-13.6°$ is obtained, and the principal values turn out to be $S_{x'x'}=S_{xx}=-0.1162$ and $S_{z'z'}=\sin^2\omega S_{yy}+\cos^2\omega S_{zz}-\sin(2\omega)S_{yz}=0.2090$. Therefore, z' axis orients most preferrably perpendicular to the solvent molecule as shown in Fig. 2. The principal axes of the moment of inertia (A, B, and C) are also depicted in Fig. 2 (I_A=406.4, I_B=3068.6, and I_C=3371.1 amu Å^2). By comparing Fig. 2 with Fig. 2 in Ref. 1, following tendency is noticed: substitution of Cl atoms for Br atoms makes z' and C axes inclined much toward the Cl atoms in conformity with the smallness in size and weight of the Cl atoms, also it reduces slightly the discrepancy between the two principal axis systems determined for the order tensor and for the moment of inertia. Such a steric effect of substituent was already observed in cases of the stereoisomers of 1,2,3,4,5,6-hexachlorocyclohexane.[10] The absolute value of $S_{x'x'}/S_{z'z'}$ is equal to 0.56 for the dichloro derivative, which is smaller than the value of 0.61 for the dibromo derivative. This is in accordance with the trend in size of the substituents.

The author (H.F.) is grateful to Professor Kensuke Takahashi of Nagoya Institute of Technology for facilities for the NMR measurements.

References

1) H. Fujiwara, M. Watanabe, T. Takagi, and Y. Sasaki, *Bull. Chem. Soc. Jpn.*, **61**, 369 (1988).

2) J.-P. Malrieu and B. Pullmann, *Theor. Chim. Acta*, **2**, 293 (1964).

3) J. J. H. McDowell, *Acta Crystallogr., Sect. B*, **32**, 5 (1976).

4) A. Saupe, *Mol. Cryst.*, **1**, 527 (1966).
5) J. Nehring and A. Saupe, *Mol. Cryst. Liq. Cryst.*, **8**, 403 (1969).
6) E. Sachmann, P. Krebs, H. U. Rega, J. Voss, and H. Mowald, *Mol. Cryst. Liq. Cryst.*, **24**, 283 (1973).
7) T. Vaananen, J. Jokisaari, and J. Lounila, *J. Magn. Reson.*, **49**, 73 (1982).
8) H. Fujiwara and Y. Sasaki, *J. Phys. Chem.*, **91**, 481 (1987).
9) J. M. Anderson, *J. Magn. Reson.*, **4**, 231 (1971).
10) H. Fujiwara, N. Shimizu, T. Takagi, and Y. Sasaki, *Magn. Reson. Chem.*, **24**, 71 (1986).
11) M. Strell and M. Rupprecht, Ger. Patent 938669 (1959).
12) P. Diehl, P. M. Henrichs, and W. Niederberger, *Mol. Phys.*, **20**, 139 (1971).
13) QCPE No. 178, Indiana University. A correction was made as described in Ref. 1. In the original version, initial coordinates were rotated oppositely to the correct direction in obtaining the transposed coordinates in the pricipal axis system.
14) L. Pohl, R. Eidenschink, J. Krause, and G. Weber, *Phys. Lett.*, **65A**, 169 (1978).

 © 1988 The Chemical Society of Japan Bull. Chem. Soc. Jpn., 61, 1095—1101 (1988)

Effects of Supporting Electrolyte and pH on Charge Transport within Electropolymerized Poly(*o*-phenylenediamine) Films Deposited on Graphite Electrodes

Noboru OYAMA,* Takeo OHSAKA, Kazuyuki CHIBA, and Katsuhiko TAKAHASHI
Department of Applied Chemistry for Resources, Tokyo University of Agriculture and Technology, Koganei, Tokyo 184
(Received October 3, 1987)

The homogeneous charge-transport process within electropolymerized electroactive poly(*o*-phenylenediamine) (PPD) films on graphite electrodes in various supporting electrolytic solutions (i.e., NaCl, $NaClO_4$, Na_2SO_4, LiCl, CF_3COONa, tetraethylammonium chloride (TEACl) and sodium *p*-toluenesulfonate (NaPTS)) at various pH's was examined by potential-step chronoamperometry and chronocoulometry. The overall charge-transport process was found to obey Fick's diffusion laws and thus the apparent diffusion coefficients (D_{app}) for the diffusion-like charge-transport process were estimated. The D_{app} values for the oxidation and reduction processes (i.e., D^a_{app} and D^c_{app}) were almost the same at pH 1.0 irrespective of the thickness of PPD films and were actually independent of the supporting electrolytes except for NaPTS. As pH was increased from 1 to 7, the D^a_{app} values decreased slightly from ca. 5.6×10^{-8} to 1.6×10^{-8} $cm^2\,s^{-1}$ and the D^c_{app} values did more largely from ca. 5.6×10^{-8} to 2.2×10^{-9} $cm^2\,s^{-1}$. This behavior was essentially common to all the supporting electrolytes examined. Such pH dependences of D^a_{app} and D^c_{app} are discussed on the basis of the fact that the charge-transport process within PPD films involves the intrinsic electron-transfer process between adjacent electroactive sites as well as the proton addition-elimination process, the charge-compensating counterion motion, the motion of solvent and the segmental motion of the polymeric chain. Especially, it is demonstrated that in this system the proton addition-elimination process must necessarily occur in order for the charge-transport process to proceed.

A large amount of work is devoted at present to a new class of organic polymers (in most cases obtained as films on electrode surfaces) produced by electropolymerization of various kinds of aromatic compounds (e.g., NH_2 and/or OH groups-containing aromatic compounds, heterocyclic aromatic compounds, polynuclear aromatic compounds and vinyl group-containing aromatic compounds), owing to the large field of potential applications of the resulting polymers themselves as well as the "composite" electrode materials composed of electrode substrates and the polymer films.[1] The property-dependent applications of electropolymerized film-coated electrodes have been suggested in various fields.[1]

On the other hand, some basic problems concerning electropolymerizations and the resulting films remain to be fully understood, e.g., the chemical composition and structure of films, the conductivity of films, the mechanism of electropolymerization and the rate of charge (ion and/or electron) transport through films. Especially in the case where polymer film-coated electrodes are used under a "wet" state (e.g., as electron-transfer catalysts (or mediators) for the redox reaction of a dissolved redox species) the rate of charge transport within films is one of the important factors which define the usefulness of film-coated electrodes as materials or devices with desired properties.

This paper deals with a potential-step chronoamperometric and chronocoulometric study of the charge transport within electroactive poly(*o*-phenylenediamine) (PPD) films which can be prepared by electropolymerization of *o*-phenylenediamine in an acidic solution.[2] There are relatively many papers concerning the functions of PPD films, e.g., protection against photo-corrosion of n-type semiconductor electrodes,[3] anticorrosion of metals,[4] pH response,[5-7] permselectivity,[8] and electrochemical diode property.[9] Such different properties of PPD films depend on the electrolytic conditions in their preparation. Recently, we[10] have examined the kinetics of the electrode reaction of PPD films deposited on graphite electrodes in an aqueous supporting electrolytic solution, and reported that the heterogeneous electron-transfer reaction obeys the conventional Butler-Volmer equation and the homogeneous charge-transport process within films can be treated as a Fickian diffusion process. Also, we have revealed that the PPD prepared from an acidic aqueous solution is a ladder polymer with phenazine rings.[2] The rates of the charge-transport within PPD films in aqueous solutions containing various supporting electrolytes at various pH's have been estimated as apparent diffusion coefficients (D_{app}) for the diffusion-like charge transport within the films. The results reveal that the proton addition-elimination process involved in the oxidation-reduction reaction of the PPD film as well as the motion of supporting electrolyte ions which is necessarily, for charge neutrality, coupled to electron transfer are closely related to the rate of the overall charge-transport process within the films.

Experimental

Materials. *o*-Phenylenediamine (Tokyo Kasei Co.) was purified three times by recrystallization from water and dried under reduced pressure. Sodium chloride (NaCl), sodium sulfate (Na_2SO_4), sodium perchlorate ($NaClO_4$) (Wako Chemical Co.), lithium chloride (LiCl), tetraethylammonium chloride (TEACl), sodium *p*-toluenesulfonate (PTSNa) (Kanto Chemical Co.), and sodium trifluoroacetate

(CF_3COONa) (Aldrich), which were reagent grade, were used as supporting electrolytes without further purification. In each supporting electrolytic solution, the concentration of supporting electrolyte was 0.2 M (1M=1 mol dm^{-3}). At pH<2, no buffer solutions were used and at pH 3—7, a citric acid-disodium hydrogenphosphate buffer (20 mM) was used. The basal plane pyrolytic graphite (BPG) (Union Carbide Co.) disk electrodes (area: 0.2 cm^2) were prepared and mounted into glass tube with heat-shrinkable polyolefin tube. Fresh electrode surfaces were produced by cleaving the disk with a scalpel. Aqueous solutions were prepared from doubly distilled water. All other chemicals were reagent grade and were used as received.

Preparation of Poly(*o*-phenylenediamine) (PPD) Films. The PPD films were prepared on BPG or In-Sn oxide conducting glass (ITO) electrodes by scanning (at 50 mV s^{-1}) the electrode potential between −0.8 and 1.2 V vs. SSCE in a 0.5 M Na_2SO_4-H_2SO_4 solution (pH 1.0) containing 50 mM *o*-phenylenediamine, as previously described.[2] The films prepared on BPG (or ITO) electrodes were rinsed with H_2SO_4 solution (pH 1.0) and then with distilled water, and used for further study without removing them from the electrode surfaces. The thicknesses of the films were controlled by the amount of charge passed during the electrochemical polymerization. The film thicknesses (ϕ) were measured with a Surfcom 550 A (Surface Texture Measuring Instrument, Tokyo Seimitsu Co.) as previously described.[2,9]

Apparatus and Procedures. A standard three-electrode electrochemical cell was used for all electrochemical experiments. The electrode assembly consisted of a bare or PPD-coated BPG (or ITO) as working electrode, a sodium chloride saturated calomel electrode (SSCE) as reference electrode and a spiral platinum electrode as counter electrode.

The surface concentration (Γ_p°) of the electroactive site in PPD films was estimated in mol cm^{-2} by measuring the area of cyclic voltammograms (for the oxidation-reduction reaction of PPD films themselves) obtained at scan rate of 2 mV s^{-1} in a 0.2 M $NaClO_4$-$HClO_4$ solution (pH 1.0). The molar concentration (C_p°) (in mol cm^{-3}) of the electroactive site was calculated from the Γ_p° thus obtained using the thicknesses (ϕ) of the films. It was found that there is a linear relationship between ϕ and Γ_p° at $\Gamma_p^\circ < 1.0\times10^{-7}$ mol cm^{-2} and that the C_p° values are $(7.8\pm0.8)\times10^{-4}$ mol cm^{-3} irrespective of ϕ at $\phi < 2\times10^{-4}$ cm.

For cyclic voltammetry, potential-step chronoamperometry and potential-step chronocoulometry, a home-made instrument was employed along with a Nicolet digital oscilloscope (model 3091) and X-Y recorder (Graphtec Co., Tokyo). Positive feedback circuitry was employed to compensate the resistances (these were typically ca. 20—50 Ω) associated with the polymer coatings as much as possible. All experiments were run under nitrogen atmosphere at laboratory temperature (25±1 °C). Potentials were measured and are quoted with respect to SSCE.

Results

Figure 1 shows a typical cyclic voltammogram representing the electrochemical response for the oxidation-reduction reaction of the PPD film deposited on BPG electrode in a 0.2 M $NaClO_4$-$HClO_4$ aqueous solution (pH 1.0). The wave shape resembles that for the ordinary electrode reaction of a solution-phase redox species at an uncoated electrode,[11] that is, the wave has "diffusion tails" and its shape is unsymmet-

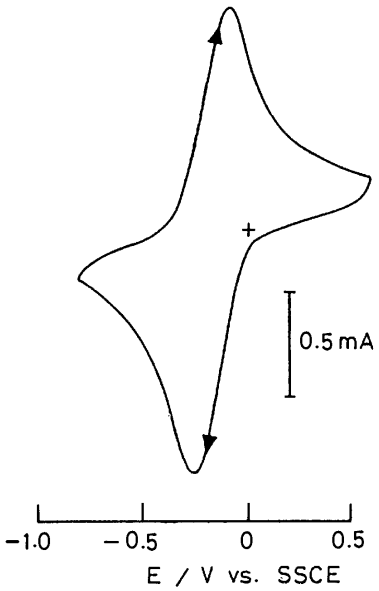

Fig. 1. A typical cyclic voltammogram for the oxidation-reduction reaction of the PPD film deposited on BPG electrode in a 0.2 M $NaClO_4$+$HClO_4$ solution (pH 1.0) at 500 mV s^{-1}. Film thickness: 1.9 μm. C_p°: 7.8×10^{-4} mol cm^{-3}.

Table 1. Apparent Diffusion Coefficients for the Diffusional Charge-Transport Process within PPD Films in a 0.2 M $NaClO_4$+$HClO_4$ Solution (pH 1.0)[a]

ϕ[b] / μm	$10^8\Gamma_p^\circ$[c] / mol cm^{-2}	Reaction[d]	Method[e]	$10^8 D_{app}$ / $cm^2 s^{-1}$
0.19±0.02	1.5±0.2	Ox	CA	2.3±0.2
		Ox	CC	1.9±0.2
		Red	CA	2.6±0.3
		Red	CC	3.0±0.4
0.38±0.04	3.0±0.3	Ox	CA	1.7±0.2
		Ox	CC	1.6±0.2
		Red	CA	1.9±0.2
		Red	CC	2.3±0.2
0.59±0.02	4.6±0.2	Ox	CA	2.9±0.3
		Ox	CC	2.6±0.3
		Red	CA	3.2±0.3
		Red	CC	3.3±0.3
1.08±0.02	8.4±0.2	Ox	CA	3.6±0.4
		Ox	CC	3.2±0.3
		Red	CA	3.1±0.3
		Red	CC	3.1±0.3
1.40±0.03	10.9±0.3	Ox	CA	3.2±0.3
		Ox	CC	2.9±0.3
		Red	CA	2.8±0.3
		Red	CC	2.9±0.3

a) Values averaged with several electrodes. b) Film thicknesses. c) Surface concentrations of the electroactive site in PPD films. d) Ox: oxidation process, Red: reduction process. e) CA: potential-step chronoamperometry, CC: potential-step chronocoulometry.

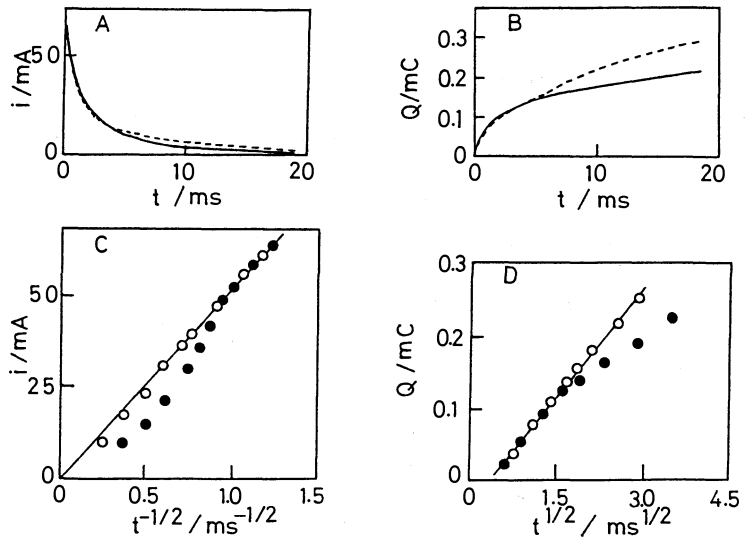

Fig. 2. (A) Potential-step chronoamperometric current–time responses for the oxidation and reduction processes of the PPD film. (B) Potential-step chronocoulometric charge–time responses corresponding to the current–time responses in A. (C) Cottrell plots of i vs. $t^{-1/2}$ for the data in A. (D) Cottrell plots of Q vs. $t^{1/2}$ for the data in B. Supporting electrolyte: 0.2 M $NaClO_4$+$HClO_4$ (pH 1.0). Film thickness: 0.20 μm. C_p°: 7.8×10^{-4} mol cm^{-3}. (----, ○): reduction process; (——, ●): oxidation process. The electrode potentials were stepped from −0.50 V to 0.40 V vs. SSCE and from 0.40 V to −0.50 V vs. SSCE for the oxidation and reduction processes, respectively.

Table 2. Apparent Diffusion Coefficients for the Diffusional Charge-Transport Process within PPD Films in Various Supporting Electrolytic Solutions of pH 1.0[a,b]

Supporting electrolyte	$10^8\,\Gamma_p^\circ$[c] / mol cm^{-2}	$10^4\,C_p^\circ$[f] / mol cm^{-3}	Reaction[d]	Method[e]	$10^8\,D_{app}$ / cm^2 s^{-1}
$NaClO_4$	2.8±0.3	7.8±0.8	Ox	CA	3.2±0.4
			Ox	CC	2.9±0.3
			Red	CA	4.0±0.4
			Red	CC	3.7±0.4
NaCl	2.8±0.3	7.8±0.8	Ox	CA	6.0±0.7
			Ox	CC	5.7±0.6
			Red	CA	4.8±0.5
			Red	CC	4.6±0.5
CF_3COONa	2.3±0.3	6.4±0.7	Ox	CA	4.1±0.4
			Ox	CC	3.4±0.4
			Red	CA	4.0±0.4
			Red	CC	3.5±0.4
Na_2SO_4	2.2±0.2	6.1±0.6	Ox	CA	4.4±0.4
			Ox	CC	4.0±0.4
			Red	CA	6.0±0.6
			Red	CC	5.9±0.6
PTSNa	1.7±0.2	4.7±0.5	Ox	CA	1.7±0.2
			Ox	CC	2.1±0.2
			Red	CA	2.5±0.2
			Red	CC	2.2±0.2

a) Values averaged with several electrodes. b) Film thicknesses (ϕ) of the PPD films: 0.36±0.03 μm. c—e) see Table 1 for the definitions of column headings. f) Volume concentrations of the electroactive site in PPD films were calculated as Γ_p°/ϕ.

ric, although in general electropolymerized electroactive polymer films display the complicated redox responses as being reported for the electropolymerized polyaniline film.[12,13] Based on our recent studies[2] concerning the structure of the PPD film, the electroactive sites in PPD films are considered to be phenazine rings.

In order to estimate the kinetic parameters characterizing the charge-transport process within the films, the potential-step chronoamperometric and chronocoulometric responses for the oxidation and reduction of the PPD films were examined. A typical example of such an examination is shown in Fig. 2. The Cottrell plots (i.e., i-$t^{-1/2}$ and Q-$t^{1/2}$ plots) are linear at short times. The deviation from the linearity indicates that currents in longer times become controlled by finite diffusion.[14,15] These facts indicate that the charge-transport process within the PPD films follows Fickian diffusion laws. Thus, the slopes of the linear plots shown in Fig. 2 yielded the apparent diffusion coefficients (D_{app}) for the diffusion-like charge-transport process within the films. The obtained D_{app}'s are summarized in Tables 1 and 2 and Fig. 3. The D_{app}

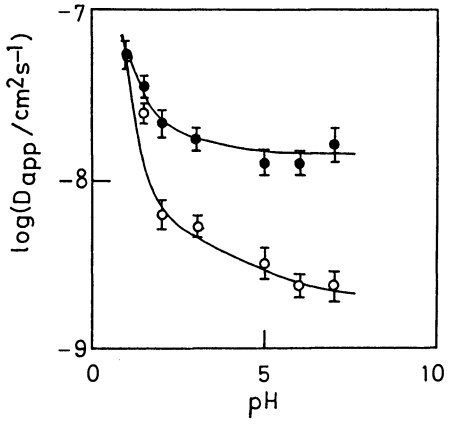

Fig. 3. pH dependences of D^{a}_{app} and D^{c}_{app}. (●): for the oxidation process (D^{a}_{app}); (○): for the reduction process (D^{c}_{app}). Supporting electrolyte: 0.2 M NaCl. At pH<2, no buffer solutions were used and at pH 3—7 a citric acid-disodium hydrogenphosphate buffer (20 mM) was used.

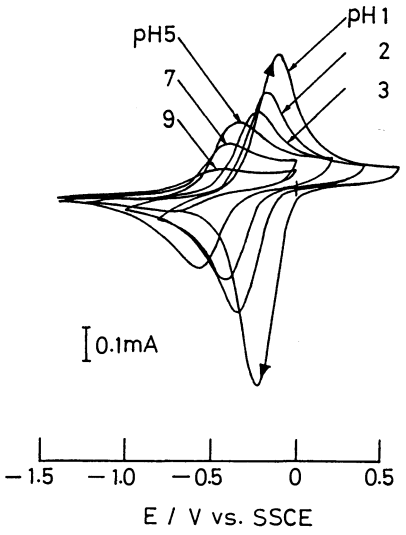

Fig. 4. Typical cyclic voltammograms for the oxidation-reduction reaction of the PPD film in buffered aqueous solutions of various pH's. Supporting electrolyte: 0.2 M NaCl. Film thickness: 0.36 μm. Scan rate: 200 mV s^{-1}.

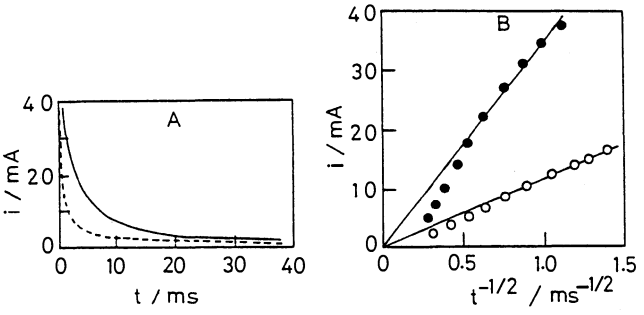

Fig. 5. (A) Typical potential-step chronoamperometric current-time curves for the oxidation and reduction processes of the PPD film deposited on BPG electrode in a 0.2 M NaCl+20 mM CH_3COONa/CH_3COOH solution (pH 5.0). (B) Cottrell plots of i vs. $t^{-1/2}$ for the data in A. The electrode potentials were stepped from −0.8 V to 0.10 V vs. SSCE and from 0.0 V to −0.90 V vs. SSCE for the oxidation and reduction processes, respectively. Film thickness: 0.34 μm. C^{o}_{p}: 7.8×10^{-4} mol cm^{-3}. (----, ○): reduction process; (——, ●): oxidation process.

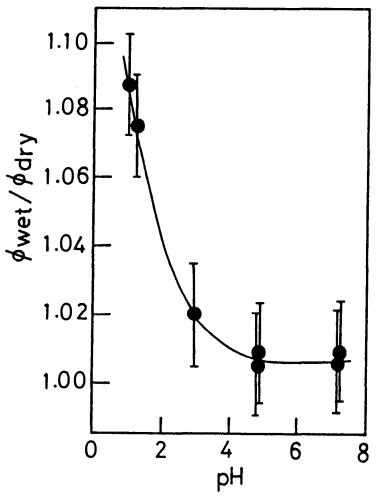

Fig. 6. pH dependence of the swelling of PPD films. The PPD films were prepared on ITO electrodes by a potential-sweep electrolysis between −0.6 and 1.2 V vs. SSCE at 50 mV s^{-1} in 0.5 M Na_2SO_4 solution (pH 1.0) containing 50 mM *o*-phenylenediamine. The dry thicknesses (ϕ_{dry}) of the PPD films: 0.32 μm. The wet thicknesses (ϕ_{wet}) were measured after the immersion of each of the PPD film-coated electrodes in 0.2 M NaCl solutions of various pH's for an hour. The citric acid-phosphate solution (20 mM) was used as a buffer solution except at pH 1.0.

Table 3. Apparent Diffusion Coefficients for the Diffusional Charge-Transport Process within PPD Films in Various Supporting Electrolytic Solutions of pH 5.0[a,b]

Supporting electrolyte	$10^8\,\Gamma_p^{o}$ [c] / mol cm^{-2}	$10^4\,C_p^{o}$ [f] / mol cm^{-3}	Reaction[d]	Method[e]	$10^8\,D_{app}$ / cm^2 s^{-1}
$NaClO_4$	2.7±0.3	7.9±0.7	Ox	CA	2.9 ±0.3
			Ox	CC	2.5 ±0.3
			Red	CA	0.43±0.04
			Red	CC	0.37±0.04
NaCl	2.0±0.2	5.9±0.6	Ox	CA	3.6 ±0.4
			Ox	CC	2.9 ±0.3
			Red	CA	0.37±0.04
			Red	CC	0.29±0.03
CF_3COONa	2.1±0.2	6.2±0.6	Ox	CA	2.7 ±0.3
			Ox	CC	2.4 ±0.2
			Red	CA	0.42±0.04
			Red	CC	0.31±0.03
Na_2SO_4	1.9±0.2	5.6±0.5	Ox	CA	2.5 ±0.3
			Ox	CC	2.2 ±0.2
			Red	CA	0.62±0.06
			Red	CC	0.50±0.05
PTSNa[g]	1.9±0.2	5.6±0.5	Red	CA	0.21±0.02
			Red	CC	0.19±0.02
LiCl	2.4±0.2	7.1±0.7	Ox	CA	1.7 ±0.2
			Ox	CC	1.2 ±0.1
			Red	CA	0.27±0.03
			Red	CC	0.21±0.02
TEACl	2.2±0.2	6.5±0.6	Ox	CA	2.2 ±0.2
			Ox	CC	1.5 ±0.2
			Red	CA	0.24±0.02
			Red	CC	0.19±0.02

a) Values averaged with several electrodes. b) Film thicknesses (ϕ) of the PPD films: 0.34±0.03 μm. c—f) see Tables 1 and 2 for the definitions of column headings. g) For the oxidation process, the linear i-$t^{-1/2}$ and Q-$t^{1/2}$ plots were not obtained.

values (i.e., D_{app}^{a} and D_{app}^{c}) for anodic and cathodic processes in an acidic solution are almost the same irrespective of the film thicknesses and supporting electrolytes examined.

Figure 4 shows typical cyclic voltammograms of the PPD film at different pH's. As reported previously,[2] the anodic and cathodic peak potentials (E_p^{a} and E_p^{c}) shifted to negative values with increasing pH and the slopes of the formal redox potential ($E^{o\prime}$), estimated as the average of E_p^{a} and E_p^{c} values, vs. pH plots were about −60 mV pH^{-1} in the examined range of pH 1 to 7. This suggests that the overall electrode reaction of the PPD film is a H^+/e^- (1/1) reaction. Then, the peak currents decreased slightly with an increase in pH. This was found to be not due to the decrease of the electroactive site number (N_{active}) in the PPD film, but due to the decrease in the apparent rate of the diffusion-like charge transport in the film. The concentrations (C_p^{o}) of the electroactive site were almost constant (7.8×10^{-4} mol cm^{-3}) within experimental error irrespective of pH in the examined range of pH 1 to 7. In this case, N_{active}, i.e., C_p^{o} values at various pH's were determined by the graphical integration of the cyclic voltammograms as described in Experimental section. Such a decrease of peak currents with increasing pH was found to be clearly reflected in the potential-step chronoamperometric (and chronocoulometric) behavior and as a result in the D_{app} values. The results are shown in Fig. 3. It is apparent that as pH increases both D_{app}^{a} and D_{app}^{c} decrease. Further, we can see that the difference between D_{app}^{a} and D_{app}^{c} values becomes larger with increasing pH. A typical example of the potential-step chronoamperometric data demonstrating the largely different D_{app} values for the oxidation and reduction processes at pH 5.0 is shown in Fig, 5. The slope of the i vs. $t^{-1/2}$ plot for the oxidation process is significantly larger than that for the reduction process, and thus in contrary to the D_{app}'s obtained in more acidic solutions (e.g., at pH 1.0) the D_{app}^{a} value is much larger than the D_{app}^{c} value. The related data are summarized in Table 3.

pH dependence of the swelling of PPD films was examined by measuring the wet thickness (ϕ_{wet}) of the films swollen in 0.2 M NaCl aqueous solutions of various pH's. The result is shown in Fig. 6. The ϕ_{wet}/ϕ_{dry} values (ϕ_{dry}: dry thickness) decreased largely with an increase in pH in the range of pH 1 to 3, and at higher pH's they decreased slightly with increasing pH. This behavior is associated with the protonation of PPD film, as mentioned below.

Discussion

From Table 1, it is apparent that Γ_p^o's are proportional to ϕ. This indicates that C_p^o values which are estimated as Γ_p^o/ϕ are constant irrespective of ϕ, that is, the distribution of the electroactive sites in the PPD films is homogeneous. Further, we can see that the values of D_{app}^a and D_{app}^c are actually independent of ϕ in the examined range of ϕ from 0.19 to 1.4 μm and the D_{app}^a and D_{app}^c values are almost the same ($(2.7\pm 1.1)\times10^{-8}$ $cm^2 s^{-1}$).

Table 2 shows the D_{app} values measured in different supporting electrolytic solutions at pH 1.0. The Γ_p^o values seem to slightly change with supporting electrolytes, probably suggesting the partially inhomogeneous distribution of the electroactive sites and the formation of electroinactive regions. Similar results have been also observed for other polymeric film-coated electrodes.[16,17] $D_{app}^a \approx D_{app}^c$ for a given supporting electrolyte. The D_{app} 's obtained in $NaClO_4$, NaCl, CF_3COONa, and Na_2SO_4 electrolytic solutions are almost the same and those in PTSNa solution seem to be a little smaller. This may reflect the different rates of the diffusional motion of electrolytic ions which is necessarily coupled to electron transfer, as can be expected from the Stokes radii (γ_s) of the electrolytic ions used: $\gamma_s(PTS^-) > \gamma_s(Na^+) \approx \gamma_s(CF_3COO^-) \approx \gamma_s(SO_4^{2-}) > 2\gamma_s(Cl^-) \approx 2\gamma_s(ClO_4^-)$.[18]

Table 3 shows the D_{app}'s obtained in various supporting electrolytes containing 20 mM CH_3COONa/CH_3COOH buffer solution (pH 5.0). For all the supporting electrolytes examined, D_{app}^a's are largely different from D_{app}^c's. For example, in the case of NaCl and TEACl electrolytes D_{app}^a's are about one order of magnitude larger than D_{app}^c's. This remarkable fact demonstrates the significantly different rates of the homogeneous charge transports within the films during the reduction and oxidation processes, and seems to be associated with the low concentration (i.e., 10^{-5} M) of hydrogen ion. The more detailed pH responses of D_{app}^a and D_{app}^c values are shown in Fig. 3. Both D_{app}^a's and D_{app}^c's decrease with increasing pH and the degree of the decrease is different each other: As pH was increased from 1 to 7, D_{app}^a's decreased from ca. 5.6×10^{-8} to 1.6×10^{-8} $cm^2 s^{-1}$ and D_{app}^c's from 5.6×10^{-8} to 2.2×10^{-9} $cm^2 s^{-1}$. Such essentially different pH dependences of D_{app}^a and D_{app}^c may be ascribable to the fact that a proton addition-elimination process is involved in the homogeneous charge-transport process in the PPD films which can be regarded as a homogeneous oxidation-reduction process between electroactive sites, as mentioned below.

On the basis of the fact that PPD is a ladder polymer with phenazine rings[2] and that the slope of the $E^{o\prime}$ .vs. pH plot is ca. -60 mV pH^{-1} in the range of pH 1—7, and with the assumption that the protonation constant (pK_a) of PPD is ca. 1 based on the pK_a values of phenazine ($pK_{a_1}=1.2$ and $pK_{a_2}=-4.3$),[19,20] the heterogeneous electron-transfer reaction of PPD in aqueous solutions of pH ca. 1—7 may be written as:

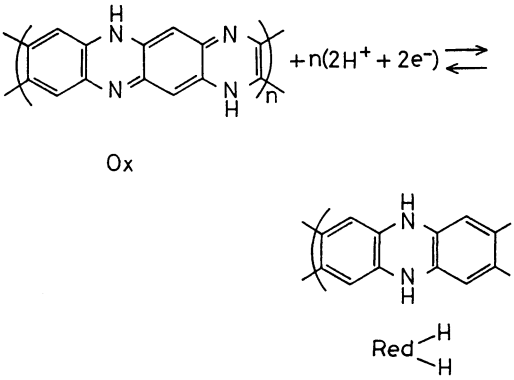

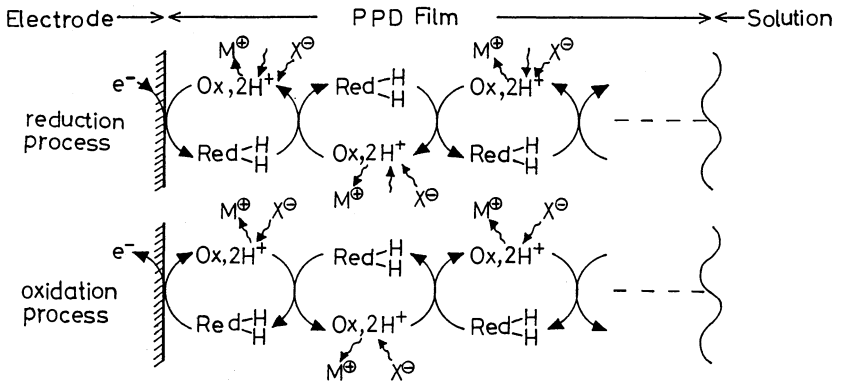

Fig. 7. Schematic depiction of homogeneous charge-transport process within PPD films on electrodes. The symbols Ox and Red represent the oxidized and reduced forms (see text), respectively, of the PPD, and $M^{\oplus}$ and $X^{\ominus}$ indicate supporting electrolytic cations and anions, respectively. H^+ is hydrogen ion. The symbol $\rightsquigarrow$ shows the diffusional motion of H^+, $M^{\oplus}$ and $X^{\ominus}$. The symbols $\curvearrowright$ and $\curvearrowleft$ show the homogeneous oxidation-reduction (electron self-exchange) reaction between adjacent electroactive sites.

From the analogy with the heterogeneous electron-transfer reaction (Eq. 1), the mechanism of the homogeneous charge (ion and electron)-transport process within solvent-swollen PPD films undergoing electrolysis (i.e., oxidation and reduction of the electroactive sites) can thus be schematically represented as in Fig. 7. The charge-transport process is considered to involve the intrinsic electron-transfer process between adjacent electroactive sites, the proton addition-elimination process, the charge-compensating counterion motion, the motion of solvent and the segmental motion of the polymeric chain. The charge-transport rate, which will be determined by only the slower of these various processes, is characterized by the D_{app}'s mentioned throughout the paper.

The D^{a}_{app}'s tend to decrease slightly with increasing pH, especially in the range of pH between 1 and ca. 2 and are almost constant at pH 2—7. This may be explained as follows: The pK_a of PPD may be assumed to be ca. 1 as mentioned above. Thus, the degree of the protonation of PPD is thought to change with pH in the pH range where the decreasing of D^{a}_{app} with an increase in pH was observed. Further, the swelling of the PPD film is associated with the protonation: The higher the degree of the protonation of PPD is, the larger is the swelling of its film (see Fig. 6). In a more swollen film, the motions of supporting electrolytic ions and solvents and/or the segmental motion of polymeric chains become easier and as a result larger D^{a}_{app} values are obtained at lower pH's.

The same explanation seems to be also applicable to the decreasing of D^{c}_{app}'s with increasing pH. However, in this case, another important factor should be taken into account. That is to say, in order for the charge-transport process during the reduction process to proceed more rapidly, hydrogen ions are necessary to be sufficiently present in the vicinity of the oxidized sites (symbolized by "Ox" in Fig. 7). The apparent rate of the charge transport during the reduction process should decrease with decreasing the concentration of hydrogen ion. Thus, the D^{c}_{app} values decrease with increasing pH.

This work was partially supported by Grant-in-Aid for Scientific Research on Priority Area of "Dynamic Interactions and Electronic Processes of Macromolecular Complexes" No. 62612504, for N. Oyama, from the Ministry of Education, Science and Culture, Japan.

References

1) See, for example: T. Ohsaka and N. Oyama, *Maku*, **11**, 261, 334 (1986).
2) K. Chiba, T. Ohsaka, Y. Ohnuki, and N. Oyama, *J. Electroanal. Chem.*, **219**, 117 (1987).
3) H. S. White, H. D. Abruna, and A. J. Bard, *J. Electrochem. Soc.*, **129**, 265 (1982).
4) A. Volkov, G. Tourillon, P. C. Lacaze, and J. E. Dubois, *J. Electroanal. Chem.*, **116**, 279 (1980).
5) W. R. Heineman, H. J. Wieck, and A. M. Yacynych, *Anal. Chem.*, **52**, 345 (1980).
6) G. Cheek, C. P. Wales, and R. J. Nowak, *Anal. Chem.*, **55**, 380 (1983).
7) I. Rubinstein, *Anal. Chem.*, **56**, 1135 (1984).
8) Y. Ohnuki, H. Matsuda, T. Ohsaka, and N. Oyama, *J. Electroanal. Chem.*, **158**, 55 (1983).
9) N. Oyama, K. Chiba, Y. Ohnuki, and T. Ohsaka, *Nippon Kagaku Kaishi*, **1985**, 1172.
10) K. Chiba, T. Ohsaka, and N. Oyama, *J. Electroanal. Chem.*, **217**, 239 (1987).
11) For example, A. J. Bard and L. R. Faulkner, "Electrochemical Methods, Fundamentals and Applications," Willey, New York (1980).
12) A. F. Diaz and J. A. Logan, *J. Electroanal. Chem.*, **111**, 111 (1980).
13) T. Ohsaka, Y. Ohnuki, N. Oyama, G. Katagiri, and K. Kamisako, *J. Electroanal. Chem.*, **161**, 399 (1984).
14) K.-N. Kuo and R. W. Murray, *J. Electroanal. Chem.*, **131**, 37 (1982).
15) N. Oyama, S. Yamaguchi, Y. Nishiki, K. Tokuda, H. Matsuda, and F. C. Anson, *J. Electroanal. Chem.*, **139**, 371 (1982).
16) T. Ohsaka, N. Oyama, K. Sato, and H. Matsuda, *J. Electrochem. Soc.*, **132**, 1871 (1985) and references therein.
17) N. Oyama, K. Hirabayashi, and T. Ohsaka, *Bull. Chem. Soc. Jpn.*, **59**, 2071 (1986).
18) R. A. Robinson and R. H. Stokes, "Electrolyte Solutions," Butterworth, London (1959).
19) H. H. Perkampus and H. Kohler, *Z. Electrochem.*, **64**, 365 (1960).
20) S. Wawzonek, *Anal. Chem.*, **28**, 638 (1956).

 © 1988 The Chemical Society of Japan Bull. Chem. Soc. Jpn., 61, 1103—1108 (1988)

Equations-of-Motion Method for the Electronic Transitions to Compound (1p-1h)+(2p-2h) States

Tai-ichi SHIBUYA,* Tadashi FUNADA,§ and Haruo GOTOH
Department of Chemistry, Faculty of Textile Science and Technology, Shinshu University, Ueda, Nagano-ken 386
(Received October 6, 1987)

The equations-of-motion (EOM) method proposed by Shibuya and McKoy (*Phys. Rev.*, **A2**, 2208 (1970); *J. Chem. Phys.* **58**, 500 (1973)) has been extended to include (2p-2h)-state creation and annihilation operators in the excitation operator $O_\lambda^\dagger$.

The equations-of-motion (EOM) method proposed by Shibuya and McKoy[1] has been successfully applied to ab initio calculations of the transition energies and oscillator strengths of small molecules like C_2H_4, CO, N_2, C_6H_6, H_2O, and CH_4.[2,3] The EOM method has the advantage that the equations are set up directly for the electronic transitions, i.e. for the difference between the ground and the excited states, while in the traditional CI method the equation is solved for each of the states separately.

The basic idea of the EOM method is to find an excitation operator $O_\lambda^\dagger$ which creates an excited state $|\lambda>$ by its action on the ground state $|0>$:

$$|\lambda>=O_\lambda^\dagger|0> \quad (\text{and } O_\lambda|0>=0). \tag{1}$$

As was shown by Sinanoğlu,[4] the major part of the closed-shell ground state correlation consists of doubly-excited configurations, i.e. 2p-2h states. Thus, it is natural to construct the $O_\lambda^\dagger$ as a linear combination of 1p-1h creation and annihilation operators. The coefficients of the linear combination are determined in such a way that the excitation operator $O_\lambda^\dagger$ satisfies the equation

$$[H,O_\lambda^\dagger]|0>=\omega_\lambda O_\lambda^\dagger|0>, \tag{2}$$

which takes the same form as the equation of motion for a boson creation operator. In this equation ω_λ is the energy difference between $|0>$ and $|\lambda>$.

The low-lying excited states of molecules are usually well described as the linear combinations of 1p-1h states. However, some of the important valence states of conjugated molecules are essentially of 2p-2h states. The well-known example is the 2^1Ag state of linear polyenes.[5] For these states, the perturbative treatment proposed earlier[1b] is not adequate and the whole EOM-Hamiltonian matrix including those elements of 2p-2h states must be diagonalized to give correct solutions of the excitation operator. In the present work, we provide all the matrix elements needed for this type of the EOM calculations. Recently Oddershede and coworkers[6] have developed the perturbative propagator methods which are essentially equivalent to our perturbative treatment.[1b] Many references in relation with the propagator methods and the EOM methods are found in a recent review by Oddershede.[7]

§ Present address: Yashiro High School, Koshoku, Nagano-ken 387.

The EOM for 1p-1h States

In this section, we begin with a summary of the previously developed EOM method for 1p-1h states.[1] Let us consider the excitation of an electron from the occupied orbital γ to the unoccupied orbital m. The excited electron may take the spin state of α or β. Thus, if the molecule is initially in the closed-shell ground state, its final state may be either singlet ($S=0$) or triplet ($S=1$). Therefore, the creation operators of the particle-hole pairs are written[1a]

$$\left.\begin{aligned} C_{m\gamma}^\dagger(00) &= (2^{-1/2})[c_{m\alpha}^+ c_{\gamma\alpha} + c_{m\beta}^+ c_{\gamma\beta}] \\ C_{m\gamma}^\dagger(1M) &= \begin{cases} -c_{m\alpha}^+ c_{\gamma\beta} & (M=+1) \\ (2^{-1/2})[c_{m\alpha}^+ c_{\gamma\alpha} - c_{m\beta}^+ c_{\gamma\beta}] & (M=0) \\ c_{m\beta}^+ c_{\gamma\alpha} & (M=-1) \end{cases} \end{aligned}\right\} \tag{3}$$

where $c_{i\alpha}^+$ and $c_{i\alpha}$ are the creation and the annihilation operators of an elcctron in the state of orbital i and spin α, respectively, and they satisfy the anticommutation relations of fermions. Inspecting the structure of the correlated ground state $|0>$ according to Sinanoğlu's many-electron theory,[4] we have proposed that the excited state $|\lambda>$ of spin-symmetry S, M may be obtained by the action of the excitation operator

$$O^\dagger(\lambda SM)=\sum_{m\gamma}\{Y_{m\gamma}(\lambda S)\,C_{m\gamma}^\dagger(SM)-Z_{m\gamma}(\lambda S)\,C_{m\gamma}(\overline{SM})\} \tag{4}$$

on the ground state $|0>$. In this expression,

$$C_{m\gamma}(\overline{SM})=(-)^{S+M}\,C_{m\gamma}(S,-M) \tag{5}$$

annihilates the (m, γ) pair and gives a state of spin-symmetry S, M. Note that $C_{m\gamma}(SM)$ is the adjoint operator of $C_{m\gamma}^\dagger(SM)$.

Solutions of Eq. 2 are readily found by solving the variational equation[8]

$$<0|[\delta O_\lambda, H, O_\lambda^\dagger]|0>=\omega_\lambda<0|[\delta O_\lambda, O_\lambda^\dagger]|0>, \tag{6}$$

where the double commutator is defined as

$$[a,H,b]=\frac{1}{2}([a,[H,b]]+[[a,H],b]). \tag{7}$$

The problem here is to find the eigenvector (Y,Z) in Eq. 4 and the eigenvalue ω_λ. We have shown[1] that the

substitution of Eq. 4 into 6 leads to the matrix equation

$$\begin{bmatrix} A & B \\ -B & -A \end{bmatrix} \begin{bmatrix} Y(\lambda) \\ Z(\lambda) \end{bmatrix} = \omega_\lambda \begin{bmatrix} D & 0 \\ 0 & D \end{bmatrix} \begin{bmatrix} Y(\lambda) \\ Z(\lambda) \end{bmatrix} \tag{8}$$

where

$$\left.\begin{aligned} A_{m\gamma,n\delta}(S) &= <0|[C_{m\gamma}(SM), H, C_{n\delta}^{\dagger}(SM)]|0> \\ B_{m\gamma,n\delta}(S) &= -<0|[C_{m\gamma}(SM), H, C_{n\delta}(\overline{SM})]|0> \\ D_{m\gamma,n\delta} &= <0|[C_{m\gamma}(SM), C_{n\delta}^{\dagger}(SM)]|0> \end{aligned}\right\} \tag{9}$$

Note that A and B are independent of M, and D is independent of S and M. We shall henceforth denote unoccupied orbitals (particle states) by m, n, p, or q, and occupied orbitals (hole states) by γ, δ, μ, or ν. In expanding these elements explicitly, we first let

$$<0|0>=1. \tag{10}$$

Then, in the level of the 2nd-order perturbation theory of the ground-state correlation, we obtain[1]

$$\left.\begin{aligned} A_{m\gamma,n\delta}(S) &= A^{\circ}_{m\gamma,n\delta}(S) \\ &\quad + \delta_{\gamma\delta}\left[T_{mn} - \frac{1}{2}(\varepsilon_m + \varepsilon_n - 2\varepsilon_\gamma)\rho_{mn}\right] \\ &\quad - \delta_{mn}\left[T_{\gamma\delta} - \frac{1}{2}(2\varepsilon_m - \varepsilon_\gamma - \varepsilon_\delta)\rho_{\gamma\delta}\right] \\ B_{m\gamma,n\delta}(S) &= B^{\circ}_{m\gamma,n\delta}(S) + (-1)^S S_{m\gamma,n\delta} \\ D_{m\gamma,n\delta} &= \delta_{mn}\,\delta_{\gamma\delta} + \delta_{mn}\,\rho_{\gamma\delta} - \delta_{\gamma\delta}\,\rho_{mn}, \end{aligned}\right\} \tag{11}$$

where A° and B° are the RPA matrices, i.e.

$$\left.\begin{aligned} A^{\circ}_{m\gamma,n\delta}(S) &= \delta_{mn}\,\delta_{\gamma\delta}(\varepsilon_m - \varepsilon_\gamma) - V_{m\delta n\gamma} + (\delta_{S0})\,2V_{m\delta\gamma n} \\ B^{\circ}_{m\gamma,n\delta}(S) &= -(-1)^S V_{mn\delta\gamma} + (\delta_{S0})\,2V_{mn\gamma\delta}. \end{aligned}\right\} \tag{12}$$

ε_k is the HF orbital energy and

$$V_{ijkl} \equiv <i(1)j(2)|(r_{12})^{-1}|k(1)l(2)>. \tag{13}$$

T and S are correction terms linear in the ground-state correlation coefficients. ρ is quadratic in the correlation coefficients. They are explicitly written as

$$\left.\begin{aligned} S_{m\gamma,n\delta} &= -\sum_{p\mu}[V_{m\mu\delta p}\,C_{p\mu,n\gamma}(0) + V_{n\mu\gamma p}\,C_{p\mu,m\delta}(0)] \\ T_{mn} &= -\frac{1}{2}\sum_{q\mu\nu}[V_{mq\mu\nu}\,C_{q\nu,n\mu}(0) + V_{\mu\nu nq}\,C_{m\mu,q\nu}(0)] \\ T_{\gamma\delta} &= \frac{1}{2}\sum_{pq\nu}[V_{pq\gamma\nu}\,C_{q\nu,p\delta}(0) + V_{\delta\nu pq}\,C_{p\gamma,q\nu}(0)] \end{aligned}\right\} \tag{14}$$

and

$$\left.\begin{aligned} \rho_{mn} &= \frac{1}{2}\sum_{p\mu\nu}\sum_{S=0,1} C'_{p\mu,m\nu}(S)\,C_{n\nu,p\mu}(S) \\ \rho_{\gamma\delta} &= -\frac{1}{2}\sum_{pq\mu}\sum_{S=0,1} C'_{p\mu,q\gamma}(S)\,C_{q\delta,p\mu}(S), \end{aligned}\right\} \tag{15}$$

where

$$C'(0) = \frac{1}{4}[3C(0) + C(1)];\quad C'(1) = \frac{1}{4}[C(0) + 3C(1)]. \tag{16}$$

To the first order in the Rayleigh-Schrödinger perturbation theory the ground-state correlation coefficients are given by

$$C_{m\gamma,n\delta}(S) \cong -B^{\circ}_{m\gamma,n\delta}(S)/(\varepsilon_m + \varepsilon_n - \varepsilon_\gamma - \varepsilon_\delta). \tag{17}$$

Finally, in the diagonalization approximation

$$D_{m\gamma,n\delta} \cong \delta_{mn}\delta_{\gamma\delta}(1 + \rho_{\gamma\gamma} - \rho_{mm}) \equiv \delta_{mn}\,\delta_{\gamma\delta}\,g_{m\gamma}^2, \tag{18}$$

Eq. 8 becomes

$$\begin{bmatrix} \mathscr{A} & \mathscr{B} \\ -\mathscr{B} & -\mathscr{A} \end{bmatrix} \begin{bmatrix} \mathscr{Y}(\lambda) \\ \mathscr{Z}(\lambda) \end{bmatrix} = \omega_\lambda \begin{bmatrix} \mathscr{Y}(\lambda) \\ \mathscr{Z}(\lambda) \end{bmatrix}, \tag{19}$$

where

$$\left.\begin{aligned} \mathscr{A}_{m\gamma,n\delta} &\equiv g_{m\gamma}^{-1}\,A_{m\gamma,n\delta}\,g_{n\delta}^{-1} \\ &= \delta_{mn}\,\delta_{\gamma\delta}(\varepsilon_m - \varepsilon_\gamma) \\ &\quad + \{-[V_{m\delta n\gamma} + \delta_{mn}\,T_{\gamma\delta} - \delta_{\gamma\delta}\,T_{mn}] \\ &\quad + (\delta_{S0})\,2V_{m\delta\gamma n}\}/g_{m\gamma}\,g_{n\delta}) \\ \mathscr{B}_{m\gamma,n\delta} &\equiv g_{m\gamma}^{-1}\,B_{m\gamma,n\delta}\,g_{n\delta}^{-1} \\ &= \{-(-1)^S[V_{mn\delta\gamma} - S_{m\gamma,n\delta}] \\ &\quad + (\delta_{S0})\,2V_{mn\gamma\delta}\}/(g_{m\gamma}\,g_{n\gamma}) \\ \mathscr{Y}_{m\gamma} &\equiv g_{m\gamma}\,Y_{m\gamma};\quad \mathscr{Z}_{m\gamma} \equiv g_{m\gamma}\,Z_{m\gamma}. \end{aligned}\right\} \tag{20}$$

The EOM for (1p-1h)+(2p-2h) States

The excitation operator in Eq. 4 is now extended to include 2p-2h creation and annihilation operators:

$$\begin{aligned} O^{\dagger}(\lambda SM) &= \sum_{m\gamma}\{Y_{m\gamma}(\lambda S)\,C_{m\gamma}^{\dagger}(SM) - Z_{m\gamma}(\lambda S)\,C_{m\gamma}(\overline{SM})\} \\ &\quad + \sum_{(m\gamma,n\delta)}\{Y^{(2)}_{(m\gamma,n\delta)}(\lambda S)\,\Gamma^{\dagger}_{(m\gamma,n\delta)}(SM) \\ &\qquad - Z^{(2)}_{(m\gamma,n\delta)}(\lambda S)\,\Gamma_{(m\gamma,n\delta)}(\overline{SM})\}, \end{aligned} \tag{21}$$

where $\Gamma^{\dagger}_{(m\gamma,n\delta)}(SM)$ are 2p-2h creation operators. The second summation in Eq. 21 runs over all the independent 2p-2h states, not over $m\gamma$ and $n\delta$ separately. In general, $\Gamma^{\dagger}_{(m\gamma,n\delta)}(SM)$ is a linear combination of $C_{m\gamma}^{\dagger}(SM)C_{n\delta}^{\dagger}(00)$, $C_{n\delta}^{\dagger}(SM)C_{m\gamma}^{\dagger}(00)$, $C_{m\delta}^{\dagger}(SM)C_{n\gamma}^{\dagger}(00)$, and $C_{n\gamma}^{\dagger}(SM)\,C_{m\delta}^{\dagger}(00)$.

The substitution of Eq. 21 into Eq. 6 gives

$$\begin{bmatrix} A & B & A^{(1,2)} & B^{(1,2)} \\ -B & -A & -B^{(1,2)} & -A^{(1,2)} \\ A^{(2,1)} & B^{(2,1)} & A^{(2,2)} & B^{(2,2)} \\ -B^{(2,1)} & -A^{(2,1)} & -B^{(2,2)} & -A^{(2,2)} \end{bmatrix} \begin{bmatrix} Y(\lambda) \\ Z(\lambda) \\ Y^{(2)}(\lambda) \\ Z^{(2)}(\lambda) \end{bmatrix} = \omega_\lambda \begin{bmatrix} D & 0 & 0 & 0 \\ 0 & D & 0 & 0 \\ 0 & 0 & D^{(2,2)} & 0 \\ 0 & 0 & 0 & D^{(2,2)} \end{bmatrix} \begin{bmatrix} Y(\lambda) \\ Z(\lambda) \\ Y^{(2)}(\lambda) \\ Z^{(2)}(\lambda) \end{bmatrix}, \tag{22}$$

where the matrix elements of A, B, and D are already given above, and the matrix elements of $A^{(1,2)}$, $B^{(1,2)}$, $A^{(2,2)}$, $B^{(2,2)}$, and $D^{(2,2)}$ are defined by

Table 1. The Orthonormal 2p-2h Creation Operators $\Gamma^{\dagger}_{(m\gamma,n\delta)}$

$S=M=0$	
$\Gamma^{\dagger}_{(m\gamma,m\gamma)}=c_{m\alpha}{}^{+}c_{m\beta}{}^{+}c_{\gamma\beta}c_{\gamma\alpha}=C_{m\gamma}{}^{\dagger}(00)C_{m\gamma}{}^{\dagger}(00)$	
$\Gamma^{\dagger}_{(m\gamma,n\gamma)}=(1/\sqrt{2})(c_{m\alpha}{}^{+}c_{n\beta}{}^{+}+c_{n\alpha}{}^{+}c_{m\beta}{}^{+})c_{\gamma\beta}c_{\gamma\alpha}=\sqrt{2}C_{m\gamma}{}^{\dagger}(00)C_{n\gamma}{}^{\dagger}(00)$	$(m\neq n)$
$\Gamma^{\dagger}_{(m\gamma,m\delta)}=(1/\sqrt{2})c_{m\alpha}{}^{+}c_{m\beta}{}^{+}(c_{\delta\beta}c_{\gamma\alpha}+c_{\gamma\beta}c_{\delta\alpha})=\sqrt{2}C_{m\gamma}{}^{\dagger}(00)C_{m\delta}{}^{\dagger}(00)$	$(\gamma\neq\delta)$
$\Gamma^{\dagger}_{(m\gamma,n\delta)_1}=1/2(c_{m\alpha}{}^{+}c_{n\beta}{}^{+}+c_{n\alpha}{}^{+}c_{m\beta}{}^{+})(c_{\delta\beta}c_{\gamma\alpha}+c_{\gamma\beta}c_{\delta\alpha})=C_{m\gamma}{}^{\dagger}(00)C_{n\delta}{}^{\dagger}(00)+C_{m\delta}{}^{\dagger}(00)C_{n\gamma}{}^{\dagger}(00)$	$(m\neq n,\gamma\neq\delta)$
$\Gamma^{\dagger}_{(m\gamma,n\delta)_2}=(1/\sqrt{3})\{(c_{m\alpha}{}^{+}c_{n\alpha}{}^{+}c_{\delta\alpha}c_{\gamma\alpha}+c_{m\beta}{}^{+}c_{n\beta}{}^{+}c_{\delta\beta}c_{\gamma\beta})$ $+1/2(c_{m\alpha}{}^{+}c_{n\beta}{}^{+}-c_{n\alpha}{}^{+}c_{m\beta}{}^{+})(c_{\delta\beta}c_{\gamma\alpha}-c_{\gamma\beta}c_{\delta\alpha})\}=(1/\sqrt{3})(C_{m\gamma}{}^{\dagger}(00)C_{n\delta}{}^{\dagger}(00)-C_{m\delta}{}^{\dagger}(00)C_{n\gamma}{}^{\dagger}(00))$	$(m\neq n,\gamma\neq\delta)$
$S=1,\ M=0$	
$\Gamma^{\dagger}_{(m\gamma,n\gamma)}=(1/\sqrt{2})(c_{m\alpha}{}^{+}c_{n\beta}{}^{+}-c_{n\alpha}{}^{+}c_{m\beta}{}^{+})c_{\gamma\beta}c_{\gamma\alpha}=(1/\sqrt{2})(C_{m\gamma}{}^{\dagger}(10)C_{n\gamma}{}^{\dagger}(00)-C_{n\gamma}{}^{\dagger}(10)C_{m\gamma}{}^{\dagger}(00))$	$(m\neq n)$
$\Gamma^{\dagger}_{(m\gamma,m\delta)}=(1/\sqrt{2})c_{m\alpha}{}^{+}c_{m\beta}{}^{+}(c_{\delta\beta}c_{\gamma\alpha}-c_{\gamma\beta}c_{\delta\alpha})=(1/\sqrt{2})(C_{m\gamma}{}^{\dagger}(00)C_{m\delta}{}^{\dagger}(10)-C_{m\delta}{}^{\dagger}(10)C_{m\gamma}{}^{\dagger}(00))$	$(\gamma\neq\delta)$
$\Gamma^{\dagger}_{(m\gamma,n\delta)_1}=1/2(c_{m\alpha}{}^{+}c_{n\beta}{}^{+}-c_{n\alpha}{}^{+}c_{m\beta}{}^{+})(c_{\delta\beta}c_{\gamma\alpha}+c_{\gamma\beta}c_{\delta\alpha})$ $=1/2(C_{m\gamma}{}^{\dagger}(10)C_{n\delta}{}^{\dagger}(00)-C_{n\delta}{}^{\dagger}(10)C_{m\gamma}{}^{\dagger}(00)+C_{m\delta}{}^{\dagger}(10)C_{n\gamma}{}^{\dagger}(00)-C_{n\gamma}{}^{\dagger}(10)C_{m\delta}{}^{\dagger}(00))$	$(m\neq n,\gamma\neq\delta)$
$\Gamma^{\dagger}_{(m\gamma,n\delta)_2}=1/2(c_{m\alpha}{}^{+}c_{n\beta}{}^{+}+c_{n\alpha}{}^{+}c_{m\beta}{}^{+})(c_{\delta\beta}c_{\gamma\alpha}-c_{\gamma\beta}c_{\delta\alpha})$ $=1/2(C_{m\gamma}{}^{\dagger}(10)C_{n\delta}{}^{\dagger}(00)-C_{n\delta}{}^{\dagger}(10)C_{m\gamma}{}^{\dagger}(00)-C_{m\delta}{}^{\dagger}(10)C_{n\gamma}{}^{\dagger}(00)+C_{n\gamma}{}^{\dagger}(10)C_{m\delta}{}^{\dagger}(00))$	$(m\neq n,\gamma\neq\delta)$
$\Gamma^{\dagger}_{(m\gamma,n\delta)_3}=(1/\sqrt{2})(c_{m\alpha}{}^{+}c_{n\alpha}{}^{+}c_{\delta\alpha}c_{\gamma\alpha}-c_{m\beta}{}^{+}c_{n\beta}{}^{+}c_{\delta\beta}c_{\gamma\beta})=(1/\sqrt{2})(C_{m\gamma}{}^{\dagger}(10)C_{n\delta}{}^{\dagger}(00)+C_{n\delta}{}^{\dagger}(10)C_{m\gamma}{}^{\dagger}(00))$	$(m\neq n,\gamma\neq\delta)$

$$
\left.\begin{aligned}
&A^{(1,2)}{}_{m'\gamma';(m\gamma,n\delta)}(S)\\
&\quad=\langle 0|[C_{m'\gamma'}(SM),\ H,\Gamma^{\dagger}_{(m\gamma,n\delta)}(SM)]|0\rangle\\
&B^{(1,2)}{}_{m'\gamma';(m\gamma,n\delta)}(S)\\
&\quad=-\langle 0|[C_{m'\gamma'}(SM),\ H,\Gamma_{(m\gamma,n\delta)}(\overline{SM})]|0\rangle\\
&A^{(2,2)}{}_{(m'\gamma',n'\delta');(m\gamma,n\delta)}(S)\\
&\quad=\langle 0|[\Gamma_{(m'\gamma',\,n'\delta')}(SM),\ H,\Gamma^{\dagger}_{(m\gamma,n\delta)}(SM)]|0\rangle\\
&B^{(2,2)}{}_{(m'\gamma',n'\delta');(m\gamma,n\delta)}(S)\\
&\quad=-\langle 0|[\Gamma_{(m'\gamma',\,n'\delta')}(SM),\ H,\Gamma_{(m\gamma,n\delta)}(\overline{SM})]|0\rangle\\
&D^{(2,2)}{}_{(m'\gamma',n'\delta');(m\gamma,n\delta)}\\
&\quad=\langle 0|[\Gamma_{(m'\gamma',\,n'\delta')}(SM),\ \Gamma^{\dagger}_{(m\gamma,n\delta)}(SM)]|0\rangle
\end{aligned}\right\}\qquad (23)
$$

Note that

$$A^{(2,1)}=\tilde{A}^{(1,2)};\ B^{(2,1)}=\tilde{B}^{(1,2)}. \qquad (24)$$

Also note that $A^{(1,2)}$, $B^{(1,2)}$, $A^{(2,2)}$, and $B^{(2,2)}$ are independent of M, and that $D^{(2,2)}$ is independent of S and M.

In the present work, we shall replace the correlated ground state $|0\rangle$ in Eq. 23 by the Hartree-Fock ground state $|HF\rangle$, obtaining $A^{\circ(1,2)}$, $B^{\circ(1,2)}$, $A^{\circ(2,2)}$, $B^{\circ(2,2)}$, and $D^{\circ(2,2)}$, respectively. It is clear that $B^{\circ(1,2)}$ and $B^{\circ(2,2)}$ vanish, for the Hamiltonian H consists of only the pair creation operators $C_{ij}{}^{\dagger}(00)$ and their products $C_{ij}{}^{\dagger}(00)C_{kl}{}^{\dagger}(00)$. The matrix elements of $A^{\circ(1,2)}$ and $A^{\circ(2,2)}$ are obtained from their primitive elements given in the Appendix. The matrix $D^{\circ(2,2)}$ becomes an identity matrix when the basis set of $\Gamma^{\dagger}_{(m\gamma,n\delta)}$ is chosen such as given in Table 1. These 2p-2h creation operators were given earlier in Ref. 1b. They are reproduced here for convenience and some typographic errors involved there have been corrected. In this basis set of 2p-2h creation operators, we now have, instead of Eq. 22,

$$
\begin{bmatrix}
\mathscr{A} & \mathscr{B} & \mathscr{A}^{\circ(1,2)} & 0\\
-\mathscr{B} & -\mathscr{A} & 0 & \mathscr{A}^{\circ(1,2)}\\
\mathscr{A}^{\circ(2,1)} & 0 & A^{\circ(2,2)} & 0\\
0 & -\mathscr{A}^{\circ(2,1)} & 0 & -A^{\circ(2,2)}
\end{bmatrix}
\begin{bmatrix}\mathscr{Y}\\ \mathscr{Z}\\ Y^{(2)}\\ Z^{(2)}\end{bmatrix}
=\omega
\begin{bmatrix}\mathscr{Y}\\ \mathscr{Z}\\ Y^{(2)}\\ Z^{(2)}\end{bmatrix}, \qquad (25)
$$

where $\mathscr{A}$, $\mathscr{B}$, $\mathscr{Y}$, and $\mathscr{Z}$ are already given in the preceding section, and

$$\mathscr{A}^{\circ(1,2)}{}_{m'\gamma';\,(m\gamma,n\delta)}=A^{\circ(1,2)}{}_{m'\gamma';\,(m\gamma,\,n\delta)}/g_{m'\gamma'}. \qquad (26)$$

In order to reduce the matrix size of Eq. 25, we first write it as

$$
\begin{bmatrix}
\mathscr{A}-\mathscr{B} & \mathscr{A}^{\circ(1,2)}\\
\mathscr{A}^{\circ(2,1)} & A^{\circ(2,2)}
\end{bmatrix}
\begin{bmatrix}\mathscr{Y}-\mathscr{Z}\\ Y^{(2)}-Z^{(2)}\end{bmatrix}
=\omega
\begin{bmatrix}\mathscr{Y}+\mathscr{Z}\\ Y^{(2)}+Z^{(2)}\end{bmatrix}, \qquad (27a)
$$

$$
\begin{bmatrix}
\mathscr{A}+\mathscr{B} & \mathscr{A}^{\circ(1,2)}\\
\mathscr{A}^{\circ(2,1)} & A^{\circ(2,2)}
\end{bmatrix}
\begin{bmatrix}\mathscr{Y}+\mathscr{Z}\\ Y^{(2)}+Z^{(2)}\end{bmatrix}
=\omega
\begin{bmatrix}\mathscr{Y}-\mathscr{Z}\\ Y^{(2)}-Z^{(2)}\end{bmatrix}. \qquad (27b)
$$

Multiplication of the matrix

$$
\begin{bmatrix}
\mathscr{A}-\mathscr{B} & \mathscr{A}^{\circ(1,2)}\\
\mathscr{A}^{\circ(2,1)} & A^{\circ(2,2)}
\end{bmatrix}
$$

from the left on both sides of Eq. 27b gives

$$
\begin{bmatrix}
\mathscr{A}-\mathscr{B} & \mathscr{A}^{\circ(1,2)}\\
\mathscr{A}^{\circ(2,1)} & A^{\circ(2,2)}
\end{bmatrix}
\begin{bmatrix}
\mathscr{A}+\mathscr{B} & \mathscr{A}^{\circ(1,2)}\\
\mathscr{A}^{\circ(2,1)} & A^{\circ(2,2)}
\end{bmatrix}
\begin{bmatrix}\mathscr{Y}+\mathscr{Z}\\ Y^{(2)}+Z^{(2)}\end{bmatrix}
=\omega^2
\begin{bmatrix}\mathscr{Y}+\mathscr{Z}\\ Y^{(2)}+Z^{(2)}\end{bmatrix}. \qquad (28)
$$

Similarly we also have

$$
\begin{bmatrix}
\mathscr{A}+\mathscr{B} & \mathscr{A}^{\circ(1,2)}\\
\mathscr{A}^{\circ(2,1)} & A^{\circ(2,2)}
\end{bmatrix}
\begin{bmatrix}
\mathscr{A}-\mathscr{B} & \mathscr{A}^{\circ(1,2)}\\
\mathscr{A}^{\circ(2,1)} & A^{\circ(2,2)}
\end{bmatrix}
\begin{bmatrix}\mathscr{Y}-\mathscr{Z}\\ Y^{(2)}-Z^{(2)}\end{bmatrix}
=\omega^2
\begin{bmatrix}\mathscr{Y}-\mathscr{Z}\\ Y^{(2)}-Z^{(2)}\end{bmatrix}. \qquad (29)
$$

Solving either Eq. 28 or 29 may suffices if one is only interested in finding the transition energy ω. For the evaluation of the transition moments, however, both eigenvectors of Eqs. 28 and 29 are needed. In any case, the order of the matrix to be diagonalyzed has been reduced to the half.

The Transition Moment

In deriving the explicit expressions of the matrix elements, we have assumed the normalization condition of Eq. 10 for the $|0>$. For excited states, we let

$$<\lambda|\lambda>=1. \tag{30}$$

Then, the transition dipole moment is written

$$\begin{aligned}\boldsymbol{D}_\lambda &=<0|(\boldsymbol{r})_{op}|\lambda> \\ &=-\sqrt{2}\sum_{ij}\boldsymbol{d}^\circ_{ij}<0|[C_{ij}{}^\dagger(00),\ O^\dagger{}_\lambda]|0>,\end{aligned} \tag{31}$$

where

$$\boldsymbol{d}^\circ_{ij}\equiv\int i(\boldsymbol{r})\,\boldsymbol{r}\,j(\boldsymbol{r})\,\mathrm{d}^3r. \tag{32}$$

The oscillator strength is given by

$$f_\lambda\equiv(2/3)\,\omega_\lambda|\boldsymbol{D}_\lambda|^2. \tag{33}$$

Employing the diagonalization approximations used in the treatment of D and $D^{(2,2)}$, we can rewrite the normalization condition Eq. 30 as

$$\begin{aligned}&\sum_{m\gamma}\{|\mathcal{Y}_{m\gamma}(\lambda S)|^2-|\mathcal{Z}_{m\gamma}(\lambda S)|^2\} \\ &\quad+\sum_{(m\gamma.n\delta)}\{|Y^{(2)}_{(m\gamma.n\delta)}(\lambda S)|^2-|Z^{(2)}_{(m\gamma.n\delta)}(\lambda S)|^2\}=1\end{aligned} \tag{34}$$

Note that the first and the second terms on the left-hand side of this equation are the scalar products of $(\mathcal{Y}+\mathcal{Z},\mathcal{Y}-\mathcal{Z})$ and $(Y^{(2)}+Z^{(2)},\ Y^{(2)}+Z^{(2)})$. These are evaluated by using eigenvectors of Eqs. 28 and 29. With the diagonalization approximation in Eq. 18, Eq. 31 leads to

$$\boldsymbol{D}_\lambda=\delta_{S0}\sqrt{2}\sum_{m\gamma}\{\mathcal{Y}_{m\gamma}(\lambda 0)+\mathcal{Z}_{m\gamma}(\lambda 0)\}\,(g_{m\gamma}\boldsymbol{d}^\circ{}_{m\gamma}). \tag{35}$$

Note that terms of $Y^{(2)}$ and $Z^{(2)}$ vanish in deriving the last expression, for in our approximation,

$$<0|[C_{ij}{}^\dagger(00),\ \Gamma^\dagger{}_{(m\gamma.n\delta)}(00)]|>=0. \tag{36}$$

Thus, $\boldsymbol{D}_\lambda$ is only indirectly affected by $Y^{(2)}$ and $Z^{(2)}$ through the normalization condition Eq. 34. When the second term bccomes large on the left-hand side of Eq. 34, $\boldsymbol{D}_\lambda$ may drastically reduce in comparison with that obtained from the (1p-1h) EOM.

Discussion

With the results obtained above, we are now able to make computations of the EOM at the level of (1p-1h)+(2p-2h). Previously we[9] analyzed the dynamical screening due to sigma-electrons in the $\pi\rightarrow\pi^*$ transition of the ethylene molecule. We showed that the N→T (triplet) transition is almost free from this kind of screenings but the N→V (singlet) transition is significantly affected. More recently we[10] have shown that in the zero-differential overlap (ZDO) approximation between sigma- and pi-orbitals, the triplet $\pi\rightarrow\pi^*$ transitions are generally unaffected by the dynamical screening. Such observations have led us[11] to propose a scheme to parametrize the EOM for $\pi\rightarrow\pi^*$ transitions. In the forthcoming papers, we propose a semi-empirical scheme of the (1p-1h)+(2p-2h) EOM for $\pi\rightarrow\pi^*$ transitions and present numerical results of its application to linear polyenes.

Appendix: The Matrix Elements of $A^{\circ(1,2)}$ and $A^{\circ(2,2)}$

The matrix elements of $A^{\circ(1,2)}$ and $A^{\circ(2,2)}$ appearing in Eqs. 25—29 are constructed on the orthonormal basis set of $\Gamma^\dagger{}_{(m\gamma.n\delta)}$ in Table 1. These elements are readily obtained from the primitive elements

$$\begin{aligned}&A^{\circ(1,2)}{}_{m'\gamma';\,m\gamma.\,n\delta}(S) \\ &\quad\equiv<HF|[C_{m'\gamma'}(SM),\ H,C_{m\gamma}{}^\dagger(SM)C_{n\delta}{}^\dagger(00)]|HF>\end{aligned} \tag{A. 1}$$

$$\begin{aligned}&A^{\circ(2,2)}{}_{m'\gamma',\,n'\delta';\,m\gamma.\,n\delta}(S) \\ &\quad\equiv<HF|[(C_{m'\gamma'}{}^\dagger(SM)\,C_{n'\delta'}{}^\dagger(00))^\dagger, \\ &\qquad H,C_{m\gamma}{}^\dagger(SM)C_{n\delta}{}^\dagger(00)]|HF>\end{aligned} \tag{A. 2}$$

To expand these primitive elements, it is convenient to have the Hamiltonian in the following form:[1a]

$$\left.\begin{aligned}&H=H(1)+H(2)+H(3); \\ &H(1)=\sum_i\varepsilon_i\sqrt{2}\,C_{ii}{}^\dagger(00), \\ &H(2)=\sum_{ij}[-\frac{1}{2}\sum_k V_{ikkj}+\sum_\gamma(V_{i\gamma\gamma j}-2V_{i\gamma j\gamma})]\,\sqrt{2}\,C_{ij}{}^\dagger(00), \\ &H(3)=\sum_{ijkl}V_{ijkl}\,C_{ik}{}^\dagger(00)\,C_{jl}{}^\dagger(00),\end{aligned}\right\} \tag{A. 3}$$

where

$$V_{ijkl}=<i(1)j(2)|(r_{12})^{-1}|k(1)l(2)>. \tag{A. 4}$$

In Eq. A. 3, γ refers to a hole orbital and i, j, k, l to any orbital, i.e., hole or particle. Cf. Ref. 1a for various relations useful in expanding the right-hand side of Eqs. A. 1 and A. 2.

First note that Eqs. A. 1 and A. 2 can be also written as

$$\begin{aligned}&A^{\circ(1,2)}{}_{m'\gamma';\,m\gamma.\,n\delta}(S) \\ &\quad=<HF|[C_{m'\gamma'}(S0),\ H]C_{m\gamma}{}^\dagger(S0)C_{n\delta}{}^\dagger(00)|HF> \\ &\quad+\frac{1}{2}<HF|HC_{m'\gamma'}(S0)C_{m\gamma}{}^\dagger(S0)\,C_{n\delta}{}^\dagger(00)|HF>\end{aligned} \tag{A. 5}$$

$$\begin{aligned}&A^{\circ(2,2)}{}_{m'\gamma',\,n'\delta';\,m\gamma.n\delta}(S) \\ &\quad=<HF|[C_{n'\delta'}(00)\,C_{m'\gamma'}(S0)[H,\ C_{m\gamma}{}^\dagger(S0)\,C_{n\delta}{}^\dagger(00)]|HF> \\ &\quad+\frac{1}{2}<HF|[C_{n'\delta'}(00)C_{m'\gamma'}(S0)C_{m\gamma}{}^\dagger(S0)\,C_{n\delta}{}^\dagger(00),\ H]|HF>.\end{aligned} \tag{A. 6}$$

In the second term of Eq. A. 5, we have

$$<HF|H(1)C_{m'\gamma'}(S0)C_{m\gamma}{}^\dagger(S0)C_{n\delta}{}^\dagger(00)|HF>=0 \tag{A. 7}$$

and

$$\begin{aligned}&<HF|H(2)C_{m'\gamma'}(S0)C_{m\gamma}{}^\dagger(S0)C_{n\delta}{}^\dagger(00)|HF> \\ &\quad=-<HF|H(3)C_{m'\gamma'}(S0)C_{m\gamma}{}^\dagger(S0)C_{n\delta}{}^\dagger(00)|HF> \\ &\quad=\sqrt{2}\sum_{p\mu}\{\frac{1}{2}(\sum_\nu V_{\mu\nu\nu p}-\sum_q V_{\mu qqp})-2\sum_\nu V_{\mu\nu p\nu}\}\times \\ &\quad<HF|C_{p\mu}(00)C_{m'\gamma'}(S0)C_{m\gamma}{}^\dagger(S0)C_{n\delta}{}^\dagger(00)|HF>.\end{aligned} \tag{A. 8}$$

In the second term of Eq. A. 6, we have

$$C_{n'\delta'}(00)C_{m'\gamma'}(S0)C_{m\gamma}{}^{\dagger}(S0)C_{n\delta}{}^{\dagger}(00)|HF\rangle$$
$$=\{\delta_{m'm}\delta_{n'n}(\delta_{\gamma'\gamma}\delta_{\delta'\delta}-\frac{1}{2}\delta_{\gamma'\delta}\delta_{\delta'\gamma})$$
$$+\delta_{m'n}\delta_{n'm}(\delta_{S0}\delta_{\gamma'\delta}\delta_{\delta'\gamma}-\frac{1}{2}\delta_{\gamma'\gamma}\delta_{\delta'\delta})\}|HF\rangle \quad \text{(A. 9)}$$

and a similar expression for $\langle HF|C_{n'\delta'}(00)C_{m'\gamma'}(S0)C_{m\gamma}{}^{\dagger}(S0)C_{n\delta}{}^{\dagger}(00)$. Hence, the second terms of Eqs. A. 5 and A. 6 vanish, and we have

$$A^{\circ(1,2)}{}_{m'\gamma';\,m\gamma,n\delta}(S)$$
$$=\langle HF|[C_{m'\gamma'}(S0),H]C_{m\gamma}{}^{\dagger}(S0)C_{n\delta}{}^{\dagger}(00)|HF\rangle \quad \text{(A. 10)}$$

$$A^{\circ(2,2)}{}_{m'\gamma',\,n'\delta';\,m\gamma,\,n\delta}(S)$$
$$=\langle HF|[C_{n'\delta'}(00)C_{m'\gamma'}(S0)[H,C_{m\gamma}{}^{\dagger}(S0)C_{n\delta}{}^{\dagger}(00)]|HF\rangle \quad \text{(A. 11)}$$

Now, it is useful to note the following equations:

$$[H(1),C_{m\gamma}{}^{\dagger}(S0)]=(\varepsilon_m-\varepsilon_\gamma)C_{m\gamma}{}^{\dagger}(S0) \quad \text{(A. 12)}$$

$$[H(2),C_{m\gamma}{}^{\dagger}(S0)]$$
$$=\sum_i\{-\frac{1}{2}\sum_k V_{ikkm}+\sum_{\gamma''}(V_{i\gamma''\gamma''m}-2V_{i\gamma''m\gamma''})\}C_{i\gamma}{}^{\dagger}(S0)$$
$$-\sum_j\{-\frac{1}{2}\sum_k V_{\gamma kkj}+\sum_{\gamma''}(V_{\gamma\gamma''\gamma''j}-2V_{\gamma\gamma''j\gamma''})\}C_{mj}{}^{\dagger}(S0) \quad \text{(A. 13)}$$

$$[H(3),C_{m\gamma}{}^{\dagger}(S0)]$$
$$=-\frac{1}{2}\sum_{ik}V_{ikkm}C_{i\gamma}{}^{\dagger}(S0)-\frac{1}{2}\sum_{jk}V_{\gamma kkj}C_{mj}{}^{\dagger}(S0)$$
$$+\sum_{ij}V_{\gamma ijm}C_{ij}{}^{\dagger}(S0)$$
$$+\sqrt{2}\sum_{kl}\{\sum_i V_{ikml}C_{kl}{}^{\dagger}(00)C_{i\gamma}{}^{\dagger}(S0)$$
$$-\sum_j V_{\gamma kjl}C_{kl}{}^{\dagger}(00)C_{mj}{}^{\dagger}(S0)\} \quad \text{(A. 14)}$$

which amounts to

$$[H,C_{m\gamma}{}^{\dagger}(S0)]$$
$$=(\varepsilon_m-\varepsilon_\gamma)C_{m\gamma}{}^{\dagger}(S0)+\sum_{ij}V_{\gamma ijm}C_{ij}{}^{\dagger}(S0)$$
$$-\sum_i(\sum_{m''}V_{im''m''m}+\sum_{\gamma''}2V_{i\gamma''m\gamma''})C_{i\gamma}{}^{\dagger}(S0)$$
$$-\sum_{j\gamma''}(V_{\gamma\gamma''\gamma''j}-2V_{\gamma\gamma''j\gamma''})C_{mj}{}^{\dagger}(S0)$$
$$+\sqrt{2}\sum_{kl}\{\sum_i V_{ikml}C_{kl}{}^{\dagger}(00)C_{i\gamma}{}^{\dagger}(S0)$$
$$-\sum_j V_{\gamma kjl}C_{kl}{}^{\dagger}(00)C_{mj}{}^{\dagger}(S0)\} \quad \text{(A. 15)}$$

Also note that

$$[H,C_{m\gamma}{}^{\dagger}(S0)C_{n\delta}{}^{\dagger}(00)]$$
$$=(\varepsilon_m+\varepsilon_n-\varepsilon_\gamma-\varepsilon_\delta)C_{m\gamma}{}^{\dagger}(S0)C_{n\delta}{}^{\dagger}(00)$$
$$+\sum_{ij}\{V_{\gamma ijm}C_{ij}{}^{\dagger}(S0)C_{n\delta}{}^{\dagger}(00)+V_{\delta ijn}C_{m\gamma}{}^{\dagger}(S0)C_{ij}{}^{\dagger}(00)\}$$
$$-\sum_i\{(\sum_p V_{ippm}+2\sum_\mu V_{i\mu m\mu})C_{i\gamma}{}^{\dagger}(S0)C_{n\delta}{}^{\dagger}(00)$$
$$+(\sum_p V_{ippn}+2\sum_\mu V_{i\mu n\mu})C_{m\gamma}{}^{\dagger}(S0)C_{i\delta}{}^{\dagger}(00)$$
$$-\sum_{p\mu}\{(V_{\gamma\mu\mu j}-2V_{\gamma\mu j\mu})C_{mj}{}^{\dagger}(S0)C_{n\delta}{}^{\dagger}(00)$$
$$+(V_{\delta\mu\mu j}-2V_{\delta\mu j\mu})C_{m\gamma}{}^{\dagger}(S0)C_{nj}{}^{\dagger}(00)\}$$
$$+\sqrt{2}\sum_{kl}[\{\sum_i V_{ikml}C_{kl}{}^{\dagger}(00)C_{i\gamma}{}^{\dagger}(S0)$$
$$-\sum_j V_{\gamma kjl}C_{kl}{}^{\dagger}(00)C_{mj}{}^{\dagger}(S0)\}C_{n\delta}{}^{\dagger}(00)$$
$$+C_{m\gamma}{}^{\dagger}(S0)\{\sum_i V_{iknl}C_{kl}{}^{\dagger}(00)C_{i\delta}{}^{\dagger}(00)$$
$$-\sum_j V_{\delta kjl}C_{kl}{}^{\dagger}(00)C_{nj}{}^{\dagger}(00)\}]. \quad \text{(A. 16)}$$

Now, from Eq. A. 15, we have

$$[C_{m'\gamma'}(S0),H]$$
$$=(\varepsilon_{m'}-\varepsilon_{\gamma'})C_{m'\gamma'}(S0)+\sum_{ij}V_{jm'\gamma'i}C_{ij}(S0)$$
$$-\sum_i(\sum_p V_{pm'ip}+2\sum_\mu V_{m'\mu i\mu})C_{i\gamma'}(S0)$$
$$-\sum_{j\mu}(V_{\mu j\gamma'\mu}-2V_{j\mu\gamma'\mu})C_{m'j}(S0)$$
$$+\sqrt{2}\sum_{kl}\{\sum_i V_{m'lik}C_{i\gamma'}(S0)C_{kl}(00)$$
$$-\sum_j V_{jl\gamma'k}C_{m'j}(S0)C_{kl}(00)\}. \quad \text{(A. 17)}$$

The substitution of this expression into Eq. A. 10 gives

$$A^{\circ(1,2)}{}_{m'\gamma';m\gamma,n\delta}(S)$$
$$=\langle HF|\sqrt{2}\sum_{kl}\{\sum_i V_{m'lik}C_{i\gamma'}(S0)C_{kl}(00)$$
$$-\sum_j V_{jl\gamma'k}C_{m'j}(S0)C_{kl}(00)\}C_{m\gamma}{}^{\dagger}(S0)C_{n\delta}{}^{\dagger}(00)|HF\rangle$$
$$=\langle HF|\sqrt{2}\sum_{q\nu}\{\sum_p V_{m'\nu pq}C_{p\gamma'}(S0)C_{q\nu}(00)$$
$$-\sum_\mu V_{\mu\nu\gamma'q}C_{m'\mu}(S0)C_{q\nu}(00)\}C_{m\gamma}{}^{\dagger}(S0)C_{n\delta}{}^{\dagger}(00)|HF\rangle$$
$$=\sqrt{2}\{\delta_{\gamma'\gamma}(V_{m'\delta mn}-\frac{1}{2}V_{m'\delta nm})$$
$$+\delta_{\gamma'\delta}(\delta_{S0}V_{m'\gamma nm}-\frac{1}{2}V_{m'\gamma mn})$$
$$-\delta_{m'm}(V_{\gamma\delta\gamma'n}-\frac{1}{2}V_{\delta\gamma\gamma'n})-\delta_{m'n}(\delta_{S0}V_{\delta\gamma\gamma'm}-\frac{1}{2}V_{\gamma\delta\gamma'm})\}. \quad \text{(A. 18)}$$

On the other hand, the substitution of Eq. A. 16 into Eq. A. 11 gives

$$A^{\circ(2,2)}{}_{m'\gamma',n'\delta';\,m\gamma,n\delta}(S)$$
$$=\langle HF|C_{n'\delta'}(00)C_{m'\gamma'}(S0)$$
$$\times[(\varepsilon_m+\varepsilon_n-\varepsilon_\gamma-\varepsilon_\delta)C_{m\gamma}{}^{\dagger}(S0)C_{n\delta}{}^{\dagger}(00)$$
$$+\sum_{p\mu}\{V_{\gamma p\mu m}C_{p\mu}{}^{\dagger}(S0)C_{n\delta}{}^{\dagger}(00)$$
$$+V_{\delta p\mu n}C_{m\gamma}{}^{\dagger}(S0)C_{p\mu}{}^{\dagger}(00)\}$$
$$-\sum_q\{(\sum_p V_{qppm}+2\sum_\mu V_{q\mu m\mu})C_{q\gamma}{}^{\dagger}(S0)C_{n\delta}{}^{\dagger}(00)$$
$$+(\sum_p V_{qppn}+2\sum_\mu V_{q\mu n\mu})C_{m\gamma}{}^{\dagger}(S0)C_{q\delta}{}^{\dagger}(00)\}$$
$$-\sum_{p\mu}\{(V_{\gamma\mu\mu\nu}-2V_{\gamma\mu\nu\mu})C_{m\nu}{}^{\dagger}(S0)C_{n\delta}{}^{\dagger}(00)$$
$$+(V_{\delta\mu\mu\nu}-2V_{\delta\mu\nu\mu})C_{m\gamma}{}^{\dagger}(S0)C_{n\nu}{}^{\dagger}(00)\}]|HF\rangle$$
$$+\langle HF|C_{n'\delta'}(00)C_{m'\gamma'}(S0)$$
$$\times\sqrt{2}\sum_{kl}[\{\sum_i V_{ikml}C_{kl}{}^{\dagger}(00)C_{i\gamma}{}^{\dagger}(S0)$$
$$-\sum_j V_{\gamma kjl}C_{kl}{}^{\dagger}(00)C_{mj}{}^{\dagger}(S0)\}C_{n\delta}{}^{\dagger}(00)$$
$$+C_{m\gamma}{}^{\dagger}(S0)\{\sum_i V_{iknl}C_{kl}{}^{\dagger}(00)C_{i\delta}{}^{\dagger}(00)$$
$$-\sum_\nu V_{\delta kvl}C_{kl}{}^{\dagger}(00)C_{n\nu}{}^{\dagger}(00)\}]|HF\rangle. \quad \text{(A. 19)}$$

The last term of this expression can be reduced as follows: (the lasst term)

$$
\begin{aligned}
&=\langle HF|C_{n'\delta'}(00)C_{m'\gamma'}(S0)\times\\
&[-\sum_{q\nu}\{V_{\delta qm\nu}C_{n\gamma}{}^{\dagger}(S0)+V_{\gamma qn\nu}C_{m\delta}{}^{\dagger}(S0)\}C_{q\nu}(00)\\
&+\sum_{q}\{\sum_{p}V_{pqmn}C_{p\gamma}{}^{\dagger}(S0)-\sum_{\nu}V_{\gamma qn\nu}C_{m\nu}{}^{\dagger}(S0)\}C_{q\delta}{}^{\dagger}(00)\\
&+\sum_{\nu}\{\sum_{\mu}V_{\gamma\delta\mu\nu}C_{m\mu}{}^{\dagger}(S0)-\sum_{q}V_{q\delta m\nu}C_{q\gamma}{}^{\dagger}(S0)\}C_{n\nu}{}^{\dagger}(00)\\
&+\{\sum_{q}(\sum_{p}V_{pqmn}+2\sum_{\nu}V_{q\nu m\nu})C_{q\gamma}{}^{\dagger}(S0)\\
&+\sum_{\mu\nu}(V_{\gamma\mu\mu\nu}-2V_{\gamma\mu\nu\mu})C_{m\nu}{}^{\dagger}(S0)\\
&+2\sum_{q\nu}(\delta_{S0}V_{\gamma qm\nu}-V_{q\gamma m\nu})C_{q\nu}{}^{\dagger}(S0)\}C_{n\delta}{}^{\dagger}(00)\\
&+C_{m\gamma}{}^{\dagger}(S0)\{\sum_{q}(\sum_{p}V_{pqnp}+2\sum_{\nu}V_{q\nu n\nu})C_{q\delta}{}^{\dagger}(00)\\
&+\sum_{\mu\nu}(V_{\delta\mu\mu\nu}-2V_{\delta\mu\nu\mu})C_{n\nu}{}^{\dagger}(00)\\
&+2\sum_{q\nu}(V_{\delta qn\nu}-V_{\delta q\nu n})C_{q\nu}{}^{\dagger}(00)\}]|HF\rangle. \qquad \text{(A. 20)}
\end{aligned}
$$

Thus, Eq. A. 19 becomes

$$
\begin{aligned}
&A^{\circ(2,2)}{}_{m'\gamma',n'\delta';\,m\gamma,n\delta}(S)\\
&=\langle HF|C_{n'\delta'}(00)C_{m'\gamma'}(S0)\times\\
&[(\varepsilon_m+\varepsilon_n-\varepsilon_\gamma-\varepsilon_\delta)C_{m\gamma}{}^{\dagger}(S0)C_{n\delta}{}^{\dagger}(00)\\
&+\sum_{q\nu}\{(2V_{\delta qn\nu}-V_{\delta q\nu n})C_{m\gamma}{}^{\dagger}(S0)C_{q\nu}{}^{\dagger}(00)\\
&+(\delta_{S0}2V_{\gamma qm\nu}-V_{q\gamma m\nu})C_{q\nu}{}^{\dagger}(S0)C_{n\delta}{}^{\dagger}(00)\\
&-\sum_{q\nu}\{V_{\delta qm\nu}C_{n\gamma}{}^{\dagger}(S0)+V_{\gamma qn\nu}C_{m\delta}{}^{\dagger}(S0)\}C_{q\nu}{}^{\dagger}(00)\\
&+\sum_{q}\{\sum_{p}V_{pqmn}C_{p\gamma}{}^{\dagger}(S0)-\sum_{\nu}V_{\gamma qn\nu}C_{m\nu}{}^{\dagger}(S0)\}C_{q\delta}{}^{\dagger}(00)\\
&+\sum_{\nu}\{\sum_{\mu}V_{\gamma\delta\mu\nu}C_{m\mu}{}^{\dagger}(S0)\\
&-\sum_{q}V_{q\delta m\nu}C_{q\gamma}{}^{\dagger}(S0)\}C_{n\nu}{}^{\dagger}(00)]|HF\rangle. \qquad \text{(A. 21)}
\end{aligned}
$$

After some tedious calculations using Eq. A. 9 in the last expression, we finally obtain

$$
\begin{aligned}
&A^{\circ(2,2)}{}_{m'\gamma',n'\delta';\,m\gamma,n\delta}(S)\\
&=\{(\varepsilon_m+\varepsilon_n-\varepsilon_\gamma-\varepsilon_\delta)\times\\
&[(\delta_{m'm}\delta_{n'n}\delta_{\gamma'\gamma}\delta_{\delta'\delta}-\frac{1}{2}\delta_{m'm}\delta_{n'n}\delta_{\gamma'\delta}\delta_{\delta'\gamma}\\
&-\frac{1}{2}\delta_{m'n}\delta_{n'm}\delta_{\gamma'\gamma}\delta_{\delta'\delta})+(\delta_{S0})\delta_{m'n}\delta_{n'm}\delta_{\gamma'\delta}\delta_{\delta'\gamma}]\\
&+(\delta_{m'm}\delta_{n'n}-\frac{1}{2}\delta_{m'n}\delta_{n'm})V_{\gamma\delta\gamma'\delta'}\\
&+((\delta_{S0})\delta_{m'n}\delta_{n'm}-\frac{1}{2}\delta_{m'n}\delta_{n'n})V_{\gamma\delta\delta'\gamma'}\\
&+(\delta_{\gamma'\gamma}\delta_{\delta'\delta}-\frac{1}{2}\delta_{\gamma'\delta}\delta_{\delta'\gamma})V_{m'n'mn}\\
&+((\delta_{S0})\delta_{\gamma'\delta}\delta_{\delta'\gamma}-\frac{1}{2}\delta_{\gamma'\gamma}\delta_{\delta'\delta})V_{n'm'mn}\}\\
&+\{[\delta_{m'm}\delta_{\gamma'\gamma}(2V_{\delta n'n\delta'})-(\delta_{m'm}\delta_{\delta'\gamma}V_{\delta n'n\gamma'}+\delta_{n'm}\delta_{\gamma'\gamma}V_{\delta m'n\delta'}\\
&+\delta_{m'n}\delta_{\gamma'\gamma}V_{\delta n'm\delta'}+\delta_{m'm}\delta_{\gamma'\delta}V_{\gamma n'n\delta'})\\
&+\frac{1}{2}(\delta_{m'm}\delta_{\delta'\delta}V_{\gamma n'n\gamma'}+\delta_{n'n}\delta_{\gamma'\gamma}V_{\delta m'm\delta'}\\
&+\delta_{m'n}\delta_{\delta'\gamma}V_{\delta n'm\gamma'}+\delta_{n'm}\delta_{\gamma'\delta}V_{\gamma m'n\delta'})]\\
&+(\delta_{S0})[2(\delta_{m'n}\delta_{\gamma'\delta}V_{\gamma n'm\delta'}\\
&+\delta_{n'm}\delta_{\delta'\gamma}V_{\delta m'n\gamma'}+\delta_{n'n}\delta_{\delta'\delta}V_{\gamma m'm\gamma'})\\
&-(\delta_{n'n}\delta_{\gamma'\delta}V_{\gamma m'm\delta'}+\delta_{m'n}\delta_{\delta'\delta}V_{\gamma n'm\gamma'})]\\
&+(\delta_{n'm}\delta_{\delta'\delta}V_{\gamma m'n\gamma'}+\delta_{n'n}\delta_{\delta'\gamma}V_{\delta m'm\gamma'})]\}\\
&+\{[-\delta_{m'm}\delta_{\delta'\delta}V_{\gamma n'\gamma'n}+\delta_{n'n}\delta_{\gamma'\gamma}V_{\delta m'\delta'm}\\
&+\delta_{m'm}\delta_{\gamma'\gamma}V_{\delta n'\delta'n}+\delta_{n'n}\delta_{\delta'\delta}V_{\gamma m'\gamma'm})\\
&+\frac{1}{2}(\delta_{m'm}\delta_{\delta'\gamma}V_{\delta n'\gamma'n}+\delta_{n'm}\delta_{\gamma'\gamma}V_{\delta m'\delta'n}+\delta_{m'n}\delta_{\gamma'\gamma}V_{\delta n'\delta'm}\\
&+\delta_{m'm}\delta_{\gamma'\delta}V_{\gamma n'\delta'n}+\delta_{n'n}\delta_{\gamma'\delta}V_{\gamma m'\delta'm}+\delta_{m'n}\delta_{\delta'\delta}V_{\gamma n'\gamma'm}\\
&+\delta_{n'm}\delta_{\delta'\delta}V_{\gamma m'\gamma'n}+\delta_{n'n}\delta_{\delta'\gamma}V_{\delta m'\gamma'm})]\\
&+(\delta_{S0})[-(\delta_{m'n}\delta_{\delta'\gamma}V_{\delta n'\gamma'm}+\delta_{n'm}\delta_{\gamma'\delta}V_{\gamma m'\delta'n}\\
&+\delta_{m'n}\delta_{\gamma'\delta}V_{\gamma n'\delta'm}+\delta_{n'm}\delta_{\delta'\gamma}V_{\delta m'\gamma'n})]\}. \qquad \text{(A. 22)}
\end{aligned}
$$

Note that all the terms in the second braces are of particle-hole "exchange integral" type and those in the third braces are of particle-hole "Coulomb integral" type.

References

1) a) T. Shibuya and V. McKoy, *Phys. Rev.*, **A2**, 2208 (1970); b) T. Shibuya, J. Rose, and V. McKoy, *J. Chem. Phys.*, **58**, 500 (1973).

2) T. Shibuya and V. McKoy, *J. Chem. Phys.*, **54**, 1738 (1971); J. Rose, T. Shibuya, and V. McKoy, *ibid.*, **58**, 74 (1973); **60**, 2700 (1974); W. Coughran, J. Rose, T. Shibuya, and V. McKoy, *ibid.*, **58**, 2699 (1973); D. L. Yeager and V. McKoy, *ibid.*, **60**, 2714 (1974); T. N. Rescigno, C. F. Bender, and V. McKoy, *Chem. Phys. Lett.*, **45**, 307 (1977).

3) G. R. J. Williams and D. Poppinger, *Mol. Phys.*, **30**, 1005 (1975).

4) O. Sinanoğlu, *Adv. Chem. Phys.*, **6**, 315 (1964); **14**, 237 (1969).

5) See, e.g., B. S. Hudson, B. E. Kohler, and K. Schulten, *Excited States*, **6**, (1982).

6) E. S. Nielsen, P. Jørgensen, and J. Oddershede, *J. Chem. Phys.*, **73**, 6238 (1980); J. Geertsen and J. Oddershede, *ibid.*, **85**, 2112 (1986).

7) J. Oddershede, *Adv. Chem. Phys.*, **69**, 201 (1987).

8) D. J. Rowe, *Rev. Mod. Phys.*, **40**, 153 (1968).

9) T. Shibuya, Y. J. I'Haya, and V. McKoy, *Int. J. Quantum Chem.*, **9**, 505 (1975).

10) T. Shibuya and T. Funada, *Chem. Phys. Lett.*, **70**, 199 (1980).

11) T. Shibuya and T. Funada, *Int. J. Quantum Chem.*, **18**, 205 (1980).

 © 1988 The Chemical Society of Japan Bull. Chem. Soc. Jpn., 61, 1109—1113 (1988)

Dielectric Loss of Dehydrated Rb_3Na_8-ZK4 Zeolite

Tatsuo OHGUSHI
Department of Materials Science, Toyohashi University of Technology, Toyohashi 440
(Received October 12, 1987)

The dielectric properties of completely dehydrated Rb_3Na_8-ZK4 zeolite were studied in the range 12—2.2×10^6 Hz and 211—705 K. Two kinds of losses, relaxation and conduction, were observed. The relaxation loss in the higher-frequency region had an activation energy of 99±2 kJ mol^{-1} and was tentatively assigned to a jump of the Rb^+ ion from an 8-ring site to a vacant 4-ring site. The loss at the lower-frequency region had an activation energy of 95±3 kJ mol^{-1} and was attributed to a movement of the Rb^+ ion on the 8-ring site beyond the unit-cell dimension.

In a recent study on the ^{18}O-exchange between CO_2 and zeolite A, it was confirmed that exchangeable cations migrate out from their normal sites and take part in the formation of an activated complex.[1] Movements of exchangeable cations in a zeolite play a decisive role in the thermal deterioration of its crystallinity and may also play an important role in catalytic processes at higher temperatures. Dielectric measurements are most appropriate for studying cation movement in zeolites, since the jump of cation produces a dielectric loss peak.

Dielectric studies of hydrated zeolites have been carried out by many workers, and various properties have been elucidated. Water in a zeolite increases its electrical conductivity.[2-5] The activation energy in a dielectric relaxation process is seriously influenced by adsorbed water.[3,6-9] However, as pointed out by Jonscher et al.,[10] the dielectric properties of completely dehydrated zeolites have been little known and, thus, the dielectric effect of cationic movements in the completely dehydrated zeolites have not been well understood.

Zeolite A is a leading zeolite for studying the physical and chemical properties of zeolites, and its nature is well-understood. In zeolite A, there exist three structurally distinct cations: those located on the sites of 8-, 6-, and 4-membered oxygen rings, respectively. These cations are abbreviated as an 8-, 6-, and 4-ring cation, respectively, in the following. The distribution of these cations had been studied in detail.[11-20] The presence of three structurally distinct cations makes it too complicate to determine which cation is responsible for a dielectric loss. On the other hand, zeolite ZK4 is isostructural with zeolite A and has two structurally distinct cations, 8- and 6-ring cations,[21] and is appropriate for determining to which cation an observed dielectric loss is to be assigned.

Experimental

Apparatus. The measurement system is shown in Fig. 1. In order to ensure a clean vacuum, parts for an ultrahigh vacuum and a turbo molecular pump were used. Methane is usually evolved, even though in small amounts, from the stainless-steel wall; therefore oxygen was continuously flowed into the system at a pressure level of 5×10^{-4} Pa in order to oxidize methane. At temperatures lower than 470 K, at which the decomposition of methane may not occure, oxygen was not introduced. At temperatures lower than room temperature, helium gas was introduced as a heat conductor, through a helium leaker of quartz kept above 670 K. Dielectric measurements were made with a Cole-Gross-type bridge.[22] A guard electrode is useful for determining the absolute value of the dielectric constant and to reduce the surface leakage current. In the present work, however, we did not require the absolute value of the dielectric constant but, rather, its frequency and temperature dependence; further, the surface leakage current was minimized by vacuum techniques, so that it was not necessary to use the guard electrode, thus avoiding unnecessary complications in the cell system.

Sample. Zeolite ZK4, supplied by Vaughan,[23] had a composition of $Na_{11.0}(AlO_2)_{11.0}(SiO_2)_{13.0}\cdot nH_2O$ (abbreviated as $Na_{11.0}$-ZK4), and was used as a starting material. The zeolite was ion-exchanged with a 0.2 mol dm^{-3} solution of CH_3COORb; its composition was determined by atomic absorption spectrometry to be $Rb_{3.0}Na_{8.0}$-ZK4. Powdery zeo-

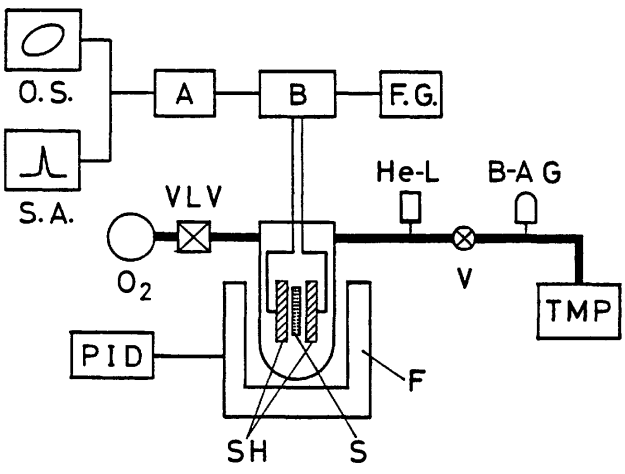

Fig. 1. Apparatus for dielectric measurements.
B: Cole-Gross type brigde, A: amplifier, FG: function generator, OS: oscilloscope, SA: spectrum analyzer, O_2: O_2 gas reservoir, VLV: valiable leak valve, He-L: He leaker, V: stop valve, B-AG, B-A gauge, TMP: turbo molecular pump, PID: PID controller of heater current, SH: sample holder, S: sample, F: electric furnace. Bold line denotes vacuum line.

lite was pressed at a pressure of 900 kg cm^{-2} (8.8×10^7 Pa) at room temperature; the obtained disk had a density of 62% of the single crystal value. The sample did not show any sign of structural damage in its X-ray diffraction pattern and in the water sorption capacity. Thin gold films were evaporated on both sides of the disk for electric contact with gold electrodes. A sample placed in the vacuum system was gently heated under pumping, the temperature being raised by a step of 50 K at an interval of 10 h and finally baked out at 670 K for one day. The back-ground pressure reached was less than 4×10^{-5} Pa. This pressure did not change upon baking out at 670 K for one more day, and was close to the back-ground pressure of the vacuum system without a sample at 670 K, ca. 3×10^{-5} Pa; thus, we judged the sample to be completely dehydrated.

Results

Complex dielectric constants ($\varepsilon^*=\varepsilon'-i\varepsilon''$) were measured as a function of the frequency, f, in the range 12—2.2×10^6 Hz and 211—705 K. Their values measured were not corrected for the packing factor, since we do not need the absolute values (as mentioned above). The sample temperature, T, was controlled, at least, within ±0.5 K of a preset temperature. Data were reproducible in a range of ±1%.

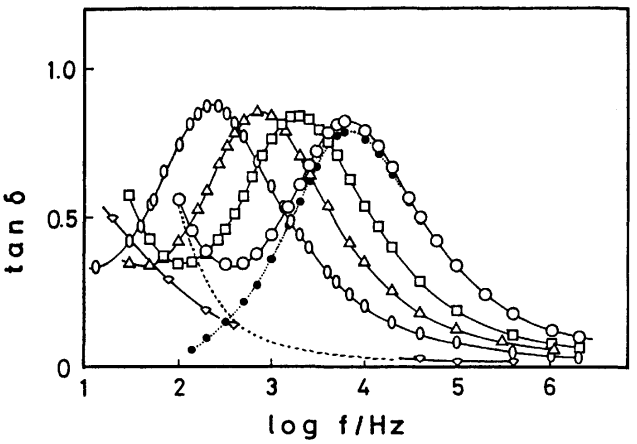

Fig. 2. Spectra of loss tangent. ○: 705.2 K, □: 656.6 K, △: 624.0 K, 0: 588.3 K, ◇: 500.3 K, broken line: loss tangent of conduction ($\tan\delta_c=\varepsilon''_c/\varepsilon'_{obs}$) at 705.2 K, calculated by using relation of $\varepsilon''_c=\sigma/2\pi f\varepsilon_o$ with σ=1.93×10^{-7} S m^{-1}, ●: loss tangent of relaxation ($\tan\delta_r$) at 705.2 K, obtained from relation of $\tan\delta_r=\tan\delta_{obs}-\tan\delta_c$. Subscript obs denotes observed value.

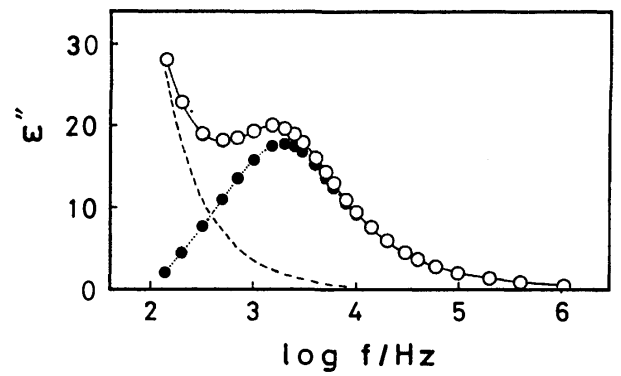

Fig. 3. Spectrum of dielectric loss. ○: observed value at 705.2 K (ε''_{obs}), broken line: conduction loss, ε''_c, calculated from $\varepsilon''_c=\sigma/2\pi f\varepsilon_o$ with σ=1.93×10^{-7} S m^{-1}, ●: relaxation loss ε''_r ($=\varepsilon''_{obs}-\varepsilon''_c$).

The spectra of the loss tangent ($\tan\delta$) and ε'' contain two kinds of losses: one a relaxation loss peak in the higher-frequency region and the other a loss in the lower-frequency region (abbreviated as the low-frequency loss), as shown in Figs. 2 and 3. Let f_{tan} be the applied frequency giving a maximum peak of the loss tangent; we can then approximately determine the activation energy in the relaxation process, E_{tan}, from Arrhenius plots of ln f_{tan} vs. $1/T$. The value obtained is given in Table 1. In the spectra of ε'' (Fig. 3), the low-frequency loss is described by the conductivity loss expressed as $\varepsilon''_c=\sigma/2\pi f\varepsilon_o$, where σ is the apparent specific d.c. conductivity and ε_o the permittivity of vacuum. The low-frequency loss gives a steep rise at higher ε' in the Cole-Cole plots (Fig. 4); this rise is a characteristic of the conduction loss.[24] The low-frequency loss has been frequently observed in zeolite systems and is attributed to the conduction loss.[2,7,25,26] Thus, the low-frequency loss in the present system is assigned to the conduction loss. The most appropriate value of σ was determined by the method described in the Appendix; contributions of the conductivity loss and the conductivity loss tangent were calculated as shown in Figs. 2 and 3. From plots of ln σ vs. $1/T$, the activation energy in the conduction process, E_c, was determined, as listed in Table 1. A relaxation loss part, ε''_r, is obtained from the relation

$$\varepsilon''_r=\varepsilon''_{obs}-\varepsilon''_c=\varepsilon''_{obs}-\sigma/2\pi f\varepsilon_o.$$

Cole-Cole plots, ε''_r vs. ε'_{obs}, are well described by a single circular arc, as shown in Fig. 4; this shows that the loss part, ε''_r, contains a single relaxation process. The

Table 1. Activation Energies and Frequency Factor

E_{tan}	$E_{\varepsilon''}$	E_c	log ω_o
99±2	99±2	95±3	11.4±0.2

E: energy in kJ mol^{-1}, ω_o: angular frequency in s^{-1}.

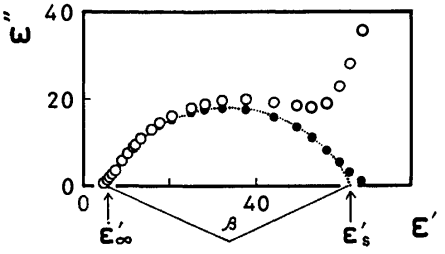

Fig. 4. Cole-Cole plots. ○: observed value at 705.2 K (ε''_{obs} vs. ε'_{obs}), ●: value corrected for conduction loss ($\varepsilon''_{obs}-\varepsilon''_c$ vs. ε'_{obs}, $\varepsilon''_c=\sigma/2\pi f\varepsilon_o$ wth σ=1.93×10^{-7} S m^{-1}) ε'_s=61.2, ε'_∞=5.6, β=108°. Subscript obs denotes observed value.

Table 2. Factors of Cole-Cole Circular Arc at Various Temperatures

T/K	ε'_s	ε'_∞	$\varepsilon'_s/\varepsilon'_\infty$	β/deg
705.2	61.2	5.6	11	108
673.9	60.7	5.3	11	109
656.6	61.9	5.6	11	107
624.0	64.0	5.7	11	106
588.3	63.3	5.8	11	102

values of ε'_s, ε'_∞, and β can be determined on the Cole-Cole plots, as shown in Fig. 4 and listed in Table 2, where ε'_s, ε'_∞, and β denote the permittivities at $f\to 0$ and $f\to\infty$, respectively, and the central angle subtended by the circular arc. The frequency, $f_{\varepsilon''}$, giving the maximum value of ε''_r was determined on the spectrum of ε''_r. From Arrhenius plots of $\ln f_{\varepsilon''}$ vs. $1/T$, the activation energy of the relaxation loss, $E_{\varepsilon''}$, and the frequency factor of the jumping cation, ω_0, were obtained as given in Table 1, where ω_0 is defined as $\ln f_{\varepsilon''} = \ln \omega_0/2\pi - E_{\varepsilon''}/RT$.

Discussion

The observed values of $E_{\tan}$ and $E_{\varepsilon''}$ agree well with each other, as shown in Table 1; this shows that $\varepsilon'_s/\varepsilon'_\infty$ and β are independent of the temperature, since their activation energies are given as[27]

$$E_{\tan} = -R\left[\frac{\mathrm{d}}{\mathrm{d}(1/T)}\ln f_{\tan}\right] = -R\left[\frac{\mathrm{d}}{\mathrm{d}(1/T)}\ln f_{\varepsilon''} + \frac{1}{2}\frac{\mathrm{d}}{\mathrm{d}(1/T)}\frac{1}{\beta}\ln\left(\frac{\varepsilon'_s}{\varepsilon'_\infty}\right)\right]$$

and

$$E_{\varepsilon''} = -R\frac{\mathrm{d}}{\mathrm{d}(1/T)}\ln f_{\varepsilon''}.$$

As can be seen from Table 2, $\varepsilon'_s/\varepsilon'_\infty$ and β are virtually independent of the temperature. Therefore, one may determine, in the present system, the activation energy of the cation jump in the relaxation process from Arrhenius plots of either $\ln f_{\varepsilon''}$ or $\ln f_{\tan}$.

The values of $E_{\varepsilon''}$ and E_c are close to each other. This suggests, as pointed out by Barrer et al.[24] and Rosseinsky et al.,[28] that the relaxation process involves the same cation jump as that in the conduction process. If a charge carrier has a same mechanism in the relaxation process and the conduction process, the dielectric relaxation frequency is related to the specific d.c. conductivity as[29,30]

$$\sigma = \frac{\pi n e^2 d^2 f_{\varepsilon''}}{3kT},$$

where n is the number density of the charge carrier per unit volume, e the elementary charge and d the jump distance. From the equation, one has

$$E_{\varepsilon''} - E_c = RT.$$

In the present experimental conditions, RT is 5—6 kJ mol^{-1} (T is 588—705 K) and the above relation is satisfied within the experimental error.

Let us consider the allowed cation jumps in the zeolite used. There is no data concerning X-ray structural analyses of the Rb_3Na_8-ZK4 zeolite. From X-ray structural analyses of zeolite A, it was found that the Na^+ ion had a stronger affinity for the 6-ring than the Rb^+ ion, and that the Rb^+ ion occupied the center of the 8-ring.[18] It is highly probable that the cations have the same site-affinities in both zeolite A and ZK4. We therefore conclude that $8Na^+$ ions occupy the 6-rings and $3Rb^+$ ions at the centers of the 8-ring in Rb_3Na_8-ZK4 (all 4-ring sites are vacant in zeolite ZK4[21]). A vacant site is necessary for a cation to move. In the above cation distribution, therefore, only three kinds of jumps are allowed. The first is a jump of the Rb^+ ion on the 8-ring to the 4-ring, called Jump I. The 6-ring has two kinds of sites near it, SI and SI', and can accommodate one cation on either site,[16,17] where SI and SI' denote the sites of the large cage side and the sodalite cage side of the 6-ring plane, respectively. The free diameter of the 6-ring is sufficiently large for a Na^+ ion to pass through the ring;[14,15,31] therefore the Na^+ ion can jump between SI and SI', called Jump II. The third is a jump of the Na^+ ion on SI to the 4-ring, called Jump III. In Jumps I—III, only Jump I can contribute to the ionic conduction, since the Rb^+ ion can go away from the unit cell dimension through the route 8-ring→4-ring→another 8-ring. The Na^+ ion has no route to escape from the cell. Consequently, we can assign Jump I to the observed low-frequency loss. This assignment is supported by the results of Haidar et al.[10] They studied the dielectric behaviors of a Ca-A zeolite which was not completely dehydrated, and observed the low-frequency loss. They assigned the loss to a movement beyond the unit-cell dimension of Ca^{2+} ion or ionic species arising from the presence of humidity. In the present zeolite, there is no humidity and, thus, humidity does not become the cause of the low-frequency loss.

If the mechanism of the relaxation loss observed in the present zeolite is same as that of the conduction loss, as suggested above, Jump I is also responsible for the relaxation loss. However, it may be necessary to confirm this assignment by other experiments.

Recently, there has been a discussion concerning the mechanism of the low-frequency loss:[10,32] two kinds, true d.c. and quasi d.c., conduction mechanisms exist. In the present system, measurements could not be made at a sufficiently low frequency range to judge which conduction mechanism was the origin of the low-frequency loss. Whether the low-frequency loss is raised by the true or the quasi d.c. conduction, the charge carrier moves beyond the unit cell dimension and, hence, the assignment of Jump I to the observed low-frequency loss is valid.

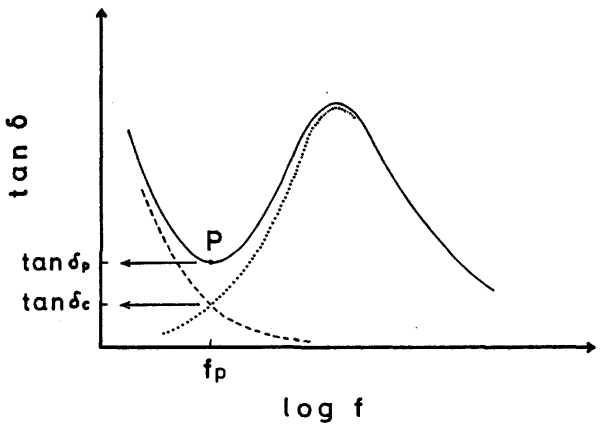

Fig. A-1. Spectrum of loss tangent. Solid line: observed loss tangent, broken line: loss tangent of conduction, dotted line: loss tangent of relaxation, P: saddle point, f_p: frequency at P, $\tan\delta_p$: observed loss tangent at f_p, $\tan\delta_c$: loss tangent of conduction at f_p.

Appendix

In the present system, the low-frequency loss overlaps the relaxation loss. It is desirable to resolve such a composite loss into individual losses in order to study the characteristics of the each loss. The low-frequency loss can be described by $\varepsilon''_c=\sigma/2\pi f\varepsilon_o$. However, there are some arbitrary choices in a determination of the σ-value. Hence, some devices may be necessary in order to determine the σ-value without any arbitrariness. In this Appendix, an approximate determining method is described.

The shape of a loss band and a saddle point clearly manifest themselves in the spectrum of tan δ more than ε''. Hence, the present method can be applied to the spectrum of tan δ. Let tan δ_p and f_p be the values of loss tangent and the frequency at the saddle point P, respectively, as shown in Fig. A-1. At the saddle point, the loss tangent of the conduction, tan δ_c, is approximately equal to the loss tangent of the relaxation, tan δ_r. Then, one has

$$\begin{aligned}\tan\delta_p &= \tan\delta_c + \tan\delta_r \\ &= 2\tan\delta_c. \end{aligned} \quad \text{(A-1)}$$

From the definition of loss tangent, tan δ_p and tan δ_c are written as

$$\tan\delta_p = \frac{\varepsilon''_p}{\varepsilon'_p} \quad \text{(A-2)}$$

and

$$\tan\delta_c = \frac{\varepsilon''_{cp}}{\varepsilon'_p}, \quad \text{(A-3)}$$

where ε'_p and ε''_p denote the observed values of the permittivity and the loss at f_p, respectively, and ε''_{cp} the conduction loss at f_p. The value of ε''_{cp} is expressed as

$$\varepsilon''_{cp} = \frac{\sigma_m}{2\pi f_p\varepsilon_o}, \quad \text{(A-4)}$$

where σ_m denotes the most appropriate value of σ. From the Eqs. A-1—A-4, one obtaines

$$\sigma_m=\pi\varepsilon_o f_p\varepsilon'_p\tan\delta_p$$

or

$$\pi\varepsilon_o f_p\varepsilon''_p.$$

The present author sincerely thanks Prof. Tetsuo Takaishi of Toyohashi University of Technology, for useful discussions, and Dr D. E. W. Vaughan of Exxon Research and Engineerring Co., who supplied ZK4 zeolite. The present work was partially supported by Grant-in-Aid for Encouragement of Young Scientists of the Ministry of Education of the Japanese Government, contract no. 60740232.

References

1) T. Takaishi and A. Endo, *J. Chem. Scoc., Faraday Trans. 1*, **83**, 411 (1987).
2) B. Morris, *J. Phys. Chem. Solids*, **30**, 73 (1969).
3) B. Morris, *J. Phys. Chem. Solids*, **30**, 103 (1969).
4) F. J. Jansen and R. A. Schoonheydt, Reunion Hispano-Berga Miner. Arcilla, An. 1970 (Pub. 1971), p. 45.
5) G. Jones, *J. Chem. Soc., Faraday Trans. 1*, **71**, 2085 (1975).
6) R. M. Barrer and P. J. Coen, *Nature (London)*, **199**, 587 (1963).
7) R. M. Barrer and E. A. Saxon-Napier, *Trans. Faraday Soc.*, **58**, 145 (1962).
8) F. J. Jansen and R. A. Schoonheydt, *Adv. Chem. Ser.*, **121**, 96 (1973).
9) G. Jones and M. Davies, *J. Chem. Soc., Faraday Trans. 1*, **71**, 1791 (1975).
10) A. R. Haidar and A. K. Jonscher, *J. Chem. Soc., Faraday Trans. 1*, **82**, 3535 (1986).
11) T. Takaishi, Y. Yatsurugi, A. Yusa and T. Kuratomi, *J. Chem. Soc., Faraday Trans. 1*, **71**, 97 (1975).
12) A. Yusa, T. Ohgushi, and T. Takaishi, *J. Phys. Chem. Solids*, **38**, 1233 (1977).
13) T. Ohgushi, A. Yusa and T. Takaishi, *J. Chem. Soc., Faraday Trans. 1*, **74**, 613 (1978).
14) J. J. Pluth and J. V. Smith, *J. Am. Chem. Soc.*, **102**, 4704 (1980).
15) V. Subramanian and K. Seff, *J. Phys. Chem.*, **81**, 2249 (1977).
16) J. J. Pluth and J. V. Smith, *J. Phys. Chem.*, **83**, 741 (1979).
17) P. C. W. Leung, K. B. Kunz, K. Seff, and I. E. Maxwell, *J. Phys. Chem.*, **79**, 2157 (1975).
18) R. L. Firror and K. Seff, *J. Am. Chem. Soc.*, **99**, 1112 (1977).
19) T. B. Vance, Jr. and K. Seff, *J. Phys. Chem.*, **79**, 2163 (1975).
20) R. L. Firror and K. Seff, *J. Am. Chem. Soc.*, **99**, 6249 (1977).
21) D. W. Breck, "Zeolite Molecular Sieves," John Wiley & Sons, New York (1974), p. 179.
22) R. H. Cole and P. M. Gross Jr., *Rev. Sci. Instr.*, **20**, 252 (1949).
23) R. H. Jarman, M. T. Melchior and D. E. W. Vaughan, "Intrazeolite Chemistry," ed by G. D. Stucky and F. G. Dwyer, Am. Chem. Soc., Washigton (1983), p 267.

24) R. M. Barrer and E. A. Saxon-Napier, *Trans. Faraday Soc.*, **58**, 156 (1962).
25) F. J. Jansen and R. A. Schoonheydt, *J. Chem. Soc., Faraday Trans. 1*, **69**, 1338 (1973).
26) R. A. Schoonheydt and W. Wild, *J. Chem. Soc., Faraday Trans. 1*, **70**, 2132 (1974).
27) K. S. Cole and R. H. Cole, *J. Chem. Phys.*, **9**, 341 (1941).
28) D. R. Rosseinsky, J. S. Tonge, J. Berthelot, and J. F. Cassidy, *J. Chem. Soc., Faraday Trans. 1*, **83**, 231 (1987).
29) D. R. Rosseinsky, J. A. Stephan, and J. S. Tonge, *J. Chem. Soc., Faraday Trans 1*, **77**, 1719 (1981).
30) S. Bone, J. Eden, P. R. C. Gascoyne, and R. Pething, *J. Chem. Soc., Faraday Trans. 1*, **77**, 1729 (1981).
31) "Handbook of Chemistry and Physics," 66th ed, CRC Press, Boca Raton, Florida (1985), p. F164.
32) A. K. Jonscher and A. R. Haidar, *J. Chem. Soc., Faraday Trans. 1*, **82**, 3553 (1986).

 © 1988 The Chemical Society of Japan Bull. Chem. Soc. Jpn., 61, 1115—1119 (1988)

Reflectance Spectra of the 1 : 1 Salts of Bis(methylenedithio)tetrathiafulvalene (BMDT-TTF): Estimation of the On-Site Coulomb Energy

Michiko YOSHITAKE, Kyuya YAKUSHI,* Haruo KURODA,* Akiko KOBAYASHI, Reizo KATO,† and Hayao KOBAYASHI†

Department of Chemistry, Faculty of Science, University of Tokyo, Hongo, Tokyo 113
†Department of Chemistry, Faculty of Science, Toho University, Funabashi, Chiba 274

(Received November 5, 1987)

Polarized reflectance spectra were measured on the single crystals of (BMDT-TTF)AsF_6 and (BMDT-TTF)SbF_6. The charge-transfer band was observed along the stacking direction in the crystals of (BMDT-TTF)AsF_6, while in the crystal of (BMDT-TTF)SbF_6 the charge-transfer band was found not only along the stacking direction but also along the S ··· S direction nearly parallel to the short axis of the BMDT-TTF molecule. The effective on-site Coulomb energies and the transfer integrals of these salts were estimated by analyzing the charge-transfer bands.

Recently organic conductors based on BEDT-TTF (bis(ethylenedithio)tetrathiafulvalene) have been extensively studied, and many metallic salts have been found one after another.[1-3] BMDT-TTF (bis(methylenedithio)tetrathiafulvalene)) is one of the derivatives of BEDT-TTF, and involves the same conjugated moiety as that of BEDT-TTF. In contrast to BEDT-TTF salts, the positive charge in BMDT-TTF radical salts tends to be localized despite two-dimensional S ··· S network is formed in these crystals like the crystals of BEDT-TTF salts.[4,5] The characteristics of such an electronic structure is probably related to the magnitude of the electron-electron Coulomb energy and the transfer integrals. In this paper, we studied the optical spectra of the (1 : 1) salts of BMDT-TTF, (BMDT-TTF)AsF_6, and (BMDT-TTF)SbF_6, for the purpose to characterize the dimensionality of the intermolecular interaction and of the electron-electron Coulomb interaction.

Experimental

BMDT-TTF was synthesized by the method described elsewhere.[4] Single crystals of (BMDT-TTF)AsF_6 and (BMDT-TTF)SbF_6 were prepared by the method of electrochemical crystallization in the 1,1,2-trichloroethane solutions of BMDT-TTF, $(n\text{-Bu})_4NAsF_6$, and $(n\text{-Bu})_4NSbF_6$ being used as electrolytes. (BMDT-TTF)AsF_6 crystallized into thin needle-like crystals elongated along the c-axis, the typical length being 1.3 mm. The single crystal of (BMDT-TTF)SbF_6 was a thin platelet developping the (100) crystal face. The crystal axes and faces were determined by the oscillation and Weissenberg photographs. The polarized reflectance spectra were measured by the use of a microspectrophotometric technique. The reflectance spectrum was measured in the spectral region from 4.2×10^3 cm^{-1} to 25×10^3 cm^{-1}.

Results and Discussion

The crystal of (BMDT-TTF)AsF_6 belongs to the triclinic system with the space group, $P\bar{1}$,[6] the unit cell containing one molecule. BMDT-TTF is stacking along the c-axis with their molecular planes parallel to each other. The neighboring molecule is shifted along the long axis of molecule, and the long axis is inclined by 34° to the c-axis. Since these molecular column is surround by AsF_6 anions, the intermolecular interaction is expected to be strongest along the c-axis. Figure 1 shows the crystal structure projected onto the (100) plane and the reflectance spectra of (BMDT-TTF)AsF_6 measured on the (100) crystal face. The dispersions of the reflectance were observed at 5×10^3 cm^{-1}, 11×10^3 cm^{-1}, and 21×10^3 cm^{-1} in the //c spectrum. Since BMDT-TTF salt is not soluble in organic solvents, we assinged these electronic transitions by comparing with the electronic spectrum of BPDT-TTF (bis(propylenedithio)tetrathiafulvalene) salts, the cation of which involves the same conjugated moiety as BMDT-TTF. The electronic transitions of the cation radical of BPDT-TTF in the 1,1,2-trichloroethane was found at 13.5×10^3 cm^{-1} (A), 18.4×10^3 cm^{-1} (B), and 22.4×10^3 cm^{-1} (C) in the visible region of the absorption spectrum.[7] Since the transition, B. is much weaker than the other transitions, the dispersion at 11×10^3 cm^{-1} and 21×10^3 cm^{-1} were assigned to these

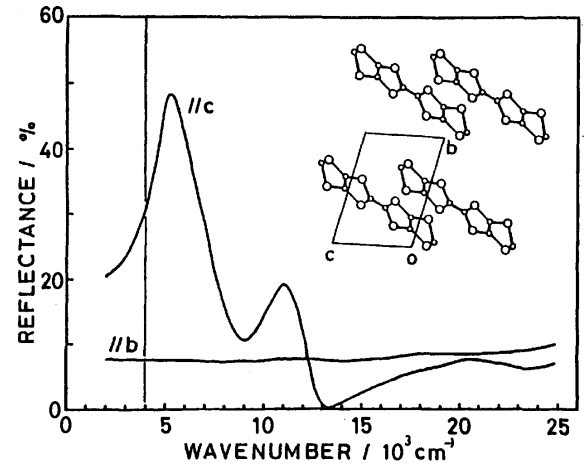

Fig. 1. Polarized reflectance spectrum of (BMDT-TTF)AsF_6 on the (100) crystal face. The reflectance curves in the region lower than 4×10^3 cm^{-1} are the extrapolated curves by the curve fittings based on the Lorentz model. The inset shows the crystal structure projected onto the (100) plane.

intramolecular transitions, A and C, respectively. Thus, the lowest excitation at 5×10^3 cm^{-1} was safely assigned to the charge-transfer (CT) transition between BMDT-TTF$^+$'s. This assignment is supported by the polarization direction which is parallel to the stacking axis of BMDT-TTF. Incidentally, the intramolecular transitions in this spectral region were found to be polarized parallel to the long axis of molecule, since the short axis of the molecule is nearly perpendicular (93°) to the c-axis.

The crystal of (BMDT-TTF)SbF_6 belongs to the triclinic system with the space group $P\bar{1}$, and $Z=1$.[8] BMDT-TTF is stacking along the b-axis such a manner as the long axis is inclined by 35° to the stacking axis. The adjacent molecule is mutually shifted to the long and short axes of molecule, so that one of the 1,3-dithiole moiety of BMDT-TTF is overlapping the same portion of the adjacent molecule. In this sense the intermolecular interaction along this stacking direction seems to be relatively weak. In contrast to the structure of (BMDT-TTF)AsF_6 the molecular columns linked by the S ··· S interaction make a sheet parallel to the (100) plane, and several short S ··· S contacts are reported between the neighboring molecules in this sheet.[8] Figure 2 shows the crystal structures and the polarized reflectance spectra measured on the (100) and (010) crystal faces. According to the spectrum of (BMDT-TTF)AsF_6 the intramolecular transitions at 11×10^3 cm^{-1} and 21×10^3 cm^{-1} are polarized parallel to the long axis of molecule. Therefore, the dispersion at 11.5×10^3 cm^{-1} in the //a spectrum and that at 20×10^3 cm^{-1} in the //b spectrum are respectively assignable to these intramolecular transitions, A and C. The assignment of the 20×10^3 cm^{-1} transition is consistent with the observed polarization dependence, since the long axis of molecule is least inclined (35°) to the b-axis among the three crystallographic axes as shown in Fig. 2. The shoulder at 17×10^3 cm^{-1} in the //b spectrum probably corresponds to the weak absroption band, B, found at 18.4×10^3 cm^{-1} in the solution spectrum of the BPDT-TTF cation radical. From the polarization direction the strongest dispersion at 5×10^3 cm^{-1} in the //c spectrum is safely assigned to the CT transition between BMDT-TTF$^+$'s through the S ··· S interaction. The dispersion at 9×10^3 cm^{-1} in the //b spectrum looks like the intramolecular transition, A, but the excitation energy does not agree with the a-component of the transition, A. Furthermore, the width of this dispersion is slightly broader than that of the CT band in the //c spectrum. Thus we assinged this 9×10^3 cm^{-1} dispersion to the superposition of the CT transition along the stacking direction parallel to the b-axis and the b-component of the intramolecular transition, A, since both transitions take place most strongly along the b-axis. This assignment was confirmed by the low-temperature spectrum, because a small shoulder was found at 11×10^3 cm^{-1} in the //b spectrum at 42 K as shown in Fig. 3. Therefore, we arrived at the most important result in this experiment that two kinds of charge-transfer transitions were observed along the S ··· S direction as well as the stacking direction in the crystal of (BMDT-TTF)SbF_6. Such a two-dimensional intermolecular interaction has been observed in many BEDT-TTF salts.[9,10] This is the first optical evidence of the two dimensionality of

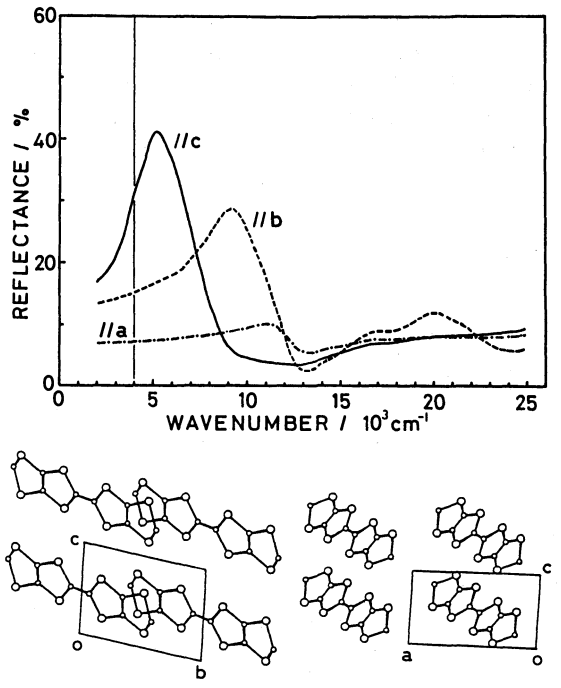

Fig. 2. Polarized reflectance spectrum and crystal structure of (BMDT-TTF)SbF_6. The //c and //b spectra were measured on the (100) crystal face, and the //a spectrum was measured on the (010) face. The reflectance curves in the region lower than 4×10^3 cm^{-1} are the extrapolated curves by the curve fittings based on the Lorentz model.

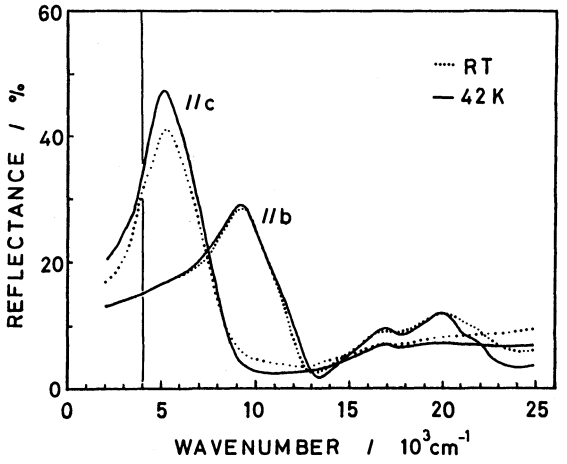

Fig. 3. Low-temperature reflectance spectrum of (BMDT-TTF)SbF_6. The room-temperature spectrum is also illustrated by a dotted line for comparison. The reflectance curves in the region lower than 4×10^3 cm^{-1} are the extrapolated curves by the curve fittings based on the Lorentz model.

BMDT-TTF salts.

Figures 4a and 4b show the optical conductivity spectra of (BMDT-TTF)AsF_6 and (BMDT-TTF)SbF_6 obtained from the Kramers-Kronig transformation of the reflectance spectra. These salts have half-filled metallic band structures, if the electron-electron correlation is fully screened. However, the appearance of the CT band shown in Fig. 4 indicates the existence of a band gap. In addition, both of these salts exhibit semiconductive behavior as regards the temperature dependence of the electrical resistivity.[6,8] These results clearly show that the strong Coulomb interaction plays an important role in these materials. As shown in the conductivity spectrum of (BMDT-TTF)SbF_6, the CT absorption bands of the //c and //b spectra show up at different wavenumbers separating about 4×10^3 cm^{-1}. The excitation energy of the CT band in the limit of a strongly correlated half-filled band is given by $U-V_i$, where U is the on-site Coulomb energy, V_i, the Coulomb energy between the neighboring sites along the i-th direction. The distance between the centers of adjacent molecules is 5.63 Å along the c-axis, whereas that is 7.50 Å along the b-axis. Therefore, the difference of the excitation energies between the CT transitions polarized along the c-and b- axes is attributed to the nearest-neighbor Coulomb interaction which depends on the distance between the adjacent molecules. The similar phenomenon was found in the single-crystal absorption spectrum of $(TTF)ClO_4$, in which two charge-transfer bands separated by 3×10^3 cm^{-1} were interpreted to be the intra-dimer and inter-dimer CT transitions.[11] This interpretation to the spectrum of (BMDT-TTF)SbF_6 means that the magnitude of the long range Coulomb energy is comparable to that of the on-site Coulomb energy, and thus the excited state is not the free-electron and free-hole state but the bound electron-hole state. In this situation charge-transfer process takes place predominantly between the adjacent molecules, so that the CT transition can be approximately analyzed by a dimer model. In the dimer model, the excitation energy and the oscillator strength of a CT band is represented by the Eqs. 1 and 2,[12]

$$E_{CT}=U_{eff}/2+(U_{eff}^2/4+4t^2)^{1/2} \quad (1)$$

$$f=(2d^2m_eN_d/N\hbar^2)(2t^2/(U_{eff}^2/4+4t^2)^{1/2}) \quad (2)$$

where E_{CT}, U_{eff}, t, f, d, m_e, N_d, and N denote the CT excitation energy, the effective on-site Coulomb energy, the transfer integral, the oscillator strength, the distance between the centers of molecules, the electron mass, the number density of a dimer, and the number density of BMDT-TTF, respectively. We set N_d/N equal to 1, since the CT interaction equivalently occurs to both side of a molecule in a regular chain. The oscillator strength, f, of the CT band was calculated by using the following equation,

$$f=(2m_e/\pi e^2N)\int\sigma(\omega)d\omega \quad (3)$$

where e and $\sigma(\omega)$ are the charge of an electron and the conductivity spectrum, respectively. Table 1 shows the effective on-site Coulomb energy, $U_{eff}=U-V$, and the transfer integral, t, which were calculated by the use of the Eqs. 1 and 2. The oscillator strength and thus the transfer integral in the //b spectrum of (BMDT-TTF)SbF_6 is the upper limit because the b-component of the intramolecular transition is involved in the 9.0×10^3 cm^{-1} band. Keeping this point in mind, the relation between the transfer integral and the overlap integral is qualitatively good in BMDT-TTF salts.

Bondeson and Soos numerically examined the systematic deviation of the excitation energy and the transition probability of a CT transition in going from a dimer to a finite chain by the aid of a diagrammatic valence bond method.[13] According to their calculation, a dimer model is a good approximation to the infinite chain only for $U_{eff}/4t>3.5$, otherwise the excitation energy predicted from a dimer model is considerably larger than that of an infinite chain. Unfortunately, the parameters, $U_{eff}/4t$, of these BMDT-TTF salt is not in the former regime, so that the actual effective on-site Coulomb energies in Table 1 is considered to be significantly larger than the values listed in Table 1. Therefore, we analyzed the CT spectrum of the one-dimensional (BMDT-TTF)AsF_6 salt by a Hubbard model, in which the long range Coulomb

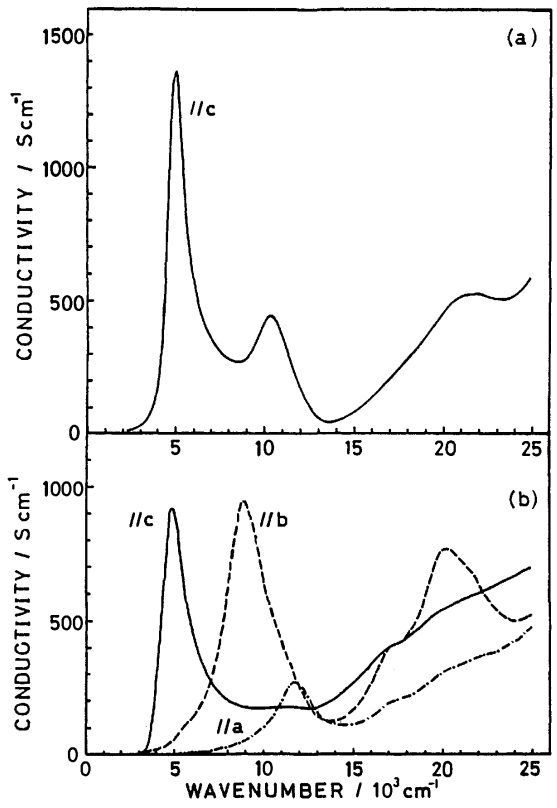

Fig. 4. Optical conductivity spectra of (a) (BMDT-TTF)AsF_6 and (b) (BMDT-TTF)SbF_6.

Table 1. Effective On-Site Coulomb Energies, U_{eff}, and Transfer Integrals, t, of (BMDT-TTF)AsF_6 and (BMDT-TTF)SbF_6 Estimated from the Dimer Model. E_{CT} and f Are the Excitation Energy and the Oscillator Strength of the Charge Transfer Band. d and S Denote the Distance between the Centers of Molecules and the Overlap Integral of the HOMO's between the Adjacent Molecules

	(BMDT-TTF)AsF_6	(BMDT-TTF)SbF_6	
	// c (stacking direction)	// c (S---S direction)	// b (stacking direction)
E_{CT}/eV	0.62	0.61	1.1
f	0.43	0.31	<0.60
d/Å	5.84	5.63	7.50
U_{eff}/eV)	0.57	0.60	1.1
t/eV	0.09	0.08	<0.11
S	-10.6×10^{-3}	-12.5×10^{-3}	-5.1×10^{-3}

energy is completely neglected. In the one-dimensional chain, the exact solutions were reported on the optical excitation energy[14] and the oscillator strength[15] as shown in the following equations.

$$E_{opt}/4t = u - 1 + 2\int_0^\infty (J_1(x)/x)(1+\exp(2ux))^{-1}\,dx \quad (4)$$

$$(f/4t)(\hbar^2/md^2) = \int_0^\infty (J_0(x)J_1(x))[x^{-1}(1+\exp(2ux))^{-1} + u(1+\cosh(2ux))^{-1}]\,dx \quad (5)$$

where E_{opt} is the absorption edge of the optical transition across the Hubbard gap, u is defined to be $U_{eff}/4t$, and $J_0(x)$ and $J_1(x)$ are the Bessel functions. The values of $E_{opt}/4t$ and $(f/4t)(\hbar^2/md^2)$, which were obtained by numerical calculation, were plotted against u in Fig. 5 together with the quantity of $(E_{opt}/f)(md^2/\hbar^2)$ which is experimentally obtainable. We defined the absorption edge, E_{opt}, as the wavenumber at which the conductivity curve takes half of the maximum value of the CT absorption band. The parameter, $u=U_{eff}/4t$, was calculated to be 1.80 from the u-dependent curve of $(E_{opt}/f)(md^2/\hbar^2)$ by the use of the experimental values, E_{opt}=0.56 eV, f=0.43, and d=5.84 Å. The parameters, t and U_{eff}, were determined to be 0.14 eV and 1.0 eV from the u-dependent curves of $(E_{opt}/4t)$ and $(f/4t)(\hbar^2/md^2)$. This is the first attempt to analyze the CT band of the regular-stack one-dimensional chain with a half-filled band on the basis of the exact solution of the Hubbard model. However, the analysis is not complete, because the appearance of the two CT bands at different wavenumbers in the polarized spectrum of (BMDT-TTF)SbF_6 indicates that the nearest-neighbor Coulomb interaction should be included in the analysis. However, the theoretical study on the optical transition of the extended Hubbard model has not been conducted in the case $u\simeq1$. Bondeson and Soos numerically examined the difference of the optical

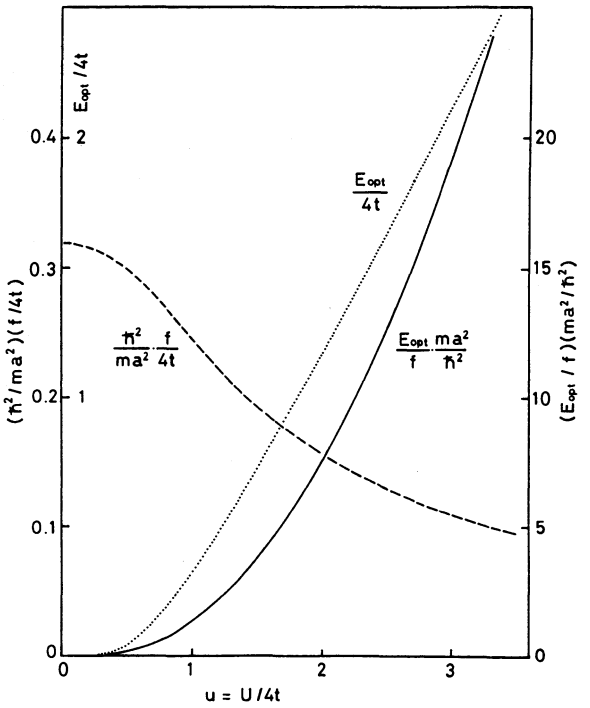

Fig. 5. Numerical calculation of the excitation energy, the oscillator strength, and their ratio which is predicted from the exact solution of the one-dimensional Hubbard model.

transition across the Hubbard gap between the extended Hubbard model and the Hubbard model. According to their calculation the excitation energy of the CT band based on the extended Hubbard model in the case $U-V_1\simeq4t$ is significantly higher than that based on the Hubbard model in the case $U_{eff}\simeq4t$ and much lower than that of the dimer model. Therefore, we consider that the effective on-site Coulomb energy, U_{eff}, is in the range between 0.6 eV and 1.0 eV. The numerical calculation by Bondeson and Soos also indicated that the transition probability of the CT band did not change significantly among the dimer model, the Hubbard model and the extended Hubbard model, so that the transfer integral, t, was estimated to be about 0.1—0.15 eV. Torrance et al. examined the band parameters of TTF salts, (TTF)X (X=$Cl_{0.80}$, $Br_{0.79}$, and $I_{0.71}$).[16] They estimated the parameters, U_{eff} and t, to be 1.25 eV and 0.28 eV, respectively. Because they used the dimer model to obtain these parameters. U_{eff} must be larger than 1.25 eV. Therefore, we conclude that the on-site Coulomb energy of BMDT-TTF salt is significantly smaller than that of TTF salts. This is in accord with the extended molecular structure of BMDT-TTF in comparison with TTF.

References

1) H. Kobayashi, R. Kato, T. Mori, A. Kobayashi, Y. Sasaki, G. Saito, T. Enoki, and H. Inokuchi, *Mol. Cryst. Liq. Cryst.*, **103**, 33 (1984).

2) R. P. Shibaeva, V. F. Kaminskii, and E. B. Yagubskii,

Mol. Cryst. Liq. Cryst., **119**, 361 (1985).
3) J. M. Williams and K. Carneiro, *Adv. Inorg. Chem. Radiochem.*, **29**, 249 (1986).
4) R. Kato, A. Kobayashi, Y. Sasaki, and H. Kobayashi, *Chem. Lett.*, **1984**, 993.
5) R. Kato, H. Kobayashi, A. Kobayashi, and Y. Sasaki, *Chem. Lett.*, **1984**, 1693.
6) R. Kato, H. Kobayashi, and A. Kobayashi, unpublished data.
7) K. Yakushi, H. Tajima, T. Ida, M. Tamura, H. Hayashi, H. Kuroda, R. Kato, H. Kobayashi, and A. Kobayashi, *Synthetic Metals*, in press.
8) R. Kato, H. Kobayashi, and A. Kobayashi, *Chem. Lett.*, **1986**, 2013.
9) H. Kuroda, K. Yakushi, H. Tajima, and G. Saito, *Mol. Cryst. Liq. Cryst.*, **125**, 135 (1985).
10) H. Tajima, H. Kanbara, K. Yakushi, and G. Saito, *Solid State Commun.*, **57**, 911 (1986).
11) K. Yakushi, S. Nishimura, T. Sugano, H. Kuroda, and I. Ikemoto, *Acta Crystallogr., Sect. B*, **36**, 358 (1980).
12) M. J. Rice, *Solid State Commun.*, **31**, 93 (1979).
13) S. R. Bondeson and Z. S. Soos, *Chem. Phys.*, **44**, 403 (1979).
14) A. Mursurkin and A. A. Ovchinnikov, *Soviet Phys. Solid State*, **12**, 2031 (1971).
15) D. Baeriswyl, J. Carmelo, and A. Luther, *Phys. Rev. B*, **33**, 7247 (1986).
16) J. B. Torrance, B. A. Scott, B. Welber, F. B. Kaufman, and P. E. Seiden, *Phys. Rev. B*, **19**, 730 (1979).

 © 1988 The Chemical Society of Japan Bull. Chem. Soc. Jpn., 61, 1121—1129 (1988)

Photoreduction of Anthraquinone by Triethylamine in Ethanol and Toluene Studied by Steady-State Photolysis and Laser Photolysis

Kumao HAMANOUE,* Toshihiro NAKAYAMA, Yoshiaki YAMAMOTO, Kazuhide SAWADA, Yoshihito YUHARA, and Hiroshi TERANISHI
Department of Chemistry, Kyoto Institute of Technology, Matsugasaki, Sakyo-ku, Kyoto 606
(Received November 14, 1987)

Photoreduction of anthraquinone (AQ) by triethylamine (TEA) in toluene and ethanol was studied by means of steady-state photolysis and laser photolysis. In toluene, addition of TEA enhanced the quantum yield of photoreduction of AQ, and the reaction was found to originate via the formation of an exciplex between ground-state TEA and the lowest triplet state of AQ: This exciplex changed to a contact ion pair followed by proton transfer, generating anthrasemiquinone radical and triethylamine radical, and 9,10-anthracenediol was obtained as the final photoproduct. Although the mechanism of the photoreduction of AQ in ethanol/TEA was essentially the same as that in toluene/TEA and the final products in ethanol/TEA were 9,10-anthracenediol and its anion, the quantum yield of photoreduction decreased with increase in TEA concentration. It was proposed that the exciplex in ethanol was quenched by ground-state TEA via the formation of a triplex of a radical anion of AQ and a radical cation of TEA dimer bonded by the three σ-electrons on two nitrogen atoms, based on the suggestion made by Hub et al. (*J. Am. Chem. Soc.*, **106**, 701 (1984); **106**, 708 (1984)).

Photoinduced electron transfer is one of the most important primary processes in a number of photochemical reactions, and the photoreductions of aromatic carbonyls in amine solutions have been investigated extensively.[1-6] Although intermediacy of a radical anion of ketones or a complex (an exciplex, a charge-transfer complex or an ion pair) of triplet ketones with ground-state amines has been proposed, the mechanism for the formation of these ionic species and the interconversion among them are generally dependent on the combination of the donor and the acceptor as well as the nature of the solvent. Moreover, the absorption spectra of these various species are generally very similar to each other. Therefore, it is very important to know the difference in the absorption spectra of the ionic species for full understanding of their formation.

Since we have observed that the quantum yields of photoreduction of anthraquinone (AQ) and haloanthraquinones (the chloro and bromo compounds) are increased by the addition of triethylamine (TEA), it is expected that ionic species mentioned above are also produced upon photolysis of anthraquinones/TEA in solution. As an extension of our study on the photophysics and photochemistry of anthraquinones,[7-12] this paper deals with the details of the photoreduction of AQ by TEA in ethanol and toluene, studied by means of steady-state photolysis and laser photolysis. Preliminary results have already been published elsewhere.[13]

Experimental

Chemicals. The details of the methods of preparation of AQ have been given in our previous paper.[7] GR-grade TEA (Wako) was refluxed over calcium hydride and distilled under nitrogen. Spectral-grade ethanol (Nakarai), and scintillation-grade benzene (Dojin) and toluene (Dojin) as the solvents were used without further purification. Unless otherwise stated, the sample solutions were degassed by several freeze-pump-thaw cycles.

Steady-State Photolysis. Photolysis of AQ/TEA in solution was carried out at room temperature using an USH-500D super-high pressure mercury lamp. Light of 313-nm monochromatic wavelength was selected by the combination of two Toshiba color glass filters (UV-29 and UV-D33S) and a filter solution ($Ni_2SO_4 \cdot 6H_2O$, 50 g dm^{-3}, path length 2 cm). Absorption spectra were taken on a Hitachi 200-20 spectrophotometer. The quantum yields of photoreduction were determined by the Hatchard-Parker's tris(oxalato)ferrate(III) actinometry method.[14]

For the identification of absorption spectra of a radical anion ($AQ^{\cdot-}$) of AQ and monoanion (AQH^-) of 9,10-anthracenediol (AQH_2), photolyses of AQ and AQH_2 in alkaline ethanol were performed using 366- and 404-nm lights, respectively, where light of 366-nm monochromatic wavelength was selected by the combination of two Toshiba color glass filters (UV-35, UV-D35) and a filter solution ($CuSO_4 \cdot 5H_2O$, 100 g dm^{-3}, path length 3 cm) and 404-nm light was selected by the combination of a Toshiba color glass filter (UV-39) and a filter solution (loc. cit.).

Laser Flash Photolysis. All transient absorption spectra were taken at room temperature. Unless otherwise stated, picosecond laser photolysis was performed using the second harmonic (347.2 nm) of a picosecond mode-locked ruby laser. The details of this laser photolysis system with a 30 ps instrumental time constant have been given elsewhere.[15] A double-beam optical arrangement was adopted and an absorption spectrum over a range of 200-nm wavelengths was obtained by two measurements: First, reference and probe light intensities without firing the exciting laser pulse, i.e., $I_O^A(\lambda)$ and $I_O^B(\lambda)$, respectively, were measured. Next, reference and probe light intensities with firing the exciting laser pulse, i.e., $I_E^A(\lambda)$ and $I_E^B(\lambda)$, respectively, were measured. Then, the absorbance $D(\lambda)$ at a given delay time was calculated by a microcomputer using the following equation;

$$D(\lambda) = \log[I_E^A(\lambda)/I_E^B(\lambda)] - \log[I_O^A(\lambda)/I_O^B(\lambda)] \quad (1)$$

where λ is the wavelength. The sample solutions in a cell of 2-mm path length were not deaerated.

To confirm a weak triplet-triplet ($T'\leftarrow T_1$) absorption of AQ at 500—600 nm, picosecond laser photolysis was also performed using the third harmonic (355 nm), with a pulse width of ≈25 ps, from a mode-locked Nd^{3+}: YAG laser of Osaka University, where the sample solutions in a cell of 10-mm path length were deaerated. The details of this laser photolysis system have been given elsewhere by Miyasaka et al.[16] The time-resolved absorption spectrum over a range of 400-nm wavelengths was calculated by

$$D(\lambda)=\log[\sum I_E^A(\lambda)/\sum I_E^B(\lambda)]-\log[\sum I_O^A(\lambda)/\sum I_O^B(\lambda)] \quad (2)$$

where spectral averaging was made five times.

The details of the Q-switched ruby laser photolysis system have also been given elsewhere.[10,17] The half-peak duration of the second harmonic (347.2 nm) was 20 ns, and the decay of the transient absorption was recorded by a combination of an HTV R666 photomultiplier with an Iwatsu TS-8123 storage oscilloscope: Time-resolved absorption spectra at delay times longer than 2 μs were recorded by the "ISD" system,[18] that is, a combination of a nanosecond ruby laser with an image sensor detector and a microcomputer, where a pulsed xenon flash lamp with a 1.7-μs full width at half-maximum intensity was used as a probe-light source. The time-resolved absorption spectrum over a range of 400-nm wavelengths was calculated by

$$D(\lambda)=\log[\sum I_O(\lambda)-\sum I_b(\lambda)]-\log[\sum I_E(\lambda)-\sum I_d(\lambda)] \quad (3)$$

where $I_b(\lambda)$ is the dark current spectrum of the detector system, and $I_d(\lambda)$ is the emission intensity due to the excited species, as measured without the probe light upon firing of the laser pulse. (Also, spectral averaging was made five times.) The sample solutions in a cell of 10-mm path length were deaerated.

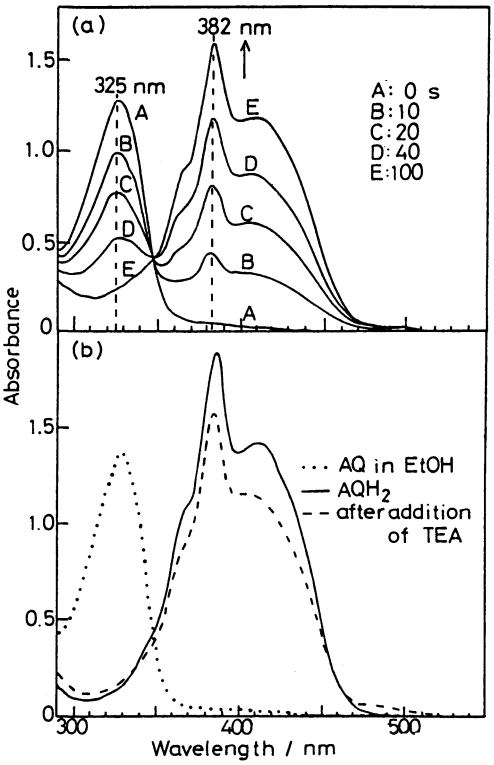

Fig. 1. Absorption spectral change of AQ/TEA (0.2 M) in ethanol upon irradiation with 313-nm light at room temperature (a), and change of the absorption spectrum of AQH_2 upon addition of TEA (b).

Results

Steady-State Photolysis. The absorption spectral change of AQ/TEA (0.2 M; 1 M=1 mol dm^{-3}) in ethanol at room temperature is shown in Fig. 1a: Upon irradiation with 313-nm light, the absorption band of AQ with λ_{max}=325 nm decreased and a new band of the photoproduct with λ_{max}=382 nm built up, accompanied by an isosbestic point at 346 nm. This reaction is essentially the same as that of AQ in the absence of TEA.[8] Thus, one can safely conclude that the absorption band with λ_{max}=382 nm is due to AQH_2. In Fig. 1a, however, one can observe a weak tail at 470—530 nm. Such an absorption was not observed in the absence of TEA. We interpret this weak tail as the absorption due to AQH^-, based on the following reasons: (1) We have already reported that the forms of 10-cyano-9-anthrol (or its anion) and 10-benzoyl-9-anthrol (or its anion) in a solution containing TEA was dependent on the basicity, polarity and rigidity of medium as well as temperature.[19] The absorption bands of the base forms were observed at longer wavelengths than those of the acid forms. (2) As shown in Fig. 1b, 313-nm photolysis of AQ in ethanol without TEA yielded AQH_2. Subsequent addition of TEA in vacuo gave rise to the same absorption spectrum as that observed in Fig. 1a. (3) Upon addition of 0.2-ml aqueous solution of NaOH (0.01 M) to 4-ml ethanol solution of AQH_2 in vacuo, spectrum A of AQH_2 changed to spectrum B as shown in Fig. 2a; the concentration of NaOH in this alkaline ethanol is 4.8×10^{-4} M. (Inserted spectrum is the absorption spectrum of AQH^- reported by Carlson and Hercules.[20]) Upon photolysis with 404-nm light, the absorption bands at 393, ca. 484, ca. 773 and ca. 860 nm increased (cf. spectra C, D, and E).

AQ in alkaline ethanol is known to be photoreduced readily to form $AQ^{\cdot-}$. Figure 2b shows the absorption spectrum of $AQ^{\cdot-}$, prepared by 366-nm photolysis of AQ in alkaline ethanol (loc. cit.). The spectrum thus obtained is essentially identical with that reported by Carlson and Hercules[20] (cf. Inserted spectrum). Comparison of the absorption spectra in Fig. 2a with those in Fig. 2b suggests that photolyses of AQH_2, AQH^-, and AQ in alkaline ethanol give rise to the formation of $AQ^{\cdot-}$ as a final product. These results differ somewhat from that of Carlson and Hercules;[20] they reported that photolysis of $AQ^{\cdot-}$ in alkaline ethanol with 350-nm light gave rise to quantitative formation of AQH^-.

Anyway, it is reasonable to conclude that AQH_2 ionizes partly to the base form in TEA/ethanol solution. Thus, the quantum yields (Φ) of photoreduction of AQ in several TEA/ethanol solutions were deter-

Table 1. Quantum Yields (ϕ) of Photoreduction of AQ and Decay Constants of Exciplex (k_1) and Ion Pair (k_2)

Solvent		Concentration of TEA/M						
		0	0.02	0.05	0.1	0.2	0.4	1
Ethanol	ϕ	1.0	0.93	—	0.81	0.77	0.71	0.60
	$k_1/10^6\,s^{-1}$	—	1.07	1.32	1.67	1.65	2.33	4.24
	$k_2/10\,s^{-1}$	—	1.2	1.2	1.3	1.3	1.3	1.3
Toluene	ϕ	0.3	0.63	0.68	0.66	0.62	0.60	0.62
	$k_1/10^6\,s^{-1}$	—	3.5	3.4	3.3	3.4	3.7	3.6
	$k_2/10^5\,s^{-1}$	—	1.9	1.9	2.0	1.9	1.9	2.1

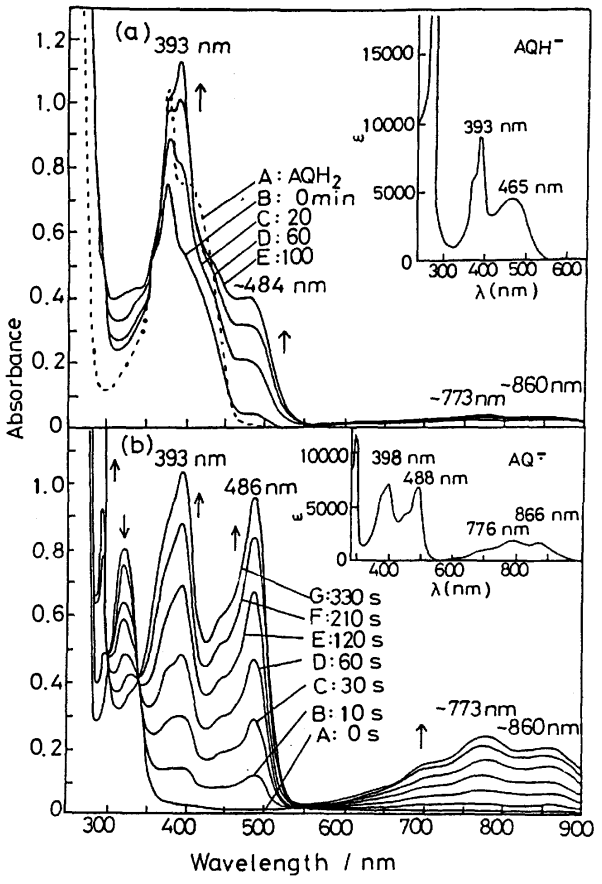

Fig. 2. Absorption spectral change of AQH_2 in alkaline ethanol ($NaOH=4.8\times10^{-4}$ M) upon irradiation with 404-nm light at room temperature (a), and absorption spectrum of $AQ^{\cdot-}$ prepared by 366-nm photolysis of AQ in alkaline ethanol at room temperature (b). Inserted spectra in (a) and (b) are the absorption spectra of AQH^- and $AQ^{\cdot-}$, respectively, reported by Carlson and Hercules.[20]

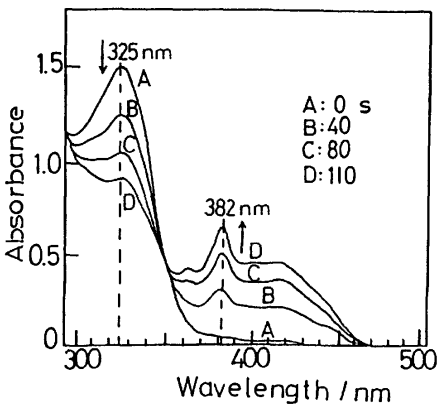

Fig. 3. Absorption spectral change of AQ/TEA (0.2 M) in toluene upon irradiation with 313-nm light at room temperature.

mined by measuring the decrease in the absorbance of AQ, and the results obtained are listed in Table 1. For comparison, we also show the value of Φ obtained in ethanol without TEA.

Photolysis of AQ/TEA (0.2 M) in toluene gave the same result as that in toluene without TEA and the final photoproduct was AQH_2 (cf. Fig. 3). No formation of AQH^- was observed. This is consistent with our previous observation[19] that the acid-base equilibrium of 10-cyano-9-anthrol and its base form (and 10-benzoyl-9-anthrol and its base form) depends on the dielectric constant of the solvent even in the presence of TEA. Thus, the values of Φ in several TEA/toluene solutions were determined by measuring the increase in the absorbance due to AQH_2, and the values obtained are also listed in Table 1 together with that in toluene without TEA.[21]

Laser Flash Photolysis. Figure 4 shows the transient absorption spectra obtained at room temperature upon picosecond laser photolyses of AQ/TEA (1 M) in ethanol (a) and toluene (b), respectively. The absorption spectra at a delay time of 40 ps in both solvents are nearly identical with the $T'\leftarrow T_1$ absorption spectrum of the lowest triplet state (T_1) of AQ, recorded at 77 K in EPA (ether/isopentane/ethanol=5:5:2 in volume ratio) without TEA (cf. Fig. 4c).[7,18]

Although the $T'\leftarrow T_1$ absorption spectra at room temperature are very weak, Manring and Peters[22] observed a strong $T'\leftarrow T_1$ absorption spectrum with a maximum absorbances at λ_{max}=623 and 677 nm, and a shoulder at 582 nm in deaerated benzene (cf. dotted line in Fig. 5b). Since this spectrum is obtained from the accumulation of at least 200 laser shots and the hydrogen-atom abstraction of triplet AQ from the solvent molecule gives rise to the formation of anthrasemiquinone radical ($AQH\cdot$),[10,11,20] the transient absorption spectrum observed by Manring and Peters might contain absorption due to $AQH\cdot$. In fact, Carlson and Hercules[20] have reported that $AQH\cdot$ has

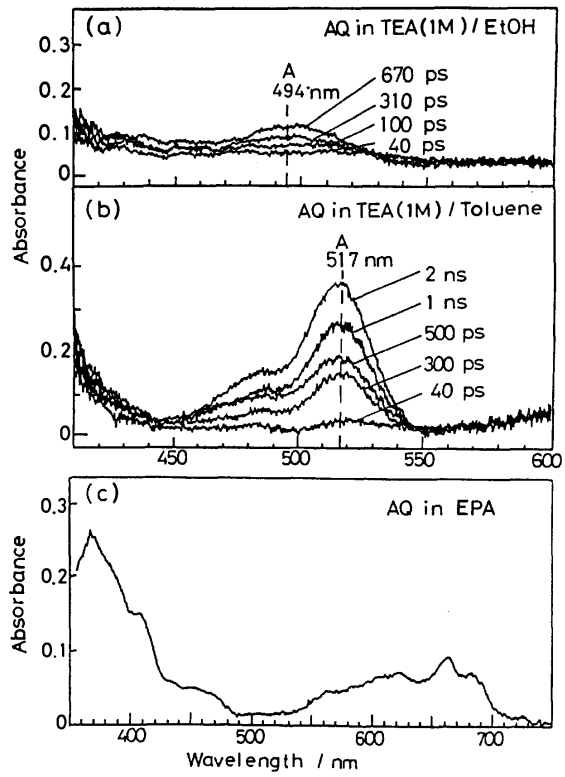

Fig. 4. Transient absorption spectra of AQ/TEA (1 M) in ethanol (a) and toluene (b) obtained by picosecond ruby laser photolysis at room temperature. The spectrum in (c) is the $T' \leftarrow T_1$ absorption spectrum of AQ at 77 K in EPA, obtained by nanosecond ruby laser photolysis.

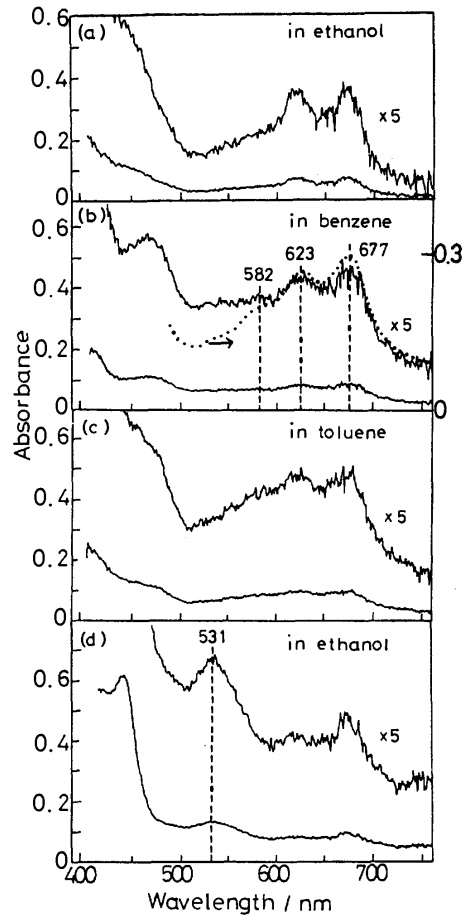

Fig. 5. The $T' \leftarrow T_1$ absorption spectra of AQ at room temperature in ethanol (a), benzene (b), and toluene (c), obtained by picosecond Nd^{3+}:YAG laser photolysis at a delay time of 100 ps. The spectra in (d) were obtained for the sample which was illuminated by 175 laser shots before the spectral measurement, and the $T' \leftarrow T_1$ absorption spectrum reported by Manring and Peters[22] is shown by a dotted line in (b).

three absorption bands at 678, 631, and 575 nm in ethanol. Thus, we have also performed picosecond laser photolyses of AQ in deaerated ethanol, benzene, and toluene using a picosecond Nd^{3+}: YAG laser of Osaka University.[16] Obviously, the spectra obtained by us (cf. Figs. 5a—c) are very weak compared with that obtained by Manring and Peters, being due to the fact that our transient spectra are not essentially accumulated as can be seen in Eq. 2. However, five times expansion of the transient spectra clearly indicates that they are identical with that obtained by Manring and Peters, even in ethanol solution in which the quantum yield of photoreduction is unity. We have also measured the transient spectra of the sample solutions which were illuminated by 175 laser shots before the spectral measurements. The spectra obtained in benzene and toluene were identical with those shown in Figs. 5b and c, although that in ethanol had an additional band at 531 nm (cf. Fig. 5d). This band is different from those of AQH· and AQH_2. (At present, we cannot assign this band.) All the results obtained so far indicate that the weak absorptions at 500—700 nm are not due to AQH· but due to triplet AQ, based on the following reasons: (1) The dominant feature of the absorption spectrum of AQH· is the existence of peaks of nearly equal intensity at 631 and 678 nm in ethanol.[20] (2) The absorption spectrum of AQH· is observed on a microsecond time scale after the excitation of AQ.[10,11,20] (3) The value of Φ is unity in ethanol, while that in toluene is smaller than 0.5 as can be seen in Table 1. However, the spectral intensities in Figs. 5a—c are almost identical.

In Fig. 4, a comparison of the $T' \leftarrow T_1$ absorption spectrum at 40 ps delay with those at delay times longer than 100 ps suggests that a new intermediate (Band A) is produced after the buildup of the T_1 state of AQ, because the time constant for the buildup of the $T' \leftarrow T_1$ absorption of AQ is less than 70 ps.[23] Upon picosecond laser photolyses of 1,8-dichloroanthraquinone (DCAQ)/TEA (1 M) in ethanol and toluene,[24] we observed that the transient absorption spectra at delay times shorter than 100 ps were identical with those observed in the absence of TEA.[12] A new intermediate (λ_{max}=540 nm in TEA/ethanol and 566 nm in TEA/toluene) similar to those in Fig. 4 built up

at the expense of the T_1 state:[24] Recently, we have confirmed that addition of 2 M TEA in toluene quenches both the second triplet (T_2) and T_1 states of DCAQ.[25]

Figure 6a shows the results of nanosecond laser photolysis of AQ/TEA (0.2 M) in ethanol: The transient absorption at 490 nm appeared within the duration of the nanosecond laser pulse and increased up to 4 μs delay, and the maximum absorbance persisted beyond 200 μs with no measurable decay. In accordance with this, the transient absorption spectrum taken immediately after the nanosecond laser pulse is identical with that observed upon picosecond laser photolysis, while those (Band B) taken at delay times longer than 2 μs are shifted to the blue by ca. 8 nm as can be seen in Fig. 6b. (The spectrum shown by open circles was obtained by separate measurements of the absorbances at a number of desired wavelengths,[13] each following a single laser shot, that is, by point-to-point observation.) On a much longer time scale, Band B decayed accompanied by the appearance of a new absorption (Band E) as shown in Fig. 6c. Band E is identical with the absorption band of AQH_2 (cf. Fig. 1a). Moreover, the rise and decay of Band B could be fitted by first-order reaction kinetics as shown in Fig. 7. In ethanol, the rate constants for the buildup of Band B increased with increasing concentration of TEA (cf. closed circles in Fig. 8). On the other hand, no concentration effect of TEA on the decay of Band B was observed. (For comparison, we also show the variation of $1/\Phi$ with the concentration of TEA by open circles.)

Similar results were also obtained in toluene as shown in Fig. 9. The transient absorption of Band A (λ_{max}=517 nm) observed upon picosecond laser photolysis also appeared within the duration of the nanosecond laser pulse (cf. dotted line in Fig. 9a). And the

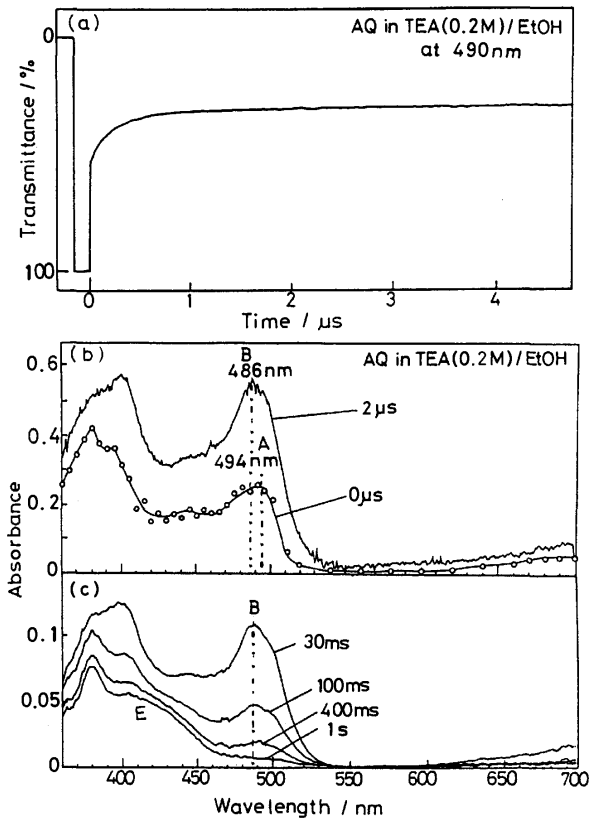

Fig. 6. Time-variation of the transient absorption at 490 nm (a) and change of the transient absorption spectra (b, c) of AQ/TEA (0.2 M) in ethanol, obtained by nanosecond ruby laser photolysis at room temperature.

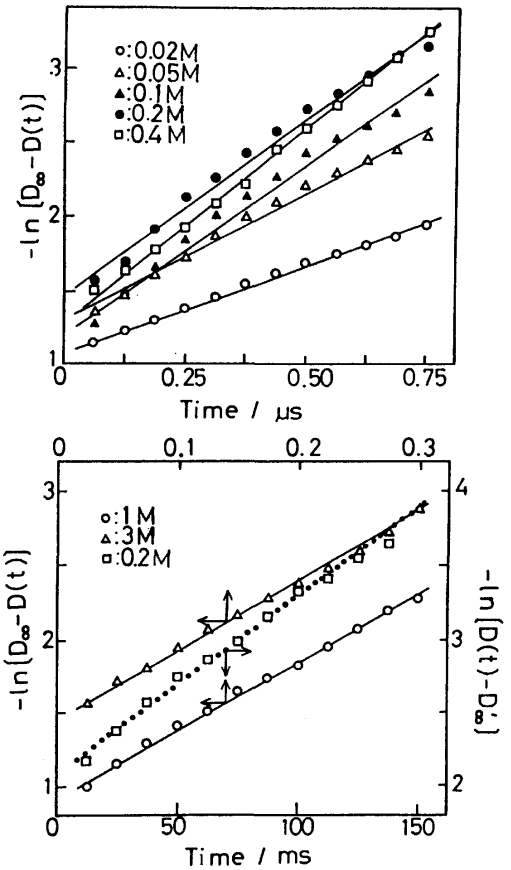

Fig. 7. First-order plots for the rise (full lines) and the decay (dotted line) of Band B in ethanol. Numbers in figures are the concentrations of TEA.

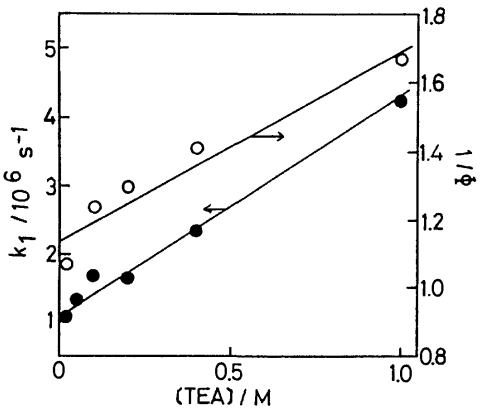

Fig. 8. Plots of k_1 (closed circles) and $1/\Phi$ (open circles) against the concentration of TEA in ethanol.

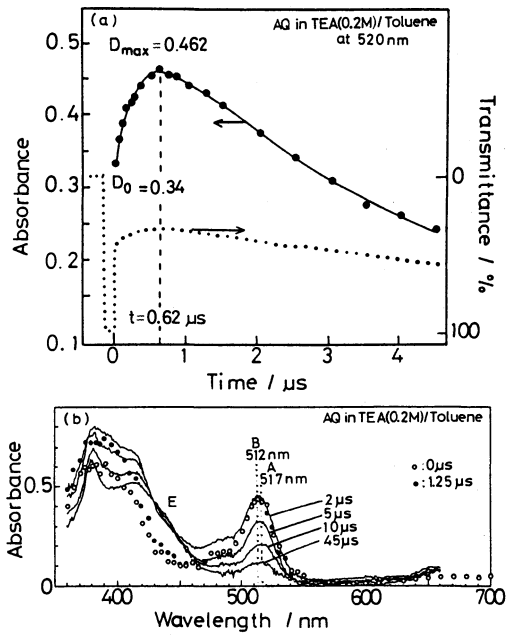

Fig. 9. Time-variation of the transient absorption at 520 nm (a, dotted line) and change of the transient absorption spectra (b) of AQ/TEA (0.2 M) in toluene, obtained by nanosecond ruby laser photolysis at room temperature. Closed circles and a full line in (a) are the absorbances and the best-fit theoretical curve, respectively.

transient absorption increased initially, followed by the spectral shift by ca. 5 nm to Band B (cf. Fig. 9b). (The spectra shown by open and closed circles were recorded by point-to-point measurement.[13]) Thus, one may say that the small spectral shift of ca. 5 nm is within the experimental error. However, the spectra recorded by the ISD system (full lines) are essentially identical with those obtained by point-to-point method. The decay of Band B was accompanied by the buildup of the new absorption due to AQH_2 (Band E at ca. 440 nm), and one can clearly observe the existence of two isosbestic points at 430 and 450 nm. The effects of the concentration of TEA on the buildup and decay of Band B were negligible.

Discussion

The results of steady-state photolysis of AQ/TEA with 313-nm light indicate the existence of a clear isosbestic point which support quantitative conversion of AQ to AQH_2 (and its anion). Exposure to oxygen caused quantitative oxidation of AQH_2 back to AQ. These results are just the same as the photoreductions of AQ and haloanthraquinones in the absence of TEA.[8,9]

Table 1 shows that the values of Φ in TEA/toluene solutions are clearly greater than 0.5, while that in toluene without TEA is 0.3. This enhancement of the photoreduction of AQ by TEA is very similar to that of benzophenone (BP) by several amines,[1-6] and the generally accepted mechanism is that an electron is transferred from amines to triplet BP, forming a radical anion of BP or a complex (an exciplex, a charge-transfer complex or an ion pair) of triplet BP with ground-state amines. It is also thought that the complex is quenched either by proton transfer, generating a benzhydrol radical and an amine radical, or by spin inversion followed by back electron transfer, yielding ground-state BP and amine. In ethanol, the quantum yields of photoreduction of AQ decreased with increase in TEA concentration. This problem will be discussed later.

Except for Band E, the transient absorption spectra in Figs. 4b, 6b—c, and 9b are very similar to those of $AQ^{\cdot-}$ which were produced upon photolysis of AQ in alkaline ethanol (cf. Fig. 2b) or γ-radiolysis of AQ in 2-methyltetrahydrofuran at 77 K.[26] Although no transient photocurrent was detected in toluene, it was observed in ethanol. However, the rise and decay of this photocurrent were different from those of Bands A and B. Moreover, the intensity of the initial photocurrent increased after repeated measurements, indicating that the photocurrent is due to some ionic species produced electrochemically.

We conclude that Bands A and B are different from the $T'\leftarrow T_1$ absorption of AQ observed by us (cf. Fig. 5) and Manring and Peters,[22] based on the following reasons: The $T'\leftarrow T_1$ absorptions in Fig. 4 are very weak compared with Bands A and B. Moreover, their spectral profile and the positions of the absorption maxima are essentially different from those of the $T'\leftarrow T_1$ absorptions.

Based on the above discussion and those for the absorption spectra of the radical anions,[27] it is reasonable to make the following conclusions: (1) The intermediate (Band A) observed by picosecond laser photolysis is identical with that produced within the duration of the nanosecond laser pulse. This intermediate may be assigned to a triplet exciplex between ground-state TEA and the T_1 state of AQ. (2) In ethanol, the exciplex generates a contact ion pair (Band B) between $AQ^{\cdot-}$ and the radical cation ($TEA^{\cdot+}$) of TEA. The contact ion pair may be relatively stable in a polar solvent such as ethanol, because no decay of the contact ion pair was observed up to 200 μs delay. Since AQH_2 was produced upon steady-state photolysis of AQ/TEA in ethanol as shown in Fig. 1a, the contact ion pair may finally disappear by proton transfer from $TEA^{\cdot+}$ to $AQ^{\cdot-}$, generating neutral $AQH\cdot$ and triethylamine radical ($TEA\cdot$). Actually the decay of Band B was accompanied by the appearance of the absorption due to AQH_2 (cf. Fig. 6c). (3) In toluene, the exciplex also generates the contact ion pair, however, it is subsequently quenched by proton transfer on a microsecond time scale.

If the mechanism mentioned above is correct, the photoreduction of AQ by TEA in ethanol and toluene may be interpreted in terms of the following consecutive reactions based on the results of photoreduction of

several anthraquinones without TEA[8-11] and BP/amines;[1-6] Triplet AQ+TEA→Exciplex→Contact ion pair→AQH·+TEA·; TEA·+AQ→AQH·; 2AQH·→AQ+AQH_2 (and its base form). AQH· may also be produced via the hydrogen-atom abstraction by ground-state AQ from TEA·, because the value of Φ in the presence of TEA are greater than 0.5 as shown in Table 1. In toluene without TEA, the value of Φ is smaller than 0.5, indicating that no AQH· is produced via the hydrogen-atom abstraction by ground-state AQ from a benzyl radical. In ethanol without TEA, the value of Φ was unity, while in TEA/ethanol solutions, Φ's were between 0.93 ([TEA]=0.02 M) and 0.60 ([TEA]=1 M). This may be due to the back electron transfer in the exciplex or ion pair. Also, quenching of the exciplex by ground-state TEA is expected to occur as will be discussed later.

From the buildup time of the exciplex of AQ/TEA, the rate constant for electron transfer from ground-state TEA to triplet AQ was estimated to be $\approx 2.5\times10^9$ M^{-1} s^{-1} in ethanol. This value is nearly equal to those for BP/TEA in benzene (3×10^9 M^{-1} s^{-1})[2] and BP/1,4-diazabicyclo[2.2.2]octane (DABCO) in ethanol (2.3×10^9 M^{-1} s^{-1}).[5] Since the transient absorption at 490 nm did not decay up to 200 μs in ethanol, the buildup of the absorbance $D(t)$ at time t can be given by

$$D(t)=D_0(1-\alpha\beta)\exp(-k_1t)+D_0\alpha\beta \quad (4)$$

where D_0 is the absorbance of the exciplex at $t=0$, α is the ratio of the extinction coefficient of the contact ion pair (Band B) to that of the exciplex (Band A), β is the efficiency of formation of the contact ion pair from the exciplex and k_1 is the decay constant of the exciplex. We determined $D_\infty=D_0\alpha\beta$ from the absorbance at 4 μs delay in Fig. 6a, and the plots of $-\ln[D_\infty-D(t)]$ against time gave the straight lines as shown by full lines in Fig. 7. Band B decayed on a much longer time scale and the decay constant (k_2) could be obtained by the first-order plot of $-\ln[D(t)-D'_\infty]$ vs. t, where D'_∞ is the absorbance due to the final product (cf. dotted line in Fig. 7). In Table 1, the decay constants of the exciplex and ion pair obtained so far are also listed.

In toluene, $D(t)$ may be expressed by

$$D(t)=D_0\left(1-\frac{\alpha\beta k_1}{k_1-k_2}\right)\exp(-k_1t)+\frac{D_0\alpha\beta k_1}{k_1-k_2}\exp(-k_2t). \quad (5)$$

We determined $\alpha\beta$ from the value of D_{max} as a function of k_1 and k_2 (cf. Fig. 9a), and the rate constants can be determined by a best fit of the theoretical curve of $D(t)$ to the experimental values. A typical curve of $D(t)$ is also shown in Fig. 9a (full line), and the best-fit values obtained so far are also listed in Table 1. (The value of $\alpha\beta$ was nearly constant, i.e., 1.53.)

Although we have proposed that triplet AQ produces exciplexes with ground-state TEA both in ethanol and toluene and there are many papers to infer the existence of triplet exciplexes,[28] direct observation of their phosphorescences is extremely rare. This may be due to the fact that the phosphorescences are generally observable only in rigid media at low temperature where diffusion is extremely slow. Since the phosphorescences can be studied only with the complexes which are present in the ground state already, and since the exciplexes mean the nonexistence of the ground-state complexes, observation of the exciplex phosphorescences may be difficult even at 77 K.

It is well known that the lifetimes of the singlet exciplexs or ion pairs are in general of the order of a few nanoseconds.[29] However, we believe that our data in Table 1 are reasonable based on the following considerations: (1) Decay constants even for singlet exciplexes are sometimes small:[29] benzene/tetracyanobenzene (TCNB), $k_1=6.8\times10^6$ s^{-1}; toluene/TCNB, $k_1=8.2\times10^6$ s^{-1}; pyrene/*N*,*N*-dimethylaniline, $k_1=5.3\times10^6$ s^{-1}. (2) The phosphorescence lifetimes (τ_p) of exciplexes at 77 K are shorter than those of the electron donors or electron acceptors.[29] For example, τ_p of TCNB complexes with benzene, toluene, mesitylene, durene, and hexamethylbenzene are 3.0, 2.4, 2.3, 1.7, and 0.76 s, respectively, and all shorter than that of TCNB itself, 3.2 s. This is consistent with our result at room temperature; the lifetime of triplet AQ in toluene is 15.3 μs, while that of AQ/TEA exciplex can be calculated from Table 1 to be ca. 0.29 μs. (3) In liquid solutions at room temperature, the triplet exciplexes with decay constants of 10^4—10^6 s^{-1} are also known.[2,30,31]

Hub et al.[32] observed that an exciplex of singlet *trans*-stilbene (TS) with several amines was quenched by ground-state amines at their higher concentrations: They interpreted this quenching in terms of the interaction of amine radical cation with neutral amine, forming a triplex of a radical anion of TS and a radical cation of amine dimer bonded by the three σ-electrons on two nitrogen atoms. Thus, it is expected that the triplet exciplex of AQ/TEA may also be quenched by the formation of a triplet triplex of $AQ^{\cdot-}/TEA_2^{+}$. In fact, the values of Φ in ethanol decreased with increase in the concentration of TEA, indicating exciplex quenching by ground-state TEA (cf. Table 1). If exciplex formation is assumed to occur irreversibly, one can give the following approximate kinetic scheme (Scheme 1).

$$\begin{array}{ccc} AQ & \xrightarrow{h\nu} & AQ(T_1) \\ & & AQ(T_1)+TEA \\ & & \downarrow \\ AQ+TEA & \xleftarrow{k_d^0} & (AQ^{\cdot-}\cdots TEA^{+})^* \xrightarrow{k_q[TEA]} Triplex \\ & & \downarrow k_{ion} \\ & & (AQ^{\cdot-}\cdots TEA^{+}) \\ & & \downarrow k_2 \end{array}$$

Scheme 1.

Under these conditions, the decay constant of the exciplex can be given by

$$k_1 = k_d^0 + k_{ion} + k_q[\mathrm{TEA}]. \quad (6)$$

A plot of k_1 against the concentration of TEA ([TEA]) gave a straight line with the quenching rate constant of 3.1×10^6 M^{-1} s^{-1} in ethanol (cf. Fig. 8). This value is about two orders of magnitude smaller than that obtained for the singlet exciplex of TS/TEA, i.e., 3×10^8 $M^{-1}s^{-1}$, but may be nearly equal to that obtained for TS/diisopropylamine, i.e., $\ll1.0\times10^7$ M^{-1} s^{-1} by Hub et al.[32] (In toluene, the value of k_q was negligibly small compared with that in ethanol.)

The approximate values of k_d^0 and k_{ion} for the exciplex of AQ/TEA in ethanol can be obtained from the dependence of $1/\Phi$ on [TEA] using the following equation;

$$\frac{1}{\Phi} = \left(\frac{k_d^0 + k_{ion}}{k_{ion}} + \frac{k_q[\mathrm{TEA}]}{k_{ion}}\right)\cdot\frac{1}{\gamma} \quad (7)$$

where γ is the efficiency of formation of AQH· from the contact ion pair. Since a plot of $1/\Phi$ against [TEA] gave a straight line (cf. open circles in Fig. 8), the values of k_d^0 and k_{ion} were determined to be 8.4×10^5 s^{-1} and 5.6×10^6 s^{-1}, respectively, on the assumption that γ is unity. In toluene, the value of Φ is independent of [TEA] as can be seen in Table 1, indicating that the value of $k_d^0+k_{ion}$ is much greater than that of k_q[TEA].

The formation of exciplexes with ground-state TEA was also observed for triplet α-haloanthraquinones both in ethanol and toluene.[13,24,26] However, our results are a little different from those of BP/amine (amine=TEA, *N*,*N*-diethylaniline, *N*,*N*-dimethylaniline, DABCO), reported by Peters et al.: In their first two papers,[4,5] they proposed that an electron was transferred from amine to triplet BP forming an exciplex. Later they changed the assignment of the exciplex to that of a solvent-separated ion pair,[6] but no explanation has been given. Presumably their assignment to the solvent-separated ion pair may be based on their finding that picosecond laser photolysis of BP/amine in acetonitrile gave rise to a new intermediate with λ_{max} of 715 nm. Since this intermediate changed to another intermediate with λ_{max} of 690 nm on a picosecond time scale, they concluded that the photoreduction proceeded via rapid electron transfer from amine to triplet BP forming the solvent-separated ion pair followed by the formation of a contact ion pair. In ethanol, the absorption maximum shifted to blue from 690 to 625 nm, and this spectral shift was attributed to the formation of a hydrogen-bonded solvent-separated ion pair from an initially formed contact ion pair.

In our present study both in ethanol and toluene, however, no spectral shift was observed on a picosecond time scale, nor in 2-methyltetrahydrofuran, acetone and dimethylsulfoxide. On a few microsecond time scale, the transient absorption shifted to blue by ca. 8 nm in ethanol and ca. 5 nm in toluene, and the shifted bands decayed following a single exponential function. Thus, we suggest that the exciplex is produced initially in both ethanol and toluene.

The spectral shifts observed by Peters et al. might be due to a special solvent effect of acetonitrile. This explanation is based on the following facts:[33] (1) Picosecond laser photolysis of AQ/TEA (1 M) in acetonitrile gave rise to the spectral change similar to those observed by Peters et al. Namely, an absorption band (Band X) with λ_{max}=540 nm built up during the first 500 ps delay and this band did not decay up to 2 ns. On the other hand, an absorption band (Band Y) with λ_{max}=515 nm increased up to 2 ns and the overall spectral profile at 2 ns delay looked like a superposition of Bands X and Y. (2) Nanosecond laser photolysis of AQ/TEA (0.2 M) in acetonitrile revealed that the absorption spectrum taken immediately after the laser pulse was similar to that observed upon picosecond laser photolysis at 2 ns delay, while those taken at delay times longer than 0.05 μs had no absorption due to Band Y. This indicates that Band Y shifted to red by ca. 25 nm: The transient absorption at 540 nm appeared within the duration of the nanosecond laser pulse, and it increased up to 1 μs delay. The maximum absorbance persisted beyond 50 μs and decayed on a much longer time scale, following second order reaction kinetics. (3) A transient photocurrent was detected in acetonitrile, and its buildup curve was identical with that of the transient absorption. (4) Nanosecond pulse radiolysis of AQ in acetonitrile without TEA gave rise to the appearance of a new absorption band similar to Band X: The rate constant for the buildup of this new absorption band was equal to that for the decay of the absorptions due to anionic species such as a solvated electron, monomeric and/or dimeric radical anion of acetonitrile.[34]

Thus, we proposed that Bands X and Y were due to a free $AQ^{\cdot-}$ and an exciplex, respectively. Since the transient absorption spectrum obtained by picosecond laser photolysis exhibited the time-dependent spectral change, the free $AQ^{\cdot-}$ and the exciplex may be produced independently from the different encounter collisional complexes between ground-state TEA and triplet AQ.[3,30] We suggested that the free $AQ^{\cdot-}$ and the exciplex in acetonitrile were produced via the T_2 and T_1 states of AQ, respectively, based on the following facts: The time constants for the internal conversion from the T_2 to T_1 states were estimated to be less than 70 ps for AQ and 1-chloroanthraquinone (1-CAQ),[23] while that for DCAQ was 0.70—0.75 ns.[12] In accordance with this, the ratio of the intensity of Band Y to that of Band X for DCAQ[35] was smaller than those for AQ[33] and 1-CAQ.[35]

We wish to express our sincere thanks to Professor Noboru Mataga and Dr. Hiroshi Miyasaka of Osaka University for the help in the measurements of the

transient absorptions using a picosecond Nd^{3+}:YAG laser. Thanks are also due to Dr. Yoshinori Hirata of Osaka University for his help in the measurements of transient photocurrents.

References

1) S. G. Cohen, A. Parola, and G. H. Parson, Jr., *Chem. Rev.*, **73**, 141 (1973).

2) S. Inbar, H. Linschitz, and S. G. Cohen, *J. Am. Chem. Soc.*, **103**, 1048 (1981), and references cited therein.

3) S. Arimitsu, H. Masuhara, N. Mataga, and H. Tsubomura, *J. Phys. Chem.*, **79**, 1255 (1975).

4) K. S. Peters, S. C. Freilich, and C. G. Schaeffer, *J. Am. Chem. Soc.*, **102**, 5701 (1980).

5) C. G. Schaeffer and K. S. Peters, *J. Am. Chem. Soc.*, **102**, 7566 (1980).

6) J. D. Simon and K. S. Peters, *J. Am. Chem. Soc.*, **103**, 6403 (1981); **104**, 6542 (1982); *J. Phys. Chem.*, **87**, 4855 (1983).

7) K. Hamanoue, Y. Kajiwara, T. Miyake, T. Nakayama, S. Hirase, and H. Teranishi, *Chem. Phys. Lett.*, **94**, 276 (1983); K. Hamanoue, T. Nakayama, Y. Kajiwara, T. Yamaguchi, and H. Teranishi, *J. Chem. Phys.*, **86**, 6654 (1987).

8) K. Hamanoue, K. Yokoyama, T. Miyake, T. Kasuya, T. Nakayama, and H. Teranishi, *Chem. Lett.*, **1982**, 1967; K. Hamanoue, K. Sawada, K. Yokoyama, T. Nakayama, S. Hirase, and H. Teranishi, *J. Photochem.*, **33**, 99 (1986).

9) K. Hamanoue, T. Nakayama, K. Sawada, Y. Yamamoto, S. Hirase, and H. Teranishi, *Bull. Chem. Soc. Jpn.*, **59**, 2735 (1986).

10) K. Hamanoue, K. Yokoyama, Y. Kajiwara, K. Nakajima, T. Nakayama, and H. Teranishi, *Chem. Phys. Lett.*, **110**, 25 (1984).

11) K. Hamanoue, T. Nakayama, A. Tanaka, Y. Kajiwara, and H. Teranishi, *J. Photochem.*, **34**, 73 (1986).

12) K. Hamanoue, K. Nakajima, Y. Kajiwara, T. Nakayama, and H. Teranishi, *Chem. Phys. Lett.*, **110**, 178 (1984); K. Hamanoue, T. Nakayama, M. Shiozaki, Y. Funasaki, K. Nakajima, and H. Teranishi, *J. Chem. Phys.*, **85**, 5698 (1986).

13) K. Hamanoue, K. Yokoyama, Y. Kajiwara, M. Kimoto, T. Nakayama, and H. Teranishi, *Chem. Phys. Lett.*, **113**, 207 (1985).

14) C. G. Hatchard and C. A. Parker, *Proc. R. Soc. London, Ser. A*, **235**, 518 (1956).

15) T. Nakayama, S. Tai, K. Hamanoue, and H. Teranishi, *Mem. Fac. Ind. Arts, Kyoto Tech. Univ., Sci. Technol.*, **29**, 46 (1980); K. Hamanoue, T. Hidaka, T. Nakayama, and H. Teranishi, *Chem. Phys. Lett.*, **82**, 55 (1981).

16) H. Miyasaka, H. Masuhara, and N. Mataga, *Laser Chem.*, **1**, 357 (1983).

17) T. Nakayama, T. Miyake, M. Okamoto, K. Hamanoue, and H. Teranishi, *Mem. Fac. Ind. Arts, Kyoto Tech. Univ., Sci. Technol.*, **29**, 35 (1980).

18) T. Nakayama, T. Yamaguchi, K. Hamanoue, H. Teranishi, T. Nagamura, A. Mugishima, and S. Sakimukai, *J. Spectrosc. Soc. Jpn.*, **36**, 126 (1987).

19) K. Hamanoue, S. Hirayama, M. Amano, K. Nakajima, T. Nakayama, and H. Teranishi, *Bull. Chem. Soc. Jpn.*, **55**, 3104 (1982); K. Hamanoue, K. Nakajima, M. Amano, T. Hidaka, T. Nakayama, and H. Teranishi, *Polym. Photochem.*, **3**, 407 (1983).

20) S. A. Carlson and D. M. Hercules, *Photochem. Photobiol.*, **17**, 123 (1973).

21) We confirmed that the values of Φ determined from the decrease of AQ absorptions matched those from the increase of AQH_2 absorptions. Since the prolonged photolysis of AQ in toluene without TEA gave rise to complicated reactions, the extinction coefficient of AQH_2 in TEA/toluene solution was determined as follows: First, AQH_2 was produced upon photolysis of AQ in ethanol without TEA, and the yield of AQH_2 was determined. Next, ethanol was removed in vacuo, and then TEA/toluene was added. Thus, one could determine the extinction coefficient of AQH_2 in TEA/toluene solution.

22) L. E. Manring and K. S. Peters, *J. Am. Chem. Soc.*, **107**, 645 (1985).

23) K. Hamanoue, unpublished data.

24) K. Hamanoue, M. Kimoto, Y. Kajiwara, T. Nakayama, and H. Teranishi, *J. Photochem.*, **31**, 143 (1985).

25) K. Hamanoue, Y. Yamamoto, T. Nakayama, and H. Teranishi, *Studies in Organic Chemistry*, **31**, 235 (1987) ("Physical Organic Chemistry 1986" ed by M. Kobayashi).

26) K. Hamanoue, unpublished data.

27) H. V. Cater, B. J. McClelland, and E. Warhurst, *Trans. Faraday Soc.*, **56**, 455 (1960); T. E. Hogen Esch and J. Smid, *J. Am. Chem. Soc.*, **87**, 669 (1965); **88**, 307 (1966); H. E. Zaugg and A. D. Schaefer, *ibid.*, **87**, 1857 (1965); J. Smid, "Ions and ion pairs in organic reactions," ed by M. Szwarc, Wiley-Interscience, New York (1972), Vol. 1, p. 85.

28) H. Beens and A. Weller, "Molecular Luminescence," ed by E.C. Lim, Benjamin, New York (1969), p. 203; C. C. Wamser, G. S. Hamond, C.T. Chang, and C. Baylor, Jr., *J. Am. Chem. Soc.*, **92**, 6362 (1970); I. G. Lopp, R. W. Hendren, P. D. Wildes, and D. G. Whitten, *ibid.*, **92**, 6440 (1970); J. K. Roy and D. G. Whitten, *ibid.*, **93**, 7093 (1971); P. De Mayo, *Acc. Chem. Res.*, **4**, 41 (1971).

29) S. Nagakura, "Excited States," ed by E. C. Lim, Academic Press, New York (1975), Vol. 2, p. 322.

30) V. A. Kuzmin, A. P. Darmanyan, and P. P. Levin, *Chem. Phys. Lett.*, **63**, 509 (1979).

31) V. L. Ivanov, S. A. Al-Ainen, and M. G. Kuzmin, *Dokl. Akad. Nauk SSSR*, **237**, 1400 (1977); J. A. Mercer-Smith, C. Sutcliff, R. H. Schmehl, and D. G. Whitten, *J. Am. Chem. Soc.*, **101**, 3995 (1979); T.-S. Fang, R. E. Brown, C. L. Kwan, and L. A. Singer, *J. Phys. Chem.*, **82**, 2489 (1978); A. Salmassi, J. Eichler, C. P. Herz, and W. Z. Schnabel, *Naturforsch. Teil A*, **35**, 1273 (1980); Ye. I. Kapinus, V. P. Stary, and I. I. Dilung, *Teor. Eksp. Kihm.*, **17**, 100 (1981); *Dokl. Akad. Nauk SSSR*, **261**, 907 (1982); B. B. Craig, A. A. Gorman, I. Hamblett, and C. W. Kerr, *Radiat. Phys. Chem.*, **23**, 111 (1984); I. V. Renge, V. A. Kuzmin, and Yu. E. Borisevich, *J. Photochem.*, **31**, 67 (1985).

32) W. Hub, S. Schneider, F. Dörr, J. D. Oxman, and F. D. Lewis, *J. Am. Chem. Soc.*, **106**, 701 (1984); **106**, 708 (1984).

33) K. Hamanoue, T. Nakayama, K. Sugiura, H. Teranishi, M. Washio, S. Tagawa, and Y. Tabata, *Chem. Phys. Lett.*, **118**, 503 (1985).

34) K. Hamanoue, T. Nakayama, K. Sawada, H. Teranishi, M. Washio, S. Tagawa, and Y. Tabata, paper is in preparation.

35) M. Shiozaki, T. Nakayama, K. Hamanoue, and H. Teranishi, abstract for the presentation at the 52nd Spring Meeting of the Chemical Society of Japan (1986), Vol. 1, p. 305.

 © 1988 The Chemical Society of Japan Bull. Chem. Soc. Jpn., 61, 1131—1134 (1988)

Rate of Solvent Extraction of Chromium(III) with Acetylacetone into Carbon Tetrachloride

Tatsuya SEKINE,* Kazuho INABA,† Tatsumu MORIMOTO, and Hidehiko AIKAWA
Department of Chemistry, Science University of Tokyo, Kagurazaka, Shinjuku-ku, Tokyo 162
†Water and Soil Environment Division, National Institute for Environmental Studies, Onogawa, Tsukuba-shi, Ibaraki 305
(Received May 2, 1987)

The rate of solvent extraction of chromium(III) in aqueous perchlorate solutions into carbon tetrachloride as the tris(acetylacetonato) complex has been determined. The rate was first order with respect to the acetylacetone concentration and inverse first order with respect to the hydrogen-ion concentration. From this information, the rate-controlling reaction is concluded to be the formation of the first complex in the aqueous phase by a reaction between $[Cr(OH)]^{2+}$ and HA.

Since the rate of solvent extraction of chromium(III) in aqueous solutions with chelating extractants is very low, this experimental method can be used only when it is enhanced, for example, by heating the aqueous solutions containing hydrated Cr^{3+} ions in the presence of the extractant[1] or by the complex formation of metal ions with a second ligand, such as fluoride ions.[2]

In the course of a series of kinetic studies on the solvent extraction of chromium(III) with β-diketones, it has been found that the rate of extraction with acetylacetone (2,4-pentanedione, HA) was much higher when the diluent was 4-methyl-2-pentanone (MIBK) than when it was carbon tetrachloride; the extraction into the latter solvent was negligible, even after two-phase agitation for 24 h, while it was measurable into the former solvent under identical conditions, except for the diluent.[3]

In the present study, the rate of extraction of Cr^{3+} in aqueous sodium perchlorate solutions into this non-polar solvent with β-diketone was measured at a much higher ligand concentration than in the previous work and the mechanism of the extraction process as well as the rate-controlling reaction was considered.

Experimental

All the experiments were carried out at 298 K. The solvent and reagents were of reagent grade. The tris(acetylacetonato)chromium(III) was obtained from Dojindo Laboratories. Sodium perchlorate was recrystallized three times from water. Carbon tetrachloride was washed twice with water before use. The aqueous solutions were 4 mol dm^{-3} sodium perchlorate constant ionic media containing 1×10^{-3} mol dm^{-3} of Cr^{3+} and 5×10^{-3} mol dm^{-3} of sulfanilic acid-sulfanilate buffer which kept the hydrogen-ion concentration from 10^{-3} to $10^{-4.5}$ mol dm^{-3}. Experiments were carried as follows: A portion of the aqueous solution and the same volume of an organic solution of acetylacetone was placed in a stoppered glass vessel. The two phases were agitated at such a speed that no increase in the rate was found upon further increasing the agitation speed for a certain time; they were then centrifuged. The content of the tris(acetylacetonato)chromium(III), CrA_3, in the organic phase was determined from the optical density at 380 nm and the chromium(III) concentration in the aqueous phase was determined by an atomic absorption method.

The distribution constant of the CrA_3 complex was determined as follows. A carbon tetrachloride solution containing 1×10^{-3} mol dm^{-3} of the complex and 1×10^{-1} mol dm^{-3} of acetylacetone was agitated with the same volume of an aqueous perchlorate solution for 3 min; then the two phases were centrifuged off. The chromium(III) content in the aqueous phase was determined by the atomic absorption method.

Results and Discussion

In the present paper, all species in the organic phase are denoted by "org" and that in the aqueous phase by using no subscript. The volumes of the two phases were the same. The hydrogen-ion concentration was always higher than 1×10^{-5} mol dm^{-3}. The pK_a of the reagent was about 10.1[4] and was in large excess to the metal ions. Under these conditions, the following equation may be written for the extractant in the aqueous phase:

$$[HA]_{total}=[HA]+[A^-]+\sum a[CrA_a^{3-a}]. \quad (1)$$

The value of distribution constant of the CrA_3 complex, $K_{dm}=[CrA_3]_{org}/[CrA_3]$, was obtained to be $10^{2.24}$.

It was found that the rate of solvent extraction was not affected by the speed of the two-phase agitation. There was no difference in the rate of solvent extraction when the two phases in the vessel were continuously agitated using a mechanical shaker and when they were agitated by hand for a few minutes after they were left standing in the dark after an initial agitation of the two phases. Furthermore, when an aqueous solution which contained the metal ions, acetylacetone, and the buffer was left standing in the dark for a certain time and agitated with a carbon tetrachloride solution of acetylacetone for 30 min, the amount extracted was similar to that when the two phases were continuously agitated. These results indicate that the rate controlling reaction is the complex formation in the aqueous phase and that it is neither a reaction on the interface nor in the organic phase.

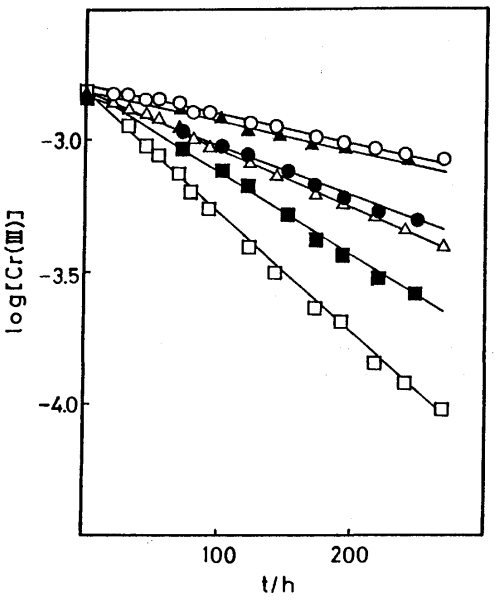

Fig. 1. Amount of extracted Cr(III) as tris(acetylacetonato) complex into carbon tetrachloride as a function of standing time of the system. The pH of solution is; 3.42 (○), 3.93 (△), 4.46 (□), 3.89 (●), 3.45 (▲), and 4.32 (■).

Figure 1 shows the decrease in the chromium(III) concentration in the aqueous phase upon solvent extraction as a function of time. As can be seen from Fig. 1, each set of data can be represented by a straight line and, thus, the rate of extraction should be first order with respect to the total chromium(III) concentration in the aqueous phase. The rate of solvent extraction, V_{se}, can be given by the decrease in the chromium(III) concentration in the aqueous phase, [Cr(III)], and can be written

$$V_{se} = -\mathrm{d}[\mathrm{Cr(III)}]/\mathrm{d}t = k_{obsd}[\mathrm{Cr(III)}]. \quad (2)$$

Figure 2 gives a log k_{obsd} vs. log [HA] plot for a $-\log[H^+]$ of 3.6. As can be seen from Fig. 2, the values of k_{obsd} are first order with respect to [HA] and, thus, the formation of the first complex should be the rate-determining step.

Figure 3 gives the dependence of k_{obsd} on the hydrogen-ion concentration. In this figure, the value of $k_{obsd}/[HA]$ is given on the basis of the results in Fig. 2 in order to compare the data at different extractant concentrations. The plot in Fig. 3 is not a straight line but a curve. After trials, the following equation was found to fit well with the experimental data when $C_1=10^{-8.9}$ and $C_2=10^{-4.3}$:

$$\log(k_{obsd}/[HA]) = \log(C_1/(C_2+[H^+])). \quad (3)$$

The above values of C_1 and C_2 are introduced into Eq. 3. The broken line in Fig. 3 is calculated by using this data. Thus, Eq. 2 can be rewritten as

$$V_{se} = C_1[\mathrm{Cr(III)}][HA]/([H^+]+C_2). \quad (4)$$

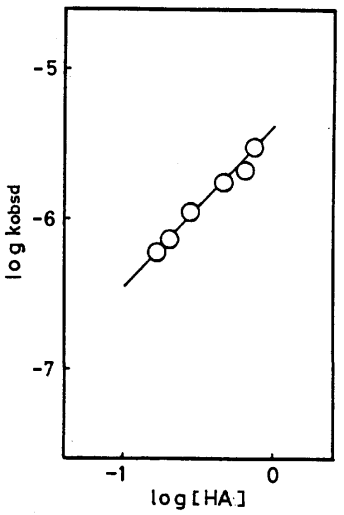

Fig. 2. Rate of complex formation as a function of concentration of acetylacetone in undissociated form in aqueous phase. The slope of the line is +1.

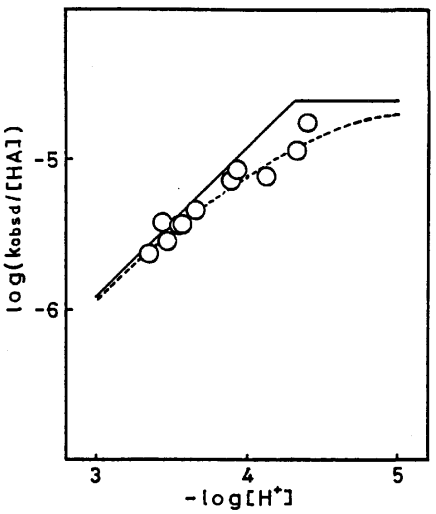

Fig. 3. Rate of solvent extraction of Cr(III) into carbon tetrachloride as a function of hydrogen ion concentration. Aqueous phase: 4 mol dm^{-3} $NaClO_4$. The broken line is the calculated curve by using Eq. 3 with $C_1=10^{-8.9}$ and $C_2=10^{-4.3}$. Each asymptote give the value when $[H^+]\to\infty$ and $[H^+]\to 0$.

When the rate-controlling reaction is the formation of the first complex in the aqueous phase, it can be given by one or both of the following equations:

$$[\mathrm{Cr(OH)}]^{2+} + \mathrm{HA} \quad (5)$$

and/or

$$\mathrm{Cr}^{3+} + \mathrm{A}^-. \quad (6)$$

The rate of complex formation, V_{cf}, may be given by

$$V_{cf} = k_1[\mathrm{Cr(OH)}^{2+}][HA] + k_2[\mathrm{Cr}^{3+}][\mathrm{A}^-]. \quad (7)$$

When only the following hydrolysis is taken into the account,

$$[\mathrm{Cr(H_2O)_6}]^{3+} \rightleftarrows [\mathrm{Cr(OH)(H_2O)_5}]^{2+} + \mathrm{H}^+$$

and

$$K_h=[Cr(OH)^{2+}][H^+]/[Cr^{3+}], \quad (8)$$

the total amount of uncomplexed chromium(III) can be given as

$$[Cr(III)]_{uncomp} = [Cr^{3+}]+[Cr(OH)^{2+}] = [Cr^{3+}](1+K_h/[H^+]). \quad (9)$$

The formation of polymerized species such as $[Cr_2(OH)_2]^{4+}$, $[Cr_2(OH)_3]^{3+}$, and $[Cr_2(OH)_4]^{2+}$ by the hydrolysis of chromium(III) has been pointed out.[5] For example, when $-\log[H^+]$ is 4 and the total chromium(III) concentration is 1×10^{-3} mol dm^{-3}, the formation of polymerized species after 10 days can be calculated by using the constants;[5] this value was found to be about 10%. Thus, effects due to the polymerized species could be neglected in the considerations of the rate in the early stage of the reaction. By using Eq. 8, Eq. 7 can be written as

$$V_{cf}=(k_1K_h+k_2K_a)[Cr^{3+}][HA]/[H^+], \quad (10)$$

where K_a is the acid dissociation constant, $K_a=[H^+][A^-]/[HA]$, and K_h is the hydrolysis constant in Eq. 8. The value of the constant in the literature is[4] $K_a=10^{-10.1}$. The value of K_h in the literature ranges[6] from $10^{-3.5}$ to $10^{-4.2}$; a value of $10^{-4.3}$ was reported in a recent paper.[5]

On the basis of Eq. 9, Eq. 10 can be rewritten as

$$V_{cf}=(k_1K_h+k_2K_a)[Cr(III)]_{uncomp}[HA]/([H^+]+K_h). \quad (11)$$

When $[Cr(III)]_{uncomp}$ is almost the same as [Cr(III)], it should be regarded from Eqs. 4 and 11 that $C_1=(k_1K_h+k_2K_a)$ and $C_2=K_h$.

In this data analysis, it was assumed that $[Cr(III)]_{uncomp}$ is equal to [Cr(III)]; that is, the total concentration of the acetylacetonato complex species, $[CrA^{2+}]+[CrA_2^+]+[CrA_3]$, is negligible compared to $[Cr(III)]_{uncomp}$. Separate experiments were made in order to examine this as follows. A portion of the aqueous phase was separated from the organic phase after two-phase agitation for a certain time. This was again agitated for a certain time with the same volume of carbon tetrachloride containing the same concentration of the extractant, but with no chromium(III). It was found that no chromium(III) in the aqueous phase was extracted by this second extraction. When the $[CrA]^{2+}$ and/or $[CrA_2]^+$ species are present in appreciable amounts in this separated aqueous phase, each should react with the ligand at a higher rate than of the rate-controlling reaction to form the CrA_3 species, which is extracted well as the K_{dm} value indicates. For this reason, the amounts of these species and of the CrA_3 species is, for all practical purposes, negligible compared to the amount of Cr^{3+} or $[Cr(OH)]^{2+}$ in this aqueous solution.

Due to a proton ambiguity, it is generally impossible to conclude whether Eq. 5 or 6 is the rate-controlling reaction. However, the former seems to control the whole process; if the former was the controlling reaction, the value of k_1K_h would be calculated to be $10^{-8.9}$ (s^{-1}) and, consequently, the value of k_1 would be obtained as $10^{-4.6}$ ($mol^{-1}\,dm^3\,s^{-1}$). The keto-enol equilibrium of the β-diketone should be taken into account. Since the enol form of acetylacetone is only 20% of the undissociated form,[7] ($K_e=[HA]_{enol}/[HA]_{keto}=10^{-0.63}$), the rate constant should be about 5-times higher if only the enol form of the β-diketone reacts in the way given by Eq. 5. However, it still is seen that the rate constant, k_1, is about 10^{-4} ($mol^{-1}\,dm^3\,s^{-1}$). If the latter would control the extraction, the value of k_2K_a should be equal to $10^{-8.9}$ (s^{-1}). As pointed out, K_a in these ionic media is $10^{-10.1}$ (mol dm^{-3}) and, consequently, k_2 is calculated to be $10^{1.2}$ ($mol^{-1}\,dm^3\,s^{-1}$).

In the literature,[8,9] the rate constant for the complex formation of hydrated Cr^{3+} with various ligands is in the range 10^{-5} to 10^{-7} ($mol^{-1}\,dm^3\,s^{-1}$), while that of $[Cr(OH)]^{2+}$ is in a range 10^{-3} to 10^{-5} ($mol^{-1}\,dm^3\,s^{-1}$). The present results, $k_1\simeq10^{-4}$ ($mol^{-1}\,dm^3\,s^{-1}$), suggest that the complex formation in the system studied proceeds through a reaction of the $[Cr(OH)]^{2+}$ species with the undissociated form of acetylacetone, HA.

The mechanism of water exchange of hydrated Cr^{3+} and $[Cr(OH)]^{2+}$ was considered from the viewpoint of the activation volume of the reaction.[8] It was concluded that the water exchange from the Cr^{3+} species proceeded through an I_a mechanism while the reaction for that from the $[Cr(OH)]^{2+}$ species had a dissociative character. The difference of the rate constant for the complex formation of the hydrated Cr^{3+} and $[Cr(OH)]^{2+}$ species may possibly be explained by the difference in the reaction mechanism. However, the conclusion does not seem to be definite.

The ratio of the total amount of the complexes formed in the system and the amount extracted is given as

$$R = [CrA_3]_{org}/([CrA^{2+}]+[CrA_2^+]+[CrA_3]+[CrA_3]_{org}) = K_{dm}\beta_3[A^-]^3/(\beta_1[A^-]+\beta_2[A^-]^2+\beta_3[A^-]^3+K_{dm}\beta_3[A^-]^3), \quad (12)$$

where β_n is the stability constant of the "n-th" complex. Since the value of K_{dm} is $10^{2.24}$, it can be concluded that nearly all of the complexes formed are extracted as the CrA_3 species into the organic phase when this ratio is approximately unity; however, if R is to some extent smaller than unity, the complexed chromium(III) which remains in the aqueous phase cannot be neglected.[10]

It was reported that the rate constant for the complex formation with the same ligand obtained by the data of solvent extraction into MIBK is several orders higher than the present value.[4] This problem will be considered in another paper.

The authors are grateful to Mr. Takashi Kurihara for his valuable discussion and experimental aids.

References

1) J. P. MacKaveney and H. Freiser, *Anal. Chem.*, **30**, 1965 (1958).

2) O. M. Petrukhin, L. A. Izosenkova, I. N. Marov, Yu. N. Durov, and Yu. A. Zolotov, *Zh. Neorg. Khim.*, **12**, 1407 (1967).

3) T. Sekine and H. Inagaki, *J. Inorg. Nucl. Chem.*, **42**, 115 (1980).

4) T. Sekine, K. Inaba, and O. Takahashi, *Polyhedron*, **3**, 780 (1984).

5) H. Stünzi and W. Marty, *Inorg. Chem.*, **22**, 2145 (1983); H. Stünzi, F. Rotzinger, and W. Marty, *ibid.*, **23**, 2160 (1984); F. Rotzinger, H. Stünzi, and W. Marty, *ibid.*, **25** 489 (1986).

6) L. G. Sillén and A. Martell, "Stability Constants," Spec. Pub. No. 17, The Chemical Society, London (1964).

7) O. Kammori, K. Sato, T. Takimoto, and K. Arakawa, *Bunseki Kagaku*, **15**, 5621 (1966).

8) F-C. Xu, H. Krouse, and T. Swaddle, *Inorg. Chem.*, **24**, 267 (1985).

9) For example; C. Postmus and L. King, *J. Phys. Chem.*, **59**, 1208 and 1217 (1955); R. E. Hamm, R. L. Johnson, R. H. Perkins, and R. E. Davis, *J. Am. Chem. Soc.*, **80**, 4469 (1958); M. Kimura and J. Shirai *J. Inorg. Nucl. Chem.*, **40**, 1085 (1978).

10) T. Sekine and K. Inaba, *Bull. Chem. Soc. Jpn.*, **55**, 3773 (1982).

 © 1988 The Chemical Society of Japan Bull. Chem. Soc. Jpn., 61, 1135—1139 (1988)

Effects of Compositional Changes of Hot Spring Water upon Mineral Precipitate. I. Changes in Chemical Composition and Crystal Growth Rate of Pb-Bearing Barite (Hokutolite) from Tamagawa Hot Spring Waters

Nobuyuki SASAKI* and Kunihiko WATANUKI†

Department of Chemistry, Faculty of Education, Kagawa University, Saiwai-cho, Takamatsu 760

†Department of Chemistry, The College of Arts and Sciences, The University of Tokyo, Komaba, Meguro-ku, Tokyo 153

(Received May 30, 1987)

Changes in the chemical compositions of Tamagawa Hot Spring waters and Pb-bearing barite (hokutolite) were examined. Samples were obtained from various locations and various time in Tamagawa Hot Spring. The relationships between the hot spring waters and the minerals were expressed as partition equations and phenomenological equations; then, the partition coefficients and phenomenological coefficients were calculated. The apparent partition coefficients of Pb^{2+} and of Sr^{2+} between the two phases were found to have increased, from 0.14 to 0.30(0.31) and from 0.023 to 0.035(0.042) respectively, with the decrease in the hokutolite growth rate since 1973. The reaction rate of hokutolite as calculated from the phenomenological equations was, however, about 2 times higher in 1983 than in 1965. These results were ascribed to the rise in the degree of the supersaturation of barium sulfate and also to the increase in the nucleation rate in the hot spring water.

The partition formula of a chemical element between an aqueous solution and a solid solution is often useful in expressing the relationship between these two phases. There are, however, some problems with this manner. One is the remarkable dispersion of partition coefficients[1] caused by the effect of the chemical nonequilibrium of each ion between the two phases, and the other is the difficulty of expressing the partition of the multicomponent system.[2] For the measurement of the partition coefficient of trace elements between an aqueous solution and an insoluble salt like barium sulfate, it needs a long time to reach a chemical equilibrium, so it is sometimes convenient for getting an equilibrium value to use the data of the chemical compositions of natural minerals and hot spring waters instead of the data from synthetic solids and solutions in a laboratory.[3]

As to the partition of a multicomponent system, Takano[2] proposed a formulation of a three-component system on the basis of an ion-exchange reaction, but there have been very few actual applications to experimental and natural data.

Sasaki[4] proposed a formulation of partition by utilizing phenomenological equations and applied it to the data of Tamagawa Hot Spring. To solve these phenomenological equations, however, several sets of data obtained under different conditions are needed.

In recent years conspicuous changes in chemical composition have been observed in several hot springs, including Tamagawa Hot Spring[5-7] and Kusatsu Hot Spring,[8,9] in Japan. Tamagawa Hot Spring showed remarkable increases in the SO_4^{2-} and Fe^{2-} concentrations from 1973 to 1978, from about 1200 ppm to 2600 ppm, and from about 90 ppm to 170 ppm, respectively. Sasaki[4,10] reported that these increases caused the changes in the Ba^{2+}, Pb^{2+}, and Sr^{2+} concns, of the hot spring waters. These cations are the main components of the Pb-bearing barite (hokutolite) precipitated from the hot spring waters in this district.[11] Hokutolite is a famous radioactive mineral and has been designated as a special natural monument in Japan since 1952.

The present authors[12] observed and examined the hokutolite which had been growing at Yubana fall (the end of the Yubana conduits in Tamagawa Hot Spring; shown in Fig. 1) after 1953; they also observed increases in the Pb, Sr, and Fe[a] contents (Table 1) with the decrease in the crystal growth rate (0.10 mm y^{-1} to 0.05 mm y^{-1}) after 1973. They supposed that the changes in the mineral were attributable to the decrease in the Ba^{2+} concn in the hot spring water, which might have been caused by the increase in the SO_4^{2-} concn, judging from the ionic equilibria.

The aims of present work are to ascertain the truth of this supposition formerly proposed by the present authors[12] and to clarify the relationship between the

Table 1. Chemical Composition of Pb-Bearing Barite (Hokutolite) Precipitated at Different Times at the End of the Yubana Conduit at Tamagawa Hot Spring

(a) Composition in weight percentages

Crystallization period	BaO wt%	PbO wt%	SrO wt%	CaO wt%	FeO[a] wt%
1953—1972	52.66	13.36	0.45	0.16	0.04
1973—1981	51.20	13.23	0.66	0.15	0.35

(b) Composition in mol% as barium, lead, strontium, and calcium

Crystallization period	Ba mol %	Pb mol %	Sr mol %	Ca mol %
1953—1972	83.67	14.58	1.06	0.69
1973—1981	83.02	14.73	1.58	0.66

Data cited from Sasaki and Watanuki (1983)[12] a) Iron is not situated in the crystal lattice of $BaSO_4$ (Sasaki and Watanuki, 1984).[13]

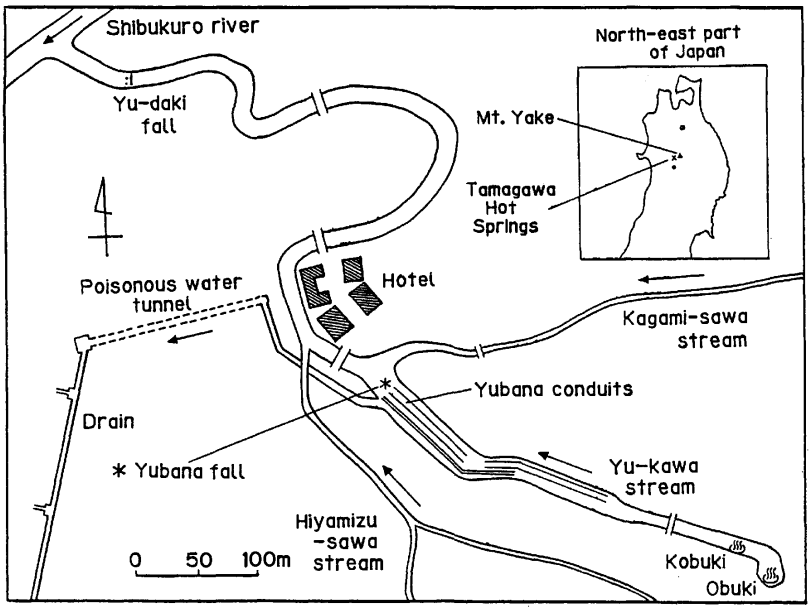

Fig. 1. Location map of Tamagawa Hot Springs. The mark * indicates Yubana fall.

changes in the chemical composition of the hot spring waters and those in the chemical composition and the crystal growth rate of mineral (hokutolite) occurring in this area.

Experimental

The hot spring water samples were collected in October, 1983, in August, 1985, and in August, 1986, at four sites, Obuki Spring and Kobuki Spring (1983, 1985, 1986), Yubana fall (1985, 1986), and the so-called poisonous water tunnel (1986) (Fig. 1).

Analytical Procedures. 1) Barium and Lead: After sampling, the Ba^{2+} and Pb^{2+} were separated immediately in situ from the other elements by coprecipitation with strontium sulfate.[14] The precipitate was brought to the laboratory, decomposed by means of hydriodic acid,[15] and analyzed. The Ba^{2+} and Pb^{2+} were determined by flame photometry and atomic-absorption spectroscopy (AAS) respectively.

2) Strontium: The Sr^{2+} was preconcentrated using Pb^{2+} and fuming nitric acid, and was determined by the use of AAS.[11]

3) Sulfate and Chloride: The SO_4^{2-} concentration was determined by the use of the gravimetric method.[16] The Cl^- concentration was measured by means of chloride-ion electrode using an ion meter (DKK, IOC-10).

Results and Discussion

The analytical results of the hot spring water are shown in Table 2. The analytical data given by Takano[14] and by Takano and Watanuki[11] for the waters sampled in 1965 are also listed in Table 2. It may be seen that the SO_4^{2-} concns in the Obuki vent were about 2100—2300 ppm in 1983, about 1600 ppm in 1985, and 1200 ppm in 1986, indicating a decrease in the SO_4^{2-} from the maximum value (ca. 2600 ppm)[6,17] in 1978.

Table 2. Barium-, Lead-, Strontium-, Sulfate-, and Chloride-Ion Concentrations of Tamagawa Hot Spring Waters ($mg \cdot dm^{-3}$)

	Obuki Spring						
	1965	1983		1985		1986	
		I[c]	II[d]	III[e]	IV[f]	V[g]	VI[h]
Ba^{2+}	0.82[a]	1.03	1.20	1.32	1.30	1.58	1.57
Pb^{2+}	1.59	0.93	1.03	0.78	0.77	0.69	0.69
Sr^{2+}	0.29	0.36	0.35	0.30	0.29	0.42	0.40
SO_4^{2-}	1242[b]	2068	2335	1577	1614	1222	1237
Cl^-	3174	3140	3160	2870	2870	2880	2780
pH	1.20	1.13	1.13	1.17	1.17	1.19	1.19

	Kobuki Spring						
	1965	1983		1985		1986	
		I[c]	II[d]	III[e]	IV[f]	V[g]	VI[h]
Ba^{2+}	0.96[a]	1.42	1.65	1.55	1.63	1.48	1.61
Pb^{2+}	1.51	1.16	1.27	1.36	1.23	0.67	0.78
Sr^{2+}	0.33	0.48	—	0.39	0.42	0.41	0.39
SO_4^{2-}	—	2144	2341	1751	1713	1443	1465
Cl^-	—	3420	3470	3150	3150	3150	3090
pH	—	1.11	1.10	1.14	1.14	1.15	1.14

a) Data cited from Takano and Watanuki (1972). b) Data cited from Takano (1969). c) I. Sampled at 8:00 a.m. on Oct. 24, 1983. d) II. Sampled at 5:00 p.m. on Oct. 24, 1983. e) III. Sampled on Aug. 3, 1985. f) IV. Sampled on Aug. 4, 1985. g) V. Sampled on Aug. 7, 1986. h) VI. Sampled on Aug. 8, 1986.

The Ba^{2+} concentrations in 1983 and in 1985 are at levels similar to or a little higher than those in 1965. This result is contrary to our estimation[12] previously mentioned. On the other hand, the Pb^{2+} concentrations have decreased, and the Sr^{2+} concns have increased, in both spring waters. The Cl^- concns are nearly invariable during the 1965—1986 period,

Table 3. Weight Ratios of Lead and Barium and of Strontium and Barium in Tamagawa Hot Spring Waters

Point No.	Obuki Spring					Kobuki Spring				
	1965	1983		1985		1965	1983		1985	
		I	II	III	IV		I	II	III	IV
Pb^{2+}/Ba^{2+}	1.94	0.90	0.86	0.59	0.59	1.57	0.82	0.77	0.88	0.75
Sr^{2+}/Ba^{2+}	0.35	0.35	0.29	0.23	0.22	0.34	0.34	—	0.25	0.26

Table 4. Apparent Partition Coefficients of Lead and Strontium between Hokutolite and Thermal Solution at Yubana Fall

	1965	1983	
		I	II
D_{Pb}	0.14	0.30	0.31
D_{Sr}	0.023	0.035	0.042

though the 1978 value (ca. 3300 ppm)[6] was a little high.

As compared with the Obuki Spring, the Kobuki Spring shows a slightly low pH value, slightly high Ba^{2+}, Pb^{2+}, and Sr^{2+} values (1983, 1985), and or Cl^- and SO_4^{2-} concns, very similar Sr^{2+}, Pb^{2+}, and Ba^{2+} (1986) concns.

The relationship between the chemical composition of a Pb-bearing barite crystal and that of Tamagawa Hot Spring water can be expressed by the following equation:

$$(M/Ba)_{crystal} = D_M\,(M/Ba)_{solution}, \quad (1)$$

where D_M denotes an apparent partition coefficient of M between the $BaSO_4$ crystal and the thermal solution on the basis of the surface equilibrium and where M refers to Pb, Sr or other minor elements. (M/Ba) indicates the weight ratio or mole ratio of two elements in each phase.

The partition of an element between the binary solid phase and the aqueous phase was formulated by Takano[2] on the basis of the ion exchange equilibrium as an example of treating a multicomponent chemical equilibrium system, but farther experimental study has not been carried out.

In this paper Eq. 1 is used.

If D_M is constant for the Tamagawa water, the chemical composition of hokutolite, (Ba, Pb, Sr)SO_4, can be calculated from the (Pb^{2+}/Ba^{2+}) and (Sr^{2+}/Ba^{2+}) ratios of the thermal solution (Obuki Spring water). Both ratios are shown in Table 3. It can clearly be seen that the (Pb^{2+}/Ba^{2+}) ratios of I in 1983 are lower than in 1965, while the (Sr^{2+}/Ba^{2+}) ratios are at similar levels between I in 1983 and in 1965 in both springs. Actually, however, the Pb/Ba and Sr/Ba ratios in hokutolite clearly increased[12] (see Table 1(b)). The apparent partition coefficients were calculated from the data in Tables 1 and 2; they are shown in Table 4. In this case, the solutions in 1965 and in 1983 were assumed to be the solutions from which the Pb-bearing barite crystals of 1953—1972 and of 1973—1981 were formed. It was found that the apparent partition coefficients of Pb and Sr both nearly doubled.

The reasons for these rises in the apparent partition coefficients seem to be profoundly interesting.

Takano[14] interpreted the variation in the Pb content of barite in terms of Pb-chloro complex formation. However, the chloro complex effect is a nondecisive factor in this case because the Cl^- concns in 1965 and in 1983 are nearly equal.

Ichikuni[18] noted that the major portion of the barium in the spring water might have been precipitated as barium sulfate within 100 m of the vent of the Obuki Spring; he also explained the increase in the Pb content in Pb-bearing barite collected at various points of the stream of Tamagawa Hot Spring. He used the homogeneous partition coefficient of Kolthoff and Noponen,[19] which is based on the solid-liquid equilibrium, as a first approximation. He calculated the crystal growth rate as 0.86 mm y^{-1}, which was considerably higher than the results of crystal growth rate obtained by Saito et al.[20] (0.09—0.25 mm y^{-1}) and by the present authors[12] (0.05—0.10 mm y^{-1}). He considered that the barium sulfate (barite) precipitates mainly in the form of minute crystals and that part of them are buried in sulfurous sinter, as was also observed by Saito et al.[20]

Takano (private communication) thought that nearly pure $BaSO_4$ is already formed as fine particles (clusters) in the upper part of the vents. To examine these ideas, the ion-activity products (IAP) of barium sulfate at several points were calculated as follows:

$$IAP = a_{Ba^{2+}} \cdot a_{SO_4^{2-}} = \frac{a_{Ba^{2+}} \cdot a_{HSO_4^-}}{a_{H^+}} K_2, \quad (2)$$

Obuki vent (100 °C) $IAP(1965) = 2.70\times10^{-10}$,
$IAP(1983) = 4.70\times10^{-10}$, (3)

Yubana fall (70 °C) $IAP(1965) = 6.15\times10^{-10}$,
$IAP(1983) = 10.8\times10^{-10}$, (4)

Yudaki fall (25 °C) $IAP(1965) = 6.35\times10^{-10}$, (5)

where K_2 is the second dissociation constant of sulfuric acid, K_2: $10^{-3.0}$ at 100 °C, $10^{-2.6}$ at 70 °C, and $10^{-2.0}$ at 25 °C.[21]

These IAP values show that Obuki Spring water is nearly saturated, or even a little supersaturated, while

Yubana fall and Yudaki fall are supersaturated with $BaSO_4$, whose solubility product, K_{sp}, is 2.82×10^{-10} (100 °C), 2.56×10^{-10} (70 °C), or 1.12×10^{-10} (25 °C).[22]

Liu et al.[23] and Sasaki and Minato[24] have shown that the rise in the degree of supersaturation, shown by the value of $IAP/K_{sp}-1$, causes the formation of many fine nuclei in the cases of $BaSO_4$ and (Ba, Pb)SO_4 crystallization. Now we can postulate that numerous barite microcrystals, which are hardly visible, are formed from three-dimensional nuclei, that they flow, drifting downstream from the upper stream, and that a large part of them no longer adhere to the crustal hokutolite crystals. This image suggests the decrease in the dissolved free Ba^{2+} concn and, therefore, the increase in Pb^{2+}/Ba^{2+} and Sr^{2+}/Ba^{2+} in the solution and the resulting increase in Pb/Ba and Sr/Ba in hokutolite crystals; at the same time, it explains the reduction of the hokutolite growth rate.

To verify this idea, the following experiments were carried out. The hot spring waters collected at Obuki and Kobuki Springs (1985) and at Yubana fall (1986) were immediately filtered with 0.1 μm membrane filters before the coprecipitation of Ba^{2+} and Pb^{2+} with strontium sulfate; then, the Ba^{2+} and Pb^{2+} concentrations were determined. The results are shown in Table 5. It was found that the Ba^{2+} and Pb^{2+} concns were nearly invariable by filtration for Obuki hot spring water, but were reduced in the Yubana fall water. These results obviate the possibility of barite microcrystals or, at least, obviate the possibility of crystals over 0.1 μm in diameter around the Obuki vent. At the Yubana fall, however, at least 20% of the Ba^{2+} had already become barite particles over 0.1 μm in diameter, although the SO_4^{2-} concn in 1986 had returned to nearly the same value as in 1965.

According to the crystal-growth (precipitation) theory, an increase in the degree of supersaturation brings about an acceleration of the crystal growth.[25] It is known that the rise in the growth rate brings about an increase in the apparent partition coefficient of a minor element in a depletion system:[26,27]

$$\lambda = \frac{I/M - k_1}{I/M - k_2}. \tag{6}$$

Table 5. Barium and Lead Concentrations of Filtered Tamagawa Hot Spring Water Compared with Non-Filtered Water (mg·dm^{-3})

Locality	Treatment	Ba^{2+}	Pb^{2+}
Obuki Spring (1985)[a]	non-filtered	1.32	0.78
	filtered	1.34	0.81
Kobuki Spring (1985)[b]	non-filtered	1.63	1.23
	filtered	1.63	1.20
Yubana fall (1986)[c]	non-filtered	1.56	0.68
	filtered	1.25	0.54

a) Sampled on Aug. 3, 1985. b) Sampled on Aug. 4, 1985. c) Sampled on Aug. 9, 1986.

Sasaki,[4] treated the partition of a multicomponent-system using the matrix formula of phenomenological equations[28,29] and assuming that the precipitation reaction proceeds under conditions close to those of chemical equilibrium. The case of a three-component system may be formulated as follows:

$$\begin{pmatrix} v_{r1} \\ v_{r2} \\ v_3 \end{pmatrix} = k_r \begin{pmatrix} x_{r1} \\ x_{r2} \\ x_{r3} \end{pmatrix} = \begin{pmatrix} L_{11} & L_{12} & L_{13} \\ L_{21} & L_{22} & L_{23} \\ L_{31} & L_{32} & L_{33} \end{pmatrix} \begin{pmatrix} A_{r1} \\ A_{r2} \\ A_{r3} \end{pmatrix} (r=1, 2, 3), \tag{7}$$

$k_r x_{ri}$ (i=1, 2, 3) is the precipitation rate of each end member, where x_{ri} (i=1, 2, 3) expresses the chemical composition (mol%) and where k_r is the reaction-rate parameter of the r'th solid phase (k_1=1 is the standard value). L_{ij} (i=1, 2, 3; j=1, 2, 3) is the phenomenological coefficient, and A_{ri} (i=1, 2, 3) is the chemical affinity of each end-member component of the r'th solid solution in the precipitation reaction.[30]

For example, A_{BaSO_4} is calculated by means of:

$$A_{BaSO_4} = RT \ln S_{BaSO_4}, \tag{8}$$

where S_{BaSO_4} is the supersaturation ratio: S_{BaSO_4}=IAP($BaSO_4$)/K_{sp}($BaSO_4$), where IAP($BaSO_4$) is an ion-activity product of Ba^{2+} and SO_4^{2-} in the spring water and where K_{sp}($BaSO_4$) is the solubility product of $BaSO_4$ at each temperature.

Using the data in Tables 1 and 2 and other sources,[11,14] following reaction-rate equations are obtained:

Yubana fall:

1965
$$k_1 \begin{pmatrix} 83.67 \\ 14.58 \\ 1.06 \end{pmatrix} = \begin{pmatrix} L_{11} & L_{12} & L_{13} \\ L_{21} & L_{22} & L_{23} \\ L_{31} & L_{32} & L_{33} \end{pmatrix} \begin{pmatrix} 0.615 \\ -2.298 \\ -5.150 \end{pmatrix}, \tag{9}$$

1983
$$k_2 \begin{pmatrix} 83.02 \\ 14.73 \\ 1.58 \end{pmatrix} = \begin{pmatrix} L_{11} & L_{12} & L_{13} \\ L_{21} & L_{22} & L_{23} \\ L_{31} & L_{32} & L_{33} \end{pmatrix} \begin{pmatrix} 0.724 \\ -2.425 \\ -4.762 \end{pmatrix}, \tag{10}$$

Yudaki fall:

1965
$$k_3 \begin{pmatrix} 81.41 \\ \\ 16.55 \end{pmatrix} = \begin{pmatrix} L_{11} & L_{12} & L_{13} \\ \\ L_{21} & L_{22} & L_{23} \end{pmatrix} \begin{pmatrix} 1.027 \\ -1.886 \\ -4.399 \end{pmatrix}. \tag{11}$$

The solution is given as follows:

L_{11}=1078.4, L_{12}=L_{21}=200.7, L_{13}=L_{31}=23.0, L_{22}=39.7, L_{23}=L_{32}=3.4, L_{33}=1.0, k_2=2.2, k_3=7.5.

These calculations indicate that the precipitation rate of hokutolite was higher in 1983 (k_2=2.2) than in 1965 (k_1=1.0), and that it was higher in the Yudaki fall (k_3=7.5) than in the Yubana fall (k_1=1.0) in 1965 with an increase in the chemical affinity of the $BaSO_4$-formation reaction. However, the actual growth rate of hokutolite was lower in 1983 (0.05 mm y^{-1}) than in 1965 (0.10 mm y^{-1}).[12] Also the growth rate in the

Yudaki fall was lower (0.09 mm y^{-1}) than in the Yubana fall (0.25 mm y^{-1}).[20]

This discrepancy seems to be explicable by taking account of the nucleation rate of lead-bearing barite, as has already been mentioned. That is, at the Yubana fall or the Yudaki fall, numerous fine (three-dimensional) nuclei of hokutolite are formed because of the high supersaturation with regard to $BaSO_4$, but a large part of them cannot adhere to the crustal hokutolite crystals in an open-flow system like Tamagawa, so the actual crystal-growth rate decreases in spite of the increase in the total precipitation rate. These relations may be roughly formulated as following:

$$v = m_1 A - m_2 \exp(-\Delta G^*/RT), \quad (12)$$

$$\Delta G^* = \frac{16\pi\gamma^3 V^2}{3A^2}, \quad (13)$$

where v: apparent growth rate, A: chemical affinity of the $BaSO_4$ formation reaction, γ: surface energy of $BaSO_4$, V: mole volume of $BaSO_4$, ΔG^*: critical free enegy of nucleus formation, m_1, m_2: constants.

The first term in Eq. 12 indicates the total precipitation rate, while the second term expresses the elimination rate of small nucleus crystals of hokutolite. It is, however, questionable whether or not nucleation formation rate of $BaSO_4$ is expressed as the second term in Eq. 12.[30] More quantitative and precise analyses will be needed to confirm this inference.

Finally, we must consider the reason for the recent changes in the Tamagawa hot spring waters mentioned above. Considering the changes in the pH, and in the Fe^{2+} and SO_4^{2-} concentrations, we can guess that a reaction like the following one might have occurred in the deep places under the Obuki vent:

$$FeS_2 + 10H_2O + 15SO_2 \rightarrow Fe^{2+} + 10H^+ + 10HSO_4^- + 6S + S^{2-}. \quad (14)$$

This reaction proceeds toward the right side with an increase in the SO_2, indicating an increase in volcanic activity.[8,31] Moreover, with the rise in the S^{2-} concn in Eq. 14, the decrease in the Pb^{2+} concn can be explained as the next reaction of PbS (galena) formation:

$$Pb^{2+} + S^{2-} \rightarrow PbS. \quad (15)$$

These reactions explain the rise in the HSO_4^- and Fe^{2+} concns and also the fall in the pH and the Pb^{2+} concn nearly quantitatively. Of course, this is only one possible reaction process to explain the compositional changes in Tamagawa hot spring waters in recent years. The presence of FeS_2 and PbS and the reaction temperature and the reaction depth have, in fact, not yet been established. Further experimental research and discussion are needed.

The authors wish to thank Dr. Bokuichiro Takano, Tokyo University, for his valuable advice and continuous encouragement.

References

1) M. Ichikuni, "Partition of elements in forming rock and minerals," No. 2, Preface (1974).
2) B. Takano, *Geochemistry*, **13**, 41 (1979).
3) M. Ichikuni, *J. Balneol. Soc. Jpn.*, **30**, 168 (1980).
4) N. Sasaki, *Mem. Fac. Educ. Kagawa Univ. II*, **36**, 53 (1986).
5) Y. Yoshiike, I. Iwasaki, S. Okamura, and T. Omori, *J. Balneol. Soc. Jpn.*, **30**, 160 (1979).
6) T. Goto, *J. Balneol. Soc. Jpn.*, **32**, 105 (1982).
7) T. Goto, Y. Umezu, and Y. Asabe, *J. Balneol. Soc. Jpn.*, **34**, 180 (1984).
8) J. Ossaka, T. Ozawa, T. Nomura, T. Ossaka, J. Hirabayashi, A. Takaesu, and T. Hayashi, *Bull. Volcanol.*, **43**, 207 (1980).
9) K. Watanuki, B. Takano, and J. Saito, *J. Balneol. Soc. Jpn.*, **32**, 133 (1982).
10) N. Sasaki, *Mem. Fac. Educ. Kagawa Univ. II*, **35**, 35 (1985).
11) B. Takano and K. Watanuki, *Geochem. J.*, **6**, 1 (1972).
12) N. Sasaki and K. Watanuki, *Miner. J.*, **11**, 297 (1983).
13) N. Sasaki and K. Watanuki, *J. Balneol. Soc. Jpn.*, **34**, 172 (1984).
14) B. Takano, *Geochem. J.*, **3**, 117 (1969).
15) B. Takano and K. Watanuki, *Bunseki Kagaku*, **21**, 1376 (1972).
16) I. M. Kolthoff and E. B. Sandell, "Textbook of Quantitative Inorganic Analysis," 3rd ed, The Macmillan Co. (1952).
17) Y. Yoshiike, S. Okamura, and I. Iwasaki, *J. Balneol. Soc. Jpn.*, **35**, 108 (1985).
18) M. Ichikuni, *Bull. Chem. Soc. Jpn.*, **39**, 898 (1966).
19) I. M. Kolthoff and G. E. Noponen, *J. Am. Chem. Soc.*, **60**, 197 (1938).
20) N. Saito, Y. Sasaki, and H. Sakai, "Geochemistry of the Tamagawa Hot Spring," Tokyo (1963), p. 182.
21) H. C. Helgeson, *Am. Jour. Sci.*, **267**, 729 (1969).
22) C. W. Blount, *Am. Mineral.*, **62**, 942 (1977).
23) S. T. Liu, G. H. Nancolass, and E. A. Gasiecki, *J. Crystal Growth*, **33**, 11 (1976).
24) N. Sasaki and H. *Minato, Miner. J.*, **11**, 365 (1983).
25) I. Sunagawa, *J. Miner. Soc. Jan*, **15**, 109 (1981).
26) W. L. McIntire, *Geochim. Cosmochim. Acta*, **27**, 1209 (1963).
27) D. H. Klein and B. Fontal, *Talanta*, **12**, 35 (1965).
28) S. R. de Groot and P. Mazur, "Non-equilibrium Thermodynamics," North Holland, Amsterdam (1962).
29) I. Prigogine, "Introduction to Nonequilibrium Thermodynamics," 3rd ed, Wiley-Interscience, New York (1967).
30) A. E. Nielsen, "Kinetics of Precipitation," Pergamon Press, New York (1964).
31) B. Takano and K. Watanuki, *Chemistry Today*, **175**, 14 (1985).

 © 1988 The Chemical Society of Japan Bull. Chem. Soc. Jpn., 61, 1141—1146 (1988)

Circular Dichroism Spectra of the Dicobalt(III) Complexes Containing Two Bridging μ-Hydroxo Ligands

Tomoharu AMA,* Hiroshi KAWAGUCHI, and Takaji YASUI
Department of Chemistry, Faculty of Science, Kochi University, Akebono-cho, Kochi 780
(Received August 1, 1987)

Five cobalt(III) complexes, $[(gly)_2Co(\mu\text{-}OH)_2Co(en)_2]^{2+}$ (two geometrical isomers), $[(edda)Co(\mu\text{-}OH)_2Co(en)_2]^{2+}$ (two geometrical isomers), and $[(nta)Co(\mu\text{-}OH)_2Co(en)_2]Cl$, were newly prepared and optically resolved. Their structures were assigned on the basis of visible and UV absorption, ^1H NMR, and circular dichroism (CD) spectral data. It was found that the CD contributions of the two different cobalt(III) chromophores are additive in the present complex systems. The vicinal CD which is induced on one of the two cobalt chromophores by the other chiral cobalt chromophore was strong ($|\Delta\varepsilon|$: ca. 2). These complexes are stable for several days in aqueous solution.

Although many reports on the preparation and characterization of dicobalt(III) complexes containing two bridging hydroxo ligands have been published, only a few reports have dealt with the complexes containing two different cobalt(III) chromophores bridged with the two hydroxo groups.[2-5] However, the complexes of this type are the fundamental polynuclear ones and are suitable for the investigation of the interaction between the two cobalt atoms. Accordingly, a reliable method to prepare many complexes of this type is required. In the pevious paper,[2] the preparation of ammine complexes such as $[(L)Co(\mu\text{-}OH)_2Co(NH_3)_4]^{2+}$ (L=$(gly)_2$, edda, or nta)[1] was reported and the following suggestion was given: the dicobalt(III) complexes with two μ-hydroxo, in which two hydrogen-bonds are formed between the amino groups on one of the two cobalt atoms and the carboxyl groups on the other cobalt atom, are preferentially produced. In order to confirm the suggestion, we tried to prepare the complexes with two ethylenediamine ligands instead of four ammine ligands (Fig. 1). In the present paper, the interaction between the cobalt(III) chromophores and the additivity rule in the CD spectra of the polynuclear complexes will be described in detail on the basis of the CD spectral data of these optically active isomers of ethylenediamine complexes. The preparation and stability of the complexes will also be described.

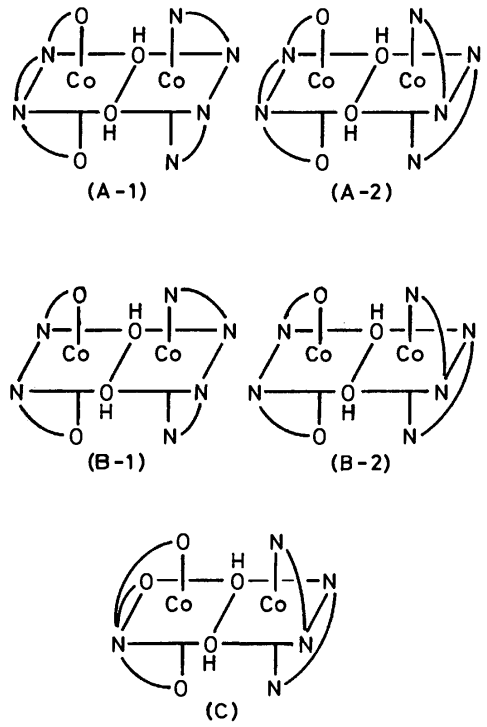

Fig. 1. Structures of the prepared complexes:
(A-1) (*Λ*, *Λ*)-$[(edda)Co(\mu\text{-}OH)_2Co(en)_2]^{2+}$ ($(+)^{CD}_{565}$**E-1**);
(A-2) (*Λ*, *Λ*)-$[(edda)Co(\mu\text{-}OH)_2Co(en)_2]^{2+}$ ($(+)^{CD}_{580}$**E-2**);
(B-1) (*Λ*, *Λ*)-$[(gly)_2Co(\mu\text{-}OH)_2Co(en)_2]^{2+}$ ($(+)^{CD}_{560}$**G-1**);
(B-2) (*Λ*, *Λ*)-$[(gly)_2Co(\mu\text{-}OH)_2Co(en)_2]^{2+}$ ($(+)^{CD}_{580}$**G-2**);
and (c) (*Λ*)-$[(nta)Co(\mu\text{-}OH)_2Co(en)_2]^{+}$ ($(-)^{CD}_{625}$**N-1**).

Experimental

Preparation of the Complexes. $[(edda)Co(\mu\text{-}OH)_2Co(en)_2]Cl_2$: In 5 cm^3 of water, $K[Co(edda)(CO_3)]\cdot H_2O$ (2.0 g)[6] was suspended and then acidified with 60% $HClO_4$ (2 cm^3). Separately, $[Co(en)_2(CO_3)]ClO_4$ (2.0 g) was suspended in 5 cm^3 of water and acidified with 60% $HClO_4$ (2 cm^3). The two solutions were mixed. The pH of the mixed solution was adjusted to 8.5 with 2 mol dm^{-3} KOH and then stirred for 60 min in a water bath at 50 °C. The reacted solution was cooled to room temperature, neutralized using 2 mol dm^{-3} $HClO_4$ and filtered. The filtrate was loaded on a column (4.7 cm×50 cm) of SP-Sephadex (K^+ form), and the adsorbed band was developed with 0.4 mol dm^{-3} KCl. The eluate from the third band (dark-violet) was transferred to another SP-Sephadex column (K^+ form) and repeatedly developed on the column using a micropump until the adsorbed band completely separated into two bands [**E-1** (earlier band) and **E-2** (later band)]. The eluate from **E-1** was evaporated to about 10 cm^3 and the KCl which deposited was filtered off. Methanol was added to the filtrate and the KCl which deposited was again filtered off. After the filtrate was evaporated almost to dryness, the residue was dissolved in 50 cm^3 of water. The solution was poured onto a column (4.7 cm×50 cm) of SP-Sephadex (K^+ form) once more. The adsorbed band was developed with 0.1 mol dm^{-3} K_2Sb_2 (*d*-tart)$_2$. This development was repeated on the column using a micropump until the adsorbed band completely separated into

two dark-violet bands. The earlier- and later-eluted bands exhibited (−) and (+) CD signs at 565 nm, respectively. Each band was eluted with 0.1 mol dm^{-3} of K_2Sb_2(*d*-tart)$_2$, and the eluted solution was concentrated to small volume under reduced pressure. To the concentrated solution, methanol was added to deposit K_2Sb_2(*d*-tart)$_2$. After the deposited K_2Sb_2(*d*-tart)$_2$ was filtered off, the filtrate was evaporated almost to dryness to exclude methanol and was diluted with a little water. The solution was reloaded on a short column (3 cm×5 cm) of QAE-Sephadex (Cl^- form) and eluted with water. The eluted solution was concentrated to small volume. Crude complex of the optically active isomer was obtained by adding methanol and acetone to the concentrated solution, which was recrystallized from water by adding methanol and acetone.

The eluate from **E-2** was optically resolved by a method similar to that employed for **E-1**. The earlier and later eluates on the development with K_2Sb_2 (*d*-tart)$_2$ were $(+)^{CD}_{580}$ and $(-)^{CD}_{580}$ forms, respectively. Found for the $(+)^{CD}_{565}$ **E-1** isomer: C, 22.14; H, 5.68; N, 15.52%. Calcd for [(edda)Co(μ-OH)$_2$-Co(en)$_2$]Cl$_2$·1.5H$_2$O=$C_{10}H_{31}N_6O_{7.5}Cl_2Co_2$: C, 22.07; H, 5.74; N, 15.44%. Found for the $(+)^{CD}_{580}$ **E-2** isomer: 21.08; H, 6.06; N, 14.82%. Calcd for [(edda)Co(μ-OH)$_2$Co(en)$_2$]Cl$_2$·3H$_2$O= $C_{10}H_{34}N_6O_9Cl_2Co_2$: C, 21.03; H, 6.00; N, 14.71%.

[(gly)$_2$Co(μ-OH)$_2$Co(en)$_2$]Br$_2$: By a method similar to that described above, this complex was prepared from K[Co-(gly)$_2$(CO$_3$)] (2.0 g)[6] and [Co(en)$_2$(CO$_3$)]ClO$_4$ (2.0 g) (reaction conditions: pH 8.0, 50 °C, 45 min). The reacted solution was cooled to room temperature, neutralized using 2 mol dm^{-3} HClO$_4$ and filtered. The filtrate was loaded on a column (4.7 cm×50 cm) of SP-Sephadex C-25 (NH_4^+ form), and the adsorbed band was developed with 0.2 mol dm^{-3} $(NH_4)_2SO_4$. The eluate from the third band (dark-violet) was transferred to another SP-Sephadex column (NH_4^+ form) and repeatedly developed on the column using a micropump until the adsorbed band separated completely into two bands [**G-1** (earlier band) and **G-2** (later band)]. An eluate from **G-1** was evaporated to about 10 cm^3 and methanol was added to the concentrated solution. After the $(NH_4)_2SO_4$ which deposited was filtered off, the filtrate was evaporated almost to dryness. The crude complex was dissolved in 50 cm^3 of water and optically resolved on the column by the same method as that described for **E-1**. The earlier- and later-eluted bands on the development with K_2Sb_2(*d*-tart)$_2$ showed (−) and (+) CD signs at 560 nm, respectively. Finally, each of the resolved **G-1** was converted to the Br^- salt using a QAE-Sephadex column (Br^- form).

The eluate from **G-2** was optically resolved by the same method as that employed for **G-1**. The earlier and later eluates on the development with K_2Sb_2(*d*-tart)$_2$ were $(+)^{CD}_{580}$ and $(-)^{CD}_{580}$ isomers, respectively. Found for the $(+)^{CD}_{560}$ **G-1** isomer: C, 15.78; H, 4.88; N, 13.82%. Calcd for [(gly)$_2$Co(μ-OH)$_2$Co(en)$_2$]Br$_2$·1.5H$_2$O=$C_8H_{29}N_6O_{7.5}Br_2Co_2$: C, 15.83; H, 4.82; N, 13.84%. Found for the $(+)^{CD}_{580}$ **G-2** isomer: C, 15.95; H, 4.67; N, 14.05%. Calcd for [(gly)$_2$Co(μ-OH)$_2$Co(en)$_2$]Br$_2$·H$_2$O=$C_8H_{28}N_6O_7Br_2Co_2$: C, 16.07; H, 4.72; N, 14.05%.

[(nta)Co(μ-OH)$_2$Co(en)$_2$]Cl: By a method similar to that described for [(edda)Co(μ-OH)$_2$Co(en)$_2$]Cl$_2$, [(nta)Co(μ-OH)$_2$-Co(en)$_2$]$^+$ (**N-1**) was prepared from K$_2$[Co(nta)(CO$_3$)] and [Co(en)$_2$(CO$_3$)]ClO$_4$ (reaction conditions: pH 8.5, 50 °C, 40 min). The reacted solution was cooled to room temperature, neutralized using 2 mol dm^{-3} HClO$_4$ and filtered. The filtrate was loaded on a column (4.7 cm×50 cm) of SP-Sephadex (K^+ form), and the adsorbed band developed with 0.2 mol dm^{-3} KCl. The eluate from the second band (dark-violet) was evaporated to about 10 cm^3 and methanol was then added to the concentrated solution. The KCl which deposited was filtered off and the filtrate was evaporated almost to dryness. The crude complex was dissolved in 50 cm^3 of water and optically resolved by the same method as that employed for **E-1**. The earlier and later eluates on the development with K_2Sb_2(*d*-tart)$_2$ were $(-)^{CD}_{625}$ and $(+)^{CD}_{625}$ isomers, respectively. Calcd for the $(+)^{CD}_{625}$ isomer: C, 22.47; H, 5.33; N, 13.06%. Calcd for [(nta)Co(μ-OH)$_2$Co(en)$_2$]Cl·2H$_2$O=C_{10}-$H_{28}N_5O_{10}ClCo_2$: C, 22.59; H, 5.30; N, 13.17%.

Spectral Measurements. The visible and UV absorption and the CD spectra were recorded on a Hitachi 557 spectrophotometer and a JASCO J-22 spectropolarimeter in aqueous soiution, respectively. ^{1}H NMR spectra were recorded on a JEOL MH-100 spectrometer using DSS as an internal standard in D$_2$O solution.

Results and Discussion

Structural Assignments and Absorption Spectra. The Complexes Containing edda: The first absorption band of the edda complex **E-1** (or **E-2**) is very broad (Fig. 2), suggesting that **E-1** (or **E-2**) contains two chromophores of different types in the complex

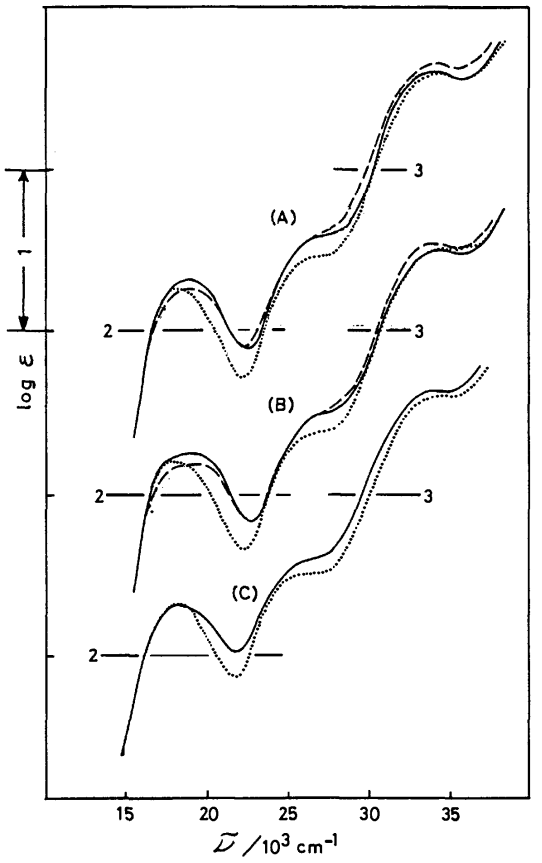

Fig. 2. Absorption spectra of the complexes: (A) **E-1** (——), **E-2** (----), and [(edda)Co(μ-OH)$_2$Co(NH$_3$)$_4$]$^{2+}$ (……); (B) **G-1** (——), **G-2** (----), and [(gly)$_2$Co(μ-OH)$_2$Co(NH$_3$)$_4$]$^{2+}$ (……); and (C) **N-1** (——) and [(nta)Co(μ-OH)$_2$(NH$_3$)$_4$]$^+$ (……). The ε values are given in mol^{-1} dm^3 cm^{-1}.

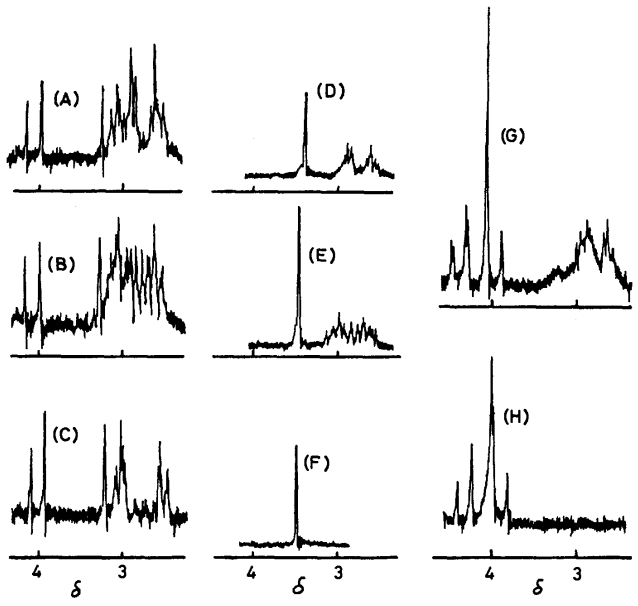

Fig. 3. ^{1}H NMR spectra of the complexes: (A) **E-1**, (B) **E-2**, (C) $[(edda)Co(\mu\text{-}OH)_2Co(NH_3)_4]^{2+}$, (D) **G-1**, (E) **G-2**, (F) $[(gly)_2Co(\mu\text{-}OH)_2Co(NH_3)_4]^{2+}$, (G) **N-1**, and (H) $[(nta)Co(\mu\text{-}OH)_2Co(NH_3)_4]^{+}$.

ion. However, the chromatographic development on an SP-Sephadex column gave only a single band, showing that the complex is cationic and not a mixture of cationic and anionic complexes. Accordingly, it is reasonable to propose that the two chromophores are bridged in the cationic complex ion.

The ^{1}H NMR spectral pattern of the glycinate protons of the coordinated edda in **E-1** (or **E-2**) resembles that in $[(edda)Co(\mu\text{-}OH)_2Co(NH_3)_4]^{2+}$ [2] (Fig. 3). That is, the glycinate methylene protons of edda in **E-1** (or **E-2**) appeared as an AB quartet signal (δ: ca 3.1 and ca. 4.0), suggesting that the two glycinate methylenes in edda are equivalent in their chemical environment; the edda takes α-cis chelation form.[9] In addition, the ethylenediamine backbones of edda appeared as multiplet signals (δ: ca. 2.7) in both the ammine and the ethylenediamine complexes. These similarities show that the present edda complexes have the same di-μ-hydroxo structure as that of $[(edda)Co(\mu\text{-}OH)_2Co(NH_3)_4]^{2+}$. The signals arising from ethylenediamine also appeared at ca. 2.7 ppm in **E-1** (or **E-2**) as a multiplet, overlapping with those arising from the backbone of edda. The intensity ratio of (quartet (δ: ca. 3.1 and 4.0))/(multiplets (δ: ca. 2.7)) was 4/12, indicating that the ratio of edda/en is 1/2. Moreover, the elemental analysis data suggest that the edda/en ratio in each complex is 1/2. Accordingly, both **E-1** and **E-2** contain (edda) and $(en)_2$ moieties.

A characteristic UV absorption band arising from the $Co(\mu\text{-}OH)_2Co$ moiety,[14] such as $[Co_2(NH_3)_8(\mu\text{-}OH)_2]^{4+}$ and $[Co_2(en)_4(\mu\text{-}OH)_2]^{4+}$,[10-12] was also observed in the present edda complexes at ca. 34000 cm^{-1} (Fig. 3). The band intensities of **E-1** and **E-2** are nearly equal to those of the complexes containing two bridging OH's. These results also suggest that **E-1** and **E-2** have the $Co(\mu\text{-}OH)_2Co$ moiety (Fig. 1).

Although the UV and visible spectral pattern of either **E-1** or **E-2** was similar to that of $[(edda)Co(\mu\text{-}OH)_2Co(NH_3)_4]^{2+}$, some minor differences were observed. The first absorption band (the d-d absorption band which appears at ca. 18000 cm^{-1}) of each ethylenediamine complex was broader than that of the ammine complex and the band maximum of the former was observed at higher energy than the latter. These observations can be explained as follows. The first absorption band maximum of the $Co(en)_2(\mu\text{-}OH)_2$ moiety can be assigned to the higher energy side with higher intensity than that of $Co(NH_3)_4(\mu\text{-}OH)_2$ moiety, since the first absorption band of $[Co(en)_2(O\text{-}O)]^+$ (O-O: $C_2O_4^{2-}$ or CO_3^{2-}) shifts to the higher energy side with higher intensity than that of $[Co(NH_3)_4(O\text{-}O)]^+$.[10,13] On the other hand, the first absorption band maximum of the $Co(edda)(\mu\text{-}OH)_2$ moiety can be assigned to the lower energy side with higher intensity than that of the $Co(en)_2(\mu\text{-}OH)_2$ or $Co(NH_3)_4(\mu\text{-}OH)_2$ moiety. Accordingly, the overlapping band due to the $Co(en)_2(\mu\text{-}OH)_2$ and $Co(edda)(\mu\text{-}OH)_2$ moieties gives a broader first absorption band in $[(edda)Co(\mu\text{-}OH)_2\text{-}Co(en)_2]^{2+}$ than the overlapping band due to the $Co(NH_3)_4(\mu\text{-}OH)_2$ and $Co(edda)(\mu\text{-}OH)_2$ moieties in $[(edda)Co(\mu\text{-}OH)_2(Co(\mu\text{-}OH)_2Co(NH_3)_4]^{2+}$.[2] The second absorption band (the d-d transition observed at ca. 25000 cm^{-1}) of these complexes appeared as a shoulder beside the strong charge-transfer band (at ca. 34000 cm^{-1}) arising from the bridging OH's.[14] The intensity of the second band of **E-1** (or **E-2**) is slightly stronger than that of $[(edda)Co(\mu\text{-}OH)_2Co(NH_3)_4]^{2+}$.

The Complexes Containing gly: The structural assignments of the glycinato complexes **G-1** and **G-2** also are made on the basis of the absorption and ^{1}H NMR spectral data. The possiblity that the $Co(gly)_2(\mu\text{-}OH)_2$ moiety in each complex has trans(N) structure can be ruled out. The shape of the absorption band of **G-1** (or **G-2**) is similar to those of **E-1** and **E-2** having C_2-*cis*(*N*)-$[Co(N)_2(O)_4]$ structure. Furthermore, the complexes do not exhibit such a shoulder band at ca. 16000 cm^{-1} as is characteristic to the *trans*-(*N*)-$[Co(N)_2(O)_4]$ type chromophore.[15,16] The possibility that the $Co(gly)_2(\mu\text{-}OH)_2$ moiety of each complex has the C_1-*cis*(*N*)-$[Co(N)_2(O)_4]$ structure is also ruled out, because the two glycinate methylene protons in the moiety appeared as a singlet signal in ^{1}H NMR (Fig. 3); this suggests that the moiety has a C_2 axis which makes the two methylenes equivalent. The two possible geometrical isomers based on the above discussion are shown in Fig. 1. The ^{1}H NMR and visible absorption spectra of **G-1** and **G-2** are similar to those of $[(gly)_2Co(\mu\text{-}OH)_2Co(NH_3)_4]^{2+}$ as those of **E-1** and **E-2** are to those of $[(edda)Co(\mu\text{-}OH)_2Co(NH_3)_4]^{2+}$.

The Complexes Containing nta: This complex **N-1** also showed the characteristic band arising from the

$Co(\mu\text{-}OH)_2Co$ moiety[14] at 34000 cm^{-1} with nearly the same intensity as that of **E-1** or **E-2**. The elemental analysis data showed that the nta/en ratio in the complex is 1/2. Accordingly, the structure $[(nta)Co(\mu\text{-}OH)_2Co(en)_2]^+$ is assigned. Only one geometrical isomer (chiral) is possible for this complex ion.

The ^1H NMR spectra of **E-1**, **E-2**, **G-1**, and **G-2** (these are ethylenediamine Complexes) resemble those of the corresponding ammine complexes respectively, while the ^1H NMR spectrum of **N-1** is slightly different from the corresponding ammine complex, $[(nta)Co(\mu\text{-}OH)_2Co(NH_3)_4]^+$. That is, the glycinate protons in nta appeared as two AB quartets and one singlet in **N-1**, while they appeared as one AB quartet (for four protons) and one singlet (for two protons) in the corresponding ammine complex (Fig. 3). This result is interpreted as follows. In the ammine complex, the two glyinate rings in nta are equivalent in chemical environment because the OH-Co-OH plane is a mirror plane. On the other hand, in **N-1**, the mirror plane is broken by the two coordinated ethylenediamines on the neighboring cobalt atom.

CD Spectra. The CD spectra of the optically active complexes are illustrated in Fig. 4. The $(+)^{CD}_{565}$ **E-1** and $(+)^{CD}_{560}$ **G-1** isomers (Fig. 4 shows the CD curve for $(-)^{CD}_{560}$ **G-1** isomer) show two intense CD bands with opposite signs in the first absorption band region. As their main CD bands in the lower energy side corresponding to the *cis*-$[Co(N)_2(O)_4]$ type chromophore are (+) sign, the configuration around the *cis*-$[Co(N)_2(O)_4]$ type chromophore is assigned to Λ.[17] On the other hand, these complexes show (−) CD in the first absorption band region of the *cis*-$[Co(N)_4(O)_2]$ type chromophore, suggesting that these complexes have Δ configurations[17] around the $Co(en)_2(\mu\text{-}OH)_2$ moieties which belong to the *cis*-$[Co(N)_4(O)_2]$ type chromophore. The deduced structures are illustrated in Fig. 1 (A-1 and B-1).

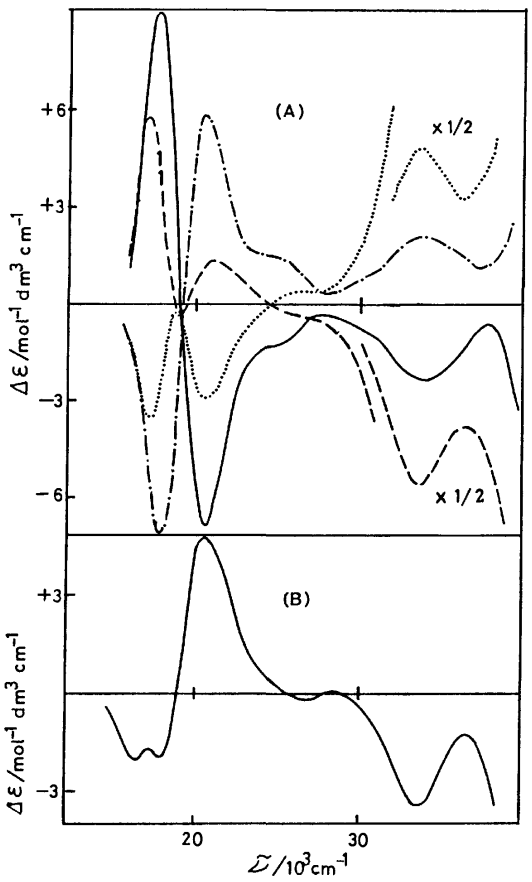

Fig. 4. CD spectra of the complexes: (A) $(+)^{CD}_{565}$**E-1** (——), $(+)^{CD}_{580}$**E-2** (----), $(-)^{CD}_{560}$**G-1** (-·-·-), and $(-)^{CD}_{580}$**G-2** (·····); and (B) $(-)^{CD}_{625}$**N-1** (——).

In contrast to these complexes, $(+)^{CD}_{580}$ **E-2** and $(+)^{CD}_{580}$ **G-2** showed two (+) CD components in the first absorption band region. Therefore, either **E-2** or **G-2** has Λ configurations in both *cis*-$[Co(N)_2(O)_4]$ and *cis*-$[Co(N)_4(O)_2]$ moieties (Fig. 1 (A-2 and B-2)).

The CD pattern of **G-1** resembles that of **E-1** in the region of 15000—38000 cm^{-1}. This result suggests that the geometrical structure of the $Co(gly)_2(\mu\text{-}OH)_2$ moiety in **G-1** is similar to that of $Co(edda)(\mu\text{-}OH)_2$ in **E-1** (*cis*(*N*)-$[Co(N)_2(O)_4]$ type), as described above. The CD spectrum of **G-2** resembles that of **E-2**.

The $(-)^{CD}_{625}$ **N-1** isomer shows three CD components in the first absorption band region (Fig. 4(B)). The small (−) CD (at 18000 cm^{-1}) and large (+) CD (at 20600 cm^{-1}) components are presumed to arise from the Λ-$Co(en)_2(\mu\text{-}OH)_2$ moiety, because the CD components of this moiety is expected to appear in a higher energy region than that of the $Co(nta)(\mu\text{-}OH)_2$ moiety. Since the $Co(nta)(\mu\text{-}OH)_2$ moiety is achiral, it is supposed that no CD is observed in the first absorption band region corresponding to the $Co(nta)(\mu\text{-}OH)_2$ moiety (near 16000 cm^{-1}). In spite of this supposition, CD was observed at 16200 cm^{-1}. This CD is the vicinal CD induced by the neighboring $Co(en)_2(\mu\text{-}OH)_2$ moiety which is chiral. It is noteworthy that the sign of this CD component is opposite from that of the main CD in the first absorption band region of $Co(en)_2(\mu\text{-}OH)_2$ moiety.

CD Additivity of the Two Neighboring Co(III) Chromophores: It has been clarified that the configurational CD of the Co(III) chromophore and the vicinal CD of the asymmetric carbon or nitrogen are additive in the d-d transition band region.[17] However, for the polynuclear complexes, there are few reports about the CD additivity of the Co(III) chromophores neighboring to one another.[18] In this work, assuming that the CD of one of the Co(III) chromophores in each di-μ-hydroxo complex is separable from that of the other Co(III) chromophore, the CD of the prepared complex is assigned to the CD contributions of the two Co(III) chromophores. The additivity is then confirmed by comparison of the analyzed data with other CD data, as described below.

The CD spectra arising from the $Co(edda)(\mu\text{-}OH)_2$ and $Co(en)_2(\mu\text{-}OH)_2$ moieties in **E-1** and **E-2** were separated by the following equations, where Δ_{en} and

Λ_{en} mean the CD contributions arising from the Δ- and Λ-Co(en)$_2$(μ-OH)$_2$ moieties, and Δ_{edda} and Λ_{edda} mean those from the Δ- and Λ-Co(edda)(μ-OH)$_2$ moieties, respectively.

$$\Lambda_{en} = \frac{1}{2}\{(\Lambda_{edda}, \Lambda_{en}) - (\Lambda_{edda}, \Delta_{en})\}$$

$$= \frac{1}{2}\{((+)^{CD}_{580}\ \textbf{E-2}) - (+)^{CD}_{565}\ \textbf{E-1})\} \quad (1)$$

$$\Delta_{en} = -\Lambda_{en} \quad (2)$$

$$\Lambda_{edda} = \frac{1}{2}\{(\Lambda_{edda}, \Lambda_{en}) + (\Lambda_{edda}, \Delta_{en})\}$$

$$= \frac{1}{2}\{((+)^{CD}_{580}\ \textbf{E-2}) + ((+)^{CD}_{565}\ \textbf{E-1})\} \quad (3)$$

$$\Delta_{edda} = -\Lambda_{edda} \quad (4)$$

The CD curves for the calculated Λ_{edda} coincide well with the observed CD curve of Λ-[(edda)Co(μ-OH)$_2$-Co(NH$_3$)$_4$]$^{2+}$. This result suggests that the CD contributions arising from the Co(edda)(μ-OH)$_2$ moieties are similar to each other in the complexes having the same type chromophore ([Co(N)$_4$(O)$_2$] type) in the vicinity of Co(edda)(μ-OH)$_2$ moiety, showing the CD additivity of the two Co(III) chromophores. Similar additivity of the CD contributions of the cobalt chromophores were reported for *cis*-[Co(CN)$_2${(μ-OH)$_2$Co(en)$_2$}$_2$]$^{3+}$.[18,19]

The same discussion as described above can be applied to the glycinato complexes, **G-1** and **G-2**, based on the following equations.

$$\Lambda_{en} = \frac{1}{2}\{(\Lambda_{gly}, \Lambda_{en}) - (\Lambda_{gly}, \Delta_{en})\}$$

$$= \frac{1}{2}\{((+)^{CD}_{580}\ \textbf{G-2}) - (+)^{CD}_{560}\ \textbf{G-1})\} \quad (5)$$

$$\Delta_{en} = -\Lambda_{en} \quad (6)$$

$$\Lambda_{gly} = -\Delta_{gly} \quad (7)$$

$$\Delta_{gly} = -\frac{1}{2}\{(\Lambda_{gly}, \Lambda_{en}) + (\Lambda_{gly}, \Delta_{en})\}$$

$$= -\frac{1}{2}\{((+)^{CD}_{580}\ \textbf{G-2}) + (+)^{CD}_{560}\ \textbf{G-1})\} \quad (8)$$

In these equations, Δ_{gly} and Λ_{gly} mean the CD contributions from the Δ- and Λ-Co(gly)$_2$(μ-OH)$_2$ moieties and the Δ_{en} and Λ_{en} mean the CD contributions of Δ- and Λ-Co(en)$_2$(μ-OH)$_2$ moieties in **G-1** and **G-2**. The calculated Δ_{gly} CD curve coincides with the observed curve of Δ-[(gly)$_2$Co(μ-OH)$_2$Co(NH$_3$)$_4$]$^{2+}$ as for the edda complexes.

The CD curve for the Λ_{en} obtained from **E-1** and **E-2** is similar to that obtained from **G-1** and **G-2** in the range 15000—38000 cm^{-1} (Fig. 5). This can be interpreted in a similar manner to that described above. The cobalt(III) chromophores existing in the vicinity of the Co(en)$_2$(μ-OH)$_2$ moieties are equally *cis*-[Co(N)$_2$(O)$_4$] type in each of **E-1** and **E-2** pair or **G-1** and **G-2** pair, the CD spectra arising from the Co(en)$_2$(μ-OH)$_2$ are similar to each other. However, the CD pattern of Λ_{en} is different from that of Λ-**N-1**. This result suggests that the CD pattern of Co(en)$_2$(μ-OH)$_2$ is affected by the neighboring chromophores, that is, the chromophore exisiting in the vicinity of Co(en)$_2$(μ-OH)$_2$ belongs to the [Co(N)(O)$_5$] type in **N-1** and differs from the *cis*-[Co(N)$_2$(O)$_4$] type which is found in **E-1**, **E-2**, **G-1**, and **G-2**.

The Λ_{en} CD curve has a relatively strong (−) CD component at ca. 18500 cm^{-1} compared to the vicinal CD of the mononuclear tris(bidentate) complexes (Fig. 5).[17] It is expected that this CD component may contain the vicinal (−) CD on the [Co(N)$_2$(O)$_4$] type chromophore induced by the Λ-Co(en)$_2$(μ-OH)$_2$ moiety, since the Λ-[(nta)Co(μ-OH)$_2$Co(en)$_2$]$^+$ shows a (−) vicinal CD on the first absorption band region of the Co(nta)(μ-OH)$_2$ moiety ($\Delta\varepsilon$: ca. −2) which is induced by the chiral Co(en)$_2$(μ-OH)$_2$ moiety. In addition, it is expected that the Λ-Co(en)$_2$(μ-OH)$_2$ moiety has another (−) CD component at ca. 18000 cm^{-1} similarly to Λ-**N-1** (at 18000 cm^{-1}). Accordingly, the overlapping of the induced (−) CD and this CD may give a relatively strong CD at 18500 cm^{-1}.

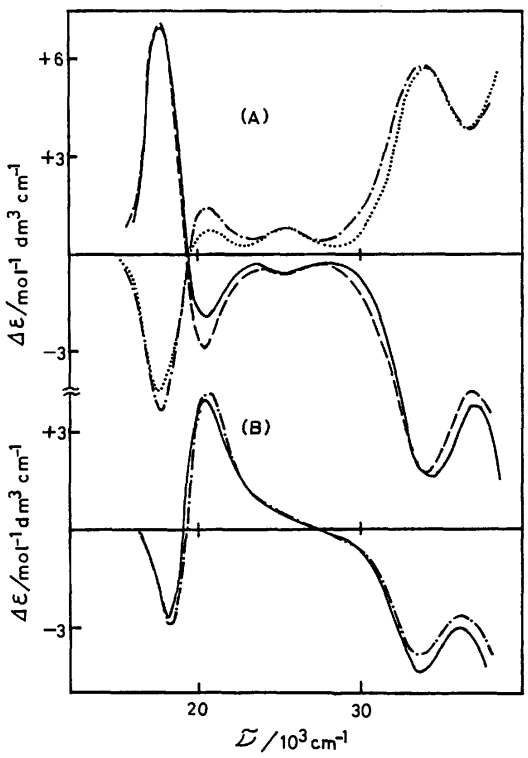

Fig. 5. Calculated and observed CD curves of the complexes: (A) Λ_{edda} in Eq. 3 (——), Λ-[(edda)Co(μ-OH)$_2$Co(NH$_3$)$_4$]$^{2+}$ (– – –), Δ_{gly} in Eq. 8 (–·–·–), and Δ-[(gly)$_2$Co(μ-OH)$_2$Co(NH$_3$)$_4$]$^{2+}$ (·····); and (B) Λ_{en} in Eq. 1 (——) and Λ_{en} in Eq. 5 (–·–·–).

In the charge transfer band region of μ-OH (ca. 34000 cm^{-1}),[14] strong CD bands are observed for the calculated CD curves. The averaged CD intensities calculated for the chiral Co(L)(μ-OH)$_2$ moieties are as follows: Λ-Co(en)$_2$(μ-OH)$_2$ (ca. -4), Λ-Co(gly)$_2$(μ-OH)$_2$ (ca. -6), Λ-Co(edda)(μ-OH)$_2$ (ca. -7), and Λ-*fac*(*O*)-Co(en)(gly)(μ-OH)$_2$ (ca. -5).[5] These values are significantly different from each other, showing that the CD intensity is affected by the ligands except for μ-OH. However, the follwing rough prediction is possible for the chiral di(μ-hydroxo)dicobalt(III) complexes: the complexes which have (Δ-Δ) or (Λ-Λ) pairs show larger CD intensities (absolute values) than those which have (Δ-Λ) or (Λ-Δ) pairs.

Stability of the Complexes. Absorption spectral changes with time were measured in the aqueous solutions of some of the di-μ-hydroxo complexes at 20 °C. Solutions of these complexes showed no spectal change for several days, while that of $[Co_2(\mu\text{-}OH)_2(NH_3)_8]Br_4$ showed an obvious change after one day. This means that these complexes are more stable than $[Co_2(\mu\text{-}OH)_2(NH_3)_8]^{4+}$, suggesting that some stabilizing factors exist in the present complexes. On the X-ray study of $[Cr_2(L\text{-}pro)_4(\mu\text{-}OH)_2]$, Oki and Yoneda[20] pointed out that the two intramolecular N-H···O hydrogen bonds (bridging two chromophores) stabilize the di-μ-hydroxo structure. Moreover, in the X-ray study of $[(en)(gly)Co(\mu\text{-}OH)_2Co(en)(gly)]^{2+}$, it was confirmed that the two hydrogen bonds which bind amino and carboxylate groups stabilize the dinuclear structure.[21] Accordingly, it is reasonable to propose two hydrogen bonds as the stabilizing factor of the present complexes. It was not easy to prepare the isomers having one or no hydrogen bonds, but it was easy to prepare those having two hydrogen bonds. This result agrees with that obtained for the isomers of $[(en)(gly)Co(\mu\text{-}OH)_2Co(en)(gly)]^{2+}$ [5] and $[(L)Co(\mu\text{-}OH)_2Co(NH_3)_4]^{n+}$ (L=(gly)$_2$, (edda), and (nta)),[2] suggesting that the hydrogen bond is important as a stabilizing factor.

References

1) The following abbreviations will be used in the present paper: H_2edda=ethylenediamine-*N*,*N*′-diacetic acid; Hgly=glycine; H_3nta=nitrilotriacetic acid; en=ethylenediamine; *d*-H_4tart=*d*-tartaric acid.

2) T. Ama, H. Kawaguchi, and T. Yasui, *Bull. Chem. Soc. Jpn.*, **60**, 1183 (1987).

3) K. Nakamoto, J. Fujita, and H. Maruta, *J. Am. Chem. Soc.*, **80**, 4817 (1958).

4) W. Hackbusch, H. H. Rupp, and K. Wieghardt, *J. Chem. Soc., Dalton Trans.*, **1975**, 1015.

5) T. Ama, A. Mukai, K. Miyauchi, H. Kawaguchi, and T. Yasui, *Mem. Fac. Sci. Kochi Univ., Ser. C*, **7**, 1 (1986).

6) M. Mori, M. Shibata, E. Kyuno, and F. Maruyama, *Bull. Chem. Soc. Jpn.*, **35**, 75 (1962).

7) M. Shibata, H. Nishikawa, and Y. Nishida, *Inorg. Chem.*, **7**, 9 (1968).

8) M. Mori, M. Shibata, E. Kyuno, and Y. Okubo, *Bull. Chem. Soc. Jpn.*, **31**, 940 (1958).

9) J. I. Legg and D. W. Cooke, *Inorg. Chem.*, **4**, 1576 (1965).

10) H. Kuroya and R. Tsuchida, *Bull. Chem. Soc. Jpn.*, **15**, 427 (1940).

11) J. Springborg and C. E. Schaffer, *Inorg. Synth.*, **18**, 75 (1978).

12) U. Inamura and Y. Kondo, *Nippon Kagaku Zasshi*, **74**, 627 (1953).

13) Y. Shimura and R. Tsuchida, *Bull. Chem. Soc. Jpn.*, **29**, 311 (1956).

14) S. F. Mason and J. W. Wood, *Chem. Commun.*, **1967**, 209.

15) H. Yamatera, *Bull. Chem. Soc. Jpn.*, **31**, 95 (1958).

16) N. Matsuoka, J. Hidaka, and Y. Shimura, *Bull. Chem. Soc. Jpn.*, **40**, 1868 (1968).

17) Y. Shimura, *Kagaku Sosetsu*, No. 13, 83 (1976).

18) S. Kaki, K. Yamanari, and Y. Shimura, *Bull. Chem. Soc. Jpn.*, **56**, 2276 (1983).

19) Y. Shimura, *Rev. Inorg. Chem.*, **6**, 149 (1984).

20) H. Oki and H. Yoneda, *Inorg. Chem.*, **20**, 3875 (1981).

21) E. Oota, K. Hamada, R. Hino, T. Fujiwara, and T. Ama, the Symposium by the Chemical Society of Japan, Matsue, November 1987, Abstr. No. 1A04.

 © 1988 The Chemical Society of Japan Bull. Chem. Soc. Jpn., 61, 1147—1151 (1988)

Studies of the Hydrous Niobium(V) Oxide Ion Exchanger. IV. The Rate of the Isotopic Exchange of Sodium Ions between the Exchanger in the Na^+ Form and Aqueous Solutions

Yasushi INOUE,* Hiromichi YAMAZAKI, and Mitsuji IKEDA
Department of Nuclear Engineering, Faculty of Engineering, Tohoku University, Aramaki, Sendai 980
(Received August 3, 1987)

The rate of the isotopic exchange of sodium ions between the hydrous niobium(V) oxide ion exchanger in the Na^+ form and aqueous solutions was determined radiochemically. Since the fractional attainment of equilibrium was independent of the sodium-ion concentration in the solutions ($\geqq$0.1 mol dm^{-3}), and inversely proportional to the square of the particle radius, the isotopic exchange rate on the hydrous niobium(V) oxide is controlled by the diffusion of the sodium ions in exchanger particles. The self-diffusion coefficients of sodium ions (D=3.1×10^{-7} cm^2 s^{-1} at 25 °C) and their activation energy (E_a=27±4 kJ mol^{-1}) were also determined.

An investigation of ion-exchange kinetics is very important for understanding the ion-exchange mechanism of hydrous metal oxides. A measurement of the rate of the isotopic exchange of cations between ion exchangers and aqueous solutions provides fundamental data which are useful for elucidating ion-exchange kinetics. As a part of the study in our series, radiochemical experiments were previously undertaken to measure the rate of the isotopic exchange of sodium ions between hydrous tin(IV) oxide in the Na^+ form and the aqueous solutions of sodium salts. The rate-controlling step of the reaction was concluded to be the diffusion of ions in the primary particles, which were formed at the initial stage of precipitation and aggregated to form the oxide gel.[1] It is especially interesting to know whether we can generalize this view regarding the isotopic-exchange rate for a variety of hydrous metal oxides.

This paper deals with the rate of the isotopic exchange of sodium ions between hydrous niobium(V) oxide in the Na^+ form and aqueous solutions and with the comparison between this and the hydrous tin(IV) oxide cases.

Experimental

Preparation of the Exchanger in the Na^+ Form Spiked with ^{22}Na. The hydrous niobium(V) oxide was prepared by a previously recommended method. The sample was classified into four particle sizes by using Japan Industrial Standerd sieves; it was then converted to the H^+ form by treating it with a 0.1 mol dm^{-3} HCl solution. After being washed with water, the exchanger was air-dried and stored in a desiccator containing a saturated NH_4Cl solution (relative humidity, 79%).[2] Table 1 shows the particle size and some properties of each sample. The average particle radius was estimated by approximating the particle shape by a sphere, from the particle-size distribution measured in a 83 wt% glycerol solution by using a Seishin Enterprise Micron-Photo-Sizer, Model SKC-2000S. The specific surface area of the sample, after being heated at 110 °C to constant weight, was determined by the BET method (N_2 adsorption at −196 °C) using a Yanagimoto Surface Area Measuring Apparatus, Model GSA-10.

The exchanger in the H^+ form was converted to the Na^+ form by treating it on a column with a Na^+ solution, followed by labeling with ^{22}Na by equilibrating with the ^{22}Na solution for 2 d at room temperature. After having been washed with a solution free from ^{22}Na, the exchanger was used for the rate measurements. The Na^+ solutions having the same chemical composition were used throughout these three procedures; the solutions prepared by the desired combinations of NaCl and NaOH were used when the rate was measured at pH 11.0, and buffer solutions, 0.1 mol dm^{-3} NaH_2PO_4 (72.2 vol%)-0.05 mol dm^{-3} $Na_2B_4O_7$ (27.8 vol%) solution and 0.1 mol dm^{-3} NaH_2PO_4 (46.5 vol%)-0.05 mol dm^{-3} $Na_2B_4O_7$ (53.5 vol%), respectively, were used when the rate was measured at pH 6.0 and 8.0.

Measurement of the Isotopic Exchange Rate. All the rate measurements were performed in a nitrogen atmosphere by using the same apparatus as descrived earlier.[3] The rate was measured in solutions with the same compositions as those

Table 1. Particle Size and Some Properties of Samples

Particle size	Average radius	Density	Ion-exchange capacity[b]	Composition[c]	Specific surface area
mesh[a]	μm	g cm^{-1}	mmol g^{-1}	molH_2O (molNb_2O_5)$^{-1}$	m^2 g^{-1}
−48+60	145±4	2.38±0.05	2.34±0.02	—	321±5
−70+80	107±3	—	—	—	314±5
−100+120	74±2	—	—	6.45±0.06	—
−145+200	52±2	2.39±0.05	2.36±0.02	—	317±5

a) Japan Industrial Standard mesh. b) Exchange capacity for Na^+ at pH 11.0 (ionic strength=0.1). c) The water content was determined from the weight loss at 850 °C.

used for converting the exchanger to the Na^+ form; otherwise, the ion-exchange reaction would occur between H^+ and Na^+ ions, since the ion-exchange capacity for Na^+ strongly depends on the pH and on the concentration of the solution. A 0.05-gram to 0.17-gram portion of the sample was placed in a cage and immersed in 200 cm^3 of a solution of the desired composition while the cage was being rotated. The frequency of the revolution was measured with a Yokogawa, Model 2607, photo tachometer. The solution had been adjusted in advance to a constant temperature within ±0.1 °C. Aliquots of the solution (0.2 cm^3) were taken out at appropriate time intervals in order to measure the radioactivity with a well-type NaI(Tl)-scintillation counter(Aroka Model ARC-361). The time of the contact of the exchanger with the solution was taken as the time elapsing between the immersion of the cage and the withdrawal of an aliquot of the solution. The fractional attainment of equilibrium, $F(t)=C_t/C_\infty$, was calculated from these results; here, C_t is the total radioactivity of the solution at time t and C_∞ at $t=\infty$. C_∞ was calculated using $C_\infty=C_iM/(M+m)$, where C_i is the initial total radioactivity of the exchanger, and m and M, the total amounts of Na^+ in the exchanger and in the solution, respectively. Although the rate was measured by a batch method, the infinite solution-volume approximation is closely obeyed under the present experimental conditions: less than 0.17 g of the exchanger per 200 cm^3 of the solution.

Results and Discussion

In order to ascertain the efficiency of agitation, the effect of the stirring rate on the half-exchange time was examined for pH-11 solutions of different NaCl concentrations. The time required for half-exchange became shorter as the revolution rate increased, and reached a constant value at 1050 min^{-1}. Furthermore, it was confirmed that no particles were broken down during the agitation of the revolution rate up to 1500 min^{-1}. On the basis of these results, a revolution rate of 1300 min^{-1} was adopted throughout the experiment.

The comparison of the isotopic exchange rates in up to 1 mol dm^{-3} solutions of different sodium salts indicated that no difference was observed in the rates between anions in the solutions (Cl^-, ClO_4^-, and SO_4^{2-}).

Figure 1 shows the results of the method called "interruption test" in 0.1 mol dm^{-3} sodium concentration; the exchangers were removed from the solution for 1 h and then reimmersed. The rate immediately after reimmersion was greater than that prior to the interruption, suggesting that the rate is controlled by particle diffusion.

When the isotopic exchange rate is controlled by the diffusion of the ions in spherical exchangers immersed in a well-stirred solution of approximately an infinite volume, the fractional attainment of equilibrium, $F(t)$, can be obtained by solving the following equation:[4]

$$F(t) = 1 - \frac{6}{\pi^2}\sum_{n=1}^{\infty}\frac{1}{n^2}\exp(-Bn^2t), \quad (1)$$

$$B=\pi^2D/r^2, \quad (2)$$

D is the self-diffusion coefficient of the ions in the exchanger and r refers to the radius of the particles. When $F(t)$ is less than about 0.4, Eq. 1 can be approximated by a simpler form:[5]

$$F(t) = \frac{6}{r}\left(\frac{Dt}{\pi}\right)^{1/2}, \quad (3)$$

which holds to a fairly good approximation. Therefore, a plot of $F(t)$ against the square root of the contact

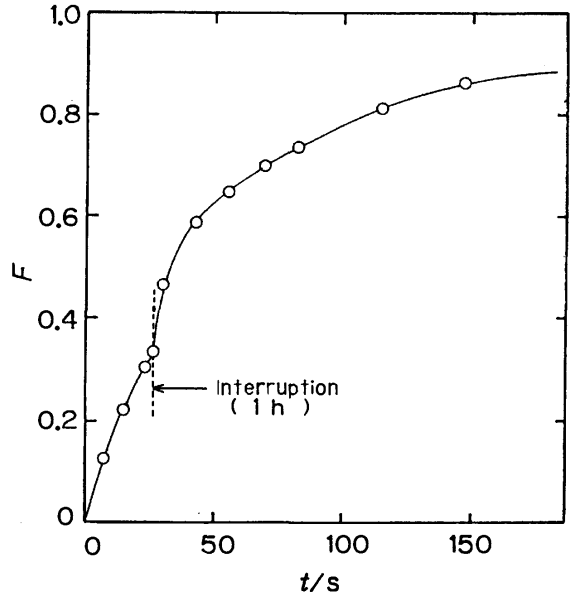

Fig. 1. Interruption test. Sample, −70+80 mesh; temperature, 5.0°C; 0.10 mol dm^{-3} Na(Cl,OH); pH, 11.0.

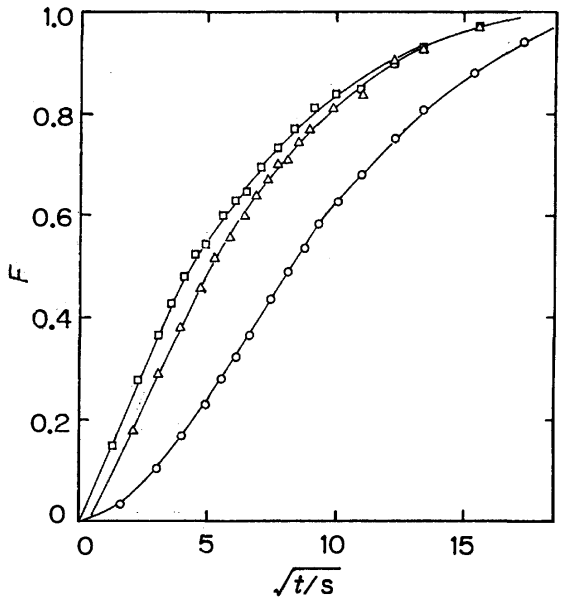

Fig. 2. Effect of Na^+ concentration on the isotopic exchange rates. Sample, −70+80 mesh; temperature, 5.2°C; pH, 11.0; Na(Cl,OH) concn/ mol dm^{-3}, ○: 0.01, △: 0.10, □: 1.0.

time must give a straight line passing through the point of origin in the region in which $F(t)$ is less than 0.4.

Figure 2 shows the influence of the sodium ion concentration on the rate. When the concentration was higher than or equal to 0.1 mol dm^{-3}, although there was very small induction period of the exchange reaction in 0.1 mol dm^{-3} solution, the rate of the exchange reaction was independent of the concentration of the solutions; the straight lines between $F(t)$ and $t^{1/2}$ had the same slope within the experimental errors. In the case of a 0.01 mol dm^{-3} solution, a linear relation did not hold between $F(t)$ and $t^{1/2}$. This cannot be understood by the film diffusion control, since a plot of $-\log(1-F(t))$ against t was sigmoid. This observation can be understood by considering that the equilibrium of sodium ion concentrations between the surface of the exchanger and in the solution was temporarily disturbed by the rinsing of the particles after the labeling, and that the surface concentration of sodium ions approaches equilibrium at a rate proportional to the concentration in the solutions when the exchanger was again immersed in the solution for the rate measurement. The result in a 0.01 mol dm^{-3} solution is ascribed to an overlapping of the rate of the reestablishment of the equilibrium surface-concentration of sodium ions and the isotopic exchange rate.

As has been previously described, this material is considered to have at least two kinds of dissociable ion-exchange sites owing to the presence of an inflection point at pH 7.3 in the cation-uptake curve.[2,6,7] This means that the sites contributing to the exchange reaction have different acidities in each side of the inflection point; only sites having high acidity effect the exchange reaction in a solution of pH lower than 7.3, and, at a higher pH, less acidic sites also participate in the exchange reaction. The exchange rate, however, was independent of pH, as is shown in Fig. 3. Consequently, the change of the electronic density on the exchange sites, which results in the difference in the acidity among the sites, has no influence on the exchange rate.

Figure 4 shows the effect of the particle size on the rate for a 0.1 mol dm^{-3} sodium ion concentration. Here, Bt values were calculated from the measured values of $F(t)$ by using the equation derived by D. Reichenberg:

$$Bt=2\pi-\frac{\pi^2}{3}F(t)-2\pi\left(1-\frac{\pi}{3}F(t)\right)^{1/2}. \quad (4)$$

This equation gives a fairly good approximation in the region where $F(t)$ is less than 0.85.[8] The reason why the Bt-t plots were used instead of Eq. 3 is because the fast rate of the exchange reaction causes a decrease in the number of experimental points falling within the limit of the validity of the equation ($F(t)<0.4$), due to a technical difficulty. When the rate is controlled by the particle diffusion, the plot of Bt against t must give a straight line passing through the point of origin, and the slope of this straight line, i.e., B, is inversely proportional to the square of the particle radius. This figure shows that the plot agrees well with this expectation, irrespective of the particle sizes. In a solution of 1.0 mol dm^{-3} sodium ion concentration, the same dependency was also obtained. Table 2 shows the relation between the particle radii(r) and B, as well as the D calculated from these values. Since D is independent

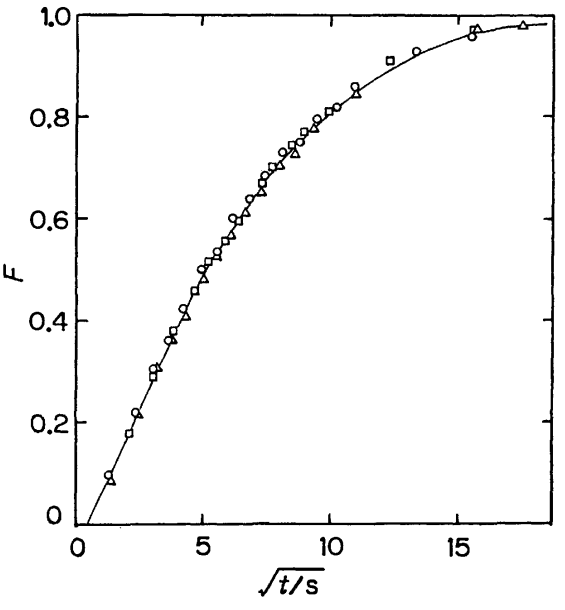

Fig. 3. Effect of pH on the isotopic exchange rates. Sample, −70+80 mesh; temperature, 5.2°C; 0.1 mol dm^{-3} Na^+; pH, ○: 6.6, △: 8.0, □: 11.0.

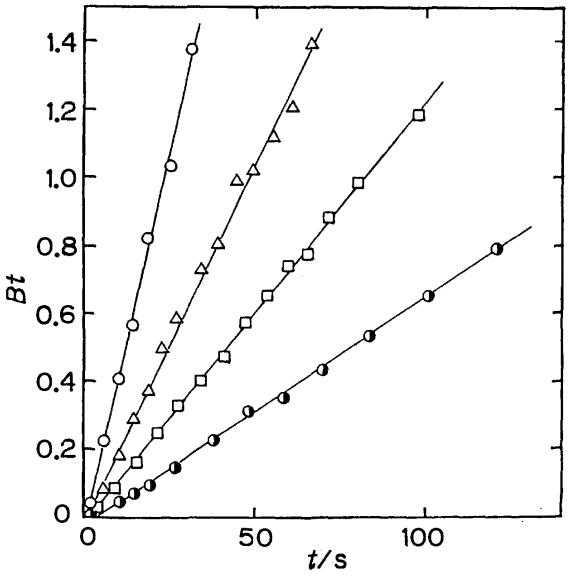

Fig. 4. Effect of particle size on the isotopic exchange rates. Temperature, 5.2°C; 0.10 mol dm^{-3} Na(Cl,OH); pH, 11.0; particle size/mesh, ◑: −48+60, □: −70+80, △: −100+120, ○: −145+200.

Table 2. Effect of Particle Size on the Isotopic Exchange Rates

Na^+ concentration in the solution	Ion-exchange capacity[a)]	Particle size	B	D
mol dm^{-3}	mmol g^{-1}	r/μm	s^{-1}	cm^2 s^{-1}
0.10	2.34±0.02	145±4	(0.67±0.02)×10^{-2}	(1.4±0.1)×10^{-7}
		107±3	(1.24±0.02)×10^{-2}	(1.4±0.1)×10^{-7}
		74±2	(2.13±0.09)×10^{-2}	(1.2±0.1)×10^{-7}
		52±2	(4.45±0.13)×10^{-2}	(1.2±0.1)×10^{-7}
1.0	2.90±0.04	145±4	(0.59±0.02)×10^{-2}	(1.3±0.1)×10^{-7}
		107±3	(1.36±0.07)×10^{-2}	(1.6±0.2)×10^{-7}
		74±2	(2.77±0.08)×10^{-2}	(1.5±0.1)×10^{-7}
		52±2	(5.64±0.29)×10^{-2}	(1.5±0.2)×10^{-7}

Temperature: 5.2±0.1 °C. a) Exchange capacity for Na^+ at pH 11.0.

Table 3. Effect of Temperature on Na^+ Self-Diffusion Coefficients

Na^+ concentration in the solution	Temperature	D	E_a	D_0
	°C	cm^2 s^{-1}	kJ mol^{-1}	cm^2 s^{-1}
0.10 mol dm^{-3}	0.2	(1.2±0.1)×10^{-7}	27±4	6.5×10^{-3}
	5.2	(1.4±0.1)×10^{-7}		
	10.2	(1.7±0.1)×10^{-7}		
	19.8	(2.3±0.2)×10^{-7}		
	29.6	(3.8±0.4)×10^{-7}		

Particle size: −48+60 mesh.

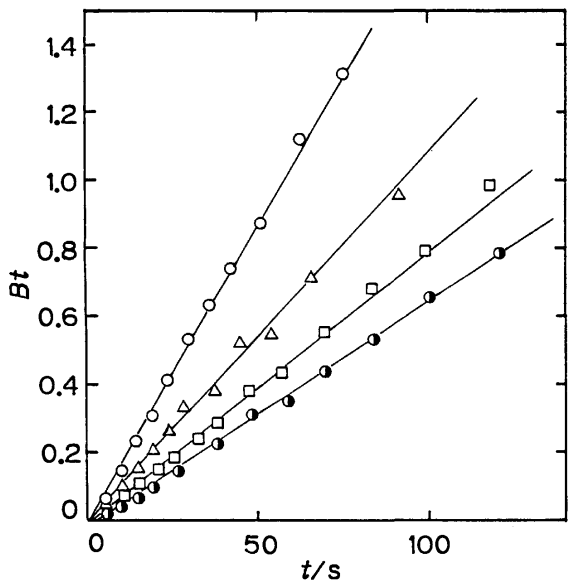

Fig. 5. Effect of temperature on the isotopic exchange rates. Sample, −48+60 mesh; 0.10 mol dm^{-3} Na(Cl,OH); pH, 11.0; temperature/ °C, ◑: 5.2, □: 10.2, △: 19.8, ○: 29.6.

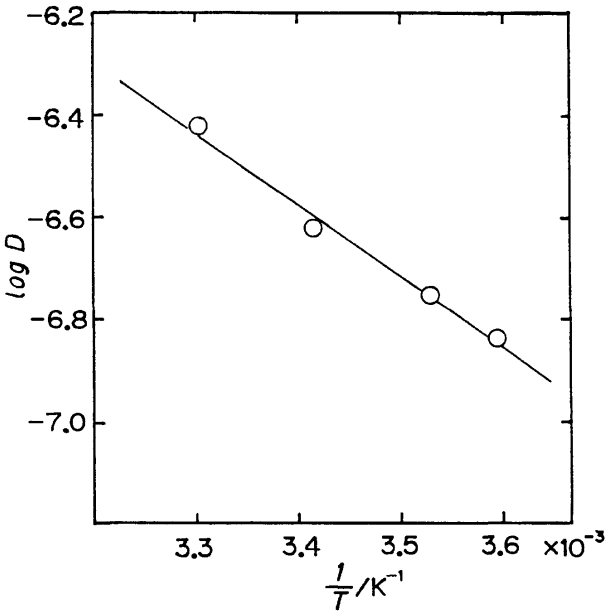

Fig. 6. Arrhenius plots of Na^+ self-diffusion coefficients. Sample, −48+60 mesh; 0.10 mol dm^{-3} Na(Cl,OH); pH, 11.0.

of the particle size, B is inversely proportional to $1/r^2$. Furthermore, since the self-diffusion coefficients of sodium ions are independent of the concentration in solutions, the mechanism of the diffusion of sodium ions in the exchanger is considered to be unchanged by the composition of the material.

When these results are combined with the preceding discussion, the isotopic exchange rate on the hydrous niobium(V) oxide in a Na^+ solution higher than 0.1 mol dm^{-3} is controlled by the diffusion of the sodium ions in the exchanger particles.

The effect of temperature on the isotopic exchange rates was studied in a 0.1 mol dm^{-3} sodium ion solution, as is shown in Fig. 5. This figure indicates that the rates of the exchange increased with temperature. The self-diffusion coefficients of sodium ions were then evaluated from the slopes of these lines by using Eq. 2. These values are summarized in Table 3. When

log D was plotted against $1/T$, a good linearity was obtained (Fig. 6). From the Arrhenius equation, $D=D_0 \exp(-E_a/RT)$, the activation energy, E_a, and the constant, D_0, were determined. The self-diffusion coeffient of sodium ions at 25 °C ($D=3.1\times10^{-7}$ cm^2 s^{-1}) and its activation energy ($E_a=27\pm4$ kJ mol^{-1}) in the hydrous niobium(V) oxide are similar to those reported for sodium ion diffusion in a sulfonated polystyrene type cation-exchange resin of 16% divinylbenzene ($D=2.7\times10^{-7}$ cm^2 s^{-1} at 25 °C, and $E_a=35$ kJ mol^{-1}).[9]

These findings shows that in the hydrous niobium(V) oxide the diffusion of the counter ions in the exchanger particles is the rate-determining step of the exchange reaction in a Na^+ solution higher than 0.1 mol dm^{-3}. This differs from the case of the hydrous tin(IV) oxide; the rate-controlling step is the diffusion of the counter ions in the primary particles, which are formed during the initial stage of precipitation and aggregate to form the hydrous tin(IV) oxide gel. We can, therefore, conclude that the rate of the ion-exchange reaction of hydrous metal oxides cannot be generally interpreted in terms of the same rate-controlling step. Hence, in the analysis of the ion-exchange rates of these materials, the rate-controlling step should be clarified for each.

References

1) Y. Inoue, H. Yamazaki, and A. Osawa, *Bull. Chem. Soc. Jpn.*, **59**, 169 (1986).
2) Y. Inoue, H. Yamazaki, and Y. Kimura, *Bull. Chem. Soc. Jpn.*, **58**, 2481 (1985).
3) Y. Inoue and Y. Yamada, *Bull. Chem. Soc. Jpn.*, **56**, 705 (1983).
4) F. Helfferich, "Ion Exchange," McGraw-Hill, New York (1963), Chap. 6.
5) G. E. Boyd, A. W. Adamson, and L. S. Myers, *J. Am. Chem. Soc.*, **69**, 2863 (1947).
6) Y. Inoue, H. Yamazaki, K. Okada, and K. Morita, *Bull. Chem. Soc. Jpn.*, **58**, 2955 (1985).
7) Y. Inoue, H. Yamazaki, and Y. Matsuda, *Bull. Chem. Soc. Jpn.*, **58**, 3225 (1985).
8) D. Reichenberg, *J. Am. Chem. Soc.*, **75**, 589 (1953).
9) G. E. Boyd and B. A. Soldano, *J. Am. Chem. Soc.*, **75**, 6091 (1953).

 © 1988 The Chemical Society of Japan Bull. Chem. Soc. Jpn., 61, 1153—1157 (1988)

Precise Measurement of Helium Isotopes in Terrestrial Gases

Yuji SANO* and Hiroshi WAKITA
Laboratory for Earthquake Chemistry, Faculty of Science, The University of Tokyo, Bunkyo-ku, Tokyo 113
(Received August 7, 1987)

Helium isotope ratios of terrestrial natural gas samples were measured using a high-precision mass spectrometer and an ultrahigh-vacuum purification line. The line is equipped with a charcoal trap held at 40 K using a helium expansion refrigerating machine. To avoid interference, Ne was completely separated from He by the trap before the gas was admitted to the mass spectrometer. Ion beams of ^{3}He and ^{4}He were measured at the same time by a double collector system. A resolving power of about 550 at the 5% level of the peak height was attained for the complete separation of ^{3}He ions from those of HD and H_3. Precision and reproducibility of the helium isotope ratio were less than 1%, examined by repeated measurements of an air standard. Accuracy of the ratio was checked by comparing observed data with reports in the literature.

Helium has two stable isotopes, of mass number 3 and 4. Most ^{3}He in terrestrial samples is considered to be a trapped component of solar nebulae at the time of the Earth's accretion (primordial He). In contrast ^{4}He is produced by radioactive decay of U and Th in crustal rocks (radiogenic He). The ^{3}He/^{4}He ratio provides useful information on the origin of He[1,2] (primordial or radiogenic). It is well-established that heliums with ^{3}He/^{4}He ratios higher than that of the air (1.40×10^{-6}) are found in gas and rock samples from volcanic and geothermal areas.[3] The helium is thought to be an emanation of the primordial He which still remains deep in the earth. On the other hand, heliums with lower ^{3}He/^{4}He ratios than the air He ratio are reported for non-volcanic regions.[4] This suggests that degassing of the primordial helium has a close relation to geotectonic activity in the region, and particularly to magmatic activity. Thus, the ^{3}He/^{4}He ratio is an important key to the study of magmatic volatiles.[5]

Precise measurements of the ^{3}He/^{4}He ratio can also provide a powerful and convenient method for analysis of environmental tritium. Using a mass spectrometer with extremely high sensitivity, it is possible to detect excess ^{3}He which has accumulated for a sufficient amount of time by in situ decay of tritium in groundwater. The method has been developed by Clarke et al.[6] and is applied to environmental and limnological studies.[7,8] In addition helium isotope ratios can be used in research on the origin of natural gases,[9] on marine ferromanganese nodules,[10] and on the problem of the atmospheric helium budget.[11,12]

In this paper we report precise measurements of ^{3}He/^{4}He and ^{20}Ne/^{4}He ratios in terrestrial natural gas samples. Since ^{20}Ne/^{4}He ratios of mantle-derived and crustal gases are significantly lower than that of air, the ^{20}Ne/^{4}He ratio of the sample can be used as an indicator of air contamination. The analytical system used included a high-precision mass spectrometer, a quadrupole mass spectrometer, a purification and separation vacuum line, and a charcoal trap equipped with a He expansion refrigerator. Performance data are also given. With its high precision and accuracy, the present ^{3}He/^{4}He measurement system is applicable to various fields of geochemistry and environmental sciences.

Experimental

Helium Purification Vacuum Line and Purification Procedure. In order to purify He and Ne from original gas samples and to separate He from Ne, an ultrahigh-vacuum line was constructed (Fig. 1). Since He permeates normal glass quickly, stainless steel was used for all parts of the line. The line consists of three purification and separation parts divided by all-metal bakable valves (V1, V3, and V4). The system in principle resembles that reported by Sano et al.,[13] but several improvements were made. A turbo molecular pump (TMP) is used for creating a rough vacuum instead of an oil diffusion pump. A quadrupole mass spectrometer (QMG112, Balzers) is used in the third part of the line to measure the ^{20}Ne/^{4}He ratio in a gas sample and to ensure adsorption of Ne in a cryogenic charcoal trap (CT3) held at 40 K. A Pirani gauge (PG) is attached to the first part to examine the vacuum when an original gas sample is being introduced.

Hot spring and natural gas samples were collected via the water displacement method in the field using a 50-cm^3 lead glass container with vacuum valves at both ends. After the container was brought back to the laboratory, it was connected directly to the inlet part of the line using an O-ring high-vacuum connector or Tygon tube. A sample of about 1 cm^3 STP was admitted to the first part, and major components such as N_2, O_2, Ar, CH_4, H_2O, and CO_2 were removed by a charcoal trap (CT1) kept at liquid nitrogen temperature (77 K). Unadsorbed components including He and Ne were expanded to the second part. Using a titanium–zirconium getter furnace (TZ1) held at 550 °C and a charcoal trap (CT2) kept at 77 K, He and Ne were purified. When the TZ1 reached room temperature, the purified fraction was introduced into the third part.

The ^{20}Ne/^{4}He ratio of the purified sample was measured by a quadrupole mass spectrometer (QMS) in the third part. No other chemical species except He and Ne were detected by QMS. Interference from doubly charged ions of ^{40}Ar with ^{20}Ne was reduced by a charcoal trap (CT2) held at 77 K and was checked by measurements of the ^{20}Ne/^{22}Ne ratio. Even in the case of a small Ne content, the ^{20}Ne/^{22}Ne ratio showed an atmospheric value of about 10, suggesting negligible contribution of the doubly-charged ^{40}Ar ions. Since the ^{20}Ne/^{4}He ratio was determined by a peak height method, uncer-

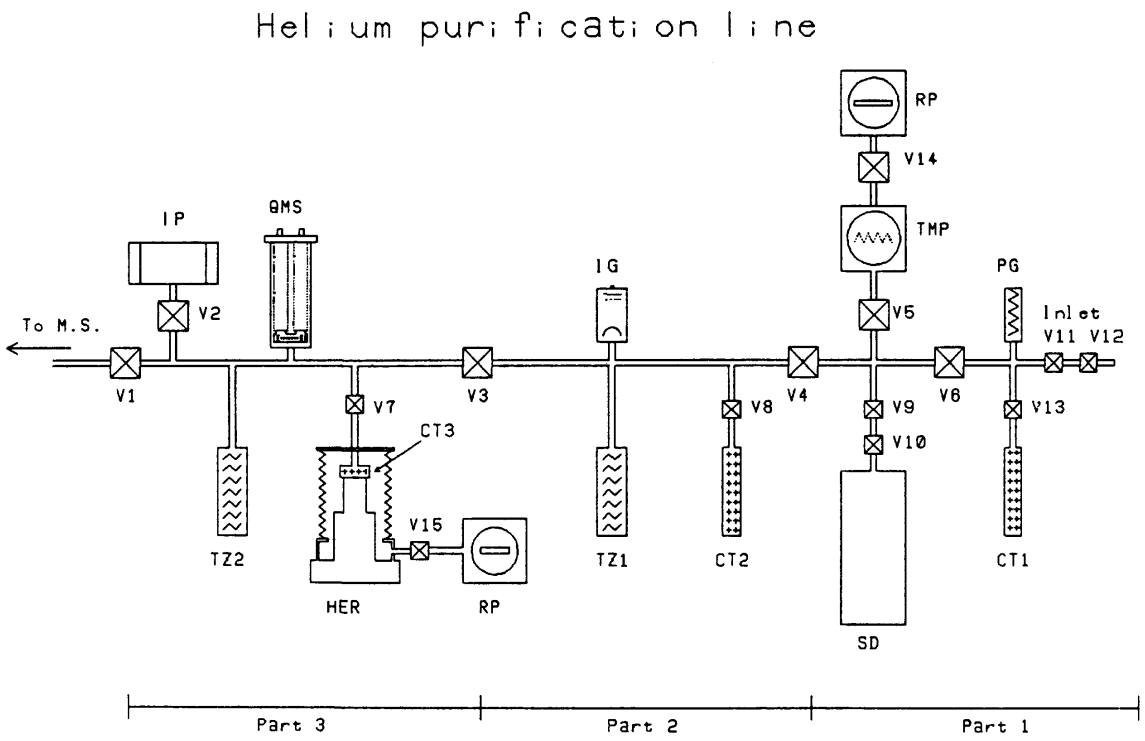

Fig. 1. Helium purification vacuum line. M.S.: mass spectrometer. V: valves, IP: sputter ion pump, QMS: quadrupole mass spectrometer, IG: ionization gauge, PG: Pirani gauge, TZ: titanium-zirconium getter, CT: charcoal trap, HER: helium expansion refrigerator, RP: rotary pump, TMP: turbo molecular pump, SD: standard gas reservoir.

tainty was about 10% at maximum.

Separation of Helium from Neon. According to Rison and Craig,[14] varying He/Ne ratios in a mass spectrometer affected the measured $^3He/^4He$ ratio by up to 10%. If atmospheric He is used as a working standard without separating the Ne, measured values on samples whose He/Ne ratios are quite different from that of air would be significantly erroneous and require major correction. Similar results were suggested by several groups[15] using special $^3He/^4He$ mass spectrometers originally designed by Clarke et al.[6] Thus, it is necessary to separate He from Ne when a precise $^3He/^4He$ ratio is required.

A cryogenic charcoal trap (CT3) was attached to the third part of the purification line (Fig. 1) in order to adsorb Ne completely. The mechanism is in principle similar to that of the improved charcoal trap reported by Reynolds et al.[16] Cooling was done by a commercial He expansion refrigerating machine (Cryomini-S, Osaka-sanso Co.), which was constantly operated at full cooling level. Temperature can be readily controlled by a feedback system (PID) composed of a variable heater and a thermometer. Since the working He in the compressor and the expansion head is sealed by a metal wall, no He leak to the laboratory air is possible.

About 2000 cm^3 STP air was introduced into the vacuum line and was purified by charcoal traps (CT1 and CT2) and a titanium zirconium getter (TZ1). The purified He and Ne were stored in a 2000 cm^3 stainless steel vessel (SD in Fig. 1) and used as a running standard gas. About 0.5 cm^3 STP of standard gas, the volume in the space between the valves (V9 and V10), was expanded into the line and the separation of He from Ne was examined. Figure 2 shows equilibrium ion currents by QMS (normalized to 100% release) versus trap

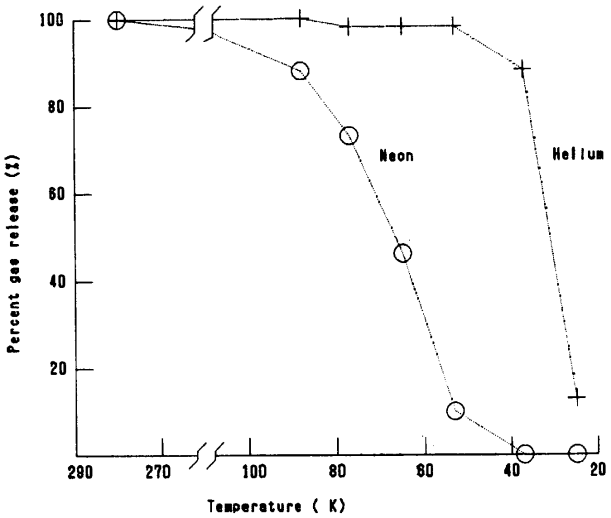

Fig. 2. Equilibrium ion currents for ^4He and ^{20}Ne versus charcoal temperature.

temperature at CT3. The sorption curves agree well with those reported by Reynolds et al.[16] An excellent separation of He from Ne is attained at approximately 40 K in our system.

Mass Spectrometer and Helium Isotope Ratio Measurement. The $^3He/^4He$ ratio was measured with a 27 cm radius extended geometry static gas mass spectrometer. Our instrument was a catalogue model, VG5400 (VG Isotopes, Winsford), modified somewhat in order to detect ^3He and ^4He ion beams simultaneously. The ^3He beam was mea-

sured by a Daly multiplier collector and the ^{4}He beam by a conventional Faraday cup. The resolving power of the Daly collector was higher than 510; that of the Faraday cup, about 200. In order to obtain coincidence of ^{3}He and ^{4}He beams—that is, simultaneous collection of the two beams—the position of the Faraday cup is adjustable by a manipulator. If the coincidence of ^{3}He and ^{4}He beams is sufficient, it is not necessary to perform the peak jumping procedure. These modifications lead to a highly precise ^{3}He/^{4}He ratio measurement. Peak heights of ^{3}He and ^{4}He ion currents were obtained simultaneously by dual-digital electrometers, and the ratio was calculated by a computer. Twenty-five measurements of the ratio were conducted in an individual run, and the ratios were extrapolated to the initial time when the sample was introduced into the mass spectrometer.

Results and Discussion

Neon Interference and Pressure Dependence of the Helium Isotope Ratio. As stated above, varying He/Ne ratios in samples may affect the measured ^{3}He/^{4}He ratio. The relation between the ^{3}He/^{4}He ratio of an air standard and co-existing Ne content, here expressed as ^{20}Ne/^{4}He ratio, is examined (Fig. 3). There is a negative correlation between the ^{3}He/^{4}He and ^{20}Ne/^{4}He ratios: the higher the ^{20}Ne/^{4}He ratio, the lower the observed ^{3}He/^{4}He ratio. The measured ^{3}He/^{4}He ratio of air He containing Ne with the ^{20}Ne/^{4}He ratio of 3.14 (which is air composition) shows a value about 11% lower than the ^{3}He/^{4}He ratio of air He without Ne. If we compare the peak heights of the ^{3}He and ^{4}He, ion currents of ^{4}He are almost constant against varying ^{20}Ne/^{4}He ratios, whereas those of ^{3}He decrease with the ^{20}Ne/^{4}He ratios. This may be attributed either to suppression of the ion beam of ^{3}He in the presence of Ne or to depression of the efficiency of the Daly multiplier by Ne.

The relation between the ^{3}He/^{4}He ratio of air He and total pressure in a mass spectrometer (6-60-SGA, Nuclide Co.) was reported by Sano et al.[13] The higher the total pressure in the mass spectrometer, the higher was the ^{3}He/^{4}He ratio. A similar relation is examined in this work in the range from about 2.0×10^{-5} to 2.5×10^{-4} Pa (Fig. 4). There is a negative correlation between the ^{3}He/^{4}He ratio and the pressure, in contrast to the previous results.[13] In the pressure range below 9×10^{-5} Pa, the ^{3}He/^{4}He ratio is almost constant within an experimental error margin. In contrast, a remarkable decrease in the ^{3}He/^{4}He ratio is observed in the pressure range of about 2×10^{-4} Pa. The discrimination is up to about 6% of the ratio. Taking into account this effect, the total pressure of He was kept lower than 9×10^{-5} Pa in the actual measurements of natural gas samples.

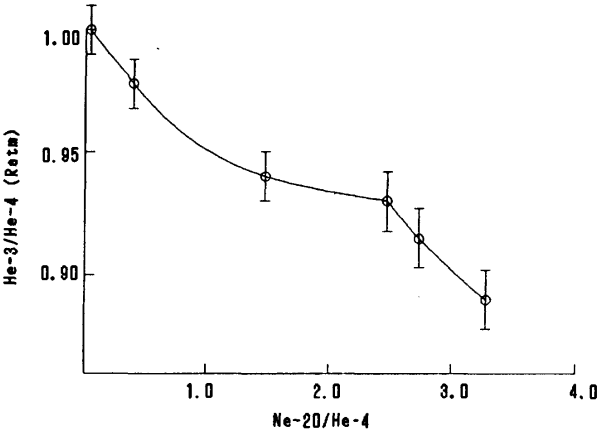

Fig. 3. Correlation between the ^{3}He/^{4}He and ^{20}Ne/^{4}He ratios.

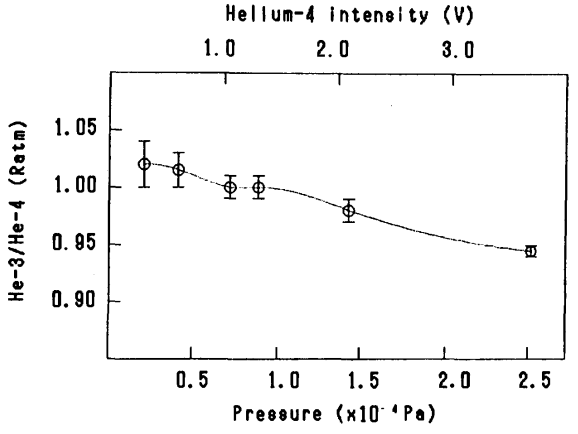

Fig. 4. Pressure dependence of the atmospheric ^{3}He/^{4}He ratios in the mass spectrometer.

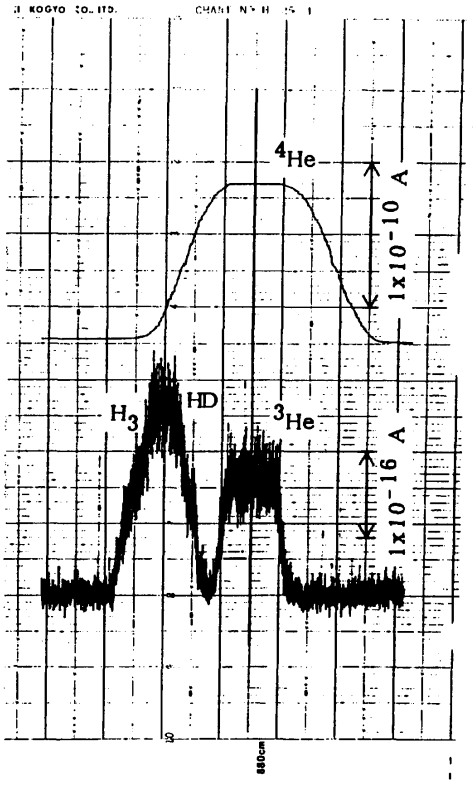

Fig. 5. A typical mass spectrum of purified He from the atmosphere of about 0.3 cm^3 STP.

Reproducibility of the Helium Isotope Ratio Measurements. Since the atmospheric $^3He/^4He$ ratio shows a constant value of $(1.40\pm0.03)\times10^{-6}$, irrespective of latitude, longitude and elevation,[17] air He is regarded as an ideal standard gas. Generally the observed $^3He/^4He$ ratio was represented as a form of the ratio to the air He.[3] The unit of R/R_{atm} is defined here to indicate the $^3He/^4He$ ratio relative to the air value of 1.40×10^{-6}. In this work accuracy and reproducibility of the $^3He/^4He$ ratio were examined by repeated measurements of air He in a standard vessel. In the process He of about 1.8×10^{-6} cm^3 STP was admitted to the mass spectrometer and the $^3He/^4He$ ratio was measured. A typical mass spectrum of ^3He and ^4He in the air standard is shown in Fig. 5. An excellent separation of ^3He from HD plus H_3 beams was observed on the Daly collector with a flat peak shape. A resolving power of about 550 at the 5% level of the peak height was attained. The sensitivity of the Faraday cup was estimated to be about 5×10^{-5} A cm^{-3} STP ^4He and that of the Daly collector to be 3×10^{-3} A cm^{-3} STP ^3He. Taking into account the noise level of the Daly collector of 2×10^{-18} A, the detection limit of ^3He is calculated to be 3×10^{-14} cm^3 STP, which is equivalent to 8×10^5 atoms and about 25 times lower than the previous system.[13]

Table 1. Repeated Measurements of Atmospheric $^3He/^4He$ Ratio

No.	Date	$^3He/^4He$ ($\times10^{-6}$)	^4He ($\times10^{-10}$A)	$^{20}Ne/^4He$
1	Oct. 23, 1986	1.518±0.007	1.09	0.680
2	Oct. 24, 1986	1.498±0.006	1.14	0.699
3	Oct. 24, 1986	1.524±0.006	1.10	0.685
4	Oct. 25, 1986	1.502±0.007	1.14	0.676
5	Oct. 27, 1986	1.489±0.006	1.14	0.676
6	Oct. 28, 1986	1.518±0.007	1.11	0.662
7	Oct. 29, 1986	1.511±0.006	1.12	0.658
8	Oct. 30, 1986	1.520±0.005	1.09	
9	Oct. 31, 1986	1.507±0.006	1.12	0.667
10	Nov. 1, 1986	1.507±0.005	1.12	0.649
11	Nov. 8, 1986	1.505±0.006	1.02	0.662
12	Nov. 13, 1986	1.520±0.007	1.09	0.662
	av.	1.510±0.011	1.11±0.03	0.671±0.014

Results of repeated measurements of the $^3He/^4He$ ratio in air are summarized in Table 1 together with the $^{20}Ne/^4He$ data obtained by QMS. The $^3He/^4He$ ratios were calculated by the observed ratio of the Daly collector's output to the Faraday's output and by the gain of the Daly over the Faraday. The gain was independently determined using different amounts of ^4He. The mass discrimination factor of the measuring system was examined by comparing the mean value of $(1.510\pm0.010)\times10^{-6}$ with the critical ratio of $(1.399\pm0.013)\times10^{-6}$. The discrimination factor of about 7.9% is smaller than that of the previous system.[13] The reproducibility of the $^3He/^4He$ ratio is 0.69% within three weeks, and the value is comparable to the precision of each individual run. The value of 0.69% is the lowest one so far reported.[13,18,19] The $^{20}Ne/^4He$ ratios were calculated using ion current ratios of ^4He to ^{20}Ne in QMS, which show almost constant values of (0.671±0.014) during this period.

Accuracy of the Helium Isotope Ratio Measurements. The $^3He/^4He$ ratios of eight volcanic and hot spring gases collected at representative sites were measured. At the time of measurement, the pressure dependency of the $^3He/^4He$ ratio was taken into account. The observed $^3He/^4He$ ratios were calibrated against that of the air standard obtained on the same day. The results are listed in Table 2 together with reference data including the institutions where the ratios were measured. The error assigned to the observed $^3He/^4He$ ratios is one standard deviation, including a statistical error of an individual run and an error of the air standard to which the $^3He/^4He$ ratio is calibrated. Thus calculated, the net uncertainty of the measurement in this study is less than 1% of the $^3He/^4He$ ratio.

The observed $^3He/^4He$ ratios range from 0.331 R/R_{atm} to 16.23 R/R_{atm}. These agree well with the reference data except for the Kakehashi sample (No. 6).

Table 2. $^3He/^4He$ Ratios of Terrestrial Gases

No.	Name	$(^3He/^4He)_{obs}$ (R/R_{atm})	$(^3He/^4He)_{ref}$ (R/R_{atm})	Ref.	Lab.
1	Mud volcano Yellowstone, USA	16.23±0.10	16.45	14	SIO
			15.8	22	UCB
2	Hakone Kanagawa, Japan	6.13±0.03	6.2	20	SIO
			6.08	25	OU
			5.92	23	UT
3	Nigorigo Gifu, Japan	6.02±0.05	6.06±0.17	21	UT
4	Shirakawa Nagano, Japan	5.21±0.04	5.18±0.07	21	UT
5	Uminokuchi Nagano, Japan	5.15±0.03	5.16±0.11	23	UT
6	Kakehashi Nagano, Japan	3.70±0.02	3.43±0.05	21	UT
7	Yuya Gifu, Japan	2.04±0.01	2.13±0.06	21	UT
8	Kashima Fukushima, Japan	0.331±0.07	0.335±0.011	24	UT

SIO: Scripps Institution of Oceanography, University of California. UCB: Berkeley, University of California. OU: Osaka University. UT: University of Tokyo.

The discrepancy observed in No. 6 is about 7% of the ratio. Excluding this sample, differences are about 4% at maximum and equivalent to the experimental errors of the reference data. This suggests that the present system gives sufficiently accurate $^3He/^4He$ ratio measurements, assuming the reliability of the reference data.

The $^3He/^4He$ ratio of the Yellowstone sample (No. 1), 16.23 R/R_{atm}, is significantly higher than the $^3He/^4He$ ratios of 8—9 R/R_{atm} in mid-ocean ridge basalt (MORB).[3] Since the composition of the MORB is considered to be representative of the Earth's upper mantle, the source region of the Yellowstone sample is more primitive than that of the upper mantle. Gas samples from the Hakone volcano (No. 2) and the Nigorigo hot spring near the Ontake volcano (No. 3) show $^3He/^4He$ ratios of about 6 R/R_{atm}, identical to those in the circum Pacific volcanic region and slightly lower than the MORB. The $^3He/^4He$ ratio of bubbling gas in a Kashima well (No. 9), situated on the forearc region of Northeast Japan, is lower than the air ratio. Radiogenic He produced in crustal rock and sediment may be dominant in the sample.

Conclusion

The present analytical system has a high sensitivity of 5×10^{-5} A cm^{-3} STP of ^4He measured with a Faraday cup, an extreme precision of less than 1%, and sufficient accuracy of $^3He/^4He$ ratio measurement. The system can be applied to various fields of geoscience research, such as mantle geology, volcanology, marine chemistry, and environmental and limnological studies.

References

1) H. Craig and J. E. Lupton, "The Sea," **7**, Wiley, New York (1981), p. 391.
2) B. A. Mamyrin and I. N. Tolstikhin, "Helium Isotopes in Nature," Elsevier, New York (1984), p. 273.
3) J. E. Lupton, *Ann. Rev. Earth Planet. Sci.*, **11**, 371 (1983).
4) I. N. Tolstikhin, "Terrestrial Rare Gases," Japan Sci. Soc. Press, Tokyo (1978), p. 33.
5) Y. Sano, Y. Nakamura, H. Wakita, A. Urabe, and T. Tominaga, *Science*, **224**, 150 (1984).
6) W. B. Clarke, W. J. Jenkins, and Z. Top, *Int. J. App. Radiat. Isot.*, **27**, 515 (1976).
7) T. Torgersen, Z. Top, W. B. Clarke, W. J. Jenkins, and W. S. Broecker, *Limnol. Oceanogr.*, **22**, 181 (1977).
8) N. Takaoka and Y. Mizutani, *Earth Planet. Sci. Lett.*, **85**, 74 (1987).
9) H. Wakita and Y. Sano, *Nature (London)*, **305**, 792 (1983).
10) Y. Sano, K. Toyoda, and H. Wakita, *Nature (London)*, **317**, 518 (1985).
11) Y. Sano, H. Wakita, and C.-W. Huang, *Nature (London)*, **323**, 55 (1986).
12) Y. Sano, *Geochem. J.*, **20**, 227 (1986).
13) Y. Sano, T. Tominaga, Y. Nakamura, and H. Wakita, *Geochem. J.*, **16**, 237 (1982).
14) W. Rison and H. Craig, *Earth Planet. Sci. Lett.*, **66**, 407 (1983).
15) P. Schlosser, *Nature (London)*, **321**, 233 (1986).
16) J. H. Reynolds, P. M. Jeffery, G. A. McCrory, and P. M. Varga, *Rev. Sci. Instrum.*, **49**, 547 (1978).
17) B. A. Mamyrin, G. S. Anufriev, I. L. Kamenskiy, and I. N. Tolstikhin, *Geochem. Int.*, **7**, 498 (1970).
18) T. Torgersen and W. J. Jenkins, *Geochim. Cosmochim. Acta*, **46**, 739 (1982).
19) R. Poreda, *Earth Planet. Sci. Lett.*, **73**, 244 (1985).
20) H. Craig, J. E. Lupton, and Y. Horibe, "Terrestrial Rare Gases," Japan Sci. Soc. Press, Tokyo (1978), p. 3.
21) Y. Sano, Y. Nakamura, H. Wakita, K. Notsu, and Y. Kobayashi, *J. Geophys. Res.*, **91**, 12291 (1986).
22) B. M. Kennedy, M. A. Lynch, J. H. Reynolds, and S. P. Smith, *Geochim. Cosmochim. Acta*, **49**, 1251 (1985).
23) Y. Sano and H. Wakita, *J. Geophys. Res.*, **90**, 8729 (1985).
24) Y. Sano, Y. Nakamura, and H. Wakita, *Chem. Geol. (Isot. Geosci. Sect.)*, **52**, 1 (1985).
25) K. Nagao, N. Takaoka, and O. Matsubayashi, *Earth Planet. Sci. Lett.*, **53**, 175 (1981).

 © 1988 The Chemical Society of Japan Bull. Chem. Soc. Jpn., 61, 1159—1162 (1988)

Interfacial Adsorption of 1,10-Phenanthroline Complexes in Solvent Extraction Systems

Hitoshi WATARAI,* Yoko HORII, and Mitsuaki FUJISHIMA
Department of Chemistry, Faculty of Education, Akita University, Akita 010
(Received August 8, 1987)

A significant adsorptivity of tris(1,10-phenanthroline)iron(II), $[Fe(phen)_3]^{2+}$, at the interface of chloroform or carbon tetrachloride/0.1M aqueous sodium chloride systems was determined by means of interfacial tension measurements at 25 °C. In the distribution systems of phen containing Zn(II) or Cu(II), a characteristic interfacial tension lowering was observed and interpreted in terms of an interfacial adsorption of metal-phen complexes.

Ion-association extraction of Fe(II) with 1,10-phenanthroline, phen, has been extensively studied not only for a colorimetric determination of iron itself, but also for an indirect determination of a variety of organic and inorganic anions which are extractable with $[Fe(phen)_3]^{2+}$.[1,2] Although the stoichiometry of the overall extraction equilibrium between bulk phases has been established, there is no available information concerning the role of the interface in an extraction with phen and its derivatives, except those which we reported recently. In this case the interfacial adsorption of protonated phen derivatives in the chloroform/acidic aqueous phase[3] and of Cu(II) and Zn(II) 4,7-diphenyl-1,10-phenanthroline complexes in the chloroform/aqueous phase systems[4] were determined by means of a high-speed stirring method. Also, a significant role of the interface was demonstrated. For the elucidation of a realistic mechanism of ion-association extraction, which should include a rational assessment on interfacial reactions, further extensive studies concerning interfacial phenomena are required.

In the present study, first the interfacial adsorptivity of $[Fe(phen)_3]^{2+}$, a very stable tris(phen) complex, was examined by means of interfacial tension measurements. Secondly, the interfacial tension in the systems containing both phen and Zn(II) or Cu(II), which include mono, bis, and tris(phen) complexes, was measured; the adsorptivity of each complex, especially of the tris(phen) complexes, is discussed based on the results of $[Fe(phen)_3]^{2+}$ system.

Experimental

Chemicals. phen, wako G.R., was used as purchased. $[Fe(phen)_3]Cl_2$ and $[Fe(phen)_3](ClO_4)_2$ were synthesized by the conventional methods and purified by recrystallization from an aqueous solution. Chloroform, Wako G.R., was washed with an equal amount of water three times prior to use. Carbon tetrachloride, Nakarai G.R., was shaken with sulfuric acid, washed with water and then fractionally distilled. Other chemicals used were of all G.R. grade. Stock solutions of Zn(II) and Cu(II) were prepared by dissolving pure zinc powder and $CuCl_2 \cdot 2H_2O$ in hydrochloric acid solution, respectively. The ionic strength of the aqueous solution was adjusted to 0.1 by sodium chloride, and the pH was controlled by hydrochloric acid and sodium acetate (0.002 M, 1 M=1 mol dm^{-3}). The use of sodium chloride completely depressed the ion-association extraction of metal-phen complexes and made conspicuous the interfacial adsorption of the complexes.

Interfacial Tension Measurements. Measurements of the interfacial tension, γ, were carried out by means of a drop-volume method at 25±1 °C. The apparatus used is schematically shown in Fig. 1. The organic and aqueous phases, 10 ml each, were shaken for 30 min and equilibrated prior to the measurements. The aqueous drop produced on the end of a glass capillary (6 mm o.d.) was slowly released after 5 min equilibration, and the volume of a detached drop was measured using a Gilmont micrometer pipet s1200 (2 μl smallest division) or s4200 (0.1 μl smallest division). The volume of one drop was determined as an average of at least 5 drops. The interfacial tension was then calculated by using the interfacial tension values of 31.5 dyn cm^{-1} and 44.55 dyn cm^{-1} for $CHCl_3$/water and CCl_4/water systems, respectively, and by applying the Lando-Oakley's equation.[5]

Distribution of phen. Distribution constants of phen in

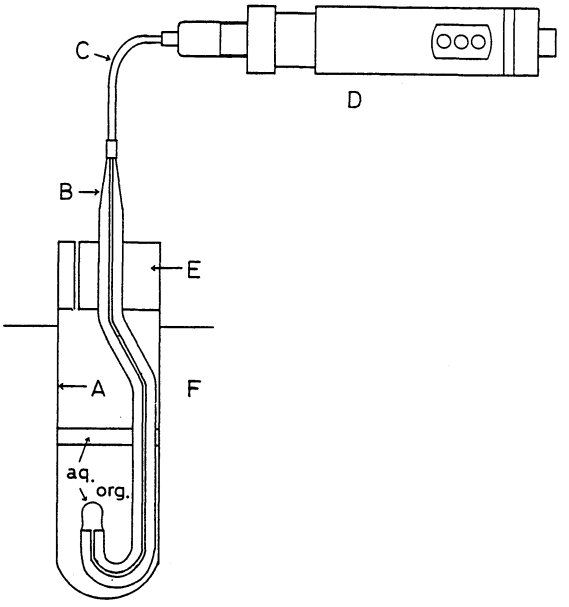

Fig. 1. Apparatus for interfacial tension measurements by drop-volume method in halomethane/water system: A, glass vessel; B, glass capillary; C, teflon tube; D, digital micrometer pipet; E, stopper with a hole; F, thermostated water bath.

$CHCl_3$/0.1 M NaCl and CCl_4/0.1 M NaCl systems were determined by a batch method. An aqueous solution of phen, 5 ml or 10 ml, was shaken with 5 ml organic solvent for 30 min by means of a mechanical shaker. The pH of the aqueous phase was controlled to higher than 6.2. From the absorbances at 265 nm of the aqueous phases before and after distribution, the distribution constant, K_D, was calculated, as listed in Table 1. Absorbance measurements were carried out by means of a Hitachi 200-20 or UVIDEC 430 spectrophotometer. The value of K_D was employed for the calculation of the concentrations of mono, bis, and tris(phen) complexes in the aqueous phases of $CHCl_3$/aqueous systems containing phen, and Zn(II) or Cu(II). An NEC PC-microcomputer was used for both calculations of the concentrations and the interfacial tensions.

Results and Discussion

Interfacial Adsorption of $[Fe(phen)_3]^{2+}$. The interfacial tension in an $CHCl_3$/0.1 M NaCl solution decreased upon the addition of $[Fe(phen)_3]^{2+}$ above a concentration of 10^{-6} M, as shown in Fig. 2. The substitution of $[Fe(phen)_3]Cl_2$ by $[Fe(phen)_3](ClO_4)_2$ did not seriously affect γ under the present conditions. When the organic solvent was changed from $CHCl_3$ to CCl_4, the concentration at which γ began to decrease was shifted to a value about 100-times higher than that in the $CHCl_3$ system (see Fig. 2).

The observed lowering in γ is attributable to an interfacial adsorption of $[Fe(phen)_3]^{2+}$, which is usually analysed according to the Gibbs equation or the Langmuir isotherm. The interfacial excess Γ of a solute is defined by the Gibbs equation:

$$\Gamma = -\frac{1}{RT}\frac{\partial\gamma}{\partial \ln C}, \quad (1)$$

where C refers to the solute concentration in aqueous phase. However, according to the Langmuir isotherm, the interfacial concentration of the solute, C_i, can be represented by

$$C_i = \frac{aK'C}{a+K'C}, \quad (2)$$

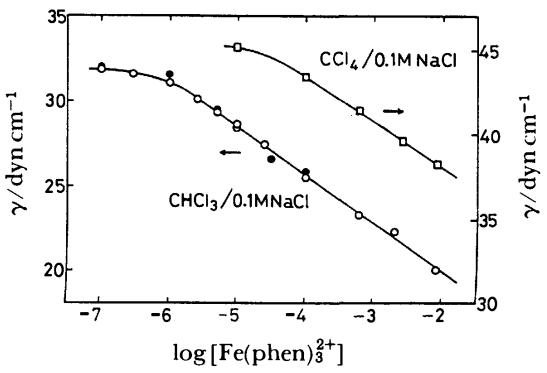

Fig. 2. Interfacial tension lowering by addition of $[Fe(phen)_3]Cl_2$ (○) or $[Fe(phen)_3](ClO_4)_2$ (●) in $CHCl_3$/0.1 M NaCl (pH=6.2) and CCl_4/0.1 M NaCl (pH=6.2).

where a refers to the interfacial concentration at saturation and K' to the equilibrium constant for adsorption of the solute from aqueous phase to interface at infinite dilution. By combining Eqs. 1 and 2 by approximating $\Gamma \fallingdotseq C_i$, and integrating the combined equation over a concentration range from zero to C, corresponding to the interfacial tension from γ_0 to γ, one obtains

$$\gamma = \gamma_0 - aRT \ln\left(1+\frac{K'C}{a}\right). \quad (3)$$

When $C \gg a/K'$, Eq. 3 becomes,

$$\gamma = \gamma_0 - aRT \ln\frac{K'}{a} - aRT \ln C. \quad (4)$$

Equation 4 represents a linear relationship between γ and log C, as observed in a higher-concentration region in Fig. 2; the slope of the straight line refers to $-2.303aRT$. In addition, the concentration C^*, at which the straight line of Eq. 4 and another straight line of $\gamma=\gamma_0$ crosses, is found to be equal to a/K'. The application of these analyses to $[Fe(phen)_3]^{2+}$ systems yields parameters a and K' for the two-solvent systems listed in Table 1. The values of the interfacial concentration at the saturation or interfacial area occupied by a single complex ion does not differ very much in two-solvent systems (see Table 1). As for the values of C^*, however, as well as those of K', there is a strong solvent dependence: K' in $CHCl_3$ system is 86-times larger than that in the CCl_4 system; this means that the $[Fe(phen)_3]^{2+}$ ion is much more adsorbable to the $CHCl_3$/water interface than the CCl_4/water interface. Ozeki et al. recently reported that $[Fe(phen)_3]^{2+}$ is never surface-active from the fact that the surface tension of a 5.0×10^{-4} M $[Fe(phen)_3](ClO_4)_2$ solution was 71.93 ± 0.1 dyn cm^{-1}, agreeing with that of pure water.[6] Consequently, the interfacial adsorptivity of $[Fe(phen)_3]^{2+}$ observed in the present systems should be ascribable to a lipophilic interaction between phen molecules coordinated to Fe(II) and the organic solvent at the interface. This idea is supported by the fact that the distribution constant of phen, which is a measure of the lipophilic interaction, is much larger in the $CHCl_3$ system (see Table 1). From the above discussion, it is concluded that tris(phen) complexes are strongly

Table 1. Parameters in the Interfacial Adsorption of $[Fe(phen)_3]^{2+}$ at 25 °C

Parameter	Organic solvent	
	CCl_4	$CHCl_3$
a/mol cm^{-2}	4.80×10^{-11} (346)[a]	4.98×10^{-11} (333)
C^*/mol l^{-1}	4.50×10^{-5}	5.40×10^{-7}
K'/l cm^{-2}	1.07×10^{-6}	9.23×10^{-5}
K_D(phen)	1.14 ± 0.07	723 ± 18

a) Values in parentheses refer to an area (Å^2) per molecule.

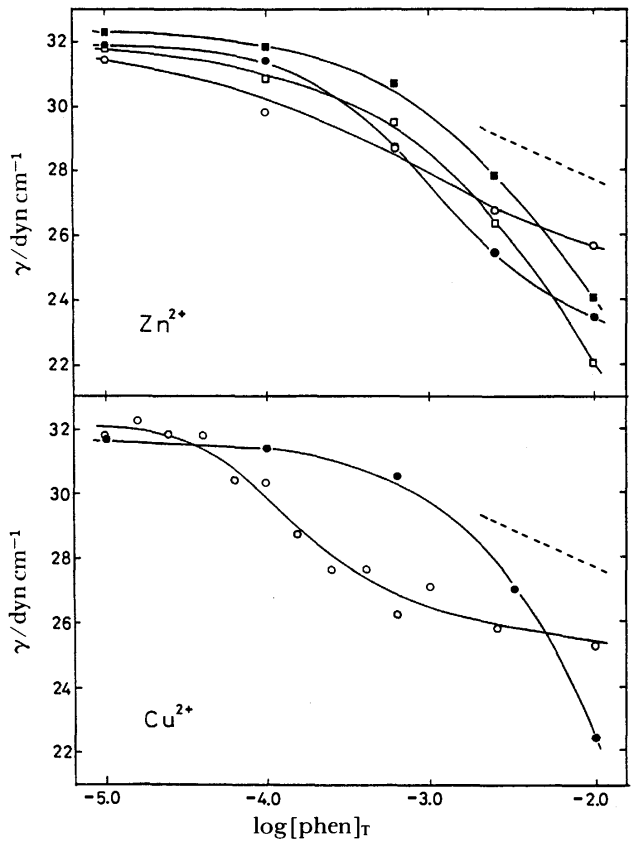

Fig. 3. Effects of zinc(II) and copper(II) on the interfacial tension of phen-$CHCl_3$/0.1 M NaCl systems: no metal ion (----); $[Zn^{2+}]_T=1.0\times10^{-4}$ M, pH=6.06 (○), 1.0×10^{-3} M, pH=5.33 (●), 5.0×10^{-3} M. pH=3.44 (□), 1.0×10^{-2} M, pH=2.68 (■); $[Cu^{2+}]_T=1.0\times10^{-4}$ M, pH=6.28 (○), 1.0×10^{-3} M. pH=6.03 (●).

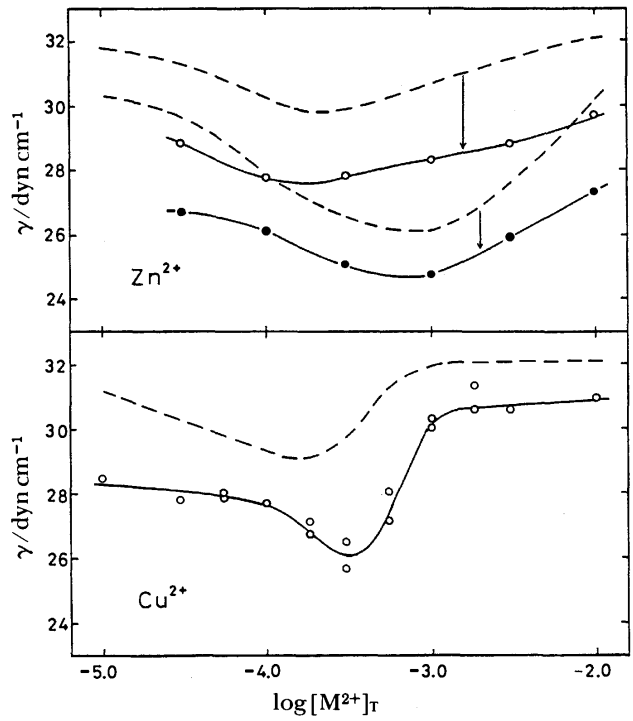

Fig. 4. Dependence of interfacial tension in $CHCl_3$ system on the zinc(II) and copper(II) concentrations at a constant phen concentration: $[phen]_T=6.21\times10^{-4}$ (○), 2.49×10^{-3} M (●), pH=6.1 in Zn(II) systems; $[phen]_T=6.24\times10^{-4}$ M (○), pH=3.91—6.02 in Cu(II) systems.

adsorbable at the $CHCl_3$/water interface.

Interfacial Adsorption of Zn(II)-phen and Cu(II)-phen Complexes. The interfacial tension in phen-$CHCl_3$/0.1 M NaCl systems containing Zn(II) or Cu(II) ions depended on both the concentrations of phen and the metal ion. In Fig. 3, the effect of the metal ions on plots of γ vs. the logarithm of the total phen concentration, log $[phen]_T$, is shown. In both systems, the following tendencies are observed: in a lower phen concentration, the lowering of γ is larger in a lower metal concentration than that in a higher metal concentration, while in a higher phen concentration the situation is reversed, more obviously in Cu(II) systems. In the region $[phen]_T=10^{-4}$—10^{-3} M, the values of γ in $[Cu^{2+}]_T=10^{-4}$ M are lower than those in $[Cu^{2+}]_T=10^{-3}$ M. This means that the species formed under the condition $[phen]_T>[Cu^{2+}]_T$ is more adsorbable than those formed under $[phen]_T<[Cu^{2+}]_T$, suggesting a preferencial adsorptivity of a bis or tris-(phen) complex than a mono(phen) complex. When the total phen concentration was fixed, the plots of γ vs. log $[M^{2+}]_T$ showed a minimum that depended on the phen concentration, as shown in Fig. 4. It is noted in Fig. 4 that the Zn(II) concentration, showing a minimum in γ, shifted toward a higher region when $[phen]_T$ was increased. These interfacial tension lowering characteristics are thought to be ascribable to the adsorption of Zn(II) or Cu(II)-phen complexes, since the adsorptivity of phen is very low.[3] In order to discuss which type of the complex is most responsible for the lowering of γ, the concentrations of mono-, bis-, and tris(phen) complexes in the aqueous phase under the given total concentrations of metal ion and phen were calculated using

$$[M^{2+}]_T = [M^{2+}](1+\beta_1[L]+\beta_2[L]^2+\beta_3[L]^3) \quad (5)$$

and

$$[L]_T = (1+\frac{[H^+]}{K_a}+K_D)[L] + [M^{2+}](\beta_1[L]+2\beta_2[L]^2+3\beta_3[L]^3), \quad (6)$$

where $[M^{2+}]$ and [L] refer to the concentrations of the free metal ion and the free ligand phen, respectively; the subscript T denotes the total concentration of the metal ion or phen. The value of the formation constants used for the calculation are log $\beta_1=6.30$, log $\beta_2=11.95$, and log $\beta_3=17.05$ for Zn(II)-phen system and log $\beta_1=8.82$, log $\beta_2=15.39$, and log $\beta_3=20.41$ for Cu(II)-phen system.[7] A calculation of $[M^{2+}]$, $[ML^{2+}]$

$[ML_2^{2+}]$, and $[ML_3^{2+}]$ was carried out by determining the best value of [L] so that the $[M^{2+}]_T$ and $[L]_T$ calculated by Eqs. 5 and 6 would agree with the experimental concentrations. The contribution of $[LH^+]$ in Eq. 6 was not serious in almost systems studied here, since pK_a=4.98 for phen.[7] Because a preliminary comparison between the calculated results and Figs. 3 and 4 suggested a significant contribution of ML_3^{2+}, a semi-quantitative comparison was attempted between the observed γ values and the estimated values using

$$\gamma = 32.1 - 1.24 \ln\left(1 + \frac{[ML_3^{2+}]}{5.40 \times 10^{-7}}\right), \quad (7)$$

which is determined for the $[Fe(phen)_3]^{2+}$ system, assuming that the adsorptivity of ML_3^{2+} is the same as that of $[Fe(phen)_3]^{2+}$. The broken lines in Fig. 4 show the γ estimated using the calculated $[ML_3^{2+}]$ and Eq. 7. Although a quantitative agreement between the calculated and observed γ's is not satisfactory, the features of the γ vs. log $[M^{2+}]_T$ profile are well-reproduced, especially in Zn(II) systems. The observed minima in Zn(II) systems correspond to the situation where $[M^{2+}]_T$: $[L]_T$=1 : 3. These results confirm that a predominant species at the interface in Zn(II) systems is $[Zn(phen)_3]^{2+}$. In Cu(II) systems, the minimum point in Fig. 4 is close to $[M^{2+}]_T$: $[L]_T$=1 : 2. Hence, the adsorption of $[Cu(phen)_2]^{2+}$ as well as $[Cu(phen)_3]^{2+}$ may take place in higher Cu(II) concentration.

The authors wish to thank the Ministry of Education, Science and Culture for a financial support, a Grant-in-Aid for Scientific Research to H.W. (No. 61470034).

References

1) Y. Yamamoto, T. Tarumoto, and E. Iwamoto, *Anal. Chim. Acta*, **64**, 1 (1973).
2) K. L. Cheng, K. Ueno, and T. Imamura, "Handbook of Organic Analytical Reagents," CRC Press, Inc., Florida, USA (1982).
3) H. Watarai, *J. Phys. Chem.*, **89**, 384 (1985).
4) H. Watarai, *Talanta*, **32**, 817 (1985).
5) J. L. Lando and H. T. Oakley, *J. Colloid Interface Sci.*, **25**, 526 (1967).
6) S. Ozeki, S. Tachiyashiki, S. Ikeda, and H. Yamatera, *J. Colloid Interface Sci.*, **91**, 439 (1983).
7) H. Irving and D. H. Miller, *J. Chem. Soc.*, **1962**, 5222.

 © 1988 The Chemical Society of Japan Bull. Chem. Soc. Jpn., 61, 1163—1167 (1988)

Association of Naphthalene and Its Methyl Derivatives with Cyclodextrins in Aqueous Medium

Motohisa FUJIKI, Toshio DEGUCHI, and Isao SANEMASA*
Department of Chemistry, Faculty of Science, Kumamoto University, Kurokami 2-39-1, Kumamoto 860
(Received September 5, 1987)

Formation constants of naphthalene and its (1- and 2-)methyl and (1,4-, 1,5-, and 1,8-)dimethyl derivatives with α-, β-, and γ-cyclodextrins (CyD) were determined in the aqueous medium in the presence of excess CyD. The technique used to study associations between host (CyD) and guest(hydrocarbon) is based on the facts that the guest molecules can be driven out to gaseous phase by introducing an inert gas at a constant flow rate into the aqueous solution and that the volatilization rate of guest decreases with increasing association with the host in aqueous solution. The 1:1 and 2:1 (host:guest) formation constants were evaluated at 25 °C. From the formation constant estimated, a host-guest spatial-fitting model for each association complex is presented.

We have recently reported a method useful for estimating association constants between volatile and nonvolatile solutes in aqueous medium.[1-2] The method is based on volatility of nonelectrolyte solute in water. Volatile molecules are driven out to gaseous phase by introducing an inert gas at a constant flow rate into the aqueous solution. The volatilization rate was measured with and without addition of nonvolatile solute which associates with the volatile solute and decreased with the degree of association between the solutes. The method is applicable to such systems where (a) one of the solute is volatile, (b) the concentration of nonvolatile solute is sufficiently high in comparison with that of volatile solute, and (c) the rate of association is rapid compared with the volatilization rate.

The method was applied to association of benzene and alkylbenzenes as guests with cyclodextrins (CyD) as hosts and 1:1 and 2:1 (host:guest) formation constants were evaluated.[3] The present work is concerned with an application of the method to association of naphthalene and its methyl derivetives with α-, β-, and γ-CyDs.

There have been reported several data concerning the naphthalene-CyD formation constant.[4-7] The data are, however, only on the β-CyD complex and little is known concerning naphthalene derivatives. The present study was undertaken to see whether or not the volatilization method is successfully applicable to naphthalene and its derivatives and to elucidate the effects of the cavity size of host and the steric hindrance of guest on the host-guest inclusion complex formation.

Experimental

Materials and Preparation of Sample Solutions. Distilled deionized water was used throughout the experiments. Aromatic hydrocarbons used as guest were of analytical reagent grade (the purity is listed in Table 1). Cyclodextrins (α-, β-, and γ-CyD) used as host were of guaranteed grade from Nakarai Chemical Co. Both guest and host reagents were used without further purification. An aqueous solution of each guest was prepared by adding an excess solid or liquid hydrocarbons to water and stirring for at least 24 h. After standing the mixture for at least 24 h, a portion of the saturated guest solution was transferred into a separatory funnel and the UV absorption of its chloroform extract was measured to determine the guest concentration, and another portion was transferred into a 2.5ϕ×25 cm cylindrical glass tube. A suitable amount of CyD, which had been dried over phosphorus pentaoxide under vacuum, was weighed and dissolved into the guest solution. The solution was then diluted to 100 cm^3 with water. Ranges of concentration of guest and host are given in Table 3.

Amberlite XAD-2 resin (Rohm and Hass) of 100—150 mesh size was used as an adsorbent of guest vapor.

Apparatus and Procedures. The apparatus and the experimental procedure were the same as those described in the previous paper with minor modifications.[3] Because the volatility of guest substances examined in this study is considerably lower than that of benzene and alkylbenzenes, a sintered glass ball was used as an N_2 bubbler to drive guest molecules effectively out of the aqueous solution at higher N_2 flow rates (Table 1). The N_2 gas leaving the sample solution was passed through an XAD resin column of 0.5ϕ×10 cm and the guest hydrocarbon adsorbed on the resin for a fixed time was eluted out with $CHCl_3$ of 6 cm^3. The amount of guest collected in an XAD column, ΔQ_ϕ, was determined by UV spectroscopy at the optimum wavelength for each guest hydrocarbon (Table 1).

Table 1. Experimental Conditions

Guest substance	Purity	λ[a]	N_2 gas flow rate
	%	nm	$cm^3 min^{-1}$
Naphthalene	G.R.[b]	276.6	50, 150, 250
1-Methyl-naphthalene	97	283.0	350
2-Methyl-naphthalene	G.R.	277.2	350
1,4-Dimethyl-naphthalene	95	243.0	700
1,5-Dimethyl-naphthalene	98.0	289.0	700
1,8-Dimethyl-naphthalene	95.0	287.6	700

a) The wavelength for determining the concentration of guest molecules after $CHCl_3$ extraction. b) Guaranteed grade reagent (the purity is not specified).

Results and Discussion

Estimation of 1 : 1 and 2 : 1 (Host : Guest) Formation Constants. Under the present experimental conditions that host molecules are always excess over guest molecules, the possible host : guest stoichiometric ratios are 1 : 1 and 2 : 1. Then, the reactions that should be taken into account are:

$$\mathrm{CyD}+\phi \rightleftarrows \mathrm{CyD}\cdot\phi,\ (K_1), \tag{1}$$

$$\mathrm{CyD}\cdot\phi+\mathrm{CyD} \rightleftarrows \mathrm{CyD_2}\cdot\phi,\ (K_2), \tag{2}$$

and

$$\phi(\mathrm{aq}) \rightarrow \phi(\mathrm{gas}),\ (k), \tag{3}$$

where ϕ refers to a guest hydrocarbon molecule, K_1 and K_2 are the corresponding stepwise formation constants, and k is the rate constant for transfer of guest molecules from aqueous to gaseous phase.

We assume that the release of guest molecules at a constant N_2 flow rate is of first-order with respect to the concentration of free species in the solution as follows:

$$dQ_\phi V^{-1}/dt = k[\phi], \tag{4}$$

where V is the volume of aqueous solution.

An equation to estimate K_1 and K_2 can be derived using the total concentrations of host (C_{CyD}) and guest (C_ϕ) and the amount of guest released from aqueous solution during the aeration time (Q_ϕ, the sum of ΔQ_ϕ from time 0 to t), in the same way as described in the previous paper as follows:[3]

$$\ln(C_\phi - Q_\phi V^{-1}) = -kt/(1+K_1C_{CyD}+K_1K_2C_{CyD}^2) + \ln C_\phi = -k't + \ln C_\phi, \tag{5}$$

where

$$k' = k/(1+K_1C_{CyD}+K_1K_2C_{CyD}^2). \tag{6}$$

Rearrangement of Eq. 6 yields:

$$1/k' = K_1K_2C_{CyD}^2/k + K_1C_{CyD}/k + 1/k. \tag{7}$$

Plots according to Eq. 5 for naphthalene-β-CyD are shown in Fig. 1. The plots give straight lines up to ca. 70% release of the guest hydrocarbon initially present in the solution. This linearity verifies the assumption that the volatilization of guest molecules follows a first-order reaction at a constant N_2 flow rate. The slopes of resulting straight lines, k' (and k), were evaluated using the least-squares method; the results for naphthalene are given in Table 2. Both k and k' values change with the N_2 flow rate, but their values

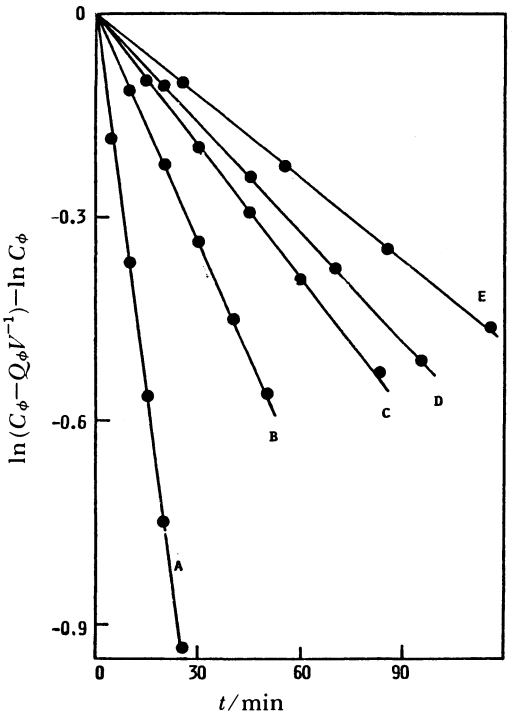

Fig. 1. Naphthalene-β-CyD system. The plots of $\ln(C_\phi - Q_\phi V^{-1}) - \ln C_\phi$ vs. t in the presence and absence of cyclodextrin. N_2 flow rate: 250 cm^3 min^{-1}; $C_{CyD}/10^{-3}$M: (A) 0, (B) 3.50, (C) 7.11, (D) 8.84, (E) 12.1; C_ϕ: 1.76×10^{-5} M.

Table 2. The Rate Constant for Transfer of Naphthalene from Aqueous to Gaseous Phase in the Presence and Absence of α-, β-, and γ-Cyclodextrin

k or k'[a]	C_ϕ[b]	Total concentration of		
		α-CyD	β-CyD	γ-CyD
10^{-2} min^{-1}	10^{-5} M	10^{-2} M	10^{-3} M	10^{-3} M
N_2 flow rate: 250 cm^3 min^{-1}				
3.53[c]	0.86—1.71			
1.22	1.94	1.50		
0.625	1.94	3.00		
0.369	2.01	4.50		
0.180	1.94	7.50		
0.112	2.01	10.2		
0.0893	1.94	11.5		
1.12	1.76		3.50	
0.648	1.76		7.11	
0.538	1.76		8.84	
0.413	1.76		12.1	
2.31	2.02			2.62
2.00	2.02			5.24
1.78	2.02			7.45
1.30	1.95			9.44
0.694	1.95			24.9
0.437	1.95			44.9
0.385	1.95			52.8
N_2 flow rate: 50 cm^3 min^{-1}				
0.971[c]	1.90			
0.439			1.90	
0.313			3.36	
0.219			5.38	
0.126			10.1	
N_2 flow rate: 150 cm^3 min^{-1}				
2.22[c]	2.05			
0.714	2.05		3.35	
0.435	2.05		6.65	
0.326	2.05		9.40	

a) $k'=k/(1+K_1C_{CyD}+K_1K_2C_{CyD}^2)$, where C_{CyD} is the total concentration of cyclodextrin. b) The initial concentration of naphthalene. c) The average of four determinations.

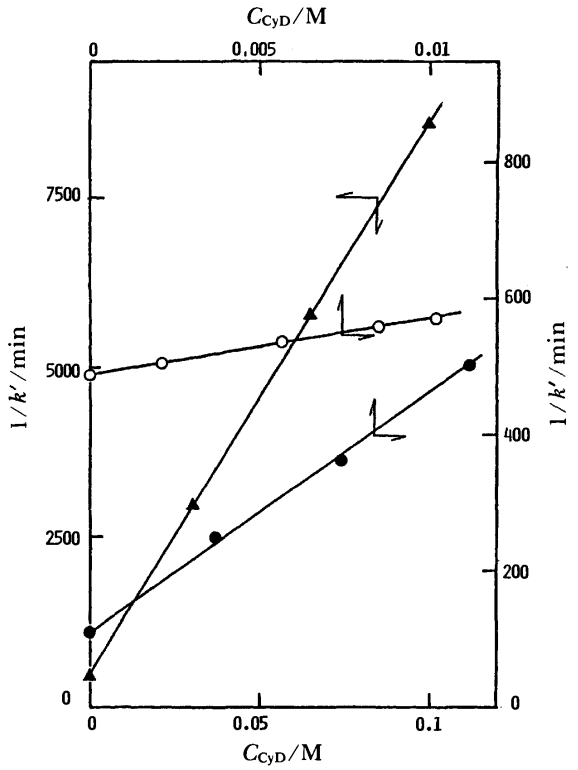

Fig. 2. The plots of $1/k'$ vs. C_{CyD}. Examples of straight line. 1-Methylnaphthalene-β-CyD (●), 1,8-dimethylnaphthalene-β-CyD (○), 1,8-dimethylnaphthalene-γ-CyD (▲).

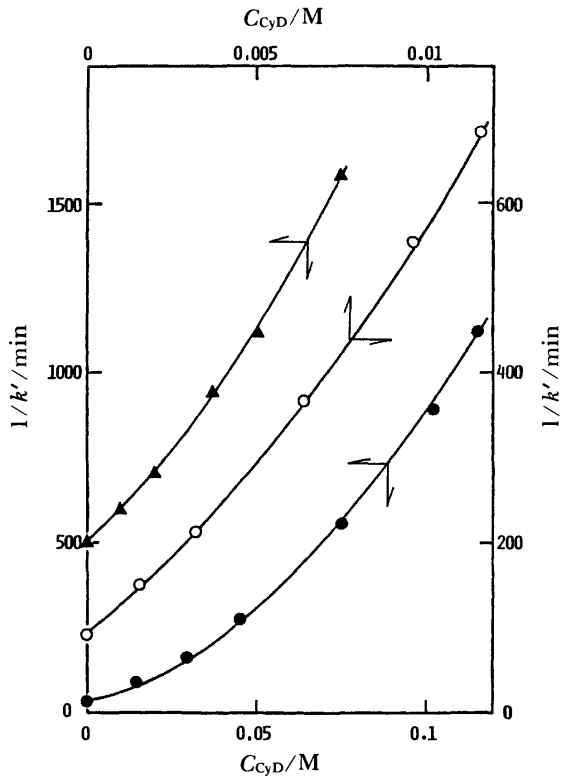

Fig. 3. The plots of $1/k'$ vs. C_{CyD}. Examples of parabolic curve. Naphthalene-α-CyD (●), 1,4-dimethylnaphthalene-β-CyD (○), 1,8-dimethylnaphthalene-α-CyD (▲).

are not significant when the N_2 flow is set at the same rate for two runs in the presence and absence of CyD. The K values determined for naphthalene-β-CyD at three different N_2 flow rates of 50, 150, and 250 cm^3 min^{-1} are found to be (6.6, 6.2, and 6.3)$\times 10^2$ M^{-1} (M≡mol dm^{-3}), respectively. Relatively large deviation inherent in the present method being considered, these K values for naphthalene-β-CyD seem to be in a reasonable agreement. This suggests that the rate of association is rapid compared with the volatilization rate; the essential requirement of the present method is fulfilled.

Figures 2 and 3 show some typical results plotted by a curve-fitting method with the aid of Eq. 7. The $1/k'$ vs. C_{CyD} plots appear to be linear (Fig. 2) or parabolic (Fig. 3) depending on the host-guest combination. The K_1 and K_2 values determined in this work are summarized in Table 3. As was pointed out in our previous paper,[3] the deviation of formation constant is relatively large, which arises from uncertainty in determining the amount of released guest; the overall error in Q_ϕ becomes large due to the accumulation of errors in ΔQ_ϕ.

The K value estimated here for naphthalene-β-CyD of 6.3$\times 10^2$ M^{-1} is consistent with the literature values,

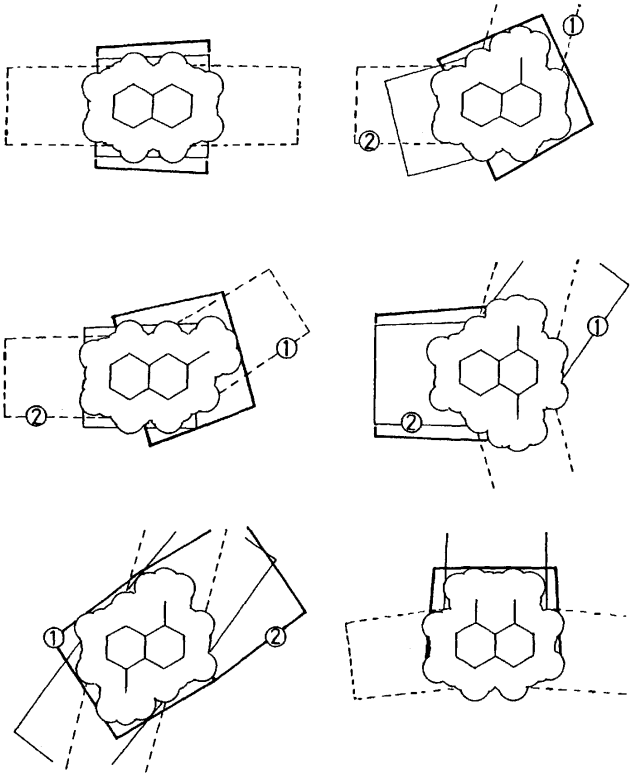

Fig. 4. Host-guest inclusion model. α-, β-, and γ-cyclodextrin cavities are drawn by dotted, thin solid, and thick solid lines, respectively. In the case of 2:1 (host:guest) complex being formed, the binding sites corresponding to K_1 and K_2 are, when necessary, are indicated respectively by the numbers, 1 and 2, in the circle.

Table 3. Concentration Ranges of Host and Guest and the Formation Constants, K_1(1 : 1) and K_2 (2 : 1) of (Host : Guest) Complexes at 25.0 °C

	Concentration		Formation constant[a]	
	C_ϕ[b]	C_{CyD}[c]	K_1	K_2[d]
	10^{-5} M	10^{-2} M	M^{-1}	M^{-1}
Naphthalene				
α-CyD	1.94—2.02	1.50 —11.5	83±3	23±6
β-CyD	1.76—2.05	0.190— 1.21	(6.3±0.4)×10²	—
γ-CyD	2.08	0.260— 9.06	(1.3±0.4)×10²	—
1-Methylnaphthalene				
α-CyD	2.61	2.62 —11.8	40±1	17±1
β-CyD	2.62	0.372— 1.32	(3.1±0.3)×10²	—
γ-CyD	2.61	1.04 —13.3	(1.3±0.5)×10²	—
2-Methylnaphthalene				
α-CyD	1.95	1.51 —11.1	22±5	12±4
β-CyD	1.93	0.377— 1.36	(7±1)×10²	—
γ-CyD	1.88	2.60 —11.7	(1.5±0.2)×10²	—
1,4-Dimethylnaphthalene				
α-CyD	0.482	1.91 — 9.52	43±8	17±7
β-CyD	0.478	0.161— 1.16	(3.5±0.2)×10²	50±8
γ-CyD	0.524	2.24 — 8.96	10±2	—
1,5-Dimethylnaphthalene				
α-CyD	0.181	2.47 —11.2	28±3	16±4
β-CyD	0.366	0.249— 1.12	(2.0±0.2)×10²	(1.1±0.4)×10²
γ-CyD	0.395	2.47 —11.2	(1.00±0.04)×10³	5±1
1,8-Dimethylnaphthalene				
α-CyD	1.37	1.01 —10.2	20±1	6±2
β-CyD	1.42	0.211— 1.01	17±1	—
γ-CyD	1.45	3.06 — 9.95	(1.7±0.1)×10²	—

a) The confidence level is set at 95%. b) The initial concentration of guest substance. c) The total concentration of cyclodextrin. d) The dash-sign indicates that K_2 was not evaluated, because $1/k'$ vs. C_{CyD} plots by Eq. 7 gave nearly straight line only.

685,[4] 730,[4] and 850 M^{-1},[6] determined by fluorescent method (the enhancement of guest fluorescence intensity in the presence of host). The UV absorption measurement, on the other hand, seems to give a lower value, 186 M^{-1}.[7]

For the naphthalene-β-CyD system, Hamai proposed 2 :2 complex formation:[4]

$$\beta\text{-CyD}\cdot\phi + \beta\text{-CyD}\cdot\phi \rightleftarrows (\beta\text{-CyD}\cdot\phi)_2. \quad (8)$$

The equilibrium constant is reported to be 4000 M^{-1}. If the 2 :2 complex exists, a 5% of the 1 : 1 complex is to be converted into the 2 : 2 form, when the initial concentration of naphthalene is 10^{-5} M and that of β-CyD is 10^{-2} M. Under the present experimental conditions, where the contribution of Reaction 8 is small, we have ignored the equilibrium of 2 : 2 complex formation in determining K.

Host-Guest Spatial-Fitting Model. The following data in Å unit were used for guests; bond length: 1.40 for the average C-C in naphthalen,[8]1.54 for C-C in alkyl group, 1.08 for C-H in naphthalene and alkyl group, van der Waals radius:[9] 1.0 for H and 1.7 for C. Concerned with hosts, we used the values; the inner diameter of cavity:[10] 4.7—5.2 for α-CyD, 6.0—6.4 for β-CyD, and 7.5—8.3 for γ-CyD (the smaller value is for the primary hydroxyl group and the larger is for the secondary hydroxyl group), the cavity depth:[11] 6.7 for α-CyD and ca. 7 for β- and γ-CyD.

By taking into account the magnitude of K_1 and K_2, inclusion models for all the host-guest combinations studied in this work are depicted in Fig. 4. When two hosts share a single guest, unambiguous assignment of K_1 and K_2 to the corresponding binding site is difficult. Then, we assumed that alkyl group is included in CyD cavity preferentially to naphthalene ring if the cavity entrance radius admits. Another assumption was made that a guest enters into CyD through wider secondary hydroxyl side.

It has been suggested that, if K_2 is large or nearly equal to K_1, the cross-section of secondary hydroxyl group sides of two CyDs are situated in parallel to each other in a suitable distance to form hydrogen bond.[12] In view of the K_2 values for the present 2 : 1 complexes being smaller than the corresponding K_1, we speculate that the distance along a naphthalene molecule is too long for two α-CyDs to cooperate with each other to form hydrogen bonds, while the distance is suitable for the second α-CyD to act to stabilize the 1 : 1 complex for benzene and also for *p*-xylene.

The cavity size of γ-CyD is sufficiently large to

include naphthalene ring, while the diameter of β-CyD cavity seems small to include a whole naphthalene molecule.[13] The cavity of β-CyD is, however, considered to suitably fit the naphthalene molecule, because K of β-CyD is larger than that of γ-CyD. The inner diameter of β-CyD we employed should be larger by 10%. According to this modification, 2-methylnaphthalene can enter the β-CyD cavity from methyl substituent. It seems, however, that 1-methyl derivative cannot be included from this substituent side due to the steric hindrance. The bulky 1,8-dimethyl groups obviously hinder the guest from entering deeply into β-CyD, but seem to exert no hindrance effect on γ-CyD. The 1,4-dimethyl groups, on the other hand, have a hindrance effect on γ-CyD. The size of γ-CyD fits most suitably 1.5-dimethylnaphthalene, and a large van der Waals stabilization works.

For benzene, alkylbenzenes, naphthalene, and its methyl derivatives, the largest formation constants observed are as follows; propylbenzene for α-CyD ($5.9\times10^2\,M^{-1}$), isopropylbenzene for β-CyD ($1.2\times10^3\,M^{-1}$), and 1,5-dimethylnaphthalene for γ-CyD ($1.00\times10^3\,M^{-1}$). From these observations, the alkyl chain seems to contribute to form more stable complexes with CyDs than an additional condensed ring does. This implies that the hydrophobic nature of guest is an important factor when the host-guest spatial-fitting requirement meets.

It should be emphasized that the inclusion models presented here are highly speculative because they are made based only on the magnitude of K_1 and K_2. Other information such as NMR, CD, and X-ray crystallographic data and thermodynamic and kinetic studies are necessary to confirm the inclusion model.

References

1) I. Sanemasa, Y. Nishimoto, A. Tanaka, and T. Deguchi, *Bull. Chem. Soc. Jpn.*, **59**, 1459 (1986).

2) I. Sanemasa, Y. Nishimoto, A. Tanaka, and T. Deguchi, *Bull. Chem. Soc. Jpn.*, **59**, 2269 (1986).

3) I. Sanemasa and Y. Akamine, *Bull. Chem. Soc. Jpn.*, **60**, 2059 (1987).

4) S. Hamai, *Bull. Chem. Soc. Jpn.*, **55**, 2721 (1982).

5) K. Kano, B. Zhou, M. Sakaguchi, H. Matsumoto, and S. Hashimoto, *Sci. Eng. Rev. Doshisha Univ.*, **25**, 33 (1985).

6) S. Hashimoto and J. K. Thomas, *J. Am. Chem. Soc.*, **107**, 4655 (1985).

7) N. Kobayashi, S. Minato, and T. Osa, *Makromol. Chem.*, **184**, 2123 (1983).

8) K. B. Lipkowitz, A. M. Naylor, and W. B. Melchior, *Tetrahedron Lett.*, **25**, 2297 (1984).

9) A. Bondi, *J. Phys. Chem.*, **68**, 441 (1964).

10) W. Saenger, *Angew. Chem., Int. Ed. Engl.*, **19**, 344 (1980).

11) M. L. Bender and M. Komiyama, "Cyclodextrin Chemistry," Springer-Verlag, New York (1978).

12) W. C. Cromwell, K. Byström, and M. R. Eftink, *J. Phys. Chem.*, **89**, 326 (1985).

13) The CyD cavity size differs from literature to literature. According to F. Cramer, W. Saenger, and H.-Ch. Spatz, *J. Am. Chem. Soc.*, **89**, 14 (1967), the inner diameter of α-, β-, and γ-CyD is 6, 7.5, and 9—10 Å, respectively. The data we employed in this paper are considerably small compared with these values.

 © 1988 The Chemical Society of Japan Bull. Chem. Soc. Jpn., 61, 1169—1174 (1988)

Crystal and Molecular Structure of Cobalt(II)mercury(II) Thiocyanate Adducts Having a New Layer Structure

Hisashi KINOSHITA* and Akira OUCHI†

Department of Chemistry, Faculty of Liberal Arts, Shizuoka University, Ohya, Shizuoka 422

†Department of Chemistry, College of Arts and Sciences, The University of Tokyo, Komaba, Meguro-ku, Tokyo 153

(Received September 29, 1987)

N-Methyl-2-piperidone adduct and dimethyl sulfoxide adduct of cobalt(II)mercury(II) thiocyanate were synthesized and their crystal and molecular structures were determined by the single-crystal X-ray diffraction technique. The former adduct is triclinic with a space group $P\bar{1}$, a=8.488(3), b=17.206(7), c=8.466(3) Å, α=103.72(1)°, β=90.00(1)°, γ=100.85(1)°, Z=2, while the latter adduct is orthorhombic with a space group $P2_12_12_1$, a=8.418(3), b=27.389(10), c=8.407(3) Å, Z=4, and the final R values obtained were 0.059 and 0.066, respectively. In these adducts each mercury atom is in the tetrahedral geometry, coordinated with four sulfur atoms of the thiocyanate (SCN) ions, and each cobalt atom is in the octahedral geometry, coordinated with four nitrogen atoms of SCN ions and two oxygen atoms of the Lewis-base molecules which occupy the trans-positions. Each pair of different kinds of metal atoms are bridged by an SCN ion forming a 16-membered ring of $Co_2Hg_2(SCN)_4$; these are linked, forming a two-dimensional network. The Lewis-base ligands are extended perpendicular to the plane on both sides. The complex layers are piled up in parallel, and there are no chemical or hydrogen bondings between the layers. This is a new type of the structure for $CoHg(SCN)_4L_2$ (L=Lewis base) type adducts.

The cobalt(II)mercury(II) thiocyanate (**1**) was found to have a diamond-like three-dimensional polymeric structure,[1] in which both kinds of the metal atoms are in the tetrahedral geometry. Each metal atom is linked with four metal atoms of another kind by one thiocyanate ion (SCN), respectively.

Previously, the present authors studied and determined the crystal and molecular structures of various Lewis base adducts of **1**.[2-6] According to our results, as well as other references, adducts with formula $CoHg(SCN)_4L_2$ (L=*N*,*N*-dimethylformamide (dmf),[7] *N*-methylformamide (mfa),[3] and pyridine (py)[8]) always have three-dimensional polymeric structures. On the other hand, complexes with formula $CoHg(SCN)_4(H_2O)_2\cdot 2L$ (L=*N*,*N*-dimethylacetamide (dma),[4] *N*-methyl-2-pyrrolidone (mpd)[5] and 2-pyrrolidone (pd)[6]) have a layer-type network structure of $[CoHg(SCN)_4(H_2O)_2]_n$: the Lewis-base molecules are not directly coordinated to any metal atoms, but are only hydrogen-bonded to the coordinated water, taking positions between the layers.

Along this line of research, we have continued to search for adducts with other linkage structures; we found two adducts of the type $CoHg(SCN)_4L_2$ in their crystalline states (L=*N*-methyl-2-piperidone (mpp) and dimethyl sulfoxide (dmso)). The former is a new compound, while the latter had already been reported by Makhija,[9] However, neither of their structures had been reported. Consequently, their crystal and molecular structures were determined by the X-ray diffraction method using their single crystals.

Experimental

Synthesis of the Adducts. (1) Bis(*N*-methyl-2-piperidone)-tetrakis(thiocyanato)cobalt(II)mercury(II) (**2**). A crystalline powder of **1** (1.0 g, 2.0 mmol) was dissolved into mpp (10 cm³), and 20 cm³ of water was added to the solution. It was left standing for several days and crystals of **2** were deposited. The pink crystals were filtered off and dried over silica gel. Yield: 0.5 g, 36%. Found: Co, 8.30; C, 26.24; H, 3.21; N, 11.55%. Calcd for $CoHgC_{16}H_{22}N_6O_2S_4$: Co, 8.21; C, 26.76; H, 3.09; N, 11.70%.

(2) Bis(dimethyl sulfoxide)tetrakis(thiocyanato)cobalt(II)-mercury(II) (**3**). Although this adduct had already been synthesized by Makhija from the tetrahydrofuran adduct of **1**,[9] we could obtain **3** more easily by the following method. A crystalline powder of **1** (1.0 g, 2.0 mmol) was dissolved into dmso(10 cm³), and 12 cm³ of water was added to the solution. It was left standing overnight and crystals of **3** were deposited. The pink-red crystals were filtered off and dried over silica gel. Yield: 0.8 g, 62%. Found: Co, 9.10; C, 14.66; H, 1.84; N, 8.61%. Calcd for $CoHgC_8H_{12}N_4O_2S_6$: Co, 9.09; C, 14.83; H, 1.87; N, 8.64%.

Intensity Data Collection. Crystals of **2** (dimensions 0.2×0.2×0.2 mm³), and of **3** (spherical, with ϕ=0.21 mm) were used for intensity data measurements.

Crystallographic data are as follows: **2**, $CoHgC_{16}H_{22}N_6O_2S_4$, *F.W.*=718.17, triclinic, with the space group of $P\bar{1}$, a=8.488(3), b=17.206(7), c=8.466(3) Å, α=103.72(1)°, β=90.00(1)°, γ=100.85(1)°, U=1178.4(6) Å³, Z=2, D_m=2.03(3) g cm⁻³, D_c=2.03 g cm⁻³, μ(Mo$K\alpha$)=7.74 mm⁻¹.

3, $CoHgC_8H_{12}N_4O_2S_6$, *F.W.*=648.12, orthorhombic with the space group of $P2_12_12_1$, a=8.418(3), b=27.389(7), c=8.407(3) Å, U=1938.3(10) Å³, Z=4, D_m=2.22(3) g cm⁻³, D_c=2.22 g cm⁻³, μ(Mo$K\alpha$)=9.57 mm⁻¹.

Reflections within the ranges of $3°<2\theta<55°$ for **2** and $3°<2\theta<60°$ for **3** were collected on a Rigaku AFC-6A automated four-circle X-ray diffractometer with graphite-monochromated Mo$K\alpha$ radiation (λ=0.71073 Å). The ω-2θ scan technique was employed (scan speed, 4° min⁻¹; scan width, 1.21+0.5tanθ° for **2** and 1.25+0.5tanθ° for **3**).

For **2**, of the 5435 independent reflections measured, 4051 $|F_o|>3\sigma(|F_o|)$ reflections were used for a structure determinaion; for **3**, of the 3271 independent reflections measured, 1953 $|F_o|>3\sigma(|F_o|)$ reflections were used. The intensities were corrected for Lorentz and polarization factors, as well as for absorption using numerical Gaussian integration.[10]

Structure Determination. The structures were solved by the heavy-atom method. The positions of the mercury and

cobalt atoms were deduced from a three-dimensional Patterson map, while the other non-hydrogen atoms were located by means of succesive Fourier syntheses. Their positional and thermal parameters (first isotropic and finally anisotropic) were refined by a block-diagonal least-squares method. The final R values obtained, applyng their anisotropic temperature parameters, were 0.059 for **2** and 0.066 for **3**.[11] (In the case of **3**, since it does not have a center of symmetry, the structure of the reversed chirality was also examined. However, since its R value was 0.069, the structure was not adopted.)

All calculations were carried out on a HITAC M-680H computer apparatus at the Computer Center of the University of Tokyo using a local version of the UNICS program system.[12] The atomic scattering factors were taken from Ref. 13.

Other Measurements. The magnetic moments of their solid samples were measured at 20 °C using a Gouy balance. The infrared absorption spectra were obtained by means of a JASCO IR810 grating infrared spectrophotometer using mineral oil and hexachloro-1,3-butadiene mull.

Results and Discussion

The final atomic parameters of the non-hydrogen atoms are listed in Tables 1 and 2, while the selected bond lengths and bond angles are shown in Tables 3 and 4, respectively.[14] Perspective drawings of both complexes around the mercury and the cobalt atoms are given in Figs. 1 and 2, together with the numbering scheme of the atoms.

Although the crystal systems as well as the space groups of **2** and **3** are different from each other (triclinic, $P\bar{1}$ for **2**, and orthorhombic, $P2_12_12_1$ for **3**), their molecular structures resemble each other. In both adducts each mercury atom is coordinated with four SCN sulfur atoms and is in a tetrahedral geometry.

Table 1. Final Atomic Coordinates ($\times 10^3$) and Equivalent Isotropic Temperature Factors (B_{eq}/Å^2) of **2** with Estimated Standard Deviations in Parentheses

Atom	x	y	z	B_{eq}/Å^2 a)
Hg	108.96(5)	251.32(3)	414.83(5)	2.9_6
Co	604.1(2)	251.1(1)	953.9(2)	2.0_3
S(1)	408.2(3)	313.4(2)	442.8(3)	3.2_9
S(2)	71.1(3)	173.2(2)	116.2(3)	3.0_0
S(3)	1062.6(4)	177.8(2)	641.8(4)	4.0_1
S(4)	903.0(4)	342.3(2)	443.1(3)	3.6_8
N(1)	492.9(10)	251.2(6)	700.9(10)	2.8_6
N(2)	379.2(11)	232.4(6)	25.5(11)	3.1_2
N(3)	827.2(10)	254.7(6)	805.5(11)	3.2_7
N(4)	728.3(11)	267.8(6)	150.7(11)	3.1_2
C(1)	455.3(11)	274.9(6)	594.8(12)	2.2_7
C(2)	254.2(13)	208.5(6)	62.4(12)	2.3_9
C(3)	922.6(11)	225.0(7)	736.2(12)	2.4_9
C(4)	799.7(12)	297.4(7)	269.3(12)	2.5_4
O(11)	602.6(10)	126.2(5)	872.4(11)	3.8_2
O(21)	616.2(10)	377.0(5)	1001.8(11)	3.7_5
N(11)	595.8(12)	−5.4(6)	766.7(12)	3.3_8
N(21)	729.1(11)	505.8(6)	1107.7(12)	3.1_8
C(11)	522.0(14)	58.5(7)	805.4(13)	2.9_1
C(12)	346.6(15)	47.2(9)	765.5(18)	4.5_4
C(13)	265(2)	−38.6(14)	686(4)	11.6_8
C(14)	346(3)	−98.2(11)	647(4)	10.8_5
C(15)	517(2)	−90.3(8)	687.7(19)	5.3_8
C(16)	773.9(16)	8.8(9)	795(2)	5.4_2
C(21)	684.9(12)	443.6(7)	979.2(13)	2.7_8
C(22)	712.6(19)	453.6(9)	810.3(16)	4.7_4
C(23)	769(3)	544.4(14)	806(2)	10.4_6
C(24)	862(3)	593.3(11)	935(3)	7.7_3
C(25)	806.4(18)	589.3(8)	1100.3(19)	4.7_3
C(26)	709.9(19)	495.3(9)	1273.2(14)	4.6_2

a) The isotropic temperature factors were computed using the following expressions: $B_{eq}=4/3(B_{11}a^2+B_{22}b^2+B_{33}c^2)$. The Bij's are defined by: $T=\exp[-(h^2B_{11}+k^2B_{22}+l^2B_{33}+2hlB_{13}+2hkB_{12}+2klB_{23})]$.

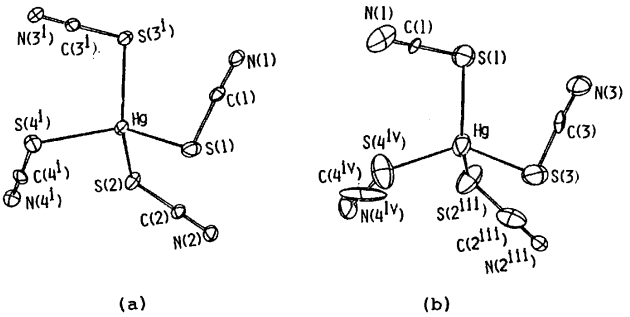

Fig. 1. The perspective drawing of the complex around a mercury atom and the included Lewis bases. (a) $CoHg(SCN)_4(mpp)_2$: (b) $CoHg(SCN)_4(dmso)_2$. Key to the symmetry operations, see Ref. 15.

Table 2. Final Atomic Coordinates ($\times 10^3$) and Equivalent Isotropic Temperature Factors (B_{eq}/Å^2) of **3** with Estimated Standard Deviations in Parentheses

Atom	x	y	z	B_{eq}/Å^2 a)
Hg	261.26(8)	624.31(4)	6.20(9)	3.3_8
Co	763.3(3)	625.2(1)	498.4(3)	2.4_0
S(1)	266.5(8)	577.0(3)	266.0(7)	4.8_5
S(2)	287.7(10)	574.6(3)	754.2(7)	4.9_2
S(3)	501.9(8)	681.0(3)	18.9(9)	4.8_0
S(4)	996.6(7)	667.5(3)	994.4(8)	4.1_3
N(1)	−10(2)	616.6(8)	393(2)	3.5_5
N(2)	537(2)	626.8(8)	613(2)	3.6_5
N(3)	652(2)	637.9(7)	276.5(19)	2.8_0
N(4)	871(2)	622.1(8)	730(2)	4.4_5
C(1)	106(3)	601.4(9)	337(2)	2.9_2
C(2)	439(3)	604.6(9)	676(5)	6.7_4
C(3)	595(3)	655.0(9)	176(3)	3.7_8
C(4)	924(2)	642.2(8)	835.5(19)	2.0_5
O(11)	792.5(16)	700.6(5)	497.5(19)	3.3_3
O(21)	738.1(18)	549.3(6)	465(2)	4.3_6
S(11)	653.6(6)	734.2(2)	502.3(10)	3.5_8
S(21)	739.7(8)	517.0(2)	614.3(8)	3.8_4
C(11)	652(4)	771.4(14)	688(4)	7.3_7
C(12)	705(4)	779.2(11)	368(3)	5.9_3
C(21)	603(4)	471.6(10)	565(4)	6.8_6
C(22)	923(3)	482.3(15)	630(3)	6.6_6

a) The isotropic temperature factors were computed using the following expressions: $B_{eq}=4/3(B_{11}a^2+B_{22}b^2+B_{33}c^2)$. The Bij's are defined by: $T=\exp[-(h^2B_{11}+k^2B_{22}+l^2B_{33}+2hlB_{13}+2hkB_{12}+2klB_{23})]$.

Table 3. Selected Bond Lengths and Bond Angles of **2** with Estimated Standard Deviations in Parentheses

Bond length	*l*/Å	Bond length	*l*/Å
Hg-S(1)	2.551(3)	Hg-S(2)	2.554(3)
Hg-S(3^{i})	2.533(4)	Hg-S(4^{i})	2.533(4)
Co-N(1)	2.111(10)	Co-N(2^{ii})	2.095(10)
Co-N(3)	2.140(9)	Co-N(4^{ii})	2.122(10)
Co-O(11)	2.087(9)	Co-O(21)	2.093(8)
S(1)-C(1)	1.660(13)	C(1)-N(1)	1.140(17)
S(2)-C(2)	1.664(11)	C(2)-N(2)	1.135(14)
S(3)-C(3)	1.663(11)	C(3)-N(3)	1.129(14)
S(4)-C(4)	1.654(11)	C(4)-N(4)	1.130(14)
O(11)-C(11)	1.238(12)	O(21)-C(21)	1.241(14)
Bond angle	**ϕ/°**	**Bond angle**	**ϕ/°**
S(1)-Hg-S(2)	102.66(9)	S(1)-Hg-S(3^{i})	104.59(11)
S(1)-Hg-S(4^{i})	120.28(10)	S(2)-Hg-S(3^{i})	121.22(11)
S(2)-Hg-S(4^{i})	103.22(11)	S(3^{i})-Hg-S(4^{i})	106.05(13)
N(1)-Co-N(2^{ii})	90.3(4)	N(1)-Co-N(4^{ii})	172.3(4)
N(1)-Co-N(3)	88.2(4)	N(2^{ii})-Co-N(3)	173.0(4)
N(2^{ii})-Co-N(4^{ii})	92.6(4)	N(1)-Co-O(11)	96.7(4)
N(1)-Co-O(21)	89.8(4)	O(11)-Co-O(21)	173.5(3)
Hg-S(1)-C(1)	97.6(5)	Hg-S(2)-C(2)	96.6(4)
Hg-S(3^{i})-C(3^{i})	98.5(4)	Hg-S(4^{i})-C(4^{i})	97.8(4)
Co-N(1)-C(1)	159.5(9)	Co-N(3)-C(3)	152.8(9)
Co-N(2^{ii})-C(2^{ii})	167.6(9)	Co-N(4^{ii})-C(4^{ii})	162.0(10)
Co-O(11)-C(11)	143.2(8)	Co-O(21)-C(21)	143.0(8)
S(1)-C(1)-N(1)	177.2(12)	S(3)-C(3)-N(3)	176.6(10)
S(2)-C(2)-N(2)	179.8(10)	S(4)-C(4)-N(4)	178.9(10)

Key to the symmetry operations: See Ref. 15.

Table 4. Selected Bond Lengths and Bond Angles of **3** with Estimated Standard Deviations in Parentheses

Bond length	*l*/Å	Bond length	*l*/Å
Hg-S(1)	2.540(7)	Hg-S(2^{iii})	2.528(7)
Hg-S(3)	2.554(7)	Hg-S(4^{iv})	2.525(6)
Co-N(1^{v})	2.123(18)	Co-N(2)	2.136(18)
Co-N(3)	2.115(17)	Co-N(4)	2.15(2)
Co-O(11)	2.080(13)	Co-O(21)	2.110(16)
S(1)-C(1)	1.63(2)	C(1)-N(1)	1.15(3)
S(2)-C(2)	1.65(3)	C(2)-N(2)	1.15(4)
S(3)-C(3)	1.70(3)	C(3)-N(3)	1.08(3)
S(4)-C(4)	1.62(2)	C(4)-N(4)	1.14(3)
O(11)-S(11)	1.488(14)	O(21)-S(21)	1.534(18)
Bond angle	**ϕ/°**	**Bond angle**	**ϕ/°**
S(1)-Hg-S(2^{iii})	116.4(2)	S(1)-Hg-S(3)	105.1(2)
S(1)-Hg-S(4^{iv})	106.8(2)	S(3)-Hg-S(4^{iv})	114.6(2)
N(1^{v})-Co-N(2)	174.5(7)	N(1^{v})-Co-N(3)	92.6(7)
N(1^{v})-Co-N(4)	89.7(8)	N(1^{v})-Co-O(11)	90.1(6)
N(2)-Co-N(3)	90.0(7)	N(2)-Co-N(4)	88.3(7)
N(1^{v})-Co-O(21)	85.7(7)	O(11)-Co-O(21)	172.1(6)
Hg-S(1)-C(1)	95.3(9)	Hg-S(3)-C(3)	98.4(9)
Hg-S(2^{iii})-C(2^{iii})	97.8(10)	Hg-S(4^{iv})-C(4^{iv})	99.3(7)
Co-N(1^{v})-C(1^{v})	165.1	Co-N(4)-C(4)	148.9(19)
Co-N(2)-C(2)	146.5(2)	Co-N(3)-C(3)	163.4(2)
Co-O(11)-S(11)	121.4(8)	Co-O(21)-S(21)	117.3(9)
S(1)-C(1)-N(1)	177(2)	S(4)-C(4)-N(4)	176.0(19)
S(2)-C(2)-N(2)	175(2)	S(3)-C(3)-N(3)	179(2)

Key to the symmetry operations: See Ref. 15.

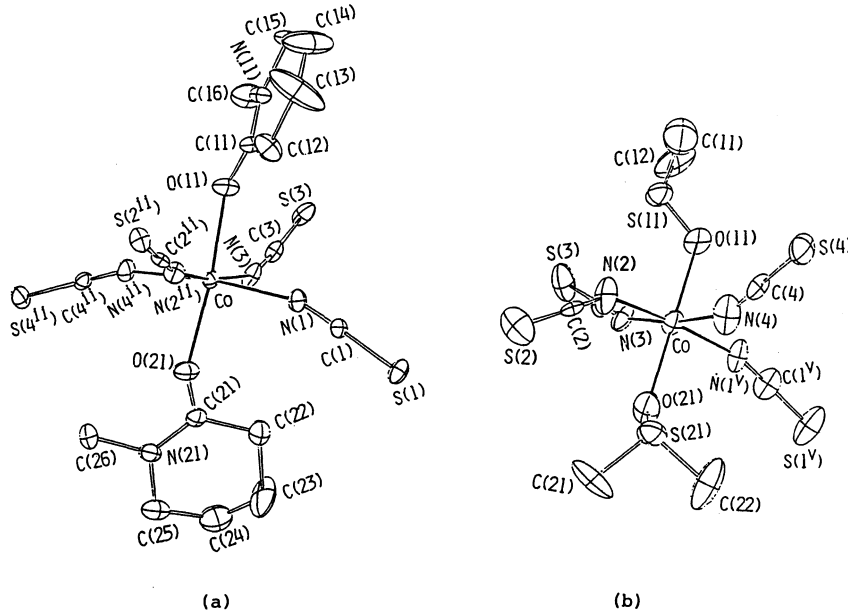

Fig. 2. The perspective drawing of the complex around a cobalt atom and the included Lewis bases. (a) $CoHg(SCN)_4(mpp)_2$: (b) $CoHg(SCN)_4(dmso)_2$. Key to the symmetry operations, see Ref. 15.

The average Hg-S lengths are 2.542 Å (maximum 2.554 and minimum 2.533 Å) for **2** and 2.537 Å (maximum 2.554 and minimum 2.525 Å) for **3**. The average bond angles around the mercury atoms of these complexes are not much different from the typical tetrahedral angles: the deviations are in the same grade as the other several mercury thiocyanates already reported.[1,16-18]

In **2** and **3**, the cobalt atom is hexa-coordinated and is in an octahedral geometry; both of the oxygen atoms of the Lewis base molecules are coordinated axially, while four SCN nitrogen atoms are coordinated equa-

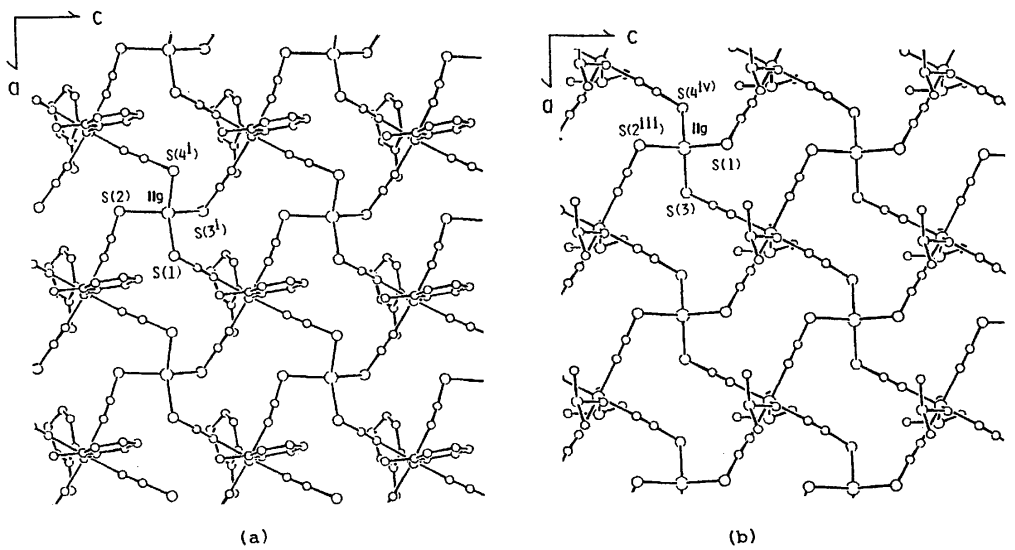

Fig. 3. The perspective drawing of the complex layer parallel to the (0 1 0) plane. (a) $CoHg(SCN)_4(mpp)_2$: (b) $CoHg(SCN)_4(dmso)_2$. Key to the symmetry operations, see Ref. 15.

torially. The average Co-N and Co-O bond lengths are 2.117 and 2.090 Å for **2** and 2.131 and 2.095 Å for **3**, respectively. They are about the same as the Co-N[19-21] and Co-O[22-24] lengths of the common octahedral cobalt(II) complexes. The average bond angles, N-Co-O and N-Co-N (between vicinal nitrogen atoms), are 90.0° and 90.2° for **2** and 90.1° and 90.2° for **3**, respectively. The angles O-Co-O are a little distorted from 180°, i.e. 173.5(3)° for **2** and 172.1(6)° for **3**, respectively. In total, the octahedral geometry of the cobalt core is not much deformed from the ideal form. The bond angles of Co-N-C, on the average, are 160.5° for **2** and 156.0° for **3**, respectively, being much deviated from 180°. Such large distortions of the angles are probably due to a steric hindrance to form the planar complex networks in the crystal.

Each pair of mercury and cobalt atoms is bridged by one SCN ion (where the sulfur atom is ligated to the mercury and the nitrogen atom to the cobalt atom). As is shown in Fig. 3, in both adducts, two mercury(II), two cobalt(II), and four SCN ions make a sixteen-membered ring which organizes the unit of a two-dimensional network. They resemble the $[CoHg(SCN)_4(H_2O)_2]_n$ network found in the $CoHg(SCN)_4(H_2O)_2 \cdot 2L$ type inclusion compounds previously reported,[4-6] although in these new complexes, Lewis base molecules are coordinated directly to the cobalt(II) atoms in place of the water molecules. As shown in Fig. 4, the complex network layers are piled up in the b-axis direction, and no chemical or hydrogen-bond bridgings exist between the layers: the interlayer space is occupied by the Lewis base molecules (mpp in **2**, dmso in **3**), which are coordinated to the cobalt(II) atoms of both side layers, respectively.

The respective complex layers found in **2** and **3** are almost in the same type structure. The y-coordinates

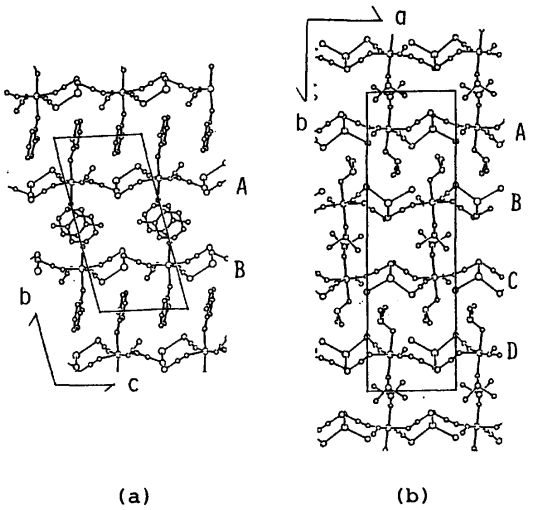

Fig. 4. The projection of the unit cell of the complex to the (1 0 0) plane (a) and to the (0 0 1) plane (b). (a) $CoHg(SCN)_4(mpp)_2$: (b) $CoHg(SCN)_4(dmso)_2$.

of all the (Co and Hg) metal atoms of one unit, sixteen-membered ring is approximately the same; the ring is regarded as being nearly in a plane, although four SCN sulfur atoms (and to a less extent the SCN carbon atoms) are located above or below the plane of the four metal atoms. The side-by-side SCN ions coordinated to one cobalt atom are extended above and beneath the respective positions of their sulfur atoms, which are above or beneath the complex plane, making a tetrahedral geometry around the mercury atom which is on the plane.

On the other hand, in $[CoHg(SCN)_4(H_2O)_2] \cdot 2L$ type complexes, cobalt atoms exist in positions slightly above and below the mercury network plane, alternately, since all four SCN ions coordinated to one

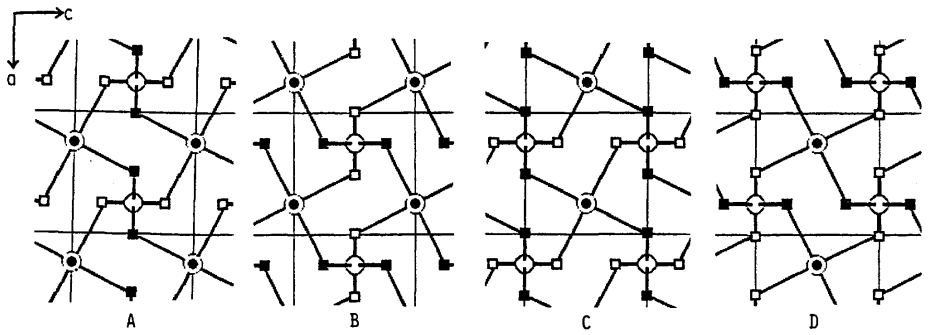

Fig. 5. Projection along b-axis of the network layers of the complex **3**. Approximate metal *y*-coordinates are: A, 0.12; B, 0.38; C, 0.62; D, 0.88. ○: Hg, ◉: Co, ■; S (above the layer plane), □: S (below the layer plane) atoms, respectively.

Table 5. Infrared Absorption Data of **1**, mpp, **2**, dmso, and **3** (in σ/cm^{-1})

1[1]	mpp[24]	**2**	dmso[25]	**3**	Tentative assignment
2150(s)		2145(s)		2145(s)	ν(CN)
	1675(s)	1610(s)			ν(CO)
			1055(s)	995(s)	ν(SO)
720(s)		725(m)		725(m)	ν(CS)
470(s)		460(s)		460(m)	δ(SCN)
447(s)		440(s)		440(s)	δ(SCN)

1, $CoHg(SCN)_4$; **2**, $CoHg(SCN)_4(mpp)_2$; **3**, $CoHg(SCN)_4(dmso)_2$.

cobalt atom are extended upward or downward. The stress around the cobalt atom may be less than that of the title complexes. (The angles of Co-C-N of the $[CoHg(SCN)_4(H_2O)_2]\cdot 2L$ type complexes are about 165—170°:[4-6] the distortions from 180° are less than the title complexes.)

The unit rings are linked two-dimensionally. In each network plane, there are two types of unit rings, I and II, which are alternately laid side by side along the [1, 0, 1] and [1, 0, −1] axes. Rings I and II are about the same in form: the latter has an arrangement of atoms which rotates unit I by 90° around an axis perpendicular to the ring plane.

In **2**, since the unit cell has a center of symmetry and Z=2, two kinds of layers, A and the reversed one B, are in a unit cell, they appear alternately along the b-axis in the crystal. As shown in Table 1, since the *y*-coordinates of the cobalt and mercury atoms are approximately the same, 0.25, all the interlayer separations (b-axis length ×0.5 $\sin\alpha$ $\sin\gamma$) are about the same, 8.21 Å. In the crystal, the same kind of metal atoms of all layers are laid in a zigzag pattern along the b-axis. As shown in Fig. 4, the respective planes of the mpp rings coordinated to the cobalt atoms of the layers above and below line up, one after another, and are arranged in the a- or c-axis direction.

Although the structure of the layers in **3** is not much different from that of **2**, some of their detailed bond lengths and bond angles are a little different from each other. Since the space group of **3** is $P2_12_12_1$, (Fig. 4), there are four such parallel complex layers in one unit cell along the b-axis; however, only one layer is crystallographically independent. As shown in Table 2, since the *y*-coordinates of the cobalt(II) and mercury(II) atoms of **3** are approximately the same, 0.62, the metal atomic *y*-coordinates of the four layers, A—D, are about, 0.12(A), 0.38(B), 0.62(C), and 0.88(D), respectively. Therefore, all interlayer separations are about the same in distances, about one-fourth of the b-axis length, 6.847 Å; they are piled up in the order D′, A, B, C, D, A″,⋯. Since the *x*- and *z*-coordinates of the cobalt and mercury atoms are approximately 0.25, 0 and 0.75, 0.50 (exactly, 0.26126, 0.00620 and 0.7633, 0.4984), the mercury and cobalt atoms of the A-layer have approximately the same *x*- and -coordinates as the cobalt and mercury atoms of the C-layer, respectively; the same relation for the metal coordinates are also found between those in the B and D layers. The positions of the metal atoms, together with the bridging SCN ions of the respective layers of **3**, are schematically shown in Fig. 5 by the projections to the ac-plane. The dmso ligands coordinated to the cobalt atoms are extended approximately perpendicular to the complex layer. The positions above and below the cobalt atom of one layer are approximately at the center of the sixteen-membered rings of the next complex layers on both sides. Therefore, no other atoms take positions very near the dmso molecules.

The positions of half of the SCN sulfur atoms overlap with the sulfur atom positions of one-side next complex layer respectively; the other half overlap with those of the other side next layer. Each pair of over-

lapping sulfur atoms of the side-by-side planes deviate above or below the network in order to decrease their interatomic distances to a value smaller than the separation of the complex layers.

Thus, these $CoHg(SCN)_4L_2$ type mixed complexes have a new characteristic layer structure, which is reported here for the first time.

Some infrared spectral data are shown in Table 5. When the wavenumbers of the peaks of **2** and **3** are compared with those of the free-ligand molecules, mpp[25] and dmso,[26] its ν(C=O) peak in **2** and ν(S=O) peak in **3** are found to be red-shifted by 60—70 cm^{-1}. Such red shifts are larger than those which have also been observed in the spectra of some amide adducts of previously reported $[CoHg(SCN)_4(H_2O)_2]\cdot 2L$ types.[4-6] This fact is due to the direct coordinate bonds of the Lewis base molecule to the cobalt atom. The wave numbers of the bands caused by the SCN ions of **1**, **2** and **3** are not very different from one another.

The magnetic moment of **2** is about 5.10 BM, and that of **3**, about 4.99 BM at 20 °C (1 BM=9.274078(36)$\times 10^{-24}$ JT^{-1}). These values are typical for the cobalt(II) ion in the octahedral geometry.

References

1) J. W. Jeffery and K. M. Rose, *Acta Crystallogr., Sect. B*, **24**, 653 (1968).

2) H. Kinoshita, M. Shimoi, and A. Ouchi, *Bull. Chem. Soc. Jpn.*, **58**, 1304 (1985).

3) H. Kinoshita and A. Ouchi, *Bull. Chem. Soc. Jpn.*, **59**, 3495 (1986).

4) H. Kinoshita, M. Shimoi, A. Ouchi, and S. Sato, *Bull. Chem. Soc. Jpn.*, **58**, 2782 (1985).

5) H. Kinoshita, M. Shimoi, and A. Ouchi, *Bull. Chem. Soc. Jpn.*, **59**, 1253 (1986).

6) H. Kinoshita and A. Ouchi, *Bull. Chem. Soc. Jpn.*, **60**, 1933 (1987).

7) M. R. Udupa and B. Krebs, *Inorg. Chim. Acta*, **42**, 37 (1980).

8) A. L. Beauchamp, L. Pazdernik, and R. Rivest, *Acta Crystallogr., Sect. B*, **32**, 650 (1976).

9) R. Makhija and R. Rivest, *J. Inorg. Nucl. Chem.*, **39**, 683 (1977).

10) W. R. Busing and H. A. Levy, *Acta Crystallogr.*, **10**, 180 (1957).

11) $R=\sum||F_o|-|F_c||/\sum|F_o|$

12) "The Universal Crystallographic Computation Program-System (UNICS)," ed by T. Sakurai, Crystallographic Society of Japan, Tokyo (1967).

13) "International Tables for X-Ray Crystallography," Kynoch Press, Birmingham (1974), Vol. IV, pp. 72, 150.

14) The final atomic and thermal parameters, and the final F_o-F_c tables are deposited as Document No. 8782 at the Office of the editor of Bull Chem. Soc. Jpn.

15) Key to the symmetry operations: for **2**, i, $-1+x,y,z$; ii, $x,y,1+z$; for **3**, iii, $x,y,-1+z$; iv, $-1+x,y,-1+z$; v, $1+x,y,z$.

16) R. C. Makhija, A. L. Beauchamp, and R. Rivest, *J. Chem. Soc., Dalton Trans.*, **1973**, 2447

17) R. C. Makhija, A. L. Beauchamp, and R. Rivest, *J. Chem. Soc., Chem. Commun.*, **1972**, 1043.

18) D. Grdenic, *Quart. Rev.*, **19**, 303 (1965).

19) H. Hartl and S. Steidl, *Z. Naturforsh.*, **B32**, 6 (1977).

20) B. Buss, P. G. Jones, R. Mews, M. Noltemeyer, and G. M. Sheldrick, *Acta Crystallogr., Sect. B*, **36**, 141 (1980).

21) H. Hartl and I. Brudgam, *Acta Crystallogr., Sect. B*, **36**, 162 (1980).

22) H. Lynton and P. Y. Siew, *Can. J. Chem.*, **51**, 227 (1973).

23) J. A. Bertrand and T. C. Hightower, *Inorg. Chem.*, **12**, 206 (1973).

24) A. Vegas, *Acta Crystallogr., Sect. B*, **37**, 1916 (1981).

25) S. E. Krikorian, T. A. Andrea, and M. Mahpour, *Spectrochim. Acta*, **32A**, 1447 (1976).

26) W. F. Currier, and J. H. Weber, *Inorg. Chem.*, **6**, 1539 (1967).

 © 1988 The Chemical Society of Japan Bull. Chem. Soc. Jpn., 61, 1175—1179 (1988)

Depletion-Mode Field Effect Semiconductor Sensor with Cation-Sensitive Polymer Membranes

Yusuke Okawa,* Mitsunori Sukigara, Shoichiro Yoshida, and Tadashi Watanabe*
Institute of Industrial Science, The University of Tokyo, 7-22-1 Roppongi, Minato-ku, Tokyo 106
(Received September 29, 1987)

Semiconductor ion sensors based on the surface conductance change due to a variation in the depletion layer thickness have been constructed. An n-SnO_2 electrode was coupled with four kinds of cation-sensitive polymer membranes (Fe^{3+}- and Cu^{2+}-exchanged Nafion membranes and poly(vinyl chloride)-supported dioctyl phthalate membranes containing a neutral carrier, valinomycin or nonactin), and its surface conductance was measured under depletion conditions as a function of the cation concentration. The sensor exhibited sensitivity to Fe^{3+}, Cu^{2+}, K^+, or NH_4^+ at levels higher than 10^{-4} mol dm^{-3} within 10 s. The sensor response was analyzed in terms of (1) the dependence of the surface conductance on the surface band bending and (2) the potential difference at solution/membrane interfaces. From the analysis, it is confirmed that the membranes show nearly Nernstian behavior and that the semiconductor acts as a potentiometric transducer. The applicability of the depletion-mode semiconductor sensor is discussed.

Semiconductor devices with low output impedance have been extensively studied recently in view of micro and multifunctional sensor fabrication. Many of such devices are of the ISFET (ion-sensitive field effect transistor) type, introduced by Bergveld,[1,2] with an insulator/semiconductor structure. The device is a modification of the MISFET (metal-insulator-semiconductor FET) and is based on the variable thickness of the inversion layer (channel) of a semiconductor substrate.[3,4] A variety of chemically sensitive membranes has been coupled with this device to develop effective sensors.[4]

There are another type of field effect devices, namely, the metal-semiconductor FET (MESFET) and junction FET (JFET), in which a change in the depletion layer thickness is utilized.[5] However, application of these devices for chemical sensor construction has scarcely been studied.

A field effect chemical sensor can be constructed also by use of semiconductor/electrolyte interfaces as follows. When an anodic bias is applied to an n-type semiconductor in contact with an electrolyte solution, a depletion layer is formed in the semiconductor. The conduction electrons are driven away from the surface region of the semiconductor. A change in the depletion layer thickness, caused for instance by ionic adsorption, alters the surface conductance of the semiconductor. Since the depletion layer acts as an insulating layer, no insulator needs to be placed on the semiconductor surface, and the device has no p-n junction in the semiconductor substrate. Thus, the structure of the sensor based upon the above principle is much simpler than that of the conventional ISFET.

In a previous paper,[6] we used n-type SnO_2 as a semiconductor and a perfluorinated sulfonate cation-exchange polymer, Nafion, as an ion-sensitive layer, to fabricate the first example of a "depletion-mode field effect sensor." The present work has been conducted to explore further the applicability of the depletion-mode sensor. By combining an SnO_2 electrode with four kinds of cation-sensitive polymer membranes, sensors for Fe^{3+}, Cu^{2+}, K^+, and NH_4^+ have been developed.

Experimental

Materials. Nafion (a 5% alcoholic solution, equivalent weight 1100), valinomycin, and nonactin were obtained from Aldrich Chemical Co., Sigma Chemical Co., and Boehringer Mannheim GmbH, respectively. Poly(vinyl chloride) (PVC, degree of polymerization 1100), dioctyl phthalate (DOP) as a plasticizer, and spectro-grade tetrahydrofuran (THF) were from Wako Pure Chemicals. $FeCl_3 \cdot 6H_2O$, $CuCl_2 \cdot 2H_2O$, KCl, NH_4Cl, LiCl, NaOH, and HCl were of reagent grade. All these chemicals were used without further purification. Distilled water, or deionized water purified with Milli Q-II (Millipore Ltd.) was used.

Preparation of Sensors. SnO_2-coated glass plates were used as semiconductor substrates. The SnO_2 layer had a thickness of about 50 nm and a donor density of 10^{21} cm^{-3}. Two terminals, W and D, were placed on the SnO_2 layer with the ohmic contacts of indium metal, which were insulated with an epoxy resin. The effective surface area of the sensor was 1×1 cm^2.

The Nafion membrane was prepared as follows.[6] A Nafion solution was spread on the SnO_2 surface and dried; the thickness of the membrane was estimated to be 1—2 μm from the weight gain. The Nafion-coated semiconductor was then immersed in a 0.2 M (1 M=1 mol dm^{-3}) $FeCl_3$ or $CuCl_2$ aqueous solution for at least 16 h to obtain ion-exchanged Nafion.

The neutral carrier-PVC membranes were cast from a THF solution containing 12 mg of PVC, 2.5 mg of a neutral carrier, and 35 μl of DOP.[7] The membrane formed on the semiconductor was air-dried overnight, then placed in a vacuum desiccator for 1 h. The thickness of the membranes was roughly 0.1 mm. The membranes were conditioned by immersing them in 0.2 M KCl and NH_4Cl aqueous solutions for valinomycin and nonactin, respectively.

The sensor construction is illustrated in Fig. 1.

Operation of Sensors. The electrical conductance of the sensor at a constant electrode potential, V_W, was measured as reported in the previous paper.[6] The electrode potential was

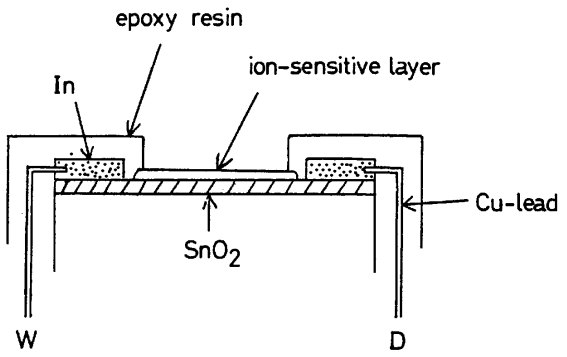

Fig. 1. Schematic representation of sensor construction.

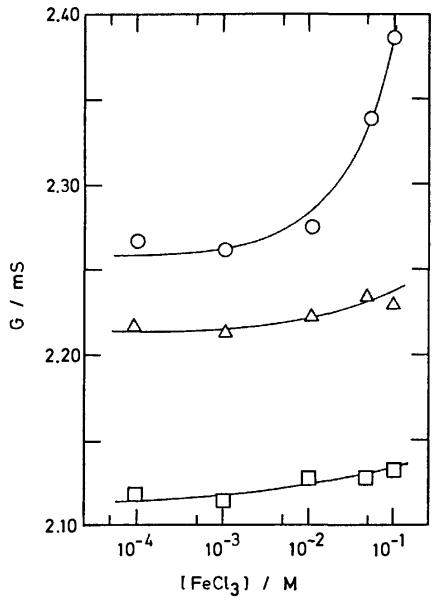

Fig. 2. Response of the Fe^{3+}-sensor (Fe^{3+}-Nafion/SnO_2). V_W=+400 (○), +500 (△), +1000 mV (□) vs. Ag/AgCl.

controlled by a Toho Technical Research potentiostat Model 2000 against an Ag/AgCl (KCl saturated) reference electrode. A small voltage (1—5 mV), V_D, was applied with a Yokogawa voltage supply Model 2553 between the two terminals, W and D, and the current, I_D, was measured by a Takeda Riken electrometer Model TR 8651. The electrical conductance, G, was calculated from the relation;

$$G = \partial I_D / \partial V_D.$$

For measurements of the time response to a concentration step, the voltage supply and the electrometer were replaced with a Yokogawa-Hewlett-Packard low frequency impedance analyzer Model 4192A operated at 1 kHz and 5 mV.

All the measurements were carried out at room temperature and in solutions flushed with nitrogen.

Results

Nafion-Based Fe^{3+}- and Cu^{2+}-Sensors. Figure 2 shows a typical response of the Fe^{3+}-sensor carrying an Fe^{3+}-exchanged Nafion membrane in the aqueous solutions containing $FeCl_3$ in the concentration range

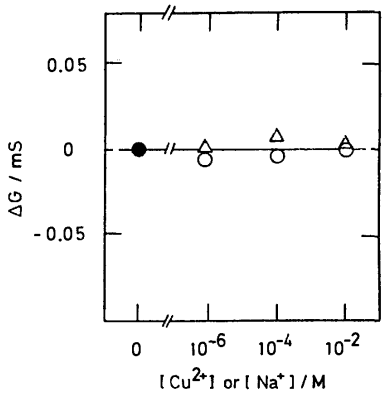

Fig. 3. Effect of coexisting Cu^{2+} (○) and Na^+ (△) on the Fe^{3+}-sensor. [$FeCl_3$]=1×10^{-3} M (pH 1.5); V_W=+400 mV vs. Ag/AgCl.

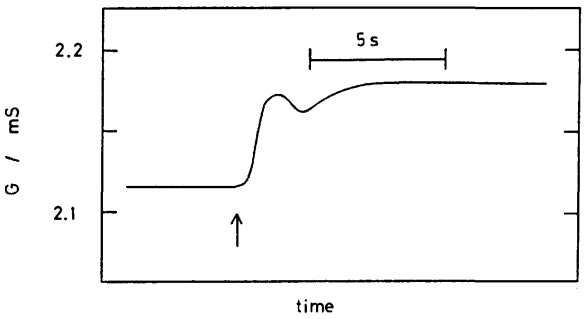

Fig. 4. Time response of the Fe^{3+}-sensor to a Fe^{3+} concentration step (0→0.1 M). V_W=+400 mV vs. Ag/AgCl.

from 10^{-4} to 10^{-1} M at pH 1.5. The conductance of the sensor changed with a change in the $FeCl_3$ concentration. The sensitivity is higher at more negative electrode potentials. At an appropriate electrode potential, the Fe^{3+}-sensor can detect Fe^{3+} ions at levels higher than 10^{-4} M.

The Fe^{3+}-sensor shows no pH dependence.[6] Addition of Na^+ or Cu^{2+} to a 10^{-3} M $FeCl_3$ test solution did not alter the sensor response, as depicted in Fig. 3, where a change in surface conductance, ΔG, upon addition of these interfering ions is plotted against their concentration. This result ensures a good selectivity of the Fe^{3+}-sensor.

Figure 4 shows a time response of the Fe^{3+}-sensor to a stepped change in Fe^{3+} concentration from 0 to 0.1 M under vigorous stirring. Though the trace is perturbed in the initial phase probably due to non-uniform mixing of the solution, the response of the sensor is completed within 10 s, which is short enough for practical use.

Use of the Cu^{2+}-exchanged Nafion membranes gave electrodes sensitive to Cu^{2+}. A typical response of the Cu^{2+}-sensor in the aqueous solutions containing $CuCl_2$ at pH 1.5 is given in Fig. 5. Similar to the Fe^{3+}-sensor, the sensitivity is higher at more negative electrode potentials. The effective potential range for

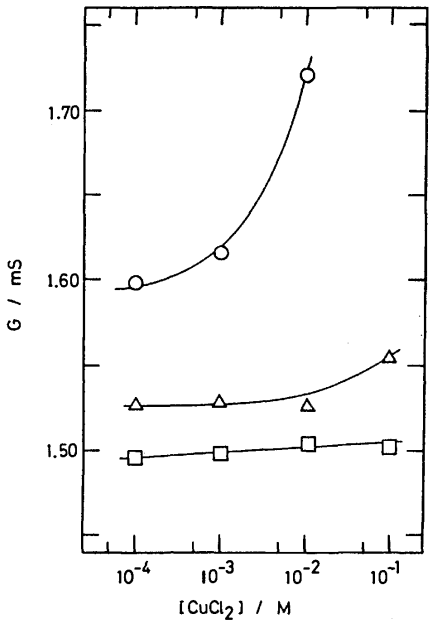

Fig. 5. Response of the Cu^{2+}-sensor (Cu^{2+}-Nafion/SnO_2). V_W=+150 (○), +300 (△), +400 mV (□) vs. Ag/AgCl.

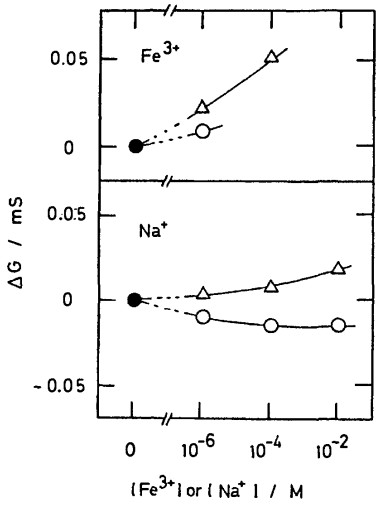

Fig. 6. Effect of coexisting Fe^{3+} and Na^+ on the Cu^{2+}-sensor. [$CuCl_2$]=1×10^{-3} M (pH 1.5); V_W=+150 (○), +300 mV (△) vs. Ag/AgCl.

the Cu^{2+}-sensor is negative of that for the Fe^{3+}-sensor.

Figure 6 shows the effect of interfering ions (Na^+ and Fe^{3+}) to the response of a Cu^{2+}-sensor (in 10^{-3} M $CuCl_2$, pH 1.5). The conductance of the sensor was affected by the addition of these ions, and hence the selectivity of the Cu^{2+}-sensor is not sufficient.

Since the semiconductor used in this work is highly doped, the depletion layer is correspondingly thin; for example, about 1.0 and 1.4 nm at electrode potentials 0.4 and 1.0 V vs. Ag/AgCl, respectively, for the case of the SnO_2 in direct contact with a pH 1.5 electrolyte solution. The conduction electrons may tunnel to the solution through the depletion layer,[8] giving rise to a

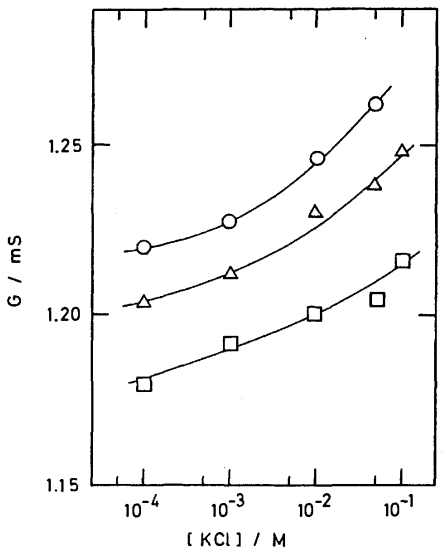

Fig. 7. Response of the K^+-sensor (valinomycin-DOP-PVC/SnO_2). V_W=−200 (○), −100 (△), +100 mV (□) vs. Ag/AgCl.

cathodic current reducing Fe^{3+} or Cu^{2+}.[9] The utilization of this current for the sensor signal was discussed in the previous work.[6] In the case of the Cu^{2+}-sensor, the current reducing Fe^{3+} was too large to carry out a stable conductance measurement, because the effective operational range for the Cu^{2+}-sensor is negative enough to reduce Fe^{3+}.[9]

Neutral Carrier-Based K^+- and NH_4^+-Sensors. Several macrolide antibiotics are known to exhibit highly selective complexing ability to certain cations.[10] Valinomycin for K^+ [11] and nonactin for NH_4^+ [12] are typical examples, and have been used as cation carriers in liquid membrane systems.[10,13] Combination of a polymer-supported liquid membrane containing a carrier and a semiconductor transducer gives an ion sensor.[14] In view of this, we have attempted to construct K^+- and NH_4^+-sensors by use of PVC-supported DOP membranes.[15]

The valinomycin-based sensor showed K^+-sensitivity, as illustrated in Fig. 7. The solution was a KCl aqueous solution containing 0.1 M NaCl (pH 6.2). The K^+-sensor did not respond to Na^+ and Li^+ at concentrations below 10^{-2} M, and to H^+ for pH value ranging from 4 to 10.

The response of a nonactin-based NH_4^+-sensor is shown in Fig. 8. Here an NH_4Cl aqueous solution containing 0.1 M NaCl was used. The sensor did not respond to Na^+ and K^+ at concentrations below 10^{-2} M.

Discussion

Under depletion conditions, the surface conductance of a semiconductor depends on the space charge layer thickness, which in turn is related to the surface band bending. This situation is described by the following equation for n-type semiconductors;[6]

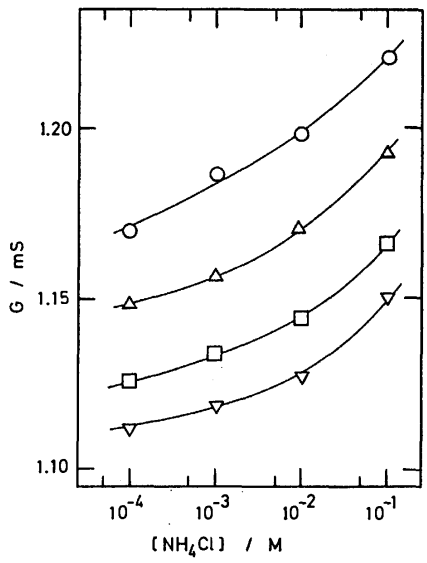

Fig. 8. Response of the NH_4^+-sensor (nonactin-DOP-PVC/SnO_2). V_W=−100 (○), +0 (△), +100 (□), +200 mV (▽) vs. Ag/AgCl.

$$\Delta\sigma_S = -(2\varepsilon e N_D \mu_e^2)^{1/2}(-V_S)^{1/2}. \quad (1)$$

Here V_S is the band bending at surface ($V_S=V_{fb}-V_W$; V_{fb} is the flatband potential), $\Delta\sigma_S$ the difference between the surface conductivity under a depletion condition ($V_S<0$) and that at the flatband state ($V_S=0$), ε the dielectric constant of the semiconductor, μ_e the mobility of the conduction electrons, N_D the donor density, and e the elementary charge.

As the potential drop in the Helmholtz layer of an oxide semiconductor surface changes in general with pH of the solution,[16] V_{fb}, and hence V_S and the surface conductance, of the semiconductor in direct contact with an electrolyte solution depend on pH of the solution under potentiostatic conditions. For the sensors developed in this work, however, the semiconductor surface is covered with an ion-sensitive polymer membrane. In such a case a change in V_S via the cation concentration change in solution should be caused by the potential difference at the membrane/solution interface. This has been confirmed previously by flatband potential measurements for the Nafion/SnO_2 system.[6] The flatband potential is generally estimated from the Mott-Schottky plot of the depletion capacitance. However, this procedure is difficult to apply to the high-resistance and low-capacitance membrane/semiconductor system as in the present study.

If the potential difference at the membrane/solution interface exhibits the Nernstian behavior, a plot of G against $[V_W-(RT/nF)\ln a]$, where n is the valency of the cation and a is its activity, should give a single curve for a variety of V_W-a combinations. The term $(RT/nF)\ln a$ is approximated by $(0.059/n)\log c$ (V) at T=300 K, where c is the cation molarity. Figures 9 and 10 show the G vs. $[V_W-(0.059/n)\log c]$ plots for the Fe^{3+}- and NH_4^+-sensors, respectively. Each plot gives a single curve, and the above-mentioned point is thus

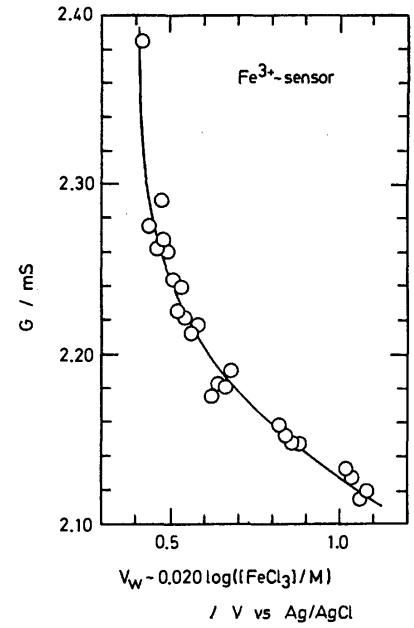

Fig. 9. Plot of the surface conductance against $V_W-(0.059/n)\log c$ for the Fe^{3+}-sensor (n=3).

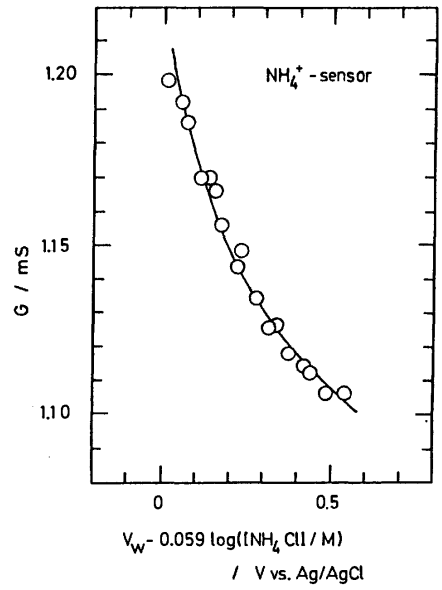

Fig. 10. Plot of the surface conductance against $V_W-(0.059/n)\log c$ for the NH_4^+-sensor (n=1).

verified. Similar results were also obtained both for Cu^{2+}- and K^+-sensors.

The dependence of the sensitivity on the electrode potential is explained with reference to Eq. 1. A more negative electrode potential gives a smaller band bending for a given cation concentration (the band edge is fixed to the solution at the given cation concentration). At a more negative potential, therefore, the change in the surface conductance is greater for a change in the cation concentration, thus resulting in higher sensitivity.

Our measurements have shown that the selectivity of the Cu^{2+}-sensor is poorer than that of the Fe^{3+}-sensor.

This could be accounted for by invoking a higher affinity of the sulfonato groups in Nafion to Fe^{3+} than to Cu^{2+}, as has been suggested also for Nafion-based ion-selective electrodes.[17] In contrast, valinomycin and nonactin are ionophores highly selective to K^+ and NH_4^+, respectively.[11,12] This is corroborated by the excellent selectivities of the K^+- and NH_4^+-sensors developed in this work.

The Nafion-based Cu^{2+}-sensor required application of a more negative electrode potential than the Fe^{3+}-sensor for the sufficient sensitivity. This observation is explained qualitatively as follows. As the affinity of the sulfonato groups is higher to Fe^{3+} than to Cu^{2+}, the difference in the chemical potential of Fe^{3+} between in Nafion and in the solution is larger than in the case of Cu^{2+}. The electrochemical potentials of the cation in Nafion and in the solution are equal at equilibrium. On a reasonable assumption that the electrical potential drop in the solution is zero, the electrical potential in Nafion is more positive for Fe^{3+} than for Cu^{2+}. Hence the band edge of the semiconductor contacting Nafion is more lowered, or V_{fb} is more positive for Fe^{3+} than for Cu^{2+}. Thus the Cu^{2+}-sensor required application of a more negative electrode potential for the sufficient sensitivity.

The performance of the sensors constructed in this work is based mainly on the properties of the membrane used, and the semiconductor is acting as a potentiometric transducer under depletion conditions. Incorporation of other chemically sensitive layers into this simple yet effective transducer may introduce new useful chemical sensors.

Further, the present system could find potential application for the electrochemical characterization of thin layers on solid substrates, including Langmuir-Blodgett films.

This work has been supported in part by Grants-in-Aid from the Ministry of Education, Science and Culture (Nos. 61103007 and 61227005).

References

1) P. Bergveld, *IEEE Trans. Biomed. Eng.*, **BME-17**, 70 (1970).
2) P. Bergveld, *IEEE Trans. Biomed. Eng.*, **BME-19**, 342 (1972).
3) P. Bergveld, N. F. DeRooij, and J. N. Zemel, *Nature (London)*, **273**, 438 (1978).
4) "Solid State Chemical Sensors," ed. by J. Janata and R. H. Huber, Academic Press, Orland (1985).
5) S. M. Sze, "Physics of Semiconductor Devices," 2nd ed., John Wiley & Sons, New York (1981).
6) M. Sukigara, Y. Aikawa, M. Kimura, and Y. Okawa, *Nippon Kagaku Kaishi*, **1987**, 484.
7) U. Fielder and J. Růžička, *Anal. Chim. Acta*, **67**, 179 (1973).
8) K. Kobayashi, Y. Aikawa, and M. Sukigara, *Bull. Chem. Soc. Jpn.*, **55**, 2820 (1982).
9) T. Sagara, Y. Aikawa, and M. Sukigara, *Nippon Kagaku Kaishi*, **1986**, 261.
10) W. E. Morf and W. Simon, "Ion-Selective Electrodes in Analytical Chemistry, Vol. 1," ed. by H. Freiser, Plenum Press, New York (1978), Chap. 3.
11) M. M. Shemyakin, Yu. A. Ovchinnikov, V. T. Ivanov, V. K. Antonov, E. I. Vinogranova, A. M. Shkrob, G. G. Malenkov, A. V. Evstratov, I. A. Laine, E. I. Melnik, and I. D. Ryabova, *J. Membr. Biol.*, **1**, 402 (1969).
12) R. P. Sholer and W. Simon, *Chimia*, **24**, 372 (1970).
13) S. Yoshida and S. Hayano, *J. Am. Chem. Soc.*, **108**, 3903 (1986).
14) R. T. McBride, J. Janata, P. A. Comte, S. D. Moss, and C. C. Johnson, *Anal. Chim. Acta*, **101**, 239 (1978).
15) G. J. Moody and J. D. R. Thomas, "Ion-Selective Electrodes in Analytical Chemistry, Vol. 1," ed. by H. Freiser, Plenum Press, New York (1978), Chap. 4.
16) D. E. Yates, S. Levine, and T. W. Healey, *J. Chem. Soc., Faraday Trans. 1*, **70**, 1807 (1974).
17) C. R. Martin and H. Freiser, *Anal. Chem.*, **53**, 902 (1981).

 © 1988 The Chemical Society of Japan Bull. Chem. Soc. Jpn., 61, 1181—1184 (1988)

Dynamic NMR as a Nondestructive Method for the Determination of Rates of Dissociation. XIII. Sulfur Inversion in 9,9-Dialkyl-10-mesitylthioxanthenium Salts[1)]

Michinori Ōki*,† and Yasuhisa Yamada
Department of Chemistry, Faculty of Science, The University of Tokyo, Bunkyo-ku, Tokyo 113
(Received July 31, 1987)

The sulfur-inversion in the title compound (alkyl=ethyl) was found to take place with the following activation parameters by dynamic NMR spectroscopy: ΔH^{*}=23.8±0.2 kcal mol^{-1}, ΔS^{*}=2.6±0.4 cal mol^{-1} K^{-1}. The significance of the near zero entropy of activation is discussed. The mesityl group in the title compounds also showed restricted rotation of which barrier to rotation was estimated to be 14 kcal mol^{-1} at 318 K for the compound where the alkyl is a methyl.

During the course of investigation by the dynamic NMR spectroscopy on the dissociation of a chemical bond, it has become clear that the entropy of activation is large positive if the ground state is ionic and the transition state is losing the electric charge, whereas it is large negative if the ground state is covalent and the transition state is of ionic character.[2)] Thus this technique may be used as a diagnostic means for the mechanism of a dynamic process of a molecule.

Sulfur-inversion in sulfonium ions is known to take place with a free energy of activation of ca. 25—30 kcal mol^{-1} (1 cal=4.184 J).[3)] In contrast to this fact, the sulfur ligand in platinum complexes inverts with much less free energy of activation,[4)] which might be an implication that the mechanism of the sulfur-inversion in the complexes is different from the true inversion: inversion after dissociation is one of the alternative possibilities.

In tackling this problem, we expected that the dynamic NMR technique would give valuable information. However, literature search indicated that the number of literatures that treated with this problem by dynamic NMR is very limited: to our knowledge, there is only one paper that reports the kinetic parameters of sulfur-inversion in sulfonium ions, this paper giving only free energy of activation.[5)] Therefore, some basic data should be accumulated in order to prove that the dynamic NMR technique is useful in discussing the mechanism of inversion of sulfur. As one of the contributions to this end, we have reported that the sulfur-inversion in a sulfonium ion, in which the C-S bond dissociation is unlikely to occur, exhibits near-zero entropy of activation by a classical method.[6)] A next problem is to prove that the dynamic NMR technique affords in fact a near-zero entropy of activation, if the mechanism of the sulfur-inversion does not involve the C-S bond dissociation followed by inversion.

The only one literature we found reported that the sulfur-inversion in 9,9-dimethyl-10-phenylthioxanthenium perchlorate takes place to show coalescence of the two methyl signals at ca. 200 °C at 60 MHz.[5)] In this compound, the C-S bonds involved are aromatic carbon-to-sulfur ones only: the involvement of the bond dissociation is unlikely in the sulfur-inversion. Since the coalescence temperature of the key signals of the reported compound would be too high for the instrument we possess (270 MHz), we decided to modify the molecule to lower the coalescence temperature.

There are two techniques to lower the coalescence temperature: one is to reduce the difference in chemical shifts of the exchanging nuclei, and the other is to raise the ground state energy so that the energy gap between the ground state and the transition state for inversion becomes small. We chose the latter method firstly. The former will be accomplished by selecting the chain length of the alkyl groups at the 9-position.

The syntheses of the compounds used in this study were carried out by the known methods. 9,9-Dialkylthioxanthene (**1**) was oxidized to the corresponding sulfoxide **2** which was treated with sulfuric acid after dissolving in mesitylene.[5)] For the synthesis of 9,9-dibenzyl compound, this method failed probably because of the presence of the phenyl ring in the benzyl group. Therefore, only the 10-phenyl derivative **5** was prepared by phenylation[7)] of 9,9-dibenzylthioxanthene (**4**).

Although it was hoped that the introduction of a mesityl group into the 10-position of the thioxanthenium ion would lower the barrier to inversion, the change in the observed line shapes of 10-mesityl-9,9-dimethylthioxanthenium perchlorate (**3**: R=CH_3, X=ClO_4) at high temperatures was not good enough for the total line shape analysis. Introduction of two benzyl groups in the 9-position of thioxanthenium ion was not satisfactory either: 9,9-dibenzyl-10-phenylthioxanthenium perchlorate (**5**) possessed a too high barrier to inversion for the measurement with our instrument, although we hoped that the steric effects of the benzyl groups would lower the barrier.

Finally we synthesized 9,9-diethyl-10-mesitylthioxanthenium tetrafluoroborate (**3**: R=C_2H_5, X=BF_4) and found the compound to be suitable for the

† Present address: Department of Chemistry, Faculty of Science, Okayama University of Science, Ridaicho, Okayama 700.

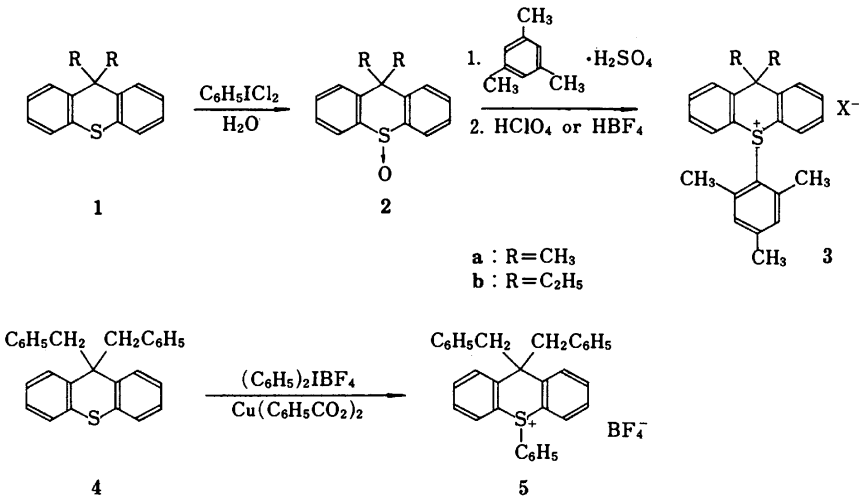

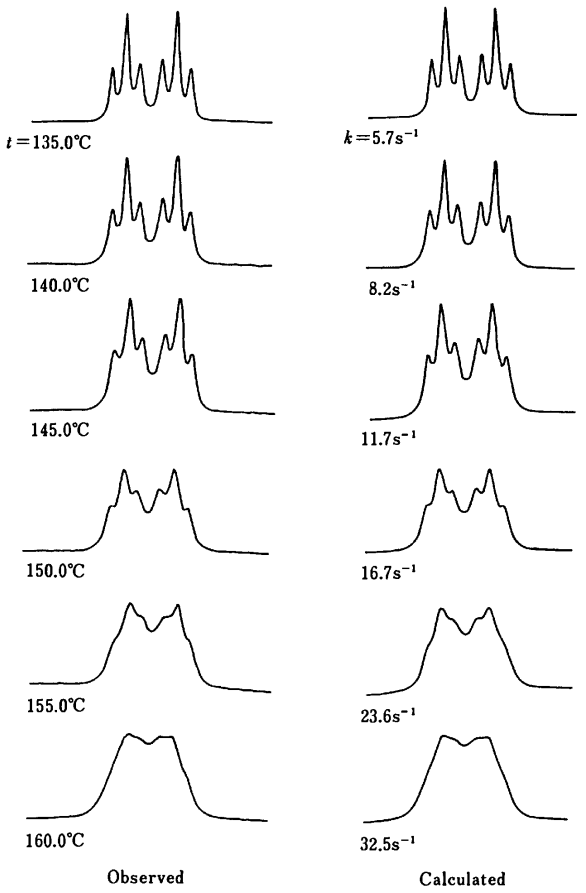

Fig. 1. Observed and calculated line shapes of the methyl protons of 9,9-diethyl-10-mesitylthioxanthenium tetrafluoroborate.

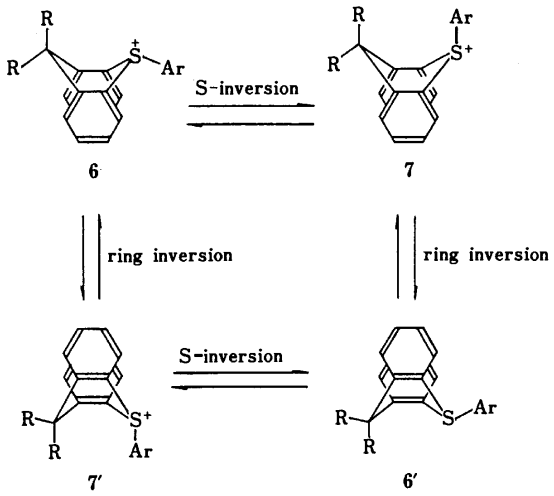

Fig. 2. Isomerization circuit.

dynamic NMR work, thanks to the steric effects given by the mesityl group and probably by the ethyl groups, in addition to the small chemical shift differences of the methyl protons in the ethyl groups. The kinetic data obtained by the total line shape analysis are given in Fig. 1, taking typical examples, together with observed and calculated line shapes for the methyl protons of the ethyl groups. The enthalpy of activation, 23.8±0.2 kcal mol^{-1}, and entropy of activation, 2.6±0.4 cal mol^{-1} K^{-1}, were obtained by putting these results into the Eyring equation. The correlation coefficient was excellent.

The feature of the kinetic parameters is the near-zero entropy of activation. Since the C-S bonds in this compound can be assumed to not dissociate under the conditions of the investigation, the sulfur-inversion must be a single step process. In such processes, the entropy of activation is near-zero in agreement with the results obtained by a classical method applied to other sulfonium compounds that do not easily dissociate at the C-S bonds. We may conclude that in those cases the dynamic NMR technique gives reliable data as was the case of internal rotation in molecules.[8]

It may be argued that, since the 9,10-dihydroanthracene and its analogs take a boat conformation in the ground state,[9] the process we observe here may not be the sulfur-inversion. We believe, however, that the process observed here is indeed the sulfur-inversion for the following reasons. The isomerization circuit is shown in Fig. 2. Firstly, the rates of ring inversion in

this type of compounds are known to be very large at room temperature.[10] Therefore, the ring inversion cannot be the rate-determining step of the observed process. Secondly, if the mesityl group is axial **7** or **7'**, then the steric interaction of the mesityl group with the alkyl group in the 9-position that opposes the mesityl group is great: the mesityl-axial conformation **7** or **7'** will be too unstable to be observed. Therefore, the ground state for the compounds in question must be the mesityl-equatorial conformation **6** and **6'**. When sulfur-inversion takes place from the stable conformation, the mesityl-axial conformation is assumed transiently but the ring inversion follows very rapidly. It also means that, if the ring inversion takes place to form the mesityl-axial conformation, the reverse process follows rapidly.

The molecular ion of 9,9-dialkyl-10-mesitylthioxanthenium showed broad peaks for the methyl protons of the mesityl group as well as the aromatic protons which are directly bonded to the mesityl-phenyl group at room temperature to indicate that the rotation of the mesityl group is fairly slow. By lowering the temperature of the solution of 9,9-dimethyl-10-mesitylthioxanthenium perchlorate (**3**: R=CH_3, X=ClO_4), we found the two methyl signals were separated (1.14 and 2.96) as well as the meta protons of the mesityl group (7.14 and 7.38). The coalescence of the methyl proton signals took place at 318 K. Because of the presence of other proton signals in the region where the coalescence of the signals took place, we abandoned the total line shape analysis and the free energy of activation for rotation was obtained as 14 kcal mol^{-1} at the coalescence temperature by assuming that the chemical shift difference is constant throughout the temperature range examined.

This barrier to rotation may be compared with that for the mesityl or 2,6-dimethylphenyl group in 9,9-dimethyl-10-(2,6-dimethylphenyl)-9,10-dihydroanthracene, 19.6 kcal mol^{-1} at 399 K,[11] and 9,9-dimethyl-10-mesitylxanthene , 17.6 kcal mol^{-1} at 298 K.[12] The lowering of the barrier to rotation in the sulfur compound (**3**: RCH$_3$, X=ClO_4) is undoubtedly caused by the large bond-lengths of the C-S bonds relative to the C-C bonds.

Experimental

NMR Measurement. The NMR data including the dynamic NMR were collected with the use of a JEOL GX-270 spectrometer unless otherwise mentioned. The temperature was calibrated by a thermometer. For the dynamic NMR measurements, a solution of ca. 40 mmol L^{-1} was used. Dimethyl-d_6 sulfoxide and chloroform-*d* were used for high and low temperature measurements, respectively.

Calculation of Rate Constants. The exchange of spins observed here is in principle $A_3X_2B_3Y_2 \rightleftarrows B_3Y_2A_3X_2$. We approximated the process to be $AX_2 \rightleftarrows BY_2$ for the convenience of calculation which was carried out by the use of DNMR3 program.[13] The coupling constants were found to be constant at several temperatures, where the exchange was negligibly slow. Thus we assumed $J_{AX}=J_{BY}=7.3$ Hz at the temperature range examined. Since the transverse relaxation time (T_2) could not be obtained from a signal within the molecule, the relaxation time was obtained by calculation that gave the best fit with the observed signals at temperatures in the slow exchange limit. T_2 was thus obtained as 0.12 s and this value was used throughout the calculation of the line shapes at various temperatures. The chemical shifts drifted as the temperature was changed. At the slow exchange limit, we observed the chemical shifts of the A, B, X, and Y protons at various temperatures to obtain the correlations between the temperature and the chemical shift. The results are shown in Table 1. These relations were extrapolated to the temperatures where the line shapes changed. The agreement between the observed and the calculated spectra was excellent, as is seen in Fig. 1. The following rate constants (s^{-1}) were obtained (temperature in °C given in parentheses): 5.7 (135.0), 6.8 (137.5), 8.2 (140.0), 9.7 (142.5), 11.7 (145.0), 13.9 (147.5), 16.7 (150.0), 19.6 (152.0), 23.6 (155.0), 28.0 (157.5), 32.5 (160.0), 38.5 (162.5). These data were put into the Eyring equation to obtain the enthalpy of activation, 23.8±0.2 kcal mol^{-1}, and entropy of activation, 2.6±0.4 cal mol^{-1} K^{-1}. The correlation coefficient was 0.999.

Table 1. Correlation between Temperature and Chemical Shifts of the Protons Involved in the Exchange

Nuclei[a]	$f(t)$[b]
A	$0.179t$ +151.41
B	$0.234t$ +170.22
X	$0.144t$ +489.97
Y	$0.0510t$+735.89

a) For A, B, X, and Y, see the text. b) $\nu=f(t)$, t being temperature in °C.

For the calculation of the free energy of activation for rotation of the mesityl group, the equation

$$k_c = \frac{\pi\Delta\nu}{\sqrt{2}}$$ [14]

was used, where $\Delta\nu$ is the chemical shift difference of the exchanging proton signals and k_c the rate constant at the coalescence temperature. The value of the rate constant was put into the Eyring equation.

9,9-Dibenzylthioxanthene (4). To a solution of 5.32 g (17.5 mmol) of 9-benzylthioxanthen-9-ol[15] in 100 mL of ether was added 30 mL of 70% perchloric acid at −78 °C with stirring. The mixture was allowed to warm up to the room temperature and the red precipitates were collected. Recrystallization from hot acetic acid gave 4.91 g of 9-benzylthioxanthylium perchlorate. To a Grignard solution prepared from 4.8 g (38 mmol) of benzyl chloride, 0.92 g (38 mmol) of magnesium and 100 mL of ether, was added 4.90 g (12.7 mmol) of the perchlorate and the mixture was refluxed for 2 h. The mixture was decomposed with aqueous ammonium chloride and the ether layer was separated. After drying over sodium sulfate, ether was removed and the residue was submitted to chromatography on silica gel with hexane as an eluent to afford 2.44 g (50.8%) of the desired product and 1.00 g of 9-benzylidenethioxanthene, identified by its melting

point, 119.0—120.0 °C (lit,[15] mp 121—122 °C), and its ^{1}H NMR spectra ($CDCl_3$, δ): 6.87 (1H, s), 6.9—7.8 (13H, m). The desired product was purified by recrystallization from dichloromethane-hexane, mp 160.0—161.0 °C. Found: C, 85.39; H, 5.80; S, 8.27%. Calcd for $C_{27}H_{22}S$: C, 85.67; H, 5.86; S, 8.47%. ^{1}H NMR ($CDCl_3$) δ=3.52 (4H, s), 6.6—7.4 (18H, m).

9,9-Dibenzyl-10-phenylthioxanthenium Tetrafluoroborate (5). A mixture of 0.55 g (1.5 mmol) of 9,9-dibenzylthioxanthene in 15 mL of chlorobenzene, 0.55 g (1.5 mmol) of diphenyliodonium tetrafluoroborate[7] and 10 mg of copper(II) benzoate was heated at 120—125 °C under a nitrogen atmosphere for 3 h. The mixture was cooled and ether was added to induce precipitation. Recrystallization of the precipitate from ethanol afforded 0.33 g (42%) of the desired product, mp 296—297 °C (decomp). Found: C, 72.79; H, 4.75; S, 6.16%. Calcd for $C_{33}H_{27}BF_4S$: C, 73.07; H, 5.02; S, 5.91%. ^{1}H NMR ($CDCl_3$) δ=3.60 (2H, s), 4.08 (2H, s), 6.02 (2H, d, J=7.2 Hz), 6.6—7.6 (17H, m), 7.96 (2H, t, J=7.2 Hz), 8.42 (2H, d, J=7.2 Hz).

10-Mesityl-9,9-dimethylthioxanthenium Perchlorate (3a: X=ClO$_4$). To a solution of 0.44 g (1.8 mmol) of 9,9-dimethylthioxanthene 10-oxide (**2a**)[5] in 5 mL of mesitylene, was added 1 mL of concentrated sulfuric acid at 0 °C with stirring. The stirring was continued for 10 d. The mixture was poured into water and shaken with ether. To the aqueous layer cooled at 0 °C, was added 2 mL of 70% perchloric acid. After stirring for 1h, the precipitates were collected and washed with water and then with ether. Recrystallization from acetone-ether afforded 0.60 g of the desired product, mp 262.0—263.5 °C. Found: C, 64.56; H, 5.90; S, 7.56; Cl, 8.08%. Calcd for $C_{24}H_{25}ClO_4S$: C, 64.78; H, 5.66; S, 7.20; Cl, 7.97%. ^{1}H NMR ($CDCl_3$, −50 °C) δ=1.14 (3H, s), 1.52 (3H, s), 2.18 (3H, s), 2.46 (3H, s), 2.96 (3H, s), 7.14 (1H, s), 7.25 (2H, d, J=7.5 Hz), 7.38 (1H, s), 7.51 (2H, d, J=7.5 Hz), 7.78 (2H, t, J=7.5 Hz), 7.91 (2H, d, J=7.5 Hz).

9,9-Diethylthioxanthene 10-Oxide (2b). To a solution of ethylmagnesium iodide prepared from 1.0 mL (13 mmol) of ethyl iodide, 0.3 g (13 mmol) of magnesium and 50 mL of ether, was added 1.85 g (5.70 mmol) of 9-ethylthioxanthylium perchlorate[16] and the mixture was heated for 2 h. The mixture was decomposed with aqueous ammonium chloride and the ether layer was separated. The ether solution was washed with water and dried over magnesium sulfate. Evaporation of the solvent afforded practically pure 9,9-diethylthioxanthene (**1b**) in 99% yield. ^{1}H NMR ($CDCl_3$) δ=0.68 (6H, t, J=7.3 Hz), 2.07 (4H, q, J=7.3 Hz), 7.1—7.5 (8H, m).

The practically pure thioxanthene **1b** was dissolved in 10 mL of pyridine and 1 mL of water. To the solution was added 1.70 g (6.18 mmol) of phenyliodonium dichloride in 7 mL of pyridine in 10 min at −40 °C and the mixture was stirred overnight. Dilute sulfuric acid was added with cooling to neutralize and the mixture was extracted with chloroform. The chloroform layer was washed with water and dried over sodium sulfate. Evaporation of the solvent and addition of hexane afforded crystals in 87.5% yield. Recrystallization of the product from hexane gave the pure sample, mp 125.0—125.5 °C. Found: C, 75.46; H, 6.84; S, 11.84%. Calcd for $C_{17}H_{18}OS$: C, 75.52; H, 6.71; S, 11.86%. ^{1}H NMR ($CDCl_3$) δ=0.61 (3H, t, J=7.5 Hz), 0.84 (3H, t, J=7.5 Hz), 1.62 (2H, q, J=7.5 Hz), 2.47 (2H, q, J=7.5 Hz), 7.4—7.6 (6H, m), 8.0—8.2 (2H, m).

9,9-Diethyl-10-mesitylthioxanthenium Tetrafluoroborate (3b: X=BF$_4$). A mixture of 0.38 g of the sulfoxide **2b**, 5 mL of mesitylene and 1 mL of concentrated sulfuric acid was stirred at room temperature for 4 d. The mixture was poured into ice-water and ether-soluble materials were removed by shaking with ether. To the aqueous layer was added 2 mL of 40% tetrafluoroboric acid with cooling and the mixture was stirred for 1 h at 0 °C. The precipitate was collected by filtration, washed with water and then with ether, and recrystallized from ethanol to afford 0.17 g of the desired product, mp 202.0—203.0 °C. Found: C, 67.83; H, 6.53; S, 6.96%. Calcd for $C_{26}H_{29}BF_4S$: C, 67.53; H, 6.40; S, 7.16%. ^{1}H NMR (DMSO-d_6) δ=0.57 (3H, t, J=7.3 Hz), 0.64 (3H, t, J=7.3 Hz), 1.38 (3H, br s), 1.86 (2H, q, J=7.3 Hz), 2.40 (3H, s), 2.73 (2H, q, J=7.3 Hz), 2.94 (3H, br s), 7.21 (1H, br s), 7.38 (2H, d, J=7.8 Hz), 7.49 (1H, br s), 7.60 (2H, t, J=7.8 Hz), 7.86 (2H, t, J=7.8 Hz), 8.09 (2H, d, J=7.8 Hz).

This work was supported by a Grant-in-Aid (No. 61134043) for Fundamental Scientific Research of the Ministry of Education, Science and Culture.

References

1) For Part XII, see S. Toyota and M. Ōki, *Bull. Chem. Soc. Jpn.*, **61**, 699 (1988).
2) T. Morita and M. Ōki, *Bull. Chem. Soc. Jpn.*, **59**, 3605 (1986) and references cited therein.
3) P. H. Laur, in "Sulphur in Organic and Inorganic Chemistry," ed by A. Senning, Mercel-Dekker, New York (1972), Vol. 3, p. 91; M. Mikolajczyk and J. Drabowicz, *Top. Stereochem.*, **13**, 333 (1982).
4) P. C. Turley and P. Haake, *J. Am. Chem. Soc.*, **89**, 4617 (1967); E. W. Abel, M. Booth, and K. G. Orrell, *J. Chem. Soc., Dalton Trans.*, **1977**, 42.
5) K. K. Andersen, M. Cinquini, and N. E. Papanikolaou, *J. Org. Chem.*, **35**, 706 (1970).
6) M. Ōki, Y. Yamada, and S. Murata, *Bull. Chem. Soc. Jpn.*, **61**, 707 (1988).
7) J. V. Crivello and J. W. Lam, *J. Org. Chem.*, **43**, 3055 (1978).
8) M. Nakamura, H. Kihara, N. Nakamura, and M. Ōki, *Org. Magn. Reson.*, **12**, 702 (1979); G. Binsch and H. Kessler, *Angew. Chem., Int. Ed. Engl.*, **19**, 411 (1980).
9) P. W. Rabideau, *Acc. Chem. Res.*, **11**, 141 (1978): see also A. L. Ternay, Jr., L. Ens, J. Herrmann, and S. Evans, *J. Org. Chem.*, **34**, 940 (1969).
10) W. B. Smith and B. A. Shoulders, *J. Phys. Chem.*, **69**, 2022 (1965).
11) M. Nakamura and M. Ōki, *Bull. Chem. Soc. Jpn.*, **53**, 2977 (1980).
12) S. V. McKinley, P. A. Grieco, A. E. Young, and H. H. Dreedman, *J. Am. Chem. Soc.*, **92**, 5900 (1970).
13) G. Binsch, *Top. Stereochem.*, **3**, 97 (1968).
14) H. S. Gutowsky and C. H. Holm, *J. Chem. Phys.*, **25**, 1228 (1956).
15) E. D. Bergman, E. Fischer, Y. Hirshberg, D. Lavie, B. Pullman, and D. Shapiro, *Bull. Soc. Chim. Fr.*, **19**, 262 (1952).
16) A. Mustafa, *J. Chem. Soc.*, **1949**, 2295.

 © 1988 The Chemical Society of Japan Bull. Chem. Soc. Jpn., 61, 1185—1190 (1988)

Dynamic NMR as a Nondestructive Method for the Determination of Rates of Dissociation. XIV. Examination of Rates of Proton-Detachment from Ammonium Ions with Multiple Probes[1)]

Toshiari Morita and Michinori Ōki*,†
Department of Chemistry, Faculty of Science, The University of Tokyo, Bunkyo-ku, Tokyo 113
(Received November 5, 1987)

The rates of proton-detachment and those of topomerization in ammonium ions of benzyldiethylammonium chloride and benzylisopropylmethylammonium chloride were determined by dynamic NMR spectroscopy, by taking advantage of loss of coupling of the benzylic methylene or the methyl protons for the former process and site-exchange of the diastereotopic protons at the ethyl-methylene, isopropyl-methyl, or benzylic methylene positions for the latter in ^{1}H NMR spectroscopy. The rates of the both processes were in good agreement with each other to indicate that the rate-limiting process in the observed topomerization is the proton-detachment. Thus it is shown that any available probes may be used for the proton-detachment or for the ivestigation of the proton affinity of amines by the dynamic NMR spectroscopy in aprotic solvents. The preference of the probes was discussed.

The knowledge on basicity of amines in aprotic solvents is important in understanding organic reactions, because most of them are carried out in organic solvents and bases are important catalysts in many cases. Although basicity of amines in aqueous solvents has well been documented[2)] and proton affinity of amines in the gas-phase has recently been discussed,[3)] the determination of basicity or proton affinity of amines in organic solvents is not straightforward and lacks general reliability.

In the series of investigation of proton affinity of amines in aprotic solvents by dynamic NMR spectroscopy, we have demonstrated that the dynamic NMR technique is a potentially very useful method in the field of determination of proton affinity of amines in aprotic solvents. In addition to the fact that the proton affinity of the series of *p*-substituted *N*,*N*-dibenzylanilines in chloroform-*d* parallels those of the series of *p*-substituted *N*,*N*-dimethylanilines in water and *p*-substituted anilines in the gas phase,[4)] we have been able to demonstrate that examination of proton affinity of anions derived from strong acids in aprotic solvents is possible by applying the same technique that utilizes a constant amine and a series of acid salts derived therefrom.[5)]

Although this technique is potentially widely applicable, there have remained two points to be clarified before claiming the general applicability. The origin of the problems is that we have used benzylic methylene proton signals, which simultaneously lose coupling and exchange sites on detachment of the proton from the anilinium ion, as a probe in ^{1}H NMR spectroscopy.

The topomerization processes involve three steps, as

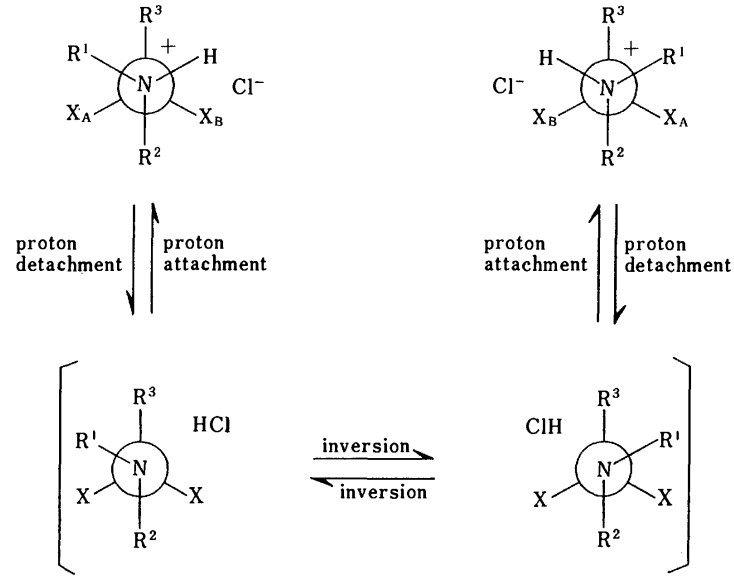

Scheme 1. Topomerization processes

† Present address: Department of Chemistry, Faculty of Science, Okayama University of Science, Ridaicho, Okayama 700.

are shown in Scheme 1: proton detachment, inversion of amine, and proton attachment. In the previous work, it was assumed that the rate-limiting step is the proton detachment because the inversion of amine is a rapid process[6] and proton atachment to amine should also be fast. However, this assumption should be confirmed.

The second problem is that, in the line shape analyses, we have assumed that the coupling constant between the ammonium proton and the benzylic methylene protons in the *N,N*-dibenzylanilinium ions is inversely proportional to the rate of proton detachment at a certain range where the rate is reasonably large, since DNMR3 program[7] does not accommodate the two processes involved. This again remains to be confirmed.

To overcome these problems, it is necessary to compare the rates of true proton-detachment with the rates of topomerization which are not affected by the coupling with the detaching proton. After establishing these rates, we may compare the rates of topomerization that are obtained by observing topomerization with concomitant loss of coupling. Thus we designed molecules that conform with these requirements. They are benzyldiethylammonium chloride (**1**) and benzylisopropylmethylammonium chloride (**2**).

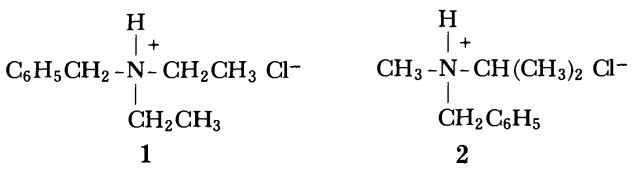

1 **2**

Compound **1** is an example of aliphatic amines that carry two probes. The benzylic methylene protons should show coupling with the ammonium proton as far as the proton sticks to the amino-nitrogen. This probe should provide the rates of proton-detachment, as has been shown by the case of *N,N*-dimethylcyclohexylamine hydrochloride.[8,9] The ethyl-methylene protons are diastereotopic when the proton-detachment is slow and show both site-exchange and loss of coupling with the ammonium proton when the process becomes fast.

Compound **2** provides three probes for the determination of the rates of the observable processes. The coupling of the *N*-methyl protons with the ammonium proton should be lost in the fast exchange limit. The isopropyl-methyls are the probe that should give information of the topomerization but has negligibly small coupling constant with the detaching ammonium proton. Compound **2** also carries benzylic methylene protons that are diastereotopic if the proton detachment is slow, exchange their site on topomerization, and show coupling, that disappears at the fast exchange limit of the ammonium proton, with the ammonium proton at the slow exchange limit. Thus this compound possesses all the necessary probes for comparison of the rate constants.

Syntheses of the compounds in question are straightforward. The hydrochlorides were purified by recrystallization to avoid any complexity arising from the excess of acid or base,[9] and dissolved in 1,1,2,2-tetrachloroethane-d_2. The observed and calculated spectra are shown in Figs. 1 and 2, where the line shapes at the same temperature are arranged along the abscissa for the convenience of comparison. The rate constants thus obtained and temperatures were put into the Eyring equation to afford activation parameters which are compiled in Table 1.

As are clear from both figures, the rate constants obtained with the two probes in **1** and those obtained from the three probes in **2** show satisfactory agreement, the disagreement in the rate constants being generally within 10%. The results confirm that the nitrogen-

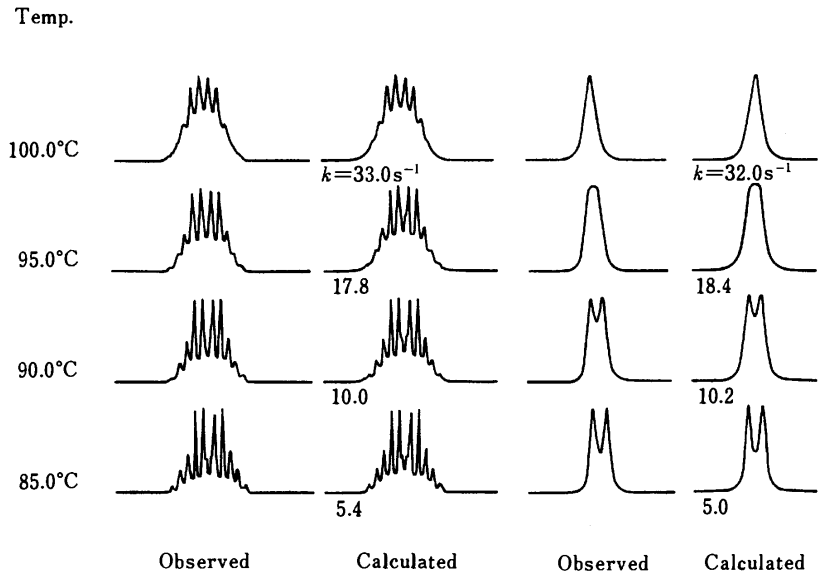

Fig. 1.

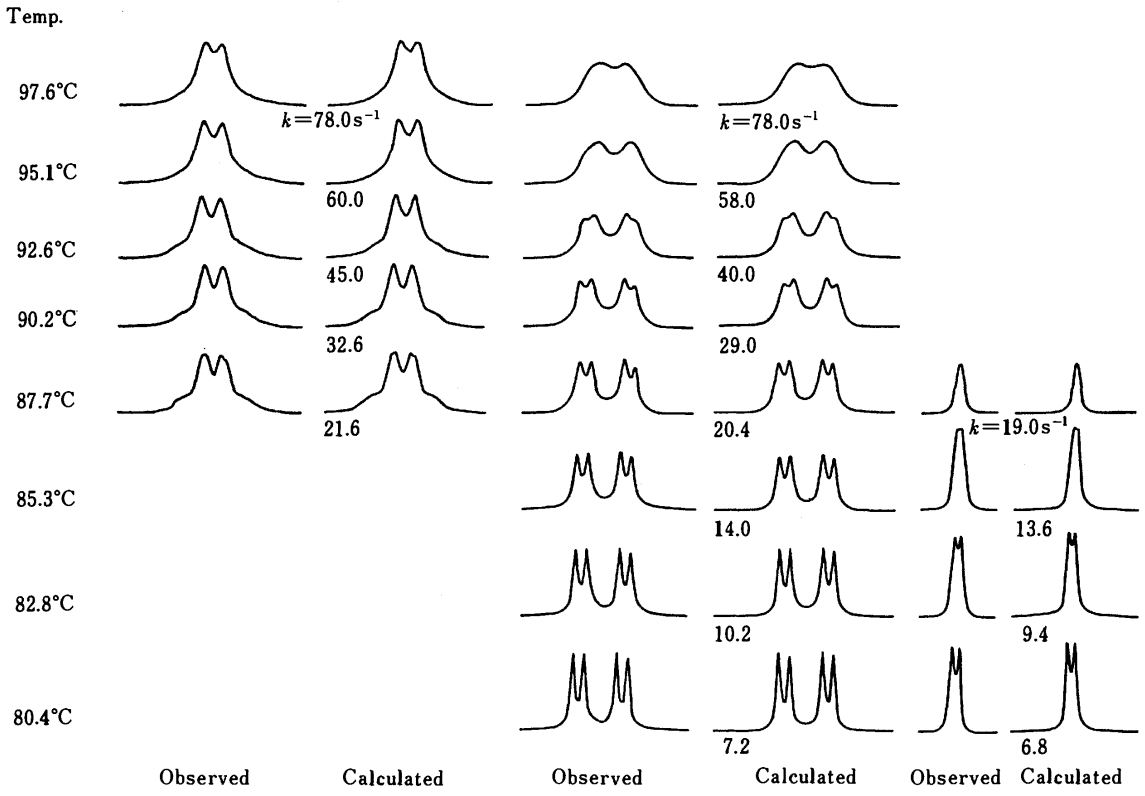

Fig. 2.

Table 1. Activation Parameters for the Rate Processes Observed in Benzyldiethylammonium Chloride (**1**) and Benzylisopropylmethylammonium Chloride (**2**) in $CDCl_2CDCl_2$

Compound	Probe	$\Delta H^{\ddagger}$[a]	$\Delta S^{\ddagger}$	$\Delta G^{\ddagger}_{363}$	r[b]
		kcal mol^{-1}	cal mol^{-1} K^{-1}	kcal mol^{-1}	
1	$CH_3\underline{CH_2}$[c]	31.2±1.8	31.5±4.8	19.7	0.9998
	$C_6H_5\underline{CH_2}$	32.0±4.8	33.7±13.0	19.7	0.9988
2	$(\underline{CH_3})_2CH$	35.7±0.8	46.1±2.1	19.0	0.9998
	$\underline{CH_3}N$	35.2±2.2	44.4±6.1	19.0	0.9998
	$C_6H_5\underline{CH_2}$	33.5±5.4	40.1±14.7	18.9	0.9962
	$C_6H_5\underline{CH_2}$[c]	34.6±2.0	43.0±5.4	19.0	0.9992

a) 1 cal=4.184 J. b) Correlation coefficient in the statistical treatment. c) Data obtained by decoupling with the ammonium proton.

inversion in these compounds is indeed fast and the rate-limiting step in the topomerization is the proton-detachment, because the proton-attachment to an amine is believed to be diffusion-controlled and is very fast.[10] They also confirm that the probe which shows both site-exchange and the loss of coupling also gives satisfactory results, although the method involves an assumption about the dependence of the coupling constants on the rate of detachment.

The results also suggest that any of the probes available in these amine hydrochlorides may be used in determining the rates of proton-detachment. This finding is quite useful and extends the scope of application of this technique, because an overlap of the line shapes of the exchanging nuclei with other signals often obscures the calculation results, some of the signals due to the exchanging nuclei may be hidden by other signals, or only one type of probes is available in a given molecule. It is now possible to use any of the probes, the loss of coupling, the site-exchange, and the combination of the both phenomena, in determining the proton affinity of amines in aprotic solvents.

A remaining problem is which probe is prefered when multiple of them are available in a given compound. Our choice is the protons of the isopropyl-methyls like in compound **2**. As is clear from Fig. 2, the change in line shapes is observable at the largest range of temperature if the isopropyl-methyl protons are used as probes. The loss of coupling of the methyl protons in **2** is treated as if the chemical shift difference corresponds to the coupling constant.[11] Since usually the coupling constant is small, i.e. ca. 5 Hz for the

CH-NH^+ protons, coalescence of the signals takes place in a rather small temperature range. In addition, the determination of the transverse relaxation times (T_2) can be problematic in this case because of the simple line shapes as is discussed later. For the diastereotopic proton pair which shows the coupling with the ammonium proton, our approximation forces us to use rather a small temperature range as well. In principle, it is possible to treat the line shapes of this kind of probes by analyzing the loss of coupling first and applying the extrapolated coupling constants to the calculation of the site exchange of the diastereotopic protons, but this procedure is tedious and does not guarantee the reliable data. The discussion presented here favors the use of isopropyl-methyl protons due to the fact that the more rate constants are available than the coupling and coupling-site-exchange cases to make the Eyring plot more reliable.

There is still another point for the preference of the isopropyl-methyl probe. That is, the more complex signals give the more reliable data in the line shape analysis owing to the multitude of checking points in the simulation.[12,13] The simpler line shapes are known to tend to produce large errors especially in entropy of activation. Since coupling with the ammonium proton gives a simple two-singlet pattern, the reliability of the line shape analysis must be considered carefully. The small errors in the activation parameters obtained from the methyl signals in **2** is rather fortuitous, The benzylic methylene signals in **2** should be better than those due to the methyl protons, but the assumption we made seems to deteriorate the quality of the data to some extent.

As the results of these factors, the kinetic parameters obtained from the isopropyl-methyl probes in **2** contain the smallest errors among those obtained here (see Table 1). The errors in the kinetic parameters obtained from the benzylic methylene probe are rather large owing to the approximation we employed. The method cannot avoid the ambiguity in determining the coupling constants and the rate constants (see Experimental part).

Compound **1** casts an additional problem to us. That is, the exchange of the sites of the methylene protons in the ethyl groups is in principle that of $ABL_3X \rightleftarrows BAL_3X$, in addition to the loss of coupling on proton-detachment. This exchange is too complicated for our program. Therefore, we irradiated the the ammonium proton to simplify the exchange to $ABX_3 \rightleftarrows BAX_3$. This operation might cause some error in the line shapes. Since this kind of operation has not been carried out, to our knowledge, in the dynamic NMR study, it was desired to confirm its reliability. If the technique does not involve problems, it will be both convenient and reliable, because the complexity of the signals will guarantee good quality of data.

In order to check the influence on the kinetic parameters given by decoupling operations, we carried out the measurement of the line shapes due to benzylic methylene protons in **2** with irradiation at the ammonium proton frequency. The rate constants were obtained as follows as the results of line shape analysis (rate constants in s^{-1} and temperatures in °C in parentheses are given): 10.0 (82.8), 15.6 (85,3), 20.6 (87.7), 28.8 (90.2), 55.0 (95.1), 76.4 (97.6). Activation parameters derived from these data are given in Table 1 as well. The agreement is excellent with those derived by using other probes and the correlation coefficient satisfactory. The results confirm that the line shape analysis using those produced by decoupling is a satisfactory method.

The feature of the kinetic parameters in Table 1 is very large, positive entropies of activation. The similar values have been obtained for *p*-substituted *N,N*-dibenzylanilinium halides[4,5] and for [*o*-(diethylaminomethyl)phenyl]halodimethylstannanes.[14] Large, positive entropies of activation seem to be general in the process when one goes from the ionic ground state to the less ionic transition state, The freedom of motion of solvent molecules must increase in the transition state in these cases.

Close examination of the data in Table 1 reveals that compond **2** gives a larger entropy of activation than **1** which in turn gives a larger entropy of activation than the *N,N*-dibenzylanilinium chloride (18—24 cal mol^{-1} K^{-1}).[4] This will probably mean that the transition state for the proton-detachment in an ammonium ion derived from a strong base is later than in that derived from a weak base. The apparent trend we have seen in the series of *N,N*-dibenzylanilinium chlorides, namely the trend that a weak base gives a larger entropy of activation for the proton-detachment than a strong,[4] is now concluded not significant. The fortuitous trend was caused by the errors involved in the line shape analysis of the benzylic methylene proton signals which simultaneously lose coupling and exchange sites on proton-detachment.

Experimental

Materials. *N,N*-Diethylbenzylamine, bp 60—62 °C/3.5 mmHg (1 mmHg=133.322 Pa) (lit,[15] bp 211—212 °C), was prepared by a standard method starting from benzyl chloride and diethylamine. ^{1}H NMR ($CDCl_3$) δ=1.01 (6H, t, J=7.0 Hz), 2.49 (4H, q, J=7.0 Hz), 7.1—7.4 (5H, m). *N*-Isopropyl-*N*-methylbenzylamine, bp 60—62 °C/3.5 mmHg, was prepared by formylation of *N*-isopropylbenzylamine by a standard method and by reduction of the resulting formyl compound with lithium tetrahydridoaluminate. ^{1}H NMR ($CDCl_3$) δ=1.07 (6H, d, J=7.0 Hz), 2.13 (3H, s), 2.86 (1H, sept, J=7.0 Hz), 3.84 (2H, s), 7.2—7.4 (5H, m).

The hydrochlorides of the amines were prepared by dissolving them in hexane and introducing hydrogen chloride gas into the solution. The precipitates thus obtained were recrystallized from tetrahydrofuran.

Benzyldiethylammonium Chloride (1), mp 182—183 °C. Found: C, 66.22; H, 8.97; N, 7.05; Cl, 17.80%, Calcd for

$C_{11}H_{18}ClN$: C, 66.15; H, 9.08; N, 7.01; Cl, 17.75%. ^1H NMR ($CDCl_3$) δ=1.46 (6H, t, J=7.3 Hz), 3.07 (4H, m), 4.16 (2H, d, J=5.3 Hz), 7.4—7.7 (5H, m), 12.43 (1H, br s).

Benzylisopropylmethylammonium Chloride (2), mp 126—127 °C. Found: C, 66.01; H, 9.02; N, 7.10; Cl, 17.65%. Calcd for $C_{11}H_{18}ClN$: C, 66.15; H, 9.08; N, 7.01; Cl, 17.75%. ^1H NMR ($CDCl_3$) δ=1.36 (3H, d, J=6.4 Hz), 1.52 (3H, d, J=6.4 Hz), 2.63 (3H, d, J=4.8 Hz), 3.49 (1H, m), 4.15 (2H, m), 7.4—7.8 (5H, m), 12.27 (1H, br s).

Dynamic NMR Spectral Study. The spectral measurement was carried out with either a JEOL FX-200 or JEOL GX-270 spectrometer. Since we used a spectrometer that operated at 60 MHz for the determination of rates of proton-detachment in *N,N*-dibenzylanilinium halides,[4,5] the 200 MHz machine was more convenient for comparison due to the fact that the 270 MHz machine gave apparently different line shapes because of the larger chemical shift differences. Samples were dissolved in 1,1,2,2-tetrachloroethane-d_2, which was dried over Molecular Sieves 4A, to make up ca. 50 mmol L^{-1} solutions.

Temperature was determined by a thermocouple. The chemical shift differences of the exchanging nuclei and coupling constants were checked at the slow exchange limits. All the coupling constants were found to be temperature-independent, whereas the chemical shift differences changed linearly with the temperature. The chemical shift differences were at least checked at four temperatures to find that they were linearly correlated with temperature, except for the isopropyl-methyl proton signals, of which chemical shift differences were temperature-independent. The results are shown in Table 2. These straight lines were extrapolated to the temperatures where the change in line shapes was observed. The simulation was carried out with the use of DNMR3 program.[7] T_2 was estimated from the line width due to the undeuterated solvent molecules and was adjusted to give the best fit in simulation for the line shapes involved in the site-exchange. Thanks to the complexity of the signals, changes in T_2 and rate constant k gave different effects on the line shapes in these cases, as were observed in other complex signals,[16] thus enabling us to determine T_2 and k uniquely.

For the simulation of the exchanging benzylic methylene proton signals, ABX⇄BAX, that lose coupling on dissociation of the ammonium proton was performed in the following way. At the coalescence temperature where the quadruplet-doublet became a broad quadruplet, the rate constant of the proton-detachment and the J_{AX} and J_{BX} values, the rough values of which were estimated from those at low temperatures, were used as variants and the T_2 and the chemical shift differences between A and B, which could be derived as above, were taken as given. The best fit values of the rate constant and the coupling constants were sought in the simulation of the line shapes. After determining the rate constant at the temperature, then the coupling constants, J_{AX} and J_{BX}, were treated as inversely proportional to the rate constant of proton-detachment. The obtained rate constants were doubled for comparison with the data obtained from the loss of coupling because the topomerization takes place only when the proton attaches to the amine after inversion of the amine and the attachment at the same configuration is not counted in the topomerization.

Table 2. Equations Correlating the Chemical Shift Differences and Temperature in Given Probes in **1** and **2**

Compound	Probe	$f(T)$[a]	External magnetic field
			MHz
1	$CH_3\underline{CH_2}$	42.9−0.040T	270
2	$(\underline{CH_3})_2CH$	26.5±0.000T	200
	$C_6H_5\underline{CH_2}$	−63.8+0.235T	200
	$C_6H_5\underline{CH_2}$[b]	−85.2+0.313T	270

a) $f(T)$ for $\Delta\nu$/Hz=$f(T)$/K. b) Decoupled with the ammonium proton.

For the simulation of the line shapes which change owing to the detachment of the ammonium proton, the principle established for methylamine in dilute hydrochloric acid[11] was used. The spin-spin coupling constants were invariant within the slow exchange limit. T_2 was estimated from the line width of the undeuterated solvent peak and this value was used throughout the simulations of the spectra at various temperatures. Since the changes in k and T_2 gave similar trends in the modification of the line shapes, there remains ambiguity in the rate constants thus obtained to some extent.

For the decoupled measurements, care was exercised for not affecting the line shapes in the slow exchange limit. The irradiation of the ammonium proton was carried out at the center of the broad signal. The irradiation power was IRATN 130.

The measurement of the ^1H NMR spectra at 200 MHz was carried out at Showa Denko Company, Ltd. We wish to thank for the permission of the use of the instrument. The work was supported by a Grant-in-Aid (No. 61134043) for Fundamental Scientific Research of the Ministry of Education, Science and Culture.

References

1) For part XIII, see M. Ōki and Y. Yamada, *Bull. Chem. Soc. Jpn.*, **61**, 1181 (1988).

2) See for example, D. D. Perrin, "Dissociation Constants of Organic Bases in Aqueous Solution," Butterworths, London (1965): Supplement (1972).

3) D. H. Aue, H. M. Webb, and M. T. Bowers, *J. Am. Chem. Soc.*, **98**, 311, 318 (1976): R. H. Staley, M. Taagapera, W. G. Henderson, I. Koppel, J. L. Beauchamp, and R. W. Taft, *ibid.*, **99**, 326 (1977).

4) M. Ōki, M. Ohira, Y. Yoshioka, T. Morita, H. Kihara, and N. Nakamura, *Bull. Chem. Soc. Jpn.*, **57**, 2224 (1984).

5) M. Ōki and M. Ohira, *Bull. Chem. Soc. Jpn.*, **57**, 3025 (1984).

6) C. H. Bushweller, S. H. Fleischman, G. L. Grady, P. McGoff, C. D. Rithner, M. R. Whalon, J. G. Brennan, R. P. Marcantonio, and R. P. Domingue, *J. Am. Chem. Soc.*, 104, 6224 (1982).

7) G. Binsch, *Top. Stereochem.*, **3**, 97 (1968).

8) F. M. Menger, T. D. Singh, and F. A. Bayer, *J. Am. Chem. Soc.*, **98**, 5011 (1976).

9) C. L. Perrin and W.-H. Wang, *J. Am. Chem. Soc.*, **104**, 2325 (1982).

10) R. A. Y. Jones, "Physical and Mechanistic Organic

Chemistry," Cambridge University Press, Cambridge (1984), pp. 257—8 and 291—2.
11) E. Grunwald, A. Loewenstein, and S. Meiboom, *J. Chem. Phys.*, **27**, 630 (1957).
12) M. Nakamura, H. Kihara, N. Nakamura, and M. Ōki, *Org. Magn. Reson.*, **12**, 702 (1979).
13) G. Binsch and H. Kessler, *Angew. Chem., Int. Ed. Engl.*, **19**, 411 (1980).
14) M. Ōki and M. Ohira, *Bull, Chem. Soc. Jpn.*, **57**, 3117 (1984).
15) V. Meyer, *Ber.*, **10**, 309 (1877).
16) T. Morita and M. Ōki, *Bull. Chem. Soc. Jpn.*, **59**, 3605 (1986).

 © 1988 The Chemical Society of Japan Bull. Chem. Soc. Jpn., 61, 1191—1194 (1988)

Dynamic NMR as a Nondestructive Method for Determination of Rates of Dissociation. XV. Dissociation of Thioether and Ether Ligands in Tin(IV) and Boron Complexes and Significance of Entropy of Activation Therein[1)]

Michinori Ōki*,† and Yasuhisa Yamada
Department of Chemistry, Faculty of Science, The University of Tokyo, Bunkyo-ku, Tokyo 113
(Received November 5, 1987)

The rates of dissociation of thioether ligands which are imbedded in organotin(IV) compounds, such as trichloro[*o*-(ethylthiomethyl)phenyl]stannane, were determined by the dynamic NMR method. The dynamic processes of the corresponding ether ligands was too fast to detect as the change in line shapes in ^{1}H NMR spectra. All the boron compounds examined, which possessed similar structures to the stannane and were of the boronate type, failed to show dissociation of a thioether or ether ligand due to their large rates of dissociation. The rates of dissociation of a thioether-tribromoboron complex were determined by the same technique. The feature of the activation parameters was that the compounds examined exhibited fairly large positive entropy of activation in accordance with other results that involve dissociation of ionic species into covalent species.

The mechanism of sulfur inversion in sulfur-ligands in platinum(II) complexes attracted interests of some investigators. It seemed generally accepted that the inversion took place without breaking the Pt-S bond.[2)] However, it was shown recently that sulfur-ligands in platinum complexes could dissociate under certain circumstances.[3)] We felt therefore that it would be worthwhile to provide a methodology of diagnosing the mechanism of sulfur-inversion in coordination compounds.

Our experience shows that, if dissociation takes place from an ionic ground state via more or less covalent transition state, the entropy of activation should be large positive, and, if the ground state is covalent and the transition state is ionic, the entropy of activation is large negative.[4)] Since thioether-platinum(II) complexes can be considered to possess an ionic ground state and the transition state for dissociation of the ligand is of covalent character, it is expected that, if the dissociation is the rate determining step in the sulfur-inversion, the entropy of activation is large positive whereas it will be near-zero, if a simple sulfur-inversion takes place.

Indeed, there is a literature that reports the entropy of activation is very small in sulfur-inversion in a platinum(II)-thioether complex.[5)] This result might be taken as evidence for the sulfur-inversion without breaking of the Pt-S bond, but there are several points to be considered before concluding in that way. Firstly, the examples that show nearly-zero entropy of activation in the sulfur-inversion in platinum-sulfur complexes are too few in literature. Secondly, the compound examined in the literature contained two thioether ligands that might affect observation of the sulfur-inversion processes. Thirdly, for not only the cases of platinum complexes, examples of reported entropy of activation are too few. Dissociation of boron-ether[6)] or boron-ketone[7)] complexes as investigated by the dynamic NMR technique has been reported, but the free energy of activation was obtained at only one point of temperature. There is also a literature that reports sulfur-inversion in a thioether-trichloroboron complex,[8)] but the results are again obtained at one temperature.

We felt on the above backgrounds that at least some examples should be provided before concluding the relationship between the entropy of activation and the mechanism of sulfur (or oxygen) inversion that is simple and causes no ambiguity about the conclusion. Thus we have examined a case that is purely sulfur-inversion that gives near-zero entropy of activation both by classical[9)] and dynamic NMR[10)] methods. In this paper we wish to report that the entropy of activation for the sulfur-inversion of which mechanism is supposed to be dissociative indeed is large, positive.

The compounds of which rates of sulfur-inversion were examined by the dynamic NMR technique were prepared in the following way. 1-Bromo-8-ethylthionaphthalene (**1**) which was prepared by a standard diazotization and substitution reaction of 8-bromo-1-naphthalenamine was lithiated with butyllithium and was then treated with tin(IV) chloride. This operation afforded dichlorobis(8-ethylthio-1-naphthyl)stannane (**2**), as are observed in other similar reactions. Com-

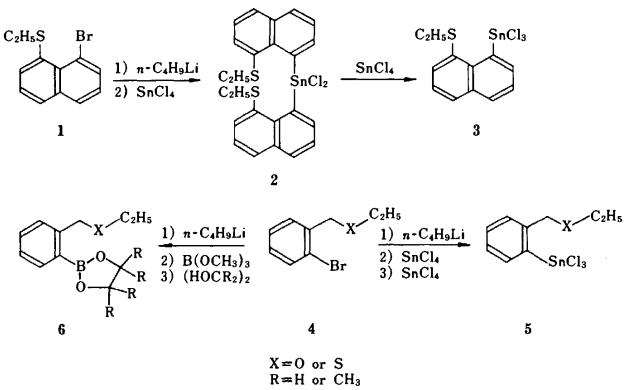

† Present address: Department of Chemistry, Faculty of Science, Okayama University of Science, Ridaicho, Okayama 700.

pound **2** was treated with excess of tin(IV) chloride to give trichloro(8-ethylthio-1-naphthyl)stannane (**3**).[11]

The syntheses of trichloro[(*o*-ethoxymethyl)phenyl]-stannane (**5**: X=O) and the thio analog (**5**: X=S) were performed similarly from *o*-bromo[ethoxy(or ethylthio)methyl]benzene (**4**). Treatment of **4** with butyllithium followed by methyl borate and then a 1,2-diol afforded 2-[*o*-ethoxy(or ethylthio)methylphenyl]-1,3,2-dioxaborolane (**6**: X=O or S, R=H or CH_3).

The selection of the compounds bases on our principle that a diastereotopic pair of protons exchange their sites on dissociation followed by racemization and recombination.[12] The methylene or gem-dimethyl protons act as probes because they are diastereotopic as far as the ligand sticks to the metalloid center. It is possible that the sulfur-inversion takes place without breaking the sulfur-metalloid bond. But if it were the case, the entropy of activation would be close to zero as were the cases of pure sulfur-inversion.[9,10,13]

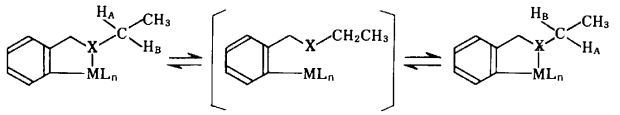

Scheme 1. A typical site-exchange process for the diastereotopic methylene protons by dissociation.

The methylene protons of the ethyl group in compound **3** showed a typical A_2 pattern of an A_2X_3 system. When the temperature was lowered to −90 °C, the signal began to broaden at 270 MHz, but the complete decoalescence of the signal was not observed. Although it is difficult to mention the exact free energy of activation for the process without knowing the chemical shift difference of the A and B protons, the rough estimate of the free energy of activation for the process is 8—10 kcal mol^{-1} (1 cal=4.184 J) at −90 °C. In contrast, compound **5** (X=S) showed the change in line shapes at and below −65 °C and the line shapes at −90 °C and below indicated that it was in the slow exchange limit. The total line shape analysis of the spectra afforded the rate constants shown in Table 1 and putting these rate constants and temperatures into the Eyring equation afforded the following kinetic parameters: $\Delta H^{\ddagger}$=12.7±0.2 kcal mol^{-1}, $\Delta S^{\ddagger}$= 13.3±1.0 cal mol^{-1} K^{-1}, $\Delta G^{\ddagger}_{273}$=9.1 kcal mol^{-1}. The low energy barrier to the process observed for **3** relative to **5** can be ascribed to the strain in the coordinated form of **3** relative to **5**, because the skeleton of the molecule is more rigid because of the presence of the naphthalene nucleus than in **5**.

The oxygen compound (**5**: X=O) failed to show any line broadening even at −50 °C where compound **5** (X=S) showed the line-broadening. We judge that the dynamic process for the oxygen-tin complex is much faster than that in the sulfur compound. This is in accordance with the fact that the $(CH_3)_2O$-$TiCl_4$ complex is less stable than the $(CH_3)_2S$-$TiCl_4$.[14]

All the boron compounds (**6**: X=O or S, R=H or CH_3) failed to show line broadening at −90 °C at 270 MHz. Therefore the barrier to the dynamic process that we expected to observe was apparently very low. We believe this observation owes to two factors. The first is that the formation of 5-membered ring will cost some energy because of the short bond distances involving the boron atom and the second is that boron acidity in boronates is lower than that of boron trihalide or trialkylborane due to the 2p-2p conjugation between the oxygen and the boron atoms.[15] The latter factor may be more effective than the former in lowering the barrier to the process, because dissociation of amine ligands in the similar compounds has been reported.[16,17]

Thus for the boron compound, we chose an intermolecular complex for the investigation, where boron which carries electronegative substituents can be easily used. As a sulfide, we used 3,3,4,4-tetramethylthiolane that had been made by us.[9] Tribromoboron was our choice because of easy handling. Thus compound **7**, 3,3,4,4-tetramethylthiolane-tribromoboron complex, was made. The reason for the selection of compound **7** is that the two pairs of the gem-dimethyl protons can be used as probes for the dissociation: although the gem-protons alpha to the sulfur atom in a sulfide can be diastereotopic on ligation of the sulfide to a boron compound, they show very complex signals because of coupling with ^{10}B and ^{11}B.

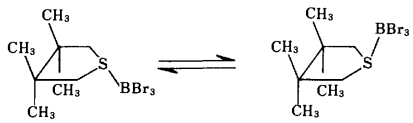

7 7'

Table 1. Rate Constants (Temperature in °C) of M-S Bond Dissociation as Determined by Dynamic NMR Spectroscopy

Compound	k/s^{-1} (Temp/°C)
5	12.0 (−80.9), 18.0 (−78.4), 28.0 (−75.9), 43.0 (−73.4), 65.0 (−70.9), 98.0 (−68.3), 142.0 (−65.8)
7[a]	3.0 (4.8), 4.3 (7.3), 6.1 (9.9), 8.7 (12.4), 12.4 (14.8), 17.1 (17.4), 23.0 (19.9), 32.4 (22.4)
7[b]	3.0 (4.8), 4.3 (7.2), 6.1 (9.8), 8.7 (12.3), 12.3 (14.8), 17.1 (17.4), 23.0 (19.8), 32.4 (22.4)

a) 20% excess of BBr_3 added. b) 10 molar excess of BBr_3 added.

Compound **7** dissociated to ca. 5% into the sulfide and tribromoboron in chloroform-*d* at −50 °C, as found by ^{1}H NMR spectrum at 270 MHz. Since excessive sulfide can cause S_N2 type substitution in addition to dissociative mechanisms, as was the case of ether-borane complexes,[6] we added excess of tribromoboron to the solution: if the excess of the boron compound affects the dissociation rates, extrapolation to the zero excess of the Lewis acid should give intrinsic rates of dissociation of the sulfur-boron complex. The results are given in Table 1, where only two extreme values are shown. At other points of excess of the boron compound, the rate constants were the same with those listed in the table. Putting these parameters to the Eyring equation, we obtain the following activation parameters: $\Delta H^{\ddagger}$=21.5±0.4 kcal mol^{-1}, $\Delta S^{\ddagger}$=21.0±1.4 cal mol^{-1} K^{-1}.

The feature of the kinetic parameters for both compounds **5** (X=S) and **7** is that the entropy of activation is both large positive, although the enthalpy of activation is different. This makes a sharp contrast to the case of pure sulfur-inversion that gives near-zero entropy of activation. The results are in agreement with others in that the entropy of activation is positive when the ground state is of ionic character and the transition state for dissociation reduces the ionic character. The generality of the rule thus encompasses the coordination complexes that contain sulfur ligands.

Experimental

Dynamic NMR Spectroscopy. All the ^{1}H NMR spectra were recorded on a JEOL GX-270 NMR spectrometer operating at 270 MHz. The temperature indicated on the temperature setting of the machine was calibrated by a thermocouple. A sample was dissolved in an appropriate solvent to make up ca. 50 mmol L^{-1} solutions. The solvent was dichloromethane-d_2 in the case of intramolecularly ligating stannane and borane compounds and it was chloroform-*d* for compound **7**. When 20% excess of tribromoboron was added to the chloroform-*d* solution of **7**, no signal attributable to the free sulfide was observed. The spin exchange was treated as AB $\rightleftarrows$ BA with no coupling for compound **7** and $ABX_3 \rightleftarrows BAX_3$ for compound **5** and the line shapes were simulated with the use of DNMR3 program.[18] The chemical shift differences of the methyl signals (A and B) in compound **7** drifted a little according to temperatures of observation and the linear relation was obtained between the former and the latter in the slow exchange limit: $\Delta\nu$/Hz=0.016t/°C+12.5 for the cases of small excess of tribromoboron and $\Delta\nu$/Hz=0.016t/°C+12.3 for the case where tribromoboron was of 10 molar excess. In the case of compound **5**, the chemical shift differences between A and B protons and between A and X protons were constant in the slow exchange limit at 99.6 and 364 Hz, respectively. The coupling constants, J_{AB} and J_{AX}=J_{BX}, for compound **5** were constant at −13.6 and 7.3 Hz, respectively, throughout the temperature range examined. These results were extended to the temperature range, where line broadening and coalescence took place, in calculation of the spectra. T_2 was estimated to be 0.10 s for compound **5** and 0.16 s for **7** and these values were used throughout the simulation of the line shapes. The best fit between the observed and the calculated spectra were obtained by visual fitting. The agreement between them was satisfactory. The rate constants thus obtained were put into the Eyring equation to produce the activation parameters.

1-Bromo-8-ethylthionaphthalene (1). 1-Amino-8-bromonaphthalene[19] (5.00 g or 22.5 mmol) was dissolved in 50 mL of water and 6 mL of concentrated hydrochloric acid by heating. To the cooled mixture, was added a solution of 1.6 g (23 mmol) of sodium nitrite in 10 mL of water with shaking. The diazotized solution was neutralized by adding aqueous sodium acetate with cooling and filtered. The solution was added at 40 °C to an aqueous solution of sodium ethanethiolate prepared from 1.0 g (25 mmol) of sodium hydroxide, 50 mL of water and 1.6 mL (22 mmol) of ethanethiol. The mixture was heated to 90 °C and stirred at that temperature for 2 h. The cooled mixture was extracted with benzene, and the extract was washed with water. After drying over magnesium sulfate, the solvent was evaporated and the residue was submitted to chromatography on silica gel with hexane as an eluent. The desired product was obtained in 46.7% yield after recrystallization from hexane, mp 47.0—48.0 °C. Found: C, 53.75; H, 4.08%. Calcd for $C_{12}H_{11}BrS$: C, 53.95; H, 4.08%. ^{1}H NMR ($CDCl_3$) δ=1.36 (3H, t, J=7.6 Hz), 2.93 (2H, q, J=7.6 Hz), 7.1—7.9 (6H, m).

Dichlorobis(8-ethylthio-1-naphthyl)stannane (2). To a solution of 2.40 g (8.98 mmol) of the bromo compound **1** in 80 mL of ether was added 7.5 mL (11 mmol) of a ca. 1.5 mol L^{-1} hexane solution of butyllithium at −30 °C under a nitrogen atmosphere. The mixture was allowed to stand so that the temperature slowly rose until the temperature became ambient. The solution was transfered to a dropping funnel through a Teflon tube and added to a solution of 2 mL (17 mmol) of tin(IV) chloride in 100 mL of benzene at room temperature. After the reaction was continued for an additional hour at the temperature, the solvent was evaporated. Recrystallization of the residue from dichloromethane-hexane afforded the desired compound, mp 225.5—226.5 °C, in 67% yield. Found: C, 50.83; H, 3.66; Cl, 12.57; S, 11.47%. Calcd for $C_{24}H_{22}Cl_2S_2Sn$: C, 51.10; H, 3.93; Cl, 12.57; S, 11.37%. ^{1}H NMR ($CDCl_3$) δ=0.89 (6H, t, J=7,7 Hz), 2.70 and 3.00 (4H, AB part of ABX_3, J_{AB}=12.0 Hz, J_{AX}=J_{BX}=7.7 Hz), 7.4—8.1 (10 H, m), 8.86 (2H, dd, J=6.9 and 1.3 Hz).

Trichloro(8-ethylthio-1-naphthyl)stannane (3). A solution of 1.70 g (3.01 mmol) of the diaryldichlorostannane (**2**) and 1 mL (9 mmol) of tin(IV) chloride in 80 mL of toluene was heated under reflux for 12 h under a nitrogen atmosphere. The solvent was evaporated and the residue was extracted with hot hexane. Cooling the hexane extract afforded crystals. Recrystallization of the product from dichloromethane-hexane gave a pure sample, mp 108.5—109.5 °C. Found: C, 34.89; H, 2.76; Cl, 25.99; S, 7.85%. Calcd for $C_{12}H_{11}Cl_3SSn$: C, 34.96; H, 2.69; Cl, 25.79; S, 7.78%. ^{1}H NMR ($CDCl_3$) δ=1.23 (3H, t, J=7.4 Hz), 2.96 (2H, q, J=7.4 Hz), 7.5—8.2 (5H, m), 8.58 (lH, d, J=7.2 Hz).

Dichlorobis[2-(ethylthiomethyl)phenyl]stannane, mp 174.5—175.5 °C, was obtained by similar treatment of 1-bromo-2-(ethylthiomethyl)benzene[20] as described in the preparation of **2** in 45% yield. Found: C, 43.44; H, 4.50; Cl, 15.42%. Calcd for $C_{18}H_{22}Cl_2S_2Sn$: C, 43.93; H, 4.51; Cl, 14.41%. ^{1}H NMR ($CDCl_3$) δ=0.99 (6H, t, J=7.5 Hz), 2.37 (4H, q, J=7.5 Hz), 4.11 (4H, s), 7.2—7.5 (6H, m), 8.2—8.3 (2H, m).

Trichloro[2-(ethylthiomethyl)phenyl]stannane (**5**: X=S), mp 108.5—109.5 °C, was similarly obtained by treating the diaryldichlorostannane with $SnCl_4$ in 79% yield. Found: C, 28.49; H, 2.95; Cl, 27.92%. Calcd for $C_9H_{11}Cl_3SSn$: C, 28.73; H, 2.95; Cl, 28.26%. ^1H NMR ($CDCl_3$) δ=1.28 (3H, t, J=7.4 Hz), 2.40 (2H, q, J=7.4 Hz), 4.10 (2H, s), 7.4—7.7 (3H, m), 8.1—8.2 (1H, m).

Dichlorobis[2-(ethoxymethyl)phenyl]stannane was similarly prepared from 1-bromo-2-(ethoxymethyl)benzene.[21] The product was recrystallized from dichloromethane-hexane to give 46% of the desired product, mp 194.0—195.0 °C. Found: C, 46.78; H, 4.92; Cl, 15.45%, Calcd for $C_{18}H_{22}Cl_2O_2Sn$: C, 47.00; H, 4.82; Cl, 15.42%. ^1H NMR ($CDCl_3$) δ=0.92 (6H, t, J=6.9 Hz), 3.37 (4H, q, J=6.9 Hz), 4.70 (4H, s), 7.1—7.5 (6H, m), 8.3 (2H, m).

Trichloro[2-(ethoxymethyl)phenyl]stannane (**5**: X=O), mp 130.5—132.0 °C, was similarly prepared as for the preparation of **3** in 67% yield. The analytical sample was obtained by recrystallization from hexane. Found: C, 29.73; H, 3.21; Cl, 29.44%. Calcd for $C_9H_{11}Cl_3OSn$: C, 30.01; H, 3.08; Cl, 29.52%. ^1H NMR ($CDCl_3$) δ=1.44 (3H, t, J=7.0 Hz), 4.15 (2H, q, J=7.0 Hz), 4.81 (2H, s), 7.4 (1H, m), 7.5—7.6 (2H, m), 8.0—8.1 (1H, m).

2-[2-(Ethylthiomethyl)phenyl]-4,4,5,5-tetramethyl-1,3,2-dioxaborolane (**6**: X=S, R=CH_3). To a solution of 4.03 g (17.4 mmol) of 1-bromo-2-(ethylthiomethyl)benzene[21] in 50 mL of ether was added 12.2 mL (18.3 mmol) of a ca. 1.5 mol L^{-1} hexane solution of butyllithium at −78 °C under a nitrogen atmosphere. The mixture was allowed to warm slowly up to room temperature and then transferred to a dropping funnel through a Teflon tube. The mixture was added to 3.4 mL (30 mmol) of trimethyl borate in 50 mL of ether at −78 °C and allowed to warm slowly up to the room temperature. Water (10 mL) and then 10 mL of dilute sulfuric acid were added to the mixture and the ether layer was separated. The aqueous layer was extracted with ether and the combined ether layers were washed with water. The solvent was evaporated and the residue was mixed with 2.0 g (17 mmol) of 2,3-dimethyl-2,3-butanediol and 150 mL of toluene. The mixture was heated with a Dean-Stark apparatus for 2 h. The mixture was then fractionally distilled to give the desired product, bp 128.0—130.0 °C/3 mmHg (1 mmHg=133.322 Pa). The yield was 1.8 g (37%). Found: C, 64.85; H, 8.51; S, 11.66%. Calcd for $C_{15}H_{23}BO_2S$: C, 64.76; H, 8.33; S, 11.52%. ^1H NMR ($CDCl_3$) δ=1.17 (3H, t, J=7.5 Hz), 2.38 (2H, q, J=7.5 Hz), 1.40 (12H, s), 4.01 (2H, s), 7.2—7.3 (3H, m), 7.7—7.8 (1H, m).

2-[2-(Ethylthiomethyl)phenyl]-1,3,2-dioxaborolane (**6**: X=S, R=H), bp 114—115 °C/3 mmHg, was similarly prepared by treating 2-(ethylthiomethyl)phenyllithium with trimethyl borate and then with acidic water followed by ethylene glycol in 55% yield. Found: C, 59.45; H, 6.94; S, 14.09%. Calcd for $C_{11}H_{15}BO_2S$: C, 59.48; H, 6.81; S, 14.09%. ^1H NMR ($CDCl_3$) δ=1.19 (3H, t, J=7.4 Hz), 2.40 (2H, q, J=7.4 Hz), 4.00 (2H, s), 4.37 (4H, s), 7.1—7.3 (3H, m), 7.7—7.8 (1H, m).

2-[2-(Ethoxymethyl)phenyl]-1,3,2-dioxaborolane (**6**: X=O, R=H), bp 95—105 °C/4 mmHg, was similarly prepared from 1-bromo-2-(ethoxymethyl)benzene[21] as for the preparation of **6** (X=S, R=CH_3) in 46% yield. The distillate solidified and was recrystallized from dichloromethane-hexane to afford a pure sample, mp 50.0—51.0 °C. Found: C, 64.23; H, 7.06%. Calcd for $C_{11}H_{15}BO_3$: C, 64.12; H, 7.34%. ^1H NMR ($CDCl_3$) δ=1.24 (3H, t, J=6.9 Hz), 4.56 (2H, q, J=6.9 Hz), 4.38 (4H, s), 4.74 (2H, s), 7.2—7.5 (3H, m), 7.8 (1H, m).

3,3,4,4-Tetramethylthiolane-Tribromoboron Complex (7). To a solution of 0.20 g (0.14 mmol) of the thiolane[9] in 1 mL of dichloromethane was added 0.15 mL (0.16 mmol) of tribromoboron at −78 °C and then dry hexane to give precipitates. The supernatant liquid was removed by a syringe and the residue was recrystallized from dichloromethane-hexane. This compound began to decompose at 118 °C, as indicated by the sublimed crystals of the thiolane, and then the decomposition was complete at 170—192 °C. Found: S, 7.76%. Calcd for $C_8H_{16}BBr_3S$: S, 8.12%. ^1H NMR ($CDCl_3$, −50 °C) δ=1.10 (6H, s), 1.14 (6H, s), 3.1—3.6 (4H, m). An additional peak attributable to free thiolane at δ 0.96 (ca. 5%) was observed under the conditions.

This work was supported by a Grant-in-Aid (No. 61134043) for Fundamental Scientific Research of the Ministry of Education, Science and Culture.

References

1) For Part XIV, see T. Morita and M. Ōki, *Bull. Chem. Soc. Jpn.*, **61**, 1185 (1988).
2) P. Haake and P. C. Turley, *J. Am. Chem. Soc.*, **89**, 4611 (1967); P. C. Turley and P. Haake, *ibid.*, **89**, 4617 (1967).
3) S. Lanza, D. Minniti, P. Moore, J. Sachinidis, R. Romeo, and M. L. Tobe, *Inorg. Chem.*, **23**, 4428 (1984): G. Alibrandi, G. Bruno, S. Lanza, D. Minniti, R. Romeo, and M. L. Tobe, *ibid.*, **26**, 185 (1987).
4) T. Morita and M. Ōki, *Bull. Chem. Soc. Jpn.*, **59**, 3605 (1986) and references cited therein.
5) E. W. Abel, M. Booth, and K. G. Orrell, *J. Chem. Soc., Dalton Trans.*, **1977**, 42.
6) A. C. Rutenberg, A. A. Palko, and J. S. Drury, *J. Am. Chem. Soc.*, **85**, 2702 (1963).
7) J. S. Hartman, P. Stilbis, and S. Forsen, *Tetrahedron Lett.*, **1975**, 3497.
8) S. Brownstein, *J. Am. Chem. Soc.*, **98**, 2663 (1976).
9) M. Ōki, Y. Yamada, and S. Murata, *Bull. Chem. Soc. Jpn.*, **61**, 707 (1988).
10) M. Ōki and Y. Yamada, *Bull. Chem. Soc. Jpn.*, **61**, 1181 (1988).
11) R. C. Poller, *J. Chem. Soc.*, **1963**, 706.
12) M. Ōki and M. Ohira, *Bull. Chem. Soc. Jpn.*, **54**, 3117 (1984).
13) R. Scartazzini and K. Mislow, *Tetrahedron Lett.*, **1967**, 2719.
14) S. J. Ruzicka, C. M. P. Favez, and A. E. Merbach, *Inorg. Chim. Acta*, **23**, 239 (1977).
15) E. W. Abel, W. Gerrard, M. F. Lappert, and R. Shafferman, *J. Chem. Soc.*, **1958**, 2895.
16) H. Kessler, G. Zimmermann, H. Frietze, and H. Möhrle, *Chem. Ber.*, **111**, 2605 (1978).
17) T. Bergmeister, R. Grobe-Einsler, R. Grotstollen, A. Mannschreck, and G. Wulff, *Chem. Ber.*, **114**, 3403 (1981).
18) G. Binsch, *Top. Stereochem.*, **3**, 97 (1968).
19) L. F. Fieser and A. M. Seligman, *J. Am. Chem. Soc.*, **61**, 136 (1939).
20) G. Bähr and K. H. Thiele, *Chem. Ber.*, **90**, 1578 (1957),
21) F. G. Holliman and F. G. Mann, *J. Chem. Soc.*, **1942**, 737.

 © 1988 The Chemical Society of Japan Bull. Chem. Soc. Jpn., 61, 1195—1200 (1988)

Rotational Isomerism in Fluorene Derivatives. X.[1] The Conformational Equilibria of 9-Substituted 9-(2-Methylthiophenyl)- and 9-Substituted 9-(2-Methylsulfinylphenyl)fluorene Derivatives

Akiko NISHIDA, Michinao TAKAMUKU, Shizuo FUJISAKI, and Shoji KAJIGAESHI*
Department of Industrial Chemistry, Faculty of Engineering, Yamaguchi University, Tokiwadai, Ube 755
(Received June 6, 1987)

Several 9-substituted 9-(2-methylthiophenyl)fluorene derivatives and their oxidation products, 9-substituted 9-(2-methylsulfinylphenyl)fluorene derivatives were prepared. Each equilibrium constant was investigated and the conformational equilibria *ap* ⇄ *sp* of these compounds were discussed on the basis of nonbonding intramolecular interactions (attraction or repulsion) between 2-substituents in phenyl moieties (methylthio or methylsulfinyl) and fluorene ring or 9-substituents. It was found that the conformational equilibria were effected by the electronic properties of methylthio and methylsulfinyl groups. Kinetic data for internal rotation of a few compounds were shown.

9-(2-Substituted phenyl)fluorene derivatives have been the subject of recent interest because of their high barriers to rotation about the C(9)-C(Ar) bond; many important stereochemical effects have been found in these systems.[2,3] We have also investigated the restricted rotation about the C(9)-C(Ar) bonds in 9-substituted 9-(2-methylphenyl)fluorene derivatives[4] and 9-(2-methoxyphenyl)fluorene derivatives.[5] In the present paper, we wish to report on the syntheses of some 9-substituted 9-(2-methylthiophenyl)fluorene derivatives and their oxidation products, 9-substituted 9-(2-methylsulfinylphenyl)fluorene derivatives, and to discuss the conformational equilibria of these compounds on the basis of nonbonding intramolecular interactions between 9-substituents and the 2-methylthio or 2-methylsulfinyl group.

Results and Discussion

Preparation of 9-Substituted 9-(2-Methylthiophenyl)-fluorene Derivatives. The treatment of fluorenone with 2-methylthiophenyllithium, which was prepared by the reaction of 2-methylthiobromobenzene[6] and butyllithium in ether, followed by hydrolysis, afforded 9-(2-methylthiophenyl)-9-fluorenol (**1**). Bubbling hydrogen bromide into a solution of **1** in acetic acid gave 9-bromo-9-(2-methylthiophenyl)fluorene (**2**); then, **2** was refluxed in methanol or ethanol to give 9-methoxy- (**3a**) or 9-ethoxy-9-(2-methylthiophenyl)-fluorene (**3b**), respectively. The reduction of **1** with hydriodic acid gave 9-(2-methylthiophenyl)fluorene (**4**). 9-Lithio compound **5** was obtained from **4** and butyllithium, and then converted directly to 9-methyl- (**6a**) or 9-ethyl-9-(2-methylthiophenyl)fluorene (**6b**) by treating with methyl iodide or ethyl iodide, respectively. 9-(2-Methylthiophenyl)-9-fluorenecarboxylic acid (**7**) was prepared by the treatment of **5** with Dry Ice in ether. After heating **7** with thionyl chloride at 50 °C, methanol was added to afford 9-methoxycarbonyl-9-(2-methylthiophenyl)fluorene (**8**). Upon continuous heating of **7** with thionyl chloride at 80 °C, a ring compound, spiro[benzo[*b*]thiophene-3(2*H*),9′-fluoren]- 2-one (**10**) was obtained. 9-Acetyl- (**9a**) and 9-benzoyl-9-(2-methylthiophenyl)fluorene (**9b**) were obtained by the treatment of **5** with acetic anhydride and benzoyl chloride in ether, respectively. 9-Substituted 9-(2-methylthiophenyl)fluorene derivatives **1**—**9** are shown in Scheme 1.

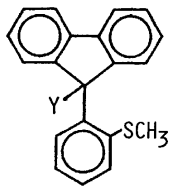

	Y
1	OH
2	Br
3a	OCH_3
3b	OC_2H_5
4	H
6a	CH_3
6b	C_2H_5
7	COOH
8	$COOCH_3$
9a	$COCH_3$
9b	COPh

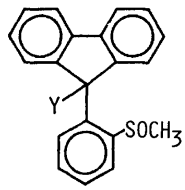

	Y
11	OH
12a	OCH_3
12b	OC_2H_5
13	H
14	CH_3
15a	$COCH_3$
15b	COPh

Scheme. 1.

Preparation of 9-Substituted 9-(2-Methylsulfinylphenyl)fluorene Derivatives. Some of the 9-substituted 9-(2-methylthiophenyl)fluorene derivatives were converted to 9-substituted 9-(2-methylsulfinylphenyl)-fluorene derivatives by oxidation with nitric acid (d=1.38). That is, 9-(2-methylsulfinylphenyl)-9-fluorenol (**11**) was prepared by the reaction of **1** with nitric acid in acetic acid at 10—20 °C. In this case, when the reaction temperature was raised to 50 °C, a ring closed compound, spiro[3*H*-2,1-benzoxathiole-3,9′-fluorene] 1-oxide (**16**), was obtained. The reactions of **3a** and **3b** with nitric acid in acetic acid at 10—20 °C afforded 9-methoxy- (**12a**) and 9-ethoxy-9-(2-methylsulfinylphenyl)fluorene (**12b**), respectively. Then, **4** was treated with nitric acid under the same reaction conditions to give 9-(2-methylsulfinylphenyl)fluorene (**13**). Furthermore, the oxidation of **6a** by nitric acid was

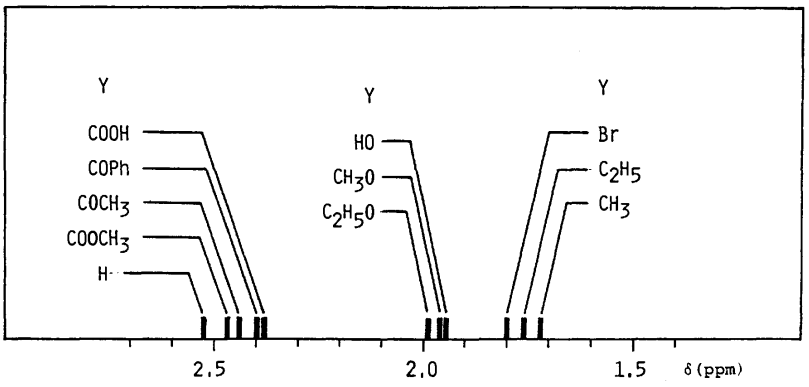

Fig. 1. The δ values for 2-SCH_3 of 9-substituted 9-(2-methylthiophenyl)fluorenes in $CDCl_3$ at room temperature.

Table 1. Oxidation of 9-Substituted 9-(2-Methylthiophenyl)fluorenes by Nitric Acid (d=1.38)

Material (2.0 mmol)	Reaction condition		Solvent (10 ml)	Product	Yield
	Time/h	Temp/°C			%
1	3	10—20	AcOH	**11**	75
1	1	150	AcOH	**16**	40
3a	5	10—20	AcOH	**12a**	93
3b	3	10—20	AcOH	**12b**	33
4	7	10—20	AcOH	**13**	82
6a	5	35—45	AcOH	**14**	78
9a	8	35—40	AcOH	**15a**	21
9b	24	40	AcOH	**15b**	12

carried out at 35—45 °C in acetic acid to afford 9-methyl-9-(2-methylsulfinylphenyl)fluorene (**14**). Reactions of **9a** and **9b** with nitric acid in acetic acid were carried out at 35—45 °C to give 9-acetyl-(**15a**) and 9-benzoyl-9-(2-methylsulfinylphenyl)fluorene (**15b**), respectively. These results are shown in Table 1.

Conformational Equilibria of 9-Substituted 9-(2-Methylthiophenyl)fluorene Derivatives. Previously, we discussed the conformations of 9-substituted 9-(2-methylphenyl)- and 9-substituted 9-(2-methoxyphenyl)fluorene derivatives on the basis of their 2-methyl and 2-methoxyl signals in ^1H NMR at low or room temperature.

In this case, the conformations of 9-(2-methylthiophenyl)fluorene derivatives were investigated on the basis of 2-methylthio signals in ^1H NMR at 50—40 °C. The NMR data for these signals are illustrated in Fig. 1. These compounds can be clearly classified into three groups: The first group includes compounds **2**, **6a**, and **6b** in which the signals for methylthio groups appear at a high field; the second includes compounds, **4**, **7**, **8**, **9a**, and **9b** in which the signals for methylthio groups are observed in a low field; the third contains the compounds, **1**, **3a**, and **3b** in which the signals for methylthio groups are found in a middle field.

The compounds that belong to the third group (9-substituents: OH, OCH_3, OC_2H_5) showed a broad singlet for methylthio protons at room temperature. As

ap-form *sp*-form

Y: OH, OCH_3, OC_2H_5

Fig. 2. Isomerization processes between *sp* and *ap* forms in **1**, **3a**, and **3b**.

the temperature was lowered, these signals gradually changed to broad two singlets; then, the signal of **1** showed two sharp singlets at δ 1.88 and 2.55 (2.0 : 1) at −30 °C, whereas that of **3a** showed two sharp singlets at δ 1.89 and 2.51 ppm (2.3 : 1) at −30 °C. The methylthio signal at the higher field corresponds to a conformation of the *ap*-form and the other at a lower field to that of the *sp*-form. It is known that the 2-substituent of the *ap* conformation is located in a shielding zone of the fluorene ring. Thus, the substituent gives an ^1H NMR signal at a higher field than that of the *sp* conformation, which is located in a deshielding zone of the fluorene ring. We have already reported that in 9-(2-methoxyphenyl)-9-fluorenol the *sp*-form was only observed because of its high stabilization, which was caused by an intramolecular hydrogen bond between the oxygen atom of the 2-methoxyl group and the hydrogen atom of the 9-hydroxyl group. However, in compound **1**, the hydrogen bond between the sulfur atom of the 2-methylthio group and the hydrogen atom of the 9-hydroxyl group could not be recognized by its IR spectra in several solvents. This may be due to the weakness of the electronegativity of the sulfur atom compared with that of the oxygen atom. The steric repulsion between the methylthio group and the hydroxyl group may unstabilize the *sp*-form of **1**. After all, third-group compounds predominantly existed as the *ap*-form (Fig. 2).

Furthermore, the rotational barriers about the C(9)–C(Ar) bonds in **1** and **3a** were obtained by line-shape analyses of methylthio signals in their DNMR spec-

Table 2. Activation Free Energies for Rotation about C(9)–(Ar) Bonds and *ap*/*sp* Ratios of the Compounds **1**—**15**

9-Substituent	2-SCH_3				2-$SOCH_3$			
	Compd.	$\Delta G^{\neq}_{sp\to ap}$[a] kcal mol^{-1}	$\Delta G^{\neq}_{ap\to sp}$[a] kcal mol^{-1}	$K(ap/sp)$	Compd.	$\Delta G^{\neq}_{sp\to ap}$[a] kcal mol^{-1}	$\Delta G^{\neq}_{ap\to sp}$[a] kcal mol^{-1}	$K(ap/sp)$
OH	**1**	14.0	14.3	2.0/1	**11**	14.3	13.5	1/4.0
OCH_3	**3a**	13.6	14.1	2.3/1	**12a**	14.5	12.9	1/15
H	**4**			*sp*[b]	**13**	15.5	15.3	1/1.5
Br	**2**			*ap*[c]	—			
R	**6**[d]			*ap*[c]	**14**[e]			*ap*[c]
COR	**7**—**9**[f]			*sp*[b]	**15**[g]			*sp*[b]

a) 1 cal=4.18 J. b) *sp*-Form was predominant. c) *ap*-Form was predominant. d) R=CH_3, C_2H_5. e) R=CH_3. f) R=OH, OCH_3, CH_3, Ph. g) R=CH_3, Ph.

Table 3. NMR Spectral Data of 9-Substituted 9-(2-Methylsulfinylphenyl)fluorene Derivatives **11**—**15** at Room Temperature

Compd.	NMR ($CDCl_3$): δ/ppm			
	$SOCH_3$	6-H	9-Substituent	Aromatic proton
11	2.52br.s		4.10br.s	6.22—8.18m
12a	2.93br.s	6.45br.d	2.93s	7.00—8.20m
12b	3.00br.s	6.74br.s	1.14t 3.18q	7.04—8.03m 8.42d
13	1.79br.s 3.00br.s	6.62br.d	5.35br.s	7.02—7.94m 8.24d
14	1.60s		1.82s	7.00—8.10m
15a	2.85s	6.66d	1.73s	7.0—8.01m 8.23d
15b	2.98s	6.62d		6.90—8.04m 8.24d

tra.[7] The results are tabulated together with those of compounds in which the equilibria were onesided, in Table 2.

In first-group compounds (Y: Br, CH_3, C_2H_5), the chemical shifts for these methylthio protons appeared at δ 1.72—1.80. These chemical shifts have been approximated to those for the *ap*-methylthio proton (roughly δ=1.9) in third-group compounds; these methylthio signals do not split, even at −50 °C. These results indicate that a steric repulsion between the 9-substituents and the 2-methylthio group in first-group compounds makes the equilibria *ap*⇄*sp* incline to the *ap*-form, exclusively.

The chemical shifts (δ 2.28—2.53) for methylthio protons in the compounds (Y: H, CO_2CH_3, $COCH_3$, COPh, and CO_2H) that belong to the second group, have been approximated to those for *sp*-methylthio group in third-group compounds (roughly δ=2.5); no split of these signals occured until −50 °C. It is then shown that the equilibria *ap*⇄*sp* lies very far to the *sp* side, contrary to the case of the first group.

We have described that in the 9-substituted 9-(2-methoxyphenyl)- and 9-substituted 9-(2-methylphenyl)fluorene derivatives, the compounds in which 9-substituents bear carbonyl groups have an intramolecular attractive interaction between the carbonyl group and the methoxyl or methyl group. Furthermore, Ōki and his coworkers have proposed that the same interaction existed in several 1,4-dimethyl-9-(carbonylmethyl)triptycene.[8] It is reasonable that in compounds **7**—**9** a dipole-electric charge interaction between the carbonyl and methylthio group makes the *sp*-conformation more predominant (Fig. 3).

ap-form *sp*-form

Fig. 3. Isomerization processes between *sp* and *ap* forms in 9-carbonyl compounds **7**—**9**.

Conformational Equilibria of 9-Substituted 9-(2-Methylsulfinylphenyl)fluorene Derivatives. Regarding 9-(2-methylsulfinylphenyl)fluorene derivatives, their conformations are discussed in terms of the chemical shifts for the 2-methylsulfinyl proton in their ^{1}H NMR.

These NMR data are listed in Table 3. The equilibrium constants, or predominant conformers, are tabulated in Table 2. Regarding compound **13**, two signals (δ 1.72 and 3.00) appeared at room temperature, the former being assigned to methylsulfinyl protons of the *ap*-form; the latter was assigned to those of the *sp*-form (*ap*/*sp*=1/1.5). On the contrary, only the *sp*-form was observed in **4**. The *sp*-form was fairly unstabilized by means of a steric repulsion between the 9-

hydrogen and methylsulfinyl group; then, two conformers existed in equilibria. Table 3 also shows that the signals for methylsulfinyl protons in most compounds, except **14**, can be approximated to that for methylsulfinyl protons in the *sp*-form of **13** (δ 3.0). It is suggested that the *sp*-form exists predominantly in these compounds.

When **11** was measured in the NMR spectra at low temperatures, the signal of methylsulfinyl protons split into two singlets at δ 1.24 (*ap*-form) and 2.64 (*sp*-form), and its ratio was 1/4. The conformational equilibria of **11** was different from that of **1**. The *sp*-form was predominant due to a dipole-electric charge interaction between the methylsulfinyl and hydroxyl groups rather than hydrogen bond. An attempt to measure the FT-IR spectra of **11** in CCl_4 failed because of the insolubility of **11** in the solvent.

In compound **12a**, with a methoxyl group at the 9-position, the signal for the methylsulfinyl proton appeared as a broad singlet at room temperature, and split into two singlets at δ 1.66 and 3.18 (*ap*/*sp*=1/15) at −33 °C. Accordingly, the *sp*-form must be exclusively predominant. The favorable conformation has also been reversed compared with the case of sulfides, **3a** and **3b**. It can be considered that an attractive (dipole-electric charge) interaction operates between the methylsulfinyl and alkoxyl groups.

The chemical shifts for the methylsulfinyl proton in **15a** and **15b** have approximated to that for the methylsulfinyl proton of the *sp*-form in **13**. The signal in **15a** appeared as a sharp singlet in the temperature range −50 to 30 °C. The predominance of the *sp*-conformation stemmed from an attractive interaction between the methylsulfinyl and carbonyl group.

The signal for the methylsulfinyl group in **14** was observed as a sharp singlet at δ 1.56 near to the value of the *ap*-form of **13**. The steric strain between the methylsulfinyl and methyl groups results in a predominance of the *ap*-from.

The activation free energies of the internal rotation (*ap*⇄*sp*) of **11**, **12a**, and **13** are shown in Table 2. The higher barrier of **13**, compared to that of **11**, may be attributed to a lowering of the ground state of **13**.

Formation of Ring-Closed Compounds 10 and 16. As described above, an attempted esterification of **7** and an oxidation of **1** under severe conditions gave ring closed compounds **10** and **16**, respectively. These mechanisms are considered to be as follows. Acid chloride **17** was obtained by the reaction of **7** with thionyl chloride and converted to cyclic sulfonium salt **18** at a higher temperature (80 °C); then **10** should have been obtained by the elimination of methyl chloride from this unstable intermediate **18**. The oxidation of **1** by nitric acid afforded **11**, which is ring closed to intermediate **19**; then **19** eliminates methane to give **16**. These reactions are shown in Scheme 2.

Experimental

All melting points are uncorrected. The ^1H NMR spectra were recorded on a JEOL-MH-100 spectrometer with a JEOL model JES-VT-3 variable temperature controller. The chemical shifts are expressed in ppm, with tetramethylsilane as an internal standard. Dynamic NMR spectra were analyzed by using a modified version of the computer program DNMR3. The IR spectra were measured on a IRA-1 spectrometer as potassium bromide pellets.

9-(2-Methylthiophenyl)-9-fluorenol (1). To a solution of *o*-bromophenyl methyl sulfide (27.4 g, 0.14 mol) in dry ether (80 ml) was added a solution of commercial butyllithium in hexane (82.2 ml) at −40 °C. After the reaction mixture was stirred for 1.5 h, a solution of fluorenone (24.3 g, 0.14 mol) in dry benzene was added dropwise. The reaction mixture was stirred for 15 min and allowed to warm at room temperature. The mixture was hydrolyzed by dil. hydrochloric acid, extracted with benzene, washed with water, dried ($MgSO_4$) and concentrated in vacuo to give a solid which was recrystallized first from benzene and then ethanol to give **1** as colorless needles; yield: 25.2 g (61%); mp 141 °C. ^1H NMR ($CDCl_3$) δ=1.95 (3H, br. s, SCH_3), 2.52 (1H, br.s, OH), and 6.92—8.36 (12H, m, H_{arom}). Found: C, 79.05; H, 5.26%. Calcd for $C_{20}H_{16}OS$: C, 78.91; H, 5.30%.

9-Bromo-9-(2-methylthiophenyl)fluorene (2). Into a solution of **1** (1.83 g, 6 mmol) in acetic acid (20 ml) was

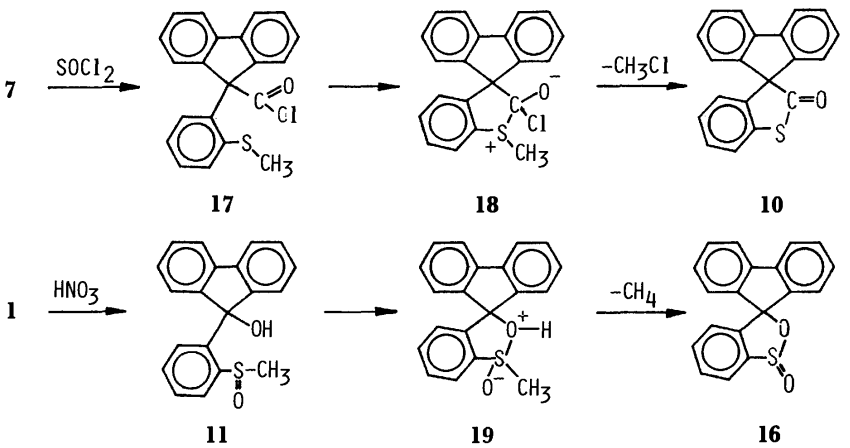

Scheme 2.

bubbled hydrogen bromide gas generated from tetralin and bromine for 30 min. After being stirred for 1 h, the precipitated solid was filtered and washed with water. The crude product was recrystallized from hexane–benzene (1 : 4) to give **2** as slight yellow prisms; yield: 2.03 g (92%); mp 167 °C (decomp). ^{1}H NMR ($CDCl_3$) δ=1.80 (3H, s, SCH_3), 6.92—7.69 (11H, m, H_{arom}), and 8.46—8.62 (1H, m, 6′-H). Found: C, 65.58; H, 4.10%. Calcd for $C_{20}H_{15}BrS$: C, 65.40; H, 4.12%.

2-Methoxy-9-(2-methylthiophenyl)fluorene (3a). A solution of **2** (0.55 g, 1.5 mmol) in methanol (5 ml) was refluxed for 1.5 h. After cooled, the product **3a** was filtered and pure enough for analysis; colorless prisms; yield: 0.46 g (97%; mp 96—97 °C. ^{1}H NMR ($CDCl_3$) δ=1.96 (3H, br. s, SCH_3), 2.78 (3H, s, OCH_3), and 7.00—8.12 (12H, m, H_{arom}). Found: C, 78.86; H, 5.68%. Calcd for $C_{21}H_{18}OS$: C, 79.21; H, 5.70%.

2-Ethoxy-9-(2-methylthiophenyl)fluorene (3b). Compound **2** (0.55 g, 1.5 mmol) was treated with ethanol instead of methanol and the reaction mixture was worked up as described for the preparation of **3a** to give **3b** as colorless crystals; yield: 0.38 g (76%); mp 127—128 °C. ^{1}H NMR ($CDCl_3$) δ=1.04 (3H, t, $CH_2C\underline{H}_3$), 1.99 (3H, br.s, SCH_3), 2.89 (2H, q, CH_2), and 7.0—8.0 (12H, m, H_{arom}). Found: C, 79.44; H, 6.08%. Calcd for $C_{22}H_{20}OS$: C, 79.48; H, 6.06%.

9-(2-Methylthiophenyl)fluorene (4). Hydriodic acid (57%, 15 g, 70 mmol) was added dropwise to a solution of **1** (6.08 g, 20 mmol) in acetic acid (150 ml), and refluxed for 1.5 h. The reaction mixture was poured into water and $NaHSO_3$ powder was added to the above mixture. The solution was extracted with benzene. The benzene solution was washed with Na_2CO_3 solution and water, and then dried with $MgSO_4$. The solution was evaporated in vacuo, leaving a residue which was recrystallized from benzene–acetone (1 : 2) to give **4** as colorless needles; yield: 4.54 g (79%); mp 118—119 °C. ^{1}H NMR ($CDCl_3$) δ=2.53 (3H, s, SCH_3), 5.74 (1H, s, 9-H), 6.32 (1H, d, 6′-H), and 6.64—7.78 (11H, m, H_{arom}). Found: C, 83.40; H, 5.61%. Calcd for $C_{20}H_{16}S$: C, 83.29; H, 5.59%.

9-Methyl-9-(2-methylthiophenyl)fluorene (6a). 9-Lithio-(2-methylthiophenyl)fluorene (**5**) was prepared from the reaction of **4** (0.5 g, 1.73 mmol) in dry ether (50 ml) and a solution of commercial butyllithium in hexane (1.7 ml) under a N_2 atmosphere.

To the above solution was added methyl iodide (0.22 ml, 3.46 mmol) dropwise, stirred for 30 min. The reaction mixture was poured into water, extracted with benzene, and dried with $MgSO_4$. The solution was evaporated in vacuo, leaving a residue which was column-chromatograhed on alumina using benzene as an eluent to give **6a**; yield: 0.38 g (73%); colorless needles; mp 149—151 °C (from hexane). ^{1}H NMR ($CDCl_3$) δ=1.72 (3H, s, SCH_3), 1.76 (3H, s, CH_3), and 6.87—7.84 (12H, m, H_{arom}). Found: C, 83.66; H, 5.99%. Calcd for $C_{21}H_{18}S$: C, 83.40; H, 6.00%.

9-Ethyl-9-(2-methylthiophenyl)fluorene (6b). Compound **5** prepared for **1** (0.5 g, 1.7 mmol) was treated with ethyl iodide (1.0 ml, 12.5 mmol) instead of methyl iodide and the reaction mixture was worked up as described for the preparation of **6a**, to give **6b** as colorless crystals; yield: 0.38 g (76%); mp 69—73 °C. ^{1}H NMR $CDCl_3$) δ=0.30 (3H, t, $CH_2C\underline{H}_3$), 1.76 (3H, s, SCH_3), 2.32 (2H, q, CH_2), and 6.80—7.86 (12H, m, H_{arom}). Found: C, 83.35; H, 6.35%. Calcd for $C_{22}H_{20}S$: C, 83.50; H, 6.37%.

9-(2-Methylthiophenyl)-9-fluorenecarboxylic Acid (7). A solution of compound **5** from **1** (2.6 g, 9 mmol) in ether was poured into crushed Dry Ice and stirred for 30 min. The reaction mixture was poured into a ice-water. The precipitated solid was filtered and recrystallized from ethyl acetate to give **7** as colorless crystals; yield: 1.93 g (64%); mp 180 °C (decomp). IR (KBr): 1680 cm^{-1} (CO), 3070 (OH); ^{1}H NMR ($CDCl_3$) δ=2.38 (3H, s, SCH_3), and 6.43—7.81 (12H, m, H_{arom}). Found: C, 75.54; H, 4.91%. Calcd for $C_{21}H_{16}O_2S$: C, 75.87; H, 4.85%.

9-Carboxymethyl-9-(2-methylthiophenyl)fluorene (8). A mixture of **7** (0.2 g, 0.6 mmol), thionyl chloride (5 ml), and *N,N*-dimethylformamide (3 drops) were heated at 50—60 °C for 1 h. To the reaction mixture was added methanol (10 ml); the precipitated solid was then extracted with benzene. The benzene solution was washed with $NaHCO_3$ solution, dried with $MgSO_4$, and concentrated in vacuo. The crude product was recrystallized from acetone to give **8** as colorless prisms; yield: 0.05 g (24%); mp 132—135 °C. IR (KBr): 1700 cm^{-1} (CO); ^{1}H NMR ($CDCl_3$) δ=2.47 (3H, s, SCH_3), 3.59 (3H, s, $COOCH_3$), 6.42 (1H, d, 6′-H), and 6.53—7.75 (11H, m, H_{arom}). Found: C, 75.98; H, 5.33%. Calcd for $C_{22}H_{18}O_2S$: C, 76.27; H, 5.24%.

9-Acetyl-9-(2-methylthiophenyl)fluorene (9a). To a solution of **5** prepared from **1** (0.6 g, 2 mmol) in ether was added a solution of acetic acid anhydride (0.3 ml) in ether (1 ml) dropwise at room temperature. After being stirred for 1 h, the reaction mixture was poured into water, extracted with benzene, washed with water, and dried with $MgSO_4$. The solvent was distilled off in vacuo, leaving a residue which was recrystallized from benzene to give **9a** as colorless plates; yield: 0.25 g (36%); mp 174—175 °C. IR (KBr): 1680 cm^{-1} (CO); ^{1}H NMR ($CDCl_3$) δ=1.88 (3H, s, $COCH_3$), 2.44 (3H, s, SCH_3), 6.55 (1H, d, 6′-H), and 6.72—7.85 (11H, m, H_{arom}). Found: C, 80.04; H, 5.51%. Calcd for $C_{22}H_{18}OS$: C, 79.96; H, 5.49%.

9-Benzoyl-9-(2-methylthiophenyl)fluorene (9b). Compound **5** prepared from **1** (1.0 g, 3.5 mmol) was reacted with benzoyl chloride (0.74 g, 5 mmol) instead of acetic anhydride; the reaction mixture was worked up as described for the preparation of **9a**, to give **9b** as colorless prisms; yield: 1.27 g (92%); mp 181—182 °C (from acetone). IR (KBr): 1645 cm^{-1} (CO); ^{1}H NMR ($CDCl_3$) δ=2.39 (3H, s, SCH_3), 6.51 (1H, d, 6′-H), and 6.63—7.86 (16H, m, H_{arom}). Found: C, 82.25; H, 5.09%. Calcd for $C_{27}H_{20}OS$: C, 82.62; H, 5.14%.

Spiro[benzo[*b*]thiophene-3(2*H*),9′-fluorene]-2-one (10). A mixture of **7** (0.5 g, 1.5 mmol), thionyl chloride (3 ml), and *N,N*-dimethylformamide (3 drops) was refluxed for 2 h. Thionyl chloride was distilled off in vacuo and methanol (15 ml) was added to the above residue. The mixture was refluxed for another 1 h. The solution was concentrated in vacuo, leaving a crude product which was recrystallized from benzene to give **10** as colorless crystals; yield: 0.1 g (20%); mp 139—140 °C. IR (KBr): 1710 cm^{-1} (CO); ^{1}H NMR ($CDCl_3$) δ=6.31—7.79 (12H, m, H_{arom}). Found: C, 80.26; H, 4.12%. Calcd for $C_{20}H_{12}OS$: C, 79.97; H, 4.03%.

9-Substituted 9-(2-Methylsulfinylphenyl)fluorenes (11—15). General Procedure: To a solution of **1** (0.61 g, 2.0 mmol) in acetic acid (10 ml) was added nitric acid (d=1.38, 1 ml) dropwise at 18 °C with stirring. After being stirred at 10—20 °C for 3 h, the reaction mixture was poured into water. The precipitated solid was extracted with benzene. The benzene solution was washed with a $NaHCO_3$ solution and water, and then dried with $MgSO_4$. The solvent was distilled off to obtain a residue which recrystallized from benzene and

then ethanol to give **11** as colorless needles; yield; 0.48 g (75%); mp 214—216 °C (decomp). IR (KBr): 1020 cm^{-1} (SO), 3080 (OH); ^1H NMR ($CDCl_3$) δ=2.52 (3H, br.s, $SOCH_3$), 4.10 (1H, br.s, OH), and 6.22—8.18 (12H, m, H_{arom}). Found: C, 74.82; H, 5.05%. Calcd for $C_{20}H_{16}O_2S$: C, 74.97; H, 5.03%.

9-Methoxy-9-(2-methylsulfinylphenyl)fluorene (12a). This compound was obtained as colorless crystals; yield: 93%; mp 222—223 °C (from methanol). IR (KBr): 1050 cm^{-1} (SO). Found: C, 75.49; H, 5.45%. Calcd for $C_{21}H_{18}O_2S$: C, 75.42; H, 5.43%.

9-Ethoxy-9-(2-methylsulfinylphenyl)fluorene (12b). This compound was obtained as colorless prisms; yield: 32%; mp 201—203 °C (from ethanol). IR (KBr): 1050 cm^{-1} (SO). Found: C, 76.08; H, 5.79%. Calcd for $C_{22}H_{20}O_2S$: C, 75.83; H, 5.79%.

9-(2-Methylsulfinylphenyl)fluorene (13). This compound was obtained as colorless needles; yield: 82%; mp 233—235 °C (from benzene). IR (KBr): 1050 cm^{-1} (SO). Found: C, 79.25; H, 5.46%. Calcd for $C_{20}H_{16}OS$: C, 78.91; H, 5.30%.

9-Methyl-9-(2-methylsulfinylphenyl)fluorene (14). This compound was obtained as colorless crystals (from benzene-hexane); yield: 78%; mp 177—178 °C. IR (KBr): 1050 cm^{-1} (SO). Found: C, 78.95; H, 6.03%. Calcd for $C_{21}H_{18}OS$: C, 79.21; H, 5.70%.

9-Acetyl-9-(2-methylsulfinylphenyl)fluorene (15a). This compound was obtained as slight yellow prisms (from benzene-hexane); yield: 41%; mp 184—186 °C. IR (KBr): 1055 cm^{-1} (SO). Found: C, 76.32; H, 5.29%. Calcd for $C_{22}H_{18}O_2S$: C, 76.27; H, 5.24%.

9-Benzoyl-9-(2-methylsulfinylphenyl)fluorene (15b). This compound was obtained as colorless crystals; yield: 12%; mp 186—189 °C (from benzene). IR (KBr): 1055 cm^{-1} (SO). Found: C, 79.15; H, 5.03%. Calcd for $C_{27}H_{20}O_2S$: C, 79.38; H, 4.94%.

Spiro[3*H*-2,1-benzoxathiole-3,9′-fluorene] 1-Oxide (16). To a solution of **1** (0.6 g, 2 mmol) in acetic acid (10 ml) was added nitric acid (d=1.38, 2 ml) dropwise. After being stirred at 50—60 °C for 30 min, the reaction mixture was poured into water. The mixture was extracted with benzene, and worked up as described for the preparation of **11** to give **16** as colorless prisms; yield: 0.23 g (38%); mp 161—162 °C (from acetone and then ethanol). IR (KBr): 1120 cm^{-1} (SO); ^1H NMR ($CDCl_3$) δ=6.38—8.10 (12H, m, H_{arom}). Found: C, 74.99; H, 4.12%. Calcd for $C_{19}H_{12}O_2S$: C, 74.98; H, 3.97%.

The authers wish to thank Professor Masashi Tashiro, Institute of Advances Material Study, Kyushu University, for the elemental analyses, and are grateful for the financial support of this work by Research Grant-in-Aid from the Ministry of Education, Science and Culture (No. 60470023).

References

1) Part IX of this series: S. Kajigaeshi, A. Nishida, and S. Fujisaki, *Bull. Chem. Soc. Jpn.*, **58**, 1967 (1985).
2) M. Ōki, *Angew. Chem., Int. Ed. Engl.*, **15**, 87 (1976).
3) M. Ōki, *Top. Stereochem.*, **14**, 1 (1983).
4) A. Nishida, S. Watanabe, S. Fujisaki, H. Hara, and S. Kajigaeshi, *Nippon Kagaku Kaishi*, **1983**, 1148.
5) A. Nishida, S. Shiwaku, S. Fujisaki, and S. Kajigaeshi, *Nippon Kagaku Kaishi*, **1984**, 574.
6) H. Gilman and G. A. Martin, *J. Am. Chem. Soc.*, **74**, 5317 (1952).
7) G. Binsch, *J. Am. Chem. Soc.*, **91**, 1304 (1969); H. Kihara, *JAPC*, **4**, 9 (1983).
8) M. Ōki, G. Izumi, G. Yamamoto, and N. Nakamura, *Bull. Chem. Soc. Jpn.*, **55**, 159 (1982).

 © 1988 The Chemical Society of Japan Bull. Chem. Soc. Jpn., 61, 1201—1206 (1988)

Infrared Spectroscopic Conformational Analysis of Polystyrene Resin-Bound Human Proinsulin C-Peptide Fragments.[1] β-Sheet Aggregation of Peptide Chains during Solid-Phase Peptide Synthesis

Mitsuaki NARITA,* Shinya HONDA, Hiroshi UMEYAMA, and Toshihiko OGURA
Department of Industrial Chemistry, Faculty of Technology, Tokyo University of Agriculture and Technology, Koganei 184
(Received August 1, 1987)

Conformational analysis of human proinsulin C-peptide fragments bound to cross-linked and soluble polystyrene resin matrices was performed using IR absorption spectroscopy. The conformational analysis of octa- and tridecapeptides in the swollen and solid states revealed that both peptides easily interacted with each other through intermolecular hydrogen bonding to form a β-sheet aggregation even at a low loading of peptide chains on the matrices. The high potential of the resin-bound peptides for the β-sheet formation was compatible with that of the corresponding peptides free from macromolecular protecting groups and was predicted using the average coil conformational value, $\langle P_c \rangle$, of each peptide. The significance of the results is discussed in connection with solid-phase peptide synthesis. Effects of shear stress on conformational transformations of resin-bound peptides was also examined in the solid state.

Peptide synthesis by fragment condensation on cross-linked and soluble polymer supports has been expected to be one of the most promising methods for syntheses of large peptides and proteins.[2,3] However, a serious problem in the method is the low yields in some fragment condensation reactions on resin supports.[4] In previous papers,[5-7] we demonstrated that decrease in coupling yields occurred on a copoly(styrene-2% divinylbenzene) support due to the restricted permeability of carboxyl-component peptides into resin matrices. We also verified that the permeability was further restricted by additional cross-linking caused by a β-sheet formation of amino-component peptides on resin matrices. Thus, the conformational analysis of cross-linked polystyrene resin-bound oligopeptides is of utmost importance in connection with solid-phase peptide synthesis. However, very few investigations have been reported of the conformational analysis of cross-linked polystyrene resin-bound oligopeptides.[8-10] In order to elucidate the hydrogen-bonding behavior of resin-bound oligopeptides, we studied the conformational properties of cross-linked polystyrene resin-bound oligo(Leu)s and showed that the peptide chains had various conformations depending on the peptide chain length.[8,9]

In this paper, we report IR absorption spectroscopic analysis of cross-linked and soluble polystyrene resin-bound human proinsulin C-peptide fragments and demonstrate that a β-sheet aggregation through intermolecular hydrogen bonds is commonly achieved in solid-phase peptide synthesis. The resin-bound oligopeptides used in this study are illustrated in Fig. 1. Cross-linked and soluble resin-bound peptides **1a** and **1b**, **2a** and **2b**, and **3a** and **3b** correspond to human proinsulin C-peptide (9-13), (6-13), and (1-13), respectively. The numbers in parentheses in the following C-peptide represent the positions of the first and last amino acids from the N-terminal in human proinsulin C-peptide.[11]

Experimental

Materials. Copoly(styrene-1% divinylbenzene) beads of 200—400 mesh, Bio-Beads S-X1, were purchased from Bio-

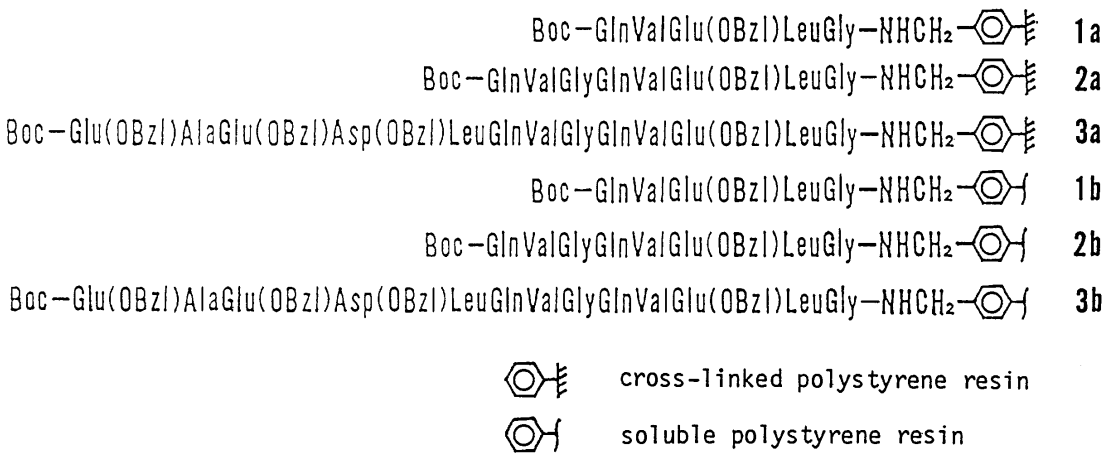

Fig. 1. The cross-linked and soluble polystyrene resin-bound peptides **1a**—**3a** and **1b**—**3b**.

Rad Laboratories. The aminomethylation was performed according to the method described previously.[12] Soluble aminomethylated polystyrene was prepared by the copolymerization of styrene and a mixture of *m*- and *p*-(phthalimidomethyl)styrene, followed by hydrazinolysis.[13] Human proinsulin C-peptide fragments, Boc-Gln-Val-Glu(OBzl)-Leu-Gly-OH, Boc-Gln-Val-Gly-OH, and Boc-Glu(OBzl)-Ala-Glu(OBzl)-Asp(OBzl)-Leu-OH, were those prepared before.[14] These peptide fragments were successively coupled with aminomethylated polystyrene resins in a mixture of dichloromethane and *N*-methylpyrrolidone (1/1, v/v) using DCC as a coupling reagent in the presence of HOBt.[2,8] The reaction using DCC and HOBt as coupling reagents is well-known to be nearly free from racemization.[15] Amino acid analyses of acid hydrolysates of the resin-bound peptides showed that the mole ratios of the component amino acid are close to the values calculated (Table 1).

IR Measurements. The IR absorption spectra of resin-bound peptides were recorded at room temperature with a JEOL Model JIR-100 FT-IR spectrometer. IR measurements in the swollen state were performed by holding the samples between potassium bromide windows after resin-bound peptides were swollen in each solvent overnight. IR measurements in solution were recorded by employing 0.1 mm path length cells with potassium bromide windows. The concentration of the solution was kept near 50 mg ml^{-1}. Only the soluble resin-bound peptide **1b** was soluble in dichloromethane and tetrahydrofuran, and the soluble resin-bound peptides **2b** and **3b** were insoluble in both solvents. The peptides **1b—3b** were insoluble in carbon tetrachloride, and the IR absorption spectra of these insoluble peptides were obtained in the swollen state. IR measurements in the solid state for the soluble resin-bound peptides **1b—3b** were carried out on films cast from their dichloromethane solution or gel in dichloromethane. IR absorption spectra without influence of shear stress (Fig. 6) were obtained using these samples. IR absorption spectra of the cross-linked resin-bound peptides **1a—3a** in the solid state under slight shear stress (Fig. 6) were obtained in a Nujol mull after the solid samples were weakly pulverized with Nujol by hand using an agate mortar.[8,16] The IR absorption spectra of the peptides **1a—3a** and **1b—3b** after application of shear stress (Fig. 7) were also obtained in a Nujol mull after the solid samples were strongly pulverized without Nujol by hand using an agate mortar.[8,16]

Amino Acid Analyses. The amino acid composition of acid hydrolysate was determined using Shimadzu HPLC LC-3A all amino acid analysis system. The conditions of acid hydrolyses of resin-bound peptides were the same to those described before.[14]

Results and Discussion

Oligopeptides Bound to Cross-Linked and Soluble Polystyrene-Resin Matrices. The copoly(styrene-1% divinylbenzene) resin support (Bio-beads S-X1), used as a starting resin bead, has commonly been used for solid-phase peptide synthesis, and the aminomethylated form is expected to have a uniform distribution of aminomethyl groups, based on the reaction mechanism of aminomethylation.[12] Soluble aminomethylated polystyrene was prepared by the copolymerization of styrene and a mixture of *m*- and *p*-(phthalimidomethyl)styrene, followed by hydrazinolysis.[13] The aminomethyl groups are also thought to be randomly distributed on the basis of the copolymerization curve. The first peptide, Boc-Gln-Val-Glu(OBzl)-Leu-Gly-OH, was directly coupled with aminomethyl groups using DCC and HOBt as coupling reagents. The peptide contents were 106 $\mu mol\,g^{-1}$ of resin (ca. 1.1 mol-% per styrene unit) for the cross-linked resin-bound peptide **1a** and 104 $\mu mol\,g^{-1}$ of resin for the soluble resin-bound peptide **1b**, respectively. These initial peptide contents were selected in order to get rational information for peptide chain interactions in the conventional solid-phase method.

Conformational Analysis of the Cross-Linked and Soluble Resin-Bound Peptides Swollen or Soluble in Dichloromethane. The IR absorption spectra of the cross-linked resin-bound peptides **1a—3a** swollen in dichloromethane are presented in Fig. 2 in the most significant spectral regions for conformational assignments (3500—3100 cm^{-1}, amide A; 1800—1600 cm^{-1}, amide I). Figure 3 illustrates those of the soluble resin-bound peptides **1b—3b** soluble or swollen in dichloromethane. The peptide **1b** dissolved in dichloromethane, while the peptides **2b** and **3b** were in a gel. Except for the soluble resin-bound peptide **1b**, the resin-bound peptides **1a—3a**, **2b**, and **3b** show strong bands around 3280 cm^{-1} in the amide A region and 1630 cm^{-1} in the amide I region, assigned to a β-sheet structure.[8,9,17-19] The results of the cross-linked resin-bound peptides **1a—3a** indicate that cross-linked resin-bound peptides swollen in dichloromethane, a most common solvent in conventional solid-phase peptide synthesis, can easily interact with each other through

Table 1. Amino Acid Analyses of the Resin-Bound Peptides **1a—3a** and **1b—3b**[a]

Resin-bound peptide	Asp	Glu(Gln)[b]	Gly	Ala	Val	Leu
1a	—	1.79 (2)	1.08 (1)	—	0.98 (1)	1.00 (1)
2a	—	2.96 (3)	1.90 (2)	—	2.03 (2)	1.00 (1)
3a	0.97 (1)	4.84 (5)	2.12 (2)	0.92 (1)	2.28 (2)	2.00 (2)
1b	—	1.88 (2)	1.08 (1)	—	1.00 (1)	1.06 (1)
2b	—	2.75 (3)	1.86 (2)	—	2.00 (2)	1.15 (1)
3b	0.93 (1)	4.74 (5)	2.06 (2)	0.90 (1)	2.17 (2)	2.00 (2)

a) The values in parentheses are the calculated ones. b) The values are the total ones of Glu and Gln residues.

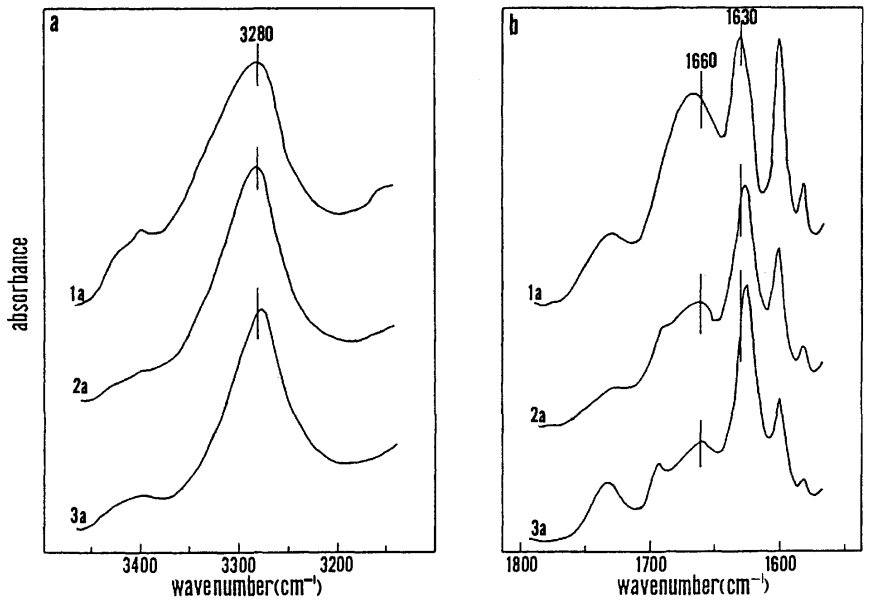

Fig. 2. IR absorption spectra in the amide A (a) and amide I (b) regions of the cross-linked resin-bound peptides **1a**—**3a** swollen in dichloromethane. The absorption band at 1603 cm^{-1} is due to aromatic rings of the polystyrene supports.

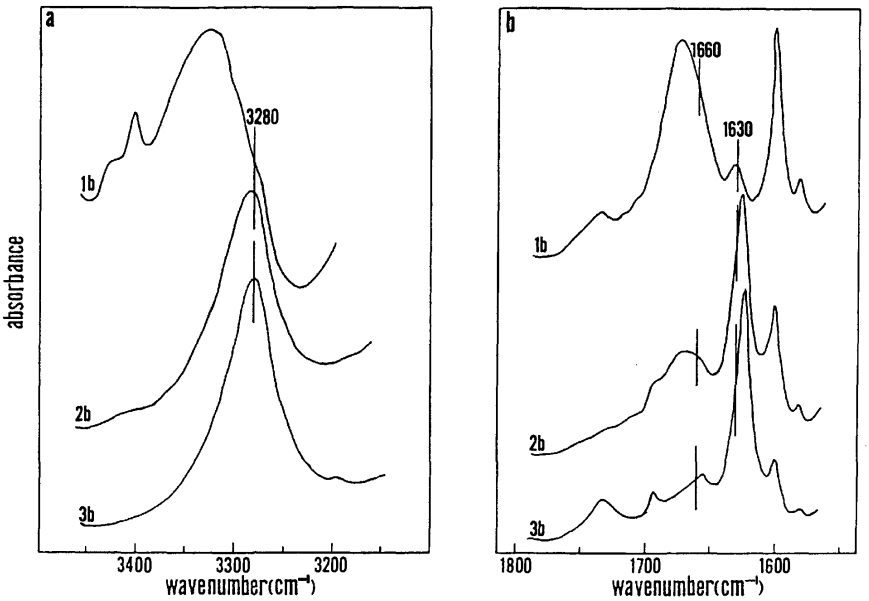

Fig. 3. IR absorption spectra in the amide A (a) and amide I (b) regions of the soluble resin-bound peptides **1b**—**3b** soluble or swollen in dichloromethane. For assignment of the absorption band at 1603 cm^{-1}, see Fig. 2.

peptide main chains to form intermolecular hydrogen bonds even at a low loading of peptide chains on the matrices. Especially, the result of the peptide **1a** clearly shows that the intraresin site separation of the peptide chains is not achieved even at a pentapeptide level. The conformational behavior of the soluble resin-bound peptides **2b** and **3b** is essentially the same as that of the cross-linked resin-bound peptides **2a** and **3a**. On the other hand, the soluble resin-bound peptide **1b** shows a weak band at 1630 cm^{-1} and a strong band at 1675 cm^{-1}in the amide I region, indicating that the resin-bound peptide **1b** is nearly free from intermolecular hydrogen bonds. As pointed out before,[8,9] the high potential for the β-sheet formation of the cross-linked resin-bound peptide **1a** swollen in dichloromethane is attributed to cross-linking by divinylbenzene, that is, the cross-linking has a concentrating effect. The conformational behavior of the cross-

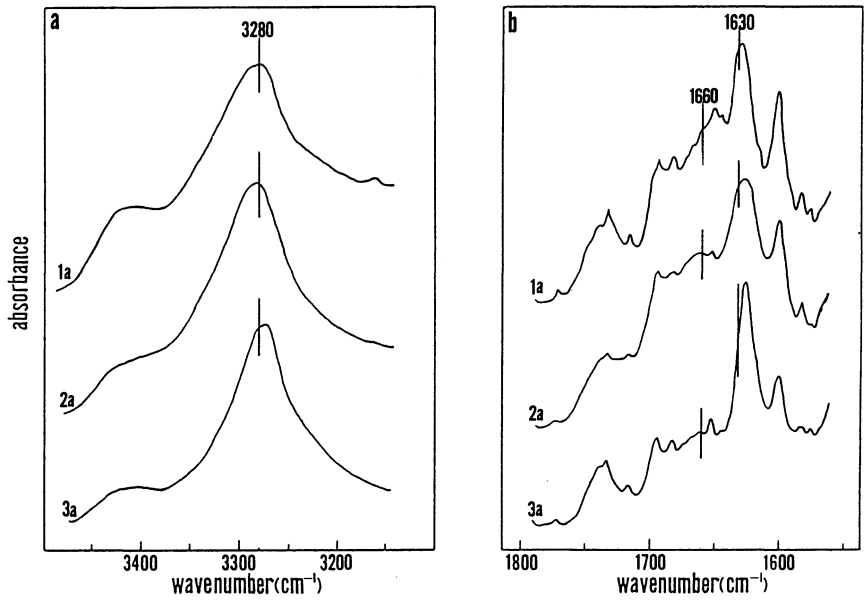

Fig. 4. IR absorption spectra in the amide A (a) and amide I (b) regions of the cross-linked resin-bound peptides **1a—3a** swollen in carbon tetrachloride. For assignment of the absorption band at 1603 cm^{-1}, see Fig. 2.

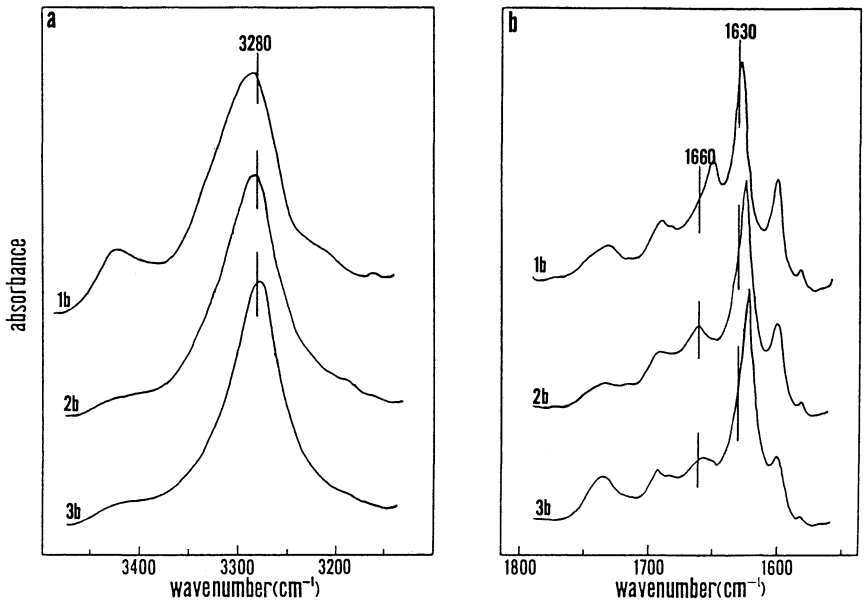

Fig. 5. IR absorption spectra in the amide A (a) and amide I (b) regions of the soluble resin-bound peptides **1b—3b** swollen in carbon tetrachloride. For assignment of the absorption band at 1603 cm^{-1}, see Fig. 2.

linked and soluble resin-bound peptides **1a—3a** and **1b—3b** in tetrahydrofuran (not shown) is essentially the same as that in dichloromethane, and the β-sheet aggregation in tetrahydrofuran is also easily achieved at a pentapeptide level in a cross-linked resin-bound peptide. Although it had been assumed that the cross-linked resin matrix isolated the growing peptide chains at a low loading, these results show that site-site reactions between pendant peptide chains do occur even at a pentapeptide level in solid-phase peptide synthesis.

The results obtained for the human proinsulin C-peptide fragments bound to resin matrices are essentially the same as those obtained for resin-bound oligo (Leu)s[9] and the corresponding human proinsulin C-peptide fragments free from macromolecular protecting groups,[18] indicating that polar side chains can not disturb the formation of the β-sheet structure in solid-

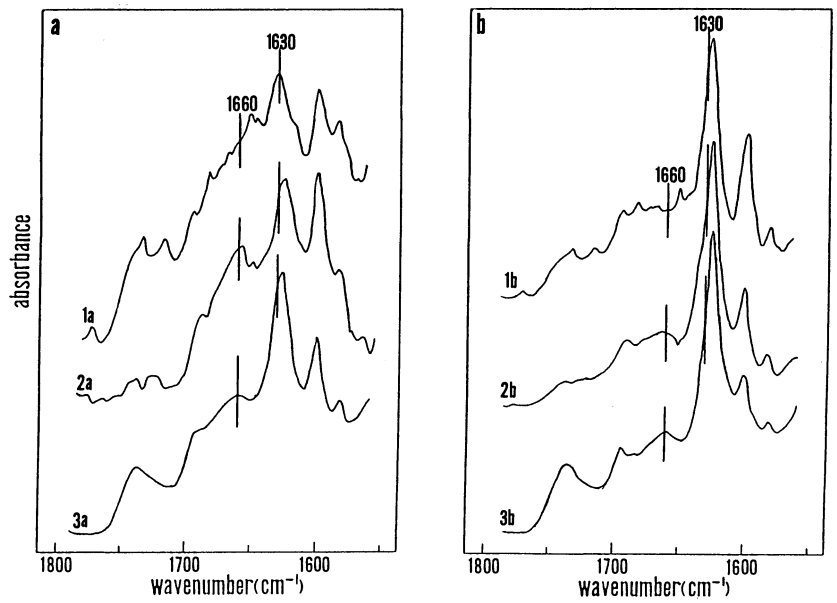

Fig. 6. IR absorption spectra in the amide I regions of the cross-linked resin-bound peptides **1a—3a** (a) and the soluble resin-bound peptides **1b—3b** (b) in the solid state. For assignment of the absorption band at 1603 cm^{-1}, see Fig. 2.

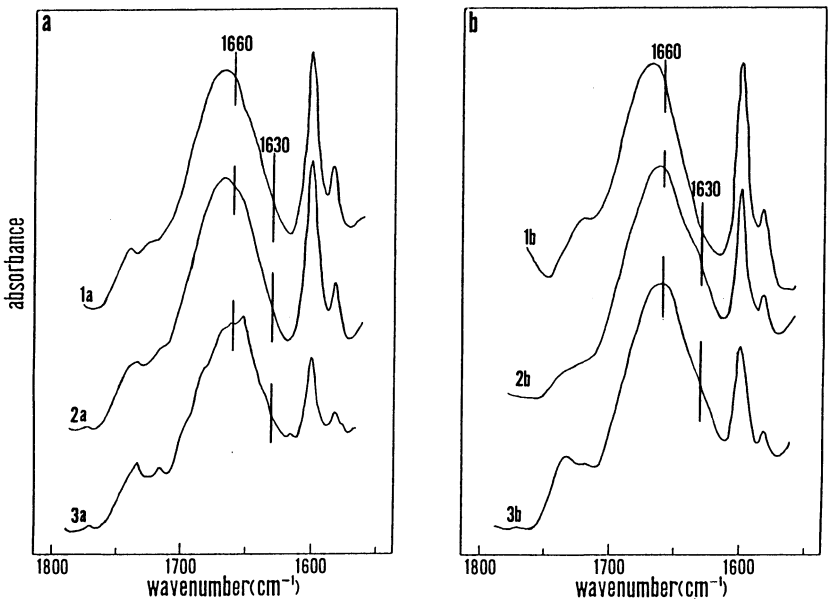

Fig. 7. IR absorption spectra in the amide I regions of the cross-linked resin-bound peptides **1a—3a** (a) and the soluble resin-bound peptides **1b—3b** (b) in the solid state after application of strong shear stress. For assignment of the absorption band at 1603 cm^{-1}, see Fig. 2.

phase peptide synthesis. Since the potential for a β-sheet formation of peptide fragments has successfully been predicted using an average coil conformational value, $\langle P_c \rangle$, calculated from the coil conformation parameter, P_c, for each amino acid,[18,20,21] the potential for a β-sheet formation of resin-bound peptides can be predicted by this method.

Conformational Analysis of the Cross-Linked and Soluble Resin-Bound Peptides Swollen or Soluble in Carbon Tetrachloride. Figures 4 and 5 illustrate the IR absorption spectra in the amide A and amide I regions of the peptide resins **1a—3a** and **1b—3b**, respectively. All of the peptides show strong bands around 3280 and 1630 cm^{-1}, assigned to a β-sheet structure.[8,9,16-18] The conformational behavior of the soluble resin-bound pentapeptide **1b** swollen in carbon tetrachloride is different from that in dichloromethane and tetrahydrofuran. It is attributed to the high poten-

tial of carbon tetrachloride for promoting a β-sheet formation of peptides. The β-sheet formation of the resin-bound peptides **1a—3a** and **1b—3b** in carbon tetrachloride indicates that the peptide phase aggregated through intermolecular hydrogen bonding behaves like a suspended crystalline, while the polystyrene part swells well in carbon tetrachloride. The conformational behavior of the resin-bound peptides **1a—3a**, **2b**, and **3b** in dichloromethane and tetrahydrofuran also indicates that a microphase separation occurs in the solvents. These results indicate that the insolubility of the peptide part in these solvents, causing the restricted permeability of carboxyl components and incomplete coupling reactions, becomes a serious problem in solid-phase peptide syntheses as well as in the classical solution method, although the insolubility of the peptide phase has been out of consideration in solid-phase peptide synthesis.

Conformational Analysis of Cross-Linked and Soluble Resin-Bound Oligopeptides in the Solid State. Figure 6 shows the IR absorption spectra of the peptide resins **1a—3a** and **1b—3b** in the amide I region. The spectra of the soluble resin-bound peptides **1b—3b** show a strong band at 1630 cm^{-1} characteristic of a β-sheet structure.[8,9,17—19] They are accompanied by weak shoulder bands around 1660 cm^{-1}, assigned to other conformations or amide carbonyl groups of Gln residues: those of the cross-linked resin-bound peptides **1a—3a** are accompanied by stronger shoulder bands around 1660 cm^{-1}. The latter spectra are resemble those of the corresponding oligopeptides free from macromolecular protecting groups.[17] The difference in the conformational behavior between the peptides **1a—3a** and **1b—3b** may be caused by added shear-stress in preparing IR samples. In fact, the β-sheet structures of the cross-linked and soluble resin-bound peptides **1a—3a** and **1b—3b** are easily disrupted by application of strong shear stress as shown in Fig. 7. The easy disruption of the β-sheet structure for the resin-bound peptides **1a—3a** and **1b—3b** reflects the potential of the peptide parts for the formation of an α-helical structure.[16]

The conformational behavior of the peptide resins **1a—3a** and **1b—3b** in the solid state resembles that of resin-bound oligo (Leu)s.[8] The easy formation of the β-sheet structure for the resin-bound peptides **1a—3a** and **1b—3b** in the solid state also indicates that resin-bound peptide chains having polar side chains can easily interact with each other through peptide main chains to form intermolecular hydrogen bonds even in polymer networks as well as in resin-bound hydrophobic peptide chains.

The authors are indebted to the financial support of the Asahi Glass Foundation for Industrial Technology. We also wish to thank Ajinomoto Co., Ltd., for the generous gift of various amino acids.

References

1) This paper forms Part III of "Syntheses and Properties of Resin-Bound Oligopeptides" series. For part II of this series, see M. Narita, Y. Tomotake, S. Isokawa, T. Matsuzawa, and T. Miyauchi, *Macromolecules*, **17**, 1903 (1984). The abbreviations for amino acids are those recommended by the IUPAC-IUB Commission on Biochemical Nomenclature, *J. Biol. Chem.*, **247**, 977 (1972). Amino acid symbols denote the *L*-configuration. Additional abbreviations used are the following: OBzl, benzyl ester; Boc, *t*-butoxycarbonyl; DCC, dicyclohexylcarbodiimide; HOBt, 1-hydroxy-1*H*-benzotriazole.

2) M. Narita, *Bull. Chem. Soc. Jpn.*, **51**, 1477 (1978); M. Narita, S. Itsuno, M. Hirata, and K. Kusano, *ibid.*, **53**, 1028 (1980).

3) H. Yajima and S. Funakoshi, *Yuki Gosei Kagaku Kyokai Shi*, **43**, 1083 (1985).

4) H. Yajima and Y. Kiso, *Chem. Pharm. Bull.*, **22**, 1087 (1974).

5) S. Isokawa, N. Kobayashi, R. Nagano, and M. Narita, *Makromol. Chem.*, **185**, 2065 (1984).

6) M. Narita, S. Isokawa, T. Matsuzawa, and T. Miyauchi, *Macromolecules*, **18**, 1363 (1985).

7) M. Narita, S. Isokawa, S. Nagasawa, and T. Ishijima, *Macromolecules*, **20**, 2306 (1987).

8) M. Narita, S. Isokawa, Y. Tomotake, and S. Nagasawa, *Polym. J.*, **15**, 25 (1983).

9) M. Narita, Y. Tomotake, S. Isokawa, T. Matsuzawa, and T, Miyauchi, *Macromolecules*, **17**, 1903 (1984).

10) A. G. Ludwick, L. W. Jelinski, D. Live, A. Kintanar, and J. J. Dumais, *J. Am. Chem. Soc.*, **108**, 6493 (1986) and references cited therein.

11) P. E. Oyer, S. Cho, J. D. Perterson, and D. F. Steiner, *J. Biol. Chem.*, **246**, 1375 (1971).

12) A. R. Mitchell, S. B. H. Kent, M. Engelhard, and R. B. Merrifield, *J. Org. Chem.*, **43**, 2845 (1978).

13) M. Narita, K. Enomoto, H. Ishii, A. Munakata, and S. Isokawa, "Peptide Chemistry 1980," ed by K. Ohkawa, Protein Research Foundation, Osaka (1981), p. 47.

14) M. Narita, T. Ogura, K. Sato, and S. Honda, *Bull. Chem. Soc. Jpn.*, **59**, 2433 (1986).

15) W. König and R. Geiger, *Chem. Ber.*, **103**, 788 (1970).

16) M. Narita, M. Doi, and H. Takegahara, *Bull. Chem. Soc. Jpn.*, **60**, 2445 (1987).

17) T. Miyazawa and E. J. Blout, *J. Am. Chem. Soc.*, **83**, 712 (1961).

18) M. Narita, T. Ogura, K. Sato, and S. Honda, *Bull. Chem. Soc. Jpn.*, **59**, 2439 (1986).

19) M. Narita, T. Ogura, K. Sato, and S. Honda, *Bull. Chem. Soc. Jpn.*, **59**, 2445 (1986).

20) M. Narita, K. Ishikawa, J.-Y. Chen, and Y. Kim, *Int. J. Peptide Protein Res.*, **24**, 580 (1984).

21) M. Narita, J.-Y. Chen, Y. Sato, and Y. Kim, *Bull. Chem. Soc. Jpn.*, **58**, 2494 (1985); M. Narita, M. Doi, K. Kudo, and Y. Terauchi, *ibid.*, **59**, 3553 (1986); M. Narita, M. Doi, and T. Nakai, *ibid.*, **60**, 3255 (1987).

 © 1988 The Chemical Society of Japan Bull. Chem. Soc. Jpn., 61, 1207—1211 (1988)

Synthetic Studies on Germacranolides: Synthesis of Optically Active 3-Benzoyloxy-6-oxo-13-nor-12,8-heliangolide

Akiko UTAGAWA,† Hiroshi HIROTA,* Shigeru OHNO, and Takeyoshi TAKAHASHI††
Department of Chemistry, Faculty of Science, The University of Tokyo, Hongo, Bunkyo-ku, Tokyo 113
(Received August 6, 1987)

Optically active (3*R*,7*R*,8*R*,1(10)*E*,4*Z*)-3-benzoyloxy-6-oxo-13-nor-1(10),4-germacradieno-12,8-lactone, a key synthetic intermediate for naturally occurring hiyodorilactone A, was prepared from (−)-carvone.

A group of sesquiterpene lactones with germacrane skeleton, named generically as "germacranolides," have been isolated from various plants.[1] Among them, 1(10)-*trans*-4-*cis*-germacranolides are called as "heliangolide." We have already reported several synthetic studies on 3-oxygenated heliangolides,[2] such as (−)-4,5-*cis*-3β-hydroxygermacranolide (**1**)[2c] isolated from *Tanacetum tanacetioides*, starting from optically active carvone using oxy-Cope rearrangement to construct the ten-membered ring. Since most of naturally occurring heliangolides possess acyloxyl group at C-8 position, which may enhance biological activities, we planned to synthesize 3,8-dihydroxylated heliangolide derivatives, such as hiyodorilactone A (**2**) which was isolated from *Eupatorium sachalinense* Makino by our group and showed a strong inhibitory activity in vivo against Ehrlich ascites carcinoma.[3] This compound **2** has already been synthesized by Still et al., who introduced the oxygen functional group at C-8 position by Baeyer-Villiger oxidation of a cyclobutanone ring under drastic conditions (anhydrous H_2O_2).[4]

In this paper, we would like to report another method to introduce oxygen functional group at C-8 position of the germacrane skeleton and the preparation of (3*R*, 7*R*, 8*R*, 1(10)*E*, 4*Z*)-3-benzoyloxy-6-oxo-13-nor-1(10),4-germacradieno-12,8-lactone (**3**) from (−)-carvone (**4**). The compound **3** is the antipode of **5**, which was a key intermediate on the total synthesis of hiyodorilactone A (**2**) by Still's group, except for the difference in the protecting group of the alcohol at C-3 position. If (+)-carvone, which is also commercially available at a higher price, is used as the starting material, the antipodal compound of **3** could be obtained. To construct the ten-membered ring, both we and Still's group had applied oxy-Cope rearrangemet to compounds **6** and **7**, respectively.

In order to introduce an oxygen functional group at C-8 position, we must use a compound which possesses a substituent (X) on the terminus of vinyl group of **6** as a substrate for oxy-Cope rearrangement to be able to transform into oxygen functional group at later stages. As a model compound, we first tried to prepare a compound **8** having ethoxyl group as X from isopiperitenone (**9**) and 2-ethoxyvinyllithium,[5] but it became clear that **8** decomposed via deethanolization upon purification and/or under the reaction conditions of oxy-Cope rearrangement. Then we decided to use 1-methylethylidene group, which could be transfered into oxygen by ozonolysis as X group of **6**. To determine the reaction conditions of oxy-Cope rearrangement, allenyl alcohol **10a** was prepared from isopiperitenone (**9**) and 3,3-dimethylallenyllithium (generated from 1,1-dimethylallene and methyllithium)[6] in 79% yield. When **10a** was refluxed with potassium hydride and 18-crown-6 in THF for 30 min (anionic oxy-Cope rearrangement),[2,4,7] piperitenone (**11**), which would be produced by the removal of dimethylallene followed by double bond isomerization, was obtained as a major product. When trimethylsilyl ether derivative of **10a** was heated at 150 °C without solvent under nitrogen atmosphere (siloxy-Cope rearrangement),[8] no reaction took place after 1 h. When **10a** was heated with almost ten equivalent moles of 1-methyl-2-pyrrolidinone at 120—130 °C for about 10 h (solvent-assisted oxy-Cope rearrangement),[9] the desired compound **12a** was produced (isolation yield: 25%) together with approximately the same amounts of the starting material **10a** and a bicyclic compound **13a**. The structure of **13a** was deduced from ^{1}H NMR spectrum, and **13** would be formed via ene reaction.

Since the ten-membered-ring compound **12a** could be obtained in considerable yield, solvent-assisted oxy-Cope rearrangement reaction was applied to the compound **10b** having an additional hydroxyl group of a benzoylated form. The benzoyloxyl group was considered to be stable under the transformation reactions of **12b** into **3**.

The benzoyloxy ketone **14**, which was obtained from (−)-carvone (**4**) via carveol and carvyl benzoate, was treated with 3,3-dimethylallenyllithium[6] to afford **10b** in 29% yield. The alcohol **10b** was rearranged into the ten-membered-ring compound **12b** in 32% yield on heating with 1-methyl-2-pyrrolidinone at about 100 °C for 22 h. Other products, such as the bicyclic compound **13b**, were also formed, but these were not fully characterized. Ozonolysis of **12b** at −30 °C, adjusting the amount of ozone as less than 1 equivalent mole by pre-adsorption on a proper amount of silica gel, gave the desired diketone **15** in 21% yield. The diketone **15**

† Present name and address: Akiko KAKIZAKI; Tokyo Metropolitan Hino High School, Ishida 190, Hino, Tokyo 191.
†† Present address: Department of Agricultural Chemistry, College of Agriculture and Veterinary Medicine, Nihon University, Shimouma, Setagaya-ku, Tokyo 154.

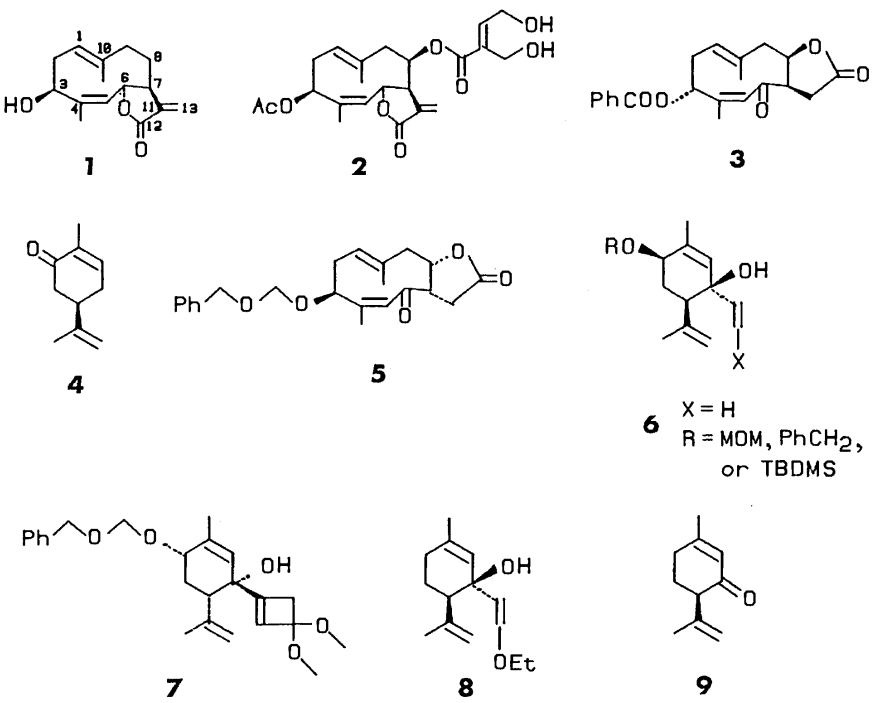

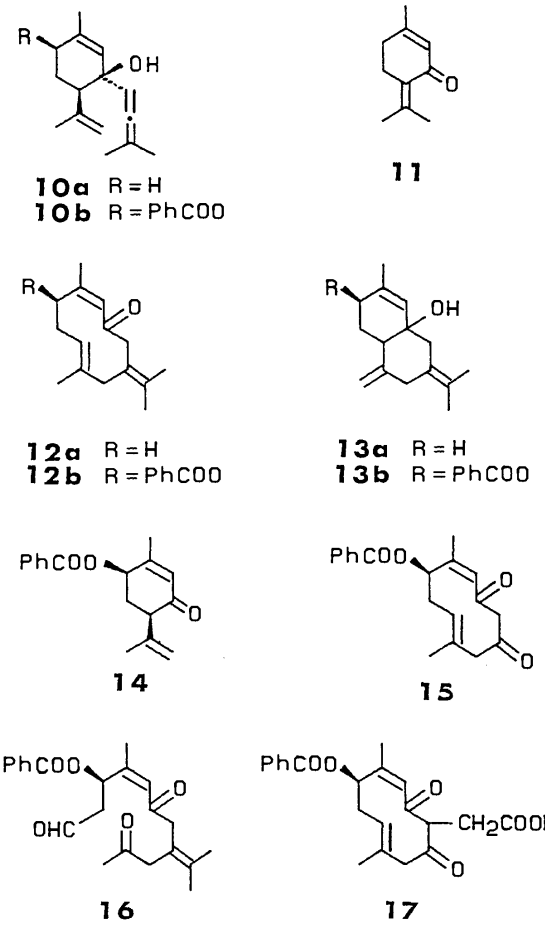

was accompanied by almost the same amount of a compound, which would have structure **16**, formed by cleavage of the non-conjugated trisubstituted double bond of **12b**. Signals of ^{1}H NMR showed that diketone **15** existed as approximately 1 : 1 mixture of two conformational isomers at room temperature.

Table 1. Main Proton Signals of **3** and **5** at 270 MHz ^{1}H NMR

Position	3			5[a]		
	δ		J/Hz	δ		J/Hz
1-H	5.1	m[b]		4.94	dd	12 and 5
3-H	6.48	dd	11.6 and 4.2	5.31	dd	12 and 4
5-H	6.14	br s		6.09	br s	
7-H	3.63	td	12.6 and 8.1	3.56	td	13 and 8
8-H	5.11	m[b]		5.04	ddd	13, 8, and 3
11-H	2.41	dd	18.1 and 8.1	2.36	dd	18 and 8
	3.25	dd	18.1 and 12.6	3.19	dd	18 and 13

a) Analyzed a copy of spectral chart sent from Prof. Still. b) Overlapped each other.

Diketone **15** was treated with sodium hydride followed by ethyl bromoacetate to give a diketo ester **17** in 44% yield. This compound **17** was also observed as a 1 : 2 mixture of two conformers by ^{1}H NMR at room temperature. When temperature was raised up to 45 °C, a set of olefinic methyl signals (δ ca. 1.95) having smaller chemical shift differences at room temperature coalesced into a singlet in the 270 MHz ^{1}H NMR spectrum. Stereochemistry at C-7 of **17** was assumed as 7α-H by considering the reaction pathway. That is, the enolate ion generated with sodium hydride would have a more stable 6Z-double bond, and the electrophile would attack from the peripheral side of the ten-membered ring to give 7α-H configuration compound. Similar argument has also been made in previous papers.[2] This stereochemical assignment was confirmed by subsequent transformation into γ-lactone **3**.

Treatment of **17** with sodium borohydride in ethanol gave a γ-lactone (**3**; $\nu_{C=O}$ 1780 cm^{-1}) as a major product (45% yield). The stereostructure of **3** was deduced to 8*R* or *cis*-lactone from Dreiding model consideration. It was very difficult to construct *trans*-lactone by Dreiding model, while it was fairly easy to make *cis*-lactone. This stereochemical assignment was confirmed by direct comparison of 270 MHz ^1H NMR spectra of **3** and **5**. In Table 1 were listed assignments, chemical shifts, and coupling constants of the main proton signals of **3** and **5** for comparison.

Thus the structure of **3** was shown to be (3*R*, 7*R*, 8*R*,1(10)*E*,4*Z*)-3-benzoyloxy-6-oxo-13-nor-1(10),4-germacradieno-12,8-lactone.

Experimental

General Procedures. All melting points were measured on a Mel-temp capillary melting point apparatus (Laboratory Devices) and uncorrected. Optical rotation was determined on a JASCO polarimeter DIP-181. Ultraviolet absorption (UV) and infrared (IR) spectra were measured on a Hitachi 340 and a Hitachi 260-30 spectrometer, respectively. Proton nuclear magnetic resonance (^1H NMR) spectra were taken using a Varian EM390 (90 MHz) and a JEOL GX270 (270 MHz) at ambient temperature, unless otherwise noted. Chemical shifts were expressed in δ (ppm) downfield from tetramethylsilane as an internal standard and coupling constants in Hz. Mass spectra (MS) were run on a JEOL JMS-D300 mass spectrometer operating at 70 eV. Thin-layer chromatography (TLC) including preparative one was carried out on Kieselgel 60 GF_{254} coated in 0.25 mm-thickness. Wakogel C-200 (Wako) was used for silica-gel column chromatography.

(+)-3-Methyl-1α-(3-methyl-1,2-butadienyl)-6β-(1-methylethenyl)-2-cyclohexen-1β-ol (10a). To an ether solution of methyllithium (0.58 M (1M=1mol dm^{-3}); 23.5 mL) was added diisopropylamine (0.05 mL) followed by 4.2 mL of a mixture (4:7) of 3-methyl-1,2-butadiene and tetrahydrofuran (THF), dropwisely at room temperature under nitrogen atmosphere, and the mixture was stirred for 4 h. At −78 °C, (±)-isopiperitenone (1.25 g) in ether (5 mL) was added dropwise. After stirring for about 2 h at room temperature and addition of saturated brine, the reaction mixture was extracted with ether. Usual work-up afforded 1.77 g of oily residue. Pure **10a** (1.426 g) was obtained by Kugel-Rohr distillation (80 °C/0.05 mmHg; 1 mmHg=133.322 Pa): an oil, IR (neat) 3460, 1670, 1635, 965, and 890 cm^{-1}; ^1H NMR (CCl_4; 90 MHz) δ=1.70 (9H, br s), 1.80 (3H, br s), 4.72 (1H, br s), 4.84 (1H, br s), 4.97 (1H, sept), and 5.28 (1H, br s); MS *m/z* (%) 218 (M^+, 6), 203 (5), 200 (100), 185 (55), 157 (57), and 143 (72); Found: *m/z* 218.1659. Calcd for $C_{15}H_{22}O$: M, 218.1669.

(2*Z*,6*E*)-3,7-Dimethyl-9-(1-methylethylidenyl)-2,6-cyclodecadien-1-one (12a). A solution of allenyl derivative (**10a**; 544 mg) in 6 mL of 1-methyl-2-pyrrolidinone was heated at 120—130 °C (bath temperature) for about 10 h under argon atmosphere. After cooling and addition of ether, the mixture was poured into water, and was extracted with ether as usual. ^1H NMR showed that the residue was consisted from three compounds, that is, the starting material **10a**, the objective ten-membered ketone **12a**, and a bicyclic compound **13a**, the ratio of which was almost 3:2:2, respectively. The residue was separated by column and preparative thin-layer chromatographies (solvent: hexane-ethyl acetate). **12a** (139 mg): white amorphous solid; IR (nujol) 1680, 1633, 1210, 1085, and 992 cm^{-1}; ^1H NMR (CCl_4; 90 MHz) δ=1.35 (3H, br s), 1.77 (9H, br s), 4.94 (1H, br t, *J*=8 Hz), and 5.77 (1H, br s); MS *m/z* (%) 218 (M^+, 100), 200 (71), and 185 (49); Found: *m/z* 218.1666. Calcd for $C_{15}H_{22}O$: M, 218.1669. **13a**: an oil; IR (neat) 3350, 1660, 1640, 1255, 1090, and 965 cm^{-1}; ^1H NMR (CCl_4; 90 MHz) δ=1.70 (9H, br s), 2.68 (1H, dd, *J*=14 and 3 Hz), 3.28 (1H, dd, *J*=14 and 3 Hz), 4.51 (1H, br s), 4.77 (1H, br s), and 5.27 (1H, br s); MS *m/z* (%) 218 (M^+, 20), 200 (61), 185 (35), 175 (100), and 157 (50); Found: *m/z* 218.1662. Calcd for $C_{15}H_{22}O$: M, 218.1669.

(−)-*cis*-Carvyl Benzoate ((3*R*, 5*R*)-3-Benzoyloxy-2-methyl-5-(1-methylethenyl)cyclohexene) and (4*R*, 6*R*)-4-Benzoyloxy-3-methyl-6-(1-methylethenyl)-2-cyclohexen-1-one (14). A solution of (−)-carvone (**4**; 50 g) in dry ether (150 mL) was added dropwise over 30 min to a stirring suspension of lithium aluminium hydride (6.5 g) in dry ether (300 mL) at about 0 °C. After additional 30 min stirring at room temperature, water and 2 M hydrochloric acid were added, successively. Ether extraction followed by removal of the solvent was performed as usual to afford carveol.[10] Benzoyl chloride (60 mL) was added to a solution of carveol in pyridine (300 mL) at about 0 °C, and the mixture was stirred at room temperature for 8 h. After addition of methanol (100 mL) followed by saturated brine, organic solvents were removed in vacuo, and the reaction mixture was extracted with ether as usual to afford crude carvyl benzoate. Kugel-Rohr distillation (170 °C, 0.5 mmHg) of a part of this crude material afforded the analytical sample of carvyl benzoate: $[\alpha]_D^{22}$ +13.3° (*c* 1.25, EtOH); UV (EtOH) 229.5 nm (ε 14280); IR (neat) 1725, 1645, 1270, and 1115 cm^{-1}; ^1H NMR ($CDCl_3$; 270 MHz) δ=1.71 (3H, br s), 1.74 (3H, s), 4.74 (2H, s), 5.6—5.8 (2H, m), 7.4—7.6 (3H, m), and 8.0—8.1 (2H, m); MS *m/z* (%) 256 (M^+, 5), 213 (15), 134 (14), 119 (19), and 105 (100); Found: C, 79.48%; H, 7.72%; and *m/z* 256.1466. Calcd for $C_{17}H_{20}O_2$: C, 79.65%; H, 7.86%; and M, 256.1464.

A solution of the crude carvyl benzoate in carbon tetrachloride (50 mL) was added to a carbon tetrachloride solution (700 mL) of *t*-butyl chromate (prepared from 130 g of chromium(VI) oxide). Acetic anhydride (200 mL) and acetic acid (70 mL) was added, and the whole was refluxed for 16 h. After filtration and addition of a solution of oxalic acid (160 g) in 1.2 L of water and then solid oxalic acid (50 g), the reaction mixture was extracted with ether. The ether layer was washed with aqueous sodium hydrogensulfite, saturated sodium hydrogencarbonate aqueous solution, and saturated brine, successively, and dried over anhydrous sodium sulfate. After evaporation of solvent, the residue was chromatographed on a column of silica gel (800 g). Elution with hexane-ethyl acetate (8:1) afforded 28 g of the unreacted carvyl benzoate and 21 g of the objective allyl-oxidation product **14**: an oil, $[\alpha]_D^{22}$ +27.9° (*c* 0.143, EtOH); UV (EtOH) 232.5 nm (ε 27600); IR (neat) 1725, 1680, 1645 (sh), 1265, and 1115 cm^{-1}; ^1H NMR ($CDCl_3$; 270 MHz) δ=1.75 (3H, s), 2.02 (3H, br s), 4.85 (1H, br s), 5.00 (1H, br s), 5.95—6.05 (2H, m), 7.4—7.7 (3H, m), and 8.05—8.15 (2H, m); MS *m/z* (%) 270 (M^+, 1.5), 202 (3), 148 (7), 105 (100), and 77 (25); Found: C, 75.31; H, 6.87, and *m/z* 270.1262. Calcd for $C_{17}H_{18}O_3$: C, 75.53; H, 6.71, and M, 270.1256.

(1*R*,4*R*,6*R*)-4-Benzoyloxy-3-methyl-1-(3-methyl-1,2-butadienyl)-6-(1-methylethenyl)-2-cyclohexen-1-ol (10b). To a

mixture of butyllithium (1.2 mL; 1.8 M hexane solution), THF (3 mL), and several drops of diisopropylamine was added a mixture (3 : 1) of 3-methyl-1,2-butadiene and THF, dropwise at room temperature. After stirring for 1 h, the mixture was added dropwise into a solution of **14** (280 mg) in THF (5 mL) at −78 °C, and was stirred for 1 h at −60 °C and then 10 min at 0 °C. Saturated ammonium chloride aqueous solution was added, and the reaction mixture was exracted with ether as usual. After evaporation, the residue was separated by column chromatography (SiO_2 16 g). Elution with hexane-ether (20 : 1) afforded the objective compound **10b** (100 mg): an oil, $[\alpha]_D^{19}$ +83.0° (*c* 1.73, EtOH), IR (neat) 3530, 1715, 1640, and 1275 cm^{-1}; ^1H NMR ($CDCl_3$; 270 MHz) δ=1.71 (3H, d, *J*=3 Hz), 1.74 (3H, d, *J*=3 Hz), 1.76 (3H, br s), 1.86 (3H, br s), 4.82 (1H, br s), 5.00 (1H, br s), 5.09 (1H, sept, *J*=3 Hz), 5.58 (1H, br s), 5.62 (1H, dd, *J*=10 and 7 Hz), 7.4—7.65 (3H, m), and 7.95—8.1 (2H, m); MS *m/z* (%) 338 (M^+, 0.6), 320 (0.8), 271 (5), 216 (5), 122 (7), and 105 (100); Found: *m/z* 338.1852. Calcd for $C_{22}H_{26}O_3$: M, 338.1880.

(4*R*, 2*Z*, 6*E*)-4-Benzoyloxy-3,7-dimethyl-9-(1-methylethylidenyl)-2,6-cyclodecadien-1-one (12b). A solution of **10b** (277 mg) in 2.8 mL of 1-methyl-2-pyrrolidinone was heated at 105 °C (bath temperature) for 22 h under argon atmosphere. After cooling to room temperature and the addition of ether, the whole was poured into water and was extracted as usual. After evaporation, the residue was separated by silica gel (15 g) column chromatography. Elution with hexane-ether (20 : 1) afforded 153 mg of recovered starting material **10b** and 40 mg of the objective ketone **12b**. **12b**: white crystals, mp 153—155.5 °C (recrystallized from ether); $[\alpha]_D^{19}$ −150° (*c* 0.44, $CHCl_3$); UV (EtOH) 230 nm (ε 21100); IR (KBr) 1720, 1690, 1645, and 1280 cm^{-1}; ^1H NMR ($CDCl_3$; 270 MHz) δ=1.61 (3H, br s), 1.79 (3H, br s), 1.86 (3H, s), 1.93 (3H, br s), 5.15 (1H, br t, *J*=8 Hz), 6.11 (1H, dd, *J*=11 and 6 Hz), 6.13 (1H, br s), 7.35—7.6 (3H, m), and 8.0—8.1 (2H, m); MS *m/z* 338 (M^+, 10), 320 (3), 295 (2), 233 (2), 216 (23), 198 (25), 173 (22), 122 (17), and 105 (100); Found: C, 78.03; H, 7.52; and *m/z* 338.1875. Calcd for $C_{22}H_{26}O_3$: C, 78.07; H, 7.74; and M, 338.1880.

Quantification of an Amount of Ozone. Some known amount of silica gel, which had been activated for several hours at 110 °C, was packed into a U-shaped glass tube, one end of which was connected with an ozonator and the other end was introduced into potassium iodide aqueous solution. At −78 °C, ozone was passed through the tube to be adsorbed on the silica-gel surface. When the potassium iodide solution was colored, the silica gel was judged to be saturated with ozone. Nitrogen stream was passed through the tube at room temperature to liberate the adsorbed ozone, which was then introduced into 2% aqueous solution of potassium iodide for titration. The potassium iodide solution containing iodide was acidified with sulfuric acid, and was titrated with standard sodium thiosulfate aqueous solution. As the result, it was turned out that 1.16% (w/w) ozone was adsorbed on the silica gel.[11]

(3*R*, 1(10)*E*, 4*Z*)-3-Benzoyloxy-11,12,13-trinor-1(10),4-germacradiene-6,8-dione (15). A solution of ketone **12b** (64 mg) in methanol (2 mL) and dichloromethane (1 mL) was stirred at −30 °C with introduction of ozone which was liberated from the saturated surface of 510 mg of the silica gel by nitrogen stream. (Calculated amount of ozone was 6.1 mg; 0.68 equivalent mole.) Acetic acid (0.2 mL) and zinc powder (ca. 50 mg) were added, and the mixture was stirred at 0 °C to room temperature for 15 min. After removal of excess zinc powder by filtration, the reaction mixture was diluted with ether, poured into water, and then was exracted with ether as usual. After evaporation, the residue was separated by preparative TLC (benzene-ether (5 : 1)). Together with the unreacted material **12b** (8.7 mg; R_f 0.7) and a compound (probably **16**; 8 mg; R_f 0.2), 10.8 mg of diketone (**15**; R_f 0.3) was obtained. **15**: an oil, $[\alpha]_D^{18}$ −130° (*c* 0.27, $CHCl_3$); UV (EtOH) 230 nm (ε 18100); IR (neat) 1730, 1720, 1680, 1640, and 1280 cm^{-1}; ^1H NMR (CCl_4; 90 MHz) δ=1.48 (1.5H, br s), 1.74 (1.5H, br s), 1.90 (1.5H, br s), 1.98 (1.5H, br s), ca. 5.3 (1H, m), 6.02 (1H, br s), 6.22 (0.5H, dd, *J*=11 and 5 Hz), 6.41 (0.5H, dd, *J*=11 and 4 Hz), ca. 7.4 (3H, m), and ca. 8.0 (2H, m); MS *m/z* (%) 312 (M^+, 4.5), 190 (7), 172 (11), 122 (7), and 105 (100); Found: *m/z* 312.1356. Calcd for $C_{19}H_{20}O_4$: M, 312.1350.

Ethyl (3*R*, 7*R*, 1(10)*E*, 4*Z*)-3-Benzoyloxy-6,8-dioxo-13-nor-1(10),4-germacradien-12-oate (17). To a mixture of 5 mg of 50% sodium hydride in oil dispersion and 1 mL of THF was added a solution of diketone **15** (19.6 mg) in THF (1 mL) at 0 °C. After stirring for 30 min at room temperature, large excess amount of ethyl bromoacetate (0.03 mL) was added at 0 °C, and the mixture was stirred for 1.5 h at room temperature. Saturated brine was added, and the reaction mixture was extracted with ether as usual. After evaporation, the residue was separated by preparative TLC (hexane-ether (1 : 2)). Together with the starting material **15** (3.3 mg, R_f 0.4), 9.2 mg of diketo ester **17** (R_f 0.6) was obtained. **17**: white crystals, mp 148—149.5 °C (recrystallized from ether); $[\alpha]_D^{14}$ −160° (*c* 0.18, $CHCl_3$); UV (EtOH) 230 nm (ε 21300); IR (KBr) 1725, 1680, 1635, and 1280 cm^{-1}; ^1H NMR ($CDCl_3$; 270 MHz) δ=1.25 (3H, t, *J*=7 Hz), 6.29 (1H, br s), ca. 7.5 (3H, m), and ca. 8.0 (2H, m). Other signals could be assigned to one of two conformational isomers, the ratio of which was almost 2 : 1. The major isomer: δ=1.72 (3H, br s), 1.96 (3H, br s), 2.45 (1H, q, *J*=11.7 Hz), 2.90, 2.95, 3.44, and 3.49 (2H, ABq, *J*=13.7 Hz), 4.02 (1H, t, *J*=7.1 Hz), 4.12 (2H, q, *J*=7.1 Hz), 5.11 (1H, br dd, *J*=12 and 5 Hz), and 6.35 (1H, dd, *J*=11.7 and 3.8 Hz). The minor isomer: δ=1.65 (3H, br s), 1.98 (3H, br s), 2.17 (1H, ddd, *J*=12, 12, and 7.8 Hz), 3.00, 3.04, 3.21, and 3.26 (2H, ABq, *J*=11.5 Hz), 4.24 (1H, dd, *J*=8.5 and 5.9 Hz), 4.13 (2H, q, *J*=7.1 Hz), 5.50 (1H, br t, *J*=8 Hz), and 6.25 (1H, dd, *J*=12 and 5.7 Hz). MS *m/z* (%) 398 (M^+, 8), 276 (11), 212 (25), 122 (28), and 105 (100); Found: *m/z* 398.1723. Calcd for $C_{23}H_{26}O_6$: M, 398.1729.

(3*R*, 7*R*, 8*R*, 1(10)*E*, 4*Z*)-3-Benzoyloxy-6-oxo-13-nor-1(10),4-germacradieno-12,8-lactone (3). To a solution of diketo ester **17** (4.4 mg) in ethanol (2 mL) and dichloromethane (0.1 mL) was added sodium borohydride (1 mg) at 0 °C, and the mixture was stirred for 1 h. After addition of acetone to destroy the excess hydride reagent, the reaction mixture was acidified by addition of dil. HCl. After concentration of the solution in vacuo, ether extraction as the usual work-up, and evaporation, the residue was separated by preparative TLC (hexane-ethyl acetate (2 : 1)). Togethr with the unreacted material **17** (0.9 mg, R_f 0.6), lactone **3** (1.4 mg, R_f 0.3) was obtained. **3**: white crystals, mp 149—150.5 °C (recrystallized from $CHCl_3$); $[\alpha]_D^{19}$ −190° (*c* 0.14, $CHCl_3$); UV (EtOH) 232 nm (ε 18100); IR (Nujol) 1780, 1730, 1710, 1680, 1620, 1275, and 1170 cm^{-1}; ^1H NMR ($CDCl_3$, 270 MHz) δ=1.57 (3H, br s), 1.94 (3H, br s), ca. 2.4 (2H, m), 2.41 (1H, dd, *J*=18.1 and 8.1 Hz), ca. 2.6 (2H, m), 3.25 (1H, dd, *J*=18.1 and 12.6 Hz), 3.63 (1H, td, *J*=12.6 and 8.1 Hz), 5.1 (2H, m), 6.14 (1H, br s), 6.48 (1H, dd, *J*=11.6 and 4.2 Hz), 7.4—7.7 (3H, m), and 8.0—8.15

(2H, m); MS *m/z* (%) 354 (M^+, 2), 232 (7), 214 (13), 122 (11), and 105 (100); Found: *m/z* 354.1481. Calcd for $C_{21}H_{22}O_5$: M, 354.1467.

The authors wish to thank Professor W. Clark Still, Columbia University, for the kind sending of a copy of 270 MHz ^1H NMR spectrum of their synthetic intermediate **5**.

References

1) e.g., B. M. Frage, *Natural Product Reports*, **3**, 273 (1986); **2**, 147 (1985); J. S. Roberts and I. Bryson, *ibid.*, **1**, 105 (1984).

2) a) C. Kuroda, H. Hirota, and T. Takahashi, *Chem. Lett.*, **1982**, 249; b) C. Kuroda, T. Nakamura, H. Hirota, K. Enomoto, and T. Takahashi, *Bull. Chem. Soc. Jpn.*, **58**, 146 (1985); c) T. Nakamura, H. Hirota, C. Kuroda, and T. Takahashi, *Chem. Lett.*, **1986**, 1879. Literatures of other synthetic works on germacranolides are listed in these references.

3) T. Takahashi, H. Eto, T. Ichimura, and T. Murae, *Chem. Lett.*, **1978**, 1345.

4) W. C. Still, S. Murata, G. Revial, and K. Yoshihara, *J. Am. Chem. Soc.*, **105**, 625 (1983).

5) K. S. Y. Lau and M. Schlosser, *J. Org. Chem.*, **43**, 1595 (1978); G. Stork and M. Tomasz, *J. Am. Chem. Soc.*, **86**, 471 (1964).

6) X. Creary, *J. Am. Chem. Soc.*, **99**, 7632 (1977); W. S. Bailey and C. R. Pfeifer, *J. Org. Chem.*, **20**, 95 (1955).

7) D. A. Evans and A. M. Golob, *J. Am. Chem. Soc.*, **97**, 4765 (1975).

8) R. W. Thies, *J. Chem. Soc., Chem. Commun.*, **1971**, 237.

9) T. Onishi, Y. Fujita, and T. Nishida, *Synthesis*, **1980**, 651; and references cited therein.

10) R. Grandi, U. M. Pagnoni, R. Trave, and L. Garanti, *Tetrahedron*, **30**, 4037 (1974).

11) On a literature (Z. Cohen, E. Keinan, Y. Mazur, and T. H. Varkony, *J. Org. Chem.*, **40**, 2141 (1975)), ca. 4% of ozone could be adsorbed on the surface of silica gel at −78 °C.

 © 1988 The Chemical Society of Japan Bull. Chem. Soc. Jpn., 61, 1213—1220 (1988)

Metal(II) *d*-Tartrates Catalyzed Asymmetric Ring Opening of Oxiranes with Various Nucleophiles

Hiroyuki YAMASHITA
Central Research Institute, Mitsui Toatsu Chemicals, INC., Kasama-cho, Sakae-ku, Yokohama 247
(Received August 13, 1987)

The asymmetric ring opening of *meso*-2,3-disubstituted oxiranes with thiols, aniline, and trimethylsilyl azide was studied by the use of metal(II) *d*-tartrates as heterogeneous chiral Lewis acid catalysts. The enantioselectivity varied widely with the combination of oxirane, nucleophile, and metal(II) *d*-tartrate, and Zn(II) *d*-tartrate gave the best enantioselectivity in the respective reactions of 1,2-epoxycyclohexane with 1-butanethiol, aniline, and trimethylsilyl azide to afford the corresponding adducts in 85, 58, and 42% ee, respectively. Furthermore, the kinetic resolution of racemic oxiranes with thiols catalyzed by Zn(II) *d*-tartrate was studied.

Catalytic asymmetric synthesis has attracted much attention because a large quantity of optically active compound can be effectively produced by using a small quantity of chiral source.

Although various types of catalytic asymmetric synthesis have been reported, only a little have been known about catalytic enantiotopos differentiating reaction, namely, the differentiation between two equivalent moieties in a symmetrical molecule by a chiral catalyst. To our knowledge, the asymmetric reduction of cyclic anhydride to lactone[1] and the asymmetric oxidation of *cis*-1,2-bis(hydroxymethyl)-cycloalkane to lactone[2] by a chiral ruthenium complex have been reported in this category, but their enantioselectivities were not satisfactory.

Only a few chiral Lewis acid catalysts have been known, for example, alkoxydichloroaluminium[3] and dialkoxydichlorotitanium[4] in the Diels-Alder reaction, and diphenoxyzinc[5] in the cyclization of unsaturated aldehyde. Optically active alkoxyl or phenoxyl group is involved in these catalysts as a chiral source and they were used by in situ preparation because of their instabilities.

In the course of our studies on the preparation of optically active polyfunctionalized synthetic building blocks by asymmetric synthesis starting from symmetrical compounds,[6] we recently communicated the asymmetric ring opening reaction of *meso*-2,3-disubstituted oxiranes with some nucleophiles catalyzed by Zn(II) *d*-tartrate or Cu(II) *d*-tartrate.[7] This reaction is classified as a catalytic enantiotopos differentiating reaction. These metal(II) *d*-tartrates act as heterogeneous chiral Lewis acid catalysts which have the advantages of the stability to air, moisture, and heat, and the easy recovery from reaction mixture simply by filtration.

Results and Discussion

Various metal(II) *d*-tartrates such as BeT·H_2O,[8] MgT·H_2O,[9] CaT·H_2O,[10] SrT·H_2O,[10] BaT,[10,11] MnT,[12] FeT,[12] CoT,[12,13] NiT·H_2O,[12,14] CuT,[15] ZnT,[12,16] CdT,[12,17] HgT,[12,18] SnT, and PbT[12] (T=*d*-tartrate) were examined as chiral catalysts by the use of 10 mol% of metal(II) *d*-tartrate in dichloromethane at room temperature in the reactions of 1,2-epoxycyclohexane with thiols such as *p*-toluenethiol, phenylmethanethiol, and 1-butanethiol to give the corresponding optically active *trans*-2-substituted cyclohexanols. In these reactions, active metal ions were Zn^{2+} and Mn^{2+} which have almost same electronegativities,[19] 8.0 and 7.5, respectivery. Other metal ions with lower or higher electronegativities exhibited no catalytic activities.

Next, instead of thiols, we tried various nucleophiles in the presence of 15 metal(II) *d*-tartrates described above, and found that aniline and trimethylsilyl azide gave optically active *trans*-2-anilinocyclohexanol and *trans*-1-azido-2-(trimethylsilyloxy)cyclohexane, respectively. In the reaction with aniline, MnT, FeT, ZnT, CoT, SnT, and CuT were active, and the electronegativities of these metal ions ranged from 7.5 to 9.5. When trimethysilyl azide was employed as a nucleophile, ZnT, CuT, MnT, SnT, CdT, FeT, and MgT·H_2O were active, and the electronegativities of these metal ions ranged widely from 6.0 to 9.5. Other nucleophiles such as benzylamine, ammonia, phenol, benzyl alcohol, methanol, benzoic acid, phenylacetic acid, and acetic acid resulted in no reactions by the use of metal(II) *d*-tartrates screened.

Reaction of *meso*-Oxiranes with Thiols. The results of the asymmetric ring opening of 1,2-epoxycyclohexane, 1,2-epoxycyclopentane, and *cis*-2,3-dimethyloxirane catalyzed by ZnT or MnT are summerized in Table 1. Comparing the chemical yields in the reactions for 5 d, the reactivity of oxiranes decreased in the order of 1,2-epoxycyclohexane > *cis*-2,3-dimethyloxirane > 1,2-epoxyclopentane with each thiol. No reaction took place in the cases of 1,2-epoxycyclooctane and *exo*-2,3-epoxynorbornane probably because of their steric hindrance around their oxirane rings. The same steric effects had been noticed in the reduction of oxiranes with lithium aluminium hydride[20] or sodium borohydride.[21]

The reactivity of thiols decreased in the order of *p*-toluenethiol > phenylmethanethiol > 1-butanethiol

Table 1. Reaction of *meso*-Oxiranes with Thiols[a)]

Oxirane	Thiol	Catalyst	Product	Yield %	$[\alpha]_D^{23}$ °b)	ee %	Abs. Conf.[c)]
	p-TolSH	ZnT	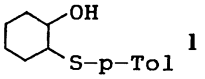 **1**	96	−45.0	68	(1*R*, 2*R*)
		MnT		95	+21.8	33	(1*S*, 2*S*)
	$PhCH_2SH$	ZnT	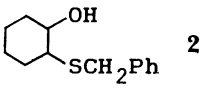 **2**	88	−34.4	77	(1*R*, 2*R*)
		MnT		56	−10.1	23	(1*R*, 2*R*)
	n-BuSH	ZnT	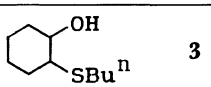 **3**	82	−44.7	85	(1*R*, 2*R*)
		MnT		14	+10.5	20	(1*S*, 2*S*)
	p-TolSH	ZnT	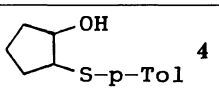 **4**	85	−8.0	45	(1*R*, 2*R*)
		MnT		72	0.0	0	
	$PhCH_2SH$	ZnT	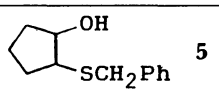 **5**	43	−7.8	50	(1*R*, 2*R*)
		MnT		Trace			
	n-BuSH	ZnT	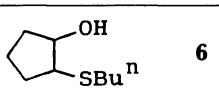 **6**	30	−15.1	72	(1*R*, 2*R*)
		MnT		Trace			
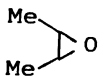	*p*-TolSH	ZnT	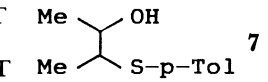 **7**	98	−25.8	60	(2*R*, 3*R*)
		MnT		65	−17.3	40	(2*R*, 3*R*)
	$PhCH_2SH$	ZnT	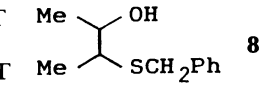 **8**	70	−18.5	75	(2*R*, 3*R*)
		MnT		Trace			
cis	*n*-BuSH	ZnT	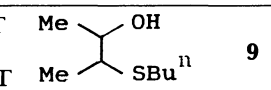 **9**	58	−29.0	71	(2*R*, 3*R*)
		MnT		Trace			

a) The mixture of oxirane (2 mmol), thiol (2 mmol), and catalyst (0.2 mmol) in CH_2Cl_2(5 cm^3) was stirred at room temperature for 5 d. b) (*c* 5.0, CH_2Cl_2). c) Absolute configuration.

with each oxirane. This order can be ascribed to the reverse order of the electron densities on their sulfur atoms.

When MnT was used as a catalyst, these orders were clearly observed. While 1,2-epoxycyclohexane reacted with *p*-toluenethiol to give the corresponding product in an excellent yield, the combination of less reactive oxiranes such as 1,2-epoxycyclopentane and *cis*-2,3-dimethyloxirane and less reactive thiols such as phenylmethanethiol and 1-butanethiol resulted in almost no reactions.

Compared with ZnT, MnT showed less catalytic activity and enantioselectivity, but exibited the following interesting feature, that is, MnT varied the stereoselectivity according to the combination of oxiranes and thiols to give (1*S*,2*S*)-**1**,**3**, (1*R*,2*R*)-**2**, and (2*R*,3*R*)-**7**, while ZnT gave (1*R*,2*R*) or (2*R*,3*R*)-product in all cases.

In the reaction of 1,2-epoxycyclohexane with *p*-toluenethiol, the salts such as Zn(II) (2*R*,3*R*)-2,3-dimethoxysuccinate (ZnDMS),[22)] Zn(II) (2*R*,3*R*)-2-hydroxy-3-methoxysuccinate (ZnHMS),[23)] Zn(II) (*S*)-2-hydroxysuccinate (ZnHS), and Zn(II) (*S*)-2-methoxysuccinate (ZnMS)[24)] were catalytically active but scarcely selective.

Table 2. Reaction of 1,2-Epoxycyclohexane with Aniline[a)]

Catalyst	**10**			
	Yield/%	$[\alpha]_D^{23}$/° b)	ee/%	Abs. Conf.[c)]
MnT	68	−24.6	24	(1*R*, 2*R*)
FeT	43	+ 1.38	1	(1*S*, 2*S*)
ZnT	28	−52.6	52	(1*R*, 2*R*)
CoT	18	−28.3	28	(1*R*, 2*R*)
SnT	16	− 2.48	3	(1*R*, 2*R*)
CuT	9	+24.5	24	(1*S*, 2*S*)

a) The mixture of 1,2-epoxycyclohexane (2 mmol), aniline (2 mmol), and catalyst (0.2 mmol) in CH_2Cl_2 (5 cm^3) was stirred at room temperature for 7 d. b) (*c* 2.0, CH_2Cl_2). c) Absolute configuration.

In order to confirm the absolute configurations of ring opening products, *trans*-2-(arylthio or alkylthio)-cyclohexanols **1**—**3**, -cyclopentanols **4**—**6**, and *threo*-3-(arylthio or alkylthio)-2-butanols **7**—**9** were converted into optically active 2-cyclohexen-1-ol,[25)] 2-cyclopenten-1-ol,[26)] and 3-buten-2-ol,[27)] respectively, by oxidation with *m*-chloroperbenzoic acid and successive thermal decomposition of the resulting *S*-oxides with-

out the formation of ketones. The enantiomeric exesses (ee) of **1—9** were determined by ^{19}F NMR measurements of their esters of (+)-α-methoxy-α-(trifluoromethyl)phenylacetic acid (MTPA).[28]

Reaction of *meso*-Oxiranes with Aniline. The results of the asymmetric ring opening of 1,2-epoxycyclohexane with aniline are summerized in Table 2. The salts such as ZnT, MnT, CoT, and SnT gave (1*R*,2*R*)-2-anilinocyclohexanol (**10**), while CuT and FeT gave (1*S*,2*S*)-**10**.

The enantiomeric excess of **10** was determined by ^{19}F NMR measurement of the MTPA ester of 2-(*N*-methylanilino)cyclohexanol (**11**) derived from **10** by *N*-methylation with Me_2SO_4. In order to confirm the absolute configuration, **11** was oxidized with *m*-chloroperbenzoic acid and the resulting *N*-oxide was transformed into optically acitve 2-cyclohexen-1-ol by thermal decomposition.

Compared with the reaction of 1,2-epoxycyclohexane with thiols, the chemical and optical yields were rather low in the reaction with aniline. One of the reasons could be considered that the amino alcohol **10** thus formed tightly coordinated to metal ion as a basic bidentate to decrease both catalytic activity and enantioselectivity of the salt. This possibility was clarified by the examination of the relationship between chemical yield and optical yield. As shown in Table 3, when 10 mol% of ZnT was used, the ee values were almost constant throughout the reaction in the case of *p*-toluenethiol. On the other hand, in the case of aniline, the ee values were gradually decreased and the reaction stopped completely after 28 d. When 50 mol% of ZnT was used, the reaction completed (95% yield) within 7 d, however, the enantioselectivity was not improved (37% ee).

Reaction of *meso*-Oxiranes with Trialkylsilyl Azide. The results of the reactions of 1,2-epoxycyclohexane, 1,2-epoxycyclopentane, and *cis*-2,3-dimethyloxirane with trimethylsilyl azide are summerized in Table 4. Throughout the experiments, (1*R*,2*R*)-products were produced in almost all cases except in the combination of 1,2-epoxycyclohexane and MnT resulting in the formation of (1*S*,2*S*)-product. The chemical yield was satisfactory, however, the optical yield was only 42% ee at best.

We screened several trialkylsilyl azides in place of trimethylsilyl azide to improve the enantioselectivity. When *t*-butyldimethylsilyl azide and triethylsilyl azide were employed, almost no products were obtained due to their severe steric hindrance, while ethyldimethylsilyl azide and isopropyldimethylsilyl azide gave the corresponding ring opening products **15—20** though in poor optical yields. These results are summerized in Table 5.

Table 3. Relation between Yield and Enantiomeric Excess[a]

Nucleophile	Reaction Time/d	Product	Yield %	ee %
p-TolSH	1	**1**	28	67
	2		51	66
	3		72	68
	4		88	68
	5		96	68
$PhNH_2$	3	**10**	19	58
	7		28	52
	14		42	45
	21		51	34
	28		53	32

a) The mixture of 1,2-epoxycyclohexane (2 mmol), nucleophile (2 mmol), and ZnT (0.2 mmol) in CH_2Cl_2 (5 cm^3) was stirred at room temperature.

Table 4. Reaction of *meso*-Oxiranes with Trimethylsilyl Azide[a]

Oxirane	Catalyst	Product	Yield %	$[\alpha]_D^{23}$ °[b]	ee %	Abs. Conf.[c]
	ZnT	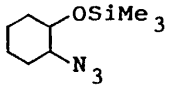 **12**	96	+10.9	42	(1*R*, 2*R*)
	CuT		96	+5.45	21	(1*R*, 2*R*)
	MnT		94	−2.95	11	(1*S*, 2*S*)
	SnT		95	0.0	0	
	CdT		92	+2.16	9	(1*R*, 2*R*)
	CoT		64	+1.00	4	(1*R*, 2*R*)
	FeT		41	+2.29	9	(1*R*, 2*R*)
	$MgT \cdot H_2O$		95	+1.29	5	(1*R*, 2*R*)
	ZnT	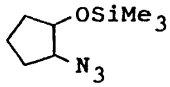 **13**	88	−8.86	27	(1*R*, 2*R*)
	CuT		85	−10.1	31	(1*R*, 2*R*)
	MnT		22	0.0	0	
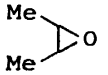 cis	ZnT	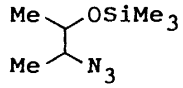 **14**	85	−1.47	17	(2*R*, 3*R*)
	CuT		80	−3.35	40	(2*R*, 3*R*)
	MnT		52	−2.15	26	(2*R*, 3*R*)

a) The mixture of oxirane (10 mmol), trimethylsilyl azide (12 mmol), and catalyst (1 mmol) in benzene (5 cm^3) was stirred at room temperature for 14 d. b) (*c* 2.0, CH_2Cl_2). c) Absolute configuration.

Table 5. Reaction of *meso*-Oxiranes with Trialkylsilyl Azides[a]

Oxirane	Azide	Catalyst	Product		Yield %	$[\alpha]_D^{23}$ °[b]	ee %	Abs. Conf.[c]
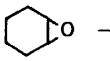	$EtMe_2SiN_3$	ZnT	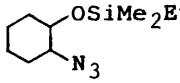	**15**	97	+2.40	15	(1*R*, 2*R*)
		CnT			58	+0.40	2	(1*R*, 2*R*)
	i-$PrMe_2SiN_3$	ZnT	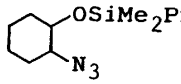	**16**	85	+0.38	15	(1*R*, 2*R*)
		CuT			72	+0.30	12	(1*R*, 2*R*)
	$EtMe_2SiN_3$	ZnT	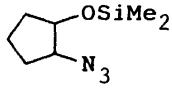	**17**	94	−9.08	24	(1*R*, 2*R*)
		CuT			85	−8.70	23	(1*R*, 2*R*)
	i-$PrMe_2SiN_3$	ZnT	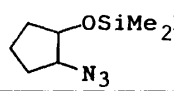	**18**	73	−7.44	21	(1*R*, 2*R*)
		CuT			67	−7.87	22	(1*R*, 2*R*)
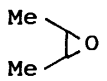 cis	$EtMe_2SiM_3$	ZnT	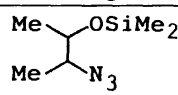	**19**	80	−3.56	20	(2*R*, 3*R*)
		CuT			50	−1.97	11	(2*R*, 3*R*)
	i-$PrMe_2SiN_3$	ZnT	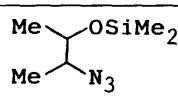	**20**	82	−9.45	32	(2*R*, 3*R*)
		CuT			80	−3.59	12	(2*R*, 3*R*)

a) The mixture of oxirane (10 mmol), trialkylsilyl azide (12 mmol) and catalyst (1 mmol) in benzene (5 cm^3) was stirred at room temperature for 14 d. b) (*c* 2.0, CH_2Cl_2). c) Absolute configuration.

Table 6. Kinetic Resolution of Racemic Oxiranes[a]

Oxirane	Thiol	Reaction Time/d[c]	Recovered Oxirane		
			Yield/%[d]	ee/%	Abs. Conf.[f]
	p-TolSH	2	35	5	*R*
	$PhCH_2SH$	2	39	6	*R*
	n-BuSH	3	37	4	*R*
	t-BuSH	7	38	15	*R*
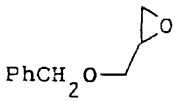	*t*-BuSH	5	43	27	*R*
trans	*p*-TolSH	14	47[e]	43[e]	(2*S*, 3R)[e]
	p-TolSH[b]	14	9[e]	72[e]	(2*S*, 3*R*)[e]

a) The mixture of oxirane (4 mmol), thiol (2 mmol), and ZnT (0.2 mmol) in CH_2Cl_2 (10 cm^3) was stirred at room temperature. b) 0.4 mmol. c) Complete consumption time of thiol checked by thin-layer chromatography. d) Based on oxirane. e) Ring opening product **21**. f) Absolute configuration.

These *O*-silylated β-azido alcohols **12—20** were desilylated by refluxing with methanol in the presence of a catalytic amount of concd HCl, and successive catalytic hydrogenolysis with 10% Pd-C resulted in the formation of corresponding *trans*-β-amino alcohols whose absolute configurations and maximum optical rotations have been known.

Kinetic Resolution of Racemic Oxiranes. As a model study, we examined the kinetic resolution of racemic oxiranes with thiols catalyzed by ZnT. At first, the reaction of 2-phenyloxirane with half molar equivalents of various thiols were carried out until thiols were completely consumed. When bulky 2-methyl-2-propanethiol was used as a nucleophile, (*R*)-2-phenyloxirane[29] was recovered in 15% ee. In the same reaction of 1-benzyloxy-2,3-epoxypropane, (*R*)-oxirane[30] was recovered in 27% ee. When *trans*-2,3-dimethyloxirane was treated with half molar equivalents of *p*-toluenethiol, (2*S*,3*R*)-3-(*p*-tolylthio)-2-butanol (**21**) was obtained in 43% ee, and in the case of 10 mol% of *p*-toluenethiol, the product **21** showed 72% ee. The recovery of unreacted *trans*-2,3-dimethyloxirane was failed because the separation from solvent (CH_2Cl_2) by distillation was difficult, however, (2*R*, 3*R*)-2,3-dimethyloxirane might be remained judging from the configuration of the ring opening product **21**.

The combination of *trans*-2,3-dimethyloxirane and less reactive thiols such as phenylmethanethiol, 1-butanethiol, and 2-methyl-2-propanethiol resulted in no reactions. These results are summerized in Table 6.

In all these reactions catalyzed by ZnT, thiols attacked the back side of the asymmetric carbon having *S*-configuration faster than that of *R*-configuration. These results were in good accordance with the intramolecular enantioselectivity in the reaction of *meso*-oxiranes with thiols catalyzed by ZnT, that is, thiols attacked the side of *S*-configuration and (1*R*,2*R*)-β-substituted alcohols were obtained.

Structure of Metal (II) *d*-Tartrate. The salts such as $CaT \cdot 4H_2O$,[31,32] $SrT \cdot 3H_2O$,[31] $CuT \cdot 3H_2O$,[33] and $Ni_2T_2 \cdot 5H_2O$[34] are known to have common polymeric structures stabilized by three dimensional networks of hydrogen bonds, but their detailed coordination structures are different in every salts. Furthermore, the structure of anhydrous ZnT has been reported to be X-ray crystallographycally amorphous.[35] Considering these structural variations, it is difficult to simply presume the structures of the other metal(II) *d*-tartrates employed in the present experiments.

The catalytically active metal ions existed in a certain range of electronegativity in accordance with thiols, aniline, and trialkylsilyl azide, and highly basic nucleophiles such as benzylamine and ammonia resulted in no reactions. The enantioselectivity was varied according to the combination of oxirane, nucleophile, and metal(II) *d*-tartrate. Based on these results, it may be possible to consider that both oxirane and nucleophile coordinate simultaneously to metal (II) *d*-tartrate which acts as a heterogeneous Lewis acid catalyst to activate the oxirane, and the entropically advantageous state enables the enantioselective ring opening reaction to proceed smoothly. The detailed mechanism of the enantiotopos differentiation is remained unknown at present.

Experimental

All the boiling points and the melting points were uncorrected. The IR spectra were recorded with a JASCO IRA-2 spectrometer. The ^1H NMR spectra were measured with a JEOL JNM-3H-60 spectrometer or a JEOL JNM-PMX-60SI spectrometer with tetramethylsilane as an internal standard, and ^{19}F NMR spectra were taken with a Varian EM-390 spectrometer. The optical rotations were measured with a Union Giken PM-101 polarimeter or a JASCO DIP-181 polarimeter. Kugelrohr distillation was carried out with a Sibata GTO-250RS distilling apparatus. Column chromatography was performed on silica gel (Wakogel C-200). Dichloromethane and benzene were stored over Molecular Sieves 4A.

Preparation of Metal(II) Dicarboxylates. Typical Procedures for the Preparation of ZnT. Method A. To an aqueous solution (100 cm^3) of $ZnCl_2$ (13.6 g, 0.10 mol) was added an aqueous solution (100 cm^3) of potassium sodium *d*-tartrate tetrahydrate (28.2 g, 0.10 mol). The mixture was stirred at room temperature for 1 h and was left overnight. The precipitated white powder was collected by filtration, washed with water (100 cm^3) and methanol (50 cm^3), and dried at 150 °C/1 Torr (1 Torr≈133.322 Pa) for 5 h to afford ZnT (21 g, 98%). Found: C, 22.49; H, 1.93; Zn, 30.27%. Calcd for $C_4H_4O_6Zn$: C, 22.51; H, 1.89; Zn, 30.63%.

Method B. An aqueous solution (100 cm^3) of Zn $(OAc)_2 \cdot 2H_2O$ (27.9 g, 0.10 mol) was added to an aqueous solution (100 cm^3) of *d*-tartaric acid (15.0 g, 0.10 mol). The mixture was stirred for 1 h, and was left over night followed by the same work-up as Method A to give ZnT (21 g, 98%). Found: C, 22.53; H, 1.92; Zn, 30.32%. Calcd for $C_4H_4O_6Zn$: C, 22.51; H, 1.89; Zn, 30.63%.

The other salts such as $BeT \cdot H_2O$, $CaT \cdot H_2O$, $SrT \cdot H_2O$, BaT, MnT, FeT, and CuT were prepared from the corresponding metal(II) chlorides and potassium sodium *d*-tartrate by method A, and $MgT \cdot H_2O$, CoT, $NiT \cdot H_2O$, CdT, HgT, and PbT were prepared from the corresponding metal(II) diacetates and *d*-tartaric acid by method B.

The salts such as ZnDMS, ZnHMS, ZnHS, and ZnMS were prepared from $Zn(OAc)_2 \cdot 2H_2O$ and the corresponding dicarboxylic acids by method B with a slight modification. These salts were very soluble in water. The aqueous reaction mixture was evaporated in vacuo, and the residual salt was washed with methanol and dried.

The yields and analytical data for metal(II) dicarboxylates: $BeT \cdot H_2O$ (54%), Found: C, 27.05; H, 3.62%. Calcd for $C_4H_6O_7Be$: C, 27.44; H, 3.45%. $MgT \cdot H_2O$ (37%), Found: C. 24.98; H. 3.42%. Calcd for $C_4H_6O_7Mg$: C, 25.23; H, 3.18%. $CaT \cdot H_2O$ (94%), Found: C, 23.14; H, 3.11%. Calcd for $C_4H_6O_7Ca$: C, 23.30, H, 2.93%. $SrT \cdot H_2O$ (82%), Found: C,19.01; H, 2.22%. Calcd for $C_4H_6O_7Sr$: C, 18.94; H, 2.38%. BaT (98%), Found: C, 16.18; H, 1.58%. Calcd for $C_4H_4O_6Ba$: C, 16.83; H, 1.41%. MnT (94%), Found: C, 23.28; H, 2.09%. Calcd for $C_4H_4O_6Mn$: C, 23.43; H, 1.97%. FeT (86%), Found: C, 23.52; H, 2.06%. Calcd for $C_4H_4O_6Fe$: C, 23.56; H, 1.98%. CoT (71%), Found: C, 23.54; H, 2.06%. Calcd for $C_4H_4O_6Co$: C, 23.21; H, 1.95%. $NiT \cdot H_2O$ (77%), Found: C, 21.11; H, 2.82%. Calcd for $C_4H_6O_7Ni$: C, 21.37; H, 2.69%. CuT (99%), Found: C,22.69; H, 2.01%. Calcd for $C_4H_4O_6Cu$: C, 22.70; H, 1.91%. CdT (88%), Found: C,18.43; H, 1.50%. Calcd for $C_4H_4O_6Cd$: C, 18.44; H, 1.55%. HgT (92%), Found: C, 13.77; H,1.11%. Calcd for $C_4H_4O_6Hg$: C, 13.78; H, 1.16%. PbT (96%), Found: C, 13.29; H, 1.04%. Calcd for $C_4H_4O_6Pb$: C, 13.52; H, 1.13%. SnT (90%), Found: C, 17.94; H, 1.60%. Calcd for $C_4H_4O_6Sn$: C, 18.01; H, 1.51%. ZnDMS (96%), Found: C, 29.75; H, 3.46%. Calcd for $C_6H_8O_6Zn$: C, 29.84; H, 3.34%. ZnHMS (92%), Found: C, 26.43; H, 2.81%. Calcd for $C_5H_6O_6Zn$: C, 26.40; H, 2.66%. ZnHS (85%), Found: C, 24.14; H, 2.19%. Calcd for $C_4H_4O_5Zn$: C, 24.33; H, 2.04%. ZnMS (95%), Found: C, 28.35; H, 2.93%. Calcd for $C_5H_6O_5Zn$: C, 28.40; H, 2.86%.

General Procedure for the Reaction of *meso*-Oxiranes with Thiols. To a dichloromethane (5 cm^3) solution of oxirane (2 mmol) and thiol (2 mmol) was suspended metal(II) *d*-tartrate (0.2 mmol). The heterogeneous mixture was stirred at room temperature for 5 d. After filtration of metal(II) *d*-tartrate, the filtrate was concentrated and purified by column chromatography on silica gel (hexane:ethyl acetate=10:1) to give *trans*-β-(alkylthio or arylthio) alcohol. The isolated yields, optical rotations, and enantiomeric excesses of the adducts **1—9** in the various combination of oxiranes thiols, and metal(II) *d*-tartrates are listed in Table 1. Spectral and analytical data for **1—9** are as follows.

(1*R*,2*R*)-2-(*p*-Tolylthio)cyclohexanol (1): IR (neat) 3450, 800 cm^{-1}; ^1H NMR (CCl_4) δ=1.02—1.48 (4H, m), 1.52—1.83

(2H, m), 1.83—2.12 (2H, m), 2.32 (3H, s), 2.43—2.78 (1H, m), 2.90 (1H, s), 2.98—3.39 (1H, m), 7.04 (2H, d, J=8 Hz), 7.32 (2H, d, J=8 Hz). Found: C, 70.03; H, 8.27; S, 14.37%. Calcd for $C_{13}H_{18}OS$: C, 70.22; H, 8.16; S, 14.42%.

(1*R*,2*R*)-2-(Benzylthio)cyclohexanol (2): IR (neat) 3450, 690 cm^{-1}; ^{1}H NMR (CCl_4) δ=1.02—1.48 (4H, m), 1.50—1.82 (2H, m), 1.72—2.12 (2H, m), 2.15—2.42 (1H, m), 2.83 (1H, s), 3.08—3.36 (1H, m), 3.62 (2H, s), 7.18 (5H, s). Found: C, 69.93; H, 8.10; S, 14.38%. Calcd for $C_{13}H_{18}OS$: C, 70.22; H, 8.16; S, 14.42%.

(1*R*,2*R*)-2-(Butylthio)cyclohexanol (3): IR (neat) 3450, 730 cm^{-1}; ^{1}H NMR (CCl_4) δ=0.93 (3H, t, J=8 Hz), 1.00—2.25 (12H, m), 2.52 (2H, t, J=7 Hz), 2.25—2.50 (1H, m), 2.80 (1H, s), 3.08—3.45 (1H, m). Found: C, 63.50; H, 10.59; S, 16.95%. Calcd for $C_{10}H_{20}OS$; C, 63.77; H, 10.70; S, 17.03%.

(1*R*,2*R*)-2-(*p*-Tolylthio)cyclopentanol (4): IR (neat) 3410, 780 cm^{-1}; ^{1}H NMR (CCl_4) δ=1.10—2.38 (6H, m), 2.27 (3H, s), 3.16—3.37 (1H, m), 3.45 (1H. s), 3.80—4.18 (1H, m), 7.00 (2H, d, J=8 Hz), 7.25 (2H, d, J=8 Hz). Found: C, 68.93; H, 8.03; S. 15.05%. Calcd for $C_{12}H_{16}OS$: C, 69.19; H, 7.74; S, 15.39%.

(1*R*,2*R*)-2-(Benzylthio)cyclopentanol (5): IR (neat) 3410, 690 cm^{-1}; ^{1}H NMR (CCl_4) δ=1.10—2.30 (6H, m), 2.60—2.84 (1H, m), 3.19 (1H, s), 3.66 (2H, s), 3.78—4.04 (1H, m), 7.26 (5H, s). Found: C, 69.25; H, 8.03; S, 15.10%. Calcd for $C_{12}H_{16}OS$: C, 69.19; H, 7.74; S. 15.39%.

(1*R*,2*R*)-2-(Butylthio)cyclopentanol (6): IR (neat) 3410 cm^{-1}; ^{1}H NMR (CCl_4) δ=0.96 (3H, t, J=6 Hz), 1.05—2.38 (10H, m), 2.17 (1H, s), 2.53 (2H, t, J=7 Hz), 2.65—2.96 (1H, m), 3.87—4.18 (1H. m). Found: C, 62.28; H, 10.26; S, 18.21%. Calcd for $C_9H_{18}OS$: C. 62.02, H, 10.41; S, 18.39%.

(2*R*,3*R*)-3-(*p*-Tolylthio)-2-butanol (7): IR (neat) 3430, 810 cm^{-1}; ^{1}H NMR (CCl_4) δ=1.87 (3H, d, J=7 Hz), 1.24 (3H, d, J=7 Hz),2.35 (3H, s), 2.43 (1H, s). 2.67—3.08 (1H, m), 3.32—3.75 (1H, m), 7.07 (2H, d, J=8 Hz), 7.32 (2H, d, J=8 Hz). Found: C, 67.14; H, 7.99; S, 16.43%. Calcd for $C_{11}H_{16}OS$: C, 67.30; H, 8.22; S, 16.33%.

(2*R*,3*R*)-3-(Benzylthio)-2-butanol (8): IR (neat) 3430, 690 cm^{-1}; ^{1}H NMR (CCl_4) δ=1.15 (3H, d, 7 Hz), 1.21 (3H, d, J=7 Hz), 2.29 (1H, s), 2.37—2.65 (1H, m), 3.40—3.66 (1H, m), 3.74 (2H, s), 7.34 (5H, s). Found: C. 67.56; H, 8.38; S, 16.21%. Calcd for $C_{11}H_{16}OS$: C, 67.30; H, 8.22; S, 16.33%.

(2*R*,3*R*)-3-(Butylthio)-2-butanol (9): IR (neat) 3430 cm^{-1}; ^{1}H NMR (CCl_4) δ=0.94 (3H, t, J=7 Hz), 1.09 (3H, d, J=6 Hz), 1.33 (3H, d, J=7 Hz), 1.34—1.82 (4H, m), 2.03 (1H, s), 2.38—2.69 (1H, m), 2.35 (2H, t, J=7 Hz), 3.32—3.58 (1H, m). Found C, 59.43; H, 10.97; S, 19.58%. Calcd for $C_8H_{18}OS$: C, 59.21; H, 11.18; S, 19.75%.

Reaction of 1,2-Epoxycyclohexane with Aniline Catalyzed by ZnT. To a dichloromethane (5 cm^3) solution of 1,2-epoxycyclohexane (196 mg, 2 mmol) and aniline (186 mg, 2 mmol) was suspended ZnT (43 mg, 0.2 mmol). The heterogeneous mixture was stirred at room temperature for 7 d. After filtration of ZnT, the filtrate was concentrated and purified by column chromatography on silica gel ($CHCl_3$) to afford 108 mg (28% yield) of (1*R*,2*R*)-2-anilinocyclohexanol (**10**): $[\alpha]_D^{23}$ −52.6° (*c* 2.0, CH_2Cl_2); mp 78—81 °C; IR (KBr) 3370, 3450, 1590, 1280 cm^{-1}; ^{1}H NMR ($CDCl_3$) δ=1.00—1.52 (4H, m), 1.55—1.88 (2H, m), 1.88—2.24 (2H, m), 2.86—3.45 (2H, m), 3.34 (2H, s), 6.48—6.51 (3H, m), 6.96—7.23 (2H, m). Found: C, 75.12; H, 8.86; N, 7.48%. Calcd for $C_{12}H_{17}NO$: C, 75.36, H, 8.96, N, 7.32%. The isolated yields, optical rotations, and enantiomeric excesses of **10** in the use of various metal(II) *d*-tartrates are listed in Table 2.

Preparation of Trialkylsilyl Azide. Trimethylsilyl azide was commercially available (Tokyo Kasei) and was used without further purification. The following trialkylsilyl azides were prepared from the corresponding trialkylsilyl chlorides and sodium azide according to the literature for the preparation of trimethylsilyl azide.[36]

Ethyldimethylsilyl Azide: Yield 56%; bp 72 °C/150 Torr; IR (neat) 2160 cm^{-1}; ^{1}H NMR (CCl_4) δ=0.14 (6H, s), 0.72 (2H, q, J=8 Hz), 1.04 (3H, t, J=8 Hz). Found: C, 37.29; H, 8.51, N, 32.40%. Calcd for $C_4H_{11}N_3Si$: C, 37.18; H, 8.58; N, 32.51%.

Isopropyldimethylsilyl Azide: Yield 72%; bp 75 °C/90 Torr; IR (neat) 2140 cm^{-1}; ^{1}H NMR (CCl_4) δ=0.23 (6H, s), 1.04 (6H, d, J=5 Hz), 1.03 (1H, q, J=5 Hz). Found: C, 41.73; H, 9.04; N, 29.45%. Calcd for $C_5H_{13}N_3Si$: C, 41.91; H, 9.15; N, 29.33%.

***t*-Butyldimethylsilyl Azide:** Yield 84%; bp 78 °C/67 Torr; IR (neat) 2140 cm^{-1}; ^{1}H NMR (CCl_4) δ=0.22 (6H, s), 0.97 (9H, s). Found: C, 45.90; H, 9.75; N, 26.47%. Calcd for $C_6H_{15}N_3Si$: C, 45.81; H, 9.61; N, 26.72%.

Triethylsilyl Azide: Yield 80%; bp 82 °C/35 Torr; IR (neat) 2130 cm^{-1}; ^{1}H NMR (CCl_4) δ=0.79 (6H, q, J=9 Hz), 1.05 (9H, t, J=9 Hz). Found: C, 45.82; H, 9.75; N, 26.51%. Calcd for $C_6H_{15}N_3Si$: C, 45.81; H, 9.61; N, 26.72%.

General Procedure for the Reaction of *meso*-Oxiranes with Trialkylsilyl Azides. To a benzene (5 cm^3) solution of oxirane (10 mmol) and trialkylsilyl azide (12 mmol) was suspended metal(II) *d*-tartrate (1 mmol). The heterogeneous mixture was stirred at room temperature for 14 d. After filtration of metal(II) *d*-tartrate, the filtrate was concentrated and purified by Kugelrohr distillation to afford *trans*-*O*-trialkylsilyl β-azido alcohol. The isolated yields, optical rotations, and enantiomeric excesses of the adducts in the various combination of oxiranes, trialkylsilyl azides, and metal(II) *d*-tartrates are listed in Tables 4 and 5. Spectral and analytical data of the adducts **12—20** are as follows.

(1*R*,2*R*)-1-Azido-2-(trimethylsilyloxy)cyclohexane (12): Bp 110 °C/5 Torr; IR (neat) 2110 cm^{-1}; ^{1}H NMR ($CDCl_3$) δ=0.16 (9H, s), 1.02—1.05 (4H, m), 1.55—2.20 (4H, m), 3.00—3.60 (2H, m). Found: C, 50.58: H, 8.93; N, 19.83%. Calcd for $C_9H_{19}N_3OSi$: C, 50.65; H, 8.98; N, 19.70%.

(1*R*,2*R*)-1-Azido-2-(trimethylsilyloxy)cyclopentane (13): Bp 105 °C/5 Torr; IR (neat) 2100 cm^{-1}; ^{1}H NMR (CCl_4) δ=0.12 (9H, s), 1.23—2.25 (6H, m), 3.40—3.76 (1H, m), 3.78—4.10 (1H, m). Found: C, 48.01, H, 8.47; N, 21.32%. Calcd for $C_8H_{17}N_3OSi$: C, 48.20: H, 8.60, N. 21.08%.

(2*R*,3*R*)-2-Azido-3-(trimethylsilyloxy)butane (14): Bp 100 °C/5 Torr; IR (neat) 2100 cm^{-1}; ^{1}H NMR (CCl_4) δ=0.13 (9H, s), 1.15 (3H, d, J=10 Hz), 1.16 (3H, d, J=10 Hz), 2.98—3.40 (1H, m), 3.50—3.89 (1H, m). Found: C, 44.72; H, 8.98; N, 22.51%. Calcd for $C_7H_{17}N_3OSi$: C, 44.88; H, 9.15; N, 22.43%.

(1*R*,2*R*)-1-Azido-2-(ethyldimethylsilyloxy)cyclohexane (15): Bp 120 °C/6 Torr; IR (neat) 2100 cm^{-1}; ^{1}H NMR (CCl_4) δ=0.10 (6H, s), 0.58 (2H, q, J=8 Hz), 0.96 (3H, t, J=8 Hz), 1.02—2.35 (8H, m), 2.70—3.63 (2H, m). Found: C,52.69; H, 9.13; N, 18.40%. Calcd for $C_{10}H_{21}N_3OSi$: C, 52.82; H, 9.31; N, 18.48%.

(1*R*,2*R*)-1-Azido-2-(ethyldimethylsilyloxy)cyclopentane (17): Bp 105 °C/5 Torr; IR (neat) 2100 cm^{-1}; ^{1}H NMR (CCl_4) δ=0.10 (6H, s), 0.58 (2H, q, J=8 Hz), 0.96 (3H, t, J=8 Hz); 1.16—2.24 (6H, m), 3.48—3.82 (1H, m), 3.84—4.19 (1H,

m). Found: C, 50.51; H, 8.79%; N, 19.79%. Calcd for $C_9H_{19}N_3OSi$: C, 50.65; H, 8.98; N, 19.70%.

(2*R*,3*R*)-2-Azido-3-(ethyldimethylsilyloxy)butane (19): Bp 100 °C/5 Torr; IR (neat) 2100 cm^{-1}; ^1H NMR (CCl_4) δ=0.09 (6H, s), 0.58 (2H, q, J=8 Hz), 0.97 (3H, t, J=8 Hz), 1.13 (3H, d, J=6 Hz), 1.15 (3H, d, J=6 Hz), 3.02—3.42 (1H, m), 3.44—3.86 (1H, m). Found: C, 47.76; H, 9.38; N, 20.98%. Calcd for $C_8H_{19}N_3OSi$: C, 47.72; H, 9.51; N, 20.87%.

(1*R*,2*R*)-1-Azido-2-(isopropyldimethylsilyloxy)cyclohexane (16): Bp 135 °C/5 Torr; IR (neat) 2100 cm^{-1}; ^1H NMR (CCl_4) δ=0.09 (6H, s), 0.92 (1H, q, J=5 Hz), 0.97 (6H, d, J=5 Hz), 1.00—2.32 (8H, m), 2.83—3.85 (2H, m). Found: C, 54.71; H, 9.48; N, 17.46%. Calcd for $C_{11}H_{23}N_3OSi$: C, 54.72; H, 9.60; N, 17.41%.

(1*R*,2*R*)-1-Azido-2-(isopropyldimethylsilyloxy)cyclopentane (18): Bp 120 °C/5 Torr; IR (neat) 2100 cm^{-1}; ^1H NMR (CCl_4) δ=0.07 (6H, s), 0.92 (1H, q. J=5 Hz), 0.97 (6H, d, J=5 Hz), 1.35—2.32 (6H, m), 3.40—3.83 (1H, m), 3.84—4.17 (1H, m). Found: C, 52.91; H, 9.57; N, 18.47%. Calcd for $C_{10}H_{21}N_3OSi$: C, 52.82; H, 9.31; N, 18.48%.

(2*R*,3*R*)-2-Azido-3-(isopropyldimethylsilyloxy)butane (20): Bp 110 °C/5 Torr; IR (neat) 2100 cm^{-1}; ^1H NMR (CCl_4) δ=0.08 (6H, s), 0.92 (1H, q, J=5 Hz), 0.97 (6H, d, J=5 Hz), 1.17 (3H, d, J=9 Hz), 1.26 (3H, d, J=9 Hz); 3.02—3.83 (2H, m). Found: C, 50.46; H, 9.63; N, 19.47%. Calcd for $C_9H_{21}N_3OSi$: C, 50.19: H, 9.83; N, 19.51%.

Kinetic Resolution of *trans*-2,3-Dimethyloxirane. To a dichloromethane (100 cm^3) solution of *trans*-2,3-dimethyloxirane (2.88 g, 40 mmol) and *p*-toluenethiol (2.48 g, 20 mmol) was suspended ZnT (0.43 g, 2 mmol). This heterogeneous mixture was stirred at room temperature for 14 d. After filtration of ZnT, the filtrate was concentrated and purified by column chromatography on silica gel (hexane : ethyl acetate=10 : 1) to afford (2*S*,3*R*)-3-(*p*-tolylthio)-2-butanol (**21**) (3.70 g, 47%). $[\alpha]_D^{23}$ +2.16° (*c* 5.00, CH_2Cl_2). IR (neat) 3440, 800 cm^{-1}. ^1H NMR (CCl_4) δ=1.16 (3H, d, J=8 Hz), 1.27 (3H, d, J=8 Hz), 2.08 (1H, s), 2.37 (3H, s), 2.96—3.27 (1H, m), 3.50—3.86 (1H, m), 7.07 (2H, d, J=8 Hz), 7.30 (2H, d, J=8 Hz). Found: C, 67.07; H, 8.26; S, 16.39%. Calcd for $C_{11}H_{16}OS$: C, 67.30; H, 8.22; S, 16.33%.

Typical Procedures for the Conversion of (1*R*,2*R*)-1 into (*R*)-2-Cyclohexen-1-ol. Oxidation of 1. To a $CHCl_3$ (50 cm^3) solution of **1** (4.04 g, 20 mmol, $[\alpha]_D^{23}$ −45.0°, (*c* 5.00, CH_2Cl_2)) was added *m*-chloroperbenzoic acid (5.2 g, 30 mmol) little by little on ice cooling with stirring. Afer stirring for 30 min at room temperature, the reaction mixture was washed with 20 cm^3 of 5% aqueous $KHCO_3$ three times, dried over Na_2SO_4, concentrated, and purified by column chromatography on silica gel ($CHCl_3$: MeOH=50 : 1) to afford the corresponding S-oxide (4.4 g, 92%). Mp 135—139 °C. IR (KBr) 3380, 1020 cm^{-1}.

Thermal Decomposition of *S*-Oxide of 1. The mixture of *S*-oxide of **1** (3.2 g, 13 mmol) and $CaCO_3$ (1.3 g, 13 mmol) was heated at 150 °C/10 Torr for 3 h. During the thermal decomposition, the distillate was collected in a reciever with Dry Ice-acetone cooling, and was purified by Kugelrohr distillation (100 °C/15 Torr) to give (*R*)-2-cyclohexen-1-ol (0.90 g, 69%, $[\alpha]_D^{23}$ +92.4° (*c* 0.60, $CHCl_3$)).

By the same way, (1*R*,2*R*)-**2** ($[\alpha]_D^{23}$ −34.4°) and (1*R*,2*R*)-**3** ($[\alpha]_D^{23}$ −44.7°) were transformed into (*R*)-2-cyclohexen-1-ol ($[\alpha]_D^{23}$ +102.7 and +110.8°) in 41 and 58% yields, respectively.

The 2-substituted cyclopentanols such as (1*R*,2*R*)-**4** ($[\alpha]_D^{23}$ −7.97°), (1*R*,2*R*)-**5** ($[\alpha]_D^{23}$ −7.80°), and (1*R*,2*R*)-**6** ($[\alpha]_D^{23}$ −15.1°) were converted into (*R*)-2-cyclopenten-1-ol ($[\alpha]_D^{23}$ +46.8, +52.3, and +81.9° (*c* 1.0, $CHCl_3$)) in 80, 62, and 48% yields, respectively.

The 3-substituted 2-butanols such as (2*R*,3*R*)-**7** ($[\alpha]_D^{23}$ −25.8°), (2*R*,3*R*)-**8** ($[\alpha]_D^{23}$ −18.5°), and (2*R*,3*R*)-**9** ($[\alpha]_D^{23}$ −29.0°) were converted into (*R*)-3-buten-2-ol ($[\alpha]_D^{23}$ −16.9, −23.1, and −21.8° (neat)) in 57, 41, and 53% yields, respectively. Furthermore, (2*S*,3*R*)-**21** ($[\alpha]_D^{23}$ +2.16°) was also converted into (*S*)-3-buten-2-ol ($[\alpha]_D^{23}$ −14.1° (neat)) in 51% yield.

Conversion of (1*R*,2*R*)-10 into (*R*)-2-Cyclohexen-1-ol. *N*-Methylation of 10. To a methanol (50 cm^3) solution of (1*R*,2*R*)-**10** (4.2 g, 22 mmol, $[\alpha]_D^{23}$ −52.6° (*c* 5.0, CH_2Cl_2)) was added 50 cm^3 of 25% aqueous K_2CO_3, and Me_2SO_4 (12.6 g, 100 mmol) during 2 h with vigorous stirring. After adding 10 cm^3 of 5% aqueous NaOH, the reaction mixture was extracted with 50 cm^3 of ethyl acetate, dried over Na_2SO_4, cocentrated, and purified by column chromatography on silica gel (hexane : ethyl acetate=6 : 1) to yield (1*R*,2*R*)-**11** (4.2 g, 94%,). $[\alpha]_D^{23}$ +46.4° (*c* 5.0, CH_2Cl_2). IR (neat) 3450 cm^{-1}. ^1H NMR ($CDCl_3$) δ=1.10—1.85 (8H, m), 2.18 (1H, s), 2.76 (3H, s), 3.20—3.85 (2H, m), 6.60—7.38 (5H, m). Found: C, 76.18; H, 9.28; N, 6.86%. Calcd for $C_{13}H_{19}NO$: C, 76.06; H, 9.33; N, 6.82%.

Oxidation of (1*R*,2*R*)-11. To a dichloromethane (50 cm^3) solution of **11** (4.2 g, 20 mmol) was added *m*-chloroperbenzoic acid (4.0 g, 23 mmol) little by little. After being stirred for 1 h at room temperature, the mixture was washed with 50 cm^3 of 10% aqueous K_2CO_3 three times, dried over Na_2SO_4, concentrated, and purified by column chromatography on silica gel ($CHCl_3$: MeOH=20 : 1) to afford the corresponding *N*-oxide (3.7 g, 82%). Mp 123—125 °C. IR (KBr) 3420, 1450, 1110 cm^{-1}.

Thermal Decomposition of *N*-Oxide. The *N*-oxide of **11** (1.0 g, 4.5 mmol) was heated at 140 °C/20 Torr for 3 h. The distillate was collected in a reciever with Dry Ice-acetone cooling, and was purified by Kugelrohr distillation to yield (*R*)-2-cyclohexen-1-ol (0.30 g, 67%, $[\alpha]_D^{23}$ +69.3° (*c* 0.60, $CHCl_3$).

Desilylation of *O*-Trialkylsilyl β-Azido Alcohols 12—20. Typical Procedure for the Desilylation of (1*R*,2*R*)-12 into (1*R*,2*R*)-2-Azidocyclohexanol. A methanol solution (8 cm^3) of (1*R*,2*R*)-**12** (2.13 g, 10 mmol, $[\alpha]_D^{23}$ +10.9° (*c* 2.0, CH_2Cl_2)) and 0.05 cm^3 of concd HCl was refluxed for 2 h. After being concentrated in vacuo, the residue was purified by Kugelrohr distilation (105 °C/4.5 Torr) to give (1*R*,2*R*)-2-azidocyclohexanol (1.4 g, 92%). $[\alpha]_D^{23}$ −30.8° (*c* 2.0, CH_2Cl_2). IR (neat) 3320, 2100 cm^{-1}. ^1H NMR ($CDCl_3$) δ=1.00—2.28 (8H, m), 2.26 (1H, s), 3.00—3.70 (2H, m). Found: C, 50.89; H, 7.64; N, 29.71%. Calcd for $C_6H_{11}N_3O$: C, 51.05; H, 7.85; N, 29.77%.

By the same way, (1*R*,2*R*)-**15** and **16** ($[\alpha]_D^{23}$ +2.40 and +0.38°) were transformed into (1*R*,2*R*)-2-azidocyclohexanol ($[\alpha]_D^{23}$ −10.5 and −11.1°) in 85 and 87%, respectively.

Desilylation of (1*R*,2*R*)-**13**, **17**, and **18** ($[\alpha]_D^{23}$ −10.1, −9.08, and −7.44° (*c* 2.0, CH_2Cl_2)) were similarly carried out to afford (1*R*,2*R*)-2-azidocyclopentanol ($[\alpha]_D^{23}$ −21.0, −16.5, and −14.3° (*c* 2.0, CH_2Cl_2)) in 91, 88, and 86%. Bp 105 °C/5 Torr (Kugelrohr distillation). IR (neat) 3290, 2120 cm^{-1}. ^1H NMR ($CDCl_3$) δ=1.30—2.56 (6H, m), 3.36 (1H, s), 3.40—3.78 (1H, m), 3.80—4.42 (1H, m). Found: C.47.30; H, 7.09; N, 33.12%. Calcd for $C_5H_9N_3O$: C, 47.22; H, 7.13, N, 33.05%.

Desilylation of (2*R*,3*R*)-**14**,**19**, and **20** ($[\alpha]_D^{23}$ −3.35, −3.56, and −9.45° (*c* 2.0, CH_2Cl_2)) yielded (2*R*,3*R*)-3-azido-2-butanol ($[\alpha]_D^{23}$ −37.8, −18.3, and −29.2° (*c* 2.0, CH_2Cl_2)) in

86, 86, 81%, respectively. Bp 100 °C/5 Torr (Kugelrohr distillation). IR (neat) 3370, 2100 cm^{-1}. ^1H NMR ($CDCl_3$) δ=1.12 (2H, d, J=12 Hz), 1.25 (2H, d, J=12 Hz), 2.30 (1H, s), 3.03—3.79 (2H, m). Found: C, 41.79; H, 7.67; N, 36.42%. Calcd for $C_4H_9N_3O$: C, 41.72; H, 7.88; N, 36.42%.

Hydrogenolysis of Azido Alcohols. Typical Procedure for the Hydrogenolysis of (1*R*,2*R*)-2-Azidocyclohexanol. The catalytic hydrogenolysis of (1*R*,2*R*)-2-azidocyclohexanol (1.3 g, 9.2 mmol, $[\alpha]_D^{23}$ −30.8° (*c* 2.0, CH_2Cl_2)) was carried out in methanol (12 cm^3) with 10% Pd-C (0.1 g) under atmospheric pressure at room temperature for 1 h. The catalyst was filtered off, and the filtrate was concentrated and purified by Kugelrohr distillation (165 °C/5 Torr) to afford (1*R*,2*R*)-2-aminocyclohexanol (1.2 g, 86%). $[\alpha]_D^{23}$ −15.9° (*c* 1.3, H_2O), (lit,[37] $[\alpha]_D^{22}$ −37.6°).

In a similar manner, the catalytic hydrogenolysis of (1*R*,2*R*)-2-azidocyclopentanol and (2*R*,3*R*)-3-azido-2-butanol ($[\alpha]_D^{23}$ −21.0 and −37.8° (*c* 2.0, CH_2Cl_2)) gave (1*R*,2*R*)-2-amonocyclopentanol (95% yield, $[\alpha]_D^{23}$ −10.2° (*c* 1.7, EtOH lit,[38] $[\alpha]_D^{20}$ −33.3°) and (2*R*,3*R*)-3-amino-2-butanol (95% yield, $[\alpha]_D^{23}$ −6.84° (neat); lit,[39] $[\alpha]_D^{25}$ −17.05°), respectively.

We wish to express our thanks to Professor Teruaki Mukaiyama of Tokyo Science University for correcting the manuscript and encouragement.

References

1) K. Osakada, M. Obana, T. Ikaria, M. Saburi, and S. Yoshikawa, *Tetrahedron Lett.*, **22**, 4297 (1981); T. Ikariya, Y. Ishii, H, Kawano, T. Arai, M. Saburi, S. Yoshikawa, and S. Akutagawa, *J. Chem. Soc., Chem. Commun.*, **1985**, 922.

2) Y. Ishii, K. Osakada, T. Ikariya, M. Saburi, and S. Yoshikawa, *Chem. Lett.*, **1982**, 1179.

3) S. Hashimoto, N. Komeshima, and K. Koga, *J. Chem. Soc., Chem. Commun.*, **1979**, 437.

4) K. Narasaka, M. Inoue, and T. Yamada. *Chem. Lett.*, **1986**, 1967.

5) S. Sakane, K. Maruoka, and H. Yamamoto, *Tetrahedron Lett.*, **26**, 5535 (1985); S. Sakane, K. Maruoka, and H. Yamamoto, *Tetrahedron*, **42**, 2203 (1986).

6) T. Mukaiyama, H. Yamashita, and M. Asami, *Chem. Lett.*, **1983**, 385; H. Yamashita and T. Mukaiyama, *ibid.*, **1985**, 363.

7) H. Yamashita and T. Mukaiyama, *Chem. Lett.*, **1985**, 1643; H. Yamashita, *ibid.*, **1987**, 525.

8) A. Atterberg, *Svenska Akad. Handl.*, **12**, 37 (1873): A. Rosenheim and H. Itzig, *Ber.*, **32**, 3430 (1899).

9) K. P. Chatterjee and N. R. Dhar, *J. Phys. Chem.*, **28**, 1021 (1924); S. U. Pickering, *J. Chem. Soc.*, **109**, 235 (1916).

10) W Herz and G. Muhs, *Ber.*, **36**, 3715 (1903).

11) J. A. Broomhead, F. P. Dwyer, and W. Hogarth, *Inorg. Synth.*, **6**, 183 (1960).

12) S. U. Pickering, *J. Chem. Soc.*, **109**, 235 (1916).

13) H. B. Jonassen, J. C. Bailer, and E. H. Huffman, *J. Am. Chem. Soc.*, **70**, 756 (1948); J. A. Broomhead, F. P. Dwyer, and F. W. Hogarth, *Inorg. Synth.*, **6**, 186 (1960).

14) O. F. Tower, *J. Am. Chem. Soc.*, **22**, 501 (1900).

15) O. Masson and B. D. Steele, *J. Chem. Soc.*, **75**, 725 (1899).

16) G. Spacu and P. Viochescu, *Z. Anorg. Allg. Chem.*, **227**, 129 (1936).

17) G. Spacu and P. Viochescu, *Z. Anorg. Allg. Chem.*, **227**, 385 (1936).

18) T. Sugita, Y. Yamasaki, O. Ito, and K. Ichikawa, *Bull. Chem. Soc. Jpn.*, **47**, 1945 (1974).

19) K. Tanaka, A. Ozaki, and K. Tamaru, *Shokubai*, **6**, 262 (1964).

20) M. Lj. Mihailovic, V. Andrejevic. J. Milovanovic, and J. Jankovic, *Helv. Chim. Acta*, **59**, 2305 (1976).

21) A. Ookawa, H. Hiratsuka, and K. Soai, *Bull. Chem. Soc. Jpn.*, **60**, 1813 (1987).

22) (2*R*,3*R*)-2,3-Dimethoxysuccinic acid (mp 147—148 °C, $[\alpha]_D^{23}$ +84.8° (*c* 1.0, EtOH)) was prepared according to the following literature: I. Felner and K. Schenker, *Helv. Chim. Acta*, **53**, 754 (1970).

23) (2*R*,3*R*)-2-Hydroxy-3-methoxysuccinic acid (mp 171— 173 °C, $[\alpha]_D^{23}$ +50.8° (*c* 1.0, EtOH)) was obtained by acid hydrolysis of the corresponding dimethyl ester prepared according to the following literature: F. Smith, *J. Chem. Soc.*, **1944**, 510.

24) (*S*)-2-Methoxysuccinic acid (mp 88—90 °C, $[\alpha]_D^{23}$ −31.3° (*c* 2.0, H_2O)) was prepared according to the following literature: G. Fodor and F. Sóti, *J. Chem. Soc.*, **1965**, 6830.

25) R. K. Hill and J. W. Morgan, *J. Org. Chem.*, **33**, 927 (1968); S. Yamada, N. Takamura, and T. Mizoguch, *Chem. Pharm. Bull.*, **23**, 2539 (1975); T. Sato, M. Watanabe, N. Honda, and T. Fujisawa, *Chem. Lett.*, **1984**, 829.

26) R. K. Hill and A. G. Edwards, *Tetrahedron Lett.*, **1964**, 3239; T. Sato, Y. Gotoh, Y. Wakabayashi, and T. Fujisawa, *Tetrahedron Lett.*, **24**, 4123 (1983).

27) K. L. Oliver and W. G. Young, *J. Am. Chem. Soc.*, **81**, 5811 (1959); W. G. Young and F. F. Caserio, Jr., *J. Org. Chem.*, **26**, 245 (1961); R. H. Pickard and J. Kenyon, *J. Chem. Soc.*, **1913**, 1938.

28) J. A. Dale, D. L. Dull, and H. S. Mosher, *J. Org. Chem.*, **34**, 2543 (1969).

29) C. R. Johnson and C. W. Schrock, *J. Am. Chem. Soc.*, **95**, 7418 (1973).

30) G. Hirth and R. Barner, *Helv. Chim. Acta*, **65**, 1059 (1982).

31) G. K. Ambady, *Acta Crystallogr., Sect. B*, **24**, 1548 (1968).

32) F. C. Hawthorne, I. Borys, and R. B. Ferguson, *Acta Crystallogr., Sect. B*, **38**, 2461 (1982).

33) C. K. Prout, J. R. Carruthers. and F. J. C. Rossotti, *J. Chem. Soc. A*, **1971**, 3336.

34) L. J. Bostelaar, R. A. G. Graaff, F. B. Hulsbergen, J. Reedijk, and W. M. H. Sachtler, *Inorg. Chem.*, **23**, 2294 (1984).

35) V. Frei and V. Cáslavská, *Collect. Czech. Chem. Commun.*, **29**, 1418 (1964); V. Frei and K. Mach, *ibid.*, **30**, 777 (1965).

36) L. Birkofer and A. Ritter, *Angew. Chem.*, **77**, 414 (1965).

37) T. Suami, S. Ogawa, and S. Umezawa, *Bull. Chem. Soc. Jpn.*, **36**, 459 (1963); S. Umezawa, T. Tsuchiya, and K. Tatsuta, *ibid.*, **39**, 1235 (1966).

38) A. A. Barr, I. Frencel, and J. B. Robinson, *Can. J. Chem.*, **55**, 4180 (1977).

39) F. H. Dickey, W. Fickett, and H. J. Lucas, *J. Am. Chem. Soc.*, **74**, 944 (1952).

One-Pot Ortho Hydroxylations of 2-(1-Hydroxyalkyl)-naphthalenes and (1-Hydroxyalkyl)benzenes[1)]

Yasuhiro TANOUE, Akira TERADA,* Iwao SETO, Yasuo UMEZU, and Otohiko TSUGE†
Department of Chemistry, Kyushu Institute of Technology, Tobata, Kitakyushu, Fukuoka 804
†Institute of Advanced Material Study, Kyushu University, Kasugakoen, Kasuga, Fukuoka 816
(Received August 20, 1987)

Hydroxylations of 2-(1-hydroxyalkyl)-1,4,5,8(or 1,4,5,6,8)-tetra(or penta)methoxynaphthalenes and 2-(1-hydroxyalkyl)-1,4-dimethoxybenzenes at the 3-position were accomplished by a one-pot procedure. The same procedure has been found to be applicable to 2-(1-hydroxyalkyl)naphthalenes and (1-hydroxyalkyl)benzenes having no methoxyl substituent.

Our synthetic route of Erythrostominone (**1**)[2)] requires a polymethoxynaphtol **2** which has a possibility of being converted into **1** by using our method.[3)] During synthetic studies involving naphthoquinone derivatives, we have found a new one-pot procedure that introduces a phenolic hydroxyl group into type-**3** compounds at the ortho position of the hydroxyalkyl to give type-**2** compounds in good yields.

Usually, the hydroxylations of aromatic rings by the oxidation of the corresponding Grignard or organolithium compounds required two steps,[4)] except for the synthesis of 2,2′-dimethoxy-3,3′-dihydroxybiphenyl from 2,2′-dimethoxybiphenyl by Gilman et al.[5)] That is to say, the first step should be a halogenation of the starting aromatic compounds and the second an oxidative hydroxylation of the Grignard or lithium compounds obtained from the halides.

The lithiation of aromatic rings having both methoxyl and hydroxymethyl groups at 1- and 3-positions has already been reported.[6)] Also, aromatics bearing either a methoxyl or hydroxymethyl group could be ortho lithiated.[7)] However, no information has been found in the literature concerning one-pot hydroxylation at the 2-position of aromatic rings having methoxyl and hydroxyalkyl groups at both the 1- and 3-positions, or about one-pot ortho hydroxylation of aromatics bearing only one hydroxyalkyl. In this paper, we report one-pot ortho hydroxylations of 2-(1-hydroxyalkyl)naphthalenes and (1-hydroxyalkyl)benzenes.

Results and Discussion

The substrates **3a—3f** in THF were first treated with butyllithium, then with butylmagnesium bromide and at last oxidized by dry oxygen. A decomposition of the system by an addition of dil HCl or aq NH_4Cl resulted in the formation of naphthols **2a—2f** (Table 1).

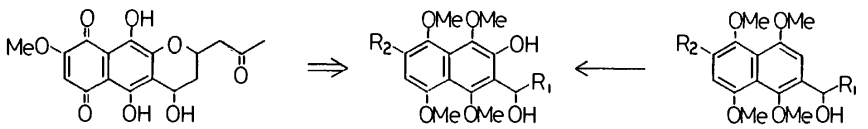

1 2 3

Table 1. Hydroxylation of 2-(1-Hydroxyalkyl)-1,4,5,8(or 1,4,5,6,8)-tetra(or penta)methoxynaphthalene

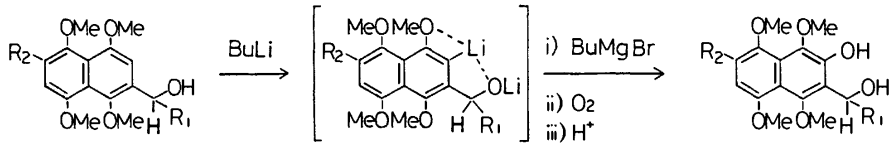

3a~3f 2a~2f

Substrate	Product	Yield/%
3a: R_1=R_2=H	**2a**	36[53][a)]
3b: R_1=H, R_2=OMe	**2b**	59
3c: R_1=C_4H_9, R_2=H	**2c**	39[46][a)]
3d: R_1=C_4H_9, R_2=OMe	**2d**	73
3e: R_1=CH_2CH=CH_2, R_2=H	**2e**	45
3f: R_1=CH_2CH=CH_2, R_2=OMe	**2f**	78

a) Conversion yield.

Table 2. Hydroxylation of 2-(1-Hydroxyalkyl)naphthalene

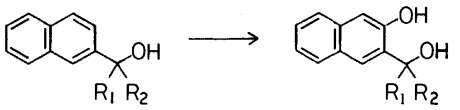

4a.b 5a.b

Substrate	Product	Yield/%
4a: R_1=R_2=H	**5a**	15[76][a]
4b: R_1=H, R_2=C_4H_9	**5b**	22[69][a]

a) Conversion yield.

Table 3. Hydroxylation of 2-(1-Hydroxyalkyl)benzene

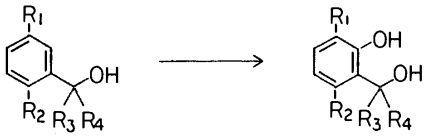

6a~6f 7b~7f

Substrate	Product	Yield/%
6a: R_1=R_2=OMe, R_3=R_4=H	**7a**	51[68][a]
6b: R_1=R_2=OMe, R_3=H, R_4=C_4H_9	**7b**	58[98][a]
6c: R_1=OMe, R_2=R_3=R_4=H	**7c**	19[73][a]
6d: R_1=OMe, R_2=R_3=H, R_4=C_4H_9	**7d**	22[72][a]
6e: R_1=R_2=R_3=R_4=H	**7e**	26[66][a]
6f: R_1=R_2=R_3=H, R_4=C_4H_9	**7f**	19[93][a]

a) Conversion Yield.

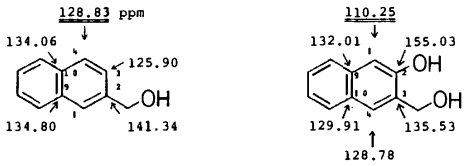

4a 5a

This hydroxylation procedure was applicable to syntheses of the 2-naphthols **5a** and **5b** from 2-(1-hydroxyalkyl)naphthalenes **4a** and **4b** having no methoxyl group (Table 2). The reactions were usually carried out in the presence of *N,N,N′,N′*-tetramethylethylenediamine in an ether solvent. Even if a large excess of *n*-BuLi was used for the reactions, a part of the starting materials was always recovered.

It was clearly proved by ^{13}C NMR that the newly introduced hydroxyl group had occupied the 3-position in the substrats **4a** and **4b**. It is well-known that the ^{13}C-chemical shift of the ortho positional carbon atom adjacent to the carbon atom bearing the hydroxyl group in an aromatic ring moves upfield to an appreciable extent.[8] The chemical shift of C_1 (δ 110.25) in product **5a** was observed more upfield than that of C_4 (δ 128.83) in 2-hydroxymethylnaphthalene (**4a**). Since this C_1 peak (δ 110.25) of the singlet changed into a doublet upon a proton off-resonace decoupling operation, this carbon atom must be a tertiary one of C_1. Therefore, the newly introduced

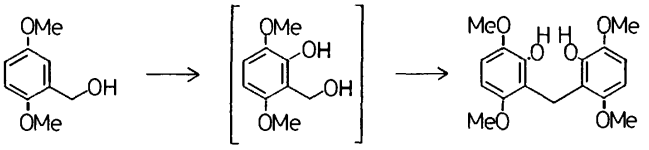

6a 7a

hydroxyl group occupied the 2-position in **5a**.

In the similar fashion, the benzenes **6a—6f** were also ortho-hydroxylated to give phenols **7a—7f** (Table 3).

A product from **6a** was concluded to have the structure **7a** and the formation process might be as shown in the following chart. This is one of the typical Bakelite formation reactions. Martin,[9] for example, has reported that the formation of his diphenylmethanes could be explained best by a loss of one mole of water and one mole of formaldehyde between two moles of hydroxymethylphenols; he confirmed a loss of formaldehyde in this experiment. These kinds of condensations were easily carried out in the presence of lithium hydroxide.[10] Dean et al.[11] also reported that a change of 1-hydroxymethyl-2-naphthol into 1,1′-methylenedi-2-naphthol occured at 25 °C in ethanol containing of HCl during 1 min, along with an elimination of formaldehyde.

Experimental

^{1}H and ^{13}C NMR spectra were taken on a JEOL JNM-60. MS was obtained with a JEOL DX-300, IR with a Hitachi 260-30. Column chromatography was carried out on silica gel (Wakogel C-200) or alumina gel (Sumitomo, KCG-30) with chloroform as eluent. Melting points were determined with a Yanagimoto micromelting point apparatus and uncorrected. High-performance liquid chromatography (HPLC) was performed with a EYELA PLC-10 using TC-ODS 1171.

Materials. The substrates **3a—3f** were prepared by reductions or by Grignard reactions of 2-formyl-1,4,5,8-tetramethoxynaphthalene (see Ref. 12) and of 2-formyl-1,4,5,6,8-pentamethoxynaphthalene (see Ref. 3).

3a: A cream-colored solid (99% yield); mp 104—105 °C (from hexane-benzene); IR (KBr) 3520 (OH) and 1060 cm^{-1} (OCH_3, OH); ^{1}H NMR ($CDCl_3$) δ=2.42 (s, 1H, OH), 3.76, 3.88, 3.90, 3.92 (each s, 3H, OCH_3), 4.84 (s, 2H, CH_2), 6.80 (s, 2H, ArH), and 6.91 (s, 1H, ArH); MS, *m/z* 278 (M^+), 263, and 245. Calcd for $C_{15}H_{18}O_5$: C, 64.74; H, 6.52%. Found: C, 64.39; H, 6.57%.

3b: It was prepared as shown in Ref. 12.

3c: Colorless viscous oil (99% yield); IR (neat) 3450 (OH), 1600, and 1070 cm^{-1}; ^{1}H NMR ($CDCl_3$) δ=0.89 (t, *J*=6.6 Hz, 3H, CH_3), 1.1—1.9 (m, 6H, CH_2), 2.42 (broad, 1H, OH), 3.74, 3.88 (each s, 3H, OCH_3), 3.92 (s, 6H, OCH_3), 5.22 (t, *J*=6.0 Hz, 1H, CH), 6.80 (s, 2H, ArH), and 6.97 (s, 1H, ArH); MS, *m/z* 334 (M^+), 316 ($M^+ - H_2O$), 301, 270, 231, and 137; HRMS, Calcd for $C_{19}H_{26}O_5$: M, 334.1781. Found: *m/z* 334.1784.

3d: Colorless viscous oil (89% yield); IR (neat) 3450 (OH), 1600, 1360, 1070 cm^{-1}; ^{1}H NMR ($CDCl_3$) δ=0.90 (t, *J*=6.0 Hz, 3H, CH_3), 1.1—1.9 (m, 6H, CH_2), 2.18 (broad, 1H, OH), 3.74, 3.81, 3.94 (each s, 3H, OCH_3), 3.97 (s, 6H, OCH_3), 5.22 (t, *J*=6.9 Hz, 1H, CH), 6.73 (s, 1H, ArH), and 6.92 (s, 1H, ArH);

MS, m/z 364 (M^+), 346 ($M^+ - H_2O$), 331, and 152; HRMS, Calcd for $C_{20}H_{28}O_6$: M, 364.1862. Found: m/z 364.1885.

3e: Colorless viscous oil (97% yield); IR (neat) 3470 (OH), 1640 (C=C), 1605, 1070, 995 (vinyl), and 915 cm^{-1} (vinyl); ^1H NMR ($CDCl_3$) δ=2.20 (broad, 1H, OH), 2.57 (t, J=6.9 Hz, 2H, CH_2), 3.75, 3.88 (each s, 3H, OCH_3), 3.92 (s, 6H, OCH_3), 4.9—5.4 (m, 3H, CH, $=CH_2$), 5.9 (m, 1H, -CH=), 6.81(s, 2H, ArH), and 7.00 (s, 1H, ArH); MS, m/z 318 (M^+), 300 ($M^+ - H_2O$), 285, 277, and 262; HRMS, Calcd for $C_{18}H_{22}O_5$: M, 318.1467. Found: m/z 318.1472.

3f: Cream-colored crystals (98% yield); mp 90—91 °C (from hexane); IR (KBr) 3460 (OH), 1640 (C=C), 1600, 1070, 995 (vinyl), and 915 cm^{-1} (vinyl); ^1H NMR ($CDCl_3$) δ=2.20 (broad, 1H, OH), 2.56 (t, J=6.8 Hz, 2H, CH_2), 3.75, 3.81, 3.95 (each s, 3H, OCH_3), 3.98 (s, 3H, OCH_3), 4.9—5.4 (m, 3H, CH, $=CH_2$), 5.9 (m, 1H, -CH=), 6.73, 6.95 (each s, 1H, ArH); MS, m/z 348 (M^+), 330 ($M^+ - H_2O$), 315, and 269. Calcd for $C_{19}H_{24}O_6$: C, 65.50; H, 6.94%. Found: C, 65.25; H, 7.01%.

Substrates **4a** and **4b** were obtained by a treatment of 2-formylnaphthalene with $NaBH_4$ or with butylmagnesium bromide.

4a: White crystals; mp 82—83 °C (lit,[13a] mp 81—82 °C); ^{13}C NMR ($CDCl_3$) δ=125.90 (C_3), 126.48, 126.68, 127.17, 128.98 (C_4, C_5, C_8), 134.06 (s, C_{10}), 134.80 (s, C_9), 141.34 (s, C_2).

4b: A white solid (96% yield); mp 50—51 °C; IR (KBr) 3300 (OH), 1600, 1050, and 1010 cm^{-1}; ^1H NMR ($CDCl_3$) δ=0.88 (t, J=5.1 Hz, 3H, CH_3), 1.1—2.1 (m, 7H, OH, CH_2), 4.82 (t, J=7.1 Hz, 1H, CH), and 7.3—7.9 (m, 7H, ArH); ^{13}C NMR ($CDCl_3$) δ=124.19 (C_3), 124.63, 125.70, 126.05, 127.71, 127.95, 128.19 (C_4), 132.99 (s, C_{10}), 133.28 (s, C_9), 142.32 (s, C_2); MS, m/z 214 (M^+), 196 ($M^+ - H_2O$), 157, and 129. Calcd for $C_{15}H_{18}O$: C, 84.07; H, 8.47%. Found: C, 83.55; H, 8.54%.

Substrates **6a** and **6e** were commercially available, and **6b**, **6c**, **6d**, and **6f** were prepared by reductions of Grignard reactions of the corresponding aldehydes.

6b: White crystals (92% yield); mp 52—53 °C (from hexane); IR (KBr) 3360 (OH), 1600, 1220, and 1050 cm^{-1}; ^1H NMR ($CDCl_3$) δ=0.89 (t, J=5.3 Hz, 3H, CH_3), 1.1—1.9 (m, 7H, OH, CH_2), 2.57 (d, J=5.9 Hz, 1H, OH), 3.76, 3.80 (each s, 3H, OCH_3), 4.82 (q, J=5.9 Hz, 1H, CH), and 6.7—7.0 (m, 3H, ArH); MS, m/z 224 (M^+), 206 ($M^+ - H_2O$), 177, and 167. Calcd for $C_{13}H_{20}O_3$: C, 69.61; H, 8.99%. Found: C, 69.65; H, 9.06%.

6c: Colorless viscous oil (99% yield); IR (neat) 3300 (OH), 1600, 1260, and 1040 cm^{-1}; ^1H NMR ($CDCl_3$) δ=2.60 (t, J=5.2 Hz, 1H, OH), 3.76 (s, 3H, OCH_3), 4.59 (d, J=5.2 Hz, 2H, CH_2), and 6.6—7.3 (m, 4H, ArH); MS, m/z 138 (M^+), 109, and 77; HRMS, Calcd for $C_8H_{10}O_2$: M, 138.0682. Found: m/z 138.0696.

6d: Colorless viscous oil (98% yield); IR (neat) 3350 (OH), 1600, 1265, and 1040 cm^{-1}; ^1H NMR ($CDCl_3$) δ=0.88 (t, J=5.3 Hz, 3H, CH_3), 1.0—2.0 (m, 7H, OH, CH_2), 3.80 (s, 3H, OCH_3), 4.62 (t, J=6.6 Hz, 1H, CH), and 6.7—7.3 (m, 4H, ArH); MS, m/z 194 (M^+), 176 ($M^+ - H_2O$), 137, and 109; HRMS, Calcd for $C_{12}H_{18}O_2$: M, 194.1306. Found: m/z 194.1301.

6f: Colorless viscous oil (93% yield); IR (neat) 3380 (OH), 1500, 1455, and 1040 cm^{-1}; ^1H NMR ($CDCl_3$) δ=0.88 (t, J=5.1 Hz,3H, CH_3), 1.0—1.9 (m, 6H, CH_2), 2.11 (broad, 1H, OH), 4.62 (t, J=5.6 Hz, 1H, CH), and 7.30 (s, 5H, ArH); MS, m/z 164 (M^+), 163, 107, and 79; HRMS, Calcd for $C_{11}H_{16}O$: M, 164.1200. Found: m/z 164.1196.

General Procedure for Hydroxylations of the Substrates 3a—3f. A solution of a substrate (1 mmol) in THF (10 ml) was cooled to −15 °C in an ice bath, then allowed to react with n-BuLi (7 mmol, 10 w/v% in hexane), stirred at −15 °C for 2 h. To the system, a dark red solution, was added a solution of butylmagnesium bromide in THF (Mg: 8 mmol; BuBr: 8 mmol; THF: 10 ml) at −15 °C. After 1 h, dry oxygen was bubbled into the system for 1 h at such a rate as to keep the temperature below 0 °C. The reaction mixture was decomposed upon the addition of dil HCl or aq NH_4Cl, extracted with chloroform, washed with brine, dried over Na_2SO_4, and concentrated. Purification of the crude products by silica-gel chromatography with chloroform as eluent gave the hydroxylated products **2a—2f**. The purity of the oily products isolated by chromatography was determined by HPLC.

General Procedure for Hydroxylations of 4a, 4b, and 6a—6f. n-BuLi (7.5 mmol) was added under cooling to −15 °C to a solution of a substrate (3 mmol) and *N,N,N',N'*-tetramethylethylenediamine (7.5 mmol) in ether (15 ml) and stirred at room temperature for 3 h. To the system was added a solution of butylmagnesium bromide (9 mmol) in THF (15 ml) at −10 °C. Oxidation, decomposition, and purification procedures were carried out in the same manner as the above mentioned general procedure.

2a: Viscous oil (contained ca. 20% of **3a**); IR (neat) 3400 (OH), 1605, 1370, 1075, and 1050 cm^{-1}; ^1H NMR ($CDCl_3$) δ=2.38 (broad, 2H, OH), 3.74, 3.77, 3.90, 3.92 (each s, 3H, OCH_3), 4.84 (s, 2H, CH_2), 6.68 (d, J=5.7 Hz, 1H, ArH), and 6.76 (d, J=5.7 Hz, 1H, ArH); MS, m/z 294 (M^+), 279, and 233; HRMS, Calcd for $C_{15}H_{18}O_6$: M, 294.1102. Found: m/z 294.1093.

2b: Viscous oil (a pure); IR (neat) 3400 (OH), 1600, 1355, and 1050 cm^{-1}; ^1H NMR ($CDCl_3$) δ=2.21 (broad, 2H, OH), 3.79, 3.85, 3.86, 3.97, 4.06 (each s, 3H, OCH_3), 4.85 (s, 2H, CH_2), and 6.74 (s, 1H, ArH); MS, m/z 324 (M^+), 309, 291, 279, and 263; HRMS, Calcd for $C_{16}H_{20}O_7$: M, 324.1208. Found: m/z 324.1206.

2c: Viscous oil (contained ca. 20% of **3c**); IR (neat) 3400 (OH), 1603, 1365, and 1050 cm^{-1}; ^1H NMR ($CDCl_3$) δ=0.90 (t, J=6.0 Hz, 3H, CH_3), 1.1—1.9 (m, 6H, CH_2), 2.28 (broad, 2H, OH), 3.72, 3.76, 3.89, 3.93 (each s, 3H, OCH_3), 5.21 (t, J=6.0 Hz, 1H, CH), 6.69 (d, J=6.3 Hz, 1H, ArH), and 6.78 (d, J=6.3 Hz, 1H, ArH); MS, m/z 350 (M^+), 332 ($M^+ - H_2O$), 317, and 301; HRMS, Calcd for $C_{19}H_{26}O_6$: M, 350.1730. Found: m/z 350.1755.

2d: Viscous oil (a pure); IR (neat) 3400 (OH), 1600, 1355, and 1050 cm^{-1}; ^1H NMR ($CDCl_3$) δ=0.91 (t, J=6.0 Hz, 3H, CH_3), 1.1—1.9 (m, 6H, CH_2), 2.22 (broad, 1H, OH), 3.75, 3.83, 3.86, 3.97, 4.04 (each s, 3H, OCH_3), 5.23 (t, J=7.2 Hz, 1H, CH), 6.22 (broad, 1H, OH), and 6.77 (s, 1H, ArH); MS, m/z 380 (M^+), 362 ($M^+ - H_2O$), 347, and 309; HRMS, Calcd for $C_{20}H_{28}O_7$: M, 380.1835. Found: m/z 380.1847.

2e: Viscous oil (contained ca. 10% of **3e**); IR (neat) 3430 (OH), 1640 (C=C), 1605, 1370, 1050, 995 (C=C), and 920 cm^{-1} (C=C); ^1H NMR ($CDCl_3$) δ=2.22 (broad, 2H, OH), 2.58 (t, J=6.7 Hz, CH_2), 3.75, 3.76, 3.89, 3.93 (each s, 3H, OCH_3), 4.9—5.5 (m, 3H, CH, $=CH_2$), 5.9 (m, 1H,-CH=), 6.73 (d, J=11.0 Hz, 1H, ArH), and 6.91 (d, J=11.0 Hz, 1H, ArH); MS, m/z 334 (M^+), 316 ($M^+ - H_2O$), 300, and 277; HRMS, Calcd for $C_{18}H_{22}O_6$: 334.1417. Found: m/z 334.1429.

2f: Viscous oil (a pure); IR (neat) 3400 (OH), 1640 (C=C), 1600, 1355, 1050, 990 (C=C), 915 cm^{-1} (C=C); ^1H NMR

($CDCl_3$) δ=2.30 (broad, 1H, OH), 2.58 (t, J=6.8 Hz, 2H, CH_2), 3.76, 3.83, 3.86, 3.97, 4.04 (each s, 3H, OCH_3), 4.9—5.5 (m, 3H, CH, $=CH_2$), 5.9 (m, 1H, -CH=), 6.30 (broad, 1H, OH), and 6.81 (s, 1H, ArH); MS, m/z 364 (M^+), 346 ($M^+ -H_2O$), 331, and 323; HRMS, Calcd for $C_{19}H_{24}O_7$: M, 364.1523. Found: m/z 364.1538.

5a: Cream-colored crystals; mp 191—192 °C (from hexane-ethanol); IR (KBr) 3430 (OH), 3150 (OH), 1630, 1600, 1245, and 870 cm^{-1}; ^1H NMR ($(CD_3)_2CO$) δ=4.45 (q, J=4.9 Hz, 1H, OH), 4.89 (d, J=4.9 Hz, 2H, CH_2), 7.0—8.0 (m, 6H, ArH), and 8.75 (s, 1H, OH); ^{13}C NMR ($(CD_3)_2CO$) δ=62.24 (CH_2OH), 110.25 (d, C_1), 124.29 (C_6), 126.93 (C_8), 127.07 (C_5), 127.36 (C_7), 128.78 (C_4), 129.91 (s, C_{10}) 132.01 (s, C_9), 135.53 (C_3), and 155.03 (C_2); MS, m/z 174 (M^+), 156, and 128. Calcd for $C_{11}H_{10}O_2$: C, 75.84; H, 5.79%. Found: C, 75.41; H, 5.86%.

5b: Cream-colored crystals; mp 81—82 °C (from hexane); IR (KBr) 3450 (OH), 3100 (OH), 1630, 1600, 1230, 1170, 875, and 750 cm^{-1}; ^1H NMR ($CDCl_3$) δ=0.89 (t, J=5.0 Hz, 3H, CH_3), 1.1—2.1 (m, 6H, CH_2), 2.72 (broad, 1H, OH), 4.96 (t, J=6.9 Hz, 1H, CH), 7.1—7.9 (m, 6H, ArH), and 7.98 (s, 1H, OH); ^{13}C NMR ($CDCl_3$) δ=14.08, 22.59, 28.11, 36.91, 76.42, 111.67 (d, C_1), 123.65 (C_6), 126.34 (C_5, C_7, C_8), 127.61 (C_4), 128.19 (s, C_{10}), 129.95 (s, C_9), 134.26 (C_3), and 153.66 (C_2); MS, m/z 230 (M^+), 212 ($M^+ -H_2O$), 183, and 157. Calcd for $C_{15}H_{18}O_2$: C, 78.23; H, 7.88%. Found: C, 77.69; H, 7.87%.

7a: White crystals; mp 209.5—210.5 °C (from hexane-ethanol); IR (KBr) 3370 (OH), 1600, 1230, and 1045 cm^{-1}; ^1H NMR ($CDCl_3$) δ=3.75, 3.76 (each s, 6H, OCH_3), 3.80 (s, 2H, CH_2), 5.49 (s, 2H, OH), 6.56, 6.61 (each s, 2H, ArH); ^{13}C NMR ($(CD_3)_2NCDO$) δ=29.04 (CH_2), 56.13 (C_3-OMe), 57.30 (C_6-OMe), 101.06 (C_5), 116.37 (C_4), 120.03 (C_1), 141.99 (C_3), 146.68 (C_2), and 152.64 (C_6); MS, m/z 320 (M^+), 305, 289, and 153. Calcd for $C_{17}H_{20}O_6$: C, 63.74; H, 6.29%. Found: C, 63.36; H, 6.45%.

7b: Viscous oil (contained ca. 16% of **6b**); IR (neat) 3550 (OH), 3430 (OH), 1610, 1200, and 1050 cm^{-1}; ^1H NMR ($CDCl_3$) δ=0.88 (t, J=5.4 Hz, 3H, CH_3), 1.1—2.0 (m, 7H, OH, CH_2), 3.74, 3.84 (each s, 3H, OCH_3), 4.62 (t, J=6.5 Hz, 1H, CH), 5.64 (s, 1H, ArOH), 6.53 and 6.92 (each s, 1H, ArH); MS, m/z 240 (M^+), 239, 222 ($M^+ -H_2O$), 193, and 161; HRMS, Calcd for $C_{13}H_{20}O_4$: 240.1362. Found: m/z 240.1396.

7c: White crystals; mp 115—116 °C (from hexane); IR (KBr) 3440 (OH), 3150 (OH), 1600, 1265, 1235, 1030, and 995 cm^{-1}; ^1H NMR ($CDCl_3$) δ=1.57 (s, 1H, OH), 3.90 (s, 3H, OCH_3), 4.61 (s, 2H, CH_2), 5.60 (s, 1H, ArOH), and 6.87 (m, 3H, ArH); MS, m/z 154 (M^+), 137, 93, and 65. Calcd for $C_8H_{10}O_3$: C, 62.33; H, 6.54%. Found: C, 62.37; H, 6.66%.

7d: A semisolid; IR (neat) 3400 (OH), 1600, 1270, and 1035 cm^{-1}; ^1H NMR ($CDCl_3$) δ=0.87 (t, J=5.4 Hz, 3H, CH_3), 1.1—1.9 (m, 6H, CH_2), 2.35 (broad, 1H, OH), 3.85 (s, 3H, OCH_3), 4.62 (t, J=4.4 Hz, 1H, CH), 5.80 (broad, 1H, ArOH), and 6.80 (m, 3H, ArH); MS, m/z 210 (M^+), 153, 125, and 93; HRMS, Calcd for $C_{12}H_{18}O_3$: M, 210.1257. Found: m/z 210.1278.

7e: White crystals, mp 82.5—83.5 °C (from hexane-ethanol) (lit, [13b] mp 80 °C).

7f: Viscous oil (a pure); IR (neat) 3300 (OH), 1590, 1240, and 750 cm^{-1}; ^1H NMR ($CDCl_3$) δ=0.90 (t, J=5.9 Hz, 3H, CH_3), 1.1—2.0 (m, 6H, CH_2), 2.53 (broad, 1H, OH), 4.82 (t, J=5.6 Hz, 1H, CH), 6.7—7.4 (m, 4H, ArH), and 7.93 (s, 1H, ArOH); MS, m/z 180 (M^+), 162 ($M^+ -H_2O$), 133, and 77; HRMS, Calcd for $C_{11}H_{16}O_2$: 180.1150. Found: 180.1119.

References

1) Synthesis of Naphthoquinone Derivatives. 6. For 5, Y. Tanoue and A. Terada, *Bull. Chem. Soc. Jpn.*, **60**, 3039 (1987).

2) R. H. Thomson, "Naturally Occurring Quinones," 2nd ed, Academic Press, London (1971), p. 297.

3) Y. Tanoue, A. Terada, T. Tsuboi, T. Hayashida, and O. Tsuge, *Bull. Chem. Soc. Jpn.*, **60**, 2927 (1987).

4) For example, R. L. Kidwell, M. Murphy, and S. D. Darling, *Org. Synth.*, Coll. Vol. V, 918 (1973); M. Seehan and D. J. Cram, *J. Am. Chem. Soc.*, **91**, 3544 (1969).

5) H. Gilman, J. Swiss, and L. C. Cheney, *J. Am. Chem. Soc.*, **62**, 1963 (1940).

6) M. Uemura, S. Yokuyama, and T. Sakan, *Chem. Lett.*, **1975**, 1195; B. M. Trost, G. T. Rivers, and J. M. Gold, *J. Org. Chem.*, **45**, 1835 (1980).

7) N. S. Narashimhan and R. S. Mali, *Synthesis*, **1983**, 957.

8) E. Breitmaier and W. Voelter, "^{13}C NMR Spectroscopy," 2nd ed, Verlag Chemie, New York (1978), p. 213; L. Ernst, *Chem. Ber.*, **108**, 2030 (1975).

9) R. W. Martin, *J. Am. Chem. Soc.*, **73**, 3952 (1951).

10) S. Seto and H. Horiuchi, *Kogyokagaku Zasshi*, **56**, 354, 815 (1953).

11) M. S. Chauhan, F. M. Dean, D. Matkin, and M. L. Robinson, *J. Chem. Soc., Perkin Trans. 1*, **1973**, 120.

12) A. Terada, Y. Tanoue, A. Hatada, and H. Sakamoto, *Bull. Chem. Soc. Jpn.*, **60**, 205 (1987).

13) a) S. Coffey, "Rodd's Chemistry of Carbon Compounds," Elsevier Sci. Publ., Amsterdam (1978), III G, p. 149; b) *idem*, III D, p. 147.

 © 1988 The Chemical Society of Japan Bull. Chem. Soc. Jpn., 61, 1225—1230 (1988)

Cycloaddition Reactions of 2-Hydroxy-, 2-Amino-, and 2-Mercapto-1-azaazulenes with Reactive Acetylenes

Noritaka ABE* and Toshiyuki TAKEHIRO
Department of Chemistry, Faculty of Science, Yamaguchi University, Yamaguchi 753
(Received August 28, 1987)

The reaction of 1-methyl-1-azaazulen-2(1*H*)-one (**1a**) with dimethyl acetylenedicarboxylate (DMAD) or dibenzoylacetylene (DBA) in refluxing acetonitrile gave 1,2-disubstituted azulene (**2**), 2-methylcyclopent[*de*]isoquinolin-3(2*H*)-ones, 1-methyl-1-azacyclopent[*cd*]azulen-2(1*H*)-ones, and 3-substituted 1-methyl-1-azaazulen-2(1*H*)-ones, whereas in refluxing *t*-butylbenzene, compound **2** and 6,8-etheno-1-methylcyclohepta[*b*]pyrrol-2(1*H*)-one were obtained as major products. The reactions proceeded periselectively depending on the temperature. 2-Hydroxy-1-azaazulene behaved as 1-azaazulen-2(1*H*)-one and the reaction with DMAD gave similar result as for **1a**. The reaction of 2-amino-1-azaazulene with DMAD gave methyl 2,4a-dihydro-2-oxo-1,4a-diazabenz[*a*]azulene-4-carboxylate and tetramethyl 4,5-dihydro-1*H*-1,11-diazacyclohept[*a*]azulene-2,3,4,5-tetracarboxylate. The reaction of 2-mercapto-1-azaazulene with DMAD gave tetramethyl 4,4a-dihydro-4a-azabenz[*a*]azulene-1,2,3,4-tetracarboxylate in moderate yield. The reaction mechanisms of these reactions are discussed.

We have studied the cycloadditions of 1-azaazulenes with reactive acetylenes and found that the acetylenes first attaked the N-1 position of 1-azaazulenes and give dipolar intermediates.[1,2] As a continuation of our work, we have advanced the reaction to 2-hydroxy-, 2-amino-, and 2-mercapto-1-azaazulenes. It is known that 2-hydroxy-1-azaazulene is a tautomer of 1-azaazulen-2(1*H*)-one and reacts toward electrophile at the C-3 position as well as the N-1 position.[3-9] Therefore, it is expected that 2-hydroxy-1-azaazulene with reactive acetylenes undergoes another type of cycloaddition reaction. Therefore, we first investigated the reaction of 1-methyl-1-azaazulen-2(1*H*)-one[9] in order to understand the reaction of the keto-form.[10] We then investigated the reaction of 2-hydroxy-, 2-amino-, and 2-mercapto-1-azaazulenes.

A treatment of **1a** with dimethyl acetylenedicarboxylate (DMAD) in refluxing acetonitrile for 120 h gave dimethyl 1,2-azulenedicarboxylate[11,12] (**2a**) (9%), dimethyl 2-methyl-2,3-dihydro-3-oxocyclopent[*de*]-

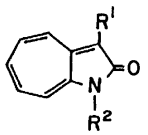

1a: R^1=H, R^2=Me
1b: R^1=CO_2Et, R^2=Me
1c: R^1=R^2=H
1d: R^1=CO_2Et, R^2=H
1e: R^1=CO_2Et, R^2=(*E*)-CCO_2Me=$CHCO_2$Me

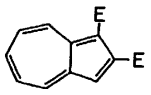

2a: E=CO_2Me
2b: E=COPh

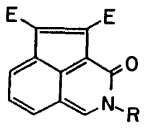

3a: R=Me, E=CO_2Me
3b: R=Me, E=COPh
3c: R=H, E=CO_2Me

4a: R=Me, E=CO_2Me
4b: R=Me, E=COPh
4c: R=H, E=CO_2Me

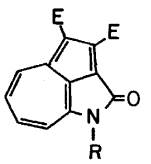

5a: R=Me, E=CO_2Me
5b: R=Me, E=COPh
5c: R=H, E=CO_2Me

6a: R=Me, E=CO_2Me
6b: R=Me, E=COPh
6c: R=H, E=CO_2Me

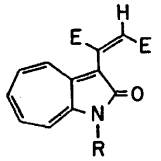

7a: R=Me, E=CO_2Me
7b: R=Me, E=COPh
7c: R=H, E=CO_2Me

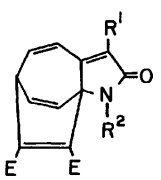

8a: R^1=H, R^2=Me, E=CO_2Me
8b: R^1=CO_2Et, R^2=Me, E=CO_2Me
8c: R^1=H, R^2=Me, E=COPh

isoquinoline-4,5-dicarboxylate (**3a**) (11%), dimethyl 1-methyl-1,2,2a,3-tetrahydro-2-oxo-1-azacyclopent[*cd*]-azulene-3,4-dicarboxylate (**4a**) (11%), dimethyl 1-methyl-1,2-dihydro-2-oxo-1-azacyclopent[*cd*]azulene-3,4-dicarboxylate (**5a**) (7%), dimethyl 1-methyl-1,2-dihydro-2-oxo-1-azaazulene-3-maleate (**6a**) (17%), and dimethyl 1-methyl-1,2-dihydro-2-oxo-1-azaazulene-3-fumarate (**7a**) (21%). These structures were determined on the basis of the spectroscopic data as well as on elemental analyses. Compound **3a** was a stable fused 3(2*H*)-isoquinolinone derivative. In its ^{1}H NMR spectrum, a signal of the 1H singlet assignable to H-1 can be seen at δ 8.73 , which is a reasonable value as 3(2*H*)-isoquinolinone.[13] In the ^{1}H NMR spectrum of **4a**, AB doublets can be seen at δ 3.10 and 4.32 (J=9.2 Hz), and in the ^{13}C NMR spectrum, two methine signals at δ 43.14 and 50.09. The dehydrogenation of **4a** by tetrachloro-*o*-benzoquinone (TCQ) gave **5a** in 47% yield. The result assists with the structure.

When the above reaction was carried out in refluxing *t*-butylbenzene for 3 h, compounds **2a** (21%), **3a** (5%), **5a** (0.8%), and dimethyl 6,8a-etheno-1-methyl-1,2-dihydro-2-oxocyclohepta[*b*]pyrrole-7,8-dicarboxylate (**8a**) (49%) were isolated. In the ^{13}C NMR spectrum of **8a**, signals assignable to sp^3 carbons can be seen at δ 38.70 (d, C-6) and 71.55 (s, C-8a), and in its ^{1}H NMR spectrum, methine proton can be observed at δ 4.46 (ddd, J=8.5, 6.7, and 1.2 Hz, H-6). Further evidence supporting the structure of **8a** is provided by its mass spectrum which displays an intense peak at m/z 159 (98%) associated with the loss of DMAD.

Ethyl 1-methyl-1,2-dihydro-2-oxo-1-azaazulene-3-carboxylate (**1b**) did not react with DMAD in refluxing benzene or acetonitrile, but gave **8b** (66%) in refluxing *t*-butylbenzene.

In a similar treatment, the reaction of **1a** with dibenzoylacetylene (DBA) in refluxing acetonitrile gave **2b** (9%), **3b** (3%), **4b** (50%), **5b** (6%), and **7b** (6%), and in refluxing *t*-butylbenzene **2b** (60%), **3b** (19%), and **8c** (15%). Dehydrogenation of **4b** with TCQ gave **5b** in a 70% yield.

The reaction of 1,2-dibenzoylazulene **2b** with hydrazine hydrate gave the corresponding pyridazino derivative **9**.

The reaction of 2-hydroxy-1-azaazulene with DMAD in refluxing acetonitrile gave **2a** (7%), **3c** (35%), **5c** (5%), **6c** (21%), and **7c** (30%). The result was similar to that of **1a**; it is therefore considered that 2-hydroxy-1-azaazulene behaved as 1-azaazulen-2(1*H*)-one (**1c**). The observation that compound **1b** exists in exactly the keto form in the ^{1}H NMR spectrum in $CDCl_3$ is in agreement with the above consideration. The structures obtained from the above reaction were assigned on the basis of spectroscopic data as well as on elemental analyses.

Compound **3c** was acetylated with acetic anhydride to give **10**. In the IR spectrum of **10**, three ester carbonyl signals were observed at 1756, 1730, and 1700 cm^{-1}, whereas the amide carbonyl signal was not. We therefore assigned **10** as an *O*-acetylated compound. In the ^{1}H NMR spectrum of **10**, an H-1 proton was observed at δ 8.92. The ^{1}H NMR spectrum of **3c** in DMSO-d_6 shows a signal of H-1 at δ 8.91, which is

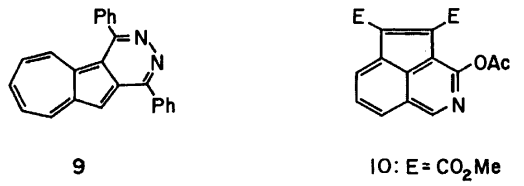

9

10: E = CO_2Me

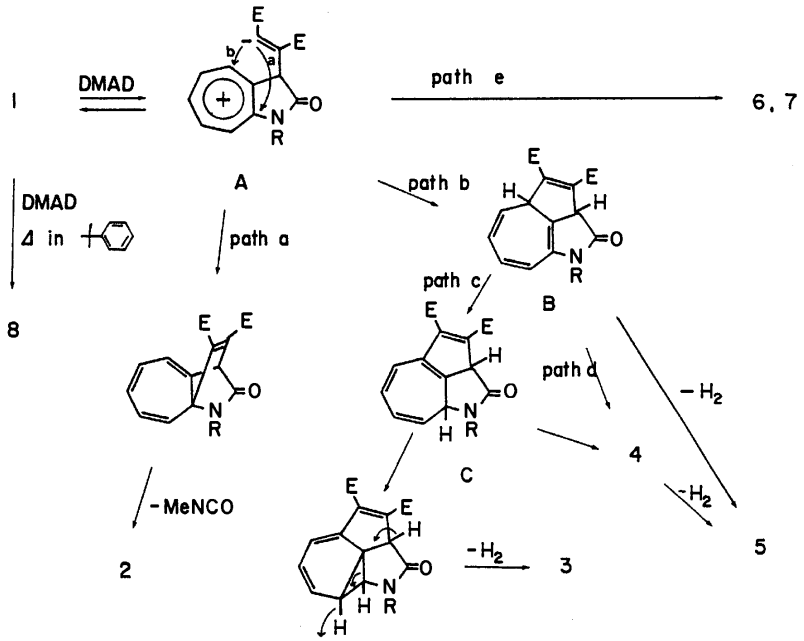

Scheme 1.

comparable with that of **10**. Therefore, we considered that compound **3c** would exist in an enol form in DMSO-d_6.

Previously, we reported that ethyl 1,2-dihydro-2-oxo-1-azaazulene-3-carboxylate (**1d**) reacted with DMAD to give **1e**.[2] Different from this, the corresponding fumarate was not obtained upon the reaction of **1c**. This result suggested that the C-3 position of **1c** is more reactive than the N-1 position.

A plausible mechanism is shown in Scheme 1. When DMAD attacks the C-3 position of **1**, which is a reactive site towards electrophile, a dipolar species **A** should be produced. A cyclization on the C-8a position of **A** and a successive elimination of MeNCO furnishes **2** (path a). A cyclization on the C-4 position of **A** gives **B** (path b), and several successive 1,5-hydrogen shifts of **B** produces **C** (path c) and **4** (path d). Dehydrogenation of **B** and/or **4** affords **5**. A tautomerization of **C** and a subsequent dehydrogenation leads to **3** (path c). A protonation and aromatization of **A** gave Michael adducts **6** and **7** (path e). Through a reaction at a higher temperature a Diels-Alder reaction occurs on a seven-membered ring and **8** is produced, in addition to the cycloaddition-cycloreversion product **2**. It is considered that the activation energy of the formation of **8** is higher than that of **A**. Consequently, compound **A** is favorably produced at lower temperatures. A similar periselectivity dependence on the temperature is known regarding the reaction of 5-azaazulene with reactive acetylenes.[14]

The treatment of 2-amino-1-azaazulene (**11**) with DMAD in refluxing acetonitrile for 5 h gave methyl 2,4a-dihydro-2-oxo-1,4a-diazabenz[*a*]azulene-4-carboxylate (**12**) and tetramethyl 4,5-dihydro-1*H*-1,11-diazacyclohept[*a*]azulene-2,3,4,5-tetracarboxylate (**13**) in 18.5% and 19% yield, respectively. These structures were assigned on the basis of the spectroscopic data as well as elemental analyses. The ^{1}H NMR spectrum of **12** shows protons at δ 4.04 (s, Me), 7.09 (s, H-10), 7.19 (s, H-3), 7.25—7.45 (m, H-6, 7, and 8), 7.94 (d, J=10.4 Hz, H-9), and 9.84—9.96 (H-5). In the ^{1}H NMR of 4-oxo compound **14**,[15] proton at C-5 was observed at δ 10.05—10.30. Different from the 4-oxo compound, deesterification of **12** gave no distinct compound. We therefore assigned **12** as being a 2-oxo compound. The ^{1}H NMR spectrum of **13** showed a pair of AB doublets (J=4.9 Hz) at δ 4.97 and 5.21. In its ^{13}C NMR spectrum, sp^3 carbon appeared at δ 43.47 (d) and 45.43 (d).

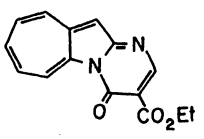

14

A plausible mechanism is shown in Scheme 2. When DMAD attacks the N-1 position of amino-form **11**, compound **12** should be produced. An attack of DMAD at the C-3 position of imino-form **11A** and a successive reaction of another molecule of DMAD furnishes **13**. In the ^{1}H NMR spectrum of **11** in $CDCl_3$, equilibrium (80% of **11**, 20% of **11A**) was observed.

The treatment of 2-mercapto-1-azaazulene (**15**) with DMAD in refluxing acetonitrile for 17 h gave a complex mixture and only **16** was isolated in 38% yield. Compound **16** was analyzed as $C_{21}H_{19}NO_8$ from HRMS and elemental analysis, and assigned as tetramethyl 4,4a-dihydro-4a-azabenz[*a*]azulene-1,2,3,4-tetracarboxylate. The ^{1}H NMR spectrum of **16** shows protons at δ 6.41 (s, H-4), 7.10—7.20 (m, H-6, 7, 8, and 9), 7.45 (s, H-10), and 7.63 (d, J=11.0 Hz, H-5), in addition of four methyl singlets. In its ^{13}C NMR spectrum, one sp^3 carbon was observed at δ 54.74 (d).

A plausible mechanism is shown in Scheme 3. In the ^{1}H NMR spectrum of **15** in $CDCl_3$, a predominant existance of the thione form **15A** (over 95%) was observed. This suggests that the reaction of **15A** with DMAD (considered as soft electrophile) would first occur on sulfur, which is a most soft atom, and gives 1-azaazulene **D**. A second molecule of DMAD attacks

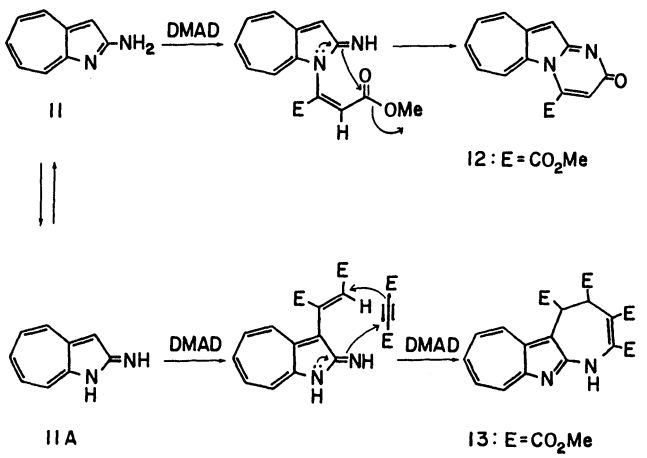

Scheme 2.

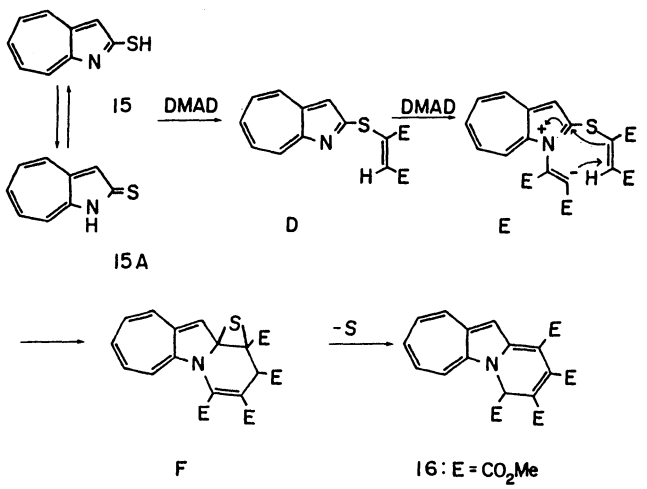

Scheme 3.

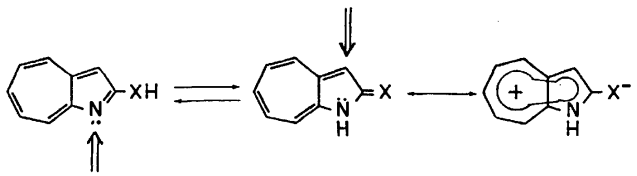

G H I

the N-1 position of **D** and gives a dipolar intermediate **E**. A cyclization of **E** affords **F**, and a desulfurization of **F** furnishes **16**.

All these results show that DMAD first attacks the N-1 position of the 1-azaazulene form **G**, whereas DMAD first attacks the C-3 position or soft atom of 1,2-dihydro-1-azaazulen-2-ylidene form **H**. The reason for the difference in the reaction is considered to be as follows. In form **G**, the N-1 atom is most electron rich,[16] and a lone pair on nitrogen would have more nucleophilicity than C-3 carbon. On the other hand, in form **H**, the nucleophilicity of a lone pair on nitrogen would decrease owing to the contribution to the 10-π aromatic resonance as form **I**. The observation that the reaction occures on the N-1 position (**1d**) or not at all (**1b**) at lower temperatures, whereas the Diels-Alder reaction on seven membered ring is predominant at higher temperature (**1b**), when 3-position is blocked in form **H**, assists in the above consideration.

Experimental

Melting points are uncorrected. ^{1}H NMR sapctra (250 MHz) and ^{13}C NMR spectra (62.87 MHz) were recorded on a Hitachi R-250H spectrometer using deuteriochloroform as a solvent with tetramethylsilane as an internal standard, unless otherwise stated. IR spectra were recorded on a Hitachi 270-50 infrared spectrophotometer for Nujol mulls. Mass spectra were determined with a JEOL JMS-01SG-2 spectrometer (70 eV). Kieselgel 60 was used for column chromatography unless otherwise stated.

Reaction of 1 with DMAD. a) A solution of **1a** (0.510 g) and DMAD (1.367 g) in dry acetonitrile (30 ml) was refluxed for 120 h and evaporated. The residue was chromatographed. Elution with benzene gave **2a** (0.072 g, 9%), which was recrystallized from hexane to give violet needles, mp 53—54 °C (lit,[12] mp 45 °C, lit,[11] oil); ^{1}H NMR δ=3.96 (3H, s, OMe), 3.99 (3H, s, OMe), 7.48 (1H, s, H-3), 7.48 (1H, t, J=9.8 Hz, H-5), 7.57 (1H, t, J=9.8 Hz, H-7), 7.87 (1H, t, J=9.8 Hz, H-6), 8.50 (1H, d, J=9.8 Hz, H-4), and 9.44 (1H, d, J=9.8 Hz, H-8); IR 1732 and 1698 cm^{-1} (ester C=O); MS m/z (rel intensity) 244 (M$^+$; 81), 213 (100), 186 (11), 183 (14), 127 (14), and 126 (10); Anal. ($C_{14}H_{12}O_4$) C, H. Elution with benzene–chloroform (4 : 1) gave a 1 : 1-mixture (from the integration of the ^{1}H NMR) of **3a** and **4a** (0.216 g, 22%). Fractional recrystallization of the mixture from cyclohexane gave **3a** [0.055 g, yellow needles, mp 168—169 °C, ^{1}H NMR δ=3.40 (3H, s, NMe), 3.99 (3H, s, OMe), 4.11 (3H, s, OMe), 6.95 (1H, dd, J=6.1 and 1.2 Hz, H-6), 7.45—7.60 (2H, m, H-7 and 8), and 8.73 (1H, s, H-1); ^{13}C NMR δ=26.36 (q), 52.84 (q), 53.08 (q), 106.85 (d), 120.59 (d), 123.86 (s), 126.08 (s), 127.81 (s), 127.99 (s), 130.21 (d), 130.50 (s), 134.04 (d), 139.85 (s), 165.30 (s), 165.38 (s), and 166.64 (s); IR 1738, 1722, and 1700 (ester C=O), 1638 (amide C=O), and 795 cm^{-1} (1,2,3-trisubstituted benzene); MS m/z (rel intensity) 299 (M$^+$; 100), 268 (62), 196 (16), 183 (39), 182 (21), 181 (26), 127 (13); Anal. ($C_{16}H_{13}NO_5$) C, H, N.] and **4a** [0.030 g, yellow prisms, mp 151—152 °C, ^{1}H NMR δ=3.08 (3H, s, NMe), 3.10 (1H, d, J=9.2 Hz, H-2a), 3.86 (3H, s, OMe), 3.88 (3H, s, OMe), 4.32 (1H, d, J=9.2 Hz, H-3), 5.66 (1H, d, J=6.1 Hz, H-8), 6.40—6.50 (2H, m, H-5 and 6), and 6.65—6.75 (1H, m, H-7); ^{13}C NMR δ=27.14 (q), 43.14 (d), 50.09 (d), 52.33 (q), 52.55 (q), 98.33 (d), 122.19 (d), 124.69 (d), 124.75 (s), 130.83 (s), 131.29 (d), 134.43 (s), 134.68 (s), 162.86 (s), 164.40 (s), and 170.73 (s); MS m/z (rel intensity) 301 (M$^+$; 100), 241 (26), 210 (26), 200 (26), 154 (11), 140 (13), 127 (12), 115 (10), and 114 (11); IR 1720 and 1706 (ester C=O), and 1628 cm^{-1} (amide C=O); Anal. ($C_{16}H_{15}NO_5$) C, H, N.]. Elution with chloroform gave **5a** (0.065 g, 7%), which was recrystallized from cyclohexane-dichloromethane to give red needles, mp 190—191 °C, ^{1}H NMR δ=3.52 (3H, s, NMe), 3.94 (3H, s, OMe), 4.05 (3H, s, OMe), 7.48 (1H, d, J=9.8 Hz, H-8), 7.72 (1H, t, J=9.8 Hz, H-6), 8.15 (1H, t, J=9.8 Hz, H-7), and 9.16 (1H, d, J=9.8 Hz, H-5); ^{13}C NMR δ=26.55 (q), 51.67 (q), 52.72 (q), 113.74 (d), 114.03 (s), 115.22 (s), 128.29 (d), 135.17 (s), 137.11 (s), 138.93 (s), 140.87 (d), 141.40 (d), 149.96 (s), 162.79 (s), 164.23 (s), and 167.63 (s); IR 1734, 1708, and 1700 (ester C=O), and 1620 cm^{-1} (amide C=O); MS m/z (rel intensity) 299 (M$^+$; 35), 268 (76), 240 (22), 238 (22), 210 (36), 209 (39), 196 (47), 182 (40), 153 (51), 152 (50), 126 (100), 114 (75). Anal. ($C_{16}H_{13}NO_5$) C, H, N. Further elution gave **6a** (0.164 g, 17%), which was recrystallized from cyclohexane–dichloromethane to give red prisms, mp 123.5—124 °C, ^{1}H NMR δ=3.58 (3H, s, NMe), 3.79 (3H, s, OMe), 3.96 (3H, s, OMe), 7.00 (1H, s, H-vinyl), 7.05—7.40 (4H, m, H-5, 6, 7, and 8), and 7.76 (1H, d, J=11.0 Hz, H-4); IR 1715 and 1656 (ester C=O), and 1620 cm^{-1} (amide C=O); Anal. ($C_{16}H_{13}NO_5$) C, H, N. Elution with chloroform–ethyl acetate (1 : 1) gave **7a** (0.206 g, 21%), which was recrystallized from cyclohexane–dichloromethane to give red prisms, mp 150—151 °C, ^{1}H NMR δ=3.58 (3H, s, NMe), 3.68 (3H, s, OMe), 3.81 (3H, s, OMe), 6.90—7.30 (5H, m, H-4, 5, 6, 7, and 8), and 7.15 (1H, s, H-vinyl), IR 1728 and 1672 (ester C=O), and 1630 cm^{-1} (amide C=O); Anal. ($C_{16}H_{15}NO_5$) C, H, N.

b) A solution of **1a** (0.200 g), and DMAD (0.536 g) in t-butylbenzene (6 ml) was refluxed for 3 h and evaporated. The residue was chromatographed. Elution with benzene gave **2a** (0.064 g, 21%). Elution with benzene–chloroform (1 : 1) gave **3a** (0.019 g, 5%) and **5a** (0.003 g, 0.8%), successively. Elution with chloroform gave **8a** (0.185 g, 49%), which was recrystallized from cyclohexane to give colorless scales, mp 156—158 °C, ^{1}H NMR δ=3.05 (3H, s, NMe), 3.77 (3H, s, OMe), 3.78 (3H, s, OMe), 4.46 (1H, ddd, J=8.5, 6.7, and 1.2 Hz, H-6), 5.95 (1H, s, H-3), 6.06 (1H, d, J=10.4 Hz, H-4), 6.21 (1H, dd, J=7.9 and 1.2 Hz, H-9), 6.41 (1H, dd, J=10.4 and 8.5 Hz, H-5), and 6.66 (1H, dd, J=7.9 and 6.7 Hz, H-10); ^{13}C NMR δ=26.47 (q), 38.70 (d), 52.64 (q×2), 71.55 (s), 120.57 (d), 121.16 (d), 129.47 (d), 132.62 (d), 133.26 (d), 134.23 (s), 145.64 (s), 147.03 (s), 163.07 (s), 164.95 (s), and 171.28 (s); IR 1735, 1720, and 1688 (ester C=O), and 1622 (amide C=O); MS m/z (rel intensity) 301 (M$^+$; 100), 270 (19), 269 (13), 242 (88), 241 (35), 210 (45), 198 (16), 183 (47), 159 (98), 154 (26), 130 (16), and 127 (12); Anal. ($C_{16}H_{15}NO_5$) C, H, N.

c) A mixture of **1b** (0.075 g) and DMAD (0.1 g) in t-butylbenzene (5 ml) was refuxed for 7 h and evaporated. The

residue was chromatographed with chloroform to give **8b** (0.08 g, 66%), which was recrystallized from hexane to give colorless prisms, mp 99—101 °C, ^{1}H NMR δ=1.36 (3H, t, J=7.0 Hz, Me), 3.06 (3H, s, NMe), 3.77 (3H, s, OMe), 3.78 (3H, s, OMe), 4.34 (2H, q, J=7.0 Hz, OCH_2), 4.57 (1H, ddd, J=7.9, 6.7, and 1.2 Hz, H-6), 6.23 (1H, dd, J=7.9 and 1.2 Hz, H-9), 6.69 (1H, dd, J=11.0 and 7.9 Hz, H-5), 6.78 (1H, dd, J=7.9 and 6.7 Hz, H-10), and 6.84 (1H, d, J=11.0 HZ, H-4); IR 1748, 1720, and 1710 (ester C=O), and 1688 cm^{-1} (amide C=O); Anal. ($C_{19}H_{19}NO_7$) C, H, N.

d) A solution of **1c** (0.250 g) and DMAD (0.75 g) in dry acetonitrile (30 ml) was refluxed for 45 h and evaporated. The residue was chromatographed. Elution with benzene gave **2a** (0.029 g, 7%). Elution with chloroform gave **3c** (0.180 g, 35%), which was recrystallized from cyclohexane-dichloromethane to give orange prisms, mp 176—178 °C, ^{1}H NMR δ=4.00 (3H, s, OMe), 4.12 (3H, s, OMe), 7.11 (1H, d, J=6.7 Hz, H-6), 7.56 (1H, dd, J=7.9 and 6.7 Hz, H-7), 7.63 (1H, d, J=7.9 Hz, H-8), 8.59 (1H, bs, exch., OH), and 8.81 (1H, s, H-1). δ (DMSO-d_6)=3.93 (6H, s, OMe×2), 7.15 (1H, d, J=6.7 Hz, H-6), 7.64 (1H, dd, J=8.5 and 6.7 Hz, H-7), 7.79 (1H, d, J=8.5 Hz, H-8), 8.91 (1H, s, H-1), and 11.13 (1H, s, exch., OH); IR 3188 (OH), 1750, 1722, and 1702 (ester C=O), 1638 (amide C=O), and 795 cm^{-1} (1,2,3-trisubstituted benzene); Anal. ($C_{15}H_{11}NO_5$) C, H, N. Further elution gave **5c** (0.026 g, 5%), which was recrystallized from cyclohexane-dichloromethane to give orange needles, mp 250—251 °C, ^{1}H NMR δ (DMSO-d_6)=3.86 (3H, s, OMe), 3.90 (3H, s, OMe), 7.72 (1H, d, J=9.8 Hz, H-8), 7.90 (1H, t, J=9.8 Hz, H-6), 8.37 (1H, t, J=9.8 Hz, H-7), 9.08 (1H, d, J=9.8 HZ, H-5), and 11.48 (1H, s, exch., NH); IR 3284 (NH), 1730, 1704, and 1684 (ester C=O), and 1625 cm^{-1} (amide C=O); MS Found: m/z 285.0617. Calcd for $C_{15}H_{11}NO_5$: M, 285.0638. Elution with chloroform-ethyl acetate gave **6c** (0.106 g, 21%), which was recrystallized from cyclohexane-dichloromethane to give red micro needles, mp 248—249 °C, ^{1}H NMR δ=3.80 (3H, s, OMe), 3.98 (3H, s, OMe), 7.05 (1H, s, H-vinyl), 7.10 (1H, dd, J=11.5 and 9.5 Hz, H-5), 7.30—7.42 (3H, m, H-6, 7, and 8), 7.80 (1H, d, J=11.5 Hz, H-4), and 11.27 (1H, s, exch., NH), δ (DMSO-d_6)=3.70 (3H, s, OMe), 3.86 (3H, s, OMe), 7.03 (1H, s, H-vinyl), 7.22 (1H, dd, J=11.6 and 9.8 Hz, H-5), 7.30—7.50 (3H, m, H-6, 7, and 8), 7.60 (1H, d, J=11.6 Hz, H-4), and 12.20 (1H, s, exch., NH); IR 3100—2600 (broad, NH), 1736 and 1704 (ester C=O), and 1652 cm^{-1} (amide C=O); Anal. ($C_{15}H_{13}NO_5$) C, H, N. Elution with ethyl acetate gave **7c** (0.150 g, 30%), which was recrystallized from cyclohexane-dichloromethane to give orange needles, mp 165—167 °C, ^{1}H NMR δ=3.67 (3H, s, OMe), 3.82 (3H, s, OMe), 7.03 (1H, dd, J=9.16 and 9.14 Hz, H-5), 7.10—7.32 (3H, m, H-6, 7, and 8), 7.19 (1H, s, H-vinyl), 7.35 (1H, d, J=9.16 Hz, H-4), and 12.43 (1H, s, exch., NH); IR 3150—2600 (broad, NH), 1730 (ester C=O), and 1644 cm^{-1} (amide C=O); Anal. ($C_{15}H_{13}NO_5$) C, H, N.

Reaction of 1 with DBA. a) A solution of **1a** (0.461 g) and DBA (1.357 g) in dry acetonitrile (30 ml) was refluxed for 72 h and evaporated. The residue was chromatographed. Elution with benzene gave **2b** (0.083 g, 8.5%), which was recrystallized from hexane to give blue prisms, mp 133—134 °C, ^{1}H NMR δ=7.10—7.52 (11H, m, H-5 and phenyl×2), 7.54 (1H, dd, J=10.4 and 9.8 Hz, H-7), 7.63 (1H, s, H-3), 7.89 (1H, dd, J=10.4 and 9.8 Hz, H-6), 8.60 (1H, d, J=9.8 Hz, H-4), and 9.19 (1H, d, J=10.4 Hz, H-8); IR 1670 cm^{-1} (C=O); Anal. ($C_{24}H_{16}O_2$) C, H. Elution with benzene-chloroform (1 : 1) gave **3b** (0.037 g, 3%), which was recrystallized from cyclohexane-dichloromethane to give yellow prisms, mp 204—205 °C, ^{1}H NMR δ=3.67 (3H, s, NMe), 7.03 (1H, dd, J=5.5 and 2.5 Hz, H-6), 7.4—7.7 (8H, m, H-7, 8, and m,p-phenyl×2), 7.83 (2H, d, J=7.3 Hz, H-o-phenyl), 7.88 (2H, d, J=7.3 Hz, H-o-phenyl), and 8.30 (1H, s, H-1); IR 1700, 1672, and 1652 (C=O), and 1632 cm^{-1} (amide C=O); Anal ($C_{26}H_{17}NO_3$) C, H, N. Further elution gave **4b** (0.568 g, 50%), which was recrystallized from cyclohexane to give orange micro needles, mp 100—102 °C, ^{1}H NMR δ=3.13 (3H, s, NMe), 3.32 (1H, bd, J=9.2 Hz, H-2a), 4.92 (1H, d, J=9.2 Hz, H-3), 5.73 (1H, bd, J=6.1 Hz, H-8), 6.35—6.45 (2H, m, H-5 and 6), 6.72 (1H, dd, J=9.8 and 6.1 Hz, H-7), 7.05—7.52 (10 H, m, phenyl×2); IR 1716 and 1662 (C=O), and 1638 cm^{-1} (amide C=O); Anal. ($C_{26}H_{19}NO_3$) C, H, N. Elution with chloroform gave **5b** (0.063 g, 6%), which was recrystallized from cyclohexane-dichloromethane to give red needles, mp 246—247 °C, ^{1}H NMR δ=3.55 (3H, s, NMe), 7.05—7.52 (8H, m, phenyl), 7.53 (1H, d, J=9.8 Hz, H-8), 7.61 (2H, d, J=7.3 Hz, H-o-phenyl), 7.74 (1H, t, J=9.8 Hz, H-6), 8.20 (1H, t, J=9.8 Hz, H-7), and 8.96 (1H, d, J=9.8 Hz, H-5); IR 1718 and 1654 (C=O) and 1624 cm^{-1} (amide C=O); Anal. ($C_{26}H_{17}NO_3$) C, H, N. Further elution gave **7b** (0.064 g, 6%), which was recrystallized from cyclohexane-dichloromethane to give red prisms, mp 201—203 °C, ^{1}H NMR δ=3.66 (3H, s, NMe), 7.00—7.20 (3H, m, H-5, 6, and 7), 7.30—7.60 (7H, m, H-8 and m,p-phenyl ×2), 7.88 (1H, d, J=11.0 Hz, H-4), 8.04 (2H, d, J=6.7 Hz, H-o-phenyl), 8.07 (2H, d, J=6.7 Hz, H-o-phenyl), and 8.59 (1H, s, H-vinyl); IR 1664 (C=O) and 1638 cm^{-1} (amide C=O); Anal. ($C_{26}H_{19}NO_3$) C, H, N.

b) A solution of **1a** (0.200 g) and DBA (1.472 g) in t-butylbenzene (10 ml) was refluxed for 1 h and evaporated. The residue was chromatographed. Elution with benzene gave recovered DBA (0.884 g) and **2b** (0.638 g, 60%). Elution with benzene-chloroform (1 : 1) gave **3b** (0.231 g, 19%). Elution with chloroform gave **8c** (0.188 g, 15%), which recrystallized from cyclohexane to give colorless prisms, mp 174—174.5 °C, ^{1}H NMR δ=2.88 (3H, s, NMe), 4.42 (1H, ddd, J=8.5, 6.7, and 1.2 Hz, H-6), 6.02 (1H, s, H-3), 6.29 (1H, d, J=10.4 Hz, H-4), 6.36 (1H, dd, J=7.9 and 1.2 Hz, H-9), 6.48 (1H, dd, J=10.4 and 8.5 Hz, H-5), 6.86 (1H, dd, J=7.9 and 6.7 Hz, H-10), and 7.14—7.50 (10H, m, phenyl ×2); IR 1688 and 1662 (C=O), and 1646 cm^{-1} (amide C=O); Anal. ($C_{26}H_{19}NO_3$) C, H, N.

Dehydrogenation of 4. a) A mixture of **4a** (0.030 g) and TCQ (0.080 g) in dry benzene (20 ml) was refluxed for 2 h and evaporated. The residue was chromatographed on alumina. Elution with chloroform gave **5a** (0.014 g, 47%).

b) A mixture of **4b** (0.440 g) and TCQ (1.200 g) in dry benzene (50 ml) was refluxed for 1 h and evaporated. The residue was chromatographed on alumina with chloroform to give **5b** (0.308 g, 70%).

Synthesis of 9. A solution of **2b** (0.184 g) and 80% hydrazine hydrate (1 ml) in ethanol (20 ml) was refluxed for 30 min and evaporated. The residue was chromatographed with chloroform to give **9** (0.081 g, 45%), which was recrystallized from cyclohexane-dichloromethane to give blue prisms, mp >300 °C, ^{1}H NMR δ=7.14 (1H, dd, J=1.0 and 7.9 Hz, H-6), 7.31 (1H, dd, J=9.8 and 8.6 Hz, H-8), 7.55—7.70 (7H, m, H-7 and m,p-phenyl ×2), 7.74 (1H, s, H-10), 7.80—7.88 (2H, m, H-o-phenyl), 8.15—8.21 (2H, m, H-o-phenyl), 8.40 (1H, d, J=9.8 Hz, H-9), and 8.44 (1H, d, J=7.9 Hz, H-5); IR no carbonyl absorption; MS m/z (rel intensity) 332 (M^+; 100), 331 (64), 302 (91), 300 (50), 276 (52), 226 (52), 202 (24), 200

(25), 151 (57), 150 (50), 138 (41), 126 (28), and 77 (71); Anal. ($C_{24}H_{16}N_2$) C, H, N.

Acetylation of 3c. A mixture of **3c** (0.080 g), acetic anhydride (10 ml), and conc. sulfuric acid (1 drop) was refluxed for 1 h and poured into water (100 ml). The mixture was neutralized with sodium hydrogencarbonate, extracted with chloroform, washed with water, dried over sodium sulfate, and evaporated. The residue was recrystallized from cyclohexane to give **10** (0.035 g, 38%) as yellow prisms, mp 174—176 °C, ^{1}H NMR δ=2.80 (3H, s, Me), 4.01 (3H, s, OMe), 4.13 (3H, s, OMe), 7.71 (1H, dd, J=8.6 and 6.7 Hz, H-7), 7.83 (1H, d, J=8.6 Hz, H-8), 8.32 (1H, d, J=6.7 Hz, H-6), and 8.92 (1H, s, H-1); IR 1756, 1730, and 1700 cm^{-1} (ester C=O). HRMS Found: m/z 327.0750. Calcd for $C_{17}H_{13}NO_6$: M, 327.0744.

Reaction of 2-Amino-1-azaazulene with DMAD. A solution of **11** (0.577 g) and DMAD (0.85 g) in acetonitrile (50 ml) was refluxed for 5 h and evaporated. The residue was chromatographed. Elution with chloroform gave **12** (0.188 g, 18.5%), which was recrystallized from cyclohexane-dichloromethane to give violet needles, mp 223—225 °C, ^{1}H NMR δ=4.04 (3H, s, OMe), 7.09 (1H, s, H-10), 7.19 (1H, s, H-3), 7.25—7.45 (3H, m, H-6, 7, and 8), 7.94 (1H, d, J=10.4 Hz, H-9), and 9.84—9.96 (1H, m, H-5); Anal. ($C_{14}H_{10}N_2O_3$) C, H, N. Elution with chloroform-ethyl acetate (1 : 1) gave **13** (0.325 g, 19%), which was recrystallized from ethyl acetate to give orange prisms, mp 182—183 °C, ^{1}H NMR δ=3.45, 3.61, 3.63, and 3.79 (each 3H, s, OMe), 4.97 (1H, d, J=4.9 Hz, H-4), 5.21 (1H, d, J=4.9 Hz, H-5), 7.60—7.80 (3H, m, H-7, 8, and 9), 8.12 (1H, bs, NH, exch.), and 8.20—8.38 (2H, m, H-6 and 10); ^{13}C NMR δ=43.47 (d), 45.43 (d), 52.38 (q), 52.49 (q×2), 52.75 (q), 105.64 (s), 106.37 (s), 128.74 (d), 129.83 (d), 130.85 (d), 131.77 (d), 134.04 (d), 139.79 (s), 145.84 (s), 156.02 (s), 159.08 (s), 165.20 (s), 167.71 (s), 169.81 (s), and 170.84 (s); IR 3230 (NH), 1750, 1740, 1730, and 1704 cm^{-1} (ester C=O); Anal. ($C_{21}H_{20}N_2O_8$) C, H, N.

Reaction of 2-Mercapto-1-azaazulene with DMAD. A mixture of **15** (0.350 g), DMAD (0.82 g), and acetonitrile (50 ml) was refluxed for 5 h, then evaporated. The residue was chromatographed. Elution with chloroform gave **16** (0.347 g, 35%), which was recrystallized from cyclohexane to give violet needles, mp 188—189 °C, ^{1}H NMR δ=3.64, 3.81, 3.83, 3.96 (each 3H, s, OMe), 6.41 (1H, s, H-4), 7.10—7.20 (4H, m, H-6, 7, 8, and 9), 7.45 (1H, s, H-10), and 7.63 (1H, d, J=11.0 Hz, H-5); ^{13}C NMR δ=51.16 (q), 52.03 (q), 52.38 (q), 53.03 (q), 54.74 (d), 91.40 (s), 101.02 (s), 110.71 (d), 115.76 (d), 131.50 (d), 132.13 (d), 132.60 (d), 133.04 (d), 142.73 (s), 143.65 (s), 146.39 (s), 152.22 (s), 164.23 (s), 164.94 (s), 167.52 (s), and 168.53 (s); IR 1740, 1690, 1676, and 1665 cm^{-1} (ester C=O); MS m/z (rel intensity) 413 (M^+; 2), 412 (7), 382 (5), 354 (100), and 178 (6). Found: C, 60.53; H, 4.58; N, 3.16%. Calcd for $C_{21}H_{19}NO_8$: C, 61.02; H, 4.63; N, 3.39%. HRMS Found: m/z 413.1109. Calcd for $C_{21}H_{19}NO_8$: M, 413.1109.

We thank Dr. Masafumi Yasunami (Tohoku University) and Dr. Akira Mori (Kyushu University) for the measurements of the mass spectra and elemental analyses.

References

1) N. Abe, Y. Tanaka, and T. Nishiwaki, *J. Chem. Soc., Perkin Trans. 1*, **1978**, 429.
2) N. Abe and T. Nishiwaki, *Bull. Chem. Soc. Jpn.*, **54**, 1277 (1981).
3) T. Nozoe, S. Seto, S. Matsumura, and T. Terasawa, *Chem. Ind.*, **1954**, 1356.
4) H. Nakao, N. Soma, Y. Sato, and G. Sunagawa, *Chem. Pharm. Bull.*, **13**, 473 (1985).
5) T. Toda, S. Seto, and T. Nozoe, *Bull. Chem. Soc. Jpn.*, **41**, 2102 (1968).
6) T. Toda, *Bull. Chem. Soc. Jpn.*, **40**, 590 (1967).
7) A. Sato, S. Nozoe, T. Toda, S. Seto, and T. Nozoe, *Bull. Chem. Soc. Jpn.*, **46**, 3530 (1973).
8) T. Toda, S. Ryu, Y. Hagiwara, and T. Nozoe, *Bull. Chem. Soc. Jpn.*, **48**, 82 (1975).
9) C.-R. Wu and P.-W. Yang, *Hua Hsueh*, **1977**, 45.
10) Preliminary report: N. Abe and T. Takehiro, *Heterocycles*, **26**, 1727 (1987).
11) W. von E. Doering and D. W. Wiely, *Tetrahedron*, **11**, 183 (1960).
12) I. Kawamoto, Y. Sugimura, N. Soma, and Y. Kishida, *Chem. Lett.*, **1972**, 931.
13) H. Fukumi and H. Kurihara, *Heterocycles*, **9**, 1197 (1978).
14) K. Hafner and J. Haring, *Erdoel Kohle, Erdgas, Petrochem.*, **32**, 136 (1979).
15) N. Abe, *Bull. Chem. Soc. Jpn.*, **60**, 1053 (1987).
16) H. Kon, *Sci. Rept. Tohoku Univ., Ser. I*, **38**, 67 (1954).

 © 1988 The Chemical Society of Japan Bull. Chem. Soc. Jpn., 61, 1231—1235 (1988)

Synthesis of Substituted 1,3-Dienes by the Reaction of Alkenesulfonyl Chlorides with Olefins Catalyzed by a Ruthenium(II) Complex

Masayuki KAMEYAMA, Hiroshi SHIMEZAWA, Takeshi SATOH, and Nobumasa KAMIGATA*
Department of Chemistry, Faculty of Science, Tokyo Metropolitan University, Fukazawa, Setagaya-ku, Tokyo 158
(Received August 31, 1987)

Alkenesulfonyl chlorides reacted with vinylarenes in the presence of a catalytic amount of dichlorotris(triphenylphosphine)ruthenium(II) to give substituted 1 : 1 adducts, which were dehydrochlorinated and desulfonylated successively to form substituted (*E,E*)-1,3-dienes in good yield.

We have previously reported that the reaction of alkane- and arenesulfonyl chlorides with olefins catalyzed by dichlorotris(triphenylphosphine)ruthenium(II) (**1**) under mild conditions affords 1 : 1 adducts in high yield.[1] We recently found that alkenesulfonyl chlorides reacted with olefins in the presence of the ruthenium(II) catalyst **1** to form 1 : 1 adducts, which were dehydrochlorinated and desulfonylated successively by raising the reaction temperature from 80 to 150 °C to give (*E,E*)-1,4-diaryl-1,3-butadienes in high yield.[2,3] However, these reactions were limited to the formation of 1,3-butadienes substituted with aryl groups at the 1- and 4-positions. Here, we report on the formation of substituted 1,3-dienes by the reaction of alkenesulfonyl chlorides with styrenes catalyzed by the ruthenium(II) complex **1**.

The reaction of (*E*)-2-phenyl-1-propene-1-sulfonyl chloride (**2b**) with styrene was carried out in benzene, in the presence of a catalytic amount of dichlorotris(triphenylphosphine)ruthenium(II) (**1**), by heating the reaction mixture at 80 °C under a nitrogen atmosphere to give 1 : 1 adduct **3d** in 89% yield. Similarly, (*E*)-2-phenylethene-, (*E*)-2-phenyl-1-propene-1-, and (*E*)-1-phenyl-1-propene-2-sulfonyl chloride (**2a—c**) were added to substituted vinylarenes using **1** as a catalyst at 80—100 °C to afford 1 : 1 adducts **3** in high yield. The results are summarized in Table 1. Thus, the ruthenium(II)-phosphine catalyzed addition reaction of styrenesulfonyl chlorides possessing methyl group at α- and β-position (**2b** and **2c**) to α- and β-methylstyrenes was found to give 1 : 1 adducts in good yield.

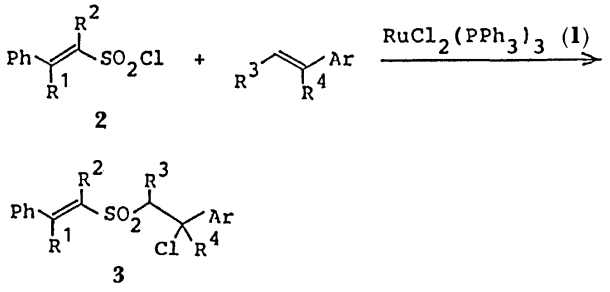

The reaction of (*E*)-2-phenyl-1-propene-1-sulfonyl-chloride with styrene catalyzed by **1** was also carried out in benzene upon raising the reaction temperature from 80 to 150 °C, to give unsymmetrical 1,4-diphenyl-1,3-pentadiene (**4b**) in 51% yield. Similarly, several alkenesulfonyl chlorides **2a—c** were reacted with substituted vinylarenes in order to study the scope and limitation of the formation of substituted 1,3-dienes. The results are summarized in Table 2.

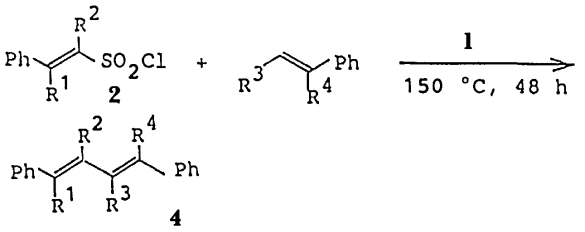

We have previously reported that the reaction of (*E*)-2-phenylethenesulfonyl chloride with *p*-methylstyrene catalyzed by **1** proceeds successively via an addition, dehydrochlorination, and desulfonylation to give (*E*)-2-chloro(*p*-tolyl)ethyl styryl sulfone, (*E,E*)-*p*-methylstyryl sulfone, and (*E,E*)-1-phenyl-4-(*p*-tolyl)-1,3-butadiene, respectively, by studying the time course. Moreover, it was also found that a ruthenium(II) catalyst was effected in each of the three steps.[3] Therefore, the formation of substituted 1,3-diene **4** could be accounted for by the following path-way, as shown in Scheme 1. Alkenesulfonyl chlorides **2** react with the olefins catalyzed by the ruthenium(II) complex **1** to give 1 : 1 adducts **3** during the initial step. Dehydrochlorination and desulfonylation from adducts **3** take place, successively, in the presence of the ruthenium complex **1** to afford substituted 1,3-dienes **4**.

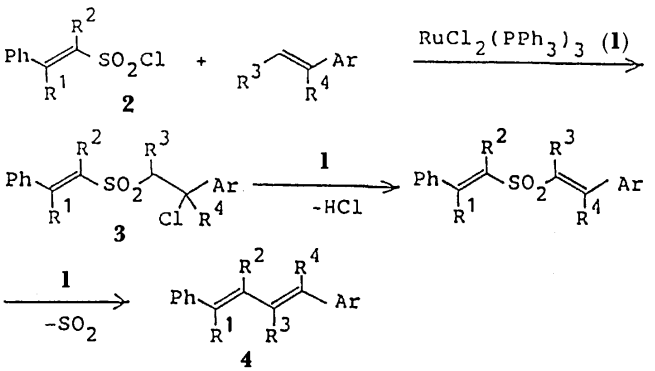

Scheme 1.

There are a number of methods for the preparation of 1,3-dienes;[4-6] however, some of them can prepare

Table 1. Reaction of Alkenesulfonyl Chloride with Olefin Catalyzed by $RuCl_2(PPh_3)_3$ (**1**)

Sulfonyl chloride	Olefin	Temp/°C	Time/h	Product	Yield/%
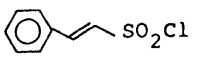 **2a**	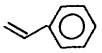	80	70	**3a**	88
	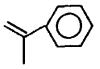	100	36	**3b**	46[21]
	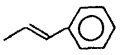	100	24	**3c**	23
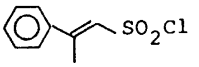 **2b**	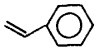	80	24	**3d**	89
	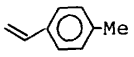	80	21	**3e**	81
	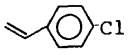	80	13	**3f**	95
	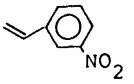	80	24	**3g**	70
	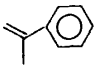	100	36	**3h**	80[21]
	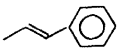	100	24	**3i**	61
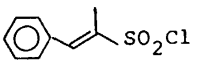 **2c**	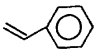	80	24	**3j**	84
	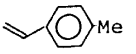	80	37	**3k**	74
	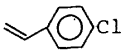	80	37	**3l**	76
	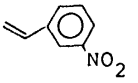	80	72	**3m**	70
	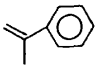	100	36	**3n**	80[21]
	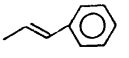	100	24	**3o**	53

only symmetrical 1,3-dienes[7-12] and others require sophisticated organometallic reagents.[13-17] On the other hand, the present method can be used to prepare symmetrical and unsymmetrical 1,3-dienes in good yield by the reaction of easily available sulfonyl chlorides with olefin. The reaction of **2c** with 2-phenyl-1-propene afforded 2-methyl-1,4-diphenyl-1,3-pentadiene (**4e**) and (*E*)-2-chloro-2-phenylpropyl 1-methyl-2-phenylethenyl sulfone (**3n**) in 15% and 63% yields, respectively (Run 8 in Table 2). This indicates that the adduct **3n** was not readily dehydrochlorinated and desulfonylated to 1,3-diene **4e** when ethenesulfonyl chloride has a substituent at the β-position, probably by the steric effect of the methyl group.

A reaction of (*E*)-1-propene-1-sulfonyl chloride with styrene was carried out at 150 °C using the ruthenium(II) complex **1** while expecting the formation of 1-phenyl-1,3-pentadiene. Unfortunately, the expected 1,3-diene was not obtained, though various transition metal complexes, such as $NiCl_2(PPh_3)_2$, $Pd(PPh_3)_4$, $PdCl_2(PPh_3)_2$, $Pt(PPh_3)_4$, $RhCl(PPh_3)_3$, and $RuCl_2(PPh_3)_3$, were used as catalysts. The results show that

Table 2. Formation of (*E,E*)-1,3-Dienes by the Reaction of (*E*)-Alkenesulfonyl Chlorides with Olefin Catalyzed by the Ruthenium(II) Complex **1**

Run	Sulfonyl chloride	Olefin	Product	Yield/%
1	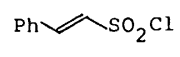 **2a**		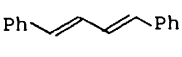 **4a**	91
2			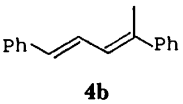 **4b**	56
3		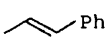	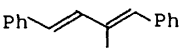 **4c**	38
4	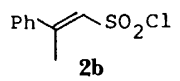 **2b**		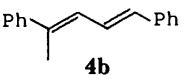 **4b**	51
5			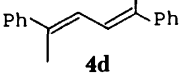 **4d**	80
6		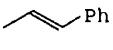	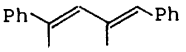 **4e**	23[a]
7	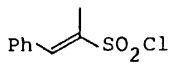 **2c**		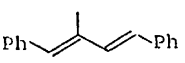 **4c**	21
8			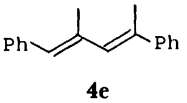 **4e**	15[b]
9		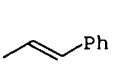	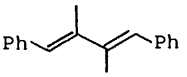 **4f**	10[c]

a) Isomer of **4e** was isolated in 17% yield. b) Adduct **3n** was formed in 63% yield. c) Isomer of **4f** and adduct **3o** were isolated in 6% and 16% yield respectively.

the reaction of alkenesulfonyl chlorides without an aryl group with vinylarenes did not afford 1,3-dienes, although the reason has not yet been clarified.

In conclusion, symmetrically and unsymmetrically substituted 1,4-diaryl-1,3-dienes were formed by the reaction of alkenesulfonyl chlorides with olefins catalyzed by the ruthenium(II) complex. The present method involves a very excellent one-pot synthesis of symmetrical and unsymmetrical (*E,E*)-1,4-diaryl-1,3-dienes, since substituted ethenesulfonyl chloride can be prepared very easily by treating vinylarenes with sulfuryl chloride in *N,N*-dimethylformamide.[18] The present reaction can be regarded as an oxidative coupling reaction of each terminal carbon atom of two kinds of vinylarenes by using sulfuryl chloride and ruthenium(II) catalyst. Since a direct oxidative coupling of vinylarenes is impossible, the present reaction offers a novel and convenient synthetic method of symmetrical and unsymmetrical (*E,E*)-1,4-diaryl-1,3-dienes.

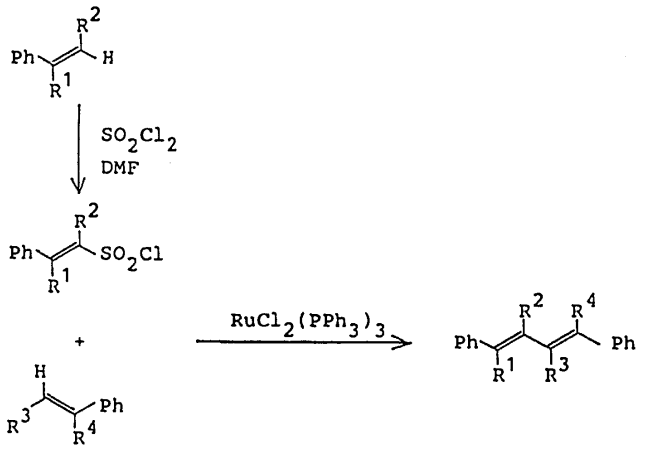

Experimental

Measurement. Melting points and boiling points were uncorrected. The infrared absorption spectra were determined on a Hitachi Model 260-10 spectrophotometer with samples as either neat liquids or KBr disks. The proton magnetic resonance spectra were recorded at 60 MHz by using a JMX-PMX 60 SI spectrometer with Me_4Si as an internal standard in $CDCl_3$. Mass spectra were determined with a JEOL JMX-DX 300 mass spectrometer with JEOL 5000 Mass Data System at an ionizing voltage of 20—70 eV. The gel-permeation chromatography was accomplished on a JAI LC-08 liquid chromatograph with a JAIGEL-1H column (20ϕ×600 mm×2) using chloroform as an eluent.

Materials. Dichlorotris(triphenylphosphine)ruthenium-(II) (**1**) was prepared according to a procedure described in the literature.[19] (*E*)-2-Phenylethenesulfonyl chloride (**2a**) was prepared from styrene by treatment with sulfuryl chloride in *N,N*-dimethylformamide by the method described in the literature:[18] yield 50%; mp 87—88 °C (from ethanol–hexane; lit, mp 89—90 °C). (*E*)-2-Phenyl-1-propene-1-sulfonyl chloride (**2b**) or (*E*)-1-phenyl-1-propene-2-sulfonyl chloride (**2c**) were prepared from 2-phenyl-1-propene or 1-phenyl-1-propene by treating with sulfuryl chloride in *N,N*-dimethylformamide–dichloromethane and then with triethylamine in ether: (**2b**) yield 29%; bp 96—98 °C/0.2 mmHg (1 mmHg=133.322 Pa); IR (neat) 1370 and 1170 cm^{-1}; ^1H NMR ($CDCl_3$) δ=2.65 (3H, s), 6.90 (1H, s), and 7.40 (10H, s); MS *m/z* 216 (M^+): (**2c**) yield 68%; bp 95—96 °C/0.2 mmHg; IR (neat) 1370, 1355, and 1170 cm^{-1}; ^1H NMR ($CDCl_3$) δ=2.45 (3H, s), 7.35 (5H, s), and 7.65 (1H, s); MS *m/z* 216 (M^+). (*E*)-1-Propene-1-sulfonyl chloride was prepared from propylene oxide by treatment with sodium hydrogensulfite, phosphorus pentachloride, and then triethylamine in ether according to the literature:[20] yield 68%; bp 88—89 °C/21 mmHg. Styrene, *p*-methylstyrene, *p*-chlorostyrene (Tokyo Kasei Chemicals), *m*-nitrostyrene (Aldrich Chemicals), 2-phenyl-1-propene, and 1-phenyl-1-propene (Wako Chemicals) were purified by distillation prior to use.

Formation of 1:1 Adducts by the Reaction of Alkenesulfonyl Chlorides with Olefins. To a solution of 1.0 mmol of alkenesulfonyl chloride and 1.5 mmol of olefin in 2.0 cm^3 of benzene or toluene was added 0.01 mmol of dichlorotris(triphenylphosphine)ruthenium(II) (**1**) and heated at 80—100 °C under a nitrogen atmosphere. The reaction mixture was chromatographed on florisil by using benzene as an eluent to separate polar substances. Nonpolar substances were purified by gel-permeation chromatography using chloroform as an eluent to isolate 1:1 adducts **3a—o**.

The physical and spectral data of compounds **3a—o** are as follows:

(*E*)-2-Chloro-2-phenylethyl Styryl Sulfone (3a): Mp 97—98 °C; IR (KBr) 1310 and 1130 cm^{-1}; ^1H NMR ($CDCl_3$) δ=3.78 (1H, d, J=7.8 Hz), 3.82 (1H, d, J=7.8 Hz), 5.33 (1H, t, J=7.8 Hz), 6.33 (1H, d, J=15 Hz), 7.10—7.40 (10H, m), and 7.35 (1H, d, J=15 Hz); MS m/z 306 (M^+).

(*E*)-2-Chloro-2-phenylpropyl Styryl Sulfone (3b): IR (neat) 1310 and 1130 cm^{-1}; ^1H NMR ($CDCl_3$) δ=4.20 (2H, s), 5.42 (1H, s), 5.60 (1H, s), 6.43 (1H, d, J=16 Hz), 7.00—7.30 (10H, m), and 7.32 (1H, d, J=16 Hz);[21] MS m/z 321 (M^+ +1);[22] HRMS, Found m/z 320.0743, Calcd for $C_{17}H_{17}O_2SCl$: M, 320.0637.

(*E*)-2-Chloro-1-methyl-2-phenylethyl Styryl Sulfone (3c): Mp 95—96 °C; IR (KBr) 1310 and 1130 cm^{-1}; ^1H NMR ($CDCl_3$) δ=1.53 (3H, d, J=8.0 Hz), 3.22—3.63 (1H, m), 5.59 (1H, d, J=4.0 Hz), 6.38 (1H, d, J=15 Hz), 7.27 (10H, s), and 7.38 (1H, d, J=15 Hz); MS m/z 320 (M^+); HRMS, Found: m/z 319.0577, Calcd for $C_{17}H_{16}O_2SCl$: M, 319.0559.

(*E*)-2-Chloro-2-phenylethyl 2-Phenyl-1-propenyl Sulfone (3d): Mp 95—96 °C; IR (KBr) 1305 and 1120 cm^{-1}; ^1H NMR ($CDCl_3$) δ=2.40 (3H, s), 3.70—3.85 (2H, m), 5.36 (1H, t, J=6.0 Hz), 6.07 (1H, s), and 7.00—7.80 (10H, m); MS m/z 320 (M^+); HRMS, Found: m/z 320.0644, Calcd for $C_{17}H_{17}O_2SCl$: M, 320.0637.

(*E*)-2-Chloro-2-(*p*-tolyl)ethyl 2-Phenyl-1-propenyl Sulfone (3e): IR (neat) 1310 and 1130 cm^{-1}; ^1H NMR ($CDCl_3$) δ=2.17 (3H, s), 2.37 (3H, s), 3.79 (2H, d, J=6.0 Hz), 5.33 (1H, t, J=6.0 Hz), 5.93 (1H, s), and 6.70—7.70 (9H, m); MS m/z 298 (M^+ −HCl); HRMS, Found: m/z 298.0993, Calcd for $C_{18}H_{17}O_2S$: M, 298.1027.

(*E*)-2-Chloro-2-(*p*-chlorophenyl)ethyl 2-Phenyl-1-propenyl Sulfone (3f): Mp 58—60 °C; IR (neat) 1310 and 1130 cm^{-1}; ^1H NMR ($CDCl_3$) δ=2.43 (3H, s), 3.76—3.85 (2H, m), 5.36 (1H, t, J=6.0 Hz), 6.06 (1H, s), and 7.00—7.50 (9H, m); MS m/z 354 (M^+); HRMS, Found m/z 354.0222, Calcd for $C_{17}H_{16}O_2SCl_2$: M, 354.0248.

(*E*)-2-Chloro-2-(*m*-nitrophenyl)ethyl 2-Phenyl-1-propenyl Sulfone (3g): Mp 101—102 °C; IR (KBr) 1540, 1350, 1310, and 1120 cm^{-1}; ^1H NMR ($CDCl_3$) δ=2.48 (3H, s), 3.75—3.90 (2H, m), 5.47 (1H, t, J=6.0 Hz), 6.13 (1H, s), and 7.18—8.21 (9H, m); MS m/z 365 (M^+); HRMS, Found: m/z 365.0523, Calcd for $C_{17}H_{16}O_4NSCl$: M, 365.0488.

(*E*)-2-Chloro-2-phenylpropyl 2-Phenyl-1-propenyl Sulfone (3h): IR (neat) 1305 and 1130 cm^{-1}; ^1H NMR ($CDCl_3$) δ=2.33 (3H, s), 4.13 (2H, s), 5.39 (1H, s), 5.57 (1H, s), 6.30 (1H, m), and 6.70—7.40 (10H, m);[16] MS m/z 335 (M^+ +1);[17] HRMS, Found: m/z 299.1125, Calcd for $C_{18}H_{19}O_2S$: M, 299.1105.

(*E*)-2-Chloro-1-methyl-2-phenylethyl 2-Phenyl-1-propenyl Sulfone (3i): IR (neat) 1300 and 1130 cm^{-1}; ^1H NMR ($CDCl_3$) δ=1.36 (1H, d, J=7.0 Hz), 1.54 (2H, d, J=7.0 Hz), 2.48 (3H, s), 3.10—3.65 (1H, m), 5.40—5.64 (1H, m), 6.00—6.10 (1H, m), and 6.90—7.30 (10H, s); MS m/z 335 (M^+ +1);[17] HRMS, Found: m/z 299.1105, Calcd for $C_{18}H_{19}O_2S$: M, 299.1105.

(*E*)-2-Chloro-2-phenylethyl 1-Methyl-2-phenylethenyl Sulfone (3j): Mp 93—95 °C; IR (neat) 1300 and 1140 cm^{-1}; ^1H NMR ($CDCl_3$) δ=2.20 (3H, d, J=1.2 Hz), 3.76 (2H, d, J=6.0 Hz), 5.26 (1H, t, J=6.0 Hz), and 7.00—7.40 (11H, m); MS m/z 320 (M^+); HRMS, Found: m/z 284.0831, Calcd for $C_{17}H_{16}O_2S$: M, 284.0871.

(*E*)-2-Chloro-2-(*p*-tolyl)ethyl 1-Methyl-2-phenylethenyl Sulfone (3k): Mp 91—92 °C; IR (neat) 1305 and 1140 cm^{-1}; ^1H NMR ($CDCl_3$) δ=2.09—2.15 (6H, m), 3.77 (2H, d, J=6.0 Hz), 5.26 (1H, t, J=6.0 Hz), and 7.00—7.30 (10H, m); MS m/z 334 (M^+); HRMS, Found: m/z 298.1036, Calcd for $C_{18}H_{17}O_2S$: M, 298.1027.

(*E*)-2-Chloro-2-(*p*-chlorophenyl)ethyl 1-Methyl-2-phenylethenyl Sulfone (3l): Mp 91—92 °C; IR (KBr) 1310 and 1140 cm^{-1}. ^1H NMR ($CDCl_3$) δ=2.14 (3H, s), 3.75 (2H, d, J=6.0 Hz), 5.28 (1H, t, J=6.0 Hz), and 7.10—7.40 (10H, m); MS m/z 354 (M^+); HRMS, Found: m/z 354.0267, Calcd for $C_{17}H_{16}O_2SCl_2$: M, 354.0248.

(*E*)-2-Chloro-2-(*m*-nitrophenyl)ethyl 1-Methyl-2-phenylethenyl Sulfone (3m): IR (neat) 1540, 1360, 1310, and 1140 cm^{-1}; ^1H NMR ($CDCl_3$) δ=2.21 (3H, s), 3.73—3.88 (2H, m), 5.41 (1H, t, J=6.0 Hz), and 7.00—8.20 (10H, m); MS m/z 365 (M^+); HRMS, Found: m/z 365.0452, Calcd for $C_{17}H_{16}O_4NSCl$: M, 365.0488.

(*E*)-2-Chloro-2-phenylpropyl 1-Methyl-2-phenylethenyl Sulfone (3n): IR (neat) 1300 and 1140 cm^{-1}; ^1H NMR ($CDCl_3$) δ=2.40 (3H, s), 4.13 (2H, s), 5.04 (1H, s), 5.20 (1H, s), and 6.90—7.30 (11H, m);[16] MS m/z 335 (M^+ +1);[17] HRMS, Found: m/z 299.1167, Calcd for $C_{18}H_{19}O_2S$: M, 299.1105.

(*E*)-2-Chloro-1-methyl-2-phenylethyl 1-Methyl-2-phenylethenyl Sulfone (3o): Mp 112—113 °C; IR (KBr) 1300 and 1140 cm^{-1}. ^1H NMR ($CDCl_3$) δ=1.25 (1H, d, J=7.0 Hz), 1.55 (2H, d, J=7.0 Hz), 2.10—2.30 (3H, m), 3.28—3.86 (1H, m), 5.14—5.53 (1H, m), and 7.00—7.60 (10H, m); MS m/z 335 (M^+ +1);[17] HRMS, Found: m/z 334.0762, Calcd for $C_{18}H_{19}O_2SCl$: M, 334.0794.

The Formation of 1,3-Dienes by the Reaction of Alkenesulfonyl Chlorides with Olefins. A solution containing of 1.0 mmol of alkenesulfonyl chloride, 1.5 mmol of olefin, and 0.01 mmol of the ruthenium(II) complex **1** in 2.0 cm^3 of benzene was degassed and heated in a sealed tube at 150 °C for 48 h. Gel-permeation chromatography using chloroform as an eluent was performed to isolate 1,3-dienes.

The physical and spectral data of the compounds **4a—f** are as follows:

(*E,E*)-1,4-Diphenyl-1,3-butadiene (4a): Mp 148—149 °C (lit,[23] mp 149.7 °C); IR (KBr) 3010, 1490, 1440, 990, 740, and 690 cm^{-1}; ^1H NMR ($CDCl_3$) δ=6.10—6.80 (4H, m) and 6.90—7.40 (10H, m); MS m/z 206 (M^+).

(*E,E*)-1,4-Diphenyl-1,3-pentadiene (4b): Mp 95—96 °C (lit,[24] mp 95.5—97 °C); IR (KBr) 3030, 1595, 1490, 1440, 970, 750, and 690 cm^{-1}; ^1H NMR ($CDCl_3$) δ=2.21 (3H, s), 6.36—6.89 (2H, m), and 7.00—7.50 (11H, m); MS m/z 220 (M^+).

(*E,E*)-2-Methyl-1,4-diphenyl-1,3-butadiene (4c): Mp 76—77 °C (lit,[5] mp 78—80 °C); IR (KBr) 3020, 1490, 1440, 960, 740, and 695 cm^{-1}; ^1H NMR ($CDCl_3$) δ=2.08 (3H, s) and 6.17—7.40 (13H, m); MS m/z 220 (M^+).

(*E,E*)-2,5-Diphenyl-2,4-hexadiene (4d): Mp 130—132 °C (lit,[8] mp 136—137.5 °C); IR (KBr) 3030, 2960, 1495, 1445, 760, and 700 cm^{-1}; ^1H NMR ($CDCl_3$) δ=2.20 (6H, s), 6.70 (2H, s), and 7.03—7.50 (10H, m); MS m/z 234 (M^+).

(*E,E*)-2-Methyl-1,4-diphenyl-1,3-pentadiene (4e): IR (neat) 3030, 2850, 1600, 1490, 1440, 1380, 1025, 880, 750, and 690 cm^{-1}; ^1H NMR ($CDCl_3$) δ=2.27 (6H, s), 6.81 (2H, m), and 7.15—7.60 (10H, m); MS *m/z* 234 (M^+); HRMS, Found: *m/z* 234.1408, Calcd for $C_{18}H_{18}$: M, 234.1408.

(*E,E*)-2,3-Dimethyl-1,4-diphenyl-1,3-butadiene[13] (4f): IR (neat) 2900, 1490, 1450, 750, and 700 cm^{-1}; ^1H NMR ($CDCl_3$) δ=1.79 (6H, s) and 6.80—7.40 (12H, m); MS *m/z* 234 (M^+); HRMS, Found: *m/z* 234.1404, Calcd for $C_{18}H_{17}$: M, 234.1408.

References

1) N. Kamigata, H. Sawada, and M. Kobayashi, *J. Org. Chem.*, **48**, 3793 (1983); N. Kamigata, H. Sawada, N. Suzuki, and M. Kobayashi, *Phosphorus and Sulfur*, **19**, 199 (1984); N. Kamigata, N. Suzuki, and M. Kobayashi, *ibid.*, **20**, 139 (1984).

2) N. Kamigata, J. Ozaki, and M. Kobayashi, *Chem. Lett.*, **1985**, 705.

3) N. Kamigata, J. Ozaki, and M. Kobayashi, *J. Org. Chem.*, **50**, 5045 (1985).

4) G. Wilke and H. Muller, *Justus Liebigs Ann. Chem.*, **629**, 222 (1960); G. Zweifel and R. L. Miller, *J. Am. Chem. Soc.*, **92**, 6678 (1970).

5) W. Fischetti, K. T. Mak, F. G. Stakem, J. I. Kim, A. L. Rheingold, and R. F. Heck, *J. Org. Chem.*, **48**, 948 (1983).

6) E. Wenkert, M. H. Leftin, and E. L. Michelotti, *J. Chem. Soc., Chem. Commun.*, **1984**, 617; S. Yamada, H. Ohsawa, T. Suzuki, and H. Takayama, *J. Org. Chem.*, **51**, 4934 (1986).

7) R. C. Larock, *J. Org. Chem.*, **41**, 2241 (1976).

8) R. Levene, J. Y. Becker, and J. Klein, *J. Organomet. Chem.*, **67**, 467 (1974).

9) Y. Yamamoto, H. Yatagai, K. Maruyama, A. Sonoda, and S-I. Murahashi, *J. Am. Chem. Soc.*, **99**, 5652 (1977).

10) K. Tamao, H. Matsumoto, T. Kakui, and M. Kumada, *Tetrahedron Lett.*, **1979**, 1137, 1141.

11) W. P. Weber, R. A. Felix, A. K. Willard, and K. E. Koenig, *Tetrahedron Lett.*, **1971**, 4701.

12) M. F. Semmelhack, P. M. Helquist, and J. D. Gorzynski, *J. Am. Chem. Soc.*, **94**, 9234 (1972).

13) J. J. Eisch and W. C. Kaska, *J. Am. Chem. Soc.*, **88**, 2213 (1960).

14) A. Suzuki, *Pure. Appl. Chem.*, **57**, 1749 (1985) and references cited therein.

15) E. Negishi, *Acc. Chem. Res.*, **15**, 340 (1982) and references cited therein; E. Negishi, T. Takahashi, S. Baba, D. E. Van Horn, and N. Okukado, *J. Am. Chem. Soc.*, **109**, 2393 (1987).

16) N. Jabri, A. Alexakis, and J. F. Normant, *Tetrahedron Lett.*, **22**, 959 (1981) and references cited therein.

17) J. K. Stille and B. L. Groh, *J. Am. Chem. Soc.*, **109**, 813 (1987).

18) B. M. Culbertson and S. Dietz, *J. Chem. Soc. C*, **1968**, 992.

19) T. A. Stephenson, G. Wilkinson, *J. Inorg. Nucl. Chem.*, **28**, 945 (1966); T. A. Stephenson, G. Wilkinson, *J. Chem. Soc. A*, **1970**, 2497; P. S. Hallam, T. A. Stephenson, and G. Wilkinson, *Inorg. Synth.*, **12**, 238 (1972).

20) A. Goldberg, *J. Chem. Soc.*, **1945**, 464; C. S. Rondestvedt, *J. Am. Chem. Soc.*, **76**, 1926 (1954); C. S. Rondestvedt and P. K. Chang., *ibid.*, **77**, 6532 (1955).

21) The adduct formed was readily dehydrochlorinated on working up by elution chromatography to give divinyl sulfone, therefore the spectral data are shown the dehydrochlorinated divinyl sulfone. The mass spectrum was obtained by the crude product and showed the parent peak of the adduct. The yield of the adduct was caluculated from the isolated divinyl sulfone.

22) We often observed the parent peak of sulfones showed $M^+ + 1$.

23) B. B. Corson, *Org. Synth.*, Coll. Vol. II, 229 (1943).

24) L. A. Paquett, R. P. Henzel, and S. E. Wilson, *J. Am. Chem. Soc.*, **94**, 7780 (1972).

 © 1988 The Chemical Society of Japan Bull. Chem. Soc. Jpn., 61, 1237—1245 (1988)

New Application of Solid Acid to Carbon-Carbon Bond Formation Reactions: Clay Montmorillonite-Catalyzed Aldol Reactions of Silyl Enol Ethers with Aldehydes and Acetals

Motomitsu KAWAI, Makoto ONAKA,* and Yusuke IZUMI
Department of Synthetic Chemistry, Faculty of Engineering, Nagoya University, Furo-cho, Chikusa-ku, Nagoya 464
(Received September 16, 1987)

A new attempt of utilizing solid acid to the cross aldol reaction of silyl enol ethers with aldehydes or acetals has been investigated. Among solid acids employed, the reaction is promoted most effectively by a catalytic amount of aluminium ion-exchanged montmorillonite (Al-Mont). Simple diastereoselection is significantly sensitive to the nature of the reaction solvent used in the Al-Mont-catalyzed reaction. When the aluminium ions in Al-Mont were replaced by protons or titanium ions in order to investigate the cation effect, almost the same results were observed on simple diastereoselectivity and diastereofacial selectivity. This fact suggests that the metal cations in montmorillonite do not work as Lewis acid in the present aldol reaction. The acid catalysis of montmorillonite in the present aldol reaction is discussed in comparison with the catalytic behavior of some homogeneous acids.

The use of a preformed metal enolate has become a general method for the directed cross aldol reactions.[1] Especially, silyl enol ethers are widely utilized as enolates owing to their isolable properties, and undergo directed aldol reactions with carbonyl compounds in the presence of acidic promoters or by treatment of fluoride ions. As acidic promoters, not only a stoichiometric amount of Lewis acid like $TiCl_4$[2a] but also a catalytic amount of $CF_3SO_3SiMe_3$,[2b] Ph_3CClO_4,[2c] or Me_2AlCl[2d] are used to activate aldehydes or acetals electrophilically. These promoters are soluble in the reaction media, but there is few reports on the aldol reaction using a solid acid as a promoter under heterogeneous conditions.[3]

Recently we demonstrated that the allylation of acetals and carbonyl compounds with allylic silanes was catalyzed by solid acids in a heterogeneous system.[4] Especially clay montmorillonite was found to be the most efficient catalyst among the solid acids of mica, zeolite, silica-alumina, and ion-exchange resin. This experiment is the first example of an inorganic solid acid-catalyzed carbon-carbon bond-formation reaction using organosilicon reagents.[5]

Clay montmorillonite is a layered silicate possessing ion-exchange ability.[6a] Acid property of montmorillonite can be easily altered by replacing interlayered cations in the montmorillonite without any change of the crystalline structure. Although several works using montmorillonite have been done for the acid-catalyzed organic reactions,[6] the application of montmorillonite to C-C bond-formation reactions under mild conditions is quite rare. For example, montmorillonite was reported to promote the Friedel-Crafts type alkylations,[7a] the Diels-Alder reactions,[7b] and the condensation of acetals with alkyl vinyl ethers.[7c]

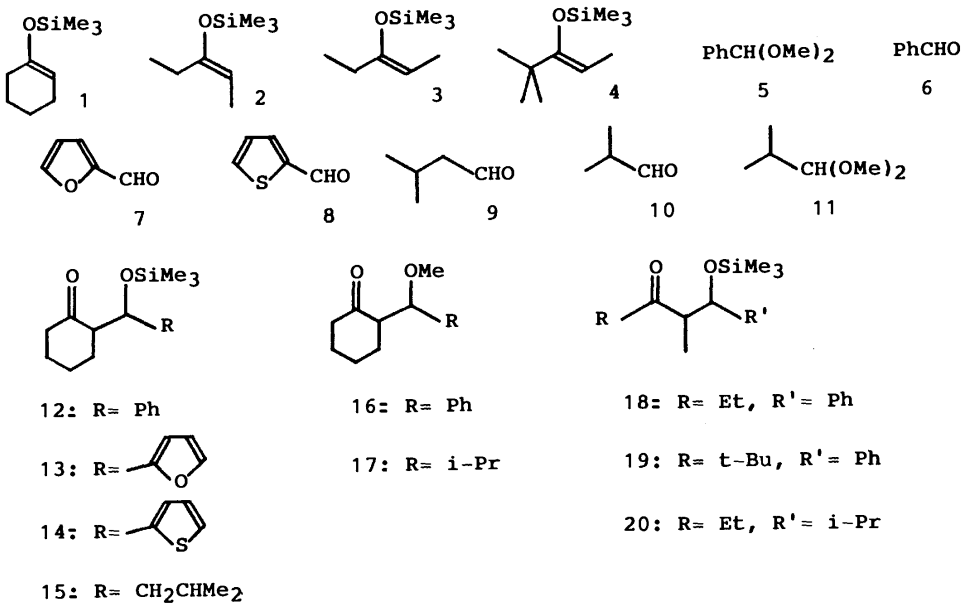

Our objectives are to utilize inorganic solid acids instead of liquid acids to complete C-C bond-formation reactions and to compare catalysis between heterogeneous and homogeneous acids. A montmorillonite-catalyzed allylation reaction is one of them.[4] We have also showed that aluminium ion-exchanged montmorillonite (Al-Mont) is an effective catalyst for the aldol reactions of silyl enol ethers or silyl ketene acetals with carbonyl compounds or acetals.[8] Here we describe additional examples of the aldol reactions and clarify the catalysis of the montmorillonite.

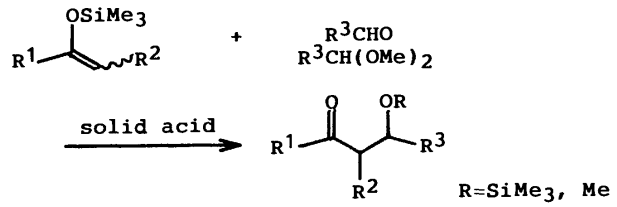

Results and Discussion

Simple Diastereoselection. The reaction of silyl enol ether **1** with an acetal **5** was examined in the presence of various solid acids and the results are listed in Table 1. The reaction proceeded smoothly with the aid of solids even under heterogeneous conditions to afford the corresponding aldol adducts in good yield (Entries 1—5, 7). Among solid acids, aluminium ion-exchanged montmorillonite (Al-Mont) showed the highest catalytic activity (Entries 1, 2) and good diastereoselectivity for an erythro adduct especially in 1,2-dimethoxyethane (DME) (Entry 2).

Next, the reaction of **1** with an aldehyde **6** was examined with respect to catalytic activity and diastereoselectivity affected both by reaction solvents and by exchangeable cations in the montmorillonite (Table 2, Entries 1—6). Al-Mont showed slightly higher activity than proton- or titanium ion-exchanged montmorillonite (described as H-Mont and Ti-Mont, respectively) (Entries 1, 2, 5, 6). Al-Mont also showed higher diastereoselectivity since the reaction proceeded at lower temperature.

The use of solid acids in liquid-phase organic reactions provides an advantage of a much more simple work-up procedure compared with that of liquid acids. As work up, only filtering a reaction mixture through a Celite pad is required in order to separate a solid catalyst from organic products. Thus the aldol adduct **12** was obtained in the form of trimethylsilyl ether.

Table 1. The Aldol Reaction of **1** with **5**[a]

Entry	Catalyst	Condition Temp/°C (Time/h)	Yield/ %[b]	Threo: Erythro
1	Al-Mont	−78(1), −50(0.2)	84	45:55
2	Al-Mont[b]	−60(0.5), −50(1.5)	93	13:87
3	SiO_2-Al_2O_3	−50(0.3), −30(1)	73	30:70
4	SiO_2-Al_2O_3[b]	−20(6)	79	21:79
5	CaY	0(2)	73	23:77
6	CaY[b]	0(1), 15(70)	0	—
7	Nafion-117[c]	−20(1), 0(1)	69	23:77
8	CF_3SO_3H[d]	−78(0.5)	80	9:91
9	CH_3SO_3H[e]	20(18)	0	—
10	$CF_3SO_3SiMe_3$[f]	−78(0.5)	89	7:93
11	BF_3-OEt_2[g]	−78(0.5)	78	22:78

a) **1** (1 mmol), **5** (1 mmol), solid acid (0.2 g), solvent (CH_2Cl_2). b) DME was used as solvent. c) An ion exchange resin which contains 1 mmol·g^{-1} of proton. Nafion 117 (0.1 g) was used. d) 0.01 mmol. e) 0.12 mmol. f) 0.01 mmol. This result is quoted from Ref. 2b. g) 1 mmol.

Table 2. The Aldol Reaction of **1** with **6**[a]

Entry	Catalyst	Solvent	Condition temp/°C (Time/h)	Yield/%	Threo: Erythro
1	H-Mont	$PhCH_3$	−50(2.5), −30(2)	75	68:32
2	Al-Mont	$PhCH_3$	−78(0.5), −50(1)	82	71:29
3	Al-Mont	CH_2Cl_2	−95(2.5)	91	63:37
4	Al-Mont	Et_2O	−50(0.1), −30(1)	82	44:56
5	Al-Mont	DME	−60(6.5)	81	21:79
6	Ti-Mont	DME	−50(0.3), −30(1)	76	28:72
7	SiO_2-Al_2O_3	$PhCH_3$	−30(0.3), −20(0.5)	54	48:52
8	SiO_2-Al_2O_3	CH_2Cl_2	−30(0.5), −10(0.5)	40	50:50
9	SiO_2-Al_2O_3	DME	0(0.3), 25(0.5)	14	32:68
10	CaY	CH_2Cl_2	20(12)	70	51:49
11	CF_3SO_3H[b]	$PhCH_3$	−20(0.2), 25(1)	0	—
12	CF_3SO_3H[c]	CH_2Cl_2	−78(0.5)	74	44:56
13	CF_3SO_3H[d]	DME	−78(0.5), −50(0.5)	58	44:56
14	CH_3SO_3H[b]	CH_2Cl_2	20(18)	0	—
15	$CF_3SO_3SiMe_3$[c]	CH_2Cl_2	−78(0.5)	84	51:49
16	BF_3·OEt_2[e]	$PhCH_3$	−78(0.5)	60	39:61
17	BF_3·OEt_2[e,f]	CH_2Cl_2	−78(1)	80	74:26
18	BF_3·OEt_2[e]	DME	−78(0.5), −40(0.5)	60	50:50

a) **1** (1 mmol), **6** (1 mmol), montmorillonite (0.2 g), SiO_2-Al_2O_3 (0.2 g), CaY (0.5 g). b) 0.1 mmol. c) 0.003 mmol. d) 0.008 mmol. e) 1 mmol. f) This result is quoted from Ref. 2a.

Table 3. The Reactions of Silyl Enol Ethers with Aldehydes or Acetals Catalyzed by Al-Mont[a)]

Entry	Silyl enol ether	Aldehyde or acetal	Solvent	Condition Temp/°C (Time/h)	Yield/%[b)]	Threo: Erythro
1	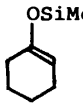		$PhCH_3$	−78(0.5), −50(1)	82	71:29
2		PhCHO	CH_2Cl_2	−95(2.5)	91	63:37
3	**1**	**6**	DME	−60(6.5)	81	21:79
4	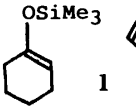		$PhCH_3$	−50(1), −40(1)	58[c)]	41:59
5			CH_2Cl_2	−78(1), −50(1)	85	67:33
6	**1**	**7**	DME	−50(1)	65	20:80
7	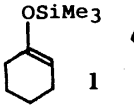		$PhCH_3$	−70(1), −40(1.5)	71[c)]	74:26
8			CH_2Cl_2	−78(0.6)	83	62:38
9	**1**	**8**	DME	−50(0.2), −30(1)	56	29:71
10	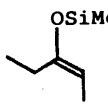		$PhCH_3$	−60(0.5)	97	76:24
11	d)	PhCHO	CH_2Cl_2	−78(0.5)	93	59:41
12	**2**	**6**	DME	−50(1), −30(1)	76	56:44
13	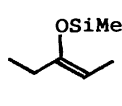		$PhCH_3$	−70(1), −60(2)	85	63:37
14	e)	PhCHO	CH_2Cl_2	−78(1)	89	53:47
15	**3**	**6**	DME	−50(1), −30(1)	73	50:50
16	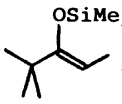	PhCHO	CH_2Cl_2	−78(0.3), −60(2)	78	96: 4
17	**4**	**6**	DME	−30(1), 0(1)	40	90:10
18	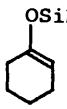		$PhCH_3$	−50(3), −30(2)	94	49:51
19		$PhCH(OMe)_2$	CH_2Cl_2	−60(0.5), −50(0.2)	84	45:55
20	**1**	**5**	DME	−65(0.5), −50(1.5)	93	13:87
21	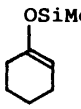		$PhCH_3$	−40(1), −30(4)	22[f)]	43:57
22			CH_2Cl_2	−78(0.5), −50(1)	86	62:38
23	**1**	**9**	DME	−30(0.5), −20(1)	29[g)]	43:57
24	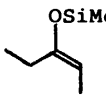	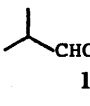	$PhCH_3$	−30(2), −20(2)	57	72:28
25	d)		CH_2Cl_2	−65(1), −50(1.5)	69	46:54
26	**2**	**10**	DME	−40(0.5), −20(2)	22[f)]	74:26
27	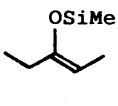	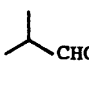	$PhCH_3$	−30(0.5), −20(2)	68	41:59
28	e)		CH_2Cl_2	−50(1), −30(1)	64	37:63
29	**3**	**10**	DME	−30(0.5), −20(2)	14[f)]	42:58
30	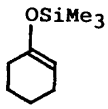	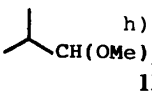	$PhCH_3$	−50(0.5), −30(2)	77	30:70
31		h)	CH_2Cl_2	−50(1), −30(1)	75	30:70
32	**1**	**11**	DME	−55(0.2), −30(1)	55[f)]	25:75

a) Silyl enol ether (1 mmol), aldehyde (1 mmol), and Al-Mont (0.2 g) were used. b) Isolated yield. c) 2 mmol of aldehyde was used. d) E/Z=83/17. e) E/Z=10/90. f) Unidentified by-products were obtained. g) The major by-product was cyclohexanone. h) 1.3 mmol of aldehyde or acetal was used.

The diastereoselectivity in the montmorillonite-catalyzed aldol reaction of **1** and **6** was considerably dependent on the nature of solvent.[9)] A threo isomer was preferentially formed in toluene (Table 2, Entries 1, 2), while an erythro isomer was dominant in DME (Table 2, Entries 5, 6).

The solvent effect on the diastereoselectivity was also observed with other substrates in Table 3. Generally, when aromatic aldehydes (benzaldehyde, furfural,[10)] 2-thiophenecarbaldehyde) and benzaldehyde dimethyl acetal were used, the ratio of threo to erythro increased in the following order of the solvent except Entry 4: DME < CH_2Cl_2 < $PhCH_3$ (Entries 1—3, 5—20). In the case of an aliphatic aldehyde and its acetal (Entries 21—32), however, the orderly solvent effects were not observed.

The dependence of diastereoselection upon solvents was not specific to the montmorillonite-catalyzed aldol reactions, but also recognized in the reactions promoted by a solid acid of SiO_2-Al_2O_3 (Table 2, Entries 7—9) and a homogeneous liquid acid of $BF_3 \cdot OEt_2$ (Table 2, Entries 16—18) though to a lesser extent. However no common pattern for the solvent effect was observable.

Acid strength of Al-Mont was measured in various solvents by use of Hammett indicators, and the result is listed in Table 4. In CH_2Cl_2 or $PhCH_3$, strongly acidic sites ($H_0 \leqq -8.2$) were detected on Al-Mont.[11] On the other hand, the acid strength of Al-Mont was weakened to $-5.6 < H_0 \leqq -3.0$ in 1,2-dimethoxyethane (DME). DME is relatively basic and thus interacts with the acid sites on montmorillonite to reduce their acid strength. We assume that the diastereoselectivity of the aldol reaction catalyzed by Al-Mont relates with the acid strength of Al-Mont since the interaction between aldehydes (acetals) and acid sites on Al-Mont is depending on the acid strength of the acid sites, and influences the stabilities of transition states of the reaction.

Diastereofacial Selection. In addition to simple diastereoselection, we also investigated diastereofacial selection in Al-Mont-catalyzed aldol reactions.

Reetz and his co-workers found that good asymmetric induction was observed in the Lewis acid-mediated aldol reactions of α- and β-alkoxy aldehydes with silyl enol ethers.[12] The diastereofacial preferences were explained with a chelation model having coordination between the two oxygens of an alkoxy aldehyde and a metal of Lewis acid. We examined whether chelation control is possible for metal cations in montmorillonite. In contrast to $TiCl_4$ which induced exclusively a chelation-controlled product **23a**,[13] various metal ions-exchanged montmorillonites showed only a slight preference for **23a** over **23b** and almost the same ratio of **23a** to **23b** irrespective of a metal cation (Table 5). The reaction of **21** with silyl ketene acetal **24** was also examined, but the diastereoselectivity was low.

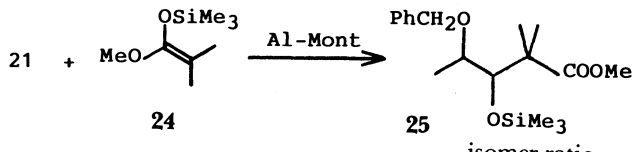

24 **25**

isomer ratio =54:46

These facts suggest that exchangeable ions in montmorillonite do not work as Lewis acid. Moreover, proton-exchanged montmorillonite (H-Mont) showed similar activity and diastereoselectivity to those of Al-Mont (Table 2, Entry 1,2; Table 5). Thus we assume that Brönsted acid sites (protons) generated by the dissociation of hydrated water in Al-Mont[14] actually play an important role in promoting the present aldol reaction.

$$M^{n+}(H_2O) \rightarrow (M\text{-}OH)^{(n-1)+} + H^+$$

Secondly, we chose an aldehyde **26** to investigate whether Cram's rule is applicable. In analogy with $BF_3 \cdot OEt_2$-mediated reactions of *t*-butyldimethylsilyl enol ether,[15] Al-Mont showed high asymmetric induction in the reaction of **26** with **22** to afford **27a** (a Cram product) selectively (Table 6).

Comparison of Catalysis between Al-Mont and Trifluoromethanesulfonic Acid (CF_3SO_3H). As homogeneous acid catalysts, we chose CF_3SO_3H and its silylated form, trimethylsilyl trifluoromethanesulfonate ($CF_3SO_3SiMe_3$) so as to compare the acid catalysis between heterogeneous and homogeneous acids. $CF_3SO_3SiMe_3$ was reported to be ineffective for the aldol reactions of aldehydes with silyl enol ethers.[2b] In our hands, however, the reaction of **1** with **6** smoothly proceeded even at low temperature in the presence of $CF_3SO_3SiMe_3$ as well as CF_3SO_3H[16] (Table 2, Entries 12, 13, 15). CF_3SO_3H also promoted the reaction of **1** with an aliphatic aldehyde.

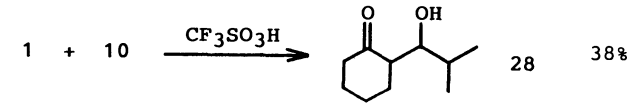

The catalytic behavior of $CF_3SO_3SiMe_3$ and CF_3SO_3H with respect to both the yield and the diastereoselectivity of **12** was found to be almost the same (Table 1, Entries 8, 10; Table 2, Entries 12, 15). CF_3SO_3H is known to be transformed to $CF_3SO_3SiMe_3$ on treatment with a silylating reagent.[17] On the basis of these facts, it seems likely that CF_3SO_3H is silylated by silyl enol ether to generate an active species of $CF_3SO_3SiMe_3$ which is in turn involved in an acid catalysis cycle[2b] of the aldol reaction.

Similarly, in the case of Al-Mont, we speculate that an active species is not a Brönsted acid site (proton) itself but a trimethylsilyl cation species derived from the reaction of Al-Mont and silyl enol ethers.[18]

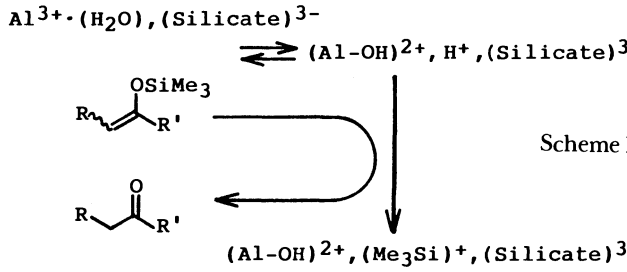

Scheme 1.

Table 4. Acid Strength of Al-Mont in Various Solvents

Indicator (H_0)	AQ (−8.2)	BAP (−5.6)	DCA (−3.0)	Maximum acid strength
$PhCH_3$	+	+	+	$H_0 \leqq -8.2$
CH_2Cl_2	+	+	+	$H_0 \leqq -8.2$
DME	−	−	+	$-5.6 < H_0 \leqq -3.0$

AQ=anthraquinone, BAP=benzylideneacetophenone, DCA=dicinnamylideneacetone.

Table 5. The Aldol Reaction of **21** with **22**

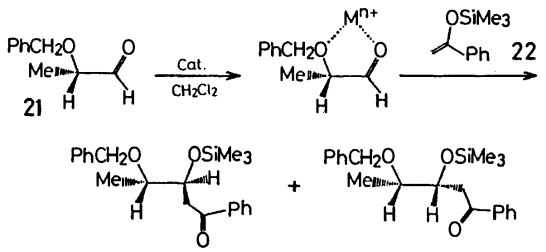

23a (chelation) **23b** (non chelation)

Catalyst	Temp/°C (Time/h)	Yield/%	**23a**:**23b**
Al-Mont	−65(1)	36	65:35
H-Mont	−50(1)	23	66:34
Ti-Mont	−20(1)	31	64:36

Reaction conditions: **21** (1 mmol), **22** (1 mmol), montmorillonite (0.2 g), solvent (CH_2Cl_2).

Table 6. The Aldol Reaction of **22** with **26**

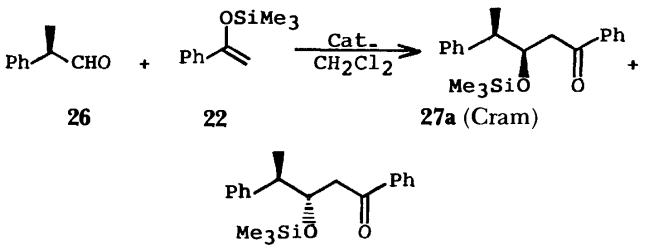

26 **22** **27a** (Cram)

27b (anti Cram)

Catalyst	Temp/°C (Time/h)	Yield/%	**27a**:**27b**
Al-Mont	−65(1)	65	93:7
H-Mont	−50(1)	54	92:8

Reaction conditions: **22** (1 mmol), **26** (1 mmol), montmorillonite (0.2 g), solvent (CH_2Cl_2).

Consideration about Acid Strength of Al-Mont. Both Al-Mont and CF_3SO_3H (a super acid[19]) promote the aldol reaction of **1** and **5**, while CH_3SO_3H (a strong acid) is completely ineffective (Table 1, Entry 9; Table 2, Entry 14). Therefore the acid strength of Al-Mont is considered to be stronger than CH_3SO_3H. Moreover, Al-Mont promoted the allylation reaction of 4-*t*-butylcyclohexanone with allyltrimethylsilane (80% yield)[4] but CF_3SO_3H failed.[20] Thus Al-Mont has higher catalytic activity than CF_3SO_3H.

Although acid strength of montmorillonite (dried at 120—130 °C in air) has been estimated to be rather low ($-8.2 < H_0 \leqq -3.0$) by several groups,[14,21] we observed that the sample of Al-Mont which was dried at 25 °C/0.5 Torr (1 Torr=133.322 Pa) for 24 h showed maximum acid strength of $-8.2 < H_0 \leqq -5.6$ in CH_2Cl_2, and the sample which was dried at 120 °C/0.5 Torr for 3 h possessed very strong acid sites of $H_0 \leqq -8.2$ in CH_2Cl_2 (Table 4). Judging from our results concerning the allylation[4] and the aldol reactions, Al-Mont (dried at 120 °C/0.5 Torr for 3 h) is one of the strongest solid acids.

Table 7. Poisoning Experiments[a]

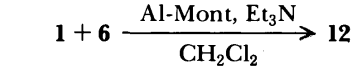

Entry	Et_3N (mol%)[b]	Yield of **12**/%	Threo: Erythro
1	0	93	61 : 39
2	0.05	95	62 : 38
3	0.15	58	64 : 36
4	0.5	1[c]	—
5	4.7	0[c]	—

a) **1** (1 mmol), **6** (1 mmol), Al-Mont (0.2 g), solvent (CH_2Cl_2), −78 °C, 0.5 h. b) Mol% of Et_3N based on **6**. c) Estimated by GC.

The Amount of Active Sites on Montmorillonite for Aldol Reactions. In order to confirm that Al-Mont acts catalytically in promoting the aldol reaction, the number of active site on Al-Mont was estimated by a poisoning experiment. After a part of acid sites on Al-Mont was deactivated by addition of triethylamine, the standard aldol reaction of **1** with **6** was performed, and judged from the change in the yield of **12**. The results are listed in Table 7. Surprisingly, only 0.5 mol% of the amine based on an aldehyde **6** is enough completely to prevent the reaction at −78 °C (Entry 4). It is concluded that a very small amount (less than 0.025 meq/g · Al-Mont) of acid sites on Al-Mont acts as an efficient catalyst in the aldol reaction.

Experimental

Measurement. ^1H NMR spectra were recorded in $CDCl_3$ with a Hitachi R-600 (60 MHz) spectrometer. ^{13}C NMR spectra were measured in $CDCl_3$ with a JEOL FX-60 spectrometer at 15 MHz or a JEOL JNM GX-400 spectrometer at 100 MHz. The chemical shifts (δ) are expressed in parts per million downfield from an internal standard of tetramethylsilane. Infrared spectra were recorded in CCl_4 on a JASCO IRA-2 spectrometer. Analytical gas-liquid chromatography (GC) was done with a Shimadzu GC-8A instrument with a flame ionization detector and nitrogen carrier gas. The following capillary columns were used: OV-1 Bonded, 25 m×0.25 mm; PEG-HT Bonded, 25 m×0.25 mm. The flow rate of carrier gas was 1—2 ml min^{-1} (0.5—1.0 kg cm^{-2}). Preparative thin-layer chromathography (TLC) was done on 20×20 cm glass plates coated with 1 mm thickness of Merck silica gel PF_{254}.

Solvents and Reagents. Dichloromethane was distilled from P_2O_5 and stored over Molecular Sieves 3A. Toluene was dried over Molecular Sieves 3A. 1,2-Dimethoxyethane (DME) and ether were distilled from $LiAlH_4$ prior to use. Triethylamine, $CF_3SO_3SiMe_3$, and pyridine were distilled from CaH_2. $BF_3 \cdot OEt_2$, 4-*t*-butylcyclohexanone, and Hammett indicators [anthraquinone (AQ), benzylideneacetophenone (BAP), and dicinnamylideneacetone (DCA)] were purchased and used without further purification. Silyl enol ethers, **1**,[22] **2** (*E*:*Z*=87:13),[23] **3** (*E*:*Z*=10:90),[24] **4** (*Z* isomer

only),[23] and **22**[22] were prepared according to the literature and the isomeric ratio of these substrates was determined by GC. Silyl ketene acetal **24** was prepared according to the literature.[25] Aldehydes **6**—**10**, **26** and CF_3SO_3H were commercially available and distilled before use. Aldehyde **21** was prepared according to the literature.[26] Acetals **5** and **11** were prepared by a conventional procedure.

Preparation of Ion-Exchanged Montmorillonites. The montmorillonite used in this study was purified Na^+ ion-exchanged montmorillonite, "Kunipia F" (cation-exchange capacity=1.19 meq. g^{-1}) supplied by Kunimine Industries Co. Aluminium ion exchange was effected by the addition of the powdered sodium ion-exchanged montmorillonite (Na-Mont, 100 g) to an aqueous solution (800 ml) of $Al(NO_3)_3 \cdot 9H_2O$ (150 g, 0.4 mol) with vigorous stirring at rt for 2 h. The resultant suspension was filtered on a Büchner funnel by suction. The clay was collected, suspended again in deionized water (500 ml) with stirring at rt for 1 h, filtered on a suction funnel, and washed with deionized water (200 ml). The clay collected was again suspended in a mixture of deionized water (200 ml) and methanol (200 ml) with stirring at rt for 1 h and filtered. This procedure was repeated twice. The washed clay was predried at 20 °C/1 Torr for 6 h, and the agglomerated clay was then ground and passed through a 60 mesh screen. The resultant powdery clay was dried at 20 °C/0.5 Torr for 24 h, and stored in a desiccator over anhydrous silica gel until use.

Similarly titanium ion exchange was conducted using 10 g of Na-Mont and aqueous $TiCl_3$ and the grinding of the Ti-excanged montmorillonite was performed under nitrogen atmosphere. Proton exchange was done using 5 g of Na-Mont and 100 ml of 1 mol dm^{-3} HCl.

Other Solid Acids. SiO_2–Al_2O_3 is a reference catalyst provided by Catalysis Society of Japan: JRC-SAL-2 (Al_2O_3 content: 13.75%). Zeolite CaY (the content of cations: Ca^{2+} 45%, Na^+ 55%) was prepared by treatment of NaY (Shokubai Kasei Co.: ZCP-50) with aqueous $CaCl_2$.[27] SiO_2–Al_2O_3 and CaY was predried at 400 °C in air for 3 h, stored in a desiccator, and then dried over flames at ca. 350 °C/0.5 Torr for 10 min or dried over an electric furnace at 400 °C/0.5 Torr for 3 h (Table 2, Entries 7—9) in a reaction vessel prior to use.

Nafion-117 [a perfluorinated resin of sulfonic acid (1 meq. g^{-1}, Du Pont)] was immersed in dry methanol overnight, washed with dry methanol, dried at 25 °C and 0.5 Torr for 30 min, and used for the reaction of **1** with **5**.

General Procedure for Clay Montmorillonite-Catalyzed Aldol Reactions of Silyl Enol Ethers with Aldehydes and Acetals. Montmorillonite (0.2 g) in a 20 ml round-bottomed flask was dried at 120 °C and 0.5 Torr for 3 h in an oil bath, and cooled under nitrogen. A solution of an aldehyde or an acetal (1 mmol) in a solvent (3 ml) was added. After the mixture being stirred for 1 min, a solution of silyl enol ether (1 mmol) in a solvent (1 ml) was added at −78 °C. The temperature was raised, the mixture was stirred under the conditions listed in tables. As work-up, cold ether (−50 °C, 5 ml) was added, the montmorillonite was filtered off through a Celite pad and washed with ether. The organic layer was evaporated and distilled on a Kugelrohr apparatus to yield aldol products.

General Procedure for Liquid Acid Promoter-Mediated Reactions (Table 1, Entries 8—11). To a stirred solution of **1** (1 mmol) and **5** (1 mmol) in CH_2Cl_2 (3 ml) was added an appropriate amount of an acid promoter in CH_2Cl_2 (1 ml) under a nitrogen atmosphere at −78 °C. After the mixture being stirred, aqueous $NaHCO_3$ was added, the resulting mixture was extracted with ether. An organic layer was dried over Na_2SO_4, and distilled on a Kugelrohr apparatus to yield **16**.

General Procedure for CF_3SO_3H and $CF_3SO_3SiMe_3$-Mediated Reactions of Aldehydes with Nucleophiles. To a stirred solution of an aldehyde (1 mmol) and a nucleophile (1 mmol) in CH_2Cl_2 (3 ml) was added an acid promoter (0.003 mmol) in CH_2Cl_2 (1 ml) under a nitrogen atmosphere at −78 °C. When the reaction was slow, the temperature was raised and/or the acid promoter was supplemented. The mixture was quenched with a few drops of pyridine, diluted with ether, and poured into an aqueous $NaHCO_3$ solution, and then the organic solvent was evaporated. Organic products were extracted with ether. The extract was washed with water and dried over Na_2SO_4, and products were purified by distillation or by TLC.

$BF_3 \cdot OEt_2$-Mediated Reaction of 1 and 6 (Table 2, Entries 16—18). To a stirred solution of **6** (1 mmol) in a solvent (2 ml) at −78 °C was added a solution (1 ml) of $BF_3 \cdot OEt_2$ (1 mmol) under a nitrogen atmosphere. Then **1** (1 mmol) in a solvent (1 ml) was added. After the mixture being stirred under conditions listed in Table 2, the reaction was quenched by injecting aqueous $NaHCO_3$. The mixture was warmed to room temperature and the mixture was extracted with ether. The organic layer was dried over Na_2SO_4 and the solvent was removed. The crude product was treated with *N*-(trimethylsilyl)imidazole (1 mmol) and one drop of chlorotrimethylsilane in ether for 0.5 h at room temperature. The reaction mixture was washed with water and the organic layer was dried over Na_2SO_4. The organic layer was evaporated and distilled on a Kugelrohr apparatus to yield **12**.

Poisoning Experiments of Al-Mont with Triethylamine. Al- Mont (0.2 g) in a 20 ml round-bottomed flask was dried at 120 °C and 0.5 Torr for 3 h in an oil bath, cooled to −78 °C under nitrogen, and dipped with CH_2Cl_2 (1 ml). Then a solution of triethylamine (0.0005—0.047 mmol) in CH_2Cl_2 (1 ml) was added. After the mixture was stirred for 10 min, a solution of **6** (1 mmol) in CH_2Cl_2 (1 ml) was added. After 5 min, a solution of **1** (1 mmol) in CH_2Cl_2 (1 ml) was added dropwise over 0.5 min and the mixture was stirred for 30 min at −78 °C and cold ether (5 ml) was added. Al-Mont was filtered off through a Celite pad and washed with ether. The organic layer was evaporated and distilled on a Kugelrohr apparatus to yield **12**.

Measurement of Acid Strength of Al-Mont.[21] Al-Mont (0.05 g) was dried at 120 °C and 0.5 Torr for 3 h. This sample was immersed in a solvent (1 ml). Then a few drops of a 0.1 wt% benzene solution of a Hammett indicator was added and the color of the indicator on the sample was judged with naked eyes.

Stereochemistry of Products. The assignment of relative configuration (threo or erythro) of the aldol products derived from **12**—**15** was made with ^1H NMR analysis of the $J_{threo} > J_{erythro}$ relationship[1b,28] and ^{13}C NMR analysis based on the upfield chemical shifts of the carbinol carbon and the methine carbon in the erythro isomer compared with those in the threo isomer.[29] Othe products were identified according to the literatures.[2a,2b,13,15,23,29,30] Diastereomer ratios were determined by GC except for **18**.

2-[Phenyl(trimethylsiloxy)methyl]cyclohexanone (12).[2a]

A mixture of diastereomers (threo : erythro=3 : 1): bp 140 °C (bath temp)/0.3 Torr; ^{1}H NMR ($CDCl_3$) δ=0.01 and 0.05 (two s, 3 : 1 ratio, 9H, CH_3Si), 1.3—2.6 (br, 9H, aliphatic CH), 5.10 (d, J=7.9 Hz, CHO, threo), 5.38 (d, J=3.9 Hz, CHO, erythro), and 7.28 (s, 5H, C_6H_5); IR (CCl_4) 1713 cm^{-1} (C=O); GC (OV-1, 25 m, 180 °C, 0.5 kg cm^{-2}) t_R 12.8 min (threo), 13.2 min (erythro).

2-(Phenylhydroxymethyl)cyclohexanone. A mixture of diastereomers obtained from **12** by hydrolysis: ^{1}H NMR ($CDCl_3$) δ=1.2—2.7 (br, 9H, aliphatic CH), 4.78 (d, J=8.7 Hz, CHO, threo), 5.37 (d, J=2.3 Hz, CHO, erythro), and 7.30 (s, 5H, C_6H_5), ^{13}C NMR ($CDCl_3$) δ=57.0 and 57.2 (1 : 3 ratio, O=C<u>C</u>H), 70.3 and 74.4 (1 : 3 ratio, CHO); IR (CCl_4) 1700 (C=O) and 3560 cm^{-1} (OH).

2-[(2-Furyl)trimethylsiloxymethyl]cyclohexanone (13). A mixture of diastereomers (threo : erythro=1 : 4): bp 140 °C (bath temp)/0.3 Torr; ^{1}H NMR ($CDCl_3$) δ=0.01 and 0.04 (two s, 1 : 4 ratio, 9H, CH_3Si), 1.4—3.1 (br, 9H, aliphatic CH), 5.14 (d, J=8.2 Hz, CHO, threo), 5.28 (d, J=6.0 Hz, CHO, erythro), 6.3 (m, 2H, CH=C), and 7.4 (m, 1H, C=CH-O); IR (CCl_4) 1714 cm^{-1} (C=O); GC (PEG-HT, 150 °C, 1.0 kg cm^{-2}; t_R 6.8 min (erythro), 7.4 min (threo).

2-[(2-Furyl)hydroxymethyl]cyclohexanone. Obtained from **13** by hydrolysis. ^{13}C NMR ($CDCl_3$) δ=54.5 and 54.9 (4 : 1 ratio, O=C<u>C</u>H), 66.4 and 68.0 (4 : 1 ratio, CHO). Each diastereoisomer was separated by preparative TLC (3 : 1 ether-hexane, developed 2 times). **A Threo Isomer:** R_f 0.42; ^{1}H NMR ($CDCl_3$) δ=1.4—3.2 (br, 9H, aliphatic CH), 3.9 (br, 1H, OH), 4.85 (d, J=8.2 Hz, CHO), 6.30 (m, 2H, CH=C), and 7.38 (m, 1H, C=CH-O); IR (CCl_4) 1702 (C=O) and 3560 cm^{-1} (OH). Found: C, 67.72; H, 7.27%. Calcd for $C_{11}H_{14}O_3$: C, 68.02; H, 7.23%. **An Erythro Isomer:** R_f 0.48; ^{1}H NMR ($CDCl_3$) δ=1.4—3.2 (br, 10H, aliphatic CH and OH), 5.24 (d, J=3.0 Hz, 1H, CHO), 6.30, (m, 2H, CH=C) and 7.33 (m, 1H, C=CHO); IR (CCl_4) 1968 (C=O) and 3580 cm^{-1} (OH).

2-[(2-Thienyl)trimethylsiloxymethyl]cyclohexanone (14). A mixture of diastereomers (threo : erythro=3 : 1): bp 150 °C (bath temp)/0.5 Torr; ^{1}H NMR ($CDCl_3$) δ=0.01 and 0.04 (two s, 3 : 1 ratio, 9H, CH_3Si), 1.4—2.6 (br, 9H, aliphatic CH), 5.39 (d, J=6.8 Hz, CHO, threo), 5.55 (d, J=4.8 Hz, CHO, erythro), 6.9 (m, 2H, CH=C), and 7.2 (m, 1H, C=CHS); IR (CCl_4) 1708 cm^{-1}(C=O); GC (OV-1, 170 °C, 1.0 kg cm^{-2}) t_R 9.1 min (threo), 9.6 min (erythro).

2-[(2-Thienyl)hydroxymethyl]cyclohexanone. A mixture of diastereomers obtained from **14** by hydrolysis: ^{1}H NMR ($CDCl_3$) δ=1.4—2.9 (br, 9H, aliphatic CH), 3.8 (br, 1H, OH), 5.07 (d, J=8.3 Hz, CHO, threo), 5.53 (d, J=3.0 Hz, CHO, erythro), 7.0 (m, 2H, CH=C), and 7.3 (m, 1H, C=CHS); ^{13}C NMR ($CDCl_3$) δ=57.2 and 57.8 (1 : 3 ratio, O=C<u>C</u>H), 68.2 and 70.6 (1 : 3 ratio); IR (CCl_4) 1702 (C=O) and 3560 cm^{-1} (OH). Found: C, 62.81; H, 6.83%. Calcd for $C_{11}H_{14}O_2S$: C, 62.83; H, 6.71%.

2-(3-Methyl-1-trimethylsiloxybutyl)cyclohexanone (15). bp 130 °C (bath temp)/0.5 Torr; GC (PEG-HT, 120 °C, 0.5 kg cm^{-2}) t_R 10.8 min (erythro), 11.1 min (threo). Each diastereoisomer was separated by preparative TLC (15 : 1 hexane-ether, developed 5 times). **A Threo Isomer:** R_f 0.59; ^{1}H NMR ($CDCl_3$) δ=0.12 (s, 9H, CH_3Si), 0.94 (d, J=6.0 Hz, 6H, CHC<u>H</u>$_3$), 1.2—2.5 (br, 9H, aliphatic CH), and 4.15—4.45 (m, 1H, CHO); IR (CCl_4) 1712 cm^{-1} (C=O). **An Erythro Isomer:** R_f 0.63; ^{1}H NMR ($CDCl_3$) δ=0.12 (s, 9H, CH_3Si), 0.92 (d, J=6.0 Hz, 6H, CHC<u>H</u>$_3$), 1.2—2.5 (br, 9H, aliphatic CH), and 4.20—4.50 (m, 1H, CHO); IR(CCl_4) 1712 cm^{-1} (C=O).

2-(1-Hydroxy-3-methylbutyl)cyclohexanone. Obtained from **15** by hydrolysis. A mixture of diastereomers (threo : erythro=3 : 2): ^{13}C NMR; δ=55.4 and 56.7 (2 : 3 ratio, O=C<u>C</u>H), 67.0 and 69.8 (2 : 3 ratio, CHO). Found: C, 71.71; H, 10.83%. Calcd for $C_{11}H_{20}O_2$: C, 71.70; H, 10.94%. **A Threo Isomer:** ^{1}H NMR ($CDCl_3$) δ=0.90 and 0.92 (two d, J=6.1, 6.1 Hz, 6H, CH_3), 1.2—2.5 (br, 13H, aliphatic CH), 3.79 (ddd, J=9.0, 7.0, 4.5 Hz, 1H, CHO), and 4.6 (s, 1H, OH); IR (CCl_4) 1708 cm^{-1} (C=O). **An Erythro Isomer:** ^{1}H NMR ($CDCl_3$) δ=0.92 (d, J=6.0 Hz, 6H, CH_3), 1.2—2.5 (br, 14H, aliphatic CH and OH), 4.21 (ddd, J=9.0, 3.6, 2.7 Hz, 1H, CHO), and 4.6 (s, 1H, OH); IR (CCl_4) 1708 cm^{-1} (C=O).

2-(Methoxyphenylmethyl)cyclohexanone (16).[2b] A mixture of diastereomers (threo : erythro=1 : 6): bp 145 °C (bath temp)/0.8 Torr; ^{1}H NMR ($CDCl_3$) δ=1.4—2.6 (br, 9H, aliphatic CH), 3.20 and 3.27 (two s, 1 : 6 ratio, 3H, OCH_3), 4.56 (d, J=8.6 Hz, CHO, threo), 4.79 (d, J=4.1 Hz, CHO, erythro), and 7.30 (s, 5H, C_6H_5); IR (CCl_4) 1712 cm^{-1} (C=O); GC (OV-1, 180 °C, 0.5 kg cm^{-2}) t_R 9.9 min (erythro), 10.2 min (threo).

2-(1-Methoxy-2-methylpropyl)cyclohexanone (17).[2b] bp 110 °C (bath temp)/2 Torr; GC PEG-HT (110 °C, 1.0 kg cm^{-2}) t_R 6.4 min (erythro), 8.5 min (threo). Each diastereoisomer was separated by preparative TLC (5 : 1 hexane-ether, developed 2 times). **A Threo Isomer:** R_f 0.42; ^{1}H NMR ($CDCl_3$) δ=0.91 and 0.94 (two d, J=6.7, 6.7 Hz, 6H, CH_3), 1.4—2.6 (br, 10H, aliphatic CH), 3.3—3.5 (m, 1H, CHO), and 3.43 (s, 3H, OCH_3); IR (CCl_4) 1712 cm^{-1} (C=O). **An Erythro Isomer:** R_f 0.58; ^{1}H NMR ($CDCl_3$) δ=0.88 and 0.93 (two d, J=6.5, 6.5 Hz, 6H, CH_3), 1.4—2.6 (br, 10H, aliphatic CH), 3.43 (s, 3H, OCH_3), and 3.4—3.6 (m, 1H, CHO); IR (CCl_4) 1708 cm^{-1} (C=O).

2-Methyl-1-phenyl-1-trimethylsiloxy-3-pentanone (18). A mixture of diastereomers (threo : erythro=3.2 : 1): bp 110 °C/0.4 Torr; ^{1}H NMR ($CDCl_3$) δ=−0.08 and 0.02 (two s, 3.2 : 1 ratio, 9H, CH_3Si), 0.73 (d, J=8.0 Hz, 3H, CHC<u>H</u>$_3$), 1.08 (t, J=8.9, Hz, 3H, CH_2C<u>H</u>$_3$), 1.9—3.2 (m, 3H, CH and CH_2), 4.65 (d, J=9.3 Hz, CHO, threo), 4.81 (d, J=8.0 Hz, CHO, erythro), 7.24 and 7.29 (two s, 5H, C_6H_5); IR (CCl_4) 1714 cm^{-1} (C=O). These diastereomers were inseparable by GC. The isomer ratio was determined by NMR.

1-Hydroxy-2-methyl-1-phenyl-3-pentanone.[30] Obtained from **18** by hydrolysis: ^{1}H NMR ($CDCl_3$) δ=0.8—1.2 (m, 6H, CH_3), 2.3—3.0 (m, 3H, C<u>H</u>$_2$COC<u>H</u>), 3.1 (br, 1H, OH), 4.73 (dd, J=8.3, 2.7 Hz, CHO, threo), 5.00 (d, J=4.8 Hz, CHO, erythro), and 7.31 (s, 5H, C_6H_5); IR (CCl_4) 1712 (C=O) and 3500 cm^{-1} (OH).

2,4,4-Trimethyl-1-phenyl-1-trimethylsiloxy-3-pentanone (19).[23] **A Threo Isomer:** bp 135 °C (bath temp)/0.3 Torr; ^{1}H NMR ($CDCl_3$) δ=−0.13 (s, 9H, CH_3Si), 0.73 (d, 3H, J=7.0 Hz, CHC<u>H</u>$_3$), 1.20 (s, 9H, t-Bu), 3.2 (m, 1H, C<u>H</u>CH$_3$), 4.71 (d, 1H, J=9.8 Hz, CHO), and 7.29 (s, 5H, C_6H_5); IR (CCl_4) 1703 cm^{-1}; GC (OV-1, 160 °C , 0.85 kg cm^{-2}) t_R 8.9 min (erythro), 9.3 min (threo). An authentic sample of an erythro isomer was prepared according to the literature.[23]

4,6-Dimethyl-5-trimethylsiloxy-3-heptanone (20). A mixture of diastereomers (threo : erythro=3 : 1): bp 125 °C (bath temp)/15 Torr; ^{1}H NMR ($CDCl_3$) δ=0.02 and 0.06 (two s, 3 : 1 ratio, 9H, CH_3Si), 0.8—1.2 (m, 12H, CH_3), 1.6 (m, 1H, $CHMe_2$), 2.3—2.9 (m, 3H, C<u>H</u>$_2$COC<u>H</u>), and 3.6—3.9 (m, 1H, CHO); IR (CCl_4) 1713 cm^{-1} (C=O); GC (PEG-HT, 80 °C, 1.0 kg cm^{-2}) t_R 5.1 min (threo), 6.0 min (erythro).

5-Hydroxy-4,6-dimethyl-3-heptanone.[29] Obtained from **20** by hydrolysis. A mixture of diastereomers (threo : eryth-

ro=3:1): ^{1}H NMR ($CDCl_3$) δ=0.8—1.2 (m, 12H, CH_3), 1.7 (m, 1H, $CHMe_2$), 2.3—2.9 (m, 3H, $C\underline{H}_2COC\underline{H}$), 2.6 (s, 1H, OH) and 3.3—3.6 (m, 1H, CHO); IR (CCl_4) 1697 (C=O), and 3520 cm^{-1} (OH); ^{13}C NMR ($CDCl_3$) δ=47.5 and 48.3 (1:3 ratio, O=CCH), 76.4 and 78.4 (1:3 ratio, CHO).

4-Benzyloxy-1-phenyl-3-trimethylsiloxy-1-pentanone (23). A mixture of diastereomers (**23a**:**23b**=2:1) purified by TLC. ^{1}H NMR ($CDCl_3$) δ=0.05 and 0.08 (two s, 2:1 ratio, 9H, CH_3Si), 1.27 (d, J=6.0 Hz, 3H, CH_3), 3.20 (d, 2H, J=6.2 Hz, CH_2CO), 3.6 (m, 1H, CHOSi), 4.4 (m, 1H, $C\underline{H}OCH_2Ph$), 4.6 (m, 2H, CH_2Ph), 7.3 (s, 5H, $CH_2C_6\underline{H}_5$), and 7.4—8.1 (m, 5H, C_6H_5CO); IR (CCl_4) 1692 cm^{-1} (C=O); GC (OV-1, 220 °C, 1.0 kg cm^{-2}) t_R 10.1 min (**23a**), 10.4 min (**23b**). An authentic sample of **23a** was prepared using a $TiCl_4$-mediated reaction.[13]

Methyl 4-Benzyloxy-2,2-dimethyl-3-trimethylsiloxypentanoate (25). A solution of **21** (1 mmol) and **24** (1 mmol) in CH_2Cl_2 (4 ml) was treated with Al-Mont (0.2 g) at 25 °C for 1 h to afford **25** in 62% yield. A mixture of diastereomers (isomer ratio =54:46): bp 180 °C (bath temp)/0.5 Torr; ^{1}H NMR ($CDCl_3$) δ=0.12 and 0.16 (two s, 1:1 ratio, 9H, CH_3Si), 1.1—1.3 (m, 9H, CCH_3), 3.39 and 3.60 (two s, 1:1 ratio, 3H, CH_3O), 3.3—3.6 (m, 1H, $CH_3C\underline{H}O$), 3.96 and 4.00 (two d, 1:1 ratio, J=5.2, 6.0 Hz, 1H, CHOSi), 4.44 and 4.47 (two d, 1:1 ratio, J=5.1, 4.7 Hz, 2H, $PhCH_2$), and 7.31 (s, 5H, C_6H_5); IR (CCl_4) 1730 cm^{-1} (C=O); GC (OV-1, 180 °C, 1.0 kg cm^{-2}) t_R 10.7 min, 11.2 min.

1,4-Diphenyl-3-trimethylsiloxy-1-pentanone (27). A mixture of diastereomers purified by TLC: ^{1}H NMR ($CDCl_3$) δ=−0.08 (s, 9H, CH_3Si), 1.33 (d, J=7.0 Hz, 3H, CH_3), 2.7—3.2 (m, 3H, CH_2 and PhCH), 4.56 (ddd, J=7.3, 6.6, 4.0 Hz, 1H, CH), 7.27 (s, 5H, $C_6\underline{H}_5CH$), and 7.3—8.0 (m, 5H, C_6H_5CO); IR (CCl_4) 1686 cm^{-1} (C=O); GC (OV-1, 180 °C, 1.0 kg cm^{-2}) t_R 24.9 min (**27b**), 25.6 min (**27a**). An authentic sample of **27a** was prepared from **21** and acetophenone by use of LDA.[15]

2-(1-Hydroxy-2-methylpropyl)cyclohexanone (28).[2a] A solution of **1** (1 mmol) and **10** (1.5 mmol) in CH_2Cl_2 (4 ml) was treated with CF_3SO_3H (0.02 mmol) at −30 °C for 0.5 h. Hydrolysis of the silylated aldol product with 1 mol dm^{-3} HCl gave **28** in 38% yield. A mixture of diastereomers (isomer ratio =57:43): ^{1}H NMR ($CDCl_3$) δ=0.7—1.0 (m, 6H, CH_3), 1.3—2.6 (m, 10H, aliphatic CH and OH), and 3.2—3.8 (m, 1H, CHO); IR (CCl_4) 1712 (C=O) and 3500 cm^{-1} (OH); GC (OV-1, 110 °C, 0.8 kg cm^{-2}) t_R 12.0, 12.3 min.

References

1) Review: a) T. Mukaiyama, *Org. React.*, **28**, 203 (1982). b) C. H. Heathcock, "Asymmetric Synthesis," ed by J. D. Morrison, Academic Press, Inc. (1984), Vol. 3, p. 111.

2) a) T. Mukaiyama, K. Banno, and K. Narasaka, *J. Am. Chem. Soc.*, **96**, 7503 (1974). b) S. Murata, M. Suzuki, and R. Noyori, *J. Am. Chem. Soc.*, **102**, 3248 (1980); R. Noyori, S. Murata, and M. Suzuki, *Tetrahedron*, **37**, 3899 (1981). c) T. Mukaiyama, S. Kobayashi, and M. Murakami, *Chem. Lett.*, **1985**, 447, 1759; S. Kobayashi, M. Murakami, and T. Mukaiyama, *ibid.*, **1985**, 1535. d) Y. Naruse, J. Ukai, N. Ikeda, and H. Yamamoto, *Chem. Lett.*, **1985**, 1451.

3) Trityl perchlorate was also used in a polymer-supported form. T. Mukaiyama and H. Iwakiri, *Chem. Lett.*, **1985**, 1363.

4) M. Kawai, M. Onaka, and Y. Izumi, *Chem. Lett.*, **1986**, 381.

5) The application of an inorganic solid with high surface area to organic synthesis is mainly a support for reagents. Review: A. McKillop and D. W. Young, *Synthesis*, **1979**, 401, 481; A. Cornelis and P. Laszlo, *ibid.*, **1985**, 909. For the purpose of carbon-carbon bond formation for organic synthesis, acidic ion-exchange resin is most widely used among solid acids. Review: G. A. Olah, P. S. Iyer, and G. K. S. Prakash, *Synthesis*, **1986**, 513.

6) a) J. M. Thomas, "Intercalation Chemistry," ed by M. S. Whittingham and A. J. Jacobson, Academic Press, New York (1982), p. 55. b) J. A. Ballantine and J. H. Purnell, *J. Mol. Catal.*, **27**, 157 (1984).

7) a) P. Laszlo and A. Mathy, *Helv. Chim. Acta.*, **70**, 577 (1987). b) P. Laszlo and J. Lucchetti, *Tetrahedron Lett.*, **25**, 2147 (1984). c) D. Fishman, J. T. Klug, and A. Shani, *Synthesis*, **1981**, 137.

8) M. Kawai, M. Onaka, and Y. Izumi, *Chem. Lett.*, **1986**, 1581. M. Onaka, R. Ohno, M. Kawai, and Y. Izumi, *Bull. Chem. Soc. Jpn.*, **60**, 2689 (1987). Al-Mont is also a good catalyst for the Michael addition of silyl enol ethers to α,β-unsaturated carbonyl compounds: M. Kawai, M. Onaka, and Y. Izumi, *J. Chem. Soc., Chem. Commun.*, **1987**, 1203.

9) The diastereoselectivity of the reaction was independent of the amount of Al-Mont used. The dependence of diastereoselectivity on solvent has not been reported in the aldol reaction using silyl enol ether.

10) Furfural (**7**) is so labile under acidic conditions that the reaction of **1** with **7** gave a complex mixture by use of $TiCl_4$. A $BF_3 \cdot OEt_2$-mediated reaction in CH_2Cl_2 gave lower yield of the aldol product (64%, threo:erythro=40:60) than an Al-Mont-mediated reaction in CH_2Cl_2.

11) A sample of Al-Mont was dried under the same conditions as those for the aldol reaction. Detailed discussion with respect to maximum acid strength is mentioned later in this paper.

12) Review: M. T. Reetz, *Angew. Chem., Int. Ed. Engl.*, **23**, 556 (1984).

13) M. T. Reetz, K. Kesseler, S. Schmidtberger, B. Wenderoth, and R. Steinbach, *Angew. Chem. Suppl.*, **1983**, 1511.

14) Frenkel, *Clays Clay Miner.*, **22**, 435 (1974), and references cited therein.

15) C. H. Heathcock and L. A. Flippin, *J. Am. Chem. Soc.*, **105**, 1667 (1983).

16) This is the first example of aldol reactions of silyl enol ether with an aldehyde catalyzed by a Brönsted acid.

17) For example, the reaction of CF_3SO_3H with allyltrimethylsilane yielded $CF_3SO_3SiMe_3$: T. Morita, Y. Okamoto, and H. Sakurai, *Synthesis*, **1981**, 745.

18) Silyl enol ethers are consumed via the raction in Scheme 1. However the amount of active sites in Al-Mont is too small to deteriorate the yield of aldol products. Concerning the amount of active sites in Al-Mont, see the last paragraph in this text.

19) CF_3SO_3H is a super acid of H_0=−14.1, while H_0 of H_2SO_4 is −11.9 : J. Grondin, R. Sagnes, and A. Commeyras, *Bull. Soc. Chim. Fr.*, **1976**, 1778; R. D. Howells and J. D. McCown, *Chem. Rev.*, **77**, 69 (1977), and references cited therein.

20) $CF_3SO_3SiMe_3$ also failed to promote this reaction: T. Tsunoda, M. Suzuki, and R. Noyori, *Tetrahedron Lett.*, **21**, 71 (1980).

21) H. A. Benesi, *J. Am. Chem. Soc.*, **78**, 5490 (1956).

22) H. O. House, L. J. Czuba, M. Gall, and H. D. Olmstead, *J. Org. Chem.*, **34**, 2324 (1969).
23) C. H. Heathcock, C. T. Buse, W. A. Kleschick, M. C. Pirrung, J. E. Sohn, and J. Lampe, *J. Org. Chem.*, **45**, 1066 (1980).
24) R. E. Ireland, R. H. Mueller, and A. K. Willard, *J. Am. Chem. Soc.*, **98**, 2868 (1976).
25) C. Ainsworth, F. Chen, and Y.-N Kuo, *J. Organomet. Chem.*, **46**, 59 (1972).
26) C. H. Heathcock, M. C. Pirrung, J. Lampe, and S. D. Young, *J. Org. Chem.*, **46**, 2290 (1981).
27) An ion exchange procedure: M. Onaka, M, Kawai, and Y. Izumi, *Bull. Chem. Soc. Jpn.*, **59**, 1761 (1986).
28) H. O. House, D. S. Crumrine, A. Y. Teranishi, and H. D. Olmstead, *J. Am. Chem. Soc.*, **95**, 3310 (1973).
29) C. H. Heathcock, M. C. Pirrung, and J. E. Sohn, *J. Org. Chem.*, **44**, 4294 (1979).
30) C. H. Heathcock, S. K. Davidsen, K. T. Hug, and L. A. Flippin, *J. Org. Chem.*, **51**, 3027 (1986).

Chemistry of Germanium Atoms. II. Reactions of Thermally Evaporated Germanium Vapor with Organic Halides[1,2]

Kunio MOCHIDA,* Kumiko TASHIRO, Yasuhiro YOSHIDA, and Yasuhisa MIZUNO
Department of Chemistry, Faculty of Sciences, Gakushuin University, 1-5-1 Mejiro, Tokyo 171
(Received September 18, 1987)

Thermally generated germanium atoms were found to react with organic halides by insertion into carbon-halogen bonds. The resulting germylenes abstracted halogens from organic halides to form trihalogermyl derivatives. Tetrahalogermanes were also formed by the abstraction of halogens with germanium atoms.

The study of a group 4B element-vapor reaction has been of considerable interest in organometallic chemistry and organic synthesis during the last few decades.[3] With this method, it is proving feasible to synthesize organometallic compounds containing group 4B elements which would be difficult, if not impossible, to prepare by other methods and to study their reactive intermediates. The study of carbon and silicon atoms as homologue of the germanium atom has been fairly well investigated, while the chemical properties of germanium atoms have been little studied.[4-8] In this paper, we report on the reactions of thermally evaporated germanium vapor (atoms) with organic halides.

The reactions of carbon atoms and silicon atoms with compounds containing carbon-halogen bonds for good trapping agents have been reported.[9,10] Under these circumstances, we have undertaken a co-condensation of germanium atoms with organic halides. The present finding is valuable for understanding not only the chemical properties of germanium atoms but also organogermanium intermediates in solutions.

Results and Discussion

The apparatus described in the Experimental section was used. Germanium metal was evaporated at a temperature of ca. 1200—1300 °C using a filament of tungsten in vacuo (ca. 5×10^{-3} Torr, 1 Torr=133.322 Pa) at a rate of ca. 10 mg min^{-1}.[11] During the vaporization of germanium metal, an excess of organic halide was introduced, as vapor, into a reaction flask. Germanium atoms and organic halide vapor was co-condensed on the walls of the reaction vessel which was cooled at 77 K. The color of co-condensation product, thus prepared, was muddy brown. After the germanium evaporation and introduction of the organic halide were completed, the reaction flask was warmed to room temperature. The co-condensation product of germanium atoms and organic halide vapor turned black. The products were identified by comparing their GC-MS and retention times on GLC with those of authentic samples. The yields of products were calculated by GLC with an internal standard.

The reactions of thermally vaporized germanium atoms with organic halides were examined. The products containing germanium are summarized in Table 1.

The reaction of germanium atoms with CCl_4 produced $GeCl_4$ (<10%), CCl_3GeCl_3 (7.0%), CCl_3CCl_3 (6.5%), and several high-boiling-point products (No. 1). The high-boiling-point products obtained did not contain germanium atoms. McGlinchey and Tan reported on a similar co-condensation of germanium atoms with CCl_4, but did not observe the formation of $GeCl_4$.[7] The yields of products were increased when a mixture of germanium atoms/copper atoms and germanium atoms/chromium atoms was used (Nos. 2 and 3, respectively). The formation of CCl_3GeCl_3 shown in Table 1 is explained by the insertion of germanium atoms into C-Cl bonds of CCl_4 to form $ClGeCCl_3$. The resulting germylene is known to abstract chlorines.[12] The compound $GeCl_4$ presumably arises as a result of abstraction of four chlorine atoms from CCl_4 by germanium atoms in a stepwise manner. The reason for increased yields of products for germanium atoms/copper atoms and germanium atoms/chromium atoms is not clear.

Other tetrahalomethanes showed a similar behavior; the reactions of germanium atoms with $CFCl_3$ and $BrCCl_3$ gave mainly $CFCl_2GeCl_3$ (1.6%) and CCl_3GeBr_3 (7.8%), respectively (Nos. 4 and 5).

The reaction of germanium atoms with $CHCl_3$ gave $CHCl_2GeCl_3$ (8.0%) as trihalogermyl compounds (No. 6). When CH_2Cl_2 and CH_2Br_2 were used as substrate, the trihalogermyl compounds formed were $CH_2ClGeCl_3$ (0.3%) and $CH_2BrGeBr_3$ (0.7%), respectively (Nos. 7 and 8).

Taking the results (Nos. 1—8) shown in Table 1 into consideration, the order of decreasing reactivity towards carbon-halogen insertion by germanium atoms is C-Br>C-Cl≫C-F. This may be a reflection of the carbon-halogen bond strengths.

The reaction of germanium atoms with MeI produced GeI_4 (14.0%), $MeGeI_3$ (11.0%), and Me_2GeI_2 (0.5%) (No. 9). Other alkyl iodides showed a similar behavior; the reactions of germanium atoms with EtI, *n*-PrI, *i*-PrI, and *n*-BuI gave $EtGeI_3$ (2.8%) (No. 10), *n*-$PrGeI_3$ (2.7%) (No. 11), *i*-$PrGeI_3$ (5.3%) (No. 12), and *n*-$BuGeI_3$ (1.0%) (No. 13), respectively. Compound GeI_4 was also produced in all reactions of germanium atoms with alkyl iodides. No reactions occurred with

alkyl monobromides and alkyl monochlorides.

On the other hand, the reaction of germanium atoms with PhBr produced Ph_2GeBr_2 (0.05%) and Ph_3GeBr (0.01%) (No. 16). With PhCl, germanium atoms reacted to give only PhH and Ph-Ph. The reactivity observed for polyhalomethanes and alkyl iodides is not consistent with those for aryl halides used in this study. The reactions of germanium atoms with aryl halides may involve a radical-initiated process.[13]

Blank experiments were carried out under identical conditions. As a result, the products shown in Table 1 were attributable to the interaction of germanium atoms with the starting organic halides.

A probable pathway for the products shown in Table 1 is outlined in Scheme 1. Thermally evaporated germanium atoms possess a ^3P ground state. ^3P germanium atoms inserted into a carbon-halogen bond of organic halides to form triplet divalent species (germylenes) (Eq. 1). The intially formed triplet germylenes rapidly relax to the singlet state (Eq. 2). The ground state of R_2Ge (R=H, Me) and GeI_2 has been shown to be a singlet by quantum chemical calculations and chemical reactions.[14-16] The singlet germylenes abstract halogens from organic halides in a stepwise manner characteristic of germyl radicals (Eq. 3). Halogen abstraction has also been reported for singlet germylenes.[12]

Table 1. The Reaction of Germanium Atoms with Organic Halides[a]

No.	Substrate	Products (Yield/%[b])
1	CCl_4	$GeCl_4$ (<10[c]), CCl_3GeCl_3 (7.0)
2[d]	CCl_4	$GeCl_4$ (<10[c]), CCl_3GeCl_3 (12.0)
3[e]	CCl_4	$GeCl_4$ (<10[c]), CCl_3GeCl_3 (10.4)
4	$CFCl_3$	$GeCl_4$ (0.6), $CFCl_2GeCl_3$ (1.6)
5	$BrCCl_3$	$GeCl_4$ (5.8), $GeBrCl_3$ (0.6), $GeBrCl_3$ (0.6), $GeBr_4$ (0.7), $CCl_3GeBrCl_2$ (0.6), CCl_3GeBr_3 (7.8)
6	$CHCl_3$	$GeCl_4$ (15.0), $CHCl_2GeCl_3$ (8.0)
7	CH_2Cl_2	$GeCl_4$ (1.6), $CH_2ClGeCl_3$ (0.3)
8	CH_2Br_2	$GeBr_4$ (2.0), $CH_2BrGeClBr_3$ (0.7)
9	MeI	GeI_4 (14.0), $MeGeI_3$ (11.0), Me_2GeI_2 (0.5)
10	EtI	GeI_4 (17.0), $EtGeI_3$ (2.8)
11	*n*-PrI	GeI_4 (3.0), *n*-$PrGeI_3$ (2.7)
12	*i*-PrI	GeI_4 (5.1), *i*-$PrGeI_3$ (5.3)
13	*n*-BuI	GeI_4 (1.0), *n*-$BuGeI_3$ (1.0)
14	*n*-BuBr	No product
15	*n*-BuCl	No product
16	PhBr	Ph_2GeBr_2 (0.05), Ph_3GeBr (0.01)
17	PhCl	No product

a) Reactions were performed at room temperature for 1.5 h. b) Yields of products were determined on the basis of the amount of the germanium metal consumed on the assumption that all of the vaporized germanium metal completely reacted with organic halides. c) The retention time of $GeCl_4$ on GLC was overlapped with that of CCl_4. The yields of $GeCl_4$ could not be accurately determined by GLC. d) A mixture of germanium atoms and copper atoms. e) A mixture of germanium atoms and chromium atoms.

$$\dot{G}e\text{:}\ (^3P) + R\text{-}X \longrightarrow {}^3[R\text{-}\dot{G}e\text{-}X] \quad (1)$$

$$^3[R\text{-}\dot{G}e\text{-}X] \longrightarrow {}^1[R\text{-}\dot{G}e\text{-}X] \quad (2)$$

$$^1[R\text{-}\dot{G}e\text{-}X] \xrightarrow{R\text{-}X} R\dot{G}eX_2 \xrightarrow{R\text{-}X} RGeX_3 \quad (3)$$

$$^1[R\text{-}\dot{G}e\text{-}X] \xrightarrow{R\text{-}X} R_2GeX_2 \quad (4)$$

Scheme 1. The mechanism for germylene intermediates.

On the other hand, singlet germylenes also undergo double insertions (Eq. 4).

C-X bonds of organic halides may also be activated by clusters rather than germanium atoms.

Experimental

^1H NMR spectra were recorded on a Varian FT 80A with tetramethylsilane as an internal-standard. GC-MS spectra were obtained on a JEOL JMS-DX 303 mass spectrometer. Infrared spectra were recorded on a Hitachi 260-10 spectrometer. Gas chromatography was performed on a Shimadzu GC-6A and 8A with 1 m 5% and 20% SE30 columns.

Materials. Organic halides are commercially available and purified prior to use. Copper metal, chromium metal, $GeCl_4$, and GeI_4 are commercially available. CCl_3GeCl_3,[17] $MeGeI_3$,[18] Me_2GeI_2,[18] $EtGeI_3$,[19] *n*-$PrGeI_3$,[19] *n*-$BuGeI_3$,[19] Ph_2GeBr_2,[20] Ph_3GeBr,[21] were prepared as described in the cited references.

Reactions of Germanium Atoms with Organic Halides. As a typical example, the reaction of germanium atoms with chloroform ($CHCl_3$) is described. Germanium atoms were produced by using essentially the same apparatus as described in the literature.[1] Germanium metal (0.5 g, 6.9 mmol) was vaporized at a temperature of 1200—1300 °C by using a resistively heated, alumina-coated tungsten spiral crucible at 6.0—7.0 V, 15A, which was connected to copper electrodes, in vacuo (ca. 5×10^{-3} Torr) at a rate of 10 mg min^{-1}. During vaporization of the germanium metal, $CHCl_3$ (ca. 15 cm^3) was co-condensed on the walls of a quartz reaction flask containing crucible and a perforated inlet tube through which $CHCl_3$ was introduced as vapor. The crucible was maintained at 1200—1300 °C and the reaction flask immersed in liquid nitrogen during germanium vaporization and the introduction of $CHCl_3$. After germanium vaporization and the introduction of $CHCl_3$ were completed, the reaction flask was warmed to room temperature and allowed to stand for 1.5 h. Products were identified by comparing their GC-MS and retention times on GLC with those of authentic samples. The amounts of products were calculated by GLC with an internal-standard method. $GeCl_4$ (15.0%), $CHCl_2GeCl_3$ (8.0%), and several high boiling products were produced. The high boiling products were confirmed to exclude germanium atoms by GC-MS. The yields of products were determined on the basis of the germanium metal consumed by supposing that the germanium metal except for germanium metal that remained in the crucible completely reacted with $CHCl_3$ vapor. Therefore, by taking into consideration that the unreacted germanium metal attaches on the walls of a reaction flask, the yields of products may be underestimated.

Identification of Products. The known compounds were identified by comparing their GC-MS and retention times on GLC with those of authentic samples. The unknown compounds were carefully identified by comparing their GC-MS with those of similar samples and by parent peaks and cleavage patterns considering the natural abundance of germanium (ratio, $^{70}Ge/^{72}Ge/^{73}Ge/^{74}Ge/^{76}Ge=56/75/21/100/21$). $^{74}Ge,^{79}Br^{35}Cl_3$ (parent ion peak at $m/z=258$), $m/z=222$ (22), 179 (22), 153 (15), and 74 (17). $^{74}Ge^{79}Br_3{}^{35}Cl$ (parent ion peak at $m/z=346$), $m/z=347$ (10), 268 (60), 153 (54), 109 (80), and 74 (7). $CF^{35}Cl_2{}^{74}Ge^{35}Cl_3$ (parent ion peak at $m/z=280$), $m/z=245$ (18), 179 (26), 101 (100), 82 (36), and 66 (6). $C^{35}Cl_3{}^{74}Ge^{79}Br_3$ (parent ion peak at $m/z=428$), $m/z=428$ (1), 395 (12), 350 (4), 312 (100), 231 (8), 153 (53), 119 (50), 82 (30), and 74 (10). $C^{79}Br^{35}Cl_2{}^{74}Ge^{79}Br_3$ (parent ion peak at $m/z=474$), $m/z=475$ (0.4), 440 (1), 394 (11), 350 (3.5), 312 (22), 231 (3), 163 (100), 153 (27), and 74 (6). $CH^{35}Cl_2{}^{74}Ge^{35}Cl_3$ (parent ion peak at $m/z=262$), $m/z=227$ (2), 179 (18), 144 (2), 109 (18), and 83 (100). $CH_2{}^{35}Cl^{74}Ge^{35}Cl_3$ (parent ion peak at $m/z=228$), $m/z=194$ (17), 179 (65), 159 (100), 144 (12), 109 (65), and 74 (20). $CH_2{}^{79}Br^{74}Ge^{79}Br_3$ (parent ion peak at $m/z=404$), $m/z=405$ (24), 327 (77), 313 (100), 232 (26), 153 (44), and 74 (6).

The authors thank professor Yoshihito Takeuchi and Mr. Katsumi Shimoda of Tokyo University for a gift of $GeBr_4$. We also thank Mitsubishi Metal Corporation for a gift of germanium metal. This work was supported in part by Grant-in-Aid for Special Project Research (Nos. 61125004 and 62115003) provided by the Ministry of Education, Science and Culture.

References

1) For paper I see: K. Mochida and K. Tashiro, *Nippon Kagaku Kaishi*, **1987**, 1168.

2) Preliminary results of this study see: K. Mochida and K. Tashiro, *Chem. Lett.*, **1987**, 1105.

3) For example: J. R. Blackborow, "Metal Vapor Synthesis in Organomeatllic Chemistry," Springer-Verlag, New York (1979); K. J. Klabunde, "Chemistry of Free Atoms and Particles," Academic Press, New York (1980); K. J. Klabunde, "Reactive Intermediates," ed by R. A. Abramovitch, Plenum Press, New York.

4) P. P. Gasper, C. A. Levy, J. J. Frost, and S. A. Bock, *J. Am. Chem. Soc.*, **91**, 1573 (1969).

5) P. P. Gasper and J. J. Frost, *J. Am. Chem. Soc.*, **95**, 6567 (1973).

6) A. Bos, *J. Chem. Soc., Chem. Commun.*, **1972**, 26.

7) M. J. McGlinchey and T.-S. Tan, *Inorg. Chem.*, **14**, 1209 (1975).

8) R. T. Conlin, S. H. Lockhart, and P. P. Gasper, *J. Chem. Soc., Chem. Commun.*, **1975**, 825.

9) P. S. Skell and R. F. Harris, *J. Am. Chem. Soc.*, **87**, 5807 (1965); P. S. Skell, J. J. Havel, and M. J. McGlinchey, *Acc. Chem. Res.*, **6**, 97 (1973).

10) K. J. Klabunde, "Chemistry of Free Atoms and Particles," Academic Press, New York (1980), Chap. 8, p. 188.

11). K. Mochida and H. Ogawa, *J. Organomet. Chem.*, **243**, 131 (1983).

12) J. Kocher and M. Lehnig, *Organometallics*, **3**, 937 (1984).

13) F. Glockling, "The Chemistry of Germanium," Academic press, New York (1969), p. 125.

14) J.-C. Barthelat, B. S. Roch, G. Tringquir, and J. Satgé, *J. Am. Chem. Soc.*, **102**, 4080 (1980).

15) G. Olbrich, *Chem. Phys. Lett.*, **73**, 110 (1980).

16) M. Schriewer and W. P. Newman, *J. Am. Chem. Soc.*, **105**, 897 (1983).

17) M. J. McGlinchey, J. D. Odom, T. Reynoldson, and F. G. A. Stone, *J. Chem. Soc.*, **1970**, 31.

18) K. Moedritzer, *J. Organomet. Chem.*, **6**, 282 (1966).

19) R. Zablotna, K. Akerman, and A. Szuchnik, Pol. Patent 51899; *Chem. Abstr.*, **67**, 108762x (1967).

20) O. H. Johnson and D. M. Harris, *J. Am. Chem. Soc.*, **72**, 5564 (1950).

21) E. H. Brooks and F. Glockling, *J. Chem. Soc. A*, **1966**, 1241.

 © 1988 The Chemical Society of Japan Bull. Chem. Soc. Jpn., 61, 1251—1258 (1988)

Palladium-Catalyzed Double-Carbonylation of Alkenyl Halides with Secondary Amines To Give α-Keto Amides

Tae-il Son, Hisayoshi Yanagihara, Fumiyuki Ozawa, and Akio Yamamoto*
Research Laboratory of Resources Utilization, Tokyo Institute of Technology, Nagatsuta, Midori-ku, Yokohama 227
(Received September 28, 1987)

The double-carbonylation reaction of alkenyl halides with diethylamine in the presence of palladium catalysts has been examined in detail. The reaction gives α-keto amide together with amide, the single-carbonylation by-product. The yield of α-keto amide is strongly dependent on the nature of alkenyl halide. Alkenyl bromides or iodides having phenyl group(s) as substituent(s) on the vinyl group are successfully double-carbonylated under appropriate reaction conditions and the corresponding α-keto amides are obtained in good to modest yields together with amides. In contrast, the reactions of alkenyl halides without a phenyl group give amides exclusively. In order to clarify the reason for the substrate-specificity in the reaction, series of alkenyl- and alkenoylpalladium(II) complexes, the presumed intermediates in the catalytic reactions, have been prepared and their reactions with secondary amines, carbon monoxide, and alkenyl halides were examined. The study suggests the operation of three types of processes for amide formation in the catalytic reactions. Possible mechanisms for amide as well as α-keto amide formation are discussed.

Recently novel double-carbonylation reactions of organic halides catalyzed by palladium complexes have been discovered.[1-3]

$$RX + 2CO + 2R'_2NH \xrightarrow{[Pd]} RCOCONR'_2 + R'_2NH_2X \quad (R = \text{aryl, alkenyl; } X = Br, I; R' = \text{alkyl}) \quad (1)$$

$$ArX + 2CO + ROH + Et_3N \xrightarrow{[Pd]} ArCOCOOR + Et_3NHX \quad (Ar = \text{aryl; } X = I, (Br); R = \text{alkyl}) \quad (2)$$

$$ArI + 2CO + H_2O + Base \xrightarrow{[Pd]} ArCOCOOH + Base \cdot HI \quad (Base = Et_3N, Ca(OH)_2) \quad (3)$$

Double-carbonylation reactions of aryl halides have been extensively examined and a variety of aryl bromides and iodides were shown to be converted into α-keto amides,[1] α-keto esters,[2] and α-keto acids[3] in good to modest yields by proper choice of nucleophiles used in the catalytic systems. On the other hand, double-carbonylation reactions of other types of organic halides have been explored less extensively.

In this study we examined the double-carbonylation reaction of alkenyl halides in detail. Alkenyl halides can be successfully double-carbonylated only by process (1) using secondary amines. Further study has revealed that yield of α-keto amide in process (1) is strongly dependent on the kind of alkenyl halide. Namely, alkenyl halides having phenyl group(s) as substituent(s) on the vinyl group give α-keto amides together with amides, whereas in the reactions of alkenyl halides without phenyl groups, only amides are formed without any α-keto amide formation. For getting information regarding the substrate-specificity in the double-carbonylation, we prepared alkenyl- and alkenoylpalladium(II) complexes as models of intermediates assumed in the catalytic reactions and examined their reactivity toward secondary amines, carbon monoxide, and alkenyl halides.

Results

Catalytic Reaction. First we sought appropriate conditions for double-carbonylation of alkenyl halides by using styryl bromide and diethylamine as starting materials. Based on the previous results regarding the double-carbonylation of aryl halides,[1] diethylamine was chosen as the most suitable secondary amine for getting α-keto amides. Table 1 summarizes catalytic activities of palladium complexes having several kinds of tertiary phosphine ligands. No product other than α-keto amide and amide was observed in the reactions as confirmed by GLC. Among the complexes examined, the palladium complex coordinated with 1,4-bis(diphenylphosphino)butane (dppb) was found to serve as the most effective catalyst regarding the selectivity for α-keto amide formation as well as conversion of the bromide.

The highest selectivity for α-keto amide formation was achieved at moderate reaction temperatures of 50 °C (Table 1, Runs 5, 8, and 9). Higher CO pressure caused increase in selectivity for α-keto amide formation but significantly retarded the progress of reaction (Runs 5—7). The similar trend of the effect of CO pressure has been observed in the double-carbonylation of aryl bromides and secondary amines.

Although styryl bromide was used as a mixture of *Z* and *E* isomers, only (*E*)-α-keto amide was obtained as double-carbonylation product, presumably for a thermodynamic reason. In contrast, amide, the single-carbonylation by-product, was formed as a mixture of the both isomers.[4]

Table 2 summarizes the results of double carbonylation of various alkenyl halides. In the double-carbonylation of alkenyl bromides and iodides having phenyl group(s), α-keto amides were formed in good to modest selectivities (Runs 1—6). In contrast, no α-keto amide formation was observed when alkenyl halides without phenyl group were employed as starting materials (Runs 7—12).

Table 1. Double-Carbonylation of Styryl Bromide and Et_2NH Promoted by Palladium Catalysts[a]

Run	Catalyst[b]	p(CO)/atm[c]	Temp/°C	Time/h	Product ratio		Conversion of RBr/%
					α-keto amide	amide	
1	$PdCl_2(PMePh_2)_2$	50	50	40	44[d]	56[e]	91
2	$PdCl_2(PEtPh_2)_2$	50	50	67	27[d]	73[f]	100
3	$PdCl_2(PMe_2Ph)_2$	50	50	67	70[d]	30[g]	76
4	$PdCl_2(PEt_2Ph)_2$	50	50	67	50[d]	50[h]	100
5	$PdCl_2$(dppb)	50	50	67	70[d]	30[i]	100
6	$PdCl_2$(dppb)	25	50	24	58[d]	42[j]	97
7	$PdCl_2$(dppb)	10	50	16	14[d]	86[k]	96
8	$PdCl_2$(dppb)	50	40	40	49[d]	51[j]	45
9	$PdCl_2$(dppb)	50	100	20	3[d]	97[l]	100

a) Reactions were carried out by using 6 mmol of styryl bromide (Z/E=1/6.5) without solvent. PhCH=CHBr/Et_2NH/catalyst=1/6/0.01 (molar ratio). b) dppb=$Ph_2P(CH_2)_4PPh_2$. c) Initial value measured at room temperature. Z/E ratio: d) E only; e), 1/5.1; f), 1/8.7; g), 1/5.8; h), 1/3.4; i), 1/9.9; j), 1/6.5; k), 1/7; l), 1/9.6.

Table 2. Reactions of Alkenyl Halides (R^1R^2C=CR^3X) and Et_2NH under CO Pressure in the Presence of Palladium Catalyst[a]

Run	Alkenyl halide				Catalyst[b]	p(CO)[c]	Temp	Time	Conversion[d] of RX (%)	Yield (%/RX)[d]	
	R^1	R^2	R^3	X		atm	°C	h		α-keto amide	amide
1	Ph	H	H	Br[g]	A	50	50	67	100	70[h]	30[j]
2	Ph	H	H	I[h]	B	70	25	70	100	93[h]	7[h]
3	Ph	Ph	H	Br	A	25	60	67	80	51	29
4	Ph	Ph	H	Br	C	40	80	18	100	43	54
5	Ph	Ph	Ph	Br	A	30	100	67	93	33	55
6	Ph	Me	H	Br[h]	A	10	60	164	98	32[h]	54[h]
7	H	H	H	Br	A	40	60	96	100	0	100[f]
8	Me	H	H	Br[i]	A	10	60	115	e)	0	50[k]
9	Me	Me	Me	Br	A	10	100	45	0	0	0
10	H	H	Bu	Br	A	10	60	67	48	0	48
11	H	H	Bu	I	A	40	40	67	100	0	100
12	COOH	Me	H	Br	A	10	60	67	79	0	30

a) Reactions were carried out by using 6 mmol of alkenyl halides without solvent; alkenyl halide/Et_2NH/catalyst=1/6/0.01 (molar ratio). b) A, $PdCl_2(Ph_2P(CH_2)_4PPh_2)$; B, $PdMe_2(PMePh_2)_2$; C, $PdCl_2(PMePh_2)_2$. c) Initial value measured at room temperature. d) Confirmed by means of GLC. e) Not measured. f) Obtained as $Et_2NCH_2CH_2CONEt_2$. Z/E ratio: g), 1/6.5; h), E only; i), 1/3; j), 1/9.9; k), 1/6.1.

Preparation of Alkenyl- and Alkenoylpalladium(II) Complexes. Series of alkenylpalladium(II) complexes having $PMePh_2$ ligands **1a—1d** were prepared as possible intermediates in the catalytic systems.

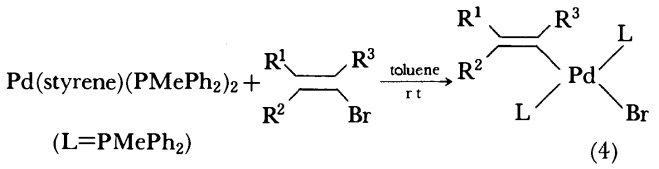

1a: R^1=R^2=R^3=H
1b: R^1=Me, R^2=R^3=H
1c: R^1=Ph, R^2=R^3=H
1d: R^1=R^2=Ph, R^3=H

Reactions of $Pd(styrene)(PMePh_2)_2$[5] with phenyl-substituted vinyl bromides proceeded smoothly in toluene at room temperature to give alkenyl complexes **1c**[6] and **1d** in good yields. In contrast, treatment of $Pd(styrene)(PMePh_2)_2$ with vinyl bromide or 1-propenyl bromide under the same conditions gave $PdBr_2(PMePh_2)_2$ instead of the desired alkenyl complex **1a** or **1b**. Formation of butadiene and 2,4-hexadiene was also noted in the reactions. The reactions may involve the alkenyl complexes **1a** and **1b** as intermediates, which undergo further interaction with alkenyl bromides to give dibromopalladium and butadiene derivatives. Indeed, the reaction of isolated **1b** with 1-propenyl bromide in toluene at room temperature afforded $PdBr_2(PMePh_2)_2$ and 2,4-hexadiene. Addition of free $PMePh_2$ to the reaction systems containing $Pd(styrene)(PMePh_2)_2$ and the alkenyl halides, effectively retarded the formation of the dibromide complex, and **1a** and **1b** could be isolated in good yields.

The alkenyl complexes thus prepared underwent CO insertion into the Pd-C bond in solution to form corresponding alkenoylpalladium complexes **2a—2d** with retention of the trans configuration.

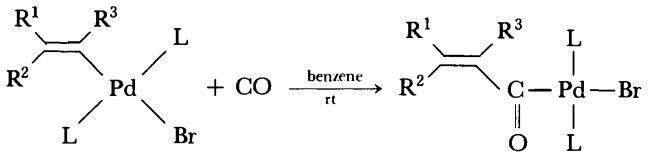

(L=$PMePh_2$)

2a: $R^1=R^2=R^3=H$
2b: $R^1=Me$, $R^2=R^3=H$
2c: $R^1=Ph$, $R^2=R^3=H$
2d: $R^1=R^2=Ph$, $R^3=H$ (5)

The alkenyl- and alkenoylpalladium(II) complexes were characterized by means of elemental analysis and spectroscopy (see Experimental section).

Reactions of the Alkenyl- and Alkenoylpalladium(II) Complexes with Secondary Amines under CO Pressure. 1. Effect of Amine. Reactions of the isolated alkenyl- and alkenoylpalladium(II) complexes with secondary amines under CO pressure smoothly proceeded in solution at room temperature to give corresponding α-keto amides and amides together with ammonium salts. The relative yields of α-keto amide and amide markedly varied with the nature of amine employed for the reaction.

Table 3. Reactions of the Styrylpalladium Complex **1c** with Various Secondary Amines under CO Pressure[a)]

Run	Amine	Product ratio		Total yield (%/Pd)
		α-keto amide	amide	
1	Pr_2NH	51	49	26
2	Et_2NH	87	13	55
3	piperidine	25	75	100
4	pyrrolidine	2	98	100

a) Reactions were carried out by using **1c** (0.05 mmol) and amine (1 mmol) in benzene (3 cm^3) under 50 atm of CO at room temperature for 2 h.

Table 4. Reactions of the Cinnamoylpalladium Complex **2c** with Various Secondary Amines under CO Pressure

Run	Amine	Product ratio		Total yield (%/Pd)
		α-keto amide	amide	
1	Pr_2NH	46	54	30
2	Et_2NH	87	13	46
3	piperidine	100	0	100
4	pyrrolidine	99	1	80

a) Reactions were carried out by using **2c** (0.05 mmol) and amine (1 mmol) in benzene (3 cm^3) under 50 atm of CO at room temperature for 2 h.

Tables 3 and 4 show effects of amines on the reactions of styryl and cinnamoyl complexes **1c** and **2c**. The reactions listed in the tables were carried out for 2 h under the same reaction conditions. In the reactions of the styryl complex **1c** (Table 3), selectivity for α-keto amide formation decreased in the order of diethylamine > dipropylamine > piperidine > pyrrolidine. The order is approximately similar to the selectivity order of these amines in the catalytic double-carbonylation of aryl halides to the α-keto amides except for the reversal of the order of diethylamine and dipropylamine. The selectivity order is inversely related with the previously observed reactivity order of the secondary amines in the reaction of *trans*-$PhCOPdI(PMePh_2)_2$ with the amines under CO.[1a)] The reactivity order of the amines is also reflected in the values of the total yields in Table 3,[7)] namely the reaction proceeds at higher rate with the more compact and reactive amines, such as piperidine and pyrrolidine, to give more amides rather than α-keto amides. However, examination of the reaction of the amines with the cinnamoylpalladium complex **2c** (Table 4) revealed that the reactivity of the alkenoyl complex differs from that of the aroyl complex.[1a,8)] Whereas the reaction of the benzoylpalladium complex with the amines and CO gave only α-keto amides, the reactions of the cinnamoylpalladium complex **2c** afforded also considerable amounts of amides when less reactive diethylamine and dipropylamine were used even under 50 atm of CO, although at higher pressure over 70 atm of CO the amide formation from **2c** became negligible.

2. Effect of Alkenyl Halide. Similarly to the reactions of **1c** and **2c**, reactions of 1-propenyl- and crotonoylpalladium complexes **1b** and **2b** derived from 1-propenyl bromide with diethylamine were found to give α-keto amide in relatively high selectivity under CO pressure (Table 5, Runs 1 and 4). These results are in contrast with those obtained in the catalytic reactions of 1-propenyl bromide, where no α-keto amide formation was observed (Table 2). Since the difference

Table 5. Reactions of Propenyl (**1b**) and Crotonoylpalladium Complex **2b** with Et_2NH under CO Pressure in the Absence and Presence of Propenyl Halides[a)]

Run	Complex	Additive (equiv/Pd)	Product ratio		Total yield (%/Pd)
			α-keto amide	amide	
1	**1b**	—	65	35	45
2	**1b**	MeCH=CHBr (50)	0	100	88
3	**1b**	MeCH=CHI (10)	0	100	250
4	**2b**	—	62	38	43
5	**2b**	MeCH=CHBr (50)	0	100	41

a) Reactions were carried in benzene under 50 atm of CO at room temperature for 2 h. Initial conditions: complex (ca. 0.05 mmol), Et_2NH (1 mmol), and benzene (3 cm^3).

in the reaction conditions between the stoichiometric and the catalytic reactions is the presence of the excess amount of 1-propenyl bromide in the catalytic systems, we next examined effect of 1-propenyl bromide on the reactions of **1b** and **2b** with diethylamine under CO pressure.

As seen from Table 5, in the presence of 1-propenyl bromide, the α-keto amide formation was completely suppressed and only amide was produced (Runs 2 and 5). Furthermore, in the presence of 1-propenyl iodide, **1b** yielded more than a stoichiometric amount of amide without formation of α-keto amide. The observation strongly suggests that 1-propenyl halides may interact with an intermediate species for α-keto amide formation derived from **2b**, carbon monoxide, and diethylamine to alter the reaction course into amide formation.

Kinetic Study on Amide Formation from Cinnamoylpalladium Complex 2c and Diethylamine in the Absence of Carbon Monoxide. The alkenoyl complexes prepared in the present study were found to have higher tendency to afford amides on interaction with amines than the previously reported aroylpalladium complexes.[1a,8] Therefore, we carried out kinetic examination of the amide formation process using cinnamoyl complex **2c** and diethylamine to get further information on the reaction mechanism.

$$\underset{(\mathbf{2c})}{PhCH=CHCOPd(Br)L_2} + 2HNEt_2 \xrightarrow[\text{toluene}]{\text{dmm}} PhCH=CHCONEt_2 + Pd(dmm)L_2 + H_2NEt_2Br \quad (6)$$

(L=$PMePh_2$, dmm=dimethyl maleate[9])

The reaction of **2c** and diethylamine in toluene containing dimethyl maleate[9] under N_2 atmosphere at 40 °C proceeded obeying the first-order kinetics up to 80% conversion of **2c** and gave a quantitative amount of amide. The first-order rate constant (k_{obsd}) increased with increase in the concentration of Et_2NH, while the reaction was effectively retarded by addition of free $PMePh_2$ to the system (Table 6). The k_{obsd} value was inversely proportional to [$PMePh_2$], the concentration of added $PMePh_2$ (Fig. 1).

Table 6. First-Order Rate Constants (k_{obsd}) for the Reaction of *trans*-Pd(COCH=CHPh)Br($PMePh_2$)$_2$ (**2c**) and Et_2NH in Toluene Containing Dimethyl Maleate at 40 °C[a]

Run	[$HNEt_2$]/ mol l^{-1}	[$PMePh_2$]/ mol l^{-1}	$10^4\,k_{obsd}$/s^{-1}	r[b]
1	0.097	0.0	0.68	0.999
2	0.17	0.0	1.05	0.997
3	0.24	0.0	1.43	0.997
4	0.48	0.0	1.73	0.990
5	0.48	0.0011	0.55	0.993
6	0.48	0.0021	0.32	0.999
7	0.48	0.0053	0.27	1.000
8	0.48	0.016	0.19	0.999
9	0.48	0.027	0.15	0.996

a) Initial conditions: [**2c**]=0.025 mol l^{-1}, [dimethyl maleate]=0.20 mol l^{-1}. b) Correlation coefficient for the first-order plot up to 70% conversion of **2c**.

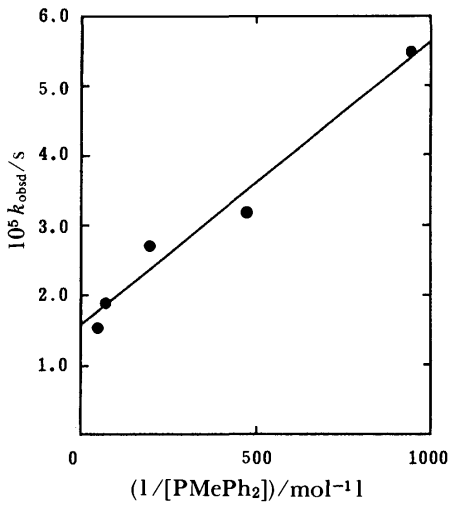

Fig. 1. Plot of k_{obsd} vs. 1/[$PMePh_2$] in the reaction of *trans*-Pd(COCH=CHPh)Br($PMePh_2$)$_2$ (**2c**) and Et_2NH to give amide.

Discussion

The results obtained in the present study regarding reactivity of the isolated alkenyl- and alkenoylpalladium complexes toward CO and amines support the involvement of these organopalladium species as intermediates in the catalytic system for the α-keto amide formation. Scheme 1 represents a catalytic cycle for the α-keto amide formation proposed on the basis of the present study together with information derived in the previous studies.

The alkenyl complex **1**, which is formed by oxidative addition of alkenyl halide to a [Pd(0)L_2] species, undergoes CO insertion into the Pd-C bond to give an alkenoyl complex **2**. Interaction of **2** with CO and amine gives an alkenoyl(carbamoyl)palladium species **3**, which reductively eliminates α-keto amide accompanied by reproduction of a [Pd(0)L_2] species as a carrier of the subsequent catalytic cycle. Since the oxidative addition of alkenyl halide (process (a) in Scheme 1) and the CO insertion (process (b)) are known to proceed with retention of the original configuration at the alkenyl group,[10] the *Z* to *E* isomerization of the alkenyl group observed in the doublecarbonylation of styryl bromide should occur after formation of **3**. It is likely that the highly electron-withdrawing $COCONR'_2$ group induces the *Z* to *E* isomerization after formation of the α-keto amide.

In the previous studies where the aryl halides have been carbonylated in the presence of CO and amines to give α-keto amides and amides, the formation of α-keto amide was accounted for by a scheme analogous to Scheme 1, whereas the formation of amide was accounted for most reasonably by assuming the reac-

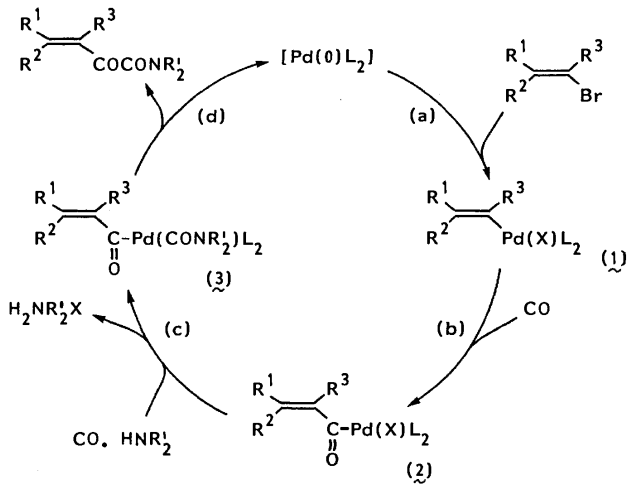

Scheme 1. Proposed mechanism for the palladium-catalyzed double-carbonylation of alkenyl halides and secondary amines to give α-keto amides.

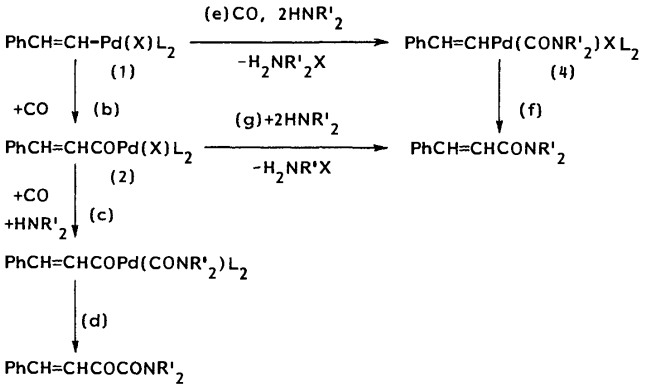

Scheme 2. Possible processes for amide formation in the reaction of alkenylpalladium with secondary amine.

tion of a CO-coordinated arylpalladium complex with amine to give an aryl-carbamoylpalladium complex that subsequently reductively eliminates amide. The results shown in Table 3 regarding the reaction of the styrylpalladium complex **1c** with various amines and CO suggest the operation of similar two routes to give α-keto amide (route b→c→d in Scheme 2) and amide (route e→f).

The formation of α-keto amides in higher yields in the reactions of styryl complex **1c** with amines and CO when less reactive amines are used can be accounted for reasonably by assuming the competitive two routes as in the reaction of the corresponding arylpalladium complexes with CO and the amines. When the reactive amine such as piperidine and pyrrolidine is employed the reaction of the styrylpalladium complex gives amide through the reaction paths (e) and (f), whereas the less reactive amine such as diethylamine and dipropylamine allows the CO insertion to take place through path (b) giving the cinnamoyl complex. Then the reaction of amine with the cinnamoyl complex under CO gives the α-keto amide through paths

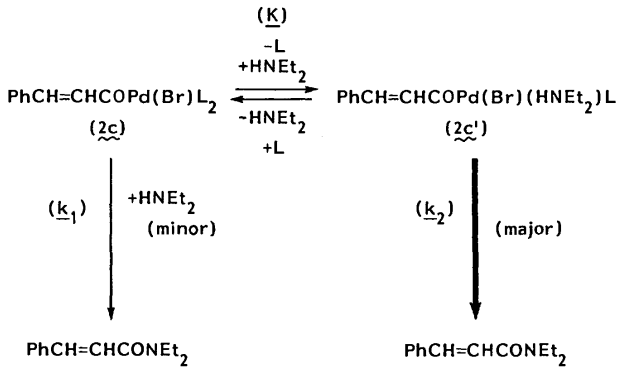

Scheme 3. Proposed mechanism for the amide formation in the reaction of *trans*-Pd(COCH=CHPh)-Br(PMePh$_2$)$_2$ (**2c**) and Et$_2$NH.

(c) and (d) as shown in Scheme 2.

However, the results shown in Table 4 and the kinetic studies of the cinnamoylpalladium complex **2c** with the secondary amines indicate that the amides can be formed by the reaction of the cinnamoyl complex with amines, whereas the corresponding reaction of the benzoylpalladium complex with amines and CO gave α-keto amides exclusively.[1a,8] Thus we have to consider another pathway to give amide from the cinnamoyl complex reacting with the amines as shown by path (g) included in Scheme 2.

In fact the kinetic study of the reaction of the cinnamoyl complex **2c** with diethylamine showed that amide can be readily formed in the reaction of **2c** with diethylamine in the absence of CO, the reaction being retarded in the presence of tertiary phosphine. The results of the kinetic study can be accounted for by assuming Scheme 3 where partial dissociation of the tertiary phosphine ligand from **2c** is involved.

In the major path to give the cinnamoyl amide from **2c** on reaction with HNEt$_2$, participation of an amine-coordinated species **2c′** is assumed. The retardation of the amide formation by addition of L suggests that one of the two tertiary phosphine ligands in **2c** is dissociated. The amide formation from the amine-coordinated intermediate complex **2c′** constitutes the main pathway. As indicated by observation of the intercept in Fig. 1, addition of an excess of L does not inhibit the amide formation completely. Thus we have to assume the presence of a minor pathway to give the amide directly from **2c** without partial dissociation of L.

Assumption of a rapid equilibrium between **2c** and **2c′**[11] and the rate-determining formation of amide from **2c** and **2c′** in Scheme 3 leads to the kinetic expressions given by Eqs. 7 and 8, where $K=[\mathbf{2c'}][L]/[\mathbf{2c}][HNEt_2]$ and $[PdCOR]=[\mathbf{2c}]+[\mathbf{2c'}]$.

$$\frac{d[\text{amide}]}{dt} = \frac{k_1[L]+k_2[K]}{[L]+K[HNEt_2]}[HNEt_2][PdCOR] \quad (7)$$

$$k_{obsd} = \frac{k_1[L]+k_2[K]}{[L]+K[HNEt_2]}[HNEt_2] \quad (8)$$

If one can assume [**2c**]≫[**2c'**] in the reaction solution containing an excess amount of added L, k_{obsd} value should be expressed by Eq. 9, because $[L]+K[HNEt_2] = [L](1+[\mathbf{2c'}]/[\mathbf{2c}]) \approx [L]$.

$$k_{obsd} = k_1[HNEt_2] + \frac{k_2 K[HNEt_2]}{[L]} \quad (9)$$

Equation 9 is compatible with the kinetic observation as shown in Fig. 1.

The behavior of the crotonoylpalladium complex **2b** with CO and Et_2NH shows a striking difference from that of the cinnamoyl complex as shown in Table 5 in that addition of propenyl halides to the reaction of **2b** with CO and Et_2NH completely inhibits the formation of α-keto amide.

$$\text{MeCH=CHCOPd(X)L}_2 \xrightarrow{+\text{CO, HNEt}_2} \text{MeCH=CHCOCONEt}_2 + \text{MeCH=CHCONEt}_2$$
$$\text{MeCH=CHCOPd(X)L}_2 \xrightarrow[+\text{MeCH=CHX (X=Br, I)}]{+\text{CO, HNEt}_2} \text{only MeCH=CHCONEt}_2 \quad (10)$$

Exclusive formation of amide in the catalytic conversion of alkenyl halides without a phenyl substituent (Table 2) is compatible with the behavior of the alkenoyl complex with CO and $HNEt_2$ in the presence of alkenyl halide. The exact reason for diversion of the reaction course that gives considerable amount of α-keto amide in the reaction of the alkenoyl complex with CO and $HNEt_2$ in the absence of alkenyl halide to that giving only amide is presently unclear and merits the further study.

Experimental

Infrared spectra were measured on a Hitachi 295 spectrometer by using KBr pellets for solid and KBr plates for liquid samples. NMR spectra were measured on JEOL FX-100 and PS-100 spectrometers by Dr. Y. Nakamura and Ms. R. Ito of our laboratory. ^{1}H NMR signals are referred to Me_4Si as internal standard and $^{31}P\{^1H\}$ NMR signals to PPh_3 as external standard. Microanalysis (C, H, N, and halogen) was carried out by Mr. T. Saito and Dr. M. Tanaka of our laboratory by using Yanagimoto CHN Autocorder Type MT-2 and Yazawa Halogen Analyzer. Mass spectra were measured on a Hitachi M-80 GC-mass spectrometer.

Solvents and amines were dried in the usual manner, distilled, and stored under a nitrogen atmosphere. Vinyl bromide, 1-propenyl bromide, and styryl bromide were used as purchased without further purification. $Ph_2C{=}CHBr$,[12] $Ph_2C{=}C(Ph)Br$,[13] $Ph(Me)C{=}CHBr$,[14] $Me_2C{=}C(Me)Br$,[15] $CH_2{=}C(Bu)I$,[16] $CH_2{=}C(Bu)Br$,[16] $BrCH{=}C(Me)COOH$,[17] $PhCH{=}CHI$,[18] $MeCH{=}CHI$[18] were prepared according to the methods in literature. Dichlorobis(tertiary phosphine)-palladium(II) complexes were prepared by the reactions of $PdCl_2(PhCN)_2$ with corresponding tertiary phosphines.

Catalytic Double-Carbonylation Reactions. A typical procedure (Table 1, Run 5) is as follows: styryl bromide (*Z*/*E*)=1/6.5; (1.0 g, 5.6 mmol) and diethylamine (3.6 cm^3, 34 mmol) were added to a 100 cm^3 stainless steel pressure bottle containing $PdCl_2(Ph_2P(CH_2)_4PPh_2)$ (0.034 g, 0.057 mmol) under nitrogen atmosphere. After evacuation of the system, 50 atm of CO gas was introduced at room temperature, and the mixture was magnetically stirred at 50 °C for 67 h. After purging the CO gas, the reaction solution was analyzed by means of GLC (Shimadzu GC-6A; column, PEG 20M 1 m) by using *o*-terphenyl as internal standard. The GLC analysis revealed the formation of $PhCH{=}CHCOCONEt_2$ (*E*-form; 70%/styryl bromide) and $PhCH{=}CHCONEt_2$ (*Z*/*E*= 1/10; 30%) at 100% conversion of styryl bromide. The α-keto amide and amide produced were isolated by column chromatography (Merck, Lobar column, LiChroprep Si 60; hexane-Et_2O) after removal of palladium catalyst by bulb-to-bulb distillation (Shibata GTO-250R), and identified by means of elemental analysis, IR and NMR spectroscopy, and mass spectrometry. (*E*)-$PhCH{=}CHCOCONEt_2$: IR (KBr plate) 1640 cm^{-1} (vs); ^{1}H NMR ($CDCl_3$) δ=1.19 (3H, t, *J*=7 Hz, CH_3), 1.24 (3H, t, *J*=7 Hz, CH'_3), 3.28 (2H, q, *J*=7 Hz, CH_2), 3.25 (2H, q, *J*=7 Hz, CH'_2), 6.85 (1H, d, *J*=16 Hz, =CH), 7.58 (1H, d, *J*=16 Hz, =CH'), and 7.2—7.6 (5H, m, Ph). Found: C, 72.6; H, 7.4; N, 6.0%; M$^+$, 231. Calcd for $C_{14}H_{17}NO_2$. C, 72.7; H, 7.4; N, 6.1%; M, 231. $PhCH{=}CHCONEt_2$: Found: C, 76.7; H, 8.5; N, 6.8%; M$^+$, 203. Calcd for $C_{13}H_{17}NO$: C, 76.8; H, 8.4; N, 6.9%; M, 203.

α-Keto amides and amides prepared in this study gave satisfactory analytical and spectroscopic data. The data for α-keto amides are as follows. $Ph_2C{=}CHCOCONEt_2$: mp 80 °C; IR (KBr disk) 1640 cm^{-1} (vs); ^{1}H NMR (CCl_4) δ=0.89 (3H, t, *J*=7 Hz, CH_3), 1.16 (3H, t, *J*=7 Hz, CH'_3), 3.08 (2H, q, *J*=7 Hz, CH_2), 3.11 (2H, q, *J*=7 Hz, CH'_2), 6.72 (1H, s, =CH), and 7.1—7.4 (10H, m, Ph). Found: C, 78.2; H, 6.8; N, 4.6%; M$^+$, 307. Calcd for $C_{20}H_{21}NO_2$: C, 78.1; H, 6.9; N, 4.6%; M$^+$, 307. $Ph_2C{=}C(Ph)COCONEt_2$: mp 118—120 °C; IR (KBr disk) 1680 (s) and 1640 cm^{-1} (vs); ^{1}H NMR (CCl_4) δ=0.64 (3H, t, *J*=7 Hz, CH_3), 1.16 (3H, t, *J*=7 Hz, CH'_3), 2.98 (2H, q, *J*=7 Hz, CH_2), 3.05 (2H, q, *J*=7 Hz, CH'_2), and 7.0—7.4 (15H, m, Ph). Found: C, 81.5; H, 6.4; N, 3.7%; M$^+$, 383. Calcd for $C_{26}H_{25}NO_2$: C, 81.4; H, 6.4; N, 3.7%; M$^+$, 383. (*E*)-$Ph(Me)C{=}CHCOCONEt_2$: IR (KBr plate) 1680 (s) and 1650 cm^{-1} (vs); ^{1}H NMR (CCl_4) δ=1.18 (3H, t, *J*=7 Hz, CH_3), 1.23 (3H, t, *J*=7 Hz, CH'_3), 2.61 (3H, s, $=CCH_3$), 3.33 (2H, q, *J*=7 Hz, CH_2), 3.42 (2H, q, *J*=7 Hz, CH'_2), 6.74 (1H, s, =CH), 7.1—7.6 (5H, m, Ph). Found: C, 72.5; H, 7.9; N, 5.6%; M$^+$, 245. Calcd for $C_{15}H_{19}NO_2$: C, 73.4; H, 7.8; N, 5.7%; M, 245.

Preparation of *trans*-Pd(CH=CH$_2$)Br(PMePh$_2$)$_2$ (1a). To a Schlenk tube containing *trans*-$PdEt_2(PMePh_2)_2$[19] (2.12 g, 3.75 mmol) were added toluene (3 cm^3) and styrene (1.7 cm^3, 15 mmol) at −30 °C under nitrogen atmosphere. The heterogeneous white mixture was stirred at 30 °C for 2 h to give a homogeneous pale yellow solution of $Pd(styrene)(PMePh_2)_2$ with evolution of quantitative amounts of ethane and ethene.[5] After cooling the system to −30 °C, $PMePh_2$ (0.34 cm^3, 3.75 mmol) and vinyl bromide (1 cm^3, 15 mmol) were added to the solution. On stirring the system at room temperature, a white precipitate was gradually formed from the solution. After 3 h the system was concentrated to almost dryness and 15 cm^3 of Et_2O was added at −30 °C to give a white solid. The solid formed was recrystallized from CH_2Cl_2-Et_2O to yield a white crystalline powder of **1a** (2.03 g, 88%): decomp 122—124 °C; ^{1}H NMR ($CDCl_3$, −40 °C) δ=2.13 (6H, t(br), PCH_3), 4.43 (1H, dt, $^3J_{HH}$=16.6 Hz, $^4J_{HP}$=2.5 Hz, =CH cis to Pd), 5.03 (1H, dt, $^3J_{HH}$=8.8 Hz, $^4J_{HP}$=6.1 Hz, =CH trans to Pd), 5.98 (1H, ddt, $^3J_{HH}$=16.6 and

8.8 Hz, $^3J_{HP}$=10.3 Hz, =CH geminal to Pd), 7.3—7.7 (20H, m, PPh); $^{31}P\{^1H\}$ NMR ($CDCl_3$, −40 °C) 15.1 ppm (s). Found: C, 54.9; H, 4.9; Br, 12.5%. Calcd for $C_{28}H_{29}P_2BrPd$: C, 54.8; H, 4.8; Br, 13.0%.

Complex **1b** was similarly prepared by using 1-propenyl bromide instead of vinyl bromide (54%): decomp 117—120 °C; ^1H NMR ($CDCl_3$, −50 °C) δ=2.14 (6H, t(br), PMe), 1.06 (3H, m, =CMe), 4.43 (1H, m, =CH cis to Pd), 5.10 (1H, dtq, $^3J_{HH}$=14.9 Hz, $^3J_{HP}$=10.3 Hz, $^4J_{HH}$=1 Hz), 7.3—7.8 (20H, m, PPh); $^{31}P\{^1H\}$ NMR ($CDCl_3$, −50 °C) 15.8 ppm (s). Found: C, 55.4; H, 4.5; Br, 12.2%. Calcd for $C_{29}H_{31}P_2BrPd$: C, 55.5; H, 5.0; Br, 12.7%.

Preparation of *trans*-Pd(CH=CHPh)Br(PMePh$_2$)$_2$ (1c). To a homogeneous toluene solution of Pd(styrene)-(PMePh$_2$)$_2$ (3.50 mmol, 3 cm^3)[5] was added (*E*)-styryl bromide (1.8 cm^3, 14 mmol)[6] at −30 °C under nitrogen atmosphere. On stirring the system at room temperature, a white precipitate was gradually formed from the solution. After 2 h 10 cm^3 of hexane was added to the system, and the white precipitate formed was collected by filtration, washed with hexane (10 cm^3) and then Et_2O (10 cm^3), and dried in vacuo. The crude product was recrystallized from CH_2Cl_2-Et_2O to yield white crystals of **1c** (2.0 g, 84%): decomp 132—134 °C; ^1H NMR ($CDCl_3$, −40 °C) δ=2.12 (6H, t, *J*=3.4 Hz, PMe), 5.51 (1H, dt, $^3J_{HH}$=15.9 Hz, $^4J_{HP}$=2 Hz, =CH cis to Pd), 6.41 (1H, dt, $^3J_{HH}$=15.9 Hz, $^3J_{HP}$=9.6 Hz, =CH geminal to Pd), 6.3—6.4 (2H, m, =CPh), 7.0—7.1 (3H, m, =CPh), 7.3—7.7 (20H, m, PPh); $^{31}P\{^1H\}$ NMR ($CDCl_3$, −40 °C) 15.5 ppm (s). Found: C, 58.9; H, 4.9; Br, 12.4%. Calcd for $C_{34}H_{33}P_2BrPd$: C, 59.2; H, 4.8; Br, 11.6%.

Complex **1d** was similarly prepared by using Ph_2C=CHBr instead of styryl bromide (81%): decomp 178—182 °C; ^1H NMR ($CDCl_3$, −40 °C) δ=2.00 (6H, t(br), PMe), 6.62 (1H, t, $^3J_{HP}$=9.4 Hz, =CH), 6.4—6.5 (2H, m, =CPh), 7.0—7.6 (28H, m, PPh and =CPh); $^{31}P\{^1H\}$ NMR ($CDCl_3$, =40 °C) 14.6 ppm (s). Found: C, 62.0; H, 5.1; Br, 11.1%. Calcd for $C_{40}H_{37}P_2BrPd$: C, 62.7; H, 4.9; Br, 10.4%.

Preparation of *trans*-Pd(COCH=CH$_2$)Br(PMePh$_2$)$_2$ (2a). To a Schlenk tube containing *trans*-Pd(CH=CH$_2$)Br(PMe-Ph$_2$)$_2$(**1a**; 0.27 g, 0.45 mmol) was added benzene (3 cm^3) under nitrogen atmosphere. After evacuating the system, atmospheric pressure of CO gas was introduced, and the resulted colorless solution was magnetically stirred at room temperature. The color of the solution was quickly changed into yellow. After 2 h, the CO gas was purged and the system was concentrated to almost dryness. Addition of 20 cm^3 of Et_2O to the system at −30 °C gave a yellow precipitate, which was collected by filtration, washed with Et_2O (15 cm^3×3), and dried in vacuo. The yellow powder thus obtained was recrystallized from CH_2Cl_2-Et_2O to yield yellow crystals of **2a** (0.21 g, 67%): decomp 122—125 °C; IR (KBr) 1635 cm^{-1} (vs), ^1H NMR ($CDCl_3$, room temperature) δ=2.11 (6H, t, *J*=3.7 Hz, PMe), 5.19 (1H, ddt, $^3J_{HH}$=17 and 8 Hz, $^4J_{HP}$=1 Hz, =CH geminal to CO), 5.46 (1H, dd, $^3J_{HH}$=8 Hz, $^2J_{HH}$=1 Hz, =CH trans to CO), 6.08 (1H, dd, $^3J_{HH}$=17 Hz, $^2J_{HH}$=1 Hz, =CH cis to CO), 7.2—7.8 (20H, m PPh); $^{31}P\{^1H\}$ NMR ($CDCl_3$, room temperature) 8.9 ppm (s). Found: C, 53.7; H, 4.6; Br, 13.5%. Calcd for $C_{29}H_{29}OP_2BrPd$: C, 54.3; H, 4.6; Br, 12.5%.

Similarly prepared were *trans*-Pd(COCH=CHMe)Br-(PMePh$_2$)$_2$ (**2b**; 53%) and *trans*-Pd(COCH=CHPh)Br-(PMePh$_2$)$_2$ (**2c**; 75%). **2b**: decomp 131—135 °C; IR (KBr) 1633 cm^{-1} (vs); ^1H NMR ($CDCl_3$, room temperature) δ=2.10 (6H, t, *J*=3.4 Hz, PMe), 1.34 (3H, dd, $^3J_{HH}$=6.8 Hz, $^4J_{HH}$=1.5 Hz, =CMe), 4.91 (1H, dq, $^3J_{HH}$=15.4 Hz, $^4J_{HH}$=1.5 Hz, =CH geminal to CO), 6.68 (1H, dq, $^3J_{HH}$=15.4 Hz, $^3J_{HH}$=6.8 Hz, =CH trans to CO), 7.2—7.9 (20H, m, PPh); $^{31}P\{^1H\}$ NMR ($CDCl_3$, room temperature) 8.7 ppm (s). Found: C, 55.6; H, 4.9; Br, 12.9%. Calcd for $C_{30}H_{31}OP_2BrPd$: C, 54.9; H, 4.8; Br, 12.2%. **2c**: decomp 132—134 °C; IR (KBr) 1640 cm^{-1} (vs); ^1H NMR ($CDCl_3$, room temperature) δ=2.12 (6H, t, *J*=3.5 Hz, PMe), 5.48 (1H, dt, $^3J_{HH}$=15.9 Hz, $^4J_{HP}$=1.5 Hz, =CH geminal to CO), 7.1—7.2 (2H, m, =CPh), 7.3—8.1 (24H, m, PPh, =CPh, and =CH cis to CO); $^{31}P\{^1H\}$ NMR ($CDCl_3$, room temperature) 9.0 ppm (s). Found: C, 57.9; H, 4.6; Br, 11.2%. Calcd for $C_{35}H_{33}OP_2BrPd$: C, 58.6; H, 4.6; Br, 11.1%.

Preparation of *trans*-Pd(COCH=CPh$_2$)Br(PMePh$_2$)$_2$ (2d). To a test tube containing *trans*-Pd(CH=CPh$_2$)Br(PMePh$_2$)$_2$ (**1d**; 0.21 g, 0.28 mmol) was added 3 cm^3 of benzene under nitrogen atmosphere. The test tube was placed in a 100 cm^3 stainless steel pressure bottle, and 10 atm of CO gas was introduced at room temperature. After the system was stirred for 8 h at room temperature, the CO gas was purged and the resulted reddish yellow solution was replaced into a Schlenk tube. The solution was concentrated to ca. half in volume. Addition of 20 cm^3 of hexane to the system yielded a yellow powder, which was recrystallized from CH_2Cl_2-Et_2O to give yellow crystals of **2d** (0.43 g, 43%): decomp 179—183 °C; IR (KBr) 1651 cm^{-1}; ^1H NMR ($CDCl_3$, room temperature) δ= 2.12 (6H, t, *J*=3 Hz, PMe), 6.60 (1H, s, =CH), 6.33 (2H, dd, *J*= 8 and 1 Hz, =CPh), 6.72 (2H, dd, *J*=8 and 1 Hz, =CPh′), 6.9—7.8 (26H, m, =CPh, =CPh′ and PPh); $^{31}P\{^1H\}$ NMR ($CDCl_3$, room temperature) 7.7 ppm (s). Found: C, 62.0; H, 5.1; Br, 11.1%. Calcd for $C_{41}H_{37}OP_2BrPd$: C, 62.0; H, 4.7; Br, 10.1%.

Reactions of Organopalladium Complexes with CO and Amines. General Procedure. To a test tube containing an organopalladium complex (ca. 0.05 mmol) were added benzene (3 cm^3), amine (1 mmol), and/or the additive under nitrogen atmosphere. The test tube was placed in a 100 cm^3 stainless steel pressure bottle, and CO gas was introduced at room temperature. After the system was magnetically stirred at room temperature for 2 h, the CO gas was quickly purged and the reaction solution was analyzed by means of GLC.

Kinetic Study on the Amide Formation from 2c and Et$_2$NH. To a Schlenk tube containing **2c** (ca. 25 mmol) and *o*-terphenyl (ca. 0.17 mmol) as an internal standard for GLC analysis, were added toluene (10 cm^3) and adequate amounts of Et_2NH and $PMePh_2$ under argon atmosphere. The Schlenk tube was placed in a thermostated bath (HAAKE F2) controlled to 40.0±0.5 °C. At intervals, a part of the reaction solution (ca. 0.1 cm^3) was sampled and quickly added into an aqueous HCl solution (ca. 1 mol dm^{-1}, 0.5 cm^3) for quenching the reaction. The organic layer separated out from the aqueous solution was analyzed by means of GLC.

The present work was supported by a Grant-in-Aid for Developmental Scientific Research from the Ministry of Education, Science and Culture (No. 62850147).

References

1) a) F. Ozawa, H. Soyama, H. Yanagihara, I. Aoyama, H. Takino, K. Izawa, T. Yamamoto, and A. Yamamoto, *J. Am. Chem. Soc.*, **107**, 3235 (1985); b) F. Ozawa, H. Yanagihara, and A. Yamamoto, *J. Org. Chem.*, **51**, 415 (1986); c) F. Ozawa, H. Soyama, T. Yamamoto, and A. Yamamoto, *Tetrahedron Lett.*, **23**, 3383 (1982); T. Kobayashi and M.

Tanaka, *J. Organomet. Chem.*, **233**, C64 (1982).

2) F. Ozawa, N. Kawasaki, H. Okamoto, T. Yamamoto, and A. Yamamoto, *Organometallics*, **6**, 1640 (1987); F. Ozawa, N. Kawasaki, T. Yamamoto, and A. Yamamoto, *Chem. Lett.*, **1985**, 567; M. Tanaka, T. Kobayashi, T. Sakakura, H. Itatani, S. Danno, and K. Zushi, *J. Mol. Catal.*, **32**, 115 (1985); B. Morin, A. Hirschauer, F. Hugues, D. Commereuc, and Y. Chauvin, *ibid.*, **34**, 317 (1986).

3) M. Tanaka, T. Kobayashi, and T. Sakakura, *J. Chem. Soc., Chem. Commun.*, **1985**, 837; T. Kobayashi, T. Sakakura, and M. Tanaka, *Tetrahedron Lett.*, **28**, 2721 (1987).

4) A. Schoenberg and R. F. Heck, *J. Org. Chem.*, **39**, 3327 (1974); A. Schoenberg, I. Bartoletti, and R. F. Heck, *ibid.*, **39**, 3318 (1974).

5) F. Ozawa, T. Ito, Y. Nakamura, and A. Yamamoto, *J. Organomet. Chem.*, **168**, 375 (1979).

6) M. K. Loar and J. K. Stille, *J. Am. Chem. Soc.*, **103**, 4174 (1981).

7) Since it has been confirmed that the reactions with less reactive Et_2NH and Pr_2NH yield quantitative amounts of α-keto amide and amide at extended reaction time, the values of total yields obtained after the reactions for 2 h at room temperature can be used as a measure of the reactivity of the amines.

8) F. Ozawa, T. Sugimoto, Y. Yuasa, M. Santra, T. Yamamoto, and A. Yamamoto, *Organometallics*, **3**, 683 (1984).

9) In the absence of dimethyl maleate (dmm), Reaction 6 did not proceed according to the first-order kinetics, probably due to interference by a $[Pd(0)L_2]$ species generated in the reaction. Since dmm serves as a good trapping agent of$[Pd(0)L_2]$ species to from stable $Pd(dmm)L_2$ complex,[5] the reaction was followed in the presence of dmm to get a well behaved kinetic results.

10) J. K. Stille and K. S. Y. Lau, *Acc. Chem. Soc.*, **10**, 434 (1977); T. C. Flood, "Stereochemistry of Reactions of Transition Metal-Carbon Sigma Bonds," in "Topics in Stereochemistry, Vol. 12," ed by G. L. Geoffroy, N. L. Allinger, and E. L. Eliel, Wiley, New York (1981), p. 37.

11) Occurrence of the rapid equilibrium between **2c** and **2c'** has been confirmed by observing the ^1H NMR spectrum of **2c** at room temperature in toluene-d_8. In the absence of Et_2NH, methyl protons of $PMePh_2$ ligands in **2c** gave a triplet due to virtual coupling of the phosphorus nuclei, while the PMe-protons were observed as a broad singlet in the presence of Et_2NH.

12) E. P. Kohler and M. Tishler, *J. Am. Chem. Soc.*, **57**, 217 (1935).

13) C. F. Koelsch, *J. Am. Chem. Soc.*, **54**, 2045 (1932).

14) D. R. Davis and J. R. Roberts, *J. Am. Chem. Soc.*, **84**, 2252 (1962).

15) J. I. Kim, B. A. Patel, and R. F. Heck, *J. Org. Chem.*, **46**, 1067 (1981).

16) B. A. Patel, J. I. Kim, D. D. Bender, L. C. Kao, and R. F. Heck, *J. Org. Chem.*, **46**, 1061 (1981).

17) C. Kolbe, *J. Prakt. Chem.*, **25**, 382 (1882).

18) K. Takagi, N. Hayama, and S. Inokawa, *Chem. Lett.*, **1978**, 1435.

19) T. Ito, H. Tsuchiya, and A. Yamamoto, *Bull. Chem. Soc. Jpn.*, **50**, 1319 (1977).

 © 1988 The Chemical Society of Japan Bull. Chem. Soc. Jpn., 61, 1259—1263 (1988)

Studies on Lignan Lactone Antitumor Agents. IV. Synthesis of Glycosidic Lignan Variants Related to α-Peltatin

Hitoshi SAITO, Yoshio NISHIMURA,* Shinichi KONDO, Tomio TAKEUCHI, and (the late) Hamao UMEZAWA
Institute of Microbial Chemistry, 3-14-23 Kamiosaki, Shinagawa-ku, Tokyo 141
(Received October 12, 1987)

Glycosidic variants of 1-β-hydroxy-α-peltatin and 1-β-hydroxy-8-*O*-methyl-α-peltatin were synthesized by glycosidation of 4′,8-di-*O*-benzyloxycarbonyl-1-β-hydroxy-α-peltatin or 4′-*O*-benzyloxycarbonyl-1-β-hydroxy-8-*O*-methyl-α-peltatin with the corresponding glucopyranose or 2-amino-2-deoxyglucopyranose derivatives. Among synthesized compounds, cyclic acetal of 1-*O*-β-(β-D-glucopyranosyl)-8-*O*-methyl-α-peltatin showed antitumor activity in mice with leukemia L-1210.

The lignan lactone antitumor agents, VP-16-213 (etoposide, **1**) and VM-26 (teniposide, **2**), are used for cancer chemotherapy.[1,2] Due to their clinical efficacy, the synthesis of new active analogues of podophyllotoxin glycoside has been of considerable interest. We have previously reported the syntheses of new active aminoglycosidic variants of podophyllotoxin **3**—**5**, which were found to have the superior activities to **1**.[3,4]

The hitherto-known structural modifications of podophyllotoxin glycoside on sugar or on lignan moiety suggested that the following factors played an important role in increasing the antitumor activity; a) the glucose configuration, b) β-glycosidic linkage, c) 4″,6″-*O*-cyclic acetal group, d) β-configuration at C-1, e) trans-fused lactone and f) 4′-phenolic hydroxyl group. In connection with our interest in investigation on the relationship between structure and antitumor activity among lignan lactone glycosides, we undertook the syntheses of glucosidic analogues of α-peltatin **11**, **17**, and **20**. The starting aglycone, 4′,8-di-*O*-benzyloxycarbonyl-1-β-hydroxy-α-peltatin (**7**) was prepared from α-peltatin.[1] Several methods were examined to introduce 1-β-hydroxyl group by a direct bromination and a subsequent substitution of the bromine with a hydroxyl group. The bromination at C-1 of α-peltatin by treatment with *N*-bromosuccinimide (NBS) in THF[5] failed, affording the dibrominated product on both of the aromatic ring B and E which was simultaneously demethylated on the ring E. The attempts of bromination of 4′,8-di-*O*-benzyloxycarbonyl-α-peltatin (**6**) with NBS in THF, and with that in the presence of benzoyl peroxide[6] were also unsuccessful. Finally, an introduction of 1-β-hydroxyl group into **6** was successfully carried out by two-step sequences (bromination and hydrolysis) in a one-pot procedure. Treatment of **6** with bromine in a mixture of aqueous barium carbonate solution and carbon tetrachloride in the presence of α,α′-azobis(isobutyronitrile) (AIBN)[7] gave **7** and an aromatized product **8** in a yield of 58 and 10%, respectively. Condensation of **7** with 2,3-di-*O*-chloroacetyl-4,6-*O*-ethylidene-β-D-glucopyranose (**9**)[8] in dichloromethane in the presence of boron trifluoride diethyl etherate[9] afforded 1-*O*-β-(2,3-di-*O*-chloroacetyl-4,6-*O*-ethylidene-β-D-glucopyranosyl)-4′,8-di-*O*-benzyloxycarbonyl-α-peltatin (**10**) as a sole product in a yield of 72%. The reaction was carried out stereoselectively by the same fashion through a benzyl cation at C-1 of the aglycone moiety generated by BF_3 as has been reported in the previous synthesis.[3,4,8,9] The stereochemistry of the glycoside was also controlled by the anomeric configuration of the original pyranose moiety. Removal of protecting groups in **10** by catalytic hydrogenolysis followed by the treatment with ethylenediamine in pyridine yielded 1-*O*-β-(4,6-*O*-ethylidene-β-D-glucopyranosyl)-α-peltatin (**11**).

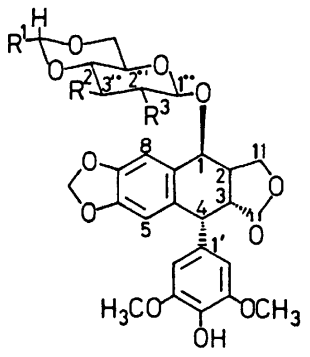

1 : R^1=CH_3, R^2=R^3=OH (Etoposide)
2 : R^1= , R^2=R^3=OH (Teniposide)
3 : R^1=CH_3, R^2=OH, R^3=NH_2
4 : R^1=CH_3, R^2=NH_2, R^3=OH
5 : R^1=CH_3, R^2=OH, R^3=$N(CH_3)_2$

Fig. 1.

Compound **11** showed no antitumor activity against mouse leukemia L-1210 (Table 1). Compound **10** was transformed into 1-β-methoxy-α-peltatin (**12**) having no antitumor activity under the conditions employed in the synthesis of podophyllotoxin glycoside[8] to remove chloroacetyl group [$Zn(OAc)_2$, CH_3OH, reflux]. These results suggested that the glycosidic bond was easily hydrolyzed by the electronic effect of the neighbouring hydroxyl group at C-8.[10] In order to improve its stability, we undertook the synthesis of the methylated compound at C-8, 1-*O*-β-(4,6-*O*-ethylidene-β-D-glucopyranosyl)-8-*O*-methyl-α-peltatin (**17**). Catalytic hydrogenolysis of **7** with 10% palladium on carbon in

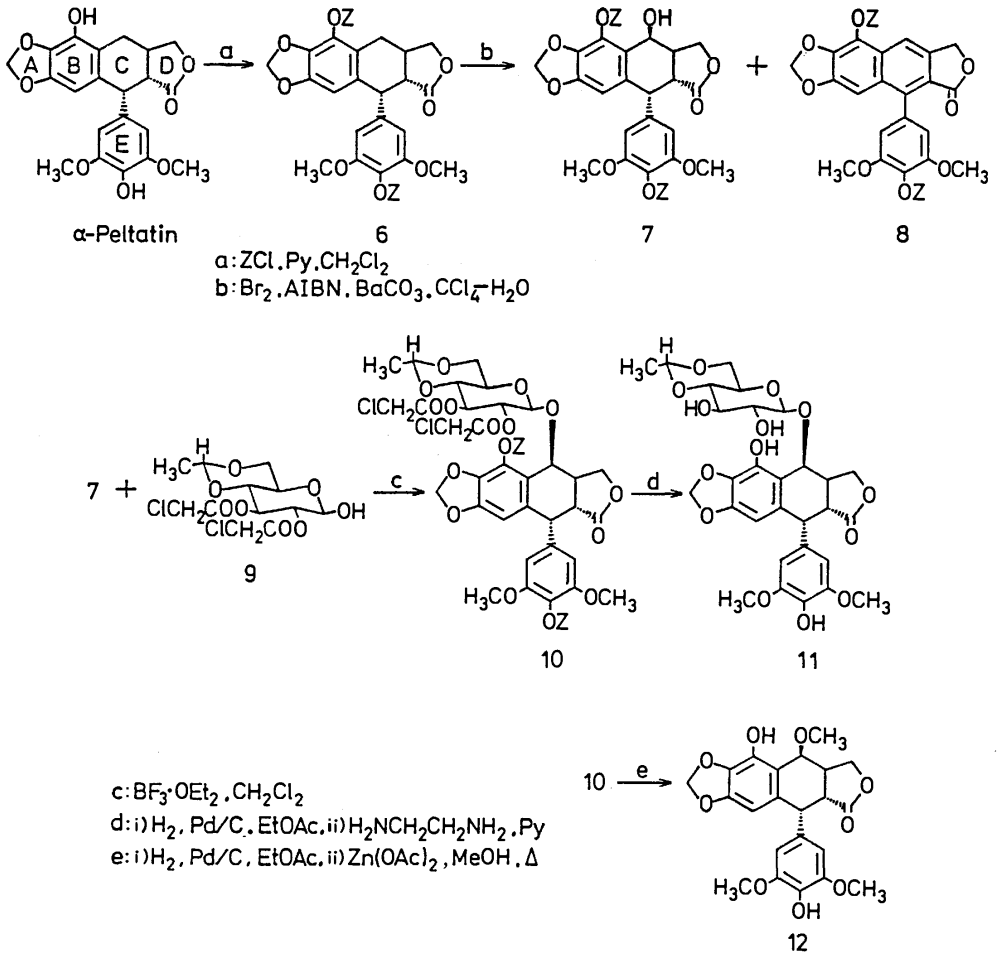

Scheme 1.

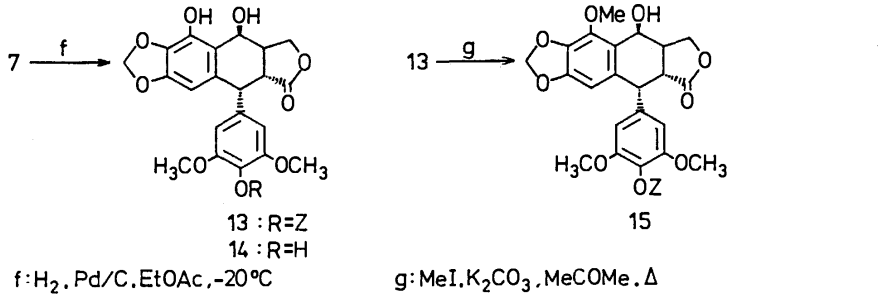

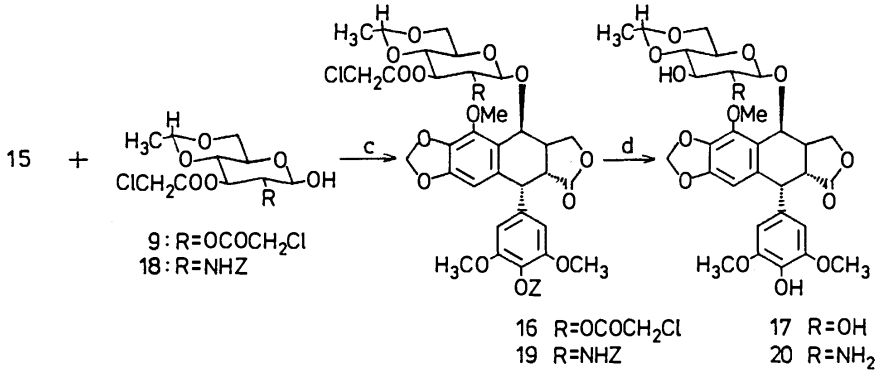

Scheme 2.

Table 1. The Antitumor Activities of α-Peltatin Analogues (T/C%)

Dose (μg/mouse)	Compound No.			
	11	**12**	**17**	**20**
25	105	128	156	119
6.25	117	103	100	95

The T/C values are the percentage ratios of the mean survival period of five treated mice to the mean survival period of the control group. L-1210 cells (10^6 cells) were inoculated intraperitoneally and the intraperitoneal treatment was started on day 1 and continued for 10 days.

ethyl acetate at −20 °C gave 4′-*O*-benzyloxycarbonyl-1-β-hydroxy-α-peltatin (**13**) and 1-β-hydroxy-α-peltatin (**14**) in 70 and 25% yield, respectively. When the same catalytic hydrogenolysis was carried out at room temperature, **14** was obtained as a sole product. Compound **13** was methylated with methyl iodide in the presence of potassium carbonate in acetone to afford quantitatively 4′-*O*-benzyloxycarbonyl-1-β-hydroxy-8-*O*-methyl-α-peltatin (**15**). Condensation of **15** with **9** followed by removal of protecting groups by the same procedure as mentioned above gave **17** in a good yield. Compound **17** was found to have the superior antitumor activity to **11**.

In relation to these syntheses, we were interested in the replacement of the sugar moiety of **17** with an amino sugar. Condensation of **15** with 2-benzyloxycarbonylamino-3-*O*-chloroacetyl-4,6-*O*-ethylidene-β-D-glucopyranose (**18**)[8] and a successive deprotection of the masking groups were carried out by the similar sequences described above to afford 1-*O*-β-(2-amino-2-deoxy-4,6-*O*-ethylidene-β-D-glucopyranosyl)-8-*O*-methyl-α-peltatin (**20**) in an excellent yield. Compound **20** showed no antitumor activity (Table 1). Further study for antitumor activity of synthesized compounds is in progress.

Experimental

General Methods. Melting points were determined with a Yamato apparatus and were uncorrected. IR spectra were determined on a Hitachi Model 260-10 and Jasco IR-810 spectrophotometers. Optical rotations were measured with a Perkin-Elmer Model 241 polarimeter. ^{1}H NMR spectra were recorded with Varian EM-390, Jeol GX-270 and Jeol GX-400 spectrometers. Chemical shifts are expressed in δ values (ppm) with tetramethylsilane as an internal standard. The mass spectra were taken by a Hitachi RMN-7M for field-desorption (FD) and a Jeol D-300 for fast atom bombardment (FAB). Natural α-peltatin was provided by Nippon Kayaku Co., Ltd.

4′,8-Di-*O*-benzyloxycarbonyl-α-peltatin (6). To a solution of α-peltatin (800 mg) in dichloromethane (5 ml) containing pyridine (400 mg) was added a solution of benzyloxycarbonyl chloride (800 mg) in dichloromethane (1 ml) at 0 °C, and the mixture was stirred for 1 h. The solution was washed with water and dried over $MgSO_4$. Evaporation of the solvent gave a solid. The solid was subjected to column chromatography on silica gel. Elution with acetone–toluene (1 : 19) gave **6** (1.1 g, 82%), which was recrystallized from methanol: mp 98—99 °C; $[\alpha]_D^{24}$ −90° (*c* 0.69, $CHCl_3$); IR (KBr) 1770, 1602, 1240, and 1128 cm^{-1}; ^{1}H NMR ($CDCl_3$, 270 MHz) δ=2.40 (1H dd, *J*=5 and 15 Hz, H-1), 2.65 (1H m, H-2), 2.72 (1H dd, *J*=4.7 and 13.7 Hz, H-3), 3.01 (1H dd, *J*=5 and 15 Hz, H-1), 3.69 (6H s, 2×OCH_3), 3.87 (1H t, *J*=9 Hz, H-11), 4.43 (1H dd, *J*=6.6 and 9 Hz, H-11), 4.64 (1H d, *J*=4.7 Hz, H-4), 5.26 and 5.31 (2H each s, 2×$C\underline{H}_2$Ph), 6.01 (2H s, methylene), 6.36 (2H s, H-2′ and 6′), 6.50 (1H s, H-5) and 7.3—7.5 (10H m, 2×Ph); MS (FAB) *m/z* 669 (M^+ +H), 533, and 381.

4′,8-Di-*O*-benzyloxycarbonyl-1-β-hydroxy-α-peltatin (7). To a suspension of **6** (334 mg), AIBN (200 mg) and $BaCO_3$ (500 mg) in a mixture of water (5 ml) and carbon tetrachloride (30 ml) was added bromine (33 μl), and the mixture was stirred at room temperature for 2 h. After evaporation, the mixture was dissolved in a mixture of acetone (30 ml) and water (1 ml), and the solution was stirred at 40 °C for 2 h. The insoluble matter was filtered off, and the filtrate was evaporated to give an oil. The oil was chromatographed on silica gel with the solvent system of acetone–toluene (1 : 5) to give solids of **7** (200 mg, 58%) and **8** (33 mg, 10%). Each solid was recrystallized from ethanol. **7**: mp 105—106 °C. $[\alpha]_D^{23}$ −78° (*c* 0.46, $CHCl_3$); IR (KBr) 1772, 1602, 1482, 1240, 1210 cm^{-1}; ^{1}H NMR ($CDCl_3$, 270 MHz) δ=2.72 (1H m, H-2), 3.32 (1H dd, *J*=5 and 14 Hz, H-3), 3.68 (6H s, 2×OCH_3), 4.37 (2H m, H-11), 4.66 (1H d, *J*=5 Hz, H-4), 5.02 (1H d, *J*=3.4 Hz, H-1), 5.26 and 5.33 (2H each s, 2×$C\underline{H}_2$Ph), 6.04 and 6.06 (2H each d, *J*=1.3 Hz, ethylidene), 6.29 (2H s, H-2′ and 6′), 6.52 (1H s, H-5) and 7.3—7.5 (10H m, 2×Ph); MS (FD) *m/z* 684 (M^+), 640, 599, and 550. **8**: mp 215—216 °C; $[\alpha]_D^{23}$ 0° (*c* 0.5, $CHCl_3$); IR (KBr) 1788, 1615, 1280, and 1228 cm^{-1}; ^{1}H NMR ($CDCl_3$, 270 MHz) δ=3.79 (6H s, 2×OCH_3), 5.33 (2H s, $C\underline{H}_2$Ph), 5.36 (2H s, H-11), 5.38 (2H s, $C\underline{H}_2$Ph), 6.15 (2H s, methylene), 6.55 (2H s, H-2′ and 6′), 7.08 (1H s, H-5), 7.3—7.5 (10H m, 2×Ph), and 7.81 (1H s, H-1); MS (FD) *m/z* 664 (M^+) and 529.

1-*O*-β-(2,3-*O*-Chloroacetyl-4,6-*O*-ethylidene-β-D-glucopyranosyl)-4′,8-di-*O*-benzyloxycarbonyl-α-peltatin (10). To a solution of a mixture of **7** (200 mg) and 2,3-di-*O*-chloroacetyl-4,6-*O*-ethylidene-β-D-glucose (130 mg, **9**) in dichloromethane (5 ml) was added dropwise boron trifluoride etherate (200 μl) at −20 °C, and the mixture was stirred at −20 °C for 1.5 h, then quenched with pyridine (200 μl). Dichloromethane (20 ml) was added, and the solution was washed with water, dried over $MgSO_4$, and filtered. The filtrate was evaporated to give a solid, which was subjected to column chromatography on silica gel. Elution with toluene–acetone (9 : 1) gave a solid of **10** (214 mg, 72%), which was recrystallized from ethanol: mp 116—117 °C, $[\alpha]_D^{23}$ −81° (*c* 0.55, $CHCl_3$); IR (KBr) 1772 and 1240 cm^{-1}; ^{1}H NMR ($CDCl_3$, 90 MHz) δ=1.34 (3H d, *J*=5 Hz, CH_3 of ethylidene), 3.66 (6H s, 2×OCH_3), 6.1 (2H s, methylene), 6.23 (2H s, H-2′ and 6′), 6.50 (1H s, H-5), and 7.2—7.6 (10H m, 2×Ph); MS (FAB) *m/z* 1025 (M^+ +H) and 890.

1-*O*-β-(4,6-*O*-Ethylidene-β-D-glucopyranosyl)-α-peltatin (11). A solution of **10** (180 mg) in ethyl acetate (10 ml) was stirred with 10% Pd/C (10 mg) under atmosphere of hydrogen at room temperature for 2 h. The catalyst was filtered off, and the filtrate was evaporated to give a solid (100 mg). The solid was dissolved in pyridine (1 ml), and to the solution was added ethylenediamine (25 μl) at 0 °C, and then the mixture was stirred at 0 °C for 1.5 h. The mixture was di-

luted with chloroform (30 ml), and washed with 5% aqueous $KHSO_4$ solution and water. The chloroform solution was dried over Na_2SO_4, and evaporated to give a solid. The solid was chromatographed on silica gel with the solvent system of toluene–acetone (2:1) to afford a solid of **11** (72 mg, 68%). The solid was recrystallized from chloroform: mp 208—209 °C (decomp); $[\alpha]_D^{25}$ −96° (*c* 0.3, CH_3OH); IR (KBr) 1758, 1625, 1482, and 1062 cm^{-1}; ^1H NMR ($CDCl_3$, 400 MHz) δ=1.44 (3H d, *J*=5 Hz, CH_3 of ethylidene), 3.26 (1H m, H-2), 3.55 (1H dd, *J*=5 and 14 Hz, H-3), 3.69 (2H m, H-4″ and 5″), 3.75 (6H s, 2×OCH_3), 4.04 (1H t, *J*=8 Hz, H-2″), 4.32 (1H t, *J*=8 Hz, H-3″), 4.38 (1H t, *J*=8 Hz, H-11), 4.80 (1H dd, *J*=9 and 11 Hz, H-11), 4.88 (1H d, *J*=5 Hz, H-4), 4.91 (1H q, *J*=5 Hz, CH of ethylidene), 5.74 (1H d, *J*=3.5 Hz, H-1), 5.76 (1H d, *J*=8 Hz, H-1″), 5.84 and 5.91 (2H ABq, *J*=1 Hz, methylene), 6.45 (1H s, H-5), and 6.86 (2H s, H-2′ and 6′); MS (FD) *m/z* 604 (M^+) and 398.

1-β-Methoxy-α-peltatin (12). A solution of debenzyloxycarbonylated compound of **10** (54 mg) in methanol (5 ml) was refluxed in the presence of zinc acetate (25 mg) for 4 h. After being diluted with chloroform (10 ml), the solution was washed with water, dried over $MgSO_4$, and filtered. Evaporation of the filtrate gave a solid, which was subjected to preparative thin-layer chromatography on silica gel developed with chloroform–methanol (1:5). Compound **12** was obtained as a solid in a yield of 66%. **12** was recrystallized from acetone to give a colorless crystal: mp 209—211 °C (decomp); $[\alpha]_D^{20}$ −92° (*c* 0.57, $CHCl_3$); IR (KBr) 1772, 1630, 1518, 1478, 1217, 1113 and 1062 cm^{-1}; ^1H NMR (90 MHz, $CDCl_3$) δ=2.70 (1H m, H-2), 3.28 (1H dd, *J*=5 and 14 Hz, H-3), 3.53 (3H s, OCH_3), 3.78 (6H s, 2×OCH_3), 4.35 (2H m, H-11), 4.60 (1H d, *J*=5 Hz, H-11), 4.86 (1H d, *J*=3 Hz, H-1), 5.40 (1H s, OH), 5.61 (1H s, OH), 5.96 (2H m, methylene), 6.22 (1H s, H-5), and 6.28 (2H s, H-2′ and 6′); MS (FD) *m/z* 430 (M^+).

4′-O-Benzyloxycarbonyl-1-β-hydroxy-α-peltatin (13). A solution of **7** (200 mg) in ethyl acetate (20 ml) was stirred under atmosphere of hydrogen in the presence of 10% Pd/C (10 mg) at −20 °C for 1 h. Catalyst was removed by filtration, and the filtrate was evaporated to give a solid. The solid was subjected to preparative thin-layer chromatography on silica gel developed with toluene–acetone (4:1). Compound **13** and 1-β-hydroxy-α-peltatin (**14**) were obtained as solids in yields of 70 and 25%, respectively. Each solid was recrystallized from methanol. **13**: mp 172—174 °C; $[\alpha]_D^{20}$ −55° (*c* 0.34, $CHCl_3$); IR (KBr) 1780, 1618, 1268, and 1140 cm^{-1}; ^1H NMR ($CDCl_3$, 270 MHz) δ=2.75 (1H m, H-2), 3.25 (1H dd, *J*=5 and 14 Hz, H-3), 3.69 (6H s, 2×OCH_3), 4.36 (1H t, *J*=8 Hz, H-11), 4.47 (1H dd, *J*=8 and 11 Hz, H-11), 4.63 (1H d, *J*=5 Hz, H-4), 5.21 (1H d, *J*=4.3 Hz, H-1), 5.26 (2H s, $C\underline{H}_2Ph$), 5.98 (2H s, methylene), 6.24 (1H s, H-5), 6.34 (2H s, H-2′ and 6′) and 7.3—7.5 (5H m, Ph); MS (FD) *m/z* 550 (M^+), 532 and 398. **14**: mp 212—214 °C; $[\alpha]_D^{20}$ −74° (*c* 0.25, $CHCl_3$); IR (KBr) 1778, 1615, and 1110 cm^{-1}; ^1H NMR ($CDCl_3$ 270 MHz) δ=2.77 (1H m, H-2), 3.23 (1H dd, *J*=4.7 and 14 Hz, H-3), 3.78 (6H s, 2×OCH_3), 4.34 (1H t, *J*=8 Hz, H-11), 4.46 (1H dd, *J*=8 and 11 Hz, H-11), 4.61 (1H d, *J*=4.7 Hz, H-4), 5.23 (1H broad s, H-1), 5.99 (2H s, methylene), 6.26 (1H s, H-5), and 6.32 (2H s, H-2′ and 6′), MS (FD) *m/z* 416 (M^+) and 398.

4′-O-Benzyloxycarbonyl-1-β-hydroxy-8-O-methyl-α-peltatin (15). A solution of **13** (168 mg) in acetone (5 ml) was refluxed with methyl iodide (150 μl) in the presence of potassium carbonate (140 mg) for 1 h, and the mixture was further refluxed with an additional methyl iodide (100 μl) for 1 h. Evaporation of the solvent gave an solid, which was dissolved in chloroform. The solution was washed with water, dried over Na_2SO_4, and filtered. The solvent was evaporated to give a solid. The solid was subjected to preparative thin-layer chromatography on silica gel developed with toluene–acetone (2:1). Compound **16** was obtained as a solid (174 mg) quantitatively. The solid was recrystallized from methanol: mp 107—108 °C $[\alpha]_D^{27}$ −57° (*c* 0.55, $CHCl_3$); IR (KBr) 1770, 1256, 1218, and 1130 cm^{-1}; ^1H NMR ($CDCl_3$, 90 MHz) δ=2.72 (1H m, H-2), 3.27 (1H dd, *J*=5 and 14 Hz, H-3), 3.70 (6H s, 2×OCH_3), 4.17 (3H s, OCH_3), 4.40 (2H m, H-11), 4.62 (1H d, *J*=5 Hz, H-4), 5.15 (1H d, *J*=3.5 Hz, H-1), 5.26 (2H s, $C\underline{H}_2Ph$), 5.95 (2H s, methylene), 6.29 (1H s, H-5), 6.37 (2H s, H-2′ and 6′), and 7.3—7.5 (5H m, Ph); MS (FAB) *m/z* 565 (M^++H), 547 and 429.

1-O-β-(2,3-Di-O-chloroacetyl-4,6-O-ethylidene-β-D-glucopyranosyl)-4′-O-benzyloxycarbonyl-8-O-methyl-α-peltatin (16). Procedure used was similar to that used for the preparation of **10** from **7** and **9** (78% yield). **16**: mp 129—130 °C; $[\alpha]_D^{23}$ −63° (*c* 0.53, $CHCl_3$); IR (KBr) 1775, 1480, 1258, 1206, and 1130 cm^{-1}; ^1H NMR ($CDCl_3$, 90 MHz) δ=1.35 (3H d, *J*=5 Hz, CH_3 of ethylidene), 2.73 (1H m, H-2), 3.67 (6H s, 2×OCH_3), 4.16 (3H s, OCH_3), 5.96 (2H s, methylene), 6.29 (3H s, H-5, 2′ and 6′), and 7.3—7.5 (5H m, Ph); MS (FAB) *m/z* 905 (M^+ +H), 770, and 547.

1-O-β-(4,6-O-Ethylidene-β-D-glucopyranosyl)-8-O-methyl-α-peltatin (17). Procedures used were similar to those used for the preparation of **11** from **10** (69% yield). **17**: mp 221—222 °C; $[\alpha]_D^{23}$ −91° (*c* 0.54, $CHCl_3$); IR (KBr) 1777, 1618, 1220 and 1118 cm^{-1}; ^1H NMR ($CDCl_3$, 400 MHz), δ=1.39 (3H d, *J*=5 Hz, CH_3 of ethylidene), 2.53 (1H broad s, 2″-OH), 2.70 (1H broad s, 3″-OH), 2.75 (1H m, H-2), 3.19 (1H dd, *J*=5.5 and 14 Hz, H-3), 3.38 (1H t, *J*=8 Hz, H-2″), 3.55 (1H m, H-6″), 3.77 (6H s, 2×OCH_3), 4.14 (3H s, OCH_3), 4.17 (1H dd, *J*=8 and 9 Hz, H-11), 4.46 (1H dd, *J*=9 and 11 Hz, H-11), 4.58 (1H d, *J*=5.5 Hz, H-4), 4.75 (1H q, *J*=5 Hz, CH of ethylidene), 4.84 (1H d, *J*=8 Hz, H-1″), 5.15 (1H d, *J*=3.5 Hz, H-1), 5.40 (1H s, 4′-OH), 5.94 and 5.96 (2H ABq, *J*=1.5 Hz, methylene), 6.26 (1H s, H-5), and 6.26 (2H s, H-2′ and 6′), MS (FAB) *m/z* 618 (M^+) and 413.

1-O-β-(2-Benzyloxycarbonylamino-3-chloroacetyl-2-deoxy-4,6-O-ethylidene-β-D-glucopyranosyl)-4′-O-benzyloxycarbonyl-8-O-methyl-α-peltatin (19). Procedure used was similar to that used for the preparation of **10** from **7** and **9** (92% yield). **19**: mp 219—220 °C; $[\alpha]_D^{18}$ −53° (*c* 0.52, $CHCl_3$); IR (KBr) 1790, 1775, 1700, 1246, 1211, and 1132 cm^{-1}; ^1H NMR ($CDCl_3$, 90 MHz) δ=1.33 (3H d, *J*=5 Hz, CH_3 of ethylidene), 2.73 (1H m, H-2), 3.67 (6H s, 2×OCH_3), 4.31 (3H s, OCH_3), 5.62 and 5.86 (1H each s, methylene), 6.24 (1H s, H-5), 6.29 (2H s, H-2′ and 6′) and 7.2—7.5 (10 H m, 2×Ph); MS (FAB) *m/z* 984 (M^+ +Na), 828, and 547.

1-O-β-(2-Amino-2-deoxy-4,6-O-ethylidene-β-D-glucopyranosyl)-8-O-methyl-α-peltatin (20). A solution of **19** (40 mg) in a mixture of dichloromethane (2 ml) and pyridine (1 ml) was stirred in the presence of ethylenediamine (30 μl) at 0 °C for 2 h. The mixture was diluted with chloroform (5 ml), and the solution was washed with 5% aqueous $KHSO_4$ solution and water. The chloroform layer was dried over Na_2SO_4, and filtered. The solvent was evaporated to give a crude solid (40 mg). The solid was dissolved in ethyl acetate–ethanol (3:2, 2 ml), and the solution was stirred under atmosphere of hydrogen in the presence of 10% Pd/C (10 mg)

at room temperature for 1 h. After removal of catalyst, the solvent was evaporated to afford a solid, which was subjected to preparative thin-layer chromatography on silica gel developed with chloroform–methanol (9 : 1). Compound **20** was obtained as a solid in a yield of 66%. The solid was recrystallized from methanol: mp 215—220 °C (decomp); $[\alpha]_D^{20}$ −82° (*c* 0.84, $CHCl_3$); IR (KBr) 1778, 1615, 1480, and 1100 cm^{-1}; ^1H NMR ($CDCl_3$, 270 MHz) δ=1.38 (3H d, *J*=5 Hz, CH_3 of ethylidene), 2.61 (1H dd, *J*=8 and 10 Hz, H-2″), 2.74 (1H m, H-2), 3.22 (1H dd, *J*=5.5 and 14 Hz, H-3), 3.77 (6H s, 2×OCH_3), 4.13 (3H s, OCH_3), 4.16 (1H dd, *J*=8 and 9 Hz, H-11), 4.45 (1H dd, *J*=9 and 11 Hz, H-11), 4.58 (1H d, *J*=5.5 Hz, H-4), 4.75 (1H d, *J*=8 Hz, H-1″), 4.75 (1H q, *J*=5 Hz, CH of ethylidene), 5.14 (1H d, *J*=3.5 Hz, H-1), 5.94 and 5.96 (2H, ABq, *J*=1.5 Hz, methylene), and 6.26 (3H s, H-5, 2′ and 6′); MS (FAB) *m/z* 618 (M^+ +H) and 413.

References

1) For review: See I. Jardine, "Podophyllotoxins in Anticancer Agents Based on Natural Products Models," Academic Press, Inc., New York (1980), pp. 319—351.

2) For review: See B. F. Issell, *Cancer Chemother. Pharmacol.*, **7**, 87 (1982).

3) H. Saito, H. Yoshikawa, Y. Nishimura, S. Kondo, T. Takeuchi, and H. Umezawa, *Chem. Pharm. Bull.*, **34** (9), 3733 (1986).

4) H. Saito, H. Yoshikawa, Y. Nishimura, S. Kondo, T. Takeuchi, and H. Umezawa, *Chem. Pharm. Bull.*, **34** (9), 3741 (1986).

5) R. H. Mitchell, Yee-Hing Lai, and R. V. Williams, *J. Org. Chem.*, **44**, 4733 (1979).

6) H. Yamaguchi, M. Arimoto, S. Nakajima, M. Tanoguchi, and Y. Fukada, *Chem. Pharm. Bull.*, **34** (5), 2056 (1986).

7) H. Umezawa, Y. Takahashi, M. Kinoshita, H. Naganawa, K. Tatsuta, and T. Takeuchi, *J. Antibiotics*, **33**, 1581 (1980).

8) H. Saito, Y. Nishimura, S. Kondo, and H. Umezawa, *Chem. Lett.*, **1987**, 799.

9) M. Kuhn and A. von Wartburg, *Helv. Chim. Acta*, **51**, 1631 (1968).

10) G. Kohnstam and D. L. H. Williams, "Directive and Activating Effects of Alkoxy and Aryloxy Groups in Aromatic and Aliphatic Reactions" in "The Chemistry of the Ether Linkage" in a series of "THE CHEMISTRY OF FUNCTIONAL GROUPS," ed by S. Patai, John Wiley & Sons, New York (1967), p. 81. An ortho-oriented hydroxyl group in **10** might accelerate the hydrolysis of the glycosidic bond.

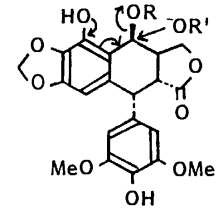

Disulfide Linkages in a Heat-Stable Enterotoxin (ST_p) Produced by a Porcine Strain of Enterotoxigenic *Escherichia coli*

Yuji HIDAKA, Hirokazu KUBOTA, Shoko YOSHIMURA, Hideaki ITO,†
Yoshifumi TAKEDA,† and Yasutsugu SHIMONISHI*
Institute for Protein Research, Osaka University, Yamada-oka 3-2, Suita, Osaka 565
†The Institute of Medical Science, The University of Tokyo, Shirokanedai, Minato-ku, Tokyo 108
(Received October 12, 1987)

Heat-stable enterotoxins, produced by various enteric bacteria such as enterotoxigenic *Escherichia coli*, *Yersinia enterocolitica*, and *Vibrio cholerae* non-01, have common segments consisting of 13 amino acid residues (T. Takao et al., *FEBS Lett.*, **193**, 250 (1985)). These segments have full enterotoxigenic activity and are bound by three intramolecular disulfide bonds. The linkages of these three disulfide bonds in a heat-stable enterotoxin (ST_p) produced by a porcine strain of enterotoxigenic *E. coli* were determined to be

Cys-Cys-Glu-Leu-Cys-Cys-Asn-Pro-Ala-Cys-Ala-Gly-Cys

by stepwise and selective formation of disulfide bonds using different types of removable protecting groups for Cys residues. These disulfide linkages were identical with those of a heat-stable enterotoxin (ST_h) produced by a human strain of enterotoxigenic *E. coli* (Y. Shimonishi et al., *FEBS Lett.*, **215**, 165 (1987)).

Pathogenic enteric bacteria such as enterotoxigenic *Escherichia coli, Yersinia enterocolitica,* and *Vibrio cholerae* non-01 produce heat-stable enterotoxins (STs), which cause acute diarrhea in children in developing countries in the tropics. We and others purified STs to homogeneity from the culture supernatants of these pathogenic enteric bacteria and determined their primary structures,[1-5] as shown in Fig. 1. On the basis of chemical syntheses of various analogues of the STs and measurements of their toxicities, we found that a segment with 13 amino acid residues containing 6 half-cystines (Fig. 1) has the full enterotoxigenic activity of STs.[6] On the other hand, reduction of the three disulfide linkages of the STs resulted in loss of their enterotoxigenic activities. These results indicated that the structural element(s) required for the toxicities of STs is located on the three dimensional structure formed by the three disulfide bonds in the segment with 13 amino acid residues. Recently, we determined that the disulfide bonds of an ST (ST_h) produced by a human strain of enterotoxigenic *E. coli*[7] were as shown in Fig. 7. We also found that these disulfide bonds in ST_h were very important for its toxicity. This observation prompted us to examine whether other STs have the same disulfide linkages as those in ST_h and to investigate the effect of amino acid substitution on the mode of disulfide bond formation or construction of the three dimensional structure and toxicity of ST_h.

In this work, we examined the mode of disulfide bond formation in an ST (ST_p) produced by a porcine strain of enterotoxigenic *E. coli*, in which the primary structure in the common 13 amino acid residues differs from that of ST_h only at position 15. The mode of three disulfide bond formation in ST_p was the same as that in ST_h of a human strain of enterotoxigenic *E. coli*, indicating that other STs produced by enteric bacteria have the same mode of disulfide bond formation.

Experimental

The general and analytical methods used were as described previously.[6] All chemicals used for synthetic experiments were of reagent grade, while those used for analysis were of guaranteed grade and solvents were distilled before use. All amino acids except glycine were of the L-configuration and Boc-amino acid derivatives were purchased from the Peptide Institute Inc. (Minoh, Osaka). A reversed-phase resin (YMC-ODS,s-5) was purchased from Yamamura Chemical Laboratories Co. (Kyoto) and packed into a column of 8×300 mm

| | | |

for analytical and preparative purposes in our laboratory. The abbreviations used in this paper are those recommended by the IUPAC-IUB [*J. Biol. Chem.*, **261**, 1 (1986)]. Additional abbreviations are: Acm, acetamidomethyl; HONSu, *N*-hydroxysuccinimide; DMF, *N,N*-dimethylformamide; MBzl, *p*-methylbenzyl; TFA, trifluoroacetic acid; TEA, triethylamine; DMSO, dimethyl sulfoxide.

General Procedures for Peptide Synthesis in Solution. As a typical procedure the coupling of compound **4** with compound **8** to give compound **9** is described as follows : Compound **4** (1.6 g, 0.75 mmol) was stirred with TFA (10 ml) at room temperature for 30 min and concentrated to a syrup. Meanwhile, compound **8** (0.82 g, 0.85 mmol) was dissolved in DMF (5 ml), cooled below −20 °C, and mixed with 6.72 M HCl (1M=1 mol dm^{-3}) in dioxane (0.88 ml) and isopentyl nitrite (0.13 ml). The solution was stirred at −20 °C for 25 min and mixed with a solution of the above syrup in DMF (10 ml) and TEA (0.94 ml). The mixture was further stirred at 0 °C for 1 day. The precipitate formed in the reaction mixture was separated by filtration and the filtrate was concentrated to a syrup under reduced pressure. The syrup was triturated to a solid in chilled 0.1M HCl. The recrystallization of the solid from EtOH gave **9** (1.40 g).

The deprotection of Z groups, hydrazinolysis of peptide esters, and formation of peptide bonds by an active ester method were carried out as described previously.[6]

Solid-Phase Peptide Synthesis. Peptide synthesis by the solid-phase method[9] was performed as described in a previous paper.[7]

Removal of Protecting Groups by HF and Oxidation by Iodine. The protected peptides (25 μmol each) were treated with anhydrous liquid hydrogen fluoride[10] and air-oxidized as described previously.[6c] The solutions containing the air-oxidized peptides were partially concentrated by lyophilization and purified by HPLC, as described below. The purified peptides with an intramolecular disulfide bond(s) and Acm groups were oxidized by iodine at a peptide-to-iodine molar ratio of 1 : 40 in a mixture of MeOH and 0.1 M HCl as described in a previous paper.[7] The iodine-oxidized peptides were directly purified by HPLC, as described below.

High-Performance Liquid Chromatography (HPLC). The HPLC apparatus consisted of a Waters M600 multisolvent delivery system (Milford, MA) connected with a Hitachi UV 655A variable wavelength UV monitor and D-2000 chromato-integrator (Tokyo, Japan). The HPLC column was equilibrated with 10% CH_3CN in 0.05% TFA or 0.01M ammonium acetate (pH 5.7) and after injection of the sample solution, was developed with a linear-gradient of 10—40% CH_3CN with increase in CH_3CN of 0.5 or 1% min^{-1} at a flow rate of 2 ml min^{-1}. Eluates were monitored for absorption at 220 nm.

Amino Acid Analysis and Fast Atom Bombardment (FAB) Mass Spectrometry. The amino acid compositions and molecular weights of purified peptides were determined as described previously.[3]

Biological Assay. Toxicity of synthetic peptides was assayed in suckling mice of 2 days old (1.7±0.1 g) as described previously.[11]

Results and Discussion

Previously,[7] to determine the mode of disulfide bond formation in ST_h (Fig. 7) we adopted a synthetic procedure in which disulfide bonds in ST_h were formed stepwise and selectively using different types of removable protecting groups for Cys residues. We found that this synthetic procedure was suitable for determination of disulfide bond formation in ST_h. Therefore, in the present work we applied this procedure for determination of the positions of disulfide linkages in ST_p.

The three disulfide linkages in ST_h between Cys^6 and Cys^{11}, Cys^7 and Cys^{15}, and Cys^{10} and Cys^{18}, are shown in Fig. 7. These disulfide linkages were expected to be similar in ST_p, because the 13 amino acid sequence including 6 half Cys residues in ST_p differs only at Ala at the fourth position from the C-terminus from that in ST_h and has almost the same biological activity as the corresponding ST_h peptide. Accordingly, we synthesized three kinds of protected linear peptides with the segment from Cys^5 to Cys^{17} of ST_p with two Cys residues at Cys^5 and Cys^{10} or Cys^6 and Cys^{14} or Cys^9 and Cys^{17} protected by an Acm group and the other four Cys residues protected by an MBzl group, which correspond to the sequence from Cys^6 to Cys^{18} in ST_h, as shown in Figs. 2—4. Table 1 summarizes data on protected peptides **1**—**21**. The protected linear peptides thus obtained were treated with liquid

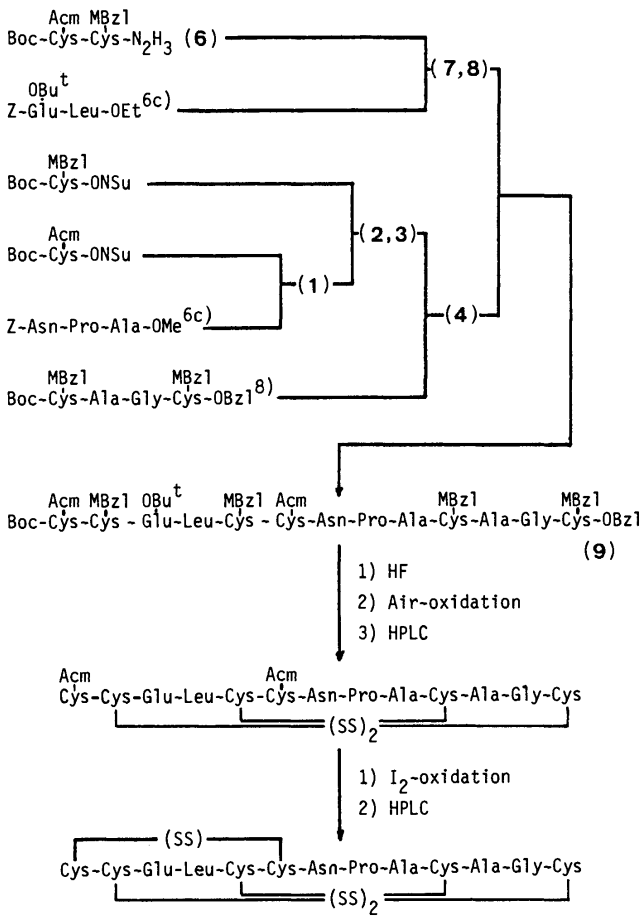

Fig. 2. Scheme for synthesis of a shorter peptide of ST_p linked by a disulfide bond between Cys^5 and Cys^{10}.

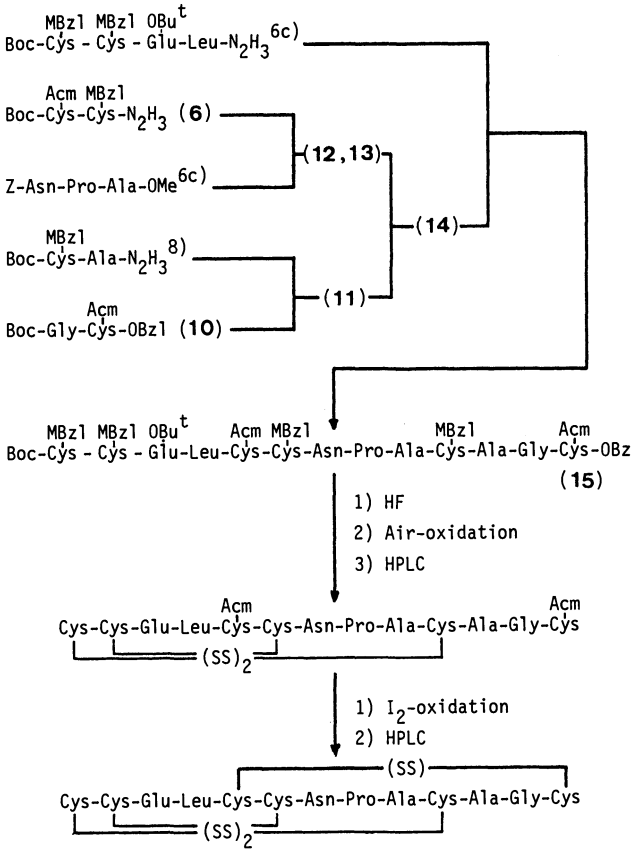

Fig. 3. Scheme for synthesis of a shorter peptide of ST_p linked by a disulfide bond between Cys^9 and Cys^{17}.

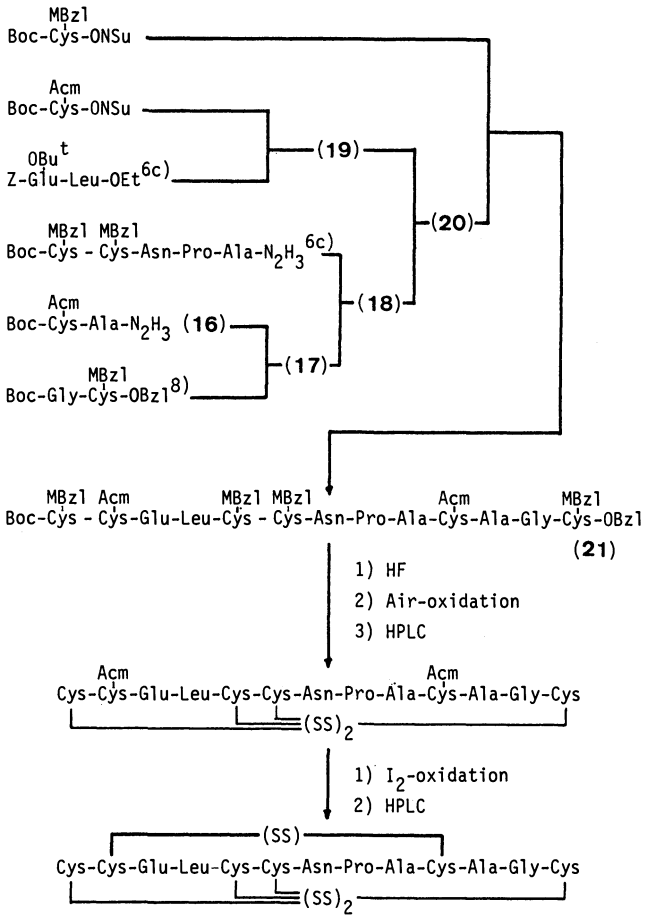

Fig. 4. Scheme for synthesis of a shorter peptide of ST_p linked by a disulfide bond between Cys^6 and Cys^{14}.

anhydrous hydrogen fluoride to remove all the protecting groups except Acm groups and air-oxidized to form intramolecular disulfide bonds between the four Cys residues, which had been protected by MBzl groups. The air-oxidized products were purified by HPLC on a reversed-phase column, as shown in Figs. 5a—5c. On the bases of amino acid and molecular weight analyses of the separated fractions, peptides with two disulfide bonds were concluded to be eluted in the peak fractions shown by asterisks (*) in Figs. 5a—5c. The yields of these peptides, for example those in Fig. 5a, were 14, 20, and 16% in order of their elution on the basis of the protected linear peptide. In this treatment, three kinds of peptides with two intramolecular disulfide bonds should theoretically be obtained. Figure 6 illustrates the HPLC profile of peak *2 in Fig. 5a, which was reduced by dithiothreitol and reoxidized spontaneously in air. Three peptide fractions were obtained similarly to those shown in Fig. 5a except for their peak ratios. However, peptides with a disulfide bond between two vicinal Cys residues were presumably formed with difficulty. In fact, when two disulfide bonds were formed in peptides **15** and **21**, only two of three possible peptides could be isolated by HPLC, as shown in Figs. 5b and 5c. The amino acid compositions, mass values, and biological activities of these peptides with two disulfide bonds are summarized in Table 2.

Then, these monomeric peptides with two disulfide bonds were selectively oxidized by iodine to form a third disulfide linkage at the two Cys residues that had been protected by Acm groups. The peptides with three disulfide linkages were separated and compared by HPLC with standard ST_p peptide, which consists of 13 amino acid residues including 6 Cys residues and has the same disulfide bond formation as native ST_p.[6b] Selective formation of a third disulfide bond between Cys^5 and Cys^{10} or Cys^9 and Cys^{17} in peptides *1 and *5 in Figs. 5a and 5b, respectively, yielded peptides that were identical with standard ST_p peptide on HPLC, as shown by arrows in Figs. 5e and 5f. Peptides *2, *3, and *4 in Figs. 5a and 5b, respectively, did not yield a peptide that was identical with standard ST_p peptide. The results indicated that the disulfide bonds in ST_p were linked between Cys^5 and Cys^{10} and Cys^9 and Cys^{17}, and therefore that the remaining disulfide bond should be between Cys^6 and Cys^{14}. However, when the third disulfide bond was linked between Cys^6

and Cys^{14} in two peptides *6 and *7 prepared from peptide **21** (Fig. 5c), no peptide was detected with the same retention time on HPLC as standard ST_p peptide. Figure 5g shows an HPLC profile of the peptide which was prepared by reaction of peptide *7 with iodine. Then, the three disulfide bonds were linked in reverse order; that is, we synthesized a protected linear peptide with two Cys residues at Cys^6 and Cys^{14} protected by an MBzl group and the remaining four Cys residues protected by an Acm group by a solid-phase procedure. The first disulfide bond was formed between Cys^6 and Cys^{14}, and then the second and third disulfide bonds were formed between the remaining four Cys residues, as shown in Figs. 5d and 5h, respectively. When the peak fraction indicated by an asterisk in Fig. 5d was oxidized by iodine, the peak fraction *16 shown by an arrow in Fig. 5h was eluted in the same position as standard ST_p peptide by HPLC. The amino acid compositions and mass values of the peptides in the peak fractions shown by asterisks in Figs. 5e—5h are summarized in Table 3. The peptides eluted by HPLC in the same position as standard ST_p peptide shown in Figs. 5e, 5f, and 5h showed toxicities at doses of 0.8—1.0 ng/mouse, which were almost the same as that of standard ST_p peptide (0.7 ng), as described in Table 3. Thus, we concluded that the three intramolecular disulfide bonds of ST_p were between Cys^5 and Cys^{10}, Cys^6 and Cys^{14}, and Cys^9 and Cys^{17}, as shown in Fig. 7. Other disulfide bond linkages except those described above were not examined, because the positions of the disulfide bonds of ST_p determined above were the same as those of ST_h.[7]

When a third disulfide bond was linked between Cys^5 and Cys^{10} and Cys^9 and Cys^{17} in peptides *1 and *5 in Figs. 5a and 5b, respectively, they gave two peak fractions on HPLC, as shown in Figs. 5e and 5f, respectively. On HPLC one of them was eluted at the same position as standard ST_p peptide, while the other was eluted earlier. When a third disulfide bond was linked between Cys^6 and Cys^{14} in peptide *7 in Fig. 5c, interestingly it gave only a peak fraction with the same retention time as peaks *9 and *11 in Figs. 5e and 5f, respectively. Moreover, these two peak fractions showed different circular dichroism spectra from each other in the range from 190 nm to 260 nm (not shown). These two peptides were not interconvertible, but stable on storage for a long time in a refrigerator. These findings suggested that two topologically stable and different conformers are present in peptides with the same three disulfide linkages and also that only one or both the two conformers are produced dependent upon the order of disulfide bond formation.

While peptide *1 was eluted as a single peak under the conditions for Fig. 5a, it was separated into two broad peak fractions on HPLC under different conditions from that in Fig. 5a, as depicted in Fig. 8. Each fraction showed the same profile on repeated HPLC as that before separation (not shown). Peptides in the

Table 1. Yields, Melting Points,[a] Solvents for Recrystallization, Optical Rotations, and Analytical Data of Intermediates

Compound	Yield	Mp	Solvent for recrystallization	$[\alpha]_D^{25}$[b]	Found (%)			Calcd (%)		
	%	θ_m/°C		degree	C	H	N	C	H	N
1	91.8	79—80	$CHCl_3$-hexane	−46.5						
2[c]	67.0	148—149	AcOEt-EtOH-ether	−70.5	52.65	6.77	12.27	52.82	6.71	12.32
3[d]	97.7	92—94	EtOH-ether	−64.3	50.21	6.87	15.53	50.17	6.80	15.49
4	93.1	169—171	EtOH-ether	−67.8	56.79	6.57	11.01	57.01	6.54	10.76
5[e]	94.1	126—127	AcOEt-hexane	−36.4	54.18	7.00	8.29	53.79	6.87	8.18
6	91.6	168—169	MeOH-ether	−23.8	51.13	6.86	13.52	51.45	6.87	13.64
7[f]	94.2	128—129.5	AcOEt-ether-hexane	−25.9	56.53	7.79	8.40	56.71	7.69	8.48
8[g]	94.7	148—149	MeOH-ether	−15.7	54.59	7.59	12.12	54.73	7.57	12.08
9	89.2	211—212	EtOH	−52.0[h]	57.14	6.99	10.42	57.35	6.74	10.70
10	88.1	94—95	AcOEt-hexane	−21.1	54.78	6.64	9.61	54.66	6.65	9.56
11	96.3	161—162	EtOH-ether	−18.1	56.49	6.61	9.80	56.89	6.60	9.76
12[i]	70.5	152—153	EtOH-$CHCl_3$-ether	−59.0	52.64	6.82	12.21	52.82	6.71	12.32
13[j]	90.5	105—106	EtOH-ether	−43.8	49.97	6.85	16.00	50.17	6.80	15.49
14	83.3	177—178	EtOH	−60.2	54.25	6.43	12.10	54.77	6.42	12.17
15	83.8	225 (decomp)	EtOH	−64.2[h]	57.02	6.77	10.67	57.35	6.74	10.70
16	62.7		MeOH-ether	−6.1	44.13	7.25	18.50	44.55	7.21	18.56
17	89.4	148—149	AcOEt-hexane	−23.1	56.72	6.63	9.69	56.89	6.60	9.76
18	92.2	170—172	EtOH	−64.1	56.68	6.48	10.81	57.01	6.54	10.76
19	82.8	163—164.5	MeOH-ether	−16.6	49.56	7.83	16.06	49.04	8.22	15.40
20	84.1	202—203	EtOH-AcOEt	−47.7[k]	56.21	6.82	11.26	56.10	6.83	11.03
21	84.5	197—198	EtOH	−59.6[h]	55.80	6.46	11.32	56.07	6.57	10.90

a) Melting points were uncorrected. b) c=1.0 in DMF. c) Boc-Cys(MBzl)-Cys(Acm)-Asn-Pro-Ala-OMe. d) Boc-Cys(MBzl)-Cys(Acm)-Asn-Pro-Ala-N_2H_3. e) Boc-Cys(Acm)-Cys(MBzl)-OMe. f) Boc-Cys(Acm)-Cys(MBzl)-Glu(OBu^t)-Leu-OEt. g) Boc-Cys(Acm)-Cys(MBzl)-Glu(OBu^t)-Leu-N_2H_3. h) c=0.5 in DMSO. i) Boc-Cys(Acm)-Cys(MBzl)-Asn-Pro-Ala-OMe. j) Boc-Cys(Acm)-Cys(MBzl)-Asn-Pro-Ala-N_2H_3. k) c=1.0 in DMSO.

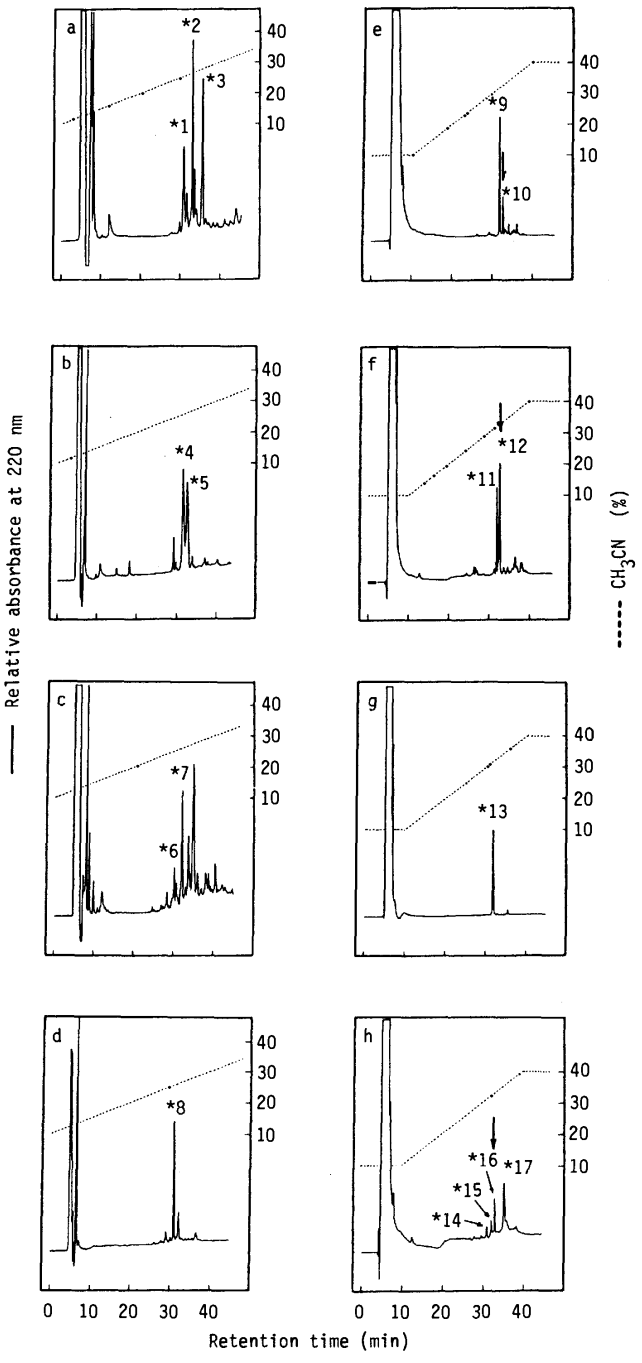

Fig. 5. HPLC profiles of: a) a deprotected and air-oxidized solution of peptides with two disulfide bonds at four Cys residues other than Cys^5 and Cys^{10} (Fig. 2), b) a deprotected and air-oxidized solution of peptides with two disulfide bonds at four Cys residues other than Cys^9 and Cys^{17} (Fig. 3.), c) a deprotected and air-oxidized solution of peptides with two disulfide bonds at four Cys residues other than Cys^6 and Cys^{14} (Fig. 4), d) a deprotected and air-oxidized solution of a peptide with a disulfide bond between Cys^6 and Cys^{14}, e) an I_2-oxidized solution of peak *1 in a), f) an I_2-oxidized solution of peak *5 in b), g) an I_2-oxidized solution of peak *7 in c), and h) an I_2-oxidized solution of peak *8 in d). Peaks *10, *12, and *16 shown by arrows were eluted at the same retention time as standard ST_p peptide.

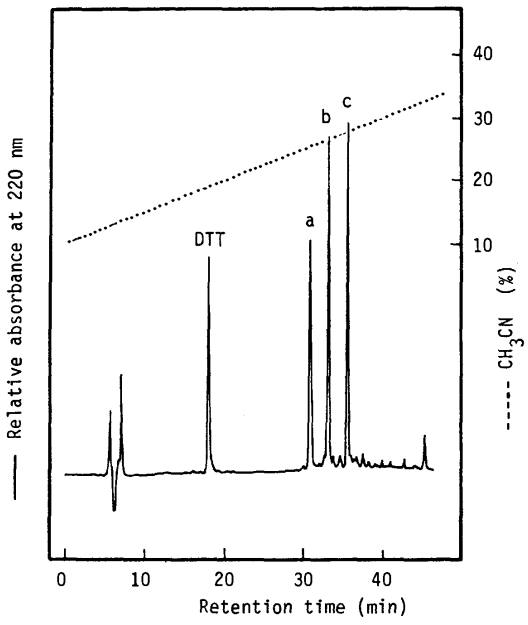

Fig. 6. HPLC profile of peptide *2 in Fig. 5a, which was reduced and reoxidized by air. Peaks a, b, and c had the same retention times as those of peaks *1, *2, and *3 in Fig. 5a, respectively.

two peak fractions 1 and 2 shown in Fig. 8 were oxidized by iodine immediately after their elution from an HPLC column. The peptide in the first fraction gave two peaks like that shown in Fig. 9a, one of which was identical with standard ST_p peptide, whereas the peptide in the second fraction gave only a peptide that was not identical with standard ST_p peptide, as shown in Figs. 9b and 9c, respectively. These findings suggested that peptide *1 consisted of two components, which were rapidly interconvertible and therefore were in equilibrium. These peptides are presumed to be two conformers with cis and trans configurations around the peptide bond between Asn^{11} and Pro^{12}, one of them corresponding to a peptide in the first fraction, and the other to a peptide in the second fraction in Fig. 8. One of the two conformers yielded two peptides, and the other only one peptide, when they were oxidized by iodine. Since peptide *5 gave two peak fractions on treatment with iodine (Fig. 5f), it was considered to consist of two components like peptide *1. However, peptide *5 could not be separated by HPLC under the same conditions as for peptide *1 in Fig. 8. The two conformers in peptide *1 might have dissimilar physicochemical properties and those in peptide *5 similar properties, or they might be rapidly equilibrated, because on reversed-phase HPLC peptide *1 could be separated but peptide *5 could not be separated.

Houghten et al.[12] proposed the mode of disulfide bond formation of ST_p from an experiment on the reoxidation kinetics of ST_p, which they synthesized according to the amino acid sequence proposed previously,[13] although the amino acid sequence was later revised to the sequence shown in Fig. 1.[2] The pro-

Table 2. Amino Acid Composition,[a] Mass Values,[b] and Toxic Activities[c] of Synthetic Peptides with One or Two Disulfide Bonds[d]

	*1	*2	*3	*4	*5	*6	*7	Theoretical value	*8	Theoretical value
Asp	0.99	1.01	1.02	1.17	1.03	1.15	1.12	1	1.07	1
Glu	0.98	0.98	1.01	1.01	1.00	1.07	1.01	1	1.02	1
Gly	0.94	0.98	0.98	1.01	0.97	1.13	1.05	1	1.02	1
Ala	2	2	2	2	2	2	2	2	2	2
1/2 Cys	5.11	3.99	6.47	5.18	5.65	6.19	6.61	6	4.34	6
Leu	0.95	0.96	0.98	1.02	1.01	1.06	1.04	1	1.01	1
Pro	1.17	0.99	1.12	1.10	1.00	1.24	1.19	1	1.14	1
$[M+H]^{+}$ [b]	1427.3	1427.1	1427.1	1427.3	1427.1	1427.0	1427.0	1427.4	1572.0	1571.5
MED/ng[c]	290	840	$\simeq 10\times10^3$	400	790	620	$>10\times10^3$		$>10\times10^3$	

a) Values are those in acid hydrolysates (110 °C, 24 h) of synthetic peptides and are shown in mol/mol of Ala. b) $[M+H]^{+}$, mass values of quasi-molecular ion. c) MED, minimum effective dose. d) *1, *2, etc. correspond to those in Fig. 5.

Table 3. Amino Acid Composition,[a] Mass Values,[b] and Toxic Activities[c] of Synthetic $ST_p(5—17)$[d]

	*9	*10	*11	*12	*13	*14	*15	*16	*17	Theoretical value
Asp	1.19	1.02	1.05	1.00	1.02	1.34	1.10	1.30	1.05	1
Glu	1.12	0.97	1.26	0.98	1.08	1.26	1.07	1.00	1.03	1
Gly	1.19	0.99	1.14	0.87	1.02	1.47	1.03	0.97	1.03	1
Ala	2	2	2	2	2	2	2	2	2	2
1/2 Cys	2.95	4.86	4.56	4.78	4.87	5.13	4.41	5.65	5.08	6
Leu	1.04	1.07	1.04	1.02	1.01	1.12	1.06	1.01	1.01	1
Pro	1.17	0.99	1.18	1.10	1.03	1.18	1.04	1.00	1.03	1
$[M+H]^{+}$[b]	1282.9	1283.0	1283.2	1283.0	1283.1	1282.8	1282.8	1283.0	1282.8	1283.3
MED/ng[c]	14	1.0	11	0.8	15	138	14	0.8	61	0.7

a) Values are those in acid hydrolysates (110 °C, 24 h) of synthetic peptides and are shown as mol/mol of Ala. b) $[M+H]^{+}$, mass values of quasi-molecular ion. c) MED, minimum effective dose per mouse. d) *9, *10, etc. correspond to those in Fig. 5.

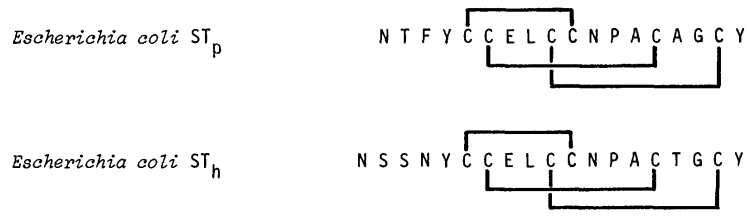

Fig. 7. Modes of three disulfide linkages of heat-stable enterotoxins (ST_p and ST_h[7]) of porcine and human strains, respectively, of enterotoxigenic *E. coli*.

posed disulfide bonds were between Cys^5 and Cys^{14}, Cys^6 and Cys^{10}, and Cys^9 and Cys^{17}. This disulfide bond formation is not consistent with that determined in this work. That is, the partners of Cys^5 and Cys^6 in disulfide bond formation are reversed. These mismatched pairings of disulfide linkages might be because they used a peptide with a different amino acid sequence from that shown in Fig. 1. If they had used a peptide with the correct amino acid sequence, they might have obtained the same results as ours.

Recently, we determined the mode of disulfide bond formation of ST_h produced by a human strain of enterotoxigenic *E. coli*, as shown in Fig. 7, and also of ST produced by *Vibrio-mimicus*.[5] The positions of the disulfide linkages were identical with those of ST_p examined in this work. These results imply that the three dimensional structure in the common 13 amino acid region as shown in Fig. 1 is very similar in all ST's examined to date. Further elucidation of this spatial structure should be useful in understanding the structure-activity relation of ST and its mechanism of binding to receptor proteins on the membranes of

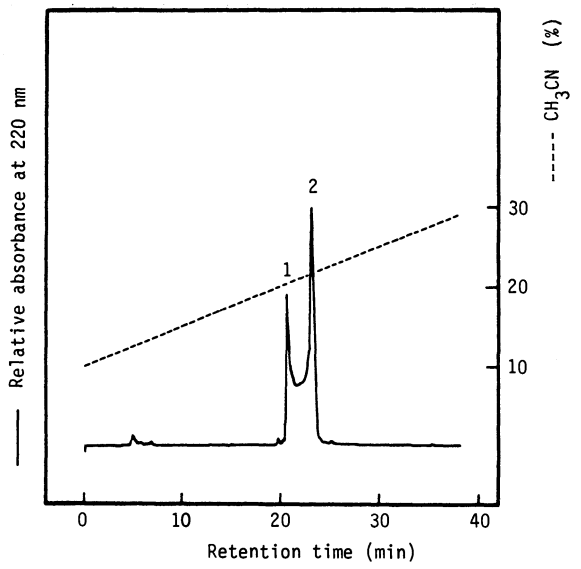

Fig. 8. HPLC profile of peptide *1 in Fig. 5a eluted with a linear-gradient of 10—30% CH_3CN concentration with increase in CH_3CN of 0.5% min^{-1} in 0.01 M ammonium acetate (pH 5.7).

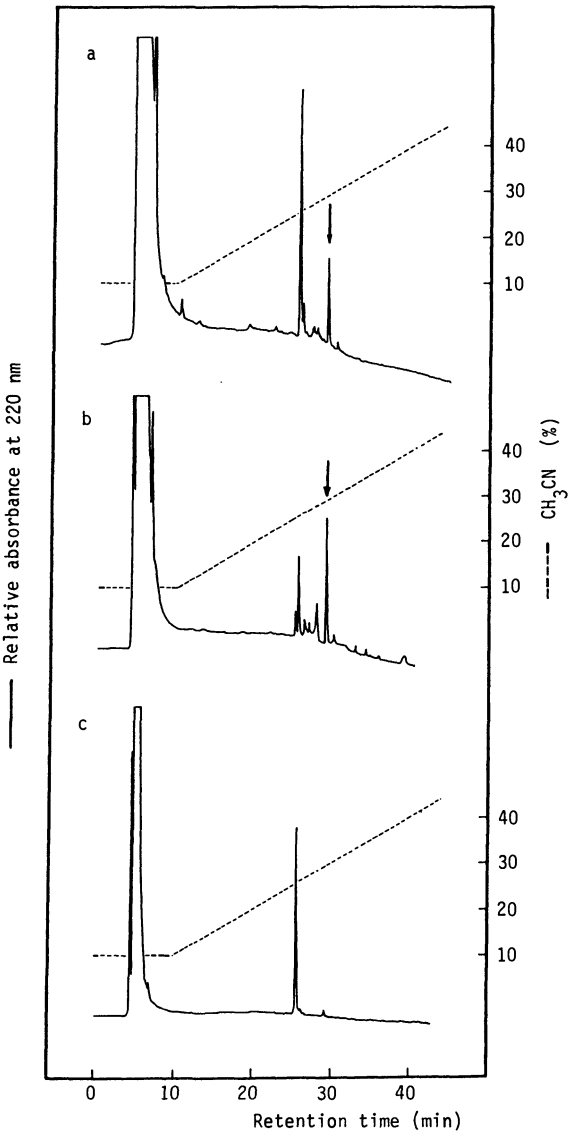

Fig. 9. HPLC profile of peak fractions eluted in Fig. 8 and oxidized by iodine: a) a mixture of peak fractions 1 and 2, b) peak fraction 1, and c) peak fraction 2. Peaks shown by arrows had the same retention times as standard ST_P peptide.

intestinal cells.

This work was supported in part by a Scientific Research Grant (No. 62470022 to Y. S) from the Ministry of Education, Science and Culture and in part by a grant from the Naito Foundation. We are indebted to Mrs. Noriko Mizoguchi for amino acid analysis and also to Mrs. Aiko Kobatake for elemental analysis and preparation of the manuscript.

References

1) S. Aimoto, T. Takao, Y. Shimonishi, S. Hara, T. Takeda, Y. Takeda, and T. Miwatani, *Eur. J. Biochem.*, **129**, 257 (1982).

2) a) T. Takao, T. Hitouji, S. Aimoto, Y. Shimonishi, S. Hara, T. Takeda, Y. Takeda, and T. Miwatani, *FEBS Lett.*, **152**, 1 (1983); b) M. R. Thompson and R. A. Giannella, *Infect. Immun.*, **47**, 834 (1985).

3) T. Takao, N. Tominaga, Y. Shimonishi, S. Hara, T. Inoue, and A. Miyama, *Biochem. Biophys. Res. Commun.*, **125**, 845 (1984); T. Takao, N. Tominaga, S. Yoshimura, Y. Shimonishi, S. Hara, T. Inoue, and A. Miyama, *Eur. J. Biochem.*, **152**, 199 (1985).

4) T. Takao, Y. Shimonishi, M. Kobayashi, O. Nishimura, M. Arita, T. Takeda, T. Honda, and T. Miwatani, *FEBS Lett.*, **193**, 250 (1985).

5) T. Takao, Y. Hidaka, M. Kobayashi, O. Nishimura, M. Arita, T. Takeda, H. Imaishi, T. Honda, T. Miwatani, and Y. Shimonishi, the manuscript in preparation.

6) a) S. Yoshimura, T. Takao, H. Ikemura, S. Aimoto, Y. Shimonishi, S. Hara, T. Takeda, Y. Takeda, and T. Miwatani, *Bull. Chem. Soc. Jpn.*, **57**, 1381 (1984); b) S. Yoshimura, H. Ikemura, H. Watanabe, S. Aimoto, Y. Shimonishi, S. Hara, T. Takeda, T. Miwatani, and Y. Takeda, *FEBS. Lett.*, **181**, 138 (1985); c) H. Ikemura, S. Yoshimura, S. Aimoto, Y. Shimonishi, S. Hara, T. Takeda, Y. Takeda, and T. Miwatani, *Bull. Chem. Soc. Jpn.*, **57**, 2550 (1984).

7) Y. Shimonishi, Y. Hidaka, M. Hane, M. Koizumi, S. Aimoto, T. Takeda, T. Miwatani, and Y. Takeda, *FEBS Lett.*, **215**, 165 (1987).

8) S. Yoshimura and Y. Shimonishi, *Bull. Chem. Soc. Jpn.*, **58**, 2805 (1985).

9) R. B. Merrifield, *J. Am. Chem. Soc.*, **85**, 2149 (1963).

10) S. Sakakibara, Y. Shimonishi, Y. Kishida, M. Okada, and H. Sugihara, *Bull. Chem. Soc. Jpn.*, **40**, 2164 (1967).

11) Y. Takeda, T. Takeda, T. Yano, K. Yamamoto, and T. Miwatani, *Infect. Immun.*, **25**, 978 (1979).

12) R. A. Houghten, J. M. Ostresh, and F. A. Klipstein, *Eur. J. Biochem.*, **145**, 157 (1984).

13) S. K. Chan and R. A. Giannella, *J. Biol. Chem.*, **256**, 7744 (1981).

A General Method for the Synthesis of Both Enantiomers of Optically Pure β-Hydroxy Esters from (*S*)-(*p*-Chlorophenylsulfinyl)acetone Easily Obtainable by Kinetic Resolution with Bakers' Yeast

Tamotsu FUJISAWA,* Atsushi FUJIMURA, and Toshio SATO
Chemistry Department of Resources, Mie University, Tsu, Mie 514
(Received October 15, 1987)

Both enantiomers of various optically pure (*R*)- and (*S*)-β-hydroxy esters were generally synthesized from (*S*)-(*p*-chlorophenylsulfinyl)acetone obtained by kinetic resolution with bakers' yeast, followed by γ-alkylation, diastereoselective reduction, subsequent introduction of ester group and reductive elimination of the sulfinyl group. The key step of the diastereoselective reduction of (*S*)-β-keto sulfoxides was performed with diisobutylaluminum hydride to give (*R*)c-(*S*)s-β-hydroxy sulfoxides or after complexation with zinc chloride followed by addition of diisobutylaluminum hydride to give (*S*)c-(*S*)s-β-hydroxy sulfoxides which were easily separated in an optically pure form by easy crystallization or separation by silica-gel chromatography due to the *p*-chlorophenyl moiety in the β-hydroxy sulfoxides. The utility of the present method could be successfully demonstrated in the synthesis of both (+)- and (−)-corynomycolic acids from optically pure methyl esters of (*R*)- and (*S*)-3-hydroxyoctadecanoic acid by alkylation with tetradecyl iodide at α-position and hydrolysis.

Optically active β-hydroxy esters are well-known as important intermediates for the synthesis of various natural products. They are prepared by a number of procedures; for example, asymmetric aldol reaction[1] by use of chiral α-sulfinyl esters,[2] lithium enolates,[3] zirconium enolates,[4] boron enolates,[5] tin enolates, and chiral diamines,[6] the Reformatsky reaction using sparteine,[7] regioselective epoxide ring opening,[8] cleavage of oxetanones,[9] and asymmetric reduction of β-keto ester with bakers' yeast.[10] Most of them give optically active β-hydroxy esters in high yields with very high optical purity, but they can not give both of the enantiomers from the same starting material. We report here a general method for the synthesis of both enantiomers of optically pure β-hydroxy ester **6** starting from (*S*)-(*p*-chlorophenylsulfinyl)acetone (**S-1**), which is easily obtainable by kinetic resolution of the corresponding racemic sulfinylacetone **1**, followed by γ-alkylation, diastereoselective reduction, subsequent introduction of ester group, and reductive elimination of the sulfinyl group. By use of the present method, both (+)- and (−)-corynomycolic acids **10** were synthesized in optically pure state.

Recently diastereoselective reduction of chiral β-keto tolyl sulfoxides with diisobutylaluminum hydride has been reported to give both diastereomers of β-hydroxy sulfoxides.[11] In spite of many attempts, we have found that it is quite difficult to isolate each diastereomer. In the case of *p*-chlorophenyl group combined to sulfinyl group, however, each diastereomer of the corresponding β-hydroxy sulfoxide was found to be easily isolated in an optically pure state, which could apply to the synthesis of optically pure β-hydroxy esters (vide infra).

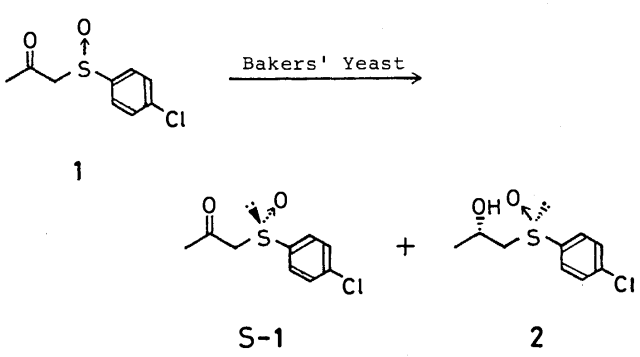

Scheme 1.

Racemic (phenylsulfinyl)acetone is known to be resolved to (*S*)-(phenylsulfinyl)acetone by bakers' yeast.[12] In the reduction of racemic (*p*-chlorophenylsulfinyl)acetone (**1**) with bakers' yeast, one enantiomer was reduced to (*S*)c-(*R*)s-2-hydroxypropyl *p*-chlorophenyl sulfoxide (**2**) and (*S*)-(*p*-chlorophenylsulfinyl)-acetone (**S-1**) remained intact. This keto sulfoxide **S-1** could be separated from the hydroxy sulfoxide by silica-gel chromatography more easily than (phenylsulfinyl)acetone is separated from the corresponding alcohol. The optically pure acetone derivative **S-1** was easily obtained by recrystallization from benzene-hexane in a yield of 38% from the racemate. Methylation at γ-position of **S-1** was carried out by use of sodium hydride and butyllithium in THF to generate the dianion, followed by addition of methyl iodide at 0 °C to yield 2-oxobutyl sulfoxide **3a**(R=CH_3) in 67% yield.[13] The β-keto sulfoxide **3a** was reduced with diisobutylaluminum hydride at −90 °C in THF to give optically active (*R*)c-(*S*)s-alcohol **4a** in 80% yield, which was easily recrystallized from benzene-hexane to give optically pure (*R*)c-(*S*)s-alcohol **4a** in 50% yield. Various β-hydroxy sulfoxides **4** were obtained by alkylation of **S-1**, with allyl bromide, benzyl bromide, benzyloxymethyl chloride, and tetradecyl iodide, respectively, followed by diastereoselective reduction with diisobutylaluminum hydride. All of these β-hydroxy sulfoxides except **4e**(R=$C_{14}H_{29}$), which was recrystallized from methanol, were recrystallized from benzene-hexane to give optically pure ones in 50—58% yields. Then carboxylation at α-position by treatment of **4a** with two

equivalents of methyllithium in THF at 0 °C to produce the dianion of **4a**, followed by pouring them into powdered Dry Ice, then esterification with diazomethane in methanol gave ester **5a**. Elimination of the sulfinyl group from **5a** by treatment with aluminum amalgam[14] in THF-water furnished optically pure methyl (*R*)-3-hydroxypentanoate (**R-6a**). Yields and values of physical properties of various optically pure methyl ester of (*R*)-β-hydroxy acids **R-6**, synthesized by the present method, were listed in Table 1.

On the other hand, when the β-keto sulfoxide **3** was reduced with diisobutylaluminum hydride in the presence of zinc chloride in THF, (*S*)c-(*S*)s-β-hydroxy sulfoxide **7** was mainly obtained. In the case of the diastereomeric mixtures of methyl- and allyl-substituted hydroxy sulfoxides **7a** and **7b**, which are oily and not crystallized, each diastereomers of them were isolated by use of silica-gel chromatography to give optically pure **7**. The (*S*)c-(*S*)s-isomers of β-hydroxy sulfoxides substituted with benzyl, and benzyloxymethyl group, **7c** and **7d**, were easily recrystallized from benzene-hexane, and substituted one with tetradecyl group **7e** was recrystallized from methanol in an optically pure state. Then introduction of ester group to prepare **8**

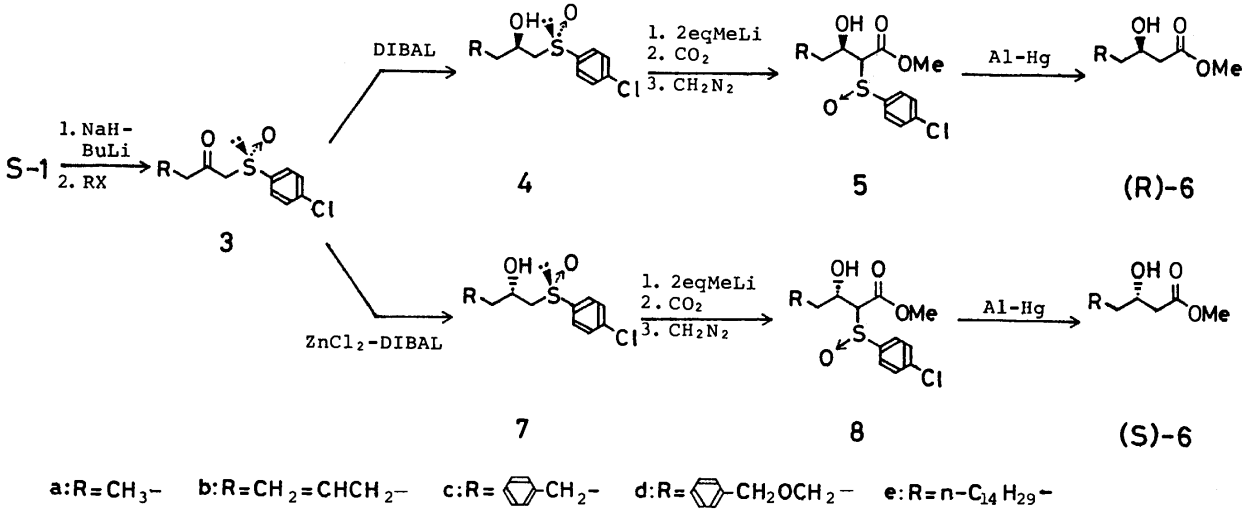

Scheme 2.

Table 1. Synthesis of (*R*)-β-Hydroxy Esters **R-6**

R	**4**		Optically pure **4**			**R-6**	
	Yield/%	*SS*/*RS*[a]	Yield/%	Mp θ_m/°C	$[\alpha]_D^{23}$/°[b]	Yield/%[c]	$[\alpha]_D^{23}$/°[d]
CH_3	80	8/92	50[e]	96—98	−233	38	−37.0[g]
CH_2=$CHCH_2$	85	6/94	58[e]	77—79	−237	50	−22.3[h]
-CH_2	80	3/97	56[e]	69—71	−192	56	−12.2
-CH_2OCH_2	87	5/95	54[e]	74—75	−174	54	−11.5
n-$C_{14}H_{29}$	81	11/89	58[f]	76—77	−146	48	−15.1[i]

a) Determined by HPLC (Finepak SIL C_{18}). b) *c* ca. 1.0, MeOH. c) Yield from **4** via **5**. d) *c* ca. 0.5, $CHCl_3$. e) Recrystallized from benzene-hexane. f) Recrystallized from methanol. g) Lit,[15] $[\alpha]_D$ −36.9° ($CHCl_3$). h) Lit,[16] $[\alpha]_D$ −22.1° ($CHCl_3$). i) Lit,[17] $[\alpha]_D$ −15° ($CHCl_3$).

Table 2. Synthesis of (*S*)-β-Hydroxy Esters **S-6**

R	**7**		Optically pure **7**			**S-6**	
	Yield/%	*SS*/*RS*[a]	Yield/%	Mp θ_m/°C	$[\alpha]_D^{23}$/°[b]	Yield/%[c]	$[\alpha]_D^{23}$/°[d]
CH_3	91	96/4	87[e]	—	−137	54	+36.7
CH_2=$CHCH_2$	94	95/5	89[e]	—	−135	49	+22.1
-CH_2	87	98/2	42[f]	59—61	−91.0	55	+12.2
-CH_2OCH_2	83	96/4	60[f]	66—67	−73.6	50	+11.6
n-$C_{14}H_{29}$	87	92/8	55[g]	84—85	−71.7	37	+14.8

a) Determined by HPLC (Finepak SIL C_{18}). b) *c* ca. 1.0, MeOH. c) Yield from **7** via **8**. d) *c* ca. 0.5, $CHCl_3$. e) Isolated by silica-gel chromatography. f) Recrystallized from benzene-hexane. g) Recrystallized from methanol.

and elimination of the sulfinyl group in the same manner as above gave methyl esters of (*S*)-β-hydroxy acids **S-6** (Table 2).

Corynomycolic acid **10** is one of the mycolic acids produced from coryne bacteria and its trehalose 6,6'-diester has various biological activities such as adjuvant, antibacterial, antitumor, and antiparasitic.[18] Optically active (+)-corynomycolic acid has been prepared in one report,[19] but (−)-comycolic acid has not been synthesized so far. The precursor of both enantiomers of corynomycolic acids is methyl 2-hydroxyoctadecanoate which can be easily prepared by the present method. Tetradecyl iodide was added to the dianion of β-keto sulfoxide **S-1** to furnish β-keto sulfoxide **3e** (R=$C_{14}H_{29}$) in 61% yield and reduction with diisobutylaluminum hydride afforded (*R*)c-(*S*)s-alcohol **4e** in 81% yield. Recrystallization from methanol gave optically pure **4e**. Subsequent carboxylation and esterification afforded ester **5e** and elimination of sulfinyl group gave methyl (*R*)-3-hydroxyoctadecanoate (**6e**). Then alkylation at α-position with tetradecyl iodide by Fráter's method[20] gave (2*R*,3*R*)-β-hydroxy ester **9** in 67% yield with (2*R*,3*R*):(2*S*,3*R*) ratio of 92:8, which was determined by HPLC of the corresponding β-benzoyloxy esters. After hydrolysis and recrystallization from methanol-hexane, optically pure (+)-corynomycolic acid (+)-**10** was obtained in 85% yield. Similarly the reduction of β-keto sulfoxide **3e** (R=$C_{14}H_{29}$) with diisobutylaluminum hydride in the presence of zinc chloride gave (*S*)c-(*S*)s-alcohol **7e** in 87% yield, and recrystallization from methanol afforded optically pure alcohol **7e**. In the same manner as above, (2*S*,3*S*)-β-hydroxy ester **11** with a (2*S*,3*S*):(2*R*,3*S*) ratio of 91:9 was hydrolyzed and recrystallized to give optically pure (−)-corynomycolic acid (−)-**10**.

In conclusion, each diastereomer of β-hydroxyalkyl *p*-chlorophenyl sulfoxides obtained by kinetic resolution of (*p*-chlorophenylsulfinyl)acetone with bakers' yeast followed by γ-alkylation and diastereoselective reduction, was easily separated to an optically pure form, and both enantiomers of optically pure (*R*)- and (*S*)-β-hydroxy esters were conveniently synthesized by using the present method.

Experimental

Melting points were uncorrected. The IR spectra were recorded on JASCO IR 810. The ^{1}H NMR spectra were recorded on JEOL JNM-PMX60si. High-pressure liquid chromatography was performed on Finepak SIL or Finepak SIL C_{18} using JASCO UVIDEC-100V. Elemental analyses were carried out by Yanaco CHN CORDER MT-3. Optical rotations were determined at ambient temperature with Union PM-101. Tetrahydrofuran (THF) was freshly distilled on sodium benzophenone ketyl.

(*S*)-(*p*-Chlorophenylsulfinyl)acetone (S-1). To a mixture of 450 ml of water and 70 g of sucrose with rapid stirring was added 45 g of bakers' yeast (Oriental Yeast Co.). After stirring for 0.5 h at ambient temperature, the solution of 4.4 g (20 mmol) of racemic (*p*-chlorophenylsulfinyl)acetone (**1**) in 40 ml of ethanol was added dropwise. After the mixture was stirred vigorously for 12 h, 200 ml of ethyl acetate was added. Stirring was continued for 0.5 h, then 40 g of celite was added, and the mixture was filtered. The solids were washed

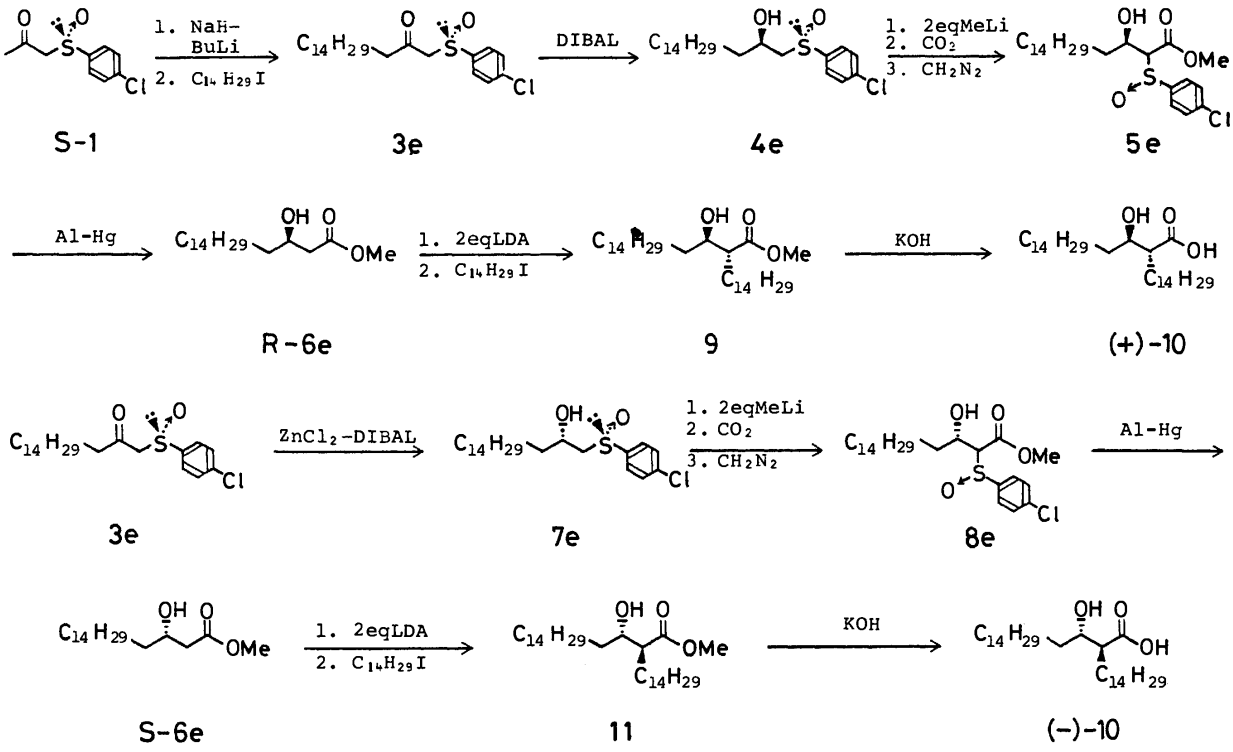

Scheme 3.

with ethyl acetate, and the combined filtrate was extracted with ethyl acetate. The organic layer was dried with sodium sulfate and concentrated. The crude material was purified by chromatography on silica gel (eluent; ethyl acetate : hexane=1 : 3) to give 1.73 g (8.0 mmol) of **S-1** (40% yield) $[\alpha]_D^{23}$ −219 ° (*c* 1.00, MeOH). Recrystallization of **S-1** from benzene–hexane afforded 1.65 g (7.6 mmol) of optically pure **S-1** (38% yield); mp 109—110 °C; $[\alpha]_D^{23}$ −231 ° (*c* 1.16, MeOH).

General Procedure for the Preparation of (*S*)-β-Keto Sulfoxide (3).[13] To a suspension of sodium hydride (1.1 mmol) in THF (2 ml) at 0 °C was added 216 mg (1 mmol) of (*S*)-(*p*-chlorophenylsulfinyl)acetone (**S-1**) in THF (3 ml). Then 1.57 mol dm^{-3} hexane solution of butyllithium (0.7 ml) was added to the reaction mixture. After stirring for 30 min at the same temperature, alkyl halide (1.1 mmol) in THF (3 ml) was added to the reaction mixture. After stirring for 3 h at 0 °C, saturated aqueous NH_4Cl was added to the reaction mixture and extracted with ethyl acetate. The organic layer was dried over sodium sulfate and the solvent was evaporated. The crude material was purified by chromatography on silica gel (eluent; ethyl acetate : hexane=1 : 3) to give (*S*)-β-keto sulfoxide.

(*S*)-1-(*p*-Chlorophenylsulfinyl)-2-butanone (3a): 67% yield; $[\alpha]_D^{23}$ −201° (*c* 0.99, MeOH); mp 96—98 °C; IR ($CHCl_3$) 1010, 1050, 1090, 1390, 1470, 1710, and 2970 cm^{-1}; ^{1}H NMR ($CDCl_3$) δ=1.04 (t, *J*=7.2 Hz, 3H), 2.55 (q, *J*=7.1 Hz, 2H), 3.83 (s, 2H), and 7.55 (s, 4H). Found: C, 52.14; H, 4.80%. Calcd for $C_{10}H_{11}SO_2Cl$: C, 52.11; H, 4.77%.

(*S*)-1-(*p*-Chlorophenylsulfinyl)-5-hexen-2-one (3b): 63% yield; $[\alpha]_D^{23}$ −206° (*c* 0.34, MeOH); mp 104—105 °C; IR ($CHCl_3$) 1090, 1385, 1470, 1705, 2900, and 3000 cm^{-1}. ^{1}H NMR ($CDCl_3$) δ=2.03—2.91 (m, 4H), 3.85 (s, 2H), 4.73—5.26 (m, 2H), 5.34—6.06 (m, 1H), and 7.57 (s, 4H). Found: C, 56.33; H, 5.25%. Calcd for $C_{12}H_{13}SO_2Cl$: C, 56.20; H, 5.07%.

(*S*)-1-(*p*-Chlorophenylsulfinyl)-4-phenyl-2-butanone (3c): 52% yield; $[\alpha]_D^{23}$ −168° (*c* 1.01, $CHCl_3$); mp 119—120 °C; IR ($CHCl_3$) 1000, 1095, 1470, 1720, 2925, and 3000 cm^{-1}; ^{1}H NMR ($CDCl_3$) δ=2.84(s, 4H), 3.78(s, 2H), and 6.81—7.80(m, 9H). Found: C, 62.60; H, 5.17%. Calcd for $C_{16}H_{15}SO_2Cl$: C, 62.68; H, 4.89%.

(*S*)-1-(*p*-Chlorophenylsulfinyl)-4-benzyloxy-2-butanone (3d): 54% yield; $[\alpha]_D^{23}$ −111° (*c* 1.08, $CHCl_3$); mp 56—58 °C; IR ($CHCl_3$) 1005, 1025, 1050, 1090, 1360, 1390, 1480, 1700, 2900, 3025, and 3050 cm^{-1}; ^{1}H NMR ($CDCl_3$) δ=2.72 (t, *J*=6.0 Hz, 2H), 3.71(t, *J*=5.9 Hz, 2H), 3.84(s, 2H), 4.45(s, 2H), 7.11(s, 5H), and 7.71(s, 4H). Found: C, 60.98; H, 5.17%. Calcd for $C_{17}H_{17}SO_3Cl$: C, 60.68; H, 5.05%.

(*S*)-1-(*p*-Chlorophenylsulfinyl)-2-heptadecanone (3e): 61% yield; $[\alpha]_D^{23}$ −121° (*c* 1.04, $CHCl_3$); mp 95—97°C; IR ($CHCl_3$) 1005, 1040, 1705, 2850, and 2950 cm^{-1}; ^{1}H NMR ($CDCl_3$) δ=0.61—1.90 (m, 29H), 2.47 (t, *J*=6.0 Hz, 2H), 3.80 (s, 2H), and 7.25—7.81 (m, 4H). Found: C, 66.90; H, 9.10%. Calcd for $C_{23}H_{37}SO_2Cl$: C, 66.98; H, 8.98%.

General Procedure for the Preparation of (*R*)c-(*S*)s-β-Hydroxy Sulfoxides 4. To a solution of (*S*)-β-keto sulfoxide **3** (1 mmol) in THF (4 ml) was dropwise added 1.4 ml of a 1.5 mol dm^{-3} solution of diisobutylaluminum hydride in hexane at −90 °C. After stirring for 5 h at −90 °C, 2 mol dm^{-3} HCl solution (3 ml) was added to the reaction mixture and the products were extracted with ethyl acetate. The organic layer was dried over sodium sulfate and the solvent was evaporated. The crude material was purified by chromatography on silica gel (eluent; CH_2Cl_2) to give (*R*)c-(*S*)s-β-hydroxy sulfoxide **4**. The yields, the diastereomeric ratios and the yields of optically pure **4** recrystallized from benzene–hexane were listed in Table 1.

(2*R*)-1-[(*S*)-*p*-Chlorophenylsulfinyl]-2-butanol (4a): $[\alpha]_D^{23}$ −233° (*c* 1.02, MeOH); mp 96—98 °C; IR ($CHCl_3$) 1020, 1090, 1120, 1450, 2950, 3000, and 3400 cm^{-1}; ^{1}H NMR ($CDCl_3$) δ=0.94 (t, *J*=6.6 Hz, 3H), 1.58 (m, 2H) 2.70 (dd, *J*=3.2, 13.2 Hz, 1H) 3.06 (dd, *J*=9.6, 13.2 Hz, 1H), 3.79—4.40 (m, 2H), and 7.62(s, 4H). Found: C, 51.43; H, 5.56%. Calcd for $C_{10}H_{13}SO_2Cl$: C, 51.66; H, 5.59%.

(2*R*)-1-[(*S*)-*p*-Chlorophenylsulfinyl]-5-hexen-2-ol (4b): $[\alpha]_D^{23}$ −237° (*c* 1.03, MeOH); mp 77—79 °C; IR ($CHCl_3$) 1005, 1020, 1090, 1475, 2950, and 3350 cm^{-1}; ^{1}H NMR ($CDCl_3$) δ=1.38—1.87 (m, 2H), 1.95—2.47 (m, 2H), 2.80 (dd, *J*=4.0, 13.4 Hz, 1H), 3.04 (dd, *J*=8.4, 13.4 Hz, 1H), 4.26 (m, 2H), 4.77—5.28 (m, 2H), 5.46—6.26 (m, 1H), and 7.64 (s, 4H). Found: C, 55.67; H, 6.04%. Calcd for $C_{12}H_{15}SO_2Cl$: C, 55.77; H, 5.80%.

(2*R*)-1-[(*S*)-*p*-Chlorophenylsulfinyl]-4-phenyl-2-butanol (4c): $[\alpha]_D^{23}$ −192° (*c* 1.02, MeOH); mp 69—71 °C; IR ($CHCl_3$) 1005, 1040, 1090, 1260, 1390, 1450, 1480, 2900, 3000, and 3400 cm^{-1}; ^{1}H NMR ($CDCl_3$) δ=1.92 (t, *J*=6.0 Hz, 2H), 2.49—3.18 (m, 4H), 3.94—4.45 (m, 2H), and 7.19 (s, 5H), 7.44 (s, 4H). Found: C, 62.51; H, 5.71%. Calcd for $C_{16}H_{17}SO_2Cl$: C, 62.28; H, 5.51%.

(2*R*)-1-[(*S*)-*p*-Chlorophenylsulfinyl]-4-benzyloxy-2-butanol (4d): $[\alpha]_D^{23}$ −174° (*c* 0.92, MeOH); mp 74—75 °C; IR ($CHCl_3$) 1000, 1090, 1470, 2850, 3000, and 3450 cm^{-1}; ^{1}H NMR ($CDCl_3$) δ=1.9 (t, *J*=6.0 Hz, 2H), 2.76 (dd, *J*=3.6, 13.6 Hz, 1H), 3.07 (dd, *J*=7.2, 13.6 Hz, 1H), 3.65 (t, *J*=5.7 Hz, 2H), 4.16—4.70 (m, 2H), 4.53 (s, 2H), 7.08 (s, 5H), and 7.73 (s, 4H). Found: C, 60.40; H, 5.57%. Calcd for $C_{17}H_{19}SO_3Cl$: C, 60.32; 5.61%.

(2*R*)-1-[(*S*)-*p*-Chlorophenylsulfinyl]-2-heptadecanol (4e): $[\alpha]_D^{23}$ −146° (*c* 0.52, MeOH); mp 76—77 °C; IR ($CHCl_3$) 1000, 1040, 1095, 1390, 1460, 2850, 2900, and 3400 cm^{-1}; ^{1}H NMR ($CDCl_3$) δ=0.65—1.80 (m, 31H), 2.70 (dd, *J*=3.2, 13.6 Hz, 1H), 3.03 (dd, *J*=8.8, 13.6 Hz, 1H), 3.94—4.50 (m, 2H), and 7.73 (s, 4H). Found: C, 66.70; H, 9.54%. Calcd for $C_{23}H_{39}SO_2Cl$: C, 66.66; H, 9.41%.

General Procedure for the Preparation of (*S*)c-(*S*)s-β-Hydroxy Sulfoxides 7.[11] To a suspension of anhydrous zinc chloride (1.1 mmol) in THF (2 ml) was added (*S*)-β-keto sulfoxide **3** (1 mmol) in THF (4 ml). After stirring for 30 min at room temperature, the reaction mixture was cooled to −90 °C, and 1.4 ml of 1.5 mol dm^{-3} solution of diisobutylaluminum hydride in hexane was added. After stirring for 5 h at −90 °C, the reaction mixture was treated with 2 mol dm^{-3} HCl solution and extracted with ethyl acetate. The organic layer was dried with sodium sulfate and the solvent was evaporated. The crude material was purified by chromatography on silica gel (eluent; CH_2Cl_2) to give (*S*)c-(*S*)s-β-hydroxy sulfoxide. The yields, the diastereomeric ratio and the yields of optically pure **7** were listed in Table 2.

(2*S*)-1-[(*S*)-*p*-Chlorophenylsulfinyl]-2-butanol (7a): $[\alpha]_D^{23}$ −137° (*c* 0.87, MeOH); IR (neat) 1020, 1090, 1120, 1450, 2950, 3000, and 3400 cm^{-1}; ^{1}H NMR ($CDCl_3$) δ=0.96 (t, 7.4 Hz, 3H), 1.72 (m, *J*=7.4 Hz, 2H), 2.77 (dd, *J*=4.0, 12.8 Hz, 1H), 3.10 (dd, *J*=8.0, 12.8 Hz, 1H), 3.58—4.39 (m, 2H), and 7.63 (s, 4H). Found: C, 51.37; H, 5.59%. Calcd for $C_{10}H_{13}SO_2Cl$: C, 51.66; H, 5.59%.

(2*S*)-1-[(*S*)-*p*-Chlorophenylsulfinyl]-5-hexene-2-ol (7b): $[\alpha]_D^{23}$ −135° (*c* 1.03, MeOH); IR (neat) 1005, 1070, 1090, 1475, 2950, and 3350 cm^{-1}: ^{1}H NMR ($CDCl_3$) δ=1.23—1.92 (m,

2H), 1.92—2.44 (m, 2H), 2.78 (dd, J=4, 12.6 Hz, 1H), 3.02 (dd, J=7.6, 12.6 Hz, 1H), 3.80—4.51 (m, 2H), 4.79—5.28 (m, 2H), 5.46—6.19 (m, 1H), and 7.63 (s, 4H). Found: C, 55.69; H, 5.70%. Calcd for $C_{12}H_{15}SO_2Cl$: C, 55.77; H, 5.80%.

(2*S*)-1-[(*S*)-*p*-Chlorophenylsulfinyl]-4-phenyl-2-butanol (7c): $[\alpha]_D^{23}$ −91.0° (*c* 1.01, MeOH); mp 59—61 °C; IR ($CHCl_3$) 1005, 1040, 1090, 1260, 1390, 1450, 1480, 2900, 3000, and 3400 cm^{-1}. ^1H NMR ($CDCl_3$) δ=1.93 (t, J=6.1 Hz, 2H), 2.56—3.11 (m, 3H), 3.67 (s, 1H), 4.08—4.49 (m, 2H), 7.23 (s, 5H), and 7.53 (s, 4H). Found: C, 62.42; H, 5.41%. Calcd for $C_{16}H_{17}SO_2Cl$: C, 62.28; H, 5.51%.

(2*S*)-1-[(*S*)-*p*-Chlorophenylsulfinyl]-4-benzyloxy-2-butanol (7d): $[\alpha]_D^{23}$ −73.6° (*c* 1.02, MeOH); mp 66—67 °C; IR ($CHCl_3$) 1000, 1090, 1470, 2850, 3000, and 3450 cm^{-1}, ^1H NMR ($CDCl_3$) δ=1.83 (t, J=5.6 Hz, 2H), 2.83 (dd, J=4.8, 13.2 Hz, 1H), 3.14 (dd, J=7.2, 13.2 Hz, 1H), 3.65 (t, J=5.4 Hz, 2H), 3.90—4.60 (m, 2H), 4.46 (s, 2H), 7.10 (s, 5H), and 7.53 (s, 4H). Found: C, 60.59; H, 5.45%. Calcd for $C_{17}H_{19}SO_3Cl$: C, 60.32; H, 5.61%.

(2*S*)-1-[(*S*)-*p*-Chlorophenylsulfinyl]-2-heptadecanol (7e): $[\alpha]_D^{23}$ −71.7° (*c* 0.51, MeOH); mp 84—85 °C; IR ($CHCl_3$) 1000, 1040, 1095, 1390, 1460, 2850, 2900, and 3400 cm^{-1}, ^1H NMR ($CDCl_3$) δ=0.67—1.79 (m, 31H), 2.77 (dd, J=3.6, 12.8 Hz, 1H), 3.03 (dd, J=7.6, 12.8 Hz, 1H), 3.94—4.58 (m, 2H), and 7.75 (s, 4H). Found: C, 66.48; H, 9.59%. Calcd for $C_{23}H_{39}SO_2Cl$: C, 66.66; H, 9.41%.

General Procedure for the Preparation of Esters. To a solution of β-hydroxy sulfoxide **4** or **7** (1 mmol) in THF (2 ml) at −5 °C was added 1.48 ml (2 mmol) of a 1.35 mol dm^{-3} solution of methyllithium in ether. After stirring for 1 h at 0 °C, the reaction mixture was cooled to −70 °C, then poured onto 20 g of powdered Dry Ice, and shaken for 15 min. The reaction mixture was acidified with 5 ml of 2 mol dm^{-3} HCl solution and extracted with ethyl acetate. The organic layer was dried over sodium sulfate and the solvent was evaporated. The residue was dissolved in 5 ml of methanol and 0.3 mol dm^{-3} diazomethane solution in ether was added until the yellow color of the solution did not fade. After removal of the solvent, the crude material was purified by chromatography on silica gel (eluent; ethyl acetate : hexane=1 : 2) to give 3-hydroxy-2-sulfinyl ester **5** or **8**.

Methyl (3*R*)-2-[(*S*)-*p*-Chlorophenylsulfinyl]-3-hydroxypentanoate (5a): 50% yield; $[\alpha]_D^{23}$ −180.9° (*c* 1.06, MeOH); mp 110—111 °C; IR ($CHCl_3$) 1040, 1090, 1380, 1450, 1740, 2950, 2975, and 3300 cm^{-1}: ^1H NMR ($CDCl_3$) δ=0.73—1.23 (m, 3H), 1.25—2.67 (m, 2H), 3.23—4.03 (m, 5H), 4.29 (s. 1H), and 7.64 (m, 4H). Found: C, 49.64; H, 5.24%. Calcd for $C_{12}H_{15}SO_4Cl$: C, 49.62; H, 5.16%.

Methyl (3*R*)-2-[(*S*)-*p*-Chlorophenylsulfinyl]-3-hydroxy-6-heptenoate (5b): 68% yield; $[\alpha]_D^{23}$ −134° (*c* 1.26, MeOH); mp 85—87 °C; IR ($CHCl_3$) 1010, 1090, 1300, 1730, 2950, and 3400 cm^{-1}: ^1H NMR ($CDCl_3$) δ=1.34—1.91 (m, 2H), 2.01—2.56 (m, 2H), 3.29—3.87 (m, 4H), 4.28 (s, 2H), 4.76—5.40 (m, 2H), 5.44—6.26 (m, 1H), and 7.04—7.94 (m, 4H). Found: C, 52.96; H, 5.54%. Calcd for $C_{14}H_{17}SO_4Cl$: C, 53.13; H, 5.37%.

Methyl (3*R*)-2-[(*S*)-*p*-Chlorophenylsulfinyl]-3-hydroxy-5-phenylpentanoate (5c): 70% yield; $[\alpha]_D^{23}$ −119 ° (*c* 1.15, MeOH); mp 82—83 °C; IR ($CHCl_3$) 1010, 1090, 1300, 1350, 1730, 2850, 2940, and 3450^{-1}; ^1H NMR ($CDCl_3$) δ=1.67—2.17 (m, 2H), 2.58—3.07 (m, 2H), 3.16—4.43 (m, 6H), 7.20 (s, 5H), and 7.50 (s, 4H). Found: C, 59.22; H, 5.28%. Calcd for $C_{18}H_{19}SO_4Cl$: C, 58.98; H, 5.18%.

Methyl (3*R*)-2-[(*S*)-*p*-Chlorophenylsulfinyl]-3-hydroxy-5-(benzyloxy)pentanoate (5d): 69% yield; $[\alpha]_D^{23}$ −98° (*c* 1.16, MeOH); mp 82—84 °C; IR ($CHCl_3$) 1005, 1095, 1485, 1730, 2350, 3000, and 3450 cm^{-1}. ^1H NMR ($CDCl_3$) δ=1.57—2.10 (m, 2H), 3.33—3.93 (m, 8H), 4.57 (s, 2H), and 7.00—7.76 (m, 9H). Found: C, 57.81; H, 5.33%. Calcd for $C_{19}H_{21}SO_5Cl$: C, 57.56; H 5.30%.

Methyl (3*R*)-2-[(*S*)-*p*-Chlorophenylsulfinyl]-3-hydroxyoctadecanoate (5e): 65% yield; $[\alpha]_D^{23}$ −146.7° (*c* 0.51, MeOH); mp 76—79 °C; IR ($CHCl_3$) 1095, 1310, 1460, 1718, 2850, 2950, and 3400 cm^{-1}; ^1H NMR ($CDCl_3$) δ=0.64—1.78 (m, 31H), 3.25—4.19 (m, 6H), and 7.53 (s, 4H). Found: C, 63.55; H, 8.52%. Calcd for $C_{25}H_{41}SO_4Cl$: C, 63.69; H, 8.70%.

Methyl (3*S*)-2-[(*S*)-*p*-Chlorophenylsulfinyl]-3-hydroxypentanoate (8a): 69% yield; $[\alpha]_D^{23}$ −164° (*c* 0.96, MeOH); mp 53—55 °C; IR ($CHCl_3$) 1040, 1090, 1380, 1450, 1740, 2950, 2975, and 3300 cm^{-1}. ^1H NMR ($CDCl_3$) δ=0.93—1.21 (m, 3H), 1.25—2.23 (m, 2H), 3.44—4.71 (m, 6H), and 7.61 (m, 4H). Found: C, 49.73; H, 5.43%. Calcd for $C_{12}H_{15}SO_4Cl$: C, 49.62; H, 5.16%.

Methyl (3*S*)-2-[(*S*)-*p*-Chlorophenylsulfinyl]-3-hydroxy-6-heptenoate (8b): 62% yield; $[\alpha]_D^{23}$ −102° (*c* 1.54, MeOH); mp 42—43 °C; IR ($CHCl_3$) 1010, 1090, 1300, 1730, 2950, and 3400 cm^{-1}: ^1H NMR ($CDCl_3$) δ=1.39—1.94 (m, 2H), 2.03—2.60 (m, 2H), 3.31—4.04 (m, 3H), 4.47 (s, 1H), 4.79—5.41 (m, 2H), 5.46-6.31 (m, 1H), 7.07—7.82 (m, 4H). Found: C, 53.32; H, 5.39%. Calcd for $C_{12}H_{15}SO_4Cl$: C, 53.13; H, 5.37%.

Methyl (3*S*)-2-[(*S*)-*p*-Chlorophenylsulfinyl]-3-hydroxy-5-phenylpentanoate (8c): 70% yield; $[\alpha]_D^{23}$ −102° (*c* 1.02, MeOH); mp 68—70 °C; IR ($CHCl_3$) 1010, 1090, 1300, 1350, 1730, 2850, 2940, and 3450 cm^{-1}; ^1H NMR ($CDCl_3$) δ=1.82—2.13 (m, 2H), 2.61—3.15 (m, 2H), 3.20—4.48 (m, 5H), 7.31 (s, 5H), and 7.61 (s, 4H). Found: C, 58.71; H, 5.35%. Calcd for $C_{18}H_{19}SO_4Cl$: C, 58.98; H, 5.18%.

Methyl (3*S*)-2-[(*S*)-*p*-Chlorophenylsulfinyl]-3-hydroxy-5-(benzyloxy)pentanoate (8d): 65% yield; $[\alpha]_D^{23}$ −85 ° (*c* 1.2, MeOH); mp 76—78 °C; IR ($CHCl_3$) 1005, 1095, 1485, 1730, 2350, 3000, and 3450 cm^{-1}; ^1H NMR ($CDCl_3$) δ=1.68—2.23 (m, 2H), 3.47—3.93 (m, 8H), 4.57 (s, 2H), 7.17—7.80 (m, 9H). Found: C, 57.60; H, 5.22%. Calcd for $C_{19}H_{21}SO_5Cl$: C, 57.56; H, 5.30%.

Methyl (3*S*)-2-[(*S*)-*p*-Chlorophenylsulfinyl]-3-hydroxyoctadecanoate (8e): 60% yield; $[\alpha]_D^{23}$ −83.2 ° (*c* 0.59, MeOH); mp 95—97 °C; IR ($CHCl_3$) 1095, 1310, 1460, 1718, 2850, 2950, and 3400 cm^{-1}; ^1H NMR ($CDCl_3$) δ=0.65—2.07 (m, 31H), 3.27—4.72 (m, 6H), and 7.54 (s, 4H). Found: C, 63.63; H, 8.61%. Calcd for $C_{25}H_{41}SO_4Cl$: C, 63.69; H, 8.70%.

General Procedure for the Preparation of β-Hydroxy Esters 6.[14] To a solution of 3-hydroxy-2-sulfinyl ester (1 mmol) in 10% aqueous THF (10 ml) was added 0.2 g of aluminum amalgam at 0 °C. The reaction mixture was stirred at room temperature in hydrogen atmosphere. After stirring for 3 h, the reaction mixture was filtered and washed with ether, and the product was extracted with ether. The organic layer was dried over sodium sulfate, and the solvent was evaporated. The crude material was purified by chromatography on silica gel (eluent; ethyl acetate : hexane=1 : 4) to give methyl β-hydroxy ester **6**.

Methyl (*R*)-3-Hydroxypentanoate (*R*-6a): 75% yield; $[\alpha]_D^{23}$ −37.0° (*c* 2.00, $CHCl_3$) (lit,[15] $[\alpha]_D$ −36.9°).

Methyl (*R*)-3-Hydroxy-6-heptenoate (*R*-6b): 74% yield; $[\alpha]_D^{23}$ −22.3° (*c* 0.7, $CHCl_3$) (lit,[16] $[\alpha]_D$ −22.1°); IR (neat) 1100, 1285, 1640, 1740, 2900, and 3500 cm^{-1}; ^1H NMR (CCl_4) δ=1.19—2.56 (m, 6H), 3.69 (s, 3H), 4.24 (m, 2H),

4.77—5.33 (m, 2H), and 5.59—5.95 (m, 6H). Found: C, 45.52; H, 6.58%. Calcd for $C_{18}H_{14}O_3$: C, 45.61; H, 6.33%.

Methyl (*R*)-3-Hydroxy-5-phenylpentanoate (*R*-6c): 80% yield; $[\alpha]_D^{23}$ −12.2° (*c* 1.16, $CHCl_3$); IR (neat) 1100, 1280, 1310, 1720, 2900, and 3500 cm^{-1}; ^1H NMR (CCl_4) δ=1.43—1.82 (m, 2H), 2.34—3.03 (m, 4H), 3.67 (s, 3H), 3.81—3.97 (m, 2H), and 6.97 (s, 5H). Found: C, 69.06; H, 7.65%. Calcd for $C_{12}H_{16}O_3$: C, 69.26; H, 7.67%.

Methyl (*R*)-3-Hydroxy-5-(benzyloxy)pentanoate (*R*-6d): 78% yield; $[\alpha]_D^{23}$ −11.5° (*c* 2.5, $CHCl_3$). The ^1H NMR and IR spectra were in agreement with the literature.[21]

Methyl (*R*)-3-Hydroxyoctadecanoate (*R*-6e): 74% yield; $[\alpha]_D^{23}$ −15.1° (*c* 0.56, $CHCl_3$) (lit,[17] $[\alpha]_D$ −15°).

Methyl (*S*)-3-Hydroxypentanoate (*S*-6a): 78% yield; $[\alpha]_D^{23}$ +36.7° (*c* 0.60, $CHCl_3$).

Methyl (*S*)-3-Hydroxyheptenoate (*S*-6b): 79% yield; $[\alpha]_D^{23}$ +22.1° (*c* 0.60, $CHCl_3$); IR (neat) 1100, 1285, 1640, 1740, 2900, and 3500 cm^{-1}; ^1H NMR (CCl_4) δ=1.18—2.58 (m, 6H), 3.68 (s, 3H), 4.33 (m, 2H), 4.91—5.36 (m, 2H), and 5.43—5.97 (m, 1H). Found: C, 45.44; H, 6.58%. Calcd for $C_{18}H_{14}O_3$: C, 45.61; H, 6.33%.

Methyl (*S*)-3-Hydroxy-5-phenylpentanoate (*S*-6c): 79% yield; $[\alpha]_D^{23}$ +12.2° (*c* 0.98, $CHCl_3$). IR (neat) 1100, 1280, 1310, 1720, 2900, and 3500 cm^{-1}; ^1H NMR (CCl_4) δ=1.43—1.96 (m, 2H), 2.36—3.04 (m, 4H), 3.59 (s, 3H), 3.75—4.05 (m, 2H), 7.07 (s, 5H). Found: C, 69.33; H, 7.71%. Calcd for $C_{12}H_{16}O_3$: C, 69.26; H, 7.67%.

Methyl (*S*)-3-Hydroxy-5-(benzyloxy)pentanoate (*S*-6d): 77% yield; $[\alpha]_D^{23}$ +11.6° (*c* 2.6, $CHCl_3$). The ^1H NMR and IR spectra were in agreement with the literature.[21]

Methyl (*S*)-3-Hydroxyoctadecanoate (*S*-6e): 62% yield; $[\alpha]_D^{23}$ +14.8° (*c* 0.55, $CHCl_3$).

Corynomycolic Acids ((+)- and (−)-10). To a solution of diisopropylamine (100 mg, 1 mmol) in THF (0.5 ml) was added 0.65 ml of an 1.54 mol dm^{-3} solution of butyllithium in hexane at 0 °C. The solution of lithium diisopropylamide was cooled to −50 °C, and 150 mg (0.48 mmol) of methyl 3-hydroxyoctadecanoate (**6e**) in THF (2 ml) was added. After stirring for 1 h at the same temperature, a solution of tetradecyl iodide (162 mg, 0.5 mmol) in 1 g of HMPA was added, and the mixture was stirred for 3 h at −30 °C. The mixture was poured on ice-water and extracted with ether. The ethereal layer was dried over sodium sulfate, and the solvent was evaporated. The crude material was purified by chromatography on silica gel (eluent; ethyl acetate: hexane=1 : 3) to give methyl corynomycolate **9** or **11**.

Methyl (2*R*,3*R*)-3-Hydroxy-2-tetradecyloctadecanoate (9): 67% yield; $[\alpha]_D^{23}$ +4.2° (*c* 0.53, $CHCl_3$); mp 58—60 °C.

Methyl (2*S*,3*S*)-3-Hydroxy-2-tetradecyloctadecanoate (11): 65% yield; $[\alpha]_D^{23}$ −4.0° (*c* 0.52, $CHCl_3$); mp 58—60 °C.

To a solution of methyl corynomycolate **9** or **11** (510 mg, 1 mmol) in 50 ml of methanol was added 5 ml of an 1 mol dm^{-3} solution of potassium hydroxide in methanol at 30 °C. After stirring for 5 h, the solvent was evaporated. The residue was dissolved into water (20 ml) and washed with ether. After acidification with 2 mol dm^{-3} HCl solution (10 ml), the acid was extracted with ether. The organic layer was dried over sodium sulfate and the solvent was evaporated. The residue was recrystallized from methanol–petroleum ether to give optically pure corynomycolic acid (**10**).

(+)-Corynomycolic Acid ((+)-10): 85% yield; $[\alpha]_D^{23}$ +7.2° (*c* 0.40, $CHCl_3$) (lit,[18] $[\alpha]_D$ +7.2°); mp 68—70 °C (lit,[18] mp 70 °C).

(−)-Corynomycolic Acid ((−)-10): 83% yield; $[\alpha]_D^{23}$ −7.3° (*c* 0.50, $CHCl_3$); mp 68—69 °C.

Methyl 2-Tetradecyl-3-(benzoyloxy)octadecanoate. To a solution of **9** or **11** (51 mg, 0.1 mmol) and catalytic amount of 4-dimethylaminopyridine (2 mg) in pyridine (2 ml) was added benzoylchloride (30 mg, 0.2 mmol) at room temperature. After stirring for 15 h, 2 mol dm^{-3} HCl solution (2 ml) was added to the reaction mixture. The products were extracted with dichloromethane, dried over sodium sulfate and evaporated. The crude material was purified by chromatography on silica gel (eluent; ethyl acetate : hexane=5 : 1) to give methyl 2-tetradecyl-3-(benzoyloxy)octadecanoate.

Methyl (2*R*,3*R*)-2-Tetradecyl-3-(benzoyloxy)octadecanoate; 85% yield. The ratio of (2*R*,3*R*) : (2*S*,3*R*) was determined to be 92 : 8 by HPLC on a Finepak SIL column using hexane : 2-propanol=600 : 1. IR (neat) 1275, 1460, 1720, 2850, and 2925 cm^{-1}; ^1H NMR ($CDCl_3$) δ=0.95—1.35 (m, 60H), 2.20 (m, 1H), 3.65 (m, 4H), and 7.30 (m, 5H).

Methyl (2*S*,3*S*)-2-Tetradecyl-3-(benzoyloxy)octadecanoate; 90% yield. The ratio of (2*S*,3*S*) : (2*R*,3*S*) was determined to be 91 : 9 by HPLC on a Finepak SIL column using hexane : 2-propanol=600 : 1. IR (neat) 1260, 1500, 1720, 2850, and 2920 cm^{-1}; ^1H NMR ($CDCl_3$) δ=0.98—1.35 (m, 60H), 2.21 (m, 1H), 3.70 (m, 4H), and 7.38 (m, 5H).

References

1) T. Mukaiyama, "Organic Reactions," John Wiley & Sons, New York (1982), Vol. 28, p. 203; M. Braun, *Angew. Chem., Int. Ed. Engl.*, **26**, 24 (1987).

2) C. Mioskowski and G. Solladié, *J. Chem. Soc., Chem. Commun.*, **1977**, 162.

3) C. H. Heathcock, M. C. Pirrung, and J. E. Sohn, *J. Org. Chem.*, **44**, 4294 (1979); C. H. Heathcock, C. T. Buse, W. A. Kleschick, M. C. Pirrung, J. E. Sohn, and J. Lampe, *ibid.*, **45**, 1066 (1980); C. H. Heathcock, *ibid.*, **45**, 1727 (1980).

4) D. A. Evans and L. R. McGee, *J. Am. Chem. Soc.*, **103**, 2876 (1981).

5) S. Masamune, W. Choy, F. A. J. Kerdesky, and B. Imperiali, *J. Am. Chem. Soc.*, **103**, 1566 (1981); S. Masamune, M. Hirama, S. Mori, S. A. Ali, and D. S. Garvey, *ibid.*, **103**, 1568 (1981); S. Masamune, T. Kaiho, and D. S. Garvey, *ibid.*, **104**, 5521 (1982); S. Masamune, L. D. L. Lu, W. P. Jackson, T. Kaiho, and T. Toyoda, *ibid.*, **104**, 5523 (1982).

6) N. Iwasawa and T. Mukaiyama, *Chem. Lett.*, **1982**, 1441; **1983**, 297.

7) M. Guette, J. Capillon, and J. P. Guette, *Tetrahedron*, **29**, 3659 (1973).

8) H. J. Carlsen, T. Katsuki, V. S. Martin, and K. B. Sharpless, *J. Org. Chem.*, **46**, 3936 (1981); J. M. Chong and K. B. Sharpless, *Tetrahedron Lett.*, **26**, 4683 (1985).

9) H. Wynberg and E. G. J. Staring, *J. Am. Chem. Soc.*, **104**, 166 (1982).

10) K. Mori, *Tetrahedron*, **37**, 1341 (1981); M. Hirama, M. Shimizu, and M. Iwashita, *J. Chem. Soc., Chem. Commun.*, **1983**, 599; G. Fráter, *Helv. Chim. Acta*, **63**, 1383 (1980); K. Nakamura, K, Ushio, S. Oka, and A. Ohno, *Tetrahedron Lett.*, **25**, 3979 (1984); T. Fujisawa, T. Itoh, and T. Sato, *ibid.*, **25**, 5083 (1984).

11) H. Kosugi, H. Konta, and H. Uda, *J. Chem. Soc., Chem. Commun.*, **1985**, 211; G. Solladié, G. Demailly, and C. Grec, *Tetrahedron Lett.*, **26**, 435 (1985).

12) S. Iriuchijima and N. Kojima, *Agric. Biol. Chem.*, **42**, 451 (1978); R. L. Crumbie, B. S. Deol, J. E. Nemorin, and D. D. Ridley, *Aust. J. Chem.*, **31**, 1965 (1978).
13) I. Kuwajima and H. Iwasawa, *Tetrahedron Lett.*, **1974**, 107; P. A. Grieco and C. S. Poganowski, *J. Org. Chem.*, **39**, 732 (1974).
14) E. J. Corey and M. Chaykovsky, *J. Am. Chem. Soc.*, **86**, 1639 (1964).
15) K. Mori and M. Ikunaka, *Tetrahedron*, **40**, 3471 (1984).
16) M. Hirama, M. Shimizu, and M. Iwashita, *J. Chem. Soc., Chem. Commun.*, **1983**, 599.
17) A. P. Tulloch and J. F. T. Spencer, *Can. J. Chem.*, **42**, 830 (1964).
18) A. Diara and J. Pudles, *Bull. Soc. Chim. Biol.*, **41**, 481 (1959); E. Lederer, *J. Med. Chem.*, **23**, 819 (1980).
19) Y. Kitano, Y. Kobayashi, and F. Sato, *J. Chem. Soc., Chem. Commun.*, **1985**, 498.
20) G. Fráter, M. Müller, and W. Günther, *Tetrahedron*, **40**, 1269 (1984).
21) B. H. Lee, A. Biswas, and M. J. Miller, *J. Org. Chem.*, **51**, 106 (1986).

 © 1988 The Chemical Society of Japan Bull. Chem. Soc. Jpn., 61, 1281—1283 (1988)

The Synthesis of a Double-Layered Annulene with 10π-Rings. 1,1 : 2,2-Bis([10]annulene-1,6-diyl)ethylene

Koji YAMAMOTO,* Jūro OJIMA,†,* Noboru MORITA,†† and Toyonobu ASAO††
Department of Chemistry, Faculty of Engineering Science, Osaka University, Toyonaka, Osaka 560
†Department of Chemistry, Faculty of Science, Toyama University, Gofuku, Toyama 930
††Department of Chemistry, College of General Education, Tohoku University, Kawauchi, Sendai 980
(Received October 17, 1987)

The synthesis of the title compound, a double-layered annulene with 10π-rings, is described. The examination of ^{1}H NMR and electronic spectra suggests that the layered compound exhibits appreciable interaction between two [10]annulene rings.

A progress in the annulene chemistry stimulates our interest in the layered annulenes made up of a various ring size to investigate the transannular interaction between the annulene rings. Although the two annulenophanes, [2]paracyclo[2](2,7)(1,6-methano[10]-annuleno)phane (**1**) and [2](1,5)naphthaleno[2](2,7)-(1,6-methano[10]annuleno)phane (**2**) which consist of the benzenoid ring and 1,6-methano[10]annulene, have been synthesized by Matsumoto et al.[1] and it has been shown that the compound **2** shows appreciable transannular interaction between 1,6-methano[10]-annulene ring and naphthalene ring, none of the layered annulenes has been reported.

On the other hand, 11-methylene-1,6-methano[10]-annulene (**3**) and 1,6-methano[10]annulen-11-one (**4**) were prepared by Vogel et al.[2] and by Itô et al.,[3] respectively, and both the compounds **3** and **4** proved to be like the parent 1,6-methano[10]annulene[4] and to show no interaction between the p_z orbitals of the bridge and peripheral 10π-electron system.[2,3]

1

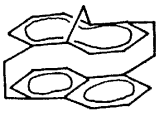

2

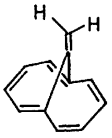

3

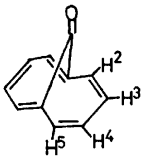

4

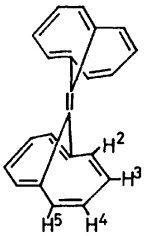

5

In this paper, we describe the first synthesis of the novel double-layered annulene **5**[5] which has two [10]annulene rings held together symmetrically with one ethylenic bridge.

Results and Discussion

The ketone **4** was initially thought to be a key intermediate for the synthesis of the title compound **5**, since **4** has a convenient carbonyl "hand" on the central position of [10]annulene ring for an intermolecular reductive coupling by McMurry method.[6] However, the attempted coupling of **4**, prepared according to the procedure of Itô et al.,[3] employing $TiCl_3$ and $LiAlH_4$ in THF[7] did not give the desired dimeric product **5**, but gave only naphthalene. We reasoned that the failure to obtain **5** from **4** is ascribed to the instability of the ketone **4** under the reaction conditions, as has been observed by us in the couplings of several fully conjugated polyenediynedials.[8] Then we directed our efforts to a two-stage approach which involves an initial coupling of the more stable ketone **6** and a subsequent dehydrogenation of the resulting dimeric hydrocarbon. Thus the reductive coupling of the ketone **6** as before[7] afforded the dimer, 1,1 : 2,2-bis(cyclodeca-2,4,8-triene-1,6-diyl)ethylene, as a mixture of syn- (**7a**) and anti-isomer (**7b**), which could not be separated by column chromatography on silica gel. When a mixture of **7a**, **b** and 2,3-dichloro-5,6-dicyano-*p*-benzoquinone (DDQ) in benzene was heated in a sealed tube under nitrogen atmosphere at 110—120 °C for 24 h, dehydrogenation took place to afford the title compound **5** as stable yellow crystals in 5.9% yield, which was isolated by column chromatography on silica gel.

The ^{1}H NMR and electronic spectral data of **5** are listed in Table 1, together with those of the reference model compounds **3** and **4**. As shown in Table 1, the ring protons of **5** resonate in A_2B_2-type as similar to the cases of **3** and **4**,[2,3] and do in lower field than the olefinic protons of **7a**, **b** (Experimental), revealing that the annulene rings of **5** sustain diamagnetic ring current. Comparison of the central chemical shifts of the annulene protons among **3**, **4**, and **5** indicates that the protons of **5** (δ 6.96) resonate in higher field than those of **3** (δ 7.20) and **4** (δ 7.46). This high-field shift of the annulene protons observed in **5** is reasonably ascribed to diamagnetic anisotropy of the opposite annulene ring. Thus, this suggests that the two annulene rings in **5** are very suitable to overlap to each other.

The electronic absorption spectra, taken in cyclohexane, are illustrated in Fig. 1. As is seen from Fig. 1, all the spectra exhibit three bands which arise from [10]annulene chromophore[9] and which is characteris-

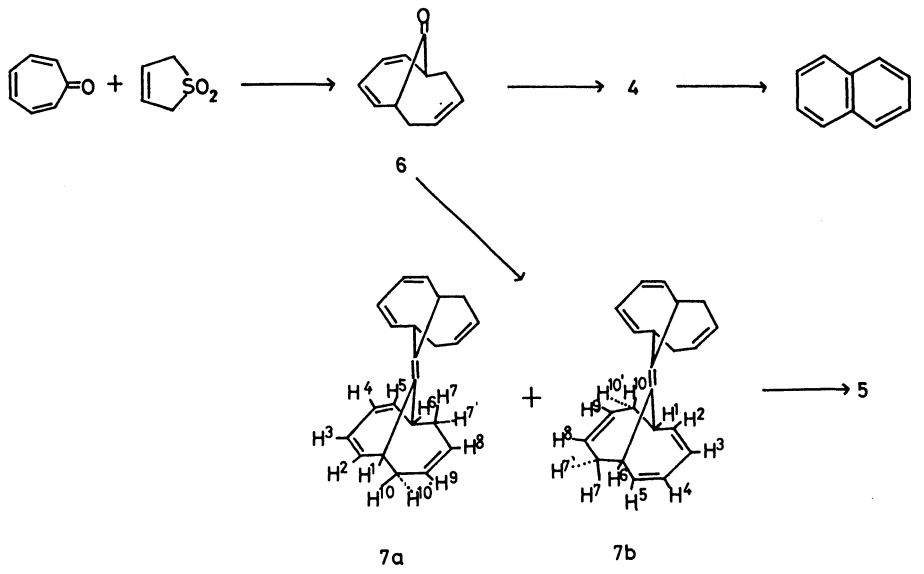

Table 1. Spectral Data of **3**—**5**

Compd		Spectral data
3[a]	^{1}H NMR (CCl_4):	δ 7.2 (center, A_2B_2-system, 8H), 3.2 ($=CH_2$, 2H);
	UV (cyclohexane):	λ_{max} 258 (67500), 300 (6700), 368 (135), 377 (170), 385 (190), 394 (184), 408 nm (180)
4[b]	^{1}H NMR ($CDCl_3$):	δ 7.55 (H^2, H^5, H^7, H^{10}, 4H), 7.36 (H^3, H^4, H^8, H^9, 4H) (A_2B_2-system, center 7.46);
	UV (cyclohexane):	λ_{max} 250.5 (77500), 296 (7000), 352 (92), 362 (124), 371 (169), 379 (228), 391 (275), 402 nm (326)
5	^{1}H NMR ($CDCl_3$):	δ 7.21—7.15 (H^2, H^5, H^7, H^{10}, 8H), 6.76—6.72 (H^3, H^4, H^8, H^9, 8H) (A_2B_2-system, center 6.96) (J_{23}=8.27 Hz, J_{34}=10.48 Hz, J_{24}=0.58 Hz, J_{25}=1.16 Hz)
	UV (cyclohexane):	λ_{max} 253 (141000), 306 sh (10900), 374 sh (481), 405 (577), 418 (513), and 432 nm (353)

a) See Ref. 2. b) See Ref. 3.

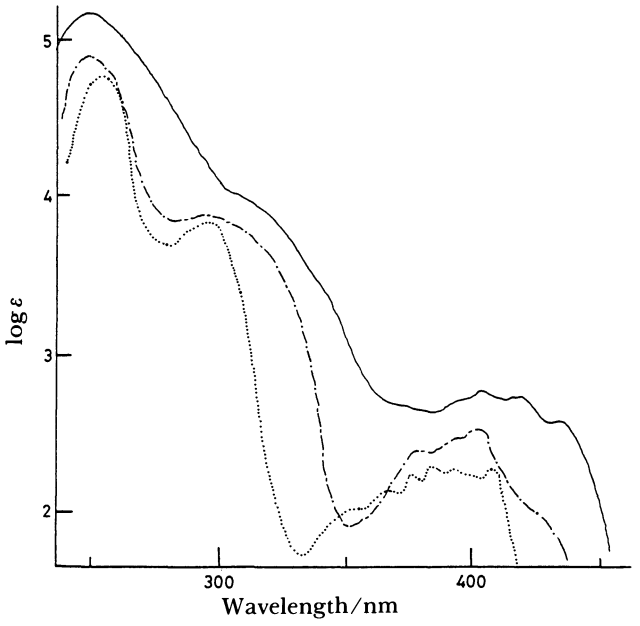

Fig. 1. Electronic spectra of **3** (----), **4**, (-·-·-), and **5** (——) in cyclohexane.

tic of $[4n+2]\pi$-electrons.[10] However, the longest wavelength band of **5** shows a remarkable bathochromic shift (20—30 nm) (Table 1), when compared with those of **3** and **4**, demonstrating that the transition associated with the longest wavelength band of [10] annulene chromophore is affected by the transannular interaction between the two annulene rings.

Experimental

Melting points are uncorrected. IR spcctra were measured on Hitachi 260-10 spectrophotometer as KBr disc; only significant maxima are reported. Electronic spectra were recorded on Hitachi 220-A spectrophotometer in nm, in cyclohexane solution. Mass spectra were measured with JEOL JMX-303 spectrometer at 70 eV using a direct inlet system. ^{1}H NMR spectra were taken on JEOL GX-500 (500 MHz) spectrometer, and refer to solutions in $CDCl_3$, in δ-values with TMS as an internal standard. The coupling constants (J) are given in Hz. Silica gel (Merck) was used for column chromatography.

The Reductive Coupling of the Ketone 4. $LiAlH_4$ (95 mg, 2.5 mmol) was added in one portion to titanium trichlo-

ride ($TiCl_3$) (0.77 g, 5 mmol) in dry THF (300 ml) under argon. The resultant black mixture was heated under reflux for 30 min. To the mixture, a soln of the ketone **4** (350 mg, 2.24 mmol) in dry THF (25 ml) was added dropwise during 30 min and then the mixture was stirred under reflux for further 4 h. Then after addition of ethanol (10 ml), the mixture was filtered through Hyflo Super-Cel under suction to remove inorganic materials and was washed with THF. The filtrate was concentrated under reduced pressure and the residue was chromatographed on silica gel (30 g). The fractions eluted with hexane afforded naphthalene (55 mg).

1,1:2,2-Bis(cyclodeca-2,4,8-triene-1,6-diyl)ethylene (7a,b). To the refluxing mixture of $LiAlH_4$ (0.92 g, 24.2 mmol) and $TiCl_3$ (7.50 g, 48.4 mmol) in dry THF (200 ml), prepared as described above, was added dropwise a soln of the ketone **6** (3.50 g, 21.8 mmol) in dry THF (200 ml) under argon and the mixture was stirred under reflux for further 4 h. After work-up as described above, the residue was chromatographed on silica gel (120 g). The initial fractions eluted with hexane gave a colorless liquid (310 mg) which proved to be a complex mixture of hydrocarbons by analysis of gas chromatography. The structures of the hydrocarbons are not established. The later fractions eluted with the same solvent afforded the desired dimer **7a,b** (100 mg, 3.1%) as a solid. Recrystallization from hexane afforded colorless needles: mp 138—139 °C; MS *m/z* 288 (M^+, 70%) and 234 (100); mol wt 288.4; IR 1595 (C=C), 710 and 705 cm^{-1} (cis C=C); UV λ_{max} (cyclohexane) 250 (9500), 261 (9800), and 273 nm sh (8600); ^1H NMR δ=5.93—5.88 (m, H^3, H^4, 4H), 5.77—5.73 (m, H^2, H^5, 4H), 5.57—5.55 (m, H^8, H^9, 4H), 3.79—3.76 (m, H^1, H^6, 4H), 2.56—2.50 (m, H^7, H^{10} or $H^{7'}$, $H^{10'}$, 4H), 2.19—2.13 (m, H^7, H^{10} or $H^{7'}$, $H^{10'}$, 4H).

Found: C, 91.29; H, 8.45%. Calcd for $C_{22}H_{24}$: C, 91.61; H, 8.39%.

1,1:2,2-Bis([10]annulene-1,6-diyl)ethylene (5). A mixture of the hydrocarbons **7a,b** (70 mg, 0.243 mmol) and DDQ (270 mg, 1.2 mmol) in dry benzene (4 ml) was heated in a sealed tube under nitrogen atmosphere at 110—120 °C for 24 h. After removing insoluble materials by filtration under suction and washing with benzene, the filtrate was concentrated. The residue was chromatographed on silica gel (10 g). The fractions eluted with hexane afforded the layered annulene **5** (4.0 mg, 5.9%) as a solid. Recrystallization from hexane-benzene afforded pale yellow needles: mp 245—247 °C; MS *m/z* 280 (M^+, 100%); mol wt 280.3; IR 750 cm^{-1} (cis C=C); UV: see Table 1 and Fig. 1; ^1H NMR: see Table 1.

Found: C, 93.69; H, 5.87%. Calcd for $C_{22}H_{16}$: C, 94.25; H, 5.75%.

The authors thank Professor Shô Itô, Tohoku University, for providing us the details for preparing the ketone **4** and helpful suggestions, Professor Yoshiteru Sakata, Osaka University, for helpful discussion, and Professor E. Vogel, Köln University, for providing us the electronic spectrum of **3**.

References

1) M. Matsumoto, T. Otsubo, Y. Sakata, and S. Misumi, *Tetrahedron Lett.*, **1977**, 4425.
2) E. Vogel, F. Weyres, H. Lepper, and V. Rautenstrauch, *Angew. Chem.*, **78**, 754 (1966).
3) S. Itô, M. Ohtani, S. Naruta, and H. Honma, *Tetrahedron Lett.*, **1972**, 2223.
4) E. Vogel and H. D. Roth, *Angew. Chem.*, **76**, 145 (1964).
5) K. Yamamoto, J. Ojima, N. Morita, and T. Asao, *J. Chem. Soc., Chem. Commun.*, **1987**, 1851.
6) J. E. McMurry, *Acc. Chem. Res.*, **7**, 281 (1974); **16**, 405 (1983).
7) A. L. Baumstark, C. J. McCloskey, and K. E. Witt, *J. Org. Chem.*, **43**, 3609 (1978).
8) J. Ojima, K. Yamamoto, T. Kato, K. Wada, Y. Yoneyama, and E. Ejiri, *Bull. Chem. Soc. Jpn.*, **59**, 2209 (1986).
9) E. Vogel, *Chimia*, **22**, 21 (1968).
10) M. Nakagawa, *Pure Appl. Chem.*, **44**, 885 (1975).

 © 1988 The Chemical Society of Japan Bull. Chem. Soc. Jpn., 61, 1285—1289 (1988)

Electron Coupled Proton Transport Mediated by $[Fe_4S_4(SC_6H_4\text{-}p\text{-}n\text{-}C_8H_{17})_4]^{2-}$ in Liquid Membrane

Koji TANAKA,* Mari MASANAGA, and Toshio TANAKA*
Department of Applied Chemistry, Faculty of Engineering, Osaka University, Yamada-Oka, Suita, Osaka 565
(Received October 28, 1987)

Electrochemical reduction of $[Fe_4S_4(SC_6H_4\text{-}p\text{-}n\text{-}C_8H_{17})_4]^{2-}$ ($[4\text{-Fe}]^{2-}$) dissolved in a CH_2Cl_2 phase of the CH_2Cl_2/H_2O two phase system is followed by protonation to give $[4\text{-Fe}]^{3-}\text{-}H^+$ when the pH of the H_2O phase is lower than 7.0, and protonated and deprotonated $[4\text{-Fe}]^{3-}$ exist as an equilibrium mixture in the CH_2Cl_2 phase. On the other hand, no protonation takes place upon the reduction of $[4\text{-Fe}]^{2-}$ in the CH_2Cl_2 phase contacting with the H_2O phase with the pH higher than 7.0. The electron transport conducted in a liquid membrane composed of the H_2O (W_1), CH_2Cl_2, and H_2O (W_2) phases containing sodium dithionite as an electron donor, $(n\text{-}Bu_4N)_2[4\text{-Fe}]$ as a mediator, and disodium anthraquinone-1,5-disulfonate (Na_2AQS) as an electron acceptor, respectively, revealed that protonated $[4\text{-Fe}]^{3-}\text{-}H^+$ mediates electron coupled proton transport in the liquid membrane, while the deprotonated cluster has no ability of electron transport in the same system.

Electron transport across a cell membrane plays key roles not only in various biological redox reactions but also in ATP synthesis in mitochondria or chloroplasts. Model studies for the electron transport have, therefore, widely been conducted by using bilayer lipid membranes[1-5] or liquid membranes.[6-9] Electron transport in biological membranes takes place according to an electrochemical proton gradient, where electrons and protons are transported from the high proton concentration side to the low proton concentration side across a biomembrane.[10-14] A pH dependence of the redox potential of an oxidation-reduction component in a biomembrane provides evidence for a proton participation in the redox reaction. Mitochondrial cytochromes which show the shift of −60 mV/pH for their half-reduction potentials have, therefore, been considered to take part in electron coupled-proton transport.[15-17] The intermediary which plays in such a role at negative potentials more than the redox reactions of cytochromes, however, has not been elucidated so far.

Iron-sulfur proteins widely distributed in plants, bacteria, and mammals are considered soley to function as electron transfer catalysts in various biological redox reactions such as nitrate reduction, CO_2- and N_2-fixation, H_2-evolution, and so on.[18] In accordance with this, the redox potentials of most Fe-S proteins show a relatively small shift (0 to −24 mV/pH) with the change of pH,[19-21] while that of the mitochondrial Fe-S Center N-2 shows a slope of −60 mV/pH,[22,23] implying a stoichiometric one electron and one proton participation in the redox reaction. Mitochondrial Fe-S Center N-2, therefore, has been proposed to function not only as electron but also as proton carriers in biomembranes.[22]

The interactions between synthetic Fe_4S_4 clusters and protons have also been studied; the pK_a values determined spectrophotometrically[24,25] and electrochemically[26-30] fall in the range 3.9 to 9.0. We have, recently, elucidated that reduction-linked proton binding to $[Fe_4X_4(YC_{12}H_{25})_4]^{3-}$ (X, Y=S and Se) takes place at the sulfur or selenium atom of the Fe_4X_4 core rather than that of terminal alkanethiolate and -selenolate ligands on the basis of their pK_a values in aqueous Triton X-100 micellar solutions.[31] The ability of proton binding to the Fe_4S_4 cluster solubilized in hydrophobic spheres in aqueous micellar solutions suggests that the synthetic Fe_4S_4 cluster can be used as a mediator of the electron coupled proton transport in a liquid membrane. In fact, $[Fe_4S_4(SPh)_4]^{3-}$ prepared by reduction of $[Fe_4S_4(SPh)_4]^{2-}$ with Cr^{II} in a toluene/water two phase system is protonated and releases the proton upon reoxidation with methylviologen.[32] This paper describes electron coupled proton transport from aqueous sodium dithionite ($Na_2S_2O_4$) to disodium anthraquinone-1,5-disulfonate solutions across a CH_2Cl_2 phase containing $[Fe_4S_4(SC_6H_4\text{-}p\text{-}n\text{-}C_8H_{17})_4]^{2-}$.

Experimental

General. All manipulations were carried out under an N_2 atmosphere. The iron-sulfur cluster $(n\text{-}Bu_4N)_2[Fe_4S_4(SC_6H_4\text{-}p\text{-}n\text{-}C_8H_{17})_4]$ ($(n\text{-}Bu_4N)_2[4\text{-Fe}]$) was prepared according to the literature.[28]

Physical Measurements. Cyclic voltammograms were obtained by the use of a Hokuto Denko potentialstat HB-401, a Hokuto Denko function generator HB-107, and a Yokogawa Electric X-Y recorder 3077. The electrolysis cell was equipped with a nozzle for bubbling N_2. The concentrations of Na^+ in aqueous solutions were determined by the use of a Nippon Jarrell-Ash atomic absorption spectrophotometer AA-8500.

Cyclic Voltammetry of $[4\text{-Fe}]^{2-}$ in an H_2O/CH_2Cl_2 Two Phase System. An aqueous H_3PO_4-NaOH buffer (0.1 mol dm^{-3}) solution (pH 9.4 or 6.5, 20 cm^3) containing $n\text{-}Bu_4NBr$ (0.6 g, 1.8 mmol) was poured in a CH_2Cl_2 solution (20 cm^3) containing $(n\text{-}Bu_4N)_2[4\text{-Fe}]$ (20 mg, 12 μmol) and $n\text{-}Bu_4NBr$ (0.6 g, 1.8 mmol), and the mixture was stirred by bubbling N_2 for several minutes. Then, the cell was allowed to stand until the CH_2Cl_2 and H_2O phases were separated completely. The proton concentration in the H_2O phase was adjusted by addition of a small amount of either aqueous NaOH or H_3PO_4 solution to the H_2O phase, followed by

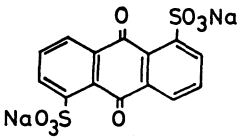

AQS^{2-} : $E_{1/2}$ = -0.43 V (pH 7.0)

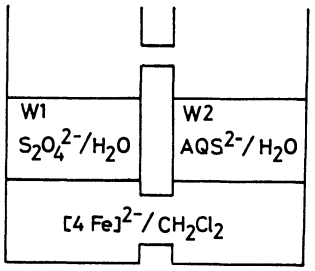

Fig. 1. A liquid membrane cell.

stirring the mixture by the same method. The pH of the H_2O phase was measured with a Toa Electronics pH meter HM-7B. The cyclic voltammogram of $(n\text{-}Bu_4N)_2$[4-Fe] solubilized in the CH_2Cl_2 phase was obtained by using a Yanaco glassy carbon disk electrode GC-2P, a Pt auxiliary electrode, and a luggin capillary of a reference electrode (SCE), all of which were immersed into the CH_2Cl_2 phase.

Electron Coupled Proton Transport across a Liqid Membrane. The electron coupled proton transport across a liquid membrane, mediated with $(n\text{-}Bu_4N)_2$[4-Fe] was conducted by using a liquid membrane cell (16 mm inner diameter) (Fig. 1). After the cell was thoroughly flushed with N_2 to remove air, a CH_2Cl_2 solution (20 cm^2) of $(n\text{-}Bu_4N)_2$[4-Fe] (2.5—20 mg, 1.5—12 μmol) was charged into the cell with syringe techniques through a septum cap attached to the top of the cell. Then, aqueous H_3PO_4-NaOH buffer solutions (0.1 mol dm^{-3}, 5 cm^3) of $Na_2S_2O_4$ (0.108 g, 0.62 mmol) and of disodium anthraquinone-1,5-disulfonate (Na_2AQS) (4.9—25 mg, 0.12—0.61 mmol) were introduced into the cell as an electron donor (W_1 phase) and an electron acceptor (W_2 phase), respectively, and the CH_2Cl_2 layer was stirred magnetically at 20 °C for 16 h in the dark owing to instability of Na_2AQS toward light. Electron transport from the W_1 to the W_2 phases through the CH_2Cl_2 phase was monitored by the change of an absorption band centered around 450 nm due to the reduced species of AQS^{2-} formed in the W_2 phase, and the electrons transported from the W_1 phase to the W_2 phase were determined from the absorbance at 450 nm. In the present study, the 450 nm band has been assigned to a two-electron reducticon product of AQS^{2-}, though several reduced species of AQS^{2-} exist as an equilibrium mixture in aqueous solutions.[33] The apparent amount of the reduced species of AQS^{2-} was calculated from the absorbance at 450 nm upon dissolving a given amount of $Na_2S_2O_4$ (as a two electron donor) in aqueous Na_2AQS solutions with the same concentration as the W_2 phase at various pH.

Results and Discussion

The Redox Behavior of $(n\text{-}Bu_4N)_2[Fe_4S_4(SC_6H_4\text{-}p\text{-}n\text{-}C_8H_{17})_4]$ in an H_2O/CH_2Cl_2 Two Phase System. As reported previously, redox potentials of the $[Fe_4S_4(SC_6H_4\text{-}p\text{-}n\text{-}C_8H_{17})_4]^{2-/3-}$ ([4-Fe]$^{2-/3-}$) couple in aqueous micellar[27,28,30] and lecithin vesicle solutions[29] are largely influenced by proton concentrations owing to the redox-linked protonation of the cluster. Thus, the redox behavior of the same cluster dissolved in the CH_2Cl_2 phase of a CH_2Cl_2/H_2O two phase system was examined with the intention of applying to an electron coupled proton transfer catalyst in a liquid membrane. The cyclic voltammogram of $(n\text{-}Bu_4N)_2$[4-Fe] in a CH_2Cl_2/H_2O (pH 9.40) two phase system shows a pair of cathodic and anodic waves due to the [4-Fe]$^{2-/3-}$ redox couple at −0.99 and −0.85 V vs. SCE, respectively, at the sweep rate 10 mV s^{-1} (Fig. 2). The cathodic and anodic peak potentials are moved in dif-

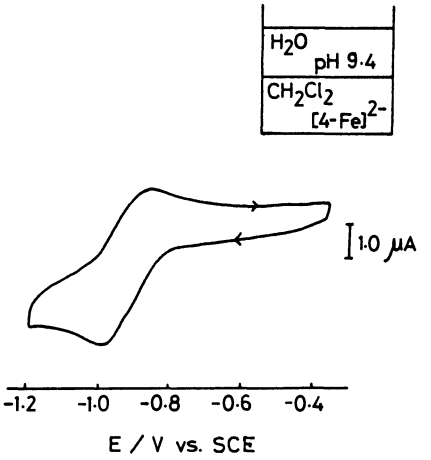

Fig. 2. Cyclic voltammogram of $(n\text{-}Bu_4N)_2[Fe_4S_4(SC_6H_4\text{-}p\text{-}n\text{-}C_8H_{17})_4]$ solubilized in the CH_2Cl_2 layer (0.60 mmol dm^{-3}) in the H_2O/CH_2Cl_2 two phase system; dE/dt=10 mV s^{-1}.

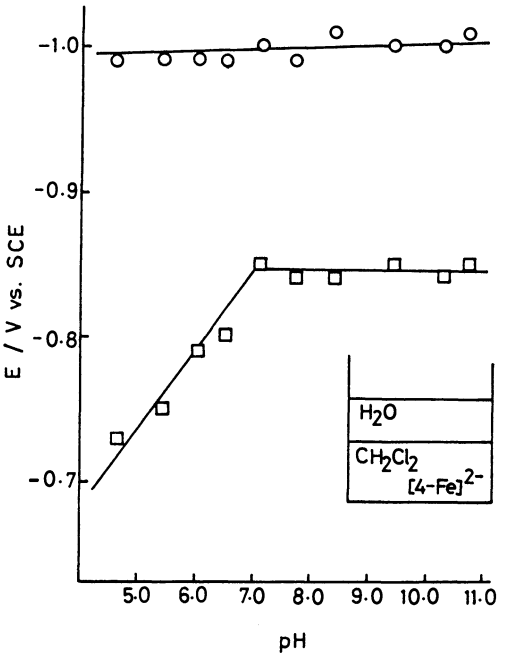

Fig. 3. Plots of the cathodic (○) and anodic peak potentials (□) of the [4-Fe]$^{2-/3-}$ redox couple in the H_2O/CH_2Cl_2 system vs. pH of the H_2O phase.

ferent fashions from each other upon change of the proton concentration in the H_2O phase (Fig. 3); the cathodic peak potential is almost independent of pH of the H_2O phase in the pH range 4.6 to 11.0 (circles in Fig. 3), suggesting that no proton transport is involved in the reduction of $[4\text{-Fe}]^{2-}$ in the H_2O-saturated CH_2Cl_2 phase. On the other hand, the anodic peak potential of the redox couple varies with a slope −55 mV/pH in the pH range 4.6 to 7.0, while it is independent of pH in the range higher than 7.0 (squares in Fig. 3). Such characteristic pH dependences of the cathodic and anodic peak potentials of the $[4\text{-Fe}]^{2-/3-}$ couple in the H_2O-saturated CH_2Cl_2 layer may be explained by assuming Eqs. 1—4. The cluster in the

$$[4\text{-Fe}]^{2-} + e^- \longrightarrow [4\text{-Fe}]^{3-} \quad (1)$$

$$[4\text{-Fe}]^{3-} + H^+ \overset{pH<7}{\rightleftharpoons} [4\text{-Fe}]^{3-}\text{-}H^+ \quad (2)$$

$$[4\text{-Fe}]^{3-} - H^+ \overset{pH<7}{\longrightarrow} [4\text{-Fe}]^{2-} + e^- + H^+ \quad (3)$$

$$[4\text{-Fe}]^{3-} \overset{pH>7}{\longrightarrow} [4\text{-Fe}]^{2-} + e^- \quad (4)$$

CH_2Cl_2 phase undergoes one-electron reduction to afford $[4\text{-Fe}]^{3-}$ (Eq. 1), followed by protonation, probably at the sulfur atom of the Fe_4S_4 core[31] in the CH_2Cl_2 phase when pH of the H_2O phase is lower than 7, where protonated and deprotonated clusters exist as an equilibrium mixture (Eq. 2). Upon subsequent oxidation, the protonated cluster $[4\text{-Fe}]^{3-}\text{-}H^+$ may release the proton owing to decreasing electron density of the Fe_4S_4 core (Eq. 3). On the other hand, the cluster may be subject to the redox reaction without undergoing protonation (Eqs. 1 and 4) in the pH range of the H_2O phase higher than 7.0, explaining the anodic peak potential being almost invariant in that pH range (squares in Fig. 3). The pK_a value 7.0 of $[4\text{-Fe}]^{3-}\text{-}H^+$ obtained from the turning point of the anodic peak potential[34] (Fig. 3) is smaller than that in aqueous micellar solutions (pK_a 9.0).[27,28] This result may partly be due to low proton concentrations in the H_2O-saturated CH_2Cl_2 phase compared with those in hydrophobic spheres in micells.

Electron Coupled Proton Transport across a Liquid Membrane Mediated with (n-Bu_4N)$_2$[4-Fe]. A proton binding to $[4\text{-Fe}]^{3-}$ in the CH_2Cl_2/H_2O two phase system suggests that the present cluster has an ability of the electron coupled proton transport. Thus, the electron transport mediated with the cluster was conducted by using a liquid membrane (Fig. 1); aqueous buffer solutions (H_3PO_4-NaOH) of sodium dithionite (W_1 phase) and of disodium anthraquinone-1,5-disulfonate (Na_2AQS) (W_2 phase) were used as an electron donor and an electron acceptor, respectively, on the CH_2Cl_2 phase containing (n-Bu_4N)$_2$[4-Fe]. The pH values of the W_1 (pH_1) and W_2 (pH_2) phases were adjusted at 6.2 and 10.7, respectively. Electron transport conducted by stirring the CH_2Cl_2 phase results in the occurrence of a strong absorption band centered around 450 nm due to the reduced species of AQS^{2-} in the electronic spectrum of the W_2 phase (a solid line in Fig. 4). On the other hand, no absorption band appears around 450 nm in the absence of (n-Bu_4N)$_2$-[4-Fe] in the CH_2Cl_2 phase under otherwise the same conditions (a broken line in Fig. 4). Thus, the iron-sulfur cluster in the CH_2Cl_2 phase mediates electron coupled H^+ or Na^+ transport from the W_1 to the W_2 phases, since no other counter cation is involved in this system. In view of the fact that protonation to $[4\text{-Fe}]^{3-}$ takes place only in the pH region lower than 7.0 of the H_2O phase in the CH_2Cl_2/H_2O two phase system, the electron coupled proton transport mediated

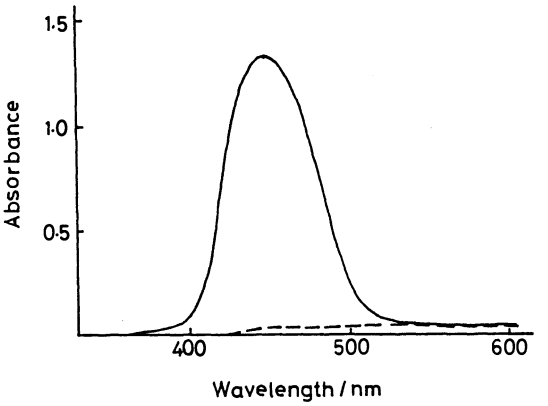

Fig. 4. Electronic absorption spectra of the reduced species of AQS^{2-} formed in the W_2 phase in the absence (----) and the presence of (n-Bu_4N)$_2$[4-Fe] (10 μmol) (——) in the CH_2Cl_2 (20 cm^3) phase after electron transport for 16 h; the concentrations of both $Na_2S_2O_4$ in the W_1 (H_2O, 5 cm^3; pH 6.2) and Na_2AQS in the W_2 (H_2O, 5 cm^3; pH 10.7) phases are 1.2×10^{-1} mol dm^{-3}.

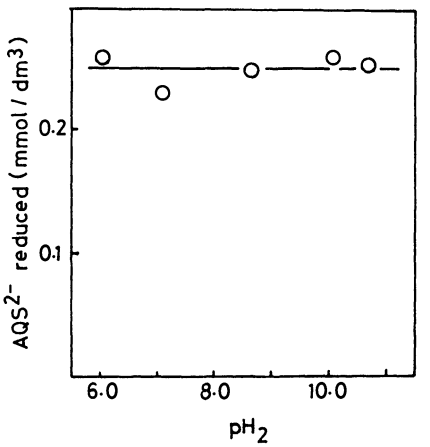

Fig. 5. Amounts of the reduced species of AQS^{2-} formed in the electron transport mediated with $[4\text{-Fe}]^{2-}$ at various pH of the W_2 phase for 16 h; the concentrations of $Na_2S_2O_4$ in the W_1 (H_2O, 5 cm^3; pH 6.2), (n-Bu_4N)$_2$[4-Fe] in the CH_2Cl_2 (20 cm^3), and Na_2AQS in the W_2 (H_2O, 5 cm^3) phases are 1.2×10^{-1}, 1.5×10^{-4}, and 1.2×10^{-1} mol dm^{-3}, respectively.

with $[4\text{-Fe}]^{3-}$ across the CH_2Cl_2 phase may largely be influenced by proton concentrations of the H_2O phase.

The amounts of the reduced species of AQS^{2-} formed in the W_2 phase is essentially constant irrespective of pH of this phase (pH) as far as pH of the W_1 phase (pH_1) is kept to be lower than 7; Fig. 5 is an example at pH_1 6.2. Thus, pH of the W_2 phase (pH_2) little influences the electron transfer from the reduced species of the cluster to AQS^{2-} at the CH_2Cl_2/W_2 interface. On the other hand, pH_1 largely influences on the formation of the reduced species of AQS^{2-} in the W_2 phase with pH_2 10.7; the amount of the reduced species of AQS^{2-} is rapidly decreased with increasing the pH value of the W_1 phase (Fig. 6). The agreement of the turning point (pH_1 7.0) in Fig. 6 with the pK_a value of $[4\text{-Fe}]^{3-}$-H^+ obtained from the plot of the anodic peak potential of the cluster vs. pH in the CH_2Cl_2/H_2O two phase system (Fig. 3) suggests that $[4\text{-Fe}]^{3-}$-H^+ rather than deprotonated cluster $[4\text{-Fe}]^{3-}$ mediates the electron transport from the W_1 phase to the W_2 phase. As an electron carrier, $[4\text{-Fe}]^{3-}$-H and $[4\text{-Fe}]^{3-}$ may exhibit a fairly different behavior from each other, since the former may have an ability of the electron coupled proton transport, while the latter mediates electron coupled Na^+ transport. The active species, $[4\text{-Fe}]^{3-}$-H^+ or $[4\text{-Fe}]^{3-}$, which mediates the electron transport from the W_1 to W_2 phases may, therefore, be assigned by determining the amount of Na^+ transported into the W_2 phase accompanied by the electron transport. The electron transport conducted by using $NaOH$-H_3PO_4 and KOH-H_3PO_4 buffer solutions in the W_1 and the W_2 phases, respectively, also produced

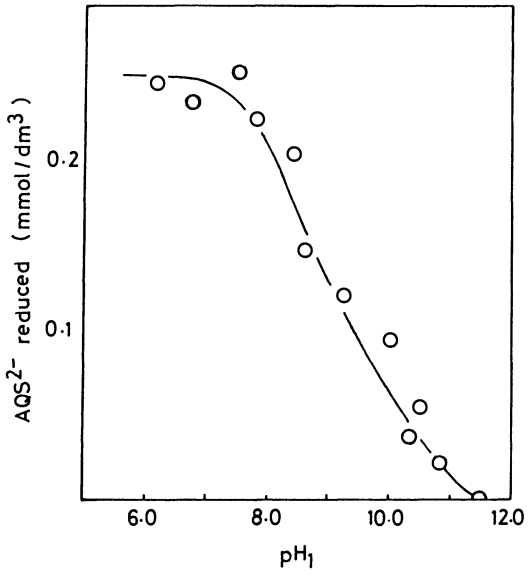

Fig. 6. The amount of the reduced species of AQS^{2-} formed in the electron transport mediated with $[4\text{-Fe}]^{2-}$ at various pH_1 (W_1 phase) for 16 h; the concentrations of $Na_2S_2O_4$ in the W_1 (H_2O, 5 cm³), $(n\text{-}Bu_4N)_2[4\text{-Fe}]$ in the CH_2Cl_2 (20 cm³), and Na_2AQS in the W_2 (H_2O, 5 cm³; pH 10.7) phases are 1.2×10^{-1}, 1.5×10^{-4}, and 1.2×10^{-1} mol dm^{-3}, respectively.

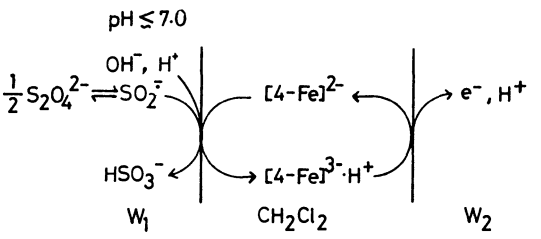

Scheme 1.

the same amounts of the reduced species of AQS^{2-} in the W_2 phase as those in Fig. 6.[35] In addition, no appreciable change of the amount of Na^+ in the W_2 phase (resulting from Na_2AQS) was observed between before and after the electron transport. It may, therefore, be concluded that no appreciable Na^+ transport from the W_1 phase to the W_2 phase takes place in the present study. Thus $[4\text{-Fe}]^{3-}$-H^+ functions as an electron carrier in the liquid membrane. The maximum electrons transported in the present study was 2.0 on the basis of the amount of $(n\text{-}Bu_4N)_2[4\text{-Fe}]$ in the CH_2Cl_2 phase for 16 h.[36] Such a low value may be resulted from an endothermic electron transfer from $S_2O_4^{2-}$ (E=−0.90 V vs. SCE in H_2O at pH 9.0)[37] to $[4\text{-Fe}]^{2-}$ (E_{red}=−0.99 V in CH_2Cl_2) at the W_1/CH_2Cl_2 interface.

Electron Pathway in the Liquid Membrance. A most possible electron pathway for the present electron coupled proton transport mediated with $(n\text{-}Bu_4N)_2$-[4-Fe] is depicted in Scheme 1; a partial dissociation $S_2O_4^{2-} \rightleftarrows 2SO_2^{\cdot-}$ in the W_1 phase generates the active reductant $SO_2^{\cdot-}$ [37] which may reduce $[4\text{-Fe}]^{2-}$ at the W_1/CH_2Cl_2 interface to afford $[4\text{-Fe}]^{3-}$ and SO_2. The former undergoes a protonation probably at sulfur of the Fe_4S_4 core[31] in the CH_2Cl_2 phase when pH_1 is lower than 7.0, and the latter reacts with OH^- to afford HSO_3^- in the W_1 phase. The protonated $[4\text{-Fe}]^{3-}$-H^+ thus formed in the CH_2Cl_2 phase is oxidized by AQS^{2-} at the CH_2Cl_2/W_2 interface with liberating the proton into the W_2 phase. The resulting oxidized cluster $[4\text{-Fe}]^{2-}$ moves back to the W_1/CH_2Cl_2 interface, regenerating $[4\text{-Fe}]^{3-}$-H^+. When pH_1 is higher than 7.0, however, the reduction of $[4\text{-Fe}]^{2-}$ hardly takes place at the W_1/CH_2Cl_2 interface unless a strong hydrophilic Na^+ in the W_1 phase migrates into the CH_2Cl_2 phase to cancel the extra negative charge of $[4\text{-Fe}]^{3-}$. Thus, protons are much more superior to Na^+ as a counter ion of the electron transport in the liquid membrane system. The mechanism proposed in Scheme 1[38] reasonably explains the vectrial electron flow from a high proton concentration side to a low proton concentration side in biomembrane, since the reverse electron transport is effectively suppressed so long as the pK_a value of the cluster is smaller than the pH value of the low proton concentration side. The present study strongly suggests that some of iron-sulfur proteins participate in the transport of protons as well as electrons in biomembrane.

The authors are grateful to the Ministry of Education for support of this work through Grant-in-Aid for Scientific Research (Grant No. 61226007).

References

1) H. T. Tien, *Nature (London)*, **219**, 272 (1968).
2) G. Hauska, *FEBS Lett.*, **79**, 345 (1977).
3) W. E. Ford, J. W. Otvos, and M. Calvin, *Nature (London)*, **274**, 507 (1978).
4) M. S. Tunuli and J. H. Fendler, *J. Am. Chem. Soc.*, **103**, 2507 (1981).
5) I. Tabushi, T. Nishiya, M. Shimomura, T. Kunitake, H. Inokuchi, and T. Yagi, *J. Am. Chem. Soc.*, **106**, 219 (1984).
6) S. S. Anderson, I. G. Lyle, and R. Paterson, *Nature (London)*, **259**, 147 (1976).
7) T. Shinbo, K. Kurihara, Y. Kobatake, and N. Kano, *Nature (London)*, **270**, 277 (1977).
8) J. J. Grimaldi, and J. M. Lehn, *J. Am. Chem. Soc.*, **101**, 1333 (1979).
9) T. Sugimoto, J. Miyazaki, T. Kokubo, S. Tanimoto, M. Okano, and M. Matsumoto, *J. Chem. Soc., Chem. Commun.*, **1981**, 210.
10) J. Devault, *J. Theor. Soc.*, **62**, 115 (1976).
11) P. Mitchell, "Mitochondria/Biomembranes," ed by S. G. Bergh, North Holand, Amsterdam (1972), Vol. 28, p. 358.
12) P. Gerland, R. A. Clegg, J. A. Downie, T. A. Gray, H. G. Lawford, and J. Skyrme, "Mitochondria/Biomembranes," ed by S. G. Bergh, North Holand, Amsterdam (1972), Vol. 28, p. 105.
13) E, Racker and W, Stockenius, *J. Biol. Chem.*, **249**, 662 (1974). N. Sone, Y. Takeuchi, M. Yoshida, and K. Ono, *J. Biochem. (Tokyo)*, **82**, 1751 (1977).
14) P. C. Malony and F. C. Hansen, J. Membr. Biol., **66**, 63 (1982).
15) D. F. Wilson, J. S. Erecinska, and M. Koppelman, *Arch. Biochem. Biophys.*, **151**, 112 (1972).
16) D. F. Wilson, J. G. Lindsay, and E. S. Brockehust, *Biochim. Biophys. Acta*, **256**, 277 (1972).
17) R. F. Urban and M. Klingenberg, *Eur. J. Chem.*, **9**, 519 (1969).
18) "Iron-Sulfur Proteins," ed by T. G. Spiro, Wiley Interscience, New York (1982), Vol. IV.
19) N. A. Stombaugh, J. E. Sundquist, R. H. Burris, and W. H. Orme-Johnson, *Biochemistry*, **15**, 2633 (1976).
20) E. T. Lode, C. L. Murray, and J. C. Rabinowitz, *J. Biol. Chem.*, **251**, 1683 (1976).
21) J. A. Fee, S. G. Mayhew, and G. Palmer, *Biochim. Biophys. Acta*, **245**, 196 (1971).
22) W. J. Ingledew and T. Ohnishi, *Biochem. J.*, **186**, 111 (1980).
23) T. Ohnishi, *Eur. J. Biochem.*, **64**, 91 (1976).
24) R. C. Job and T. C. Bruice, *Proc. Natl. Acad. Sci. U.S.A.*, **72**, 2478 (1975).
25) T. C. Bruice, R. Maskiewicz, and R. C. Job, *Proc. Natl. Acad. Sci. U.S.A.*, **72**, 231 (1975).
26) B. Odell and P. J. Geary, *J. Chem. Soc., Dalton Trans.*, **1984**, 29.
27) K. Tanaka, T. Tanaka, and I. Kawafune, *Inorg. Chem.*, **23**, 516 (1984).
28) K. Tanaka, M. Moriya, and T. Tanaka, *Inorg. Chem.*, **25**, 835 (1986).
29) K. Tanaka, M. Masanaga, and T. Tanaka, *J. Am. Chem. Soc.*, **108**, 5448 (1986).
30) M. Masanaga, K. Tanaka, and T. Tanaka, *Chem. Lett.*, **1986**, 1531.
31) M. Nakamoto, K. Tanaka, and T. Tanaka, *J. Chem. Soc., Chem. Commun.*, **1986**, 1669.
32) H. Tsai, W. V. Sweeney, and C. L. Coley, *Inorg. Chem.*, **24**, 2796 (1985).
33) Hydroquinone (QH_2) dissociates into QH^-, Q^{2-}, and H^+ in aqueous neutral and alkaline solutions, where Q^{2-} and QH^- may be oxidized by quinone (Q), if it exists, to produce QH · and $Q^{\cdot-}$. Thus, those six species exist as an equilibrium mixture in solutions.
34) The turning point of pH 7.0 in the plot of pH vs. anodic peak potentials has not been changed in the range of sweep rates 10 to 200 mV s^{-1}.
35) The electron transport was conducted at pH_1 6.20 ($NaOH-H_3PO_4$) and pH_2 10.7 ($KOH-H_3PO_4$), and at pH_1 10.7 ($NaOH-H_3PO_4$) and pH_2 10.7 ($KOH-H_3PO_4$).
36) The concentrations of $Na_2S_2O_4$ in the W_1 phase (pH 6.5), $(n\text{-}Bu_4N)_2$[4-Fe] in the CH_2Cl_2 phase, and Na_2AQS in the W_2 phase (pH 10.5) were 1.2×10^{-1}, 7.2×10^{-5}, and 1.0×10^{-1} mol dm^{-3}, respectively.
37) S. G. Mayhew, *Eur. J. Biochem.*, **85**, 535 (1978).
38) The determination of the ratio of e^-/H^+ transported in the present study has been unsuccessful, since a part of SO_2 formed at the W_1/CH_2Cl_2 interface migrates into the W_2 phase through the CH_2Cl_2 phase and reacts with OH^- to afford of a weak acid HSO_3^- (pK_a=7.18) in the W_2 phase, resulting in a difficulty in determination of the amount of H^+ transported owing to significant pH_2 change when the solutions are not buffered.

 © 1988 The Chemical Society of Japan Bull. Chem. Soc. Jpn., 61, 1291—1297 (1988)

Practical Syntheses of Immunologically Relevant β-Glycosides of 2-Acetamido-2-deoxy-D-mannopyranose. Methyl *N*-Acetyl-β-D-mannosaminide, *N*-Acetyl-β-D-mannosaminyl-(1→6)-D-galactose, and Methyl *N*-Acetyl-β-D-mannosaminyl-(1→4)-α-D-glucopyranoside

Eisuke KAJI,* Frieder W. LICHTENTHALER,† Takashi NISHINO, Aya YAMANE, and Shonosuke ZEN
School of Pharmaceutical Sciences, Kitasato University, Shirokane, Minato-ku, Tokyo 108
†Institut für Organische Chemie der Technischen Hochschule Darmstadt, D-6100 Darmstadt, West Germany
(Received October 29, 1987)

Highly stereoselective, expedient syntheses are described for three immunologically relevant β-glycosides of *N*-acetyl-D-mannosamine, i.e. β-D-Man*p*NAc-1-OMe (**8**), β-D-Man*p*NAc-(1→6)-D-Gal (**15**), and β-D-Man*p*NAc-(1→4)-α-D-Glc*p*-1-OMe (**23**). Basic mannosamine progenitor in each case is 3,4,6-tri-*O*-benzoyl-2-(benzoyloxyimino)-2-deoxy-α-D-*arabino*-hexopyranosyl bromide (**1a**), which via the three step-sequence β-selective glycosidation → hydroboration → deblocking is converted to **8**, **15**, and **23** in overall yields of 61, 56, and 39% for the glycosyl acceptors methanol, 1,2:3,4-di-*O*-isopropylidene-α-D-galactose, and methyl 2,3,6-tri-*O*-benzyl-α-D-glucopyranoside, respectively.

β-Glycosidically linked 2-acetamido-2-deoxy-D-mannopyranose (*N*-acetyl-β-D-mannosamine) carries a type-specific immunogeneity in various bacteria associated with invasive diseases.[1,2] Even simple alkyl glycosides such as methyl *N*-acetyl-β-D-mannosaminide acts as a specific hapten against the immunoglobulin of IgA class originated from a mouse myeloma MOPC 406;[3] more complex *N*-acetyl-β-D-mannosaminides constitute a number of bacterial K antigens of capsular polysaccharides[2] as well as O antigens of lipopolysaccharides.[4]

Investigations directed towards the molecular design of artificial antigens require as a principal prerequisite preparatively useful, chemical procedures for the practical construction of oligosaccharides containing *N*-acetyl-β-D-mannosamine. Such procedures are still lacking despite of the possibility of using 2-azido-2-deoxy-D-mannopyranosyl halides,[5,6] which are accessible in syrupy form via low yield, multistep reaction sequences, and furthermore, require careful optimization of glycosidation conditions to reach useful β-selectivities.[5] A similarly laborious approach[7] comprises the *a priori* construction of the respective disaccharide for example, and the *a posteriori* introduction of the 2-amino function via oxidation of a 2-hydroxyl group, oximation and subsequent reduction.[7]

Our approach to the problem of a practical synthesis for β-D-mannosaminides, that has been elaborated on lactose-derived derivatives,[8,9] comprises 2-(benzoyloxyimino)glycosyl bromides of type **1** as the key compounds readily accessible from glucose[10,11] or disaccharides[8] in a few high-yielding steps and in crystalline form. These key building blocks **1** are ideal β-D-mannosamine progenitors, since β-selective glycosidation, reduction of the benzoyloxyimino function to amino group, and deprotection yielding β-D-mannosamine-containing oligosaccharides, a protocol, which combines high stereoselectivity with efficiency of operation and large-scale adaptability

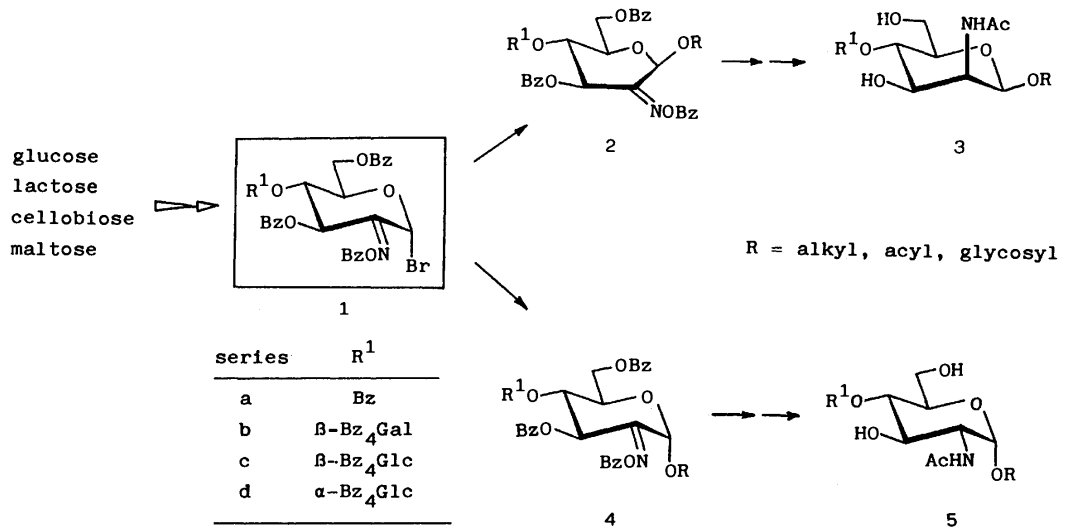

Scheme 1.

(Scheme 1).

In complementation of previous work concentrating on trisaccharides with central β-D-mannosamine units,[9] we here wish to describe[12] the utilization of the D-glucose-derived monosaccharide building block **1a** for the preparation of disaccharides with a nonreducing *N*-acetyl-β-D-mannosamine residue, of which one, i.e. **23**, constitutes a disaccharide unit of the capsular polysaccharide from *Streptococcus pneumoniae* type 9N[2] and 19F.[13]

Methyl *N*-Acetyl-β-D-mannosaminide (8) A preparatively reliable synthesis of methyl *N*-acetyl-β-D-mannosaminide (**8**), as of now, is not available, since direct glycosidation of 2-acetamido-2-deoxy-D-mannose with methanol in the presence of acid (Fischer method) results in a mixture of the four possible methyl *N*-acetyl-D-mannosaminides from which the β-D-pyranoside (**8**) is isolable in yields of 1—2% only.[14] The major isomers were α-D-pyranoside (9%), α-D-furanoside (8%), and β-D-furanoside (2—3%).

Our synthesis of **8** involves methanolysis of the building block **1a**, reduction of the resultant β-glycoside **6** to mannosaminide, *N*-acetylation, and *O*-debenzoylation, so that the synthetic efficiency depends on the β-selective methanolysis and manno-selective reduction (Scheme 2).

The glycosidation of **1a** with excess methanol (ten-fold molar amount) in the presence of several kinds of condensation promotors are summarized in Table 1. Of a variety of reaction conditions examined, only silver carbonate in dichloromethane resulted in good yield (93%) and high stereoselectivity (α:β≃5:95). Other conditions employed, such as silver triflate-tetramethylurea or 2,4,6-collidine-I_2 (cf. Runs 2—5,

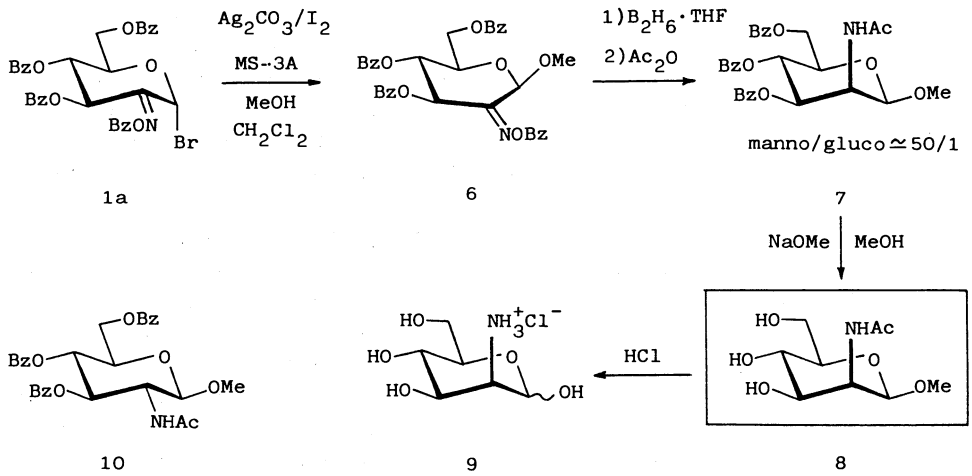

Scheme 2.

Table 1. Glycosidation of Tri-*O*-benzoyl-2-benzoyloxyimino-2-deoxy-α-D-*arabino*-hexopyranosyl Bromide (**1a**) with Methanol and Partially Protected Sugars

Run	Alcohol	Molar Ratio (Alcohol/**1a**)	Promotor	Solvent	Time h	Yield %	α:β[a]
1	MeOH	10.0	Ag_2CO_3/I_2	CH_2Cl_2	72	93	5:95
2	MeOH	10.0	AgOTf/TMU[b]	CH_2Cl_2	24	87	20:80
3	MeOH	10.0	AgOTf/TMU	Dioxane	24	83	40:60
4	MeOH	10.0	2,4,6-Collidine/I_2	Dioxane	72	75	35:65
5	MeOH	10.0	$Hg(CN)_2$	Dioxane	72	17	35:65
6	6-OH Gal iP_2[c]	1.1	Ag_2CO_3/I_2	CH_2Cl_2	24	86	5:95
7	6-OH Gal iP_2	1.1	Ag_2CO_3/I_2	CH_2Cl_2	72	94	5:95
8	6-OH Gal iP_2	1.1	AgOTf/TMU	Dioxane	16	89	70:30
9	4-OH Glc Bz_3[d]	1.1	Ag_2CO_3/I_2	CH_2Cl_2	72	<24	e)
10	4-OH Glc Bz_3	1.1	$AgClO_4$/TMU	CH_2Cl_2	24	<50	e)
11	4-OH Glc Bz_3	1.1	AgOTf/TMU	Dioxane	16	<16	e)
12	4-OH Glc Bn_3[f]	1.1	Ag_2CO_3/I_2	CH_2Cl_2	48	52	5:95
13	4-OH Glc Bn_3	2.0	Ag_2CO_3/I_2	CH_2Cl_2	48	55	5:95
14	4-OH Glc Bn_3	1.1	$AgClO_4$/TMU	CH_2Cl_2	48	<24	e)
15	4-OH Glc Bn_3	1.1	Ag_2O/I_2	CH_2Cl_2	48	<44	e)
16	4-OH Glc Bn_3	1.5	Ag-silicate	CH_2Cl_2	48	<28	e)

a) Estimated on the basis of ^1H NMR signals for the anomeric protons. b) Silver trifluoromethanesulfonate/1,1,3,3-tetramethylurea. c) 1,2:3,4-Di-*O*-isopropylidene-α-D-galacto-pyranose (**11**). d) Methyl 2,3,6-tri-*O*-benzoyl-α-D-glucopyranoside (**17**). e) Contaminated with by-products that impeded the estimation of α:β ratio. f) Methyl 2,3,6-tri-*O*-benzyl-α-D-glucopyranoside (**16**).

Table 1) gave anomeric mixtures with only partial predominance of β-anomers. β-Glycoside **6** was then subjected to hydroboration with twelve-fold molar excess diborane in tetrahydrofuran to afford on *N*-acetylation methyl *N*-acetyl-tri-*O*-benzoyl-β-D-mannosaminide (**7**) in 88% yield. The corresponding β-D-gluco isomer **10** was isolated in only 1.3% yield, so that the preference for the β-D-manno form is in the remarkable, practically very useful range of around 50 : 1. The subsequent *O*-debenzoylation of **7** was cleanly effected with 0.05 M sodium methoxide (1 M=1 mol dm^{-3}) in methanol (Zemplén method) to furnish methyl *N*-acetyl-β-D-mannosaminide (**8**) in 87% yield. Furthermore, **8** was hydrolyzed with 1 M hydrochloric acid giving D-mannosamine hydrochloride **9** in quantitative yield, which was unequivocally identified by comparison with an authentic sample.

The following stereochemical aspects are worthy of note: β-oriented methyl 2-(benzoyloxyimino)glycoside **6** seems to be distorted towards the twist-boat form as indicated in the formula considering from relatively small coupling constant of $J_{3,4}=J_{4,5}=5.7$ Hz. In contrast, **1a** and **7** prefer $^4C_1$ coformation, as evidenced by $J_{3,4}$ and $J_{4,5}$ values of 8.4—9.6 Hz. This may be attributed to substantial steric congestion caused by the 2-benzoyloxyimino and anomeric methoxyl groups in **6**. Similar conformational propensity for 2-(benzoyloxyimino)-β-glycosides were observed previously.[8,9]

^1H and ^{13}C NMR spectra of methyl β-D-mannosaminide **8** were fully elucidated with the aid of ^1H-^1H and ^1H-^{13}C shift correlated two-dimentional (2D) NMR spectra. ^1H-^1H coupling of $J_{1,2}=1.5$ and $J_{2,3}=4.5$ Hz cogently reflect β-D-manno configuration, and a $J_{C1,H1}$ coupling of 163.6 Hz agrees well with that (ca. 160 Hz) of methyl β-glycopyranosides with axial H-1.[15] A calculation of differences of ^{13}C-chemical shifts ($\Delta\delta_c$) by $\delta_{gluco}-\delta_{manno}$ between methyl *N*-acetyl-β-D-mannosaminide and the corresponding glucosaminide[16] showed that major differences appeared at C-2 ($\Delta\delta_c=-4.1$ ppm) and C-4 (−3.2), whilst they are less pronounced at C-3 (−2.0), C-1 (−1.5), C-5 (+0.5), and C-6 (−0.4). These findings were found to be helpful in the structural elucidation of β-D-mannosamine-containing oligosaccharides.

***N*-Acetyl-β-D-mannosaminyl-(1→6)-D-galactose (15) and Methyl *N*-Acetyl-β-D-mannosaminyl-(1→4)-α-D-glucopyranoside (23).** Replacement of the glycosyl acceptor in the above glycosidation **1a**→**6** by suitably blocked sugar alcohols similarly gave the desired disaccharide derivatives in preparatively highly useful fashion. Thus, glycosylation of 1,2 : 3,4-di-*O*-isopropylidene-D-galactose (**11**)[17] with (benzoyloxyimino)glycosyl bromide **1a** in the presence of silver carbonate-iodine in dichloromethane (Run 7 in Table 1) cleanly gave the β-glycoside **12** in the satisfactory yield of 94% (Scheme 3). In contrast, silver triflate in dioxane (Run 8) gave rise to α-predominance (α : β≈70 : 30), a distinct promotor-dependent inversion, that was also observed in the glycosylation of **11** with the disaccharide donor **1b**.[9] The β-glycoside **12** was then subjected to hydroboration and subsequent *N*-acetylation as described for **7** to give **13** in 74% yield, whereby the presence of the β-D-gluco epimer could not be detected. *O*-Debenzoylation of **13** followed by removal of isopropylidene groups with 95% aqueous trifluoroacetic acid gave *N*-acetyl-β-D-mannosaminyl-(1→6)-D-galactose (**15**) in 81% yield. The structure of **15** was confirmed by ^{13}C NMR spectroscopy.

Scheme 4 depicts the synthetic pathway to methyl *N*-acetyl-β-D-mannosaminyl-(1→4)-α-D-glucopyranoside (**23**). Glycosidations of **1a** with partially protected methyl glucopyranosides with a free C-4 hydroxyl group were somewhat troublesome because of the low reactivity of the secondary hydroxyl function. After

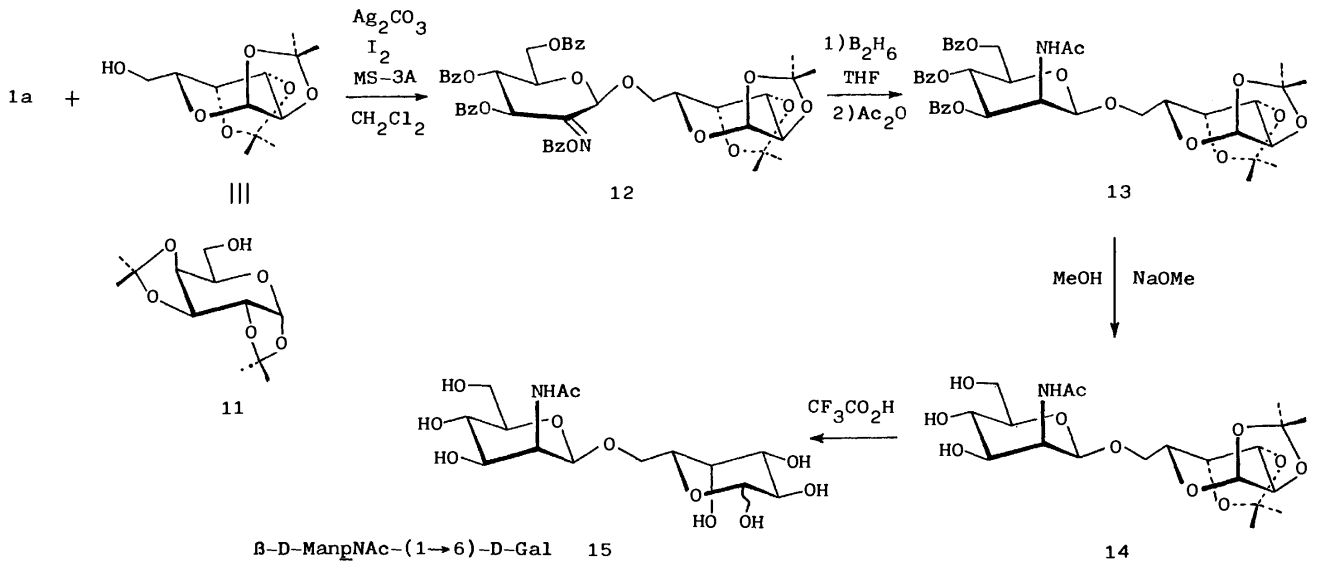

Scheme 3.

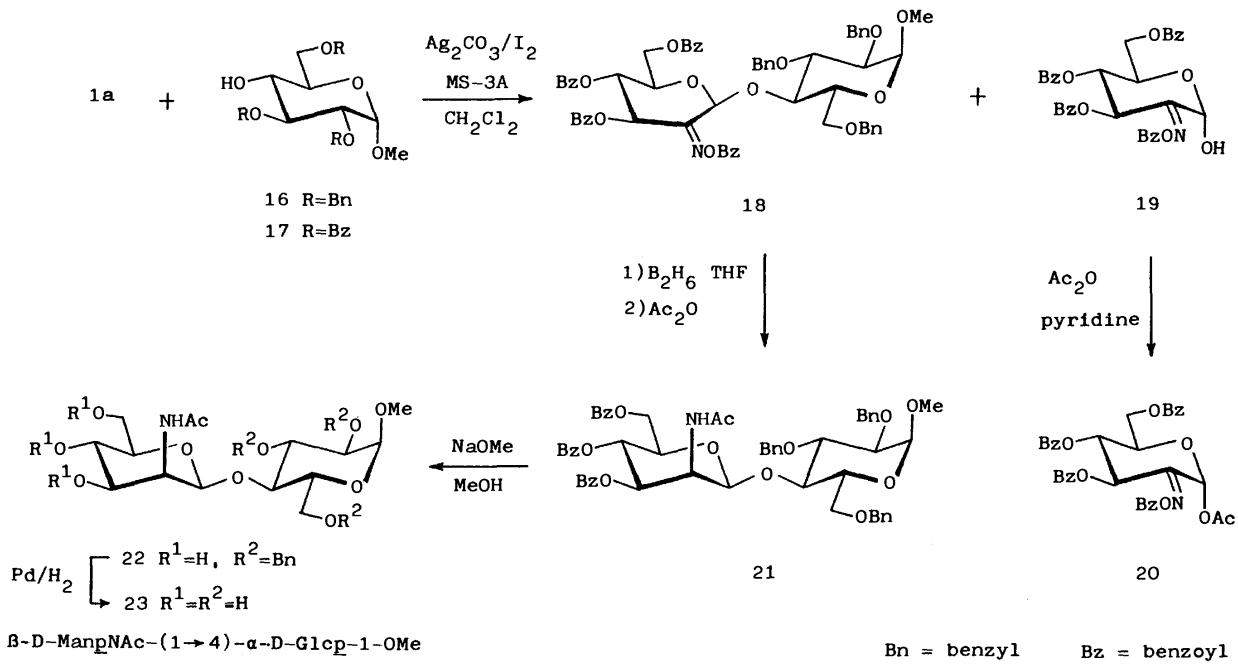

Scheme 4.

much attempts shown in Table 1, the $\beta(1\rightarrow4)$-glycoside (**18**) could be secured in 55% yield (Run 13 in Table 1) by the use of methyl 2,3,6-tri-*O*-benzyl-α-D-glucopyranoside (**16**)[18] as an acceptor and silver carbonate-iodine as the promotor, whilst methyl 2,3,6-tri-*O*-benzoyl-α-D-glucopyranoside (**17**)[19] afforded multi-component mixtures in all the cases tested (Runs 9—11). Other glycosylation catalysts, such as silver oxide, silver perchlorate, or the allegedly highly superior[20] silver silicate were noneffective (Runs 14—16).

Under the conditions of Run 13, i.e. glycosylation of **16** with two molar equivalents of **1a** and Ag_2CO_3 in dichloromethane, substantial amounts of 1-hydroxy derivative **19** was generated, its identity being established by its conversion into the 1-acetate **20α**, that in turn was unequivocally identified by comparison with an authentic sample prepared by reaction of **1a** with sodium acetate in dioxane. Hydroboration of **18** was carried out as for **6**→**7**, yet proceeded in an essentially stereospecific manner, to provide the protected *N*-acetyl-β-D-mannosaminide (**21**) in a yield of 81%. Subsequent debenzoylation readily gave **22** (96% yield), which was catalytically hydrogenated over palladium/carbon to quantitatively afford desired methyl *N*-acetyl-β-D-mannosaminyl-(1→4)-α-D-glucopyranoside (**23**).

The concise, practical route reported here for the chemical synthesis of methyl or glycosyl *N*-acetyl-β-D-mannosaminides, as of now, appears to be the most straightforward methodology for the construction of heterooligosaccharides with a terminal β-D-mannosamine unit; it can be expected to find application for the immunologically relevant repeating units of *Streptococcus pneumoniae*-derived capsular polysaccharide and a series of others, some of which we hope to report in due course.

Experimental

General. Melting points were determined on a Yamato MP-1 apparatus and are uncorrected. Spectral data were recorded on the following instruments; IR; Jasco IR-810 spectrophotometer; $[\alpha]_D$: Jasco DIP-180 digital polarimeter; MS: JMS D-100 Spectrometer; ^{1}H NMR: Varian EM-390 (90 MHz), VXR-300 (300 MHz), or XL-400 (400 MHz) spectrometers in chloroform-*d* solution unless otherwise noted. ^{1}H-^{1}H and ^{1}H-^{13}C shift correlated 2D NMR and ^{13}C NMR: Varian VXR-300 or XL-400 spectrometer. TLC was carried out on silica gel 60 F_{254} (Merck Art. 5735) developed with the same solvent systems as described for column chromatography in the individual experimental section. The spots were detected by UV light (254 nm) or charring with 10% aq. sulfuric acid. Column chromatography was achieved on a silica gel 60 (Merck Art. 7734). Paper chromatography (PC) was carried out on Toyo filter paper No. 525 and detected with 0.2% ninhydrin in pyridine solution at 100 °C for 10 min.

Methyl 3,4,6-Tri-*O*-benzoyl-2-(benzoyloxyimino)-2-deoxy-β-D-*arabino*-hexopyranoside (6). (Benzoyloxyimino)glycosyl bromide **1a**[10] (135 mg, 0.2 mmol) was added to a mixture of methanol (0.08 ml, 2 mmol), silver carbonate (279 mg, 1 mmol), and iodine (51 mg, 0.2 mmol) in dry dichloromethane (2 ml) containing Molecular Sieves 3A (100 mg, powder). The mixture was stirred in the dark at room temperature for 3 days, whereafter all the educt had been consumed (TLC). Dilution with dichloromethane (10 ml), filtration through Celite, consecutive washing of the filtrate with saturated aq. $NaHCO_3$ (10 ml) and water (3×10 ml), drying (Na_2SO_4) and evaporation to dryness in vacuo gave a residue which was eluted from a silica-gel column with toluene-ethyl acetate (8:1). The major fraction was concentrated and crystallized from diethyl ether–pentane: 116 mg (93%) of

6; mp 57—65 °C (decomp); $[\alpha]_D^{20}$—42.8° (*c* 1.0, $CHCl_3$); ^1H NMR (400 MHz) δ=3.70 (3H, s, CH_3), 4.51 (1H, m, H-5), 4.77 (1H, dd, H-6a), 4.84 (1H, dd, H-6b), 5.92 (1H, dd, H-4), 5.93 (1H, s, H-1), 6.25 (1H, d, H-3), 7.3—8.1 (aromatic H); $J_{3,4}=J_{4,5}=J_{5,6a}=5.5$, $J_{5,6b}=7.0$, $J_{6a,6b}=11.5$ Hz; ^{13}C NMR (100 MHz) δ=57.02 (OMe), 64.64 (C-6), 68.42 (C-3), 68.61 (C-4), 73.24 (C-5), 93.98 (C-1), 128.2—133.7 (phenyl C), 156.56 (C-2), 162.29, 164.52, 164.74, and 165.82 (benzoyl C=O).

Found: C, 67.09; H, 4.61; N, 2.36%. Calcd for $C_{35}H_{29}NO_{10}$: C, 67.41; H, 4.69; N, 2.25%.

Methyl 2-Acetamido-3,4,6-tri-*O*-benzoyl-β-D-mannopyranoside (7). A 1 M solution of diborane in tetrahydrofuran (15.5 ml) was added to a solution of **6** (807 mg, 1.3 mmol) in tetrahydrofuran (15 ml) at −10 °C under atmosphere of nitrogen. The mixture was stirred at −10 °C for 0.5 h and at ambient temperature for 2 h. Excess reductant was quenched with methanol (15 ml) followed by addition of acetic anhydride (8 ml) for *N*-acetylation. After stirring for 1 h at ambient temperature, the mixture was passed through a basic resin (Amberlite IR-45), and washed with methanol. The eluate was concentrated in vacuo and the residue was purified by elution from a silica-gel column with chloroform-ethyl acetate (1 : 1). The major fraction was concentrated and the residue crystallized from ethyl acetate-diethyl ether (1:2)-pentane to give 622 mg (88%) of **7**: mp 95—105 °C; $[\alpha]_D^{22}$ −55.8 ° (*c* 0.5, $CHCl_3$); IR (KBr) 3450, 3380 cm^{-1} (NH); ^1H NMR (400 MHz) δ=2.03 (3H, s, $COCH_3$), 3.55 (3H, s, OCH_3), 4.11 (1H, td, H-5), 4.57 (1H, dd, H-6a), 4.64 (1H, dd, H-6b), 4.79 (1H, d, H-1), 4.98 (1H, td, H-2), 5.47 (1H, dd, H-4), 5.87 (1H, d, NH), 7.3—8.1 (aromatic H); $J_{1,2}=2.0$, $J_{2,3}=4.0$, $J_{2,NH}=8.5$, $J_{3,4}=9.5$, $J_{4,5}=9.0$, $J_{5,6a}=6.0$, $J_{5,6b}=3.5$, $J_{6a,6b}=12.0$ Hz; ^{13}C NMR (100 MHz) δ=23.38 ($COCH_3$), 50.19 (C-2), 57.15 (OCH_3), 63.46 (C-6), 67.45 (C-4), 71.92 (C-3), 72.60 (C-5), 100.12 (C-1), 128.2—133.5 (phenyl C), 165.32, 165.53, and 165.86 (3×C=O), 170.28 (NHCO).

Found: C, 65.70; H, 5.35; N, 2.84%. Calcd for $C_{30}H_{29}NO_9$: C, 65.80; H, 5.34; N, 2.56%.

On concentration of the minor fraction, dissolution of the residue in diethyl ether, and addition of pentane, β-D-gluco isomer **10** was obtained in a yield of 9.4 mg (1.3%): mp 80—88 °C; $[\alpha]_D^{22}$ +8.8° (*c* 0.25, $CHCl_3$); ^1H NMR (90 MHz) δ=1.85 (3H, s, $COCH_3$).

Methyl 2-Acetamido-2-deoxy-β-D-mannopyranoside (8). A solution of **7** (212 mg, 0.39 mmol) in 0.05 M methanolic sodium methoxide (20 ml) was stirred at ambient temperature for 20 h and was subsequently neutralized with a dry acidic resin (Dowex 50W×8) and filtered. The filtrate was evaporated to dryness and the residue was partitioned between dichloromethane (30 ml) and water (30 ml). The aqueous layer was separated, washed with dichloromethane (2×40 ml), and concentrated to dryness. The residue was purified by elution from a silica-gel column with chloroform-methanol (1 : 1), followed by concentration and crystallization from methanol-diethyl ether to give 71 mg (74%) of **8** as 1/2 hydrate: mp 123—127 °C; $[\alpha]_D^{23}$−70° (*c* 0.25, H_2O; lit,[14] $[\alpha]_D^{24}$ −68 °(*c* 1.5, H_2O)); ^1H NMR (D_2O, 400 MHz) δ=1.95 (3H, s, $COCH_3$), 3.29 (1H, td, H-5), 3.29 (3H, s, OCH_3), 3.40 (1H, dd, H-4), 3.69 (1H, dd, H-3), 3.70 (1H, dd, H-6a), 3.80 (1H, dd, H-6b), 4.37 (1H, dd, H-2), 4.58 (1H, d, H-1); $J_{1,2}=1.5$, $J_{2,3}=4.5$, $J_{3,4}=J_{4,5}=9.5$, $J_{5,6a}=5.0$, $J_{5,6b}=2.5$, $J_{6a,6b}=12.0$ Hz; ^{13}C NMR (D_2O, 100 MHz), δ=22.82 ($COCH_3$), 53.83 (C-2), 57.81 (OCH_3), 61.24 (C-6), 67.60 (C-4), 72.83 (C-3), 77.22 (C-5), 101.24 (C-1), 176.24 (NHCO); $J_{C1,H1}=163.6$ Hz.

Found: C, 44.23; H, 7.22; N, 5.62%. Calcd for $C_9H_{17}NO_6$ 1/2H_2O: C, 44.26; H, 7.43; N, 5.73%.

The monohydrate of **8** was also isolated in a yield of 13 mg (14%) along with the 1/2 hydrate; Found: C, 42.84; H, 7.61; N, 5.40%. Calcd for $C_9H_{17}NO_6$ H_2O: C, 42.68; H, 7.56; N, 5.53%.

2-Amino-2-deoxy-D-mannopyranose Hydrochloride (9). Methyl *N*-acetyl-β-D-mannosaminide (**8**) 1/2 hydrate (30 mg, 0.124 mmol) was dissolved in 1 M HCl (10 ml) and heated at 95 °C for 2 h. After concentration of the solution, the residue crystallized from methanol-diethyl ether to afford 27 mg (quantitative yield) of **9** as colorless crystals: mp 173—175 °C (decomp); $[\alpha]_D^{24}$−4.2° (*c* 0.5, H_2O), (lit,[21] mp 178—180 °C, $[\alpha]_D^{23}$−3.0° (*c* 2.0, H_2O)); PC (*n*-BuOH-pyridine-H_2O, 6 : 4 : 3 v/v): R_{Glc}=0.73 (cf., authentic D-Man*p*N HCl: R_{Glc}=0.73, D-Glc*p*N HCl: R_{Glc}=0.68).

6-*O*-[3,4,6-Tri-*O*-benzoyl-2-(benzoyloxyimino)-2-deoxy-β-D-*arabino*-hexopyranosyl]-1,2 : 3,4-di-*O*-isopropyridene-α-D-galactopyranose (12). A mixture of diacetonegalactose (**11**)[17] (573 mg, 2.2 mmol), silver carbonate (2.76 g, 10 mmol), iodine (508 mg, 2.0 mmol), and (benzoyloxyimino)glycosyl bromide **1a** (1.35 g, 2.0 mmol) in dry dichloromethane (20 ml) with Molecular Sieves 3A (2.0 g, powder) was stirred in the dark at ambient temperature for 3 days. Subsequent dilution with dichloromethane (50 ml), filtration through celite, washing of the filtrate with 1 M aqueous $Na_2S_2O_3$ (50 ml), water (50 ml), saturated aqueous $NaHCO_3$ (50 ml), and water (3×100 ml) was followed by drying (Na_2SO_4) and evaporation to dryness. The residue was eluted through a silica-gel column with toluene-ethyl acetate (6 : 1). Concentration of the major fraction, followed by crystallization from diethyl ether-pentane gave 1.61 g (94%) of **12**: mp 83—86 °C; $[\alpha]_D^{22}$ −95.6° (*c* 0.5, $CHCl_3$); ^1H NMR (400 MHz) δ=1.27, 1.28, 1.35, and 1.40 (each 3H, s, 2×Me_2C), 3.90 (1H, dd, H-6a), 4.04 (1H, td, H-5), 4.12 (1H, dd, H-4), 4.24 (1H, dd, H-6b), 4.28 (1H, dd, H-2), 4.47 (1H, m, H-5′), 4.54 (1H, dd, H-3), 4.84 (2H, m, H-6′a,b), 5.46 (1H, d, H-1), 5.92 (1H, t, H-4′), 6.09 (1H, s, H-1′), 6.25 (1H, d, H-3′), 7.3—8.2 (aromatic H); $J_{1,2}=5.0$, $J_{2,3}=2.5$, $J_{3,4}=8.0$, $J_{4,5}=2.0$, $J_{5,6a}=6.8$, $J_{5,6b}=5.5$, $J_{6a,b}=9.7$, $J_{3',4'}=J_{4',5'}=5.3$ Hz; ^{13}C NMR (100 MHz) δ=24.32, 24.89, 25.88, and 25.96 (2×Me_2C), 64.55 (C-6′), 66.74 (C-5), 68.65 (C-3′), 68.86 (C-4′ and 6), 70.45 (C-2), 70.60 (C-3), 70.89 (C-4), 73.03 (C-5′), 93.19 (C-1′), 96.22 (C-1), 108.65 and 109.45 (2×$Me_2\underline{C}$), 128.0—134.0)phenyl C), 156.21 (C-2′), 162.68, 164.70, 164.92, and 165.91 (4×C=O).

Found: C, 64.60; H, 5.29; N, 1.59%. Calcd for $C_{46}H_{45}NO_{15}$: C, 64.86; H, 5.32; N, 1.64%.

6-*O*-(2-Acetamido-3,4,6-tri-*O*-benzoyl-2-deoxy-β-D-mannopyranosyl)-1,2 : 3,4-di-*O*-isopropylidene-α-D-galactopyranose (13). A solution of the disaccharide **12** (426 mg, 0.5 mmol) in dry tetrahydrofuran (6 ml) was treated with a 1 M solution of diborane in tetrahydrofuran (6 ml) as described for **6**→**7**. Termination with methanol (6 ml) and subsequent *N*-acetylation with acetic anhydride (3 ml) followed by processing of the mixture as described for **7** gave a syrup, which crystallized from ethyl acetate-diethyl ether (1 : 2)-pentane providing 288 mg (74%) of **13**: mp 171—173 °C; $[\alpha]_D^{22}$ −66.1° (*c* 0.5, $CHCl_3$); ^1H NMR (90 MHz) δ=1.29 and 1.40 (each 6H, s, 2×Me_2C), 1.98 (3H, s, $COCH_3$), 4.27 (1H, dd, H-2), 4.53 (1H, dd, H-3), 4.55—4.70 (2H, m, H-6a,b), 4.90 (1H, td, collapsed to dd on deuteration), 7.2—8.1 (aromatic H), 3.7—4.2 (other protons); $J_{1,2}=5.1$, $J_{2,3}=2.4$, $J_{3,4}=7.8$, $J_{1',2'}=3.0$, $J_{2',3'}=3.6$,

$J_{2',NH}$=8.4, $J_{3',4'}$=7.2, $J_{4',5'}$=7.8 Hz.

Found: C, 63.23; H, 5.81; N, 1.64%. Calcd for $C_{41}H_{45}NO_{14}$: C, 63.48; H, 5.85; N, 1.81%.

6-*O*-(2-Acetamido-2-deoxy-β-D-mannopyranosyl)-D-galactopyranose (15). A solution of **13** (343 mg, 0.44 mmol) in 0.05 M methanolic sodium methoxide (20 ml) was stirred at ambient temperature for 20 h. Subsequent neutralization (Dowex 50 W×8), filtration through Celite, and evaporation to dryness gave a residue, which was eluted through a silica-gel column with chloroform–methanol (4:1). Concentration of the major fraction gave debenzoylated product **14** as a colorless syrup (200 mg, quantitative), which was subjected to further deblocking of the isopropylidene groups without further purification.

The syrup was dissolved in 95% aqueous trifluoroacetic acid (3 ml) and stirred at ambient temperature for 20 min. Evaporation of the mixture was followed by co-evaporation with methanol to give a residue, which crystallized from ethanol–diethyl ether affording 140 mg (81%) of **15** as a monohydrate: mp 170 °C (decomp, with sintering at 115 °C): $[\alpha]_D^{21}$ −14° (*c* 0.25, H_2O): ^{1}H NMR (D_2O, 90 MHz) δ=1.90 (3H, s, $COCH_3$), 7.73 (1H, d, NH); ^{13}C NMR (D_2O, 25.4 MHz) δ=22.8 ($CO\underline{C}H_3$), 53.9 (C-2′), 61.3 (C-6′), 67.6 (C-4′), 69.1 and 69.6 (C-6 for respective anomers), 77.3 (C-5′), 93.2 (C-1 for α-anomer), 97.3 (C-1 for β-anomer), 101.6 (C-1′), 176.5 (NHCO). The anomeric carbon signals of the reducing end suggested that the ratio of the anomers was estimated as α:β=ca. 2:3.

Found: C, 41.68; H, 6.50; N, 3.38%. Calcd for $C_{14}H_{25}NO_{11}$ H_2O: C, 41.89; H, 6.78; N, 3.49%.

Methyl 4-*O*-[3,4,6-Tri-*O*-benzoyl-2-(benzoyloxyimino)-2-deoxy-β-D-*arabino*-hexopyranosyl]-2,3,6-tri-*O*-benzyl-α-D-glucopyranoside (18). Silver carbonate (138 mg, 0.5 mmol) and iodine (25 mg, 0.1 mmol) were added to a stirred solution of methyl 2,3,6-tri-*O*-benzyl-α-D-glucopyranoside (**16**)[18] (93 mg, 0.2 mmol) in dry dichloromethane (1 ml) containing Molecular Sieves 3A (100 mg, powder) and then stirred in the dark for 1 h under atmosphere of nitrogen. A solution of (benzoyloxyimino)glycosyl bromide **1a** (67 mg, 0.1 mmol) in dry dichloromethane (1 ml) was added and the mixture was further stirred at ambient temperature for 2 days. The mixture was diluted with dichloromethane (10 ml) and filtered through Celite. The filtrate was washed with saturated aqueous $NaHCO_3$ (10 ml) and water (3×15 ml). Drying (Na_2SO_4) and evaporation in vacuo gave a syrup, which was eluted through a silica-gel column with toluene–ethyl acetate (6:1). The major fraction eluted first was concentrated and the residue crystallized from diethyl ether–pentane to give 58 mg (55%) of **18**: mp 57—59 °C; $[\alpha]_D^{20}$+21.8° (*c* 0.5, $CHCl_3$); ^{1}H NMR (90 MHz), δ=3.29 (3H, s, OCH_3), 4.98 (1H, s, H-1), 5.92 (1H, t, H-4′), 6.22 (1H, d, H-3′), 6.74 (1H, s, H-1′), 3.4—4.9 (15H, other protons), 6.9—8.2 (aromatic H); $J_{3',4'}$=$J_{4',5'}$=5.4 Hz.

Found: C, 70.51; H, 5.44; N, 1.33%. Calcd for $C_{62}H_{57}NO_{15}$: C, 70.69; H, 5.20; N, 1.30%.

The minor fraction eluted next was treated as above to give 10.5 mg (18%) of **19** as 1/2 hydrate: mp 177—179 °C (decomp); $[\alpha]_D^{20}$ +32.4° (*c* 0.25, $CHCl_3$); IR (KBr) 3400 cm^{-1} (OH); ^{1}H NMR (DMSO-d_6, 90 MHz), δ=4.5—4.7 (2H, m, H-6a,b), 4.75 (1H, m, H-5), 5.87 (1H, t, H-4), 6.36 (1H, d, H-3), 6.50 (1H, t, H-1), 8.27 (1H, d, OH, disappeared on deuteration), 7.3—8.2 (aromatic H); $J_{1,OH}$=6.0, $J_{3,4}$=$J_{4,5}$=10.5 Hz.

Found: C, 66.29; H, 4.42; N, 2.19%. Calcd for $C_{39}H_{27}NO_{10}$ 1/2H_2O: C, 66.02; H, 4.56; N, 2.26%.

Acetylation of **19** with acetic anhydride–pyridine in a usual manner gave the corresponding 1-acetate **20α** which proved to be identical with the product obtained by acetylation of **1a** as described below.

1-*O*-Acetyl-3,4,6-tri-*O*-benzoyl-2-(benzoyloxyimino)-2-deoxy-α-D-*arabino*-hexopyranose (20α) and Its β-Anomer (20β). A mixture of (benzoyloxyimino)glycosyl bromide **1a** (1.0 g, 1.5 mmol), sodium acetate (369 mg, 4.5 mmol), and Molecular Sieves 3A (1 g, powder) in dry dioxane (20 ml) was stirred at ambient temperature for 3 days. The resulting mixture was diluted with dichloromethane (50 ml) and filtered through Celite. The filtrate was washed with water (3×50 ml), dried (Na_2SO_4), and evaporated to dryness. Elution of the residue through a silica-gel column with toluene–ethyl acetate (6:1) provided both anomeric isomers, which crystallized from diethyl ether–pentane to afford 365 mg (37%) of **20α** and 200 mg (20%) of the corresponding β-anomer **20β**.

20α: Mp 75—77 °C; $[\alpha]_D^{22}$ +53.4° (*c* 0.3, $CHCl_3$); ^{1}H NMR (90 MHz) δ=2.25 (3H, s, $COCH_3$), 4.4—4.7 (2H, m, H-6a,b), 4.68 (1H, m, H-5), 5.98 (1H, dd, H-4), 6.44 (1H, d, H-3), 7.2—8.2 (H-1 and aromatic H); $J_{3,4}$=9.6, $J_{4,5}$=9.0 Hz.

Found: C, 66.46; H, 4.49; N, 2.18%. Calcd for $C_{36}H_{29}NO_{11}$: C, 66.36; H, 4.49; N, 2.15%.

20β: Mp 64—66 °C (with sintering at 60 °C); $[\alpha]_D^{23}$ −43.2° (*c* 0.5, $CHCl_3$); ^{1}H NMR (90 MHz) δ=4.5—5.0 (3H, m, H-5 and 6a,b), 5.88 (1H, dd, H-4), 6.28 (1H, d, H-3), 7.2—8.2 (H-1 and aromatic H); $J_{3,4}$=5.1, $J_{4,5}$=4.8 Hz.

Found: C, 66.74; H, 4.46; N, 2.21%. Calcd for $C_{36}H_{29}NO_{11}$: C, 66.36; H, 4.49; N, 2.15%.

Methyl 4-*O*-(2-Acetamido-3,4,6-tri-*O*-benzoyl-2-deoxy-β-D-mannopyranosyl)-2,3,6-tri-*O*-benzyl-α-D-glucopyranoside (21). A solution of **18** (618 mg, 0.59 mmol) in dry tetrahydrofuran (8 ml) was treated with a 1 M solution of diborane in tetrahydrofuran (7.1 ml) as described for **6**→**7**. Subsequent acetylation with acetic anhydride (4 ml) followed by processing of the mixture as described for **7** gave 461 mg (81%) of syrupy **21**. Crystallization from diethyl ether afforded 411 mg of **21** as colorless prisms: mp 163—164 °C (decomp); $[\alpha]_D^{22}$ −21.2° (*c* 0.25, $CHCl_3$); IR (KBr) 3430 (NH), 1720 (ester C=O), 1685 cm^{-1} (amide C=O); ^{1}H NMR (300 MHz) δ=1.83 (3H, s, $COCH_3$), 3.37 (3H, s, OCH_3), 3.48 (1H, m, H-5′), 3.49 (1H, dd, H-2), 3.65—3.75 (3H, m, H-5 and H-6a,b), 3.88 (1H, t, H-3), 4.01 (1H, t, H-4), 4.24 (1H, dd, H-6′a), 4.39 (1H, dd, H-6′b), 4.55, 4.72, and 4.91 (each 2H, dd, 3×$C\underline{H}_2$Ph), 4.61 (1H, d, H-1), 4.81 (1H, td, H-2′), 4.86 (1H, d, H-1′), 5.12 (1H, dd, H-3′), 5.49 (1H, t, H-4′), 5.70 (1H, d, NH), 7.2—8.0 (aromatic H); $J_{1,2}$=3.5, $J_{2,3}$=$J_{3,4}$=$J_{4,5}$=9.3, $J_{1',2'}$=1.5, $J_{2',NH}$=8.7, $J_{2',3'}$=4.0, $J_{3',4'}$=$J_{4',5'}$=10.0, $J_{5',6'a}$=5.0, $J_{5',6'b}$=3.5, $J_{6'a,b}$=12.0 Hz; ^{13}C NMR (75 MHz) δ=23.05 ($CO\underline{C}H_3$), 51.09 (C-2′), 55.29 (OCH_3), 63.25 (C-6′), 67.26 (C-4′), 68.45 (C-6), 69.35 (C-5), 72.34 (C-5′) 72.43 (C-3′), 73.44, 73.56, and 75.00 (3×$\underline{C}H_2$Ph), 76.51 (C-4), 79.38 (C-2), 80.41 (C-3), 98.27 (C-1), 98.87 (C-1′), 126.6—139.2 (aromatic C), 165.64, 165.64, and 165.90 (3×C=O), 170.34 (NHCO).

Found: C, 70.00; H, 5.87; N, 1.42%. Calcd for $C_{57}H_{57}NO_{14}$: C, 69.85; H, 5.86; N, 1.43%.

Methyl 4-*O*-(2-Acetamido-2-deoxy-β-D-mannopyranosyl)-2,3,6-tri-*O*-benzyl-α-D-glucopyranoside (22). A 0.05 M solution of sodium methoxide in dry methanol (18 ml) was added to **21** (352 mg, 0.36 mmol). The solution was stirred at

ambient temperature for 20 h, neutralized with acidic resin (Dowex 50W×8), and filtered through Celite. The filtrate was concentrated in vacuo to give a residue, which was eluted through a silica-gel column with chloroform–methanol (8:1). Concentration of the major fraction, followed by recrystallization from methanol–pentane gave 210 mg (87%) of **22** as colorless needles: mp 170—172 °C; $[\alpha]_D^{22}$ +14.2° (*c* 0.5, CH_3OH); IR (KBr) 3400—3300 (NH and OH), 1640 cm^{-1} (amide C=O); ^1H NMR (DMSO-d_6, 90 MHz) δ=1.83 (3H, s, $COCH_3$), 3.29 (3H, s, OCH_3), 7.04 (1H, s, NH), 7.1—7.5 (aromatic H), 2.8—5.1 (other protons).

Found: C, 64.98; H, 6.89; N, 2.04%. Calcd for $C_{36}H_{45}NO_{12}$: C, 64.75; H, 6.79; N, 2.10%.

Methyl 4-*O*-(2-Acetamido-2-deoxy-β-D-mannopyranosyl)-α-D-glucopyranoside (23). A solution of **22** (172 mg, 0.26 mmol) in acetic acid (10 ml) was hydrogenated in the presence of 10% palladium on carbon (85 mg) under atmosphere of hydrogen (3.45×10^5 Pa) for 24 h. The mixture was filtered through Celite and the filtrate was concentrated in vacuo to give a syrup, which was purified by elution from a silica-gel column with chloroform–methanol (1:2). The major fraction was concentrated and the residual solid was washed with diethyl ether to give 110 mg (quantitative) of **23** as 1/2 hydrate: mp 190 °C (decomp, with sintering at 110 °C); $[\alpha]_D^{23}$ +45.2° (*c* 0.25, H_2O); ^{13}C NMR (D_2O, 25.4 MHz) δ=22.8 ($CO\underline{C}H_3$), 54.1 (C-2′), 55.8 (OCH_3), 60.9 and 61.3 (C-6 and 6′), 67.5 (C-4′), 70.8 (C-2), 71.9, 72.5, and 72.8 (C-3, C-3′, and C-5), 77.4 (C-5′), 79.6 (C-4), 99.2 (C-1), 100.2 (C-1′), 176.4 (CONH).

Found: C, 44.62; H, 7.13; N, 3.16%. Calcd for $C_{15}H_{27}NO_{11}$ $1/2H_2O$: C, 44.33; H, 6.94; N, 3.45%.

References

1) J. B. Robbins, *Immunochemistry*, **15**, 839 (1978).

2) H. J. Jennings, *Adv. Carbohydr. Chem. Biochem.*, **41**, 155 (1983).

3) L. Rovis, E. A. Kabat, and M. Potter, *Carbohydr. Res.*, **23**, 223 (1972).

4) P.-E. Jansson, B. Lindberg, and Lindquist, *Carbohydr. Res.*, **95**, 73 (1981).

5) H. Paulsen, J. P. Lorentzen, and W. Kutschker, *Carbohydr. Res.*, **136**, 153 (1985).

6) H. Paulsen and J. P. Lorentzen, *Liebigs Ann. Chem.*, **1986**, 1586.

7) E. Micheli, F. Nicotra, L. Panza, F. Ronchetti, and L. Toma, *Carbohydr. Res.*, **139**, C1 (1985).

8) F. W. Lichtenthaler, E. Kaji, and S. Weprek, *J. Org. Chem.*, **50**, 3505 (1985).

9) F. W. Lichtenthaler and E. Kaji, *Liebigs Ann. Chem.*, **1985**, 1659.

10) F. W. Lichtenthaler and P. Jarglis, *Angew. Chem., Int. Ed. Engl.*, **21**, 625 (1982).

11) F. W. Lichtenthaler, P. Jarglis, and W. Hempe, *Liebigs Ann. Chem.*, **1983**, 1959.

12) A part of this work has been presented at the 12th International Carbohydrate Symposium, Utrecht, July, 1984, Abstr. A 2.16, and at the 9th Japanese Carbohydrate Symposium, Tokyo, July, 1986, Abstr. B 08.

13) H. J. Jennings, K.-G. Rosell, and D. J. Carlo, *Can. J. Chem.*, **58**, 1069 (1980); N. Ohno, T. Yadomae, and T. Miyazaki, *Carbohydr. Res.*, **80**, 297 (1980).

14) S. Beychock, G. Ashwell, and E. A. Kabat, *Carbohydr. Res.*, **17**, 19 (1971).

15) K. Bock and C. Pedersen, *J. Chem. Soc., Perkin Trans. 2*, **1974**, 293: The $J_{C1,H1}$ of methyl *N*-acetyl-β-D-glucosaminide also shows a similar value as 163 Hz.

16) S. J. Perkins, L. N. Johnson, and D. C. Phillips, *Carbohydr. Res.*, **59**, 19 (1977).

17) H. Ohle and G. Behrend, *Ber.*, **58**, 2585 (1925); available commercially from Aldrich Chemical Co. Inc.

18) J. W. Küster and I. Dyong, *Liebigs Ann. Chem.*, **1975**, 2179; P. J. Garegg and H. Hultberg, *Carbohydr. Res.*, **93**, C10 (1981).

19) T. Ogawa and M. Matsui, *Tetrahedron*, **37**, 2363 (1981).

20) H. Paulsen and O. Lockhoff, *Chem. Ber.*, **114**, 3102 (1981).

21) R. U. Lemieux and T. L. Nagabhushan, *Can. J. Chem.*, **46**, 401 (1968).

 © 1988 The Chemical Society of Japan Bull. Chem. Soc. Jpn., 61, 1299—1312 (1988)

Three-Component Coupling Synthesis of Prostaglandins: The Aldol Route[1)]

Masaaki SUZUKI, Toshio KAWAGISHI, Akira YANAGISAWA, Takehiko SUZUKI, Noriaki OKAMURA,[2)] and Ryoji NOYORI*
Department of Chemistry, Nagoya University, Chikusa, Nagoya 464
(Received November 13, 1987)

A one-pot, high yield construction of the whole prostaglandin (PG) skeleton is accomplishable by combination of the copper-mediated conjugate addition of an ω side-chain unit to a 4*R*-oxygenated 2-cyclopentenone derivative and aldol condensation of the in situ generated enolate with an α side-chain aldehyde. Subsequent removal of the 7-hydroxyl group from the adducts and deblocking of the protective groups give PGs of E series. PGE_1 has been prepared in 56% overall yield through the five-step sequence. Selective transformation of the PGE to PGD structure can be realized simply by appropriate selection of the hydroxyl protective groups in the five-membered ring and ω side-chain units. The vicinal carba-condensation using methyl 6-formyl-5-hexynoate as the α side-chain aldehyde unit followed by deoxygenation from the aldol products gives the 5,6-didehydro-PGE_2 derivatives which serve as key intermediates in the general synthesis of various natural PGs. An efficient method for resolution of 4-hydroxy-2-cyclopentenone is also described.

The prostaglandin (PG) skeleton is constituted by the oxygenated cyclopentanone ring and the seven-and eight-carbon (α and ω, respectively) side-chains. Obviously, the three-component coupling process, viz., consecutive nucleophilic/electrophilic introduction of the two side-chain units to (*R*)-4-hydroxy-2-cyclopentenone derivatives, is regarded as the simplest converging synthesis (Scheme 1).[3)] One may anticipate that well-known organocuprate conjugate addition of the ω side-chain unit to the enone followed by reaction with alkyl halides completes the desired vicinal carba-condensation.[4,5)] However, extensive studies along this line have revealed that such direct vicinal carba-condensation is not easy to achieve.[5p,6,7)] The difficulty is presumably attributable to the complex nature of the reaction system which causes a facile double-bond migration of the initially formed enolate,[3,5p)] causing concomitant dehydration to give the cyclopentenone products. The slow alkylation reaction cannot compete with such side sequences.[8)] However, use of highly reactive electrophiles is capable of suppressing the undesired reaction and the successful trapping has indeed been achieved with acyl chlorides[5n,o,9)] and ketene bis(methylthio)acetal monoxide, a strong Michael acceptor.[5p)] The aldol route is even more attractive.[5l,m,q-v,10)] Stork and Isobe thus employed very reactive formaldehyde as a trapping agent to introduce hydroxymethyl group at C-2 regiospecifically,[5k)] and constructed the full prostanoic acid skeleton by supplementing a six-carbon unit forming the full α side chain and the rectification of the oxidation state of the functional groups. They synthesized natural $PGF_{2\alpha}$ in 9% overall yield from a racemic 4-cumyloxy-2-cyclopentenone.[5k)] We intended to realize a one-pot construction of the full PG skeleton by the aldol strategy.[11)]

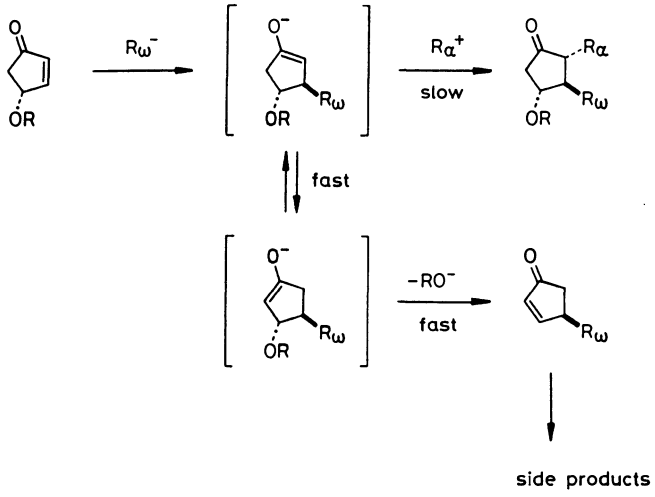

Scheme 1.

Results and Discussion

A. Vicinal Carba-Condensation of α,β-Unsaturated Ketones via the Tandem Organocopper Conjugate Addition/Aldol Reaction. We recently found a new recipe for the organocopper conjugate addition to α,β-unsaturated ketones using an organolithium (RLi), copper(I) iodide, and tributylphosphine in 1:2—3 mole ratio.[12)] The organocopper reagents undergo the conjugate addition to enones smoothly by employing 1:1 R/enone ratio and, in addition, the regio-defined enolate intermediates can be trapped effectively with equimolar amounts of aldehydes (Scheme 2). This stoichiometry-controlled, high-yield combination of the organometallic reagents and enone substrates, unlike under ordinary reaction conditions using excess organometallics, generates enolate species as only strong nucleophile present in the reaction system and, therefore, the latter reacts cleanly with one equivalent of the aldehyde trap, giving the aldol products. The results of the reaction of 2-cyclopentenone or -hexenone, the butylcopper reagent, and aldehydes are summarized in Table 1. The three-component joining effected with 1:1:1 molar ratio was general for a wide range of aldehydes including formaldehyde, simple alkanals, and α,β-unsaturated or aromatic aldehydes.

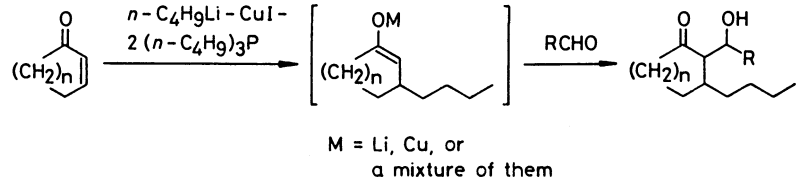

Scheme 2.

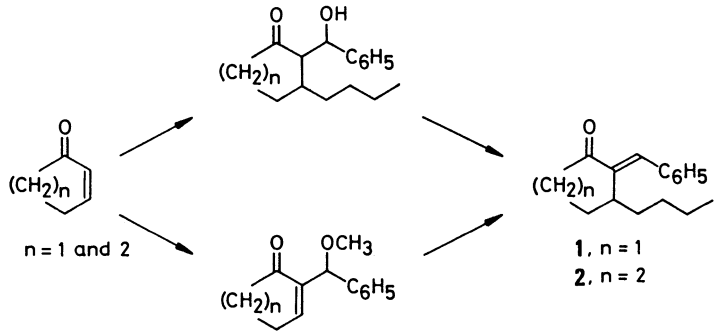

Scheme 3.

Table 1. Vicinal Carba-Condensation with α,β-Unsaturated Ketones via the Organocopper/Aldehyde Joining Process[a]

Entry	Enone	Aldehyde trapping	Aldol product Yield/%[b]
1	2-Cyclopentenone	Formaldehyde[c]	66[d]
2	2-Cyclopentenone	Butanal	98[e]
3	2-Cyclopentenone	2-Methylpropanal	93[e]
4	2-Cyclopentenone	2,2-Dimethylpropanal	71[e]
5	2-Cyclopentenone	Benzaldehyde	91[f]
6	2-Cyclopentenone	(*E*)-Cinnamaldehyde	94[f]
7	2-Cyclopentenone	2-Hexynal	72[f]
8	2-Cyclohexenone	Formaldehyde[c]	60[e]
9	2-Cyclohexenone	Acetaldehyde	91[f]
10	2-Cyclohexenone	Butanal	88[e]
11	2-Cyclohexenone	2-Methylpropanal	94[e]
12	2-Cyclohexenone	Benzaldehyde	96[f,g], 89
13	2-Cyclohexenone	(*E*)-Cinnamaldehyde	92[f]

a) The butylcopper phosphine complex was prepared in situ by mixing coppe(I) iodide, butyllithium, and tributylphosphine in 1:1:2 mole ratio at −78 °C in ether. The conjugate addition was conducted at −40 to −78 °C. Enolate trapping was carried out at −78 °C for 5—60 min. b) Yield after silica-gel column chromatography. c) Introduced with an argon stream after cracking of paraformaldehyde. d) A 59:1 stereomixture. e) A single isomer. f) A mixture of stereoisomers. g) Yield determined by ^{1}H NMR analysis.

Alkanals as the trapping agent tend to produce single coupling adducts, whereas acetaldehyde and aromatic or other α,β-unsaturated aldehydes give rise to a mixture of stereoisomers.

The two side chains are incorporated in the vicinal positions in a regiospecific manner via kinetically defined, nonequilibrating enolates. This is confirmed, for examples, by comparison of the samples of 2-benzylidene-3-butylcycloalkanones, **1** and **2**, derived from the corresponding aldols by dehydration and those prepared by an unambiguous method consisting of the combination reaction of α-alkoxyalkylation[13] and organocopper conjugate addition (Scheme 3). No α′,β-condensation products associated with possible enolate equilibration were detected in the reaction mixture.

B. Chiral Building Blocks. The optically active building blocks requisite for convergent PG synthesis are accessible in various ways.[3a] The ω side-chain alcohol having S configuration, **3**, is available by optical resolution,[14a] kinetic resolution by asymmetric epoxidation,[14b] or asymmetric reduction of the corresponding enone by chemical,[14c] or enzymatic[14d] method. The R cyclopentenone derivative, **6**, is obtainable by chemical[15a,b] or chromatographic resolution,[15c] transformation from D-tartaric acid ((2*S*,3*S*)-(−)-tartaric acid),[15d] chemical kinetic resolution of racemic 4-hydroxy-2-cyclopentenone,[15e] enzymatic kinetic resolution of the acetate,[15f] and asymmetric reduction of 2-cyclopentene-1,3-dione,[14c] etc. We now found that **6** was obtainable by efficient optical resolution of the racemate[16] using the resolving agent **9** derived from chrysanthemic acid.[17] Thus condensation of (±)-**6** with **9** in the presence of pyridinium *p*-toluenesulfonate gave the two diastereomeric mixture **10** in 99% yield based on **9**. The diastereomers separated by silica-gel column chromatography were subjected to hydrolysis in aqueous dioxane at 70 °C to give desired (*R*)-4-hydroxy-2-cyclopentenone (**6**) and its antipode in 88% and 82% of theory, respectively. No racemization was observed under these conditions. The resolving reagent **9** was recovered in >75% yield and could be recycled for the resolution precedure. The hydroxyl group of **6** was protected by a silyl or tetrahydropyranyl group by conventional methods[18]

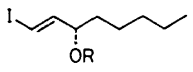

3, R = H
4, R = $Si(CH_3)_2$-*t*-C_4H_9
5, R = THP

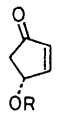

6, R = H
7, R = $Si(CH_3)_2$-*t*-C_4H_9
8, R = THP

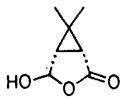

9

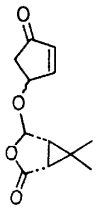

10

for the purpose of the organometallic operation.

C. A Short Synthesis of PGE_1 and PGD_1. When organocopper reagent formed from **4** was coupled with (*R*)-siloxy enone **7**, a single adduct **11** was obtained after aqueous work-up.[3a] The C-3/C-4 trans relationship was established simply by nonbonded interaction between the siloxy moiety and the entering organometallic. Encouraged by the clean trans stereochemistry induced in the conjugate addition step, we then moved to the aldehyde trapping of the enolate intermediate. The conjugate addition using the enone **8** and the organocopper reagent formed from the alkenyl iodide **5** was followed by aldol trapping of the enolate with one equivalent of methyl 6-formylhexanoate. As expected, the desired aldol **12** (a threo/erythro[19] mixture) possessing the whole PG framework was obtained in 83% yield.[20] The undesired β-elimination leading to the PGA type structure could not be observed. Removal of the C-7 hydroxyl group from **12** was accomplished via the enone **14** formed by dehydration with methanesulfonyl chloride and 4-(dimethylamino)pyridine (92% yield). Exposure of **14** to excess zinc dust in a 95:5 2-propanol-acetic acid mixture gave the saturated PGE_1 derivative **16** in 84% yield. Heating of **14** with tributyltin hydride in the presence of a catalytic amount of di-*t*-butyl peroxide increased the product yield up to 90%. Deblocking the tetrahydropyranyl protective groups gave PGE_1 methyl ester (**18**) in 92% yield. The spectroscopic and chromatographic behavior was identical with that of authentic PGE_1 methyl ester. Hydrolysis of the ester function by porcine liver esterase (86% yield)[22] completes the synthesis of natural PGE_1. Thus PGE_1 was synthesized in 56% overall yield through the five-step sequence from the starting enone **8**. PGE_1 possesses four asymmetric carbons. Here the absolute configuration at C-11 and C-15 is inherently determined at the stage of the starting enone and ω side-chain components, and the mutual trans relationship of the three ring substituents at C-11, C-12, and C-8 is established automatically through the vicinal carba-condensation and the following functional group manipulation.

PGD_1 was also accessible by fundamentally the same strategy. PGD_1, like PGE_1, has the β-hydroxycyclopentanone structure but bears a hydroxyl group at C-9 and a keto function at C-11. The choice of proper hydroxyl protective groups in the starting five-membered ring and ω side-chain units allows ready arrangement of such functional groups. Trialkylsilyl protection of 4-hydroxy-2-cyclopentenone and tetrahydropyranyl blocking of the ω side-chain alcohol were the best choice in view of their different profiles of the removal conditions. Thus the vicinal carba-condensation of the enone **7** under our standard conditions by using **5** and methyl 6-formylhexanoate as side-chain components gave the aldol **13** (a threo/erythro[19] mixture) in 70% yield. Treatment of **13** with methanesulfonyl chloride and 4-(dimethylamino)pyridine gave the dehydration product **15** in 75% yield, which upon exposure to excess tributyltin hydride and di-*t*-butyl peroxide catalyst afforded **17** in 88% yield. The oxidation states of the C-9 and C-11 positions was easily rectified as follows. Requisite stereoselective reduction of the 9-keto group was accomplished with L-Selectride (lithium tri-*s*-butylborohydride) in THF to

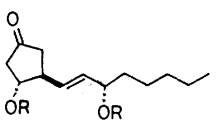

11, R = $Si(CH_3)_2$-*t*-C_4H_9

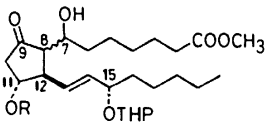

12, R = THP
13, R = $Si(CH_3)_2$-*t*-C_4H_9

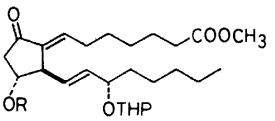

14, R = THP
15, R = $Si(CH_3)_2$-*t*-C_4H_9

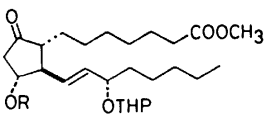

16, R = THP
17, R = $Si(CH_3)_2$-*t*-C_4H_9

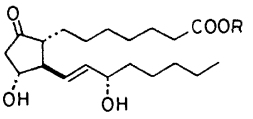

18, R = CH_3
19, R = H

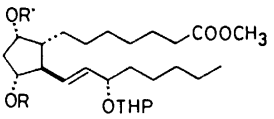

20, R = $Si(CH_3)_2$-*t*-C_4H_9; R' = H
21, R = $Si(CH_3)_2$-*t*-C_4H_9; R' = THP
22, R = H; R' = THP

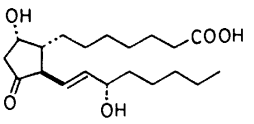

23

give the 9α alcohol **20** exclusively in 92% yield. After tetrahydropyranylation of 9-hydroxyl in **20** under standard conditions leading to **21** (94%), removal of the silyl protective group with tetrabutylammonium fluoride gave **22** in 84% yield. Alkaline hydrolysis of the methyl ester, Jones oxidation of the C-11 hydroxyl function, and final deblocking of the tetrahydropyranyl protective groups completed the synthesis of PGD_1 (**23**) as crystals in 61% overall yield from **22**. These three operations were conducted successively without purification of the intermediates. The ester hydrolysis at the stage of 9,15-*O*-bis(tetrahydropyranyl)-$PGF_{1\alpha}$, rather than the final step, turned out to be more appropriate in view of the instability of PGD_1 causing dehydration.

D. Synthesis of 5,6-Didehydro-PGE_2 Derivatives. Introduction of the unsaturation at the C-5 and C-6 positions (PG numbering) using methyl 6-formyl-5-hexynoate, an acetylenic aldehyde, as the α side-chain unit leads to a promising, general way to PGs. The tandem conjugate addition/aldol reaction was conducted by using the enone **7**, an (*E*)-alkenylcopper reagent derived from **4**, and methyl 6-formyl-5-hexynoate in ether to give the aldol adduct **24** (a 1 : 1 mixture of the C-7 epimers[23]) in 50% yield. This yield has been improved up to 83% by conducting the conjugate addition in THF, followed by addition of one equivalent of boron trifluoride etherate prior to the treatment with the aldehyde. Although attempts to remove the C-7 hydroxyl function in **24** by the above described dehydration/reduction procedure failed, the Barton deoxygenation[26] of secondary alcohols proved useful for this purpose. Thus treatment of the aldol **24** with thiobenzoyl chloride and 4-(dimethylamino)-pyridine afforded the thiobenzoate **26** in 71% yield, which upon heating at 50 °C with tributyltin hydride with a catalytic amount of di-*t*-butyl peroxide gave a single deoxygenated compound **28**[27] in 98% yield. The successful removal of the thiobenzoate moiety relies heavily on the presence of the 5,6-triple bond which effects propargylic resonance stabilization to the radical intermediate.[28] The acetylenic compound **28** acts as a key intermediate for synthesis of various naturally occuring PGs including prostacyclin.[3a]

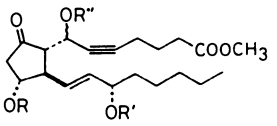

24, R = R′ = $Si(CH_3)_2$-*t*-C_4H_9; R″ = H
25, R = $Si(CH_3)_2$-*t*-C_4H_9; R′ = THP; R″ = H
26, R = R′ = $Si(CH_3)_2$-*t*-C_4H_9; R″ = C(=S)C_6H_5
27, R = $Si(CH_3)_2$-*t*-C_4H_9; R′ = THP; R″ = C(=S)C_6H_5

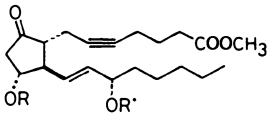

28, R = R′ = $Si(CH_3)_2$-*t*-C_4H_9
29, R = $Si(CH_3)_2$-*t*-C_4H_9; R′ = THP

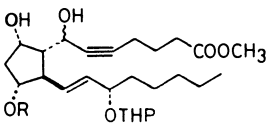

30, R = $Si(CH_3)_2$-*t*-C_4H_9

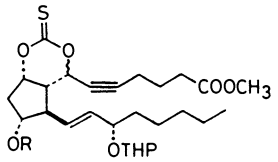

31, R = $Si(CH_3)_2$-*t*-C_4H_9

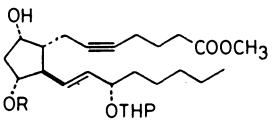

32, R = $Si(CH_3)_2$-*t*-C_4H_9

This method also allows the preparation of PGD intermediates. The aldol **25** (a mixture of the C-7 epimers) was available by the vicinal carba-condensation of the silylated hydroxycyclopentenone **7** with equimolar amounts of the tetrahydropyranylated ω side-chain unit **5** and methyl 6-formyl-5-hexynoate in 65% yield. Application of the Barton deoxygenation procedure[26] to this aldol product gave **29** in 66% yield via the corresponding thiobenzoate **27**. Removal of the C-7 hydroxyl function in **25** was also realized via the cyclic thiocarbonate intermediate.[31] Thus reduction of the more polar isomer of **25** with sodium borohydride gave the diol **30** stereoselectively in 77% yield (9α : 9β=97.5 : 2.5). Treatment of **30** with 1,1′-thiocarbonyldiimidazole and 4-(dimethylamino)pyridine afforded the cyclic thiocarbonate **31** in 92% yield. Then exposure of **31** to tributyltin hydride and di-*t*-butyl peroxide followed by alkaline treatment gave the C-7 deoxygenated compound **32** in 77% yield. The same compound was also derived in 35% overall yield from the less polar isomer of **30** via the corresponding thiocarbonate intermediate. It should be added that reduction of the less polar isomer of **30** with sodium borohydride gave a mixture of the 9α and 9β alcohols in 54 and 14% yield, respectively.

This expeditious tandem conjugate addition/aldol reaction sequence is synthetically flexible enough to apply to the synthesis of a variety of natural and unnatural PG derivatives. A range of artificial PGs can be prepared by using the 7-hydroxyl group as trigger functionality. The aldol product **24** is an important synthetic intermediate of stable PGI_2 analogues, (7*R*)- and (7*S*)-fluoro-PGI_2.[3a,32] It should be added that **12**, **13**, and the 11,15-*O*-bis-silylated analogue serve as synthetic precursors of Δ^7-PGA_1, an artificial strong antineoplastic prostaglandin.[33]

Experimental

General. (a) Spectrometers: IR spectra were obtained with a JASCO IRA-1 spectrometer. NMR spectra were determined on a JEOL PMX-60, FX-90Q, Varian HA-100, or NEVA NV-21 spectrometer. Chemical shifts are reported as δ vaules in parts per million relative to tetramethylsilane (δ=0). Splitting patterns are indicated as s, singlet; d, doublet; t, triplet; q, quartet; m, multiplet, and br means a broad

signal. Mass spectra (MS) were obtained with a JEOL D-10 mass spectrometer under an ionization potential of 75 eV. High-resolution mass spectra (HRMS) were recorded with a JEOL TMS-DX 300 spectrometer. Optical rotation was measured on a JASCO DIP-4 or DIP-181polarimeter. (b) Chromatography: R_f values on TLC were recorded on E. Merck precoated (0.25 mm) Silica Gel 60 F_{254} plates. The plates were sprayed with a solution of 2% *p*-anisaldehyde in 5% ethanolic sulfuric acid and then heated until the spots became clearly visible. Column chromatography was conducted under Florisil (Nakarai, M7P4145), silica gel (E. Merck, 7734, 70—230 mesh, or Fuji Devison, BW-80, 80—200 mesh), or deactivated silica gel (E. Merck) by mixing with water (6—9 wt%). Column chromatography at low temperature (0 °C) was conducted using a glass column equipped with a cold jacket. High-performance liquid chromatography (HPLC) was conducted on Waters 6000A instrument using a column packed with Develosil 100-5 (3.8 mmϕ×250 mm). (c) Solvents: Dry ether, THF, toluene, and benzene were prepared by distillation over Na-benzophenone ketyl under argon. Dry dichloromethane was prepared by distillation over P_4O_{10}. Dry hexamethylphosphoric triamide (HMPA), *N,N*-dimethylformamide (DMF), acetonitrile, *t*-C_4H_9OH, and dimethyl sulfoxide (DMSO) were prepared by distillation from CaH_2. The solution obtained after extraction was dried over anhydrous Na_2SO_4 or $MgSO_4$ and evaporated by a rotary evaporator under aspirator pressure. (d) Reagents and materials: Copper(I) iodide (CuI) (Nakarai) was continuously extracted with THF in a Soxhlet extractor overnight and dried in vacuo at room temperature for several hours. Tributylphosphine (Nakarai) was purified by distillation before use. *n*-C_4H_9Li (Mitsuwa or Nakarai), *t*-C_4H_9Li (Aldrich), and a THF solution of L-Selectride (Aldrich) were used directly from the bottles. Molarity of alkyllithiums were determined by titration[34] and stored at 4 °C. Zn powder was used after treatment with 2% HCl aqueous solution followed by drying in vacuo. Formaldehyde was generated from paraformaldehyde (excess) by flash heating with a heat gun and introduced into a enolate system with a stream of agron. Jones reagent was prepared by mixing CrO_3 (26.72 g) and concd sulfuric acid (23 mL) in water (50 mL). Methyl 6-formylhexanoate was prepared by ozonolysis of 1-methoxycycloheptene[35] or cycloheptene.[36] Ozonolysis of 1-methoxycycloheptene: Ozone was introduced into a mixture of 1-methoxycycloheptene (24 g, 0.19 mol) and methanol (150 mL) at −78 °C for 3 h. Remaining ozone dissolved in the solution was excluded by introducing argon into the mixture for 10 min at this temperature. To this was added dimethyl sulfide (20 mL) at −78 °C and then the mixture was slowly warmed up to room temperature over a period of 2 h. After stirring for 2 days at room temperature, the mixture was concentrated under reduced pressure and the residual oil was dissolved in a 1 : 1 mixture of ether and petroleum ether (100 mL) and the mixture was washed with water (50 mL) and dried. After evaporation of the solvent using a rotary evaporator, the residual oil was distilled under reduced pressure to give methyl 6-formylhexanoate (20.5 g, bp 82—86 °C/5 mmHg,† 68% yield) as colorless oil: ^{1}H NMR (CCl_4) δ=1.3—1.9 (m, 6H, 3 CH_2), 2.2—2.6 (m, 4H, 2 CH_2CO), 3.60 (s, 3H, OCH_3), 9.68 (br s, 1H, CHO). Methyl 6-formyl-5-hexynoate was prepared by the Swern oxidation[37] of the corresponding propargylic alcohol:[38] In a 100-mL two-necked round-bottomed flask were placed CH_2Cl_2 (20 mL) and DMSO (3.0 mL, 42 mmol) and the atmosphere was replaced with argon. After cooling to −78 °C, to this was added trifluoroacetic anhydride (4.5 mL, 32 mmol) over a period of 10 min and the mixture was stirred at this temperature for 20 min. To this mixture was added a solution of methyl 7-hydroxy-5-heptynoate (3.30 g, 21.1 mmol) in CH_2Cl_2 (5 mL) at −78 °C over a period of 15 min and the mixture was stirred for 30 min at this temperature, followed by the addition of triethylamine (9.1 mL, 65 mmol) over a period of 10 min. The mixture was stirred for 10 min at the same temperature and the cold bath was removed. After stirring for 1 h, the mixture was poured into satd $NaHCO_3$ aqueous solution (50 mL) and the resulting mixture was extracted three times with CH_2Cl_2 (30 mL each). The combined extracts were dried and evaporated. The residual material was subjected to column chromatography on silica gel (100 g) using a 5 : 1 mixture of hexane and ethyl acetate as eluant to give methyl 6-formyl-5-hexynoate (2.31 g, 71%) as colorless oil: IR (neat) 2280, 2200, 1740, 1670 cm^{-1}; ^{1}H NMR ($CDCl_3$) δ=1.7—2.7 (m, 6H, 3 CH_2), 3.70 (s, 3H, OCH_3), 9.20 (s, 1H, CHO). HRMS Found: *m/z* 153.0522. Calcd for $C_8H_{13}O_3$: M−H, 153.0552. (*S,E*)-3-Hydroxy-1-iodo-1-octene (**3**) was prepared by optical resolution of the racemate[14a] or asymmetric reduction[14c] of the corresponding enone followed by the purification through the crystalline salt of the corresponding hydrogen phthalate and (−)-α-methylbenzylamine.[14a] Silylated **4**, $[\alpha]_D^{23}$ −37.5° (*c* 0.97, CH_3OH) and tetrahydropyranylated **5**, $[\alpha]_D^{22}$ −65.9° (*c* 1.05, CH_3OH), were used in the reaction. These optically pure compounds were supplied from Teijin Co. Racemic 4-hydroxy-2-cyclopentenone was prepared by our previous procedure,[16a] acid-catalyzed rearrangement of furfuryl alcohol,[39] or oxidative dimethoxylation of 2-methylfuran[40] followed by phosphate-buffer treatment.[41] (*R*)-4-Hydroxy-2-cyclopentenone (**6**) was obtained by optical resolution using the lactol **9**.

Optical Resolution of 4-Hydroxy-2-cyclopentenone. In a 1-L one-necked round-bottomed flask equipped with a Dean-Stark water separator were placed (1*R*,2*S*)-cis-2-formyl-3,3-dimethylcyclopropane-1-carboxylic acid (**9**)[17] (a cyclic hemiacylal form) (71 g, 0.50 mol, mp 116 °C, $[\alpha]_D^{20}$−102° (*c* 0.5, C_2H_5OH), >97% ee), racemic 4-hydroxy-2-cyclopentenone (69 g, 0.70 mol), pyridinium *p*-toluenesulfonate (63 g, 0.25 mol), and dry benzene (500 mL). When the mixture was heated at reflux under stirring for ca. 5 h, the theoretical amount of water (9 mL) was collected in the separatory condenser. After removal of benzene on a rotary evaporator, the residual material was dissolved in ethyl acetate (500 mL) and washed twice with water, once with satd $NaHCO_3$ aqueous solution (200 mL),[42] and three times with water. The organic solution was dried and concentrated on a rotary evaporator to give a crude mixture of the condensation product **10** (110 g, 99% yield based on **9**).[43] Chromatography of this material on silica-gel column using a 1 : 1 mixture of hexane and ethyl acetate as eluant afforded the less polar material (41 g, 37% yield based on **9**) and more polar one (44 g, 40% yield based on **9**). The less polar material: mp 89.0—90.5 °C; $[\alpha]_D^{23}$−45° (*c* 0.36, CH_3OH); IR (KBr) 1775, 1760, 1725 cm^{-1}; ^{1}H NMR ($CDCl_3$) δ=1.16 (s, 3H, CH_3), 1.18 (s, 3H, CH_3), 2.04 (s, 2H, 2 CH), 2.27 (dd, 1H, *J*=18 and 2.5 Hz, a proton of CH_2), 2.72 (dd, 1H, *J*=18 and 5.5 Hz, a proton of CH_2), 4.9—5.0 (m, 1H, CHO), 5.27 (s, 1H, OCHO),

†1 mmHg≈133.322 Pa.

6.21 (dd, 1H, J=6 and 1.5 Hz, CH=CHCO), 7.58 (dd, 1H, J=6 and 2 Hz, CH=CHO). The more polar material: mp 97.5—98 °C; $[\alpha]_D^{22.6}$—222° (c 0.71, CH_3OH), IR (KBr) 1776 (shoulder), 1760, 1710 cm^{-1}; ^1H NMR ($CDCl_3$) δ=1.15 (s, 3H, CH_3), 1.17 (s, 3H, CH_3), 2.03 (s, 2H, 2 CH), 2.37 (dd, 1H, J=19 and 3 Hz, a proton of CH_2), 2.82 (dd, 1H, J=19 and 5.5 Hz, a proton of CH_2), 4.8—5.1 (m, 1H, CHO), 5.30 (s, 1H, OCHO), 6.25 (dd, 1H, J=6 and 1 Hz, CH=CHCO), 7.55 (dd, 1H, J=6 and 2.5 Hz, CH=CHCO).

A mixture of the less polar material (41 g, 0.18 mol) obtained above, dioxane (50 mL), and water (100 mL) was placed in a 500-mL one-necked round-bottomed flask and heated at 80 °C for 1 h under stirring. After cooling, the mixture was mixed with toluene (100 mL) and concentrated on a rotary evaporator. To the aqueous residue was added satd $NaHCO_3$ aqueous solution (100 mL) and then $NaHCO_3$ powder until the system became basic. The aqueous mixture was extracted five times with ethyl acetate (200 mL each). The combined extracts were dried and evaporated to afford (*R*)-4-hydroxy-2-cyclopentenone (**6**) (16 g, 88% yield, $[\alpha]_D^{22}$ +90.1° (c 0.43, CH_3OH), >97% ee) as a colorless oil. The optical purity was assayed by ^1H NMR analysis of the corresponding α-methoxy-α-(trifluoromethyl)phenylacetate.[44] Recovery of the resolving agent **9**: After acidification of the $NaHCO_3$ solution with 4 mol dm^{-3} HCl, the mixture was extracted with ethyl acetate (500 mL). The organic solution was washed twice with water, dried and evaporated, giving a crude hemiacylal resolving agent which was recrystallized from ether to afford pure hemiacylal **9** in 75% yield. Hydrolysis of the polar material (44 g, 0.20 mol) under similar conditions gave (*S*)-4-hydroxy-2-cyclopentenone (16 g, 82% yield). (4*R*)-4-(Tetrahydropyran-2-yloxy)-2-cyclopentenone (**8**), $[\alpha]_D^{22}$ +90.3° (c 1.02, CH_3OH), and (*R*)-4-(*t*-butyldimethylsiloxy)-2-cyclopentenone (**7**), $[\alpha]_D^{22}$ +67.4° (c 0.4, CH_3OH), were used for the synthesis of PGs. These optically pure materials were supplied from Teijin Co.

Standard Procedure for Vicinal Carba-Condensation via Organocopper Conjugate Addition/Aldol Condensation. Prior to introduction of solvents and materials, the reaction vessel was evacuated and dried by heating in vacuo with a heat gun and then, after cooling, the system was replaced with argon. Addition or transfer of the materials in the reaction was conducted under argon atmosphere. The typical procedure is illustrated in the synthesis of 3-butyl-2-(1-hydroxy-2-methylpropyl)cyclopentanone (Entry 3 in Table 1): In a 150-mL ampule was placed CuI (390 mg, 2.05 mmol) under argon atmosphere. To this was added successively dry ether (20 mL) and tributylphosphine (1.02 mL, 4.10 mmol) under stirring. The suspension was further stirred at room temperature until giving a clear solution (ca. 10 min). After cooling to −78 °C, to this was added a solution of butyllithium (1.64 mol dm^{-3}, 1.25 mL, 2.05 mmol) in hexane by using a glass syringe under stirring. After 5 min at −78 °C, a solution of 2-cyclopentenone (164 mg, 2.0 mmol) in dry ether (5 mL) was added over a period of 5 min at this temperature under stirring. After 10 min at −78 °C, a solution of 2-methylpropanal (148 mg, 2.05 mmol) in dry ether (5 mL) was added at −78 °C. After stirring for 10 min at this temperature, the mixture was quenched with satd aqueous NH_4Cl solution (50 mL) at −78 °C under vigorous shaking. The organic layer was separated and the aqueous layer was extracted with ether (10 mL). The combined ethereal extracts were dried and evaporated. The residue was subjected to column chromatography on silica gel (50 g), eluted with a 4 : 1 mixture of hexane and ethyl acetate, to give the aldol (396 mg, 93% yield) as a colorless oil: R_f 0.42 (5 : 1 benzene/ethyl acetate); IR (neat) 3450, 1735 cm^{-1}; ^1H NMR ($CDCl_3$) δ=0.8—1.1 (m, 6H, 2 CH_3), 1.2—2.0 (m, 13H, 6 CH_2 and CH), 2.2—2.4 (m, 3H, CH_2CO and CHCO), 2.68 (br, 1H, OH), 3.73 (dt, 1H, J=7.2 and 4.4 Hz, CHO). Found: C, 73.36; H, 11.49%. Calcd for $C_{13}H_{24}O_2$: C, 73.54; H, 11.39%.

Unless otherwise stated, the reaction indicated in Table 1 was conducted by a similar procedure.

3-Butyl-2-(hydroxymethyl)cyclopentanone (Entry 1). A 59 : 1 stereomixture. Liquid chromatography (LC): SiO_2, 2 : 1 petroleum ether/ethyl acetate as eluant. IR (neat) 3440, 3738 cm^{-1}; ^1H NMR (CCl_4) δ=0.8—2.5 (m, 15H, 5 CH_2, 2 CH, and CH_3), 2.78 (m, 1H, OH), 3.3—4.0 (m, 2H, CH_2O); ^{13}C NMR ($CDCl_3$) (major stereoisomer) δ=14.1, 22.9, 27.3, 29.5, 34.4, 38.4 (2C), 57.3, 59.7, 221.2. Found: C, 70.35; H, 10.69%. Calcd for $C_{10}H_{18}O_2$: C, 70.54; H, 10.66%.

3-Butyl-2-(1-hydroxybutyl)cyclopentanone (Entry 2). LC: SiO_2, 10 : 1 benzene/ethyl acetate as eluant. TLC R_f 0.42 (5 : 1 benzene/ethyl acetate); IR (neat) 3450, 1735 cm^{-1}; ^1H NMR ($CDCl_3$) δ=0.8—1.1 (m, 6H, 2 CH_3), 1.2—2.0 (m, 13H, 6 CH_2 and CH), 2.2—2.4 (m, 3H, CH_2CO and CHCO), 2.68 (br, 1H, OH), 3.73 (dt, 1H, J=7.2 and 4.4 Hz, CHO). Found: C, 73.36; H, 11.49%. Calcd for $C_{13}H_{24}O_2$: C, 73.54; H, 11.39%.

3-Butyl-2-(2,2-dimethyl-1-hydroxypropyl)cyclopentanone (Entry 4). LC: SiO_2, 6 : 1 hexane/ethyl acetate as eluant. TLC R_f 0.35 (4 : 1 hexane/ethyl acetate); IR (neat) 3450, 1729 cm^{-1}; ^1H NMR ($CDCl_3$) δ=0.8—1.1 (m, 12H, 4 CH_3), 1.1—2.4 (m, 13H, 5 CH_2, 2 CH, and OH), 3.31 (s, 1H, CHO). Found: C, 74.21; H, 11.66%. Calcd for $C_{14}H_{26}O_2$: C, 74.29; H, 11.58%.

3-Butyl-2-(hydroxyphenylmethyl)cyclopentanone (Entry 5). LC: SiO_2, 5 : 1 petroleum ether/ether as eluant. TLC R_f 0.41 (1 : 1 petroleum ether/ether); IR (neat) 3440, 1730, 694 cm^{-1}; ^1H NMR ($CDCl_3$) δ=0.7—2.5 (m, 15H, 5 CH_2, 2 CH, and CH_3), 3.39 (d, 0.36H, J=6.2 Hz, OH), 4.28 (d, 0.64H, J=1.5 Hz, OH), 4.75 (dd, 0.63H, J=7.8 and 1.5 Hz, CHO), 5.20 (dd, 0.37H, J=6.2 and 3.0 Hz, CHO), 7.32 (m, 5H, phenyl). HRMS Found: m/z 246.1594. Calcd for $C_{16}H_{22}O_2$: M, 246.1619.

3-Butyl-2-(1-hydroxy-3-phenyl-2-propenyl)cyclopentanone (Entry 6). LC: SiO_2, 4 : 1 hexane/ethyl acetate as eluant. TLC R_f 0.41 and 0.36 (2 : 1 hexane/ethyl acetate); IR (neat) 3480, 1723, 962 cm^{-1}; ^1H NMR ($CDCl_3$) δ=0.90 (m, 3H, CH_3) 1.1—1.9 (m, 8H, 4 CH_2), 1.9—2.6 (m, 4H, CH_2CO and 2 CH), 3.35 (d, 0.33H, J=8.0 Hz, OH), 3.45 (d, 0.67H, J=3.0 Hz, OH), 4.48 (m, 0.67H, CHO), 4.63 (m, 0.33H, CHO), 6.19 (dd, 0.33H, J=16.0 and 6.6 Hz, vinyl), 6.32 (dd, 0.67H, J=16.0 and 6.8 Hz, vinyl), 6.60 (d, 1H, J=16.0 Hz vinyl), 7.32 (m, 5H, phenyl). HRMS Found: m/z 272.1755. Calcd for $C_{18}H_{24}O_2$: M, 272.1776.

3-Butyl-2-(1-hydroxy-2-heptynyl)cyclopentanone (Entry 7). LC: SiO_2, 3 : 1 hexane/ether as eluant. TLC R_f 0.31 (1 : 1 hexane/ether); IR (neat) 3450, 2230, 1739 cm^{-1}; ^1H NMR ($CDCl_3$) δ=0.8—1.0 (m, 6H, 2 CH_3), 1.2—1.8 (m, 12H, 6 CH_2), 1.8—2.5 (m, 7H, 2 CH_2, 2 CH, and OH), 4.63 (m, 1H, CHO). Found: C, 76.75; H, 10.50%. Calcd for $C_{16}H_{26}O_2$: C, 76.75; H, 10.47%.

3-Butyl-2-(hydroxymethyl)cyclohexanone (Entry 8). LC: SiO_2, 2 : 1 petroleum ether/ether as eluant. TLC R_f 0.23 (1 : 1 petroleum ether/ether); IR (neat) 3400, 1700 cm^{-1}; ^1H NMR ($CDCl_3$) δ=0.93 (t, 3H, CH_3), 1.1—2.5 (m, 14H, 6 CH_2 and 2 CH), 2.6 (br, 1H, OH), 3.5—4.1 (m, 2H, CH_2O); ^{13}C NMR

($CDCl_3$) δ=14.0, 22.9, 25.7, 28.2, 30.3, 33.2, 40.1, 41.9, 56.9, 59.5, 214.8. Found: C, 71.63; H, 10.99%. Calcd for $C_{11}H_{20}O_2$: C, 71.70; H, 10.94%.

3-Butyl-2-(1-hydroxyethyl)cyclohexanone (Entry 9). LC: SiO_2, 10:1 benzene/ethyl acetate as eluant. TLC R_f 0.43 and 0.40 (2:1 benzene/ethyl acetate); IR (neat) 3430, 1709 cm^{-1}; ^1H NMR (CCl_4) δ=0.90 (t, 3H, CH_3), 1.1—2.5 (m, 17H, 6 CH_2, 2 CH, and CH_3), 2.78 (br, 1H, OH), 4.0 (br, 1H, CHO). Found: C, 72.77; H, 11.09%. Calcd for $C_{12}H_{22}O_2$: C, 72.68; H, 11.18%.

3-Butyl-2-(1-hydroxybutyl)cyclohexanone (Entry 10). LC: SiO_2, 3:1 petroleum ether/ether as eluant. TLC R_f 0.31 (1:1 petroleum ether/ether); IR (neat) 3400, 1698 cm^{-1}; ^1H NMR ($CDCl_3$) δ=0.93 (m, 6H, 2 CH_3), 1.1—3.0 (m, 19H, 8 CH_2, 2 CH, and OH), 3.8 (m, 1H, CHO). Found: C, 74.19; H, 11.63%. Calcd for $C_{14}H_{26}O_2$: C, 74.28; H, 11.58%.

3-Butyl-2-(1-hydroxy-2-methylpropyl)cyclohexanone (Entry 11). LC: SiO_2, 8:1 to 6:1 hexane/ethyl acetate as eluant. TLC R_f 0.31 (1:1 ether/petroleum ether); IR (neat) 3480, 1697 cm^{-1}; ^1H NMR (CCl_4) δ=0.8—1.0 (m, 9H, 3 CH_3), 1.1—2.2 (m, 12H, 5 CH_2 and 2 CH), 2.2—2.4 (m, 3H, CH_2CO and CHCO), 3.16 (dd, 1H, J=8.4 and 3.2 Hz, CHO). Found: C, 74.05; H, 11.72%. Calcd for $C_{14}H_{26}O_2$: C, 74.29; H, 11.58%.

3-Butyl-2-(hydroxyphenylmethyl)cyclohexanone (Entry 12). LC: SiO_2, 4:1 hexane/ethyl acetate as eluant. The less polar isomer: 18% yield; TLC R_f 0.48 (2:1 hexane/ethyl acetate); IR ($CHCl_3$) 3600, 3490, 1701 cm^{-1}; ^1H NMR ($CDCl_3$) δ=0.8—2.6 (m, 17H, CH_3, 6 CH_2, CH, and OH), 2.64 (dd, 1H, J=5.7 and 5.7 Hz, CHCO), 5.13 (d, 1H, J=5.5 Hz, CHO), 7.33 (m, 5H, phenyl). The more polar isomer: 71% yield; TLC R_f 0.32 (2:1 hexane/ethyl acetate); IR ($CHCl_3$) 3595, 3530, 1697 cm^{-1}; ^1H NMR ($CDCl_3$) δ=0.85 (t, 3H, CH_3), 1.0—2.1 (m, 11H, 5 CH_2 and CH), 2.3—2.5 (m, 2H, CH_2CO), 2.63 (dd, 1H, J=5.9 and 5.9 Hz, CHCO), 3.05 (br, 1H, OH), 4.96 (d, 1H, J=5.9 Hz, CHO), 7.35 (m, 5H, phenyl). Found: C, 78.38; H, 9.30%. Calcd for $C_{17}H_{24}O_2$: C, 78.42; H, 9.29%.

3-Butyl-2-(1-hydroxy-3-phenyl-2-propenyl)cyclohexanone (Entry 13). LC: SiO_2, 8:1 hexane/ethyl acetate as eluant. TLC R_f 0.16 and 0.10 (4:1 hexane/ethyl acetate); IR (neat) 3400, 1704, 964, 740, 685 cm^{-1}; ^1H NMR ($CDCl_3$) δ=0.91 (m, 3H, CH_3), 1.2—2.2 (m, 11H, 5 CH_2 and CH), 2.2—2.7 (m, 3H, CH_2CO and CHCO), 3.01 (br, 0.7H, OH), 3.56 (br, 0.3H, OH), 4.50 (br, 1H, CHO), 6.37 (dd, 1H, J=15.8 and 6.2 Hz, vinyl), 6.59 (dd, 1H, J=15.8 and 2.0 Hz, vinyl), 7.1—7.6 (m, 5H, phenyl). Found: M, 286.1938; M−H_2O, 268.1844. Calcd for $C_{19}H_{26}O_2$: M, 286.1933; M−H_2O, 268.1844.

***(E)*-2-Benzylidene-3-butylcyclopentanone (1).** To a solution of 3-butyl-2-(hydroxyphenylmethyl)cyclopentanone (49.2 mg, 0.20 mmol) in CH_2Cl_2 (2 mL) was added 4-(dimethylamino)pyridine (73 mg, 0.60 mmol) and the mixture was cooled to 0 °C. To this was added methanesulfonyl chloride (23 μL, 0.30 mmol) at 0 °C and the mixture was stirred for 2 h at 25 °C. Additional 4-(dimethylamino)-pyridine (146 mg, 1.20 mmol) and methanesulfonyl chloride (46 μL, 0.60 mmol) were added to the mixture and the mixture was further stirred for 10 h. The resulting mixture was poured into satd $NaHCO_3$ aqueous solution and extracted twice with CH_2Cl_2 (15 mL each). The combined extracts were washed successively with dil HCl and satd brine and dried. After evaporation of the solvent, the residual material was subjected to column chromatography on silica gel (5 g) using a 4:1 mixture of hexane and ether as eluant to give the enone **1** (33 mg, 77% yield): TLC R_f 0.55 (1:1 hexane/ether); IR (neat) 1717, 1618, 751, 687 cm^{-1}; ^1H NMR ($CDCl_3$) δ=0.91 (t, 3H, CH_3), 1.1—1.7 (m, 6H, 3 CH_2), 1.8—2.1 (m, 2H, CH_2), 2.1—2.5 (m, 2H, CH_2CO), 3.17 (br, 1H, CH), 7.2—7.6 (m, 6H, vinyl and phenyl); MS m/z: 228 (M^+). Found: C, 84.18; H, 9.11%. Cacld for $C_{16}H_{20}O$: C, 84.16; H, 8.83%. The compound **1** prepared here was identical in all respects with the product derived from the regio-controlled authentic synthesis[14] starting from 2-cyclopentenone as follows: To a solution of phenyl trimethylsilyl selenide (1.70 g, 7.42 mmol) in CH_2Cl_2 (15 mL) was added successively a solution of trimethylsilyl trifluoromethanesulfonate (0.097 mol dm^{-3}, 1.55 mL, 0.15 mmol) in CH_2Cl_2 and a solution of 2-cyclopentenone (609 mg, 7.42 mmol) in CH_2Cl_2 (5 mL) at −78 °C with stirring under argon atmosphere. After stirring at this temperature for 1 h, to this was added a solution of benzaldehyde dimethyl acetal (1.16 g, 7.62 mmol) in CH_2Cl_2 (5 mL) at −78 °C. The mixture was stirred −78 °C for 1 h and then −27 °C for 17 h. After successive addition of pyridine (0.5 mL) and 30% H_2O_2 (4.5 mL, 40 mmol), the mixture was stirred at −20 to 0 °C for 20 min and then quenched with water. The organic extract was evaporated and the residual material was subjected to column chromatography on silica gel (50 g) using a 10:1 mixture of benzene and ethyl acetate as eluant to afford 2-methoxyphenylmethyl-2-cyclopentenone (301 mg, 20% yield). IR (neat) 1703 cm^{-1}; ^1H NMR ($CDCl_3$) δ=2.3—2.5 (m, 2H, CH_2), 2.5—2.7 (m, 2H, CH_2) 3.33 (s, 3H, OCH_3), 5.02 (dd, 1H, J=2 Hz, CHO), 7.33 (br, 5H, phenyl), 7.51 (dt, 1H, J=3.0 and 1.5 Hz, vinyl). MS m/z: 202 (M^+). The butylcopper phosphine complex was prepared by the standard procedure[12b] using CuI (200 mg, 1.05 mmol), tributylphosphine (0.52 mL, 2.10 mmol), butyllithium (1.55 mol dm^{-3}, 0.68 mL, 1.05 mmol), and dry ether (15 ml) under argon atmosphere. To this solution was added a solution of 2-methoxyphenylmethyl-2-cyclopentenone (202 mg, 1.00 mmol) in ether (3.5 mL) at −78 °C over a period of 5 min. After stirring at −78 °C for 10 min and −40 °C for 10 min, the mixture was quenched with satd NH_4Cl aqueous solution (15 mL) with vigorous shaking. The organic layer was separated and the aqueous layer was extracted twice with ether (10 mL each). The combined ethereal extracts were dried and evaporated. Column chromatography on silica gel (20 g) using a 6:1 mixture of hexane and ether as eluant gave a mixture of **1** and 3-butyl-2-(methoxyphenylmethyl)-cyclopentanone (90.4 mg). This mixture was further treated with 1.8-diazabicyclo[5.4.0]undec-7-ene (DBU) (0.29 mL, 1.91 mmol) in benzene (4.5 mL) under reflux for 44 h. After being diluted with benzene (20 mL), the mixture was washed with dil HCl (36 mL×2) and then satd brine (36 mL). The solution was dried over magnesium sulfate and evaporated. Column chromatography on silica gel (18 g) using a 8:1 mixture of petroleum ether and ether gave a pure **1** (63.5 mg) as colorless oil.

***(E)*-2-Benzylidene-3-butylcyclohexanone (2).** To a solution of the more polar stereoisomer (R_f 0.32) of 3-butyl-2-(hydroxyphenylmethyl)cyclohexanone (313 mg, 1.20 mmol) and triethylamine (1.67 mL, 12 mmol) in CH_2Cl_2 (10 mL) was added methanesulfonyl chloride (0.46 mL, 6.0 mmol) at 0 °C. After being stirred at 0 °C for 30 min and 25 °C for 3 h, the mixture was diluted with ether (10 mL) and then washed twice with 1 mol dm^{-3} HCl (10 mL each). The ethereal layer was dried and evaporated. The residual material was dissolved in benzene (20 mL) and the mixture was heated with DBU (0.36 mL, 2.40 mmol) under reflux for 2 h. The mix-

ture was dissolved in benzene (20 mL) and washed with 1 mol dm^{-3} HCl (15 mL). The organic layer was dried over magnesium sulfate and evaporated. Column chromatography on silica gel (15 g) using a 4:1 mixture of hexane and ethyl acetate as eluant afforded **2** (187 mg, 64% yield) as colorless oil: TLC R_f 0.61 (2:1 hexane/ethyl acetate); IR (neat) 1689, 1599, 757, 691 cm^{-1}; ^1H NMR (CCl_4) δ=0.85 (m, 3H, CH_3), 1.0—2.0 (m, 10H, 5 CH_2), 2.1—2.6 (m, 2H, CH_2CO), 3.23 (br, 1H, CH), 7.08 (s, 1H, vinyl), 7.29 (m, 5H, phenyl); MS *m/z*: 242 (M^+). Found: C, 84.45; H, 9.22%. Calcd for $C_{17}H_{22}O$: C, 84.25; H, 9.15%. The compound prepared here was identical in all respects with the product derived from 2-cyclohexenone by the regio-controlled synthesis.[14]

7-Hydroxy-11,15-bis-*O*-(tetrahydropyran-2-yl)PGE$_1$ Methyl Ester (12). In a 20-mL test tube equipped with a septum rubber was placed (*E*,3*S*)-3-(tetrahydropyran-2-yloxy)-1-iodo-1-octene (**5**), (744 mg, 2.20 mmol) and the atmosphere was replaced with argon. Dry ether (10 mL) was added and the mixture was cooled to −95 °C. A solution of *t*-butyllithium (3.19 mL, 4.40 mmol) in pentane was added to this mixture at this temperature and then the resulting mixture was stirred at −78 °C for 3 h, giving the white suspension containing (*E*,3*S*)-3-(tetrahydropyran-2-yloxy)-1-octenyllithium. In a separated 150-mL ampule equipped with a septum rubber was placed CuI (419 mg, 2.20 mmol) and the system was evacuated under heating in vacuo. After cooling, the system was replaced with argon. To this was added dry ether (40 mL) and tributylphosphine (1.43 mL, 5.72 mmol) and the mixture was stirred until the suspension became a clear solution. The solution was cooled to −78 °C and to this was added the ethereal suspension containing (*E*,3*S*)-3-(tetrahydropyran-2-yloxy)-1-octenyllithium prepared above at −78 °C through a stainless steel cannula under argon atmosphere. The test tube was rinsed with an additional dry ether (10 mL) and this ethereal solution was added to the reaction mixture. After stirring the mixture for 10 min at this temperature, a solution of 4-(tetrahydropyran-2-yloxy)-2-cyclopentenone (**8**) (364 mg, 2.00 mmol) in dry ether (20 mL) was slowly added along the cooled (−78 °C) wall of the reaction vessel over a period of 35 min under stirring. After stirring the mixture for 15 min, a solution of methyl 6-formylhexanoate (348 mg, 2.20 mmol) in dry ether (5 mL) was added at −78 °C under stirring. The mixture was stirred at this temperature for 15 min and quenched with satd NH_4Cl aqueous solution (40 mL) and shaken vigorously. The organic layer was separated and the aqueous layer was extracted twice with ether (25 mL each). The combined organic extracts were dried and evaporated. The residual material was subjected to column chromatography on deactivated silica gel (30 g) using a 3:1 to 1:1 mixture of hexane and ethyl acetate as eluant to give the aldol product **12** (919 mg, 83% yield, a mixture of two stereoisomers) as a colorless oil: TLC R_f 0.17 (2:1 hexane/ethyl acetate); IR (neat) 3480, 1746, 974 cm^{-1}; ^1H NMR ($CDCl_3$) δ=0.89 (t, 3H, CH_3), 1.0—1.9 (m, 29H, 14 CH_2 and OH), 2.2—2.5 (m, 5H, 2 CH_2 and CH), 2.78 (dd, 1H, *J*=18.0 and 7.4 Hz, CH), 3.68 (s, 3H, OCH_3), 3.2—4.3 (m, 7H, 2 CH_2O and 3 CHO), 4.68 (br, 2H, 2 OCHO), 5.4—5.8 (m, 2H, vinyls); $[\alpha]_D^{22}$ −52.3° (*c* 1.02, CH_3OH). HRMS Found: *m/z* 384.2488. Calcd for $C_{21}H_{36}O_6$: M−$C_{10}H_{16}O_2$, 384.2512.

(7*E*)-7,8-Didehydro-11,15-bis-*O*-(tetrahydropyran-2-yl)-PGE$_1$ Methyl Ester (14). To a solution of the 7-hydroxy derivative **12** (480 mg, 0.87 mmol) in dry CH_2Cl_2 (5 mL) was added 4-(dimethylamino)pyridine (531 mg, 4.35 mmol) and the atmosphere was replaced with argon. To this was added methanesulfonyl chloride (0.17 mL, 2.17 mmol) at 18 °C and then stirred at 18 °C for 15 min and at 40 °C for 20 min. The mixture was diluted with CH_2Cl_2 (20 mL) and washed with satd $NaHCO_3$ aqueous solution (15 mL), 1 mol dm^{-3} HCl (15 mL), and satd brine (15 mL). After the mixture was dried and evaporated, the residual material was subjected to column chromatography on deactivated silica gel (10 g) using a 4:1 mixture of hexane and ethyl acetate as eluant to give the dehydrated product **14** (429 mg, 92% yield) as colorless oil: TLC R_f 0.40 (2:1 hexane/ethyl acetate); IR (neat) 1736, 1728, 1646, 974 cm^{-1}; ^1H NMR ($CDCl_3$) δ=0.88 (t, 3H, CH_3), 1.0—2.0 (m, 26H, 13 CH_2), 2.0—2.6 (m, 6H, 2 CH_2CO and CH_2C=), 3.68 (s, 3H, OCH_3), 3.3—4.3 (m, 7H, 2 CHO, 2 CH_2O, and CHC=), 4.5—4.8 (br, 2H, OCHO), 5.29 (d, 1H, *J*=14.0 and 7.9 Hz, vinyl), 5.63 (ddd, 1H, *J*=14.0, 6.3, and 3.2 Hz, vinyl), 6.75 (dt, 1H, *J*=9.7 and 1.9 Hz, vinyl); $[\alpha]_D^{22}$ +29.5° (*c* 1.01, CH_3OH). HRMS Found: *m/z* 330.2194. Calcd for $C_{21}H_{30}O_3$: M−$C_{10}H_{20}O_4$, 330.2195.

11,15-Bis-*O*-(tetrahydropyran-2-yl)PGE$_1$ Methyl Ester (16). Method A: The mixture of the enone **14** (12.0 mg, 0.022 mmol), (n-C_4H_9)$_3$SnH (0.5 mL), and di-*t*-butyl peroxide (4 mg, 0.027 mmol) was stirred at 110 °C for 25 min under argon. After cooling to room temperature, the mixture was directly chromatographed on a column of silica gel (3 g) by using a 12:2:1 mixture of hexane, benzene, and ethyl acetate as eluant to give **16** (10.8 mg, 90% yield) as colorless oil. Method B: To a solution of **14** (161 mg, 0.30 mmol) in a 95:5 mixture of 2-propanol and CH_3COOH (4 mL) was added zinc powder (1.46 g, 22.3 mmol) in several portions over a period of 2 h. The mixture was filtered through Celite 545 and the Celite was washed successively with ethyl acetate (10 mL) and ether (15 mL). The combined filtrates were washed with satd $NaHCO_3$ aqueous solution (15 mL) and then satd brine (15 mL), dried, and evaporated. Column chromatography on deactivated silica gel (6 g) using a 4:1 mixture of hexane and ethyl acetate as eluant gave **16** (126 mg, 78% yield) as a colorless oil: TLC R_f 0.41 (2:1 hexane/ethyl acetate); IR (neat) 1750, 974 cm^{-1}; ^1H NMR ($CDCl_3$) δ=0.89 (t, 3H, CH_3), 1.0—2.0 (m, 30H, 15 CH_2), 2.0—2.6 (m, 5H, 2 CH_2CO and CHCO), 2.76 (dd, 1H, *J*=18.0 and 7.2 Hz, CHC=), 3.68 (s, 3H, OCH_3), 3.3—4.4 (m, 6H, 2 CHO and 2 CH_2O), 4.70 (br, 2H, 2 OCHO), 5.4—5.8 (m, 2H, vinyls); $[\alpha]_D^{22}$ −85.4° (*c* 0.99, CH_3OH); HRMS Found: *m/z* 434.3029. Calcd for $C_{26}H_{42}O_5$: M−$C_5H_{10}O_2$, 434.3033.

PGE$_1$ Methyl Ester (18). The mixture of the tetrahydropyranylated derivative **16** (17.2 mg, 0.032 mmol) and a 3:1:1 mixture of acetic acid, water, and THF (2 mL) was stirred at 19 °C for 18 h. Then the mixture was placed in vacuo to evaporate the volatile materials. The resulting residual material was further co-evaporated three times with toluene under reduced pressure and then subjected to column chromatography on silica gel (1.7 g) using a 1:3 mixture of hexane and ethyl acetate as eluant to give PGE$_1$ methyl ester (**18**) (10.9 mg, 92% yield): TLC R_f 0.22 (1:3 hexane/ethyl acetate); IR (neat) 3390, 1748, 970 cm^{-1}; ^1H NMR ($CDCl_3$) δ=0.89 (t, 3H, CH_3), 1.1—1.8 (m, 18H, 9 CH_2), 1.8—2.6 (m, 7H, 2 CH_2CO, CHCO, and 2 OH), 2.73 (dd, 1H, *J*=18.0 and 7.6 Hz, CHC=), 3.68 (s, 3H, OCH_3), 3.9—4.3 (m, 2H, 2 CHO), 5.63 (m, 2H, vinyls); ^{13}C NMR ($CDCl_3$) δ=14.0 (C-20), 22.6, 24.8, 25.1, 26.6, 27.8, 28.8, 29.3, 31.7, 34.0, 37.4, 45.9 (C-10), 51.4 (OCH_3), 54.5 (C-12), 54.8 (C-8), 72.0 (C-11), 73.0 (C-15),

131.8 (C-13), 136.9 (C-14), 174.2 (C-1), 214.4 (C-9); $[\alpha]_D^{22}$ −53.8° (*c* 1.04, CH_3OH).

Reaction of commercial PGE_1 with diazomethane followed by HPLC (Develosil, hexane:ethyl acetate: CH_3OH= 1 : 9 :0.05 as eluant) afforded a sample indicating $[\alpha]_D^{23}$−54.0° (*c* 1.08, CH_3OH). The spectral data (IR, ^1H and ^{13}C NMR) and chromatographic behavior of **18** were identical with those of this authentic material.

11-*O*-(*t*-Butyldimethylsilyl)-7-hydroxy-15-*O*-(tetrahydropyran-2-yl)PGE_1 Methyl Ester (13). This compound was synthesized by the similar reaction procedure to the synthesis of **12**. (*E*,3*S*)-3-(tetrahydropyran-2-yloxy)-1-octenyllithium was prepared by adding a solution of *t*-butyllithium (3.21 mL, 4.40 mmol) in pentane to a solution of (*E*,3*S*)-3-(tetrahydropyran-2-yloxy)-1-iodo-1-octene (**5**) (744 mg, 2.20 mmol) in dry ether (10 mL) at −95 °C and then by stirring the mixture at −78 °C for 1.5 h. The organocopper complex was prepared by adding the organolithium compound prepared above to a solution of CuI (491 mg, 2.20 mmol) and tributylphosphine (1.43 mL, 5.72 mmol) in ether (50 mL) at −78 °C. The conjugate addition reaction was conducted by slow addition of a solution of (*R*)-4-(*t*-butyldimethylsiloxy)-2-cyclopentenone (**7**) (425 mg, 2.00 mmol) in dry ether (20 mL) to the organocopper complex prepared above at −78 °C over a period of 40 min. The aldehyde trapping of the enolate were conducted by addition of a solution of methyl 6-formylhexanoate (348 mg, 2.20 mmol) in dry ether (15 mL) at −78 °C. The reaction mixture was quenched with satd ammonium acetate aqueous solution (40 mL) with vigorous shaking at −78 °C. The organic layer was separated and aqueous layer was extracted twice with ether (20 mL each). The combined organic extracts were washed with a 20 : 5 : 1 mixture of water, benzene, and DMSO (52 mL) and then with satd brine (40 mL). After the solvent was dried and evaporated, the residual material was chromatographed at 0 °C on a two-layer column filled with Florisil (10 g, upper portion) and deactivated silica gel (100 g, lower portion) by using a 6 : 1 : 1 mixture of hexane, ethyl acetate, and benzene as eluant to give the aldol **13** (811 mg, 70%, four stereoisomers) as a pale yellow oil: TLC R_f 0.44 (2 : 1 hexane/ethyl acetate); IR ($CHCl_3$) 3600—3300, 1730 cm^{-1}; ^1H NMR ($CDCl_3$) δ=0.06 (s, 6H, 2 $SiCH_3$), 0.7—1.1 (m, 12H, $SiC(CH_3)_3$ and CH_3), 1.1—2.9 (m, 29H, 13 CH_2, 2 CH, and OH), 3.1—4.2 (m, 8H, OCH_3, 3 CHO, and CH_2O), 4.63 (m, 1H, OCHO), 5.4—5.7 (m, 2H, vinyls); $[\alpha]_D^{20}$ +14.3° (*c* 1.74, CH_3OH). HRMS Found: *m*/*z* 480.3283. Calcd for $C_{27}H_{48}O_5Si$: M−$C_5H_{10}O_2$, 480.3271.

(7*E*)-11-*O*-(*t*-Butyldimethylsilyl)-7,8-didehydro-15-*O*-(tetrahydropyran-2-yl)PGE_1 Methyl Ester (15). To a solution of **13** (348 mg, 0.60 mmol) in dry CH_2Cl_2 (20 mL) was added 4-(dimethylamino)pyridine (728 mg, 6.96 mmol) at 0 °C and the atmosphere was replaced with argon. To this was added methanesulfonyl chloride (0.23 mL, 2.97 mmol) at 0 °C and the mixture was stirred at 24 °C for 29 h. The reaction mixture was washed with satd $NaHCO_3$ aqueous solution (15 mL) and then satd brine (15 mL). After the organic layer was dried and evaporated, the residual oil was chromatographed on a column of deactivated silica gel (35 g) by using a 12:1 mixture of hexane and ethyl acetate as eluant to give **15** (255 mg, 75%) and its 7*Z*-isomer (9.2 mg, 2.7%). 7*E*-isomer **15**: TLC R_f 0.37 (4 : 1 hexane/ethyl acetate); IR (neat) 1742, 1642 cm^{-1}; ^1H NMR ($CDCl_3$) δ=0.05 (s, 6H, 2 $SiCH_3$), 0.7—1.0 (m, 12H, $SiC(CH_3)_3$ and CH_3), 1.0—2.7 (m, 26H, 13 CH_2), 3.3—4.3 (m, 8H, OCH_3, 2 CHO, CH_2O, and CH), 4.60 (m, 1H, OCHO), 5.0—5.8 (m, 2H, vinyls); 6.73 (dt, 1H, *J*=6.7 and 2.0 Hz, vinyl); $[\alpha]_D^{20}$ +16.0° (*c* 0.80, CH_3OH). HRMS Found: *m*/*z* 507.3141. Calcd for $C_{28}H_{47}O_6Si$: M−C_4H_9, 507.3142.

11-*O*-(*t*-Butyldimethylsilyl)-15-*O*-(tetrahydropyran-2-yl)-PGE_1 Methyl Ester (17). The mixture of the enone **15** (169.3 mg, 0.30 mmol), $(n\text{-}C_4H_9)_3SnH$ (1.0 mL, 3.72 mmol), and di-*t*-butyl peroxide (5 mg, 0.034 mmol) was heated at 110 °C for 15 min under argon. After cooling to room temperature, the reaction mixture was directly chromatographed on a column of deactivated silica gel (20 g) by using a 15 : 2 : 1 mixture of hexane, benzene, and ethyl acetate as eluant to give **17** (149 mg, 88%) as a colorless oil: TLC R_f 0.48 (4 : 1 hexane/ethyl acetate); IR ($CHCl_3$) 1740, 1735 cm^{-1}; ^1H NMR ($CDCl_3$) δ=0.05 (s, 6H, 2 $SiCH_3$), 0.7—1.0 (m, 12H, $Si(CH_3)_3$ and CH_3), 1.0—2.8 (m, 30H, 14 CH_2 and 2 CH), 3.3—4.2 (m, 7H, OCH_3, 2CHO, and CH_2O), 4.68 (m, 1H, OCHO), 5.4—5.6 (m, 2H, vinyls); $[\alpha]_D^{23}$ −66.2° (*c* 0.60, CH_3OH). MRMS Found: *m*/*z* 566.4015. Calcd for $C_{32}H_{58}O_6Si$: M, 566.4003.

11-*O*-(*t*-Butyldimethylsilyl)-15-*O*-(tetrahydropyran-2-yl)-$PGF_{1\alpha}$ Methyl Ester (20). In a 10-mL Schlenk tube was placed **17** (38.5 mg, 0.0679 mmol) and dissolved in dry THF (3 mL). After cooling to −78 °C, a solution of L-Selectride in THF (0.081 mL, 0.0815 mmol) was added at this temperature. After stirring at −78 °C for 20 min, 3% aqueous H_2O_2 solution (2mL) was added to the mixture at −78 °C with vigorous shaking and then diluted with ether (4 mL). The organic layer was separated and the aqueous layer was extracted with ether (4 mL). After the combined organic extracts were dried and evaporated, the residual oil was chromatographed on a column of silica gel (4 g) by using a 1 : 5 mixture of ethyl acetate and hexane as eluant to give **20** (35.4 mg, 92%) as a colorless oil: TLC R_f 0.25 (1 : 4 ethyl acetate/hexane); IR ($CHCl_3$) 3600—3320, 1725 cm^{-1}; ^1H NMR ($CDCl_3$) δ=0.04 (s, 6H, 2 $SiCH_3$), 0.7—1.1 (m, 12H, $SiC(CH_3)_3$ and CH_3), 1.1—2.7 (m, 31H, 14 CH_2, 2 CH, and OH), 3.3—4.3 (m, 8H, OCH_3, 3 CHO, and CH_2O), 4.67 (m, 1H, OCHO), 5.2—5.6 (m, 2H, vinyls); $[\alpha]_D^{20}$ −13.8° (*c* 0.62, CH_3OH). HRMS Found: *m*/*z* 511.3423. Calcd for $C_{28}H_{51}O_6Si$: M−C_4H_9, 511.3455.

11-*O*-(*t*-Butyldimethylsilyl)-9,15-bis-*O*-(tetrahydropyran-2-yl)$PGF_{1\alpha}$ Methyl Ester (21). In a 10-mL test tube was placed **20** (102.8 mg, 0.181 mmol) and the atmosphere was replaced with argon. Dry CH_2Cl_2 (1 mL) was added and the mixture was cooled to 0 °C. To this were added 3,4-dihydro-2*H*-pyran (33.4 mg, 0.398 mmol) and then pyridinium *p*-toluenesulfonate (13.5 mg, 0.0543 mmol) at 0 °C. After being stirred for 10 min at 0 °C and then 5 h at 30 °C, the mixture was diluted with CH_2Cl_2 (5 mL), followed by the addition of satd brine (10 mL). After shaking, the organic layer was separated and the aqueous layer was extracted twice with CH_2Cl_2 (10 mL each). After the combined organic extracts were dried and evaporated, the residual material was chromatographed on a column of silica gel (12 g) by using a 1 : 10 mixture of ethyl acetate and hexane as eluant to give **21** (110.8 mg, 94%) as a colorless oil: TLC R_f 0.54 (1 : 4 ethyl acatate/hexane); IR ($CHCl_3$) 1730 cm^{-1}; ^1H NMR ($CDCl_3$) δ=0.01 (s, 6H, 2 $SiCH_3$), 0.7—1.0 (m, 12H, $SiC(CH_3)_3$ and CH_3), 1.1—2.5 (m, 36H, 17 CH_2 and 2 CH), 3.3—4.2 (m, 10H, OCH_3, 3 CHO, and 2 CH_2O), 4.5—4.8 (m, 2H, 2 OCHO), 5.40 (m, 2H, vinyls); $[\alpha]_D^{25}$ +15.9° (*c* 0.37, CH_3OH). HRMS Found: *m*/*z* 550.4028. Calcd for $C_{32}H_{58}O_5Si$: M−$C_5H_{10}O_2$,

550.4054.

9,15-Bis-*O*-(tetrahydropyran-2-yl)PGF$_{1\alpha}$ Methyl Ester (22). In a 10-mL round-bottomed flask was placed **21** (103.5 mg, 0.158 mmol) and dissolved with THF (1 mL). To this was added a solution of tetrabutylammonium fluoride (1 mol dm^{-3}, 1.58 mL, 1.58 mmol) in THF at 23 °C and the mixture was stirred for 5 h at this temperature. THF (5 mL) and satd brine (5 mL) were added and the mixture was shaken vigorously. The organic layer was separated and the aqueous layer was extracted twice with ethyl acetate (5 mL each). After the combined extracts were dried and evaporated, the residual material was chromatographed on a column of silica gel (10 g) by using a 1 : 4 to 1 : 1 mixture of ethyl acetate and hexane as eluant to give **22** (71.7 mg, 84%) as a colorless oil: TLC R_f 0.17 (1 : 4 ethyl acetate/hexane); IR ($CHCl_3$) 3620—3280, 1730 cm^{-1}; ^{1}H NMR ($CDCl_3$) δ=0.88 (t, 3H, J=4.5 Hz, CH_3), 1.1—2.5 (m, 37H, 17 CH_2, 2 CH, and OH), 3.3—4.3 (m, 10H, OCH_3, 3 CHO, and 2 CH_2O), 4.5—4.8 (m, 2H, 2 OCHO), 5.45 (m, 2H, vinyls); $[\alpha]_D^{25}$ +0.65° (*c* 0.59, CH_3OH). HRMS Found: *m/z* 436.3165. Calcd for $C_{26}H_{44}O_5$: M−$C_5H_{10}O_2$, 436.3189.

PGD$_1$ (23). In a 10-mL test tube was placed **22** (15.6 mg, 0.0290 mmol) and dissolved in CH_3OH (1 mL). After cooling to 0 °C, 20% NaOH aqueous solution (1 mL) was added. The mixture was stirred for 3.7 h at 25 °C and acidified by 1 mol dm^{-3} aqueous oxalic acid solution (5 mL). The resulting mixture was extracted three times with ethyl acetate (10 mL each) and the organic extracts were washed with satd brine (10 mL), dried, and evaporated. The residual oil was placed in a 10-mL test tube and dissolved in acetone (0.8 mL). After cooling to −30 °C, Jones reagent (2.4 mol dm^{-3}, 18.1×10^{-3} mL, 0.0434 mmol) was added slowly to the mixture. The mixture was stirred for 40 min at this temperature and then ethyl acetate (10 mL) and satd $NaHCO_3$ aqueous solution (10 mL) were added. The mixture was neutralized by 1 mol dm^{-3} aqueous oxalic acid (10 mL) and the organic layer was separated. The aqueous layer was extracted twice with ethyl acetate (10 mL each). After the combined extracts were dried and evaporated, the residual oil was dissolved in a 3 : 1 : 1 mixture of acetic acid, water, and THF (2 mL) and the mixture was stirred at 25 °C for 23 h. The mixture was concentrated by exposing in vacuo and the residual material was dissolved in toluene. The toluene solution was evaporated under reduced pressure and this azeotropic operation was repeated three times. The residual oil was subjected to column chromatography on silica gel (1.5 g) using a 4 : 2 1 mixture of cyclohexane, ethyl acetate, and acetone and then pure acetone as eluant to give (+)-PGD$_1$ (**23**) (6.3 mg, 61%) as a white crystal: mp 64.5—65 °C; TLC R_f 0.14 (4 : 1 ethyl acetate/hexane); IR ($CHCl_3$) 3720—2300, 1740, 1715 cm^{-1}; ^{1}H NMR ($CDCl_3$) δ=0.88 (t, 3H, J=6.0 Hz, CH_3), 1.1—2.1 (m, 19H, 9 CH_2 and CH), 2.35 (t, 2H, J=6.4 Hz, CH_2C=O), 2.44 (d, 2H, J=2.6 Hz, CH_2C=O), 2.1—3.4 (br m, 4H, CHC=O, 2 OH, and CO_2H), 4.12 (br q, 1H, J=6.0 Hz, CHO), 4.51 (m, 1H, CHO), 5.53 (m, 2H, vinyls); $[\alpha]_D^{26}$ +9.8° (*c* 0.17, THF).

11,15-Bis-*O*-(*t*-butyldimethylsilyl)-5,6-didehydro-7-hydroxy-PGE$_2$ Methyl Ester (24). In a 150-mL ampule equipped with a spiral tube was placed (*E*,3*S*)-3-(*t*-butyldimethylsiloxy)-1-iodo-1-octene (**4**) (1.41 g, 3.83 mmol) and the atomsphere was replaced with argon. Dry ether (15 mL) was added and the mixture was cooled to −95 °C. To this was added a solution of *t*-butyllithium (4.41 mL, 7.80 mmol) in pentane at this temperature and the resulting mixture was further stirred at −78 °C for 3 h, giving the white suspension containing (*E*,3*S*)-3-(*t*-butyldimethylsiloxy)-1-octenyllithium. In a separaed 50-mL test tube equipped with a septum rubber was placed CuI (729 mg, 3.83 mmol) and the atmosphere was replaced with argon. To this was added dry ether (15 mL) and tributylphosphine (2.48 mL, 9.95 mmol) and the mixture was stirred until the suspension became a clear solution. After cooling to −78 °C, to this was added the suspension containing (*E*,3*S*)-3-(*t*-butyldimethylsiloxy)-1-octenyllithium prepared above through a stainless steel cannula under argon atmosphere. The test tube was rinsed with dry ether (15 mL) and the ethereal solution was added to the reaction mixture. After stirring the mixture at −78 °C for 5 min, a solution of 4-(*t*-butyldimethylsiloxy)-2-cyclopentenone (**7**) (796 mg, 3.75 mmol) in dry THF (30 mL) was slowly added at −78 °C along the cooled (−78 °C) wall of the reaction vessel over a period of 30 min under stirring. After stirring the mixture for 1 h, boron trifluoride etherate (0.461 mL, 3.75 mmol) was added at −78 °C and the mixture was stirred at −78 °C for 3 h. The mixture was cooled to −95 °C and then a solution of methyl 6-formyl-5-hexynoate (637 mg, 4.13 mmol) in dry ether (15 mL) was added at this temperature. The mixture was stirred at −78 °C for 1 h and quenched with satd NH_4Cl aqueous solution (30 mL) under vigorous shaking. The organic layer was separated and the aqueous layer was extracted twice with ether (20 mL each). The combined ethereal extracts were washed with a 1 : 5 : 20 mixture of DMSO, benzene, and water (52 mL) and then satd brine (20 mL). After the organic layer was dried and evaporated, the residual oil was chromatographed at 0 °C on a two-layered column filled with Florisil (10 g, upper layer) and deactivated silica gel (70 g, lower layer) by using a 1 : 10 : 2 mixture of ethyl acetate, hexane, and benzene and then a 1 : 5 mixture of ethyl acetate and hexane as eluants to give the aldol product **24** (1.90 g, 83%, a mixture of two stereoisomers) as a slightly yellow oil: The less polar material: TLC R_f 0.44 (3 : 1 hexane/ethyl acetate); IR (neat) 3630—3180, 1743 cm^{-1}; ^{1}H NMR ($CDCl_3$) δ=0.02, 0.03, 0.06 and 0.07 (s each, 12H, 4 $SiCH_3$), 0.89 (s, 18H, 2 $SiC(CH_3)_3$), 0.8—0.9 (hidden in this region, 3H, CH_3), 1.2—3.0 (m, 18H, 8 CH_2 and 2 CH), 3.68 (s, 3H, OCH_3), 3.86 (d, 1H, J=10 Hz, OH), 4.10 (m, 2H, 2 CHO), 4.46 (m, 1H, CHO), 5.59 (m, 2H, vinyls); ^{13}C NMR ($CDCl_3$) δ=−4.5 (3C), −4.1, 13.9, 18.1, 18.4 (2C), 22.6, 24.2 25.0, 25.9 (3C), 26.0 (3C), 32.0, 33.0, 38.7, 48.3, 50.9, 51.4, 59.1, 62.1, 73.0, 73.6, 80.2, 85.9, 128.2, 136.9, 173.2, 214.8; $[\alpha]_D^{19}$ −34.3° (*c* 0.91, CH_3OH). HRMS Found: *m/z* 608.3931. Calcd for $C_{33}H_{60}O_6Si_2$: M, 608.3929. The more polar material: TLC R_f 0.40 (3 : 1 hexane/ethyl acetate); IR (neat) 3620—3200, 1745 cm^{-1}; ^{1}H NMR ($CDCl_3$) δ=0.02, 0.04, 0.06 and 0.07 (s each, 12H, 4 $SiCH_3$), 0.87 and 0.88 (s each, 18H, 2 $SiC(CH_3)_3$), 0.8—0.9 (hidden in this region, 3H, CH_3), 1.2—3.0 (m, 19H, 8 CH_2, 2 CH, and OH), 3.68 (s, 3H, OCH_3), 4.10 (m, 2H, 2 CHO), 4.66 (m, 1H, CHO), 5.63 (m, 2H, vinyls); ^{13}C NMR ($CDCl_3$) δ=−4.5 (3C), −4.1, 14.0, 18.1, 18.4 (2C), 22.6, 24.1, 25.0, 25.9 (3C), 26.1 (3C), 32.0, 33.0, 38.7, 48.0, 51.4 (2C), 59.4, 62.9, 73.0, 73.6, 80.1, 85.9, 129.3, 136.7, 173.2, 213.7; $[\alpha]_D^{19}$ −15.1° (*c* 1.03, CH_3OH).

The two isomers of **24** were converted independently to the corresponding 7-benzoyloxy-PGE$_2$ derivative by the catalytic hydrogenation using Lindlar catalyst followed by benzoylation with benzoyl chloride in the presence of pyridine.[45] The benzoate derivative from the less polar isomer of **24**: CD

(cyclohexane) λ_{ext} 226 nm ($\Delta\varepsilon$+10.5°). The benzoate from the more polar isomer of **24**: CD (cyclohexane) λ_{ext} 226 nm ($\Delta\varepsilon$ −7.37°). These results indicate that the benzoyl derivative from the less polar isomer of **24** has 7*R* configuration and the other possesses 7*S* configuration. Turning back to the starting hydroxy derivatives, the less polar and the more polar isomers of **24** proved to have 7*S* and 7*R* configurations, respectively. This assignment was confirmed chemically by transformation to 7-hydroxy PGI_2 derivatives.[25]

11,15-Bis-*O*-(*t*-butyldimethylsilyl)-5,6-didehydro-7-thiobenzoyloxy-PGE$_2$ Methyl Ester (26). To a solution of the aldol **24** (126 mg, 0.21 mmol) in dry CH_2Cl_2 (2.5 mL) was added 4-(dimethylamino)pyridine (55 mg, 0.45 mmol) and then a solution of thiobenzoyl chloride (65 mg, 0.41 mmol) in CH_2Cl_2 (0.5 mL) at 21 °C under stirring. After stirring at this temperature for 70 min, the mixture was diluted with CH_2Cl_2 (20 mL) and washed successively with satd $NaHCO_3$ aqueous solution (20 mL), dil HCl (20 mL), and satd brine (20 mL) and then dried over magnesium sulfate. After evaporation of the solvent, the residual material was chromatographed on a column of silica gel (15 g) by using a 10:1 mixture of hexane and ethyl acetate as eluant to give the thiobenzoate **26** (108 mg, 71% yield, two stereoisomers at C-7) as yellow-brown oil: TLC R_f 0.29 (5:1 hexane/ethyl acetate); IR (neat) 2230, 1743, 1596, 1210 cm^{-1}; ^{1}H NMR ($CDCl_3$) δ= −0.09, −0.04, 0.07, and 0.08 (s, each, 12H, 4 $SiCH_3$), 0.8—1.0 (m, 21H, 7 CCH_3), 1.1—3.2 (m, 18H, 8 CH_2 and 2 CH), 3.65 and 3.66 (s each, 3H, OCH_3), 3.9—4.3 (m, 2H, 2 CHO), 5.4—5.9 (m, 2H, vinyls), 6.28 and 6.60 (br, 0.5H each, CHOC(=S)), 7.3—7.7 (m, 3H, aromatic), 8.1—8.4 (m, 2H, aromatic); $[\alpha]_D^{22}$+2.64° (*c* 1.21, CH_3OH). Found: C, 65.83; H, 8.78%. Calcd for $C_{40}H_{64}O_6SSi$: C, 65.88; H, 8.85%.

11,15-Bis-*O*-(*t*-butyldimethylsilyl)-5,6-didehydro-PGE$_2$ Methyl Ester (28). A mixture of the thiobenzoate **26** (93 mg, 0.13 mmol), (n-C_4H_9)$_3$SnH (0.7 mL, 2.65 mmol), and di-*t*-butyl peroxide (4 mg) was heated at 50 °C under argon atmosphere for 30 min. The mixture was directly subjected to column chromatography on a column of silica gel (5 g) using a 1:20:5 mixture of ethyl acetate, hexane, and benzene as eluant to give **28** (74.2 mg, 98% yield) as colorless oil: TLC R_f 0.50 (5:1 hexane/ethyl acetate); IR (neat) 1746, 1246, 827, 767 cm^{-1}; ^{1}H NMR ($CDCl_3$–CCl_4) δ=0.04 and 0.06 (s each, 12H, 4 $SiCH_3$), 0.89 (s, 18H, 2 $SiC(CH_3)_3$), 0.92 (t, 3H, J=6.5 Hz, CH_3), 1.1—1.5 (m, 8H, 4 CH_2), 1.7—2.9 (m, 12H, 2 CH_2CO, 2 CH_2C=, 2 CH, and CH_2), 3.65 (s, 3H, OCH_3), 4.05 (m, 2H, 2 CHO), 5.4—5.7 (m, 2H, vinyls); ^{13}C NMR ($CDCl_3$) δ=−4.7, −4.5 (2C), −4.2, 13.6, 14.0, 16.9, 18.0, 18.2, 22.6, 24.2, 25.0, 25.8 (3C), 25.9 (3C), 31.9, 32.7, 38.6, 47.7, 51.4, 51.9, 52.9, 72.7, 73.1, 77.3, 80.8, 128.2, 136.8, 173.4, 213.4; $[\alpha]_D^{21}$−13.9° (*c* 1.59, CH_3OH); HRMS Found: m/z 592.3956. Calcd for $C_{33}H_{60}O_5Si_2$: M, 592.3979. Spectral data (IR and ^{1}H NMR) of **28** were identical with those of the authentic sample gifted from Dr. C. H. Lin of Upjohn Co.

11-*O*-(*t*-Butyldimethylsilyl)-5,6-didehydro-7-hydroxy-15-*O*-(tetrahydropyran-2-yl)PGE$_2$ Methyl Ester (25). This compound was synthesized by similar reaction and work-up procedures to those of the synthesis of **13**. (*E*,3*S*)-3-(tetrahydropyran-2-yloxy)-1-octenyllithium was prepared by adding a *t*-butyllithium pentane solution (2.87 mL, 3.93 mmol) to a solution of (*E*,3*S*)-3-(tetrahydropyran-2-yloxy)-1-iodo-1-octene (**5**) (664 mg, 1.96 mmol) in ether (10 mL) at −95 °C and then stirring the mixture −78 °C for 1.5 h. The organocopper complex was prepared by adding the lithium compound prepared above to a solution of CuI (374 mg, 1.96 mmol) and tributylphosphine (1.27 mL, 5.10 mmol) in ether (40 mL) at −78 °C. The conjugate addition was conducted by slow addition of a solution of (*R*)-4-(*t*-butyldimethylsiloxy)-2-cyclopentenone (**7**) (379 mg, 1.78 mmol) in ether (20 mL) to the organocopper reagent prepared above and at −78 °C. The aldehyde trapping of the enolate was conducted by addition of a solution of methyl 6-formyl-5-hexynoate (303 mg, 1.96 mmol) in ether (15 mL) at −78 °C. After work-up, column chromatography was performed at 0 °C on a two-layer column filled with Florisil (10 g, upper layer) and deactivated silica gel (100 g, lower layer) by using a 6:1:1 mixture of hexane, ethyl acetate, and benzene and then a 3:1 mixture of hexane and ethyl acetate as eluants to give **25** (670.2 mg, 65%, two stereoisomers) as a pale yellow oil. The less polar material: TLC R_f 0.45 (1:2 ethyl acetate/hexane); IR ($CHCl_3$) 3720—3000, 1735 cm^{-1}; ^{1}H NMR ($CDCl_3$) δ=0.0—0.1 (m, 6H, 2 $SiCH_3$), 0.7—1.1 (m, 12H, $SiC(CH_3)_3$ and CH_3), 1.1—3.2 (m, 25H, 11 CH_2, 2 CH, and OH), 3.3—4.8 (m, 9H, OCH_3, CH_2O, 3 CHO, and OCHO), 5.51 (m, 2H, vinyls); $[\alpha]_D^{26}$ −80.2° (*c* 0.5, CH_3OH). HRMS Found: m/z 521.2950. Calcd for $C_{28}H_{45}O_7Si$: M−C_4H_9, 521.2935. The more polar material: TLC R_f 0.41 (1:2 ethyl acetate/hexane); IR ($CHCl_3$) 3700—3000, 1735 cm^{-1}; ^{1}H NMR ($CDCl_3$) δ=0.0—0.1 (m, 6H, 2 $SiCH_3$), 0.7—1.1 (m, 12H, $SiC(CH_3)_3$ and CH_3), 1.1—3.1 (m, 25H, 11 CH_2, 2 CH, and OH), 3.4—4.2 (m, 8H, OCH_3, CH_2O, and 3 CHO), 4.68 (m, 1H, OCHO), 5.57 (m, 2H, vinyls); $[\alpha]_D^{26}$ −26.2° (*c* 0.19, CH_3OH).

11-*O*-(*t*-Butyldimethylsilyl)-5,6-didehydro-15-*O*-(tetrahydropyran-2-yl)-7-thiobenzoyloxy-PGE$_2$ Methyl Ester (27). To a solution of **25** (100 mg, 0.173 mmol) in dry CH_3CN (10 mL) was added 4-(dimethylamino)pyridine (69.8 mg, 0.571 mmol) and then a solution of thiobenzoyl chloride (81.3 mg, 0.519 mmol) in CH_3CN (4 mL) at −40 °C under stirring. After stirring at −30 °C for 18 h, the mixture was diluted with CH_2Cl_2 (20 mL) and washed with satd $NaHCO_3$ aqueous solution (10 mzL), dil HCl (10 mL), and then satd brine (10 mL). After the mixture was dried and evaporated, the residual material was chromatographed on a column of silica gel (10 g) by using a 10:1 mixture of hexane and ethyl acetate as eluant to give **27** (93.2 mg, 77%) as brown oil: TLC R_f 0.62 and 0.57 (2:1 hexane/ethyl acetate); IR ($CHCl_3$) 1730, 1600 cm^{-1}; ^{1}H NMR ($CDCl_3$) δ=−0.1—0.2 (m, 6H, 2 $SiCH_3$), 0.7—1.1 (m, 12H, $SiC(CH_3)_3$ and CH_3), 1.1—3.2 (m, 24H, 11 CH_2 and 2 CH), 3.2—4.3 (m, 7H, OCH_3, 2 CHO, and CH_2O), 4.5—4.8 (m, 1H, OCHO), 5.1—5.8 (m, 2H, vinyls), 6.3—7.2 (m, 1H, CHOC(=S)), 7.2—8.3 (m, 5H, phenyl). HRMS Found: m/z 596.2962. Calcd for $C_{34}H_{48}O_5SSi$: M−$C_5H_{10}O_2$, 596.2992.

11-*O*-(*t*-Butyldimethylsilyl)-5,6-didehydro-15-*O*-(tetrahydropyran-2-yl)PGE$_2$ Methyl Ester (29). A mixture of thiobenzoate **27** (34.3 mg, 0.0491 mmol), (n-C_4H_9)$_3$SnH (0.5 mL, 1.86 mmol), and di-*t*-butyl peroxide (4 mg) was heated at 50 °C for 7.5 h under argon atmosphere. The reaction mixture was directly chromatographed on a column of silica gel (3 g) by using a 1:15:2 mixture of ethyl acetate, hexane, and benzene as eluant to give **29** (23.4 mg, 85%) as colorless oil: TLC R_f 0.31 (4:1 hexane/ethyl acetate); IR (neat) 1740 cm^{-1}; ^{1}H NMR ($CDCl_3$) δ=0.0—0.1 (two s, 6H, 2 $SiCH_3$), 0.7—1.0 (m, 12H, $SiC(CH_3)_3$ and CH_3), 1.0—3.0 (m, 26H, 2 CH_2CO, 10 CH_2, and 2 CH), 3.3—4.3 (m, 7H, OCH_3, 2 CHO, and CH_2O), 4.69 (m, 1H, OCHO), 5.4—5.7 (m, 2H, vinyls); $[\alpha]_D^{26}$−46.1° (*c* 0.38, CH_3OH). HRMS Found: m/z 505.2967.

Calcd for $C_{28}H_{45}O_6Si$: M−C_4H_9, 505.2986.

11-*O*-(*t*-Butyldimethylsilyl)-5,6-didehydro-7-hydroxy-15-*O*-(tetrahydropyran-2-yl)-PGF$_{2\alpha}$ Methyl Ester (30). To a solution of the more polar isomer of **25** (R_f 0.41, 1:2 ethyl acetate/hexane) (226.1 mg, 0.39 mmol) in CH_3OH (15 mL) was added $NaBH_4$ (147.8 mg, 3.9 mmol) at 0 °C under stirring. After 5 min at this temperature, the mixture was poured into satd NH_4Cl aqueous solution (15 mL) at 0 °C under stirring. After the evolution of H_2 gas ceased, the mixture was extracted three times with ethyl acetate (20 mL each). After the combined organic extracts were dried and evaporated, the residual material was chromatographed on a column of silica gel (20 g) by using a 1:3 mixture of ethyl acetate and hexane as eluant to give the diol **30** (174.2 mg, 77%) as colorless oil: TLC R_f 0.62 (1:1 hexane/ethyl acetate); IR ($CHCl_3$) 3720—3300, 1730 cm^{-1}; ^{1}H NMR ($CDCl_3$) δ=0.0—0.1 (m, 6H, 2 $SiCH_3$), 0.7—1.1 (m, 12H, $SiC(CH_3)_3$ and CH_3), 1.1—3.0 (m, 26H, CH_2CO, 10 CH_2, 2 CH, and 2 OH), 3.3—4.2 (m, 7H, OCH_3, 2 CHO, and CH_2O), 4.3—4.7 (m, 3H, 2 CHO and OCHO), 5.3—5.6 (m, 2H, vinyls); $[\alpha]_D^{26}$−38.4° (*c* 0.50, CH_3OH). HRMS Found: *m/z* 523.3063. Calcd for $C_{28}H_{47}O_7Si$: M−C_4H_9, 523.3091.

11-*O*-(*t*-Butyldimethylsilyl)-5,6-didehydro-7-hydroxy-7,9-*O*-thiocarbonyl-15-*O*-(tetrahydropyran-2-yl)PGF$_{2\alpha}$ Methyl Ester (31). To a solution of the diol **30** (57.6 mg, 0.0992 mmol) in dry CH_3CN (3 mL) were added 1,1′-thiocarbonyldiimidazole (26.5 mg, 0.149 mmol) and 4-(dimethylamino)-pyridine (36.4 mg, 0.298 mmol) at 0 °C under stirring. After stirring at 25 °C for 12 h, the mixture was diluted with CH_2Cl_2 (7 mL) followed by the addition of satd NH_4Cl aqueous solution (10 mL). The organic layer was separated and the aqueous layer was extracted twice with CH_2Cl_2 (10 mL each). The combined extracts were washed with satd brine (10 mL), dried, and evaporated. The residual material was chromatographed on a column of silica gel (5 g) by using a 1:5:1 mixture of ethyl acetate, hexane, and benzene as eluant to give the thiocarbonate **31** (56.7 mg, 92%) as yellow oil: TLC R_f 0.49 (2:1 hexane/ethyl acetate); IR ($CHCl_3$) 1730 cm^{-1}; ^{1}H NMR ($CDCl_3$) δ=0.04 (two s, 6H, 2 $SiCH_3$), 0.7—1.1 (m, 12H, $SiC(CH_3)_3$ and CH_3), 1.1—2.8 (m,, 24H, CH_2CO, 10 CH_2, and 2 CH), 3.3—4.2 (m, 7H, OCH_3, 2 CHO, and CH_2O), 4.63 (m, 1H, OCHO), 4.9—5.1 (m, 2H, 2 CHO), 5.4—5.6 (m, 2H, vinyls); $[\alpha]_D^{27}$−7.66° (*c* 0.32, CH_3OH). HRMS Found: *m/z* 565.2643. Calcd for $C_{29}H_{45}O_7SiS$: M−C_4H_9, 565.2656.

11-*O*-(*t*-Butyldimethylsilyl)-5,6-didehydro-15-*O*-(tetrahydropyran-2-yl)PGF$_{2\alpha}$ Methyl Ester (32). A mixture of the thiocarbonate **31** (41.5 mg, 0.0666 mmol), (n-C_4H_9)$_3$SnH (0.4 mL, 1.49 mmol), and di-*t*-butyl peroxide (4 mg) was heated at 50 °C for 1.5 h under argon atmosphere. To this mixture was added a 1 mol dm^{-3} solution of CH_3ONa in CH_3OH (1 mL) and dry THF (1 mL) and the mixture was stirred at 20 °C for 14.5 h. To this were added THF (10 mL) and then satd NH_4Cl aqueous solution (10 mL). The organic layer was separated and the aqueous layer was extracted twice with ethyl acetate (10 mL). After the combined organic extracts were dried and evaporated, the residual oil was chromatographed on a column of silica gel (2.5 g) by using a 1:6 mixture of ethyl acetate and hexane as eluant to give **32** (29.0 mg, 77%) as colorless oil: TLC R_f 0,53 (2:1 hexane/ethyl acetate); IR ($CHCl_3$) 3720—3300, 1730 cm^{-1}; ^{1}H NMR ($CDCl_3$) δ=0.03 (two s, 6H, 2 $SiCH_3$), 0.6—1.1 (m, 12H, $SiC(CH_3)$ and CH_3), 1.1—2.7 (m, 27H, CH_2CO, 11 CH_2, 2 CH, and OH), 3.3—4.4 (m, 8H, OCH_3, 3 CHO, and CH_2O), 4.66 (m, 1H, OCHO), 5.2—5.6 (m, 2H, vinyls); $[\alpha]_D^{26}$−28.8° (*c* 1.30, CH_3OH). HRMS Found: *m/z* 564.3828. Calcd for $C_{32}H_{56}O_6Si$: M, 564.3846.

A generous gift of chrysanthemic acid from Sumitomo Chemical Co. for the preparation of **9** is acknowledged. We deeply appreciate Ono Pharmaceutical Co. for the supply of precious samples of PGE_1, PGD_1 and for the identification of PGD_1 by 200-MHz ^{1}H NMR measurement. We also thank Dr. C. H. Lin of Upjohn Co. for sending us IR and ^{1}H NMR spectra of **28**. We also indebted to Teijin Co. for generous supply of the homochiral 4-hydroxy-2-cyclopentenone and side-chain units.

References

1) Prostaglandin Synthesis 17. Part 16: M. Suzuki, A. Yanagisawa, and R. Noyori, *J. Am. Chem. Soc.* in press.

2) Institute for Bio-Medical Research, Teijin Ltd., Tokyo.

3) a) R. Noyori and M. Suzuki, *Angew. Chem., Int. Ed. Engl.*, **23**, 847 (1984), and references cited therein; b) R. J. K. Taylor, *Synthesis*, **1985**, 364.

4) This term was suggested by Professor B. M. Trost (July, 1980). Since the entering groups are not limited to simple and functionalized alkyls, this term is more groups are not limited to simple and functionalized alkyls, this term is more appropriate than the conventionally used "vicinal alkylation".

5) Nucleophilic reactions of enolates generated from enones and lithium homocuprates: [alkyl halides] a) R. K. Boeckman, Jr., *J. Org. Chem.*, **38**, 4450 (1973); b) G. H. Posner, C. E. Whitten, and J. J. Sterling, *J. Am. Chem. Soc.*, **95**, 7788 (1973); c) R. M. Coates and L. O. Sandefur, *J. Org. Chem.*, **39**, 275 (1974); d) G. H. Posner, J. J. Sterling, C. E. Whitten, C. M. Lentz, and D. J. Brunelle, *J. Am. Chem. Soc.*, **97**, 107 (1975); e) G. H. Posner and C. M. Lentz, *Tetrahedron Lett.*, **1977**, 3215; f) G. H. Posner C. E. Whitten, J. J. Sterling, D. J. Brunelle, C. M. Lentz, A. W. Runquist, and A. Alexakis, *Ann. N. Y. Acad. Sci.*, **295**, 249 (1977); g) G. H. Posner and C. M. Lentz, *J. Am. Chem. Soc.*, **101**, 934 (1979); h) G. H. Posner, M. J. Chapdelaine, and C. M. Lentz, *J. Org. Chem.*, **44**, 3661 (1979); i) G. H. Posner, J. P. Mallamo, and K. Miura, *J. Am. Chem. Soc.*, **103**, 2886 (1981); j) G. H. Posner, J. P. Mallamo, M. Hulce, and L. L. Frye, *ibid.*, **104**, 4180 (1982); [aldehydes] k) G. Stork and M. Isobe, *J. Am. Chem. Soc.*, **97**, 6260 (1975); l) K. K. Heng and R. A. J. Smith, *Tetrahedron*, **35**, 425 (1979); m) K. K. Heng, J. Simpson, R. A. J. Smith, and W. T. Robinson, *J. Org. Chem.*, **46**, 2932 (1981); [acyl chlorides] n) T. Tanaka, S. Kurozumi, T. Toru, M. Kobayashi, S. Miura, and S. Ishimoto, *Tetrahedron Lett.*, **1975**, 1535; o) *idem*, *Tetrahedron*, **33**, 1105 (1977); [ketene bis(methylthio)acetal monoxide] p) R. Davis and K. G. Untch, *J. Org. Chem.*, **44**, 3755 (1979), and other nucleophilic reactions are also cited in this literature. Trapping with aldehydes of enolates generated from enone and Grignard reagents in the presence of catalytic amounts of copper salts; q) G. Stork and J. d'Angelo, *J. Am. Chem. Soc.*, **96**, 7114 (1974); r) F. Näf and R. Decorzant, *Helv. Chim. Acta*, **57**, 1317 (1974); s) F. Näf, R. Decorzant, and W.

Thommen, *ibid.*, **58**, 1808 (1975); for the excellent review, see t) J. d'Angelo, *Tetrahedron*, **32**, 2979 (1976); for some similar aldol reactions of enolates generated by the conjugate reaction of other organometallics and enones, see u) A. Hosomi, H. Hashimoto, H. Kobayashi, and H. Sakurai, *Chem. Lett.*, **1979**, 245; v) J. Schwartz, M. J. Loots, and H. Kosugi, *J. Am. Chem. Soc.* **102**, 1333 (1980).

6) J. W. Patterson, Jr., and J. H. Fried, *J. Org. Chem.*, **39**, 2506 (1974).

7) For such reason, they first trapped the enolate with the trimethylsilyl chloride and then alkylated the lithium enolate which was regenerated from the resulting enol silyl ether with lithium amide in liquid ammonia.

8) For a direct solution to this problem: M. Suzuki, A. Yanagisawa, and R. Noyori, *J. Am. Chem. Soc.*, **107**, 3348 (1985).

9) 7-Oxo-PGE_1 was synthesized via the one-pot combination of diorganocuprate conjugate addition of the enone and the acyl chloride trapping by a Teijin research group. See Ref. 5n and 5o.

10) a) G. Stork, *Pure Appl. Chem.*, **17**, 383 (1968); b) G. Stork, G. A. Kraus, and G. A. Garcia, *J. Org. Chem.*, **39**, 3459 (1974); c) G. Stork and G. A. Kraus, *J. Am. Chem. Soc.*, **98**, 6747 (1976).

11) Preliminary reports of this paper: a) M. Suzuki, T. Kawagishi, T. Suzuki, and R. Noyori, *Tetrahedron Lett.*, **23**, 4057 (1982); b) M. Suzuki, T. Kawagishi, and R. Noyori, *ibid.*, **23**, 5563 (1982); c) M. Suzuki, A. Yanagisawa, and R. Noyori, *ibid.*, **25**, 1383 (1984); See also Ref. 3a.

12) a) M. Suzuki, T. Suzuki, T. Lawagishi, and R. Noyori, *Tetrahedron Lett.*, **21**, 1247 (1980); b) M. Suzuki, T. Kawagishi, T. Suzuki. Y. Morita, and R. Noyori, *Isr. J. Chem.*, **24**, 118 (1984).

13) M. Suzuki, T. Kawagishi, and R. Noyori, *Tetrahedron Lett.*, **22**, 1809 (1981).

14) a) A. F. Kluge, K. G. Untch, and J. H. Fried, *J. Am. Chem. Soc.*, **94**, 7827 (1972); J. Fried, C. Lin, M. Mehra, W. Kao, and P. Dalven, *Ann. N.Y. Acad. Sci.*, **180**, 38 (1971); R. Pappo, P. Collins, and C. Jung, *ibid.*, **180**, 64 (1971); C. J. Sih, R. G. Salomon, P. Price, R. Sood, and G. Peruzzotti, *J. Am. Chem. Soc.*, **97**, 857 (1975); b) S. Okamoto, T. Shimazaki, Y. Kobayashi, and F. Sato, *Tetrahedron Lett.*, **28**, 2033 (1987); Y. Kitano, T. Matsumoto, S. Okamoto, T. Shimazaki, Y. Kobayashi, and F. Sato, *Chem. Lett.*, **1987**, 1523; c) R. Noyori, I. Tomino, and M. Nishizawa, *J. Am. Chem. Soc.*, **101**, 5843 (1979); R. Noyori, I. Tomino, M. Yamada, and M. Nishizawa, *ibid.*, **106**, 6717 (1984); See also M. M. Midland, D. C. McDowell, R. L. Hatch, and A. Tramontano, *ibid.*, **102**, 867 (1980); J. P. Vigneron and V. Bloy, *Tetrahedron Lett.*, **21**, 1735 (1980); T. Mukaiyama and K. Suzuki, *Chem. Lett.*, **1980**, 255; d) C. J. Sih, J. B. Heather, R. Sood, P. Price, G. Peruzzotti, L. F. H. Lee, and S. S. Lee, *J. Am. Chem. Soc.*, **97**, 865 (1975).

15) a) M. Gill and R. W. Rickards, *J. Chem. Soc., Chem. Commun.*, **1979**, 121; b) M. Gill and R. W. Rickards, *Tetrahedron Lett.*, **1979**, 1539; c) Y. Okamoto, R. Aburatani, M. Kawashima, K. Hatada, and N. Okamura, *Chem. Lett.*, **1986**, 1767; d) K. Ogura, M. Yamashita, and G. Tsuchihashi, *Tetrahedron Lett.*, **1976**, 759; e) M. Kitamura, K. Manabe, R. Noyori, and H. Takaya, *Tetrahedron Lett.*, **28**, 4719 (1987); f) I. Dohgane, H. Yamachika, and M. Minai, *Yuki Gousei Kagaku*, **41**, 896 (1983); see also T. Tanaka, S. Kurozumi, T. Toru, S. Miura, M. Kobayashi, and S. Ishimoto, *Tetrahedron*, **32**, 1713 (1976); Y.-F. Wang, C.-S. Chen, G. Girdaukas, and C. J. Sih, *J. Am. Chem. Soc.*, **106**, 3695 (1984); K. Laumen and M. Schneider, *Tetrahedron Lett.*, **25**, 5875 (1984); D. R. Deardoff, A. J. Matthews, D. S. McMeekin, and C. L. Craney, *ibid.*, **27**, 1255 (1986).

16) a) M. Suzuki, Y. Oda, and R. Noyori, *J. Am. Chem. Soc.*, **101**, 1623 (1979); b) *idem, Tetrahedron Lett.*, **22**, 4413 (1981), and references cited in Ref. 3a.

17) J. Martel, Japanese Patent 46-24694; Japan Kokai 54-130556, 54-130557; French Patent 159066.

18) Reviews: T. W. Greene, "Protective Groups in Organic Synthesis," John Wiley & Sons, New York (1981); J. F. W. McOmie, "Protective Groups in Organic Chemistry," Plenum Press (1973).

19) For the reasonable threo/erythro nomenclature, see R. Noyori, I. Nishida, and J. Sakata, *J. Am. Chem. Soc.*, **103**, 2106 (1981); **105**, 1598 (1983).

20) Now the aldol product is obtainable in 70—80% yield also by using one equivalent of the lithium (*E*)-alkenyl-1-pentynylcuprate (a mixed cuprate)[21] under certain optimized reaction conditions.

21) E. J. Corey and D. J. Beames, *J. Am. Chem. Soc.*, **94**, 7210 (1972).

22) A. Hazato, T. Tanaka, T. Toru, N. Okamura, K. Bannai, S. Sugiura, K. Manabe, and S. Kurozumi, *Nippon Kagaku Kaishi*, **1983**, 1390.

23) The stereochemistry of the C-7 hydroxyl group of these stereoisomers was determined by the exciton chirality method[24] after converting to the 7-benzoyloxy-PGE_2 derivatives.[25]

24) N. C. Gonnella, K. Nakanishi, V. S. Martin, and K. B. Sharpless, *J. Am. Chem. Soc.*, **104**, 3775 (1982).

25) S. Sugiura, T. Toru, T. Tanaka, N. Okamura, A. Hazato, K. Bannai, K. Manabe, and S. Kurozumi, *Chem. Pharm. Bull.*, **32**, 1248 (1984).

26) D. H. R. Barton and S. W. McCombie, *J. Chem. Soc., Perkin Trans. 1*, **1975**, 1574.

27) C. H. Lin, S. J. Stein, and J. E. Pike, *Prostaglandins*, **11**, 377 (1976).

28) It is well-known that simple β-oxoalkyl radicals undergo facile skeletal rearrangement via the tautomeric cyclopropyloxyl radicals.[29] Actually we have observed such skeletal rearrangement in the reaction of xanthate[30] of 3-butyl-2-(1-hydroxybutyl)cyclopentanone with tributyltin hydride (1.2 equiv) and azobisisobutyronitrile (0.2 equiv) at 70 °C for 2 h in toluene leading to 4-butyl-2-propylcyclohexanone (51% yield) and 3-butyl-2-butylcyclopentanone (17% yield).

29) B. Giese and H. Horler, *Tetrahedron Lett.*, **24**, 3221 (1983); B. Giese, *Angew. Chem., Int. Ed. Engl.*, **24**, 553 (1985); D. A. Lindsay, J. Lusztyk and K. U. Ingold, *J. Am. Chem. Soc.*, **106**, 7087 (1984); P. Dowd and S.-C. Choi, *ibid.*, **109**, 3493 (1987).

30) Review: W. Hartwig, *Tetrahedron*, **39**, 2609 (1983).

31) D. H. R. Barton and R. Subramanian, *J. Chem. Soc., Perkin Trans. 1*, **1977**, 1718.

32) (7*S*)-Fluoro-PGI_2: see Ref. 25 and T. Toru, S. Sugiura, and S. Kurozumi, Japan Kokai 59-10577 (1984); K. Bannai, T. Toru, T. Ōba, T. Tanaka, N. Okamura, K. Watanabe, A. Hazato, and S. Kurozumi, *Tetrahedron*, **39**, 3807 (1983); G. W. Holland and H. Maag, Ger. Offen DE3208880 (1982). (7*R*)-Fluoro-PGI_2: A. Yasuda, T. Arai, M. Kato, K. Uchida, and M. Yamabe, Kyoto Conference on Prostaglandins;

Kyoto, 1984; Abstracts, pp. 4—5. Japanese Patent Janan Kokai 59-227888.

33) a) S. Sugiura, T. Toru, T. Tanaka, A. Hazato, N. Okamura, K. Bannai, K. Manabe, S. Kurozumi, and R. Noyori, *Chem. Pharm. Bull.*, **32**, 4658 (1984); b) T. Kato, M. Fukushima, S. Kurozumi, and R. Noyori, *Cancer Research*, **46**, 3538 (1986).

34) W. G. Kofron and L. M. Baclawski, *J. Org. Chem.*, **41**, 1879 (1976); M. F. Lipton, C. M. Sorensen, A. C. Sadler, and R. H. Shapiro, *J. Organomet. Chem.*, **186**, 155 (1980).

35) R. A. Wohl, *Synthesis*, **1974**, 38.

36) S. L. Schreiber, R. E. Claus, and J. Reagan, *Tetrahedron Lett.*, **23**, 3867 (1982).

37) K. Omura, A. K. Sharma, and D. Swern, *J. Org. Chem.*, **41**, 957 (1976).

38) J. Martel, Japanese Patent 45-28153; Japan Kokai 46-5625.

39) M. Minai, Japanese Patent, 55-138502; Japan Kokai, 57-62236.

40) Review: N. Elming, "Adv. Org. Chem.," ed by R. A. Raphael, E. C. Taylor, and H. Wynberg, Interscience Publishers, Inc., New York (1960), Vol. 2, pp. 67—115.

41) T. Tanaka, Japanese Patent, 54-163510; Japan Kokai, 56-86128.

42) An unreacted hemiacylal was removed by this operation. This solution was combined with the sodium hydrogencarbonate solution obtained after hydrolysis of **10** for recovery of the resolving agent **9**.

43) For the stereochemistry, see J. J. Martel, J. P. Demonte, A. P. Tèche, and J. R. Tissier, *Pestic. Sci.*, **11**, 188 (1980).

44) J. A. Dale, D. L. Dull, and H. S. Mosher, *J. Org. Chem.*, **34**, 2543 (1969).

45) Contribution of Mr. S. Sugiura of Teijin Co. is greately appreciated.

 © 1988 The Chemical Society of Japan Bull. Chem. Soc. Jpn., 61, 1313—1317 (1988)

Enhancement of Sulfation of CaO by Fe_2O_3 in the Oxidative-Sorption Process for SO_2 Removal Using Fe_2O_3/CaO Binary Sorbents

Yukinori DAIRAKU, Satoshi SATO, Toshiaki SODESAWA, and Fumio NOZAKI*
Department of Industrial Chemistry, Faculty of Engineering, Chiba University, Yayoi-cho, Chiba 260
(Received May 8, 1987)

For the oxidative sorption of SO_2 using Fe_2O_3/CaO binary sorbents prepared by the usual impregnation method, reactivities and capacities for SO_2 removal have been investigated with TG measurements at temperatures near 500 °C in a stream of air containing SO_2 in concentration from 2 to 11%. Both the reactivities and the capacities of the sorbents were exceedingly enhanced by addition of Fe_2O_3 into CaO such small amounts as 0.1—0.8wt%, and further Fe_2O_3-loading over 1.0wt% resulted in a lowering in promoting effects. The changes in surface area and pore-size distribution with a variation of Fe_2O_3 content were also measured in order to discuss the correlation between chemical reactivity for SO_2 removal and physical property of the Fe_2O_3/CaO sorbents. In addition, Fe_2O_3-CaO mechanically mixed sorbents and the other binary sorbents such as Fe_2O_3/MgO or V_2O_5/CaO were tested to compare with the Fe_2O_3/CaO sorbents.

A large number of investigations has been made to develop process for waste gas desulfurization. Wet processes, such as alkali or limestone scrubbing, are being predominantly developed on a commercial scale. However, dry recovery processes are not always worthless since they would produce a usefull product and would avoid both flue gas reheating and the crystallization phenomena usually encountered in flue gas scrubbing.

In one of the dry recovery processes the waste gas is brought into contact with CaO or limestone, where upon SO_2 reacts with O_2 to produce $CuSO_4$ through the chemical reaction $SO_2+1/2O_2+CaO \rightarrow CaSO_4$.[1-3] However, in the cases of these investigations, such high temperatures as 700—1000 °C are required to facilitate the desulfurization reaction.

It has been reported that chemical activation of the limestone sorbent can be achieved by the addition of small amounts of Fe_2O_3 into the limestone.[4,5] These investigations were, however, made from the standpoint of practical technology for clean combustion of coal at the high temperature as 900 °C and the experimentals were not systematic.

In preliminary experiments, we have observed that Fe_2O_3/CaO sorbents exhibit high reactivities for SO_2 removal even at low temperatures near 500 °C. In this paper, details of the experimental results are reported together with a discussion of the relationship between chemical reactivity for SO_2 removal and physical property of the Fe_2O_3/CaO sorbents. In addition, we describe informations regarding Fe_2O_3-CaO mechanically mixed sorbents and the other binary sorbents such as Fe_2O_3/MgO or V_2O_5/CaO.

In this report, however, as a matter of convenience in experiments, sulfation tests of the sorbents were carried out by using the reactant gas containing SO_2 in

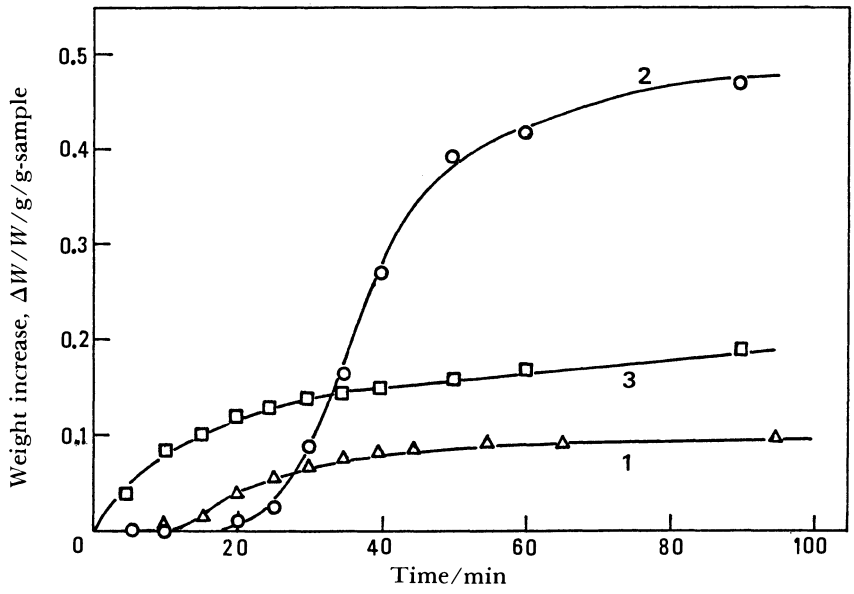

Fig. 1. Weight increase curves of various sorbents. 1: CaO, 2: Fe_2O_3 (0.11 wt%)/CaO, 3: Fe_2O_3 (0.95 wt%)/CaO. Reaction temperature: 500 °C, SO_2 concentration in the gas phase: 10.7%.

high concentration from 2 to 11%, instead of using such as a reactant gas with low concentration of SO_2 and with high concentration of CO_2 and H_2O as simulated combution gas.

Experimental

Materials. Commercial available powder of CaO reagent (Wako Pure Chemical Industries Ltd.,) was used as the sorbent after calcined at 500 °C for 2 h in a stream of air. The binary Fe_2O_3/CaO sorbent was prepared by the usual impregnation method: The prescribed mounts of $Fe(NO_3)_3$ aqueous solution were impregnated with the powders of CaO. The resulting mixture was air-dried at 120 °C, and calcined at 500 °C for 2 h in a stream of air. Several samples of Fe_2O_3/CaO sorbents differing the Fe_2O_3 content in the range of 0.1 to 3wt% were prepared by the same procedure. Mechanically mixed samples of Fe_2O_3-CaO were also prepared for the comparison with the Fe_2O_3/CaO samples prepared by the impregnation method. In the preparation of mechanically mixed Fe_2O_3-CaO sorbents, the measured amounts of Fe_2O_3, which was obtained by the calcination of $Fe(NO_3)_3$ at 500 °C, were throughly mixed with CaO powders by using agate mortar and pestle. The resulting mixtures were calcined again at 500 °C before use.

All the samples of sorbents used in this study were 12—20 mesh size. The other chemicals used were reagent grade and the gases were prepurified grade.

Apparatus and Experimental Procedure. The reactivity and capacity of various sorbents were measured in a TG reactor. The TG measurements were performed at 1 atm total pressure using a thermobalance equipped with quartz-spring which had a sensitivity of 50 μg. A small quartz boat with an area of about 1.3 cm^2 was used as the sample holder. About 200 mg of the sorbent sample was spread into a thin layer on the holder. The sample was heated to 500 °C in a stream of air and then allowed to stand for at least 30 min until there was no further weight loss. At the same temperature of 500 °C, the sufation reaction immediately followed in a flowing gas mixture of 10.7% SO_2 and the balance air, unless otherwise specified. Flow rates of the sulfating gas for the reaction were 170 ml (STP) min^{-1}, corresponding to a linear velocity of about 2 cm s^{-1}. The velocity was predetermined to be high enough to minimize gas-film diffusion resistance.

Results and Discussion

Time Course of Sulfation and Reaction Rates. Typical examples of weight increase with reaction time were illustrated in Fig. 1. Figure 1 indicates clearly that both the reactivity and the capacity of CaO reacting with SO_2 are appreciably increased by small amounts of Fe_2O_3 impregnated: CaO alone (curve 1) is usually very slow to react and its sulfation has an induction period of the order of 10 min. In contrast, CaO impregnated with about 1.0 wt% Fe_2O_3 (curve 3) is readily sulfated and there is no induction period. Fe_2O_3(0.11 wt%)/CaO sorbent (curve 2) exhibits a characteristic behavior that both the reactivity and the capacity for SO_2 removal are exceedingly enhanced by the impregnation of Fe_2O_3 such small amounts as 0.11 wt%, although the induction period has been elongated up to about 25 min.

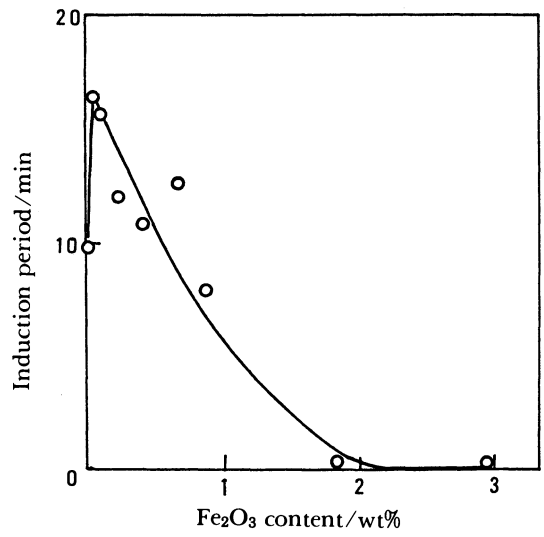

Fig. 2. Change in the induction period with Fe_2O_3 content.

As is shown in Fig. 2, the induction period in the sulfation reaction has been found to become progressively greater as the Fe_2O_3 content decreases, although the value shows some scatter. The reasons for occurrence of the induction period and for its mode of variation with the Fe_2O_3 content are still uncertain.

After the sulfation of sorbent was allowed to continue for about 100 min, X-ray diffractogram of the sorbent sample showed the pattern which was identified as those of the mixture consisting of CaO, $CaSO_4$, and Fe_2O_3. In addition, the X-ray diffractograms have proved that sulfated products such as $CaSO_3$ or $Fe_2(SO_4)_3$ are not present even in trace amounts. Thus we have tentatively speculated the reaction pathway of sulfation as the following consecutive steps:

$$SO_2\,(g) + 1/2\,O_2\,(g) \rightarrow SO_3\,(g) \quad (1)$$

$$SO_3\,(g) + CaO\,(s) \rightarrow CaSO_4\,(s) \quad (2)$$

where the oxidation step (1) of SO_2 proceeds catalytically over the surface of Fe_2O_3 and subsequent sulfation step (2) of CaO results in the formation of $CaSO_4$, accompanying weight increase in the sorbent sample.

In the weight increase-vs.-time relationship, the S-shaped curves have been observed in certain cases in which there are induction period between the start of sulfation process and the main acceleration of sulfation reaction. In these cases, the sulfation rates were varied complicatedly with the passage of time. Thus, the reactivities (the sulfation rates) were, for convenience, expressed in terms of the maximum slope of the TG measurement curves.

The sulfation rates (r) varied with SO_2 concentration of feed gas in such a way that the first-order kinetics can be roughly approximated on the basis of the data shown in Fig. 3.

Thus, it may be represented as

$$r = \left[\frac{d(\Delta W/W)}{dt}\right]_{max} = k'C_{SO_2} \quad (3)$$

where k'=apparent first-order rate constant (min^{-1} $\%^{-1}$), C_{SO_2}=SO_2 concentration in the gas phase (%).

Effects of Fe_2O_3 Content upon the Sulfation. The reactivities of sorbents were extremely affected by the variation of Fe_2O_3 content. The rate constants k' calculated from Eq. 3 are shown in Fig. 4 as a function of the Fe_2O_3 content.

As is shown in Fig. 1, the weight increase during the course of sulfation depicts a steep rise within 90 min and then levels off. Thus, it can be accepted that the conversion of CaO into $CaSO_4$ beyond reaction times of 90 min is nearly equal to the maximum conversion being expected as the sulfation process of sorbent has been saturated. Figure 5 shows the dependence of the maximum conversion of CaO with the Fe_2O_3 content.

Figures 4 and 5 show a complete similarity of shape which tends to vary from sharp peak to rounded hump. From these results, it has been found that the Fe_2O_3 content favorable to rapid sulfation and large capacity for SO_2 removal lies in the vicinity of 0.3 to 0.7 wt%. The exact mechanism for such complicated changes in the reactivity and capacity with the Fe_2O_3 content is still not understood, however, we have tentatively speculated as follows: In the case of sorbent with a low Fe_2O_3 content below 0.3 wt%, the oxidation step of SO_2 over the surface of Fe_2O_3, Eq. 1 is a rate-limiting step in the reaction sequence and thus the over-all rate of sulfation is increased with an increase in the Fe_2O_3 content. In contrast, in the samples of sorbents with a high Fe_2O_3 content above 0.7 wt%, a rate-determining step is probably allowed to move from the catalytic oxidation step of SO_2 to the diffusion step of SO_2 or SO_3 through micro-pores of Fe_2O_3/CaO binary sorbent. The diameter of the micro-pores and/or the porosity of Fe_2O_3/CaO sorbent samples seem to be reduced with an increase in the amount of Fe_2O_3 coating surface of CaO sorbent, and subsequently a fraction of the entrances to a micro-pore is blocked with an additional deposition of Fe_2O_3 when Fe_2O_3/CaO sorbent is prepared by the impregnation method. Thus, the global rates in the sulfation of Fe_2O_3/CaO sorbents with a high Fe_2O_3 content is allowed to be rapidly lowered with increasing of the Fe_2O_3 content.

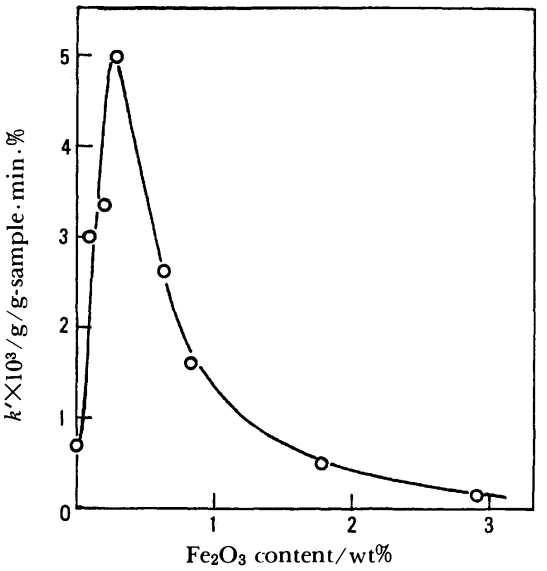

Fig. 4. Variation in rate constant k' at 500°C with Fe_2O_3 content.

The sulfation of CaO into $CaSO_4$ is well-known to be heterogeneous solid-gas reaction accompanying a change in volume of solid phase.[2] With the passage of

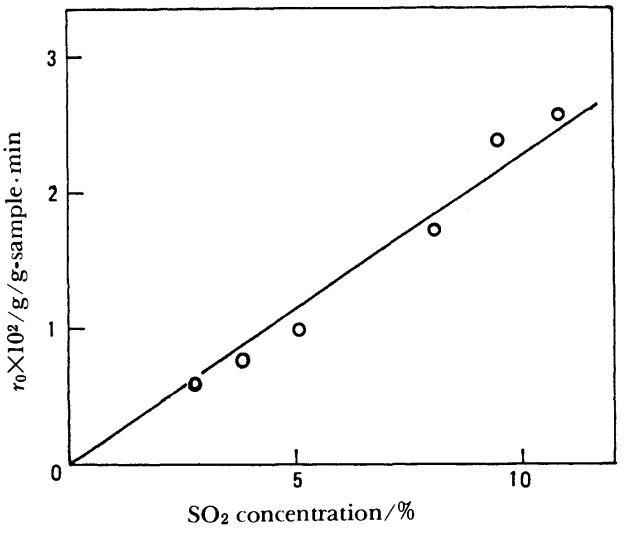

Fig. 3. Initial rates in the sulfation of Fe_2O_3 (0.11 wt%)/CaO as a function of SO_2 concentration in the gas phase. Reaction conditions are the same as for Fig. 1.

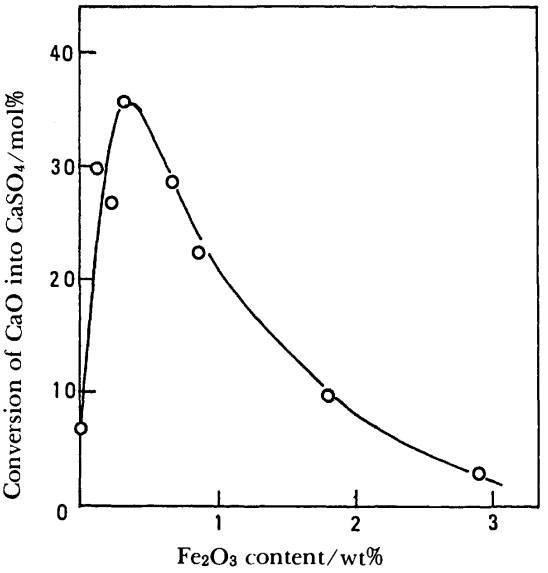

Fig. 5. Dependence of the maximum conversion of CaO with Fe_2O_3 content.

sulfation process the pore closing arises from the formation of product layer. The fraction conversion of CaO into $CaSO_4$ is ultimately limited, therefore, to the level of less than 40%, as is shown in Fig. 5.

Reactivities of Mechanically Mixed Fe_2O_3-CaO Sorbents. The sulfation experiments using mechanically mixed Fe_2O_3-CaO sorbents were separately conducted in order to compare with Fe_2O_3/CaO sorbents prepared by the impregnation method. The data of the rate constant and the conversion of CaO are shown in Fig. 6 as a function of Fe_2O_3 wt%. Figure 6 indicates that the data increase monotonically up to about 2 wt% of Fe_2O_3 content and then go up to a constant value. The shape of curves is simple and distinct clearly from such complicated curves shown in Figs. 4 and 5. However, the saturated values in both the rate constant and the conversion of CaO are close to the maximum values in Figs. 4 and 5, respectively. This fact suggests that the sulfation process proceeds consecutively through the catalytic oxidation step, Eq. (1), and the sulfation step, Eq. (2), as mentioned in the previous section. In addition, application of physically mixed Fe_2O_3-CaO sorbents is also anticipated to provide a simple and convenient method for SO_2 removal, although much larger quantities of Fe_2O_3 should be mixed with CaO in comparison with the case of sorbents prepared by the impregnation method.

Surface Area, Pore-Size Distribution and SEM-Photograph of the Sorbents Prepared by Impregnation Method. The change in surface areas of sorbents differing the Fe_2O_3 content was depicted in Fig. 7. The surface areas were determined by BET method using N_2 as the adsorbate. Figure 7 indicates that surface area of Fe_2O_3/CaO binary sorbent results in a steep rise in a very narrow interval of Fe_2O_3 content ranging from 0.1 to 0.2 wt% and then is allowed to decrease rapidly to about one-half its value in the Fe_2O_3 content of 1.0 wt% or more. The steep rise in surface area of

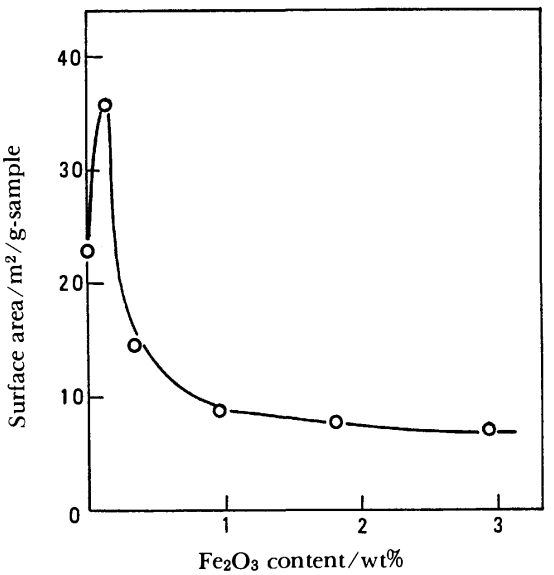

Fig. 7. Change in surface areas of Fe_2O_3/CaO samples with Fe_2O_3 content.

Fe_2O_3/CaO sorbents with a low content of Fe_2O_3 is probably due to overlapping of the surface areas of CaO itself and Fe_2O_3 finely deposited on the surface of CaO. On the other hand, the decrease in surface area in the sorbents with a high content of Fe_2O_3 over 1.0 wt% is possibly ascribed to pore closing in micro-pores of CaO by the further deposition of much larger quantities of Fe_2O_3.

The pore-size distribution measured with a mercury porosimeter is shown in Fig. 8. From the data shown in Fig. 8, it can be speculated that deposition of Fe_2O_3 trends to shrink or clog smaller pores in preference to large pores.

The scanning electron microscopic (SEM) measurements of various sorbents have clearly demonstrated that, as the amount of Fe_2O_3 impregnated is increased, fine particles constituting of solid phase of

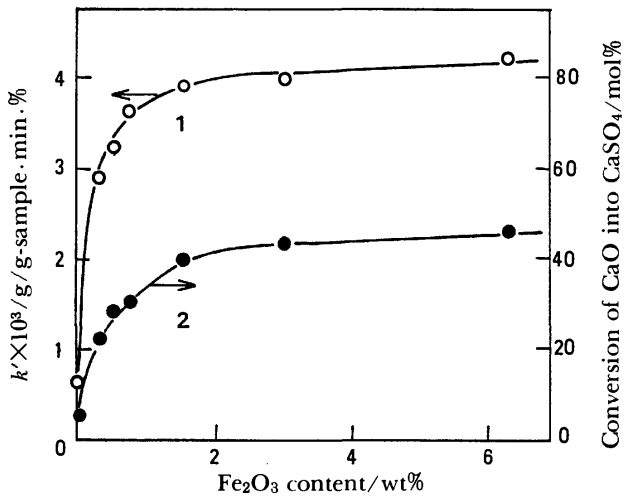

Fig. 6. Sulfation data relating to mechanically mixed Fe_2O_3-CaO samples. Reaction conditions are the same as for Fig. 1.

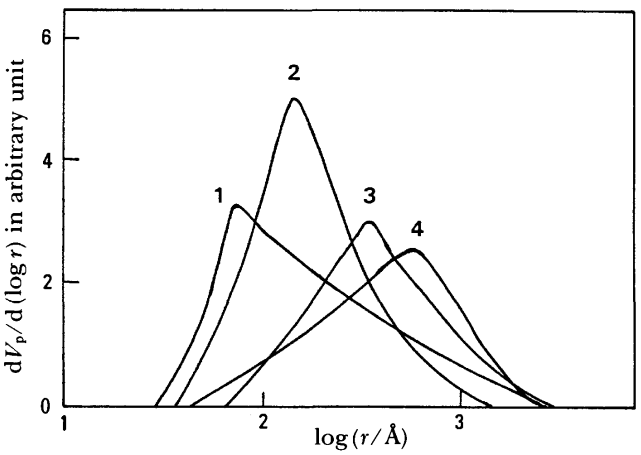

Fig. 8. Pore-size distribution in the samples. 1: CaO, 2: Fe_2O_3 (0.22 wt%)/CaO, 3: Fe_2O_3 (0.31 wt%)/CaO, 4: Fe_2O_3 (0.95 wt%)/CaO. r: pore radius in Å, V_p: pore volume.

sorbent become progressively greater in the range of about several microns to twenty microns. Similarly it has been revealed that the grain size of sorbent is allowed to appreciably enlarge by the product layer of sulfation reaction.

Other Promoters and Sorbents for Catalyzed Sulfation. In the previous sections, only the binary system consisting of Fe_2O_3 and CaO has been investigated as the sorbent. In this section, we will describe experimental results with respect to the other promoters and sorbents.

Various metal oxides such as V_2O_5, MnO_2, NiO, or CoO, other than Fe_2O_3, have been also loaded into CaO in the content of 0.3 wt% by the similar impregnation method as for Fe_2O_3/CaO sorbent. All of these oxides exhibited more or less the promotive action for catalyzed sulfation of CaO. The promoting action decreased in the order: $MnO_2 > V_2O_5 > Fe_2O_3 \gg NiO \cong CoO$. Two kinds of oxides, MnO_2 and V_2O_5, have catalytic properties somewhat superior to that of Fe_2O_3, however, application of these oxides must be avoided in the practical point of view and their high costs.

In analogy with CaO, alkaline earth oxides such as MgO or BaO are to be expected for a suitable sorbent. The sulfation tests using Fe_2O_3/MgO or Fe_2O_3/BaO have been made in order to compare their reactivities with that of Fe_2O_3/CaO.

The sorbent samples of Fe_2O_3/MgO or Fe_2O_3/BaO with a different Fe_2O_3 content were prepared by the similar impregnation method as that of Fe_2O_3/CaO. The commercial reagents of $Mg(OH)_2$ and $BaCO_3$ were used as the starting material in the preparation of the respective sorbent. These two powders of reagents were calcined at 500 °C for 2 h in a stream of air, and then were impregnated with the prescribed amount of $Fe(NO_3)_3$ aqueous solution. The resulting mixtures were hereinafter treated with the similar manner as that of the preparation of Fe_2O_3/CaO sorbent.

In the experiments used Fe_2O_3/MgO as the sorbent, the sulfation rates and the conversion of MgO into $MgSO_4$ were altered with the Fe_2O_3 content as shown in Fig. 9. Figure 9 indicates that both the rate constant k' and the conversion of MgO are lowered about one order of magnitude compared to the values of Fe_2O_3/CaO sorbent. In addition, it can be seen from Fig. 9 that capacities for SO_2 removal are increased monotonically with a low ratio by increasing Fe_2O_3 content. These facts seem to be due to poor chemical reactivity of MgO with SO_3 to the formation of $MgSO_4$. In the sulfation reaction using Fe_2O_3/MgO sorbents, the induction period was completely missing and this was also distinct from the cases of Fe_2O_3/CaO sorbents.

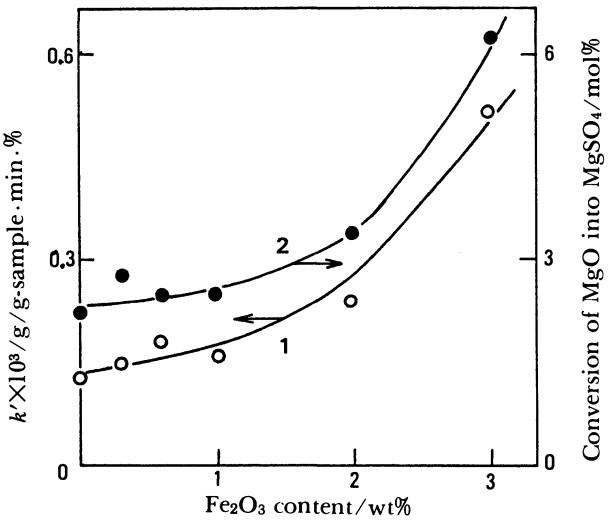

Fig. 9. Sulfation data relating to Fe_2O_3/MgO samples. Reaction conditions are the same as for Fig. 1.

The reactivities and the capacities for SO_2 removal of Fe_2O_3/BaO or Fe_2O_3/SrO sorbents were substantially comparable to that of Fe_2O_3/MgO. Consequently, the adoptability of sorbents for SO_2 removal can be summarized as $Fe_2O_3/CaO > Fe_2O_3/MgO \cong Fe_2O_3/SrO > Fe_2O_3/BaO$.

References

1) R. L. Pigford and G. Sliger, *Ind. Eng. Chem., Process Des. Dev.*, **12**, 85 (1973).

2) M. Hasatani, M. Yuzawa, and N. Arai, *Kagaku Kogaku Ronbunshu*, **8**, 45 (1982); **10**, 300 (1984).

3) L.-S. Fan, S. Satija, B. C. Kim, and H. Nack, *A. I. Ch. E. J.*, **30**, 21 (1984).

4) R. T. Yang, *Fuel*, **57**, 709 (1978).

5) N. J. Desal and R. T. Yang, *Ind. Eng. Chem., Process Des. Dev.*, **22**, 119 (1983).

The Oxidative Polymerization of 2-Methyl-6-(3,7-dimethyl-2,6-octadienyl)phenol

Sang-Heon HYUN, Hiroyuki NISHIDE, Eishun TSUCHIDA,* and Shigetoshi YAMADA†
Department of Polymer Chemistry, Waseda University, Tokyo 160
†Junior College of Technology, Shizuoka University, Hamamatsu 432
(Received September 10, 1987)

2-Methyl-6-(3,7-dimethyl-2,6-octadienyl)phenol (MGP) was prepared by the reaction of *o*-cresol and 1-chloro-3,7-dimethyl-2,6-octadiene in the presence of sodium. This MGP was then oxidatively polymerized with a copper-pyridine catalyst to yield poly[oxy[3-methyl-5-(3,7-dimethyl-2,6-octadienyl)-1,4-phenylene]]. The MGP and 2,6-dimethylphenol (DMP) copolymerized with a similar reactivity to form copolymer. The properties of the polymers were also studied.

The oxidative polymerization of 2,6-disubstituted phenols with a copper-pyridine complex as a catalyst produces poly[oxy(3,5-disubstituted phenylene)] under an oxygen atmosphere at room temperature.[1-3] Phenolic derivatives bearing isoprenoid substituents exist in nature. They are also interesting as monomers of the oxidative polymerization because they provide poly(oxyphenylene) with bulky and rigid isoprenoid groups. For example, poly[oxy(3,5-dimethyl-1,4-phenylene)] is known to show a high permselectivity of oxygen in preference to nitrogen in spite of its low permeability. Thus, it is interesting to study the effect of the bulky isoprenoid group of poly(oxyphenylene) on its gas permeability.

The present authors have previously reported the preparation of 2,6-diprenylphenol and 2-methyl-6-butenylphenol and their oxidative polymerization,[4,5] and preliminarily reported the preparation of 2-methyl-6-(3,7-dimethyl-2,6-octadienyl) phenol (2-methyl-6-geranylphenol, MGP).[6] The present paper will describe the preparation and oxidative polymerization of MGP and the copolymerization of MGP with 2,6-dimethylphenol (DMP). The reactivity of the 3,7-dimethyl-2,6-octadienyl group in the copolymer and the polymerization mechanism will also be reported.

Experimental

Materials: MGP was prepared as follows; *o*-cresol (1.08 g, 0.01 mol) was dissolved in dry diethyl ether (15 ml), and then metallic sodium (0.3 g, 0.013 g, atom) was added at room temperature. After 0.5 h, 1-chloro-3,7-dimethyl-2,6-octadiene (1.73 g, 0.01 mol) was slowly stirred into the mixture, and the mixture was refluxed for 1.5 h. After a usual work-up, a light yellow oil (2.68 g) was distilled i.vac.; bp 111—113 °C/0.2 mmHg (1 mmHg=133.322 Pa); yield, 71% (1.72 g). ^{1}H NMR of MGP (CCl_4, TMS standard): δ=1.60, 1.66 (s, 6H, =C(CH_3)$_2$), 1.72 (s, 3H, =(CH_3)-), 2.05 (m, 4H, -CH_2CH_2-), 2.19 (s, 3H, Ar-CH_3), 4.42 (d, J=7 Hz, 2H, O-CH_2-), 5.0 (m, 1H, -CH=C), 5.42 (t, 1H, -CH=) and 6.53—7.0 (m, 4H, Ar-H).

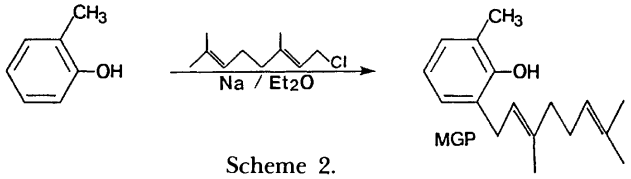

Scheme 2.

The DMP was a commercial one which was purified by recrystallization from hexane. the copper(I) chloride was prepared by the reduction of copper(II) chloride. The pyridine was purified by distillation after having been dried over KOH.

Preparative Polymerization. The polymerization of MGP was carried out in a benzene solution with the copper-pyridine complex as follows: CuCl (25 mg, 0.25 mmol) was dissolved in pyridine (5 ml) in a sealed flask equipped with an oxygen inlet tube, a dropping bottle, and a magnetic stirrer, and then 30 ml of benzene was added. This solution was vigorously stirred under an oxygen atmosphere to oxidize

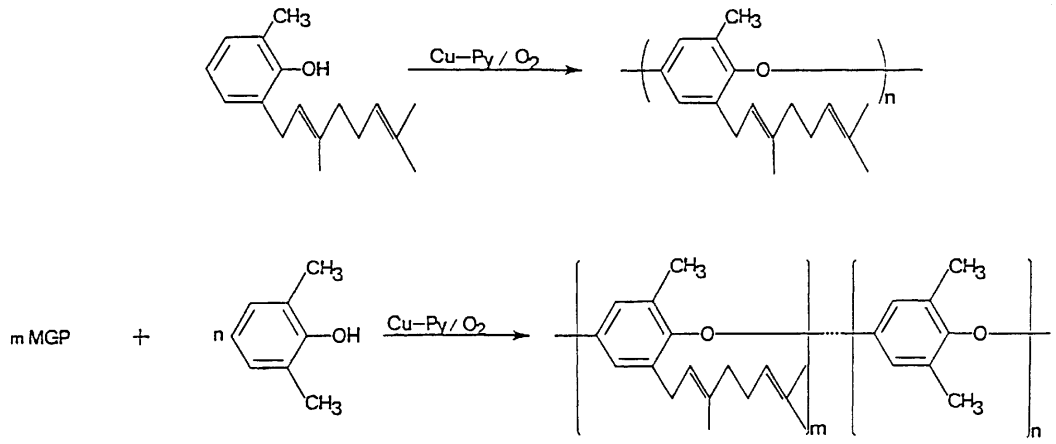

Scheme 1.

the Cu(I) ion to Cu(II) and to obtain deep-green colored copper-pyridine complex catalytic solution. A benzene solution (15 ml) of MGP (1.22 g, 5 mmol) was then added to this catalytic solution, after which the mixture was stirred for 1 h at room temperature. The reaction mixture was then stirred into 500 ml of methanol containing a small amount of hydrochloric acid; the viscous, light brown polymer thus obtained was washed with methanol and dried i. vac. Yield, 94%.

The structure of the polymer was confirmed by NMR, IR, and elemental analysis. ^{1}H NMR of the polymer ($CDCl_3$, TMS standard): δ=1.57, 1.69 (9H, $-CH_3$), 1.94 (4H, $-CH_2CH_2-$), 2.0 (3H, $-CH_3$), 3.12 (2H, $-CH_2-$), 5.08 (2H, -CH), and 6.34—6.63 (2H, Ar-H). The intrinsic viscosity of the toluene solution of the polymer was measured at 25 °C. The content of double bonds in the polymer was determined by the method of Wijs by adding an excess of ICl to the polymer solution in the dark and by titrating the excess with $Na_2S_2O_3$. It was ascertained by the titration that no replacement reaction of the phenol ring occurred.

The copolymerization of MGP and DMP was carried out in the same way. The light yellow powder thus precipitated was filtered, washed with methanol, and dried i. vac. Yield, 91%. H NMR ($CDCl_3$, TMS standard): δ=1.59, 1.70 (9H, $-CH_3$), 1.95 (4H, $-CH_2CH_2-$), 2.1 (9H, $-CH_3$), 3.12 (2H, $-CH_2-$), 5.08 (2H, -CH=) and 6.45 (4H, Ar-H). The fraction of the MGP residue in the copolymer was determined by means of the NMR spectra.

Measurement of the Polymerization Rate. The polymerization rate was followed by means of the oxygen uptake, as the oxidation of Cu(I) was very fast under the polymerization conditions. The oxygen uptake was measured with a Warburg apparatus.

Spectroscopic Measurement. The visible absorption spectrum of the mixture of the copper-pyridine complex and phenol was measured in a pyridine solution at room temperature under an oxygen-free atmosphere.

Oxidative-Peak-Potential Measurement. The oxidative peak potential of the phenols vs. Ag/AgCl was measured by means of a cyclic voltammogram in methanol, with potassium hydroxide as the supporting electrolyte.

Addition of Bromine. One gram of the copolymer was dissolved in 50 ml of CCl_4, and then 0.2 g of bromine was stirred, drop by drop, into the solution in the dark. After 1 h, the reaction mixture was poured into methanol, and the precipitate was filtered and dried i. vac. The amount of bromine introduced to the copolymer was determined by the Volhard method.

Permeation Measurement. A membrane of the MGP copolymer was prepared by casting a chloroform solution of the copolymer on a Gore-tex film and dried i. vac. at room temperature over a two-day period before measurement. The oxygen and nitrogen permeation coefficients were measured with a low-vacuum permeation apparatus (Rika Seiki Inc. Model K-315 N-031) and were calculated from the slopes of the steady-state straight lines of the permeation curves.

Results and Discussion

The oxygen-uptake curve of the polymerization of the MGP catalyzed by the copper-pyridine complex is shown in Fig. 1. After mixing the solution of MGP with a solution of a catalytic amount of the copper-pyridine complex, a linear oxygen uptake with time is observed after an induction period. The reaction is in a stationary state, the oxygen uptake being based on the oxidation of MGP. The oxygen uptake corresponds to the polymerization of MGP, since the polymer is the only reaction product.

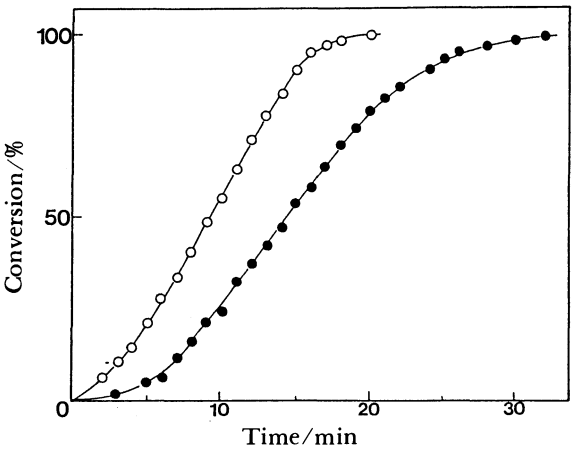

Fig. 1. Polymerization curves of MGP and DMP in benzene solution. ○: MGP, ●: DMP at 30 °C under oxygen atmosphere [Cu]=0.01 mol·l^{-1}, Pyridine 20 vol% in benzene solution.

The IR spectra of the polymers showed that the new absorptions at 990 and 1180 cm^{-1}, assigned to an ether bond, and the absorption at 3400 cm^{-1} corresponding to the hydroxyl group has almost disappeared. The ^{1}H NMR spectra were in complete agreement with those of MGP (see Experimental section).

MGP was also copolymerized with DMP. The fraction of MGP units in the copolymers and the intrinsic viscosity of the copolymers are shown in Fig. 2. Figure 2 indicates that MGP is copolymerized with DMP with a similar reactivity, but that the molecular weight of

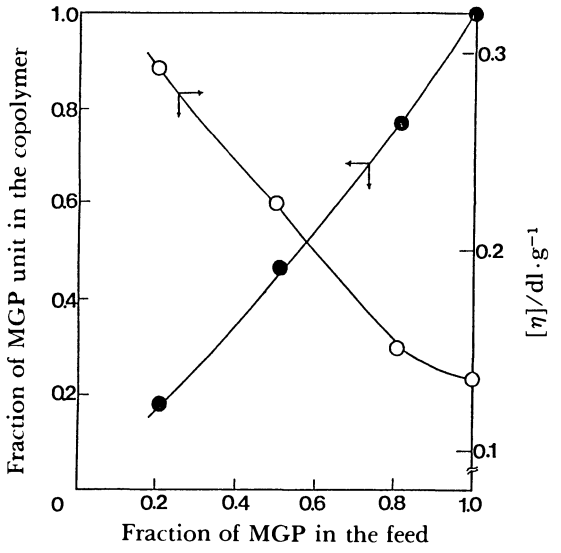

Fig. 2. Effect of the feed fraction of MGP on the composition and the intrinsic viscosity of the copolymer.

the copolymer decreases with the increase in the fraction of MGP units.

The initiation mechanism of the oxidative polymerization of phenols with the copper-pyridine complex is considered to be the following:[2] the coordination step of the phenol to the Cu(II) catalyst, the electron-transfer step from the coordinated phenol to the Cu(II) ion, the dissociation step of the activated phenol from the catalyst, and the reoxidation step of Cu(I). The previous authors have also reported[2] that the polymerization of the phenols proceeds according to a Michaelis-Menten mechanism; the following kinetic constants are estimated: the intermediate formation constants of phenol and the catalyst, K (the reciprocal of the Michaelis constant), and the reaction-rate constant, k:

$$\text{Phenol} + \text{Cu(II)} \overset{K}{\rightleftarrows} \text{Phenol-Cu} \overset{k}{\rightarrow} \text{Activated phenol} + \text{Cu(I)} \quad (1)$$

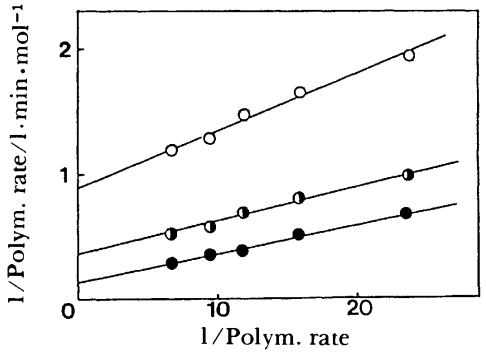

Fig. 3. Lineweaver-Burk plots for the polymerization. ○: DMP, ○: DMP-MGP (feed fraction 0.5), ●: MGP, [Cu]=1 mmol·l^{-1}, in benzene solution at 30°C under oxygen atmosphere.

The polymerization rates in a steady state for MGP and DMP were plotted with the feed phenol concentrations; their reciprocals (Lineweaver-Burk plot) show linear relationships, as in Fig. 3, supporting this mechanism. The K and k values calculated from the slopes and intercepts of the straight lines are given in Table 1.

The K value for MGP is smaller than that for DMP because the bulky 2-substituted geranyl group hinders the coordination of MGP to the copper catalyst. However, the k for MGP is larger than for DMP, leading to the relatively high polymerization rate of MGP.

Table 1. Kinetic Parameters for the Polymerization of MGP and DMP

Feed monomer fraction of MGP	K / l mol^{-1}	k / min^{-1}	k_e / min^{-1}
0	1.0	0.14	0.31
0.5	0.69[a]	0.25[a]	—
1	0.10	0.67	0.46

a) Apparent values.

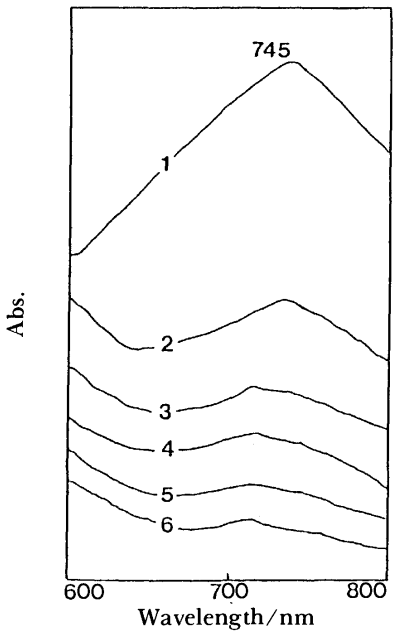

Fig. 4. Visible spectral change of the reaction mixture with time [Cu]=5 mmol·l, [MGP]=0.1 mol·l, in pyridine solution 1; without MGP, 2: 0.5 min, 3: 1.5 min, 4: 3.5 min, 5: 5,5 min, 6: 13.5 min.

This high reactivity of MGP was further studied spectroscopically. The deep-green color of the catalyst solution is based on the Cu(II) complex. After the addition of the phenol to the catalyst solution, it turned brown, which corresponds to the Cu(I) complex formation or the electron transfer from the phenol to the Cu(II) catalyst. The change in the visible absorption is shown in Fig. 4. The measurement of the decrease in d-d absorption at 745 nm under an oxygen-free atmosphere provides the rate constant (electron transfer step: k_e). The k_e value given also in Table 1 is larger for MGP, which agrees with the result for k. This behavior is consistent with the overall polymerization as has been shown in Fig. 1. The step represented by k or k_e is the rate-determining step in this polymerization.

The oxidation-peak potential of the phenols was measured by cyclic voltammetry and is given in Table 2. This indicates that MGP is more readily oxidized than DMP, a finding which agrees with the kinetic and spectroscopic results. The electron-donating 3,7-dimethyl-2,6-octadienyl group probably reduces the oxidation peak-potential of phenol and enhances its reactivity in the polymerization.

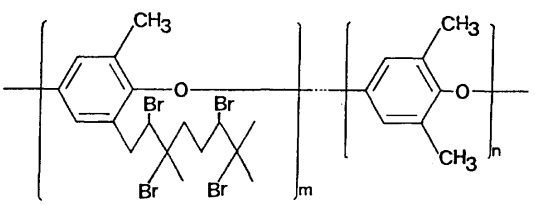

Scheme 3.

Table 2. Oxidation-Peak Potential

Phenol	Volt
MGP	0.34
DMP	1.6

The 3,7-dimethyl-2,6-octadienyl groups in the polymer showed enough chemical reactivity, e.g. for the addition of bromine. Two bromine molecules were introduced per monomer unit of the polymer; i.e., >98% of the geranyl group was reacted with bromine. The brominated polymer is interesting for its self-extinguishing property.

The oxygen- and nitrogen-permeability coefficients are given in Table 3. The gas permeability of the MGP copolymer is comparable with that of poly[oxy-(3,5-dimethyl-1,4-phenylene)], and the copolymer shows a good permselectivity.

This work was partially supported by a Grant-in-Aid from the Ministry of Education, Science and Culture.

Table 3. Gas Permeablility (P, cm^3(STP)$cm/cm^2 \cdot s \cdot cmHg$) of the MGP Copolymer Membrane[a)]

Membrane	$10^{10} \cdot P_{O_2}$	$10^{10} \cdot P_{N_2}$	P_{O_2}/P_{N_2}
MGP copolymer	5.4	1.1	4.9
Poly[oxy(3,5-dimethyl-1,4-phenylene)][b)]	15.8	3.8	4.2

a) Fraction of MGP units in the copolymer; 80 mol%.
b) H. Yasuda and Kj. Rosengren, *J. Appl. Polym. Sci.*, **14**, 2839 (1970).

References

1) A. S. Hay, *Adv. Polymer. Sci.*, **4**, 496 (1967).
2) E. Tsuchida, M. Kaneko, and H. Nishide, *Makromol. Chem.*, **151**, 235 (1972).
3) E. Tsuchida, H. Nishide, and T. Nishiyama, *Makromol. Chem.*, **176**, 1349 (1975).
4) H. Nishide, Y. Suzuki, E. Tsuchida, and S. Yamada, *Makromol. Chem.*, **182**, 2361 (1981).
5) H. Nishide, T. Minakata, E. Tsuchida, and S. Yamada, *Makromol. Chem.*, **183**, 1889 (1982).
6) S. H. Hyun, H. Nishide, E. Tsuchida, and S. Yamada, *Polym. Bull.*, **18**, 283 (1987).

 © 1988 The Chemical Society of Japan Bull. Chem. Soc. Jpn., 61, 1323—1329 (1988)

Equilibrium and Kinetic Studies of the Interaction between Orange I and Bovine Serum Albumin

Kiyofumi MURAKAMI
Department of Chemistry, Faculty of Science, Yamaguchi University, Yoshida 1677-1, Yamaguchi 753
(Received July 20, 1987)

The interaction between Orange I (sodium 4-[(4-hydroxy-1-naphthalenyl)azo]benzenesulfonate) and bovine serum albumin (BSA) at pH=7.0 and 25 °C has been studied by equilibrium dialysis, spectrophotometry, and the temperature-jump method. Equilibrium dialysis has revealed the existence of sixteen equivalent binding sites with the binding constant of $K=9.7\times10^3$ M^{-1}. All of them were found to be equivalent also in the sense of spectrophotometry. That is, Orange I interacts with BSA in a typically nonspecific manner. Five relaxations were found by the temperature-jump measurements. These relaxation times, distributed over the time range from 10 μs to 0.1 s, were determined over a wide range of reactant concentrations. The fastest relaxation becomes slow, but the four slower ones become fast, with the increase in the concentration of the free ligand. The data were interpreted by means of a combination of the bimolecular binding processes and the four isomerization modes of BSA. The results were discussed in the light of the role of the configurational adaptability of albumin molecules in the ligand-binding mechanism.

A unique property of serum albumin is its capacity to bind reversibly a variety of ions and organic molecules, such as metal ions, fatty acids, bilirubin, hormones, amino acids, and drugs. This enables albumin molecules to play their inherent role as the carrier and the reservior of those ligands in blood. The physicochemical origin of this unique property has been thought attributable to (1) configurational adaptability:[1] binding sites on albumin molecule can assume a large number of configurations in equilibrium with each other and can, in the presence of a ligand, adopt the configuration which is most suitable for interaction or to (2) pronounced flexibility:[2] a ligand molecule, during the binding process, is able to modify the configuration of a binding region in such a way that a greater congruence between the ligand molecule and parts of the region is achieved.

In recent years, many kinetic studies of albumin-ligand binding have been performed in order to elucidate the binding mechanism.[3-8] The general conclusion of these studies is that the ligand binding occurs through several steps: the first step is probably the diffusion-controlled bimolecular binding reaction, while the subsequent ones are the stabilization processes of the complex. This conclusion seems to be in harmony with the concept of the pronounced flexibility of albumin molecules. However, the kinetic studies have been concerned only with specific ligands which have one or few strong primary sites and several weak secondary sites and with a concentration range where only primary bindings occur. If nonspecific ligands, which have only one kind of relatively weak binding site, are used, we may obtain different features of the ligand-binding mechanism of albumin molecules.

The present paper will describe the equilibrium and the kinetics of the interaction between Orange I and bovine serum albumin (BSA) and will suggest that the configurational adaptability is also operative for albumin-ligand binding.

Experimental

Materials. The albumin (fraction V from bovine serum) was purchased from Armour and was defatted by means of charcoal treatment in an acid solution,[9] lyophilized, and stored at 4 °C. The molar concentration of BSA was determined from the absorbance at 280 nm ($E^{1\%}_{1cm}=6.6$[10]), assuming the molecular weight of 67000. The Orange I (sodium 4-[(4-hydroxy-1-naphthalenyl)azo]benzenesulfonate) was purchased from Wako Pure Chemical Industries, purified by repeated recrystallization from sodium acetate and aqueous ethanol solutions, and dried at 110 °C in a vacuum for 20 hours. All the other chemicals used were reagent-grade. All the sample solutions were prepared in a 0.1 M† phosphate buffer at pH=7.00±0.02.

Methods. The extent of binding was determined by the use of the equilibrium dialysis technique. Visking dialysis tubing (24/32) cut to a length of 9 cm was treated with a 1% $NaHCO_3$ aqueous solution at 100 °C for 60 min, soaked in a 0.3% EDTA solution, and then exhaustively rinsed with distilled water. 5 ml of the BSA solution ([BSA]=5×10^{-5} M) placed inside the dialysis tubing was dialysed against 10 ml of the dye solution at 25 °C for 24 h. After equilibration, the concentration of the Orange I solution was determined spectrophotometrically using a molar-extinction coefficient, $\varepsilon_{475}=3.24\times10^4$ $M^{-1}cm^{-1}$.

The spectrophotometric measurements were carried out with Shimadzu UV-200S and UV-100 spectrophotometers.

The kinetic experiments were performed with a Unisoku TF-102 fluorescence temperature-jump spectrophotometer. The details of the apparatus have been reported elsewhere.[11] The data were obtained at the temperature-rise intervals of 5 °C. All the experiments were performed at 25±0.2 °C.

Results and Discussion

Binding Parameters. Figure 1 illustrates a Scatchard plot[12] of the interaction of Orange I with BSA at pH=7.0 and 25 °C. The well-defined linearity of the plot shows that the binding sites of Orange I on BSA can be regarded as identical and independent. The binding parameters for the interaction were determined using the Scatchard equation:

† 1 M=1 mol dm^{-3}.

$$\frac{\bar{\nu}}{L} = nK - \bar{\nu}K \quad (1)$$

where $\bar{\nu}$ is the number of moles of the ligand bound per molecule of the protein, L is the free ligand concentration, and n and K are the number of binding sites and the association constant respectively. n and K were determined from the slope and the intercept of the plot as n=15.6 and K=9.7×10^3 M^{-1}. That is, Orange I binds nonspecifically to sixteen sites on BSA.

Spectrophotometric Titration. Figure 2 shows the absorption spectra of Orange I in the presence of BSA at several concentrations. The absorbance around 475 nm is reduced with the increase in the concentration of BSA, showing approximate isosbestic points at 415 nm and 525 nm. The existence of the isosbestic points suggests the following equilibrium between free and bound forms of the ligand:

$$\mathbf{L} + \mathbf{S} \rightleftharpoons \mathbf{C} \quad (2)$$

where **L**, **S**, and **C** denote the free ligand, the free binding site, and the complex between them respectively. The apparent molar-extinction coefficient at a given wavelength can be expressed by:

$$\varepsilon = (\varepsilon_F - \varepsilon_B)\alpha + \varepsilon_B \quad (3)$$

where ε_F and ε_B are the molar-extinction coefficients of the free and bound ligands respectively and where α is the free fraction of the ligand. α can be estimated from n, K, and the initial concentrations of the ligand and the protein (L_0 and P_0) as:

$$\alpha = \frac{-\{K(nP_0 - L_0)\} + [\{K(nP_0 - L_0)\}^2 + 4KL_0]^{1/2}}{2KL_0} \quad (4)$$

If all the sixteen sites determined by the equilibrium dialysis contribute equally to the spectral change (Fig. 2), the ε vs. α plot (Eq. 3) must be a straight line, and the ε_B's, which can be determined independently from the slope and the intercept of the plot, must agree with each other. The plots shown in Fig. 3 for 460, 475, and 490 nm indicate a good linearity. Furthermore, the values of ε_B (ε_{460}=1.96×10^4 M^{-1}cm^{-1}, ε_{475}=2.15×10^4 M^{-1}cm^{-1}, and ε_{490}=2.08×10^4 M^{-1}cm^{-1}) determined from the slope agree well with those (ε_{460}=1.94×10^4 M^{-1}cm^{-1}, ε_{475}=2.14×10^4 M^{-1}cm^{-1}, and ε_{490}=2.08×10^4 M^{-1}cm^{-1}) determined from the intercept. These results suggest that the sixteen sites are spectrophotometrically equivalent with each other.

Temperature-Jump Relaxations. The temperature-jump measurements revealed that the interaction between Orange I and BSA was characterized by five relaxation processes. Some typical relaxation curves

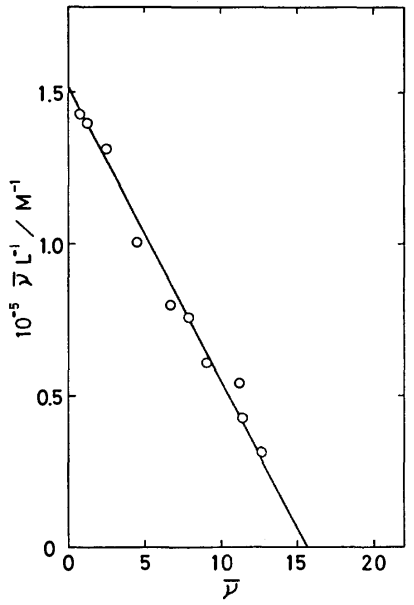

Fig. 1. Scatchard plot of the interaction of Orange I with BSA at 25°C and pH=7.0. The solid line represents the least-square fit to the data.

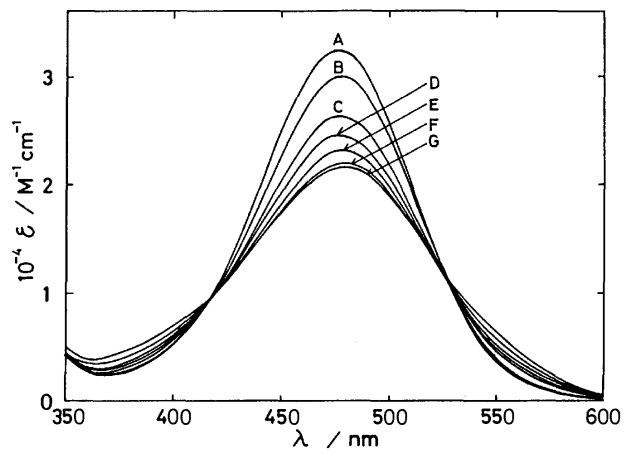

Fig. 2. Absorption spectra of Orange I in the presence of BSA at several concentrations. The data were obtained at 25°C, pH=7.0 and L_0=1.00×10^{-5}M. A: dye only, B: P_0=1.82×10^{-6}M, C: P_0=9.10×10^{-6}M, D: P_0=1.82×10^{-5} M, E: P_0=3.64×10^{-5}M, F: P_0=9.10×10^{-5}M, G: P_0=1.82×10^{-4}M.

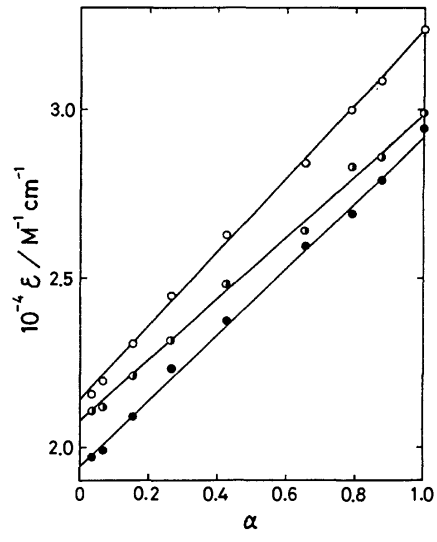

Fig. 3. Plots of ε vs. α at 460 nm (●), 475 nm (○), and 490 nm (◑). The solid lines represent least-square fits to the data.

observed at L_0/P_0 (ligand to protein ratio)=2 are shown in Fig. 4. The data were obtained at either 475 nm or 555 nm so as to give a good signal-to-noise ratio. The fastest relaxation (Fig.4(A)) was characterized by a single relaxation time (τ_1), while the second (Fig. 4(B): τ_2 and τ_3) and the third (Fig. 4(C): τ_4 and τ_5) were

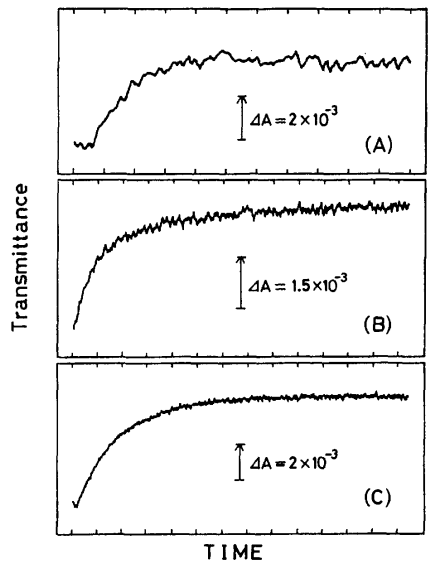

Fig. 4. Typical relaxation curves observed for the Orange I-BSA system at 25°C , pH=7.0, P_0= 5×10^{-5} M, and L_0/P_0=2. (A) λ=555 nm, 5 μs per division, (B) λ=555 nm, 1 ms per division, (C) λ=475 nm, 20 ms per division. The arrow designated for each curve shows the magnitude and the direction of the positive absorbance change.

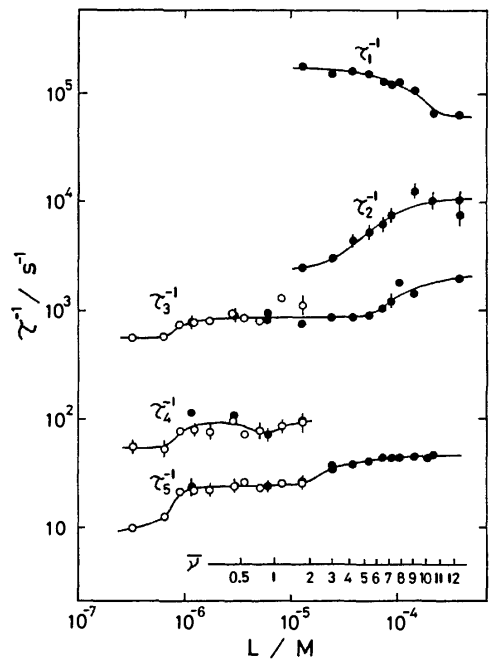

Fig. 5. Plots of τ^{-1} vs. L. The data were collected for two kinds of concentration dependence: (○) P_0/L_0 dependence (from 0.2 to 20) at $L_0=2\times10^{-5}$ M, (●) L_0/P_0 dependence (from 0.2 to 20) at $P_0=5\times10^{-5}$ M. The scale of $\bar{\nu}$ is also designated at the bottom of the figure.

double relaxations. To cover a wide range of reactant concentrations, the relaxation time of each process was determined for two kinds of concentration dependence: (1) P_0/L_0 dependence at $L_0=2\times10^{-5}$ M and (2) L_0/P_0 dependence at $P_0=5\times10^{-5}$ M. Figure 5 shows a plot of the reciprocal relaxation times versus the free-ligand concentration (L) as well as versus the $\bar{\nu}$ values, which were calculated using the values of n and K determined from the equilibrium dialysis measurement. It can be seen from this figure that the reciprocal relaxation times are increasing functions of L, except in the case of τ_1^{-1}. Furthermore, it can be seen that τ_4^{-1} disappears above $\bar{\nu}=2$ and that, in the same region, τ_2^{-1} becomes observable.

Reaction Scheme. Although the scheme of Eq. 2 is consistent with the equilibrium dialysis and the spectrophotometric data, it is obvious that this scheme is too simple to interpret the observed multiple relaxation and that it is not applicable to the present kinetic data.

Almost all the kinetic studies of albumin-ligand interaction have been concerned with specific ligands, such as bilirubin,[3,4] hemin,[7] fatty acids,[5] warfarin,[6] and Bromphenol Blue,[8] which have one strong or extremely strong primary binding site on the albumin molecule. Moreover, the data were collected over the reactant concentration range where only the primary binding occurs. A common feature of the schemes established by these studies is that a rapid bimolecular binding is followed by subsequent unimolecular stabilizations of the complex. That is,

$$\mathrm{L+S} \rightleftarrows \mathrm{C_1} \rightleftarrows \mathrm{C_2} \rightleftarrows \cdots \rightleftarrows \mathrm{C_m} \qquad (5)$$

This type of scheme predicts the reciprocal relaxation time for the i th isomerization as:[13]

$$\tau_i^{-1} = k_i + k_{-i} \qquad (6)$$

in the case of a rapid isomerization between slow ones or:

$$\tau_i^{-1} = k_i \frac{E\,(L+S)}{1+F\,(L+S)} + k_{-i} \qquad (7)$$

in the case of an isomerization slower than the preceding steps. In these equations, k_i and k_{-i} are the forward and backward rate constants of the ith step respectively, while E and F are functions of the equilibrium constants of the preceding steps. According to these equations, the reciprocal relaxation time for any of the isomerization steps must be concentration-independent or an increasing function of $L+S$. Based on a calculation using the binding parameters determined from the dialysis measurements, it can be seen that $L+S$ decreases with the increase in L at $L<7\times10^{-4}$ M, the area where almost all the relaxations were measured. Therefore, Fig. 5 shows that the reciprocal relaxation times of the four slower processes are decreasing functions of $L+S$. That is, Eq. 5 also is not applicable to the present system.

To obtain an insight into the binding scheme, we must take notice of the fact that the reciprocal relaxation times (τ_3^{-1}, τ_4^{-1}, τ_5^{-1}) are functions of only L. This fact suggests the following basic scheme for one of the relaxation times:[14]

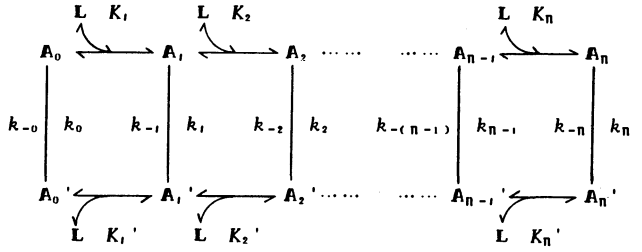

(8)

where $\mathbf{A}_i$ and $\mathbf{A}_i'$ are two isomeric forms of BSA which bind i ligands and where K_i and K_i' are association constants to form two ith complexes, $\mathbf{A}_i$ and $\mathbf{A}_{i-1}$, from $\mathbf{A}_{i-1}$ and $\mathbf{A}_{i-1}$ respectively, and where n is the maximum number of bound ligands. The equilibrium between $\mathbf{A}_0$ and $\mathbf{A}_0'$ ($\mathbf{A}_0 \rightleftharpoons \mathbf{A}_0'$) represents a mode of isomerization in the absence of a ligand, which shifts to $\mathbf{A}_1 \rightleftharpoons \mathbf{A}_1'$, $\mathbf{A}_2 \rightleftharpoons \mathbf{A}_2'$, ·····, and finally to $\mathbf{A}_n \rightleftharpoons \mathbf{A}_n'$ with the increase in the number of bound ligands. k_i and k_{-i} are the forward and backward rate constants of the ith isomerization. Assuming that bimolecular bindings are rapid compared with the isomerizations and that the concentration changes of L are negligible during the slow isomerizations, the reciprocal relaxation time for the slow steps becomes:[14]

$$\tau^{-1} = \frac{k_0 + k_1K_1L + k_2K_1K_2L^2 + \cdots\cdots + k_nK_1K_2\cdots K_nL^n}{1 + K_1L + K_1K_2L^2 + \cdots\cdots + K_1K_2\cdots K_nL^n} + \frac{k_{-0} + k_{-1}K_1'L + k_{-2}K_1'K_2'L^2 + \cdots + k_{-n}K_1'K_2'\cdots K_n'L^n}{1 + K_1'L + K_1'K_2'L^2 + \cdots\cdots + K_1'K_2'\cdots K_n'L^n} \quad (9a)$$

$$= \frac{k_0A_0 + k_1A_1 + k_2A_2 + \cdots\cdots + k_nA_n}{A_0 + A_1 + A_2 + \cdots\cdots + A_n} + \frac{k_{-0}A_0' + k_{-1}A_1' + k_{-2}A_2' + \cdots\cdots + k_{-n}A_n'}{A_0' + A_1' + A_2' + \cdots\cdots + A_n'} \quad (9b)$$

As can be seen in Eq. 9a, τ^{-1} is expressed as a function of L alone, in agreement with the present data (Fig. 5). On the other hand, Eq. 9b shows that τ^{-1} is the apparent rate constant of the isomerization , averaged over the existing complex species. At the limit of dilution, Eq. 9a can be approximated by k_0+k_{-0}. With an incease in L, the terms of the higher powers of L in both the numerator and the denominator in Eq. 9a become significant. If the terms of the ith power of L are predominant, Eq. 9a can be approximated as $\tau^{-1}=k_i+k_{-i}$ (apparent rate constant of the isomerization of the ith complex). That is, the τ^{-1} of Eq. 9 follows the rate of the isomerization of predominantly existing complexes at a given ligand concentration.

On the basis of these considerations, we may construct a scheme applicable to the present kinetic data:

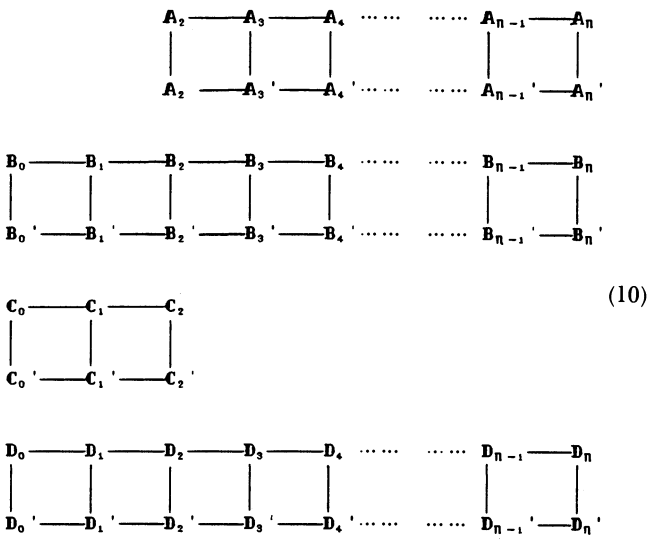

(10)

where $\mathbf{A}_i \rightleftharpoons \mathbf{A}_i'$, $\mathbf{B}_i \rightleftharpoons \mathbf{B}_i$, $\mathbf{C}_i \rightleftharpoons \mathbf{C}_i'$, and $\mathbf{D}_i \rightleftharpoons \mathbf{D}_i'$ represent the four modes of isomerization which are characterized by the relaxation times of τ_2, τ_3, τ_4, and τ_5 respectively. The horizontal lines are steps of the ligand binding, where the symbols associated with the ligand (see Eq. 8) are dispensed with. According to this scheme, the observed data may be interpreted as follows.

In the absence of a ligand, there are three intrinsic modes of isomerization, designated by $\mathbf{B}_0 \rightleftharpoons \mathbf{B}_0'$, $\mathbf{C}_0 \rightleftharpoons \mathbf{C}_0'$, and $\mathbf{D}_0 \rightleftharpoons \mathbf{D}_0'$. The apparent rate constants of these modes can be evaluated from the asymptotic values of τ_3^{-1}, τ_4^{-1}, and τ_5^{-1} within the limits of the diluted ligand concentrations (Fig. 5) as 570, 55, and 7—8 s^{-1} respectively. With an increase in the concentration of free ligands, these modes shift toward those of the complex species, accompanying the increase in the apparent rate constants. At the ligand concentration where $\bar{\nu}>2$, Mode C ceases to be observable; instead, Mode A appears at a very rapid rate. This implies that the binding of two ligands freezes Mode C by displacing the equilibrium almost completely to either of the isomers or, by inducing some kind of conformational change in the complex, alternatively causes another fast mode (Mode A). With a further increase in L, the apparent rate constants increase further and reach plateau values. It may be worth noting that the relaxation amplitude of each mode has a maximum at a $\bar{\nu}$ value between 4 and 6.5 and that this relaxation amplitude decreases (Modes B and D) or increases (Mode A) with a further increase in L, suggesting that Mode A is the most predominant mode at high $\bar{\nu}$ values.

Contrary to the case of the slower relaxations, τ_1^{-1} decreases with the increase in L (Fig. 5); that is, it increases with $L+S$. Considering the very rapid rate as well, this behavior may be interpreted by attributing the relaxation to the bimolecular binding step between the free ligand and the free binding site, such as in Eq. 2. The reciprocal relaxation time for the binding step

becomes:

$$\tau_1^{-1} = k_a(L+S) + k_d \quad (11)$$

where k_a and k_d are the rate constants of association and dissociation respectively. Figure 6 shows the plot of τ_1^{-1} vs. $L+S$, which was calculated using these binding parameters: $n=16$ and $K=9.7\times10^3$ M^{-1}. In agreement with Eq. 11, the plot shows a linear dependency in the region where τ_1^{-1} is larger than 1.2×10^5 s^{-1} and where $\bar{\nu}$ is smaller than 8. The deviation from the linearity at $\bar{\nu}>8$ may arise from interactions between sites attributable to some kind of conformational change in the complex. The slope and the intercept of the plot yield $k_a=2.4(\pm0.5)\times10^8$ $M^{-1}s^{-1}$ and $k_d=1.0(\pm2.9)\times10^4$ s^{-1} respectively. From these values, the binding constant can be calculated as $K=k_a/k_d=2.4\times10^4$ M^{-1}. Considering the estimated errors, this value may be regarded as consistent with the binding constant used for this analysis. This self-consistency confirms the present assignment for τ_1.

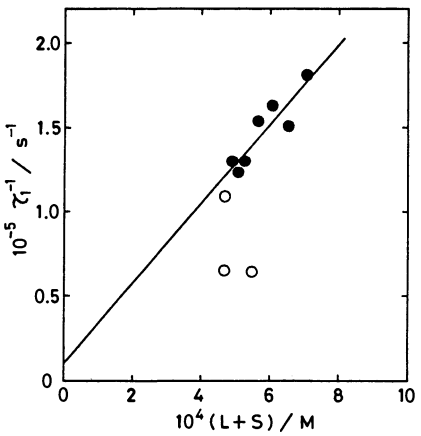

Fig. 6. Plot of τ_1^{-1} vs. $L+S$. The solid line represents the least-square fit to the data (filled circles) in the region where $\bar{\nu}<8$. Open circles show the data observed at $\bar{\nu}>8$.

Role of Isomerization Modes in Ligand-Binding Mechanism. Karush,[1] in 1950, proposed a concept of the "configurational adaptability" of albumin molecules in order to interpret their unique capability in the binding of diverse kinds of ligands. By this term, he meant that an albumin molecule in an aqueous solution is not a single form but an ensemble of many structural species in equilibrium with each other and of approximately equal energies. In the presence of a ligand, the isomeric form is stabilized by preferential interaction with the ligand, resulting in a stable complex. On the other hand, Kragh-Hansen, in his review[2] of ligand binding to serum albumin, pointed out another possibility for the binding mechanism. Many previous kinetic studies have revealed this general binding scheme (Eq. 5): a very rapid bimolecular binding, followed by sequential stabilization processes. This scheme has led him to propose a "pronounced flexibility" mechanism: a ligand molecule is, during the binding process, able to modify the configuration of a binding region so as to produce a greater congruence between the ligand molecule and parts of the region. The present scheme (Eq. 10), however, shows that BSA has, in the absence of a ligand, three modes of conformational change between isomeric forms in equilibrium. The addition of a ligand shifts the set of modes toward that of the complex species accompanying rate change, mode freezing, and the production of another mode. This behavior may be interpreted as the response of the system aimed at acquiring the most stable state as the pressure of the

Table 1. Rates of Isomerization Steps Observed for Albumin-Ligand Systems

System[a]	Rate/s^{-1}				Condition		Ref.
	(Mode A)	(Mode B)	(Mode C)	(Mode D)	T/°C	pH	
BPB-BSA		400—600	40	1—3	25	7.0	8
BCP-BSA		100—600			25	5.3—6.8	15
PR-BSA	5×10^3			3	30	7.35	16
			10—50	4—6		7.0	16
HABA-BSA		200			25	7.0	17
Long-chain fatty acid-HSA				3			5
ANS-BSA		125			25	7.0	18
Warfarin-HSA			60		25	8.7	19
			55	2.5—5	25	6.0	20
			74			9.0	20
			10—60		25	6—9	21
Bilirubin-BSA				8.5	23	7.4	22
Hemin-HSA				6.3	24	7.0	7
BPA E,F→N			50	4	25		23
BSA CD change				4—10	22	7.5—9	24
Orange I-BSA	2.5×10^3—10^4	570	55	7—8	25	7.0	This work

a) Abbreviations: BPB=Bromphenol Blue, BCP=Bromcresol Purple, PR=Phenol Red, HABA=2-(4-hydroxyphenylazo)benzoic acid, HSA=human serum albumin, ANS=8-anilino-1-naphthalenesulfonic acid, BPA=bovine plasma albumin, E,F→N=pH-jump from E and F states to the N state of albumin.

ligand concentration increases. This seems to be just the case with the configurational adaptability in the sense of Karush.

Table 1 lists the rates of the isomerization steps of complex formation reported for albumin-ligand systems at around 25 °C and in the neutral-pH region, as well as those of conformational transitions observed under similar conditions. It can be seen from this table that (1) there are four modes of isomerization, which may be classified according to the rate as: A (10^3—10^4 s^{-1}), B (10^2—10^3 s^{-1}), C (10—10^2 s^{-1}), and D (1—10 s^{-1}); (2) the number of observable modes depends on the ligand species, and finally (3) the rates, i.e., the activation free energies, which belong to a mode for different ligands are all similar to each other, regardless of the structure of the ligand. Kuwajima et al.,[23] by studying the pH-jump from the E and F states to the N state[25] of albumin molecules, observed time-dependent absorbance changes at 296 nm which are characteristic of the ionization states of tyrosyl residues. The rates of these changes (50, 4 s^{-1}), listed in Table 1, agree well with those classified in Mode C and Mode D for albumin-ligand systems. Using a pressure-jump technique with circular dichroism (CD) detection, Gruenewald and Knoche[24] observed a CD change at 222 nm. Its rate (4—10 s^{-1}) is classifiable in Mode D (Table 1). This fact suggests that Mode D is an isomerization which accompanies a change in the helix content of albumin molecules. From the pH-dependence of the rates of Mode D in the Phenol Red-BSA system,[16] Mode C in the warfarin-HSA system,[21] and the Mode D observed by the pressure-jump CD measurement,[24] it can be seen that these modes are closely related to the N⇄B transition[25] of albumin molecules. Mode A and Mode B have not been well characterized from the point of view of the conformational state of the protein. Because Mode A was observed only at high L_0/P_0 values, it is not necessarily attributable to an isomerization of native albumin, but seems to arise from the albumin-ligand complex. There may also be another slow mode of isomerization ($\tau^{-1}<1$ s^{-1}),[23,26] but it is not discussed in the present paper.

These observations suggest that the modes of isomerization of pure albumin molecules are closely related to the ligand-binding mechanism. In the absence of a ligand, albumin molecules are distributed among many structural species, each of which is characterized by a set of isomers of those modes, and the structures of the albumin molecules fluctuate between those species on several time scales and to several spatial extents. Immediately after the addition of a ligand, and before the fastest mode of isomerization takes place, the ligand molecules will at first come into a rapid binding equilibrium with the instantaneous structural species. In this stage, extremely fast (faster than, or comparable to, the relaxation time of the diffusion-controlled bimolecular binding process) rearrangements of the side chains and mobile segments in the vicinity of the binding site slightly stabilize each of the isomeric forms and also slightly alter the free-energy profile of each mode. Because of the time limitation, possible structural changes must be restricted to a very local region of the protein molecule. The alteration is, therefore, probably so small that the free-energy profile and the distribution of albumin molecules among the structural species are essentially the same as those in the pure albumin solution. In the second stage, the ligand molecules will come into an equilibrium with the fastest mode of isomerization. At this stage, albumin molecules are able to use slower and larger structural changes than those in the previous step to establish a preferable interaction with ligand molecules. Each of the isomers of the fastest mode may be stabilized by the structural changes, but they may be destabilized if such a preferable interaction can not be attained because of structural restrictions, resulting in an alteration of the free-energy profile along the reaction coordinate of the fastest mode. If the activation free energy is lowered, the rate of the isomerization becomes fast and the redistribution of the complex species among the isomers is achieved through the altered mode. On the other hand, if the activation free energy becomes large, the rate becomes slow and the redistribution will be achieved mainly through the mode of pure albumin. Within the limits of a large activation free energy, however, this mode is practically prohibited. Furthermore, it may also be possible that a strong interaction between ligand and binding site causes some kinds of conformational transitions of albumin molecules and extinguishes the mode of isomerization, alternatively causing another, new isomerization mode. In each subsequent equilibration step, similar changes will occur along another reaction coordinate in still larger spatial and slower time scales, keeping the equilibrium in the faster modes. When all the modes come into an equilibrium with the ligand molecules, a stable distribution of the complexes is established. In the case of the present system, it is likely that the activation free energy of each mode is progressively lowered with the increase in the number of bound ligands and that some kinds of conformational change take place when two ligand molecules are bound. Some kinds of ligand molecules may interact selectively with either of the isomers. Even in such a case, though, it is also possible that the stabilization of the complex takes place through the reaction coordinates of the isomerization modes; that is, a bimolecular binding step is followed by subsequent unimolecular isomerizations (Eq. 5). This may correspond to the case of the interaction between albumin and such specific ligands as bilirubin.[3,4] In this way, the existence of the isomerization modes of albumin molecules may be closely connected with the formation of stable albumin-ligand complexes.

References

1) F. Karush, *J. Am. Chem. Soc.*, **72**, 2705 (1950).
2) U. Kragh-Hansen, *Pharmacol. Rev.*, **33**, 17 (1981).
3) T. Faerch and J. Jacobsen, *Arch. Biochem. Biophys.*, **184**, 282 (1977).
4) R. D. Gray and S. D. Stroupe, *J. Biol. Chem.*, **253**, 4370 (1978).
5) W. Scheider, *Proc. Natl. Acad. Sci. U.S.A.*, **76**, 2283 (1979).
6) N. Rietbrock and A. Laßmann, *Naunyn-Schmiedeberg's Arch. Pharmacol.*, **313**, 269 (1980).
7) P. A. Adams and M. C. Berman, *Biochem. J.*, **191**, 95 (1980).
8) K. Murakami, T. Sano, and T. Yasunaga, *Bull. Chem. Soc. Jpn.*, **54**, 862 (1981).
9) R. F. Chen, *J. Biol. Chem.*, **242**, 173 (1967).
10) E. J. Cohn, W. L. Huges, Jr., and J. H. Weare, *J. Am. Chem. Soc.*, **69**, 1753 (1947).
11) K. Murakami, K. Mizuguchi, Y. Kubota, and Y. Fujisaki, *Bull. Chem. Soc. Jpn.*, **59**, 3393 (1986).
12) G. Scatchard, *Ann. N. Y. Acad. Sci.*, **51**, 660 (1949).
13) C. F. Bernasconi, "Relaxation Kinetics," Academic Press, New York (1976), p. 40.
14) H. Strehlow and W. Knoche, "Fundamentals of Chemical Relaxation," in "Monographs in Modern Chemistry," ed by H. F. Ebel, Verlag Chemie, New York(1977), Vol. 10, pp. 85—90.
15) Z. Horiuchi, M. Nakao, S. Abe, K. Takahashi, and T. Yasunaga, *J. Sci. Hiroshima Univ., Ser. A*, **39**, 37 (1975).
16) D. E. Goldsack and P. M. Waern, *Can. J. Biochem.*, **49**, 1267 (1971).
17) K. Murakami, T. Sano, T. Tsuchie, and T. Yasunaga, *Biophys. Chem.*, **21**, 127 (1985).
18) H. Nakatani, M. Haga, and K. Hiromi, *FEBS Lett.*, **43**, 293 (1974).
19) J. Wilting, J. M. H. Kremer, A. P. Ijzerman, and S. G. Schulman, *Biochim. Biophys. Acta*, **706**, 96 (1982).
20) A. Laßmann and N. Rietbrock, *Naunyn-Schmiedeberg's Arch. Pharmacol.*, **320**, 189 (1982).
21) J. M. H. Kremer, G. Bakker, and J. Wilting, *Biochim. Biophys. Acta*, **708**, 239 (1982).
22) R. F. Chen, *Arch. Biochem. Biophys.*, **160**, 106 (1974).
23) K. Kuwajima, T. Matsushima, K. Nitta, and S. Sugai, *Biopolymers*, **23**, 1347 (1984).
24) B. Gruenewald and W. Knoche, *Rev. Sci. Instrum.*, **49**, 797 (1978).
25) J. F. Foster, "Albumin Structure, Function and Uses," ed by V. M. Rosenoer, M. Oratz, and M. A. Rothschild, Pergamon Press, New York (1977), pp. 53—84.
26) E. S. Benson, B. E. Hallaway, and R. W. Lumry, *J. Biol. Chem.*, **239**, 122 (1964).

 © 1988 The Chemical Society of Japan Bull. Chem. Soc. Jpn., 61, 1331—1334 (1988)

Gamma-Irradiation Effect on the Catalytic Behavior of Binary Oxide Catalysts

E. A. Hassan,* K. M. Abd El-Salaam, and A. A. Said
Chemistry Department, Faculty of Science, Assiut University, Assiut, Egypt
(Received February 18, 1986)

Decomposition of hydrogen peroxide in aqueous solution was used for testing the effect of gamma radiation on the catalytic activity of $Co_xFe_{3-x}O_4$, with $0 \leqslant x \leqslant 3.0$. The activity variation was interpreted in terms of the catalysts electronic structure. The presence of Co^{2+} on octahedral sites is superior to Fe^{2+} in the catalytic process. However, γ-irradiation can produce a considerable effect on the catalytic activity due to its influence on the active site concentration and cation distribution.

Results of most studies[1-3] on H_2O_2 decomposition indicate that among the decisive factors governing the catalytic activity is the presence of ions in various valency state as a catalytically active component. Cobalt-iron spinel oxides which can be represented as Co_x-$Fe_{3-x}O_4$ with $0 \leqslant x \leqslant 3.0$ were reported[4] to possess an activity towards H_2O_2 decomposition. As the activity can be explained in terms of intrinsic factors such as the electronic structure of the catalysts, the sensitivity of catalysts to ionizing radiation can be account.

Effect of γ-irradiation on the activity of various catalysts has been studied by several workers.[5-7] Caffrey and Allen[5] have found that the catalytic activity of silica gel in the decomposition of pentane was increased by γ-irradiation. Kohn and Taylor[7] have reported that these changes in the catalytic activities of silica gel and alumina in deuterium-hydrogen exchange were related to changes in the internal pore structures of the irradiated catalysts.

The present study is devoted to the effects of γ-irradiation on the catalytic behavior of cobalt iron oxides, in which intrinsic factors are taken into account.

Experimental

Cobalt-iron oxides over the complete composition range of the system ($0 \leqslant x \leqslant 3.0$) were prepared using analar basic cobalt(II) carbonate, iron(III) carbonate, and freshly prepared iron(II) carbonate. Iron(II) carbonate in molar ratio $(1-x)$ was added in the composition range $0 \leqslant x \leqslant 1.0$. The appropriate amounts of the carbonates were suspended in distilled water, stirred well, evaporated to dryness and then dried at 110 °C. The preparations were calcined in air at 300 °C for 4 h. The x values were 0, 0.5, 1.0, 1.5, 2.0, 2.5, and 3.0.

All samples calcined at 300 °C for 4 h, were γ-irradiated at ambient temperature with gamma rays using ^{60}Co cell with a dose rate of 27 rad s^{-1} for 70 h.

X-Ray diffraction patterns (XRD) for unirradiated and γ-irradiated samples were obtained with the aid of philips unit, type PW 2103100 using a Cu target and Ni filter.

Infrared spectra for specimens were recorded using the KBr technique in the range of 1000—200 cm^{-1} with the aid of infrared spectrophotometer Model 599B, Perkin Elmer.

The activity of the catalysts towards H_2O_2 decomposition was evaluated in the liquid phase using the gasometric technique of Cota et al.[8] Catalyst samples (100 mg) were introduced into a thermostated reaction vessel containing standardized 25 ml of 0.4 M H_2O_2 (1 M=1 mol dm^{-3}).

Results

The XRD patterns (Fig. 1) show that cobalt-iron spinel oxides have indeed been formed at 300 °C. The existence of XRD lines corresponding to d-values of 2.53, 1.48, and 1.61 Å as the more intensive lines in the spinels after γ-irradiation reveals that, at our experimental conditions, γ-irradiation preserves the spinel structure of all samples.

The recorded IR spectra for unirradiated and γ-irradiated cobalt-iron oxides are shown in Fig. 2. The expected absorption bands for the ferrites have two intense broad frequency bands sited in the region of 550—600 cm^{-1} (ν_1) and 370—390 cm^{-1} (ν_2) depending

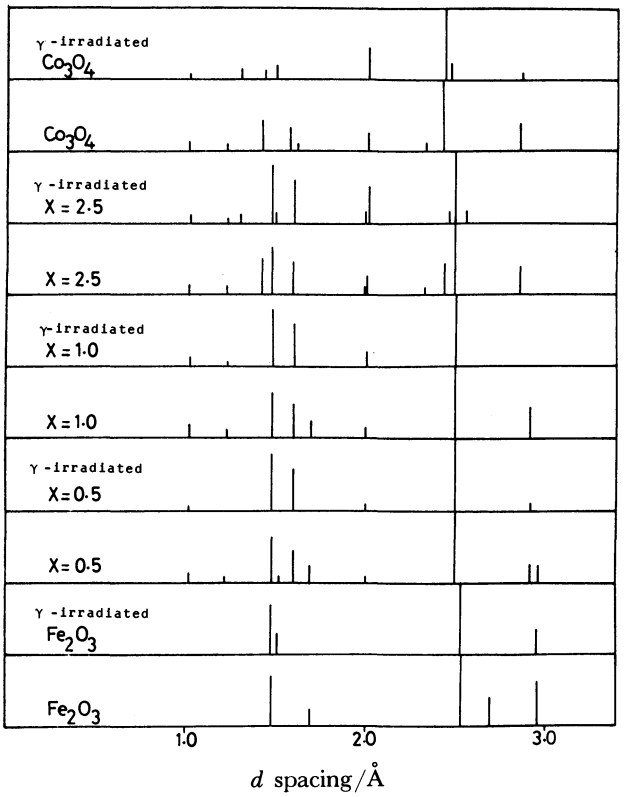

Fig. 1. XRD for unirradiated and γ-irradiated samples.

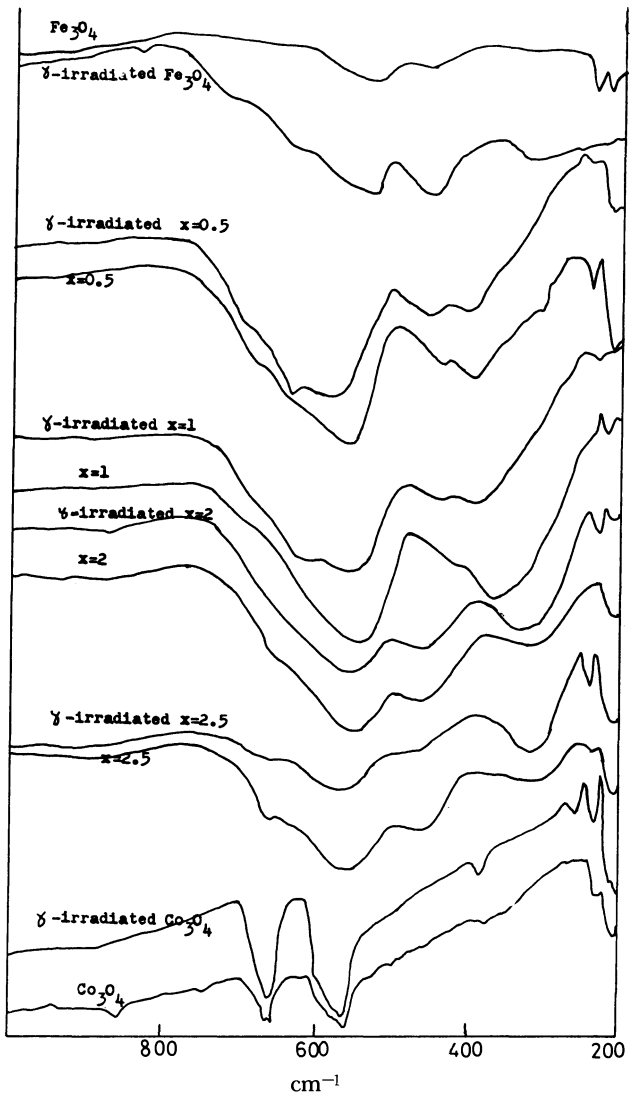

Fig. 2. IR spectra for unirradiated and γ-irradiated cobalt–iron oxides.

on the composition. At 330—350 cm^{-1} there is other band (ν_3) appeared with high concentration of cobalt (x=2.0, 2.5). At 260 cm^{-1} a small band (ν_4) was assigned. Waldron[9] attributed the ν_1-band to the intrinsic vibration of the tetrahedral groups and ν_4 to the octahedral groups. The ν_3-band was reported[9] to be assigned to the vibrations of the bivalent metal ion-oxygen complex. Preudhomme and Tarte[10] reported that ν_4 depends on the mass of bivalent tetrahedral cations. The presence of two-side band around 400 cm^{-1} in rich-iron specimens, in the present study, reveals the presence of Fe^{2+} ions in octahedral sites as confirmed in $Ni_{1-x-y}Fe_x^{2+}Zn_yFe_2^{3+}O_4$.[11]

When cobalt-iron spinels were treated with gamma rays, a displacement of the frequency bands was observed. This displacement can be attributed to gamma-induced different metal valencies and/or cation redistribution. The appearance of ν_3 in both Co_3O_4 and Fe_3O_4 informed an increase in the crystallinity of Co_3O_4 and Fe_3O_4 after γ-irradiation.

The reactivity of the unirradiated and γ-irradiated

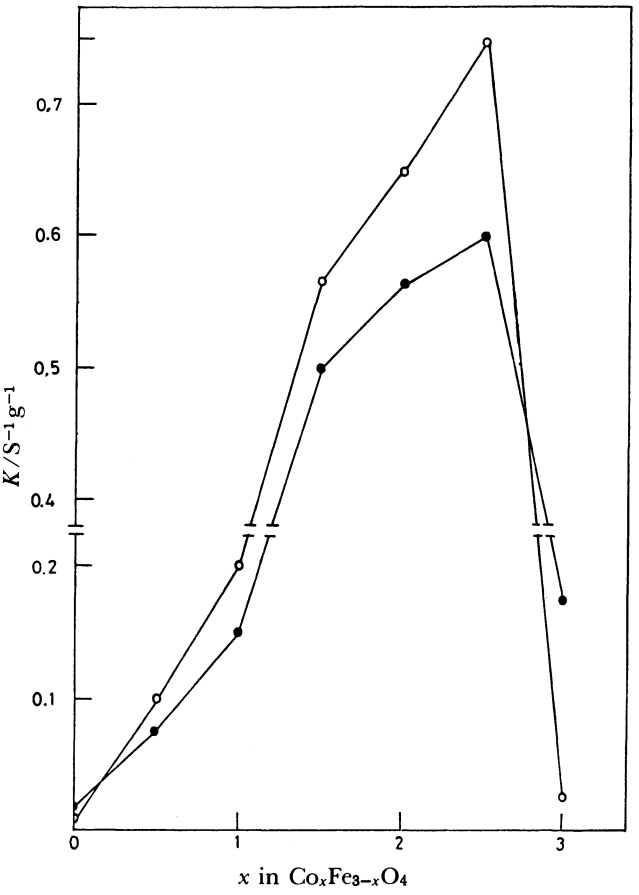

Fig. 3. Initial rate for H_2O_2 decomposition over unirradiated and γ-irradiated $Co_xFe_{3-x}O_4$, at 30°C. ●: Unirradiated, ○: γ-irradiated.

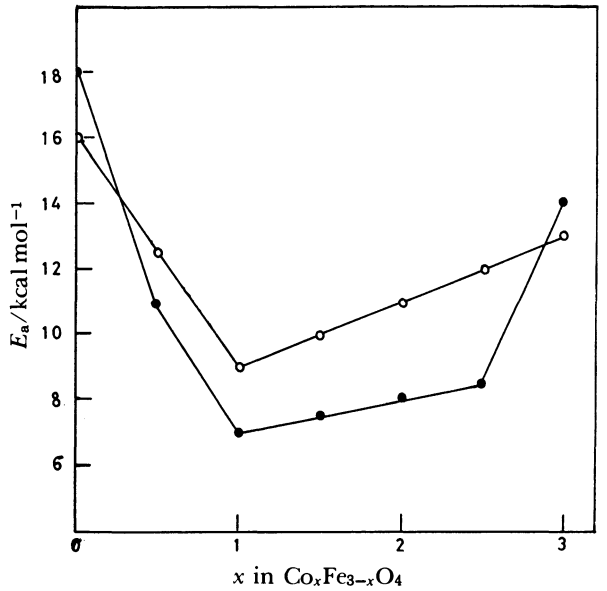

Fig. 4. Activation energy for H_2O_2 decomposition versus composition for unirradiated and γ-irradiated $Co_xFe_{3-x}O_4$. ●: Unirradiated, ○: γ-irradiated.

spinels is illustrated in Figs. 3 and 4. The H_2O_2 decomposition kinetics were found to follow a first order rate equation with respect to H_2O_2, with induced

correction for self decomposition at the experimental conditions. Gamma-irradiation increased the specific rate constants for $0 \leqslant x \leqslant 3.0$ and decreased that of $x=3.0$ sample.

Since the initial rates are dependent on the catalyst microstructure, surface morphology[12] and activation energy was selected independently. As shown in Fig. 4, γ-irradiation induces a marked change in E_a for the catalytic decomposition of H_2O_2 over $Co_xFe_{3-x}O_4$.

Discussion

In cobalt iron oxides, there are two types of bivalent ions readily promoted to the trivalent state, i.e., Fe^{2+} and Co^{2+}. The electronic structures of Co_3O_4 and Fe_3O_4 were reported as $(Co^{2+})_t[Co_2^{3+}]_oO_4$[13] and $(Fe_t^{3+})_t[Fe_t^{2+}Fe_t^{3+}]_oO_4$[14] respectively. Although Co^{2+} in Co_3O_4 is positioned on isolated tetrahedral sites, it has greater activity in H_2O_2 decomposition than octahedral Fe^{2+} ion in the inverse spinel Fe_3O_4, as seen in Fig. 4. Moreover Hart et al.[15] reported that p-type semiconducting oxides are more active catalysts for H_2O_2 decomposition than n-type which is confirmed in the present study. Jonker reported an n-type behavior for $x \leqslant 1.0$ in the $Co_xFe_{3-x}O_4$ system, while those with composition of $x \geqslant 1.0$ were p-type semiconductors. The fact that there is a contradiction between the trend of rate variation in Fig. 3 and activation energy values, reveals that the microstructure parameter controls the rate values. Cota et al.,[8] when normalized H_2O_2 decomposition rates to unit BET surface area yields intrinsic catalytic activities, which follow the trend of activation energy. Thus, the intrinsic factor in the present study is the activation energy.

Considering the spinel electronic structure as Co_x-$Fe_{3-x}O_4$, when cobalt ions are substituted into the Fe_3O_4 lattice, they first replace Fe^{2+} ions on the octahedral sites (B sites), while the Fe^{3+} ions still occupy the tetrahedral sites (A sites). In cobalt-rich region with $x \geqslant 2.0$, Co^{2+} ions occupy only the A sites as represents in Table 1.

The effect of γ-irradiation on the catalytic activity is shown in Fig. 4 can be interpreted according to the induced ionization of the ions (Co^{2+} and Fe^{2+}) with formation of free change carriers (electrons). The negative effect of γ-irradiation on the activity of p-type Co_3O_4 can be attributed to the creation of anionic vacancies, while the same effect for n-type Fe_3O_4 is attributed to the cation random distribution such as $(Fe_{1-\alpha}^{3+}Fe_\alpha^{2+})_t[Fe_{1-\alpha}^{2+}Fe_{1+\alpha}^{3+}]_oO_4$ as detected by ν_2-band lowering.

The catalytic behavior for γ-irradiated mixed oxides can be ascribed to the electron diffusion from the bulk to the surface, and recombining with the higher-valency states (Fe^{3+} and Co^{3+}). Hence the concentration of the active centers (Fe^{2+} and Co^{2+}) increased. For cobalt-rich spinels, ν_1- and ν_2-band intensities and increasing in ν_3-band intensity induced by X-irradiation suggest partially inverse structure, i.e., some Co^{3+} ions on B sites invert with Co^{2+}, giving a distribution of the form $(Co_{1-\alpha}^{2+}Co_\alpha^{3+})_t[Co_\alpha^{2+}Co_{2-x\cdot\alpha}^{3+}Fe^{3+}]_oO_4$ instead of the simple distribution $(Co_t^{2+})_t[Co_{2-x}^{3+}Fe_x^{3+}]_oO_4$. In iron-rich region, highering of ν_1- and ν_2-bands by γ-irradiation reveals formation of lower-valency states as the active sites on both A and B sites, with larger ionic radius leading to an activity increase as predicted.

References

1) I. Mochida and K. Takeshita, *J. Phys. Chem.*, **78**, 1653 (1974).
2) V. A. Sadykov and P. G. Grulnikov, *Kinet. Katal.*, **18**, 137 (1977).
3) V. Múcka, *Collect. Czech. Chem. Commun.*, **46**, 1876 (1981).
4) J. R. Goldstein and C. C. Tseung, *J. Catal.*, **32**, 452 (1974).
5) J. M. Caffrey and A. O. Allen, *J. Phys. Chem.*, **62**, 33 (1958).
6) Y. Saito and Y. Makishima, *Nature (London)*, **183**, 388 (1959).
7) H. W. Kohn and E. H. Taylor, *J. Phys. Chem.*, **63**, 966 (1959).
8) H. M. Cota, J. Katan, M. Chin, and J. F. Schoenweis, *Nature (London)*, **203**, 1281 (1964).
9) R. D. Waldron, *Phys. Rev.*, **99**, 1727 (1955).
10) J. Preudhomme and P. Tarte, *Spectrochim. Acta, Part A*, **27**, 1817 (1971).
11) V. A. Potakova, N. D. Zverv, and V. P. Romanov, *Phys. Status. Solidi A*, **12**, 623 (1972).
12) W. C. Schumb, C. N. Salterfield, and R. L. Wentworth,

Table 1. Properties of Cobalt Iron Oxides

Composition	Cation distribution[a]	E_a for unirrad. kcal mol^{-1}	E_a for γ-irradiated kcal mol^{-1}
$Co_0Fe_3O_4$	$(Fe_t^{3+})_t[Fe_t^{2+}Fe_t^{3+}]_oO_4^{2-}$	16.0	18.0
$Co_{0.5}Fe_{2.5}O_4$	$(Fe_t^{3+})_t[Co_{0.5}^{2+}Fe_{0.5}^{2+}Fe_t^{3+}]_oO_4^{2-}$	12.5	11.0
$Co_1Fe_2O_4$	$(Fe_t^{3+})_t[Co_t^{2+}Fe_t^{3+}]_oO_4^{2-}$	9.0	7.0
$Co_{1.5}Fe_{1.5}O_4$	$(Co_{0.5}^{2+}Fe_{0.5}^{3+})_t[Co_{0.5}^{2+}Co_{0.5}^{3+}Fe_{1.0}^{3+}]_oO_4^{2-}$	10.0	7.5
$Co_2Fe_1O_4$	$(Co_t^{2+})_t[Co_t^{3+}Fe_t^{3+}]_oO_4^{2-}$	11.0	8.0
$Co_{2.5}Fe_{0.5}O_4$	$(Co_t^{2+})_t[Co_{1.5}^{3+}Fe_{0.5}^{3+}]_oO_4^{2-}$	12.0	8.5
$Co_3Fe_0O_4$	$(Co_t^{2+})_t[Co_t^{3+}Co_t^{3+}]_oO_4^{2-}$	13.0	14.0

a) Cation distribution from Ref. 4.

"Hydrogen Peroxide," Reinhold, New York (1955), Chap. 8, pp. 472, 476.
13) J. P. Suchet, "Chemical Physics of Semiconductors," Van Nostrand, Amsterdam (1965), p. 77.
14) E. Verwey, *Philips Res. Rep.*, **5**, 173 (1950).
15) A. B. Hart, J. McFadyen, and R. A. Ross, *Trans. Faraday Soc.*, **59**, 1458 (1963).

 © 1988 The Chemical Society of Japan Bull. Chem. Soc. Jpn., 61, 1335—1337 (1988)

Charge-Transfer Complexes of Nitrones. VI. Molecular Complexes of Nitrones with Iodine

Ahmed M. Nour EL-DIN* and Abdel-Razak TAWFIK†
Chemistry Department, Faculty of Science, El-Minia University, El-Minia, A. R. Egypt
†Chemistry Department, Faculty of Education, Ain Shams University, Cairo, A. R. Egypt
(Received April 30, 1986)

Charge-transfer (CT) complexes between some α-aryl and α-(heterocyclic substituted)nitrones and iodine as σ-acceptor in dichloromethane have been investigated spectrophotometrically. From the energies of the charge-transfer transitions, the ionization potentials of the nitrones have been obtained. The stoichiometry of the complexes has been determined. All the results are in agreement with the n-σ* nature of these complexes with some involvement of the π-orbital of the donor.

In our earlier reports,[1-4] it has been shown that nitrones form 1 : 1 CT complexes with the π-acceptors like tetracyanoethylene (TCNE), 7,7,8,8-tetracyanoquinodimethane (TCNQ), and 2,3-dichloro-5,6-dicyanobenzoquinone (DDQ). The results indicate also that, these complexes are weak in nature and the Ph-CH=N→O moiety is responsible for the complexation with π-acceptors. Therefore, it seemed interesting to investigate the ability of nitrones to form CT complexes with σ-acceptors like iodine.

This work reports the spectrophotometric results for CT complexes of some α-aryl and α-(heterocyclic substituted) nitrones **1a—f**, **2**, and **3a,b** as donors and iodine as σ-acceptor. The role of the nitrone group, >C=N→O, as well as the aryl and heterocyclic moieties of the electron donors on the formation and stabilization of the CT complexes with iodine have been discussed. The stoichiometry and formation constant values of the different CT complexes studied have been determined. Furthermore, the ionization potentials (I.P) of the donors under investigation have been calculated.

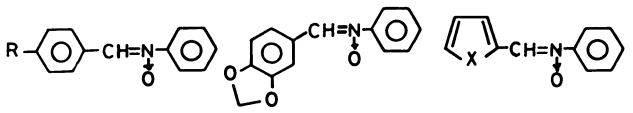

1a—f **2** **3a, b**

1a: R = OC_2H_5; **1b**: R = OCH_3; **3a**: X = S;
1c: R = CH_3; **1d**: R = H; **3b**: X = O.
1e: R = Cl; **1f**: R = NO_2.

Fig. 1.

Experimental

E. Merck G. R. quality iodine was resublimed under reduced pressure. The nitrones **1a—f**, **2**, and **3a**, **b** were prepared according to the literature.[5] Dichloromethane was purified following Vogel[6] dried and distilled. The formation constants K_{ct} and the stoichiometry of the CT complexes were determined utilizing the Benesi-Hildebrand equation[7] and the conventional continuous variation method[8] (Job's method), respectively. For the purpose of determining the formation constants, the concentration of I_2 was 7.505×10^{-5} M (1M=1 mol dm^{-3}), while those of the donors **1a—f**, **2**, and **3a**, **b** ranged from 3×10^{-3} to 1.5×10^{-2} M. However, for the determination of the soichiometry, stock solutions (3×10^{-3} M) of donors and acceptors were prepared. The electronic spectra were recorded from 200—750 nm with a Beckman spectrophotometer model 26, using 5 cm stoppered silica cells.

Results and Discussion

A new band in the visible region (484—499 nm) is observed on mixing dichloromethane solutions of each of nitrones **1a—f**, **2**, as well as **3a**, **b** and iodine. This broad band is attributed to the formation of CT complexes, since neither the nitrones nor the iodine alone absorb in this region. However, after standing overnight, the violet color of the solutions varied to a more yellowish hue, and sometimes a fine brownish precipitation was produced. This behavior may be ascribed to a chemical reaction between the nitrones (reactive 1,3-dipoles) and iodine. Similar behavior was observed in the CT complexes of nitrones with the π-acceptor TCNE.[3,9]

According to the electronic structure of nitrones[10] **1a—f**, **2**, and **3a**, **b**, the formation of CT complexes with iodine can be attributed to either n-σ* or π-σ* interactions. In other words, n-electrons of oxygen atom of the nitrone functional group (>C=$\overset{+}{N}$-$\overline{O}$) or π-electrons of the aromatic rest can be involved in the CT complexation process. Information on this could come from the observation of the substituent effect on λ_{max} and K_{ct} of the CT complexes formed.[11] Data in Table 1 show that, the effect of different substituent on λ_{max} s and K_{ct} s is relatively small. Although there is a great difference in both inductive and mesomeric effects between the moieties which attached to the nitrone functional group, e.g. thienyl and *p*-nitrophenyl moieties, the λ_{max} values of the CT complexes lie in a narrow range (484—499 nm). In addition, a plot of transition energies of the substituted nitrones **1a—f** against the Hammett σ_p constants[12] gave a linear fit with slope (ρ)=0.42 and shows that the substituents (OC_2H_5, OCH_3, CH_3, H, Cl, and NO_2) exert weak electronic effects upon the transition energies of the CT complexes. This result indicates that, the transmission of the substituent effect in the nitrone-iodine

Table 1. Maximum Absorption Wavelengths λ_{max} (nm), Transition Energies E (kcal mol^{-1}), Molar Extinction Coefficients ε (l mol^{-1} cm^{-1}) and Formation Constants K_{ct} (l mol^{-1}) for the CT Complexes between the Nitrones **1a—f**, **2**, and **3a**, **b** and Iodine in CH_2Cl_2 at 25 °C, as well as the Ionization Potentials I.P (eV) of the Donors **1a—f**, **2**, and **3a**, **b**

Donor	λ_{max}/nm	E	ε	K_{ct}	I.P
		kcal mol^{-1}	l mol^{-1} cm^{-1}	l mol^{-1}	eV
1a	499	57.31	3395	23.27	6.69
1b	498	57.43	3360	22.19	6.70
1c	496	57.66	3291	21.10	6.71
3a	495	57.77	2950	21.15	6.72
2	493	58.01	3385	20.11	6.73
1d	492	58.13	3188	19.69	6.74
1e	491	58.25	2922	19.12	6.75
3b	491	58.25	2560	18.55	6.75
1f	484	59.09	2265	16.83	6.80

complexes is small and implies that the interaction between the nitrone and iodine may be ascribed to the lone pair electrons of the oxygen atom of the nitrone functional group, i.e. the n-σ^* nature of these CT complexes. On the other hand, comparison of this ρ value with the corresponding value of the analogous π-σ^* complexes[7] shows that, the nitrone **1a—f**-I_2 complexes exhibits low ρ value and give an evidence for the n-σ^* nature. Moreover, the formation constant K_{ct} values of the CT complexes (Fig. 2) follow the same pattern as λ_{max} and gives another evidence for the n-σ^* nature of the CT complexes. Hence, it can be inferred that the complexation process between the nitrones and iodine is due to the lone-pair electrons of oxygen atom. In addition, the extra negative charge on the oxygen atom should make it a better electron donor according to charge transfer theory[7,13] and consequently the center reasonably seems to be the oxygen atom. However, as was stated previously,[13] 2p π electrons of the oxygen atom in nitrones are conjugated with the rest of the π-electron system and the N-O bond has about 30% of double bond character.[14] Thus, it can be concluded that, the complexation process between the nitrones and iodine can be attributed to n-σ^* interaction, with small involvement of the π-orbital of the aromatic rest of the nitrones.

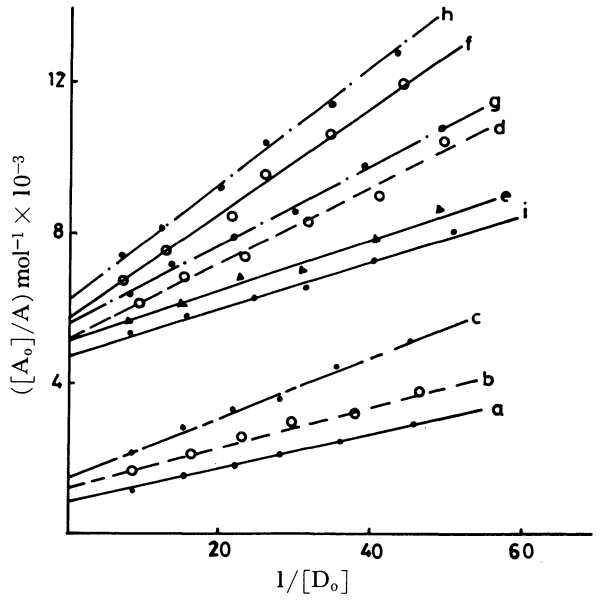

Fig. 2. Typical plots employed in the calculation of formation constants of complexes: (a) **1a**-I_2, (b) **1b**-I_2, (c) **1c**-I_2, (d) **3c**-I_2, (e) **2**-I_2, (f) **1d**-I_2, (g) **1e**-I_2, (h) **3b**-I_2, (i) **1f**-I_2; $[A_o]=7.505\times10^{-5}$ M and $[D_o]=3\times10^{-3}$ to 1.5×10^{-2} M. Dichloromethane used as solvent.

The ionization potential values listed in Table 1 were estimated from the energies of the CT bands applying the following empirical equation:[7,11]

$$\text{I.P (eV)} = 2.90 + 1.89\times10^{-4}\,\tilde{\nu}_{I_2}\,(\text{cm}^{-1})$$

Recently,[15] the complexation process between α-aryl nitrones and π-acceptors (TCNE and 1,4-benzoquinones) has been attributed to π-π^* interaction. A comparison of the I.P values of the nitrones **1b—e** in the case of iodine complexes with those values in cases of DDQ and TCNE complexes indicates that there is a reasonable difference between both I.P values (Table 2). Such difference suggests that the orbital of nitrones involved in the interaction with iodine acceptor is different from that involved in cases of DDQ and TCNE. Again, this result reinforces the suggestion of the n-σ^* nature of the nitrones-iodine complexes.

The stoichiometry of the molecular complexes formed were determined by application of Job's method[8] (continuous variation method). The plots of the intensity of the CT band maxima against the mole fraction of the donors (Fig. 3) furnished symmetrical curves with maxima at mole fraction 0.5 indicating

Table 2. Ionization Potentials of the Nitrones **1b—e** as obtained from Transition Energies of CT Complexes with DDQ, TCNE, and Iodine

Nitrone	I.P/eV DDQ[a]	I.P/eV TCNE[a]	Iodine
1b	8.02	8.07	6.70
1c	8.27	8.16	6.71
1d	8.40	8.29	6.74
1e	8.40	8.47	6.75

a) Data are taken from Ref. 16.

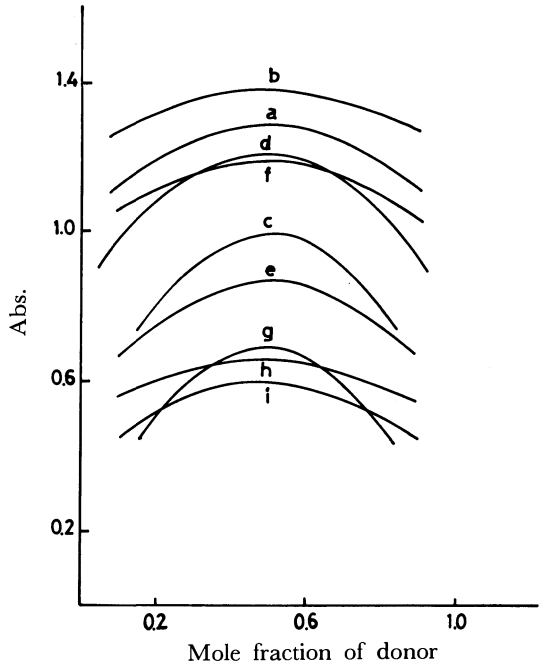

Fig. 3. Job's method for the CT complexes of I_2 with: a) **1a**; λ_{max}=499 nm, b) **1b**; λ_{max}=498 nm, c) **1c**; λ_{max}=496 nm, d) **3a**; λ_{max}=495 nm, e) **2**; λ_{max}=493 nm, f) **1d**; λ_{max}=492 nm, g) **1e**; λ_{max}=491 nm, h) **3b**; λ_{max}=491 nm, i) **1f**; λ_{max}=484 nm, total concentration=2×10^{-3} M. Dichloromethane used as solvent.

1 : 1 stoichiometric ratio for all CT complexes studied.

References

1) A. M. Nour El-Din and A. E. Mourad, *Bull. Soc. Chim. Belg.*, **91**, 539 (1982).
2) A. M. Nour El-Din and A. E. Mourad, *Monatsh. Chem.*, **114**, 211 (1983).
3) A. M. Nour El-Din and D. Döpp, *Bull. Soc. Chim. Belg.*, **93**, 891 (1984).
4) A. M. Nour El-Din, *Spectrochim. Acta, Part A.* **41**, 721 (1985).
5) W. Rundel, "Methoden der Organischen Chemie," Houben-Wely-Müller, Thieme, Stuttgart (1968), Bd. Xi4, S. 309.
6) A. I. Vogel, "Textbook of Practical Organic Chemistry," 3rd ed., Longman, London (1957).
7) R. Foster, "Organic Charge Transfer Complexes," Academic Press, London (1969).
8) P. Job, *Ann. Chim.*, **10**, 113 (1928).
9) D. Döpp and A. M. Nour El-Din, *Chem. Ber.*, **111**, 3952 (1978).
10) R. Huisgen, *J. Org. Chem.*, **41**, 403 (1976).
11) G. G. Aloisi and S. Pignataro, *J. Chem. Soc., Faraday Trans. 1*, **69**, 534 (1973).
12) H. H. Jaffe, *Chem. Rev.*, **53**, 222 (1953).
13) R. S. Mulliken, *J. Am. Chem. Soc.*, **74**, 811 (1952).
14) G. Tsoucaris, *J. Chim. Phys.*, **58**, 619 (1961).
15) A. M. Nour El-Din, *Bull. Soc. Chim. Belg.*, (1986), submitted for publication.
16) A. M. Nour El-Din, *Indian J. Chem.*, **24A**, 511 (1985).

Condensation and Cyclization Reactions of 2-Hydrazinobenzimidazole, -benzoxazole, and -benzothiazole

M. Z. A. Badr,* A. M. Mahmoud, S. A. Mahgoub, and Z. A. Hozien
Chemistry Department, Faculty of Science, Assiut University, Assiut, Egypt
(Received June 16, 1986)

2-Hydrazinobenzoxazole (**1**), -benzimidazole (**2**), and benzothiazole (**3**) were condensed with ethyl chloroformate and/or diethyl oxalate to produce, 1,2,4-triazolo- and 1,2,4-triazino-fused ketones of the title azoles respectively. Condensation of **1** and **2** with aromatic aldehydes and/or acetic anhydride produced, 3-aryl- and 3-methyl-substituted 1,2,4-triazolo-fused azoles respectively. The hydrazines **1** and **2** cyclized with acetylacetone to produce the corresponding 2-(1-pyrazolyl) derivatives. 2-Acetylthiazolobenzimidazole reacted with hydroxylamine and/or alkylamines, to produce the corresponding condensation products. Also it condensed with aromatic aldehydes to give the chalcones. When reacted with benzenediazonium salt, it gave the corresponding 2-arylazo-substituted compounds.

Thiazolo[3,2-*a*]benzimidazole derivatives have long been known for their antibacterial activity[1] and their quaternary salts as hypoglycaemicagents.[2] Fungicidal,[2,3,5] herbicidal,[4] insecticidal,[5] and plant-growth-regulating[6] properties of thiazolobenzimidazoles have also been reported. On the other hand, benzimidazoles have been reported to be used as anthelmintics,[7] for treatment of *Echinoccus granulosus* or *Tinea hydatigena*[8] and as antiabesity together with other variable applications.

In the present paper we report new procedures for synthesis of new benzimidazoles, benzoxazoles, and benzothiazoles and the thiazolo[3,2-*a*]benzimidazoles through variable condensation and cyclization reactions.

Results and Discussion

As a continuation for our studies[9] on synthesis of fused heterocyclic ring systems constituting triazolo, triazino, and tetrazolo moiety, through cyclization

Table 1. Physical and Analytical Data of 3-Aryltriazolobenzoxazoles (**4a—f**) and 3-Aryltriazolobenzimidazoles (**5a—f**)

Compd[a]	Mp(θ_m/°C) (Solvent)	Yield/%	Molecular Formula	Anal. (Calcd / Found)/%		
				C	H	N
4a	92 (EtOH)	60	$C_{14}H_9N_3O$	71.49 71.50	3.83 3.80	17.87 17.85
4b	315 (AcOH)	75	$C_{14}H_8N_4O_3$[b]	60.00 60.00	2.86 2.89	20.00 20.02
4c	219 (AcOH)	67	$C_{14}H_8N_3OCl$	62.22 62.25	2.96 3.00	15.56 15.54
4d	162 (AcOH)	54	$C_{15}H_{11}N_3O_2$	67.93 67.98	4.15 4.18	15.85 15.82
4e	249 (AcOH)	48	$C_{16}H_{14}N_4O$[b]	69.07 69.05	5.04 5.08	20.14 20.15
4f	233 (AcOH)	43	$C_{15}H_{11}N_3O$	72.29 72.30	4.42 4.41	16.87 16.83
5a	270 (aq. EtOH)	62	$C_{14}H_{10}N_4$	71.80 71.83	4.27 4.30	23.93 23.96
5b	318 (AcOH)	78	$C_{14}H_9N_5O_2$	60.22 60.26	3.23 3.26	25.09 25.08
5c	288 (EtOH)	70	$C_{14}H_9N_4Cl$	62.45 62.46	3.35 3.31	20.82 20.85
5d	245 (aq. EtOH)	58	$C_{15}H_{12}N_4O$	68.18 68.20	4.55 4.53	21.21 21.26
5e	255 (EtOH)	55	$C_{16}H_{15}N_5$	69.31 69.35	5.46 5.50	25.27 25.31
5f	257 (AcOH)	50	$C_{15}H_{12}N_4$	72.58 72.60	4.84 4.80	22.58 22.60

a) IR(KBr); **4a**, 1610 (C=N), 1150 (C-O-C), 1615, 1610, 1570 cm^{-1} (oxazole); **4b**, 1660 (C=N), 1100 (C-O-C), 1615, 1610, 1585 (oxazole), 1550, 1370 cm^{-1} (NO_2); **4c**, 1615 (C=N), 1080 (C-O-C), 1600, 1585, 1575 (oxazole), 690 cm^{-1} (Cl); **4d**, 1615 (C=N), 1110 (C-O-C), 1580, 1570 cm^{-1} (oxazole), **4e**, 1660 (C=N), 1105 (C-O-C), 1600, 1545, 1540 (oxazole), **4f**, 1680 (C=N), 1090 (C-O-C), 1630, 1610, 1590 (oxazole), 1450, 1310 cm^{-1} (CH_3); **5a**, 1650 (C=N), 3410 cm^{-1} (NH), **5b**, 1630 (C=N), 3400 (NH), 1560, 1330 cm^{-1} (NO_2); **5c**, 1650 (C=N), 3420 (NH), 370 cm^{-1} (Cl); **5d**, 1650 (C=N), 3390 (NH), 1125 cm^{-1} (OCH_3); **5e**, 1650 (C=N), 3510 (NH), 800 cm^{-1} ($N(CH_3)_2$); **5f**, 1700 (C=N), 3420 (NH), 1450 cm^{-1} ($-CH_3$). b) Molecular ions, **4b**, *m/z* 280; **4e**, *m/z* 296.

Table 2. Physical and Analytical Data of (2-Benzoxazolyl)hydrazones (**6a—f**) and (2-Benzimidazolyl)hydrazones (**7a—f**)

Compd[a]	Mp(θ_m/°C) (Solvent)	Yield/%	Molecular formula	Anal. (Calcd / Found)/%			Ref.
				C	H	N	
6a	204.5 (EtOH)	60	—	—	—	—	8
6b	245 (EtOH)	75	$C_{14}H_{10}N_4O_3$	59.58 59.50	3.55 3.65	19.86 19.99	—
6c	248 (DMF)	91	—	—	—	—	19
6d	207 (EtOH)	89	—	—	—	—	19
6e	224 (aq. DMF)	83	—	—	—	—	19
6f	215 (EtOH)	51	$C_{15}H_{13}N_3O$	71.71 71.75	5.18 5.23	16.73 16.66	—
7a	291 (EtOH)	63	$C_{14}H_{12}N_4$	71.19 71.15	5.09 5.00	23.71 23.75	—
7b	283 (EtOH)	68	—	—	—	—	20
7c	270 (EtOH)	70	$C_{14}H_{11}N_4Cl$	61.99 62.03	4.06 4.00	20.66 20.70	—
7d	212 (EtOH)	58	—	—	—	—	20
7e	245 (EtOH)	49	—	—	—	—	20
7f	277 (EtOH)	50	$C_{15}H_{14}N_4$	72.00 72.11	5.6 5.62	22.40 22.35	—

a) Compound **6a**, ^{1}H NMR ($CDCl_3$) δ=7.40—7.45 (m, 5H, Ar), 7.70—7.85 (m, 4H, Ar), 8.60 (s, 1H, -CH=N- and NH proton is downfield: **6b**, IR(KBr), 1700 (C=N), 3420 (NH), 3020 cm^{-1} (NH, imidazole); ^{1}H NMR (DMSO), δ=2.40 (s, 3H, CH_3), 7.1—7.55 (m, 8H, Ar), 7.65—7.80 (s, 2H, 2NH), 8.15 (s, 1H, -N=CH-).

Table 3. Physical and Analytical Data of Compound **8—12** and **15—19**

Compd[a]	Mp(θ_m/°C) (Solvent)	Yield/%	Molecular formula	Anal. (Calcd / Found)/%			
				C	H	N	S
8	218 (EtOH)	55	$C_8H_5N_3O_2$	54.86 54.98	2.86 2.96	24.00 24.13	—
9	173 (EtOH)	43	$C_8H_6N_4O$	55.17 55.23	3.45 3.54	32.18 32.13	—
10	176 (EtOH)	50	$C_8H_5N_3OS$	50.26 50.18	2.62 2.60	21.99 21.88	16.76 16.75
11	110 (Benzene)	89	$C_9H_9N_3O_2$	56.55 56.60	4.71 4.78	21.99 22.01	—
12	273 (AcOH)	85	$C_9H_{10}N_4O$	56.84 56.98	5.26 5.32	29.47 29.41	—
15	360 (EtOH)	85	$C_9H_5N_3O_3$	53.20 53.35	2.46 2.49	20.69 20.75	—
16	360 (abs EtOH)	80	$C_9H_6N_4O_2$	53.47 53.61	2.97 3.01	27.72 27.68	—
17	340 (EtOH)	82	$C_9H_5N_3O_2S$	49.32 49.38	2.28 2.25	19.19 19.23	14.61 14.53
18	120—121 (EtOH)	60	$C_{12}H_{11}N_3O$	67.59 67.61	5.20 5.30	19.71 19.72	—
19	175 (EtOH)	48	$C_{12}H_{12}N_4$	67.92 68.10	5.66 5.70	26.42 26.42	—

a) Compound **8**, IR(KBr) 3385 (NH), 1710 (C=O enolic), 1660 (C=N), 1100 (C-O-C), 1610, 1590, 1560 cm^{-1} (oxazole); **10**, IR(KBr) 3300 (NH), 1590 (C=O), 1640 (C=N), 1240 cm^{-1} (C-O-C); **11**, IR(KBr) 3310 (NH), 1725 cm^{-1} (C=O), **12**, IR(KBr) 3315 (NH), 1670 cm^{-1} (C=O), ^{1}H NMR ($CDCl_3$) δ=2.50 (s, 3H), 7.40 (m, 4H) δ of NH is downfield; **15**, IR(KBr) 1695, 1645 (COCONH), 1610 (C=N), 1605, 1585, 1555 (oxazole), 1090 cm^{-1} (C-O-C); **16**, IR(KBr) 1710, 1703 (COCONH), 1675 (C=N), 3220 (NH), 1185 cm^{-1} (C-N); **17**, IR (KBr) 1590 (COCONH), 1620 (C=N), 3300 (NH), 1200 cm^{-1} (C-S-C); **18**, ^{1}H NMR ($CDCl_3$) δ=2.60 (s, 3H), 3.20 (s, 3H), 7.3—8.0 (m, 5H, 4HAr+1H, C=CH); **19**, ^{1}H NMR ($CDCl_3$) δ=2.15 (s, 3H), 2.35 (s, 3H), 7.15—7.77 (m, 5H, 4HAr+1H, C=CH), 11.50 (1H, NH).

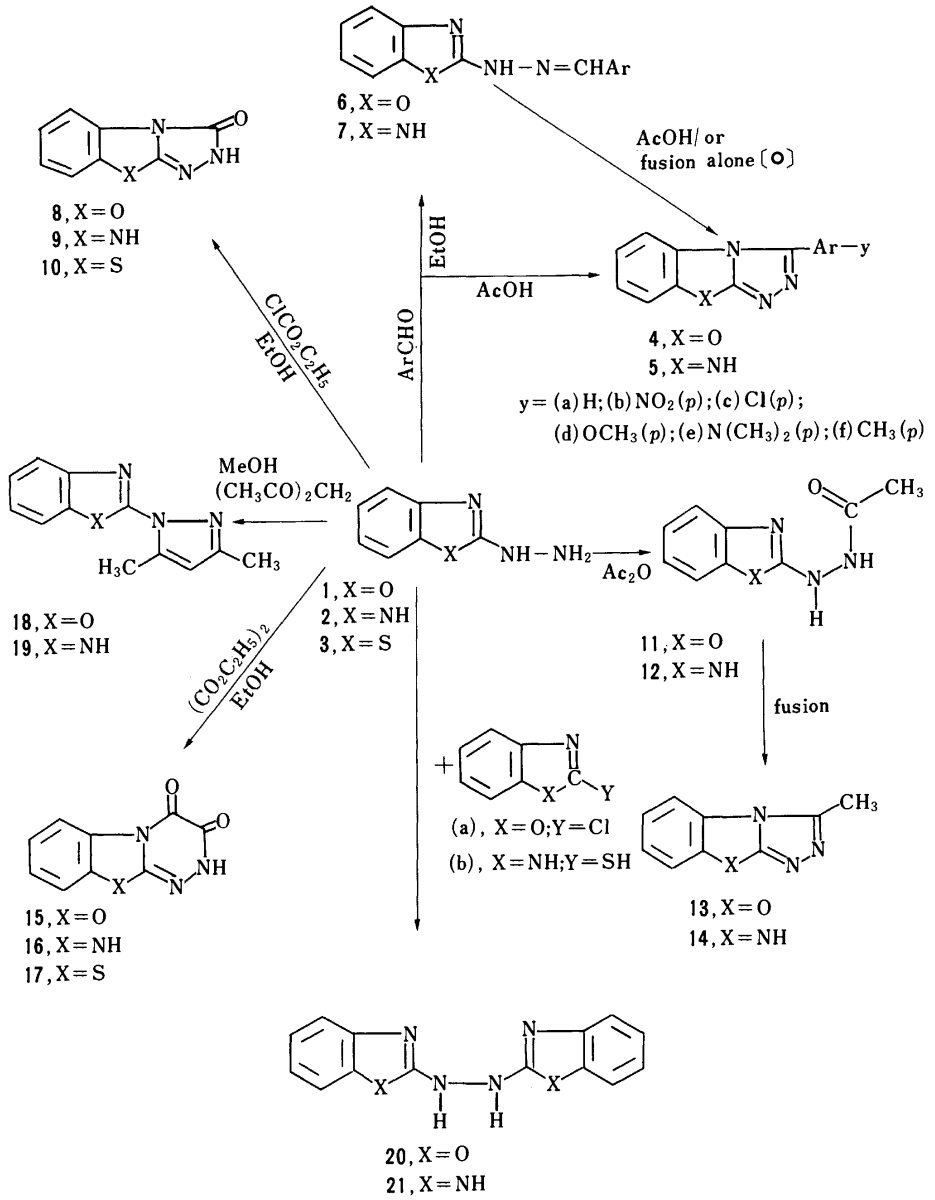

Scheme 1.

reactions, we had discussed the synthesis of comparable heterocycles constituting benzoxazoles, benzimidazoles, and benzothiazoles and thiazolobenzimidazole ring systems.

Reaction of 2-hydrazinobenzoxazole (**1**)[10] and/or 2-hydrazinobenzimidazole (**2**)[10] with benzaldehyde and its *p*-nitro, *p*-chloro, *p*-methoxy, *p*-dimethylamino, and *p*-methyl derivatives in glacial acetic acid gave the corresponding 3-aryl-1,2,4-triazolo[4,3-*b*]benzoxazoles (**4a—f**) and 3-aryl-1,2,4-triazolo[4,3-*a*]benzimidazoles (**5a—f**) respectively. The IR spectra (Table 1) of **4** and **5** showed no (NH_2) bands at 3300, 3200, and 3350, 3250 cm^{-1}, but exhibited (C=N) bands at 1610—1680 and 1650—1700 cm^{-1} together with other characteristic bands. The NMR spectrum of (**5a**) (in DMSO-d_6) showed multiplet at δ 7.1—7.45 (9H, aromatic protons) and broad singlet at δ 9.1—9.85 (1H, NH proton). Compounds **4** and **5** were further produced through ring closure reactions of the corresponding aldehyde (2-benzoxazolyl)hydrazones (**6a—f**) and/or aldehyde (2-benzimidazolyl)hydrazones (**7a—f**) by their refluxing with glacial acetic acid or by its fusion through air oxidation[9,11] (Table 2).

Refluxing **1**, **2**, and **3** with ethyl chloroformate in absolute ethanol produced 1,2,4-triazolo[4,3-*b*]benzoxazol-3(2*H*)-one (**8**); 9*H*-1,2,4-triazolo[4,3-*a*]benzimidazol-3(2*H*)-one (**9**) and/or 1,2,4-triazolo[4,3-*b*]benzothiazol-3(2*H*)-one (**10**) respectively (Table 3).

Refluxing **1** and/or **2** with acetic anhydride produced the corresponding monoacetyl derivatives (**11** and **12**) which cyclized on heating over its melting points into 3-methyl-1,2,4-triazolo[4,3-*b*]benzoxazole (**13**) and 3-methyl-9*H*-1,2,4-triazolo[4,3-*a*]benzimidazole (**14**) respectively in comparable cyclization mechanism as recorded before.[9,12] The IR spectra of both **11** and **12** showed disappearance of (NH_2) bands

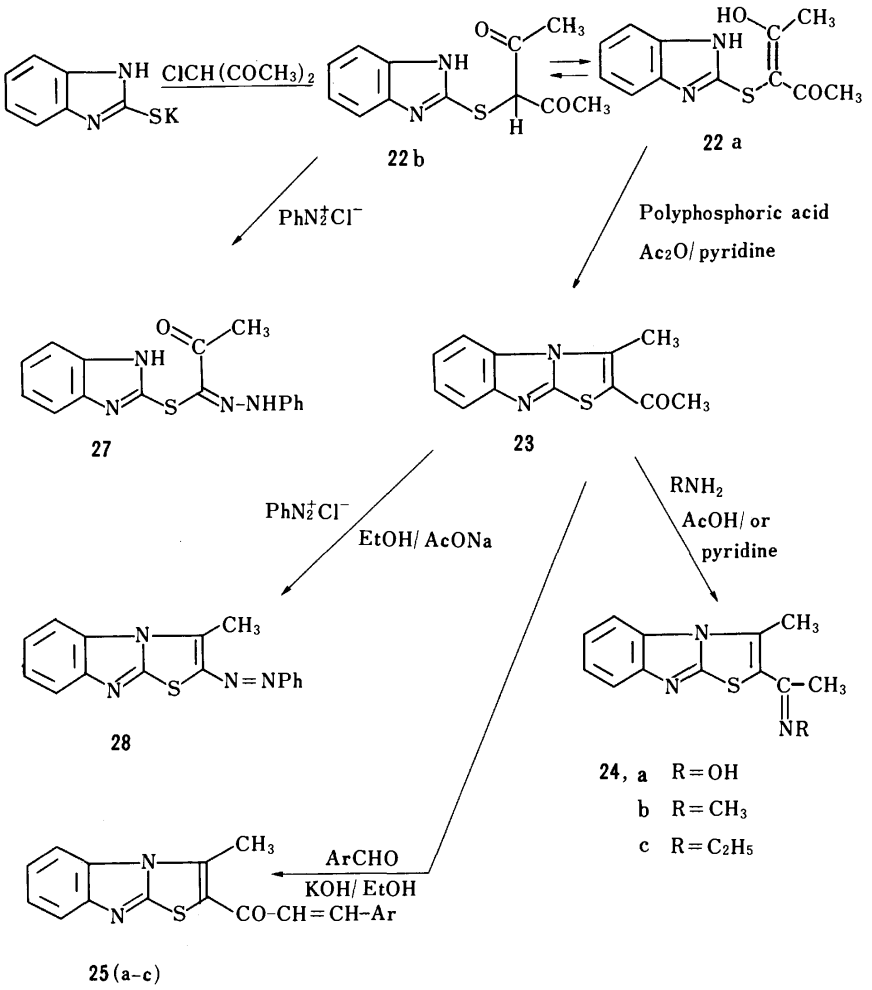

Scheme 2.

and the presence of (NH) group which was also characterized by other spectral means (Table 3).

Similarly, refluxing **1**, **2**, and **3** with diethyl oxalate in absolue ethanol produced the cyclization products, 2*H*-1,2,4-triazino[4,3-*b*]benzoxazole-3,4-dione (**15**), 1,2,4-triazino[4,3-*a*]benzimidazole-3,4-dione (**16**) and 1,2,4-triazino[4,3-*b*]benzothiazole-3,4-dione (**17**) respectively. The IR spectra showed characteristic bands (Table 2). On the other hand, refluxing **1** and **2** with 2,4-pentanedione in methanol produced, 2-(3,5-dimethyl-1-pyrazolyl)benzoxazole (**18**) and 2-(3,5-dimethyl-1-pyrazolyl)benzimidazole (**19**) respectively in similar cyclization step as before,[13,14] which showed characteristic NMR spectra (Table 3). Moreover, refluxing **1** with 2-chlorobenzoxazole and refluxing **2** with benzimidazole-2-thiol in absolute ethanol produced 2,2′-hydrazobis(benzoxazole) dihydrochloride (**20**) and 2,2′-hydrazobis(benzimidazole) (**21**) respectively. Their IR spectra showed disappearance of (NH_2) bands at 3300, 3200 and 3350, 3250 cm^{-1}.

Heating of 3-(2-benzimidazolylthio)-2,4-pentanedione (**22b**) with polyphosphoric acid or refluxing in acetic anhydride-pyridine mixture produced 2-acetyl-3-methylthiazolo[3,2-*a*]benzimidazole (**23**).[15] Its IR spectrum showed the disappearance of the (enolic OH) and (NH) bands at 3370 and 3350 cm^{-1}. Its NMR (in $CDCl_3$) showed singlet at δ 2.48 (3H, CH_3), singlet at δ 3.03 (3H, $COCH_3$) and multiplet at δ 7.05—8.15 (4H, aromatic protons).

Coupling of compounds **22b** and **23** with benzenediazonium salt and sodium acetate in ethanol had resulted into a Japp-Klingemann type reaction[16] producing the corresponding products, 1-(2-benzimidazolylthio)-1-(arylhydrazono)-2-propanone (**27**) and 2-phenylazo-3-methylthiazolo[3,2-*a*]benzimidazole (**28**) respectively. The IR spectrum of **27** showed appearance of bands at 1650 (C=O) and 3150 cm^{-1} (NH), while that of **28** showed disappearance of (C=O) band at 1645, and appearance of (N=N) band at 1640 cm^{-1} together with other characteristic bands.

Refluxing **23** with hydroxylamine, methylamine, and/or ethylamine hydrochloride in acetic acid or in pyridine produced the corresponding oxime **24a** and/or Schiff's bases **24b** and **c**. Higher aliphatic alkyl and aromatic amines were unsuccessfully condensed under variaty of conditions which may be attributed to steric factors. The IR spectra of **24a—c** showed no (C=O) band at 1645, but (C=N) band at 1610 and a broad (OH) band at 3450 cm^{-1} in the oxime **24a** spectrum.

Table 4. Physical and Analytical Data of Compound **24** and **25**

Compd[a]	Mp(θ_m/°C) (Solvent)	Yield/%	Molecular formula	Anal. (Calcd / Found)/%			
				C	H	N	S
24a	285 (AcOH)	75	$C_{12}H_{11}N_3OS$	58.78 58.76	4.49 4.50	17.14 17.20	13.06 13.10
24b	160 (EtOH)	62	$C_{13}H_{13}N_3S$	64.20 64.25	5.35 5.38	17.28 17.30	13.17 13.15
24c	175 (EtOH)	50	$C_{14}H_{15}N_3S$	65.37 65.40	5.84 5.86	16.34 16.30	12.45 12.48
25a	188 ($AcOH/H_2O$)	90	$C_{19}H_{14}N_2OS$	71.70 71.68	4.41 4.39	8.81 8.84	10.06 10.10
25b	200 (EtOH)	52	$C_{19}H_{13}N_3O_3S$	62.81 62.85	3.58 3.53	11.57 11.55	8.82 8.86
25c	180 (AcOH)	50	$C_{12}H_{19}N_3OS$	69.81 69.85	5.26 5.22	11.63 11.63	8.86 8.88

a) Compound **25a**, ^{1}H NMR (DMSO) δ=2.5 (s, 3H), 6.9—7.8 (m, 11H, 9HAr+2H, HC=CH); **25b**, ^{1}H NMR (DMSO) δ=2.51 (s, 3H, CH_3), 7.2—8.5 (m, 10H, 8HAr+2H, CH=CH).

Condensation of **23** with benzaldehyde and its *p*-nitro and *p*-dimethylamino substituents in ethanolic KOH produced the corresponding 2-(3-aryl-1-oxo-2-propenyl)-3-methylthiazolo[3,2-*a*]benzimidazoles (**25a—c**) (Table 4).

Experimental

Melting points were uncorrected. Infrared spectra were recorded on Unicam SP 200 g. Perkin-Elmer 599B and Shimadzu infrared spectrophotometers using potassium bromide Wafer technique. Ultraviolet spectra in ethanol were measured on Shimadzu 200S spectrophotometer and NMR spectra were recorded on Varian A60 and EM-390 (90MHz). MS were recorded on AEI MSI2 spectrophotometer at 70 eV.

Reactions of 2-Hydrazinobenzoxazole and 2-Hydrazinobenzimidazole (1 and 2) with Aromatic Aldehydes: i) (2-Benzoxazolyl)hydrazones (6a—f) and (2-Benzimidazolyl)hydrazones (7a—f): The hydrazino compounds[10] **1** and/or **2** (0.1 mol) and aromatic aldehydes (0.01 mol), namely benzaldehyde (**a**) and *p*-nitro- (**b**), *p*-chloro- (**c**), *p*-methoxy- (**d**), *p*-dimethylamino- (**e**), and *p*-methylbenzaldehyde (**f**) were refluxed in ethanol. The solids were separated on cooling, filtered and recrystallized from the proper solvent to give the corresponding hydrazones **6** and **7** which show characteristic mps as listed in Table 2.

ii) 3-(*p*-Substituted phenyl)-1,2,4-triazolo[4,3-*b*]benzoxazoles (4) and 3-(*p*-Substituted phenyl)-1,2,4-triazolo[4,3-*a*]benzimidazole:[5] **General Procedure:** A mixture of the hydrazino compound **1** and/or **2** (0.01 mol) and the aromatic aldehydes (0.01 mol) was refluxed in glacial acetic acid. After cooling, the separated solid was recrystallized from proper solvent, which gave the characteristic mps as shown in Table 1. The same compounds were produced from the corresponding hydrazones **6** and **7** on refluxing in glacial acetic acid for 8 h or on heating over their mp for 10 min.

1,2,4-Triazolo[4,3-*b*]benzoxazol-3(2*H*)-one (8), 9*H*-1,2,4-Triazolo[4,3-*a*]benzimidazol-3(2*H*)-one (9), and 1,2,4-Triazolo-[4,3-*b*]benzothiazol-3(2*H*)-one (10): A mixture of corresponding hydrazino compounds **1—3** (0.01 mol) and ethyl chloroformate (0.1 mol) in absolute ethanol (10 ml) was refluxed for 4 h. The solid separated was filtered and recrystallized from proper solvent to separate the corresponding triazolo compounds in Table 3.

3-Methyl-1,2,4-triazolo[4,3-*b*]benzoxazole (13) and 3-Methyl-9*H*-1,2,4-triazolo[4,3-*a*]benzimidazole (14): i) A mixture of hydrazino compounds **1** and **2** (0.1 mol) and acetic anhydride was refluxed for 8 h. The solid separated on cooling, filtered, and recrystallized from proper solvent to give the corresponding monoacetyl compounds **11** and **12** respectively as in Table 3.

ii) The monoacetyl compounds **11** and **12** were heated over their melting points for 30 min, cooled and recrystallized from 1-butanol to produce the corresponding methyltriazoles **13** and mp 170 °C and **14** mp 231 °C[17] respectively. Found: C, 62.42; H, 4.10; N, 24.33%. Calcd for $C_9H_7N_3O$ (**13**): C, 62.43; H, 4.05; N, 24.3%.

2*H*-1,2,4-Triazino[4,3-*b*]benzoxazole-3,4-dione (15), 1,2,4-Triazino[4,3-*a*]benzimidazole-3,4-dione (16), and 1,2,4-Triazino[4,3-*b*]benzothiazole-3,4-dione (17): A mixture of the corresponding hydrazino compounds (0.1 mol) and diethyl oxalate (0.1 mol) in absolute ethanol (10 ml) refluxed for 3 h. The solid separated on cooling was filtered and recrystallized from proper solvent to give corresponding triazino compounds as in Table 3.

2-(3,5-Dimethyl-1-pyrazolyl)benzoxazole (18) and 2-(3,5-Dimethyl-1-pyrazolyl)benzimidazole (19): A mixture of the corresponding hydrazino compounds (0.1 mol) and 2,4-pentanedione (0.1 mol) in methanol (20 ml) was refluxed for 3 h. The solid separated on cooling, filtered and recrystallized from proper solvent into the corresponding pyrazolyl compounds **18**[18] and **19** respectively as in Table 3.

2,2′-Hydrazinobis(benzoxazole) (20): A mixture of **1** (0.1 mol) and 2-chlorobenzoxazole (0.1 mol) in absolute ethanol was refluxed for 2 h. The solid separated on cooling, filtered, and recrystallized from ethanol as white crystals of **20** as hydrochloride; yield 60%, mp 198 °C. Found: C, 49.50; H, 3.48; N, 16.40; Cl, 20.88%. Calcd for $C_{14}H_{10}N_4O_2 \cdot 2HCl$: C, 49.41; H, 3.59; N, 16.47; Cl, 21.17%.

2,2′-Hydrazinobis(benzimidazole) (21): A mixture of **2** (0.1 mol) and 2-mercaptobenzimidazole (0.1 mol) was heated at 290—300 °C for 5 h. After cooling, the solid separated filtered and recrystallized from ethanol as colorless crystals, yield 52%, mp 257 °C. Found: C, 63.60; H, 4.60; N, 31.91%. Calcd for $C_{14}H_{12}N_6$: C, 63.64; H, 4.55; N, 31.82%.

2-Acetyl-3-methylthiazolo[3,2-*a*]benzimidazole (23): i) A mixture of 2-mercaptobenzimidazole (1.5 g) and KOH 85%

(0.75 ml) in ethanol (12 ml) was heated at 80 °C for 10 min. To the cooled reaction mixture was added 3-chloro-2,4-pentanedione (1.4 ml) and stirred for 4 h. The separated solid from ice-water mixture was filtered and recrystallized from ethanol as pale brown crystals of 3-(2-benzimidazolylthio)-2,4-pentanedione (**22**), yield 52%, mp 218 °C. Spectral analysis confirm the tautomeric enol form **22a** where the IR spectrum showed (OH) strong band at 3370 cm^{-1}. The ^1H NMR spectrum (in DMSO) showed signals at δ=2.4 (s, 6H, $2CH_3$), 3.4 (br, 2H, NH-OH), and 7.1—7.6 (m, 4H, Ar). Found: C, 58.18; H, 4.90; N, 11.31; S, 12.88%. Calcd for $C_{12}H_{12}N_2O_2S$: C, 58.07; H, 4.84; N, 11.29; S, 12.09%.

ii) A mixture of **22** (2 g) and polyphosphoric acid (10 g) was heated at 100 °C for 1 h, then at 125 °C for 15 min. The solid separated with ice-water, was filtered and recrystallized from ethanol into white crystals of **23**, yield 49%, mp 169—170 °C. The same compound was separated in 90% yield or refluxing **22** with acetic anhydride-pyridine (2:3) mixture for 2 h. Found: C, 62.65; H, 4.39; N, 12.20; S, 13.96%. Calcd for $C_{12}H_{10}N_2OS$: C, 62.61; H, 4.35; N, 12.17; S, 13.91%.

Reaction of Benzenediazonium Salt with Compounds 22 and 23: To ice-cooled mixture of **22** (1.3 g) and/or **23** (1.3 g) and sodium acetate (3 g) in ethanol (20 ml) was added benzenediazonium chloride (from 1.3 g aniline) while stirring, then left for 1 h and poured on cooled water. The separated solid was filtered and recrystallized from benzene into corresponding yellow compounds, 1-(2-benzimidazolylthio)-1-(arylhydrazone)-2-propanone (**27**), yield 50%, mp 99 °C and 2-phenylazo-3-methylthiazolo[3,2-*a*]benzimidazole (**28**), yield 68%, mp 183 °C respectively. **27**: Found: C, 61.98; H, 4.50; N, 18.01; S, 10.36%. Calcd for $C_{16}H_{14}N_4OS$: C, 61.94; H, 4.52; N, 18.07; S, 10.32%. **28**: Found: C, 65.80; H, 4.07; N, 19.20; S, 10.97%. Calcd for $C_{16}H_{12}N_4S$: C, 65.75; H, 4.11; N, 19.18; S, 10.96%.

Reactions of 23 with the Appropriate Amino Compounds: General Procedure: A mixture of **23** (1 mol) and the aliphatic amines (1.1 mol), namely, hydroxylamine, methylamine, and/or ethylamine hydrochloride, ether in glacial acetic acid or in pyridine, was refluxed, and cooled. The separated solid filtered and recrystallized from proper solvent into the corresponding oxime and/or Schiff's bases (**24a—c**) respectively as in Table 4.

2-(3-Aryl-1-oxo-2-propenyl)-3-methylthiazolo[3,2-*a*]benzimidazoles (25a—c): A mixture of **23** (0.1 mol) and aromatic aldehydes (0.01 mol), benzaldehyde and its *p*-nitro and *p*-dimethylamino derivatives together with KOH solution (10 ml, 4%) in ethanol (50 ml). The mixture was kept overnight, acidified with dilute acetic acid. The separated chalcones filtered and recrystallized from proper solvent as in Table 4.

M. Z. A. Badr is thankful to Dr. Kevin S. Peters of Harvard University, U.S.A., for his assistance with some NMR and mass spectral analyses.

References

1) V. K. Chadha, H. S. Chaudhary, and H. K. Piyari, *Indian J. Chem.*, **7**, 769 (1969).

2) D. E. Kuhla, U. S. Patent, 3860718; *Chem. Abstr.*, **82**, 140133 (1975).

3) K. C. Joshi, V. N. Pathak, and P. Arya, *Agric. Biol. Chem.*, **41**, 543 (1977); *Chem. Abstr.*, **87**, 53140 (1977); H. S. Chaudhary, C. S. Parda, and H. K. Pujari, *Indian J. Chem.*, **8**, 10 (1970); J. Mohan, V. K. Chadha, H. S. Chaudhary, B. D. Sharma, H. K. Pujari, and L. N. Mohapatra, *Indian J. Exp. Biol.*, **10**, 37 (1972).

4) J. J. D'Amico, U. S. Patent, 3225059; *Chem. Abstr.*, **64**, 8193 (1966).

5) H. J. School, E. Klauke, F. Grewe, and I. Hammann, Ger. Patent, 2062348; *Chem. Abstr.*, **77**, 114391 (1972).

6) G. Hasegawa and A. Kotani, Jpn. Patent, 7495997; *Chem. Abstr.*, **82**, 156299 (1975).

7) P. N. Peterson; *Chem. Rev.*, **74**, 279 (1974).

8) M. A. Gammell, S. N. Paramter, and R. Sutton, *J. Kan., Ngaire Z. Parasitenked.*, **64**, 135 (1981).

9) M. Z. A. Badr, H. A. H. Elsherief, G. M. El-Naggar, and S. A. Mahgoub, *J. Heterocycl. Chem.*, **21**, 471 (1984); S. A. Mahgoub, A. M. Fahmy, M. M. Aly, and M. Z. A. Badr, *Acta Chim. Hung.*, **116**, 267 (1984).

10) O. Bayer, E. Herdieckeboff, and H. Schindelm (to I. G. Farbenind. A-G), U. S. Patent, 2073600; *Chem. Abstr.*, **31**, 3299 (1937).

11) H. Zimmer, J. McManus, T. Novinson, E. V. Hess, and H. Litwin, *Anzneim Forsch.*, **20**, 1586 (1970).

12) J. W. Schneller and D. G. Bartholomew, *J. Heterocycl. Chem.*, **15**, 439 (1978).

13) H. A. Zaher, H. Jahine, O. Sherif, and R. Mohammady, *Indian J. Chem.*, **18B**, 316 (1979).

14) M. Z. A. Badr, S. A. Mahgoub, A. M. Fahmy, and F. F. Abdel-Latif, *Acta Chim. Hung.*, **124** (3), 413 (1987).

15) J. J. D'Amico, R. M. Compbell, and E. C. Guinn, *J. Org. Chem.*, **29**, 865 (1964).

16) Japp-Klingemann Reaction, *Org. Reac.*, **10**, 143 (1959).

17) J. A. Van Allan, U. S. Patent, 2891862; *Chem. Abstr.*, **54**, 4224 (1960).

18) T. P. Sycheva, I. D. Kiseleva, and M. N. Shchukina, *Khim. Geterotsikl. Soedin*, **1**, 43 (1967); *Chem. Abstr.*, **67**, 64274 (1967).

19) K. Katz, *J. Am. Chem. Soc.*, **75**, 712 (1953).

20) M. V. Provstyanoi, E. V. Logachev, P. M. Kochergin, and Yu. I. Beilis, *Izv. Vyssh. Uchebn, Zaved., Khim. Tekhnol.*, **19**, 708 (1976); *Chem. Abstr.*, **85**, 78051 (1976).

 © 1988 The Chemical Society of Japan Bull. Chem. Soc. Jpn., 61, 1345—1349 (1988)

Synthesis and Application of Some 1-[8-Hydroxy-5(or 7)-quinolinyl]-alkylidene-Substituted Heterocycles as Bactericides, Funjicides, and Bioregulator

Zarif Haleem KHALIL, Amal Sabet YANNI,* Ali Ali KHALAF, Ali Ali ABDEL-HAFEZ, and Raafat Foaad ABDO
Chemistry Department, Faculty of Science, Assiut University Assiut, Egypt
(Received December 2, 1986)

Interaction of 5-acetyl-8-quinolinol, corresponding 1-ethylquinolinium iodides, and 8-hydroxyquinoline-7-carbaldehyde with diethylmalonate under basic condition gave the corresponding of **4—6**. Further reaction of **4—6** with hydrazine, phenyl hydrazine, hydroxylamine, urea, and/or thiourea gave the corresponding 1-[8-hydroxy-5(7)-quinolinyl]alkylidene-substituted heterocyclic derivatives (**7—16**) and corresponding 1-ethylquinolinium iodides (**17—21**). The structure of the synthesized compounds was confirmed by elemental and spectral analysis. The biological activity of 5-substituted 8-quinolinol was tested as microbicidal and bioregulator agents, the results obtained were interpreted according to their structure-activity relationships.

The biological activity of azoles and barbituric acid derivatives is of interest.[1-3] Pharmacological studies showed that some of these compounds possessed hypolipidimic central nervous system depressant[4] and antitumor activities.[5] In this work 5(7)-heteroarylidenemethyl-8-hydroxyquinolines were prepared to evaluate the effect of substitution on the biological activity of 8-quinolinol nucleus as antimicrobial and bioregulator agents. Structure activity relationships has also been studied to detect the preferable structures required for such purposes.

Results and Discussion

The reaction of 5-acetyl-8-quinolinol (**1**), its corresponding 1-ethylquinolinium iodide (**2**), and 8-hydroxyquinoline-7-carbaldehyde (**3**) with diethyl malonate in the presence of sodium ethoxide gave the corresponding ethyl 2-ethoxycarbonyl-3-(8-hydroxy-5-quinolinyl)-2-butenoate (**4**), corresponding 1-ethylquinolinium iodide (**5**), and ethyl 2-ethoxycarbonyl-3-(8-hydroxy-7-quinolinyl)-2-propenoate (**6**) respectively.

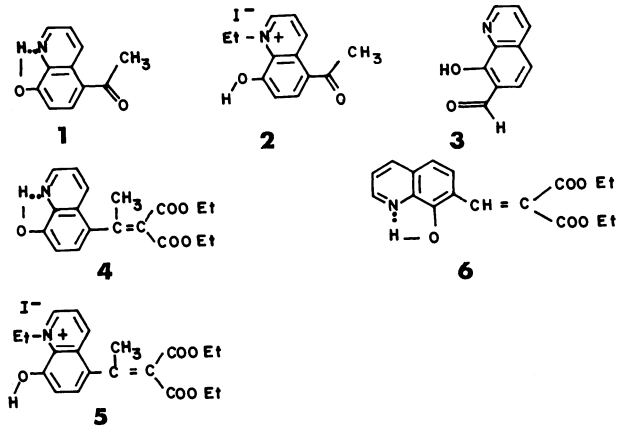

Further reaction of **4—6** with hydrazine hydrate, phenylhydrazine, hydroxylamine hydrochloride, urea, and thiourea gave the corresponding 4-[1-(8-hydroxy-5-quinolinyl)ethylidene]-3,5-pyrazolidinedione (**7**), 4-[1-(8-hydroxy-5-quinolinyl)ethylidene]-1-phenyl-3,5-pyrazolidinedione (**8**), 4-[1-(8-hydroxy-5-quinolinyl)-ethylidene]-3,5-isoxazolidinedione (**9**), 5-[1-(8-hydroxy-5-quinolinyl)ethylidene]barbituric acid (**10**), 5-[1-(8-hydroxy-5-quinolinyl)ethylidene]-2-thiobarbituric acid (**11**); corresponding 1-ethylquinolinium iodides (**17—21**); and 4-[(8-hydroxy-7-quinolinyl)methylene]-3,5-pyrazolidinedione (**12**), 4-[(8-hydroxy-7-quinolinyl)-methylene]-1-phenyl-3,5-pyrazolidinedione (**13**), 4-[(8-hydroxy-7-quinolinyl)methylene]-3,5-isoxazolidinedione (**14**), 5-[(8-hydroxy-7-quinolinyl)methylene]barbituric (**15**) and 2-thiobarbituric acid (**16**). The structures of the synthesized compounds were confirmed by elemental and spectral analysis. The infrared and ultraviolet spectral data are given in Table 3. All of the synthesized compounds 1-[8-hydroxy-5(or 7)-quinolinyl]alkylidene-substituted heterocyclic compounds showed the presence of ν_{-NH} group at 3100—3190 cm^{-1} and the lack of ν_{-NH_2}. The NMR ($CDCl_3$) of compound **11** showed signals at δ 2.7 (3H, CH_3, s), 6.8—7.7 (5H, aromatic, m), and 11.3—11.5 (2H, NH, s).

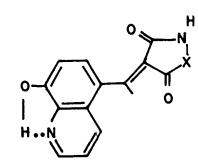

7, X=NH
8, X=N-C_6H_5
9, X=O

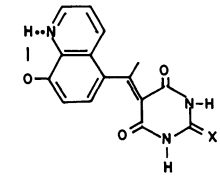

10, X=O
11, X=S

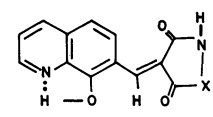

12, X=NH
13, X=N-C_6H_5
14, X=O

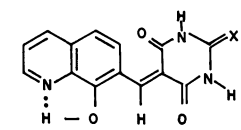

15, X=O
16, X=—S

The role of hydrogen bonding, 5-acetyl group and ring size of the 5-substituted 8-quinolinol are essential factors on the biological activity of the synthesized

Table 1. Physical and Analytical Data of Compounds **4**—**11**

Compd	Solvent of crystallization	Yield %	Mp(θ_m/°C)	R_f value	Molecular formula	Calcd/Found(%)[f]			
						C	H	N	S
4	Ethanol	78	340	0.34[a]	$C_{18}H_{19}NO_5$	69.90	6.15	4.26	—
						70.12	6.30	4.30	—
5	Ethanol	70	245—247 (decomp)	0.7[b]	$C_{20}H_{24}NO_5I$	49.48	4.95	2.90	—
						49.63	5.10	2.80	—
6	Dioxane	63	258—260	—	$C_{17}H_{17}NO_5$	69.15	5.76	4.44	—
						69.33	5.84	4.51	—
7	Ethanol	63	323—325 (decomp)	0.4[c]	$C_{14}H_{11}N_3O_3$	62.45	4.09	15.61	—
						62.60	4.21	15.57	—
8	Methanol	61	218—220	0.46[c]	$C_{20}H_{15}N_3O_3$	69.56	4.34	12.17	—
						69.80	4.52	12.22	—
9	Ethanol	63	327—329 (decomp)	0.43[c]	$C_{14}H_{10}N_2O_4$	62.22	3.70	10.37	—
						62.48	3.92	10.46	—
10	Ethanol	67	210—212	0.51[c]	$C_{15}H_{11}N_3O_4$	60.60	3.70	14.40	—
						60.83	3.88	13.09	—
11	Ethanol	57	258—260	0.56[c]	$C_{15}H_{11}N_3O_3S$	57.51	3.51	13.42	10.22
						57.83	3.68	13.11	10.30
12	Ethanol	43	288—290	0.38[c]	$C_{13}H_9N_3O_3$	61.18	3.53	16.47	—
						61.32	3.70	16.39	—
13	Ethanol	45	220—222 (decomp)	0.45[c]	$C_{19}H_{13}N_3O_3$	68.88	3.93	12.69	—
						69.05	4.11	12.75	—
14	Ethanol	55	279—280 (decomp)	0.41[c]	$C_{13}H_8N_2O_4$	60.94	3.12	10.94	—
						61.16	3.35	11.02	—
15	Ethanol	46	228—230	0.49[c]	$C_{14}H_9N_3O_4$	59.36	3.18	14.84	—
						59.50	3.22	14.91	—
16	Dioxane	40	330—332 (decomp)	0.53[c]	$C_{14}H_9N_3O_3S$	56.19	3.01	14.05	10.70
						56.24	3.30	14.20	10.61
17	Ethanol	66	328—329 (decomp)	0.63[d]	$C_{16}H_{16}N_3O_3I$	45.17	3.76	9.88	—
						45.35	3.95	9.93	—
18	Ethanol	54	345—347 (decomp)	0.58[d]	$C_{22}H_{20}N_3O_3I$	52.69	3.99	8.38	—
						52.77	4.12	8.45	—
19	Ethanol	54	268—270 (decomp)	0.61[d]	$C_{16}H_{15}N_2O_4I$	45.70	3.52	6.57	—
						45.90	3.70	6.61	—
20	Benzene	62	99—100	0.55[e]	$C_{17}H_{16}N_3O_4I$	45.03	3.53	9.27	—
						44.90	3.28	9.33	—
21	Benzene	47	113	0.66[e]	$C_{17}H_{16}N_3O_3SI$	43.50	3.41	8.96	6.82
						43.78	3.50	9.00	6.91

a) Benzene-ethanol (2:1). b) Benzene-ethanol (1:1). c) Benzene-ethanol (3:1). d) Benzene-ethanol (4:1). e) Toluene-ethanol (2:1). f) All compounds gave satisfactory C, H results.

Table 2. Antifungal and Antibacterial Screening

Compd	Inhibition zones (mm) Fungi						Inhibition zones (mm) bacteria		
	Penicillium notatum 100 ppm	*Aspergillus flavus* 100 ppm	*Stachybotrys atra*				*Bacillus subtilis*	*Micrococcus luteus*	*Serratia sp.*
			100 ppm	50 ppm	25 ppm	12.5 ppm			
1	30	35	71	55	40	35	22	19	23
2	25	22	65	48	35	—	—	—	20
4	20	—	52	45	32	—			
5	20	—	58	—	—	—			
10	20	21	53	—	—	—			
11	—	19	52	—	—	—			
15	20	21	53	—	—	—			
16	—	19	52	—	—	—			
17	25	—	50	—	—	—			
18	30	21	65	50	45	35	20		20
19	—	—	53	—	—	—			
20	22	—	57	46	32	—			
21	20	23	56	50	35	—	—		23

The compounds **3**, **6**—**9**, and **12**—**14** have no effect for all the fungi used. The compounds **3**—**21** have no effect for all the bacteria used (except **18** and **21**).

compounds. Thus 5-acetyl-8-quinolinol (**1**) is quite potent as fungicides especially *Stachybotrys atra* (71 mm inhibition zone at 100 ppm, cf. Table 2). Quaternization of **1** decreases its potency. Substitution of 5-acetyl by a butenoate moiety decreases its potency. 6-Membered barbituric and thiobarbituric heterocycles are more effective as fungicides than 5-membered (azoles) ones. On the other hand the above compounds are less potent as bactericides. The results are given in Table 2. Water-soluble compounds were choosen as bioregulator for *Vicia faba* seeds. Germination as expressed in the seedling height after 14 days versus the concentration with respect to the control was studied. It is clear that some of these compounds e.g. (**2**, **7**, **10**, **11**, **17**) enhance the seedling growth. The results are shown in Fig. 1.

More than one shoot per seedling was observed with percentage of 10% at the concentration of 100 ppm for compounds **1** and **7**; 50 and 1000 ppm for compound **17** and 500 ppm for compounds **10** and **11**. The difference in seedling height and the multishooted per seedling phenomena in the treated seeds led us to the

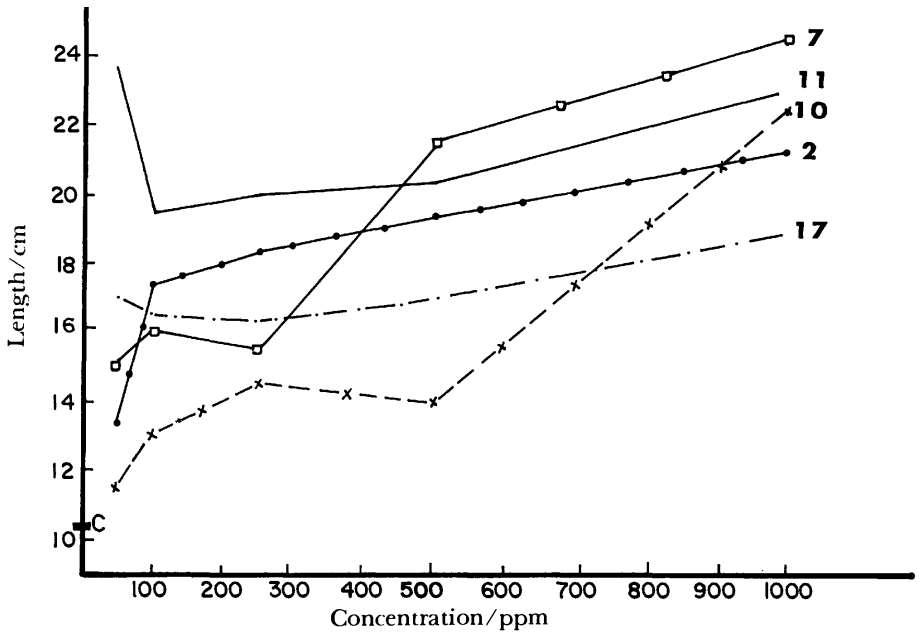

Fig. 1. Germination of *Vicia faba* seeds as expressed in seedling height after 14 days versus the concentration with respect to the control C.

Table 3. IR and UV Spectral Data of Compounds **4**—**21**

Compd	ν_{OH} cm^{-1}	ν_{NH} cm^{-1}	ν_{CO} cm^{-1}	λ_{max} (ε)		
4	3325(s)	—	1725(s)	—	320(5500)	404(2400)
5	3350(s)	—	1630(m), 1730(s)	280 (8700)	305(5800)	392(7000)
6	3345(s)	—	1630(m), 1670(m)		310(4900)	
7	3400	3190(s)	1700(b)	260 (9500)	335(7300)	380(6200)
8	3400(s)	3190(s)	1710(s)	285(15400)	340(7600)	380(5800)
9	3350(s)	3170(s)	1715(s)	260 (9500)	290(6300)	400(2400)
10	3430	3185(s)	1712(s), 1718	280 (6000)	336(7900)	402(3500)
11	3180	3100(s)	1715(s), 1720	285 (7100)	338(9600)	400(1000)
12	3320(b)	3100(b)	1700(m)		314(1900)	
13	3330(b)	3100(b)	1720(m)		312(3600)	
14	3320(b)	3090(s)	1720(m)		313(8200)	
15	3325(b)	3100(m)	1715(s)		310(5900)	
16	3330(b)	3100(m)	1715(s)		320(1000)	
17	3350(s)	3100(m)	1640(m)	—	310(4300)	391(3600)
18	3340(s)	3100(m)	1640(m)	—	306(7200)	394(8100)
19	3335(s)	3100(m)	1650(m)	—	328(5800)	392(3600)
20	3300(s)	3130(m)	1650(s)	—	326(7700)	392(3300)
21	3300(s)	3130(m)	1640(s)	—	328(9400)	390 (800)

(a) Control (b) Bridge formation

(c) More bridge formed (d) Fragment produced

Fig. 2. Chromosomal aberrations of the root-tips of the treated *Vicia faba* seeds as bridge and/or fragments with respect to the control.

cytological examination in the anatelophase. Rootless of the treated seeds showed chromosomal aberation as bridge and/or fragments with respect to the control. This chromosomal aberation is responsible for this behavior of the treated *Vicia faba* seeds (Fig. 2).

Experimental

All melting points are uncorrected. Infrared spectra were determined with a Perkin-Elmer 599 B spectrophotometer using the KBr wafer technique. NMR spectra were carried out in $CDCl_3$ using a Varian EM 390 (90 MHz). UV spectra were recorded in ethanolic solutions using a Cary 219 spectrophoto-meter.

5-Acetyl-[6] and 7-formyl-8-quinolinol[7] were prepared according to literature method reported earlier.

Synthesis of 5-Acetyl-1-ethyl-8-hydroxyquinolinium Iodide (2): A mixture of 10 g (0.054 mol) of 5-acetyl-8-quinolinol[6] (**1**) and 15 ml of ethyl iodide was heated in a sealed tube at 105 °C for 7 h. The product was filtered off, air dried and recrystallized from ethanol to give 19.4 g (82%) of the product

2 in the form of yellowish brown crystals, mp 285—287 °C. Found: N, 4.15%. Calcd for $C_{13}H_{14}NO_2I$: N, 4.08%.

Synthesis of Ethyl 2-Ethoxycarbonyl-3-(8-hydroxy-5-quinolinyl)-2-butenoate (4), Its Ethiodide (5), and Ethyl 2-Ethoxycarbonyl-3-(8-hydroxy-7-quinolinyl)-2-propenoate (6): Diethylmalonate (1.6 g, 0.01 mol) was added to ethanolic sodium ethoxide solution (0.1 g Na in 30 ml absolute ethanol) and the mixture was stirred at room temperature for 1 h. To the resulting sodiomalonate was added an equivalent amount of ethanolic solution from 5-acetyl-8-quinolinol[6] (**1**, 1.9 g in 30 ml), or its ethiodide (**2**, 3.4 g in 50 ml), or 8-hydroxy-7-quinolinecarbaldehyde (**3**, 1.7 g in 30 ml) in one portion. The reaction mixture was heated under reflux for 7 h, cooled and neutralized with acetic acid. The precipitated solid was filtered by suction and air dried. Physical and analytical data are given in Table 1.

Synthesis of 1-[8-Hydroxy-5(or 7)-quinolinyl]alkylidene-Substituted Azolidinediones and Barbituric Acid Derivatives (7—16), and Their Ethiodides (17—21). A mixture of **4**, **5**, or **6** (0.01 mol), hydrazine hydrate, phenylhydrazine, urea, or thiourea (0.01 mol) in ethanolic sodium ethoxide solution (0.1 g Na in 30 ml absolute ethanol) was heated under reflux for 7 h. The reaction mixture was filtered while hot and the filtrate was cooled and neutralized with acetic acid. The precipitated solid was filtered with suction and air dried. Physical and analytical data are given in Table 1.

Biological Activity of Selected New Synthesized Compounds as Antimicrobial and Plant Growth Regulator. The Antimicrobial Activity: The selected new synthesized compounds were dissolved in ethylene glycol (10 mg/100 ml, 100 ppm) and transfered to filter paper disc (15 mm), diffusion plate method.[8] The antifungal activity was determined against *Penicillium notatum*, *Aspergillus flavus*, and *Stachybotrys atra*. The antibacterial effect of the same compounds was determined against *Bacillus subtilis*, *Micrococcus luteus*, and *Serratia Sp*.

Bacterial suspension was prepared by adding 10 ml of sterile distilled water to 10 d old culture of the test bacteria grown on a nutrient agar of NA.[9] The culture consisted of beef extract (10 $g L^{-1}$), peptone (10 $g L^{-1}$), NaCl (5 $g L^{-1}$), and agar (10 $g L^{-3}$) at pH 7.4. One milliliter aliquots of the bacterial suspension were added to NA Petri dishes (one plate/test compound). The excess liquid has removed and filter paper disc (15 mm diameter) containing the test compound was placed on the plate. Plates were then incubated at 37 °C, and the diameter of the inhibition zones were measured after 24 h. These experiments were repeated thrice. The results are given in Table 2.

Spore suspension was prepared by adding 10 ml of sterile distilled water to 10-d-old culture of the test fungus grown on potato-D-glucose-agar (PDA) potatose (peeled and sliced, 200 $g dm^{-3}$), D-glucose (20 $g dm^{-3}$), and agar (17 $g dm^{-3}$) at pH 6.5.[10] One ml aliquots of the spore suspension were added to PDA Petri dishes (plate/test compound). The excess liquid was removed and filtered paper disc containing the tested compound was placed on the plate, then the plate is incubated at 37 °C and the inhibition zones were measured after 3 d. The experiments were carried out in triplicate. The results are given in Table 2.

Biological Effects on the Germination of *Vicia faba* (Variety Giza 2) Seeds: Materials and Methods: Seeds of *Vicia faba* (variety Giza 2) were treated with five concentrations 50, 100, 250, 500, and 1000 ppm of the selected compounds. Fresh solution of the required concentration were prepared using distilled water. A total of 100 seeds were used for each of the five treatments and the control. Seeds were immersed in the solution at room temperature of 25±2 °C for 4 h. Control seeds were treated with distilled water. After treatment, the seeds were washed thoroughly with distilled water to eliminate the solution traces. The seeds of each concentration was germinated on wet germinating papers in the Petri dishes for estimating the germination percentage, seedling height and for cytological studies. After 14 d, germinating and nongerminating seeds were counted and the percentage of germination was determined for each treatment and the number of seeds with more than one shoot were counted for each concentration. The results are shown in Fig. 1.

Cytological Examination: Secondary rootlets of 5—10 mm in length were excised and fixed in a 3:1 ethanol-glacial acetic acid mixture for 12 h and stored in 70% ethanol in a refrigerator. Fixed rootlets were prepared for cytological examination by the acetocarmine Smear technique.[11] For each treatment, preparations from 4 seedling were examined. The chromosomal aberrations were determined in the anaphase stage as bridges and fragments. The experiment was repeated twice and the results are shown in Fig. 2.

References

1) W. O. Foye, "Principles of Medicinal Chemistry," Lee and Fibiger Philadelphia (1974).

2) A. I. Eid, M. I. Kira, and H. H. Fahmy, *J. Pharm. Belg.*, **33**, 5, 303 (1973).

3) A. R. Katritzky, "Advances in Heterocyclic Chemistry," Academic Press, New York (1966), Vol. 6, p. 345.

4) P. Vainilavicius, S. Tumkevicius, A. Deniene, V. Rucka, and N. Laucuviene, *Khim.-Farm. Zh.*, **18**, 1335, (1984); *Chem. Abstr.*, **102**, 131987 (1985).

5) G. R. Glushkov, A. L. Nikolaeva, V. O. Kozlova, N. L. Dronova, *Khim.-Farm. Zh.*, **18**, 674 (1984); *Chem. Abstr.*, **102**, 6372 (1985).

6) G. V. Villenal'd, N. N. Anshets, *J. A. Osodchii, USSR*, 579, 271 (01c070 215/24), 05 No. 1977, Appl. 2, 362, 762, 19 May 1976.

7) R. N. Sen and S. K. Ray, *J. Indian Chem. Soc.*, **9**, 178 (1932).

8) Y. H. Loo, P. S. Shell, T. Ehruch, J. Mecurie, G. M. Savage, and J. C. Sylvester, *J. Bacteriol.*, **50**, 701 (1945).

9) E. T. Knudsen and G. W. Rotinson, *Lancet* (1945).

10) A. S. Riker and R. S. Riker, "Introduction to Research on Plant Diseases," Joh Swift (1936).

11) C. D. Darlington and L. F. La Cour, "The Handling of Chromosomes," 4th ed, George Allend Uniwin Ltd., London (1962).

 © 1988 The Chemical Society of Japan Bull. Chem. Soc. Jpn., 61, 1351—1355 (1988)

Behavior of the Enthalpy of Mixing in the Ternary Systems Lead-Antimony-Tin, Bismuth-Lead-Tin, and Bismuth-Cadmium-Tin at 950 K. I. Experimental Investigation

Walid Ahmad Badawi
Department of Chemistry, Faculty of Science, Al-Fateh University, Tripoli, Libya
(Received October 29, 1986)

Calorimetric studies on the enthalpies of mixing in the ternary systems Pb-Sb-Sn, Bi-Pb-Sn, and Bi-Cd-Sn have been carried out at 950 K. The partial enthalpy of mixing in the system Pb-Sb-Sn at quasi-binary section drawings goes through positive and negative regions. The partial enthalpy of mixing of lead is positive, while that of antimony is negative and takes a minimum between the quasi-binary section drawings $x_{Sn}=0$ and $x_{Sn}/x_{Pb}=6/4$. The partial molar enthalpy of mixing of bismuth in the ternary systems Bi-Cd-Sn and Bi-Pb-Sn shows level minima and the same behavior as observed for the partial enthalpy of mixing of antimony in the related system Pb-Sb-Sn. The partial enthalpy of mixing of tin in the system Bi-Pb-Sn is positive, while that of lead takes positive and negative values. Also the partial molar enthalpy of mixing of Cd in the system Bi-Cd-Sn shows a level minimum.

The binary systems of metals and metalloids have been studied in details.[1-3] In fact we have also contributed in this area.[4,5] However it appears that ternary systems have not received similar attention. Thus, the study of ternary systems from both theoretical and experimental approaches seemed of interest.

The measurements of enthalpy of mixing for binary systems and their correlation to the factors which determine the excess function behavior proved to be useful in getting insight into the behavior of such systems. It is expected that a similar approach to the ternary systems will yield better understanding of these systems. Hence we have been studying the systems Bi-Pb-Sn, Cd-Bi-Sn, and Pb-Sb-Sn in our adiabatic shield calorimeter. The experimental results of the enthalpy of mixing determinations are reported in the present paper. The analysis of the experimental results and theoretical approach to ternary solutions form the subject matter of another paper.

Experimental

Sample. The metals used were: lead of extra purity grade (E. Merck Company), 99.8 mass percent antimony (Schuchardt Company, Germany) and zone-refined 99.9999 mass percent pure tin (Koch-Light Laboratories, Ltd. England). The mixture of metals with a total mass of 149.213 g was sealed in the sample container of silica glass together with about 50 cm of 2.5 diameter silica cord. The silica cord was coiled spirally in the sample space and its purpose was to prevent breakage of the container on fusion and thermal cycling of the sample.

Calorimetric Technique. The slightly modified calorimetric apparatus was described before.[1] The calorimeter is operated with primary indirect provision of energy under adiabatic conditions. The procedures adopted were similar to those used earlier.[6,7] The 30 cm^3 sample container of silica glass has holes for heater, stirrer (made of ceramic) and a Pt-to-(Pt+10 mass per cent Rh) thermopile, axially located in the cylindrical silver calorimeter. The calorimeter-sample assembly is suspended inside a thermostat of steel (Thermax 10 FAL, production no. 4742, Germany). Below the thermostat is a heated guard system also of silver. The whole assembly is placed in a vertical tube furnace which in turn was protected by another larger one in order to obtain a double thermostat principle.

The temperature differences between the calorimeter and thermostat were measured by means of a set of fifteen differential Pt-PtRh thermopiles. These were serial connected and calibrated on a standard Pt-PtRh thermopile. The accuracy of the temperature values obtained was found to be ±0.1 K. The temperature of the guard body is kept automatically 0.2 K below that of the shield, while the temperature of the furnace is kept 5 K lower to secure satisfactory operation of the control units.

Heat capacity measurements of the empty calorimeter and thermostat were carried out in a seperate series of experiments. The C_p of the calorimeter was found to be 300 $J K^{-1}$ and that of the thermostat 5 $kJ K^{-1}$. The calibration of the calorimeter occured on exactly measured enthalpy of a standard sample of tin.[1] The time needed to reach equilibrium was registered to 430 s. The short-term fluctuation of the null point was measured to 0.3×10^{-3} K min^{-1}. The "interchange of heat constant" of the calorimeter at 973 K was estimated to 0.55 $W K^{-1}$. The sensibility of the calorimeter was measured to 630 $\mu V K^{-1}$. The thermometer resistence was measured with a Mueller bridge (Leeds & Northrup Model 8072), automated locally with stepping motors and a gated null detector, operated by a computer (Hewlett-Packard 2114B). The derived temperatures are judged to correspond with the IPTS-68 to within 0.01 K at 500 K and 0.1 K at 1000 K. In fact, the temperature increments were precisely measured to 0.0003 K.

The computer-operated energy imputs from a constant-current supply (John Fluke Current Calibrator Model 382 A) were measured with an integrating voltmeter (Hewlett-Packard Model 2401 C).

Results and Discussion

The data have been treated with the computer program Algol which searches for a set of parameters that minimizes the error square sum $h^m=(h^m_{calc}-h^m_{exp})^2$. The selected measurements comprise 36 data points corresponding the schema:

$x_1=0, 1\ j; x_2=1\ k; x_3=0\ 1\ l;$

$j, k, l=1 \cdots\cdots 8; j+k+l=10.$

These were symmetrical distributed in the Gibbs Triangle (x_1, x_2, and x_3 are the mole fractions of component 1, 2, and 3, respectively).

In order to save computer time, the measurement points and the values belonging to them are expressed as adjustable polynomial functions:

$$Y^e = Y^e(x_i, x_j) = \sum_{k,l} a_{kl}\, x_i^k\, x_j^l = \sum_{i,j} b_{ij}\, x_3^i\, x_1^j, \quad (1)$$

where i, j=1, 2 or 2, 3 or 3, 1. In this case, the following condition must be satisfied:

$$a_{00} = \sum_k a_{k0} = \sum_i a_{01} = 0. \quad (2)$$

Table 1. Enthalpy of Mixing in the System Pb-Sb-Sn at 950 K in J mol^{-1}. Estimated Standard Deviations in Parenthesis

x_1	x_2	x_3	h^m	x_1	x_2	x_3	h^m	x_1	x_2	x_3	h^m
0	0	X	0	5	1	4	897(5)	0	8	2	−787(2)
1	0	9	496(1)	4	2	4	349(21)	9	0	1	539(1)
0	1	9	−483(6)	3	3	4	−134(6)	8	1	1	409(1)
2	0	8	888(3)	2	2	4	−569(17)	7	2	1	231(12)
1	1	8	−5(21)	1	5	4	−989(9)	6	3	1	103(14)
0	2	8	−883(2)	0	6	4	−1299(2)	5	4	1	−37(9)
3	0	7	1168(4)	7	0	3	1202(2)	4	5	1	−170(9)
2	1	7	421(4)	6	1	3	875(16)	3	6	1	−231(11)
1	2	7	−379(19)	5	2	3	428(5)	2	7	1	−323(6)
0	3	7	−1172(3)	4	3	3	71(24)	1	8	1	−371(3)
4	0	6	1342(2)	3	4	3	−319(1)	0	9	1	−410(0)
3	1	6	709(12)	2	5	3	−650(12)	X	0	0	0(0)
2	2	6	42(15)	1	6	3	−890(10)	9	1	1	−10(0)
1	3	6	−718(7)	0	7	3	−1092(0)	8	2	0	−40(1)
0	4	6	−1343(0)	8	0	2	937(4)	7	3	0	−49(0)
5	0	5	1403(1)	7	1	2	701(2)	6	4	0	−59(1)
4	1	5	850(3)	6	2	2	380(10)	5	5	0	−59(1)
3	2	5	239(10)	5	3	2	100(7)	4	6	0	−60(0)
2	3	5	−379(0)	4	4	2	−129(5)	3	7	0	−29(1)
1	4	5	−934(5)	3	5	2	−359(7)	2	8	0	−11(1)
0	5	5	−1379(4)	2	6	2	−521(12)	1	9	0	1(2)
6	0	4	1361(0)	1	7	2	−671(2)	0	X	0	0(0)

x_1, x_2, and x_3 indicate 10 x the mole fraction of antimony, lead, and tin, respectively. The point 631 (for example) means x_1=0.6, x_2=0.3, x_3=0.1. X means 1.0.

The calculations of the coefficients b_{ij} from those a_{kl} occur by means of Algol program.

Results of the enthalpy of mixing determinations in the ternary system Pb-Sb-Sn are presented in Table 1. A number within parenthesis is the estimated standard deviation (esd.) calculated by the program. The average error of the individual measurement was found to be 1%. In fact the accuracy of the measurement results is considerably better since the enthalpy of mixing in the region near the pair Pb-Sb is small and this yields a large percentage error. To the best of our knowledge, there does not seem to be any report on the data for the enthalpy of mixing in the ternary system Pb-Sb-Sn. However, data for the binary systems Sb-Pb, Sb-Sn, and Pb-Sn with an accuracy of 1—2% have been reported earlier.[2-3,7] These date are in reasonable agreement with those obtained (for the above given pairs) in the present study on the ternary system Pb-Sb-Sn. The molar enthalpy of mixing, h^m, and the partial one of antimony at the quasi-binary section drawings Sb-Pb and Sb-Sn in the system Pb-Sb-Sn are shown in Fig. 1. The adjustable values of the integral enthalpy of mixing at the quasi-binary section drawing Pb-Sb beginning from the apex Sn are given in Table 2.

In Tables 3—5 are collected the values of the partial enthalpy of mixing of Pb, Sb, and Sn at the section

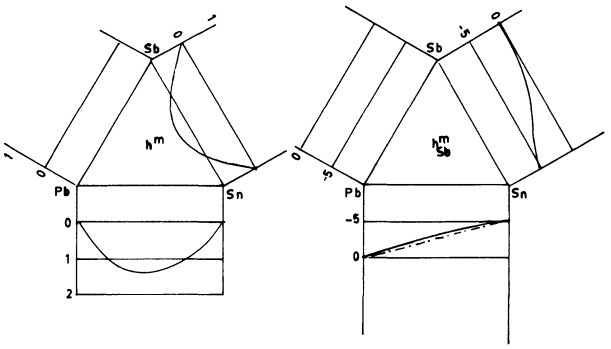

Fig. 1. The molar enthalpy of mixing, h^m, the partial one, h^m_{Sb} at the quasi-binary section drawings Sb-Pb and Sb-Sn in the system Pb-Sb-Sn at 950 K.

Table 2. Adjustable Values of the Enthalpy of Mixing (at Quasi-Binary Section Drawings Beginning from the Apex Tin) at 950 K in the System Pb-Sb-Sn in J mol^{-1}

x_{Sn}	Section drawing										
	Pb-Sn	1	2	3	4	5	6	7	8	9	Sb-Sn
0.0	0	−14	−44	−46	−51	−59	−55	−40	−13	4	0
0.1	533	437	279	141	4	−192	−193	−271	−379	−377	−422
0.2	936	749	520	282	51	−304	−304	−470	−603	−721	−801
0.3	1204	956	691	401	107	−160	−393	−599	−802	−971	−1100
0.4	1363	1107	799	491	168	−121	−399	−664	−911	−1131	−1299
0.5	1407	1139	849	538	237	−83	−381	−663	−931	−1167	−1393
0.6	1339	1097	833	547	271	−33	−319	−889	−863	−1101	−1353
0.7	1167	958	741	503	262	7	−241	−491	−714	−939	−1167
0.8	887	734	553	383	203	14	−171	−353	−526	−714	−879
0.9	486	401	301	199	99	5	−89	−201	−301	−402	−485
1.0	0	0	0	0	0	0	0	0	0	0	0

Table 3. Partial Enthalpy of Mixing of Lead (at Quasi-Binary Section Drawings Beginning from the Apex Pb) at 950 K in the System Pb-Sb-Sn in J mol^{-1}

x_{Pb}	Section drawing										
	Sn-Pb	1	2	3	4	5	6	7	8	9	Sn-Pb
0.0	317	237	561	1139	1921	2735	3564	4347	5022	5401	5165
0.1	−121	402	933	1494	2097	2714	3298	3871	4331	4632	4583
0.2	−217	361	903	1403	1891	2353	2771	3132	3451	3642	3641
0.3	−181	304	753	1182	1575	1925	2222	2563	2617	2714	2733
0.4	−132	246	612	963	1272	1534	1727	1865	1963	1984	2014
0.5	−93	186	473	756	973	1174	1296	1391	1431	1441	1438
0.6	−39	163	354	553	697	815	898	943	974	969	993
0.7	−22	121	242	334	434	501	543	554	581	573	600
0.8	5	57	121	163	201	222	241	253	247	255	265
0.9	8	21	31	40	46	52	46	49	61	54	58
1.0	0	0	0	0	0	0	0	0	0	0	0

Table 4. Partial Enthalpy of Mixing of Antimony (at Quasi-Binary Section Drawings Beginning from the Apex Sb) at 950 K in the System Pb-Sb-Sn in J mol^{-1}

x_{Sb}	Section drawing										
	Sn-Sb	1	2	3	4	5	6	7	8	9	Pb-Sb
0.0	−5501	−3891	−4431	−3991	−3571	−3163	−2702	−2151	−1455	−669	−43
0.1	−5496	−5572	−5591	−5472	−5214	−4814	−4706	−3910	−2923	−1725	−271
0.2	−5651	−5964	−6114	−6037	−5661	−5113	−4432	−3627	−2693	−1585	−321
0.3	−5713	−6042	−6144	−5598	−5646	−5113	−4437	−3640	−2691	−1585	−294
0.4	−5582	−5791	−5791	−5573	−5165	−4603	−3922	−3153	−2286	−1341	−244
0.5	−5122	−5234	−5160	−4913	−4507	−3982	−3363	−2681	−1917	−1107	−169
0.6	−4595	−4417	−4327	−4124	−3796	−3375	−2854	−2285	−1634	−900	−38
0.7	−3472	−3464	−4400	−3270	−3051	−2747	−2364	−1900	−1322	−620	250
0.8	−2550	−2490	−2423	−2330	−2193	−1990	−1700	−1284	−760	−70	814
0.9	−1863	−1641	−1450	−1246	−1037	−800	−490	−90	431	1063	1880
1.0	0	0	0	0	0	0	0	0	0	0	0

Table 5. Partial Enthalpy of Mixing of Tin (at Quasi-Binary Section Drawings Beginning from the Apex Tin) at 950 K in the System Pb-Sb-Sn in J mol^{-1}

x_{Sn}	Section drawing										
	Pb-Sn	1	2	3	4	5	6	7	8	9	Sb-Sn
0.0	5950	5084	3681	2203	990	−242	−1240	−2221	−3204	−4081	−4350
0.1	4803	3881	2753	1590	484	−518	−1432	−2248	−2299	−3633	−3998
0.2	3617	2904	2133	1304	462	−371	−1137	−1871	−2521	−3091	−3540
0.3	2647	2181	1668	1130	524	−86	−714	−1318	−1901	−2432	−2913
0.4	1922	1614	1302	950	555	107	−360	−830	−1293	−1738	−2197
0.5	1363	1151	952	730	481	194	−131	−454	−794	−1142	−1504
0.6	902	751	602	482	317	163	−33	−231	−441	−665	−894
0.7	511	397	325	244	163	83	−21	−120	−230	−343	−480
0.8	215	162	119	83	50	11	−33	−70	−114	−155	−199
0.9	44	33	20	8	−5	−9	−20	−31	−40	42	−60
1.0	0	0	0	0	0	0	0	0	0	0	0

drawings Sb-Sn, Sn-Pb, and Pb-Sb beginning with the apices Pb, Sb, and Sn, respectively. From these data one may observe that h^m_{Sb} takes only negative values, h^m_{Pb} is positive while h^m_{Sn} goes through positive and negative regions. Figure 2 shows the partial enthalpy of mixing of antimony at the quasi-binary section drawing Sn-Pb beginning from the apex Sb in the system Pb-Sb-Sn. It is clearly observable that h^m_{Sb} takes a minimum between the quasi-binary section drawings $x_{Sn}=0$ and $x_{Sn}/x_{Sb}=6/4$.

It is expected that the partial molar enthalpy of mixing of bismuth in the ternary systems Bi-Cd-Sn and Bi-Pb-Sn shows the same behavior as observed for h^m_{Sb} in the related system Pb-Sb-Sn. In order to decide this, we have also been studying these two systems. In Tables 6 and 7 are presented the values of h^m_{Bi} at quasi-binary section drawings in the systems Bi-Pb-Sn and Bi-Cd-Sn beginning from the apex Bi. Figure 3 shows the integral enthalpy of mixing, h^m, at the quasi-binary section drawings in the system Bi-Pb-Sn. h^m_{Si} is also shown in this figure. The integral enthalpy of mixing takes positive values in the pairs Pb-Sn and

Sn-Bi, while h^m is negative in the pair Bi-Pb. This was also recognized by Wittig in his study on these binary systems.[1,2] A somewhat surprising observation is that h^m_{Bi} in Bi-Pb-Sn indicates a level minimum in the region between the quasi-binary section drawings $x_{Sn}=0$ and $x_{Pb}/x_{Sn}=6/4$. As indicated in Fig.4, h^m_{Sn} takes positive values while h^m_{Pb} goes through positive and negative regions.

Figure 5 shows the integral enthalpy of mixing, h^m, and the partial molar one of Bi, h^m_{Bi}, at the quasi-binary

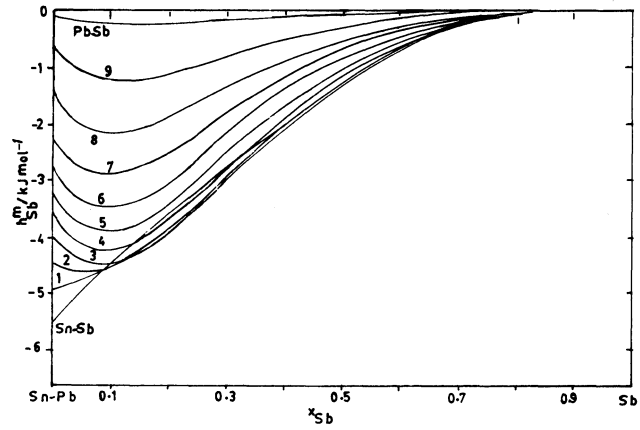

Fig. 2. Partial enthalpy of mixing of antimony at the quasi-binary section drawing Sn-Pb beginning from the apex Sb in the system Pb-Sb-Sn at 950 K.

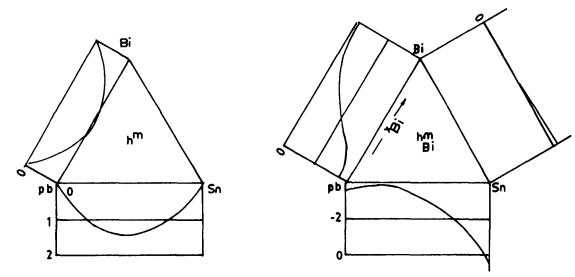

Fig. 3. Partial enthalpy of mixing of bismuth at quasi-binary section drawings in the system Bi-Pb-Sn and the integral enthalpy of mixing at 950 K.

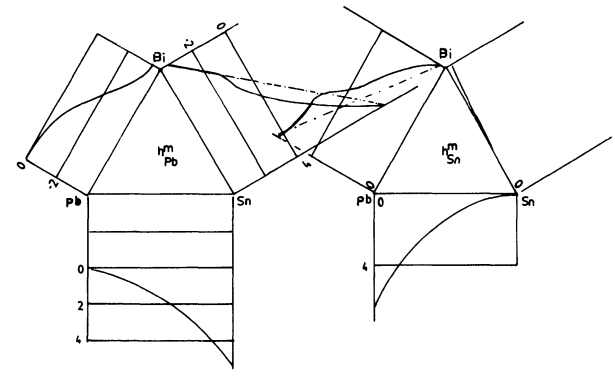

Fig. 4. Partial enthalpy of mixing of Pb and Sn at quasi-binary section drawings in the system Bi-Pb-Sn at 950 K.

Table 6. Partial Molar Enthalpy of Mixing of Bismuth (at Quasi-Binary Section Drawings Beginning from the Apex Bi) at 950 K in the System Bi-Pb-Sn in J mol^{-1}

x_{Bi}	Section drawing										
	Bi-Pb	1	2	3	4	5	6	7	8	9	Bi-Sn
0.0	−3705	−3298	−2976	−2679	−2397	−2121	−1820	−1450	−979	−344	392
0.1	−3572	−3166	−3041	−2976	−2836	−2624	−2334	−1950	−1447	−826	351
0.2	−3006	−2566	−2630	−2399	−2482	−2285	−2016	−1388	−1252	−675	301
0.3	−2510	−1990	−2023	−1978	−1861	−1685	−1460	−884	−882	−418	149
0.4	−2015	−1410	−1400	−1348	−1228	−1110	−946	−590	−552	−239	96
0.5	−1009	−842	−829	−824	−756	−667	−515	−373	−321	−189	75
0.6	−852	−460	−356	−282	−202	−178	−166	−154	−142	−131	71
0.7	−753	−202	−157	−125	−91	−82	−71	−64	−55	−43	58
0.8	−251	−156	−125	−101	−75	−64	−60	−51	−48	−39	48
0.9	−75	−72	−72	−62	−58	−54	−51	−42	−38	−34	41
1.0	0	0	0	0	0	0	0	0	0	0	0

Table 7. Partial Molar Enthalpy of Mixing of Bismuth (at Quasi-Binary Section Drawings Beginning from the Apex Bi) at 950 K in the System Bi-Cd-Sn in J mol^{-1}

x_{Bi}	Section drawing										
	Cd-Bi	1	2	3	4	5	6	7	8	9	Sn-Bi
0.0	9420	8398	7580	6825	6108	5407	4642	3699	2500	1135	381
0.1	7620	8063	7746	7582	7228	6690	5955	4976	3696	2112	364
0.2	6190	6537	6700	6113	6327	5828	5145	4227	3198	1727	392
0.3	4905	5070	5155	5041	4744	4298	3727	3046	2253	1325	294
0.4	3440	3570	3570	3436	3130	2833	2415	1940	1412	822	146
0.5	1988	2240	2207	2100	1927	1702	1438	1143	823	470	73
0.6	1207	1213	1187	1129	1040	924	784	764	547	245	69
0.7	536	535	524	502	469	411	364	345	298	94	57
0.8	415	413	418	405	387	372	352	337	216	88	56
0.9	381	381	379	376	365	351	339	316	199	78	32
1.0	0	0	0	0	0	0	0	0	0	0	0

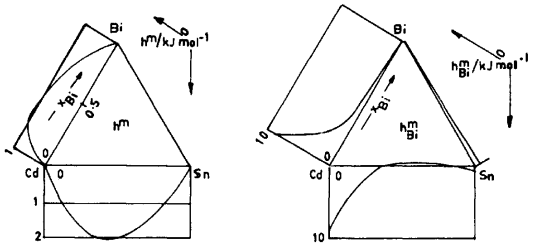

Fig. 5. Integral enthalpy of mixing and partial enthalpy of mixing of bismuth at quasi-binary section drawings in the system Bi-Cd-Sn at 950 K.

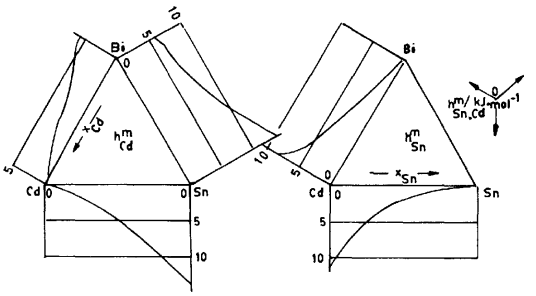

Fig. 6. Partial enthalpy of mixing of Cd and Sn at quasi-binary section drawings in the system Bi-Cd-Sn at 950 K.

section drawings Bi-Cd and Bi-Sn in the system Bi-Cd-Sn. It is clearly observable that h^m takes a maximum at $x_{cd}=x_{Sn}=0.5$. h^m is also positive in the pairs Bi-Cd and Sn-Bi. As we have expected, h^m_{Sb} takes also a striking level minimum in the region $x_{Sn}=0$ to $x_{Cd}/x_{Sn}=6/4$. This means that there exists a general property for ternary systems.

Figure 6 shows the partial molar enthalpy of mixing of Cd and Sn at the quasi-binary section drawings Bi-Cd and Bi-Sn. h^m_{Cd} exhibits also a level minimum. However, the level minimum of Cd and the bend joined to this minimum disappear rapidly when the mole fraction of Sn increases. At the same time the bend of h^m_{Bi} in the pairs Bi-Cd and Bi-Sn shows always positive trends.

On the basis of our discussion, we come to the following conclusion: There exists a general property which predicts the behavior of mixing in ternary systems. This property could be overlapped by other ones belonging to the pairs of components in the ternary systems. In fact, this property is recognized in the present study and will be reported together with the theoretical analysis of the experimental results in the second part of this work.

References

1) F. E. Wittig and E. Gehring, *Z. f. Naturforschung*, **18a**, 351 (1963).
2) F. E. Wittig, *Z. Electrochem.*, **63**, 327 (1959).
3) F. E. Wittig and E. Gehring, *Ber. Bunsenges. Phys. Chem.*, **70**, 717 (1966).
4) W. A. Badawi, *Bull. Chem. Soc. Jpn.*, (in press).
5) W. A. Badawi and A. E. Eid, *Bull. Chem. Soc. Jpn.*, **60**, 3771 (1987).
6) F. E. Wittig and F. Huber, *Z. Electrochem*, **60**, 1181 (1956).
7) F. E. Wittig and W. Schmatz, *Z. Electrochem*, **63**, 470 (1959).

 © 1988 The Chemical Society of Japan Bull. Chem. Soc. Jpn., 61, 1357—1362 (1988)

Sorption of Uranyl Ions on Hydrous Oxides. A New Surface Hydrolysis Model

Anand Ram GUPTA* and Balakrishnan VENKATARAMANI
Chemistry Division, Bhabha Atomic Research Centre, Bombay 400085, India
(Received July 24, 1986)

Sorption of uranyl ions on hydrous titanium oxide(HTiO), magnetite(MAG), and hydrous thorium oxide(HThO) has been studied as a function of pH. Hydrous oxides have been characterized by their pH-titration curves, intrinsic dissociation constants(pK_{ai}^*) and point of zero charge (pH_{pzc}). The fraction of protonated surface hydroxyl groups as well as the surface pH(pH_{surf}) as a function of solution pH have been computed. The distribution of various hydrolyzed species of uranyl ions with solution pH have been compared with uranyl sorption isotherm on these oxides. Sorption edge in all the cases occurs when free hydroxyl groups are available on the surface and pH_{surf} is sufficiently high to favor the formation of dimer-like species on the surface. A new model for the sorption process, called surface hydrolysis model, which explains these and other features of uranyl sorption on hydrous oxides has been proposed. The model visualizes the sorption process as linking of uranyl ions with two adjacent free surface hydroxyl groups without deprotonation (provided the surface pH is high for the hydrolysis of uranyl ions) and formation of dimer-like structures on the surface. The new model has been successfully applied to the present and other available data on uranyl ion sorption on hydrous oxides.

There has been a great interest in the study of the sorption of hydrolysable metal ions on hydrous oxides. Though many features of the sorption behavior are well-understood, a complete picture is still not available. The sorption process depends upon the properties of the metal ions (e.g. hydrolysability), characteristics of the oxide surface (e.g. point of zero charge, pzc) and experimental conditions (e.g. pH of the solution) Dugger et al.[1] viewed the sorption of transition metal ions on hydrous oxides as an ion exchange reaction between the surface hydroxyl groups and the metal ions:

$$m(\mathrm{SOH}) + \mathrm{M}^{m+} \rightleftarrows (\mathrm{SO})_m\,\mathrm{M} + m\mathrm{H}^+, \qquad (1)$$

where (SOH) is the surface hydroxyl group and M is the metal ion being sorbed. The variation in the sorption of different metal ions was attributed to the strength of the M-O bond which was correlated with the stability constants of monohydroxo complexes of cations.[1] This was applicable when the solution pH was such that hydrolysis of metal ions did not take place. In the sorption isotherms, an abrupt increase was observed as a function of pH, James and Healy[2] suggested that ionic charge on the sorbing metal ion was lowered by hydrolysis or ligand complex formation, facilitating closer approach to the interface and the sorption process.

More recently, the sorption process has been looked upon as surface complexation of metal ions by suface hydroxyl groups, so that the hydrolysis of metal ions in solution was not a pre-requisite of the sorption mechanism.[3,4] The deprotonation of the surface groups accompanied the sorption of the metal ions. In general, the soption of metal ions is viewed[5] as a competition between the surface hydroxyl groups and any ligand present in solution for the complexation of free metal ion. The sorption of ligands or anions of the oxide surface is also taken into consideration[6] to explain the sorption data. Recently, a precipitation model[7] for the sorption of metal ions on hydrous oxides has been proposed to account for the non-limiting sorption capacities of the oxides. Essentially the model is based on Eq. 1 but allows for precipitation of sorbing metal ion and solid solution formation, provided the solubility product of the sorbing metal cation is exceeded on the surface.

The above models, however, do not explain satisfactorily the observation that the abrupt increase in the sorption of metal ions on hydrous oxides occurs at a pH where the oxide surface is positively charged. These models also fail to explain the observed incease in the positive charge and the shift in pzc of the oxide as a result of sorption.[2,8] With a view to understand the sorption process on hydrous oxides, we had undertaken a detailed study of the sorption of metal cations on different hydrous oxides. In this communication we are presenting our results on the sorption of uranyl ions on hydrous titanium and thorium oxides and hydrous magnetite. A new sorption mechanism which accounts for all the features of the sorption process (including the hitherto unexplained ones) is proposed.

Experimental

Peparation of the Hydrous Oxides. Hydrous Titanium Oxide (HTiO): HTiO was prepared by adding 2 mol dm^{-3} NaOH to a hot solution of Ti(IV) in concd H_2SO_4 under constant stirring. The precipitate was digested in the mother liquor at 353 K for 4 h, allowed to cool and stand for 2 d. It was then filtered, washed free of alkali and air dried. The product, which is the same used in an earlier study,[9] did not contain any sulfate but sodium ions were present making the material alkaline. The sodium ions incorporated in it were removed by repeatedly treating it with dil $HClO_4$ and washing with water. This was continued till the pH of the water in contact with HTiO was neutral.

Hydrous Thorium Oxide (HThO): HThO was prepared by adding 1 mol dm^{-3} NaOH to a hot solution of thorium (IV) nitrate in HNO_3. The precipitate was later digested in

Table 1. Characteristics of the Hydrous Oxides

Hydrous oxide	Capacity (C) / mmol g^{-1}	$pK_a=pK_a^*+m\cdot q$	$pH_{pzc}=\frac{1}{2}(pK_{a1}^*+pK_{a2}^*)$
HTiO	0.65	$pK_{a1}=4.79-0.43\times10^4 q$	
		$pK_{a2}=8.3-0.26\times10^4 q$	6.55
HThO	0.23	$pK_{a1}=3.18+0.88\times10^3 q$	
		$pK_{a1}=10.4-0.35\times10^4 q$	6.79
MAG	0.14	$pK_{a1}=2.88+0.48\times10^4 q$	
		$pK_{a1}=10.05-0.45\times10^4 q$	6.47

hot condition, aged for 2 d, filtered, washed, and air dried.

Hydrous Magnetite (MAG): MAG was prepared by the method of Benton and Horsfall.[10] To a hot 5L solution containing sulfuric acid, 25 g KNO_3 and 90 g $FeSO_4\cdot7H_2O$, NaOH was added under constant stirring. The green precipetate initially formed turned black. The precipitate was digested in hot condition, aged for 2 d, filtered, washed and air dried.

All the air dried hydrous oxides were broken in water, washed, dried and finally crushed and sieved. For sorption experiments −100 BSS samples were used. X-Ray analysis of the oxides showed that HTiO and HThO were amorphous; and MAG was crystalline.

pH Titration. Continuous pH titration were carried out with 0.4 g of the air dried samples in 50 cm^3 of 0.1 mol dm^{-3} $NaNO_3$ with 0.1 mol dm^{-3} HNO_3 or NaOH. The pH of the slurry was measured using Elico Digital pH-meter. After the addition of acid or alkali, solutions were stirred continuously for 10 min before pH measuement.

Sorption Experiments. All sorption experiments were done at a total ionic strength of about 0.1 mol dm^{-3} $NaClO_4$. 0.1 g of the oxide was equilibrated with 25 cm^3 of the solution of 10^{-4} mol dm^{-3} uranyl nitrate in $NaClO_4$, preadjusted to a known pH using $HClO_4$ or NaOH. The solid-solution mixture was equilibrated for 4 h at constant room temperature (298±1 K). Later the pH of the supernatant solution was measured. The uranium in the equilibrated solution was estimated spectrophotometrically using H_2O_2 at 400 nm.[11] The difference in the uranium concentration before and after equilibration gave the amount sorbed on the oxide.

Results and Discussion

Characteristics of the Hydrous Oxides. Capacity Determination: The capacity of the hydrous oxide is the ion sorption capacity of the material (mmol g^{-1}). It is equal to the total number of hydroxyl groups taking part either in Reaction 2 or 3. It has been determined as the limiting value of H^+ ions consumed in the acid region of the pH-titration curve or the limiting value of OH^- ions consumed in the alkaline region of the titration curve. Its value has also been estimated from the limiting amounts of Na^+ or Cl^- ions sorbed by the oxides. The values for capacities obtained by different procedures were in reasonable agreement with one another and are listed in Table 1.

Analysis of pH-Titration Curves: The pH-titration curves of the three oxides in the acidic as well as alkaline regions are given in Fig. 1. The steep rise (alkaline region) and decline (acidic region) of pH in the titration curve of HThO and MAG compared to HTiO reflect their lower capacities vis-a-vis HTiO. As the hydrous oxides are amphoteric in character, the following reactons take place:

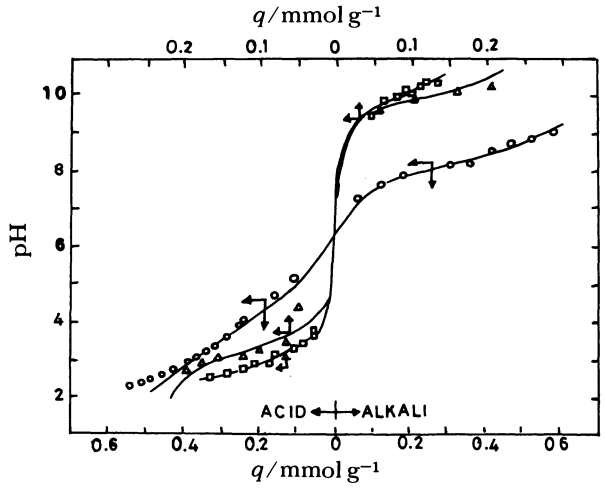

Fig. 1. pH-titration curves of hydrous oxides (○): HTiO; (△): HThO; (□): Magnetite. Solid lines based on pK_{a1} and its dependence on q (Table 1).

$$\text{acidic rigion: } SOH_2^+ \rightleftharpoons SOH + H^+, \quad (2)$$

$$\text{alkaline region: } SOH \rightleftharpoons SO^- + H^+. \quad (3)$$

The coresponding equilibrium constants are given by:

$$K_{a1} = N_{(SOH)}\, m_{H^+}/N_{(SOH_2^+)}, \quad (4)$$

$$K_{a2} = N_{(SO^-)}\, m_{H^+}/N_{(SOH)}, \quad (5)$$

where m_{H^+}, $N_{(SOH_2^+)}$, $N_{(SOH)}$, and $N_{(SO^-)}$ are molality of H^+ in solution and mole fractions of protonated, undissociated and dissociated surface hydroxyl groups in the oxide.

These equilibrium constants can be computed from the pH-titration curves by the method given by Schindler and Gamsjaeger.[12] Similar procedures have been recommended by other workers also.[13] The function q defined by $q=[SOH_2^+]-[SO^-]$, is computed from:

$$q = \frac{V(H-h)}{a} \quad (\text{mol } g^{-1}). \quad (6)$$

Where V is the volume of the solution taken for titration (dm^3); H is the amount of acid or base added

(mol dm^{-3}); h is the equilibrium H^+ concentration in solution (mol dm^{-3}); and a is the amount of hydrous oxides used (g). Assuming that SOH_2^+ is zero in alkaline region and SO^- is zero in acidic region, the equilibrium constants are:

$$K_{a1} = \frac{h(C-q)}{q} = \frac{h(1-\alpha)}{\alpha} \quad \text{(acidic region)}, \quad (7)$$

$$K_{a2} = \frac{h \cdot q}{C-q} = \frac{h(\alpha)}{(1-\alpha)} \quad \text{(alkaline region)}, \quad (8)$$

where C(mol g^{-1}) is the capacity of the hydrous oxide, and $\alpha = q/C$, is the fraction of the surface hydroxyl groups in either SOH_2^+ (Eq. 7) or SO^- (Eq. 8) form. The values of the equilibrium constants vary with q. A plot of pK_{ai} ($=-\log_{10} K_{ai}$, i=1 or 2) versus q were straight lines. The y-intercept gives the intrinsic dissociation constant (pK_{ai}^*) of the surface groups of the hydrous oxides. The slopes of the linear plots ('m') were either positive or negative. The equations describing the linear relationship between pK_{a1} and q are given in Table 1. Using these equations the pH-titration curves of the three hydrous oxides were calculated, which were in good agreement with experimental data (Fig. 1). The point of zero charge, pH_{pzc}, is the pH where the net surface charge is zero, implying that $[SOH_2^+]$ and $[SO^-]$ are equal at this point. pH_{pzc} is calculated from the relation:

$$pH_{pzc} = \frac{1}{2}(pK_{a1}^* + pK_{a2}^*). \quad (9)$$

The values of pK_{ai}^* and pH_{pzc} for HTiO and MAG are in the range reported for these oxides.[2,12-17]

The surface hydrogen ion concentration, h^*, is given by the relations:

$$K_{a1}^* = \frac{h^*(C-q)}{q} = \frac{h^*(1-\alpha)}{\alpha} \quad \text{(acidic region)}, \quad (10)$$

$$K_{a2}^* = \frac{h^* q}{C-q} = \frac{h^*(\alpha)}{(1-\alpha)} \quad \text{(alkaline region)}. \quad (11)$$

Using these equations surface pH, pH_{surf}, ($=-\log_{10} h^*$) for different α values have been evaluated.

Sorption of Uranium. Sorption isotherms of uranium as a function of pH on the three hydrous oxides are given in Fig. 2(A). An abrupt increase in the sorption within a narrow pH range is observed in all the three cases. The sorption edge, however, occurs at different solution pH (pH_{soln}) for the three hydrous oxides. As pH_{pzc} of these oxides are higher than the sorption edge pH, the sorption of uranyl ions occurs on positively charged surfaces.

For a particular value of $\alpha(=q/C)$, the value of K_{a1} can be calculated with the help of data given in Table 1. Using this value of K_{a1}, the value of the solution pH ($=-\log_{10} h$) was calculated from Eq. 7. Plots of α vs. solution pH for the SOH_2^+ group present on the three hydrous oxides are given in Fig. 2(C). The plots clearly show that the sorption edge for HTiO (Fig. 2A) occurs when 90% of the surface hydroxyl groups are in SOH_2^+ form. In HThO and MAG, 20% and 15% of surface hydroxyl groups, respectively, are in SOH_2^+ form at the sorption edge.

Earlier models[18] regarded the sorption process as surface complexation accompanied by the dissociation of surface hydroxyl groups, even at pH lower than their pH_{pzc}, just as the deprotonation of hydroxyl groups of the ligands on complex formation with metal cations. Such a model does not account for the data in Fig. 2, in particular for HTiO where more than one proton per hydroxyl group has to be released for forming a single $SO\text{-}UO_2^{2+}$ link, i.e. the formation of oxo bridges between uranyl ions and the surface is ruled out. Another aspect of the earlier models, namely the participation of hydrolyzed metal ion species in the sorption process, was also examined. For this purpose, the distribution of hydrolyzed species of uranium as a function of pH at a total uranium concentration of 10^{-4} mol dm^{-3}, was computed using the following stability constants:[1]

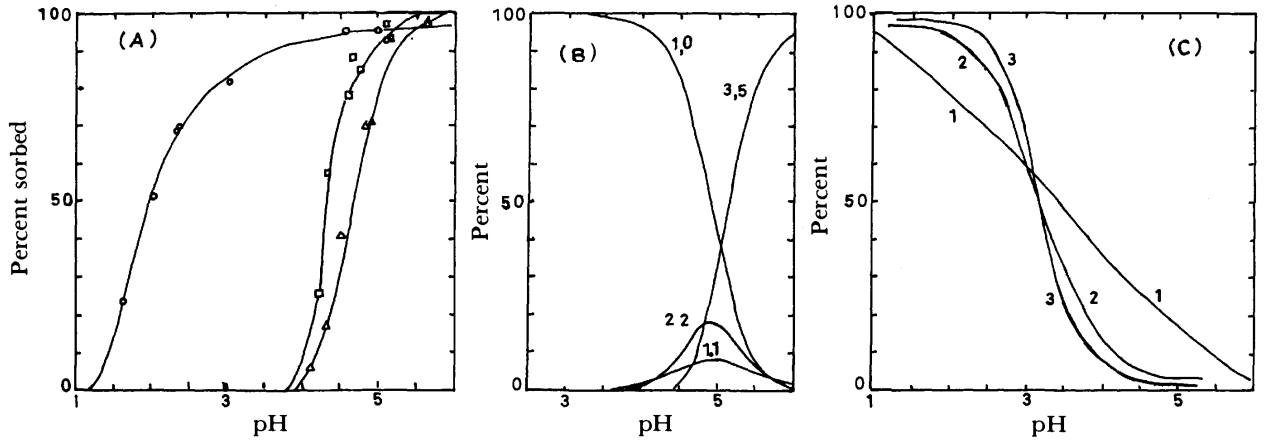

Fig. 2. (A) Uranyl sorption isotherm on hydrous oxides $\sum U = 10^{-4}$ mol dm^{-3}. (○) HTiO; (□) HThO; (△) Magnetite. (B) Distribution of hydrolyzed uranyl species vs. pH. (1,0)=UO_2^{2+}; (1,1)=$(UO_2)(OH)^+$; (2,2)=$(UO_2)_2(OH)_2^{2+}$; (3,5)=$(UO_2)_3(OH)_5^+$. (C) Percent of SOH_2^+ groups vs. pH; (1) HTiO; (2) HThO; (3) Magnetite.

$$UO_2^{2+} + H_2O \rightleftharpoons UO_2OH^+ + H^+;\ \log \beta_{11} = -5.7, \quad (12)$$

$$2UO_2^{2+} + 2H_2O \rightleftharpoons (UO_2)_2(OH)_2^{2+} + 2H^+;\ \log \beta_{22} = -5.92, \quad (13)$$

$$3UO_2^{2+} + 5H_2O \rightleftharpoons (UO_2)_3(OH)_5^+ + 5H^+;\ \log \beta_{35} = -16.5. \quad (14)$$

Distribution plots for various species in Fig. 2(B) demonstrate that uranium is present only as UO_2^{2+} at the sorption edge for HTiO and hydrolysis of uranyl ions starts only after 90% of uranium has been absorbed. In the case of HThO and MAG sorption edge occurs at a pH where the hydrolysis of uranium has not started and uranium is essentially present as uranyl ions.

The New Model-Surface Hydrolysis Model. The above analysis clearly demonstrates that the sorption of uranium on the three hydrous oxides, studied in this investigation, can not be accounted for by the existing models. Neither the hydrolyzed species of uranium participate in the sorption process nor does the sorption takes place under conditions where the surface complexation and conversion of surface hydroxyl groups to oxo groups would be a likely process. Sorption occurs on positively charged surfaces which are, as in HTiO, predominantly in SOH_2^+ form. Besides another feature of the sorption process observed in earlier studies,[2,18,20] namely, the increase in the positive charge of the oxide surface as a result of the sorption of metal ions, can not be explained by any of the existing models. In order to account for these features of the sorption process, a new model for the sorption of hydrolyzable metal cations on hydrous oxides is proposed.

Essential Features of the Model Are: 1) The main postulate of the model is that the sorption of metal ions on the surface of hydrous oxides occurs by attachment to surface hydroxyl groups without deprotonation of hydroxyl groups. On positively charged surfaces having SOH_2^+ groups, sorption of metal ions occurs only on free hydroxyl groups, i.e. SOH groups. The availability of free SOH groups is, thus, an essential requirement of the sorption process. (Fig. 3, A)

Schematically, the sorption process according to the new surface hydrolysis model is shown in Fig. 3.

2) In order to overcome the coulombic repulsion between positively charged metal ions and positively charged surfaces as well as to make the sorption process to be energetically favorable in comparison with the protonation of surface hydroxyl groups, it is further postulated that metal ion is simultaneously attached to two adjacent surface hydroxyl groups forming bridged hydroxo complexes with the surface in much the same manner as in dimerized hydroxo species, $(M^{+z}\langle^{OH}_{OH}M^{+z})^{2z-2}$ formed during the hydrolysis of metal cations (B).

3) For the sorption process described in postulate (2), to be thermodynamically feasible, the model requires that the surface pH of the oxide at the sorption edge, as distinct from the solution pH, which defines the sorption edge, should correspond to the pH where dimerized hydroxo species are formed in solution, i.e. pH_D.

4) As surface pH increases, dimer or trimer-like species can be formed on the surface (C). pH_T is the pH at which trimeric species are formed in solution. In the limit when pH_{surf} approaches precipitation pH, i.e. pH_{ppt}, precipitation of the metal cation on the surface and solid solution formation takes place (E).

5) When $pH_{surf} \geqslant pH_{pzc}$, sorption process is governed by Eq. 1 (D). (In Fig. 3, pH_{surf} is indicated as pH_{su}).

The model thus predicts that the surface becomes more positively charged as a consequence of the adsorption process—a feature hitherto unexplained by the existing models of the sorption process. The validity of the various postulates of the model has been tested by analyzing the present data on the sorption of uranyl ions on the three hydrous oxides. Subse-

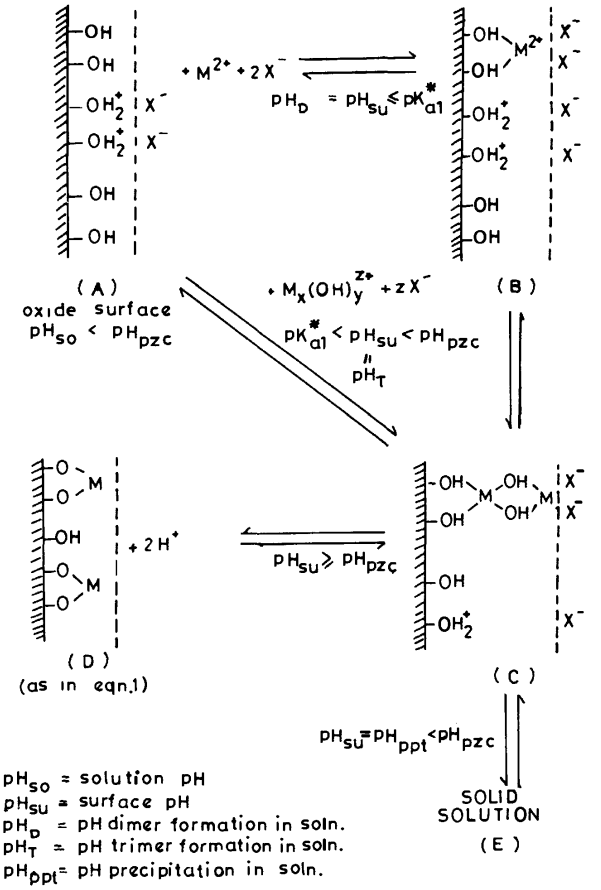

Fig. 3. Schematic representation of the surface hydrolysis model.
(A) Positively charged oxide surface having SOH_2^+ groups. (B) Dimer-like structure formed by the unhydrolyzed metal ion on the surface. (C) Trimer-like structure formed by the hydrolyzed dimeric species on the surface. (D) Negatively charged oxide surface. (E) Solid solution formation.

quently, the model has been applied to those studies on uranyl sorption on other hydrous oxides where data required for the application of the model are available.

Hydrous Titanium Oxide. Besides the sorption isotherms of uranyl ions as a function of solution pH, the model also requires information about the variation of the fraction of surface hydroxyl groups in SOH_2^+ form with solution pH. Such data plotted in Fig. 2(C) clearly show that at sorption edge pH (1.3) free SOH groups are available for the sorption of uranyl ion. Then the oxide surface corresponds to A in Fig 3. At this pH, uranyl ions in the solution phase exist only as unhydrolyzed uranyl ions. In order to apply the model, surface pH, pH_{surf}, is also required. This has been computed using Eq. 10. pH_{soln} as a function of α were calculated using Eq. 7. Table 2 lists values of pH_{surf} and pH_{soln} for various values of α. It is seen that pH_{surf} for HTiO is considerably higher than pH_{soln}. For this oxide, at the sorption edge pH_{soln} is 1.3, SOH_2^+ is 90%, and pH_{surf} is 3.9. The distribution diagram of various hydrolyzed uranium species shows that the hydrolysis of uranyl ions starts at pH 3.5 (formation of monomeric $UO_2(OH)^+$ (1, 1) in Fig. 2(B)) and at pH 3.8, (pH_D in Fig. 3) formation of dimeric species ((2, 2) in Fig. 2(B)), $(UO_2)_2(OH)_2^{2+}$, starts. At the sorption edge, pH_{surf} is very close to this. Thus, at the sorption edge, when solution pH is 1.3 and only free UO_2^{2+} (aq) ions exists in solution, conditions on the surface are favorable for the process A→B to occur (Fig. 3), which results in the formation of dimer-like species on the surface. In the dimeric species in solution, two OH groups form two bridges between two uranyl ions, $[UO_2\overset{OH}{\underset{OH}{<}}UO_2]_{sol}$. In the dimer-like species on the surface, two OH groups form two bridges between a uranyl ion and the surface $[\overset{-OH}{\underset{-OH}{>}}UO_2]_{surf}$. Thus the uranyl ions are sorbed without the dissociation of OH groups, with the formation of dimer-like structures on the surface.

The fact that sorption edge occurs when pH_{surf} is 3.9 and not at 3.5, when UO_2OH^+ species or structures resembling such species (in the same sense as dimer-like structures) could exist on surface implies that sorption process corresponds to A→B (Fig. 3). Such a sorption mechanism, that is, attachment of uranyl ions on hydroxyl groups to form dimer-like structures, is supported by a recent Raman study of the interaction of uranyl ions with Th(IV) hydrolyzed polymer networks[21] in homogeneous systems.

As the solution pH increases, the solution contains hydrolyzed (dimeric) species of uranyl ions and pH_{surf} approaches pH_T (solution pH when trimecic species are formed in solution) and the condition on surface becomes favorable for A→C or B→C (Fig. 3) $[\overset{-OH}{\underset{-OH}{>}}UO_2\overset{OH}{\underset{OH}{<}}UO_2]_{surf}$. If precipitation pH, pH_{ppt}, is less than pH_{pzc}, process C→E can occur, otherwise, C→E occurs when pH_{surf} exceeds pH_{pzc}.

Table 2. pH_{sol} and pH_{surf} as a Function of α

α	HTiO		HThO		MAG	
	pH_{sol}	pH_{surf}	pH_{sol}	pH_{surf}	pH_{sol}	pH_{surf}
0.1	5.4	5.7	4.1	4.13	3.95	3.83
0.2	4.8	5.39	3.8	3.78	3.6	3.48
0.3	4.3	5.16	3.6	3.55	3.45	3.25
0.4	3.8	4.97	3.4	3.36		
0.5	3.4	4.79				
0.6	2.95	4.61				
0.7	2.4	4.42				
0.8	1.9	4.19				
0.9	1.3	3.89				

Hydrous Thorium Oxide and Magnetite. The sorption isotherms of uranyl ions on these two oxides are very similar. The data (Fig. 2(A)) show that the sorption edge in both the oxides occur at about pH_{soln} 3.9, which is also the pH at which dimeric species, $(UO_2)_2(OH)_2^{2+}$, are formed in solution. The surface pH for both the oxides (Table 2) is nearly equal to solution pH. On both the oxides nearly 90% of the surface groups are in the undissociated SOH form (Fig. 2(C)). Thus, in these oxides A→C (Fig. 3) is likely to be the preferred process.

To summarize, the present data indicate that uranyl ions are sorbed on positively charged oxide surface. The sorption edge occurs when pH_{surf} is favorable for the formation of dimer-like or trimer-like structures on the oxide surface. At the sorption edge, undissociated surface hydroxyl groups are present and sorption of uranyl ion involves simultaneous attachment to two adjacent undissociated surface groups. Thus, our data conforms to the basic postulates of the surface hydrolysis model.

Application of the Model to Other Oxides. Haematite: In a recent study of the sorption of uranyl ions on haematite,[22] Ho and Doern correlated the sorption edge at pH ≈5.0 with the marked increase of $(UO_2)_3(OH)_5^+$ species in solution phase at that pH and concluded that the trimer species are the sorbed species on the surface.

Their electrophoretic mobillity data on pure haematite (no uranyl sorption) clearly show that electrophoretic mobility remains constant between pH 3 and 5 and decreases beyond pH 5. This indicates that below pH 5 surface hydroxyl groups are totally in SOH_2^+ form and only after pH 5 free SOH groups become available on the surface. Even at pH 4 the dimeric species of uranyl ions will be present in solution.

The striking feature of the data of Ho and Doern.[22] is that though solution conditions are favorable for the sorption of uranyl ions even at pH 4, the sorption edge on haematite occurs only after pH 5.0 due to non-availability of free surface hydroxyl groups at pH<5.0 thus satisfying one of the prime requirement of the surface hydrolysis model for the sorption of uranyl

ions. In this case, reaction A→C (Fig. 3) is likely to be the preferred process.

γ-Alumina: In another study,[23] Mikami et al. have studied the sorption of uranyl ions on γ-alumina by pressure jump technique. γ-Alumina used had a pK_{al}^*=6.8, pH_{pzc}=8.5 and sorption edge was at $pH_{soln} \geqslant 4.0$. They also concluded that $(UO_2)_3(OH)_5^+$ species are sorbed on the oxide.

Based on their pK_{al}^* value, it is found that for all values of α between 0.9—0.1, pH_{surf} is greater than 6.0. This indicates that the surface pH conditions are favorable for the formation of trimer-like species (reaction A→C Fig. 3). The sorption edge occurs in the decreasing part of the ξ-potential curve, which indicates that some SOH_2^+ groups have already deprotonated to give free SOH groups. Though the solution pH conditions are not favorable for trimeric species, the pH_{surf} favors the formation of trimer-like species on the surface (reaction A→C in Fig. 3) as soon as free surface hydroxyl groups become available.

Conclusion

In contrast to the above two oxides, free surface hydroxyl groups are available on MAG and HThO even at pH 3 (Fig. 2(C)), but sorption of uranyl ions on MAG and HThO occrts only when pH_{surf} approaches 4 when dimer-like species can be formed on the surface. Hence it is the characteristics of the oxide surface, (pK_{al}^*, pH_{surf}) and availability of free SOH groups which govern the sorption of uranyl ions. Sorption is not governed by the presence or absence of hydrolyzed uranyl species in the solution. This point is strikingly demonstrated by HTiO where the sorption edge occurs when uranium is present only as unhydrolyzed uranyl ion in solution.

Authors wish to thank Dr V. K. Kelkar for his help in computer calculations.

References

1) D. L. Dugger, J. H. Stanton, B. N. Irby, B. L. McConnell, W. W. Cummings, and R. W. Maatman, *J. Phys. Chem.*, **68**, 757 (1964).
2) R. O. James and T. W. Healy, *J. Colloid Interface Sci.*,**40**, 42, 53, 65 (1972).
3) H. Hohl and W. Stumm, *J. Colloid Interface Sci.*, **55**, 281 (1976).
4) D. W. Schindler, B. Fuerst, R. Dick, and P. W. Wolf, *J. Colloid Interface Sci.*, **55**, 469 (1976).
5) J. A. Davis and J. O. Leckie, *J. Colloid Interface Sci.*, **67**, 90 (1978).
6) M. M. Benjamin and J. O. Leckie, *Environ. Sci. Technol.*, **15**, 1050 (1981).
7) K. J. Farley, D. A Dzombak, and F. M. M. Morel. *J. Colloid Interface Sci.*, **106**, 226 (1985).
8) G. R. Wise and T. W. Healy, *J. Colloid Interface Sci.*, **51**, 434 (1975).
9) B. Venkataramani and A R. Gupta, Proc. Int. Meeting on the Recovery of Uranium from Sea Water (IMRUS-83), Tokyo, Japan, Oct. 17—19, 1983 (At. Energy. Soc. Japan, 1984), p. 313.
10) D. P. Benton and G. A. Horsfall, *J. Chem. Soc.*, **1962**, 3899.
11) E. B. Sandell, "Colorimetric Determination of Traces of Metals," 3rd ed, Inter Sceince, New York (1959), p. 915.
12) P. W. Schindler and H. Gamsjaeger, *Kolloid Z. Z. Polymere*, **250**, 759 (1972).
13) J. A. Davis, R. O. James, and J. O. Leckie, *J Colloid Interface Sci.*, **63**, 480 (1976).
14) A. Foissy, A. M. 'Pandou, J. M. Lamarche, and N. Jaffrezic-Renault, *Colloids Surf*, **5**, 363 (1982).
15) P. H. Tewari and A. W. McLean, *J Colloid Interface Sci.*, **40**, 267 (1972).
16) H. Tamura, E. Matijevic, and L. Meites, *J. Colloid Interface Sci.*, **92**, 303 (1983).
17) M. A. Blesa, N. M. Figliola, A. J. G. Maroto, and A. E. Regazzoni, *J. Colloid Interace Sci.*, **101**, 410 (1984).
18) G. A. Parks, *Chem. Aust.*, **49**, 389 (1982).
19) C. F. Baes Jr, and R. E. Mesmer, "Hydrolysis of Cations," John-Wiley and Son, New York (1976), p. 177.
20) N. Jaffrezic-Renault, H. Poirer-Andrade, and D. H. Trang, *J. Chromatogr.*, **201**, 187 (1980).
21) L. M. Toth, H. A. Friedman, G. M. Begun, and S. E. Dorris, *J. Phys. Chem.*, **88**, 5574 (1984).
22) C. H. Ho and D. C. Doern, *Can. J. Chem.*, **63**, 1100 (1985).
23) N. Mikami, M. Sasaki, K. Hachiya, and T. Yasunaga, *J. Phys. Chem.*, **87**, 5478 (1983).

 © 1988 The Chemical Society of Japan Bull. Chem. Soc. Jpn., 61, 1363—1367 (1988)

Peroxy Acid Oxidations. II.† A Kinetic and Mechanistic Study of Oxidation of α-Diketones

Radhasyam PANDA,* Akhil Krishna PANIGRAHI, Chakrapani PATNAIK, Sabita Kumari SAHU, and Sabita Kumari MAHAPATRA
Department of Chemistry, Khallikote College, Berhampur 760001, Orissa, India
(Received November 11, 1986)

The kinetics of Baeyer-Villiger oxidation of biacetyl and benzil by peroxomonophosphoric acid and peroxomonosulfuric acid have been studied in different pH ranges at 308 K. The reactions are second order; first order each in peroxy acid and in diketone concentrations at constant pH. The oxidation rate is strongly pH-dependent; the rate increases with increase in pH. From the pH-rate data the reactivity of different peroxo species, in the oxidation, has been determined. A mechanism consistent with rate-determining nucleophilic attack of peroxo species on carbonyl carbon of the diketone molecule has been proposed. Acetic acid and benzoic acid are respectively found to be the products of oxidation of biacetyl and benzil.

Oxidation of α-diketones by peroxidic reagents[1] have been reported to yield carboxylic acids. These reactions are known to involve the intermediary formation of anhydrides which on hydrolysis yield corresponding carboxylic acids. In the reaction[2] of benzil with H_2O_2, in benzene, Leffler isolated benzoic anhydride, which gave benzoic acid on hydrolysis. The first kinetic study on the oxidation of benzils by peracetic acid in the presence of H_2SO_4 was reported by Furuya et al.[3] They described this reaction as a sort of Baeyer-Villiger reaction; both the acid-catalyzed and uncatalyzed oxidations have been discussed. Foote and Sawaki,[4] in the oxidation of benzil by alkaline H_2O_2, have ruled out the dioxetane and epoxide mechanisms basing on high energy requirements, product and isotopic studies; the acyclic Baeyer-Villiger type mechanism was supported.

Although peroxomonophosphoric acid and peroxomonosulfuric acid are known to be potential Baeyer-Villiger reagents, there have been only a few reports on the oxidation of carbonyl compounds using these peroxy acids. Recently we reported our studies[5] on the oxidation of acetylacetone by peroxomonophosphoric acid in alkaline pH.

As part of an effort to study the oxidation of dicarbonyl compounds by peroxy acids, we wish to report here the kinetic studies on the Baeyer-Villiger oxidation of α-diketones by peroxomonophosphoric acid (PMPA) and peroxomonosulfuric acid (PMSA) in aqueous and in aqueous-acetonitrile solution of different pH. The study has enabled us to estimate the relative reactivities of different peroxo species.

It is of interest that the pH dependence of the oxidation rate is quite contrary to that observed in the acetylacetone oxidation[6] in acid pH.

Experimental

PMPA solutions were prepared by acid hydrolysis[7,8] of $K_4P_2O_8$. The potassium salt of Caro's acid, oxone ($2KHSO_5 \cdot KHSO_4 \cdot K_2SO_4$), was obtained from Dupont Chemical Co., U. S. A., and was used to prepare PMSA solutions. All other chemicals used were of AnalaR grade. Biacetyl (Riedel) was distilled just before use (bp 89—91 °C). Benzil was prepared by means[9] of benzoin obtained from benzaldehyde, and was recrystallized from ethanol, mp 94 °C (lit, mp 94—96 °C). Acetonitrile was distilled over P_2O_5 (bp 80—82 °C). Sodium perchlorate, prepared in situ by neutralizing perchloric acid with carbonate-free sodium hydroxide, was used for adjusting ionic strength of the medium. All the solutions were prepared in doubly distilled water, the second distillation being from $KMnO_4$. Acidity of the solution was maintained by adding calculated amounts of $HClO_4$ or standard buffers. Measurements of pH were made on a Systronics Digital pH Meter 335.

The kinetics was followed by measuring the rate of disappearance of peroxy acid, the estimation of which was made iodometrically using standard thiosulfate; PMPA estimation was done in an acetate buffer of pH 4—5 with a drop of ammonium molybdate solution.[10] The observed second-order rate constant (k_2' obs) was calculated by dividing pseudo-first-order rate constant with respect to peroxy acid disappearance by the substrate concentration. The rate constants were reproducible to ±5%. The self-decomposition of PMPA or PMSA was found to be either nil or negligibly small under our experimental conditions. The temperature was constant to within ±0.1 °C. Computations were done with a DCM Micro System 1121.

Product Study. A solution of PMSA (1.2×10^{-4} mol) in water (10 ml) was added to a solution of benzil (5×10^{-4} mol) in acetonitrile (10 ml). Before the addition was started the pH was adjusted to 10. The reaction mixture was allowed to stand for 12 h at room temperature. It was then poured into water (100 ml) and acidified with dil HCl. The product extracted with chloroform was identified as benzoic acid (mp 122 °C).

In the oxidation of biacetyl, the product acetic acid was detected by spot tests.[11]

The stoichiometry of the PMSA-biacetyl reaction with excess PMSA over biacetyl was determined by estimating the left over PMSA when the reaction was complete (PMSA= 27.5×10^{-4} mol dm^{-3}, biacetyl=9.84×10^{-4} mol dm^{-3}, pH= 4.08, 308 K). The biacetyl: PMSA ratio for the reaction was found to be 0.91. The overall reaction can, hence, be represented as,

$$HSO_5^- + CH_3COCOCH_3 + H_2O \rightarrow 2CH_3COOH + HSO_4^-.$$

†Part I, Ref. 5.

Results and Discussion

The kinetics of oxidation of biacetyl and benzil by peroxomonophosphoric acid and by peroxomonosulfuric acid have been investigated at 308 K. The reactions, at constant pH and ionic strength, I, were shown to exhibit second-order kinetics; first order each in peroxy acid concentration and in diketone concentration (Tables 1 and 2), the rate law being,

$$\text{Rate} = k_2' \text{ [Peroxy acid]}_t \text{ [Diketone]},$$

where k_2' is the observed second-order rate constant and 't' denotes total concentration.

The rate was not influenced by ionic strength. Addition of acrylamide also had no effect on the oxidation rate (Tables 1 and 2).

The kinetics of oxidation of biacetyl and benzil by PMPA have been investigated in the pH ranges 0—5.5 and 7.2—11 respectively, and that by PMSA in the pH ranges 0.3—4 and 5—9.7. The influence of pH on the oxidation rate are presented in Tables 3 and 4, and shown in Fig. 1.

It is observed, in both PMPA and PMSA reactions with biacetyl, that variation of pH in the lower range (0—1.3 in PMPA and 0—0.7 in PMSA oxidation) did not significantly change the rate. However, the rate increased linearly with pH in the range 2.1—5.5 in PMPA oxidation, and 1—4 in PMSA oxidation. Such an observation is quite contrary to that made in the oxidation of acetylacetone,[6] a β-diketone, by PMPA in the pH range 0.4—7.75, where the rate first decreased with increase of pH in the range 0.4—3, and then increased (pH range 4—7.75).

In case of benzil, the rate (in both PMPA and PMSA oxidations) increased with increase of pH. The reactions were instantaneous at pH values higher than the

Table 1. Oxidation of Biacetyl by Peroxomonophosphoric Acid[a]

10^3[diketone] / mol dm^{-3}	10^4[PMPA] / mol dm^{-3}	$10^3 k'_2$[b] / dm^3 mol^{-1} s^{-1}
5.01	7.51	14.3
9.82	8.88	16.8
20.0	7.51	16.2
10.9	2.29	18.4
10.9	10.7	15.6
10.3	6.10	14.7[c]
10.3	5.89	15.7[d]
11.2	6.03	15.9[e]

a) [H$^+$]=0.1 mol dm^{-3}, I=0.3 mol dm^{-3}, aqueous, 308 K. b) Observed second-order rate constant. c) I=0.15 mol dm^{-3}. d) I=0.5 mol dm^{-3}. e) [Acrylamide]=5.0×10^{-3} mol dm^{-3}.

Table 2. Oxidation of Biacetyl by Peroxomonosulfuric Acid[a]

10^3[diketone] / mol dm^{-3}	10^4[PMSA] / mol dm^{-3}	$10^3 k'_2$ / dm^3 mol^{-1} s^{-1}
11.0	3.85	27.0
10.5	5.47	26.4
10.2	11.6	27.0
10.6	28.1	32.2
7.07	6.09	26.9
10.5	5.47	26.4
22.1	5.9	28.6
40.9	5.76	31.8
10.5	5.72	27.5[b]
10.5	5.29	33.3[c]
10.5	5.24	44.6[d]

a) [H$^+$]=0.1 mol dm^{-3}, I=0.3 mol dm^{-3}, aqueous, 308K, b) I=0.2 mol dm^{-3}, c) I=0.5 mol dm^{-3}, d) I=0.5 mol dm^{-3}.

Table 3. Oxidation of Biacetyl by Peroxy Acids: Effect of pH[a]

Peroxy acid	pH	$10^2 k'_2$ / dm^3 mol^{-1} s^{-1}	$10^2 k'_2$(calcd) / dm^3 mol^{-1} s^{-1}
PMPA	0.7	1.78	2.49
	1.0	1.68	3.88
	1.3	1.66	5.40
	2.11	2.20	8.42
	2.78	5.19	11.0
	3.53	20.1	22.5
	3.64	24.7	26.5
	4.38	137	99.3
	4.85	212	235
	5.47	300	557
PMSA	0.3	2.05	2.01
	0.7	2.02	2.29
	1.0	2.64	2.77
	1.3	4.47	3.72
	1.6	8.17	5.62
	1.83	8.87	11.3
	3.08	124	116
	4.08	765	1145

a) Aqueous, I=0.3 mol dm^{-3}, 308 K.

Table 4. Oxidation of Benzil by Peroxy Acids: Effect of pH[a]

Peroxy acid	pH	$10^2 k'_2$ / dm^3 mol^{-1} s^{-1}	$10^2 k'_2$(calcd) / dm^3 mol^{-1} s^{-1}
PMPA	7.19	0.419	0.716
	7.94	0.864	0.90
	8.25	2.15	1.12
	10.02	27.5	27.5
	10.96	89.5	232
PMSA	5.03	0.50	1.47
	6.07	2.71	2.79
	6.8	9.94	9.12
	7.05	14.1	15.1
	7.1	20.7	16.8
	9.5	1101	1757
	9.7	1660	2063

a) CH_3CN: water=40 : 60 (v/v), I=0.2 mol dm^{-3}, 308 K.

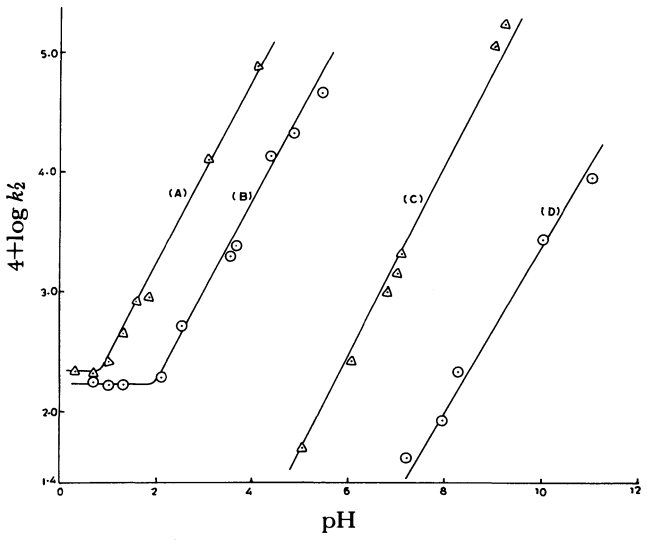

Fig. 1. Plots of $\log k_2'$ vs. pH.
A; PMSA-biacetyl, B; PMPA-biacetyl, C; PMSA-benzil, D; PMPA-benzil.

reported range.

Our attempt to collect a few kinetic runs with H_2O_2 in the presence of H^+, for comparison purpose, was frustrated owing to no definite kinetic order with respect to H_2O_2 disappearance.

PMPA is a tribasic acid having the following dissociation equilibria in solution.[7]

$$H_3PO_5 \overset{K_1}{\rightleftharpoons} H_2PO_5^- + H^+, \quad (1)$$

$$H_2PO_5^- \overset{K_2}{\rightleftharpoons} HPO_5^{2-} + H^+, \quad (2)$$

$$HPO_5^{2-} \overset{K_3}{\rightleftharpoons} PO_5^{3-} + H^+. \quad (3)$$

The dissociation constants K_1, K_2, and K_3 are 8.0×10^{-2}, 4.2×10^{-6}, and 1.6×10^{-13} mol dm^{-3} respectively at 298 K and I=0.2 mol dm^{-3}.

In the pH range 0—5.5 PMPA exists[7,8] as H_3PO_5, $H_2PO_5^-$, and HPO_5^{2-}. The reaction scheme for biacetyl oxidation in this pH range can, therefore, be presented by Eqs. 4—6.

$$H_3PO_5 + \text{biacetyl} \xrightarrow{k_1} \text{products}, \quad (4)$$

$$H_2PO_5^- + \text{biacetyl} \xrightarrow{k_2} \text{products}, \quad (5)$$

$$HPO_5^{2-} + \text{biacetyl} \xrightarrow{k_3} \text{products}, \quad (6)$$

which lead to the rate expression,

$$-\frac{d[PMPA]_t}{dt} = (k_1[H_3PO_5] + k_2[H_2PO_5^-] + k_3[HPO_5^{2-}])[\text{biacetyl}], \quad (7)$$

where $[PMPA]_t$ represents the total stoichiometric concentration of PMPA, and can be expressed by Eq. 8.

$$[PMPA]_t = [H_3PO_5] + [H_2PO_5^-] + [HPO_5^{2-}] \quad (8)$$

From Eqs. 1, 2, and 8 we get,

$$[H_3PO_5] = \frac{[H^+]^2[PMPA]_t}{K_1K_2 + K_1[H^+] + [H^+]^2}, \quad (9)$$

$$[H_2PO_5^-] = \frac{K_1[H^+][PMPA]_t}{K_1K_2 + K_1[H^+] + [H^+]^2}, \quad (10)$$

and

$$[HPO_5^{2-}] = \frac{K_1K_2[PMPA]_t}{K_1K_2 + K_1[H^+] + [H^+]^2}. \quad (11)$$

Substituting Eqs. 9, 10, and 11 in Eq. 7, we get,

$$-\frac{d[PMPA]_t}{dt} = \left\{\frac{k_1[H^+]^2 + k_2K_1[H^+] + k_3K_1K_2}{K_1K_2 + K_1[H^+] + [H^+]^2}\right\} \times [PMPA]_t[\text{biacetyl}], \quad (12)$$

or

$$k_2' = \frac{k_1[H^+]^2 + k_2K_1[H^+] + k_3K_1K_2}{K_1K_2 + K_1[H^+] + [H^+]^2}. \quad (13)$$

The values of k_2 and k_3, calculated by a method of least-squares using Eq. 13, are 0.087 and 10.0 dm^3 mol^{-1} s^{-1} respectively. The value of k_1 is small and negative and hence, could be approximated to zero. This allows us to rule out the path involving H_3PO_5 (Eq. 4). These values of k_1, k_2, and k_3 have been used to obtain k_2' calcd, which are presented in Table 3.

The PMPA species contributing to the rate of oxidation of benzil, in the pH range 7—11, are HPO_5^{2-} and PO_5^{3-}. Hence, the steps of the oxidation can be written as,

$$HPO_5^{2-} + OH^- \overset{K_4}{\rightleftharpoons} PO_5^{3-} + H_2O, \quad (14)$$

$$HPO_5^{2-} + \text{benzil} \xrightarrow{k_4} \text{products}, \quad (15)$$

$$PO_5^{3-} + \text{benzil} \xrightarrow{k_5} \text{products}. \quad (16)$$

The rate law is,

$$-\frac{d[PMPA]_t}{dt} = (k_4[HPO_5^{2-}] + k_5[PO_5^{3-}])[\text{benzil}], \quad (17)$$

$$= \left\{\frac{k_4K_h + k_5[OH^-]}{K_h + [OH^-]}\right\}[PMPA]_t[\text{benzil}], \quad (18)$$

where

$$[PMPA]_t = [HPO_5^{2-}] + [PO_5^{3-}], \quad (19)$$

and

$$K_h = [H_2O]/K_4. \quad (20)$$

Equation 18 can be rearranged to give Eq. 21

$$k_2' = \frac{k_4K_h + k_5[OH^-]}{K_h + [OH^-]}, \quad (21)$$

which has been used to calculate the rate constant k_2' (calcd) in Table 4.

The K_h value for PMPA species, as determined from Eq. 22 using the literature reported K_3 value, is 6.25×10^{-2} mol dm^{-3}.

$$K_h = K_w/K_3 \tag{22}$$

The statistical analysis of Eq. 21 was repeated by allowing the K_h value to vary until optimal values of k_4 and k_5 were obtained. These values are K_h=7.35×10^{-2} mol dm^{-3}, k_4=6.77×10^{-3} dm^3 mol^{-1} s^{-1} and k_5=188 dm^3 mol^{-1} s^{-1}.

The structure of peroxomonosulfuric acid has been shown[10] to be

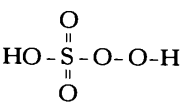

of which one proton is a sulfuric acid proton and the other is a hydrogen peroxide proton. The pK_a value of the sulfuric acid proton lies in the high acidity region, while the hydrogen peroxide proton has a pK_a value[12] of 9.4.

In aqueous solution PMSA exists as HSO_5^- and SO_5^{2-}

$$HSO_5^- \overset{K_5}{\rightleftharpoons} SO_5^{2-} + H^+,\ K_5 = 4\times10^{-10}\ \text{mol dm}^{-3}. \tag{23}$$

For the oxidation of α-diketones by PMSA, in the range of pH studied, the dependence on pH can be explained by a mechanism in which the diketone molecule reacts simultaneously with HSO_5^- and SO_5^{2-} in two parallel reactions.

For biacetyl oxidation, in the pH range 0.3—4, the reaction steps are,

$$HSO_5^- + \text{biacetyl} \xrightarrow{k_6} \text{products}, \tag{24}$$

$$SO_5^{2-} + \text{biacetyl} \xrightarrow{k_7} \text{products}, \tag{25}$$

which follow the rate expression,

$$-\frac{d[PMSA]_t}{dt} = \left\{k_6[HSO_5^-] + k_7[SO_5^{2-}]\right\}[\text{biacetyl}], \tag{26}$$

from which we get,

$$-\frac{d[PMSA]_t}{dt} = \frac{k_6[H^+] + k_7K_5}{K_5 + [H^+]}[PMSA]_t[\text{biacetyl}], \tag{27}$$

where

$$k_2' = \frac{k_6[H^+] + k_7K_5}{K_5 + [H^+]}. \tag{28}$$

In the pH range 0.3—4,

$$K_5 \ll [H^+]. \tag{29}$$

Equation 28 may, therefore, be written as,

$$k_2' = \frac{k_6[H^+] + k_7K_5}{[H^+]}. \tag{30}$$

Equation 30 has been used to determine the reactivity of HSO_5^- and SO_5^{2-} in biacetyl oxidation. The values of k_6 and k_7 are respectively found to be 1.82×10^{-2} dm^3 mol^{-1} s^{-1} and 2.39×10^6 dm^3 mol^{-1} s^{-1}.

The reaction steps for benzil oxidation, in pH range 5—9.7 are postulated as,

$$HSO_5^- + OH^- \overset{K_6}{\rightleftharpoons} SO_5^{2-} + H_2O, \tag{31}$$

$$HSO_5^- + \text{benzil} \xrightarrow{k_8} \text{products}, \tag{32}$$

$$SO_5^{2-} + \text{benzil} \xrightarrow{k_9} \text{products}. \tag{33}$$

Equations 31—33 lead to the rate equation,

$$k_2' = \frac{k_8K_h' + k_9[OH^-]}{K_h' + [OH^-]}, \tag{34}$$

where K_h'=K_w/K_5.

A least squares solution of Eq. 34, using K_h'=K_w/K_5, gave us the values of k_8 and k_9. These values are k_8=1.34×10^{-2} dm^3 mol^{-1} s^{-1} and k_9=30.9 dm^3 mol^{-1} s^{-1}, which have been used to calculate k_2' calcd. in Table 4.

Peroxo species which participate in the reaction with α-diketones are $H_2PO_5^-$, HPO_5^{2-}, and PO_5^{3-} in PMPA oxidation, and HSO_5^- and SO_5^{2-} in PMSA oxidation. From the magnitude of rate constants (Table 5) for these species, it is evident that the reaction is facilitated by the more nucleophilic peroxo species; the reactivity of H_3PO_5 is negligible in the oxidation. The reactivity of SO_5^{2-} is approximately eight orders of magnitude higher than that of HSO_5^- in biacetyl oxidation. The reduced reactivity of benzil might be due to the decrease in electrophilic character of the carbonyl carbon.

Baeyer-Villiger reaction of aldehydes or ketones with hydrogen peroxide or peroxy acids are well-known.[1] Acid catalysis is an important feature of these oxidations.

The fundamental step in the reaction of carbonyl compounds with peroxides is rapid addition[13] of the peroxide molecule to the carbonyl group to give 'Criegee intermediate' of type I,

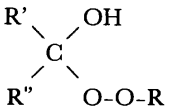

(I)

which then rearranges to give the product. The rate-determining step, in these reactions, may be either addition of peroxy acid to >C=O or migration from adduct depending on the substrate.

In the oxidation[14] of acetophenones by PMPA, cata-

Table 5. Comparison of Second-Order Rate Constants for the Oxidation of α-Diketones by Various Peroxo Species at 308 K

Oxidant	k'_2/dm^3 mol^{-1} s^{-1}	
	Biacetyl	Benzil
H_3PO_5	≈0	
$H_2PO_5^-$	8.7×10^{-2}	
HPO_5^{2-}	10.0	6.77×10^{-3}
PO_5^{3-}	Very fast	188
HSO_5^-	1.82×10^{-2}	1.34×10^{-2}
SO_5^{2-}	2.39×10^6	30.9

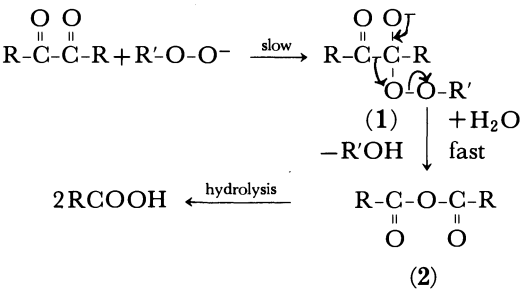

(R=CH_3 or C_6H_5, and R'OO^-=$H_2PO_5^-$, HPO_5^{2-}, PO_5^{3-}, HSO_5^-, or SO_5^{2-}).

Scheme 1.

lyzed by H_2SO_4, the migration step was shown to be rate determining, while in perbenzoic acid oxidation[15] the rate-determining step was the acid-catalyzed addition of peroxy acid to >C=O.

α-Diketones have been shown to react readily with Baeyer-Villiger reagents in both acid and alkaline media.[1] The product was either an anhydride or a carboxylic acid depending on the nature of solvent used.

The oxidation of benzil by peracetic acid was reported[3] to be acid-catalyzed. The acid catalysis has been traced to protonation of the carbonyl group, which was then attacked by peroxy acid in a rate-determining step.

In the oxidation of benzil by alkaline H_2O_2, from both product and isotopic studies, it has been established[4] that the reaction involves a Baeyer-Villiger type acyclic mechanism. Even though the migratory aptitude of the acyl group is very low in carbon-to-carbon migrations,[16] the acyl shift to peroxide oxygen has been shown to be facile.[17]

A significant observation, in the present study, is that the reactions are not acid-catalyzed. The increased reactivity in higher pH points to the nucleophilic behavior of peroxo species in the oxidation.

The initial step in the reactions of α-diketones by PMPA or PMSA is now believed to be the rate-determining nucleophilic addition of peroxy acid to the carbonyl carbon to form an adduct **1**. This adduct, can, then rearrange to the anhydride **2**, which is hydrolyzed, under reaction conditions, giving the corresponding carboxylic acid (Scheme 1).

The authors are grateful to Professor G. P. Panigrahi, Department of Chemistry, Berhampur University for helpful discussions. They are also grateful to Professor S. C. Padhi, Department of Chemistry, Khallikote College, for providing necessary facilities, and encouragement. A financial help from UGC, New Delhi is gratefully acknowledged.

References

1) C. H. Hassall, *Org. React.*, **9**, 73 (1957).
2) J. E. Leffler, *J. Org. Chem.*, **16**, 1785 (1951).
3) Y. Furuya and I. Urasaki, *Bull. Chem. Soc. Jpn.*, **41**, 660 (1968).
4) Y. Sawaki and C. S. Foote, *J. Am. Chem. Soc.*, **101**, 6292 (1979); **105**, 5035 (1983).
5) R. S. Panda, A. K. Panigrahi, S. N. Mohapatro, and C. P. Patnaik, *Bull. Chem. Soc. Jpn.*, (in press).
6) R. S. Panda and C. P. Patnaik, unpublished results.
7) C. J. Battaglia and J. O. Edwards, *Inorg. Chem.*, **4**, 552 (1965).
8) R. S. Panda, Ph. D. Thesis, Berhampur University (1980).
9) R. Adams and C. S. Marvel, *Org. Synthe.*, Coll. Vol. I, 94 (1956).
10) G. P. Panigrahi and R. S. Panda, *Bull. Chem. Soc. Jpn.*, **53**, 2366 (1980).
11) F. Feigl, "Spot Tests in Organic Analysis," Elsevier, New York (1960), p. 515.
12) D. L. Ball and J. O. Edwards, *J. Am. Chem. Soc.*, **78**, 1125 (1956).
13) M. F. Hawthorne and W. D. Emmons, *J. Am. Chem. Soc.*, **80**, 6398 (1958).
14) Y. Ogata, K. Tomizawa, and T. Ikeda, *J. Org. Chem.*, **43**, 2417 (1978).
15) S. L. Friess and A. H. Soloway, *J. Am. Chem. Soc.*, **73**, 3968 (1951).
16) C. A. Bunton, "Peroxide Reaction Mechanisms," ed by J. O. Edwards, Interscience, New York (1962), p. 11.
17) Y. Sawaki and T. Ogata, *J. Am. Chem. Soc.*, **100**, 856 (1978).

 © 1988 The Chemical Society of Japan Bull. Chem. Soc. Jpn., 61, 1369—1373 (1988)

Synthesis, Ion-Exchange Properties, and Analytical Applications of Anilinium Tin(IV) Phosphate

Dhruv Kumar SINGH* and Anjana DARBARI
Department of Chemistry, Harcourt Butler Technological Institute, Kanpur-208002, India
(Received January 13, 1987)

A new inorganic ion-exchanger anilinium tin(IV) phosphate (ATP) has been synthesized under varying conditions. The effects of mixing ratio of reagents and the pH of the mixture on the properties of the material have been studied. The sample ATP_1 has been chosen for detailed studies, such as ion-exchange capacity, chemical and thermal stabilities, chemical composition, pH titration, break-through curve, and IR analysis. Distribution coefficients of 16 metal ions have been studied in water, hydrochloric acid and acetone-hydrochloric acid media. On the basis of K_d values some analytically important separations of metal ions have been achieved on the small columns of anilinium tin(IV) phosphate.

There have been continuous efforts to improve the chemical, thermal, and mechanical stabilities of ion-exchangers and to make them highly selective for particular metal ions. Hahn and Klein[1] introduced organic ammonium ions in place of inorganic ammonium ion in ammonium hexacyanoferrate(II) compound of cobalt(II) and reported that the ammonium compounds have excellent exchange properties for ^{137}Cs. Ammonium tin(II) hexacyanoferrate(II),[2] ammonium tin(IV) hexacyanoferrate(II),[3] tin(IV) diethanolammonium,[4] iron(III) diethanolammonium,[5] and tin(IV) phosphate[6,7] have already been reported and utilized for the separations of metal ions. Anilinium tin(IV) phosphate has not been studied so far. The present paper summarizes the synthesis, ion-exchange properties and analytical applications of anilinium tin(IV) phosphate as a new inorganic ion-exchanger.

Experimental

Reagants. Tin(IV) chloride pentahydrate (Poland), aniline, and orthophosphoric acid (BDH, India) were used. All other reagents were of analytical grade.

Apparatus. Bausch and Lomb Spectronic 20 for spectrophotometry, Systronic digital pH meter for pH measurements and Perkin Elmer model 599 B Spectrophotometer for IR studies, were used. An electric rotary shaking machine IEC-56 was used for shaking purpose.

Synthesis. An excess of aniline (ca. 5 cm^3) was added dropwise to 10 cm^3 of 1 mol dm^{-3} orthophosphoric acid solution with constant stirring to prepare dianilinium hydrogenphosphate $[(C_6H_5NH_3)_2HPO_4]$. It was dissolved in demineralized water (DMW) and diluted up to 200 cm^3. This solution was added to 0.1 mol dm^{-3} tin(IV) chloride solution with constant stirring as outlined in Table 1. The pH of the sample solution in each case was adjusted by adding hydrochloric acid solution dropwise. After 24 h the product was filtered, washed with DMW and dried at 40 °C. The material broke into small particles when immersed in DMW and was converted into H^+ form on treatment with 1 mol dm^{-3} nitric acid for 24 h with occasional shaking and renewal of the acid. The excess of the acid was removed after several washings with DMW. The samples were dried at 40 °C.

Ion-Exchange Capacity. The ion-exchange capacity of various samples of anilinium tin(IV) phosphate was determined by the column method (Tables 1 and 2). One gram exchanger in H^+ form was taken in the column of 7.2 mm (i.d.). The H^+ ions were eluted by percolating the required 1 mol dm^{-3} cationic solution through the column. The feed was passed until its pH became equal to that of the effluent collected. The hydrogen ions so eluted were titrated against standardized 0.1 mol dm^{-3} NaOH. The neutral salt decomposition capacity with different uni- and bivalent ions is reported in Table 3.

Chemical Composition. The well-powdered material (0.5 g) was fused with a 1 : 1 mixture of potassium and sodium carbonates. The fused mixture was extracted with hot water, the undissolved portion was ignited and weighed as SnO_2. The diphosphorus pentoxide present in the dissloved portion was precipitated as ammonium molybdophosphate, filtered and determined gravimetrically.[8] For the determination of aniline, another 0.5 g sample of the exchanger was introduced into a Kjeldahl digestion flask. After digestion 25 cm^3 potassium hydroxide solution (50%) was added dropwise. The amine distilled into 50 cm^3 boric acid solution (1%) was titrated with 0.1 mol dm^{-3} HCl using a mixed indicator (Bromocresol Green and Methyl Red).[9]

Chemical Stability. A 0.2 g of the material (sample ATP_1) was shaken with 20 cm^3 of the solution concerned at 30±2 °C for 6 h. Tin, phosphorus, and aniline were determined spectrophotometrically with phenylfluorone,[10] molybdovanadophosphoric acid,[11] and iron(III) nitrate[12] respectively.

pH Titration. Topp and Peppers'[13] method was used for pH titrations using NaOH-NaCl system. A quarter gram samples of dry exchanger (ATP_1) in H^+ form were shaken with 25 cm^3 portions of 0.1 mol dm^{-3} (NaCl+NaOH) cationic solution in different conical flasks at 30±1 °C. The concentration ratio of NaCl/NaOH was varied from 0.096 mol dm^{-3}/0.004 mol dm^{-3} to 0.004 mol dm^{-3}/0.096 mol dm^{-3} in the equilibrating solution of the flasks. After 24 h pH of the supernatant solution of each flask was recorded and plotted against the mEq of OH^- added per 0.25 g of dry exchanger (Fig. 1).

Break-through Curve. The break-through curves[14] were observed for Zn^{2+}, Cd^{2+}, and Hg^{2+} by passing 0.02 mol dm^{-3} solution (pH≈6) of each metal ion through a glass column, i.d. 7.2 mm and 30 cm length packed with 4 g of anilinium thin(IV) phosphate in H^+ form (Sample ATP_1). The flow rate was maintained 1 cm^3 min^{-1}. The results are presented in Fig. 3.

Table 1. Synthesis and Properties of Anilinium Tin(IV) Phosphate[a, b]

Sample No.	Volume of 0.1 mol dm^{-3} Tin(IV) chloride/cm^3	pH	Ion-exchange capacity for K^+ meq (dry g)$^{-1}$	Composition Sn: $C_6H_5NH_2$: PO_4^{3-}	Yield g
ATP_1	50	1	1.68	4:2:1	1.06
ATP_2	100	1	1.52	—	—
ATP_3	200	1	1.40	—	—
ATP_4	50	2	1.53	—	—
ATP_5	50	3	1.44	4.6:2:1	—
ATP_6	50	5	1.30	5:2:1	—

a) Tin(IV) chloride solution was added to 200 cm^3 of 5×10^{-2} mol dm^{-3} $(C_6H_5NH_3)_2HPO_4$ solution. b) Appearance of precipitate was white gelatinous and appearance of beads after drying at 40 °C was white.

Table 2. Reproducibility of the Synthesis

Batch No.	Ion-exchange capacity for K^+ meq (dry g)$^{-1}$	Composition Sn : $C_6H_5NH_2$: PO_4^{3-}
1	1.68	4 : 2 : 1
2	1.70	4 : 2 : 1
3	1.68	4.02 : 2 : 1
4	1.66	4 : 2 : 1
5	1.70	4.02 : 2 : 1

Distribution Coefficient. Distribution coefficients (K_d values) of a number of metal ions in water, hydrochloric acid and acetone-hydrochloric acid systems were determined by a batch process.[15] A quarter gram of the exchanger in H^+ form (50—100 mesh) was equilibrated with 25 cm^3 cation solutions (4×10^{-3} mol dm^{-3}) at 30±1 °C for 6 h in a 100 cm^3 Erlenmeyer flask. The amount of cation in the solution after and before the treatment with the exchanger was determined by EDTA titration except Pt^{4+} which was determined with tin(II) chloride[16] spectrophotometrically. K_d values were calculated from

$$K_d(\text{cm}^3\,\text{g}^{-1}) = \frac{\text{Amount of metal ion in exchanger phase per gram}}{\text{Amount of metal ion in solution phase per cm}^3}$$

The results are presented in Table 5.

Quantitative Separations. Quantitative separations of some important metal ions of analytical utility were achieved on the columns of anilinium tin(IV) phosphate. Two grams of the exchanger in H^+ form (50—100 mesh) was taken into a glass column of i.d. 3.9 mm. The column was first washed with about 20 cm^3 of 80% acetone-hydrochloric acid (0.01 mol dm^{-3}) and then the mixture of metal ions having concentration 0.644 to 1.044 mg/10 cm^3 was introduced into the column and allowed to be adsorbed. The metal ions were then eluted separately using suitable eluting reagents and determined by EDTA titrations except Pt^{4+} which was determined spectrophotometrically.[16] The flow rate was maintained about 0.2 cm^3 min^{-1} throughout the elution process. Results of separations achieved have been reported in Table 6.

Results and Discussion

The ion-exchange capacities and the compositions of the samples of anilinium tin(IV) phosphate are presented in Table 1. In the synthesis of anilinium tin(IV) phosphate, increased pH and volume of 0.1 mol dm^{-3} tin(IV) chloride results in decreased ion-exchange capacity. The maximum ion-exchange capacity (1.7 meq (dry g)$^{-1}$) is observed for sample ATP_1 prepared by mixing 50 cm^3 of 0.1 mol dm^{-3} tin(IV) chloride solution to the anilinium phosphate solution at pH 1. The ion-exchange capacity of ATP_1 is higher than the reported capacity, 1.4 meq (dry g)$^{-1}$

Table 3. Ion-Exchange Capacity of Anilinium Tin(IV) Phosphate (Sample ATP_1) for Various Cations

Cation[a]	pH	Hydrated radii/nm	I.E.C. meq (dry g)$^{-1}$
Li^+	6.8	0.340	1.28
Na^+	6.8	0.276	1.64
K^+	6.8	0.232	1.70
Mg^{2+}	6.5	0.700	1.00
Ca^{2+}	6.5	0.630	1.46
Sr^{2+}	6.2	—	1.50
Ba^{2+}	6.2	0.590	1.62

a) Used as chloride (1 mol dm^{-3}).

Table 4. Chemical Stability of Anilinium Tin(IV) Phosphate (ATP_1)

Solvent	Solubility (mg/20 cm^3)		
	Sn released	$C_6H_5NH_2$ released	P released
Demineralized water	0.00	0.02	0.06
1 mol dm^{-3} Nitric acid	0.06	0.04	0.12
4 mol dm^{-3} Nitric acid	1.30	0.84	1.86
1 mol dm^{-3} Hydrochloric acid	0.20	0.37	0.28
4 mol dm^{-3} Hydrochloric acid	2.58	2.14	3.60
0.1 mol dm^{-3} Sodium hydroxide	0.04	3.00	1.62
Acetone	0.00	0.00	0.10
Methanol	0.00	0.04	0.16

of tin(IV) phosphate.[6,7] ATP_1 shows reproducible properties as is evident from data presented in Table 2.

The ion-exchange capacity measured for various cations is given in Table 3. The data show that ion-exchange capacity for alkali metals are higher than alkaline earths. In both cases the capacity increases with the decrease in hydrated radii of ions. The effect of drying temperature on the ion exchange capacity was studied. The results shown in Fig. 2 indicate that this exchanger can be used up to 100 °C without loss in ion-exchange capacity; above 100 °C there is a decrease in ion-exchange capacity but the decrease is much less than in anilinium hexacyanoferrate(II) of tin(II) and tin(IV).

The results of chemical stability measurements (Table 4) indicate that the product is fairly stable in water, acetone, ethanol, 0.1 mol dm^{-3} NaOH and up to 1 mol dm^{-3} nitric acid and hydrochloric acid.

Analytical data of sample ATP_1 are as follows: amount of exchanger taken, 1.000g; $C_6H_5NH_2$ obtained after distillation, 0.217±0.003 g (2.333 mmol); amount o Sn(IV) found, 0.544±0.002 g (4.583 mmol); amount of PO_4^{3-} found, 0.108±0.002 g (1.137 mmol); molar ratio of Sn(IV): $C_6H_5NH_2$: PO_4^{3-}, 4 : 2 : 1. The products prepared at pH values greater than one contained more tin.

The capacity which is utilized until break-through occurs is called break-through capacity. The break-through behavior of anilinium tin(IV) phosphate for Zn^{2+}, Cd^{2+}, and Hg^{2+} was studied. The results are plotted in Fig. 3.

The results of pH titrations indicate that ATP_1 in

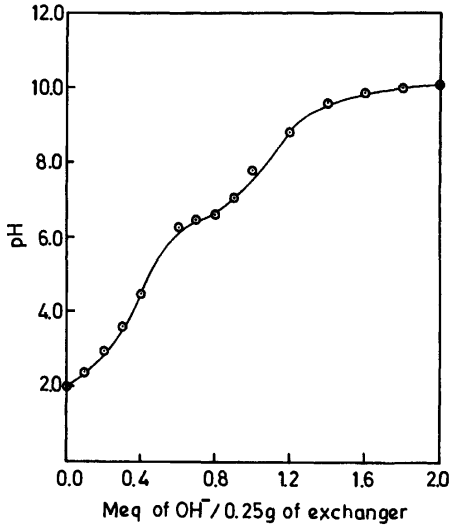

Fig. 1. pH-titration curve of anilinium tin(IV) phosphate(H^+) (Sample ATP_1).

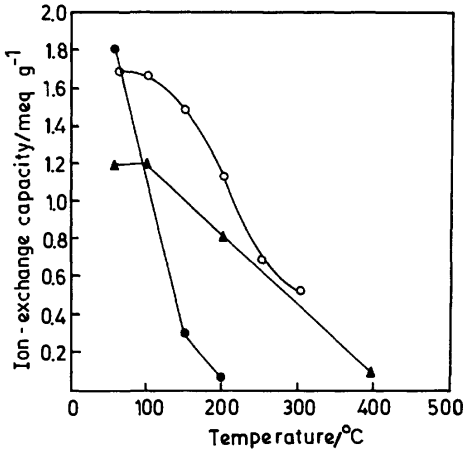

Fig. 2. Ion-exchange capacity of various aniline complexes as a function of drying temperature.
▲ Anilinium tin(II) hexacyanoferrate(II).
● Anilinium tin(IV) hexacyanoferrate(II).
○ Anilinium tin(IV) phosphate (Sample ATP_1).

Table 5. Distribution Coefficients of Some Metal Ions on Anilinium Tin(IV) Phosphate

Metal ion	K_d/cm^3 g^{-1}						
	Water	0.01 mol dm^{-3} HCl	0.1 mol dm^{-3} HCl	80% 0.01 mol dm^{-3} HCl–20% acetone	60% 0.01 mol dm^{-3} HCl–40% acetone	20% 0.01 mol dm^{-3} HCl–80% acetone	Acetone
Zn^{2+}	40	11	3	6	9	13	39
Cd^{2+}	87	49	11	51	81	190	380
Hg^{2+}	580	370	280	1200	5700	7900	9800
Mn^{2+}	40	26	6	21	28	40	63
Fe^{3+}	58	42	26	53	68	110	220
Co^{2+}	69	59	50	350	440	580	900
Ni^{2+}	68	56	43	68	78	110	220
Cu^{2+}	70	17	9	160	250	260	370
Pb^{2+}	410	350	320	360	410	430	500
Mg^{2+}	19	7	1	9	11	26	78
Ca^{2+}	99	55	20	70	95	130	300
Ba^{2+}	110	50	28	86	100	150	330
Al^{3+}	85	60	44	300	470	900	1200
Th^{4+}	22	19	10	35	79	98	110
Pt^{4+}	780	—	210	—	600	750	1300
Zr^{4+}	310	220	130	230	300	—	510

Table 6. Quantitative Separations of Metal Ions on Anilinium Tin(IV) Phosphate (Sample ATP_1) Columns

Sample No.	Separation	Amount fed to the column / μg	Amount found after elution / μg	Percent of metal ions eluted	Total elution volume / cm^3	Eluent used
1	Zn^{2+}	327	326	99.7	30	60% 0.01 mol dm^{-3} HCl-40% acetone
	Cd^{2+}	225	223	99.4	50	80% 0.01 mol dm^{-3} HCl-20% acetone
	Hg^{2+}	400	388	97.0	70	80% 0.5 mol dm^{-3} HCl-20% acetone
2	Zn^{2+}	327	326	99.6	30	60% 0.01 mol dm^{-3} HCl-40% acetone
	Ni^{2+}	427	421	98.7	50	80% 0.2 mol dm^{-3} HCl-20% acetone
	Pt^{4+}	145	141	96.8	70	80% 0.5 mol dm^{-3} HCl-20% acetone
3	Zn^{2+}	327	326	99.7	30	60% 0.01 mol dm^{-3} HCl-40% acetone
	Cu^{2+}	317	313	98.9	40	80% 0.1 mol dm^{-3} HCl-20% acetone
	Hg^{2+}	400	389	97.2	70	80% 0.5 mol dm^{-3} HCl-20% acetone
4	Zn^{2+}	327	326	99.7	30	60% 0.01 mol dm^{-3} HCl-40% acetone
	Fe^{3+}	280	275	98.2	40	80% 0.2 mol dm^{-3} HCl-20% acetone
	Pb^{2+}	401	394	98.4	50	80% 0.5 mol dm^{-3} HCl-20% acetone
5	Mg^{2+}	243	242	99.8	30	80% 0.01 mol dm^{-3} HCl-20% acetone
	Th^{4+}	232	230	99.1	40	80% 0.1 mol dm^{-3} HCl-20% acetone
	Pt^{4+}	380	372	97.9	70	80% 0.5 mol dm^{-3} HCl-20% acetone
6	Th^{4+}	232	230	99.0	40	80% 0.1 mol dm^{-3} HCl-20% acetone
	Zr^{4+}	450	441	98.0	60	80% 0.5 mol dm^{-3} HCl-20% acetone
7	Mn^{2+}	540	536	99.3	30	60% 0.1 mol dm^{-3} HCl-40% acetone
	Co^{2+}	431	424	98.5	50	80% 0.5 mol dm^{-3} HCl-20% acetone
8	Mg^{2+}	243	242	99.8	30	80% 0.01 mol dm^{-3} HCl-20% acetone
	Ca^{2+}	401	394	98.4	50	80% 0.2 mol dm^{-3} HCl-20% acetone

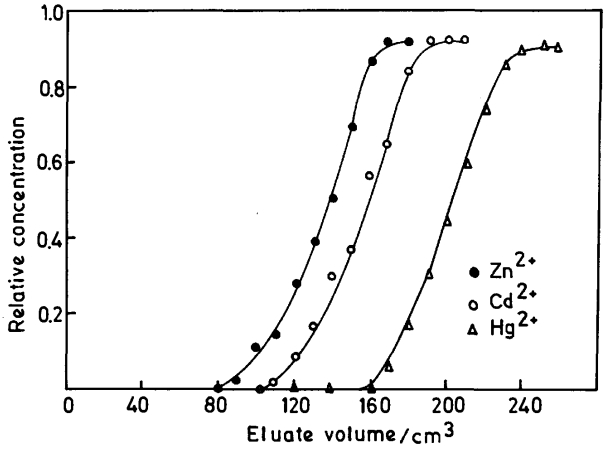

Fig. 3. Break-through curves of ATP_1 for three bivalent cations.

H^+ form behaves as a diprotic acid (Fig. 1). The total ion-exchange capacity is 3.6 meq g^{-1} calculated at the neutralization point. This gives the maximum number of replaceable counter ions and is independent of the nature of the cation.

The IR spectrum of anilinium tin(IV) phosphate is in accord with the proposed composition.

In order to study the analytical potentialities of the ion-exchanger the distribution coefficients of 16 metal ions in seven systems were determined, the results are shown in Table 5. Anilinium tin(IV) phosphate shows selective behavior (higher K_d values) for Hg^{2+}, Pb^{2+} and Pt^{4+}. The data in Table 5 show that K_d values decrease with the increase in concentration of hydrochloric acid and increase in solutions with greater percentage of acetone. On the basis of this behavior (K_d values) separations were tried. Those experimentally successfully achieved are reported in Table 6. The relative order of elution for Zn^{2+}-Cd^{2+}-Hg^{2+} is similar to that of break-through curves (Fig. 3). It is interesting that no significant tailing was observed during the elution of various metal ions and only small volumes of eluents were required to give compact chromatograms.

Mg^{2+} is eluted ahead of Ca^{2+} (binary separation of Mg^{2+}-Ca^{2+}) with suitable hydrochloric acid-acetone solution, hence the columns of anilinium tin(IV) phosphate may be utilized to separate magnesium from calcium in dolomite.[17] Usually, 0.1 to 0.5% cadmium is present in zincblende (Sphalerite) and Calamine.[18] The ternary separation of Zn^{2+}-Cd^{2+}-Hg^{2+} may be utilized to recover Cd^{2+} from these ores using suitable eluents. Zircon contains usually less than 1 per cent of thorium oxide.[19] The binary separation of Th^{4+}-Zr^{4+} can be applied for the recovery of Th^{4+} from Zr^{4+}. Iron and lead occur in major to trace concentrations in zinc bearing ores.[20] Zn^{2+}, Fe^{3+}, and Pb^{2+} can be eluted by different hydrochloric acid-acetone solutions using anilinium tin(IV) phosphate columns.

Authors thank Prof. A. K. Vasishtha, Director and Prof. R. S. Tewari, Head, Department of Chemistry, H. B. Technological Institute, Kanpur for research facilities. Financial assistance from U.G.C. is also gratefully acknowledged.

References

1) R. B. Hahn and H. C. Klein, *Anal. Chem.*, **40**, 1135 (1968).
2) K. G. Varshney and S. Naheed, *J. Inorg. Nucl. Chem.*, **39**, 2075 (1977).
3) K. G. Varshney, A. A. Khan, and S. S. Varshney, *Indian J. Chem.*, **21A**, 398 (1982).
4) J. P. Rawat and M. Iqbal, *Ann. Chimica*, **1981**, 431.
5) D. K. Singh, R. R. Bhatnagar, and A. Darbari, *Indian J. Tech.*, **24**, 45 (1986).
6) Y. Inoue, *J. Inorg. Nucl. Chem.*, **26**, 2241 (1964).
7) Y. Inoue, *Bull. Chem. Soc. Jpn.*, **36**, 1316 (1963).
8) N. H. Furman, "Standard Methods of Chemical Analysis," 5th ed, (1939), Vol. 1, p. 694.
9) J. J. Mitchell, I. M. Kolthoff, E. S. Proskauer, and A. Weisberger, "Organic Analysis," Interscience, New York (1956), Vol. 3, p. 140.
10) E. B. Sandell, "Colorimetric Determination of Traces of Metals," Interscience, New York (1959), p. 862.
11) F. B. David, "Colorimetric Determination of Non-metals, Chemical Analysis," Interscience, New York (1958), Vol. 8, p. 36.
12) J. P. Rawat and J. P. Singh, *Anal. Chem.*, **47**, 738 (1975).
13) N. E. Topp and Pepper, *J. Chem. Soc.*,**1949**, 3299.
14) J. Inczedy, "Analytical Applications of Ion-Exchangers," Pergamon Press (1966), p. 126.
15) J. P. Rawat and D. K. Singh, *Anal. Chim. Acta*, **87**, 157 (1976).
16) E. B. Sandell, "Colorimetric Determination of Traces of Non-metals," Interscience, New York (1959), p. 726.
17) N. H. Furman, "Standard Methods of Chemical Analysis," 6th ed, D. Van Nostrand, Inc., Princeton, New Jersey (1962), Vol. 1, p. 585.
18) I. M. Kolthoff, P. J. Elving, and E. B. Sandell, "Treatise on Analytical Chemistry," Interscience Publishers, New York, London (1961), Part 2, Vol. 3, p. 173.
19) Ref. 18, Vol. 5, p. 143.
20) Ref. 18, p. 99.

 © 1988 The Chemical Society of Japan Bull. Chem. Soc. Jpn., 61, 1375—1377 (1988)

Nitriles in Organic Synthesis. The Chemical Behavior of [1-(2-Furyl)-ethylidene]- and [1-(2-Thienyl)ethylidene]malononitriles

Mohamed Abdallah EL-MAGHRABY,† Kamal Usef SADEK,†† Maghraby Ali SELIM,† and Mohamed Hilmy ELNAGDI*
Department of Chemistry, Faculty of Science, Cairo University, A. R. Egypt
†Department of Chemistry, Faculty of Science, Aswan University
††Department of Chemistry, Faculty of Science, Minia University
(Received January 26, 1987)

The chemical behavior of [1-(2-furyl)ethylidene]- and [1-(2-thienyl)ethylidene]malononitriles **1a** and **b** toward electrophilic reagents, active methylene reagents and (arylmethylene)malononitriles is described.

The chemistry of nitriles has received considerable recent attention.[1,2] A variety of new systems has been efficiently synthesized utilizing simple nitriles as starting components.[3,4] In conjunction with our program directed for developing utility of polycyano compounds in organic synthesis we have recently reported a novel synthesis of pyridazines and 3,5-disubstituted-2,6-dicyanoanilines utilizing (1-phenylethylidene)malononitrile (**1c**) as starting material.[5] In order to see if reactions of the type reported above can be extended to constitute general route for the synthesis of pyridazines and 3,5-disubstituted-2,6-dicyanoanilines , we report here the results of our investigations to conduct similar reactions with [1-(2-furyl)], and [1-(2-thienyl)ethylidene]malononitriles (**1a** and **b**).

In contrast to the reported formation of [1-phenyl-2-(phenylhydrazono)ethylidene]malononitrile on coupling **1c** with benzenediazonium chloride, compounds **1a** and **b** coupled with the same reagent to yield (phenylazo)malononitrile (**2**). The formation of **2** in this reaction is assumed to proceed via coupling of benzenediazonium chloride with malononitrile, the latter is assumed to be formed via action of water on **1a** or **b** (cf. route (a)). Possible formation of **2** via route (b) seems unlikely, although it cannot be ruled out. The difference in behavior between **1a,b** and **1c** can be attributed to a decrease in the acidity of the methyl group in **1a** and **b** by the effect of the electron-rich heterocycles which counterbalance the electron-attracting effect of the two cyano functions.[6]

Compound **1a** reacted with (arylmethylene)malononitriles 3**a**—**c** to yield products of condensation via HCN elimination. Two isomeric structures seemed possible for the reaction product (cf. structures **4** and **5**). Structures **4a**—**c** were established for the reaction products based on their syntheses via reactions of **6** with malononitrile. Compounds **6** were obtained in turn via reaction of **1a, b** with furfural and 2-thiophenecarbaldehyde. Compound **4a** was also found identical with authentic sample prepared as has been previously described.[5] Similarly, compound **1b** rected with (arylmethylene)malononitriles **3a** and **b** to yield the 3,5-disubstituted-2,6-dicyanoanilines **4c** and **d**. In contrast, compound **1b** reacted with **3c** to yield 1 : 1 adduct. The pyridine structure **7** was established for the reaction product based on its analytical and spectral data (cf. Experimental).

The behavior of **1a** and **b** toward malononitrile was also investigated. It has been found that **1a** reacted with malononitrile to yield a compound of molecular formula $C_{12}H_8ON_4$ (M^+=224; m/z). This compound can be formulated as the pyridine derivative **8** or the isomeric benzene derivative **9**. Structure **8** was readily eliminated based on ^{1}H NMR which revealed the absence of CH_2 function. Thus, structure **9** was considered for the reaction product. Attempts at addition of **1b** to malononitrile under the same experimental conditions were unsuccessful. The reactants were recovered almost unchanged after reflux in sodium-dioxane mixture.

In contrast to the reported addition of **1c** to trichloroacetonitrile,[5] attempts at addition of **1a** and **b** to the same reagents has failed.

The results obtained in our investigation clearly reveal the effect of C-1 substituent on the reactivity of methyl grorup in [1-substitutedethylidene]malononitriles. Electron-rich substituents counterbalance the electron-attracting force of the cyano groups which result in the decrease of the reactivity of methyl group.

Experimental

All melting points were uncorrected. IR spectra were recorded (potassium bromide) on a Shimadzu-408 spectrophotometer. ^{1}H NMR were measured in DMSO on a Varian EM-390 spectrophotometer at 90 MHz with TMS as internal reference and chemical shifts were expressed as δ (ppm). Microanalytical data (C, H, N, S.) were obtained from the Microanalytical Data Unit at Cairo University.

[1-(2-Furyl)ethylidene]- and [1-(2-Thienyl)ethylidene]-malononitriles (1a and b). General Procedure: Malononitrile (0.01 mol) was added to a suspension of 2-acetylfuran or 2-acetylthiophene (0.01 mol) in a mixture of benzene-acetic acid (50 : 5) in the presence of β-alanine (2 g). The reaction miture was heated under reflux in the presence of a water separator until complete removal of water (2 h) then evaporated in vacuo. The solid product, so formed, was collected by filtration and crystallized from the appropriate solvent (see Table 1).

Coupling of Compounds 1a and b with Benzenediazonium Chloride: An ice cold solution of 0.01 mol of benzenediazonium chloride (prepared from 0.01 mol of aniline

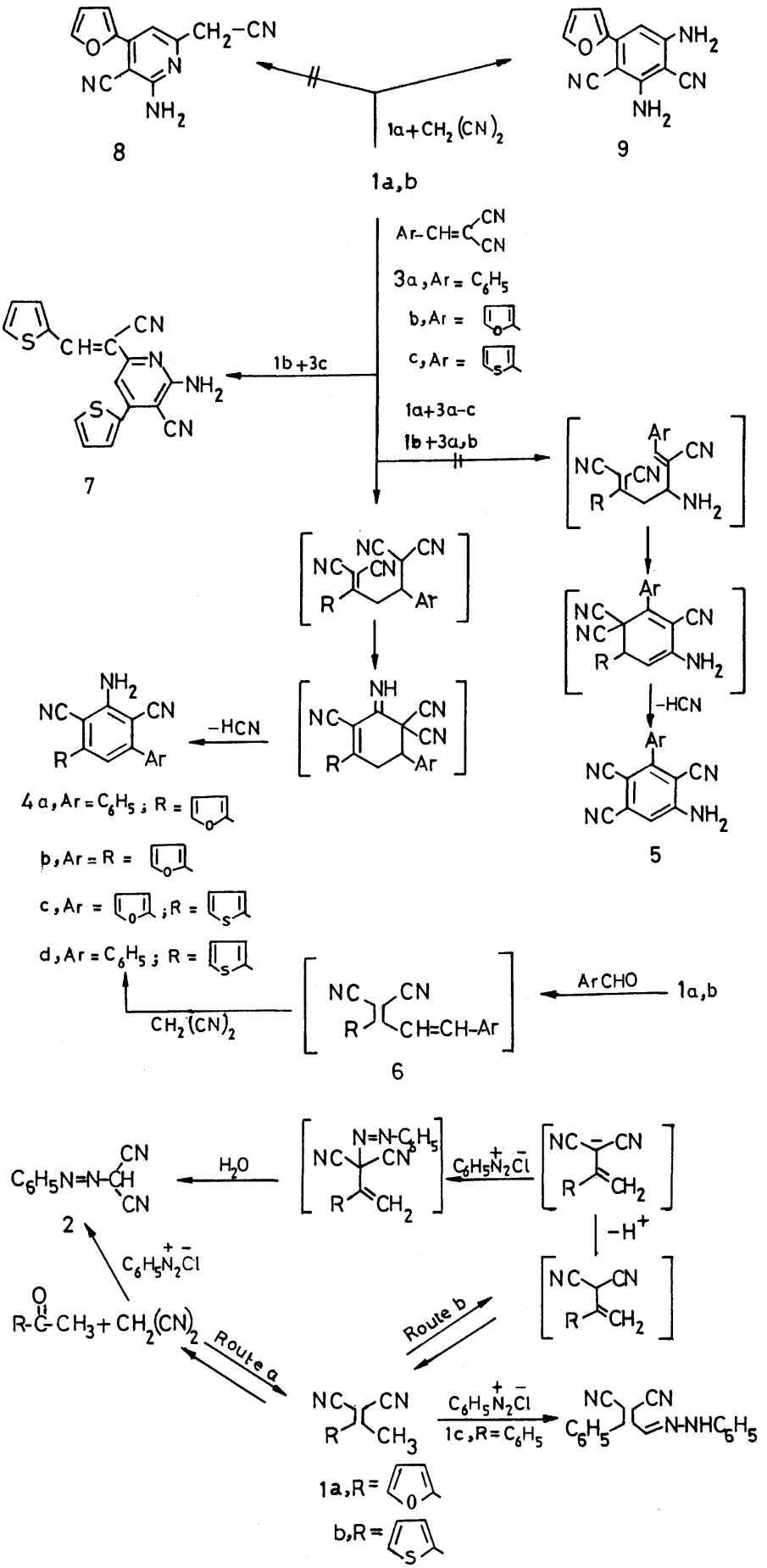
8
9
1a+CH2(CN)2
1a,b
Ar-CH=C(CN)CN
3a, Ar = C6H5
b, Ar =
c, Ar =
1b+3c
1a+3a-c
1b+3a,b
7
-HCN
4a, Ar = C6H5 ; R =
b, Ar = R =
c, Ar = ; R =
d, Ar = C6H5 ; R =
5
-HCN
ArCHO
1a,b
CH2(CN)2
6
H2O
2
C6H5N2Cl
-H+
Route a
Route b
1c, R = C6H5
1a, R =
b, R =

Table 1. List of the Newly Synthesized Compounds

Compd.	Cryst. solvent	Mp θ_m/°C	Yield %	Mol. form. mol. Wt.	Calcd (Found)/% C	H	N	S	ν_{max}/cm^{-1}	δ_H
1a	Methanol	75	70	$C_9H_6N_2O$ (158.15)	68.35 (68.2	3.82 3.6	17.71 17.8)		2970(CH_3), 2190, 2200(CN bands), and 1580(C=C)	1.3(s, 3H, CH_3), 7.3—8.2(m, 3H$_{furan}$)
1b	Methanol	82	72	$C_9H_6N_2S$ (174.15)	62.07 (62.6	3.47 3.5	16.09 16.2	18.37 18.1)	2900(CH_3), 2190, 2200(CN bands), and 1550(C=C)	1.2(s, 3H, CH_3), 7.0—7.66(m, 3H$_{thiophene}$)
4a	Ethanol	235	82	$C_{18}H_{11}N_3O$ (285.29)	75.78 (75.7	3.89 3.8	14.73 14.5)		3350(NH_2), 2200(CN bands), and 1630(δ NH_2)	3.7(br, 2H, NH_2), 7.2—8.2(m, 9H, aromatic protons)
4b	Acetone	255	85	$C_{16}H_9N_3O_2$ (275.26)	69.81 (69.7	3.30 3.2	15.27 15.5)		3390(NH_2), 2190, 2200(CN bands), and 1635(δ NH_2)	3.5(br, 2H, NH_2), 6.8—8.2(m, 7H, aromatic protons)
4c	Acetone	250	83	$C_{16}H_9N_3OS$ (291.26)	65.97 (66.4	3.11 3.5	14.43 14.4	11.0 11.0)	3350(NH_2), 2190, 2200(CN bands), and 1630(δ NH_2)	3.3(s, 2H, NH_2), 6.8—8.0(m, 7H, aromatic protons)
4d	Ethanol	237	75	$C_{18}H_{11}N_3S$ (301.29)	71.75 (71.5	3.68 3.5	13.95 14.0	10.62 10.8)	3340(NH_2), 2190, 2200(CN bands), and 1635(δ NH_2)	3.4(br, 2H, NH_2), 7.0—7.9(m, 9H, aromatic protons)
7	Acetone	270	75	$C_{17}H_{10}N_4S_2$ (334.28)	61.08 (61.1	3.02 3.5	16.76 16.9	19.15 19.1)	3350(NH_2), 2200(CN bands), and 1640(δ NH_2)	3.8(br 2H, NH_2), 6.2(s, 1H, ylidene CH), 7.2—8.0(m, 7H, aromatic protons)
9	Ethanol-water	228	77	$C_{12}H_8ON_4$ (224.22)	64.29 (64.8	3.60 3.5	24.99 25.0)		3350, 3150(NH_2 bands), 2200 (CN bands)	3.3(br 4H, $2NH_2$), 6.6—8.2(m, 4H, aromatic protons)

and the appropriate amount of sodium nitrite and hydrochloric acid) was added to a solution of **1a** or **b** (0.01 mol) in ethanol (50 ml) containing sodium acetate (5 g). The precipitate was filtered off and crystallized from ethanol. The product was identical with authentic sample of (phenylazo)malononitrile.

Condensation of Compounds 1a and b with (Arylmethylene)malononitrile Derivatives 3a—c. General Procedure: A solution of compound **1a** or **b** (0.01 mol) and the appropriate (arylmethylene)malononitrile derivatives **3a—c** (0.01 mol) in ethanol (50 ml) was treated with piperidine (1.0 ml). The reaction mixture was heated under reflux for 3 h and then evaporated in vacuo. The solid product, so formed, was collected by filtration and recrystallized from the appropriate solvent (see Table 1).

The same products were obtained by the follwing procedure: To a solution of compound **1a** or **b** (0.01 mol) in ethanol (50 ml) was added to the appropriate aromatic aldehyde in the presence of piperidine (1.0 ml). The reaction mixture was heated under reflux for 1—2 h (TLC monitor). To this solution, malononitrile (0.01 mol) was added and the reaction mixture was heated under reflux for additional 2 h. The solvent was then evaporated in vacuo and the solid product, so formed, was collected by filtration.

Compound **4a** was also found identical with authentic sample prepared as was previously described.[5]

Reaction of 1a with Malononitrile. Equimolecular amounts (0.01 mol) of **1a** and malononitrile were heated under reflux in 50 ml of dioxane with 0.01 mol of sodium metal for 4 h. The mixture was then evaporated in vacuo and neutralized with HCl. The solid product, so formed was collected by filtration and recrystallized from the appropriate solvent (see Table 1).

References

1) F. Freeman, *Synthesis*, **1981**, 925.

2) F. M. Abdelrazek, A. W. Erian, and K. M. H. Hilmy, *Synthesis*, **1986**, 74.

3) G. E. H. Elgemeie, H. A. Elfahham, S. Elgamal, and M. H. Elnagdi, *Heterocycles*, **23**, 1999. (1985).

4) M. H. Elnagdi, M. R. H. Elmoghayar, E. A. A. Hafez, and H. H. Alnima, *J. Org. Chem.*, **40**, 2604, (1975).

5) N. S. Ibrahim, F. M. Abdel-Galil, Z. E. Kandeel, R. M. Abdel-Motaleb, and M. H. Elnagdi, *Liebigs Ann. Chem.*, **1987** (in press).

6) K. U. Sadek, M. A. EL-Maghraby, M. A. Selim, and M. H. Elnagdi, *Bull. Chem. Soc. Jpn.* (1987) (in press).

 © 1988 The Chemical Society of Japan Bull. Chem. Soc. Jpn., 61, 1379—1381 (1988)

Alkylation of Phenol by C_9 and C_{12} Olefins

Rajeev Anand RAJADHYAKSHA* and Dilip Devidas CHAUDHARI
Department of Chemical Technology, University of Bombay, Matunga, Bombay 400019, India
(Received November 17, 1986)

Alkylation of phenol by 1-dodecene, propylene tetramer and trimer is investigated using a variety of acid catalysts. The catalytic activity of perfluorinated sulfonic acid resin Nafion-H, the recently described 'sulfate treated' zirconia and trifluoromethanesulfonic acid is compared with that of cation exchange resin (CER) catalyst which is commonly employed in industrial practice. The activity of zirconia is observed to be comparable to CER and Nafion-H. In view of its low cost and higher thermal and structural stability, this catalyst shows considerable promise for practical application.

Alkylation of phenol with higher olefins in C_8 to C_{15} range does not take place as readily as with the lower olefins.[1] Among these alkylated phenols, nonyl- and dodecylphenol are of considerable commercial importance, especially in the manufacture of surfactants and lube oil additives.[2] Propylene oligomers have branched chain structure and the resultant alkylphenols are nonbiodegradable. Hence, for use in biodegradable surfactants linear α-olefins such as 1-dodecene, 1-nonene, or linear olefins with internal double bond are preferred.

These alkylation reactions have been studied on a variety of acid catalysts such as *p*-toluenesulfonic acid, boron trifluoride, boron trifluoride etherate, hydrofluoric acid, aluminium chloride-sulfuric acid,[3] hydrofluoric acid-carbon dioxide,[4] cation exchange resin,[5] bentonite clay,[6] zinc chloride-hydrochloric acid,[7] and silica-alumina.[8] Most of the literature is in the form of patents and hence provides limited information. Most of the catalysts mentioned above suffer from various drawbacks such as problems of separation from reaction products, corrosion and nonreusability. Boron trifluoride and CER catalysts seem to be preferred in industrial practice. Use of solid catalysts has clear advantage due to the ease of separation from the products and noncorrosive nature of reaction medium. In the present work, catalytic activity of a variety of solid acid catalysts is investigated for alkylation of phenol with 1-dodecene, propylene tetramer and trimer. The catalysts include the perfluorinated sulfonic acid resin Nafion-H, and the 'sulfate treated' zirconia recently described by Arata and Hino.[9-11] The catalytic activity of these catalysts is compared with that of CER catalysts. Trifluoromethanesulfonic acid (triflic acid) is one of the strongest acids known and unlike many other super acids, it is stable in a variety of reaction media and is also reusable.[1,2] The catalytic activity of this acid was also investigated.

Experimental

Materials. Phenol, 1-dodecene Fluka, zirconium dichloride oxide of A.R. grade, while propylene trimer (135—137 °C, ρ=0.739 g cm^{-3}) and propylene tetramer (187—188 °C, ρ=0.770 g cm^{-3}) were used in the present study.

Catalysts. The superacid catalysts Nafion-H and triflic acid [$\geqslant$98%] were obtained from Du Pont and Fluka respectively. The 'sulfate treated' zirconia was prepared by treating zirconium hydroxide with 0.5 M sulfuric acid (1 M=1 mol dm^{-3}) followed by drying and calcination at 650 °C for 3 h. This zirconium hydroxide was prepared from zirconium dichloride oxide by hydrolysis with aq ammonia.[9] 98% Sulfuric acid of A.R. grade was used. The CER [Polystyrene-DVB crosslinked resin sulfonic acid, Indion-130] was procured from Ion Exchange India. The solid catalysts were dried at 110 °C for 1 h just before use.

General Reaction Procedure and Analysis. The reactor consisted of a flat bottom glass vessel of 5.0 cm i.d. and 200 ml volume. The reactor was equipped with baffles and was stirred by a glass turbine stirrer at 1000 rpm. The reactor was kept in a constant temperature bath. In a typical run, 29 g of phenol (0.31 mol) was brought to the required temperature under agitation and 0.73 g of catalyst [2.5% (w/w) of phenol] and 34.7 g of 1-dodecene [0.207 mol] were added. This was considered as zero time. Samples of the reaction mixture (0.5 ml) were withdrawn from time to time. Samples were analyzed by gas chromatography using a s.s. column containing 5% SE-30 on Chromosorb-W [HP] as stationary phase and flame ionization detector.

Results and Discussion

In all experiments, the alkylated product consisted of the para isomer exclusively.

Alkylation of Phenol with 1-Dodecene. Alkylation of phenol with 1-dodecene was studied in the temperature range of 100—145 °C using zirconia catalyst. The conversions observed at different reaction time are given in Table 1. The data could be fitted to a simple

Table 1. Alkylation of Phenol with 1-Dodecene
Effect of Temperature on Activity

Time	% Conversion of 1-dodecene at temp			
min	100 °C	115 °C	130 °C	145 °C
15	8	23	30	35
30	13	33	49	51
60	27	48	62	65
90	37	55	75	77
120	45	68	77	79

Mole ratio, phenol: 1-dodecene=1.5: 1.
Loading of zirconia=2.5% (w/w) of phenol.

Table 2. Alkylation of Phenol with 1-Dodecene Effect of Mole Ratio on Activity

Mole ratio phenol: 1-dodecene	% Conversion of 1-dodecene at time in min					
	15	30	45	60	120	180
1 : 1	10	25	32	38	60	70
1.5 : 1	35	49	53	64	78	
1 : 1.5	2	11	17	20	27	31

Temperature 130 °C. Loading of zirconia 2.5% (w/w) of phenol.

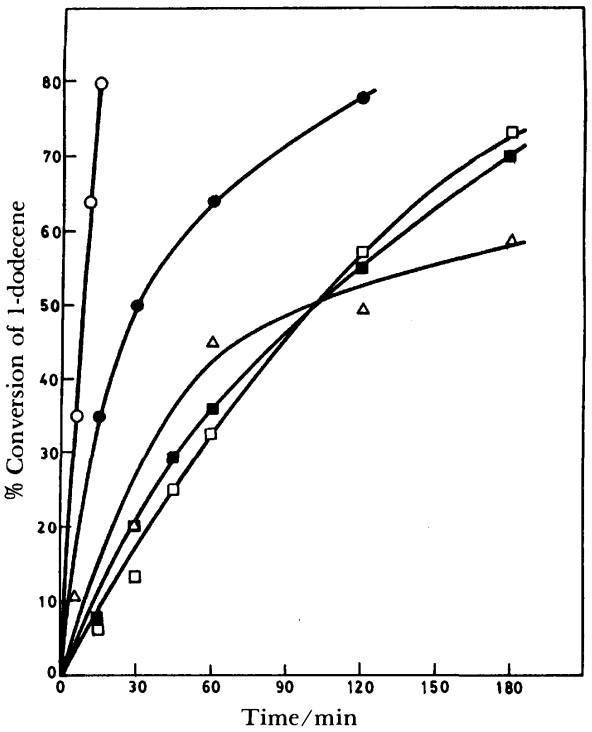

Fig. 1. Alkylation of phenol with 1-dodecene; comparison of activity of different catalysts. Mole ratio of phenol:1-dodecene 1.5:1, 130°C, catalyst 2.5% (w/w) of phenol: ● zirconia, ■ Nafion-H, ○ triflic acid, □ CER, △ 98% sulfuric acid.

second-order kinetic expression. The activation energy was found to be 7.5 kcal mol^{-1}. The reaction was also carried out using different initial mole ratio of reactants. The results are give in Table 2.

Figure 1 compares the catalytic activities of Nafion-H, triflic acid, CER, 98% sulfuric acid, and zirconia. Equal weights of all the catalysts were employed in these experiments. Triflic acid exhibited highest activity while sulfuric acid showed lowest activity. The product was deeply colored when these two homogeneous acids were used. The three solid acid catalysts showed comparable activity. Repetitive experiments were carried out to investigate the reusability of these catalysts. No change of activity could be observed after two recycles.

Alkylation of Phenol with Propylene Tetramer. Alkylation of phenol with propylene tetramer was observed to be considerably slower than that with 1-dodecene and hence much higher loading of the catalysts had to be employed. The tetramer has branched skeletal structure and the double bond is located anywhere in the skeleton. This probably results in steric hindrance in the reaction between the tetramer and phenol. Table 3 shows the progress of the reaction at different temperatures. The data were fitted to a simple second-order kinetic expression. The variation of the rate constants with temperature gave an activation energy of 8.0 kcal mol^{-1}.

The activity of different catalysts is compared in Fig.

Table 3. Alkylation of Phenol by Propylene Tetramer: Effect of Temperature on Activity

Time	% Conversion of propylene tetramer at temp			
min	100 °C	115 °C	130 °C	145 °C
15	8	19	27	30
30	20	25	48	50
60	32	41	60	67
90	43	52	70	78
120	48	61	78	80

Mole ratio: phenol, propylene tetramer=1.5: 1. Loading of zirconia: 15% (w/w) of phenol.

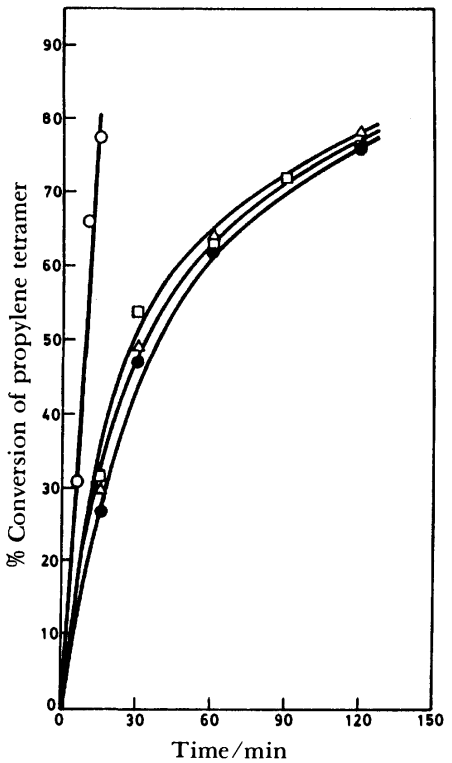

Fig. 2. Alkylation of phenol with propylene tetramer. Comparison of activity of different catalysts. Mole ratio of phenol: propylene tetramer, 1.5:1, 130°C. Catalyst [%(w/w) of phenol]: ● Zirconia [15%], □ Nafion-H [15%], ○ triflic acid [2.5%], △ CER [15%].

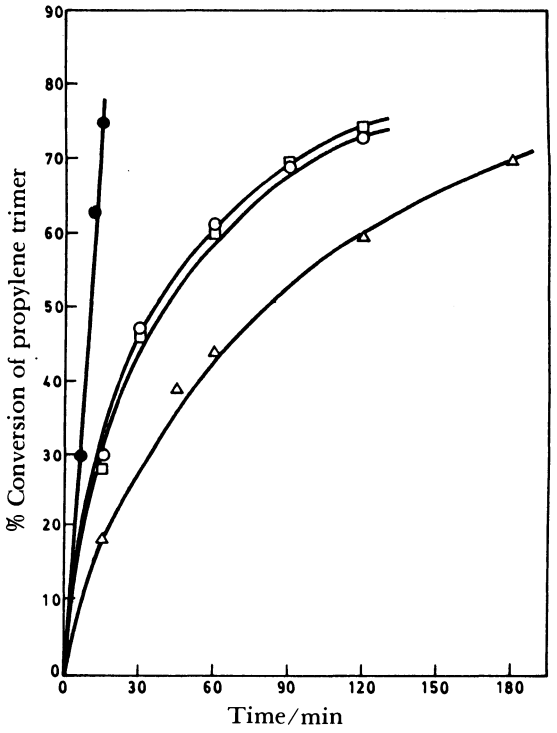

Fig. 3. Alkylation of phenol with propylene trimer. Comparison of activity of different catalysts. Molar ratio of phenol: propylene trimer 1.5:1, 130°C. Catalyst [%(w/w) of phenol]: △ Zirconia [20%], ○ Nafion-H [20%], ● triflic acid [2.5%], □ CER [20%].

2. The order of activity for the different catalysts is similar to that observed in alkylation with 1-dodecene.

Alkylation of Phenol with Propylene Trimer. The reaction was observed to be slower than that in the case of propylene tetramer. Comparable conversions were obtained at 20% [(w/w) of phenol] loading of zirconia and hence subsequent experiments were carried out at this loading. In the temperature range of 100—130 °C, the activation energy was found to be 10.3 kcal mol^{-1}.

The comparison of the activities of the different catalysts is shown in Fig. 3. Once again the order of activity is similar to that observed with the previous systems. Among the solid acid catalysts, zirconia showed somewhat lower activity than Nafion-H and CER.

Conclusion

Triflic acid exhibits the highest activity for the reactions, however, its use always results in deeply colored products and hence this catalyst appears unsuitable for practical use. Nafion-H is considerably more expensive as compared to CER and zirconia and exhibits similar activity. The zirconia catalyst, on the other hand, can be relatively inexpensive as compared to the polymer resin catalyst and at the same time has higher thermal and structural stability. Thus the present work demonstrates the promise of this novel catalyst for an industrially useful class of reactions.

One of us (DDC) wishes to thank CSIR, New Delhi, for the award of a Senior Research Feffowship.

References

1) R. H. Rosenwald, "Kirk Othmer Encyclopedia of Chemical Technology," ed by M. Grayson, John Wiley and Sons, New York (1978), 3rd ed, Vol. 2, p. 65.

2) H. W. B. Reed,"Kirk Othmer Encyclopedia of Chemical Technology," ed by M. Grayson, John Wiley and Sons, New York (1987), 3rd ed, Vol. 2, pp. 90, 92.

3) B. S. Friedman, S. H. Patinkin, "Friedel Crafts and Related Reactions," ed by G. A. Olah, Interscience Publishers, London (1964), Vol. II, Part 1, p. 86.

4) G. L. Hervert, (Universal Oil Products Co.), U. S. Patent 3929912 (1975); *Chem. Abstr.*, **84**, 73895 q.

5) R. Y. Mixer and J. W. Wagner, (Richfield Oil Corp.), Fr. Patent 1322509 (1963); *Chem. Abstr.*, **59**, 11388 g.

6) H. K. Kaplan, (General Aniline and Film Corp.), U.S. Patent, 3287422 (1966), *Chem. Abstr.*, **66**, 57610 r.

7) J. Beck and H. Spaening, (Badische-Anilin- and Soda Fabrik A.-G.) Brit. Patent 906219 (1962); *Chem. Abstr.*, **58**, 8972 h.

8) J. B. Roddey, (Universal Oil Products Co.), Fr. Patent 1344636 (1963); *Chem. Abstr.*, **60**, 11944 c.

9) K. Arata and M. Hino, *J. Chem. Soc., Chem. Commun.*, **18**, 851 (1980).

10) K. Arata and M. Hino, *React. Kinet. Catal. Lett.*, **19**, 101 (1982).

11) K. Arata and M. Hino, *Chem. Lett.*, **12**, 1671 (1981).

12) R. D. Howell and J. D. McCown, *Chem. Rev.*, **77**, 69 (1977).

 © 1988 The Chemical Society of Japan Bull. Chem. Soc. Jpn., 61, 1383—1389 (1988)

Reaction Network for Selective Oxidation of Propene on a (Mo-Pr-Bi)O/SiO_2 Catalyst

J. M. López Nieto, J. M. D. Tascón,† and G. Kremenić*
Instituto de Catálisis y Petroleoquímica, C. S. I. C., Serrano 119, 28006 Madrid, Spain
†Instituto Nacional del Carbón y sus Derivados, C. S. I. C., Apartado 73, 33080 Oviedo, Spain
(Received December 25, 1986)

Oxidation of propene on a $Mo_4Pr_{0.5}Bi_{0.5}O_x/SiO_2$ catalyst was studied in order to establish the reaction network. In the temperature range 598—653 K the primary reaction products were propenal (main product), acetone, acetaldehyde, and carbon dioxide. Other products (mainly aldehydes and acids) could be classified as secondary reaction products. From studies of oxidation of the primary unstable products and the kinetics of formation of minor primary products it is concluded that both, acetaldehyde and carbon dioxide, are formed through parallel and consecutive reactions. Acetone formation is strongly influenced by reaction temperature, probably due to changes in the active centers of the catalyst.

Catalytic oxidation of olefins gives rise to a large number of products, and only a close control of catalyst characteristics and/or operation conditions may selectively favor a given type of reaction: allylic oxidation, oxyhydration, or scission reactions.[1,2]

A limited amount of published work has dealt with establishment of the overall reaction network in olefin selective oxidation processes. For allylic oxidation of propene only propenal and carbon oxides formation pathways have generally been taken into account.[3-5] However, many other products are usually originated in this process through parallel and/or consecutive reactions. For different catalytic systems, various authors[6-8] have proposed that propenal forms directly form propene while acetaldehyde and carbon oxides are formed through both, parallel and consecutive reactions; the origin of acetaldehyde and carbon oxides is not clear. Margolis[9] proposed that acetaldehyde forms directly by oxidation of the double bond, while Keulks et al.[10] suggested that acetaldehyde comes almost exclusively from propenal oxidation. In the case of CO_2, the situation is much more complicated since, depending on the catalyst used, parallel-consecutive pathways by propene and propenal oxidation,[11] as well as only consecutive reactions from propenal[9,10] have been proposed.

In a previous work, the kinetics of propene and isobutene oxidation at 653 K were studied on a (Mo-Pr-Bi)O/SiO_2 catalyst. It was deduced that similar mechanisms operate for both reactants,[12] and that propenal is formed from propene through a redox mechanism.[13] The aim of the present work is to establish the reaction network for propene oxidation on the same catalyst, from analysis of: i) Products distribution; ii) oxidation of primary reaction products; iii) influence of operation conditions on formation of minor primary products; and iv) kinetics of formation of minor primary products.

Experimental

Catalyst Preparation and Characterization. The catalyst was prepared by sequential impregnation of BASF D-11-11 silica particles. Impregnations were carried out respectively with an aqueous solution of $(NH_4)_6Mo_7O_{24}\cdot 4\,H_2O$ (Merck, p.a.) and with an acid solution of $Bi(NO_3)_3$ (Koch Light) and $Pr(NO_3)_3\cdot 5\,H_2O$ (Fluka, a.g.). The final calcination was carried out at 823 K for 16 h.[13]

The atomic ratio in the oxide catalyst was Mo:Pr:Bi=4:0.5:0.5, with a concentration of MoO_3 of 20 wt%. The BET surface area was 55.6 $m^2\,g^{-1}$ the pore volume being 1.31 $cm^3\,g^{-1}$ and the mean pore radius 40 nm. X-Ray diffraction showed the presence of three crystalline phases: MoO_3, α-Bi_2O_3, and Bi_2MoO_6. By means of Analytical Electron Microscopy the presence of highly dispersed praseodimium on the catalyst surface was observed.

Methods. The flow system and calculations used for catalytic activity and selectivity determination have been described previously.[14] Catalyst samples with a particle size of 0.042—0.059 cm, in amounts from 0.2 to 0.8 g, were diluted with carborundum (0.059 cm particle size) in order to keep a constant catalytic bed volume (5.6 cm^3). Blank tests were carried out with a reaction mixture of molar composition $C_3H_6:O_2:He:H_2O$=20:30:30:20. In the absence of catalyst, total conversion at 673 K was lower than 0.3% (molar). No diffusion effects on reaction rate were found at 653 K for propene flows greater than 1.1×10^{-2} mol h^{-1} and catalyst particle sizes lower than 0.141 cm. Prior to each experiment, the catalyst was placed in the reactor and heated to 573 K in a helium stream. Then, the reaction mixture was introduced while heating until reaching the reaction temperature. The system was left to reach stead-state conditions for 1.5 h before analyzing the reaction products. Duplicated experiments showed the constancy of catalytic activity with time.

Results

Nature and Stability of Products. In Fig. 1 the influence of contact time, W/F (g cat. h mol^{-1} C_3H_6) on total propene conversion at different temperatures (593—653 K) for a mixture containing a molar ratio $C_3H_6:O_2:He:H_2O$=20:30:30:20 is shown. From yields to the different products selectivity curves, as proposed by Corma et al.,[15,16] were obtained. The plots corresponding to a temperature of 653 K are given in Fig. 2 (qualitatively similar results were

obtained at the other temperatures studied).

We detected a number of products in propene oxidation on our catalyst. They originate either from partial oxidation, partial degradation or total oxidation reactions. From the shape of selectivity curves one can establish the nature and stability of the different products.[15] It can be deduced from plots in Fig. 2 that propenal, acetone, and acetaldehyde are primary products, while acrylic acid, acetic acid, formic acid, and ethylene are secondary products. In the case of CO and CO_2 it is not possible from Fig. 2 to differentiate clearly if they are either primary or secondary products.

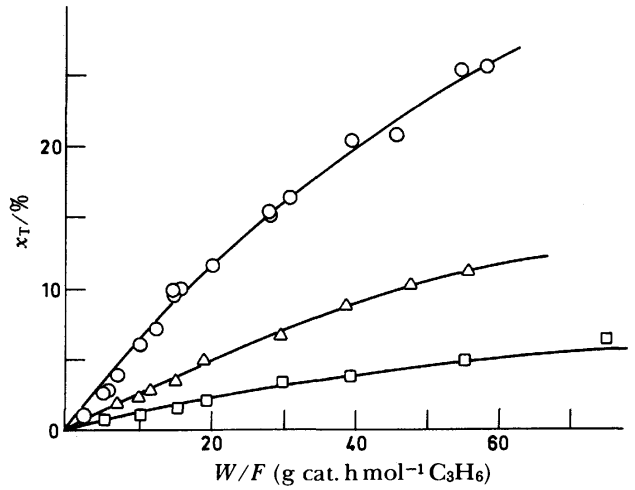

Fig. 1. Effect of contact time, W/F, on total conversion at 593 K (○), 623 K (△), and 653 K (□). Molar composition of the reaction mixture: 20% propene, 30% oxygen, 30% helium, and 20% water.

From plots of selectivity to each product (S_i) vs. total conversion (Fig. 3) it can be observed that selectivities decrease with increasing total conversion in the case of propenal, acetone, and acetaldehyde, thus clearly showing that these products are unstable. In the case of CO and CO_2 it is deduced that, while CO_2 is a primary+secondary product (with a selectivity of 6% at $x_T \rightarrow 0$), CO is merely a secondary product (selectivity at $x_T \rightarrow 0$ equal to zero or very small). On the other hand, at lower temperatures and/or for propene-poor reaction mixtures, the presence of CO was not detected at total conversions lower than 5%.

In the case of acetic acid, formic acid, and ethylene, selectivities initially increase with total conversion and afterwards remain constant or diminish. This shows

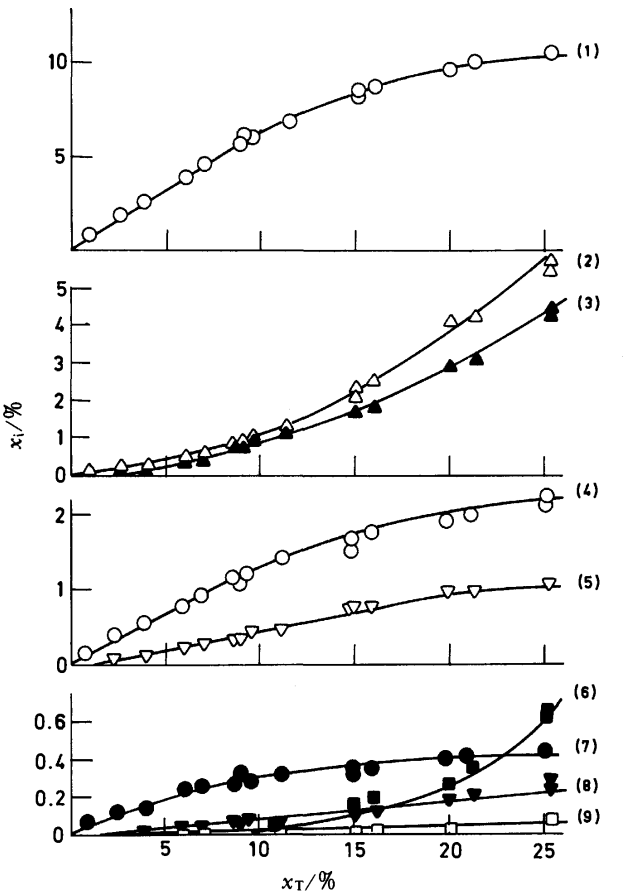

Fig. 2. Variation of yields to the different reaction products of propene oxidation with total conversion at 653 K. Same reaction conditions as for Fig. 1. (1), propenal; (2), CO_2; (3), CO; (4), acetaldehyde; (5), acetic acid; (6), acrylic acid; (7), acetone; (8), formic acid; (9), ethylene.

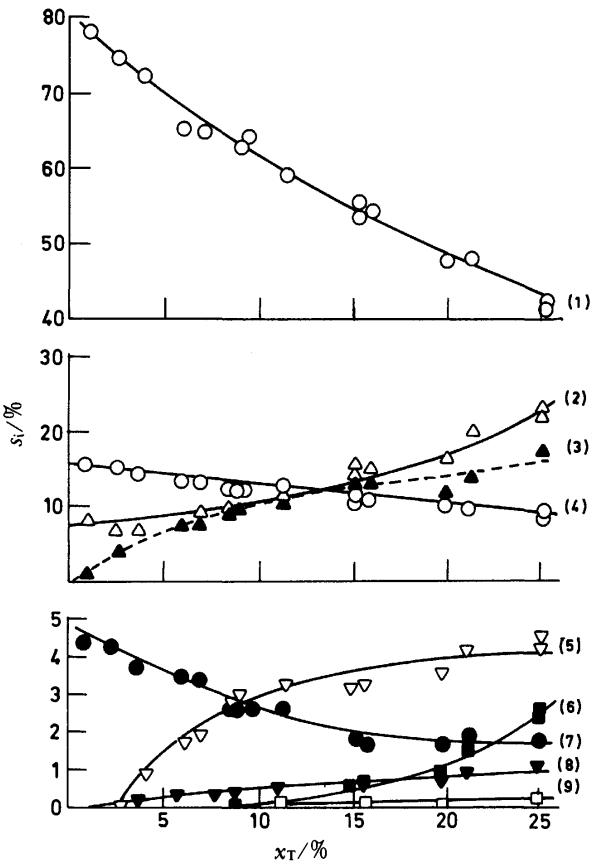

Fig. 3. Variation of selectivities to the different reaction products of propene oxidation with total conversion at 653 K. Same reaction conditions and symbols as for Fig. 2.

the stable character of these products. The very low yield of acrylic acid make it difficult to evaluate the stability of this product, especially at high temperatures and/or high conversions.

Oxidation of Primary Products. Experiments to study oxidation of unstable primary products were carried out in reaction conditions similar to those used for propene oxidation, i.e. at 653 K and molar ratio reactant: O_2 : He : H_2O=20 : 30 : 30 : 20.

In propenal and acetaldehyde oxidations it was observed that homogeneous reaction takes place in a large extent, it being thus impossible to carry out a quantitative study on the nature and type of reaction products. However, the remarkable differences between homogeneous and catalytic reaction permit to make a qualitative study. The results obtained for both, propenal and acetaldehyde, are shown in Table 1.

Propenal: In homogeneous oxidation of propenal, CO appears as the main reaction product. The other products (in a decreasing selectivity order) are CO_2, acetic acid, ethylene, formic acid, acetaldehyde, and small amounts of acrylic acid. However, a significant increase in selectivity to acrylic acid and acetaldehyde is observed for the catalytic reaction in addition to a moderate increase for acetic acid and CO_2 and an important decrease in CO production. Consequently, it seems that propenal oxidation leads preferentially to formation of acrylic acid as well as degradation products: acetaldehyde, acetic acid, CO, and CO_2.

Acetaldehyde: In homogeneous oxidation of acetaldehyde, carbon oxides, and formic acid predominates as reaction products while an increase of CO_2, acetic acid, ethylene, methane, and formaldehyde formation and a decrease of formic acid and CO production are observed in the catalyzed reaction. In catalytic reaction conditions, oxidation to acetic acid could take place simultaneously with two degradation pathways, the one leading to formaldehyde and methane and the other to total oxidation products.

Acetone: No homogeneous oxidation was detected in the case of acetone. Study of the nature of oxidation products was carried out by varying the contact time, W/F. CO_2, CO, formic acid, and acetaldehyde were the main reaction products in addition to small amounts of butandione, propenal, and ethylene.

In Table 2 the results obtained at 653 K for different contact times are given. From these results it can be concluded that both, CO and CO_2, are primary+secondary stable products; formic acid, acetaldehyde, and acetic acid are primary, unstable products, while ethylene, propenal, and butandione are secondary, unstable products.

Influence of Operation Conditions on Primary Products Formation. For the study of influence of reaction temperature and/or oxygen: propene ratio in the reaction mixture, changes in yield to the different reaction products and in initial selectivities (i.e., selectivities for $x_T \rightarrow 0$) to the primary reaction products were monitored. This study was carried out at temperatures ranging from 593 to 653 K, and oxygen: propene ratios varying from 1.5 to 6. The corresponding results are shown in Table 3.

No changes in nature of the primary reaction products were found. An increase of reaction temperature led to increase of initial selectivity to propenal and to an important decrease of initial selectivities to acetone and CO_2, the decrease being less marked the case of acetaldehyde. On the other hand, increase of oxygen: propene ratio in the reaction mixture caused a decrease of initial selectivities to propenal and acetone, and an increase of selectivities to acetaldehyde and CO_2.

Kinetics of Minor Primary Products Formation. The detailed kinetic analysis of propenal formation

Table 1. Propenal and Acetaldehyde Oxidation[a)]

Reactant	Type of reaction	x_T	S_i/%								
		%	CH_2=CHCOOH	CH_3CHO	CH_3COOH	HCOOH	HCHO	C_2H_4	CH_4	CO	CO_2
CH_2=CHCHO	Homogeneous	4.03	0.9	3.1	8.2	4.6	0	5.9	0	66.2	11.1
	Catalytic[b)]	6.32	15.1	20.2	12.1	4.8	0	4.6	0	32.4	10.8
CH_3CHO	Homogeneous	2.10	0	t[c)]	3.1	10.8	0.4	0.7	2.5	64.9	17.6
	Catalytic[b)]	4.05	0	t[c)]	6.2	5.3	2.1	3.1	6.8	47.1	29.4

a) Experimental conditions in text. b) W/F=1.00 g cat. h mol^{-1} C_3H_4O (or C_2H_4O). c) $CH_3COCOCH_3$. t=traces.

Table 2. Acetone Oxidation[a)]

W/F (g cat. h mol^{-1} C_3H_6)	X_T	S_i/%							
	%	$CH_3COCOCH_3$	CH_2=CHCHO	CH_3COOH	CH_3CHO	C_2H_4	HCOOH	CO_2	CO
0.30	5.34	0	0	33.9	11.1	0	4.0	37.8	13.3
0.92	9.94	t	t	29.3	9.8	0	4.6	43.5	13.1
1.62	17.45	0.9	0.3	27.6	8.1	t	5.0	43.7	14.4
4.31	42.87	1.0	1.4	23.8	7.5	0.4	2.8	44.6	18.5

a) Experimental conditions in text. t=traces.

Table 3. Initial Selectivities to Primary Products in the Oxidation of Propene on Mo-Pr-Bi-O/SiO_2

Product	S_i/%					
	A[a]			B[b]		
	593 K	623 K	653 K	593 K	623 K	653 K
CH_2=CHCHO	42	65	80	37	60	75
CH_3COCH_3	33	13	6	30	11	3.5
CH_3CHO	18	17	12	23	18.5	15.5
CO_2	7	5	2	10	7.5	6

a) Mixture A: oxygen/propene=1.5. b) Mixture B: oxygen/propene HL=6.0.

during propene oxidation over the same catalyst used in the present work was carried out previously and published elsewhere.[13] However, the important differences found among the kinetics of formation of the rest of products justified to undertake a more detailed analysis, which was made by the initial rates technique, i.e., at total converisons lower than 7%. Influence of the main operation variables (temperature, contact time, and partial pressure) was examined. For studying the influence of reaction mixture composition, the conventional technique of modifying the concentration of one reactant while keeping constant the concentration of the rest of reactants was used.

Kinetic measurements were carried out in the following ranges: propene partial pressure, 0.047—0.374 atm (with oxygen partial pressure constant and equal to 0.280 atm); oxygen partial pressure, 0.065—0.470 atm (with propene partial pressure constant and equal to 0.190 atm); reaction temperature, 593—653 K. In all cases a constant water partial pressure of 0.190 atm was kept, as well as a helium partial pressure balance to 1 atm.

For the study of dependence of the rates of formation of the different reaction products on composition of the reaction mixture an empirical rate equation was used:

$$\ln r_i = \ln k_i + a \ln p_H + b \ln p_O, \quad (1)$$

where k_i is the rate constant for formation of product i, and a and b are the apparent reaction orders for propene and oxygen, respectively. From plots of ln r_i vs. ln p_H or ln p_O (p_H and p_O being the partial pressures of propene and oxygen, respectively), straight lines were obtained whose slopes gave the apparent reaction order for a given reactant (Table 4).

In the cases of acetaldehyde and CO_2 and at temperatures of 593 and 623 K two different reaction orders for propene were found: at pressures lower than 0.19 atm the apparent order was greater than unity, while it was lower than 1 at pressures greater than 0.19 atm. This kind of behavior was not observed in the case of oxygen.

Values of k_i were determined by linear fitting of experimental and calculated rate values for the different products at 593, 623, and 653 K; they are given with their 95% confidence intervals (in parenthesis) in Table 4. In the case of acetaldehyde and CO_2 the values reported were determined at reaction temperatures of 593 and 623 K from results obtained at propene partial pressures lower than 0.19 atm, while at 653 K results correspond to the whole partial pressure range (0.047—0.374 atm). Finally, from plots of ln k_i vs. $1/T$, apparent activation energies for each product were calculated. Their values are given in Table 5.

Table 4. Power Law Model Parameters (k_i, a, b, with r in 10^{-4} mol g^{-1} h^{-1})

Product	Temp / K	$k_i \times 10^3$	a	b
CH_3COCH_3	593	1.34(0.02)	0.93	0.26
	623	1.37(0.04)		
	653	1.38(0.01)		
CH_3CHO	593	4.50(0.04)[a]	1.05[a]	0.75
			0.42[b]	
	623	8.23(0.04)[a]	1.20[a]	0.52
			0.81[b]	
	653	16.6(0.1)	1.26	0.50
CO_2	593	3.67(0.01)[a]	1.31[a]	0.26
			0.47[b]	
	623	6.75(0.03)[a]	1.31[a]	0.34
			0.73[b]	
	653	16.08(0.05)	1.41	0.29

a) p_H=0.047—0.190 atm. b) p_H=0.190—0.370 atm.

Table 5. Apparent Activation Energies for the Formation of Primary Products (593—653 K)

Product	E_a/KJ mol^{-1}
CH_2=CHCHO	117.0±15.5
CH_3COCH_3	1.7±1.3
CH_3CHO[a]	69.4±10.2
CO_2[a]	78.6±11.3

a) Calculated for $p_H \leqslant 0.19$ atm.

Discussion

Reaction Network. From the results of selectivity curves (Figs. 2 and 3), a first scheme can be drawn for propene oxidation:

propene → propenal + acetone + acetaldehyde + CO_2.

Primary products containing three carbon atoms (propenal and actone) are both unstable. Therefore, increase of temperature influences unequally selectivities to these products (Table 3). Propenal is usually

obtained at temperatures above 523 K, while acetone forms below this temperature.[1] This effect of reaction temperature on selectivities probably depends on the different ways of oxygen incorporation to the catalyst surface. In a previous study carried out in this laboratory, oxygen adsorption experiments were carried out on the same catalyst used in the present work in the temperature range corresponding to the catalytic reaction.[13] The oxygen adsorption isobar exibited an ascending branch; for example, oxygen coverages at 25 mmHg (1 mmHg=133.322Pa) increased from 0.05% (572 K) to 1.39% (621 K). This increase of oxygen adsorption with temperature is probably associated with the appearance of dissociative adsorption.

If both, oxyhydration and allylic oxidation reactions are competitive, selectivities to acetone or propenal will depend on the relative formation rates of these products.[17] The reactivity of either adsorbed species or oxygen ions present in the catalyst will monotonically increase with reaction temperature. Consequently, as reaction temperature increases, a change in the nature of reactive centers and, hence, in the reaction mechanism will take place.[18,19]

From results of studying catalytic oxidation of propenal, secondary reactions may be summarized as follows:

$$\text{propenal} \rightarrow \text{acrylic acid} + \text{acetic acid} + \text{acetaldehyde} + CO_2 + CO.$$

Margolis[9] proposed that propenal oxidation leads preferentially to formaldehyde and carbon oxides. Cathala and Germain[6] found carbon oxides and acetaldehyde when this reaction was carried out on Mo-Bi-O catalysts. Indeed, reactions of propene methatesis are well characterized on MoO_3/SiO_2 catalysts working at high temperature, ethylene being formed.[20] The auto-oxidation processes proposed by Semenov[21] may explain formation of the different products. Finally, it is clear that acetic acid proceeds from propenal consecutively.

Catalytic oxidation of acetone leads to the following products:

$$\text{acetone} \rightarrow \text{acetic acid} + \text{acetaldehyde} + \text{formaldehyde} + CO + CO_2.$$

Acetone forms by propene oxidation; however, 2-propanol was not detected, contrary to reports of some authors[22,23] concerning both, propene and acetone oxidation. This absence of 2-propanol may be due either to a small yield to acetone in propene oxidation, and/or to a rapid conversion of this alcohol into ketone.[22,24]

Acetaldehyde is a primary product (from propene degradation), but it also forms by decomposition of C_3-oxygenated products. Different possible pathways have been suggested for acetaldehyde formation, either from propene via allylic intermediate,[9] or by double-bond break[25] and/or by propenal oxidation.[6,26] In catalytic oxidation of acetaldehyde:

$$\text{acetaldehyde} \rightarrow \text{acetic acid} + \text{formic acid} + CO + CO_2,$$

carbon oxides formation seems to be the main reaction pathway, and takes place through decomposition of the different secondary products.[6,27]

In summary, carbon oxides seem to be the only stable reaction products. However, while CO_2 is a primary+secondary product, CO is merely a secondary product (Fig. 3). On the other hand, the possibility that at higher temperatures CO may be produced directly from propene cannot be discarded. In any case, CO production at high temperatures by consecutive reaction is higher than that of CO_2; this fact could explain why, at high conversions, the amount of CO produced is higher than that of CO_2.

Concerning the main secondary reaction products, formation of acrylic acid may be ralated to propenal oxidation on the catalyst surface; this is in agreement with IR spectroscopic studies of propenal adsorption on different catalysts.[28] Acetic acid comes from oxidation of primary products,[23,24] but the most favorable route is acetaldehyde oxidation. Finally, the presence of large amounts of acetic acid can be explained as due to consecutive oxidation of acetaldehyde.

From the above consideration, the overall reaction network given in Fig. 4 is proposed. Formation of ethylene and methane was not taken into account in this scheme because these products appeared in very minor concentrations. Formation of these products seems to take place through a pathway very different from those observed for the rest of reaction products. Their appearance could be explained on the basis of auto-oxidation processes of propenal and acetaldehyde, respectively.[6,10,21]

Kinetic Results. In a previous work[13] the activation energy for propenal formation from propene oxi-

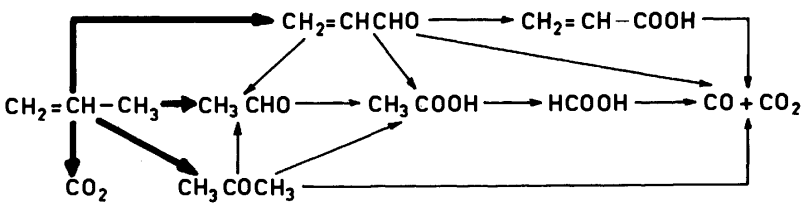

Fig. 4. Simplified reaction network for the oxidation of propene on $Mo_4Pr_{0.5}Bi_{0.5}O_x/SiO_2$ catalyst. ➡, primary reactions; →, secondary reactions.

dation over the $Mo_4Pr_{0.5}Bi_{0.5}O_x/SiO_2$ catalyst was determined, its value being similar to that one obtained for USb_3O_{10}[5] but much lower than that one reported for bismuth molybdate.[29]

An important feature is the low activation energy (1.7 kJ mol^{-1}) found for acetone formation, in contrast to values obtained for the rest of products. This can be interpreted as due to a decrease of the number of active centers present in catalyst surface with increasing temperatures. Moreover, increase of reaction temperature favorises acetone elimination via secondary reactions. The poor fit obtained for the influence of temperature on the rate constant, for acetone formation is due to the combined effect of these two phenomena.

Apparent reaction orders for acetaldehyde and CO_2 formation were strongly dependent on the hydrocarbon partial pressure; only at a temperature of 653 K constant values were obtained for the apparent reaction orders along the whole propene partial pressure range, their values being 1.26 for acetaldehyde and 1.41 for CO_2. It is rather unusual to obtain values for reaction orders greater than unity; however, such values have been previously reported in both, acetaldehyde[7] and carbon oxides[4,30] formation. This fact could be explained by simultaneous presence of both, consecutive and parallel pathways in propene degradation. However, this fact alone cannot explain the effect observed if a value of 1 is considered for the reaction order corresponding to both pathways.

It seems logical to conclude that acetaldehyde and CO_2 formation on our catalyst follow similar pathways, namely both, consecutive reaction (from primary products), and parallel reaction (from propene). Consequently, a complex kinetic equation results taking into account these two different pathways. On the other hand, the similarity of values obtained for activation energies for acetaldehyde and CO_2 formation (69.4 and 78.6 kJ mol^{-1}, respectively) is a further evidence for the similarity of these phenomena.

Finally, it seems convenient to recall some characterization results in order to compare our catalyst with the well-known bismuth molybdate catalyst. The $Mo_4Pr_{0.5}Bi_{0.5}O_x$ catalyst shows a high selectivity for propene oxidation to propenal[13] (redox mechanism) but a low selectivity for 2-methyl propene oxidiation to 2-methyl propenal[31,32] (competitive redox and stationary state of adsorption mechanism). The most active and selective binary Mo-Pr oxide catalysts (i.e., those with Mo/Pr=4—6.7) for propene oxidation contain Pr_2O_3 instead of Pr_6O_{11}, as well as a highly dispersed MoO_3 phase.[33] For a Mo/Pr ratio equal to 4, the most active and selective ternary Mo-Pr-Bi catalysts (those with Mo/Bi=13.3) show the highest surface acidity in this series.[34] The increase of selectivity is ascribable to the well-known ability of bismuth to active propene in the form of allylic species.[35] On the other hand, ESR studies on Mo-Pr-Bi/SiO_2 catalysts, indicate that the presence of Pr in the Mo/Bi catalysts increase the dispersion of bismuth molybdates.[36] Additional work is in progress in our laboratories in order to get some further insight on the role of praseodimium in selective oxidation catalysts.

References

1) G. W. Keulks, L. D. Krenzke, and T. M. Notermann, *Adv. Catal.*, **27**, 183 (1978).

2) D. J. Hucknall, "Selective Oxidation of Hydrocarbons," Academic Press, London (1974); C. F. Cullis and D. J. Hucknall, "Catalysis," ed by G. C. Bond and G. Webb, Vol. 5, Chap. 7; The Chemical Society, London (1982).

3) I. Aso, S. Furukawa, N. Yamazoe, and T. Seiyama, *J. Catal.*, **64**, 29 (1980).

4) J. R. Monnier and G. W. Keulks, *J. Catal.*, **68**, 51 (1981).

5) G. W. Keulks, Z. Yu, and L. D. Krenzke, *J. Catal.*, **84**, 38 (1983).

6) M. Cathala and J. E. Germain, *Bull. Soc. Chim. Fr.*, **1971**, 2167.

7) M. Crozart and J. E. Germain, *Bull. Soc. Chim. Fr.*, **1973**, 3077.

8) G. W. Godin, C. C. McCain, and E. A. Porter, Proc. 4th. Intern. Congr. Catal., Vol. 1, p. 271; Akadémiai Kadó, Budapest (1971).

9) L. Ya. Margolis, *J. Catal.*, **21**, 93 (1971).

10) G. W. Keulks, M. P. Rosynek, and C. Daniel, *Ind. Eng. Chem., Prod. Res. Dev.*, **10**, 138 (1971).

11) C. R. Adams, H. H. Voge, C. Z. Morgan, and W. E. Armstrong, *J. Catal.*, **3**, 379 (1964).

12) G. Kremenić, V. Cortés Corberán, and J. M. López Nieto, Proc. 9th. Iberoam. Symp. Catal., Lisbon (1984), Vol. 2, p. 908.

13) G. Kremenić, J. M. L. Nieto, J. M. D. Tascón, L. G. Tejuca, and S. W. Weller, *Ind. Eng. Chem. Res.* (in press).

14) G. Kremenić, J. M. López Nieto, and S. Mendioroz, *Bull. Chem. Soc., Perú*, **53**, 73 (1984).

15) A. Corma and B. W. Wojciechowski, *Catal. Rev. Sci. Eng.*, **24**, 1 (1982).

16) V. Cortés Corberán, A. Corma, and G, Kremenić, *Ind. Eng. Chem., Prod. Res. Dev.*, **23**, 546 (1984).

17) Y. Moro-oka, Y. Takita, and A. Ozaki, *J. Catal.*, **27**, 177 (1972).

18) S. Tan, Y. Moro-oka, and A. Ozaki, *J. Catal.*, **17**, 132 (1970).

19) Y. Takita, Y. Moro-oka, and A. Ozaki, *J. Catal.*, **52**, 95 (1978); M. Ai and A. Ozaki, *Bull. Chem. Soc. Jpn.*, **52**, 1454 (1979).

20) J. C. Mol and J. A. Moulijn, *Adv. Catal.*, **24**, 131 (1975); T. Sodesawa, E. Ogata, and Y. Kamiya, *Bull. Chem. Soc. Jpn.*, **52**, 1661 (1979).

21) N. N. Semenov, "Some Problems in Chemical Kinetics," Princeton University Press (1958), Vol. 2.

22) Y. Takita, K. Nita, T. Machara, N. Yamazoe, and T. Seiyama, *J. Catal.*, **50**, 364 (1977).

23) J. Buiten, *J. Catal.*, **13**, 373 (1969); **27**, 232 (1972).

24) T. G. Alkhazov, K. Yu. Adzhamov, and A. K. Khanmamedova, *Russ. Chem. Rev.*, **51**, 542 (1982).

25) J. L. Portefaix, F. Figueras, and M. Forissier, *J. Catal.*, **63**, 307 (1980).

26) C. C. McCain and G. W. Godin, *Nature (London)*, **202**, 692 (1964).

27) T. Seiyama, K. Nita, T. Machara, N. Yamazoe, and Y. Takita, *J. Catal.*, **49**, 164 (1977).
28) R. Grabowski, J. Haber, and J. Sloczýnski, *React. Kinet. Catal. Lett.*, **12**, 119 (1979).
29) L. D. Krenzke and G. W. Keulks, *J. Catal.*, **64**, 295 (1980).
30) J. M. Baryshevaskaya, K. M. Kholyavenko, and M. Ya. Rubanik, *Ukr. Khim. Zh.*, **35**, 702 (1969); **35**, 805 (1980).
31) J. M. López Nieto, J. M. D. Tascón, G. Kremenić, and L. González Tejuca, Proc. 6th. Intern. Symp. Heterog. Catal., Sofia, 1987 (in press).
32) G. Kremenić, J. M. López Nieto, J. M. D. Tascón, and L. González Tejuca, *Less Common Met.*, (in press).
33) J. M. López Nieto, J. L. G. Fierro, L. González Tejuca, and G. Kremenić, *J. Catal.*, (in press).
34) G. Kremenić, J. M. López Nieto, J. L. G. Fierro, and L. González Tejuca, *J. Less-Common Met.*, (in press).
35) B. Grzybowska, J. Haber, and J. Janas, *J. Catal.* **49**, 150 (1977).
36) G. Kremenić, J. M. López Nieto, J. Soria, and J. Martî, "New Frontiers in Rare Earth Science and Applications," ed by Xu Guangxian and Xiao Kimei, Vol. 1, p. 614; Science Press, Beijing, People's Republic of China (1985).

Synthesis of [5$_2$](1,2)Ferrocenophane

Masao HISATOME,* Rin-ichi YAMASHITA, Jun WATANABE, and Koji YAMAKAWA
Faculty of Pharmaceutical Sciences, Science University of Tokyo, 12 Ichigaya-Funagawara, Shinjuku-ku, Tokyo 162
(Received October 31, 1987)

Synopsis. The title compound **1** has been synthesized via bridge enlargement of compound **2** which was formed by cyclization of [5]ferrocenophane-2-propionic acid. By this study the structure of **2**, which was discrepantly described by two groups, has been established as [5]-α-oxo[3](1,2)ferrocenophane.

In the previous papers,[1,2] we reported on the synthesis of [5$_2$](1,3)-, [5$_3$](1,2,4)-, and [5$_4$](1,2,3,4)ferrocenophanes[3,4] multi-bridged with pentamethylene chains. However, [5$_2$](1,2)ferrocenophane (**1**) bridged with two chains at the neighboring positions each other has not yet been synthesized. The compound **1** might be derived from [5]-α-oxo[3](1,2)ferrocenophane (**2**) by application of a general method that we developed for insertion of two methylene units into the trimethylene bridge of ferrocenophanes.[1,2]

Brown and Winstead[5] described that the compound **A** (77%, mp 156—158 °C) given in the cyclization of [5]ferrocenophane-2-propionic acid was phane **2**, but Struchkov et al.[6] claimed for the structure of the compound **A** to be revised. They obtained a dibridged compound **B** (2.5%, mp 149—151 °C) as a by-product in the reaction of [5]ferrocenophane with acryloyl chloride and $AlCl_3$, and assigned the compound **B** to [5](1,1′)-α-oxo[3](3,2′)ferrocenophane (**3**), a slantwise dibridged ferrocenophane. They mentioned that Brown's compound **A** was phane **3**, because **B** was almost identical with **A** in melting point and spectral data. Both groups described the chemical shift values of the cyclopentadienyl (Cp) ring proton signals in ^{1}H NMR spectra but not the multiplicities and coupling constants of the signals. Accordingly, the proper structure of **A** or **B** cannot be judged only by their descriptions.

In the first place, we reinvestigated the reaction reported by Brown and Winstead in order to solve the discrepancy between the descriptions of the two groups. [5]Ferrocenophane-2-propionic acid was treated with trifluoroacetic anhydride in dichloromethane to give two products **2** (75%, mp 163—163.5 °C) and **3** (6.3%, mp 75—78 °C) which both showed the molecular ion peak at m/z 308 in the mass spectra. The melting point of **2** is close to those of compounds **A** and **B**, and the chemical shift values of **2** are also almost similar to the data of **A** and **B**. Accordingly, the phane **2** definitely corresponds to **A** and **B**. In the ^{1}H NMR spectra, the two triplet signals of the Cp ring protons of **2** at δ 4.24 and 4.38 are split by 2.4 and 2.6 Hz, respectively, whereas two triplets of **3** at δ 4.08 and 4.78 have the coupling constants of 2.4 and 1.4 Hz. The usual ortho and meta coupling constants in multibridged ferrocenophanes are 2.0—3.1 and 1.0—1.6 Hz, respectively.[1,2,7,8] Therefore, the three protons appearing as triplet with a larger coupling constant have hydrogens at two ortho positions in the Cp rings, and only one proton of **3** has hydrogens at two meta positions. The spectra indicate that compound **2** have a symmetrically bridged structure at 1,2-positions and **3** is a slantwise bridged ferrocenophane.

Bridge enlargement of **2** with diazomethane and BF_3 etherate according to the method used in the synthesis of multibridged [5$_n$]ferrocenophanes[1,2] afforded two enlarged ketones **4** and **5**. The mass spectra of **4** and **5** indicated that they were produced by insertion of one and two units of methylene group, respectively. Reduction of **5** with $LiAlH_4$ and $AlCl_3$ afforded compound **1**. The C_{2v} symmetric structure of **1** was deter-

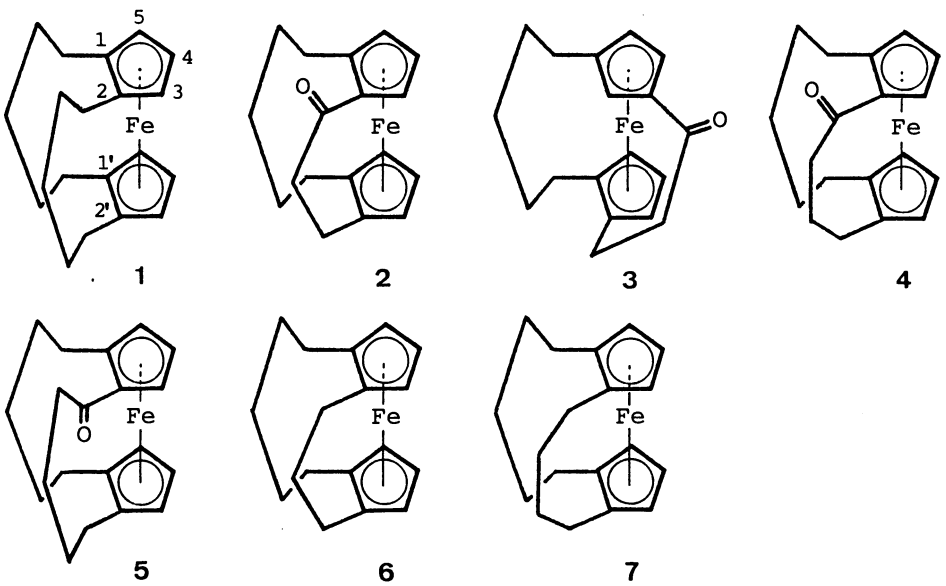

1 2 3 4

5 6 7

mined by NMR spectrometry. The Cp ring protons of **1** appear as only two signals at δ 3.93(d) and 4.18(t). The ^{13}C NMR spectrum of **1** shows a simple pattern which consists of only three methylene carbon and three ring carbon signals.

The NMR spectra of **6** and **7** obtained by reduction of **2** and **4**, respectively, indicate their C_s symmetric structure. The melting point (153—153.5 °C) and the chemical shift values of the Cp ring protons of **6** are almost similar to those of reduction product (mp 153—154 °C[5]) of compound **A**. Therefore, it has been confirmed that the description by Brown and Winstead was correct.

Experimental

All melting points were uncorrected. Spectra were measured on the same instruments as those used in the synthesis of [5$_4$]ferrocenophane.[2] All reactions were carried out according to the procedures described in the previous reports.[1,2]

Bridging Reaction of [5]Ferrocenophane-2-propionic Acid (8). The starting material **8** was prepared by condensation of 2-formyl[5]ferrocenophane[1] with malonic acid and piperidine in pyridine followed by hydrogenation with H_2/Pd-C in acetone. The acid **8** (260 mg) was treated with trifluoroacetic anhydride (550 mg) in dichloromethane (20 ml). The crude product was column-chromatographed over silica gel with benzene. The first band yielded [5]-α-oxo[3](1,2)ferrocenophane (**2**) (177 mg, 75%), which was recrystallized from ethyl acetate to give orange rodlike crystals; mp 163—163.5 °C (lit, mp 156—158 °C,[5] 149—151 °C[6]). IR (KBr) 1665 (C=O) cm^{-1}; ^{1}H NMR ($CDCl_3$) δ=1.30—3.50 (14H, m, -CH_2-), 3.70 (1H, dd, J=1.4 and 2.4 Hz, 3'- or 5'-H), 4.04 (1H, dd, J=1.4 and 2.6 Hz, 3- or 5-H), 4.24 (1H, t, J=2.4 Hz, 4'-H), 4.38 (1H, t, J=2.6 Hz, 4-H), 4.54 (1H, dd, J=1.4 and 2.4 Hz, 3'- or 5'-H), 4.78 (1H, dd, J=1.4 and 2.6 Hz, 3- or 5-H); MS m/z (rel intensity) 308 (100, M$^+$).

The second band yielded [5](1,1')-α-oxo[3](3,2')ferrocenophane (**3**) (15 mg, 6.3%), which was recrystallized from ethyl acetate to give orange prisms; mp 75—78 °C. IR(KBr) 1650 (C=O) cm^{-1}; ^{1}H NMR ($CDCl_3$) δ=1.50—3.80 (14H, m, -CH_2-), 3.94 (1H, dd, J=1.5 and 2.4 Hz, 3'- or 5'-H), 4.08 (1H, t, J=2.4 Hz, 4'-H), 4.16 (1H, dd, J=1.4 and 2.4 Hz, 5-H), 4.30 (1H, dd, J=1.5 and 2.4 Hz, 3'- or 5'-H), 4.47 (1H, dd, J=1.4 and 2.4 Hz, 4-H), 4.78 (1H, t, J=1.4 Hz, 2-H); MS m/z (rel intensity) 308 (100, M$^+$).

Found: m/z 308.0847. Calcd for $C_{18}H_{20}OFe$: M, 308.0862.

Bridge Enlargement of Ketone 2. Ketone **2** (900 mg) in benzene (150 ml) was allowed to react with alcohol-free diazomethane (50 ml of an ether solution) in the presence of BF_3 etherate (1.0 ml). The crude product was column-chromatographed over silica gel with benzene–ethyl acetate (50:1). The first band yielded [5]-β-oxo[4](1,2)ferrocenophane (yellow crystals, 161 mg, 17%). IR(KBr) 1695 (C=O) cm^{-1}. The β-ketone was contaminated with further enlarged products, and could not be purified.

The second band yielded [5]-α-oxo[5](1,2)ferrocenophane (**5**) (333 mg, 35%), which was recrystallized from ethyl acetate to give red plates; mp 134—135 °C. IR(KBr) 1648 (C=O) cm^{-1}; ^{1}H NMR ($CDCl_3$) δ=1.30—3.20 (18H, m, -CH_2-), 3.85 (1H, t, J=2.0 Hz, 4'-H), 4.15 (2H, m, Cp-H), 4.27 (1H, t, J=2.0 Hz, 4-H), 4.57 (2H, m, Cp-H); MS m/z (rel intensity) 336 (100, M$^+$), 308 (6), 322 (2).

Found: C, 71.51; H, 7.12; m/z 336.1191. Calcd for $C_{20}H_{24}OFe$: C, 71.44; H, 7.19; M, 336.1175.

The starting material **2** (98 mg, 11%) was yielded from the third band. The fourth band yielded [5]-α-oxo[4](1,2)ferrocenophane (**4**) (216 mg, 23%), which was recrystallized from ethyl acetate to give orange needles; mp 157—158 °C. IR (KBr) 1645 (C=O) cm^{-1}; ^{1}H NMR ($CDCl_3$) δ=1.20—3.00 (16H, m, -CH_2-), 3.95 (2H, m, Cp-H), 4.15 (1H, t, J=2.5 Hz, 4'-H), 4.27 (1H, t, J=2.0 Hz, 4-H), 4.51 (2H, m, Cp-H); MS m/z (rel intensity) 322 (100, M$^+$), 298 (5).

Found: C, 70.80; H, 6.81; m/z 322.1019. Calcd for $C_{19}H_{22}OFe$: C, 70.82; H, 6.88; M, 322.1018.

[5][3](1,2)Ferrocenophane (6). Ketone **2** (40 mg) was reduced with $LiAlH_4$ (20 mg) and $AlCl_3$ (70 mg) in ether (10 ml). Phane **6** (35 mg, 92%), isolated from the crude product by column chromatography over silica gel with benzene, was recrystallized from hexane to give yellow needles; mp 153—153.5 °C (lit, mp 153—154 °C[5]). ^{1}H NMR ($CDCl_3$) δ=1.20—3.20 (16H, m, -CH_2-), 3.78 (4H, d, J=2.4 Hz, 3,3',5,5'-H), 4.14 (2H, t, J=2.4 Hz, 4,4'-H); ^{13}C NMR ($CDCl_3$) δ=21.10, 21.44, 22.27, 26.46, and 34.65 (methylene-C), 66.58, 68.09, and 69.35 (unsubstd. Cp-C), 83.20 and 85.78 (substd. Cp-C); MS m/z (rel intensity) 294 (100, M$^+$); λ_{max} (THF) 442 nm (ε=221).

[5][4](1,2)Ferrocenophane (7). Ketone **4** (40 mg) was reduced with $LiAlH_4$ (20 mg) and $AlCl_3$ (70 mg) in ether (10 ml). Phane **7** (38 mg, quant.) was isolated by column chromatography over alumina with benzene and recrystallized from ethyl acetate to give yellow needles; 137—138 °C. ^{1}H NMR ($CDCl_3$) δ=1.30—3.00 (18H, m, -CH_2-), 3.82 (2H, dd, J=1.4 and 3.2 Hz, 3,3'-H), 3.97 (2H, dd, J=1.4 and 3.2 Hz, 5,5'-H), 4.04 (2H, t, J=3.2 Hz, 4,4'-H); ^{13}C NMR ($CDCl_3$) δ=22.27, 22.86, 25.39, 26.37, and 26.71 (methylene-C), 65.65, 67.06, and 68.77 (unsubstd. Cp-C), 85.88 and 86.12 (substd. Cp-C); MS m/z (rel intensity) 308 (100, M$^+$); λ_{max} (THF) 444 nm (ε=110).

Found: C, 74.12; H, 7.82; m/z 308.1213. Calcd for $C_{19}H_{24}Fe$: C, 74.40; H, 7.85; M, 308.1225.

[5$_2$](1,2)Ferrocenophane (1). Ketone **5** (39 mg) was reduced with $LiAlH_4$ (18 mg) and $AlCl_3$ (62 mg) in ether (10 ml). Phane **1** (35 mg, 95%) was isolated by column chromatography over alumina with benzene and recrystallized from ethyl acetate to give orange plates; mp 130—132 °C. ^{1}H NMR ($CDCl_3$) δ=1.20—3.00 (20H, m, -CH_2-), 3.93 (4H, d, J=2.4 Hz, 3,3',5,5'-H), 4.18 (2H, t, J=2.4 Hz, 4,4'-H); ^{13}C NMR ($CDCl_3$) δ=22.42, 22.81, and 25.78 (methylene-C), 66.72 and 67.55 (unsubstd. Cp-C), 85.14 (substd. Cp-C); MS m/z (rel intensity) 322 (100, M$^+$); λ_{max} (THF) 446 nm (λ=109).

Found: C, 74.14; H, 8.00; m/z 322.1379. Calcd for $C_{20}H_{26}Fe$: C, 74.54; H, 8.13; M, 322.1382.

References

1) M. Hisatome and M. Hillman, *J. Organomet. Chem.*, **212**, 217 (1981).

2) M. Hisatome, J. Watanabe, R. Yamashita, and K. Yamakawa, 18th Symposium on Structural Organic Chemistry, Toyama, Oct. 1985, Abstr. No. B2-08; M. Hisatome, R. Yamashita, J. Watanabe, K. Yamakawa, and Y. Iitaka, *Bull. Chem. Soc. Jpn.*, in press.

3) The nomenclature of ferrocenophanes[2] in the present work is a modification of that presented by Vögtle and Neumann.[4]

4) F. Vögtle and P. Neumann, *Tetrahedron*, **26**, 5847 (1970).

5) A. D. Brown, Jr. and J. A. Winstead, *J. Org. Chem.*, **36**, 2832 (1971).

6) Y. T. Struchkov, G. G. Aleksandrov, A. Z. Kreindlin, and M. I. Rybinskaya, *J. Organomet. Chem.*, **210**, 237 (1981).

7) M. Hisatome, T. Sakamoto, and K. Yamakawa, *J. Organomet. Chem.*, **107**, 87 (1976).

8) M. Hisatome, N. Watanabe, T. Sakamoto, and K. Yamakawa, *J. Organomet. Chem.*, **125**, 79 (1977).

^{35}Cl NQR Study and Addition Reactions to Cyclohexene of Cyclic *N*-Chloro Amides (Imides)

Yoshitaka NAGAO* and Shigeyoshi KATAGIRI
Department of Chemistry, Faculty of Science, Hirosaki University, Bunkyo-cho, Hirosaki 036
(Received April 11, 1987)

Synopsis. ^{35}Cl NQR frequencies were measured for *N*-chloro-2-pyrrolidinone, *N*-chloro-4,4-dimethyl-2-oxazolidinone, *N*-chloro-2-oxazolidinone, *N*-chloroglutarimide, and *N*-chlorosuccinimide. The ionicities of the N-Cl bonds were estimated on the basis of those measurements. These ionicities were related to the total yields of the 1,2-addition in the photochemical reaction with cyclohexene. When the value of the ionicity neared zero, the total yield increased.

N-Chloro imides are effective reagents for the chlorination and the oxidation of olefins, alcohols, and carbonyl compounds. Thus, it seems that it would be interesting to investigate the character of the N-Cl bonds in *N*-chloro amides (imides). It is worth while to measure the ^{35}Cl NQR frequencies of *N*-chloro amides (imides), because these frequencies give information on the bond character of N-Cl bonds. If the quadrupole coupling constant is obtained from the observed ^{35}Cl NQR frequency, the bond ionicity may be evaluated. In a previous paper,[2] the ^{35}Cl NQR frequencies for some *N*-chloro imides were observed, and the N-Cl bond ionicities of these compounds were evaluated. The ionicities were related to the reactivities of these compounds. If the value of the ionicity is near zero, the chlorine radical is produced easily and a high yield can be expected in a radical reaction.

In this study, we observed the ^{35}Cl NQR frequencies for the cyclic *N*-chloro amides(imides) shown below and estimated the ionicities of these compounds. The ionicities were then compared with the yields of 1,2-addition in the photochemical reaction of these compounds with cyclohexene.

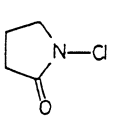

1

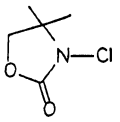

2

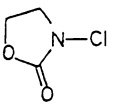

3

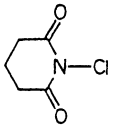

4

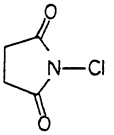

5

Experimental

The *N*-chloro amides(imides) were prepared as follows: *N*-Chloro-2-oxazolidinone (**3**) and *N*-chloro-4,4-dimethyl-2-oxazalidinone (**2**) were obtained by the method of Kosugi et at.[4] after the corresponding amides had been prepared by Homeyer's method.[5] The *N*-chloro-3-pyrrolidinone (**1**) was prepared by passing chlorine gas into 2-pyrrolidinone dissolved in water containing sodium hydrogencarbonate.[6] The *N*-chloroglutarimide (**4**) was obtained by the reaction of glutarimide with a bleaching-powder solution[7] after the glutarimide had been prepared by the reaction of glutaric anhydride with aqueous ammonia.[8] These compounds were purified several times by recrystallization.

The NQR spectrometer described by Dean was employed.[9] The signals were modulated by the reference signal from a lock-in amplifier (FM Circuit Design Block Co., Ltd., Model LI-572B) and were displayed on a CRO screen (National, VP-5250). The frequency measurement was made by a method described previously.[2,3] All the measurements were made at the temperature of liquid nitrogen. Glass vessels containing 8—10 g of the samples were used.

Results and Discussion

The ^{35}Cl NQR frequencies of the *N*-chloro compounds at the temperature of liquid nitrogen are given in Table 1. The resonance lines appear in the region from 52.7 to 54.1 MHz. This region lies in the ^{35}Cl NQR frequency range of the N-Cl bond with a tr^1 tr^1 tr^1 π^2 hybridized nitrogen atom proposed by Hart and Whitehead.[1] The resonance frequency of **3** is higher than that of **1**. This difference results from the fact that **3** has an oxygen which is electron-attractive instead of the methylene group in **1**. In the cases of **2** and **3**, the latter has a higher frequency than the former. The presence of methyl groups is responsible for the decrease in the resonance frequency of **2**, for the methyl group is electron-donative. The resonance frequency of **5** is higher than that of **1** because of having another electron-attractive carbonyl group on the ring. Cyclic compounds show an increase in the nuclear quadrupole resonance frequency which rises with an increase in the ring strain.[10] This tendency is observed in the cases of both **4** and **5**.

The pure quadrupole resonance frequency can be expressed as functions of the quadrupole coupling constant, e^2Qq/h, and the asymmetry parameter, η, of the field gradient. These two parameters cannot be determined uniquely from the observed frequencies. However, if it is assumed that $\eta=0$, the coupling constant is equal to twice the resonance frequency for the chlorine atom with a 3/2 nuclear spin. On this assumption, we have calculated the coupling constants given in Table 1. The adequacy of this assumption for the compounds cited in Table 1 is supported by a consideration of the resonance structures, for the most probable main factor leading to the asymmetry of the field gradient in molecules of this type is the π-bond character of the nitrogen-chlorine bond and the axially symmetric charge distribution of σ-electrons does not contribute to the parameter. The calculated quadrupole coupling constants for *N*-chloro compounds are lower than that of the chlorine atom (109.74 MHz for ^{35}Cl). This indicates that the chlorine

Table 1. ^{35}Cl NQR Parameters of *N*-Chloro Compounds at the Temperature of Liquid Nitrogen and the Total Yield of the 1,2-Addition Reaction to Cyclohexene

Compound	ν/MHz	e^2Qq/h	i[a]	Yield/%[d]
N-Chloro-2-pyrrolidinone	51.732	103.46	−0.06	9
N-Chloro-4,4-dimethyl-2-oxazolidinone	52.244	104.49	−0.05	
N-Chloro-2-oxazolidinone	52.805	105.61	−0.04	34
	52.914			
N-Chloroglutarimide	53.096			
	(53.005)[c]	106.01	−0.03	
N-Chloroglutarimide	54.095[b]	108.19	−0.01	54

a) The minus sign indicates that the chlorine atom has a negative fractional charge. b) From Ref. 1. c. 2. c) Averaged values. d) From Ref. 1. c. 12.

atom of the *N*-chloro compound cited in Table 1 has a negative fractional charge. According to Dailey and Townes,[11] $(e^2Qq)_{mol}$ is expressed by:

$$(e^2Qq)_{mol}=(1-i)(e^2Qq)_{atom}$$

where i stands for the bond ionicity and where $(e^2Qq)_{atom}$ denotes the e^2Qq value of the atomic chlorine. In this equation, the contribution from the s character of the bonding orbital of chlorine is assumed to be zero, for the electronegativity of chlorine is practically the same as that of nitrogen. The contribution from the d character is ignored because it is always less than 5% for the chlorine atom. The ionic characteristics of the N-Cl bonds shown in Table 1 were calculated from this relation.

Lessard et al.[12] investigated the total yield of 1,2-addition in the photochemical reaction of cyclic *N*-chloro amides (imides) with cyclohexene. They proposed that 1,2-addition occurs through a radical-chain mechanism as follows:

$$\text{-CO-N-Cl} \xrightarrow{h\nu} \text{-CO-N}\cdot + \text{Cl}\cdot \quad (1)$$

$$\text{-CO-N}\cdot + \text{C=C} \longrightarrow \text{-CO-N-C-C}\cdot \quad (2)$$

$$\text{-CO-N-C-C}\cdot + \text{Cl-N-CO-} \longrightarrow \text{-CO-N-C-C-Cl} + \cdot\text{N-CO-} \quad (3)$$

They also suggested that the total yield of the 1,2-addition reaction increases when the *N*-chloro compound in Reaction 3 is a good chlotine-atom donor. When the *N*-chloro compound is a good chlorine-atom donor, the value of the ionicity of the N-Cl bond should be near zero. Thus, we compared the total yield of the 1,2-addition with the ionicity of the *N*-chloro compound. The total yield for the photochemical addition to cyclohexene is shown in Table 1. *N*-Chlorosuccinimide (**5**) gives rise to the highest yield and has the nearest value to zero for the ionicity. When the value of the ionicity is far from zero, the yield decreases.

References

1) R. M. Hart and M. A. Whitehead, *Trans. Faraday Soc.*, **67**, 1569 (1971).
2) Y. Nagao and S. Katagiri, *Bull. Chem. Soc. Jpn.*, **59**, 641 (1986).
3) Y. Nagao and S. Katagiri, *Sci. Rep. Hirosaki Univ.*, **33**, 69 (1986).
4) M. Kosugi, J. J. Kaminski, S. H. Selk, I. H. Pitman, N. Bodor, and J. Higuchi, *J. Pharm. Sci.*, **65**, 1743 (1976).
5) A. H. Homeyer, U. S. Pat. 2399188 (1946); *Chem. Abstr.*, **40**, 4081 (1946).
6) J. Lessard, M. Mondon, and D. Touchard, *Can. J. Chem.*, **59**, 431 (1981).
7) C. Beard and J. Hickinbotton, *J. Chem. Soc.*, **1958**, 2982.
8) W. A. Noyes and P. K. Porter, *Org. Synth.*, Coll. Vol. II, 457 (1956).
9) C. Dean and M. Pollak, *Rev. Sci. Instrum.*, **29**, 630 (1958).
10) H. G. Fitzky, "Advances in Nuclear Quadrupoleresonance," Vol. 1, ed by J. A. S. Smith, Heyden and Son (1974), p. 86.
11) T. P. Das and E. L. Hahn, "Nuclear Quadrupole Resonance Spectroscopy," Academic Press, New York (1958), p. 142.
12) J. Lessard, Y. Couture, M. Mondon, and D. Touchard, *Can. J. Chem.*, **62**, 105 (1984).

Optical Resolution of α-Ethylbenzylamine and Its Application as a Resolving Agent

Hiroyuki NOHIRA,* Misako NOHIRA, Shin-ichi YOSHIDA,
Ayako OSADA, and Daiyo TERUNUMA
Department of Applied Chemistry, Faculty of Engineering, Saitama University, Shimo-ohkubo, Urawa 338
(Received September 8, 1987)

Synopsis. (±)-α-Ethylbenzylamine ((±)-**1**) was efficiently resolved into a pair of enantiomers by fractional crystallization as its *cis*-2-benzamidocyclohexanecarboxylic acid (**2**) salt. Moreover, it was found that each of both enantiomers was obtained by mutual resolution between (±)-**1** and (±)-**2**. The optically active amine (**1**) was substantially capable of resolving a variety of chiral carboxylic acids.

Among the many synthetic resolving agents, optically active α-methylbenzylamine is widely used for resolving chiral carboxylic acids. But the amine is not necessarily an effective resolving agent for all chiral carboxylic acids. Especially, it is not so effective for resolving such chiral carboxylic acids as chrysanthemic acid (**3**)[1] and pantolactone (**4**). We therefore intend to report on the optical resolution and effective application of **1** as a new synthetic resolving agent which can be used widely.

Optically active α-ethylbenzylamine (**1**) is expected to be as effective as α-methylbenzylamine on account of their structural similarity. Although many attempts have been made so far for resolving (±)-**1** by fractional crystallization as the salts with (*S*)-(−)-malic acid and (2*R*, 3*R*)-(+)-tartaric acid,[2] and *N*-acetyl-3,5-dibromo-L-tyrosine,[3] no successful method have been reported since a recrystallization of the diastereomeric salt must be repeated several times. Moreover, optically active amine **1** as a resolving agent remains unexplored.

(±)-**1** is readily synthesized from propiophenone, which is commercially available in large quantities by reductive amination with ammonia and hydrogen in the presence of a Raney nickel catalyst.

After primary examinations looking for a suitable resolving agent for (±)-**1**, it was found that optically active *cis*-2-benzamidocyclohexanecarboxylic acid (**2**)[4] gave almost pure (+)- and (−)-**1** in good yields without any recrystallization.

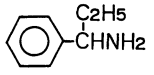

1

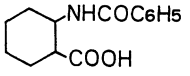

2

In the process of the optical resolution described above, such physical properties as the melting point and solubility, infrared spectra of the less soluble salts ((+)-**1**·(−)-**2** and (−)-**1**·(+)-**2**) and those of the racemic salt ((±)-**1**·(±)-**2**) were determined. The less soluble salts did have higher melting points (mp 190—191 °C) and lower solubilities toward methanol than the racemic salt (mp 156—157 °C), and their infrared spectra were found to be identical. These results indicate that crystals of the racemic salt are deposited as a conglomerate and that the racemic salt is resolvable by preferential crystallization, namely mutual resolution.

Actually, (+)-**1**·(−)-**2** salt could be cleanly crystallized from a supersaturated solution of (±)-**1**·(±)-**2** salt in methanol when (+)-**1**·(−)-**2** salt was seeded in the solution. Alternate seeding of (−)-**1**·(+)-**2** or (+)-**1**·(−)-**2** salt to the supersaturated solution gave (−)-**1**·(+)-**2** or (+)-**1**·(−)-**2** salt in moderate to high optical purity. Then, crystals having the same sign of optical rotation were combined, recrystallized, and decomposed with an alkaline solution and hydrochloric acid to give optically pure (+)-**1**, (−)-**2** and (−)-**1**, (+)-**2**, respectively.

The optical purities of the resolved amines were determined by measuring the ^{1}H NMR spectra of the diastereoisomeric amides (**5**) derived from (+)-**1** or (−)-**1** and (+)-(benzylmethylphenylsilyl)acetic acid.[5]

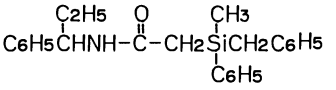

5

Then, the optically active amine (**1**) was applied in order to resolve such chiral carboxylic acids as chrysanthemic acid (**3**), pantolactone (**4**), and *N*-carbamoylmethionine(**6**), which were not efficiently resolved using α-methylbenzylamine.

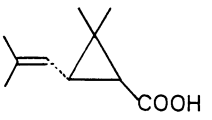

3

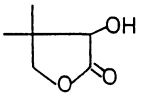

4

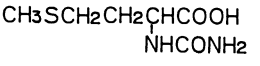

6

As summarized in Table 1, the amine (**1**) have apparently clear advantages for the optical resolution of the above-mentioned chiral carboxylic acids.

Experimental

All melting points were measured by a Laboratory Devices MEL-TEMP apparatus and are uncorrected. Optical rotations were measured on a JASCO DIP-360 Digital Polarime-

Table 1. Resolution of Racemic Carboxylic Acids Using (+)- or (−)-**1**

Salt					Liberated acid			
	Recrystallization solvent	Mp/°C	$[\alpha]_D$/° a) (°C)			Total yield/%b)	$[\alpha]_D$/° (°C)	Optical purity (%)
(−)-**3**·(+)-**1**	MeOH	138—140	−9.5	(20)	(−)-**3**	28	−13.1 (16) (*c* 1.0, EtOH)	94c)
(+)-**4′**·(−)-**1**	MEK	123—125	+22.2	(21)	(−)-**4**	56	−40.7 (25) (*c* 1.0, H_2O)	80d)
(−)-**4′**·(+)-**1**	MEK	125—127	−25.3	(25)	(+)-**4**	60	+47.8 (24) (*c* 1.0, H_2O)	95d)
(+)-**6**·(+)-**1**	H_2O	191—195	+3.3	(19)	(+)-**5**	42	+17.4 (19) (*c* 1.0, EtOH)	100e)

a) (*c* 1.0, MeOH). b) Based on half the amount of (±)-carboxylic acid used. c) Based on $[\alpha]_D^{25}$−14.01° (*c* 1.535, EtOH) from Merk Index. d) Based on $[\alpha]_D^{25}$−50.7° (*c* 2.05, H_2O) and $[\alpha]_D^{25}$+50.1° (*c* 2.0, H_2O) from Merk Index. e) Based on $[\alpha]_D^{26}$+17.4° (*c* 1.0, EtOH), optically active *N*-carbamoylmethionine derived from optically pure methionine.

ter. The ^1H NMR spectra were recorded with a JEOL FX-90Q spectrometer. The IR spectra were determined on a JASCO A-302 spectrophotometer.

Fractional Crystallization of 1·2 Salt. A clear solution of (±)-**1** (20.25g, 150 mmol) and (+)-**2** (29.68 g, 120 mmol) in methanol (150 ml) at an elevated temperature was allowed to cool slowly at room temperature and stand overnight. The white precipitates which appeared were collected by filtration to give almost pure (−)-**1**·(+)-**2** salt (20.97 g, 54.8 mmol) without any recrystallization: Mp 187—190 °C: $[\alpha]_D^{26}$+27.4° (*c* 1.00, MeOH).

Found: C, 72.07; H, 7.84; N, 7.30%. Calcd for $C_{23}H_{30}N_2O_3$: C, 72.22; H, 7.90; N, 7.23%.

To the salt was added a 1M NaOH solution (65 ml) in order to decompose the salt. The liberated amine was extracted with ether (2×45 ml), and the ethereal extracts were combined, dried over potassium hydroxide pellets, and concentrated under reduced pressure to give (−)-**1** (7.26 g, 53.7 mmol): $[\alpha]_D^{24}$−6.27° (*c* 1.276, EtOH); optical purity 95% ee.

The plus enriched amine recovered from the mother liquor (12.4 g, 92.2 mmol) was similarly reacted with (−)-**2** (22.80 g, 92.2 mmol) in methanol on heating. Cooling the solution at room temperature gave (+)-**1**·(−)-**2** salt (18.17 g, 47.5 mmol): Mp 187—191 °C ; $[\alpha]_D^{20}$−26.2° (*c* 1.098, MeOH). The similar treatment of the salt gave (+)-**1** (6.16 g, 45.6 mmol): $[\alpha]_D^{8}$+5.98° (*c* 1.00, EtOH); 91% ee.

Preferential Crystallization of (±)-1·(±)-2 Salt. A refluxed clear solution of an equimolar amount of (±)-**1** (3.53 g) and (±)-**2** (6.47 g) in methanol (35 ml) was allowed to cool at about 40 °C, seeded with (−)-**1**·(+)-**2** salt (41 mg, Mp 190—191 °C, $[\alpha]_D^{30}$+28.8° (*c* 1.00, MeOH)) and kept overnight at room temperature. The precipitates which appeared were collected by filtration, washed with a small amount of methanol, and dried over P_2O_5 to give 0.25 g of (−)-**1**·(+)-**2** salt ($[\alpha]_D^{28}$+24.6° (*c* 0.85, MeOH)). Successively, (±)-**1**·(±)-**2** salt (0.30 g) was added to the filtrate and dissolved at an elevated temperature. The solution was similarly cooled, seeded with (+)-**1**·(−)-**2** salt (46 mg, Mp 190—191 °C, $[\alpha]_D^{27}$−28.8° (*c* 1.00, MeOH)) and kept overnight at room temperature to yield 0.29 g of (+)-**1**·(−)-**2** salt ($[\alpha]_D^{26}$−27.1° (*c* 0.96, MeOH)). The process was repeated in a similar manner by supplying about 0.50 g of (±)-**1**·(±)-**2** salt in each run to give 0.30—0.63 g of optically active **1**·**2** salt. From the initial six runs, 1.34 g of (+)-**1**·(−)-**2** salt and 0.93 g of (−)-**1**·(+)-**2** salt were obtained, and recrystallized from methanol to give 0.98 g of (+)-**1**·(−)-**2** salt (Mp 190—191 °C, $[\alpha]_D^{27}$−28.8° (*c* 1.11, MeOH)) and 0.65 g of (−)-**1**·(+)-**2** salt (Mp 189—191 °C, $[\alpha]_D^{27}$+28.2° (*c* 1.00, MeOH)). Decomposition of the salts gave (+)-**1** (0.29 g), (−)-**2** (0.60 g) and (−)-**1** (0.21 g), (+)-**2** (0.40 g) respectively.

(+)-**1**: $[\alpha]_D^{30}$+6.6° (*c* 1.49, EtOH); 100 % ee.

(−)-**2**: Mp 205—207 °C; $[\alpha]_D^{26}$−36.4° (*c* 1.00, EtOH); 100% ee.

(−)-**1**: $[\alpha]_D^{30}$−6.5° (*c* 2.00, EtOH); 98% ee.

(+)-**2**: Mp 202—205 °C; $[\alpha]_D^{31}$+35.6° (*c* 0.86, EtOH); 98% ee.

Resolution of (±)-Pantolactone ((±)-4) with (−)-1 and (+)-1. A solution of 6.50 g (50 mmol) of (±)-**4** in water (25 ml) was treated with sodium hydroxide (2.24 g) and heated to 80—90 °C to hydrolyze the lactone. After cooling the the solution, the pH of the solution was adjusted to 8.5 with 2M HCl (1M=1 mol dm^{-3}). To the solution was added 6.76 g (50 mmol) of (−)-**1**, which was dissolved in 2M HCl (25 ml). The solution was concentrated under reduced pressure and the organic salts were extracted with 2-butanone (MEK) (60 ml). The extract was concentrated (10 ml) and allowed to stand overnight. The white precipitates which appeared were collected by filtration and dried over P_2O_5 to yield the salt (4.27 g, 15.1 mmol) of (+)-2,4-dihydroxy-3,3-dimethylbutyric acid ((+)-**4′**) and (−)-**1**: Mp 123—125 °C; $[\alpha]_D^{21}$+22.2° (*c* 1.00, MeOH).

After treating the salt with 1M NaOH (18 ml), the liberated amine was extracted with ether (2×10 ml). To the aqueous layer was added 2M HCl (10 ml); the solution was then evaporated in vacuo. The residue was then extracted with ether (2×5 ml) and dried over Na_2SO_4; the solvent was evaporated to give (−)-**4** (1.82 g, 14.0 mmol): Mp 84—87 °C; $[\alpha]_D^{25}$−40.7° (*c* 1.00, H_2O); 80.3% ee.

A similar treatment of the plus enriched lactone recovered from the mother liquor with (+)-**1** (4.72 g, 34.9 mmol) gave (−)-**4′**·(+)-**1** salt (4.54 g, 16.0 mmol): Mp 125—127 °C; $[\alpha]_D^{25}$−25.3° (*c* 1.00, MeOH). Decomposition of the salt gave (+)-**4** (1.96 g, 15.1 mmol): Mp 85—88 °C; $[\alpha]_D^{24}$+47.8° (*c* 1.00, H_2O); 95.4% ee.

Results of the resolution of (±)-**3** and (±)-**5** with (+)-**1** are shown in Table 1.

The authors thank Daicel Chemical Industries Ltd. for a gift of racemic α-ethylbenzylamine.

References

1) H. Nohira, *Farumashia*, **19**, No. 4, 356 (1983).
2) A. J. Little, J. M'Lean, and F. J. Wilson, *J. Chem. Soc.*, **1940**, 336.
3) H. D. Dewitt and A. W. Ingersoll, *J. Am. Chem. Soc.*, **73**, 5782 (1951).
4) H. Nohira, K. Watanabe, and M. Kurokawa, *Chem. Lett.*, **1976**, 229.
5) D. Terunuma, M. Kato, M. Kamei, H. Uchida, and H. Nohira, *Chem. Lett.*, **1985**, 13.

Polarographic and Cyclic Voltammetric Reduction of *p*-Chlorobenzaldehyde Isonicotinoylhydrazone

Papammagari Raveendra REDDY† and Sukuru Brahmaji RAO*
Department of Chemistry, Sri Krishnadevaraya University, Anantapur-515 003, India
†Lecturer in Chemistry, SSBN College, Anantapur-515 001, India
(Received January 8, 1987)

Synopsis. *p*-Chlorobenzaldehyde isonicotinoylhydrazone (*p*-Cl-BAINH) exibits a single wave in acid buffered solutions (pH 2—6) and two waves in alkaline buffered solutions (pH 7—9). However, the compound exhibits three cathodic peaks in acid solution and two cathodic peaks in alkaline solutions. The electrode reactions are attributed to the reductive cleavage of =N-N- linkage and the reduction of the amide formed in the cleavage.

Isonicotinohydrazide derivatives of carbonyl compounds are used extensively as theraptic agents.[1-4] *p*-Chlorobenzaldehyde isonicotinoylhydrazone (*p*-Cl-BAINH) with the following structure

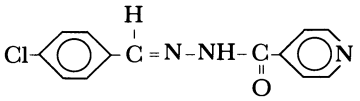

p-Cl-BAINH

is one of such compounds. This compound offers interesting features for electrochemical reduction studies since it possesses more than one reducible sites in its molecule. The authors have therefore undertaken polarographic and cyclic voltammetric studies in solutions of pH 2 to 9. The results are communicated here.

Experimental

p-Cl-BAINH was prepared by refluxing a mixture (1 : 1) of *p*-chlorobenzaldehyde and isonicotinohydrazide for 2 h. The product was purified by repeated recrystallization from hot aqueous ethanol. The compound was characterized by infrared spectral data and melting point (measured value 217 °C, lit, 217—218 °C). All the other chemicals used in the investigations were of analytical reagent grade.

Current-voltage curves were recorded in Britton-Robinson buffers (pH 2—9) with a DC pen recording polarograph (CL 25, ELICO, India). The dropping mercury electrode had the following characteristics: t=3.0 s, m=1.93 mg s^{-1} at a height of 85 cm of mercury column in water under open circuit conditions. Cyclic voltammograms were recorded with a polarographic analyzer (model 174 A, Applied Research Company of Princeton, USA) coupled with an X-Y recorder (model RE 0074) and universal programmer (model 175). Hanging mercury drop electrode (HMDE, Metrohm model 9323), platinum wire electrode and SCE were used as working electrode, counter electrode, and reference electrode respectively. The results are presented in Tables 1 and 2.

Results and Discussion

Electrochemical Reduction in Acid Solutions. *p*-Cl-BAINH exhibits a single polarographic wave in acid solutions (pH 2—6). Semi-logarithemic analysis of the wave reveals that the wave is irreversible. The limiting current varied linearly with the concentration of the hydrazone and with the square root of the mercury column height indicating that the wave is diffusion-controlled. Half-wave potential shifts towards more negative values with increase in pH. This indicates that protons are taking part in the reduction process.

Table 1. Polarographic Reduction Waves of *p*-Cl-BAINH (4×10^{-4} M[a])in 20% Aqueous *N*,*N*-Dimethylformamide

pH	$-E_{1/2}$/V vs. SCE	
	First wave	Second wave
2.0	0.78	—
3.0	0.87	—
4.0	0.89	—
5.0	0.97	—
6.0	1.03	—
7.0	1.08	1.25
8.0	1.14	1.28
9.0	1.18	1.29

a) 1 M=1 mol dm^{-3}.

Table 2. Cyclic Voltammetric Peak Potentials of *p*-Cl-BAINH (4×10^{-4} M) in 20% Aqueous *N*,*N*-Dimethylformamide.

Sweep rate / V s^{-1}	$-E_{pc}$ I/V	$-E_{pc}$ II/V	$-E_{pc}$ III/V
	pH 4.0		
0.020	0.84	0.89	0.95
0.050	0.85	0.91	0.96
0.100	0.86	0.92	0.97
	pH 8.0		
0.020	1.15	1.28	—
0.050	1.16	1.30	—
0.100	1.17	1.31	—

The cyclic voltammogram of the hydrazone shows three cathodic peaks in acid solutions in the forward scan. In the reverse scan, no peak is observed. This indicates the irreversible nature of the electrode process. This is also confirmed by the negative shift in the peak potentials with increasing sweep rates.

The total number of electrons involved in the polarographic process is established experimentally to be 8. On the basis of the three peaks observed in cyclic voltammogram and the number of electrons involved in the single reduction wave noticed and on the basis of the reported behavior in the literature[5] of semicarbazones (compounds bearing structural relationship with the present hydrazone) it is proposed that the single polarographic wave observed is a composite wave representing the reductive cleavage of =N-N-

linkage and the reduction of the imine and the amide formed in the cleavage. The appearance of a single wave suggests that these reduction steps take place at potentials very close to each other. This is clear from the almost same potentials of the peaks in the cyclic voltammogram. Bulk electrolysis and subsequent chemical identification of the products in acid solutions revealed the presence of amine and alcohol. The electrolysis was carried out in solutions of pH 4 at an applied voltage of −1.2 V vs. SCE with mercury pool as cathode. The catholyte after electrolysis was concentrated and extracted with ether. The extract responded to the tests for the primary amine (diazotization and coupling with 2-naphthol) and for the primary alcohol (oxidation and condensation with 2,4-dinitrophenylhydrazine).

E_1 *p*-Cl-BAINH $+ 2H^+ + 2e \rightarrow$

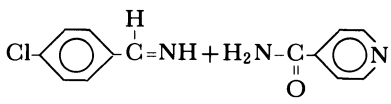

Peak 1

E_2

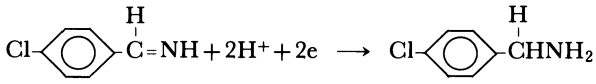

Peak 2

E_3

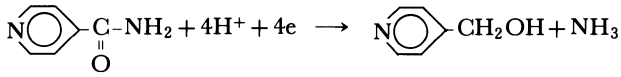

Peak 3

$E_1 \approx E_2 \approx E_3$ in acidic solutions
E_1, E_3 in alkaline solutions
(E: Half-wave potential).

Electrochemical Reduction in Alkaline Solutions. *p*-Cl-BAINH exhibits two polarographic waves in alkaline solutions. The effect of mercury column height and concentration on the wave height suggests that the waves are diffusion-controlled. The wave is found irreversible by the semi-logarithemic analysis.

The cyclic voltammogram of the compound exhibits two cathodic peaks in the forward scan. In the reverse scan, no peak is observed. This fact indicates the irreversible nature of the electrode process. This is also confirmed by the negative shift in the peak potentials with increasing sweep rates.

It was reported that semicarbazones undergo reductive cleavage of =N-N- linkage and the imine formed in the cleavage is resistant to further reduction.[6] Imine undergoes reduction only in the protonated form. The absence of imine reduction in alkaline solution can therefore be attributed to the significant decrease in the recombination rate. It was reported that amides undergo reduction to the corresponding alcohols.[7] Bulk electrolysis and subsequent identification reveal the formation of alcohol as well as the aldehyde in alkaline solutions. The aldehyde, formed is attributed to the decomposition of Ar-CH=NH to Ar-CHO in alkaline solution. The two waves appeared therefore indicate the =N-N- cleavage (first wave) and the amide reduction (second wave), respectively. The reduction of the amide being made difficult in alkaline solutions is understood since protonated amide alone is susceptible to reduction. The appearence of two peaks with potentials similar to the half-wave potentials supports the mechanism proposed.

One of the authors (PRR) is thankful to the authorities of Sri Krishnadevaraya University, Anantapur for providing the necessary facilities.

References

1) L. Monti and G. Simonett, *Chim. Ital.*, **70**, 369 (1940).
2) R. Walker, *Food Cosmet. Toxicol.*, **8**, 659 (1970).
3) H. G. Garg and P. P. Singh, *J. Med. Chem.*, **13**, 1250 (1970).
4) E. J. Modest, H. N. Scheein, and G. E. Foley, *J. Pharmacol.*, **9**, 68 (1957).
5) P. Zuman, "Topics in Organic Polarography," Plenum Press, London-New York (1970). p. 384.
6) H. Lund, *Acta Chem. Scand.*, **13**, 249 (1959); H. Lund, *Discuss. Faraday Soc.*, **45**, 193 (1968); H. Lund and E. T. Tensen, *Acta Chem. Scand.*, **25**, 2727 (1971); H. Lund, *Electrochim. Acta*, **28**, 395 (1983); H. Lund. "Chemistry of Carbon Nitrogen Double Bond," ed by S. Patai, Wiley, New York (1970), pp. 543—550.
7) H. Lund, *Acta Chem. Scand.*, **17**, 2325 (1963); T. Nonaka, T. kato, and T. Fuchigami, *Electrochim. Acta*, **26**, 887 (1981) and lits. cited therein.

Temperaturabhängigkeit der Fluoreszenz von Gd^{3+} in Wässriger Lösung

Markus BAUMANN
Alvenslebenstr. 20, D-1000 Berlin 30, B. R. D.
(Received December 8, 1986)

Synopsis. The effects of pressure and temperature on the fluorescence of aqueous Gd^{3+} solution have been studied, the following results being obtained: (a) The pressure up to 100 MPa gives no influence on emission. (b) The fluorescence diminishes with temperature rise, nearly disappearing at 200 °C.

Die Temperaturabhängigkeit der Fluoreszenzeigenschaften wässriger Lanthanoidlösungen ist Gegenstand mehrerer Untersuchungen.[1-6] In den Arbeiten sind Unterschiede in der Temperaturabhängigkeit der Fluoreszenz wässriger Lanthanoidlösungen (zum Teil) bis zu 98 °C aufgezeigt und diskutiert. Eine Literaturrecherche in den Chemical Abstracts, Publikationen bis 1985 umfassend, ergab keine Anhaltspunkte, daß der Meßbereich erweitert wurde. Der Grund liegt wahrscheinlich in den bis zu dieser Temperatur apparativ leicht zugänglichen Versuchsbedingungen.

In dieser Arbeit wird untersucht, wie sich die Fluoreszenzemission des Gadoliniumions in heißer wässriger Lösung bei Temperaturen bis zu 200 °C verhält. Für die in-situ-Analytik hydrothermaler (geochemisch relevanter) Lanthanoidlösungen mittels fluorimetrischer Methoden erweist sich die Kenntnis über das Ausmaß des Fluoreszenzquenching, verursacht durch die Temperatur der Lösung, als unerläßlich.

Ergebnisse und Diskussion

In einer Hochdrucksichtzelle wurde bei Temperaturen bis zu 200 °C und einem Druck von 100 MPa die Fluoreszenzemission von wässrigen Gadolinium(III)-Lösungen vermessen. Die Lösungen wurden zunächst mit dem Druck von 100 MPa beaufschlagt und auf Änderungen der Emissionseigenschaften hin untersucht, anschließend bei konstant gehaltenem Druck bis auf 200 °C erhitzt.

Es wurde gefunden, daß ein Druck von 100 MPa ohne Einfluß auf die Fluoreszenzeigenschaften ist. Einzuschränken ist, daß ungünstige optische Bedingungen, durch die Hochdruckanordnung verursacht, es nicht zuließen, Intensitätsänderungen von weniger als 5% als signifikant anzusehen.

Bewirkt eine hohe Druckbelastung keine Beeinträchtigung der Fluoreszenz, so führt jedoch eine Temperaturerhöhung zu einer erheblichen Verminderung der Emission. Bei 100 °C können nur noch 45% des Ausgangswertes unter Normalbedingungen, bei 200 °C 10% der ursprünglichen Intensität gemessen werden (siehe auch Abb. 1).

Eine Aussage über die unterschiedliche Beeinflussung der übergänge $^6P_{5/2}$-$^8S_{7/2}$ (306 nm) und $^6P_{7/2}$-$^8S_{7/2}$ (312 nm) war nicht möglich. Die zur Unterscheidung dieser Banden erforderliche optische Auflösung konnte, wegen der geringen Intensitäten bei höher Temperatur, nicht vorgenommen werden.

Das aufgezeigte Fluoreszenzverhalten des Gadoliniumions unterscheidet sich erheblich von den unter vergleichbaren Bedingungen gemessenen Terbium(III)- und Samarium(III)-Lösungen.[2,8] Bei diesen Lanthanoiden bringt eine Temperaturerhöhung auch bis zu 200 °C keine Verminderung der Fluoreszenz. Diese Untersuchungsergebnisse unterstreichen die Bedeutung des energetischen Abstandes zwischen den beiden ersten Fluoreszenzniveaus der Seltenen Erden für temperaturbedingtes Fluoreszenzquenching.[1-6]

Abschließend sei erwähnt, daß auch ein (für die Analytik oft unvorteilhaftes) Fluoreszenzquenching einer praktischen Nutzung zugeführt werden kann, und zwar in der Verwendung der Temperaturabhängigkeit der Fluoreszenz als Temperatursensor.[9]

Experimentelles

Meßlösungen. Die untersuchten Lösungen waren 0,01 molar an Gd^{3+}, 1 M an NaCl sowie 1 M an HCl (1 M=1 mol dm^{-3}).

Probenbehälter. Während der Messung befand sich die Lösung in einem Probenbehälter bestehend aus den Materialien Saphir und PTFE. Zur Temperatur- und Druckbeaufschlagung wurde diese Probekammer in eine mit Saphirfenstern ausgestattete Hochdrucksichtzelle gestellt. Der Stahlkörper dieses Druckbehälters (ohne Saphirfenster)

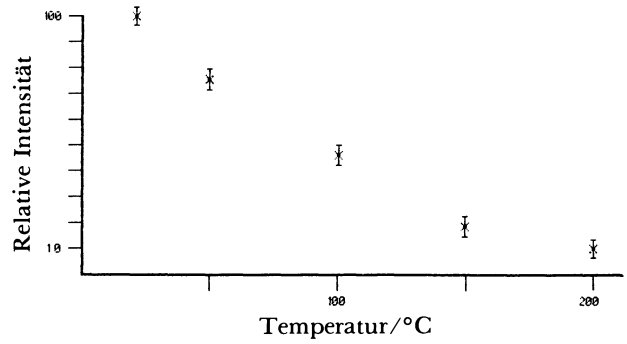

Abb. 1. Fluoreszenintensität in Abhängigkeit von der Temperatur in System: Gd^{3+} 0.01 M, HCl 1 M, NaCl 1 M; Druckbelastung 100 (±3) MPa bei allen Temperaturen.

*Die Durchsicht der Literatur sowie eigene Erfahrungen im Umgang mit heißen wässrigen Lanthanoidlösungen veranlassen dazu anzumerken, daß bei fluorimetrischen Untersuchungen an solchen Lösungen der Bildung von Hydrolyseprodukten vermehrte Beachtung geschenkt werden muß. Ein bei Normaltemperatur sonst unkritischer pH-Wert um 5 führt auch bei wenig erhöhter Temperatur zur teilweisen Hydrolyse des Lanthanoidions, wobei die Fluoreszenzeigenschaften, d.h. Intensität und Lebensdauer der Fluoreszenz der betreffenden Lanthanoidspezies, vergleichsweise zu der des Aqua-Ions, verschlechtert werden können. Neben dem pH-Wert ist auch die Standzeit der Lösung bei der betreffenden Untersuchungstemperatur von Bedeutung.

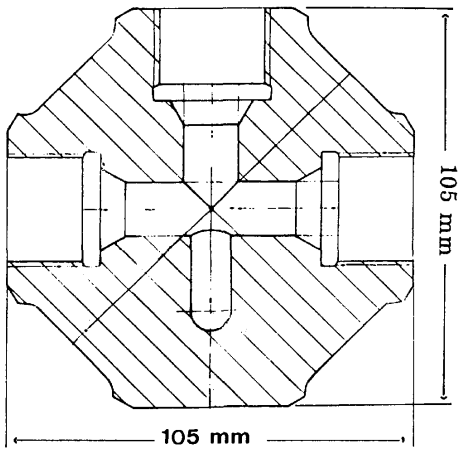

Abb. 2. Autoklavenkörper zur Druck- und Temperaturbeaufschlagung mit den Maßen: 105 mm (Höhe), 70 mm (Breite).

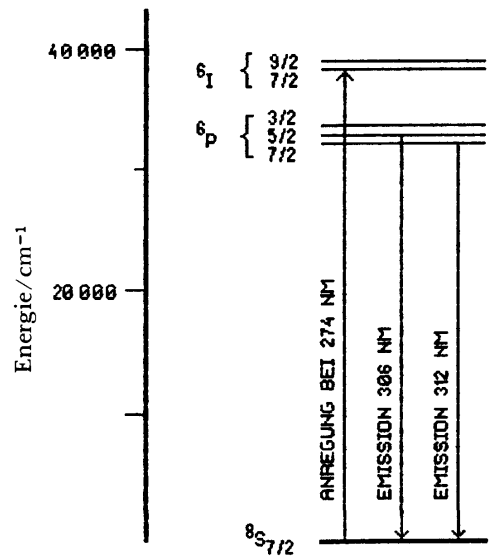

Abb. 3. Partielles Termschema von Gd^{3+}; Energiewerte aus CARNALL et al. (1968).[7]

ist in Abb. 2 widergegeben. In den Stahlkörper sind neben den Öffnungen für die optischen Fenster jeweils noch eine Bohrung zur Druckübertragung und zur Temperaturmessung eingelassen (nicht aus der Zeichnung ersichtlich). Zur Druckerzeugung diente ein Kompressor mit Argon als Druckmedium. Eine geregelte Widerstandsheizung (Heizdrähte in einen dem Stahlkörper angepaßten Kupfermantel eingebettet) sorgte für die Temperierung. Es sei noch angemerkt, daß eine Berechnung der maximalen Druckbelastung bei dem aufgezeigten Zellentyp schwierig ist. Es empfiehlt sich bei sehr hohen Drücken eine zylindrische Form für den Autoklavenkörper zu wähen.

Optische Auswertung. Die optische Verbindung zwischen Sichtzelle und Spektrometer erfolgte mit Quarzlichtleitern, da aus Sicherheitsgründen die Zelle in einem Stahlbehältnis untergebracht war. Die Messung der Fluoreszenzemission erfolgte mit einem Fluoreszenzspektrometer der Fa. SPEX, USA (Modell: Fluorolog II) bei einer Anregungswellenlänge von 274 nm. Zur Auswertung kam die Emission bei 312 nm, siehe auch partielles Termschema des Gd^{3+} in Abb. 3 .

Die vorliegende Arbeit beruht auf experimentellen Ergebnissen des Verfassers während seines Aufenthaltes am Hahn-Meitner-Institut für Kernforschung GmbH, Berlin. Die Hochdrucksichtzelle ist eine Konstruktion von A. Truong, Hahn-Meitner-Institut für Kernforschung GmbH, Berlin.

Literaturen

1) J. L. Kropp und W. R. Dawson, *J. Chem. Phys.*, **45**, 2419 (1966).
2) M. Baumann und B. A. Bilal, *Z. Naturforsch.*, **41a**, 974 (1986).
3) Y. Haas, G. Stein, und E. Würzberg, *J. Chem. Phys.*, **58**, 2777 (1973),
4) Y. Haas, G. Stein, und E. Würzberg, *J. Chem. Phys.*, **60**, 258 (1974)
5) G.Stein und E. Würzberg, *J. Chem. Phys.*, **62**, 208 (1975).
6) V. S. Tachin, V L. Ermolaev, und E. N. Bodunov, *Zhur. Neog. Khim.*, **20**, 189 (1975)
7) W. T. Carnall, P. R. Fields, und K. Rajnak *J. Chem. Phys.*, **49**, 4443 (1968).
8) M. Baumann, unveröffentlichte Messungen in Hahn-Meitner-Institut für Kernforschung GmbH, Berlin (1984).
9) M. Baumann, D. B. P., 3600660 (1986).

Halogenation Using Quaternary Ammonium Polyhalides. IX.[1] One-Step Syntheses of Acylureas and Carbamates from Amides by Use of Tetrabutylammonium Tribromide and DBU

Shizuo FUJISAKI, Kazushi TOMIYASU, Akiko NISHIDA, and Shoji KAJIGAESHI*
Department of Industrial Chemistry, Faculty of Engineering, Yamaguchi University, Tokiwadai, Ube 755
(Received June 15, 1987)

Synopsis. The reaction of amides with tetrabutylammonium tribromide (TBA Br_3) (0.5 equiv) and DBU (one equiv) in dichloromethane at room temperature gave *N*-substituted acylureas in fairly good yields. In the presence of alcohols, the reaction of amides with TBA Br_3 (one equiv) and DBU (two equiv) gave *N*-substituted carbamates.

Tetraalkylammonium polyhalides have recently been reported to act as useful, selective halogenating reagents.[2] In this paper, we wish to report on a one-step synthesis of *N*-substituted acylureas and carbamates from amides by the use of tetrabutylammonium tribromide[2a] (TBA Br_3) in the presence of a base, 1,8-diazabicyclo[5.4.0]undec-7-ene (DBU).

Results and Discussion

Recently, it has been noted that acylureas reveal the physiological actitivities of insects. That is, derivatives of *N*-benzoyl-*N'*-phenylurea are known to inhibit a formation of the epidermis of insects during their ecdyses.[3]

Rand et al. have already reported that a treatment of *N*-chlorobenzamide with potassium fluoride gave *N*-benzoyl-*N'*-phenylurea. In this case, they showed that an initial proton abstraction by the fluoride followed by a Hofmann-type rearrangement gave intermadiate phenyl isocyanate; then, the addition of residual *N*-chlorobenzamide to the isocyanate with a subsequent hydrolysis yielded the product.[4]

$$\text{Ph-CONH-Cl} \xrightarrow[\text{benzene}]{\text{KF}} [\text{Ph-N=C=O}] \xrightarrow{\text{PhCONHCl}}$$

$$\text{Ph-NH-CO-N(Cl)-COPh} \xrightarrow{H_2O} \text{PhNHCON(H)-COPh} \quad (1)$$

The reaction of amides with TBA Br_3 (half equiv) and DBU (one equiv) in commercially available dichloromethane (contained a catalytic amount of methanol) gave *N*-substituted acylureas in fairly good yields. In these cases, isocyanates should also be produced as reaction intermadiates. Since the presence of methanol considerably promotes the reaction,[5] it is assumed that the main active species is probably methyl hypobromite produced from the reaction of TBA Br_3 with methanol.[2b] Therefore, the reaction which affords acylureas can be presented in the following equations:

$$(C_4H_9)_4NBr_3 + CH_3OH + DBU \rightarrow CH_3OBr + (C_4H_9)_4N^+Br^- + DBU(HBr), \quad (2)$$

$$\underset{\mathbf{1}}{RCONH_2} + CH_3OBr \rightarrow \underset{\mathbf{2}}{RCONH\text{-}Br} + CH_3OH, \quad (3)$$

$$\mathbf{2} + DBU \rightarrow \underset{\mathbf{3}}{R\text{-}N=C=O} + DBU(HBr), \quad (4)$$

$$\mathbf{3} + \mathbf{2} \rightarrow \underset{\mathbf{4}}{RNHCON(Br)\text{-}COR}, \quad (5)$$

and

$$\mathbf{4} + \mathbf{1} \rightarrow \underset{\mathbf{5}}{RNHCONH\text{-}COR} + \mathbf{2}. \quad (6)$$

Equation 7 can be derived from Eqs. 2—6.

$$2\underset{\mathbf{1}}{RCONH_2} + (C_4H_9)_4NBr_3 + 2DBU \rightarrow \underset{\mathbf{5}}{RNHCONHCOR} + 2DBU(HBr) + (C_4H_9)_4NBr. \quad (7)$$

Table 1. Acylureas from Amides by Use of TBA Br_3 and DBU

$$\underset{\mathbf{1}}{2R\text{-}CONH_2} \xrightarrow[CH_2Cl_2{}^{a)}\ rt]{(C_4H_9)_4N^+Br_3^-,\ DBU} \underset{\mathbf{5}}{R\text{-}NHCONHCO\text{-}R}$$

	R	Reaction time/h	Yield[b] %	Mp θ_m/°C Found	Mp θ_m/°C Reported
a		0.5	70	206—207	206—208[4]
b	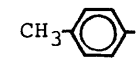	0.5	73	230—232	216.2—219.8[8]
c		0.5	77	213—215	—
d	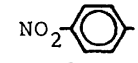	0.5	70	261—263	—
e		0.5	65	208—211	—
f	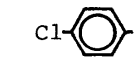	0.5	87	253—254	—
g		1.0	93	211—212	—
h		1.0	50	214—216	—
i	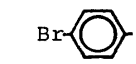	1.0	50	264—266	—
j	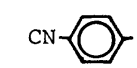	1.0	83	270—273	—
k	CH_3CH_2-	0.5	87	100—102	—
l	$CH_3(CH_2)_4$-	0.5	45	99—101	—

a) Commercially available dichloromethane (containing methanol (0.5 vol%) as a stabilizer) was used. b) Yield of isolated product.

Table 2. Carbamates from Amides by Use of TBA Br_3 and DBU

$$\text{R-CONH}_2 \xrightarrow[\text{CH}_2\text{Cl}_2{}^{a)}\ \text{rt}]{(C_4H_9)_4N^+Br_3^-,\ \text{DBU},\ \text{R'-OH}} \text{R-NHCO}_2\text{-R'}$$

1 7

	R	R'	Reaction time/h	Yield[b] %	Mp θ_m/°C Found	Mp θ_m/°C Reported
a		CH_3-	1.0	65	47—48.5	48[9]
b		CH_3CH_2-	1.5	69	49—50.5	51[10]
c		$CH_3CH_2CH_2$-	1.5	80	54—55	57—59[11]
d		$CH_3(CH_2)_3$-	1.5	77	62	65.5[12]
e		CH_3-	1.5	97	61—62	60—61[13]
f	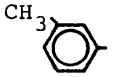	CH_3-	1.5	88	70—72	67.5—69[13]
g	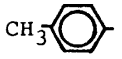	CH_3-	1.5	79	99—101	98.5—99.5[13]
h	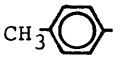	CH_3CH_2-	1.5	78	49—51	51—52[13]
i		CH_3-	1.5	76	115—117	115[14]
j	CH_3CH_2-	CH_3CH_2-	1.5	54	Bp 174—176	Bp 175[15]

a) Purified dichloromethane was used. b) Yield of isolated product.

The results are summarized in Table 1.

In the presence of a large excess of alcohols (≫20 equiv), the reaction of amides with TBA Br_3 (one equiv) and DBU (two equiv) in dichloromethane gave carbamates as main products.[6] That is, as shown in the following Eq. 8, intermediary isocyanates react with alcohols to afford carbamates:[7]

$$\underset{\mathbf{3}}{\text{R-N=C=O}} + \underset{\mathbf{6}}{\text{R'-OH}} \rightarrow \underset{\mathbf{7}}{\text{RNH-CO}_2\text{R'}}. \quad (8)$$

Equation 9 can be obtained from Eqs. 2—4 and 8.

$$\underset{\mathbf{1}}{\text{RCONH}_2} + (C_4H_9)_4NBr_3 + \underset{\mathbf{6}}{\text{R'OH}} + 2\text{DBU} \rightarrow \underset{\mathbf{7}}{\text{RNHCO}_2\text{R'}} + (C_4H_9)_4NBr + 2\text{DBU(HBr)}. \quad (9)$$

The results are summarized in Table 2.

These methods would be useful in the preparation of **5** or **7** from the readily available starting materials **1** and TBA Br_3 by one-step under mild conditions.

Experimental

All melting points are uncorrected. The ^{1}H NMR spectra were recorded on a JMN-MH-100 spectrometer with tetramethylsilane as an internal standard. The IR spectra were obtained on a JASCO IRA-1 spectrometer.

***N*-Benzoyl-*N'*-phenylurea (5a). Typical Procedure.** To a solution of benzamide (0.48 g, 4.0 mmol) and TBA Br_3 (1.00 g, 2.07 mmol) in commercially available dichloromethane (contained a catalytic amount of methanol) (20 ml) was added DBU (0.64 g, 4.2 mmol) in dichloromethane (5 ml) at room temperature. After the mixture was stirred for 30 min the solvent was distilled in vacuo. To the residue was added a small amount of ether and water; then the precipitate obtained was filtered and washed with ether and water to give **5a** as colorless crystals; yield 0.33 g (70%); mp 206—207 °C (lit,[3] mp 206—208 °C).

***N*-(2-Nitrobenzoyl)-*N'*-(2-nitrophenyl)urea (5c).** Compound **5c** was prepared similarly: Yield 77%; pale yellow crystals; mp 213—215 °C; IR (KBr) 3210 (ArN-H), 3100 (N-H), 1700 (ArC=O), and 1680 cm^{-1} (C=O); ^{1}H NMR (DMSO-d_6) δ=7.38—8.68 (8H, m, 2Aromatics), and 11.60—12.00 (2H, m, 2NH). Found: C, 50.66; H, 3.25; N, 17.06%. Calcd for $C_{14}H_{10}O_6N_4$: C, 50.91; H, 3.05; N 16.97%.

***N*-(4-Nitrobenzoyl)-*N'*-(4-nitrophenyl)urea (5d).** Yield 70%; pale yellow crystals; mp 261—263 °C; IR (KBr) 3220 (ArN-H), 3100 (N-H), 1690 (ArC=O), and 1670 cm^{-1} (C=O). Found: C, 50.68; H, 3.20; N, 16.90%. Calcd for $C_{14}H_{10}O_6N_4$: C, 50.91; H, 3.05; N, 16.97%.

***N*-(3-Chlorobenzoyl)-*N'*-(3-chlorophenyl)urea (5e).** Yield 65%; colorless crystals; mp 208—211 °C; IR (KBr) 3200 (ArN-H), 3110 (N-H), 1700 (ArC=O), and 1660 cm^{-1} (C=O); ^{1}H NMR (DMSO-d_6) δ=7.20—8.27 (8H, m, 2Aromatics), 10.88 (1H, br.s, Ar-NH-), and 11.28 (1H, br.s, -NH-). Found: C, 54.52; H, 3.38; N, 9.15%. Calcd for $C_{14}H_{10}O_2N_2Cl_2$: C, 54.39;

H, 3.26; N, 9.06%.

***N*-(4-Chlorobenzoyl)-*N'*-(4-chlorophenyl)urea (5f).** Yield 87%; colorless crystals; mp 253—254 °C; IR (KBr) 3100 (N-H), 1680 (ArC=O), and 1650 cm^{-1} (C=O); ^1H NMR (DMSO-d_6) δ=7.40—8.18 (8H, m, 2Aromatics), 10.90 (1H, br.s, ArNH-), and 11.23 (1H, br.s, -NH-). Found: C, 54.35; H, 3.35; N, 9.06%. Calcd for $C_{14}H_{10}O_2N_2Cl_2$: C, 54.39; H, 3.26; N, 9.06%.

***N*-(2-Bromobenzoyl)-*N'*-(2-bromophenyl)urea (5g).** Yield 93%; colorless crystals; mp 211—212 °C; IR (KBr) 3230 (ArN-H), 3130 (N-H), and 1710 cm^{-1} (C=O); ^1H NMR (DMSO-d_6) δ=6.92—8.40 (8H, m, 2Aromatics), 10.93 (1H, br.s, ArNH-), and 11.42 (1H, br.s, -NH-). Found: C, 42.15; H, 2.45; N, 7.12%. Calcd for $C_{14}H_{10}O_2N_2Br_2$: C, 42.24; H, 2.53; N, 7.04%.

***N*-(3-Bromobenzoyl)-*N'*-(3-bromophenyl)urea (5h).** Yield 50%; colorless crystals; mp 214—216 °C; IR (KBr) 3220 (ArN-H), 3140 (N-H), and 1720 cm^{-1} (C=O); ^1H NMR (DMSO-d_6) δ=7.36—8.44 (8H, m, 2Aromatics), 10.87 (1H, br.s, ArNH-), and 11.28 (1H, br.s, -NH-). Found: C, 42.03; H, 2.43; N, 7.12%. Calcd for $C_{14}H_{10}O_2N_2Br_2$: C, 42.24; H, 2.53; N, 7.04%.

***N*-(4-Bromobenzoyl)-*N'*-(4-bromophenyl)urea (5i).** Yield 50%; colorless crystals; mp 264—266 °C; IR (KBr) 3200 (ArN-H), 3120 (N-H), 1700 (PhC=O), and 1660 cm^{-1} (C=O); ^1H NMR (DMSO-d_6) δ=7.68—8.10 (8H, m, 2Aromatics), 10.90 (1H, br.s, ArNH-), and 11.26 (1H, br.s, -NH-). Found: C, 42.07; H, 2.45; N, 7.15%. Calcd for $C_{14}H_{10}O_2N_2Br_2$: C, 42.24; H, 2.53; N, 7.04%.

***N*-(4-Cyanobenzoyl)-*N'*-(4-cyanophenyl)urea (5j).** Yield 83%; colorless crystals; mp 270—273 °C; IR (KBr) 3200 (ArN-H), 2200 (C=N), 1680 (PhC=O), and 1660 cm^{-1} (C=O); ^1H NMR (CF_3CO_2H) δ=7.92—8.34 (8H, m, 2Aromatics). Found: C, 65.87; H, 3.65; N, 19.48%. Calcd for $C_{16}H_{10}O_2N_4$: C, 66.20; H, 3.47; N, 19.30%.

***N*-Ethyl-*N'*-propionylurea (5k).** Yield 87%; colorless crystals; mp 100—102 °C; IR (KBr) 3200 (N-H), and 1680 cm^{-1} (C=O); ^1H NMR ($CDCl_3$) δ=1.10—1.34 (6H, m, $2CH_3$), 2.44 (2H, q, $COCH_2$-), 3.40 (2H, m, -$NHCH_2$-), 8.58 (1H, br.s, CH_2NHCO), and 9.92 (1H, br.s, CONHCO). Found: C, 49.99; H, 8.37; N, 19.49%. Calcd for $C_6H_{12}O_2N_2$: C, 49.98; H, 8.36; N, 19.43%.

***N*-Hexanoyl-*N'*-pentylurea (5l).** Yield 45%; colorless crystals, mp 99—101 °C; IR (KBr) 3200 (N-H), and 1660 cm^{-1} (C=O); ^1H NMR ($CDCl_3$) δ=0.80—1.10 (6H, m, $2CH_3$), 1.28—2.00 (12H, m, $2(CH_2)_3$), 2.40 (2H, br.t, $COCH_2$), 3.38 (2H, m, $NHCH_2$-), 8.68 (1H, br.s, -CH_2NHCO), and 9.94 (1H, br.s, CONHCO). Found: C, 62.97; H, 10.72; N, 12.41%. Calcd for $C_{12}H_{24}O_2N_2$: C, 63.12; H, 10.60; N, 12.27%.

Methyl Phenylcarbamate (7a). Typical Procedure. To a solution of benzamide (0.61 g, 5.0 mmol) and TBA Br_3 (2.50 g, 5.18 mmol) in dichloromethane (15 ml)-methanol (40 ml, 1 mol) was added DBU (1.70 g, 11.2 mmol) in dichloromethane (5 ml) at room temperature. After the mixture was stirred for 1 h the solvent was distilled in vacuo and the obtained precipitate was extracted with ether. The ether layer was dried with magnesium sulfate and evaporated. A crude product was purified by column chromatography on silica gel (3:1 hexane-benzene) to afford **7a** as colorless crystals; yield 0.49 g (65%); mp 47—48.5 °C (lit,[9] mp 48 °C).

The authors wish to thank Professor Masashi Tashiro, Institute of Advanced Material Study, Kyushu University, for the elemental analyses.

References

1) Part VIII of this series: S. Kajigaeshi, T. Kakinami, M. Moriwaki, S. Fujisaki, and T. Okamoto, *Tech. Rep. Yamaguchi Univ.*, **4**, 65 (1987).

2) a) S. Kajigaeshi, T. Kakinami, T. Okamoto, and S. Fujisaki, *Bull. Chem. Soc. Jpn.*, **60**, 1159 (1987); b) S. Kajigaeshi, T. Kakinami, H. Tokiyama, T. Hirakawa, and T. Okamoto, *Chem. Lett.*, **1987**, 627; c) S. Kajigaeshi, T. Kakinami, H. Tokiyama, T. Hirakawa, and T. Okamoto, *Bull. Chem. Soc. Jpn.*, **60**, 2667 (1987).

3) J. J. van Daalen, J. Meltzer, R. Mulder, and K. Wellinga, *Naturwissenschaften*, **56**, 132 (1972).

4) L. Rand and R. J. Dolinski, *J. Org. Chem.*, **30**, 48 (1965).

5) In the case of the absence of methanol, the reaction of benzamide (**1a**) with half equiv of TBA Br_3 and one equiv of DBU in dichloromethane for 0.5 h at room temperature gave **5a** in only 35% yield.

6) When about 10—15 equiv of methanol was previously added to the reaction mixtures, the resultant acylureas were obtained in equally good yields. In these cases, methyl carbamates expected were hardly obtained.

7) J. March, "Advanced Organic Chemistry: Reactions, Mechanisms, and Structure," McGraw-Hill, New York (1968), p. 663.

8) S. Nagai, N. Goto, and T. Ueno, *Kogyo Kagaku Zasshi*, **69**, 1561 (1966).

9) J. W. Backer and J. B. Holdsworth, *J. Chem. Soc.*, **1947**, 713.

10) D. Pharmazent, *Ber.*, **71**, 1797 (1938).

11) H. Roemer, *Ber.*, **6**, 1011 (1873).

12) F. D. Chattaway and E. Saerens, *J. Chem. Soc.*, **117**, 708 (1920).

13) S. Shulman and J. A. Griepentrog, *Microchem. J.*, **6**, 179 (1962).

14) W. Siefken, *Liebigs Ann. Chem.*, **562**, 75 (1949).

15) M. Barker, L. Hunter, and N. G. Rrynolds, *J. Chem. Soc.*, **1948**, 874.

Effects of Aryl Substituents on Electron-Transfer-Mediated Photochemical Addition of Alcohol to 1,1,2-Triarylcyclopropanes

Hideo TOMIOKA* and Osamu INOUE
Department of Industrial Chemistry, Faculty of Engineering, Mie University, Tsu, Mie 514
(Received July 16, 1987)

Synopsis. Direct irradiation of 1,1,2-triarylcyclopropanes in alcohol resulted in the formation of all possible products arising from trimethylene biradicals, while DCB-sensitized irradiation gave a novel "anti-Markownikoff" addition product of alcohol almost exclusively. In order to get insight into the nature and fate of intermediates in the reactions, the effects of nucelophiles and aryl substituents are examined.

Since the early 1980s the scope of cyclopropane photochemistry[1] was greatly broadened through electron transfer sensitized reaction. Among the important features of electron-transfer sensitization are higher reactivity and anomalous but simpler product distributions.[2] Thus, Hixson et al.[3] found that 1,4-dicyanobenzene (DCB)-sensitized photolysis of several phenylcyclopropanes in methanol-acetonitrile resulted in a novel "anti-Markownikoff" addition of methanol to the cyclopropane ring. The reactions are rationalized as proceeding via initial electron transfer from the cyclopropane to the excited DCB to give the cyclopropane cation radicals.

As a part of our program of work on the photochemical generation of ionic intermediates,[4] we became interested in the nature of intermediates that are involved in the electron-transfer-sensitized reaction of cyclopropanes. Thus, we have irradiated several 1,1,2-triarylcyclopropanes in the presence of sensitizers (electron acceptors) in alcohols and examined the effects of nucleophiles and aryl substituents on the product distributions.

Results and Discussion

Irradiation of 1,1,2-triphenylcyclopropane (**1c**) in ethanol-acetonitrile with a light of 300W Hg lamp through quartz was monitored by GC which revealed the gradual disappearance of the starting cyclopropane along with the formation of at least five products. Separation followed by characterization of each components demonstrated that these products are diphenylethoxymethane (**2c**, R=Et), 1,1,3-triphenylpropene (**3c**), 1,1,3-triphenylpropane (**4c**), 1,1,3-triphenyl-1-ethoxypropane (**5c**, R=Et), and 1,1,3-triphenyl-3-ethoxypropane (**6c**, R=Et), all of which are the most commonly observed photoproducts of arylcyclopropanes in alcohols as a result of ring opening.[5] In a marked contrast, similar irradiation of **1** in the presence of *p*-dicyanobenzene (DCB) resulted in a rapid disappearance of **1c** and concurrent appearance of single major product which was assigned as polar addition product **6c** (R=Et) of the OH bond across the ring in "anti-Markownikoff" fashion.

Similar marked enhancement of photoreactivity of the triphenylcyclopropane caused by DCB was also observed when other alcohols are employed as a trapping reagent although yield of anti-Markownikoff addition product decreased in *t*-butyl alcohol (Table 1). In 2,2,2-trifluoroethanol (TFE), **1c** was equally rapidly photolyzed in the presence of DCB, but the addition product was formed in only 12% yield. This

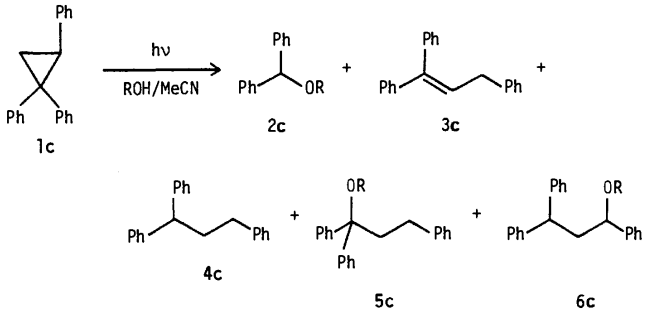

Table 1. Irradiation of **1c** in Various Alcohols[a]

ROH	Condition[b]	Irradiation time/h	Conversion %	Yield/%[c] 2c	3c	4c	5c	6c
MeOH	D	16	68.7	15.8	28.2	<1	<1	<1
	S	2	98.1	5.3	0	0	0	75.0
EtOH	D	16	75.9	15.9	4.6	<1	5.6	3.1
	S	2	95.2	4.3	0	0	0	85.3
^{i}PrOH	D	16	65.0	18.4	26.1	<1	0	0
	S	2	96.8	3.2	0	0	0	87.2
^{t}BuOH	D	16	70.4	9.4	12.9	<1	0	0
	S	2	95.0	1.5	0	0	0	51.8
CF_3CH_2OH	D	16	70.4	19.5	18.7	<1	0	0
	S	2	93.9	0	0	0	0	12.1

a) Direct irradiations were conducted on 10 mM solution of **1c** in ROH/MeCN (1 : 4) at 10 °C in quartz tubes. For sensitized run, *p*-DCB (10 mM) was added to the solution. b) D refers to direct irradiation while S refers to sensitized run. c) Determined by GC.

Table 2. Effect of Aryl Substituents on DCB-Sensitized Photoreaction of 1,1,2-Triarylcyclopropane in EtOH/MeCN[a)]

1	X	Y	OX $E_{1/2}/V^{b)}$	ΔG/kJ·mol$^{-1c)}$	Conversion %	6/%
a	MeO	H	0.98	−138.2	96.8	72.3
b	Me	H	1.25	−112.7	98.1	57.5
c	H	H	1.25	−112.7	95.2	85.3
d	CN	H	1.40	−97.8	30.2	23.6
e	NO_2	H	1.47	−91.3	4.8	0
f[d)]	H	MeO	1.17	−120.7	96.1	63.4
g[d)]	H	CN	1.39	−99.0	90.7	44.6
h[d)]	H	NO_2	1.41	−97.1	2.4	0

a) All irradiations were conducted on 10 mM solution of **1** in the presence of 10 mM of *p*-DCB in EtOH/MeCN (1 : 4) for 2 h in quartz tubes. Yields were determined by GC. b) Oxidation potentials were obtained by cyclic voltammetry: Pt electrode, tetraethylammonium perchlorate (0.1 mol dm^{-3}) in acetonitrile solution, vs. Ag/Ag$^+$. c) Calculated using Eq. 1. d) Roughly 1 : 1 cis-trans mixtures were used.

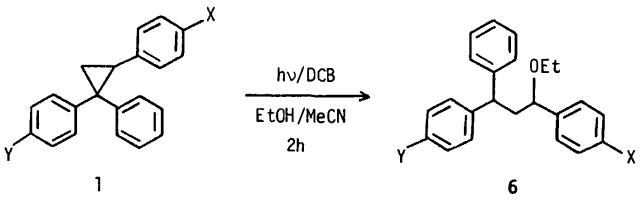

1 6

suggests that an intermediate generated by the interaction of excited DCB with **1c** is not efficiently trapped by TFE presumably due to its decreased nucleophilicity. Complete absence of addition products in the direct run, however, indicates that the intermediate formed in the DCB-sensitized run should be considerably electrophilic.

A series of *p*-monosubstituted triphenylcyclopropanes (**1a,b,d—h**) were prepared by conventional method and the effect of these substituents on the electron-transfer-mediated photoreaction was investigated. The results summarized in Table 2 suggest that the introduction of strongly electron-withdrawing group (i.e., nitro) suppressed the reaction almost completely. It is also noted that the reaction is somewhat more sensitive to the substituent (X) on 2-phenyl ring than that (Y) on 1-phenyl ring. Thus, the reaction was essentially unaffected by *p*-cyano group on 1-phenyl ring while the same group on 2-phenyl ring considerably suppressed the reaction.

The foregoing observations are explained in terms of the mechanism involving electron transfer originally proposed by Hixson.[3)] Thus, excitation of the sensitizer is followed by electron transfer from the cyclopropane to the sensitizer[6)] to give the geminate sensitizer anion radical-cyclopropane cation radical pair. The initially formed radical cation has the three-membered ring intact since it has been suggested that the electron has been taken from a phenyl ring.[7)] This radical ion pair can either deactivate by back electron transfer, or dissociate to separated radical ions, where the radical cation is attacked by alcohol followed by proton loss to afford diphenylmethyl radical (**7**).

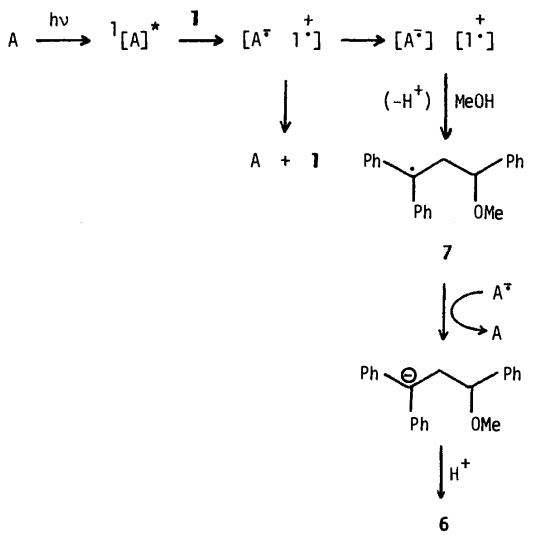

Reduction of **7** with the sensitizer anion radical ($A^{-\cdot}$) leads to the adduct **6**.

What is the origin of the effect of ring substituents, then? A possible explanation would be that electron transfer becomes less feasible as more electron withdrawing groups are introduced on phenyl ring. The free energy change (ΔG) associated with the electron-transfer process can be estimated using Wellers' equation[8)] originally proposed to account for fluorescence quenching by electron-transfer mechanism,

$$\Delta G(\mathrm{kJ\,mol^{-1}}) = 96.8[E(\mathrm{D/D^+})_v - E(\mathrm{A/A^-})_v - e^2/(\varepsilon a)] - Es \quad (1)$$

where $E(\mathrm{D/D^+})$ and $E(\mathrm{A/A^-})$ are the oxidation potentials of the donor (in this case the cyclopropanes) and the reduction potential of the acceptor (in this case the sensitizer), respectively. Thus, the oxidation potential of **1** were measured by cyclic voltammetry and the free energy of electron transfer to DCB (Es=408.4 kJ mol^{-1}, $E_{1/2}^{red}$=2.00 eV)[9)] from various cyclopropanes **1a—h** in MeCN was estimated (Table 3). In all cases ΔG is significantly negative. This means that the electron transfer process should be spontaneous for all cyclopropanes employed.

Complete lack of reactivity of the cation radical from *p*-nitro derivatives, then, can be interpreted as indicating that the lifetime of the cation radical is too short, due to the strongly destabilizing effect of *p*-nitro group, to be trapped by alcohol and hence it undergoes the back electron transfer in the geminate pair before it dissociates and/or is intercepted by alcohol.[10)]

Experimental

Instrumentation. UV spectra were recorded on a Hitachi 220-S spectrophotometer. IR spectra were measured on a JASCO A-100 spectrometer and ^{1}H NMR spectra were determined with JEOL JNM-MH-100 NMR spectrometer in CCl_4 with Me_4Si as an internal reference. Mass spectra were recorded on Shimadzu QP-1000 mass spectrometer (70 eV). Oxidation potentials were measured on Yanaco polarographic analyzer P-1100.

Materials. All 1,1,2-triarylcyclopropanes (**1a—h**) were prepared by the reaction of the corresponding diaryldiazomethanes with styrenes in refluxing benzene, followed by

column chromatography. The data are shown below.

1a: Yield 24.7%; mp 109—112 °C (lit,[11a] 111—112 °C).

1b: Yield 78.1%; Liquid; ^{1}H NMR δ=7.10—6.96 (10H, m), 6.79—6.56 (4H, m), 2.74 (1H, dd), 2.19 (3H, s), 1.93—1.63 (2H, m); MS *m/z* 284.

1c: Yield 73.5%; mp 47—48.5 °C (lit,[11b] 49.5—50.0 °C).

1d: Yield 55.5%; mp 111.0—112.0 °C; ^{1}H NMR δ=7.20—6.45 (14H, m), 2.92—2.70 (1H, m), 2.02—1.68 (2H, m); MS *m/z* 295.

1e: Yield 76.4%; mp 97.2—99.8 °C; ^{1}H NMR δ=7.79 (2H, d), 7.40—6.80 (12H, m), 2.85 (1H, dd), 2.10—1.80 (2H, m); MS *m/z* 315.

1f: Yield 79.0%; mp 57.0—59.5 °C; ^{1}H NMR δ=7.10—6.40 (14H, m), 3.60 and 3.56 (each s, 3H), 2.76—2.60 (1H, m), 1.87—1.54 (2H, m); MS *m/z* 300.

1g: Yield 53.5%; mp 55.0—57.0 °C; ^{1}H NMR δ=7.40—6.60 (14H, m), 2.90—2.60 (1H, m), 2.10—1.60 (2H, m); MS *m/z* 295.

1h: Yield 85.3%; mp 120.0—121.0 °C; ^{1}H NMR δ=8.10—7.80 (2H, m), 7.40—6.80 (12H, m), 3.10—2.80 (1H, m), 2.20—1.70 (2H, m); MS *m/z* 315.

Authentic samples of **3c—5c** were prepared according to the literature procedures.[5,12] The ethers **6** were isolated from the DCB-sensitized photolytic mixtures by preparative TLC and characterized spectroscopically. ^{1}H NMR data are shown below.

6a (R=Et): ^{1}H NMR δ=7.2—6.6 (14H, m), 4.12 (1H, dd), 3.94 (1H, dd), 3.58 (3H, s), 3.35—2.87 (2H, m), 2.56—2.02 (2H, m), 1.06 (3H, t).

6b (R=Et): ^{1}H NMR δ=7.1—6.5 (14H, m), 4.10 (1H, dd), 3.80 (1H, dd), 3.38—2.90 (2H, m), 2.54—2.00 (2H, m), 2.18 (3H, s), 1.05 (3H, t).

6c (R=Me): ^{1}H NMR δ=7.6 (15H, bs), 4.10 (1H, dd), 3.82 (1H, dd), 3.03 (3H, s), 2.60—2.05 (2H, m).

6c (R=Et): ^{1}H NMR δ=7.5—6.8 (15H, m), 4.17 (1H, dd), 3.87 (1H, dd), 3.30—2.95 (2H, m), 2.46—2.00 (2H, m), 1.08 (3H, t).

6c (R=^{i}Pr): ^{1}H NMR δ=7.4—6.9 (15H, m), 4.12 (1H, dd), 3.95—3.40 (2H, m), 2.52—2.00 (2H, m), 1.20 (3H, d).

6c (R=^{t}Bu): ^{1}H NMR δ=7.6 (15H, bs), 4.12 (1H, dd), 3.90 (1H, dd), 2.75—2.00 (2H, m), 1.20 (9H, s).

6c (R=CH_2CF_3): ^{1}H NMR δ=7.4—6.8 (15H, m), 4.15 (1H, dd), 3.98 (2H, q), 3.90 (1H, dd), 2.50—2.09 (2H, m).

6d (R=Et): ^{1}H NMR δ=7.4—6.6 (14H, m), 4.12 (1H, dd), 3.85 (1H, dd), 3.32—2.87 (2H, m), 2.55—2.00 (2H, m), 1.08 (3H, t).

6f (R=Et): ^{1}H NMR δ=7.3—6.5 (14H, m), 4.2—4.0 (1H, m), 4.0—3.8 (1H, m), 3.66, 3.63, (3H, s), 3.5—2.8 (2H, m), 2.6—2.1 (2H, m), 1.10 (3H, t).

6g (R=Et): ^{1}H NMR δ=7.5—7.0 (14H, m), 4.14 (1H, dd), 3.85 (1H, dd), 3.4—2.9 (2H, m), 2.5—2.1 (2H, m), 1.09 (3H, t).

Irradiation for Product Identification. In a typical run, a solution of **1** (1 mmol) and *p*-DCB (1 mmol) in ROH (10 dm^3)-MeCN (40 dm^3) was placed in a quartz tube and irradiated using a high pressure, 300W, Hg lamp with a water-cooled quartz jacket. The progress of the reaction was monitored by TLC. After irradiation of 5 h, the irradiation mixtures were concentrated on a rotary evaporator and chromatographed on preparative TLC (silica gel) eluted with chloroform-hexane.

Irradiation for Analysis Purposes. All irradiations outlined in Tables were carried out on 10 mM solutions of **1** in a quartz tube of 5 dm^3 capacity at 15 °C. The yields were conveniently determined by standard GC techniques, and the identity of the products was confirmed by GC-MS comparison with authentic samples prepared as above.

Authors wish to thank Professor Yasuji Izawa of Aichi Institute of Technology and Dr. Kazuhiko Mizuno of Osaka Prefectural University for their helpful discussion and Professor Katsuhiko Takagi of Nagoya University for the measurement of cyclic voltammetry.

References

1) A general overview of photochemistry of arylcyclopropanes in solution phase is given by S. S. Hixson in "Organic Photochemistry," ed by A. Padwa, Marcel Dekker, New York (1979), Vol. 4, p. 191.

2) See for reviews; S. L. Mattes and S. Farid, "Organic Photochemistry," ed by A. Padwa, Marcel Dekker, New York (1983), Vol. 6, p. 233; K. Mizuno, *Yuki Gosei Kagaku Kyokaishi*, **44**, 1010 (1986); Y. Otsuji and K. Mizuno, *Rep. Asahi Glass Found. Ind. Technol.*, **49**, 215 (1986).

3) V. R. Rao and S. S. Hixson, *J. Am. Chem. Soc.*, **101**, 6458 (1979).

4) a) Y. Izawa, H. Tomioka, M. Natsume, S. Beppu, and H. Tsujii, *J. Org. Chem.*, **45**, 4835 (1980); b) Y. Izawa, K. Ishiguro, and H. Tomioka, *Bull. Chem. Soc. Jpn.*, **56**, 951, 1490 (1983); c) Y. Izawa, M. Takeuchi, and H. Tomioka, *Chem. Lett.*, **1983**, 1297; d) Y. Izawa, Y. Watoh, and H. Tomioka, *Chem. Lett.*, **1984**, 33; e) Y. Izawa, M. Takeuchi, Y. Watoh, and H. Tomioka, *J. Chem. Soc. Jpn., Chem. Ind. Chem.*, **1984**, 98.

5) Similar results have been reported by C. S. Irving, R. C. Pefferson, I. Sarkar, H. Krisfinsson, C. S. Aaron, G. W. Griffin, and G. J. Boudreaux, *J. Am. Chem. Soc.*, **88**, 5675 (1966).

6) That the reaction takes place via initial excitation of the sensitizer was indicated by the fact that the irradiation of **1** using 1,4-dicyanonaphthalene as an electron acceptor with long wavelength light (>300 nm) which is not absorbed by **1** also resulted in increase in the yield of **6**.

7) P. C. Wong and D. R Arnold, *Tetrahedron Lett.*, **1979**, 2101.

8) D. Rehm and A. Weller, *Isr. J. Chem.*, **8**, 259 (1970).

9) D. Arnold and A. J. Maroulis, *J. Am. Chem. Soc.*, **98**, 5931 (1976).

10) Control experiments using either cis or *trans*-**1h** showed that **1h** underwent photoisomerization under these conditions in a rate comparable to that observed in direct irradiation.

11) a) A. Sonoda and I. Moritani, *Bull. Chem. Soc. Jpn.*, **43**, 3522 (1979); b) G. W. Griffin, A. F. Marcantonio, H. Kristinsson, R. C. Peterson, and C. S. Irving, *Tetrahedron Lett.*, **1965**, 2951.

12) A. W. Fort and J. D. Roberts, *J. Am. Chem. Soc.*, **78**, 584 (1956).

Synthesis of 2-Benzylidene-3(2*H*)-benzofuran-3-ones (Aurones) by Oxidation of 2′-Hydroxychalcones with Mercury(II) Acetate

Haruo SEKIZAKI
Faculty of Pharmaceutical Science, Higashi Nippon Gakuen University, Ishikari-Tobetsu, Hokkaido 061-02
(Received August 7, 1987)

Synopsis. The reaction of 2′-hydroxychalcones with mercury(II) acetate in acetic acid gives predominantly 2-benzylidene-3(2*H*)-benzofuran-3-ones (aurones) in 28—62% yield accompanied by flavanones in 5—21% yield.

2′-Hydroxychalcones are one of the important intermediates for the synthesis of flavonoids, and afford various products (flavone, flavonol, 3-hydroxyflavanone and aurone) according to the different oxidizing agents.[1] Hydrogen peroxide is the most historical reagent for the oxidation of 2′-hydroxychalcones to flavonols or aurones, but 6′-methoxyl group is necessary for the synthesis of aurones.

On the other hand, the oxidation of 2′-hydroxychalcones with selenium(IV) oxide,[1] palladium(II) lithium chloride,[2] 2,3-dichloro-5,6-dicyano-1,4-benzoquinone (DDQ),[3] thallium(III) nitrate trihydride[4] and a combination of nickel chloride, zinc powder and potassium iodide[5] provide only flavones. While, Kurosawa et al.,[6,7] reported that the oxidation of 2′-hydroxychalcones with lead(IV) acetate or manganese(III) acetate in acetic acid gave the aurones as main products, but Ollis et al.,[8] reported that thallium(III) acetate gave the rearranged products. Thus oxidation of 2′-hydroxychalcones with metal acetates afford different products depending on the metal.

This report deals with the synthesis of aurones by the oxidation of 2′-hydroxychalcones with mercury(II) acetate in acetic acid. These results are similar to those of Kurosawa described above but a chalcone (**1c**) having hydroxyl group at 4-position also afforded the product **2c** as a pure crystal. The results are shown in Table 1.

2′-Hydroxychalcones **1a—i** were prepared by the usual potassium hydroxide-catalyzed condensation of the corresponding 2′-hydroxyacetophenones and benzaldehyde or its derivatives. The products **1a—i** were identified by their physical properties and spectroscopic analyses.

2′-Hydroxychalcones **1** were dehydrogenatively cyclized to the aurones **2** on heating at 90—95 °C for 8 h with two equivalents of mercury(II) acetate in acetic acid. The reaction mixture was separated by the addition of saturated sodium chloride solution followed by extraction with ethyl acetate and column chromatography on silica gel to give aurone **2** accompanied by flavanone **3** produced from acid-catalyzed cyclization of 2′-hydroxychalcone **1**. The aurones **2a—i** and flav-

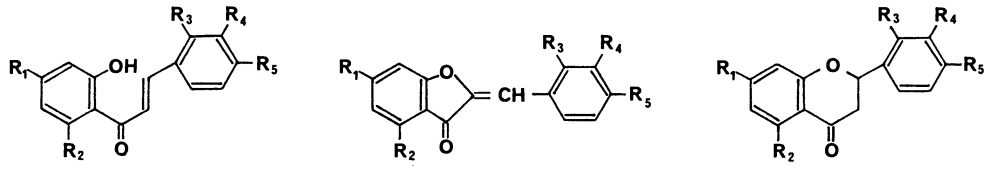

1 **2** **3**

a $R_1=R_2=R_3=R_4=R_5=H$
b $R_1=OMe$, $R_2=R_3=R_4=R_5=H$
c $R_1=R_2=R_3=R_4=H$, $R_5=OH$
d $R_1=R_2=OMe$, $R_3=R_4=R_5=H$
e $R_1=R_2=R_3=OMe$, $R_4=R_5=H$
f $R_1=R_2=R_4=OMe$, $R_3=R_5=H$
g $R_1=R_2=OMe$, $R_3=R_4=H$, $R_5=OCH_2Ph$
h $R_1=R_2=R_3=R_5=OMe$, $R_4=H$
i $R_1=R_2=R_4=OMe$, $R_3=H$, $R_4=OCH_2Ph$

Fig. 1.

Table 1.

Chalcone			Aurone				Flavanone			
No.	Mp (lit) θ_m/°C	Ref.	No.	Yield %	Mp (lit) θ_m/°C	Ref.	No.	Yield %	Mp (lit) θ_m/°C	Ref.
1a	86—8 (88—9)	9	**2a**	51	108—9 (108)	15	**3a**	6	75—6 (75—6)	21
1b	108—9 (107—8)	10	**2b**	40	147—8 (145—6)	16	**3b**	21	86—7 (89)	22
1c	158—9 (162)	11	**2c**	28	238—9 (242)	17	**3c**	9	186—7 (186—7)	11
1d	89—90 (91)	12	**2d**	62	152—3 (151—2)	18	**3d**	5	168—9 (152—3)	23
1e	113—4 (106—8)	13	**2e**	42	220—1 (214—6)	19	**3e**	11	130 (124—5)	24
1f	96.5—7 (—)	—	**2f**	54	194—5 (190—1)	19	**3f**	7	102—3 (—)	—
1g	163—4 (—)	—	**2g**	62	205—6 (197)	20	**3g**	10	168—9 (—)	—
1h	171—3 (128)	14	**2h**	55	215—7 (211—7)	19	**3h**	12	165—6 (167—8)	25
1i	123—4 (—)	—	**2i**	31	191—2 (—)	—	**3i**	14	128 (—)	—

anones **3a—i** were identified by their physical properties and spectroscopic analyses.

Experimental

The melting points were determined on a Yanaco micro-melting point apparatus and are uncorrected. The IR spectra were taken on a Hitachi 270-30 infrared spectrophotometer. The ultraviolet spectra were determined by a Shimadzu UV-210 digital spectro-photometer. The ^{1}H NMR spectra were recorded on a JEOL FX 90Q spectrometer. Chemical shifts are given on the δ (ppm) scale with tetramethylsilane as an internal standard (s, singlet; d, doublet; t, triplet; m, multiplet). The MS were taken on a Shimadzu LKB-9000 and a JEOL JNM-PM-60 spectrometer by the direct inlet method; ionization voltage 70 eV.

Preparation of Chalcones. A solution of an equimolar amount of 2′-hydroxychalcone and benzaldehyde in a small volume of ethanol was treated with 10% ethanolic potassium hydroxide with stirring at 35—40 °C for 12 h. The reaction mixture was poured into ice-water and acidified with dilute hydrochloric acid. The resulting precipitate was collected by filtration and washed with water. The crude product was purified by column chromatography on silica gel and recrystallized from ethanol. **1f:** IR (KBr) 1635 and 1584 cm^{-1}. UV (C_2H_5OH) 250 (log ε 4.04) and 345 nm (4.30). ^{1}H NMR ($CDCl_3$) δ=3.84 (3H, s, OCH_3), 3.85 (3H, s, OCH_3), 3.91 (3H, s, OCH_3), 5.96 (1H, d, J=2.2 Hz, H-3′), 6.10 (1H, d, J=2.2 Hz, H-5′), 6.80—7.30 (4H, m, H-2, 4, 5 and 6), and 7.80 (2H, d, J=4.4 Hz, H-α and β). MS m/z (rel intensity 314 (M^+; 96), 297 (20), 286 (17), 207 (100), and 180 (29). High MS Found: m/z 314.1145, Calcd for $C_{18}H_{18}O_5$: M, 314.1152. **1g**: IR (KBr) 1632, 1622, and 1581 cm^{-1}. UV (C_2H_5OH) 250 (log ε 4.10) and 365 nm (4.54). ^{1}H NMR ($CDCl_3$) δ=3.83 (3H, s, OCH_3), 3.91 (3H, s, OCH_3), 5.11 (2H, s, -C$\underline{H}_2$Ph), 5.93 (1H, d, J=2.2 Hz, H-3′), 6.01 (1H, d, J=2.2 Hz, H-5′), 6.96 (2H, d, J=8.8 Hz, H-3 and 5), 7.39 (5H, s, PhH), 7.52 (2H, d, J=8.8 Hz, H-2 and 6), and 7.78 (2H, s, H-α and β). MS m/z (rel intensity) 390 (M^+; 22), 271 (18), 181 (22), and 91 (100). High MS Found: m/z 390.1489, Calcd for $C_{24}H_{22}O_5$: M, 390.1466. **1i**: IR (KBr) 1629 and 1581 cm^{-1}. UV (C_2H_5OH) 245 (log ε 4.00) and 371 nm (4.50). ^{1}H NMR ($CDCl_3$) δ=3.82 (6H, s, 2×OCH_3), 3.93 (3H, s, OCH_3), 5.20 (2H, s, -C$\underline{H}_2$Ph), 5.92 (1H, d, J=2.2 Hz, H-3′), 6.10 (1H, d, J=2.2 Hz, H-5′), 6.90 (1H, d, J=8.4 Hz, H-2 or 3), 7.15 (1H, d, J=2.2 Hz, H-6), 7.40 (6H, m, PhH and H-2 or 3), and 7.68 (2H, s, H-α and β). MS m/z (rel intensity) 420 (M^+; 34), 181 (42), 180 (31), and 91 (100). High MS Found: m/z 420.1563, Calcd for $C_{25}H_{24}O_6$: M, 420.1571.

Mercury(II) Acetate Oxidation of Chalcones. A solution of chalcone (**1**) (5 mol dm^{-3}) and mercury(II) acetate (10 mol dm^{-3}) in 100 cm^3 of acetic acid was heated at 90—95 °C for 8 h. After removal of the acetic acid in vacuo, the resulting solid was treated with saturated sodium chloride solution and then extracted with ethyl acetate. The ethyl acetate layer was separated and evaporated. The residue was dissolved in a small amount of a mixture of benzene-ethyl acetate (6/1 volume ratio) and separated by silica-gel column chromatography with a mixture of benzene-ethyl acetate (6/1 volume ratio) as eluant. Aurones **2** were obtained as the first fraction and flavanones **3** were obtained as the second fraction. **2i**: IR (KBr) 1692, 1673, 1614, and 1595 cm^{-1}. UV (C_2H_5OH) 252 (log ε 3.68), 265 (sh, 3.62), 380 (sh, 4.08), and 395 nm (4.15). ^{1}H NMR ($CDCl_3$) δ=3.93 (3H, s, OCH_3), 3.95 (6H, s, 2×OCH_3), 5.24 (2H, s, -C$\underline{H}_2$Ph), 6.12 (1H, d, J=1.8 Hz, H-5), 6.29 (1H, d, J=1.8 Hz, H-7), 6.68 (1H, s, H-10), 6.93 (1H, d, J=8.4 Hz, H-5′), and 7.45 (7H, m, PhH, H-2′ and 6′). MS m/z (rel intensity) 418 (M^+; 42), 327 (41), 299 (14), 181 (31), and 91 (100). High MS Found: m/z 418.1406, Calcd for $C_{25}H_{22}O_6$: M, 418.1414. **3f**: IR (KBr)1674, 1608, and 1566 cm^{-1}. UV (C_2H_5OH) 282 (log ε 4.29) and 310 nm (sh, 3.67). ^{1}H NMR ($CDCl_3$) δ=2.91 (2H, m, H-3), 3.85 (3H, s, OCH_3), 3.86 (3H, s, OCH_3), 3.92 (3H, s, OCH_3), 5.38 (1H, d,d, J=15.6 and 4.0 Hz, H-2), 6.11 (1H, d, J=2.4 Hz, H-6), 6.19 (1H, d, J=2.4 Hz, H-8), and 6.97 (4H, m, H-2′, 3′, 4′, and 6′). MS m/z (rel intensity) 314 (M^+; 55), 207 (29), and 180 (100). High MS Found: m/z 314.1168, Calcd for $C_{18}H_{18}O_5$: M, 314.1153. **3g**: IR (KBr) 1680, 1608, and 1569 cm^{-1}. UV (C_2H_5OH) 282 (log ε 3.93) and 310 nm (sh, 3.14). ^{1}H NMR ($CDCl_3$) δ=2.39 (2H, m, H-2), 3.18 (3H, s, OCH_3), 3.87 (3H, s, OCH_3), 5.08 (2H, s, -C$\underline{H}_2$Ph), 5.34 (1H, d,d, J=13.3 and 4.0 Hz, H-2), 6.08 (1H, d, J=2.4 Hz, H-6), 6.13 (1H, d, J=2.4 Hz, H-8), 7.00 (2H, d, J=9.8 Hz, H-3′ and 5′), 7.38 (2H, d, J=9.8 Hz, H-2′ and 6′), and 7.39 (5H, s, PhH). MS m/z (rel intensity) 390 (M^+; 22), 299 (8), and 91 (100). High MS Found: m/z 390.1491, Calcd for $C_{22}H_{22}O_5$: M, 390.1476, **3i**: IR (KBr) 1674, 1608, and 1572 cm^{-1}. UV (C_2H_5OH) 283 (log ε 4.29) and 311 nm (sh, 3.68). ^{1}H NMR ($CDCl_3$) δ=2.27 (2H, m, H-3), 3.81 (3H, s, OCH_3), 3.89 (6H, s, 2×OCH_3), 5.16 (2H, s, -C$\underline{H}_2$Ph), 5.28 (1H, d,d, J=16.0 and 4.0 Hz, H-2), 6.09 (1H, d, J=2.2 Hz, H-6), 6.12 (1H, d, J=2.2 Hz, H-8), 6.95 (3H, m, H-2′, 3′, and 6′), and 7.38 (5H, m, PhH). MS m/z (rel intensity) 420 (M^+; 43), 181 (45), 105 (45), and 91 (100). High MS Found: m/z 420.1559, Calcd for $C_{25}H_{24}O_6$: M, 420.1576.

The auther is indebted to Dr. Hideo Tanino and Mr. Katsuyoshi Masuda at the Faculty of Pharmacy, Meijo University for the high resolution MS measurements.

References

1) J. B. Harborne, T. J. Mabry, and H. Mabry, "The Flavonoids," Chapman and Hall, London (1975).
2) A. Kasahara, T. Izumi, and M. Oshima, *Bull. Chem. Soc. Jpn.*, **47**, 2526 (1974).
3) T. Tanaka, K. Iwashima, and S. Matsuura, *Yakugaku Zasshi*, **104**, 1306 (1984).
4) M. Meyer-Dayan, B. Bodo, C. Deschamps-Vallent, and D. Molho, *Tetrahedron Lett.*, **1978**, 3359.
5) S. M. Ali, J. Iqbal, and M. Liyas, *J. Chem. Res. (S)*, **1984**, 236.
6) K. Kurosawa, *Bull. Chem. Soc. Jpn.*, **42**, 1456 (1969).
7) K. Kurosawa and J. Higuchi, *Bull. Chem. Soc. Jpn.*, **45**, 1132 (1972).
8) W. D. Ollis, K. L. Ormand, and I. O. Sutherland, *J. Chem. Soc. C*, **1970**, 119.
9) J. Buckingham, "Dictionary of Organic Compounds," Chapman and Hall, London (1982), p. 3220.
10) S. Matsueda, K. Sannohe, and Y. Saito, *Bull. Chem. Soc. Jpn.*, **36**, 1528 (1963).
11) T. A. Geissman and R. O. Clinton, *J. Am. Chem. Soc.*, **68**, 697 (1946).
12) R. Haensel, G. Ranft, and R. Baehr, *Z. Naturforch*, **18b(5)**, 370 (1963).
13) J. Buckingham, "Dictionary of Organic Compounds," Chapman and Hall, London (1982), p. 3227.
14) "Beilstein's Handbuch der Organishen Chemie," Vol. 8, p. 543.
15) W. Feuerstein and St. von Kostanecki, *Ber.*, **31**, 1759 (1898).
16) S. K. Grover, V. N. Gupta, A. C. Jain, and T. R. Seshadri, *J. Sci Ind. Res. (Indian)*, **19B**, 258 (1960).
17) "Beilstein's Handbuch der Organishen Chemie," Vol. 10, p. 61.
18) R. N. Goel, V. B. Mahesh, and T. R. Seshadri, *Proc. Indian Acad. Sci., Sect. A*, **47**, 184 (1958).
19) V. D. Vittorio, *Rent. Ist. Super Sanita*, **21**, 418 (1958).
20) F. Lor and G. Agnes and N. Mihaly, *Acta Chem. (Budapest)*, **53**, 311 (1968).

21) H. Ryan and G. Cruess-Callaghan, *Proc. R. Ir. Acad.*, **39**, 124 (1919).
22) J. Shinoda, *Yakugaku Zasshi*, **48**, 214 (1928).
23) M. Hasegawa and T. Shirato, *J. Am. Chem. Soc.*, **79**, 450 (1975).
24) "Beilstein's Handbuch der Organischen Chemie," Vol. 18, p. 395.
25) "Beilstein's Handbuch der Organischen Chemie," Vol. 10, p. 209.

Stereoselective Synthesis of 3,5-Alkadienoic Esters from 2,4-Dienoic Isomers

Sadao TSUBOI,* Jun-ichi SAKAMOTO, Akihisa KURODA, Masanori UTAKA, and Akira TAKEDA
Department of Synthetic Chemistry, School of Engineering, Okayama University, Tsushima, Okayama 700
(Received August 19, 1987)

Synopsis. The treatment of (2*E*,4*Z*)-2,4-alkadienoic esters with lithium diisopropylamide (LDA) at −80 °C gave (3*E*,5*E*)-isomers with 81—98% stereoselectivity. In contrast, the treatment of (2*E*,4*E*)-isomers under the same conditions gave (3*E*,5*Z*)-isomers with 72—80% stereoselectivity. The application to the synthesis of megatomoic acid is described. Carbon-13 NMR data regarding these 3,5-dienoates were obtained.

Some natural products containing a 3,5-dienoic acid moiety are reported. For example, an antibiotic mycomycin **1**[1] and an insect pheromone, megatomoic acid **2**,[2] are well-known.

$HC{\equiv}C\text{-}C{\equiv}C\text{-}CH{=}C{=}CH\text{-}CH{=}CHCH{=}CHCH_2CO_2H$
mycomycin **1**

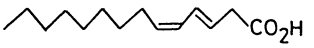

megatomoic acid **2**

Conjugated diene groupings are useful for the synthesis of natural products via a Diels-Alder reaction.[3] To our knowledge, synthetic methods for 3,5-alkadienoic esters are quite limited. The conventional method consists of the combination of a Wittig reaction and a hydrogenation of triple bonds. On the other hand, Chiusoli reported the synthesis of 3,5-alkadienoates via the isomerization of 2,5-alkadienoates.[4] Krebs[5] and Kende et al.[6] reported that deconjugative alkylation of (*E*)- and (*Z*)-2-alkenoates with strong bases, such as lithium diisopropylamide (LDA) or potassium hexamethyldisilazide, gave, respectively, (*Z*)- and (*E*)-3-alkenoate with high stereoselectivities. We recently reported the highly stereo- and regioselective alkylation of alkylidenemalonates.[7] This paper reports a detailed description of the previous communication[8] concerning the deconjugative protonations of (2*E*,4*Z*)- and (2*E*,4*E*)-2,4-alkadienoates with LDA.[9]

In 1982 we reported a convenient synthesis of (2*E*,4*Z*)-alkadienoic esters **3** by the stereoselective rearrangement of β-allenic esters promoted with alumina.[10] As a result of our continuous interest in the chemistry of **3**,[11] we treated **3** with LDA at −80 °C. The reaction gave (3*E*,5*E*)-isomers **4** in good yield. On the other hand, a treatment of (2*E*,4*E*)-2,4-alkadienoates **5** with LDA afforded (3*E*,5*Z*)-isomers **6**. Various alkadienoates **3** and **5** were prepared and treated with LDA in THF/hexamethylphosphoric triamide (HMPA). These results were tabulated in Tables 1 and 2. The transformation of **3** to **4** proceeded with 81—98% stereoselectivity, while that of **5** to **6** proceeded with 72—80%. To improve the stereoselectivity, various lithium amides such as lithium dicyclohexylamide, lithium bis(trimethylsilyl)amide, and lithium diethylamide were used as a base. However, a notable improvement could not be established. The stereoselectivity decreased slightly as the substituent became larger. The geometry of the rearrangement products was determined by ^1H NMR spectral data with the aid of a shift reagent Eu(dpm)$_2$ and a proton decoupling technique. For example, both $J_{3,4}$ and $J_{5,6}$ in ethyl (3*E*,5*E*)-3,5-decadienoate (**4c**) were 15 Hz, which shows a trans geometry. The coupling constants of ethyl (3*E*,5*Z*)-3,5-decadienoate were $J_{3,4}$=15.4 Hz and $J_{5,6}$=10.8 Hz. The ^{13}C NMR spectra of compounds prepared in this work were measured and tentatively assigned as shown in Table 3. In general, signals of cis olefinic carbons of **6** appeared at a higher field than those of trans, trans-olefins **4** as a result of a steric effect.[12] These data afford an additional support for the structural assignment of **4** and **6**.

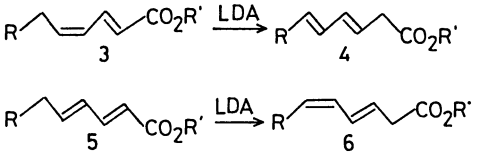

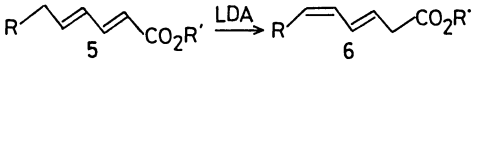

Table 1. Transformation of (2*E*,4*Z*)-2,4-Alkadienoates **3** to (3*E*,5*E*)-Isomers **4**

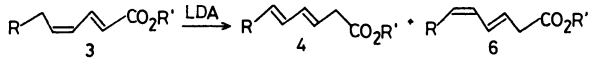

	3		Yields of products/%[a]			Stereoselectivity
No.	R	R′	3	4	6	4/6(%)
a	C_2H_5	CH_3	2	77	3	96
b	n-C_3H_7	CH_3	0	56	1	98
c	n-C_4H_9	C_2H_5	0	87	10	90
d	n-C_7H_{15}	C_2H_5	0	68	12	85
e	n-C_8H_{17}	CH_3	23	62	15	81

a) Analyzed by GLC fitted with Golay column (SE-30 silicone gum rubbers, 0.5 mm×45 m) or 10% SE-30 on Chromosorb W column (3 mm×1 m).

Table 2. Transformation of (2*E*,4*E*)-2,4-Alkadienoates **5** to (3*E*,5*Z*)-Isomers **6**

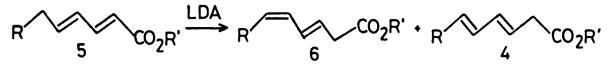

	5		Yields of products/%[a]		Stereoselectivity
No.	R	R′	6	4	6/4(%)
a	C_2H_5	CH_3	51	13	80
b	n-C_3H_7	CH_3	66	22	75
c	n-C_4H_9	C_2H_5	72	28	72
e	n-C_8H_{17}	CH_3	75	19	80

a) Analyzed by GLC fitted with Golay column (SE-30 silicone gum rubbers, 0.5 mm×45 m) or 10% SE-30 on Chromosorb W column (3 mm×1 m).

The stereochemical outcome in the present transformation can be explained by the assumption of carbanion intermediates[6] (**3′**, **3″**, **5′**, and **5″**), as shown in Chart 1. The deprotonation of **3** directly yields the minimum energy carbanion stereoisomer **3′**, which gives rise to the observed (3*E*,5*E*)-product. The alternative carbanion **3″** is unfavorable because of a severe 1,3-allylic strain between R and $CH{=}CHCO_2Et$. The deprotonation of **5** gives carbanion intermediates **5′** and **5″**, leading to the (3*E*,5*Z*)-and (3*E*,5*E*)-products, respectively. The formation of the carbanion **5′** leading to (3*E*,5*Z*)-product is favorable, since the cis form for the crotyl anion system is usually more stable than the trans form.[6] A higher stereoselectivity in the transformation of **3** to **4** than that of **5** to **6** is attributable to a larger energy difference between **3′** and **3″** than that between **5′** and **5″**.

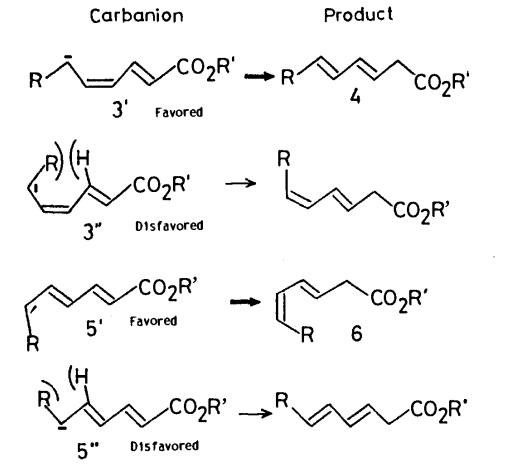

Chart 1.

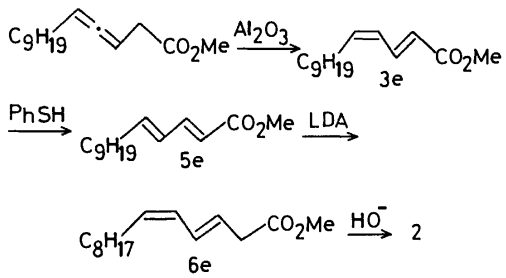

Scheme 1.

The present system was applied for the synthesis of megatomoic acid **2**, the sex attractant of the black carpet beetle.[2] The reaction sequence is shown in Scheme 1. The starting material, (2*E*,4*E*)-2,4-tetradecadienoate (**3e**), was prepared in 70% yield by a highly stereoselective rearrangement of methyl 3,4-tetradecadienoate, promoted with alumina, as reported previously.[7] The conversion of **3e** to methyl (2*E*,4*E*)-2,4-tetradecadienoate (**5e**) was established in 81% yield by a thermal treatment catalyzed by thiophenol and 2,2′-azobis(isobutyronitrile)(AIBN).[13] The treatment of **5e** with LDA gave a mixture of methyl (3*E*,5*Z*)-3,5-tetradecadienoate (**6e**) and the (3*E*,5*E*)-isomer **4e** (75:19). Spectral data were consistent with those reported previously.[11a] It has been reported that the hydrolysis of **6e** purified with GLPC gave megatomoic acid.[11a]

The present method will be useful for the stereoselective synthesis of polyenoic compounds, such as insect pheromones and leukotrienes.

Experimental

The boiling points are uncorrected. Elemental analyses were carried out by Mr. Eiichiro Amano of our laboratory. Analytical determinations by GLC were performed on a Hitachi Model 163 gas chromatograph fitted with 10% Silicone SE-30 on Chromosorb W column (3 mm×1 m) or Golay column (SE-30 silicone gum rubbers, 0.5 mm×45 m). IR spectra were taken on a JASCO Model A-102 spectrometer. ^1H NMR spectra (60 MHz) were recorded with a JEOL JNM-PMX60SI apparatus. ^{13}C NMR spectra (25 MHz) were obtained with a JEOL JNM-FX100 apparatus, using $CDCl_3$ as a solvent. Column chromatography was accomplished with 100—200 mesh Wakogel C-200. High-performance liquid chromatography (HPLC) was obtained with Yanagimoto liquid chromatograph L-2000 fitted with Yanapak SA-I (6 mm×250 mm). Tetrahydrofuran (THF) was distilled from sodium benzophenone ketyl under an atmosphere of nitrogen. Hexamethylphosphoric triamide (HMPA) was distilled from CaH_2 under reduced pressure. All experiments of the isomerization were carried out under an atmosphere of argon.

(2*E*,4*Z*)-2,4-Alkadienoates **3** was prepared according to the procedure reported previously.[10] (2*E*,4*E*)-2,4-Alkadienoates **5** was obtained from **3** by the procedure of the literature[13] and purified by preparative TLC (SiO_2, hexane/ethyl acetate=15/1) developed twice. The sample was purified by preparative TLC (SiO_2, hexane/ethyl acetate=15/1) developed twice. Some representative preparation of **4** and **6** are described below.

Table 3. ^{13}C NMR Data of (3*E*,5*E*)-3,5-Alkadienoates **4** and (3*E*,5*Z*)-3,5-Alkadienoates **6**

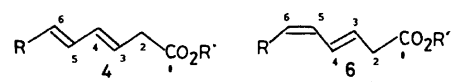

Compd	C_1	C_2	C_3	C_4	C_5	C_6	C_7	C_8	C_9	C_{10}	C_{11}	C_{12}	C_{13}	C_{14}
4a	171.9	38.0	122.4	134.2	128.4	136.4	25.6	13.5						
4b	172.1	37.9	122.3	134.7	129.7	134.2	34.7	22.4	13.7					
4c	171.8	38.2	122.5	134.8	129.6	134.1	29.1	31.4	22.3	14.0				
4e	172.1	37.8	122.2	134.4	129.4	134.1	28.3	29.5*	29.3*	28.5*	28.5*	31.9	22.7	14.1
6a	171.9	38.2	124.6	134.0	127.2	129.3	21.2	14.3						
6b	172.1	38.1	124.5	132.1	127.9	129.3	29.8	22.8	13.7					
6c	171.8	38.2	123.9	132.4	126.9	128.0	28.3	31.7	22.3	14.0				
6e	172.0	38.1	124.5	132.4	127.7	129.5	27.8	29.3*	29.3*	29.6*	29.6*	31.9	22.7	14.1

* May be exchangeable.

Methyl (3*E*,5*E*)-3,5-Octadienoate (4a). To a solution of diisopropylamine (0.289 ml, 2.10 mmol) in THF (4.5 ml) was added dropwise 1.18 ml of 1.65 M BuLi (1M=1 mol dm^{-3}) at 0 °C. After 30 min, HMPA (0.4 ml) was added and the mixture was cooled to −80 °C. A solution of **3a** (236 mg, 0.992 mmol) in THF (1.5 ml) was added dropwise; then, the mixture was stirred for 1 h and poured into ice water. After the mixture was acidified with dil. HCl, the organic materials were extracted with ether. The combined extracts were washed with water, dried over $MgSO_4$, and concentrated. The residual oil was chromatographed on SiO_2 to give 189 mg of an oil, of which GLC analysis (golay column, 130 °C) showed two peaks at R_t 3.2 and 3.4 min in a ratio of 4:96. Each component was separated by preparative GLC. The major fraction was identified as **4a**.[13] The minor fraction gave **6a**:[14] IR (neat) 1640 and 1600 cm^{-1}; ^1H NMR (CCl_4) δ=0.95 (t, 3H, CH_3), 2.16 (m, 2H, CH_2CH_3), 3.05 (d, 2H, J=7 Hz, CH_2CO), 3.59 (s, 3H, CO_2CH_3), 5.05—6.48 (m, 4H, $(CH{=}CH)_2$).

Ethyl (3*E*,5*E*)-3,5-Decadienoate (4c). To a solution of 0.046 ml (0.38 mmol) of dicyclohexylamine in 2 ml of dry THF was added at −15 °C 0.208 ml (0.38 mmol) of 1.65 M butyllithium in hexane. After 20 min, 0.1 ml of HMPA was added and then a solution of 65 mg (0.33 mmol) of **3c** in 2.5 ml of THF was added dropwise at −80 °C. The mixture was stirred for 1 h at −80 °C and then poured into ice water. The organic materials were extracted with ether, washed with water, dried over $MgSO_4$, and the solvent was evaporated. Analysis of the residual oil (67 mg) with GLC [column, SE-30 (3 mm×1 m), 120 °C; carrier gas, N_2 (0.5 kg cm^{-2})] gave two peaks. The structure was determined by comparison of the retention time with that of the authentic sample. The peaks, compounds, retention times, and integrated percentages were as follow: 1, **6c**, 3.9, 10%; 2, **4c**,[15] 4.1, 87%.

Methyl (3*E*,5*Z*)-3,5-Tetradecadienoate (6e). A solution of **5e** (98 mg, 0.41 mmol) in THF (0.1 ml) was treated with LDA prepared from diisopropylamine (0.069 ml, 0.5 mmol), 1.65 M butyllithium (0.273 ml, 0.5 mmol), and HMPA (0.15 ml) at −72 °C for 1 h, as shown in the preparation of **4c**. The mixture was worked up as usual and a crude product was obtained as an oil (93 mg) which was analyzed by GLC [column: SE-30 (3 mm×1 m), 170 °C; carrier gas, N_2 (0.5 kg cm^{-2})]. The peaks, retention times, and integrated peak areas are as follows: 1, 3.7 min, 80%; 2, 4.4 min, 20%. Component 1 was identified as **6e** (75% yield) by comparison of spectral data and the retention times with those of an authentic sample.[11a] Component 2 was identified as **4e** (19% yield) by a comparison of the spectral data and the retention time with those of a sample prepared from **3e**.

References

1) a) W. D. Celmer and I. A. Solomons, *J. Am. Chem. Soc.*, **74**, 2245 (1952); b) W. D. Celmer and I. A. Solomons, *ibid.*, **74**, 1870 (1952); c) W. D. Celmer and I. A. Solomons, *ibid.*, **75**, 1372 (1953).

2) R. M. Silverstein, J. O. Rodin, W. E. Burkholder, and J. E. Gorman, *Science*, **157**, 85 (1967).

3) a) R. V. Stevens, R. E. Cherpeck, B. L. Harrison, J. Lai, and R. Lapalme, *J. Am. Chem. Soc.*, **98**, 6317 (1976); b) P. A. Grieco, K. Yoshida, and Z. He, *Tetrahedron Lett.*, **25**, 5715 (1984).

4) G. P. Chiusoli, *Angew. Chem.*, **72**, 750 (1960).

5) E.-P. Krebs, *Helv. Chim. Acta*, **64**, 1023 (1981).

6) A. S. Kende and B. H. Toder, *J. Org. Chem.*, **47**, 163 (1982).

7) S. Tsuboi, K. Muranaka, T. Sakai, and A. Takeda, *J. Org. Chem.*, **51**, 4944 (1986).

8) S. Tsuboi, A. Kuroda, T. Masuda, and A. Takeda, *Chem. Lett.*, **1984**, 1541.

9) In the course of our study, Yamamoto et al. reported the isomerization of (2*E*,4*E*)-2,4-tetradecadienoate to (3*E*, 5*Z*)-3,5-tetradecadienoate: Y. Ikeda, J. Ukai, N. Ikeda, and H. Yamamoto, *Tetrahedron*, **43**, 743 (1987).

10) a) S. Tsuboi, T. Masuda, H. Makino, and A. Takeda, *Tetrahedron Lett.*, **23**, 209 (1982); b) S. Tsuboi, T. Masuda, and A. Takeda, *J. Org. Chem.*, **47**, 4478 (1982).

11) a) S. Tsuboi, T. Masuda, and A. Takeda, *Bull. Chem. Soc. Jpn.*, **56**, 3521 (1983); b) S. Tsuboi, Y. Nooda, and A. Takeda, *J. Org. Chem.*, **49**, 1204 (1984); c) S. Tsuboi, S. Maeda, and A. Takeda, *Bull. Chem. Soc. Jpn.*, **59**, 2050 (1986).

12) D. E. Dorman, M. Jautelat, and J. D. Roberts, *J. Org. Chem.*, **36**, 2757 (1971).

13) R. A. Amos and J. A. Katzenellenbogen, *J. Org. Chem.*, **43**, 555 (1978).

14) G. P. Chiusoli, *Angew. Chem.*, **72**, 750 (1960).

15) F. Warnaar, *Phytochemistry*, **20**, 89 (1981).

Synthesis and Epoxidation of Methyl *trans*-5,6-Diacetoxy-1,3-cyclohexadiene-1-carboxylate

Seiichiro OGAWA* and Tohei TAKAGAKI
Department of Applied Chemistry, Faculty of Science and Technology, Keio University, Hiyoshi, Yokohama 223
(Received October 3, 1987)

Synopsis. The (±)-methyl 1,3-cyclohexadiene-1-carboxylate, a useful intermediate for synthesis of derivatives of shikimic acid, was prepared by bromination of (±)-methyl (1,3/2)-2,3-diacetoxy-4-cyclohexene-1-carboxylate, followed by debromination of the major dibromide obtained with zinc dust. Epoxidation of the diene with peracid gave selectively two 3,4-monoepoxides.

Shikimic acid (**1**) occupies an important position in biosynthesis (shikimate pathway) of aromatic amino acids in nature.[1,2] On the other hand, some related compounds derived from **1**, viz. glyoxalase I inhibitor,[3] rancinamycins,[4] dioxolamycin,[5] etc., have been known to possess an interesting biological activity. We now describe a synthesis of the title compound, substituted (±)-methyl 1,3-cyclohexadiene-1-carboxylate, a versatile precursor for preparation of derivatives[2,6] of shikimic acid and analogs of naturally occurring cyclohexene oxides.[7]

Bromination of (±)-methyl (1,3/2)-2,3-diacetoxy-4-cyclohexene-1-carboxylate[8] (**2**) with 2 molar equiv of *N*-bromosuccinimide (NBS) in carbon tetrachloride in the presence of a trace amount of α,α'-azobisisobutyronitrile (AIBN) at reflux temperature for 2 h produced one major and four minor components. The products were separated by chromatography on silica gel to give two monobromides **3** (5%) and **5** (4%), and three dibromides **4**[9] (2%), **6** (50%), and **7**[10] (7%). Their structures were deduced on the basis of the previous results[11] on the reaction of the corresponding benzoyloxy and bromomethyl derivatives[12] with NBS, and finally confirmed by the ^{1}H NMR spectra (data in Experimental).

Mechanistically, four monobromides **3**, **5**, **8a**, and **8b** are considered to be formed initially by allylic bromination. The highly unstable isomer **8a**, in which the bromo group exists in quasi-axial position and cis to the 1-methoxycarbonyl group, readily undergoes elimination of hydrogen bromide to yield a diene **9**, which rapidly reacts with bromine generated in situ to give the dibromides **6** and **7**. The formation of the dibromide **4** might be deduced that the monobromide **3** possibly reacts with bromine to give a tribromide **10** which is convertible to **4** by elimination of hydrogen bromide under these reaction conditions or during chromatography on a silica-gel column.

Debromination of **6** was effected by treatment with zinc dust in acetic acid to give 83% yield of the diene **9**[13] as crystals. When ethanol was used as a solvent, partial *O*-deacetylation occurred to produce a mixture of two monoacetates and dihydroxy compound, together with a low yield of **9**. Since racemic **2** can readily be optically resolved,[14] and the absolute configurations of both enantiomers have already been established, it may be possible to provide optically active **9**.

In order to demonstrate the reactivity of the diene system, oxidation of **9** with equimolar *m*-chloroperbenzoic acid (MCPBA) was carried out in dichloromethane in the presence of phosphate buffer (pH 8) at room temperature. Two monoepoxides **11** (13%) and **12** (45%) were obtained selectively, and the structures were confirmed on the basis of the ^{1}H NMR spectra. The favored conformation of **11**, deduced by consideration of $J_{2,3}$ (7.5 Hz), would adopt the twist form with the 2- and 3-OAc groups being oriented in diequatorial positions. On the other hand, two acetoxyl groups of **12** seems to situate in diaxial positions ($J_{2,3}$=2.3 Hz). Each conformation is compatible with that of the corresponding benzoyloxymethyl derivatives.[11]

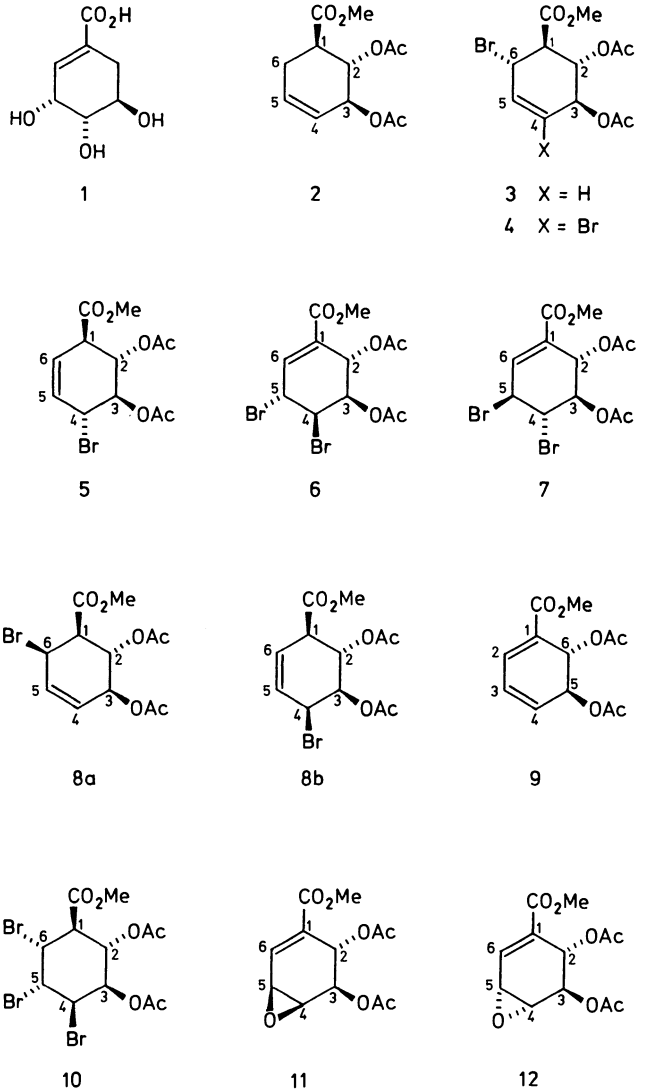

Experimental

Melting points were determined in an open capillary tube in a MEL-TEMP melting point apparatus and are uncorrected. ^{1}H NMR spectra were recorded in chloroform-*d* solution with tetramethylsilane as an internal standard. The peak positions are given in δ values. TLC was performed on precoated silica gel 60 F-254 (E. Merck, Darmstadt; 0.2 mm thickness). The silica gel used for column chromatography was Wakogel C-300 (Wako Co., Osaka; 300 mesh). Organic solutions were concentrated below 30 °C under reduced pressure.

Bromination of (±)-Methyl (1,3/2)-2,3-Diacetoxy-4-cyclohexene-1-carboxylate (2) with NBS. A mixture of **2**[8] (0.50 g, 2.0 mmol), NBS (0.71 g, 4.0 mmol), AIBN (5 mg), and carbon tetrachloride (10 ml) was refluxed under nitrogen atmosphere for 2 h. TLC (2-butanone-toluene 1 : 5) showed a disappearance of **2** (R_f 0.46), and a formation of one major (R_f 0.56) and several minor components (R_f 0.67, 0.63, 0.50, and 0.46). Succinimide formed was removed by filtration and the filtrate was concentrated. The residue (0.98 g) was chromatographed on silica gel (50 g) with 2-butanone-toluene (1 : 20) as eluent to give as the first fraction (±)-methyl (1,3/2,6)-2,3-diacetoxy-4,6-dibromo-4-cyclohexene-1-carboxylate (**4**) (22 mg, 2%) as crude crystals (from ethanol): Mp 112—113 °C. ^{1}H NMR ($CDCl_3$) δ=2.03 (3H, s) and 2.07 (3H, s) (OAc), 3.44 (1H, dd, $J_{1,2}$=9 Hz, $J_{1,6}$=7.2 Hz, H-1), 3.75 (3H, s, CO_2Me), 5.00 (1H, ddd, $J_{3,6}$=2.3 Hz, $J_{5,6}$=3.3 Hz, H-6), 5.36 (1H, dd, $J_{2,3}$=6 Hz, H-2), 5.66 (1H, ddd, $J_{3,5}$=1.3 Hz, H-3), 6.49 (1H, dd, H-5).

The above mother liquid of **4** was concentrated and the residue was rechromatographed on silica gel (8 g) with acetone-hexane (1 : 15) as eluent to give (±)-methyl (2,4/3,5)-2,3-diacetoxy-4,5-dibromo-6-cyclohexene-1-carboxylate (**7**) (57 mg, 7%) as a syrup contaminated with an unidentified compounds. ^{1}H NMR ($CDCl_3$) δ=2.03 (3H, s) and 2.10 (3H, s) (OAc), 3.81 (3H, s, CO_2Me), 4.54 (1H, dd, $J_{3,4}$=7.5 Hz, $J_{4,5}$=5.3 Hz, H-4), 5.01 (1H, br dd, $J_{5,6}$=3 Hz, H-5), 5.32 (1H, dd, $J_{2,3}$=4.5 Hz, H-3), 5.87 (1H, br dd, $J_{2,6}$=1.5 Hz, H-2), 7.13 (1H, br dd, H-6).

The second fraction (R_f 0.56) gave a syrup which crystallized from ethanol to give (±)-methyl (2,5/3,4)-2,3-diacetoxy-4,5-dibromo-6-cyclohexene-1-carboxylate (**6**) (0.40 g, 50%) as prisms: Mp 115—116 °C. ^{1}H NMR ($CDCl_3$) δ=2.07 (3H, s) and 2.12 (3H, s) (OAc), 3.80 (3H, s, CO_2Me), 4.57 (1H, dd, $J_{3,4}$=2.7 Hz, $J_{4,5}$=4 Hz, H-4), 4.97 (1H, t, $J_{5,6}$=4 Hz, H-5), 5.49 (1H, dd, $J_{2,3}$=6.5 Hz, H-3), 6.03 (1H, d, H-2), 7.10 (1H, d, H-6).

Found: C, 34.97; H, 3.45; Br, 38.83%. Calcd for $C_{12}H_{14}Br_2O_6$: C, 34.81; H, 3.41; Br, 38.60%.

The third fraction (R_f 0.50) gave a syrup which crystallized from ethanol to give (±)-methyl (1,3/2,4)-2,3-diacetoxy-4-bromo-5-cyclohexene-1-carboxylate (**5**) (27 mg, 4%) as needles: Mp 91.5—93 °C. ^{1}H NMR ($CDCl_3$) δ=2.03 (3H, s) and 2.08 (3H, s) (OAc), 3.53 (1H, ddd, $J_{1,2}$=8.8 Hz, $J_{1,5}$=2.5, $J_{1,6}$=1.8 Hz, H-1), 3.74 (3H, s, CO_2Me), 4.06 (1H, ddd, $J_{3,4}$=7 Hz, $J_{4,5}$=2.5 Hz, $J_{4,6}$=1.8 Hz, H-4), 5.38—5.47 (2H, m, H-2 and H-3), 5.72 (1H, dt, $J_{5,6}$=10 Hz, H-6), 5.99 (1H, dt, H-5).

Found: C, 43.13; H, 4.59; Br, 23.97%. Calcd for $C_{12}H_{15}BrO_6$: C, 43.01; H, 4.51; Br, 23.84%.

The last fraction was concentrated to give a syrup (0.22 g) which was rechromatographed on silica gel (13 g) with acetone-hexane (1 : 5) as eluent to give as a major component (±)-methyl (1,3/2,6)-2,3-diacetoxy-6-bromo-4-cyclohexene-1-carboxylate (**3**) (32 mg, 5%) as needles (from benzene-hexane): Mp 78—79 °C. ^{1}H NMR ($CDCl_3$) δ=2.03 (6H, s, 2 OAc), 3.29 (1H, dd, $J_{1,2}$=10.5 Hz, $J_{1,6}$=9 Hz, H-1), 3.75 (3H, s, CO_2Me), 5.01 (1H, ddd, $J_{4,6}$=1.5 Hz, $J_{5,6}$=2.7 Hz, H-6), 5.24 (1H, dd, $J_{2,3}$=7.2 Hz, H-2), 5.47—5.66 (2H, m, H-3 and H-4), 6.03 (1H, dt, $J_{3,5}$=2.7 Hz, $J_{4,5}$=10 Hz, H-5).

Found: C, 43.22; H, 4.57; Br, 23.90%. Calcd for $C_{12}H_{15}BrO_6$: C, 43.01; H, 4.51; Br, 23.84%.

(±)-Methyl *trans*-5,6-Diacetoxy-1,3-cyclohexadiene-1-carboxylate (9). To a stirred solution of **6** (100 mg, 0.24 mmol) in acetic acid (1.0 mL) was added portionwise zinc dust (63 mg, 0.96 matom) at room temperature. After 10 min, TLC (2-butanone-toluene 1 : 5) showed a disappearance of **6** and formation of a single component (R_f 0.41). An insoluble material was removed by filtration and washed with ether (15 ml). The filtrate and washing were combined and washed successively with water, saturated sodium hydrogen carbonate, and aqueous sodium chloride, dried, and concentrated. The residual syrup (80 mg) was crystallized from aqueous ethanol to give **9** (52 mg, 83%) as prisms: Mp 80—81 °C. ^{1}H NMR ($CDCl_3$) δ=2.04 (6H, s, 2 OAc), 3.80 (3H, s, CO_2Me), 5.27 (1H, dd, $J_{4,5}$=4.5 Hz, $J_{5,6}$=1.7 Hz, H-5), 5.92 (1H, d, H-6), 6.33 (2H, m, H-3 and H-4), 7.28 (1H, dd, $J_{2,3}$=4.5, $J_{2,4}$=1.5 Hz, H-2).

Found: C, 56.46; H, 5.53%. Calcd for $C_{12}H_{14}O_6$: C, 56.69; H, 5.55%.

Epoxidation of 9 with MCPBA. A mixture of **9** (110 mg, 0.43 mmol), MCPBA (0.13 g, ca. 0.43 mmol), dichloromethane (3 ml), and phosphate buffer (pH 8, 3 ml) was stirred vigorously at room temperature for 3 d. TLC (ethyl acetate-hexane 1 : 3) showed a formation of one major (R_f 0.20) and one minor component (R_f 0.23). The mixture was diluted with dichloromethane (20 ml) and the solution was washed with aqueous 10% sodium thiosulfate, saturated sodium hydrogencarbonate, and water, and dried and concentrated. The residual syrup (0.11 g) was chromatographed on silica gel (5 g) with ethyl acetate-hexane (1 : 4) as eluent to give as a first fraction (±)-methyl 2,3-di-*O*-acetyl-4,5-anhydro-(2/3,4,5)-2,3,4,5-tetrahydroxy-6-cyclohexene-1-carboxylate (**11**) (15 mg, 13%) as prisms: Mp 82—84 °C (from ethanol). ^{1}H NMR ($CDCl_3$) δ=2.00 (3H, s) and 2.13 (3H, s) (OAc), 3.53 (1H, t, $J_{4,5}$= $J_{5,6}$=3.3 Hz, H-5), 3.64 (1H, dd, $J_{3,4}$=1.5 Hz, H-4), 3.74 (3H, s, CO_2Me), 5.33 (1H, dd, $J_{2,3}$=7.5 Hz, H-3), 5.88 (1H, dd, $J_{2,6}$=2.3 Hz, H-2), 7.05 (1H, dd, H-6).

Found: C, 53.36; H, 5.24%. Calcd for $C_{12}H_{14}O_7$: C, 53.34; H, 5.22%.

The second fraction gave (±)-methyl 2,3-di-*O*-acetyl-4,5-anhydro-(2,4,5/3)-2,3,4,5-tetrahydroxy-6-cyclohexene-1-carboxylate (**12**) (53 mg, 45%) as needles (from ethanol): Mp 104—105.5 °C. ^{1}H NMR ($CDCl_3$) δ=2.07 (6H, s, 2 OAc), 3.51 (1H, t, $J_{4,5}$= $J_{5,6}$=3.8 Hz, H-5), 3.72 (1H, dt, $J_{2,4}$= $J_{3,4}$=2.3 Hz, H-4), 3.80 (3H, s, CO_2Me), 5.46 (1H, t, $J_{2,3}$=2.3 Hz, H-3), 5.82 (1H, t, H-2), 7.50 (1H, d, H-6).

Found: C, 53.62; H, 5.30%.

We thank Mr. Saburo Nakada and Mr. Akio Takahashi for their elemental analyses.

References

1) B. A. Bohm, *Chem. Rev.*, **1965**, 435.
2) B. Ganem, *Tetrahedron*, **34**, 3353 (1978).
3) K. Tatsuta, T. Tsuchiya, N. Mikami, S. Umezawa, H. Naganawa, Y. Muraoka, Y. Okami, and H. Umezawa, *J. Antibiot.*, **27**, 579 (1974).
4) A. D. Argoudelis, R. W. Sprague, and T. Pyke, *J. Antibiot.*, **29**, 777 (1976); A. D. Argoudelis, R. W. Sprague, and S. A. Mizsak, *ibid.*, **29**, 787 (1976).
5) B. Zhu, M. Morioka, H. Nakamura, S. Umezawa, H. Umezawa, and H. Naganawa, *J. Antibiot.*, **37**, 673 (1984).
6) Recent synthetic work on shikimic acid: P. A. Bartlet and L. A. McQuaid, *J. Am. Chem. Soc.*, **106**, 7854(1984); H. Posner and D. G. Wettlaufer, *ibid.*, **108**, 7373 (1986).

7) C. Thebtaranonth and Y. Thebtaranonth, *Acc. Chem. Res.*, **19**, 84 (1986).
8) S. Ogawa, Y. Yato, K. Nakamura, M. Takata, and T. Takagaki, *Carbohydr. Res.*, **148**, 249 (1986).
9) This compound was not isolable in a pure form.
10) This compound was not obtained in a pure form and not stable enough for further purification.
11) S. Ogawa, T. Toyokuni, M. Ara, M. Suetsugu, and T. Suami, *Chem. Lett.*, **1980**, 379; *Bull. Chem. Soc. Jpn.*, **56**, 1710 (1983).
12) S. Ogawa, T. Toyokuni, T. Kondoh, Y. Hattori, S. Iwasaki, M. Suetsugu, and T. Suami, *Bull. Chem. Soc. Jpn.*, **54**, 2739 (1981).
13) Compound **9** was shown to be readily converted into **6** by treatment with bromine.
14) S. Ogawa, K. Nakamura, and T. Takagaki, *Bull. Chem. Soc. Jpn.*, **59**, 2956 (1986).

Ring Size Effect on [2+2] Photochemical Cycloaddition of Enones with Cyclic Olefins

Masahiro TADA* and Yuuki NIEDA
Tokyo University of Agriculture and Technology, Laboratory of Bio-organic Chemistry, Fuchu, Tokyo 183
(Received October 3, 1987)

Synopsis. Photochemical reaction of 3-substituted 2-cyclohexen-1-ones with methyl 1-cyclohexene-1-carboxylate gave only head-to-tail, cis-transoid-cis photoadduct. The photoadducts of 3-methyl-2-cyclohexen-1-one with methyl 1-cyclopentene-1-carboxylate and with methyl 1-cyclobutene-1-carboxylate had head-to-head, cis-transoid-cis ring systems.

Photochemical [2+2] cycloaddition of enones with olefins is one of the most famous photochemical reactions. The application of this reaction for the synthesis of natural products has been well-documented.[1] Corey et al.[2] and Loutfy and De Mayo[3] investigated the mechanism of photocycloaddition of enones with olefins in an attempt to explain the regio- and stereoselectivity. Weedon made a general statement concerning the stereochemistry of enone photochemical cycloaddition.[4] Wender reported that irradiation of 3-methyl-2-cyclohexen-1-one (**1**) with methyl 1-cyclobutene-1-carboxylate (**2**) produced a head-to-head, cis-transoid-cis photoadduct **3** in dichloromethane.[5] Lange obtained a similar head-to-head, cis-transoid-cis photoadduct **5** by the photochemical reaction of enone **1** with methyl 1-cyclopenetene-1-carboxylate (**4**) in toluene.[6] In the course of our synthetic investigation of natural products using photochemical cycloaddition, we found that the products of 3-substituted 2-cyclohexen-2-ones with methyl 1-cyclohexene-1-carboxylate have a head-to-tail, cis-transoid-cis ring system. We report here that the regiochemistry of the photoadducts of enone with cycloolefins is dependent on the ring size of the cycloolefins.

Results and Discussion

A dichloromethane solution of equimolar mixture of 3-methyl-2-cyclohexen-1-one (**1**) and methyl 1-cyclohexene-1-carboxylate (**6**) was irradiated by a 100 W high-pressure Hg-lamp for 8 hours. The photoadduct **7** was obtained in 74.4% yield along with unreacted starting materials. The same adduct was also obtained as a major product by the photochemical reaction of **1** with **6** in methanol, or in CH_3CN. The structure of the compound **7** was determined as follows. The compound **7** showed the M^+ at m/z 250 by mass spectrum and was found to have a ketone and an ester group by IR spectrum (1726, 1697, 1223. and 1155 cm^{-1}). The ^{13}C NMR spectrum of the compound **7**, showed the signals assigned to a ketone, a methyl ester, two methyls, 7 methylenes, 2 methines, a quaternary carbon and no C=C double bond. In the ^1H-^1H COSY of the compound **7** spectrum,[7] a large coupling (J=10.8 Hz) between the C-12H (δ 2.50, d, J=10.8 Hz) and the C-12H (δ 2.96, ddd, J=2.1, 5.2, 10.8 Hz) was observed. The coupling constants ($J_{1,12}$=10.8, $J_{12,11}$=5.2, and $J_{12,11}$=2.1 Hz) of compound **7** could be satisifactorily assigned only by one of the conformations of the cis-transoid-cis ring system. In the NOESY spectrum[8] of the compound **7**, cross peaks were appeared between C-6Me and C-1H. Whereas no NOE was observed between C-12H and C-1H, between C-12H and C-6Me and between C-12H and the ester methyl. Finally, the compound **7** was converted to a hydroxy ketone **8** by the successive treatment of acetalization, reduction, and hydrolysis (acetone-TsOH). The signal of C-12H of compound **8** was observed at higher chemical shift (δ 2.36, dd, J=5.0, 10.2 Hz) compared to that of the compound **3**, whereas no remarkable change of chemical shifts were observed on C-1H and C-6Me in ^1H NMR. These results reveal that the photoadduct **7** has a head-to-tail, cis-transoid-cis ring system.

The regiochemistry of the photoadduct **7** is different from that of the photoadducts **3** and **5**. The photochemical reaction of the other six-membered ring compounds were examined from the mechanistic interest.

The photochemical reaction of the enone **1** with 1-cyclohexene-1-carboxylic acid (**9**) gave a major product **10** under the similar conditions in CH_2Cl_2. The major product **10** was converted to the compound **7** by methylation with diazomethane showing that the major product of the photochemical reaction of the enone **1** with the acid **9** is a similar head-to-tail, cis-transoid-cis adduct **10** (9.3%). The photochemical reaction of the enone **1** with 1-cyclohexenylmethanol was very slow and no photoadduct obtained under similar conditions. Irradiation of the CH_2Cl_2 solution of the 2-cyclohexen-1-one (**11**) and the ester **6** for **5** hours gave a major product **12** (7.4%) with unreacted starting materials. The structure of **12** was clarified by the NMR spectra (^1H, ^{13}C NMR, and ^1H-^1H COSY) as in the case of the compound **7**. No photochemical reaction product was obtained by the irradiation of the CH_2Cl_2 solution of 3-methoxy-2-cyclohexen-1-one (**13**) and the ester **6** for 16 hours. Acetophenone (1%) was thus, used for a photosensitizer and the solution was irradiated for 8 hours to give a head-to-tail, cis-transoid-cis compound (**14**) in a yield of 10.5%. The structure proof of the product **14** was obtained from the NMR experiments (^1H, ^{13}C NMR, ^1H-^1H COSY, and NOESY). The signal of the C-12H (δ 2.47, ddd, J=2.5, 5.4, 10.8 Hz) of compound **14** was appeared in very similar splittung pattern as that of compound **7**.

In summary, photochemical cycloaddition of 3-substituted 2-cyclohexen-1-one with cyclohexene-1-carboxylic acid and with its ester gave head-to-tail, cis-transoid-cis compounds. The regiochemistry of the adduct **7**, **10**, **12**, and **14** are opposite to the photoadducts **3** and **5**. These results suggest that the difference of the regiochemistry of the photoadducts depends on

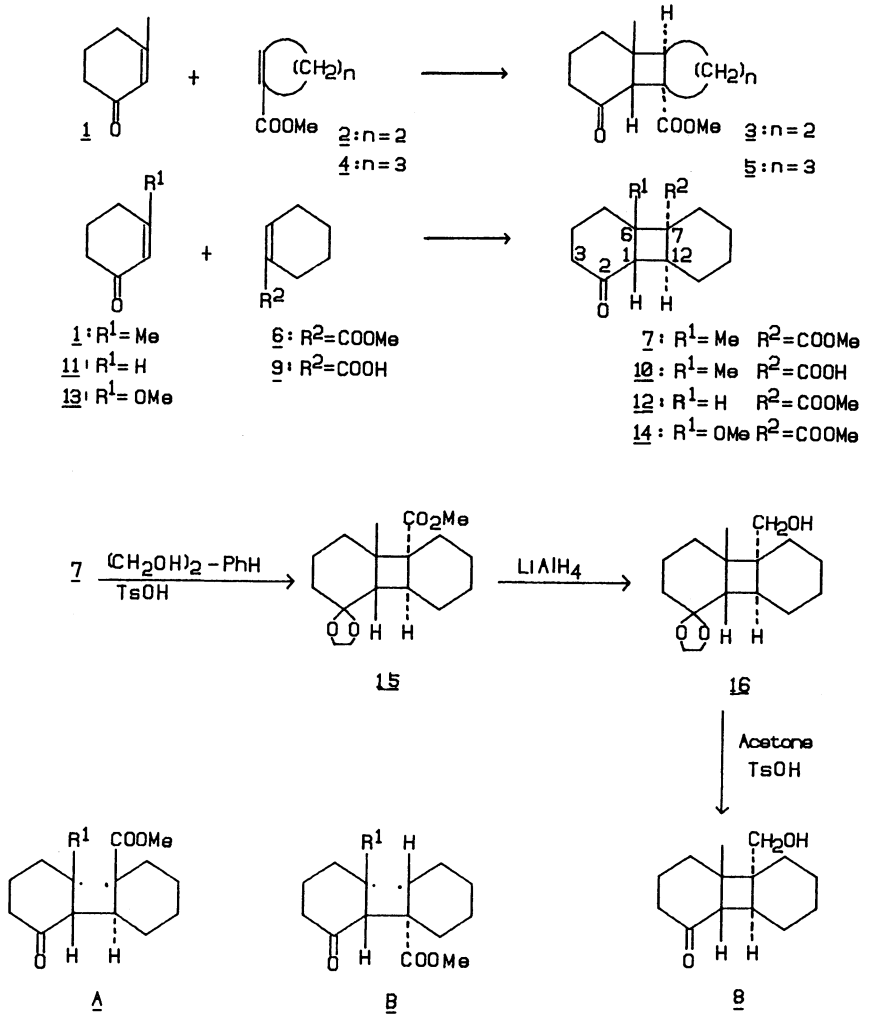

Fig. 1.

the ring size of the cyclic olefinic esters.

The photoadducts **7**, **10**, **12**, and **14** should be produced via the more stable biradical **A** rather than the less stable biradical **B**. The unambigious mechanistic explanation for the ring size effect could not be accomplished yet.

Experimental

NMR spectra were measured with a JEOL GX-270 spectrometer in $CDCl_3$ solution containing tetramethylsilane as an internal standard. IR spectra measured on JASCO IR-810 spectrometer. HPLC was performed on JASCO BIP-1 HPLC system with RI detector (RID-300) and silica-gel column (LiChrosorb Si-60 10 μm, 7,5 *500 mm). Thin-layer chromatography was carried out on Kieselgel GF_{254} (Merck) in 0.25 mm thickness. Wakogel C-200 (Wako Pure Chemical Industries) was used for column chromatography.

General Procedures for Irradiation of Enone with Olefin. The enone **1** (1 m mol, 110 mg) and the ester **6** (1 m mol, 140 mg) were dissolved in 50 ml of CH_2Cl_2, and the mixture was irradiated through Pyrex glass vessel for 8 h under nitrogen atmosphere with 100 W high-pressure Hg-lamp. The reaction mixture was concentrated, and the residue was column chromatographed on silica gel eluted with hexane-EtOAc and purified by HPLC to give 186.0 mg (74.4%) of **7**: IR (neat) 1726, 1697, 1223, 1155 cm^{-1}; ^1H NMR ($CDCl_3$) δ=3.72 (3H, s), 2.96 (1H, ddd, J=2.1, 5.2, 10.8 Hz), 2.50 (1H, d, J=10.8 Hz), 1.14 (3H, s); ^{13}C NMR ($CDCl_3$) δ=20.51(q), 21.15(t), 21.24(t), 21.59(t), 23.54(t), 27.54(t), 31,39(t), 36.83(d), 38.14(t), 44.92(s), 49.64(s), 50.17(d), 51.16(q), 175.70(s), 211.79(s); MS m/z 250.

Photochemical reaction of the other enones with olefins were performed by the similar procedures. The acid **10** was methylated with a ether solution of diazomethane as usual procedures before the separation. Acetophenone (1 mg) was added to the benzene (50 ml) solution of the enone **13** (117.5 mg) and the ester **6** (126.3 mg) as a photosensitizer before the irradiation. Compound **12**: ^1H NMR ($CDCl_3$) δ=3.70 (3H, s), 3.07 (1H, dd, J=5.4, 10.8 Hz), 2.90 (1H, dd, J=7.0, 10.8 Hz); ^{13}C NMR ($CDCl_3$) δ=21.29, 21.93, 22.32, 24.10, 24.32, 32.64, 38.79, 38.90, 41.51, 44.06, 46.81, 51.53, 175.56, 212.55; compound **14**: IR 1723, 1698 cm^{-1}; ^1H NMR ($CDCl_3$) δ=3.75 (3H, s), 3.31 (3H, s), 2.66 (1H, d, J=10.8 Hz), 2.47 (1H, ddd, J=2.5, 5.4, 10.8 Hz); ^{13}C NMR ($CDCl_3$) δ=19.18, 20.94, 21.15, 23.45, 25.08, 25.26, 23.03, 38.54, 50.34, 51.72, 51.88, 52.97, 80.52, 175.55, 210.78.

Acetalization of the Photoadduct 7. A mixture of **7** (96.6 mg), ethylene glycol (1 g), TsOH (5 mg), and benzene (20 ml) was refluxed for 12 h with Dean-Stark water trap. The raction mixture was poured into brine, and extracted with ether. The organic layer was washed with aqueous sodium carbonate (5%) and brine, dried over sodium sulfate and concentrated. The residue was column chromatographed on silica gel eluted with EtOAc to give the acetal **15** (70.4 mg, 62%): IR(neat) 1725, 1225, 1207 cm^{-1}; ^1H NMR ($CDCl_3$) δ= 1.08 (3H, s), 2.63 (1H, dd), 3.65 (1H, s), 3.9 (4H, m); ^{13}C NMR

($CDCl_3$) δ=19.93(t), 20.48(q), 21.88(t), 22.08(t), 24.06(t), 27.78(t), 31.70(t), 32.25(t), 33.78(d), 42.92(s), 43.36(d), 49.94(s), 51.00(q), 64.10(t), 64.14(t), 109.42(s), 176.68(s).

Reduction of Acetal 15. A solution of the acetal **15** (262.6 mg) in ether (10 ml) was added dropwise to a stirred slurry of lithium aluminum hydride (75 mg) in ether (10 ml). After being stirred for 3 h, saturated aqueous sodium sulfate solution was added and the product was extracted with ether. The ether solution was washed with brine, dried over sodium sulfate and evaporated. The silica-gel column chromatographed of the residue afforded the hydroxy acetal **16** (198 mg, 83.4%): IR (neat) 3450 (br.), 1093 cm^{-1}; ^1H NMR ($CDCl_3$) δ=1.05 (3H, s), 3.58 (1H, d, J=10.5 Hz), 3.67 (1H, d, J=10.5 Hz), 3.9 (4H, m); ^{13}C NMR ($CDCl_3$) δ=20.07, 21.63, 22.10, 22.14, 24.74, 25.57, 30.08, 32.28, 34.43, 41.10, 43.16, 43.58, 64.08, 64.12, 64.89, 109.83.

Deprotection of the Hydroxy Acetal 16. A solution of the hydroxy acetal **16** (53 mg) and TsOH (50 mg) in acetone (15 ml) was stirred for 16 h at room temperature. The reaction mixture was evaporated and the residue was disolved in EtOAc. The solution was washed with 5%-Na_2CO_3 and brine, and evaporated. The product was purified with HPLC to give the hydroxy ketone **8** (33 mg, 75%): IR (neat) 3480, 1680 cm^{-1}; ^1H NMR ($CDCl_3$) δ=3.73 (1H, d, J=11.1 Hz), 3.66 (1H, d, 11.1 Hz), 2.57 (1H, d, J=10.2 Hz), 2.36 (1H, dd, J=5.0, 10.2 Hz), 1.13 (3H, s); ^{13}C NMR ($CDCl_3$) δ=21.16, 21.28, 21.84, 22.06, 24.35, 25.70, 29.59, 37.77, 38.76, 43.12, 43.44, 50.84, 64.36, 213.54.

References

1) G. Desimoni, G. Tacconi, A Barco, and G. P. Pollini, "[2+2] cycloadditions" in "Natural Products Synthesis Through Pericyclic Reactions," American Chemical Society, Washigton, D.C. (1983), p. 33.

2) E. J. Corey, J. D. Bass, R. LeMahieu, and R. B. Mitra, *J. Am. Chem. Soc.*, **86**, 5570, (1964).

3) R. O. Loutfy and P. De Mayo, *J. Am. Chem. Soc.*, **99**, 3559 (1977).

4) A. C. Weedon, "Enone Photochemical Cycloaddition in Organic Synthesis" in "Synthetic Organic Photochemistry," ed by W. M. Horspool, Plenum Press, New York (1984), p. 92.

5) P. A. Wender and J. C. Hubbs, *J. Org. Chem.*, **45**, 365, (1980).

6) G. L. Lange, C. Decicco, and M. Lee, *Tetrahedron Lett.*, **28**, 2833 (1987).

7) W. P. Aue, E. Bartholdi, and R. R. Ernst, *J. Chem. Phys.*, **64**, 2229 (1976).

8) B. H. Meier and R. R. Ernst, *J. Am. Chem. Soc.*, **101**, 6441 (1979).

Unusual Concentration-Rate Profiles for Oxidation of a Pair of Associating Thiols

Jun-ichi KATO, Masato M. ITO, Kazuomi HAGINO, Narumi NAITOH, Makoto MISAKA, Einosuke FUJISHIRO, and Tadashi ENDO*

Department of Chemistry, College of Science and Engineering, Aoyama Gakuin University, Chitosedai, Setagaya-ku, Tokyo 157

(Received October 5, 1987)

Synopsis. In base-catalyzed oxidation of a pair of associating thiols [$HSCH_2$-CONHCONH-Ph and $HSCH_2CH_2$-NHCONHCO-C_6H_{13}] with oxygen, there are concentration regions where initial rates decrease with increasing concentrations of the thiols. For a pair of nonassociating thiols [$HSCH_2CO_2C_2H_5$ and $HSCH_2CH_2OH$], initial rates increase linearly with concentrations of the thiols.

Intermolecular association plays a very important role in controlling chemical reactions.[1-3] Recently, it has been found that, in oxidation of a pair of associating thiols (**1** and **2**), rate enhancement with time occurs in protic media.[4] We report here the unusual behavior of initial rates toward concentrations of the associating thiols in their oxidation.

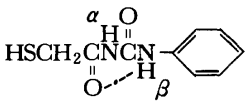

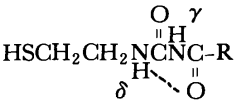

1 **2a** R = $(CH_2)_3CH_2CH_2CH_3$

b R = $(CH_2)_3CH(CH_3)_2$

c R =

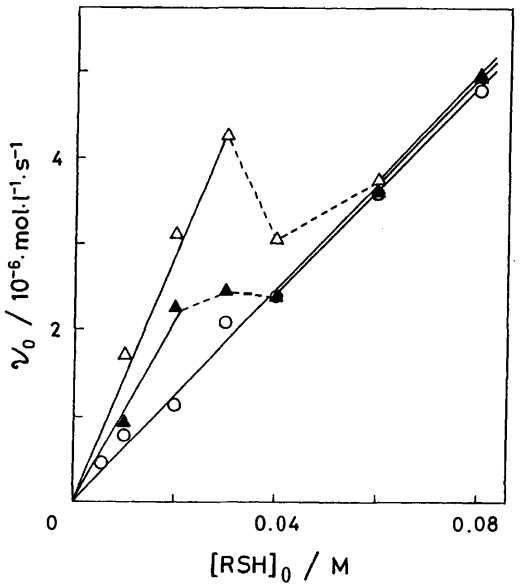

Fig. 1. Dependence of overall initial rates (v_0) for oxidation of 1:1 mixtures of **1** and **2** on initial concentrations of the thiols ([RSH]$_0$) in MeCN at 35.0°C. [RSH]$_0$=[**1**]$_0$+[**2**]$_0$; [Et_3N]=2.0×10^{-3} M. ▲, **1** and **2a**; △, **1** and **2b**; ○, **1** and **2c**.

Figure 1 plots the overall initial rates (v_0) — average rates until 5% consumption of thiols — for oxidation of 1:1 mixtures of **1** and **2** against the initial concentrations of the thiols ([RSH]$_0$) in oxygen-saturated acetonitrile (MeCN) at the fixed concentration of triethylamine (Et_3N) as a catalyst (35.0 °C). The v_0 for a cyclohexyl (c-C_6H_{11}) group used as R increases linearly with increasing [RSH]$_0$. On the other hand, for n-hexyl and isohexyl groups as R there exist concentration regions where the v_0 remains almost unaltered with [RSH]$_0$ (0.02—0.04 M (1 M=1 mol dm^{-3})) and decreases with increasing [RSH]$_0$ (0.03—0.04 M), respectively.

The concentration-initial rate profiles were further investigated in ethanol (Fig. 2). The v_0 for R=n-C_6H_{13} has proved to decrease with increasing [RSH]$_0$ in the 0.02—0.03 M range. In contrast, for R=c-C_6H_{11} the v_0 seems not to show appreciable changes in the 0.02—0.04 M range.

It appears that a deviation from a straight line in the concentration-initial rate profiles (Figs. 1 and 2) becomes more remarkable in EtOH than in MeCN: for R=c-C_6H_{11} a "normal linear" profile in MeCN changes into a "plateau" one in EtOH, for R=n-C_6H_{13} a "plateau" profile in MeCN changing into a "decrease" one in EtOH.

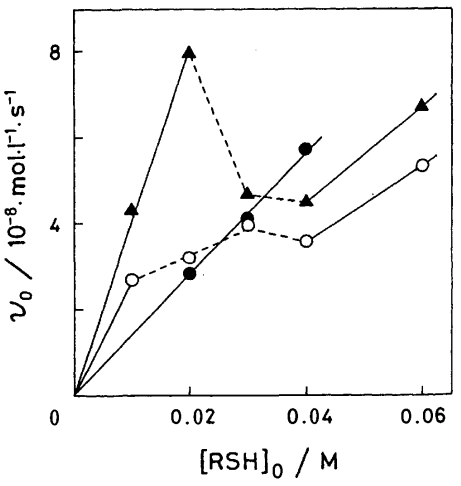

Fig. 2. Dependence of overall initial rates (v_0) for oxidation of 1:1 mixtures of **1** and **2** (or **3** and **4**) on initial concentrations of the thiols ([RSH]$_0$) in EtOH at 35.0°C. [RSH]$_0$=[**1**]$_0$+[**2**]$_0$ (or [**3**]$_0$+[**4**]$_0$); [Et_3N]=2.0×10^{-3} M. ▲, **1** and **2a**; ○, **1** and **2c**; ●, **3** and **4**.

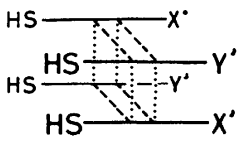

5

Fig. 3. Association scheme in a typical tetramer **5**. ----, Hydrogen bonds in dimers; ·····, noncovalent weak interactions responsible for stabilization of tetramers. The symbols X' and Y' represent Ph and R, respectively.

The $[RSH]_0$-v_0 plot for a pair of nonassociating thiols (**3** and **4**) shows a straight line in EtOH (Fig. 2). This control experiment demonstrates that "rate decrease" occurs for the associating thiols (**1** and **2**).

$HSCH_2CO_2C_2H_5$ $HSCH_2CH_2OH$

3 **4**

Thiols **1** and **2** have been shown to associate strongly with each other as well as with themselves in $CDCl_3$ via two NH···O intermolecular hydrogen bonds between the inner -NHCO- units in the -CONHCONH- group to form tetramers (reaction intermediates) such as **5** (Fig. 3).[1b,1c,5] In an attempt to elucidate the relationship between intermolecular association and the observed kinetic behavior, the following two experiments were carried out. First, NMR spectra of 1:1 mixtures of thiols **1** and **2b** were measured under nearly the same conditions as for the oxidation [i.e., at total concentrations of **1** and **2b** ($[RSH]$)=0.020, 0.030, and 0.040 M in CD_3CN at 35 °C].[6] The chemical shifts for the NH^{β} and NH^{δ} protons, which participate in intramolecular hydrogen bonds, remain constant [δ 10.28 (H^{β}) and 8.54 (H^{δ})] with [RSH], whereas the NH^{α} and NH^{γ} protons, which participate in intermolecular hydrogen bonds, undergo slight downfield shifts with increasing [RSH] from δ 8.69 to 8.74 (H^{α}) and from 8.27 to 8.33 (H^{γ}). Second, plots of $\ln([RSH]/[RSH]_0)$ against time in MeCN at 35.0 °C (Fig. 4) have revealed that oxidation of **1** and **2b** at $[RSH]_0$=0.020[4] and 0.030 M follows pseudo first-order kinetics, whereas at $[RSH]_0$=0.040 M an upward curvature is observed.[7] Though these results appear to be related to the unusual kinetic behavior mentioned above, it is difficult to explain the behavior by them.

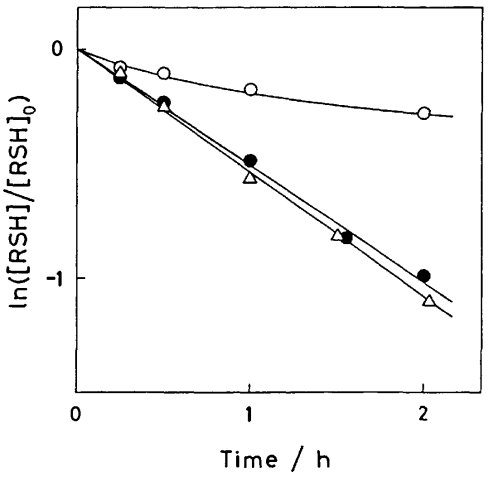

Fig. 4. First-order kinetic plots for oxidation of 1:1 mixtures of **1** and **2b** in MeCN at 35.0 °C. $[RSH]_0$=$[\mathbf{1}]_0$+$[\mathbf{2}]_0$; $[Et_3N]$=2.0×10^{-3} M. △, $[RSH]_0$=2.0×10^{-2} M; ●, $[RSH]_0$=3.0×10^{-2} M; ○, $[RSH]_0$=4.0×10^{-2} M.

From the experimental evidence presented here, it seems reasonable to conclude that intermolecular association is responsible for the unusual concentration-initial rate profiles for the oxidation.

Experimental

The melting points were uncorrected. ^1H NMR (270 MHz) spectra were measured on a JEOL GX-270 spectrometer using tetramethylsilane as an internal standard. The mass spectra were taken on a Hitachi RMU-6M mass spectrometer.

Materials. Organic solvents were dried by proper procedures,[8] and purified by distillation. Water was purified through Millipore Milli-Q water purification system followed by distillation. The iodine solution (0.001 M) containing potassium iodide (0.005 M) was titrated with 1.00×10^{-3} M aqueous sodium arsenite standard solution before use.

Thiol **1** was prepared as described previously,[1b] recrystallized from benzene-hexane, and had the following properties: Mp 127—128 °C; ^1H NMR (CD_3CN) δ=2.34 (1H, s), 3.34 (2H, s), 7.11 (1H, t, J=7 Hz), 7.33 (2H, dd, J=7 and 8 Hz), 7.51 (2H, d, J=8 Hz), 8.70 (1H, s, NH^{α}), 10.27 (1H, s, NH^{β}). Found: C, 51.32; H, 4.77; N, 13.21; S, 15.24%; M^+, 210. Calcd for $C_9H_{10}N_2O_2S$: C, 51.41; H, 4.79; N, 13.32; S, 15.25%; M, 210.

Thiols **2** were prepared as described before,[1b,9] and had the following properties.

2b: Mp 102.5—103.0°C (hexane-ether); ^1H NMR (CD_3CN) δ=0.88 (6H, d, J=6 Hz), 1.15—1.24 (2H, m), 1.50—1.65 (4H, m), 2.27 (2H, t, J=7 Hz), 2.60—2.68 (2H, m), 3.35—3.42 (2H, m), 8.38 (1H, s, NH^{γ}), 8.53 (1H, s, NH^{δ}). Found: C, 51.98; H, 8.55; N, 12.09; S, 13.99%; M^+, 232. Calcd for $C_{10}H_{20}N_2O_2S$: C, 51.70; H, 8.68; N, 12.06; S, 13.78%; M, 232.

2c: Mp 147—148 °C (ether); ^1H NMR (CD_3CN) δ=1.23—2.30 (11H, m), 2.60—2.68 (2H, m), 3.34—3.42 (2H, m), 8.34 (1H, s), 8.58 (1H, s). Found: C, 52.22; H, 7.94; N, 12.14; S, 13.80%; M^+, 230. Calcd for $C_{10}H_{18}N_2O_2S$: C, 52.15; H, 7.88; N, 12.16; S, 13.92%; M, 230.

Other thiols and Et_3N were purified by distillation through a fractionating column.

Kinetics. Equimolar amounts of the two thiols [**1** and **2** (or **3** and **4**)] were weighed into a two-necked flask, and dissolved in 10.00 ml of the reaction solvent. The solution was stirred under an oxygen atmosphere for at least 4 h in a well-stirred water bath thermostated to ±0.1 °C. Oxidation of thiols was negligible in the absence of Et_3N. At time zero, 2.0×10^{-5} mol of Et_3N was added to the solution with a microsyringe, and time measurement was begun. At appropriate time intervals, a 0.50 ml portion of the reaction mixture was pipetted out, and quenched in 5 ml of a 1:9 mixture of 3 M hydrochloric acid with the solvent. The amount of remaining thiols in the quenched solution was then determined by titration with the 0.001 M iodine solution. Each plot in Figs. 1 and 2 represents the average of generally six, or more runs.

References

1) a) T. Endo, A. Kuwahara, H. Tasai, T. Murata, M. Hashimoto, and T. Ishigami, *Nature (London)*, **268**, 74 (1977); b) T. Endo, A. Okubo, Y. Kaneko, M. Uehara, H.

Tasai, A. Sato, K. Nikki, N. Nakagawa, and S. Kamei, *Bull. Chem. Soc. Jpn.*, **55**, 2224 (1982); c) T. Endo, *Top. Curr. Chem.*, **128**, 91 (1985).

2) R. A. Moss, Y.-C. P. Chiang, and Y. Hui, *J. Am. Chem. Soc.*, **106**, 7506 (1984); R. Ueoka, R. A. Moss, S. Swarup, Y. Matsumoto, G. Strauss, and Y. Murakami, *ibid.*, **107**, 2185 (1985).

3) H. Pervez, L. Rees, and C. J. Suckling, *J. Chem. Soc., Chem. Commun.*, **1985**, 512.

4) M. M. Ito, T. Ogikubo, H. Ueda, K. Hagino, and T. Endo, *Bull. Chem. Soc. Jpn.*, **59**, 1263 (1986).

5) T. Endo, Y. Takeda, T. Orii, Y. Kaneko, and M. Kondo, *Chem. Lett.*, **1979**, 1455.

6) The NH protons were assigned on the basis of (i) comparison between chemical shifts for the NH protons of the 1 : 1 mixture and those of **1** and **2b** themselves (experimental section) and (ii) comparison of the concentration dependence of chemical shifts for the NH protons of the 1 : 1 mixtures with one another.

7) The rate of this type of Et_3N-catalyzed oxidation is shown to follow the equation $v=k_{1.7}[RSH][Et_3N]^{0.7}$ in aqueous MeCN (mole fraction of water=0.42) at 35.0 °C: T. Endo, M. Hashimoto, T. Orii, and M. M. Ito, *Bull. Chem. Soc. Jpn.*, **57**, 1562 (1984).

8) J. A. Riddick and W. B. Bunger, "Organic Solvents," 3rd ed, Wiley, New York (1970).

9) T. Endo, T. Ueda, T. Isago, J. Kato, T. Suzuki, M. Misaka, and M. M. Ito, *Bull. Chem. Soc. Jpn.*, **60**, 2298 (1987).

The Structure of Galantinamic Acid, a New Amino Acid in a Peptide Antibiotic Galantin I

Tateaki WAKAMIYA, Shin-ichi TERASHIMA, Mitsuyasu KAWATA, Tadashi TESHIMA, and Tetsuo SHIBA*
Department of Chemistry, Faculty of Science, Osaka University, Toyonaka, Osaka 560
(Received October 9, 1987)

Synopsis. A new amino acid named galantinamic acid was found as one of the constituent amino acids in a peptide antibiotic galantin I. The primary structure of galantinamic acid was determined chemically and spectrometrically to be 6,10-diamino-2,3,5-trihydroxydecanoic acid.

A peptide antibiotic galantin I was isolated from a culture broth of *Bacillus pulvifaciens* by Shoji et al.[1] The structure of galantin I was determined as shown in Fig. 1, in which we recognized two new amino acids, i.e., galantinic acid (**1**) and galantinamic acid (**2**).[2] An absolute structure of galantinic acid was determined chemically, spectrometrically,[3] and finally synthetically[4] to be (2*S*,4*S*,5*S*)-5-amino-2-carboxymethyl-4-hydroxytetrahydropyran. In this paper, we describe the determination of primary structure of galantinamic acid.

An isolation of galantinamic acid was carried out by ion-exchange column chromatography of the acid hydrolyzate of galantin I. For preparation of galantinamic acid, the acid hydrolysis of the peptide was ceased for 10 h in order to avoid an easy decomposition of this amino acid during the hydrolysis.[5] The observed pK_a values, 3.2, 8.7, and 10.5, for galantinamic acid suggested that this amino acid must be a diamino monocarboxylic acid but not an α-amino acid whose pK_1' value is generally around 2.4. The molecular formula of galantinamic acid was deduced to be $C_{10}H_{22}N_2O_5$ from the results of an elemental analysis and a determination of molecular weight by FD-MS spectrometry (m/z=251 $(M+H)^+$). This fact suggested the presence of three hydroxyl, two amino and one carboxyl groups in the molecule.

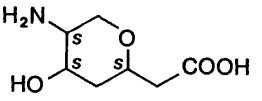

1 Galantinic acid

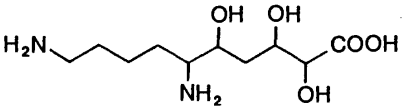

2 Galantinamic acid

The result of ^{1}H NMR analysis of galantinamic acid was summarized in Table 1. Four methine carbon atoms must carry OH or NH_2 as judged from the values of chemical shifts of their protons. Of these methine proton signals, a characteristic one appearing as doublet at δ 3.91 was first assigned to be α-methine proton connected to a carboxyl group suggesting us a presence of a partial structure such as -CH(**Y**)-CH(**X**)-COOH (**X**,**Y**=OH or NH_2). Since galantinamic acid is not an α-amino acid as described above, **X** is now deduced to be OH. The other proton at the highest field (δ 3.39) was assigned to be -CH(NH_2)-, since an irradiation to this proton caused a collapse at regions of two methine protons centered at δ 4.13 and of methylene protons centered at about δ 1.8 corresponding to -C-CH_2-C-. However, this proton did not couple with α-methine proton at δ 3.91. Thus, we could assign OH for **Y** to lead another partial structures of -C-CH_2-CH(NH_2)-CH(OH)- as well as -CH(OH)-CH(OH)-COOH. Furthermore, methylene signal at δ 3.01 was assigned to be NH_2CH_2- adjacent to -CH_2-C- type of methylene from the value of chemical shift and the coupling mode.

When we prepared *N*-benzoyl derivative of galantinamic acid, the IR spectrum of the derivative showed the absorption at 1735 cm^{-1} corresponding to ester or δ-lactone. Since there was no possibility of ester formation, δ-lactone was assumed to be formed under the acidic conditions after the *N*-benzoylation. Therefore, a partial structure can now be extended to -CH(OH)-

Table 1. ^{1}H NMR of Galantinamic Acid in D_2O

δ	Multiplicity	Supposed partial structure
1.8 (8H)	Multiplet	-C-**CH_2**-C- (×4)
3.01 (2H)	Triplet	-C-**CH_2**-N-
3.39 (1H)	Multiplet	-**CH_2**-N-
3.91 (1H)	Doublet	-CH-**CH**-COOH
4.13 (2H)	Multiplet	-**CH**-O- (×2)

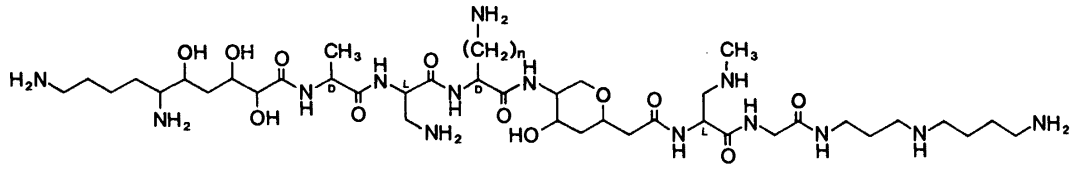

Fig. 1. The structure of galantin I which is a mixture of two congeners. Lysine (n=4) and ornithine (n=3) are found in a ratio of 9:1.

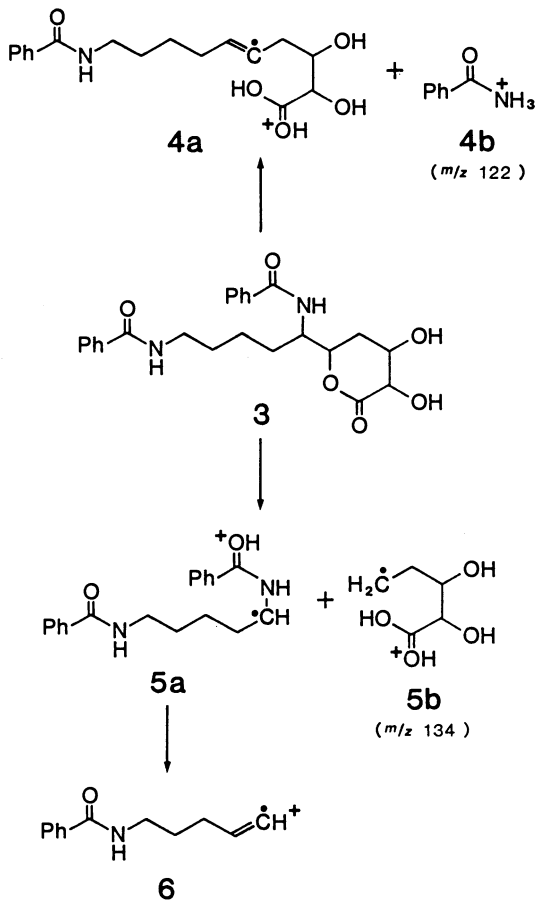

Fig. 2. Significant fragment ions observed in EI-MS spectrum of *N,N'*-dibenzoylgalantinamic acid lactone (**3**). The masses of fragments **4a**, **5a**, and **6** were exactly measured by high resolution method as summarized in Table 2.

Table 2. The Results of High-Resolution Mass Sprctrometry of Fragments **4a**, **5a**, and **6**.

Fragment	Molecular formula	EI-MS	
		Observed (*m/z*)	Calcd (M)
4a	$C_{17}H_{23}NO_5$	321.1590	321.1577
5a	$C_{19}H_{22}N_2O_2$	310.1710	310.1683
6	$C_{12}H_{14}NO$	188.1055	188.1076

C-CH(OH)-CH(OH)-COOH. As the results of above considerations, we can propose a following whole structure of galantinamic acid:

$NH_2CH_2CH_2CH_2CH_2CH(NH_2)$-
$CH(OH)CH_2CH(OH)CH(OH)COOH$.

The proposed structure was then confirmed chemically and spectrometrically. First, periodic acid oxidation followed by permanganate oxidation produced 5-aminovaleric acid which was derived from a part of $NH_2CH_2CH_2CH_2CH_2CH(NH_2)CH(OH)$-. Secondly, a study of high resolution EI-mass spectrometry of *N,N'*-dibenzoylgalantinamic acid lactone (**3**) gave quite important informations as shown in Fig. 2 and Table 2. For example, a fragment ion **5a** corresponding to $PhCONHCH_2CH_2CH_2CH_2CHNHC(=OH)^+Ph$ (*m/z* 310.1710) showed consistency with the molecular weight calculated as $C_{19}H_{22}N_2O_2$ (*m/z* 310.1683). Another two fragments, **4a** and **6**, also supported the proposed structure.

As described above, we could determine the primary structure of galantinamic acid, albeit the absolute structure was not assigned yet.[6]

Experimental

The NMR spectra were obtained with Varian XL-100-15 spectrometer for ^1H and JEOL JNM-FX-90Q spectrometer for ^{13}C in D_2O or CD_3OD. Sodium 2,2-dimethyl-2-silapentane-5-sulfonate was used as an external standard in D_2O or tetramethylsilane as an internal standard in CD_3OD. The chemical shifts were given in δ-value (ppm) from the standard. FD and EI mass spectra were measured with a JEOL JMS-O1SG-2 mass spectrometer. Amino acid analysis was carried out with a Hitachi KLA-5 amino acid analyzer.

Isolation of Galantinamic Acid. The acid hydrolyzate of galantin I (1.76 g)[3] was subjected to column chromatography over Amberlite IRC-50 (100—200 mesh, NH_4^+ form, 1.5×140 cm). Neutral amino acids were first eluted from the column by a gradient elution with 0.1—1.5% aqueous ammonia (1L). Basic amino acids were next separated by use of 1.5—5.6% aqueous ammonia (1L). The fractions containing galantinamic acid were concentrated in vacuo to obtain 160 mg of the crude material as hygroscopic powder. A part of crude galantinamic acid (110 mg) was dissolved in water and pH of the solution was adjusted to 6.5 with 0.01M HCl (1M=1 mol dm^{-3}). The neutralized solution was once concentrated in vacuo. To a solution of the residue in a small amount of water was added methanol. The methanolic solution was kept in a refrigerator to precipitate crystalline hydrochloride of galantinamic acid, yield 78 mg, mp 207.5—209 °C (decomp), $[\alpha]_D^{22}$ −0.4° (*c* 0.5, 1M HCl), amino acid analysis: 34 min (7.5 cm column, Hitachi #2611 resin, 0.35M citrate buffer (pH 5.28)). ^{13}C NMR (D_2O) δ=22.72 (C_8), 26.89 (C_9), 27.16 (C_7), 35.28 (C_4), 39.73 (C_{10}), 56.56 (C_6), 67.57 (C_5), 68.96 (C_3), 74.36 (C_2), 176.07 (C_1).

Found: C, 41.53; H, 8.23; N, 9.64; Cl, 12.10%. Calcd for $C_{10}H_{22}N_2O_5 \cdot HCl$: C, 41.88; H, 8.10; N, 9.77; Cl, 12.36%.

***N,N'*-Dibenzoylgalantinamic Acid δ-Lactone.** To a solution of free galantinamic acid (33 mg, 0.13 mmol) in water (4 mL) were added aqueous Na_2CO_3 (110 mg in 2 mL of H_2O) and benzoyl chloride gradually. A progress of the reaction was checked by TLC and addition of reagents was continued until the starting material disappeared. The alkaline solution was extracted with ether and ethyl acetate. Aqueous layer acidified with 1M HCl was extracted with ether twice and then concentrated in vacuo until colorless crystals deposited out. Crude product thus obtained was recrystallized from water, yield 42 mg (70%), mp 117.5—119.5°C. FD-MS: *m/z* 441 $[(M+H)^+]$, ^1H NMR(CD_3OD) δ=1.4—2.0 (m, 2H×4); 3.40 (t, 2H); 3.8—4.3 (m, 1H×4); 7.4 (m, 6H); 7.8 (m, 4H), IR (KBr): 1540, 1635, 1735 cm^{-1}.

Periodic-Permanganate Oxidation of Galantinamic Acid. To a solution of galantinamic acid (1.3 mg, 5.2 μmol) in 0.5 ml of water was added periodic acid ($HIO_4 \cdot 2H_2O$, 3.0 mg, 13 μmol) and the mixture was allowed to stand overnight at room temperature. To the solution was added 0.2% potassium permanganate solution until pale purple color remained. A small amount of MnO_2 was filtered off and the filtrate was used for TLC or amino acid analysis.

The authors wish to express their thanks to Dr. Junichi Shoji, Shionogi Research Laboratory,

Shionogi & Co. Ltd., for his generous supply of galantin I. We are grateful to Dr. Yasufumi Ohfune, Suntory Institute for Bioorganic Research, for his kind information about the synthetic study of galantinamic acid.

References

1) J. Shoji, R. Sakazaki, Y. Wakimasu, K. Koizumi, M. Mayama, and S. Matsuura, *J. Antibiot.*, **28**, 122 (1975).

2) T. Ando, S. Terashima, M. Kawata, T. Teshima, T. Wakamiya, and T. Shiba, "Peptide Chemistry 1980," ed by K. Okawa, Protein Research Foundation, Osaka (1981), p. 113.

3) T. Wakamiya, T. Ando, T. Teshima, and T. Shiba, *Bull. Chem. Soc. Jpn.*, **57**, 142 (1984).

4) Y. Ohfune and N. Kurokawa, *Tetrahedron Lett.*, **25**, 1587 (1984).

5) Hydrolysis for 24 h as a general condition caused a decomposition of more than 50% of galantinamic acid.

6) Recently, (2*R*,3*S*,5*S*,6*R*)-configuration for galantinamic acid was suggested from the synthetic study by Dr. Y. Ohfune (private communication).

Asymmetric Catalytic Hydrogenations of Oximes and Benzylimino Derivatives of Chiral Pyruvamides

Toratane MUNEGUMI and Kaoru HARADA*
Department of Chemistry, University of Tsukuba, Tennoudai, Tsukuba, Ibaraki 305
(Received November 6, 1987)

Synopsis. Oximes and benzylimino derivatives of chiral pyruvamides were hydrogenated over palladium hydroxide on charcoal in several solvents. Oximes of pyruvamides containing (*R*)-α-ethylbenzylamine as a chiral source gave (*S*)-alanine in excess (up to 70% e.e.) through the hydrolyses of the hydrogenated products.

In the previous study,[1] oximes of benzoylformamides whose chiral centers were (*S*)-α-methylbenzylamine, were hydrogenated over palladium on charcoal and then hydrolyzed to afford (*S*)-phenylglycine in a low e.e. (5.5%). On the other hand, the catalytic hydrogenations of chiral pyruvamides have given *N*-(*S*)-lactoyl-(*S*)-α-alkylbenzylamine with good asymmetric yields (up to 62%).[2] In the asymmetric catalytic hydrogenations, it was found that α-alkylbenzylamines were useful chiral moieties to stabilize the "chelated intermediates"[3] as shown in Fig. 1. However, asymmetric catalytic hydrogenations of oximes and Schiff bases of pyruvamides whose chiral centers are α-alkylbenzylamines have not been studied.

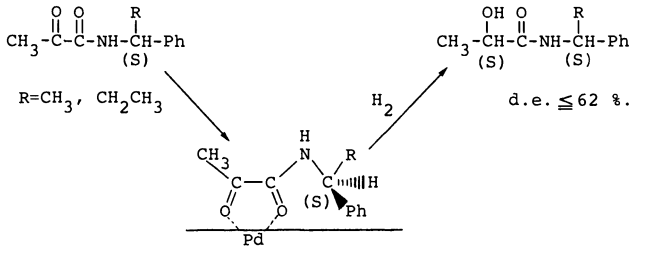

Fig. 1. Possible steric course in the catalytic hydrogenations of chiral pyruvamides **3a**, **b**.[3] d.e.: diastereoisomeric excess.

In this paper, we wish to report on the results of the asymmetric catalytic hydrogenations of oximes **5a—c** and Schiff bases **5d—f** of pyruvamides over palladium hydroxide on charcoal. Substrates **5a—f** were prepared as shown in Scheme 1. The catalytic hydrogenations were carried out in several solvents at 30 °C. After hydrolyses of the hydrogenated products, the chemical yields of alanine were determined by amino acid analyses and the enantiomeric excess (e.e.) were determined by gas chromatographic separation of the derivatized DL-alanine[*N*-(trifluoroacetyl)alanine isopropyl ester].

Results and Discussion

The results of the catalytic hydrogenations are shown in Table 1. Substrates **5a**, **b** whose chiral sources were (*S*)-amine and (*R*)-amine, gave (*R*)-alanine and (*S*)-alanine in excess respectively after hydrolyses of hydrogenated products. Substrate **5b** gave higher e.e. (up to 70%) than **5a** gave. Substrate **5c** whose chiral source was (*R*)-amine gave (*S*)-alanine with low e.e. These results suggested that the asymmetric induction was affected by the difference of the bulkiness between H and R groups bonded to the chiral carbon in the substrate molecules. There are two possible steric courses through which oximes **5a** give (*R*)-alanine. Those are steric course A (non-chelation mechanism) and B (chelation mechanism) as shown in Fig. 2.[4] In the first step (A-1) of the steric course A, the carbonyl and the imino groups take s-trans conformation owing to their electrostatic repulsion, and the H and R groups which are bonded to the chiral carbon interpose the NH group. The substrate molecule taking

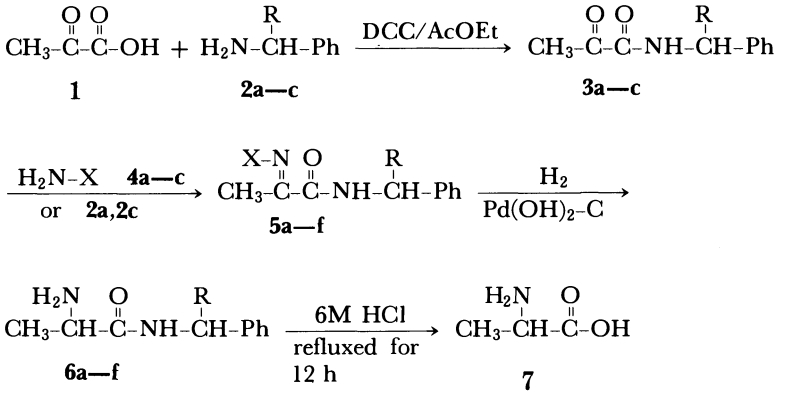

Scheme 1. **2a**, **3a**: R=Me (*S*); **2b**, **3b**: R=Et (*R*); **2c**, **3c**: R=Me (*R*); **4a**: X=OH; **4b**: X=OCH_2Ph; **4c**: X=CH_2Ph; **5a**: X=OH, R=Me (*S*); **5b**: X=OH, R=Et (*R*); **5c**: X=OCH_2Ph, R=Me (*R*); **5d**: X=CH_2Ph, R=Me (*R*); **5e**: X=—CH(Me)Ph (*S*); R=Me (*R*); **5f**: X=—CH(Me)Ph (*R*), R=Me (*R*).

Table 1. Asymmetric Catalytic Hydrogenations of Oximes and *N*-Benzylimino Derivatives at 30 °C

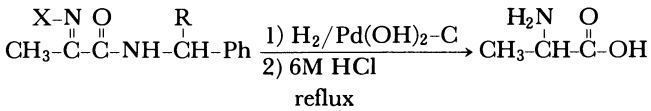

Substrate	R	X	Config.[a]	Solvent	Yield of Ala %	e.e. of Ala %	Config.[b]
5a	Me	OH	*S*	MeOH	52	47	*R*
			S	EtOH	31	34	*R*
			S	Pr^{i}OH	11	36	*R*
			S	AcOEt	42	15	*R*
5b	Et	OH	*R*	MeOH	58	70	*S*
			R	EtOH	21	45	*S*
			R	Pr^{i}OH	19	38	*S*
			R	AcOEt	25	20	*S*
5c	Me	OCH_2Ph	*R*	MeOH	39	15	*S*
5d	Me	OCH_2Ph	*R*	MeOH	61	3.7	*S*
5e		Me (S) -CHPh	*R*	MeOH	57	12	*S*
5f		Me (R) -CHPh	*R*	MeOH	61	0.3	*R*

a) Configuration of chiral amine in the amide moiety. b) Configuration of alanine.

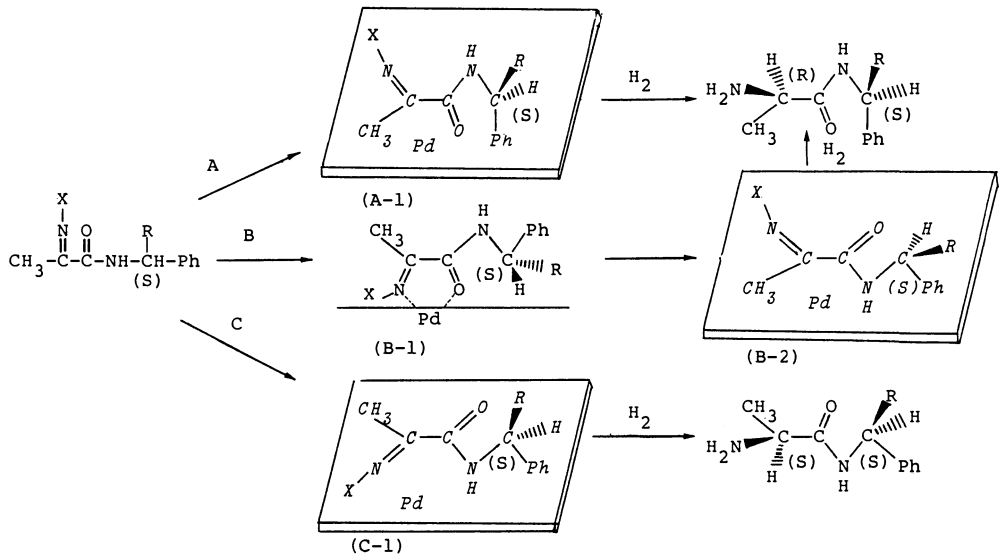

Fig. 2. Possible steric courses in the catalytic hydrogenations of oximes **5a—c** and *N*-benzylimino derivatives **5d, f.** X=OH, OCH_2Ph, CH_2Ph, CH(Me)Ph.

this conformation could be adsorbed on the palladium surface at the less bulky side of the molecule, and be hydrogenated from the catalyst side to give (*R*)-alanyl-(*S*)-amine. However, the steric course A seemed to contribute little to the asymmetric induction, since A-1 would be unstable due to the steric repulsion between C=O and Ph groups.

On the other hand, the steric course B could explain the stereochemistry of the catalytic hydrogenations. In the first step (B-1), the substrate molecule would stand on the catalyst surface by the carbonyl and oxime groups to form the "chelated intermediate," and the H and R groups interpose the carbonyl group as shown in Fig. 2. In the second step (B-2), the intermediate would be adsorbed at the less bulky side of the substrate on the catalyst, and then hydrogenated from the catalyst side to afford (*R*)-alanyl-(*S*)-amine. The steric course B could explain that the asymmetric induction in the catalytic hydrogenations was caused by the difference of the bulkiness between H and R groups of the asymmetric moiety.

The conformation around the N-C (chiral carbon)

bond of the "chelated intermediate" (B-1) is different from that in Fig. 1, which has been proposed[3] for the hydrogenation of pyruvamides **3a**, **b**. Since the bond length of α-carbonyl group(-C=O) of **3a**, **b** is shorter than that of oxime group (-C=N-OH) of **5a**, **b**, the space between the catalyst and the asymmetric moiety of **5a**, **b** is smaller than that of **3a**, **b**. Therefore, the H and R groups would prefer to interpose the amide carbonyl as shown in B-1 in Fig. 2. The low ee of alanine obtained from substrates **5c**, **d** could also be explained by the steric course B and C. The population of the substrate molecule which passes through the steric course B could be much smaller in the hydrogenations of substrates **5c**, **d** than **5a**, **b**, because the OCH_2Ph and CH_2Ph groups in the imino moiety would disturb the formation of the stable "chelated intermediates." And a part of the substrate molecules would pass through the steric course C rather than B, and afford (*S*)-alanine with low ee.

Although substrates **5e**, **f** have two chiral centers in the amide moiety(*R*) and the imino moiety[(*S*) or (*R*)], these substrates **5e**, **f** gave alanine with low ee. These low ee could also be explained by the instabilization of the "chelated intermediate" like in substrates **5c**, **d**.

In this study, the steric course in the catalytic hydrogenations of oximes **5a**, **c** and *N*-benzylimino derivatives **5d**, **f** of the chiral pyruvamides could be explained by the chelation mechanism. And a maximum ee (70%) of (*S*)-alanine was obtained in the hydrolysis of the hydrogenated product of substrate **5b** in methanol.

Experimental

The melting points were uncorrected. The optical rotations were measured with a Jasco DIP-181 Digital Polarimeter. The gas chromatographic analyses were carried out with a Hitachi 163 gas chromatograph, and the peaks on the chromatograms were integrated with a Sic Chromatocoda II. NMR spectra were measured with a Hitachi R-24 High Resolution NMR spectrometer. IR spectra were measured with a Hitachi 260-50 infrared spectrometer. Palladium hydroxide (10%) on charcoal were prepared by the similar manner in the literature.[5]

Materials. Chiral amines **2a** and **2c** were purchased from Aldrich chemical Co. **2a**. $[\alpha]_D^{20}$ −39.0 (neat), 96% ee[6] **2c**. $[\alpha]_D^{20}$ +39.0 (neat), 96% ee[6] **2b**. $[\alpha]_D^{17}$ +19.0 (neat) 95% ee.[7]

***N*-Pyruvoyl Amines 3a, b.** **3a**, **b** were prepared by the manner in the literature.[2]

Oximes of *N*-Pyruvoyl Amines 5a—c. Pyruvamides **3a** (1.03 g, 10 mmol) and hydroxylamine hydrochloride (2.08 g, 30 mmol) were dissolved in a mixture of ethanol and pyridine. The solution was refluxed for 3 h. The reaction mixture was evaporated in vacuo to dryness. The residue was redissolved in water (20 ml) and the solution was extracted with three 20 ml portions of ethyl acetate. The ethyl acetate layer was dried with anhydrous magnesium sulfate and was evaporated to give oily product. The oily product was purified with silica-gel column chromatography (benzene-ethyl acetate (5 : 1)) to give 1.13 g **5a** (55%). Mp 51—52 °C ^{1}H NMR ($CDCl_3$) δ=1.85 (3H, d, *J*=7Hz), 2.40 (3H, s), 5.40 (1H, m), 7.20 (1H, br), 7.45 (5H, s), 9.34 (1H, s). IR (KBr) 1530, 1650, 3400 cm^{-1}. Calcd for $C_{11}H_{14}N_2O_2$: C, 64.06; H, 6.84; N, 13.58%. Found: C, 63.82; H, 7.02; N, 13.17%. $[\alpha]_D^{29}$ +24.4 (*c* 1.05, methanol). **5b**. Yield, 37% (oil). ^{1}H NMR ($CDCl_3$) δ=0.90 (3H, t, 7.3 Hz), 1.80 (2H, q, 7.3 Hz), 2.05 (3H, s), 4.90 (1H, q, 7.3 Hz), 7.0—7.1 (1H, br), 7.28 (5H, s). IR (KBr) 1530, 1650, 3400 cm^{-1}. Calcd for $C_{12}H_{16}N_2O_2$: C, 65.43; H, 7.32; N, 12.71%. Found: C, 64.79; H, 7.42; N, 12.53%. $[\alpha]_D$ −14.7 (*c* 1.01, methanol). **5c**, Yield, 52%. Mp, 70—71 °C. ^{1}H NMR ($CDCl_3$) δ=1.50 (3H, d, 6.8 Hz), 2.05 (3H, s), 4.98—5.28 (1H, m), 5.20 (2H, s), 6.80—7.10 (1H, br), 7.31 (5H, s), 7.34 (5H, s). IR (KBr) 1530, 1650, 3400 cm^{-1}. Calcd for $C_{18}H_{20}N_2O_2$: C, 72.94; H, 6.80; N, 9.45%. Found: C, 72.87; H, 6.83; N, 9.41%. $[\alpha]_D^{20}$ −63.4 (*c* 1.03, methanol).

***N*-(2-Imino-1-oxopropyl) Amines 5d—f.** *N*-Pyruvoylamines **3c**, **d** (20 mg, 0.1 mmol) and benzylamine (50 μl, 0.46 mmol) were dissolved in dry benzene. The solution was stirred over anhydrous magnesium sulfate (600 mg) for 24 h. After drying agent was filtered off, the resulting filtrate was evaporated to dryness.

Catalytic Hydrogenation of Substrates 5a—f. Substrates **5a—f** (0.1 mmol) were dissolved in 3 ml of methanol, ethanol, 2-propanol, and ethyl acetate, and were hydrogenated over 10% palladium hydroxide on charcoal. After one to seven day's reaction at 30°C, the catalyst was filtered off and the filtrate was evaporated to dryness. The residue was used for hydrolysis without further purification.

Hydrolysis of Hydrogenated Products. The residue obtained by the evaporation of the hydrogenated product was hydrolyzed in 6M HCl (1M=1 mol dm^{-3}) for 12 h.

Determination of Chemical Yield and Enantiomeric Excess of Alanine. Chemical yields of alanine were determined by means of an amino acid analyzer. Enantiomeric excess of alanine was determined by the resolution of derivatized enatiomers of alanine [*N*-(trifluoroacetyl)alanine isopropyl ester) using a gas liquid chromatography equipped with a chiral glass capillary column (Chirasil-Val).[8]

References

1) K. Harada and K. Matsumoto, *J. Org. Chem.*, **32**, 1794 (1967).

2) K. Harada and T. Munegumi, *Bull. Chem. Soc. Jpn.*, **57**, 3203 (1984).

3) K. Harada, Asymmetric Heterogeneous Catalytic Hydrogenation, "Asymmetric Synthesis," ed by J. D. Morrison, Academic Press, New York (1985), Vol. 5, pp. 345—383.

4) T. Munegumi, M. Fujita, T. Maruyama, S. Shiono, M. Takasaki, and K. Harada, *Bull. Chem. Soc. Jpn.*, **60**, 249 (1987).

5) A. Skita and W. A. Meyer, *Ber.*, **45**, 3579 (1912).

6) A. J. Little, J. M. Lean, and F. J. Wilson, *J. Chem. Soc.*, **1940**, 336.

7) W. Theilaker and H. G. Winkler, *Chem. Ber.*, **87**, 691 (1954).

8) H. Frank, G. J. Nicolson, and E. Bayer, *J. Chromatogr.*, **146**, 197 (1978).

Catalytic Activity of *catena*-μ-Cyano-(phthalocyaninato)cobalt(III) for the Cathodic Reduction of Oxygen

Osamu IKEDA,†,* Shuji ITOH, and Hiroshi YONEYAMA*
Department of Applied Chemistry, Faculty of Engineering, Osaka University, 2-1 Yamadaoka, Suita, Osaka 565
(Received August 28, 1987)

Synopsis. *catena*-μ-Cyano-(phthalocyaninato)cobalt(III) showed a 4-electron reducibility for the cathodic reduction of oxygen at low overpotentials, which was not observed for (phthalocyaninato)cobalt(II) and chloro(phthalocyaninato)-cobalt(III).

Many of metal complexes of phthalocyanine, porphyrin and tetraazaannulene possess electrocatalytic activities for the cathodic reduction of oxygen. However, most of them catalyze the 2-electron pathway ($O_2+H_2O+2e^-\rightarrow HO_2^-+OH^-$). Therefore, the conversion of the 2-electron pathway to the 4-electron pathway ($O_2+2H_2O+4e^-\rightarrow 4OH^-$) has been tried by means of molecular designs; The preparations of face-to-face or cofacial porphyrins[1,2] and a planar binuclear complex[3] are typical examples. In the present study, catalytic activities of *catena*-μ-cyano-(phthalocyaninato)-cobalt(III) ($[Co^{III}(pc)CN]_n$), which has a stacked structure bridged by cyanide ions[4] as shown in Fig. 1, have been investigated to examine the effect of molecular designs.

Experimental

$[Co^{III}(pc)CN]_n$ was prepared from $Co^{II}(pc)$ via dichloro-(phthalocyaninato)cobal(III) $[Co^{III}(pc)(Cl)_2]$ and then via dicyano (phthalocyaninato)cobalt(III) $[Co^{III}(pc)(CN)_2]$.[4] $Co^{III}(pc)Cl$ was obtained by the thermal decomposition of $[Co^{III}(pc)(Cl)_2]$ in Ar atmosphere at 320 °C.[5] The formation of catenary $[Co^{III}(pc)CN]_n$ was confirmed by an IR spectrum ($\nu_{C\equiv N}$=2158 cm^{-1}) and a high conductivity ($\sigma=2\times10^{-3}$ $S\,cm^{-1}$)[5] of the resulting powders.

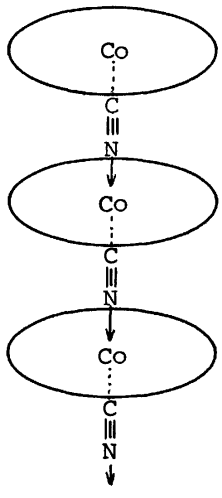

Fig. 1. Stacked structure of $[Co^{III}(pc)CN]_n$. Ellipses represent the phthalocyanine ring (pc(−2)).

(Phthalocyaninato)cobalt-coated disc electrodes were prepared by coating with use of a microsyringe *N,N*-dimethylacetamide (DMA) solutions containing either one of the above-mentioned (phthalocyaninato)cobalts onto a top surface of a glassy carbon rod (Tokai Carbon GC20; 6 mm diameter and 10 mm length) preheated to 80 °C on a hot plate. The amount of coating was 2×10^{-7} mol cm^{-2} for all cases. The GC rod was then installed into the disc cavity of a ring-disc electrode. The potential of the Pt ring was fixed to 0.3 V vs. SCE, where diffusion limiting currents due to oxidation of peroxide ions (HO_2^-) as a reduction intermediate of oxygen were observed. Aqueous 1 M (=mol dm^{-3}) KOH was used as the electrolytic solution.

Results and Discussion

Axial ligands of metallomacrocycles are apt to exchange with other competing ligands. In fact, $[Co^{III}(pc)CN]_n$ is known to be decomposed by organic bases (L) such as pyridine and piperadine to give monemeric $Co^{III}(pc)(CN)L$.[4] Since the catalytic activities for oxygen reduction were studied in an alkaline solution, it was then examined whether or not the phthalocyanines used were decomposed in contact with hydroxide ions. For this purpose, visible light absorption spectra were measured before and after addition of 1 M KOH to the DMA solutions of $Co^{III}(pc)Cl$ and $[Co^{III}(pc)CN]_n$, and before and after immersion of $[Co^{III}(pc)CN]_n$ and $Co^{III}(pc)Cl$-coated quartz plates into 1 M KOH. $Co^{III}(pc)Cl$ showed a spectrum change both in the DMA solution and in the coated films, suggesting that $Co^{III}(pc)Cl$ changed into $Co^{III}(pc)OH$ in the presence of OH^-. On the other hand, the spectra of $[Co^{III}(pc)CN]_n$ were little changed by contact with OH^-, suggesting that the Co-CN-Co bond is stable against OH^-. The stability of the axial ligand or the strength of the ligand-metal bond seems to roughly correspond to spectrochemical series for Co^{III}-complexes ($Cl^-<OH^-\ll CN^-$).

Figure 2 shows disc currents and ring currents of the rotating ring-disc electrodes as a function of the disc potential in oxygen-saturated 1 M KOH. There are differences in the electrochemical behaviors of the three kinds of (phtalocyaninato)cobalts at rising portion of the disc currents. In the case of $Co^{II}(pc)$ and $Co^{III}(pc)Cl$, though the actual form of the latter will be $Co^{III}(pc)OH$, disc and ring currents have the same onset potential. In the case of $[Co^{III}(pc)CN]_n$, however, there are negligible ring currents in an onset potential region of the disc currents. The results seem to suggest that oxygen is reduced to OH^- through the 4-electron pathway at the $[Co^{III}(pc)CN]_n$ but not at the $Co^{II}(pc)$ and $Co^{III}(pc)Cl$ electrodes.

In order to evaluate the 4-electron reducibility of the three kinds of (phtalocyaninato)cobalts, the apparent

† Present address: Department of Chemistry, College of Liberal Arts, Kanazawa University, 1-1 Marunouchi, Kanazawa 920.

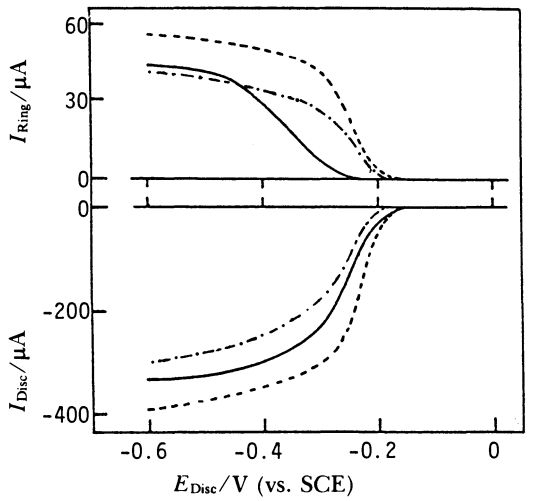

Fig. 2. Disc currents and ring currents at the ring(Pt)-disc(GC) coated with (----) Co^{II}(pc), (-·-·-) Co^{III}(pc)Cl, and (——) $[Co^{III}(pc)CN]_n$ electrodes as a function of disc potential in O_2-saturated 1 M KOH. Rotation rate, 1000 rpm; ring potential, 0.3 V vs. SCE; sweep rate at the disc, 20 mV s^{-1}; the disc area, 0.28 cm^2.

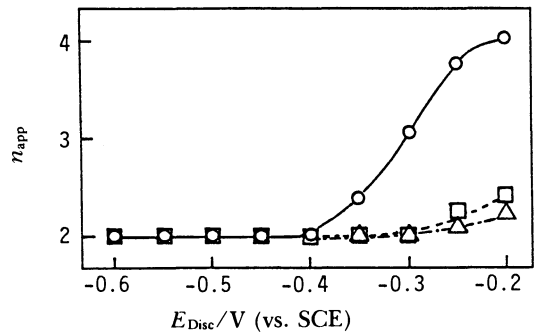

Fig. 3. Variation of n_{app} (apparent number of electrons involved in O_2 reduction) with disc potential for (○) $[Co^{III}(pc)CN]_n$, (△) Co^{III}(pc)Cl, and (□) Co^{II}(pc), respectively.

number of electrons involved in the oxygen reduction (n_{app}) was determined as a function of the disc electrode potentials. In the determination n_{app}, it was assumed that the O_2 reduction at the disc consisted of a mixed reaction of the 2-and 4-electron pathways. Thus, n_{app} was evaluated by the next relation: $n_{app}=4I_{Disc}/(I_{Disc}+I_{Ring}/N_{corr})$, where I_{Disc} and I_{Ring} are the disc and ring currents at a potential, respectively, and N_{corr} is the collection efficiency for HO_2^-, corrected for a deviation from coplanality between the Pt ring and the (phtalocyaninato)cobalt-coated disc.[4] The results are shown in Fig. 3. It is obvious from this figure that catenary $[Co^{III}(pc)CN]_n$ has a high 4-electron reducibility compared with monomeric Co^{II}(pc) and Co^{III}-(pc)Cl for oxygen reduction at low overpotentials.

In order to clarify the participation of redox of metal sites in the above oxygen reduction, the electrochemistry of Co^{II}(pc), Co^{III}(pc)Cl and $[Co^{III}(pc)CN]_n$ was studied by means of cyclic voltammetry of these (phtalocyaninato)cobalt-coated glassy carbon electrodes in deaerated 1 M KOH. However, clear redox peaks were not observed in the cyclic voltammograms between 0 V and −0.6 V vs. SCE for all catalysts. Furthermore, no detectable change was observed in visible absorption spectra of Co^{II}(pc), Co^{III}(pc)Cl, and $[Co^{III}(pc)CN]_n$ on an optically transparent electrode (In_2O_3/quartz) between 0 V and −0.6 V vs. SCE. Each spectrum was almost the same as that at open circuit in 1 M KOH. These results suggest that the oxygen reduction mechanism in the present catalysts is not controlled by the redox of metal sites.

Therefore, the results for oxygen reduction in Figs. 2 and 3 are discussed on the basis of d-electron configuration of cobalt ions and molecular conformation of the phtalocyanines as follows. The effective magnetic moment μ_{eff} of Co^{II}(pc) has been reported to be 2.7 μ_B (Bohr Magneton),[7] and the d-electron configuration of Co(II) is estimated to be $(d_{xy})^2(d\pi)^4(d_z^2)^1$.[8] Exerimental values of μ_{eff} for Co^{III}(pc)Cl and $[Co^{III}(pc)CN]_n$ were 3.1 and 1.0 μ_B, respectively. The spin only equation for magnetically diluted substances roughly predicts that the number of unpaired electrons is 2 for Co^{III}(pc)Cl and 0 for $[Co^{III}(pc)CN]_n$. Consequently, the d-electron configuration of Co^{III}(pc)OH which will be the actual form of Co^{III}(pc)Cl in 1 M KOH, will be the same as that of Co^{III}(pc)Cl, because the ligand field strength would not be so different between Cl^- and OH^-.

Both Co^{II}(pc) and Co^{III}(pc)Cl have an unpaired electron on d_z^2 orbital of the central cobalt ions, which facilitates an interaction with the oxygen $1\pi_g^*$ orbital. This interaction leads to the 2-electron pathway for oxygen reduction through its end-on coordination.[9] The cobalt ion in $[Co^{III}(pc)CN]_n$ has an empty d_z^2 orbital, which offers a favorable condition for the 4-electron pathway, because the σ-coordination of the oxygen $1\pi_u$ electron to the empty cobalt d_z^2 orbital and the π-back donation of d_π electrons to the oxygen $1\pi_g^*$ orbital facilitate the side-on coordination of oxygen.[10] However, such a side-on coordination is expected only at the terminal cobalt ions in the stacked structure of $[Co^{III}(pc)CN]_n$. In order to obtain the observed peculiar effect of the Co-CN-Co bridge for the 4-electron reduction of oxygen, we have to assume that an oxygen makes a bridge type coordination between two cobalt ions.[11] The intermetallic distance separated by the cyanide ions of $[Co(pc)CN]_n$ was estimated to be 4—5 Å, which is fitted well in making the bridge type coordination of oxygen.[1] However, the interaction between a filled d_π orbital or paired electrons and the oxygen $1\pi_g^*$ orbital electron seems to be weak, because the latter has a radical character. The μ_{eff} of $[Co(pc)CN]_n$ was not real zero but 1.0 μ_B, suggesting that there is a small unparing character in the d_π orbital. Probably, this unpairing character allows the bridge type coordination of oxygen leading to the 4-electron pathway, but it may disappear with increasing the overpotential. Thus, the 2-electron pathway becomes predominant.

The potential dependence of n_{app} for $[Co^{III}(pc)CN]_n$ was reproduced even after 100 potential sweep cycles between 0 V and −0.6 V vs. SCE. The result suggests that the molecular conformation of $[Co^{III}(pc)CN]_n$ is

also stable against the potential sweep cycles.

References

1) J. P. Collman, M. Marrocco, C. Koval, and F. C. Anson, *J. Am. Chem. Soc.*, **103**, 6027 (1980).
2) H. Y. Liu, M. Weaver, C. Wang and C. Chang, *J. Electroanal. Chem. Interfacial Electrochem.*, **145**, 439 (1983).
3) E. Yeager, *Electrochim. Acta*, **29**, 1527 (1984).
4) J. Metz, and M. Hanack, *J. Am. Chem. Soc.*, **105**, 828 (1983).
5) M. Hanack, *Mol. Cryst. Liq. Cryst.*, **105**, 133 (1984).
6) O. Ikeda, H. Fukuda, and H. Tamura, *J. Chem. Soc., Farady Trans. 1*, **82**, 1561 (1986).
7) R. L. Carlin, "Transition Metal Chemistry," Marcel Dekker, New York (1965), Vol. 1, p. 30.
8) G. A. Williams and B. N. Figgis, *J. Chem. Soc., Dalton Trans.*, **1981**, 734.
9) L. Pauling, *Nature (London)*, **203**, 182 (1964).
10) J. S. Griffith, *Proc. R. Soc. London, Ser. A*, **235**, 23 (1956).
11) E. Yeager, *J. Electrochem. Soc.*, **128**, 160C (1981).

New Description of the Substituent Effect on Electronic Spectra by Means of Substituent Constants. V. n-π^* Transition of Aliphatic Carbonyl Groups

Bunji UNO, Kenji KANO, Noriya HOSOI, and Tanekazu KUBOTA*
Gifu Pharmaceutical University, 5-6-1, Mitahora-higashi, Gifu 502
(Received August 31, 1987)

Synopsis. The substituent (X) effect on the carbonyl n-π^* band of CH_3COX is discussed on the basis of a general equation, theoretically derived in order to express the substituent effect on electronic spectra using substituent constants. The results have been successful and are supported by MO calculations.

In this series[1] we have reported a new description of the substituent effect on the electronic spectra by means of substituent constants, since the theoretical background of this kind study has so far been ambiguous.[1] We have used Eqs. 1 and 2 by focusing special attention on the fact that the substituent effect on the electronic ground and excited states is very different:[2]

$$^{1,3}E^{UV}_{ho\rightarrow lu} = aF + bR + c \quad (1)$$

and

$$^{1,3}E^{UV}_{ho\rightarrow lu} = \alpha\sigma_i + \beta\sigma_\pi^+ + \gamma\sigma_\pi^- + c. \quad (2)$$

Here, F and R are Swain's substituent constants,[3] and σ_i, σ_π^+, and σ_π^- are Yukawa-Tsuno-Sawada's substituent constants.[4] Singlet or triplet transition energy is expressed by $^{1,3}E^{UV}_{ho\rightarrow lu}$, which is mainly contributed from the HOMO→LUMO transition and has the same spectral character in a series of substituents. These equations were derived as an extension of Eq. 3, discussed previously:[5]

$$(E^{oxd}_{1/2} - E^{red}_{1/2}) = k_1 \cdot {}^{1,3}E^{UV}_{ho\rightarrow lu} + k_2. \quad (3)$$

It is noteworthy to point out that the substituent dependence of half-wave oxidation ($E^{oxd}_{1/2}$) and reduction ($E^{red}_{1/2}$) potentials is quite different,[1,5] just as a different behaviour is observed for the substituent effect on the electronic ground and excited states.[2] An important condition is that the various kinds of substituent constants (σ_p, σ_m, σ^+, σ^-, σ^* etc.) reported hitherto can be expressed in the form $[fF+rR+c]$ for aromatic and aliphatic systems, or by $[l\sigma_i+m\sigma_\pi^+ + n\sigma_\pi^-]$ for π-electron systems. The former and the latter are satisfied by employing the substituent constants proposed by Swain[3] and Yukawa-Tsuno-Sawada,[4] respectively. In addition to our foregoing results that the HOMO→LUMO type π-π^* bands, n-π^* bands of aromatic systems, and charge-transfer spectra of EDA complexes well satisfy Eqs. 1 and 2, we report here that the n-π^* band of aliphatic carbonyl groups of the type CH_3COX is also well described by the application of Eq. 1.

Experimental

Samples. Here, we have used substances of the type CH_3COX, where X is H, CH_3, C_2H_5, $C(CH_3)_3$, CF_3, Cl, Br, OH, OCH_3, OC_2H_5, $O(CH_2)_2CH_3$, NH_2, $COCH_3$, $COOC_2H_5$. All the samples are commercially available. Special guaranty reagents or spectrograde purity reagents of X=CH_3, C_2H_5, $C(CH_3)_3$, OCH_3, OC_2H_5, $O(CH_2)_2CH_3$ were repeatedly distilled in normal or reduced pressure under a nitrogen atmosphere. Analyzed-grade acetic acid for precise analytical chemistry was used without further treatment. The other samples (X=H, Cl, Br, $COCH_3$, $COOC_2H_5$, CF_3) were all special guaranty reagents and were employed for spectral measurements without further treatment.

Spectral Measurements. These were performed in the usual manner with a Hitachi spectrophotometer, Model 323, at room temperature. In order to make it possible to record the spectra at shorter wavelengths (as much as possible), the inside air in the spectrometer and the cell compartment was replaced with N_2 gas, and a gas stream was maintained during measurements. Although 10- and 2-mm matched quartz cells were usually used for spectral measurements, in the case of samples having a hydrogen bond formation ability, just like acetic acid, we also used quartz cells with long pass lengths, so that diluted solutions of the samples would be possible for recording the spectra; also, the hydrogen bonding effect on n-π^* bands was diminished, since this kind of effect brings about a blue shift of the bands.[2] Nevertheless, the concentration of acetic acid was about 3×10^{-3} mol dm^{-3}. The dimer formation constant of acetic acid was reported as being 2370 in CCl_4,[6] so that about 67% of 3×10^{-3} mol dm^{-3} was still in the dimer form. We then excluded acetic acid from the present regression study. Also, CH_3CONH_2 was not employed here, since it is not only insoluble in heptane, but its n-π^* band is not clearly recorded in CH_3CN, since that band is hidden in the tail of the strong carbonyl π-π^* band.[7] Solvents used were heptane and acetonitrile of spectrograde purity, which were dried over CaH_2 and then carefully distilled.

Molecular Orbital (MO) Calculation. In order to analyze the character of the n-π^* bands of the carbonyl groups we performed a MO calculation by means of the CNDO/S method proposed by the Jaffé and Duke groups.[8] Such parameter values as the Slater exponent (μ), bonding constant ($-\beta_X^0$), one-center repulsion integral (γ_{XX}), ($I_P^S+E_A^S$), and ($I_P^P+E_A^P$) are the same as those employed in our previous papers.[1] The molecular geometries were assumed to be as follows. When X in CH_3COX is alkyl or alkoxyl groups the carbon or oxygen atom in the substituent X, which bonds directly to the C=O group carbon atom, is put in the same plane as that of (H_3)**C-C=O**, where the carbonyl group carbon atom is in sp^2 hybridization ($\angle120°$). The conformation was assumed to be staggerd, as in Form I, and such substitu-

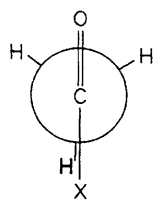

Form I

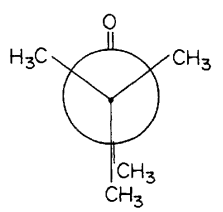

Form II

ents (X) as *O*-alkyl, $OCOCH_3$, $COCH_3$, $COOC_2H_5$, and alkyl groups are linearly extended in a zig-zag type arrangement, which seems to be in the most reduced steric hindrance. In the case of $X=C(CH_3)_3$ the configuration of Form II was used. All the bond lengths are taken from Ref. 9. The bond angles used are 109°28′, except for the sp^2 carbon atoms with 120°. The substituent effect on n- and π-orbital energies was also checked by ab initio calculations using the 4-31G basis set under the same molecular geometries as mentioned above. CNDO/S calculations were carried out with a FACOM M-382 computer in the Nagoya University Computation Center, the 4-31G ab initio calculations being made with a HITAC M-680 Computer at the Institute for Molecular Science (IMS) using the IMS library program "IMSPACK".

Results and Discussion

The Nature of n-π* Bands of Aliphatic Carbonyl Substances. Aliphatic carbonyl compounds are typical examples that show clearly weak n-π* bands in a near UV region; thus many studies have been made and reported. Nagakura, Baba, McMurry, Kasha, and McConnell first interpreted the electronic structures and spectra of carbonyl substances by means of molecular orbital theory and discussed the substituent and solvent effects on the n-π* bands.[10] They thus gave a theoretical background regarding the experimental facts that n-π* bands bring about a blue shift by the introduction of electron donating substituents, like OH and NH_2, and also in solvents with a hydrogen bonding ability. Many subsequent investigations have supported these results. We discuss the above substituent effect from the viewpoint of substituent constants. The aliphatic ketones employed here clearly exhibit an n-π* band in the near UV region (200—400 nm) with $\varepsilon=10$—60, some typical spectra in heptane being illustrated in Fig. 1. In Table 1 are listed the spectral data and the orbital energies of the n-HOMO and π*-LUMO calculated by an ab initio 4-31G basis set and

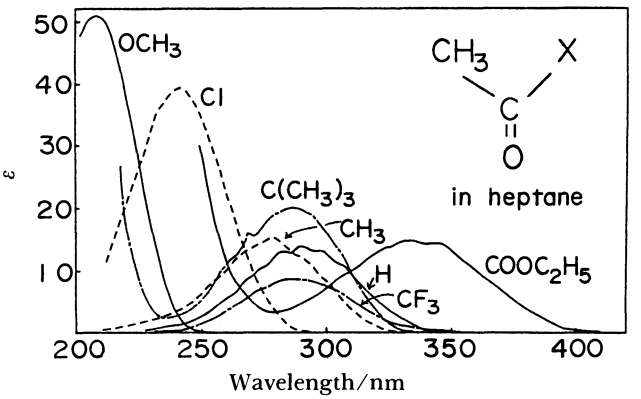

Fig. 1. Absorption spectra of carbonyl n-π* bands of CH_3COX with various substituents X.

the CNDO/S method. The character of the n-π* band of ketones studied was checked by a CNDO/S-CI calculation, which clearly showed that the above-mentioned n-π* bands are strongly (more than 90%) localized in a single configuration contributed from the transition to a π-type LUMO from an n-type HOMO and, thus, having a similar spectral nature. Exceptional compounds are, however, $X=COCH_3$ and $COOC_2H_5$. These have two carbonyl groups in a molecule, so that nonbonding orbitals localized in the two carbonyl group oxygen atoms interact with each other; there therefore occur two n-type occupied MO's, localized mainly at the carbonyl group oxygen atoms. Consequently, the second n-π* configuration is mixed in the first n-π* transition, that is the main configuration, and the longest wavelength n-π* band is quite red shifted.[11] The correlation of the observed n-π* band energies ($E^{obs}_{n-\pi^*}$) to the CNDO/S calculated ones ($E^{calcd}_{n-\pi^*}$) is however relatively good: $E^{obs}_{n-\pi^*}=1.82E^{calcd}_{n-\pi^*}-1.50$ in eV unit with a correlation coefficient $r=0.914$ (sample number $n=11$: see Table 1).

Table 1. Observed First n-π* Transition Energies and Calculated n-HOMO and π*-LUMO Energies for Aliphatic Ketones CH_3COX

X	Obseved n-π* band[a]				Calculated orbital energy/eV			
	in heptane		in CH_3CN		CNDO/S		ab initio 4-31G	
	E/eV	ε_{max}	E/eV	ε_{max}	n-HOMO	π*-LUMO	n-HOMO	π*-LUMO
H	4.283	14.0	4.343	15.7	−12.221	−0.625	−11.536	3.974
CH_3	4.455	14.6	4.522	15.2	−11.650	−0.305	−11.074	4.163
C_2H_5	4.460	16.8	4.500	18.0	−11.553	−0.279	−11.030	4.160
$C(CH_3)_3$	4.313	20.1	4.353	22.4	−11.241	−0.167	−10.786	4.120
Cl	5.130	39.6	5.205	43.4	−12.569	−1.108	−12.234	3.240
Br	5.134	99.5	—[b]	—[b]				
OH	5.939[c]	43.8[c]	—[d]	—[d]	−12.596	−0.720	−12.268	4.496
OCH_3	5.871	51.3	5.952	56.4	−12.357	−0.559	−12.133	4.622
OC_2H_5	5.848	58.0	5.915	60.3	−12.275	−0.522	−12.041	4.653
$O(CH_2)_2CH_3$	5.868	58.0	5.924	55.7	−12.254	−0.507	−12.004	4.532
CF_3	4.298	8.75	4.360	14.1	−12.444	−1.222	−12.879	2.255
$COOC_2H_5$	3.718	14.8	3.774	19.9				
$COCH_3$	2.959	2.61	2.994	2.45				

a) ε_{max} means molar absorption coefficient at the wavenumber of the maximum absorption. b) Acetonitrile solution of acetylbromide is unstable and gradually turns out to be yellow. c) This spectral data are not for the monomer alone, but for the mixture of dimer and monomer of acetic acid. See experimental section in the text. d) The spectra of acetic acid was not recorded because of the end absorption of CH_3CN.

Application of Substituent Constants to the n-π* Band of Aliphatic Ketones. The conditions discussed in the foregoing section necessarily lead to the conclusion that the carbonyl n-π* bands can be explained using Eq. 1, except for diketones. The results of a multiregression analysis for the spectral data in heptane is given in Fig. 2. The agreement between the observed and calculated n-π* band energies is very good. Experimental data in CH_3CN (see Table 1) also gave a regression equation similar to that given in Fig. 2: i. e. $^1E^{UV}_{n-\pi^*}=0.960F-0.629R+4.28$ ($n=9$, $r=0.996$). In these regression equations the fact that the contribution of the F term is larger than that of the R term seems to be reasonable (as discussed below). The n and π* orbital energies are listed in Table 1. Regression equations using the F and R constants for 4-31G calculation results are as follows: $\varepsilon_n=-1.941F-0.243R-11.255$ ($n=9$, $r=0.952$) for the n-orbitals, and $\varepsilon_{\pi^*}=-1.206F-0.881R+3.800$ ($n=9$, $r=0.992$) for the π*-LUMO orbitals. It is understood that both the n and π* orbital energies are well described by the two substituent constants, but that the contribution from the F term is extraordinarily large for the ε_n values, showing that the field and inductive effect is predominant for the substituent effect on the nonbonding orbital. The same conclusion as these was also obtained from an analysis utilizing the CNDO/S orbital energies. This is of course reflected in the regression equation in Fig. 2. Kobayashi and Nakamoto[12] discussed in 1949 the substituent effect on aliphatic carbonyl n-π* bands as a function of the charge density at the alpha-atom of >C=O group. Later, Rao et al.[13] studied only the alkyl (X) group substituent effect on the CH_3COX n-π* bands using the Taft σ* constant. In principle, however, attention was only payed to the substituent effect on the ground state, and the effect on n-π* excited states was explicitly disregarded. Our present treatment makes it possible for the first time to describe the ground and excited states by the same substituent constants; also, the present results applied to the carbonyl n-π* bands are quite good and are compatible with the results from the MO calculations. The correlation equation given in Fig. 2 leads to 6.16 eV (201 nm) for the n-π* band of CH_3CONH_2 in heptane. We think that the accurate singlet n-π* band position of CH_3CONH_2 has still not been reported,[7] and that the data estimated by some authors are contradictory to each other.[7,14-17] Our present estimation shows that the n-π* band is at a shorter wavelength than that (211 nm in heptane) of CH_3COOCH_3; this is in agreement with Nagakura's opinion,[7] who says that the n-π* band of CH_3CONH_2 may occur at a shorter wavelength than 200 nm on the basis of an MO consideration.

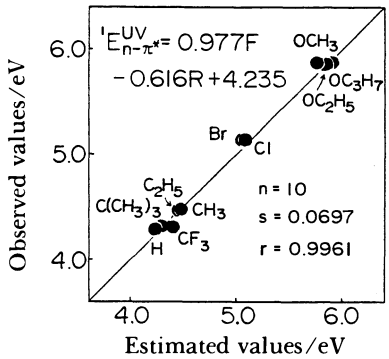

Fig. 2. Linear-least-squares correlation of observed n-π* band energies to the estimated ones using Swain's substituent constants.

References

1) B. Uno, Y. Ninomiya, K. Kano, and T. Kubota, *Spectrochim. Acta*, **43A**, 955 (1987), and the other our papers cited therein.

2) N. Mataga and T. Kubota, "Molecular Interactions and Electronic Spectra," Marcel Dekker, Inc., New York (1970).

3) C. G. Swain, S. H. Unger, N. R. Rosenquist, and M. S. Swain, *J. Am. Chem. Soc.*, **105**, 492 (1983).

4) M. Sawada, M. Ichimura, Y. Yukawa, T. Nakachi, and Y. Tsuno, *Bull. Chem. Soc. Jpn.*, **53**, 2055 (1980).

5) T. Kubota, H. Miyazaki, M. Yamakawa, K. Ezumi, and Y. Yamamoto, *Bull. Chem. Soc. Jpn.*, **52**, 1588 (1979), and the other papers given therein.

6) A. Ben-Naim, "Hydrophobic Interactions," Plenum Press, New York, London (1980), p. 83; J. Wenograd and R. A. Spurr, *J. Am. Chem. Soc.*, **79**, 5844 (1957).

7) S. Nagakura, *Rep. Inst. Sci. Technol., Tokyo Univ.*, **6**, No. 1, 5 (1952); S. Nagakura (chief editor), "Electronic Spectra," in Jikken Kagaku Koza, Zoku 11, ed by the Chemical Society of Japan, Maruzen, Tokyo, 1965, p. 280; K. Kaya and S. Nagakura, *Theoret. Chim. Acta (Berl.)*, **7**, 117 (1967); S. Nagakura, *Mol. Phys.*, **3**, 105 (1960).

8) R. L. Ellis, G. Kuehnlenz, and H. H. Jaffé, *Theor. Chim. Acta*, **26**, 131 (1972); C. B. Duke and N. O. Lipari, *J. Chem. Phys.*, **63**, 1758 (1975).

9) J. A. Pople and D. L. Beveridge, "Approximate Molecular Orbital Theory," McGraw-Hill, New York (1970).

10) H. Baba, *Nippon Kagaku Zasshi*, **72**, 74, 341 (1951); H. Baba and S. Nagakura, *Nippon Kagaku Zasshi*, **72**, 72 (1951); S. Nagakura, *Bull. Chem. Soc. Jpn.*, **25**, 164 (1952); M. Kasha, *Discuss. Faraday Soc.*, **9**, 14 (1950); G. J. Brealey and M. Kasha, *J. Am. Chem. Soc.*, **77**, 4462 (1955); H. L. McMurry, *J. Chem. Phys.*, **9**, 231, 241 (1941); H. McConnell, *J. Chem. Phys.*, **20**, 700 (1952).

11) J. W. Sidman, *Chem. Revs.*, **58**, 689 (1958).

12) M. Kobayashi and K. Nakamoto, *Nippon Kagaku Zasshi*, **70**, 243 (1949).

13) C. N. R. Rao, G. K. Goldman, A. Balasubramanian, *Chem. Ind.*, **1960**, 1025; C. N. R. Rao, G. K. Goldman, A. Balasubramanian, *Can. J. Chem.*, **38**, 2508 (1960).

14) For example, Jaffé and Orchin[15] reported 214 nm in water for the n-π* band position of CH_3CONH_2, but Nielsen and Schellman[16] found that no n-π* band appears in the above wavelength region in water and the band may occur at more shorter wavelength. Ab initio CI calculation with double excitations led to 5.85 eV for the n-π* band of $CH_3CONHCH_3$.[17]

15) H. H. Jaffé and M. Orchin, "Theory and Applications of Ultraviolet Spectroscopy," John Wiley, New York (1962), p. 180.

16) E. B. Nielsen and J. A. Schellman, *J. Phys. Chem.*, **71**, 2297 (1967).

17) L. E. Nitzshe and E. R. Davidson, *J. Am. Chem. Soc.*, **100**, 7203 (1978).

The Crystal Structure of the β'_1 Form of Optically Active α-Monostearin

Midori GOTO,* Kozo KOZAWA,† and Tokiko UCHIDA†
National Chemical Laboratory for Industry, 1-1, Higashi, Tsukuba, Ibaraki 305
†Department of Industrial Chemistry, Faculty of Science and Technology, Science University of Tokyo, 2641, Yamazaki, Noda, Chiba 274
(Received September 5, 1987)

Synopsis. The crystal structure of the β'_1 form of (*R*)-α-monostearin has been determined. The space group is $P2_12_12_1$, with a=4.943(1), b=8.858(2), c=101.05(1)Å, and Z=8. The two independent molecules in the title compound have different conformations.

The polymorphism of the α-monoglycerides has been reported mainly in racemic forms.[1] The modifications named the sub-α, α, β', and β forms (β_1, β_2) have been known.[1,2] The β_1 form is a stable form and the structure has been determined in α-monolaurin.[3]

The pioneer work on the optically active α-monoglycerides was carried out by Larsson. Four modifications, the α, β'_1, β'_2, and β forms were found. He described the lattice constants and the space groups of two β' forms of monostearin, but did not solve their structures.[2] Recently Iwahashi et al. reported the thermodynamic behavior, infrared and NMR spectra of optically active monoglycerides.[4] The present authors obtained a single crystal of the β'_1 form of (*R*)-α-monostearin and undertook an X-ray crystal structure analysis.

Experimental and Structure Determination

The (*R*)-α-monostearin was obtained from Fluka AG-(Switzerland). The phase of the β'_1 form can be made from solvents as precipitates and is considered the stable form at room temperature. A crystal for the X-ray work could be obtained by slow evaporation at 20 °C from a acetone–chloroform mixed solution (1 : 1 volume ratio). A crystal with dimensions of 0.3×0.3×0.1 mm^3 was used. The unit cell parameters and intensities were measured on a Rigaku-Denki AFC-4 four-circle diffractometer by using graphite monochromated Cu $K\alpha$ radiation (λ=1.54184 Å). 4020 independent reflections within the range of $5°<2\theta<120°$ were collected by the $2\theta/\omega$ scan mode, with a scan width ω of $0.7+0.35\tan\theta$, and a scan speed of 4° min^{-1}. The standard reflections, monitored every 50 reflections showed no decline. 1855 independent reflections with $|F_o|\geq 3\sigma(|F_o|)$ were used for the analysis. The 1 0 0 reflection (F_o=15.5) was observed. Attempts to refine the structure in the $P2P2_1P2_1$ space group remained unsatisfactory. Therefore, it was concluded that the existence of the 1 0 0 reflection might be due to some disorders in the lattice, and so this reflection was excluded from the reflection data. Crystal data: $C_{21}H_{42}O_4$, M=358.6, orthorhombic, $P2_12_12_1$, a=4.943(1), b=8.858(2), c=101.05(1) Å, cell volume=4424.2(11) Å^3, Z=8, D_c=1.08 g cm^{-3}, μ=5.76 cm^{-1}. The structure could be solved by MULTAN 84.[5] The hydrogen atoms of the carbon chains were placed at the calculated positions. The structural parameters were refined by a block-diagonal least-squares method, using scattering factors from the International Tables for X-ray Crystallography (1974).[7] Anisotropic thermal parameters were assumed for the non-hydrogen atoms, and isotropic parameters for the hydrogen atoms. All the calculations except MULTAN 84 were carried out in a Facom M-380 Computer, using the UNICS III system.[7] The final refinement led to the R value of 0.110 (W=1.0). The maximum and minimum heights on the final difference Fourier map were 0.28 and −0.32 e Å^{-3} respectively; no other significant features were observed.

Results and Discussion

The numbering of the atoms in the molecules is shown in Fig. 1, while the final atomic coordinates are given in Table 1.[8]

The asymmetric unit contains two crystallographically independent molecules, which differ in the conformation of their glycerol parts. They will hereafter be named A and B. The differences in conformation are illustrated in Fig. 1, while the dihedral angles are shown in Table 2, together with the case of racemic α-monolaurin. The larger temperature factors of the O1A and O1B atoms might be due to the disorder.

The packing of the molecules in the crystal is shown in Fig. 2. In the packing of the hydrocarbon chains, every second hydrocarbon plane is approximately perpendicular to the other chain planes. This packing is common in fatty acids or paraffin crystals (named O⊥

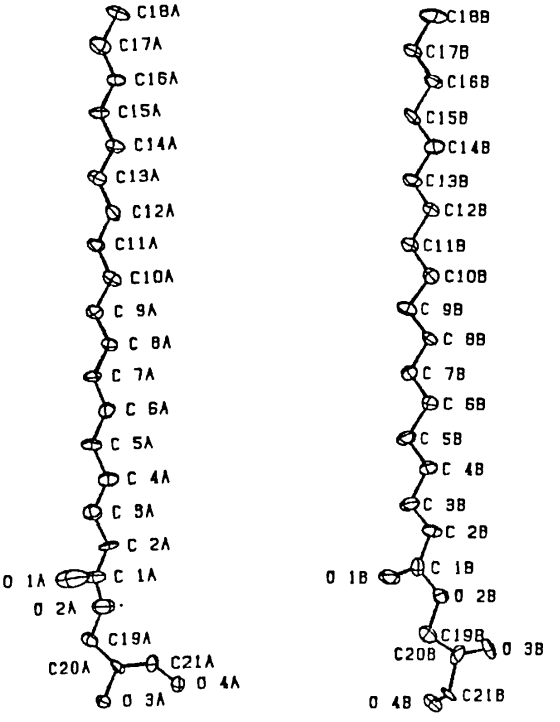

Fig. 1. ORTEP drawing and the numbering systems of atoms. The ellipsoids are drawn to enclose 40% probability.

Table 1. Fractional Atomic Coordinates ($\times 10^4$) and Thermal Parameters for Non-hydrogen Atoms
$B_{eq}=4/3\ \sum_i\sum_j a_i a_j$

Atom	X	Y	Z	B_{eq}/A^2
C1A	4486(41)	10106(21)	8092(2)	4.6(6)
C2A	5889(40)	8883(20)	8166(2)	4.0(5)
C3A	4494(41)	8730(20)	8304(2)	4.2(5)
C4A	5838(40)	7401(21)	8380(2)	4.3(6)
C5A	4437(39)	7243(19)	8522(2)	3.9(5)
C6A	5711(41)	5923(19)	8600(2)	4.0(5)
C7A	4258(47)	5686(20)	8736(2)	4.7(6)
C8A	5842(34)	4330(17)	8805(2)	2.8(5)
C9A	4661(40)	4125(18)	8942(2)	3.8(5)
C10A	5804(33)	2755(17)	9017(2)	3.4(5)
C11A	4655(44)	2552(18)	9157(2)	4.2(5)
C12A	5707(44)	1184(18)	9229(2)	4.4(6)
C13A	4427(49)	969(19)	9373(2)	5.1(6)
C14A	5685(36)	−401(18)	9440(2)	3.4(5)
C15A	4665(41)	−602(19)	9580(2)	4.0(5)
C16A	5838(36)	−1959(18)	9650(2)	3.3(5)
C17A	4832(46)	−2141(20)	9793(2)	5.2(6)
C18A	5855(50)	−3530(21)	9861(2)	6.1(7)
C19A	4668(44)	11685(18)	7904(2)	4.4(6)
C20A	5553(40)	11275(15)	7763(2)	3.4(5)
C21A	4205(44)	9955(18)	7704(2)	4.6(6)
O1A	2743(48)	10946(23)	8132(2)	12.5(9)
O2A	5646(34)	10456(15)	7983(1)	6.6(5)
O3A	5020(25)	12593(10)	7679(1)	3.2(3)
O4A	5287(28)	9508(11)	7585(1)	4.1(4)
C1B	368(41)	14936(18)	8082(2)	4.1(5)
C2B	−816(39)	13852(20)	8172(2)	4.0(5)
C3B	451(48)	13785(22)	8302(2)	5.2(6)
C4B	−696(47)	12510(21)	8385(2)	5.0(6)
C5B	647(45)	12314(22)	8522(2)	4.9(6)
C6B	−707(41)	10936(19)	8594(2)	4.0(5)
C7B	528(40)	10719(18)	8730(2)	3.6(5)
C8B	−477(41)	9360(19)	8806(2)	4.1(5)
C9B	824(36)	9194(18)	8947(2)	3.8(5)
C10B	−347(47)	7785(19)	9011(2)	4.7(6)
C11B	874(35)	7571(18)	9152(2)	3.4(5)
C12B	−430(41)	6225(17)	9230(2)	3.8(5)
C13B	691(42)	5985(17)	9361(2)	4.1(5)
C14B	−582(50)	4645(21)	9431(2)	5.6(7)
C15B	895(39)	4399(18)	9571(2)	4.2(6)
C16B	−368(44)	3059(21)	9647(2)	4.9(6)
C17B	913(37)	2835(18)	9785(2)	3.7(5)
C18B	−343(59)	1537(25)	9861(2)	7.8(8)
C19B	1007(41)	15879(19)	7845(2)	4.4(6)
C20B	−329(47)	15486(17)	7725(2)	4.5(6)
C21B	390(37)	16605(16)	7609(2)	3.5(5)
O1B	2517(34)	15676(17)	8100(1)	7.7(6)
O2B	−494(25)	14899(13)	7949(1)	4.0(3)
O3B	−155(29)	13969(11)	7688(1)	5.1(4)
O4B	3314(26)	16536(12)	7609(1)	4.3(4)

Table 2. Dihedral Angles (φ/°)

	Racemic		Active	
	A2	B2	A	B
O2−Cn−Cn+1−Cn+2	−52(3)	53(3)	68(2)	167(1)
O2−Cn−Cn+1−O3	174(2)	−58(3)	−171(2)	−61(2)
O3−Cn+1−Cn+2−O4	60(3)	171(3)	67(2)	−78(2)

Racemic α-monolaurin (β_1) n=13.
Active α-monolaurin (β'_1) n=19.

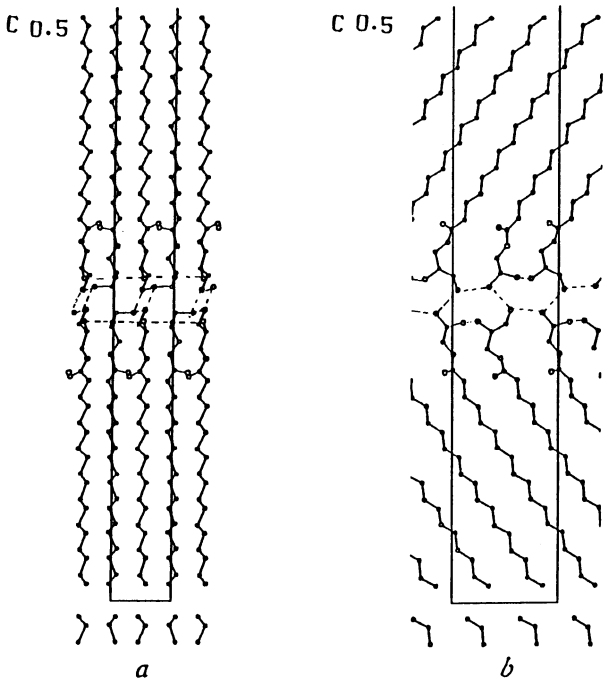

Fig. 2. Molecular arrangement. a) Viewed along the b axis. b) Viewed along the a axis.

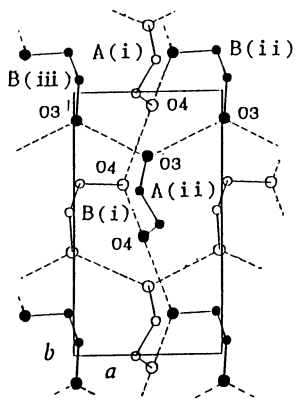

Fig. 3. Illustration of the hydrogen bond net work viewed along the c-axis. O3A(ii)-O3B(ii) 2.68(2)Å, O3A(ii)-O3B(iii) 2.84(2), O4A(i)-O4B(ii) 2.74(2), O4A(i)-O4B(i) 2.82(2). Symmetry code; A(i) $x,y+1,z$; B(ii) $1-x,y-1.5,1.5-z$; B(i) $x,y-1,z$; B(iii) $1-x,y-1.5,1.5-z$; A(ii) $1-x,y-0.5,1.5-z$. Upper layer atoms ●, Lower layer atoms ○.

packing). The dimensions of the subcell are; a_s=7.42 Å, b_s=4.94 Å, and c_s=2.54 Å. These are nearly the same as those of the B and C forms of fatty acids.[9,10] The molecules are linked by the hydrogen bonds shown in Fig. 3. Only the hydroxyl groups participate in the hydrogen-bond system. The average hydrogen-bond distance is 2.77 Å.

We are indebted to Dr. Toshio Sakurai and Miss Kimiko Kobayashi of the Institute of Physical and Chemical Research for the UNICS III programs used in this work; we also wish to thank Dr. Kazumasa Honda of National Chemical Laboratory for help with the experimental work.

References

1) T. Maruyama, I. Niiya, M. Imamura, M. Okada, and T. Matsumoto, *Yukagaku*, **22**, 85 (1973); R. T. O'Conner, "Fatty Acids," ed by K. S. Markley, Intersci. Pub., (1960), Part 1, p. 330; E. S. Lutton, *J. Am. Oil Chem. Soc.*, **48**, 778; (1971).

2) K. Larsson, *Ark. Kemi*, **23**, 29 (1964).

3) M. Goto and T. Takiguchi, *Bull. Chem. Soc. Jpn.*, **58**, 1319 (1985).

4) M. Iwahashi, Y. Watanabe, T. Watanabe, and M. Muramatsu, *Bull. Chem. Soc. Jpn.*, **57**, 1446 (1984).

5) P. Main, M. M. Woolfson, and G. Germain, MULTAN, "A Computer Programme for the Automatic Solution of Crystal Structures," Univ. of York, England, and Univ. de Louvain, Leuven, Belgium (1984); Rigaku Rasa-5P Software Package.

6) International Tables for X-Ray Crystallography Birmingham: Kynoch Press (1974).

7) T. Sakurai and K. Kobayashi, *Rikagaku Kenkyusho Hokoku*, **55**, 69 (1978).

8) The lists of the structure factors, the atomic parameters for the hydrogen atoms, and the anisotropic thermal parameters for the non-hydrogen atoms are deposited at the Office of the Chemical Society of Japan. (Document No. 8786).

9) E. von Sydow, *Ark. Kemi*, **9**, 231 (1951).

10) D. Chapmann, "The Structure of Lipids," London: Methuen and Co (1965).

The Photocyclization of *N,N*-Dialkyl β-Oxo Amides Adsorbed on Silica Gel

Tadashi HASEGAWA,* Jun-ichi MORIBE, and Michikazu YOSHIOKA†
Department of Chemistry, Tokyo Gakugei University, Nukuikitamachi, Koganei, Tokyo 184
†Department of Chemistry, Saitama University, Shimooukubo, Urawa, Saitama 338
(Received June 13, 1987)

Synopsis. β-Oxo amides 1 adsorbed on silica gel underwent photocyclization via δ-hydrogen abstraction to give the five-membered lactams **2**. No severe restrictions on the molecular motion could be observed in the photoreaction on the silica-gel surface. However, the relative photoreactivity of *N,N*-dibenzyl-2-benzoylacetamide (**1a**) to *N,N*-dibenzyl-2-benzoylpropionamide (**1b**) increased greatly on the silica-gel surface compared to that in solution, probably because of the greater keto content on the surface.

The photochemistry and photophysics of organic molecules adsorbed on silica gel have been studied well and compared with their solution counterparts.[1-5] The mobility of excited molecules or radical pair intermediates has received particularly much attention because they are unique surface probes.[3d] Most of the photochemical studies have, however, been concerned with photodecompositions via radical-pair intermediates, and much less attention has been focussed on the intramolecular photoreactions of organic molecules on the dry silica gel surface.[5] We will report here as the photocyclization of *N,N*-dialkyl β-oxo amides via intramolecular δ-hydrogen abstraction by the excited carbonyl group on a dry silica-gel surface.

Experimental

Materials. Silica gel (Merck Kiesel Gel 60, Art. #9385) was used as received. The β-oxo amides **1a—d** were prepared according to a previously described method.[6] Valerophenone was purified by fractional distillation with a Taika SM-NB spinning-band distilation apparatus. Phenanthrene (Tokyo Kasei Co.), a calibrant for the HPLC analysis, was recrystallized from ethanol. Hexadecane (Tokyo Kasei Co.), a calibrant for the GC analysis, was purified by passing it through silica gel.

General Procedure. Preparative Irradiation of the β-Oxo Amides 1 on Dry Silica Gel: The β-oxo amide **1** (ca. 0.1 mmol) in 5 cm^3 of dichloromethane was added to 2 g of silica gel in a Pyrex tube (30×200 mm). The mixture was sonicated for 5 min, and then the solvent was evaporated under reduced pressure. The tube was rotated and irradiated for 10 h with a 100 W high-pressure mercury lamp (Taika Co.). Acetonitrile (10 cm^3) was then added to the mixture, the mixture was sonicated, and the adsorbed material was extracted with acetonitrile.[7] After the removal of the solvent, the residue was chromatographed on silica gel. Elution with a mixture of benzene-ethyl acetate (10/1 (v/v)) gave the unreacted β-oxo amide **1** and the lactam **2**. The structures of **2a—d** were determined by comparison with authentic samples.[6,8] The yields of the lactam **2** are summarized in Table 1.

The Quantitative Photolysis of the β-Oxo Amides 1 on Dry Silica Gel: The β-oxo amide **1** (ca. 0.03 mmol) in 1 cm^3 of dichloromethane was added to 0.5 g of silica gel in a Pyrex tube (18×180 mm). In the quenching experiments, appropriate amounts of 2,5-dimethyl-2,4-hexadiene in dichloromethane were added. The mixture was sonicated for 5 min, and then the solvent was evaporated under reduced pressure. The tubes were rotated and irradiated with a 100 W high-pressure mercury lamp. The adsorbed material was sonicated and extracted with acetonitrile. To the acetonitrile solution was added 1 cm^3 of an acetonitrile solution containing a known amount of phenanthrene (ca. 0.001 mmol) as a calibrant for the HPLC analyses. The analyses were performed using a Gasukuro Kogyo 570B high-pressure liquid chromatograph with a Model 511 single-wave UV detector (254 nm). A Unishil QC18 column (4×250 mm) was used, and a mixture of methanol-water (7/3 (v/v)) was employed as the moving phase at a flow rate of 0.7 ml min^{-1}.

Photolysis of Valerophenone on Dry Silica Gel: Valerophenone (ca. 0.03 mmol) in 1 cm^3 of dichloromethane was adsorbed on 0.5 g of silica gel and irradiated as has been described above. After the extraction with acetonitrile, 1 cm^3 of an acetonitrile solution containing a known amount of hexadecane (ca. 0.001 mmol) as a calibrant was added. The mixture was then analyzed using a Shimazu GC-4B gas chromatograph equipped with a flame ionization detector. Analysis was performed on a 2 m×4 mm column packed with 5% DCQF-1 and 1% EGS on Chromosorb P.

Results and Discussion

The irradiation of *N,N*-dibenzyl-2-benzoylacetamide (**1a**) adsorbed on silica gel with a 100 W high-pressure mercury lamp gave a five-membered lactam, 1-benzyl-

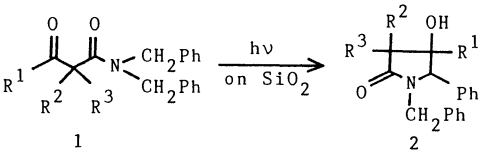

1 2

Scheme 1.

Table 1. Yields of the Photoproduct **2** and the Reaction Conditions

	Starting material			Yield of **2**/%	
	R^1	R^2	R^3	In benzene	On silica gel
1a	Ph	H	H	80[a]	83
1b	Ph	Me	H	90[a]	91
1c	Ph	Me	Me	65[a]	63
1d	2-Naphthyl	H	H	50[b]	7

a) Ref. 8, b) Ref. 6.

4-hydroxy-4,5-diphenyl-2-pyrrolidinone (**2a**), in an 83% yield. Similarly, the irradiation of two β-oxo amides, **1b** and **1c**, on dry silica gel gave the lactam **2b** and **2c** in 91 and 63% yield respectively. The yields of the lactams **2a**—**c** from photolyses of the β-oxo amides **1a**—**c** on silica gel are similar to those in photoreactions in solution[8] (Table 1). The formation of the lactams **2a**—**c** on silica gel can be explained in terms of the intramolecular δ-hydrogen shift to the carbonyl oxygen, as in photoreactions in solution.[6] The rates at which the β-oxo amides **1** adsorbed on silica gel undergo conformational change should be as fast as the rate at which they react chemically from their electronically excited states.

The β-oxo amide **1a** exhibits the keto-enol tautomerism. We have previously reported that the enol-form of the β-oxo amides 1 acted as an internal filter in solution photochemistry; the quantum yield for the production of the lactam from **1a** in benzene was 33 times lower than that from 1b (ϕ_{2a}/ϕ_{2b}=0.03).[6] The enol tautomer may reduce the photoreactivity of the β-oxo amides **1** on silica gel. However, the rate of the disappearance of the β-oxo amide **1a** on silica gel was equal to that of **1b** (Fig. 1). This result may be explained in two ways; the efficiency of the photoreaction of **1a** may be increased, or that of 1b may be decreased, by the steric effect of the 2-methyl group. However, it seems that the latter possibility can be excluded because the quantum yield for the production of **2b** from **1b**[6] is comparable to that for acetophenone formation from valerophenone[9] in solution photochemistry (Φ_{2b}/Φ_{PhCOMe}=0.79). The reaction rate for the production of **2b** from **1b** on the silica gel surface relative to that of acetophenone formation from valerophenone on the surface was also comparable (Φ_{2b}/Φ_{PhCOMe}=0.56). This result indicates that the photoreactivity of **1a** on the silica gel surface is increased to the same level as that of **1b**. The efficient photoreactivity of **1a** might indicate that the β-oxo amide **1a** exists nearly completely as in the keto form on the surface. The enol content of **1a** in a solution depends on the solvent polarity. The enol content of **1a** as well as other β-oxo amides[10] decreases with an

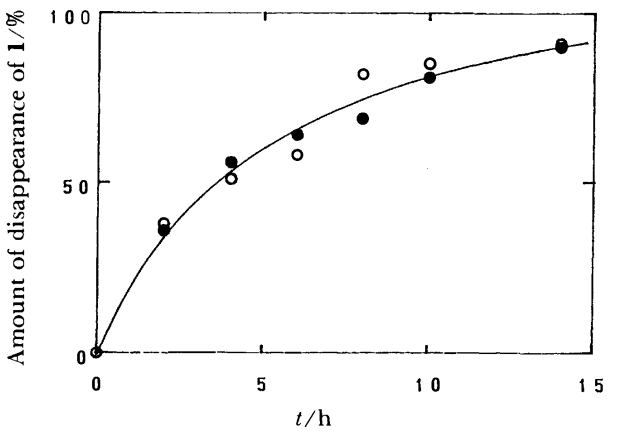

Fig. 1. Disappearance of the β-oxo amide **1a** (○) and **1b** (●) on silica gel. In each case 0.028 mmol of the oxo amides was used.

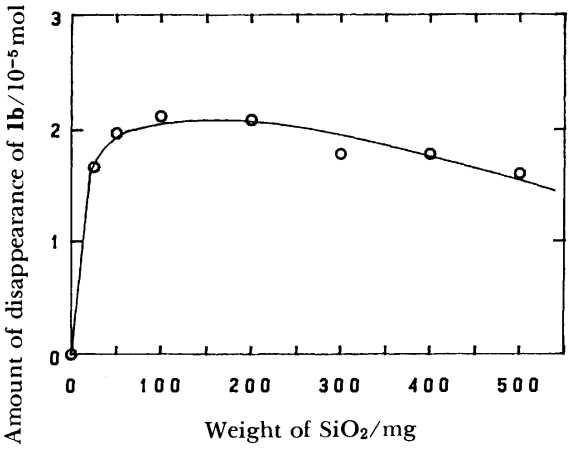

Fig. 2. Efficiency of the photoreaction of **1b** on silica gel. In each case 0.028 mmol of **1b** was used.

increase in the solvent polarity.[8] The increment of the keto form of **1a** may be due to the polar property of the silica-gel surface. The surface of silica gel is presumed to be a suitable field for a photoreaction from only the keto tautomer of β-dicarbonyl compounds.

The rate of the disappearance of the β-oxo amides **1** on silica gel depended on the amounts of the β-oxo amides adsorbed on a unit gram of silica gel (Fig. 2). The amount of **1b** (0.028 mmol) which disappeared increased with the increase in the amounts of silica gel and reached its maximum at about 100 mg of silica gel. This suggests that 100% coverage is achieved with 0.028 mmol of **1b** per 100 mg of silica gel. This idea was supported by the following calculation. The surface area of silica gel (Merck Kiesel Gel 60, Art #9385) was 444 $m^2\ g^{-1}$. Consequently, the surface area occupied by one molecule can be calculated to be 2.6×10^{-18} m^2. The longest molecular chain of **1b** was calculated to be 15Å by using the values of bond lengths and bond angles.[11] From the experimental results described above, it was expected that the molecule of the β-oxo amides **1** on the silica gel surface could change its conformation within the lifetime of the excited state. Therefore, the surface area occupied by one molecule of the β-oxo amide **1b** can be approximated by the square model (15×15 $Å^2=2.3\times10^{-18}$ m^2). This value is almost entirely consistent with the experimental value. Therefore, 0.028 mmol of **1b** per 100 mg of silica gel corresponds to 100% monomolecular-layer coverage. When the ratio of the β-oxo amide **1b** to silica gel is over 0.028/100 mmol/mg, multiple layers might be formed. The molecules of the β-oxo amides on the monomolecular layer might act as filter for the β-oxo amide molecules in the layer.

The irradiation of **1b** in the solid state without silica gel under the same conditions resulted in the formation of a trace of the lactam **2b**, and more than 95% of the starting material was recovered.[12] The use of silica gel as an adsorbent effectively promotes the photoreaction of the β-oxo amides because silica gel has a wide surface area and because the β-oxo amide can be widespread on the silica-gel surface.

The quenching of the photoreaction of the β-oxo amides **1** on silica gel with 2,5-dimethyl-2,4-hexadiene

was attempted. Scarecely no quenching was observed on **1a**, while the photoreaction of **1b** was remarkably quenched. These results are consistent with the photochemical behavior of the β-oxo amides in solution. The photoreaction of **1a** is presumed to occur through the charge-transfer intermediate. The $k_q\tau$ values could not be determined from the slopes in the Stern-Volmer plots because the diene was consumed during the irradiation.[13]

The π,π^* excited state of ketones is generally not sensitive to direct hydrogen abstraction, while the n,π^* state is sensitive to it.[14] The irradiation of the β-oxo amide **1d**, which is expected to have the π,π^* configuration in its lowest excited state, on silica gel also gave the lactam **2d** in a 7% yield. This result also suggests that electron transfer from nitrogen to the carbonyl group occurs prior to the hydrogen shift, even on silica gel, while the yield of **2d** is low.

The authors are grateful to Dr. Yoshimasa Inoue of the Central Research Laboratory, Sumitomo Metal Mining Co., for the surface-area determination.

References

1) P. A. Leermakers, H. T. Thomas, L. D. Weis, and F. C. James, *J. Am. Chem. Soc.*, **88**, 5075 (1966).

2) a) J. R. Leffler and J. J. Zupancic, *J. Am. Chem. Soc.*, **102**, 259 (1980); b) J. E. Leffler and J. T. Barbas, *ibid.*, **103**, 7768 (1981).

3) a) L. J. Johnston, P. de Mayo, and S. K. Wong, *J. Chem. Soc., Chem. Commun.*, **1982**, 1106; b) P. de Mayo, *Pure Appl. Chem.*, **54**, 1623 (1982); c) L. J. Johnston, P. de Mayo, and S. K. Wong, *J. Org. Chem.*, **49**, 20 (1984); d) P. de Mayo , L. V. Natarajan, and W. R. Ware, in "Organic Phototransformations in Nonhomogeneous Media," ed by M. A. Fox, ACS Symposium Ser 14 (1985), pp. 1—19 and the references cited therein.

4) B. H. Baretz and N. J. Turro, *J. Am. Chem. Soc.*, **105**, 1309 (1983).

5) H. Aoyama, K. Miyakami, M. Sakamoto, and Y. Omote, *Chem. Lett.*, **1983**, 1583.

6) T. Hasegawa, H. Aoyama, and Y. Omote, *J. Chem. Soc., Perkin Trans. 1*, **1979**, 963.

7) More than 95% of the organic material could be extracted by this method.

8) T. Hasegawa, H. Aoyama, and Y. Omote, *J. Chem. Soc., Perkin Trans. 1*, **1976**, 2054.

9) P. J. Wagner, *Acc. Chem. Res.*, **4**, 168 (1971).

10) W. R. Oliver and L. R. Hamilton, *Tetrahedron Lett.*, **1971**, 1837.

11) A. J. Gordon and R. A. Ford, "The Chemist's Companion," John Wiley, New York (1972), pp. 107—111.

12) The numbers of photons absorbed by **1b** were not corrected.

13) The structures of the photoproducts from the diene could not be determined.

14) N. J. Turro, "Modern Molecular Photochemistry," Benjamin, Menlo Park (1978), pp. 388—389.

Synthesis of 1,2,5a-Triazacyclohept[*a*]azulen-5(2*H*)-ones

Noritaka ABE* and Yoshifumi EMOTO
Department of Chemistry, Faculty of Sciences, Yamaguchi University, Yamaguchi 753
(Received August 24, 1987)

Synopsis. Reactions of 2-hydrazino-1-azaazulenes with acetylacetone gave 2-(3,5-dimethyl-1-pyrazolyl)-1-azaazulenes. Cyclizations of diethyl (1-azaazulen-2-yl)hydrazinomethylenemalonates in refluxing *t*-butylbenzene or on silica gel gave 1,2,5a-triazacyclohept[*a*]azulen-5(2*H*)-ones.

The chemistry of azaazulenes has attracted considerable attention because of their interesting chemical behavior and physicochemical properties.[1] Although many studies regarding hetero-annulated 1-azaazulenes have been made,[2-9] azepine-annulated 1-azaazulene, which would have a 16π-electronic antiaromaticity, has not been synthesized. In this paper, an attempt to synthesize of 1,2,5a-triazacyclohept[*a*]azulene is described. Although the conversion to a full conjugated 16π-electronic system was not successful, the publication of the synthesis of a novel tricyclic 1,2,5a-triazacyclohept[*a*]azulen-5(2*H*)-one seemed worthwhile, which is considered to be precursor of 1,2,5a-triazacyclohept[*a*]azulene.

It is known that hydrazino-substituted heterocycles have often been used in the synthetic design of annulated triazepines.[10-12] We therefore employed 2-hydrazino-1-azaazulenes[13] (**1**) as starting materials.

The treatment of **1a** and **1b** with acetylacetone (AA) gave 2-(3,5-dimethyl-1-pyrazolyl)-1-azaazulenes (**2a** and **2b**) in good yields, respectively. Compounds **2a** and **2b** were identical with the products derived from 2-chloro-1-azaazulenes (**3a** and **3b**) and 3,5-dimethylpyrazole, respectively.

Reaction of **1a** with ethyl acetoacetate (EAA) gave **4** as orange prisms in 63% yield, which was assigned as 2-(3-methyl-5-oxo-3-pyrazolin-1-yl)-1-azaazulene on the basis of the spectroscopic data as well as elemental analysis.

Since a direct construction of the triazepine ring using **1** and AA or EAA was unsuccessful, we carried out the synthesis and cyclizations of diethyl (1-azaazulen-2-yl)hydrazinomethylenemalonate (**5**).

The treatment of **1** with diethyl ethoxymethylenemalonate (DEEM) in refluxing ethanol gave **5** in good yields. Heating of **5a** in *t*-butylbenzene under reflux for 30 min gave **6a** in 92.5% yield, which was assigned as ethyl 2,5-dihydro-5-oxo-1,2,5a-triazacyclohept[*a*]-azulene-4-carboxylate on the basis of the spectroscopic data as well as HRMS. Compound **6a** was also obtained in 56% yield through a treatment of **5a** with silica gel for 7 d. In the ^{1}H NMR spectrum of **6a**, a low-field resonated 1H multiplet, owing to a deshielding effect of C-5 carbonyl, was observed at δ 9.20—9.27, which could be assigned to the C-6 proton. Other signals were observed at δ 7.23 (s, H-11), 7.75—7.95 (m, H-3, 7, 8, and 9), and 8.41 (d, J=10.4 Hz, H-10) together with ethyl ester signals.[14]

The treatment of **5b** in refluxing *t*-butylbenzene gave **6b**, but a treatment of **5b** with silica gel did not.

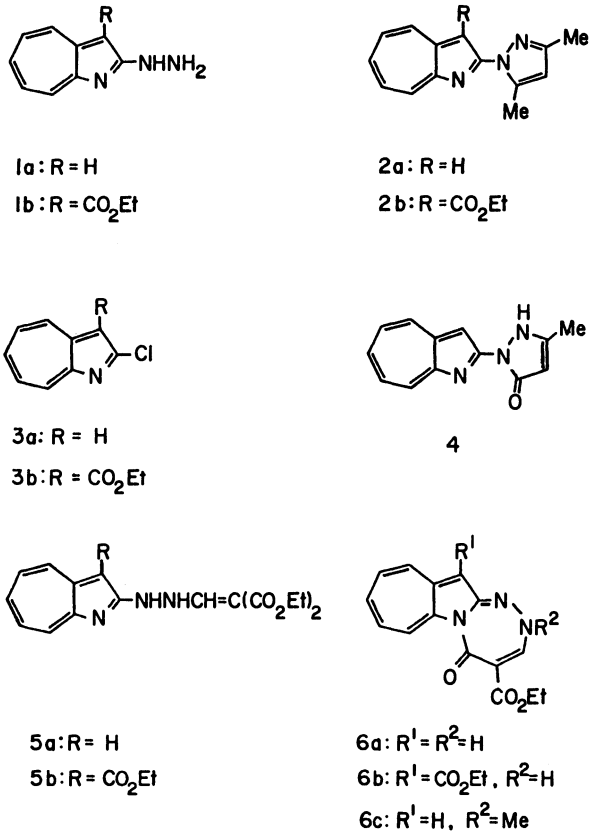

Fig. 1.

In the ^{13}C NMR spectrum of **6b**, signals of seven membered carbons (C-6, 7, 8, 9, and 10) are observed at δ 134—140. In its ^{1}H NMR spectrum, signals of H-6 and 10 were observed at δ 8.96 (dd, J=6.8 and 2.4 Hz) and 9.01 (d, J=12.2 Hz), respectively, which were deshielded by the carbonyl group at C-5 and ester group at C-11, respectively. Other signals of seven-membered ring protons (H-7, 8, and 9) were observed at δ 7.90—8.15 (m). Although these observations suggest that **6b** should be fundamentally aromatic, the large divergence of the coupling constants ($J_{6\text{-}7}$—$J_{9\text{-}10}$=5.4 Hz) shows that the contribution of heptafulvene form should be considerably large.

Compounds **6a** and **6b** were somewhat decomposed and changed to unidentified reddish violet compounds by prolonged heating or prolonged contact with silica gel.

For leading to full conjugated system, acetylation and methylation of **6a** were attempted. The treatment of **6a** with acetic anhydride gave no distinct product. The treatment of **6a** with methyl iodide in the presence of a base gave **6c**, which was assigned as an *N*-methylated product on the basis of the spectroscopic data; no *O*-methylated compound was obtained. *N*-Methyl protons appeared at δ 4.11 in the ^{1}H NMR

spectrum of **6c** and *N*-methyl carbon at δ 41.2 in its ^{13}C NMR spectrum.

Reactions and successive cyclizations of diethyl ethoxymethylenemalonate and heterocycles have been exclusively used for the preparation of fused pyrimidines.[9,15,16] Now we extended the reaction for the preparation of fused triazepine, as described above.

Experimental

Melting points were uncorrected. ^1H NMR spectra (250 MHz) and ^{13}C NMR spectra (62.87 MHz) were recorded on a Hitachi R-250H spectrometer using deuteriochloroform as a solvent (tetramethylsilane as an internal standard), unless otherwise stated. IR spectra were recorded for Nujol mulls with a Hitachi 270-50 infrared spectrophotometer. Mass spectra were determined with a JEOL-01SG-2 spectrometer at 70 eV of ionization energy. High-resolution mass spectra were obtained on the same instrument. Column chromatography was performed on Kieselgel 60.

Reaction of 1 with AA. a) A mixture of **1a** (318 mg, 2 mmol) and AA (405 mg, 4 mmol) in ethanol (30 ml) was refluxed for 3 h and evaporated. Chromatography of the residue with chloroform–ethyl acetate (1 : 1) gave **2a** (430 mg, 96%), which was crystallized from cyclohexane to give orange needles (359 mg, 80%), mp 86—88 °C, ^1H NMR δ=2.36 (3H, s, Me), 2.87 (3H, s, Me), 6.06 (1H, s, H-4′), 7.58 (1H, s, H-3), 7.50—7.75 (3H, m, H-5, 6, and 7), 8.39 (1H, d, J=9.8 Hz, H-4), 8.45—8.53 (1H, m, H-8). Found: C, 75.45; H, 5.94; N, 18.65%. Calcd for $C_{14}H_{13}N_3$: C, 75.31; H, 5.87; N, 18.82%.

When above reaction was carried out in refluxing benzene or acetic acid, **2a** was obtained in 95% and 91%, respectively.

b) A mixture of **1b** (463 mg, 2 mmol), AA (452 mmol, 4.5 mmol), and trifluoroacetic acid (0.1 ml) in ethanol (30 ml) was refluxed for 20 h and evaporated. Chromatography of the residue with chloroform gave **2b** (512 mg, 87%) as yellow oil. ^1H NMR (60 MHz) δ=1.25 (3H, t, Me), 2.32 (3H, s, Me), 2.47 (3H, s, Me), 4.28 (2H, q, OCH_2), 5.96 (1H, s, H-4′), 7.58—7.96 (3H, m, H-5, 6, and 7), 8.45—8.70 (1H, m, H-8), 9.05—9.25 (1H, m, H-4); IR 1702 cm^{-1} (ester C=O). Picrate of **2b**, yellow scales (from ethanol), mp 151—153 °C, Found: C, 52.61; H, 3.77; N, 16.13%. Calcd for $C_{23}H_{20}N_6O_9$: C, 52.67; H, 3.84, N, 16.02%.

Reaction of 3 with 3,5-Dimethylpyrazole. A mixture of **3a** (146 mg, 1mmol) and 3,5-dimethylpyrazole (120 mg, 1.25 mmol) in 1-butanol was refluxed for 17 h and evaporated. To the residue water was added, and the mixture was neutralized with sodium hydrogencarbonate and extracted with chloroform. The extract was dried (Na_2SO_4) and evaporated. Chromatography of the residue with chloroform gave **2a** (38%).

Similar treatment of **3b** with 3,5-dimethylpyrazole gave **2b** in a 54% yield.

Reaction of 1a with EAA. A solution of **1a** (318 mg, 2 mmol) and EAA (390 mg, 3 mmol) in ethanol (30 ml) was refluxed for 5 h and evaporated. Chromatography of the residue with ethyl acetate gave **4** (0.284 mg, 63%), which was crystallized from hexane to give orange prisms (37%), mp 198—200 °C; ^1H NMR δ=2.31 (3H, s, Me), 5.46 (1H, s, H-4′), 7.46 (1H, s, H-3), 7.60—7.80 (3H, m, H-5, 6, and 7), 8.35—8.41 (1H, m, H-4), 8.41 (1H, d, J=9.8 Hz, H-8);[14] IR 3250—2800 (NH), 1646 cm^{-1} (amido C=O). Found: C, 69.48; H, 4.96; N, 18.71%. Calcd for $C_{13}H_{11}N_3O$: C, 69.32; H, 4.92; N, 18.65%.

Reaction of 1 with DEEM. A solution of **1a** (318 mg, 2 mmol) and DEEM (451 mg, 2.1 mmol) in ethanol (30 ml) was refluxed for 1 h and evaporated. The residue was crystallized from cyclohexane–dichloromethane to give **5a** (602 mg, 92%) as red needles, mp 163—165 °C; ^1H NMR δ=1.25 (3H, t, J=7.0 Hz, Me), 1.38 (3H, t, J=7.0 Hz, Me), 4.19 (2H, q, J=7.0 Hz, OCH_2), 4.30 (2H, q, J=7.0 Hz, OCH_2), 6.28 (1H, s, H-3), 6.63—7.00 (4H, m, H-4, 5, 6, and 7), 7.23 (d, J=11.6 Hz, H-8), 8.46 (d, J=10.4 Hz, =CHNH), 11.60 (bd, J=10.4 Hz, =CHNH, exch.);[14] IR 3200—2650 (NH), 1674 (ester C=O), and 1634 cm^{-1} (C=N). Found: C, 62.13; H, 5.90; N, 12.71%. Calcd for $C_{17}H_{19}N_3O_4$: C, 62.00; H, 5.81; N, 12.76%.

In a similar manner, reaction of **1b** (463 mg, 2.0 mmol) and DEEM (895 mg, 4.14 mmol) in refluxing ethanol (40 ml) for 30 min gave **5b** (774 mg, 96%), which was crystallized to give yellow needles (592 mg, 74%), mp 119—121 °C; ^1H NMR δ=1.35 (3H, t, J=7.3 Hz, Me), 1.40 (3H, t, J=6.7 Hz, Me), 1.52 (3H, t, J=7.3 Hz, Me), 4.36 (2H, q, J=6.7 Hz, OCH_2), 4.40 (2H, q, J=7.3 Hz, OCH_2), 4.53 (2H, q, J=7.3 Hz, OCH_2), 7.75—7.85 (3H, m, H-5, 6, and 7), 8.28—8.35 (1H, m, H-8), 8.81 (1H, d, J=3.1 Hz, =CHNH), 8.96 (1H, d, J=3.1 Hz, =CHNH), 9.20 (1H, d, J=9.15 Hz, H-4), 10.09 (1H, bs, NH); IR 3328 (NH), 3200—2650 (NH), 1714 and 1664 (ester C=O), and 1604 cm^{-1} (C=N). Found: C, 59.91; H, 5.83; N, 10.28%. Calcd for $C_{20}H_{23}N_3O_6$: C, 59.84; H, 5.77; N, 10.47%.

Cyclization of 5a. a) A solution of **5a** (1.00 g, 3.04 mmol) in *t*-butylbenzene (10 ml) was refluxed for 30 min and evaporated. The residue was chromatographed with acetone to give **6a** (796 mg, 92.5%), which was crystallized from cyclohexane–dichloromethane to give red needles (650 mg, 76%), mp 232—234 °C; ^1H NMR δ=1.18 (3H, t, J=6.7 Hz, Me), 4.14 (2H, q, J=6.7 Hz, OCH_2), 7.23 (1H, s, H-11), 7.75—7.95 (3H, m, H-7, 8, and 9), 7.87 (1H, s, H-3), 8.41 (1H, d, J=10.4 Hz, H-10), 9.20–9.27 (1H, m, H-6);[14] IR 3150 (NH), 1722 (ester C=O), 1630 (amido C=O), and 1615 (C=N); MS *m/z* (rel intensity) 283 (M^+; 100), 238 (77), 237 (68), 211 (55), 129 (16), and 102 (36). HRMS Found: *m/z* 283.0954. Calcd for $C_{15}H_{13}N_3O_3$: M, 283.0956.

b) A mixture of **5a** (250 mg, 0.76 mmol) and silica gel (5.0 g) in chloroform (50 ml) was left to stand at room temperature for 7 d and then chromatographed. Elution with chloroform–ethyl acetate (1 : 1) gave recovered **5a** (25 mg, 10%). Elution with acetone gave **6a** (120 mg, 56%).

Cyclization of 5b. A solution of **5b** (402 mg, 1.00 mmol) and *t*-butylbenzene (10 ml) was refluxed for 40 min and cooled. The precipitate was collected by filtration to give **6b** (262 mg, 74%), which was crystallized from cyclohexane–dichloromethane to give red needles (185 mg, 52%), mp 186—188 °C; ^1H NMR δ=1.34 (3H, t, J=7.3 Hz, Me), 1.39 (3H, t, J=7.3 Hz, Me), 4.31 (2H, q, J=7.3 Hz, OCH_2), 4.48 (2H, q, J=7.3 Hz, OCH_2), 7.90—8.15 (3H, m, H-7, 8, and 9), 7.99 (1H, s, H-3), 8.96 (1H, dd, J=6.8 and 2.4 Hz, H-6), 9.01 (1H, d, J=12.2 Hz, H-10), and 9.50 (1H, bs, NH); ^{13}C NMR δ=14.14 (q), 14.55 (q), 59.34 (t), 61.53 (t), 93.18 (s), 106.34 (s), 134.45 (d), 134.72 (d), 134.87 (d), 135.80 (d), 139.47 (d), 144.03 (s), 146.31 (d), 149.45 (s), 151.51 (s), 162.06 (s), 163.26 (s), 163.84 (s); IR 3200—2650 (NH), 1734, 1710 (ester C=O), 1630 (amido C=O), and 1610 cm-1 (C=N); MS *m/z* (rel intensity) 355 (M^+; 100), 310 (22), 309 (38), 264 (71), 237 (94), 129 (22), and 110 (31). HRMS Found: *m/z* 355.1087. Calcd for $C_{18}H_{17}N_3O_5$: M, 355.1167.

Methylation of 6a. To the mixture of **6a** (100 mg, 0.35 mmol) and potassium hydroxide 180 mg, 3.2 mmol) in 90% aq ethanol (50 ml), methyl iodide (500 mg) was added, and the mixture was refluxed for 16 h and evaporated. The residue was dissolved in water, neutralized with 1M hydrochloric acid (1M=1 mol dm^{-3}), and extracted with chloroform. The extract was dried over sodium sulfate and evaporated. The residue was chromatographed with chloroform–ethyl acetate (1 : 1) gave **6c** (25 mg, 24%), which was crystallized from hexane–dichloromethane to give orange needles (18 mg, 17%), mp 173—174 °C, ^1H NMR δ=1.38 (3H, t, J=7.3 Hz, Me), 4.11 (3H, s, NMe), 4.35 (2H, q, J=7.3 Hz, OCH_2), 7.63—7.83 (3H, m, H-7, 8, and 9), 7.97 (1H, s, H-11), 8.10 (1H, s,

H-3), 8.52 (2H, d, J=9.2 Hz, H-6 and 10); ^{13}C NMR δ=14.42 (q), 41.21 (q), 60.11 (t), 100.25 (s), 104.84 (d), 129.32 (d), 129.77 (d), 134.15 (d), 134.61 (d), 135.98 (d), 146.75 (s), 148.21 (d), 154.76 (s), 155.53 (s), 160.85 (s), 162.01 (s); IR 1716 (ester C=O) and 1668 cm-1 (amido C=O); MS m/z (rel intensity) 297 (M^+; 65), 268 (20), 224 (55), 223 (42), 195 (100), 184 (74), 171 (78), 144 (44), 129 (53), and 102 (29). HRMS Found: m/z 297.1112. Calcd for $C_{16}H_{15}N_3O_3$: M, 297.1109.

We thank Dr. Masafumi Yasunami (Tohoku University) and Dr. Akira Mori (Kyushu University) for the measurements of the Mass spectra and elemental analyses.

References

1) T. Nishiwaki and N. Abe, *Heterocycles*, **15**, 547 (1981).
2) K. Yamane, K. Fujimori, and T. Takeuchi, *Chem. Lett.*, **1981**, 293.
3) K. Fujimori, N. Hirako, and K. Yamane, *Bull. Chem. Soc. Jpn.*, **56**, 1247 (1983).
4) N. Abe, T. Nishiwaki, H. Yamamoto, and N. Kunishige, *Bull. Chem. Soc. Jpn.*, **56**, 3703 (1983).
5) B. Abarca, R. Ballesteros, and G. Jones, *J. Heterocyclic Chem.*, **21**, 1585 (1984).
6) T. Nishiwaki and N. Kunishige, *J. Chem. Res. (S)*, **1985**, 363.
7) K. Yamane, H. Yamamoto, A. Satoh, Y. Tamura, and T. Nozoe, *Bull. Chem. Soc. Jpn.*, **59**, 3326 (1986).
8) N. Abe, *Heterocycles*, **26**, 51 (1987).
9) N. Abe, *Bull. Chem. Soc. Jpn.*, **60**, 1053 (1987).
10) M. L. Jain and R. P. Soni, *Heterocycles*, **16**, 1077 (1981).
11) N. P. Peet, S. Sunder, and R. J. Barbuch, *J. Heterocyclic Chem.*, **19**, 747 (1982).
12) J.-C. Lancelot, D. Laduree, H. E. Kashef, and M. Robba, *Heterocycles*, **23**, 909 (1985).
13) T. Nozoe, S. Seto, S. Matsumura, and T. Terasawa, *Chem. Ind.*, **1954**, 1357.
14) One NH proton is not observed.
15) I. Hermecz and Z. Meszaros, *Adv. Heterocyclic Chem.*, **33**, 241 (1983).
16) I. Hermecz, A. Horvath, L. Vasvari-Debreczy, and Z. Meszaros, *Synthesis*, **1984**, 152.

The Adsorption of Cholesterol and Egg-Lecithin from Solutions on Active Carbon

Zhenguo ZHAO,* Aiyin WU, Tiren GU, and Yuanming MA†
Laboratory of Surface and Colloid Chemistry, Department of Chemistry, Peking University, Beijing, China
†Department of Pharmacology, Shanghai Medical University, Shanghai, China
(Received December 1, 1986)

Synopsis. The adsorption isotherms of cholesterol from ethanol and cyclohexane (at 25 and 35 °C), and of egg-lecithin from ethanol and ethanol-water mixed solvent (at 25 °C) onto active carbon have been determined. The isotherms can be represented by Dubinin-Radushkevich equation. The results indicate that the adsorption of cholesterol and lecithin from solutions onto active carbon can be explained by the mechanism of micropore filling.

The model biological membrance is of great theoretical and practical importance. The model lipid monolayer formed on solid surface by adsorption method has been studied by Poltorak and Chukhrai,[1] Kamyshnyi et al.,[2] Benko et al.[3] Tamamushi[4] studied the adsorption of lipids from solutions. The adsorbents used in these studies were mostly nonporous or had macro-pores. In the present work the adsorption of cholesterol and lecithin from ethanol, cyclohexane, and ethanol-cyclohexane mixtures on active carbon has been studeid. The effect of solvents on the adsorption and the mechanism of the adsorption are discussed.

The egg-lecithin was extracted from egg yolk. The MS analysis showed that the molecular weight of the egg-lecithin obtained was 701. The purity of the egg-lecithin was examined by means of thin-layer chromatography. Pure cholesterol was supplied by E. Merck Co. The melting point was 148.5 °C, in agreement with literature.[5] The granular active carbon GH was supplied by Guang Hua Wood Factory and was treated further with acetic acid and hydrofluoric acid repeatedly. The excess acids were washed out with hot water and finally the active carbon was dried in air at 120 °C. The BET surface area from the N_2 adsorption method was 1410 $m^2 \cdot g^{-1}$, the pore volume was 0.609 $cm^3 \cdot g^{-1}$ by the saturated CCl_4 vapor adsorption method, and the average pore radius was 8.6 Å.

The adsorption experiments were carried out with a shaker-bath, at 25 or 35 °C (±0.5 °C), using 25 cm^3 flasks, with 0.1g active carbon samples, 10.0 cm^3 solution and a 24 h shaking time (previous experiments showed that equilibrium was achieved within 12 h). After settling, the supernatant liquid was analyzed by UV absorption. The adsorbed amount (a $g \cdot g^{-1}$) was calculated according to

$$a = \frac{V\Delta C}{m},$$

where ΔC ($g \cdot dm^{-3}$) is the change in concentration of solute coused by adsorption, V is the total volume of solution, and m is the mass of adsorbent.

The adsorption isotherms of cholesterol from the solution of ethanol and cyclohexane (both at 25 and 35 °C), and of lecithin from ethanol and mixed solvent of ethanol-water (volume ratio 4 : 1) (at 25 °C) are plotted in Figs. 1 and 2, respectively. Figure 1 shows that the adsorbed amount of cholesterol from ethanol is smaller than that from cyclohexane in the experimental concentration range. Figure 2 shows that the adsorbed amount of lecithin from the mixed solvent is smaller than that from ethanol when the concentration is higher than 2 $g \cdot dm^{-3}$.

For porous adsorbents, particularly active carbon with micropores whose radius is smaller than 1 nm, the effect of increasing adsorption potentials as a result of overlapping of the fields of opposite walls of the pores is prominent. The characteristic adsorption isotherm due to Dubinin and Radushkevich,[6] which

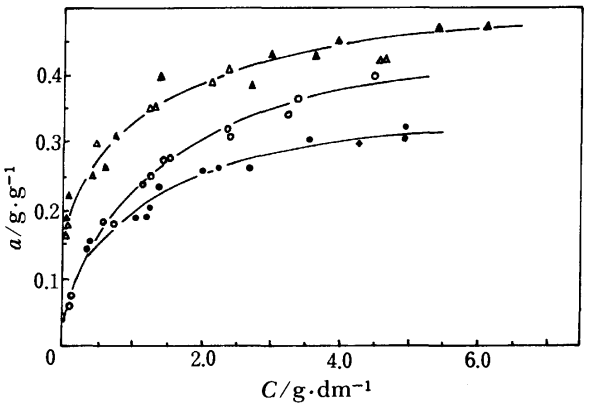

Fig. 1. Adsorption isotherms of cholesterol from ethanol (○, 25 °C; ●, 35 °C) and cyclohexane (△, 25 °C; ▲, 35 °C) on active carbon GH.

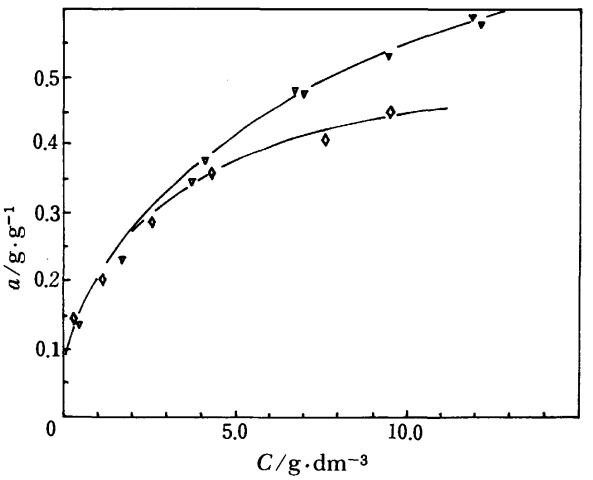

Fig. 2. Adsorption isotherms of egg-lecithin from ethanol (▽, 25 °C) and ethanol-water (volume ratio 4:1) mixed solvent (◇, 25 °C) on active carbon GH.

Table 1. Adsorption of Cholesterol and Lecithin on Active Carbon GH

Adsorbate	Cholesterol				Lecithin	
Solvent	Ethanol		Cyclohexane		Ethanol	Ethanol–water
Temperature/°C	25	35	25	35	25	25
Pore volume of the adsorbent, W_0/ml · g^{-1}	0.609	0.609	0.609	0.609	0.609	0.609
Maximumm volume of adsorbed solute, W_m/ml · g^{-1}	0.439	0.356	0.498	0.492	0.573[a)]	0.454
W_m/W_0	0.72	0.58	0.82	0.81	0.94	0.75

a) This value is calculated from maximum adsorbed amount, as the solubility data are not available.

was later modified by Dubinin and Zaverina,[7] can be written in the form,

$$\ln W - \ln W_0 = -A\varepsilon^2, \quad (1)$$

where W is the volume of adsorbed substance, W_0 is the total volume of adsorption space that represents the volume of micropores of the active carbon, parameter the A is a kind of distribution function of volume of the pores according to sizes, and ε is the Polanyi potential. According to the Polanyi theory of adsorption, ε is the work required to transfer a molecule from the gas phase at pressure P to the liquid phase at saturated pressure P_0

$$\varepsilon = kT \ln(P_0/P), \quad (2)$$

and k is the Boltzmann constant. Relationship 1, which is known as the DR equation,[8] together with its extension,[9] is used to describe pore filling as pressure increases. When dealing with the adsorption from solutions, the DR equation can be written as

$$\log a - \log a_m = -B\left(\log \frac{C_0}{C}\right)^2, \quad (3)$$

where a and a_m are the amount and maximum amount of the adsorbed substance, respectively, C and C_0 are the equilibrium concentration and saturated concentration of adsorbate, respectively, and B is a constant. A plot of $\log a$ against $(\log C_0/C)^2$ should give a straight line with an intercept $\log a_m$ and a slope $-B$, from which the two constant a_m and B can be evaluated.

Figure 3 gives the plots illustrating the applicability of the DR equation to the adsorption of cholesterol and lecithin from solution on active carbon. It should be noted that the constant B in Eq. 3 depends not only on the adsorbent but also on the solute and solvent. The maximum volume of the adsorbed solute, W_m, can be calculated from a_m and the density of the solute. Table 1 shows that the maximum adsorbed volume of cholesterol and lecithin from solutions are 58—82% and 75—94% of the total pore volume of the adsorbent, respectively. Obviously, the rest of the pore volume should be filled with the solvent. Similar results have been obtained by Koganovskii and Levchenko[10] for the adsorption of 1-propanol, 1-butanol, and 1-hexanol from aqueous solution onto active carbon.

It is well-known that the adsorption of the solute must be accompanied by a displacement of the solvent.

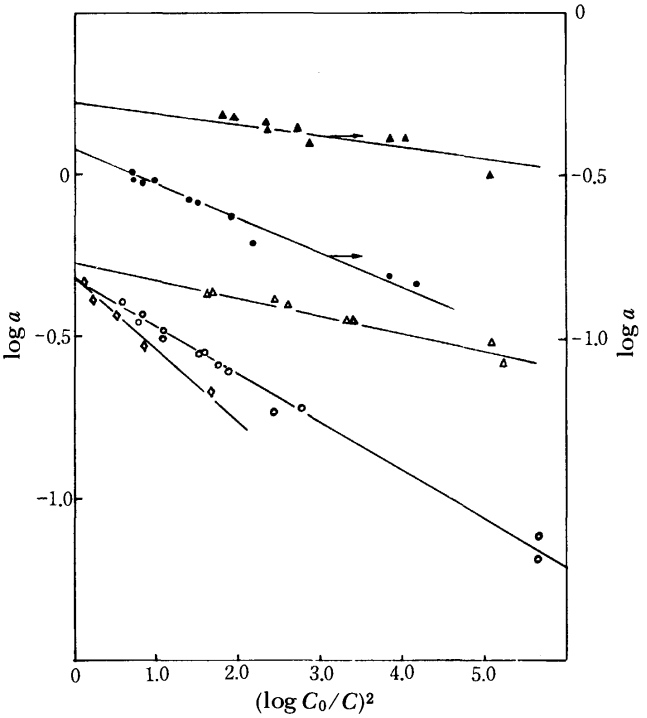

Fig. 3. Adsorption isotherms of cholesterol and lecithin from solutions on active carbon GH, Legend as in Figs. 1 and 2.

Based on the thermodynamics, the free energy of this displacement becomes progressively greater as the interface interaction and the number of solvent molecules on the surface or in the pore space becomes less.[11] In other words, the solvent molecules cannot be completely displaced from the solid surface (pore space).

It should be noted that one of the main reasons for the failure of attempts to predict W_m has been the failure to account for solvent remaining in the adsorbed phase. Only when the solubility of the solute in solvent or the miscibility of the solute with solvent is very low and the interaction between the solute and solid surface is very strong, the maximum adsorption volume of solute should be approximately equal to the pore volume of adsorbent. An example is the adsorption of *p*-chlorophenol, *p*-chloroaniline, nitrobenzene, chloroform, and benzene from aqueous solution onto active carbon by Koganokvskii et al.[12]

References

1) O. M. Poltorak and Ye. S. Chukhrai, *Zh. Fiz. Khim.*, **40**, 1665 (1966).
2) A. L. Kamyshnyi, Ye. S. Chukhrai, and O. M. Poltorak, *Vestn. Mosk. Univ., Khim.*, **13**, 275 (1972).
3) Ye. M. Benko, A. L. Kamyshnyi, Ye. S. Chukhrai, and O. M. Poltorak, *Koll. Zh.*, **41**, 211 (1979).
4) Bun-ichi Tamamushi, "Adsorption from Solution," ed by R. H. Ottewill, C. H. Rochester, and A. L. Smith, Academic Press, London (1983).
5) "CRC Handbood of Chemistry and Physics," ed by R. C. Weast, 63rd ed, CRC press, Inc. Boca Raton, Florida (1983), c-231.
6) M. M. Dubinin and L. V. Radushdevich, *Dokl. Akad. Nauk. USSR*, **55**, 331 (1947).
7) M. M. Dubinin and E. D. Zaverina, *Zh. Fiz. Khim.*, **23**, 1129 (1949).
8) G. F. Cerofolini, "Colloid Science," Vol. 4, ed by D. H. Everett, The Chemical Society, London (1983), Chap. 2.
9) M. M. Drbinin, "Adsorption-Desorption Phenomena," ed by F. Ricca, Academic Press, London (1972), p. 3.
10) A. M. Koganovskii and T. M. Levchenko, *Zh. Fiz. Khim.*, **46**, 1789 (1972).
11) Y. Fu, R. S. Hansen and F. E. Bartell, *J. Phys. Colloid Chem.*, **52**, 374 (1948).
12) A. M. Koganovskii, T. M. Levchenko, "Adsorbtsiya Rastvorennykh Veshchestv" (Adsorption of Dissolved Substances), Naukova Dumka, Kiev, USSR (1977).

Chlorothionitrene Complexes of Tungsten. Synthesis, Characterization, and Chemical Behavior of Tungsten(VI) Thionitrene Complexes

Jyoti SETH, Minu GUPTA, and U. C. AGARWALA*
Department of Chemistry, I. I. T., Kanpur, India
(Received January 20, 1987)

Synopsis. The syntheses of Tungsten(VI) chlorothionitrene complexes have been described and their chemical behavior was studied. The compounds were characterized by microanalyses, vibrational, electronic, ESR, NMR spectral and other Chemical studies.

Although the chemistry of metal nitrosyls has been extensively studied,[1,2] it is only recently that there has been considerable interest in the study of the reactivity of NSCl with various transition metal complexes for the syntheses of thionitrosyls.[3-9] Characterization of its interaction products indicates that S-N species formed from NSCl and bonded to the metal center are quite diverse. Due to this intriguing behavior of thionitrosyl chloride, many investigations have been devoted to study such complexes. In addition, our efforts in recent years have been in a direction to search the possibility of using trimeric thionitrosyl chloride as a thionitrosylating agent for the synthesis of metal thionitrosyls,[3-5,10,11] a field which is still in an embryonic state. While making these efforts, the reactions of $(NSCl)_3$ with substituted tungsten(II) carbonyl complexes having 2,2′-bipyridine or 1,10-phenanthroline as coligand afforded complexes in which NSCl is bonded to W(VI) in the form of chlorothionitrene group $M{=}N{=}S\diagdown_{Cl}$, a bonding mode which has been fairly studied. This paper focuses on the detailed syntheses and characterization of these componds.

Experimental

Materials and Methods. All the chemicals used were of reagent or AnalaR grade. Tungsten hexacarbonyl, tungsten hexachloride, 2,2′-bipyridine and 1,10-phenanthroline, and Sephadex LH-20 resin were purchased from the Aldrich Chemical Company and were used as such. The starting materials $[W(CO)_3(L\text{-}L)X_2]$ (L-L=bpy or *o*-phen; X=Br or I), $[W(NSCl)Cl_4)]_2$ and trimeric thionitrosyl chloride were prepared by the literature methods.[12-14] Solvents were purified and dried by standard methods.[15] and degassed prior to use. All experiments were performed under nitrogen atmosphere. Details of the physicochemical methods are given elsewhere.[16]

Preparations. (A) Reaction Medium-Dichloromethane. (a) Reaction of $(NSCl)_3$ with $[W(CO)_3(L\text{-}L)X_2]$ (L-L=bpy or *o*-phen; X=Br or I). A solution of $(NSCl)_3$ (ca. 0.03 mmol) in 10 ml of dichloromethane was added to a stirred solution of $[W(CO)_3(L\text{-}L)X_2]$ (ca. 0.1 mmol) in 15 ml of dichloromethane. After the mixture was stirred for approximately 1 h and gas evolution had ceased, the resulting solution was concentrated under reduced pressure to about 5 ml. The product (I) was precipitated from the concentrate with light petroleum ether, which was filtered and washed with a little of benzene and then with copious amounts of petroleum ether. The product was recrystallized from dichloromethane-petroleum ether. The recrystallized product was further purified by column chromatography using Sephadex LH-20 column (25 cm×2.5 cm) and 1 : 1 mixture of dichloromethane and chloroform as the eluent (elution rate, approximately 1—2 ml min^{-1}). A broad brown band formed on the column top was eluted by CH_2Cl_2 and the eluent was concentrated under reduced pressure to about 5 ml and kept at 0 °C for a few days for crystallization. Thereby microcrystals (II) were deposited on the sides of the flask. These were collected washed with a little benzene, petroleum ether, dried under vacuum. The same compound was also obtained by precipitating it from the concentrated eluent with light petroleum ether and drying it under vacuum (yield 50%). The compounds I and II were found to be identical as has been found from chemical analysis, mp, mixed mp, IR and UV-visible spectral data. The compound has the formulation $[W(NSCl)Cl_3X'\ (L\text{-}L)]$ (X′=Cl or Br).

(b) (Reactions of 2,2′-Bipyridine and 1,10-Phenanthroline with $[W(NSCl)Cl_4]_2$. A stoichiometric amount of bpy or *o*-phen was added to a stirred suspension of $[W(NSCl)Cl_4]_2$ (ca. 0.1 mmol) in 25 ml of dichloromethane and stirring was continued for 1 h when the solution attained brown color. It was filtered and the filtrate was concentrated under reduced pressure. The concentrate was processed as described in A(a) (yield 60%).

(B) Reaction Medium-Tetrahydrofuran. The reactions were carried out by the same procedure as described in A(a) and A(b) except that tetrahydrofuran was used as the reaction medium in the place of dichloromethane. The working up of the reaction product, recrystallization of the compounds and their purification by column chromatography were done as described in (A).†

(C) Thermolysis of $[W(NSCl)Cl_3X'\ (L\text{-}L)]$ (L-L=bpy or *o*-phen; X′=Cl or Br). Thermolysis of $[W(NSCl)Cl_3X'\text{-}(L\text{-}L)]$ (exactly weighed) was carried out at about 250 °C for 4 h in a two necked flask having an inlet and outlet tube. Through the inlet tube a slow stream of nitrogen gas was allowed to pass slowly, while the gaseous products coming out of the outlet tube were bubbled into water. The hydrolyzed products were then analyzed for sulfur and chloride ion. The compound after thermolysis changed to pinkish grey color and was analyzed for $[WNCl_2X'\ (L\text{-}L)]_n$ (III).

In another experiment, the known weight of $[W(NSCl)\text{-}Cl_3X'\ (L\text{-}L)]$ was heated at 250 °C for 4 h over a watch glass. After cooling the change in weight was recorded. The loss in weight of the complex corresponded approximately to one mole of SCl_2 per mole of the complex.

Results and Discussion

The reactions of trimeric thionitrosyl chloride with $[W(CO)_3(L\text{-}L)X_2]$ yielded the novel compounds of empirical formula $[W(NSCl)Cl_3X'(L\text{-}L)]$ (**1**) (cf. Table 1). Apart from being a ligand linked to the metal ion as $(NSCl)^{-2}$, the trimeric thionitrosyl chloride oxidizes tungsten from II to VI oxidation state. In

† In THF, compounds became oily during recrystallization process.

Table 1. Color, Mp,[a] Microanalysis, Thermolysis, and UV-Visible Data of Complexes

Sample No.	Compound	Color[b]	Elemental analysis in % Exptl (Calcd)					Thermolysis % loss Exptl (Calcd)			UV-visible data λ_{max}/nm
			C	H	N	S	X	% loss in wt.	% S	% Cl	
1	$[W(NSCl)Cl_4$ bipy]	GR	21.6 (21.2)	1.8 (1.4)	7.2 (7.4)	5.9 (5.7)	30.9 (31.4)	19.4 (18.2)	5.2 (5.7)	13.2 (12.6)	250, 310, 380, 475, 510
2	$[W(NSCl)Cl_3Br$ bipy]	O	19.2 (19.7)	1.9 (1.3)	6.4 (6.9)	5.6 (5.2)	36.1 (36.4)	18.2 (16.9)	5.0 (5.2)	13.0 (11.6)	255, 320, 375, 480, 515
3	$[W(NSCl)Cl_4$ *o*-phen]	YB	24.7 (24.5)	1.4 (1.3)	6.8 (7.1)	5.1 (5.4)	29.8 (30.1)	18.9 (17.5)	5.0 (5.4)	12.5 (12.0)	250, 315, 380, 475, 510
4	$[W(NSCl)Cl_3Br$ *o*-phen]	B	22.4 (22.7)	1.7 (1.2)	6.3 (6.6)	4.9 (5.0)	34.8 (35.0)	17.8 (16.3)	4.2 (5.0)	12.0 (11.2)	248, 320, 375, 475, 520
5	$[W(NSCl)Cl_4$ bipy]·THF	RB	26.9 (26.4)	2.8 (2.5)	6.2 (6.6)	4.8 (5.0)	27.2 (27.8)	28.2 (27.5)	4.0 (5.0)	11.8 (11.1)	250, 310, 380, 485, 515
6	$[W(NSCl)Cl_3Br$ bipy]·THF	OY	24.2 (24.6)	3.1 (2.3)	6.0 (6.2)	5.0 (4.7)	32.2 (32.6)	26.3 (25.7)	4.1 (4.7)	11.4 (10.4)	250, 315, 375, 480, 520
7	$[W(NSCl)Cl_4$ *o*-phen]·THF	Y	28.9 (29.1)	2.1 (2.4)	6.5 (6.3)	5.1 (4.8)	26.4 (26.8)	28.0 (26.5)	4.2 (4.8)	11.2 (10.7)	255, 310, 380, 475, 510
8	$[W(NSCl)Cl_3Br$ *o*-phen]·THF	B	26.9 (27.2)	2.8 (2.3)	6.2 (5.9)	4.2 (4.5)	31.1 (31.5)	26.1 (24.8)	3.5 (4.5)	11.0 (10.1)	250, 320, 375, 480, 520

a) All the compounds decomposed around 230 °C. b) GR=greenish red, O=orange, YB=yellow brown, B=brown, RB=reddish brown, OY=orangish yellow, Y=yellow.

Table 2. IR Spectra of Representative Complexes[a]

$[W(NSCl)Cl_3X'(L\text{-}L)]$		$[WNCl_2X'(L\text{-}L)]$	
910 (m)		999 (VS)	
940 (m)	ν_{as} (WNS)	900 (m)	ν_{as} (W≡N)
970 (m)			
500 (w)	ν (SCl)	450 (s)	
430 (w)	ν_s (WNS)		
340 (s)		370 (m)	ν (WCl)
320 (m)	ν (WCl)	340 (m)	
270 (w)	δ (NSCl)		

a) IR bands due to coordinated 2,2′-bipyridine and 1,10-phenanthroline were observed in the expected region.

iodo complexes, both the iodide ions and in bromo ones only one bromide ion were substituted by the chloride ions in their respective products. The approximate amount of liberated iodine during the reaction was iodometrically estimated which conformed to two moles of iodide ions per mole of the complex.

The compounds are soluble in halo-substituted solvents and decompose in methanol to yield polymeric nitrido compound of empirical formula $[W_2N(L\text{-}L)\text{-}S_2Cl_5]$ as suggested by analytical and IR data. These when solubilized in $POCl_3$ yielded the moisture sensitive adduct $[W(NSCl)Cl_3X'(L\text{-}L)]\cdot POCl_3$ similar to the behavior of $[W(NSCl)Cl_4]_2$.

The compounds in general were preserved at low temperature (0 °C) as they undergo slow decomposition at room temperature yielding a pinkish grey compound. This was further corroborated by the results of the thermolysis experiments (vide infra). The gaseous products obtained by pyrolyzing the compound were hydrolyzed by bubbling in water and the halogen and sulfur contents were estimated. The results corresponded to the loss of a molecule of SCl_2 per molecule of the compound, as also suggested by the loss of weight of the compound after thermolysis. It appears that the complexes lose a molecule of SCl yielding pink nitrido complexes from which another chloride ion could be lost to preserve the charge balance similar to the earlier reported $M{=}N{=}S\diagdown_{Cl}$ complexes.[6] These may further be reduced partially to other polymeric tungsten nitrides in +V oxidation state.

The infrared spectra of all the compounds showed three medium to intense bands in the region 1000—900 cm^{-1} assignable to the stretching modes of M≡N=S moiety.[6,14,17,18] The bonding mode of NSCl moiety is further corroborated by the following chemical evidence.

The coordinatively unsaturated compound $[W(NSCl)\text{-}Cl_4]_2$ had been shown to have $[W{=}N{=}S\diagdown_{Cl}]$ unit by X-ray crystal structure studies. The reaction of this compound with bpy or *o*-phen yielded compounds of the type $[W(NSCl)Cl_4(L\text{-}L)]$ which were found to be identical to the compounds synthesized by the procedure A(a). The identical nature of these complexes, as also shown by X-ray powder patterns, gives one sufficient reason to believe that the (NSCl) moiety in our compounds have a $[M{=}N{=}S\diagdown_{Cl}]$ type of bonding, assuming reactions of bpy or *o*-phen do not affect the bonding mode of (NSCl).[19] Further the bands due to ν(WNS) of $[W(NSCl)Cl_3X'(L\text{-}L)]$ disappeared in the vibrational spectra of the pinkish grey thermolysis product and an intense band appeared at 990 cm^{-1}, assigned to ν(W≡N).[20,21] The shift of ν(W≡N) band position to lower wave numbers compared to that of W(VI) nitrido compounds (viz. 1040 cm^{-1}) could be attributed to the partial reduction of W(VI) to W(V)[20,21] (vide infra). The assignments of bands due to lack of crystal structure are somewhat tentative and additional studies are required to confirm their

identity.

The electronic spectral features of the compounds are given in Table 1. The spectra showed a band at around 250 nm, assigned to $\pi(X) \rightarrow d\pi(W(VI))$ charge transfer transition.[23] The band at around 500 nm was found to be split in general and one of its components along with 380 nm band could be attributed to the π(bpy or *o*-phen)$\rightarrow d\pi(W(VI))$ charge transfer transition. Preliminary solvent dependent studeis indicated the solvatochromism[23,24] associated with one of the components of the band at around 500 nm and this was utilized as a criterion for differentiating the charge transfer band. Its other component may possibly arise due to intraligand transition involving $=N=S\diagdown_{Cl}$ moiety or due to charge transfer transition of the $[M=N=S\diagdown_{Cl}]$ unit. All the compounds were found to be diamagnetic and their ESR spectra were recorded, wherein no signal was obtained. This indicates the presence of tungsten in VI oxidation state, substantiating further the linkage of NSCl as $M=N=S\diagdown_{Cl}$.

In the compounds preparted in tetrahydrofuran the solvated formulation viz. $[W(NSCl)Cl_3X'(L\text{-}L)]\cdot$ THF could be preferred over the coordinated one based on the following observations.

(i) The NMR spectra showed practically no shift in the resonances of the THF protons as compared to that of the free THF molecule.

(ii) The color and the mp's of the compounds were almost similar to those of the compounds prepared in dichloromethane.

(iii) The compounds were analyzed to $[W(NSCl)Cl_4(L\text{-}L)]\cdot$THF. The efforts to remove the solvated THF completely by different means were unsuccessful.

On the basis of the foregoing discussions the compounds were assigned the heptacoordinate structure $[W(NSCl)Cl_3X'(L\text{-}L)]$ with the metal ion in VI oxidation state. Although seven coordination is commonly not encountered in compounds of tungsten in higher oxidation states, it is however not unlikely.[25]

One of the authors (Ms. J. Seth) thanks CSIR, New Delhi, India for the award of Senior Research Fellowship.

References

1) B. F. G. Johnson and J. A. McCleverty, *Prog. Inorg. Chem.*, **7**, 27 (1966).
2) N. G. Connelly, *Inorg. Chim. Acta, Rev.*, **6**, 47 (1972).
3) K. K. Pandey, D. M. K. Raju, H. L. Nigam, and U. C. Agarwala, *Proc. Indian Natl. Sci. Acad.*, **48**, 16 (1982).
4) H. W. Roesky and K. K. Pandey, *Adv. Inorg. Chem. Radiochem.*, **26**, 337 (1982).
5) P. F. Kelly and J. D. Woollins, *Polyhedron*, **5** (3), 607 (1986).
6) U. Kynast and K. Dehnicke. *Z. Anorg. Allg. Chem.*, **502**, 29 (1983).
7) H. Wadle and K. Dehnicke, *Z. Naturforsch. B*, **40**, 1314 (1985).
8) H. Wadle, E Conradi, U. Muller, and K. Dehnicke, *Z. Naturforsch. B*, **40**, 1626 (1985).
9) H. Wadle, E. Conradi, U. Muller, and K. Dehnicke, *Z. Naturforsch. B*, **40**, 429 (1986).
10) K. K. Pandey, S. Datta, and U. C. Agarwala, *Z. Anorg. Allg. Chem.*, **468**, 228 (1980).
11) Minu Gupta, R. F. N. Ashok, Anjali Mishra, V. B. S. Chauhan, and U. C. Agarwala, *J. Chem. Soc., Dalton Trans.*, **1985**, 2449.
12) M. H. B. Stiddard, *J. Chem. Soc. A*, **1966**, 317.
13) K. D. Magiure, J. J. Smith, and W. L. Jolly, *Chem. Ind. (London)*, **39**, 334 (1963).
14) U. Kynast, U. Muller, and K. Dehnicke, *Z. Anorg. Allg. Chem.*, **508**, 26 (1984).
15) A. I. Vogel, "A Textbook of Practical Organic Chemistry," IV ed, Longmans Green Co,, London (1980), p. 264.
16) K. M. Rao, L. Mishra, and U. C. Agarwala, *Polyhedron*, **5**, 1491 (1986).
17) U. Kynast, P. Klingelhofer, U. Muller, and K. Dehnicke. *Z. Anorg. Allg. Chem.*, **515**, 61 (1984).
18) W. Heller, J. Hohyla, J. Stahle, H. G. Hauck, and K. Dehnicke, *Z. Anorg. Allg. Chem.*, **514**, 72 (1984).
19) R. Christophersen, P. Klingenlhofer, U. Muller, K. Dehnicke, and D. Rehder. *Z. Naturforsch. B*, **40**, 1631 (1985).
20) J. Chatt and J. R. Dilworth, *J. Chem. Soc., Chem. Commun.*, **1974**, 517.
21) N. Kruger and K. Dehnicke, *Z. Naturforsch. B*, **34**, 1343 (1979).
22) M. L. Larson and F. W. Moore, *Inorg. Chem.*, **5**, 801 (1966).
23) A. B. P. Lever, "Inorganic Electronic Spectroscopy," II ed, Elsevier, New York (1984) p. 227.
24) C. Overton and J. A. Connor, *Polyhedron*, **1**, 53 (1982).
25) Zvi Dori, *Prog. Inorg. Chem.*, **28**, 239 (1981).

 © 1988 The Chemical Society of Japan Bull. Chem. Soc. Jpn., 61, 1451—1454 (1988)

Thermodynamic Stability of Polycyclic Aromatic Hydrocarbons Detected in Our Environment

Jun-ichi AIHARA
Department of Chemistry, Faculty of Science, Shizuoka University, Oya, Shizuoka 422
(Received June 16, 1987)

Various polycyclic aromatic hydrocarbons (PAHs) are distributed widely in our environment. Diesel particulate extract contains many larger PAHs. All these PAHs have a percent resonance energy larger than 2.50. Dibenzo[def,mno]chrysene and anthracene constitute the most unstable PAHs among them. A couple of reaction paths to the formation of ovalene are discernible in flames by inspecting the combustion products. It seems likely that a similar type of reactions take place in the envelopes of carbon stars to give large compact PAHs and graphite.

Polycyclic aromatic hydrocarbons (PAHs) are formed abundantly by incomplete combustion of organic matter and fossil fuel.[1,2] As a result, they are distributed virtually everywhere in our environment. Although reaction mechanisms in flames remain very elusive, formation of many PAHs has been confirmed by means of chromatographic and spectroscopic methods.[1,2] Recently, Jinno et al. elaborately analyzed the Diesel particulate extract, and identified many very large PAHs.[3-6] Most PAHs detectable both in our environment and in the Diesel particulate extract are devoid of side chains and substituents. PAHs can nowadays be detected in the interstellar medium.[7,8] In this paper we attempt to find a rationale for the presence of such PHAs not only in our environment but also in the combustion products.

We previously defined the percent resonance energy (%RE) of a given molecule[8-11] as 100 times the graph-theoretically defined resonance energy,[9,12-15] divided by the total π-electron energy of the olefinic reference structure.[8-11] Many examples indicate that the %RE is an excellent index for determining the thermodynamic stability of a cyclic conjugated system. We first estimate the degree of thermodynamic stability for widely detectable PAHs by evaluating the %REs. We then seek for the formation mechanisms of PAHs in incomplete combustion. Analysis of combustion processes might give an important clue to the question as to why there are large compact PAHs and graphite in the interstellar medium.[7,8] Simple Hückel theory is used to calculate %REs.

Results and Discussion

The %REs of all PAHs investigated are listed in Table 1. The PAHs distributed widely in air, water, soil, and tissue are classified as group-A PAHs.[1,2] They are usually formed by incomplete combustion of fossil fuel, organic matter, and plants, polluting our entire environment. It is noteworthy that all group-A PAHs have a %RE larger than 2.50 in the ground electronic state. Group-B PAHs are the ones identified in the Diesel Particulate extract by Jinno et al.[5,6] These very large PAHs again have a %RE larger than 2.50. Most of the group-A PAHs are of course detectable in the Diesel Particulate extract.[3,4] Thus, automobile exhaust is full

Table 1. Percent Resonance Energies of Polycyclic Aromatic Hydrocarbons

PAH	RE/β	%RE	PAH	RE/β	%RE
Group A			Benzo[*rst*]pentaphene (**19**)	0.861	2.60
Naphthalene (**1**)	0.389	2.92	Dibenzo[*b,def*]chrysene (**20**)	0.844	2.55
Anthracene (**2**)	0.475	2.52	Naphtho[8,1,2-*bcd*]perylene (**21**)	0.950	2.63
Phenanthrene (**3**)	0.546	2.89	Naphtho[1,2,3,4-*ghi*]perylene (**22**)	1.015	2.81
Pyrene (**4**)	0.598	2.73	Dibenzo[*cd,lm*]perylene (**23**)	0.942	2.61
Fluoranthene (**5**)	0.578	2.64	Benzo[*a*]coronene (**24**)	1.118	2.85
Benz[*a*]anthracene (**6**)	0.643	2.63	Benzo[*pqr*]naphtho[8,1,2-*bcd*]-perylene (**25**)	1.095	2.79
Chrysene (**7**)	0.688	2.81			
Benzo[*a*]pyrene (**8**)	0.725	2.64	Naphtho[8,1,2-*abc*]coronene (**26**)	1.162	2.75
Benzo[*e*]pyrene (**9**)	0.791	2.87	Ovalene (**27**)	1.224	2.70
Benzo[*b*]fluoranthene (**10**)	0.734	2.67			
Benzo[*j*]fluoranthene (**11**)	0.700	2.54	Others		
Benzo[*k*]fluoranthene (**12**)	0.696	2.53	Naphtho[2,1-*a*]pyrene (**28**)	0.878	2.65
Perylene (**13**)	0.740	2.69	Triphenylene (**29**)	0.739	3.01
Dibenzo[*def,mno*]chrysene (**14**)	0.766	2.51	Dibenzo[*fg,op*]naphthacene (**30**)	0.983	2.96
Benzo[*ghi*]perylene (**15**)	0.853	2.79	Azulene (**31**)	0.151	1.14
Indeno[1,2,3-*cd*]pyrene (**16**)	0.785	2.57	Azupyrene (**32**)	0.217	0.99
Coronene (**17**)	0.947	2.82	Acenaphthylene (**33**)	0.354	2.18
			Cyclopenta[*cd*]pyrene (**34**)	0.565	2.27
Group B			Pyracylene (**35**)	0.106	0.55
Naphtho[1,2,3,4-*def*]chrysene (**18**)	0.925	2.79			

of PAHs. Dibenzo[*def,mno*]chrysene (**14**) and anthracene (**2**) constitute the most unstable PAHs among them.

Schmidt stressed that the thermodynamic stability of PAHs plays only a secondary role in determining the composition of combustion products.[16] This never means that the composition of the PAHs found in our environment are not governed by any thermodynamic factor. There are many PAHs which are less stable than dibenzo[*def,mno*]chrysene (**14**) and anthracene (**2**).[17,18] However, they have not been detected around us. Therefore, we might say that some thermodynamic factor indeed operates in the combustion process and in our environment.

Labile PAHs may be formed in substantial amounts in flames, but readily degrade thereafter. Therefore, the %REs of group-A and group-B PAHs give a good criterion for choosing PAHs which have a possibility of surviving in our environment. In other words, the %RE of 2.50 marks a borderline between stable and unstable PAHs. If a given PAH has a %RE larger than 2.50, it would not degrade readily. Such PAHs are being accumulated in our environment, polluting air, soil, water, and food.[1,2] In the polyacene series, the %REs of naphthacene and higher members are smaller than 2.50.[8] They are missing not only in the Diesel exhaust but also in our environment.[1-6]

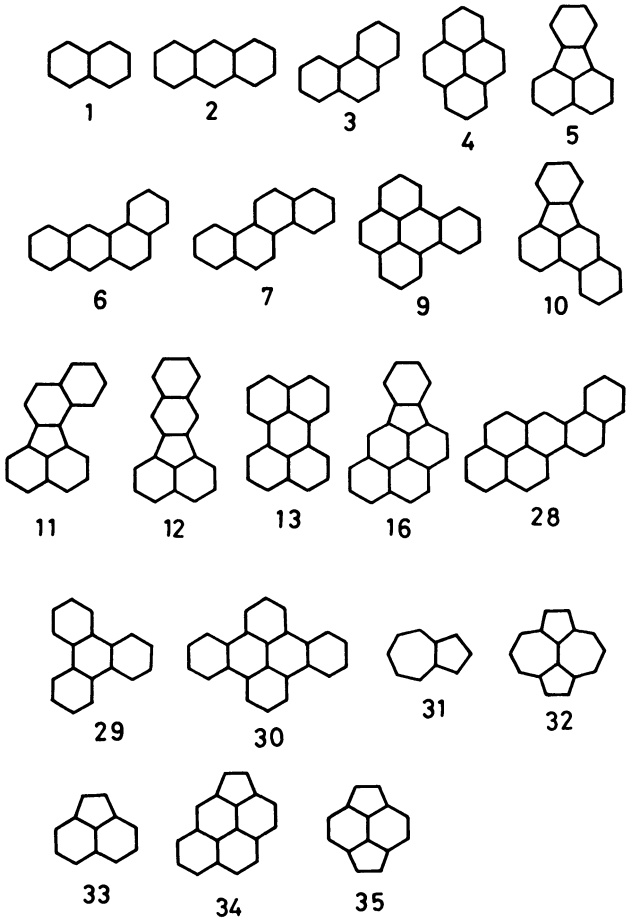

Let us briefly review the formation mechanism of PAHs in incomplete combustion. Numerous intermediate species are involved whose sequential formation and destruction give a progression to decreasing amounts of larger species.[19-26] The largest amounts of species being produced and consumed in combustion are acetylene, 1,3-butadiyne (diacetylene), and 1-buten-3-yne (vinylacetylene).[20,21,25] These unsaturated aliphatics have been identified as important species for the growth of PAH and soot by addition reactions with aromatic radicals. Specifically, the combined presence of aromatic radicals and acetylene is particularly favorable to the growth of PAHs.[20,25]

In a hydrogen-deficient environment, rather compact PAHs with a low H/C ratio are produced preferentially. Non-compact PAHs provide active bonding sites for the attachment of smaller unsaturated species in Diels-Alder and cycloaddition reactions.[16] Compact PAHs must be less reactive in flames full of acetylenic species than non-compact ones. In this sense, the stability of compact PAHs are not only thermodynamic but also kinetic in nature. Compact PAHs, such as pyrene (**4**), dibenzo[*def,*

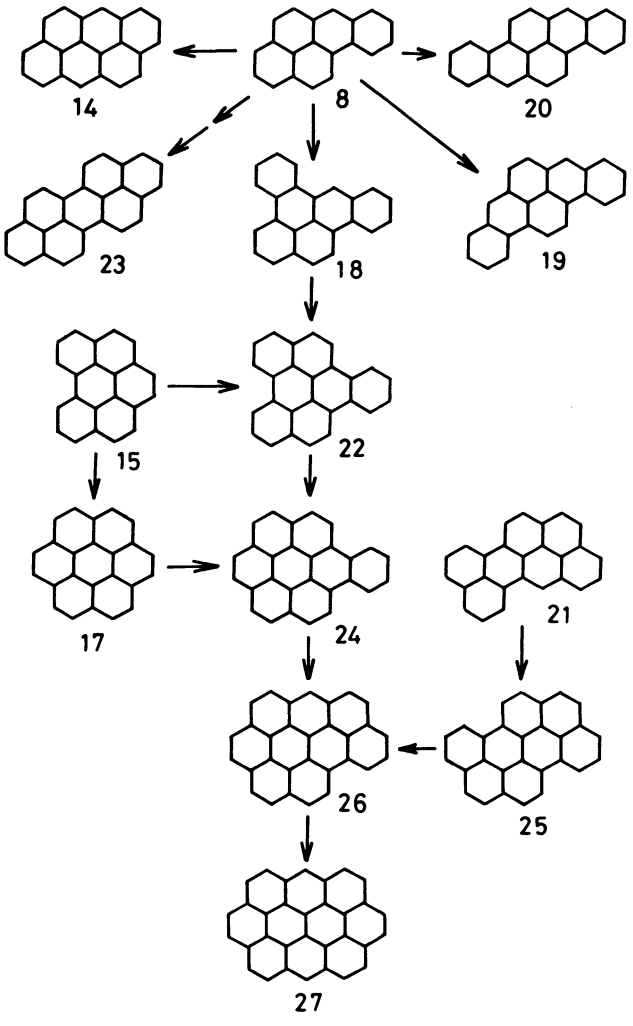

Fig. 1. Possible reaction paths in a Diesel engine.

mno]chrysene (**14**), coronene (**17**), and ovalene (**27**), are neither mutagenic nor carcinogenic.[1,27] Lack of carcinogenicity coincides with the non-existence of L and bay regions.

With such combustion chemistry in mind, possible reactions in a Diesel engine[3–6] can be inferred from the composition of combustion products. As shown in Fig. 1, most group-B PAHs can be arranged in such a manner that they constitute a couple of thermodynamically favored routes for building up ovalene (**27**), a typical large compact PAH. According to the reaction scheme of Stein[23] and Bockhorn et al.,[25] each PAH in this figure represents addition of one ring at a time. Starting with benzo[*a*]pyrene (**8**) and naphtho-[8,1,2-*bcd*]perylene (**21**), individual rings are added by the formal addition of either C_4H_2 or C_2 units. Since most group-B PAHs can be arranged in this manner, it is highly probable that they are formed consecutively according to the analogous reaction scheme. Many other reaction pathways are in principle possible.

It is known that individual PAHs themselves serve to accelerate the formation of larger members of the group.[26] This further rationalizes the reaction scheme given in Fig. 1. Benzo[*ghi*]perylene (**15**) and coronene (**17**) coexist fairly abundantly in the automobile exhaust.[19] Therefore, air in Los Angeles is rich in **15** and **17**.[28] Such a comparative study supports the existence of a reaction route along which **17** is formed from **15**. There is a discontinuity between benzo[*a*]-pyrene (**8**) and dibenzo[*cd,lm*]perylene (**23**) in Fig. 1. Naphtho[2,1-*a*]pyrene (**28**) must intervene between them. Although this PAH was not detected in the Diesel exhaust, it has been detected in the hard-coal combustion effluents.[16]

Various dimerization products are obtained by pyrolysis of naphthalene (**1**), among which are benzo-[*j*]fluoranthene (**11**), benzo[*k*]fluoranthene (**12**), and perylene (**13**).[29] Thus, there are reaction paths along which small PAHs grow into larger ones through dimerization with elimination of hydrogen. By analogy, fluoranthenes (**5**, **10**, **11**, **12**) and indeno[1,2,3-*cd*]pyrene (**16**) are presumably prepared by the condensation of two smaller aromatics.

Fully benzenoid hydrocarbons are the PAHs whose Clar structures consist of aromatic sextets only.[30] They are the PAHs of supreme thermodynamic stability.[8,17,18] Triphenylene (**29**) and dibenzo[*fg,op*]-naphthacene (**30**) belong to the PAH family of this type. However, such PAHs are scarcely detected in the Diesel particulate extract and in our environment.[1–6] It was this fact that convinced Schmidt that thermodynamic factors are of secondary importance in combustion processes.[16] Fully benzenoid hydrocarbons have three or more bay regions, which are susceptible at high temperatures to reaction with acetylenic species.

In general, the carbon skeleton of a benzenoid PAH is stable towards isomerization and cleavage. Azulene (**31**) and azupyrene (dicyclopenta[*ef,kl*]heptalene) (**32**) thermally isomerize to naphthalene (**1**) and pyrene (**4**), respectively.[31,32] However, no reverse reaction occurs. This is why such nonbenzenoid PAHs are not found in our environment.[1–6] This is also why Fig. 1 consists of benzenoid PAHs alone. Semibenzenoid PAHs, such as fluoranthenes (**5**, **10**, **11**, and **12**) and indeno[1,2,3-*cd*]pyrene (**16**), seem to be free from this type of isomerization. Bay regions adjacent to a five-membered ring of a fluoranthene-type molecule appear to be much less reactive toward dienophiles.

Recently, infrared (IR) astronomy revealed that a set of discrete IR lines are emitted from many astronomical objects, such as reflection nebulae and active galaxies.[7] In 1984 Léger and Puget proposed that these IR bands can be assigned reasonably to fundamental vibrations of large compact PAHs in the interstellar medium.[33–36] These PAHs are presumably placed in the intense radiation field since they must be excited electronically in advance of IR emission. In a previous paper,[8] we supported the view of Léger and Puget by showing that many large compact PAHs have large %REs both in the ground and excited states.

Formation mechanisms of PAHs and graphite in the interstellar medium have not been clarified yet.[7] There is no evidence for the existence of small PAHs in the astronomical IR spectra. We showed that small PAHs are photochemically very unstable.[8] Then, the most plausible formation mechanism of PAHs in the intense radiation field is shattering of graphitic carbon grains in shocks.[34,37,38] However, if interstellar matter is rather dense, and if it is not exposed to hard UV radiation, the growth of PAHs and graphite from small molecular pieces is possible. This condition might be satisfied in such places as envelopes of carbon stars.[22,34]

In case PAHs are formed from smaller molecules in space, the combustion processes discussed above will give an important clue to the details of their formation mechanism. There are abundant acetylenic hydrocarbons not only in flames but also in the interstellar medium.[7] Reactions in flames must resemble those in the interstellar medium, in that large compact PAHs are formed preferentially. Thus, the formation of graphitic carbon grains and PAHs and their injection into the interstellar medium is explainable.[22,34]

Concluding Remarks

The PAHs which are formed in incomplete combustion and survive in our environment were found to be thermodynamically fairly stable. In general, the %REs of widely detectable PAHs are greater than 2.50. The PAHs with the %REs$<$2.50 presumably degrade rapidly in our environment. Some PAHs with the

%RE>2.50 are missing or very scanty in our environment, which may imply that they are scarcely formed in flames. For example, perylene (**13**) is very scanty in our environment for a very stable PAH.[1)]

Acenaphthylene (**33**) has been detected in flames.[16,20)] Cyclopenta[cd]pyrene (**34**) was isolated exceptionally from carbon black.[39)] These PAHs have an olefinic C-C double bond, and their %REs are much less than 2.50. Since these PAHs are not very stable, it seems unlikely that they can survive long in our environment. Pyracylene (cyclopent[*fg*]acenaphthylene) (**35**) is essentially olefinic with a very small positive %RE. It has been reported that this compound is also formed in flames.[20,22)] Synthetic pyracylene is stable only in solution, and far from isolable.[40,41)]

Most of group-A and group-B PAHs are photochemically unstable with negative or small positive %REs in the electronically excited state.[8)] This implies that the photochemical instability is not a crucial factor for determining the composition of combustion products. This is in marked contrast to the situation in the interstellar medium, where photochemically stable PAHs alone are probably abundant due to strong UV radiation.[8)]

Helpful discussion with Prof. Kiyokatsu Jinno (Toyohashi Univ. Technol.) is gratefully acknowledged.

References

1) "Polycyclic Hydrocarbons and Cancer," ed by H. V. Gelboin and P. O. P. Tso, Academic Press, New York (1978), Vols. 1 and 2.
2) "Polynuclear Aromatic Hydrocarbons: Formation, Metabolism and Measurement," ed by M. Cooke and A. J. Dennis, Battelle Press, Columbus (1983).
3) K. Jinno, and M. Kuwajima, *Chromatographia*, **21**, 622 (1986).
4) K. Jinno, T. Hoshino, T. Hondo, M. Saito, and M. Senda, *Anal. Chem.*, **58**, 2696 (1986).
5) K. Jinno, J. C. Fetzer, and W. R. Biggs, *Chromatographia*, **21**, 274 (1986).
6) J. C. Fetzer, W. R. Biggs, and K. Jinno, *Chromatographia*, **21**, 439 (1986).
7) "Polycyclic Aromatic Hydrocarbons and Astrophysics," ed by A. Léger, L. d'Hendecourt, and N. Boccara, Reidel, Dordrecht, The Netherlands (1987).
8) J. Aihara, *Bull. Chem. Soc. Jpn.*, **60**, 3143 (1987).
9) J. Aihara, *Pure Appl. Chem.*, **54**, 1115 (1982).
10) J. Aihara, *Bull. Chem. Soc. Jpn.*, **52**, 2202 (1979).
11) J. Aihara, *Bull. Chem. Soc. Jpn.*, **53**, 2689 (1980).
12) J. Aihara, *J. Am. Chem. Soc.*, **98**, 2750 (1976).
13) J. Aihara, *Netsu Sokutei*, **12**, 61 (1985).
14) I. Gutman, M. Milun, and N. Trinajstić, *J. Am. Chem. Soc.*, **99**, 1692 (1977).
15) N. Trinajstić, "Chemical Graph Theory," CRC Press, Boca Raton, Florida (1983), Vol. II, Chap. 1.
16) W. Schmidt in Ref. 7, pp. 149—164.
17) B. A. Hess, Jr., and L. J. Schaad, *J. Am. Chem. Soc.*, **93**, 2413 (1971).
18) J. Aihara, *J. Am. Chem. Soc.*, **99**, 2048 (1977).
19) E. J. Baum in Ref. 1, Vol. 1, Chap. 2.
20) J. B. Howard and J. P. Longwell in Ref. 2, pp. 27—62.
21) S. J. Harris and A. M. Weiner, *Annu. Rev. Phys. Chem.*, **36**, 31 (1985).
22) R. Keller in Ref. 7, pp. 387—397.
23) S. E. Stein, *J. Phys. Chem.*, **82**, 566 (1978).
24) W. C. Gardiner, Jr., *Sci. Am.*, **246 (2)**, 110 (1982).
25) H. Bockhorn, F. Fetting, and H. W. Wenz, *Ber. Bunzenges. Phys. Chem.*, **87**, 1067 (1983).
26) L. F. Lang, H. Buffleb, and M. Zander, *Erdöl Kohle*, **16**, 944 (1963).
27) D. D. Morgan, D. Warshawsky, and T. Atkinson, *Photochem. Photobiol.*, **25**, 31 (1977).
28) R. J. Gordon, *Environ. Sci. Technol.*, **10**, 370 (1976).
29) K. F. Lang, H. Buffleb, and J. Kalowy, *Chem. Ber.*, **90**, 2888 (1957).
30) E. Clar, "The Aromatic Sextet," Wiley, London (1972).
31) L. T. Scott, *Acc. Chem. Res.*, **15**, 52 (1982).
32) A. G. Anderson, Jr., and L. G. Kao, *J. Org. Chem.*, **47**, 3589 (1982).
33) A. Léger and J. L. Puget, *Astron. Astrophys.*, **137**, L5 (1984).
34) A. Léger and L. d'Hendecourt in Ref. 7, pp. 223—254.
35) L. J. Allanamdola, A. G. G. M. Tielens, and J. R. Barker, *Astrophys. J.*, **290**, L25 (1985).
36) L. J. Allanamdola, A. G. G. M. Tielens, and J. R. Barker in Ref. 7, pp. 255—271.
37) A. Omont, *Astron. Astrophys.*, **164**, 159 (1986).
38) W. W. Duley in Ref. 7, pp. 373—386.
39) A. Gold, *Anal. Chem.*, **47**, 1469 (1975).
40) B. M. Trost and G. M. Bright, *J. Am. Chem. Soc.*, **89**, 4244 (1967).
41) B. M. Trost, G. M. Bright, C. Frihart, and D. Brittelli, *J. Am. Chem. Soc.*, **93**, 737 (1971).

The Crystal Structure and Intramolecular Electron Transfer of 1′,1‴-Diethylbiferrocenium Triiodide at 298 and 140 K

Michiko KONNO* and Hirotoshi SANO†,*
Department of Chemistry, Faculty of Science, Ochanomizu University, Otsuka, Bunkyo-ku, Tokyo 112
†Department of Chemistry, Faculty of Science, Tokyo Metropolitan University, Fukasawa, Setagaya-ku, Tokyo 158
(Received September 3, 1987)

The crystal structure of 1′,1‴-diethylbiferrocenium triiodide, $(EtFcFcEt)^+ I_3^-$, was determined by means of X-ray diffraction. The crystals at 298 and 140 K are found to be monoclinic, with the $P2_1/c$ space group and with $Z=2$. At 298 K, $a=9.7557(10)$, $b=9.9772(12)$, $c=13.8216(13)$ Å, $\beta=107.625(9)°$, and $U=1282.18(23)$ Å^3, while at 140 K, $a=9.6931(17)$, $b=9.8065(22)$, $c=13.7373(19)$ Å, $\beta=107.642(15)°$, and $U=1244.4(4)$ Å^3. The structures are refined to $R=0.049$ at 298 K and $R=0.036$ at 140 K. The $(EtFcFcEt)^+$ cations and I_3^- anions sit on a crystallographic center of symmetry both at 298 and at 140 K, and the two ferrocenyl(Fc) units are crystallographically equivalent. The ethyl group in each ethylcyclopentadienyl(EtCp) group is not parallel to the fulvalene moiety, but the terminal CH_3 group moves away with the 60° inclination from the Cp plane. An appreciable interaction seems to exist between the Cp ring of the cation and the I_3^- anion along the $a+c/2$ direction, but the interaction among the cations along the a axis seems to be so weak as to be negligible.

Recently, a number of monooxidized salts of binuclear ferrocene derivatives have been studied in order to clarify the mechanism of the intramolecular electron transfer between the metal atoms through the bridged ligands by measurements of the ^{57}Fe-Mössbauer, IR, and EPR spectra. It has been reported[1,2] that biferrocenium and 1′,1‴-dialkylbiferrocenium (alkyl=ethyl, propyl, butyl) triiodides show the temperature dependences of the valence state of iron atoms. We ourselves have previously reported[3] that the crystal structure of 1′,1‴-dipropylbiferrocenium($Pr^nFcFcPr^n$) triiodide changes from the state of an equivalent set of two Fc units and a triiodide anion with a symmetric I–I–I structure at 298 K to the state of an unequivalent set of ferrocene- and ferrocenium-like units and a triiodide anion with an unsymmetric structure I–I···I, showing positional disorder in the triiodide anions on the (110) plane at 110 K. These results agree with the Mössbauer spectroscopic data, which show a change from two doublets to one doublet around 240 K. On the other hand, 1′,1‴-dihalobiferrocenium salts[4] show no temparature dependence of the valence state of iron atoms. A comparison of the crystal structures of 1′,1‴-diiodo- or 1′,1‴-dibromobiferrocenium cations, which show an averaged valence state, with the structure of 1′,1‴-dichlorobiferrocenium$^+$ cations, which show a trapped valence state, suggests that the valence state of iron atoms is greatly affected by the symmetric or unsymmetric interaction of the triiodide anions with the cations. The Mössbauer spectra of biferrocenium salts[5] show that the transition temperature is lowered by 150 K when the I_3^- anions are replaced with Br_2I^- anions. The crystal structure of biferrocenium triiodide, which shows a trapped valence state at 296 K, indicates that the two Fc units are crystallographically equivalent. The 1′,1‴-diethylbiferrocenium (EtFcFcEt) triiodide shows a transition from the trapped to the averaged valence state around 270 K, as $(Pr^nFcFcPr^n)^+I_3^-$ does around 240 K in the Mössbauer spectra. In the present paper, we will report the crystal structures of $(EtFcFcEt)^+I_3^-$ at 298 and 140 K and discuss the differences in the crystal structures and IR spectra between $(EtFcFcEt)^+I_3^-$ and $(Pr^nFcFcPr^n)^+I_3^-$ in order to elucidate the infuluence of molecular packing and the effects of the triiodide anion and of different substituted groups on the intramolecular electron transfer in the cations and, therefore, on the valence state of iron atoms.

Experimental

X-Ray Measurements. The crystals of $(EtFcFcEt)^+I_3^-$ were kindly supplied by Dr. Seiichi Iijima. A dark-green thin plate crystal was sealed into a Lindemann-glass capillary for the intensity measurements. Preliminary oscillation and Weissenberg photographs taken at room temperature by means of Cu $K\alpha$ radiation showed that the crystal is monoclinic with the space group of $P2_1/c$. The final lattice constants were determined by the least-squares procedure based on the θ values of 33 reflections at 298 K and of 20 reflections at 140 K measured by a diffractometer using Ag $K\alpha$ radiation. The crystal specimen was cooled by a stream of cold N_2 gas surrounded by a warmer N_2 gas curtain. The temperature was controlled electrically at 140±2 K by monitoring with a chromel-almel thermocouple throughout the experiment. The intensities were collected on a Rigaku automated four-circle diffractometer using graphite-monochromated Ag $K\alpha$ radition ($\lambda=0.5609$ Å). Three standard reflections ($10\bar{2}$ 300 020) were measured for every fifty reflections. The intensity data were corrected for Lorentz and polarization effects, but no corrections for absorption and extinction were made. The crystal data and experimental conditions are summarized in Table 1.

Infrared Measurements. The infrared spectra were recorded on a Fourier-transform spectrometer (NICOLET 7199). All samples were prepared as KBr pellets 13 mm in diameter. For the low-temperature measurements, the sample mounted in a holder was cooled by means of a copper plate linked to liquid nitrogen in a Dewar apparatus with KRS-5 windows.

Table 1. Crystal Data
$(Fe_2C_{24}H_{26})^+I_3^-$, M.W. 806.88

Temperature/K	298 Monoclinic	140 Monoclinic
Space group	$P2_1/c$	$P2_1/c$
a/Å	9.7557(10)	9.6931(17)
b/Å	9.9772(12)	9.8065(22)
c/Å	13.8216(13)	13.7373(19)
β/°	107.625(9)	107.642(15)
U/Å^3	1282.18(23)	1244.4(4)
Z	2	2
D_x/g·cm^{-3}	2.090	2.153
μ(Ag $K\alpha$)/mm^{-1}	2.48	2.55
Crystal size/mm	0.08×0.20×0.28	0.075×0.23×0.31
Scan method	ω–2θ	ω
$\sin\theta/\lambda_{max}$	0.753	0.682
Independent reflections ($\|F_o\| \geq 3\sigma(F_o)$)	2420	2698
Maximum repeating number	3	1
$R=\sum\|\|F_o\|-\|F_c\|\|/\|F_o\|$	0.049	0.036
$R_2=\{\sum(\|F_o\|-\|F_c\|)^2/\sum\|F_o\|^2\}^{1/2}$	0.070	0.056

Table 2. Positional Parameters for Non-Hydrogen (×10^4, for I, Fe ×10^5) and Hydrogen Atoms (×10^3) in $(EtFcFcEt)^+I_3^-$ at 298 K
For Non-Hydrogen Atoms, $U_{eq}=1/3\sum_i\sum_j U_{ij}a^*_i a^*_j \boldsymbol{a}_i\cdot\boldsymbol{a}_j$

	x	y	z	10^4U_{eq}/Å^2 (298 K)	10^4U_{eq}/Å^2 (140 K)
I(1)	0(0)	0(0)	50000(0)	452(3)	192(2)
I(2)	29658(8)	−8282(8)	59762(5)	605(3)	246(1)
Fe	13387(13)	4562(13)	18701(8)	351(4)	151(2)
C(1)	71(11)	−1120(10)	1165(6)	451(32)	207(17)
C(2)	−324(11)	−706(11)	2038(7)	499(35)	235(18)
C(3)	−731(10)	663(10)	1907(7)	455(32)	215(17)
C(4)	−638(9)	1111(10)	951(6)	423(30)	195(17)
C(5)	−171(9)	−2(9)	471(5)	368(25)	181(16)
C(6)	3430(11)	−157(12)	2201(8)	564(38)	232(18)
C(7)	3052(17)	94(21)	3106(12)	670(54)	255(18)
C(8)	2685(11)	1401(14)	3131(8)	593(42)	251(18)
C(9)	2819(11)	2011(11)	2247(8)	536(37)	241(18)
C(10)	3298(10)	1036(11)	1681(7)	507(34)	213(17)
C(11)	3589(23)	1300(31)	683(14)	876(78)	340(24)
C(12)	5129(17)	1689(20)	832(12)	1188(87)	539(37)
				10^3U/Å^2	
H(C1)	35(10)	−205(10)	107(7)	51(28)	
H(C2)	−19(13)	−154(13)	277(9)	101(43)	
H(C3)	−91(11)	130(11)	234(8)	67(32)	
H(C4)	−83(10)	199(10)	65(7)	49(27)	
H(C6)	386(14)	−82(14)	195(10)	99(47)	
H(C7)	305(17)	−18(17)	336(10)	68(61)	
H(C8)	232(11)	185(11)	351(8)	70(35)	
H(C9)	260(8)	298(9)	212(6)	33(22)	
H(C11a)	360(13)	50(12)	41(10)	72(43)	
H(C11b)	323(19)	176(18)	40(13)	125(87)	

Structure Determination

The position of the Fe and I atoms were deduced from three-dimensional sharpened Patterson maps. The electron density Fourier maps using the phases calculated on the basis of the coordinates of these atoms revealed the position of all the C atoms. Difference Fourier maps were used to locate the position of all the H atoms. The structure was refined by a full-matrix least-squares program RADIEL[6] on the basis of F magnitudes with unit weight for all the reflections. Anisotropic thermal parameters and isotropic thermal parameters were applied to the non-hydrogen atoms and the hydrogen atoms respectively. Atomic scattering factors for the non-hydrogen atoms were taken from International Table for X-Ray Crystallography,[7] and those for H atoms, from the data reported by Stewart et al.[8] The initial atomic

coordinates at 140 K were readily deduced from those at 298 K. Refinements at 140 K were carried out in the same way as those at 298 K. The *R* factors converged to 0.049 at 298 K and to 0.036 at 140 K. The final atomic parameters are given in Table 2.††

Results and Discussion

Description of the Crystal Structure. The projections of the structure along the a and b axes at 140 K are shown in Figs. 1 and 2 respectively. The $(EtFcFcEt)^+$ cations have a trans-configuration, with the two iron atoms on opposite sides with respect to the fulvalene moiety. Both the $(EtFcFcEt)^+$ cations and the I_3^- anions sit on a crystallographic center of symmetry at 298 and 140 K. The presence of the center of symmetry requires two Fc units in a cation which are crystallographically equivalent at both temperatures. The interplanar distances between the two five-membered rings in each Fc unit in the cation and their dihedral angles are, respectively, 3.351 Å and 4.8° at 298 K and 3.355 Å and 4.6° at 140 K. The distances from the iron to the least-squares planes of the two

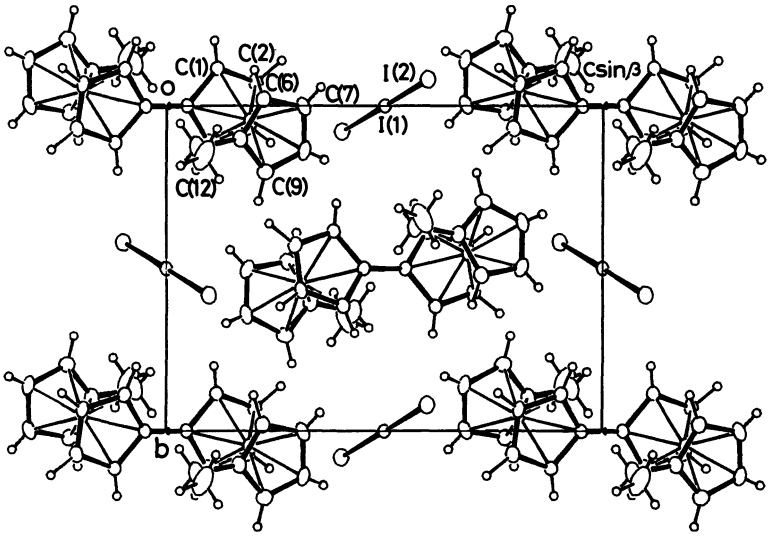

Fig. 1. The projection of the structure at 140 K along the a axis.

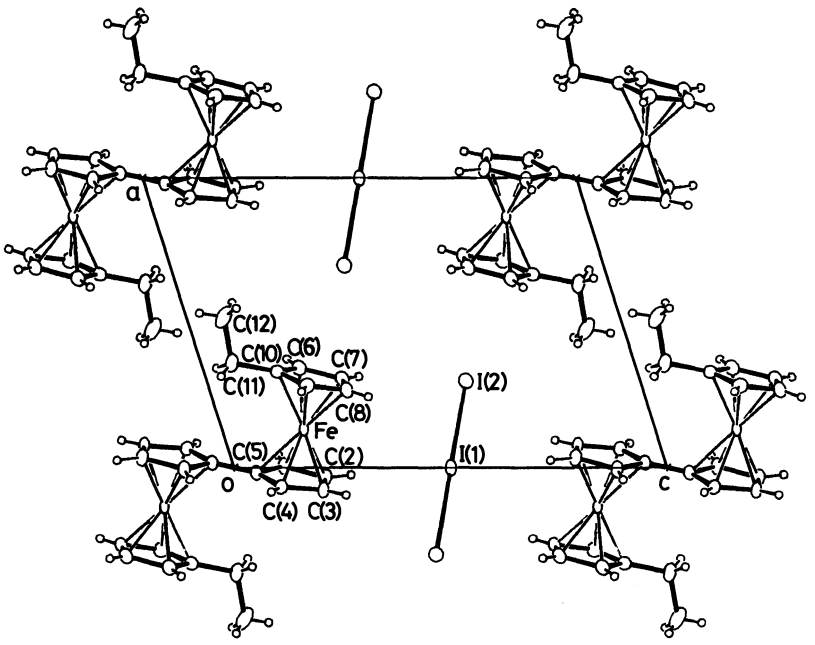

Fig. 2. The projection of the structure at 140 K along the b axis.

†† Lists of the structure factors and anisotropic thermal parameters at 298 and 140 K and the atomic coordinates at 140 K are kept in the Chemical Society of Japan as Document No. 8788.

Table 3. Bond Distances and Bond Angles with e.s.d.'s in Parentheses

(a) Bond distances at 298 and 140 K

	l/Å	l/Å		l/Å	l/Å
Temperature/K	298	140		298	140
I(1)-I(2)	2.917(1)	2.921(1)	C(2)-C(3)	1.418(14)	1.413(9)
Fe-C(1)	2.054(9)	2.062(6)	C(3)-C(4)	1.423(13)	1.422(8)
Fe-C(2)	2.063(11)	2.051(7)	C(4)-C(5)	1.437(13)	1.432(9)
Fe-C(3)	2.046(10)	2.053(6)	C(1)-C(5)	1.443(12)	1.443(8)
Fe-C(4)	2.068(8)	2.079(5)	C(5)-C(5′)	1.439(16)	1.443(12)
Fe-C(5)	2.096(7)	2.094(5)	C(6)-C(7)	1.429(21)	1.438(9)
Fe-C(6)	2.045(11)	2.063(6)	C(7)-C(8)	1.356(25)	1.403(10)
Fe-C(7)	2.028(14)	2.049(5)	C(8)-C(9)	1.406(17)	1.421(9)
Fe-C(8)	2.065(10)	2.064(6)	C(9)-C(10)	1.413(16)	1.431(9)
Fe-C(9)	2.075(10)	2.089(6)	C(6)-C(10)	1.376(16)	1.407(9)
Fe-C(10)	2.088(10)	2.097(6)	C(10)-C(11)	1.513(24)	1.499(10)
C(1)-C(2)	1.435(14)	1.433(9)	C(11)-C(12)	1.504(29)	1.501(14)

(b) Bond angles at 298 K

	φ/°		φ/°
C(2)-C(1)-C(5)	107.8(8)	C(7)-C(6)-C(10)	107.3(12)
C(1)-C(2)-C(3)	107.8(9)	C(6)-C(7)-C(8)	109.3(12)
C(2)-C(3)-C(4)	109.1(9)	C(7)-C(8)-C(9)	107.4(13)
C(3)-C(4)-C(5)	107.7(8)	C(8)-C(9)-C(10)	108.5(10)
C(1)-C(5)-C(5′)	124.6(8)	C(6)-C(10)-C(9)	107.5(10)
C(4)-C(5)-C(5′)	127.5(8)	C(6)-C(10)-C(11)	127.8(12)
		C(10)-C(11)-C(12)	112.1(15)

Primed and unprimed atoms are related by the inversion center at the center of the molecule.

five-membered rings are 1.670(7) and 1.683(3) Å at 298 K and 1.674(3) and 1.684(1) Å at 140 K for inner or fulvalene and outer or ethylcyclopentadienyl(EtCp) rings respectively. The bond distances (298 and 140 K) and bond angles (298 K) are given in Table 3. The mean Fe-C distances are estimated to be 2.065 and 2.060 Å at 298 K and 2.068 and 2.072 Å at 140 K for the inner and the outer rings respectively. These values agree well with the mean Fe-C distances of 2.059, 2.071, and 2.060 Å observed in the $(Pr^nFcFcPr^n)^+$,[3] 1′,1‴-diiodobiferrocenium$^+$,[4] and biferrocenium$^+$[2] cations respectively. The C-C bond distances in the fulvalene moiety are distributed from 1.418(14) to 1.443 (12) Å, with the mean bond distance of 1.431 Å, while those in the cyclopentadienyl(Cp) ring are found in the range from 1.356(25) of C(7)-C(8) to 1.429(21) Å of C(6)-C(7) at 298 K. These large deviations found in the Cp ring are to be ascribed to the interaction between the Cp ring and the I_3^- anion along the $a+c/2$ direction; that is, the linear I_3^- anions come close to the Cp rings, with distances of 3.709 Å (298 K) and 3.641 Å (140 K) from the Cp plane and inclinations of 60.3° (298 K) and 61.1° (140 K) to its plane pointing to the middle of the C(6)-C(7) bond.

It has previously been reported that two Mössbauer doublets converge to one doublet above 270 and 240 K in $(EtFcFcEt)^+I_3^-$ and $(Pr^nFcFcPr^n)^+I_3^-$ respectively, revealing that a trapped valence state, Fe(II) and Fe(III), at low temperatures become an averaged valence state with two iron atoms which cannot be distinguished in the Mössbauer time scale, ca. 10^{-7} s, above the transition temperatures. The results of the Mössbauer spectra of $(EtFcFcEt)^+I_3^-$ require two kinds of valence states of Fe atoms in the Fc units below 140 K in the Mössbauer time scale, while the crystal structure at 140 K indicates that $(EtFcFcEt)^+$ cations sit on the center of symmetry and are crystallographically equivalent, contradicting the results of the Mössbauer spectra. If an electron was hopping between the two Fc units more slowly than the Mössbauer time scale, ca. 10^{-7} s, or was localized in a static state to form Fe(II) and Fe(III), disordering the cations in space, it should be reflected in an unusually high thermal motion and a large anisotropy of each atom, especially those of the Cp rings in the cations. The thermal parameters are, however, very well defined, with equivalent thermal parameters, U_{eq}, in the range from 0.0181(16) to 0.0255(18) Å^2 for C atoms in Cp rings and fulvalene moieties and 0.0192(2) and 0.0246(1) Å^2 for I atoms at 140 K, in comparison with the range from 0.0368(25) to 0.0670(54) Å^2 for C atoms and 0.0452(3) and 0.0605(3) Å^2 for I atoms at 298 K. These values for the C atoms at 140 K correspond to the root mean-square amplitudes from 0.13 to 0.16 Å. The anisotropic temperature factors of U_{11} and U_{22} for all the atoms except the C(9) and C(10) atoms are larger than those of U_{33} at 140 and 298 K respectively, and their U_{11}/U_{33} and U_{22}/U_{33} rations at 140 K become slightly larger than those at 298 K. In 1′,1‴-dibutylbiferrocenium$^+I_3^-$ and 1′,1‴-dichlorobiferrocenium$^+I_3^-$, both with a trapped valence state, Fe(II)-Fe(III), the interplanar distances between two five-membered rings in ferrocene- and ferrocenium-like units are found to be 3.313 and 3.390 Å for the 1′,1‴-dibutylbiferrocenium salt[2] and 3.26 and 3.38 Å for the 1′,1‴-dichlorobiferrocenium salt[4] respectively.

The difference between ferrocene- and ferrocenium-like units is about 0.10 Å, therefore, the displacement in the position of the Cp rings between ferrocene- and ferrocenium-like units is estimated to be about 0.05 Å. The overall amplitude of about 0.15 Å due to the thermal motion of the molecules and the mosaicity of the crystal may sufficiently smear this positional difference.

In $(Pr^nFcFcPr^n)^+I_3^-$, the cations and the anions sit on the crystallographic center of symmetry at 298 K, while the center of symmetry is lost on the (110) plane and two unequivalent Fc units are observed at 110 K. However, if the whole crystal has no center of symmetry, a dipole moment will remain in only one direction. Hence, one ordered structure on the (110) plane and its reversely ordered structure, in which Fe(II) and Fe(III) units in a cation and an I_3^- anion are inverted in relative to the former structure, are stacked at random or in an orderly manner along the $\boldsymbol{a}+\boldsymbol{b}$ direction, and the whole structure should have a center of symmetry. The comparison of the molecular structure and the packing in $(EtFcFcEt)^+I_3^-$ with those in $(Pr^nFcFcPr^n)^+I_3^-$ or biferrocenium$^+I_3^-$ gives an important suggestion with regard to investigating the effect of anions on the electron-transfer process between the two Fc units. The packings of the cations and anions on the (100) plane of $(EtFcFcEt)^+I_3^-$ and biferrocenium$^+I_3^-$ and on the (001) plane of $(Pr^nFcFcPr^n)^+I_3^-$ are the same as that on the (100) plane of the NaCl type, but different inclinations of the two ions in the direction perpendicular to these planes are found because substituent groups give rise to different stacking modes on the (010) plane for $(EtFcFcEt)^+I_3^-$, the $(\bar{1}11)$ plane for biferrocenium$^+I_3^-$, and the (110) plane for $(Pr^nFcFcPr^n)^+I_3^-$ as is shown in Fig. 3. In the $(EtFcFcEt)^+$ cations, the ethyl group of ethylcyclopentadienyl(EtCp) is found not to be parallel to the fulvalene moiety, but the terminal CH_3 moves away with the 60° inclination from the Cp plane, as observed in neutral 1′,1‴-diethylbiferrocene.[9] The ethyl groups in a cation contact ethyl groups in adjacent cations along the a axis in a longer distance than the van der Waals' contact, hence, the intermolecular interaction among cations along the a axis should be very weak, while an appreciable interaction between the Cp ring of a cation and an I_3^- anion is found along the $\boldsymbol{a}+\boldsymbol{c}/2$ direction. In $(Pr^nFcFcPr^n)^+$ cations, the propyl groups of Pr^nCp go parallel to the fulvalene moiety, and a π–π interaction between the Cp rings between the adjacent cations along the c axis is found to exist with the interplanar distance of 3.47 Å, providing a segregated column structure of cations and anions along the c axis. In biferrocenium$^+I_3^-$, an interaction between the Cp rings of adjacent cations and an overlapping between a fulvalene moiety of the cation and an I_3^- anion are observed on the $(\bar{1}11)$ plane. If one Fc unit in a cation has a more positive charge, one of the I atoms in an I_3^- anion in the vicinity of the cation along the $-\boldsymbol{a}+\boldsymbol{b}$ direction will have a more negative charge and one of the I–I bonds in the anion will get a longer bond distance, such as I(1)–I(2)=2.948 Å and I(2)–I(3)=2.902 Å at 110 K in $(Pr^nFcFcPr^n)^+I_3^-$, whereas a symmetric relative position is found with respect to a Fc unit and an I_3^- anion along the $\boldsymbol{c}$ and $\boldsymbol{b}+\boldsymbol{c}$ directions, putting a more negative charge in the central I atom in the I_3^- anion in both $(EtFcFcEt)^+I_3^-$ and biferrocenium$^+I_3^-$. The intermolecular distances between iron and iodine atoms given in Table 4 show the symmetric relative position in $(EtFcFcEt)^+I_3^-$.

The segregated column structrue and the presence of a rotational disorder of propyl group in a Pr^nCp in $(Pr^nFcFcPr^n)^+I_3^-$ may provide the driving force for an ordered structure on the (110) plane with the distinguishable Fe(II) and Fe(III) states observed at 110 K. On the other hand, the presence of isolated cations and the weak interaction between the cations and anions may bring about a disordered symmetric structure of the cations at low temperatures in $(EtFcFcEt)^+I_3^-$.

Infrared Spectroscopy. It is difficult to judge whether both the ground states of the $(EtFcFcEt)^+$ and

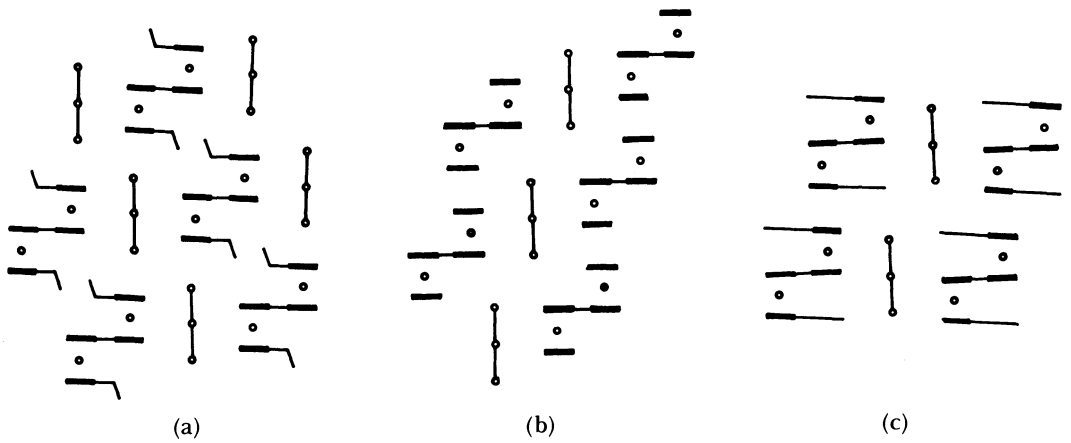

Fig. 3. The stacking models for (a) $(EtFcFcEt)^+I_3^-$, (b) biferrocenium$^+I_3^-$, and (c) $(Pr^nFcFcPr^n)^+I_3^-$.

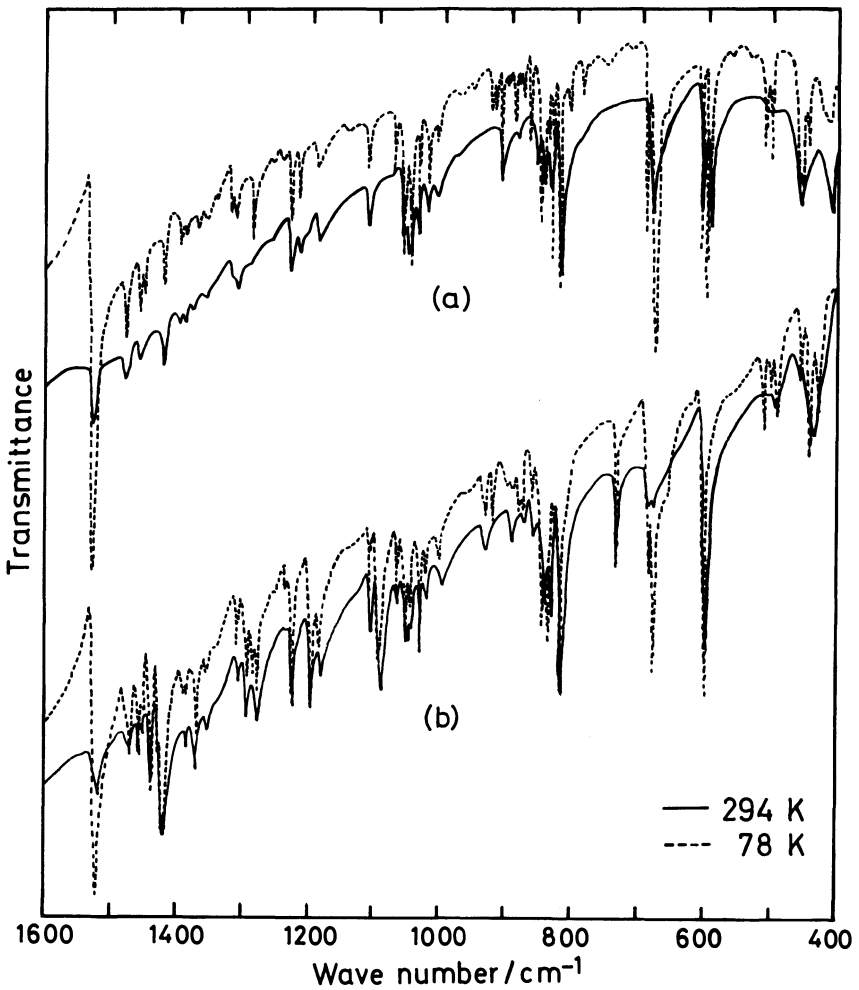

Fig. 4. IR spectra of KBr pellets of (a) 1′,1‴-diethylbiferrocenium$^+I_3^-$ and (b) 1′,1‴-dipropylbiferrocenium$^+I_3^-$.

Table 4. Intermolecular Distances between Iron and Iodine Atoms

Symmetry code
None x, y, z (i) $1-x$, $-y$, $1-z$
(ii) x, $1/2-y$, $1/2+z$ (iii) $-x$, $1/2+y$, $1/2-z$

	l/Å	l/Å
Temperature/K	298	140
I(1)···Fe	4.904(1)	4.843(1)
I(2)···Fe	5.560(1)	5.492(1)
I(2^i)···Fe	5.464(1)	5.395(2)
I(1)···Fe^{ii}	5.186(1)	5.127(1)
I(2)···Fe^{ii}	5.828(2)	5.747(2)
I(2^i)···Fe^{ii}	6.070(1)	6.050(1)
I(1)···Fe^{iii}	5.998(1)	5.912(2)
I(2^i)···Fe^{iii}	5.153(1)	5.114(2)

$(Pr^nFcFcPr^n)^+$ cations at 300 K are to be ascribed to the complete delocalization of the electrons or to the rapid intramolecular electron hopping. The IR spectra of $(EtFcFcEt)^+I_3^-$ and $(Pr^nFcFcPr^n)^+I_3^-$ at 294 and 78 K are illustrated in Fig. 4. Strong, new bands are observed in the vicinity of 680 and 1525 cm^{-1} in the IR spectra when the neutral $Pr^nFcFcPr^n$, EtFcFcEt, 1′,1‴-diiodo-, 1′,1‴-dibromo-, and 1′,1‴-dichlorobifferocene[4] are monooxidized. Moreover, the intensities of these two bands are very strong in their trapped valence states, while they become weak in their averaged valence states, judging from the Mössbauer spectra. The single bands at 700 and 703 cm^{-1}, observed in the IR spectra[10] of fulvalene(Cp_2) and carbene(Cp) respecively, are assigned to an out-of-plane C–H deformation. Two new bands around 680 cm^{-1} may be the same bands as those for the Cp and fulvalene moieties. The intensity of the single band at 1525 cm^{-1} is unusually strong in the trapped valence states. The C=C skeletal stretching vibrations are observed from near 1500 to 1600 cm^{-1} in aromatic compounds. The fulvalene has a center of symmetry in the unoxidized compounds, but loses it in monooxidized cations if the cations are not in a delocalized ground state. Hence, the band at 1525 cm^{-1} may be assigned to a C=C stretching mode of the fulvalene ring, and the coupling of this vibration mode with the electrons distributed unsym-

metrically in the fulvalene moiety may be considered to give rise to the unusually strong intensity at 78 K. On the other hand, this band does not vanish at 294 K. This indicates that the hole of the cation in the averaged-valence state is not completely delocalized.

Conclusion

Alkyl groups in the monooxidized biferrocenium derivatives affect the packing between the cations and anions, and the different interaction of anions with cations gives a different phase transition temperature. The electronic state of cations will couple with a phonon mode because a positive charge of a cation and a negative charge of an anion attract each other. However, in 1′,1‴-dibromo- and 1′,1‴-diiodobiferrocenium$^+I_3^-$, a strong intramolecular interaction resulting from the overlap between the iodine or bromine group and one of the Cp rings of the fulvalene moiety will generate an averaged valence state, even at a low temperature.

References

1) S. Iijima, R. Saida, I. Motoyama, and H. Sano, *Bull. Chem. Soc. Jpn.*, **54**, 1375 (1981).

2) T.-Y. Dong, D. N. Hendrickson, K. Iwai, M. J. Cohn, S. J. Geib, A. L. Rheingold, H. Sano, I. Motoyama, and S. Nakashima, *J. Am. Chem. Soc.*, **107**, 7996 (1985).

3) M. Konno, S. Hyodo, and S. Iijima, *Bull. Chem. Soc. Jpn.*, **55**, 2327 (1982).

4) T.-Y. Dong, D. N. Hendrickson, C. G. Pierpont, and M. F. Moore, *J. Am. Chem. Soc.*, **108**, 963 (1986).

5) M. J. Cohn, T.-Y. Dong, D. N. Hendrickson, S. J. Geib, and A. L. Rheingold, *J. Chem. Soc., Chem. Commun.*, **1985**, 1095.

6) P. Coppens, T. N. Guru-Row, P. Leung, E. D. Stevens, P. J. Becker, and Y. W. Yang, *Acta Crystallogr., Sect. A*, **35**, 63 (1979).

7) "International Tables for X-Ray Crystallography," Kynoch Press, Birmingham (1974), Vol. IV, pp. 73—86.

8) R. F. Stewart, E. R. Davidson, and W. T. Simpson, *J. Chem. Phys.*, **42**, 3175 (1965).

9) Z. Kałuski, *Bull. Acad. Polon. Sci., Ser. Sci. Chim.*, **13**, 355 (1965).

10) M. S. Baird, I. R. Dunkin, N. Hacker, M. Poliakoff, and J. J. Turner, *J. Am. Chem. Soc.*, **103**, 5190 (1981).

NQR of ^{35}Cl, ^{127}I, and ^{121}Sb in $I_3Cl_2SbCl_6$ and ICl_2SbCl_6

Mitsuo MISHIMA* and Tsutomu OKUDA†
Department of Chemistry, Shimane Medical University, Izumo 693
†Department of Chemistry, Faculty of Science, Hiroshima University, Hiroshima 730
(Received September 7, 1987)

NQR spectra due to ^{35}Cl, ^{127}I, and ^{121}Sb in $I_3Cl_2SbCl_6$ and ICl_2SbCl_6 have been observed in the temperature range 77 K to melting point. The Zeeman effect on the single crystals of these complexes has been examined. In $I_3Cl_2SbCl_6$ the η-values for the I atoms contributing to the higher and the lower NQR frequencies are 0.73 to 0.09, respectively, whereas in ICl_2SbCl_6 the η-value for the I atom is 0.15. In these complexes the ^{35}Cl NQR lines which yield large η-values (0.42 to 0.56) are assigned to the bridging Cl atoms. The η-values for the other Cl atoms, except the Cl atoms in the ICl_2^+ ion which have η-values of 0.13 to 0.15, are negligibly small. The Sb atoms in both complexes have considerably large η-values (0.39). The orbital populations have been calculated from the NQR parameters. The bonding in the cations is explained on the basis of an approximation using only p orbitals of the I atom.

The NQR investigations on a number of polyhalogen anions shed light on the charge distribution and the interaction between these anions and the surrounding cations.[1-8] Above all, the bonding in trihalides was satisfactorily explained in terms of a three-center four-electron (3c-4e) bond or a resonance hybrid X-Y $X^- \longleftrightarrow X^-$ Y-X. On the other hand, polyhalogen cations are less stable,[9] and the crystal structures of a few compounds were determined by X-ray analysis. The NQR data on the polyhalogen cations were reported for the first time by Evans and Lo,[10] who assigned the ^{35}Cl resonance lines in ICl_2AlCl_4 roughly to the ICl_2^+ and the $AlCl_4^-$ ions. Merryman et al.[9,11] observed the resonances of ^{35}Cl and ^{127}I in $I_2ClSbCl_6$, $I_2ClAlCl_4$, I_3AlCl_4, and I_5AlCl_4, and estimated atomic charges and bond populations. From the known crystal structures of polyhalogen derivatives,[12-16] it is inferred that bridging halogen atoms construct infinite chains of cations and anions. It is therefore important to elucidate the bond character in detail.

Birchall and Myers[14] reported the crystal structure of $I_3Cl_2SbCl_6$ and threw doubt on the presence of $I_2ClSbCl_6$ on the basis of the unit cell parameters and the Raman spectrum. They followed the method of Shamir and Lustig[17] in an attempt to prepare $I_2ClSbCl_6$. It is of interest to know whether this complex is present or not. Although ICl_2SbCl_6 is one of the first compounds in which the presence of the polyhalogen cation was well established by crystallographic study,[12] this complex has not been investigated by NQR yet, so far as we know.

In this paper we describe the results of the NQR Zeeman investigations on single crystals of the complexes $I_3Cl_2SbCl_6$ and ICl_2SbCl_6. The choice of the $SbCl_5$-complexes was favored since the resonances of ^{35}Cl, ^{127}I, and ^{121}Sb could be observed in the course of the experiment. Furthermore a comparison of the Zeeman data with the structural ones was considered to yield useful information on the assignment of the NQR lines and charge distribution.

Experimental

Complexes of $I_3Cl_2SbCl_6$ and ICl_2SbCl_6 were prepared in the manner described in the literatures.[14,18] These were identified by the melting points and the halogen contents. The procedure of Merryman and Corbett[11] was followed in an attempt to prepare $I_2ClSbCl_6$. The NQR spectra of this complex were essentially, except for some parts, identical with those in the literature.[11] Single crystals were grown by Bridgman's method.

A superregenerative spectrometer of Dean's type and a superregenerative parallel transmission line spectrometer were used for detecting the NQR lines. The absorption lines were observed on an oscilloscope. The resonance frequencies were determined with a frequency counter, TR-4142G, of Takeda Riken Co. The Zeeman effect was measured by means of the zero-splitting cone method. The Zeeman field was supplied by means of a Helmholtz coil. Temperature was measured by the use of a copper-constantan thermocouple.

Results

The NQR frequencies for ^{35}Cl, ^{121}Sb, and ^{127}I in $I_3Cl_2SbCl_6$ and ICl_2SbCl_6 are listed in Tables 1 and 2, respectively. Figures 1 and 2 show the temperature dependence of the resonance frequencies for ^{35}Cl

Table 1. ^{35}Cl, ^{127}I, and ^{121}Sb NQR Parameters in $I_3Cl_2SbCl_6$ at Room Temperature

Atom	Frequency/MHz		η/%[a]	e^2Qqh^{-1}/MHz[a]
	77 K	297 K		
Cl_1	21.007	20.784	42.6	40.361
Cl_2	25.175	24.839	1.9	49.675
Cl_3	26.135	25.702	3.2	51.395
Cl_4	38.620	38.293	4.9	76.555
I_1 ν_1	432.065	429.13	8.8	2837.0
I_2 ν_1	529.30	522.63	73.4	2373.1
Sb ν_1	22.688	21.054	38.0	122.49
ν_2	36.966	35.730	(38.0)[b]	

a) These values correspond to 297 K. b) Obtained from the frequency ratio of ν_2/ν_1.

Table 2. ^{35}Cl, ^{127}I, and ^{121}Sb NQR Parameters in ICl_2SbCl_6 at 233 K

Atom	Frequency/MHz			η/%	e^2Qqh^{-1}/MHz
	77 K	233 K	298 K		
Cl_1	19.363	19.198	19.114	56.7	36.490
Cl_2	20.522	20.447	—	48.3	39.409
Cl_3	25.476	25.444	25.127	5.2	50.420
Cl_4	26.059	25.793	25.66[b]	3.6	50.555
Cl_5	27.145	26.832	25.67[b]	4.5	53.806
Cl_6	27.159	26.912	26.78[b]	2.9	53.817
Cl_7[a]	38.654	38.405	38.270	15.4	76.261
Cl_8[a]	40.053	39.829	39.691	13.8	79.155
I[a] ν_1	462.569	457.52	454.70	14.9	2962.2
Sb[a] ν_1	17.896	17.870	17.857	39.5	102.91
ν_2	30.954	30.337	29.975	(39.5)[c]	

a) The values of η and e^2Qqh^{-1} for these atoms correspond to 298 K. b) Very weak and broad. c) Obtained from the frequency ratio of ν_2/ν_1.

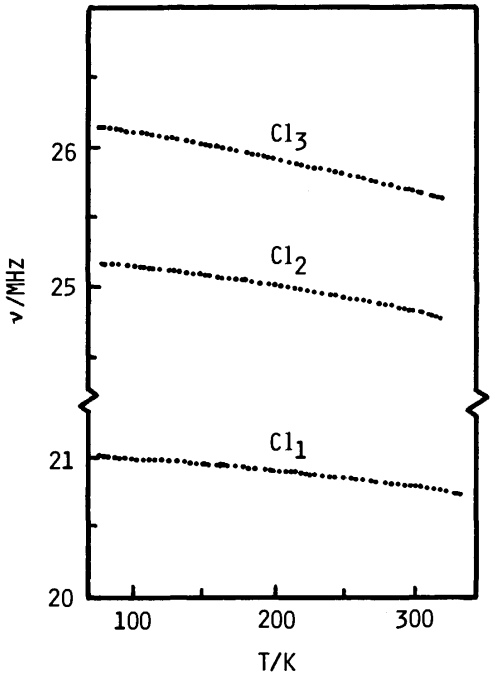

Fig. 1. Temperature dependence of ^{35}Cl NQR frequencies in $I_3Cl_2SbCl_6$.

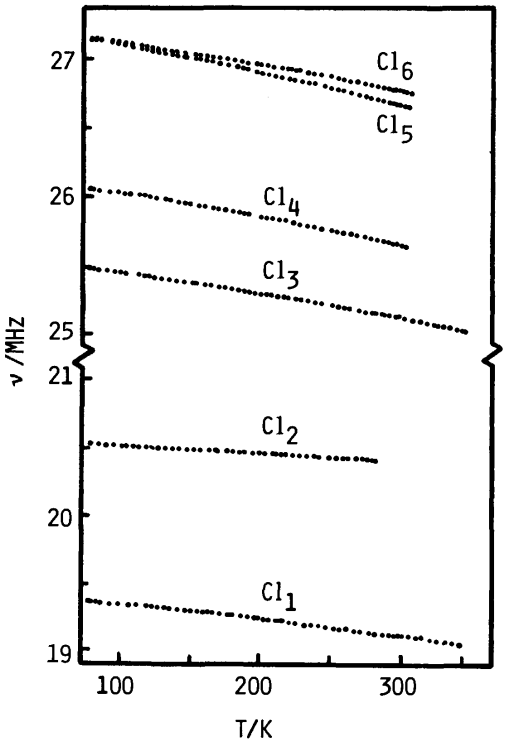

Fig. 2. Temperature dependence of ^{35}Cl NQR frequencies in ICl_2SbCl_6.

bonded to the Sb atom in $I_3Cl_2SbCl_6$ and ICl_2SbCl_6, respectively, in the temperature range from 77 K to the melting points. In $I_3Cl_2SbCl_6$, the NQR lines of the Cl_2 and Cl_3 atoms faded out at around 320 K, whereas the resonance of the Cl_1 atom could be detected up to the melting point. In ICl_2SbCl_6, similarly, the resonance lines of the Cl_1 and Cl_3 atoms could be detected up to near 350 K, and those of the other Cl atoms faded out in the range from 280 to 300 K. This suggests that the Sb–Cl_1 bond in $I_3Cl_2SbCl_6$ and the Sb–Cl_1 and Sb–Cl_3 bonds in ICl_2SbCl_6 are nearly parallel to the reorientational axis of the $SbCl_6$ group.[19,20] The other lines due to ^{35}Cl, ^{127}I, and ^{121}Sb in these complexes were observed up to their melting points.

The Zeeman effect on ^{35}Cl, ^{123}Sb, and ^{127}I in $I_3Cl_2SbCl_6$ was examined at room temperature. The zero-splitting loci are shown in Fig. 3. A single pattern was obtained for each resonance line. This is in agreement with the crystal structure which belongs to the space group $P\bar{1}$.[14] The calculated asymmetry parameters (η) are listed in Table 1 along with the coupling constants (e^2Qqh^{-1}). The Cl_1, I_2, and Sb atoms are characterized by their large η-values. The assignment of the NQR lines on the Cl atoms is based on a comparison of orientation of the efg axis at the

resonant nucleus with the corresponding bond directions, as seen in Table 3. The I_1 and I_2 atoms cannot be unequivocally assigned because of the parallelism of their efg axes and because of unreliability in the intensity ratio of the resonance lines. The assignment of these was decided by considering the relationship between the orientation of the efg axes and the charge distribution, as described below. The efg axes at the atoms Cl_2, Cl_3, and Cl_4 coincide in direction with the bond axes. The

Table 3. Angles between efg Axes and Bond Angles in $I_3Cl_2SbCl_6$

Bond	Cl_1–Sb	Cl_2–Sb	Cl_3–Sb	Cl_4–I_2
Cl_2–Sb	87.25°			
	(89.56)			
Cl_3–Sb	85.80	89.63		
	(89.71)	(89.97)		
Cl_4–I_1	63.95	51.52	46.26	
	[69.3][b]	[51.6]	[46.0]	
I_1 z-axis	93.51	140.55	50.53	90.11
x-axis	65.0	52.5	44.7	1.7
I_2 z-axis	63.40	51.51	46.6	0.58
x-axis	94.1	139.2	49.0	90.2
I_1–I_2	[92.6]	[141.9]	[52.2]	(92.62)

a) The value in parentheses is the corresponding bond angle. b) The value in brackets was calculated from the atomic positions (Ref. 14).

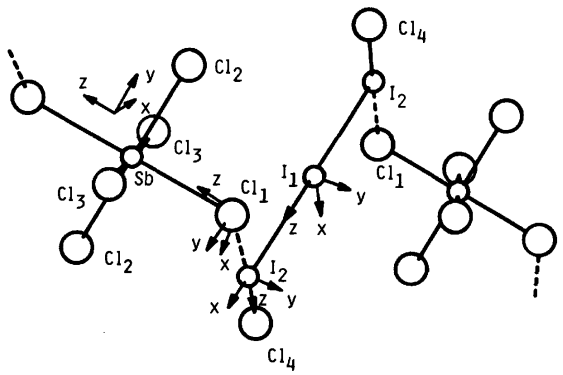

Fig. 4. Molecular shape of $I_3Cl_2SbCl_6$.

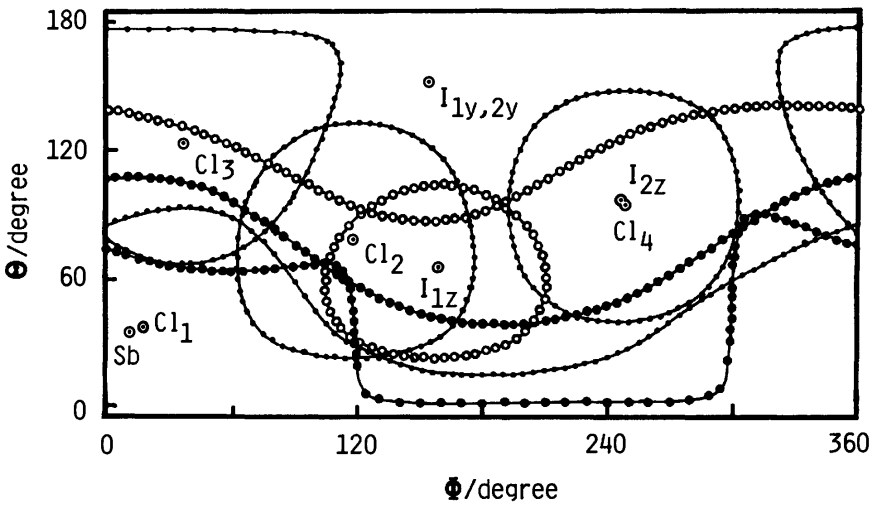

Fig. 3. Zero-splitting loci of ^{35}Cl, ^{127}I, and ^{121}Sb (ν_1, ν_2) Zeeman lines in $I_3Cl_2SbCl_6$.

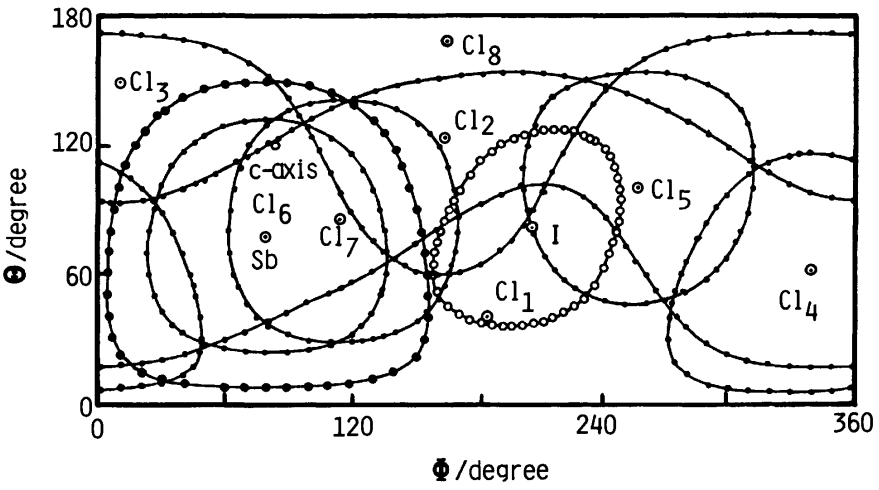

Fig. 5. Zero-splitting loci of ^{35}Cl, ^{127}I, and ^{121}Sb (ν_2) Zeeman lines in ICl_2SbCl_6. Cl_8 indicates the direction of the efg z axis calculated from the other crystal sites.

z axis at the bridging atom Cl_1 deviates from the Sb–Cl bond axis by ca. 6°, as shown in Fig. 4.

In ICl_2SbCl_6, forty zero-splitting loci for ^{35}Cl, ^{127}I, and ^{121}Sb are expected to be observed from its crystal structure, which belongs to the tetragonal space group $P4_1$.[12] However, only thiry-one loci could be found, since some efg z axes are nearly parallel to the rf field. The Zeeman effect on the Cl atoms bonded to the Sb atom was observed at 233 K, and that for the other atoms was observed at room temperature. The zero-splitting loci relating to one of the crystal sites are shown in Fig. 5. The NQR parameters are listed in Table 2. The η-value for the Cl_1 atom at room temperature was 0.6 percent less than that at 233 K. The efg axes and the corresponding bond directions are compared in Table 4, and the significant efg axes are shown in Fig. 6. The coupling constant of the I atom is comparable to the value of 3066±37 MHz at 4.2 K obtained from the ^{127}I Mössbauer effect.[13]

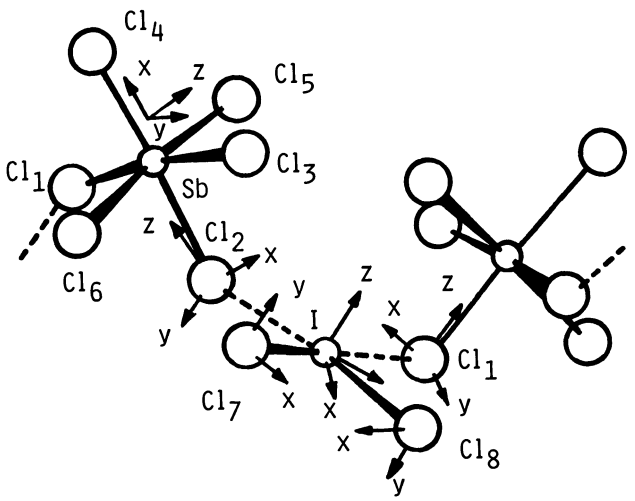

Fig. 6. Molecular shape of ICl_2SbCl_6.

Discussion

$I_3Cl_2SbCl_6$. The NQR spectrum is very similar to that reported previously for $I_2ClSbCl_6$,[11] except for some parts. The sample prepared by the method of Merryman and Corbett[11] exhibited the same spectrum as $I_3Cl_2SbCl_6$. This is verified by examining some samples. They reported that the absorption line due to ^{35}Cl was veiled by the very broad ^{121}Sb line and the corresponding ^{37}Cl line. These lines could not be seen, although the NQR spectrum was examined at various temperatures. The other parts of the spectrum in $I_3Cl_2SbCl_6$ were identical with that reported for $I_2ClSbCl_6$, except that the resonance frequency for the I_2 atom was somewhat different.

The I–I–I bond in the centrosymmetric planar $I_3Cl_2^+$ ion is completely linear. The I–I distance (2.906 Å) is considerably longer than a covalent I–I distance,[14] and is comparable to that in a symmetrical I_3^- ion of $(C_6H_5)_4AsI_3$ (2.90 Å).[21] In the present study the bonding in the I_3 part of the $I_3Cl_2^+$ ion was interpreted in terms of the 3c-4e bond. The atoms Cl_1, Cl_4, I_1, and I_2 are almost coplanar. The bridging $Cl_1\cdots I_2$ bond and the terminal Cl_4–I_2 bond make angles of 89.55° and 92.62°, respectively, to the I_1–I_2 bond. The $Cl_1\cdots I_2$–Cl_4 bond is almost linear and is orthogonal to the I–I–I bond. The $Cl_1\cdots I_2$ distance (2.94 Å) is considerably shorter than the sum of van der Waals radii (3.9 Å), although the Cl_4–I_2 distance (2.33 Å) is nearly equal to the sum of the covalent radii. The $Cl_1\cdots I_2$–Cl_4 bond can therefore be regarded as an asymmetrical three-center bond.

Taking the Sb–$Cl_1\cdots I_2$ angle of 109.75° into account, the orbitals on the bridging Cl atom can be approximated by sp^3 hybridization. The orbital directed toward the Sb atom (ϕ_1) is nonequivalent to that directed toward the I_2 atom (ϕ_2). The latter is

Table 4. Angles between efg Axes and Bond Angles in ICl_2SbCl_6

Bond	Cl_1–Sb	Cl_2–Sb	Cl_3–Sb	Cl_4–Sb	Cl_5–Sb	Cl_6–Sb	Cl_7–I
Cl_2–Sb	86.78°						
	(81.6)[a]						
Cl_3–Sb	169.31	95.19					
	[172.4][b]	(91.3)					
Cl_4–Sb	96.71	175.38	91.36				
	(91.0)	[173.3]	(95.2)				
Cl_5–Sb	81.18	87.20	91.39	90.36			
	(88.9)	(86.5)	(92.4)	(93.1)			
Cl_6–Sb	84.45	89.03	91.60	91.67	176.34		
	(86.5)	(88.3)	(91.5)	(91.6)	[173.6]		
Cl_7–I	79.18	59.34	77.54	55.10	38.64	35.03	
	[72.7]	[55.1]	[78.4]	[57.4]	[40.3]	[34.2]	
Cl_8–I	51.49	44.4	41.46	49.46	80.12	79.41	93.41
	[46.9]	[53.3]	[39.7]	[46.9]	[79.7]	[79.8]	(92.5)
Sb z-axis	83.2	88.5	89.7	91.1	2.2	1.5	
x-axis	78.7	13.1	71.7	16.8	89.5	89.9	

a) The value in parentheses is the corresponding bond angle. b) The value in brackets was calculated from the atomic positions (Ref. 12).

presumed to be intermediate between ϕ_1 and the lone pair orbitals (ϕ_3 and ϕ_4). The orbital populations of ϕ_1 and ϕ_2 cannot be determined unequivocally. The populations, however, can be estimated by considering the following extremes: in one extreme ϕ_2 is equivalent to ϕ_1 (C_{2v} symmetry) and in another ϕ_2 is equivalent to the lone pair orbitals (C_{3v} symmetry). The hybrid orbitals belonging to the symmetry C_{2v} are expressed as follows;

$$\begin{aligned}
\phi_1 &= s\psi_s + (1 - s^2)^{1/2}\psi_{p_z},\\
\phi_2 &= s\psi_s + (1 - s^2)^{1/2}\{\psi_{p_z}\cos\theta + \psi_{p_x}\sin\theta\},\\
\phi_3 &= \{(1 - 2s^2)/2\}^{1/2}\psi_s\\
&\quad - s\{\psi_{p_z}\cos(\theta/2) + \psi_{p_x}\sin(\theta/2)\} + 2^{-1/2}\psi_{p_y},\\
\phi_4 &= \{(1 - 2s^2)/2\}^{1/2}\psi_s\\
&\quad - s\{\psi_{p_z}\cos(\theta/2) + \psi_{p_x}\sin(\theta/2)\} - 2^{-1/2}\psi_{p_y},
\end{aligned} \tag{1}$$

where $s^2=2^{-1}\{1-\cot(\theta/2)\}$ and θ is the angle between the bonds Sb–Cl_1 and $Cl_1\cdots I_2$. The z axis is taken along the Sb–Cl_1 and the x axis in the plane $SbCl_1I_2$, although the efg z axis deviates slightly from the Sb–Cl_1 bond. If ϕ_1 and ϕ_2 are occupied by a and b electrons, respectively, then the coupling constant data may be analyzed by the equations;

$$\begin{aligned}
&(2 - a)\cos^2(\theta/2) = \eta U_p/3,\\
&(2 - a) + (2 - b)\{1 - (3/2)\sin^2\theta\} = 2U_p\sin^2(\theta/2),
\end{aligned} \tag{2}$$

where $U_p=(e^2Qq)_{obs}/(e^2Qq)_{atom}$.

The hybrid orbitals belonging to the symmetry C_{3v} are given by[22]

$$\begin{aligned}
\phi_1 &= s_1\psi_s + (1 - s_1^2)^{1/2}\psi_{p_z},\\
\phi_2 &= s_2\psi_s + (1 - s_2^2)^{1/2}(\psi_{p_z}\cos\theta + \psi_{p_x}\sin\theta),\\
\phi_3 &= s_2\psi_s + (1 - s_2^2)^{1/2}\{\psi_{p_z}\cos\theta - (1/2)\psi_{p_x}\sin\theta\\
&\qquad + (3^{1/2}/2)\psi_{p_y}\sin\theta\},\\
\phi_4 &= s_2\psi_s + (1 - s_2^2)^{1/2}\{\psi_{p_z}\cos\theta - (1/2)\psi_{p_x}\sin\theta\\
&\qquad - (3^{1/2}/2)\psi_{p_y}\sin\theta\},
\end{aligned} \tag{3}$$

where $s_1^2=2\cot^2\theta$ and $s_2^2=1-2/(3\sin^2\theta)$, and therefore

$$\begin{aligned}
&2 - b = \eta U_p,\\
&\{(2 - a) - (2 - b)/3\}(1 - 2\cot^2\theta) = U_p.
\end{aligned} \tag{4}$$

Using the experimental bond angle, the values of a=1.46 and b=1.84 are obtained for the symmetry C_{2v}, and those of a=1.45 and b=1.84, for the symmetry C_{3v}. Even when the deviation of the z axis on the Cl_1 atom from the Sb–Cl_1 axis is taken into account, the variations in the populations of ϕ_1 and ϕ_2 are less than 0.5 percent.

Each I atom in the $I_3Cl_2^+$ ion is positively charged. The efg components can be written in terms of the population N_i on the i-th p orbital as follows;

$$\begin{aligned}
q_{ii} &= [N_i - (N_j - N_k)/2]q_{atom}(1 + \varepsilon)^{\rho},\\
&\quad i, j, k = x, y, z
\end{aligned} \tag{5}$$

where ρ is the charge at the I atom and ε is the correction parameter for the ionization of the I atom. The value of ε=0.12 was used for the I atom.[23] If only the p_z and p_x orbitals on the I atom participate on bonding and the p_y orbital is completely filled, the charge on the I atom is approximated by

$$\rho = [U_p(1 + \eta) - 1]/[U_p\varepsilon(1 + \eta) + 1]. \tag{6}$$

The populations deduced from Eqs. 1—6 are listed in Table 5.

The electron numbers for the I_2–I_1–I_2 and $Cl_1\cdots I_2$–Cl_4 bonds are 3.83 and 3.88, respectively, assuming that the s character for the bonding orbital of the Cl_4 atom is 0.15. These values are close to the expected value 4, notwithstanding neglect of the s and d character of the central I atom, and accordingly these bonds can be explained essentially in terms of the 3c-4e bond. The total charges of the I_1 and I_2 atoms are estimated to be +0.30 and +0.66, respectively. These values are comparable to the values of +0.2 and +0.5 which were calculated by using the relationship between bond length and bond order.[14,24]

Table 5. Electronic Distributions of Polyhalogen Cations and Surrounding Chlorine Atoms in $I_3Cl_2SbCl_6$ and ICl_2SbCl_6

Compound	Atom	N_x[a]	N_y[a]	N_z[a]	N_σ[b]	
$I_3Cl_2SbCl_6$	Cl_1	1.90	(2)	1.58	$1.45<a<1.46$	(Sb)
					$b=1.84$	(I_2)
	Cl_4	(2)	(2)	1.20	1.18	
	I_1	1.93	(2)	0.77		
	I_2	1.53	(2)	0.81		
ICl_2SbCl_6	Cl_1	1.87	(2)	1.58	$1.48<a<1.53$	(Sb)
					$1.78>b>1.75$	(I)
	Cl_2	1.88	(2)	1.58	$1.42<a<1.44$	(Sb)
					$b=1.81$	(I)
	Cl_7	1.93	(2)	1.27	1.14	
	Cl_8	1.93	(2)	1.25	1.11	
	I	0.95	0.84	(2)		

a) The value in the parentheses is assumed to be 2. b) The population in the bonding atomic orbital. The symbols in parentheses indicate the atom toward which the hybrid orbital directs.

ICl_2SbCl_6. According to X-ray analysis,[12] the atoms I, Cl_1, Cl_2, Cl_7, and Cl_8 are almost coplanar. The z axis for the I atom is normal to this plane, and the x axis almost coincides with the bisector of the angle $\angle Cl_7ICl_8$. The z axes at the Cl_1 and Cl_2 atoms are nearly parallel to the corresponding Sb–Cl bond (see Table 4). The z axis at each bridging atom lies in the Sb-Cl···I plane. According to the ^{127}I Mössbauer effect, the value e^2Qqh^{-1} is positive.[13] This is in agreement with the results of the Zeeman effect of NQR.

The angles $\angle SbCl_7I$ and $\angle SbCl_8I$ are 116.8° and 114.8°, respectively. The valence orbitals at these bridging Cl atoms can be approximated by sp^2 hybridization. The wave functions can be written as follows:

$$\begin{aligned}\phi_1 &= s_1\psi_s + s_2\psi_{p_z},\\ \phi_2 &= (1/2)s_2\psi_s + 2^{-1/2}s_1\psi_{p_z} + 2^{-1/2}\psi_{p_x},\\ \phi_3 &= (1/2)s_2\psi_s + 2^{-1/2}s_1\psi_{p_z} + 2^{-1/2}\psi_{p_x},\\ \phi_4 &= \psi_{p_y},\end{aligned} \tag{7}$$

where $s_1=\cot\theta$ and $s_2=(1-\cot^2\theta)^{1/2}$. If the populations in ϕ_1 and ϕ_2 are set equal to a and b, respectively, the relations between the NQR parameters and the orbital populations are given by

$$\begin{aligned}2 - b &= (4/3)\eta U_p,\\ \{(2 - a) - (2 - b)/2\}(1 - \cot^2\theta) &= (1 - \eta/3)U_p.\end{aligned} \tag{8}$$

The ranges of the orbital populations can be estimated in a similar manner as above. These are listed in Table 5. According to X-ray analysis,[12] the distances of the bonds Sb–Cl_1, Sb–Cl_2, Cl_1···I, and Cl_2···I are 2.33, 2.29, 2.85, and 3.00 Å, respectively. The values of a and b correlate to the corresponding bond distance, as can be seen in Table 5. The populations of the valence p orbitals were calculated by assuming $N_z=2$. The net charge on the I atom is estimated to be +1.21. This is comparable to the value (+1.26) for I_2Cl_6[10] and that (+1.13) calculated for the isolated ICl_2^+ ion.[24]

If sp^3 hybridization with C_{2v} symmetry is adopted to the I atom, the interorbital angle is calculated to be 92.6° by using the relation $\eta=-3\cos\theta$.[25] This value is in good agreement with the crystallographically known angle of $\angle Cl_7ICl_8$ (92.5°).[12] The shortness of the distances I···Cl_1 and I···Cl_2 suggests that the interaction between the I atom and the surrounding Cl atoms cannot be described by simple sp^2 hybrid orbitals at the I atom.

The atomic arrangement around the I atom can be represented as a resonance $ICl_2^+SbCl_6^- \longleftrightarrow ICl_4^-SbCl_4^+$, and is similar to that in the ICl_4^- ion.[12] The bonding in the ICl_4^- ion and I_2Cl_6 could be satisfactorily explained by considering only the valence p orbitals.[3,10] If this is the case for the ICl_4 part in ICl_2SbCl_6, the total number of electrons that take part in σ-bonding is 8. Examination of Table 5 reveals that the total electron number is about 7.6. Although this is somewhat smaller than the expected value, it is considered that the I atom in this complex presents essentially only the p orbitals for bonding, as well as the $I_3Cl_2^+$ ion. The comparatively large η-values for the terminal Cl atoms may be ascribed to the π-interaction of the p_x orbital at each Cl atom with the p_x and p_y orbitals at the I atom.

The η-values of ^{121}Sb in $I_3Cl_2SbCl_6$ and ICl_2SbCl_6 are significantly large. There is no experimental atomic coupling constant for ^{121}Sb. If the calculated value of 1300 or 945 MHz is used for $(e^2Qqh^{-1})_{atom}$,[26,27] the imbalance in the orbital population is estimated to be at most 0.02 to 0.03. Hence, a slight imbalance in the population of the p orbitals brings about the large η-value. This is ascribable to the large ionic character of the Sb atom.

References

1) C. D. Cornwell and R. S. Yamasaki, *J. Chem. Phys.*, **27**, 1060 (1957).
2) Y. Kurita, D. Nakamura, and N. Hayakawa, *Nippon Kagaku Zasshi*, **79**, 1093 (1958).
3) R. S. Yamasaki and C. D. Cornwell, *J. Chem. Phys.*, **30**, 1265 (1959).
4) A. Sasane, D. Nakamura, and M. Kubo, *J. Phys. Chem.*, **71**, 3249 (1967).
5) G. L. Breneman and R. D. Willet, *J Phys. Chem.*, **71**, 3684 (1967).
6) G. A. Bowmaker and S. Hocobian, *Aust. J. Chem.*, **21**, 551 (1968).
7) Y. Kume and D. Nakamura, *J Magn. Reson.*, **21**, 235 (1976).
8) T. Okuda, I. Tomoyasu, K. Yamada, and H. Negita, *Bull. Chem. Soc. Jpn.*, **50**, 1695 (1977).
9) D. J. Merryman, J. D. Corbett, and P. A. Edwards, *Inorg. Chem.*, **14** 428 (1975).
10) J. C. Evans and G. Y-S. Lo, *Inorg. Chem.*, **6**, 836 (1967).
11) D. J. Merryman and J. D. Cornwell, *Inorg. Chem.*, **13**, 1258 (1974).
12) C. G. Vonk and E. H. Wiebenga, *Acta Crystallogr.*, **12**, 859 (1959).
13) T. Birchall and R. D. Myers, *Inorg. Chem.*, **20**, 2207 (1981).
14) T. Birchall and R. D. Myers, *Inorg. Chem.*, **21**, 213 (1982).
15) T. Birchall and R. D. Myers, *Inorg. Chem.*, **22**, 1751 (1983).
16) J. Passmore, G. Sutherland, and P. S. White, *Inorg. Chem.*, **20**, 2169 (1981).
17) J. Shamir and M. Lustig, *Inorg. Chem.*, **12**, 1108 (1973).
18) C. G. Vonk and E. H. Wiebenga, *Recl. Trav. Chim. Pays-Bas*, **78**, 913 (1959).
19) J. Rupp-Bensadon and E. A. C. Lucken, *J. Chem. Soc., Dalton Trans.*, **1983**, 19.
20) M. Mishima, *J. Sci. Hiroshima Univ.*, **A46**, 41 (1982).
21) J. C. Slater, *Acta Crystallogr.*, **12**, 197 (1959).
22) T. P. Das and E. L. Hahn, "Nuclear Quadrupole

Resonance Spectroscopy," Academic Press, New York, London (1958), Chap. 3, p. 151.
23) J. P. Dailey and C. H. Townes, *J. Chem. Phys.*, **23**, 118 (1955).
24) E. H. Wiebanga and D. Kracht, *Inorg. Chem.*, **8**, 738 (1969).
25) P. A. Casabella, P. J. Bray, and R. G. Barnes, *J. Chem. Phys.*, **30**, 1393 (1959).
26) G. A. Jeffrey and T. Sakurai, *Progr. Solid State Chem.*, **1**, 380 (1964).
27) E. A. C. Lucken, "Nuclear Quadrupole Coupling Constants," Academic Press, London, New York (1969), Chap. 12, p. 276.

Hydrodynamic Characterization of Amylose-SDS Complex by Viscosity Measurement

Masako YAMAMOTO,* Shoji HARADA,† Thoru NAKATSUKA,† and Takayuki SANO†
Department of Life Science, Kure Women's Junior College, Agaminami, Kure 737
†Department of Materials Science, Faculty of Science, Hiroshima University, Higashisenda-machi, Nakaku, Hiroshima 730
(Received September 8, 1987)

The hydrodynamic behavior of amylose with and without sodium dodecyl sulfate (SDS) has been examined by viscosity measurements. Two distinct viscosity phenomena have been observed by complexation; one is the increase at the first stage of binding of SDS, which disappears by an addition of salt, and the other is the subsequent decrease in the region of further binding of SDS. These results are interpreted by an idea that the expansion of the complex occurs by an electrostatic repulsion of the bound SDS molecules and the contraction of the complex by a hydrophobic interaction of cooperatively bound SDS molecules. This idea was confirmed further by experiments using amyloses of different length and homologous surfactants of SDS.

It is known that surfactants interact with amylose in the same way as iodine, aliphatic acids, and alcohols, forming complexes where these guest molecules are included in the amylose helix.[1-4] The helical conformation of amylose has been established in the solid state, while the conformation of amylose in solution still remains uncertain. Three models have so far been proposed for the structure of amylose in solution, i.e., (1) entirely random coil model, (2) interrupted helical model, and (3) entirely helical model.[5,6] Banks and Greenwood claimed that the conformation of amylose is the model (1)[7] and Szejtli et al. proposed the model (2),[8] and Senior et al. proposed a model which is characterized by the regions of loose and extended helices which alternate with shorter random coil regions.[9] We also conducted a series of studies on the complex formation of amylose and proposed a model similar to the model (2) and revealed the properties of the cooperative binding of guest molecules to amylose.[10-13] These results indicate a probability of structural change of the amylose by the complexation.

In the present study, the viscosity of the amylose solution with and without SDS was investigated in connection with the cooperative binding and is discussed from a viewpoint of the structural changes of the amylose by the complexation.

Experimental

Materials. Potato amylose, purchased from Pierce Chemicals, was purified by precipitation three times from 1-butanol. Its average degree of polymerization (DP) was estimated to be 1100 by gel filtration. Amyloses of small DPs were prepared as described in the previous paper.[10] Wet 1-butanol complex of amylose was dissolved in water and 1-butanol was subsequently removed by distillation for 30 min in a boiling water bath with bubbling nitrogen gas. After cooling, the solution was filtered through a G3 sintered glass filter. The concentration was determined by the phenol-sulfuric acid method.[14] Sodium alkyl sulfates were synthesized according to the method of Dreger et al.[15] Other chemicals used were of guaranteed grade.

Measurements. Amylose solutions were prepared in the concentration range of 0.10—1.50 mg ml^{-1} for the amyloses of DP 100, 300, and 1100 and 10—15 mg ml^{-1} for those of DP 42 and 57. Fresh amylose solutions were pipetted into the viscometer and the same volume of 2 mM surfactant solution (1 M=1 mol dm^{-3}) was added. The mixed solution was held for 30 min in the water bath before runs. Since the amylose-surfactant complexation is rapid all the reactions were presumed to be fully equilibrated on this time scale.[16] The viscosity was measured by Ubbelohde type viscometers at 20.0±0.1 °C. The efflux times of pure water were around 180—240 s and the kinetic energy corrections were negligible. The measurements were repeated for solutions prepared by subsequent addition of surfactant solution. The concentration of bound surfactants was determined potentiometrically as described in the previous paper.[12] To rule out any effect due to the micellization, the concentration of surfactant was kept below the critical micelle concentration.

Results

The specific viscosity, η_{sp}, was measured for the amylose solution in the absence or in the presence of SDS and the reduced viscosity, η_{sp}/C_p, was obtained for the concentration of amylose, C_p. The reduced viscosity was constant for free amylose or SDS solutions. For the amylose-SDS system, on the other hand, the value of η_{sp}/C_p increases rapidly in the first stage and then decreases with the SDS concentration as seen in Fig. 1.

These results are indicative of two-step hydrodynamic changes of the amylose complex, and systematic experiments were carried out by changing various experimental factors as follows. Firstly, the viscosity of the SDS-amylose solution was measured by changing the concentration of amylose under the constant concentration of SDS. As seen in Fig. 2, the η_{sp}/C_p value was independent of the concentration of amylose in the concentration range of 0.10 to 0.50 mg ml^{-1} for various concentrations of SDS. Secondly, the viscosity was measured for the SDS-amylose solution in the presence of NaCl and the results are shown in Fig. 3. Here, the experiments were carried out at relatively low NaCl concentration in order to avoid

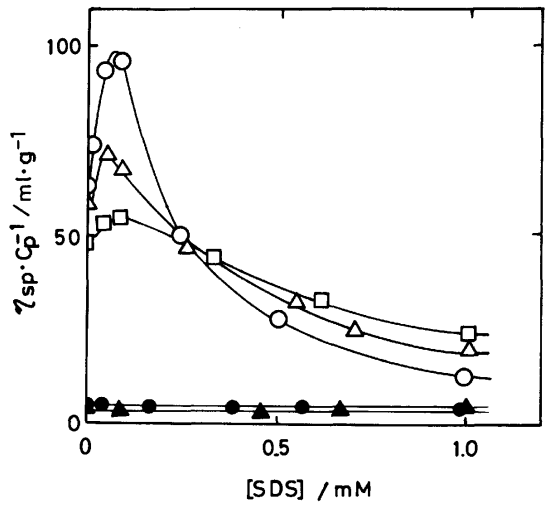

Fig. 1. SDS concentration dependence of reduced viscosity. (○) DP 1100; 0.42 mg ml^{-1}, (△) DP 300; 0.50 mg ml^{-1}, (□) DP 100; 1.00 mg ml^{-1}, (●) DP 57; 5.0 mg ml^{-1}, (▲) DP 42; 5.0 mg ml^{-1}.

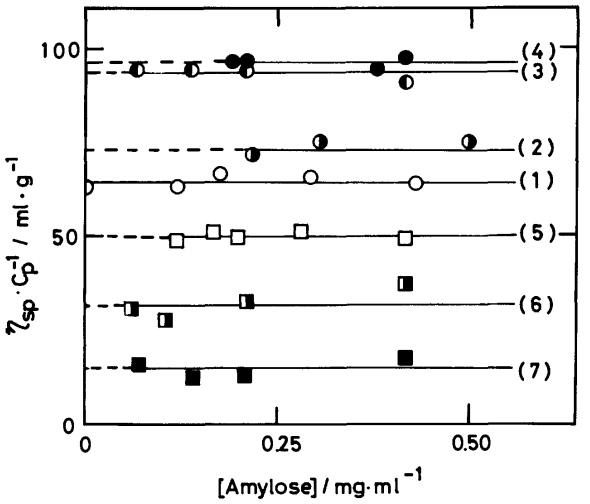

Fig. 2. Amylose concentration dependence of reduced viscosity at various SDS concentrations. (1) 0 mM, (2) 0.01 mM, (3) 0.05 mM, (4) 0.1 mM, (5) 0.2 mM, (6) 0.5 mM, (7) 1.0 mM.

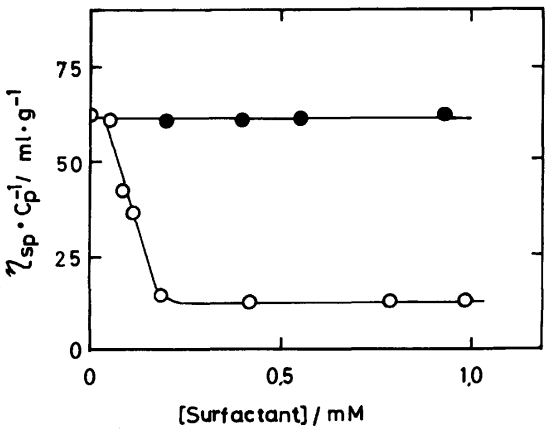

Fig. 3. Surfactant concentration dependence of reduced viscosity in the presence of 10.7 mM NaCl. (●) C_8, (○) C_{12} (=SDS). Amylose concentration was in the range of 0.46 to 1.38 mg ml^{-1}.

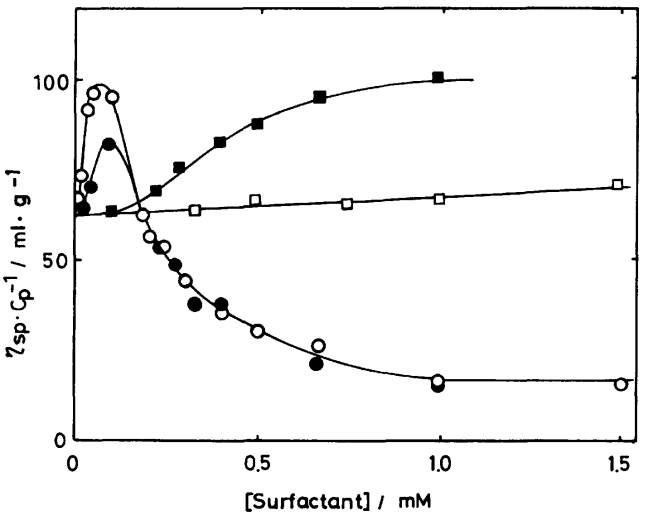

Fig. 4. Surfactant concentration dependence of reduced viscosity for sodium alkyl sulfate-amylose systems in the absence of NaCl. (□) C_8, (■) C_{10}, (○) C_{12} (=SDS), (●) C_{14}. Amylose concentration was in the range of 0.46 to 1.38 mg ml^{-1}.

aggregation of the complex. As seen in the figure, the characteristic increase of the viscosity in the first stage disappeared, i.e., the viscosity was constant in the range of [SDS]<0.03 mM, and above this concentration, the viscosity decreased uniformly with increase of SDS. Thirdly, the viscosity was measured by changing the surfactant to the homologues of SDS, i.e., $C_nH_{2n+1}SO_4Na$ (n=8—14). As seen in Fig. 4, the concentration dependency behavior of η_{sp}/C_p differs greatly between the surfactants of C_8 and C_{10} and those of C_{12} and C_{14}. In the former systems, only the increase of the viscosity was observed with increase of the surfactant concentration and the viscosity decreasing process is absent. While in the latter systems, the viscosity increases at first and then decreases. The increasing behavior observed for the surfactant-amylose systems disappeared on an addition of salt. Fourthly, the viscosity of the solutions of SDS and amyloses of small DP was examined in the same way as that of amylose of DP 1100 system studied above. The values of η_{sp}/C_p for the amyloses of DP 42 and DP 57 were independent of the SDS concentration (Fig. 1), and the result is in contrast to the behavior of the amylose of DP 1100. Those of the amyloses of DP 100 and 300 are similar.

The amount of bound surfactant was measured by potentiometric titration. As seen in Fig. 5, the amount of bound SDS does not change on the addition of salt under the present experimental concentration range.

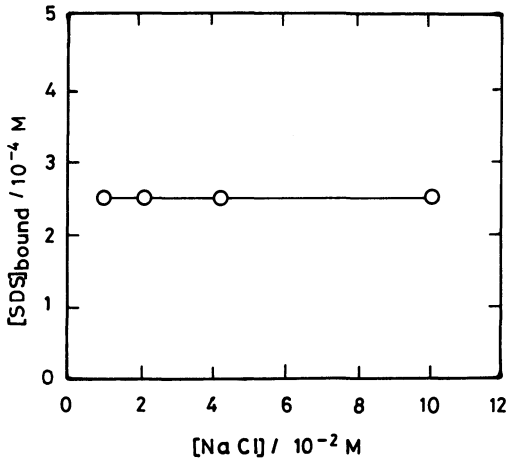

Fig. 5. NaCl concentration dependence of the maximum amount of bound SDS to amylose (DP 1100). [Amylose]=0.46 mg ml^{-1}.

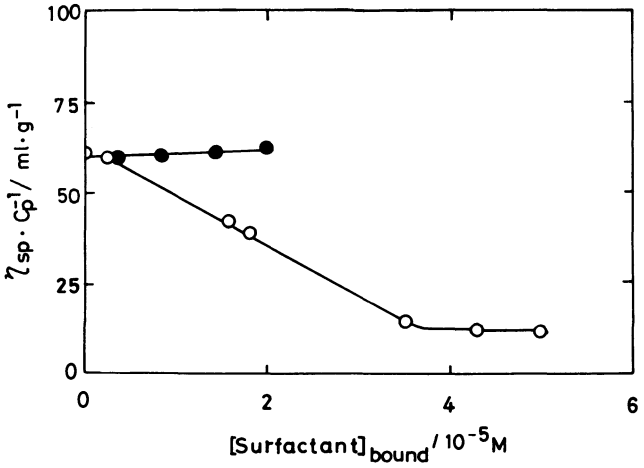

Fig. 6. The dependence of the viscosity on the amount of bound surfactant. (●) C_8, (○) C_{12} (=SDS). Amylose concentration was in the range of 0.46 to 1.38 mg ml^{-1}.

Discussion

As the origin of the characteristic viscosity behavior observed above, two effects may be considered. One is the intermolecular effect of amylose or its SDS complex. This may be discounted, because the viscosity of the solution of amylose or its complex was independent of their concentration. The result suggests that the amylose retains the same binding state irrespective of the amylose concentration as long as the SDS concentration is constant. This suggestion was supported by the fact that the amount of bound SDS was proportional only to the amylose concentration under the present experimental condition. The other possibility is the intramolecular effect which has been proposed by some workers.

Rao et al. have observed the viscosity decrease on complexation for the SDS-amylose system and ascribed it to the propagation of the helix.[17] According to them, SDS first binds to the originally helical part of amylose, which is not accompanied by any change of viscosity. Further binding induces a helix propagation accompanying a decrease of viscosity. Their idea is applicable to our data for SDS-amylose system (Fig. 6) indicating the original helical part of amylose corresponds to about 5% of the total amount of SDS binding. If their interpretation is applied to the binding of C_8 surfactant system, similar viscosity behavior to those of SDS system is expected since the amount of its binding exceeds fully that for the originally helical part of amylose.[12] However, this expectation was not satisfied as seen in Fig. 6 and the idea of Rao et al., therefore, is questionable. For a complexation of amylose with iodine, Banks et al. observed a decrease of viscosity and ascribed it to the conformational change of amylose from a random coil to a helix.[7] While, Senior et al. insisted that the decrease is due to a shortening of the linear dimension of the polymer chain.[9] All these experiments have been performed in the presence of electrolyte, and only the decrease in viscosity by complexation has been observed. Therefore, these interpretations cannot be applied satisfactorily to either the lack of decrease of viscosity in C_8 and C_{10} surfactant systems or the increase of viscosity in C_{12} and C_{14} surfactant systems. Recently, Francois et al. observed an increase in viscosity on the complexation of poly(oxyethylene) with SDS and claimed that the polymer complexes with SDS micelles.[18] However, this idea is not applicable to the present system where the surfactant concentration is much lower than the critical micelle concentration. As a consequence, we developed our own idea in the following way.

It is said that amylose is composed of several segments which are composed of about 60 anhydroglucose units; there is however some discrepancy in the literature values.[10,19-21] Taking this fact into consideration, the amyloses of DP 42 and 57 are composed of a single segment and DP 100, 300, and 1100 of several segments. These facts show that the characteristic viscosity behavior appears when the amylose is composed of more than two segments. So, segment-segment interactions of the SDS complex are the origins of the increase and/or the decrease of viscosity.

Further information on these interactions are derived from the salt effects on the viscosity. Since the binding of SDS was not affected appreciablely by the presence of salt, the disappearance of the viscosity increasing behavior on the addition of salt should not be ascribed to the decomposition of the complex. Instead it implies that the segment-segment interaction contributing to the viscosity increase is interrupted by the addition of salt, i.e., the interaction may

be an electrostatic one. Therefore, the viscosity increase indicates an expansion of the complex by electrostatic repulsion among the segments charged by the initial binding of SDS. On the other hand, the interaction contributing to the viscosity decrease may be nonelectrostatic since the viscosity decrease process was not affected by the addition of salt.

We have investigated the binding isotherm of surfactant to amylose by the potentiometric titration and clarified that (i) SDS binds to isolated binding sites in the region of [SDS]$<$0.03 mM while it binds cooperatively in the region of 0.03 mM$\leqq$[SDS]$\leqq$0.20 mM, (ii) the cooperativity is approved for the bindings of C_{12} and C_{14} surfactants but not for those of C_8 and C_{10} surfactants, (iii) the cooperativity is approved for amyloses composed of more than two segments, i.e., it is related to the segment-segment interaction.[12] These facts, together with the viscosity data, indicate that the boundary concentrations of SDS in the viscosity behavior shown in Fig. 3 are in good agreement with those observed in the binding curve, respectively. The viscosity constant region in the first stage of SDS binding also corresponds to the binding on the isolated sites while the decreasing behavior in the subsequent stage corresponds to the cooperative binding. Therefore, it is clear that the viscosity decrease indicates a contraction of the complex by the nonelectrostatic segment-segment interaction induced by the additional binding of SDS. In accordance with this conclusion, it is interesting to see that the cooperativity is observed also for the iodine-amylose system, and the viscosity decrease observed by Banks et al.[7] and Senior et al.[9] will be due to the contraction of the complex induced by the cooperative binding of iodine. Furthermore, lack of the viscosity decrease process in the binding of the C_8 and C_{10} surfactants to amylose (DP 1100) is also compatible with the lack of the cooperativity in their bindings.

These characterization of viscosity behavior supports a model previously proposed for the SDS-amylose complex, where SDS molecules are binding at each end of the helical segment and the cooperativity is ascribed to the hydrophobic interaction between the alkyl chains of bound SDS.[12] Based on this model, we conclude that the viscosity increase observed at the first stage of the SDS binding is due to the expansion of the complex by electrostatic repulsion between the charged head groups of SDS bound to the isolated sites of the helical segments. The viscosity decrease observed in the second stage is due to the contraction of the amylose complex induced by the hydrophobic interaction of the bound SDS.

The above interpretation is also applicable to the results for the C_8 and C_{10} surfactant systems and to those for SDS-amyloses of low DPs. The C_8 and C_{10} surfactants bind to amylose non-cooperatively due to their somewhat shorter alkyl chain, and the bindings do not induce the contract of the complex because the electrostatic repulsion among the segments with charged surfactants is predominant. Hence, only the viscosity increase process is observed and the decrease process is not observed in their bindings. In the binding of SDS to amyloses of DP 42 and 57, the interaction between the segments in the complex and the cooperativity are not expected because they consist of a single segment. Therefore, any characteristic hydrodynamic behavior is not observed.

References

1) F. F. Mikus, R. M. Hixon, and R. E. Rundle, *J. Am. Chem. Soc.*, **68**, 1115 (1946).
2) T. Takagi and T. Isemura, *Bull. Chem. Soc. Jpn.*, **33**, 437 (1960).
3) Y. J. Kim and R. J. Robinson, *Staerke* **31**, 293 (1979).
4) Y. Hui, J. C. Russell, and D. G. Whitten, *J. Am. Chem. Soc.*, **105**, 1374 (1983).
5) O. Kratky and G. Porod, *Recl. Trav. Chim. Phys-Bas*, **68**, 1106 (1949).
6) Q. T. Nguyen, P. Aptel, and J. Neel, *Biopolymers*, **15**, 2097 (1976).
7) W. Banks and C. T. Greenwood, *Staerke*, **23**, 300 (1971).
8) J. Szejtli, M. Richter, and S. Augustat, *Biopolymers*, **5**, 5 (1967).
9) M. B. Senior and E. Hamori, *Biopolymers*, **12**, 65 (1973).
10) M. Yamamoto, T. Sano, and T. Yasunaga, *Bull. Chem. Soc. Jpn.*, **55**, 1886 (1982).
11) M. Yamamoto, T. Sano, S. Harada, and T. Yasunaga, *Bull. Chem. Soc. Jpn.*, **55**, 3702 (1982).
12) M. Yamamoto, T. Sano, S. Harada, and T. Yasunaga, *Bull. Chem. Soc. Jpn.*, **56**, 2643 (1983).
13) M. Yamamoto, S. Harada, T. Sano, T. Yasunaga, and N. Tatsumoto, *Biopolymers*, **23**, 2082 (1984).
14) M. Dubois, K. A. Gilles, J. K. Hamilton, P. A. Rebers, and F. Smith, *Anal. Chem.*, **28**, 350 (1956).
15) E. E. Dreger, G. I. Keim, G. D. Miles, L. Shedlovsky, and J. Ross, *Ind. Eng. Chem.*, **36**, 610 (1944).
16) S, V, Bhide, M, S, Karve, and N, R, Kale, *Am. Chem. Soc. Symp. Ser.*, No. 50, pp. 491—511 (1981).
17) V. S. R. Rao and J. F. Foster, *Biopolymers*, **1**, 527 (1963).
18) J. Francois, J. Dayantis and J. Sabbadin, *Eur. Polym. J.*, **21**, 165 (1985).
19) J. Szejtli, M. Richter, and S. Augustat, *Biopolymers*, **6**, 27 (1968).
20) T. Watanabe, K. Ogawa, and S. Ono, *Bull. Chem. Soc. Jpn.*, **43**, 950 (1970).
21) K. Hiromi, T. Shibaoka, and S. Ono, *J. Biochem.*, **68**, 205 (1970).

Mixed Surfactant Bilayers on Monodispersed Ferric Hydro Sols

Kunio Esumi,* Yuichi Sakamoto, Keiko Yoshikawa, and Kenjiro Meguro
Department of Applied Chemistry, Institute of Colloid and Interface Science,
Science University of Tokyo, Kagurazaka, Shinjuku-ku, Tokyo 162
(Received September 9, 1987)

The properties of mixed surfactant bilayers on monodispersed ferric hydro sol were studied by measuring the amount of surfactant adsorbed, particle size, and pyrene fluorescence spectra. The positively charged sols flocculated upon addition of sodium dodecyl sulfate (SDS) or lithium perfluoro-1-octanesulfonate (LiFOS) were redispersed by further addition of poly(oxyethylene) nonyl phenyl ether (NP7.5) due to the formation of a mixed surfactant bilayer on the sols. The mixed surfactant bilayer of SDS–NP7.5 on the sols was more easily formed than LiFOS–NP7.5. Fluorescence fine structure of pyrene gave information on the polarity of the microenvironment in the mixed surfactant layer on the sols.

The dispersion behavior of particles upon addition of surfactants has been extensively investigated[1-7] in order to elucidate the interaction between surfactants and particles and further to apply to many fields such as flotation, oil recovery, and paints etc. It has been demonstrated[1] in the past by measuring the zeta potential and particle size that positively charged particles flocculate upon addition of anionic surfactants and that on further addition, the particles redisperse due to formation of surfactant bilayers.

Recently, the structural characteristics of the surfactant layer on solids have been elucidated by fluorescence[8-11] and electron spin resonance probing methods.[12] Chandar et al.[8] have reported that highly organized surfactant aggregates of sodium dodecyl sulfate at alumina–water interface are formed by the association of hydrocarbon chains from pyrene and dinaphthylpropane fluorescence probes. A similar experiment for Triton X-100-silica has been studied.[11]

On the other hand, Meguro et al.[13] have demonstrated that positively charged particles flocculated upon addition of an anionic surfactant can be redispersed upon addition of another surfactant owing to the formation of a mixed surfactant adsorbed layer. Their results have not, however, been discussed in detail.

In this work we studied the formation of mixed surfactant layers on monodispersed ferric hydro sols by measurements of the zeta potential, particle size, adsorbed amount, and fluorescence probe. The surfactants used were two different mixed systems: sodium dodecyl sulfate–poly(oxyethylene)nonyl phenyl ether and lithium perfluoro-1-octanesulfonate–poly(oxyethylene) nonyl phenyl ether.

Experimental

Materials. As surfactants, sodium dodecyl sulfate (SDS), lithium perfluoro-1-octanesulfonate (LiFOS), and poly(oxyethylene) nonyl phenyl ether having average oxyethylene chains of 7.5(NP7.5) were used. SDS and LiFOS were synthesized in our laboratory and purified. NP7.5 was obtained from Nikko Chemical Co. Ltd. and used without further purification. The cmc's of these surfactants in the presence of 10 mmol·dm^{-3} nitrates were 3.0 for SDS, 3.4 for LiFOS, and 3.0×10^{-2} mmol·dm^{-3} for NP-7.5, respectively. The water used in all experiments was purified by passing through a Milli-Q system until its specific conductivity fell below $10^{-7}\,\Omega^{-1}\,cm^{-1}$.

Hydro sols consisting of spherical hematite particles with a narrow size distribution were prepared by essentially the same procedure as Matijević et al.[14] described. The final stock sol had a concentration of 3.17 mg·cm^{-3}, as determined directly by dry-weight measurement, and was kept at pH 5.8. The mean particle size was determined by a Particle analyser (Autosizer Model 700, Malvern Co. Ltd.); the average diameter was 160 nm with a polydispersity of 0.03. Alumina was supplied by Showa Denkou Co. The surface area and the average diameter of the alumina particles were 10.1 m^2·g^{-1} and 500 nm, respectively.

Methods. As the ferric hydro sol had an isoelectric point of pH 7.9, the ferric hydro sol was allowed to flocculate upon addition of LiFOS or SDS at pH 3.5. Then, NP7.5 was added into the flocculated sol. The concentration of the sol in all the experiments except the fluorescence measurement was 3.17 mg/5 cm^3. In order to keep the ionic strength constant, all the measurements were carried out in 10 mmol·dm^{-3} sodium nitrate or lithium nitrate solution at 25 °C. Nitric acid was used to adjust the pH of the mixtures.

For the fluorescence experiments, pyrene dissolved in ethanol was first introduced into a flask and the solvent allowed to evaporate. Then, the ferric hydro sol (the concentration of the sol; 0.32 mg/5 cm^3) was added and sonificated.

Measurements. The amount of anionic surfactants adsorbed on the ferric hydro sol was determined from the difference in concentrations before and after the adsorption. The concentration of anionic surfactants was determined by means of isotachophoresis (Shimadzu Co. Ltd.). That of NP7.5 was also determined by means of a UV spectrophotometer (200A, Hitachi Co.). The zeta potential of the ferric hydro sol was measured by means of an electrophoresis apparatus Laser-Zee meter Model-500 (Pen Kem Inc.).

Steady-state emission spectra were obtained using a Hitachi 650-10S fluorescence spectrophotometer. A portion of the dispersion sample was transferred to a 1 cm quartz cell. The concentration of pyrene ranged from 1×10^{-6} to 1×10^{-7} mol·dm^{-3}. The pyrene containing samples were excited at 335 nm.

Results and Discussion

In order to characterize the ferric hydro sols, the zeta potential was measured as a function of pH. Since the isoelectric point of the sol was estimated to be pH 7.9, the interaction between the sol and the anionic surfactants due to electric attraction forces plays an important role in the range below pH 7.9. Accordingly, in this study, all the measurements were conducted at pH 3.5 where the zeta potential of the ferric hydro sols was about +25 mV.

Figure 1 shows the adsorption isotherms of anionic surfactants on the ferric hydro sols. In both cases, the amount adsorbed increased gradually and then sharply, following a plateau level. This behavior has been observed by other workers.[8,15] At the same time, the dispersion behavior of the ferric hydro sols was observed: the sol flocculated upon addition of SDS or LiFOS (flocculation region pointed by the arrow) and then redispersed by further addition of the same surfactant.[16] Here, the optimum additive concentration for the flocculation of ferric hydro sol was about 0.2 mmol·dm^{-3} for both cases, although the amount of SDS adsorbed was twice that of LiFOS.

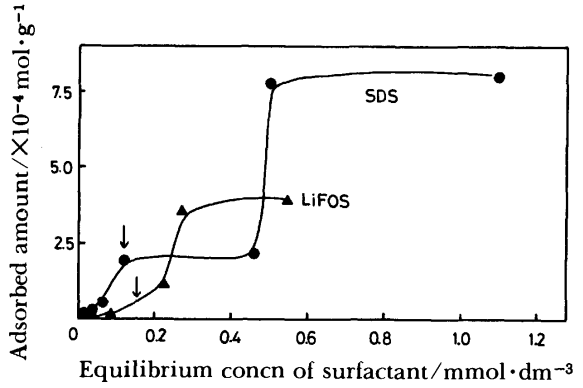

Fig. 1. Adsorption isotherms of anionic surfactants on ferric hydro sols at pH 3.5 in 10 mmol·dm^{-3} nitrates.

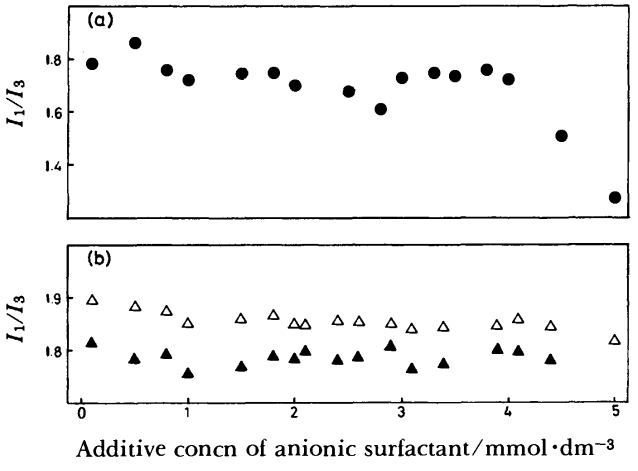

Fig. 2. (a) I_1/I_3 ratio of pyrene in SDS-ferric hydro sols. (b) I_1/I_3 ratio of pyrene in LiFOS-ferric hydro sols: ▲, in dispersion; △, in supernatant.

The pyrene fluorescence fine structure has been found to be remarkably dependent on the solvent: the intensity ratio of I_1/I_3(I_1, first vibrionic and I_3 third vibrionic bands at 373 and 383 nm, respectively) is sensitive to the solvent polarity.[17] This fluorescence method was applied to the dispersion system in order to obtain the polarity of environment of surfactant adsorbed layer on the ferric hydro sol. The change in intensity ratio of, I_1/I_3, of pyrene in SDS-sol and LiFOS-sol dispersion as a function of additive concentration of anionic surfactant is given in Fig. 2. In the case of SDS-ferric hydro sol, no pyrene was detected in the supernatants of the dispersion, which suggests that pyrene is almost solubilized in the adsorbed layer. The I_1/I_3 values of the probe were constant up to 4 mmol·dm^{-3} SDS, corresponding to the region of the cmc, and then decreased rapidly to a value of 1.30. The above result suggests that the solubilization site for pyrene above 4 mmol·dm^{-3} SDS is probably the hydrocarbon region which is formed by association of SDS hydrocarbon chains on the surface. A similar result has been reported on SDS-alumina system using pyrene steady-state fluorescence.[8] On the other hand, in the LiFOS-ferric hydro sol, the I_1/I_3 values were almost constant(1.80) over the whole concentration region of LiFOS, whose values coincide with that for pyrene in water. The I_1/I_3 values in the supernatants were also constant (1.86). This indicates that the pyrene is only very weakly solubilized in the fluorocarbon chain layer of LiFOS on the sol. This speculation is also supported by the fact that the I_1/I_3 value of pyrene solubilized into the LiFOS micelles is about 1.51[18] and the amount of adsorbed pyrene in the adsorbed layer is negligibly low.

In order to elucidate the interaction of the anionic surfactant and NP7.5 on the ferric hydro sols, NP7.5 was added to the sol which had been flocculated upon addition of 0.2 mmol·dm^{-3} anionic surfactant.

Figure 3 shows the amount of the anionic surfactant adsorbed and of NP7.5 on the ferric hydro sols as a function of the additive concentration of NP7.5. As can be seen, the amount of the anionic surfactant adsorbed on the sols is almost constant even after addition of different concentrations of NP7.5. This indicates that the anionic surfactant required for flocculation is adsorbed strong enough on the sol due to the electric attraction between the charged head group of the surfactant and the charged site of the sol. Upon addition of NP7.5, the amount of NP7.5 adsorbed increased for both the SDS-NP7.5 and the LiFOS-NP7.5 systems, although the amount adsorbed was larger for SDS-NP7.5 than for LiFOS-NP7.5. This result can be interpreted as follows: In

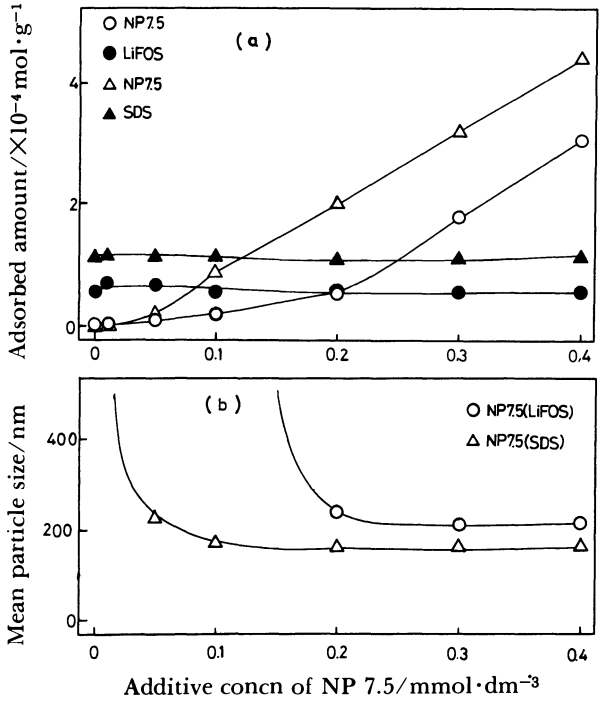

Fig. 3. (a) Amount adsorbed of anionic surfactant and of NP7.5 on ferric hydro sol in presence of 0.2 mmol·dm^{-3} of anionic surfactant as a function of additive concentration of NP7.5. (b) Particle size of ferric sols flocculated by addition of anionic surfactant (0.2 mmol·dm^{-3}) as a function of additive concentration of NP7.5.

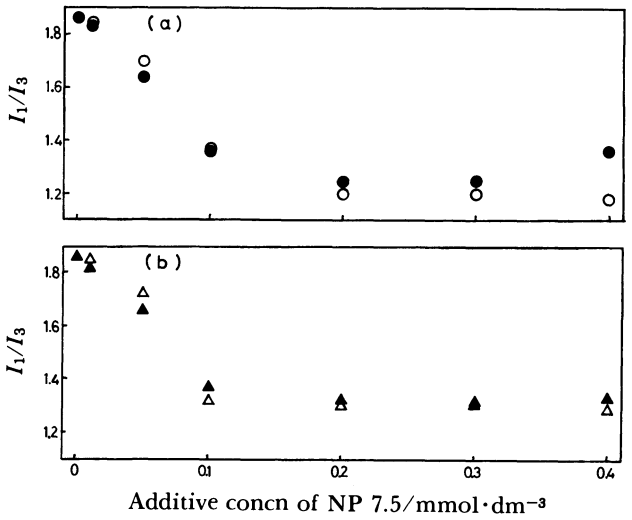

Fig. 4. I_1/I_3 ratio of pyrene for systems shown in Fig. 3. (a) SDS-NP7.5-ferric hydro sols: ●, in dispersion; O, in supernatant. (b) LiFOS-NP7.5-ferric hydro sols: ▲, in dispersion; △, in supernatant.

SDS-NP7.5, the flocculated ferric sol, upon addition of SDS is fully covered with SDS molecules, orienting their hydrocarbon chain to the aqueous solution. This dense hydrocarbon layer allows the adsorption of NP7.5 easily where the hydrocarbon chains of NP7.5 forms hydrophobic bond with the hydrocarbon layer of SDS, resulting in the formation of a mixed surfactant bilayer. Scamehorn et al.[19] studied the adsorption of mixtures of anionic and nonionic hydrocarbon surfactants on kaolinite and alumina and they reported the adsorption amount of mixed surfactant, but not the interaction between the mixed bilayer. On the other hand, due to a lower adsorption density of LiFOS, NP7.5 can not easily be adsorbed on the LiFOS layer. Further, since it is known[20] that the interaction between the hydrocarbon and fluorocarbon is weaker than that between hydrocarbon and hydrocarbon, this factor also governs the magnitude in the adsorption of NP7.5 on LiFOS layer.

In order to examine the dispersing state of ferric hydro sols for SDS-NP7.5 and LiFOS-NP7.5, the particle size of the sol was also measured (Fig. 3). Upon addition of SDS or LiFOS to the positively charged sol, the sol flocculated and its particle size became too large to detect by the Autosizer. When NP7.5 was added to the flocculated sol, the particle size decreased remarkably upon addition of more than some concentration of NP7.5: 0.05 mmol·dm^{-3} for SDS-NP7.5 and 0.2 mmol·dm^{-3} for LiFOS-NP7.5. These concentrations of NP7.5 were above the cmc of NP7.5(3.0×10^{-2} mmol·dm^{-3}). The decrease in the particle size corresponds to the redispersion state of the sol. Compared to the amount of NP7.5 adsorbed required to attain the redispersion of the sol, the amount for SDS-NP7.5 decreases to one third of that for LiFOS-NP7.5. This result also supports the view that the hydrocarbon-hydrocarbon interaction is preferred to the fluorocarbon-hydrocarbon interaction.

The properties of the mixed surfactant adsorbed layer on the sol were also examined using the pyrene probe method. Figure 4 shows the changes in intensity ratio of I_1/I_3 of pyrene in the SDS-NP7.5 and LiFOS-NP7.5 containing sols. The I_1/I_3 values decreased and then became constant (1.34) above 0.1 mmol·dm^{-3} NP7.5 for both cases. This value is almost the same as that in micelles of NP7.5. Accordingly, pyrene is solubilized into mainly hydrocarbon chains of NP7.5 for both cases, but there is no strict distinction whether pyrene is solubilized in aqueous micelles of NP7.5 or in mixed bilayer on the sols. So, in order to clarify this point, a highly concentrated dispersion system is necessary to obtain information from the bilayer on the solids. In this case, we used an alumina instead of a ferric hydro sol because alumina does not significantly scatter fluorescence light, compared with ferric hydro sol. Figure 5 shows the I_1/I_3 ratios of pyrene for SDS-NP7.5-alumina and LiFOS-NP7.5-alumina. Here, the amount of alumina used was 0.3 g/10 ml. The I_1/I_3 values for pyrene in SDS-NP7.5-alumina ranged between 1.05 and 1.34

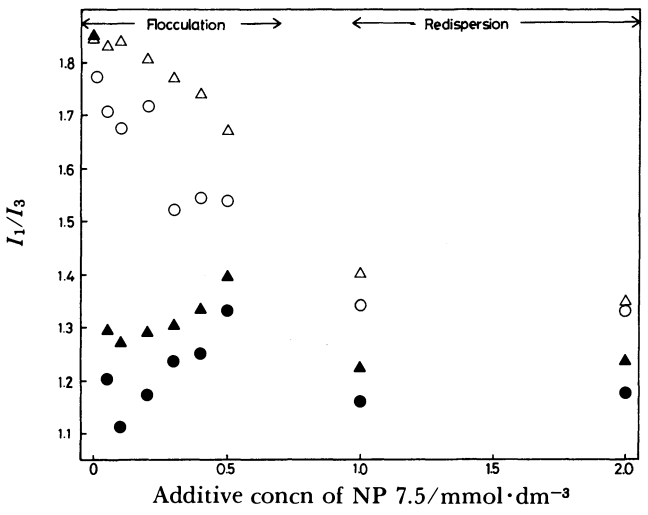

Fig. 5. I_1/I_3 ratio of pyrene for SDS-NP7.5-alumina (●, ○) and LiFOS-NP7.5-alumina (▲, △): filled symbols, in dispersion; empty symbols, in supernatant.

where the alumina particles were flocculated. Above 1 mmol·dm^{-3} of NP7.5, the alumina particles were redispersed due to formation of a mixed bilayer on the alumina and the I_1/I_3 values became constant (1.17). On the other hand, the I_1/I_3 values in the supernatants decreased with an increase of concentration of NP7.5 and reached a constant value (1.34). This suggests that the mixed bilayer of SDS and NP7.5 on the alumina is more densely compact than that of their mixed micelles. In the case of LiFOS-NP7.5-alumina, the I_1/I_3 values of pyrene decreased steeply from 1.85 to 1.30 upon an addition of 0.05 mmol·dm^{-3} NP7.5 and ranged between 1.27 and 1.39 below 0.5 mmol·dm^{-3} NP7.5 where the alumina particles were flocculated. Upon further addition of NP7.5, the alumina particles were redispersed and the I_1/I_3 values decreased to 1.23. The I_1/I_3 values in the supernatants decreased with an increase of concentration of NP7.5 and reached a value of 1.35. The I_1/I_3 value of pyrene(1.17) in SDS-NP7.5-alumina, for the redispersion state is smaller than that (1.23) in LiFOS-NP7.5-alumina, suggesting that pyrene is solubilized in the higher polarity environment of the mixed bilayer for LiFOS-NP7.5-alumina than for SDS-NP7.5-alumina. The isoelectric points of alumina and ferric hydro sol are 9.0 and 7.9, and the zeta potential values at pH 3.5 are +30 mV for the former, +25 mV for the latter. It might be expected from these values that alumina and ferric hydro sol would show a similar interaction behavior against the surfactants. Consequently, these microenvironment results obtained from the dispersion systems containing alumina would reflect the dispersion system containing ferric hydro sol.

From the above results, it is concluded that ferric hydro sols flocculated upon addition of SDS or LiFOS redisperse by further addition of NP7.5 due to formation of a mixed surfactant bilayer and the difference in mixed surfactant bilayer on the sols between SDS-NP7.5 and LiFOS-NP7.5 are characterized by measuring the amount adsorbed and the pyrene fluorescence spectra.

References

1) K. Ogihara, S. Tomioka, K. Esumi, and K. Meguro, *Shikizai Kyokaishi*, **55**, 546 (1982).
2) H. Kuno, R. Abe, and S. Tahara, *Kolloid-Z.*, **198**, 77 (1964).
3) S. Fukushima and S. Kumagai, *J. Colloid Interface Sci.*, **42**, 539 (1973).
4) N. Moriyama, *J. Colloid Interface Sci.*, **50**, 80 (1975).
5) J. M. Corkill, J. F. Goodman, and J. R. Tate, *Trans. Faraday Soc.*, **62**, 979 (1966).
6) E. Matijević and R. H. Ottewill, *Trans. Faraday Soc.*, **62**, 750 (1966).
7) J. F. Scamehorn, R. S. Schecter, and W. H. Wade, *J. Colloid Interface Sci.*, **85**, 463 (1982).
8) P. Chandar, P. Somasundaran, and N. J. Turro, *J. Colloid Interface Sci.*, **117**, 31 (1987).
9) P. Somasundaran, N. J. Turro, and P. Chandar, *Colloids Surf.*, **20**, 145 (1986).
10) K. Viaene, J. Caigui, R. A. Schoonheydt, and F. C. De Schryver, *Langmuir*, **3**, 107 (1987).
11) P. Levitz, H. Van Damme, and D. Keravis, *J. Phys. Chem.*, **88**, 2228 (1984).
12) P. Chandar, P. Somasundaran, K. C. Waterman, and N. J. Turro, *J. Phys. Chem.*, **91**, 148 (1987).
13) K. Meguro, S. Tomioka, N. Kawashima, and K. Esumi, *Prog. Colloid Polym. Sci.*, **68**, 97 (1983).
14) E. Matijević and P. Scheiner, *J. Colloid Interface Sci.*, **63**, 509 (1978).
15) P. Somasundaran and D. W. Fuerstenau, *J. Phys. Chem.*, **70**, 90 (1966).
16) A. Nakajima, *Bull. Chem. Soc. Jpn.*, **44**, 3272 (1971).
17) K. Esumi, Y. Ono, M. Ishizuka, and K. Meguro, *Colloids Surf.* in press.
18) Y. Muto, K. Esumi, K. Meguro, and R. Zana, *J. Colloid Interface Sci.*, **120**, 162 (1987).
19) J. F. Scamehorn, R. S. Schechter, and W. H. Wade, *J. Colloid Interface Sci.*, **85**, 494 (1982).
20) P. Mukerjee, *JAOCS*, **59**, 573 (1982).

 © 1988 The Chemical Society of Japan Bull. Chem. Soc. Jpn., 61, 1479—1483 (1988)

A Simulation of Bromate-Cerium-Oxalic Acid Oscillations

Yoshihiro SASAKI
Institute for Chemical Research, Kyoto University, Uji, Kyoto 611
(Received September 9, 1987)

The oscillation behavior of the bromate-cerium-oxalic acid system was simulated within the FKN framework with bromine-hydrolysis control, where a radical-chain reaction of HOBr with oxalic acid and the formation of $HCO_2\cdot$ by the reduction of Ce(IV) were assumed. When $[(COOH)_2]=0.03$ mol dm^{-3} and $k_{13}=0.075$ s^{-1} (k_{13}: the rate constant of bromine removal), the oscillation behavior was qualitatively consistent with the experimental results. Excitability in the reduced and oxidized steady states, induced by a sudden change in the concentration of bromine, was simulated. No bistability was found. When $[(COOH)_2]=0.03$ mol dm^{-3}, no hysteresis near the bifurcation points was observed. However, when $[(COOH)_2]=0.001$ mol dm^{-3}, hysteresis was observed in the transition between the oxidized steady state and the oscillatory state.

The FKN mechanism seems widely accepted at present as a qualitatively adequate description of the exotic Belousov-Zhabotinskii (BZ) oscillation.[1] In the mechanism, bromide is a control intermediate, and a stoichiometric factor is used in order to simplify the complicated processes of the reduction of Ce(IV) and the formation of bromide by malonic acid and its brominated compound.[2,3] The BZ oscillation in the presence of silver ions could also be simulated within the FKN framework.[4]

Recently Noszticzius et al.[5,6] reported characteristic oscillation behavior of the bromate-cerium-oxalic acid system under batch conditions, and Gáspár and Galambosi,[7] in the CSTR mode. In this system, the bromine had to be removed physically or chemically in order to sustain the oscillations between the explicit oxidized steady state and the reduced steady state, and the time period of the oscillations depended on the magnitude of the bifurcation parameters. Moreover, excitability in the steady states and bistability were observed.

Field and Boyd simulated the oscillation of the bromate-cerium-oxalic acid-acetone system by using the Oregonator model with bromine-hydrolysis control,[8] supporting the idea that bromide is an intermediate in the system as well. Gáspár and Galambosi also reported a simulation for the bromate-cerium-oxalic acid system within a revised Oregonator model.[7] However, these simulations did not reproduce the oscillation behavior described above. The inconsistency seems to be ascribable to the excessive simplification of the reduction process of HOBr by oxalic acid. The bromate-cerium-oxalic acid system is one of the simplest BZ-type oscillations because oxalic acid cannot be brominated. Thus, when we simulate the oscillation behavior of this system, we have to take account of the processes of the reduction of Ce(IV) and of the formation of bromide in detail. Noyes,[9] as well as Field and Boyd,[8] has proposed the formation of $HCO_2\cdot$ and $Br\cdot$ radicals in the processes of the reduction of Ce(IV) by oxalic acid and the formation of bromide. In this paper, we will simulate the oscillation behavior of the bromate-cerium-oxalic acid system by using the FKN mechanism with bromine-hydrolysis control and by assuming the formation of $HCO_2\cdot$ and $Br\cdot$ radicals, according to the proposals of Noyes and of Field and Boyd.

Reaction Mechanism and Method of Calculation

Bromate and oxalic acid react in the presence of a cerium catalyst to give bromine and CO_2:[5]

$$2BrO_3^- + 5(COOH)_2 + 2H^+ \longrightarrow 10CO_2 + Br_2 + 6H_2O \quad (a)$$

In this study, the following mechanism will be assumed for Reaction a:

$$Br^- + BrO_3^- + 2H^+ \longrightarrow HOBr + HBrO_2 \quad (1)$$

$$Br^- + HOBr + H^+ \rightleftharpoons Br_2 + H_2O \quad (2)$$

$$Br^- + HBrO_2 + H^+ \longrightarrow 2HOBr \quad (3)$$

$$BrO_3^- + HBrO_2 + H^+ \rightleftharpoons 2BrO_2\cdot + H_2O \quad (4)$$

$$BrO_2\cdot + Ce(III) + H^+ \rightleftharpoons Ce(IV) + HBrO_2 \quad (5)$$

$$2HBrO_2 \longrightarrow HOBr + BrO_3^- + H^+ \quad (6)$$

$$HOBr + (COOH)_2 \longrightarrow HCO_2\cdot + Br\cdot + H_2O + CO_2 \quad (7)$$

$$Ce(IV) + (COOH)_2 \longrightarrow Ce(III) + HCO_2\cdot + CO_2 + H^+ \quad (8)$$

$$HCO_2\cdot + HOBr \longrightarrow Br\cdot + H_2O + CO_2 \quad (9)$$

$$Br\cdot + (COOH)_2 \longrightarrow HCO_2\cdot + Br^- + CO_2 + H^+ \quad (10)$$

$$Br\cdot + Br\cdot \longrightarrow Br_2 \quad (11)$$

$$HCO_2\cdot + HCO_2\cdot \longrightarrow (COOH)_2 \quad (12)$$

$$Br_2 \longrightarrow Br_2(gas) \quad (13)$$

Table 1. Rate Constants Used in the Calculations

k_1	$2.1\ M^{-3}\ s^{-1}$	k_6	$4.0\times10^7\ M^{-1}\ s^{-1}$
k_2	$8.0\times10^9\ M^{-2}\ s^{-1}$	k_7	$25\ M^{-1}\ s^{-1}$
k_{-2}	$110\ s^{-1}$	k_8	$27.5\ M^{-1}\ s^{-1}$
k_3	$2.0\times10^9\ M^{-2}\ s^{-1}$	k_9	$2.0\times10^7\ M^{-1}\ s^{-1}$
k_4	$1.0\times10^4\ M^{-2}\ s^{-1}$	k_{10}	$2000\ M^{-1}\ s^{-1}$
k_{-4}	$2.0\times10^7\ M^{-1}\ s^{-1}$	k_{11}	$1.0\times10^8\ M^{-1}\ s^{-1}$
k_5	$6.0\times10^5\ M^{-2}\ s^{-1}$	k_{12}	$1.2\times10^9\ M^{-1}\ s^{-1}$
k_{-5}	$5.0\times10^7\ M^{-1}\ s^{-1}$		

(1 M=1 mol dm^{-3})

The mechanism consisted of the FKN mechanism with bromine-hydrolysis control and the formation of $HCO_2\cdot$ and $Br\cdot$ radicals in a reaction between HOBr and oxalic acid. That is, HOBr reacted with oxalic acid to give $HCO_2\cdot$ and $Br\cdot$ radicals, and the radicals consumed HOBr and oxalic acid according to a radical-chain reaction composed of Reactions 9 and 10 or vanished according to Reactions 11 and 12. Reaction 14 was ignored because it was thought to make no contribution to the BrO_3^-–oxalic acid reaction:[8]

$$Br\cdot + HCO_2\cdot \longrightarrow Br^- + CO_2 + H^+ \quad (14)$$

Ce(IV) was assumed to give $HCO_2\cdot$ according to Reaction 8 and was thus explicitly concerned with the consumption of HOBr. Reaction 13 represents a process of the first order, where the bromine produced was removed from the BrO_3^-–Ce–$(COOH)_2$ system.[6,7] Reaction 15, which is a part of the FKN mechanism, is not important because it is very slow ($k_{15}=9.6\ mol^{-1}\ s^{-1}$ and $k_{-15}=1.3\times10^{-4}\ mol^{-3}\ s^{-1}$):[10]

$$Ce(IV) + BrO_2\cdot + H_2O \rightleftharpoons Ce(III) + BrO_3^- + 2H^+ \quad (15)$$

The rate constants of Reactions 1—12 are shown in Table 1. The k_1—k_{-4} and k_6 rate constants are according to Bar-Eli and Ronkin,[10] and k_5 and k_{-5}, according to Tyson.[11] The other rate constants agreed with those estimated by Field and Boyd.[8] Ce(IV) is reduced to Ce(III) by oxalic acid according to Reactions 8 and 16:[12,13]

$$Ce(IV) + HCO_2\cdot \longrightarrow Ce(III) + CO_2 + H^+ \quad (16)$$

We ignored Reaction 16 and assumed a larger k_8 value than that obtained experimentally.[8]

The numerical integration of the differential equations generated from Reactions 1—13 was performed using the Gear algorithm.[14] In the calculations we assumed that $[H^+]=1$ mol dm^{-3} and that $[Ce]_{total}(=[Ce(III)]+[Ce(IV)])=0.0005$ mol dm^{-3}, while k_{13} and $[BrO_3^-]$ were regarded as bifurcation parameters.

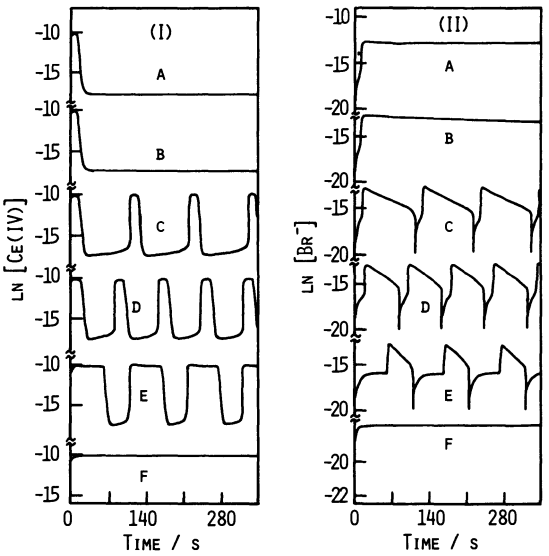

Fig. 1. The change in the oscillation pattern with k_{13}. $[BrO_3^-]=0.03$ mol dm^{-3}, $[(COOH)_2]=0.03$ mol dm^{-3}. k_{13} A: 0.001 s^{-1}, B: 0.005 s^{-1}, C: 0.05 s^{-1}, D: 0.075 s^{-1}, E: 0.1 s^{-1}, F: 0.25 s^{-1}.

Results and Discussion

When $[(COOH)_2]=0.03$ mol dm^{-3}. Figure 1 shows the change in the oscillation pattern with k_{13}. When $k_{13}=0.001\ s^{-1}$, the bromate–cerium–oxalic acid system stayed at a reduced steady state (steady-state LO by Noszticzius et al.[6]) characterized by a small concentration of Ce(IV). On the other hand, when $k_{13}=0.25\ s^{-1}$, the system stayed at an oxidized steady state (steady-state HI) characterized by a large concentration of Ce(IV). When $0.005\ s^{-1}\leq k_{13}\leq 0.1\ s^{-1}$, the system exhibited sustained oscillations between the two steady states. The time period of the oscillations, T, and the time that the system spent in either steady state, τ, depended on the value of k_{13}.

Figure 2 shows the relationship between the oscillation pattern and the concentration of bromate. When $[BrO_3^-]=0.006$ mol dm^{-3}, the system existed in a reduced steady state, and when $[BrO_3^-]=0.045$ mol dm^{-3}, in an oxidized steady state. When 0.007 mol $dm^{-3}\leq[BrO_3^-]\leq 0.0425$ mol dm^{-3}, the sustained oscillations between the two steady states appeared. T and τ depended on the value of $[BrO_3^-]$, but the amplitude of the oscillations was approximately constant. Hysteresis was not observed in the transitions from the monostable steady states to the oscillatory state, or vice versa.

Figure 3 shows the excitability of a reduced steady state induced by a sudden decrease in the concentration of bromine. The value of $[Br_2]$ at the steady state was 1.2857×10^{-8} mol dm^{-3}. When $[Br_2]=1.02\times10^{-8}$ mol dm^{-3}, the system returned to the reduced steady state with a damped oscillation. When $[Br_2]=1.01\times$

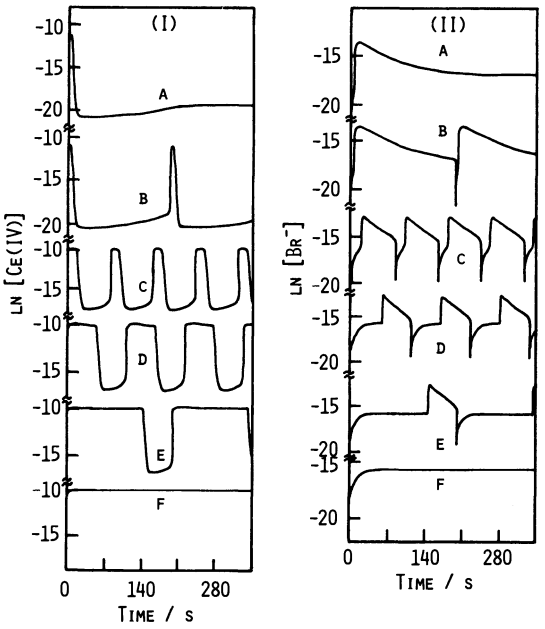

Fig. 2. The change in the oscillation pattern with $[BrO_3^-]$.
$[(COOH)_2]=0.03$ mol dm^{-3}, $k_{13}=0.075$ s^{-1}. $[BrO_3^-]$ A: 0.006 mol dm^{-3}, B: 0.007 mol dm^{-3}, C: 0.03 mol dm^{-3}, D: 0.04 mol dm^{-3}, E: 0.0425 mol dm^{-3}, F: 0.045 mol dm^{-3}.

10^{-8} mol dm^{-3}, the system started to vary after ca. 15 s and then returned to the reduced steady state after ca. 240 s. When $[Br_2]=5.0\times10^{-9}$ mol dm^{-3}, the system immediately started to vary.

Figure 4 shows the excitability of an oxidized steady state induced by a sudden increase in the concentration of bromine. When $[Br_2]=1.3079\times10^{-4}$ mol dm^{-3}, the system returned to the oxidized steady state with a damped oscillation. When $[Br_2]=1.3080\times10^{-4}$ mol dm^{-3}, the system started to vary after ca. 8 s and returned to the oxidized steady state after ca. 150 s.

Figures 3 and 4 reveal that, when the change in the concentration of bromine is below a certain threshold, [Ce(IV)] and $[Br^-]$ undergo modest changes, while the change in $[Br_2]$ exceeds the threshold, [Ce(IV)] and $[Br^-]$ undergo major changes.

When $[(COOH)_2]=0.001$ mol dm^{-3}. As is shown in Fig. 5, when $[BrO_3^-]=0.002$ mol dm^{-3}, [Ce(IV)] gave rise to a jagged oscillation. When $[BrO_3^-]=0.0003$ mol dm^{-3}, the system stayed much larger in the reduced steady state. The time period of the oscillations was much larger than that when $[(COOH)_2]=0.03$ mol dm^{-3}. The amplitude of the oscillations depended on the concentration of bromate.

Figure 6 depicts the bifurcation diagram of the system studied here. The system could exist in both

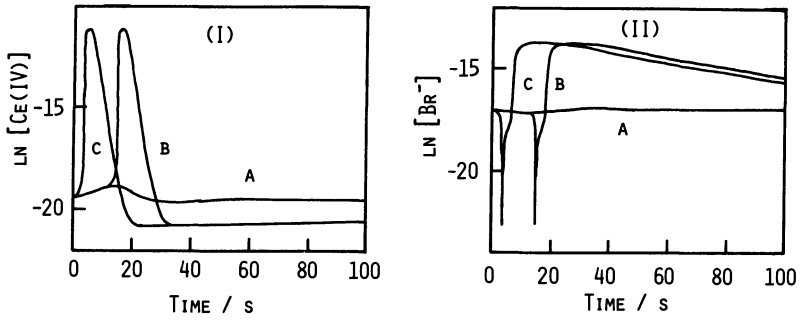

Fig. 3. The excitability of the reducd steady state induced by the changes in $[Br_2]$.
$[BrO_3^-]=0.006$ mol dm^{-3}, $[(COOH)_2]=0.03$ mol dm^{-3}, $k_{13}=0.075$ s^{-1}, $[Br_2]_{ss}=1.2857\times10^{-8}$ mol dm^{-3}. $[Br_2]$ A: 1.02×10^{-8} mol dm^{-3}, B: 1.01×10^{-8} mol dm^{-3}, C: 5.00×10^{-9} mol dm^{-3}.

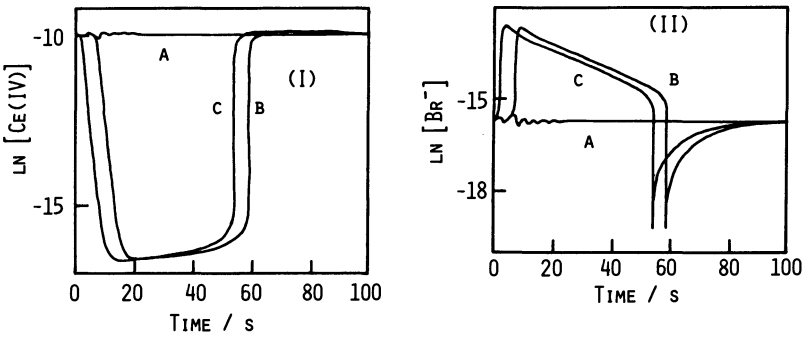

Fig. 4. The excitability of the oxidized steady state induced by the changes in $[Br_2]$.
$[BrO_3^-]=0.045$ mol dm^{-3}, $[(COOH)_2]=0.03$ mol dm^{-3}, $k_{13}=0.075$ s^{-1}, $[Br_2]_{ss}=1.2751\times10^{-4}$ mol dm^{-3}. $[Br_2]$ A: 1.3079×10^{-4} mol dm^{-3}, B: 1.3080×10^{-4} mol dm^{-3}, C: 1.3250×10^{-4} mol dm^{-3}.

reduced and oxidized steady states and in the oscillatory state, but no bistability was found in the system.

Figure 7 shows the relationship between the concentration of bromate and the time period of the oscillations. Up to now, the bromate-cerium-oxalic acid system has been simulated by using Reactions 17 and 18 instead of Reactions 7—12:[7,8]

$$HOBr + (COOH)_2 \longrightarrow Br^- + 2CO_2 + H_2O + H^+ \quad (17)$$

$$Ce(IV) + (COOH)_2 \longrightarrow Ce(III) + \text{inert products} \quad (18)$$

The model did not reproduce the characteristic oscillations of the system. That is, it has been reported that the experimental value of τ is dependent on the bifurcation parameters, such as k_{13} and $[BrO_3^-]$,[6,7] but the τ estimated from the model depended little on the parameters. Figure 7(A), which was obtained according to the model, was also not consistent with the experimental results reported by Gáspár and Galambosi.[7] Figures 7 (B) and 7 (C) were obtained on the basis of Reactions 1—13. The dependency of the time period of the oscillations on $[BrO_3^-]$ (Fig. 7(B)), as well as that of τ on the bifurcation parameters (Figs. 1 and 2) and the excitability (Figs. 3 and 4), were qualitatively consistent with the experimental results. However, the bistability could not be reproduced, and the rate constant of the bromine removal (k_{13}) and the amplitudes of the oscillations in Figs. 1 and 2 were larger than the values obtained experimentally. The failure to reproduce the bistabi-

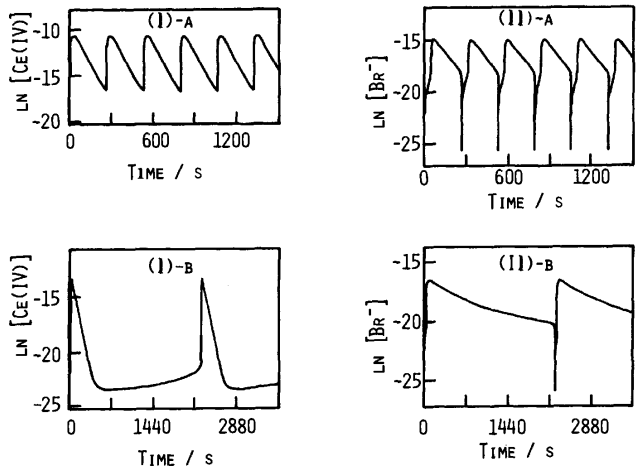

Fig. 5. The oscillations when $[(COOH)_2]=0.001$ mol dm^{-3} and $k_{13}=0.075$ s^{-1}.
A: $[BrO_3^-]=0.002$ mol dm^{-3}, B: $[BrO_3^-]=0.0003$ mol dm^{-3}.

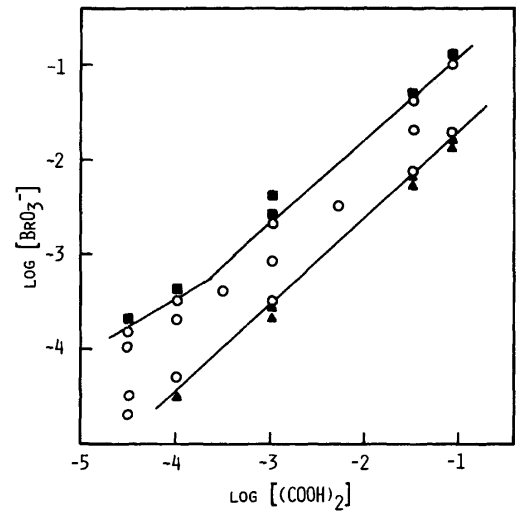

Fig. 6. The bifurcation diagram when $k_{13}=0.075$ s^{-1}.
■: oxidized steady state, ▲: reduced steady state, ○: oscillatory state.

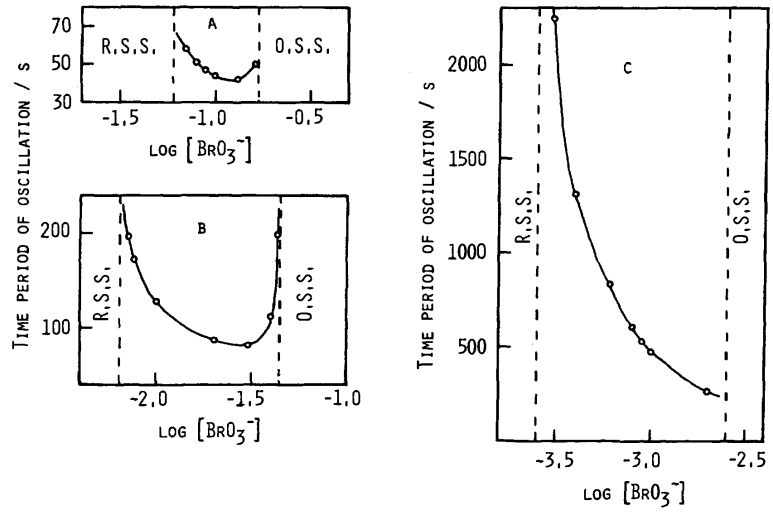

Fig. 7. The relationship between the time period of the oscillations and $[[BrO_3^-]$.
A: $[(COOH)_2]=0.05$ mol dm^{-3}, $k_{13}=0.13$ s^{-1}. Calculated by using Reactions 1—6, 13, 17, and 18.
B: $[(COOH)_2]=0.03$ mol dm^{-3}, $k_{13}=0.075$ s^{-1}. C: $[(COOH)_2]=0.001$ mol dm^{-3}, $k_{13}=0.075$ s^{-1}.

lity may be ascribed to inaccuracy in the rate constants in Table 1, for it seems difficult to determine the values of all the rate constants precisely. For the FKN mechanism, a revised set of the rate constants was developed.[15]

Maselko proposed four fundamental possibilities for bifurcation, leading from a steady state to a stable periodic orbit, and vice versa, in chemical systems.[16] There is a controversy as to the bifurcations in the classical BZ reaction.[17,18] In the bromate-cerium-oxalic acid system, the transitions from the monostable steady states to the oscillatory state have been reported to occur via saddle-node infinite-period (SNIPER) bifurcation.[6,7] The simulation in this study gave suggestions as to the bifurcations in the system. That is, the results in Figs. 1, 2, and 7(B) (the time period and the amplitude of the oscillations), and the fact that there is no hysteresis near the bifurcation points when $[(COOH)_2]=0.03$ mol dm^{-3}, were consistent with SNIPER bifurcation. On the other hand, when $[(COOH)_2]=0.001$ mol dm^{-3}, hysteresis was observed in the transition between the oxidized steady state and the oscillatory state, and not in the transition between the reduced steady state and the oscillatory state. These and the oscillation patterns in Fig. 5 suggest that the former transition occurs via subcritical Hopf bifurcation, and the latter transition, via SNIPER bifurcation.

In the reaction mechanism used in this study, HOBr is reduced by oxalic acid through both Reactions 17 and 19, under the stationary-state approximation for $HCO_2\cdot$ and Br$\cdot$ radicals:[19]

$$2HOBr + (COOH)_2 \longrightarrow Br_2 + 2CO_2 + 2H_2O \quad (19)$$

It is interesting that we can simulate the oscillation patterns of the bromate-cerium-oxalic acid system when the mechanism presented here is used, but not when Reactions 17 and 18 are used instead of Reactions 7—12. In bromate-cerium-oxalic acid-cyclohexanone system, more complicated bifurcation phenomena were observed.[20] Thus, the oscillation behavior in the bromate-cerium-oxalic acid system seems to be sensitive to the feed-back part of the reaction mechanism.

References

1) "Oscillations and Traveling Waves in Chemical Systems," ed by R. J. Field and M. Burger, Wiley-Interscience, New York (1985).

2) R. J. Field, E. Körös, and R. M. Noyes, *J. Am. Chem. Soc.*, **94**, 8649 (1972).

3) R. M. Noyes, *J. Chem. Phys.*, **80**, 6071 (1984).

4) B. Schwitters and P. Ruoff, *J. Phys. Chem.*, **90**, 2497 (1986).

5) Z. Noszticzius and J. Bódiss, *J. Am. Chem. Soc.*, **101**, 3177 (1979).

6) Z. Noszticzius, P. Stirling, and M. Wittmann, *J. Phys. Chem.*, **89**, 4914 (1985).

7) V. Gáspár and P. Galambosi, *J. Phys. Chem.*, **90**, 2222 (1986).

8) R. J. Field and P. M. Boyd, *J. Phys. Chem.*, **89**, 3707 (1985).

9) R. M. Noyes, *J. Am. Chem. Soc.*, **102**, 4644 (1980).

10) K. Bar-Eli and J. Ronkin, *J. Phys. Chem.*, **88**, 2844 (1984).

11) J. J. Tyson, "Oscillations and Traveling Waves in Chemical Systems," ed by R. J. Field and M. Burger, Wiley-Interscience, New York (1985), p. 95.

12) Y. A. El-Tantawy and G. A. Rechnitz, *Anal. Chem.*, **36**, 1774 (1964).

13) B. D. Kansal, N. Singh, and H. Singh, *J. Indian Chem. Soc.*, **55**, 304 (1978).

14) C. W. Gear, "Numerical Initial Value Probrems in Ordinary Differential Equations," Prentice-Hall, Englewood Cliffs, N. J. (1971), Chap. 11.

15) R. J. Field and H.-D. Försterling, *J. Phys. Chem.*, **90**, 5400 (1986).

16) J. Maselko, *Chem. Phys.*, **67**, 17 (1982).

17) Z. Noszticzius, M. Wittmann, and P. Stirling, *J. Chem. Phys.*, **86**, 1922 (1987).

18) K. Bar-Eli and R. M. Noyes, *J. Chem. Phys.*, **86**, 1927 (1987).

19) When $k_{11}=0$ and $k_{12}=0$, only Reaction 17 occurs, but when $k_9=0$ and $k_{10}=0$, only Reaction 19 occurs.

20) R. P. Rastogi and G. P. Mirsa, *J. Phys. Chem.*, **91**, 3007 (1987).

 © 1988 The Chemical Society of Japan Bull. Chem. Soc. Jpn., 61, 1485—1490 (1988)

Molecular and Crystal Structure of the Lipid-Model Amphiphile, Dioctadecyldimethylammonium Bromide Monohydrate

Kenji Okuyama,* Yoshie Soboi, Naomi Iijima, Kiyoshi Hirabayashi, Toyoki Kunitake,† and Tisato Kajiyama†
Faculty of Technology, Tokyo University of Agriculture and Technology, Koganei, Tokyo 184
†Faculty of Engineering, Kyushu University, Fukuoka 812
(Received September 14, 1987)

Dioctadecyldimethylammonium bromide monohydrate ($2C_{18}N^+2C_1Br^-\cdot H_2O$), $C_{38}H_{80}NBr\cdot H_2O$, was crystallized from its solution in chloroform and hexane. The crystals are triclinic with the space group $P\bar{1}$, $Z=2$, a (normal to the bilayer surface)=3.811(2), b=0.7890(2), c=0.7418(2) nm, α=104.37(3), β=103.06(4), and γ=74.93(3)°. The structure was solved by the direct method and refined by the block-diagonal least-squares procedure: R=0.08 for 3121 observed reflections. The crystal structure consists of bimolecular layers stacking regularly along the a-direction. The two amphiphile molecules in the unit cell are related by centrosymmetry and pack tail to tail in a bilayer structure with tilting hydrocarbon chains by about 45° to the bilayer surface. The packing cross section per molecule in the layer plane is 0.567 nm². The hydrocarbon chains pack with an triclinic ($T//$) subcell with dimensions of a_s=0.42, b_s=0.49, c_s=0.26 nm, α_s=88, β_s=104, and γ_s=111°. One of the two alkyl chains bends near the nitrogen atom and conforms a part of a head region. Two water oxygen atoms with half occupancies were found in an asymmetric unit and accomodated statistically in a unit cell. These water molecules are linked with bromide anions by hydrogen bonds with the distance of about 0.34 nm. Bromide anions and ammonium cations are on the same plane parallel to the bilayer surface.

Dialkyldimethylammonium bromide, $2C_nN^+2C_1Br^-$, is a first totally synthetic amphiphile which conforms the biological membrane-like bilayer structure.[1,2] Their bilayer structures have been studied by electron microscopy,[1,2] differential scanning calorimetry and wide- and small-angle X-ray analysis,[3] and it has shown that the similarity of the molecular assembly of $2C_nN^+2C_1Br^-$ to those of phospholipids found in biological membranes. In the case of $2C_{18}N^+2C_1Br^-$, the electron micrograph showed the multilamellar liposome with mean thickness of 4.2 nm when the amphiphile solution was sonicated in the presence of uranyl acetate. The small-angle X-ray diffraction pattern taken at 25 °C (the crystal liquid-crystal transition temperature, T_c=51 °C) showed the long period of about 3.6 nm, independent of the water concentration.[3] This long period seems to correspond to the lamellar periodicity of the electron-dense striations in the electron micrograph. Since the extended bimolecular length of $2C_{18}N^+2C_1Br^-$ is about 5.0 nm on the assumption of the planar zigzag conformation of two dioctadecyl groups, it was speculated that the hydrocarbon chains of $2C_{18}N^+2C_1Br^-$ inclined at 47° to the lamellar surface in the bimolecular structure.[3]

Recently, the totally synthetic amphiphiles become important because of their ability to conform desired bilayer assemblies in the form of the single crystals, casting films and Langumuir-Blogett films. For a proper understanding of the physicochemical properties of these molecular assemblies, detailed structural information on an atomic level is required. In the cases of $2C_nN^+2C_1Br^-$ (n=18 and 16), single crystals suitable for X-ray analysis were obtained as the first example for the totally synthetic amphiphiles which could conform bimolecular layer.[4] In this paper, we discuss the structure of $2C_{18}N^+2C_1Br^-$ determined by X-ray single crystal analysis. Since this compound is chemically simple as a lipid-model able to conform the biological membrane-like bilayer structure, the precise structure on the atomic level will be useful for the better understanding of the physicochemical properties for more complicated amphiphilic compounds.

Experimental and Structure Determination

Dioctadecyldimethylammonium bromide, $2C_{18}N^+2C_1Br^-$, was prepared by stepwise alkylation of dimethylamine.[1] $2C_{18}N^+2C_1Br^-$ (50 mg) was dissolved in 2 ml of chloroform. After complete dissolution, 8 ml of hexane was added. Transparent, plate-like crystals formed at the bottom of the vessel by keeping the solution for several days at room temperature (ca. 20 °C). The size of the large crystals reached 5 mm×5 mm×0.1 mm. Many of them were usually multiple crystals with the common axis normal to the plate surface. Large plate-like crystals were cut into small pieces in order to obtain those with suitable dimensions for X-ray analysis. After many trials of X-ray investigation of such crystals, single crystals available for X-ray diffraction study were found. Approximate dimensions of the crystal used in this analysis were 0.8 mm×0.5 mm×0.01 mm.

Lattice parameters and diffraction intensities were measured on a Rigaku four-circle diffractometer with Ni-filtered Cu $K\alpha$ radiation (λ=0.154184 nm). The lattice parameters were refined by the least-squares fit using 25 reflections in the 2θ range of 19°—65°. By using the ω-scan mode at a scan rate of 10° min^{-1}, intensities of 3919 reflections were measured up to 100° in 2θ. The scan width was $\Delta\omega=(1.8+0.15\tan\theta)°$. Three reference reflections monitored every 50 reflections showed no significant intensity deterioration during the data collection. Corrections were made for the Lorentz and polarization factors, but not for absorption and extinction effects. However, the (h00) reflections with $h<12$ were excluded from the data set

because of an absorption effect on these reflections as shown in the later. A total of 3121 reflections greater than $3\sigma(F_o)$ were used in the following analysis.

Density was measured by flotation method using aqueous solution of sodium chloride. On the basis of the measured density and a unit cell volume, the unit cell contains two $2C_{18}N^+2C_1Br^-$ molecules and seems to contain one or two water molecules. While the elemental analysis showed the monohydrated structure of this amphiphile (Calcd for $C_{38}H_{80}NBr \cdot H_2O$: C, 70.33; H, 12.74; N, 2.16%. Found: C, 70.18; H, 12.75; N, 2.12%.). Further, the result of X-ray structure analysis also supported monohydrated structure as shown below.

Crystal Data: $C_{38}H_{80}NBr \cdot H_2O$, F.W.=648, triclinic, space group $P\bar{1}$, Z=2, a=3.811(2), b=0.7890(2), c=0.7418(2) nm, α=104.37(3), β=103.06(4), γ=74.93(3)°, V=2.055(2) nm^3, D_x=1.047, D_m=1.04 g cm^{-3}, ρ(Cu $K\alpha$)=10.2 cm^{-1}.

Determination and Refinement of the Structure. The direct method with the MULTAN 78 program[5] was applied for $P1$ and $P\bar{1}$ space groups. Only for the latter space group, two planar zigzag alkyl chains could be readily discerned. The vector between two bromide anions related by the centrosymmetric operation for the $P\bar{1}$ space group was clearly appeared in the three-dimensional Patterson map, which also supported this space group for the $2C_{18}N^+2C_1Br^- \cdot H_2O$ crystal. After several cycles of block-diagonal least-squares refinement starting from the coordinates of all the non-hydrogen atoms of the amphiphile obtained by the direct method, difference Fourier syntheses revealed the several peaks, which was assumed to be oxygen atoms of water molecules. After several refinement cycles including these newly found water positions, it was found that two water molecules with half occupancies were able to be accomodated statistically in an asymmetric unit in terms of

Table 1. Fractional Coordinates and Equivalent Isotropic Temperature Factors[16] for Non-Hydrogen Atoms of $2C_{18}N^+2C_1Br^- \cdot H_2O$ with Estimated Standard Deviations in Parentheses

Atom	x	y	z	$B_{eq} \times 10^4$/nm^2
Br	0.0537(0)	0.2000(1)	0.3716(2)	541
N	0.0606(2)	0.8896(10)	0.8116(10)	388
C(1)	0.0280(2)	1.0379(13)	0.7951(14)	520
C(2)	0.0530(3)	0.7640(14)	0.9164(14)	536
C(31)	0.0671(2)	0.7940(12)	0.6139(12)	384
C(32)	0.0987(3)	0.6286(12)	0.6019(13)	449
C(33)	0.1101(3)	0.5701(13)	0.4083(13)	501
C(34)	0.1258(3)	0.7049(12)	0.3528(12)	430
C(35)	0.1620(2)	0.7456(12)	0.4770(12)	436
C(36)	0.1730(2)	0.8926(12)	0.4184(13)	428
C(37)	0.2100(3)	0.9350(12)	0.5337(13)	440
C(38)	0.2193(2)	1.0903)12)	0.4773(13)	458
C(39)	0.2564(3)	1.1309(12)	0.5850(13)	455
C(310)	0.2651(3)	1.2877(13)	0.5286(13)	470
C(311)	0.3026(3)	1.3286(12)	0.6334(13)	465
C(312)	0.3109(3)	1.4847(13)	0.5760(13)	476
C(313)	0.3486(3)	1.5243(13)	0.6811(14)	491
C(314)	0.3573(3)	1.6808(13)	0.6246(14)	512
C(315)	0.3949(3)	1.7189(13)	0.7317(15)	533
C(316)	0.4037(3)	1.8762(14)	0.6752(15)	578
C(317)	0.4415(3)	1.9117(15)	0.7801(17)	701
C(318)	0.4513(4)	2.0678(19)	0.7225(21)	990
C(41)	0.0944(2)	0.9560(12)	0.9324(12)	404
C(42)	0.1045(2)	1.0986(12)	0.8587(13)	433
C(43)	0.1406(2)	1.1406(12)	0.9728(12)	422
C(44)	0.1507(2)	1.2888(12)	0.9121(13)	435
C(45)	0.1879(2)	1.3315(12)	1.0158(12)	413
C(46)	0.1966(2)	1.4851(12)	0.9564(13)	410
C(47)	0.2339(2)	1.5271(12)	1.0601(13)	434
C(48)	0.2421(2)	1.6843(12)	1.0026(13)	440
C(49)	0.2793(2)	1.7253(12)	1.1079(13)	442
C(410)	0.2873(2)	1.8844(12)	1.0516(13)	458
C(411)	0.3250(2)	1.9237(12)	1.1561(13)	460
C(412)	0.3332(3)	2.0818(13)	1.1003(14)	478
C(413)	0.3706(3)	2.1212(13)	1.2039(14)	497
C(414)	0.3790(3)	2.2785(13)	1.1475(14)	514
C(415)	0.4169(3)	2.3136(13)	1.2482(15)	560
C(416)	0.4254(3)	2.4722(15)	1.1906(15)	611
C(417)	0.4631(3)	2.5045(16)	1.2873(19)	789
C(418)	0.4723(4)	2.6601(20)	1.2295(21)	994
OW(1)	−0.0004(5)	0.4159(18)	0.6982(23)	838
OW(2)	0.0251(6)	0.5303(23)	0.1079(29)	1187

stereochemistry and hydrogen bonding scheme. After an anisotropic refinement of non-hydrogen atoms, hydrogen atoms located on their calculated positions with isotropic temperature factors were included in the refinement. The quantity minimized was $\Sigma w(|F_o|-|F_c|)^2$ with $w=1.0$ for reflections with $F_o \leqq 50.0$ or with $w=0.5$ for other reflections. After several cycles some hydrogen atoms with unacceptable geometry were excluded from further calculations.

At this stage, all the magnitudes of the observed structure factors for the ($h00$) reflections with $h<12$ were consistenly smaller than those of the calculated ones. Especially, the pronounced discrepancy was observed for (100) reflection. The main reason of these systematic disagreement between the observed and calculated structure factors was most likely due to the absorption effect originated from the plate-like crystal shape and its long lattice constant a (3.811 nm) directed normal to the plate surface of the crystal. Therefore, these reflections were excluded from the reflection data set in the further refinement, which decreased the R-value by about 1%. The final R value was 0.070 (R_w=0.084) for all non-hydrogen atoms and 71 hydrogen atoms. The final atomic parameters for non-hydrogen atoms are given in Table 1.[6]

The atomic scattering factors were taken from International Tables for X-Ray Crystallography, Vol. IV.[7] Computations were done on an ACOS 700S computer at the Crystallographic Research Center, Institute for Protein Research, Osaka University and on a HITAC M-280H computer at the Computer Center, University of Tokyo.

Results and Discussion

Molecular Conformation of $2C_{18}N^+2C_1Br^-$. The molecular structure is shown in Fig. 1 with bond lengths, bond angles and dihedral angles together with atomic labelling for non-hydrogen atoms. One of the two hydrocarbon chains is bent at almost right angles at the C(33) atom. After this bending both chains have a trans zigzag conformation with their zigzag plains parallel to each other. Dihedral angles of the folding part, C(42)-C(41)-N-C(31), C(41)-N-C(31)-C(32), N-C(31)-C(32)-C(33), C(31)-C(32)-C(33)-C(34), and C(32)-C(33)-C(34)-C(35) are 64, 60, −165, 64, and 64°, respectively (Figs. 1 and 4). This folding pattern (G, G, T, G, G) has been known as the short folding model on the lamella surface of the polyethylene single crystal. To make stable packing of hydrocarbon chains in the bilayer structure, the $2C_{18}N^+2C_1Br^-$ molecule adopts the most simple and compact folding pattern. In the rest of the molecule, all the dihedral angles are within the range of 180±3°, with exception of N-C(41)-C(42)-C(43) (−173°) and C(33)-C(34)-C(35)-C(36) (−175°). The two zigzag planes are arranged in parallel fashion (Fig. 1 (b) and (c)) with about 0.40—0.43 nm separation. One zigzag chain (C(41), C(42), C(43), ···, C(418))

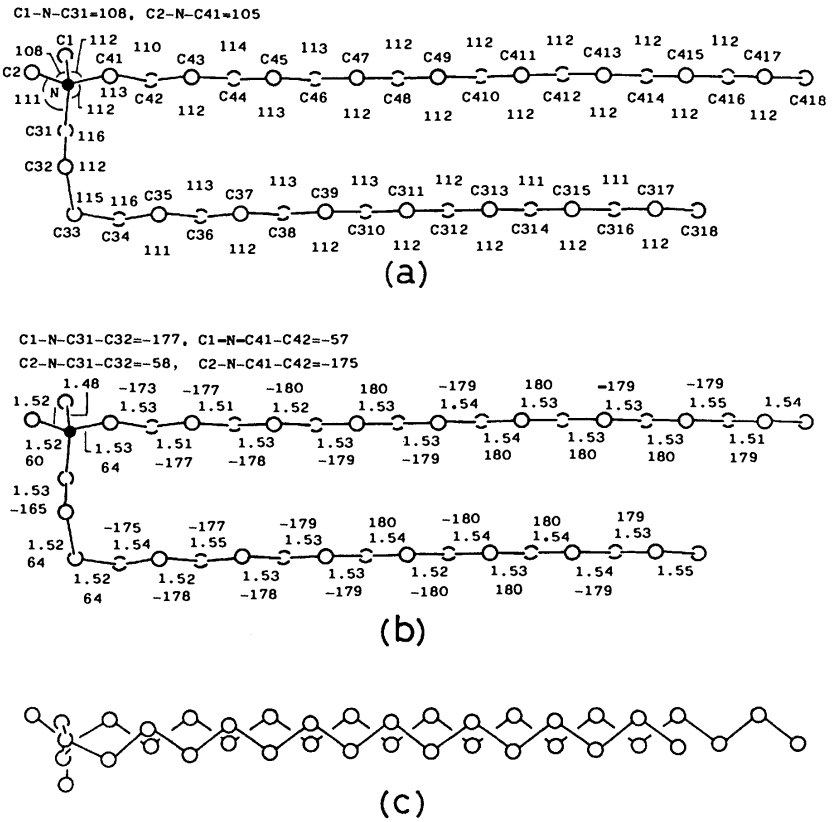

Fig. 1. (a) Atomic labelling and bond angles (ϕ/°), and (b) bond lengths (l×10/nm) and dihedral angles (ϕ/°) in $2C_{18}N^+2C_1Br^-$. Maximum estimated standard deviations for bond lengths, bond angles and dihedral angles are 0.002 nm, 1° and 1°, respectively. (c) Molecular conformation viewed from the direction normal to the zigzag plane.

is translated by three methylene unit along the chain axis to the other (C(33), C(34), C(35), ···, C(318)) (Fig. 1(c)). The average C–C bond length and C–C–C bond angle in the molecule are 0.153(1)nm and 112(1)°, respectively. There are in good agreement with values previously found in the long hydrocarbon chains of the other related amphiphilic compounds.[8,9]

Crystal Structure of $2C_{18}N^{+}2C_1Br^{-}$. The two $2C_{18}N^{+}2C_1Br^{-}$ molecules of the unit cell are related by centrosymmetry and pack tail to tail in a bimolecular layer with tilting long hydrocarbon chains (Fig. 2). The packing cross section per molecule in the layer plain (0.567 nm²) is determined by the space requirements of the hydrophilic part of the molecule, bromide anion and water molecule and coincides with the *bc*-plain of the unit cell. The dimethylammonium moiety has a chemically very simple structure compared with the hydrophilic parts of the natural amphiphilic compounds, such as phosphatidylethanolamine and phosphatidylcholine. The cross-sectional area of hydrophilic part of $2C_{18}N^{+}2C_1Br^{-}$, however, is comparatively larger than those of the above phospholipids, because of the conformationally fixed bulky dimethylammonium moiety and a bromide anion. Since the cross section of one hydrocarbon chain is about 0.20 nm², two hydrocarbon chains of $2C_{18}N^{+}2C_1Br^{-}$ molecule are tilted by 45° (=$\cos^{-1}(0.40/0.567)$) in order to accomodate to the large area of 0.567 nm² of the hydrophilic part (Fig. 2). Because of this tilting, two methyl carbon atoms at the tail end of the long alkyl chains are aligned parallel to the bilayer surface.

During the refinement procedure, statistically four water molecules with half occupancies were found in a unit cell. This number of water molecule is in good agreement with the results from chemical analysis and density measurement. Because of a short contact between OW1 and OW2 (0.18 nm), it is not possible to accomodate these four water molecules within the same unit cell. Figure 3 shows four types of their occurence and hydrogen bonding networks with bromide anions. Each unit cell in Fig. 3 contains two water molecules with full occupancy. Types A and B have no centrosymmetric relationships between water oxygens. In both cases, the water oxygen OW1 links to bromide anions by hydrogen bonds with lengths of 0.327 and 0.337 nm. Another water oxygen OW2 links to a bromide anion and a water oxygen OW1 in the

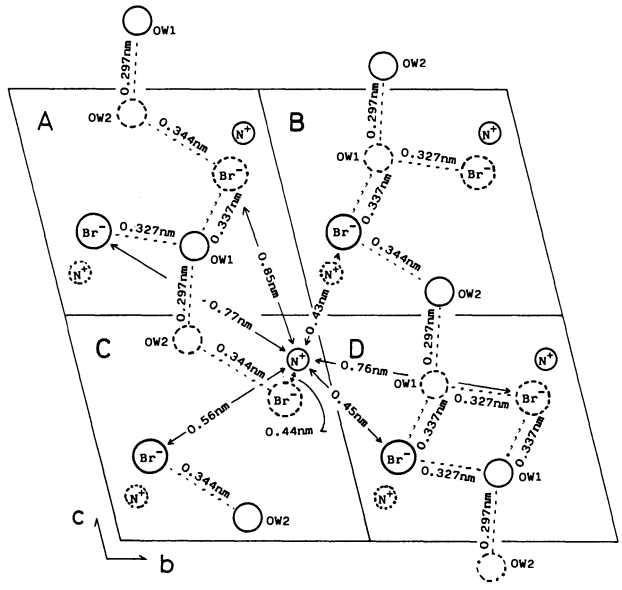

Fig. 3. Schematic illustration of hydrophillic layer of $2C_{18}N^{+}2C_1Br^{-}\cdot H_2O$ projected onto the *bc*-plane. Two water oxygen atoms are accomodated in a unit cell. Each unit cell, A, B, C, and D, has a different pair of water oxygens and hydrogen bonding scheme. Hydrogen bonds between bromide anions and water oxygen atoms are indicated by broken lines together with their bond lengths. Solid and broken circles represent atoms on the upper and lower side of the hydrophillic layer, respectively.

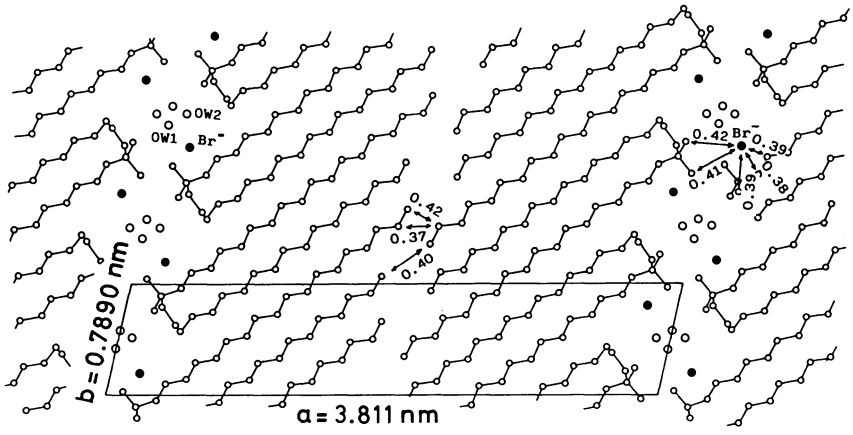

Fig. 2. Packing of $2C_{18}N^{+}2C_1Br^{-}\cdot H_2O$ projected onto the *ab*-plane (ORTEP[15] drawing). Four water oxygen atoms, OW1 and OW2 and their centrosymmetrical mates, are located on their positions in the unit cell. Distances (*l*/nm) between arrowed atoms are indicated short contacts in the structure.

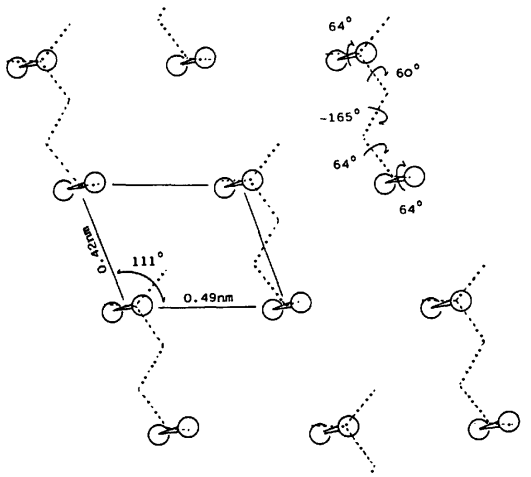

Fig. 4. The triclinic packing ($T//$) of the hydrocarbon chains in $2C_{18}N^{+}2C_1Br^{-}$. The chain axis C_s is a normal to the figure. The dotted lines denote the folding part and dimethyl groups in the molecule.

neighbouring unit cell with bond lengths 0.344 and 0.297 nm, respectively. Types C and D have a pair of oxygen atoms OW2 and OW1, respectively. In these cases, oxygen atoms are related by a centrosymmetry at the center position of each unit cell. The combination of the unit cells of AA, BB, BD, and DA along the c-axis makes a continuous hydrogen bond network along this direction within a hydrophilic layer. While the combination of BA, CA, BC, and CC is not possible because of a short OW2···OW2 contact (0.23 nm). The rest of the combination gives a discontinuous hydrogen bond network. Although there are many ways to accomodate water molecules in a unit cell, as a statistical point of view, one asymmetric unit contains two water oxygen atoms OW1 and OW2 with half occupancies as a whole.

The short intermolecular contacts between carbon atoms at the tail portions are 0.37 (C(417)···C(417)), 0.40 (C(318)···C(418)), 0.42 (C(417)···C(418)), 0.42 (C(317)···C(417)), and 0.43 nm (C(418)···C(418)) (Fig. 2). Rest of them are more than 0.48 nm. The short distances between carbon atoms in the adjacent alkyl chains are in the range of 0.39—0.43 nm including those between chains in the same molecule. On the other hand, there are several strong interactions in the hydrophilic region. Bromide anions link to water molecules by a hydrogen bonding with a distance of about 0.34 nm as mentioned above. Other short contacts of the bromide anion are with methyl carbons of C(1)(0.41 nm), C(2)(0.42 nm) and alkyl carbons of C(31)(0.39 nm), C(32)(0.40 nm), C(33)(0.40 nm), C(41) (0.38 nm), and C(42)(0.39 nm). Thus, the bromide anion is very neatly nestled among the head portions of the amphiphiles and water molecules.

Ammonium cations and bromide anions make a plane parallel to the bilayer surface within the deviation of 0.013 nm (Table 1). Two such planes are contained in one hydrophilic layer (Fig. 2). This kind of planarity among charged atoms have been reported in many other amphiphilic salt crystals.[10-13] A nitrogen cation is surrounded by six bromide anions (four on the same plane and two on the other plane in the same hydrophilic layer) (Fig. 3). Three of them are located at the place with somewhat long distances (0.56—0.77 nm) from a nitrogen cation because of the hydrogen-bonded water molecules with these bromide anions. The distances from the rest of bromide anions are rather short (0.43—0.45 nm). Therefore, the plus charge on the ammonium cation seems to be canceled exclusively by these three bromide anions.

The hydrocarbon chains pack latterally according to the triclinic ($T//$) packing mode.[14] The subcell dimensions are: a_s=0.42, b_s=0.49, c_s=0.26 nm, α_s=88, β_s=104 and γ_s=111° (Fig. 4). The packing cross section per chain perpendicular to its long chain axis is 0.193 nm^2, giving a well packed chain matrix. It is remarkable that all the hydrocarbon chains pack identically as it were no folding part in the amphiphile molecule.

The authors wish to express their deep thanks to Professor Yukiteru Katsube and co-workers at the Crystallographic Research Center, Institute for Protein Research, Osaka University for the use of a four-circle diffractometer and an ACOS 700S computer.

References

1) T. Kunitake, Y. Okahata, K. Tamaki, F. Kumamaru and M. Takayanagi, *Chem. Lett.*, **1977**, 387.

2) T. Kunitake and Y. Okahata, *J. Am. Chem. Soc.*, **99**, 3860 (1977).

3) T. Kajiyama, A. Kumano, M. Takayanagi, Y. Okahata, and T. Kunitake, "Contemporary Topics in Polymer Science," ed by W. J. Bailey and T. Tsuruta, Plenum (1984), Vol. 4, pp. 829—854.

4) K. Okuyama, Y. Soboi, K. Hirabayashi, A. Harada, A. Kumano, T. Kajiyama, M. Takayanagi, and T. Kunitake, *Chem. Lett.*, **1984**, 2117.

5) P. Main, S. E. Hull, L. Lessinger, G. Germain, J. P. Declercq, and M. M. Woolfson, MULTAN 78. "A System of Computer Programs for the Automatic Solution of Crystal Structures from X-ray Diffraction Data," Univs. of York, England, and Louvain, Bergium (1978).

6) Tables of anisotropic thermal parameters, coordinates of hydrogen atoms, and observed and calculated structure factors are kept at the Chemical Society of Japan, Document No. 8793.

7) International Tables for X-ray Crystallography, Vol. IV, Kynoch Press, Birmingham (1974), p. 71.

8) S. Abrahamsson, B. Dahlen, and I. Pascher, *Acta Crystallogr., Sect. B*, **33**, 2008 (1977).

9) I. Pascher and S. Sundell, *Chem. Phys. Lipids*, **20**, 175 (1977).

10) J. H. Dumbleton and T. R. Lomer, *Acta Crystallogr.*, **19**, 301 (1965).

11) V. Vand, T. R. Lomer, and A. Lang, *Acta Crystallogr.*, **2**, 214 (1949).
12) K. Okuyama, H. Watanabe, M. Shimomura, K. Hirabayashi, T. Kunitake, T. Kajiyama, and N. Yasuoka, *Bull. Chem. Soc. Jpn.*, **59**, 3351 (1986).
13) H. Watanabe, K. Okuyama, H. Ozawa, K. Hirabayashi, M. Shimomura, T. Kunitake, and N. Yasuoka, *Nippon Kagaku Kaishi*, **1987**, 550.
14) S. Abrahamsson, B. Dahlén, H. Löfgren, and I. Pascher, *Prog. Chem. Fats other Lipids*, **16**, 125 (1978).
15) C. K. Johnson, ORTEP II, Report ORNL-5138, Oak Ridge National Laboratory, Tennessee (1976).
16) W. C. Hamilton, *Acta Crystallogr.*, **12**, 609 (1959).

Preparation of SnO_2 and Nb_2O_5 Supported Vanadium Oxide Catalysts by a Column-Exchange Adsorption Method and Dispersed States of Vanadia Species

Yoshiya KERA* and Takahiro KAWASHIMA
Department of Applied Chemistry, Faculty of Science and Engineering, Kinki University, Higashiosaka, Osaka 577
(Received September 16, 1987)

SnO_2 and Nb_2O_5-supported monolayer or sub monolayer vanadium oxide catalysts were prepared by an impregnation method such as the column-exchange adsorption of oxovanadium ion at various pH(=2, 4, and 7). The deposited states of the vanadia species on SnO_2 and Nb_2O_5 surfaces were examined by ESR spectrometry using V^{4+} ion as a probe. The catalytic features were studied by measuring the 2-propanol decomposition rate as a test reaction. The deposited states of the vanadia species differed to a small extent between SnO_2 and Nb_2O_5 carriers depending upon the difference in the symmetry of the surface field. The deposited states, however, did not vary with pH upon impregnation, although the amounts of vanadium oxide deposited (coverage, θ) were much affected by the pH. The activation energy (E_a) for the dehydration of 2-propanol over these catalysts was linearly related to the reciprocal of the coverage ($1/\theta$). When both curves were extended to $1/\theta=0$, they crossed at around 5—6 kcal·mol^{-1} which was the minimum value, although the inclination differed largely between the carriers. This low activation energy was regarded as an intrinsic value that was caused by the multi-layered vanadium oxide deposited on the carriers. Through the discussion it is clearly shown that the most effective catalyst, a monolayer catalyst, was prepared on impregnation at pH=2 and the vanadia species were dispersed widely, keeping a weak interaction with the SnO_2 and Nb_2O_5 surfaces.

A column-exchange adsorption method [1] has been reported as an effective method for preparing vanadium oxide monolayer catalysts that have a superior activity and the selectivity for hydrocarbon oxidations, especially in titania-supported vanadia catalysts.[2-4] Previously the deposited state of a monolayer or sub monolayer vanadium oxide was shown to depend greatly upon the crystalline symmetry of the support. This in turn depends upon the crystal field symmetry around the cation on the surface. ESR analysis has been applied to vanadia deposited on rutile and anatase[5] by such an exchange-adsorption method. Many investigators have studied the binary V_2O_5-SnO_2 catalyst system because it has a high activity and selectivity for ammoxidation and various hydrocarbon oxidations.[6-13] The effect of pH on vanadium oxide monolayer catalysts deposited on SnO_2 (the crystal structure of which belongs to rutile type[14]) were examined by the column-exchange adsorption method. We also prepared vanadium oxide monolayer catalysts deposited on Nb_2O_5 which have a V_2O_5 type crystal structure.[15] We were interested specially in the interaction between vanadia species and Nb_2O_5 surfaces and in comparing the result with those of SnO_2 and titania (rutile and anatase). Recently many people have payed attention to Nb_2O_5 as a catalyst carrier bacause it shows a higher Strong-Metal-Support Interaction (SMSI) than TiO_2 or ZrO_2 carriers.[16]

ESR analysis for V^{4+} ion showed that vanadia deposited on SnO_2 and Nb_2O_5 appeared to interact more weakly with those carrier surfaces than TiO_2 (rutile). The interaction was similar in extent to that of TiO_2 (anatase). Of special interest is the linear relation between the apparent activation energy(E_a) for 2-propanol decomposition on the catalysts and the reciplocal of the surface coverage(θ) of the vanadia species. The E_a vs. $1/\theta$ curves for V_2O_5/SnO_2 and Nb_2O_5, which were extrapolated to $1/\theta$ both gave the lowest E_a=5—6 kcal·mol^{-1}. This should be regarded as the intrinsic activation energy for 2-propanol decomposition over the multi-layered vanadium oxide on SnO_2 and Nb_2O_5. Such a low value appeared to arise only from the vanadium oxide dispersed widely on the carrier surface with a weak interaction.

Experimental

1) **Materials and Preparation Procedures.** Four grams of Nb_2O_5 powder (Nakarai Chem. Co., Ltd., guaranteed grade) was packed into a glass column (o.d.=15 mm). About 0.5 wt% of NH_4VO_3 (Kanto Chem. Co., Ltd., guaranteed grade) aqueous solution, the pH of which were exactly adjusted at 2, 4, and 7 by adding HNO_3 and aqueous ammonia, were poured into the column to make the oxovanadium ion adsorb. Each 3 ml of the effluent solution was collected to measure the changes in the pH and the concentration of oxovanadium ion (V-ion) while passing through the column.

For the SnO_2 carrier (Kanto Chem. Co., Ltd., guaranteed grade), about 4 g were packed into the column; the NH_4VO_3 solution was added until both the pH and V-ion concentration had recovered to the original values. Those pH and V-ion concentrations were determined by the use of a pH-meter, TOA model HM-7B and the usual Mohr-titration method, respectively. After the adsorption, the samples were dried at 110 °C for 8 h, and then calcined at 400 °C for 2 h in order to prepare Nb_2O_5 and SnO_2 supported vanadium oxide catalysts, V_2O_5/Nb_2O_5 and V_2O_5/SnO_2.

2) Measurements and Computer Simulation. The surface areas of V_2O_5/Nb_2O_5 and SnO_2 were determined by N_2 gas adsorption at 77 K according to a convenient method.[17] The deposited states of the vanadia species were examined by ESR spectrometry. The ESR spectrometer used was a Nippon Denshi Model JES-PE (X-band, 9.3 GHz and 100 kHz modulation). Computer simulation of the ESR spectrum was performed using an IBM 4381 system. The catalytic activities for 2-propanol decomposition, as a test reaction, were measured in a closed circulation system (ca. 0.5 dm^3) connected directly to the gaschromatograph with a Porapac-Q column (1 m). 20 mg of the catalysts were spread widely over the bottom of the vassel and preheated at the reaction temperature in air for one hour before the reaction. The vessel containing 2-propanol was cooled by an ice-water bath during the reaction in order to maintain the vapor pressure constant at 8.4 mmHg (1 mmHg≈133.322 Pa). The intensity of the GC-peak of the main product, (that was confirmed to be propylene) was measured at intervals of 2 min. The decomposition rate was determined from the intensity change for the initial 20 min. The reaction temperature was controlled within ±0.5 °C in the range 270—350 °C.

Results

1) The Amounts of Vanadium Oxide Deposited on SnO_2 and Nb_2O_5 Carriers. When the NH_4VO_3 aqueous solutions with different pH were poured into the glass column packed with SnO_2 carrier, the pH and vanadium ion (V-ion) concentration of the effluent solution varied as shown in Fig. 1. The pH initially increased from 2 to about 4 or more in a run of pH=2 and increased only slightly in a run at pH=4, while in a run at pH=7 it decreased to near 6. The pH finally returned to the original values in all runs. Accompanied by the pH-changes, the V-ion concentrations initially decreased and then gradually recovered to the original values. The amounts of the adsorbed vanadium ion were estimated, based on these V-ion concentration vs. effluent-volume cruves. The adsorbed amounts of oxovanadium ion, which were estimated on the assumption that they were deposited in the form of V_2O_5, are given in the 3rd and 4th column of Table 1 (in units of $mg(V_2O_5)\cdot g\text{-carrier}^{-1}$ and $mg(V_2O_5)\cdot m^{-2}$, respectively). The surface area and surface coverage are also given in the 2nd and 5th column in Table 1, respectively. The coverage was estimated on the assumption that the V–O–V network of V_2O_5 extends two-dimensionally on the SnO_2 carrier and the V–O bond distance is 2.0 Å.[18]

With respect to the Nb_2O_5 carrier, the changes in the pH and the V-ion concentration of the effluent solutions are shown in Fig. 2. The pH change is small in all pH runs. The V-ion concentration initially

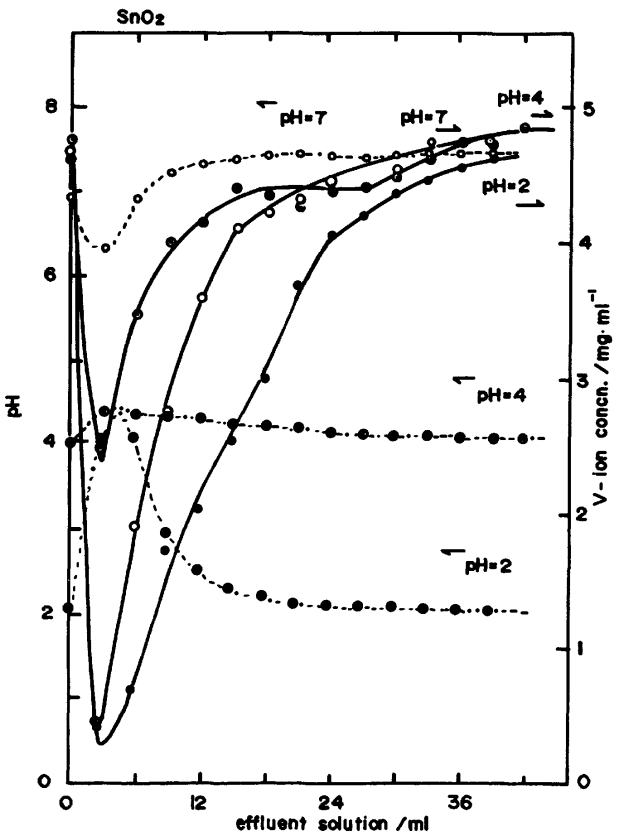

Fig. 1. The variations of pH and vanadium ion concentration in ammonium metavanadate effluent solution during passing through SnO_2-packed column for various pH runs. ----: pH change and —: V-ion concentration change.

Table 1. Surface Areas, the Amounts of Vanadium Oxide Deposited (Reduced to V_2O_5), and the Surface Coverages of V_2O_5/SnO_2 and V_2O_5/Nb_2O_5

Catalyst	Surface area	Deposited amounts		Surface coverage
	$m^2\cdot g^{-1}$	$mg(V_2O_5)\cdot g\text{-car.}^{-1}$	$mg\cdot m^{-2}$	(θ)
SnO_2 carrier	32	—	—	—
V_2O_5/SnO_2 (pH=2)	36	29	0.80	0.42
V_2O_5/SnO_2 (pH=4)	39	10	0.25	0.14
V_2O_5/SnO_2 (pH=7)	35	15	0.42	0.22
Nb_2O_5 carrier	3.9	—	—	—
V_2O_5/Nb_2O_5 (pH=2)	3.6	9.5	2.6	1.4
V_2O_5/Nb_2O_5 (pH=4)	3.4	5.9	1.7	0.90
V_2O_5/Nb_2O_5 (pH=7)	3.7	1.4	0.38	0.19
V_2O_5 powder	8.5	—	—	—

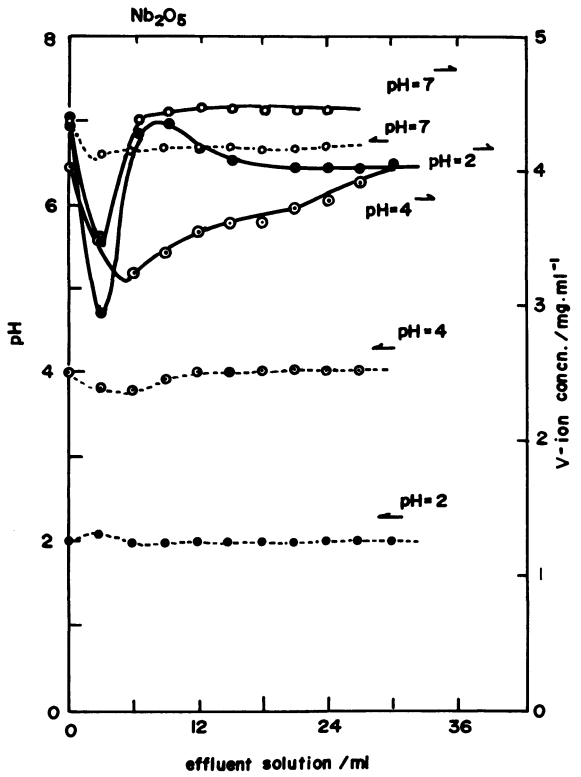

Fig. 2. The variations of pH and vanadium ion concentration in ammonium metavanadate effluent solution during passing through Nb_2O_5-packed column for various pH runs. ----: pH change and —: V-ion concentration change.

decreases slightly relative to the case of SnO_2 because of the small surface area. The concentration curve does not fully return to the original value except for a run at pH=7. The adsorbed amounts of vanadium ion were similarly estimated as given in the 3rd and 4th column of Table 1. The surface areas and the coverage are also given in the 2nd and 5th column of Table 1, respectively.

2) **ESR Spectra of V(IV) Ion on V_2O_5/SnO_2 and Nb_2O_5.** The ESR spectrum of the supported vanadia catalysts did not basically differ with the pH upon impregnation. The ESR spectra for V_2O_5/SnO_2 impregnated at pH=2 and 7, which were measured at 77 K after the evacuation at room temperature, are illustrated in Fig. 3-a and b, respectively. The spectrum for V_2O_5/SnO_2(pH=7), which was measured at 77 K after the evacuation at 400 °C, is shown in Fig. 3-c. The spectrum is considered to contain 8 hf-lines due to the ^{51}V-nucleus (I=7/2). After heat treatment at 400 °C, however, the spectrum varies in a complex manner; the other ESR species are added to the original one. V_2O_5/SnO_2 (pH=2) shows a composite spectrum even upon pretreatment at room temperature.

The ESR spectra for V_2O_5/Nb_2O_5 impregnated at pH=2 and 7, which are measured at 77 K after evacuation at room temperature, are illustrated in Figs. 4-a and b. The spectrum of V_2O_5/Nb_2O_5(pH=2), the surface coverage (θ) of which is larger than unity, shows specially unresolved hfs upon evacuation at

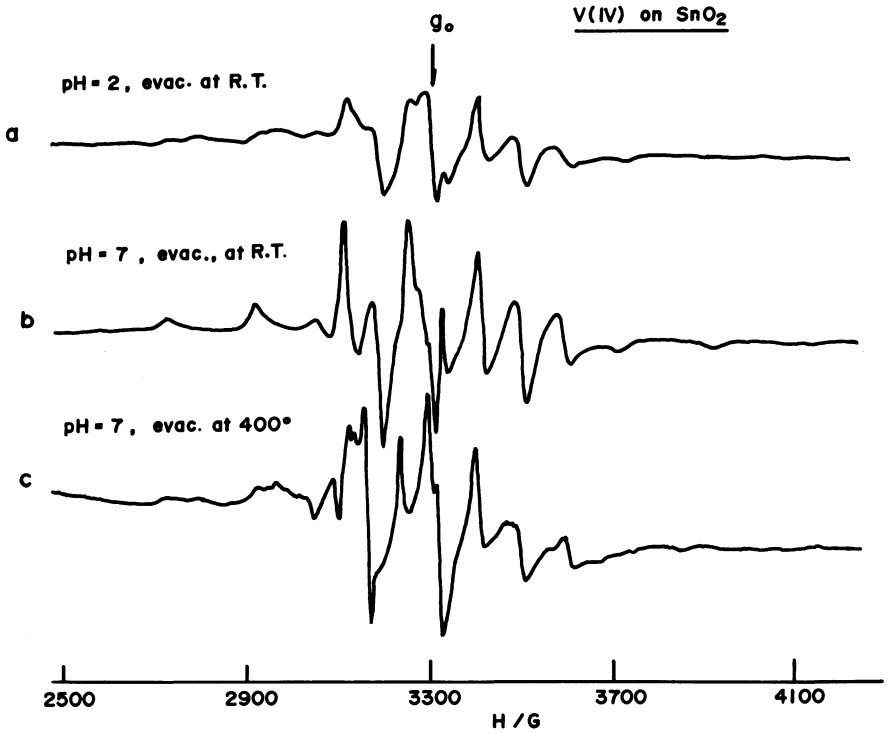

Fig. 3. ESR spectra for V(IV) ion on V_2O_5/SnO_2 prepared at pH=2 and 7. a: on V_2O_5/SnO_2 (pH=2), which was measured at 77 K after evacuating at room temperature, b: on V_2O_5/SnO_2 (pH=7), which was measured at 77 K after evacuating at room temperature, and c: on V_2O_5/SnO_2 (pH=7) measured at 77 K after evacuating at 400 °C.

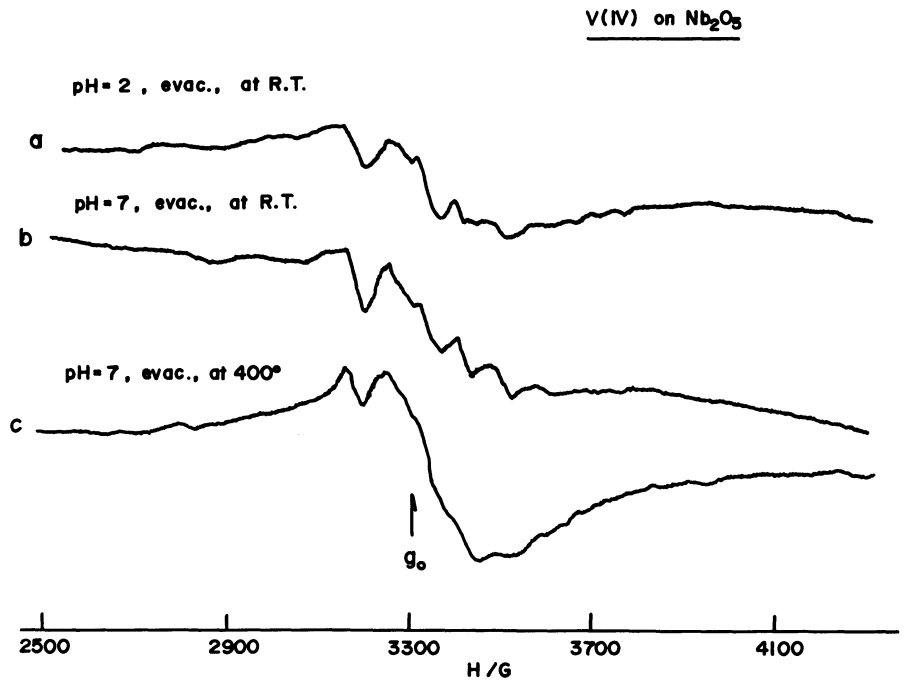

Fig. 4. ESR spectra for V(IV) ion on V_2O_5/Nb_2O_5 prepared at pH=2 and 7. a: on V_2O_5/Nb_2O_5 (pH=2) which was measured at 77 K after evacuating at room temperature, b: on V_2O_5/Nb_2O_5 (pH=7) which was measured at 77 K after evacuating at room temperature, and c: on V_2O_5/Nb_2O_5 (pH=7) which was measured at 77 K after evacuating at 400 °C.

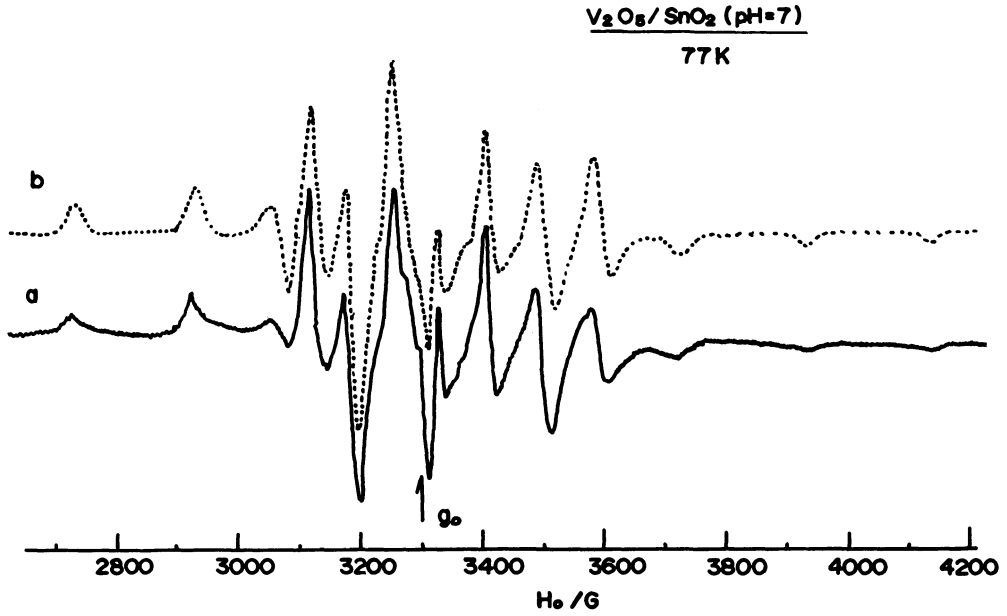

Fig. 5. The ESR spectrum for V_2O_5/SnO_2 (pH=7) and the best fit spectrum simulated. —: observed and ----: simulated.

room temperature. V_2O_5/Nb_2O_5(pH=7) shows a relatively clear hfs upon evacuation at room temperature, but after evacuation at 400 °C the hfs completely disappeared and a very broad spectrum appeared.

A computer simulation was applied to the spectra of Figs. 3-b and 4-b which were measured for V_2O_5/SnO_2 and Nb_2O_5 impregnated at pH=7 at 77 K after evacuation at room temperature. The first derivative curve was calculated according to the usual simulation method at intervals of 10 G (1 G=10^{-4} T) in a magnetic field of 2600—4300 G, as described previously.[5] The intensity of the microwave absorption at each resonance field was obtained by numerical inte-

Table 2. The Best Fitting Parameters Used for Simulating the ESR Spectra of V(IV) Ion on V_2O_5/SnO_2 and V_2O_5/Nb_2O_5 Catalysts Evacuated at Room Temperature

Catalyst	Species	g value		A value		Line width
		$g_{//}$	$g_{\perp}$	$A_{//}$/G	$A_{\perp}$/G	d/G
V_2O_5/SnO_2	V(IV)	1.9265	1.9807	200.5	74.0	27
V_2O_5/Nb_2O_5	V(IV)	1.9100	1.9780	200.0	70.0	40

Table 3. Arrhenius Parameters of 2-Propanol Decomposition over V_2O_5/SnO_2 and V_2O_5/Nb_2O_5 Catalysts Impregnated at pH=2, 4, and 7

Catalyst	$\log V_o$ molecules·m^{-2} s^{-1}	E_a kcal·mol^{-1}
SnO_2 carrier	23.7	16.2
V_2O_5/SnO_2 (pH=2)	21.3	9.6
V_2O_5/SnO_2 (pH=4)	24.0	17.0
V_2O_5/SnO_2 (pH=7)	22.8	13.0
Nb_2O_5 carrier	26.4	20.0
V_2O_5/Nb_2O_5 (pH=2)	22.0	7.2
V_2O_5/Nb_2O_5 (pH=4)	22.2	8.0
V_2O_5/Nb_2O_5 (pH=7)	25.9	18.2

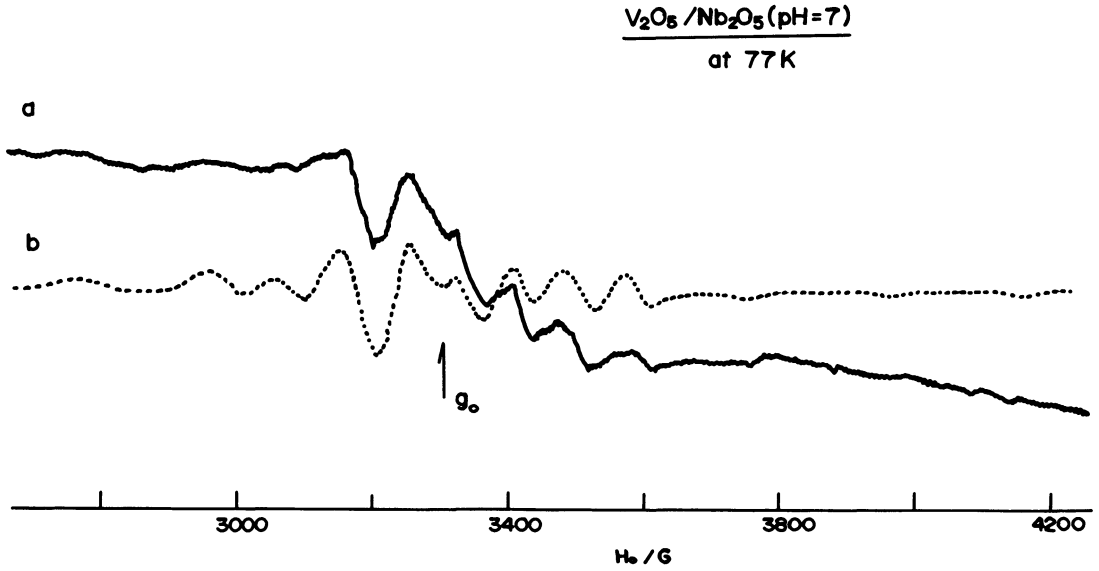

Fig. 6. The ESR spectrum for V_2O_5/Nb_2O_5 (pH=7) and the best fit spectrum simulated. —: observed and ----: simulated.

grations at intervals of 1.5° to θ and ϕ for all directions under the assumption of a Gaussian shape function and 27 G of the half width for V_2O_5/SnO_2 and 40 G for V_2O_5/Nb_2O_5. The best-fit parameters are given in Table 2 and the simulated spectra are shown by the broken line in Figs. 5-b and 6-b.

3) **Decomposition Rates of 2-Propanol over V_2O_5/SnO_2 and Nb_2O_5.** The reaction rates of 2-propanol decomposition over the SnO_2 and Nb_2O_5-supported vanadium oxide catalysts were determined from changes in the GC-peak intensity for the produced propylene in the temperature range 270—350 °C. Arrhenius plots for the initial mean rates, thus obtained, are summarized in Fig. 7(Arrhenius relation: $V=V_o\exp(-E_a/RT)$ and $\log V=\log V_o-E_a/RT$). Arrhenius parameters, $\log V_o$ and E_a, estimated from those plots, are given in Table 3. The minimum activation energy was found to be 7.2 kcal·mol^{-1} for V_2O_5/Nb_2O_5 prepared at pH=2, while the maximum was 18.2 kcal·mol^{-1} for V_2O_5/Nb_2O_5 prepared at pH=7. The activation energy tends to decrease with the amounts of vanadium oxide deposited in any series of catalysts.

The reaction rates in units of molecules·m^{-2}·s^{-1} and molecules·mg$(V_2O_5)^{-1}$·s^{-1}, which were estimated at 300 °C in Fig. 7, are shown in Figs. 8 and 9, respec-

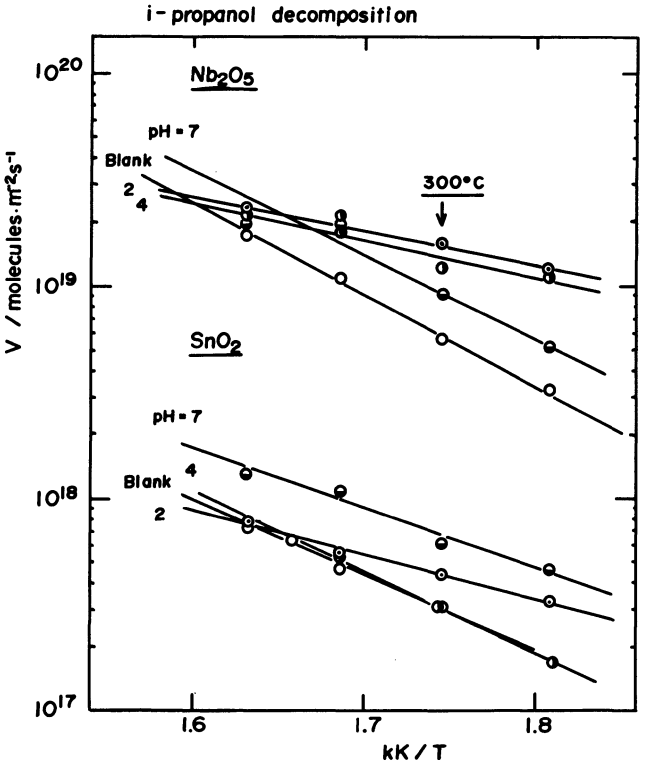

Fig. 7. Arrhenius plots for the 2-propanol decomposition rates over V_2O_5/SnO_2, Nb_2O_5 prepared at various pH and carrier themselves.

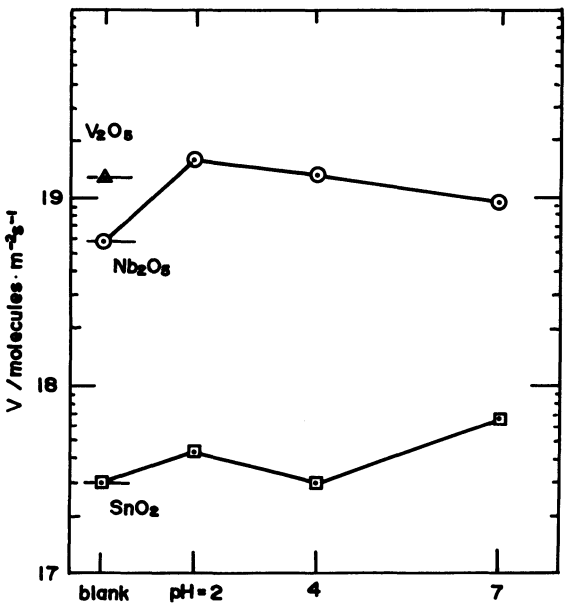

Fig. 8. Comparison of the activity per m^2 and per second for 2-propanol decomposition among V_2O_5 powder, the carrier themselves, and the supported vanadium oxide catalysts at 300°.

tively. In Fig. 8, the activity per m^2 of V_2O_5 powder is higher than those of the carriers, Nb_2O_5 and SnO_2, and the activity is accelerated 2—3 times in V_2O_5/Nb_2O_5 catalysts and twice or less in V_2O_5/SnO_2 relative to the carrier themselves. In Fig. 9, the activity per

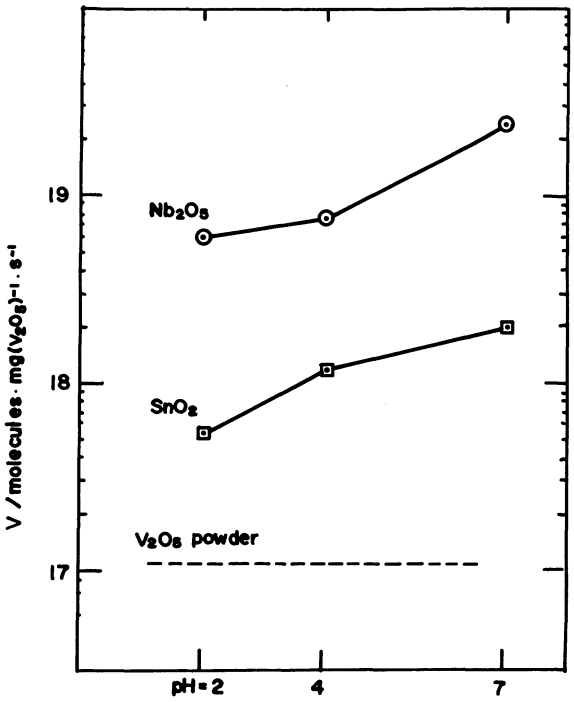

Fig. 9. Comparison of activity per $mg(V_2O_5)$ and per second for 2-propanol decomposition among V_2O_5 powder and the supported catalysts at 300°C.

$mg(V_2O_5)$ generally increases with the pH upon the impregnation and the maximum activity was attained at pH=7 in both carriers. It should be specially noted that the activity is 50—200 times higher in V_2O_5/Nb_2O_5 and 5—20 times higher in V_2O_5/SnO_2 than that of V_2O_5 powder itself. Thus, it is evident that the vanadia species spread widely over the carrier surfaces.

Discussion

Deposited States of Vanadium Oxide on SnO_2 and Nb_2O_5. The deposited states of vanadium oxide on titania (rutile and anatese) have been successfully studied through the analysis of the ESR spectra using the surface V(IV) ion as a probe. The deposited state is greatly affected by the crystal structure of the original carrier; the vanadia species on rutile differed from that on anatase.[5] SnO_2 belongs to the rutile type structure, although the radius ratio $r_{cation}:r_{anion}$ is slightly larger in $SnO_2(r_c/r_a=0.53)$ than in rutile (0.45).[14] Thus, we can also estimate the d-orbital splitting of V(IV) ion from the g-value by Eq. 1.[19]

$$g_{//} = g_o + 8\lambda/\Delta \text{ and } g_\perp = g_o + 2\lambda/\delta \quad (1)$$

where Δ and δ are the crystal field splitting constants and λ the spin-orbit coupling constant which is assumed reasonably to be 250 cm^{-1}.[20]

With respect to V(IV) ion doped into SnO_2 crystalline lattice, the coordination model and d-orbital splitting that was estimated from a reported

g-value[21] by Eq. 1 are shown in Fig. 10-a. For V(IV) ion in the vanadia species deposited on SnO_2, the $g_\perp$ component in Table 2 is large and the $g_{//}$ small ralative to those for the doped sample. The differences in the g-values indicate that the d-orbital splitting Δ, decreases and the δ increases when the V(IV) ion located in the inner bulk is brought to the top of the surface. A similar change was found in the titania-vanadia system:[5] Previously, we showed that the field symmetry around the V(IV) ion replacing the Ti ion site on the rutile surface was similar to that around the V(IV) ion placed in a distorted square pyramidal field. The V(IV) ion doped into a rutile crystal was subject to an octahedral field. Thus, accompanied by removing the V(IV) ion from inner bulk to the top of the rutile surface, the crystal field around V(IV) ion changes from octahedral to a distorted square pyramid. The coordination model and the d-orbital splittings for V_2O_5/SnO_2 are shown analogously in Fig. 10-b. However, V(IV) ion placed on an SnO_2 surface is subject to a weaker field than that on rutile, because the ratio of r_c/r_a is larger in SnO_2 than TiO_2.[14] In fact, the splitting constant, Δ and δ, for V(IV) ion deposited on SnO_2 are smaller than those on rutile (Δ=38 and δ=26 kcm^{-1}).[5] Moreover, the extent of the interaction between vanadia species and carrier surfaces can be compared, based on the hf-coupling constant for the V(IV) ion as a probe, as previously pointed out;[5] since $A_{//}$ and $A_\perp$ for V_2O_5/SnO_2 are 200.5 and 74 G, respectively, while those for $V_2O_5/R\text{-}TiO_2$ 173.1 and 55 G, the interaction for V_2O_5/SnO_2 is understood to be weaker than that for $V_2O_5/R\text{-}TiO_2$. The extent of the hf-splittings of V_2O_5/SnO_2 is similar to those of $V_2O_5/A\text{-}TiO_2$ described in the previous paper(Δ=22 and δ=24 kcm^{-1}), in which the V(IV) ion was assumed to be placed only near the Ti ion vacant site.[5]

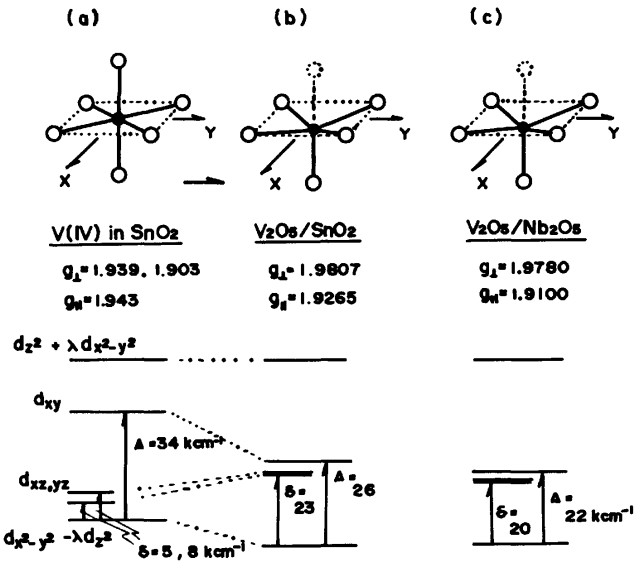

Fig. 10. Coodination model and crystal field splitting for the surface V(IV) ion in V_2O_5/SnO_2 and Nb_2O_5. Analysis for the data of V(IV) ion doped in SnO_2 lattice[21] is shown in (a) for comparison.

The spectrum for V_2O_5/SnO_2 sharpens considerably but remains complicated, after the evacuation at 400 °C, as illustrated in Fig. 3-c. Some reduced vanadia species might be formed by such evacuation treatment and spread over the surface without interacting with each other. Thus, no reduced phase was detected even upon the high temperature evacuation.

Nb_2O_5 belongs to a V_2O_5 type crystal but the oxygen ion coordination around the Nb ion is closer to octahedral symmetry than that of V_2O_5, because the ionic radius of Nb(1.43 A) is larger than that of V(1.32 A).[15] The g-value for the V(IV) ion on Nb_2O_5 surface is almost the same as on an SnO_2 surface, and also close to that for the V_2O_5 inner lattice.[22] Thus, the coordination model and the splitting constants are close to those of V_2O_5/SnO_2, as Fig. 10-c shows. When the V_2O_5/Nb_2O_5 catalyst was evacuated at 400 °C, the spectrum with hfs changed to a broad one as Fig. 4-c illustrated. The broadening might be caused by a dipole-dipole interaction between a reduced vanadia species produced by such a high temperature evacuation.

Catalytic Properties of V_2O_5/SnO_2 and Nb_2O_5. A good compensation relation was found between log V_o and E_a for 2-propanol decomposition over the titania-supported vanadia catalysts, V_2O_5/R- and $A\text{-}TiO_2$, prepared by the column-exchange adsorption of oxo-vanadium ion under different pH(=2, 4, and 7).[5] Based on such a compensation relation,[23] we could discuss the best conditions for the catalyst preparation. A compensation relation also holds between log V_o and E_a in Table 3 for the catalysts , V_2O_5/SnO_2 and Nb_2O_5, impregnated at different pH(=2, 4, and 7), as shown in Fig. 11. The lowest activation energy was obtained for both SnO_2 and Nb_2O_5 carriers on impregnation at pH=2. The most desirable conditions, thus, is impregnation at pH=2.

E_a tends to decrease with increase in the coverage, θ, as indicated previously. In fact, the E_a vs. $1/\theta$ plot gives a good linear curve, as shown in Fig. 12. The inclination of the curve for SnO_2 differs to some extent from that for Nb_2O_5, but both curves cross at around E_a=5—6 kcal·mol^{-1} upon extrapolation to $1/\theta$=0. The E_a value should correspond to such activation energy as caused by the multilayered vanadium oxide piled on SnO_2 and Nb_2O_5 surfaces; it might indicate an intrinsic activation energy for pure vanadium oxide crystallite. We have never found any linear relation between E_a and $1/\theta$ in vanadia-titania[5] and -zirconia[24] systems. With these carriers, not only the coverage (θ) but also the deposited states would be affected by the pH upon preparation, although the difference in the deposited states could never be detected by ESR-measurement.

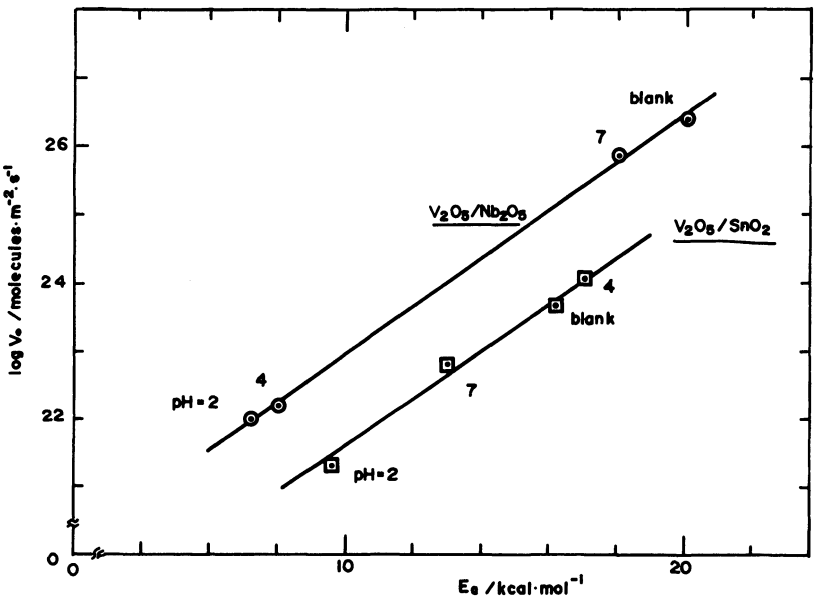

Fig. 11. Relationship between the pre-exponential factor ($\log V_0$) and the activation energy (E_a) for 2-propanol decomposition over the SnO_2- and Nb_2O_5-supported vanadium oxide catalysts.

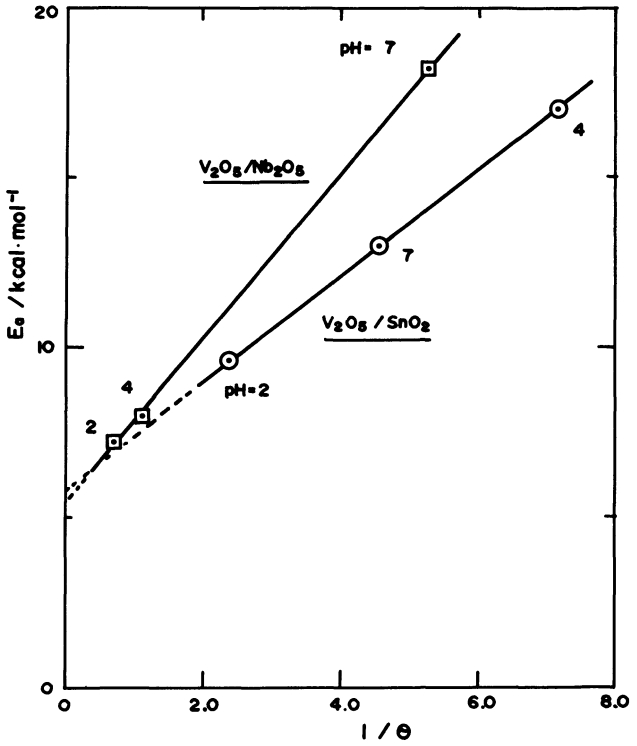

Fig. 12. Relationship between the activation energy and the reverse of the surface coverage ($1/\theta$) of vanadium oxide dispersed on SnO_2 and Nb_2O_5 carriers, see text in detail.

Hernadi et al.[12] showed that the maximum selectivity for 1-butene oxidation was obtained in the composition interval $3:1<V_2O_5:SnO_2<2:1$. Ai[9] showed that the highest activity was obtained for the V_2O_5–SnO_2 catalyst with atomic ratio V:Sn=1:1 and it was the most effective composition for production of maleic anhydride. Andersson[6] suggested in the study on ammonxidation of 3-methylpyridine on V_2O_5/SnO_2 that the catalyst with both V_2O_5 and V_6O_{13} phases is especially active and selective and that the effective catalyst has the composition $V_{0.03}Sn_{0.97}O_2$, in which the V=O bond is weakened by the incorporation of Sn^{4+} ion into the V_2O_5 lattice. Hauffe et al.[10] gave a similar suggestion for the effective working state of various metal oxide supported V_2O_5 catalysts. These authors were also concerned with the fused binary V_2O_5–SnO_2 catalyst, and the effective species were suggested to be formed by the incoporation of Sn^{4+} ion into vanadium oxide lattice. Ono et al.[11] investigated the rates of oxidation of C_3H_6, C_2H_4, C_3H_8, and CO over V-Sn oxides of various compositions. The rates showed two maxima at V/Sn= 2/1 and 1/8. Their ESR, IR, and X-ray measurements suggested that the former rate maximum arises from the formation of an amorphous compound and the latter is associated with the presence of a V^{4+} ion dissolved into SnO_2.[21,25] We have had no evidence for either the incorporations of Sn^{4+} and Nb^{5+} ions into the vanadia species or of V^{4+} ion into SnO_2 and Nb_2O_5 carriers. With the present impregnated catalysts, since the vanadia species were clearly shown to be deposited on SnO_2 and Nb_2O_5 surfaces in the same manner as vanadium ion (V^{4+}) is placed near the Sn^{4+} and Nb^{5+} vacant sites. However we can not directly compare the surface state with those of their fused catalysts. However, the V-O bond can surely be considered to be weakened in such vanadia species as are interacting with the carrier surface, even though quite weakly, as

was discussed for the titania–vanadia system in the previous paper.[5]

Finally, it should be noted that the weak interaction of vanadia species with Nb_2O_5 contrasts with the SMSI in metal supported Nb_2O_5 catalyst.[16] These V_2O_5/SnO_2 and Nb_2O_5 catalysts will be tested for ammoxidation and hydrocarbon oxidation in the near future.

References

1) F. Roozeboom, T. Fransen, P. Mars, and P. J. Gellings, *Z. Anorg. Allg. Chem.*, **449**, 25 (1979); F. Roozeboom, J. Medema, and P. J. Gellings, *Z. Phys. Chem., NF*, **111**, 215 (1978); F. Roozeboom, P. D. Cordingely, and P. J. Gellings, *J. Catal.*, **68**, 464 (1981); F. Roozeboom, M. C. Mittelmeijer-Hazeleger, J. A. Moulijn, J. Medema, V. H. J. de Beer, and P. J. Gellings, *J. Phys. Chem.*, **84**, 2783 (1980).

2) G. C. Bond and K. Brukman, *Faraday Discuss. Chem. Soc.*, **72**, 235 (1981); G. C. Band and P. Konig, *J. Catal.*, **77**, 309 (1982).

3) M. Rusiecka, B. Grzybowska, and M. Gasior, *Appl. Catal.*, **10**, 101 (1984).

4) I. E. Wachs, R. Y. Saleh, S. S. Chan, and C. C. Chersich, *Appl. Catal.*, **15**, 339 (1985); R. Y. Saleh, I. E. Wachs, S. S. Chan, and C. C. Chersich, *J. Catal.*, **98**, 102 (1986).

5) Y. Kera and Y. Matsukaze, *J. Phys. Chem.*, **90**, 5752 (1986); Y. Kera, T. Inoue, and Y. Matsukaze, *Bull. Chem. Soc. Jpn.*, **61**, 761 (1988).

6) A. Andersson, *J. Catal.*, **69**, 465 (1981).

7) K. L. Madhok, *React. Kinet. Catal. Lett.*, **25**, 159 (1984).

8) P. J. Pomonis and J. C. Vickerman, *J. Chem. Soc., Faraday Discuss.*, **72**, 247 (1981); *J. Catal.*, **90**, 305 (1984).

9) M. Ai, *J. Catal.*, **40**, 318 (1975).

10) K. Hauffe and H. Raveling, *Ber. Bunsenges. Phys. Chem.*, **84**, 912 (1980).

11) T. Ono, Y. Nakagawa, and Y. Kubokawa, *Bull. Chem. Soc. Jpn.*, **54**, 343 (1981); T. Ono and Y. Kubokawa, *Bull. Chem. Soc. Jpn.*, **55**, 1748 (1982).

12) K. Hernadi, J. Halasz, K. Varga, and P. Fejes, *Acta Phys. Chem.*, **30**, 97 (1984).

13) Yu. D. Panakratiev, L. N. Kurina, T. V. Lazareva, and S. P. Rabota, *React. Kinet. Catal. Lett.*, **27**, 173 (1985).

14) W. Huckel, "Structural Chemistry of Inorganic Compounds(II)," Elsevior Sci., New York (1951), p. 581.

15) R. Kiriyama and H. Kiriyama, "Structural Inorganic Chemistry," 2nd ed, Kyoritsu, Tokyo (1964). p. 142.

16) K. Tanabe and T. Iizuka, *Hyomen*, **23**, 471 (1985).

17) V. M. Samoilov and A. N. Ryabov, *Kinet. Katal.*, **19**, 250 (1978).

18) A. Bystrom, K. Wilhelmi, and O. Brotzen, *Acta Chem. Scand.*, **4**, 1119 (1950).

19) B. A. Goodman and J. B. Bayer, *Advan. Inorg. Chem. Radiochem.*, **13**, 135 (1970).

20) G. C. Pake, "Paramagnetic Resonance," W. A. Benjanin, New York (1962).

21) C. Kikuchi, I. Chen, W. H. From, and P. B. Dorain, *J. Chem. Phys.*, **42**, 181 (1965).

22) Y. Kera and K. Kuwata, *Bull. Chem. Soc. Jpn.*, **52**, 1268 (1979).

23) Y. Kera and M. Negoro, *J. Catal.*, **99**, 198 (1986).

24) Y. Kera and T. Kamada, unpublished data.

25) P. H. Kasai, *Phys. Lett.*, **7**, 5 (1963).

The ^1H and ^{13}C NMR of 9,10-Bis(phenylethynyl)anthracene Dianion

Masatoshi HIRAYAMA,* Masaaki KOBAYASHI, and Hiroshi YAMAMOTO†
Department of Chemistry, Faculty of Science, Ibaraki University,
2-1-1 Bunkyo, Mito 310

†Faculty of Education, Ibaraki University, 2-1-1 Bunkyo, Mito 310
(Received September 18, 1987)

The formation of 9,10-bis(phenylethynyl)anthracene dianion by contact of tetrahydrofuran-d_8 solution of its precursor with sodium in vacuo, is confirmed by the ^1H and ^{13}C NMR spectra and its reactivity. The excess π-charge-density distribution estimated by the CNDO/2 calculation for the dianion, is consistent with the observed ^1H and ^{13}C chemical shift values.

The NMR studies of the π-dianions of polycyclic aromatics and annulenes have so far been largely served to investigate the electronic structures of these π-conjugated systems,[1] as well as ESR studies on the corresponding anion radicals. It has been suggested that the ease of the formation of π-dianion correlates well with the resonance energy per atom in a dianion molecule.[2] However, in practice the line broadening due to spin exchange with a corresponding anion radical in equilibrium with dianion in solution often prevents an observation of high-resolution NMR signals of dianion. On the other hand, it may be significant that a substituent effect on π-conjugated system can be discussed in terms of the excess charge distribution of the corresponding π-dianion. However, a discussion from this point of view has not generally been of interest. In the anthracene dianion, excess charge relative to its neutral precursor has been known to be extraordinarily large at the 9 and 10 positions;[3] this observation prompted us to discuss the effect of several kinds of substituents at these positions on the excess charge distribution.

The present paper reports on the formation of the dianion of 9,10-bis(phenylethynyl)anthracene (**1**) as a unique anthracene derivative and on its electronic structure on the basis of an observation of its ^1H and ^{13}C NMR and charge density distribution estimated by a MO calculation.

Experimental

Compound **1** (Aldrich Co. Ltd.) was used without further purification and tetrahydrofuran-d_8 (THF-d_8) (Canada MSD Co. Ltd.) was vacuum-distillated after drying with sodium/potassium alloy in a high-vacuum tube. 1 ml of a 0.2 mol dm^{-3} THF-d_8 solution of **1** was introduced into a 10 mm Pyrex tube connected to high-vacuum line and degassed. A small amount of sodium metal was placed in the upper part of an NMR tube connected to the vacuum line. After the solution was transferred into the sample tube, the tube was cut off from the vacuum line. By turning the tube, the solution was brought into contact with the metal at room temperature for controlled periods of time. The NMR spectra were measured on a Varian VXR-300 pulsed FT spectrometer operating at 300 and 75 MHz for ^1H and ^{13}C, respectively, at room temperature. The ESR spectra and mass spectra were recorded on a JES-FE1XG ESR spectrometer (X-band, 100 kHz modulation) and a JMS DX-300 mass spectrometer, respectively. A calculation of the charge density distribution was performed by the MO method with Y4CB04 of the library programs in the Computer Center of the University of Tokyo on HITAC M-240H of Ibaraki University.

Results and Discussion

Immediately after the contact of the THF-d_8 solution of **1** with sodium metal in vacuo at room temperature, the solution turned green, which gave an ESR spectrum of the anion radical of **1**. Upon further contact, the color of the solution gradually became purple, while the ESR disappeared and new NMR lines developed. The ^1H spectrum of the purple

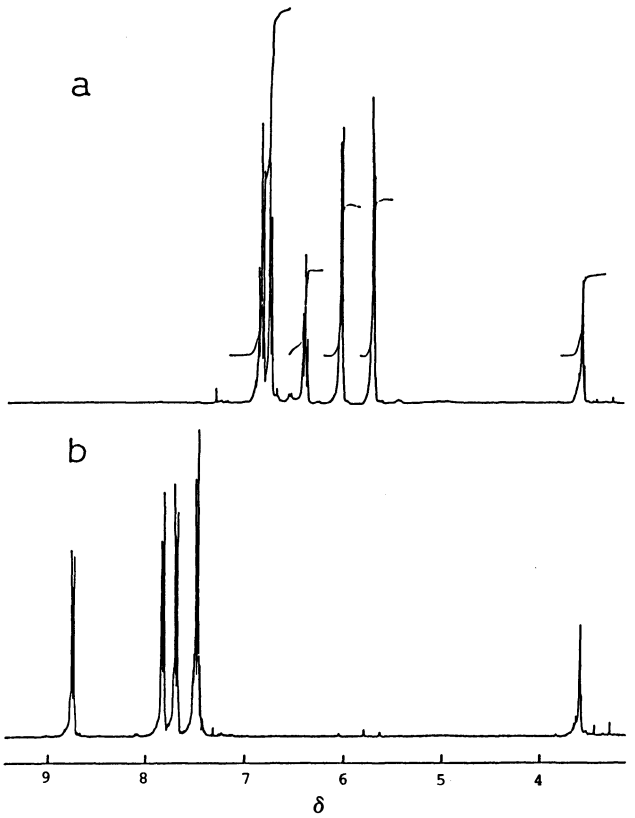

Fig. 1. ^1H NMR spectra of $\mathbf{1}^{2-}$ (a) and its neutral precursor (b) in THF-d_8.

solution measured after contact for 24 h is shown in Fig. 1, together with that of the neutral precursor **1** in THF-d_8. This spectrum exhibited the same pattern as that of **1**, which consists of an AA'BB' and an AA'BB'C systems. The center of gravity of ^{1}H signals was shifted toward 1.53 ppm higher than that for **1**. Furthermore, in order to investigate whether this species is a diamagnetic monoanion formed by subtracting a proton from the solvent or not, after a purple solution was prepared in THF with the same technique, THF was excluded by evaporation and a resulting purple residue was solved in THF-d_8. The ^{1}H spectrum of the resulting purple solution was completely identical with that produced first by contact with sodium metal in THF-d_8; that is, the latter spectrum has no other lines than the former. One can thus rule out the possibility of the formation of a monoanion. The ^{13}C spectrum of the purple species (Fig. 2) is consistent with that expected from the ^{1}H spectrum, consisting of lines of five tertiary and five quaternary carbons as well as those of **1**. The high-field shift of the center of gravity of ^{13}C signals from **1** to the purple species is 5.26 ppm.[4] Thus, from these results, one may anticipate that the purple species is identified to a π-dianion of **1**, $\mathbf{1}^{2-}$ (or a disodium salt of dianion ($\mathbf{1}^{2-}\cdot 2Na^+$)).

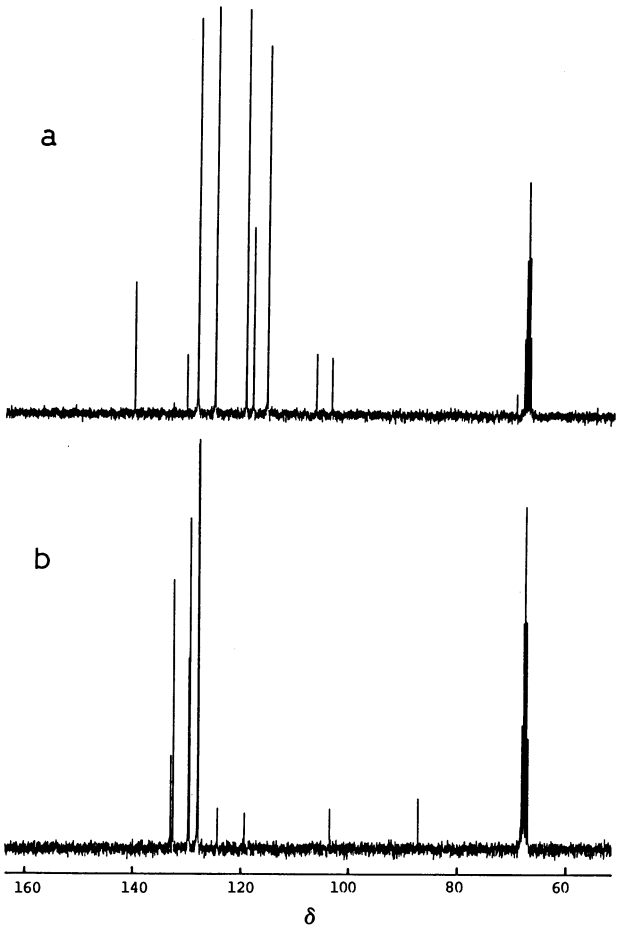

Fig. 2. ^{13}C NMR spectra of $\mathbf{1}^{2-}$ (a) and its neutral precursor (b) in THF-d_8.

For the ^{1}H spectrum of **1**, the lower-field group of the AA'BB' system was assigned to H_1, in analogy with the case of 9,10-diphenylanthracene,[5] which is similar to **1** in view of containing π-type substituents at the 9 and 10 positions. The *o*-, *m*-, and *p*-protons of phenyl groups could be straightforwardly assinged due to their coupling patterns. For the ^{1}H spectrum of $\mathbf{1}^{2-}$, the lower-field group of the AA'BB' pattern was assigned to H_1 on the basis of a combination of a C–H shift correlation 2D NMR (Fig. 4) and the ^{13}C assignment determined from a comparison of shift difference from **1** ($\Delta\delta$) with the calculated excess

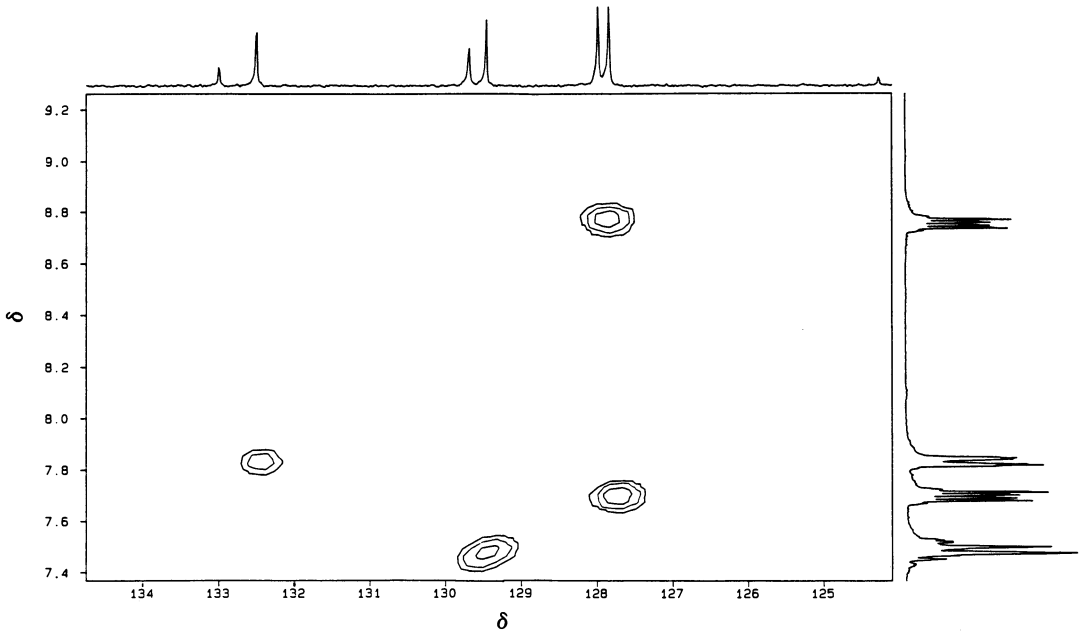

Fig. 3. H–C shift correlation 2D NMR of **1**.

charge (Δq_c^{π}) described later. The phenyl protons was easily assigned as well as **1**. For both **1** and $\mathbf{1}^{2-}$, all of tertiary carbons were assigned on the basis of the C–H shift correlation 2D NMR (Figs. 3 and 4) and ^{1}H assignments. Since assignments of the quaternary carbons of both **1** and $\mathbf{1}^{2-}$ are quite difficult, they were tentatively made by analogy with those of several phenyl derivatives of acetylene and by a comparison with the calculated excess π-charge-densities Δq_c^{π}'s (Table 1).

It was then confirmed by measuring the ESR that addition of a reducible aromatic compound, *m*-dinitrobenzene, to the purple solution in vacuo gives the anion radical of this compound. A quenching experiment with oxygen afforded a neutral precursor, while with water and deutrium oxide the dihydro (*m/z* 380) and dideuterio derivatives (*m/z* 382) of **1** were formed, respectively, as shown by mass spectrometry. All these results strongly support the above expectation that the purple species is a π-dianion of **1** or its disodium salt.

The observed mean high-field ^{13}C shift, 5.26 ppm, of $\mathbf{1}^{2-}$ from **1** is only about a half of 10.67 ppm estimated by using a commonly used value of k_c, 160 ppm/electron, in the correlation of ^{13}C shift with charge density, $\Delta\delta_c = k_c \cdot \Delta q_c^{\pi}$.[6] Recently, it was found by Eliasson et al.[7] that for 4nπ-systems the anisotropic high-field shift of a ring proton due to a paratropic ring current correlates well with a k_c value for ring carbons determined experimentally and that the anomalous deshielding of ring carbons for such a system is explained in terms of the average electronic excitation energy. For the anthracene dianion, 89 ppm/electron is given as k_c from their analysis. Since in our present system about 80% of the total excess π-charge occupies the anthracene moiety as calculated later, it may be plausible to consider that the anthracene ring carbons are affected by such the anomalous deshielding effect. Thus, this reason may explain the considerable reduction in the high-field shift of the center of gravity of ^{13}C signals from 10.67 ppm.

The MO calculations of electron density distributions were then performed on **1** and $\mathbf{1}^{2-}$ by the CNDO/2 method.[8] Since an available crystal structure of **1** has not been found in the literature, a possible molecular geometry for **1** was estimated by a combination of the crystal structures of diphenylacet-

Table 1. Observed ^{1}H and ^{13}C Chemical Shifts for **1** and $\mathbf{1}^{2-}$ [a]

	δ_N	δ_D	$\Delta\delta_{obsd}$
H_1	8.75	6.05	−2.70
H_2	7.70	5.72	−1.98
H_{18}	7.83	6.76	−1.07
H_{19}	7.49	6.86	−0.63
H_{20}	7.49	6.42	−1.07
C_1	128.00	115.48	−12.52
C_2	127.85	119.39	−8.46
C_9[b]	133.00	69.40	−63.60
C_{11}[b]	103.56	106.50	2.94
C_{15}[b]	119.31	132.00	12.69
C_{16}[b]	86.97	103.60	16.63
C_{17}[b]	124.27	140.12	15.85
C_{18}	132.51	125.15	−7.36
C_{19}	129.47	128.41	−1.06
C_{20}	129.70	118.10	−11.60

a) Measured in ppm relative to the lower-field multiplet of THF and referred to TMS. δ_N and δ_D are shifts for **1** and $\mathbf{1}^{2-}$, respectively. $\Delta\delta_{obsd}$ is shift of $\mathbf{1}^{2-}$ relative to that of **1**. Positive signs denote low field shifts. b) Assigned tentatively.

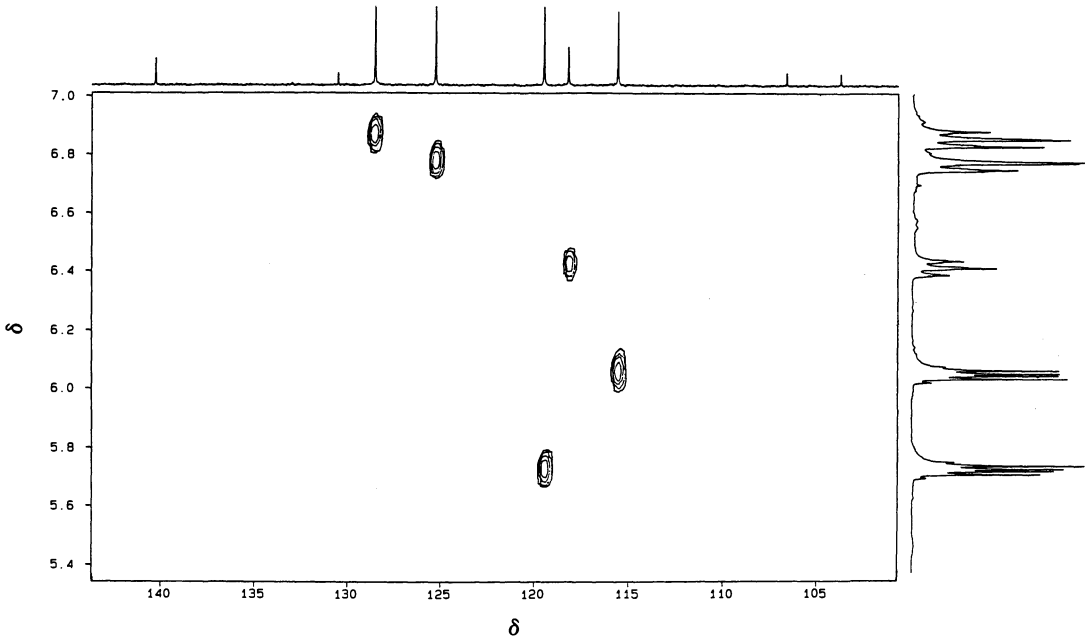

Fig. 4. H–C shift correlation 2D NMR of $\mathbf{1}^{2-}$.

Table 2. Comparison of Changes of Calculated and Observed ^1H and ^{13}C Shifts of 1^{2-} from 1[a]

		Δq_c[b]	$\Delta\delta_{calcd}$[c]	$\Delta\delta_{obsd}$
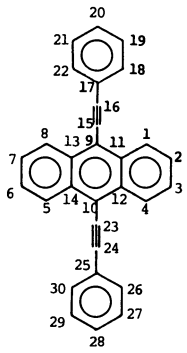	H_1		−0.92	−2.70
	H_2		−0.46	−1.98
	H_{18}		−0.58	−1.07
	H_{19}		−0.04	−0.63
	H_{20}		−1.17	−1.07
	C_1	0.0858	−13.73	−12.52
	C_2	0.0429	−6.86	−8.46
	C_9	0.4700	−75.20	−63.60
	C_{11}	0.0349	−5.58	2.94
	C_{15}	−0.0458	(7.33)[d]	12.69
	C_{16}	0.1318	(−21.09)[d]	16.63
	C_{17}	−0.1037	16.59	15.85
	C_{18}	0.0543	−8.69	−7.36
	C_{19}	0.0041	−0.66	−1.06
	C_{20}	0.1090	−17.44	−11.60

a) In ppm. Positive signs denote low-field shifts. b) Excess π-charge density of 1^{2-} relative to that of **1**. c) Shifts of 1^{2-} from those of **1** calculated using k_H=10.7 ppm/electron and k_c=160 ppm/electron in $\Delta\delta_H=-k_H\cdot\Delta q_c^\pi$ and $\Delta\delta_c=-k_c\cdot\Delta q_c^\pi$, respectively. d) Shift values in parentheses are not reliable because the standard k_c value (160 ppm/electron) may not be applied to sp-hybridized carbons.

ylene[9] and anthracene[10] as a planar structure.[11] The distance between C_9 and C_{15}, R_{9-15}, was taken as the equal magnitude to R_{16-17}, by taking into account the considerable stability of the anthracene moiety.[12] The electron density at the $2p_z$ orbital of carbon is denoted by q_c^π and its change from **1** to 1^{2-} by Δq_c^π. ^1H and ^{13}C chemical shifts of 1^{2-} relative to those of **1**, $\Delta\delta_{calcd}$, were estimated using the relation $\Delta\delta_H=k_H\cdot\Delta q_c^\pi$[13] and $\Delta\delta_c=k_c\cdot\Delta q_c^\pi$, respectively. As can be seen from Table 2, the observed shifts of 1^{2-} from **1**, $\Delta\delta_{obsd}$, for the anthracene ring protons are anomalously larger (3—4 times) than $\Delta\delta_{calcd}$ obtained using the standard k_H value, 10.7 ppm/electron, in contrast to those of the phenyl protons. This may be ascribed to a contribution of the partially paratropic ring current effect of the anthracene moiety.[14] It may be plausible to consider that the change of the anisotropy of the triple bond from **1** to 1^{2-} scarecely affects the $\Delta\delta_{obsd}$ of all the ring protons owing to its location far from protons. On the other hand, for C_1 and C_2 $\Delta\delta_{obsd}$ corresponds comparatively well to $\Delta\delta_{calcd}$; this seems to imply that an anomalous deshielding was not remarkably observed. Also for C_{18}, C_{19}, and C_{20}, the pattern of $\Delta\delta_{obsd}$ approximately corresponds to that of $\Delta\delta_{obsd}$. Since for the sp-hybridized C_{15} and C_{16}, a relevant k_c value has been unknown so far, the shifts of these carbons can not sufficiently be discussed here. For C_{17}, $\Delta\delta_{obsd}$ corresponds well to $\Delta\delta_{calcd}$; while for both C_9 and C_{11} $\Delta\delta_{obsd}$ is much smaller than $\Delta\delta_{calcd}$; that is, these two carbons are much more subject to the anomalous paramagnetic ring current than the other ring carbons. On the other hand, the calculation result that most of the excess π-charge in the anthracene moiety is concentrated on the central ring of anthracene allows us to consider that the central ring may contribute considerably to the partial paratropicity of the anthracene moiety. Thus, all the shifts, except for C_{15} and C_{16}, could be consistently explained, though qualitatively, with tentative assignments for the quaternary carbons.

References

1) a) K. Müllen, *Chem. Rev.*, **84**, 603 (1984) and references therein; b) K. Müllen, W. Huber, T. Meul, M. Nakagawa, and M. Iyoda, *J. Am. Chem. Soc.*, **104**, 5403 (1982); c) K. Müllen, W. Huber, T. Meul, M. Nakagawa, and M. Iyoda, *Tetrahedron*, **39**, 1575 (1983); d) A. Minsky, A. Y. Meyer, and M. Rabinovitz, *J. Am. Chem. Soc.*, **104**, 2475 (1982); e) K. Müllen, *Pure Appl. Chem.*, **58**, 177 (1986).

2) R. B. Bates, B. A. Hess, Jr., C. A. Ogle, and L. J. Schaad, *J. Am. Chem. Soc.*, **103**, 5052 (1981).

3) R. G. Lawler and C. V. Ristagno, *J. Am. Chem. Soc.*, **91**, 1534 (1969).

4) The value (5.26 ppm) seems to correspond to the formation of a monoanion by subtracting a proton or deuterium from the solvent, when the standard k_c value (160 ppm/electron) is applied to all the carbons. However, this correspondence is only incidental and the ^{13}C shift values will be precisely discussed later.

5) R. Biehl, K. Hinrichs, H. Kurreck, W. Lubitz, U. Mennenga, and K. Roth, *J. Am. Chem. Soc.*, **99**, 4278 (1977).

6) H . Spiesecke and W. G. Schneider, *Tetrahedron Lett.*, **1961**, 468; G. A. Olah and G. D. Mateescu, *J. Am. Chem. Soc.*, **92**, 1430 (1970).

7) B. Eliasson, U. Edlund, and K. Müllen, *J. Chem. Soc., Perkin Trans. 2*, **1986**, 937.

8) J. A. Pople, D. C. Beveridge, and P. A. Dobosh, *J. Am. Chem. Soc.*, **90**, 4201 (1968).

9) V. D. Samarskaya, R. M. Myasnikova, and A. I. Kitaigorodskij, *Kristallografiya*, **13**, 616 (1968).

10) D. W. J. Cruickshank, *Acta Crystallogr.*, **9**, 915 (1956).

11) The geometric parameters used for CNDO/2 calculations are as follows: C_1C_2=1.3639 Å, C_2C_3=1.4180 Å, C_1C_{11}=1.4312 Å, C_9C_{11}=1.3968 Å, $C_{11}C_{12}$=1.4340 Å, C_9C_{15}=1.4384 Å, $C_{15}C_{16}$=1.1911 Å, $C_{16}C_{17}$=1.4384 Å, $C_{17}C_{18}$=1.3890 Å, $C_{18}C_{19}$=1.3907 Å, $C_{19}C_{20}$=1.3854 Å, $\angle C_1C_2C_3$=120.68°, $\angle C_{11}C_1C_2$=120.59°, $\angle C_1C_{11}C_{12}$=118.73°, $\angle C_9C_{11}C_{12}$=121.12°, $\angle C_{11}C_9C_{13}$=120.88°, $\angle C_{18}C_{17}C_{22}$=119.80°, $\angle C_{17}C_{18}C_{19}$=120.09°, $\angle C_{18}C_{19}C_{20}$=119.84°, $\angle C_{19}C_{20}C_{21}$=120.32°.

12) In order to examine an effect of excess π-electrons on the conjugated system, an attempt was then made of calculation of Δq_c^π with slight changes of each value of R_{9-15} and R_{15-16}. It was then found that Δq_c^π pattern is very sensitive to each of these two distances all through the molecule. However, no set of these two distances afforded Δq_c^π pattern which explaines $\Delta\delta_{obsd}$ better than original values of distances (R_{9-15}=1.4384 Å and R_{15-16}=1.1911 Å).

13) T. Schaefer and W. G. Schneider, *Can. J. Chem.*, **41**, 966 (1963).

14) H. W. Vos, Y. W. Bakker, C. MacLean, and N. H. Velthorst, *Org. Magn. Reson.*, **6**, 245 (1974); H. W. Vos, C. MacLean, and N. H. Velthorst, *Mol. Phys.*, **35**, 329 (1978); U. Edlund and B. Eliasson, *J. Chem. Soc., Chem. Commun.*, **1982**, 950.

Adsorbing-Particle Flotation of Hg^{2+} by Combined Use of Charcoal, Polyacrylamide, and Cationic Surfactant

Tadahiko KIDOKORO,* Kotaro MATSUI, Satoshi ISHIWATA, Toshiyuki SASAKI, and Tsunetaka SASAKI
Department of Chemistry, Faculty of Science, Tokai University, 1117 Kitakaname, Hiratsuka 259-12
(Received September 24, 1987)

Adsorbing-particle flotation of Hg^{2+} ions by using active charcoal as an adsorbent, Polyacrylamide (PAA) as a coagulant, and hexadecyltrimethylammonium chloride (HTAC) as a frother was carried out. The floatability exceeded 90% in a wide range of pH and nearly 98% of Hg^{2+} ions was floated from 2.1×10^{-4} mol dm^{-3} solution by adding 2500 ppm of active charcoal, 24 ppm of PAA, 81 ppm of HTAC and with shaking. Stepwise and double flotations were further attempted which proved to distinctly increase the floatability, while sodium sulfide treatment of active charcoal showed only a slight increase and the coexistence of chloride ions showed no effect. The mechanism of adsorbing-particle flotation was discussed.

The adsorbing-particle or colloid flotation has been known as one of the effective methods to remove or concentrate dissolved ions in solution, because it enables the flotation of various organic and inorganic ions and molecules by selecting suitable adsorbent, coagulant, and surfactant as a collector and/or a frother. With regard to the practical application of such a technique, Grieves[1] published a general review in which we confirm that adsorbents mainly used are oxides, hydroxides or sulfides of Fe^{3+}, Al^{3+}, Cd^{2+}, Hg^{2+}, Mn^{4+}, and Th^{4+}. However, one of the present authors has drawn attention to different group of ion adsorbents of particulate or powder type, such as bentonite,[2,3] charcoal,[4] and poly(ethyleneimine),[5] confirming that these effectively remove inorganic and organic anions and cations. Among them charcoal is particularly promising since it can be used widely as an adsorbent. But published reports are rather scanty although the possibility of its application has been suggested.[6]

In the present study, removal of Hg^{2+} ions was attempted by using charcoal as an adsorbent, Polyacrylamide as a coagulant, and hexadecyltrimethylammonium chloride (HTAC) as a surfactant. The stepwise and double flotations were worked out to improve the flotation efficiency.

Experimental

Materials. Active charcoal mainly used as an adsorbent was the product of Wako Pure Chemicals, labelled "Chemical Activated." Some other charcoals of different origin were used for comparison. Polyacrylamides mainly used as coagulants were the products of Mitsubishi Chemical Industries, DCLE MA-3000L (DL), DCLE MA-3000H (DH), and DCLE MA-3000-3H (D3H), molecular weight being about 10^7 and the content of sodium polyacrylate 10, 20, and 30% respectively. Other coagulants used were the products of Toagosei Chemical Industries, sodium polyacrylate (AR) of molecular weight of $2-6\times10^6$ and PAA derivatives of Sanyokasei Industries, anionic Sanfloc AH (SA), nonionic Sanfloc N (SN), and cationic Sanfloc CH (SC) of molecular weight of 1.7×10^7 for the former two and 7×10^6 for the latter. Surfactants used were the commercial products of cationic HTAC and anionic sodium dodecyl sulfate (SDS).

Measurement. To carry out the flotation measurement, 20 cm^3 of an aqueous solution of nitric acid containing 2.1×10^{-4} mol dm^{-3} Hg^{2+} ions, 2500 ppm charcoal of different origins, coagulant and surfactant in different amounts, and NaOH for controlling the pH, was introduced into a stoppered test tube of 1.6 cm in inner diameter and 29 cm in length, equipped with a stopcock at the bottom. The test tube was gently turned upside down repeatedly for 2 min and then vigorously shaken ten times by hand to complete the flotation.

Concentration of Hg^{2+} ions in the underlying solution was determined by Hitachi Atomic Absorption Spectrometer 508 at wavelength of 248.3 nm. The floatability F (%) was calculated by the following equation:

$$F = \frac{C_0 - C}{C_0} \times Fc \times 100\%, \quad (1)$$

where C_0 and C express concentrations of solution before and after the flotation respectively, and Fc fraction of active charcoal floated.

The stepwise flotation was worked out similarly to the previous study[2] to improve the flotation efficiency. In this technique, charcoal was added to the solution at a time but coagulant and surfactant were added in two steps. After the first addition of coagulant and surfactant, flotation was carried out and the suspension below the scum was transferred to another test tube, into which remaining portions of coagulant and surfactant were added and the second flotation was conducted. From the concentration of Hg^{2+} and the amount of active charcoal in the solution after the second flotation, floatability of Hg^{2+} was calculated. A similar stepwise flotation but without transferring the solution to another test tube was carried out to simplify the operation. This procedure is called the double flotation to distinguish it from the stepwise flotation.

All the measurements were done at room temperature.

Results and Discussion

According to the preliminary measurements and the former study,[4] concentrations of coagulant and surfactant favorable for charcoal flotation were pre-

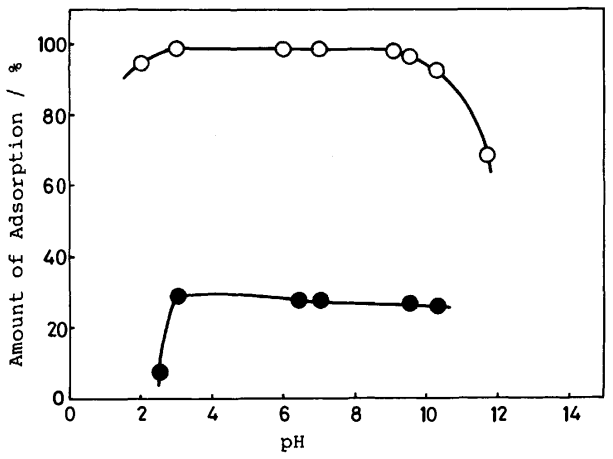

Fig. 1. Adsorption of Hg^{2+} by charcoal.
Hg^{2+}: 2.1×10^{-4} mol dm^{-3}. Charcoal ○: 2500 ppm, ●: 400 ppm.

sumed to be in the ranges of 20 to 200 ppm and 50 to 500 ppm, respectively, for 2500 ppm of charcoal. The optimum concentration range varies with the adsorbent to be used and ions to be floated.[2-5]

Adsorption of Hg^{2+} Ions by Charcoal. In order to confirm the proper amount of active charcoal required for the Hg^{2+}-ion flotation, adsorption of Hg^{2+} ions by active charcoal was measured for the solution containing various amounts of charcoal and at different pH. Figure 1 shows two such instances. Here the amount of Hg^{2+} ions adsorbed is expressed not as per unit weight of charcoal but conventionally as percent of initial Hg^{2+} concentration in agreement with $(C_0-C)/C_0$ term in Eq. 1. The figure shows a flat maximum of adsorption exceeding 98% for a wide range of pH at charcoal concentration of 2500 ppm. From this result, the concentration of charcoal was kept constant to 2500 ppm throughout the present study. It should be noted that although all of the charcoals used in the present study which are not listed here exhibited a good adsorption towards Hg^{2+} and most of them also showed a good floatability as reported in a previous paper,[4] the floatability of Hg^{2+}-adsorbed charcoal was often unsatisfactory. In the present study, the product of Wako, Charcoal Activated, was eventually used exclusively.

Adsorbing-Particle Flotation of Hg^{2+} (Simple Flotation). Adsorbing particle flotation of Hg^{2+} ions was carried out for various combinations and compositions of charcoal, coagulant, and surfactant. Figure 2 shows some results of floatability of Hg^{2+} plotted against pH. Floatability appeared to exceed 90% in a wide range of pH for the coagulant of various types of Polyacrylamide and 98% floatability was seen for the system using D3H as a coagulant. Wide pH range of high floatability is seen which is favorable because the flotation of Hg^{2+} ions has been often conducted under the conditions of excess chloride ions and low pH.[7]

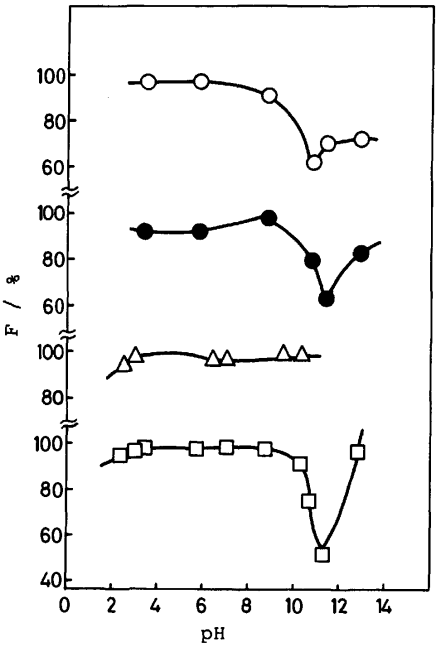

Fig. 2. Flotation of Hg^{2+} by different coagulants.
Hg^{2+}: 2.1×10^{-4} mol dm^{-3}. Charcoal: 2500 ppm. HTAC: 540 ppm. Coagulants ○: DL 210 ppm, ●: DH 160 ppm, △: D3H 210 ppm, □: SA 210 ppm.

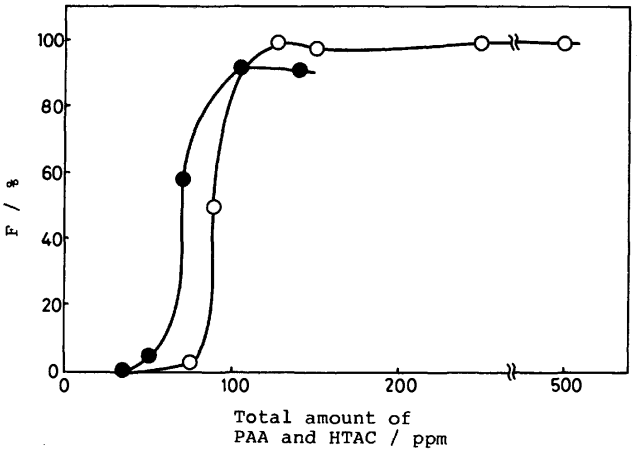

Fig. 3. Floatability vs. concn of PAA+HTAC.
Hg^{2+}: 2.1×10^{-4} mol dm^{-3}. Charcoal: 2500 ppm. ○: DL-HTAC system, weight ratio of DL/HTAC=0.388 ●: DH-HTAC system, weight ratio of DH/HTAC= 0.296.

The floatability seems to increase as a whole with the degree of both the polymerization and hydrolysis of Polyacrylamide as far as the present study is concerned.

We further attempted to reduce the amount of coagulant and surfactant without considerable decrease in the floatability. Figure 3 shows the results for DL-HTAC and DH-HTAC systems. The figure expresses the relation between the floatability of Hg^{2+} ions and the total concentration of coagulant and surfactant at a constant ratio between them and at

constant pH. As seen in Fig. 3, amounts of both coagulant and surfactant could be reduced to 35 and 90 ppm respectively for DL–HTAC system and 24 and 81 ppm respectively for DH–HTAC system without noticeable decrease in floatability.

Effects of Na_2S-Treatment of Charcoal and Coexistence of Chloride Ions on Floatability. In order to enhance the floatability of Hg^{2+}, active charcoal was immersed in an aqueous solution of 1 mol dm^{-3} sodium sulfide for 6 h, then washed with distilled water until the supernatant became neutral and dried. An instance of the floatability of Hg^{2+} ions using Na_2S-treated charcoal is shown in Fig. 4, together with the result using charcoal without the Na_2S-treatment. The increase of floatability due to the treatment was observed, but the effect was not so distinct as had been expected. Further the effect of the coexistence of chloride ions upon the floatability was examined, because halogen ions have been reported to increase the adsorption of Hg^{2+} ions by charcoal.[7,8] But such an effect did not appear as far as the present study is concerned.

Dependence of Floatability on Hg^{2+} Concentration. The effect of Hg^{2+} ion concentration upon the floatability was examined and the result is shown in Fig. 5. The coagulant AR used there was somewhat different in the degree of polymerization from that used in the previous experiments, so the results were unable to compare strictly with each other but general tendency is seen that the floatability increases slightly in the concentration range of 10^{-5} to 10^{-6} mol dm^{-3} of Hg^{2+} ions.

Ionic Interaction Between Coagulant and Surfactant. In order to examine the ionic interaction between coagulant and surfactant, which supposedly contributes to the flotation, the floatability of Hg^{2+} ions was further measured by using SA, SN, and SC as anionic, nonionic, and cationic coagulants respectively and HTAC and SDS as cationic and anionic surfactants. The results are shown in Fig. 6. As seen in Fig. 6, among the systems using cationic surfactant HTAC, the system with anionic coagulant SA exhibited most pronounced floatability in a wide range of pH, the value was distinctly small for nonionic coagulant SN and zero for cationic coagulant SC in a wide range of pH. Thus the ionic interaction between coagulant and surfactant is evident. Large floatability shown by the system of SC–SDS also confirms this fact.

Stepwise and Double Flotations. Some of the results of stepwise and double flotations are shown in Table 1, together with the simple one-step flotation hitherto mentioned. In this table we can see a general tendency of enhanced floatability of stepwise and double flotations compared with that of simple foltation, similarly to the case of stepwise flotation using bentonite as an adsorbent.[2] It is noted that the floatability increases as a whole in the order of double flotations applying stepwise additions for surfactant alone, coagulant alone and for both of them, and

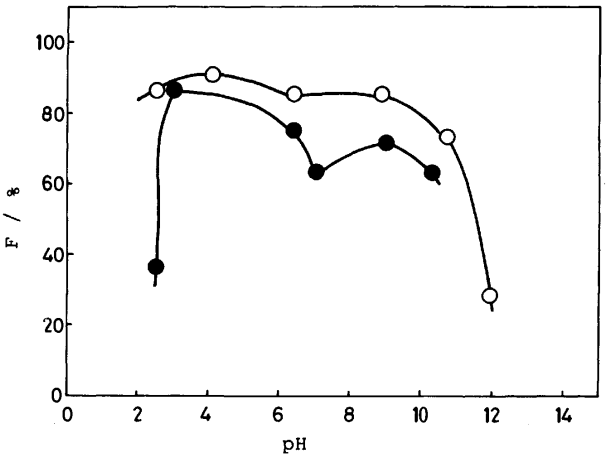

Fig. 4. Effect of Na_2S treatment on floatability.
Hg^{2+}: 2.1×10^{-4} mol dm^{-3}. Charcoal: 2500 ppm. DL: 24—25 ppm. HTAC: 63—64 ppm. ○: Na_2S-treated charcoal, ●: charcoal without treatment.

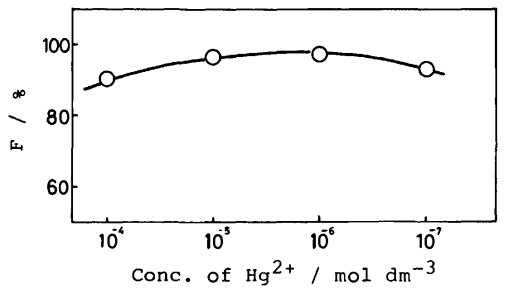

Fig. 5. Floatability vs. Hg^{2+} concentration.
Hg^{2+}: 2.1×10^{-4} mol dm^{-3}. Charcoal: 2500 ppm. AR: 60 ppm. HTAC: 540 ppm. pH: 6—7.5.

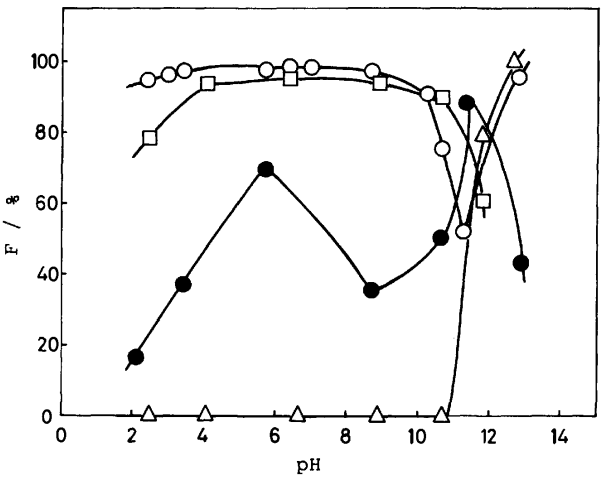

Fig. 6. Ionic interaction between coagulant and surfactant.
Hg^{2+}: 2.1×10^{-4} mol dm^{-3}. Charcoal: 2500 ppm. ○: SA 210 ppm, HTAC 540 ppm. ●: SN 210 ppm, HTAC 540 ppm. △: SC 210 ppm, HTAC 540 ppm. □: SC 210 ppm, SDS 450 ppm.

Table 1. Simple, Double, and Stepwise Flotations

SA added/ppm[a] First	SA added/ppm[a] Second	HTAC added/ppm First	HTAC added/ppm Second	F(%)
		Simple flotation		
250	0	300	0	91.7
		Double flotation		
250	0	240	60	94.8
200	50	300	0	98.5
200	50	240	60	99.3
		Stepwise flotation		
200	50	240	90	99.7

a) Amount of addition is expressed by the increase of concentration. Hg^{2+}: 2.1×10^{-4} mol dm^{-3}, charcoal: 2500 ppm, pH: 7.5—9.5.

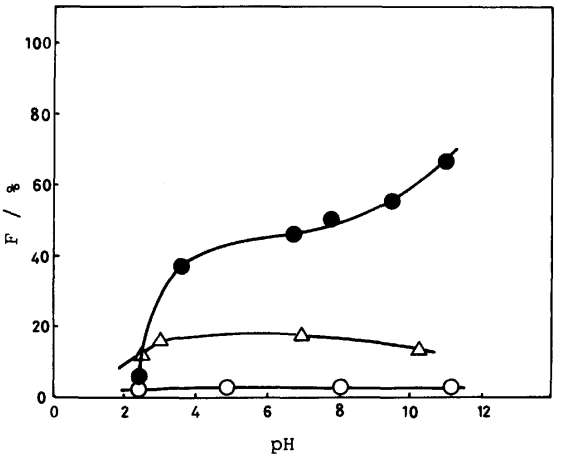

Fig. 7. Flotation without charcoal and/or coagulant. Hg^{2+}: 2.1×10^{-4} mol dm^{-3}. ○: Charcoal 2500 ppm, DL 0, HTAC 540 ppm. ●: Charcoal 0 ppm, DL 210, HTAC 540 ppm, △: Charcoal 0 ppm, DL 0, HTAC 540 ppm.

stepwise flotation. Thus, both the stepwise and double flotations are confirmed to be equally effective compared with the simple flotation. In the case of practical application, the double flotation is considered preferable compared with the stepwise one.

Mechanism of Adsorbing-Particle Flotation. In order to confirm the action of each component contributing to the adsorbing-particle flotation, flotation measurement of Hg^{2+} using HTAC without the addition of charcoal and/or coagulant was carried out. The results are show in Fig. 7. It is evident in this figure that charcoal, coagulant, and surfactant is indispensable for the adsorbing-particle flotation of Hg^{2+} ions, because the absence of any one of them results in a poor flotation. Thus the mechanism of adsorbing-particle flotation of Hg^{2+} ions is considered to be similar to the case of flotation using poly(ethyleneimine) as an adsorbent reported in a preceding paper.[5] Figure 8 illustrates the scum structure composed of Hg^{2+} ions, charcoal, anionic coagulant, and cationic surfactant together with an air bubble to which the sum is attached.

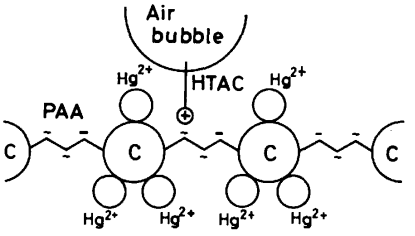

Fig. 8. Structure of scum consisting of Hg^{2+}, charcoal, PAA and HTAC. C: Charcoal.

References

1) R. B. Grieves, "Recent Development in Separation Science," Vol. 5, ed by N. N. Li, CRC Press, West Palm Beach, Florida, USA (1979), p. 55.

2) K. Kobayashi, H. Sato, K. Kachi, M. Nakamura, and T. Sasaki, *Bull. Chem. Soc. Jpn.*, **48**, 3533 (1975).

3) T. Inakazu, K. Kobayashi and T. Sasaki, *Bull. Chem. Soc. Jpn.*, **48**, 3008 (1975); K. Kobayashi, N. Watabe, and T. Sasaki, *ibid.*, **9**, 2701 (1976); K. Kobayashi, K. Natori, M. Kamaya, and T. Sasaki, *ibid.*, **51**, 439 (1978); K. Kobayashi, Y. Shimizu, and T. Sasaki, *ibid.*, **53**, 2448 (1980); T. Sasaki, K. Matsubara, and I. Machida, *ibid.*, **54**, 3153 (1981).

4) T. Sasaki, K. Mochizuki, and S. Ishiwata, *Bull. Chem. Soc. Jpn.*, **55**, 3717 (1982).

5) T. Sasaki, H. Kurosawa, K. Miyasaka, and M. Mizushima, *Bull. Chem. Soc. Jpn.*, **53**, 2506 (1980).

6) R. B. Grieves and E. F. Chouinard, *J. Appl. Chem.*, **19**, 60 (1969).

7) W. Walkowiak, D. Bhattacharyya, and R. B. Grieves, *Anal. Chem.*, **48**, 975 (1976).

8) S. Nishi, R. Kobayashi, Y. Horimoto, and M. Mito, *Nippon Kagaku Kaishi*, **1978**, 171.

Reactions of Cobalt Complexes of 5,10,15,20-Tetraphenylporphyrin with Peroxide Radicals Generated from Organic Peroxides and Unsaturated Fatty Acids

Masahiro KOHNO
JEOL Ltd., Akishima, Tokyo 196
(Received September 25, 1987)

The title reactions in aerated benzene solutions were investigated by using ESR and optical-absorption spectrometers. It was found that (1) a benzyl peroxide radical, bpox·, generated photochemically from dibenzoyl peroxide (DBPO) oxidizes [Co^{II}(tpp)] to produce, successively, a five-coordinate cobalt(III) complex, [Co^{III}(bpox)(tpp)]; a π cation radical, [Co^{III}(tpp)$^{+}$](bpox)$_2$, and isoporphyrin; (2) a *t*-butyl peroxide radical, bupox·, generated from di-*t*-butyl peroxide (DBuPO) oxidizes [Co^{II}(tpp)] to give only a six-coordinate cobalt(III)complex, [Co^{III}(bupox)(tpp)(dbupo)]; (3) lipid peroxide radicals (lpox·: oapox·, lapox·, lnapox·, and aapox·) produced from unsaturated fatty acids, oleic acid (OA), linoleic acid (LA), linolenic acid (LNA), or arachidonic acid (AA), do not react with [Co^{II}(tpp)]; (4) all the peroxide radicals (pox·: lpox·, bpox·, bupox·) react with [Co^{III}(Cl)(tpp)] to produce π cation radicals, [Co^{III}(tpp)$^{+}$](Cl)(pox), and (5) bpox· and lapox· react further with the π cation radicals to give isoporphyrins. Finally, the present reactions were compared with the reactions of horseradish peroxidase.

It has been well-known that horseradish peroxidase, chloroperoxidase, and cytochrome c peroxidase react with alkyl hydroperoxide, and peroxycarboxylic acid to· form intermediates, enzyme-bound-high-valent iron porphyrins (Compounds I and II).[1] It has also been known that active oxygens including hydroperoxide decompose metalloproteins both in vivo and in vitro.[2] As model reactions, a number of studies of the redox reactions of metal porphyrins have been carried out.[3-5]

Recently, we reported[6] on the reactions of a system composed of chloro(5,10,15,20-tetraphenylporphyrinato)cobalt(III), [Co^{III}(Cl)(tpp)], and its π cation radical, [Co^{III}(tpp)$^{+}$](Cl)$_2$, with several phenols. The phenols were oxidized to phenoxyl radicals. Concomitantly, the cobalt complexes were reduced in different manners, depending on the oxidation potentials of the phenols. The phenols investigated were classified into two groups after taking into account the differences in their reaction activities and their redox potentials: the phenols mainly reacting with [Co^{III}(tpp)$^{+}$](Cl)$_2$, and those reacting with both [Co^{III}(tpp)$^{+}$](Cl)$_2$ and [Co^{III}(Cl)(tpp)]. The reaction schemes of cobalt porphyrins [Co^{II}(tpp)], [Co^{III}(Cl)(tpp)], and [Co^{III}(tpp)$^{+}$](Cl)$_2$ with phenols showed a clear correspondence to the oxidation reactions of horseradish peroxidase (HRP).

In this study, we will investigate the inverse reactions of cobalt porphyrins ([Co^{II}(tpp)] and [Co^{III}(Cl)(tpp)]) with organic peroxides and unsaturated fatty acids in aerated benzene solutions by using ESR and optical absorption techniques. As the results, the reaction mechanisms between the cobalt porphyrins and the peroxide radicals will be presented. Finally, the reaction mechanisms of cobalt porphyrins with the peroxide radicals will be discussed in comparison with the formation mechanism of Compound I, and Compound II of HRP.[7]

Experimental

Materials. The chloro(5,10,15,20-tetraphenylporphyrinato)cobalt(III), [Co^{III}(Cl)(tpp)], and (5,10,15,20-tetraphenylporphyrinato)cobalt(II), [Co^{II}(tpp)],[8] were provided by Dr. Kiyoko Yamamoto of the Institute of Physical and Chemical Research.

The dibenzoyl peroxide (DBPO) and di-*t*-butyl peroxide (DBuPO) were supplied by Nakarai Chemical Industries. 99%-pure oleic acid (OA), linoleic acid (LA), linolenic acid (LNA), and arachidonic acid (AA) were supplied from the Sigma Chemical Co., Ltd., and were used without further purification. The nitrosodurene, a spin-trapping reagent, was supplied by Mr. Naohiro Takahashi of the Sumitomo Chemical Co., Ltd.

Preparation of Sample Solutions. Benzene was used as the solvent throughout this study.

The [Co^{II}(tpp)] and [Co^{III}(Cl)(tpp)] were dissolved in 2×10^{-3} mol dm^{-3} in the cases of reactions with all peroxide radicals except DBuPO. The solution of [Co^{III}(Cl)(tpp)] contains 2.7×10^{-5} mol dm^{-3} of the π cation radical, [Co^{III}(tpp)$^{+}$](Cl)$_2$.[6] In the case of the reaction with DBuPO, [Co^{II}(tpp)] and [Co^{III}(Cl)(tpp)] were dissolved in 2×10^{-4} mol dm^{-3}. DBPO, DBuPO, OA, LA, LNA, and AA were dissolved just before use (DBPO, 2×10^{-3} mol dm^{-3}; DBuPO, 1×10^{-1} mol dm^{-3}; OA, LA, LNA, and AA, 10%).

Measurements. The ESR spectra were measured by means of a JEOL FE-2XG spectrometer equipped with a Takeda Riken TR-5211 microwave counter. The ESR spectra of the π cation radical, [Co^{III}(tpp)$^{+}$](x)(y), measured in this work show the pair of the maximum and the minimum separated by a wide plateau. Such spectra are due to eight unresolved, hyperfine lines. In this work, therefore, the *g* values were determined from the midpoint of the maximum and the minimum of the spectra. The spacings between maximum and minimum points, ΔH, are the measure of the hyperfine line of cobalt:

$$\Delta H \simeq 7 \times a_{Co^{III}} + \Delta H_{msl}, \quad (1)$$

where ΔH_{msl} is the intrinsic line width. Hereafter, we will

adopt these values as the ESR parameters.

For a quantitative analysis of the π cation radicals, a computer system of JES ES-PRIT23 was used. The optical absorption spectra were measured by means of a Hitachi 330 spectrophotometer using quartz cells with optical path lengths of 1 and 0.1 cm.

Simultaneous measurements of the ESR and the optical absorption spectra were carried out by using an ESRET system combining a Spectro Multi-Channel Photo Detector MCPD-100 (Otsuka Electronics) with a JES FE-2XG apparatus equipped with a transmission cavity, ES-MCX-3B.[9] By the use of the ESRET, one can measure simultaneously both the ESR and the optical spectra of a sample solution under the same conditions. This apparatus is very useful for mesurement of a solution containing an unstable sample or a small amount of a sample. A quartz cell with an optical path length of 0.3 mm, 10 mm in width, and 40 mm in height, was used for the ESRET measurements. To 0.1 cm^3 of a [Co^{II}(tpp)] or [Co^{III}(Cl)(tpp)] solution was added 0.1 cm^3 of a peroxide or fatty-acid solution. The ESR and absorption spectra of the mixed solution were simultaneously measured at intervals of 1 min after mixing. The absorption spectra obtained from the ESRET were checked with those obtained by means of a Hitachi 330 spectrophotometer. The time dependent ESR spectra were measured using a rapid detection system.[6] 0.2 cm^3 of neat unsaturated fatty acids were added to 0.2 cm^3 of a [Co^{III}(Cl)(tpp)] solution, which was bubbled in by dry nitrogen gas.

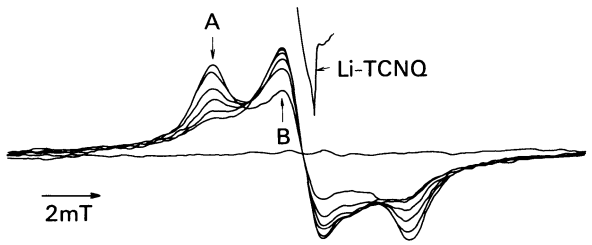

Fig. 1a. ESR spectra measured before and after (the interval of 1 min) addition of DBPO to [Co^{II}(tpp)] in a benzene solution. A: [Co^{III}(tpp)$^+$](bpox)$_2$, B: bpox·. Li-TCNQ is internal standard, g=2.0026.

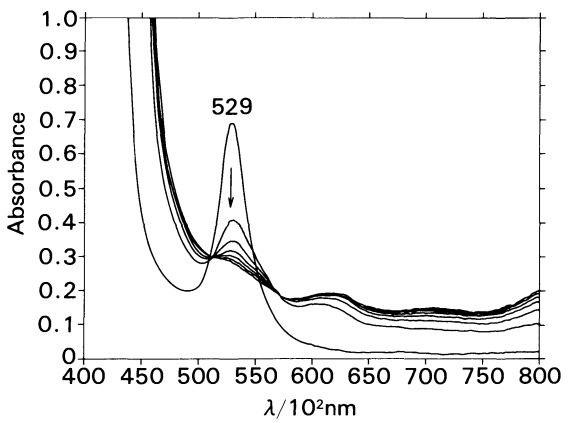

Fig. 1b. Absorption spectra measured before and after (the interval of 1 min) addition of DBPO to [Co^{II}(tpp)] in a benzene solution.

Results and Discussion

Reaction of [Co^{II}(tpp)] with DBPO or DBuPO. To a benzene solution of [Co^{II}(tpp)] were added the same amount of a DBPO solution; the ESR and the optical absorption spectra of the mixed solution were then measured by using the ESRET apparatus at intervals of 1 min after adding DBPO to the [Co^{II}(tpp)]. The ESR spectra thus measured are shown in Fig. 1a. The solution of [Co^{II}(tpp)] gave no ESR signals at room temperature because of the short relaxation time. One minute after the addition of DBPO, two signals, A and B, appeared. The ESR parameters of the A signal are g=2.0048 and ΔH=6.89 mT. This signal was assigned to a π cation radical, [Co^{III}(tpp)$^+$](bpox)$_2$ on the basis of the ESR parameters.[10,11] The ESR parameters of the B signal are g=2.0082 and ΔH=0.65 mT. It is well-known that DBPO decomposes easily to produce the peroxide radical under these ambient conditions: natural light, air, and room temperature. In order to confirm the B signal, DBPO in an aerated benzene solution was irradiated by using a mercury lamp as a light source without a filter; the ESR spectrum was then measured at 5 °C. An ESR signal of g=2.0155(±0.0002) and ΔH=0.75 mT was obtained. The g value is typical of peroxide radicals,[12,13] so the signal was identified as a peroxede radical of DBPO (bpox·: $C_6H_5(CO)OO\cdot$). The same signal was observed for a deaerated benzene solution of irradiated DBPO. The g value of the B signal is somewhat smaller than that of bpox· obtained in neat benzene by irradiation. This might be because of an interaction between the radical and the tpp ligand of [Co^{II}(tpp)]. With an increase in the time, the intensity of the A signal decreased, while that of the B signal increased. This suggests that bpox· successively generated oxidizes [Co^{II}(tpp)] to produce [Co^{III}(tpp)$^+$](bpox)$_2$ and then further decomposes the π cation radical. The corresponding optical absorption spectra are shown in Fig. 1b. With an increase in the time, the characteristic absorption band at 529 nm of [Co^{II}(tpp)] decreased in intensity, while weak and broad bands appeared at longer wavelengths. The bands in the near infrared-region are interpreted as being due to the formation of isoporphyrin,[14-16] because the optical-absorption spectrum measured for the solution by means of the Hitachi 330 spectrophotometer showed absorption maxima at 700 and 800 nm. The absorption bands in the visible region may be due to those of [Co^{III}(tpp)]$^+$ and the π cation radical of Co^{III}(tpp). From both the ESR and the optical-absorption-spectral changes, it is concluded that bpox· oxidizes [Co^{II}(tpp)] to produce [Co^{III}(tpp)]$^+$, then the π cation radical, and finally isoporphyrin.

The optical-absorption spectra observed for the reaction mixture of [Co^{II}(tpp)] and DBuPO by using the

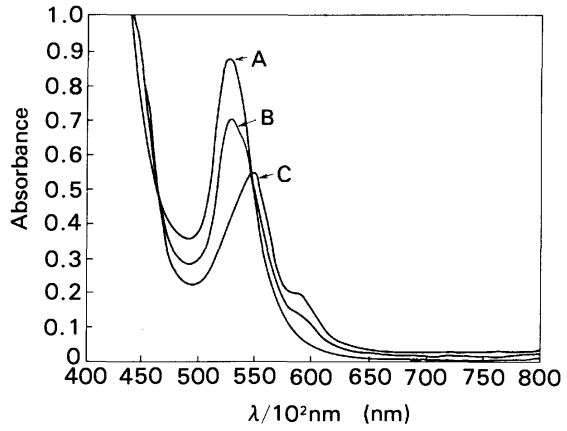

Fig. 2. Absorption spectra measured beore (A) and after (B: 7 min, C: 15 min) addition of DBuPO to [Co^{II}(tpp)] in a benzene solution.

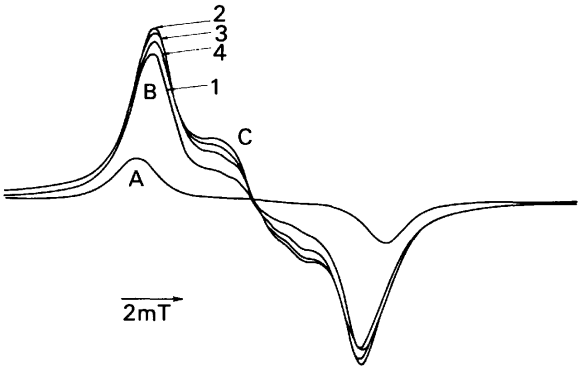

Fig. 3a. ESR spectra measured beore (A) and after (B: 1, 2, 3, 4) addition of BPO to [Co^{III}(Cl)(tpp)] in a benzene solution at the interval of 1 min.
A: [Co^{III}(tpp^{+}](Cl)$_2$, B: [Co^{III}(tpp)$^{+}$](Cl)(bpox$_2$), C: bpox·.

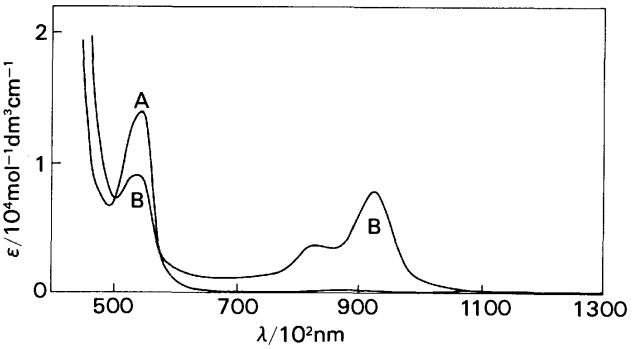

Fig. 3b. Absorption spectra measured beore (A) and after (B) addition of BPO to [Co^{III}(Cl)(tpp)] in a benzene solution.

ESRET apparatus are shown in Fig. 2. The reaction mixture gave no ESR spectrum of the π cation radical. Upon the addition of DBuPO to [Co^{II}(tpp)] in a benzene solution, the intensity of the absorption band of [Co^{II}(tpp)] at 529 nm (A) decreased and the absorption maximum shifted towards longer wavelengths, showing one set of isosbestic points at 465 and 545 nm, and new bands appeared at 550 and 590 nm. The absorption spectrum represents the characteristic absorption of the six-coordinate [Co^{III}-(tpp)]$^{+}$ complex.[17] The spectrum was an unchanged with the increase in time. It is also well-known that DBuPO decomposes under ambient conditions. DBuPO in an aerated benzene solution was irradiated by using a mercury lamp as a light source without a filter, and the ESR spectrum was measured at 5 °C. The ESR signal of g=2.0155(±0.0002) and ΔH=0.3 mT appeared; it was identified as a peroxide radical, bupox·(C_4H_9OO·), on the basis of the g value. From the results of the optical-absorption-spectral change and the lack of any ESR spectra, it is concluded that [Co^{II}(tpp)] is oxidized by bupox· to produce five-coordinate [Co^{III}(bupox)(tpp)]; then excess DBuPO coordinates as the 6th ligand to form a six-coordinate complex, [Co^{III}(bupox)(tpp)(dbupo)].

The reactions of [Co^{II}(tpp)] with unsaturated fatty acids, OA, LA, LNA, and AA, in aerated benzene solutions gave no ESR or absorption-spectral changes.

Reaction of [Co^{III}(Cl)(tpp)] with DBPO, DBuPO, OA, LA, LNA, and AA. The ESR spectra measured for a mixed solution of [Co^{III}(Cl)(tpp)] and DBPO are shown in Fig. 3a. Signal A in Fig. 3a represents the signal of [Co^{III}(tpp)$^{+}$](Cl)$_2$ (g=2.0047 and ΔH=8.98 mT) that is contained in the solid [Co^{III}(Cl)(tpp)].[18] In the ESR spectrum obtained after the addition of DBPO, the signal of [Co^{III}(tpp)$^{+}$](Cl)$_2$ disappeared, and new two signals, B and C, appeared. The ESR parameters of the B signal are g=2.0062 and ΔH= 6.37 mT. This showed the species to be a π cation radical, [Co^{III}(tpp)$^{+}$](Cl)(bpox), on the basis of the ESR parameters. The C signal represents the signal of bpox·. When an increase in the time, the signal intensity of B decrease, while that of C increases, as in the case of the reaction of [Co^{II}(tpp)] with DBPO.

The optical-absorption spectra observed before and after the addition of DBPO, (A) and (B), respectively, are shown in Fig. 3b. The characteristic absorption band of [Co^{III}(Cl)(tpp)] at 540 nm decrease in intensity upon the addition of DBPO, and new bands appeared at 815 and 915 nm. The bands in the near-infrared region are attributed to isoporphyrin. From the results of the ESR and the absorption spectra, it is concluded that bpox· oxidizes [Co^{III}(Cl)(tpp)] to [Co^{III}-(tpp)$^{+}$](Cl)(bpox) and then to isoporphyrin, while [Co^{III}(tpp)$^{+}$](Cl)$_2$ is oxidized to isoporphyrin.

The ESR spectra and optical absorption spectra of a reaction mixture of [Co^{III}(Cl)(tpp)] and DBuPO were measured as in the case of the reaction with DBPO. The ESR spectra showed that the signal of [Co^{III}-(tpp)$^{+}$](Cl)$_2$ disappeared and a new signal appeared. Based on the ESR parameters obtained from the spectrum, the B signal, g=2.0062 and ΔH=7.78 mT, can be interpreted as being to the formation of a π cation

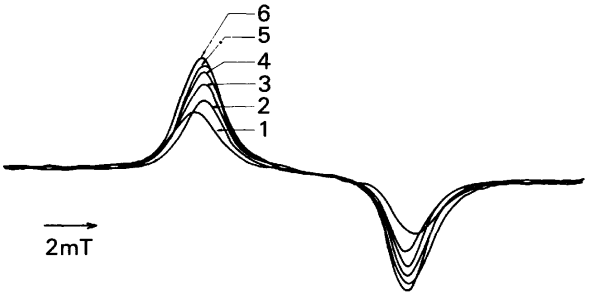

Fig. 4a. ESR spectra measured after addition of OA (1: 0%, 2: 2%, 3: 4%, 4: 6%, 5: 8%, and 6: 10%) to [Co^{III}(Cl)(tpp)] in a benzene solution.

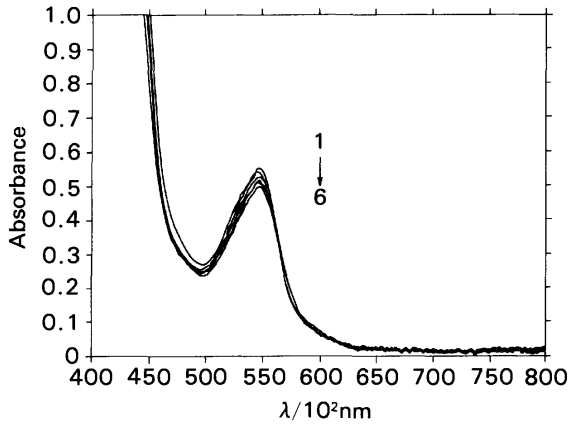

Fig. 4b. Absorption spectra measured after addition of OA (1: 0%, 2: 2%, 3: 4%, 4: 6%, 5: 8%, and 6: 10%) to [Co^{III}(Cl)(tpp)] in a benzene solution.

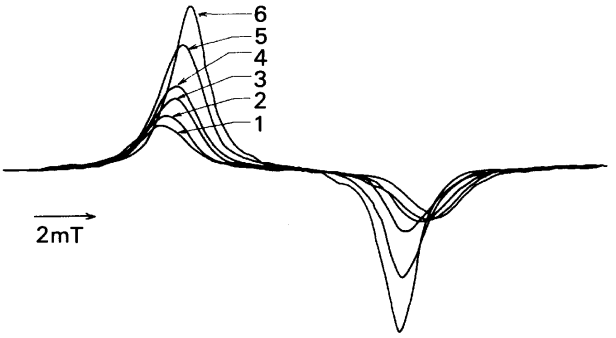

Fig. 5a. ESR spectra measured after addition of LA (1: 0%, 2: 1.25%, 3: 2.5%, 4: 5%, 5: 10%, and 6: 20%) to [Co^{III}(Cl)(tpp)] in a benzene solution.

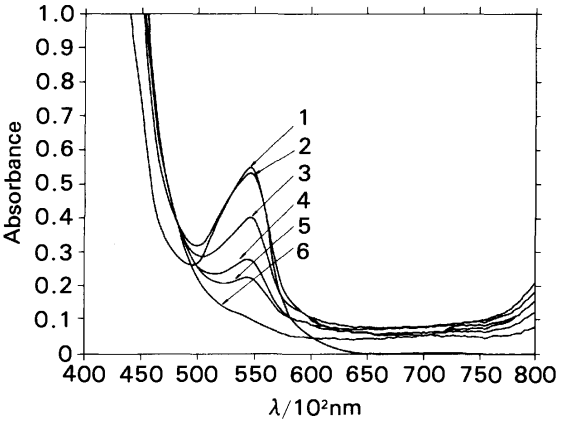

Fig. 5b. Absorption spectra measured after addition of LA (1: 0%, 2: 1.25%, 3: 2.5%, 4: 5%, 5: 10%, and 6: 20%) to [Co^{III}(Cl)(tpp)] in a benzene solution.

radical, [Co^{III}(tpp)$^{+}$](Cl)(bupox). The corresponding optical-absorption spectra showed that, with an increase in the time, the intensities of the characteristic absorption bands of [Co^{III}(Cl)(tpp)] at 406 and 540 nm decrease and a new shoulder appears at 436 nm which may be attributable to the formation of a π cation radical.[19] The ESR and optical-absorption-spectral changes suggest that [Co^{III}(Cl)(tpp)] reacts with DBuPO to form a π cation radical, [Co^{III}(tpp)$^{+}$](Cl)(bupox).

The ESR spectra measured for aerated benzene solutions of [Co^{III}(Cl)(tpp)] with various amounts of OA (0, 2, 4, 6, 8, and 10%) are shown in Fig. 4a. Upon the addition of OA, the signal (1 in the figure) due to [Co^{III}(tpp)$^{+}$](Cl)$_2$ disappeared and a new signal (2—6) appeared. The new signal is identified as a π cation radical, [Co^{III}(tpp)$^{+}$](Cl)(oapox), due to the ESR parameters obtained from the spectrum. With the increase in the amount of OA, the intensity of the signal increased. The concentration of [Co^{III}(tpp)$^{+}$](Cl)(oapox) produced by the addition of 10% of OA is 8×10^{-5} mol dm^{-3}. The corresponding optical absorption spectra showed only a slight decrease in the absorption intensity of [Co^{III}(Cl)(tpp)] at 540 nm (Fig. 4b). The ESR and optical absorption spectral changes suggest that [Co^{III}(Cl)(tpp)] is oxidized by a peroxide radical (oapox·) generated from OA under the ambient conditions (to be described below) to produce [Co^{III}(tpp)$^{+}$](Cl)(oapox). The reactions of [Co^{III}(Cl)(tpp)] with LNA and AA also gave rise to the formation of π cation radicals, [Co^{III}(tpp)$^{+}$](Cl)(lnapox) and [Co^{III}(tpp)$^{+}$](Cl)(aapox) respectively.

The ESR and optical-absorption spectra of aerated benzene solutions of [Co^{III}(Cl)(tpp)] with various amounts of LA (0, 1.25, 2.5, 5, 10, and 20%) were also measured. The spectra are shown in Fig. 5a. Upon the addition of LA, the signal (1 in the figure) of [Co^{III}(tpp)$^{+}$](Cl)$_2$ disappeared and a new signal (2—6) appeared. The new signal is identified as a π cation radical, [Co^{III}(tpp)$^{+}$](Cl)(lapox), on the basis of the ESR parameters obtained from the spectrum. With the increase in the amount of LA, the intensity of the signal increased. The concentration of [Co^{III}(tpp)$^{+}$](Cl)(lapox) produced by the addition of 10% of OA is ca. 6×10^{-5} mol dm^{-3}. The corresponding optical-absorption spectra (Fig. 5b) obtained by using ESRET apparatus showed that the intensity of the absorption band of [Co^{III}(Cl)(tpp)] at 540 nm rapidly decreased and the new bands appeared at 825 and 912 nm

attributable to the formation of isoporphyrin. The ESR and optical-absorption-spectral changes lidicate that the peroxide radical of lapox· oxidizes [Co^{III}(Cl)(tpp)] to [Co^{III}(tpp)$^{+}$](Cl)(lapox) and then afterward to isoporphyrin.

The ESR parameters of the π cation radicals obtained are summarized in Table 1.

Reaction Rates. In the reactions of [Co^{III}(Cl)(tpp)] (2×10^{-3} mol dm^{-3}) with unsaturated fatty acids (10^{-1} mol dm^{-3}) in aerated benzene solutions, the formation rate of the π cation radical, [Co^{III}(tpp)$^{+}$](Cl)(lpox), was estimated by using a rapid-detection system.[6] In Fig. 6, the concentrations of the π cation radicals formed are plotted against the reaction time. In the cases of the reactions with OA, LNA, and AA, the amounts of the π cation radicals, [Co^{III}(tpp)$^{+}$](Cl)(oapox), [Co^{III}(tpp)$^{+}$](Cl)(lnapox), and [Co^{III}(tpp)$^{+}$](Cl)(aapox), increase with the time in the early stage of the reaction. However, in the case of the reaction with LA, the amount of [Co^{III}(tpp)$^{+}$](Cl)(lapox) is the largest, though it decreases rapidly. The reaction rates were estimated from the linear portion in Fig. 6, the reaction rates were obtained as 3.5×10^{-5}, 2.5×10^{-5}, and 3×10^{-6} mol s^{-1} for OA, LNA, and AA respectively. The rate for LA was larger than 2.4×10^{-4} mol s^{-1}. The decrease in the π cation radicals which may be seen in Fig. 6 may show that lpox· oxidizes the π cation radicals further to isoporphyrin and also that the oxidation activity of lapox· is distinctly large among lpox··. It should also be noted here that the formation rates of the π cation radical, [Co^{III}(tpp)$^{+}$](Cl)(lpox), are not ralated to the autooxidation rates of unsaturated fatty acids (OA<LA<LNA<AA),[21] but rather with the oxidation potentials of unsaturated fatty acids, as in the reactions between cobalt porphyrins and phenols.[6]

Table 1. The ESR Parameters of the π Cation Radicals Obtained, [Co^{III}(tpp)$^{+}$](x)(y), in Benzene

x	y	g (±0.0002)	ΔH[a] / mT
Cl	Cl	2.0047	8.98
Cl	bpox	2.0062	6.37
Cl	bupox	2.0058	7.78
Cl	oapox	2.0054	7.63
Cl	lapox	2.0063	6.93
Cl	lnapox	2.0047	7.73
Cl	aapox	2.0047	7.72
bpox	bpox	2.0082	6.89

a) Peak-to-peak width.

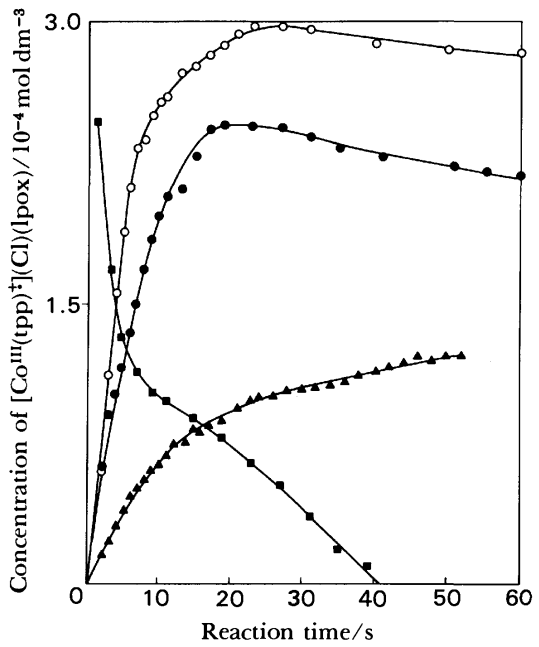

Fig. 6. Concentration decay of [Co^{III}(tpp^{+}](Cl)(lpox) generated from the reaction of [Co^{III}(Cl)(tpp)] with unsaturated fatty acids (○: OA, ■: LA, ●: LNA, and ▲: AA) against reaction time.

Detection of Peroxide Radicals Generated from Unsaturated Fatty Acids under Ambient Conditions. It has been well-known that unsaturated fatty acids, when subjected to autooxidation in air, produce peroxide radicals. The active species generated from unsaturated fatty acids were investigated by using the spin-trapping method. Nitrosodurene (3 mg) was added to neat OA (and LA), after which the solution was irradiated under degassed conditions by using a mercury lamp as a light source; then the ESR spectrum was measured. A signal with an anisotropic pattern in the high magnetic field was obtained, as is shown in Fig. 7. The ESR parameters obtained from the spectrum are a_N=1.36 mT and a_H=0.64 mT. These parameters coincide with the values of the adduct with the alkyl radicals (R·).[20] In order to examine the effect of air, nitrosodurene dissolved in OA was irradiated under aerated condition and the ESR spectrum was measured. The spectrum showed the same radical; however, the amount of spin adducts observed was smaller than that observed in degassed conditions, as is shown in Fig. 8. This is interpreted as showing

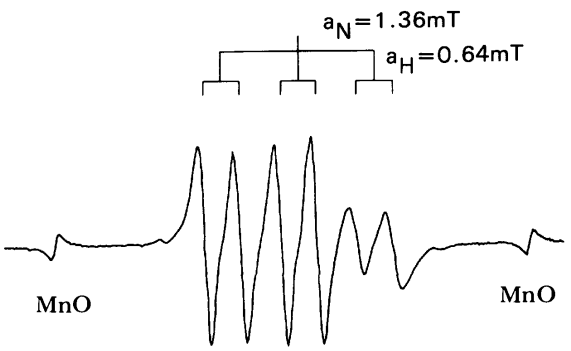

Fig. 7. ESR spectrum of spin adduct of nitrosodurene with alkyl radical of OA. MnO is internal standard signal.

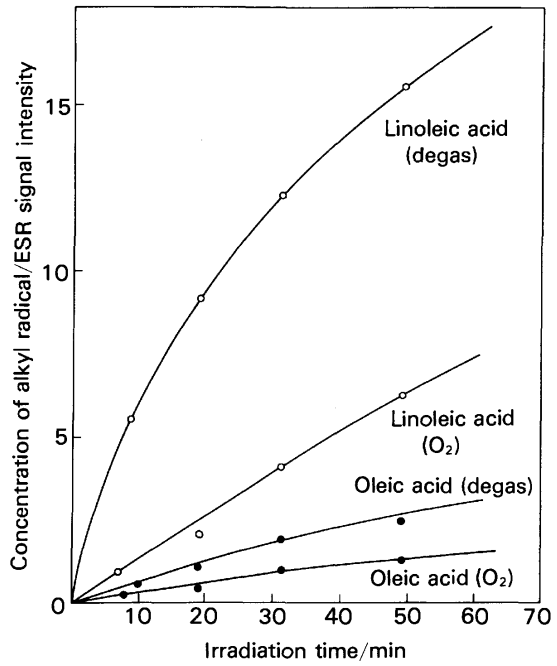

Fig. 8. Effect of oxygen molecule on concentration of formed spin adducts of nitrosodurene with alkyl radical of OA or LA in aerated and deaerated conditions.

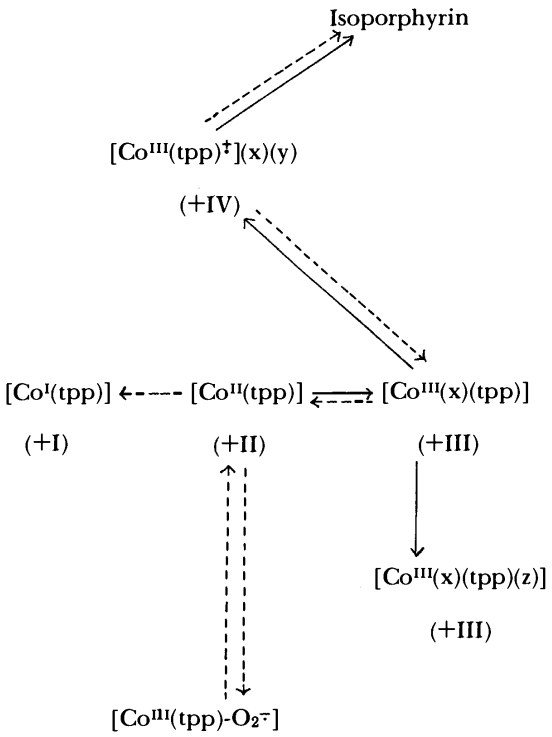

Scheme 1. Redox system of cobalt porphyrins. —: present oxidation process, -----: reduction and oxidation process as previously reported.[6,22]

that the alkyl radicals generated from unsaturated fatty acids combine with oxygen molecules to form stable peroxide radicals (lpox·).

The present reactions may be summarized as follows: (1) the bpox· oxidizes both [Co^{II}(tpp)] and [Co^{III}(Cl)(tpp)] to π cation radicals; (2) the bupox· oxidizes [Co^{II}(tpp)] to [Co^{III}(bupox)(tpp)(dbupo)], while the cobalt(III) species is not subjected to any further oxidation of the bupox·; however, [Co^{III}(Cl)-(tpp)] is oxizided to form π cation radicals; (3) the lpox· (oapox·, lapox·, lnapox·, and aapox·) oxidizes [Co^{III}(Cl)(tpp)], but not [Co^{II}(tpp)], to π cation radicals and (4) the bpox· and the lapox· further react with π cation radicals to give isoporphyrins. These results indicate that the oxidation reactions proceed depending on the oxidation potentials of both cobalt porphyrins and peroxide radicals.

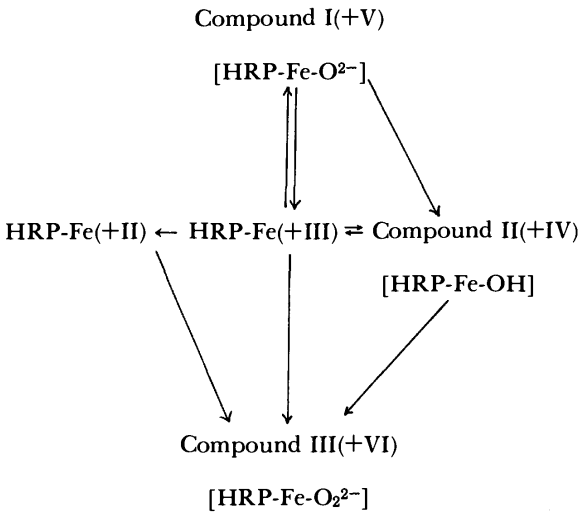

Scheme 2. Redox system of HRP.[7]

Cobalt tpp and Horseradish Peroxidase(HRP)

We will now compare our results with the reaction of a typical enzyme, HRP. The function of cobalt porphyrins, [Co^{II}(tpp)] and [Co^{III}(Cl)(tpp)], and the enzymatic reaction of HRP are written in Schemes 1 and 2. The numbers in parentheses in these schemes represent the apparent oxidation states estimated on the basis of data from earlier studies.[6,7] [Co^{III}(tpp)$^{+}$]$^{2+}$ and Compound I of HRP are both π cation radicals. Here, we assume a correspondence (1) of [Co^{II}(tpp)] to native HRP, (2) of [Co^{III}(tpp)]$^{+}$ to Compound II, and (3) of [Co^{III}(tpp)$^{+}$]$^{2+}$ to Compound I.

In the HRP system, it has been known that native HRP is subjected to two-electron oxidation to produce Compound I, and also that Compound I reacts with such substrates as phenol derivatives and is reduced to native HRP through Compound II. In the present study, we found that peroxide radicals oxidize [Co^{II}(tpp)] to produce, successively, [Co^{III}(tpp)]$^{+}$, [Co^{III}(tpp)$^{+}$]$^{2+}$, and isoporphyrin. This fact suggests that, in the system of HRP and alkyl hydroperoxide, Compound I is formed by the successive oxidation of native HRP with the peroxide radicals (·OOR).

Furthermore, Compound II has been known to be [HRP-Fe-OH] which is coordinated with the OH generated from hydroperoxide or alkyl hydroperoxide. Taking into account the fact that [Co^{II}(tpp)] is oxidized by a peroxide radical (bpox·) to produce [Co^{III}(bpox)(tpp)], it is considered that the Compound II formed in the system of HRP and alkyl hydroperoxide may be [HRP-Fe-OOR]. The formation of isoporphyrins in the reactions suggests that the degradation of HRP is caused by the peroxide radicals formed in the process of the autooxidation of lipids.

The author wishes to express his deep gratitude to Professor Hiroaki Ohya-Nishiguchi of Kyoto University and Dr. Kiyoko Yamamoto of The Institute of Physical and Chemical Research for their helpful discussion during the course of this study.

References

1) W. D. Hewson and L. P. Hager, "Peroxidases, Catalases, and Chloroperoxidase," in "The Porphyrines," ed by D. Dolphin, Academic Press, New York (1979), Vol. 7, p. 295, and the other references cited therein.

2) C. C. Winterboun, *Environmental Health Perspectives*, **64**, 321 (1985).

3) W. A. Lee and T. C. Bruice, *Inorg. Chem.*, **25**, 131 (1986).

4) K. Tajima, K. Ishizu, H. Sakurai, and H. Ohya-Nishiguchi, *Biochem. Biophys. Res. Commun.*, **135**, 972 (1986).

5) S. Sano and Y. Sugiura, *J. Chem. Soc., Chem. Commun.*, **1982**, 750.

6) M. Kohno, *Bull. Chem. Soc. Jpn.*, **59**, 2053 (1986).

7) I. Yamasaki and K. Yokota, *Mol. Cell. Biochem.*, **2**, 39 (1973).

8) K. Yamamoto, *Sci. Papers Inst. Phys. Chem. Res.*, **71**, 111 (1977).

9) H. Ohya-Nishiguchi, K. Kohno, K. Mitsuta, and S. Tsuboyama, Proceeding of the 36th Annual Meeting of Coordination Chemistry, 1986, p. 127.

10) H. Ohya-Nishiguchi, K. Kohno, and K. Yamamoto, *Bull. Chem. Soc. Jpn.*, **54**, 1923 (1981).

11) K. Ichimori, H. Ohya-Nishiguchi, N. Hirota, and K. Yamamoto, *Bull. Chem. Soc. Jpn.*, **58**, 623 (1985).

12) B. Kalyanaraman, C. Mottley, and R. P. Mason, *J. Bio. Chem.*, **258**, 3855 (1983).

13) A. Tkac, K. Vesely, and L. Omelka, *J. Phy. Chem.*, **75**, 2575, 2580 (1971).

14) A. Gold, W. Ivey, G. E. Toney, and R. Sangaiah, *Inorg. Chem.*, **23**, 2932 (1984).

15) D. Dolphin, R. H. Felton, D. C. Borg, and J. Fajer, *J. Am. Chem. Soc.*, **92**, 743 (1970).

16) J. A. Guzinski and R. H. Felton, *J. Chem. Soc., Chem. Commun.*, **1973**, 715.

17) K. Yamamoto and S. Tonomura, *Sci. Papers Inst. Phys. Chem. Res.*, **58**, 122 (1964).

18) M. Kohno, H. Ohya-Nishiguchi, K. Yamamoto, and T. Sakurai, *Bull. Chem. Soc. Jpn.*, **56**, 822 (1983).

19) K. Yamamoto, M. Hoshino, M. Kohno, and H. Ohya-Nishiguchi, *Bull. Chem. Soc. Jpn.*, **59**, 351 (1986).

20) T. Chiba, K. Fujimoto, and T. Kaneda, *J. Am. Oil Chem. Soc.*, **58**, 587 (1981).

21) M. Uchida, M. Matsuo, and M. Sagai, "Kasanka-Shishitsu to Seitai," Gakkai-Shuppan Senta, Tokyo (1985), Chap. 1.

22) F. A. Walker, *J. Am. Chem. Soc.*, **92**, 4235 (1970).

Study of Ion Transport across Amphoteric Ion-Exchange Membrane.[1] V. Nonequilibrium Thermodynamic Analyses of Ion Selectivity

Kozue KAIBARA,* Hiroyoshi INOUE, Shigeru TSURUYAMA, and Hideo KIMIZUKA
Department of Chemistry, Faculty of Science, Kyushu University,
Hakozaki, Higashi-ku, Fukuoka 812
(Received September 28, 1987)

Ion-transport processes across an amphoteric ion-exchange membrane were investigated by means of estimating the membrane permeability matrix, a set of modified linear phenomenological coefficients, from the electrochemical and the ion flux data. Systematic comparisons of phenomenological analyses on an amphoteric ion-exchange membrane system with those on an ordinary cation-exchange membrane system were carried out to investigate the correlations of singly- and binary-charged membrane structures to characteristic transport properties. The modes of ion permselectivity of an amphoteric ion-exchange membrane in the metal chloride concentration-cell systems are characterized by the potentiometric selective response due to the ion-sieve effect, the low membrane conductance, and the large ion flux, while those of an ordinary cation-exchange membrane are characterized by the totally charge-dependent potential response, the high conductance, and the extremely small ion flux. The cross elements of the membrane permeability matrix, which represent the partial contributions of cation-anion interactions to the membrane permselectivity, are positive for an amphoteric membrane and negative for a cation-exchange membrane. The positive cross matrix elements act deceleratively on the membrane permeability, whereas the negative elements do acceleratively. It was pointed out based on the nonequilibrium thermodynamic theory that the preferable and efficient permeation mechanism is the simple diffusion process in an amphoteric ion-exchange membrane, whereas the electroconductive process in a cation-exchange membrane.

The linear phenomenological analysis is a powerful tool to characterize membrane transport processes on the basis of the nonequilibrium thermodynamics (see e.g., Refs. 2, 3). A variety of nonequilibrium thermodynamic theories on the membrane transport processes have been developed to investigate meterial transport phennomena arising across membranes. These membrane theories are useful to describe quantitatively the selective transport performance in some particular membrane samples by evaluating the linear phenomenological coefficients from the available experimental data. However, there seem to be some uncertain factors, even now, in the generalized correlations of phenomenological coefficients with membrane properties such as permeability, selectivity, polymeric and charged structures, and phase behavior of membrane substances. Therefore, it is still worth to examine differences in the linear phenomenological coefficients between the membrane systems showing distinguishable transport characteristics with each other.

As shown in earlier reports of this series, an amphoteric ion-exchange membrane, in which almost equal amounts of positively and negatively charged sites are homogeneously and regularly dispersed at high densities, shows unique transport characteristics different from those of a uniform ion-exchange membrane. By introducing equal amounts of positively and negatively charged sites into the membrane phase, the permselectivities to cations or anions are deteriorated inevitably; however, potentiometric permselectivities were demonstrated even for ions of the same charge as the most interesting transport properties of the homogeneous type amphoteric ion-exchange membrane, unlike the usual uniform ion-exchange membrane.[1,4] It has been pointed out that a useful amphoteric ion-exchange membrane should have the membrane structure in which both the cation- and anion-exchange regions are as small as possible[5] and also that the transport phenomena specific to an amphoteric ion-exchange membrane are observed when the ratio of cationic to anionic exchange capacity ranges from 0.8 to 1.[6] Recently developed amphoteric ion-exchange membranes, in which cationic and anionic exchange sites are distributed homogeneously over the functionalized polymer network in microscopic dimensions with high density, are proved to be applicable to the processes separating organic compounds of low molecular weight from inorganic electrolyte mixtures.[7,8]

In the present investigations, ion transport characteristics of an amphoteric ion-exchange membrane are examined by means of estimating the membrane permeability matrix as a principal membrane permselectivity parameter. The transport process analyses utilizing the membrane permeability matrix, of which element is recognized as a modified linear phenomenological coefficient describing a partial contribution of correlation between permeating ions on the membrane selectivity to respective ions, provide a quantitative description of ion transport process on the basis of nonequilibrium thermodynamics.[9–11] The estimated membrane permeability matrix of an amphoteric ion-exchange membrane was compared with that of an ordinary cation-exchange membrane, since the present discussion also aims at inspecting how the charged membrane structure reflects on

qualitative and quantitative aspects of the phenomenological coefficients.

Experimental

An amphoteric membrane used in the present experiments is 1.0-PA-29 amphoteric ion-exchange membrane (Kanegafuchi Chemical Industry Co., Ltd.) and CK-1, 1.0t cation-exchange membrane (Asahi Chemical Industry Co., Ltd.) was used as a reference membrane sample of ordinary highly selective cation-exchange membrane. Fundamental physicochemical properties and an outline of preparation procedures of these membranes were described in earlier papers.[1,4,7,10] Both the ion-exchange membranes have the same cation-exchange site, usual sulfonic acid type, and comparable ion-exchange capacities, ca. 1.7—2.0 eq·(kg wet-membrane)$^{-1}$. Accordingly, systematic and generalized discussions are available to investigate substantial differences in the ion transport characteristics of a binary-charged amphoteric ion-exchange membrane as compared with those of an ordinary singly-charged cation-exchange membrane.

Electrochemical properties, such as transmembrane potential and conductance, and inter-compartmental ion fluxes were measured for the concentration-cell systems to evaluate the membrane transport parameters based on the nonequilibrium thermodynamic theory. Experimental systems consisted of solution phase I, in which electrolyte concentration was varied from 10^{-1} to 10^{-3} mol dm^{-3}, and phase II with a fixed concentration of 10^{-2} mol dm^{-3} separated by a membrane phase. Electrolyte used in the present measurements included metal chlorides such as CsCl, KCl, NaCl, LiCi, $CaCl_2$, and $SrCl_2$. Electrolyte solutions were prepared from extra-pure salts with conductivity water. Measurements were carried out with a setup, essentially the same as reported in an earlier paper.[10] A high-input-impedance digital voltmeter (TR6877D, Takeda Riken Co.) and impedance measuring equipments (YHP4255A and YHP4440B, Yokogawa-Hewlett-Packard Co.; KC-530, Kokuyo Electric Co.) were employed to measure the electrochemical properties of the concentration-cell systems with the ion-exchange membrane by the ordinary methods. Inter-compartmental ion flux was estimated by means of tracing the time changes in solution conductivities of the solution phases I and II. All the measurements were carried out at regulated temperature, 25.0±0.1 °C, using a water-jacket glass-made measurement cell throughout the present experiments.

Results and Discussion

Membrane Transport Phenomena. Figure 1 summarizes the results obtained in the present experiments. Transmembrane potential data in Fig. 1-A indicate that the 1.0-PA-29 amphoteric ion-exchange membrane reveals potentiometric selectivities even to permeant metal cations of the same charge. It has been pointed out that these potentiometric selectivities are due to an "ion-sieve effect" to hydrated permeant ion demonstrated for all ions regardless of the electrolyte species and of positive or negative charges.[1,4] The ion-sieve effect responsible for shifting out the hydrated cations and anions permeating across the 1.0-PA-29 amphoteric ion-exchange membrane was suggested to be dependent upon the three-dimensional-array ion-exchange groups with an alternately charged regular arrangement.

Providing that equal numbers of the cation- and anion-exchange sites are introduced into the membrane phase and that both the ion-exchange sites

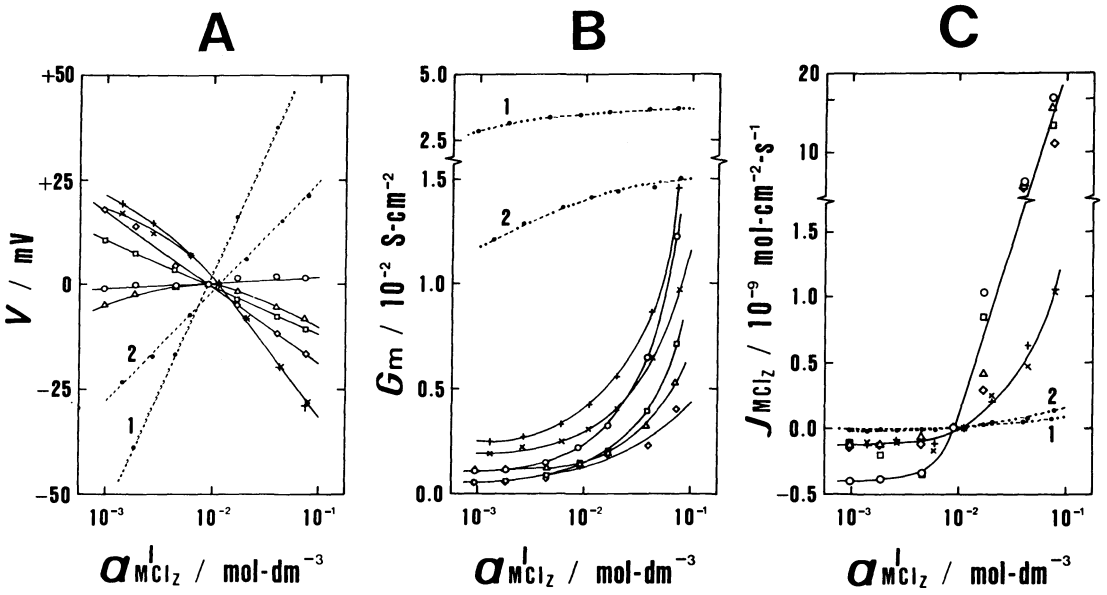

Fig. 1. Transmembrane potential (A), membrane conductance (B), and inter-compartmental ion flux (C) as a function of the mean electrolyte activity of phase I for a variety of aqueous metal chloride concentration-cell systems with an amphoteric ion-exchane membrane, 1.0-PA-29. ○: CsCl; △: KCl; □: NaCl; ◇: LiCl; ×: $CaCl_2$; +: SrCl. The broken lines 1 and 2 refer to the data for NaCl and $CaCl_2$ systems with a cation-exchange membrane, CK-1, 1.0t.

interact equivalently with oppositely charged permeant ions, the zero transmembrane potential should be observed for a 1–1 electrolyte system as an ideal amphoteric ion-exchange membrane potential, since the membrane permeabilities to cation and anion are identical with each other. In the present case, the CsCl system, in which transport numbers to Cs^+ and Cl^- are estimated at 0.51 and 0.49, respectively, from the membrane potential data, realizes apparently these situations as can be seen in Fig. 1-A. The Cs^+/Cl^- hydrated radius ratio is 0.99. The 1.0-PA-29 membrane also demonstrated almost ideal potential responses for an amphoteric ion-exchange membrane in the $NaClO_3$ concentration-cell systems, in which transport numbers to Na^+ and ClO_3^- are 0.51 and 0.49, and the Na^+/ClO_3^- hydrated radius ratio is 1.05.[1)] In case of KCl systems composed of cation and anion with comparable hydrated radii, the 1.0-PA-29 membrane exhibited a biphasic ion selectivity in which cations are more permeable than anions at lower electrolyte concentrations, but at higher concentrations, the ion permselectivity is reversed. Transport numbers to cations are decreased with an increasing radius of hydrated cation as: K^+ (transport number, 0.43—0.54), Na^+ (0.40), and Li^+ (0.35). In the 1.0-PA-29 membrane, the ionic selectivity balance leans slightly toward an anion-selective side (see also Refs. 1 and 4).

Similar situations, such as the cation transport number sequence depending upon the hydrated ionic radius, the slight unbalance of ionic permselectivity shifted to anion selective side, and the resultant potentiometric selective response to 1–1 metal chloride systems, were observed also in the different samples of an amphoteric ion-exchange membrane fabricated by the block copolymerization method.[12)] In this amphoteric ion-exchange membrane composed of a pentablock copolymer having sulfonic acid type and quaternary ammonium type ion-exchange sites, it was reported that the permeabilities to cation and anion are balanced well in the KCl concentration-cell systems with an external electrolyte concentration ratio of 2 and that the transport numbers to cation decrease as: $K^+ > Na^+ > Li^+$.

The practical cation to anion permselectivity balance of an amphoteric ion-exchange membrane seems to be controlled by a variety of factors, such as the specific interactions of cation and anion with oppositely charged ion-exchange sites, detailed balance in numbers of cation- and anion-exchange sites, properties of functionalized network polymer, etc. Furthermore, it is one of the most interesting characteristics of an amphoteric ion-exchange membrane that the permselectivities to cations and anions shift either side depending upon the external electrolyte species and their concentrations.

In case that the permeating cation is bivalent, the 1.0-PA-29 amphoteric ion-exchange membrane showed more anion selective transport properties than the case of univalent cation as shown in Fig. 1-A. Transport numbers to Ca^{2+} and Sr^{2+} ranged from 0.27 to 0.45. Attractive interactions of permeating ions with the oppositely charged exchange sites, as well as repulsive interactions with equally charged sites, within the binary-charged amphoteric ion-exchange membrane phase are expected to be improved as an increase in the charge of permeating ions. Accordingly, the modes of ionic permselectivity of an amphoteric ion-exchange membrane are affected inevitably and definitely by ionic charges of permeants, as a common property of ion transport process across charged membranes. The present results suggest that the repulsive interactions of bivalent metal cations with fixed sites of the same charge exceed the attractive interactions with oppositely charged fixed sites (see also Ref. 1).

Membrane conductance and inter-compartmental ion flux data of the concentration-cell systems for a series of metal chlorides are given in Figs. 1-B and 1-C. The membrane conductances were larger in the bivalent cationic systems, while the inter-compartmental cationic flux was larger in the univalent cationic systems. External electrolyte concentration dependences of these data, increasing with an increasing external concentration, were observed also in the singly-charged ion-exchange membrane. Interesting and substantial differences in these transport properties, as well as in the membrane potential responses mentioned above, between the binary-charged amphoteric ion-exchange membrane, 1.0-PA-29, and the singly-charged cation-exchange membrane, CK-1, 1.0t, are discussed in a latter part of this section.

Membrane Permeability Matrix. A variety of the membrane transport theories based on the nonequilibrium thermodynamics provide an appropriate set of the linear phenomenological coefficients describing the transport phenomena across membranes. The membrane permeability matrix theory is shown to be useful to analyze quantitatively the permselective ion transport across a charged membrane.[9–11,13)] According to these theoretical formulations, the membrane permeability matrix, which is introduced to describe partial contributions of correlations between the permeating ions on the membrane permselectivity to ions, can be expressed for the concentration-cell systems containing Z-valent metal cation M and chloride ion as:

$$\begin{bmatrix} J_M \\ J_{Cl} \end{bmatrix} = -\begin{bmatrix} P_{M\cdot M} & P_{M\cdot Cl} \\ P_{Cl\cdot M} & P_{Cl\cdot Cl} \end{bmatrix} \times \begin{bmatrix} a_M^{II}\exp(ZFV/2RT) - a_M^{I}\exp(-ZFV/2RT) \\ a_{Cl}^{II}\exp(-FV/2RT) - a_{Cl}^{I}\exp(FV/2RT) \end{bmatrix} \quad (1)$$

where J is the ionic flux, V is the transmembrane

potential, a is the ionic activity, F is the Faraday constant, R is the gas constant, and T is the absolute temperature; the superscripts I and II indicate the two solution phases separated by the membrane phase, respectively; the subscripts M and Cl refer to metal cation and chloride ion, respectively. The 2×2 matrix in Eq. 1 is the membrane permeability matrix. Each element represents a partial contribution on the permselective transport process due to the correlations between permeating ion species indicated by the subscript index. The cross coefficients of membrane permeability matrix, $P_{M\cdot Cl}$ and $P_{Cl\cdot M}$, are related with each other as:[9]

$$\frac{P_{M\cdot Cl}}{P_{Cl\cdot M}} = \frac{(a_M^I a_M^{II})^{1/2}}{(a_{Cl}^I a_{Cl}^{II})^{1/2}} \times \frac{\sinh[ZF(V-V_M)/2RT]/[ZF(V-V_M)/2RT]}{\sinh[-F(V-V_{Cl})/2RT]/[-F(V-V_{Cl})/2RT]} \quad (2)$$

The electroconductive membrane permeabilities to metal cation M and to Cl^-, P_M and P_{Cl}, are defined as a function of the elements of the 2×2 membrane permeability matrix and estimated from the transmembrane potential and conductance data as:

$$P_M = P_{M\cdot M} - (1/Z)P_{Cl\cdot M} = \frac{t_M G_m RT}{Z^2F^2(a_M^I a_M^{II})^{1/2}} \frac{[ZF(V-V_M)/2RT]}{\sinh[ZF(V-V_M)/2RT]} \quad (3)$$

$$P_{Cl} = P_{Cl\cdot Cl} - ZP_{M\cdot Cl} = \frac{t_{Cl} G_m RT}{F^2(a_{Cl}^I a_{Cl}^{II})^{1/2}} \frac{[-F(V-V_{Cl})/2RT]}{\sinh[-F(V-V_{Cl})/2RT]} \quad (4)$$

where t is the transport number, G_m is the membrane conductance; V_M and V_{Cl} is the Nernstian equilibrium membrane potentials to metal cation M and Cl^-, respectively.

In a special case where total electric current across membrane is zero, Eq. 1 can be reduced to the next modified phenomenological equation:

$$\begin{bmatrix} J_M \\ J_{Cl} \end{bmatrix}_{I=0} = -\begin{bmatrix} P_M^0 & 0 \\ 0 & P_{Cl}^0 \end{bmatrix} \times \begin{bmatrix} a_M^{II}\exp(ZFV_0/2RT) - a_M^I\exp(-ZFV_0/2RT) \\ a_{Cl}^{II}\exp(-FV_0/2RT) - a_{Cl}^I\exp(FV_0/2RT) \end{bmatrix} \quad (5)$$

where V_0 is the transmembrane potential in absence of membrane electric current. The diffusional membrane permeabilities to M^{z+} and to Cl^-, P_M^0 and P_{Cl}^0, which can be estimated directly from the transmembrane potential and inter-compartmental ion flux data, are expressed as a function of the membrane permeability matrix elements:

$$P_M^0 = (P_{M\cdot M}P_{Cl\cdot Cl} - P_{M\cdot Cl}P_{Cl\cdot M})/P_{Cl} \quad (6)$$

$$P_{Cl}^0 = (P_{M\cdot M}P_{Cl\cdot Cl} - P_{M\cdot Cl}P_{Cl\cdot M})/P_M \quad (7)$$

The electroconductive and diffusional membrane permeabilities are related with each other as:

$$P_M^0/P_M = P_{Cl}^0/P_{Cl} = 1 + (P_{Cl\cdot M}/ZP_M) + (ZP_{M\cdot Cl}/P_{Cl}) \quad (8)$$

The electroconductive membrane permeability defined by Eqs. 3 and 4 should be discriminated on the basis of nonequilibrium thermodynamics from the diffusional membrane permeability defined by Eqs. 6 and 7.[9-11,13] The electroconductive permeability as a function of the ionic mobility across membrane phase represents the electrical conductive process of membrane transport, whereas the diffusional permeability as a function of the diffusion coefficient across membrane phase represents the ionic diffusion process. As discussed in latter part of this section, relative magnitudes of these two permeabilities prescribe characteristics of the modes of ion migration across

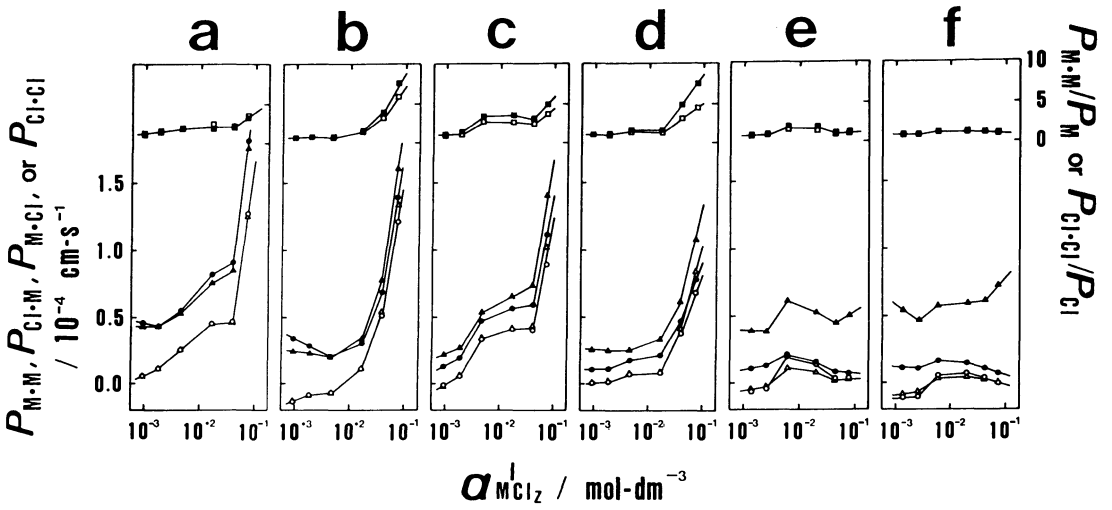

Fig. 2. Membrane permeability matrix elements and, $P_{M\cdot M}/P_M$ and $P_{Cl\cdot Cl}/P_{Cl}$ ratios as a function of the mean electrolyte activity of phase I for the 1.0-PA-29 amphoteric ion-exchange membrane systems. ●: $P_{M\cdot M}$; ○: $P_{Cl\cdot M}$; △: $P_{M\cdot Cl}$; ▲: $P_{Cl\cdot Cl}$; ■: $P_{M\cdot M}/P_M$; □: $P_{Cl\cdot Cl}/P_{Cl}$. a: CsCl; b: KCl; c: NaCl; d: LiCl; e: $CaCl_2$; f: $SrCl_2$.

membrane and also provide a practical index indicating the efficient way of the membrane utilization.

The membrane permselectivity parameters, such as the permeability matrix elements, $P_{M\cdot M}$, $P_{Cl\cdot M}$, $P_{M\cdot Cl}$, and $P_{Cl\cdot Cl}$, electroconductive permeabilities, P_M and P_{Cl}, and diffusional permeabilities, P^0_M and P^0_{Cl}, can be estimated from the membrane potential, the membrane conductance, and the inter-compartmental ion flux data based on these thermodynamic relationships, Eqs. 2—8. These parameters indicate the membrane permselectivities to respective ions by referring the apparent permeation speed across membrane. The membrane potential can be expressed as a function of the membrane permeability ratio or relative membrane permebility, $P_{Cl}/P_M(=P^0_{Cl}/P^0_M)$.[1,11,13] The membrane conductance and the ionic membrane conductance, product of the transport number and membrane conductance, are proportional directly to the electroconductive membrane permeability as indicated in Eqs. 3 and 4, while the diffusional membrane permeability is proportional to the ionic flux under the conditions of $ZJ_M=J_{Cl}$.

Figure 2 summarizes the values of membrane permeability matrix elements for a series of metal chlorides. In case of the univalent metal chloride systems, all the four membrane permeability matrix elements increased with increasing external concentrations, while in the bivalent metal systems, the matrix elements remained at almost constant levels. A sequence in the matrix element was $P_{Cl\cdot Cl}\geqq P_{M\cdot M}>P_{Cl\cdot M}$, $P_{M\cdot Cl}$; however, differences in the matrix element values between the terms based on a correlation of equally charged ions and those of oppositely charged ions are quite small. As indicated by Eqs. 3 and 4, the positive $P_{Cl\cdot M}$ and $P_{M\cdot Cl}$ contribute deceleravively to the respective permeabilities to metal cation and chloride ion. The positive values of these cross elements, in addition, result in the situations where the diffusional permeabilities exceed the electroconductive permeabilities as illustrated in Fig. 3. As expected from the results of transmembrane potential measurements, the 1.0-PA-29 amphoteric ion-exchange membrane is, in general, more permeable to chloride ions than to respective metal cations. Detailed discussion on the characteristic ion transport process across an amphoteric ion-exchange membrane is carried out in the following part of this section based on these membrane permeability parameters.

Comparisons with an Ordinary Singly-Charged Cation-Exchange Membrane. Systematic comparisons of the transport parameters for the 1.0-PA-29 membrane systems with those for the CK-1, 1.0t membrane are useful to investigate further the ionic transport processes across an amphoteric ion-exchange membrane. It is also interesting to clarify substantial differences in the ionic transport processes between singly- and binary-charged ion-exchange membranes.

In Fig. 1, the transmembrane potential, conductance, and ion flux data for the NaCl and $CaCl_2$ concentration-cell systems with the CK-1, 1.0t cation exchange membrane are presented as typical examples of 1–1 and 2–1 electrolyte systems. As discussed already, the 1.0-PA-29 amphoteric ion-exchange membrane reveals potentiometric selectivities even to ions of the same charge due to the ion-sieve effect based on the binary-charged membrane structure, in which the alternately charged sites seem to form the networks of three-dimensional-array ion-exchange groups responsible for shifting out the cations and anions. On the contrary to the potentiometric selective responses of the 1.0-PA-29 membrane, the CK-1, 1.0t membrane demonstrated a strictly charge-dependent potential response. An almost ideal

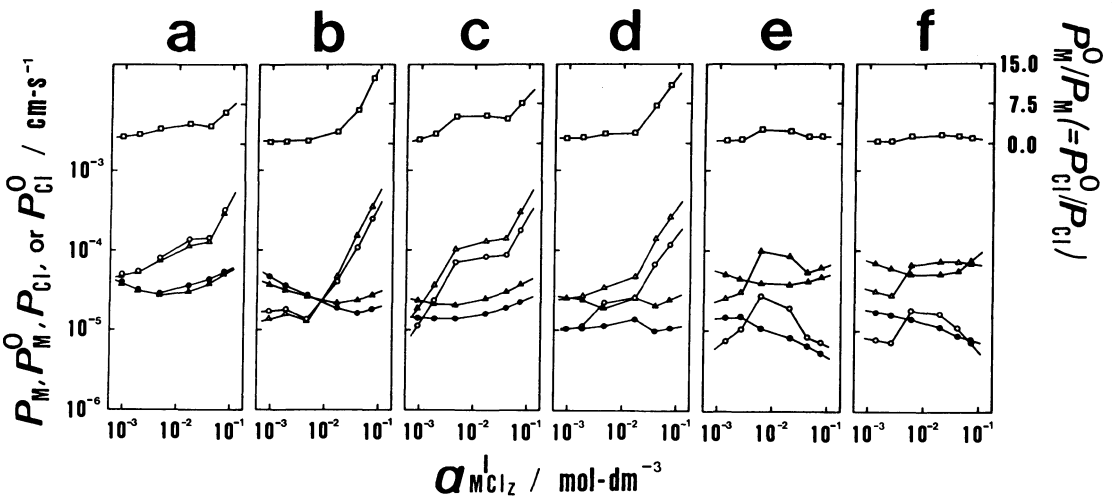

Fig. 3. Electroconductive and diffusional membrane permeabilities and diffusional/conductive permeability ratio as a function of the mean electrolyte activity of phase I for the 1.0-PA-29 amphoteric ion-exchange membrane systems. ●: P_M; ○: P^0_M; ▲: P_{Cl}; △: P^0_{Cl}; □: P^0_M/P_M $(=P^0_{Cl}/P_{Cl})$. a: CsCl; b: KCl; c: NaCl; d: LiCl; e: $CaCl_2$; f: $SrCl_2$.

Nernstian potential response was observed for the concentration-cell systems with the CK-1, 1.0t membrane containing univalent cations, even for the system containing bulky cations such as tetrabutylammonium cation. The transport number of the CK-1, 1.0t membrane to univalent cation estimated from the potential data for a variety of systems is ranged from 0.97 to 0.99 regardless of the electrolyte species in the concentration range studied, 10^{-1}—10^{-3} mol dm^{-3}. These situations are the same as in an ordinary highly permselective anion-exchange membrane system. An almost ideal Nernstian potential response was observed in simple inorganic univalent anion systems as well as in univalent long-hydrocarbon-chain surfactant anion systems.[14-16] The CK-1, 1.0t membrane developed for a desalination process is less permeable to bivalent cations than univalent cations. The membrane potential response showing the transport number of 0.90—0.98 to bivalent cations were observed in the concentration-cell systems containing $CaCl_2$, $SrCl_2$, or $MgCl_2$. In case of the $LaCl_3$ concentration-cell systems with the CK-1, 1.0t membrane, the transport number to La^{3+} was suppressed further to 0.72—0.83.

As seen in Figs. 1-B and 1-C, there is a great difference in the membrane conductance and inter-compartmental ion flux data between the 1.0-PA-29 and CK-1, 1.0t membrane systems. The membrane conductance changes in the 1.0-PA-29 membrane depending upon the external concentration are due to the fact that the membrane-solution distribution factors of ions (cation concentration within membrane phase [mol·(kg-wet membrane)$^{-1}$]/cation concentration in external solution [mol·dm^{-3}]) are almost unity in the concentration ranges studied.[17] Whereas high and relatively constant conductance values of the CK-1, 1.0t membrane are caused from the high and constant cation concentrations within membrane phase corresponding to the ion-exchange capacity. One of the objects to develop an amphoteric ion-exchange membrane was to get a large salt flux by means of the specific and unique transport mechanisms based on the binary-charged membrane structure.[5,18] On the other hand, only a fairly small ion flux can be observed across the singly-charged CK-1, 1.0t membrane as shown in Fig. 1-C, since the membrane systems are close to the equilibrium conditions as expected from the membrane potential data. Considering the thickness of these two membranes (1.0-PA-29: 0.1 mm; CK-1, 1.0t: 1.09 mm), the membrane conductance and inter-compartmental ion flux of the 1.0-PA-29 membrane are less than 1/10—1/100 and more than 10—100 times of those of the CK-1, 1.0t membrane, respectively.

Figures 4 and 5 summarizes the permselectivity parameters estimated for the NaCl and $CaCl_2$ concentration-cell systems with the CK-1, 1.0t cation-exchange membrane, corresponding to Figs. 2 and 3 for the 1.0-PA-29 amphoteric ion-exchange membrane system. Calculated results of other univalent metal chloride systems were comparable with those of the NaCl system in Figs. 4-a and 5-a, and the $SrCl_2$ system, with the $CaCl_2$ system in Figs. 4-b and 5-b. The sequences in the membrane permeability matrix elements were $P_{M\cdot M} \gg P_{Cl\cdot Cl} > P_{M\cdot Cl} > P_{Cl\cdot M}$ in the CK-1, 1.0t membrane system, since the exchange-sites-bound cations come up to 99% of the total cation concentrations within the

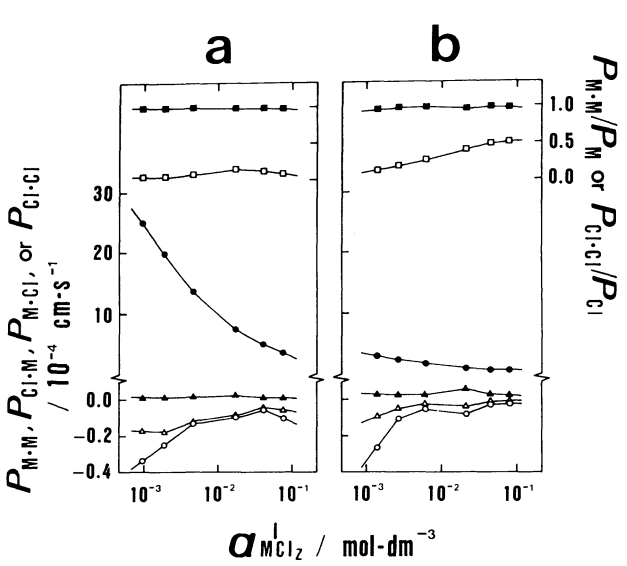

Fig. 4. Membrane permeability matrix elements and, $P_{M\cdot M}/P_M$ and $P_{Cl\cdot Cl}/P_{Cl}$ ratios as a function of the mean electrolyte activity of phase I for the CK-1, 1.0t cation-exchange membrane systems. Symbols are the same as those in Fig. 2. a: NaCl; b: $CaCl_2$.

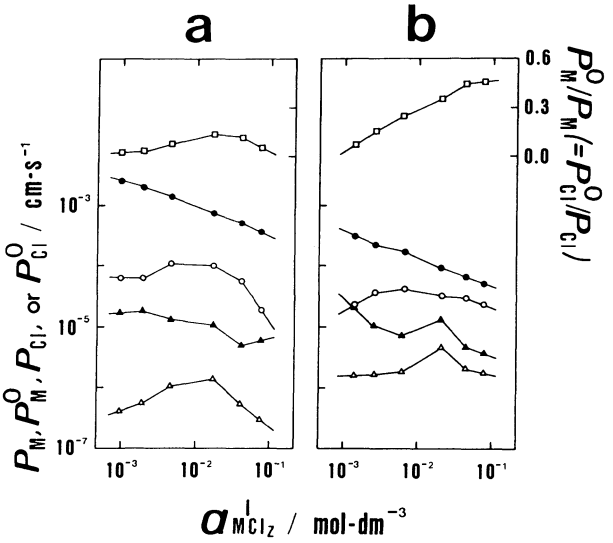

Fig. 5. Electroconductive and diffusional membrane permeabilities and diffusional/conductive permeability ratio as a function of the mean electrolyte activity of phase I for the CK-1, 1.0t cation-exchange membrane systems. Symbols are the same as those in Fig. 3. a: NaCl; b: $CaCl_2$.

membrane and chloride ions are almost perfectly excluded from the membrane phase.[17] In case of the binary-charged 1.0-PA-29 membrane, almost equal amounts of cations and anions are distributed within the membrane phase, so the four permeability matrix elements contribute comparably to the permselective ion transport process as $P_{Cl\cdot Cl} \cong P_{M\cdot M} > P_{Cl\cdot M}, P_{M\cdot Cl}$. The membrane permeability to metal cation is dependent upon the major contributions of the cation-cation correlation term, $P_M \cong P_{M\cdot M}$, as indicated in Fig. 4 and negative values of cross elements, $P_{Cl\cdot M}$ and $P_{M\cdot Cl}$, act acceleratively on the permeabilities to cation and anion as expected from Eqs. 3 and 4 in the singly-charged CK-1, 1.0t membrane system.

Drastic increases in the membrane/solution partition factor of cations in the CK-1, 1.0t membrane with decreasing external concentration cause an improvement of permselectivity with decreasing external concentrations. As discussed in an earlier part, the cross matrix elements are positive in the 1.0-PA-29 membrane, and accordingly, the permselective transport process across a binary-charged membrane depends upon the accelerative contributions based on the correlations between equally charged ions and upon the decelerative contributions based on the correlations between oppositely charged ions. Both of these positive and negative contributions in the 1.0-PA-29 membrane system containing univalent metal chlorides, as seen in Fig. 2, increased with increasing ion concentration of the membrane phase which are proportional to the external concentrations. Then, almost constant electroconductive permeabilities to cation and anion are revealed in the 1.0-PA-29 membrane system.

It has been a theoretically and experimentally established concept that the ionic permselectivity across charged membrane is a function of the permeation speed across membrane and of the membrane/solution partition factor of respective ions. The binary-charged membrane structure results in the totally different situations of ions in membrane phase from those in the singly-charged membrane phase as an origin of the unique ion transport characteristics of an amphoteric ion-exchange membrane.[17] Nonequilibrium thermodynamic analyses on the electrolyte transport process in free aqueous media pointed out that the correlation terms between cation and anion contribute negatively to the transport process similarly as in the binary-charged 1.0-PA-29 membrane.[19]

Equation 8 deduces that the signs of $P_{Cl\cdot M}$ and $P_{M\cdot Cl}$ prescribe a preferential transport mechanism across membranes, the electroconductive or diffusional processes. If these two cross elements are zero, namely none of the interactions between cation and anion exists, both the membrane permeabilities coincide with each other.[9,13] The diffusional/conductive membrane permeability ratio, $P^0_M/P_M (=P^0_{Cl}/P_{Cl})$, can be recognized as a practical index judging whether the electro-dialytic or mechano-dialytic application is efficient for some membrane samples. As shown in Fig. 3, these ratios were larger than unity and increased with an increasing external concentration in the univalent metal chloride system with the 1.0-PA-29 membrane, and in case of the bivalent metal chloride system, these ratios charged from 0.5 to 2.5 depending upon the external concentration. On the other hand in the CK-1, 1.0t membrane system as seen in Fig. 5, the diffusional/conductive membrane permeability ratios were smaller than unity, 0.025—0.17 for univalent metal chloride system and 0.07—0.5 for bivalent system. Whether the diffusional/conductive membrane permeability ratio is larger than or smaller than unity, the sign of the cross elements of membrane permeability matrix is dependent upon the balance of magnitudes of electrical membrane conductance and ionic flux.

Transmembrane potential can be expressed, in general, as a function of the membrane permeability ratio between permeating ions. According to the present membrane transport theory, the following equation for the membrane potential in absence of electric membrane current is obtained from Eqs. 1, 3, and 4:

$$Za^{II}_M \exp[(Z+1)FV_0/2RT] + (P_{Cl}/P_M)a^I_{Cl}\exp(FV_0/RT) - Za^I_M \exp[-(Z-1)FV_0/2RT] - (P_{Cl}/P_M)a^{II}_{Cl} = 0 \quad (9)$$

Identical equation for P^0_{Cl}/P^0_M can be also derived from Eq. 5. In case of the univalent metal chloride systems, Eq. 9 is reduced to the next equation, which is equivalent in form to the well known membrane potential equations for a symmetrical electrolyte such as the Goldman equation, Eisenman equation, etc.:[3]

$$V_0 = -(RT/F)\ln[(a^{II}_M + (P_{Cl}/P_M)a^I_{Cl})/(a^I_M + (P_{Cl}/P_M)a^{II}_{Cl})] = -(RT/F)\ln[(a^{II}_M + (P^0_{Cl}/P^0_M)a^I_{Cl})/(a^I_M + (P^0_{Cl}/P^0_M)a^{II}_{Cl})]. \quad (10)$$

Figure 6 summarizes the chloride ion/metal cation membrane permeability ratios, P_{Cl}/P_M $(=P^0_{Cl}/P^0_M)$, estimated for the 1.0-PA-29 and CK-1, 1.0t membrane systems. As expected from the membrane potential data and Eqs. 9 and 10, the P_{Cl}/P_M values varied with electrolyte species in the 1.0-PA-29 membrane system. As shown in Fig. 3, the electroconductive membrane permeabilities to univalent metal cations and chloride ion are decreased as $P_{Cs} \cong P_K \cong P_{Cl} > P_{Na} > P_{Li}$ with increasing radius of the hydrated ion due to the ion-sieve effect (see also Ref. 1). It has been an established concept that the permeant ion size is one of the dominant factors to control the membrane permselectivity.[20] Indeed also in the CK-1, 1.0t membrane system, the permeability sequences to univalent metal cations were the same as those in the 1.0-PA-29 membrane. However the P_{Cl} values were also changed

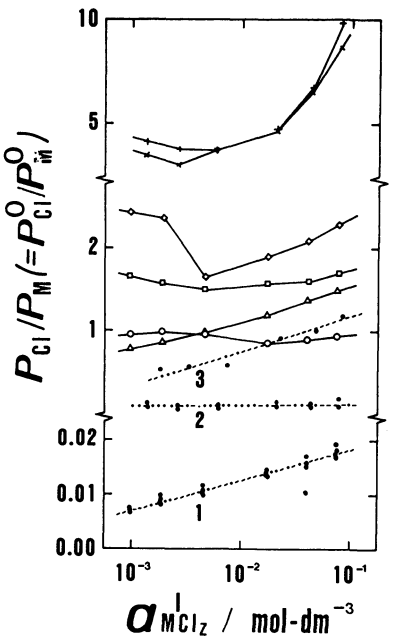

Fig. 6. Chloride ion/metal cation membrane permeability ratio, P_{Cl}/P_M, as a function of the mean electrolyte activity of phase I for the 1.0-PA-29 amphoteric ion-exchange membrane. Symbols are the same as those in Fig. 1. The broken lines 1, 2, and 3 refer to P_{Cl}/P_M values for univalent metal (Cs, K, Na, and Li) chloride, bivalent metal (Ca and Sr) chloride, and $LaCl_3$ concentration-cell systems with the CK-1, 1.0t cation-exchange membrane, respectively.

proportionally with the changes in P_M values as expected from Eq. 10, since the CK-1, 1.0t membrane shows an identical Nernstian response to all the univalent cation systems. Membrane permeability sequences for the Ck-1, 1.0t membrane are as: $P_{Cs}>P_K>P_{Na}>P_{Li}\gg P_{Cl(Cs)}>P_{Cl(K)}>P_{Cl(Na)}>P_{CL(Li)}$, where $P_{Cl(M)}$ indicates the chloride permeability in 1-1 electrolyte, MCl, system. Accordingly, the ion transport process across the binary-charged 1.0-PA-29 membrane is characterized as: the permeabilities both to cation and to anion depend upon the size of the hydrated ions and the permeability to a given ion has a definite value regardless of the electrolyte species. On the contrary, a highly selective cation transport across the CK-1, 1.0t membrane is characterized by the quite low anion/cation permeability ratio, in which the ion size effects on membrane permselectivity are shielded due to tight interactions between oppositely charged ion and fixed site, and accordingly, a potentiometric response to ions of the same charge cannot be observed.

In the ion transport processes across charged membranes, whether the singly- or binary-charged membranes, interactions between permeating ions and fixed ion-exchange sites control the permselectivity as a primary physicochemical factor. Therefore, in a nontreated singly-charged ion-exchange membrane, it has been well-known that the permeability and selectivity parameters to multivalent ions exceed those of univalent ions. In case of the singly-charged membrane developed for the concentration processes of sea water such as the CK-1, 1.0t cation-exchange membrane, the membrane surface was treated by polycationic substance to suppress the permeation of multivalent cations to prevent from $CaSO_4$ scale formation. Figure 6 shows a stepwise increase in P_{Cl}/P_M values with an increasing cation valency from 1 to 3. Once a large amount of multivalent cation has penetrated into the membrane phase; however, the multivalent cations are more permselective than univalent cations due to the tight interaction with oppositely charged exchange sites, as reported in the NaCl-$CaCl_2$, NaCl-$LaCl_3$, and $CaCl_2$-$LaCl_3$ biionic systems with the CK-1, 1.0t membrane.[11,21] As already discussed, the permeability to bivalent metal cation in the binary-charged 1.0-PA-29 membrane is decelerated due to the repulsive interactions with positively charged exchange site, while the permeability to Cl^- is accelerated almost as twice as those in the univalent metal chloride system (see also Ref. 1).

Present results suggest that a qualitative improvement of the membrane permselectivity to ions can be provided by means of introducing the carefully selected pairs of oppositely charged ion-exchange sites into the membrane phase with high densities. Further investigations on the detailed aspects of ion transport process across a binary-charged amphoteric ion-exchange membrane will be achieved by examining the ion conditions within membrane phase such as membrane/solution partition and diffusion process of permeating ions.[17] These studies contribute also to the developments of more useful and efficient membrane-related processes.

The authors wish to thank the Ministry of Education, Science and Culture of Japan for a Grant-in-Aid for Scientific Research. One of the authors (K. K.) is also grateful to the Kurata Foundation for supporting the research grant. We also wish to thank Asahi Chemical Industry Co., Ltd. and Kanegafuchi Chemical Industry Co., Ltd. for providing the ion-exchange membranes used in this work.

References

1) Part IV of this series: K. Kaibara, Y. Nagata, T. Kimotsuki, and H. Kimizuka, *J. Membr. Sci.*, **29**, 37 (1986).

2) A. Katchalsky and P. F. Curran, "Nonequilibrium Thermodynamics in Biophysics," Harvard University Press, Cambridge, Mass., USA (1965).

3) N. Lakshminarayanaiah, "Equations of Membrane Biophysics," Academic Press, New York, NY. USA (1984).

4) K. Kaibara, H. Sonoda, Y. Nagata, and H. Kimizuka, *Bull. Chem. Soc. Jpn.*, **56**, 1346 (1983).

5) J. N. Weinstein, B. J. Bunow, and S. R. Caplan, *Desalination*, **11**, 341 (1972).

6) T. Yamabe, K. Umezawa, S. Yoshida, and N. Takai, *Desalination*, **15**, 127 (1974).
7) T. Eguchi, S. Mori, and M. Shimokawa, *Membrane*, **3**, 289 (1978).
8) T. Fujimoto, K. Ohkoshi, Y. Miyaki, and M. Nagasawa, *J. Membr. Sci.*, **20**, 313 (1984).
9) H. Kimizuka, K. Kaibara, E. Kumamoto, and M. Shirozu, *J. Membr. Sci.*, **4**, 81 (1978).
10) K. Kaibara and H. Kimizuka, *Bull. Chem. Soc. Jpn.*, **55**, 1743 (1982).
11) K. Kaibara, H. Inoue, and H. Kimizuka, *Bull. Chem. Soc. Jpn.*, **60**, 3175 (1987).
12) M. Tasaka, T. Okano, and T. Fujimoto, *J. Membr. Sci.*, **19**, 273 (1984).
13) H. Kimizuka and K. Kaibara, *J. Colloid Interface Sci.*, **52**, 516 (1975).
14) K. Kaibara, T. Nakahara, I. Satake, and R. Matuura, *Mem. Fac. Sci., Kyushu Univ., Ser. C*, **7**, 1 (1970).
15) K. Shirahama, *Kolloid Z. Z. Polym.*, **250**, 620 (1972).
16) T. Sasaki, M. Hattori, J. Sasaki, and K. Nukina, *Bull. Chem. Soc. Jpn.*, **48**, 1397 (1975).
17) H. Inoue, K. Kaibara, and H. Kimizuka, The 1987 International Congress on Membranes and Membrane Processes, Tokyo, Japan, June 8-12, 1987, Abstr. No. 1-P14.
18) J. Shorr and F. B. Leitz, *Desalination*, **14**, 11 (1974).
19) D. G. Miller, *J. Phys. Chem.*, **70**, 2639 (1966).
20) G. Eisenman, "The Elementary Atomic Origin of Equilibrium Ionic Specificity," in "Membrane Transport and Metabolism," ed by A. Kleinzeller and A. Kotyk, Academic Press, New York (1961), p. 163.
21) K. Kaibara, J. Nakajima, Y. Nagata, and H. Kimizuka, *Mem. Fac. Sci., Kyushu Univ., Ser. C*, **14**, 239 (1984).

ESR Study on the Reactions of 1,3-Diene Cation Radicals in Low-Temperature Matrices

Jun FUJISAWA, Toshiyuki TAKAYANAGI, Shin SATO,* and Kazuo SHIMOKOSHI†
Research Laboratory for Nuclear Reactors, Tokyo Institute of Technology, Ookayama, Meguro-ku, Tokyo 152
†Department of Chemistry, Tokyo Institute of Technology, Ookayama, Meguro-ku, Tokyo 152
(Received October 3, 1987)

The reactions of the cation radicals of 1,3-butadiene, *cis*- and *trans*-1,3-pentadienes, 2-methyl-1,3-butadiene, and 2,3-dimethyl-1,3-butadiene have been investigated by low-temperature matrix ESR. The cation radicals produced in the irradiated solid solutions of CCl_2FCCl_2F were found to react with their neutral parents at temperatures above ca. 110 K, forming radicals with allylic ends. On the other hand, 1,3-pentadiene cation radicals in the matrices of CCl_4, CCl_3F, and CCl_3CF_3 were found to isomerize into cyclopentene cation radicals, irrespective of the cis and trans forms. The possible mechanisms for the reactions and their implications in the cationic polymerization of dienes are discussed.

The primary process in radiation-induced polymerization has long been a subject in radiation chemistry.[1] Traditional approaches, however, have mostly been confined to speculation about the mechanisms, since the high reactivity of the cation radicals prohibited any spectroscopic detection of the primary processes.

The method of radiolytic generation and stabilization of cation radicals in Freons has now widely been applied to a variety of organic compounds.[2] By measuring the ESR spectra of the cation radicals, thus prepared over a wide temperature range, direct information concerning their reactions has often been obtained.[3,4]

This technique, as it applies to the cation radicals of unsaturated hydrocarbons, is of special interest since some of them are supposed to initiate polymerization.[1] In fact, we have found that the cation radicals of ethylene and isobutene easily associate with their neutral parents to form chain end radicals.[5,6] This is in remarkable contrast to the deprotonation observed for the cation radicals of other olefins[6] and paraffins[3] giving neutral radicals.

In the present study, we have examined the reactions of a series of 1,3-diene cation radicals by the same method mentioned above. The isolated cation radicals of 1,3-pentadienes and 2,3-dimethyl-1,3-butadiene were newly observed by ESR, as well as those of 1,3-butadiene and 2-methyl-1,3-butadiene. The ESR observation for the formations of chain end allylic radicals from these cation radicals and the isomerization found for the cation radicals of 1,3-pentadiene are described.

Experimental

1,3-Butadiene from Takachiho Kagaku Kogyo Co., 2-methyl-1,3-butadiene, 2,3-dimethyl-1,3-butadiene, and cyclopentene from Tokyo Kasei Co. were used as received. Cis and trans isomers of 1,3-pentadiene were kindly supplied by Nippon Zeon Co. Ltd. All the dienes, except for 1,3-butadiene, can polymerize easily, even at room temperature. About 30 ppm of a polymerization inhibitor was kept incorporated with these compounds. Preliminary measurements using samples from which the inhibitor had been removed immediately before preparation gave the same results as described in this paper. The high purity (>97%) of each isomer was checked by NMR spectroscopy. Commercially available halocarbons (CCl_4, CCl_3F, CCl_3CF_3, and CCl_2FCCl_2F from Tokyo Kasei Co.) were used as a matrix media without further purification.

The procedure of sample preparation and ESR measurement have been described previously.[4-6] Solid solutions containing small amounts of the dienes (0.2—0.5 mol%) in various halocarbons were prepared in quartz tubes at 77 K, then irradiated to generate the cation radicals. The ESR measurement was carried out with a JES FE-2XG spectrometer calibrated with an NMR probe and a digital frequency counter. The sample temperature was regulated with a temperature controller, and the spectra were recorded at temperatures between 77 K and the melting point of each matrix with suitable intervals.

Results

1,3-Butadiene. The spectrum shown in Fig. 1a was recorded at 77 K after the irradiation of a solid solution of 1,3-butadiene in CCl_3CF_3. The spectrum consists of a quintet with an hfc (hyperfine coupling) constant of 10.4 G (1 G=10^{-4} T), which can readily be assigned to the cation radical of 1,3-butadiene. Essentially the same spectrum was observed for the solutions of CCl_3F and CCl_2FCCl_2F at 77 K. The cation radical of 1,3-butadiene in other matrices has been studied by several workers.[7-9] The present result is in good agreement with the previous results, as shown in Table 1.

The 1,3-butadiene cation radicals in CCl_3F and CCl_3CF_3 were found to remain isolated up to about 145 K. A further elevation of the temperature resulted in a uniform decay of the cation radical without giving any new paramagnetic species. This may be attributed to the neutralization between the cation radical and the chloride anion. On the other hand, the irradiated solution of 1,3-butadiene in CCl_2FCCl_2F

showed an irreversible change at around 110 K from the initial spectrum of the cation radical to a new one. Figure 1b shows the spectrum observed upon warming to 128 K. The spectrum was well reproduced by the simulation shown in Fig. 1c when an allylic structure **1** was assumed.[7]

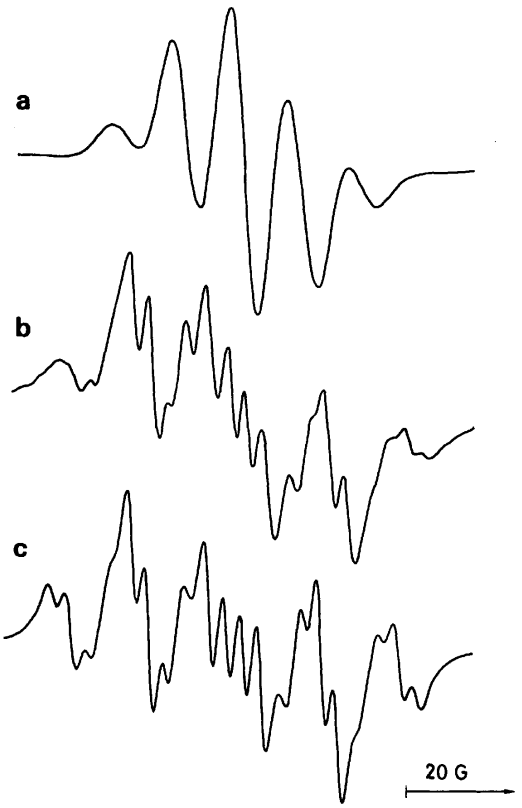

Fig. 1. (a) ESR spectrum of the cation radical of 1,3-butadiene in CCl_3CF_3 at 77 K. (b) ESR spectrum of the irradiated CCl_2FCCl_2F solution of 1,3-butadiene at 128 K, showing the features assigned to the allylic end **1**. (c) Simulation for (b) using the parameters given in Table 2 and a Lorentzian line width of ΔH_{msl}=5.0 G.

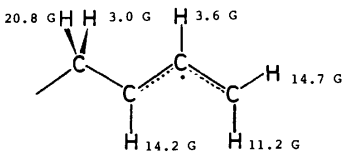

1

At elevated temperatures, it has often been observed that an irradiated CCl_2FCCl_2F solution allows molecular diffusion which may cause ion-molecule reactions.[4-6] The irreversible change of the spectrum, therefore, strongly suggests that the cation radical reacts with its neutral parents to form species whose radical end has an allylic structure **1**.

***cis*- and *trans*-1,3-Pentadienes.** The irradiated solutions of *cis*- and *trans*-1,3-pentadienes in CCl_2FCCl_2F exhibited the spectra shown in Figs. 2a and 3a, respectively. The former was successfully analyzed by using hfc constants of 15.2 G (3H), 10.4 G (3H), and 5.9 G (1H), as shown in Fig. 2b. Based on the results of INDO calculations (values in the parentheses in the diagrams **2**, **5**, and **6**),[10] the species giving the spectrum was assigned to the cation radical of *cis*-1,3-pentadiene (**2**). The analysis of the spectrum for the trans isomer (Fig. 3a) is less straightforward because of its low resolution. It was found, however, that the essential features of the spectrum closely resemble those of the cis isomer. This suggests the formation of

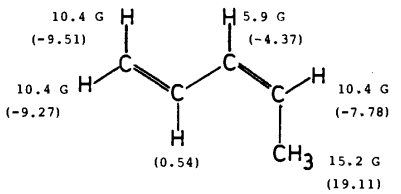

2

Table 1. Isotropic ESR Parameters of Diene Cation Radicals

Cation radical	Matrix	Temp/K	hfc constant/G			Ref.
			a(CH)	a(CH_2)	a(CH_3)	
CH_2=CHCH=CH_2^+	CCl_3CF_3	77		10.4		
	CCl_2FCCl_2F	77		11.4		
	Silica gel	77	3.2	11.4		7)
	CCl_4	130		10.1		8)
	CCl_3F	77	2.0	12.2		9)
CH_3CH=CHCH=CH_2^+ (cis isomer)	CCl_2FCCl_2F	108	5.9 10.4	10.4	15.2	
CH_2=C(CH_3)CH=CH_2^+	CCl_3CF_3	128		8.7 13.1	4.3	
	CCl_4	163	3.2	9.2 13.0	4.9	12)
CH_2=C(CH_3)C(CH_3)=CH_2^+	CCl_4	183		9.9	5.0	

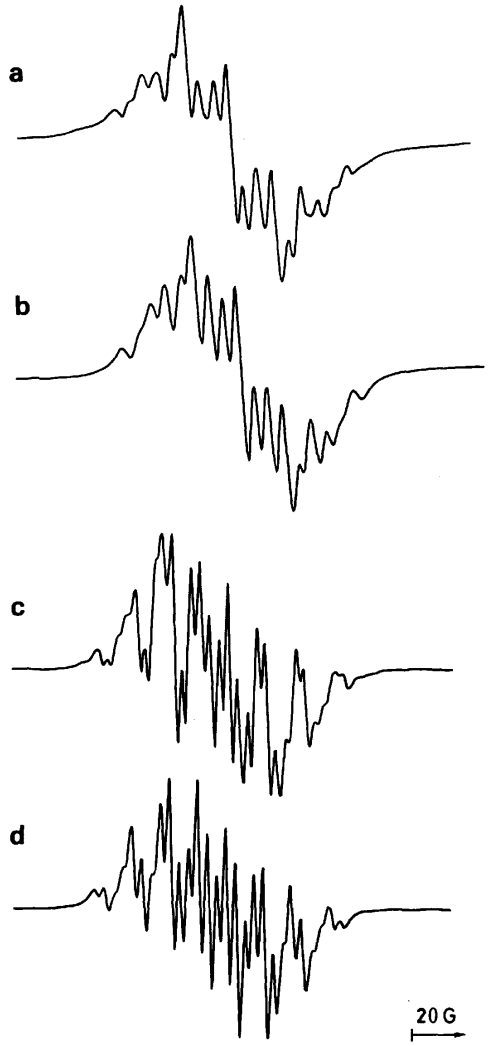

Fig. 2. (a) ESR spectrum of the cation radical of *cis*-1,3-pentadiene in CCl_2FCCl_2F at 108 K. (b) Simulation for (a) using the parameters given in Table 1 and a Lorentzian line width of ΔH_{msl}= 8.4 G. (c) Same as (a) at 143 K, showing the features assigned to the allylic end **3**. (d) Simulation for (c) using the parameters given in Table 2 and a Lorentzian line width of ΔH_{msl}=5.0 G.

a *tarns*-1,3-pentadiene cation radical, though the cause of the apparent difference in the resolution between the isomers is not clear.

The essential differences between cis and trans isomers of the cation radicals were characterized by their reactions. Upon warming, the spectra of these cation radicals changed irreversibly into different patterns, as shown in Figs. 2c and 3b, respectively. Taking the small variations of the hyperfine interaction into account, both could be reproduced by simulations, as shown in Figs. 2d and 3c. Such a variation has often been observed for allylic radicals with different conformations;[6,11] the spectra can consistently be assigned to the allylic ends with cis **3** and trans **4** skeletons.

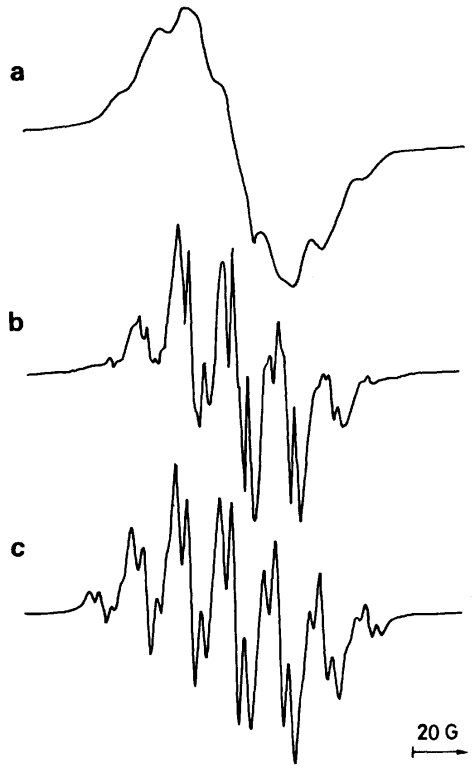

Fig. 3. (a) ESR spectrum of the cation radical of *trans*-1,3-pentadiene in CCl_2FCCl_2F at 77 K. (b) Same as (a) at 128 K, showing the features assigned to the allylic end **4**. (c) Simulation for (b) using the parameters given in Table 2 and a Lorentzian line width of ΔH_{msl}=5.2 G.

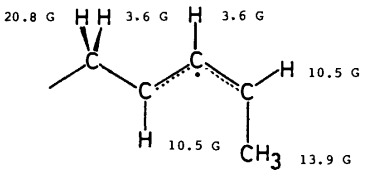

3

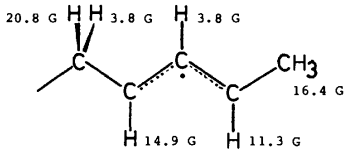

4

When the matrix of CCl_4, CCl_3F, or CCl_3CF_3 was used instead, a completely different spectral pattern was observed. The spectrum shown in Fig. 4a was recorded at 77 K immediately after the irradiation of a solution of a *cis*-1,3-pentadiene in CCl_3F. Upon warming, the resolution of the spectrum was improved to give the spectrum shown in Fig. 4b at 128 K. Essentially the same spectra were obtained for *trans*-1,3-pentadiene, as shown in Figs. 4c and 4d. The spectra shown in Fig. 4 closely resemble that of a cyclopentene cation radical, reported by Shida and co-

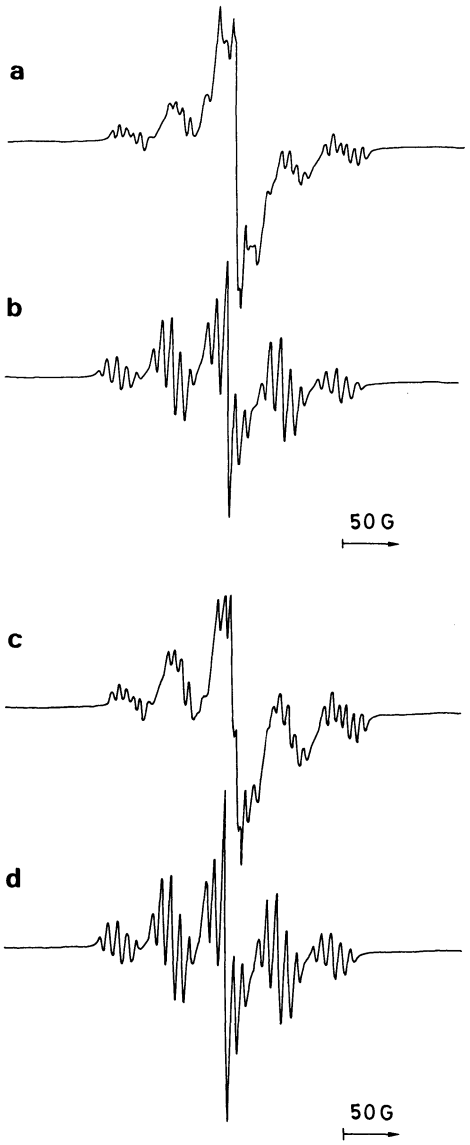

Fig. 4. (a) ESR spectrum of the irradiated CCl_3F solution of *cis*-1,3-pentadiene at 77 K, showing the features assigned to the cation radical of cyclopentene. (b) Same as (a) at 128 K. (c) Same as (a) for *trans*-1,3-pentadiene. (d) Same as (c) at 123 K.

workers.[9] We performed the same experiment and confirmed that these spectra coincide almost exactly with the spectra from cyclopentene. Therefore, it may be concluded that the cation radical of cyclopentene was formed immediately after the irradiation of the CCl_3F solutions of *cis*- and *trans*-1,3-pentadienes. The employment of other matrices of CCl_4 and CCl_3CF_3 also gave similar results.

2-Methyl- and 2,3-Dimethyl-1,3-butadienes. The irradiated 2-methyl-1,3-butadiene in CCl_3CF_3 yielded the spectrum shown in Fig. 5a at 128 K. The spectrum is quite similar that previously observed in CCl_4.[12] The hfc constants of 13.1 G (2H), 8.7 G (2H), and 4.3 G (3H) were derived from the simulation shown

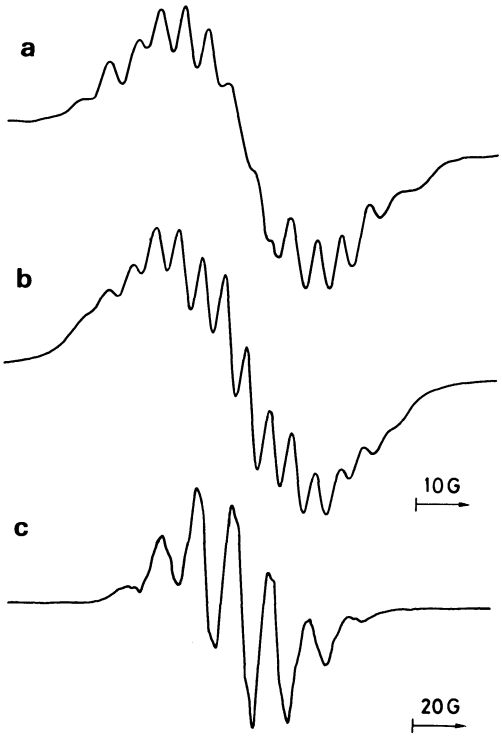

Fig. 5. (a) ESR spectrum of the cation radical of 2-methyl-1,3-butadiene in CCl_3CF_3 at 128 K. (b) Simulation for (a) using the parameters given in Table 1 and a Lorentzian line width of ΔH_{msl}=7.5 G. (c) ESR spectrum of the irradiated CCl_2FCCl_2F solution of 2-methyl-1,3-butadiene at 133 K, showing the features assigned to the allylic end **7**.

in Fig. 5b and were ascribed to the 2-methyl-1,3-butadiene cation radical (**5**).

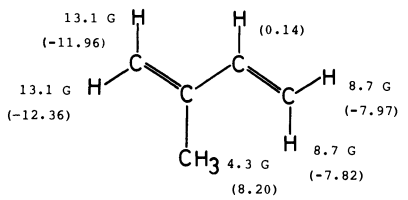

5

For an irradiated solution of 2,3-dimethyl-1,3-butadiene in CCl_3CF_3, a poorly resolved spectrum was obtained. Well-resolved structures were observed by using CCl_4 instead (Fig. 6a). Although some background signals due to the matrix radicals[13] are superimposed at the low-field side of the spectrum, the main spectral pattern can easily be identified as a quintet of septets with hfc constants of 9.9 G (4H) and 5.0 G (6H) (Fig. 6b); those agree well with the values expected for the cation radical of 2,3-dimethyl-1,3-butadiene (**6**).

Irreversible spectral changes were also observed for these systems upon warming. Figure 5c shows the spectrum observed for an irradiated CCl_2FCCl_2F solution of 2-methyl-1,3-butadiene at 118 K. The

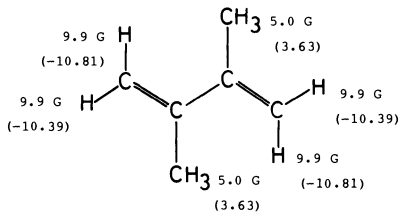

6

septet structure separated by about 13 G may be assigned to the allylic end **7**, though possible differences in hfc constants among six protons are not clear from the spectrum. A similar septet pattern was also obtained for an irradiated solution of 2,3-dimethyl-1,3-butadiene at 128 K (Fig. 6c). The formation of another type of allylic end **8** may be responsible.

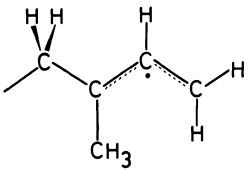

7

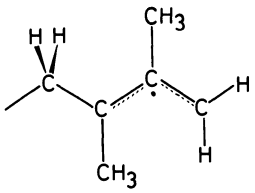

8

The observed ESR parameters for the cation radicals of dienes and the allylic end radicals are summarized in Tables 1 and 2, respectively.

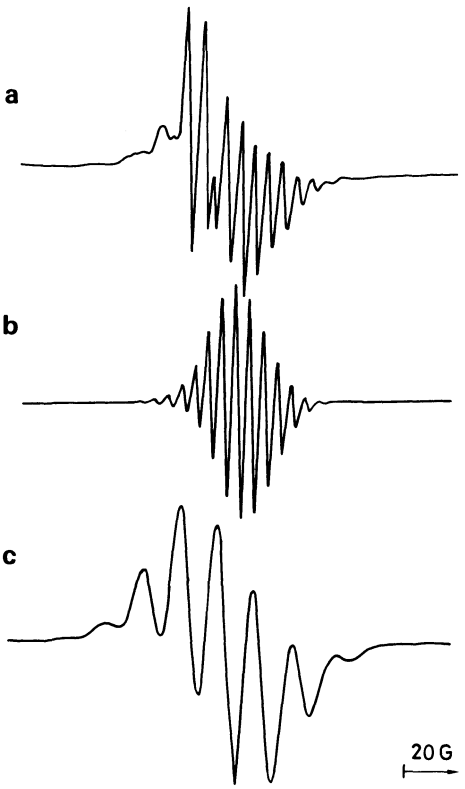

Fig. 6. (a) ESR spectrum of the cation radical of 2,3-dimethyl-1,3-butadiene in CCl_4 at 183 K. (b) Simulation for (a) using the parameters given in Table 1 and a Lorentzian line width of ΔH_{msl}=3.0 G. (c) ESR spectrum of the irradiated CCl_2FCCl_2F solution of 2,3-dimethyl-1,3-butadiene at 128 K, showing the features assigned to the allylic end **8**.

Table 2. Isotropic ESR Parameters of Allylic End Radicals

Chain end	Monomer	Temp/K	hfc constant/G			Ref.
			a(CH)	a(CH_2)	a(CH_3)	
$\dot{C}H_2CH{=}CHCH_2$-	$CH_2{=}CHCH{=}CH_2$[a]	128	3.6	11.2		
			14.2	14.7		
				3.0		
				20.8		
	$CH_2{=}CHCH{=}CH_2$[b]	195	4.2	13.8		7
			14.9	13.8		
				12.8		
				12.8		
$(CH_3)\dot{C}HCH{=}CHCH_2$- (cis isomer)	$CH_3CH{=}CHCH{=}CH_2$[a] (cis isomer)	143	3.6	3.6		
			10.5	20.8	13.9	
			10.5			
$(CH_3)\dot{C}HCH{=}CHCH_2$- (trans isomer)	$CH_3CH{=}CHCH{=}CH_2$[a] (trans isomer)	128	3.8	3.8		
			11.3	20.8	16.4	
			14.9			

a) In a CCl_2FCCl_2F matrix. b) Adsorbed on silica gel.

Discussion

The cation radicals of 1,3-butadiene and its methyl and dimethyl derivatives were stabilized in halocarbon matrices upon irradiation at 77 K. From the results of ESR measurements (Table 1), it can be seen that the coupling constants of CH_2 protons vary little among the species. This indicates that the cation radicals of 1,3-dienes possess essentially the same π-structures as that of 1,3-butadiene, where an unpaired electron is located mainly on the terminal (1,4-position) carbons.

The radicals derived from these cation radicals were characterized by their allylic ends, which reflect the conformations of the corresponding parent cation radicals. In particular, cis and trans isomers of 1,3-pentadiene cation radicals in CCl_2FCCl_2F were found to give allylic ends with cis and trans skeletons, respectively. This indicates that the radicals formed by reactions, as well as the parent cation radicals, retain their geometrical identities of neutral dienes. A similar stereospecificity has also been found for reactions of the *cis*- and *trans*-2-butene cation radicals.[6]

Regardings the ESR parameters of the radical from the 1,3-butadiene cation radical, there is a noticeable difference between the present result and the previous one;[7] i.e., large inequivalence between the two β-methylene proton couplings, 20.3 and 3.0 G, has not been previously observed (see Table 2). The difference may be ascribed to the lower temperature at which the present measurement was carried out. In this case, the motional averaging between two protons may be prohibited. Such an inequivalence of β-methylene proton couplings has been observed for other allylic end radicals,[14] and the present values seem to be appropriate for this type of radical.

So far, a number of studies have been reported concerning the primary processes in the radiation-induced polymerization of 1,3-butadiene.[1a,7,8,15] The formation of primary cation radicals or allylic end radicals has been observed, depending on the conditions. The concentration effect on the processes was investigated by Lund et al.[7] for the irradiated 1,3-butadiene adsorbed on silica gel. They reported that the cation radical was observable at a low 1,3-butadiene content, but absent when the allylic end radical occurred at high concentrations. The following reaction scheme has been proposed for 1,3-butadiene:[7,8,15c]

$$CH_2{=}CH{-}CH{=}CH_2 \longrightarrow CH_2{=}CH{-}CH{=}CH_2^{\ddagger} + e^-, \quad (1)$$

$$CH_2{=}CH{-}CH{=}CH_2^{\ddagger} + CH_2{=}CH{-}CH{=}CH_2 \longrightarrow \dot{C}H_2{-}CH{=}CH{-}CH_2{-}CH_2{-}CH{=}CH{-}CH_2^+, \quad (2)$$

$$\dot{C}H_2{-}CH{=}CH{-}CH_2{-}CH_2{-}CH{=}CH{-}CH_2^+ + n[CH_2{=}CH{-}CH{=}CH_2] \longrightarrow \dot{C}H_2{-}CH{=}CH{-}CH_2\text{-}(CH_2{-}CH{=}CH{-}CH_2)_n CH_2{-}CH{=}CH{-}CH_2^+. \quad (3)$$

In the present study, the formation of the allylic end was characterized as the ion-molecule reaction of 1,3-butadiene cation radical. This may be considered as direct evidence for the initiation reaction 2. During the subsequent step, the polymerization has been thought to proceed cationically as in reaction 3. The present result is compatible with this scheme in that the spectra of allylic end radicals can be assigned without taking into account any branched structures which often occur in radical propagation.

The reaction scheme implies two possible candidates for species with an allylic end: i.e., the dimer cation radical from reaction 2 and the propagating radical formed by reaction 3. Though the ESR measurement does not provide any direct information about this, the latter seems more probable since reaction 3 is known to take place with a nominal activation energy and, hence, at low temperature.[1a,15a]

The results suggest that similar mechanisms are also applicable to the methyl and dimethyl derivatives of 1,3-butadiene. This was demonstrated by the formation of radicals with the specific conformations of methyl groups, as expected from the 1,4-addition reactions. The observed hfc constants of all the diene cation radicals indicate that the unpaired electron is mainly located on positions 1 and 4, which also accords well with this scheme.

For reactions of the cation radicals of 1,3-pentadienes and 2-methyl-1,3-butadiene, there are two possible structures in forming allylic ends, as illustrated in Fig. 7. These two structures are

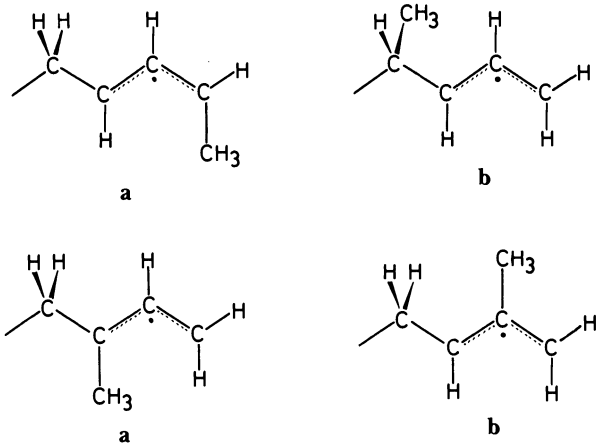

Fig. 7. Two possible structures of the allylic ends which may be formed by the polymerization of *cis*-1,3-pentadiene and 2-methyl-1,3-butadiene. Only the structures (a) were observed (see text). Similar scheme is applicable also to the reaction of *trans*-1,3-pentadiene cation radical.

distinguishable from their ESR spectra. The results indicate that a specific structure **a** is formed exclusively for both of the cation radicals. This may be explained in terms of possible differences in hyperconjugative effects; i.e., the formation of the allylic ends **a** may be preferable because of their higher conjugation in π-systems.

As for the reactions of the cation radicals of 1,3-pentadienes, an alternative possibility of cation radical Diels–Alder reaction[16] has been discussed by Shiga and Okamura.[12] They observed a spectrum with a quintet structure separated by as much as 48.5 G for an irradiated CCl_4 solution of *cis*-1,3-pentadiene at 77 K and assigned it to a vinylcyclohexene-type cation radical. We obtained a similar spectra for irradiated solutions of *cis*- and *trans*-1,3-pentadienes in CCl_4, CCl_3F, and CCl_3CF_3 but found that these spectra could more reasonably be assigned to the cation radical of cyclopentene. Therefore, the absence of the primary cation radicals in these systems should be considered as being due to unimolecular isomerizations of the cation radicals of 1,3-pentadiene into the cation radical of cyclopentene.

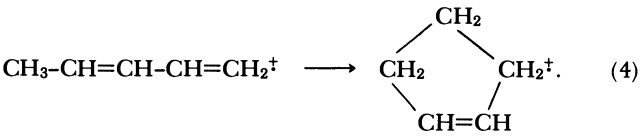

It is noteworthy that the above reaction took place irrespective of the cis and trans forms of 1,3-pentadiene. They, in turn, have two possible conformations around the single bond: s-cis and s-trans. In forming the cyclopentene ring, however, the s-cis conformations seem preferable to s-trans conformations for both forms. In this case, the following mechanisms could illustrate the processes.

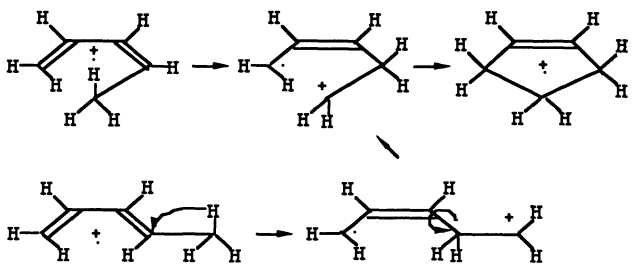

These mechanisms include 1,2-hydrogen atom shifts in froming the cation radical of cyclopentene. Another possible mechanism is a 1,4-hydrogen atom shift process. However, the necessary rearrangement of the carbon skeleton for the trans form is not conceivable in that case because of the double-bond nature of the 2,3-bond. Since isomerization was observed for both forms, the 1,2-hydrogen atom shift process is more appropriate.

As for the neutral molecules of 1,3-pentadienes, it is known that the s-trans is more stable from the results of the microwave spectra[17] and UV spectra.[18] In order to elucidate the stable conformations for the cation radicals of 1,3-pentadienes, we calculated the energies of these cation radicals by using the INDO method.[10] The result shows that the s-trans is more stable than s-cis conformation by ca. 10 kcal mol^{-1}. In a low-temperature matrix, nevertheless, these cation radicals might possibly have s-cis conformations as a result of matrix effects. In fact, it has been reported that the cation radicals of some alkanes do not have extended conformations but have less stable gauche conformations in the matrices of CCl_3F and CCl_3CF_3.[3,19] Therefore, we tentatively considered that the cation radicals of 1,3-pentadiene in CCl_4, CCl_3F, and CCl_3CF_3 specifically have s-cis conformations and are subject to the immediate isomerization into cyclopentene cation radicals. On the other hand, the cation radicals of 1,3-pentadiene in CCl_2FCCl_2F might remain as they are because of their s-trans conformations.

References

1) a) W. S. Anderson, *J. Phys. Chem.*, **63**, 765 (1959); b) P. C. Chang, N. C. Yang, and C. D. Wagner, *J. Am. Chem. Soc.*, **81**, 2060 (1959); c) K. Takeda, H. Yoshida, K. Hayashi, and S. Okamura, *Memo. Fac. Eng. Kyoto Univ.*, **32**, 213 (1966). d) K. Tsuji, H. Yoshida, K. Hayashi, and S. Ogasawara, *Polym. Lett.*, **5**, 313 (1967).

2) T. Shida, E. Haselbach, and T. Bally, *Acc. Chem. Res.*, **17**, 180 (1984).

3) K. Toriyama, K. Nunome, and M. Iwasaki, *J. Chem. Phys.*, **77**, 5891 (1982).

4) J. Fujisawa, S. Sato, K. Shimokoshi, and T. Shida, *Bull. Chem. Soc. Jpn.*, **58**, 1267 (1985).

5) J. Fujisawa, S. Sato, and K. Shimokoshi, *Chem. Phys. Lett.*, **124**, 391 (1986).

6) J. Fujisawa, S. Sato, K. Shimokoshi, and T. Shida, *J. Phys. Chem.*, **89**, 5481 (1985).

7) T. Shiga, A. Lund, and P-O. Kinell, *Int. J. Rad. Phys. Chem.*, **3**, 131 (1971).

8) A. Lund, T. Shiga, and P-O. Kinell, *Nobel Symp.*, **22**, 95 (1972).

9) T. Shida, Y. Egawa, H. Kubodera, and T. Kato, *J. Chem. Phys.*, **73**, 5963 (1980).

10) The INDO calculations were performed using the program coded by one of the authors (KS) (K. Shimokoshi, J. Fujisawa, K. Nakamura, S. Sato, and T. Shida, *Chem. Phys. Lett.*, **99**, 483 (1983).). The standard geometries of the neutral 1,3-dienes were used for the calculations.

11) J. K. Kochi and P. J. Krusic, *J. Am. Chem. Soc.*, **90**, 7157 (1968).

12) T. Shiga and S. Okamura, *Polym. J.*, **6**, 7 (1974).

13) T. Shida and Y. Takemura, *Red. Phys. Chem.*, **21**, 157 (1983).

14) T. Ohmori, T. Ichikawa, and M. Iwasaki, *Bull. Chem. Soc. Jpn.*, **46**, 1383 (1973).

15) a) Y. Tabata, H. Sobue, and E. Oda, *J. Phys. Chem.*, **65**, 1645 (1961); b) T. Shiga, A. Lund, and P-O. Kinell, *Int. J.*

Rad. Phys. Chem., **3**, 145 (1971); c) T. Shiga, T. Matsuyama, H. Yamaoka, and S. Okamura, *Makromol. Chem.*, **175**, 217 (1974); d) T. Shiga and S. Okamura, *Polym. J.*, **6**, 1 (1974).

16) a) N. L. Bauld, D. J. Bellville, R. Pabon, R. Chelsky, and G. Green, *J. Am. Chem. Soc.*, **105**, 2378 (1983); b) D. J. Bellville, D. D. Wirth, and N. L. Bauld, *J. Am. Chem. Soc.*, **103**, 718 (1981); c) P. G. Gassman and D. A. Singleton, *J. Am. Chem. Soc.*, **106**, 7993 (1984).

17) S. L. Hsu and W. H. Flygare, *J. Chem. Phys.*, **52**, 1053 (1970).

18) H. Booker, L. K. Evans, and A. E. Gillam, *J. Chem. Soc.*, **1940**, 1453.

19) G. Dolivo and A. Lund, *J. Phys. Chem.*, **89**, 3977 (1985).

 © 1988 The Chemical Society of Japan Bull. Chem. Soc. Jpn., 61, 1535—1538 (1988)

H_2 Evolution from Various Aqueous Solutions over Thermally Reduced TiO_2 and Pt-TiO_2 Powder

Akihiko KUDO, Kazunari DOMEN, Ken-ichi MARUYA, and Takaharu ONISHI*
Research Laboratory of Resources Utilization, Tokyo Institute of Technology,
4259 Nagatsuta, Midori-ku, Yokohama 227
(Received October 5, 1987)

The reduction of H_2O (or H^+) to form H_2 by reduced TiO_2 and Pt-TiO_2 was studied in distilled water and aqueous solutions of HCl, H_2SO_4, HNO_3, and NaOH. Over the reduced TiO_2 powder, H_2 evolved moderately in distilled water and Ti^{3+} ions on the surface were presumed to be active sites for the reaction. The reaction in aqueous NaOH solution proceeded similarly to that in water while it was strongly suppressed in aqueous HCl and H_2SO_4 solutions. It was found that the suppression of H_2 evolution is due to protons in the solution. Over reduced Pt-TiO_2, H_2 evolved rapidly from all solutions, except HNO_3. In aqueous HNO_3 solution, NO_3^- was reduced to NH_3 over reduced TiO_2 and Pt-TiO_2.

Recently TiO_2 has been extensively studied from several view points. It is well-known that TiO_2 has a photocatalytic activity under the band gap irradiation.[1] For example, the partial oxidation of hydrocarbons by O_2 on TiO_2 powder,[2,3] the photo-Kolbe reaction of acetic acid in aqueous media on platinized TiO_2,[4,5] the evolution of H_2 from aqueous solution of organic compounds,[6,7] and the photodecomposition of water on Pt-TiO_2[8] and NiO-TiO_2[9] were reported. The photoelectrochemical cell which consisted of a TiO_2 photoanode and a Pt cathode was also proved to decompose water into H_2 and O_2.[10,11] Although detailed mechanisms of these reactions have not been well-understood, the initiation of each reaction is recognized to generate an excited electron-hole pair by the absorption of a photon (>3 ev) in TiO_2. The generation of e^- and h^+ would be also regarded as the formation of Ti^{3+} and O^- species in TiO_2.

TiO_2 has been widely used also as supports for various heterogeneous catalysts, especially in recent years for the purpose of the study of the so-called strong metal support interaction (SMSI).[12] This phenomenon occurs when metals such as Ni and Pt supported on TiO_2 are reduced at high temperatures (>773 K). It is interpreted that the SMSI state is caused by the generation of Ti^{3+} by the high temperature reduction,[13-15] the migration of titanium oxide to metal surfaces[16-19] and so on.

Thus Ti^{3+} ions play an important role in the chemistry of TiO_2. The nature of Ti^{3+} produced by the band gap irradiation[20-25] and also by the thermal reduction[26-28] was investigated by some workers. However, few studies have been reported on the reaction of Ti^{3+} on TiO_2 powder in a liquid phase. In this paper, the behavior of H_2 evolution over thermally reduced TiO_2 and Pt-TiO_2 in various aqueous solutions, liquid water and water vapor was studied in order to reveal the activity of Ti^{3+} on the surface under the dark condition.

Experimental

TiO_2 powder (aerosil; P-25) used was a mixture of rutile and anatase, and its surface area was 53 $m^2 \cdot g^{-1}$. Pt(1 wt%)-TiO_2 was prepared by mechanical mixing of Pt black (Kojima Chemical, purity; 99.99%) and TiO_2.

Pretreatments of TiO_2 and Pt(1 wt%)-TiO_2, and reactions with various solutions were carried out in a closed gas circulation system connected to a vacuum line. TiO_2 or Pt(1 wt%)-TiO_2 (1 g) was dispersed on a flat bottom reaction cell made of quartz. They were reduced by H_2 (ca. 40 kPa) at 773 K for 1 h and then H_2 was evacuated at the same temperature. The aqueous solution was degassed thoroughly and then introduced onto the reduced powder in the reaction cell without exposing to air.

The amount of evolved H_2 was determined by gas chromatography (Ar carrier, MS-5A column) directly connected to the circulation system.

Results and Discussion

H_2 Evolution in the Reaction of Reduced TiO_2 and Pt-TiO_2 with Water. Behavior of H_2 evolution at 300 K from liquid and vapor water over reduced TiO_2 and Pt(1 wt%)-TiO_2 is shown in Fig. 1. The Pt-TiO_2 powder shows higher activity than TiO_2 and there is almost no difference in the activity between the reactions of liquid and vapor water. The evolution of H_2 on reduced TiO_2 is slow while that on reduced Pt-TiO_2 occurs immediately after the introduction of water. It is well-known that the reduced TiO_2 powder has Ti^{3+} ions and oxygen vacancies. When H_2 evolved from H_2O over the reduced TiO_2 powder the oxygen vacancies would be occupied by oxygen derived from H_2O. Therefore, a mechanism of H_2 evolution over the reduced TiO_2 surface is proposed as follows;

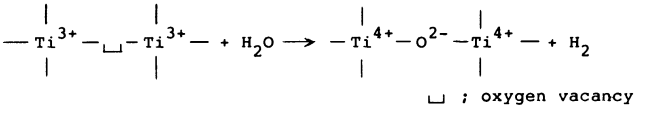

and/or

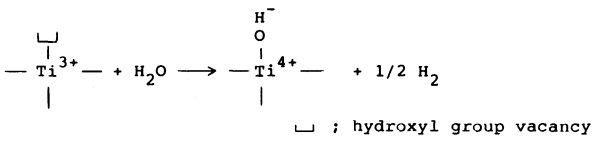

The driving forces are the reducing power of Ti^{3+} ions and stabilization energy of oxygen from water into the lattice oxygen. When TiO_2 powder is irradiated in aqueous solution containing a reducing agent such as alcohol, it is often observed that the color of TiO_2 changes from white to blue or gray, and a small amount of H_2 evolves. In this case, TiO_2 was reduced by a reducing agent with formation of oxygen vacancies on the surface and H_2 seems to evolve by a similar mechanism as stated above. On the other hand, in the case of Pt-TiO_2, the evolution of H_2 proceeds on the Pt surface after the electron transfers from reduced TiO_2 to Pt. This phenomenon is similar to that of the photocatalytic reaction for H_2 evolution from aqueous solutions. It was reported that the SMSI state of the Pt-TiO_2 system disappears when water exists.[29,30] This phenomenon may be explained by the oxidation of reduced TiO_2 by water via a similar process.

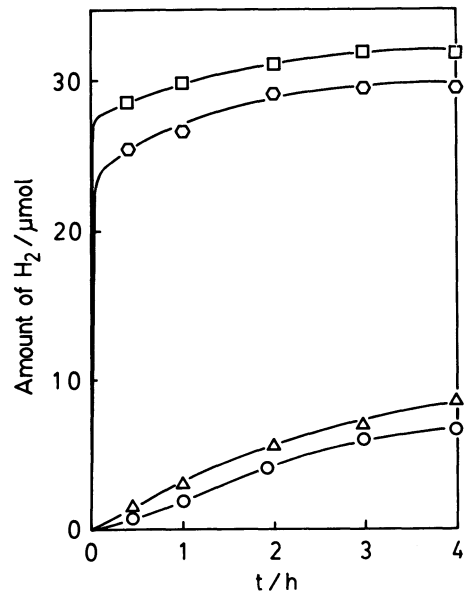

Fig. 1. H_2 evolution from liquid (10 ml) and vapor (3.2 kPa) water over reduced TiO_2 (1 g) and Pt(1 wt%)-TiO_2 (1 g) at room temperature.
□; liquid and ○ ; vapor over Pt-TiO_2, ○; liquid and △; vapor over TiO_2.

In Table 1, the amount of consumed H_2 by the reduction at 773 K and that of evolved H_2 from water are summarized. The extent of the reduction of TiO_2 by H_2 is different from that of Pt-TiO_2. In both cases, the amount of evolved H_2 is less than that of H_2 consumed during the reduction. The rate of H_2 evolution and the total amount of evolved H_2 increased with increasing the reaction temperature. The color of reduced TiO_2 was blue indicating the existence of Ti^{3+}, which was confirmed by ESR. After the reaction, the color was not completely recovered to original white at room temperature and even at 773 K. Furthermore, the evolution of H_2 was completely suppressed by the contact with O_2 (ca. 40 kPa) for 5 min at room temperature. The color was still blue in this case while it was rapidly turned into white by exposing to O_2 at 773 K. These results suggest that only Ti^{3+} existing close to the surface can react with H_2O, and the most of Ti^{3+} accompanied by oxygen vacancies in the bulk remains unchanged at room temperature. On the other hand, Ti^{3+} in the bulk can also react partially at 773 K. The apparent activation energy calculated from the initial rate of H_2 evolution over reduced TiO_2 was about 21 kJ·mol^{-1} below 473 K and about 50 kJ·mol^{-1} above 473 K. The activation energy is probably required for the H_2 evolution on reduced TiO_2 and the diffusion of a lattice oxygen from H_2O into the oxygen vacancy of the bulk respectively.

H_2 Evolution from the Reactions over Reduced TiO_2 and Pt-TiO_2 with Various Aqueous Solutions. The evolution of H_2 on the reactions of distilled water and aqueous solutions of NaOH, HCl, H_2SO_4, and HNO_3 over reduced TiO_2 is shown in Fig. 2. The evolution of H_2 from acidic solutions is much slower than those from distilled water and aqueous alkaline solution.

The rates of H_2 evolution at various concentrations of NaOH over reduced TiO_2 are shown in Fig. 3. The rate of H_2 evolution is moderately suppressed with increacing the NaOH concentration. On the contrary, in the case of reduced Pt-TiO_2, a large amount of H_2 evolves at the beginning of the reaction.

The evolution of H_2 from aqueous HCl solution

Table 1. The Amount of Ti^{3+} and That of Evolved H_2

	Consumed H_2 by the reduction at 773 K	Degree of reduction	Ti^{3+} total	Ti^{3+} surface[a]	Evolved H_2	
					at r.t.	at 773 K
	μmol	%	μmol	μmol	μmol	μmol
TiO_2	70	1.1	140	9	7	33
Pt-TiO_2	130	2.1	260	17	30	52

a) The amount of titanium ions on the surface was estimated to be ca. 800 μmol g^{-1} from a surface area by assuming a rutile (110) surface.

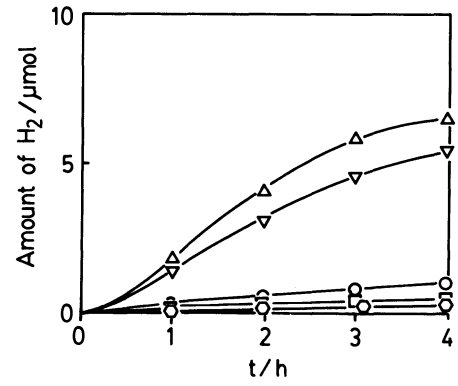

Fig. 2. H_2 evolution from various aqueous solutions (10 ml) over reduced TiO_2 (1 g) at room temperature. △; distilled water, ▽; 0.1 mol·dm^{-3} NaOH, ○; 0.1 mol·dm^{-3} HCl, □; 0.1 mol·dm^{-3} HNO_3, ○; 0.1 mol·dm^{-3} H_2SO_4.

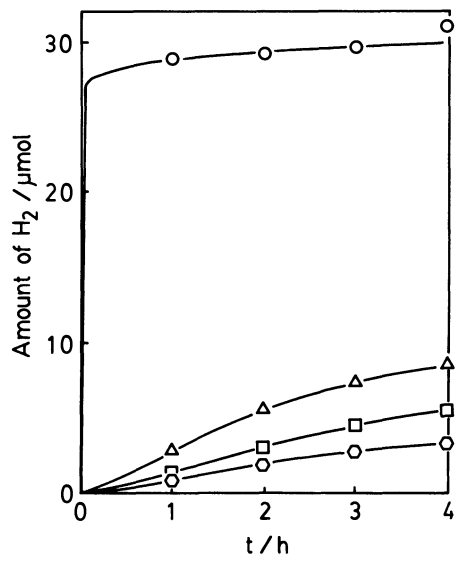

Fig. 3. H_2 evolution from aqueous NaOH solutions (10 ml) over reduced TiO_2 (1 g) and Pt(1 wt%)-TiO_2 (1 g) at room temperature.
○; 1 mol·dm^{-3} over Pt-TiO_2, △; 0.01 mol·dm^{-3}, □; 0.1 mol·dm^{-3}, ○; 1 mol·dm^{-3} over TiO_2.

over reduced TiO_2 and Pt(1 wt%)-TiO_2 is shown in Fig. 4. It was found that the reaction over reduced TiO_2 is strongly suppressed by HCl. Only a small amount of H_2 evolves in aqueous HCl solution (1 mol·dm^{-3}). The suppression effect of HCl on H_2 evolution is more remarkable than that of NaOH. The reaction in aqueous NaCl solution shows similar behavior to that in distilled water, which means the suppression was not owing to Cl^- ions. To examine the effect of HCl in more detail, the neutralization of aqueous HCl solution by NaOH solution was carried out during the reaction as shown in Fig. 5. Over reduced TiO_2 only a small amount of H_2 evolved in aqueous HCl solution (1 mol·dm^{-3}) in contrast to Pt which is a better catalyst for H_2 evolution. As soon as

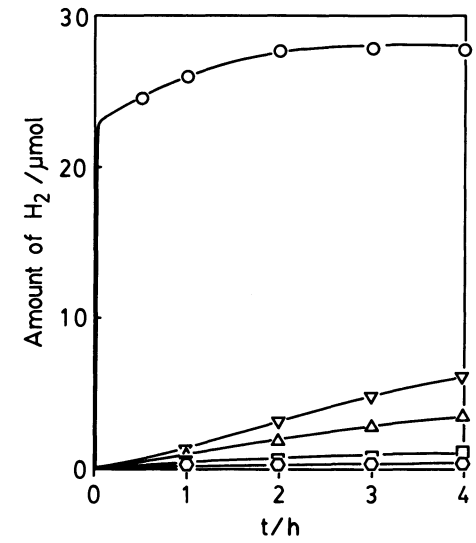

Fig. 4. H_2 evolution from aqueous HCl solutions (10 ml) over reduced TiO_2 (1 g) and Pt(1 wt%)-TiO_2 (1 g) at room temperature.
○; 1 mol·dm^{-3} over Pt-TiO_2, ▽; 0.01 mol·dm^{-3} (NaCl), △; 0.01 mol·dm^{-3}, □; 0.1 mol·dm^{-3}, ○; 1 mol·dm^{-3} over TiO_2.

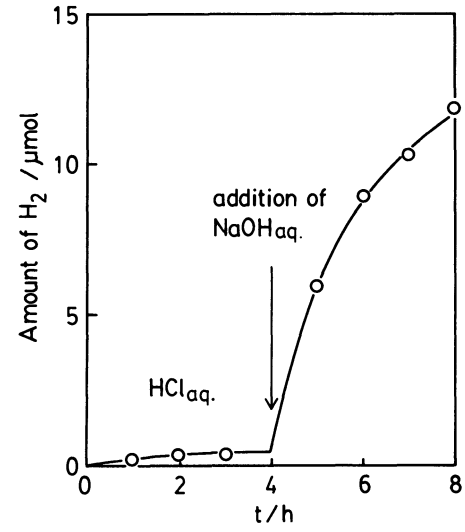

Fig. 5. Effect of addition of aqueous NaOH solution (1 mol·dm^{-3}, 10 ml) on H_2 evolution from aqueous HCl solution (1 mol·dm^{-3}, 5 ml) over reduced TiO_2 (1 g).

aqueous NaOH solution (1 mol·dm^{-3}) was added into the system, H_2 evolved rapidly. The resultant solution was in alkaline condition. From these results, it is inferred that H^+ suppresses the H_2 evolution over reduced TiO_2. Excess protons seem to poison the basic site which works as an electron donar center for H_2 evolution. Grätzel et al.[16] reported that Ti^{3+} species are produced when colloidal TiO_2 in acidic and alkaline solutions are irradiated, and ESR signals are different in acidic and in alkaline solutions. On the basis of these results it is concluded that the state of

Ti^{3+} on TiO_2 in acidic solution differs from that in alkaline solution. However, the detailed mechanism of the suppression of H_2 evolution by protons is not clear at present.

The reactions of aqueous HNO_3 solution over reduced TiO_2 and Pt(1 wt%)-TiO_2 were quite different from those of aqueous HCl and H_2SO_4 solutions. Instead of H_2 evolution, NH_3 was detected by the Nessler reagent in the solution after the reactions in both cases. This means that NO_3^- was preferentially reduced to NH_3 by Ti^{3+}. The photocatalytic reduction of NO_3^- into NH_3 by water over Pt-TiO_2 powder has already been reported.[31]

References

1) M. A. Grätzel, "Energy Resources through Photochemistry and Catalysis," Academic Press, Inc., New York (1983).
2) M. Formenti, F. Juillet, and S. J. Teichner, *C. R. Acad. Sci.*, **C270**, 138 (1970).
3) M. Formenti, F. Juillet, P. Meriaudeau, and S. J. Teichner, *Chem. Tech.* **1971**, 680.
4) B. Kraeutler and A. J. Bard, *J. Am. Chem. Soc.*, **100**, 2239 (1978).
5) B. Kraeutler and A. J. Bard, *J. Am. Chem. Soc.*, **100**, 5985 (1978).
6) T. Kawai and T. Sakata, *Nature (London)*, **286**, 474 (1980).
7) T. Kawai and T. Sakata, *Chem. Lett.*, **1981**, 81.
8) K. Yamaguchi and S. Sato, *J. Chem. Soc., Faraday Trans. 1*, **81**, 1237 (1985).
9) A. Kudo, K. Domen, K. Maruya, and T. Onishi, *Chem. Phys. Lett.*, **133**, 517 (1987).
10) A. Fujishima and K. Honda, *Nature (London)*, **238**, 37 (1972).
11) M. S. Wrighton, D. S. Ginley, P. T. Wolczanski, A. B. Ellis, D. L. Morse, and A. Linz, *Proc. Natl. Acad. Sci. U. S. A.*, **72**, 1518 (1975).
12) S. J. Tauster, S. C. Fung, and R. L. Garten, *J. Am. Chem. Soc.*, **100**, 170 (1978).
13) S. C. Fung, *J. Catal.*, **76**, 225 (1982).
14) J. M. Herrmann and P. Pichat, *J. Catal.*, **78**, 425 (1982).
15) J. M. Herrmann, *J. Catal.*, **89**, 404 (1984).
16) D. E. Resasco and G. L. Haller, *J. Catal.*, **82**, 279 (1983).
17) H. R. Sadeghi and V. E. Henrich, *J. Catal.*, **87**, 279 (1984).
18) S. Takatani and Y.-W. Chung, *J. Catal.*, **90**, 75 (1984).
19) J. A. Dumesic, S. A. Stevenson, R. D. Sherwood, and R. T. K. Baker, *J. Catal.*, **99**, 79 (1986).
20) W. J. Lo, Y. W. Chung, and G. A. Somorjai, *Surf. Sci.*, **71**, 199 (1978).
21) S. Ferrer and G. A. Somorjai, *Surf. Sci.*, **94**, 41 (1980).
22) F. T. Wagner, S. Ferrer, and G. A. Somorjai, *Surf. Sci.*, **101**, 462 (1980).
23) M. Anpo, T. Shima, and Y. Kubokawa, *Chem. Lett.*, **1985**, 1799.
24) R. F. Howe and M. Grätzel, *J. Phys. Chem.*, **89**, 4495 (1985).
25) J. Kiwi, *J. Phys. Chem.*, **90**, 1493 (1986).
26) P. C. Gravelle, F. Juillet, P. Meriaudeau, and S. J. Teichner, *Disc. Faraday Soc.*, **52**, 140 (1971).
27) S. Sato and J. M. White, *J. Phys. Chem.*, **85**, 592 (1981).
28) S. Ferrer and G. A. Somorjai, *J. Phys. Chem.*, **85**, 1464 (1981).
29) K. Kunimori, H. Abe, E. Yamaguchi, S. Matsui, and T. Uchijima, The Proc. of the 8 th International Congress on Catalysis (Berlin), *V*, 251 (1984), Verlag Chemie.
30) K. Kunimori, S. Matsui, and T. Uchijima, *Chem. Lett.*, **1985**, 359.
31) A. Kudo, K. Domen, K. Maruya, and T. Onishi, *Chem. Lett.*, **1987**, 1019.

Structure of Platinum Particles Deposited on Titanium Dioxide (110) Surface Studied by X-Ray Photoelectron Diffraction

Koji TAMURA,* Masanori OWARI, and Yoshimasa NIHEI
Institute of Industrial Science, University of Tokyo,
7-22-1 Roppongi, Minato-ku, Tokyo 106
(Received October 9, 1987)

Platinum atoms deposited on a TiO_2 (110) surface were studied by X-ray photoelectron diffraction, and the structure of the platinum particles was clarified. It was found that after annealing at 823 K for 30 min the platinum particles coalesced and that the structural model of platinum particles based on the (111) surface of the fcc crystal explained the experimental XPED patterns very well.

Small metal particles are an interesting subject in the field of chemistry and physics.[1] Especially, the structure and the chemical state of noble metal particles on metal oxides are important in connection with supported metal catalysts.[2,3]

In general, in order to obtain structural information about small metal particles, transmission electron microscopy (TEM) or extended X-ray absorption fine structure (EXAFS) have been used. In order to obtain a TEM micrograph or microdiffraction pattern, the irradiation of small metal particles by an electron beam is essential. However, the damage caused by the high energy electron beam is serious. Iijima has studied ultrafine particles of gold by electron microscopy, and emphasized that the structure of the gold particles became unstable because of charge fluctuations when they were exposed to intense electron-beam irradiation.[4] It is also difficult for TEM measurement to use a well defined single crystal sample as a support. From EXAFS measurements, information on the surrounding atoms about a particular type of atom is obtained such as the number of neighboring atoms and their distance from the reference atom. This information is, however, insufficient to create a three dimensional structural model or determine the directional relation between overlayer and substrate.

X-Ray photoelectron diffraction (XPED) has been shown to be a promising new method for surface structural and chemical state analysis,[5,6] and does not have these drawbacks. The advantages of XPED measurement compared with other surface analytical methods are summarized as follows: 1) the charging of a sample does not prevent obtaining clear diffraction patterns; 2) long-range ordering is not necessary to obtain structural information; 3) the contribution as an emitter atom from each component can be distinguished. From these features, XPED measurement is considered to be a more desirable method to analyze the metal particles deposited on insulating materials like metal oxides than other conventional methods. Kudo et al. have applied XPED measurement to gold atoms evaporated on a semiconductor, namely, GaAs(110), (001), Ge(110), and GaSb(110), and characterized the surface layer of metal-semiconductor contacts.[7]

In this study, the XPED patterns for platinum atoms deposited on a TiO_2 (110) surface were obtained, and the structure of the platinum particles was analyzed by a theoretical calculation. This sample was studied as a well-defined model system of Pt/TiO_2 catalyst which is one of the most important systems among supported metal catalysts. When one attemps to explain catalysis, the phenomenon becomes ambiguous for practical catalysts, because of uncertainty about the impurities, or atomic structure of the substrate etc. To clarify the essential nature of catalysis, the investigation of model catalysts is very useful.

Experimental

All experiments were performed with an angle-resolved X-ray photoelectron spectrometer, which was equipped with a hemi-spherical electron energy analyzer and computer controlled multichannel detection system.[8] Aluminum $K\alpha$ radiation was used to excite photoelectrons. The base pressure of the system was less than 2.7×10^{-8} Pa.

A (110) oriented TiO_2 rutile single crystal, obtained from the Nakazumi Crystal Laboratory, was aligned to within $\pm0.5°$ of the desired orientation. This was checked by the Laue back reflection. The crystal was then mechanically polished, and chemically etched. Before measurements, the sample was cleaned by Ar^+-ion bombardment (700 eV) and annealing (1010 K) cycles. The temperature was monitored with a chromel-alumel thermocouple spotwelded to the sample holder. Since oxygen atoms diffused out from the bulk of the sample because of the annealing treatment, the surface stoichiometry change caused by the selective sputtering was sufficiently restored. This was checked from the shape of Ti2p spectra and the valence spectra. The cleanliness of substrate surface was checked by X-ray photoelectron spectroscopy, and no carbon nor other impurities were detected.

The platinum was evaporated in vacuum by resistively heating from a pure platinum ribbon onto the titanium dioxide. The deposition rate of platinum was approximately 0.08 Å min^{-1}. To eliminate the apparent shift caused by the charging of the sample, the binding energy of platinum 4f was calibrated from the $Ti2p_{3/2}$ peak (458.8 eV).

Results and Discussion

The azimuthal dependences of Ti2p emission from TiO_2 (110) at a polar angle θ=50° relative to the surface normal are shown in Fig.1(a). The XPED pattern exhibited much fine structure, which indicated that the crystal regularity was sufficiently restored after the annealing treatment. The XPED pattern was mirror symmetric about the azimuthal angle ϕ=0° ([1$\bar{1}$0] direction of TiO_2) and 90° ([001] direction), which reflected the crystal structure. Though it was impossible to obtain full 360° azimuthal dependences by one scan with our system, different part of the azimuthal dependences which are not shown in this figure was checked by another experiment. These results indicated that the XPED pattern of TiO_2(110) has two-fold symmetry.

Figure 2 shows the XPS signal intensity (a) and the binding energy (b) of the Pt4f level as a function of the metal coverage. It was evident from these results that the binding energy of $Pt4f_{7/2}$ level decreased as the metal coverage increased. The decrease of the binding energy was caused mainly by the change of the degree of the screening of a core-hole by the electrons of

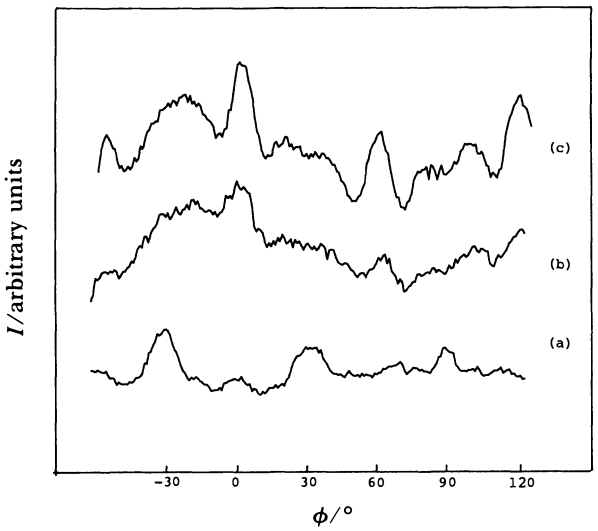

Fig. 1. (a) Azimuthal pattern of Ti2p at θ=50° from TiO_2(110). (b) Azimuthal pattern of Pt4f at θ=53° deposited on TiO_2(110) to a thickness of about 15.8 Å. (c) Azimuthal pattern of Pt4f at θ=53° after annealing at 823 K for 30 min.
ϕ: Azimuthal angle. I: Intensity.

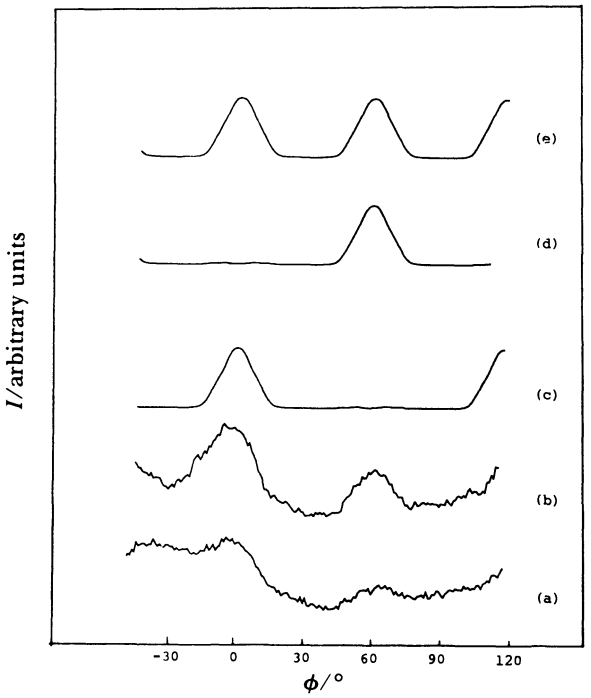

Fig. 3. (a) Azimuthal pattern of Pt4f at θ=33° deposited on TiO_2(110) to a thickness of about 15.8 Å. (b) Azimuthal pattern of Pt4f at θ=33° after annealing at 823 K for 30 min. (c) Calculated pattern of Pt4f from platinum No. 1. (d) Calculated pattern from platinum No. 2. (e) Calculated pattern when two types of particles exist.

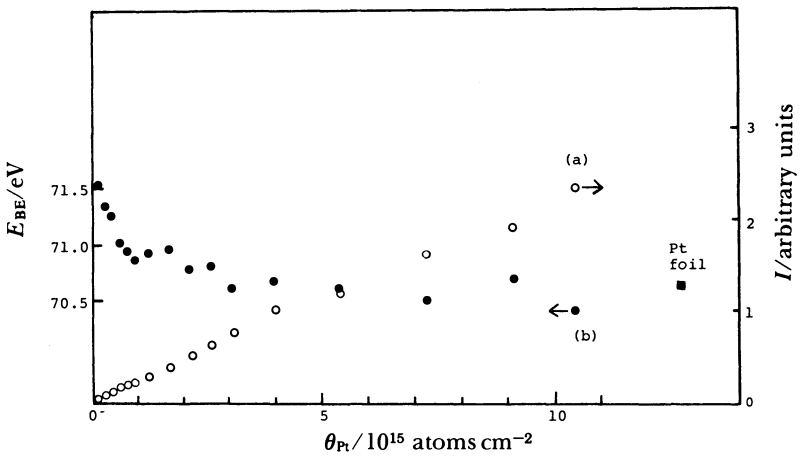

Fig. 2. (a) XPS signal intensity of Pt4f. (b) Binding energy of $Pt4f_{7/2}$ as a function of Pt coverage.
θ_{Pt}: Pt coverage. E_{BE}: Binding energy.

neighboring atoms.[3] In larger particles, since there were more neighboring electrons, the screening was more effective than in smaller particles, and the binding energy lowered. The amount of platinum deposited after the final step of the deposition was equivalent to the layer 15.8 Å in thickness, if layer growth was assumed. This thickness was roughly estimated from the XPS signal intensity ratio of Pt4f peak to Ti2p peaks assuming that the mean free path is 20 Å. XPED patterns were measured at this final point.

The azimuthal dependences of Pt4f emission at polar angles θ=53° (Fig.1(b)) and θ=33° (Fig. 3(a)) just after deposition were obtained. As can be seen in these XPED patterns, the photoelectron intensity maxima were already observed at ϕ=0°, 60°, 120°, which indicated that the platinum had structural regularity to some degree.

The sample was then annealed at 823 K for 30 min, which caused some significant changes. First, the XPS intensities for titanium and oxygen atoms relative to platinum atoms increased. Thus, the average thickness of the platinum, determined from the XPS signal intensity ratio, decreased to 7.6 Å. Second, as shown in Fig. 1 (c) for θ=53° and Fig. 3 (b) for θ=33°, the modulation of the XPED patterns increased and the patterns became clear. The amplitude of the anisotropy, defined as the ratio of (maximum−minimum)/maximum for θ=53°(Fig. 1 (b), (c)), increased from 16% to 29%. In contrast to the pattern from the titanium atom (Fig.1 (a)), these patterns can be regarded as having six-fold symmetry rather than two-fold symmetry.

These results indicated that most of platinum particles coalesced and became larger (metal agglomeration) on heat treatment, and simultaniously the degree of crystallization of the Pt particles and the degree of epitaxial relation between overlayer and substrate increased. Since the exposed area of the substrate surface increased on coalescence of the platinum particles, the XPS intensity from the substrate increased. On the other hand, since the exposed surface area of the platinum particles decreased on coalescence, the intensity from overlayer decreased. As a result, the Pt/Ti signal ratio decreased.

The diffusion of platinum atoms into the substrate may also decrease the Pt/Ti signal ratio, but this contribution was not so large, because 1) the chemical state of the platinum atom in the substrate must be different from that on the substrate, and these differences must be reflected in the platinum spectra. But no significant changes were observed in the platinum 4f spectral region. 2) if platinum atoms diffused into the substrate, the XPED pattern shows two-fold symmetry (selective incorporation case) or smaller modulation (random incorporation case), which were different from the experimental observation.

Assuming the coalescence is due to annealing only, the degree of coalescence could be estimated roughly based on a simple model as follows. The model is shown in Fig. 4 (a),(b). Hemi-spherical particles were assumed on the basis of the experimental observation by electron microscopy that the platinum particles grew in an island-like fashon on TiO_2.[9] The highly dispersed particles (a) just after deposition coalesced and became larger particles (b) because of annealing. Based on this model, the XPS signal intensity of the platinum atom for normal exit angle after annealing was written as

$$I_{Pt} = 2\pi I^{\infty}_{Pt}\left[\frac{1}{2}N^{2/3}a^2 - \int_0^{N^{1/3}a} r\cdot\exp(-\sqrt{N^{2/3}a^2 - r^2}/\lambda)\mathrm{d}r\right]. \quad (1)$$

The XPS intensity of the titanium atom in the exposed substrate was written as

$$I_{Ti}(1) = I^{\infty}_{Ti}(2\sqrt{3}N - \pi N^{2/3})a^2, \quad (2)$$

and the intensity of the titanium under the platinum particle was

$$I_{Ti}(2) = 2\pi I^{\infty}_{Ti}\left[\int_0^{N^{1/3}a} r\cdot\exp(-\sqrt{N^{2/3}a^2 - r^2}/\lambda)\mathrm{d}r\right], \quad (3)$$

where I^{∞}_{Pt} and I^{∞}_{Ti} were the XPS intensities of platinum and titanium from a semi-infinite platinum and TiO_2 layer, respectively; λ was the attenuation length, and a

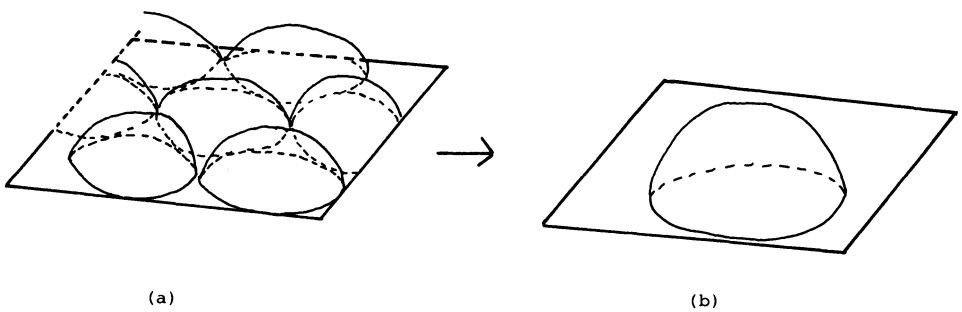

Fig. 4. Schematic representation of platinum particles on TiO_2(110) (a) just after deposition and (b) after annealing at 823 K for 30 min.

the radius of a particle just after deposition. N was the number of particles which gathered and became one larger particle because of the annealing treatment. Thus, the relative intensity of Pt to Ti after annealing became (1)/((2)+(3)), and the degree of coalescence N could be determined from the experimental signal ratio. It was estimated from the experimental XPS data that because of the heat treatment the volume of a particle increased about 26 times, and the exposed surface area of the platinum particles decreased to about 34% of that before annealing.

Ocal et al. have observed that annealing at 800 K in vacuum, which was almost the same treatment as our study, caused the suppression of CO adsorption for a Pt/TiO_2 sample and the uptake of CO per Pt atom was reduced by a factor of 2.[10] They suggested its relation to, what is called, strong metal-support interaction (SMSI), which recently attracted much interests in the field of catalysis.[11] The predominant model to explain this phenomenon is called the migration or decoration model, in which, titanium sub-oxide TiO_x migrates from a substratum and covers the surface area of the dispersed metal.[12] This may also decrease the Pt/Ti signal ratio. Ocal et al. also observed the Ti^{3+} state after vacuum annealing of a Pt/TiO_2 sample at 800 K, and the relative concentration of Ti^{3+} to Ti^{4+} ion was about 20%.[10] Greenlief et al. have observed the Ti^{3+} state after the vacuum annealing of TiO_2 overlayer on Pt at 1300 K,[13] which was higher than our temperature. They suggested a model in which the reduced titania species diffused into the platinum layer. Figure 5 shows the experimental spectra of Ti2p emission before platinum deposition (a) and after the annealing treatment (b). The height of these spectra was normalized and all of the spectra were smoothed. After annealing under these experimental conditions, namely, platinum deposited on TiO_2 (110) single crystal annealed in UHV at 823 K for 30 min, a small amount of a lower binding energy state did appear. But even if it covered the surface of the Pt particle because of migration, its contribution to the decrease of the Pt/Ti signal intensity ratio after the annealing was small. This indicated that the large decrease of the Pt/Ti ratio was not caused by the migration of sub-oxide onto the Pt particle.

The structural analysis of the platinum particles was next investigated by theoretical calculations. The calculations were performed within the double scattering approximation, in which the total photoelectron wave was expressed as a sum of a direct wave, a single-scattering wave and a double-scattering wave. The scattering amplitude for the double-scattering wave was a product of each scattering amplitude. Inelastic damping factors were derived from a sum of each path. Elastic scattering amplitudes were obtained from tabular form data.[14] The cluster of atoms used in this calculation consisted of a hemi-spherical platinum cluster 15 Å in radius

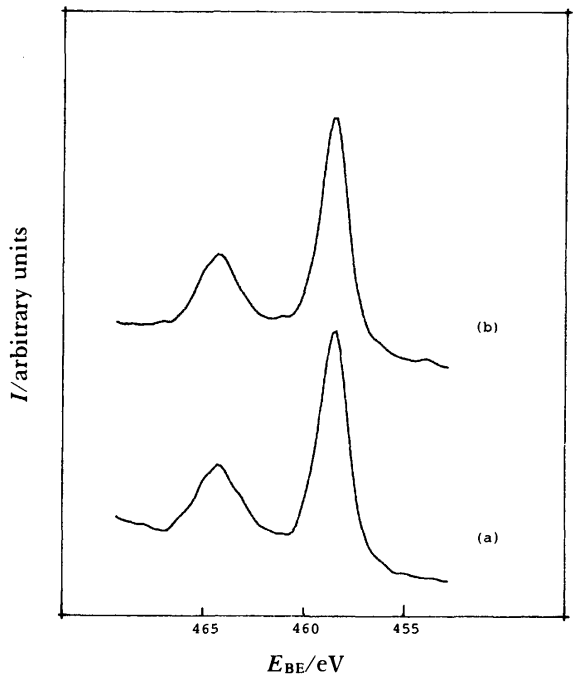

Fig. 5. XPS spectra of Ti2p from (a) clean TiO_2(110) surface and (b) Pt/TiO_2(110) annealed at 823 K for 30 min.

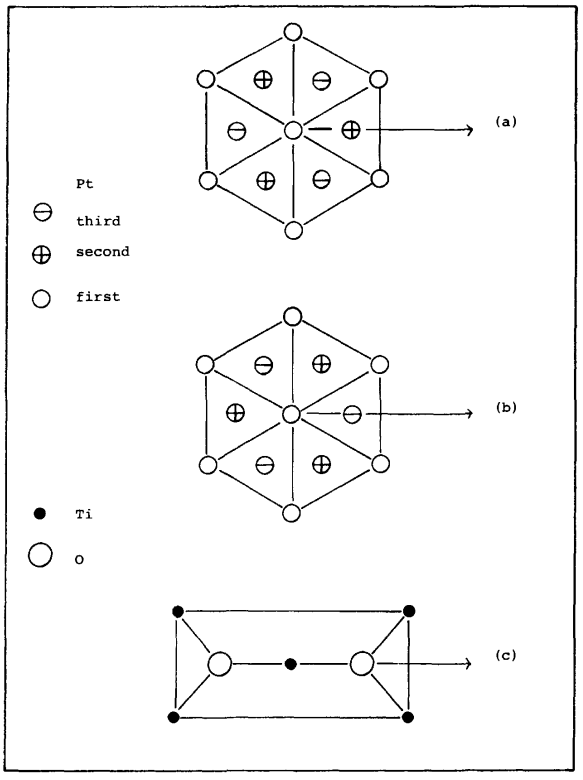

Fig. 6. (a), (b) Structural model of platinum particles No. 1 and No. 2. (c) Structural model of TiO_2(110) surface.

and a substrate cluster whose atoms were within 10 Å to the emitter atom. Since the six-fold symmetry of the experimental results was explained by the multiple of two fold-symmetry of the substrate and three-fold symmetry of the overlayer, it was sufficient to assume only the structural model based on the (111) plane of fcc platinum crystal. Two cluster models No. 1 and No. 2 were assumed and they are shown in Fig. 6(a),(b). The cluster model No. 1 is expressed as follows; (111) plane of platinum is parallel to the (110) surface of titanium dioxide (Fig. 6(c)) and [$\bar{2}$11] direction of the former is parallel to [1$\bar{1}$0] direction of the latter. The cluster model No. 2 is mirror symmetric with the model No. 1 about the (1$\bar{1}$0) plane of the substrate. The calculated patterns obtained from model No. 1 and No. 2 are shown in Fig. 7(b) and (c), respectively, for θ=53°, together with corresponding experimental pattern (a). For θ=33° Fig. 3(c) and (d) show the calculated patterns from model No. 1 and No. 2, respectively. These platinum patterns were three-fold symmetric and did not agree with the experimental pattern. These two models were equivalent from the standpoint of the structural relationships between substrate and overlayer. When two clusters exist with equal probability on the surface of titanium dioxide, corresponding patterns were obtained as shown in Fig. 7(d) for θ=53° and Fig. 3(e) for θ=33°. From the comparison, it was found that the calculated patterns at θ=53° and θ=33° agreed well with the experimental pattern. This model also explained other experimental results very well which were obtained by the different angular scans. Since the XPED pattern is sensitive to the crystal structure, it was concluded from the XPED analysis that after the platinum deposition the two orientations of clusters based on the (111) surface of the fcc crystal existed with equal probability on the TiO_2(110) surface.

The amplitude of the anisotropy for the calculated pattern for θ=53° was 96%, and was much larger than that of the experimental pattern. This deviation was explained as follows. First, in this calculation, thermal vibration of the platinum lattice was neglected. Second, emitter atoms were assumed to exist only in the center of the cluster. As a result, the contributions from the platinum atoms, which existed in the near surface region of the platinum particle, were not included. Since the intensity modulation for these platinum atoms is less than that of in the center, the modulation of the calculated pattern was overestimated. On the other hand, the degree of ordering of the real platinum particles was possibly lower than that of ideal bulk crystal, which diminished the modulation of the experimental pattern.

Figure 7(e) shows the calculated pattern which involved only a single scattering of the electrons. From the comparison it was found that the agreement of the pattern was worse and the double scattering was proved to be more accurate.

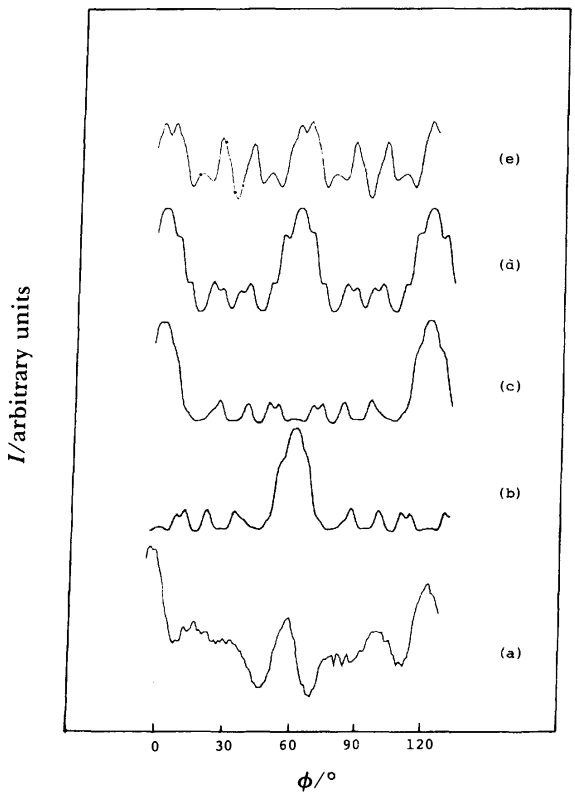

Fig. 7. (a) Azimuthal pattern of Pt4f at θ=53° after annealing at 823 K for 30 min. (b) Calculated pattern from platinum No. 1 considering double scattering. (c) Calculated pattern from platinum No. 2. (d) Calculated pattern when two types of particles exist. (e) Calculated pattern considering only single scattering.

Wang et al. have observed by transmission electron microscopy (TEM) that Pt particles on SiO_2 were produced with predominantly (100) and (110) planes if grown and treated in H_2, contrary to the prospect from surface free energy.[15] Our experimental results, however, showed that, when annealed in UHV, the (111) plane was the most favored, as expected for an ideal surface structure of a fcc crystal. Since the modulation of the XPED pattern of platinum after annealing was large, the contributions from the different structural particles or randomly oriented particles were small, and the structure of most of the particles was expressed by the model shown in Fig. 6. Also, the dynamic movement of the platinum particles, such as gold particles under the TEM observation, did not occur, because clear XPED patterns could not be obtained from the unstable particles.

As shown above, the structure of platinum particles deposited on a TiO_2 (110) surface was determined by XPED measurements. Moreover, the XPED analysis proved to be a useful technique for structural analysis

of the dispersed metal particles on the metal oxide, which were very difficult to analyze by any other technique.

We thank Dr. Masahiro Kudo for his technical assistance and for useful discussion.

References

1) W. D. Knight, K. Clemenger, W. A. de Heer, W. A. Sounders, M. Y. Chou, and M. L. Cohen, *Phys. Rev. Lett.*, **52**, 2141 (1984); I. Katakuse, T. Ichihara, Y. Fujita, T. Matsuo, T. Sakurai, and H. Matsuda, *Int. J. Mass Spectrom. Ion Phys.*, **67**, 229 (1985).

2) R. T. K. Baker, E. B. Prestridge, and R. L. Garten, *J.Catal.*, **56**, 390 (1979).

3) T. Huizinga, H. F. J. Vant' Blik, J. C. Vis, and R. Prins, *Surf. Sci.*, **135**, 580 (1983).

4) S. Iijima and T. Ichihashi, *Phys. Rev. Lett.*, **56**, 616 (1986).

5) Y. Nihei, M. Owari, M. Kudo, and H. Kamada, *Jpn. J. Appl. Phys.*, **20**, L420 (1981); N. Koshizaki, M. Kudo, M. Owari, Y. Nihei, and H. Kamada, *ibid.*, **19**, L349 (1980); M. Kudo, N. Koshizaki, M. Owari, Y. Nihei, and H. Kamada, *Hyoumen Kagaku*, **1**, 48 (1980).

6) K. Tamura, M. Owari, M. Kudo, and Y. Nihei, *Bull. Chem. Soc. Jpn.*, **58**, 1873 (1985).

7) M. Kudo, Pei-Xun Jien, M. Owari, N. Koshizaki,H. Kamada, and Y. Nihei, *Nippon Kagaku Kaishi*, **1985**, 1223.

8) M. Owari, M. Kudo, and Y. Nihei, *J. Electron Spectrosc.*, **22**, 131 (1981); M. Owari, M. Kudo, Y. Nihei, and H. Kamada, *J. Electron Spectrosc. Relat. Phenom.*, **34**, 215 (1984).

9) H. Nakamatsu, T. Kawai, A. Koreeda and S. Kawai, *J. Chem. Soc., Faraday Trans. 1*, **82**, 527 (1985).

10) C. Ocal and S. Ferrer, *J. Chem. Phys.*, **84**, 6474 (1986).

11) S .J. Tauster, S. C. Fiung and R. L. Gartern, *J. Am. Chem. Soc.*, **100**, 170 (1978).

12) H. R. Sadeghi, V. E. Henrich, *J. Catal.*, **87**, 279 (1984); A. J. Simoens, R. T. K. Baker, D. J. Dwyer, C. R. F. Lund, and J. R. Madon, *J. Catal.*, **86**, 359 (1984).

13) C. M. Greenlief, J. M. White, C. S. Ko, and R. J. Gorte, *J. Phys. Chem.*, **89**, 5025 (1985).

14) M. Fink and A. C. Yates, *At. Data*, **1**, 385 (1970); M. Fink and J. Ingram, *ibid.*, **4**, 129 (1972); D. Gregory and M. Fink, *At. Data Nucl. Data Tables*, **14**, 39 (1974).

15) T. Wang, C. Lee, and L. D. Schmidt, *Surf. Sci.*, **163**, 181 (1985).

 © 1988 The Chemical Society of Japan Bull. Chem. Soc. Jpn., 61, 1545—1550 (1988)

Effect of Counterionic Species on the Adsorption of Tetradecyltrimethylammonium Ion at the Polarized Nitrobenzene-Water Interface

Takashi KAKIUCHI, Miki KOBAYASHI, and Mitsugi SENDA*
Department of Agricultural Chemistry, Faculty of Agriculture, Kyoto University, Sakyo-ku, Kyoto 606
(Received October 16, 1987)

The effect of counterions, F^-, Cl^-, and Br^- on the adsorption of the hexadecyltrimethylammonium ion ($HTMA^+$) at the polarized nitrobenzene-water interface has been studied by measuring electrocapillary curves. The interfacial tension in the negative branch of the electrocapillary curve, where the interface is polarized such that the potential in the aqueous phase is negative with respect to that in the nitrobenzene phase, was lowered due to the specific adsorption of $HTMA^+$ ion at the interface. The magnitude of interfacial tension depression in the negative branch became larger in the order F^-, Cl^-, and Br^-, indicating a specific counterion binding at the interface in this order. The adsorption free energy of the $HTMA^+$ ion, ΔG_a^0, for the adsorption of $HTMA^+$ ion at the interface from the nitrobenzene phase was found to depend markedly on the anionic species present in the aqueous side of the interface. This ΔG_a^0 values can be taken as a quantitative measure of the counterion specificity at the interface. The meaning of the fact that the change in the shape of the electrocapillary curves depends on the counterion species is discussed in detail in terms of the thermodynamics of the oil-water interface.

The counterion specificity in interfacial chemistry and colloid chemistry has long been recognized. For example, the critical micelle concentration of cationic surfactants with different counterionic species decreases, while its micelle size increases, in accordance with the Hofmeister series of counterions.[1] A similar counterion specificity has been observed in a wide variety of surface phenomena, including surface pressure-area curves at air-water interfaces,[2] flocculation of colloidal particles,[3] and the rate of a chemical reaction at the interface.[4] However, only a few attempts have been made to quantitatively estimate the counterion specificity on the surface activity of surfactants.[5-7] Particular attention has recently been focused on the counterion binding at micelle surfaces in relation to micellar catalysis.[8] In these studies, the micelle was treated as a pseudophase and the relative affinity of counterions to the micelle surface has been estimated in terms of the ion-exchange constants of counterions.[8] In the previous paper we reported on the adsorption behavior of hexadecyltrimethylammonium ion at the polarized nitrobenzene-water interface, where an electrical double layer structure can be studied in the well defined electrical conditions of the interface.[9] This type of an interface provides us with a useful means to study the effect of counterion specificity to the surface properties of ionic surfactants. The present paper deals with the effect of counterion species on the adsorption of hexadecyltrimethylammonium ion ($HTMA^+$) at the polarized nitrobenzene-water interface. The advantage of this approach is that the counterion specificity can be quantitatively estimated through the adsorption free energy, which is obtainable as a function of the potential drop across the interface. Furthermore, in this approach the surfactant and its counterion to be studied reside in separate phases; they interact with each other only at the interface. This makes the interpretation of the experimental data much simpler, since the effect of the counterionic species in the bulk phase, e.g., salting out effect which may exists when both of them are in the same phase, needs not be considered.

Experimental

The interfacial tension of the nitrobenzene-water interface was measured with the drop time method using a dropwise ascending electrolyte solution electrode.[10] This electrode was also used to record current vs. potential curves using a four-electrode potentiostat with a positive feedback circuit for iR compensation. Details of the measurements and the method of calculation to convert the drop time into the interfacial tension value have been described previously.[10] All measurements were made at 25.00±0.05 °C. Methods for the preparation of hexadecyltrimethylammonium tetraphenylborate(HTMATPB), tetrapentylammonium tetraphenylborate(TPnATPB), and lithium tetraphenylborate (LiTPB) have been described elsewhere.[9,11] Lithium bromide and lithium fluoride were of Spurpur grade(Merck). Nitrobenzene was distilled under reduced pressure and then treated with active alumina. Triply distilled water was used to prepare the aqueous solutions.

Results and Discussion

The electrochemical cells used in the present study are represented by:

I	II	III	IV	V
Ag	AgCl	1 mM LiCl	1 mM LiTPB	(0.1−x)M TPnATPB x M HTMATPB
		(W)	(W)	(NB)

VI	VII	VIII	IX	
satd. LiF (W)	satd. KCl (W)	AgCl	Ag	(I)

and

I	II	III	IV	V	
Ag	AgCl	1 mM LiCl (W)	1 mM LiTPB (W)	(0.1−x)MTPnATPB x M HTMATPB (NB)	

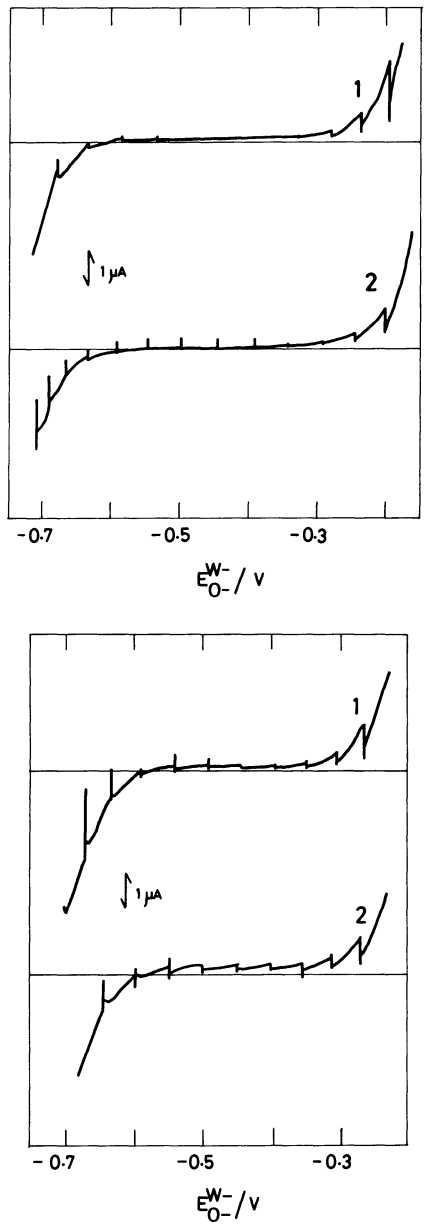

Fig. 1. a) Current vs. potential curves for the interface between aqueous solution of 0.05 mol dm^{-3} LiF and 0.1 mol dm^{-3} TPnATPB(1) or 0.1 mol dm^{-3} HTMATPB(2). b) Current vs. potential curves for the interface between aqueous solution of 0.05 mol dm^{-3} LiBr and nitrobenzene solution of 0.1 mol dm^{-3} TPnATPB(1) or 0.1 mol dm^{-3} HTMATPB(2).

VI	VII	VIII	
0.5 M LiBr (W)	AgBr	Ag	(II)

where M=mol dm^{-3}. The saturated solution of LiF whose concentration is 0.499 mol dm^{-3} at 25 °C[12] was used for the aqueous phase in Cell (I). The concentration of HTMATPB was varied from 0 to 0.1 mol dm^{-3} while keeping the total concentration of TPnATPB and HTMATPB in the nitrobenzene phase constant at 0.1 mol dm^{-3}. This mixed electrolyte method[13] has been conveniently used for obtaining a specifically adsorbed amount of $HTMA^+$ ion from the electrocapillary curves.[9]

The potential of the right-hand side of the Cells (I) and (II) with respect to the left is indicated as E^{W-}_{O-}, where the super- and subscripts indicate that the reference electrodes in the aqueous phase and the nitrobenzene phase are reversible to the anion (Cl^-) and the anion (TPB^-), respectively.[9] Figures 1a and 1b show the current vs. potential curves recorded for Cells (I) and (II). The polarized potential ranges for Cell (I) in the presence and the absence of HTMATPB

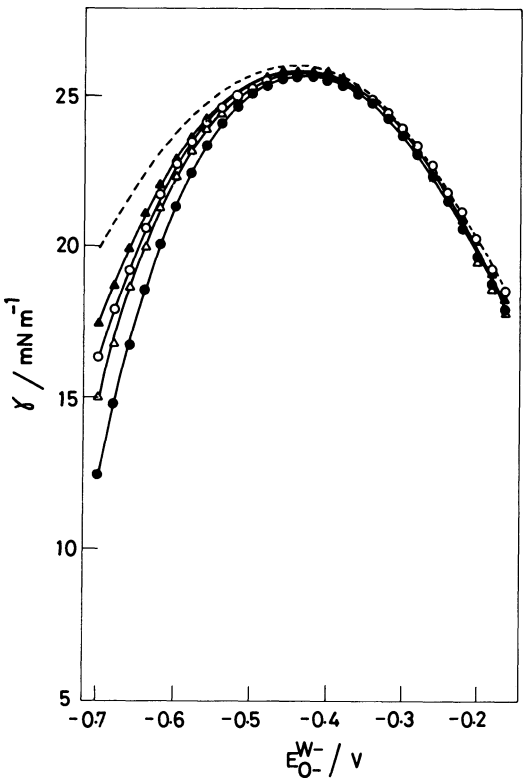

Fig. 2. Electrocapillary curves for the interface between aqueous solution of 0.05 mol dm^{-3} LiF and nitrobenzene solution of (0.1−a) mol dm^{-3} TPnATPB and a mol dm^{-3} HTMATPB, where a=0(-----), 0.01(−△−), 0.02(−○−), 0.04(−△−), and 0.10(−●−).

in the nitrobenzene phase were the same (Fig. 1a). On the other hand, the polarized potential range for Cell (II) was narrower in comparison with those for Cell (I) irrespective of the presence of HTMATPB (Fig. 1b). This is probably due to the transfer of Br^- ions from the aqueous phase to the nitrobenzene phase in the negative extreme range of the polarized potential. The standard ion transfer potential of Br^- ion is -0.295 V and is at least 30 mV more positive than that of Cl^- ion.[11] Figure 1b shows that there still remains a polarized potential range of about 300 mV. The electrocapillary measurements for Cells (I) and (II) were made within these polarizable potential ranges.

The electrocapillary curves were recorded at intervals of 20 mV for seven different concentrations of HTMATPB, from $x=0$ to 0.1. Some of the results are shown in Figs. 2 and 3. For both cases the interfacial tension was lowered with the increase of the HTMATPB concentration in the negative branch, i.e., $E^{w-}_{o-}-E_{pzc}<0$, where E_{pzc} is the potential of zero charge at $x=0$. This lowering of the interfacial tension indicates the existence of the specific adsorption of $HTMA^+$ ion at the interface.[9]

The electrocapillary curves at $x=0.1$ mol dm^{-3} for LiF, LiCl, and LiBr as the electrolyte in aqueous phase are compared in Fig. 4, in which the potential scale is relativized with respect to the E_{pzc} obtained with different reference electrodes. The degree of interfacial tension depression was larger in the sequence of LiF, LiCl, and LiBr. The result in Fig. 4 indicates that the specific adsorption of $HTMA^+$ ion is enhanced in this order. Since in the negative branch the potential of the aqueous phase is negative with respect to the nitrobenzene phase and the anionic species (F^-, Cl^-, or Br^-) exceeds the cationic species in the vicinity of the aqueous side of the interface, this enhancement of the adsorption strongly suggests the existence of a specific interaction between the charged head group of the adsorbed $HTMA^+$ ions and the anions in the aqueous side of the interface. This anion effect ensures that the polar head groups of the adsorbed $HTMA^+$ molecules are exposed to the aqueous phase so that it can interact with the counterion in the aqueous phase. The trend of the counterion effect in Fig. 4 is in marked contrast with the results reported by Watanabe et al.[6] They studied the adsorption of $HTMA^+$ ion at the methyl isobutyl ketone–water interface under the less polarized conditions compared with Cells(I) and (II) and found that the interfacial tension in the negative branch was decreased in the order, I^-, Br^-, Cl^-, and F^-.

The specifically adsorbed amount of the $HTMA^+$

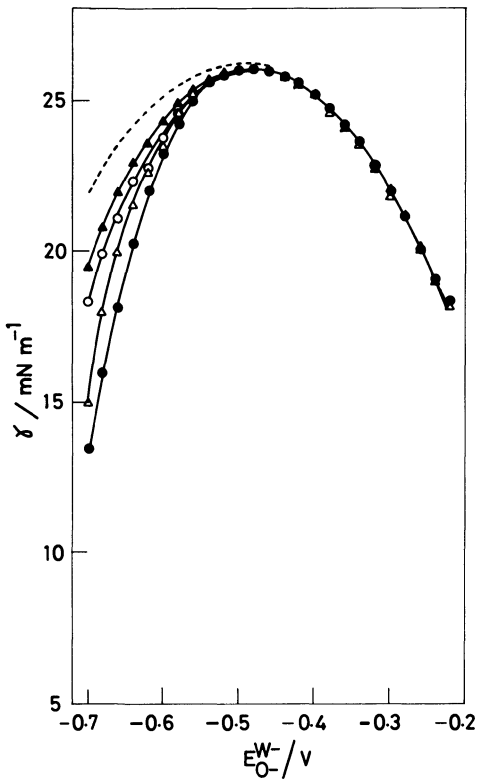

Fig. 3. Electrocapillary curves for the interface between aqueous solution of 0.05 mol dm^{-3} LiBr and nitrobenzene solution of (0.1−a) mol dm^{-3} TPnATPB+a mol dm^{-3} HTMATPB, where a= 0(-----), 0.02(−△−), 0.03(−○−), 0.05(−△−), and 0.10(−●−).

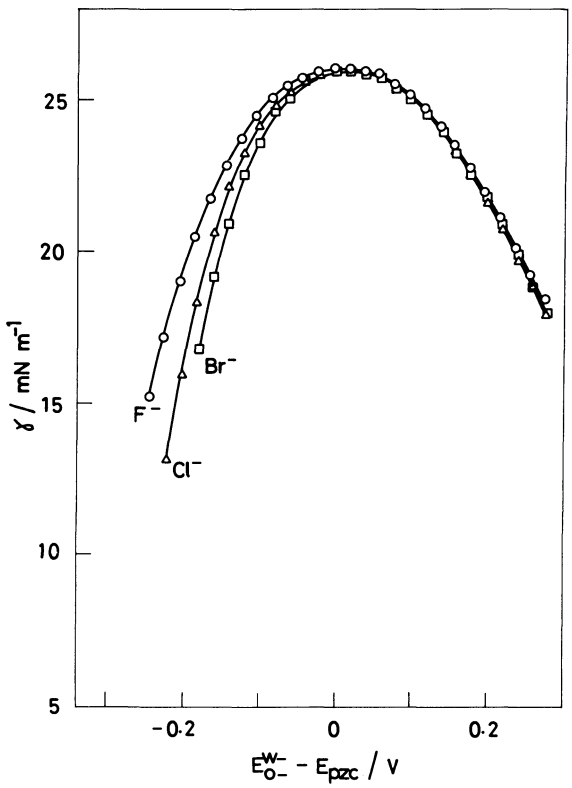

Fig. 4. Comparison of the electrocapillary curves for the interface between nitrobenzene solution of 0.1 mol dm^{-3} HTMATPB and aqueous solution of 0.05 mol dm^{-3} LiF(−○−), LiCl(−△−), or LiBr(−□−).

ions at a given potential was obtained from the electrocapillary curves by applying the electrocapillary equation modified for mixed electrolyte method.[9] The adsorption isotherms for both cases were well described by the Vorotyntsev's isotherm[14] which is a virial type isotherm of the form:

$$\ln(c/q^*) = \frac{\Delta G_a^0}{RT} + 2vq^*, \quad (1)$$

In Eq. 1, c is the bulk concentration of the surface active compound, v is the interaction parameter, and q^* is the adsorbed amount expressed in $\mu C\,cm^{-2}$ and is defined by $F\Gamma$, where F is Faraday and Γ the surface concentration. The adsorption free energy of $HTMA^+$ ion, ΔG_a^0, referrs to the standard states of 1 mol dm^{-3} and 1 $\mu C\,cm^{-2}$ for the nitrobenzene solution and the adsorption layer, both based on infinite dilution. From the intercepts of $\ln(c/q^*)$ vs. q^* plots at the different potentials, ΔG_a^0's were obtained (Fig. 5). The results for LiCl reported previously are also included in Fig. 5. ΔG_a^0's were linearly dependent on the potential difference, which was also the case for LiCl. The slopes of the straight lines were 5.0×10^4, 5.0×10^4, and 3.8×10^4 C mol^{-1} for F^-, Cl^-, and Br^-, respectively. Thus, the curves for F^- and Cl^- are in parallel with each other, suggesting that the effect of the applied voltage on the ΔG_a^0 value is essentially in electrostatic nature.[9] The slope for Br^- is smaller than these, but the difference is not very significant because of the experimental uncertainty. The vertical distance between these straight lines in Fig. 5 at a given potential can be seen as a direct and quantitative measure of the relative affinity of the polar head group of the $HTMA^+$ ion with the counterion in the aqueous phase. The difference in ΔG_a^0, $\Delta\Delta G_a^0$, is a quantitative measure of the affinity of the trimethylammonium head group of $HTMA^+$ ion with a counterion at the interface, provided that the maximum adsorptions of $HTMA^+$ for various counterions are the same. The maximum adsorption of the $HTMA^+$ ion is not likely to depend on the counterionic species. $\Delta\Delta G_a^0$'s at $E_{O-}^{W-}-E_{pzc}=-0.2$ V are shown in Table 1. $\Delta\Delta G_a^0$ for F^-–Br^- pair is four times greater than $\Delta\Delta G_a^0$ for F^-–Cl^- pair, suggesting the strong affinity of the trimethylammonio group and Br^- ion at the interface. Larsen and Magid have found that the enthalpy change of Br^- with respect to F^- for the transfer of ion from water to 0.1 mol dm^{-3} $HTMA^+$ aqueous solution is also four times larger than the corresponding value of Cl^- ion transfer.[15] This correspondence suggests the enthalpic nature of the factor that determines the counterion specificity.

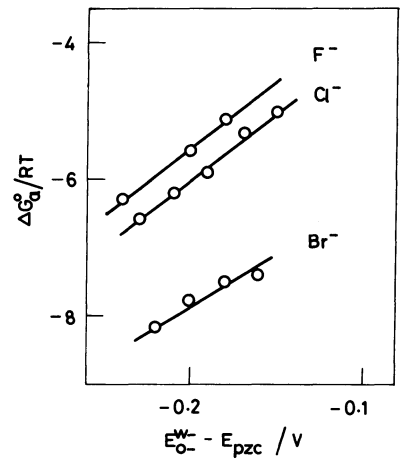

Fig. 5. Dependence of ΔG_a^0 of $HTMA^+$ ion on the potential drop across the interface between nitrobenzene and aqueous solution containing 0.05 mol dm^{-3} LiF, LiCl, or LiBr.

Table 1. Difference in Specific Interaction Energy of Halide Ions with Alkyltrimethylammonium Ions at Oil-Water Interfaces

Ion	$\Delta\Delta G_a^0$/kJ mol^{-1}			
	I[a]	II[b]	III[c]	IV[d]
F^-–Cl^-	2.2	—	2.5	1.2
F^-–Br^-	—	2.9	8.7	4.6

a) Davies.[5] b) Watanabe et al.[6] c) Goddard et al.[7] d) Present results.

Table 1 also includes the energies of the interaction between the counterion and the trimethylammonio head group of alkyltrimethylammonium ion surfactant in the monolayer estimated from various methods by Davies,[5] Watanabe et al,[6] and Goddard et al.[7] As shown in Table 1 all values obtained from three independent methods have the same order of magnitude. However, quantitatively there are discrepancies between them. Davies calculated the value from surface viscosity of the octadecyltrimethylammonium ion monolayer at the air-water interface. The value, therefore, involves the simplified assumptions which became necessary in order to estimate the interaction energies from kinetic data. Goddard et al. used the change in the surface pressure vs. area curves of docosyltrimethylammonium ion at the air-water interface at various subphase compositions. Their data also show the strong affinity of the trimethylammonio head group with Br^-. However, the values of $\Delta\Delta G_a^0$ are twice larger than ours. They assumed that the decrease of the surface pressure due to the specific interaction of $HTMA^+$ with the counterion was realized equivalently by increasing the ion concentration exhibiting no specific interaction with the head group. Since the specific adsorption, if any, cannot be solely attributed to the surface concentration term, their assumption is not likely to be valid in general.

Watanabe et al. calculated the ΔG_a^0 value employing the electrocapillary equation. It is interesting that they obtained a trend for ΔG_a^0 similar to ours, in spite of the fact that the effect of counterion on the surface tension depression in the electrocapillary curves they

found was reverse to the present result as described above. They interpreted the lesser degree of interfacial tension depression in the negative branch as a decrease in the surface charge density caused by the counterion binding with the head group of the adsorbed surfactant. However, their interpretation contradicts the following thermodynamic reasoning of the surface charge density obtained from an electrocapillary curve. At constant temperature, pressure, and the potential, the electrocapillary equation may be written in the integral form:

$$\gamma^0 - \gamma = RT\int_0^c \Gamma \mathrm{d}\ln c, \tag{2}$$

where Γ is the surface excess, γ is the interfacial tension, and c is the concentration of a surface active substance. Thus, the magnitude of the interfacial tension depression is directly related to the adsorbed amount of the surfactant, rather than to the amount of ion-pairs formed at the interface. Secondly, the change in the surface charge density accompanied by the adsorption of a surface active substance can generally be expressed in terms of the adsorbed amount of the substance at the interface without resorting to the concept of counterion binding. It is known that the adsorption of most of the surface active substances at an electrified interface follows an adsorption isotherm of the form:[16]

$$\Gamma = \Gamma(\beta c) \tag{3}$$

where β is the adsorption coefficient and is related to ΔG_a^0 through $\Delta G_a^0 = -RT\ln\beta$. Then the change in the surface charge density, q, due to the adsorption of a surface active substance can be expressed through[17]

$$q - q^0 = RT\frac{\mathrm{d}\ln\beta}{\mathrm{d}E}\Gamma \tag{4}$$

where E is the electrical potential difference. Since $\mathrm{d}\ln\beta/\mathrm{d}E$ is not much different for F^-, Cl^-, and Br^- in the present results, the change in the slope of the electrocapillary curves can be attributed to the difference in the adsorbed amount of $HTMA^+$ ion and is not directly related to the counterion binding.

Further insight concerning counterion binding may be obtained from the electrocapillary equation in the presence of ion-pair formation at the interface. Suppose that a cation $\bar{i}$ in the oil phase and an anion $\bar{q}$ in the aqueous phase form a neutral species $\bar{i}_{\nu_{\bar{i}q}^+}\bar{q}_{\nu_{\bar{i}q}^-}$ due to ion-pair formation,

$$\nu_{\bar{i}q}^+(\bar{i}) + \nu_{\bar{i}q}^-(\bar{q}) = (\bar{i})_{\nu_{\bar{i}q}^+}(\bar{q})_{\nu_{\bar{i}q}^-}, \tag{5}$$

where $\nu_{\bar{i}q}^+$ and $\nu_{\bar{i}q}^-$ are the stoichiometric numbers. If we assume for simplicity that the ion-pair exists only at the interface and is present neither in the oil phase nor in the aqueous phase, the following additional terms appear in the right-hand side of the basic electrocapillary equation for oil-water interface (Eq. 16 in Ref. 18):

$$\Gamma_{\bar{i}q}\left[\frac{\nu_{\bar{i}q}^+}{\nu_{\bar{i}\bar{j}'}^+}\mathrm{d}\mu_{\bar{i}\bar{j}'} + \frac{\nu_{\bar{i}q}^-}{\nu_{\bar{p}\bar{q}}^-}\mathrm{d}\mu_{\bar{p}'\bar{q}} - \frac{\nu_{\bar{i}q}^+ z_{\bar{j}}}{\nu_{\bar{i}'\bar{j}'}^-|z_{\bar{j}'}|}\mathrm{d}\mu_{\bar{i}'\bar{j}'} - \frac{\nu_{\bar{i}q}^-|z_{\bar{q}}|}{\nu_{\bar{p}'q'}^+ z_{\bar{p}'}}\mathrm{d}\mu_{\bar{p}'q'}\right]$$
$$+ z_{\bar{i}}\nu_{\bar{i}q}^+\Gamma_{\bar{i}q}\left(\frac{1}{z_{\bar{i}'}}\mathrm{d}\tilde{\mu}_{\bar{i}'} + \frac{1}{|z_{q'}|}\mathrm{d}\tilde{\mu}_{q'}\right), \tag{6}$$

where $\tilde{\mu}$ is the chemical potential and z is the ionic charge. Equation 16 in Ref. 18 as well as these additional terms are derived for the case in which the reference electrodes in the oil phase and aqueous phase are reversible to the ions i' and q', respectively. The last term in the above expression shows that the term $z_{\bar{i}}\nu_{\bar{i}q}^+\Gamma_{\bar{i}q}$ contributes to the derivative of γ with respect to the potential, i.e.,

$$-\frac{1}{F}\left(\frac{\partial\gamma}{\partial E_{O-}^{W-}}\right)_{T,P,\mu} = \sum_p z_p\Gamma_p - \sum_q z_q\Gamma_q - z_{\bar{i}}\nu_{\bar{i}q}^+\Gamma_{\bar{i}q} \tag{7}$$

where p and q represent cations and anions in the aqueous phase. The first two terms on the r.h.s. of this equation represent the excess surface charge density in the aqueous phase. The surface charge density in the aqueous phase is negative in the potential range where the adsorption of the $HTMA^+$ ion takes place. Therefore, the additional term $z_{\bar{i}}\nu_{\bar{i}q}^+\Gamma_{\bar{i}q}$ contributes in this case to the derivative such that the decrease of the surface charge density due to ion-pair formation at the interface is compensated for. Thus, the ion-pair formation does not necessarily lead to the decreae of the apparent surface charge density given by the slope of the electrocapillary curve. Equation 7 shows that the slope of the electrocapillary curve at a given potential cannot be an unequivocal measure of the ion-pair formation at the interface, as was claimed by Watanabe et al.[6] The importance of the possible ion-pair formation at the oil-water interface was first pointed out by Girault and Schiffrin.[19]

Equation 7 also shows that when the ion-pair formation occurs at the interface, the second derivative of an electrocapillary curve with respect to the potential, $-\partial^2\gamma/\partial(E_{O-}^{W-})^2$, does not generally accord with the double layer capacitance defined by $\partial q/\partial E$, where q is the excess free surface charge density.[20] The decrease of the excess free surface charge density caused by the ion-pair formation thus leads to a decrease in the double layer capacitance in comparison with that in the absence of the charge neutralization. In other words, the differential capacitance can be a useful means for detecting the ion-pair formation at the interface, if one combines the capacitance data with the electrocapillary curve data.

This work as supported by Grant-in-Aid for Scientific Research No. 60211017 and Grant-in-Aid for Scientific Research on Priority Areas "Macromolecule-Complexes (No. 62612003)" from the Ministry of Education, Science and Culture.

References

1) C. Tanford, "The Hydrophobic Effect: Formation of Micelles and Biological Membranes," 2nd ed, Chap. 8, John Wiley&Sons, New York(1980).

2) E. H. Lucassen-Reynders, "Progress in Surface and Membrane Science,"ed by D. A. Cadenhead and J. F. Danielli, Vol. 10, p. 253, Academic Press, New York (1977).

3) J. Th. G. Overbeek, "Colloid Science," ed by H. R. Kruyt Elsevier, Amsterdam (1952), Vol. 1, p. 302.

4) M. Almgren and R. Rydholm, *J. Phys. Chem.*, **83**, 360 (1979); J. B. S. Bonilha, G. Chiericato, Jr., S. M. Martins-Franchetti, E. J. Ribaldo, and F. H. Quina, *J. Phys. Chem.*, **86**, 4941 (1982); L. S. Romsted, *J. Phys. Chem.*, **89**, 5107 (1985).

5) J. T. Davies and E. K. Rideal, "Interfacial Phenomena," 2nd ed, p. 87, Academic Press, New York(1963).

6) A. Watanabe, M. Matsumoto, H. Tamai, and R. Gotoh, *Kolloid Z. Z. Polym.*, **221**, 47 (1967).

7) E. D. Goddard, O. Kao, and H. C. Hung, *J. Colloid Interface Sci.*, **27**, 616 (1968).

8) F. H. Quina and H. Chaimovich, *J. Phys. Chem.*, **83**, 1844 (1979); H. Chaimovich, J. B. S. Bonilha, M. J. Politi, and F. H. Quina, *J. Phys. Chem.*, **83**, 1851 (1979); D. Bartet, C. Camboa, and L. Sepulveda, *J. Phys. Chem.*, **84**, 272 (1980); C. Gamboa, L. Sepulveda, and R. Soto, *J. Phys. Chem.*, **85**, 1429 (1981); E. A. Lisa, E. B. Abuin, L. Sepulveda, and F. H. Quina, *J. Phys. Chem.*, **88**, 81 (1984).

9) T. Kakiuchi, M. Kobayashi, and M. Senda, *Bull. Chem. Soc. Jpn.*, **60**, 3109 (1987).

10) T. Kakiuchi and M. Senda, *Bull. Chem. Soc. Jpn.*, **56**, 1322 (1983).

11) T. Kakiuchi and M. Senda, *Bull. Chem. Soc. Jpn.*, **60**, 3099 (1987).

12) W. F. Linke, "Solubilities," Vol. II, p. 412, American Chemical Society, Washington, DC (1965).

13) H. D. Hurwitz, *J. Electroanal. Chem. Interfacial Electrochem.*, **11**, 100 (1966).

14) M. A. Vorotyntsev, *J. Res. Inst. Catalysis Hokkaido Univ.*, **30**, 167 (1982).

15) J. W. Larsen and L. J. Magid, *J. Am. Chem. Soc.*, **96**, 5774 (1974).

16) B. B. Damaskin, O. A. Petrii, and V. V. Batrakov, "Adsorption of Organic Compounds on Electrodes," Chap. 3, Plenum Press, New York (1971).

17) R. Parsons, *Trans. Faraday Soc.*, **55**, 999 (1959).

18) T. Kakiuchi and M. Senda, *Bull. Chem. Soc. Jpn.*, **56**, 2912 (1983).

19) H. H. Girault and D. J. Schiffrin, *J. Electroanal. Chem. Interfacial Electrochem.*, **170**, 127 (1984).

20) A. N. Frumkin, O. A. Petrii, and B. B. Damaskin, "Comprehensive Treatise of Electrochemistry," ed by J. O'M. Bockris, B. E. Conway, and E. Yeager, Vol. 1, Chap. 5, Plenum Press, New York(1980).

 © 1988 The Chemical Society of Japan Bull. Chem. Soc. Jpn., 61, 1551—1555 (1988)

Transfer of Homologous Alkanols from Water to Fluorocarbon and Hydrocarbon Surfactant Micelles

Masahiro MANABE,* Hideo KAWAMURA,† Gohsuke SUGIHARA,†† and Mitsuru TANAKA††
Department of Industrial Chemistry, Niihama National College of Technology, Niihama, Ehime 792
††Department of Chemistry, Faculty of Science, Fukuoka University, Fukuoka 814-01
(Received October 27, 1987)

The critical micelle concentration, cmc, of sodium perfluorooctanoate, SPFO, and sodium dodecyl sulfate, SDS, in the presence of two homologous series of alkanols (1-alkanols and ω-phenyl-1-alkanols) at very low concentrations of the alkanols C_a, was measured by a differential specific conductivity method. The free energy of transfer per CH_2 group in the alkanols from water to the respective micelles, $\Delta G°(CH_2)$, has been estimated from a linear relation of the rate of cmc-decrease, $\Delta cmc/\Delta C_a$, with the number of carbon atoms in the alkyl chain of alkanols. The respective values of $\Delta G°(CH_2)$ obtained for two series of homologues added to a given surfactant are in good agreement with each other: $\Delta G°(CH_2)$ is -1.73 kJ mol^{-1} in the SPFO system and -2.30 kJ mol^{-1} in the SDS system. The former has been found to be smaller in magnitude than the latter. On the basis of $\Delta G°(CH_2)$, a thermodynamic parameter has been proposed which characterizes the degree of modification of a medium from its pure liquid state to surfactant micelles or to interfaces composed of a hydrocarbon or a fluorocarbon.

Fluorocarbons are unique in their phobicity not only to water but also to hydrocarbons. Mixtures of a fluorocarbon and a hydrocarbon exhibit a positive deviation from the ideal solution behavior and there occurs partial miscibility as can be seen, for example, in n-C_4F_{10}–n-C_4H_{10} system.[1] The unique properties have tempted some workers to study the mixed micelle formation of a fluorocarbon surfactant and a hydrocarbon surfactant,[2-8] and the solubilization of hydrocarbon derivatives in fluolocarbon surfactant solutions.[9] One of the interesting results obtained is that the relation of the critical micelle concentration, cmc, with the composition of surfactants gives a maximum,[2-4,7] or a minimum.[8] It has been ascribed to the nonideality of mixing, i.e., to the coexistence of two types of mixed micelles in mutual solution; the regular solution theory has been applied to explain cmc data.[3]

It is known that the standard free-energy change of transfer of some homologous series of hydrocarbon derivatives from water to various environments, such as oil phases, micelles, and interfaces, has a linear dependence on the number of carbon atoms in the homologues; the transfer free energy per CH_2 group, $\Delta G°(CH_2)$, gives information about the interaction of the hydrocarbon chain with the respective environments.[10] However, few studies on $\Delta G°(CH_2)$ between water and fluorocarbon media have so far been made.[11] Such studies will afford a better understanding of the nonideal behavior of mixed surfactant solutions of fluorocarbon and hydrocarbon surfactants.

In the present study, the initial rate of decrease of the cmc of a fluorocarbon surfactant and a hydrocarbon surfactant upon the addition of two homologous series of alkanols has been determined in order to estimate $\Delta G°(CH_2)$ between water and the respective surfactant micelles.

Experimental

Materials. Sodium perfluorooctanoate, SPFO, was prepared as follows. Commercially available perfluorooctanoic acid (P.C.R Research Chemicals, U.S.A.) was recrystallized twice from CCl_4. Its aqueous solution was neutralized with NaOH; then, the crude crystals obtained were recrystallized twice from water and then dried in a vacuum. Sodium dodecyl sulfate, SDS, was synthesized and purified using the same procedure as described elsewhere.[12] Each surfactant gave no minimum around its critical micelle concentration, cmc, in a plot of the surface-tension against concentration. Purchased 1-alkanols (C_2—C_7; Tokyo Kasei, Japan) and ω-phenyl-1-alkanols ($C_6H_5(CH_2)_mOH$: m=1—3; Tokyo Kasei) were used as additives after fractional distillation; the phenylalkanols (m=4, 5: 99%; Aldrich, U.S.A.) were used without further purification. The water for solvent was purified by means of ion exchange and distillation. Its specific conductivity was lower than 2 μS cm^{-1} at 298.15 K.

Conductivity Measurements for cmc Determination. An aqueous solution with a given concentration of each alkanol was prepared and used as a solvent. A portion of the solvent was poured into a conductivity cell (cell constant: 0.4743 cm^{-1}). A concentrated surfactant solution was prepared with the other portion of the solvent, and successively added into the conductivity cell. Upon each addition, the conductivity of the solution was measured on a conductivity metel (Model MY-8; Yanagimoto, Japan). The temperature of the water bath was controlled at 298.15±0.005 K.

Results and Discussion

In order to determine the critical micelle concentration, cmc, of the surfactants in the presence of alkanols, the differential specific conductivity method[2,13] was applied. Figure 1 illustrates the dependence of the differential conductivity, $\Delta\kappa/\Delta C_s$, on the mean concentration of surfactants, $\bar{C}_s$, just around the cmc, in an SPFO–1-hexanol system. At a given concentration of alkanol, C_a, $\Delta\kappa/\Delta C_s$ decreases slowly and

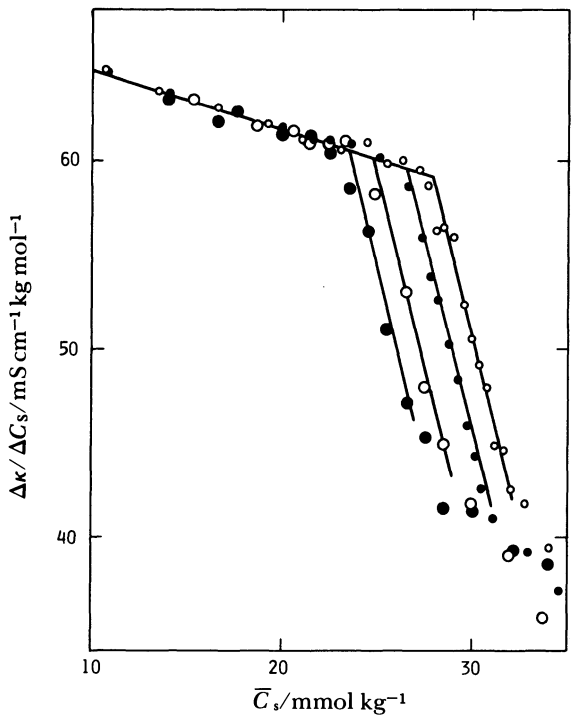

Fig. 1. The dependence of differential specific conductivity on the mean concentration of SPFO. Concentration of 1-hexanol in mmol kg^{-1}: 0 (○); 4.995 (●); 10.60 (○); 15.00 (●).

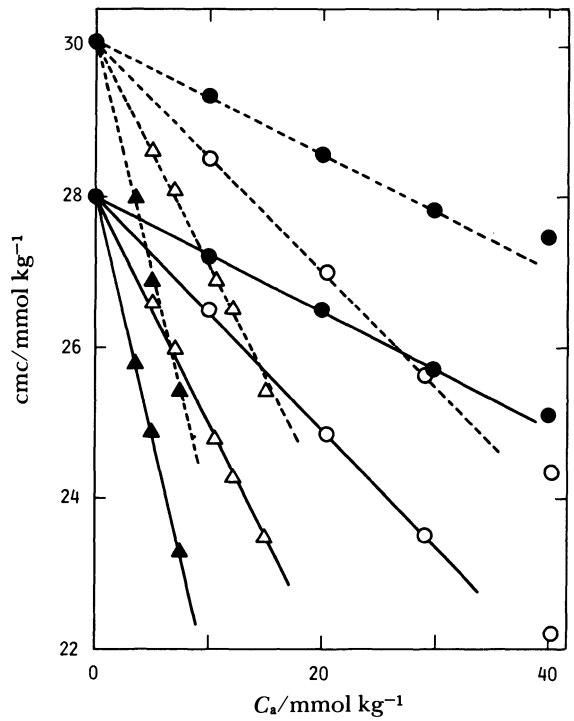

Fig. 2. The dependence of cmc of SPFO on 1-alkanol concentration. cmc determination method: equivalent conductivity (broken line); differential conductivity (solid line). Added 1-alkanols: 1-butanol (●); 1-pentanol (○); 1-hexanol (△); 1-heptanol (▲).

linearly until a break point; then it decreases sharply in a linear fashion whthin a narrow region of $\overline{C}_s$. The value of $\overline{C}_s$ at the intersection of the two straight lines is taken as the cmc. It is apparent that the points of $\Delta\kappa/\Delta C_s$ below the cmc fall on the same line, at any C_a studied, whereas the lines above the cmc are regarded as being parallel to each other. The latter finding indicates that the break remains clear, even if C_a increases; this is in marked contrast to a plot of the equivalent conductivity against the square root of the surfactant concentrations, C_s, (equivalent conductivity method) and a plot of specific conductivity against C_s (specific conductivity method), which are often employed for cmc determinations. In the latter two plots, as is well-known, the break around cmc becomes less distinct with increasing C_a. Therefore, it is claimed that the differential conductivity method is better for a cmc determination than those other conductivity methods, especially in the presence of some additives.

The cmc of SPFO determined by the differential conductivity method and the equivalent conductivity method is plotted in Fig. 2 against C_a of 1-alkanols, where the cmc value by the former method can be ascertained with more accuracy than by the latter method because of the more distinct break in Fig. 1. It is obvious that at a definite C_a of a certain alkanol, the cmc values are different from each other determined by the respective methods: the values are higher in the order of those by the specific, equivalent, and differential conductivity method, although cmc by the specific conductivity method is not shown in Fig. 2. In line with the reported results,[14,15] the cmc decreases linearly with C_a up to a certain C_a; this decreasing tendency becomes more marked with an increase in the alkyl-chain length of alkanols. The limiting slopes, Δcmc/ΔC_a, shown by the straight lines, are found to be almost identical, irrespective of the determination methods. The values of Δcmc/ΔC_a estimated from the cmc data by the differential conductivity method are listed in Table 1.

Table 1. Δcmc/ΔC_a and $\Delta G°(CH_2)$ for 1-Alkanols and ω-Phenyl-1-alkanols Added in SDS and SPFO at 298.15 K

	$-\Delta$cmc/ΔC_a				
m_n	SDS[a]	SPFO	m_p	SDS	SPFO
4	0.028	0.0767	1	0.0667	0.0663
5	0.078	0.155	2	0.113	0.134
6	0.21	0.300	3	0.255	0.258
7	0.53	0.634	4	0.553	0.500
			5	1.40	1.15
$-\Delta G°(CH_2)$[b]	2.45	1.74		2.19[c]	1.73

a) Taken from Ref. 15. b) In kJ mol^{-1} unit. c) Determined at m_p=3—5.

The relation between log ($-\Delta$cmc/ΔC_a) and the

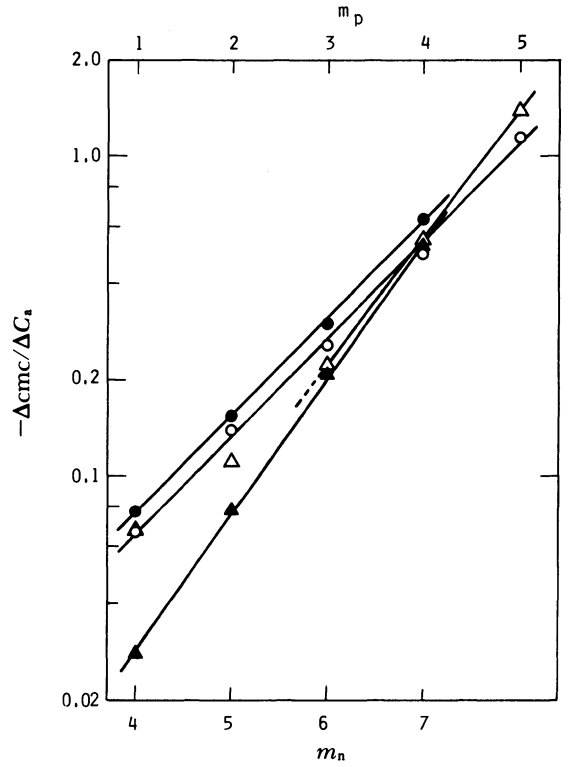

Fig. 3. The dependence of $\log(-\Delta cmc/\Delta C_a)$ on the number of carbon atoms in the alkylchain of added alkanols. Surfactant: SPFO (circle); SDS (triangle). Alkanol: 1-alkanol (closed mark); ω-phenyl-1-alkanol (open mark).

number of carbon atoms in the alkyl chain of added homologous alkanols (denoted by m_n for 1-alkanols, and m_p for ω-phenyl-1-alkanols) is shown in Fig. 3 where literature data for the SDS-1-alkanol systems[15] are also plotted. It is apparent that, as has been known in other systems,[14,15] a linear relation holds in each system, except for some short-chain alkanols (m_p=1, 2). It is perceived that the respective straight lines of 1-alkanols and phenylalkanols for each surfactant are parallel to each other and that the slopes of the straight lines for SPFO are less steep than those for SDS.

It is found that at a given value of $\Delta cmc/\Delta C_a$ for each surfactant, m_p is higher by about 3 than m_n, i.e., $m_p=m_n+3$. This result implies that the phenyl group is hydrophobic and its hydrophobicity corresponds to that of three methylene groups in the alkyl-chain. The difference of 3 is in agreement with that assigned to the phenyl group in a homologous series of sodium alkylbenzenesulfonates by comparison in cmc with homologous sodium alkanesulfonates.[16]

Manabe et al.[17] described the relation between $\Delta cmc/\Delta C_a$ and K_x (partition coefficient of a solubilizate between the bulk water and micelle phases, in mole fraction unit). When C_a is very low, the relation is expressed as

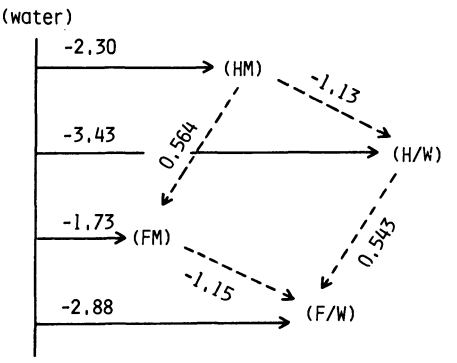

Fig. 4. Free energy of transfer per CH_2 group at 298.15 K. Values are in kJ mol^{-1}. Data for H/W and F/W are taken from Ref. 11.

$$-\Delta cmc/\Delta C_a = (cmc_0/n_w)\theta K_x, \quad (1)$$

where cmc_0, n_w, and θ refer to the cmc in water (in molality unit), the mole number of water, and a constant, respectively. In the SDS-1-alkanol systems (m_n=4—7), the value of θ (0.69,[17] 0.82[18]) was reported to be independent of the chain-length of alkanols. Assuming that θ is constant in each present system, the standard free-energy change of transfer per CH_2 group in the alkanols from the bulk water to micelles, $\Delta G°(CH_2)$, can be calculated through Eq. 1 as

$$\Delta G°(CH_2) = -RT\, d\ln(-\Delta cmc/\Delta C_a)/dm. \quad (2)$$

Here, R, T, and m are the gas constant, the absolute temperature, and the carbon number (m_n or m_p), respectively. The values of $\Delta G°(CH_2)$ calculated by Eq. 2 from the linear relation in Fig. 3 are shown in Table 1. It is noticed that $\Delta G°(CH_2)$ for the respective homologous series with a given surfactant are in agreement, as can also be seen in Fig. 3; also the value for SPFO (mean value, −1.73 kJ mol^{-1}) is smaller in magnitude than that for SDS (−2.30 kJ mol^{-1}). These figures indicate that a hydrocarbon derivative is more difficult to be solubilized in fluorocarbon surfactant micelles than in hydrocarbon surfactant ones. This is consistent with the fact that a liquid hydrocarbon is partially miscible with a liquid fluorocarbon, as observed in the n-C_4H_{10}-n-C_4F_{10} system.[1]

Mukerjee and Handa[11] measured the interfacial tension of dilute aqueous solutions of some homologous sodium alkyl sulfates as well as some sodium perfluoroalkanoates at air-water (A/W), hydrocarbon-water (H/W), and fluorocarbon-water (F/W) interfaces, and estimated the free-energy change for a CH_2 group as well as a CF_2 group in the surfactant molecules transferring from water (W) to each interface. For the CH_2 group, their data are schematically compared in Fig. 4 with the present data for $\Delta G°$ (CH_2) in the transferring process from W to hydrocarbon surfactant micelles (HM) and to fluorocarbon surfactant micelles (FM). Figure 4 suggests that

the oil-water interface has a greater affinity for the CH_2 group than the micelle when both media consist of the same substance (hydrocarbon or fluorocarbon). Further, it is apparent that the difference of the free energy of transfer between HM and H/W (1.13 kJ mol^{-1}) is in agreement with the difference between FM and F/W (1.15 kJ mol^{-1}). In addition, the difference between HM and FM (0.564 kJ mol^{-1}) is also regarded as being identical with that between H/W and F/W (0.543 kJ mol^{-1}). Accordingly, the four broken lines in Fig. 4 form a parallelogram. The parallelogrammic relation suggests that the modification of a type of medium, such as micelle or interface, characterizes a unique affinity for the CH_2 group.

The difference, 0.543 kJ mol^{-1}, between F/W and H/W in Fig. 4 was attributed by Mukerjee and Handa[11] to a nonideality of the mixing of hydrocarbon and fluorocarbon, by a comparison with the following excess free energy. By the regular solution approach, the incremental change per methylene group in the partial molar excess free energy of homologous hydrocarbons dissolved at infinite dilution in perfluorohexane was estimated to be 0.585 kJ mol^{-1}, which was in agreement with the value 0.543 kJ mol^{-1}. It should be noted that in the calculation for the respective free energies, different standard states of the solute were used, i.e., an extrapolated state from a limiting dilution for the adsorption free energy and the pure state of solute for the excess free energy. Then, we will propose an alternative explanation for the thermodynamic relation between the different standard states.

We consider a solute such as a hydrocarbon derivative distributed between two phases, α and β, at mole fractions of the solute, x^α and x^β, in respective phases. At a certain temperature and pressure, the chemical potential of the solute in each phase, μ^α and μ^β, can be expressed on the basis of two different reference systems. The one is that the activity coefficient (γ) of the solute is equal to unity in its pure liquid state (so called, Raoult's reference system) and the other is that the activity coefficient (f) of the same solute approaches unity as the solution becomes more and more dilute (Henry's reference system). Representing standard chemical potentials in, e.g., α phase as $\mu^{\alpha 0}$ and $\mu^{\alpha\ominus}$ by respective reference systems, the chemical potentials can be expressed as

$$\mu^\alpha = \mu^{\alpha 0} + RT\ln(\gamma^\alpha) + RT\ln(x^\alpha)$$
$$= \mu^{\alpha\ominus} + RT\ln(f^\alpha) + RT\ln(x^\alpha)$$

and

$$\mu^\beta = \mu^{\beta 0} + RT\ln(\gamma^\beta) + RT\ln(x^\beta)$$
$$= \mu^{\beta\ominus} + RT\ln(f^\beta) + RT\ln(x^\beta). \quad (3)$$

It should be noticed that in the above equations $\mu^{\alpha 0}$ is identical with $\mu^{\beta 0}$ since they concern the same pure solute. When in equilibrium, $\mu^\alpha = \mu^\beta$; therefore, from Eq. 3,

$$\mu^{\beta 0} - \mu^{\alpha 0} = 0 = -RT\ln(\gamma^\beta/\gamma^\alpha) - RT\ln(x^\beta/x^\alpha)$$

and

$$\mu^{\beta\ominus} - \mu^{\alpha\ominus} = -RT\ln(f^\beta/f^\alpha) - RT\ln(x^\beta/x^\alpha). \quad (4)$$

Under the conditions of infinite dilution of the solute in both phases, both f^α and f^β can be taken to be unity. Form Eq. 4, it follows that

$$\mu^{\beta\ominus} - \mu^{\alpha\ominus} = -RT\ln(x^\beta/x^\alpha) = RT\ln(\gamma^\beta/\gamma^\alpha). \quad (5)$$

This equation reveals a significant point that the standard free energy change, $\mu^{\beta\ominus} - \mu^{\alpha\ominus}$, for an ideal solution based on Henry's system is correlated with the excess free-energy change on Raoult's system.

These considerations can be applied to the present data as follows. The standard free energy of transfer, corresponding to $\mu^{\beta\ominus} - \mu^{\alpha\ominus}$ in Eq. 5, between any pair of media in Fig. 4 is calculated as the difference of $\Delta G°(CH_2)$. The quantity of $\Delta G°(CH_2)$ in the transferring process from water to each medium is denoted by $\Delta G°(CH_2{:}W)$; the values are arranged according to the order of magnitude in Table 2. When the CH_2 group transfers from a hydrocarbon medium to another one, the free energy of transfer, denoted by $\Delta G°(CH_2{:}H)$, may be given as the difference between $\Delta G°(CH_2{:}W)$ and -3.59 kJ mol^{-1} determined from the partition coefficients of homologous 1-alkanols between water and dodecane at infinite dilution at 298.15 K.[19] The values of $\Delta G°(CH_2{:}H)$ are also

Table 2. Thermodynamic Quantities for CH_2 Group in Transfering Processes at 298.15 K

Medium	$-\Delta G°(CH_2{:}W)$ / kJ mol^{-1}	$\Delta G°(CH_2{:}H)$[b] / kJ mol^{-1}	γ^ω	$((RT\ln(\gamma^\omega))/\bar{V})^{1/2}$ / (cal cm^{-3})$^{1/2}$[c]
H	3.59[a]	0	1	0
H/W	3.43	0.040	1.07	1.55
F/W	2.88	0.711	1.33	3.19
A/W	2.59	1.00	1.50	3.80
HM	2.30	1.30	1.69	4.33
FM	1.73	1.86	2.12	5.18
W	0	3.59	4.27	7.20

Notations are defined in text. a) From Ref. 19. b) $\Delta G°(CH_2{:}H) = \Delta G°(CH_2{:}W) - (-3.59)$. c) 1 cal = 4.184 J.

shown in Table 2. If the hydrocarbon medium and another one are represented by superscripts h and ω instead of α and β in the above equations, respectively, $\Delta G°(CH_2{:}H)$ can be rewritten along with Eq. 5 as

$$\Delta G°(CH_2{:}H) = \mu^{\omega\ominus} - \mu^{h\ominus} = RT\ln(\gamma^{\omega}/\gamma^{h}). \quad (6)$$

Assuming that the hydrocarbon solution of the CH_2 group is a perfect solution, γ^h as well as f^h may be regarded to be unity. Then, we obtain

$$\Delta G°(CH_2{:}H) = RT\ln(\gamma^{\omega}). \quad (7)$$

This equation is in line with that derived by Butler et al.[20] The values of γ^{ω} calculated by Eq. 7 are listed in Table 2. It is recognized that the medium with a higher value of γ^{ω} has a lower affinity to the CH_2 group. Therefore, the activity coefficient, γ^{ω}, based on Raoult's reference system, is a parameter which numerically characterizes each type of media (the degree of modification of a solvent), such as micelle or interface, in which the CH_2 group is dissolved.

According to the regular solution theory by Hildebrand,[21] the activity coefficient of a solute (γ^R) which is originally related to the energy of mixing is expressed by the quantities, i.e., solubility parameters of a solute (δ_2) and a solvent (δ_1), molar volume of the solute (V_2), and volume fraction of the solvent (ϕ_1), as $RT\ln(\gamma^R)=V_2\phi_1^2(\delta_2-\delta_1)^2$. Present data concerning γ^{ω} and the literal value of the partial molar volume of the CH_2 group, $\overline{V}$, 16.6 $cm^3\,mol^{-1}$,[22] which is the incremental change of partial molar volumes of homologous alkanols in a hydrocarbon, allow us to estimate the quantity $(RT\ln(\gamma^{\omega})/\overline{V})^{1/2}$, which corresponds to the difference of the solubility parameter, $|\delta_2-\delta_1|$. The values of $|\delta_2-\delta_1|$ for some representative substances (hexane($\delta_1=\delta_2=7.3$),[23] perfluorohexane ($\delta_1=5.9$),[23] and water ($\delta_1=24$)[24]) are 0, 1.4, and 16.7, respectivelly. It is seen that this order is consistent with that of $(RT\ln(\gamma^{\omega})/\overline{V})^{1/2}$ in Table 2. In the regular solution theory, the activity coefficient of a solute depends only on the properties of the solute and solvent in their pure states. However, for a given solute (CH_2 group), γ^{ω} reflects the characteristics of its solvent not only in the pure state but also in the modified states such as micelle or interface. In this respect, it is claimed that γ^{ω} is more useful than γ^R in the regular solution approach. Further, the parallelogram relation in Fig. 4 suggests that the modification of the solvent is uniquely determined and the degree of modification is reflected on γ^{ω}.

Thanks are due for the partial support by a research grant from the Ministry of Education, Culture and Science (No. 60470011).

References

1) J. H. Hildebrand and R. L. Scott, "Regular Solutions," Prentice-Hall, Englewood Cliffes, New Jersey (1962), p. 17.
2) P. Mukerjee and A. Y. S. Yang, *J. Phys. Chem.*, **80**, 1388 (1976).
3) K. Shinoda and T. Nomura, *J. Phys. Chem.*, **84**, 365 (1980).
4) N. Funasaki and S. Hada, *J. Phys. Chem.*, **84**, 736 (1980).
5) T. Suzuki, M. Ueno, and K. Meguro, *JAOCS*, **1981**, 801.
6) T. Asakawa, S. Miyagishi, and M. Nishida, *J. Colloid Interface Sci.*, **104**, 279 (1985).
7) G. Sugihara, D. Nakamura, M. Ōkawauchi, S. Sakai, K. Kuriyama, M. Tanaka, and Y. Ikawa, *Fukuoka Univ. Sci. Reports*, **17**, 31 (1987).
8) G. Sugihara, M. Yamamoto, Y. Wada, Y. Murata, and Y. Ikawa, *J. Solution Chem.*, in press.
9) J. Carlfors and P. Stilbs, *J. Colloid Interface Sci.*, **103**, 332 (1985).
10) C. Tanford, "The Hydrophobic Effects," Johon Wiley & Sons, New York (1980).
11) P. Mukerjee and T. Handa, *J. Phys. Chem.*, **85**, 2298 (1981).
12) M. Manabe, K. Shirahama, and M. Koda, *Bull. Chem. Soc. Jpn.*, **49**, 2904 (1976).
13) M. Manabe, H. Kawamura, A. Yamashita, and S. Tokunaga, *J. Colloid Interface Sci.*, **115**, 147 (1987).
14) K. Shinoda, *J. Phys. Chem.*, **58**, 1136 (1954).
15) M. Manabe and M. Koda, *Bull. Chem. Soc. Jpn.*, **51**, 1599 (1978).
16) K. Shinoda, T. Nakagawa, B. Tamamushi, and T. Isemura, "Colloidal Surfactants," Academic Press, New York (1963), p. 50.
17) M. Manabe, M. Koda, and K. Shirahama, *J. Colloid Interface Sci.*, **77**, 189 (1980).
18) K. Hayase and S. Hayano, *J. Colloid Interface Sci.*, **63**, 446 (1978).
19) M. Manabe, M. Koda, and K. Shirahama, *Bull. Chem. Soc. Jpn.*, **48**, 3553 (1975).
20) J. A. V. Butler, D. W. Thomson, and W. H. Maclennan, *J. Chem. Soc.*, **1933**, 674.
21) Ref. 1, p. 22.
22) M. Sakurai and T. Nakagawa, *J. Chem. Thermodynamics*, **16**, 171 (1984).
23) Ref. 1, p. 172.
24) K. Shinoda, "Principles of Solution and Solubility," Marcel Dekker, New York (1978), p. 85.

 © 1988 The Chemical Society of Japan Bull. Chem. Soc. Jpn., 61, 1557—1563 (1988)

Proton and Carbon-13 NMR Study of Dimer Dianions Produced from 1,1-Diphenylethylene Derivatives

Yukihiro YOKOYAMA, Masahiro USHIO, Kenji GOTO, Mikio TAKAKI, Kensuke TAKAHASHI,* and Ryuzo ASAMI
Department of Applied Chemistry, Nagoya Institute of Technology, Gokiso-cho, Showa-ku, Nagoya 466
(Received October 28, 1987)

^{1}H and ^{13}C NMR spectra have been observed for the carbanions produced from 1,1-diphenylethylene derivatives. Among five precursors, three have been reduced to corresponding dimer dianions in contact with alkali metal in THF; however, the rest could not be dimerized. Failure in dimerization is controlled by a steric effect of substituents at the 2-position. DNMR measurements were also carried out for 1,1-di-*p*-tolylpropene dimer dianions. The results are discussed in terms of two internal rotations around the bonds between the C_1 and C_2, and the C_1 and C_i atoms.

Many NMR studies have been carried out in order to obtain structural information concerning benzyl-type carbanions which are important in synthetic chemistry. Throughout these studies, NMR parameters have been shown to vary with carbanion structures, cations, solvents and temperatures.[1)]

The dimerization of the radical anions produced from styrene, α-methylstyrene, or 1,1-diphenylethylene has been studied by ESR with dynamic stopped-flow techniques.[2)] The NMR parameters of these dimeric anions have also been partly reported.[3)] The NMR method is especially effective for structural studies of these carbanions since they are unstable when in contact with air or moisture. However, there have not yet been any systematic NMR studies concerning the formations and structures of these dimeric carbanions. This study was aimed at obtaining the NMR parameters of three dimeric carbanions produced from the 1,1-diphenylethylene derivatives. In the measurements of the two dianions at lower temperatures, two phenyl rings were not equivalent because of a hindered rotation around the bond between the C_1 and C_2 atoms. This situation is shown in Scheme 1, where

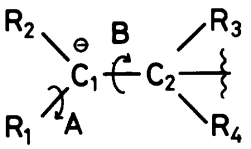

$R_1=R_2=C_6H_4X$
(X=H or p-CH_3)
R_3, R_4=H or CH_3

Scheme 1.

the two restricted internal rotations are differentiated as A and B. Several articles have been written concerning rotations, such as A,[4–11)] but not on those, such as B, in carbanions.

Experimental

Five starting materials, 1,1-di-*p*-tolylpropene (**1a**), 1,1-diphenylpropene (**2a**), 1,1-di-*p*-tolylethylene (**3a**), 1,1-dimethyl-2,2-di-*p*-tolylethylene (**5a**), and 1,1-dimethyl-2,2-diphenylethylene (**6a**), were prepared using a conventional method involving reactions of Grignard reagents produced from the corresponding alkyl bromides or iodides with substituted benzophenones. The solvents used for the preparation, THF, THF-d_8, and DME, were refluxed upon sodium metal, distilled, degassed, and finally kept on a sodium-potassium alloy.

An example of the preparation of the carbanions is as follows: 0.95 g of 1,1-diphenylpropene (**2a**) was melted, degassed in vacuum, and dissolved in 10 ml of dried THF. The solution was in contact with a sodium-potassium alloy in vacuum at room temperature. Immediately after contact, the solution became colored dark red. After standing for 24 h, the colored solution was filtered and sealed in an NMR tube and in a stocking glass container with a breakable seal. The concentration of the carbanion solution was about 0.5 or 1 M (1 M=1 mol dm^{-3}).

In order to obtain a chemical evidence, the potassium salt of 1,1-diphenylpropene dimer dianion (**2**) in THF was quenched by water. The quenched product was shown to have a structure consistent with 2,3-dimethyl-1,1,4,4-tetraphenylbutane, based on its ^{1}H NMR parameters ($\delta(CH_3)$= 0.92, δ(2-CH)=2.64, δ(1-CH)=3.91, and $\delta(C_6H_5)$=7.2—7.5 in THF-d_8).

The NMR spectra were measured with a Hitachi R-20B or with a Varian XL-200 FT NMR spectrometer. Variable-temperature spectra were measured in the range from 60 to −110 °C. The ^{1}H and ^{13}C NMR chemical shifts were evaluated from the solvent peak used as an internal reference and then converted to δ_H and δ_C values from TMS, by taking δ_H 1.79 and δ_C 26.4 for THF, δ_H 3.28 and δ_C 58.8 for DME, and δ_H 2.58 and δ_C 37.0 for HMPA.

Results and Discussion

Formation of Dimer Dianions. Typical NMR spectra of the carbanions obtained in this study are given in Figs. 1, 2, and 3, together with spectra of the neutral precursors. From these spectra, each carbanionic sample solution was found to consist of mainly a single species. When the precursors of **1a**, **2a**, and **3a** reacted with alkali metal in THF solutions they produced their dimer dianions, **1**, **2**, and **3**, which were ascertained by their NMR spectra. The same was true

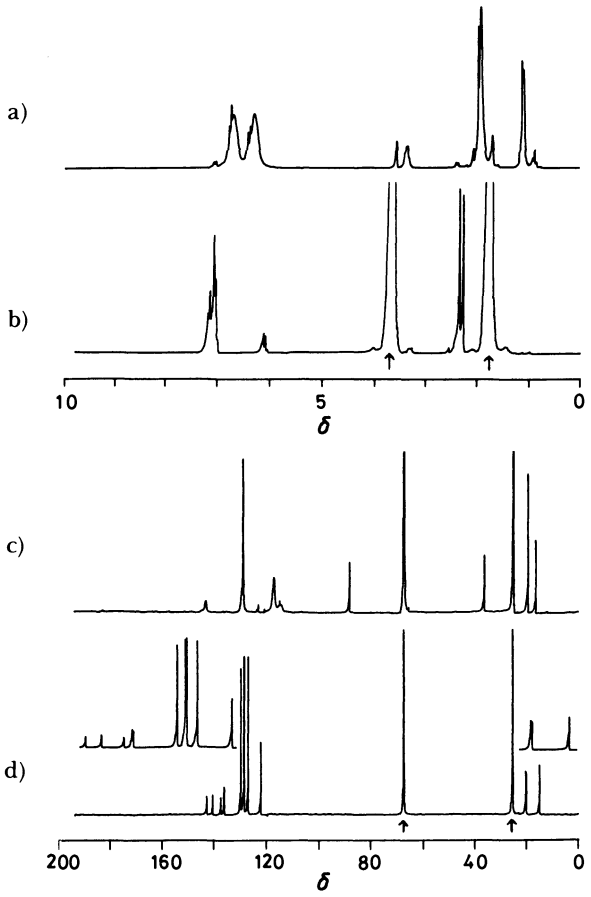

Fig. 1. ^{1}H and ^{13}C NMR spectra of **1** and **1a**. (a) ^{1}H spectrum of **1** in THF-d_8, (b) ^{1}H spectrum of **1a** in THF at 200 MHz and 25 °C, (c) ^{13}C spectrum of **1** in THF, and (d) ^{13}C spectrum of **1a** in THF at 50.3 MHz and 25 °C. The signals of the solvent were denoted by arrows.

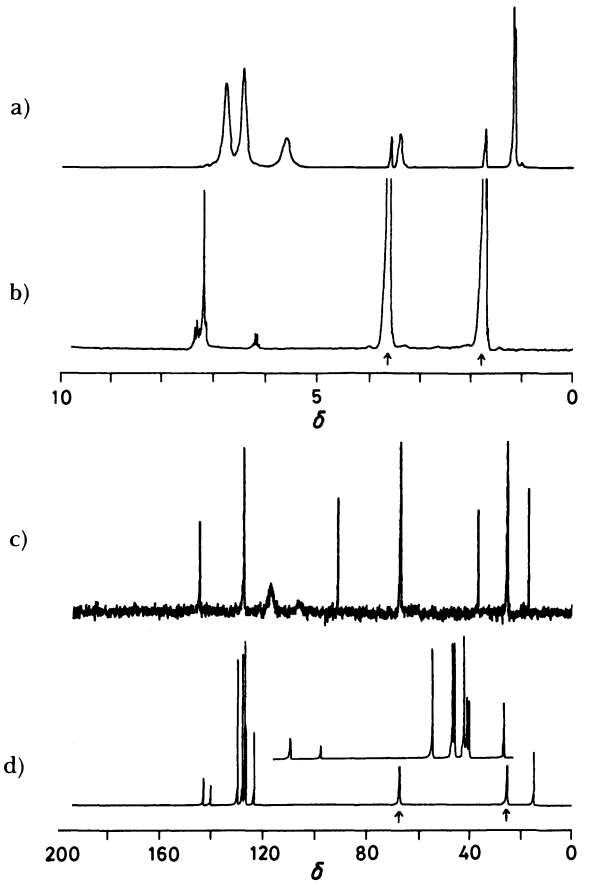

Fig. 2. ^{1}H and ^{13}C NMR spectra of **2** and **2a**. (a) ^{1}H spectrum of **2** in THF-d_8, (b) ^{1}H spectrum of **2a** in THF at 200 MHz and 25 °C, (c) ^{13}C spectrum of **2** in THF, and (d) ^{13}C spectrum of **2a** in THF at 50.3 MHz and 25 °C.

of 1,1-diphenylethylene (**4a**); we have already reported on its dimer dianion **4**.[3] The situation, however, was different for **5a** or **6a** in which the NMR spectrum of a solution treated similarly with metal was complex and its quenched product was multiplex. In every case, an anionic radical species is produced immediately after a precursor is dissolved in THF and comes into contact with metal. The reactant solution changes in color from colorless to dark red. When a C_2 atom of a precursor is substituted by a group, such as a phenyl ring, the radical anion is easily reduced further and becomes a monomeric dianion, as does tetraphenylethylene.[12]

When a substituent at C_2 is a hydrogen or a methyl group, which is not an effective electron-delocalizable group, two-electron reduction does not occur; instead, dimerization occurs between the anion radicals. The latter case has occurred in reactions of **1a**, **2a**, **3a**, and **4a**. In the cases of **5a** and **6a** such dimerization has not occurred. The reason seems to be due to their steric circumstances around the C_2 atoms. The dimerization of the radical anions is known to be an essentially reversible process which can be controlled thermodynamically.[2] The ^{1}H NMR spectra of the dianions observed in this study show that the anions are stable at room temperature and that their line widths are narrow. In this respect the equilibrium between the dimer dianion and the radical anion is largely shifted to the former.

Further, both the dianions **1** and **2** have two asymmetric carbons in a molecule. Therefore, it is a problem whether they are in either racemic or meso form. In the NMR spectra of several 2,3-disubstituted butanes, the two forms are differentiated in their chemical shifts. For example, the differences in ^{13}C chemical shifts between the two forms of 2,3-dichlorobutanes are reported to be 1.09 and 1.99 ppm for the C_1 and C_2 in the backbone butane skeleton.[13] As shown in Table 2, the C_1 and C_2 chemical shifts of **1** and **2** are attributed to those of a single species. It is therefore estimated that **1** or **2** exists either as the racemic or meso form. This may be controlled sterically. As stated before, dimerization did not occur in the cases of **5a** and **6a**. In other words, two methyl

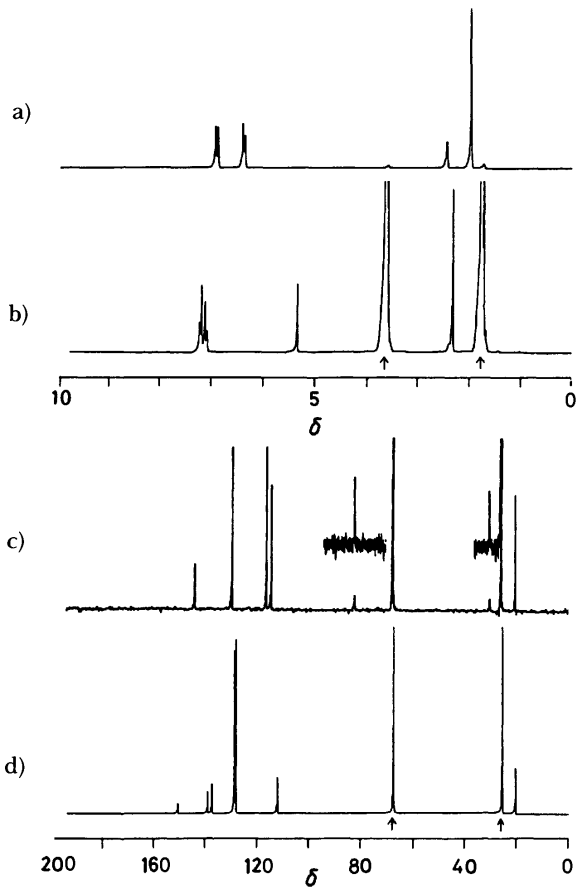

Fig. 3. ^{1}H and ^{13}C NMR spectra of **3** and **3a**. (a) ^{1}H spectrum of **3** in THF-d_8, (b) ^{1}H spectrum of **3a** in THF at 200 MHz and 25 °C, (c) ^{13}C spectrum of **3** in THF, and (d) ^{13}C spectrum of **3a** in THF at 50.3 MHz and 25 °C.

groups at the C_2 of **5a** and **6a** inhibited the dimerization. Therefore, one methyl group at the C_2 of **1a** and **2a** can be said to control the way of dimerization, sterically. This is one reason why only a racemic or meso form of **1** or **2** is prepared. The racemic form is more probable because of a steric reason. However, this is not clear at present and must be studied in the future. Anyhow, it is considered that the anion, **1** or **2**, is in a highly crowded situation.

^{1}H and ^{13}C NMR Parameters. The NMR parameters obtained for the anions and their precursors are summarized in Tables 1 and 2. All the ^{1}H chemical shifts of the anions are shielded by about 0.3 to 3.0 ppm, as compared with those of the precursors. This tendency is consistent with that reported previously.[1] However, the protons attached to the C_2 atoms are shifted upfield by about 3 ppm. This large shift is attributed to a hybridization change of the C_2 atom from sp^2 to sp^3, accompanied with dimerization. This fact has also been verified from changes in the ^{13}C NMR parameters. The changes of the chemical shifts of the C_2 are about 82—90 ppm. The values are similar to those observed for triphenyl- and diphenylmethanide ions (92 and 97 ppm).[14] However, a corresponding change of the ^{13}C NMR parameters for the carbons of the anions without hybridization change is about 17 ppm in the case of 1,1,4,4-tetraphenylbutadiene dianion (**7**).[15] Therefore, from the viewpoint of the chemical shift parameters, the C_2 of **1**, **2**, and **3** are considered to be sp^3-hybridized. Additional evidence of hybridization of the C_2 is given by measuring the one-bond J_{CH} coupling constants, which are about 123, 121, and 122 Hz for **1**, **2**, and **3**, respectively. These

Table 1. ^{1}H NMR Chemical Shifts of Dimer Dianions and Their Precursors

Compd	Solvent	Temp	Assignment					
		°C	ortho	meta	para	2-H	*p*-CH_3	2-CH_3
1	THF-d_8	20	6.68[a]	6.24[a]	—	3.59[a]	1.97	1.15
		−70	6.81	6.36	—	3.39[a]	1.88	1.12
			6.70	6.16			2.02	
2	THF-d_8	23	6.81[a]	6.48[a]	5.65[a]	3.42[a]	—	1.18
3	THF-d_8	23	6.93	6.41	—	2.46	2.00	—
4[b]	THF	31.5	7.01	6.55	5.67	2.48	—	—
1a	THF-d_8	25	7.08	7.03	—	6.10	2.28	1.72
			7.04	7.17			2.35	
	THF	23	7.12	7.06	—	6.14	2.31	c)
			7.07	7.20			2.38	
	DME	25	7.08	7.02	—	6.10	2.27	1.72
			7.04	7.16			2.34	
2a	THF	23	7.4[d]	7.2[d]	7.2[d]	6.22	—	1.75[e]
3a	THF	23	7.25	7.15	—	5.39	2.36	—
4a	THF	23	7.3[d]	7.3[d]	7.3[d]	5.48	—	—
5a	THF	31.5	7.00	7.00	—	—	2.29	c)
	CCl_4	31.5	6.92	6.92	—	—	2.29	1.77
6a	HMPA	23	7.10	7.34	7.22	—	—	1.78
	CCl_4	31.5	7.08	7.08	7.08	—	—	1.78

a) Broad. b) Cited from Ref. 3a. c) Overlapped with large solvent peaks. d) With large uncertainty because of the signal overlapping. e) The value is given for a CCl_4 solution.

Table 2. ^{13}C NMR Chemical Shifts of Dimer Dianions and Those Precursors

Compd	Solvent	Temp	Assignment							
		°C	C_i	C_o	C_m	C_p	C_1	C_2	p-CH_3	2-CH_3
1	THF	25	143.94	117.84[a]	129.84	115.06[a]	89.15	37.67	20.77	17.78
		−70	142.81	117.63	129.06	114.37	88.50	36.43	21.25	17.56
			145.56	118.04	129.81	114.15			20.93	
	DME	25	144.38	117.95[a]	129.68	114.65[a]	88.76	37.31	20.80	18.06
2	THF	23	145.61	118.49[a]	128.87	107.84[a]	92.82	37.79	—	18.05
3	THF	24	144.19	116.43	129.81	114.62	82.90	30.61	20.89	—
4[b]	THF	31.5	145.8	117.5	129.25	108.05	86.9	30.45	—	—
1a	THF-d_8	25	143.36	127.94	129.60	137.11	138.26	123.10	21.36	15.91
			141.38	129.41	130.76	136.93			21.01	
	THF	25	143.48	127.87	129.53	137.04	138.20	123.02	21.30	15.85
			141.31	129.34	130.69	136.86			21.16	
2a	THF	23	143.82	127.94	129.00	127.70	140.97	124.29	—	15.98
			143.74	128.80	130.81	127.50				
3a	THF	23	139.78	128.92	129.56	138.08	151.11	112.94	21.31	—
4a	THF	25	142.45	128.98	128.98	128.47	151.40	114.30	—	—
5a	THF	23	141.57	129.17	130.49	136.13	129.67	129.49	22.64	21.17
6a	HMPA	23	143.57	128.52	130.01	126.74	130.67	137.99	—	22.55

a) Broad signals because of coalescence. b) Cited from Ref. 3c.

Table 3. Comparison of ^{13}C Chemical Shift Changes and Charge Distributions of **1**, **2**, **3**, and **4**[a]

Compd	$\Delta\delta C_i$	$\Delta\delta C_o$	$\Delta\delta C_m$	$\Delta\delta C_p$	$\Delta\delta C_1$	$\Delta\delta C_2$	S_1[b]	S_2[c]
1	−1.55	10.77	0.27	21.89	49.05	85.35	218.23	132.88
	(−0.01)[d]	(0.07)	(0.00)	(0.14)	(0.31)			(0.83)
2	−1.83	9.88	1.04	19.76	48.15	86.50	212.12	125.62
	(−0.01)	(0.06)	(0.01)	(0.12)	(0.30)			(0.79)
3	−4.41	12.49	−0.25	23.46	68.21	82.33	237.60	155.27
	(0.04)	(0.08)	(0.00)	(0.15)	(0.43)			(0.97)
4	−3.35	11.48	−0.27	20.42	64.5	83.85	226.2	142.36
	(−0.02)	(0.07)	(0.00)	(0.13)	(0.40)			(0.89)
7[e]	−2.96	7.11	1.53	15.96	57.82	17.40	135.78	
	(−0.02)	(0.04)	(0.01)	(0.10)	(0.36)	(0.11)	(0.85)	

a) The values for the methyl carbons are not shown in the table because of their small values, but they are included into the evaluation of S_1 and S_2. b) A total sum for a monomer unit. c) $S_2=S_1-\Delta\delta C_2$. d) The value in parentheses is the excess electron density on the carbon atom, which was evaluated by a method used in Ref. 18. e) The values are cited from Ref. 15 for the sodium salt.

values are consistent with those of typically sp^3-hybridized carbons.[16] The excess charge distribution of the anions can be evaluated from the differences of the chemical shifts between the anions and the corresponding precursors (Table 3), using an equation proposed by Fraenkel et al.[17] and a factor presented by Spiesecke and Schneider.[18] In a total sum for a monomer unit, S_1 has an uncertainty due to the hybridization change of the C_2 atom of the anion, **1**, **2**, **3**, or **4**. Therefore S_2 is evaluated as a total sum for a monomer unit, except for the difference of the C_2 atom. It is considered that the hybridization of the C_1 atom of the anion does not change from that of the precursor, as disscussed previously.[14] The S_2 values of **3** and **4** are larger than those of **1** and **2**. This is mainly ascribed to the difference of the C_1 chemical shift. This means that **3** or **4** has a larger electron density at the C_1 than **1** and **2** has, suggesting that the counter-cation is nearer to the C_1 for **3** or **4** than for **1** or **2**. This is ascribed to a steric effect of the 2-methyl group for **1** and **2**. The S_2 values are approximately 139 ppm as a mean. This is nearly equal to the S_1 value of **7**. Thus, the excess charge of the dimer dianions is mostly delocalized into the phenyl rings and on the C_1 (or C_4) carbon.

Temperature Dependency of the Chemical Shifts. For three carbanions (**1**, **2**, and **3**), there are two different internal rotations, A and B, as shown in Scheme 1. The ^1H NMR signals of the H_o, H_m, and p-CH_3 hydrogens of **1** were broad at 25 °C, as shown in Fig. 1a. When the temperature was lowered, each signal split into two. Similarly, all ^{13}C signals of the phenyl groups of **1** were split into two at −70 °C. Therefore, two geminal phenyl rings of **1** are not magnetically equivalent at this temperature. The chemical shift values at −70 °C are also given in Tables 1 and 2. The values arranged in the same line are those for the protons or carbons belonging to the same phenyl ring.

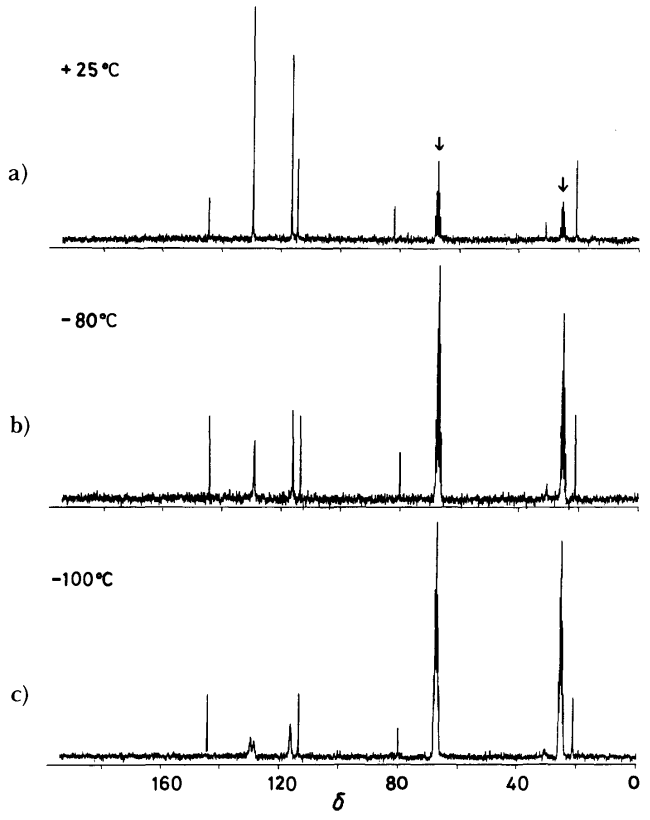

Fig. 4. ^{13}C NMR spectral changes of **3** in THF-d_8 at 50.3 MHz. (a) At 25 °C, (b) at −80 °C, and (c) at −100 °C.

Similarly, the splittings of the signals were also observed at a lower temperature in **2** but not **3**. Therefore, the cause of the nonequivalence is attributed to the presence of a methyl group at the C_2 and to hindered rotation around the bond between the C_1 and C_2 atoms, which is denoted as B in Scheme 1. When the temperature was lowered, **3** showed a broad C_o signal and two broad split C_m signals at −100 °C, as shown in Fig. 4. The peak heights of the C_o and C_m signals are low as compared with those of other carbon signals (C_i and C_p). Therefore, the signal splitting is considered to be caused by the restriction of rotation about the bond between the C_1 and C_i, which is denoted as A in Scheme 1. Even at −110 °C, the C_o signals were not separated into two. Therefore, the thermodynamic parameters of this hindered rotation could not be obtained. The temperature-dependent ^{13}C chemical shifts of **1** are given in Fig. 5. In the figures the vertical line at each temperature shows an approximate line width of each signal. Coalescences were observed for the signals of all carbons in two phenyl rings in the temperature range from −20 to 20 °C, accompanied by signal broadening. This is due to the rotation B. The chemical shift changes of the C_o and C_p carbons of **1** behave in a strange manner. For example, the C_p signals of **1** showed another coalescence phenomenon at −80 °C. This coalescence is quite different from those at higher temperatures. It was not accompanied by broadening of the signals like that as shown at a temperature near 0 °C in Fig. 5. The same is true for the C_o signals. Therefore, this coalescence is explained by temperature-dependent chemical shift changes. However, the origin of this chemical shift change is not clear at present. It seems to be concerned with the active center of the anion: that is, the C_1 atom. Thus, the difference of the chemical shifts is the largest at the C_i which is the nearest carbon from the active center. It must be noted, however, that two C_p atoms have the same chemical shift value at −100 °C, though they have different chemical shifts at −20 °C. The chemical shift differences of the two split signals are about 2.1, 1.0, 0.8, and 1.8 ppm for C_i, C_o, C_m, and C_p atoms at −20 °C, respectively. The difference is larger for the C_i and C_p than for the C_o and C_m. Therefore, the two former carbons are more sensitive to their circumstances than the two latter carbons. This behavior is characteristic in the ^{13}C chemical shifts of monosubstituted benzenes.[19] Another reason for these relative magnitudes is considered to be due to the rotation A, which causes an averaging of the chemical shifts for the C_o and C_m. Thus, the C_p and C_i atoms are on the axis of the rotation A, but the C_o and C_m atoms are not. Further, evidence of the presence of the rotation A in **1** is as follows: the line widths of the C_o and C_m resonances of **1** are about twice those of the C_p and C_i atoms at −70 °C. An effect of the methyl substituent can be evaluated from a comparison of the ^{13}C spectra of **1** and **2**. However, the effect could not be obtained quantitatively. Visually, the signal widths of the ring carbons of **2** are quite larger than those of **1** at about −80 °C. This suggests that a temperature of −80 °C is near the coalescence temperature of **2**, but far from that of **1**. Therefore, the methyl group lowers the potential barrier of the rotation A of **1**, as expected from the electron-donating property of substituent, as reported by Bushweller et al.[8] As a conclusion two internal rotations, A and B, are differentiated for **1**. The former does not stop, even at −100 °C, though the latter stops approximately at −20 °C. The phenomenon observed for **1** at about 0 °C was explained by the restricted rotation B. However, it may be considered to be explained by any other reasons such as the presence of two different aggregation states or two different species (for example, racemic and meso forms). These explanations, however, were denied for the following two reasons. First, two split signals were observed only for the atoms concerning the aromatic rings. Second, they appeared with equal intensity.

Line-Shape Analyses. The temperature-dependent ^1H and ^{13}C NMR spectra were analyzed as simple two-site exchanging problems. The line widths were

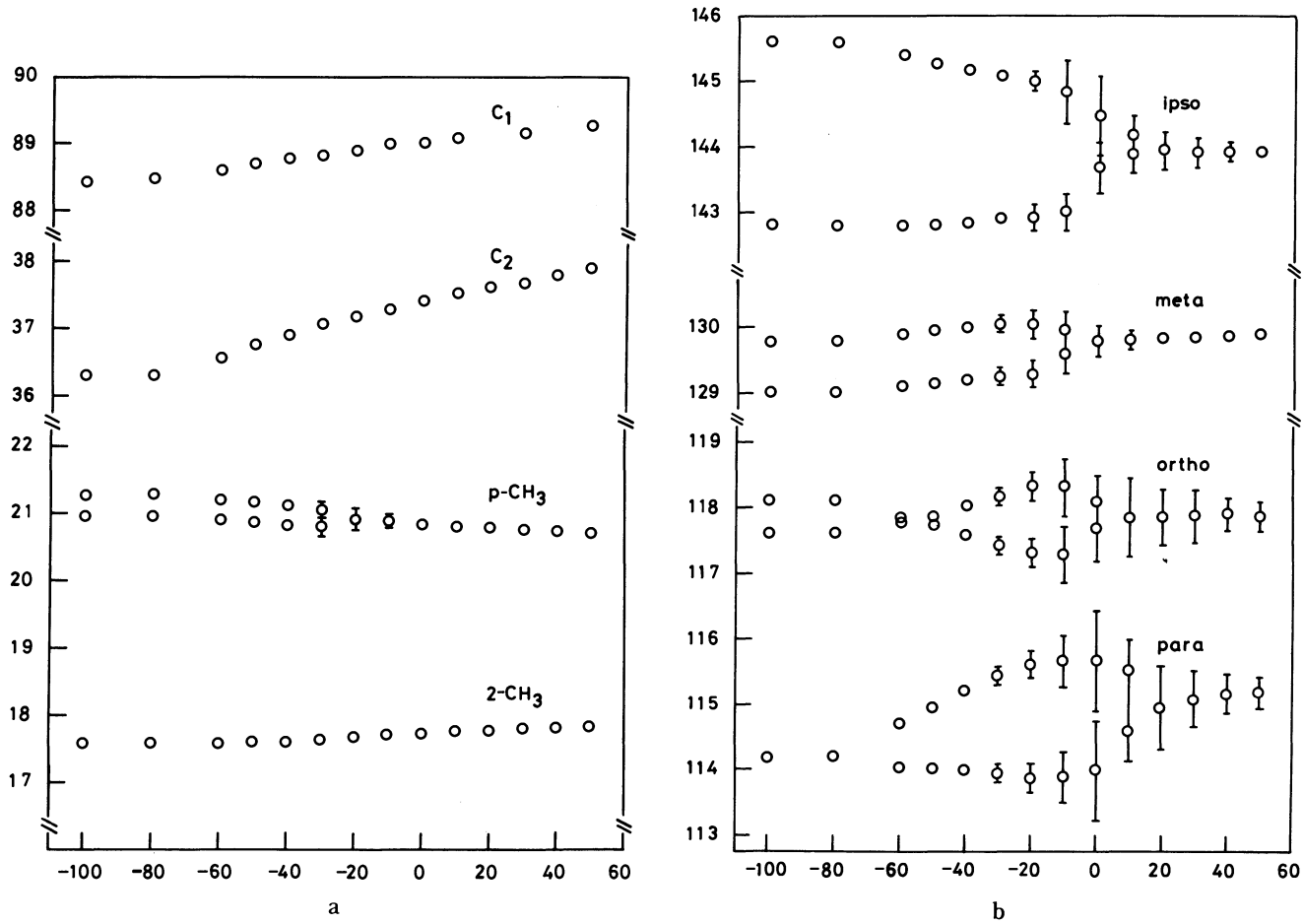

Fig. 5. ^{13}C chemical shifts (ordinate in ppm) of **1** in THF as a function of temperature (abscissa in °C) at 50.3 MHz, (a) Aliphatic and (b) aromatic carbon regions.

Table 4. Thermodynamical Parameters for the Internal Rotation Around the C_1–C_2 Bond of **1** in THF-d_8

E_a/kJ mol^{-1}	log A	ΔH^*/kJ mol^{-1}	ΔS^*/J K^{-1} mol^{-1}
43.0±0.6	9.8±0.1	40.5±0.6	−66.4±2.1

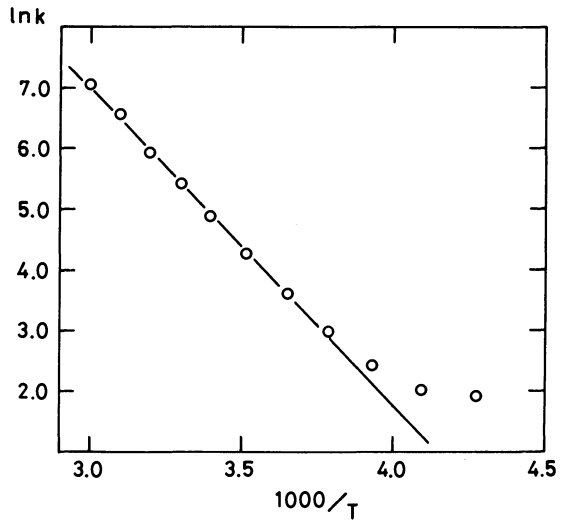

Fig. 6. An Arrhenius plot for the rotation B of **1** in THF.

estimated from the observed spectra. The calculated and experimental line shapes were compared visually. The thermodynamical parameters for the rotation (B) were obtained by Arrhenius and Eyring plots. An example of the analyses is shown in Fig. 6 for an Arrhenius plot of the kinetic parameters obtained for the exchange of the two *p*-CH_3 protons of **1**. However, the plotted points are divergent at the temperatures lower than −20 °C. A reason for this divergence seems to be due to an interaction between the two rotations, A and B, in the molecule. It must also be noted that errors in the DNMR method will become appreciable at two extremes of the range.[20] Therefore, although several trials were carried out, the parameters for other peaks could not be obtained unambiguously, except for the *p*-CH_3 protons. The thermodynamical parameters are given in Table 4, which were obtained for the temperature ranges between −10 and 60 °C

concerning the rotation, B. The coalescence temperature can be used to evaluate the change in the free energy of activation for the rotation in the molecule using the following equation:

$$\Delta G_c^{\ddagger} = aT_c[9.972 + \log(T_c/\Delta\nu)],$$

where T_c, $\Delta\nu$, and a are the coalescence temperature, the chemical-shift difference of two exchanging sites, and a constant of 19.14 J mol^{-1} respectively.[21] In the case of **1**, the $\Delta G_c^{\ddagger}$ value is 58.3 kJ mol^{-1} when the values of T_c and $\Delta\nu$ are adopted as ca. 278 K and 28.5 Hz. This value is consisent with that calculated from the parameters given in Table 4.

References

1) a) R. N. Young, *Progr. in NMR Spectr.*, **12**, 261 (1979); b) D. H. O'Brien, "Comprehensive Carbanion Chemistry," ed by E. Buncel and T. Durst, Elsvier, New York (1980), p. 271.

2) M. Szwarc, "Carbanions, Living Polymer and Electron Transfer Processes", John Wiley, New York (1968), p. 367.

3) a) K. Takahashi and R. Asami, *Bull. Chem. Soc. Jpn.*, **41**, 231 (1968); b) K. Takahashi, M Takaki, and R. Asami, *J. Phys. Chem.*, **75**, 1062 (1971); c) K. Takahashi, K. Yamada, K. Wakata, and R. Asami, *Org. Magn. Reson.*, **6**, 62 (1974).

4) V. R. Sandel, S. V. McKinley, and H. H. Freedman, *J. Am. Chem. Soc.*, **90**, 495 (1968).

5) S. Brownstein and D. J. Worsfold, *Can. J. Chem.*, **50**, 1246 (1972).

6) G. Fraenkel, J. G. Russell, and Y.-H. Chen, *J. Am. Chem. Soc.*, **95**, 3208 (1973).

7) G. Fraenkel and J. M. Geckle, *J. Am. Chem. Soc.*, **102**, 2869 (1980).

8) C. H. Bushweller, J. S. Sturges, M. Cipullo, S. Hoogasian, M. W. Gabriel, and S. Bank, *Tetrahedron Lett.*, **1978**, 1359.

9) G. A. Olah and M. I. Watkins, *Proc. Natl. Acad. Sci. U. S. A.*, **77**, 703 (1980).

10) K. Matsuzaki, Y. Shinohara, and T. Kanai, *Makromol. Chem.* **181**, 1923 (1980); **182**, 1533 (1981).

11) M. Morikawa, H. Matsui, A. Yoshino, K. Takahashi, and G. Miyajima, *Bull. Chem. Soc. Jpn.*, **57**, 3327 (1984).

12) K. Takahashi, Y. Inoue, and R. Asami, *Org. Magn. Reson.*, **3**, 349 (1971).

13) C. J. Carman, A. R. Tarpley,Jr., and J. H. Goldstein, *J. Am Chem. Soc.*, **93**, 2864 (1971).

14) K. Takahashi, Y. Kondo, R. Asami, and Y. Inoue, *Org. Magn. Reson.*, **6**, 580 (1974).

15) Y. Yokoyama and K. Takahashi, *Chem. Lett.*, **1987**, 589.

16) J. L. Marshall, "Carbon-Carbon and Carbon-Proton NMR Couplings" Deerfield Beach, Verlag Chemie International, Inc. (1983).

17) G. Fraenkel, R. E. Carter, A. McLachlan, and J. H. Richard, *J. Am. Chem. Soc.*, **82**, 5846 (1960).

18) H. Spiesecke and W. G. Schneider, *Tetrahedron Lett.*, **1961**, 468.

19) H. Spiesecke and W. G. Schneider, *J. Chem. Phys.*, **35**, 731 (1961).

20) G. Binsch, *Top. Streochem.*, **3**, 97 (1968).

21) J. Sandström, "Dynamic NMR Spectroscopy," Academic Press, London (1982), p. 96.

Effect of Polyethylene Glycol Monoalkyl Ethers on Phase Transition Temperature of Dipalmitoylphosphatidylcholine Vesicle Membrane

Tohru INOUE,* Kohsuke FUKUSHIMA, and Ryosuke SHIMOZAWA
Department of Chemistry, Faculty of Science, Fukuoka University,
Nanakuma, Jonan-ku, Fukuoka 814-01
(Received October 28, 1987)

The gel-to-liquid-crystalline phase transition temperature of a dipalmitoylphosphatidylcholine vesicle membrane was measured in the presence of polyethylene glycol monoalkyl ethers (C_nE_m) of various chain lengths of hydrophobic (n) and hydrophilic (m) groups. All of the surfactants, except of $C_{12}E_1$, depressed the transition temperature almost linearly with the concentration. The depression of the phase-transition temperature was analyzed by applying the van't Hoff model for the freezing-point depression; also, the partition coefficients of the surfactants between bulk water and the membrane phase were estimated. Discussions were given concerning the dependence of the partition coefficients on the chain lengths of both oxyethylene and alkyl groups.

The interaction of surfactants with a phospholipid bilayer has been investigated in relation to the solubilization[1,2] or fusion[2-4] of biological membranes and to the preparation of lipid vesicles by detergent removal method.[5-7] Most of these studies deal with the mixed micelles formed by the addition of surfactants at a concentration higher than the critical micelle concentration. Recently, Goñi et al.[8] have paid attention to the effect of surfactants on the structure and properties of the lipid bilayer at rather lower concentration range. Such studies may have a significance different from the above-mentioned practical interest. Surfactants are typical amphiphiles, and the amphiphilicity can be readily controlled by combining various types of head groups and hydrocarbon tails. Hence, the surfactant-lipid bilayer system may provide a useful model system for us to understand the biologically significant interaction between amphiphilic ligands and a biological membrane.

Along the line of this interest, we have been studying the interaction of surfactants with model membranes in terms of their effect on the membrane properties.[9-11] As an extension of this series of studies, in the present work we investigated the effect of polyethylene glycol monoalkyl ethers, nonionic surfactants, on the gel-to-liquid-crystalline phase transition of dipalmitoylphosphatidylcholine vesicle membrane. Interest was focused on the dependence of the effect on both the alkyl and oxyethylene chain lengths.

Experimental

Synthetic dipalmitoylphosphatidylcholine (DPPC) was obtained from Sigma. The following polyethylene glycol monoalkyl ethers with homogeneous chain lengths were used (abbreviated as C_nE_m, where n and m represent the carbon number of alkyl chain and the number of oxyethylene unit, respectively): n=10, m=6, 8; n=12, m=1, 3, 4, 5, 6, 7, 8; n=14, m=6, 8. All the surfactants were obtained from Nikko Chemicals Co.

A stock suspension of DPPC vesicle in water was prepared by sonication in the cup-horn of a Branson Sonifier Model 185 at 45 °C for about 30 min. The sample suspension was prepared by mixing the DPPC suspension and surfactant solution to give the desired surfactant concentration, and by sonicating again at 45 °C for about 5 min. The sizes of vesicles were estimated from quasielastic light-scattering measurements to be about 160 nm in diameter; taking into account the size and the phase-transition pattern,[12] these vesicles may be regarded as being multilamellar. The DPPC concentration was kept at about 5×10^{-4} M† throughout the experiments.

The gel-to-liquid-crystalline phase transition of a DPPC vesicle membrane was followed by the scattered-light intensity from the vesicle suspension. Details concerning the procedure have been described previously.[9] Typical traces of the scattered-light intensity with temperature are

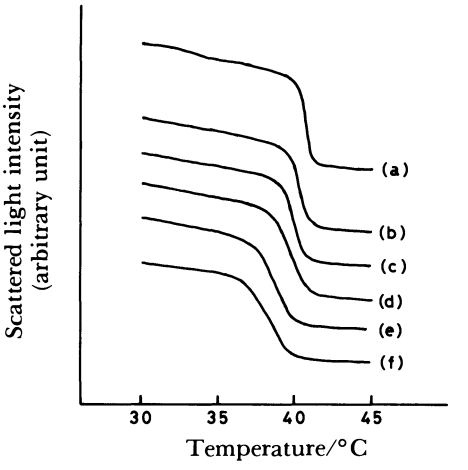

Fig. 1. Typical traces of the change in scattered light intensity at 400 nm with the temperature rise observed with DPPC–$C_{12}E_5$ system. Heating rate is 0.5 °C min^{-1}. DPPC concentration is 5.2×10^{-4} M. $C_{12}E_5$ concentrations (10^{-5} M) are (a) 0, (b) 2.52, (c) 3.37, (d) 5.05, (e) 6.73, and (f) 8.42.

† 1 M=1 mol dm^{-3}.

shown in Fig. 1. A drastic change in the scattered-light intensity was found corresponding to the phase transition. The transition temperature, T_m, was taken as the temperature at the half-height between two intersections of a line drawn through the steep portion of the transition region and the two lines drawn through the rather flat portions above and below the transition. The measurements were repeated at least three times for a given sample; a good reproducibility (typically within ±0.1 °C) was obtained for the transition temperature.

Results and Discussion

Figure 1 illustrates the effect of added $C_{12}E_5$ on the phase transition of a DPPC vesicle membrane. It can be seen that the transition temperature decreases with increasing $C_{12}E_5$ concentration. It was observed that at a higher concentration of the surfactant, the change in the scattered-light intensity at the transition region became small accompanied with the deformation of the transition curve; a further increase in the concentration led to an extremely low intensity of the scattered-light, probably due to the formation of a mixed micelle. This was also the case for other surfactants. Thus, the concentration ranges of added surfactants were limited to those where normal phase-transition patterns were observed.

Some examples of the relation between the transition temperature and the surfactant concentration are shown in Figs. 2a—c. In these figures, the depression of the transition temperature, $-\Delta T = -(T_m - T_{m0})$, is plotted against the surfactant concentration, where T_m and T_{m0} are the transition temperatures with and without the surfactants. As can be seen in these figures, $-\Delta T$ increases linearly with increasing added surfactant concentration.

The depression of the phase-transition temperature of lipid bilayers induced by additives of the small molecule has been successfully analyzed by applying the van't Hoff model for the freezing-point depression.[13-15] This model describes the transition temperature as being depressed as a result of the lowering of the chemical potential of lipid molecule in a liquid-crystalline phase due to the mixing with the additive molecules. According to this interpretation, ΔT is proportional to the mole fraction of additives in the lipid bilayer for the case of a sufficiently low additive concentration, which in turn allows an estimation of the partition coefficient of the additives between bulk water and a lipid bilayer when the additives are partitioned between these phases. Based on this treatment, ΔT is related to the partition coefficient, K, by the following equation:[9]

$$-\Delta T = \frac{RT_{m0}^2}{\Delta H} \cdot \frac{K}{55.5 + C_L K} C_A^0, \qquad (1)$$

where ΔH is the enthalpy change associated with the phase transition, R the gas constant, and C_L and C_A^0 the total concentrations of lipid and additives in molarity scale, respectively. K is defined as $K = x_A'/x_A$, where x_A' and x_A are the mole fractions of the additives in membrane and water phases, respectively.

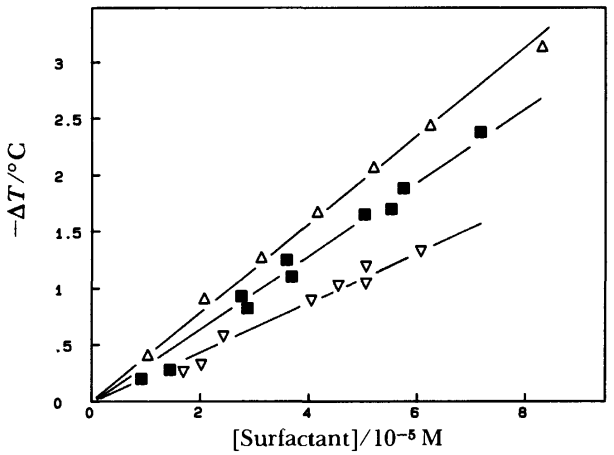

Fig. 2a. Plot of the depression of the phase transition temperature, $-\Delta T$, against the concentration of added surfactants. Surfactants are $C_{12}E_4$ (△), $C_{12}E_6$ (■), and $C_{12}E_8$ (▽).

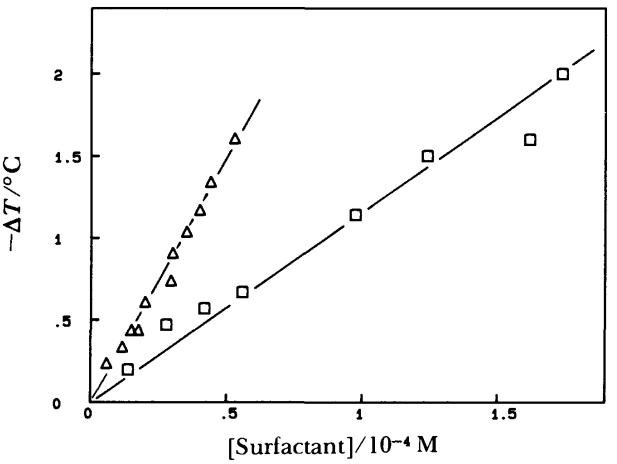

Fig. 2b. Plot of $-\Delta T$ against the added concentration of $C_{10}E_6$ (□) and $C_{14}E_6$ (△).

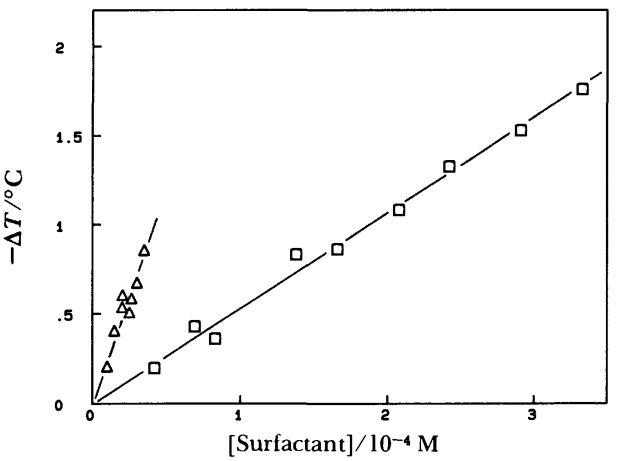

Fig. 2c. Plot of $-\Delta T$ against the added concentration of $C_{10}E_8$ (□) and $C_{14}E_8$ (△).

Equation 1 predicts a linear relationship between $-\Delta T$ and C_A^0, and allows an evaluation of the partition coefficient, K, from the slope. The partition coefficients of C_nE_m were estimated from the slopes of straight lines, as shown in Figs. 2a—c, using the values of T_{m0}=314 K and ΔH=36.4 kJ mol^{-1}.[16] Below, we examine the dependence of these K values on the oxyethylene chain length and the alkyl chain length.

Dependence of K on the Oxyethylene Chain Length. In Fig. 3, log K obtained with $C_{12}E_m$ is plotted against the number of oxyethylene unit, m. It can be seen that log K decreases almost linearly with increasing m in the range from m=4 to 8. The slope of this straight line provides $0.46RT$ as the contribution of an oxyethylene unit to the standard free energy change for the transfer of the surfactants from bulk water to the lipid bilayer. The critical micelle concentration (cmc)[17] of $C_{12}E_m$ is also shown in Fig. 3 for comparison. log cmc exhibits very weak dependence on m. This means that the contribution of oxyethylene unit to the standard free energy of micelle formation is negligibly small. For DPPC–surfactant systems previously studied,[9,11] there observed a good correlation between K and cmc; log K vs. log cmc plot gives straight lines with the slope of -1, the intercept of which weakely depends on the type of hydrophilic group. Comparing the present results for $C_{12}E_m$ with those for other surfactant systems, it is a wonder why the effect of oxyethylene chain length appears only in the partitioning into the lipid bilayer but not in the micelle formation. It is reasonable to consider that when surfactant molecules are incorporated in the lipid membrane, the hydrophilic head group of the surfactant is anchored at the membrane surface and the alkyl chain intercalates between the acyl chains of the lipid. The difference in the dependence on the oxyethylene chain length between K and cmc may be ascribed to a difference in the environment between the bilayer surface and the micellar surface.

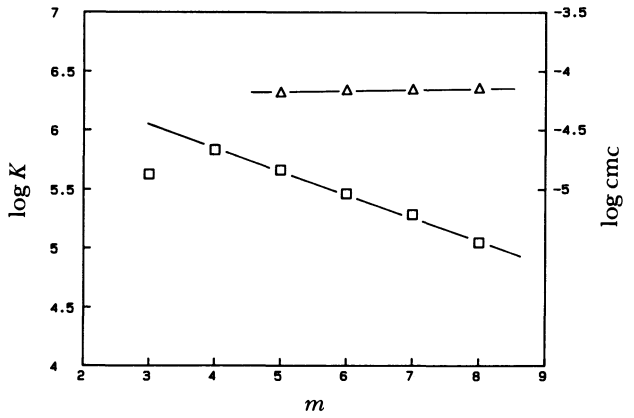

Fig. 3. Plot of log K (□, left scale) and log cmc (△, right scale) against the number of oxyethylene unit, m, for $C_{12}E_m$.

Considering the fact that the interior of lipid bilayer consists of the hydrocarbon region, it is of interest to compare the present partition data between water and lipid bilayer with those between water and hydrocarbon. Some partition data for nonionic surfactants with an oxyethylene chain between water and the hydrocarbon media are available in the literature.[18–20] From values of the partition coefficients, the free energies of the transfer from water to isooctane[18] and from water to cyclohexane[19,20] per oxyethylene unit are estimated to be $1.08RT$ and $0.96RT$, respectively. These are larger by a factor of about 2 than those of the transfer from water to DPPC bilayer. This difference may be attributed to the environmental difference between the partitions into the bulk hydrocarbon (water–hydrocarbon system) and into the water/hydrocarbon interface (water-bilayer system). The oxyethylene chain of the surfactants incorporated in the lipid bilayer locates at the bilayer surface and may be exposed to interfacial water; hence, the free energy loss may become less compared with the partition into the bulk hydrocarbon.

Another remarkable feature in Fig. 3 is the downward deviation of $C_{12}E_3$ from a straight line. This may be interpreted as follows. Equation 1 is based on the assumption that the amount of additives partitioned into the gel state bilayer is much smaller than those into the liquid-crystalline state, or even though the additives are incorporated substantially in gel phase, they are not randomly mixed but dispersed as aggregates (phase separation). It is likely that when the hydrophilicity of additives is reduced, the affinity to gel state bilayer becomes substantial, and the partitioning and mixing in gel state membrane becomes appreciable. In this case, Eq. 1 gives an underestimate of the partition coefficient. It may be

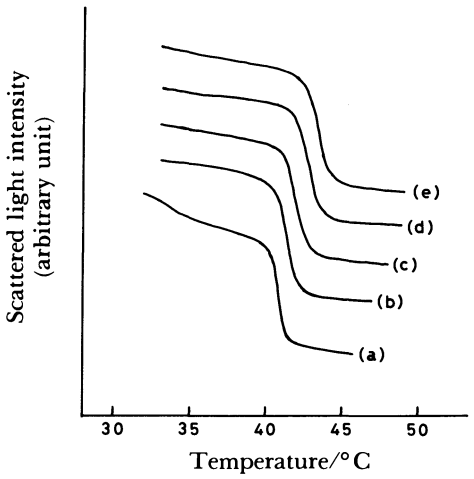

Fig. 4. Phase transition curves obtained with DPPC–$C_{12}E_1$ system. DPPC concentration is 5.0×10^{-4} M. $C_{12}E_1$ concentrations (10^{-4} M) are (a) 0, (b) 1.25, (c) 1.54, (d) 2.56, and (e) 3.42.

regarded that the K value obtained with $C_{12}E_3$ by applying Eq. 1 is not correct, but underestimated. When the oxyethylene chain length is further reduced, the effect of an additive on the phase transition becomes reversed; $C_{12}E_1$ elevated the transition temperature, as shown in Fig. 4. According to the van't Hoff model (described above) the elevation of the transition temperature can be interpreted as being due to the partitioning and mixing of the additives in the gel state bilayer, exceeding that in the liquid-crystalline state. A similar behavior of the additives concerning the phase-transition temperature of phosphatidylcholine vesicle membrane is well known for 1-alkanols; long-chain 1-alkanols with an alkyl chain length exceeding about 10 carbon atoms elevate the transition temperature, although shorter 1-alkanols depress it.[21–23] This suggests that the smaller hydrophilicity of 1-alkanols with longer alkyl chains favors their distribution in the gel state bilayer rather than liquid-crystalline state. The present results demonstrate that a similar reverse effect on the transition temperature is also induced by decreasing the hydrophilic oxyethylene chain length as the effect observed for 1-alkanol by increasing the hydrophobic chain length. Thus, the following general feature may be drawn for long-chain amphiphilic additives; reducing the hydrophilicity of the amphiphile below a certain critical level, it tends to partition into the gel state bilayer and mix with gel state lipids.

Dependence of K on the Alkyl Chain Length. Figure 5 shows the relation between $\log K$ and the carbon number of alkyl chain, N_c, obtained with C_nE_6 and C_nE_8. The increments of $\log K$ with N_c on going from 10 to 12 are similar for C_nE_6 and C_nE_8, which provide about 1 RT for the transfer free energy from the bulk water to the lipid bilayer per methylene unit. This increment of $\log K$ per methylene unit in alkyl chain is just the same as that obtained with other nonionic long-chain amphiphiles,[10] and the contribution of methylene unit to the transfer free energy is comparable to the free energy per methylene unit for the hydrophobic interaction.[24] On the contrary, from N_c=12 to 14, the increments of $\log K$ with N_c fall down for both C_nE_6 and C_nE_8, the extent of which is larger for C_nE_6 than C_nE_8. This deviation of $\log K$ for N_c=14 from the extraporated values from the lower N_c may be explained by the same way as the deviation of $C_{12}E_3$ from the linear relationship between $\log K$ and m in a series of $C_{12}E_m$ (Fig. 3). The hydrophilicity of $C_{14}E_6$ and $C_{14}E_8$ is weakened, relatively, due to their increased alkyl chain length, hence the partitioning and mixing in the gel state bilayer may occur substantially, and the K values obtained with these surfactants may be underestimated. The larger deviation for $C_{14}E_6$, whose hydrophilicity is less than $C_{14}E_8$, is consistent with this interpretation; i.e., the extent of underestimation of K is larger when the relative hydrophilicity is lower. A similar deviation of $\log K$ with increasing alkyl chain length was also observed for alkyltrimethylammonium salts.[9,11]

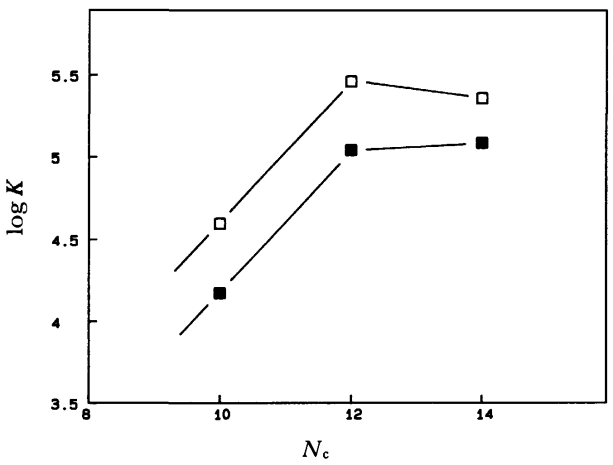

Fig. 5. Plot of $\log K$ against the carbon number in alkyl chain, N_c, for C_nE_6 (□) and C_nE_8 (■).

Conclusion

In this study, the partition coefficients of C_nE_m between bulk water and a DPPC bilayer were estimated from the depression of the phase transition temperature of a DPPC vesicle membrane by applying the van't Hoff model. The conclusion derived by examining the chain-length dependence of K is summarized as follows: (i) For a series of $C_{12}E_m$, $\log K$ decreased linearly with increasing m in the range between m=4 and 8. This suggests that the bilayer surface provides an energetically unfavorable fields for oxyethylene group compared with bulk water. (ii) $C_{12}E_3$ deviates from the linear plot of $\log K$ vs. m. $C_{14}E_6$ and $C_{14}E_8$ deviate from the linear plot of $\log K$ vs. N_c plot. These findings, along with the observation that $C_{12}E_1$ elevated the transition temperature, suggest that the decrease in the relative hydrophilicity of long-chain amphiphilic additives leads to partitioning into a gel state bilayer and mixing with the gel state lipids.

The authors wish to thank Mr. Akira Ogawa for his assistance in the experimental work. This work was supported in part by funds from the Central Research Institute of Fukuoka University.

References

1) D. Lichtenberg, R. J. Robson, and E. A. Dennis, *Biochim. Biophys. Acta*, **737**, 285 (1983).

2) A. Alonso, M-A. Urbaneja, F. M. Goñi, F. G. Carmona, F. G. Cánovas, and J. C. Gómez-Fernández, *Biochim. Biophys. Acta*, **902**, 237 (1987).

3) A. Alonso, R. Saez, A. Villena, and F. M. Goñi, *J. Membr. Biol.*, **67**, 55 (1982).

4) R. Saez, F. M. Goñi, and A. Alanso, *FEBS Lett.*, **179**,

311 (1985).
5) M. Ueno, C. Tanford, and J. A. Reynolds, *Biochemistry*, **23**, 3070 (1984).
6) P. Schurtenberger, N. Mazer, and W. Känzig, *J. Phys. Chem.*, **89**, 1042 (1985).
7) S. Almog, T. Kushnir, S. Nir, and D. Lichtenberg, *Biochemistry*, **25**, 2597 (1986).
8) F. M. Goñi, M-A. Urbaneja, J. L. R. Arrondo, A. Alonso, A. A. Durrani, and D. Chapman, *Eur. J. Biochem.*, **160**, 659 (1986).
9) T. Inoue, K. Miyakawa, and R. Shimozawa, *Chem. Phys. Lipids*, **42**, 261 (1986).
10) T. Inoue, T. Iwanaga, K. Fukushima, and R. Shimozawa, *Chem. Phys. Lipids*, **46**, 25 (1988).
11) T. Inoue, Y. Muraoka, K. Fukushima, and R. Shimozawa, *Chem. Phys. Lipids*, **46**, 107 (1988).
12) H. Takemoto, S. Inoue, T. Yasunaga, M. Sukigara, and Y. Toyoshima, *J. Phys. Chem.*, **85**, 1032 (1981).
13) M. W. Hill, *Biochim. Biophys. Acta*, **356**, 117 (1974).
14) H. Kamaya, S. Kaneshina, and I. Ueda, *Biochim. Biophys. Acta*, **646**, 135 (1981).
15) S. Kaneshina, H. Kamaya, and I. Ueda, *J. Colloid Interface Sci.*, **93**, 215 (1983).
16) S. Mabrey and J. M. Sturtevant, *Proc. Natl. Acad. Sci. U. S. A.*, **73**, 3862 (1976).
17) Data sheet from Nikko Chemicals Co.
18) E. H. Crook, D. B. Fordyce, and G. F. Trebbi, *J. Colloid Sci.*, **20**, 191 (1965).
19) F. Harusawa, T. Saitō, H. Nakajima, and S. Fukushima, *J. Colloid Interface Sci.*, **74**, 435 (1980).
20) F. Harusawa, H. Nakajima, and M. Tanaka, *J. Soc. Cosmet. Chem.*, **33**, 115 (1982).
21) A. W. Elliasz, D. Chapman, and D. F. Ewing, *Biochim. Biophys. Acta*, **448**, 220 (1976).
22) A. G. Lee, *Biochemistry*, **15**, 2448 (1976).
23) H. Kamaya, N. Matubayasi, and I. Ueda, *J. Phys. Chem.*, **88**, 797 (1984).
24) C. Tanford, "The Hydrophobic Effect," 2nd ed, John Wiley & Sons, New York (1980), Chap. 7.

 © 1988 The Chemical Society of Japan Bull. Chem. Soc. Jpn., 61, 1571—1576 (1988)

Preparation and Characterization of (Tetrabenzoporphyrinato)nickel Hexafluoroarsenate, $(NiTBP)_3(AsF_6)_2(C_{10}H_7Cl)$. A New Type of Metallomacrocyclic Radical Salts

Kyuya YAKUSHI,* Michiko YOSHITAKE, Haruo KURODA, Atsushi KAWAMOTO,†
Jiro TANAKA,† Tadashi SUGANO,†† and Minoru KINOSHITA††
Department of Chemistry, Faculty of Science, the University of Tokyo, Hongo, Tokyo 113
†Department of Chemistry, Faculty of Science, Nagoya University,
Furocho, Chikusa-ku, Nagoya 474
††Institute for Solid State Physics, the University of Tokyo, Roppongi, Tokyo 106
(Received November 5, 1987)

Single crystals of a (tetrabenzoporphyrinato)nickel hexafluoroarsenate, $(NiTBP)_3(AsF_6)_2$ were prepared by the use of an electrochemical technique. NiTBP is stacked one-dimensionally with a periodic unit composed of three macrocycles. This stacking mode is a new type among the one-dimensionally stacked macrocyclic complexes. The experimental results on reflectance spectrum and ESR indicate that this material is a one-dimensional semiconductor with a small electron correlation.

Study on highly conducting quasi-one-dimensional solids of metallomacrocyclic compounds has been extensively conducted by the group of Northwestern University.[1-7] They explored mainly iodine complexes by changing the central metals from Fe to Zn. They also studied on (tetrabenzoporphyrinato)nickel iodide. The family of the one-dimensionally stacked macrocycles will be expanded by selecting the combination of the central metals, the porphyrin ligands, and the counter anions. We have prepared metallic (phthalocyaninato)nickel salts by the use of an electrochemical technique to change the counter anions, and found a new complexes with a different chemical composition from iodine complexes.[8,9] This time we prepared a one-dimensional complex by using a (tetrabenzoporphyrinato)nickel as a macrocycle and several octahedral, tetrahedral, and linear anions as counter anions. In this paper we present the crystal structure, electrical, optical, and magnetic properties of $(NiTBP)_3(AsF_6)_2(C_{10}H_7Cl)$, and briefly describe the preliminary results on the other salts.

Experimental

NiTBP was synthesized by exchanging the central metal of ZnTBP according to the method given by Martinsen et al.,[6] and was purified by means of vacuum sublimation. The result of the chemical analysis was as follows; Found: C, 76.07; H, 3.42; N, 9.79, Calcd for $C_{36}H_{20}N_4Ni$: C, 76.22; H, 3.55; N, 9.88. Single crystals of the NiTBP radical salts were grown by oxidizing NiTBP electrochemically in the 1-chloronaphthalene solution, $(n\text{-}Bu)_4X$ (X=BF_4, ClO_4, ReO_4, PF_6, AsF_6, SbF_6, Br_3, I_3) being used as the supporting electrolytes. 1-Chloronaphthalene were refluxed with CaH_2 under the Ar atmosphere and then distilled in vacuum. The electrolytes were recrystallized from methanol solution for several times. The electrochemical oxidation were performed at 120±2 °C with a constant current of 2—5 μA for about two weeks. The concentrations of NiTBP and the electrolytes were 2×10^{-4} mol l^{-1} and 1.6×10^{-3} mol l^{-1}, respectively. NiTBP is more soluble to 1-chloronaphthalene than NiPc ((phthalocyaninato)nickel), and almost all NiTBP seems to be consumed after two weeks because the deep color of the starting material disappeared. The needle-

Table 1. Crystal Data

Compound	$(NiTBP)_3(AsF_6)_2(C_{10}H_7Cl)$
Formula	$(NiC_{36}H_{20}N_4)_3(AsF_6)_2(C_{10}H_7Cl)$
Formula wt.	2242.23
Cell parameters a	16.019(2) Å
b	16.470(3) Å
c	9.853(5) Å
α	108.30(2)°
β	96.10(3)°
γ	66.06(1)°
Cell volume V	2255.0 Å^3
Number of formula unit Z	1
Density: calcd.	1.65 g cm^{-3}
Density: obsd.	1.57 g cm^{-3}
Space group	$P\bar{1}$
Radiation	Cu $K\alpha$
Linear absorption coefficient	25.5 cm^{-1}
Crystal shape	needle-like elongated along c-axis
Number of reflections ($F_o > 3(\sigma(F_o))$)	6202
R-factor	0.083

Table 2. Fractional Coordinates ($\times 10^4$) and Equivalent Temperature Factors ($B_{eq}=(4/3)\sum_{ij}\beta_{ij}a_ja_i$)

	x	y	z	B_{eq}
NiTBP molecule A				
Ni(1)	0	0	0	1.8
N(2)	−641(3)	−854(3)	−594(5)	1.8
N(3)	1173(3)	−1073(4)	−95(5)	1.8
C(4)	−1565(4)	−621(4)	−805(6)	2.1
C(5)	−1772(5)	−1451(5)	−1253(7)	2.4
C(6)	−2604(5)	−1553(6)	−1589(9)	3.6
C(7)	−2545(6)	−2478(6)	−1996(10)	4.3
C(8)	−1712(6)	−3230(6)	−2053(10)	4.0
C(9)	−881(5)	−3113(5)	−1716(8)	3.1
C(10)	−952(5)	−2197(5)	−1314(7)	2.4
C(11)	−256(4)	−1801(4)	−898(6)	2.0
C(12)	655(4)	−2360(5)	−845(7)	2.3
C(13)	1321(4)	−2000(4)	−469(6)	2.0
C(14)	2276(4)	−2581(5)	−403(7)	2.4
C(15)	2739(5)	−3541(5)	−707(8)	3.2
C(16)	3694(5)	−3878(6)	−549(9)	4.0
C(17)	4149(5)	−3269(6)	−115(9)	3.8
C(18)	3682(5)	−2304(5)	176(8)	3.2
C(19)	2727(4)	−1978(5)	20(7)	2.4
C(20)	2037(4)	−1050(5)	204(6)	2.1
C(21)	2224(4)	−263(5)	625(7)	2.2
NiTBP molecule B				
Ni(22)	−317(1)	196(1)	3282(1)	2.0
N(23)	−1604(3)	345(4)	2924(5)	2.0
N(24)	65(3)	−1160(4)	2790(5)	1.9
N(25)	963(4)	41(4)	3648(5)	2.0
N(26)	−711(4)	1563(4)	3774(5)	2.1
C(27)	−2354(4)	1166(5)	3020(7)	2.6
C(28)	−3180(5)	976(5)	2636(7)	2.8
C(29)	−4087(5)	1570(7)	2535(10)	4.5
C(30)	−4710(6)	1136(7)	2088(12)	5.5
C(31)	−4437(6)	171(7)	1780(11)	4.8
C(32)	−3539(5)	−408(6)	1877(9)	4.0
C(33)	−2909(5)	24(5)	2311(7)	2.7
C(34)	−1926(5)	−361(5)	2482(7)	2.5
C(35)	−1419(5)	−1292(5)	2245(7)	2.5
C(36)	−485(5)	−1660(5)	2378(7)	2.3
C(37)	58(5)	−2653(5)	2101(7)	2.6
C(38)	−180(6)	−3426(6)	1663(9)	3.7
C(39)	535(6)	−4285(6)	1445(10)	4.2
C(40)	1446(6)	−4398(6)	1667(9)	4.1
C(41)	1673(5)	−3613(5)	2142(8)	3.3
C(42)	953(5)	−2750(5)	2348(7)	2.5
C(43)	943(4)	−1815(5)	2770(7)	2.2
C(44)	1727(5)	−1649(5)	3108(7)	2.4
C(45)	1720(4)	−762(5)	3503(6)	2.3
C(46)	2551(5)	−587(5)	3822(7)	2.6
C(47)	3466(5)	−1181(6)	3752(8)	3.5
C(48)	4112(6)	−779(7)	4047(10)	4.5
C(49)	3822(6)	194(7)	4418(10)	4.5
C(50)	2904(5)	799(6)	4516(8)	3.6
C(51)	2274(5)	371(5)	4180(7)	2.6
C(52)	1291(5)	760(5)	4067(6)	2.3
C(53)	773(5)	1686(5)	4330(7)	2.4
C(54)	−148(5)	2050(5)	4167(7)	2.5
C(55)	−687(5)	3036(5)	4405(7)	2.8
C(56)	−426(6)	3807(5)	4753(9)	4.0
C(57)	−1115(7)	4665(6)	4802(11)	5.0
C(58)	−2038(7)	4783(6)	4540(10)	4.6
C(59)	−2289(6)	4024(5)	4221(9)	3.8
C(60)	−1590(5)	3150(5)	4156(7)	2.7
C(61)	−1586(5)	2216(5)	3764(7)	2.5
C(62)	−2364(5)	2042(5)	3429(7)	2.6
AsF_6 anion				
As(63)	3119(1)	3286(1)	8073(2)	7.1
F(64)	3080(13)	3134(9)	6350(13)	20.5
F(65)	3042(13)	3511(9)	9781(13)	22.2
F(66)	2147(9)	4222(8)	8167(16)	17.0
F(67)	4013(9)	2383(8)	7937(22)	22.9
F(68)	3593(13)	3982(11)	8259(24)	26.3
F(69)	2561(9)	2639(10)	7970(22)	22.1
1-Chloronaphthalene				
Cl(70)	−5986(8)	3985(9)	3008(16)	10.5
C(71)	−5000	5000	5000	9.4
C(72)	−4541(14)	3864(12)	6828(21)	5.4
C(73)	−4363(11)	4489(13)	7077(20)	12.6
C(74)	−5305(19)	3758(17)	5226(35)	10.6
C(75)	−4095(15)	5192(20)	7319(30)	10.1
C(76)	−5454(17)	4144(20)	4380(28)	11.1
C(77)	−4900(18)	4302(22)	5787(35)	11.2
C(78)	−4438(19)	5234(22)	6303(32)	11.5

like crystal was elongated to the c-axis developing {100}, {010}, and {110} planes. The chemical analysis of Ni and As in the crystal were conducted by the use of the ICP atomic emission spectrometer, Jarrel Ash ICAP-575II.

The intensities of X-ray diffraction were collected with a Rigaku automated diffractometer using Cu $K\alpha$ radiation monochromatized with a graphite plate. The crystal data were listed in Table 1. The structure was solved by the heavy atom method and was refined by the block-diagonal least-squares method. All hydrogen atoms were neglected in the analysis. The absorption collection was made with a program ACACA written by C. T. Prewitt. R-value was 11.7% without a solvent molecule. The difference synthesis map revealed that solvent molecules are included in the crystal and the solvent molecule was located around (1/2, 1/2, 1/2) in the unit cell. Since the solvent molecule was disordered around the center of symmetry, two atoms, Cl(70) and C(71), overlap other carbon atoms related by the inversion symmetry. In order to avoid the divergence of the overlapped atoms, we refined Cl(70) by using an average atomic scattering factor between chlorine and carbon, and fixed the positional parameters of C(71) at the inversion center. Therefore, the geometry of 1-chloronaphthalene was determined to be heavily distorted. The final R-value decreased to 8.3% by refining the parameters of 1-chloronaphthalene. The molecular geometry of NiTBP did not change significantly before and after including a solvent molecule in the analysis. The temperature factor of fluorine atoms of AsF_6 is very large probably due to the orientational disorder, so that the positions of fluorine atoms could not be accurately determined. Since we are mainly interested in the column structure of NiTBP, we stopped the analysis at this

stage. The final atomic coordinates were shown in Table 2. The computer program used in this analysis was the UNICS system.[10]

The electrical resistivity was measured along the needle axis by using a two-probe method. The contact between the sample and the 20 μm gold wire were made by carbon paint. The polarized reflectance spectrum of the single crystal were measured in the spectral region from 2000 cm^{-1} to 25000 cm^{-1} by using a microspectro-photometric technique.[11,12] ESR were measured with JEOL, JES-FElXG by the use of X-band.

Results and Discussion

$(NiTBP)_3(AsF_6)_2(C_{10}H_7Cl)$. The ratio of the chemical composition between NiTBP and AsF_6 was determined to be 1.4±0.1:1 by means of ICP atomic emission spectrometry of Ni and As atoms. The 3:2 composition was supported also by crystal structure analysis. This chemical composition between a macrocycle and a counter anion is a new one in the family of the radical salts based on the metallo-macrocyclic compounds. Figure 1 shows the side view of the molecular columns of NiTBP. NiTBP's are stacking along the c-axis with their molecular planes parallel to each other. The unit of this molecular column is a trimer of NiTBP which is composed of a molecule, A, on the center of symmetry and two molecules, B and B′, which are interrelated by the center of symmetry. The dihedral angle between the molecules A and B is 0.6°. Table 3 shows the mean bond lengths which were calculated by averaging the chemically equivalent bonds. Significant difference in the molecular geometry was not observed between the molecules A and B, and also between the molecules of $(NiTBP)_3(AsF_6)_2(C_{10}H_7Cl)$ and NiTBPI.[6] The neighboring molecules within the trimer is overlapping with a twisted angle of 45.0° as shown in

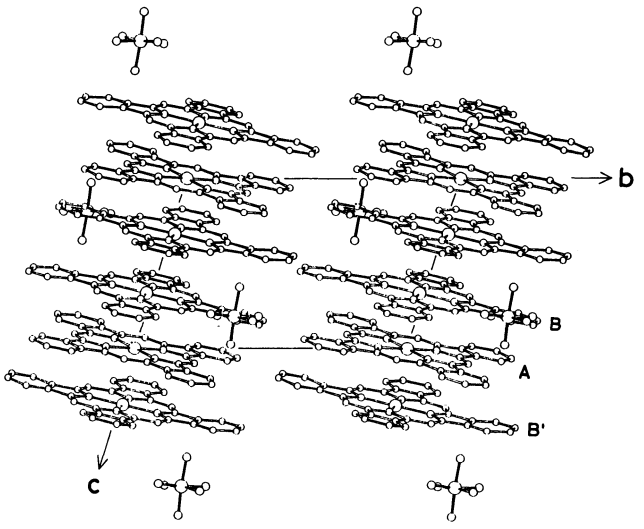

Fig. 1. Side view of the molecular columns of NiTBP. The solvent molecule included in the crystal at (1/2, 1/2, 1/2) is not drawn in this figure.

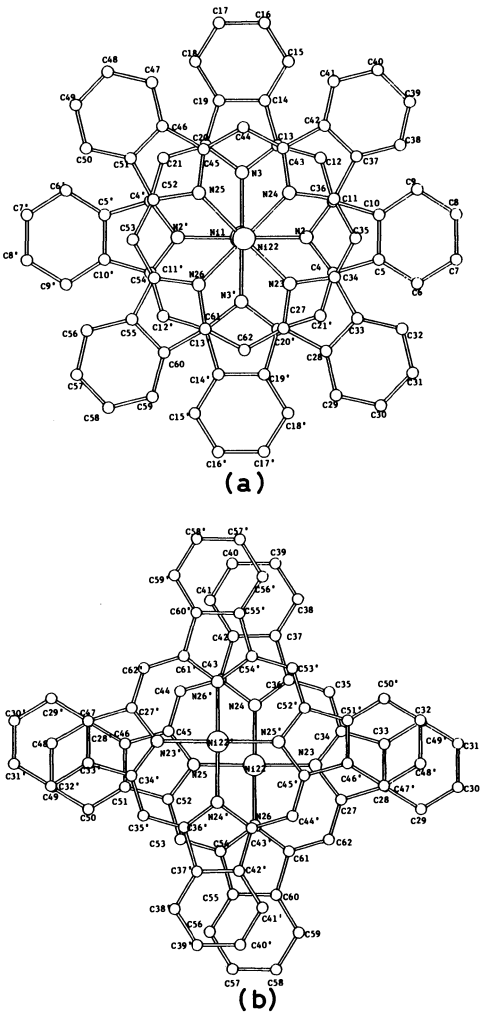

Fig. 2. Overlapping mode of NiTBP's between (a) A and B and (b) B and B′, where A is on the center of symmetry, and B and B′ are interrelated by the center of symmetry.

Table 3. Mean Bond Distances of NiTBP Calculated by Averaging the Chemically Equivalent Bonds

	Molecule A	Molecule B	NiTBPI
Ni–Np	1.976(6)	1.975(6)	1.966(9)
Np–Ca	1.381(11)	1.385(11)	1.391(13)
Ca–Cb	1.455(11)	1.456(12)	1.460(15)
Ca–Cm	1.377(12)	1.367(12)	1.340(15)
Cb–Cb	1.386(11)	1.384(11)	1.391(15)
Cb–Cc	1.405(14)	1.406(14)	1.387(15)
Cc–Cd	1.409(15)	1.395(16)	1.390(16)
Cd–Cd	1.401(15)	1.404(16)	1.391(17)

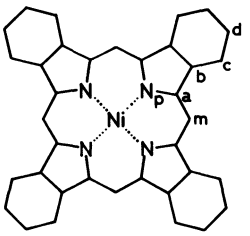

Fig. 2a. This type of overlap is commonly found in the metallo-phthalocyanine iodide (MPcI)[1-3,5] and NiTBP iodide (NiTBPI).[6] The interplanar distance is 3.16 Å, and the Ni-Ni distance is 3.221(2) Å. The molecular overlap between the adjacent trimer is shown in Fig. 2b. The porphyrin skeleton is not twisted but shifted with the interplanar distance of 3.45 Å. This overlapping mode is found in the α-modification of platinum phthalocyanine.[13] The Ni-Ni distance is 3.608(2) Å. The intermolecular atomic distances shorter than 3.4 Å were listed in Table 4. These distances suggest that a charge-transfer interaction exists not only between the molecules A and B but also between B and B'. Figure 3 shows the arrangement of the molecular columns viewed nearly along the c-axis. The NiTBP column is packed pseudo-hexagonally and this packing mode is quite different from those of MPcI and NiTBPI complexes and $(NiPc)_2SbF_6$.[8] The 1-chloronaphthalene molecule is not drawn in Figs. 1 and 3 not to complicate the figure. The solvent molecule is located at the central space, (1/2, 1/2, 1/2) in Fig. 3, the molecular plane making an angle of 57.2° against the NiTBP molecule. The molecular geometry, the an-

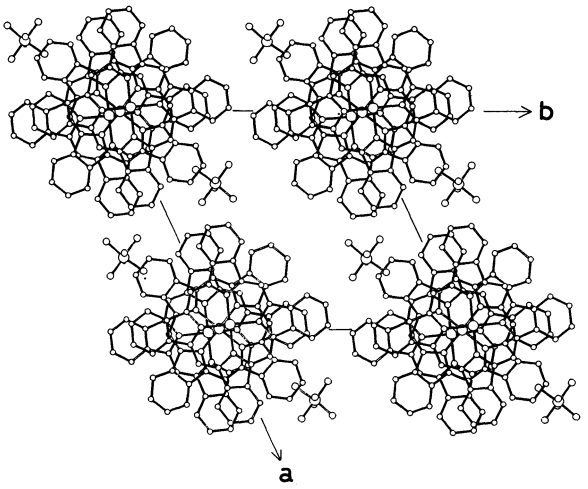

Fig. 3. Projection of the molecules viewed along the c-axis. The solvent molecule which is included in the crystal at around (1/2, 1/2, 1/2) is not drawn in this figure.

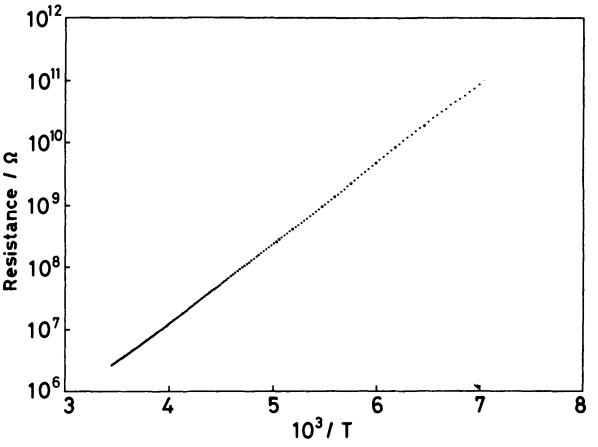

Fig. 4. Temperature dependence of the electrical resistivity.

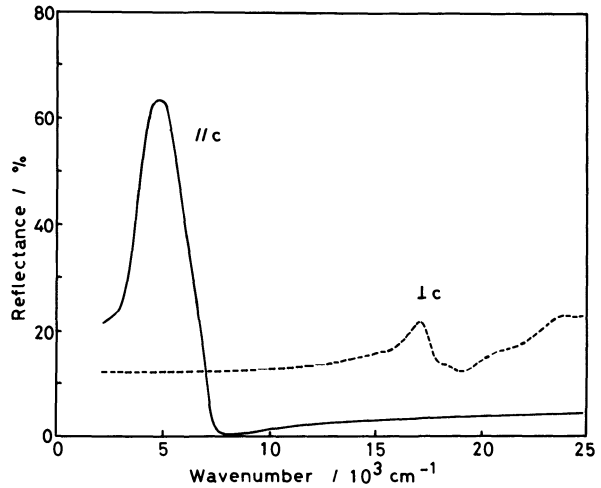

Fig. 5. Polarized reflectance spectrum of $(NiTBP)_3(AsF_6)_2(C_{10}H_7Cl)$.

Table 4. Intermolecular Atomic Distances Shorter than 3.4 Å

		A-B	
Ni(1)-Ni(22)	3.221(2)	C(4)-C(34)	3.214(10)
C(4')-C(52)	3.215(10)	C(10)-C(35)	3.383(9)
C(11)-C(36)	3.213(10)	C(11')-C(54)	3.219(10)
C(12)-C(37)	3.379(12)	C(12)-C(42)	3.352(11)
C(12')-C(55)	3.329(9)	C(12')-C(60)	3.371(10)
C(13)-C(43)	3.209(10)	C(13')-C(61)	3.208(10)
C(14)-C(44)	3.364(9)	C(14')-C(62)	3.399(11)
C(15')-C(59)	3.368(11)	C(19)-C(44)	3.379(11)
C(19')-C(62)	3.362(10)	C(20)-C(45)	3.198(9)
C(20')-C(27)	3.205(10)	C(21)-C(46)	3.310(11)
C(21)-C(51)	3.328(9)	C(21')-C(28)	3.356(10)
C(21')-C(33)	3.388(12)		
		B-B'	
N(23)-C(45')	3.380(8)	N(26)-C(43')	3.341(9)
C(34)-C(51')	3.399(11)	C(36)-C(53')	3.340(11)

isotropic temperature factors, and F_o-F_c data are deposited as Document No. 8791 at the Office of the Editor of Bull. Chem. Soc. Jpn.

The electrical resistivity along the c-axis was 400—1000 ohm cm at room temperature. Figure 4 shows a typical example of the temperature dependence, which indicates the semiconductive behavior. The activation energy of the electrical resistivity was obtained to be 0.26—0.28 eV. If we assume that it is equal to twice the activation energy, the band-gap is estimated to be 0.52—0.56 eV. Figure 5 shows the reflectance spectrum polarized parallel and perpendicular to the c-axis. The //c spectrum exhibited a strong dispersion at about 5000 cm^{-1}, the excitation energy of which is much lower than the lowest intramolecular transition (Q-band) which shows up at 17000 cm^{-1} in the $\perp$c spectrum. Furthermore, this dispersion is completely polarized to the stacking direction. Therefore, this electronic transition is assignable to the charge-transfer (CT) transition. The appearance of the CT transition indicates directly the presence of a strong CT interaction along the stacking direction, in addition to the short intermolecular atomic distances shown in Table 3. Figure 6 shows the optical conductivity spectrum calculated through the Kramers-Kronig transformation of the reflectance spectrum. The FWHM of the CT band is about 1000 cm^{-1} at room temperature, which is extraordinary narrow as compared with organic radical salts.[14-16] The sharp line shape of the CT band means that the electron-molecular vibration coupling is very small. In other words, the distortion of the molecular geometry accompanying the charge transfer is very small. The oscillator strength of the CT absorption band was calculated to be 0.75 per one cation by integrating the conductivity spectrum. This value is considerably larger than the corresponding values: 0.34 for $(BPDT\text{-}TTF)_3(PF_6)_2$[17] and 0.35 of Cs_2TCNQ_3.[18]

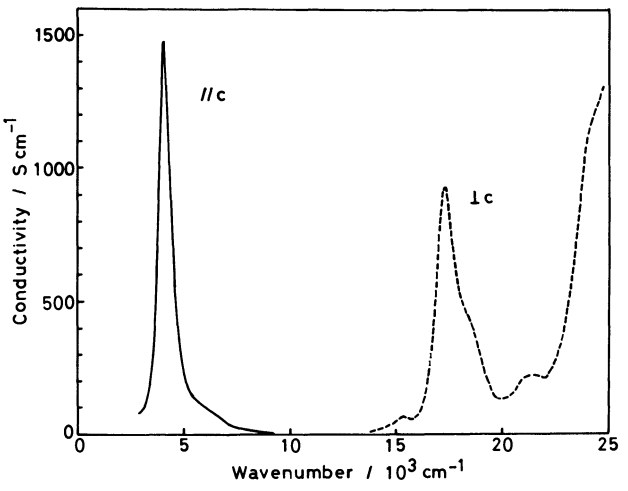

Fig. 6. Optical conductivity spectrum of $(NiTBP)_3(AsF_6)_2(C_{10}H_7Cl)$.

The oscillator strength of the CT band is the measure of the transfer integral. The average transfer integral of $(NiTBP)_3(AsF_6)_2(C_{10}H_7Cl)$ was roughly estimated to be larger than 0.3 eV.[17] A weak ESR signal with a Lorentzian line shape was observed. The g-values were $g//=2.0035$ and $g\perp=2.0014$, and the line widths were $\Gamma//=4.2$ G and $\Gamma\perp=8.0$ G (1G=10^{-4} T), where the static magnetic field was applied parallel and perpendicular to the c-axis. Angle dependence of g-value around the c-axis was very small, and neither g-value nor line width were dependent on temperature. The temperature dependence of the intensity of this signal was Curie-like. The concentration of the unpaired electrons estimated from the temperature dependence of the ESR intensity was 1/1000 molecule^{-1}. Therefore, the large majority of spins on NiTBP forms pairs making non-magnetic ground state, and the origin of the ESR signal is probably attributed to the unpaired electrons trapped at the lattice defects. The g-value of NiTBPI were reported to be $g//=2.060$ and $g\perp=2.018$, and the half width, $\Gamma//=110$ G and $\Gamma\perp=75$ G.[6] In the case of NiTBPI, the unpaired electrons are located both at the Ni atom and at the TBP ligand. The small g-value and the narrow half width of ESR signal in $(NiTBP)_3(AsF_6)_2$-$(C_{10}H_7Cl)$ indicate that the unpaired electrons are located at the TBP ligand. Since the orbital energy of the d_{z^2} is expected to be pressed up by the Ni-Ni interaction, the oxidation part depends probably on the Ni-Ni distance. However, the Ni-Ni distance of this material is almost the same as that (3.217 Å) of NiTBPI.[6] Thus the Madelung energy may also contribute to determine the oxidation part.

The experimental results on the optical spectrum and ESR are quite different from those of organic radical salts like $(BPDT\text{-}TTF)_3(PF_6)_2$[17] and Cs_2-$TCNQ_3$, which are expected to have equivalent electronic structures. For example, Cs_2TCNQ_3 exhibits two CT bands at about 4000 cm^{-1} and 10000 cm^{-1},[18] and presents an ESR signal at room temperature which is attributed to a thermally excited triplet exciton.[19] The appearance of the CT band at higher wavenumber and the small excitation energy of the triplet exciton comes from the large on-site Coulomb energy ($U/4t>1$).[20] However, this material does not exhibit the second CT band despite that the unpaired electrons are making pairs. Therefore, the electronic structure of this material should be understood on the basis of an uncorrelated one-dimensional band model. In this model the CT transition is reinterpreted to be an interband transition and the magnetic activation energy is given by the band gap. This model is in accord with the fact that the band gap estimated from the electrical resistivity agrees quite well with the excitation energy of the optical spectrum. Therefore, we consider that this material have a small on-site Coulomb energy

Table 5. Crystal Growth of Ni(TBP) Complexes by Electrochemical Oxidation

Anion shape	Octahedral	Tetrahedral	Linear
	PF_6 ○	BF_4 ○	Br_3 □
	AsF_6 ○	ClO_4 ○	I_3 □
	SbF_6 □	ReO_4 ○	

○: Single crystal, the typical dimension of which is (0.02—0.09)×(0.02—0.09)×(1—4) mm³. □: Microcrystal, the dimension of which is less than 0.01×0.01×0.5 mm³.

($U/4t<1$), which is related to the large size of the TBP ligand and the large transfer integral.

Other Radical Salts. We prepared several radical salts by using other counter anions. The results on the preparative experiment are shown in Table 5. We examined the structural, electrical, and magnetic properties of the large size of single crystals (X=PF_6, BF_4, ClO_4, and ReO_4) shown in Table 5. The X-ray oscillation photographs showed that the periodic unit along the needle axis were about 9.6 Å. All of these salts are semiconductors with the specific resistivities of 10^3—10^4 ohm cm, and exhibited no ESR signal. These properties quite resembles $(NiTBP)_3(AsF_6)_2$-$(C_{10}H_7Cl)$ which we characterized in this paper. Therefore, we consider that the NiTBP radical salts with octahedral and tetrahedral counter anions shown in Table 5 belong to the same family with $(NiTBP)_3$-$(AsF_6)_2(C_{10}H_7Cl)$.

We deeply thank Prof. Hiroki Haraguchi, Department of Chemistry, the University of Tokyo, and Mr. Yoshimasa Kasahara, Japan Jarrel Ash, Co., for the elemental analysis of Ni and As by means of ICP atomic emission spectroscopy. We are grateful to Prof. Takeshi Miyamoto, Department of Chemistry, the University of Tokyo, for kindly providing us 2-acetylbenzoic acid which is the starting material to synthesize NiTBP.

References

1) C. J. Schramm, R. P. Scaringe, D. R. Stojakovic, B. M. Hoffman, J. A. Ibers, and T. J. Marks, *J. Am. Chem. Soc.*, **102**, 6702 (1980).

2) T. E. Phillips, R. P. Scaringe, B. M. Hoffman, and J. A. Ibers, *J. Am. Chem. Soc.*, **102**, 3435 (1980).

3) J. Martinsen, L. J. Pace, T. E. Phillips, B. M. Hoffman, and J. A. Ibers, *J. Am. Chem. Soc.*, **104**, 83 (1982).

4) J. Martinsen, S. M. Palmer, J. Tanaka, R. C. Greene, and B. M. Hoffman, *Phys. Rev. B*, **30**, 6269 (1984).

5) S. M. Palmer, J. L. Stanton, N. K. Jaggi, B. M. Hoffman, J. A. Ibers, and L. H. Schwartz, *Inorg. Chem.*, **24**, 2040 (1985).

6) J. Martinsen, J. L. Stanton, R. L. Greene, J. Tanaka, B. M. Hoffman, and J. A. Ibers, *J. Am. Chem. Soc.*, **107**, 6915 (1985).

7) T. Inabe, S. Nakamura, W. B. Liang, T. J. Marks, R. L. Burton, C. R. Kannewurf, and K. Imaeda, *J. Am. Chem. Soc.*, **107**, 7224 (1985).

8) K. Yakushi, M. Sakuda, H. Kuroda, A. Kawamoto, and J. Tanaka, *Chem. Lett.*, **1986**, 1161.

9) K. Yakushi, M. Sakuda, I. Hamada, H. Kuroda, A. Kawamoto, J. Tanaka, T. Sugano, and M. Kinoshita, *Synthetic Metals*, **19**, 769 (1987).

10) T. Sakurai and K. Kobayashi, *Rep. Inst. Phys. Chem. Res.*, **55**, 69 (1979).

11) Y. Iyechika, K. Yakushi, and H. Kuroda, *Bull. Chem. Soc. Jpn.*, **53**, 603 (1980).

12) H. Tajima, K. Yakushi, H. Kuroda, G. Saito, and H. Inokuchi, *Solid State Commun.*, **49**, 769 (1984).

13) J. M. Robertson and I. Woodward, *J. Phys. Chem.*, **1940**, 36.

14) K. Yakushi, S. Miyajima, T. Kusaka, and H. Kuroda, *Chem. Phys. Lett.*, **114**, 168 (1985).

15) C. S. Jacobsen, D. B. Tanner, and K. Bechgaard, *Phys. Rev. B*, **28**, 7019 (1983).

16) K. Yakushi, S. Aratani, K. Kikuchi, H. Tajima, and H. Kuroda, *Bull. Chem. Soc. Jpn.*, **59**, 363 (1986).

17) K. Yakushi, H. Tajima, T. Ida, M. Tamura, H. Hayashi, H. Kuroda, A. Kobayashi, H. Kobayashi, and R. Kato, *Synthetic Metals*, in press.

18) K. Yakushi and H. Hayashi, unpublished data.

19) D. B. Chesnut and P. Arthur, Jr., *J. Chem. Phys.*, **36**, 2969 (1962).

20) Z. G. Soos and D. J. Klein, "Molecular Association, Vol. 1," ed by R. Foster, Academic Press, London (1975), p. 1.

 © 1988 The Chemical Society of Japan Bull. Chem. Soc. Jpn., 61, 1577—1585 (1988)

Formation of Graphite Single Crystal from Iron Solution by the Slow Cooling Method

Yoshihiro SUMIYOSHI, Masumi USHIO,* and Sadao SUZUKI
Department of Applied Chemistry, Faculty of Engineering, Gunma University,
Tenjin-cho, Kiryu-shi 376
(Received April 10, 1987)

Graphite single crystals with maximum dimensions of 40 mm in diameter and 0.04-mm thick were prepared from an iron solution by a slow-cooling method. The cell parameters of the product were a_o=2.462±0.002 and c_o=6.708±0.001 Å. A flux of 200 g of electrolytical iron and 8 g of graphite were charged in the graphite crucible. The iron melt, saturated with carbon, was slowly cooled from maximum temperatures ranging between 1800 and 2500 °C to near 1150 °C at cooling rates ranging from 5 to 30 °C min^{-1}. Large graphite single-crystal films of better quality were formed after quick cooling rather than slow cooling. Large graphite crystal films were formed at above 1850 °C; temperatures greater than 1950 °C were needed in order to grow the crystal films with good quality. From in-situ observations through a hole, the growth of the small graphite crystals was seen to occur on the surface of the melt at about 1550 °C; these were gathered in a constant direction, initiating the incorporation of small crystals. The incorporation of the small crystals was promoted at about 1700 °C and the surface of the melt was covered with a single-crystal film. For the formation mechanism of the graphite single-crystal film, a heating process was played an important role.

In recent years, industrial carbon materials have entered the spotlight because of the following interesting properties. Such structures are unique, including amorphous carbon to graphite single crystals; the electrical resistances vary from 10^5—10^6 Ω cm, close to that of a semiconductor to about 10^{-4} Ω cm, comparable with that of a metal. The thermal conductivity of carbon materials expand from ones larger than that of the steel to ones close to that a thermal insulator. The melting point of carbon is 3800 °C and is thus a material having resistance against high temperatures.

These special characteristics are depend on the chemical bonding form of carbon atoms and the crystal structure of graphite based on the carbon atom. Therefore, in order to study such properties as chemical, physical, and mechanical, it is necessary to study the formation of graphite single crystals and to clarify the formation mechanism.

Studies on the formation of graphite single crystals have been reported by many researchers. These formation methods are as follows: (1) A method in which graphite is directly melted and then cooled while crystallizing.[1-3] (2) A method in which graphite is crystallized from a metal melt which is saturated with carbon.[4-9] (3) A method involving the thermal decomposition of metal carbides.[10-12]

In these methods, (2) is most suitable for the formation of large graphite single crystals. Nickel, iron, and many other metals are used as a flux. In these metals, since graphite is highly soluble in iron and iron is more economical than other metals, iron is used as a flux in this experiment.

Studies on the formation of graphite single crystals from an iron melt have been reported by Austerman et al.[7] and Noda et al.[8,9] Austerman et al. synthesized graphite single crystals by slow cooling an iron melt which was saturated with carbon using an electric precision furnace with a temperature gradient control. Noda et al. grew graphite single crystal films of about 30 mm in diameter and about 0.06-mm thick in which the c-axis was parallel to the surface of the iron melt, by slow cooling the iron melt with 1 wt% Si. However, the formation of these large graphite single crystal films was hard to reproduce and the formation conditions have not yet been clearly understood.

The purpose of this study was to clarify the formation conditions and mechanisms of large single crystal films and to elucidate the formation conditions under which graphite single-crystal films become thickened in the direction of the c-axis. The reproducibility was also investigated. Grown graphite single-crystal films were examined by the X-ray Laue photograph method.

Experimental

In the present experiment, carbon-saturated iron was slowly cooled from a maximum temperature ranging between 1800 and 2500 °C, to nearly 1150 °C at a cooling rate ranging between 5 and 30 °C min^{-1}.

An outline of the experimental apparatus is shown in Fig. 1. A Tunman furnace (1.5 kW, Max.current 1000 A) was used as a heating apparatus; it could obtain a maximum temperature of 2500 °C after supplying an electric current to a graphite heater. The dimension of the graphite heater was 260-mm long, 60-mm inner diameter, and 5-mm thick. The graphite crucible (40-mm inner diameter, 5-mm thick, and 50-mm high) was made from a graphite rod by machining. A graphite tube (12-mm inner diameter, 4-mm thick, and 200-mm long) used for observations was made and installed in the graphite crucible.

The surface temperature of the melt was measured using a pyrometer through this graphite tube. Temperature errors were within ±20 °C.

Iron prepared electrolytically (purity above 98%) was used

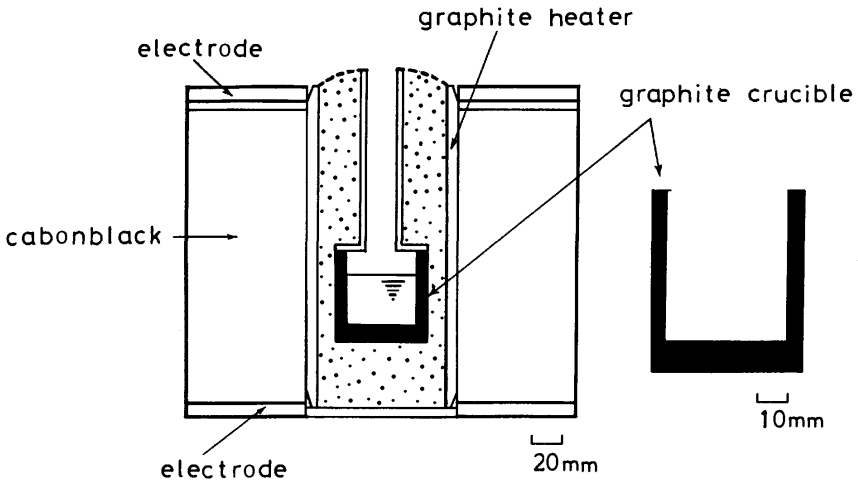

Fig. 1. Arrangement of an electric furnace for the growth of graphite single-crystal film.

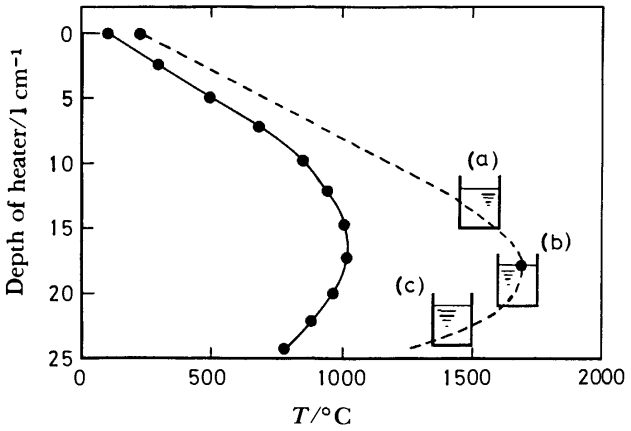

Fig. 2. Temperature distribution in an electric furnace and the positions of the graphite crucibles. -----; estimated curve, —; measured curve, ●; measured value.

as the flux. Graphite powder under 100 mesh, which shaved the graphite rod, was added because the graphite crucible became eroded by the iron melt. The lattice parameters of graphite added in a quantity of about 4 wt% were a_o=2.483±0.002 Å and c_o=6.727±0.002 Å. Powdered iron (200 g) and graphite (8 g) were charged in the graphite crucible.

The experimental process was divided into three steps: a heating process, a constant-temperature process, and a cooling process. The formation conditions of graphite single-crystal films were investigated by considering these three processes.

Temperature Distribution in the Melt. The temperature distribution in the melt significantly affected the formation of a graphite single-crystal film. However, since the graphite heater was fixed at a certain position, the required temperature distribution in the melt was obtained by varing the position of the crucible. The temperature distributions inside the graphite heater and in the melt were measured by a Pt-Pt 13%Rh thermocouple in order to determine the position of the maximum temperature in the heater. The experimental results are shown in Fig. 2. Since the limits of use of the thermocouple is below about 1500 °C, a higher temperature distribution of this experiment can be gained from measurements using a pyrometer. In an experiment involving a slow-cooling method, the crucible was placed at three positions (a, b, and c) as shown in Fig. 2. In the a-position, the lower part of the melt was located at a position of maximum temperature in the heater. On the other hand, the higher part of the melt was located as a position of maximum temperature for the b- and c-positions. In the former, the bottom of the graphite crucible was liable to erode. However, since a thermal convection current was produced in the melt since the lower part of the melt was located at a position of higher temperature, the temperature of the inside of the crucible was liable to make it uniform. On the other hand, for the b- and c-positions, the wall of the graphite crucible was liable to erode; it is therefore thought that a temperature difference between the lower and the higher parts of the melt was generated.

Results

Growth of Graphite Single-Crystal Film. The grown graphite single-crystal films can be classified roughly into the following classes: a large graphite single-crystal film, a small graphite single crystal, and a fine crystal in a solidified flux brick.

In the case of growing a large graphite single-crystal film all over the surface of the melt, it was shown the state of graphite formation as shown in Fig. 3. In this appearance, a graphite single-crystal film could be easily separated from the brick of iron flux.

In the case in which a cooling experiment was carried out at the a-position, a flux brick was created which was supposed to spout from the inside of the crucible through the center of the graphite crystal film, as shown in Fig. 4. Since it was difficult to grow a large graphite single-crystal film and to prevent this phenomenon, the graphite crucible was put in the temperature distribution at the b- and c-positions instead of the a-position. In the b- and c-positions of the crucible, solidification of the melt occured from

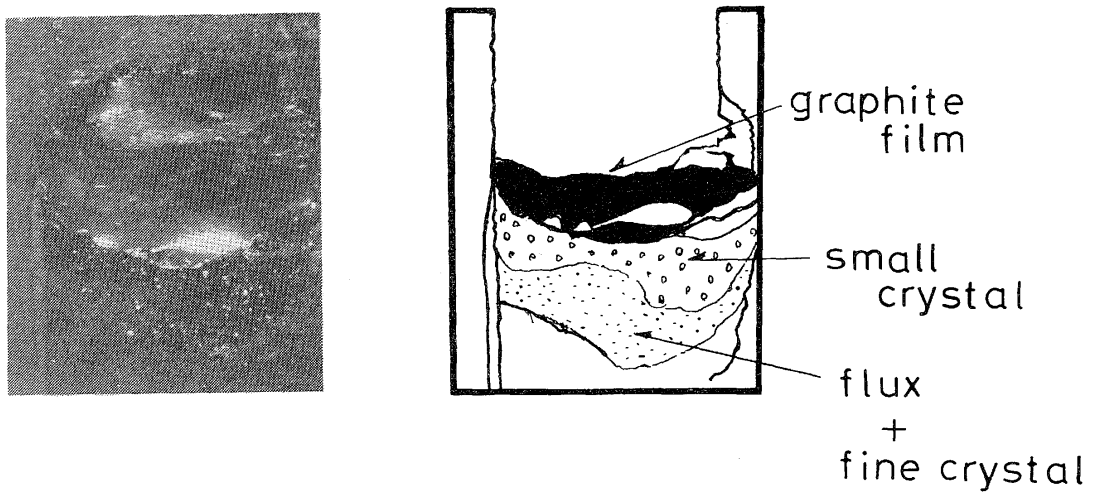

Fig. 3. Typical appearance after the growth of graphite single-crystal film.

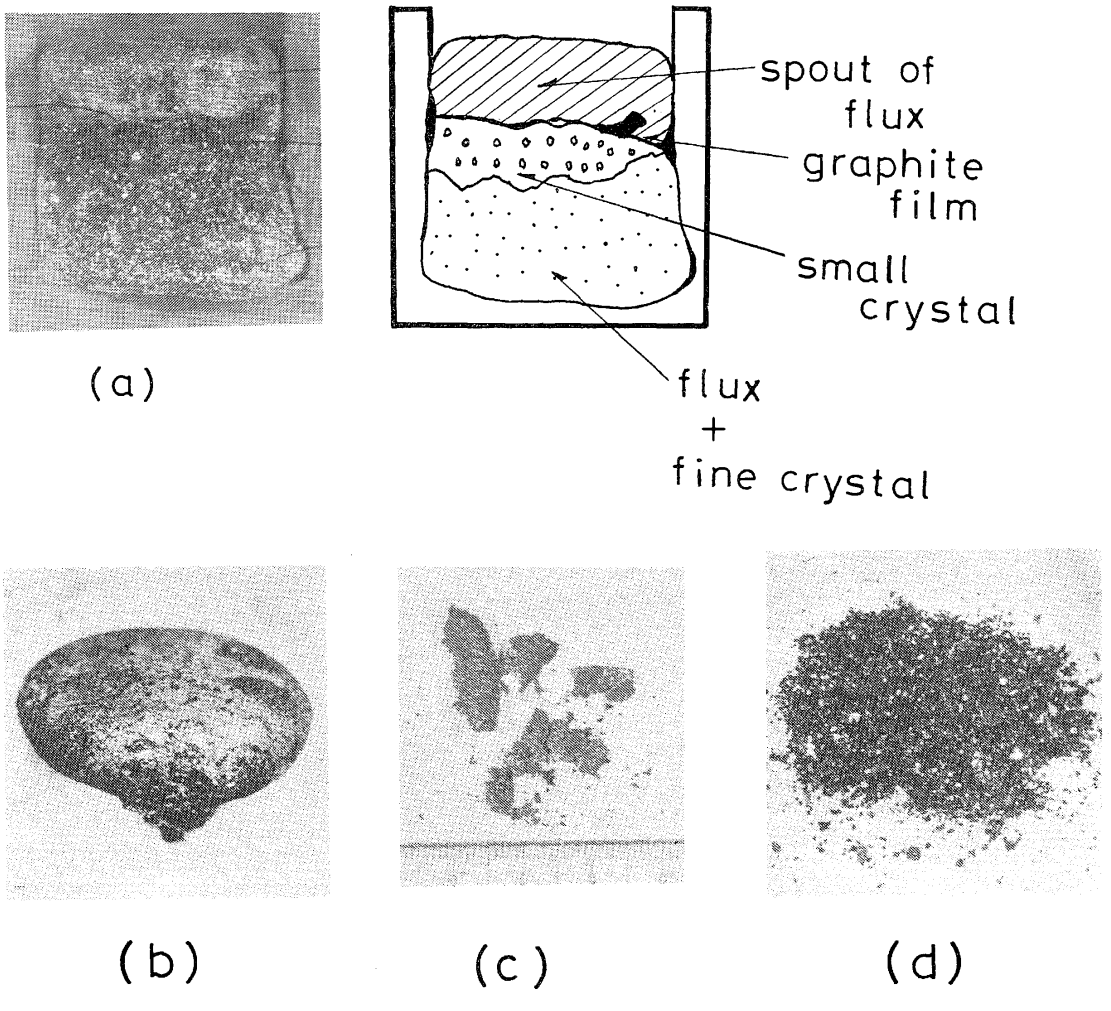

Fig. 4. Typical appearance after the growth of graphite single-crystal film.
(a) The spout of the flux through the center of graphite single-crystal film. (b) Spout of the flux. (c) Graphite single-crystal film. (d) Small graphite crystal.

the lower part, since the temperature at the higher part was higher than at the lower part; thus, the eutectic melt was not spouted out on the graphite single-crystal film. In this case, the single-crystal film could easily be separated from the solidified flux.

The experimental results using the slow-cooling method are shown in Table 1. In this table, the heating rate results from dividing the temperature difference between 1400 °C and the maximum temperature T_m by the time (minute) taken to heat; the cooling rate results from dividing the temperature difference between the maximum temperature T_m and 1400 °C by the cooling time. In order to obtain precise values, it is necessary to use temperature-time relation curves.

In this table, the double circles represent the case in which a large graphite single-crystal film (greater than 2.5 cm in diameter) was grown; the circle represents the case in which small single crystals (less than 1 cm in diameter) were prepared. As is evident from Table 1, when the heating rate was comparatively slow, a large graphite single-crystal film could not be grown at above a heating rate of 10 °C min^{-1}. On the other hand, heating rates between 5 and 9 °C min^{-1} were closely related to the growth of graphite single-crystal films. Regarding the position of the crucible, a large graphite single-crystal film could more easily be grown at the b-position than the a-position.

Table 1. Experimental Results by the Slow Cooling Method

Run No.	Position of crucible	Flux weight	Maximum temperature	Cooling rate	Heating rate	Graphite single-crystal film	Quality of graphite single-crystal film
		g	°C	°C min^{-1}	°C min^{-1}		
S-1-2	a	189	1900	7	8	○	Poor
S-1-3	a	209	1950	14	9	○	Poor
S-1-4	a	213	2000	20	10	○	Poor
S-1-9	b	221	1800	10	7	○	Poor
S-1-6	b	221	1850	15	9	◎	Poor
S-1-12	b	212	1950	5	4	◎	Good
S-1-5	b	221	1950	11	9	◎	Good
S-1-7	b	221	1950	18	22	○	Poor
S-1-11	b	221	2000	5	9	○	Poor
S-1-15	b	212	2000	6	8	○	Poor
S-1-14	b	212	2000	13	5	◎	Good
S-1-8	b	221	2000	17	16	○	Poor
S-1-10	b	221	2000	20	8	○	Good
S-1-17	b	210	2050	30	6	◎	Good
S-1-16	b	216	2100	5	5	◎	Good
S-1-13	b	212	2100	9	14	○	Poor
S-1-19	b	205	2200	11	7	◎	Poor
S-1-22	c	205	1800	7	20	○	Poor

○: Small film below 1 cm dia. ◎: Large film above 2.5 cm dia. Graphite powder of 8 g was added in the graphite crucible.

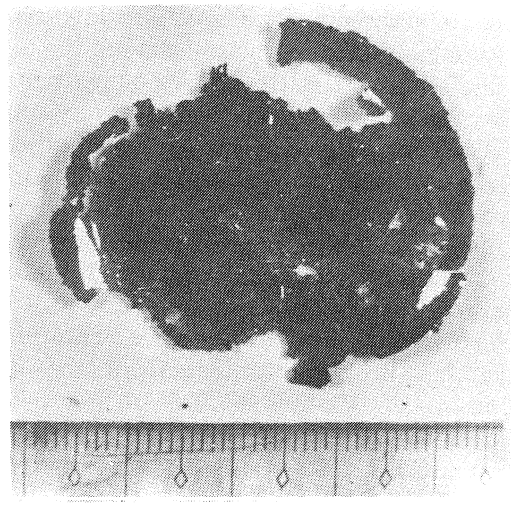

Fig. 5. Grown graphite single-crystal film for Run No. (S-1-14).

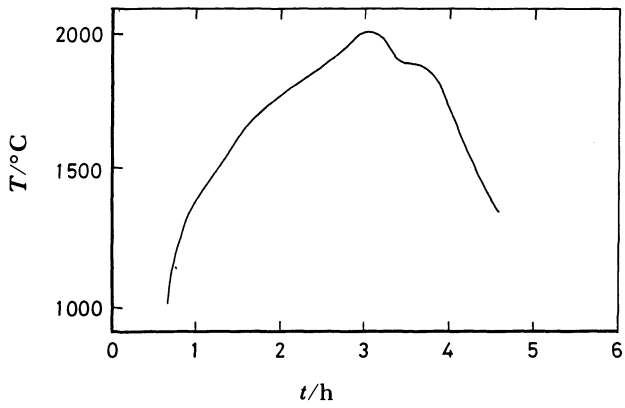

Fig. 6. A heating curve during the growth of graphite single-crystal film for Run No. (S-1-14).

Fig. 7. An appearance of the graphite crucible just after the growth of graphite single-crystal film for Run No.(S-1-17).

The photograph of a single-crystal film obtained from Run No. (S-1-14) and the heating curve are shown in Figs. 5 and 6, respectively. A large single-crystal film with a metallic luster and the dimensions of 4 mm in diameter and 0.03_5 mm thick, could be grown. The circumference of this single-crystal film curved at a state of meniscus. The grown graphite single-crystal film had good quality, judging from the Laue X-ray pattern.

A photograph of experimental Run No. (S-1-17) and the heating curve are shown in Fig. 7. The spout of a flux melt was formed through a single-crystal film with metallic luster. This depended on quick cooling: that is, a cooling rate of 30 °C min^{-1}.

Laue X-Ray Photographs and Electron Diffraction Patterns. From a Laue X-ray photograph of the product of Run No. (S-1-5), it was presumed that the grown graphite single-crystal film had a good quality, judging from the spots of hexagonal symmetry. Though the grown single-crystal film from Run No.

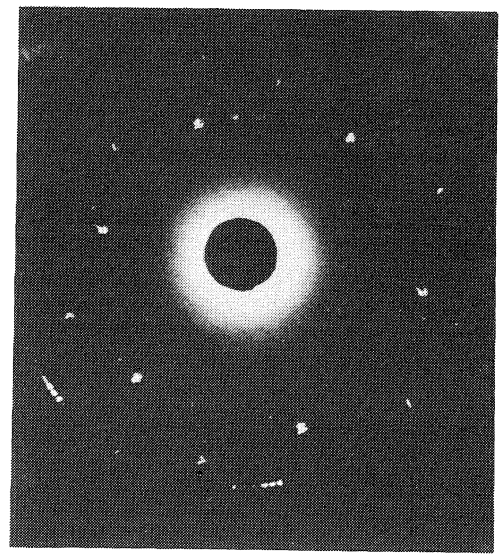

Fig. 8. Laue photograph of the graphite single-crystal film for Run No. (S-1-14).

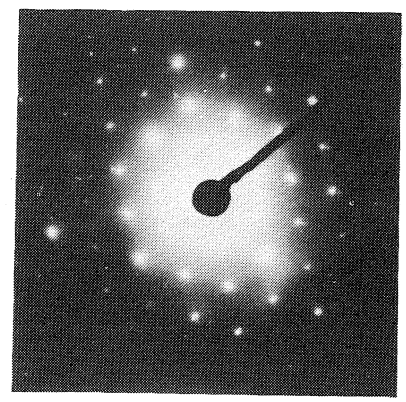

Fig. 9. An electron diffraction pattern of the graphite single-crystal film for Run No. (S-1-14).

(S-1-6) had good crystallinity, it was hard to say whether it was a single crystal from a Laue X-ray photograph and the electron diffraction pattern.

A Laue X-ray photograph and an electron diffraction pattern of the single-crystal film from Run No. (S-1-14) are shown in Figs. 8 and 9. It appears that the grown crystal had very a good quality.

Discussion

The reason that the flux spout formed above the graphite single crystal film (Fig. 4) is thought to be due to a solidification of the melt that occured from its surface. The internal pressure resulted from a contraction of iron flux upon solidifying; then, the eutectic melt of the flux plus graphite gushed out to the surface of the single-crystal film.

Formation Condition and Mechanism of a Graphite Single-Crystal Film. Graphite single-crystal films with good quality were obtained from Runs No. (S-1-5), (S-1-6), (S-1-10), (S-1-12), (S-1-14), (S-1-16), and (S-1-17), as is shown in Table 1. From these results, the formation conditions and mechanism of graphite single-crystal films are discussed in detail.

In an experiment involving the slow-cooling method, it was widely noted that the iron-flux method saturated when the graphite was cooled; it then separated the saturated graphite as crystals. This process, which separated the crystals from the iron flux, can be classified into two classes: the nucleation and the crystal growth. These two phenomena were strongly dependent on the temperature. The rate of nucleation was generally faster as the cooling rate increased, and the growth rate of crystal was faster as the temperature increased. Consequently, it is necessary to grow a single crystal in which nucleation occurs as much as possible and the crystals grow. As described above, the experimental process was thought to classified into three large steps: heating, constant-temperature and cooling processes. The correlation between these processes and the formation of a large graphite single-crystal film was investigated.

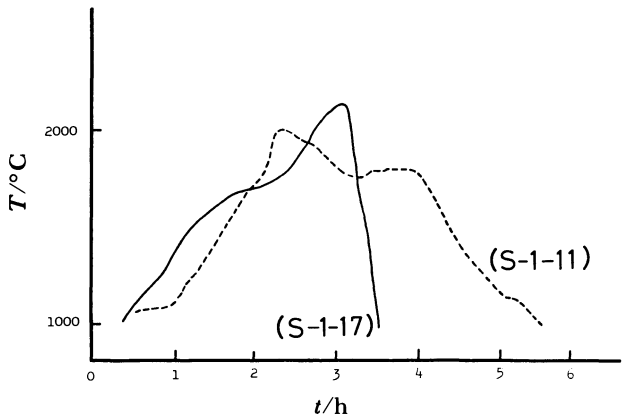

Fig. 10. Comparison of Run No. (S-1-17) quenched quickly with Run No. (S-1-11) cooled slowly.

Cooling Process. The cooling process, which was believed to be very important and a strong governing factor, was examined in terms of the cooling method. Figure 10 summarizes the results of both the temperature curves of an experiment involving rapid cooling (Run No. (S-1-17)) and an experiment involving slow cooling (Run No. (S-1-11)). Although it is generally said that for a slower cooling rate the better is the graphite single-crystal film quality, a large graphite single crystal with good quality was formed for Run No. (S-1-17), compared to Run No. (S-1-11) involving slow cooling. The assumption was compatible with these results. Note that a large

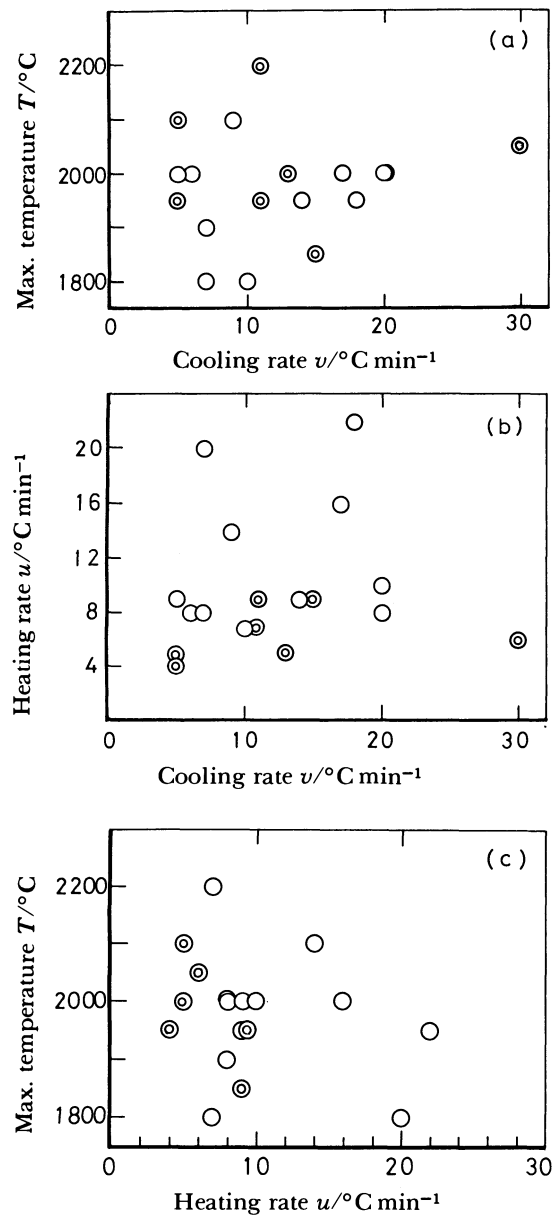

Fig. 11. Relationship among the growth ease of the graphite single-crystal film and the cooling rate, the heating rate, and the maximum temperature.
O: small film below 1 cm dia., ◎: large film above 2.5 cm dia.

graphite could be formed, even if the slow cooling was fairly well controlled. An adequate correlation based upon the cooling rate could not be found, as is shown in Fig. 11. Thus, there was little possibility of a factor which determines the formation of a graphite single-crystal film. In the cooling process, small crystals were formed below the graphite single-crystal film. Therefore, an apparatus that could control the cooling process was used; small crystals were thought to grow to some degree. A cooling process was far from a factor influenced to the growth of graphite single-crystal film.

A Constant Temperature Process. The next factor examined was the influence of the maximum temperature and its holding time. The experimental results are shown in Table 1. The influence of the maximum temperature are not shown to have a certain correlation. A large graphite single-crystal film could be formed if the maximum temperature was above 1850 °C as shown in Table 1.

We could not determine the correlation in terms of the holding time at the maximum temperature (Fig. 12). However, this constant-temperature process shows a very attractive tendency, which is obvious by comparing the temperature curves of Run No. (S-1-5) and Run No. (S-1-6), as shown in Fig. 13. In the case of Run No. (S-1-5), the temperature was held constant at a value which fell slightly from the maximum temperature (1950 °C); under this condition a graphite single-crystal film with good quality was formed. However, in Run No. (S-1-6) with a constant temperature of 1850 °C, a graphite single-crystal film of good quality could not be grown.

Generally, in the case of the type as shown in Fig. 14(a), a single-crystal film with good quality could form (Run No. (S-1-5), (S-1-14), and (S-1-16)). On the other hand, as for the temperature curve of the type shown in Fig. 14(b), Runs No. (S-1-7), (S-1-10), and (S-1-13), large graphite single-crystal films of good quality could not be formed. From these results, it appears to act as the annealing if the constant temperature, which lowered slightly from the maximum temperature, held. However, it seems to be true that another dominant factor existed.

A Heating Process. Finally, the more important factor was the heating process. The experimental results are shown in Fig. 11. In case that the heating rate was below 9 °C min^{-1}, a large graphite single crystal with good quality could form. The relation between graphite single-crystal film growth and the heating process could be determined by observing the surface of the melt from a hole. The experimental results are schematically shown in Fig. 15. It was observed that graphite single crystals rose to the surface of the melt at a temperature of about 1550 °C, and gathered in the constant direction; then, the incorporation of crystals was initiated. This incor-

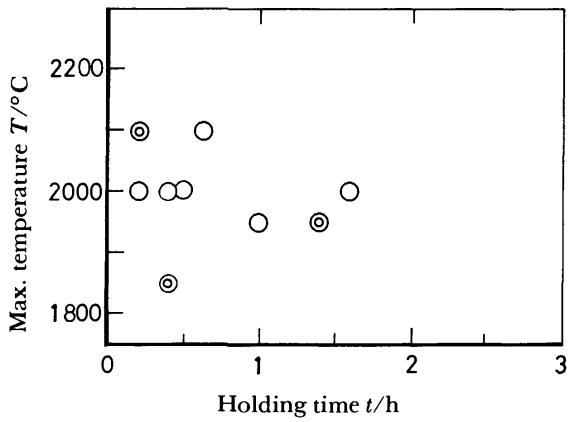

Fig. 12. Relationship among the growth ease of graphite single-crystal film and the holding time, and the maximum temperature, O: small film below 1 cm dia., ◎: large film above 2.5 cm dia.

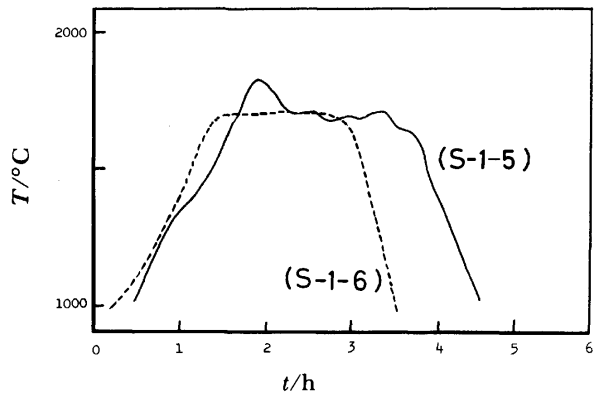

Fig. 13. Comparison of the holding times for Run No. (S-1-5) with for Run No. (S-1-6).

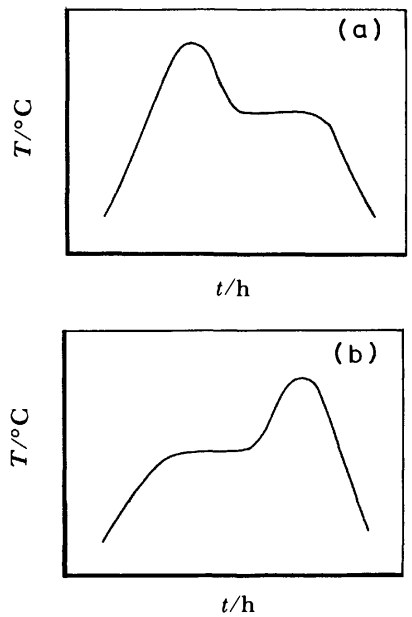

Fig. 14. Typical heating curves for the growth of the graphite single-crystal films.

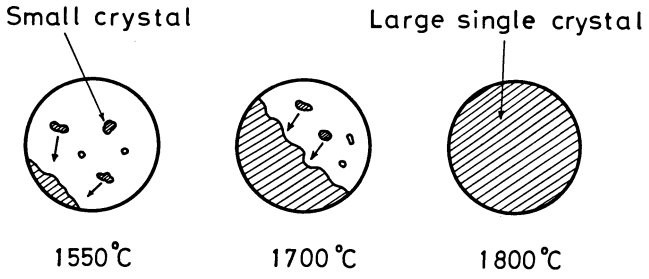

Fig. 15. Observation of the growth process of the graphite single-crystal film on the surface of the melt.

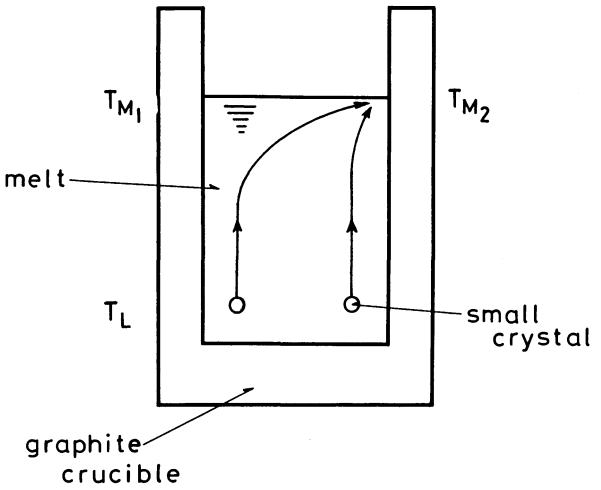

Fig. 16. The deposition process of the small graphite single crystals in the melt.

poration was promoted at about 1700 °C and the graphite single crystal covered the surface areas. Also, wrinkled patterns on the surfaces of the grown small graphite crystals were observed. These patterns were in agreement with that of a grown single-crystal film observed after the experiment. It was thus found that a single-crystal film is formed during the heating processes.

This formation mechanism of graphite single-crystal films is new and quite different from the so-called mechanism of the crystal growth by slow-cooling.

As previously stated, small graphite crystals were observed to gather in a constant direction, as is shown in Fig. 15. To investigate the cause, the temperature distribution in the horizontal direction of the graphite heater was observed. As a result, the temperature difference between sides in the central sections of the heater was several 10 °C. It seems that the graphite heater was wasted unequally during many repeated experiments; consequently, a temperature difference in the horizontal direction of the heater was produced. Accordingly, it is obvious that a temperature difference was produced in the horizontal direction in the same manner in the vertical direction as the temperature was increased.

The crystal growth of graphite is considered to be as follows. As is shown in Fig. 16, the graphite became saturated from the melt while precipitating and migrating from the lower-temperature (T_L) parts to the high-temperature (T_M) parts, owing to a difference in the specific gravities. It then floated to the surface of the melt. Then, graphite crystals were incorporated the opposite side (T_{M_2}) of the crucible wall (T_{M_1}), where the graphite heater was fairly wasted. A graphite single-crystal film with good quality was obtained by holding these incorporated crystals at a constant temperature.

From this point of view, the heating process was very significant. Therefore, the incidence of a nucleus could be slightly lowered by the decreasing the temperature difference, thus, decreasing the heating rate within 6 °C min^{-1}. It is possible that a large graphite single-crystal film with good quality was obtained by increasing the growth rate of the crystal as the temperature increased, within the scope of the heating process. In conclusion, when making use of a temperature difference in both horizontal and vertical directions, by controlling the heating rate to be 6 °C min^{-1}, and holding the maximum temperature above about 1950 °C, a large graphite single-crystal film was obtained with good reproducibility. Such hitherto performed experiments as the slow-cooling method are described; however, from a practical point of view it could be called a sort of temperature-gradient method which made use of the both temperature difference between in the horizontal and vertical directions.

Transmission Laue Photograph and Electron Diffraction Patterns. The graphite single-crystal films formed were examined by X-ray and electron diffraction methods as to whether these crystals had good quality or not.

The crystal structure of graphite has a stratified layer structure. The regular hexagonal rings of the carbon atoms are numerously linked together and make the enormous network plane. These alternate layers fall vertically above one another. Owing to the way these layers are piled, the graphite structure has two polytypes: a hexagonal system with an ABABAB structure (2H) and a rhombohedral system with an ABCABCABC structure (3R). The hexagonal system is the most common in graphite crystals with a unit cell of a_o=2.4612 Å and c_o=6.708 Å; the 3R-type unit cell is a_o=2.4612 Å and c_o=10.062 Å, by expressing it by the hexagonal cell. In the grown graphite single-crystal films with the high crystallinity, the Laue spots show a 6-fold axis of symmetry of the distinct {101} and {112} forms.

In the case of experimental Run No. (S-1-14), as

shown in Fig. 8, a Laue pattern of the distinct 6-fold axis of hexagonal symmetry was obtained, indicating that a graphite single-crystal film with good quality was obtained.

The indices of these spots were evaluated by making use of a gnomonic projection method. By closely observing the Laue spots of the graphite single-crystal film for Run No. (S-1-14), it is obvious that these spots were split. When an electron diffraction photograph of the same graphite single-crystal film was taken and magnified, the spots were certainly split. In this case, the split spots of a graphite single-crystal film should be based on either twised two sheet-like networks or on the incompatibility of these networks in the a- and the b-directions. Perhaps, we suppose that the small crystals were adhered to the surface of the graphite single-crystal films.

Conversely, there was also a case in which the spots on a concentric circle were not split; the split spots appeared at the inside or outside of the circle. There is a reason that the graphite crystal was expected as a single one; however, graphite single-crystal films were piled up and the spots of the Laue photograph were split and then appeared at the inside or outside of the concentric circle, or small crystals adhered to the surface of the single-crystal film.

When we examine the Laue spots of the graphite single-crystal film curved to meniscus for Run No. (S-1-14), many spots could be recognized at the insides and outsides of the spots of 6-fold symmetry, except that of the 6-fold symmetry for {101} and {112} groups. These many spots could not index with a hexagonal system. From data of the powdered X-ray diffraction patterns, the Laue photograph, etc., we determined that these many spots corresponded to a rhombohedral structure and also that many spots on a concentric circle, except for the 6-fold symmetry, corresponded to a twisted structure like the aberration of the positions of card as a spiral stairs. There are a few cases in which a rhombohedral structure was created by a shear-stress deformation.[13]

In the present experiment, the outside circumference of the graphite single-crystal film was curved by accepting a deformation stress during the cooling time; it was also thought that a rhombohedral structure was partially created.

It is recognized that a rhombohedral structure existed several per cent in a natural graphite crystal as well as in an artificial graphite crystal with good quality. Therefore, it could be thought that the rhombohedral structure also partly existed in the large graphite single-crystal film with good quality.

Unit Cell Parameters of a Graphite Single-Crystal Film. The parameters, a_0 and c_0 values, of the graphite single-crystal film were 2.462±0.002 Å and 6.708±0.001 Å, respectively, according to the present data from the powdered X-ray diffraction method and agreed with that of a natural graphite crystal.

References

1) M. J. Basset, *J. Phys. Radium.*, **10**, 217 (1937).
2) T. Noda and H. Matuoka, *Kogyo Kagaku Zasshi*, **63**, 456 (1960).
3) T. Noda and H. Kato, *Carbon*, **3**, 289 (1965).
4) K. Niwa and G. Shimaoka, *J. Metal.*, **9**, 431 (1957).
5) P. C. Li, *Nature (London)*, **192**, 864 (1961).
6) H. J. C. Tulloch and D. A. Young, *Nature (London)*, **211**, 730 (1966).
7) S. B. Austerman, S. M. Myron, and J. W. Wagner, *Carbon*, **5**, 549 (1967).
8) T. Noda, Y. Sumiyoshi, and N. Ito, *Carbon*, **6**, 813 (1968).
9) T. Noda, *Carbon*, **6**, 125 (1968).
10) L. M. Foster, G. Long, and H. C. Stumpt, *Am. Mineral.*, **43**, 285 (1958).
11) D. V. Badam, *Carbon*, **3**, 53 (1965).
12) T. Ishii, *Denki Kogyo Kagaku Zasshi*, **35**, 688 (1967).
13) E. J. Freise and A. Kelly, *Philos. Mag.*, **8**, 1519 (1963); G. E. Bacon, *Acta Crystallogr.*, **4**, 558 (1951).

Liquid-Liquid Extraction of Some Class *b* Metal Ions with a Thiacrown Compound, 1,4,7,10,13,16-Hexathiacyclooctadecane

Eiichi SEKIDO,* Hideo KAWAHARA, and Kaoru TSUJI
Department of Chemistry, Faculty of Science, Kobe University, Rokkodai, Nada-ku, Kobe 657
(Received July 20, 1987)

The liquid-liquid extraction of various metal ions, especially of soft class *b* metal ions with a thiacrown compound, 1,4,7,10,13,16-hexathiacyclooctadecane (HTCO) using picrate ion (Pic^-) was examined and compared with that of 1,4,8,11-tetrathiacyclotetradecane (TTCT). Although the extraction behavior of the class *a*, *ab*, and *b* metals with HTCO is fundamentally similar to that with TTCT, that of some metals belonging to class *b* metals with HTCO is different from that with TTCT. The extraction percentages of copper(II) and palladium(II) with HTCO are a few times larger than those with TTCT. Copper(I) and silver(I) are extracted with HTCO as the 1:1 complexes such as $[Cu(htco)]^+Pic^-$ and $[Ag(htco)]^+Pic^-$, respectively, regardless of the relative concentration of the ligand to the metal. On the other hand, copper(I) and silver(I) complexes with TTCT are extracted with different compositions depending upon the relative concentration of the ligand to the metal.

The extraction behavior of various metal ions, especially of the class *b* metal ions, with the thiacrown compound, 1,4,8,11-tetrathiacyclotetradecane (TTCT) was examined using perchlorate ion as the counter anion and dichloroethane or chloroform as the extraction solvent.[1,2] It was found that class *a* metal ions were not extracted at all, and *ab* metal ions, except the copper(II) ion, were hardly extracted but class *b* metal ions were extracted.

Although the formation of the metal thiacrown cation complex might be primarily governed by the softness of the metal ion to bond with the sulfur atom in a thioether type ligand (R-S-R), it will depend also on the size ratio of the metal ion to the cavity of the thiacrown ligand and on the favourable stereochemistry of the metal ion with minimal strain of the cyclic ligand molecule. Moreover, the extraction of the metal ion is associated with the formation of the ion pair between the formed metal complex cation and the counter anion and also with the affinity of the generated ion pair for the organic solvent. Consequently, it is interesting to investigate how the extraction behavior of various metals alters (especially the *b* metals) according to the number of sulfur atoms and to the number of the constituent atoms in the cyclic thiacrown ligand. This can help to separate the class *b* metals by the solvent extraction with thiacrown compounds.

In this paper, the extraction behavior of metal ions with 1,4,7,10,13,16-hexathiacyclooctadecane (HTCO) which has six sulfur atoms in its 18-membered ring is examined and compared with that of 1,4,8,11-tetrathiacyclotetradecane (TTCT) which has four sulfur atoms in its 14-membered ring.

Experimental

Reagents. The reagent, HTCO, was synthesized according to the method by Black and McLean,[3] and recrystallized twice from ethyl acetate-hexane. The reagent, TTCT, synthesized according to the method by Rosen and Bush[4] was recrystallized three times from chloroform-ethanol. HTCO as well as TTCT were dissolved in 1,2-dichloroethane immediately prior to use. Metal sulfates (guaranteed-reagent grade) were used except for thallium(I) nitrate and the 1×10^{-2} mol dm^{-3} stock solution of each metal ion was prepared. The concentration of each metal was determined by potentiometric titration with chloride. 1,2-Dichloroethane was shaken three times with 2 mol dm^{-3} potassium hydroxide and with distilled water, dried with calcium chloride and distilled. Other reagents were of guaranteed-reagent grade.

Apparatus. A Taiyo M incubator was used for shaking the solutions. A Seiko SAS-725 atomic absorption spectrophotometer was used for the determination of metal ions. UV and visible absorption spectra were measured with a Shimadzu UV-240 recording spectrophotometer. The IR spectra of isolated metal thiacrown complexes were taken with a Hitachi 207 EPI-G2 type grating IR spectrophotometer. The pH of the aqueous phase was measured with a Hitachi-Horiba H-5 pH meter.

Liquid-Liquid Extraction of Various Metals. Ten ml of the aqueous solution containing 5×10^{-5} mol dm^{-3} metal ion, 1×10^{-3} mol dm^{-3} picrate ion and 1×10^{-2} mol dm^{-3} acetate buffer, were kept at an ionic strength of 0.1 with sodium sulfate. This solution was kept in a stoppered 50 ml glass cylindrical tube. For the copper(I) solution, hydroxylammonium sulfate was added to copper(II) sulfate solution to give 0.1 mol dm^{-3} hydroxylamine solution. To the resulting aqueous solution 10 ml of 5×10^{-3} or 5×10^{-4} mol dm^{-3} HTCO or TTCT 1,2-dichloroethane solution was added and the mixture was shaken for 30 min on 200 strokes/min at 25±0.1 °C. The mixture was then centrifuged for 5 min at 2000 rpm, the pH of the aqueous phase was measured and the concentration of the picrate ion in the aqueous phase was determined spectrophotometrically at 354 nm. The concentrations of the metal ion in the aqueous and organic phases were determined by atomic absorption spectrophotometry. The metal concentration in an organic phase was determined as follows: A definite quantity of the organic phase was allowed to evaporate, the

residue was treated with small amounts of concentrated nitric acid and diluted with water to a standard volume and the concentration of the metal was then determined by atomic absorption spectrophotometry.

Isolation of Metal-HTCO and -TTCT Complexes. **Copper(I)-HTCO Complex:** Twenty ml of an aqueous solution containing copper sulfate (1×10^{-2} or 5×10^{-3}), hydroxylammonium sulfate (0.1 mol dm^{-3}), sodium picrate (1×10^{-2} mol dm^{-3}) and acetic acid-sodium acetate buffer (0.1 mol dm^{-3}, pH 4.4—5.0) was stirred with 20 ml of HTCO 1,2-dichloroethane solution (1×10^{-2} mol dm^{-3}) for 30 min at 25 °C in a 50 ml separation funnel. The yellow-orange deposit which formed between the two phases was filtered, washed with ethanol and 1,2-dichloroethane and dried in vacuo.

Silver(I)-HTCO Complex: The silver(I)-HTCO complex was extracted by the same method described in the isolation of copper(I)-HTCO complex, using silver nitrate instead of copper sulfate. After stirring, the mixed solution was centrifuged. When carbon tetrachloride was added to the separated organic phase, a yellow deposit was obtained. The filtered deposit was washed with ethanol and dried in vacuo.

Silver(I)-TTCT Complex: Twenty ml of the aqueous solution adjusted with acetic acid-sodium acetate to pH 5.0 containing silver sulfate (1×10^{-2} or 5×10^{-3} mol dm^{-3}) and sodium picrate (2×10^{-2} mol dm^{-3}) was placed in a 50 ml separation funnel and stirred with 20 ml of HTCO 1,2-dichloroethane solution (1×10^{-2} mol dm^{-3}) for 30 min at 25 °C. After centrifugation of the mixed solution, the organic phase was separated. On addition of 40 ml of carbon tetrachloride to the organic phase, a yellow solid deposit was obtained. It was washed with carbon tetrachloride and dried in vacuo.

Determination of the Composition of Metal Thiacrown Complexes. In order to determine the amount of the picrate ion contained in copper(I) and silver(I) thiacrown complexes, a definite amount of each complex was dissolved in DMF and the concentration of the picrate ion was spectrophotometrically determined by measuring the absorbance at 378 nm. To determine each metal ion concentration, metal thiacrown complexes were dissolved in DMF or were decomposed with sulfuric acid and then the resulting solution was then adequately diluted and the concentration of each metal was determined by atomic absorption spectrophotometry. The contents of HTCO and TTCT in the copper(I) and silver(I) complexes were estimated by subtracting of the amounts of both the metal and picrate ion from the initial amounts of the complex.

Results and Discussion

Liquid-Liquid Extraction of Various Metals with HTCO. The following metals were examined: Na(I) and Mg(II) as the class *a* metal; Mn(II), Co(II), Ni(II), Cu(II), Zn(II), and Tl(I) as the class *ab* metal; Cd(II), Cu(I), Ag(I), and Pd(II) as the class *b* metal. The results are shown in Table 1 with those for the extraction with TTCT.[1] It was found that the extraction

Table 1. Data for the Extraction of Various Metal Ions in the Presence of the Picrate Ion with HTCO and TTCT in 1,2-Dichloroethane Solution

Metal ion 5×10^{-5} mol dm^{-3}	Group of metal by Ahrland[a]	α value[b]	pH	Extraction (%)		
				HTCO		TTCT[c]
				5×10^{-4} mol dm^{-3}	5×10^{-3} mol dm^{-3}	5×10^{-3} mol dm^{-3}
Na(I)	*a*	~0	3.9	0		0
			5.4	0		0
Mg(II)	*a*	~0	3.9	0		0
			5.4	0		0
Mn(II)	*ab*	1.04	3.9	~0		0.5
			5.4	~0		0.8
Co(II)	*ab*	1.39	3.9	~0		0.8
			5.3	~0		0.8
Ni(II)	*ab*	1.41	3.9	~0		0.8
			5.3	~0		0.7
Cu(II)	*ab*	1.64	3.9	3	13	7.5
			5.4	4	24	5.9
Zn(II)	*ab*	1.25	3.9	~0		0.4
			5.3	~0		0.5
Tl(I)	*ab*	1.24	3.9	~0		2.2
			5.4	~0		1.0
Cd(II)	*b*	1.66	3.9	~0		0.6
			5.4	~0		0.8
Cu(I)	*b*	3.92	4.0	99		99.4
			5.4	100		99.4
Ag(I)	*b*	3.60	3.9	100		99.9
			5.4	100		99.9
Pd(II)	*b*	5.33	3.9	10	42	12.7
			5.4	11	45	14.3

a) Ref. 6. b) Ref. 7. c) Ref. 1.

behavior of the class *a*, *ab*, and *b* metal groups with HTCO is fundamentally similar to that with TTCT. That is, Na(I) and Mg(II) were not extracted at all, Mn(II), Co(II), Ni(II), Zn(II), Tl(I), and Co(II) were very weakly extracted Cu(II) and Pd(II) were extracted in some degree and Cu(I) and Ag(I) were extracted very well. The increases of both the constituent atoms of the thiacrown ring from 14 members for TTCT to 18 for HTCO and the sulfur ligand atoms from 4 for TTCT to 6 for HTCO had hardly any effect on the extraction behavior of the class *a* and *ab* metals. This fact means that the class *a* and *ab* metals except for copper(II), do not bind at all or very little with the sulfur atoms of the thioether type (R-S-R), regardless of other factors such as the number of sulfur atoms in the ligands, the number of constituent ring atoms, the molecular structure of the ligand, the kinds of the counter anion and the extraction solvent. However, the extraction behavior of some metals belonging the class *b* metals and copper(II) with HTCO is different from that with TTCT. For example, it was found that the percent extraction of Cu(II) and Pd(II) with HTCO is a few times larger than that with TTCT.

Extraction of Copper(I) and Silver(I). Copper(I) and silver(I) are almost completely extracted at pH 4.0 and 5.4 as shown in Table 1. Further, the dependence on pH and on the concentrations of the ligand and the picrate ion on the extraction of copper(I) and silver(I) were examined.

Dependence on pH: Plots of the logarithmic distribution ratio of copper(I) and silver(I) with HTCO against the pH of the aqueous phase are shown in Fig. 1. The decrease of the copper(I) extraction below pH 4 can be attributed to the decrease of the reducing power of hydroxylamine in acidic medium as well as in the case of Cu(I) extraction with TTCT.[1)]

Dependence on the Concentration of the Ligand and Picrate: If the species extracted into an organic phase is represented by $M(htco)_mPic_n$ (Pic^-: picrate ion), the extraction equilibrium and the extraction constant, K_{ex}, are given by Eqs. 1 and 2, respectively,

$$M^n + m\,htco(o) + nPic^- \overset{K_{ex}}{\rightleftharpoons} M(htco)_m(Pic)_n(o) \quad (1)$$

$$K_{ex} = [M(htco)_m(Pic)_n]_o/[M^{n+}][htco]_o^m[Pic]^n \quad (2)$$

where (o) and subscript o indicate the species in the organic phase. The logarithm of the distribution ratio of a metal, $\log D_M$ is represented by the Eq. 3.

$$\log D_M = \log K_{ex} + m\log[htco]_o + n\log[Pic^-] \quad (3)$$

The extraction of copper(I) and silver(I) at pH 4.4 was examined at various concentrations of picrate ion under constant concentration of HTCO, 5×10^{-4} mol dm^{-3}. The relationships between the logarithmic distribution ratio of copper(I) and silver(I), $\log D_M$, and the logarithm of the picrate concentration in the aqueous phase, $\log[Pic^-]$, are shown in Fig. 2. Two straight lines were obtained with slopes close to +1.0, indicating that $n=1$.

Similarly, the value of "*m*" in Eq. 3 should be given by the slope of the straight line obtained by the plots of $\log D_M$ vs. $\log[htco]$. However, these plots gave a straight line which is independent of [htco]. As examples, plots of $\log D_{Ag}$ vs. $\log[htco]$ in various organic

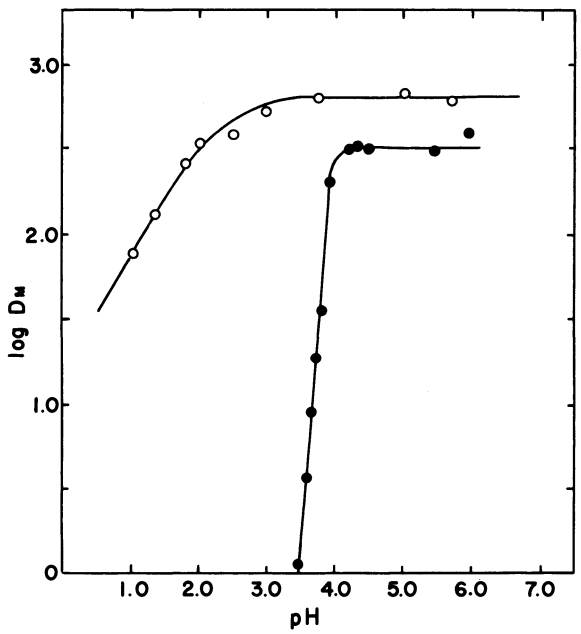

Fig. 1. Plots of distribution ratio of copper(I) (●) and silver(I) (○) vs. pH. Initial concentration: HTCO; 5×10^{-3} mol dm^{-3}, copper(I) and silver(I); 5×10^{-5} mol dm^{-3}.

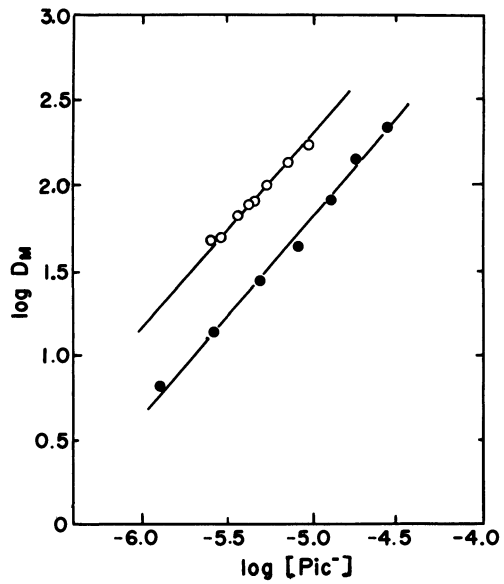

Fig. 2. Plots of $\log D_M$ vs. $\log[Pic^-]$ for copper(I) (●) and silver(I) (○). Initial concentration: HTCO; 5×10^{-4} mol dm^{-3}, copper(I) and silver(I); 5×10^{-5} mol dm^{-3}. pH 4.4.

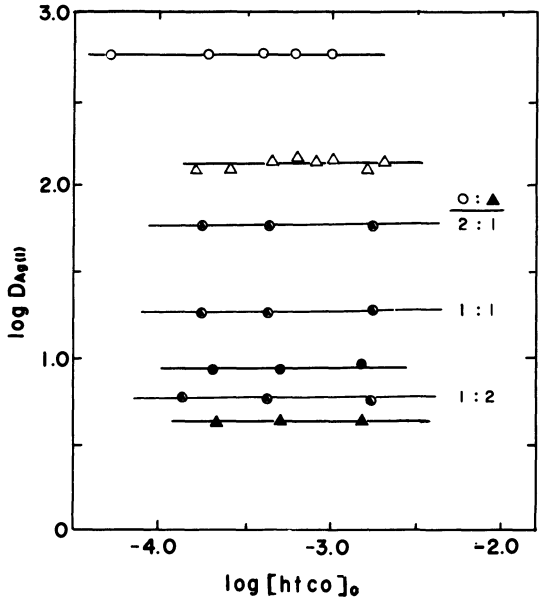

Fig. 3. Plots of $\log D_{Ag(I)}$ vs. $\log[htco]_o$ for various organic solvents. Initial concentration: silver(I); 5×10^{-5} mol dm^{-3}, picrate; 5×10^{-4} mol dm^{-3}. Organic solvent: O; 1,2-dichloroethane, △; chloroform, ●; benzene, ▲; carbon tetrachloride, ◭; mixture of 1,2-dichloroethane and carbon tetrachloride. pH: 5.4.

solvents such as 1,2-dichloroethane, chloroform, benzene and carbon tetrachloride, are shown in Fig. 3. The straight lines are independent of the concentration of HTCO and the values of $\log D_{Ag}$ increase in the order of 1,2-dichloroethane>chloroform>benzene> carbon tetrachloride, which is the order of their dielectric constants. The reason that values of the $\log D_{Ag}$ are below 1.0 for benzene and carbon tetrachloride will be owing to the formation of the yellow precipitate on the boundary of two layers. It is thought that the solubility of their ion-pair compound, $[M(htco)_m]^+Pic^-$, is limited in solvents having a low dielectric constant. This supposition is also supported by the facts that the values of the $\log D_{Ag}$ in a mixture of 1,2-dichloroethane and carbon tetrachloride do not vary with the concentration of HTCO and that their values decrease with the increase of the fraction of carbon tetrachloride in the mixture as shown in Fig. 3. The reason why the values of $\log D_M$ for copper(I) and silver(I) do not depend on the concentration of HTCO can be explained as follows. The ability of the complex formation of HTCO to copper(I) and silver(I) is so high that the equilibrium of

$$M^+ + m\,htco \rightleftharpoons [M(htco)_m]^+ \quad (4)$$

lies far to the right. Therefore, it is considered that the concentration of uncomplexed copper(I) or silver(I) in the aqueous phase is too low to be determined by atomic absorption spectrophotometry. Thus, the

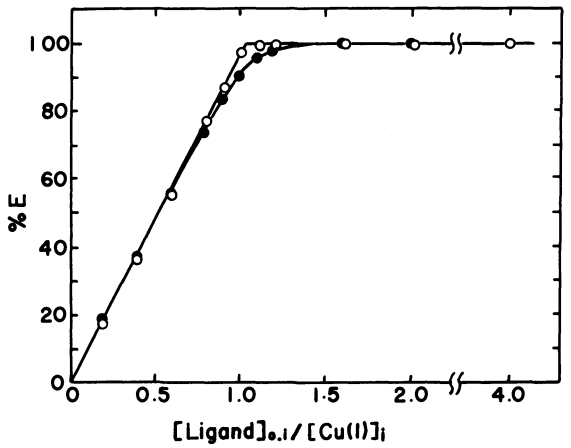

Fig. 4. Molar ratio study for copper complexes with HTCO (O) and TTCT (●). Initial concentration: copper(I); 5×10^{-5} mol dm^{-3}, picrate; 5×10^{-4} mol dm^{-3}. pH: 4.0.

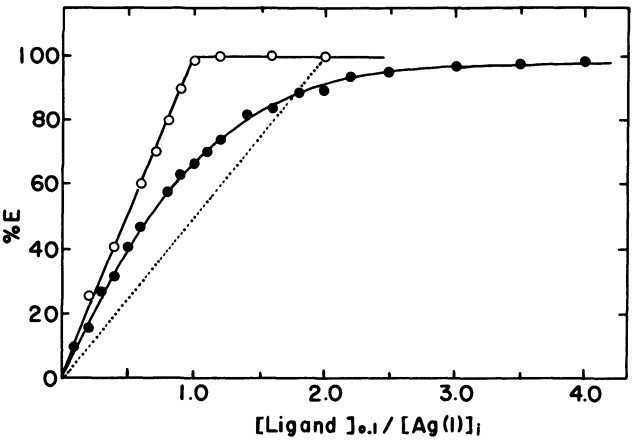

Fig. 5. Molar ratio study for silver(I) complexes with HTCO (O) and TTCT (●). Initial concentration: silver(I); 5×10^{-5} mol dm^{-3}, picrate; 5×10^{-4} mol dm^{-3}. pH: 4.0 Dotted line represents the case of formation of the stable 1:2 complex alone.

extractions of these metals appear to depend only upon the distribution of the ion-pair complex, $M(htco)_m^+Pic_n^-$.

In order to determine the value of m, the molar ratio method was tried. The plots of the %E for copper(I) vs. the ratio of $[htco]_{o,i}$ or $[ttct]_{o,i}$ to $[Cu(I)]_i$ and similar plots for silver(I) are shown in Figs. 4 and 5, respectively. The subscript i represents the initial concentration. In Fig. 4, the %E of copper(I) increases linearly with the increase of the ratio, $[htco]_{o,i}/[Cu(I)]$, and reaches almost 100% at the ratio=1. The distinct break point at $[htco]_{o,i}/[Cu(I)]_i=1$ means $m=1$. It is obvious that copper(I) forms the very stable 1:1 cationic complex, $[Cu(htco)]^+$, and the ion pair, $[Cu(htco)]^+Pic^-$, which is effectively extracted into 1,2-dichloroethane. The fact that the break point for HTCO is clearer than for TTCT as shown in Fig. 4

Table 2. Composition of Copper(I) and Silver(I) Complexes with HTCO

Metal	Initial condition	Metal:HTCO:Pic (Found)	Proposed formula
Cu(I)	Cu : HTCO = 1 : 1	1.0 : 1.0 : 0.9	[Cu(htco)]Pic
	Cu : HTCO = 1 : 2	1.0 : 1.1 : 0.9	[Cu(htco)]Pic
Ag(I)	Ag : HTCO = 1 : 1	1.0 : 0.9 : 0.9	[Ag(htco)]Pic
	Ag : HTCO = 1 : 2	1.0 : 0.8 : 0.9	[Ag(htco)]Pic

Table 3. Composition of Copper(I) and Silver(I) Complexes with TTCT

Metal	Initial condition	Metal:TTCT:Pic (Found)	Proposed formula
Cu(I)	Cu : TTCT = 1 : 1	1.0 : 1.3 : 1.0	[Cu(ttct)]Pic
	Cu : TTCT = 1 : 2	1.0 : 1.6 : 0.9	[Cu(ttct)]Pic + [Cu(ttct)$_2$]Pic
Ag(I)	Ag : TTCT = 1 : 1	1.0 : 0.4 : 0.8	[Ag$_2$(ttct)]Pic$_2$
	Ag : TTCT = 1 : 2	1.0 : 0.6 : 0.8	[Ag$_2$(ttct)]Pic$_2$ + [Ag(ttct)]Pic

indicates the copper(I)-HTCO complex is more stable than the copper(I)-TTCT complex. From both Eq. 3 and the result shown in Fig. 2, log K_{ex}=8.7±0.4 for the extraction of copper(I) with HTCO was estimated, of which value is larger than the value, 7.3±0.3 for copper(I)-TTCT.[1]

As shown in Fig. 5, the results of the molar ratio study for silver(I) to HTCO and TTCT seem to be different. In the case of HTCO, a distinct break point is found at $[htco]_{o,i}/[Ag(I)]=1$, which indicates that the extracted species is [Ag(htco)]Pic. On the other hand, in the case of TTCT, it seems to form the more stable [Ag(ttct)$_2$]Pic than [Ag(ttct)]Pic which may form on the ratio of $[ttct]_{o,i}/[Ag(I)]<1$. This estimation accords with the previous report[5] that silver(I) is extracted as the ion-pair complex compound, [Ag(ttct)$_2$]$^+$Pic$^-$, under the presence of the excess TTCT. The composition of the extracted silver(I) complex species seems to be different between TTCT and HTCO. The comparison of the curves of silver(I)-HTCO and -TTCT in Fig. 5, indicates that the 1:1 silver(I)-HTCO complex is more stable than the 1:1 or 1:2 silver(I)-TTCT complex.

Isolated Copper(I) and Silver(I) Complexes with HTCO and TTCT. The results of the determination of the compositions of copper(I) and silver(I)-HTCO and -TTCT complexes isolated from their extracts into 1,2-dichloroethane solution are shown in Table 2 for HTCO complexes and Table 3 for TTCT complexes. As seen in Table 2, regardless of the initial concentration ratios of copper(I) to HTCO, the molar ratio of copper(I), HTCO and picrate ion of the isolated complex is 1:1:1, corresponding to a proposed formula [Cu(htco)]Pic. This accords with the results of the above mentioned solvent extraction. Similarly, the composition of silver(I)-HTCO complex is [Ag(htco)]Pic, regardless of the initial concentration ratio of silver(I) to HTCO. However, as seen in Table 3, the composition of the copper(I) and silver(I)-TTCT complexes was not simple. Increasing the initial concentration of TTCT increases the content of TTCT and the complex seems to be a mixture of [Cu(ttct)]Pic and [Cu(ttct)$_2$]Pic. According to the study of the extraction equilibria for the copper(I)-TTCT-Pic complex,[1] it was estimated that copper(I) is extracted as the 1:1:1 complex, [Cu(ttct)]$^+$Pic$^-$, into 1,2-dichloroethane solution, regardless of the initial concentration of TTCT. Probably, the extracted 1:1:1 complex transforms to the 1:2:1 complex, [Cu(ttct)$_2$]$^+$Pic$^-$, under the condition of the excess TTCT in the 1,2-dichloroethane solution.

In the case of silver(I), the obtained complexes will be the mixture of [Ag$_2$(ttct)]Pic$_2$ and [Ag(ttct)]Pic. The complex, [Ag(ttct)$_2$]Pic could not be obtained.

References

1) K. Saito, Y. Masuda, and E. Sekido, *Anal. Chim. Acta*, **151**, 447 (1983).

2) K. Saito, Y. Masuda, and E. Sekido, *Bull. Chem. Soc. Jpn.*, **57**, 189 (1984).

3) D. St. C. Black and I. A. McLean, *Tetrahedron Lett.*, **1969**, 3961.

4) W. Rosen and D. H. Bush, *J. Am. Chem. Soc.*, **91**, 4694 (1969).

5) E. Sekido, K. Saito, Y. Naganuma, and H. Kumazaki, *Anal. Sci.*, **1**, 363 (1985).

6) S. Ahrland, J. Chatt, and N. R. Davies, *Quart. Rev., London*, **12**, 265 (1958).

7) S. Yamada and M. Tanaka, *J. Inorg. Nucl. Chem.*, **37**, 587 (1975).

 © 1988 The Chemical Society of Japan Bull. Chem. Soc. Jpn., 61, 1593—1600 (1988)

Reactions of Bis(β-diketonato)platinum(II) and -palladium(II) with Diphosphines $Ph_2PCHRPPh_2$ (R=H, Me): Unexpected Formation of the Homoleptic Bis(diphenylphosphino)-methanido and Related Complexes

Hiromasa HASHIMOTO, Seichi OKEYA,† and Yukio NAKAMURA*
Department of Chemistry, Faculty of Science, Osaka City University, Sumiyoshi-ku, Osaka 558
†Department of Chemistry, Faculty of Education, Wakayama University, Sakaedani, Wakayama 640
(Received August 12, 1987)

The reactions of $[M(\beta\text{-dik})_2]$ (M=Pt(II), Pd(II); β-dik=acetylacetonate (acac), dipivaloylmethanate (dpm), hexafluoroacetylacetonate (hfac) ions) with dppm (dppm=$Ph_2PCH_2PPh_2$) and mdppm (mdppm=$Ph_2PCH(Me)PPh_2$) have been investigated. $[M(hfac)_2]$ complexes react with dppm to afford the stable cationic complexes, $[M(dppm)_2](hfac)_2$. By contrast, $[M(acac)_2]$ complexes react to give the homoleptic bis(diphenylphosphino)methanido complexes, $[M(Ph_2PCHPPh_2)_2]$, through deprotonation of dppm by the displaced acac anions. The analogous complexes, $[M(Ph_2PC(Me)PPh_2)_2]$, are obtained using mdppm, instead of dppm. A complete reaction scheme leading to these products is proposed, based on the IR and ^1H, ^{13}C, and ^{31}P NMR spectral data. Some consideration is given to the dependence of these reactions on the metals and the β-diketonate ligands, employed.

Bis(diphenylphosphino)methane, dppm, is known to act as a monodentate ligand, as a chelating bidentate ligand, or as a bridging ligand, and hence extensive studies have been made on structures and reactivities of complexes containing dppm as a ligand.[1] This ligand, when free, is readily deprotonated by a strong base to give $Ph_2PCHPPh_2^-$ and the resulting anion can also serve as a ligand towards transition metals with a variety of bonding modes, including P,P′-chelated,[2] P,P′- or P,C-bidentate bridged,[3,4] and P,P′,C-tridentate bridged[5] forms, thus constituting recent interesting chemistry. These hitherto isolated complexes are mostly obtained by deprotonation of a coordinated dppm with a strong base such as *n*-BuLi, if $Li(Ph_2PCHPPh_2)$ is not used as a reactant.

Here we describe the novel reactions of $[M(\beta\text{-dik})_2]$, especially $[M(acac)_2]$ (M=Pt(II) (**1a**), Pd(II) (**1b**)), with dppm, during which the coordinated dppm is readily deprotonated without strong bases. A preliminary report of this work was published in a short communication.[6]††

Experimental

Infrared spectra were obtained in Nujol mulls with a JASCO DS701G infrared spectrophotometer. Proton NMR spectra were recorded on a JEOL MH100 (100 MHz) or a GX400 (400 MHz) spectrophotometer. Carbon-13 and phosphorus-31 NMR spectra were recorded on a JEOL FX60Q instrument operating at 15 and 24 MHz, respectively. Chemical shifts are described in ppm relative to tetramethylsilane (for ^1H, ^{13}C) and 85% phosphoric acid (for ^{31}P).

†† In this paper, dppm−H and mdppm−H represent bis(diphenylphosphino)methanide ($Ph_2PCHPPh_2^-$) and 1,1-bis(diphenylphosphino)ethanide ($Ph_2PC(Me)PPh_2^-$) ions, respectively.

Preparation of Complexes. Bis(diphenylphosphino)-methane, dppm, was purchased from Strem Co. and used without further purification.· 1,1-Bis(diphenylphosphino)-ethane, mdppm,[7] was prepared according to the literature. The starting complexes, **1a**, **1b**, $[Pt(hfac)_2]$, $[Pd(hfac)_2]$, and $[Pd(dpm)_2]$, were prepared by the methods described in the previous papers.[8] Diphosphine complexes, $[PdCl_2(dppm)]$[9] and $[Pd(dppm)_2]X_2$ (X=Br, PF_6),[10] were prepared according to the literature. Solvents were dried over an appropriate drying agent and distilled under an atmosphere of argon before use.

Bis[bis(diphenylphosphino)methanido]platinum(II), [Pt(dppm−H)$_2$] (3a): When dppm (0.600 g, 1.56 mmol) was added to a solution of **1a** (0.305 g, 0.776 mmol) in dichloromethane (3 cm^3) at room temperature, a yellow precipitate began to deposit after a while. The mixture was stirred for 2—3 h under reflux and the precipitate was filtered, washed with acetone, and dried in vacuo (yield 0.70 g, 94%). The product was insoluble in common organic solvents such as benzene, acetone, diethyl ether, and haloalkanes.

Found: C, 62.12; H, 4.40%. Calcd for $C_{50}H_{42}P_4Pt$: C, 62.44; H, 4.37%.

Similarly, bis[1,1-bis(diphenylphosphino)ethanido]platinum(II), [Pt(mdppm−H)$_2$] (**3c**), was prepared as a yellow powder, using mdppm instead of dppm (yield 51%). The product was also insoluble in common organic solvents described above.

Found: C, 62.89; H, 4.59%. Calcd for $C_{52}H_{46}P_4Pt$: C, 63.09; H, 4.65%.

[Pd(dppm−H)$_2$] (3b): A solid dppm (0.602 g, 1.57 mmol) was added to a solution of **1b** (0.239 g, 0.785 mmol) in dichloromethane (5 cm^3) at room temperature. The resulting solution was stirred for a few minutes and petroleum ether was added to deposit a yellowish orange solid, which was filtered, washed with petroleum ether, and dried in vacuo (yield 0.58 g, 85%). The product was slightly soluble in chloroform but after a while equilibrated in the solvent with other species, as evidenced by ^{31}P NMR spectroscopy. $^{31}P\{^1H\}$ NMR ($CDCl_3$) δ=−36.7 (s).

Found: C, 68.31; H, 4.91%. Calcd for $C_{50}H_{42}P_4Pd$: C, 68.78; H, 4.85%.

[Pd(mdppm−H)$_2$] (3d): A solid mdppm (0.379 g, 0.952 mmol) was added to a solution of **1b** (0.145 g, 0.476 mmol) in dichloromethane (5 cm^3), and the resulting solution was stirred for 10 min to separate out reddish orange crystals, which were filtered, washed with dichloromethane, and dried in vacuo (yield 0.30 g, 70%). The product was slightly soluble in common organic solvents such as benzene and haloalkanes. ^{1}H NMR (C_6D_6, 400 MHz)[11] δ=1.78 (quintet, J_B(PH)=7.8 Hz, 3H, CH_3). ^{31}P{^{1}H} NMR (C_6D_6) δ=−25.5 (s).

Found: C, 69.40; H, 5.07%. Calcd for $C_{52}H_{16}P_4Pd$: C, 69.30; H, 5.14%.

Acetylacetonato[bis(diphenylphosphino)methanido]palladium(II), [Pd(acac)(dppm−H)] (2b): Method A: After dissolving dppm (0.633 g, 1.65 mmol) in a solution of **1b** (0.500 g, 1.64 mmol) in dichloromethane (5 cm^3), the resulting solution was diluted with pentane (30 cm^3) and allowed to stand in a freezer (ca. −5 °C). The yellow orange plates which separated out were filtered, washed with diethyl ether, and dried in vacuo. During the filtration, the crystals changed to a yellow powder with devitrification (yield 0.438 g). On standing the washing in a freezer, another crop was separated out as a reddish orange crystalline solid including no solvent of crystallization. Total yield: 0.581 g (50%). The melting point and the NMR and analytical data for the reddish orange crystals were as follows: mp: 157—159 °C. ^{1}H NMR ($CDCl_3$, 400 MHz) δ=5.27 (s, 1H, acac-CH), 2.56 (br, 1H, PCHP), and 1.94 (s, 6H, acac-CH_3). ^{13}C NMR (CD_2Cl_2)[11] δ=187.2 (t, J_A=1 Hz, CO), 99.4 (s, acac-CH), 28.1 (t, J_A=4.5 Hz, acac-CH_3), and 16.8 (t, J(PC)=65 Hz, ^1J(CH)=177 Hz, PCHP). ^{31}P{^{1}H} NMR ($CDCl_3$) δ=−55.7 (s).

Found: C, 61.27; H, 4.82%. Calcd for $C_{30}H_{28}O_2P_2Pd$: C, 61.19; H, 4.79%.

Method B: Thallium(I) acetylacetonate (0.243 g, 0.801 mmol) was added to a suspension of [$PdCl_2$(dppm)] (0.225 g, 0.401 mmol) in dichloromethane (50 cm^3). After being stirred for 20 min at room temperature, the mixture was filtered, the filtrate was concentrated to dryness, and then the residue was extracted with toluene. The solvent was evaporated to dryness and the product was washed with pentane, and dried in vacuo (yield 0.20 g, 85%).

[Pd(acac)(dppm)](PF_6): To a dichloromethane solution (8 cm^3) containing **2b** (0.050 g, 0.085 mmol) and *p*-toluenesulfonic acid monohydrate ($TsOH\cdot H_2O$, 0.017 g, 0.089 mmol) was added a methanol solution (4 cm^3) of potassium hexafluorophosphate (0.016 g, 0.087 mmol). The resulting KOTs was removed by filtration, pentane was added to the filtrate, and then the solution was kept in a freezer to deposit yellowish orange needles, which were collected, washed with diethyl ether, and air-dried (yield 0.028 g, 45%). ^{1}H NMR ($CDCl_3$) δ=5.62 (s, 1H, acac-CH), 4.67 (t, J(PH)=12 Hz, 2H, PCH_2P), and 2.16 (s, 6H, acac-CH_3). ^{13}C NMR ($CDCl_3$)[11] δ=187.2 (t, J_A=1.5 Hz, CO), 100.2 (s, acac-CH), 33.7 (t, J(PC)=32 Hz, PCH_2P), and 27.7 (t, J_A=5 Hz, acac-CH_3). ^{31}P{^{1}H} NMR (CD_2Cl_2) δ=−52.3 (s, dppm) and −144.0 (heptet, J(FP)=711 Hz, PF_6). The same compound was also obtained as an orange red precipitate on addition of pentane to an equimolar mixture of [Pd(acac)-(Et_2NH)$_2$](PF_6) (vide infra) and dppm in dichloromethane (yield 49%).

[Pt(dppm−H)(dppm)](PF_6): A solid dppm (0.138 g, 0.359 mmol) was added to a solution of [Pt(acac)(PPh_3)$_2$]-(PF_6) (vide infra) (0.157 g, 0.160 mmol) in dichloromethane (3 cm^3). The resulting solution was diluted with pentane and kept in a freezer to deposit yellow needles, which were filtered, washed with diethyl ether, and dried in vacuo (yield 0.120 g, 64%). Mp: 233—235 °C (decomp). Inclusion of one molecule of dichloromethane per platinum atom as solvent of crystallization was confirmed by the ^{1}H NMR spectroscopy. ^{1}H NMR ($CDCl_3$, 400 MHz) δ=5.33 (s, 2H, CH_2Cl_2), 5.07 (br, t, J(PH)=11 Hz; J(PtH)=indiscernible, 2H, PCH_2P), and 3.85 (br, t, J(PH)=7 Hz; J(PtH)=171 Hz, 1H, PCHP). ^{31}P{^{1}H} NMR (CD_2Cl_2) δ=−144.2 (heptet, J(FP)=711 Hz, PF_6). The signal assigned to (dppm+dppm−H) appeared as a AA'BB' spin system, of which the center was located at δ=−42.2 (J(PtP)=ca. 1916 Hz.).

Found: C, 52,18; H, 3.82%. Calcd for $C_{50}H_{43}F_6P_5Pt\cdot CH_2Cl_2$: C, 51.35; H, 3.80%.

The corresponding BF_4 salt was obtained in a similar manner using [Pt(acac)(PPh_3)$_2$](BF_4) as a starting material, which was readily synthesized by the reactions of **1a** with triphenylphosphine and sodium tetrafluoroborate in methanol. In this case, chloroform was used as a solvent and the product included one molecule of chloroform per platinum atom as solvent of crystallization. Yellow fine needles (yield 83%). Mp: 152—154 °C (decomp). ^{1}H NMR ($CDCl_3$) δ=5.16 (br, t, J(PH)=8 Hz; J(PtH)=48 Hz, 2H, PCH_2P) and 3.86 (br, t, J(PH)=5 Hz; J(PtH)=171 Hz, 1H, PCHP). The ^{31}P{^{1}H} NMR spectrum in $CDCl_3$ showed a signal assignable to (dppm+dppm−H) with a AA'BB' spin system, of which the center was located at δ=−41.9 (J(PtP)=ca. 1916 Hz).

Found: C, 52.74; H, 3.83%. Calcd for $C_{50}H_{43}BF_4P_4Pt\cdot CHCl_3$: C, 52.39; H, 3.79%.

[Pt(acac)(PPh_3)$_2$](PF_6): Compound **1a** (0.222 g, 0.565 mmol) was dissolved in hot methanol (10 cm^3) and allowed to react with triphenylphosphine (0.296 g, 1.13 mmol) under continued heating for 30 min. After cooling to room temperature, ammonium hexafluorophosphate (0.276 g, 1.69 mmol) was added and the resulting solution was further stirred for 30 min. The solution was concentrated and diethyl ether was added to deposit a white solid, which was filtered, washed with water, and dried in vacuo (yield 0.40 g, 72%). Recrystallization from dichloromethane–pentane gave the product including one fourth of dichloromethane molecule per platinum atom as solvent of crystallization.

Found: C, 50.38; H, 3.85%. Calcd for $C_{41}H_{37}F_6O_2P_3Pt\cdot 1/4CH_2Cl_2$: C, 50.30; H, 3.84%.

[Pd(acac)(Et_2NH)$_2$](PF_6): The compound was prepared by adding [Pd(acac)(Et_2NH)$_2$](acac)[12] (0.177 g, 0.393 mmol) to an aqueous solution (2 cm^3) of potassium hexafluorophosphate (0.089 g, 0.48 mmol). The yellow precipitate which separated out of the chilled solution was filtered, washed with methanol and diethyl ether, successively, and air-dried (yield 0.16 g, 81%). Recrystallization from dichloromethane–diethyl ether gave yellow plates. ^{1}H NMR ($CDCl_3$) δ=5.45 (s, 1H, acac-CH), 3.53 (br, 2H, NH), 2.72 (m, 8H, Et_2NH-CH_2), 2.01 (s, 6H, acac-CH_3), and 1.55 (t, J(HH)=7 Hz, 12H, Et_2NH-CH_3). ^{13}C NMR ($CDCl_3$) δ=186.6 (s, CO), 101.2 (s, acac-CH), 47.2 (s, Et_2NH-CH_2), 26.0 (s, acac-CH_3), and 14.1 (s, Et_2NH-CH_3).

Found: C, 31.53; H, 5.92; N, 5.68%. Calcd for $C_{13}H_{29}F_6N_2O_2PPd$: C, 31.43; H, 5.88; N, 5.64%.

[M(dppm)$_2$](hfac)$_2$ (M=Pd(II), Pt(II)): A solid dppm (0.268 g, 0.697 mmol) was added to a solution of [Pd(hfac)$_2$] (0.179 g, 0.344 mmol) in dichloromethane (2 cm^3). The

resulting solution was diluted with pentane and kept in a freezer to deposit a white or colorless crystalline solid, $[Pd(dppm)_2](hfac)_2$,[13] which was filtered and washed with diethyl ether, and air-dried (yield 0.28 g, 63%). ^1H NMR (CD_3CN)[11] δ=5.40 (s, 2H, hfac-CH) and 5.16 (quintet, J_B=5 Hz, 4H, PCH_2P). ^{13}C NMR (CD_3CN)[11] δ=172.9 (quartet, J(FC)=28 Hz, CO), 119.4 (quartet, J(FC)=293 Hz, hfac-CF_3), 82.5 (s, hfac-CH), and 38.4 (quintet, J_B=13 Hz, ^1J(CH)=141 Hz, PCH_2P). $^{31}P\{^1H\}$ NMR (CD_3CN) δ=−33.6 (s).

Found: C, 55.47; H, 3.57%. Calcd for $C_{60}H_{46}F_{12}O_4P_4Pd$: C, 55.90; H, 3.60%.

Starting from $[Pt(hfac)_2]$, $[Pt(dppm)_2](hfac)_2$ was prepared, analogously (yield 88%).

Found: C, 51.84; H, 3.36%. Calcd for $C_{60}H_{46}F_{12}O_4P_4Pt$: C, 52.30; H, 3.36%.

$[M(dppm)_2](OTs)_2$ (M=Pd(II), Pt(II)): The Pd(II) salt was obtained by adding acetone solutions (1 cm^3) of $TsOH\cdot H_2O$ (0.072 g, 0.38 mmol) and dppm (0.12 g, 0.32 mmol), successively, to a solution of $[Pd(dpm)_2]$ (0.075 g, 0.16 mmol) in dichloromethane (1 cm^3). The white solid which separated out was filtered, washed with diethyl ether, and dried in vacuo (yield 0.11 g, 56%). Recrystallization from methanol–diethyl ether gave colorless cubes, which changed to a white powder on vacuum drying.

Found (for powder): C, 62.78; H, 4.73%. Calcd for $C_{64}H_{58}O_6P_4PdS_2$: C, 63.13; H, 4.80%.

Starting from **1a**, $[Pt(dppm)_2](OTs)_2$ was obtained as a white powder, analogously.

Formation of the Cationic Complexes, $[Pt(dppm)_2]X_2$ (X=Cl, BF_4, NO_3), by Protonation of 3a. $[Pt(dppm)_2]Cl_2$: To a suspension of **3a** in ethanol was added an excess of 6 M hydrochloric acid (1 M=1 mol dm^{-3}), and the mixture was stirred for 1 h prior to evaporation of the solvent. The dichloromethane-extract of the residue was concentrated and pentane was added to produce a white precipitate, which was filtered, washed with pentane, and dried in vacuo. The compound included one molecule of dichloromethane per platinum atom as solvent of crystallization.

Found: C, 54.35; H, 4.19%. Calcd for $C_{50}H_{44}Cl_2P_4Pt\cdot CH_2Cl_2$: C, 54.71; H, 4.14%.

$[Pt(dppm)_2](BF_4)_2$: An excess of 42% tetrafluoroboric acid was added to a suspension of **3a** in ethanol and the mixture was stirred for 1 h to produce a white precipitate, which was collected, washed with water, and dried in vacuo.

Found: C, 52.44; H, 3.88%. Calcd for $C_{50}H_{44}B_2F_8P_4Pt$: C, 52.80; H, 3.90%.

$[Pt(dppm)_2](NO_3)_2$: Similarly, a suspension of **3a** in ethanol was allowed to react with an excess of 16 M nitric acid for 1 h. The solvent was evaporated to produce a white precipitate, which was filtered, washed with water, and dried in vacuo.

Found: C, 54.83; H, 4.02; N, 2.60%. Calcd for $C_{50}H_{44}N_2O_6P_4Pt$: C, 55.20; H, 4.08; N, 2.58%.

Yields of all these products were almost quantitative.

Regeneration of 3a and 3b by the Reactions of $[M(dppm)_2]^{2+}$ (M=Pt(II), Pd(II)) with Tl(acac) and Some Aqueous Bases. With Tl(acac): When two equivalents of Tl(acac) were allowed to react with $[Pt(dppm)_2]Cl_2$ in dichloromethane, a yellow precipitate was produced immediately, together with that of TlCl. The IR spectrum of the product confirmed the formation of **3a** by the appearance of its characteristic bands (vide infra). Similarly, $[Pd(dppm)_2]Br_2$ reacted with two equivalents of Tl(acac). After removal of the precipitated TlBr, organic soluble **3b** was isolated from the filtrate by the addition of hexane. The formation of **3b** was also confirmed by the IR data.

With Aqueous Bases: To a suspension of $[Pt(dppm)_2](NO_3)_2$ in methanol was added an excess of 5% aqueous solution of sodium carbonate as a base, and the mixture was stirred for 35 min at room temperature. The solvent was evaporated completely and the residue was extracted with dichloromethane. The extract was concentrated to dryness to leave a yellow powder, which was collected, washed with water and pentane, successively, and dried in vacuo. The yield was almost quantitative and the IR spectrum was in accord with that of **3a**. The use of triethylamine and sodium methoxide as bases was also effective on deprotonation of the coordinated dppm to produce **3a**.

Equimolar Reaction between 1a and dppm. When a dichloromethane solution (2 cm^3) containing equimolar amounts of **1a** (0.156 g, 0.400 mmol) and dppm (0.154 g, 0.400 mmol) was stirred for 30 min, a yellow precipitate began to deposit. Stirring was further continued for 3.5 h until no further precipitation occurred. The yellow precipitate obtained was filtered, washed with dichloromethane, and dried in vacuo. This product was identified as **3a** by IR assay. The yield was 0.155 g (0.161 mmol). The filtrate was evaporated to dryness and the residue was washed with diethyl ether to leave a deep yellow solid (0.067 g). This crude product was placed on the column (silica gel, 200 mesh) and eluted with dichloromethane. The eluate was again evaporated to dryness to give a yellow crystalline solid. This solid was identified as **1a** by IR spectroscopy. The recovered **1a** was 0.055 g (0.140 mmol), 35% of **1a** employed.

Another experiment was performed to confirm the intermediate species in this reaction. Equimolar amounts of **1a** and dppm were dissolved in CD_2Cl_2 in an NMR tube and the reaction was followed by $^{31}P\{^1H\}$ NMR spectroscopy at room temperature. Signal intensities were accumulated from 20 min after the initiation of the reaction over a 34-min period and from 60 min over a 90-min period, and those spectral data were recorded. These results are shown in Fig. 1.

Results and Discussion

Reactions of $[M(\beta\text{-dik})_2]$ (M=Pt(II), Pd(II)) with dppm and mdppm in the 1:2 Mole Ratio. In dichloromethane, $[M(hfac)_2]$ reacted with dppm to afford the stable cationic complexes, $[M(dppm)_2](hfac)_2$, by displacement of the coordinated hfac ligands (Eq. 1), whereas $[M(acac)_2]$ (M=Pt(II) (**1a**), Pd(II) (**1b**)) gave the homoleptic bis(diphenylphosphino)methanido complexes, $[M(dppm-H)_2]$ (M=Pt(II) (**3a**), Pd(II) (**3b**)) (Eq. 2), which were previously prepared from $[MCl_2(PMe_3)_2]$ and $Li(Ph_2PCHPPh_2)$[2d] or from $K_2[PtCl_4]$, dppm, and KOH.[2f]

$$[M(hfac)_2] + 2dppm \longrightarrow [M(dppm)_2](hfac)_2 \quad (1)$$

$$[M(acac)_2] + 2dppm \longrightarrow [M(dppm-H)_2] + 2acacH \quad (2)$$

Table 1. IR Bands (cm^{-1}) Characteristic of the Deprotonated dppm and mdppm Complexes[a]

Complex	dppm−H/mdppm−H	ν(C=O)+ν(C=C)
[Pd(acac)(dppm−H)] (**2b**)	1007(s), 853(vs), 553(vs)	1578(vs), 1510(vs)
[Pt(dppm−H)$_2$] (**3a**)	1113(vs), 889(vs), 858(vs), 558(w)	
[Pd(dppm−H)$_2$] (**3b**)	1117(vs), 882(s), 866(vs), 546(vs)	
[Pt(mdppm−H)$_2$] (**3c**)	1110(s), 847(vs)	
[Pd(mdppm−H)$_2$] (**3d**)	1110(s), 851(vs)	

a) In Nujol; v=very, s=strong, w=weak.

The IR spectra of **3a** and **3b** showed no absorption bands assignable to ν(C=O), but exhibited new bands which had not appeared for free or coordinated dppm. Table 1 lists these IR bands, which are characteristic of deprotonated dppm complexes. Protonation of **3a** with an acid HX (X=Cl, BF_4, or NO_3) in ethanol led to the formation of a cationic complex [Pt(dppm)$_2$]X$_2$ (Eq. 3), of which the IR spectrum coincided with that of the authentic sample,[14] demonstrating that the diphosphines in **3a** were certainly deprotonated.

$$[Pt(dppm-H)_2] + 2HX \longrightarrow [Pt(dppm)_2]X_2 \quad (3)$$

A reverse reaction, i.e., deprotonation of [Pt(dppm)$_2$]X$_2$ to give **3a**, readily occurred by Tl(acac) (Eq. 4), as well as some other bases like NEt_3, NaOMe, and Na_2CO_3, suggesting that the acac anion was working as a base to deprotonate.

$$[Pt(dppm)_2]Cl_2 + 2Tl(acac) \longrightarrow [Pt(dppm-H)_2] + 2acacH + 2TlCl \quad (4)$$

When mdppm instead of dppm was allowed to react with [M(acac)$_2$], analogous complexes [M(mdppm−H)$_2$] (M=Pt(II) (**3c**), Pd(II) (**3d**)) were obtained. The characteristic IR bands are also listed in Table 1.

Although the platinum complexes **3a** and **3c** were insoluble in common organic solvents probably because of their polymeric nature as reported previously,[2d] the palladium complexes **3b** and **3d** prepared by us were organic soluble and the $^{31}P\{^1H\}$ NMR spectra of these complexes showed a single resonance line, disclosing the existence of four magnetically equivalent phosphorus atoms. No useful ^1H NMR data were obtained for **3b** because of its low solubility in any appropriate solvent. However, the methyl-substituted complex **3d** showed the methyl proton resonance as a quintet due to virtual coupling to the four phosphorus atoms, thus indicating that the complex is a symmetric bis-chelate.

As described in the Experimental section, the $^{31}P\{^1H\}$ NMR spectrum of **3b** in $CDCl_3$ gradually changed with time, although no appreciable change was observed for that of **3d** in C_6D_6. After about 45 min, the signal originally assigned to **3b** completely disappeared and many other weak signals appeared, instead. This spectral change was not elucidated further, but the reaction of the coordinated bis(diphenylphosphino)methanido carbanions with the haloalkane solvent employed to form the cationic species like [Pd(dppm−H)(Ph$_2$PCHRPPh$_2$)]Cl and [Pd(Ph$_2$PCHRPPh$_2$)$_2$]Cl$_2$ (R=$CDCl_2$) might be assumed, since the carbanions in **3a** are methylated by excess methyl iodide to give similar cationic species.[15]

Characterization of Some Reaction Intermediates. Although the equimolar reaction between **1a** and dppm afforded **3a** exclusively, leaving about 35% of **1a** employed as unreacted, we succeeded, in the palladium case, in isolating the intermediate species, [Pd(acac)(dppm−H)] (**2b**), in high yield. This was fully characterized by elemental analysis and ^1H, ^{13}C, and ^{31}P NMR spectroscopy (see the Experimental section). When the dipivaloylmethanido complex, [Pd(dpm)$_2$], was allowed to react with an equimolar amount of dppm in $CDCl_3$, the same type of complex, [Pd(dpm)(dppm−H)], was also formed in solution as evidenced by its NMR data.[16] The IR spectrum of **2b** exhibited the absorption bands characteristic of both the *O,O'*-chelated acac and deprotonated dppm ligands as represented in Table 1.

In order to elucidate what kind of platinum-containing intermediate is formed in solution, we followed the reaction of **1a** with dppm in the 1:1 mole ratio by $^{31}P\{^1H\}$ NMR spectroscopy as described in the Experimental section. A yellow precipitate of **3a** began to deposit within 10 min after mixing both reactants in CD_2Cl_2. Figure 1 shows two spectra recorded at an appropriate time (see the figure caption) after the initiation of the reaction. The first spectrum (Fig. 1A) exhibited a sharp and most intense resonance line at δ −22.8. This coincided with the chemical shift of free dppm, suggesting that significant amounts of dppm still remained unreacted in this stage of the reaction. The spectrum also revealed the existence of two kinds of intermediates. One of them appeared at δ −5.4 (P_A) and −29.2 (P_B) as two doublets coupled each other with $^2J(P_A\text{-}P_B)$=73 Hz, each being flanked by the ^{195}Pt satellites with $^1J(Pt\text{-}P_A)$=4457 and $^3J(Pt\text{-}P_B)$=53 Hz, whereas the other showed a broad resonance line, of which the center was located at δ −42.3, with $^1J(PtP)$=1912 Hz. In the second spectrum (Fig. 1B), the signals of the intermediates increased in their intensities, whereas the free dppm disappeared. Based on both the signal pattern described above and the similarity of the $^1J(Pt\text{-}P_A)$ value to that of [Pt(tfac)(tfac-*O*){P(*o*-tolyl)$_3$}][17] (tfac=trifluoroacetylaceton-

ate ion) or [Pt(acac)(acac-*O*){P(C_6H_{11}}$_3$)],[18] the former intermediate was supposed to be of the type **A-2** (see Scheme 1). It seems reasonable to assume that the latter intermediate will be formed in the course of reaction process from **2** to **3**. If this is true, the intermediate would be expected to be of the type **B-3** because the strong trans effect of a phosphorus atom makes the existence of the *O*-unidentate acac intermediate of the type **B-2** very unlikely (see Scheme 1). In fact, the signal of the latter intermediate coincided both in chemical shift and in coupling constant, ^1J(PtP), with that of [Pt(dppm−H)(dppm)](PF_6), which was isolated incidentally from the reaction mixture of [Pt(acac)(PPh_3)$_2$](PF_6) and dppm in the mole ratio of 1:2.24 in CH_2Cl_2.

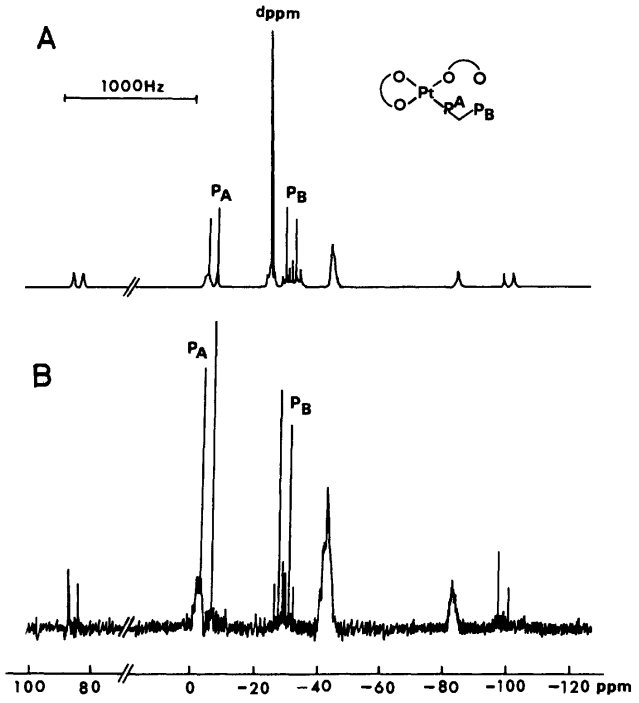

Fig. 1. ^{31}P NMR spectra obtained in the equimolar reaction between **1a** and dppm in CD_2Cl_2 at room temperature. The signal intensities accumulated from 20 min after the initiation of the reaction over a 34-min period (in A) and from 60 min over a 90-min period (in B) are shown. The signal for the final product, [Pt(dppm−H)$_2$] (**3a**), is not observed due to the insoluble character of the complex in CD_2Cl_2.

The Proposed Reaction Mechanism. On the basis of the results described above we can propose the processes represented in Scheme 1 as the likely mechanism for formation of [M(acac)(dppm−H)] and [M(dppm−H)$_2$] by the reactions of [M(acac)$_2$] (M=Pt(II), Pd(II)) with dppm. Although no intermediates of **A-1** to **A-3** were isolated in the present case, complexes of these types including the central-carbon-bonded β-diketonato complexes have been obtained by the reactions of [M(β-dik)$_2$] (M=Pt(II), Pd(II)) containing various β-dik ligands with unidentate tertiary phosphines.[17,19]

Isolation of the mixed ligand complex **2b** is especially noteworthy since the reactions of **1a** and **1b** with tricyclohexylphosphine and triphenylphosphine, respectively, in the 1:2 mole ratios in aprotic solvents such as benzene and diethyl ether afforded complexes of the type [M(acac)(acac-*O*)L] (L=unidentate tertiary phosphines), alone.[19b,c] However, when **1a** and **1b** were allowed to react with two equivalents of triphenylphosphine in methanol, the almost quantitative formation of [M(acac)(PPh_3)$_2$](acac) (M=Pt(II), Pd(II)) was recognized in situ by NMR probe.[20] Although we failed in isolating the acac salts, the PF_6 salt with M=Pt(II) was isolated from the reaction mixture and utilized as a starting complex for the preparation of [Pt(dppm−H)(dppm)](PF_6) (see the Experimental section). The formation of the latter com-

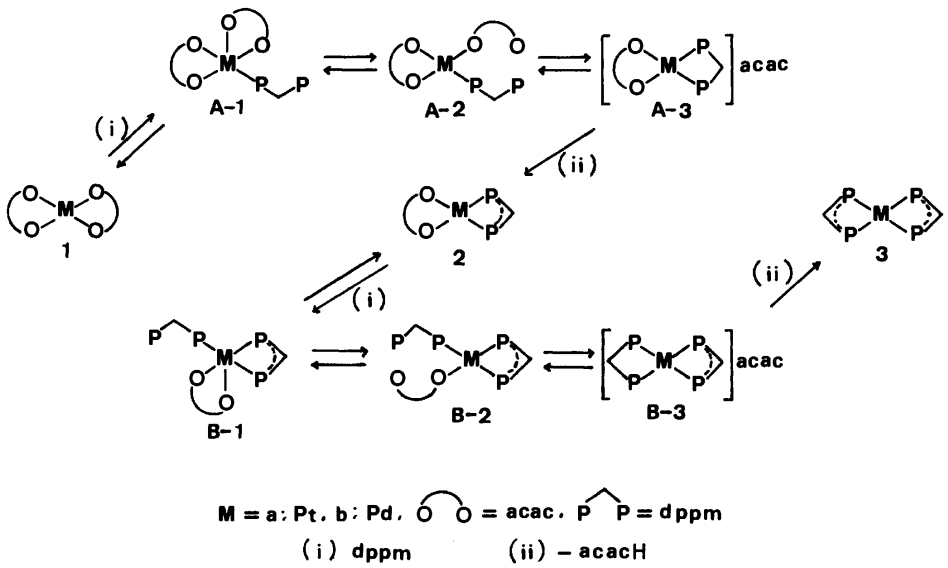

Scheme 1.

plex was also recognized in situ when $[Pt_2(PPh_3)_2(\mu\text{-dppm})_2](PF_6)_2$ was treated with **3a**, but its isolation was not attempted.[4]

The most important step to form the bis(diphenylphosphino)methanido complexes **2** and **3** is the deprotonation process from intermediate **A-3** to **2** or from **B-3** to **3**. This key step will be discussed in a succeeding paragraph.

Ligand and Metal Control in the Key Step. Deprotonation of the coordinated dppm by the acac anion is particularly interesting from the view point of the relative acidity of acacH and free dppm, whose pK_a values are 9.0[21] and 29.9,[22] respectively. Therefore, the above-mentioned chemical change is probably due to the electronic effect caused by coordination of dppm to the metal atom (vide infra).

In order to examine how the stability of intermediates of the type **A-3** varies with different β-dik ligands and with different metals, we conducted equimolar reactions of $[M(\beta\text{-dik})_2]$ with dppm in $CDCl_3$ and determined the species produced in solution by NMR spectroscopy. The effect of the β-dik ligand on the key step appeared as follows. When $[M(hfac)_2]$ was a starting complex, deprotonation of the coordinated dppm never occurred and either the stable product, [Pd(hfac)(dppm)](hfac)[23] or $[Pt(dppm)_2](hfac)_2$, was obtained, whereas for $[M(acac)_2]$, the deprotonation was effected, giving **2b** or **3a**, unless some strong acids were present. These results are clearly attributable to the difference in pK_a between hfacH (pK_a=4.3) and acacH (pK_a=9.0).[21] The reaction forming **2b** from $[PdCl_2(dppm)]$ and two equivalents of Tl(acac) also seems to take place via the precursor complex, [Pd(acac)(dppm)](acac) (Eq. 5).

$$[PdCl_2(dppm)] + 2Tl(acac) \xrightarrow{-2TlCl} [Pd(acac)(dppm)](acac) \xrightarrow{-acacH} \mathbf{2b} \qquad (5)$$

The relative thermodynamic stability of the intermediates depends on the metal. As noted above, a treatment of $[Pd(hfac)_2]$ with dppm in $CDCl_3$ resulted in the quantitative formation of [Pd(hfac)(dppm)](hfac) in an NMR tube,[23] while $[Pt(hfac)_2]$ did not afford [Pt(hfac)(dppm)](hfac) but $[Pt(dppm)_2](hfac)_2$ in a 50% yield. In the case of platinum(II), it is conceivable that the intermediate of type **A-3** is thermodynamically unstable, and hence the reaction proceeds ultimately to give the bis(dppm)-chelate. A similar situation was encountered in the reactions of **1a** and **1b** with dppm. Thus **1b** reacted with dppm to form **2b**, while **1a** afforded **3a** via intermediates of types **A-2** and **B-3**. In this case, the partially produced **2a** may be attacked by the second dppm to result in the formation of **3a**. In any event, it is certain that in contrast with the strong M–O bonds of **1**, those of the type-**A-3** intermediate and **2** are destabilized by the trans phosphorus donor atoms.

We may note here that, although complexes of the type **A-3** were never isolated, protonation of **2b** with a strong acid $TsOH\cdot H_2O$ led to the quantitative formation of [Pd(acac)(dppm)](OTs) in situ as evidenced by the NMR data.[24] The PF_6 salt was also readily isolated in the presence of potassium hexafluorophosphate.

Relationship between Diphosphine Coordination Modes and NMR Spectra. Mono(chelating dppm) Complexes: The PCH_2P protons in complexes of the type $[Pd(\beta\text{-dik})(dppm)]X$ resonated at δ 4.7—5.0 as a triplet with $J(PH)$=12 Hz and the corresponding carbon did at δ 32—34 as a triplet with $J(PC)$=32—33 Hz. For the ^1H-nondecoupled ^{13}C spectra of these complexes, the $^1J(CH)$ coupling constant was found to be 146 Hz, reflecting the situation of sp^3 carbon.

Bis(chelating dppm) Complexes: For complexes of the type $[M(dppm)_2]X_2$, the PCH_2P proton signal appeared at δ 4.9—5.7 as a quintet with J_B=5 Hz[11] and the corresponding carbon signal at δ 38—43 as a quintet with J_B=13—17 Hz. The $^1J(CH)$ of ca. 140 Hz, observed for these complexes, is also appropriate to sp^3 carbon. The quintet pattern comes from the virtual coupling with the second dppm-phosphorus-31 atoms. If $^4J(PH)$ and $^3J(PC)$ are considered negligibly small compared with $^2J(PH)$ and $^1J(PC)$, respectively, the latter coupling constants are evaluated to be ca. 10 and 28 Hz, respectively, according to the equation defined in Ref. 11. The values are comparable to those for the mono(chelating dppm) complexes, indicating that the M–P bonding characters of both types of complexes resemble each other.

Mono(chelating dppm–H) Complexes: In the case of $[Pd(\beta\text{-dik})(dppm{-}H)]$, we could not observe a well-resolved signal for the PCHP proton, but the corresponding carbon signal appeared at δ 15—17 as a clear triplet with $J(PC)$=65 Hz. The $^1J(CH)$ was found to be ca. 176 Hz. The signal is largely shifted to the higher-field compared with that of the above-mentioned PCH_2P carbon. This upfield shift reflects an increase in net electron density on the carbon atom caused by deprotonation. The coupling constant $J(PC)$ becomes twice in the value and the $^1J(CH)$ is also increased by ca. 30 Hz. These results reflect an increase in double-bond character of the P–C bonds, as well as increased sp^2 character of the carbon atom.

Complexes Bearing Both Chelating dppm and dppm–H: The PCH_2P protons in complexes of the type $[Pt(dppm{-}H)(dppm)]X$ resonated at δ 5.1—5.2 as a triplet with $J(PH)$=8—11 Hz, both the chemical shift and the coupling constant being close to those for the dppm complexes described above. In contrast with the case of $[Pd(\beta\text{-dik})(dppm{-}H)]$, the PCHP proton of the $[Pt(dppm{-}H)(dppm)]X$ complexes resonated at δ 3.86 as a well-resolved triplet with $J(PH)$=5—7 Hz. It is interesting to note that three bond coupling ($^3J(PtH)$=171 Hz) of the PCHP proton

Table 2. The CH_2-Proton Chemical Shifts of the Various dppm Complexes with Palladium in the Different Oxiation Numbers[a)]

Complex	Solvent	$\delta(CH_2)$	Lit
dppm	c)	2.80	g)
	Oxidation Number 0		
$[Pd_2(dppm)_3]$	d)	3.00	h)
	Oxidation Number 1		
$[Pd_2Br_2(dppm)_2]$	d)	4.22	h)
	Oxidation Number 2		
$[PdBr_2(dppm)]$	d)	4.33	h)
$[Pd(acac)(dppm)](PF_6)$	c)	4.67	g)
$[Pd(acac)(dppm)](OTs)$[b)]	c)	5.13	g)
$[Pd(hfac)(dppm)](hfac)$[b)]	c)	5.60	g)
$[Pd(dppm)_2]Br_2$	c)	4.26	g)
$[Pd(dppm)_2](PF_6)_2$	e)	4.92	g)
$[Pd(dppm)_2](hfac)_2$	e)	5.16	g)
$[Pf(dppm)_2](OTs)_2$	f)	ca. 5.3	g)

a) δ in ppm from internal TMS. b) Not isolated. c) $CDCl_3$. d) CD_2Cl_2. e) CD_3CN. f) CD_3OD. g) This work. h) H. C. Hunt and A. L. Balch, *Inorg. Chem.*, **20**, 2267 (1981).

to the platinum atom is more than three times as large as that ($^3J(PtH)$=48 Hz for X=BF_4) of the PCH_2P protons. It seems reasonable to assume that the bis(diphenylphosphino)methanido ligand coordinates more strongly to the central metal atom than does the neutral dppm.

Estimation of the Coordination Effect on Deprotonation of dppm. In order to estimate to what extent the C–H bond in dppm is activated when the diphosphine is coordinated to a metal, we examined the CH_2-proton chemical shifts of the various dppm complexes with palladium in the different oxidation states and compared those with that of free dppm. As shown in Table 2, the chemical shifts move to lower field on coordination of dppm to the metal and with increasing oxidation number of the metal, especially for the cationic complexes. These results imply that the CH_2 protons are largely deshielded in the cationic complexes with palladium(II), thus facilitating deprotonation of the dppm ligand. Although the counteranion dependence of the CH_2-proton chemical shift does not appear so clearly because the chemical interaction between the cation and the anion may be conceivable,[25)] the CH_2 signal of the $[Pd(dppm)_2]X_2$ complexes tends to cause a downfield shift with decreasing acidity of the conjugate acid HX.

We can not compare the CH_2 chemical shift data for complexes with X=hfac and acac since even if $[Pd(dppm)_2](acac)_2$ is formed in solution, it will be deprotonated immediately to give **3b**. Although the behavior of $[Pd(tfac)_2]$ towards dppm is particularly interesting for pK_a of tfacH is intermediate between those of hfacH and acacH, the reaction profile is not so simple and the details will be reported separately.

The authors wish to express their thanks to Professor Kiyoshi Isobe of Institute for Molecular Science for his helpful discussion, and to Mr. Junichi Gohda for elemental analyses. This work was supported by a Grant-in-Aid for Scientific Research No. 59470036 from the Ministry of Education, Science and Culture.

References

1) For the latest reviews of this subject, see: a) A. L. Balch, "Binuclear, Phosphine-Bridged Complexes: Progress and Prospects," in "Homogeneous Catalysis with Metal Phosphine Complexes," ed by L. H. Pignolet, Plenum Press, New York (1983), Chap. 5; b) R. Puddephatt, *J. Chem. Soc. Rev.*, **12**, 99 (1983).

2) a) K. Issleib and H. P. Abicht, *J. Prakt. Chem.*, **312**, 456 (1970); b) K. Issleib, H. P. Abicht, and H. Winkelmann, *Z. Anorg. Allg. Chem.*, **388**, 89 (1972); c) H. Schmidbaur and J. R. Mandl, *Angew. Chem.*, **89**, 679 (1977); d) J.-M. Bassett, J. R. Mandl, and H. Schmidbaur, *Chem. Ber.*, **113**, 1145 (1980); e) J. Browning, G. W. Bushnell, and K. R. Dixon, *J. Organomet. Chem.*, **198**, C11 (1980); f) M. P. Brown, A. Yavari, L. Manojlovic-Muir, K. W. Muir, R. P. Moulding, and K. R. Seddon, *J. Organomet. Chem.*, **236**, C33 (1982); g) S. Al-Jibori and B. L. Shaw, *J. Chem. Soc., Chem. Commun.*, **1982**, 286; h) R. Uŝon, A. Laguna, M. Laguna, B. R. Manzano, P. G. Jones, and G. M. Sheldrick, *J. Chem. Soc., Dalton Trans.*, **1984**, 839.

3) a) H. Schmidbaur, J. R. Mandl, J.-M. Bassett, G. Blaschke, and B. Zimmer-Gasser, *Chem. Ber.*, **114**, 433 (1981); b) C. E. Briant, K. P. Hall, and D. M. P. Mingos, *J. Organomet. Chem.*, **229**, C5 (1982).

4) M. P. Brown, A. Yavari, L. Manojlović-Muir, and K. W. Muir, *J. Organomet. Chem.*, **256**, C19 (1983).

5) a) A. Camus, N. Marsich, G. Nardin, and L. Randaccio, *J. Organomet. Chem.*, **60**, C39 (1973); b) J. W. A. van der Velden, F. A. Vollenbroek, J. J. Bour, P. T. Beurskens, J. M. M. Smits, and W. P. Bosman, *Recl. Trav. Chim. Pays-Bas.*, **100**, 148 (1981); c) R. Uŝon, A. Laguna, M. Laguna, B. R. Manzano, P. G. Jones, and G. M. Sheldrick, *J. Chem. Soc., Dalton Trans.*, **1985**, 2417; d) G. M. Dawkins, M. Green, J. C. Jeffery, C. Sambale, F. G. A. Stone, *J. Chem. Soc., Dalton Trans.*, **1983**, 499; e) R. R. Sharp and Y.-W. Ge, *J. Am. Chem. Soc.*, **109**, 3796 (1987).

6) H. Hashimoto, Y. Nakamura, and S. Okeya, *Inorg. Chim. Acta*, **120**, L25 (1986).

7) C. S. Kraihanzel and P. K. Maples, *J. Organomet. Chem.*, **117**, 159 (1976).

8) a) S. Okeya, S. Ooi, K. Matsumoto, Y. Nakamura, and S. Kawaguchi, *Bull. Chem. Soc. Jpn.*, **54**, 1085 (1981); b) S. Okeya and S. Kawaguchi, *Inorg. Synth.*, Vol. XX, 65 (1980).

9) W. L. Steffen and G. J. Palenik, *Inorg. Chem.*, **15**, 2432 (1976).

10) J. Chatt, F. A. Hart, and H. R. Watson, *J. Chem. Soc. A*, **1962**, 2537. For the PF_6 salt, $NaPF_6$ instead of NaBr was used as a reagent.

11) Notations of J_A and J_B denote the average coupling constants represented by the following equations, respectively. $J_A=1/2|{}^nJ(P_{cis}\text{-H or } P_{cis}\text{-C})+{}^nJ(P_{trans}\text{-H or } P_{trans}\text{-C})|$ and $J_B=1/2|{}^nJ(\text{PH or PC})+{}^{n+2}J(\text{PH or PC})|$.

12) S. Okeya, H. Sazaki, M. Ogita, T. Takemoto, Y. Onuki, Y. Nakamura, B. K. Mohapatra, and S. Kawaguchi, *Bull. Chem. Soc. Jpn.*, **54**, 1978 (1981).

13) The compound was previously synthesized; A. R. Siedle and L. H. Pignolet, *Inorg. Chem.*, **21**, 135 (1982).

14) M. P. Brown, J. R. Fisher, R. H. Hill, R. J. Puddephatt, and K. R. Seddon, *Inorg. Chem.*, **20**, 3516 (1981).

15) H. Hashimoto, Y. Nakamura, and S. Okeya, *Inorg. Chim. Acta*, **122**, L9 (1986).

16) ^{1}H NMR (CD_2Cl_2) δ=5.70 (s, 1H, dpm-CH) and 1.15 (s, 18H, dpm-CH_3). The dppm-CH signal was indiscernible. ^{13}C NMR (CD_2Cl_2)[11] δ=196.5 (t, J_A=1.5 Hz, CO), 90.0 (s, dpm-CH), 42.0 (t, J_A=4 Hz, dpm-*C*(CH_3)$_3$), 28.9 (s, dpm-C(*C*H_3)$_3$) and 15.1 (t, J(PC)=65 Hz, ^1J(CH)=176 Hz, PCHP).

17) For [Pt(tfac)(tfac-*O*){P(*o*-tolyl)$_3$}], the observed coupling constants were as follows; ^1J(PtP)=4410 Hz for cis(Me, P), 4380 Hz for trans(Me, P). See, S. Okeya, Y. Nakamura, and S. Kawaguchi, *Bull. Chem. Soc. Jpn.*, **54**, 3396 (1981).

18) For [Pt(acac)(acac-*O*){P(C_6H_{11})$_3$}], the coupling constant ^1J(PtP) was found to be 4176 Hz; S. Okeya and Y. Nakamura, unpublished results.

19) a) S. Kawaguchi, *Coord. Chem. Rev.*, **70**, 51 (1986) and references cited therein; b) S. Okeya, T. Miyamoto, S. Ooi, Y. Nakamura, and S. Kawaguchi, *Bull. Chem. Soc. Jpn.*, **57**, 395 (1984); c) T. Ito, T. Kiriyama, and A. Yamamoto, *Chem. Lett.*, **1976**, 835.

20) The NMR data for [M(acac)(PPh_3)$_2$](acac) (M=Pt(II), Pd(II)) will be presented in the subsequent paper in preparation.

21) T. Sekine, Y. Hasegawa, and N. Ihara, *J. Inorg. Nucl. Chem.*, **35**, 3968 (1973).

22) T. G. Bordwell, W. S. Matthews, and N. R. Vanier, *J. Am. Chem. Soc.*, **97**, 442 (1975).

23) ^{1}H NMR δ=6.38 (s, 1H, chelated hfac-CH), 6.06 (s, 1H, hfac$^-$-CH), and 5.60 (t, J(PH)=12 Hz, 2H, PCH_2P). ^{13}C NMR δ=176.0 (quartet, J(FC)=39 Hz, chelated hfac-CO), 175.1 (quartet, J(FC)=33 Hz, hfac$^-$-CO), 117.9 (quartet, J(FC)=288 Hz, hfac$^-$-CF_3), 114.7 (quartet, J(FC)=283 Hz, chelated hfac-CF_3), 93.8 (s, chelated hfac-CH), 88.4 (s, hfac$^-$-CH), and 32.4 (t, J(PC)=33 Hz, ^1J(CH)=146 Hz, PCH_2P). ^{31}P NMR δ=−53.6 (s).

24) ^{1}H NMR ($CDCl_3$) δ=5.60 (s, 1H, acac-CH), 5.13 (t, J(PH)=12 Hz, 2H, PCH_2P), and 2.16 (s, 6H, acac-CH_3). ^{13}C NMR ($CDCl_3$)[11] δ=187.1 (t, J_A=1.7 Hz, CO), 100.1 (s, acac-CH), 33.9 (t, J(PC)=32 Hz, PCH_2P), and 27.8 (t, J_A=5 Hz, acac-CH_3). ^{31}P NMR ($CDCl_3$) δ=−53.6 (s).

25) Recently, the halide salts of the Pt(II) analogue were found to exist as the five-coordinate cation [Pt(dppm)$_2$X]$^+$ in solution. See, M. C. Grossel, R. P. Moulding, K. R. Seddon, and F. J. Walker, *J. Chem. Soc., Dalton Trans.*, **1987**, 705.

 © 1988 The Chemical Society of Japan Bull. Chem. Soc. Jpn., 61, 1601—1606 (1988)

S-Bridged Polynuclear Complexes. II. Formation and Some Properties of [M{Co(L-cys-*N*,*S*)$_3$}$_2$]-Type Complexes (M=Fe(III), Co(III), and Ni(II); L-cys=L-cysteinate)

Sen-ichi AIZAWA,* Ken-ichi OKAMOTO, Hisahiko EINAGA,† and Jinsai HIDAKA
Department of Chemistry, University of Tsukuba, Tsukuba, Ibaraki 305
†Institute of Materials Science, University of Tsukuba, Tsukuba, Ibaraki 305
(Received August 29, 1987)

Three trinuclear complexes with Δ_{LLL}- and/or Λ_{LLL}-*fac*(*S*)-[Co(L-cys-*N*,*S*)$_3$] terminals, $\Delta_{LLL}\Delta_{LLL}$-, $\Delta_{LLL}\Lambda_{LLL}$-, and $\Lambda_{LLL}\Lambda_{LLL}$-[Fe{Co(L-cys-*N*,*S*)$_3$}$_2$]$^{3-}$, $\Delta_{LLL}\Lambda_{LLL}$-[Co{Co(L-cys-*N*,*S*)$_3$}$_2$]$^{3-}$, and $\Delta_{LLL}\Delta_{LLL}$-[Ni{Co(L-cys-*N*,*S*)$_3$}$_2$]$^{4-}$, were newly prepared. These complexes were characterized from their electronic absorption, CD, and ^{13}C NMR spectra. Each reaction of Δ_{LLL}-*fac*(*S*)-[Co(L-cys-*N*,*S*)$_3$]$^{3-}$ with Fe(II) and Co(II) was accompanied by the inversion of the absolute configuration of the one or both terminals to give the $\Delta_{LLL}\Lambda_{LLL}$ and $\Lambda_{LLL}\Lambda_{LLL}$ isomers, while the reaction with Fe(III), Co(III), or Ni(II) proceeded with the retention of the terminal to give the $\Delta_{LLL}\Delta_{LLL}$ isomer. The voltammetric study revealed that the formal potential of $\Delta_{LLL}\Delta_{LLL}$-[Fe{Co(L-cys-*N*,*S*)$_3$}$_2$]$^{3-}$ (−0.16 V) is more anodic than that of $\Delta_{LLL}\Delta_{LLL}$-[Co{Co(L-cys-*N*,*S*)$_3$}$_2$]$^{3-}$ (−0.43 V). These redox potentials are discussed in relation to the formation ratios of the isomers for the trinuclear complexes.

A few transition metal complexes with thiolate type ligands, such as 2-aminoethanethiolate (aet) and L-cysteinate (L-cys), have some unique properties in an aqueous solution. For example, the sulfur donor atoms of the ligands bridge two metal ions to give trinuclear complexes with μ-thiolato structure.[1-10] We previously reported that $\Lambda_{LLL}\Lambda_{LLL}$-[Co{Co(L-cys-*N*,*S*)$_3$}$_2$]$^{3-}$ was formed selectively by the reaction of Δ_{LLL}-*fac*(*S*)-[Co(L-cys-*N*,*S*)$_3$]$^{3-}$ with an excess amount of Co(II).[9,10] The inversion of the absolute configuration of the terminals seems to be related to the redox property of the central metal. From this point of view, the present authors have attempted to introduce a transition metal such as iron and nickel as the central metal of the trinuclear complex. In the present work, the formations of the trinuclear complexes, $\Delta_{LLL}\Delta_{LLL}$-, $\Delta_{LLL}\Lambda_{LLL}$-, and $\Lambda_{LLL}\Lambda_{LLL}$-[Fe{Co(L-cys-*N*,*S*)$_3$}$_2$]$^{3-}$, $\Delta_{LLL}\Lambda_{LLL}$-[Co{Co(L-cys-*N*,*S*)$_3$}$_2$]$^{3-}$, and $\Delta_{LLL}\Delta_{LLL}$-[Ni{Co(L-cys-*N*,*S*)$_3$}$_2$]$^{4-}$, were confirmed by the reaction of Δ_{LLL}-*fac*(*S*)-[Co(L-cys-*N*,*S*)$_3$]$^{3-}$ with Fe(III), Fe(II), Co(II), and Ni(II) respectively. These complexes are characterized on the basis of their electronic absorption, CD, and ^{13}C NMR spectral behavior. The configurational inversions, which were observed for each reaction of Δ_{LLL}-*fac*(*S*)-[Co(L-cys-*N*,*S*)$_3$]$^{3-}$ with Fe(II) and Co(II), are discussed in relation to the redox properties of these trinuclear complexes.

Experimental

Preparation of Complexes. 1) Δ_{LLL}-*fac*(*S*)-K$_3$[Co(L-cys-*N*,*S*)$_3$]·9H$_2$O·0.5KCl: This complex was prepared by the method described in the literature.[11]

2) $(+)^{CD}_{600}\cdot(+)^{CD}_{530}$-$\Delta_{LLL}\Delta_{LLL}$-K$_3$[Fe{Co(L-cys-*N*,*S*)$_3$}$_2$]·9H$_2$O·0.25KCl: To a solution containing 0.6 g (2.2 mmol) of $FeCl_3\cdot6H_2O$ in 40 cm^3 of water was added a solution containing 2.8 g (3.8 mmol) of Δ_{LLL}-*fac*(*S*)-K$_3$[Co(L-cys-*N*,*S*)$_3$]·9H$_2$O·0.5KCl in 50 cm^3 of water, whereupon the color of the solution immediately turned from deep green to reddish brown. The solution was then stirred at room temperature for 15 min. To this was added a large amount of ethanol in an ice bath. the resultant complex was recrystallized twice from water by adding ethanol in an ice bath. It was found, from the QAE-Sephadex A-25 column chromatographic technique and from absorption and CD spectral measurements, that the complex contained only $(+)^{CD}_{600}\cdot(+)^{CD}_{530}$-$\Delta_{LLL}\Delta_{LLL}$-[Fe{Co(L-cys-*N*,*S*)$_3$}$_2$]$^{3-}$. Found: C, 18.19; H, 4.08; N, 7.14%. Calcd for $C_{18}H_{48}N_6O_{21}S_6Cl_{0.25}K_{3.25}FeCo_2$: C, 18.22; H, 4.08; N, 7.08%.

3) $(-)^{CD}_{600}\cdot(-)^{CD}_{530}$-$\Delta_{LLL}\Delta_{LLL}$-H$_3$[Fe{Co(L-cys-*N*,*S*)$_3$}$_2$]·5H$_2$O·3HCl: To a solution containing 0.19 g (0.68 mmol) of $FeSO_4\cdot7H_2O$ in 10 cm^3 of water was added a solution containing 1.0 g (1.36 mmol) of Δ_{LLL}-*fac*(*S*)-K$_3$[Co(L-cys-*N*,*S*)$_3$]·9H$_2$O·0.5KCl in 30 cm^3 of water. The mixture was stirred at room temperature for 15 min and then poured onto a column of QAE-Sephadex A-25 (Cl^- form, 3.5 cm×90 cm). After the column had been swept with water, the adsorbed band was eluted with a 0.1 mol dm^{-3} aqueous solution of NaCl. A large amount of the brownish red band (B-1) and small amounts of the brownish green (B-2) and brown (B-3) ones were eluted in this order. The B-2 eluate showed absorption and CD spectra identical with those of $(-)^{CD}_{600}\cdot(-)^{CD}_{360}$-$\Delta_{LLL}\Delta_{LLL}$-[Co{Co(L-cys-*N*,*S*)$_3$}$_2$]$^{3-}$,[9,10] while the B-1 and B-3 eluates contained $(-)^{CD}_{600}\cdot(-)^{CD}_{530}$-$\Delta_{LLL}\Lambda_{LLL}$-[Fe{Co(L-cys-*N*,*S*)$_3$}$_2$]$^{3-}$ and a by-product respectively. The B-1 eluate was concentrated to ca. 50 cm^3 with a rotary evaporator below 25 °C. This solution was adjusted to pH 2—3 by adding a 1 mol dm^{-3} hydrochloric acid in an ice bath. The resultant complex was collected by filtration and washed with ethanol and ether. Found: C, 19.76; H, 4.13; N, 7.59%. Calcd for $C_{18}H_{46}N_6O_{17}S_6Cl_3FeCo_2$: C, 19.82; H, 4.25; N, 7.70%.

4) $(-)^{CD}_{600}\cdot(+)^{CD}_{530}$-$\Delta_{LLL}\Lambda_{LLL}$-H$_3$[Fe{Co(L-cys-*N*,*S*)$_3$}$_2$]·5H$_2$O·3HCl·0.5NaCl: This complex was prepared and chromatographed by a procedure similar to that used in **3**) under dilute conditions ($FeSO_4\cdot7H_2O$ 0.095 g (0.34 mmol)), water 160 cm^3; the starting Δ_{LLL}-*fac*(*S*) complex 0.50 g (0.68 mmol), water 160 cm^3). The four bands, reddish brown (C-1), brownish red (C-2), brownish green (C-3), and brown (C-4), were eluted in this order. The C-2 and C-3 eluates showed absorption and CD spectra identical with $(-)^{CD}_{600}\cdot(-)^{CD}_{530}$-$\Lambda_{LLL}\Lambda_{LLL}$-[Fe{Co(L-cys-*N*,*S*)$_3$}$_2$]$^{3-}$ and $(-)^{CD}_{600}\cdot(-)^{CD}_{360}$-$\Delta_{LLL}\Delta_{LLL}$-

$[Co\{Co(L\text{-}cys\text{-}N,S)_3\}_2]^{3-}$ [9,10] respectively. The C-1 and C-4 eluates contained $(-)^{CD}_{600}\cdot(+)^{CD}_{530}$-$\Delta_{LLL}\Delta_{LLL}$-$[Fe\{Co(L\text{-}cys\text{-}N,S)_3\}_2]^{3-}$ and a by-product respectively. The formation ratio of $\Delta_{LLL}\Delta_{LLL}$- and $\Lambda_{LLL}\Lambda_{LLL}$-$[Fe\{Co(L\text{-}cys\text{-}N,S)_3\}_2]^{3-}$ was about 37:63. After moving only the C-1 eluate into another column of QAE-Sephadex A-25 (Cl^- form, 3.5 cm×25 cm), the adsorbed band was eluted with a saturated aqueous solution of NaCl. The eluate was immediately adjusted to pH 2—3 by adding a 1 mol dm^{-3} hydrochloric acid in an ice bath. The resultant complex was collected by filtration and washed with ethanol and ether. Found: C, 19.09; H, 3.91; N, 7.61%. Calcd for $C_{18}H_{46}N_6O_{17}Na_{0.5}S_6Cl_{3.5}FeCo_2$: C, 19.30; H, 4.14; N, 7.50%.

5) $(-)^{CD}_{600}\cdot(+)^{CD}_{360}$-$\Delta_{LLL}\Delta_{LLL}$-$K_3[Co\{Co(L\text{-}cys\text{-}N,S)_3\}_2]\cdot 8.5H_2O$: This complex was prepared and chromatographed by a procedure similar to that used in **3**), but using $CoCl_2\cdot 6H_2O$ instead of $FeSO_4\cdot 7H_2O$ ($CoCl_2\cdot 6H_2O$ 0.082 g (0.34 mmol), water 40 cm^3; the starting Δ_{LLL}-*fac*(*S*)-complex 0.50 g (0.68 mmol), water 40 cm^3). After the eluate had been circulated in the same column twice, three bands, brown (A-1), brownish green (A-2), and a small amount of brownish green (A-3), were eluted in this order. The A-2 and A-3 eluates showed absorption and CD spectra identical with those of $(+)^{CD}_{600}\cdot(+)^{CD}_{360}$-$\Delta_{LLL}\Delta_{LLL}$- and $(-)^{CD}_{600}\cdot(-)^{CD}_{360}$-$\Delta_{LLL}\Delta_{LLL}$-$[Co\{Co(L\text{-}cys\text{-}N,S)_3\}_2]^{3-}$ respectively,[9,10] while the A-1 eluate contained $(-)^{CD}_{600}\cdot(+)^{CD}_{360}$-$\Delta_{LLL}\Delta_{LLL}$-$[Co\{Co(L\text{-}cys\text{-}N,S)_3\}_2]^{3-}$. The formation ratio of the three isomers, A-1, A-2, and A-3, was about 23:72:5. The A-1 eluate was concentrated to a small volume with a rotary evaporator below 25 °C. The deposited NaCl was then filtered off, and the filtrate was passed through columns of Sephadex G-10 (3.5 cm×90 cm) and then SP-Sephadex C-25 (K^+ form, 3.5 cm×25 cm) by elution with water. The eluate was then concentrated to a small volume again. To this was added a large amount of ethanol in an ice bath. The resultant complex was collected by filtration and washed with ethanol and ether. Found: C, 18.57; H, 4.14; N, 7.22%. Calcd for $C_{18}H_{47}N_6O_{20.5}S_6K_3Co_3$: C, 18.60; H, 4.08; N, 7.22%.

When the above reaction was carried out under a nitrogen atmosphere and the reaction solution was oxidized by exposure to air, the $\Delta_{LLL}\Delta_{LLL}$ isomer was formed selectively.

6) $(+)^{CD}_{600}$-$\Delta_{LLL}\Delta_{LLL}$-$H_4[Ni\{Co(L\text{-}cys\text{-}N,S)_3\}_2]\cdot 3H_2O\cdot 2HCl$: To a solution containing 0.087 g (0.37 mmol) of $NiCl_2\cdot 6H_2O$ in 5 cm^3 of water was added a solution containing 0.50 g (0.68 mmol) of Δ_{LLL}-*fac*(*S*)-$K_3[Co(L\text{-}cys\text{-}N,S)_3]\cdot 9H_2O\cdot 0.5KCl$ in 20 cm^3 of water, whereupon the color of the solution immediately turned from deep green to brownish green. The solution was stirred at room temperature for 10 min and then filtered. The filtrate was adjusted to pH 2—3 by adding a 1 mol dm^{-3} hydrochloric acid in an ice bath. The resultant complex was collected by filtration and washed with ethanol and ether. It was found, from the QAE-Sephadex A-25 column chromatographic technique and the absorption and CD spectral measurements, that the complex contained only $(+)^{CD}_{600}$-$\Delta_{LLL}\Delta_{LLL}$-$[Ni\{Co(L\text{-}cys\text{-}N,S)_3\}_2]^{4-}$. Found: C, 21.06; H, 4.14; N, 8.24%. Calcd for $C_{18}H_{42}N_6O_{15}S_6Cl_2Co_2Ni$: C, 21.15; H, 4.14; N, 8.22%.

Formation Ratio of Isomers. a) It was found, under the same reaction conditions as those described in **5**), that the formation ratio of the three isomers of $[Co\{Co(L\text{-}cys\text{-}N,S)_3\}_2]^{3-}$ depends on the concentration of Co(II). That is, when 0.162 g (0.68 mmol) and 0.324 g (1.36 mmol) of $CoCl_2\cdot 6H_2O$ were used instead of 0.081 g (0.34 mmol) in **5**), the formation ratios of $\Delta_{LLL}\Delta_{LLL}$-, $\Delta_{LLL}\Lambda_{LLL}$-, and $\Lambda_{LLL}\Lambda_{LLL}$-$[Co\{Co(L\text{-}cys\text{-}N,S)_3\}_2]^{3-}$ were about 0:9:91 and 0:6:94 respectively.

The formation ratio for the isomers of $[Fe\{Co(L\text{-}cys\text{-}N,S)_3\}_2]^{3-}$ was confirmed by using 0.095 g (0.34 mmol) of $FeSO_4\cdot 7H_2O$ instead of $CoCl_2\cdot 6H_2O$ as in **5**); the ratio of $\Delta_{LLL}\Delta_{LLL}$-, $\Delta_{LLL}\Lambda_{LLL}$-, and $\Lambda_{LLL}\Lambda_{LLL}$-$[Fe\{Co(L\text{-}cys\text{-}N,S)_3\}_2]^{3-}$ was 0:5:95.

b) In an acidic solution (40 cm^3) adjusted to ca. pH 1 by the addition of a 1 mol dm^{-3} hydrochloric acid was suspended 0.50 g (0.68 mmol) of Δ_{LLL}-*fac*(*S*)-$K_3[Co(L\text{-}cys\text{-}N,S)_3]\cdot 9H_2O\cdot 0.5KCl$. To this was then added an acidic solution (ca. pH 1) containing an excess amount of $CoCl_2\cdot 6H_2O$ (0.324 g, 1.36 mmol) in 40 cm^3 of water. While the mixture was stirred for 15 min, the starting complex was gradually dissolved and the color of the solution turned to deep greenish brown. The solution was chromatographed in the same manner as in **5**). The formation ratio of $\Delta_{LLL}\Delta_{LLL}$-, $\Delta_{LLL}\Lambda_{LLL}$-, and $\Lambda_{LLL}\Lambda_{LLL}$-$[Co\{Co(L\text{-}cys\text{-}N,S)_3\}_2]^{3-}$ was 62:38:0.

Measurements. The electronic absorption spectra were recorded with JASCO UVIDEC-1 and JASCO UVIDEC-610C spectrophotometers, and the CD spectra with a JASCO J-20 spectropolarimeter. The ^{13}C NMR spectra were recorded with a JEOL JNM-FX-100 or FX-90Q NMR spectrometer at the probe temperature in D_2O solvent. Sodium 2,2-dimethyl-2-silapentane-5-sulfonate (DSS) was used as an internal reference. The pH of the aqueous solution was measured with a Hitachi-Horiba pH meter, model F7-SS, equipped with a glass and saturated calomel electrodes. The cyclic voltammograms were recorded with a Hokuto Denko potentiogalvanostat, model HA-201, to which a linear potential scanner, model HB-103, was attached. A hanging Hg drop microelectrode or a Pt working electrode, a Pt wire counter electrode with a sufficiently large surface area, and a 3.33 mol dm^{-3} KCl calomel reference electrode were used for the potentiostatic measurements in a 0.01 mol dm^{-3} sodium nitrate solution at room temperature (25±1 °C). The electrode potential data were corrected to those for the standard hydrogen electrode (SHE).

Results and Discussion

Structural Assignment. Three isomers, $\Delta_{LLL}\Delta_{LLL}$, $\Delta_{LLL}\Lambda_{LLL}$, and $\Lambda_{LLL}\Lambda_{LLL}$, are expected for $[M\{Co(L\text{-}cys\text{-}N,S)_3\}_2]$-type complexes (M=Fe(III) and Ni(II)), considering the absolute configuration of the two terminal moieties, *fac*(*S*)-$[Co(L\text{-}cys\text{-}N,S)_3]$ (Fig. 1), as in the case of $[Co\{Co(aet)_3\}_2]^{3+}$ and $[Co\{Co(L\text{-}cys\text{-}N,S)_3\}_2]^{3-}$.[3,9,10] The absorption and CD spectra of the isomers are shown in Figs. 2—4, and their data are summarized in Table 1. Of the two isomers, $(+)^{CD}_{600}\cdot(+)^{CD}_{360}$ and $(-)^{CD}_{600}\cdot(+)^{CD}_{360}$, which were obtained by the reaction of Δ_{LLL}-*fac*(*S*)-$[Co(L\text{-}cys\text{-}N,S)_3]^{3-}$ with a stoichiometric amount of Co(II), the $(+)^{CD}_{600}\cdot(+)^{CD}_{360}$ isomer exhibits absorption and CD spectra identical with those of the isomer determined to be $\Delta_{LLL}\Delta_{LLL}$-$[Co\{Co(L\text{-}cys\text{-}N,S)_3\}_2]^{3-}$ by X-ray structure analysis[10] (Fig. 2). The $(-)^{CD}_{600}\cdot(+)^{CD}_{360}$ isomer exhibits an absorp-

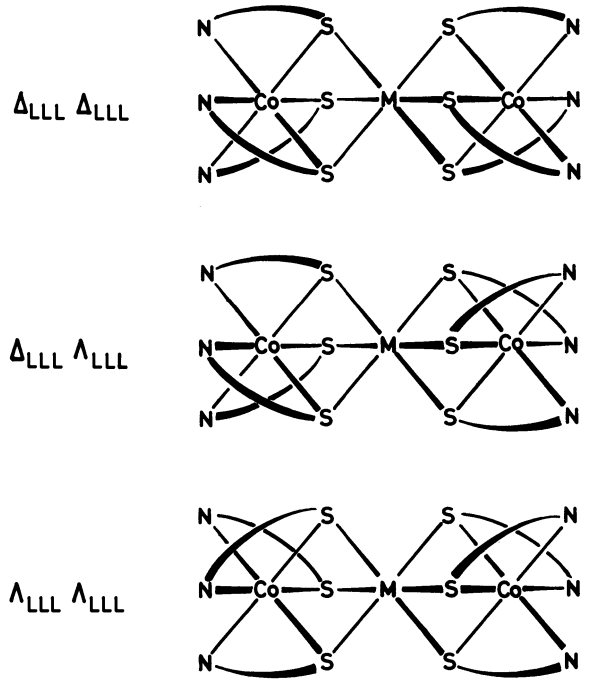

Fig. 1. Three isomers expected for [M{Co(L-cys-*N*,*S*)$_3$}$_2$]-type complexes.

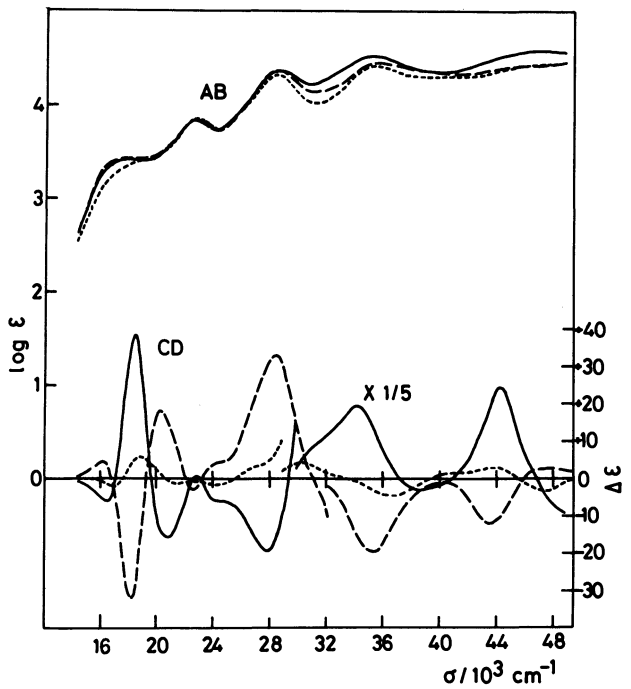

Fig. 2. Absorption and CD spectra of [Co{Co(L-cys-*N*,*S*)$_3$}$_2$]$^{3-}$; $(-)^{CD}_{600}\cdot(-)^{CD}_{360}$- (——), $(+)^{CD}_{600}\cdot(+)^{CD}_{360}$- (-----), and $(-)^{CD}_{600}\cdot(+)^{CD}_{360}$- (·····).

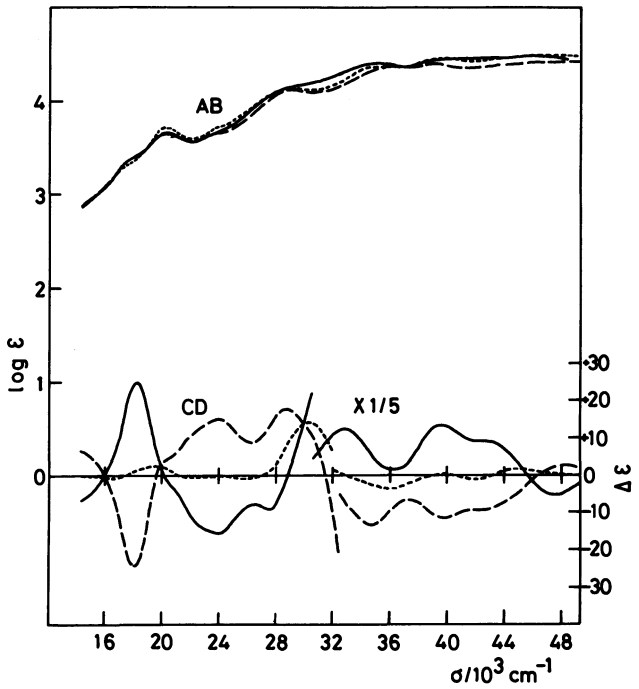

Fig. 3. Absorption and CD spectra of [Fe{Co(L-cys-*N*,*S*)$_3$}$_2$]$^{3-}$; $(+)^{CD}_{600}\cdot(+)^{CD}_{530}$- (——), $(-)^{CD}_{600}\cdot(-)^{CD}_{530}$- (-----), and $(-)^{CD}_{600}\cdot(+)^{CD}_{530}$- (·····).

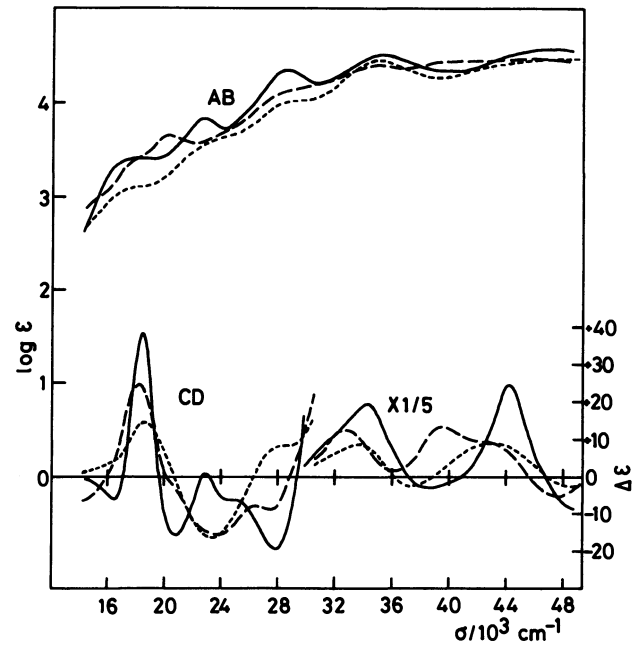

Fig. 4. Absorption and CD spectra of $\Delta_{LLL}\Delta_{LLL}$ isomers; $(-)^{CD}_{600}\cdot(-)^{CD}_{360}$-[Co{Co(L-cys-*N*,*S*)$_3$}$_2$]$^{3-}$ (——), $(+)^{CD}_{600}\cdot(+)^{CD}_{530}$-[Fe{Co(L-cys-*N*,*S*)$_3$}$_2$]$^{3-}$ (-----), and $(+)^{CD}_{600}$-[Ni{Co(L-cys-*N*,*S*)$_3$}$_2$]$^{4-}$ (·····).

tion spectrum quite similar to that of $\Delta_{LLL}\Delta_{LLL}$-[Co{Co(L-cys-*N*,*S*)$_3$}$_2$]$^{3-}$, but it exhibits quite a different CD spectrum from $\Delta_{LLL}\Delta_{LLL}$- and $\Delta_{LLL}\Delta_{LLL}$-[Co{Co(L-cys-*N*,*S*)$_3$}$_2$]$^{3-}$ [9,10] (Fig. 2). Furthermore, the ^{13}C NMR spectrum of the $(-)^{CD}_{600}\cdot(+)^{CD}_{360}$ isomer exhibits six resonance lines (38.2, 38.8, 63.3, 66.4, 178.0, and 179.0 ppm) due to the methylene, methine, and carboxylato carbon atoms, whereas each of the $\Delta_{LLL}\Delta_{LLL}$ and $\Delta_{LLL}\Delta_{LLL}$ isomers exhibits three resonance lines (D_3 symmetry).[9,10] According to the model construction, the symmetry of the $\Delta_{LLL}\Delta_{LLL}$ isomer is lower than or equal to C_3, therefore, this isomer can be expected to exhibit six or more resonance lines. These facts

Table 1. Absorption and CD Data of $[M\{Co(L\text{-cys-}N,S)_3\}_2]^{n-}$ (M=Fe(III), Co(III), and Ni(II))

	Absorption maxima $\sigma/10^3\,cm^{-1}$ ($\log \varepsilon/mol^{-1}\,dm^3\,cm^{-1}$)	CD extrema $\sigma/10^3\,cm^{-1}$ ($\Delta\varepsilon/mol^{-1}\,dm^3\,cm^{-1}$)
$(+)^{CD}_{600}\cdot(+)^{CD}_{530}$-$[Fe\{Co(L\text{-cys-}N,S)_3\}_2]^{3-}$	17.54 (3.35sh)	18.18 (+24.8)
	20.24 (3.64)	23.81 (−15.7)
	28.57 (4.12sh)	27.32 (−9.0)
	35.34 (4.39)	32.79 (+61.9)
	40.00 (4.42sh)	39.37 (+66.0)
	46.73 (4.47)	42.7 (+46.0sh)
		47.62 (−26.3)
$(-)^{CD}_{600}\cdot(+)^{CD}_{530}$-$[Fe\{Co(L\text{-cys-}N,S)_3\}_2]^{3-}$	17.24 (3.29sh)	16.44 (−0.8)
	20.20 (3.70)	19.68 (+2.4)
	29.07 (4.11)	22.83 (−0.4)
	35.46 (4.35sh)	25.77 (−0.8)
	39.68 (4.44)	30.40 (+14.0)
		35.71 (−16.7)
		39.68 (+1.3)
		41.66 (−5.0)
		44.64 (+7.75)
$(-)^{CD}_{600}\cdot(-)^{CD}_{530}$-$[Fe\{Co(L\text{-cys-}N,S)_3\}_2]^{3-}$	17.24 (3.33sh)	18.02 (−24.5)
	20.12 (3.66)	23.81 (+14.9)
	29.07 (4.11)	28.74 (+17.6)
	36.23 (4.36)	34.72 (−65.9)
	39.06 (4.38)	39.68 (−57.6)
		43.1 (−45.0sh)
		48.31 (+13.2)
$(-)^{CD}_{600}\cdot(+)^{CD}_{360}$-$[Co\{Co(L\text{-cys-}N,S)_3\}_2]^{3-}$	18.02 (3.36sh)	16.77 (−2.1)
	22.83 (3.85)	18.79 (+5.5)
	28.41 (4.31)	21.55 (−1.3)
	35.46 (4.39)	24.21 (−1.7)
	48.08 (4.43)	26.9 (+3.2sh)
		30.30 (+19.4)
		36.76 (−22.3)
		40.3 (+5.74sh)
		43.85 (+13.2)
		47.39 (−16.2)
$(+)^{CD}_{600}$-$[Ni\{Co(L\text{-cys-}N,S)_3\}_2]^{4-}$	17.54 (3.08sh)	18.59 (+14.4)
	23.26 (3.58sh)	23.36 (−16.2)
	28.57 (4.05sh)	28.41 (+8.3)
	34.97 (4.43)	33.67 (+42.1)
		37.45 (−13.2)
		43.10 (+43.4)

sh denotes a shoulder.

suggest that the $(-)^{CD}_{600}\cdot(+)^{CD}_{360}$ isomer is $\Lambda_{LLL}\Lambda_{LLL}$-$[Co\{Co(L\text{-cys-}N,S)_3\}_2]^{3-}$.

The three isomers which were obtained by the reaction of Δ_{LLL}-*fac*(*S*)-$[Co(L\text{-cys-}N,S)_3]^{3-}$ with Fe(III) or Fe(II) exhibit absorption spectral behavior quite similar to one another (Fig. 3 and Table 1), as in the case of $[Co\{Co(L\text{-cys-}N,S)_3\}_2]^{3-}$. The two isomers, $(+)^{CD}_{600}\cdot(+)^{CD}_{530}$ and $(-)^{CD}_{600}\cdot(-)^{CD}_{530}$, exhibit intense CD bands which are almost enantiomeric over the whole region, while the remaining one, $(-)^{CD}_{600}\cdot(+)^{CD}_{530}$, exhibits weak CD bands (Fig. 3). The CD spectral pattern of the $(+)^{CD}_{600}\cdot(+)^{CD}_{530}$ isomer approximately coincides with that of $\Delta_{LLL}\Delta_{LLL}$-$[Co\{Co(L\text{-cys-}N,S)_3\}_2]^{3-}$,[9,10] except for the ambiguity around 20—27×10³ cm^{-1} (Fig. 3). On the other hand, the $(-)^{CD}_{600}\cdot(-)^{CD}_{530}$ isomer exhibits a CD spectral pattern similar to that of $\Lambda_{LLL}\Lambda_{LLL}$-$[Co\{Co(L\text{-cys-}N,S)_3\}_2]^{3-}$ [9,10] (Fig. 3). These facts suggest that the $(+)^{CD}_{600}\cdot(+)^{CD}_{530}$ isomer is $\Delta_{LLL}\Delta_{LLL}$-$[Fe\{Co(L\text{-cys-}N,S)_3\}_2]^{3-}$ and that the $(-)^{CD}_{600}\cdot(-)^{CD}_{530}$ isomer is the $\Lambda_{LLL}\Lambda_{LLL}$ one. Accordingly, the remaining $(-)^{CD}_{600}\cdot(+)^{CD}_{530}$ siomer can be assigned to $\Delta_{LLL}\Lambda_{LLL}$-$[Fe\{Co(L\text{-cys-}N,S)_3\}_2]^{3-}$.

The reaction of Δ_{LLL}-*fac*(*S*)-$[Co(L\text{-cys-}N,S)_3]^{3-}$ with Ni(II) formed only the $(+)^{CD}_{600}$ isomer, exhibiting intense absorption bands over the whole region similar to those of $[Co\{Co(L\text{-cys-}N,S)_3\}_2]^{3-}$ and $[Fe\{Co(L\text{-cys-}N,S)_3\}_2]^{3-}$ (Fig. 4). Furthermore, the CD spectral behavior of the $(+)^{CD}_{600}$ isomer agrees with that

of $\Delta_{LLL}\Delta_{LLL}$-[Fe{Co(L-cys-*N*,*S*)$_3$}$_2$]$^{3-}$ (Fig. 4). Accordingly, the $(+)^{CD}_{600}$ isomer is tentatively assigned to $\Delta_{LLL}\Delta_{LLL}$-[Ni{Co(L-cys-*N*,*S*)$_3$}$_2$]$^{4-}$.

CD Spectra. In the energy region higher than ca. 32×10^3 cm^{-1}, the CD spectral patterns of the three $\Delta_{LLL}\Delta_{LLL}$-[M{Co(L-cys-*N*,*S*)$_3$}$_2$]$^{n-}$ complexes (M=Fe(III), Co(III), and Ni(II)) are similar to that of the mononuclear complex, Δ_{LLL}-*fac*(*S*)-[Co(L-cys-*N*,*S*)$_3$]$^{3-}$, as in the case of their absorption spectral patterns (Figs. 4 and 5). The absorption bands at ca. 34×10^3 cm^{-1} are probably related to the sulfur-to-metal charge transfer bands[12-14] in the terminals, and the CD bands in the corresponding region are commonly positive. Though the overall CD spectral patterns resemble one another in the region of $14-32\times10^3$ cm^{-1}, some absorption and CD spectral deviations are observed in the region of $20-30\times10^3$ cm^{-1}. The deviations in this region are probably due to the characteristic chromophore, FeS_6, CoS_6, or NiS_6, at the center of $\Delta_{LLL}\Delta_{LLL}$-[M{Co(L-cys-*N*,*S*)$_3$}$_2$]$^{n-}$ (M=Fe(III), Co(III), or Ni(II)), besides the common chromophore, CoS_3N_3, in the terminals.

The similarity in the CD spectral patterns of the present trinuclear complexes led us to attempt a CD curve analysis on the assumption that the CD contributions of the chiralities in the trinuclear complexes are additive, as in the case of the mononuclear cobalt(III) complexes.[15-17] The trinuclear complexes in this work formally have the following three CD contributions; (1) the configurational chirality (Δ or Λ) arising from the skew pair of the chelate rings in the terminals, (2) the chirality due to the asymmetric carbon atoms in the L-cys ligands, and (3) the chirality (*R* or *S*) due to the asymmetric sulfur donor atoms bridging the two metal ions. Of the three types of chiralities, the three asymmetric sulfur donor atoms in the Δ_{LLL}-*fac*(*S*)-[Co(L-cys-*N*,*S*)$_3$] terminal are regulated to the *R* configuration for the Fe(III) trinuclear complex and to the *S* configuration for the Co(III) one, while those in the Λ_{LLL}-*fac*(*S*)-[Co(L-cys-*N*,*S*)$_3$] terminal are regulated to the *S* configuration for the Fe(III) complex and to the *R* configuration for the Co(III) one. Accordingly, the CD contributions due to the asymmetric sulfur donor atoms of both terminals in $\Delta_{LLL}\Delta_{LLL}$ trinuclear complex cancell each other out, as in the case of the configurational chiralities, Δ and Λ. Taking this assumption into consideration, the observed CD curves of $\Delta_{LLL}\Delta_{LLL}$-[M{Co(L-cys-*N*,*S*)$_3$}$_2$]$^{3-}$ (M=Fe(III) and Co(III)) seem to exhibit only a vicinal CD contribution due to the asymmetric carbon atoms in the L-cys ligands. In fact, the calculated vicinal CD curves, $1/2\{\Delta\varepsilon(\Delta_{LLL}\Delta_{LLL})+\Delta\varepsilon(\Lambda_{LLL}\Lambda_{LLL})\}$, for the Fe(III) and Co(III) trinuclear complexes are, over the whole region, quite similar to the observed curves of $\Delta_{LLL}\Delta_{LLL}$-[Fe{Co(L-cys-*N*,*S*)$_3$}$_2$]$^{3-}$ and $\Delta_{LLL}\Delta_{LLL}$-[Co{Co(L-cys-*N*,*S*)$_3$}$_2$]$^{3-}$ respectively, as is shown in Fig. 6. These results indicate that the observed CD curves of the $\Delta_{LLL}\Delta_{LLL}$ complexes are composed mainly of the contribution due to the asymmetric carbon atoms of the L-cys ligands, and probably suggest that the additivity on the CD curve is substantiated for the present trinuclear complexes.

Inversion and Redox Reaction. The reaction of Δ_{LLL}-*fac*(*S*)-[Co(L-cys-*N*,*S*)$_3$]$^{3-}$ with Co(III),[9,10] Fe(III), or Ni(II) proceeded with a retention of the Δ_{LLL}-*fac*(*S*) configuration to give $\Delta_{LLL}\Delta_{LLL}$-[M{Co(L-cys-*N*,*S*)$_3$}$_2$]$^{n-}$. By contrast, the reaction with Co(II) or Fe(II) was accompanied by the inversion to the Λ_{LLL} of the Δ_{LLL}-

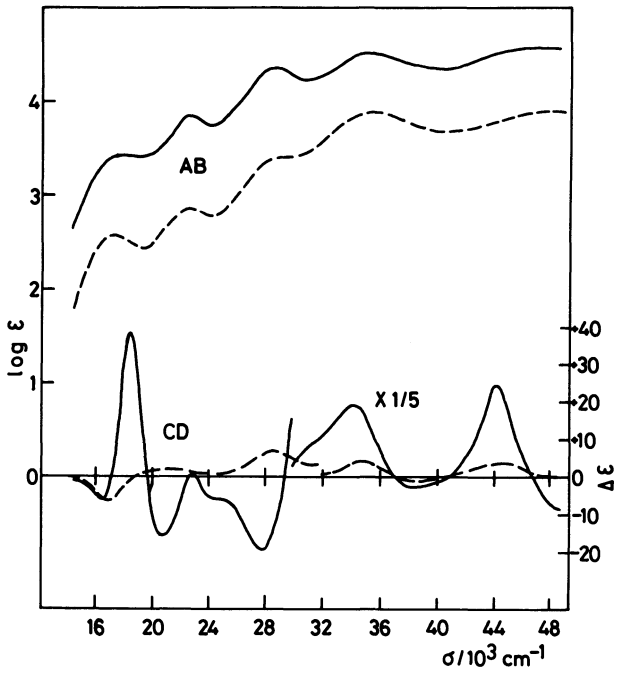

Fig. 5. Absorption and CD spectra of $\Delta_{LLL}\Delta_{LLL}$-[Co{Co(L-cys-*N*,*S*)$_3$}$_2$]$^{3-}$ (—) and Δ_{LLL}-*fac*(*S*)-[Co(L-cys-*N*,*S*)$_3$]$^{3-}$ (-----).

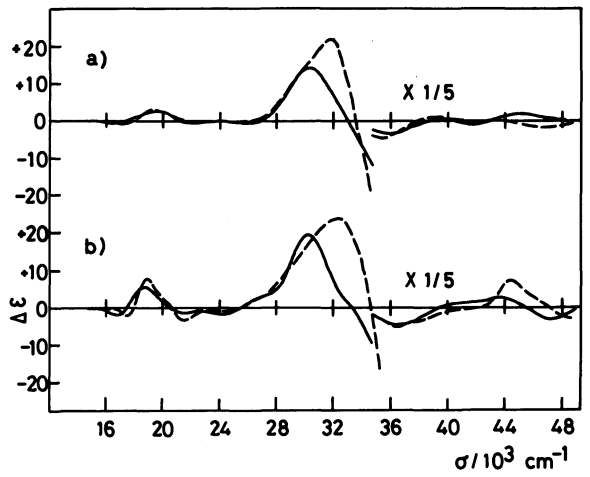

Fig. 6. The observed CD curves of $\Delta_{LLL}\Delta_{LLL}$-[M{Co(L-cys-*N*,*S*)$_3$}$_2$]$^{3-}$ (—) and the calculated CD curves for $1/2\{\Delta\varepsilon(\Delta_{LLL}\Delta_{LLL})+\Delta\varepsilon(\Lambda_{LLL}\Lambda_{LLL})\}$ (-----); a) M=Fe and b) M=Co.

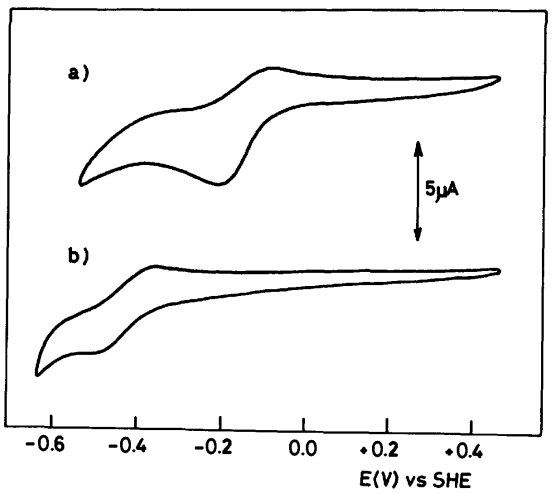

Fig. 7. Cyclic voltammograms of $\Delta_{LLL}\Delta_{LLL}$-[M{Co(L-cys-N,S)$_3$}$_2$]$^{3-}$: scan rate, 10 mV s^{-1}; 0.01 mol dm^{-3} $NaNO_3$ soln.; Hg electrode; 25 °C; a) M=Fe, $E°$=−0.16 V, ΔE_p=100 mV and b) M=Co, $E°$=−0.43 V, ΔE_p=90 mV.

fac(S)-[Co(L-cys-N,S)$_3$] terminals. The inversion ratio runs parallel to the concentration of Co(II) or Fe(II) in the reaction, and under a nitrogen atmosphere these reactions are completely accompanied by the inversion to give only $\Delta_{LLL}\Delta_{LLL}$-[Co{Co(L-cys-N,S)$_3$}$_2$]$^{3-}$. It is obvious that Fe(II) and Co(II) promote the inversion of the Δ_{LLL}-*fac*(S)-[Co(L-cys-N,S)$_3$] terminals, consequently, the $\Delta_{LLL}\Delta_{LLL}$ isomer forms easily.

The reaction of Δ_{LLL}-*fac*(S)-[Co(L-cys-N,S)$_3$]$^{3-}$ with Fe(II) was accompanied by a more remarkable inversion to Δ_{LLL} than that with Co(II). In order to elucidate the difference in inversion for the reactions with Fe(II) and Co(II), the redox potentials of $\Delta_{LLL}\Delta_{LLL}$-[M{Co(L-cys-N,S)$_3$}$_2$]$^{3-}$ (M=Fe(III) and Co(III)) were measured in a 0.01 mol dm^{-3} sodium nitrate solution at the hanging Hg drop microelectrode. All the potentials were referred to the SHE, and the symbols denote the following: E_{pa} is the anodic peak potential, E_{pc} is the cathodic peak potential, and ΔE_p is (E_{pa}−E_{pc}). The formal potential, $E°_{298}$, is taken as the average of E_{pa} and E_{pc}. $\Delta_{LLL}\Delta_{LLL}$-[Fe{Co(L-cys-N,S)$_3$}$_2$]$^{3-}$ and $\Delta_{LLL}\Delta_{LLL}$-[Co{Co(L-cys-N,S)$_3$}$_2$]$^{3-}$ display a quasi-reversible (ΔE_p=90—100 mV) cyclic response in different potential ranges, and no other redox process is observed in the potential range of −0.6—+0.9 V (Fig. 7). These results are interpreted in terms of the following one-electron redox reaction.

$$[M^{III}\{Co(L\text{-}cys\text{-}N,S)_3\}_2]^{3-} + e^- \rightleftharpoons [M^{II}\{Co(L\text{-}cys\text{-}N,S)_3\}_2]^{4-} \quad (M = Co \text{ or } Fe)$$

The formal potential of [Fe{Co(L-cys-N,S)$_3$}$_2$]$^{3-}$ (−0.16 V) is more anodic than that of [Co{Co(L-cys-N,S)$_3$}$_2$]$^{3-}$ (−0.43 V). This relationship corresponds to that of the formal potentials for the $Co^{III}N_6$- and $Fe^{III}N_6$-type complexes with the cyclic amine ligands.[18,19] These facts indicate that the central metal M is presumably redox active and that the redox potential of the Fe(II) center is more anodic than that of the Co(II) center. Taking these electrochemical properties into consideration, it is suggested that, in the formation process of the trinuclear complex by the reaction with the bivalent metal ion, the Fe(II) bridged with sulfur donor atoms of Δ_{LLL}-*fac*(S)-[Co(L-cys-N,S)$_3$]$^{3-}$, namely, $Fe^{II}(S_3CoN_3)$, has a lower oxidation tendency than the Co(II) one, $Co^{II}(S_3CoN_3)$. This suggestion is consistent with the fact that the formation of the $\Delta_{LLL}\Delta_{LLL}$ isomer is promoted more remarkably by the reaction of Δ_{LLL}-*fac*(S)-[Co(L-cys-N,S)$_3$] with Fe(II) than by that with Co(II), because the Δ_{LLL}-*fac*(S) terminals in the reaction with Fe(II) are labilized more than those in the reaction with Co(II).

References

1) D. C. Jicha and D. H. Busch, *Inorg. Chem.*, **1**, 872, 878 (1962).
2) D. H. Busch and D. C. Jicha, *Inorg. Chem.*, **1**, 884 (1962).
3) G. R. Brubaker and B. E. Douglas, *Inorg. Chem.*, **6**, 1562 (1967).
4) C. H. Wei and L. F. Dahl, *Inorg. Chem.*, **9**, 1878 (1970).
5) R. E. DeSimone, T. Ontko, L. Wardman, and E. L. Blinn, *Inorg. Chem.*, **14**, 1313 (1975).
6) E. L. Blinn, P. Bulter, K. M. Chapman, and S. Harris, *Inorg. Chim. Acta*, **24**, 139 (1977).
7) P. R. Bulter and E. L. Blinn, *Inorg. Chem.*, **17**, 2037 (1978).
8) M. J. Heeg, E. L. Blinn, and E. Deutsch, *Inorg. Chem.*, **24**, 1118 (1985).
9) T. Konno, S. Aizawa, K. Okamoto, and J. Hidaka, *Chem. Lett.*, **1985**, 1017.
10) K. Okamoto, S. Aizawa, T. Konno, H. Einaga, and J. Hidaka, *Bull. Chem. Soc. Jpn.*, **59**, 3859 (1986).
11) M. P. Schubert, *J. Am. Chem. Soc.*, **55**, 3336 (1933).
12) K. Yamanari, J. Hidaka, and Y. Shimura, *Bull. Chem. Soc. Jpn.*, **50**, 2299 (1977).
13) R. C. Elder, G. J. Kennard, M. D. Payne, and E. Deutsch, *Inorg. Chem.*, **17**, 1296 (1978).
14) M. Kojima and J. Fujita, *Bull. Chem. Soc. Jpn.*, **56**, 139 (1983).
15) C. T. Liu and B. E. Douglas, *Inorg. Chem.*, **3**, 1356 (1964).
16) B. E. Douglas and S. Yamada, *Inorg. Chem.*, **4**, 1561 (1965).
17) J. I. Legg, D. W. Cooke, and B. E. Douglas, *Inorg. Chem.*, **6**, 700 (1967).
18) K. Wieghardt, W. Schidt, W. Herrmann, and H.-J. Kuppers, *Inorg. Chem.*, **22**, 2953 (1983).
19) K. Wieghardt, I. Tolksdorf, and W. Herrmann, *Inorg. Chem.*, **24**, 1230 (1985).

Syntheses, and Crystal and Molecular Structures of [Enneakis(chloroacetato)-tetrakis(dimethyl sulfoxide)trineodymium(III)], $[Nd_3(ClCH_2CO_2)_9\{(CH_3)_2SO\}_4]$, and of the Isomorphous Lanthanum(III) and Praseodymium(III) Salts

Yoshihiko SUGITA and Akira OUCHI*
Department of Chemistry, College of Arts and Sciences, The University of Tokyo, Komaba, Meguro-ku, Tokyo 153
(Received September 11, 1987)

The crystal and molecular structures of the chloroacetato-dimethyl sulfoxide (dmso) mixed complex of neodymium(III) indicated in the title were determined by the single-crystal X-ray diffraction method. The crystal is monoclinic, space group $P2_1/n$, a=21.106(21), b=15.871(8), c=15.748(7) Å, β=93.29(5)°, Z=4 (including 12 metal atoms in a unit cell). There are three kinds of crystallographically independent metal atoms, Nd(1), Nd(2), and Nd(3): Nd(1) and Nd(3) are ennea-coordinated (approximately tricapped trigonal-prism geometry), and Nd(2) is deca-coordinated (approximately bicapped square-antiprism geometry) including a slightly long M–O bonding. All dmso molecules are directly coordinated to the metal atoms as unidentate, while all the carboxylate ions bridge metal atoms acting as bidentate or tridentate ligands. The bridging atoms are arranged in a chain which is approximately formed along the [101] axis. Also, the isomorphous lanthanum(III) and praseodymium(III) complexes were obtained and their structures were elucidated.

The variety of polymeric structures as well as the high coordination numbers of the metal atoms are characteristic of carboxylato complexes of lanthanoids.[1-10] Among them, the structures of the hydrated chloroacetates of more than half the lanthanoids and yttrium, as well as of the scandium salt (anhydride) have been reported in previous papers.[1-3] The light lanthanoids (La—Eu), the heavy lanthanoids (Gd—Yb) and yttrium, and the scandium salts have the respective types of chain structures.

It is well-known that many transition metals can form Lewis base adducts of their salts. Many of them are mixed complexes in which Lewis base molecules are also directly coordinated to the metal atoms; however, in the other adducts, the base molecules are not bonded to the metal atoms directly. In cases of lanthanoid complexes, although a great variety of adducts have already been synthesized,[11-16] only a few reports have so far been published concerning their structures.

On the line of our structural research concerning the lanthanoid(III) carboxylates, we could synthesize the dimethyl sulfoxide (dmso) adducts of some lanthanoid(III) chloroacetates, which did not include water.

It is interesting to compare their structures with those of the hydrated salts, which have already been elucidated, as well as of other carboxylates. Therefore, the authors have tried to determine the structures of the title complexes by the single-crystal X-ray diffraction method.

Experimental

Synthesis of the [Enneakis(chloroacetato)tetrakis(dimethyl sulfoxide)trineodymium(III)], $[Nd_3(ClCH_2CO_2)_9\{(CH_3)_2SO\}_4]$, and its Isomorphous Complexes. The hydrated neodymium(III) chloroacetate, $Nd(ClCH_2CO_2)_3 \cdot 5/3H_2O$ (0.90 g, 2.5 mmol)[1] were dissolved into ethanol (10 cm³), then dmso (0.40 g, 5.1 mmol) as well as benzene (10 cm³) were added to it. The solution was evaporated off by a vacuum rotary evaporator at about 80 °C. To the gummy residue, 15 cm³ of the ethanol–benzene mixture (1:1=v/v) was added and was evaporated once more in the same way. The residue was dissolved into 10 cm³ of methanol, and left standing in a desiccator over silica gel until about two-thirds of the solvent was evaporated off. The deposited crystals were separated, washed with a small portion of methanol, and dried in a silica gel desiccator. Yield, 0.9 g (6.7 mmol, 68%). By the same method, the isomorphous praseodymium(III) and lanthanum(III) mixed complexes were obtained (the yields of the lanthanum and praseodymium complexes were, 1.1 g (2.1 mmol, 75%) and 1.8 g (3.4 mmol, 85%), starting at 1.0 g (2.8 mmol) and 1.4 g (4.0 mmol) of the respective hydrated salts).

Analyses of the complexes (the calculated values were obtained assuming the formula of $M_3C_{26}H_{42}O_{22}Cl_9S_4$): M=Nd, Found, Nd, 27.36; C, 19.40; H, 2.59%. Calcd, Nd, 27.27; C, 19.68; H, 2.67%. M=La, Found, La, 26.70; C, 19.70; H, 2.59%. Calcd, La, 26.53; C, 19.88; H, 2.70%. M=Pr, Found, Pr, 26.68; C, 19.77; H, 2.68%. Calcd, Pr, 26.81; C, 19.81; H, 2.69%.

Single Crystal X-Ray Structure Analysis. Their crystallographic data are shown in Table 1, together with some experimental conditions regarding the collection of intensity data. The reflections were collected on a Rigaku AFC-6A automated 4-circle X-ray diffractometer with graphite-monochromated Mo $K\alpha$ radiation (λ=0.71073 Å; scan speed, 4° min⁻¹ (θ)). During the preliminary intensity data-collection process, since some (though only a few) peaks were found to overlap partially with the vicinal ones, the ω-scan technique was used.

Structure Determination. The structure of the neodymium(III) complex was solved by the heavy-atom method. The positions of metal and some chlorine atoms were deduced from a three-dimensional Patterson map, while all the other non-hydrogen atoms were located by means of successive Fourier syntheses, and refined by a block-diagonal least-squares method. In the last-cycle of the

Table 1. Crystallographic Data and Some Experimental Conditions to Obtain Their Intensity Data of Lanthanum(III), Praseodymium(III), and Neodymium(III) Chloroacetate Dimethyl Sulfoxide, $[M_3(ClCH_2CO_2)_9\{(CH_3)_2SO\}_4]$ Monoclinic; Space Group, $P2_1/n$

	La	Pr	Nd
F. W.	1570.66	1576.65	1586.65
$a(l/Å)$	21.169(12)	21.125(14)	21.106(21)
$b(l/Å)$	15.965(8)	15.888(7)	15.871(8)
$c(l/Å)$	15.885(6)	15.788(5)	15.748(7)
$\beta(\phi/°)$	93.12(4)	93.27(4)	93.29(5)
$U(v/Å^3)$	5361(5)	5290(5)	5267(8)
Z	4	4	4
$D_m(d/g\,cm^{-3})$	1.96(3)	1.97(3)	1.98(3)
$D_x(d/g\,cm^{-3})$	1.95	1.98	2.00
μ(Mo $K\alpha$)(n/cm^{-1})	30.4	33.8	36.0
Number of reflection measured	9882	7372	10513
Reflections used for the calculation[a]	7757	5093	7155
Measured range $(2\theta/°)$	3—50	3—45	3—50
Scan width $(\theta/°)$	1.08	1.03	1.00
Size of the crystal (v/mm^3)	0.28×0.25×0.22	0.30×0.27×0.15	0.35×0.30×0.20
R[b]	0.057	0.061	0.048

a) Reflections with $|F_o|>3\sigma(|F_o|)$ were used. b) $R=\sum||F_o|-|F_c||/\sum|F_o|$.

Table 2. Final Atomic Coordinates ($\times10^4$) of the Non-Hydrogen Atoms and Their Equivalent Isotropic Temperature Factors of the Neodymium(III) Complex (Estimated Standard Deviations in Parentheses)

Atom	x	y	z	$B_{eq}/Å^2$[a]	Atom	x	y	z	$B_{eq}/Å^2$[a]
Nd(1)	2989.5(2)	7627.6(3)	163.2(3)	2.1_5	O(31)	4916(3)	6490(4)	629(4)	3.9_9
Nd(2)	6426.2(2)	7109.1(3)	3137.0(3)	2.3_2	O(32)	4202(3)	7452(4)	249(4)	2.9_5
Nd(3)	4617.8(2)	7459.0(3)	1821.1(3)	2.2_0	O(33)	3813(3)	6371(4)	1786(4)	3.5_8
S(1)	2240(1)	7800(2)	2127(2)	3.9_6	O(34)	3252(3)	6177(4)	566(4)	3.4_3
S(2)	6837(2)	5677(2)	1483(2)	5.1_0	O(35)	4371(3)	8986(4)	1773(5)	3.7_1
S(3)	4343(1)	8020(2)	4001(2)	4.1_5	O(36)	3534(3)	8219(4)	1479(4)	2.7_0
S(4)	3694(2)	9228(2)	−1094(2)	4.7_6	C(1)	2455(6)	7150(8)	3031(7)	5.1_5
Cl(11)	6846(2)	4442(3)	5692(3)	9.7_7	C(2)	1390(6)	7779(10)	2172(9)	6.2_7
Cl(12)	8164(2)	7858(5)	1286(3)	12.9_9	C(3)	7365(6)	4799(8)	1465(9)	6.1_6
Cl(13)	5616(2)	9090(3)	5570(2)	6.9_8	C(4)	6126(5)	5171(9)	1105(8)	5.7_9
Cl(21)	4975(3)	4445(4)	3858(4)	16.1_1	C(5)	3610(7)	8370(11)	4409(8)	7.3_9
Cl(22)	6103(2)	8362(2)	−602(2)	6.7_8	C(6)	4568(6)	7221(9)	4785(7)	5.4_5
Cl(23)	5865(2)	10455(2)	3317(2)	4.9_7	C(7)	4433(7)	9698(10)	−792(11)	7.4_4
Cl(31)	5321(2)	6089(3)	−1071(2)	7.7_9	C(8)	3222(7)	10148(9)	−1327(9)	6.5_5
Cl(32)	2875(2)	4424(2)	931(2)	6.4_4	C(11)	7037(4)	5930(6)	4879(6)	2.8_0
Cl(33)	3609(3)	10312(3)	2540(3)	10.2_0	C(12)	6664(6)	5104(7)	4811(7)	5.2_5
O(1)	2366(3)	7237(4)	1378(4)	3.8_0	C(13)	8026(4)	7645(6)	2988(5)	2.9_3
O(2)	6739(4)	5825(5)	2427(4)	4.3_4	C(14)	8518(6)	7786(12)	2325(7)	7.2_2
O(3)	4134(3)	7535(5)	3205(4)	3.9_4	C(15)	6506(4)	8191(6)	4756(5)	3.0_0
O(4)	3449(3)	8931(4)	−265(4)	3.5_3	C(16)	6410(5)	8967(7)	5295(7)	4.1_5
O(11)	7287(3)	6182(5)	5566(4)	3.8_4	C(21)	5291(5)	5922(6)	3146(6)	3.2_1
O(12)	7082(3)	6327(4)	4194(4)	3.1_6	C(22)	4805(6)	5223(8)	3117(9)	6.0_5
O(13)	8266(3)	7722(4)	3724(4)	3.5_1	C(23)	5992(4)	7732(6)	1026(6)	2.9_3
O(14)	7469(3)	7474(5)	2777(4)	4.0_9	C(24)	6399(5)	7726(8)	259(7)	4.9_2
O(15)	7072(3)	8095(4)	4553(4)	3.3_1	C(25)	5744(4)	8756(6)	2996(5)	2.6_1
O(16)	6072(3)	7721(4)	4498(4)	3.2_0	C(26)	5380(4)	9535(6)	3199(7)	3.5_3
O(21)	5702(3)	6028(5)	3733(4)	4.0_6	C(31)	4622(4)	6901(6)	76(6)	2.9_4
O(22)	5264(3)	6386(4)	2515(4)	3.9_9	C(32)	4727(5)	6839(8)	−869(7)	4.8_2
O(23)	6250(4)	7346(5)	1645(4)	4.6_4	C(33)	3462(4)	5960(6)	1281(6)	2.8_5
O(24)	5471(3)	8083(5)	993(4)	3.6_3	C(34)	3270(6)	5109(8)	1670(8)	5.4_9
O(25)	6322(3)	8729(4)	3009(4)	3.1_7	C(35)	3795(4)	8918(6)	1635(5)	2.7_4
O(26)	5408(3)	8098(4)	2880(4)	2.8_3	C(36)	3357(5)	9682(7)	1673(7)	4.4_0

a) The equivalent isotropic temperature factors were computed using the following expression: $B_{eq}=4/3(B_{11}a^2+B_{22}b^2+B_{33}c^2+B_{13}ac\cos\beta)$. The B_{ij}'s are defined by: $T=\exp[-(h^2B_{11}+k^2B_{22}+l^2B_{33}+2hlB_{13}+2klB_{23}+2hkB_{12})]$.

refinement with anisotropic temperature factors for all the non-hydrogen atoms, all the parameter-shifts were less than one-third of the corresponding standard deviations. All hydrogen atoms were excluded from the structure factor calculations. The structures of the isomorphous complexes were solved by starting with the final parameters of the neodymium(III) complex, and were refined in the same way. All of their parameters converged within one-third of the respective standard deviations, too.

Some chlorine atoms of the ligands were found to have relatively large thermal parameters, and some Cl-C bond lengths were a little shorter than the sum of the Pauling's covalent bonding radii (1.76 Å),[17] although the average of the all Cl-C bond lengths of all the three complexes is not short, 1.76 Å. We tried to divide the positions of some such chlorine atoms into disordered structures, but failed. Probably their large temperature factors are due to their low positional restrictions: no atoms are very near such chroline atoms in the crystal. Such a phenomenon has also been found in other lanthanoid complexes, about the atoms in the tail part of the coordinating ligands.[18,19]

All the calculations were carried out on a HITAC M-682H apparatus at the Computer Center of the University of Tokyo, using the local version of the UNICS program.[20] The atomic scattering factors are taken from Ref. 21.

Infrared Spectrum Measurements. Their infrared spectra were obtained by means of a JASCO A202 grating infrared spectrophotometer, using liquid paraffin or hexachloro-1,3-butadiene mull.

Results and Discussion

The final atomic parameters of the neodymium(III) complex are listed in Table 2, while selected bond lengths and bond angles as well as some inter-metal-atomic distances are tabulated in Table 3.[22] The perspective drawing of the neodymium(III) complex around the metal atoms (Nd(1), Nd(2), and Nd(3)), as well as the numbering scheme of the atoms are shown in Figs. 1—3, and the projection of the unit cell to the ac-plane in Fig. 4, respectively.

The Nd(1) and Nd(3) atoms are ennea-coordinated being approximately in a tricapped trigonal-prism geometry, while the Nd(2) atom is deca-coordinated being approximately in a cis-bicapped square-antiprism geometry;[24] however, Nd(2)-O(15) (2.988(8) Å) is a little longer than the other Nd-O bonds. The averages of the Nd-O bond lengths, together with those of the other isomorphous complexes are summarized in Table 4. The average Nd-O bond lengths around Nd(1) and Nd(3) atoms (2.513 and 2.499 Å) are not much different from each other, and they are approximately the same as the sum of the Shannon's ionic radii, 2.51 Å (where the coordination number of the Nd atoms is 9).[25] The Nd(1,3)-O(dmso)$_{av.}$ (from now on, "av." means the average of the values) is

Table 3. Selected Bond Lengths and Bond Angles of the Neodymium Complex, with the Standard Deviations in Parentheses

Bond length	(l/Å)	Bond length	(l/Å)
Nd(1)-O(1)	2.461(9)	Nd(1)-O(4)	2.399(7)
Nd(1)-O(32)	2.570(6)	Nd(1)-O(34)	2.444(7)
Nd(1)-O(36)	2.495(8)	Nd(1)-O(11^{i})[a]	2.506(7)
Nd(1)-O(12^{i})	2.901(6)	Nd(1)-O(13^{i})	2.437(9)
Nd(1)-O(15^{i})	2.403(7)	Nd(2)-O(2)	2.434(8)
Nd(2)-O(12)	2.442(7)	Nd(2)-O(14)	2.376(8)
Nd(2)-O(15)	2.988(8)	Nd(2)-O(16)	2.505(9)
Nd(2)-O(21)	2.515(8)	Nd(2)-O(22)	2.832(8)
Nd(2)-O(23)	2.387(10)	Nd(2)-O(25)	2.588(7)
Nd(2)-O(26)	2.673(6)	Nd(3)-O(3)	2.462(10)
Nd(3)-O(22)	2.405(7)	Nd(3)-O(24)	2.489(8)
Nd(3)-O(26)	2.505(7)	Nd(3)-O(31)	2.534(9)
Nd(3)-O(32)	2.579(8)	Nd(3)-O(33)	2.420(7)
Nd(3)-O(35)	2.479(7)	Nd(3)-O(36)	2.614(6)
M(1)···M(3)	4.203(3)	M(3)···M(2)	4.274(4)
M(1)···M(2^{i})	4.476(3)		
Bond angle	**(ϕ/°)**	**Bond angle**	**(ϕ/°)**
Nd(1)-O(11^{i})-C(11^{i})	104.5(7)	Nd(1)-O(12^{i})-C(11^{i})	85.1(7)
Nd(2)-O(12)-C(11)	140.5(7)	Nd(1)-O(13^{i})-C(13^{i})	137.5(8)
Nd(2)-O(14)-C(13)	150.6(7)	Nd(1)-O(15^{i})-C(15^{i})	135.0(7)
Nd(2)-O(15)-C(15)	81.7(6)	Nd(2)-O(16)-C(15)	105.3(6)
Nd(2)-O(21)-C(21)	103.2(7)	Nd(2)-O(22)-C(21)	87.9(7)
Nd(3)-O(22)-C(21)	141.9(7)	Nd(2)-O(23)-C(23)	151.8(9)
Nd(3)-O(24)-C(23)	118.0(7)	Nd(2)-O(25)-C(25)	96.6(5)
Nd(2)-O(26)-C(25)	91.4(5)	Nd(3)-O(26)-C(25)	140.8(7)
Nd(3)-O(31)-C(31)	93.8(7)	Nd(1)-O(32)-C(31)	139.4(6)
Nd(3)-O(32)-C(31)	90.3(6)	Nd(3)-O(33)-C(33)	141.4(7)
Nd(1)-O(34)-C(33)	124.3(7)	Nd(3)-O(35)-C(35)	97.1(5)
Nd(1)-O(36)-C(35)	132.1(7)	Nd(3)-O(36)-C(35)	89.9(5)

a) Key to the symmetry operation: $-0.5+x$, $1.5-y$, $-0.5+z$.

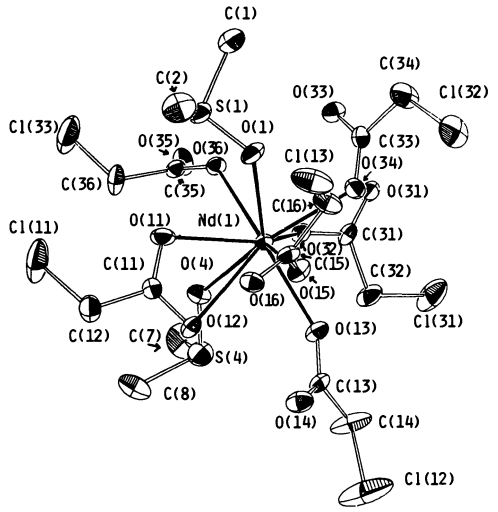

Fig. 1. A perspective drawing of the neodymium(III) complex around the Nd(1) atom. Here the atoms of the acidato ligands including Cl(11), Cl(12), and Cl(13) are the ones symmetry operated by $-0.5+x$, $1.5-y$, $-0.5+z$.

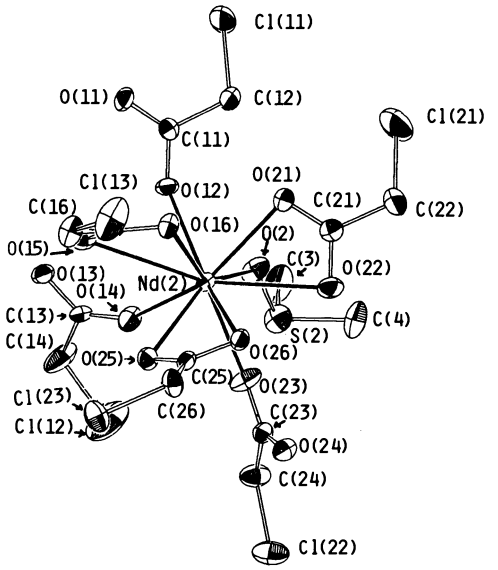

Fig. 2. A perspective drawing of the neodymium(III) complex around the Nd(2) atom.

Table 4. Comparison of the M-O Bondings of the Complexes (l/Å)

M=	La	Pr	Nd
M(1)-O(all)$_{av.}$[a]	2.562	2.526	2.513
M(3)-O(all)$_{av.}$	2.556	2.515	2.499
M(2)-O(all except 15)$_{av.}$	2.586	2.540	2.528
M(2)-O(all)$_{av.}$	2.618	2.584	2.574
M(1,3)-O(dmso)$_{av.}$	2.486	2.457	2.441
M(1,3)-O(acid)$_{av.}$	2.573	2.534	2.519
M(2)-O(acid)$_{av.}$	2.632	2.601	2.590
Sum of Shannon's ionic radii[b]			
M(IX)-O(II)	2.57	2.53	2.51
M(X)-O(II)	2.62	(2.58)	(2.56)

a) av. means the average of the M-O bond lengths between the metal atom and the group of coordinating oxygen atoms. b) See Ref. 25. II, X, IX means their coordination number.

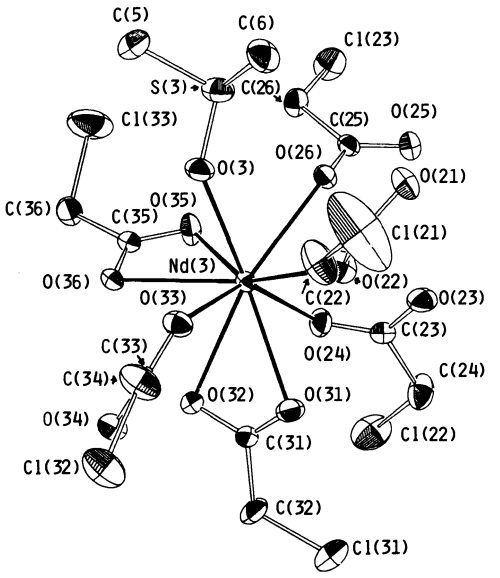

Fig. 3. A perspective drawing of the neodymium(III) complex around the Nd(3) atom.

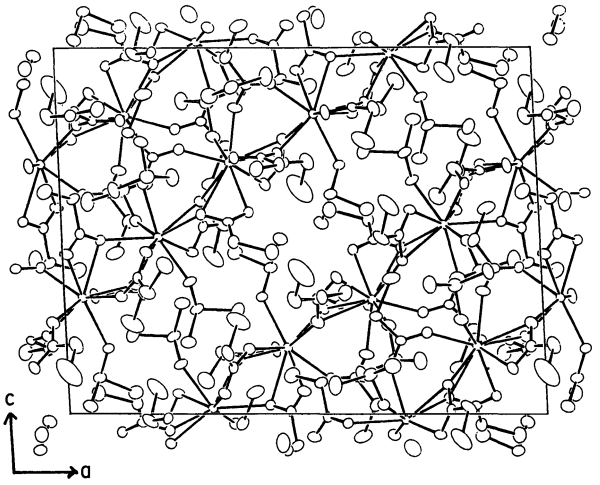

Fig. 4. A projection of the unit-cell to the ac-plane.

2.441 Å, which is shorter than the Nd(1,3)-O(acid)$_{av.}$, 2.519 Å. Therefore, in these complexes, the former bonds are likely to be stronger than the latter ones.

The average of all ten Nd-O bond lengths around the Nd(2) atom is 2.574 Å, which is longer than the sum of the Shannon's ionic radii, 2.56 Å (the coordination number of the Nd atom is 10).[25] Even when the longest bond, Nd(2)-O(15), is rejected, the average of the other nine bond lengths is 2.528 Å, which is longer than the average Nd-O bond lengths around the ennea-coordinated Nd(1) or Nd(3) atoms. Therefore, atom O(15) should be regarded as the ligating atom, or at least, it also affects the coordination geometry around the Nd(2) atom. The Nd-(2)-O(2) (dmso oxygen atom) is 2.434 Å, which is much shorter than the Nd(2)-O(acid)$_{av.}$, 2.590 Å. Consequently, the Nd-O(dmso) bond is stronger than the

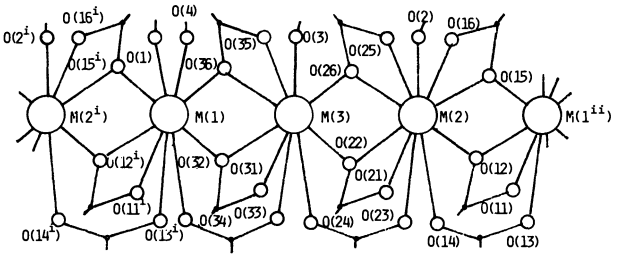

Fig. 5. A schematic presentation of the bridgings between the metal atoms.[23]

Nd–O(acid) bonds around the deca-coordinated Nd(2) atom, too.

The metal atoms are arranged approximately along the [101] axis in the order of Nd(1^{ii}), Nd(2), Nd(3), Nd(1), Nd(2^{i})···,[23] as shown schematically in Fig. 5. The interatomic distance is 4.317 Å (on the average); this is shorter than the average inter-metal-atomic distance of the chain in the hydrated neodymium chloroacetate, 4.435 Å.[1]

It is very interesting that this dmso adduct has an average M···M′ distance of the complex chain shorter than that of the hydrate, though the dmso adduct has a larger unit-cell, and smaller density (5267(8) Å^3 and 2.00 g cm^{-3} for the dmso adduct, and 3986(2) Å^3 and 2.27 g cm^{-3} for the hydrate). Moreover, since the Nd–O(dmso)$_{av.}$ lengths are shorter than the Nd–O(acid)$_{av.}$ lengths in the dmso adduct, while the Nd–O(water)$_{av.}$ lengths are about the same as the Nd–O(acid)$_{av.}$ lengths in the hydrate, the approaching dmso ligands in this adduct are expected to prevent any approaching of neighboring complexes in the linear polymer: however this expectation did not prove to be correct.

Probably, the dmso methyl groups in this adduct, which are non-polar and are intercalated between complex chains, act to pack the chain in the limited space between the hydrophobic layers of the hydrocarbon groups: the inter-chain separations are kept large, but the inter-metal atomic distances in the chains are shortened.

The bridging structure, the numbers and the types of the bridging carboxylate ions between respective neighboring metal atoms in the chain of the title dmso adduct, is much different from that of the hydrated salt of the same metal;[1] this type of chain structure has not yet been found in any other linear polymeric chains of the other lanthanoid carboxylates. In the titled complex, all the pairs of the neighboring metal atoms are bridged by three carboxylate ions respectively: one in bidentate (approximately in the *Z,Z*-type, but some of them are quite deformed), and two in the tridentate types.[26] In some deformed bidentate bridges between Nd(1) and Nd(3), as well as Nd(3) and Nd(2), one of the C–O–M angles in very small, only about 110—125°, and some atomic positions are much deviated from the mean-square plane of the MOCO′M′ bridging. All the tridentate bridges of these complexes are also more or less deformed from the ideal form (here the ideal form means the bridge, where the three metal-oxygen bondings, M–O, M–O′, and M′–O′, are about the same in their lengths, and the bond angles of M–O–C as well as M–O′–C are about the same (95—100°), while that of M′–O′–C is larger (150—160°)).[26]

Although there are no fundamental differences between their structures, the isomorphous lanthanum(III) and praseodymium(III) complexes have larger unit cells than the neodymium(III) complex: their cell dimensions decrease depending on the atomic number of the central metal atom. The decrease of the cell-volume is mainly caused by packing the coordination sphere around the central metal atom: the M–O bond lengths decrease. Therefore, as shown in Table 4, almost all M–O bond lengths are generally shorter in a higher atomic number metal complex, although the lengths of some weak bonds, such as M(1)–O(15) and M(1)–O(12^{i}), rather increase with the metal atomic number.

The infrared spectra of these complexes were examined, but there are almost no differences between them. The ν_{as}(COO) and ν_{s}(COO) peaks appear as the respective doublets of the maximum wavenumbers of 1598, 1573 cm^{-1}, and of 1418, 1402 cm^{-1}, respectively. In the spectra of the hydrated chloroacetates of lanthanum(III), and neodymium(III), these bands appear at about 1580 and 1415—1420 cm^{-1}, respectively. Therefore, these peak maximum wavenumbers of both types of complexes are not much different from each other.

The ν(SO) band of the titled complexes appear at about 1000 cm^{-1} as a sharp strong peak, while the band of free dmso appears at about 1050 cm^{-1} as a broad band: the peak of the complexes is much red-shifted. This fact corresponds with the strong M–O(dmso) bond in the complexes, as was expected from the results of the X-ray structure analysis.

The authors wish to thank Shin-Etsu Ind. Co., Ltd., for presenting us with the highly pure lanthanoid oxides.

References

1) T. Imai, M. Shimoi, and A. Ouchi, *Bull. Chem. Soc. Jpn.*, **60**, 159 (1987).

2) Y. Sugita and A. Ouchi, *Bull. Chem. Soc. Jpn.*, **60**, 171 (1987).

3) Y. Sugita, Y. Ohki, Y. Suzuki, and A. Ouchi, *Bull. Chem. Soc. Jpn.*, **60**, 3441 (1987).

4) A. S. Antsyshkina, M. A. Porai-Koshits, I. V. Arkhangel'skii, V. N. Ostrikova, and A. Z. Amanov, *Dokl. Akad. Nauk. AZ. SSR*, **36**, 47 (1980).

5) G. G. Sadikov, G. A. Kukina, and M. A. Porai-Koshits, *Zh. Strukt. Khim.*, **8**, 551 (1967).

6) M. C. Favas, D. L. Kepert, B. W. Skelton, and A. H.

White, *J. Chem. Soc., Dalton Trans.*, **1980**, 454.
7) R. Wenk, *Z. Kristallogr.*, **154**, 137 (1981).
8) T. Imai and A. Ouchi, *Bull. Chem. Soc. Jpn.*, **60**, 408 (1987).
9) Y. Koizumi, H. Sawase, Y. Suzuki, T. Takeuchi, and A. Ouchi, *Bull. Chem. Soc. Jpn.*, **57**, 1809 (1984).
10) S. Kondo, M. Shimoi, A. Ouchi, and T. Takeuchi, *Bull. Chem. Soc. Jpn.*, **57**, 2840 (1982).
11) J. C. Prado and G. Vicentini, *Inorg. Nucl. Chem. Lett.*, **55**, 2840 (1973).
12) G. Vicentini and C. Airoldi, *J. Inorg. Nucl. Chem.*, **33**, 1733 (1971).
13) G. Vicentini, M. Perrier, and J. C. Prado, *J. Inorg. Nucl. Chem.*, **31**, 825 (1969).
14) L. B. Zinner, G. Vicentini, and L. Rothschild, *J. Inorg. Nucl. Chem.*, **36**, 2499 (1974).
15) J. T. Donoghue and D. A. Peters, *J. Inorg. Nucl. Chem.*, **31**, 467 (1969).
16) E. Griesbrecht and L. D. Zinner, *Inorg. Nucl. Chem. Lett.*, **5**, 575 (1969).
17) L. Pauling, "The Nature of the Chemical Bonds," 3rd ed, Cornell Univ. Press, N. Y. (1960), pp. 246, 247.
18) T. Imai, M. Nakamura, K. Nagai, Y. Ohki, Y. Suzuki, M. Shimoi, and A. Ouchi, *Bull. Chem. Soc. Jpn.*, **59**, 2115 (1986).
19) R. Nakamura, K. Nagai, M. Shimoi, and A. Ouchi, *Bull. Chem. Soc. Jpn.*, **57**, 2919 (1984).
20) "Universal Crystallographic Computation Program System (UNICS)," ed by T. Sakurai, Crystallographic Society of Japan, Tokyo (1967).
21) "International Tables for X-Ray Crystallography," Kynoch Press, Birmingham (1974), Vol. IV, pp. 72, 150.
22) The atomic parameters of the lanthanum and praseodymium salts, the final thermal parameters and the final F_o-F_c tables of all three complexes, and some of their bond length and bond angle data are deposited as Document No. 8785 at the office of the Editor of Bull. Chem. Soc. Jpn.
23) Key to the symmetry operations: i, $-0.5+x$, $1.5-y$, $-0.5+z$; ii, $0.5+x$, $1.5-y$, $0.5+z$.
24) Around the Nd(1) atom, O(1), O(12^{i}), O(15^{i}), and O(4), O(32), O(36) atoms are at the apexes of the both side triangles of the prism, respectively, while around the Nd(3) atom, O(22), O(24), O(26), and O(32), O(33), O(36) atoms are at the respective apex positions of the both triangles. Around the Nd(2) atom, O(2), O(14), O(25), O(22), and O(12), O(15), O(16), and O(21) are at the apexes of the respective squares, while O(23) (over the former square) and O(26) (over the O(16), O(21), O(22), O(25) side face) are at the cap positions. Around the Nd(2) atom, when the O(15) atom is not regarded, tricapped trigonal-prism geometry can be assumed, where O(16), O(25), O(26), and O(2), O(16), O(22) are at the apexes of the both side triangles of the prism, respectively, while O(14), O(16), and O(22) are at the cap positions.
All of these geometries are quite deformed from the ideal shape.
25) R. D. Shannon, *Acta Crystallogr., Sect. A*, **32**, 751 (1976). The values given in the paper are as follows: Metal (Valence=3+; Coordination number=9), La, 1.216; Pr, 1.179; Nd, 1.163 Å; (Valence=3+; Coordination number=10), La, 1.27 Å. (As the ionic radii of praseodymium and neodymium of this coordination number were not given, the lengths 0.05 Å longer than the respective ionic radii of their coordination number=9 are adopted tentatively: Pr, 1.23; Nd, 1.21 Å).
26) H. Sawase, Y. Koizumi, Y. Suzuki, M. Shimoi, and A. Ouchi, *Bull. Chem. Soc. Jpn.*, **57**, 2730 (1984).

Copper(II)-Lanthanoid(III) Complexes of Binucleating Ligands Derived from 3-Formylsalicylic Acid and Diamines

Masatomi SAKAMOTO,* Minoru TAKAGI, Tomitaro ISHIMORI, and Hisashi ŌKAWA†
Department of Industrial Chemistry, Faculty of Engineering, Ehime University, Bunkyo-cho, Matsuyama 790
†Department of Chemistry, Faculty of Science, Kyushu University, Hakozaki, Higashi-ku, Fukuoka 812
(Received December 17, 1987)

Heterometal binuclear complexes, [CuLn(fsaen)(H_2O)$_n$](NO_3) (Ln=La, Pr, Nd, Sm, Eu, Gd, Tb, Dy, Ho, Er, Tm, Yb, or Lu; n=4—5) and [CuLn(fsapn)(H_2O)$_4$](NO_3) (Ln=La, Pr, Nd, Sm, Eu, Gd, Tb, or Dy) have been synthesized and characterized, where H_4fsaen and H_4fsapn denote *N,N'*-bis(3-carboxysalicylidene)ethylenediamine and *N,N'*-bis(3-carboxysalicylidene)-1,2-propanediamine, respectively. The ligand field band due to the copper(II) ion bound to the N_2O_2-site is at 18.5×10^3—19.5×10^3 cm^{-1} for [CuLn(fsaen)(H_2O)$_n$](NO_3) and 18.4×10^3—19.2×10^3 cm^{-1} for [CuLn(fsapn)(H_2O)$_4$](NO_3), which are higher frequencies than those of the mononuclear complexes, [Cu(H_2fsaen)](H_2O)$_{0.5}$ and [Cu(H_2fsapn)](H_2O)$_{0.5}$ (18.3×10^3 and 18.4×10^3 cm^{-1}, respectively). When the complexes are dissolved in pyridine (Py), dimethyl sulfoxide (DMSO), or *N,N*-dimethylformamide (DMF), the d-d band frequency decreases in the order of the solvent DMSO>DMF>Py for the binuclear complexes, whereas it decreases in the order of DMF>DMSO>Py for the mononuclear complexes. These trends were discussed in terms of the different affinities of solvent molecules for copper(II) and lanthanoid(III) ions. No significant magnetic spin-exchange interaction occurred between metal ions.

Various rare earth perovskite or garnet type compounds have been widely studied because of their growing possible use as the magnetic material, electrical semiconductor, catalysis, and so on.[1] However, the role of rare earth metal ions in these materials seems not to be still well-defined. For the understanding of their interesting properties, heterometal binuclear complexes comprising a transition metal and a lanthanoid ions are presumed to be good simple models.

A general method for obtaining heterometal binuclear complexes is the stepwise addition of two different metal ions to a coordinatively selective binucleating ligand, in which two coordinating sites differ from each other in the ligand field strength or in the stereochemistry of coordination. A number of such compartmental ligands have been synthesized[2-8] and studies on binuclear complexes with dissimilar d-transition metal ions have been developed with these ligands.[3,5,6,9-15] On the other hand, very few reports[8] are available on the heterometal binuclear complexes containing a d-transition metal ion and a lanthanoid ion.

Since Okawa et al.[3] first used *N,N'*-bis(3-carboxysalicylidene)ethylenediamine (H_4fsaen) as an excellent binucleating ligand possessing dissimilar coordination sites, this ligand and its homologs have been extensively utilized for the syntheses of homo- and heterometal binuclear complexes to investigate their magnetic, optical, electrochemical, and structural properties.[3,5,9,10,13-16] In those studies, it was revealed that physicochemical properties of the metal ion bound at N_2O_2-site (inside coordination site) are very sensitive to the second metal ion at the O_4-site (outside coordination site).[5] Since the outside coordination site seems favorable for binding lanthanoid ions, these ligands are expected to be applicable to the syntheses of heterometal binuclear complexes comprising a d-transition metal and a lanthanoid metal ions.

In this work we have prepared copper(II)-lanthanoid(III) complexes of H_4fsaen and *N,N'*-bis(3-carboxysalicylidene)-1,2-propanediamine (H_4fsapn), in which copper(II) and lanthanoid(III) ions are bound at the inside and outside coordination sites, respectively (Fig. 1). The effect of the presence of a lanthanoid(III) ion at the outside site upon the ligand field around copper (II) ion at the inside site has been discussed mainly on the basis of electronic spectra. The IR, ESR, and magnetic data of these complexes are also reported.

Experimental

Syntheses. 3-Formylsalicylic acid was prepared after the method of Duff and Bills.[17] The mononuclear copper(II) complexes, [Cu(H_2fsaen)](H_2O)$_{0.5}$ and [Cu(H_2fsapn)](H_2O)$_{0.5}$, were obtained by the method of Okawa et al.[4]

CuLn(fsaen)(NO_3)(H_2O)$_4$ and CuLn(fsapn)(NO_3)(H_2O)$_4$ (Ln=La—Nd): The corresponding mononuclear copper(II) complex (1 mmol) was dissolved in a methanolic solution (50 cm^3) of lithium hydroxide monohydrate (2 mmol). To this solution was added a methanolic solution (50 cm^3) of lanthanoid nitrate hydrate (1 mmol) with stirring. After the mixture was refluxed for 2—3 h with stirring, the precipitate formed was filtered, washed with methanol and then with diethyl ether, and dried in the open air.

CuLn(fsaen)(NO_3)(H_2O)$_n$ (Ln=Sm—Ho, n=4—5): The procedure was the same in principle as that described above, except for the use of 25 cm^3 methanol for each treatment.

CuLn(fsaen)(NO_3)(H_2O)$_5$ (Ln=Er—Lu) and CuLn(fsapn)(NO_3)(H_2O)$_4$ (Ln=Sm—Dy): These binuclear complexes were synthesized in the same way as that for the above complexes, except that the mononuclear copper(II) complex (1 mmol) was dissolved in a methanolic solution (25 cm^3) of

Table 1. Elemental Analyses of Complexes

Complex	Found(%)(Calcd (%))				
	C	H	N	Cu	Ln
$CuLa(fsaen)(NO_3)(H_2O)_4$	31.07	2.55	6.35	9.26	20.65
	(31.39)	(2.93)	(6.10)	(9.23)	(20.17)
$CuPr(fsaen)(NO_3)(H_2O)_4$	30.96	2.56	6.13	9.14	19.93
	(31.30)	(2.92)	(6.08)	(9.20)	(20.40)
$CuNd(fsaen)(NO_3)(H_2O)_4$	31.16	2.68	5.99	9.14	20.68
	(31.15)	(2.90)	(6.05)	(9.15)	(20.78)
$CuSm(fsaen)(NO_3)(H_2O)_4$	31.12	2.65	5.63	9.15	21.80
	(30.87)	(2.88)	(6.00)	(9.07)	(21.47)
$CuEu(fsaen)(NO_3)(H_2O)_4$	30.38	2.71	5.68	9.20	21.98
	(30.80)	(2.87)	(5.99)	(9.05)	(21.65)
$CuGd(fsaen)(NO_3)(H_2O)_4$	30.33	2.71	5.60	8.93	22.63
	(30.57)	(2.85)	(5.94)	(8.99)	(22.24)
$CuTb(fsaen)(NO_3)(H_2O)_5$	29.85	2.58	5.85	8.85	22.13
	(29.74)	(3.05)	(5.78)	(8.74)	(21.86)
$CuDy(fsaen)(NO_3)(H_2O)_5$	29.37	2.65	5.89	8.56	22.65
	(29.60)	(3.04)	(5.75)	(8.70)	(22.25)
$CuHo(fsaen)(NO_3)(H_2O)_5$	29.73	2.85	5.80	8.80	23.05
	(29.50)	(3.03)	(5.73)	(8.67)	(22.51)
$CuEr(fsaen)(NO_3)(H_2O)_5$	29.11	2.55	5.47	9.06	23.20
	(29.40)	(3.02)	(5.72)	(8.64)	(22.75)
$CuTm(fsaen)(NO_3)(H_2O)_5$	28.89	2.73	5.60	8.75	23.01
	(29.34)	(3.01)	(5.70)	(8.62)	(22.93)
$CuYb(fsaen)(NO_3)(H_2O)_5$	28.58	2.78	5.61	8.72	23.38
	(29.18)	(2.99)	(5.67)	(8.58)	(23.35)
$CuLu(fsaen)(NO_3)(H_2O)_5$	28.64	2.51	5.51	8.60	23.80
	(29.10)	(2.98)	(5.66)	(8.55)	(23.55)

Table 2. Elemental Analyses of Complexes

Complex	Found(%)(Calcd (%))				
	C	H	N	Cu	Ln
$CuLa(fsapn)(NO_3)(H_2O)_4$	31.64	3.08	6.03	9.02	19.96
	(32.47)	(3.15)	(5.98)	(9.04)	(19.76)
$CuPr(fsapn)(NO_3)(H_2O)_4$	31.38	3.11	6.12	8.61	20.34
	(32.38)	(3.14)	(5.96)	(9.02)	(19.99)
$CuNd(fsapn)(NO_3)(H_2O)_4$	31.97	2.99	6.06	8.96	20.56
	(32.22)	(3.13)	(5.93)	(8.97)	(20.37)
$CuSm(fsapn)(NO_3)(H_2O)_4$	31.37	3.05	5.76	8.73	21.10
	(31.95)	(3.10)	(5.88)	(8.90)	(21.15)
$CuEu(fsapn)(NO_3)(H_2O)_4$	31.37	3.05	6.14	8.58	22.12
	(31.88)	(3.10)	(5.87)	(8.88)	(21.23)
$CuGd(fsapn)(NO_3)(H_2O)_4$	31.24	3.04	5.84	8.63	21.86
	(31.64)	(3.07)	(5.83)	(8.81)	(21.80)
$CuTb(fsapn)(NO_3)(H_2O)_4$	31.34	3.05	5.92	8.75	21.57
	(31.57)	(3.07)	(5.81)	(8.79)	(21.99)
$CuDy(fsapn)(NO_3)(H_2O)_4$	30.95	3.01	5.87	8.35	22.17
	(31.41)	(3.05)	(5.78)	(8.75)	(22.37)

lithium hydroxide monohydrate (2 mmol), followed by the addition of methanolic solution (5 cm^3) of lanthanoid nitrate hydrate (1 mmol).

Elemental analyses for the complexes are given in Tables 1 and 2.

Measurements. Elemental analyses of carbon, hydrogen, and nitrogen were carried out at the Service Center of Elemental Analysis, Kyushu University or Advanced Instrumentation Center for Chemical Analysis, Ehime University. Metal contents were determined by EDTA titration. Infrared spectra were measured with a JASCO IR-G Spectrometer on KBr disks or on nujol mulls. Electronic spectra were obtained on nujol mulls and in dimethyl sulfoxide, *N,N*-dimethylformamide, or pyridine with a Shimadzu UV-VIS Recording Spectrophotometer Model 240. Magnetic susceptibilities were measured by the Gouy method or the Faraday method from liquid nitrogen temperature to room temperature. Diamagnetic correction was done using the Pascal's constants. Magnetic moments were calculated from the equation, $\mu_M=2.828\sqrt{x_M T}$, where x_M is the susceptibility per molecule. The ESR spectra were recorded with a JES-ME-3X Spectrometer by the X-band in dimethyl sulfoxide, *N,N*-dimethylformamide, or pyridine at liquid nitrogen temperature.

Results and Discussion

Infrared spectra of the binuclear complexes are essentially similar to each other as far as the same ligand is concerned. The absorption band at 1630—1640 cm^{-1} is assignable to the C=N stretching mode. The band due to the free carboxyl group was reported to appear at 1705 cm^{-1} for both $[Cu(H_2fsaen)](H_2O)_{0.5}$ and $[Cu(H_2fsapn)](H_2O)_{0.5}$.[4] However, this band disappeared in the spectra of $CuLn(fsaen)(NO_3)(H_2O)_n$ and $CuLn(fsapn)(NO_3)(H_2O)_4$. Instead a broad and strong band was observed around 1540 cm^{-1}. The binuclear d-transition metal complexes of 3-formylsalicylic acid[18] and its Schiff bases[3-5,9,19] are known to exhibit the absorption band at 1540—1580 cm^{-1} which is attributable to the C=O stretching vibration. Therefore, it seems reasonable to assign the band around 1540 cm^{-1} to the coordinated carboxylato group.

It is well-known that for the phenoxo-bridged binuclear complexes one of the skeletal vibrations (near 1540 cm^{-1}) is by 15—20 cm^{-1} higher than that of the corresponding mononuclear complexes.[2] For example, the mononuclear copper(II) complex of a macrocycle, 24,25-dihydroxy-10,22-dimethyl-3,6,14,18-tetraazatricyclo[18.3.1.1^{8,12}]pentacosa-1(24),2,6,8(25),9,11,13,18,20,22-decaene, shows the skeletal band at 1543 cm^{-1}, whereas its binuclear copper(II) complex shows the corresponding band at 1560 cm^{-1}.[2] For the present Cu(II)-Ln(III) complexes, however, such a marked shift of the skeletal band was not observed. That is, the band for the Cu(II)-Ln(III) complexes appeared around 1560 cm^{-1}, whereas the band for $[Cu(H_2fsaen)](H_2O)_{0.5}$ and $[Cu(H_2fsapn)](H_2O)_{0.5}$ appeared around 1555 cm^{-1}.

For the nitrates of lanthanoid complexes it is reported that IR bands appear around 1450—1500, 1300, 1030, and 815 cm^{-1} if the nitrate ion functions as a bidentate ligand.[8,20] Such bands could not be clearly seen in the IR spectra of the present binuclear complexes. Instead the sharp bands appeared at 1380 and 805 cm^{-1} which are characteristic of free nitrate ion.[21] Furthermore, the splitting of combination bands in the region of 1700—1800 cm^{-1}, which has been often utilized as a diagnosis of the bonding mode of nitrate ion,[22] was not recognized for the complexes. These observations indicate that the nitrate ion does not coordinate to the metal ion. The spectra on nujol mulls for the binuclear complexes showed two bands at 3350 and 3250 cm^{-1} assignable to the asymmetric and symmetric stretching vibrations of H_2O molecule, respectively, whereas $[Cu(H_2fsaen)](H_2O)_{0.5}$ and $[Cu(H_2fsapn)](H_2O)_{0.5}$ showed a band at 3400 cm^{-1} attributable to a lattice water. Judging from these facts, the present binuclear complexes can be formulated as $[CuLn(fsaen)(H_2O)_n](NO_3)$ and $[CuLn(fsapn)(H_2O)_4](NO_3)$ in which lanthanoid ions are presumably of eight or nine coordination with O_4-donor atoms of the Schiff base and four or five H_2O molecules, though the detailed structure is unclear at the present stage.

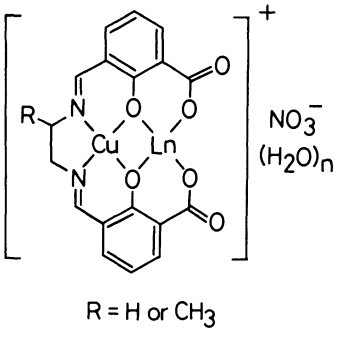

Fig. 1. The structure of copper(II)–lanthanoid(III) heterometal binuclear complexes.

Some of the electronic spectra determined on nujol mulls are shown in Fig. 2. The absorption maxima of the complexes are summarized in Figs. 3 and 4. $[Cu(H_2fsaen)](H_2O)_{0.5}$ and $[Cu(H_2fsapn)](H_2O)_{0.5}$ show the ligand field band due to the copper(II) ion at 18.25×10^3 and 18.38×10^3 cm^{-1}, respectively, which are very close to those determined by reflection on powder samples by Okawa et al.[4] The d-d band is shifted to higher frequency on binuclear complex formation. This is in accord with that $[Cu(H_2fsaen)](H_2O)_{0.5}$ and $[Cu(H_2fsapn)](H_2O)_{0.5}$ are purple while the Cu(II)-Ln(III) complexes are red-purple. Such a blue shift of the d-d band may be attributed to the enhanced

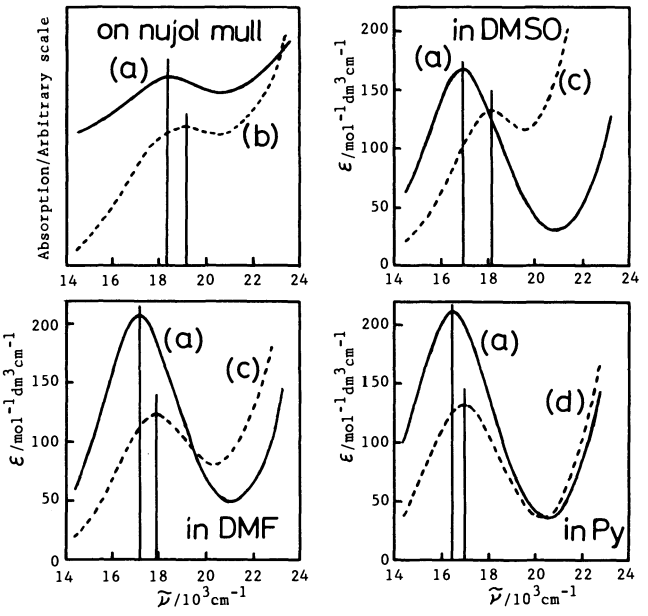

Fig. 2. The electronic spectra. (a): $[Cu(H_2fsaen)](H_2O)_{0.5}$, (b): $[CuLu(fsaen)(H_2O)_5](NO_3)$, (c): $[CuSm(fsaen)(H_2O)_4](NO_3)$, (d): $[CuGd(fsaen)(H_2O)_4](NO_3)$.

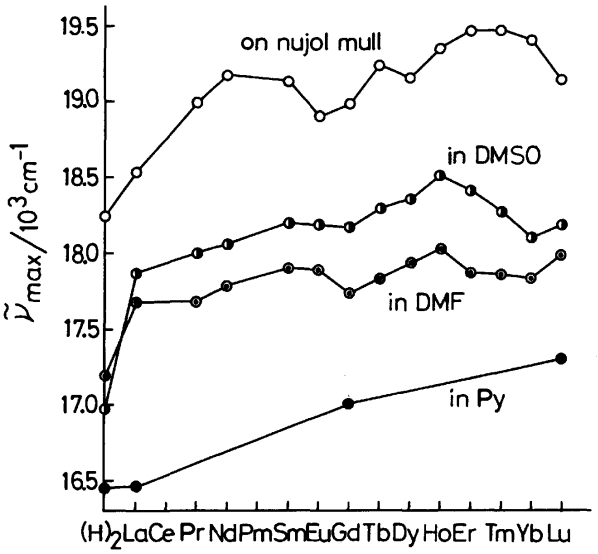

Fig. 3. The d-d band absorption maxima of [Cu(H2fsaen)](H2O)0.5 and [CuLn(fsaen)(H2O)n](NO3). (H)2, La, Pr, ···, and Lu of abscissa denote the mononuclear copper(II), copper(II)-lanthanum(III), copper(II)-praseodymium(III), ···, and copper(II)-lutetium(III) binuclear complexes, respectively.

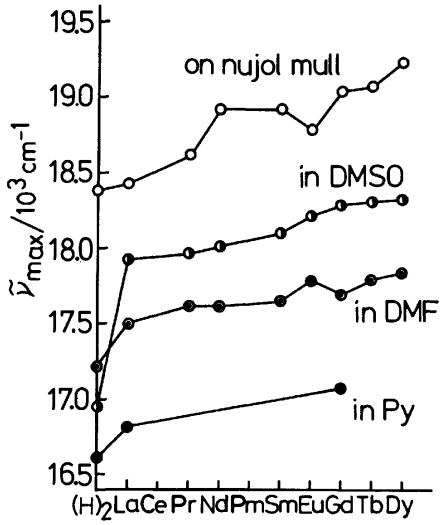

Fig. 4. The d-d band absorption maxima of [Cu(H2fsapn)](H2O)0.5 and [CuLn(fsapn)(H2O)4](NO3). (H)2, La, ···, and Dy of abscissa denote the mononuclear copper(II), copper(II)-lanthanum-(III), ···, and copper(II)-dysprosium(III) binuclear complexes, respectively.

planarity of the $[CuN_2O_2]$ chromophore on forming a binuclear complex with a lanthanoid ion at the outside coordination site as was observed for Cu(II)-M(II) (M=Co,Ni,Cu,Zn,Mg) heterometal binuclear complexes of *N,N'*-bis(3-carboxysalicylidene)-1,1-dibenzylethylenediamine.[5] The relatively small shift of the band for the CuLa complexes suggests that large lanthanum ion cannot reside in the outside coordination site and causes more or less a distortion of the $[CuN_2O_2]$ plane.

When the mononuclear copper(II) complexes were dissolved in pyridine (Py), dimethyl sulfoxide (DMSO), or *N,N*-dimethylformamide (DMF), the solutions were all blue. Their absorption spectra are given in Fig. 2. The frequency of the d-d band is in the following order of solvent: DMF>DMSO>Py(see also Figs. 3 and 4). This is quite understandable when one recalls the facts that the coordination at the apical site causes a red shift of the d-d band for planar copper(II) complexes and that the donating ability of the solvent increases in the order, DMF<DMSO<Py. On the other hand, solutions of the Cu(II)-Ln(III) complexes in Py are blue but those in DMSO or DMF purple. Accordingly, the spectra showed that the frequency of the d-d band is in the order, DMSO>DMF>Py. This may be explained by taking into consideration the difference in coordination affinity of a solvent molecule to copper(II) and lanthanoid(III) ions. Since pyridine has a higher affinity for copper(II) ion than for lanthanoid(III) ions, the pyridine molecule selectively coordinates to the copper(II) ion to result in the shift of the d-d band to lower frequency. On the other hand, DMSO and DMF have similar affinities for both copper(II) and lanthanoid(III) ions. If these solvents preferentially coordinate to the lanthanoid ion rather than the copper(II) ion to afford a high coordination number around the lanthanoid ion, then the coordinated solvent molecules block the apical part of the copper(II) ion and hence hinder the approach of other solvent molecules to the copper-(II) ion. Such a shielding must be more effective in DMSO than in DMF because the former solvent generally coordinates more strongly to lanthanoid ions. Planar copper(II) complexes of *N,N'*-disalicylideneethylenediamine and its homologs show the d-d band at 17.8×10^3—18.2×10^3 cm^{-1} in nondonative solvents.[5,24-26] These frequencies are comparable to those of the present binuclear complexes in DMSO, indicating that the coordination geometry of copper is essentially planar even in DMSO. It is presumed that the situation is nearly the same in DMF, judging from the d-d band frequency.

We have measured the ESR spectra of [Cu(H2fsaen)](H2O)0.5 and [CuLn(fsaen)(H2O)n](NO3) (Ln=La, Lu) in Py, DMSO, or DMF at liquid nitrogen temperature and found that ESR parameters, $g_{//}$ and $A_{//}$, are essentially the same for the mononuclear and binuclear complexes irrespective of the change of the solvent. This may be explained by that the axial coordination of the solvents (Py, DMSO, DMF) to the mononuclear complexes and the axial coordination of Py to the binuclear CuLn-complexes may destabilize the d_{z^2} orbital but this is not clearly detected by ESR because the d_{z^2} orbital is EPR-innocent.

The magnetic moments of the Cu(II)-Ln(III)

Table 3. Magnetic Moments of Complexes[a)]

Complex	Magnetic moment		Complex	Magnetic moment	
	μ_M[b)]	μ_M^{calcd}[c)]		μ_M[b)]	μ_M^{calcd}[c)]
$CuLa(fsaen)(NO_3)(H_2O)_4$	1.85	1.85	$CuYb(fsaen)(NO_3)(H_2O)_5$	4.80	5.20
$CuPr(fsaen)(NO_3)(H_2O)_4$	3.81	3.87	$CuLu(fsaen)(NO_3)(H_2O)_5$	1.81	1.85
$CuNd(fsaen(NO_3)(H_2O)_4$	3.85	3.96	$CuLa(fsapn)(NO_3)(H_2O)_4$	1.85	1.84
$CuSm(fsaen)(NO_3)(H_2O)_4$	2.43	2.43	$CuPr(fsapn)(NO_3)(H_2O)_4$	3.83	3.87
$CuEu(fsaen)(NO_3)(H_2O)_4$	3.80	3.89	$CuNd(fsapn)(NO_3)(H_2O)_4$	3.84	3.95
$CuGd(fsaen)(NO_3)(H_2O)_4$	8.04	8.12	$CuSm(fsapn)(NO_3)(H_2O)_4$	2.35	2.43
$CuTb(fsaen)(NO_3)(H_2O)_5$	9.69	9.68	$CuEu(fsapn)(NO_3)(H_2O)_4$	3.82	3.88
$CuDy(fsaen)(NO_3)(H_2O)_5$	10.53	10.56	$CuGd(fsapn)(NO_3)(H_2O)_4$	8.11	8.12
$CuHo(fsaen)(NO_3)(H_2O)_5$	10.43	10.56	$CuTb(fsapn)(NO_3)(H_2O)_4$	9.74	9.68
$CuEr(fsaen)(NO_3)(H_2O)_5$	9.68	9.58	$CuDy(fsapn)(NO_3)(H_2O)_4$	10.43	10.56
$CuTm(fsaen)(NO_3)(H_2O)_5$	7.32	7.34			

a) Moments are given in Bohr magneton, $\mu_B(=9.274\times10^{-24}\,Am^2$ in SI units). b) Experimental values at 287 K. c) Calculated from the equation, $\mu_M^{calcd}=\sqrt{(\mu_{Cu})^2+(\mu_{Ln})^2}$, where μ_{Cu} denotes the values,[4)] 1.85 μ_B (294.3 K) and 1.84 μ_B (292.9 K) for $Cu(H_2fsaen)(H_2O)_{0.5}$ and $Cu(H_2fsapn)(H_2O)_{0.5}$, respectively and μ_{Ln} are those reported[27)] for the general lanthanoid(III) compounds.

complexes at room temperature are summarized in Table 3, together with the moments calculated from the equation, $\mu_M^2=\mu_{Cu}^2+\mu_{Ln}^2$ using the reported moments, μ_{Cu}, for the mononuclear complexes[4)] and the common values, μ_{Ln}, of tervalent lanthanoid ions.[27)] The moments observed coincide approximately with the calculated values. The cryomagnetic investigations down to liquid nitrogen temperature ruled out the possibility of the operation of a spin-exchange interaction in these complexes: That is, their magnetic moments were practically independent of temperature in the range 78—300 K (except for the case of Cu(II)-Sm(III) and Cu(II)-Eu(III) complexes). It is known that the magnetic spin-exchange interaction between lanthanoid ions is very weak because the 4f-electrons are shielded by the outer-shell electrons. The present work reveals that no significant magnetic spin-exchange interaction is operating also between copper(II) and lanthanoid(III) ions.

The authors wish to express their hearty thanks to Professor Sigeo Kida of Institute for Molecular Science (Present: Kyushu University) and Associate Professor Yuzo Nishida of Yamagata University for their helpful discussions. They also would like to thank Mr. Masayuki Koikawa and Mr. Toshiro Kamiusuki of Kyushu University for measuring ESR spectra and magnetic susceptibilities, respectively.

References

1) C. P. Khattak and F. F. Y. Wang, "Handbook on the Physics and Chemistry of Rare Earths," ed by K. A. Gschneider, Jr., and L. Eyring, Morth-Holland Publishing Company (1979), Chap. 29.

2) H. Okawa and S. Kida, *Bull. Chem. Soc. Jpn.*, **45**, 1759 (1972).

3) H. Okawa, M. Tanaka, and S. Kida, *Chem. Lett.*, **1974**, 987.

4) M. Tanaka, M. Kitaoka, H. Okawa, and S. Kida, *Bull. Chem. Soc. Jpn.*, **49**, 2469 (1976).

5) W. Kanda, M. Nakamura, H. Ōkawa, and S. Kida, *Bull. Chem. Soc. Jpn.*, **55**, 471 (1982).

6) B. Tomlonovic, R. L. Hough, M. D. Glick, and R. L. Lintvedt, *J. Am. Chem. Soc.*, **97**, 2925 (1975).

7) D. E. Fenton and S. E. Gayda, *J. Chem. Soc., Dalton Trans.*, **1977**, 2095; **1977**, 2101.

8) K. K. Abid and D. E. Fenton, *Inorg. Chim. Acta*, **109**, L5 (1985).

9) H. Okawa, Y. Nishida, M. Tanaka, and S. Kida, *Bull. Chem. Soc. Jpn.*, **50**, 127 (1977).

10) M. Mikuriya, H. Okawa, S. Kida, and I. Ueda, *Bull. Chem. Soc. Jpn.*, **51**, 2920 (1978).

11) D. E. Fenton and S. E. Gayda, *J. Chem. Soc., Dalton Trans.*, **1977**, 2109.

12) R. L. Lintvedt, M. D. Click, B. Tomlonovic, and D. P. Gavel, *Inorg. Chem.*, **15**, 1646 (1976); M. D. Glick, R. L. Lintvedt, D. P. Gavel, and B. Tomlonovic, *ibid.*, **15**, 1654 (1976).

13) J. Galy, J. Jaud, O. Kahn, and P. Tola, *Inorg. Chem.*, **19**, 2945 (1980).

14) O. Kahn, J. Galy, P. Tola, and H. Coudanne, *J. Am. Chem. Soc.*, **100**, 3931 (1978).

15) O. Kahn, R. Claude, and H. Coudanne, *J. Chem. Soc., Chem. Commun.*, **1978**, 1012.

16) J. P. Beale, J. A. Cunningham, and D. J. Phillips, *Inorg. Chim. Acta*, **33**, 113 (1979).

17) J. C. Duff and E. J. Bills, *J. Chem. Soc.*, **1932**, 1987.

18) M. Tanaka, H. Okawa, I. Hanaoka, and S. Kida, *Chem. Lett.*, **1974**, 71.

19) M. Tanaka, H. Okawa, T. Tamura, and S. Kida, *Bull. Chem. Soc. Jpn.*, **47**, 1669 (1974).

20) R. B. King and P. R. Heckley, *J. Am. Chem. Soc.*, **96**, 3118 (1974).

21) F. A. Miller and C. H. Wilkins, *Anal. Chem.*, **24**, 1253 (1952).

22) A. B. P. Lever, E. Mantovani, and B. S. Ramaswany, *Can. J. Chem.*, **49**, 1957 (1971).

23) M. Sakamoto, *Bull. Chem. Soc. Jpn.*, **59**, 1273 (1986).

24) A. Nakahara, H. Yamamoto, and H. Matsumoto, *Bull.*

Chem. Soc. Jpn., **37**, 1137 (1964).
25) R. H. Holm, *J. Am. Chem. Soc.*, **82**, 5632 (1960).
26) R. S. Downing and F. L. Urbach, *J. Am. Chem. Soc.*, **91**, 5977 (1969).
27) T. H. Siddall, III, "Theory and Applications of Molecular Paramagnetism," ed by E. A. Boudreaux & L. N. Mulay, Wiley-Interscience Publication, New York (1976), p. 276.

An Ab Initio Molecular Orbital Study on the Conformations of Bicyclo[3.1.0]hexane Derivatives

Renji Okazaki,* Jun Niwa,*,† and Shigeki Kato††
Department of Chemistry, Faculty of Science, The University of Tokyo, Hongo, Tokyo 113
†College of General Education, Nagoya University, Chikusa, Nagoya 464
††Department of Chemistry, College of Arts and Sciences, The University of Tokyo, Komaba, Tokyo 153
(Received June 8, 1987)

Ab initio calculations have been carried out for 2,4-dithia- (**5**), 2,4-dioxa- (**6**), 6-oxa- (**8**), 6-thiabicyclo-[3.1.0]hexanes (**9**), bicyclo[3.1.0]hexane (**7**), and some of the corresponding cyclohexane derivatives **10—12** using 3-21G, 3-21G(*), and 6-13G* basis sets. Relative total energies and geometries have been obtained for both boat and chair forms of these compounds. The calculated geometries are in good agreement with observed ones for **7—9**. The boat form is more stable than the chair form in the bicyclic systems **7—9**, while both the forms have almost equal stability for **5** and the chair form of **6** is slightly more stable than the boat form. The relative stability of the boat form in the bicyclic systems compared with that in the monocyclic cyclohexane derivatives can be explained in terms of the stabilizing orbital interaction. Inversion barriers between the boat and chair forms for **5—7** have also been estimated and are briefly discussed. A similar calculation for bicyclo[3.2.0]hept-6-ene also shows that the boat form is much more stable than the chair form contrary to the conclusion derived from the analysis of experimental results.

In our previous study on stereoselective reactions of carbanions of dithiabicyclo[3.1.0]hexanes, we performed ab initio calculations of the dithiabicyclohexanes and the corresponding dithianes and revealed that the carbanion **1** of boat form is most stable among isomeric carbanions **1—4** and that the boat and chair forms of the corresponding neutral molecules **5B** and **5C** have almost equal stability.[1] The structures of similar bicyclic systems, such as bicyclo[3.1.0]hexane (**7**),[2] 6-oxabicyclo[3.1.0]hexane (**8**),[3] and 6-thiabicyclo[3.1.0]hexane (**9**),[4] have been determined spectroscopically to be a boat form. These computational and experimental results suggest that the high stability of the boat form is a general trend in bicyclo[3.1.0]hexane systems, which stands in a sharp contrast to the well-established fact that the chair form is much more stable in the case of the corresponding monocyclic six-membered systems.[5]

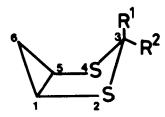

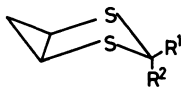

1	R^1=H, R^2=—	**3**	R^1=H, R^2=—
2	R^1=—, R^2=H	**4**	R^1=—, R^2=H
5B	R^1=R^2=H	**5C**	R^1=R^2=H

We have become interested in why the boat form in the bicyclic systems has relatively high stability in spite of the unfavorable steric interaction between inward hydrogens on C_3 and C_6, and have carried out accurate ab initio geometry optimizations on these bicyclohexane derivatives and some related compounds. The main purpose of this account is to elucidate the factors determining the stability of the boat form from the standpoint of orbital interaction. We also report on inversion barriers between boat and chair forms in some representative bicyclohexane systems.[6]

Computational Details. The geometries for all the structures considered were completely optimized by energy gradient method at the Hartree-Fock level of theory. The standard split-valence 3-21G and 3-21G(*) basis sets (including a set of d-type polarization functions for sulfur atoms) were used in these optimizations. This level of theory has been demonstrated

Table 1. Relative Energies (kcal mol^{-1}) of Compounds **5—13**

Compound	3-21G	3-21G(*)	6-31G*	Compound	3-21G	3-21G(*)	6-31G*
5B	0.1	0.0[b]	0.0[c]	**9C**	4.1	4.3	4.5
5C	0.0[a]	0.5	0.0	**10B**	7.6		7.9
6B	0.4		0.9	**10C**	0.0[m]		0.0[n]
6C	0.0[d]		0.0[e]	**11B**	5.3		6.6
7B	0.0[f]		0.0[g]	**11C**	0.0[o]		0.0[p]
7C	3.1		3.3	**12B**	4.4	5.5	5.5
8B	0.0[h]		0.0[i]	**12C**	0.0[q]	0.0[r]	0.0[s]
8C	3.9		3.8	**13B**	0.0[t]		0.0[u]
9B	0.0[j]	0.0[k]	0.0[l]	**13C**	5.8		5.4

a) −945.1732 hartree. b) −945.3897 hartree. c) −949.9442 hartree. d) −302.9175 hartree. e) −304.6136 hartree. f) −231.7045 hartree. g) −233.0001 hartree. h) −267.3151 hartree. i) −268.8144 hartree. j) −588.4676 hartree. k) −588.5693 hartree. l) −591.4921 hartree. m) −232.9169 hartree. n) −234.2076 hartree. o) −304.1405 hartree. p) −305.8302 hartree. q) −946.3860 hartree. r) −946.6008 hartree. s) −951.1499 hartree. t) −269.3375 hartree. u) −270.8410 hartree.

to be reliable in the calculation of molecular geometries for a wide variety of systems.[7] In order to obtain more reliable energy estimates we have repeated the calculations with 6-31G* basis at the 3-21G or 3-21G(*) optimized geometries.

Calculated Relative Energies and Geometries. Relative energies obtained for **5**—**12** are listed in Table 1. The pertinent points in Table 1 are as follows: (1) For monocyclic systems **10**—**12**, the chair form is much more stable than the boat form, as is well known experimentally.[5] (2) In contrast to the monocyclic systems, the boat form is definitely more stable than the chair form in the bicyclic systems **7**—**9** where the five-membered ring consists of only carbon atoms. This also agrees with the experimental results that each of them exists only as a boat-form conformation.[2-4] (3) For bicyclic compounds having heteroatoms at 2- and 4-positions, **5** and **6**, although the stability of a boat form becomes less pronounced than in the case of **7**—**9**, the boat form has the stability almost equal to the chair form in the sulfur heterocycle **5**, and the boat form of the oxygen heterocycle **6** is very slightly less stable than its chair form.

Comparison of Calculated and Observed Geometries. Calculated geometries obtained for **5**—**9** are listed in Table 2[8] along with the observed geometries for **7**—**9**. As mentioned previously each of **7**—**9** has been reported to exist as the boat conformer in keeping with the present calculations. The calculated geometries are in good agreement with the experimental ones with the only exception of C_1—C_5 bond length of **7B** where the calculated value is longer than the observed one by 0.06 Å. The reason for this discrepancy has not been clear up to the present. There are some interesting features in the geometries of these compounds. (1) The angles between the planes $C_1C_5X_6$ and $C_1X_2X_4C_5$ (X=C, O, or S) in **5**, **6**, **7**, and **9** (denoted as α hereafter) are almost constant, ca. 110°, while those for **8B** and **8C** are 103—105°. (2) The angle between the planes $C_1X_2X_4C_5$ and $X_2C_3X_4$ (X=C, O, or S) (denoted as β hereafter) is constant, 150—152°, in the boat form except for 161° in **6B**. In the chair form, however, those having carbon atoms at 2- and 4-positions have β of 161° while those having heteroatoms at these positions have a smaller β (151—154°). (3) When the boat form is more stable than the chair form, β in the boat form is always smaller than β in the chair form. Conversely, when the chair form is more stable than the boat form, β in the chair form is smaller than that in the boat form. In an intermediate case where both the boat and chair forms have a

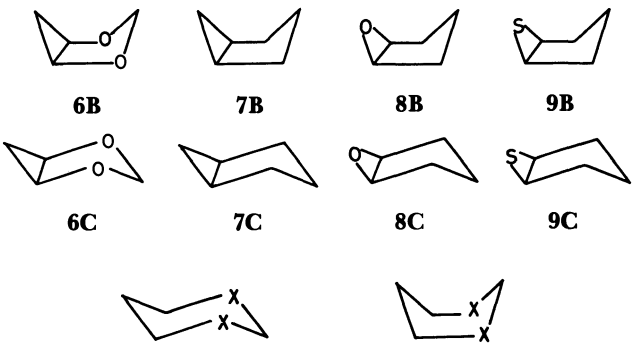

10 X=CH_2
11 X=O
12 X=S

Table 2. Bond Lengths (Å) and Bond Angles (deg) in **5**—**9** and **13** as Determined by Calculations (3-21G or 3-21G(*))[a,b]

Compd	X_2–C_1 (X_4–C_5)	X_2–C_3 (X_4–C_3)	C_1–C_6[c] (C_5–C_6)	C_1–C_5	X_6–H_3[d]	$\angle C_1X_2C_3$ ($\angle C_5X_4C_3$)	$\angle\alpha$[e]	$\angle\beta$[e]
5B	1.784	1.824	1.513	1.511	2.663	96.0	113.1	149.8
5C	1.790	1.824	1.511	1.511		96.8	110.8	149.8
6B	1.427	1.440	1.516	1.490	2.470	107.9	111.6	161.4
6C	1.432	1.438	1.510	1.499		107.1	109.3	153.6
7B	1.524	1.554	1.514	1.515	2.231	104.7	110.3	149.7
	(1.543)	(1.543)	(1.515)	(1.454)			(109.4)	(154.8)
7C	1.527	1.559	1.512	1.515		105.7	109.8	160.9
8B	1.512	1.557	1.477	1.472	2.683	103.9	104.3	151.8
	(1.513)	(1.53)	(1.443)	(1.482)		(104.0)	(104.7)	(152.3)
8C	1.516	1.561	1.477	1.475		105.0	103.4	160.6
9B	1.526	1.554	1.828	1.493	2.937	104.5	110.7	150.3
	(1.513)	(1.530)	(1.819)	(1.471)			(110—120)	(150)
9C	1.532	1.561	1.826	1.493		105.2	110.3	160.9
13B[f]	1.537	1.550	1.537	1.599		105.1	114.2	145.0
13C[f]	1.542	1.559	1.540	1.593		106.8	114.6	160.9

a) Calculations were carried out for **5** and **9** with 3-21G(*) and for **6**—**8** and **13** with 3-21G basis. b) Values in parentheses for **7B**, **8B**, and **9B** are observed values. c) C_1–C_7 for **13**. d) This represents the distance between the two inward hydrogens on C_3 and C_6 for **5B**, **6B**, and **7B**, and that between the inward hydrogen on C_3 and the heteroatom at 6-position for **8B** and **9B**. e) α and β are dihedral angles between two planes $C_1C_6C_5$ and $C_1X_2X_4C_5$ and between two planes $X_2C_3X_4$ and $C_1X_2X_4C_5$, respectively. f) C_6–C_7 is 1.326 and 1.325 Å for **13B** and **13C** respectively.

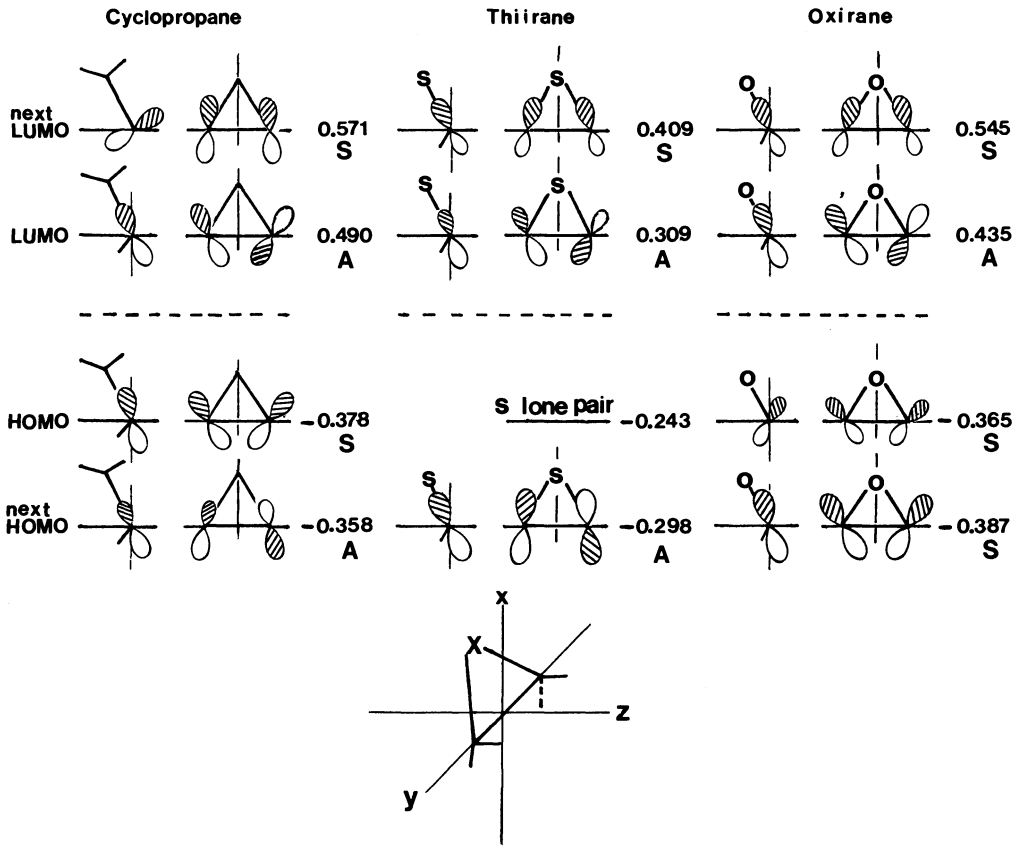

Fig. 1. Some important molecular orbitals in cyclopropane, thiirane, and oxirane.

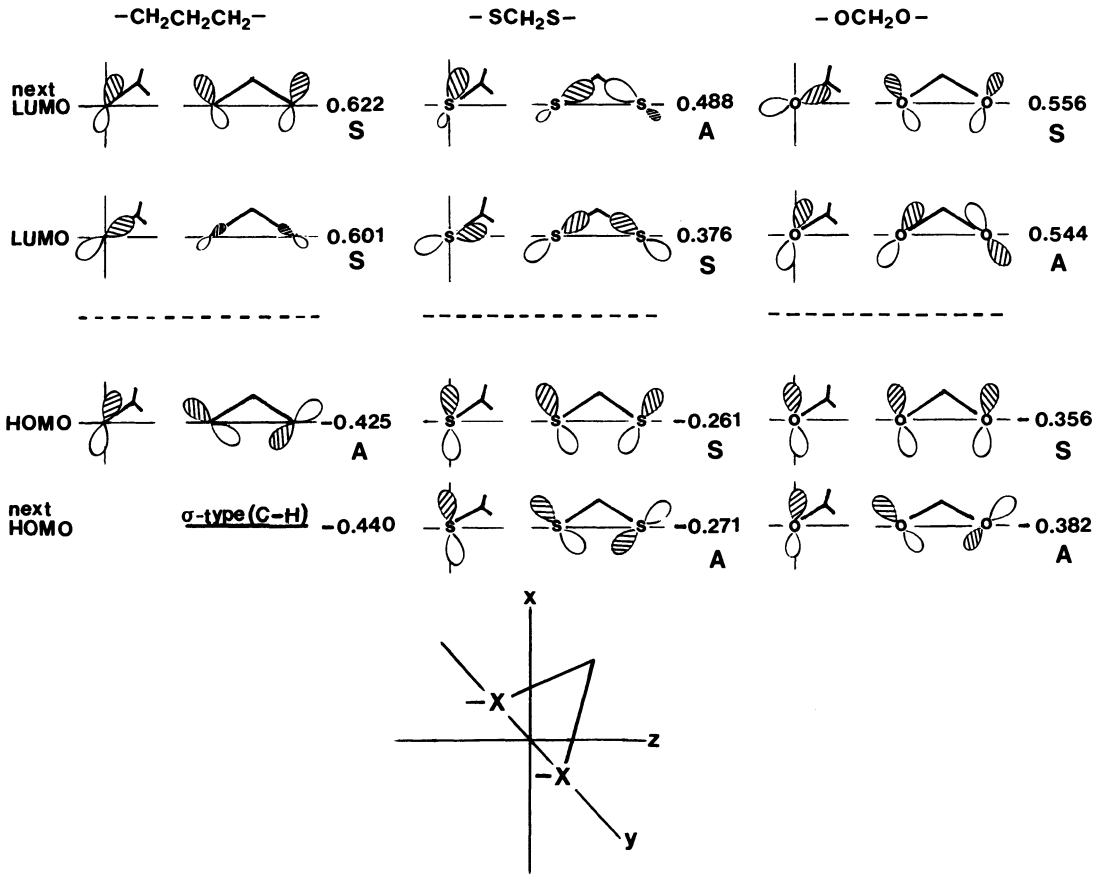

Fig. 2. Some important molecular orbitals in $HXCH_2XH$ moiety (X=CH_2, S, O).

similar stability, β's in the both forms are similar. (4) As for bond lengths, there is no essential difference between those for the boat and the chair conformers.

Rationale for the High Stability of Boat Forms. In view of the high stability of a chair form of monocyclic six-membered systems, it is remarkable that the boat form is highly stabilized in bicyclohexane systems. Although the chair form is more stable than the boat form in the case of **6**, the difference in energy between the two conformers is only 0.9 kcal mol^{-1}, which is much smaller than the corresponding difference for **11**, i.e., 6.6 kcal mol^{-1}.

In order to explain this high stabilization of the boat form, we have considered the orbital interactions between the three membered ring and the XCH_2X parts (X=CH_2, O, S). In Figs. 1 and 2 are shown some occupied and unoccupied orbitals of these parts pertinent to the following discussion.

The figures indicate that there exists an in-phase orbital interaction between LUMO of the three-membered ring and HOMO or next HOMO of the XCH_2X group. This orbital interaction mainly contributes to the relative stabilization of the boat form. On the other hand, in the chair forms such an efficient orbital interaction cannot exist, because the downside lobe of HOMO (or next HOMO) on the XCH_2X group is tilted outward in contrast with the case of the boat form as illustrated in Fig. 3 with **5** as an example.

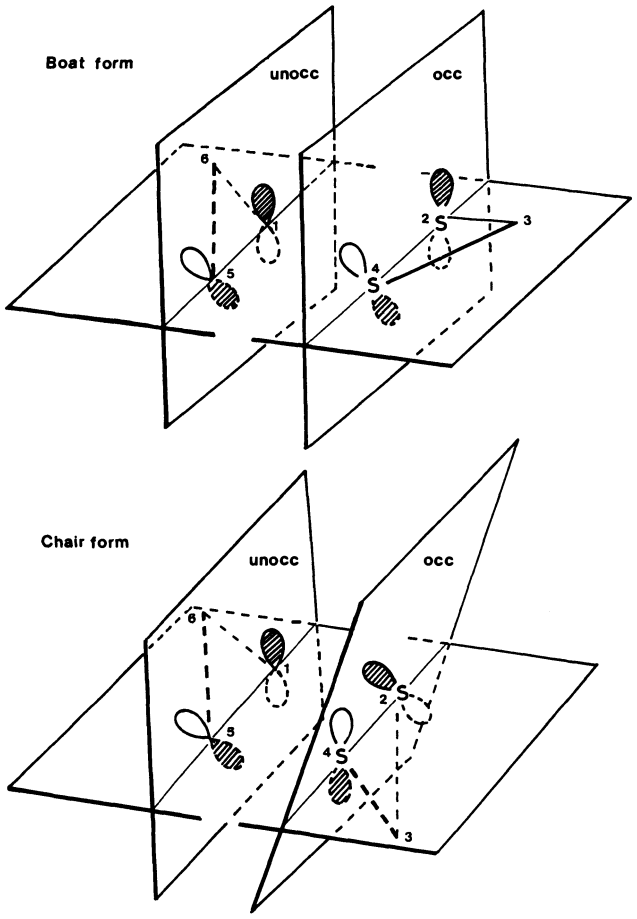

Fig. 3. Molecular orbital interaction between cyclopropane and SCH_2S moieties in **5B** and **5C**.

Dithiabicyclohexane 5B and Dioxabicyclohexane 6B: In **5B**, the most favorable interaction is that between LUMO on C_1—C_5 (antisymmetric, denoted as (A) hereafter) of the cyclopropane and the next HOMO of the lone pair on sulfur atoms, (A), of SCH_2S moiety the orbital energy of which is very close to that of HOMO (Fig. 2). The cyclopropane HOMO (S)-SCH_2S LUMO(S) interaction is also conceivable but it is not efficient because the lobe of LUMO on sulfur atoms is pointed to the direction almost perpendicular to the cyclopropane orbital.

The stabilizing interaction in **6B** is similar to that of **5B** except that the HOMO-LUMO energy difference is larger because of the higher electronegativity of oxygen. This larger difference is probably responsible for the less stability of the boat form **6B** than **5B**.

6-X-Bicyclohexanes (X=CH_2, O, S), 7B, 8B, and 9B: In **7B**, there exists an in-phase interaction between cyclopropane LUMO (A) and large back lobes (HOMO(A)) of pseudo-equatorial C-H bonds at 2- and 4-positions. The stabilization of the boat form is mainly attributed to this type of interaction. The cyclopropane HOMO(S)-$CH_2CH_2CH_2$ LUMO(S) cannot cause the stabilization, because LUMO of $CH_2CH_2CH_2$ moiety is directed toward C_1-C_2 (or C_4-C_5) bond axis(i.e., z-axis). As can be seen from HOMO and LUMO of ethylene oxide and ethylene sulfide shown in Fig. 1, the stabilizing interaction in **8B** and **9B** can be explained in a manner similar to **7B**, namely, the interaction between cyclopropane-like Walsh-type orbital and the back lobes of C-H bonds at 2- and 4-positions.

The higher stability of cyclohexane **10C** vs. **10B** has traditionally been explained in terms of the two pairs of unfavorable eclipsed interaction in the CH_2CH_2 bond and the steric repulsion between inward hydrogens of the bow and stern carbons in the boat form.[9] Inspection of the molecular model of bicyclo[3.1.0]-hexane suggests that the former type of eclipsed interaction exists between C_1H and quasi-equatorial C_2H in the chair form, **7C**, while the relationship between those hydrogens becomes gauche in the boat form, **7B**. The relative stability of **7B** vs. **7C** has exclusively been attributed to this type of unfavorable interaction in **7C**.[10] However, the latter type of steric interaction between inward hydrogens on C_1 and C_4 in **10B** should be more conspicuous in **7B** because the presence of the cyclopropane ring makes the distance between inward hydrogens on C_3 and C_6 shorter as judged by the molecular model. The calculated geometries of **10B** and **7B** also support the above argument since the distance in question is 2.355 Å in

10B and 2.231 Å in **7B** which is rather close to the sum of the van der Waals radii of two hydrogen atoms. This implies that the boat forms in **7—9** must be stabilized by some other factors in spite of this severe repulsive interaction. It is strongly suggested, therefore, that the above-mentioned stabilization due to stereoelectronic effect plays an important role in these compounds. In this connection, it is interesting that β in the boat form is always smaller than β in the chair form when the boat form is more stable than the chair form (see point (3) in the previous section). Since the HOMO-LUMO interaction becomes more effective in parallel with decrease of β in **7B**, **8B**, and **9B**, the values of β are considered to become small in spite of the repulsive interaction between C_3H-C_6H (or C_3H-X_6 lone pair). The reason for the large β value in **6B** is not very clear at present, but it is most likely that the large β is a consequence of a compromise between the HOMO-LUMO interaction and C_3H-C_6H repulsion which becomes relatively serious in this case because of shorter C-O (1.427 and 1.440 Å) than C-C bond distances (1.524 and 1.554 Å).

Conformation of Bicyclo[3.2.0]hept-6-ene. Chiang and Bauer studied the structure of bicyclo[3.2.0]hept-6-ene (**13**) by microwave spectroscopy and reported that it has a chair form.[11] In view of the above-mentioned general trend that bicyclo[3.1.0]hexane

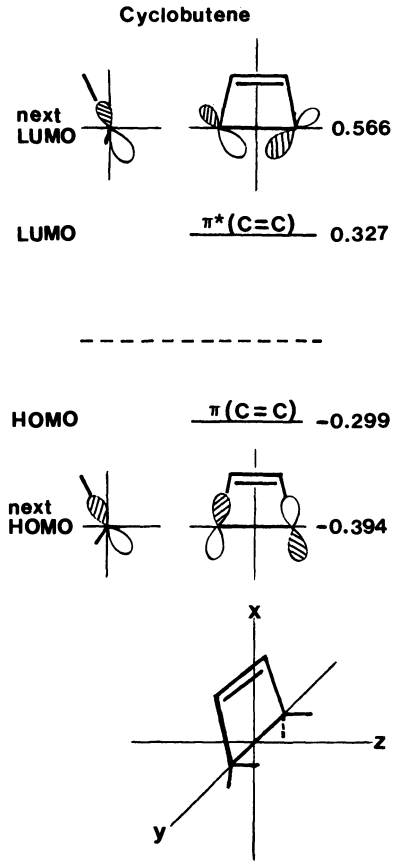

Fig. 4. Some important molecular orbitals in cyclobutene.

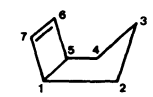

13B

13C

derivatives have a boat form, we have become interested in why the bicycloheptene **13** prefers the chair form to the boat form and have carried out ab initio calculations for this compound. The results are shown in Tables 1 and 2. The calculation indicates that the boat form is obviously more stable than the chair form, and indeed here again exists the stabilizing interaction between the cyclobutene ring and the $(CH_2)_3$ moiety similar to that for **7B** discussed above (Figs. 2 and 4). In view of the fact that the present calculations correctly reproduce experimental results both in the relative energies and geometries of **7—9**, we think that there is some room for doubt in the structual analysis of Chiang and Bauer and reexamination of the structure of **13** is highly desirable.

Energy Barrier of Boat-Chair Interconversion. In order to obtain information on the barrier of boat-chair interconversion, we have carried out ab initio calculations for the representative bicyclic systems, **5**, **6**, and **7**. In the calculations, atoms 1, 2, 4, and 5 are fixed on the same plane and atom 3 is fixed so as to be x Å apart from the plane. Under this constraint geometry optimizations have been performed at several x values. As can be seen from Fig. 5, the barrier height for the boat-chair conversion of **6** and **7** are almost zero in each case and hence it is suggested that the boat form of **6** and the chair form of **7** actually cannot exist as a stable conformer. In the case of **5** there is a definite barrier for interconversion between the boat and chair forms. However, it is so small that each conformer is considered to be able to undergo

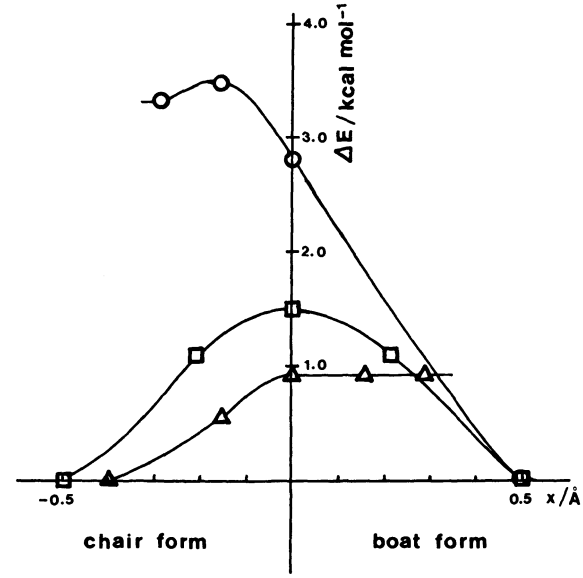

Fig. 5. Energy barrier of boat-chair interconversion in **5**, **6**, and **7**. □: **5**, △: **6**, ○: **7**.

almost free interconversion at least at ambient temperature.[12]

Conclusion

Relative energies and geometries have been calculated by ab initio method for boat and chair forms of bicyclohexane derivertives **5**—**9**. Contrary to monocyclic cyclohexane derivatives **10**—**12** which exist as a chair conformer, the stability of a boat form is much increased in the bicyclic compounds and in the case of **7**—**9** the boat conformer becomes a more stable one. The stability of the boat conformer has been found to result from the stabilizing orbital interaction between HOMO of the three-membered ring and LUMO of the $Y_3CH_2Y_4$($Y=CH_2$, O, or S) group. Calculation on bicyclo[3.2.0]-hept-6-ene has revealed that the boat conformer is preferred again in this case contrary to the conclusion derived from the experimental result, thus necessitating reexamination of the structural analysis of this compound. Calculated energy barriers for **5**—**7** have indicated that **6** and **7** exist only as the chair and boat forms, respectively, while **5** undergoes free interconversion between the boat and chair conformers.

The numerical calculations were carried out with the IMSPACK program at the Nagoya University Computation Center.

References

1) R. Okazaki, M. O-oka, T. Akiyama, N. Inamoto, J. Niwa, and S. Kato, *J. Am. Chem. Soc.*, **109**, 5413 (1987).

2) V. S. Mastryukov, E. L. Osina, L. V. Vilkov, and R. L. Hilderbrandt, *J. Am. Chem. Soc.*, **99**, 6855 (1977).

3) R. L. Hilderbrandt and J. D. Wieser, *J. Mol. Struc.*, **22**, 247 (1974).

4) P. J. Mjoberg, W. M. Ralowski, and S. O. Ljunggren, *J. Mol. Struc.*, **60**, 179 (1976).

5) F. A. Carey and R. J. Sundberg, "Advanced Organic Chemistry," Plenum Press, New York (1984), Part A. Chap. 3.

6) Part of this work was presented at 8th International Conference on Physical Organic Chemistry (August, 1986 in Tokyo, Japan).

7) See for example, D. J. DeFrees, B. A. Levi, S. K. Pollack, W. J. Hehre, J. S. Binkley, and J. A. Pople, *J. Am. Chem. Soc.*, **101**, 4085 (1979); W. J. Pietro, M. M. Francl, W. J. Hehre, D. J. DeFrees, J. A. Pople, and J. S. Binkley, *J. Am. Chem. Soc.*, **104**, 5039 (1982).

8) Ab initio calculations (4-31G) on the geometry of **7B** have been reported: P. N. Skancke, *J. Mol. Struct.*, **86**, 255 (1982). Our calculated values for **7B** are in good agreement with those reported.

9) E. L. Eliel, "Stereochemistry of Carbon Compounds," McGraw-Hill, New York (1962), Chap. 8.

10) S. Chang, D. McNally, S. Shary-Tehrany, S. M. J. Hickey, and R. H. Boyd, *J. Am. Chem. Soc.*, **92**, 3109 (1970).

11) J. F. Chiang and S. H. Bauer, *J. Am. Chem. Soc.*, **88**, 420 (1966).

12) The NMR spectra of dithiabicyclohexanes I and II[1] have indicated that there is no essential change between 20 °C and −70 °C. It suggests that freezing of the flipping of the five membered ring does not occur at least at −70 °C, consistent with the present calculations.

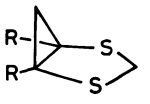

I: R = CH_3
II : RR = $(CH{=}CH)_2$

 © 1988 The Chemical Society of Japan Bull. Chem. Soc. Jpn., 61, 1625—1631 (1988)

Preparation of Fluorine-Containing Phenylacetylenes by the Method of Introduction of the Ethynyl Group Using 1,1-Dichloro-2,2-difluoroethene

Kazuo KODAIRA and Kunio OKUHARA*
Government Industrial Research Institute, Nagoya, Hirate-cho, Kita-ku, Nagoya 462
(Received June 29, 1987)

Phenylacetylenes (ArC≡CH) having fluoro- or trifluoromethyl substituents (*o*-, *m*-, *p*-F; *o*-, *m*-, *p*-CF_3; 2,4-, 2,5-, 2,6-, 3,5-$(CF_3)_2$) have been prepared from bromobenzenes (ArBr) and benzenes (ArH) using 1,1-dichloro-2,2-difluoroethene (**1**) by a two-step route: ArLi or ArMgBr→ArCF=CCl_2→ArC≡CLi. Upon careful treatment at −70 °C with **1**, *o*-fluorophenyllithium gave *o*-$FC_6H_4CF{=}CCl_2$ in good yield, together with benzyne-derived products, such as *o*-(*o*-FC_6H_4)$C_6H_4CF{=}CCl_2$. Lithiation of *m*-bis(trifluoromethyl)benzene at 0 °C for 9 h (24 h) followed by treatment with bromine gave 1-bromo-2,4-, 2,6-, and 3,5-bis(trifluoromethyl)benzene in 35 (38), 31 (36), and 8% (6%) yield, respectively.

In connection with projects to prepare polymers of fluorine-containing acetylenes and diacetylenes and to examine their applications, it became neccessary to prepare phenylacetylenes having fluoro or trifluoromethyl substituents. Previously, such phenylacetylenes were prepared mostly[1] from the corresponding acetophenones[2–4] and styrenes.[5,6] When relatively inexpensive bromofluorobenzenes and bromo(trifluoromethyl)benzenes are used as the starting material,[7] these routes require at least four steps,[5,6,8] and the overall yields of these multistep preparations are often low. Palladium-catalyzed coupling with ethynyltrimethylsilane followed by a hydrolytic removal of the trimethylsilyl group is a recently developed method for the conversion of aryl bromides (or iodide) into the corresponding arylacetylenes.[9,10] *m*-(Trifluoromethyl)-phenylacetylene was prepared by this method with an overall yield of 40%.[10]

The method of introduction of the ethynyl group using 1,1-dichloro-2,2-difluoroethene ($CF_2{=}CCl_2$, **1**), presented previously by one of us,[11,12] seemed to be easily applicable for the preparation of phenylacetylenes having fluoro or trifluoromethyl subsituents. A subsequent study has shown that not only the phenylacetylenes having *m*-F, *p*-F, *o*-CF_3, *m*-CF_3, and *p*-CF_3 as substituents are prepared in overall yields ranging from 48 to 69%, starting with the corresponding bromobenzenes, but also this method is applicable for the preparation of *o*-fluorophenylacetylene, for which the reaction of unstable *o*-fluorophenyllithium with **1** is involved. Furthermore, among the six isomeric bis(trifluoromethyl)phenylacetylenes, on which little information is available, four compounds were obtained. Considerable efforts have also been devoted toward a clarification of complications encountered in the lithiation of *m*-bis(trifluoromethyl)benzene and in the reaction of the resulting phenyllithiums with **1**.

The course of the present synthesis is given in Scheme 1. It consists of the first step: the preparation of the 2,2-dichloro-1-fluoroethenyl intermediates (**6**) and the second step: the conversion of these intermediates into the corresponding terminal acetylenes **8**.[11] The second step was carried out in good yield in every case by using the standard conditions. For the first step, however, the reaction conditions had to be examined in individual cases in order to obtain satisfactory results.

m- and *p*-$FC_6H_4CF{=}CCl_2$ (**6b** and **6c**) were prepared from *m*- and *p*-bromofluorobenzene, respectively, both via the Grignard reagents and via the corre-

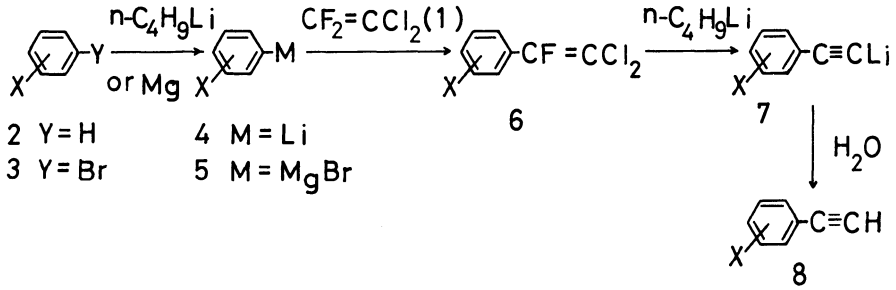

a X=*o*-F **b** X=*m*-F **c** X=*p*-F **d** X=*o*-CF_3 **e** X=*m*-CF_3 **f** X=*p*-CF_3 **g** X=2,4-$(CF_3)_2$ **h** X=2,5-$(CF_3)_2$ **i** X=2,6-$(CF_3)_2$ **j** X=3,5-$(CF_3)_2$ **k** X=*o*-(*o*-FC_6H_4)

Scheme 1. Course of preparation of fluorine-containing phenylacetylenes (**8**).

sponding organolithium reagents. The yields of **6b** and **6c** obtained via the Grignard reagents **5** were substantially higher than those obtained via the fluorophenyllithiums (**4**). The yields of **6b** and **6c** via the fluorophenyllithiums, when ethereal solutions of the fluorophenyllithiums were not kept cold before and during the addition to solutions of **1**, were even considerably lower than those given in Table 1. It appears that these fluorophenyllithiums[13] have a tendency to form polyphenyls with an elimination of lithium fluoride.

Initially, no attempt was made for the preparation of *o*-$FC_6H_4CF{=}CCl_2$ (**6a**) because of the known tendency of *o*-fluorophenyllithium (**4a**) to lose lithium fluoride to form benzyne.[14] Later, a careful low-temperature treatment of **4a** with **1** was found to give **6a** in a good yield. The method consists of the preparation of *o*-fluorophenyllithium (**4a**)[15] at −80 °C, the addition of **1** at lower temperatures, and allowing the reaction of **4a** with **1** to proceed within a temperature range between −80 and −70 °C until **4a** is mostly consumed. This reaction should be conducted on a small scale with great precaution (see the section of **6a** in Experimental). In this procedure, the formation of products **6k** and **10k** derived from *o*-(*o*-fluorophenyl)phenyllithium (**4k**), which results from a decomposition of **4a** into benzyne (**9**) followed by addition of another molecule of **4a**, was more or less unavoidable (Scheme 2). We also obtained a compound to which the structure *o*-$(CF_2{=}CCl)C_6H_4CF{=}CCl_2$ (**12**) was assigned on the basis of spectroscopic data. The formation of **12** could be explained in terms of the addition of $CF_2{=}CClLi$, which is formed from **1** by a Cl–Li exchange,[11] to **9** followed by a reaction of the resulting lithium compound **11** with **1**.

For the preparation of *o*-, *m*-, and *p*-$CF_3C_6H_4CF{=}CCl_2$ (**6d**, **6e**, and **6f**) from the respective isomers of bromo(trifluoromethyl)benzenes, both the route via the

Table 1. Isolated Yields[a,b] of Dichlorofluoroethenyl Intermediates (**6**) and Phenylacetylenes (**8**)

Starting compound (**2** or **3**)	Substituent	Yield of **6**/%		Yield of **8**/%
		via **4**	via **5**	
o-Bromofluorobenzene	**a**	75		87
m-Bromofluorobenzene	**b**	48	82 (18)	84
p-Bromofluorobenzene	**c**	62	79 (24*)	82
o-Bromo(trifluoromethyl)benzene	**d**	77 (1)	0[c] (30)	86
m-Bromo(trifluoromethyl)benzene	**e**	56	72 (21**)	80
p-Bromo(trifluoromethyl)benzene	**f**	61 (1)	61 (19**)	78
1-Bromo-2,4-bis(trifluoromethyl)benzene	**g**	67		78
p-Bis(trifluoromethyl)benzene	**h**	72		78
1-Bromo-2,6-bis(trifluoromethyl)benzene	**i**	48[d] (15*)		83
1-Bromo-3,5-bis(trifluoromethyl)benzene	**j**	80		85
(*o*-Bromofluorobenzene)	**k**	9[e]		82

a) Based on charged starting material. b) Total refluxing times (h) with **1** in ether are indicated in parentheses; continuous (unmarked), with one overnight interruption in 2 days (*), with two overnight interruptions in 3 days (**). Where no parenthesized figure is given, the reaction mixture was hydrolyzed without refluxing. c) Determined yield was 0.1%. d) Hexane–ether was used as solvent. Compound **13i** (2,6-$(CF_3)_2C_6H_3C{\equiv}CCl$) in 4% yield was also obtained. e) Yield obtained as by-product of the reaction where **6a** was the main product (75%).

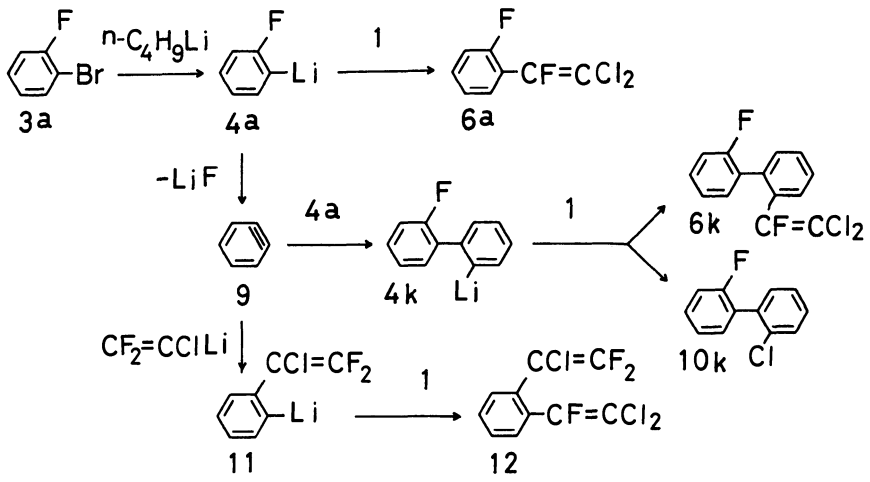

Scheme 2. Reaction of *o*-fluorophenyllithium (**4a**) with **1**.

Grignard reagents and the route via the corresponding lithium reagents were examined. In the case of the *m*-isomer **6e**, the use of the Grignard reagent gave a higher yield, as has been already reported.[11] However, the yield of the *p*-isomer **6f** obtained from the Grignard reagent was the same as that obtained from the corresponding lithium reagent. Furthermore, *o*-(trifluoromethyl)phenylmagnesium bromide (**5d**) gave no more than a trace amount of *o*-$CF_3C_6H_4CF{=}CCl_2$ (**6d**) upon treatment with **1** under reflux for 30 h, whereas *o*-(trifluoromethyl)phenyllithium (**4d**) gave **6d** in 77% yield.

The use of (trifluoromethyl)benzene (benzylidyne trifluoride: IUPAC; benzotrifluoride: trivial) as the starting material for the preparation of (trifluoromethyl)phenylacetylenes has two disadvantages: Slow lithiation and the formation of isomers.[16,17] Nevertheless, the low cost and easy availability of (trifluoromethyl)benzene makes this route worth examining. In a typical experiment, 0.9 mol of (trifluoromethyl)-benzene was refluxed for 23 h in an ethereal solution of butyllithium prepared from 1 mol of butyl bromide. A subsequent treatment with **1** afforded a mixture of **6d**, **6e**, and **6f**. Since a mutual separation of isomers at this stage was difficult, the mixture was converted into an isomeric mixture of (trifluoromethyl)phenylacetylenes (35% yield of **8d** and 15% yield of **8e**+**8f** based on unrecovered (trifluoromethyl)benzene) by a treatment with butyllithium. A fractional distillation of this isomeric mixture under reduced pressure gave nearly pure *o*-(trifluoromethyl)phenylacetylene (**8d**, higher boiling), although the *m*-isomer **8e** was obtained only as a mixture containing the *o*-isomer as well as the *p*-isomer.

The activation of the benzene ring by an additional trifluoromethyl group para to the original trifluoromethyl group makes the lithiation definitely easier. Thus, *p*-bis(trifluoromethyl)benzene was readily lithiated by a treatment with butyllithium under reflux for 4 h, and subsequent reaction with **1** afforded 2,5-$(CF_3)_2C_6H_3CF{=}CCl_2$ (**6h**) in 72% yield. The relatively high yield is attributed not only to the formation of a single isomer **4h** from the lithiation of *p*-bis(trifluoromethyl)benzene but also to the apparent high stability of **4h** in the lithiated mixture. The latter point is in sharp contrast to the instability of **4g** and **4j** in the mixture obtained from *m*-bis(trifluoromethyl)-benzene by lithiation (vide infra).

Lithiation of *m*-bis(trifluoromethyl)benzene[18,19] gives 2,4- (**4g**), 2,6- (**4i**), and 3,5-bis(trifluoromethyl)-phenyllithium (**4j**). Initial attempts to obtain the isomers of $(CF_3)_2C_6H_3CF{=}CCl_2$ (**6g**, **6i**, and **6j**) by the treatment of such lithiated mixtures with **1** were met with unpredictable and sometimes unreproducible results. After a considerable number of experiments, it was found that 3,5-bis(trifluoromethyl)phenyllithium (**4j**), first, and the 2,4-isomer **4g**, next, tended to disappear when reaction mixtures obtained by lithiation of *m*-bis(trifluoromethyl)benzene under refluxing conditions were further refluxed or left standing.[20] The nature of the reaction(s) where **4j** and **4g** are consumed is not clear at present. In addition, a considerable difference in the reactivity with **1** exists between the 2,6-isomer **4i** and the 2,4-isomer **4g** or 3,5-isomer **4j**. These facts, coupled with isomer separation problems, prompted us to examine the preparation of the three isomers **3g**, **3i**, and **3j** of bromobis(trifluoromethyl)benzene, from which individual isomers of bis(trifluoromethyl)phenyllithium are obtained.

The lithiation of *m*-bis(trifluoromethyl)benzene under ice-cooling for 9 h followed by quenching with bromine and fractional distillation gave 1-bromo-2,4-(**3g**), 2,6- (**3i**), and 3,5-bis(trifluoromethyl)benzene (**3j**) in 35, 31, and 8% yield, respectively. When the time of the lithiation was extended to 24 h under otherwise the same conditions, the yields of **3g**, **3i**, and **3j** were 38, 36, and 6%, respectively. The change in the isomer distribution of the bromobis(trifluoromethyl)benzenes seems to reflect the relative stabilities (durabilities) of the isomeric bis(trifluoromethyl)phenyllithiums in the lithiated mixture stated above. 1-Bromo-3,5-bis-(trifluoromethyl)benzene (**3j**), which was formed only in small yield in the above reactions, was commercially obtained and smoothly converted into 3,5-$(CF_3)_2C_6H_3CF{=}CCl_2$ (**6j**) in good yield via the corresponding lithium compound **4j**. The yield of the equivalent transformation of 1-bromo-2,4-bis(trifluoromethyl)benzene (**3g**) into 2,4-$(CF_3)_2C_6H_3CF{=}CCl_2$ (**6g**) was considerably lower.

The reaction of 2,6-bis(trifluoromethyl)phenyllithium (**4i**) with **1** was much slower than those of the other isomers **4g**, **4h**, and **4j** and required hours of refluxing. In initial experiments, 2,6-$(CF_3)_2C_6H_3Cl$ (**10i**) was the predominant product accompanied by a smaller proportion of 2,6-$(CF_3)_2C_6H_3CF{=}CCl_2$ (**6i**). The Cl-Li exchange represented by Eq. 2 was initially regarded as the main route of **10i** since reaction (2) is suggested to be relatively favored when the substitution reaction (1) is sterically retarded.[11] In this particular case, course (3) is also considered important in view of the formation of 2,6-$(CF_3)_2C_6H_3C{\equiv}CCl$ (**13i**) and 2,6-$(CF_3)_2C_6H_3C{\equiv}CC_6H_3(CF_3)_2$-6,2. However, in some of the initial experiments **6i** was obtained in relatively good yield. In order to elucidate the factors responsible for such a variation in the yield of **6i**, we carried out a number of experiments and finally found experimental conditions under which 2,6-$(CF_3)_2C_6H_3CF{=}CCl_2$ (**6i**) was obtained consistently in about 50% yield based on **3i** (see Experimental).

$$CF_2{=}CCl_2\ (\mathbf{1}) + ArLi\ (\mathbf{4}) \longrightarrow ArCF{=}CCl_2\ (\mathbf{6}) + LiF \quad (1)$$

$$\mathbf{1} + \mathbf{4} \longrightarrow ArCl\ (\mathbf{10}) + CF_2{=}CClLi \quad (2)$$

$$\mathbf{6} + \mathbf{4} \longrightarrow ArCF{=}CClLi + \mathbf{10} \quad (3)$$

Table 2. Physical Properties[a] and Elemental Analysis Data of Dichlorofluoroethenyl Intermediates (**6**) and Phenylacetylenes (**8**)

Compd	Bp/ °C(mm Hg)[b]	n_D^{20} or [Mp/°C][c]	^{19}F NMR δ[d] I[e]	^{19}F NMR δ[d] II[f]	^{1}H NMR δ[d] I[g]	^{1}H NMR δ[d] II[h]	IR[i]/cm^{-1}	C(%) (Calcd) Found	H(%) (Calcd) Found
6a	107(33)	1.5285	−31.0[j]	−13.2 (d9.0)		6.94—7.54	1660	(45.97) 45.96	(1.93) 1.86
6b	111(30)	1.5438	−33.0[j]	−18.6 (d2.4)		6.93—7.53	1645	(45.97) 46.05	(1.93) 1.85
6c	110—111(30)	1.5411	−30.1[j]	−17.5		7.04(t 8.7) 7.62(d8.5) (d5.0)	1645	(45.97) 46.14	(1.93) 2.14
6d	110(30)	1.4815	17.3 (d8.8)	−6.4 (q8.9)		7.45—7.86	1664	(41.73) 41.74	(1.56) 1.62
6e	110(30)	1.4974 (1.4970)[k]	15.6	−19.2		7.38—7.97	1645sh		
6f	115(30)	1.5004	15.3	−19.4		7.59(8.7)[l] 7.72(8.7)[l]	1645sh	(41.73) 41.97	(1.56) 1.74
6g	101(30)	1.4452	16.8 (d9.9) 14.9	−8.4 (q9.6)		7.70(8.5)[l] 7.87(8.5)[l] 7.98	1667	(36.72) 36.51	(0.92) 0.86
6h	96(30)	1.4422	16.5 (d9.9) 14.7	−8.1 (q9.6)		7.85[m]	1668	(36.72) 37.00	(0.92) 0.99
6i	108—111(30)	[26.5—28]	17.7 (d6.8)	−5.5 (sep6.8)		7.72(ca.8)[n] 7.96(ca.8)[n]	1667	(36.72) 36.47	(0.92) 0.83
6j	109(30)	1.4457	15.0	−20.9		7.91(1H) 8.14(2H)	1645sh	(36.72) 35.63	(0.92) 0.86
6k	ca.110(1)	1.5771	−37.9[j]	−8.4		6.98—7.60	1657	(58.97) 58.30	(2.83) 2.96
8a	59(30)	1.5252 (1.524)[o]	−31.5[j]		3.27	6.88—7.53	**2114** 3300		
8b	61(50)	1.5151 (1.514)[o]	−34.2[j]		3.06	6.78—7.27	**2107** 3300		
8c	52(30)	[ca.25] ([25—27])[p]	−31.7[j]		3.00	6.93(t 8.2) 7.39(d5.3) (d8.7)	**2110** 3295 3305sh		
8d	ca.70(40)	1.4756 (1.4775)[q]	16.2		3.31	7.20—7.66	**2118** 3303		
8e	69(53)	1.4634 (1.4672)[q]	15.3		3.09	7.27—7.77	**2112**w 3300sh 3312		
8f	56(31)	1.4652 (1.4642)[q]	15.4		3.14	7.49	**2112**w 3300 3315sh		
8g	66(30)	1.4307	15.5 15.0		3.47	7.68[r] 7.69[r] 7.84	**2116** 3314 3330sh	(50.43) 50.48	(1.69) 1.65
8h	67(30)	1.4290	15.5 14.7		3.43	7.63(8.5)[l] 7.73(8.5)[l] 7.83	**2122** 3307	(50.43) 50.43	(1.69) 1.82
8i	70(30)	[56—57]	16.2		3.67	7.48(ca.8)[n] 7.78(ca.8)[n]	**2122** 3320	(50.43) 50.62	(1.69) 1.59
8j	74(60)	1.4221	14.9		3.20	7.77(1H) 7.82(2H)	**2125** 3312	(50.43) 50.40	(1.69) 1.60
8k	ca.80(1)	1.6006	−36.3[j]		2.92	7.00—7.69	**2108** 3293 3290sh	(85.69) 85.37	(4.62) 4.63

a) All the compounds listed in the table showed the molecular peaks in mass spectroscopy. b) Not neccessarily accurate enough to give a correct boiling point order for isomers due to the uncertainty in pressure measurement in mutually independent experiments. c) Literature values given in parentheses. d) 20% solution in $CDCl_3$. ^{1}H and ^{19}F chemical shifts measured downfield relative to internal tetramethylsilane and relative to external CF_3CO_2H, respectively. Splitting pattern and (apparent) coupling constant (Hz) indicated in parentheses. e) ^{19}F chemical shift for the trifluoromethyl group and the fluorine atom on the benzene ring. f) ^{19}F chemical shift for $-CF=CCl_2$. g) ^{1}H chemical shift for $-C\equiv CH$. h) ^{1}H chemical shif for ring protons. i) ν(C=C) of $-CF=CCl_2$ and ν(C≡C) (in bold face) and ν(C–H) of $-C\equiv CH$ are given. Neat for liquid and in KBr pellet for crystals. w, weak; sh, shoulder. j) Center of complex signals spreading over 25—31 Hz (0.45—0.55 ppm). k) Ref. 11. l) AB pattern. m) A sharp signal with a broad base (δ=7.66—7.94). n) AB_2 pattern. The upper value represents A. o) Ref. 5 (n_D^{25}). p) Ref. 2. q) Ref. 6. r) Probably the center signals of an AB pattern though the outer signals are not clear.

$$ArCF{=}CClLi \longrightarrow ArC{\equiv}CCl\ (\mathbf{13}) + LiF \qquad (4)$$

Unexpectedly, the use of a freshly prepared sample of **1**[21] was found to be the most important requirement for the formation of **6i** with a reasonable yield. It appears that partially deteriolated samples of **1** contain a compound or compounds (possibly, the epoxide of **1** and/or its secondary products) which gives ArCl upon reaction with ArLi, probably by a Cl–Li exchange. Generally, the reaction of an aryllithium with such a compound is not considered important since the reaction of the aryllithium with **1** proceeds rapidly. In the case of 2,6-bis(trifluoromethyl)phenyllithium, however, the reaction with **1** giving **6i** is slow and, thus, the suspected reaction will become important. If this is the case, the use of a large excess of a (deteriolated) sample of **1** is particularly undesirable for the preparation of **6i**.

The dichlorofluoroethenyl intermediates **6** prepared as mentioned above were converted into the corresponding phenylacetylenes (**8**) in good yield in all cases by treatment with 2 equivalents of butyllithium[11] in ether at about −50 °C. Pure products **8** were isolated by vaccum distillation. For an easy isolation of pure **8** by distillation, it is essential to use a sample of $ArCF{=}CCl_2$ (**6**) free from ArCl(**10**), which is a by-product of the reaction of ArLi (**4**) with **1** and has a boiling point close to that of $ArC{\equiv}CH$ (**8**).

The present study has proved that the method of introducing the ethynyl group using **1**[11] is suitable for the laboratory preparation of fluorine-containing phenylacetylenes **8a** through **8j**. Preparations on up to a 0.5—1 mol scale were relatively easily performed with no apparent danger, except for the reaction of *o*-fluorophenyllithium (**4a**) with **1**. The inverse addition method, which is relatively safe and generally used for the preparation of the dichlorofluoroethenyl intermediates **6** as well as for their conversion into acetylenes **8** involving **8a**, is difficult to apply for the preparation of **6a** from unstable **4a**. The reaction procedure described in the experimental section of **6a**, if the temperature control fails, can be hazardous and, thus , has to be carried out with great precaution on a small scale.

The ^1H chemical shift of the acetylenic protons (Table 2) seems to be closely related to the acidity of the prepared phenylacetylenes (**8**). The trifluoromethyl group, when it is in the *o*-position, has a marked effect on the ^{19}F chemical shift of the $-CF{=}CCl_2$ group. The trifluoromethyl group present ortho to the dichlorofluoroethenyl group is also clearly indicated by a relatively large constant of coupling with the fluorine atom of the dichlorofluoroethenyl group. A clear difference was also found in the mass spectroscopy between the dichlorofluoroethenyl compounds with and without the *o*-trifluoromethyl group. For each of **6a**, **6b**, **6c**, **6e**, **6f**, and **6j**, which has no *o*-CF_3 group, the molecular peak is the strongest (100%), and the intensity of the M−Cl peak is in the range 23—45%. In contrast, for each of **6d**, **6g**, **6h**, and **6i**, which has at least one *o*-CF_3 group, the M−Cl peak is the strongest (100%), and the intensity of the molecular peak is in the range 59—85%.

Experimental

Temperature readings are uncorrected. Pressure readings are given in terms of mmHg (1 mmHg=133.322 Pa). ^{19}F NMR[22] and ^1H NMR spectra were recorded on a Hitachi R-20BK operated at 56.451 MHz and on a Hitachi R-22 operated at 90 MHz, respectively. IR spectra were recorded on a Hitachi EPI-G3 or 285H, and mass spectra on a Shimadzu GCMS-7000. For an integration of the GC peak area, a Shimadzu C-R2AX was used. Compound **1** was prepared as described previously.[11] Other fluoro chemicals were obtained from PCR Inc., Lancaster Synthesis Ltd., Fluorochem Ltd., Yarsley Research Laboratories, and Central Glass Co. Ltd. (Tokyo). All reactions of organolithium and Grignard reagents were conducted under an atmosphere of nitrogen using sodium-dried ether. Ethereal butyllitium was generally prepared from butyl bromide with cut pieces of lithium in ether under nitrogen. However, an argon atmosphere was neccessary for a smooth preparation of butyllithium from more recently obtained samples of lithium. The amount of butyllithium is calculated from the nominal concentration. In the case where a portion of the worked-up mixture was reserved, the fraction (e.g., 0.90) actually subjected to vaccum distillation is necessary for a yield calculation and is indicated as "÷0.90".

***o*-(2,2-Dichloro-1-fluoroethenyl)fluorobenzene (6a).** To a solution of *o*-bromofluorobenzene (40.0 g, 0.229 mol) in ether (300 ml) mechanically stirred and cooled between −90 °C and −100 °C in a liquid-nitrogen bath (a stainless steel Dewar), ethereal butyllithium (160 ml, 0.267 mol) was added. The temperature was then maintained at about −80 °C for 1 h, lowered to about −90 °C, and **1** (59 g, 0.44 mol) was added. The temperature of the resulting mixture was carefully watched and maintained at −70 °C (±3 °C) for 1 h by an occassional adjustment of the bath height with a lab jack. The mixture was then allowed to warm to −60 °C over 30 min and to −50 °C over another 30 min. (*Caution: The temperature should not be allowed to approach −60 °C before the reaction for at least 1 h at −70 °C (or at least 2 h at −80 °C). Otherwise, uncontrolably rapid temperature rise may be started resulting in dangerous sudden vaporization of the flask content.*) When the temperature reached −27 °C after an additional 30 min, the mixture was hydrolyzed by pouring it onto a mixture of concd hydrochloric acid (27 ml) and crushed ice. Workup and fractional distillation afforded **6a** (35.0 g, ÷0.98, 75%), bp 107 °C(30 mmHg). Also obtained were 1-(1-chloro-2,2-difluoroethenyl)-2-(2,2-dichloro-1-fluoroethenyl)benzene (**12**, 1.2 g, 2%), bp 60 °C(1 mmHg), 2-chloro-2′-fluorobiphenyl (**10k**, 0.3 g, 1%), bp ca 90 °C(1 mmHg), and 1-(2,2-dichloro-1-fluoroethenyl)-2-(*o*-fluorophenyl)benzene (**6k**, 2.9 g, 9%), bp ca. 109 °C(1 mmHg).

10k: Mp 76—77 °C. ^1H NMR δ=6.92—7.47. ^{19}F NMR δ=−34.58 (m). Found: C, 69.96; H, 3.76; M^+, 206. Calcd for

$C_{12}H_8ClF$: C, 69.74; H, 3.90; M, 206.

12: n_D^{20} 1.5289. IR (neat) 1738 (CF_2=CCl–) and 1658 cm^{-1} (CCl_2=CF–). ^1H NMR δ=7.41 (a sharp signal with a broad base: δ=7.24—7.52). ^{19}F NMR δ=−6.1 (1F, d, J=31 Hz), −9.5 (1F, dd, J=31 and 2 Hz), and −11.0 (1F). Found: C, 41.61; H, 1.31; M^+, 286. Calcd for $C_{10}H_4Cl_3F_3$: C, 41.77; H, 1.40; M, 286.

***m*-(2,2-Dichloro-1-fluoroethenyl)fluorobenzene (6b). a) Via *m*-Fluorophenyllithium (4b).** To a Dry Ice-acetone cooled solution of *m*-bromofluorobenzene (98.4 g, 0.562 mol) in ether (100 ml) was added ethereal butyllithium (380 ml, 0.63 mol) while keeping the internal temperature between −30 °C and −40 °C. The resulting solution of **4b** was kept cold until its addition to an ice-cooled solution of **1** (121 g, 0.91 mol) in ether (100 ml) was started. The addition was conducted through a dropping funnel, briefly cooled with Dry Ice over 23 min while keeping the internal temperature of the reaction flask at about 20 °C. The resulting mixture was stirred for an additional 1 h, hydrolyzed, and worked up. Fractional distillation afforded **6b** (55.9 g, ÷0.98, 48%), bp 108 °C (28 mmHg).

b) Via *m*-Fluorophenylmagnesium Bromide (5b). A solution of *m*-fluorophenylmagnesium bromide (**5b**) was prepared from *m*-bromofluorobenzene (96.7 g, 0.552 mol) and magnesium (14.5 g, 0.60 g atom) in ether (300 ml). The addition of **1** (120 g, 0.90 mol) to the solution resulted in a mild refluxing, which lasted for 2 h. The resulting mixture was refluxed for an additional 16 h by external heating and hydrolyzed by pouring it onto a mixture of conc hydrochloric acid (50 ml) and crushed ice. The workup and fractional distillation afforded **6b** (92.2 g, ÷0.97, 82%), bp 111 °C(30 mmHg).

1-(2,2-Dichloro-1-fluoroethenyl)-2-(trifluoromethyl)benzene (6d). Ethereal butyllithium (330 ml, 0.55 mol) was added to a solution of *o*-bromo(trifluoromethyl)benzene (112.5 g. 0.500 mol) in ether (100 ml) over a period of 38 min below 7 °C (internal). The resulting solution was added to a Dry Ice-acetone cooled solution of **1** (105 g, 0.79 mol) in ether (100 ml) over 28 min while keeping the internal temperature at about −25 °C. The resulting mixture was allowed to warm to room temperature, refluxed for 1 h, and poured onto a mixture of crushed ice and concd hydrochloric acid (55 ml). The ether layer was separated, washed (with water and then with aq $NaHCO_3$), and dried (Na_2SO_4). Fractional distillation afforded **6d** (98.6 g, ÷0.98, 77%), bp 110 °C (30 mmHg), together with *o*-$CF_3C_6H_4Cl$ (2.4 g, 3%), bp ca. 60 °C (30 mmHg).

1-(2,2-Dichloro-1-fluoroethenyl)-2,5-bis(trifluoromethyl)-benzene (6h). A solution obtained by the addition of ethereal butyllithium (230 ml, 0.38 mol) to a solution of *p*-bis(trifluoromethly)benzene (63.8 g. 0.298 mol) in ether (100 ml) was refluxed for 4 h. It was then added to a Dry Ice-acetone cooled solution of **1** (90 g, 0.68 mol) in ether (100 ml) over 13 min while keeping the internal temperature between −20 °C and −30 °C. The resulting mixture was stirred for an additional 1 h without cooling and then poured onto a mixture of concd hydrochloric acid (40 ml) and crushed ice. The workup and fractional distillation afforded **6h** (69.3 g, ÷0.98, 72%), bp 96 °C(30 mmHg).

Lithiation of *m*-Bis(trifluoromethyl)benzene Followed by Treatment with Bromine. A solution (ca. 600 ml) of butyllithium prepared from 1.00 mol of butyl bromide was added to an ice-cooled solution of *m*-bis(trifluoromethyl)-benzene (170 g, 0.794 mol) in ether (100 ml). Stirring and ice cooling were continued for 9 h. The reaction mixture was then cooled with Dry Ice-acetone, and bromine (165 g, 1.03 mol) was carefully added while the internal temperature was kept below −46 °C. The resulting mixture was rapidly warmed to 0 °C using a water bath, poured onto crushed ice; then aqueous sodium sulfite was added, and the whole mixture was thoroughly agitated in order to release butane. The ether layer was separated, washed with aqueous Na_2SO_3 and then with aqueous $NaHCO_3$, and dried with sodium sulfate. (The simultaneous use of $NaHCO_3$ and Na_2SO_3 was avoided since in a preliminary experiment, in which these reagents were used simultaneously, a portion of the $(CF_3)_2C_6H_3Br$ was reduced to *m*-$(CF_3)_2C_6H_4$.) The solvent was removed, and the remaining liquid was fractionally distilled using a 50-cm metal-packed column at a high reflux ratio (mostly 60:1 or 120:1) until the solid product (**3i**) came out, which was rapidly collected by vacuum distillation. The following compounds were obtained: butyl bromide, 14.5 g (13.6%); *m*-bis(trifluoromethyl)benzene, bp ca. 113 °C, 21.1 g (12.7%); 1-bromo-3,5-bis(trifluoromethyl)benzene (**3j**), bp ca. 151 °C, 17.4 g (7.6%); 1-bromo-2,4-bis(trifluoromethyl)benzene (**3g**), bp 161.5 °C, 79.1 g (34.7%); 1-bromo-2,6-bis(trifluoromethyl)benzene (**3i**), bp 86 °C (29 mmHg) (bp ca. 173 °C), 70.9 g (31.1%). The above yields include individual compounds in mixed fractions, the calculation being based on the assumed proportionality of the weight to the GC peak area. The yields of essentially purely isolated **3g** and **3i** were 31% (70.9 g) and 29% (65.6 g), respectively. Compound **3j** was obtained at a purity of less than 88%. In another run, during which the time of the lithiation was extended to 24 h under otherwise the same conditions, the yields were as follows: butyl bromide, 3.6 g (3.4%); *m*-bis(trifluoromethyl)benzene, 8.4 g (5.1%); **3j**, 13.5 g (5.9%); **3g**,86.0 g (37.8%); **3i**,81.6 g (35.9%). The yields of essentially purely isolated **3g** and **3i** were 35% (80.1 g) and 34.5% (78.5 g), respectively.

3g: n_D^{20} 1.6363. ^1H NMR δ=7.60, (1H), 7.83 (1H), 7.92 (1H). The signals of the chemical shifts 7.60 and 7.83 seem to constitute an AB pattern (J=8 Hz) though the signal at 7.92 and the outer signal of the chemical shift 7.83 are unresolved. The signals of the chemical shift 7.83 show an additional splitting (d, J=2 Hz). ^{19}F NMR δ=15.33, 15.29 (partially resolved). Found: C, 32.58; H, 0.98; M^+, 292. Calcd for $C_8H_3BrF_6$: C, 32.79; H, 1.03; M, 292.

3i: Mp 51—52 °C, ^1H NMR δ=7.49 (1H), 7.81 (2H), J=ca. 8 Hz (results of approximate analysis as AB_2). ^{19}F NMR δ=16.2(s). Found: C, 32.55; H, 0.87; M^+, 292. Calcd for $C_8H_3BrF_6$: C, 32.79; H, 1.03; M, 292.

1-(2,2-Dichloro-1-fluoroethenyl)-2,6-bis(trifluoromethyl)-benzene (6i). To an ice-cooled solution of 1-bromo-2,6-bis(trifluoromethyl)benzene (**3i**, 16.1 g, 0.055 mol) dissolved in a mixed solvent of ether (50 ml) and hexane (20 ml) was added a hexane solution of butyllithium (a 1.6 mol dm^{-3} Aldrich product, 37 ml, 0.059 mol) over 1 h. After a freshly prepared sample of **1** (19 g, 0.14 mol) was added to the solution, the resulting mixture was refluxed for a total of 15 h over two days and then hydrolyzed. Fractional distillation afforded **6i** (7.9 g, ÷0.91, 48%), bp 110 °C (30 mmHg). The minor products involved 1-chloro-2,6-bis(trifluoromethyl)benzene (**10i**, 1.1 g, 9%), bp ca. 70 °C (30 mmHg), and 1-(chloroethynyl)-2,6-bis(trifluoromethyl)-benzene (**13i**, 0.6 g, 4%), bp ca. 100 °C (30 mmHg). The latter

compound was contained in the first fractions of **6i**. Samples of **6i** containing **13i** are usable for the preparation of the corresponding acetylene **8i** since **13i** is the intermediate of the conversion of **6i** into **8i** (see the section of **8i**).

***o*-Trifluoromethylphenylacetylene (8d).** To a Dry Ice-acetone cooled solution of **6d** (69.9 g, 0.27 mol) in ether (100 ml) was added butyllithium (380 ml, 0.63 mol) over 2 h while keeping the internal temperature below −50 °C. In GC monitoring, **6d** and *o*-$CF_3C_6H_4C{\equiv}CCl$ were essentially absent. The resulting mixture was stirred for an additional 1.4 h without cooling and then hydrolyzed by pouring it onto a mixture of concd hydrochloric acid (65 ml) and cushed ice. The ether layer was washed (with water and then with aq $NaHCO_3$), dried (Na_2SO_4), and distilled, giving **8d** (38.5 g, ÷0.98, 86%), bp 68 °C(30 mmHg).

2,6-Bis(trifluoromethyl)phenylacetylene (8i). This particular run was conducted starting with a sample (43.0 g, 0.130 mol) consisting of 87.2% of **6i**, 9.9% of 2,6-$(CF_3)_2$-$C_6H_3C{\equiv}CCl$ (**13i**), and 2.9% of impurities. The sample was dissolved in ether (50 ml) and treated (at about −50 °C) as above with ethereal butyllithium (200 ml, 0.334 mol). Compound **8i**, bp ca. 76 °C(29 mmHg), mp 56—57 °C, was obtained in 83% yield (24.8 g, ÷0.96).

References

1) An alternative route: *m*-Fluoro-, *p*-fluoro-, and *m*-(trifluoromethyl)phenylacetylenes were obtained from β-chlorostyrenes by treatment with phenyllithium: M. Schlosser and V. Ladenberger, *Chem. Ber.*, **100**, 3901 (1967).

2) M. R. Tirpak, C. A. Hollingsworth, and J. H. Wotiz, *J. Org. Chem.*, **25**, 687 (1960).

3) A. D. Allen and C. D. Cook, *Can. J. Chem.*, **41**, 1084 (1963).

4) D. A. Dawson and W. F. Reynolds, *Can. J. Chem.*, **53**, 373 (1975).

5) I. J. Solomon and R. Filler, *J. Am. Chem. Soc.*, **85**, 3492 (1963).

6) D. Mesnard, F. Bernadou, and L. Miginiac, *J. Chem. Res. (M)*, **1981**, 3216.

7) Although the two-step conversion of acetophenones into the corresponding phenylacetylenes is a well-established procedure, commercial fluoroacetophenones and (trifluoromethyl)acetophenones are apparently too expensive to be used for the preparation of relatively large amounts of phenylacetylenes. The Friedel-Crafts acetylation, which is used for the preparation of *p*-fluoroacetophenone, is generally not applicable for the preparation of (trifluoromethyl)acetophenones since aluminium chloride reacts with the trifluoromethyl group on the benzene ring to convert it into the trichloromethyl group: A. L. Henne and M. S. Newman, *J. Am. Chem. Soc.*, **60**, 1697 (1938).

8) *m*-(Trifluoromethyl)acetophenone was prepared in 3 steps from *m*-bromo(trifluoromethyl)benzene: J. W. Corse, R. G. Jones, Q. F. Soper, C. W. Whitehead, and O. K. Behrens, *J. Am. Chem. Soc.*, **70**, 2837 (1948).

9) S. Takahashi, Y. Kuroyama, K. Sonogashira, and N. Hagihara, *Synthesis*, **1980**, 627.

10) W. B. Austin, N. Bilow, W. J. Kelleghan, and K. S. Y. Lau, *J. Org. Chem.*, **46**, 2280 (1981).

11) K. Okuhara, *J. Org. Chem.*, **41**, 1487 (1976).

12) K. Okuhara, *Bull. Chem. Soc. Jpn.*, **54**, 2045 (1981).

13) *m*-Fluorophenyllithium: H. Gilman, R. D. Gorsich, and B. J. Gaj, *J. Org. Chem.*, **27**, 1023 (1962).

14) G. Wittig, *Naturwissenschaften*, **30**, 696 (1942).

15) H. Gilman and R. D. Gorsich, *J. Am. Chem. Soc.*, **77**, 3919, (1955); **78**, 2217 (1956).

16) J. D. Roberts and D. Y. Curtin, *J. Am. Chem. Soc.*, **68**, 1658 (1946).

17) D. A. Shirley, J. R. Johnson, Jr., and J. P. Hendrix, *J. Organomet. Chem.*, **11**, 209 (1968).

18) Lithiation of *m*-bis(trifluoromethyl)benzene with butyllithium: G. Hallas, D. E. Grocock, and J. D. Hepworth, *J. Soc. Dyers Colour.*, **86**, 200 (1970).

19) Lithiation of *m*-bis(trifluoromethyl)benzene with butyllithim-TMEDA gave only 2,6-bis(trifluoromethyl)-phenyllithium as judged from the results of carbonation: D. E. Grocock, T. K. Jones, G. Hallas, and J. D. Hepworth, *J. Chem. Soc. C*, **1971**, 3305. This appears to be a result of disappearance of the 3,5-isomer **4j** and 2,4-isomer **4g** rather than preferential formation of the 2,6-isomer **4i**.

20) The tendency of disappearance of **4j** and **4g** was confirmed by the following experiment: Ethereal butyllithium (62 ml, 0.104 mol) was added to an ice-cooled solution of *m*-bis(trifluoromethyl)benzene (17.0 g, 0.079 mol) and undecane (internal standard, 5 ml) in ether (40 ml), and stirring and ice cooling were continued for 9 h. Then, with occassional monitoring, the resulting mixture was stirred for 24 h at ambient temperature (ca. 30 °C) and left standing for additional 24 h. In each case of monitoring, a 10 ml portion of the reaction mixture was transferred to a special vessel, diluted with ether, treated with bromine (2 g) under an inert atmosphere with Dry Ice-acetone cooling, and worked up. The GC peak areas changed as shown below, the peak area of *m*-$(CF_3)_2C_6H_4$ relative to that of undecane in the initial solution being taken as 100%. At 0 h (ca. 10 min after discontinuation of ice cooling), *n*-C_4H_9Br 8%, *m*-$(CF_3)_2C_6H_4$ 17%, **3j** 6%, **3g** 34%, **3i** 37%; at 3 h, *n*-C_4H_9Br 0%, *m*-$(CF_3)_2C_6H_4$ 12%, **3j** 5%, **3g** 38%, **3i** 38%; at 12 h, *m*-$(CF_3)_2C_6H_4$ 14%, **3j** 0%, **3g** 34%, **3i** 39%; at 24 h, *m*-$(CF_3)_2C_6H_4$ 18%, **3g** 19%, **3i** 38%; and at 48 h, *m*-$(CF_3)_2C_6H_4$ 22%, **3g** 4%, **3i** 38%. (Compound **4i** was unreactive to chlorotrimethylsilane, a reagent commonly used for monitoring organolithiums.)

21) Samples of **1** which were sealed soon after the preparation and have been stored at −20 °C may be used equally well.

22) The ^{19}F chemical shifts given in this paper are measured downfield relative to external CF_3CO_2H although those given in Refs. 11 and 12 are measured upfield relative to the same standard.

Thermal and Photochemical Reactions of 10-Methyl-9-phenylacridinium Chloride in Alcohols

Bin ZHOU, Koji KANO,* and Shizunobu HASHIMOTO
Department of Applied Chemistry, Faculty of Engineering, Doshisha University, Kamikyo-ku, Kyoto 602
(Received July 13, 1987)

The photoreduction of 10-methyl-9-phenylacridinium chloride in methanol containing K_2CO_3 involves the nucleophilic addition of methanol to the 9-position of the acridinium cation, the photoinduced heterolysis of the methanol adduct, and the hydride transfer from the alkoxide anion to the acridinium cation in the nonrelaxed ground states to give 9,10-dihydro-10-methyl-9-phenylacridine.

In the previous paper, we postulated the photoreduction mechanism of 10-methylacridinium chloride (MA^+Cl^-) in methanol (Scheme 1):[1]

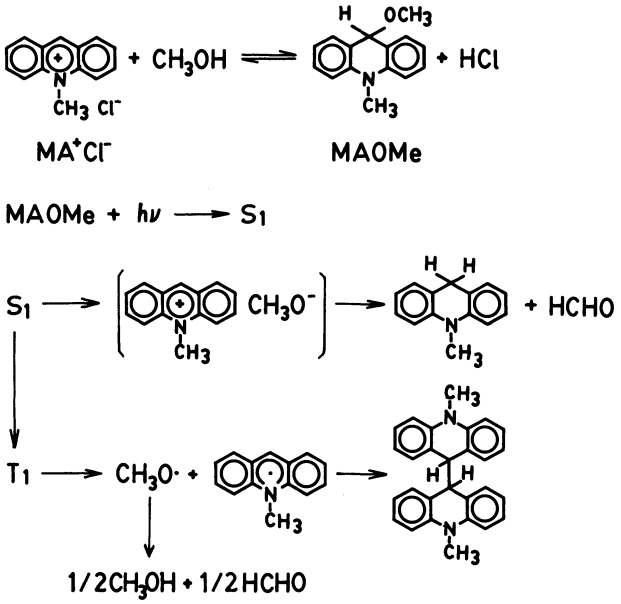

Scheme 1.

This mechanism is different from that for acridine whose n, π^* excited state can abstract a hydrogen atom from alcohols.[2] The mechanism involving the hydrogen abstraction of photoexcited acridinium cation from alcohols[3] is not understandable because the acridinium cation has no odd electrons which can participate in the n-π^* transition. Our mechanism can explain reasonably the formation of 9,10-dihydro-10-metylacridine (MAH_2) and 10,10′-dimethyl-9,9′, 10,10′-tetrahydro-9,9′-biacridinyl ($(MAH)_2$). From a different point of view, the reduction of the acridinium cation by alcohols is interesting because of its analogy with the $NADP^+$ alcohol dehydrogenase reactions. The light energy, however, needs to promote the reduction of MA^+Cl^- to MAH_2. One of the key steps to realize the $NADP^+$-mimic reaction is heterolysis of the alcohol adduct, which is formed by a nucleophilic attack of the alcohol to the carbon atom at the 9-position of the acridinium cation. A possibility to achieve spontaneous heterolysis of the alcohol adduct is utilization of strain energy at the 9-position of the acridine ring. Next we examined the reaction of 9,10-dimethylacridinium chloride (MMA^+Cl^-) with methanol.[4] Indeed, the methanol adduct provided by a K_2CO_3-catalyzed reaction of MMA^+Cl^- with methanol dissociates into MMA^+ and CH_3O^- in the dark. Unfortunately, however, a proton abstraction from the CH_3 group at the 9-position of MMA^+ of CH_3O^- proceeds to give 9,10-dihydro-10-methyl-9-methyleneacridine (Scheme 2):[4]

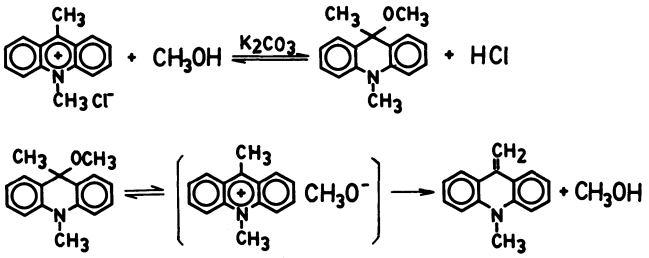

Scheme 2.

These aspects led us to study the reactions of 10-methyl-9-phenylacridinium chloride (MPA^+Cl^-) with alcohols. Although the $NADP^+$-mimic reactions could not be realized, we obtained important results which strongly support the photoreduction mechanism shown in Scheme 1.

Experimental

9-Phenylacridine (PA) was prepared by a Bernthsen method.[5] MPA^+Cl^- (mp 187—189 °C) was obtained by passing an aqueous solution of 10-methyl-9-phenylacridinium iodide, (which was prepared by the reaction of PA with methyl iodide), through a Dowex 1X8 ion-exchange column and recrystallization from water. 9,10-Dihydro-10-methyl-9-phenylacridine (mp 109—110 °C) (MPAH) was prepared according to procedures described in the literature.[6] 9,10-Dihydro-9-methoxy-10-methyl-9-phenylacridine (MPAOMe) was obtained by the following procedures. MPA^+Cl^- (1.6 g) in methanol (20 ml) was poured into methanol (50 ml) containing 1 M (1 M=1 mol dm^{-3}) NaOH and the solution was stirred for 5 min at room temperature. The colorless precipitates were filtered, washed with water, and recrystallized from hexane, giving MPAOMe (1.2 g, 74 %): mp 149—150 °C; ^1H NMR (acetone-d_6) δ=2.94 (3H, s, OCH_3), 3.57 (3H, s, N-CH_3), and 6.88—7.33 (13H, m,

aromatic); UV (C_2H_5OH) 332 (ε 4900), 319 (5100), 300 (sh), and 285 nm (19600). Found: C, 83.71; H, 6.29; N, 4.63%. Calcd for $C_{21}H_{19}NO$: C, 83.69; H, 6.35; N, 4.65%. All solvents used were of spectroscopic grades.

The absorption spectra were taken on a Shimadzu UV-200S spectrophotometer. The 400 MHz ^1H NMR spectra were measured by a JEOL JNM-GX400 spectrometer. The ESR spectrum was kindly measured by Professor K. Maruyama and Dr. T. Katagiri of Kyoto University using a JEOL PE-3X spectrometer. The methods of photolysis and analysis of the products have been described in the previous paper.[1]

Results

Nucleophilic Addition of Alcohols to MPA$^+$Cl$^-$. Bunting and Meathrel[7] reported ^1H NMR of MPAOMe obtained from the reaction of MPA$^+$Cl$^-$ with sodium methoxide without mention of mp and yield. We also isolated and purified MPAOMe as is described in the Experimental Section.

A dilute methanolic solution of MA$^+$Cl$^-$ (1×10^{-5}M) does not show the characteristic absorption spectrum of the acridinium ion because most of MA$^+$Cl$^-$ molecules are converted to MAOMe.[1] As Fig. 1 shows, however, MPA$^+$Cl$^-$ in methanol exhibits the ^1L_a, ^1L_b, and ^1B_b transition bands due to the acridinium ring. Comparing the absorption spectrum of MPA$^+$Cl$^-$ in methanol with that in acetonitrile, it was found that an additional absorption band appears at around 285 nm in methanol. The spectrum of an authentic sample suggests that the absorption band with λ_{max} at 285 nm is ascribed to MPAOMe. Upon addition of K_2CO_3, MPAOMe was formed at the expense of MPA$^+$Cl$^-$ (Fig. 1).

The pseudo-first-order rate constants for the alcohol addition (k) and the infinite yield of the alcohol adducts could be determined from the changes in the optical densities of MPA$^+$Cl$^-$ (5×10^{-5} M) in alcohols containing K_2CO_3 (5×10^{-4}). The results are summarized in Table 1. The alcohol addition was depressed in the order of methanol, ethanol, 2-propanol, and t-butyl alcohol.

Spontaneous Heterolysis of MPAOMe. When MPAOMe (5×10^{-5} M) was dissolved in methanol, the intensity of the absorption band due to MPAOMe (285 nm) gradually decreased and the bands due to 10-methyl-9-phenylacridinium methoxide (MPA$^+$MeO$^-$) appeared at 362 and 424 nm. After a definite time, the system reached a stationary state where MPAOMe and MPA$^+$MeO$^-$ coexist:

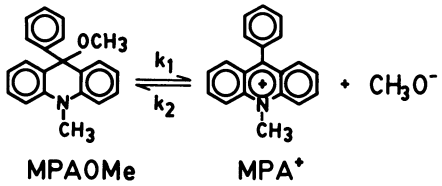

(1)

The rate constant for the dissociation of MPAOMe (k_1) could be obtained from Eq. 2:

$$\ln\frac{C_e + C(1 - C_e/C_0)}{C_e - C} = \left(\frac{2C_0}{C_e} - 1\right)k_1 t \qquad (2)$$

where C_0 is the initial concentration of MPAOMe, C_e is the MPA$^+$MeO$^-$ concentration at the equilibrium state, and C is the MPA$^+$MeO$^-$ concentration at time t. Equation 2 can be applied to the reactions in methanol and aprotic solvents. When alcohols other than methanol are used, the exchange reactions such

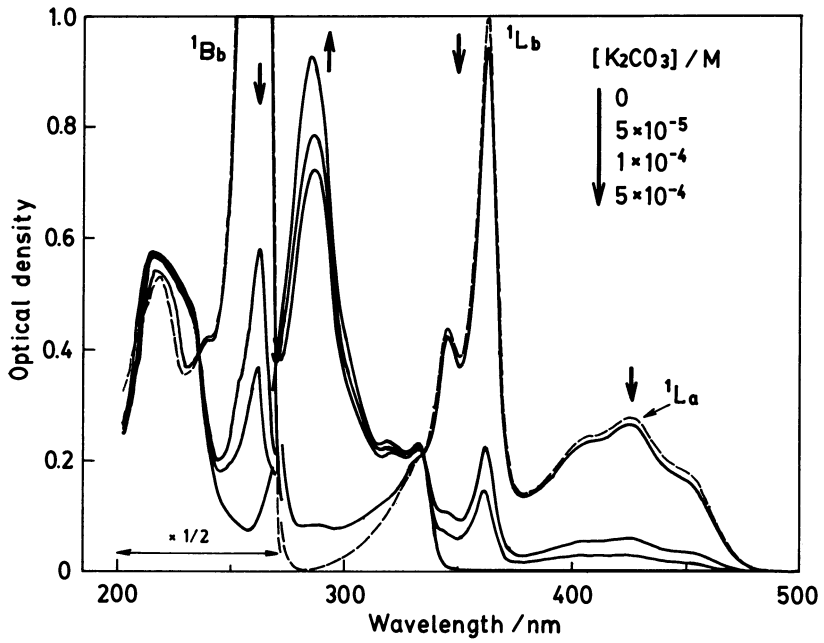

Fig. 1. Absorption spectra of MPA$^+$Cl$^-$ (5×10^{-5} M) in methanol with and without K_2CO_3 (——) and in acetonitrile (– – –) at 22 °C.

as $CH_3O^-+ROH \rightleftarrows CH_3OH+RO^-$ may take place necessitating a more complex treatment. The k_1 values in the methanol and acetonitrile are shown in Table 2 together with the yields of MPA+MeO$^-$ at the equilibrium states and the dissociation constants of MPAOMe (K_D). As Table 2 clearly indicates, the dissociation of MPAOMe occurs effectively only in methanol. This may be ascribed to the stabilization of the polar transition state and the ionic products by the polar protic solvent. A polar aprotic solvent, such as acetonitrile, is a poor solvent for dissociation because of the absence of a hydrogen bond between CH_3O^- and the solvent.

Although MPAOMe dissociates spontaneously to MPA+MeO$^-$ in methanol at room temperature, no formation of MPAH was detected by means of HPLC.

Photoinduced Heterolysis of MPAOMe. In the case of MAOMe, the photochemical dissociation of this pseudo base into MA+MeO$^-$ is observed only in a solvent matrix at 77 K[1,8] As is reported by Grigoreva et al.,[9] however, the photolysis of MPAOMe in aerated alcohols and acetonitrile at 22 °C caused the rapid formation of MPA+MeO$^-$. The relationship between the yield of MPA+MeO$^-$, which was determined by means of absorption spectroscopy, and the irradiation time is shown in Fig. 2. Figure 2 indicates that the formation of MPA+MeO$^-$ is saturated and photostationary states are reached. The yields of MPA+MeO$^-$ at the stationary states were 44% in methanol, 45% in ethanol, 49% in 2-propanol, and 17% in acetonitrile.

A 30-s irradiation of the ethanolic MPAOMe (5×10^{-5} M) solution gave MPA+MeO$^-$ in 12% yield. The dissociation was followed by a slow recombination to the alcohol adduct in the dark. After the recombination was completed, the photolyzed solution was analyzed by means of HPLC which reveals the formation of a trace amount of MPAH. For the photolysis of MAOMe in solution, we postulated the mechanism for formation of MAH_2 shown in Scheme 1.[1] If this mechanism is applicable for the photolysis of MPAOMe, it can be considered that the hydride transfer from CH_3O^- to MPA$^+$ occurs in low quantum yield. Although the 2-min irradiation of MAOMe (5×10^{-5}M) in aerated methanol provides MAH_2 and MA=O in 35 and 5% yields respectively, the yield of MPAH in the photolysis of MPAOMe under the same conditions is only <1%.

Photochemical Reactions of MPA+Cl$^-$ and MPAOMe in the Presence of K_2CO_3. Figure 3 shows the rates of MPAH formation when MPA+Cl$^-$ (5×10^{-5} M) in aerated methanol was irradiated in the absence and the presence of K_2CO_3. A slow photoreduction occurred in the absence of K_2CO_3, whereas the formation of MPAH was markedly accelerated by K_2CO_3. These results clearly indicate that MPAH is produced via

Table 1. Pseudo-First-Order Rate Constants for Nucleophilic Addition of Alcohols to MPA+Cl$^-$ (k) and Yields of Alcohol Adducts at Infinite Time at 22 °C[a]

Alcohol	$10^4\,k/s^{-1}$	Yield/%
Methanol	very fast	100
Ethanol	58.3±0.7	100
2-Propanol	7.55±0.03	100
t-Butyl alcohol[b]	4.77±0.11	58

a) The rate constants and the yields of the alcohol adducts were determined for the samples of 5×10^{-5} M MPA+Cl$^-$ in alcohols containing 5×10^{-4} M K_2CO_3. b) The concentration of K_2CO_3 was 3×10^{-4} M.

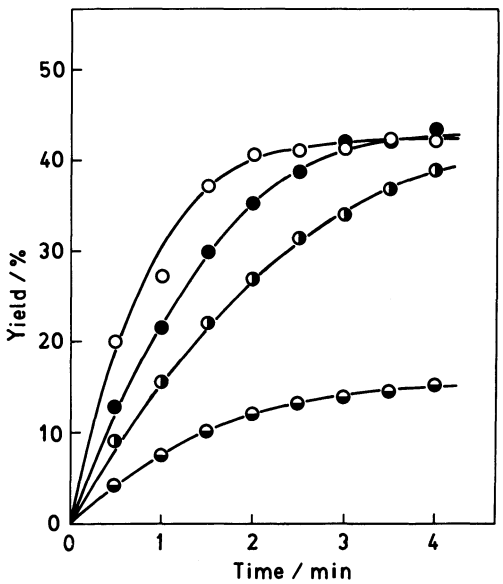

Fig. 2. Photoinduced dissociation of MPAOMe (5×10^{-5} M) to MPA+MeO$^-$ in methanol (○), ethanol (●), 2-propanol (◑), and acetonitrile (◒) without base at 22 °C. The ordinate is the yield of MPA+MeO$^-$.

Table 2. First-Order Rate Constants for Dissociation of MPAOMe to MPA+MeO$^-$ (k_1), Yields of MPA+MeO$^-$ at Equilibrium States, and Dissociation Constants of MPAOMe (K_D) in Alcohols and Acetonitrile at 22 °C[a]

Solvent	$10^7\,k_1/s^{-1}$	Yield of MPA+MeO$^-$/%	K_D/M
Methanol	7870±73	37	5000
Ethanol	(840±14)[b]	6	230
2-Propanol	(35.6±0.6)[b]	4	120
Acetonitrile	3.7±1.3	2	9

a) The initial concentration of MPAOMe was 5×10^{-5} M. b) The apparent k_1 value was obtained by assuming that the exchange reaction, $CH_3O^-+ROH=CH_3OH+RO^-$, does not occur (see text).

photolysis of MPAOMe. Under similar conditions, the photolysis of MPAOMe yielded MPAH (Fig. 4). Upon irradiation in methanol without K_2CO_3, about 50% of MPAOMe rapidly dissociated into MPA^+MeO^- which is inactive toward photoreduction. In the presence of K_2CO_3, however, the MPA^+ generated reverts instantaneously to the original MPAOMe which is the precursor of MPAH. The prolonged irradiation, therefor, seems to result in an accumulation of MPAH. The yield of MPAH was 68% when MPAOMe (5×10^{-5} M) in aerated methanol containing K_2CO_3 (5×10^{-4} M) was irradiated for 3 h. The photochemical behavior of MPAOMe in aerated ethanol was essentially the same as that in methanol (Table 3). In this case, MPA^+ photochemically generated may be attacked by surrounding ethanol to yield 9,10-dihydro-9-ethoxy-10-methyl-9-phenylacridine (MPAOEt) by the aid of K_2CO_3. MPAOEt may also be a precursor of MPAH.

As Table 3 shows, the yield of MPAH was significantly lowered during photolysis in aerated 2-propanol containing K_2CO_3. Since the nucleophilic attack of 2-propanol to MPA^+ is slower than the photoinduced heterolysis of MPAOMe (see Table 1), the formation of MPA^+MeO^- was detected by absorption spectroscopy at the initial stage of the photolysis. Prolonged irradiation caused the decomposition of MPA^+, giving small amounts of MA=O along with various unknown products. Complex photoreactions of MPAOMe also proceeded in aerated acetonitrile without K_2CO_3. From the photolyzed solution, PA and MA=O were isolated by means of a silica-gel column chromatography. These products were identified by ^1H NMR, absorption, and emission spectroscopy. The changes in the yields of MPAH, MA=O, and PA with irradiation time are shown in Fig. 5.

The yields of MPAH in the photolyses of MPAOMe decreased under anaerobic conditions (Table 3). The

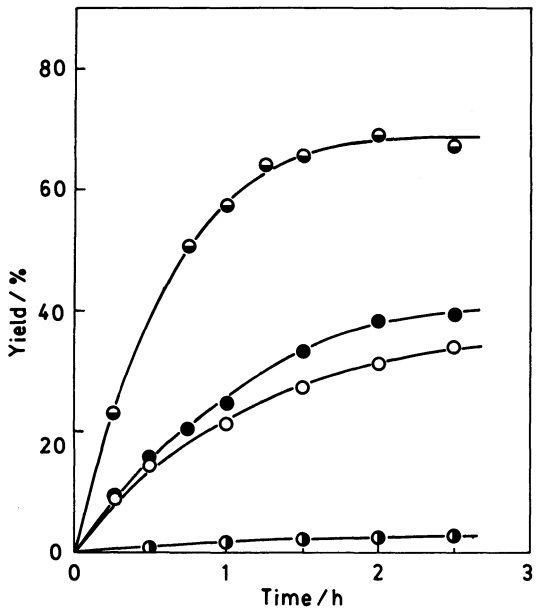

Fig. 3. Yields of MPAH in the photolyses of MPA^+Cl^- (5×10^{-5}) in aerated methanol in the absence (◑) and the presence of 5×10^{-5} (○), 1×10^{-4} (●), and 5×10^{-4} M (◒) K_2CO_3 at 22 °C.

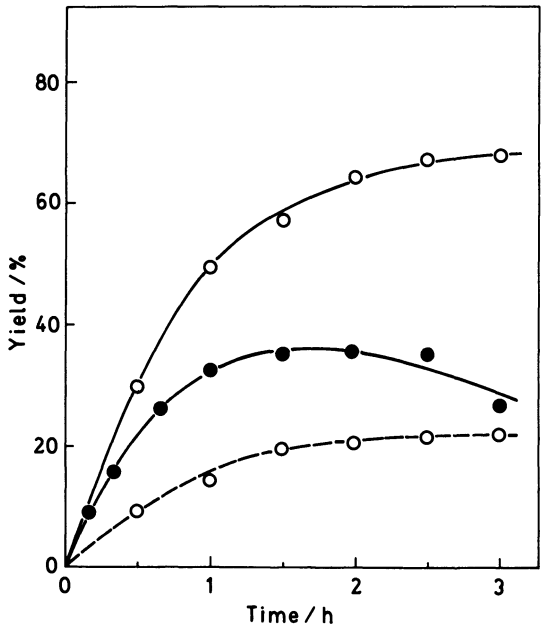

Fig. 4. Yields of MPAH in the photolyses of MPAOMe (5×10^{-5} M) in aerated (○) and deaerated methanol (●) in the absence (———) and the presence of 5×10^{-4} M K_2CO_3 (——) at 22 °C.

Table 3. Yields of MPAH, PA, and MA=O in Photolyses of MPAOMe in Solvents under Aerobic and Anaerobic Conditions and Lifetimes of MPA·(τ) Photochemically Generated at 22 °C[a]

Solvent	Irradiation time/min	Yield/%[b]			τ/min
		MPAH	PA	MA=O	
Methanol	90	66(35)	0(0)	0(0)	3.7
Ethanol	90	58(23)	0(0)	0(0)	27
2-Propanol	40	14(7)	0(0)	5(0)	55
Acetonitrile[c]	10	7(5)	15(8)	8(0)	16

a) The alcohols solutions of 5×10^{-5} M MPAOMe was irradiated in the presence of 5×10^{-4} M K_2CO_3. b) The values in parentheses represent the yields of the products obtained under anaerobic conditions. c) The MPAOMe (5×10^{-5} M) solution was irradiated in the absence of K_2CO_3.

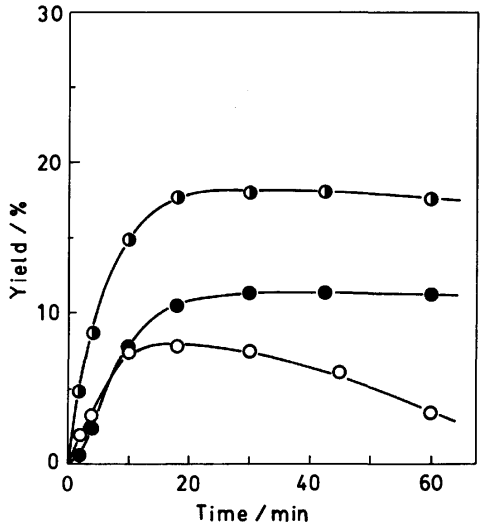

Fig. 5. Yields of MPAH (○), PA (◑), and MA=O (●) in the photolysis of MPAOMe (5×10^{-5} M) in aerated acetonitrile without base at 22°C.

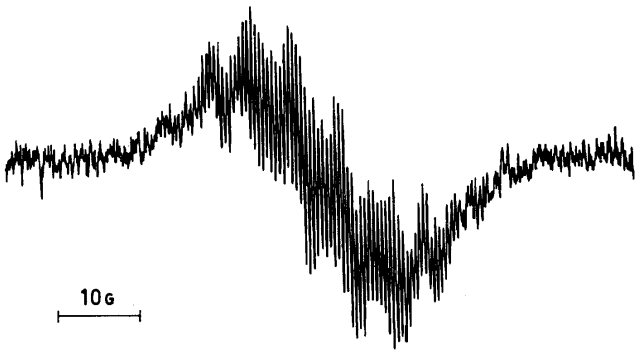

Fig. 6. ESR spectrum of MPA· generated by the photolysis of MPAOMe (5×10^{-4} M) in deaerated ethanol containing ca. 1×10^{-3} M K_2CO_3. The spectrum was measured after the solution was irradiated with a 500-W super high-pressure Hg lamp for ca. 20 s at room temperature.

formation rate of MPAH in deaerated methanol containing K_2CO_3 is shown in Fig. 4. The initial rate in deaerated methanol was slightly slower than that in aerated methanol and the subsequent photodecomposition of MPAH proceeded. The HPLC analysis of the photolyzed solution indicated that various unknown products are produced along with MPAH upon irradiation in deaerated methanol. Most of these unknown products were the same as those produced by the photolysis of MPAH. During irradiation, the photolyzed solution became red-violet (λ_{max}=518 and 487 nm) which faded upon contact with air. The ESR spectrum (Fig. 6) clearly showed that the red-violet color is due to 10-methyl-9-phenylacridinyl radical (MPA·). The ESR spectrum shown in Fig. 6 is in good agreement with that of MPA· produced by electrochemical reduction of MPA+Cl⁻.[10] MPA· gradually disappeared in the dark. The lifetimes of MPA· in alcohols and acetonitrile are listed in Table 3.

Photochemical Reaction of MPAOMe in Ethanol Matrix at 77 K. MPAOMe (5×10^{-5} M) in an ethanol matrix at 77 K was irradiated for 70 min. The absorption spectrum indicated the disappearance of MPAOMe and the appearance of an absorption band having its maximum wavelength at 360 nm, which corresponds to that of PA. The HPLC analysis showed the formation of MPAH and PA in 29 and 15% yields, respectively.

Thermal Reaction of MPAOMe in Methanol and Acetonitrile. The acetonitrile solution of MPAOMe (5×10^{-5} M) was refluxed for 3.5 h under the aerobic conditions. The reaction mixture became yellowish during heating and the formation of MPA+MeO⁻ (ca. 80% yield) was confirmed by absorption spectroscopy. Interestingly, MPAH, MA=O, and PA were also produced in 11, 2, and 8% yields, respectively. Any other products were not detected by HPLC. Under anaerobic conditions, however, no MPA+MeO⁻ was formed and MPAH (2%) was the sole product which was detectable by HPLC, while most of the MPAOMe decomposed in refluxing acetonitrile. No generation of MPA· was observed by absorption spectroscopy. Although the dissociation of MPAOMe to MPA+MeO⁻ occurred in boiling methanol under aerobic conditions, neither MPAH nor MA=O and PA were produced. In the presence of K_2CO_3, MPAOMe in boiling methanol did not react at all.

Discussion

It is well-known that the electrophilicity of 10-alkylacridinium cations is so strong that nucleophiles such as hydroxide and alkoxide anions attack the carbon atom at the 9-position of the acridinium ring to give corresponding pseudo bases.[11–19] Bunting et al.[7,17] have found that the nucleophilic addition of OH⁻ to the 9-aryl-10-methylacridinium cations occurs about 30-fold faster than that to the corresponding triphenylmethyl cation analogues and the bulky substituents at the 9-position do not seriously prevent the addition of OH⁻. In the present study, we isolated and purified the methanol adduct of MPA+Cl⁻, MPAOMe, in moderate yield (see Experimental Section). It was also found that an equilibrium shown in Eq. 3 is established in methanol even in the absence of base:

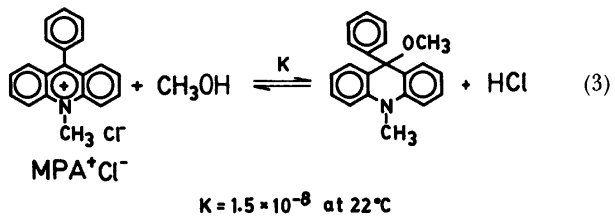

(3)

In dilute solution, MPA^+Cl^- could be converted quantitatively to MPAOMe in methanol in the presence of K_2CO_3 (see Table 1). As Table 1 shows, the addition of alcohols to MPA^+Cl^- is greatly affected by the kind of alcohol. Since the positive charge of the acridinium cation distributes in the transition state, the nucleophilic addition of alcohol is expected to be accelerated in a nonpolar solvent. The experimental results, however, are opposite to this expectation. One of the factors which dominates the alcohol addition may be a steric hindrance. The hydrogen atoms at the 1- and 8-positions as well as the phenyl substituent at the 9-position of the acridinium ring may inhibit ability to reach the transition state. Meanwhile, since the carbon atom at the 9-position of the alcohol adducts is a sp^3 orbital, the steric hindrance is greatly weakened. The alcohol adducts, therefore, are considerably more stable in the cases of the primary and secondary alcohols when a weak base is present in the system.

We expected the spontaneous heterolyses of the alcohol adducts followed by the hydride transfer from the alkoxide anions to MPA^+. The spontaneous heterolyses could be realized in alcohols and acetonitrile (see Table 2). As is expected theoretically, the dissociation of MPAOMe into MPA^+MeO^- favors a polar protic solvent such as methanol. In ethanol, 2-propanol, and acetonitrile, however, MPAOMe hardly dissociates. Since the phenyl ring at the 9-position of MPA^+ is not coplanar with the acridinium ring, the change in the hybrid orbital of the carbon atom from sp^3 to sp^2 upon dissociation of MPAOMe to MPA^+MeO^- seems to require relatively large energy. Although the spontaneous heterolysis of MPAOMe in methanol was appreciable, the hydride transfer between MPA^+ and CH_3O^- does not occur at all.

MPAH could be obtained photochemically from MPAOMe. In aerated methanol without base, the photolysis of MPAOMe led to the effective heterolysis to MPA^+MeO^- and the ineffective reduction to MPAH (see Fig. 2). In the presence of K_2CO_3, the photochemical formation of MPAH became a predominant reaction (see Fig. 4 and Table 3). Under anaerobic conditions, the formation of MPAH was depressed because of the photodecomposition of MPAH (see Fig. 4). If the photoreduction proceeds by a radical mechanism via the triplet state of MPAOMe, the rate of the MPAH formation should be faster, at least at the initial stage of the photolysis, in deaerated methanol than in aerated methanol. The experimental results disagree with this expectation (see Fig. 4). It can be concluded, therefore, that an ionic mechanism via the lowest excited singlet state of MPAOMe accounts for the formation of MPAH. In photolyses under anaerobic conditions, however, the formation of MPA· was detected by adsorption and ESR spectroscopy. In the presence of oxygen, MPA· is expected to be quenched (Eq. 4) or converted to MA=O (Eq. 5):

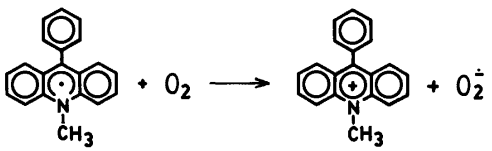

(4)

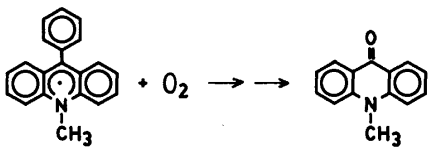

(5)

Indeed, small amounts of MA=O were produced in the photolyses of MPAOMe in aerated 2-propanol and acetonitrile (see Table 3). In neither methanol and ethanol, could MA=O be detected. Another reaction of MPAOMe in acetonitrile is the elimination of the CH_3 group at the 10-position of the acridine ring to give PA. The most plausible mechanism for the PA formation is S_N2 reaction between MPA^+ and CH_3O^- photochemically generated:

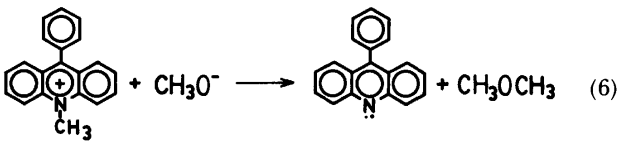

(6)

PA was not produced in alcoholic solutions (see Table 3). This may be due to the stabilization of CH_3O^- by strong solvation with alcohols through hydrogen bonding.

Important information was obtained from the photolysis of MPAOMe in an ethanol matrix at 77 K. In the rigid matrix, the formation of MPA^+MeO^- and MPA· was not observed by the absorption spectroscopy. The main photoproducts are MPAH and PA. MPA^+MeO^- photochemically generated should be a contact ion pair without solvation in the rigid matrix. Such an ion pair, therefore, is so active that the recombination to MPAOMe, the hydride transfer from CH_3O^- to MPA^+ giving MPAH and formaldehyde, and the S_N2 reaction giving PA and CH_3OCH_3 are expected to occur competitively.

Let us return to the mechanism in fluid solutions. A plausible mechanism for the photoreaction of MPA^+Cl^- in methanol is shown in Scheme 3. In the presence of base, photochemically inactive MPA^+Cl^- is converted to MPAOMe which dissociates into MPA^+MeO^- from its lowest excited singlet state. Most of the ion pairs in the Franck–Condon ground states will be solvated rapidly by a polar solvent. It seems that a part of the ion pairs in the nonrelaxed states transfers a hydride from CH_3O^- to MPA^+ to give MPAH even in very low quantum yield. Solvated MPA^+MeO^- is inactive and MPA^+ is returned to the original MPAOMe by the aid of K_2CO_3. In both 2-

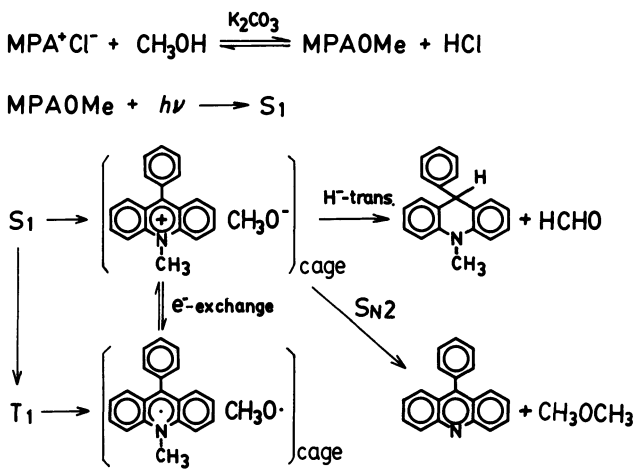

Scheme 3.

propanol and acetonitrile, the formation of the alcohol adduct is so slow that the electron transfer from CH_3O^- to MPA^+ takes place to generate MPA· and CH_3O· whose subsequent reactions may provide MA=O and unknown products. Since the electron transfer occurs through a long-distance interaction between MPA^+ and CH_3O^-, the formation of MPA· and CH_3O· may not be inhibited so sereously as hydride transfer from CH_3O^- to MPA^+ by solvation. MPA· therefore, was generated in all solvents tested in the present study under anaerobic conditions.

Another mechanism for MPAH formation is a radical mechanism which involves the homolysis of MPAOMe in the lowest excited singlet state to yield a singlet radical pair, MPA·MeO·, and subsequent hydrogen abstraction of MPA· from CH_3O· to form MPAH. This mechanism can be excluded on the basis of the results on the thermal reactions of MPAOMe in boiling methanol and acetonitrile. Although no reaction of MPAOMe occurred in aerated methanol except for the dissociation to MPA^+MeO^-, the products which are the same as those in the photolysis (MPA^+MeO^-, MPAH, MA=O, and PA) were obtained in refluxing acetonitrile. Under anaerobic conditions, heating in acetonitrile provided unknown products along with a small amount of MPAH; neither MPA^+MeO^- nor MPA· was detected. If the thermal reaction of MPAOMe to MPAH proceeds via the singlet radical pair, MPAH should also be produced in the reaction of MPAOMe in boiling methanol because the yield of MPAH photochemically formed is higher in methanol than in acetonitrile. The solvent effect on the thermal reaction of MPAOMe can be interpreted in terms of the ionic mechanism, but not the radical mechanism. Since acetonitrile is an aprotic polar solvent, the stabilization of CH_3O^- by this solvent should be much weaker than by methanol. The thermal dissociation of MPAOMe to MPA^+MeO^-, therefore, may be followed by the hydride transfer and the nucleophilic substitution to give MPAH and PA, respectively, in boiling acetonitrile. Presumably, an electron transfer from CH_3O^- to MPA^+ occurs to generate the radical pair composed of MPA· and CH_3O·. Under aerobic conditions, MPA· should be quenched by oxygen to regenerate MPA^+ (see Eq. 4). In the absence of oxygen, however, the radical species may induce complex reactions to give unknown products in refluxing acetonitrile. It can be concluded, therefore, that the radical pair, MPA·CH_3O· is not a precursor of both MPAH and PA. It is clear that the solvation to MPA^+MeO^- plays an important role to promote the subsequent hydride transfer and nucleophilic substitution reactions. In alcoholic solvents, CH_3O^- generated as a counter anion of MPA^+ is stabilized so extensively by alcohols through hydrogen bonding that neither intramolecular hydride transfer nor nucleophilic substitution of MPA^+MeO^- take place. The photochemical processes of MPAOMe, however, can provide a nonrelaxed ground state of MPA^+MeO^- to promote hydride transfer to form MPAH.

The present study was supported by Grant-in-Aids for Science Research No. 61550647 from the Ministry of Education, Science and Culture.

References

1) K. Kano, B. Zhou, and S. Hashimoto, *Bull. Chem. Soc. Jpn.*, **60**, 1041 (1987).
2) M. Koizumi, S. Kato, N. Mataga, T. Matsuura, and Y. Usui, "Photosensitized Reactions," Kagaku Dojin, Kyoto (1978), Chap. 4.
3) V. Zanker, E. Erhardt, F. Mader, and J. Z. Thies, *Naturforsch. B*, **21**, 102 (1966).
4) K. Kano, B. Zhou, S. Hashimoto, T. Sugino, and A. Torii, *Chem. Express*, **2**, 13 (1987).
5) A. Bernthsen, *Justus Liebigs Ann. Chem.*, **224**, 1 (1884).
6) A. K. Colter, G. Saito, and F. J. Sharom, *Can. J. Chem.*, **55**, 2741 (1977).
7) J. W. Bunting and W. G. Meathrel, *Can. J. Chem.*, **52**, 981 (1974).
8) K. Kano, B. Zhou, and S. Hashimoto, *Chem. Lett.*, **1985**, 791.
9) T. M. Grigoreva, V. L. Ivanov, and M. G. Kuzmin, *Zh. Org. Khim.*, **17**, 428 (1981); *Chem. Abstr.*, **95**, 6092q (1981).
10) N. W. Koper, S. A. Jonker, J. W. Verhoeven, and C. van Dijk, *Recl. Trav. Chim. Pays-Bas*, **104**, 296 (1985).
11) A. Hantzsch and M. Kalb, *Chem. Ber.*, **32**, 3109 (1899).
12) J. J. Dobbie and C. K. Tinkler, *J. Chem. Soc.*, **1905**, 269.
13) J. G. Aston, *J. Am. Chem. Soc.*, **53**, 1448 (1931).
14) R. J. Goldacre and J. N. Phillips, *J. Chem, Soc.*, **1949**, 1724.
15) F. Krohnke and H. L. Honig, *Chem. Ber.*, **90**, 2215 (1957).
16) J. Clark and M. Bakavali, *J. Chem. Soc., Perkin Trans. 1*, **1977**, 1966.

17) J. W. Bunting, V. S. F. Chew, S. B. Abhyankar, and Y. Goda, *Can. J. Chem.*, **62**, 351 (1984).
18) J. W. Bunting and G. M. Kauffman, *Can. J. Chem.*, **62**, 729 (1984).
19) S. Shinkai, T. Tsuno, and O. Manabe, *J. Chem. Soc., Perkin Trans. 2*, **1984**, 661.

Homolytic Decomposition of *t*-Alkyl 2,2-Dimethylperoxypropionates

Takeshi KOMAI, Kazuo MATSUYAMA,* and Masaru MATSUSHIMA
Chemicals & Explosives Research Laboratory, Nippon Oil & Fats Co., Ltd.,
Taketoyo-cho, Chita-gun, Aichi-ken 470-23
(Received August 3, 1987)

Decomposition rates and products of *t*-alkyl 2,2-dimethylperoxypropionates were measured in cumene at several temperatures. The peroxyesters decomposed homolytically, depending on the structure of the *t*-alkyl moiety. The relative rates of the *t*-alkyl moieties to the 1,1-dimethylethyl one were: 1,1-dimethylbutyl (1.14), 1,1-dimethylpropyl (1.19), 1,1,2-trimethylpropyl (1.85), 1,1,3,3-tetramethylbutyl (2.10), and 1,1-dimethyl-2-phenylethyl (2.34). The decomposition showed an isokinetic relationship and the importance of stabilization by hyperconjugation. Based on these data, the decomposition mechanism, which contains a slight stretching of the C_α–C_β bond to the peroxyl oxygen at the transition state is, discussed.

A large number of investigations concerning the decomposition mechanism of *t*-alkyl peroxyesters have been concerned with the relationship between the structure of the peroxyesters and the mode of decomposition.[1] However changes in the structure have been restricted to the acyl moiety. Only a few reports concerning the structure of the *t*-alkylperoxyl group exist.[2] Sheldon and Kochi indicated that there is a small influence of the *t*-alkylperoxyl group on the decomposition of di-*t*-alkyl diperoxyoxalates, and the variation of the solvent from pentane to acetonitrile enhances the rate and the formation of heterolytic decomposition products.[2a] Difficulties in studying the influence of the *t*-alkylperoxyl moiety can be attributed to the possibility that radical decompositions are accompanied by heterolytic ones.[3] It has also been known that peroxyesters are acceptable to heterolytic decompositions when the acidity of the parent acid is large.[4]

We have studied the homolytic decomposition of *t*-alkyl 2,2-dimethylperoxypropionates (**1**) which could be expected to decompose more homolytically because of the slight acidity of the parent acid. One of the compounds studied, 1,1-dimethylethyl 2,2-dimethylperoxypropionate (**1a**) has been used as a standard compound.

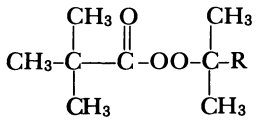

1a; R = CH_3, **1b**; R = CH_3CH_2, **1c**; R = $CH_3CH_2CH_2$, **1d**; R = $(CH_3)_2CHCH_2$, **1e**; R = $(CH_3)_2CH$, **1f**; R = $PhCH_2$

Results and Discussion

The peroxyesters were synthesized by the acylation

Table 1. Rate Constants and Activation Parameters for Decomposition of *t*-Alkyl 2,2-Dimethylpropionates at Concentration of 0.05 mol dm^{-3} in Cumene[a]

Peroxyester	Temperature	Rate constant	Activation parameter	
	°C	$10^5 k_d/s^{-1}$	ΔH^*/kJ mol^{-1}	ΔS^*/J K^{-1} mol^{-1}
1a[b]	60	2.95	118.0	23
1b	50	1.05 ±0.09	114.9±1.2	14±7
	60	3.51 ±0.08		
	70	13.09 ±0.35		
	80	42.39 ±3.61		
1c	40	0.239±0.008	116.3±0.8	18±5
	50	0.883±0.031		
	60	3.37 ±0.097		
	70	12.26 ±0.51		
	80	41.66 ±3.47		
1d	40	0.480±0.011	112.4±1.3	12±8
	50	1.797±0.053		
	60	6.18 ±0.32		
	70	23.44 ±0.76		
1e	40	0.36 ±0.11	114.2±1.5	15±9
	50	1.59 ±0.08		
	60	5.14 ±0.40		
	70	19.21 ±1.10		
1f	40	0.456±0.017	116.5±0.5	24±3
	50	1.833±0.031		
	60	6.91 ±0.20		
	70	25.1 ±0.8		

a) Rate constants and their standard deviations were calculated by the method of least squares. b) Ref. 19.

of the correspoding hydroperoxides with 2,2-dimethylpropionyl chloride in the presence of potassium hydroxide at low temperatures. The hydroperoxides were prepared from the corresponding alcohols or olefins by using 50% hydrogen peroxide in the presence of sulfuric acid.

The rates for the decomposition of the peroxyesters were measured by iodometric titration of the active oxygen. Good first-order rate constants were obtained over 10—80% conversion in all cases. Rate data concerning cumene are given in Table 1 together with calculated activation parameters; data concerning acetonitrile are given in Table 2. The decomposition products formed from the *t*-alkylperoxyl moiety in cumene were analyzed with GC and are shown in Table 3, together with the relative rates of β-scission of the corresponding alkoxyl radicals.[4,5] The total yields of the corresponding alcohol and the acetone were upper 90%. The inversion product ($C(CH_3)_3CO_2$-$C(CH_3)_2$-OR) and the hydrolysis product (ROH) from the heterolyic decomposition could not be recognized with detectable amounts. The solvent effect in cumene and acetonitrile was similar to that of *p*-substituted 1,1-dimethylethyl 2-methyl-2-phenylperoxypropionates.[1f] These facts indicate that the decomposition of **1** in cumene proceeds mainly by a homolytic path. The formation ratio of the acetone to the corresponding alcohol in Table 3 changes with the alkyl group (R), and the order of these ratios is similar to those in the decomposition of di-*t*-alkyl diperoxyoxalates and in β-scission of the corresponding alkoxyl radicals (Table 3). However, the ratios of **1d** and **1e** are considerably different in the order and size from those of the relative rate (k_β/k'_A) in the β-scission. The ratio of **1d** increases regardless of whether there is less β-scission, and the ratio of **1e** is very small, compared with the remarkable β-scission. The decomposition rates of **1** change with the *t*-alkyl group, of which the effect is not large. The ratio of the rate constant for the slowest **1a** against the fastest **1f** is 0.43 at 60 °C. This corresponds to that reported for the decomposition of di-*t*-alkyl diperoxyoxalates in pentane.

Figure 1 shows an isokinetic relationship for the decomposition of **1** in cumene. A good linear free-energy relation exists for five electron-donating alkyl substituents, except **1f** (electron-withdrawing one). This suggests that the difference of decomposition rates except **1f** (discussed later) takes place with a single interaction mechanism of the substituents.[6]

The relative rates in the decomposition of **1** in cumene are found to depend on the nature of the substituents and follow the order: **1a**<**1c**<**1b**<**1e**<**1d**<**1f** (Table 1). The data in Table I could be analyzed by the following Taft equation:[7]

$$\log (k_d/k_{d0}) = \rho^*\sigma^* + (\Delta n)h, \quad (1)$$

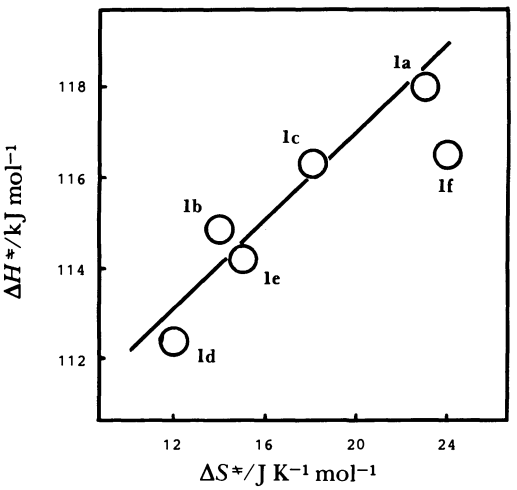

Fig. 1. Isokinetic relationship for the decomposition of *t*-alkyl 2,2-dimethylpropionates in cumene.

Table 2. Rate Constants in Acetonitrile and Relative Rates with Variation of Solvent at 60 °C[a]

Peroxyester	Rate constant $10^5 k_d/s^{-1}$	Relative rate[b]
1a	5.18±0.04	1.76
1c	7.39±0.14	2.19
1d	11.43±0.13	1.85

a) Initial concentration of peroxyester is 0.05 mol dm^{-3}.
b) Relative rate of acetonitrile against cumene.

Table 3. Decomposition Products Formed from *t*-Alkyl Moiety at 60 °C

Peroxyester	Product/mol		Ratio[a]	Ratio in peroxyoxalate[b]	k_β/k'_A in β-scission[c]
	Acetone	Corresponding alcohol			
1a	0	0.88	0	<0.02	0.053
1b	0.28	0.66	0.42	0.09	2.9
1c	0.17	0.76	0.22	—	2.4
1d	0.43	0.59	0.73	—	1.4
1e	0.54	0.38	1.42	2.92	96
1f	0.54	0.40	1.35	1.25	2.2

a) Ratio of acetone to the corresponding alcohol formed per the decomposed peroxyester **1** (mol/mol) in cumene.
b) In pentane at 40 °C.[2a] c) Relative rate of β-scission to hydrogen abstraction with cyclohexane of alkoxyl radical.[5] These values were calculated by using data in Ref. 4.

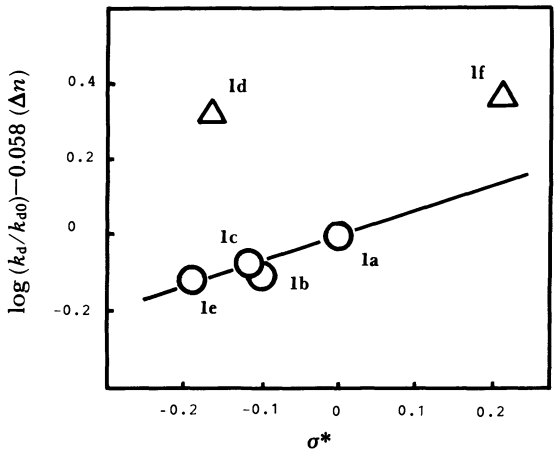

Fig. 2. A plot of [log (k_d/k_{d0})=0.058 (Δn)] against σ^* in the decomposition of *t*-alkyl 2,2-dimethylpropionates in cumene at 60°.

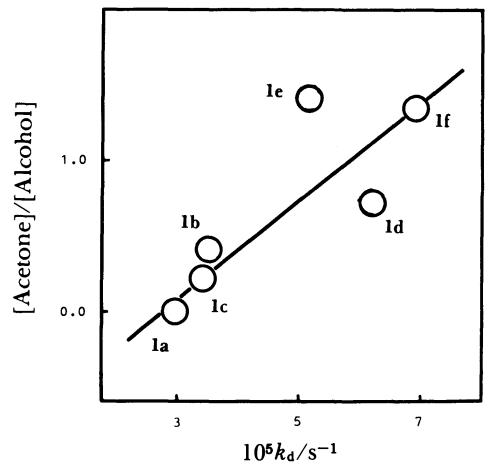

Fig. 3. A plot of [Acetone]/[Alcohol] against k_d in the decomposition of *t*-alkyl 2,2-dimethylpropionates in cumene at 60°C.

where k_d/k_{d0} is relative rate of the related peroxyester to **1a**, σ^*, the polar substituent constant by Taft, ρ^*, reaction constant, (Δn), the difference between the related peroxyester and **1a** for the number of the hydrogen atoms participating in C–H hyperconjugation, and h, an emperical constant. A plot of [log (k_d/k_{d0})−(Δn)h] vs. σ^* in Fig. 2 shows good linearity for **1a**, **1b**, **1c**, and **1e**, and the values of ρ^*= 0.67 and h=0.058 are estimated by using a least-squares method. These are interpreted in terms of C–H hyperconjugative and inductive stabilizing effects of the substituents at the transition state.

On the basis of the decomposition rates and products, the isokinetic relationship and the importance of the hyperconjugation, the following scheme for the main reactions may be considered as a decomposition mechanism of **1**:

$$\mathbf{1} \underset{k_{-1}}{\overset{k_1}{\rightleftharpoons}} [CH_3\text{-}\overset{CH_3}{\overset{|}{C}}\cdots\overset{O}{\overset{\|}{C}}\text{-}O\cdots O\text{-}\overset{CH_3}{\overset{|}{C}}\cdots R]_{cage} \quad (2)$$

2

$$[\mathbf{2}]_{cage} \xrightarrow{k_c} CH_3\text{-}\overset{CH_3}{\overset{|}{C}}\text{=}CH_2 + CO_2 + HO\text{-}\overset{CH_3}{\overset{|}{C}}\text{-}R \quad (3)$$

3

$$[\mathbf{2}]_{cage} \xrightarrow{k_{DA}} CH_3\text{-}\overset{CH_3}{\overset{|}{C}}\cdot + CO_2 + \cdot O\text{-}\overset{CH_3}{\overset{|}{C}}\text{-}R \quad (4)$$

$$[\mathbf{2}]_{cage} \xrightarrow{k_{D\beta}} CH_3\text{-}\overset{CH_3}{\overset{|}{C}}\cdot + CO_2 + O\text{=}\overset{CH_3}{\overset{|}{C}} + \cdot R \quad (5)$$

4

$$R\text{-}\overset{CH_3}{\overset{|}{C}}\text{-}O\cdot + R'H \xrightarrow{k_A} \mathbf{3} + R'\cdot \quad (6)$$

$$R\text{-}\overset{CH_3}{\overset{|}{C}}\text{-}O\cdot \xrightarrow{k_\beta} R\cdot + \mathbf{4} \quad (7)$$

$$CH_3\text{-}\overset{CH_3}{\overset{|}{C}}\cdot + R'H \longrightarrow CH_3\text{-}\overset{CH_3}{\overset{|}{C}}\text{-}H + R'\cdot \quad (8)$$

$$2R'\cdot \longrightarrow R'\text{-}R' \quad (9)$$

Here, k_1 is the rate constant for the bond homolysis, k_{-1} the rate constant for the cage return, **2** a reaction intermediate, k_c the rate constant for the disproportionation between the 1,1-dimethylethyl and the alkoxyl radicals within a solvent cage, k_{DA} the rate constant for the diffusion of the alkoxyl radical out of the solvent cage, $k_{D\beta}$ the rate constant for the outwared diffusion of the acetone formed within the solvent cage, k_A the rate constant for hydrogen abstraction of the alkoxyl radical with cumene (R'H), and k_β the rate constant for β-scission of the alkoxyl radical outside the solvent cage, respectively.

The decomposition prcducts of **1a** in cumene included isobutylene and isobutane in approximately equal amounts;[8] most of them may be considered from the

amount of 2,3-dimethyl-2,3-diphenylbutane to be formed exclusively within (Eq. 3) and outside the solvent cage (Eq. 8), respectively. The coupling products between the 1,1-dimethylethyl and the alkoxyl radicals within the solvent cage, and between these radical species outside it were negligibly small in the photodecomposition of **1**.[2c] Since the cage return (Eq. 2) can be neglected in a concerted decomposition ($k_1 \gg k_{-1}$)[9] the observed rate constant of the decomposition, k_d, is as follows:

$$k_d = k_1(k_{DA} + k_{D\beta} + k_c)/(k_{-1} + k_{DA} + k_{D\beta} + k_c) \simeq k_1, \quad (10)$$

The formation ratio of the acetone to the corresponding alcohol ([**4**]/[**3**]) in Table 3 is plotted against the decomposition rate constant, k_d, shown in Fig. 3. The decomposition of **1d** yield much more acetone than that estimated from the β-scission, compared with those of **1b** and **1c**. This can be explained by the fact that a part of the acetone is formed by the β-scission within the solvent cage or directly from the intermediate 2 (Eq. 5). Figure 3 suggests that the formation of acetone is apt to increase with the decomposition rate of **1** and is based on the direct one from the intermediate **2**. The points of **1e** and **1d** in Fig. 3 deviate greatly from a linear line (correlation coefficient=0.8676)[10] which passes through the points of **1c** and **1f**, and the corresponding alkoxyl radicals to **1c** and **1f** have the similar values of k_β/k'_A with each other (Table 3). These deviations may be understood by the difference of the β-scission outside the solvent cage.[10]

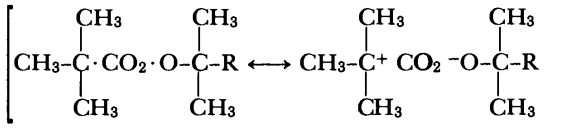

2a **2b**

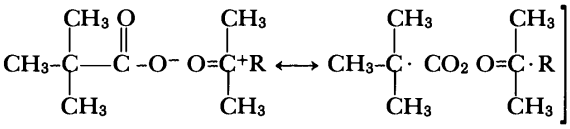

(11)

2c **2d**

The intermediates of **2a** and **2b** at the transition state had been confirmed by the relationships between the structure of the acyl group and the reactivity.[1] The positive value of ρ^* in the Taft equation (Eq. 1) shows an inductive stabilizing effect more by an electron-withdrawing substituent on the intermediate **2**. The importance of the hyperconjugation (Eq. 1) and the formation of the β-scission product from the intermediate **2** (Eq. 5) indicate that, in addition to **2a** and **2b**, there exist intermediates of **2c** and **2d** at the transition state. The intermediate of **2c** is correlated to that in the heterolytic decomposition of *t*-alkyl *p*-nitroperbenzoates.[3] Walling et al. had proposed that all of radical and ionic decomposition products arise from a common rate-determining transition state to partition into radical and ionic pairs occurring at a later stage in the decomposition of diacyl peroxides.[11] The decompositions of 1-methyl-1-phenylethyl peracetate and di-*t*-alkyl diperoxyoxalates follow heterolytic, homolytic, or their mixed pathways, depending on the polarity of the solvent and the presence of acid catalysis.[12] The similarities between the homolytic and the heterolytic decompositions (as shown in this work) support the Walling hypothesis in the same manner as diacyl peroxides. Deviations of **1f** from the isokinetic relationship and the Taft equation (Figs. 1 and 2) may probably result from the stabilization of the intermediate **2d** of which the benzyl radical is the most stable. The deviation of **1d** from the Taft equation (Fig. 2) may be understood to be similar to the rate enhancement in neopentyl solvolysis, in which γ-carbon atoms to the cationic center participate in the stabilization at the transition state.[13] Thus, the influence of the *t*-alkylperoxyl moiety could be explained by inductive and resonance effects without any consideration of steric effects. In conclution, it may be suggested that the C_α–C_β bond to the peroxyl oxygen is only slightly streched, together with the C_α–CO and O–O bonds at the transition state.

Experimental

IR and NMR spectra were recorded on JASCO A-3 and JEOL JNM-MH-100 spectrometers, respectively. GC analysis was carried out using Shimadzu GC-6A and GC-2D gas chromatography using five columns: (A), Silicone GE-30 on Shimalite (NAW), 2.4 m; (B), PEG 20M 25% on Shimalite (NAW), 2 m; (C), PEG 20M 5% on Shimalite (NAW), 2 m; (D), Sorbitol 30% on Shimalite (NAW), 3 m; (E), PEG 20 M 25% on Shimalite (NAW), 3 m.

Materials. 2,2-Dimethylpropionyl chloride was purified by the distillation (bp 103 °C) of a commercial product. Sixty-nine per cent 1,1-dimethylethyl, 90% 1,1-dimethylbutyl, and 86% 1,1,3,3-tetramethyl-butyl hydroperoxides were the products of Nippon Oil & Fats Co., Ltd. 1,1-Dimethylpropyl alcohol was prepared by the reaction of 2-methyl-1-pentene with an excess of 65% H_2O_2 for 30 min at 0—5 °C and the hydrolysis of the reaction mixture with an aqueous solution of 5% NaCl under a temperature of 10 °C. The alcohol was distilled after drying over anhydrous $MgSO_4$ (bp 66 °C/76 mmHg (1mmHg=133.322 Pa)).[14] In a similar method 1,1,3,3-tetramethylbutyl alcohol was prepared (bp 54 °C/16 mmHg).[14]

Preparation of Hydroperoxides. The purities of hydroperoxides were checked by iodometric titration and GC. The titration procedure involved the use of a mixture (20:2) of isopropyl alcohol and acetic acid as the solvent, and saturated potassium iodide as the source of iodide.[15]

1,1-Dimethylpropyl hydroperoxide was prepared from a reaction of the corresponding alcohol with 50% H_2O_2 by the method of Milas and Surgenor[16] and the purification by distillation (bp 50 °C/20 mmHg).[17] **1,1-Dimethylbutyl hydroperoxide** was purified by distillation (bp 41 °C/3 mmHg)[18] of the commercial product. **1,1,3,3-Tetramethylbutyl hydroperoxide** was purified from a commercial product by the isolation of sodium salt with sodium amide,

regeneration of the hydroperoxide with carbon dioxide and vacuum distillation (bp 46 °C/1 mmHg).

1,1,2-Trimethylpropyl hydroperoxide was prepared by the reaction of olefin with H_2O_2 in the presence of H_2SO_4 and acetonitrile. To an aquous solution of 44% H_2O_2 (115.0 g, 1.50 mol) there was added dropwise concd H_2SO_4 (80.0 g, 0.82 mol) for 30 min at 0 °C and added continuously acetonitrile (32.8 g, 0.80 mol) and chloroform (50 g). Then, to the mixture there was added dropwise 2,3-dimethyl-2-butene (67.4 g, 0.80 mol) for 30 min at 0—5 °C. The mixture was stirred for 30 min at 5 °C and continuously for 30 min at 10 °C in order to complete the reaction. After the reaction mixture was added by petroleum ether (50 g) and washed three times with an aquous solution of 40% $(NH_4)_2SO_4$, a crude product was obtained by the evaporation of the solvent at reduced pressure. Because dangerous materials (ketone peroxides) were contained in the crude product,[3] they were eliminated by a separation of the oily material from the crude product (32.2 g), which was added by petroleum ether (6.0 g) after the neutralization with 35% KOH (45.0 g) and methanol (30 cm^3). After regeneration of the hydroperoxide by carbon dioxide and washing with an aqueous solution of 40% $(NH_4)_2SO_4$, the crude product was distilled (bp 30—33 °C/2 mmHg) in the presence of polyethylene glycol oligomer ($\bar{n}$=300) to give 1,1,2-trimethylpropyl hydroperoxide (6.2 g) of 82.0% purity analyzed by GC using column A. IR (neat): ν_{O-H} 3400 cm^{-1}; ^1H NMR (CCl_4): δ=1.00 (6H, d, >C(CH_3)$_2$), 1.13 (6H, s, -C(CH_3)$_2$-), and 2.02 (H, m, >CH-).

1,1-Dimethyl-2-phenylethyl hydroperoxide was prepared by a reaction of the corresponding alcohol with 50% H_2O_2. A mixture of 1,1-dimethyl-2-phenylethyl alcohol (300.4 g, 2.0 mol) and THF (100 cm^3) was added dropwise to 72% H_2SO_4 (272.6 g, 2.0 mol) under a temperature of 10 °C to give the sulfonate. Then after the addition of 50% H_2O_2 (272.0 g, 4.0 mol) for 90 min under a temperature of 10 °C, the mixture was stirred for 3 h at 40 °C and for 2 h at 30 °C. The 15.4% crude material (623.0 g, containing 0.57 mol of the hydroperoxide) was obtained by washing with water after the addition of petroleum ether (300 g), and drying over anhydrous $MgSO_4$. The hydroperoxide (29.6 g) of 97.0% purity was obtained by the isolation of the sodium salt with sodium amide, regeneration of the hydroperoxide by carbon dioxide and recrystallization from petroleum ether. Mp 40—41 °C (lit,[3] mp 44 °C); IR (CCl_4): ν_{O-H} 3400 cm^{-1}, phenyl 1600 cm^{-1}; ^1H NMR (CCl_4): δ=1.16 (6H, s, -C(CH_3)$_2$-), 2.83 (2H, s, -CH_2-), 7.20 (5H, s, phenyl), and 8.02 (1H, s, -OOH).

Preparation of Peroxyesters. Purities of peroxyesters were checked by iodometric titration which involved the use of an acetic acid solution containing a saturated aqueous solution of NaI and a small amount of iron(III) chloride.[19]

Peroxyester 1a was prepared by a Schotten-Baumann reaction of 2,2-dimethylpropionyl chloride with the corresponding hydroperoxide. To a mixture of 69% 1,1-dimethylethyl hydroperoxide (20.9 g, 0.16 mol) and 30% KOH (30.0 g, 0.16 mol) there was added dropwise the acid chloride (16.1 g, 0.13 mol) for 30 min at 2 °C; the mixture was then stirred for 30 min to complete the reaction. After the reaction mixture was washed twice with 5% NaOH for 5 min at 0 °C, three times with water and dried with anhydrous $MgSO_4$, the peroxyester (18.5 g, yield 76.9%) of 93.8% purity was obtained. The distilled material (bp 50.5 °C/5 mmHg) was shown to be 97.0% purity. IR (CCl_4): $\nu_{C=O}$ 1762 cm^{-1}; ^1H NMR (CCl_4): δ=1.24 (9H, s, acyl t-Bu) and 1.20 (9H, s, peroxyl t-Bu).

Peroxyester 1b was prepared by a Schotten-Baumann reaction of the acid chloride with the corresponding hydroperoxide. To a mixture of 95.0% 1,1-dimethylpropyl hydroperoxide (7.7 g, 0.07 mol) and 20% KOH (25.3 g, 0.09 mol) there was added dropwise acid chloride (10.9 g, 0.07 mol) containing petroleum ether (2.5 g) for 30 min at 0—5 °C and stirred for 30 min to complete the reaction. Then, the reaction mixture was washed once with 5% NaOH, once with an aqueous solution which contained Na_2SO_4 (4.2%), sodium acetate (8.3%) and acetic acid (4.2%), and twice with water. After drying over anhydrous $MgSO_4$ and evaporation of the solvent, the crude product of 11.5 g (yield 83.0%) was obtained and further purified by distillation (bp 51 °C/3 mmHg) to give the peroxyester of 95.8% purity. IR (CCl_4): $\nu_{C=O}$ 1765 cm^{-1}; ^1H NMR (CCl_4): δ=0.94 (3H, m, peroxyl -CH_3), 1.24 (15H, s, acyl t-Bu and peroxyl t-Bu) and 1.53 (2H, q, -CH_2-).

Peroxyester 1c was prepared by the method according to 1,1-dimethylpropyl peroxyester. Yield 81.4%; purity 96.1%; IR (CCl_4): $\nu_{C=O}$ 1765 cm^{-1}; ^1H NMR (CCl_4): δ=0.95 (3H, m, peroxyl-CH_3), 1.24 (15H, s, acyl t-Bu and peroxyl -C(CH_3)$_2$-O), and 1.52 (4H, m, -CH_2CH_2-).

Peroxyester 1a was prepared by the method according to 1,1-dimethylpropyl peroxyester. The purity and yield of the crude product were 83.7 and 65.0%, respectively. The crude product was purified by flash chromatography on Merck Kieselgel 60 using hexane-ethyl acetate (95:5) as the eluent to give 93.1% purity. IR (CCl_4): $\nu_{C=O}$ 1765 cm^{-1}; ^1H NMR (CCl_4): δ=0.96 (6H, d, peroxyl >C(CH_3)$_2$), 1.20 (6H, s, peroxyl -C(CH_3)$_2$-O), 1.24 (9H, s, acyl t-Bu), and 1.88 (1H, m, >CH-).

Peroxyester 1d was prepared by a Schotten-Baumann reaction of the acid chloride with the corresponding hydroperoxide. To a mixture of 98.0% 1,1,3,3-tetramethylbutyl hydroperoxide (22.3 g, 0.15 mol) and 35% KOH (31 g, 0.23 mol) there was added dropwise the acid chloride (21.7 g, 0.18 mol) for 35 min at 0—5 °C to complete the reaction. The reaction mixture was washed once with 5% NaOH, once with an aqueous solution which contained Na_2SO_4 (4.2%), sodium acetate (8.3%) and acetic acid (4.2%), twice with water, and dried over anhydrous $MgSO_4$ to give the peroxyester of 94.7% purity (21.0 g, yield 48.9%). IR (CCl_4): $\nu_{C=O}$ 1765 cm^{-1}; ^1H NMR (CCl_4): δ=1.03 (9H, s, peroxyl t-Bu), 1.22 (9H, s, acyl t-Bu), 1.32 (6H, s, -C(CH_3)$_2$-O), and 1.60 (2H, s, -CH_2-).

Peroxyester 1f was prepared by a Schotten-Baumann reaction of the acid chloride with the corresponding hydroperoxide. To a mixture of 97.0% 1,1-dimethyl-2-phenylethyl hydroperoxide (17.1 g, 0.10 mol) there was added dropwise the acid chloride (14.5 g, 0.12 mol) for 15 min at 25 °C, and stirred for 10 min at 10 °C to complete the reaction. The reaction mixture was washed once with 5% NaOH, three times with water and dried over anhydrous $MgSO_4$. After the evaporation of the solvent under vacuum, a crude product of 90.0% purity (24.0 g, yield 72.0%) was obtained and purified by flash chromatography on Merck Kieselgel 60 using hexane-ethyl acetate (95:5) as the eluent to give the peroxyester of 94.0% purity. IR (CCl_4): $\nu_{C=O}$

1762 cm^{-1}; phenyl 1600 cm^{-1}; ^1H NMR (CCl_4): δ=1.25 (9H, s, acyl *t*-Bu), 2.83 (2H, s, $PhCH_2$-), and 7.12 (5H, s, phenyl).

Kinetic Procedure. A dilute solution of peroxyester in cumene or acetonitrile was placed in sealed tubes under vacuum and heated in a constant-temperature bath. The remaining amount of peroxyester was determined by the above-mentioned iodometric titration for peroxyester, in which the sample solutions were allowed to stand at room temperature for 15—30 min. The reaction was followed up to 70—80% decomposition and exhibited first-order kinetics.

Decomposition Products. Peroxyester at the concentration of 0.05 mol dm^{-3} in cumene was decomposed completely at 60 °C over 50 h and the solution were analyzed by GC using nonane and decane as internal standards. The following are the conditions used in determining yield of products (product, column): acetone, 1,1-dimehylethyl alcohol, 1,1-dimethylpropyl alcohol, 1,1-dimethylbutyl alcohol and 1,1,2-trimethylpropyl alcohol for **1a**, **1b**, **1c**, and **1e**, column B; acetone and 1,1-dimethyl-2-phenylethyl alcohol for **1f**, column C; 1,1,3,3-tetramethylbutyl alcohol for **1d**, column D; acetone for **1d**, column E.

References

1) a) T. Koenig, "Free Radicals, Vol. I", ed by J. K. Kochi, Wiley-Interscience, Chap. 3 (1973); b) L. A. Singer, "Organic Peroxides, Vol. I," ed. by D. Swern, Wiley-Interscience, Chap. V (1970); c) R. L. Friedman, R. N. Lewis, and R. L. Pstorio, *Mod. Plast.*, **48**, 66 (1971); d) C. Ruchardt, *Angew. Chem., Ent. Ed. Engl.*, **9**, 830 (1970); e) C. Ruchardt "23rd Int. Congress of Pure and Applied Chemistry 4," 223 (1971); f) J. P. Engstrom and J. C. DuBose, *J. Org. Chem.*, **38**, 3817 (1973); g) D. D. Tanner, H. Yabuuchi, and H. Lutzer, *Can. J. Chem.*, **55**, 612 (1977); h) T. Yamamoto, Y. Nakashio, H. Onishi, and M. Hirota, *Nippon Kagaku Kaishi*, **1986**, 224.

2) a) R. A. Sheldon and J. K. Kochi, *J. Org. Chem.*, **35**, 1223 (1970); b) R. R. Hiatt and W. M. J. Strachan, *J. Org. Chem.*, **28**, 1893 (1963); c) R. A. Sheldon and J. K. Kochi, *J. Am. Chem. Soc.*, **92**, 5175 (1970); d) A. S. Nazran and J. Warkentin, *J. Am. Chem. Soc.*, **104**, 6405 (1982).

3) E. Hedaya and S. Winstein, *J. Am. Chem. Soc.*, **89**, 1661 (1967).

4) a) C. Walling and A. Padwa, *J. Am. Chem. Soc.*, **85**, 1593 (1963); b) J. D. Bacha and J. K. Kochi, *J. Org. Chem.*, **30**, 3272 (1965).

5) C. Walling and B. B. Jacknow, *J. Am. Chem. Soc.*, **82**, 6108 (1960).

6) J. E. Leffler and E. Grunwald, "Rates and Equilibria of Organic Reactions", John Wiley & Sons (1963).

7) M. M. Kreevoy and R. W. Taft, Jr., *J. Am. Chem. Soc.*, **77**, 5590 (1955).

8) J. P. Lorand, S. D. Chodroff, and R. W. Wallance, *J. Am. Chem. Soc.*, **90**, 526 (1968); The decomposition products of **1a** in cumene were CO_2 (98%), 1,1-dimethylethyl alcohol (79%), isobutylene (40%), isobutane (30%), 2,3-dimethyl-2,3-diphenylbutane (68%) and bis(1,1-dimethylethyl) ether(2%) in the reference.

9) W. A. Pryor, E. H. Morkved, and H. T. Bickley, *J. Org. Chem.*, **77**, 1999 (1972).

10) If we can assume $k_c=k_{DA}$ from the decomposition products of **1a**,[8] the steady-state approximation in the reaction of Eqs. 2—7 leads to the following equation: $k_{D\beta}/k_{DA}=\{(2+k_\beta/k_A[R'H])[\mathbf{4}]/[\mathbf{3}]-k_\beta/k_A[R'H]/(1+k_\beta/k_A[R'H])\}$, where $k_\beta/k_A[R'H]=k_\beta/k'_A\times(1/[\text{Cyclohexane}])\times(k'_A[\text{Cyclohexane}]/k_A[R'H])$.[5] A relationship between $k_{D\beta}/(k_{DA}+k_{D\beta})$ and k_d has a good linearity with correlation coefficient of 0.9529. This can support the existence of Eq. 5.

11) C. Walling, H. P. Waits, J. Milovanovic, and C. G. Pappiannou, *J. Am. Chem. Soc.*, **92**, 4927 (1970).

12) a) J. E. Leffler and F. E. Scrivener, Jr., *J. Org. Chem.*, **37**, 1974 (1972); b) J. T. Barbas and J. E. Leffler, *J. Org. Chem.*, **50**, 705 (1985); c) Ref. 2c.

13) a) I. L. Reich, A. Diaz, and S. Winstein, *J. Am. Chem. Soc.*, **91**, 5635 (1969); b) T. Ando, H. Yamataka. H. Morisaki, J. Yamawaki, J. Kuramochi, and Y. Yukawa, *J. Am. Chem. Soc.*, **103**, 430 (1981): in this reference, it was suggested that the rate enhancement may be due to a small α–γ bond interaction (intermediate **3a**) or lenghthening of the β–γ bond to the cationic center (intermediate **3b**).

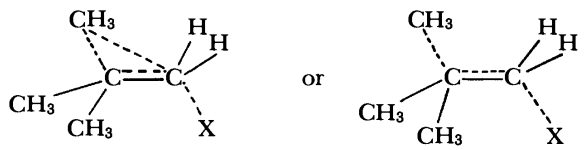

3a **3b**

14) J. J. Ritter, *J. Am. Chem. Soc.*, **70**, 4253 (1948).

15) T. Komai and K. Matsuyama, *Bull. Chem. Soc. Jpn.*, **58**, 2207 (1985).

16) N. A. Milas and D. M. Surgenor, *J. Am. Chem. Soc.*, **68**, 643 (1946).

17) M. R. Vilenskaya and T. I. Yurzhenko, *Chem. Abstr.*, **60**, 15723 (1964).

18) A. W. White, *J. Chem. Soc.*, **1953**, 1541.

19) T. Komai, H. Ishigaki, and K. Matsuyama, *Bull. Chem. Soc. Jpn.*, **58**, 2431 (1985).

Synthesis of Cyclic Polysulfides. Reactions of Dithiols and Related Compounds with Elemental Sulfur in Liquid Ammonia[1)]

Ryu SATO,* Satoru SAITO, Hiroshi CHIBA, Takehiko GOTO, and Minoru SAITO
Department of Resource Chemistry, Faculty of Engineering, Iwate University, Morioka 020
(Received August 31, 1987)

Many cyclic polysulfides, i.e., benzopentathiepins (**3a—d**), 6*H*-1,2,3,4,5-benzopentathiocin, 5*H*-1,2,3,4-benzotetrathiepin, 3*H*-1,2-benzodithiole, 1,5-dihydro-2,3,4-benzotrithiepin, 1,4-dihydro-2,3-benzodithiin, naphtho[1,8-*cd*]-1,2-dithiole, 1,2,3-trithiane, 1,2-dithiane, 2,3,4,5-tetrathiabicyclo[4.4.0]decane, and 2,3,4,5,6-pentathiabicyclo[5.4.0]undecane, were synthesized in high yields by new reactions of their corresponding dithiols and related compounds, 1,3-benzodithiole-2-thiones (**5**) and 1,3-dithiolane-2-thione, with elemental sulfur in liquid ammonia at ambient temperature. In the synthesis of **3a—d** from 1,2-benzenedithiol or **5**, considerable increase in the product yield was observed upon adding 1,3-dinitrobenzene to the solvent used in work-up.

Much interest of organic sulfur chemists has centered on cyclic polysulfides from the viewpoint of synthesis of natural products which show biological activity, such as lenthionine (**1**)[2)] and sporidesmin (**2**)[3)]. Various procedures for the synthesis of these compounds have been developed in the past few years.[4)]

1

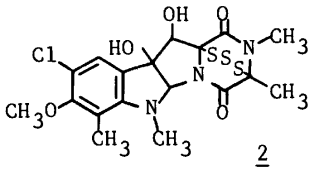

2

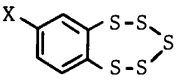

3

Scheme 1.

There have been published a few reports[5)] on the synthesis of sulfur containing compounds such as benzopentathiepins (**3**). Very recently, Chenard et al.[5)] reported the synthesis of **3** from benzothiadiazoles with elemental sulfur in the presence of 1,4-diazabicyclo[2.2.2]octane (DABCO) at high temperatures such as 180 °C in moderate yields, and **3** were shown to have acaricidal and fungicidal effects.[6)] In the course of our studies on the reactions of organic compounds with elemental sulfur in liquid ammonia,[7)] we have reported on synthesis of polysulfides from corresponding thiols.[8)] The above situation urged us to pursue a new synthesis of various cyclic polysulfides from corresponding dithiols and related compounds with elemental sulfur in liquid ammonia. Consequently, we could obtain many cyclic polysulfides **3, 7, 8, 9, 11, 12, 14, 17, 19, 21**, and **22** in moderate to excellent yields (Scheme 2). Moreover, in the case of synthesis of **3**, addition of 1,3-dinitrobenzene in the work-up procedure was found to increase the yield of **3**. This effect was explained in terms of the electron-transfer effect of thiolate species which accelerates the formation of sulfur–sulfur bond.

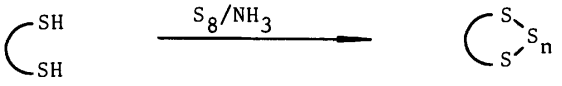

Scheme 2.

Results and Discussion

1,2-Benzenedithiols **4a** and **4b** and other dithiols **6, 10, 13, 15, 16,** and **18** or their synthetic equivalents such as 1,3-dithiole-2-thiones **5a—d** and 1,3-dithiolane-2-thione **20** were chosen as substrate for the synthesis of cyclic polysulfides and allowed to react with elemental sulfur in liquid ammonia, affording desired cyclic polysulfides together with an unidentified polymer (Scheme 3). As a typical synthesis of cyclic polysulfides, an optimization of the synthesis of **3** was studied.

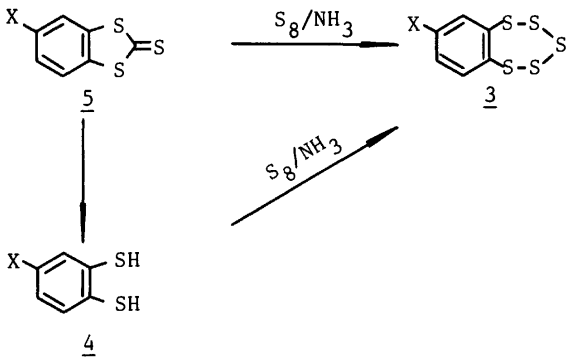

Scheme 3.

1,3-Benzodithiole-2-thione (**5a**) as a substrate gave better yields of **3** than **4** did (Runs 2, 4, 7, 12, and 13, Table 1). The quantity in equivalents of elemental sulfur used affected considerably the yields of **3**. For example, a use of 3 or 5 mg atom of elemental sulfur (6 or 10 milli equivalents, respectively) gave **3a** quantitatively (Runs 4 and 5), but in a reaction using 0.5 mg-atom of elemental sulfur the desired **3a** was

Table 1. Synthesis of Benzopentathiepins (3) with S_8/NH_3

Run	Substrate	S_8		Solvent	DNB		Yield of 3	Mp θ_m/°C (lit)
		mg-atom	milli equiv		mmol	milli equiv	%	
1	**5a**	3.0	6.0	—	0	0	**3a** Trace	64 (60)[5]
2	**5a**	3.0	6.0	CH_2Cl_2	0.5	1	**3a** 82 (64)	
3	**5a**	3.0	6.0	CH_3CN	0.5	1	**3a** 75	
4	**5a**	3.0	6.0	Benzene	0.5	1	**3a** 97 (89)	
5	**5a**	5.0	10.0	Benzene	0.5	1	**3a** 97	
6	**5a**	0.5	1.0	Benzene	0.5	1	**3a** 2	
7	**5b**	3.0	6.0	CH_2Cl_2	1.5	3	**3b** 59 (30)	87 (89)[5]
8	**5b**	3.0	6.0	Benzene	1.5	3	**3b** 41 (30)	
9	**5c**	3.0	6.0	Benzene	0.5	1	**3c** 99 (90)	101 (98)[5]
10	**5d**	3.0	6.0	Benzene	1.5	3	**3d** 91 (20)	123
11	**5e**	3.0	6.0	Benzene	0.5	1	**3e** 0	
12	**4a**	3.0	6.0	Benzene	0.5	1	**3a** 78 (5)	
13	**4b**	3.0	6.0	CH_2Cl_2	1.5	3	**3b** 54 (19)	

a) Reaction conditions: reaction temp, 20 °C; reaction time, 0.5 h; liquid ammonia, 30 ml; substrate, 0.5 mmol; solvent, 80 ml. b) These solvents were used in work up. c) 1,3-Dinitrobenzene. d) Isolated yield based on the substrate. Yields in the absence of 1.3-dinitrobenzene are shown in parentheses.

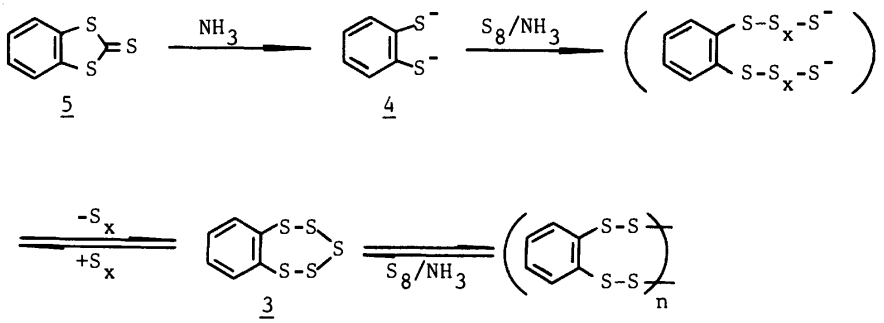

Scheme 4.

obtained only in 2% yield (Run 6). Only a trace of **3a** was obtained when no solvent was used in the work up of reaction and a use of an organic solvent such as dichloromethane or benzene significantly improved the yield of **3a** as shown in Table 1 (Runs 1—4; see Experimental). Moreover the kind of the solvent used in the work up also influenced the yield of benzopentathiepin **3**. Thus, the best yield was achieved when benzene was employed (Runs 2—4). These solvent effects may be accounted for in terms of the dilution effect of solvent which inhibits the collision of reactive species such as thiolate. A generality of the synthesis of **3** is indicated by Runs 7—11. We could not, however, obtain 5-nitro-1,2,3,4,5-benzopentathiepin (**3e**) by the present method. It should be noted that **3a** is obtained in a better yield (Run 4) from **5** than from **4** (Run 12), which is generally obtained by solvolysis of **5** (Scheme 3). In these reactions seven-membered benzopentathiepin **3a** was the sole isolated and stable product. Our further important finding is that a considerable increase in the yield of **3** was observed by addition of 1,3-dinitrobenzene to the solvent used in the work up (Runs 2, 7—10, and 12; see Experimental). In the absence of 1,3-dinitrobenzene, the amount of unidentified polymer increased. Interestingly, **3a** was also obtained by treating the polymer with elemental sulfur in liquid ammonia under similar conditions. Based on the above results, it seems that there are certain equilibriums between **3** and the polymer in both the reaction mixture and the work-up solution, and that 1,3-dinitrobenzene serves as a trapper of electron from thiolate intermediates to accelerate the formation of sulfur-linked product **3**, since it is well-known that 1,3-dinitrobenzene can trap one electron in electron-transfer systems. Plausible pathways of this reaction are depicted in Scheme 4.

To extend this method to other compounds, some dithiols, e.g., 1,2-bis(mercaptomethyl)benzene (**10**) and 1,3-propanedithiol (**16**), were treated with elemental sulfur in liquid ammonia similarly to **3**. Ten desired cyclic polysulfides **7, 8, 9, 11, 12, 14, 17, 19, 21,** and **22** were consequently obtained in moderate yields as shown in Table 2. It is noteworthy that the first two cyclic polysulfides having one benzylic methylene group were obtained by the reaction of 2-(mercaptomethyl)benzenethiol (**6**). Thus, an eight-membered ring product, 6*H*-1,2,3,4,5-benzopentathiocin (**7**), and a seven-membered ring compound, 5*H*-1,2,3,4-benzotetrathiepin (**8**), were obtained together with a five-membered ring product, 3*H*-benzo[*d*]-1,2-dithiole (**9**).

The ^{1}H NMR spectra of **8** showed a peak at δ=4.77 (AB pattern, $\Delta\delta$=0.96, J=16 Hz, 2H) characteristic of the two protons of the methylene group, whereas the methylene group in **7** appeared in a singlet peak at δ=4.41. Measurements of the molecular weights of the new compounds **7** and **8** by the Rast method gave the values of 283 and 235 respectively,[9] suggesting that the products **7** and **8** were not dimerized compounds. Similarly, a six-membered cyclic disulfide, 1,4-dihydro-2,3-benzodithiin (**12**), and 1,5-dihydro-2,3,4-benzotrithiepin (**11**) were obtained as expected when **10** was treated with elemental sulfur in liquid ammonia under similar conditions, as shown in Table 2. These results suggest that one, two, or three sulfur atoms in the molecule were incorporated from elemental sulfur to form the stable seven- or eight-membered ring compounds **7, 8, 9, 11,** and **12**. 1,8-Naphthalenedithiol (**13**) did not incorporate any sulfur atoms at all upon being treated with elemental sulfur, but naphtho[1,8-*cd*]-1,2-dithiole (**14**) was formed quantitatively. The formation of **14** may be explained on the basis of facile sulfur–sulfur bond formation to give the stable product **14**, since the two sulfur atoms in **13** lie close to each other at the peri position of the naphthalene ring. Subsequently, cyclizations of α,ω-alkanedithiols, 1,2-ethanedithiol (**15**), **16** and 1,4-butanedithiol (**18**), with elemental sulfur in liquid ammonia were carried out in a similar manner. Except the reaction of **15**, two expected six-membered cyclic polysulfides, 1,2,3-trithiane (**17**) and 1,2-dithiane (**19**), were obtained from the corresponding dithiols **16** and **18**, respectively. An unidentified polymer was mainly formed in the reaction of **15**. The results of the reactions of **16** or **18** suggest that these six-membered products are very stable in this system, in contrast to the results of the reactions of **6** or **10**.

Table 2. Synthesis of Cyclic Polysulfides **7, 8, 9, 11, 12, 14, 17, 19, 21,** and **22** with Elemental Sulfur in Liquid Ammonia

Run	Substrate	Condition	Solvent	Product (Yield/%) and Mp θ_m/°C (lit)		
1	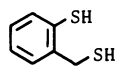 **6**	A	CH_2Cl_2	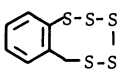 **7** (18) 61	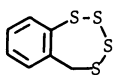 **8** (31) 49	**9** (36) oil[15]
2	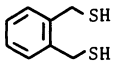 **10**	A	CH_3CN	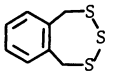 **11** (57) 101 (101)[16]	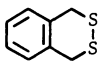 **12** (26) 78 (78)[17]	
3	**13**	B	Benzene	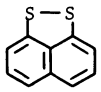 **14** (98) 122 (123)[13]		
4	HS-CH_2CH_2-SH **15**	B	Benzene	Polymer		
5	HS-$(CH_2)_3$-SH **16**	B	CH_3CN	**17** (38) 46 (46)[18]		
6	HS-$(CH_2)_4$-SH **18**	C	DMF	**19** (50) 34 (31)[19]		
7	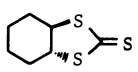 **20**	D	CH_3CN	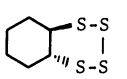 **21** (28) 88 (89)[20]	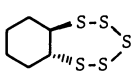 **22** (35) 68 (67)[20]	

a) Substrate, 0.5 mmol; liquid ammonia, 30 ml; solvent, 80 ml. b) Reaction conditions, A: r.t., 0.5 h, and 6 equiv of S_8. B: r.t., 2 h, and 6 equiv of S_8. C: r.t., 2 h, and 3 equiv of S_8. D: 40 °C, 3 h, and 6 equiv of S_8.

The 1,3-dithiolane-2-thione containing a cyclohexane ring, **20**, also reacted with elemental sulfur in liquid ammonia at 40 °C to give two correspoding cyclic polysulfides **21** and **22** in moderate yields (Run 7, Table 2).

In conclusion, **3** and analogous cyclic polysulfides **7**, **8**, **9**, **11**, **12**, **14**, **17**, **19**, **21**, and **22** were synthesized by this new method, which has a great advantage over precedent methods in that high yields may be obtained under mild conditions. Since these cyclic polysulfides are well known to exhibit remarkable properties and especially **3** are soluble in usual organic solvents, the use of **3** as sulfurization reagents is extensively applicable. These studies are now under progress in our laboratory.[10]

Experimental

All melting points were measured by the capillary method and uncorrected. IR spectra were obtained on a Hitachi 295 spectrophotometer, and ^{1}H NMR spectra were obtained on a Hitachi R-22 spectrometer by using tetramethylsilane as an internal standard. All reactions were monitered by TLC (Merck Kieselgel 60-GF). The silica gel used for column chromatography was Wako gel C-200. Mass spectra were taken with a Hitachi RMU-6M mass spectrometer. Elemental analyses were carried out with a Yanagimoto MT-3.

Materials. All reagents were obtained from Wako Pure Chemical Industries Ltd., Tokyo Kasei Co., Ltd., or Aldrich Chemical Co. The reagents were further purified by general methods. 1,3-Benzodithiole-2-thiones (**5**) were synthesized from 2-aminobenzenethiol by the literature method.[11] 1,2-Benzenedithiols (**4**) were obtained by hydrolysis of **5**.[11] **6** was synthesized from bis(2-carboxyphenyl) disulfide by thiation with phosphorus pentasulfide followed by reduction with lithium aluminium hydride.[12] **10** was obtained from 1,2-bis(bromomethyl)benzene by the literature method.[4] **13** was given by two-step synthesis from 1,8-dichloronaphthalene.[13] **15**, **16**, and **18** were commecially available. Hexahydro-1,3-benzodithiole-2-thione (**20**) was prepared from cyclohexene oxide with potassium hydroxide and carbon disulfide by the literature method.[14]

Reactions of Dithiols 4a-b, 6, 10, 13, 15, 16, and 18, 1,3-Benzodithiole-2-thiones 5a—e or 1,3-Dithiolane-2-thione 20 with Elemental Sulfur in Liquid Ammonia. A typical procedure is as follows: **5a** (0.5 mmol) and elemental sulfur (3.0 mg atom) were taken into a titanium autoclave (volume 50 ml) and the autoclave was evacuated. Liquid ammonia (30 ml) was charged and then the mixture was stirred at 20 °C for 0.5 h. After completion of the reaction, the reaction mixture in liquid ammonia was added dropwise to benzene (80 ml) containing 1,3-dinitrobenzene (0.5 mmol) through a needle bulb and the solution was stirred at room temperature until liquid ammonia was evaporated completely (for about 2 h). An evaporation of benzene under vacuum and a subsequent column chromatography on silica gel (Wako gel C-200) using CCl_4/hexane as an eluent gave the desired benzopentathiepin **3a** (114 mg) as yellow crystals. The products were identified with ^{1}H NMR, IR, mass spectra, and elemental analyses. In the reaction of **6** with elemental sulfur in liquid ammonia, the yields of the products, **7** and **8**, were determined by the proton ratio for methylene groups in ^{1}H NMR spectra after separation of reaction mixture by column chromatography.

7-Amino-1,2,3,4,5-benzopentathiepin (3d): Yellow crystals (ether); mp 123 °C; IR (KBr) 1020, 1235, 1570, and 1620 cm^{-1}; ^{1}H NMR (CDCl) δ=4.01 (2H, br, $-NH_2$), 6.49 (1H, dd, J=9.0 and 3.0 Hz, arom), 7.02 (1H, d, J=3.0 Hz, arom) and 7.53 (1H, d, J=9.0 Hz, arom); MS m/z 251 (M^+). Found: C, 28.42; H, 1.92%. Calcd for $C_6H_5NS_5$: C, 28.66; H, 2.00%.

7: Yellow crystals (hexane/ether); mp 61 °C; IR (KBr) 450, 540, and 1400 cm^{-1}; ^{1}H NMR ($CDCl_3$) δ=4.41(2H, s, $-CH_2-$) and 7.18—7.72(4H, m, arom); MS m/z 250 (M^+). Found: C, 33.77; H, 2.39%. Calcd for $C_7H_6S_5$: C, 33.57; H, 2.42%.

8: Yellow crystals (hexane/ether); mp 49 °C; IR (KBr) 445, 735, and 1390 cm^{-1}; ^{1}H NMR ($CDCl_3$) δ=4.28 (1H, d, J=15.0 Hz, $-CH_2-$), 5.26 (1H, d, J=15.0 Hz, $-CH_2-$) and 7.03—7.73 (4H, m, arom); MS m/z 218 (M^+). Found: C, 38.43; H, 2.74%. Calcd for $C_7H_6S_4$: C, 38.50; H, 2.77%.

Compounds 3a—c, 9, 11, 12, 14, 17, 19, 21, and 22: These were identified by comparing spectral and physical data with those of authentic samples. See Tables 1 and 2.

Reactions of Polymer obtained from 4 or 5 with Elemental Sulfur in Liquid Ammonia. The polymer (100 mg) obtained by reaction of **4a** or **5a** with elemental sulfur in liquid ammonia was taken into titanium autoclave (volume 50 ml) and then, after evacuation, liquid ammonia (30 ml) was charged into the autoclave. The mixture was allowed to react at 20 °C for 0.5 h. The reaction mixture obtained was treated in a similar manner as in the reaction of **5a** with elemental sulfur in liquid ammonia. **3a** of 53 mg was obtained.

References

1) A preliminary communication of a part of this work has already appeared: R. Sato, S. Saito, H. Chiba, T. Goto, and M. Saito, *Chem. Lett.*, **1986**, 349.

2) K. Morita and S. Kobayashi, *Chem. Pharm. Bull.*, **15**, 988 (1967); K. Morita and S. Kobayashi, *Tetrahedron Lett.*, **1966**, 573; I. W. J. Still and G. W. Kutney, *Tetrahedron Lett.*, **22**, 1939 (1981); S. J. Wratten and D. J. Faulkner, *J. Org. Chem.*, **41**, 2465 (1976).

3) For example: R. Rahman, S. Safe, and A. Taylor, *J. Chem. Soc. C*, **1969**, 1665; D. Brewer, R. Rahman, S. Safe, and A. Taylor, *J. Chem. Soc., Chem. Commun.*, **1968**, 1571.

4) For example: D. N. Harpp and R. A. Smith, *J. Am. Chem. Soc.*, **104**, 6045 (1982); R. Ballini, *Synthesis*, **1982**, 834; U. Anthoni, C. Christophersen, N. Jacobsen, and A. Svendsen, *Tetrahedron*, **38**, 2425 (1982); A. Kato, Y. Hashimoto, I. Otsuka, and K. Nakatsu, *Chem. Lett.*, **1978**, 1219; D. N. Harpp, R. A. Smith, and K. Steliu, *J. Org. Chem.*, **46**, 2072 (1981); D. N. Harpp and A. Granata, *J. Org. Chem.*, **44**, 4144 (1979); B. Milligan, B. Saville, and J. M. Swan, *J. Chem. Soc.*, **1965**, 2901; G. Goor and M. Antenius, *Synthesis*, **1975**, 329; S. Inoue, T. Tezuka, and S. Oae, *Phosphorus and Sulfur*, **4**, 219 (1978); J. Emsley and D. W. Gritfiths, *J. Chem. Soc., Perkin Trans. 1*, **1979**, 228; G. Morel, E. Marchand, and A. Foucaud, *Synthesis*, **1980**, 918; N. Yamazaki, S. Nakahama, K. Yamaguchi, and T. Yamaguchi, *Chem. Lett.*, **1980**, 1355; E. A. Chernyshev, O. K. Kuzmin, A. V. Lebedev,

A. I. Gusev, N. I. Kirillova, N. S. Nametkin, V. D. Tyurin, and A. M. Krapivin, *J. Organomet. Chem.*, **252**, 133 (1983).

5) B. L. Chenard, U. S. Patent 84/00870 [*Chem. Abstr.*, **102**, 185115g (1985)]; B. L. Chenard and T. J. Miller, *J. Org. Chem.*, **49**, 1221 (1984); B. L. Chenard, R. L. Harlow, A. L. Johnson, and S. A. Vladuchick, *J. Am. Chem. Soc.*, **107**, 3871 (1985); J. Nakayama, M. Kashiwagi, R. Yomoda, and M. Hoshino, *Nippon Kagaku Kaishi*, **1987**, 1424.

6) F. Feher and M. Langer, *Tetrahedron Lett.*, **1971**, 2125; J. L. Moriss and C. W. Ress, *J. Chem. Soc., Perkin Trans. 1*, **1987**, 211; J. Perregard, S. Sheibye, H. J. Meyer, I. Thomsen, and S. O. Lawesson, *Bull. Soc. Chim. Belg.*, **86**, 679 (1977).

7) For example: R. Sato, T. Goto, Y. Takikawa, and S. Takizawa, *Synthesis*, **1980**, 615; R. Sato, T. Etchu, Y. Takikawa, S. Takizawa, and M. Saito, *ibid.*, **1981**, 44; R. Sato, S. Chiba, Y. Takikawa, S. Takizawa, and M. Saito, *Chem. Lett.*, **1983**, 535; R. Sato, N. Saito, N. and M. Saito, *ibid.*, **1983**, 1603; R. Sato, N. Saito, Y. Takikawa, S. Takizawa, and M. Saito, *Synthesis*, **1983**, 1045; R. Sato, T. Senzaki, Y. Shikazaki, T. Goto, and M. Saito, *Chem. Lett.*, **1984**, 1423; R. Sato, K. Itoh, K. Ito, T. Goto, and M. Saito, *ibid.*, **1984**, 1913; R. Sato, M. Nakayama, Y. Yuzawa, T. Goto, and M. Saito, *Chem. Lett.*, **1985**, 1887.

8) R. Sato, T. Goto, Y. Takikawa, S. Takizawa, and S. Oae, *Phosphorus and Sulfur*, **7**, 289 (1979).

9) K. Hosaka, "Yuki-biryobunseki," Nankodo, Tokyo (1969), p. 633.

10) R. Sato, Y. Akutsu, T. Goto, and M. Saito, *Chem. Lett.*, **1987**, 2161.

11) S. Hunig and E. Fleckenstein, *Justus Liebigs Ann. Chem.*, **738**, 192 (1970).

12) A. Luttringhaus and K. Hagele, *Angew. Chem.*, **67**, 304 (1955); F. S. Fowkes and E. W. McCleland, *J. Chem. Soc.*, **1941**, 187.

13) K. Yui, Y. Aso, T. Otsubo, and F. Ogura, *Chem. Lett.*, **1986**, 551.

14) C. C. J. Culvenor, W. Davies, and K. H. Pausacker, *J. Chem. Soc.*, **1946**, 1051.

15) E. W. Mcleland, L. A. Warren, and J. H. Jackson, *J. Chem. Soc.*, **1929**, 1582; F. S. Fowes and E. W. Mcleland, *J. Chem. Soc.*, **1941**, 187.

16) S. Kabuss, A. Luttringhaus, H. Friebolin, and R. Mecke, *Z. Naturforsch., B: Anorg. Chem.*, **21**, 320 (1966).

17) P. K. Srivastava and L. Field, *J. Org. Chem.*, **37**, 4196 (1972).

18) G. Morel, E. Marchand, and A. Foucaud, *Synthesis*, **1980**, 918.

19) D. N. Harpp, S. J. Bodzay, and T. H. Chan, *Tetrahedron Lett.*, **27**, 441 (1986).

20) F. Feher and B. Degen, *Angew. Chem.*, **79**, 689 (1967).

 © 1988 The Chemical Society of Japan Bull. Chem. Soc. Jpn., 61, 1653—1659 (1988)

A Facile Synthesis of Oxetane Derivatives for Preparing Cross-Linked Polyoxetane Resins Bearing the Bromide at the Spacer End

Masatoshi MOTOI,* Hiroshi SUDA, Katsuhiko SHIMAMURA, Shinsuke NAGAHARA, Mitsuru TAKEI, and Shigeyoshi KANOH

Department of Chemistry and Chemical Engineering, Faculty of Technology, Kanazawa University, Kodatsuno, Kanazawa-shi 920

(Received September 16, 1987)

3-(6-Bromo-2-oxahexyl and 8-bromo-2-oxaoctyl)-3-methyloxetanes, and 1,8- and 1,10-bis(3-methyl-3-oxetanyl)-2,7-dioxaoctane and -2,9-dioxadecane were readily prepared in fairly good yields by the reaction of 3-hydroxymethyl-3-methyloxetane (**1**) with tetra- and hexamethylene dibromides in the presence of a phase-transfer catalyst. The formation of the mono- and disubstituted products depends upon the molar ratios of the dibromide to **1**. The optimum reaction conditions for the etherification of **1** with tetramethylene dibromide were searched. The (ω-bromo-2-oxaalkyl)oxetanes were polymerized to give soluble polyoxetanes ($\bar{M}_n$ 3500—5500) by cationic ring-opening polymerization. The use of the bisoxetanes, a new cross-linking agent, as a comonomer gave insoluble elastic polyoxetane resins having a pendant bromide at the spacer end.

In the course of our studies on the polymerization of the oxetanes and other cyclic ethers,[1-7] we hoped to synthesize oxetane derivatives for producing soft, somewhat polar polyoxetane resins; we found that the oxetane derivatives **3a**, **3b**, **4a**, and **4b** can be readily prepared by the etherification of 3-hydroxymethyl-3-methyloxetane (**1**) with α,ω-dibromoalkanes **2a** and **2b** in the presence of a phase-transfer catalyst (PTC).

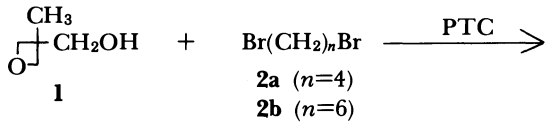

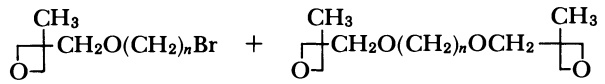

So far, several chemical reactions of the substituents attached to the oxetane rings have been reported. Chlorine of the chloromethyl group at the C-3 position of the oxetane ring was replaced into alkoxyl, aryloxyl, acetoxyl, and azido groups by displacement reactions.[8-11] Macroheterocycles bearing one or two spiro-oxetane rings were synthesized from base-induced condensations of 3,3-bis(chloromethyl)oxetane with heteropolymethylene glycols.[12] Recently, several preparation methods for the oxetane ring with various substituents have also been reported.[13-19]

Oxetanes **3a** and **3b** seem to be very useful for designing a variety of the functional polyethers since the polymers possess long spacers of oxapolymethylenes, $-CH_2O(CH_2)_n-$ where n=4 or 6, and the terminal bromine that can be readily converted into various other functional groups. It is also known that lengthening the spacers having catalytic sites is important for realizing improved catalytic activities.[20] Furthermore, the bisoxetanes **4a** and **4b** are expected to react as bifunctional monomers to give insoluble polyoxetane resins. In this paper, we describe a facile preparation of new oxetane derivatives, which give their soluble and insoluble polymers by cationic ring-opening polymerization; we also discuss reaction courses for obtaining the optimum conditions for preparing such oxetanes by phase-transfer catalysis. Related to the present study, compounds containing two oxetane rings were reported: bis[(3-methyl- and 3-ethyl-3-oxetanyl)methyl] hexanedioates[21] and 2,6-dioxaspiro[3.3]heptane.[22]

Results and Discussion

Preparation of Monomers. The monomers, **3a** and **3b**, carrying ω-bromo-2-oxaalkyl groups were synthesized by the reaction of **1** with α,ω-dibromoalkanes **2a** and **2b** in the presence of tetrabutylammonium bromide (TBAB) or hydrogen sulfate (TBHS) as PTC. **3a** and **3b** reacted further with **1** to give bisoxetanes **4a** and **4b** under the same reaction conditions. The formation of these oxetane derivatives as a main product depends on the mole ratio of the dibromide to **1**. The etherification reaction was examined under several conditions concerning the mole ratio, the PTC, and the solvent. The yield of the product was determined at a given reaction time by gas chromatography (GC) using hexadecane as an internal standard. The results are summarized in Table 1. When the reaction of **1** with a threefold molar equivalent of **2a** was carried out under refluxing in hexane and 50% aqueous NaOH with TBAB (5% molar respect to **1**), **3a** and **4a** were produced in 81.1 and 14.6% yields, respectively, indicating that more than 96% of **1** was consumed to produce the two products (Run no. 7). **2a** remained unchanged in a 29% recovery, suggesting that a considerable amount of **2a** is consumed by side reactions (vide infra). The decrease in the mole ratio was favorable for the formation of **4a**. The reaction at

Table 1. Etherification of **1** with **2a** by Phase-Transfer Catalysis[a]

Run no.	Mole ratio, **2a**/**1**	PTC[b]	Solvent		Product and yield/%[c] Reaction time/h 0.5	1.0	1.5	2.0
1	0.5	TBAB	Hexane	**3a**:	0.2	0	0	
				4a:	34.7	35.5	35.2	
2	0.8	TBAB	Hexane	**3a**:	0.8	0	0	
				4a:	49.4	52.3	52.0	
3	1.0	TBAB	Hexane	**3a**:	5.8	0.2	0[d]	
				4a:	56.8	62.0	63.1	
4	1.2	TBAB	Hexane	**3a**:	19.4	11.0	5.7	
				4a:	50.8	58.6	61.3	(63.7)
5	1.5	TBAB	Hexane	**3a**:	39.5	33.3	28.1	
				4a:	33.0	41.0	43.2	
6	2.0	TBAB	Hexane	**3a**:	60.9	60.8	59.3	
				4a:	19.4	22.1	23.0	
7	3.0	TBAB	Hexane	**3a**:	83.0[e]	81.1	(76.2)	
				4a:	14.6	14.6		
8	3.0	TBAB	Ether	**3a**:	74.0	82.8	80.2	
9	3.0	TBAB	Benzene	**3a**:	68.1	67.7		
10	3.0	TBHS	Hexane	**3a**:	74.5	76.1	77.3	
11	3.0	TBHS	Ether	**3a**:	69.1	67.9	73.8	
12	3.0	None	Hexane	**3a**:	2.6	3.4	4.9	

a) **1**, 2.06 mmol; PTC, 5% molar respect to **1**; n-$C_{16}H_{34}$ (as internal standard), 1.06 mmol; volume of organic layer was adjusted to 3 ml by adding hexane; 50% NaOH, 2.7 g; under reflux. b) Phase-transfer catalyst (PTC): TBAB and TBHS refer to tetrabutylammonium bromide and hydrogen sulfate, respectively. c) Determined by GC. Value in parenthesis indicates isolated yield of reaction using 10 or 30 g of **1**. d) After 1.5 h, **2a** was not detected and **5** was formed in 17.0% yield. e) After 0.5 h, 29.2% of **2a** fed was left unchanged and no **5** was detected.

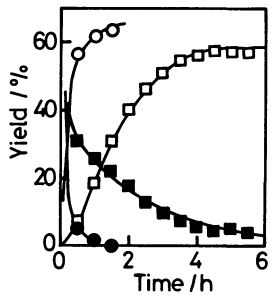

Fig. 1. Time-yield curves of **3a** (●, ■) and **4a** (○, □) in the reaction between **1** and **2a** at a 1:1 mole ratio in the presence of TBAB: (■, □) 0.7; (●, ○) 5.0 mol% to **1**.

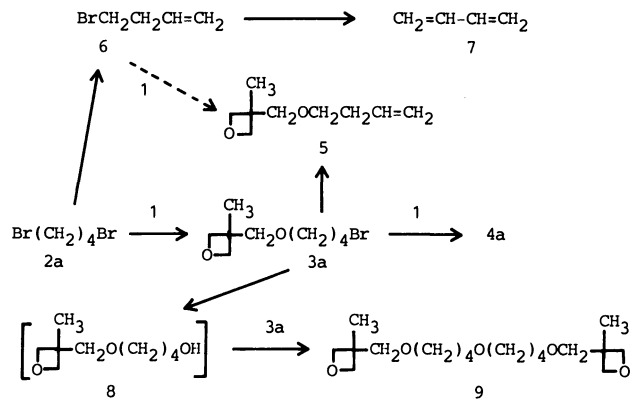

Scheme 1.

mole ratios of 1.0 to 1.2 gave **4a** in maximum yield of about 63% (Run nos. 3 and 4), which is higher than the yield of the reaction at the stoichiometric mole ratio of 0.5 (Run no. 1). At mole ratios below 1.0, all of the **2a** fed was consumed to form **4a** and by-products within at least 1.5 h. However, **1** remained, even when **2a** was completely consumed, as indicated from the following fact: when **2a** (half the amount used in the original reaction) was added into the reaction mixture upon the complete consumption of **2a** and was then allowed to react for 2 h, the yield of **4a** increased from 52 to 68% (Run no. 2). The etherification of **1** with **2a** proceeded very slowly in the absence of PTC: the yield of **3a** was only 5% after 1.5 h (Run no. 12). Therefore, PTC is obviously required for preparing oxetane derivatives. Figure 1 shows the time-product yield curves in the reaction of **1** with **2a** at a **2a**/**1** mole ratio of 1.0 in the presence of TBAB in 0.7 and 5.0 mol% to **1**. As shown in the curve of the reaction with 0.7 mol% TBAB, the yield of **4a** increases with an increase of the reaction time, while the yield of **3a**, which is produced as a main product in the early period of the reaction, decreases. This fact indicates that **3a** is an intermediate in the formation of **4a**, the rate of which can be lowered by decreasing the amount of PTC.

3-Methyl-3-(2-oxa-5-hexenyl)oxetane (**5**) was obtained as a low-boiling fraction of the reaction mixture from **1** and **2a**. Therefore, it should be considered that the such bromides as **2a** and **3a** are led to elimination products under applied phase-transfer catalytic condi-

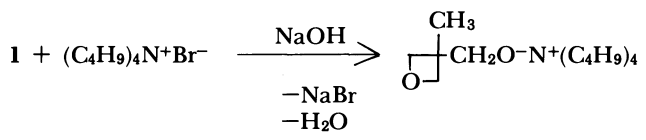

tions. The alkoxide anion of **1**, formed in a concentrated alkaline solution, transfers to an organic layer, together with a quarternary ammonium countercation. In the organic layer the alkoxide anion acts not only as a nucleophile in the substitution but also as a base in the elimination of the bromides. Actually, the odor of 1,3-butadiene (**7**) came out from the top of a water-cooled condenser during the early stage of the reaction of **1** with **2a**.

To investigate the material balance, reactions of the bromides as a substrate were carried out in hexane and 50% aqueous NaOH in the presence of TBAB (Table 2). In reactions at **3a**/**1** mole ratios of 0.5 and 1.0 (Run nos. 13 and 14), **4a** was detected in about 55% yield together with **5** in 32% yield after 1.5 h, at which time the starting material, **3a**, disappeared completely. The reaction between **3a** and **1** at a ratio of 2.0 gave **4a** in a 80.7% yield (40.4% conversion of **3a**) after 1.5 h; an additional 1-h reaction resulted in an increase of only 2% yield of **4a**, while the **3a** recovery decreased from 14.4 to 8.3% (Run no. 15). In these reactions of **3a** with **1** (Run nos. 13, 14, and 15), therefore, 13 to 21% of **3a** was consumed to produce unknown products. When **3a** was heated in a concentrated alkaline solution, no **3a** and a 32% yield of **5** were detected after 14 h, although at an early stage of the 0.5-h reaction, **5** was hardly detectable in spite of the consumption of 21% of the **3a** which was fed (Run no. 16). A pot residue of distillation from this reaction mixture was identified as being 1,13-bis(3-methyl-3-oxetanyl)-2,7,12-trioxatridecane (**9**). This product is probably formed from an etherification reaction of **3a** with the alcohol **8** derived from the bromide **3a** by its hydrolysis (Scheme 1). On the other hand, 98% of **3a** was left unchanged after heating a mixture of **3a** and threefold molar equivalent of **2a** under the same conditions as above (Run no. 17). In the absence of **1**, **2a** itself was stable under the present conditions (Run no. 18). The oxetane ring was also found to be stable under the present conditions, because the structure of 3-methyl-3-(2-oxadecyl)oxetane (**10**) was not altered upon treatment with the alkaline solution (Run no. 19). These findings lead to the following: (1) The existence of a sufficient amount of **2a** under phase-transfer catalytic conditions seems to prevent side reactions of bromide **3a**, though it is difficult at this point to explain why **2a** prevents the side reactions. (2) The reaction of **1** with 4-bromo-1-butene (**6**) is unimportant, since **5** is not produced in the reaction at a **2a**/**1** mole ratio of 3.0. Presumably, **6** is almost exclusively consumed to give **7** by an elimination reaction, but not to form **5** by a substitution reaction from **1** and **6**. (3) The elimination reaction of **3a**, which occurs during the existence of **1** (or its alkoxide anion), is also restrained by using a sufficient amount of **2a**. (4) In the reaction for preparing the bisoxetanes, the existence of an adequate amount of **2a** is required in

Table 2. Analysis of Reaction of Bromides under Phase-Transfer Catalytic Conditions[a]

Run no.	Reactant		Mole ratio, A/B	Time/h	Yield or recovery/%[b]			
	A	B			**3a**	**4a**	**5**	**2a**
13	**3a**	**1**	0.5	0.5	(0.0)	57.1		
				1.0	(0.0)	57.0		
				1.5	(0.0)	54.9	31.8	
14	**3a**	**1**	1.0	0.5	(1.9)	55.3		
				1.0	(0.0)	55.4		
				1.5	(0.0)	55.6	31.6	
15	**3a**	**1**	2.0	0.5	(24.8)	75.8		
				1.5	(14.4)	80.7		
				2.5	(8.3)	83.1	29.6	
16	**3a**	None	—	0.5	(78.9)		0.0	
				1.0	(71.4)		0.5	
				5.0	(42.3)			
				14.0	(0.5)		32.0	
17	**3a**	**2a**	3.0	0.5	(99.0)			
				1.0	(97.6)			
				2.0	(96.8)		0.0	(90.4)
18	**2a**	None	—	0.33				(90.0)
				0.66				(88.1)
19	**10**	None	—	0.5	(99.7)[c]			
				1.0	(97.7)[c]			
				2.0	(99.7)[c]			

a) Reactant A, 2.11 mmol; PTC, TBAB in 5% molar respect to reactant B (to reactant A in Run nos. 16, 18, and 19); 50% NaOH, 2.7 g; volume of organic layer was adjusted to 3 ml by addition of hexane; under reflux. b) As internal standard of GC determination, n-$C_{16}H_{34}$ (1.05 mmol) was used for **3a** and **4a**, and n-$C_{10}H_{22}$ (3.15 mmol) for **2a** and **5**. Value in parenthesis indicates recovery of the reactants. c) Value for remaining **10**.

order to avoid an elimination reaction of **3a**, until **1** is completely consumed to give **4a** from **3a** as an intermediate.

The use of ether as a solvent gave a yield of **3a** comparable to that in a reaction using hexane, though the use of benzene resulted in a lower yield (Run nos. 8 and 9). With TBHS, a slightly lower yield of **3a** was determined by GC, even when using hexane and ether (Run nos. 10 and 11).

Thus, **3a** and **4a** were isolated in 76.2 and 63.7% yields, respectively, from reactions at mole ratios of 3.0 and 1.2 on a preparative scale using 10 or 30 g of **1** and hexane as a solvent (Run nos. 7 and 4). The preparation results concerning the other ocetane derivatives are indicated in Table 3. In the same way as above, **3b** and **4b** were isolated, respectively, in 73.4 and 62.8% yields from the reactions at mole ratios of 3.0 and 1.0. Octyl bromide (**11a**) and benzyl chlorides **12a** and **12b** are used well as halides for the etherification of **1**. With the bromide **11a**, **10** was isolated in 92.9% yield, although the reaction with the chloride **11b** gave **10** in only 2% yield. The reaction of **1** with benzyl chlorides should be performed at a mole ratio of 1.0 to give sufficient yields. The use of a molar excess of benzyl chlorides toward **1** resulted in the formation of a considerable amount of dibenzyl ethers, which could hardly be removed from the desired products by fractional distillation.

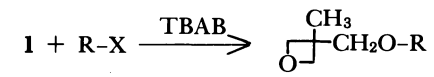

11a R=*n*-C_8H_{17}, X=Br **10** R=*n*-C_8H_{17}
11b R=*n*-C_8H_{17}, X=Cl **13a** R=$C_6H_5CH_2$
12a R=$C_6H_5CH_2$, X=Cl **13b** R=(*p*)-$CH_3C_6H_4CH_2$
12b R=(*p*)-$CH_3C_6H_4CH_2$, X=Cl

An etherification reaction of **1** with tribromide **14** did not take place to give the desired product **15**, resulting in a 86% recovery of **14**, isolated by distillation. This indicates that a nucleophilic attack of the alkoxide anion of **1** onto the α-carbon of the bromide **14** is difficult, since this α-carbon is quite similar to that of neopentyl bromide which has difficulty in being susceptible to the S_N2 reaction.

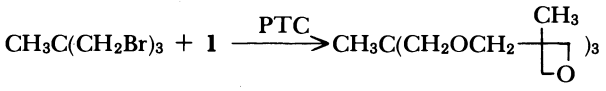

14 **15**

The etherification of **1** with **2a** gave a remarkably low yield by the Williamson synthesis using dry solvents, since the sodium alkoxide of **1**, which was prepared from **1** and sodium metal or sodium hydride, was hardly soluble in tetrahydrofuran (THF), *N,N*-dimethylformamide (DMF), and ether. On the contrary, the desired ethers were obtained in fairly good

Table 3. Preparation of Oxetane Derivatives from **1** and Halides[a]

Run no.	Halide	Mole of **1**	Mole ratio, halide/**1**	Time/h	Product	
						Yield/%[b]
20	**2b**	0.14	3.0	2.0	**3b**	73.4
21	**2b**	0.098	1.0	2.0	**4b**	62.8
22	**11a**	0.098	3.0	12.0	**10**	92.9
23	**11b**	0.098	3.0	10.0	**10**	2
24	**12a**	0.20	1.0	3.0	**13a**	85.7
25	**12b**	0.20	1.0	2.0	**13b**	73.9

a) For 98 mmol of **1**, TBAB (4.9 mmol), 50% NaOH (130 g), and hexane (100 ml) were used under reflux. b) Isolated yield.

Table 4. Cationic Ring-Opening Polymerization of Oxetane Derivatives in DCM at 0 °C for 20 h

Monomer	(mole ratio)	BF_3–THF[a] mol%	$[M]_0$[b] mol l^{-1}	Polymer Yield/%	$\overline{M}_n$[c]
3a		0.5	3.8	92	5480
3a+DMOX[d]	(49/51)	1.0	3.2	91	8380
3a+**4a**	(79/30)	1.0	3.5	95	
4a		1.0	2.2	87	
3b		0.5	1.8	86	3460
3b+**4b**	(79/21)	1.0	1.9	99	
4b+OX[d]	(32/68)	0.9	4.1	84	
13a		0.5	2.7	98	3850
13a		1.0	2.5	97	1970
13a+**10**	(78/22)	1.0	2.2	100	2400
13b		1.0	2.6	93	2890

a) Percentage to mole of ether group of oxetane ring. b) Total monomer concentration at initial time. c) By VPO (solvent, acetone) of methanol-insoluble part of product polymer. d) DMOX refers to 3,3-dimethyloxetane and OX does to oxetane.

yields by a facile operation using less expensive reagents under the present phase-transfer catalytic conditions.

Polymerization. Oxetanes, thus obtained, were polymerized to give their polymers ($\bar{M}_n$2000—5500) via a cationic ring-opening polymerization in dichloromethane (DCM) at 0 °C with trifluoroborane (BF_3)–THF complex as an initiator (Table 4). The polyoxetanes were viscous oily materials soluble in DCM, chloroform, ether, acetone, benzene, toluene, and DMF, and reprecipitated from a solution of the polymer in DCM by adding it into methanol. The IR spectra of **3a**, poly(**3a**), and poly(**4a**) are shown in Fig. 2. In Fig. 2A, the bands at 980 and 835 cm^{-1} are assignable to the cyclic ether linkage of the oxetane ring. These bands disappear in the spectra of poly(**3a**) and poly(**4a**), in which the band due to the acyclic ether linkage of the resultant polyether chain appears at 1100—1120 cm^{-1}. Methylene protons of the oxetane ring of **3a** show signals of an AB qualtet in δ 4.25—4.65; however, the signals disappear in the spectrum of poly(**3a**) (Fig. 3). Use of bisoxetanes **4a** and **4b** as a comonomer in the polymerization of **3a** and **3b** gave gel products which were insoluble in the solvents, indicating that these polymeric products have the cross-linked structures of a polyether network. These polyoxetane resins are considered to be soft, somewhat polar polymer supports bearing a bromide at the spacer end, which will be used for preparing functional polyethers according to the way employed for the functionalization of a hard, less polar, crosslinkd polystyrene having a chloromethyl group.[23–25]

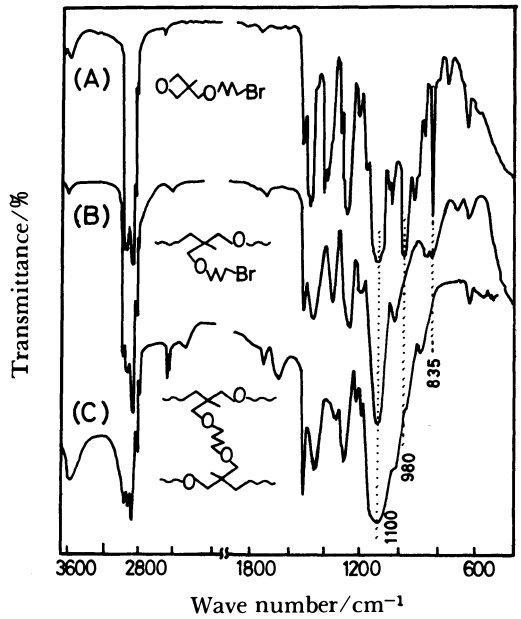

Fig. 2. IR spectra of (A) **3a**, (B) poly(**3a**), and (C) poly(**4a**).

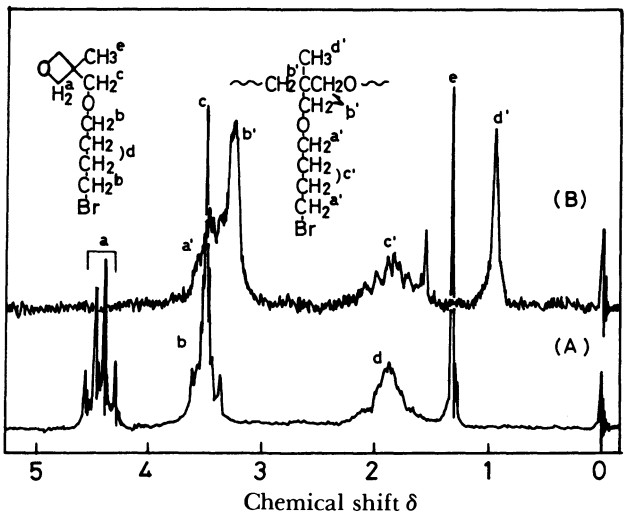

Fig. 3. ^1H NMR spectra of (A) **3a** and (B) poly(**3a**).

Experimental

Materials. 3-Hydroxymethyl-3-methyloxetane (**1**) was prepared in 60—62% yield according to a method described in the literature.[14] Oxetane (OX) and 3,3-dimethyloxetane (DMOX) were synthesized according to a method reported in the literature.[26] Halides **2a**, **2b**, **11a**, **11b**, **12a**, and **12b**, and hexane of extra pure grade reagents were used without further purification. DCM as a solvent of polymerization was twice distilled over calcium hydride in a nitrogen atmosphere. A BF_3–THF complex was obtained by passing BF_3 gas into dried THF, followed by distillation of the saturated solution: bp 87.8 °C (1.60 kPa) [lit,[27] 79.0 °C (0.96 kPa)]. Commercially available TBAB and TBHS (Tokyo Kasei Kogyo) were used as PTC without further purification.

3-(6-Bromo-2-oxahexyl)-3-methyloxetane (3a): In a three-necked flask, equipped with a mechanical stirrer, a thermometer, and a reflux condenser, a 50% aqueous NaOH solution (390 g), TBAB (4.7 g, 14.7 mmol), and hexane (300 ml) were placed and cooled in an ice-bath. A mixture of **1** (30.0 g, 0.29 mol) and **2a** (190 g, 0.88 mol) was added into it with efficient stirring and cooling. It was kept at room temperature for 30 min and then refluxed for 1.5 h. It was cooled below 5 °C and 600 ml of water was added. The organic layer, which was separated by means of separatory funnel, was dried over anhydrous Na_2SO_4. After removing the solvents and recovering **2a** (52 g) by distillation, the residue was distilled to give 53.1 g (76.2%) of **3a**: bp 110—112 °C (63—64 Pa); IR (neat) 1115 (acyclic ether), 980 and 835 (cyclic ether) cm^{-1}; ^1H NMR($CDCl_3$) δ=1.32 (3H, s, CH_3), 1.5—2.3 [4H, m, $OCH_2(C\underline{H}_2)_2CH_2Br$], 3.3—3.7 [4H, m, $OC\underline{H}_2(CH_2)_2C\underline{H}_2Br$, containing a singlet (2H) of CH_2 adjacent to oxetane ring at δ 3.49], and 4.25—4.65 (4H, q, J=6 Hz, CH_2 of oxetane ring).

Found: C, 45.77; H, 7.45; Br, 33.43%. Calcd for $C_9H_{17}BrO_2$: C, 45.58; H, 7.24; Br, 33.69%.

3-(8-Bromo-2-oxaoctyl)-3-methyloxetane (3b): 3b was prepared from **1** (14.0 g, 0.14 mol) and **2b** (100 g, 0.41 mol) in a 73.4% yield in the same way as that described for preparing **3a**: bp 95—97 °C (67 Pa); IR (neat) 1120 (acyclic ether), 985 and 840 (cyclic ether) cm^{-1}; ^1H NMR ($CDCl_3$) δ=1.22—2.22 [8H, m, OCH_2 $(C\underline{H}_2)_4CH_2Br$, containing a singlet (3H) of

CH_3 at δ 1.32], 3.30—3.70 [4H, m, $OCH_2(CH_2)_4CH_2Br$, containing a singlet (2H) of CH_2 adjacent to oxetane ring at δ 3.52], 4.33—4.63 (4H, q, J=6 Hz, CH_2 of oxetane ring).

Found: C, 50.07; H, 8.12; Br, 30.20%. Calcd for $C_{11}H_{21}BrO_2$: C, 49.81; H, 8.00; Br, 30.13%.

1,8-Bis(3-methyl-3-oxetanyl)-2,7-dioxaoctane (4a): Bis-oxetane **4a** was prepared from **1** (10.0 g, 97.9 mmol) and **2a** (25.4 g, 0.12 mol) in the same way as that described for the **3a** preparation. Working up the reaction mixture followed by distillation of the crude product gave pure **4a** in a 63.7% yield: bp 124—126 °C (69—71 Pa); IR (neat) 1110 (acyclic ether), 985 and 840 (cyclic ether) cm^{-1}; ^1H NMR ($CDCl_3$) δ=1.32 (6H, s, CH_3), 1.53—2.02 [4H, m, $OCH_2(CH_2)_2CH_2O$], 3.33—3.76 [4H, m, $OCH_2(CH_2)_2CH_2O$, containing a singlet (4H) of CH_2 adjacent to oxetane ring at δ 3.50], and 4.31—4.62 (8H, q, J=6 Hz, CH_2 of oxetane ring).

Found: C, 65.12; H, 10.20%. Calcd for $C_{14}H_{26}O_4$: C, 65.07; H, 10.16%.

1,10-Bis(3-methyl-3-oxetanyl)-2,9-dioxadecane (4b): This compound was prepared from **1** (10.0 g, 97.9 mmol) and **2b** (23.9 g, 97.9 mmol) using the same procedure as above: yield, 62.8%; bp 129—130 °C (55 Pa); IR (neat) 1110 (acyclic ether), 980 and 830 (cyclic ether) cm^{-1}; ^1H NMR ($CDCl_3$) δ=1.15—1.95 [8H, m, $OCH_2(CH_2)_4CH_2O$, containing a singlet (6H) of CH_3 at δ 1.31], 3.25—3.75 [4H, m, $OCH_2(CH_2)_4CH_2O$, containing a singlet (4H) of CH_2 adjacent to oxetane ring at δ 3.49], 4.25—4.65 (8H, q, J=6 Hz, CH_2 of oxetane ring).

Found: C, 66.80; H, 10.74%. Calcd for $C_{16}H_{30}O_4$: C, 67.08; H, 10.58%.

3-Methyl-3-(2-oxadecyl)oxetane (10): In the presence of TBAB (4.9 mmol), **1** (10.0 g, 97.9 mmol) and **11a** (56.7 g, 0.29 mol) were heated for 12 h in a 50% NaOH solution (130 g) and hexane (100 ml) with stirring under reflux. The ordinary work-up and distillation gave pure **10** in a 92.9% yield: bp 152.5—153.0 °C (2.4 kPa); IR (neat) 1110 (acyclic ether), 980 and 830 (cyclic ether) cm^{-1}; ^1H NMR ($CDCl_3$) δ=0.72—1.97 [total 18H, CH_3 adjacent to oxetane ring and $OCH_2(CH_2)_6CH_3$], 3.31—3.71 [total 4H, a singlet of CH_2 adjacent to oxetane ring and multiplet of $OCH_2(CH_2)_6CH_3$], and 4.31—4.61 (4H, q, J=6 Hz, CH_2 of oxetane ring).

Found: C, 72.68; H, 12.40%. Calcd for $C_{13}H_{26}O_2$: C, 72.83; H, 12.25%.

3-Methyl-3-(3-phenyl-2-oxapropyl)oxetane (13a): **1** (20.0 g, 0.196 mol) and **12a** (24.8 g, 0.196 mol) were allowed to react under reflux for 2 h in hexane (200 ml) and 50% NaOH in the presence of TBAB (9.8 mmol). The desired product **13a** boiling at 82—86 °C (72—83 Pa) was obtained in a 85.7% yield by fractional distillation: IR (neat) 3060, 3030, 1600, 1585, 1500 (aromatic CH and C=C), 1100 (acyclic ether), 980, 840 (cyclic ether), 740 and 700 (monosubstituted aromatic ring) cm^{-1}; ^1H NMR ($CDCl_3$) δ=1.34 (3H, s, CH_3), 3.56 (2H, s, CH_2OCH_2Ph), 4.31—4.61 [4H, q, J=5.5 Hz, CH_2 of oxetane ring, containing a singlet (2H) of CH_2Ph at δ 4.59], and 7.38 (5H, s, aromatic).

Found: C, 74.95; H, 8.41%. Calcd for $C_{12}H_{16}O_2$: C, 74.95; H, 8.40%.

3-[3-(4-Methylphenyl)-2-oxapropyl]-3-methyloxetane (13b): An equimolar mixture of **1** and **12b** in hexane was refluxed for 3 h under phase-transfer catalytic conditions. The ordinary work-up gave pure **13b** boiling at 86—88 °C (43 Pa) in a 73.9% yield: IR (neat) 1620, 1520 (aromatic C=C), 1100 (acyclic ether), 985, 840 (cyclic ether), 810 and 755 (para-substituted aromatic ring) cm^{-1}; ^1H NMR ($CDCl_3$) δ=1.27 (3H, s, aliphatic CH_3), 2.30 (3H, s, aromatic CH_3), 3.44 (2H, s, CH_2 adjacent to oxetane ring), 4.22—4.70 [4H, q, J=6 Hz, CH_2 of oxetane ring, containing a singlet (2H) of CH_2Ar at δ 4.99], and 7.28 (4H, s, aromatic).

Found: C, 75.58; H, 9.08%. Calcd for $C_{13}H_{18}O_2$: C, 75.68; H, 8.81%.

3-Methyl-3-(2-oxa-5-hexenyl)oxetane (5): This compound was contained in a low-boiling fraction of the reaction mixture from **1** and **3a**. Repeated fractional distillation of this fraction gave **5** (98% purity by GC analysis): bp 75—80 °C (2.53 kPa); IR (neat) 1640 (C=C), 1110 (acyclic ether), 980 and 830 (cyclic ether) cm^{-1}; ^1H NMR ($CDCl_3$) δ=1.30 (3H, s, CH_3), 2.13—2.57 (2H, m, $CH_2CH_2CH=CH_2$), 3.44—3.65 (2H, t, $CH_2CH_2CH=CH_2$, containing a singlet (2H) of CH_2 adjacent to oxetane ring at δ 3.50), 4.27—4.57 (4H, q, J=6 Hz, CH_2 of oxetane ring), 4.89—5.36 (2H, m, $CH=CH_2$), and 5.52—6.25 (1H, m, $CH=CH_2$).

1,13-Bis(3-methyl-3-oxetanyl)-2,7,12-trioxatridecane (9): **3a** (2.07 g, 8.73 mmol) was heated under reflux for 8 h in hexane (20 ml) and 50% NaOH (11 g) in the presence of TBAB (0.44 mmol). The contents was mixed with water (50 ml) and extracted with ether. The organic layer was separated from the aqueous layer and 0.96 g of **9** was obtained as a pot residue by distilling the organic layer at 200 °C (muximum temperature of bath)/33 Pa: IR (neat) 1115 (acyclic ether), 980 and 835 (cyclic ether) cm^{-1}; ^1H NMR ($CDCl_3$) δ=1.32 (6H, s, CH_3); 1.45—1.90 [8H, m, $OCH_2(CH_2)_2CH_2O$], 3.20—3.70 [8H, m, $OCH_2(CH_2)_2CH_2O$, containing a singlet (4H) of CH_2 adjacent to oxetane ring at δ 3.48], and 4.28—4.57 (8H, q, J=6 Hz, CH_2 of oxetane ring).

2-Bromomethyl-2-methyl-1,3-dibromopropane (14): Into powdered 1,1,1-tris(hydroxymethyl)ethane (5.96 g, 49.6 mmol) in a three-necked flask, phosphorus tribromide (20.1 g, 74.3 mmol) was added drop by drop at 80 °C and the mixture was heated at 170 °C for 10 h. After adding ice (30 g) into the reaction mixture and standing overnight, a volatile fraction was collected by steam-distillation. An organic layer of the distillate was separated and distilled to obtain **14** boiling at 105—108 °C (1.60 kPa) in 31—37% yield: IR (neat): 1460, 1420, 1375, and 1270 cm^{-1}; ^1H NMR ($CDCl_3$) δ=1.29 (3H, s, CH_3) and 3.52 (6H, s, CH_2Br).

Cationic Ring-Opening Polymerization of Oxetanes. In a ground-glass test tube, dried and flashed with dry nitrogen gas, an oxetane was introduced by using a hypodermic injection under a nitrogen atmosphere. The monomer was diluted with DCM, and chilled at −50 °C, and mixed with a catalytic amount of BF_3–THF (as a 0.27 mol l^{-1} solution in DCM). After being closed with a ground-glass stopper, the test tube was transferred to an ice-bath and allowed to stand for 20 h. The contents, in the case of soluble polymer, was poured into methanol, and, in the case of gel product, filtered and washed with 10% aqueous methanol and methanol successively. The polymer was collected and dried at 80 °C for 8 h in vacuo.

Measurement. GC analysis of the products was performed in a Shimadzu GC-8A apparatus: glass column (3.2ϕ×1 m) packed with Silicone High Vaccum Grease (30%)/celite (80—100 mesh); carrier gas, He (66 ml min^{-1}); temp, 140 or 250 °C. The IR spectra were recorded on a JASCO A-202 spectrometer and ^1H NMR on a 60 MHz instrument (Hitachi R-24B) using TMS as an internal

standard. Molecular weight measurements were made by VPO in a Corona molecular weight apparatus (model 117).

References

1) T. Saegusa, M. Motoi, S. Matsumoto, and H. Fujii, *Macromolecules*, **5**, 233 (1972).

2) T. Saegusa, S. Matsumoto, M. Motoi, and H. Fujii, *Macromolecules*, **5**, 236 (1972).

3) T. Saegusa, M. Motoi, S. Matsumoto, and H. Fujii, *Macromolecules*, **5**, 815 (1972).

4) T. Saegusa, M. Motoi, and H. Suda, *Macromolecules*, **9**, 231, 256 (1976).

5) T. Saegusa, M. Motoi, H. Suda, H. Kasai, and A. Ueyama, *Polym. J.*, **11**, 113 (1979).

6) M. Motoi, M. Kijima, Y. Kubo, and H. Suda, 33rd National Meeting of the Society of Polymer Science, Sendai, Sep. 1984, Abstr., No. G2D02.

7) Reported by the authers other than us: T. Saegusa, H. Fujii, S. Kobayashi, H. Ando, and R. Kawase, *Macromolecules*, **6**, 26, (1973).

8) A. C. Farthing, *J. Chem. Soc.*, **1955**, 3648.

9) K. Hardenstine, C. J. Murphy, R. B. Jones, L. H. Sperling, and G. E. Manser, *J. Appl. Polym. Sci.*, **30**, 2051 (1985).

10) M. B. Frankel and E. R. Wilson, U. S. Patent 383421 (1983); *Chem. Abstr.*, **98**, 160570n (1983).

11) K. Hiratani, K. Taguchi, H. Sugihara, and T. Okada, *Chem. Lett.*, **1986**, 197.

12) C. G. Krespan, *Macromolecules*, **40**, 1205 (1975); *J. Org. Chem.*, **45**, 1177 (1980).

13) K. Baum, P. T. Berkowitz, V. Grakauskas, and T. G. Archibald, *J. Org. Chem.*, **48**, 2953 (1983).

14) E. J. Corey and N. Raju, *Tetrahedron Lett.*, **24**, 5571 (1983).

15) J. T. Carlock and M. P. Mack, *Tetrahedron Lett.*, **1978**, 5153.

16) P. Picard, D. Leclercq, J.-P. Bats, and J. Moulines, *Synthesis*, **1981**, 550.

17) M. Shimizu, R. Ando, and I. Kuwajima, *J. Org. Chem.*, **49**, 1230 (1984).

18) N. Shimizu, S. Yamaoka, and Y. Tsuno, *Bull. Chem. Soc. Jpn.*, **56**, 3853 (1983).

19) E. J. Vandenberg, *J. Polym. Sci., Polym. Chem. Ed.*, **23**, 951 (1985).

20) S. L. Regen, *Angew. Chem., Int. Ed. Engl.*, **18**, 421 (1979).

21) B. P. Stark, Brit. Patent 969042 (1964); *Chem. Abstr.*, **62**, 701h (1965).

22) L. C. Hoffsommer, D. J. Glover, and N. E. Burlinson, *J. Org. Chem.*, **48**, 315 (1983).

23) T. Iizawa, T. Nishikubo, Y. Masuda, and M. Okawara, *Macromolecules*, **17**, 992 (1984).

24) M. Tomoi, Y. Hosokawa, and H. Kakiuchi, *J. Polym. Sci., Polym. Chem. Ed.*, **22**, 1243 (1984).

25) J. M. J. Fréchet, M. D. de Smet, and M. J. Farrall, *J. Org. Chem.*, **44**, 1774 (1979).

26) J. B. Rose, *J. Chem. Soc.*, **1956**, 542.

27) R. C. Osthoff, C. A. Brown, and J. A. Hawkins, *J. Am. Chem. Soc.*, **73**, 5480 (1951).

Hydrolytic Metalloenzyme Models. Effects of AOT Reverse Micelles on the Hydrolysis of *p*-Nitrophenyl Picolinate Catalyzed by Zn^{2+} and Cu^{2+} Complexes of *N*-Alkyl-2-hydroxymethylimidazoles

Tsunehisa FUJITA, Yoichi INABA, Kenji OGINO, and Waichiro TAGAKI*
Department of Applied Chemistry, Faculty of Engineering, Osaka City University, Sugimoto 3, Sumiyoshi-ku, Osaka 558
(Received September 26, 1987)

The catalytic effects of bivalent metal ion (Zn^{2+} and Cu^{2+}) complexes of *N*-alkyl-2-hydroxymethylimidazoles on the hydrolysis of *p*-nitrophenyl picolinate (PNPP) have been studied kinetically in the reverse micelles of AOT/hexane/water at 25 °C. The results were compared with those obtained in the non-micellar aqueous media and aqueous micelles. The hydrolysis was observed to occur through the acyl group transfer from PNPP to the ligand hydroxyl group in both cases of Zn^{2+} and Cu^{2+} ions and in all three non-micellar and micellar systems. However, the ligand:metal ion ratio in the kinetically active complexes was found to differ significantly in the three systems: there seems to exist general trends of 1:1, 2:1, and 4:1 stoichiometry in the ligand:metal ion ratio, depending on non-micellar aqueous media, aqueous micelles and reverse micelles, respectively. It was also noticed that the hydrolysis is always faster in micellar systems than in non-micellar aqueous media. Furthermore, a lipophilic ligand (*N*-dodecyl, Lig-12) was found to be more active than a hydrophilic ligand (*N*-methyl, Lig-1) under two micellar conditions.

The micellar catalysis has been extensively studied for the past two decades as the model of enzyme catalysis.[1] However, as for the micellar models of hydrolytic metalloenzymes, the studies appear to begin only recently.[2-7] In 1980, we reported that *N*-dodecyl-2-hydroxymethylimidazole (Lig-12) is remarkably active for the hydrolysis of *p*-nitrophenyl picolinate (PNPP) when complexed with Zn^{2+} ion and co-micelled in surfactant micelles in aqueous media.[2] Later studies revealed that Lig-12 is even more active in the presence of Cu^{2+} ion.[3]

Besides the aqueous micelles, there are also known reverse micelles in apolar solvents. Namely, certain surfactants such as sodium 1,2-bis(2-ethylhexyloxycarbonyl)ethanesulfonate (AOT) can solubilize water in apolar organic solvents to form reverse micelles.[1] In such reverse micelles, the surfactant polar heads entrap water molecules as water pools in the cores, while the surfactant hydrocarbon chains extend toward the outer bulk organic solvent. Such water pools are said to resemble somewhat those entrapped in the active sites of enzymes. Therefore, it may be interesting to see what happen when the above hydrolysis is carried out in reverse micelles. To the best of our knowledge, there has been no such a study in the literature except those in aqueous micelles[2-7] as mentioned above. We now wish to report that the bivalent metal ion (Zn^{2+} and Cu^{2+}) complexes of *N*-alkyl-2-hydroxymethylimidazoles (Lig-1 and Lig-12) are very active for the hydrolysis of PNPP in the reverse micelles of AOT/hexane/water. The results were also compared with those obtained in the previous studies in aqueous micelles.[2,3] One might ask why the two metal ions, Zn^{2+} and Cu^{2+}, are particularly selected for comparison in this work. One reason is that they are widely different in the ability to activate coordinated hydroxyl group as a nucleophile. Another and more interesting reason comes from our recent finding that Zn^{2+} ion requires a tetrahedral geometry for the activation of hydroxyl group of bis(imidazole) ligands, while Cu^{2+} ion requires square planar geometry for the activation.[8]

Results and Discussion

The metal ion salts ($Zn(NO_3)_2$ and $Cu(NO_3)_2$) could be solubilized in hexane, only in the presence of both AOT and water. The water component of reverse micelles was the acetate buffer solution (0.1 mol·dm^{-3}, pH 4.9). The use of other buffer solutions of higher pH, such as lutidine buffer (pH 7) tended to cause the

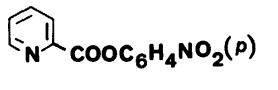

PNPP

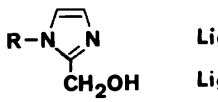

Lig−1 R = CH_3

Lig−12 R = $C_{12}H_{25}$

metal ions : Zn^{2+}, Cu^{2+}

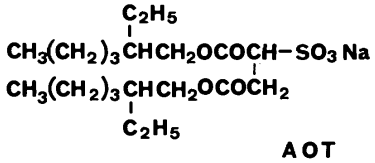

AOT

precipitation of metal ion hydroxide. Hence only acetate buffer was used in this study. Rates of hydrolysis were determined by measuring released *p*-nitrophenol spectrophotometrically at 310 nm. In all cases, under the conditions containing excess amount of ligand over the substrate (PNPP), good pseudo-first-order rate constants (k_{obsd}) were obtained up to the completion of hydrolysis.

Effects of AOT and Water. As shown in Fig. 1, the rates (k_{obsd}) increased initially up to a maximum, then decreased with increasing AOT concentration. Here the concentrations of water and Lig-12 also increased with increasing AOT, while their ratios w_o=[water]/[AOT] and [AOT]/[Lig-12] were kept constant. The curve in Fig. 1 appears to be rather common in the reactions of both aqueous and reverse micelles,[1,9-11] and may be accounted for in the following way. It is generally considered that the size of reverse micelles or

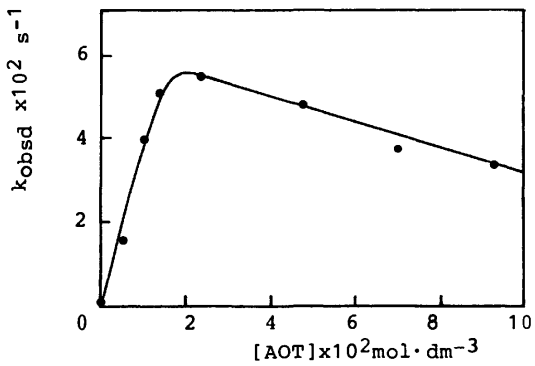

Fig. 1. Pseudo-first-order rate constants for the hydrolysis of PNPP at 25°C as the function of AOT concentration. w_o=[H_2O]/[AOT]=14.1, [AOT]/[Lig-12]=22.5, [PNPP]=5×10^{-5} mol·dm^{-3}, [Zn^{2+}]=1×10^{-4} mol·dm^{-3}.

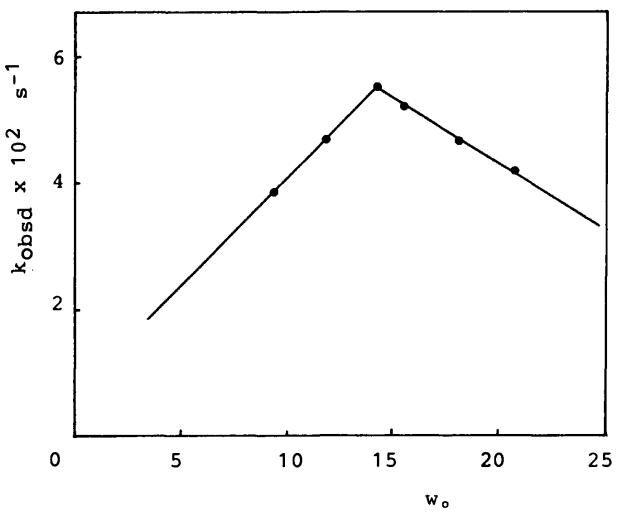

Fig. 2. Pseudo-first-order rate constants for the hydrolysis of PNPP at 25°C as the function of w_o value. [AOT]=0.022 mol·dm^{-3}, [Zn^{2+}]=1×10^{-4} mol·dm^{-3}, [PNPP]=5×10^{-5} mol·dm^{-3}, [AOT]/[Lig-12]=22.5.

the size of water pools is determined by the w_o ratio, so that at a constant w_o as in Fig. 1, the increase in AOT concentration results in the increase in micelle concentration of the same size.[1] Thus the curve of Fig. 1 shows the saturation of rates due to the saturation of incorporation of reactants into micelles (Zn^{2+} ion, Lig-12 and PNPP). A slow decrease in rates after the maximum is explained by the dilution of reactants (Zn^{2+} and PNPP) per micelle, although the concentration of Lig-12 remaines constant.

Next, the effect of w_o on the rates was examined as shown in Fig. 2. It shows the presence of an optimum value at about w_o=14. In the case of AOT, it is considered that the water molecules (in the water pools) up to perhaps w_o=6—8 are tightly bound to the head groups of the surfactant,[12,13] and above this value the water molecules become free water and the micelles swell when the water content increases.[13,14] Thus the above value w_o=14 suggests that an appropriate amount of free water is necessary for faster rates. The micellar molecular weight based on the light scattering data will be discussed later.

Stoichiometry of the Reactive Complexes. In order to know the stoichiometry of the kinetically reactive complexes, the kinetic version of Job plots[15,16] was examined by plotting the k_{obsd} values as a function of mole fraction of ligand (γ), maintaining the total concentration of ligand and metal ion constant. The results shown in Fig. 3 indicate that in the case of Zn^{2+} ion and Lig-12 the rate maximum was observed at γ=0.8 which corresponds to a stoichiometry of ligand:Zn^{2+}=4:1. The figure also indicates that the rates are very slow in the presence of metal ion

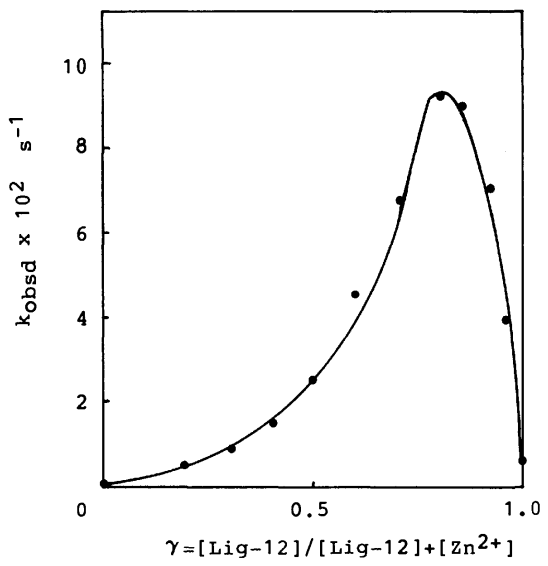

Fig. 3. Job plots for the ligand and Zn^{2+} ion complexation as measured by the rates of hydrolysis of PNPP as 25°C. [AOT]=0.022 mol·dm^{-3}, [H_2O]=0.35 mol·dm^{-3}, [PNPP]=5×10^{-5} mol·dm^{-3},([Lig-12]+[Zn^{2+}])=1× 10^{-3} mol·dm^{-3}.

or ligand alone (i.e. γ=0 or 1.0). Very similar plots were also obtained in the cases of Cu^{2+} ion as shown in Fig. 4, although the absolute values of rates were much larger than those in the case of Zn^{2+} ion. Here it should be noticed that lipophilic Lig-12 is more active than hydrophilic Lig-1.

The above 4:1 stoichiometry for Lig-12 is quite different from the 2:1 stoichiometry observed previously for Lig-12 catalysis in aqueous micelles.[2,3] In the case of a hydrophilic Lig-1, the stoichiometry in Fig. 4 is also 4:1. However, this ligand showed a 1:1

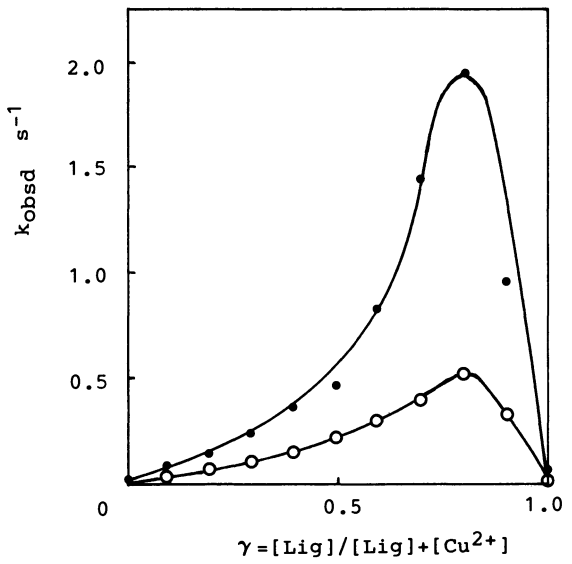

Fig. 4. Job plots for the ligand and Cu^{2+} ion complexation as measured by the rates of hydrolysis of PNPP at 25 °C. [AOT]=0.022 mol·dm^{-3}, [H_2O]=0.35 mol·dm^{-3}, [PNPP]=5×10^{-5} mol·dm^{-3}, ([Lig]+[Cu^{2+}])=5×10^{-4} mol·dm^{-3}, (○): Lig-1, (●): Lig-12.

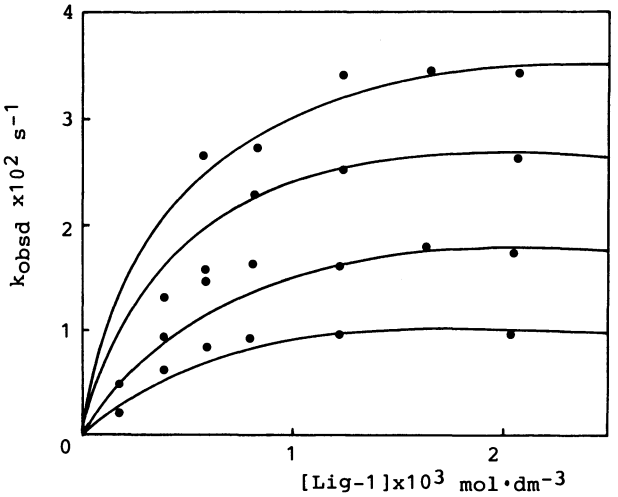

Fig. 5. Pseudo-first-order rate constants for the hydrolysis of PNPP at 25 °C as the function of Lig-1 concentration. [AOT]=0.022 mol·dm^{-3}, [H_2O]=0.35 mol·dm^{-3}, [PNPP]=5×10^{-5} mol·dm^{-3}, [Zn^{2+}]×10^4 mol·dm^{-3} from the top: 2.0, 1.5, 1.0, and 0.5.

stoichiometry in the previous catalysis in non-micellar aqueous solutions.[3,17] Thus, although it was difficult to see the stoichiometry for lipophilic Lig-12 in non-micellar aqueous media because of a low solubility of the ligand, it appears that there exist general trends of 1:1, 2:1, and 4:1 stoichiometry, depending on non-micellar aqueous media, aqueous micelles, and reverse micelles used, respectively. The reason for these differences in stoichiometry is not clear at present. It seems important to know more details about the hydration of metal ions under these different conditions before making any concrete discussions.

Second-Order Rate Constant, k_c. The k_{obsd} values were dependent on the concentrations of both Zn^{2+} ion and ligand as shown by four saturation curves in Fig. 5. These curves can be accounted for by assuming the following reaction Scheme 1.

$$M + nL \underset{}{\overset{K}{\rightleftharpoons}} \text{Complex} \quad (1)$$

$$S + \text{Complex} \xrightarrow{k_c} \text{Products} \quad (2)$$

$$S \xrightarrow{k'_o} \text{Products} \quad (3)$$

Scheme 1.

In Scheme 1, metal ion (M) and n ligand (L) form a complex with an association constant (K). Then the complex reacts with the substrate (S) to give products with the second-order rate constant (k_c). The substrate also goes to the products by other pathways with the rate constant (k'_o). The contributing pathways to k'_o may be the uncatalyzed (k_o) and the catalyzed by metal ion (k_M[M]) and ligand (k_L[L]).

The Scheme 1 leads to the rate equations, Eqs. 4—7.

Thus the pseudo-first-order rate constants, k_{obsd}, can be represented by Eq. 5. This equation would allow to obtain the k_c value if the complex concentration could be calculated.

$$\text{Rate} = k_{obsd}[S] \quad (4)$$

$$k_{obsd} = k'_o + k_c[\text{Complex}] \quad (5)$$

$$k'_o = k_o + k_L[L] + k_M[M] \quad (6)$$

$$k^{sat}_{obsd} = k'_o + k_c[M]_T \quad (7)$$

However, such was difficult because of the difficulty in determining the association constant, K in Eq. 1. Therefore, we assumed the Eq. 7 in order to calculate k_c value on the following ground. Namely, we assumed in Figs. 5 and 6 that the complex concentration at the rate saturation (k^{sat}_{obsd}) is equal to the total metal ion concentration ([M]$_T$). In the case of Zn^{2+} ion, it was also assumed that the 4:1 ligand:metal ion (n=4) complex is formed at the rate saturation. The Eq. 7 requires a straight line relationship in the plots of k^{sat}_{obsd} vs. metal ion concentration. This was

confirmed by the plots shown in Fig. 7. The k_c values obtained from the slope of these straight lines are shown in Table 1. Figure 7 also indicates k'_o, the intercepts of the straight lines, to be negligibly small.

In the case of Cu^{2+} ion, the plots of k_{obsd} vs. ligand concentration are shown in Figs. 8 and 9. The figures indicate that the rates increase steeply to a peak, then decrease sharply with increasing ligand concentration. At first glance, it seems difficult to make reasonable analysis of such complicated curves. More carefull look, however, indicates that with increasing Cu^{2+} ion concentration (from the lower to the upper), the ligand concentration at the peak position approaches to such a value to give [ligand]/[Cu^{2+}]=4. For example, in Fig. 8 the top curve of [Cu^{2+}]=2×10^{-4} mol·dm^{-3} shows the peak at [ligand]=8×10^{-4} mol·dm^{-3}. This ratio of 4 is the stoichiometry for the reactive complex (n=4 in Scheme 1) determined from Job plots (Fig. 4). Thus the decreasing in rates after the peak in Figs. 8 and 9 suggests the formation of

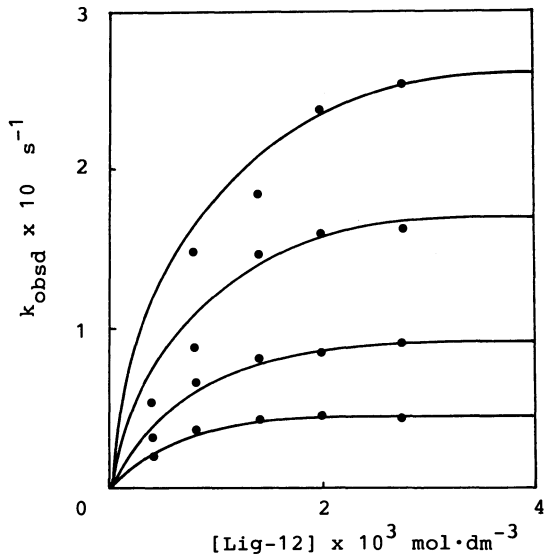

Fig. 6. Pseudo-first-order rate constants for the hydrolysis of PNPP at 25°C as the function of Lig-12 concentration. [AOT]=0.022 mol·dm^{-3}, [H_2O]=0.35 mol·dm^{-3}, [PNPP]=5×10^{-5} mol·dm^{-3}, [Zn^{2+}]×10^4 mol·dm^{-3} from the top: 3.0, 2.0, 1.0, and 0.5.

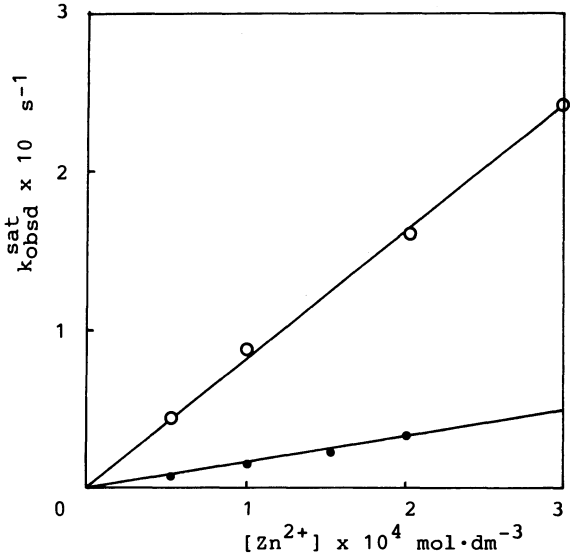

Fig. 7. Plots of k^{sat}_{obsd} in Figs. 5 and 6 as the function of Zn^{2+} ion concentration. (●): Lig-1, (○): Lig-12.

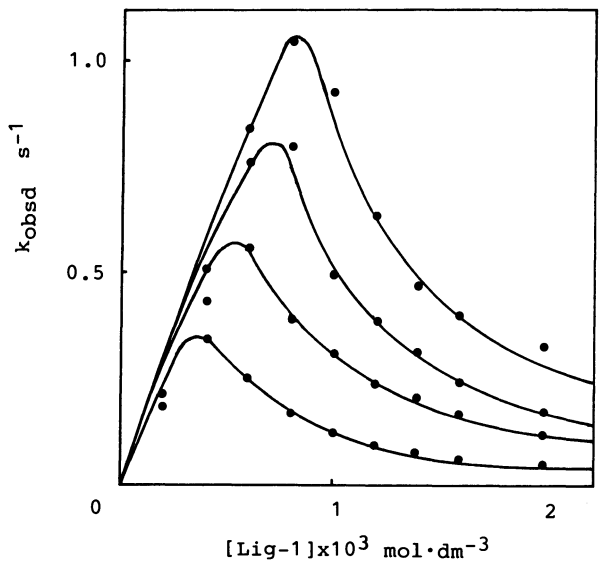

Fig. 8. Pseudo-first-order rate constants for the hydrolysis of PNPP at 25°C as the function of Lig-1 concentration. [AOT]=0.022 mol·dm^{-3}, [H_2O]=0.35 mol·dm^{-3}, [PNPP]=5×10^{-5} mol·dm^{-3}, [Cu^{2+}]×10^4 mol·dm^{-3} from the top: 2.0, 1.5, 1.0, and 0.5.

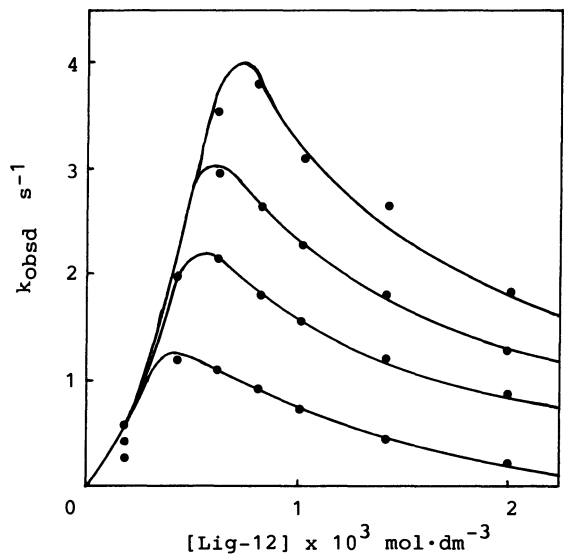

Fig. 9. Pseudo-first-order rate constants for the hydrolysis of PNPP at 25°C as the function of Lig-12 concentration. [AOT]=0.022 mol·dm^{-3}, [H_2O]=0.35 mol·dm^{-3}, [PNPP]=5×10^{-5} mol·dm^{-3}, [Cu^{2+}]×10^4 mol·dm^{-3} from the top: 2.0, 1.5, 1.0, and 0.5.

unreactive or less reactive complex(es) chelated with more than four ligands ($n>4$). It is reasonable to consider such unreactive complexes to be important for Cu^{2+} ion, but not for Zn^{2+} ion, since it is well-known that the complexation with imidazoles is much stronger for the former than for the latter metal ion. With these limitations in mind, the k_{obsd} values at the peaks (k_{obsd}^{max}) were plotted as the function of Cu^{2+} concentration to give straight lines as shown in Fig. 10. The slopes are the k_c' values of Cu^{2+} complexes which are perhaps slightly smaller than the real k_c values (see Table 1).

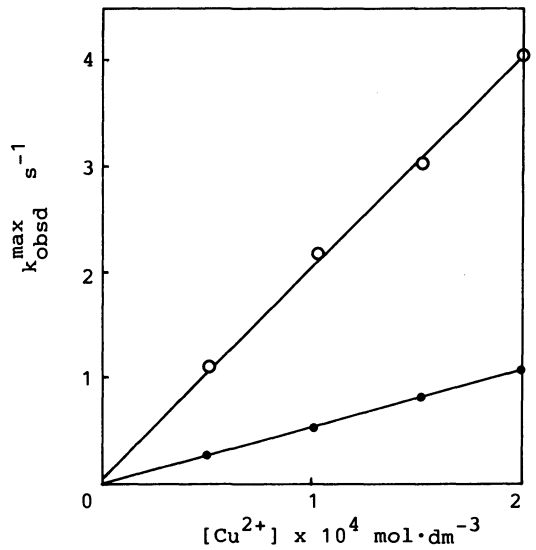

Fig. 10. Plots of k_{obsd}^{max} in Figs. 8 and 9 as the function of Cu^{2+} ion concentration. (●): Lig-1, (○): Lig-12.

General Discussion—Mechanism of Catalysis: a) Two-Step Mechanism Involving Acyl-Intermediate. The reaction occurs through the acyl group transfer from the substrate (PNPP) to the ligand hydroxyl group in both cases of Zn^{2+} and Cu^{2+} ions. This was confirmed in two ways for Lig-12 by carrying out the reaction under the conditions of excess substrate over the ligand: (1) kinetically, burst kinetics were observed as described previously,[3] and (2) the acylated intermediate (Ac-Lig-12) was detected by HPLC analysis.[8] Thus the catalytic cycle in the present reverse micelles are essentially the same as reported previously,[3,8] and as illustrated in Scheme 2.

b) The Stoichiometry in the Ligand-Metal Ion Complexation. The results are summarized in Table 1, together with those reported previously for the reactions in non-micellar aqueous media and aqueous micelles.[2,3,17] The table shows no particular difference in the stoichiometry of ligand-metal ion between Zn^{2+} and Cu^{2+} ions, regardless of the reaction conditions. However, the table clearly indicates that the reaction conditions are important in determining such stoichiometry. It seems likely that the hydration

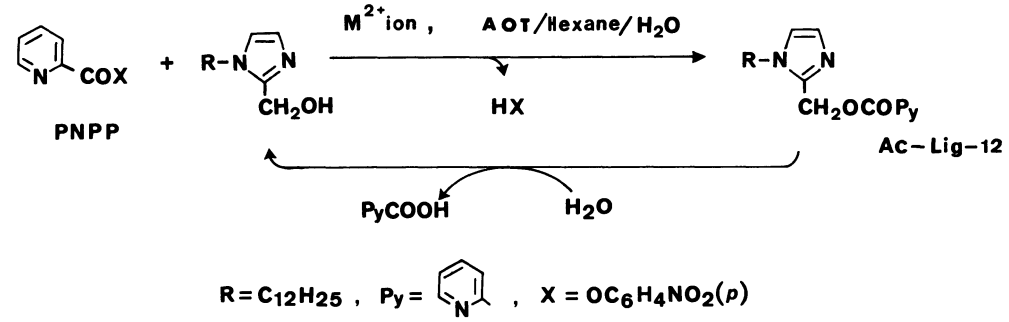

Scheme 2.

Table 1. Second-Order Rate Constants and the Stoichiometry of the Reactive Complex for the Hydrolysis of PNPP at 25 °C

Ligand	Metal ion	pH	Reactive complex Lig:M	k_c or k_c' / mol^{-1} dm^3 s^{-1}	Ref.
Reverse micelle[a]					
Lig-1	Zn^{2+}	4.9[b]	4 : 1	1.68×10^2	This work
	Cu^{2+}	4.9[b]	4 : 1	5.42×10^3	This work
Lig-12	Zn^{2+}	4.9[b]	4 : 1	0.81×10^3	This work
	Cu^{2+}	4.9[b]	4 : 1	1.92×10^4	This work
Normal micelle[c]					
Lig-12	Zn^{2+}	7.0	2 : 1	3.70×10^3	3
	Cu^{2+}	7.0	2 : 1	3.23×10^5	3
Non micelle[d]					
Lig-1	Zn^{2+}	7.0	1 : 1	1.36×10^2	3
	Cu^{2+}	7.0	1 : 1	7.69×10^3	21

a) [AOT]=0.022 mol·dm^{-3}, [H_2O]=0.35 mol·dm^{-3}. b) The pH of added acetate buffer. c) [Hexadecyltrimethylammonium bromide]=0.01 mol·dm^{-3} in aqueous buffer. d) In aqueous buffer.

of metal ions becomes weaker in the order of non-micellar aqueous media≫aqueous micelles≫reverse micelles, concomitantly with increasing number of ligand coordination. The 1:1 and 2:1 complexes may form the reactive complexes at the transition state by replacing the hydrated water with the substrate as illustrated in Fig. 11 (A and B). The situation seems to be more complicated in the cases of 4:1 complexes in reverse micelles. If they have a tetrahedral structure as generally considered for Zn^{2+} complexes, then the ligand exchange with the substrate appears to be necessary before attaining the transition state as illustrated in Fig. 12.[18]

c) The Molecular Weight of the Present AOT Reverse Micelle—an Attempt to Visualize the Catalytic Site. Self aggregation in AOT reverse micelles has been relatively well-investigated,[1] as compared to that in other surfactants. As mentioned above, it is considered that the size and the aggregation number (N) of AOT reverse micelles are determined by the w_o value. In this study, the weight average molecular weight (M_w) of AOT reverse micelles in hexane was determined by light scattering method, under the conditions of w_o=13 and by treating a composite micellar aggregate (AOT plus water) to be a single molecule. The M_w found is 8.96×10^4 which corresponds roughly to the composition of 130 of AOT molecules (N=130) and 1700 molecules of water. Day et al. reported the characterization of water-containing reverse micelles of AOT by viscosity and dynamic light scattering methods.[19] Their data indicate that there is the same straight line relationship between N and w_o in the range of w_o=3—8 for three solvents (cyclohexane, toluene, and chlorobenzene), and the extrapolated value is approximately N=170 at w_o=13 which may be in fair agreement with the present N=130. The above M_w value practically unchanged in the presence of metal ions and ligand in the present concentration range.

The above data may be used to visualize the catalytic site of the present reverse micelles as in the following way: the use of [AOT]=0.022 mol·dm^{-3} with w_o=13, [Lig]=4×10^{-4} mol·dm^{-3}, [M^{2+}]=1×10^{-4} mol·dm^{-3}, and [PNPP]=5×10^{-5} mol·dm^{-3} results in the formation of [micelle]=$0.022/130=1.7\times10^{-4}$ mol·dm^{-3} and each micelle contains about one molecule of 4:1 ligand-metal ion complex, and 0—1 molecule of substrate.

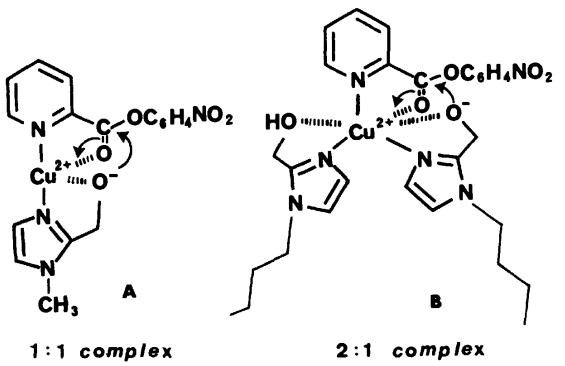

Fig. 11. Schematic illustrations of transition state structures for the non-micellar (A) and for the aqueous micellar (B) systems. (Ref. 2, 3, 17)

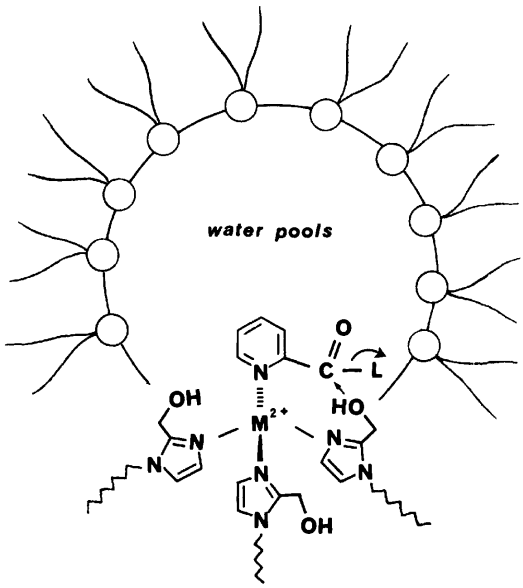

Fig. 13. Oversimplified picture of the catalytic site of AOT reverse micelles composed of bivalent metal ion-ligand complex.

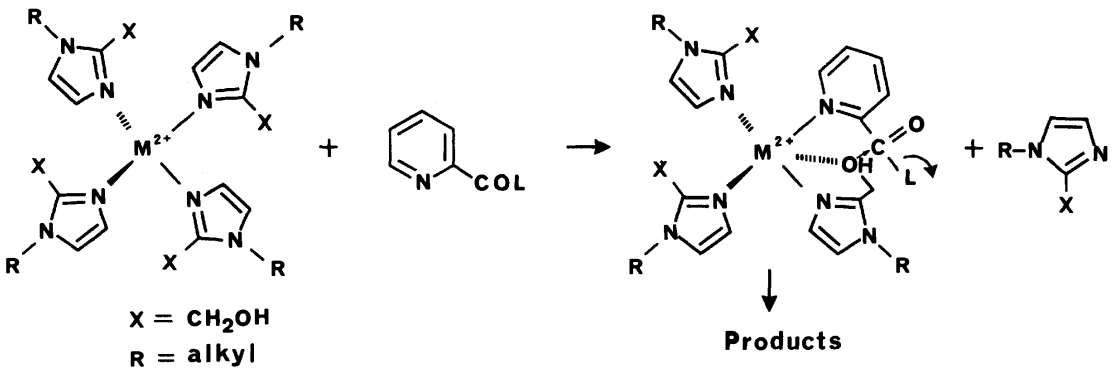

Fig. 12. Very speculative illustration of reaction pathway for 4:1 complexes.

Such a catalytic site at the transition state may be drawn schematically as in Fig. 13.

Experimental

Material. The water used for kinetics was obtained by distilling deionized water. Benzene and hexane were distilled from sodium metal (wire) before use. Acetonitrile was distilled from phosphorus pentaoxide. Buffer reagents of acetic acid and sodium acetate were commercial extra pure reagents. Commercially available metal salts, $Zn(NO_3)_2 \cdot 6H_2O$ and $Cu(NO_3)_2 \cdot 6H_2O$ were used without further purification. Commercially available sodium 1,2-bis(2-ethylhexyloxycarbonyl)ethanesulfonate (AOT, Nakarai Chemicals, Ltd.) was used without further purification. *N*-Methyl(Lig-1) and *N*-dodecyl-2-hydroxymethylimidazole (Lig-12) were prepared according to the previous method:[2,3] Lig-1, mp 118—120 °C; Lig-12, mp 56 °C.

Water Content Analysis. The water contents of the AOT solutions in hexane were determined by the Karl Fischer method, using an apparatus of Kyoto Electronics Manufacturing Co., Ltd. (MKA-3).

Examination of Micellar Aggregate by Light Scattering. The weight average molecular weight (M_w) of AOT/water aggregate in hexane was determined by light scattering photometry using Union Giken light scattering apparatus (LS-601). The light source (632.8 nm) was an Ne-He laser. The differential refractive increments of the sample solutions were measured in a Union Giken differential refractometer (RM-102). The sample solutions ([AOT]= 0.0022—0.018 mol·dm^{-3}, w_o=13) were prepared by sealing them in a quartz glass cell after optical purification by repeated filtration through 0.5 μm millipore filter (Nihon Millipore Kogyo). The M_w=8.96×10^4 (at w_o=13) was obtained by Debye plots using Rayleigh ratio, R_{90}.[20]

Kinetic Measurements.[2,3,8,17] The reaction was initiated by introducing 15 μl of a substrate stock solution in benzene into 3 ml of a reverse micellar solution of AOT in hexane/aqueous buffer containing the metal ions and the ligand of desired concentrations and maintained at 25 °C. The rate of hydrolysis of PNPP was followed by monitoring the increase of absorbance at infinite time determined for each run and by using the integrated first-order equation $k_{obsd}=(2.03/t)\log[(OD_\infty-OD_t)/(OD_\infty-OD_0)]$.

The authors thank Prof. Takayuki Ohtsu and Mr. Akikazu Matsumoto for their assistance in carrying out the light scattering experiments.

This research was supported in part by a Grant-in-Aid for Scientific Research No. 60470097 from the Ministry of Education, Science and Culture.

References

1) J. H. Fendler, "Membrane Mimetic Chemistry," Wiley, New York (1982).
2) T. Eiki, M. Mori, S. Kawada, K. Matsushima, and W. Tagaki, *Chem. Lett.*, **1980**, 1431.
3) W. Tagaki and K. Ogino, *Top. Curr. Chem.*, **128**, 145 (1985).
4) C. D Gutsche and G. C. Mei, *J. Am. Chem. Soc.*, **107**, 7965 (1985).
5) S. H. Gellman, R. Petter, and R. Breslow, *J. Am. Chem. Soc.*, **108**, 2388 (1986).
6) F. M. Menger, L. H. Gan, E. Johnson, and D. H. Durst, *J. Am. Chem. Soc.*, **109**, 2800 (1987).
7) R. Fornasier, D. Milana, P. Scrimin, and U. J. Tonellato, *J. Chem. Soc., Perkin Trans. 2*, **1986**, 233.
8) K. Ogino, N. Kashihara, T. Fujita, T. Ueda, T. Isaka, and W. Tagaki, *Chem. Lett.*, **1987**, 1303.
9) C. A. Bunton, "Reactions in micelles and similar self-organized aggregates," in "The Chemistry of Enzyme Action," ed by M. I. Page, Elsevier, Amsterdam (1984); Chap. 13, pp. 461—504.
10) P. L. Luisi, *Angew. Chem., Int. Ed. Engl.*, **24**, 439 (1985).
11) K. Martinek, A. V. Levashov, N. Klyyachko, Y. L. Khmelnitski, and V. Berezin, *Eur. J. Biochem.*, **155**, 453 (1986).
12) M. Zulauf and H. F. Eicke, *J. Phys. Chem.*, **83**, 480 (1979).
13) M. Wong, J. K. Thomas, and T. Nowak, *J. Am. Chem. Soc.*, **99**, 4730 (1977).
14) H. F. Eicke and J. Rehak, *Helv. Chem. Acta*, **59**, 2883 (1976).
15) A. Martell and S. Chabarek, "Organic Sequestering Agents," Wiley, New York (1959), p. 508.
16) D. S. Sigman and C. T. Jorgensen, *J. Am. Chem. Soc.*, **94**, 1724 (1972).
17) K. Ogino, K. Shindo, T. Minami, W. Tagaki, and T. Eiki, *Bull. Chem. Soc. Jpn.*, **56**, 1101 (1983).
18) In the cases of bis-imidazole ligands in aqueous micelles, the Cu^{2+} ion complexes with 4 imidazole units were all inactive (Refs. 3 and 8).
19) R. A. Day, B. H. Robinson, J. H. R. Clarke, and J. V. Doherty, *J. Chem. Soc., Faraday Trans. 1*, **75**, 132 (1979).
20) P. Debye, *J. Phys. Colloid Chem.*, **51**, 18 (1947).
21) K. Ogino, O. Tanaka, K. Machiya, N. Kashihara, and W. Tagaki, *J. Chem. Soc., Perkin Trans. 1*, in contribution.

Synthesis of Oligoribonucleotides by Use of 4,4′,4″-Tris(acyloxy)trityl Groups for Protection of the 6-Amino Group of Adenosine

Mitsuo SEKINE,* Reiko IWASE, Narihiro MASUDA, and Tsujiaki HATA*
Department of Life Chemistry, Tokyo Institute of Technology,
Nagatsuta, Midoriku, Yokohama 227
(Received October 17, 1987)

Two kinds of substituted trityls, i.e., 4,4′,4″-tris(benzoyloxy)trityl (TBTr) and 4,4′,4″-tris(*p*-anisoyloxy)-trityl (TAnTr), have been examined as protecting groups of the amino group of adenosine in oligoribonucleotide synthesis. The former was used for a 3′-terminal adenosine unit and the latter was introduced into an building block of internal adenosine. These protecting groups were successfully applied to the liquid-phase synthesis of pGUA and pGUAUUA which were the 5′-terminal oligoribonucleotide fragments of brome mosaic virus mRNA 4.

In the liquid-phase synthesis of oligoribonucleotides the phosphotriester approach has been most frequently adopted as a highly reproducible method to afford large quantities of target RNA oligomers required for physicochemical studies.[1] We have also employed this strategy to obtain synthetic mRNA fragments[2] which have been used as substrates for biological studies[3] of interaction with ribosomal RNAs in connection with the initiation mechanism of peptide synthesis in eukaryotic cells.[4] In order to facilitate purification of synthetic intermediates of fully protected building blocks, the 6-amino group of adenosine has been protected with the 4-methoxytrityl (MMTr)[2c,2e] or 4,4′-dimethoxytrityl[2d] (DMTr) group as an acid-labile protecting group. Especially, the former enabled us to use protic acids for selective removal of the DMTr group used for protection of the 5′-hydroxyl group so that rapid removal of the 5′-DMTr group was achieved. However, careful treatments were required for selective removal of the 5′-protecting group, since both the N^6-MMTr and 5′-*O*-DMTr groups were essentially removed under acidic conditions.[2c]

When the DMTr group was used for protection of the amino group of adenosine, it is necessary to use rather mild conditions such as 0.5 M $ZnBr_2/CH_2Cl_2$–2-propanol (85:15, v/v)[5] (1 M=1 mol dm^{-3}) for selective removal of the 5′-DMTr group.[2d] However, this Lewis acid cleaved rather slowly the 5′-terminal dimethoxytrityl ether bond when a 5′-terminal nucleoside was cytidine.[2d]

Recently, we have shown the utility of the 4,4′,4″-tris(benzoyloxy)trityl (TBTr) group as a protecting group of the amino group of deoxyadenosine.[6] The tritylating reagent TBTrBr can be prepared as crystals in a large scale from commercially available rosolic acid according to the facile procedure involving benzoylation and bromination.[7] This is one of advantageous points over the MMTr and DMTr groups. This protecting group has proved to have a unique property that it could be removed by dilute alkali via 1,6-elimination while it is rather resistant to acidic conditions.[7]

Based on these facts, we decided to apply the TBTr group to protect the amino group of adenosine to facilitate the selective removal of the 5′-DMTr group. We have chosen two 5′-terminal RNA fragments, pGUA and pGUAUUA, of brome mosaic virus mRNA 4 for synthetic targets during this study.

Results and Discussion

First, we prepared a 3′-terminal adenosine unit **4** bearing the TBTr group at the N^6 position in a manner similar to that described in the preparation of N^6-TBTr deoxyadenosine[6] as shown in Scheme 1. N^6-[4,4′,4″-Tris(benzoyloxy)trityl]adenosine (**2**) was obtained in 74% yield from adenosine (**1**). Reaction of **2** with 4,4′-dimethoxytrityl chloride gave the 5′-tritylated compound **3** in 94% yield. The successive benzoylation followed by detritylation afforded the 5′-hydroxy derivative **4** in 77% yield.

Next, in order to synthesize a key building block of adenosine unit **11**, 3′,5′-*O*-(1,1,3,3-tetraisopropyldisiloxane-1,3-diyl)adenosine (**5**)[9] was tritylated with TBTrBr in DMF in the presence of silver nitrate and lutidine. The tritylated product **6a** was obtained in 68% yield. Pyranylation of **6a** gave a fully protected adenosine derivative **7a** in 96% yield. However, when the cyclic silyl (TIPS) group was removed from **7a** by treatment with KF–Et_4NBr–H_2O/CH_3CN[2d] in the usual manner, the benzoyl group was partially eliminated from the TBTr group and the 3′,5′-diol **8a** was obtained in a low yield of 29%. This is probably because of the remaining basicity of the fluoride ion.

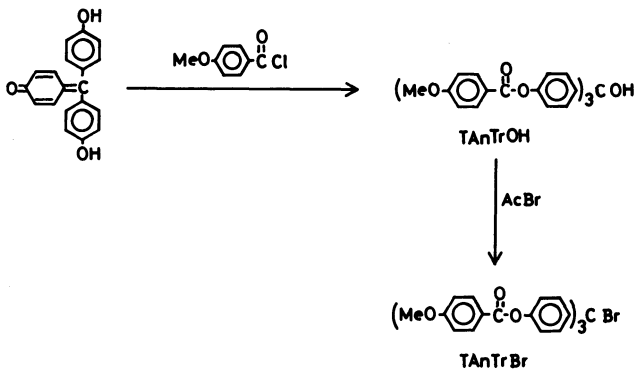

Therefore, to increase the stability of the benzoate, the benzoyl group was replaced for the *p*-anisoyl group at the 4-positions of the trityl group. The corresponding tritylating reagent 4,4′,4″-tris(anisoyloxy)trityl bromide (TAnTrBr) was synthesized in a manner similar to that described in the preparation of TBTrBr.

Similarly, compound **6b** was obtained in 54% yield by treatment of **5** with TAnTrBr. The successive pyranylation of **6b** followed by desilylation gave **8b** in 56% yield. The yields of **6b** and **8b** were unexpectedly low but this was not caused by the instability of the TAnTr group. It is due mainly to difficult separation of **6b** or **8b** from the by-products. To avoid such problems, the tetrahydropyranyl group was introduced into the 2′-oxygen prior to the N^6-tritylation. Upon the TFA-catalyzed tetrahydropyranylation of **5**, the 2′-tetrahydropyranylated adenosine derivative **9** was obtained in 74% yield. Tritylation of **9** followed by desilylation of **7b** gave **8b** as pure material in 77% yield. Furthermore, the total yield of **8b** from **5** was improved from 57% to 80%, when all the reactions (**5**–**9**–**7b**–**8b**) were in situ carried out without chromatographic separation and the tritylation was carried out at 0 °C.

An internal synthetic unit **11** of adenosine was prepared as follows. The 5′-dimethoxytritylation of **8b** gave a 5′-*O*-tritylated product **10** in 66% yield.

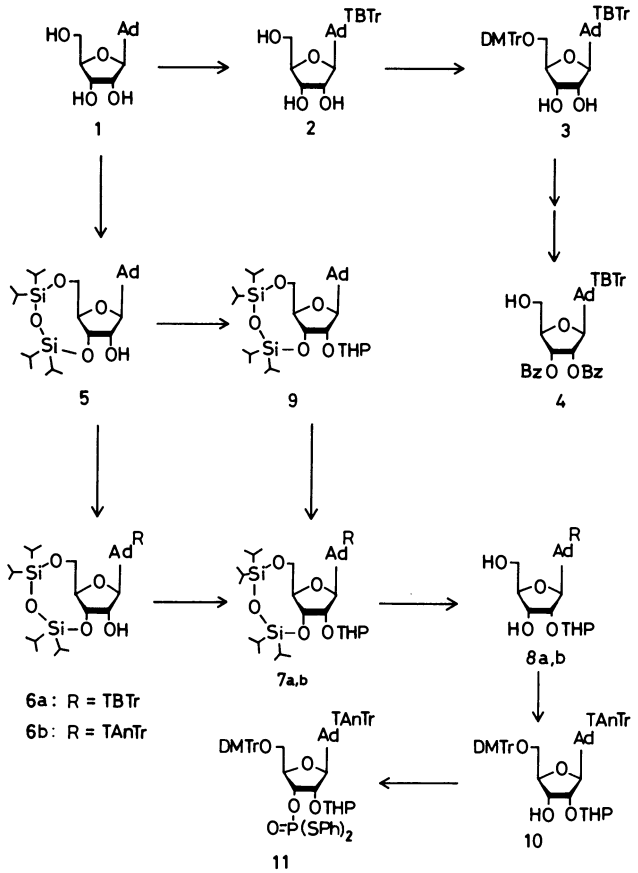

Scheme 1.

Treatment of **10** with cyclohexylammonium *S,S*-diphenyl phosphorodithioate (PPS)[10] in the presence of mesitylenedisulfonyl dichloride (MDS)[11] and tetrazole (Tet)[2f] gave the adenosine unit **11** in 85% yield.

For the synthesis of fully protected oligoribonucleotide blocks, 5′-hydroxyl and 3′-phosphodiester components **14**—**16** were prepared from the uridine and guanosine monomer units **12** and **13** by the literature method.[2d]

Next, to demonstrate the synthetic utility of **4** in oligoribonucleotide synthesis in the phosphorothioester approach[12] using *S,S*-diphenyl ribonucleoside 3′-phosphorodithioates, a fully protected UpA dimer **17** was synthesized by condensation of **4** with the phosphodiester unit **15** of uridine. A combined reagent of isodurenedisulfonyl dichloride (DDS)[11b] and 3-nitro-1,2,4-triazole (NT)[13] was employed as the condensing agent. Consequently, the dimer **17** was obtained in 88% yield. The dimer **17** could be detected as a distinct spot on TLC by spraying 10% H_2SO_4 followed by heating or by spraying dilute NaOH solution (be careful) owing to the dye character of the TBTr group. The purification was facilitated by its great lipophilicity. Treatment of **17** with TFA at 0°C for 33 min gave the 5′-hydroxyl component **18** in 82% yield. In a similar manner, a fully protected trimer **19** of GUA was obtained in 63% yield by condensation of **18** with the diester unit **16** of guanosine. In order to obtain a 5′-phosphorylated trimer **21** of pGUA, **19** was treated with TFA in CH_2Cl_2 to give the 5′-hydroxy derivative **20** in 82% yield, which was in turn phosphorylated with PSS-DDS-Tet. The fully protected pGUA (**21**) was synthesized in 88% yield.

A fully protected RNA fragment **23** of pGUAUUA was also synthesized according to the synthetic strategy as depicted in Scheme 4. The details of fragment condensation to construct this protected hexamer are shown in Table 1.

With the help of liphophilicity of the TBTr and TAnTr groups, these synthetic intermediates (fragments **1**—**6**) could be easily isolated in high yields without adsorption on silica gel. These tris(acyloxy)-trityl groups were apparently superior to the benzoyl or MMTr group in this point. At the hexamer level, the ease of its elution from silica gel was essentially

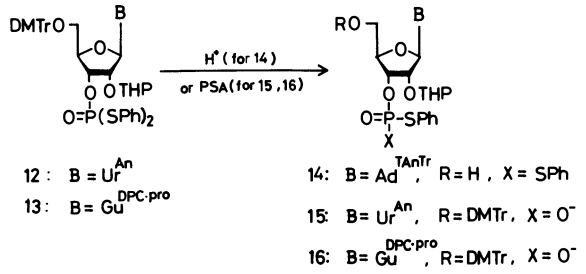

Scheme 2.

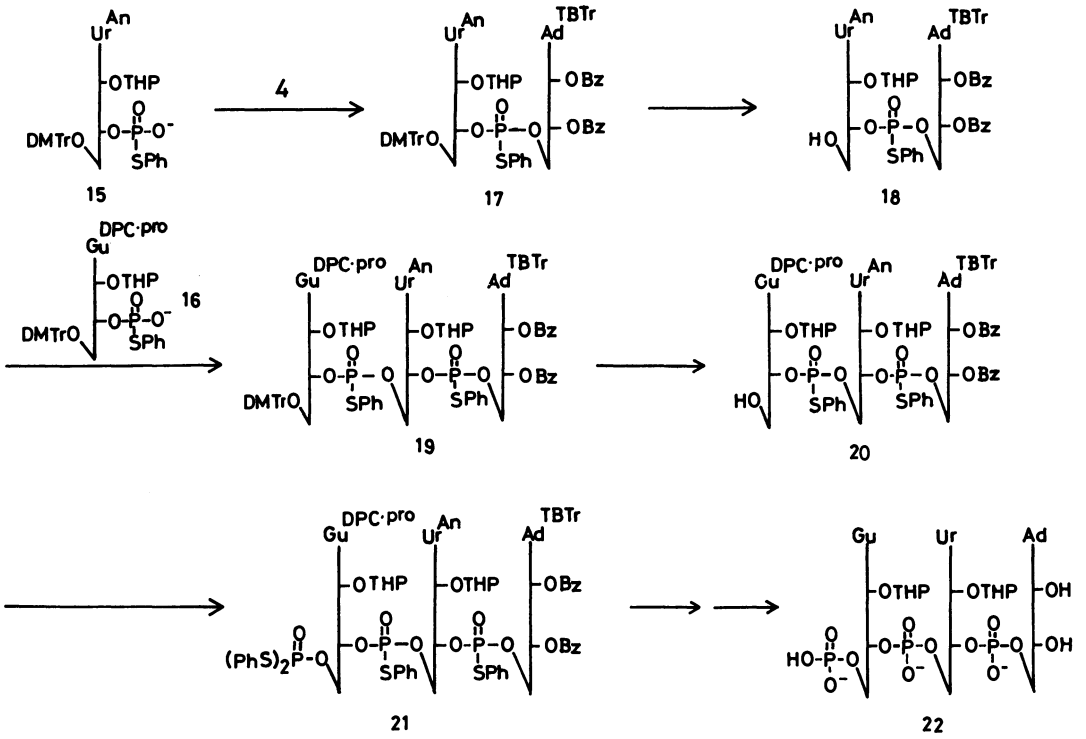

Scheme 3.

Table 1. Fragment Condensation of the Fully Protected Oligoribonucleotides **21** and **23**

Compd. No. or Frag. No.	Removal of 3′-terminal phenylthio group (40°C)			
	3′-Phosphodiester (equiv)	2 M H_3PO_2/Py	Et_3N	Time
		equiv	equiv	h
17 (=**F-1**)	U (1.3)	60	25	0.6
19	G (1.3)	60	25	2
21	PSS (1.5)			
F-2	U (1.3)	60	25	0.4
F-3	G (1.3)	60	25	2
F-4	U (1.3)	60	25	0.3
F-5	GUA (1.3)	60	25	0.5
F-6 (=**23**)	PSS (1.5)			

Compd. No. or Frag. No.	Detritylation (0°C)			Condensation	
	5′-Hydroxyl (mmol)	Time	Yield	Time	Yield
		min	%	min	%
17 (=**F-1**)	A^{TBTr} (0.1)	17 (2% TFA)	77	60	88
19	UA	33	82	60	63
21	GUA	15	82	50	88
F-2	A^{TAnTr} (2.2)	10	81	50	91
F-3	UA (0.74)	15	78	90	79
F-4	UA (0.35)	17	95	80	87
F-5	UUA (0.283)	40	92	60	73
F-6 (=**23**)	GUAUUA	28	90	40	84

the same as that of dimers. The steric hindrance of the TBTr and TAnTr groups did not affect the condensation as shown in Table 1. This is because the TBTr group is in the remote position from the condensation site, i.e., on the adenine moiety. Expectedly, it was also confirmed that the TBTr and TAnTr groups on the adenine moiety were sufficiently stable during acid treatment for removal of the 5′-

DMTr group from fully protected oligoribonucleotide derivatives so that the loss of the THP group was essentially negligible to give 5′-hydroxyl products in high yields.

Deprotection of 21 and 23. Treatment of **21** with silver nitrate in aqueous pyridine gave an unesterified trimer as a sole product. The product was in situ treated with concentrated aqueous ammonia to remove the TBTr group of adenosine and the other base-labile protecting groups. Subsequent chromatography on Whatman 3 MM papers gave the THP containing trimer **22** in 64% yield. It was observed that the THP group of **22** was somewhat unstable during the workup after the ammonical treatment. When a mixture containing **22** was coevaporated with water to remove pyridine used as the solvent, a considerable loss of the THP group was observed so that paper chromatography often gave additional two bands of pG(thp)UA (or pGU(thp)A) and pGUA. Therefore, the partial deprotection was done in the presence of pyridine through all the process to avoid the loss of the THP group. Compound **22** appeared as a set of four peaks at ca. 17 min in reversed-phase HPLC as shown in Fig. 1-A, since it has two THP groups. Upon treatment with 0.01 M HCl, the quartet peaks were changed to one major peak at 9.2 min, which was corresponding to pGUA as shown in Fig. 1-B. Finally, the unprotected trimer was obtained in 20% overall yield from **21**.

It should be noted that, during treatment with ammonia, color of the mixture due to rosolic acid liberated became deep as the TBTr group was eliminated. This change in color is also a good visible indicator for judgement if the other acyl-type of protecting groups such as diphenylcarbamoyl (DPC), propionyl, anisoyl, and benzoyl could be removed completely since they were eliminated under similar or milder conditions. The structure of the trimer was confirmed by enzyme assay with snake venom phosphodiesterase and nuclease P_1 as shown in

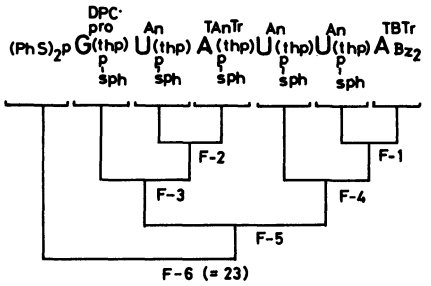

Scheme 4. The strategy for synthesis of the fully protected hexaribonucleotide (**23**).

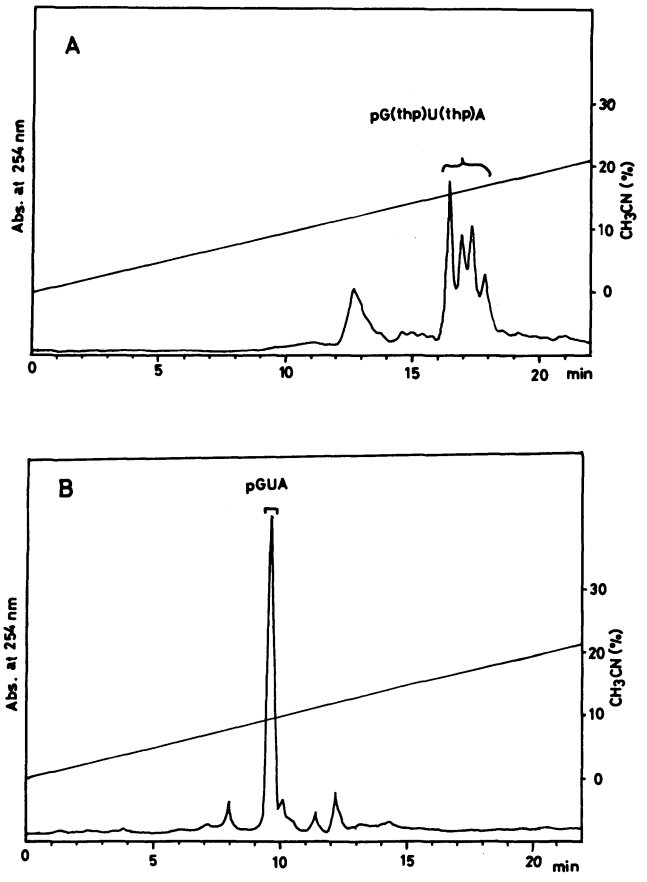

Fig. 1. A: The reverse-phase HPLC profile of pG(thp)U(thp)A (**22**) obtained by paper chromatography after partial deprotection of **21**.
B: The reverse-phase HPLC profile of crude pGUA obtained by paper chromatography after treatment of **22** with 0.01 M HCl (pH 2.0).

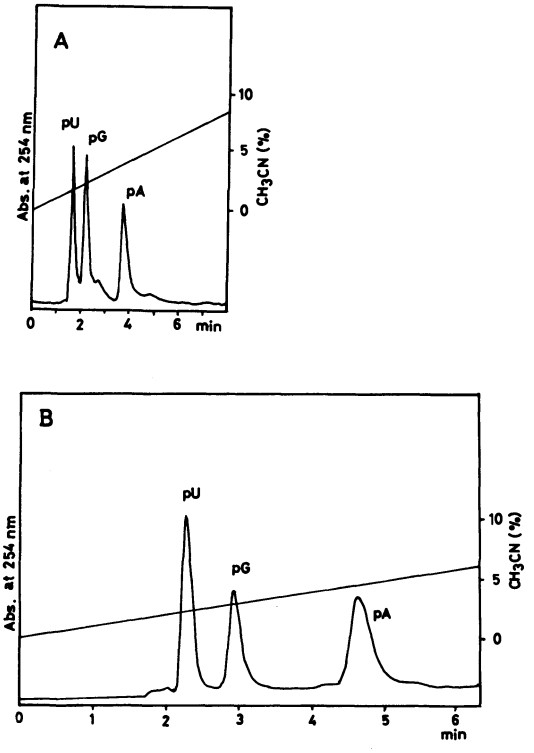

Fig. 2. The reverse-phase HPLC profile of the mixture obtained by enzyme digestion of pGUA (A) or pGUAUUA (B) with nuclease P_1.

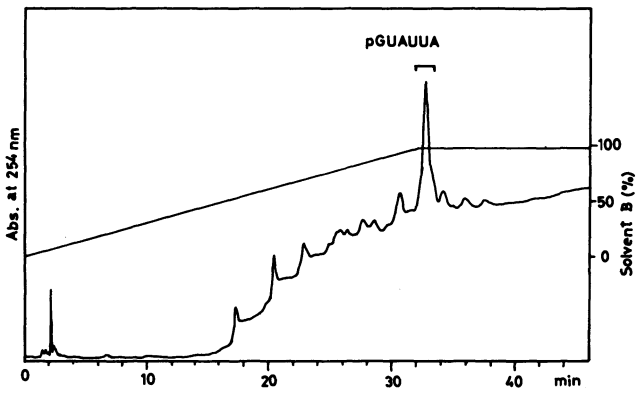

Fig. 3. The ion-exchage HPLC profile of crude pGUAUUA obtained by paper chromatography after full deprotection of **23**.

Fig. 2.

In a similar manner, pGUAUUA was obtained in 18% yield from **23** but the corresponding THP containing hexamer was not isolated and all the deprotection procedures were in situ done. In this case, the internal TAnTr group was completely removed by treatment with concentrated ammonia–pyridine (1 : 1, v/v) at room temperature for 24 h.

Purification of pGUAUUA was performed by paper chromatography followed by ion-exchange HPLC as shown in Fig. 3. The enzyme assay of the hexamer isolated is shown in Fig. 2-B.

The use of the TBTr and TAnTr groups in our approach to the synthesis of RNA fragments helped isolation of synthetic intermediates because of their great contribution to liphophilicity of the whole molecule. In addition to this merit, the choice of these protected-protecting groups also enabled us to make partially protected oligoribonucleotide derivatives which had the only THP group at each 2′-hydroxyl position of the RNA chain. Such THP containing oligoribonucleotides might be used for the synthesis of capped mRNAs if the capping reaction can be carried out in homogeneous media without protection of the exo-amino groups of A, G, and C. In this direction, we are now studying further application of partially protected oligoribonucleotides to the synthesis of capped mRNAs.

Experimental

General Remarks. ^{1}H NMR spectra were recorded at 100 MHz on a JNM-PS-100 spectrometer using ppm according to tetramethylsilane as an internal reference. UV spectra were obtained on a Hitachi 124 spectrophotometer. Column chromatography was performed with silica gel C-200 purchased from Wako Co., Ltd. Thin-layer chromatography was performed on precoated TLC plates, silica gel 60 F-254 (Merck). Reagent grade pyridine was distilled twice from *p*-toluenesulfonyl chloride and CaH_2 and then stored over Molecular Sieves 4A. Dichloromethane was dried over phosphorus pentoxide overnight, decanted, distilled from potassium carbonate and then stored over Molecular Sieves 4A.

For extraction of phosphodiester components after treatment of fully protected monomers or oligomers with phosphinic acid, two separatory funnels (A and B) were used to remove effectively the phosphinate reagent. First, the reaction mixture was diluted with dichloromethane and transferred to separatory funnel A, while CH_2Cl_2 was put in advance in separatory funnel B. The CH_2Cl_2 solution in separatory funnel A was washed with water, which was then transferred to separatory funnel B for back-extraction. After shaking, the aqueous layer was discarded from separatory funnel B. Further washing with water, 0.2 M triethylammonium hydrogencarbonate (TEAB) (×2), water (×2) was done in a similar manner when each aqueous layer was put first in separatory funnel A, transferred to separatory funnel B, and finally discarded. This extractive workup was used also for removal of excess phosphodiester components and arenedisulfonic acids after the condensation was completed but 5% sodium hydrogencarbonate was used in place of 0.2 M TEAB. The procedure was also effective for removal of DMF in the synthesis of **2**.

Ion-exchange HPLC was performed on a Partisil 10 SAX (Whatman) column using a linear gradient of 0.005 M KH_2PO_4 (pH 4.1), 20% CH_3CN to 0.5 M KH_2PO_4 (pH 4.5), 20% CH_3CN for 32 min at a flow rate of 1.5 ml ml^{-1}. Reversed-phase HPLC was performed on a μBondapak C_{18} (Waters) using a linear gradient of 0.1 M NH_4OAc to 30% CH_3CN in the same buffer for 30 min at a flow rate of 1.5 ml at 50 °C.

Elemental analysis was performed by the Microanalytical Laboratory, Tokyo Institute of Technology, at Nagatsuta.

N^6-[4,4′,4″-Tris(benzoyloxy)trityl]adenosine (2). To a solution of adenosine (2.68 g, 10 mmol) coevaporated twice with dry DMF were added 2,6-lutidine (4.86 ml, 72 mmol) and trimethylsilyl chloride (4,.56 ml, 36 mmol). After the mixture was stirred for 1 h, 2,6-lutidine (2.32 ml, 20 mmol), silver nitrate (3.40 g, 20 mmol), and TBTrBr (14.4 g, 20 mmol) were added successively to the mixture. After 1 h, 2,6-lutidine (4.17 ml, 36 mmol) and silver nitrate (6.12 g, 36 mmol) were added to complete the reaction. The mixture was stirred for 30 min, and then the resulting precipitate was removed by filtration and washed with DMF (100 ml). The filtrate and washing were combined and treated with water (32 ml). After being kept for 40 min, the solution was partitioned between dichloromethane and water for extraction, which was performed in the same manner as described in General Remarks to remove DMF completely. The organic layer was dried over sodium sulfate, filtered, and evaporated to dryness. The residue was coevaporated with six times with toluene and chromatographed on a column of silica gel (300 g) with dichloromethane–methanol. The fractions containing 2 were collected and evaporated. The residue was reprecipitated from dichloromethane into hexane to give **2** (6.41 g, 74%) as colorless powder; mp 165—170 °C; ^{1}H NMR ($CDCl_3$) δ=3.60—3.88 (2H, m, 5′-H), 4.16 (1H, m, 4′-H), 4.28 (1H, m, 3′-H), 4.82 (1H, m, 2′-H), 5.74 (d, 1H, 1′-H), 7.09 (6H, d, *J*=8 Hz, ArH), 7.46 (15H, m, ArH), 7.60 (1H, s, 2-H), 7.94 (1H, s, 8-H), 8.12 (6H, d, *J*=8 Hz).

Found: C, 68.07; H, 4.52; N, 7.62%. Calcd for $C_{50}H_{39}O_{10}N_5 \cdot H_2O$: C, 67.64; H, 4.43; N, 7.89%.

5′-*O*-(4,4′-Dimethoxytrityl)-N^6-[4,4′,4″-tris(benzoyloxy)trityl]adenosine (3). To a solution of **2** (5.90 g, 6.79 mmol), coevaporated several times with dry pyridine, in dry pyridine (19.5 ml) was added 4,4′-dimethoxytrityl chloride (2.64 g, 7.8 mmol). After being kept for 9 h, the mixture was quenched by addition of ice. The usual workup involving extraction with dichloromethane and coevaporation with toluene followed by silica-gel column chromatography (eluent: dichloromethane–methanol) gave **3**. The compound was reprecipitated from its dichloromethane solution into hexane gave pure **3** (7.45 g, 94%); mp 143.5—147 °C; ^{1}H NMR ($CDCl_3$) δ=3.72 (3H, s, OCH_3), 3.76 (3H, s, OCH_3), 4.22—4.34 (2H, m, 5′-H), 4.36 (1H, m, 4′-H), 4.64—5.00 (2H, m, 2′-H and 3′-H), 5.84 (1H, m, 1′-H), 6.77 (4H, m, ArH), 7.12 (9H, m, ArH), 7.45 (15H, m, ArH), 7.70 (s, 1H, 2-H), 8.00 (1H, s, 8-H), 8.14 (6H, d, J=8 Hz, ArH).

Found. C, 72.65; H, 5.20; N, 5.56%. Calcd for $C_{71}H_{57}O_{14}N_5 \cdot 1/2H_2O$: C, 72.19; H, 4.95; N, 5.93%.

2′,3′-*O*-Dibenzoyl-N^6-[4,4′,4″-tris(benzoyloxy)trityl]adenosine (4). Compound **3** (2.35 g, 2 mmol) was coevaporated three times with dry pyridine and finally dissolved in dry pyridine (20 ml). Benzoyl chloride (6.96 μl, 6 mmol) was added to the solution. After the mixture was stirred for 1 h, benzoyl chloride (232 μl, 2 mmol) was added. The mixture was stirred for an additional 1 h. The usual workup followed by chromatography gave the dibenzoylated product (2.96 g, quant.) as foam. This material was treated with 2% trifluoroacetic acid in dichloromethane (200 ml) at 0 °C for 17 min. After the reaction was quenched by addition of 5% sodium hydrogencarbonate (200 ml), the organic phase was collected, washed with 5% sodium hydrogencarbonate, dried over sodium sulfate, and filtered. The filtrate was evaporated and the last traces of pyridine were removed by repeated coevaporation with toluene. The residue was chromatographed on a column of silica gel with dichloromethane–methanol to give **4**. This material was reprecipitated from its dichloromethane solution into hexane to give **4** (1.65 g, 77%); mp 146.5 °C; ^{1}H NMR ($CDCl_3$) δ=4.01 (3H, m, 4′-H and 5′-H), 4.57 (1H, m, 3′-H), 6.04 (1H, m, 2′-H), 6.27 (1H, m, 1′-H), 7.12 (6H, m, ArH), 7.48 (21H, m, ArH), 7.80 (1H, s, 2-H), 7.91 (4H, m, ArH), 8.02 (1H, s, 8-H), 8.16 (6H, m, ArH).

Found: C, 70.40; H, 4.39; N, 6.31%. Calcd for $C_{64}H_{47}O_{12}N_5 \cdot H_2O$: C, 70.13; H, 4.51; N, 6.39%.

3′,5′-*O*-(1,1,3,3-Tetraisopropyldisiloxane-1,3-diyl)-N^6-[4,4′,4″-tris(benzoyloxy)trityl]adenosine (6a). Compound **5**[9] (1.02 g, 2 mmol) was rendered anhydrous by repeated coevaporation with dry DMF and dissolved finally in dry DMF (20 ml). To the solution were added successively 2,6-lutidine (463 μl, 4 mmol), silver nitrate (683 mg, 4 mmol), and TBTrBr (2.89 g, 4 mmol). After being stirred at room temperature for 25 min, the mixture was quenched with water. The resulting precipitate was removed by filtration and the filtrate was transferred to a separatory funnel. The extractive workup was done to remove DMF as described in General Marks. The combined dichloromethane layer was dried over sodium sulfate, filtered, and evaporated in vacuo. The resulting residue was chromatographed on a column of silica gel with dichloromethane–methanol. The product thus obtained was reprecipitated from dichloromethane into hexane to give a pure material (1.51 g, 68%); ^{1}H NMR ($CDCl_3$) δ=1.04 (28H, m, $C(CH_3)_2$), 3.36 (br, 1H, 2′-OH), 4.05 (3H, m, 4′- and 5′-H), 4.58 (1H, m, 3′-H), 5.08 (1H, m, 2′-H), 5.89 (1H, m, 1′-H), 6.96 (1H, s, NH), 7.14 (6H, m, ArH), 7.48 (15H, m, ArH), 7.96 (1H, s, 2-H), 8.00 (1H, s, 8-H), 8.20 (6H, m, ArH).

Found: C, 66.37; H, 5.81; N, 6.09%. Calcd for $C_{62}H_{65}O_{11}N_5Si_2 \cdot 1/2H_2O$: C, 66.41; H, 5.93; N, 6.25%.

3′,5′-*O*-(1,1,3,3-Tetraisopropyldisiloxane-1,3-diyl)-N^6-[4,4′,4″-tris(*p*-anisoyloxy)trityl]adenosine (6b). The same procedure as described in the case of **6a** was performed except for the reaction time (6 h). The yield was 54%; ^{1}H NMR ($CDCl_3$) δ=1.09 (24H, m, $C(CH_3)_2$), 1.59 (4H, m, SiCH), 3.21 (2H, m, 5′-H), 3.92 (s, 6H, OCH_3), 4.12 (1H, m, 4′-H), 4.68 (1H, m, 3′-H), 5.20 (1H, m, 2′-H), 5.94 (1H, m, 1′-H), 7.09 (6H, d, J=8.8 Hz, ArH), 7.22 (6H, d, J=8.8 Hz, ArH), 7.50 (6H, d, J=8.8 Hz, ArH), 7.92 (1H, s, 2-H), 8.04 (1H, s, 8-H), 8.20 (6H, d, J=8.8 Hz, ArH).

Found: C, 64.82; H, 5.96; N, 5.73%. Calcd for $C_{65}H_{71}O_{14}N_5Si_2$: C, 64.93; H, 5.95; N, 5.82%.

2′-*O*-(Tetrahydro-2-pyranyl)-3′,5′-*O*-(1,1,3,3-tetraisopropyldisiloxane-1,3-diyl)-N^6-[4,4′,4″-tris(benzoyloxy)trityl]adenosine (7a). To a solution of **6a** (1.17 g, 1.05 mmol) in dry dichloromethane (4.5 ml) were added Molecular Sieves 4A (1 g), 3,5-dihydro-2*H*-pyran (2.30 ml, 22.5 mmol), and trifluoroacetic acid (174 μl, 2.26 mmol). After the mixture was stirred at room temperature for 5 h, pyridine (0.5 ml) was added. The Molecular Sieves were removed by filtration and the filtrate was evaporated in vacuo. The residue was partitioned with dichloromethane and water. The organic phase was collected, dried over sodium sulfate, filtered, and evaporated to dryness. The residue was chromatographed on a silica-gel column with dichloromethane–methanol to give **7a** as foam (1.21 g, 96%); ^{1}H NMR ($CDCl_3$) δ=1.07 (24H, m, $C(CH_3)_2$), 1.56 (6H, m, THP), 1.72 (4H, m, SiCH), 3.46 (2H, m, THP), 4.18 (3H, m, 4′-H and 5′-H), 4.70 (1H, m, 3′-H), 5.00 (1H, m, 2′-H), 5.23 (1H, m, THP), 6.00 (1H, m, 1′-H), 6.93 (1H, s, NH), 7.22 (6H, m, ArH), 7.54 (15H, m, ArH), 7.95 (1H, s, 2-H), 8.04 (1H, s, 8-H), 8.20 (6H, m, ArH).

Found: C, 66.61; H, 6.12; N, 5.45%. Calcd for $C_{67}H_{73}O_{12}N_5Si_2 \cdot 1/2H_2O$: C, 66.75; H, 6.19; N, 5.81%.

2′-*O*-(Tetrahydro-2-pyranyl)-3′,5′-*O*-(1,1,3,3-tetraisopropyldisiloxane-1,3-diyl)-N^6-[4,4′,4″-tris(*p*-anisoyloxy)trityl]adenosine (7b). This compound was prepared in the same way described in the case of **7a** starting from **6b** (536 mg, 0.45 mmol) except for the reaction time (26 h). The yield was 581 mg (100%); ^{1}H NMR ($CDCl_3$) δ=1.08 (24H, m, $C(CH_3)_2$), 1.56 (6H, m, THP), 1.82 (1H, m, SiCH), 3.48 (2H, m, THP), 3.90 (9H, s, OCH_3), 4.16 (3H, m, 4′-H and 5′-H), 4.52—4.83 (2H, m, 2′-H and 3′-H), 5.24 (1H, m, THP), 6.01 (1H, m, 1′-H), 6.98 (6H, d, J=8.4 Hz, ArH), 7.14 (d, J=9 Hz), 7.48 (6H, d, J=8.4 Hz, ArH), 7.97 (1H, s, 2-H), 8.07 (1H, s, 8-H), 8.16 (6H, d, J=9 Hz, ArH).

Found: C, 65.98; H, 7.05; N, 3.92%. Calcd for $C_{70}H_{89}O_{15}N_5Si_2 \cdot 1/2H_2O$: C, 64.89; H, 7.00; N, 5.40%.

2′-*O*-(Tetrahydro-2-pyranyl)-N^6-[4,4′,4″-tris(benzoyloxy)trityl]adenosine (8a). To a solution of **7a** (506 mg, 423 μmol) in acetonitrile (2.2 ml) were added potassium fluoride (155 mg, 2.67 mmol), tetraethylammonium bromide (565 mg, 2.69 mmol), and water (48.2 μl, 2.67 mmol). The mixture was stirred at 50 °C for 3 h and then the precipitate was removed by filtration. The filtrate was evaporated and the residue was partitioned with dichloromethane and water. The organic phase was collected, dried

over sodium sulfate, filtered, and evaporated in vacuo to dryness. The residue was chromatographed on a column of silica gel with dichloromethane–methanol to give **8a**. Reprecipitation from dichloromethane into hexane gave a pure material (124 mg, 29%); ^{1}H NMR ($CDCl_3$) δ=1.60 (8H, m, THP), 3.40 (2H, m, THP), 3.82 (2H, m, 5′-H), 4.44 (2H, m, 3′-H and 4′-H), 4.88 (1H, m, 2′-H), 4.90 (1H, m, THP), 5.96 (1H, m, 1′-H), 7.22 (6H, m, ArH), 7.54 (15H, m, ArH), 7.87 (1H, s, 2-H), 8.10 (1H, s, 8-H), 8.22 (6H, d, J=8 Hz, ArH).

Found: C, 67.47; H, 5.06; N, 6.67%. Calcd for $C_{55}H_{47}O_{11}N_5 \cdot 1.5H_2O$: C, 67.34; H, 5.14; N, 7.14%.

Tris[4-(*p*-anisoyloxy)phenyl]methanol (TAnTrOH). To a solution of rosolic acid (14.5 g, 50 mmol) in dry pyridine (200 ml) was added *p*-anisoyl chloride (42.7 g, 250 mmol). The mixture was heated at 80—90 °C for 1.5 h. After being cooled to room temperature, the mixture was quenched with ice-water and extracted with CH_2Cl_2. The organic phase was washed several times with 5% $NaHCO_3$, dried over sodium sulfate, filtered, and evaporated under reduced pressure to a gum. The gummy residue was coevaporated several times with toluene to remove the last traces of pyridine. The solid material was recrystalized from benzene to give TAnTrOH (15.3 g, 44%); mp 175.5—176.5 °C; ^{1}H NMR ($CDCl_3$) δ=3.05 (1H, s, OH), 3.86 (9H, s, OCH_3), 6.88—7.38 (18H, m, ArH), 8.05 (3H, s, ArH), 8.13 (3H, s, ArH).

Found: C, 73.41; H, 4.86%. Calcd for $C_{43}H_{34}O_{10}$: C, 72.67; H, 4.82%.

4,4′,4″-Tris(*p*-anisoyloxy)trityl Bromide (TAnTrBr). To a suspension of TAnTrOH (4 g, 5.6 mmol) in dry benzene (10 ml) was added acetyl bromide (1 ml, 13.5 mmol). The mixture was refluxed for 1.5 h and the hot solution was filtered to remove a small amount of insoluble material. Dry hexane was added portionwise to the hot filtrate. After cooling, the resulting precipitate was collected by filtration and washed with dry hexane–benzene (2:1, v/v) and then with dry hexane to give TAnTrBr (3.9 g, 90%): mp 96—97 °C; ^{1}H NMR ($CDCl_3$) δ=3.88 (9H, s, OCH_3), 6.90—7.39 (18H, m, ArH), 8.02 (3H, s, ArH), 8.13 (3H, s, ArH).

Found: C, 66.59; H, 4.34; Br, 10.57%. Calcd for $C_{43}H_{33}O_9Br$: C, 66.76; H, 4.30; Br, 10.33%.

2′-*O*-(Tetrahydro-2-pyranyl)-*N*^{6}-[4,4′,4″-tris(*p*-anisoyloxy)trityl]adenosine (8b). This compound was synthesized in the same way as described in the above experiment except for the reaction time (1 h). The yield was 56%; ^{1}H NMR ($CDCl_3$) δ=1.52 (6H, m, THP), 3.90 (9H, s, OCH_3), 4.25—4.64 (4H, m, 3′,4′, and 5-H), 4.90 (1H, m, 2′-H), 5.10 (1H, m, THP), 5.92 (1H, m, 1′-H), 6.98 (6H, d, J=9 Hz, ArH), 7.16 (6H, d, J=9 Hz, ArH), 7.48 (6H, d, J=9 Hz, ArH), 7.83 (1H, s, 2-H), 8.08 (1H, s, 8-H), 8.16 (6H, d, J=9 Hz).

Found: C, 66.59; H, 5.33; N, 6.56%. Calcd for $C_{58}H_{53}O_{16}N_5$: C, 66.72; H, 5.12; N, 6.71%.

Synthesis of 8b from 5 without Purification of the Synthetic Intermediates 7b and 9. To a solution of **5**[9] (5.61 g, 11 mmol) in dry dichloromethane (110 ml) were added 3,4-dihydro-2*H*-pyran (22.5 ml, 220 mmol) and trifluoroacetic acid (1.7 ml, 22 mmol). The mixture was stirred at room temperature for 17 h. Then, additional trifluoroacetic acid (0.85 ml, 11 mmol) was added and the mixture was further stirred for 4 h. Five per cent sodium hydrogencarbonate (100 ml) was added to the mixture and the solution was extracted with dichloromethane (100 ml). The organic phase was collected, dried over sodium sulfate, filtered, and evaporated in vacuo to dryness. The residue was coevaporated several times successively with ethanol and dry DMF, and finally dissolved in dry DMF (110 ml). To the solution were added 2,6-lutidine (2.55 ml, 22 mmol), silver nitrate (3.74 g, 22 mmol), and TAnTrBr (17 g, 22 mmol) with vigorous stirring at 0 °C. The precipitate was removed by filtration and washed with dichloromethane. The filtrate and washing were combined and washed with water to remove DMF in a manner similar to that described in General Remarks. The dichloromethane layer was dried over sodium sulfate, filtered, and evaporated in vacuo to dryness. The residue was coevaporated several times with toluene and dissolved in acetonitrile (55 ml). To the solution were added potassium fluoride (3.83 g, 66 mmol), tetraethylammonium bromide (13.9 g, 66 mmol), and water (1.19 ml). The mixture was stirred at 50 °C for 1 h. The precipitate was removed by filtration. The filtrate was transferred to a separatory funnel and diluted with water. Extraction was performed with dichloromethane, in a manner similar to that described for extractive removal of DMF in General Remarks, to remove the quarternary ammonium salt. The dichloromethane phase was dried over sodium sulfate, filtered, and evaporated in vacuo to dryness. The usual workup followed by chromatography on silica gel with dichloromethane–methanol and reprecipitation gave **8b** (9.24 g, 80%).

***S,S*-Diphenyl 2′-*O*-(Tetrahydro-2-pyranyl)-5′-*O*-(4,4′-dimethoxytrityl)-*N*^{6}-[4,4′,4″-tris(*p*-anisoyloxy)trityl]adenosine 3′-Phosphorodithioate (11).** Compound **8b** (7.76 g, 7.43 mmol) was rendered anhydrous by repeated coevaporation with dry pyridine and finally dissolved in dry pyridine (22 ml). To the solution was added 4,4′-dimethoxytrityl chloride (3.03 g, 8.92 mmol). The mixture was stirred at room temperature for 1.5 h. After the usual extractive workup, chromatography on a column of silica gel with dichloromethane–methanol gave **10** (6.60 g, 66%). This compound was used in the next reaction without further characterization. Compound **10** (6.60 g, 4.9 mmol) was mixed with cyclohexylammonium *S,S*-diphenyl phosphorodithioate (2.80 g, 7.35 mmol) and 1-*H*-tetrazole (1.37 g, 19.6 mmol), and the mixture was coevaporated several times with dry pyridine and finally dissolved in dry pyridine (30 ml). To the mixture was added MDS (3.11 g, 9.8 mmol). After being stirred at room temperature for 1 h, the mixture was quenched by diluted with dichloromethane (100 ml). The solution was washed with water and 5% sodium hydrogencarbonate as described in General Remarks. The usual workup followed by chromatography (silica gel, eluent: dichloromethane–methanol) and reprecipitation from dichloromethane into hexane gave **11** (6.66 g, 85%); ^{1}H NMR ($CDCl_3$) δ=8.11 (6H, d, J=8 Hz, ArH), 8.01 (1H, s, 8-H), 7.80 (1H, s, 2-H), 6.72—7.68 (41H, m, ArH, 2H), 5.77 (d, 1H, 1′-H), 5.07—5.28 (2H, m, 2′-H and THP), 4.56 (1H, m, 3′-H), 4.18 (1H, m, 4′-H), 3.85 (9H, s, OCH_3 of TArTr), 3.75 (6H, s, OCH_3 of DMTr), 3.72 (2H, m, 5′-H), 2.85 (2H, m, THP), 1.24—1.80 (6H, m, THP).

Found: C, 69.48; H, 6.56; N, 3.88; S, 3.78%. Calcd for $C_{91}H_{80}O_{17}N_5S_2P \cdot 2.5C_6H_{14}$: C, 69.72; H, 6.35; N, 3.84; S, 3.51%.

General Procedure for Fragment Condensation. Preparation of Phosphodiester Components: An appropriately

protected monomer unit or oligomer block was rendered anhydrous by repeated coevaporation with dry pyridine and dissolved in a solution of 2 M phosphinic acid (60 equiv) in pyridine containing triethylamine as shown in Table 1. After the reaction was completed, 0.2 M TEAB was added and extracted with dichloromethane. The excess phosphinate reagent was removed by the extractive workup as described in General Remarks. In this case, washing was performed with water (×2) and 0.2 M TEAB (×2). The organic phase was dried over sodium sulfate, filtered, and evaporated in vacuo to dryness. The residue containing a mixture of the phosphodiester component and benzenethiol was used in the successive condensation without further purification.

Preparation of Hydroxyl Components: A fully protected monomer or oligomer block was dissolved in 0.5% or 0.75% (v/v) trifluoroacetic acid in dichloromethane at 0 °C. After the reaction was completed, 5% sodium hydrogencarbonate was added for neutralization. The solution was extracted with dichloromethane. The organic phase was dried over sodium sulfate, filtered, evaporated, and chromatographed on a column of silica gel for isolation of the hydroxyl component. The details of the results are listed in Table 1.

Fragment Condensation: The hydroxyl component obtained by the above procedure was mixed with the diester component and 3-nitro-1,2,4-triazole, and the mixture was rendered anhydrous by repeated coevaporation with dry pyridine and finally dissolved in dry pyridine (10 ml mmol^{-1} of hydroxyl component). DDS was added to the solution and stirring was continued until the hydroxyl component had disappeared. Then, extractive workup was performed with dichloromethane as described in General Remarks. Washing was performed each twice with water, 5% sodium hydrogencarbonate, and water. After the usual workup chromatographic separation (silica gel, eluent:dichloromethane–methanol) gave an condensation product as summarized in Table 1.

Deprotection of the Fully Protected Trimer 21. To a solution of the trimer **21** (232 mg, 0.088 mmol) in pyridine (2.25 ml) were added successively water (2.25 ml) and silver acetate (2.20 g, 13.2 mmol). The mixture was stirred vigorously at 50 °C for 5 h. After cooling to room temperature, the solution was diluted with pyridine–water (2:1, v/v, 45 ml) and treated with hydrogen sulfide gas at 0 °C for 15 min. The excess gas was removed under reduced pressure by an aspirator for 30 min. The resulting precipitate was removed by centrifugation. The supernatant was collected and passed through Dowex 50 W×2 (pyridinium form, 5 ml). The resin was washed with pyridine–water (2:1, v/v, 50 ml). The eluant and washings were combined and evaporated in vacuo after addition of pyridine (70 ml). The residue was coevaporated with pyridine (5×20 ml) to remove the last traces of acetic acid and then in dissolved pyridine (5 ml). The solution was mixed with concentrated aqueous ammonia (45 ml). The mixture was warmed at 50 °C for 5 h. After cooling, pyridine (20 ml) was added and the solution was evaporated under reduced pressure to its half volume. The concentrated solution was extracted with CH_2Cl_2 (5×20 ml). Each organic layer was washed with the same aqueous solution put in another separatory funnel. The two aqueous layers were combined and three hold of pyridine was added. The solution was evaporated in vacuo, the residue being coevaporated three times with pyridine and chromatographed on Whatman 3 MM papers with 2-propanol–concentrated aqueous ammonia–water (6:1:3, v/v/v). A broad band which moved around AMP was eluted with water to give pG(thp)pU(thp)pA (1752 OD at 260 nm, 64%). This compound was stored as its pyridine solution (5.6 μmol ml^{-1}). An aliquot of this solution (5.0 μmol) was taken and evaporated under reduced pressure. The residue was coevaporated with MeOH–toluene (1:1, v/v, 3×5 ml) and treated with 0.01 M HCl in dioxane–water which was finally adjusted to pH 2.0 by addition of 0.1 M HCl. After being stirred for 16 h, the solution was neutralized with concentrated aqueous ammonia and concentrated under reduced pressure to half the volume. The concentrate was partitioned between ether and water. The aqueous layer was collected and washed twice with ether. The aqueous solution was concentrated and applied to a column of Sephadex A-25 (triethylammonium salt, 1 ml). The column was first washed with water (50 ml) and eluted with 1 M TEAB buffer (50 ml). Fractions containing UV were combined, concentrated under reduced pressure, and the residue was covaporated several times with water to give pGUA (153 OD at 260 nm, 4.95 μmol, 98%). This compound (20 OD) was finally purified by reversed-phase HPLC (Fig. 1-B). The peak eluted at 9.2 min was collected and evaporated under reduced pressure. The residue was dissolved in water so as to adjust the concentration of ammonium acetate to less than 0.05 M and applied to a column of Sephadex A-25, 2 ml). After washing with water (100 ml), the trimer was eluted with 1 M TEAB buffer. The eluant was concentrated under reduced pressure and coevaporated repeatedly with water to give pGUA (6.4 OD at 260 nm, 0.207 μmol, 32%): UV: λ_{max}=257 nm, λ_{min}=234 nm.

Enzymatic Assay of pGUA. The trimer (1.0 OD) was incubated with shake venom phosphodiesterase (1 mg ml^{-1}, 10 μl) in 0.05 Tris–HCl buffer (pH 8.0, 50 μl) containing 1 M $MgCl_2$ (2.5 μl) at 37 °C for 3 h. The mixture was analyzed by reversed-phase HPLC, which showed three peaks of pU, pG, and pA in a ratio of 1.1:1.0:0.9.

The trimer (1.0 OD) was incubated with nuclease P_1 (2 mg ml^{-1}, 15 μl) in 0.05 M sodium acetate buffer (pH 5.4, 35 μl) at 37 °C for 30 min. A similar HPLC analysis gave a mixture of pU, pG, and pA in a ratio of 1.1:1.0:0.8.

Deprotection of the Fully Protected Hexamer 23. The fully protected hexamer **23** (25.9 mg, 5 μmol) was dissolved in pyridine (450 μl), and water (150 μl) and silver acetate (251 mg, 1.5 mmol) were successively added. The resulting mixture was vigorously stirred at 50 °C for 5 h and bubbled with hydrogen sulfide gas at 0 °C until a clear supernatant had been obtained (ca. 15 min). The excess gas was removed under reduced pressure by an aspirator. The precipitate was removed by centrifugation and the supernatant was passed through a column of Dowex 50 W×2 (Py form, 3 ml). The resin was eluted with pyridine–water (2:1, v/v, 20 ml). The eluant was evaporated under reduced pressure and coevaporated several times with pyridine to remove the last traces of acetic acid. The residue was dissolved in pyridine (25 ml) and concentrated aqueous ammonia (25 ml) was added. The mixture was stirred at room temperature for 24 h. The precipitate was removed by filtration and washed with pyridine (20 ml). The filtrate and washing were com-

bined, evaporated under reduced pressure, and coevaporated with water–dioxane (1:2, v/v, 10 ml). The residue was treated with 0.01 M HCl in water–dioxane (1:1, v/v, 10 ml) which was adjusted to pH 2.0 by addition of 0.1 M HCl. The mixture was stirred at room temperature for 1 day and then neutralized by addition of 1 M aqueous ammonia. After being evaporated under reduced pressure, the mixture was chromatographed on Whatman 3 MM papers with 2-propanol-concentrated aqueous ammonia–water (55:10:35, v/v/v) to give crude material of pGUAUUA (178 OD at 260 nm, 59%). This crude material (30 OD) was purified by anion-exchange HPLC as described in the case of the synthesis of pGUA to give pure hexamer (5.5 OD at 260 nm, 18.3%); λ_{max}=257 nm, λ_{min}=232 nm.

Enzymatic Assay of pGUAUUA. The hexaribonucleotide (0.2 OD) was incubated with nuclease P_1 (2 mg ml^{-1}, 6 μl) in 0.05 M sodium acetate (pH 5.4, 14 μl) at 37 °C for 80 min. The HPLC analysis showed a mixture of pU, pG, and pA in a ratio of 3.0:1.3:2.2.

We wish to thank The Ministry of Education, Science and Culture for its generous support (Grant-in-Aid for Scientific Research, 61470031) of our programs and also Mrs. Chieko Sugimura for preparation of this manuscript.

References

1) C. B. Reese, *Tetrahedron*, **34**, 3143 (1978).

2) a) T. Hata, N. Gokita, N. Sakairi, K. Yamaguchi, and Y. Ishido, *Bull. Chem. Soc. Jpn.*, **55**, 2949 (1982); b) K. Yamaguchi, I. Nakagawa, M. Sekine, T. Hata, K. Shimotohno, and K. Miura, *Nucleic Acid Res.*, **12**, 2939 (1984); c) S. Honda, K. Urakami, K. Koura, K. Terada, Y. Sato, K. Kohno, M. Sekine, and T. Hata, *Tetrahedron*, **40**, 153 (1983); d) T. Kamimura, K. Urakami, K. Koura, M. Sekine, K. Shinozaki, K. Miura, and T. Hata, *J. Am. Chem. Soc.*, **106**, 4552 (1984); e) M. Sekine, S. Nishiyama, T. Kamimura, Y. Osaki, and T. Hata, *Bull. Chem. Soc. Jpn.*, **58**, 850 (1985).; f) M. Sekine and T. Hata, *J. Am. Chem. Soc.*, **108**, 4581 (1986).

3) K. Yamaguchi, S. Hidaka, and K. Miura, *Proc. Natl. Acad. Sci. U.S.A.*, **79**, 1012 (1982).

4) M. Kozak, *Microbiol. Rev.*, **47**, 1 (1983).

5) R. Kierzek, H. Ito, R. Blatt, and K. Itakura, *Tetrahedron Lett.*, **22**, 376 (1981).

6) M. Sekine, N. Masuda, and T. Hata, *Tetrahedron*, **41**, 5445 (1985).

7) M. Sekine and T. Hata, *J. Org. Chem.*, **48**, 3011 (1983).

8) R. Dasgupta, D. S. Shih, C. Saris, and P. Kaesberg, *Nature (London)*, **256**, 624 (1975).

9) W. T. Markiewicz, *J. Chem. Res. (S)*, **1979**, 24.

10) a) M. Sekine, K. Hamaoki, and T. Hata, *J. Org. Chem.*, **44**, 2325 (1979); b) *idem*, *Bull. Chem. Soc. Jpn.*, **54**, 3815 (1981); c) T. Hata, K. Yamaguchi, S. Honda, and I. Nakagawa, *Chem. Lett.*, **1978**, 507.

11) a) M. Sekine, J. Matsuzaki, and T. Hata, *Tetrahedron Lett.*, **22**, 3209 (1981); b) *idem.*, *Tetrahedron*, **41**, 5279 (1985).

12) For a comprehensive review see M. Sekine and T. Hata, *Youki Gosei Kagaku Kyokai Shi*, **44**, 229 (1986).

13) C. B. Reese, R. C. Titmas, and L. Yau, *Tetrahedron Lett.*, **1978**, 2727.

Synthesis and Properties of Novel Analogs of Viologen[1)]

Toshihide KAWASHIMA,* Yutaka SHIOMI, Yasuo TOHDA, Masahiro ARIGA,
Yutaka MORI, Yoshiteru SAKATA,† and Soichi MISUMI†
Department of Chemistry, Osaka Kyoiku University, Minamikawahori-cho, Tennoji-ku, Osaka 543
†The Institute of Scientific and Industrial Research, Osaka University,
Mihogaoka, Ibaraki 567
(Received October 20, 1987)

Several viologen analogs having good coplanarity were synthesized and their redox potentials were measured by cyclic voltammetry.

A viologen has attracted much attention in various fields as it shows two reversible one-electron reductions with very ease.[2)] Recently we reported synthesis and some properties of analog **4** of methylviologen(MV^{2+}), expecting that the increased resonance in the bipyridyl system may lower the redox potential.[3)] The present paper describes the syntheses of novel analogs of viologen **4**—**11** in detail and their electronic properties.

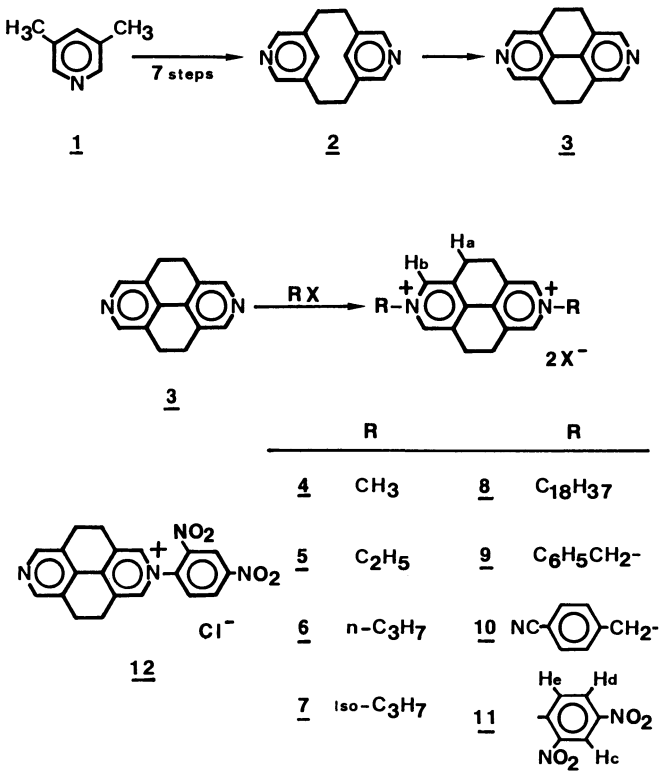

Scheme 1.

Results and Discussion

As described previously,[3)] [2.2](3,5)pyridinophane (**2**) was chosen as a starting material for our purpose. The compound **2** was prepared from the corresponding cyclic disulfone by pyrolytic procedure as reported.[4)] Pyridinophane **2** was converted into 4,5,9,10-tetrahydro-2,7-diazapyrene (**3**), a key intermediate for the following synthesis, by a transannular reaction. It is well-known that [2.2]metacyclophane is subject to the transannular reaction by treatment with various reagents, e.g. electrophiles, radical species, etc. to give tetrahydropyrene derivative.[5)] Pyridinophane **2**, on the other hand, was treated with these reagents but it produces none of the desired compound **3**. After various examinations, a modified transannular reaction with acetic anhydride, zinc dust, and $FeCl_3$ catalyst[6)] gave **3** in 53% yield, that corresponds to 2.1% in over-all yield from 3,5-lutidine (**1**). The structure of compound **3** was confirmed by elemental analysis and ^1H NMR spectroscopy. In the spectrum no other signal than two singlets (δ 2.87 and 8.39) was observed in $CDCl_3$. The former is assigned to H_a, a proton of ethylene bridge, and the latter to H_b, aromatic proton as shown in Scheme 1.

Quaternarization of **3** with alkyl halides was carried out in polar solvent, methanol or *N*,*N*-dimethylformamide (DMF), to yield the target compounds **4**—**11** in the conditions as shown in Table 1. For example,

Table 1. Reaction Conditions and Yield of Products **4**—**11**

Entry	Reagent	Solvent	Temp/°C	Time/h	Product	Yield/%
1	CH_3I	M[c)]	55—60	14.0	**4**	79
2	C_2H_5Br	D[d)]	95—100	3.0	**5**	87
3	C_3H_7Br	D	90—95	3.5	**6**	87
4	$(CH_3)_2CHBr$	D	100—105	3.0	**7**	68
5	$C_{18}H_{37}Br$	D	105—110	7.5	**8**	91
6	$C_6H_5CH_2Br$	D	105—110	13.0	**9**	Quant.
7	4-CBB[a)]	D	110—115	2.5	**10**	53
8	2,4-DNCB[b)]	M	Reflux	12.5	**11**	84
9	2,4-DNCB	M	50—55	7.0	**12**	60

a) 4-Cyanobenzyl bromide. b) 1-Chloro-2,4-dinitrobenzene. c) Methanol. d) DMF.

ethylation of **3** with ethyl bromide in DMF at 95—100 °C for 2 h gave 2,7-diethyl-4,5,9,10-tetrahydro-2,7-diazoniapyrene dibromide (**5**) in 87% yield. While arylation of **3** with 1-chloro-2,4-dinitrobenzene in methanol at 50—55 °C for 7 h gave mono-onium compound, 7-(2,4-dinitrophenyl)-4,5,9,10-tetrahydro-2-aza-7-azoniapyrene chloride (**12**) in 60% yield, the same reaction under reflux for 12.5 h afforded the desired bis-onium compound, 2,7-bis(2,4-dinitrophenyl)-4,5,9,10-tetrahydro-2,7-diazoniapyrene dichloride (**11**) in 84%. In the ^{1}H NMR spectrum of **11**, the aromatic proton appears at very low field (δ 9.35) in DMSO-d_6. The remarkable downfield shift of the aromatic protons is observed in all of the spectra of **4—11**, indicating the quaternarization of each two nitrogen atoms in the diazapyrene **3**. The redox potentials measured by cyclic voltammetry and the ^{1}H NMR characteristic shifts of **4—11** are summarized in Table 2.

Any cyclic voltammogram of the products **4—11** shows two reversible one-electron reductions except that of **11**. Cyclic voltammogram of **11**, on the other hand, shows diffusion-controlled and irreversible reduction, which is probably due to feature of nitro group. The redox potentials of **4—10** are almost equal to that of methylviologen in any case. This fact suggests that the increased resonance in the bipyridyl system and the electron-releasing effect of ethylene bridges are compensated each other in these diazoniapyrene derivatives **4—10**.

It is well-known that *N,N'*-bis(2,4-dinitrophenyl)-4,4'-bipyridinium salt is an available precursor for the other viologen derivatives by a facile ring transformation reaction with an amine.[7] From this point of view, the compounds **11** and **12** are assumed to be useful as valuable precursors for synthesis of a symmetrical and an unsymmetrical viologen analogs having good coplanarity.

Experimental

Measurements. All melting points were measured on a Yanako melting point apparatus and were uncorrected. ^{1}H NMR spectra were recorded with a Hitachi R-20B spectrometer, IR spectra with a Hitachi 260-10 spectrophotometer, and UV spectra with a Shimadzu UV-240 spectrophotometer. Cyclic voltammograms were obtained with a Yanako polarographic analyzer P-1100.

4,5,9,10-Tetrahydro-2,7-diazapyrene (3): To a mixture of 1.00 g (4.75 mmol) of [2.2](3,5)pyridinophane (**2**), 27 ml of acetic anhydride, 0.5 ml of acetic acid, and a catalytic amount of iron(III) chloride contained in a 100 ml three-necked flask was added a 136 mg portion of zinc powder(90% assay) with vigorous stirring at 30—40 °C under a nitrogen atmosphere. The temperature was maintained at 30—40 °C, an additional amount of zinc (1.362 g) was added in three portions at every half an hour. The mixture was stirred another 15 h at 30—40 °C, and then heated to 90 °C within 5 min. Upon ice-cooling to ca. 30 °C, stirring was continued further for 5 h under introduction of air. After evaporation, a little of water was added to the mixture and then neutralized till pH 9 with an aqueous solution of sodium hydroxide. The resulting mixture was stirred for additional 6 h at 40 °C. After filtration with Hyflo Super-Cel, the filtrate was extracted with chloroform. The organic layer was washed and dried over anhyd magnesium sulfate. The solvent was evaporated up to give a crystalline solid. It was purified by column chromatography on a silica gel to give 527 mg (yield: 53%) of **3**; colorless plates from acetone; mp 227.5—228.5 °C. ^{1}H NMR ($CDCl_3$) δ=2.94 (8H, s, benzylic CH_2), 8.39 (4H, s, aromatic H). Found: C, 80.98; H, 5.87; N, 13.33%; Calcd for $C_{14}H_{12}N_2$: C, 80.74; H, 5.81; N, 13.45%.

2,7-Dimethyl-4,5,9,10-tetrahydro-2,7-diazoniapyrene Diiodide (4): A solution of 118 mg (0.570 mmol) of 4,5,9,10-tetrahydro-2,7-diazapyrene (**3**) and 460 mg (3.2 mmol) of methyl iodide in methanol (5 ml) was stirred at 55 °C for 4 h. Then 460 mg (3.2 mmol, total 920 mg) of methyl iodide was added and the mixture was stirred for another 5 h. A red crystalline solid was collected by filtration and recrystallized from methanol to give 220 mg (yield: 79%) of **4** as red plates; mp>300 °C. UV(CH_3OH) 300 nm (log ε=4.14). ^{1}H NMR (DMSO-d_6) δ=3.19 (8H, s, benzylic CH_2), 4.37 (6H, s, CH_3), 9.06 (4H, s, aromatic H). Found: C, 38.76; H, 3.62; N, 5.59%; Calcd for $C_{16}H_{18}N_2I_2$: C, 39.05; H, 3.69; N, 5.69%.

2,7-Diethyl-4,5,9,10-tetrahydro-2,7-diazoniapyrene Dibromide (5): A solution of 120 mg (0.576 mmol) of **3** and 380 mg (3.46 mmol) of ethyl bromide in DMF (5 ml) was heated at 95—100 °C for an hour with magnetic stirring. After the addition of ethyl bromide (380 mg, 3.46 mmol), the mixture was further heated at 95—100 °C for 2 h. After cooling, the mixture was filtered and the collected solid was

Table 2. ^{1}H NMR Data and Redox Potentials of Products **4—11**

Compound	δ-Value[a] Ar-H	δ-Value[a] Bridge-CH_2	$E^1_{1/2}$/V[b]	$E^2_{1/2}$/V[b]
4	9.06	3.19	−0.59	−1.03
5	9.29	3.23	−0.61	−1.05
6	9.21	3.21	−0.63	−1.08
7	9.30	3.23	−0.72	−1.17
8	9.69	3.38	−0.70	−1.15
9	9.50	3.20	−0.62	−1.07
10	9.31	3.20	−0.51	−0.92
11	9.35	3.48	—	—
MV^{2+}	—	—	−0.53	−0.90

a) 60 MHz in DMSO-d_6. b) Volts vs. saturated calomel electrode at a glassy carbon electrode and the counter electrode was a Pt wire; 0.1 M Et_4NClO_4–DMF, scan rate 0.1 V s^{-1}.

recrystallized from benzene–ethanol (2:1) to give 203 mg (yield: 87%) of **5** as pale yellow fine crystals; mp 282—285 °C (decomp). UV (CH_3OH) 300 nm (log ε=4.29). ^1H NMR (DMSO-d_6) δ=1.63 (6H, t, J=7 Hz, CH_3), 3.23 (8H, s, benzylic CH_2), 4.69 (4H, q, J=7 Hz, N^+–CH_2), 9.23 (4H, s, aromatic H). Found: C, 50.75; H, 5.30; N, 6.59%; Calcd for $C_{18}H_{22}N_2Br_2$: C, 50.73; H, 5.20; N, 6.57%.

The other 2,7-disubstituted 4,5,9,10-tetrahydro-2,7-diazoniapyrene salts were prepared in a similar way to that used for **5** under the conditions as shown in Table 1.

2,7-Dipropyl-4,5,9,10-tetrahydro-2,7-diazoniapyrene Dibromide (6): Pale yellow fine crystals from benzene–ethanol (yield: 87%), mp 270—280 °C (decomp). UV (CH_3OH) 313 nm (log ε=4.49). ^1H NMR (DMSO-d_6) δ=0.95 (6H, t, J=7 Hz, CH_3), 2.05 (4H, sext, J=7 Hz, CH_2 in propyl), 3.21 (8H, br. s, benzylic CH_2), 4.60 (4H, t, J=7 Hz, N–CH_2), 9.21 (4H, s, aromatic H). Found: C, 52.85; H, 5.75; N, 6.24%; Calcd for $C_{20}H_{26}N_2Br_2$: C, 52.88; H, 5.77; N, 6.17%.

2,7-Diisopropyl-4,5,9,10-tetrahydro-2,7-diazoniapyrene Dibromide (7): Pale yellow columns from ethanol (yield: 68%), mp 270—275 °C (decomp). UV (CH_3OH) 300 nm (log ε=4.28). ^1H NMR (DMSO-d_6) δ=1.69 (6H, d, J=7 Hz, CH_3), 3.23 (8H, s, benzylic H). 5.07 (2H, hept, J=7 Hz, N–CH), 9.30 (4H, s, aromatic H). Found: C, 52.12; H, 5.62; N, 6.19%; Calcd for $C_{20}H_{26}N_2Br_2 \cdot 1/2\,H_2O$: C, 51.85; H, 5,89; N, 6.05%.

2,7-Dioctadecyl-4,5,9,10-tetrahydro-2,7-diazoniapyrene Dibromide (8): Pale yellow fine crystals from acetone–chloroform (yield: 91%), mp 261—268 °C (decomp). UV (CH_3OH) 301 nm (log ε=4.31). ^1H NMR (DMSO-d_6) δ=0.7—2.9 (66H, m, CH_3 and CH_2 in stearyl except N–CH_2), 3.38 (8H, br. s, benzylic H), 4.6—5.1 (4H, m, N–CH_2), 9.69 (4H, br. s, aromatic H). Found: C, 65.41; H, 9.54; N, 3.05%; Calcd for $C_{50}H_{86}N_2Br_2 \cdot 1/2H_2O$; C, 65.91; H, 9.97; N, 3.07%.

2,7-Dibenzyl-4,5,9,10-tetrahydro-2,7-diazoniapyrene Dichloride (9): Pale yellow fine crystals from benzene–ethanol (yield: quant.), mp 195—200 °C (decomp). UV (CH_3OH) 302 nm (log ε=4.28). ^1H NMR (DMSO-d_6) δ=3.20 (8H, s, bridge CH_2), 5.92 (4H, s, N–CH_2), 7.3—7.8 (10H, m, Aromatic H of benzene), 9.50 (4H, s, aromatic H of pyridine). Found: C, 72.12; H, 5.89; N, 5.94%; Calcd for $C_{28}H_{26}N_2Cl_2 \cdot 1/4H_2O$: C, 72.17; H, 5.74; N, 6.01%.

2,7-Bis(4-cyanobenzyl)-4,5,9,10-tetrahydro-2,7-diazoniapyrene Dibromide (10): Yellow needles from methanol (yield: 53%), mp 194—196 °C (decomp). UV (CH_3OH) 303 nm (log ε=4.30). IR(Nujol) 2240 cm^{-1} (ν_{CN}). ^1H NMR (DMSO-d_6) δ=3.20 (8H, br. s, bridge CH_2), 6.00 (4H, br. s, N–CH_2), 7.82 and 7.96 (8H, AA'BB', J_{AB}=8 Hz, aromatic H of benzene), 9.31 (4H, s, aromatic H of pyridine). Found: C, 59.33; H, 4.08; N, 9.25%; Calcd for $C_{30}H_{24}N_4Br_2 \cdot 1/2H_2O$: C, 59.13; H, 4.14; N, 9.15%.

2,7-Bis(2,4-dinitrophenyl)-4,5,9,10-tetrahydro-2,7-diazoniapyrene Dichloride (11): A mixture of 500 mg (1.33 mmol) of **4**, 3.90 g (19.2 mmol) of 1-chloro-2,4-dinitrobenzene, and methanol (2.5 ml) was refluxed with magnetic stirring for 12.5 h under a nitrogen atmosphere. After cooling, the mixture was evaporated. To the oily residue, some benzene was added. A resulting solid was collected and recrystallized from methanol to give 1.24 g (yield: 84%) of **11** as yellow prisms; mp 156—164 °C (decomp). UV (CH_3OH) 313 nm (log ε=4.49). IR(Nujol) 1550 and 1345 cm^{-1} (ν_{NO_2}). ^1H NMR (DMSO-d_6) δ=3.48 (8H, s, Ha), 8.43 (2H, d, J=8 Hz, He), 8.95 (2H, dd, J=2 and 8 Hz, Hd), 9.29 (2H, d, J=2 Hz, Hc), 9.35 (4H, s, Hb). Found: C, 50.15, H, 3.10; N, 13.46%; Calcd for $C_{26}H_{18}N_6O_8Cl_2 \cdot 1/2H_2O$: C, 50.17; H, 3.08; N, 13.50%.

7-(2,4-Dinitrophenyl)-4,5,9,10-tetrahydro-2-aza-7-diazoniapyrene Chloride (12): A mixture of 200 mg (0.96 mmol) of **4**, 1.556 g (7.68 mmol) of 1-chloro-2,4-dinitrobenzene, and methanol (1 ml) was heated at 50—55 °C with magnetic stirring for 7 h under a nitrogen atmosphere. After cooling, the mixture was evaporated up to give an oily residue and acetone was added.

Recrystallization of the resulting solid from benzene–ethanol gave 238 mg (yield: 60%) of **12** as a pale yellow powder, mp 165—170 °C (decomp). ^1H NMR (CH_3OH-d_4) δ=3.48 (8H, br. s, bridge CH_2), 8.34 (1H, d, J=8 Hz, He), 8.64 (2H, br. s, aromatic H of pyridine), 8.92 (1H, dd, J=2 and 8 Hz, Hd), 9.14 (2H, s, aromatic H of pyridinium ring), 9.26 (1H, d, J=2 Hz, Hc). Found: C, 57.36; H, 3.79; N, 13.16%; Calcd for $C_{20}H_{15}N_4O_4Cl \cdot 1/2H_2O$: C, 57.21; H, 3.84; N, 13.34%.

The authors wish to express their thanks to Dr. Kunihiko Yokoi of Osaka Kyoiku University for his kind measurement of cyclic voltammetry.

References

1) The Chemistry of Constrained Hetero Aromatics. IV.
2) C. L. Bird and A. T. Kuhn, *Chem. Soc. Rev.*, **10**, 49 (1981).
3) T. Kawashima, K. Yoshida, Y. Tohda, M. Ariga, Y. Mori, Y. Sakata, and S. Misumi, *Tetrahedron Lett.*, **25**, 1585 (1984).
4) T. Kawashima, Y. Ishizaki, Y. Tohda, M. Ariga, Y. Mori, and S. Misumi, *Mem. Osaka Kyoiku Univ.*, **35**, 139 (1986).
5) Extensive references therein: K. Nishiyama, K. Hata, and T. Sato, *J. Chem. Soc., Perkin Trans. 2*, **1974**, 557.
6) The conditions applied for dimerization of pyridine were modified; A. T. Nielsen, *J. Org. Chem.*, **29**, 2175 (1964).
7) J. G. Allen, UK Patent 1514466 (1978).

Preparation and Properties of Pyridine-Analogue of TCNQ Dianion Salt

Yoshiyuki HAMA, Yukikazu NOBUHARA, Yoshio ASO, Tetsuo OTSUBO, and Fumio OGURA*
Department of Applied Chemistry, Faculty of Engineering, Hiroshima University, Saijo, Higashi-Hiroshima 724
(Received October 23, 1987)

Bis(tetrapropyl- and tetrabutylammonium) 1,1′-(2,5-pyridinediyl)bis[dicyanomethanide] (**4a** and **4b**) were prepared in order to investigate the properties of pyridine-analogue **3** of TCNQ as a new electron acceptor and its complexation with TTF. Although **3** was not isolated, the cyclic voltammetry of the salt **4** indicated that **3** was a stronger electron acceptor than TCNQ. The charge-transfer complex of TTF and **3** was prepared by mixing TTF with **3** which was generated in situ from the electrolytic oxidation of **4** or from the oxidation of 2,5-bis(dicyanomethyl)pyridine, a precursor of **4**, with hydrogen peroxide. It consisted of 1:1 composition of donor and acceptor and showed a high electrical conductivity of 19 S cm^{-1}. The 2:1 complex was prepared by metathesis of $(TTF)_3(BF_4)_2$ and **4**, and also highly conductive.

The pyridine analogue of 7,7,8,8-tetracyanoquinodimethane (TCNQ) (**1**) attracts much attention as a modified electron acceptor with an enhanced electron affinity due to a large electronegativity of the pyridinoid nitrogen. 1-AzoniaTCNQ (**2**) has so far been studied as one example, but exists as an anionic form involving a $\overset{+}{C}-\overset{-}{N}$ ylide bond.[1] 2,5-Bis(dicyanomethylene)-2,5-dihydropyridine, so-called 2-azaTCNQ (**3**) is an intriguing candidate for the real pyridine-analogue of TCNQ. We have undertaken the synthesis of **3**, which is, however, not isolated in a neutral state but as its dianion salts **4**. The electrochemical study of **4** provides an information on the acceptor character of neutral **3**. Here we would like to report the preparation and properties of bis(tetrapropyl- and tetrabutylammonium) 1,1′-(2,5-pyridinediyl)bis[dicyanomethanide] (**4a** and **4b**) as well as charge-transfer complexation of **3** and tetrathiafulvalene (TTF).

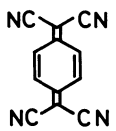
1

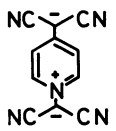
2

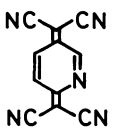
3

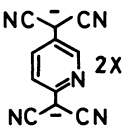
4a, X = $Pr_4\overset{+}{N}$
4b, X = $Bu_4\overset{+}{N}$

Results and Discussion

Recently Takahashi et al. developed a direct synthetic method of 2,2′-(*p*-phenylene)bis[malononitrile] from dihalobenzene and malononitrile anion.[2] We have applied a similar method for the present pyridine case (Scheme 1). First, commercially available 2,5-dibromopyridine (**5**) was treated with

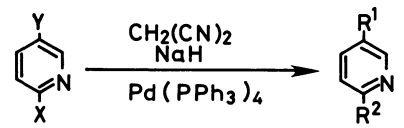

5 X=Y=Br 8 R^1 = Br, R^2 = $CH(CN)_2$
6 X=Br, Y=I 9 R^1 = $CH(CN)_2$, R^2 = Br
7 X=Y=I 10 R^1 = R^2 = $CH(CN)_2$
11 R^1 = I, R^2 = $CH(CN)_2$

Scheme 1.

malononitrile anion in the presence of tetrakis(triphenylphosphine)palladium(0) as a catalyst in refluxing tetrahydrofuran (THF), giving 5-bromo-2-(dicyanomethyl)pyridine (**8**) as a sole product in 94% yield. Neither 2-bromo-5-(dicyanomethyl)pyridine (**9**) nor 2,5-bis(dicyanomethyl)pyridine (**10**) was detected. When the reaction was carried out at a higher temperature of refluxing 1,2-dimethoxyethane (DME) for a prolonged time of 24 h, a trace of the desired 2,5-disubstituted product **10** was formed together with **8** as main product (73%). In contrast to a preliminary experiment in which 3-bromopyridine was readily convertible into 3-(dicyanomethyl)pyridine,[3] an attempted conversion of **8** into **10** failed. This suggests that **10** must have been formed via 5-substituted isomer **9**. The inertness of **8** to further substitution is probably related to its structure which exists as a tautomeric form **12** as indicated by absorptions due to

12

N–H at around 3200 cm^{-1} and conjugated C≡N at 2210 and 2186 cm^{-1} in the infrared absorption bands.[4]

Since iodoarenes are more reactive to the palladium-catalyzed substitution,[5] we next examined 2-bromo-5-iodopyridine (**6**) and 2,5-diiodopyridine (**7**), both of

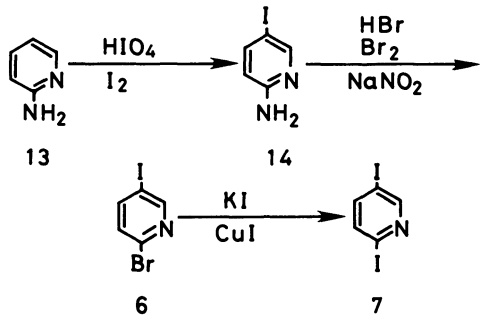

Scheme 2.

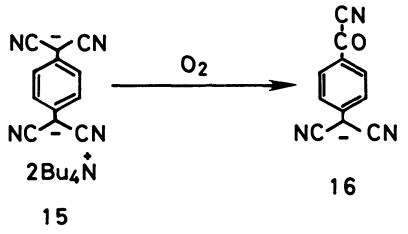

Scheme 3.

which were long known but accesible by an improved procedure as shown in Scheme 2. A similar reaction of **6** in refluxing THF gave a mixture of 5-substituted products **9** (45%) and **10** (12%), while that of **7** gave a mixture of 2-substituted products **11** (45%) and **10** (18%). Alternative treatment of either compound in refluxing DME gave a high yield of **10**. A shorter reaction time (8 h) and a somewhat higher yield (71%) for **6** than those (24 h, 64%) for **7** again support the advantage of the first substitution at 5-position for the 2,5-disubstitution.

Dehydrogenation of **10** to **3** with a common oxidizing agent, i.e., H_2O_2, chloranil, DDQ, Br_2, NBS, NCS, or $Pb(OAc)_4$ was attempted, giving only unidentified colored materials which were presumably derived from **3**. Treatment of **10** with tetrapropylammonium iodide in O_2-free aq. NaOH solution gave the ammonium salt **4a** of pyridine-analogue of TCNQ dianion in an excellent yield. The tetrabutylammonium salt **4b** was similarly obtained. They with hydrochloric acid returned to the precursor **10**. The electrolytic oxidation of **4** to **3** was furthermore attempted, but **3** was not isolated because of its air-sensitivity.

Both salts **4a** and **4b** are hydrated yellow crystals which gradually decompose on prolonged exposure to air, but are extremely sensitive to oxygen in solution, immediately turning orange. The electronic spectra of **4a** and **4b** are almost identical and have two strong absorptions at 238 and 325 nm together with a weak one at 403 nm as shown in Fig. 1. For comparison, bis(tetrabutylammonium) 7,7,8,8-tetracyanoquinodimethanide (**15**), prepared according to the literature,[6] absorbs light at 207, 244, and 326 nm. The close

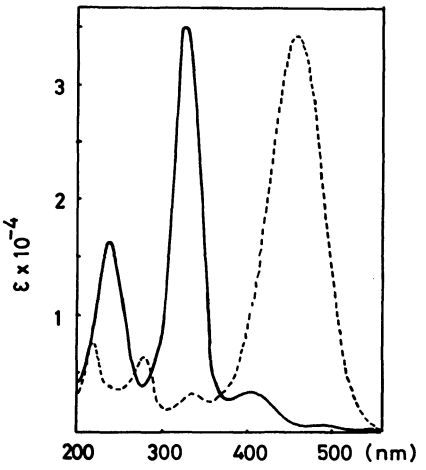

Fig. 1. Electronic absorption spectra of **4a** (—) and its decay product (------) in acetonitrile.

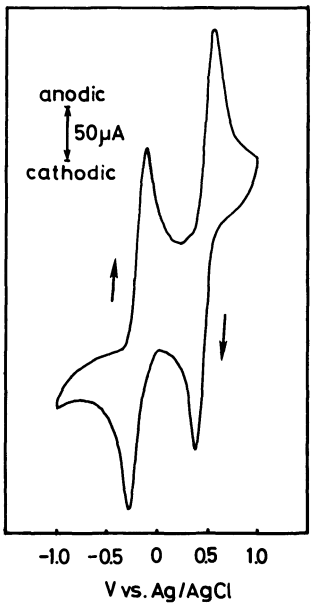

Fig. 2. Cyclic voltammogram of **4a** in 1.6 mol m^{-3} dichloromethane solution containing 0.1 mol dm^{-3} n-Bu_4NClO_4 at scan rate 0.1 V s^{-1} using a platinum working electrode and a Ag/AgCl reference electrode.

spectral resemblance of **4** and **15** reflects a similarity in their electronic structures. The light yellow solution of TCNQ dianion salt (**15**) turns orange in the presence of oxygen, too. Suchanski and Van Duyne assigned its decay product to be α,α-dicyano[*p*-(cyanocarbonyl)phenyl]methanide (**16**) (Scheme 3).[7] The considerable resemblance of both decay spectra (λ_{max} 276, 336, 458 nm from **4** and 282, 330, 480 nm from **15**) indicates that the same decay process is operative for **4**.

The cyclic voltammetry of **4** exhibits two reversible redox waves corresponding to two steps of one-electron oxidations (Fig. 2). The half-wave potentials are +0.48, −0.18 V, indicating that the neutral species

3 is a stronger electron acceptor than TCNQ ($E_{1/2}$+0.25, −0.35 V), as was expected. The charge-transfer complex of TTF and **3** was prepared by the following two methods. One used the mixing of TTF and **3** generated in situ from the electrolytic oxidation of **4** or from the dehydrogenation of **10** with hydrogen peroxide. The resulting complex consisted of 1:1 composition of donor and acceptor, and showed a high electrical conductivity of 19 S cm^{-1} which was measured on a compressed pellet at r.t. by a four probe method. Another used the metathesis of the dianion salt **4** and $(TTF)_3(BF_4)_2$.[8] In this case, the complex followed the 2:1 stoichiometry rich in donor and was also highly conductive (5.9 S cm^{-1}).

Experimental

General. Melting points are uncorrected. NMR measurements were made on a JEOL PMX-60 (60 MHz) using TMS as an internal standard. IR spectra were taken on a Hitachi 260-30 spectrophotometer, MS spectra on a Shimadzu QP-1000 spectrometer at 70 eV using a direct insertion technique, and electronic spectra on a Shimadzu UV-160 spectrophotometer.

2-Amino-5-iodopyridine (14). A mixture of 2-aminopyridine (**13**) (47.02 g, 0.50 mol), periodic acid dihydrate (22.82 g, 0.10 mol), and iodine (51.0 g, 0.20 mol) was heated in a mixed solution of acetic acid (300 cm^3), water (60 cm^3) and sulfuric acid (9 cm^3) at 80 °C for 4 h. It was then poured into aq. dil. $Na_2S_2O_3$ to remove unreacted iodine and extracted with ether. The extract was washed with aq. dil. NaOH, dried (K_2CO_3), and concentrated in vacuo. The residue was purified by column chromatography on silica gel with ethyl acetate as eluent and then recrystallization from ethanol to give colorless prisms of **14** (74.15 g, 67%): mp 132.0—132.7 °C (lit,[9] mp 129 °C).

2-Bromo-5-iodopyridine (6). Bromine (10 cm^3) and aq. solution (50 cm^3) of $NaNO_2$ (11.22 g, 0.163 mol) were succesively added into a stirred solution of 2-amino-5-iodopyridine (**14**) (13.79 g, 0.063 mol) in 47% hydrobromic acid (100 cm^3), the temperature being kept below 0 °C during the addition. The reaction was then continued for 2 h at 5—10 °C and quenched by addition of aq. solution (300 cm^3) of NaOH (36 g). The mixture was poured into aq. dil. $Na_2S_2O_3$ to remove unreacted bromine and extracted with ether. The extract was washed with water, dried (K_2CO_3), and concentrated in vacuo. The residue was purified by column chromatography on silica gel with chloroform as eluent and then recrystallization from ethanol to give colorless plates of **6** (11.65 g, 65%): mp 125—126 °C (lit,[10] mp 122.5 °C).

2,5-Diiodopyridine (7). A mixture of 2-bromo-5-iodopyridine (**6**) (2.27 g, 8.0 mmol), copper(I) iodide (7.75 g, 40.7 mmol), and potassium iodide (13.1 g, 78.5 mmol) in dry hexamethylphosphoric triamide (25 cm^3) was heated at 140—145 °C for 18 h under nitrogen. The reaction was quenched by addition of 10% HCl until the solution became neutral. Benzene (30 cm^3) was added and the insoluble copper salt was filtered off. The organic phase was separated, washed with water, dried (K_2CO_3), and evaporated. The residue was purified by column chromatography on silica gel with chloroform and then recrystallization from the same solvent to give colorless plates of **7** (1.96 g, 74%): mp 148—149.7 °C (lit,[10] mp 154 °C).

5-Bromo-2-(dicyanomethyl)pyridine (8). A solution of malononitrile (0.626 g, 9.48 mmol) in dry THF (10 cm^3) was mixed with a suspension of NaH (60% in oil, 0.667 g, 16.68 mmol) in dry THF (20 cm^3) and stirred at r.t. for 10 min in a nitrogen atmosphere. 2,5-Dibromopyridine (**5**) (0.911 g, 3.84 mmol) in dry THF (10 cm^3) and tetrakis(triphenylphosphine)palladium(0) (0.201 g, 0.174 mmol) were succesively added. The mixture was refluxed for 3 h and concentrated in vacuo. The residue was taken up with water (50 cm^3), washed with benzene, and acidified to pH 1 with 10% HCl. The resulting yellow precipitate was collected by filtration and dried. It was then purified by column chromatography on silica gel with chloroform and recrystallization from acetonitrile to give yellow prisms of **8** (0.80 g, 94%): decomp 216 °C; IR (KBr) 3200—2900 (N-H, C-H), 2210, 2186 cm^{-1} (C≡N); ^{1}H NMR (DMSO-d_6) δ=7.01 (d, J=9.6 Hz, 1H), 7.75 (dd, J=9.6 and 1.8 Hz, 1H), 7.89 (d, J=1.4 Hz, 1H); MS (70 eV) m/z 221, 223 (M$^+$). Anal. ($C_8H_4N_3Br$) C, H, N.

When the same reaction was conducted in refluxing DME for 24 h, a mixture of **8** (73%) and **10** (2%) was formed.

2-Bromo-5-(dicyanomethyl)pyridine (9), 2,5-Bis(dicyanomethyl)pyridine (10), and 2-(Dicyanomethyl)-5-iodopyridine (11). The same reaction as described in the preparation of **8** was carried out using either 2-bromo-5-iodopyridine (**6**) or 2,5-diiodopyridine (**7**) instead of **5**. The usual work-up gave a mixture of **9** (45%) and **10** (12%) from **6** and a mixture of **10** (18%) and **11** (45%) from **7**. The mixtures were separated by column chromatography on silica gel, which first eluted the monosubstituted product with chloroform and then the disubstituted one with 1:5 acetone–chloroform.

Recrystallization of **9** from acetonitrile afforded colorless prisms: decomp 142 °C; IR (KBr) 3100—3000, 2900 (C-H), 2273 cm^{-1} (C≡N); ^{1}H NMR (acetone-d_6) δ=6.17 (s, 1H), 7.80 (d, J=8.4 Hz, 1H), 8.03 (dd, J=8.4 and 3.4 Hz, 1H), 8.65 (d, J=2.6 Hz, 1H); MS (70 eV) m/z 221, 223 (M$^+$); Anal. ($C_8H_4N_3Br$) C, H, N.

Recrystallization of **10** from acetonitrile afforded yellow plates: decomp 204 °C; IR (KBr) 3100—2800 (N-H, C-H), 2214, 2188 cm^{-1} (C≡N); ^{1}H NMR (acetone-d_6) δ=5.98 (s, 1H), 7.28 (d, J=9.4 Hz, 1H), 7.85 (dd, J=8.6 and 3.0 Hz, 1H), 8.13 (d, J=2.6 Hz, 1H), 12.6—11.5 (bs, 1H); MS (70 eV) m/z 207 (M$^+$); Anal. ($C_{11}H_5N_5$) C, H, N.

Recrystallization of **11** from acetonitrile gave yellow needles: decomp. 245 °C; IR (KBr) 3200—2900 (N-H, C-H), 2222, 2198 cm^{-1} (C≡N); ^{1}H NMR (acetone-d_6+DMSO-d_6) δ=6.93 (d, J=8.6 Hz, 1H), 7.83 (dd, J=8.6 and 1.8 Hz, 1H), 7.91 (d, J=1.8 Hz, 1H); MS (70 eV) m/z 269 (M$^+$); Anal. ($C_8H_4N_3I$) C, H, N.

Bis(tetrapropyl- and tetrabutylammonium) 1,1′-(2,5-Pyridinediyl)bis[dicyanomethanide] (4a) and (4b). 2,5-Bis(dicyanomethyl)pyridine (**10**) (0.105 g, 0.51 mmol) was dissolved in 1 mol dm^{-3} NaOH solution (10 cm^3) in a nitrogen atmosphere. As soon as a solution of tetrapropylammonium iodide (0.471 mg, 1.50 mmol) in water (8 cm^3) was added, the yellow plates of **4a** precipitated. It was collected by filtration and dried in vacuo (0.264 g, 89%): decomp 133 °C; IR (KBr) 3400 (H_2O), 2974, 2888 (C-H),

2165, 2127, 2118 cm^{-1} (C≡N); Found: C, 71.61; H, 10.02; N, 15.99%. Calcd for $C_{35}H_{59}N_7 \cdot 1/2H_2O$: C, 71.63; H, 10.30; N, 16.71%. The ^1H NMR spectrum of **4a** showed some dintinct absorptions due to the propyl protons at δ 0.7—1.3 (t, 24H), 1.3—2.4 (m, 16H), 2.9—3.7 (m, 16H) and a very broad absorption due to the pyridinyl protons at δ 6.7—7.9. The latter broadening suggests that the dianion is apt to become a radical species.

The tetrabutylammonium salt **4b** was similarly obtained as yellow plates (97%): decomp 111 °C; IR (KBr) 3400 (H_2O), 2974, 2888 (C-H), 2159, 2121, 2108 cm^{-1} (C≡N); Found: C, 71.04; H, 10.92; N, 13.26%. Calcd for $C_{43}H_{75}N_7 \cdot 2H_2O$: C, 71.13; H, 10.97; N, 13.50%.

Complexation of TTF and Pyridine-Analogue 3 of TCNQ. A) Mixing Method Using Bis(tetrapropylammonium) 1,1′-(2,5-Pyridinediyl)bis[dicyanomethanide] (4a). A 20 cm^3 of H-type glass cell with a fine frit dividing the anolyte and catholyte compartments was used for electrolyses. It was equipped with platinum plates (1 cm^2 in area) as electrodes for the potentiostatic experiment and with platinum needles (3 cm in length, 1 mm in diameter) for the galvanostatic experiment. A 0.1 mol dm^{-3} solution of tetrabutylammonium perchlorate in dry acetonitrile (20 cm^3) was placed in the cell and thoroughly saturated with nitrogen gas. TTF (20.8 mg, 0.1 mmol) and **4a** (57.5 mg, 0.1 mmol) were added in the anolyte compartment and electrolyzed at +0.45 V for 1.5 h. The resulting black powder was collected, washed with dichloromethane, and dried (23.1 mg): mp>300 °C; IR (KBr) broad nitrile absorptions at 2188, 2129 cm^{-1}; σ=18.8 S cm^{-1}; Found: C, 49.68; H, 1.70; N, 16.90%. Calcd for TTF·**3**: C, 49.86; H, 1.72; N, 17.10%.

The galvanostatic electrolysis was carried out under a constant current of 0.5 mA for 12 h, giving black fine needles (14.6 mg): mp>300 °C; IR (KBr) broad nitrile absorptions at 2194, 2160, 2128 cm^{-1}; σ=19.3 S cm^{-1}; Found: C, 49.26; H, 1.63; N, 16.34%.

B) Mixing Method Using 2,5-Bis(dicyanomethyl)pyridine (10). 30% Hydrogen peroxide (2 cm^3) was added into a stirred solution of **10** (50.2 mg, 0.24 mmol) and TTF (43.1 mg, 0.21 mmol) in dry acetonitrile (5 cm^3) in a nitrogen atmosphere. After stirring for 10 min at r.t., the resulting reddish black powder was collected by filtration, washed with a small amount of acetonitrile, and dried (8.6 mg): decomp>300 °C; IR (KBr) broad nitrile absorptions at 2154, 2122 cm^{-1}; σ=1.0 S cm^{-1}; Found: C, 50.17; H, 1.74; N, 17.16%. Calcd for TTF·**3**: C, 49.86; H, 1.72; N, 17.10%.

C) Metathesis Method. A hot solution of **4a** (56 mg, 0.1 mmol) in dry acetonitrile (1.5 cm^3) was mixed with a hot solution of $(TTF)_3(BF_4)_2$ (78 mg, 0.1 mmol) in dry acetonitrile (6 cm^3) in a nitrogen atmosphere. After cooling, the resulting black powder was obtained (26.9 mg): decomp> 300 °C: IR (KBr) broad nitrile absorptions at 2187, 2156 cm^{-1}; σ=5.9 S cm^{-1}; Found: C, 45.08; H, 1.66; N, 12.32%. Calcd for $(TTF)_2 \cdot$**3**: C, 45.00; H, 1.81; N, 11.41%.

This work was partially supported by a Grant-in-Aid of Scientific Research No. 62550635 from the Ministry of Education, Science and Culture, Japan and Mazda Foundation's Research Grant.

References

1) F. Wudl, "Chemistry and Physics of One-dimensional Metals," ed by H. J. Keller, NATO Adv. Study Inst. (1977), p. 249; G. Matsubayashi, H. Tanaka, T. Tanaka, and K. Nakatsu, *Inorg. Chim. Acta*, **63**, 217 (1982); H. Tanaka, G. Matsubayashi, and T. Tanaka, *Bull. Chem. Soc. Jpn.*, **57**, 2198 (1984); H. Urayama, G. Saito, T. Inabe, T. Mori, and Y. Maruyama, *Synthetic Metals*, **19**, 469 (1987).

2) M. Uno, K. Seto, M. Masuda, W. Ueda, and S. Takahashi, *Tetrahedron Lett.*, **26**, 1553 (1985).

3) Treatment of 3-bromopyridine with malononitrile anion in the presence of catalytic $Pd(PPh_3)_4$ in refluxing THF for 7 h led to the formation of 3-(dicyanomethyl)pyridine in 58% yield.

4) H. U. Wagner and R. Gompper, *Angew. Chem., Int. Ed. Engl.*, **8**, 986 (1969).

5) M. Uno, K. Seto, and S. Takahashi, *J. Chem. Soc., Chem. Commun.*, **1984**, 932.

6) R. C. Wheland and E. L. Martin, *J. Org. Chem.*, **40**, 3101 (1975).

7) M. R. Suchanski and R. P. Van Duyne, *J. Am. Chem. Soc.*, **98**, 250 (1976).

8) F. Wudl and M. L. Kaplan, *Inorg. Synth.*, **19**, 27 (1979).

9) O. Magidson and G. Menshikow, *Ber.*, **58**, 113 (1925).

10) J. P. Wibant and G. L. Bastide, *Chem. Zentralbl., II*, **1927**, 2198.

Synthesis and X-Ray Crystal Structure of [5₄](1,2,3,4)Ferrocenophane[1)]

Masao HISATOME,* Rin-ichi YAMASHITA, Jun WATANABE, Koji YAMAKAWA, and Yoichi IITAKA†
Faculty of Pharmaceutical Sciences, Science University of Tokyo, Ichigaya-Funagawara, Shinjuku-ku, Tokyo 162
†Faculty of Pharmaceutical Sciences, The University of Tokyo, Hongo, Bunkyo-ku, Tokyo 113
(Received October 31, 1987)

The title compound bridged with four pentamethylene chains has been synthesized by stepwise construction of a pentamethylene bridge via formation of a three-carbon bridge followed by insertion of two carbon units. Crystal structure of the phane has been determined by X-ray diffraction. The compound crystallizes in the monoclinic system, space group $P2_1/n$ with unit cell parameters a=16.691(10), b=9.858(5), c=15.237(8) Å, β=112.43(6)°, and z=4. The structure parameters of the ferrocene moiety fall in normal ranges. Characteristic features are noted in the methylene bridges. The γ-methylene carbons undergo large thermal vibration, and apparent shortening of the bond lengths by oscillatory motions of atoms is seen.

A number of intramolecularly multibridged [3$_n$]- and [4$_n$]ferrocenophanes[2,3)] with tri- and tetramethylene chains have been synthesized[4,5)] since the discovery of ferrocene. Especially, recent years have seen developments in the preparation of tetra- and pentabridged ferrocenophanes,[6–10)] and symmetrically perbridged [4$_5$](1,2,3,4,5)ferrocenophane, which was named superferrocenophane, was reported by the authors[11)] in 1986. On the other hand, there have been only two reports[12,13)] on multibridged [5$_n$]ferrocenophanes (n>1) with pentamethylene chains; the one reported by Nesmeyanov et al.[12)] is [5$_2$]ferrocenophane with substituents on the bridge and the others by one of the authors[13)] are [5$_2$]- and [5$_3$]ferrocenophanes. One of the reason why [5$_n$]ferrocenophane could not be easily prepared is the difficulty of construction of additional pentamethylene bridges. Condensations between the two substituents in the two cyclopentadienyl (Cp) rings, described by several groups[12,14–17)] for the preparation of monobridged [5]ferrocenophanes, are unfavorable for synthesis of multibridged phanes, because selective substitution at the desired positions of the Cp rings is impossible. One of the authors[13)] succeeded in the formation of the pentamethylene chain by extension of α-oxotrimethylene bridge, and reported the synthesis of [5$_3$](1,2,4)ferrocenophane (**1**) via stepwise formation of pentamethylene bridges. In this paper, the synthesis of tetrabridged [5$_4$](1,2,3,4)-ferrocenophane (**2**) from **1** by application of the bridge enlargement is reported, and its molecular structure determined by X-ray diffraction is described.

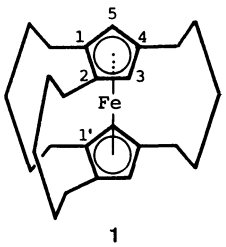

1

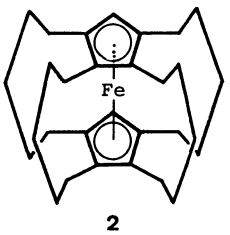

2

Results and Discussion

Synthesis. The synthetic method of [5$_4$]ferrocenophane (**2**) and the related compounds from [5$_3$]ferrocenophane (**1**) is summarized in Scheme 1. In the preparation of tribridged ferrocenophane **1**,[13)] malonic acid/piperidine and trifluoroacetic anhydride were used for condensation of formylferrocene and bridging reaction of propionic acid, respectively. However, these conventional methods were inapplicable to the construction of fourth bridge because of much more steric hindrance of the existing bridges. Accordingly, Reformatsky reaction and cyclization with polyphosphoric acid ethyl ester (PPE) were applied to these steps.

The starting material **1** was formylated according to Vilsmeyer reaction followed by Reformatsky reaction and catalytic hydrogenation to give [5$_3$]ferrocenophanepropionate (**5**) in a good yield (86% from **1**). Cyclization of propionic acid, prepared by hydrolysis of **5**, with PPE (concn 50%) in 1,2-dichloroethane under the conditions free from oxygen and moisture afforded tetrabridged compound **6** in quantitative yield. Running the reaction in the presence of a trace amount of oxygen and moisture resulted in considerable decrease in the yield of **6** (44%). Therefore, the cyclization must be carried out under strict control of reaction conditions. The signals of the Cp rings in the ^{1}H NMR spectrum of **6** appeared at δ 3.68 and 3.63 as two singlets. The NMR spectrum of phane **7** derived by reduction of **6** showed only one singlet of the Cp ring protons and eleven carbon signals of the methylene groups. The spectral pattern indicates that **7** has a C_s symmetric structure.

Treatment of ketone **6** with a large excess of diazomethane (over 10 equiv to the substrate) in the presence of BF_3 etherate (3.5 equiv) afforded three bridge-enlarged products **8**, **9**, and **10** in 35, 33, and 30% yields, respectively. β-Ketone **8** was contaminated with minor compounds, which were presumably further enlarged compounds, and attempted purification was unsuccessful. When 1.2 equivalent of BF_3 etherate to the substrate was used, the yield of α-oxo[5]ferrocenophane **10** was only 3.3%. Bridge enlargement of α-oxo[4]ferrocenophane **9** in a similar manner to the reaction of **6** also gave the desired compound **10** (42%).

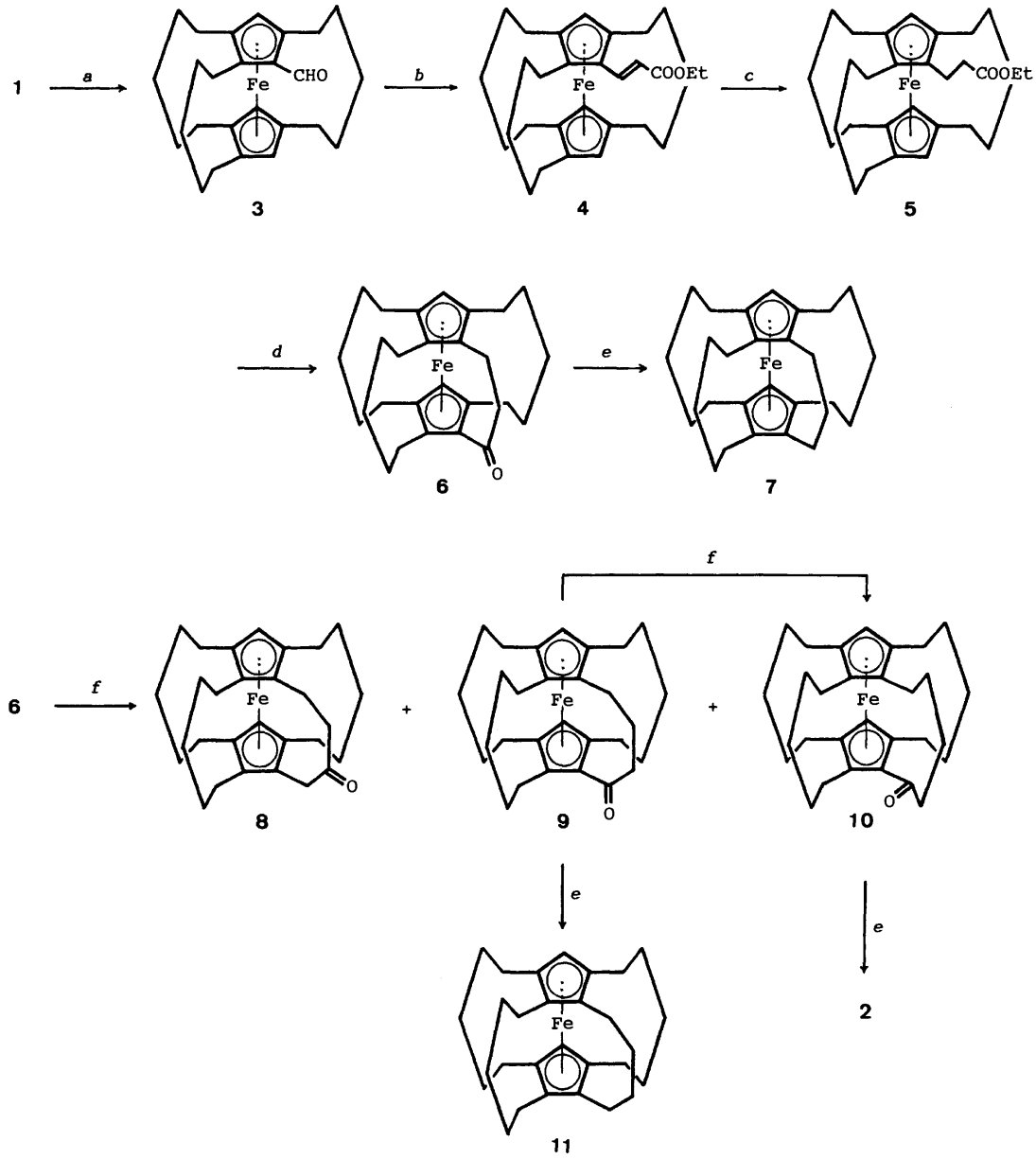

Scheme 1. Synthesis of [5$_4$](1,2,3,4)ferrocenophane (**2**) and related compounds. *a*. DMF/$POCl_3$. *b*. $BrCH_2COOEt$/Zn. *c*. H_2/Pd-C. *d*. 1) aq. NaOH, 2) PPE. *e*. $LiAlH_4/AlCl_3$. *f*. $CH_2N_2/BF_3 \cdot OEt_2$ in benzene.

Reduction of **9** and **10** with $LiAlH_4/AlCl_3$ afforded the corresponding tetrabridged ferrocenophanes **11** and **2**. In the ^1H NMR spectrum of **2**, the two protons of the Cp rings appeared as a singlet at δ 3.70. The C_{2v} symmetric structure of **2** was confirmed by observation of a simple ^{13}C NMR spectral pattern consisting of six and three signals of the methylene and Cp ring carbons, respectively.

Molecular Structure. The crystal structure of [5$_4$]ferrocenophane (**2**) was determined by X-ray diffraction. The structural parameters are given in Tables 1—6. The molecular structure and the numbering of the atoms used in this section are shown in Fig. 1.[18]

As is clear from Fig. 1, the bridging methylene chains C1···C6 and C4···C9 are in a "boat" conformation, whereas the chains C2···C7 and C3···C8 are in a "zigzag-like" conformation. In the crystal structure of tribridged phane **1** reported by Hillman et al.,[19] the conformations of the methylene chains are all boat forms. From the results it is noted that boat conformation is favorable for bridging between two Cp rings with pentamethylene chains when one of the neighboring positions of the bridge, at least, is unoccupied with other bridge. The pentamethylene chains in a boat form bend in a

Table 1. Fractional Coordinates ($\times10^5$ for Fe; $\times10^4$ for C; $\times10^3$ for H) and the Equivalent Isotropic Temperature Factor (in Å² unit) of **2** with Estimated Standard Deviations in Parentheses

Atom	x	y	z	B_{eq}	Atom	x	y	z	B_{eq}
Fe	16594(11)	15459(17)	41569(11)	3.03	H5	116(5)	301(8)	254(5)	
C1	2288(8)	1828(12)	3247(8)	3.8	H10	−5(8)	88(14)	302(9)	
C2	2882(8)	1940(12)	4200(8)	4.0	H11	254(9)	−9(15)	279(9)	
C3	2614(8)	3032(12)	4647(8)	3.6	H11′	281(7)	127(12)	225(7)	
C4	1832(8)	3575(13)	3972(8)	4.0	H12	153(13)	160(23)	125(15)	
C5	1666(8)	2843(13)	3123(8)	4.1	H12′	171(10)	4(17)	118(11)	
C6	1075(9)	−311(13)	3784(10)	4.8	H13	31(10)	51(17)	100(11)	
C7	1636(8)	−314(13)	4772(9)	4.3	H13′	59(8)	122(13)	196(9)	
C8	1297(9)	734(13)	5223(8)	4.3	H14	73(11)	−167(20)	160(13)	
C9	578(8)	1354(13)	4510(8)	4.0	H14′	−2(9)	−101(15)	191(10)	
C10	447(8)	708(13)	3631(9)	4.6	H15	106(7)	−222(12)	322(8)	
C11	2371(11)	900(15)	2519(10)	5.6	H15′	177(9)	−130(16)	310(10)	
C12	1583(10)	765(17)	1572(10)	6.2	H16	404(8)	109(14)	549(9)	
C13	716(11)	366(17)	1602(9)	6.9	H16′	409(8)	159(15)	425(9)	
C14	608(11)	−993(15)	1990(10)	7.3	H20	245(9)	−198(16)	471(10)	
C15	1152(10)	−1305(13)	3030(11)	6.2	H20′	213(8)	−183(14)	572(9)	
C16	3761(9)	1221(16)	4646(11)	6.2	H21	351(9)	451(16)	553(10)	
C17	3720(14)	−448(21)	4558(14)	10.7	H21′	369(10)	298(18)	595(12)	
C18	3925(10)	−1057(17)	5523(10)	6.5	H25	177(9)	0(15)	657(10)	
C19	3189(12)	−1001(25)	5797(19)	13.6	H25′	108(8)	135(14)	644(9)	
C20	2310(9)	−1355(15)	5284(11)	5.8	H26	162(7)	570(11)	402(8)	
C21	3176(9)	3623(16)	5638(9)	6.1	H26′	135(9)	475(15)	476(9)	
C22	2831(12)	3941(32)	6337(11)	14.9	H27	28(8)	573(14)	370(9)	
C23	2064(9)	3381(17)	6412(9)	5.9	H27′	50(10)	530(17)	273(10)	
C24	2180(20)	2025(22)	6778(11)	16.3	H28	9(8)	304(13)	293(8)	
C25	1598(11)	917(17)	6295(10)	7.0	H28′	−57(8)	431(14)	270(9)	
C26	1354(8)	4790(13)	4081(9)	4.5	H29	−72(7)	413(12)	422(8)	
C27	449(9)	5013(15)	3378(11)	5.9	H29′	−98(10)	267(18)	356(11)	
C28	−217(8)	3851(15)	3180(10)	5.7	H30	46(15)	307(26)	517(17)	
C29	−498(12)	3305(20)	3926(13)	9.0	H30′	−32(8)	184(14)	502(9)	
C30	10(9)	2420(17)	4660(10)	5.9					

Table 2. Bond Lengths (in Å) between the Heavier Atoms of **2** with Estimated Standard Deviations in Parentheses

Bond	Length	Bond	Length	Bond	Length	Bond	Length
Fe–C1	2.052(15)	C1–C5	1.401(18)	C7–C8	1.469(20)	C17–C18	1.501(26)
Fe–C2	2.053(14)	C1–C11	1.485(21)	C7–C20	1.503(18)	C18–C19	1.442(32)
Fe–C3	2.082(11)	C2–C3	1.433(18)	C8–C9	1.414(15)	C19–C20	1.418(22)
Fe–C4	2.055(13)	C2–C16	1.535(18)	C8–C25	1.525(19)	C21–C22	1.426(27)
Fe–C5	2.032(13)	C3–C4	1.423(15)	C9–C10	1.423(19)	C22–C23	1.438(28)
Fe–C6	2.050(13)	C3–C21	1.555(16)	C9–C30	1.490(21)	C23–C24	1.432(26)
Fe–C7	2.066(13)	C4–C5	1.413(17)	C11–C12	1.544(18)	C24–C25	1.460(28)
Fe–C8	2.097(15)	C4–C26	1.484(19)	C12–C13	1.517(25)	C26–C27	1.497(17)
Fe–C9	2.080(14)	C6–C7	1.438(16)	C13–C14	1.502(23)	C27–C28	1.544(20)
Fe–C10	2.046(13)	C6–C10	1.406(19)	C14–C15	1.528(20)	C28–C29	1.487(28)
C1–C2	1.415(15)	C6–C15	1.552(22)	C16–C17	1.650(26)	C29–C30	1.416(22)

manner as the γ-methylene group approaches to the ferrocene moiety. The chains C1···C6 and C4···C9 can take such a conformation, because there is no substituent at the 5- and 10 positions. However, the chains C2···C7 and C3···C8 which are surrounded with the two bridges cannot take a boat form. Therefore, the two chains are forced to have a zigzag-like conformation to avoid steric effect of the bridges in both sides.

The β- and β'-carbon atoms C17, C19, C22, and C24 of the methylene bridges undergo large thermal vibrations. The root-mean-square displacement of these atoms along the thermal ellipsoid principal axes are listed in Table 4. Most of the largest axes lie nearly along the line bisecting the bonds linking the methylene carbon atoms. This is probably due to the disorder of these bridging carbon atoms. Apparent torsion angles along each chain are listed in Table 5 which were calculated by assuming the methylene carbon atoms situated at their mean position (Table 1). It is clear that the bridging methylene chains C1···C6 and C4···C9 are much more relieved situation since there is no bridge in the neighboring position

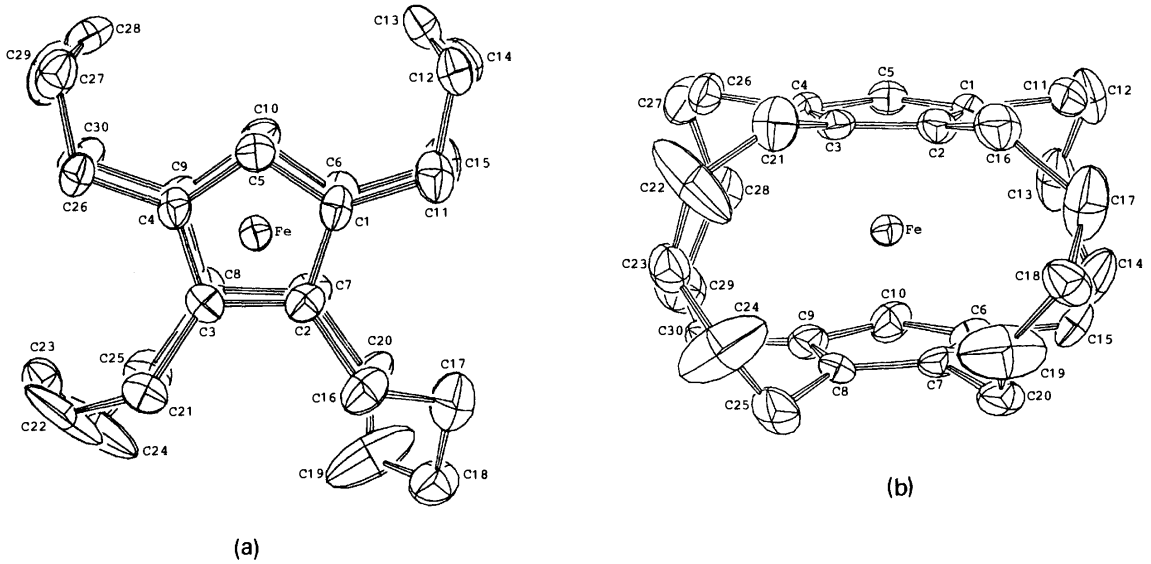

Fig. 1. (a) An ORTEP drawing[18] of the molecule viewed perpendicular to the plane formed by the two lines C1–C4 and C3–C5. The thermal ellipsoid encloses the region where the center of each atom will be found with probability 30%. Hydrogen atoms are omitted. (b) Same as (a) but rotated 90° about the horizontal line through C1 and C4.

Table 3. Bond Angles (in Degree) of **2** with Estimated Standard Deviations in Parentheses

Bond	Angle	Bond	Angle	Bond	Angle	Bond	Angle
C2-C1-C5	106.0(11)	C1-C5-C4	111.4(11)	C8-C9C-30	126.2(12)	C22-C21-C3	122.8(15)
C2-C1-C11	125.8(12)	C7-C6-C10	108.8(12)	C6-C10-C9	109.1(12)	C23-C22-C21	126.9(19)
C5-C1-C11	127.9(12)	C7-C6-C15	124.6(12)	C12-C11-C1	117.5(13)	C24-C23-C22	113.4(17)
C3-C2-C1	108.8(11)	C10-C6-C15	126.6(13)	C13-C12-C11	118.5(13)	C25-C24-C23	122.5(20)
C3-C2-C16	123.7(11)	C8-C7-C6	106.0(11)	C14-C13-C12	120.1(14)	C8-C25-C24	120.8(16)
C1-C2-C16	126.6(12)	C8-C7-C20	125.7(12)	C15-C14-C13	118.3(14)	C27-C26-C4	118.5(12)
C4-C3-C2	107.8(11)	C6-C7-C20	127.2(12)	C6-C15-C14	117.2(13)	C28-C27-C26	119.0(12)
C4-C3-C21	127.5(11)	C9-C8-C7	108.0(11)	C17-C16-C2	115.0(13)	C29-C28-C27	122.2(14)
C2-C3-C21	124.1(11)	C9-C8-C25	127.5(12)	C18-C17-C16	109.4(16)	C30-C29-C28	123.9(16)
C5-C4-C3	105.9(11)	C7-C8-C25	123.8(12)	C19-C18-C17	111.6(17)	C9-C30-C29	122.5(14)
C5-C4-C26	126.2(12)	C10-C9-C8	108.1(11)	C20-C19-C18	130.3(20)		
C3-C4-C26	127.3(11)	C10-C9-C30	125.6(12)	C7-C20-C19	122.0(15)		

Table 4. The Root-Mean-Square Displacements (in Å) of Atoms along the Three Principal Axes of the Thermal Ellipsoid. *U*1, *U*2, and *U*3 are Arranged in Order of the Magnitudes

	*U*1	*U*2	*U*3
C17	0.460	0.352	0.264
C19	0.598	0.321	0.240
C22	0.680	0.280	0.157
C24	0.704	0.296	0.189

(C5···C10) and the torsion angles along these chains are more close to those of the normal gauche conformation. Apparent shortening by oscillatory motions[20] of atoms is clearly seen in the bond lengths between the central two carbon atoms for each methylene chain (see Table 2).

Table 6 shows the planarity of the Cp rings and the deviations of atoms from the planes. The deviations of the α-methylene carbons linked directly to the Cp rings are in a direction expanding the ferrocene cage and the magnitude of the deviation is less remarkable for the above mentioned two relieved methylene chains. Based on these facts it may be clear that the pentamethylene chains are too long to accommodate between the two Cp rings, and that the chains in a boat conformation can link the ferrocene nucleus with less strain than that in a zigzag form.

The conformation of the ferrocene moiety is almost similar to that of tribridged phane **1**.[19] The two Cp rings are in an eclipsed conformation about the Cp–Fe–Cp axis. The Cp rings show a good planarity and the average value of the atomic deviations from its

Table 5. Torsion Angles (in Degree) along the Bridge Methylene Chain with Estimated Standard Deviations in Parentheses

Bond	Angle	Bond	Angle
C1-C11-C12-C13	−55.1(16)	C3-C21-C22-C23	23.2(28)
C11-C12-C13-C14	−63.3(17)	C21-C22-C23-C24	75.3(16)
C12-C13-C14-C15	62.6(16)	C22-C23-C24-C25	−127.8(19)
C13-C14-C15-C6	56.5(16)	C23-C24-C25-C8	44.0(20)
C2-C16-C17-C18	−110.6(13)	C4-C26-C27-C28	51.8(15)
C16-C17-C18-C19	78.8(16)	C26-C27-C28-C29	63.3(17)
C17-C18-C19-C20	47.3(29)	C27-C28-C29-C30	−76.5(20)
C18-C19-C20-C7	−97.5(10)	C28-C29-C30-C9	−35.9(20)

Table 6. The Least-Squares Planes of the Two Cp Rings of **2** and Deviations of Atoms (in Å) from the Planes with Estimated Standard Deviations in Parentheses

$0.5443X+0.6478Y-0.5329Z=1.233$			
C1	−0.004(11)	C11	0.093(13)
C2	−0.006(11)	C16	0.209(13)
C3	0.013(11)	C21	0.248(12)
C4	0.015(11)	C26	0.109(12)
C5	0.012(11)	Fe	−1.664(8)
$0.6036X+0.6676Y-0.4358Z=-1.409$			
C6	−0.009(12)	C15	−0.070(13)
C7	0.011(12)	C20	−0.199(13)
C8	−0.009(12)	C25	−0.236(14)
C9	0.003(11)	C30	−0.081(13)
C10	0.004(12)	Fe	1.672(8)

own least-squares plane is about 0.009 Å (root mean square). The distance between the two Cp rings through the Fe atom (3.336(16) Å) is slightly extended in comparison with that of **1** (3.293(2) Å). It is reasonable that addition of a pentamethylene chain which is too long to link between the two Cp rings results in the extension of the Cp ring distance.

Electronic Spectrum. The electronic spectrum of **2** exhibits a fairly large bathochromic shift of the d-d* absorption band in the visible region (460 nm). We have observed a linear relationship between the wavelength of the d-d* absorption and the number of tetramethylene bridges in [4$_n$]ferrocenophanes (n=0—5),[11,21,22] but there is no analogous relation in [5$_n$]ferrocenophanes. The wavelengths of the bands in mono-, di-, and tribridged phanes with pentamethylene chains are almost similar to that of ferrocene (443, 447, 446, 444, and 442 nm for ferrocene, [5]-, [5$_2$](1,2)-, [5$_2$](1,3)-, and [5$_3$](1,2,4)ferrocenophanes, respectively), but that of tetrabridged phane **2** is 18 nm higher than the same band of **1**. A linear relationship between the hypsochromic shift of the d-d* band and the compression of the Cp-Fe-Cp distance has been found in the study on the electronic spectra of various multibridged ferrocenophanes.[21] If the relation also holds for [5$_n$]ferrocenophanes, the slight elongation of the Cp-Fe-Cp distance in **2** as compared with that of **1** should result in a bathochromic shift of the band in **2**. However, we have not yet found a definitive explanation for the cause of the unusual shift in compound **2**.

The successive hypsochromic shift with the decrease of the methylene group of the 3,3′-bridge was shown in tetrabridged phanes (460, 454, and 447 nm for **2**, **11**, and **7**, respectively). Barr and Watts[23] reported that the d-d* band responded to a ring tilt deformation of the ferrocene nucleus and shifted to a long wavelength with increasing dihedral angle between the two Cp rings in ferrocenophanes. Accordingly, the shift behavior in tetrabridged phane would be reasonably explained by the "tilting effect," because the tiltings of the phanes presumably increase with the decrease of the length of the bridge at the 3,3′-position though the dihedral angles are not confirmed by structural analysis.

Experimental

All melting points were uncorrected. IR spectra were measured using a Hitachi model 215 grating infrared spectrometer. NMR spectra were measured on a JEOL JNM-FX100 spectrometer relative to tetramethylsilane as an internal standard. The figures in the parentheses of ^{13}C NMR spectral data represent the number of the peaks overlapping each other. Mass spectra were obtained with a Hitachi RMU-7M or a Hitachi M-80 double focusing mass spectrometer by electron impact ionizing technique at 70 eV. High-resolution mass spectra were analyzed on a Hitachi M-003 data processing system. Electronic spectra were measured on a Hitachi 330 spectrometer in tetrahydrofuran.

3-Formyl[5$_3$](1,2,4)ferrocenophane (3). A solution of [5$_3$](1,2,4)ferrocenophane (**1**)[13] (348 mg) and *N*,*N*-dimethylformamide (525 mg) in freshly distilled chloroform (15 ml) was stirred at 0 °C. To the cooled solution phosphoryl chloride (1.11 g) was added dropwise under a nitrogen atmosphere. The reaction mixture was stirred at 55 °C for 17 h, and then evaporated to dryness. Water was added to the residue, and the aqueous mixture was neutralized with aq. 20% NaOH. The mixture was extracted with benzene several times, and the extracts were washed with saturated aq. NaCl, dried over Na_2SO_4, and evaporated. The residue was column-chromatographed over alumina to be separated into two bands. The first band eluted with benzene yielded the starting material (44 mg, 13%). The second band eluted

with benzene-ethyl acetate (20:1) yielded aldehyde **3** (320 mg, 86%), which was recrystallized from ethyl acetate to give orange-red prisms; mp 145—148 °C. IR (KBr) 1670 (C=O) cm^{-1}; ^1H NMR ($CDCl_3$); δ=1.40—3.30 (30H, m, $-CH_2-$), 3.65 and 3.84 (each 1H, an AX system, J=1.6 Hz, 3'- and 5'-H), 4.16 (1H, s, 5-H), 10.33 (1H, s, -CHO); MS m/z (rel intensity), 418 (100, M^+), 389 (7), 388 (5).

Found: C, 74.70; H, 8.29%; m/z 418.1936. Calcd for $C_{26}H_{34}OFe$: C, 74.64; H, 8.19%; M, 418.1956.

Ethyl [5$_3$](1,2,4)Ferrocenophane-3-acrylate (4). To a solution of aldehyde **3** (100 mg) in dry benzene-ether (5:1, 6 ml) was added activated zinc (313 mg) and a small amount of iodine, and the mixture was stirred at room temperature under a nitrogen atmosphere. Ethyl bromoacetate (160 mg) was added dropwise to the suspension. The reaction mixture was refluxed on an oil bath at 110 °C for 10 min. After water was added, the mixture was extracted with benzene. The extracts were treated with concd HCl and then with aq. Na_2CO_3 containing ascorbic acid. The organic layer was washed with saturated aq. NaCl, dried over Na_2SO_4, and evaporated. The residue was eluted through a column of silica gel with benzene to yield acrylate **4** (120 mg, quant.), which was recrystallized from ethyl acetate to give red-violet flakes; mp 114—116 °C. IR (KBr) 1715 and 1625 (C=O and C=C) cm^{-1}; ^1H NMR ($CDCl_3$) δ=1.40—3.00 (30H, m, $-CH_2-$), 1.34 (3H, t, J=7 Hz, $-CH_3$), 3.49 and 3.59 (each 1H, an AX system, J=1.6 Hz, 3'- and 5'-H), 4.02 (1H, s, 5-H), 4.27 (2H, q, J=7 Hz, $-OCH_2-$), 6.08 and 7.87 (each 1H, an AX system, J=16 Hz, olefin-H); MS m/z (rel intensity) 488 (100, M^+), 460 (2).

Found: C, 73.46; H, 8.33%; m/z 488.2396. Calcd for $C_{30}H_{40}O_2Fe$: C, 73.76; H, 8.25%; M, 488.2376.

Ethyl [5$_3$](1,2,4)Ferrocenophane-3-propionate (5). Acrylate **4** (1.16 g) was reduced with H_2 gas (1 atm) and 10% Pd-C (350 mg) in acetone (80 mg) at room temperature for 24 h. The reaction mixture was evaporated and the residue was eluted through a short column of silica gel with benzene-ethyl acetate (3:1). The eluted propionate **5** (1.20 g, quant.) was recrystallized from ethyl acetate to give yellow prisms; mp 91.5—95 °C. IR (KBr) 1740 (C=O) cm^{-1}; ^1H NMR ($CDCl_3$) δ=1.40—3.00 (34H, m, $-CH_2-$), 1.27 (3H, t, J=7.5 Hz, $-CH_3$), 3.27 (1H, bs, 5-H), 3.62 (2H, bs, 3'- and 5'-H), 4.11 (2H, q, J=7.5 Hz, $-OCH_2-$); MS m/z (rel intensity) 490 (100, M^+), 4.76 (2), 461 (3), 417 (2), 388 (3).

Found: C, 73.46; H, 8.70%; m/z 490.2526. Calcd for $C_{30}H_{42}O_2Fe$: C, 73.46; H, 8.63%; M, 490.2532.

[5$_2$]-α-Oxo[3][5](1,2,3,4)ferrocenophane (6). Propionate **5** (100 mg) was dissolved into ethanol (20 ml) and the solution was added dropwise to 20% aq. NaOH (20 ml) which was heated at 90 °C. The reaction mixture was stirred at 90 °C for 10 min, and then neutralized with concd HCl. The mixture was extracted with benzene. The extracts were washed with saturated aq. NaCl, dried over Na_2SO_4, and evaporated. The residue, which was crude [5$_3$](1,2,4)ferrocenophane-3-propionic acid, was immediately used for the following reaction without further purification, because the acid was very sensitive to air.

The crude acid was dissolved into 1,2-dichloroethane, and oxygen in the solution was removed as much as possible by ultrasonic vibration. 1,2-Dichloroethane (25 ml) was added to 50% polyphosphoric acid ethyl ester (PPE) prepared in the usual way,[24] and the mixture was refluxed under an argon atmosphere for 1 h to remove oxygen in the reagent. The above solution of the acid was added dropwise to the refluxing solution of PPE, and the reaction mixture was refluxed on an oil bath at 80 °C under an argon atmosphere for 30 min. After 20% aq. NaOH containing ascorbic acid were added to be neutralized, the mixture was stirred at room temperature for 1 h and extracted with 1,2-dichloroethane. The extracts were washed with saturated aq. NaCl, dried over Na_2SO_4, and evaporated. To a solution of the residue in benzene was added a solution of diazomethane in ether. The mixture was stirred and evaporated, and the residue was dissolved into benzene again. Alumina was added to the benzene solution. The suspension was placed in a column packed with silica gel and eluted with benzene. The orange band yielded bridged product **6** (91 mg, quant.), which was recrystallized from ethyl acetate to give orange prisms; mp 225—228 °C. IR (KBr) 1665 (C=O) cm^{-1}; ^1H NMR ($CDCl_3$) δ=1.30—3.70 (34H, m, $-CH_2-$), 3.63 (1H, s, 5-H), 3.68 (1H, s, 5'-H); ^{13}C NMR ($CDCl_3$) δ=20.65, 21.24, 21.94, 22.06, 22.29, 22.41, 22.58, 23.17, 24.16, 24.34, 25.98 (3C), 26.21, 26.79, 33.35, and 47.80 (methylene-C), 70.67 and 73.30 (unsubstd. Cp-C), 70.26, 79.39, 83.54, 86.00, 86.12, 90.39, 90.68, and 93.02 (substd. Cp-C), 213.48 (C=O); MS m/z (rel intensity) 444 (100, M^+), 416 (24).

Found: C, 75.70; H, 8.13%; m/z 444.2093. Calcd for $C_{28}H_{36}OFe$: C, 75.71; H, 8.17%; M, 444.2112.

[5$_2$][3][5](1,2,3,4)Ferrocenophane (7). A solution of ketone **6** (100 mg) in absolute ether (10 ml) was added to a suspension of $LiAlH_4$ (100 mg) and $AlCl_3$ (200 mg) in ether (10 ml). The reaction mixture was stirred at room temperature for 3 h. Saturated aq. NH_4Cl was added to the mixture and the hydrolyzate was extracted with benzene. The extracts were washed with saturated aq. NaCl, dried over Na_2SO_4, and evaporated. Column chromatographic purification of the residue over alumina gave compound **7** (97 mg, quant.), which was recrystallized from ethyl acetate to give yellow prisms; mp 212—214 °C. ^1H NMR ($CDCl_3$) δ=1.20—3.20 (36H, m, $-CH_2-$), 3.56 (2H, s, Cp-H); ^{13}C NMR ($CDCl_3$) δ=18.81, 20.57, 21.05, 21.83, 22.61, 22.91, 24.61, 25.83, 26.07, 32.22, and 33.87 (methylene-C), 70.18 (unsubstd. Cp-C), 82.81, 86.41, and 91.53(2C) (substd. Cp-C); λ_{max} (THF)=447 nm (ε=245); MS m/z (rel intensity) 430 (100, M^+).

Found: C, 78.14; H, 8.88; m/z 430.2320. Calcd for $C_{28}H_{38}Fe$: C, 78.17; H, 8.90; M, 430.2320.

[5$_2$]-α-Oxo[4][5]- and [5$_2$]-α-Oxo[5][5](1,2,3,4)ferrocenophanes (9 and 10). Ketone **6** (500 mg) was dissolved into dry benzene (50 ml) and BF_3 etherate (0.7 ml) was added to the solution under a nitrogen atmosphere. The mixture was cooled on an ice-water bath. To the vigorously stirring solution of the complex was rapidly added an ether solution of alcohol-free diazomethane (50 ml), which had been prepared in the usual way[13] and stored over KOH. Water containing ascorbic acid and then 20% aq. NaOH was added and the mixture was extracted with benzene. The extracts were washed with saturated aq. NaCl, dried over Na_2SO_4, and evaporated. The residue was column-chromatographed over silica gel with benzene. The first band yielded [5$_2$]-β-oxo[4][5](1,2,3,4)ferrocenophane (**8**) (180 mg, 35%). IR (KBr) 1700 (C=O) cm^{-1}. The ketone **8** was contaminated with further enlarged products, which could not be removed by

means of various methods for purification.

The second band yielded ketone **10** (160 mg, 30%), which was recrystallized from ethyl acetate to give orange prisms; mp>300 °C. IR (KBr) 1650 (C=O) cm^{-1}; ^1H NMR ($CDCl_3$) δ=1.60—3.00 (38H, m, $-CH_2-$), 3.69 (1H, s, 5-H), 4.00 (1H, s, 5′-H); ^{13}C NMR ($CDCl_3$) δ=21.70, 22.00, 22.52, 22.70 (3C), 22.93 (3C), 24.63, 24.75, 25.16(2C), 25.57, 25.68, 25.80, 26.68, 28.37, and 39.84 (methylene-C), 69.68 and 73.07 (unsubstd. Cp-C), 81.03, 82.78, 85.47, 86.06, 87.52, 88.51, 88.92, and 89.10 (substd. Cp-C), 210.84 (C=O); MS *m/z* (rel intensity) 472 (100, M^+), 458 (7), 444 (15).

Found: C, 76.13; H, 8.29%; *m/z* 472.2420. Calcd for $C_{30}H_{40}OFe$: C, 76.30; H, 8.54%; M, 472.2426.

The third band yielded ketone **9** (170 mg, 33%), which was recrystallized from ethyl acetate to give orange prisms; mp 258—261 °C. IR (KBr) 1660 (C=O) cm^{-1}; ^1H NMR ($CDCl_3$) δ=1.40—3.00 (36H, m, $-CH_2-$), 3.68 (1H, s, 5-H), 3.91 (1H, s, 5′-H); ^{13}C NMR ($CDCl_3$) δ=21.41, 21.82, 22.23, 22.46, 22.64, 22.87, 23.05, 23.34, 23.64, 24.22, 24.45, 25.62, 25.74(2C), 26.09, 30.13, 31.01, and 43.29 (methylene-C), 69.21 and 73.25 (unsubstd. Cp-C), 79.97, 82.90, 85.12, 85.53, 86.88, 89.16(2C), and 89.74 (substd. Cp-C), 210.08 (C=O); *m/z* (rel intensity) 458 (100, M^+).

Found: C, 75.90; H, 8.21; *m/z* 458.2271. Calcd. for $C_{29}H_{38}OFe$: C, 76.01; H, 8.36; M, 458.2270.

The ketone **9** (100 mg) was converted into the desired ketone **10** (45 mg, 42%) by bridge enlargement in benzene (20 ml) with BF_3 etherate (0.14 ml) and diazomethane (ether solution 10 ml), according to the same procedure as the reaction of **6**.

[5₂][4][5](1,2,3,4)Ferrocenophane (11). Reduction of ketone **9** (100 mg) with $LiAlH_4$ (100 mg) and $AlCl_3$ (200 mg) in ether (20 ml) was carried out according to the same procedure as in the preparation of **7**. The crude product **11** (84 mg, 87%) was recrystallized from ethyl acetate to give yellow prisms; mp 242—243 °C. ^1H NMR ($CDCl_3$) δ=1.30—2.90 (38H, m, $-CH_2-$), 3.63 (2H, s, Cp-H); ^{13}C NMR ($CDCl_3$) δ=21.20, 21.69, 22.47, 22.86, 23.10, 24.32, 25.64, 26.17(2C), 27.24, and 27.78 (methylene-C), 68.67 (unsubstd. Cp-C), 81.59, 81.78, 85.83, and 87.58 (substd. Cp-C); λ_{max}(THF)=454 nm (ε=130); MS *m/z* (rel intensity) 444 (100, M^+).

Found: C, 78.34; H, 9.04%; *m/z* 444.2467. Calcd for $C_{29}H_{40}Fe$: C, 78.37; H, 9.07%; M, 444.2470.

[5₄](1,2,3,4)Ferrocenophane (2). Reduction of ketone **10** (290 mg) with $LiAlH_4$ (233 mg) and $AlCl_3$ (490 mg) in ether (10 ml) was carried out according to the same procedure as in the preparation of **7**. The crude product **2** (223 mg, 80%) was recrystallized from ethyl acetate to give yellow prisms; mp 245 °C (decomp). ^1H NMR ($CDCl_3$) δ=1.30—2.90 (40H, m, $-CH_2-$), 3.70 (2H, s, Cp-H); ^{13}C NMR ($CDCl_3$) δ=21.88, 22.76, 22.96, 25.20, 25.29, and 28.22 (methylene-C), 68.43 (unsubstd. Cp-C), 83.39 and 87.09 (substd. Cp-C); λ_{max}(THF)= 460 nm (ε=124); MS *m/z* (rel intensity) 458 (100, M^+).

Found: C, 78.88; H, 9.23%; *m/z* 458.2613. Calcd for $C_{30}H_{42}Fe$: C, 78.59; H, 9.23%; M, 458.2633.

X-Ray Crystallographic Analysis of 2. Crystals of **2** were grown in a dichloromethane–hexane solution as pale orange prisms elongated along the c axis. A specimen with approximate dimensions 0.5×0.1×0.05 mm was chosen for X-ray diffraction measurement. Crystal data and intensity data were collected on a Philips PW 1100 diffractometer using graphite monochromated Mo $K\alpha$ radiation.

Crystal data: [5₄](1,2,3,4)Ferrocenophane, $C_{30}H_{42}Fe$, MW= 458.5. Monoclinic, space group $P2_1/n$, Z=4, D_{cal}=1.314 g cm^{-3}. Lattice constants, a=16.691(10), b=9.858(5), c= 15.237(8) Å, β=112.43(6)°, U=2317 Å^3. μ for Mo $K\alpha$=6.6 cm^{-1}.

Intensities of 1710 reflections were measured as above the $2\sigma(I)$ level out of 3737 independent reflections within the 2θ angle range 6° through 50°. No absorption correction was applied.

The crystal structure was solved by the heavy atom method and refined by the block-diagonal-matrix least-squares calculations including 30 hydrogen atoms with isotropic temperature factors and dispersion terms of the atomic scattering factor of Fe for Mo $K\alpha$ radiation.[25] Twelve hydrogen atoms attached to C17, C18, C19, C22, C23, and C24 were not included because these were not found on the diffraction electron-density map due to the disorders described in results and discussion. The final R value was 0.085 for 1710 reflections. Bond lengths and bond angles calculated from the refined atomic coordinates (Table 1) are listed in Tables 2 and 3.††

References

1) This work has been presented as a preliminary report: M. Hisatome, J. Watanabe, R. Yamashita, and K. Yamakawa, 18th Symposium on Structural Organic Chemistry, Toyama, Oct. 1985, Abstr. No. B2-08.

2) The nomenclature of ferrocenophanes in the present paper is a modification of that presented by Vögtle and Neumann.[3]

3) F. Vögtle and P. Neumann, *Tetrahedron*, **26**, 5847 (1970).

4) W. E. Watts, *Organomet. Chem. Rev.*, **2**, 231 (1967).

5) A. Kasahara, *Kagaku*, **38**, 859 (1983).

6) M. Hisatome, Y. Kawajiri, K. Yamakawa, and Y. Iitaka, *Tetrahedron Lett.*, **1979**, 1777.

7) M. Hisatome, Y. Kawajiri, K. Yamakawa, Y. Harada, and Y. Iitaka, *Tetrahedron Lett.*, **23**, 1713 (1982).

8) M. Hisatome, K. Kawajiri, K. Yamakawa, K. Mamiya, Y. Harada, and Y. Iitaka, *Inorg. Chem.*, **21**, 1345 (1982).

9) M. Hisatome, J. Watanabe, K. Yamakawa, K. Kozawa, and T. Uchida, *J. Organomet. Chem.*, **262**, 365 (1984).

10) J. Watanabe, M. Hisatome, and K. Yamakawa, *Tetrahedron Lett.*, **28**, 1427 (1987).

11) M. Hisatome, J. Watanabe, K. Yamakawa, and Y. Iitaka, *J. Am. Chem. Soc.*, **108**, 1333 (1986).

12) A. N. Nesmeyanov, M. I. Rybinskaya, G. B. Schul'pin, and M. V. Tolstaya, *Dokl. Akad. Nauk SSSR*, **229**, 1124 (1976).

13) M. Hisatome and M. Hillman, *J. Organomet. Chem.*, **212**, 217 (1981).

14) T. H. Barr and W. E. Watts, *Tetrahedron*, **24**, 3219, 6111 (1968); **25**, 861 (1969).

15) J. A. Winstead, *J. Org. Chem.*, **37**, 1271 (1972).

16) S. Toma and M. Salisova, *Acta Fac. Rerum Nat. Univ. Comeninae Chim.*, **21**, 59 (1975).

†† Tables of anisotropic temperature factors, and observed and calculated structure factors are deposited as Document No. 8790 at the Office of the Editor of Bull. Chem. Soc. Jpn.

17) P. Elecko, *Acta Fac. Rerum Nat. Univ. Comeninae Chim.*, **21**, 49 (1975).
18) C. K. Johnson, ORTEP, Report ORNL-3794, Oak Ridge National Laboratory, Ork Ridge, Tennessee, U.S.A., 1965.
19) M. Hillman, E. Fujita, and H. Dauplaise, *Organometallics*, **3**, 1170 (1984).
20) D. W. J. Cruickshank, *Acta Crystallogr.*, **14**, 896 (1961).
21) M. Hisatome, J. Watanabe, K. Yamakawa, K. Kozawa, and T. Uchida, *Nippon Kagaku Kaishi*, **1985**, 572.
22) J. Watanabe, Ph. D. Thesis, Science University of Tokyo, Tokyo, 1987.
23) T. H. Barr and W. E. Watts, *J. Organomet. Chem.*, **15**, 177 (1968).
24) Y. Kawajiri, Ph. D. Thesis, Science University of Tokyo, Tokyo, 1982.
25) International Tables for X-Ray Crystallography, Kynoch Press, Birmingham, England (1974), Vol. IV, p. 149.

The Conformational Studies of 4,7,10-Trioxa-1,13-dithia[13](1,1′)ruthenocenophane and Its $PdCl_2$ Complex by X-Ray Analyses†

Sadatoshi Akabori,* Sadao Sato,*,†† Kayoko Kawazoe,†† Masaru Sato,††† and Yoichi Habata

Department of Chemistry, Faculty of Science, Toho University, Funabashi, Chiba 274
††Analytical and Metabolic Research Laboratories, Sankyo Co., Ltd., Hiromachi, Shinagawa-ku, Tokyo 140
†††Chemical Analysis Center, Saitama University, Urawa, Saitama 338

(Received November 12, 1987)

Dichlorobis(4,7,10-trioxa-1,13-dithia[13](1,1′)ruthenocenophane)palladium(II) (**6**) was obtained by the reaction of 4,7,10-trioxa-1,13-dithia[13](1,1′)ruthenocenophane (**5**) with dichlorobis(acetonitrile)palladium(II) in 72% yield. The crystal structures of the complex **6** and its metal free ligand **5** were determined by the X-ray method. The crystal data: **5**, monoclinic, $P2_1/a$, a=18.783(2), b=7.895(1), c=12.892(1) Å, β=93.53(1)°, U=1908.2 Å^3, Z=4, D_c=1.58 g cm^{-3}, μ(Mo $K\alpha$)=10 cm^{-1}. **6**, triclinic, $P\bar{1}$, a=13.956(2), b=9.174(1), c=8.770(1) Å, α=86.61(1), β=75.54(1), γ=94.37(1)°, U=1080.6 Å^3, Z=2, D_c=1.94 g cm^{-3}, μ(Mo $K\alpha$)=20 cm^{-1}. The Pd atom of **6** bonded to the two sulfur atoms of the ligand and the torsion angle (69.2°) around the z-axis of the ruthenocenophane nucleus in the metal-free ligand is much larger than the corresponding one (0.4°) in the complex. These results are completely opposite of the case of 1,4,7,10-tetrathia[10](1,1′)ruthenocenophane and its Pt complex. Furthermore, the intramolecular atomic distance (3.697 Å) between the Ru and Pd atoms in **6** suggests the absence of the Ru–Pd dative bond.

Although a number of crown, thiacrown, and azacrown ether complexes of alkali, alkaline earth, and transition metal ions have already been reported,[1] only a few complexes of platinum group metals with the above macrocyclic compounds are known.[2] Furthermore, few conformational studies of the complexes of metallocenophanes containing polyether and polythiaether moieties with metal ions by X-ray analyses have been carried out,[3–7] although many metallocenophanes have been described.[8–16] A comparison of the X-ray structures of the metal-free ligand with its metal complex can often reveal changes in the molecular conformation which is caused by complexation. In connection with the above viewpoints, we have reported the crystal structures of 1,10-dioxa-4,7-dithia- and 1,4,7,10-tetrathia[10](1,1′)ruthenocenophanes (**1** and **2**) and their platinum and/or palladium complexes (**3** and **4**).[5,6] The torsion angle (68°) between the C(1)–S(6) and S(15)–C(16) bond around the z-axis of the ruthenocene nucleus in the palladium complex **4** is much larger than the corresponding one (5.3°) in the metal-free ligand **2**, although the two Cp rings for these compounds take an eclipsed conformation and the dihedral angles between them are 2.5 and 2.4° for **2** and **4**. Also very similar results were obtained in the cases of [10](1,1′)ruthenocenophane (**1**) and its platinum complex **3**. Furthermore, we have reported on the preparation of polyoxa-1,n-dithia[n](1,1′)ruthenocenophanes by the reaction of disodium ruthenocene-1,1′-dithiolate with dihalide.[4] In this paper[17] we report the X-ray analysis of 4,7,10-trioxa-1,13-dithia[13](1,1′)ruthenocenophane (**5**) and its palladium complex **6**.

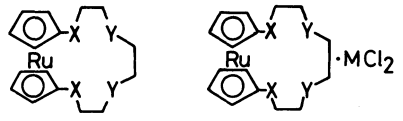

1: X=O, Y=S
2: X=Y=S
3: X=O, Y=S, M=Pd
4: X=Y=S, M=Pt

A solution of $PdCl_2\cdot(CH_3CN)_2$ in acetonitrile was reacted with a equimolar amount of **5** in acetonitrile to give 1 : 1 complex **6** in 72% yield. The melting point of the palladium complex **6** was higher than that of the corresponding metal free ligand **5**. The ^{1}H NMR spectrum of **5** in DMSO-d_6 showed a pair of triplets corresponding to the α- and β-ring protons of the ruthenocene nucleus at δ 4.64 (J=1.7 Hz, 4H) and 4.77 (J=1.7 Hz, 4H), in addition to a singlet at δ 3.75 (OCH_2CH_2O, 8H) and two triplets at δ 2.85 (J=6.6 Hz, SCH_2, 4H) and 3.60 (J=6.6 Hz, OCH_2, 4H). These results suggest that **5** in the solution takes a symmetrical structure which differs from its conformation in the solid state as described below. Furthermore, the differences in the chemical shifts between all the protons of **5** and **6** were not observed in DMSO, because the complex **6** in the solution seems to take a solvolytic form. The result is consistent with those of [10](1,1′)ruthenocenophanes and their complexes.[5,6] Measurements of the ^{1}H NMR spectra of **6** in less polar solvents such as CD_3CN and $CDCl_3$ were unsuccessful because the low solubility of the complex **6** in such solvents.

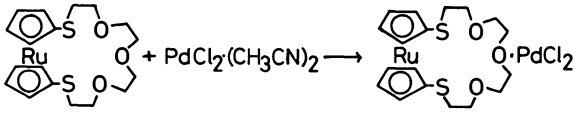

5 6

† Dedicated to Professor Michinori Ōki on the occasion of his 60th birthday.

Table 1. Fractional Atomic Coordinates ($\times 10^4$) and Thermal Parameters ($Å^2$), with Estimated Standard Deviations in Parentheses of **5**

Atom	x	y	z	B_{eq}[25]
Ru	3742.6(3)	6044.6(9)	3954.5(5)	3.08
C(1)	4518(4)	7474(11)	3101(6)	3.91
C(2)	4858(4)	6868(11)	4067(7)	4.11
C(3)	4512(5)	7645(12)	4876(7)	4.62
C(4)	3943(5)	8673(11)	4419(7)	4.97
C(5)	3956(4)	8572(10)	3313(7)	4.16
S(6)	4904(1)	7217(4)	1893(2)	6.09
C(7)	4271(5)	5899(12)	1169(6)	4.99
C(8)	4525(5)	4076(14)	1255(7)	5.79
O(9)	4030(4)	3127(8)	658(5)	6.04
C(10)	4168(5)	1352(13)	696(7)	5.90
C(11)	3509(5)	420(12)	373(7)	5.21
O(12)	3033(3)	653(8)	1165(4)	5.14
C(13)	2332(6)	108(13)	880(8)	6.45
C(14)	1866(5)	529(12)	1717(8)	6.26
O(15)	1736(3)	2333(8)	1734(5)	5.52
C(16)	1426(5)	2829(12)	2651(7)	5.19
C(17)	1303(5)	4702(12)	2628(7)	4.98
S(18)	2086(1)	6088(3)	2599(2)	4.72
C(19)	2698(4)	5021(10)	3456(6)	3.44
C(20)	3207(4)	3835(11)	3166(6)	4.03
C(21)	3579(4)	3322(10)	4119(8)	5.22
C(22)	3297(4)	4124(12)	4974(7)	4.61
C(23)	2752(4)	5217(11)	4577(6)	4.14

Table 2. Fractional Atomic Coordinates ($\times 10^4$) and Thermal Parameters ($Å^2$), with Estimated Standard Deviations in Parentheses of **6**

Atom	x	y	z	B_{eq}[25]
Ru	9028.3(4)	3395.6(6)	3220.7(6)	2.45
Pd	7464.6(4)	2650.7(5)	466.3(6)	1.80
Cl(1)	7124(2)	4688(2)	−895(2)	3.66
Cl(2)	8373(2)	1860(2)	−1862(2)	3.63
C(1)	7679(5)	4405(7)	3390(8)	2.21
C(2)	8463(5)	5329(7)	2365(9)	2.68
C(3)	9137(6)	5782(8)	3272(10)	3.43
C(4)	8750(6)	5138(8)	4845(9)	3.14
C(5)	7851(6)	4276(8)	4934(8)	2.80
S(6)	6683(1)	3379(2)	2913(2)	2.10
C(7)	5829(5)	4743(8)	2807(9)	3.00
C(8)	4877(6)	3979(10)	2645(10)	4.04
O(9)	4460(4)	3048(7)	3989(7)	4.26
C(10)	3613(7)	2110(12)	3902(14)	5.71
C(11)	3787(7)	534(11)	4059(11)	4.76
O(12)	4502(4)	212(6)	2690(7)	3.85
C(13)	4520(7)	−1351(10)	2623(11)	4.41
C(14)	5354(7)	−1662(9)	1260(11)	4.10
O(15)	6273(5)	−1430(6)	1675(7)	3.94
C(16)	7102(7)	−1353(9)	341(10)	3.96
C(17)	8009(7)	−884(8)	886(10)	3.75
S(18)	7773(1)	706(2)	2002(2)	2.39
C(19)	8931(5)	1288(8)	2323(9)	2.66
C(20)	9736(6)	2176(9)	1280(9)	3.17
C(21)	10442(6)	2543(10)	2157(11)	3.81
C(22)	10080(7)	1878(9)	3697(11)	4.19
C(23)	9140(7)	1085(8)	3828(10)	3.68

The metal free ligand **5** and its Pd complex **6** were further characterized by X-ray crystallographical studies. The final atomic parameters for **5** and **6** are listed in Tables 1 and 2, and bond lengths as well as bond and torsion angles are given in Tables 3 and 4 for **5** and **6**, respectively. The molecular structures of **5** and **6** are illustrated in Fig. 1.

In spite of the steric hindrance due to the two Cp rings the interesting selective coordination of the S(6) and S(18) atoms in **6** on the Pd atom suggests that the Pd atom has a higher complexation ability on the S atoms than the O atoms. The Pd atom bonded to the two S atoms of the oxathiacrown ether moiety has a slightly distorted cis square-planar configuration. The dihedral angle between the planes defined by S(6)–Pd–S(18) and Cl(1)–Pd–Cl(2) is 4.1(1)°. The coordination geometry of the Pd atom is similar to that found in the platinum complex of [10]ruthenocenophane **4**[6] except for the difference of the coordinated site in the macrocyclic ring. The intramolecular atomic distance between the Ru and Pd atoms is 3.697(1) Å. This value is much longer than that of the Ru–Pd dative bond (2.692(1) Å) in (1,1′-ruthenocenedithiolato-S,S′,Ru)(triphenylphosphine)palladium(II)[18] and its analogues,[19] and indicates no direct metal–metal interaction between the coordinated palladium atom and the ruthenium atom of the ruthenocene nucleus in the complex **6**. This finding is very different from the result[20] obtained in the 1:1 complex **8** of 1,4,7-trithia[7](1,1′)-ferrocenophane (**7**) with $(CH_3CN)_4 \cdot Pd(BF_4)_2$. Palladium atom was incorporated in the cavity of the macrocyclic moiety of **7** and coordinated by the three sulfur atoms to form the Fe–Pd dative bond. The absence of the Ru–Pd dative bond in **6** attributed to the strong bonding force of the Pd–Cl bond compared with Pd–B bond, because the two Pd–Cl bond length in **6** are 2.303(2) and 2.308(2) Å, respectively, which are consistent with the sum of the covalent radii[21] of Pd and Cl atoms.

The conformation of the organic ligand moiety of the complex **6** differs greatly from that of the metal-free ligand **5**. The main conformational changes are reflected in the overlapping patterns between the two Cp rings and in the torsion angles of the macrocyclic moiety. The Cp rings take an eclipsed conformation, in which the dihedral angles between them are 5.5(4) and 4.4(3)° for **5** and **6**, respectively. The torsion angle C(1)–Cp1–Cp2–C(19) (Cp1 and Cp2 are the centroids of the Cp rings) in **5** is 69.2°, although that in **6** is only 0.4°. As shown in Fig. 2, these results are just the opposite of the cases of [10](1,1′)ruthenocenophanes and their platinum and palladium complexes;[5,6] the metal-free ligand **2** has a small torsion angle (5.3°), while the torsion angle of its platinum complex is a large one (68°). The torsion angles in [3](1,1′)- and [4](1,1′)ruthenocenophanes are 14.8(2) and 1.7(2)°, respectively.[9,10] However, Cameron et al.[8] reported that the torsion angle in [4](1,1′)ferrocenophane is

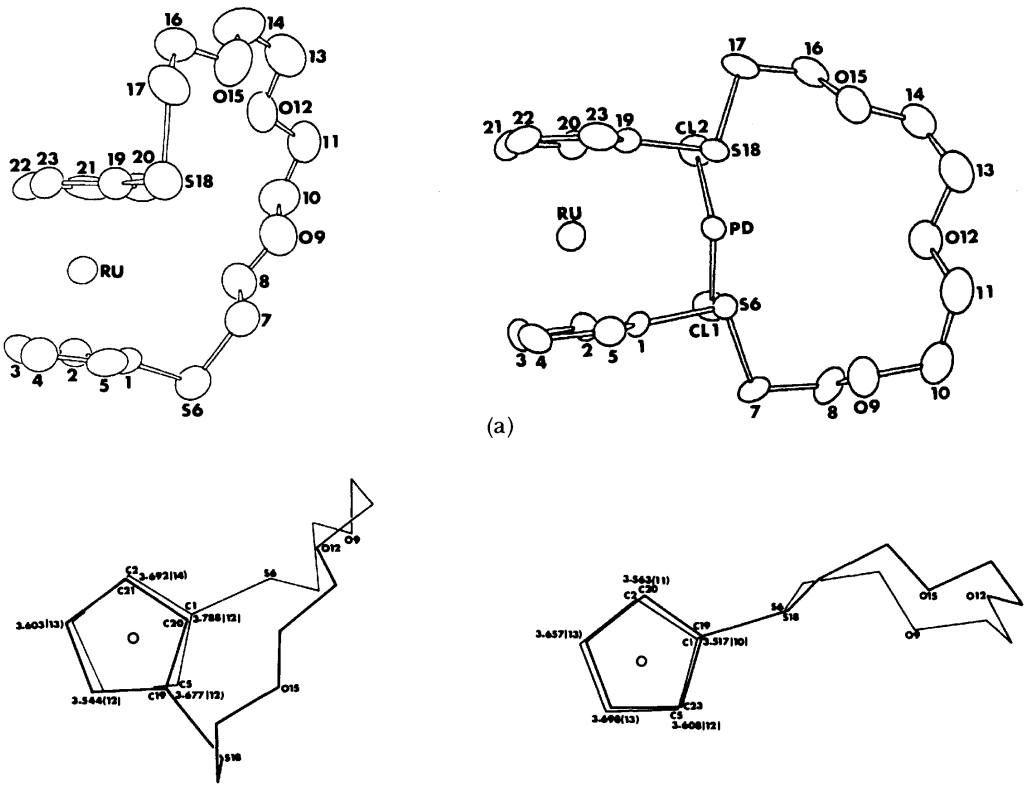

Fig. 1. (a) ORTEP (Johnson, 1965) drawings of molecules **5** and **6** with atom numbering scheme. (b) Projections of the organic ligand moieties on the Cp ring containing the C(1) atom with the C····C distances (Å) between the rings. An open circle denotes the Ru atom.

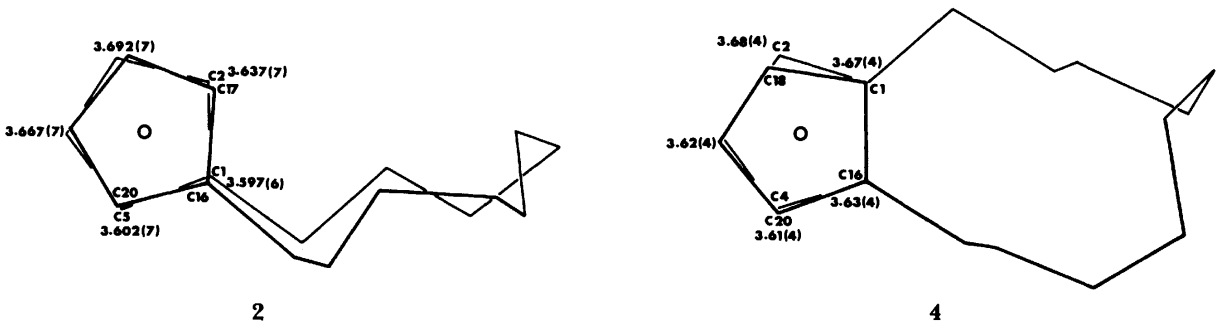

Fig. 2. Projections of the organic ligand moieties on the Cp ring containing the C(1) atom with the C····C distances (Å) between the rings. An open circle denotes the Ru atom (Ref. 5).

approximately 36°. Therefore, the conformational stability around the *z*-axis of the ruthenocene nucleus in the metal-free ligands is attributable to the ring size of the macrocyclic rings. The large rotational angle (69.2°) between the two Cp rings in the metal-free ligand **5** causes the two S atoms attached to each Cp ring to separate by more than 4.5 Å from each other, and this distance is too long to form the complex. In order to form the complex **6**, it is necessary to approach the two S atoms more closely and the lobes of lone pair electrons are rotate in the same direction. It was reported that the energy barrier of the rotation around the *z*-axis (Cpl–Ru–Cp2) of ruthenocene is only 3—6 kcal mol^{-1}.[22] Therefore, the energy of the rotation around the *z*-axis of the ruthenocene nucleus is compensated by the conformational changes of the macrocyclic moiety. Indeed, the three torsion angles, C(1)–S(6)–C(7)–C(8), S(6)–C(7)–C(8)–O(9), and C(16)–

Table 3. Bond Lengths (Å) and Bond and Torsion Angles (°) in **5**

1	2	3	4	1-2	1-2-3	1-2-3-4
Dithia-crown moiety						
S(6)	C(1)	C(2)	C(3)	1.769(9)	122.5(7)	165.2(4)
S(6)	C(1)	C(5)	C(4)		126.6(7)	−165.7(5)
C(2)	C(1)	S(6)	C(7)			117.2(8)
C(5)	C(1)	S(6)	C(7)			−78.2(9)
C(1)	S(6)	C(7)	C(8)		103.3(4)	−97.3(7)
S(6)	C(7)	C(8)	O(9)	1.798(10)	108.4(7)	−178.3(3)
C(7)	C(8)	O(9)	C(10)	1.518(14)	105.9(8)	−176.9(7)
C(8)	O(9)	C(10)	C(11)	1.390(13)	113.4(8)	160.0(7)
O(9)	C(10)	C(11)	O(12)	1.426(12)	109.4(8)	−69.1(9)
C(10)	C(11)	O(12)	C(13)	1.478(14)	106.8(8)	168.7(7)
C(11)	O(12)	C(13)	C(14)	1.410(11)	113.2(7)	−175.4(7)
O(12)	C(13)	C(14)	O(15)	1.414(12)	109.1(9)	73.0(10)
C(13)	C(14)	O(15)	C(16)	1.469(15)	110.1(9)	−167.1(8)
C(14)	O(15)	C(16)	C(17)	1.446(13)	111.5(7)	180.0(7)
O(15)	C(16)	C(17)	S(18)	1.405(12)	109.3(8)	−63.0(10)
C(16)	C(17)	S(18)	C(19)	1.497(14)	117.8(7)	−39.3(8)
C(17)	S(18)	C(19)	C(20)	1.836(10)	101.3(4)	93.9(8)
C(17)	S(18)	C(19)	C(23)			−85.5(8)
S(18)	C(19)	C(20)	C(21)	1.759(8)	125.5(6)	179.8(5)
S(18)	C(19)	C(23)	C(22)		125.2(6)	179.0(4)
Cyclopentadienyl ring						
C(1)	C(2)	C(3)	C(4)	1.445(12)	107.2(8)	2.3(10)
C(2)	C(3)	C(4)	C(5)	1.404(13)	107.9(8)	−2.0(11)
C(3)	C(4)	C(5)	C(1)	1.438(13)	108.7(8)	0.9(10)
C(4)	C(5)	C(1)	C(2)	1.429(12)	106.7(7)	0.5(10)
C(5)	C(1)	C(2)	C(3)	1.406(12)	109.5(7)	−1.8(10)
C(19)	C(20)	C(21)	C(22)	1.405(11)	105.3(8)	1.7(11)
C(20)	C(21)	C(22)	C(23)	1.434(13)	111.0(9)	−2.0(12)
C(21)	C(22)	C(23)	C(19)	1.402(14)	107.0(8)	1.4(11)
C(22)	C(23)	C(19)	C(20)	1.411(13)	107.5(8)	−0.4(10)
C(23)	C(19)	C(20)	C(21)	1.451(12)	109.3(7)	−0.7(10)

C(17)–S(18)–C(19), in **6** are remarkably changed by the complexation, compared with those of the corresponding metal-free ligand **5** as shown in Fig. 1.

Experimental

The decomposition point has not been corrected. ^{1}H NMR spectra were obtained on a JEOL FX-90Q spectrometer with TMS as an internal standard.

Materials. 4,7,10-Trioxa-1,13-dithia[13](1,1′)ruthenocenophane (**5**) was prepared according to the previously reported method.[4]

Dichlorobis(acetonitrile)palladium(II) was prepared according to methods described in the literature.[23]

Dichloro(4,7,10-trioxa-1,13-dithia[13](1,1′)ruthenocenophane)palladium(II) (**6**). A solution of 14 mg (54 mmol) of dichlorobis(acetonitrile)palladium(II) in 1 cm^3 of acetonitrile was added, dropwise, to a solution of 1 cm^3 of acetonitrile containing 23 mg (51 mmol) of **5**. The resulting precipitates were filtered and washed with a small amount of acetonitrile to give a 1:1 metal complex **6** in 72% yield. Mp 200 °C (decomp).

Found: C, 34.26; H, 3.84. Calcd for $C_{18}H_{24}O_3S_2RuPdCl_2$: C, 34.27; H, 3.84.

X-Ray Crystallography. Crystals of dimensions 0.4×0.2×0.1 mm for the metal free ligand **5** and 0.4×0.3×0.15 mm for the Pd-complex **6** were used for X-ray crystallography. Crystal data are as follows: **5**, $C_{18}H_{24}O_3S_2Ru$, M_w=456.3, Monoclinic, $P2_1/a$, a=18.783(2), b=7.895(1), c=12.892(1) Å, β=93.53(1)°, U=1908.2 Å^3, Z=4, D_x=1.58 g cm^{-3}, μ(Mo $K\alpha$)=10 cm^{-1}. **6**, $C_{18}H_{24}O_3S_2RuPdCl_2$, M_w=630.9, triclinic, $P\bar{1}$, a=13.956(2), b=9.174(1), c=8.770(1) Å, α=86.61(1), β=75.54(1), γ=94.37(1)°, U=1080.6 Å^3, Z=2, D_x=1.94 g cm^{-3}, μ(Mo $K\alpha$)=20 cm^{-1}.

Intensity data for $2\theta \leq 50°$ were recorded on a Rigaku AFC-5R with graphite-monochromatized Mo $K\alpha$ radiation. A total of 3362 (**5**) and 3424 (**6**) independent reflections were corrected for Lorentz and polarization factors but not for absorption. Both structures **5** and **6** were solved by the heavy-atom method, and refined by block-diagonal least squares methods. The positions of the hydrogen atoms were estimated using standard geometry. The final refinements with anisotropic temperature factors for the nonhydrogen atoms and isotropic temperature factors for the hydrogen atoms were lowered R values 0.054 (R_w=0.049, $w=1/\sigma(F_o)$, 2511 observed reflections with $F_o \geq 2\sigma(F_o)$) and 0.039 (R_w=0.049, $w=1/\sigma(F_o)$, 3129 observed reflections with $F_o > 2\sigma(F_o)$) for **5** and **6**, respectively. Anomalous dispersion corrections were applied to the scattering factors of Pd, Ru, Cl, and S.[24]

List of structural factors, anisotropic thermal parameters and H-atom coordinations are kept at the Chemical Society of Japan (Document No. 8792)

Table 4. Bond Lengths (Å) and Bond and Torsion Angles (°) in the Complex **6**

1	2	3	4	1-2	1-2-3	1-2-3-4
Dithia-crown moiety						
S(6)	C(1)	C(2)	C(3)	1.769(7)	128.3(5)	−173.8(4)
S(6)	C(1)	C(5)	C(4)		122.2(5)	174.6(3)
C(2)	C(1)	S(6)	C(7)			−80.4(7)
C(5)	C(1)	S(6)	C(7)			106.3(6)
C(1)	S(6)	C(7)	C(8)		102.6(4)	−171.7(5)
S(6)	C(7)	C(8)	O(9)	1.807(8)	108.3(6)	63.4(9)
C(7)	C(8)	O(9)	C(10)	1.496(13)	109.0(7)	−172.3(7)
C(8)	O(9)	C(10)	C(11)	1.386(12)	114.6(8)	118.6(9)
O(9)	C(10)	C(11)	O(12)	1.429(14)	111.7(9)	−69.0(11)
C(10)	C(11)	O(12)	C(13)	1.488(16)	108.8(9)	−166.6(8)
C(11)	O(12)	C(13)	C(14)	1.420(12)	110.3(7)	−174.1(7)
O(12)	C(13)	C(14)	O(15)	1.442(12)	109.2(8)	76.4(9)
C(13)	C(14)	O(15)	C(16)	1.504(14)	109.3(8)	−165.7(7)
C(14)	O(15)	C(16)	C(17)	1.423(12)	112.3(7)	171.7(6)
O(15)	C(16)	C(17)	S(18)	1.420(12)	107.2(8)	−49.2(9)
C(16)	C(17)	S(18)	C(19)	1.503(14)	109.0(7)	−172.0(6)
C(17)	S(18)	C(19)	C(20)	1.810(10)	104.2(4)	82.6(8)
C(17)	S(18)	C(19)	C(23)			−106.8(7)
S(18)	C(19)	C(20)	C(21)	1.758(8)	128.1(6)	170.7(4)
S(18)	C(19)	C(23)	C(22)		122.5(6)	−171.4(3)
Cyclopentadienyl ring						
C(1)	C(2)	C(3)	C(4)	1.414(10)	107.1(7)	−0.5(10)
C(2)	C(3)	C(4)	C(5)	1.430(12)	107.9(7)	0.7(10)
C(3)	C(4)	C(5)	C(1)	1.423(12)	109.0(7)	−0.6(10)
C(4)	C(5)	C(1)	C(2)	1.414(12)	106.7(7)	0.2(9)
C(5)	C(1)	C(2)	C(3)	1.433(10)	109.3(6)	0.2(9)
C(19)	C(20)	C(21)	C(22)	1.422(11)	107.1(7)	0.7(11)
C(20)	C(21)	C(22)	C(23)	1.425(12)	108.3(8)	−0.3(11)
C(21)	C(22)	C(23)	C(19)	1.402(14)	109.1(8)	−0.3(11)
C(22)	C(23)	C(19)	C(20)	1.425(14)	106.5(8)	0.7(10)
C(23)	C(19)	C(20)	C(21)	1.426(12)	108.9(7)	−0.9(10)
Pd coordination						
Cl(1)	Pd	Cl(2)		2.303(2)	90.4(1)	
Cl(2)	Pd	S(6)		2.308(2)	174.2(1)	
S(6)	Pd	Cl(1)		2.314(2)	93.8(1)	
S(18)	Pd	Cl(1)		2.303(2)	175.6(1)	
S(6)	Pd	S(18)			81.9(1)	
S(18)	Pd	Cl(2)			93.8(1)	

References

1) F. De Jong and D. N. Reinhoudt, "Stability and Reactivity of Crown-ether Complexes," Academic Press, New York (1981).

2) B. Metz, D. Moras, and R. Weiss, *J. Inorg. Nucl. Chem.*, **36**, 785 (1975); B. A. Boyce, A. Carroy, J-M. Lehn, and D. Parker, *J. Chem. Soc., Chem. Commun.*, **1984**, 1546.

3) S. Akabori, Y. Habata, and M. Sato, *Bull. Chem. Soc. Jpn.*, **57**, 68 (1984).

4) S. Akabori, H. Munegumi, Y. Habata, S. Sato, K. Kawazoe, C. Tamura, and M. Sato, *Bull. Chem. Soc. Jpn.*, **58**, 2185 (1985).

5) S. Akabori, S. Sato, T. Tokuda, Y. Habata, K. Kawazoe, C. Tamura, and M. Sato, *Chem. Lett.*, **1986**, 121; *Bull. Chem. Soc. Jpn.*, **59**, 3189 (1986).

6) S. Akabori, Y. Habata, S. Sato, K. Kawazoe, C. Tamura, and M. Sato, *Acta Crystallogr., Sect. C*, **42**, 682 (1986).

7) S. Akabori, S. Sato, K. Kawazoe, C. Tamura, M. Sato, and Y. Habata, *Chem. Lett.*, **1987**, 1783.

8) T. S. Cameron and R. E. Cordes, *Acta Crystallogr., Sect. B*, **35**, 748 (1979).

9) S. Ohba, Y. Saito, T. Ishii, S. Kamiyama, and A. Kasahara, *Acta Crystallogr., Sect. C*, **41**, 709 (1985).

10) S. Ohba, Y. Saito, S. Kamiyama, and A. Kasahara, *Acta Crystallogr., Sect. C*, **40**, 53 (1984).

11) A. G. Osborne, R. E. Hollands, R. F. Bryan, and S. Lockhart, *J. Organomet. Chem.*, **224**, 129 (1982).

12) B. R. Davis and I. Bernal, *J. Crys. Mol. Struct.*, **2**, 107 (1972).

13) M. Hillman, B. Gordon, A. J. Weiss, and A. P. Guzikowski, *J. Organomet. Chem.*, **14**, 3085 (1975).

14) A. G. Osborne, R. H. Whiteley, and R. E. Meads, *J. Organomet. Chem.*, **193**, 345 (1980).

15) H. Stoeckli-Evans, A. G. Osborne, and R. H. Whitelery, *J. Organomet. Chem.*, **194**, 91 (1980).

16) M. Hisatome, M. Yoshihashi, K. Yamakawa, and Y. Iitaka, *Bull. Chem. Soc. Jpn.*, **60**, 3474 (1987).

17) Preliminary report: S. Akabori, S. Sato, Y. Habata, K. Kawazoe, C. Tamura, and M. Sato, *Chem. Lett.*, **1987**, 787.
18) S. Akabori, T. Kumagai, T. Shirahige, S. Sato, K. Kawazoe, C. Tamura, and M. Sato, *Organometallics*, **6**, 526 (1987).
19) S. Akabori, T. Kumagai, T. Shirahige, S. Sato, K. Kawazoe, C. Tamura, and M. Sato, *Organometallics*, **6**, 2105 (1987).
20) M. Sato, K. Suzuki, and S. Akabori, *Chem. Lett.*, **1987**, 2239.
21) L. Pauling, "The Nature of the Chemical Bond," 3rd., ed by Cornell University Press, Ithaca, New York (1969).
22) L. N. Mulay and Sr. M. E. Fox, *Natureweise*, **49**, 466A (1962).
23) F. R. Hartly, S. G. Murray, W. Levason, H. E. Soutter, and C. A. McAuliffe, *Inorg. Chim. Acta*, **35**, 265 (1979).
24) "International Tables for X-Ray Crystallography," Vol. IV, Kynoch Press, Birmingham (1974), pp. 72—98 and pp. 149—150.
25) W. C. Hamilton, *Acta Crystallogr.*, **12**, 609 (1959).

Structural Requirements for the Spatial Structure and Toxicity of Heat-Stable Enterotoxin (ST_h) of Enterotoxigenic *Escherichia coli*

Shinji YAMASAKI,† Yuji HIDAKA, Hideaki ITO,† Yoshifumi TAKEDA,† and Yasutsugu SHIMONISHI*

Institute for Protein Research, Osaka University, Yamada-oka 3-2, Suita, Osaka 565
†The Institute of Medical Science, The University of Tokyo, Shirokanedai, Minato-ku, Tokyo 108

(Received October 28, 1987)

The heat-stable enterotoxin (ST_h) of enterotoxigenic *Escherichia coli* consists of 19 amino acid residues and is linked intramolecularly by three disulfide bonds between Cys^6 and Cys^{11}, Cys^7 and Cys^{15}, and Cys^{10} and Cys^{18} (Y. Shimonishi et al., *FEBS Lett.*, **215**, 165 (1987)). The syntheses and biological assays of various analogs of ST_h with one or two of the three disulfide bonds showed that a disulfide bond between Cys^7 and Cys^{15} and another between Cys^6 and Cys^{11} or Cys^{10} and Cys^{18} are necessary for construction and stabilization of the spatial structure of ST_h to express its toxicity.

Various strains of enterotoxigenic *Escherichia coli* from animal hosts produce two kinds of heat-stable enterotoxins (STI and STII) that cause acute diarrhea in man and domestic animals.[1] STI is thought to bind to membrane receptors of intestinal cells[2] and stimulate guanylate cyclase, which is coupled to or present near the receptors, resulting in the induction of fluid accumulation. The mechanism of the biological action of STII is unknown. We have been studying the primary structure of STI (ST_h and ST_p), the positions of disulfide linkages (Fig. 1), and its structure-activity relation for several years.[3–7] We have found that peptides with the same sequences as those of the 13 amino acid residues from Cys near the N-terminus to Cys near the C-terminus in ST_h and ST_p have full enterotoxigenic activities, that the three intramolecular disulfide bonds are between Cys^6 and Cys^{11}, Cys^7 and Cys^{15}, and Cys^{10} and Cys^{18} in ST_h, and that the positions of the disulfide bonds affect the extent of toxicity of ST_h. These findings prompted us to examine which of these three intramolecular disulfide bonds are important for the spatial structure of ST_h and expression of its toxicity. Studies on the toxicities of analogs of ST_h with various combinations of disulfide bonds should be helpful in elucidating the spatial structure necessary for expression of toxicity, the contribution of amino acid residues to the spatial structure of ST_h and its binding site(s) for receptors on the membrane of intestinal cells.

This paper reports that a disulfide bond between Cys^7 and Cys^{15} in ST_h is essential for expression of the toxicity of ST_h and that another disulfide bond between Cys^6 and Cys^{11} or Cys^{10} and Cys^{18} is important for stabilization of the spatial structure and expression of toxicity.

Materials and Methods

The general and analytical methods used were described in the preceeding papers.[7,9] All chemicals used for preparative experiments were of reagent grade, those used for analysis were of guaranteed grade and solvents were distilled before use. All amino acids used were of the L-configuration except glycine. The abbreviations used in this paper are those recommended by the IUPAC-IUB [*J. Biol. Chem.*, **261**, 1 (1986)]. Additional abbreviations are: MBzl, *p*-methylbenzyl; Acm, acetamidomethyl; TFA, trifluoroacetic acid.

Synthesis of Peptides. Peptides were synthesized manually by the solid-phase method.[10] Briefly, Boc-Cys(MBzl)-, Boc-Cys(Acm)-, or Boc-Ala-polystyrene (2% divinylbenzene) (0.2—0.3 mmol of amino acid per 1 g of resin) was used with the following side-chain protecting groups: Bzl for threonine and glutamic acid and MBzl or Acm for cysteine. All couplings were carried out with 4-fold excess of Boc-amino acid and DCC, and the coupling of Boc-Asn-OH was repeated twice with 2 equiv of 1-hydroxybenzotriazole. The amino acids were coupled one by one in order from the C-terminus of peptide sequences. After coupling the N-terminal amino acid,

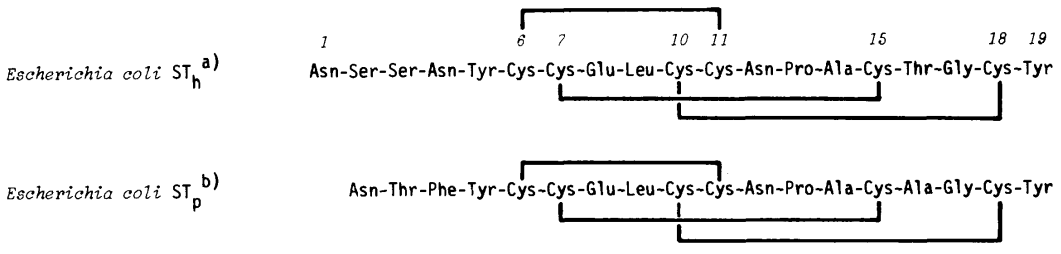

Fig. 1. Amino acid sequences and mode of disulfide bond formation of heat-stable enterotoxins produced by enterotoxigenic *Escherichia coli*: a) see Refs. 3 and 7; b) see Refs. 4 and 8.

the protected peptide-resin was removed from the reaction vessel and treated with the same amount of anisole in anhydrous hydrogen fluoride at 0 °C for 1 h. After removal of the hydrogen fluoride under reduced pressure, the peptide deprotected except for Acm on the mercapto groups of cysteine residues was extracted with 10% formic acid in an ice-water bath and washed three times with hexane. The extract was diluted with water to a final peptide concentration of 5×10^{-5} M (1 M=1 mol dm^{-3}). The solution was adjusted to pH 8.0 by adding aqueous ammonia and stood at room temperature with occasional stirring until no free mercapto groups were detectable. The crude peptide thus obtained was purified by high-performance liquid chromatography, as described below. The purified peptide with Acm groups at given Cys residues was dissolved at 5×10^{-4} M in a mixture of MeOH and H_2O (v/v, 4/1), then mixed with the same volume of a mixture of MeOH and 1M HCl (v/v, 4/1) containing iodine (40 equiv of the sample peptide), and kept for 15 min at room temperature. The reaction was stopped by adding L-ascorbic acid and the reaction product was purified by high-performance liquid chromatography, as described below.

Enzymatic Digestion. Synthetic peptides **16** and **18** were each dissolved in 0.02 M ammonium acetate (pH 7.0) and digested with aminopeptidase M (Pierce) and carboxypeptidase A (Boehringer, Mannheim), respectively, at a substrate:enzyme ratio (w/w) of 40:1 at 37 °C for 24 h.

High-Performance Liquid Chromatography (HPLC). The synthetic peptide was purified on a reversed-phase column (YMC-ODS, S-5, 8×300 mm, Yamamura Chemical Industries Ltd., Kyoto) using a high-performance liquid chromatography system consisting of a Waters M600 multisolvent delivery system (Milford, MA) and Hitachi 655A variable wavelength UV monitor and D-2000 chromato-integrator (Tokyo). The peptide was eluted with a linear gradient of 10—40% CH_3CN in 0.05% TFA or 0.01 M ammonium acetate (pH 5.7) with increase in CH_3CN of 1% min^{-1} at a flow rate of 2 ml min^{-1}. Fractions of the eluate were monitored for absorbance at 220 nm.

Amino Acid and Fast Atom Bombardment (FAB) Mass Analyses. The amino acid compositions and molecular weights of purified synthetic peptides were examined by amino acid analysis and FAB mass spectrometry, as described in Refs. 7 and 11, respectively.

Biological Assay. Toxicity was assayed in suckling mice (1.7±0.1 g) of 2 days old as described previously.[12]

Results and Discussion

To examine the effects of the three disulfide bonds on the toxicity of ST_h, we synthesized peptides with all possible combinations of two disulfide bonds, as shown in Table 1. Peptides **1—9** with two disulfide bonds other than that between the two Cys residues protected by Acm groups were synthesized as intermediates in the syntheses of peptides with three disulfide bonds in a previous study.[7] Peptides **10—15**, which had two disulfide bonds between four Cys differing for those in peptides **1—9** and in which the other two Cys were replaced by Ala, were newly synthesized in this work. That is, we synthesized protected peptide resins with the sequences listed in Table 1 where MBzl group was employed as a protecting group for mercapto groups of four Cys residues (Fig. 2). All protecting groups were removed

Table 1. Synthetic Analogs of ST_h with All Possible Combinations of Two Disulfide Bonds and Their Toxicities

No.	Peptide[a]													Toxicity[b]
	6 Cys	7 Cys	8 Glu	9 Leu	10 Cys	11 Cys	12 Asn	13 Pro	14 Ala	15 Cys	16 Thr	17 Gly	18 Cys	
1	▲	—	—	—	—	▲	—	—	—	—	—	—	—	+
2	▲	—	—	—	—	—	—	—	—	▲	—	—	—	−
3	▲	—	—	—	—	—	—	—	—	—	—	—	▲	−
4	—	▲	—	—	▲	—	—	—	—	—	—	—	—	−
5	—	▲	—	—	—	▲	—	—	—	—	—	—	—	−
6	—	▲	—	—	—	—	—	—	—	▲	—	—	—	−
7	—	▲	—	—	—	—	—	—	—	—	—	—	▲	−
8	—	—	—	—	▲	—	—	—	—	▲	—	—	—	−
9	—	—	—	—	▲	—	—	—	—	—	—	—	▲	+
10	Ala	Ala	—	—	—	—	—	—	—	—	—	—	—	−
11	Ala	—	—	—	Ala	—	—	—	—	—	—	—	—	−
12	—	—	—	—	Ala	Ala	—	—	—	—	—	—	—	−
13	—	—	—	—	—	Ala	—	—	—	Ala	—	—	—	−
14	—	—	—	—	—	Ala	—	—	—	—	—	—	Ala	−
15	—	—	—	—	—	—	—	—	—	Ala	—	—	Ala	−

a) ▲ is a Cys residue in which the thiol group is blocked by an Acm group and — is the same amino acid residue as that in the actual sequence. b) + and − indicate toxicity and no toxicity, respectively, at a dose of less than 1 μg.

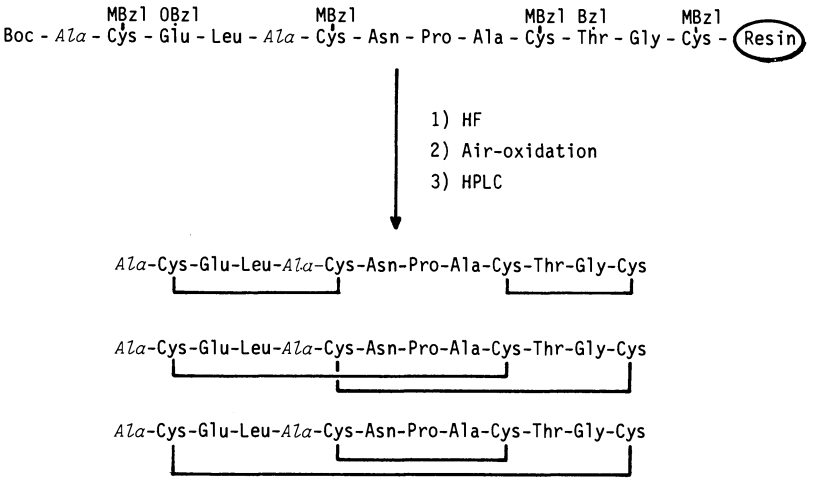

Fig. 2. Scheme for synthesis of an ST_h analog with two disulfide bonds between the four Cys other than those at positions 6 and 10, which are replaced by Ala.

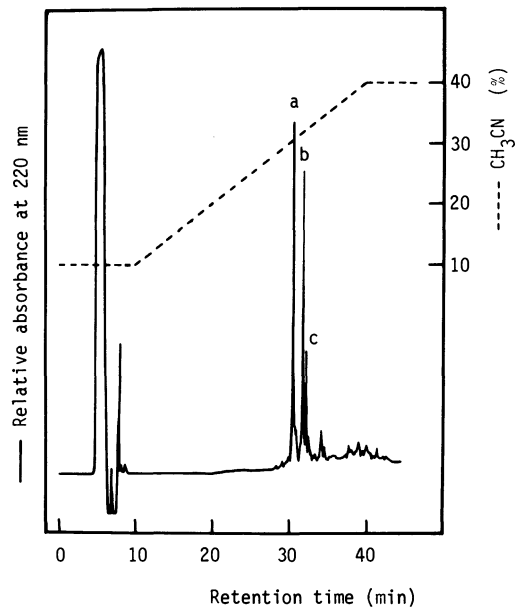

Fig. 3. Reversed-phase HPLC of peptide **11**. For chromatographic conditions, see text.

simultaneously at the stage of cleavage of peptides from the resins by their treatment with anhydrous hydrogen fluoride. The resulting free linear peptides were oxidized by air in dilute aqueous solution (5×10^{-5} M) until no free mercapto groups were detectable. Each peptide should theoretically be a mixture of monomeric peptides with three kinds of disulfide linkages. Figure 3 shows the HPLC profile of peptide **11** with two Ala at positions 6 and 10 and two disulfide bonds between four Cys at positions 7, 11, 15, and 18 (Fig. 2). By analyses of all peaks, monomeric peptides with two disulfide bonds were found in peaks a, b, and c. The results of amino acid and FAB mass spectrometric analyses of these peaks are shown in Table 2. Other peptides were synthesized by a similar procedure to that described in Fig. 2.

We examined the biological activities of all the synthetic peptides shown in Table 1 and found that peptides **1** and **9** had weak, but distinct toxicity, while the other peptides showed no toxicity at a dose of less than 1 μg. Previously[7] we found that peptides **1** and **9** yielded peptides that were identical with standard ST_h peptide in physicochemical and biological properties when the third disulfide bond was formed between Cys^6 and Cys^{11} and Cys^{10} and Cys^{18}, respectively, whereas other peptides did not yield a peptide that was identical with standard ST_h peptide when the third disulfide bond was formed. These findings indicate that peptides **1** and **9** contained peptides with the same two disulfide bonds as those in standard ST_h peptide, that they were between Cys^7 and Cys^{15} and Cys^{10} and Cys^{18} in peptide **1** and between Cys^6 and Cys^{11} and Cys^7 and Cys^{15} in peptide **9**, and that the toxicities of peptides **1** and **9** were due to peptides with these two disulfide bonds. These findings suggest that one or two of these three disulfide bonds are closely related to formation of the spatial structure of the ST_h molecule, which is necessary for expression of its toxicity.

To examine this possibility, we synthesized peptides **16—18** with two disulfide bonds at specific positions between four Cys and two Ala instead of the two remaining Cys, as shown in Table 3. Peptides **16** and **18** correspond to peptides in peptides **1** and **9**, respectively. We synthesized these peptides using two different types of protecting groups and selective and stepwise formation of disulfide bonds. Figure 4 shows the scheme for synthesis of peptide **18**, in which the two Cys at positions 10 and 18 are replaced by two Ala, the mercapto groups of the two Cys at positions 7 and 15 are protected by MBzl groups, and the mercapto groups of the two Cys at positions 6 and 11 are

Table 2. Amino Acid Compositions,[a] Mass Values, and Biological Activities of Peaks of Peptide **11**

	a[b]	b[b]	c[b]	Theoretical value
Asp	1.02	1.04	1.10	1
Thr	1.06	1.08	1.15	1
Glu	1.00	1.02	1.08	1
Pro	1.08	1.09	1.13	1
Gly	0.99	1.02	1.04	1
Ala	3	3	3	3
$\frac{1}{2}$Cys	4.15	4.04	4.39	4
Leu	1.04	1.04	1.04	1
$[M+H]^+$	1251.1	1251.1	1251.1	1251.4
MED[c] (μg)	>17	>14	>14	

a) The synthetic peptide was hydrolyzed in 6M HCl containing 1% phenol in vacuum sealed tubes at 110 °C for 24 h. b) a, b, and c correspond to peaks a, b, and c in Fig. 2. c) MED: Minimum effective dose.

Table 3. Synthetic Analogs of ST_h with One or Two Disulfide Bonds and Their Toxicities

No.	Peptide[a]	MED (pmol)[b]
	Cys-Cys-Glu-Leu-Cys-Cys-Asn-Pro-Ala-Cys-Thr-Gly-Cys	0.4
16	*Ala*-Cys-Glu-Leu-Cys-*Ala*-Asn-Pro-Ala-Cys-Thr-Gly-Cys	380
17	Cys-*Ala*-Glu-Leu-Cys-Cys-Asn-Pro-Ala-*Ala*-Thr-Gly-Cys	Inactive
18	Cys-Cys-Glu-Leu-*Ala*-Cys-Asn-Pro-Ala-Cys-Thr-Gly-*Ala*	290
19	Cys-Glu-Leu-Cys-*Ala*-Asn-Pro-Ala-Cys-Thr-Gly-Cys	150
20	Cys-Cys-Glu-Leu-*Ala*-Cys-Asn-Pro-Ala-Cys	110
21	Cys Cys-Glu-Leu-*Ala*-Cys-Asn-Pro-Ala-Cys-Thr-Gly-*Ala*	Inactive
22	Cys*-Cys*-Glu-Leu-*Ala*-Cys-Asn-Pro-Ala-Cys*-Thr-Gly-*Ala*	Inactive
23	Cys*-Cys-Glu-Leu-*Ala*-Cys*-Asn-Pro-Ala-Cys-Thr-Gly-*Ala*	Inactive
24	Cys*-*Ala*-Glu-Leu-Cys-Cys*-Asn-Pro-Ala-*Ala*-Thr-Gly-Cys	Inactive
25	Cys-Glu-Leu-*Ala*-Cys*-Asn-Pro-Ala-Cys-Thr-Gly-*Ala*	Inactive

a) Cys* denotes a Cys residue in which the thiol group is blocked by an Acm group. b) MED: Minimum effective dose.[12]

protected by Acm groups. The first disulfide bond was formed between the two Cys at positions 7 and 15 after removal of the MBzl groups by treatment with HF, and the second disulfide bond was formed between the two Cys at positions 6 and 11 by oxidation with iodine. The HPLC profile of peptide **18** is shown in Fig. 5. Other peptides were synthesized by a similar procedure. We found that peptides **16** and **18** which had two disulfide bonds between residues 7 and 15, and 6 and 11 or 10 and 18 were toxic, while peptide **17** with no disulfide bond at positions 7 and 15 was inactive, as shown in Table 3. Digestion of peptide **16** with aminopeptidase M, and of peptide **18** with carboxypeptidase A gave peptides **19** and **20**, respectively, which lack their N-terminal amino acid residue and C-terminal three amino acid residues. These peptides were about twice as toxic as their original peptides. These results indicated that a disulfide bond between Cys^7 and Cys^{15} is necessary for the toxicity of ST_h. Analytical data on peptides **16—20** are shown in Table 4.

Next, we synthesized a peptide with two disulfide bonds between Cys^6 and Cys^{11} and Cys^7 and Cys^{15}, but without the peptide bond between Cys^6 and Cys^7 (peptide **21**) and three kinds of peptides with only one disulfide bond between Cys^6 and Cys^{11}, Cys^7 and Cys^{15} or Cys^{10} and Cys^{18} (peptides **22—24**). Peptide **21** was prepared by oxidative coupling of peptide **25** and Boc-Cys(Acm)-OH followed by deprotection of the Boc group. Peptides **22** and **23** were synthesized as intermediates in the synthesis of peptide **18**, and peptide **24** as an intermediate in the synthesis of peptide **17**, by a similar procedure to that shown in Fig. 3. Analytical data on these synthetic peptides are presented in Table 4. All these peptides were inactive, as shown in Table 3. Therefore, the spatial structure of ST_h with two disulfide linkages between Cys^7 and Cys^{15}, and Cys^6 and Cys^{11} or Cys^{10} and Cys^{18} is essential for the toxicity of ST_h. In other words, the spatial structure of ST_h cannot be maintained by only one disulfide bond between Cys^7 and Cys^{15}, but requires one other disulfide bond between Cys^6 and Cys^{11} or Cys^{10} and Cys^{18}.

Figure 6 shows a CPK-model of a short peptide of ST_h with 13 amino acid residues, which was constructed from its three disulfide linkages[7] and

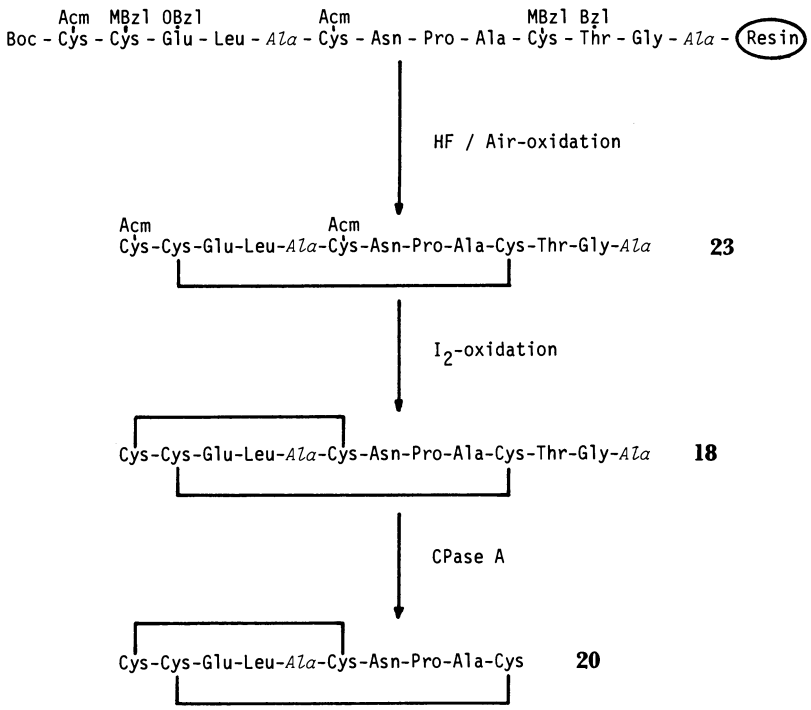

Fig. 4. Scheme for synthesis of an ST_h analog with two disulfide bonds between the Cys at positions 6 and 11 and positions 7 and 15, respectively.

Table 4. Amino Acid Compositions[a] and Mass Values[b] of Synthetic Analogs[c] of ST_h

	16	17	18	19	20	21	22	23	24	25
Asp	1.26(1)	1.00(1)	1.10(1)	0.97(1)	1.22(1)	1.07(1)	1.08(1)	1.09(1)	1.10(1)	0.98(1)
Thr	0.98(1)	1.00(1)	1.00(1)	1.00(1)	—	1.15(1)	1.12(1)	1.21(1)	1.18(1)	1.00(1)
Glu	0.99(1)	1.00(1)	0.98(1)	0.99(1)	0.98(1)	1.06(1)	1.08(1)	1.07(1)	1.03(1)	0.99(1)
Pro	1.20(1)	1.17(1)	1.01(1)	0.99(1)	1.07(1)	1.10(1)	1.16(1)	1.15(1)	1.17(1)	1.00(1)
Gly	1.00(1)	0.98(1)	0.98(1)	0.95(1)	—	1.16(1)	1.00(1)	1.03(1)	1.04(1)	0.97(1)
Ala	3 (3)	3 (3)	3 (3)	2 (2)	2 (2)	3 (3)	3 (3)	3 (3)	3 (3)	3 (3)
$\frac{1}{2}$Cys	2.22(4)	4.12(4)	3.03(4)	3.68(4)	2.77(4)	3.43(4)	3.41(4)	4.04(4)	4.23(4)	2.35(3)
Leu	0.98(1)	0.99(1)	0.98(1)	0.98(1)	1.00(1)	1.03(1)	1.04(1)	1.04(1)	1.06(1)	0.96(1)
$[M+H]^+$	1251.8 (1251.4)	1251.1 (1251.4)	1251.3 (1251.4)	1180.4 (1180.3)	1022.3 (1022.2)	1269.1 (1269.4)	1395.3 (1395.5)	1395.1 (1395.5)	1395.3 (1395.5)	1221.9 (1221.5)

a) Synthetic peptides were hydrolyzed in 6M HCl containing 1% phenol in vacuum sealed tubes at 110°C for 24 h. Numbers in parentheses are theoretical values. b) Numbers in parentheses are theoretical values. c) Numbers of peptides correspond to those in Table 3.

nuclear Overhauser effects (NOE) data measured by two-dimensional ^1H NMR spectroscopy.[13,14] The main chain of the peptide viewed from the front in Fig. 6 is seemingly folded in a twisted "8"-shape and there are two loop structures consisting of two turns between residues 9 to 11 and 12 to 15. The three disulfide linkages are located in the hinge region binding these two loops and presumably stabilize the spatial structure of ST_h. Cleavage of the disulfide bond between Cys^6 and Cys^{11} or Cys^{10} and Cys^{18} does not appreciably disrupt the spatial structure necessary for expression of toxicity, and the twisted "8"-structure shown in Fig. 6 is still maintained, at least partially. However, cleavage of the disulfide bond between Cys^7 and Cys^{15} may completely loosen the spatial conformation of ST_h, because peptide **17** was completely inactive. Cleavage of any two of the disulfide bonds shown in Fig. 6 may completely disrupt the structure fixed by the hinge region. Therefore, a twisted "8"-structure of the main chain seems important for the toxicity of ST_h or for stabilization of its spatial structure. In particular, maintenance of the spatial structure of the peptide chain from Cys^7 to Cys^{15} may be necessary for expression of the toxicity of ST_h. For further elucidation of the effect of the spatial structure of ST_h on its toxicity, attempts should be made to build a reliable molecular model of ST_h and identify the amino acid residues that bind ST_h to membrane proteins of intestinal cells.

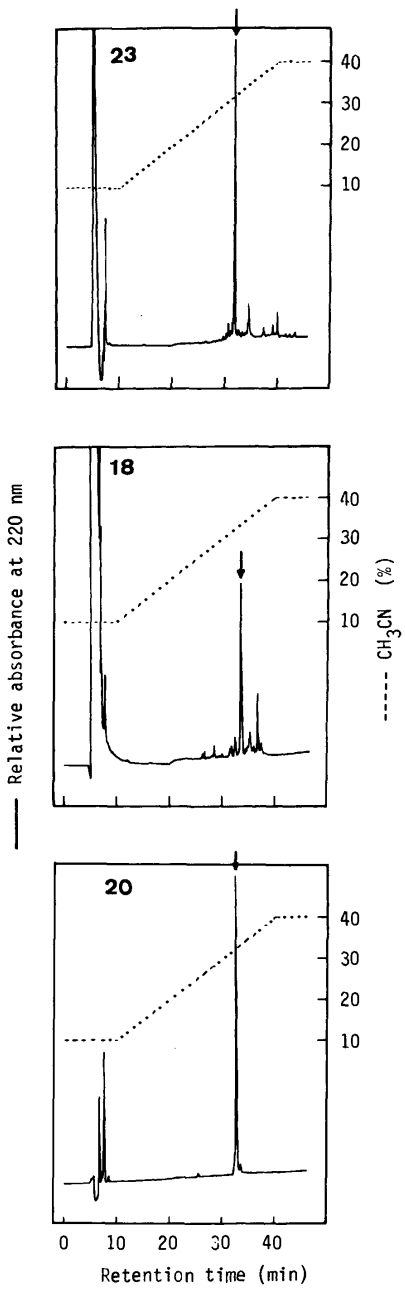

Fig. 5. HPLC profiles of peptides **23**, **18**, and **20**. For chromatographic conditions, see text.

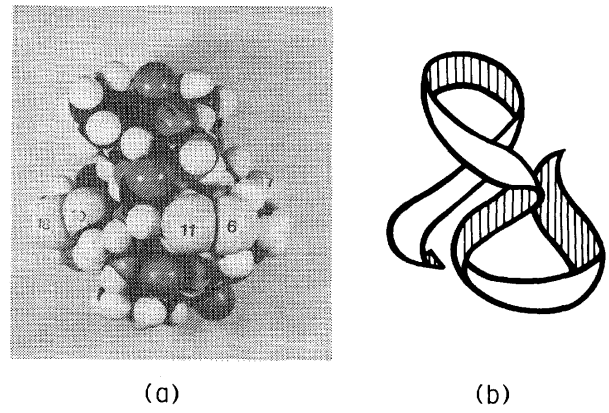

Fig. 6. A CPK-model (a) and schematic ribbon drawing of the polypeptide backbone (b) of a heat-stable enterotoxin (ST_h) consisting of 13 amino acid residues from Cys at position 6 to Cys at position 18, based on the positions of the three disulfide bonds[7] and NOE data measured by ^1H NMR spectroscopy.[13,14]

This work was supported in part by a Grant-in-Aid from the Ministry of Education, Culture and Science of Japan (Scientific Research Grant No. 62470022) and in part by a grant from the Naito Foundation. We are indebted to Mrs. Noriko Mizoguchi for amino acid analysis and to Mrs. Aiko Kobatake for preparation of the manuscript.

References

1) H. W. Smith and C. L. Gyles, *J. Med. Microbiol.*, **3**, 387 (1970).

2) J. Gariepy and G. K. Schoolnik, *Proc. Natl. Acad. Sci. U.S.A.*, **83**, 483 (1986).

3) S. Aimoto, T. Takao, Y. Shimonishi, S. Hara, T. Takeda, Y. Takeda, and T. Miwatani, *Eur. J. Biochem.*, **129**, 257 (1982).

4) T. Takao, T. Hitouji, S. Aimoto, Y. Shimonishi, S. Hara, T. Takeda, Y. Takeda, and T. Miwatani, *FEBS Lett.*, **152**, 1 (1983); M. R. Thompson an R. A. Giannella, *Infect. Immun.*, **47**, 834 (1985).

5) S. Aimoto, H. Watanabe, H. Ikemura, Y. Shimonishi, T. Takeda, Y. Takeda, and T. Miwatani, *Biochem. Biophys. Res. Commun.*, **112**, 320 (1983).

6) S. Yoshimura, H. Ikemura, H. Watanabe, S. Aimoto, Y. Shimonishi, S. Hara, T. Takeda, T. Miwatani, and Y. Takeda, *FEBS Lett.*, **181**, 138 (1985).

7) Y. Shimonishi, Y. Hidaka, M. Koizumi, M. Hane, S. Aimoto, T. Takeda, T. Miwatani, and Y. Takeda, *FEBS Lett.*, **215**, 165 (1987).

8) Y. Hidaka, H. Kubota, S. Yoshimura, H. Ito, Y. Takeda, and Y. Shimonishi, *Bull. Chem. Soc. Jpn.*, **61**, 1265 (1988).

9) S. Yoshimura and Y. Shimonishi, *Bull. Chem. Soc. Jpn.*, **58**, 2805 (1985).

10) R. B. Merrifield, *J. Am. Chem. Soc.*, **85**, 2149 (1963).

11) T. Takao, T. Hitouji, Y. Shimonishi, T. Tanabe, S. Inouye, and M. Inouye, *J. Biol. Chem.*, **259**, 6105 (1984).

12) Y. Takeda, T. Takeda, Y. Yano, K. Yamamoto, and T. Miwatani, *Infect. Immun.*, **25**, 978 (1979).

13) T. Ohkubo, Y. Kobayashi, Y. Shimonishi, K. Kyogoku, W. Braun, and M. Go, *Biopolymers*, **25**, S123 (1986).

14) J. Gariepy, A. Lane, F. Frayman, D. Wilbur, W. Robien, G. K. Schoolnik, and O. Jardetzky, *Biochemistry*, **25**, 7854 (1986).

Note Added in Proof. After submittion of this paper, Gariepy et al. (*Proc. Natl. Acad. Sci. U.S.A.*, **84**, 8907 (1987)) reported the importance of disulfide linkages in an enterotoxin and the result was the same as described here.

Syntheses and Reactions of Allylic and Homoallylic Pyrophosphate Tetraesters

Yasuo BUTSUGAN,* Kenji NAGAI, Fumitoshi NAGAYA, Hiroki TABUCHI, Katsuhisa YAMADA, and Shuki ARAKI
Department of Applied Chemistry, Nagoya Institute of Technology, Gokiso-cho, Showa-ku, Nagoya 466
(Received December 2, 1987)

Pyrophosphate tetraesters possessing allylic and homoallylic side chains were synthesized. Reaction of alkyl allyl (and 3-methyl-3-butenyl) phosphorochloridates with sodium hydrogencarbonate gave P^1,P^2-dialkyl P^1,P^2-diallyl [and P^1,P^2-bis(3-methyl-3-butenyl)] pyrophosphates. Condensation of alkyl allyl (and 3-methyl-3-butenyl) phosphorochloridates with dialkyl phosphates gave trialkyl allyl (and 3-methyl-3-butenyl) pyrophosphates. Reactions of crotyl (2-butenyl) pyrophosphates with various nucleophiles such as phenolic ethers, aromatic amines, and nitrogen-containing heterocycles in the presence of boron trifluoride etherate gave good to moderate yields of crotylated products. The crotyl pyrophosphates were found to be much more reactive than the corresponding orthophosphate esters.

In our continuous studies on the reaction of allylic phosphate esters, it has been revealed that allylic phosphates are useful and versatile reagents in synthetic chemistry.[1] They possess several advantages over allylic halides in regard to reactivity, selectivity, and ease of preparation and handling. It is well-known that naturally occurring terpenoids are biosynthesized via allylic and homoallylic pyrophosphate esters in a regio- and stereospecific manner.[2] Therefore, the use of pyrophosphates in place of orthophosphate esters is expected to improve the reactivity and selectivity in synthetic reactions. In this connection, pyrophosphate monoester salts possessing an allylic polyprenyl residue have been successfully used for enzymatic transformation to natural products.[3] However, the use of such pyrophosphate salts in preparative-scale synthesis is strictly limited owing to the difficulties in manipulation and the poor solubility in organic solvents. From these viewpoints, we were interested in the syntheses and reaction behavior of allylic and homoallylic pyrophosphate tetraesters. Although a number of workers reported the syntheses and applications of tetraalkyl pyrophosphates,[4] pyrophosphate tetraesters bearing allylic and/or homoallylic side chains have been scarcely studied.[5] In this paper, we describe the syntheses of such pyrophosphate tetraesters and discuss their reactivities toward phenolic ethers, aromatic amines, and nitrogen-containing heterocycles in comparison with that of the corresponding orthophosphate ester.

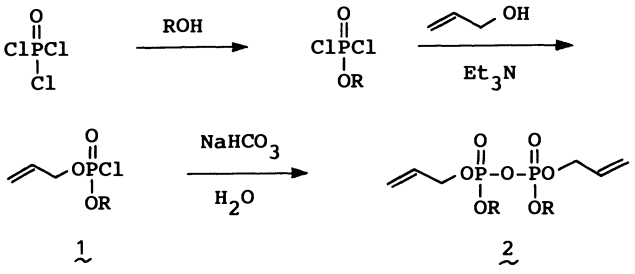

1 2

Scheme 1.

Results and Discussion

Syntheses. The synthesis of symmetrical P^1,P^2-dialkyl P^1,P^2-diallyl pyrophosphates (**2**) was achieved by the treatment of alkyl allyl phosphorochloridates (**1**) with sodium hydrogencarbonate in the presence of a catalytic amount of water.[6] The crude products were purified first by vacuum distillation and then by column chromatography on silica gel. The starting alkyl allyl phosphorochloridates (**1**) in turn were prepared by the triethylamine-induced condensation of alkyl phosphorodichloridates with allyl alcohol. The overall reaction scheme is as Scheme 1. Of the four pyrophosphate tetraesters prepared, P^1,P^2-diallyl P^1,P^2-dipropyl pyrophosphate (**2b**) is the most stable and the highest yield was achieved. The corresponding diethyl pyrophosphate **2a** is considerably unstable and all attempts to isolate P^1,P^2-diallyl P^1,P^2-dimethyl

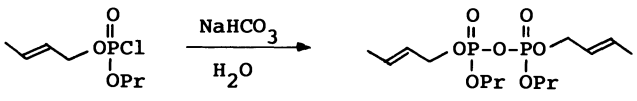

3

Scheme 2.

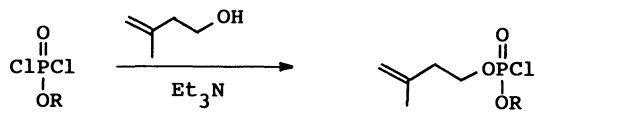

4 5

Scheme 3.

pyrophosphate failed owing to the rapid decomposition during purification. P^1,P^2-Di-2-butenyl (crotyl) P^1,P^2-dipropyl pyrophosphate (**3**) was similarly prepared from crotyl propyl phosphorochloridate in 86% yield (Scheme 2). The pyrophosphate is thermally labile and sensitive to silica gel, so it was used for next reactions without further purification.

A series of symmetrical homoallylic pyrophosphates, P^1,P^2-dialkyl P^1,P^2-bis(3-methyl-3-butenyl) pyrophosphates (**5**) were also obtained by the same method (Scheme 3). Again, the maximum yield was achieved when R=propyl.

Condensation of alkyl allyl phosphorochloridates (**1**) with dialkyl phosphates in the presence of triethylamine furnished the second type of pyrophosphate tetraesters, trialkyl allyl pyrophosphates (**6**) (Scheme 4). By this method, crotyl tripropyl pyrophosphate (**7**) was synthesized in 76% yield (Scheme 5). Pyrophosphate tetraesters (**8**) of this type bearing a homoallylic 3-methyl-3-butenyl group were analogously prepared and isolated.

Reactions. We have reported that allylic orthophosphate esters readily allylate phenolic ethers in the presence of boron trifluoride etherate.[7] In order to compare the reactivity of allylic pyrophosphates with that of allylic orthophosphates, the reactions of crotyl pyrophosphates **3** and **7** with various phenolic ethers were carried out and the yields were compared with those of the reactions of crotyl dipropyl phosphate (**9**) under the same reaction conditions. The Friedel–Crafts type alkenylations were conducted at 0—−23 °C using five-fold excess of phenolic ethers to avoid polycrotylation. Yields and product distributions were determined by GLC analysis. Results are shown in Table 1. The reactions of **3**, **7**, and **9** with anisole gave all possible four regio (α and γ) and positional isomers (ortho and para). There were no important differences in the product distributions of

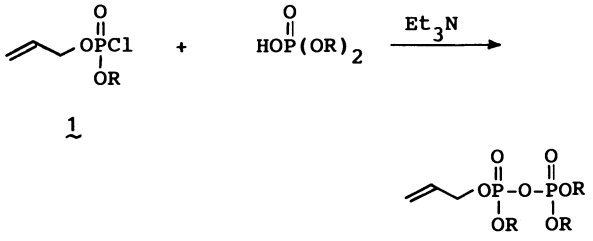

1 6

Scheme 4.

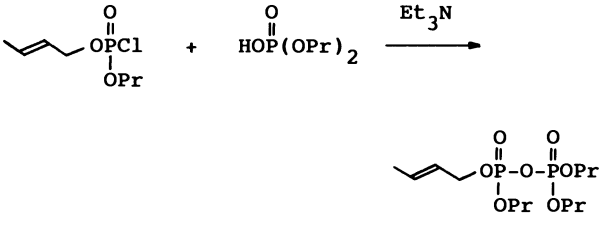

7

Scheme 5.

Table 1. Crotylation of Phenolic Ethers by Crotyl Phosphates (**3**, **7**, and **9**)

Phenol ether	Phosphate	Reaction conditions	Total yield[a]/%	Product ratio[b]/α : γ
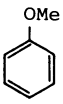	**3**	0 °C, 3.5 h	91	81 (29/57) : 14 (3/11)
	7	0 °C, 3.5 h	82	88 (30/58) : 12 (3/ 9)
	9	0 °C, 3.5 h	49	87 (38/49) : 13 (3/10)
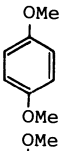	**3**	−23 °C, 4 h	76	83 : 17
	7	−23 °C, 4 h	54	84 : 16
	9	−23 °C, 4 h	4	72 : 28
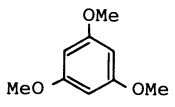	**3**	−23 °C, 4 h	97	86 : 14
	7	−23 °C, 4 h	89	91 : 9
	9	−23 °C, 4 h	27	84 : 16
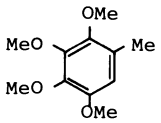	**3**	0 °C, 3 h	53	69 : 31
	7	0 °C, 3 h	61	69 : 31
	9	0 °C, 3 h	10	71 : 29
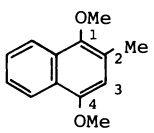	**3**	0 °C, 4 h	95	100 : 0[c]
	7	0 °C, 4 h	86	100 : 0[c]
	9	0 °C, 4 h	75	88 : 12[c]

a) Glc yield. b) Figures in parentheses refer to *o*/*p* ratio. c) The alkenylation occurred exclusively at the 3-position of the naphthalene.

the three reactions, but the yield using the orthophosphate (**9**) was largely depressed compared to those of pyrophosphate cases. It must be noted that only one crotyl group of the dicrotyl pyrophosphate (**3**) was used for alkenylation of phenolic ethers under the reaction conditions employed. The results obtained here clearly show that pyrophosphate residues are excellent leaving groups and hence the reactivity of the pyrophosphates **3** and **7** are markedly higher than that of the orthophosphate (**9**).

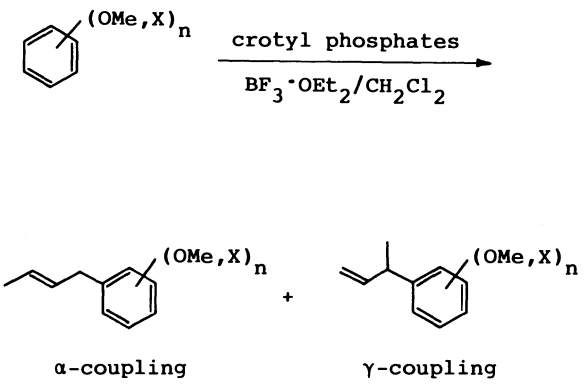

Scheme 6.

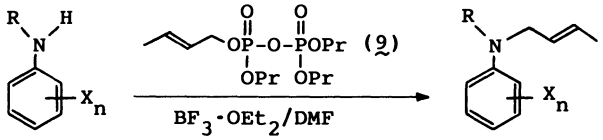

Scheme 7.

Crotyl tripropyl pyrophosphate (**7**) also allylated aromatic amines in *N,N*-dimethylformamide (DMF) in the presence of boron trifluoride etherate at room temperature. As shown in Table 2, *N*-crotylation occurred predominantly and the corresponding amines were isolated in moderate yields. In the cases of diphenylamine and 1-naphthylamine, trace amounts of nucleus-crotylated products were also obtained. Under the reaction conditions employed, crotyl orthophosphate (**9**) gave, if any, only poor yields of *N*-crotylamines,[8] owing to the lower reactivity of **9** than **7**.

Pyrrole and indole reacted with crotyl pyrophosphate (**9**) to give nucleous-crotylated products. In these reactions, *N*-crotylated products could not be found. Again, no reactions occurred when orthophosphate (**9**) was used in place of **7**.

In summary, it has been shown that allylic pyrophosphates have much higher reactivity toward various nucleophiles than the corresponding orthophosphate and that they serve as useful allylating reagents in synthetic chemistry.

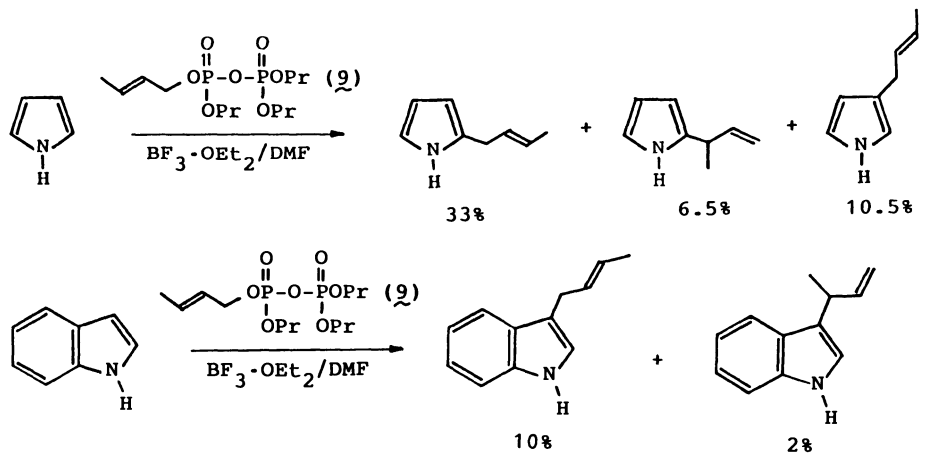

Scheme 8.

Table 2. Reaction of Crotyl Tripropyl Pyrophosphate (**7**) and Aromatic Amines

Run	Aromatic amine	Product	Yield[a]/%
1	$PhNH_2$	$PhNH(CH_2CH{=}CHCH_3)$	57 (0)
		$PhN(CH_2CH{=}CHCH_3)_2$	9 (0)
2	$Ph(CH_3)NH$	$Ph(CH_3)N(CH_2CH{=}CHCH_3)$	30 (7)
3	$4\text{-}MeOC_6H_4NH_2$	$4\text{-}MeOC_6H_4NH(CH_2CH{=}CHCH_3)$	18 (0)
		$4\text{-}MeOC_6H_4N(CH_2CH{=}CHCH_3)_2$	35 (0)
4	Ph_2NH	$Ph_2N(CH_2CH{=}CHCH_3)$	9 (0)
		$Ph_2N[CH(CH_3)CH{=}CH_2]$	5 (0)
		$PhNHC_6H_4(CH_2CH{=}CHCH_3)$	1 (0)
5	$(1\text{-Naphthyl})NH_2$	$(1\text{-Naphthyl})NH(CH_2CH{=}CHCH_3)$	22 (4)
		$(2\text{-Crotyl-1-naphthyl})NH_2$	1 (0)

a) Figures in parentheses refer to yields of the reaction with crotyl dipropyl phosphate (**9**).

Experimental

General. Infrared spectra were recorded on a JASCO IRA-102 spectrometer. ^{1}H NMR spectra were recorded on a Hitachi R-24A spectrometer (60 MHz) or on a Varian XL-200 spectrometer (200 MHz) with Me_4Si as an internal standard. ^{13}C NMR spectra were obtained on a Varian XL-200 spectrometer (50 MHz). Multiplicities refer to those of proton-decoupled spectra. Mass spectra (MS) were determined at 20 eV using a Hitachi M-52 or ESCO EMD-05B instrument. GLC analyses were performed on a Yanaco G1800 gas chromatograph. Elemental analyses were performed at the Elemental Analysis Center of Kyoto University. Dialkyl phosphates,[6] alkyl phosphorodichloridates,[9] and dialkyl phosphorochloridates[10] were prepared by the literature methods.

Alkyl Allyl (and 3-Methyl-3-butenyl) Phosphorochloridates (1 and 4). The following preparation of allyl ethyl phosphorochloridate represents the general procedure. To a solution of ethyl phosphorodichloridate (9.8 g, 60 mmol) in anhydrous ether (20 cm^3) was slowly added a mixture of allyl alcohol (3.6 g, 62 mmol) and triethylamine (6.4 g, 63 mmol) in ether (20 cm^3) with cooling in an ice-salt bath. The reaction mixture was stirred at that temperature for 4 h. Triethylammonium chloride which formed was filtered off and the filtrate was concentrated. The residue was distilled [bp 60—69 °C/1.1×10^{-3} Torr(1 Torr=133.322 Pa)] to give allyl ethyl phosphorochloridate (9.02 g, 81%) as a pale yellow liquid. Other alkyl allyl (and 3-methyl-3-butenyl) phosphorochloridates (**1** and **4**) were similarly prepared and purified by distillation. Crotyl propyl phosphorochloridate is thermally unstable, so the crude product was used for the next reactions without distillation.

Allyl ethyl phosphorochloridate (**1a**): 81% yield; bp 60—69 °C/1.1×10^{-3} Torr; IR (neat) 3100, 2990, 2950, 2930, 1650, 1415, 1395, 1370, 1300, 1165, 1030 cm^{-1}; ^{1}H NMR (CCl_4) δ=1.40 (t, J=7 Hz, 3H, Me) 3.97—4.73 (m, 4H, CH_2), 5.17—5.52 (m, 2H, =CH_2), 5.68—6.30 (m, 1H, =CH); Found: C, 32.84; H, 5.67%. Calcd for $C_5H_{10}ClO_3P$: C, 32.54; H, 5.46%.

Allyl propyl phosphorochloridate (**1b**): 82% yield; bp 54—64 °C/6.1×10^{-4} Torr; IR (neat) 3080, 2980, 2950, 2910, 2890, 1650, 1465, 1425, 1300, 1150, 1020 cm^{-1}; ^{1}H NMR (CCl_4) δ=1.01 (t, J=7 Hz, 3H, Me), 1.32—2.10 (m, 2H, CH_2), 3.79—4.36 (m, 2H, CH_2), 4.41—4.78 (m, 2H, CH_2), 5.10—5.54 (m, 2H, =CH_2), 5.59—6.30 (m, 1H, =CH); Found: C, 36.48; H, 6.31%. Calcd for $C_6H_{12}ClO_3P$: C, 36.29; H, 6.09%.

Allyl butyl phosphorochloridate (**1c**): 81% yield; bp 83—95.5 °C/1.3×10^{-4} Torr; IR (neat) 3100, 2980, 2950, 2890, 1650, 1465, 1430, 1385, 1300, 1160, 1150, 1030 cm^{-1}; ^{1}H NMR (CCl_4) δ=0.98 (t, J=7 Hz, 3H, Me), 1.30—1.85 (m, 4H, CH_2), 3.98—4.73 (m, 4H, CH_2), 5.17—5.50 (m, 2H, =CH_2), 5.68—6.29 (m, 1H, =CH); Found: C, 40.60; H, 7.00%. Calcd for $C_7H_{14}ClO_3P$: C, 39.54; H, 6.64%.

Allyl isobutyl phosphorochloridate (**1d**): 75% yield; bp 85—93 °C/2.3×10^{-3} Torr; IR (neat) 3100, 2980, 2905, 2895, 1650, 1473, 1426, 1374, 1300, 1162, 1130, 1025 cm^{-1}; ^{1}H NMR (CCl_4) δ=0.98 (d, J=6 Hz, 6H, Me), 1.59—2.28 (m, 1H, CH), 3.90 (dd, J_{HP}=8 Hz, J_{HH}=7 Hz, 2H, CH_2), 4.59 (dd, J_{HP}=10 Hz, J_{HH}=5 Hz, 2H, CH_2), 4.99—5.54 (m, 2H, =CH_2), 5.59—6.24 (m, 1H, =CH); Found: C, 39.77; H, 6.79%. Calcd for $C_7H_{14}ClO_3P$: C, 39.54; H, 6.64%.

Ethyl 3-methyl-3-butenyl phosphorochloridate (**4a**): 65% yield; bp 80 °C/1.5×10^{-3} Torr; IR (neat) 3070, 2980, 2940, 2910, 1640, 1445, 1390, 1375, 1295, 1165, 1025 cm^{-1}; ^{1}H NMR (CCl_4) δ=1.40 (t, J=7 Hz, 3H, Me), 1.87 (s, 3H, Me), 2.43 (t, J=7 Hz, 2H, CH_2), 3.86—4.52 (m, 4H, CH_2), 4.78 (s, 2H, =CH_2); Found: C, 39.79; H, 6.87%. Calcd for $C_7H_{14}ClO_3P$: C, 39.54; H, 6.64%.

3-Methyl-3-butenyl propyl phosphorochloridate (**4b**): 73% yield; bp 87—95 °C/4×10^{-4} Torr; IR (neat) 3100, 2990, 2960, 2930, 1655, 1465, 1380, 1300, 1155, 1020 cm^{-1}; ^{1}H NMR (CCl_4) δ=0.99 (t, J=7 Hz, 3H, Me), 1.51—2.00 (m, 2H, CH_2), 1.77 (s, 3H, Me), 2.41 (t, J=7 Hz, 2H, CH_2), 3.90—4.50 (m, 4H, CH_2), 4.75 (s, 2H, =CH_2); Found: C, 42.69; H, 7.35%. Calcd for $C_8H_{16}ClO_3P$: C, 42.39; H, 7.12%.

Butyl 3-methyl-3-butenyl phosphorochloridate (**4c**): 61% yield; bp 95—99 °C/4.8×10^{-4} Torr; IR (neat) 3080, 2970, 2940, 2880, 1650, 1470, 1380, 1295, 1150, 1120, 1030 cm^{-1}; ^{1}H NMR (CCl_4) δ=0.93 (bt, J=6 Hz, 3H, Me), 1.18—2.00 (m, 4H, CH_2), 1.74 (s, 3H, Me), 2.39 (t, J=7 Hz, 2H, CH_2), 3.78—4.58 (m, 4H, CH_2), 4.74 (s, 2H, =CH_2); Found: C, 44.91; H, 7.70%. Calcd for $C_9H_{18}ClO_3P$: C, 44.92; H, 7.54%.

Isobutyl 3-methyl-3-butenyl phosphorochloridate (**4d**): 62% yield; bp 90—108 °C/8.5×10^{-4} Torr; IR (neat) 3090, 2990, 2930, 2890, 1655, 1470, 1380, 1305, 1185, 1170, 1130, 1030 cm^{-1}; ^{1}H NMR (CCl_4) δ=0.98 (d, J=6 Hz, 6H, Me), 1.79 (s, 3H, Me), 1.90—2.23 (m, 1H, CH), 2.44 (t, J=7 Hz, 2H, CH_2), 3.77—4.42 (m, 4H, CH_2), 4.79 (s, 2H, =CH_2); Found: C, 45.55; H, 7.90%. Calcd for $C_9H_{18}ClO_3P$: C, 44.92; H, 7.54%.

Crotyl propyl phosphorochloridate: 88% yield; IR (neat) 2970, 2940, 2880, 2850, 1673, 1460, 1378, 1287, 1010 cm^{-1}; ^{1}H NMR (CCl_4) δ=0.99 (t, J=7 Hz, 3H, Me), 1.32—2.12 (m, 2H, CH_2), 1.75 (d, J=5 Hz, 3H, Me), 3.82—4.27 (m, 2H, CH_2), 4.52 (dd J_{HP}=10 Hz, J_{HH}=5 Hz, 2H, CH_2), 5.22—6.12 (m, 2H, =CH); ^{13}C NMR ($CDCl_3$) δ=9.9 (s, Me), 17.7 (s, Me), 23.3 (d, J=8 Hz, CH_2), 70.1 (d, J=6 Hz, CH_2), 71.3 (d, J=8 Hz, CH_2), 124.3 (d, J=7 Hz, =$\underline{C}$HCH$_2$), 133.3 (s, =$\underline{C}$HMe).

***P*^{1},*P*^{2}-Dialkyl *P*^{1},*P*^{2}-Diallyl [and *P*^{1},*P*^{2}-Bis(3-methyl-3-butenyl)] Pyrophosphates (2 and 5).** The following preparation of *P*^{1},*P*^{2}-diallyl *P*^{1},*P*^{2}-diethyl pyrophosphate (**2a**) represents the general procedure. A mixture of allyl ethyl phosphorochloridate (**1a**) (736 mg, 4 mmol), sodium hydrogencarbonate (373 mg, 4.4 mmol) and a catalytic amount (ca. 10 mol%) of water (7 mg, 0.39 mmol) was stirred for 2 h at room temperature. After sodium chloride which formed was filtered, the reaction mixture was distilled (bp 137—142 °C/4.3×10^{-3} Torr) and then column chromatographed on silica gel (eluant: ether) to give *P*^{1},*P*^{2}-diallyl *P*^{1},*P*^{2}-diethyl pyrophosphate (**2a**) (139 mg, 22%) as a viscous colorless oil. Other dialkyl diallyl [and bis(3-methyl-3-butenyl)] pyrophosphates (**2** and **5**) were similarly prepared and purified. *P*^{1},*P*^{2}-Dicrotyl *P*^{1},*P*^{2}-dipropyl pyrophosphate (**3**) is unstable and used for the next reactions without further purification.

P^1,*P*^{2}-Diallyl *P*^{1},*P*^{2}-diethyl pyrophosphate (**2a**): 22% yield; bp 137—142 °C/ 4.3×10^{-3} Torr; IR (neat) 3080, 2980, 2925, 2905, 1645, 1367, 1290, 1160, 1100, 1024, 967 cm^{-1}; ^{1}H NMR (CCl_4) δ=1.34 (t, J=7 Hz, 6H, Me), 3.80—4.80 (m, 8H, CH_2), 4.80—5.60 (m, 4H, =CH_2), 5.60—6.40 (m, 2H, =CH); ^{13}C NMR ($CDCl_3$) δ=15.9 (m, Me), 65.4 (m, CH_2), 69.2

(m, CH_2), 118.8 (s, $=CH_2$), 131.8 (m, =CH); MS *m/z* (rel intensity) 314 (M^+, 11), 189 (100); Found: C, 37.71; H, 6.66%. Calcd for $C_{10}H_{20}O_7P_2$: C, 38.22; H, 6.42%.

P^1,P^2-Diallyl P^1,P^2-dipropyl pyrophosphate (**2b**): 54% yield; bp 130—135 °C/7.7×10^{-5} Torr; IR (neat) 3080, 2975, 2945, 2910, 2880, 1650, 1465, 1425, 1295, 1155, 1025, 960 cm^{-1}; ^{1}H NMR (CCl_4) δ=0.99 (t, *J*=6 Hz, 6H, Me), 1.30—2.09 (m, 4H, CH_2), 3.83—4.38 (m, 4H, CH_2), 4.38—4.83 (m, 4H, CH_2), 5.06—5.63 (m, 4H, $=CH_2$), 5.63—6.28 (m, 2H, =CH); ^{13}C NMR ($CDCl_3$) δ=9.9 (s, Me), 23.5 (m, CH_2), 69.2 (m, CH_2), 70.8 (m, CH_2), 118.8 (s, $=CH_2$), 132.0 (m, =CH); MS *m/z* (rel intensity) 342 (M^+, 7), 217 (100); Found: C, 41.83; H, 7.18%. Calcd for $C_{12}H_{24}O_7P_2$: C, 42.11; H, 7.07%.

P^1,P^2-Diallyl P^1,P^2-dibutyl pyrophosphate (**2c**): 20% yield; bp 145—150 °C/1.5×10^{-4} Torr; IR (neat) 3090, 2970, 2945, 2880, 1650, 1470, 1425, 1385, 1295, 1155, 1030, 960 cm^{-1}; ^{1}H NMR (CCl_4) δ=0.95 (bt, *J*=6 Hz, 6H, Me), 1.18—1.88 (m, 8H, CH_2), 3.86—4.39 (m, 4H, CH_2), 4.39—4.83 (m, 4H, CH_2), 5.07—5.58 (m, 4H, $=CH_2$), 5.58—6.33 (m, 2H, =CH); ^{13}C NMR ($CDCl_3$) δ=13.5 (s, Me), 18.6 (s, CH_2), 32.1 (m, CH_2), 69.1 (m, CH_2), 69.2 (m, CH_2), 118.8 (s, $=CH_2$), 131.9 (m, =CH); MS *m/z* (rel intensity) 370 (M^+, 0.8), 99 (100); Found: C, 45.70; H, 7.62%. Calcd for $C_{14}H_{28}O_7P_2$: C, 45.41; H, 7.62%.

P^1,P^2-Diallyl P^1,P^2-diisobutyl pyrophosphate (**2d**): 23% yield; bp 146—150 °C/4.1×10^{-3} Torr; IR (neat) 3090, 2970, 2900, 2880, 1650, 1470, 1370, 1290, 1023, 960 cm^{-1}; ^{1}H NMR (CCl_4) δ=0.97 (d, *J*=6 Hz, 12H, Me), 1.70—2.35 (m, 2H, CH), 3.60—4.04 (m, 4H, CH_2), 4.30—4.90 (m, 4H, CH_2), 4.90—5.60 (m, 4H, $=CH_2$), 5.60—6.35 (m, 2H, =CH); ^{13}C NMR ($CDCl_3$) δ=18.5 (s, Me), 29.0 (m, CH), 69.2 (m, CH_2), 118.8 (s, $=CH_2$), 131.9 (m, =CH); MS *m/z* (rel intensity) 370 (M^+, 24), 259 (100); Found: C, 45.24; H, 7.72%. Calcd for $C_{14}H_{28}O_7P_2$: C, 45.41; H, 7.62%.

P^1,P^2-Diethyl P^1,P^2-bis(3-methyl-3-butenyl) pyrophosphate (**5a**): 26% yield; bp 140—150 °C/1.0×10^{-3} Torr; IR (neat) 3085, 2990, 2940, 2920, 1645, 1445, 1395, 1375, 1295, 1166, 1040, 985, 960 cm^{-1}; ^{1}H NMR (CCl_4) δ=1.35 (t, *J*=7 Hz, 6H, Me), 1.75 (s, 6H, Me), 2.39 (t, *J*=6 Hz, 4H, CH_2), 3.90—4.50 (m, 8H, CH_2), 4.75 (s, 4H, $=CH_2$); ^{13}C NMR ($CDCl_3$) δ=16.0 (m, Me), 22.4 (s, Me), 38.1 (m, CH_2), 65.3 (m, CH_2), 67.1 (m, CH_2), 112.9 (s, $=CH_2$), 140.7 (s, $-\overset{|}{C}=$); MS *m/z* (rel intensity) 370 (M^+, 0.8), 235 (100); Found: C, 45.18; H, 7.73%. Calcd for $C_{14}H_{28}O_7P_2$: C, 45.41; H, 7.62%.

P^1,P^2-Dipropyl P^1,P^2-bis(3-methyl-3-butenyl) pyrophosphate (**5b**): 66% yield; bp 135—140 °C/4.2×10^{-5} Torr; IR (neat) 3070, 2975, 2940, 2900, 1650, 1460, 1375, 1290, 1020, 960 cm^{-1}; ^{1}H NMR (CCl_4) δ=1.00 (t, *J*=7 Hz, 6H, Me), 1.40—2.10 (m, 4H, CH_2), 1.75 (s, 6H, Me), 2.40 (t, *J*=7 Hz, 4H, CH_2), 3.70—4.55 (m, 8H, CH_2), 4.73 (s, 4H, $=CH_2$); ^{13}C NMR ($CDCl_3$) δ=9.9 (s, Me), 22.4 (s, Me), 23.5 (m, CH_2), 38.1 (m, CH_2), 67.1 (m, CH_2), 70.7 (m, CH_2), 112.9 (s, $=CH_2$), 140.7 (s, $-\overset{|}{C}=$); MS *m/z* (rel intensity) 398 (M^+, 0.7), 179 (100); Found: C, 48.40; H, 8.32%. Calcd for $C_{16}H_{32}O_7P_2$: C, 48.24; H, 8.10%.

P^1,P^2-Diisopropyl P^1,P^2-bis(3-methyl-3-butenyl) pyrophosphate (**5c**): 54% yield; bp 130 °C/9.2×10^{-5} Torr; IR (neat) 3090, 2990, 2950, 1655, 1470, 1455. 1380, 1290, 1185, 1145, 1110, 1010, 960 cm^{-1}; ^{1}H NMR (CCl_4) δ=1.32 (d, *J*=7 Hz, 12H, Me), 1.76 (s, 6H, Me), 2.39 (t, *J*=7 Hz, 4H, CH_2) 3.99—4.33 (m, 4H, CH_2), 4.42—4.92 (m, 6H, CH and $=CH_2$); ^{13}C NMR ($CDCl_3$) δ=22.5 (s, Me), 23.5 (s, Me), 38.1 (m, CH_2), 66.9 (m, CH_2), 74.6 (m, CH), 112.8 (s, $=CH_2$), 140.8 (s, $-\overset{|}{C}=$); MS *m/z* (rel intensity) 398 (M^+, 0.8), 179 (100); Found: C, 48.08; H, 8.05%. Calcd for $C_{16}H_{32}O_7P_2$: C, 48.24; H, 8.10%.

P^1,P^2-Dibutyl P^1,P^2-bis(3-methyl-3-butenyl) pyrophosphate (**5d**): 50% yield; bp 140—150 °C/7.0×10^{-5} Torr; IR (neat) 3080, 2970, 2920, 2880, 1650, 1465, 1380, 1295, 1150, 1120, 1030, 965 cm^{-1}; ^{1}H NMR (CCl_4) δ=0.95 (bt, *J*=6 Hz, 6H, Me), 1.21—2.02 (m, 8H, CH_2), 1.75 (s, 6H, Me), 2.39 (t, *J*=7 Hz, 4H, CH_2), 3.82—4.42 (m, 8H, CH_2), 4.76 (s, 4H, $=CH_2$); ^{13}C NMR ($CDCl_3$) δ=13.5 (s, Me), 18.6 (s, CH_2), 22.4 (s, Me), 32.1 (m, CH_2), 38.1 (m, CH_2), 67.1 (m, CH_2), 68.9 (m, CH_2), 112.9 (s, $=CH_2$), 140.6 (s, $-\overset{|}{C}=$); MS *m/z* (rel intensity) 426 (M^+, 0.5), 179 (100); Found: C, 50.52; H, 8.72%. Calcd for $C_{18}H_{36}O_7P_2$: C, 50.70; H, 8.51%.

P^1,P^2-Diisobutyl P^1,P^2-bis(3-methyl-3-butenyl) pyrophosphate (**5e**): 64% yield; bp 130 °C/2.1×10^{-5} Torr; IR (neat) 3090, 2990, 2930, 2890, 1655, 1465, 1375, 1300, 1035, 965 cm^{-1}; ^{1}H NMR (CCl_4) δ=0.94 (d, *J*=6 Hz, 12H, Me), 1.75 (s, 6H, Me), 1.85—2.17 (m, 2H, CH), 2.38 (t, *J*=7 Hz, 4H, CH_2), 3.85 (t, J_{HH}=J_{HP}=6 Hz, 4H, CH_2), 4.19 (dd, J_{HH}=J_{HP}=7 Hz, 4H, CH_2), 4.76 (s, 4H, $=CH_2$); ^{13}C NMR ($CDCl_3$) δ=18.5 (s, Me), 22.4 (s, Me), 29.0 (m, CH), 38.1 (m, CH_2), 67.1 (m, CH_2), 74.9 (m, CH_2), 112.9 (s, $=CH_2$), 140.6 (s, $-\overset{|}{C}=$); MS *m/z* (rel intensity) 426 (M^+, 1), 68 (100); Found: C, 50.86; H, 8.80%. Calcd for $C_{18}H_{36}O_7P_2$: C, 50.70; H, 8.51%.

P^1,P^2-Dicrotyl P^1,P^2-dipropyl pyrophosphate (**3**): 86% yield; IR (neat) 3040, 2980, 2950, 2900, 2870, 1677, 1460, 1380, 1278, 1018, 968 cm^{-1}; ^{1}H NMR ($CDCl_3$) δ=0.86—1.08 (m, 6H, Me), 1.54—1.86 (m, 10H, CH_2 and Me), 3.84—4.24 (m, 4H, CH_2), 4.36—4.72 (m, 4H, CH_2), 5.50—6.00 (m, 4H, =CH); MS *m/z* (rel intensity) 370 (M^+, 3), 141 (100).

Trialkyl Allyl (and 3-Methyl-3-butenyl) Pyrophosphates (6 and 8). The following preparation of allyl triethyl pyrophosphate (**6a**) represents the general procedure. To a mixture of diethyl hydrogenphosphate (466 mg, 3 mmol) and triethylamine (0.49 cm^3, 3.5 mmol) in anhydrous ether (10 cm^3) was slowly added a solution of allyl ethyl phosphorochloridate (583 mg, 3.2 mmol) in ether (10 cm^3) with cooling in an ice-salt bath. After the addition was complete, the reaction mixture was stirred at that temperature for 2 h and then triethylammonium chloride which formed was filtered. The filtrate was concentrated and the residue was distilled (bp 155 °C/3.0×10^{-4} Torr) to give an almost pure product. This was further purified by column chromatography on silica gel (eluant: ether) to afford pure allyl triethyl pyrophosphate (**6a**) (611 mg, 67%) as a colorless oil. Other trialkyl allyl (and 3-methyl-3-butenyl) pyrophosphates (**6** and **8**) were similarly prepared and purified. Crotyl tripropyl pyrophosphate (**7**) is thermally unstable, so the crude material was used for the next reactions without further purification.

Allyl triethyl pyrophosphate (**6a**): 67% yield; bp 155 °C/3.0×10^{-4} Torr; IR (neat) 3100, 3000, 2950, 2920, 2825, 1650, 1480, 1445, 1373, 1290, 1167, 1032, 963 cm^{-1}; ^{1}H NMR (CCl_4) δ=1.38 (t, *J*=7 Hz, 9H, Me), 3.90—4.50 (m, 6H, CH_2), 4.55—4.90 (m, 2H, CH_2), 5.10—5.70 (m, 2H, $=CH_2$), 5.70—6.40 (m, 1H, =CH); ^{13}C NMR ($CDCl_3$) δ=16.0 (m, Me), 65.3 (m, CH_2), 69.2 (bt, 4 Hz, CH_2), 118.7 (s, $=CH_2$), 131.8 (bt, *J*=2 Hz, =CH); MS *m/z* (rel intensity) 302 (M^+, 6), 161 (100); Found: C, 35.65; H, 6.66%. Calcd for $C_9H_{20}O_7P_2$: C, 35.77; H, 6.67%.

Allyl tripropyl pyrophosphate (**6b**): 77% yield; bp 130—135 °C/1.4×10^{-5} Torr; IR (neat) 3090, 2980, 2950, 2920, 2890, 1650, 1465, 1425, 1380, 1295, 1155, 1030, 960 cm^{-1}; ^{1}H NMR (CCl_4) δ=0.99 (t, J=7 Hz, 9H, Me), 1.32—2.12 (m, 6H, CH_2), 3.84—4.34 (m, 6H, CH_2), 4.35—4.74 (m, 2H, CH_2), 5.05—5.54 (m, 2H, =CH_2), 5.62—6.81 (m, 1H, =CH); ^{13}C NMR ($CDCl_3$) δ=9.9 (s, Me), 23.5 (m, CH_2), 69.2 (bt, J=3 Hz, CH_2), 70.6 (m, CH_2), 118.7 (s, =CH_2), 132.0 (bt, J=3 Hz, =CH); MS m/z (rel intensity) 344 (M^+, 10), 219 (100); Found: C, 41.88; H, 7.91%. Calcd for $C_{12}H_{26}O_7P_2$: C, 41.87; H, 7.61%.

Allyl tributyl pyrophosphate (**6c**): 72% yield; bp 165—167 °C/2.0×10^{-4} Torr; IR (neat) 2975, 2950, 2925, 2890, 1650, 1467, 1383, 1293, 1153, 1120, 1033, 960 cm^{-1}; ^{1}H NMR (CCl_4) δ=0.75—1.30 (bt, J=6 Hz, 9H, Me), 1.30—2.35 (m, 12H, CH_2), 3.85—4.39 (m, 6H, CH_2), 4.39—4.75 (m, 2H, CH_2), 5.01—5.57 (m, 2H, =CH_2), 5.57—6.29 (m, 1H, =CH); ^{13}C NMR ($CDCl_3$) δ=13.5 (s, Me), 18.5 (s, CH_2), 32.1 (m, CH_2), 68.8 (m, CH_2), 68.9 (bt, J=4 Hz, CH_2), 118.7 (s, =CH_2), 131.9 (bt, J=3 Hz, =CH); MS m/z (rel intensity) 386 (M^+, 3), 179 (100); Found: C, 46.66; H, 8.65%. Calcd for $C_{15}H_{32}O_7P_2$: C, 46.63; H, 8.35%.

Allyl triisobutyl pyrophosphate (**6d**): 81% yield; bp 157 °C/3.0×10^{-4} Torr; IR (neat) 3110, 3000, 2960, 2920, 2900, 1650, 1475, 1375, 1300, 1170, 1135, 1032, 970 cm^{-1}; ^{1}H NMR (CCl_4) δ=0.98 (d, J=6 Hz, 18H, Me), 1.73—2.33 (m, 3H, CH), 3.84 (t, J_{HH}=J_{HP}=7 Hz, 6H, CH_2) 4.33—4.73 (m, 2H, CH_2), 5.03—5.53 (m, 2H, =CH_2), 5.53—6.13 (m, 1H, =CH); ^{13}C NMR ($CDCl_3$) δ=18.4 (s, Me), 28.9 (m, CH), 69.0 (bt, J=3 Hz, CH_2), 74.8 (m, CH_2), 118.6 (s, =CH_2), 131.9 (bt, J=3 Hz, =CH); MS m/z (rel intensity) 386 (M^+, 1), 219 (100); Found: C, 46.65; H, 8.53%. Calcd for $C_{15}H_{32}O_7P_2$: C, 46.63; H, 8.35%.

Triethyl 3-methyl-3-butenyl pyrophopshate (**8a**): 13% yield; bp 135—140 °C/4.0×10^{-5} Torr; IR (neat) 3080, 2990, 2940, 2920, 1650, 1480, 1445, 1395, 1370, 1295, 1065, 1030, 980, 960 cm^{-1}; ^{1}H NMR (CCl_4) δ=1.35 (t, J=7 Hz, 9H, Me), 1.75 (s, 3H, Me), 2.38 (t, J=7 Hz, CH_2), 3.81—4.48 (m, 8H, CH_2), 4.72 (s, 2H, =CH_2); ^{13}C NMR ($CDCl_3$) δ=16.0 (m, Me), 22.4 (s, Me), 38.1 (bt, J=4 Hz, CH_2), 65.2 (m, CH_2), 67.1 (bt, J=3 Hz, CH_2), 112.9 (s, =CH_2), 140.7 (s, -C=); MS m/z (rel intensity) 330 (M^+, 2), 179 (100); Found: C, 39.90; H, 7.59%. Calcd for $C_{11}H_{24}O_7P_2$: C, 40.00; H, 7.33%.

3-Methyl-3-butenyl tripropyl pyrophosphate (**8b**): 85% yield; bp 140—145 °C/7.3×10^{-5} Torr; IR (neat) 3090, 2990, 2960, 2920, 2900, 1655, 1465, 1395, 1380, 1295, 1155, 1030, 965 cm^{-1}; ^{1}H NMR (CCl_4) δ=0.99 (t, J=7 Hz, 9H, Me), 1.39—2.09 (m, 6H, CH_2), 1.77 (s, 3H, Me), 2.40 (t, J=7 Hz, 2H, CH_2), 3.88—4.44 (m, 8H, CH_2), 4.76 (s, 2H, =CH_2); ^{13}C NMR ($CDCl_3$) δ=9.9 (s, Me), 22.4 (s, Me), 23.5 (m, CH_2), 38.1 (m, CH_2), 67.1 (m, CH_2), 70.6 (m, CH_2), 112.9 (s, =CH_2), 140.7 (s, -C=); MS m/z (rel intensity) 372 (M^+, 2), 179 (100); Found: 45.27; H, 8.36%. Calcd for $C_{14}H_{30}O_7P_2$: C, 45.16; H, 8.12%.

Tributyl 3-methyl-3-butenyl pyrophosphate (**8c**): 66% yield: bp 150—155 °C/5.0×10^{-5} Torr; IR (neat) 3080, 2970, 2940, 2920, 2880, 1650, 1465, 1385, 1290, 1150, 1120, 1030, 965 cm^{-1}; ^{1}H NMR (CCl_4) δ=0.97 (bt, J=6 Hz, 9H, Me), 1.23—2.08 (m, 12H, CH_2), 1.78 (s, 3H, Me), 2.40 (t, J=7 Hz, 2H, CH_2), 3.88—4.48 (m, 8H, CH_2), 4.77 (s, 2H, =CH_2); ^{13}C NMR ($CDCl_3$) δ=13.5 (s, Me), 18.6 (s, CH_2), 22.5 (s, Me), 32.1 (m, CH_2), 38.1 (m, CH_2), 67.1 (m, CH_2), 68.9 (m, CH_2), 112.9 (s, =CH_2), 140.7 (s, -C=); MS m/z (rel intensity) 414 (M^+, 1), 179 (100); Found: C, 49.16; H, 8.85%. Calcd for $C_{17}H_{36}O_7P_2$: C, 49.26; H, 8.76%.

Triisobutyl 3-methyl-3-butenyl pyrophosphate (**8d**): 42% yield; bp 120 °C/1.8×10^{-5} Torr; IR (neat) 3090, 2980, 2890, 1655, 1475, 1365, 1300, 1185, 1170, 1135, 1030, 965 cm^{-1}; ^{1}H NMR (CCl_4) δ=0.95 (d, J=6 Hz, 18H, Me), 1.76 (s, 3H, Me), 1.87—2.19 (m, 3H, CH), 2.40 (t, J=7 Hz, 2H, CH_2), 3.84 (t, J_{HH}=J_{HP}=7 Hz, 6H, CH_2), 4.00—4.35 (m, 2H, CH_2), 4.74 (s, 2H, =CH_2); ^{13}C NMR ($CDCl_3$) δ=18.6 (s, Me), 22.4 (s, Me), 29.0 (m, CH), 38.1 (bt, J=4 Hz, CH_2), 67.1 (bt, J=3 Hz, CH_2), 74.9 (m, CH_2), 112.9 (s, =CH_2), 140.6 (s, -C=); MS m/z (rel intensity) 414 (M^+, 2), 179 (100); Found: C, 49.04; H, 8.86%. Calcd for $C_{17}H_{36}O_7P_2$: C, 49.26; H, 8.76%.

Crotyl tripropyl pyrophosphate (**7**): 76% yield; IR (neat) 2975, 2950, 2890, 2860, 1675, 1460, 1380, 1290, 1153, 1018, 957 cm^{-1}; ^{1}H NMR (CCl_4) δ=0.97 (t, J=7 Hz, 9H, Me), 1.36—1.91 (m, 9H, CH_2 and Me), 3.78—4.25 (m, 6H, CH_2), 4.31—4.71 (m, 2H, CH_2), 5.31—6.01 (m, 2H, =CH); ^{13}C NMR ($CDCl_3$) 9.9 (s, Me), 17.7 (s, Me), 23.5 (m, CH_2), 69.4 (dd, J=3, 2 Hz, CH_2), 70.6 (m, CH_2), 125.1 (dd, J=4, 2 Hz, =CH), 132.3 (s, =CH); MS m/z (rel. intensity) 358 (M^+, 15), 179 (100).

Reactions of P^1,P^2-Dicrotyl P^1,P^2-Dipropyl Pyrophosphate (3) and Crotyl Tripropyl Pyrophosphate (7) with Phenolic Ethers. Following reaction of P^1,P^2-dicrotyl P^1,P^2-dipropyl pyrophosphate (**3**) with anisole represents the general procedure. Into a mixture of anisole (1.1 cm^3, 10 mmol) and P^1,P^2-dicrotyl P^1,P^2-dipropyl pyrophosphate (**3**) (741 mg, 2 mmol) in anhydrous dichloromethane (7 cm^3) was added boron trifluoride etherate (0.25 cm^3, 2 mmol) at 0 °C, and the mixture was stirred at 0 °C for 3.5 h. The reaction was quenched by the addition of water and the products were extracted with dichloromethane. The extracts were washed with brine, and then dried over anhydrous sodium sulfate. The solvent was evaporated and the residue was analyzed by GLC using p-methylanisole as an internal standard. Pure samples of the products were isolated by preparative GLC and the structures were deduced by their spectral data.

Reactions with other phenolic ethers were similarly carried out and the products were analyzed using adequate internal standards. The reaction conditions and the results are summarized in Table 1.

(E)-1-(2-Butenyl)-2-methoxybenzene:[11] ^{1}H NMR ($CDCl_3$) δ=1.68 (d, J=6 Hz, 3H, Me), 3.33 (d, J=6 Hz, 2H, CH_2), 3.85 (s, 3H, OMe), 5.41—5.75 (m, 2H, =CH), 6.81—7.01 (m, 2H, Ar), 7.11—7.29 (m, 2H, Ar); MS m/z (rel intensity) 162 (M^+, 100).

1-Methoxy-2-(1-methyl-2-propenyl)benzene:[12] MS m/z (rel intensity) 162 (M^+, 96), 147 (100).

(E)-1-(2-Butenyl)-4-methoxybenzene:[13] ^{1}H NMR ($CDCl_3$) δ=1.68 (d, J=5 Hz, 3H, Me), 3.27 (bd, J=5 Hz, 2H, CH_2), 3.80 (s, 3H, OMe), 5.40—5.74 (m, 2H, =CH), 6.87 (d, J=9 Hz, 2H, Ar), 7.14 (d, J=9 Hz, 2H, Ar); MS m/z (rel intensity) 162 (M^+, 100).

1-Methoxy-4-(1-methyl-2-propenyl)benzene:[12] ^{1}H NMR ($CDCl_3$) δ=1.34 (d, J=7 Hz, 3H, Me), 3.34—3.54 (m, 1H, CH), 3.80 (s, 3H, OMe), 4.96—5.16 (m, 2H, =CH_2), 5.84—6.12 (m, 1H, =CH), 6.88 (d, J=9 Hz, 2H, Ar), 7.16 (d, J=9 Hz, 2H, Ar).

(E)-2-(2-Butenyl)-1,4-dimethoxybenzene:[14] IR (neat) 3030, 3000, 2950, 2920, 2860, 2840, 1590, 1503, 1465, 1286, 1220, 1177, 1155, 1048, 1027, 800 cm^{-1}; ^{1}H NMR ($CDCl_3$) δ=1.68

(d, J=6 Hz, 3H, Me), 3.30 (d, J=5 Hz, 2H, CH_2), 3.78 (s, 3H, OMe), 3.80 (s, 3H, OMe), 5.40—5.72 (m, 2H, =CH), 6.66—6.90 (m, 3H, Ar); MS m/z (rel. intensity) 192 (M^+, 100).

1,4-Dimethoxy-2-(1-methyl-2-propenyl)benzene:[14] ^1H NMR ($CDCl_3$) δ=1.31 (d, J=7 Hz, 3H, Me), 3.78 (s, 3H, OMe), 3.82 (s, 3H, OMe), 3.60—4.00 (m, 1H, CH), 5.00—5.16 (m, 2H, $=CH_2$), 5.94—6.16 (m, 1H, =CH), 6.60—6.88 (m, 3H, Ar); MS m/z (rel intensity) 192 (M^+, 100).

(*E*)-2-(2-Butenyl)-1,3,5-trimethoxybenzene: ^1H NMR ($CDCl_3$) δ=1.62 (d, J=6 Hz, 3H, Me), 3.26 (bd, J=5 Hz, 2H, CH_2), 3.82 (s, 9H, OMe), 5.35—5.71 (m, 2H, =CH), 6.17 (s, 2H, Ar); MS m/z (rel intensity) 222 (M^+, 100).

1,3,5-Trimethoxy-2-(1-methyl-2-propenyl)benzene: ^1H NMR ($CDCl_3$) δ=1.34 (d, J=7 Hz, 3H, Me), 3.80 (s, 6H, OMe), 3.81 (s, 3H, OMe), 3.98—4.18 (m, 1H, CH), 4.82—5.04 (m, 2H, $=CH_2$), 6.16 (s, 2H, Ar), 6.06—6.38 (m, 1H, =CH); MS m/z (rel. intensity) 222 (M^+, 54), 207 (100).

(*E*)-2-(2-Butenyl)-3,4,5,6-tetramethoxytoluene: IR (neat) 2960, 2940, 2860, 2830, 1645, 1463, 1350, 1258, 1195, 1073, 1040, 1010, 970 cm^{-1}; ^1H NMR ($CDCl_3$) δ=1.64 (d, J=6 Hz, 3H, Me), 2.16 (s, 3H, Me), 3.32 (d, J=5 Hz, 2H, CH_2), 3.80 (s, 3H, OMe), 3.82 (s, 3H, OMe), 3.92 (s, 3H, OMe), 3,93 (s, 3H, OMe), 5.28—5.64 (m, 2H, =CH); MS m/z (rel intensity) 266 (M^+, 100).

2,3,4,5-Tetramethoxy-6-(1-methyl-2-propenyl)toluene: ^1H NMR ($CDCl_3$) δ=1.38 (d, J=7 Hz, 3H, Me), 2.18 (s, 3H, Me), 3.78 (s, 3H, OMe), 3.80 (s, 3H, OMe), 3.90 (s, 3H, OMe), 3,92 (s, 3H, OMe), 3.60—4.08 (m, 1H, CH), 4.92—5.12 (m, 2H, $=CH_2$), 6.02—6.26 (m, 1H, =CH); MS m/z (rel intensity) 266 (M^+, 100).

(*E*)-2-(2-Butenyl)-1,4-dimethoxy-3-methylnaphthalene: IR (neat) 3075, 3030, 2940, 2850, 1590, 1450, 1375, 1353, 1263, 1197, 1097, 1067, 1015, 970, 768 cm^{-1}; ^1H NMR ($CDCl_3$) δ=1.64 (dd, 3H, J=6, 1 Hz, Me), 2.40 (s, 3H, Me), 3.50—3.66 (m, 2H, CH_2), 3.88 (s, 3H, OMe), 3.91 (s, 3H, OMe), 5.28—5.54 (m, 1H, =CH), 5.54—5.78 (m, 1H, =CH), 7.44—7.58 (m, 2H, Ar), 8.00—8.18 (m, 2H, Ar); MS m/z (rel intensity) 256 (M^+, 100).

Reactions of Crotyl Tripropyl Pyrophosphate (7) with Aromatic Amines, Pyrrole, and Indole. Following reaction of crotyl tripropyl pyrophosphate (**7**) with aniline represents the general procedure. To a mixture of aniline (225 mg, 2.4 mmol) and crotyl tripropyl pyrophosphate (**7**) (866 mg, 2.4 mmol) in DMF (8 cm^3) was added boron trifluoride etherate (0.61 cm^3, 4.8 mmol) at room temperature and the reaction mixture was stirred overnight (20 h). Saturated sodium hydrogencarbonate was added and the products were extracted with hexane. The extracts were washed with brine and dried over anhydrous sodium sulfate. The solvent was removed under reduced pressure and the residual oil was chromatographed on silica gel (eluant: benzene) to give *N*-crotylaniline (202 mg, 57%) and *N*,*N*-dicrotylaniline (21 mg, 9%).

Reactions for other aromatic amines, pyrrole, and indole were similarly carried out and the products were isolated by silica-gel column chromatography. The yields and physical data of the products are summarized in Table 2.

(*E*)-*N*-(2-Butenyl)aniline: IR (neat) 3420, 3060, 3025, 2960, 2930, 2880, 2850, 1603, 1505, 1465, 1450, 1377, 1320, 1250, 964 cm^{-1}; ^1H NMR (CCl_4) δ=1.47—1.87 (m, 3H, Me), 3.34 (bs, 1H, NH), 3.47—3.87 (m, 2H, CH_2), 5.27—5.72 (m, 2H, =CH), 6.17—6.62 (m, 3H, Ph), 6.71—7.14 (t, J=7 Hz, 2H, Ph); MS m/z (rel intensity) 147 (M^+, 68), 93 (100).

(*E*)-*N*,*N*-Di(2-butenyl)aniline: IR (neat) 3100, 3070, 3040, 2970, 2930, 2860, 1720, 1600, 1507, 1450, 1380, 1353, 1260, 966, 862, 745, 692 cm^{-1}; ^1H NMR (CCl_4) δ=1.45—1.85 (m, 6H, Me), 3.35—4.05 (m, 4H, CH_2), 5.05—5.75 (m, 4H, =CH), 6.21—7.25 (m, 5H, Ph); MS m/z (rel intensity) 201 (M^+, 81), 77 (100).

(*E*)-*N*-(2-Butenyl)-*N*-methylaniline: IR (neat) 3090, 3060, 3020, 2930, 2920, 2875, 2850, 1665, 1598, 1505, 1446, 1368, 1350, 1250, 1030, 990, 960, 935, 857, 745, 687 cm^{-1}; ^1H NMR (CCl_4) δ=1.52—1.77 (m, 3H, Me), 2.78 (s, 3H, Me), 3.57—3.92 (m, 2H, CH_2), 5.26—5.57 (m, 2H, =CH), 6.27—6.66 (m, 3H, Ph), 6.72—7.14 (m, 2H, Ph); MS m/z (rel. intensity) 161 (M^+, 80), 120 (100).

(*E*)-*N*-(2-Butenyl)-*p*-anisidine: ^1H NMR ($CDCl_3$) δ= 1.72 (d, J=4 Hz, 3H, Me), 2.60—3.00 (bs, 1H, NH), 3.65 (d, J=4 Hz, 2H, CH_2), 3.76 (s, 3H, OMe), 5.54—5.84 (m, 2H, =CH), 6.63 (d, J=8 Hz, 2H, Ar), 6.82 (d, J=8 Hz, 2H, Ar); MS m/z (rel intensity) 177 (M^+, 15), 108 (100).

(*E*)-*N*,*N*-Di(2-butenyl)-*p*-anisidine: ^1H NMR ($CDCl_3$) δ= 1.68 (d, J=4 Hz, 6H, Me), 3.70—3.90 (m, 7H, CH_2 and OMe), 5.40—5.72 (m, 4H, =CH), 6.64—6.90 (m, 4H, Ar); MS m/z (rel intensity) 231 (M^+, 56), 122 (100).

(*E*)-*N*,*N*-Diphenyl-2-butenylamine: IR (neat) 3080, 3060, 3040, 3000, 2960, 2930, 2880, 2850, 1590, 1497, 1447, 1364, 1240, 962, 745, 690 cm^{-1}; MS m/z (rel intensity) 223 (M^+, 27), 77 (100).

N,*N*-Diphenyl-1-methyl-2-propenylamine: MS m/z (rel intensity) 223 (M^+, 25), 77 (100).

(*E*)-*N*-Phenyl-4(or 2)-(2-butenyl)phenylamine: ^1H NMR ($CDCl_3$) δ=1.66—1.84 (m, 3H, Me), 3.22—3.48 (m, 2H, CH_2), 5.48—5.73 (m, 2H, =CH), 6.86—7.42 (m, 9H, Ar).

(*E*)-*N*-(2-Butenyl)-1-naphthylamine: IR (neat) 3450, 3070, 2980—2870, 1580, 1520, 1370, 1340, 1270, 965, 765 cm^{-1}; ^1H NMR ($CDCl_3$) δ=1.62—1.87 (m, 3H, Me), 3.72—4.00 (m, 2H, CH_2), 4.24 (bs, 1H, NH), 5.60—5.96 (m, 2H, =CH), 6.61 (d, J=7 Hz, 1H, Ar), 7.16—7.60 (m, 4H, Ar), 7.74—7.96 (m, 2H, Ar); MS m/z (rel intensity) 197 (M^+, 63), 115 (100).

(*E*)-2-(2-Butenyl)-1-naphthylamine: IR (neat) 3450, 3400, 3070, 3040, 2980, 2930, 2860, 1620, 1510, 1400, 970, 800 cm^{-1}; ^1H NMR ($CDCl_3$) δ=1.66—1.83 (m, 3H, Me), 3.34—3.52 (m, 2H, CH_2), 3.60—4.40 (m, 2H, NH_2), 5.46—5.80 (m, 2H, =CH), 7.20—7.55 (m, 4H, Ar), 7.76—7.94 (m, 2H, Ar); MS m/z (rel intensity) 197 (M^+, 100).

(*E*)-2-(2-Butenyl)pyrrole:[15] IR (neat) 3400, 3110, 3040, 2980, 2950, 2930, 2900, 2860, 2830, 1567, 1438, 1470, 1380, 1092, 1040, 1025, 970, 790, 717 cm^{-1}; ^1H NMR ($CDCl_3$) δ=1.71 (d, J=4 Hz, 3H, Me), 3.22—3.46 (m, 2H, CH_2), 5.48—5.72 (m, 2H, =CH), 5.86—6.03 (m, 1H, pyrrole H^4), 6.10—6.24 (m, 1H, pyrrole H^3), 6.66—6.78 (m, 1H, pyrrole H^5), 7.98 (bs, 1H, NH); MS m/z (rel intensity) 121 (M^+, 100).

2-(1-Methyl-2-propenyl)pyrrole:[15] ^1H NMR ($CDCl_3$) δ= 1.38 (d, J=7 Hz, 3H, Me), 3.40—3.56 (m, 1H, CH), 5.00—5.20 (m, 2H, $=CH_2$), 5.72—6.04 (m, 2H, =CH and pyrrole H^4), 6.10—6.20 (m, 1H, pyrrole H^3), 6.66—6.78 (m, 1H, pyrrole H^5); MS m/z (rel intensity) 121 (M^+, 76), 106 (100).

(*E*)-3-(2-Butenyl)pyrrole:[16,17] IR (neat) 3410, 3040, 2980, 2950, 2930, 2860, 2850, 1557, 1435, 1380, 1066, 1053, 970, 770, 710 cm^{-1}; H NMR ($CDCl_3$) δ=1.69 (d, J=6 Hz, 3H, Me), 3.08—3.38 (m, 2H, CH_2), 5.40—5.72 (m, 2H, =CH), 6.00—6.20 (m, 1H, pyrrole H^4), 6.54—6.70 (m, 1H, pyrrole H^5), 6.70—7.84 (m, 1H, pyrrole H^2), 8.04 (bs, 1H, NH); MS

m/z (rel intensity) 121 (M^+, 100).

(*E*)-3-(2-Butenyl)indole: ^1H NMR ($CDCl_3$) δ=1.70 (d, *J*=6 Hz, 3H, Me), 3.46 (d, *J*=4 Hz, 2H, CH_2), 5.00—5.90 (m, 2H, =CH), 7.00 (s, 1H, indole H^2), 7.08—7.28 (m, 2H, indole H^5 and H^6), 7.38 (d, *J*=8 Hz, 1H, indole H^4), 7.64 (d, *J*=8 Hz, 1H, indole H^7), 7.84—8.10 (bs, 1H, NH); MS *m/z* (rel intensity) 171 (M^+, 100).

3-(1-Methyl-2-propenyl)indole: MS *m/z* (rel intensity) 171 (M^+, 54), 156 (100).

References

1) For example: S. Araki, M. Hatano, H. Ito, and Y. Butsugan, *J. Organomet. Chem.*, **333**, 329 (1987); and references cited therein.

2) For a recent review, see: D. E. Cane, *Acc. Chem. Res.*, **18**, 220 (1985).

3) M. Kobayashi, T. Koyama, K. Ogura, S. Seto, F. J. Ritter, and I. E. M. Brüggemann-Rotgans, *J. Am. Chem. Soc.*, **102**, 6602 (1980); T. Koyama, M. Matsubara, K. Ogura, I. E. M. Brüggemann-Rotgans, and A. Vrielink, *Naturwissenschaften*, **70**, 469 (1983); T. Koyama, K. Ogura, and S. Seto, *Chem. Lett.*, **1973**, 401.

4) K. Sasse, "Organische Phosphorverbindungen" in "Methoden der Organischen Chemie," ed by E. Müller, Band XII/2.

5) For example: Sankin Industry Co. Ltd., Jpn. Patent 82-38793; *Chem. Abstr.*, **97**, 61066 (1982); Sankin Industry Co. Ltd., Jpn. Patent 82-167364; *Chem. Abstr.*, **98**, 204455 (1983).

6) A. D. F. Toy, *J. Am. Chem. Soc.*, **70**, 3882 (1948).

7) S. Araki, S. Manabe, and Y. Butsugan, *Chem. Lett.*, **1982**, 797.

8) S. Araki, S. Manabe, and Y. Butsugan, *Bull. Chem. Soc. Jpn.*, **57**, 1433 (1984).

9) T. Mizuma, Y. Minaki, and S. Toyoshima, *J. Pharm. Soc. Jpn.*, **81**, 5 (1961); *Chem. Abstr.*, **55**, 123 (1961).

10) G. Sosnovsky and E. H. Zaret, *J. Org. Chem.*, **34**, 968 (1969).

11) E. A. Vdovtsova and L. P. Yanichkin, *Zh. Org. Khim.*, **5**, 510 (1969).

12) J. Synese and H. H. Jürgen, *Chimia*, **35**, 49 (1981).

13) Japan Synthetic Rubber Co. Ltd., Jpn. Patent 81-123923; *Chem. Abstr.*, **96**, 19684 (1982).

14) M. Ochiai, E. Fujita, and M. Arimoto, *Chem. Pharm. Bull.*, **31**, 86 (1983).

15) J. M. Patterson, J. W. de Haan, M. R. Boyd, and J. D. Ferry, *J. Am. Chem. Soc.*, **94**, 2487 (1972); J. M. Patterson, L. T. Burka, and M. R. Boyd, *J. Org. Chem.*, **33**, 4033 (1968).

 © 1988 The Chemical Society of Japan Bull. Chem. Soc. Jpn., 61, 1715—1720 (1988)

Oxidoreduction between Cycloalkanols and the Corresponding Cycloalkanones in the Cultured Cells of *Nicotiana tabacum*. Simulation of the Time Courses in the Oxidoreduction

Shunsuke Izumi and Takayuki Suga*
Department of Chemistry, Faculty of Science, Hiroshima University,
Higashisenda-machi, Naka-ku, Hiroshima 730
(Received December 16, 1987)

A method for the simulation of the time courses in the oxidation of cycloalkanols and the reduction of cycloalkanones in the cultured cells of *Nicotiana tabacum* was developed on the basis of the permeability of these compounds into the cultured cells and the ^{13}C NMR chemical shift of the carbonyl carbon of the cycloalkanones. Further, the method has been applied to the simulation of the time courses in the oxidation of (+)-borneol and (+)-isopinocampheol and the reduction of (−)-carvomenthone in the cultured cells of *N. tabacum*.

Recently, we reported that the balance in the equilibrium of the oxidoreduction between 5- to 7- membered cycloalkanols and their corresponding cycloalkanones in the cultured cells of *Nicotiana tabacum* depends on the carbon number in the carbocyclic ring of the cyclic compounds.[1] It was further found that the oxidoreduction between the cycloalkanols and their corresponding cycloalkanones in the cultured cells is governed by an NAD^+-dependent alcohol dehydrogenase which is similar to the dehydrogenase from tea seeds and horse liver. We have developed a method for the simulation of the time courses in the oxidation of cycloalkanols and the reduction of cycloalkanones in the cultured cells on the basis of the permeability of these compounds into the cultured cells and the ^{13}C NMR chemical shift of the carbonyl carbon of the cycloalkanones.[2] Furthermore, the method has been applied to the oxidation of (+)-borneol (**1**) to (+)-camphor (**2**) and (+)-isopinocamphenol (**3**) to (−)-isopinocamphone (**4**) and the reduction of (−)-carvomenthone (**5**) to (+)-carvomenthol (**6**) in the cultured cells of *N. tabacum*.[3,4] The results have been partly outlined in the preliminary communications,[1-4] but we wish to describe *en bloc* details of the results together with newly obtained results.

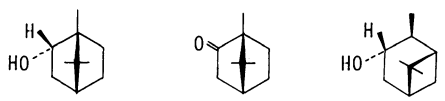

1 2 3

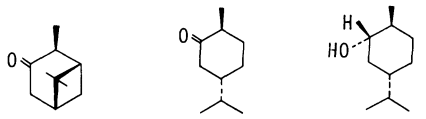

4 5 6

Results and Discussion

Reaction Rates of the Oxidoreduction of Cycloalkanols and Cycloalkanones in the Enzyme System of *N. tabacum*. Firstly, the enzyme system responsible for the oxidoreduction of cycloalkanols and their corresponding cycloalkanones in the cultured cells of *N. tabacum* was characterized. An enzyme system was partially purified prepared from the cultured cells of *N. tabacum* by treating a cell-free extract of the cells with cold acetone and then ammonium sulfate as described in the experimental section. The substrate specificity of the enzyme system was tested for the oxidation of alkanols. The alkanols used as substrate were ethanol, 1-propanol, 1-butanol, 1-pentanol, 1-hexanol, cyclopentanol, and cyclohexanol. Relative rates observed in the oxidation of these substrates are given in Table 1; ethanol was the best substrate for this enzyme system. The substrate specificity was quite similar to the specificity of alcohol dehydrogenase isolated from tea seeds[5] and horse liver.[6,7]

The reaction rates of the oxidation of cycloalkanols with this enzyme system were determined in 0.1 M† glycine-NaOH buffer (pH 9.0) by tracing the decrease in the UV absorption at 340 nm due to the reduced form of nicotinamide-adenine dinucleotide (NADH).[8] The cycloalkanols used as substrate were cyclopentanol (**7**), cyclohexanol (**8**), 2-methylcyclohexanol (**9**),

Table 1. Substrate Specificity[a]

	Relative V_{max}
Ethanol	1.0
1-Propanol	0.49
1-Butanol	0.36
1-Pentanol	0.20
1-Hexanol	0.07

a) Determined in 0.1 M glycine-NaOH buffer, pH 9.0, at 25 °C.

† 1 M=1 mol dm^{-3}.

Table 2. The Rate Constant and the Equilibrium Constant of the Oxidoreduction between Cycloalkanols and the Corresponding Cycloalkanones with the Enzyme System

Compound	k_{+1}[a)]/s^{-1}	k_{-1}[b)]/s^{-1}	K
Cyclopentanol	2.53×10^{-4}	7.09×10^{-5}	3.57
Cyclohexanol	9.52×10^{-4}	1.81×10^{-3}	0.53
2-Methylcyclohexanol	1.22×10^{-3}	5.01×10^{-3}	0.24
3-Methylcyclohexanol	1.03×10^{-3}	3.16×10^{-3}	0.33
Cycloheptanol	3.69×10^{-4}	1.20×10^{-4}	3.08

a) Determined in 0.1 M glycine–NaOH buffer, pH 9.0, at 25 °C. b) Determined in 0.1 M potassium phosphate buffer, pH 7.0, at 25 °C.

3-methylcyclohexanol (**10**), and cycloheptanol (**11**). The reaction rates of the reduction of cycloalkanones with the enzyme system were determined in 0.1 M potassium phosphate buffer (pH 7.0) by tracing the increase in the UV absorption at 340 nm due to NADH.[8] The cycloalkanones used were cyclopentanone (**12**), cyclohexanone (**13**), 2-methylcyclohexanone (**14**), 3-methylcyclohexanone (**15**), and cycloheptanone (**16**). Table 2 gives the rate constant of the oxidation of the cycloalkanols (k_{+1}), the rate constant of the reduction of the cycloalkanones (k_{-1}), and the equilibrium constant in the oxidoreduction between the cycloalkanols and the cycloalkanones (K). The equilibrium constants indicate that the equilibrium of the oxidoreduction of the 6-membered cyclic compounds shifts toward the side of the reduction, while the equilibrium of the oxidoreduction of the 5- and 7-membered cyclic compounds does toward the side of the oxidation. Such a ring-size effect on the equilibrium was quite similar to the effect on the equilibrium in the bioconversion of the cycloalkanols and the cycloalkanones in the cultured cells of *N. tabacum*.

Simulation of the Time Courses in the Oxidoreduction between the Cycloalkanols and the Corresponding Cycloalkanones in the Cultured Cells of *N. tabacum*. Figures 1 and 2 show the time courses in the oxidation of cyclohexanol to cyclohexanone and the reduction of cyclohexanone to cyclohexanol, respectively. The half lives of these substrates in the oxidation and the reduction in the cultured cells were 3 days, whereas those of the substrates in the oxidation and the reduction with the enzyme system were 10 and 45 min, respectively, as deduced from the rate constants given in Table 2. The reaction rate of the oxidoreduction in the enzyme system was much faster than that of the oxidoreduction in the cultured cells. Such a time lag is probably due to a delay arising from permeation of the cycloalkanols and the cycloalkanones into the cells. The rate of permeation is known to depend on a gradient between intra- and extracellular concentrations of the cycloalkanols;[9–12] the permeability constant can be estimated by use of Hill's equation,[11]

$$[S] = [S]_0 \cdot e^{-p \cdot t}, \quad (1)$$

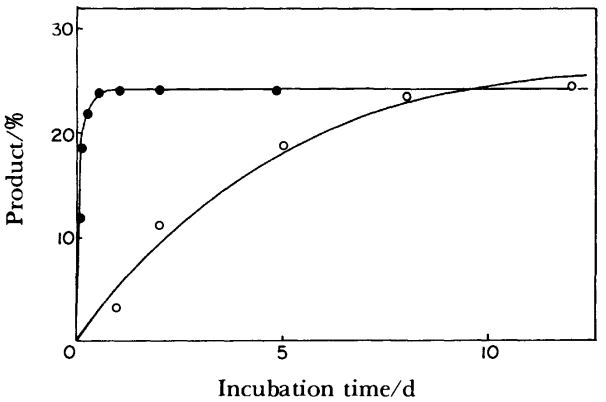

Fig. 1. Time courses in the oxidation of cyclohexanol into cyclohexanone with the enzyme system (—●—) and in the cultured cells (—○—).

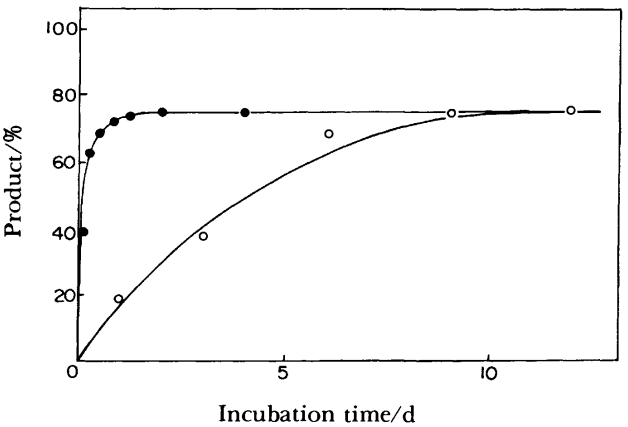

Fig. 2. Time courses in the reduction of cyclohexanone into cyclohexanol with the enzyme system (—●—) and in the cultured cells (—○—).

where [S],[S]$_0$, and p denote the concentration of the foreign substrate (cycloalkanol) at the time "t", the initial concentration of the foreign substrate, and the permeability constant, respectively. The permeability constants for permeation of the cycloalkanols and the corresponding cycloalkanones into the cultured cells were determined by substituting the data of the time courses in the bioconversion of 5- to 7-membered cycloalkanols to their corresponding cycloalkanones in the cultured cells[4] for Hill's equation; the average

of the permeability constants in the oxidation of 5- to 7-membered cycloalkanols to their corresponding cycloalkanones was 4.82×10^{-6} s^{-1}.

On the basis of the permeability constants and the rate constants, the time courses in the oxidation of the cycloalkanols in the cultured cells were simulated as follows. Temporal infinitesimal change in the concentration of the product [P] at the time "t" is given by

$$d[P] = \{[S]_0 \cdot p \cdot k_{+1}/(k_{+1} + k_{-1}) - [P] \cdot p\} \cdot dt, \quad (2)$$

where k_{+1} and k_{-1} denote the rate constant of the oxidation of the cycloalkanols and the rate constant of the reduction of the cycloalkanones, respectively. The initial term shows the infinitesimal change in the concentration of the product which is formed by oxidation of the foreign substrate and the last term shows the infinitesimal change in the concentration of the product which is permeated into the cells. The solution of this differential Eq. 2 is

$$[P] = \{[S]_0 \cdot k_{+1}/(k_{+1} + k_{-1})\}(1 - e^{-p \cdot t}). \quad (3)$$

Thus, it was established that the concentration of the product can be simulated by the permeability constant, the rate constant of the oxidation of the cycloalkanols, and the rate constant of the reduction of the cycloalkanones.

Correlation between the Reaction Rate of Enzymatic Oxidoreduction and the ^{13}C NMR Chemical Shift. The rate constants of the oxidation of the cycloalkanols (k_{+1}) and the reduction of the cycloalkanones (k_{-1}) and the equilibrium constants of the oxidoreduction between the cycloalkanols and the corresponding cycloalkanones (K) were correlated with ^{13}C NMR chemical shifts of the carbon atom bearing a hydroxyl group in the cycloalkanols and the carbonyl carbon in the cycloalkanones.[2] The correlations of ln k_{+1}, ln k_{-1}, and ln K against the ^{13}C NMR chemical shifts of the cycloalkanols are represented by the following empirical formulas (4)—(6) with r (the correlation coefficient)=0.75, 0.71, and 0.68, respectively.

Rate constants;

$$k_{+1} = \exp(-0.195\delta_{c-o} + 6.4) \quad (4)$$

$$k_{-1} = \exp(-0.515\delta_{c-o} + 29.2) \quad (5)$$

Equilibrium constant;

$$K = (k_{+1}/k_{-1}) = \exp(0.318\delta_{c-o} - 22.6) \quad (6)$$

where δ_{c-o} denotes the ^{13}C NMR chemical shift of the carbon atom bearing the hydroxyl group. However, these ^{13}C NMR chemical shifts were not well-correlated with the rate constants and the equilibrium constants.

On the other hand, a plot of ln k_{+1}, ln k_{-1}, and ln K against the ^{13}C NMR chemical shift of the carbonyl carbon yielded a straight line, as shown in Figs. 3 and 4. These correlations are represented by the following empirical formulas (7)—(9) with r (the correlation coefficient)=0.97, 0.95, and 0.94, respectively.

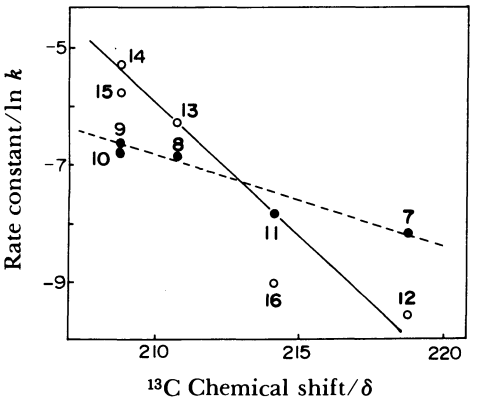

Fig. 3. Correlation of the rate constants of the oxidation of cycloalkanols (k_{+1}; --●--; cyclopentanol (**7**), cyclohexanol (**8**), 2-methylcyclohexanol (**9**), 3-methylcyclohexanol (**10**), and cycloheptanol (**11**)) and the reduction of cycloalkanones (k_{-1}; —○— cyclopentanone (**12**), cyclohexanone (**13**), 2-methylcyclohexanone (**14**), 3-methylcyclohexanone (**15**), and cycloheptanone (**16**)) with the ^{13}C NMR chemical shift of the carbonyl carbon of the cycloalkanones involved in the reaction.

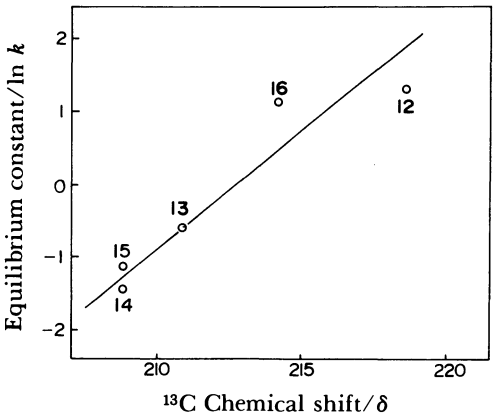

Fig. 4. Correlation of the equilibrium constant of the oxidoreduction between cycloalkanols and corresponding cycloalkanones with the ^{13}C NMR chemical shift of the carbonyl carbon of the cycloalkanones (cyclopentanone (**12**), cyclohexanone (**13**), 2-methylcyclohexanone (**14**), 3-methylcyclohexanone (**15**), and cycloheptanone (**16**)).

Rate constants;

$$k_{+1} = \exp(-0.162\delta_{c=o} + 27.1) \quad (7)$$

$$k_{-1} = \exp(-0.447\delta_{c=o} + 87.7) \quad (8)$$

Equilibrium constant;

$$K = (k_{+1}/k_{-1}) = \exp(0.284\delta_{c=o} - 60.5) \quad (9)$$

where $\delta_{c=o}$ denotes the ^{13}C NMR chemical shift of the carbonyl carbon of the cycloalkanones. The rate

constants and the equilibrium constants were predicted by the ^{13}C NMR chemical shifts of the carbonyl carbon of the cycloalkanones. This indicates a dependence of the reaction rate of the enzymatic oxidoreduction on the electron density of the carbonyl carbon of the cycloalkanones.

When we use this indication, Eq. 3 can be related with the ^{13}C NMR chemical shift of the carbonyl carbon of the cycloalkanones given in Eqs. 7 and 8. For the time courses in the oxidation of the cycloalkanols and their related compounds, the proportion of the concentration of product [P] (cycloalkanone) to the initial concentration of substrate $[S]_0$ (cycloalkanol) is found to be

$$P = [P]/[S]_0 = \{1 - \exp(-4.82 \times 10^{-6} \cdot t)\}/ \{1 + \exp(-0.284\delta_{c=o} + 60.5)\}. \quad (10)$$

The time courses in the reduction of the cycloalkanones and their related compounds were simulated in a manner similar to that described above. The simulated equation is as follows:

$$P = \{1 - \exp(-4.82 \times 10^{-6} \cdot t)\}/ \{1 + \exp(0.284\delta_{c=o} - 60.5)\}. \quad (11)$$

Therefore, the time courses in the oxidation of the cycloalkanols and the reduction of the cycloalkanones in the cultured cells were found to be simulated on the basis of the permeability of the cycloalkanols and their corresponding cycloalkanones into the cultured cells and the ^{13}C NMR chemical shift of the carbonyl carbon of the cycloalkanones or the corresponding carbonyl compounds.

Application of the Simulation to the Oxidation of (+)-Borneol and (+)-Isopinocampheol and the Reduction of (−)-Carvomenthol. The equation for the simulation of the time courses in the oxidation of the cycloalkanols was applied to the oxidation of (+)-borneol (**1**) to (+)-camphor (**2**) in the cultured cells. Figure 5 shows the time course in the bioconversion of borneol to camphor in the cultured cells[4] and the time course simulated by use of Eq. 10 with the ^{13}C NMR chemical shift of the carbonyl carbon of camphor ($\delta_{c=o}$ 218.9). The simulation curve well fits with the bioconversion curve. Furthermore, the time course in the oxidation of (+)-isopinocampheol (**3**) to (−)-isopinocamphone (**4**) was simulated by use of Eq. 10 with the ^{13}C NMR chemical shift of the carbonyl carbon of isopinocamphone ($\delta_{c=o}$ 214.3) and is shown in Fig. 6. This simulation curve well fits with the bioconversion curve of isopinocampheol in the cultured cells, as seen in Fig. 6.

On the other hand, the time course in the reduction of (−)-carvomenthone (**5**) to (+)-carvomenthol (**6**) was simulated by use of Eq. 11 with the ^{13}C NMR chemical shift of the carbonyl carbon of carvomenthone ($\delta_{c=o}$ 211.8), as shown in Fig. 7. The simulation curve also well fits with the time course in the bioconversion of carvomenthone to carvomenthol in the cultured cells.

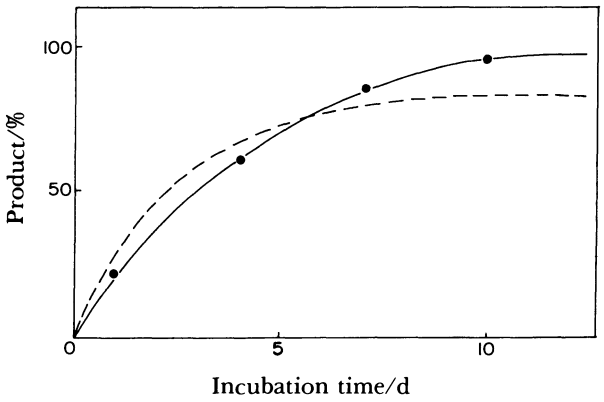

Fig. 5. Comparison of the bioconversion of (+)-borneol (**1**) into (+)-camphor (**2**) in the cultured cells (—●—) with its simulation (-----).

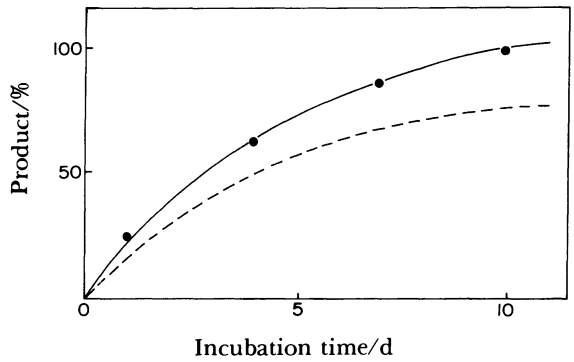

Fig. 6. Comparison of the bioconversion of (+)-isopinocampheol (**3**) into (−)-isopinocamphone (**4**) in the cultured cells (—●—) with its simulation (-----).

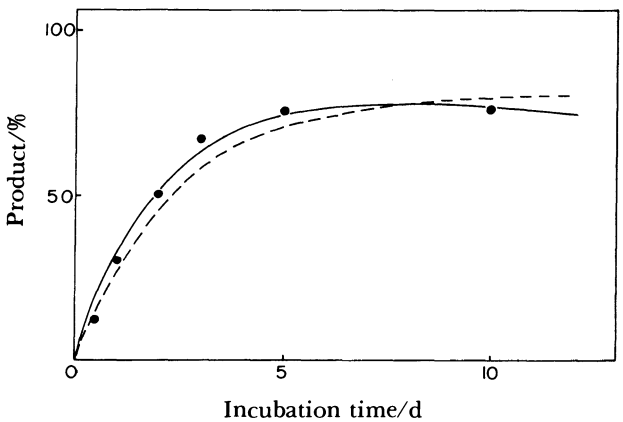

Fig. 7. Comparison of the bioconversion of (−)-carvomenthone (**5**) into (+)-carvomenthol (**6**) in the cultured cells (—●—) with its simulation (-----).

It was thus established that the time courses in the oxidation of the cycloalkanols and the related alcohols and the reduction of the cycloalkanones and the related ketones in the cultured cells can be simulated on

Table 3. The Purification of the Enzyme System

	Total protein	Total act.	Sp. act.	Purification
	mg	U	U mg^{-1}	Fold
Cell-free extract	75.6	17.8	0.23	1.0
Acetone fraction	5.0	9.8	1.92	8.3
$(NH_4)_2SO_4$ fraction	0.8	8.2	10.2	44

the basis of the permeability of the cycloalkanols, the cycloalkanones, and their related compounds into the cells and the carbonyl carbon ^{13}C NMR chemical shifts of the cycloalkanones and the related carbonyl compounds involved in the equilibrium of the oxidoreduction between the cycloalkanols and the cycloalkanones.

Experimental

GLC analyses were performed on an instrument equipped with an FID and a glass column (3 mm×2 m) packed with 15% DEGS or 2% OV-17 on Chromosorb W (AW-DMCS; 80—100 mesh), varying the column temperature over the range of 80—200 °C at the rate of 3 °C min^{-1}. ^{13}C NMR spectra were obtained at 22.6 MHz in $CDCl_3$ with tetramethylsilane as an internal reference.

Materials. Cyclopentanol, cyclohexanol, 2-methylcyclohexanol, 3-methylcyclohexanol, and cycloheptanol and their corresponding cycloalkanones were of commercial origin from Wako Pure Chemical Ind., Ltd. The chemical shifts of the carbonyl carbon of the cycloalkanones in their ^{13}C NMR spectra were 218.6, 210.8, 208.8, 208.8, and 214.2, respectively. (+)-Camphor (**2**) was purchased from Tokyo Kasei Co., Ltd. and purified by recrystallization followed by sublimation; mp 176—178 °C, $[\alpha]_D^{25}$ +42.9° (*c* 1.1, EtOH) (lit,[13] $[\alpha]_D^{25}$ −44.2°); ^{13}C NMR ($CDCl_3$) δ=218.9 (C=O). (+)-Borneol (**1**) was prepared from (+)-camphor (**2**) by reduction with $NaBH_4$ in methanol; mp 201—202 °C, $[\alpha]_D^{25}$ +37.6° (*c* 1.0, EtOH) (lit,[13] $[\alpha]_D^{25}$ +37.9°). (+)-Isopinocampheol (**3**) was synthesized from (−)-α-pinene by hydroboration;[14] mp 55—57 °C, $[\alpha]_D^{25}$ +31.6° (*c* 5.1, EtOH) (lit,[3] $[\alpha]_D^{25}$ −31.0° for the (−)-enantiomer). (−)-Isopinocamphone (**4**) was prepared from (+)-isopinocampheol (**3**) by oxidation with sodium dichromate;[15] $[\alpha]_D^{25}$ −9.8° (neat) (lit,[3] $[\alpha]_D^{25}$ −9.9°); ^{13}C NMR ($CDCl_3$) δ=214.3 (C=O). All the samples used as substrate were >99% pure on GLC.

Enzyme System from the Cultured Cells of *N. tabacum*. The cultured cells of *N. tabacum* (100 g) were homogenized in 50 mM Tris-HCl buffer (pH 7.2, 1000 ml) containing 10 mM 2-mercaptoethanol. The homogenate was stirred for 3 h at 25 °C. After filtration through several layers of cheesecloth, the filtrate was centrifuged at 13000 g for 10 min to give a cell-free extract. Into the cell-free extract, cold acetone (0 °C) was poured with vigorous stirring under ice-cooling. The soln, after standing for 30 min, was centrifuged at 17000 g for 15 min to give a precipitate, which was suspended in 50 mM Tris-HCl buffer (pH 7.2, 300 ml) containing 10 mM 2-mercaptoethanol. The suspension was treated with ammonium sulfate to give a 25—60% ammonium sulfate fraction. The salting-out product was suspended in 0.1 M potassium phosphate buffer (pH 7.0). The suspended material, after dialysis for 15 h against the same buffer solution, was centrifuged at 30000 g for 20 min. The supernatant was used as an enzyme system. The enzyme system was purified 44-fold against the cell-free extract in the activity for the conversion of ethanol to acetaldehyde by oxidation, as given in Table 3. The properties of the enzyme system were characterized as follows.

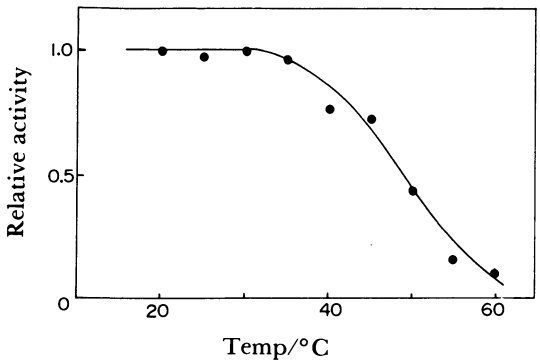

Fig. 8. Thermal stability of the enzyme system partially purified from the cultured cells of *N. tabacum*.

Substrate Specificity in the Oxidation of Alkanols. The mixture containing the enzyme system (0.6 μg protein), alkanol (0.1 M), such as ethanol, 1-propanol, 1-butanol, and 1-hexanol, and NAD^+ (0.05 mM) was diluted with 3 ml of 0.05 M Tris-HCl buffer (pH 8.5) containing 10 mM 2-mercaptoethanol and then the solution was incubated at 25 °C for 2 h. The reaction was monitored by means of UV absorption measurements. The initial rates in the oxidation of the alkanols were determined by measuring the change in the UV absorption at 340 nm for NADH. Table 1 gives the relative rates in the oxidation of the alkanols.

Thermal Stability: The enzyme system was held at various temperatures (20—60 °C) for 15 min prior to incubation. The enzyme activity in the oxidation of ethanol was determined by measuring the change in the UV absorption at 340 nm. Figure 8 shows the thermal stability of the enzyme system.

Optimum pH: The enzyme activity in the oxidation of ethanol was determined in three kinds of buffer solutions as follows: 0.1 M potassium phosphate buffer, pH 5.5—7.8; 0.1 M Tris-HCl buffer, pH 7.5—9.0; glycine-NaOH buffer, pH 8.6—11.6. Figure 9 shows the effect of pH on the enzyme activity.

Effect of 2-Mercaptoethanol: The enzyme system (5 ml, 3.0 μg protein) was dialysed for 4 days at 5 °C against (i) Tris-HCl buffer (pH 8.5) containing 10 mM 2-mercaptoethanol and (ii) Tris-HCl buffer (pH 8.5) lacking 2-mercaptoethanol. A part of each enzyme system was pipetted out at a regular time interval and the enzyme activity in the oxidation of ethanol was determined in the same manner as above. Figure 10 shows the effect of 2-

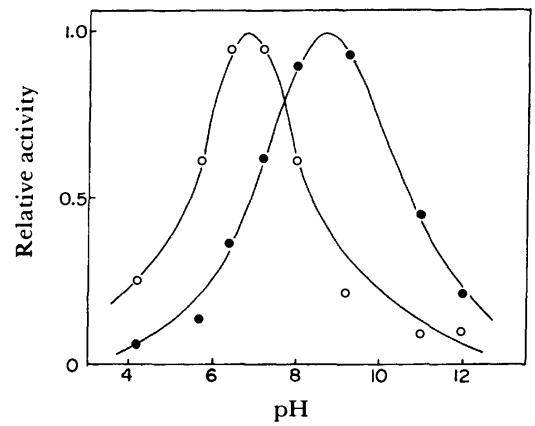

Fig. 9. Effect of pH on the activity of the enzyme system partialy purified from the cultured cells of *N. tabacum*. —○—; NADH-dependent reaction, —●—; NAD-dependent reaction.

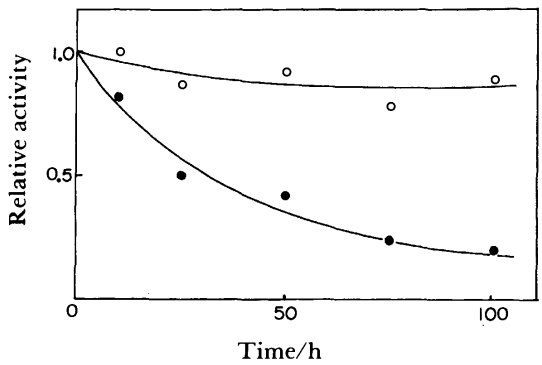

Fig. 10. Effect of dialysis on the activity of the enzyme system partially purified from the cultured cells of *N. tabacum*. —○—; Containing 10 mM 2-mercaptoethanol, —●—; Lacking 2-mercaptoethanol.

mercaptoethanol on the enzyme activity.

Oxidoreduction between Cycloalkanols and the Corresponding Cycloalkanones with the Enzyme System. The initial rates of the oxidoreduction were determined by measuring the change in the UV absorption at 340 nm for NADH and by calculating on the least square method with the Lineweaver-Burk's equation.[16]

Oxidation: To a solution of cycloalkanol (0.01—4.0 mM) and NAD^+ (0.5 mM) in 0.1 M glycine-NaOH buffer (3 ml, pH 9.0), the enzyme system (0.6 μg protein) was added. The mixture was incubated at 25 °C for 2 h. During the incubation, the reaction was monitored by means of the UV absorption measurements. Table 2 gives the rate constants of the oxidation of the cycloalkanols.

Reduction: To a solution of cycloalkanone (0.5—10 mM) and NADH (0.2 mM) in 0.1 M potassium phosphate buffer (3 ml, pH 7.0), the enzyme system (0.6 μg protein) was added. The incubation was carried out at 25 °C for 2 h under monitoring by the UV spectrometry as above. The rate constants of the reduction of the cycloalkanones are given in Table 2.

Time Courses in the Bioconversion of the Cycloalkanols in the Cultured Cells of *N. tabacum*. A suspension of the cultured cells of *N. tabacum* "Bright Yellow" was prepared as described in Refs. 2 and 17; the cells were cultured in a 300-ml conical flask containing 100 ml of Murashige and Skoog's medium[18] in each case. Each substrate (10 mg) was administered to the flask containing the precultured suspension cells (50 g fresh wt/100 ml Murashing-Skoog's medium). The culture was incubated at 25 °C for 10 days in the dark with shaking at 70 rpm. A part (10 ml) of the incubated mixture was pipetted out under sterile conditions at a regular time interval, ground in a mortar, and extracted with ether. Products in each ether extract were identified, after removal of the solvent, by GLC and co-GLC with authentic samples. Amounts of the products and the unchanged substrate were determined on the basis of the peak areas on GLC and are expressed as the relative percentage for the total amount of a whole reaction mixture obtained.

This work was in part supported by Grant-in-Aids for Developmental Scientific Research Nos. 57840030 (1982) and 59840013 (1984) from the Ministry of Education, Science and Culture.

References

1) T. Suga, H. Hamada, and T. Hirata, *Plant Cell Reports*, **2**, 66 (1983).
2) T. Suga, S. Izumi, and T. Hirata, *Chem. Lett.*, **1986**, 2053.
3) T. Suga, T. Hirata, H. Hamada, and M. Futatsugi, *Plant Cell Reports*, **2**, 186 (1983).
4) T. Suga, S. Izumi, T. Hirata, and H. Hamada, *Chem. Lett.*, **1987**, 425.
5) A. Hatanaka, T. Kajiwara, S. Tomohiro, and H. Yamashita, *Agric. Biol. Chem.*, **38**, 1835 (1974).
6) N. O. Kaplan and M. M. Ciotti, *J. Biol. Chem.*, **201**, 785 (1974).
7) J. B. Jones and M. H. Schwartz, *Can. J. Chem.*, **59**, 1574 (1981).
8) E. Racker, *J. Biol. Chem.*, **184**, 313 (1950).
9) R. Collander, *Acta Chem. Scand.*, **3**, 717 (1949).
10) T. L. Hill and O. Kedem, *J. Theor. Biol.*, **10**, 399 (1966).
11) T. L. Hill and Y. Chen, *Biophys. J.*, **11**, 685 (1971).
12) B. Hille and W. Schwary, *J. Gen. Physiol.*, **72**, 409 (1978).
13) E. Guenther, "The Essential Oils," Van Nostrand, New York (1948), pp. 239 and 429.
14) C. Zweifel and H. C. Brown, *J. Am. Chem. Soc.*, **86**, 393 (1964).
15) H. C. Brown and C. P. Garg, *J. Am. Chem. Soc.*, **83**, 2952 (1961).
16) H. Lineweaver and D. Burk, *J. Am. Chem. Soc.*, **56**, 658 (1934).
17) Y. S. Lee, T. Hirata, and T. Suga, *J. Chem. Soc., Perkin Trans. 1*, **1983**, 2475.
18) T. Murashige and F. Skoog, *Physiol. Plant.*, **15**, 473 (1962).

t-Butylsulfinyl Phenylmethyl Carbanion. Conformation in Nonpolar Solvent

Atsuyoshi Ohno,* Masato Higaki, and Shinzaburo Oka
Institute for Chemical Research, Kyoto University, Uji, Kyoto 611
(Received December 24, 1987)

^{1}H NMR spectra were studied for a carbanion derived from *t*-butyl phenylmethyl sulfoxide in tetrahydrofuran. It has been concluded that the conformation of the carbanion in solution is the same as that in a crystal. The carbanion exists in two diastereomeric dimeric forms in the presence of an equivalent amount of countercation, but it becomes a monomer when excess base exists in the solution.

A recent report on neutron diffraction crystallography on *t*-butyl phenylmethyl sulfoxide[1] casted a doubt on the configurations and reactivities of α-sulfinyl carbanions so far accepted.[2] Stereochemistry of the reaction from an α-sulfinyl carbanion changes irregularly depending on the property of attacking electrophile and the steric bulk of substituent on the sulfur atom as well as on the polarity of solvent.[2-4]

Reinvestigation of stereochemistry of the products derived from α-sulfinyl carbanions made us propose[5] that 1) the major conformation of the carbanion is determined primarily by steric bulk of the substituents on the sulfur and the carbanionic carbon atom, then 2) a conformation is preferred so that the countercation of the carbanion can maintain a maximum interaction with a lone pair on the sulfinyl oxygen. 3) An interaction between the countercation and the sulfinyl lone pair exerts a minor effect. Since solvent-separated and dissociated ion pairs become popular in polar solvents, the importance of the role of the countercation decreases in such solvents. 4) Hard electrophiles such as water and a carbonyl compound attack the carbanion from its hard face; the attacking reagent interacts with the countercation initially and the population of a particular conformation of the carbanion controls the steric course of the reaction. 5) A soft electrophiles such as an alkyl halide, on the other hand, prefer to attack the carbanion from its soft face; the carbanion lone pair anti to the lone pair on the sulfinyl sulfur becomes more polarizable due to an α-effect.[6] The reaction courses are illustrated in Scheme 1 for the protonations and methylations of carbanions derived from (*S*)-methyl phenylmethyl sulfoxide (*S*-**1**) and (*R*)-*t*-butyl phenylmethyl sulfoxide (*R*-**2**). It is important to note that the *R*,*S*-notation appears different in methyl and *t*-butyl phenylmethyl sulfoxides because of definition.

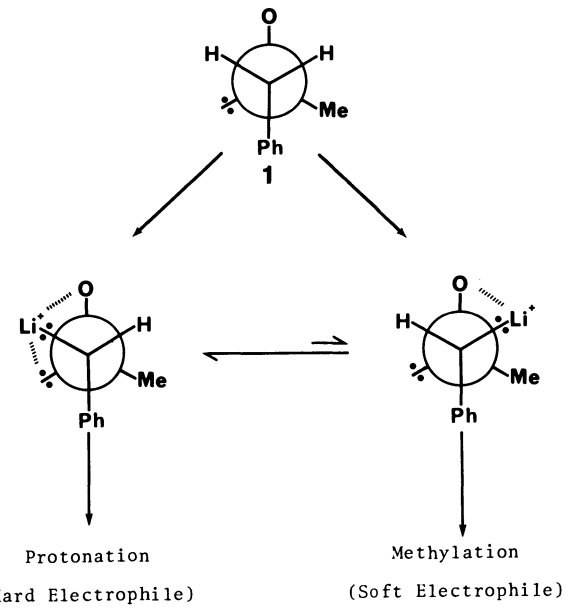

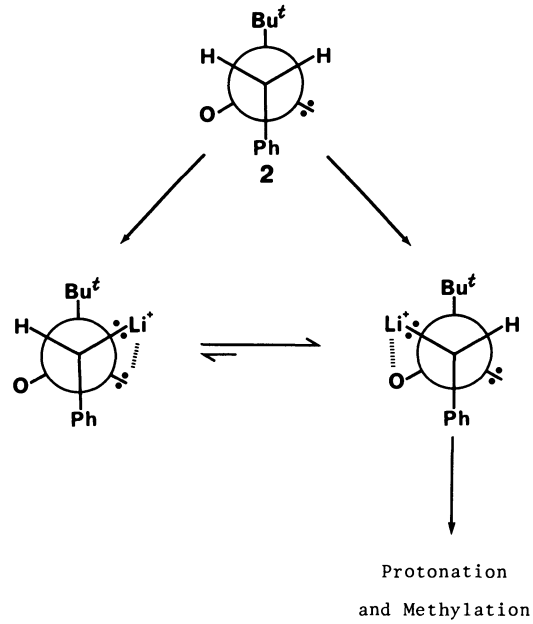

Although the proposal described above can explain the reactions of α-sulfinyl carbanions sufficiently, we have had no information on the conformation of the carbanion in solution. In order to obtain further insight into the conformation, we studied ^{1}H NMR spectroscopy of **2** in tetrahydrofuran (THF) and the results will be described in this paper. The hybridization of carbanionic carbon in α-sulfenyl, sulfinyl, and sulfonyl carbanions was extensively studied by Chassaing and Marquet by means of ^{13}C and ^{1}H NMR spectroscopies.[7,8]

Results and Discussion

When 1.2 equivalent amounts of butyllithium was added to a solution of racemic mixture of **2** in tetrahydrofuran-d_8 (THF-d_8) at −100 °C, two ^{1}H

NMR signals for the benzylic proton appeared as singlets of approximately equal intensity at δ 3.34 and 3.36 in addition to signals for the aromatic protons at 5.86 (t, para), 6.11 and 6.13 (two doublets, ortho), 6.53 (q, meta), and 6.79 (d, ortho). The spectrum is shown in Fig. 1a and hereafter this solution will be called as the standard system. As shown in Fig. 1b, however, when the same solution with optically pure *R*-**2** instead of racemic **2** was subjected to the ^{1}H NMR spectroscopy, the benzylic proton resulted in only one singlet at δ 3.34 and the doublets for ortho-protons at δ 6.11 and 6.13 converged into a single doublet at δ 6.11.

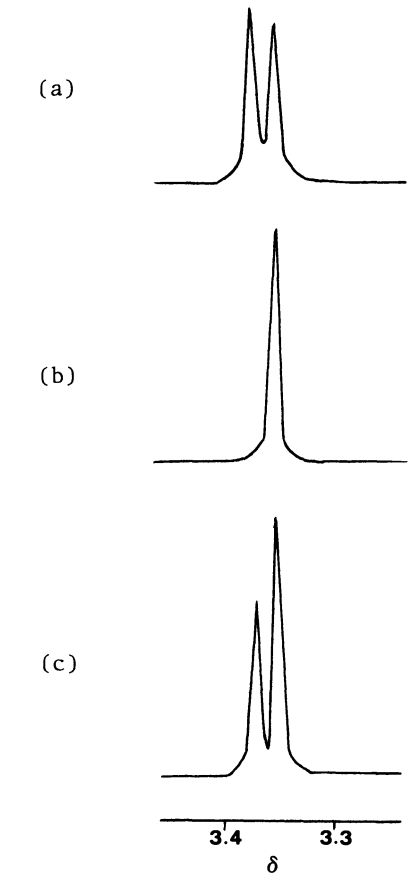

Fig. 1. ^{1}H NMR spectra of a benzylic proton of (a) racemic, (b) optically pure *R*-, and (c) 55% optically pure *R*-lithium salt of *t*-butylsulfinyl phenylmethyl carbanion in THF at −100°C.

The appearance of two singlets from the racemic system suggests the existence of two or more diastereomeric isomers. Since optically pure **2** shows only one singlet and two doublets for the benzylic proton and for the two ortho-protons, respectively, and since it has been confirmed that the abstraction of a benzylic proton in **2** by a base results in highly diastereospecific carbanion thermodynamically,[5] there is no doubt that the two singlets observed for the benzylic proton in racemic **2** is *not* due to diastereomerism of benzylic protons with respect to the chirality on a single sulfur. That is, the spectra indicate that the lithiated carbanions produced from racemic **2** in THF are dimerized[9] to form *dl* (S_RS_R and S_SS_S)- and meso (S_RS_S)-isomers (**3** and **4**, respectively), whereas those from *R*-**2** can dimerize to only one S_RS_R form. That 2-methylbutyllithium displays two ^{1}H NMR signals (quartets) for α-protons in diastereomeric hexamers has been documented as well.[10]

Although the dimer of the carbanion from 1-phenylethyl phenyl sulfoxide has been known in crystalline state[11] and the possibility of its existence in a solution was suggested,[7,8] the present result is the first one to confirm that the carbanion from **2** prefers to be in dimeric form even in a solution. It is known that benzylic carbanion tends to exist as a monomeric ion pair with a lithium cation.[12–14] The preference of the dimeric form in the present benzylic carbanion with the bridge of lithium ions seems to suggest that the coordination of lithium ion onto the lone pair of sulfinyl oxygen is more important interaction than the coordination onto the lone pair on the benzylic carbon.[7,8,15] The present result suggests that the negative charge induced on the carbanion on the

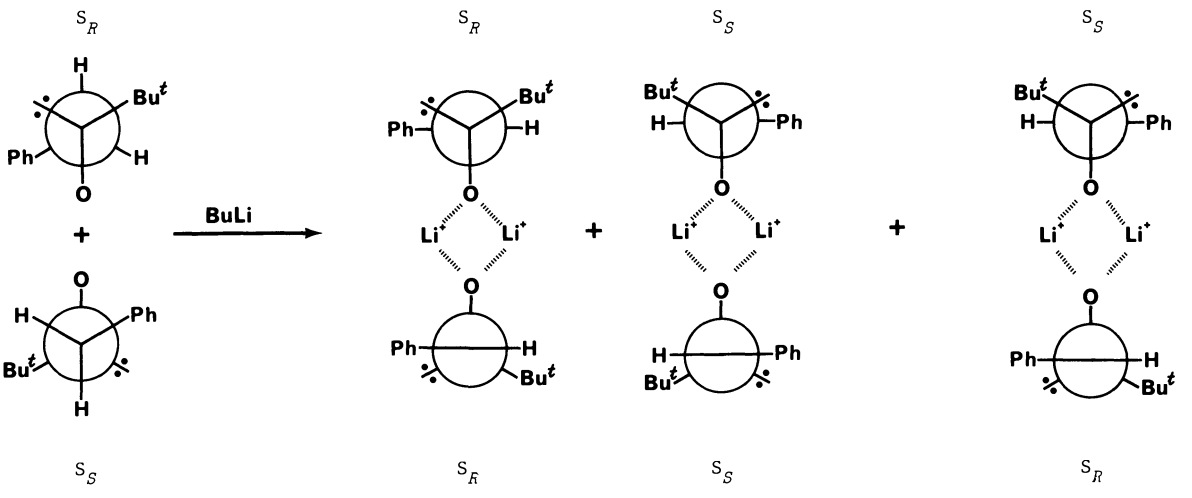

abstraction of a benzylic proton delocalizes largely onto the sulfinyl oxygen as well as on the phenyl group and the conformation of this benzylic carbon may be close to planar, in accord with the result reported previously.[7,8]

The coalescence temperature of two singlets (−40 °C) elucidates that free energy of activation for intermolecular exchange of the carbanion is 51 kJ mol^{-1}, which is almost equivalent to 56 kJ mol^{-1} for 2-methylbutyllithium.[15] Thus, the present result indicates that the SO···Li interaction in the dimer of sulfinyl carbanions is reasonably strong.

Figure 1c shows a spectrum obtained from the solution with *R*-**2** in 55% optical purity. The ratio in intensities of two singlets at δ 3.34 and 3.36 is 6:4, which is almost equivalent to the ratio of 7.5:4 calculated for the ratio in abandance of *dl*- and meso-dimers assuming random pairing of the carbanions. Thus, although thermodynamic stabilities of *dl*- and meso-dimers are equivalent in solution within experimental error, the X-ray crystallography predicted that the carbanion from a racemic mixture of 1-phenylethyl phenyl sulfoxide crystallizes as the meso-dimer.[11]

Not only the qualitative similarity in the dimeric form, but also the similarity in the conformation of individual (monomeric) carbanion can be seen between the carbanions in the solid and liquid phases; a nuclear Overhouser effect observed for the carbanion in THF at −50 °C by irradiating the signal from the methyl protons showed 13.5% increase in the intensity of the signal for the benzylic proton, whereas the effect was only 4.7% in the spectrum from the mother species, **2**.[5] This result indicates that the benzylic proton in the carbanion is set in more proximity to the *t*-butyl group than that in the original sulfoxide **2**. Thus, the conformations of carbanions derived from *S*- and *R*-**2** in THF are those shown in **3** and **4** in accord with that elucidated by X-ray crystallography.[11]

The discussion described above has been developed on the basis of assumption that the carbanion is in dimeric form in THF and not in tetramer or higher aggregate. The validity of this assumption can be tested experimentally. No change in the spectrum was observed when two equivalent amounts of *N,N,N′,N′*-tetramethylethylenediamine was added to the standard system, in contrast to the observation on butyllithium, where the presence of tetrameric aggregate is suggested.[12] Since the free energy of activation for ligand exchange in α-sulfinyl and alkyl carbanions are similar, the present observation indicates that the α-sulfinyl carbanion chelated by lithium cations are not in tetrameric or higher aggregation.[12] Instead, the sulfinyl oxygen in the dimeric form coordinates onto the lithium cation quite strongly so that the other chelating reagent can only substitute the solvent molecule on the lithium ion without destroying the dimeric form into monomers.

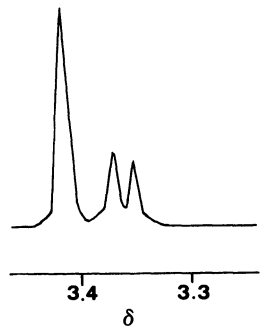

Fig. 2. ^{1}H NMR spectrum of a benzylic proton of racemic, *t*-butylsulfinyl phenylmethyl carbanion with one more equivalent excess butyllithium in THF at −100 °C.

When one more equivalent amount of butyllithium was added to the standard system, however, another singlet appeared at δ 3.40 as the signal from the benzylic proton at the sacrifice of intensities of signals from protons in the dimers. The appearance of the singlet is accompanied by the appearance of another pair of four signals from the aromatic protons (Fig. 2). That is, all the benzylic protons in the solution become magnetically equivalent by forming a new species, which means that the dimeric carbanions dissociate into monomers in the presence of excess base, or more precisely, butyllithium substituted to a half portion of the dimer forming a sulfinylalkyl mixed aggregate.

Experimental

Instruments. ^{1}H NMR spectra were recorded at 400 MHz on a JEOL GX-400 Fourier Transform NMR Spectrometer with a low-temperature equipment. δ-Values in ppm were internally related to that of the residual α-protons (δ 3.5) in the THF-d_8 solvent. The optical purity was measured on a Perkin-Elmer 241 Polarimeter. Elemental analyses were performed with a Yanako MT-3 Elemental Analyzer and gave satisfactory results for all compounds used.

Materials. (S_R)-*t*-butyl phenylmethyl sulfoxide was prepared according to the literature procedure.[16] Tetrahydrofuran-d_8 and a hexane solution of butyllithium were obtained from a commercial source.

Preparation of α-Sulfinyl Carbanion. An NMR sample tube containing 4.9 mg (0.025 mmol) of *t*-butyl phenylmethyl sulfoxide was sealed by a rubber stopper under atmosphere of nitrogen, then 700 μl of THF-d_8 was poured into the tube through a syringe. The solution was cooled to an appropriate temperature under a streem of nitrogen in order to keep the pressure inside the tube atmospheric. Since 3.57 mM dm^{-3} water was detected on the ^{1}H NMR spectrum of the solution, 1.6 μl of butyllithium in hexane was added to the solution in order to quench all the water molecule present. Then 1.2 equivalent amounts of butyllithium in hexane (19.2 μl, 0.03 mmol) was added to this solution through a syringe.

Measurement of Nuclear Overhauser Effect. The lithiated *t*-butylsulfinyl phenylmethyl carbanion (**2**) in THF-d_8 was kept at −50 °C. Irradiation on the methyl protons in the *t*-butyl group led to the enhancement in the intensity of signal from the benzylic proton in the difference NOE experiment.

References

1) Y. Iitaka, A. Itai, N. Tomioka, Y. Kodama, K. Ichikawa, K. Nishihata, M. Nishio, M. Izumi, and K. Doi, *Bull. Chem. Soc. Jpn.*, **59**, 2801 (1986).

2) T. Durst, R. Viau, and M. R. McClory, *J. Am. Chem. Soc.*, **93**, 3077 (1971).

3) J. E. Baldwin, R. E. Hacker, and R. M. Scott, *J. Chem. Soc., Chem. Commun.*, **1969**, 1415.

4) T. Durst, R. R. Fraser, M. R. McClory, R. B. Swingle, R. Viau, and Y. Y. Wigfield, *Can. J. Chem.*, **48**, 2148 (1970).

5) K. Nakamura, M. Higaki, S. Adachi, S. Oka, and A. Ohno, *J. Org. Chem.*, **52**, 1414 (1987).

6) J. O. Edwards and R. G. Pearson, *J. Am. Chem. Soc.*, **84**, 16 (1962).

7) G. Chassaing and A. Marquet, *Tetrahedron*, **34**, 1399 (1978).

8) G. Chassaing and A. Marquet, *J. Organomet. Chem.*, **232**, 293 (1982).

9) Although we do not know the molecularity in this aggregation at present, the evidence obtained from a solution with *N,N,N′,N′*-tetramethylethylenediamine elucidates the dimeric form, which will be discussed later.

10) G. Fraenkel, W. E. Beckenbaugh, and P. P. Yang, *J. Am. Chem. Soc.*, **98**, 6878 (1976).

11) M. Marsch, W. Massa, K. Harms, G. Baum, and G. Boche, *Angew. Chem., Int. Ed. Engl.*, **25**, 1011 (1986).

12) D. Seebach, R. Hässig, and J. Gabriel, *Helv. Chim. Acta*, **66**, 308 (1983).

13) R. Waack, M. A. doran, E. B. Baker, and G. A. Olah, *J. Am. Chem. Soc.*, **88**, 1057 (1969).

14) L. D. McKeever and R. Waack, *J. Organomet. Chem.*, **28**, 145 (1971).

15) C. Näjera, M. Yvs, R. Hässig, and D. Seebach, *Helv. Chim. Acta*, **67**, 1100 (1984).

16) M. Axelrod, P. Bickart, J. Facobus, M. M. Green, and K. Mislow, *J. Am. Chem. Soc.*, **90**, 4835 (1968).

 © 1988 The Chemical Society of Japan Bull. Chem. Soc. Jpn., 61, 1725—1729 (1988)

The Effect of the Heat Treatment of Pd Thin Film Alloy on the Hydrogenation of Olefins

Jun TAMAKI, Masashi YAMAMURA, and Toshinobu IMANAKA*
Department of Chemical Engineering, Faculty of Engineering Science, Osaka University, Toyonaka, Osaka 560
(Received August 31, 1987)

Pd-(B, P) thin film alloys have been prepared by an RF sputtering method. Before heat treatment, the selectivity for the partial hydrogenation of olefins increased with the increase in the B or P concentration in the Pd-(B, P) films. After the heat treatment, on the other hand, the selectivity for the partial hydrogenation was reduced over the Pd films with a low B or P concentration. However, in the case of the Pd films with a high B or P concentration, the selectivity was enhanced by the heat treatment. The high selectivity after the heat treatment was explainable in terms of the small ensemble size, the low electron density of Pd, and the appearance of a Pd_3B, $Pd_{4.8}P$, or Pd_5P_2 phase in the Pd films with a high B or P concentration. A sputtered film is known to have a columnar structure. This columnar structure was deduced to be controlled both by the alloying of Pd with B or P and by the heat treatment, so as to exhibit the high selectivity for the partial hydrogenation of olefins.

It is well-known that palladium shows a high selectivity in the hydrogenation of diolefins and acetylenes to monoolefins[1] and so is extensively utilized in industrial processes. Alloyed palladium catalysts are often used in order to enhance the properties of palladium by alloying, e.g., Pd-Pb,[2] Pd-Cu,[3-5] Pd-Au,[6] and Pd-Sn[7] alloys.

In a previous investigation,[8] boron (B) and phosphorus (P) were employed as partner elements of Pd alloys; Pd-(B, P) thin film alloys with various compositions of B or P could easily be prepared by changing the RF sputtering conditions. Since boron and phosphorus acted as the electron donor and the acceptor in the Pd alloys respectively, the electronic state of palladium could easily be modified by alloying with B or P. The palladium in the Pd-B alloys was in a high electron density, while the palladium in the Pd-P alloys was in a low density. The change in the electron density of Pd affected the selectivity for the partial hydrogenation of olefins. When the electron density of Pd was decreased by alloying by, for example, the Pd-P alloys, the selectivity was considered to be raised by the enhancement of the difference in the adsorption abilities of diene and monoene.[9] On the other hand, the ensemble effect in the alloy must be considered as well.[10] The ensemble size of Pd is invariably decreased by alloying with B or P, according to the results of investigations using the single-crystal surfaces of noble metals.[11-14] Since the small ensemble size of Pd caused a decrease in the number of adsorptive sites of hydrogen,[15] diolefins and acetylene were considered not to be readily hydrogenated up to paraffins, resulting in an enhancement of the selectivity for the partial hydrogenation. In the Pd-(B, P) alloys, the selectivity of the partial hydrogenation was controlled by the ensemble and by the ligand effect.

Thornton[16] reported that the structure of a sputtered film consisted of an aggregate of tapered columnar crystallites and that each column was separated by grain boundaries or voids so that the surface of film was not flat. The surface microstructure of the columnar crystallites is assumed to influence the catalysis by the film. Annealing by heat treatment would change the microstructure of the films. In this study, the effect of the heat treatment on the activity and the selectivity in the partial hydrogenation of olefins was examined in terms of the surface microstructure and the electronic state of the Pd film alloys.

Experimental

The Pd-(B, P) alloys were prepared using the RF sputtering method; the details of the film preparation were described in previous reports.[9,17] A Pd plate (99.95%) was used as a target for the sputtering. The boron and phosphorus sources were B_2H_6 diluted with H_2 (5.25 vol%), and PH_3 diluted with H_2 (5.37 vol%), respectively. The sputtering atmosphere was a mixed gas with a high purity of Ar (99.9995%) at a pressure of 0.05 Torr and $B_2H_6+H_2$ for the preparation of Pd-B films or a mixed gas of Ar and PH_3+H_2 for the preparation of Pd-P films. The glow discharge was carried out under various B_2H_6 or PH_3 partial pressures. The Pd thin film alloys were deposited on Pyrex glass substrates opposite the target. The average film thickness was 200 nm for all the Pd thin film alloys.

The hydrogenation of diolefins (cyclopentadiene and 1,3-butadiene) and acetylene was carried out over the Pd-(B, P) films at 273 K using a closed circulation system. The H_2/hydrocarbon ratio and the total pressure in the system were controlled to 6 and 140 Torr respectively. The products of the hydrogenation were analysed by means of a gas chromatograph (Shimadzu GC-8A) with a thermal conductivity detector. The columns used were a 3 m 2,4-dimethylsulfolane column for the hydrogenation of cyclopentadiene, a 5 m sebaconitrile column for 1,3-butadiene, and a 3 m activated charcoal column for acetylene. The heat treatment of the Pd thin film alloys was carried out at 573 K for 1 h in a vacuum ($<10^{-3}$ Torr (1 Torr=133.322 Pa)). The

surface analysis and the hydrogenation activity and selectivity were examined again after the treatment. The surface analysis was performed using a Shimadzu VD-1 X-ray diffractometer and a Shimadzu ESCA-750 X-ray photoelectron spectrometer.

Results and Discussion

Effect of the Heat Treatment on the Hydrogenation of Olefins. The highest activity in the hydrogenation was obtained over the pure Pd film. However, it steeply decreased with an increase in the B or P concentration. After the heat treatment, the hydrogenation activity decreased by about 1/3. This might be attributable to the decrease in the surface area resulting from the heat treatment.

The selectivity for the partial hydrogenation of cyclopentadiene to cyclopentene changed with the B or P concentration, as is shown in Figs. 1 and 2.

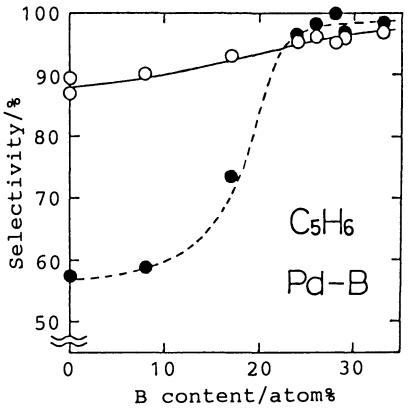

Fig. 1. Selectivity of the partial hydrogenation of cyclopentadiene as a function of the boron content.
—○—; before heat treatment. ---●---; after heat treatment.

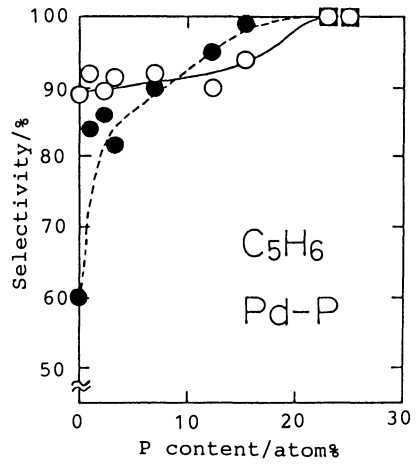

Fig. 2. Selectivity of the partial hydrogenation of cyclopentadiene as a function of the phosphorus content.
—○—; before heat treatment. ---●---; after heat treatment.

Before the heat treatment, as is shown by the solid line, the selectivity was satisfactorily high, even for the pure Pd film, and it further increased with the enhancement of the B or P concentration. The selectivity reached 96.7% for the $Pd_{67}B_{33}$ film and 100% for the $Pd_{75}P_{25}$ film. After the heat treatment, as is shown by the broken line, a selectivity drop was observed for the Pd–B films below 20 atom% of B and for the Pd–P films below 10 atom% of P. However, the selectivity increased in the region of the higher B or P concentration and reached 98.4% for the $Pd_{67}B_{33}$ film and 99.5% for even the $Pd_{85}P_{15}$ film. The selective hydrogenation of cyclopentadiene is a significant process for the utilization of the C_5 fraction in naphtha-cracking products. In the study by Hirai et al.[18] using colloidal Pd supported on a chelate resin, the selectivity for the partial hydrogenation of cyclopentadiene was 97.1% for a batch reactor in a liquid phase and 96% in a gas phase using a closed circulation system. In another study by Chaouki et

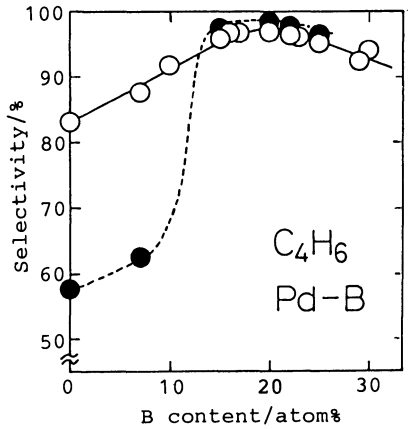

Fig. 3. Selectivity of the partial hydrogenation of 1,3-butadiene as a function of the boron content.
—○—; before heat treatment. ---●---; after heat treatment.

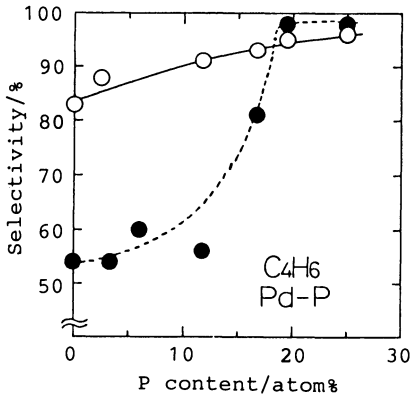

Fig. 4. Selectivity of the partial hydrogenation of 1,3-butadiene as a function of the phosphorus content.
—○—; before heat treatment. ---●---; after heat treatment.

al.[19] using the Cu/Al_2O_3 aerogel catalyst, the selectivity was about 100% for an integral plug flow reactor. Better results were obtained in our investigation in the gas phase.

The selectivity for the partial hydrogenation of 1,3-butadiene to butenes altered with the B or P concentration, as is shown in Figs. 3 and 4. Before the heat treatment, the selectivity was at its maximum at 20 atom% of B in the Pd–B films, and the maximal selectivity was 97.1%. The selectivity in the Pd–P films increased monotonously with the P concentration until it reached 96.0% for the $Pd_{75}P_{25}$ film. After the heat treatment, similar results on the hydrogenation of cyclopentadiene were observed. The selectivity was reduced below 10 atom% of B for the Pd–B films and below 17 atom% of P for the Pd–P films. However, the selectivity was enhanced in the region of a higher B or P concentration, reaching 98.3% for the $Pd_{80}B_{20}$ film and 98.0% for the $Pd_{75}P_{25}$ film.

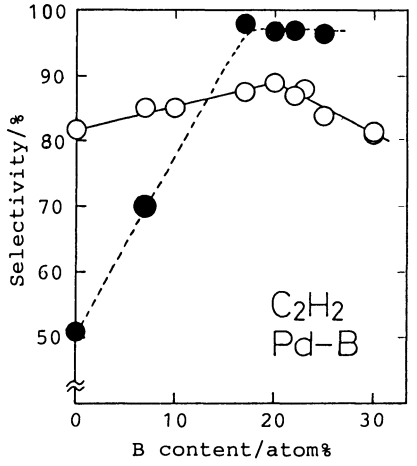

Fig. 5. Selectivity of the partial hydrogenation of acetylene as a function of the boron content.
—○—; before heat treatment. ---●---; after heat treatment.

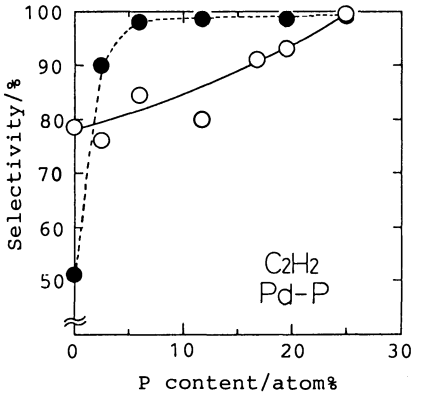

Fig. 6. Selectivity of the partial hydrogenation of acetylene as a function of the phosphorus content.
—○—; before heat treatment. ---●---; after heat treatment.

The selectivity for the partial hydrogenation of acetylene to ethylene changed with the B or P concentration, as is shown in Figs. 5 and 6. With the Pd–B films, the selectivity before the heat treatment was at its maximum at 20 atom% of B, much as in the hydrogenation of 1,3-butadiene, and the maximal selectivity was 89.0%. In the case of the Pd–P films, the selectivity increased with the increase in the P concentration. After the heat treatment, analogous to the hydrogenation of cyclopentadiene and 1,3-butadiene, the selectivity dropped in the region of a lower B or P concentration. However, it was raised in a higher B or P concentration range. The selectivity reached 98.0% for the $Pd_{84}B_{16}$ film and 99.0% for the $Pd_{75}P_{25}$ film. The partial hydrogenation of acetylene has been investigated for the sake of the commercially significant ethylene formation and the purification of ethylene by hydrogenating the acetylene contaminant. A higher selectivity of ethylene was obtained over the Pd–(B, P) films after the heat treatment in comparison to the conventional supported Pd catalysts[20] and other Pd alloy catalysts.[2–6]

Change in the Film Structure. The structure of the Pd thin film alloys was investigated by using X-ray diffraction analysis (XRD). Below 15 atom% of B in the Pd–B films, two peaks appeared at about 40 and 46 degrees; they corresponded to the Pd(111) and Pd(200) faces respectively. Below 25 atom% of P in the Pd–P films, only one peak appeared at about 40 degrees. In this region, the structure of the Pd–(B, P) films was found to be analogous to Pd fcc structure. In the higher B or P concentration range, three small peaks typically appeared at 38.6, 39.4, and 40.5 degrees in the Pd–B films (Fig. 7), while no peak was recognized in the Pd–P films (Fig. 8). The peculiar structure in the Pd–B films was found to resemble the Pd_3B crystal,

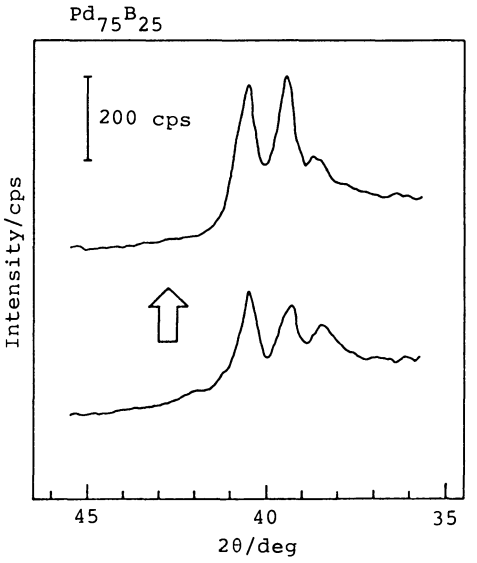

Fig. 7. Change in the X-ray diffraction pattern of $Pd_{75}B_{25}$ film by the heat treatment.

one of the stable palladium boride crystals,[21] whereas the structure of the Pd–P films was an amorphous structure.

Table 1 tabulates the changes in the peak positions and the full widths at half maximum (FWHM) of the XRD peak attributable to the Pd(111) face for the Pd–(B, P) films with the low B or P concentration upon heat treatment. After the heat treatment, the XRD peaks of the Pd fcc-like structure in the lower B or P concentration range increased in its intensity and became narrower. This indicates that Pd fcc structure develops in the Pd–(B, P) films with a low B or P concentration after the heat treatment. On the other hand, the small three peaks in the Pd–B films with a high B concentration increased a little at the same position after the heat treatment (Fig. 7). This reveals that the Pd_3B-like structure of the Pd–B film with a high B concentration grows slightly after the treatment. In the Pd–P films with a high P concentration, new six peaks appeared—at 33.0, 37.5, 38.2, 39.2, 40.0, and 43.0 degrees—after the heat treatment (Fig. 8). These peaks indicate the appearance of new crystalline Pd–P phases. The structure of the Pd–P film is assumed to be a mixed phase of the $Pd_{4.8}P$[22] and the Pd_5P_2[23] crystals, which are the stable palladium phosphide crystals. In the region of a high B or P concentration, the Pd alloy crystal was found to grow after the heat treatment, especially the amorphous structure in the Pd–P film crystallized. No growth of Pd fcc structure or separation of a Pd phase and a B or P phase were observed after the treatment in the region of a high B or P concentration.

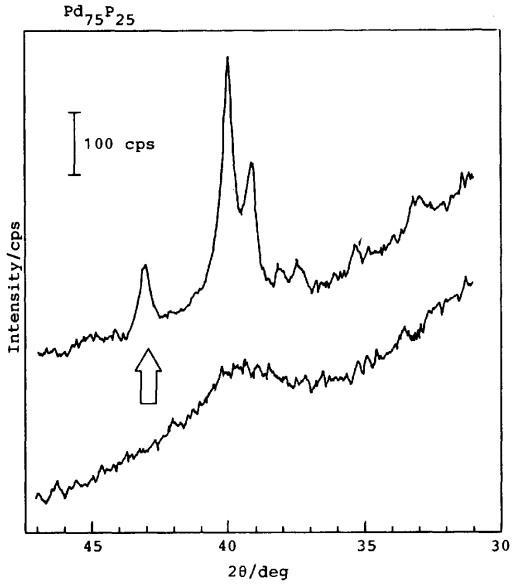

Fig. 8. Change in the X-ray diffraction pattern of $Pd_{75}P_{25}$ film by the heat treatment.

Change in the Film Composition and the Electronic State. The surface composition and the electronic state were evaluated by the use of an X-ray photoelectron spectroscope (XPS) equipped with an Ar-ion gun. The films were etched by Ar^+ for 30 sec, viz., by about 6 nm. The film composition was evaluated on the basis of the XPS peak area ratios of Pd3d5/2 to B1s or P2p level. The film composition and the binding energies (BE) of the surface and the bulk were compared before and after the heat treatment. These results are tabulated in Table 2. BE was

Table 1. Alterations in the XRD Peak Position and the Full Width at Half Maximum (FWHM) of the Pd(111) Face by the Heat Treatment

	Before		After	
	2θ/deg	FWHM/deg	2θ/deg	FWHM/deg
Pd_{100}	40.1	0.64	40.1	0.58
$Pd_{94}B_6$	40.0	0.65	40.1	0.60
$Pd_{87}B_{13}$	39.7	0.85	39.8	0.78
Pd_{100}	40.1	0.64	40.1	0.58
$Pd_{94}P_6$	39.7	0.67	39.8	0.63
$Pd_{88}P_{12}$	39.7	0.92	39.9	0.85

Table 2. Alterations in the Film Composition and the Surface Satate for Pd–(B, P) Films by the Heat Treatment

Pd–B		Surface			Bulk		
		Comp.	Pd3d5/2	B1s	Comp.	Pd3d5/2	B1s
Low	Before	$Pd_{96}B_4$	335.7	188.9	$Pd_{94}B_6$	335.7	188.8
	After	$Pd_{91}B_9$	335.6	188.8	$Pd_{93}B_7$	335.7	188.8
Middle	Before	$Pd_{68}B_{32}$	335.5	188.8	$Pd_{78}B_{22}$	335.7	188.7
	After	$Pd_{51}B_{49}$	336.0	188.9	$Pd_{64}B_{36}$	335.9	188.7
High	Before	$Pd_{35}B_{65}$	335.5	188.9	$Pd_{63}B_{37}$	335.7	189.0
	After	$Pd_{16}B_{84}$	336.6	188.2	$Pd_{31}B_{69}$	336.5	188.7
Pd–P				P2p			P2p
Low	Before	$Pd_{77}P_{23}$	335.6	130.4	$Pd_{97}P_3$	335.7	130.6
	After	$Pd_{91}P_9$	335.5	130.4	$Pd_{97}P_3$	335.7	130.7
	Before	$Pd_{66}P_{34}$	335.8	130.1	$Pd_{83}P_{17}$	336.0	130.2
	After	$Pd_{80}P_{20}$	335.9	130.4	$Pd_{83}P_{17}$	335.9	130.3
Middle	Before	$Pd_{66}P_{34}$	336.2	130.2	$Pd_{76}P_{24}$	336.2	130.2
	After	$Pd_{70}P_{30}$	336.7	130.4	$Pd_{76}P_{24}$	336.2	130.4

corrected by the use of a contaminant carbon (C1s=285.0 eV).

In the Pd–B films with a low B concentration, little enrichment of boron to the surface was observed. However, the extent of enrichment increased with the increase in the B concentration. The surface composition of Pd was only 16 atom% in a high B concentration. On the contrary, the surface enrichment of phosphorus in the Pd–P films was not as notable as that of boron. In the region of a low P concentration, the somewhat high P concentration at the surface was attributable to the adsorption of PH_3 on the surface, for the P concentration steeply reduced after only 5 s etching. It was found that the mobility of P in the film was smaller than that of B.

The BE of the Pd3d5/2 level for the Pd–B films was unchanged by the heat treatment in a low B concentration. However, the BE in a high B concentration shifted to the higher BE side after the heat treatment. This obviously indicates that the electron density of Pd in the Pd–B films with a high B concentration becomes lower after the heat treatment, although B donates electrons to Pd before the heat treatment. On the other hand, the BE of the Pd3d5/2 level for the Pd–P films was increased with the enhancement of the P concentration even before the heat treatment. After the heat treatment, it was slightly shifted to the higher BE side in a high P concentration. The electron density of Pd was also found to decrease further in the Pd–P films with a high P concentration after the heat treatment.

Model of the Pd Thin Film Alloy. The following model may explain the above results. As has been described above, the selectivity for the partial hydrogenation of olefins over the Pd alloys can be explained in terms of the ensemble and the ligand effect. The smaller ensemble size and the lower electron density of Pd for the Pd thin film alloys would result in the higher selectivity of the partial hydrogenation.

In a lower B or P concentration range, it can readily be supposed that the surface defects, i.e., the grain boundaries in the columnar structure, etc., are decreased by the heat treatment and that the columns are collapsed to large ones. Therefore, the ensemble size of Pd on the surface of the film would become larger, resulting in the decrease in the selectivity of the partial hydrogenation. Because the electronic state of Pd is unchanged by the heat treatment in a low B or P concentration, the decrease in the selectivity seems to be mainly caused by the increase in the ensemble size of Pd. In a higher B or P concentration range, B or P prevents the growth of the column during the heat treatment because the proportion of B or P is increased in the film. The ensemble size, therefore, would be almost unaltered, even after the heat treatment. This is supported by the results of XRD. The Pd_3B, $Pd_{4.8}P$, and Pd_5P_2 phases formed by the heat treatment may exhibit a high selectivity of the partial hydrogenation. Furthermore, the results of the XPS measurement suggest that the high selectivity after the heat treatment is attributable to the low electron density of Pd in the region of a higher B or P concentration.

References

1) G. C. Bond, "Catalysis by Metals," Chap. 12, Academic Press, New York (1962).
2) W. Palczewska, A. Jablonski, Z. Kaszkur, G. Zuba, and J. Wernisch, *J. Mol. Catal.*, **25**, 307 (1984).
3) A. H. Weiss, S. Leviness, V. Nair, L. Guczi, A. Sarkany, and Z. Schay, Proc. 8th Int. Conf. Catal., Vol. 5, Berlin(West) (1984), p. 591.
4) L. Guczi, Z. Schay, A. H. Weiss, V. Nair, and S. Leviness, *React. Kinet. Catal. Lett.*, **27**, 147 (1985).
5) S. Leviness, V. Nair, A. H. Weiss, Z. Schay, and L. Guczi, *J. Mol. Catal.*, **25**, 131 (1984).
6) C. Visser, J. G. P. Zuidwijk, and V. Ponec, *J. Catal.*, **35**, 407 (1974).
7) M. Masai, K. Honda, A. Kubota, S. Ohnaka, Y. Nishikawa, K. Nakahara, K. Kishi, and S. Ikeda, *J. Catal.*, **50**, 419 (1977).
8) J. Tamaki, S. Nakayama, M. Yamamura, and T. Imanaka, 59th CATSJ Meeting Abstracts, **29**, 170 (1987).
9) T. Imanaka, J. Tamaki, and S. Teranishi, *Nippon Kagaku Kaishi*, **1985**, 1064.
10) W. H. M. Sachtler and R. A. Van Santen, *Adv. Catal.*, **26**, 69 (1977).
11) Z. Karpinski, *J. Catal.*, **77**, 118 (1982).
12) Z. Karpinski, W. Juszczyk, and J. Stachurski, *J. Chem. Soc., Faraday Trans. 1*, **81**, 1447 (1985).
13) J. W. A. Sachtler and G. A. Somorjai, *J. Catal.*, **81**, 77 (1983).
14) G. A. Kok, A. Noordermeer, and B. E. Nieuwenhuys, *Surf. Sci.*, **152/153**, 505 (1985).
15) A. Noordermeer, G. A. Kok, and B. E. Nieuwenhuys, *Surf. Sci.*, **165**, 375 (1986).
16) J. A. Thornton, *J. Vac. Sci. Technol.*, **11**, 666 (1974).
17) J. Tamaki and T. Imanaka, *Chem. Lett.*, **1986**, 679.
18) H. Hirai, S. Komatsuzaki, and N. Toshima, *Bull. Chem. Soc. Jpn.*, **57**, 488 (1984).
19) J. Chaouki, C. Chavarie, D. Klvana, and G. M. Pajonk, *Appl. Catal.*, **21**, 187 (1986).
20) J. M. Moses, A. H. Weiss, K. Matusek, and L. Guczi, *J. Catal.*, **86**, 417 (1984).
21) E. Stenberg, *Acta Chem. Scand.*, **15**, 861 (1961).
22) ASTM Powder Diffraction Cards, 19—890.
23) ASTM Powder Diffraction Cards, 19—887.

Preparation of Poly(*p*-phenylene) by Electrooxidative Polymerization in Acidic Media

Kimihisa YAMAMOTO, Toshio ASADA, Hiroyuki NISHIDE, and Eishun TSUCHIDA*
Department of Polymer Chemistry, Waseda University, Tokyo 160
(Received November 5, 1987)

The electro-oxidative polymerization of benzene in the presence of strong acids yields poly(*p*-phenylene) efficiently. A strong protonic acid such as trifluoromethanesulfonic acid or Lewis acid such as an aluminum trichloride forms a complex with benzene and reduces the oxidation potential of benzene to 1.7 V, which brings about the high current efficiency. The acids act both as an electrolyte and as a catalyst in this polymerization of benzene.

There is much interest in the electrochemical preparation of aromatic conjugated polymers such as polypyrrole[1,2] polythiophene,[3,4] polyaniline,[5] poly(oxyphenylene),[6,7] poly(thiophenylene),[8] and polyazulene.[9] These polymers exhibit significant electrical conductivity and are potentially useful materials.[10,11] However, benzene is not polymerized under the same electrolytic conditions, and even under a large given potential.

Some attempts to electrooxidatively polymerize benzene to poly(*p*-phenylene) (PPP) have been reported: the electrochemical oxidation of benzene in liquid SO_2,[12] with HF,[13] with $AlCl_3$,[14] with $LiAsF_6$ and $CuCl_2$,[15] and with BF_4^-.[16] However, their yield and current efficiency were extremely low and the electrooxidative polymerization of benzene has not been studied quantitatively. We previously reported[17] that *p*-dimethoxybenzene with a lower oxidation potential is efficiently polymerized to poly(2,5-dimethoxy-1,4-phenylene) and that its polymerization proceeds via a cationic mechanism and is suppressed by basic additives. We recently found and preliminarily reported[18] that the electrooxidative polymerization of benzene is the presence of trifluoromethanesulfonic acid (FSA) gave PPP in high yield. This paper describes the efficient preparation of PPP by the electrooxidative polymerization of benzene in the presence of strong acids as well as the mechanism of this polymerization.

Experimental

Materials. Benzene was purified by distillation twice after contaminated thiophene was removed. Tetraethylammonium tosylate and other supporting electrolytes were recrystallized from ethanol–water and dried in vacuo for 1 d at 80 °C. All solvents were distilled before the electrolysis. Lewis acids, protonic acids and 9-phenylanthracene were guaranteed reagents and were used without further purification.

Electrolysis. One pair of platinum plate (2×5 cm) was set in the Cell[19] with 1 cm spacing as a working and an auxiliary electrode. The reference electrode was Ag/AgCl. The benzene solution (75 ml) of acid was kept at 20 °C under a nitrogen atmosphere in the cell. The preparative electrolysis was carried out under a controlled current with a potentiogarvanostat (Nikko Keisoku NPGS-301) without stirring. The electricity was measured by a digital coulomb meter (Nikko Keisoku NDCM-1). After the electrolysis, the adhered product was de-doped by supplying a cathodic potential at −0.1 V, and then removed from the working electrode. The product was washed with alkaline methanol and dried in vacuo for 1 d at 80 °C.

The current efficiency of the electrolysis was calculated as follows. One mole of benzene was quantitatively polymerized to PPP by two-electron oxidation. The current efficiency (%) was calculated by dividing the polymer yield by the theoretical value. Theoretical yield=$(Q/2nF)\times100$ (n: molar number, F: 96484 (c), Q: electricity (c))

Spectroscopies on the Polymer. The polymer was characterized by IR (Jasco IR-810) and Solid ^{13}C NMR (JEOL FX-100). Poly(*p*-phenylene): Solid ^{13}C NMR (ppm): 130 (broaden); IR (KBr, cm^{-1}): ν_{C-H}=3020, $\nu_{C=C}$=1600, 1480, δ_{C-H}=1000, 805.

Cyclic Voltammetry (CV). Cyclic voltammetry was carried out in a two-compartment cell. Platinum disk (0.126 cm^2), platinum wire and Ag/AgCl were used as a working, an auxiliary and a reference electrode, respectively. The concentration of benzene was 1 mmol l^{-1}. The potential was controlled with a dual potentiogarvanostat (Nikko Keisoku DPG-3) and a function generater (Nikko Keisoku NFG-3). The scanning rate of the potential was 100 mV s^{-1}. The i–E curve was recorded with a X-Y recorder.

Electrical Conductivity Measurement. After the electrolysis, PPP adhering to the anode was peeled off and washed with dry hexane. The d.c. conductivity of the PPP tablet was measured using a two-point probe method. The as-grown PPP was doped with the anions used as electrolytes and exhibited an electrical conductivity as high as 10^{-3}—10^{-4} S cm^{-1}. The doping was confirmed by the IR spectrum and fluorescence X-ray.

Results and Discussion

IR and ^{13}C NMR spectroscopic data of the de-doped sample are given in Experimental. The PPP shows the absorption band at 805 cm^{-1}, which is ascribed to a C–H out-of-plane deformation vibration of 1,4-disubstitued benzene and no strong absorptions at 840 cm^{-1} and 860 cm^{-1}, which are ascribed to trisubstituted and tetrasubstituted benzene, respectively. This IR absorption spectrum agrees with that reported for chemically prepared PPP[20,21] and indicates that the main structure of the polymer is

poly(*p*-phenylene) without crosslinking. A weak absorption of C–H out-of-plane vibration of mono-substituted phenyl rings appeared at 760 cm^{-1} in the IR spectrum. The ratio of the transmittance at the C–H out-of-plane vibration of di-substituted to that of monosubstituted one suggests that the degree of polymerization of PPP is over 7.

Table 1 shows the current efficiency for the electrooxidative polymerization of benzene in the presence of acids. The polymerization proceeds efficiently with a strong acid like FSA and a Lewis acid such as aluminum trichloride, but does not with a weak acid such as acetic acid. FSA which is one of the strongest protonic acids yields PPP with the highest current efficiency.

In the absence of acids, the electropolymerization does not sufficiently proceed with tetraethylammonium tosylate (TEATs), perchlorate, chloride or hydrogensulfate as an electrolyte. These results indicate that the polymerization of benzene is associated with the acidity of the electrolytic mixture and is retarded by the supporting electrolyte in the absence of acid.

Table 2 shows that this electropolymerization is suppressed by a strongly basic solvent such as propylene carbonate and *N*,*N*-dimethylformamide.

Table 1. Electrooxidative Polymerization[a] of Benzene in the Presence of Acids under Controlled Current

Acid	Current density	Current efficiency
	mA cm^{-2}	%
CF_3SO_3H	10	63
CF_3COOH	5	8
H_2SO_4	5	6
CCl_3COOH	5	0
CH_3COOH	5	0
HNO_3[b]	5	0
HCl[c]	5	0
$AlCl_3$	17.5	54
$BF_3 \cdot O(C_2H_5)_2$	17.5	58
$SbCl_5$	17.5	16
$FeCl_3$	17.5	10
$SnCl_4$	17.5	20
HF[13]	12.0	>1
None[d]	17.5	0
CF_3SO_3H/TEATs[e]	10	64
CF_3COOH/TEATs[e]	5	0
$AlCl_3$/TEATs[e]	17.5	54

a) Starting solutions composed: [Benzene]=1.4 mol l^{-1}, [Acid]=2.0 mol l^{-1} Electricity: 0.6 F mol l^{-1}, Solvent: Nitromethane. Polymerization in the presence of Lewis acid carried out in addition of small amount of water (1 ml) due to increase of the solution conductivity. b) 12 mol l^{-1} concd HNO_3. c) 12 mol l^{-1} concd HCl. d) The electrolyte was used as tetraethylammonium tosylate, perchlorate, chloride, or hydrogensulfate (0.2 mol l^{-1}). e) TEATs: Tetraethylammonium tosylate (0.2 mol l^{-1}).

The current efficiency was not influenced by oxygen bubbling through the electrolytic mixture, which often deactivates a radical species. These results support the idea that this polymerization proceeds via a cationic mechanism.

At a lower concentration, the polymerization is retarded probably because a reaction between benzene and an activated benzene does not easily occur. Then the current efficiency increases with the benzene concentration and becomes saturated at a concentration of 1.5 mol l^{-1}.

The above-mentioned results suggest a mechanism of this electropolymerization as given in Scheme 1. Benzene is one-electron oxidized to its cation radical. The cation radical electrophilically reacts with benzene to form a hydrodimer (**I**). It is oxidized to biphenyl accompanied by a proton elimination. The biphenyl is repeatedly oxidized to PPP.

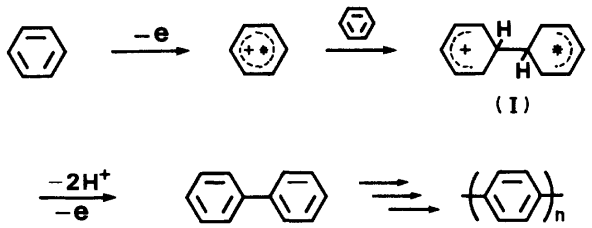

Scheme 1.

The cationic mechanism of the polymerization is consistent with the results that the polymerization is affected by a coexisting electrolyte anion and is suppressed by the basic solvent. This was further studied by UV spectroscopy and cyclic voltammetry. Since the cation radical of benzene is not stable and rapidly reacts with benzene, the effect of electrolyte species was studied by using a stable cation radical of 9-phenylanthracene[22] (9-PA) as a model for the benzene cation radical (Eq. 1). During the electrolysis

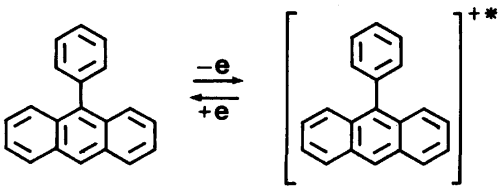

(1)

Table 2. Solvent Effect on Current Efficiency of the Electropolymerization of Benzene in the Presence of CF_3SO_3H

Solvent	Solvent donor number	Current efficiency
		%
CH_2Cl_2	—	79
CH_3NO_2	2.7	64
$C_6H_5NO_2$	4.4	56
CH_3CN	14.1	0
PC[a]	15.1	0
DMF[b]	26.6	0

a) Propylene carbonate. b) *N*,*N*-Dimethylformamide.

of 9-PA in the presence of trifluoroacetic acid or tin tetrachloride, the electrolytic solution was colored dark bluish (λ_{max}=722, 642, 569 nm), indicating the formation of the 9-PA cation radical. Immediately after a small amount addition of TEATs or DMF, the absorption of 9-PA cation radical disappeared. This suggests that the electrolyte anions and basic solvents nucleophilically react with the 9-PA cation radical.

Figure 1 shows a cyclic voltammograms of 9-PA in an acidic medium. The 9-PA cation radical is produced by a one-electron oxidation at 1.1 V, which is corresponds to the redox potential of 9-PA. The cathodic peak current coincided with the anodic one: I_{pc}/I_{pa}=1.0, which indicates that the 9-PA cation radical is stable in the acidic mixture. However, the anodic peak potential of 9-PA shifted anodically and the reduction peak of 9-PA cation radical was not observed in the presence of a small amount of such basic species as TEATs or DMF. These facts also support the observation that the 9-PA cation radical is not able to exist stable in the presence of a basic species. That is, the cation radical as an active species for the polymerization of benzene is strongly influenced by a supporting electrolyte and the acidity of the electrolytic mixture.

PPP was not given upon the addition of TEATs in a weakly acidic medium. However, in the presence of a strong acid such as FSA or $AlCl_3$, the polymerization yields PPP efficiently, even with the coexistence of an electrolyte such as TEATs and is not entirely retarded. The effect of a strong acid such as FSA and $AlCl_3$, in this polymerization process is remarkable in comparison with that of weak acids. This suggests a specific role of a strong acid in this polymerization process.

Figure 2 shows cyclic voltammograms of benzene in nitromethane. The virgin oxidation of benzene is initiated at 1.7 V and the oxidation peak potential (2.3 V) shifts toward less anodic potential in the presence of FSA, compared with a voltammogram in the absence of one (E_{pa}=2.8 V). Benzene was also oxidized above 1.7 V in the presence of $AlCl_3$. Upon the addition of benzene to strong acid solutions, the mixtures turned light brown (λ_{max}=380 nm) from colorless. Benzene is electropolymerized in the presence of these acids at a lower potential in comparison with that in the absence of ones. In the presence of a weak acid such as trifluoroacetic acid, the oxidation potential did not shift cathodically: The voltammogram was the same as in the absence of a weak acid, and the mixture remained colorless. The remarkable decrease in the oxidation potential of benzene in the presence of the strong acids can be explained as follows: Benzene forms a complex[23]

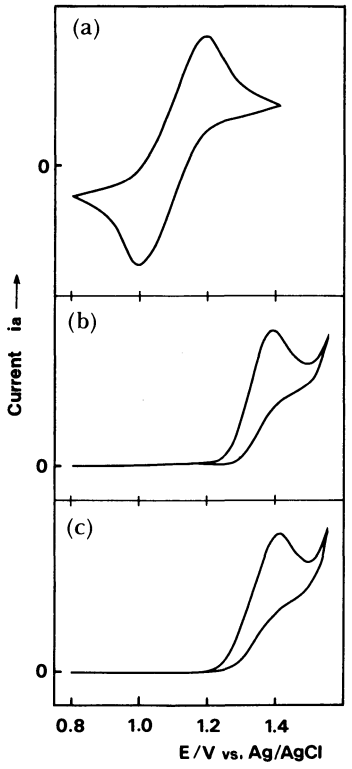

Fig. 1. Cyclic voltammograms of 9-phenylanthracene in the presence of CF_3COOH (a), tetraethylammonium tosylate (b), and DMF (c). Sweep rate: 0.1 V s^{-1}.

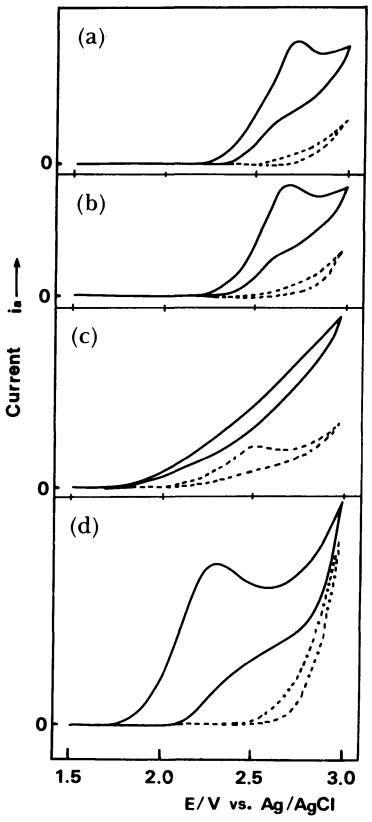

Fig. 2. Cyclic voltammograms of benzene in CH_3NO_2–TBAP (a) containing CF_3COOH (b), $AlCl_3$ (c), CF_3SO_3H (d). Dotted lines are background *i*–*E* curves in the same medium. Sweep rate: 0.1 V s^{-1}.

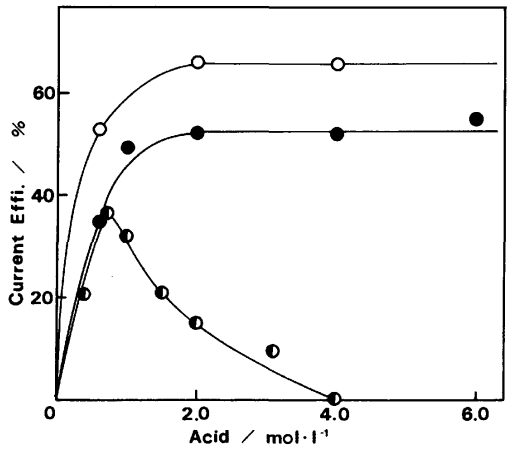

Fig. 3. Effect of the added amount of $AlCl_3$ (●), $SbCl_5$ (◐), and CF_3SO_3H (○) on the current efficiency of benzene-polymerization. [benzene] 2.0 mol l^{-1}, [tetrabutylammonium tosylate] 0.2 mol l^{-1} in nitromethane, at 17.5 mA cm^{-2}.

with a strong acid and Lewis acid such as FSA and $AlCl_3$, and the resonance stabilization of the benzene ring is reduced. That is, the oxidation potential slightly shifts toward less anodic potential in the presence of these strong acids, which corresponds to the current efficiency in the polymerization.

Figure 3 shows the effect of the concentration of FSA or $AlCl_3$. The current efficiency becomes saturated upon an equimolar addition of the acid: an equimolar addition of acid is required for a high current efficiency in PPP formation, which corresponds to the formation of a complex with an acid.

The roles of the acid for this electropolymerization of benzene are summarized as follows. The acid suppresses a nucleophilic reaction of the cation radical produced by a one-electron oxidation of benzene with basic species. The strong acid, such as FSA or $AlCl_3$, forms a cationic complex with benzene, which promotes an electrophilic attack of the cation radical to benzene and increases the polymerization efficiency. These strong acids also act as an electrolyte in this electrooxidative polymerization of benzene.

This work was partially supported by a Grant-in-Aid for Scientific Research on Priority Area of "Macromolecular Complexes" from the Ministry of Education, Science and Culture.

References

1) A. F. Diaz and K. K. Kanazawa, *J. Chem. Soc., Chem. Commun.*, **1979**, 635.
2) A. F. Diaz, J. Crowley, J. Bargon, G. P. Gardini, and J. B. Torrand, *J. Electroanal. Chem.*, **121**, 355 (1981).
3) R. J. Waltman, J. Bargon, and A. F. Diaz, *J. Phys. Chem.*, **87**, 1459 (1983).
4) A. F. Diaz, *Chem. Scr.*, **17**, 145 (1981).
5) N. Oyama, T. Ohsaka, and M. Nakanishi, *J. Macromol. Sci. Chem.*, **A24**, 375 (1987).
6) K. Yamamoto, H. Nishide, and E. Tsuchida, *Nippon Kagaku Kaishi*, **1986**, 152.
7) K. Yamamoto, H. Nishide, and E. Tsuchida, *Makromol. Chem., Rapid Commun.*, **8**, 11 (1987).
8) E. Tsuchida, H. Nishide, K. Yamamoto, and S. Yoshida, *Macromolecules*, **20**, 2315 (1987).
9) J. Bargon, S. Mohmand, and R. J. Waltman, *IBM, J. Res. Rev*, **27**, 330 (1983).
10) M. Dietrich, J. Morteuson, and J. Heinze, *J. Chem. Soc., Chem. Commun.*, **1986**, 1131.
11) K. Yoshino, M. Ozaki, and R. Sugimoto, *Jpn. J. Appl. Phys.*, **24**, L375 (1985).
12) M. Delamer, R. C. Lacaze, J. Y. Dumossau, and J. E. Dubois, *Electrochim. Acta*, **27**, 61 (1982).
13) I. Rubinstein, *J. Polym. Sci., Chem. Ed.*, **21**, 3035 (1983).
14) K. Kaeriyama, M. Sato, K. Someno, and S. Tanaka, *J. Chem. Soc., Chem. Commun.*, **1984**, 1199.
15) M. Satoh, M. Tabata, K. Kaneto, and K. Yoshino, *Polym. Commun.*, **26**, 356 (1985).
16) S. Aeiyach, J. E. Dubois, and P. C. Lacaze, *J. Chem. Soc., Chem. Commun.*, **1986**, 1668.
17) K. Yamamoto, H. Nishide, and E. Tsuchida, *Polym. Bull.*, **17**, 136 (1987).
18) E. Tsuchida, K. Yamamoto, T. Asada, and H. Nishide, *Chem. Lett.*, **1987**, 1541.
19) E. Tsuchida, H. Nishide, and T. Maekawa, *ACS Symp. Ser.*, **282**, 175 (1985).
20) C. E. Brown, M. B. Jones, and P. Kovacic, *J. Polym. Sci., Polym. Lett.*, **18**, 653 (1980).
21) G. Froyer, J. Y. Goblot, J. L. Gvilbert, T. Maurice, and Y. Pelous, *J. Physique*, **C3**, 745 (1983).
22) U. Svaiholm and V. D. Parker, *J. Am. Chem. Soc.*, **98**, 2942 (1976).
23) L. J. Andrew and R. M. Keefer, *J. Am. Chem. Soc.*, **71**, 3644 (1949).

 © 1988 The Chemical Society of Japan Bull. Chem. Soc. Jpn., 61, 1735—1742 (1988)

Relative Standard Electrode Potentials of I_3^-/I^-, I_2/I_3^-, and I_2/I^- Redox Couples and the Related Formation Constants of I_3^- in Some Pure and Mixed Dipolar Aprotic Solvents

Jayati DATTA, Abhijit BHATTACHARYA, and Kiron Kumar KUNDU*
Physical Chemistry Laboratories, Jadavpur University, Calcutta-700032, India
(Received February 12, 1987)

Standard potentials of I_3^-/I^- and I_2/I_3^- redox couples relative to that of aqueous saturated calomel reference electrode SCE (W), $E_{SCE(w)}$ have been determined in propylene carbonate (PC), *N*,*N*-dimethylformamide (DMF), acetonitrile (ACN), and their binary mixtures at 25 °C from potentiometric measurements. The results helped evaluate the standard potentials of the redox couple I_2/I^- relative to $E_{SCE(w)}$ as well as the related formation constant (K_f) of I_3^- in these solvent systems. The solvent effects on the formation equilibrium $I_2+I^- \rightleftharpoons I_3^-$ were analyzed in the light of the transfer free energies of I_2, $\Delta G_t^\circ(I_2)$, as obtained from solubility measurements of I_2 in the solvents, that of I^-, $\Delta G_t^\circ(I^-)$, as obtained earlier by use of the widely used TATB reference electrolyte assumption and that of I_3^-, $\Delta G_t^\circ(I_3^-)$, as obtained by subtracting these two contributions from the respective transfer free energies of formation equilibrium in the mixed solvents relative to a chosen reference solvent in each solvent system. The solvation behavior of these individual iodine species viz. I_2, I^-, I_3^- was interpreted in terms of involved interaction viz. Born, ion-dipole, ion-induced dipole, dispersion type soft-soft interactions, CTTS complexation and also the cavity effect as computed by the scaled particle theory (SPT).

The electrochemical behavior of the halogen/halogenide ion (X_2/X^-) redox couples in different nonaqueous media has lately become increasingly important due to their potential use in some high energy nonaqueous primary[1] and secondary batteries[1,2] and also in nonaqueous photoelectrochemical (PEC) cells.[3,4] In this context the knowledge of the intensive factor such as the standard potential (E°) of the galvanic elements X_2/X^-, and that of the involved X_3^-/X^- and X_2/X_3^- redox couples as well as the formation constant (K_f) of X_3^- in different dipolar aprotic solvents and their binary mixtures should be of particular interest. These, or at least their relative values, will be helpful to characterize the Fermi levels of these redox couples as required for the potential nonaqueous PEC cells, to elucidate their influence on the charging-discharging characteristics of the potential nonaqueous batteries and also to evaluate the kinetic parameters of the involved galvanic reactions in both the cases. This knowledge will then help judge the relative potentiality of the solvents for their use in the nonaqueous batteries or PEC cells comprising these redox couples.

Of the widely used battery fluids propylene carbonate (PC) and *N*,*N*-dimethylformamide (DMF) have attracted increasing attention.[5] Acetonitrile (ACN), though not so widely used, has got the distinction of being a protophobic dipolar aprotic solvent like PC, but nearly isodielectric to DMF. Very recently Kuznetsova et al.[6] reported the values of $E^\circ_{I_3^-/I^-}$ and $E^\circ_{I_2/I_3^-}$ and the formation constant K_f of I_3^- in DMF and its mixtures with PC at different temperatures. But their data, based on a potentiometric titration procedure using a reference half cell, Pt, I_2 solvent //, seems quest ionable, as I_2 solution without any added I^- would hardly act as a suitable redox couple. Moreover, appreciable ionization of I_2 to I^- in these aprotic solvents unlike in protic solvents like water, is somewhat doubtful, although charge transfer complex formation with these solvents cannot be ruled out. Further, the so-called electrode potential (E°) values reported, appear to be relative to the emf of the reference half-cell mentioned above. In the present paper we therefore report the standard electrode potentials (E°) of I_3^-/I^-, I_2/I_3^-, and I^-/I_2 redox couples relative to aqueous saturated calomel reference electrode SCE(w) and the related formation constant (K_f) or I_3^- in these dipolar aprotic solvents and their binary mixtures containing 25, 50, and 75 wt% of the cosolvents.

The cells used for this purpose are

$$\text{SCE(w)}//I^-(m),\ I_3^-(m),\ \text{solvent/Pt} \qquad \text{(A)}$$

$$\text{SCE(w)}//I_2(m),\ I_3^-(m),\ \text{solvent/Pt} \qquad \text{(B)}$$

where m stands for the molal concentration of I^-, I_2, and I_3^-. The emf's of the cells were measured for several values of m so that the ionic strength (μ) could be varied from 0.01 to 0.1.

Admittedly, the use of SCE(w) as the reference half-cell has resulted in the introduction of a liquid junction potential (E_j) in the final E° values of the redox couples in each solvent. While the E_j values based on TATB methods[7] are known for these pure solvents,[8] those for the mixed solvents could be estimated at least approximately by assuming linear dependence with mole per cent cosolvent composition and hence accounted for, if required (vide footnote under Table 1). Moreover, in most of the electrochemical measurements viz. cyclic voltammetry, polarography etc. the most commonly used reference half-cell is the SCE(w) itself,[9] of course with

Table 1. Standard Electrode Potentials ($E°$) (in Volt) of I_3^-/I^-, I_2/I_3^-, and I_2/I^- Redox Couples Relative to ($E_{SCE(w)}+E_j$) as well as to $E°_{SHE(w)}$ in Pure Solvents PC, ACN, DMF, and Their Binary Mixtures at 25 °C

Wt% cosolvent	$E°_{I_3^-/I^-}$	$E°_{I_2/I_3^-}$ relative to ($E_{SCE(w)}+E_j$)	$E°_{I_2/I^-}$	$E°_{I_3^-/I^-}$	$E°_{I_2/I_3^-}$ relative to $E°_{SHE(w)}$	$E°_{I_2/I^-}$
			PC+DMF mixture			
0	0.056	0.741	0.284	0.428	1.114	0.656
25	0.075	0.685	0.278	(0.470)	(1.079)	(0.673)
50	0.080	0.680	0.280	(0.493)	(1.693)	(0.693)
75	0.085	0.680	0.283	(0.513)	(1.107)	(0.711)
100	0.091	0.701	0.295	0.532	1.144	0.736
			PC+ACN mixture			
25	0.052	0.686	0.263	(0.409)	(1.043)	(0.620)
50	0.040	0.655	0.245	(0.387)	(1.002)	(0.592)
75	0.027	0.635	0.230	(0.368)	(0.976)	(0.571)
100	0.017	0.617	0.217	0.354	0.954	0.554
			ACN+DMF mixture			
25	0.055	0.604	0.238	(0.408)	(0.957)	(0.591)
50	0.076	0.650	0.267	(0.450)	(1.024)	(0.641)
75	0.078	0.667	0.274	(0.480)	(1.069)	(0.676)

The values in parentheses for the mixed solvents were tentatively estimated by assuming linear variation of E_j (TATB) values with mole percent cosolvent compositions in the respective solvent systems, the E_j (TATB) values for the pure solvents being known (Ref. 8). This assumption is however based on the fact that E_j (TATB) values caused by aqueous sat. KCl and 0.1 M Et_4N Pic at hetero-solvent interfaces comprising H_2O and methanol, ethanol, ACN, PC, DMSO, and DMF fall on a single straight line. Moreover, a recent study[26] reveals that E_j (TATB) values for the same system at interfaces, between H_2O/H_2O+ACN mixtures bear a fairly good linear relationship with mole percent ACN.

appropriate measure for minimizing the contamination of solvents across aqueous–nonaqueous interface. Thus, even if these E_j values are present, these are not likely to pose any serious problem at least from the operational point of view.

In the present study the derived formation constant (K_f) of I_3^- will be of course free from any uncertainty as the values of E_j as well as $E_{SCE(w)}$ will be eliminated. Moreover, the prime discussion being related to K_f values the contention derived thereof will have little effect on the uncertainties in E_j values.

In order to gain insight into the solvent effect on the formation equilibrium of I_3^-, $\delta[\Delta G°(I_3^-)]$ the transfer free energies $\Delta G_t°(i)$ of the involved individual species (i) from a chosen reference solvent (R) to the solvent (S) concerned are useful[10,11] as

$$\delta[\Delta G°(I_3^-)] = 2.303\,RT\,[p_S K_f(I_3^-) - p_R K_f(I_3^-)] = \Delta G_t°(I_3^-) - \Delta G_t°(I^-) - \Delta G_t°(I_2). \quad (1)$$

To facilitate the splitting, $\Delta G_t°(I_2)$ values were determined by measuring the solubilities of I_2 in the solvents, as the $\Delta G_t°(I^-)$ values based on the widely used tetraphenylarsonium tetraphenylborate (TATB)[11,12] reference electrolyte assumption:

$$\Delta G_t°(Ph_4As^+) = \Delta G_t°(Ph_4B^-) = 1/2\Delta G_t°(Ph_4\,As\,BPh_4)$$

have been evaluated earlier[13] for these solvent systems.

Experimental

PC (Koch light) was first dried over activated Molecular Sieves 4A (E. Merck) for about a week and then fractionally distilled twice under reduced pressure.[8] ACN (AR, SD) and DMF (E. Merck) were purified by methods described earlier.[8] I_2 (E. Merck) was purified by sublimation. KI (GR. E. Merck) was pretreated by heating at 150 °C for a few hours and then dried in vacuum before use.

For measuring the solubilities of I_2 in different solvents, saturated solutions of I_2 were prepared by mild shaking of the suspension of I_2 and allowed to equilibriate at 25°±0.1 °C. At 2—3 d intervals aliquots of each solution were withdrawn and I_2 concentration was estimated by titrating with a standard thiosulfate solution. The operations were repeated till two successive readings agreed within ±1%.

Stock solutions of I_2 and KI were made with the pretreated I_2 and KI in solvents of different compositions, namely 100, 75, 50, 25 wt% of each binary mixture. Solutions of cell A were prepared by adding appropriate amount of I_2 solution to known amount of standard KI solution so that $m_{I^-}=m_{I_3^-}=m$ and that of cell B by adding requisite amount of KI solution to a known amount of I_2 solution, so that $m_{I_2}=m_{I_3^-}=m$. And the solutions of different ionic strengths were prepared by appropriately diluting a suitable amount of stock mixture with the solvent.

The reference SCE(w) was of Fisher calomel reference electrode (model E 6A) with a porous ceramic junction and fitted within a jacket containing the cell solution. The jacket is connected to the rest of the cell solution through a G-2 gooch junction, similar to that used by Gritzner[14] and

the upper end allowed the insertion of the reference electrode through a tightly fitted Teflon stopper. The flow rate through the ceramic junction of the Fisher calomel reference electrode for 8 cm head being 1—5 μl per hour, the uncertainties possible for contamination of the solvents hardly affected the observed potential beyond the experimental error±1 mV.

The cell was essentially similar to the conventional[15] three necked polarographic/cyclic voltammetric cell and fitted with three standard joint mouths, through which the Pt-wire electrode as well as the jacketed reference electrode were introduced, keeping the third one closed by a standard joint stopper. The cell containing the working solution was fitted with the Pt-wire electrode and the stoppered jacket with the cell solution inside it. The system was first thermally equilibriated at 25 °C. The Fisher calomel reference electrode was then introduced into the jacket by replacing the stopper. The emf values were measured with a Kiethley Electrometer (Model 616). The equilibrium potential was attained within 15—20 min of dipping the reference electrode. Some of the readings were also checked by using Elico (India) calomel reference electrode (Type ER-70) and found to agree within the experimental error with those obtained with the jacketed reference electrode.

Results

In the case of cell (A) the half-cell reaction is essentially

$$I_3^- + 2e^- \longrightarrow 3I^-, \tag{2}$$

and the observed emf, E_A of cell is given by

$$E_A = [E^\circ_{I_3^-/I^-} - (E_{SCE(w)} + E_j)] - \frac{RT}{2F} \ln m_{I^-}^3/m_{I_3^-} - \frac{RT}{2F} \ln \gamma_{I^-}^3/\gamma_{I_3^-}, \tag{3}$$

and the extrapolation function $E_A^{\circ\prime}$ by

$$E_A^{\circ\prime} = E_A + \frac{2.3\,RT}{F} \log m - \frac{2.3\,RT}{F} S_f \mu^{1/2} = [E^\circ_{I_3^-/I^-} - (E_{SCE(w)} + E_j)] + b\mu, \tag{4}$$

where $m_{I^-} = m_{I^-} = m$, by experimental conditions, γ_i is the activity coefficient of the species i and is being computed by the limiting form of Debye-Hückel equation,[16] S_f the Debye-Hückel constant, b the emperical parameter depending upon the solvent and temperature, and the other terms are having usual significance. The extrapolation function $E^{\circ\prime}$ on extrapolation to $\mu=0$ yielded $E^\circ_{I_3^-/I^-}$ relative to $[E_{SCE(w)}+E_j]$ which on elimination of the respective E_j values as well as $E_{SCE(w)}$, furnished $E^\circ_{I_3^-/I^-}$ values in the solvents relative to $E^\circ_{SHE(w)}$.

In the case of cell (B), the half-cell reaction is essentially

$$3I_2 + 2e^- \longrightarrow 2I_3^-, \tag{5}$$

and the observed emf, E_B of the cell is given by

$$E_B = [E^\circ_{I_2/I_3^-} - (E_{SCE(w)} + E_j)] - \frac{RT}{2F} \ln m_{I_3^-}^2/m_{I_2}^3 - \frac{RT}{2F} \ln \gamma_{I_3^-}^2/\gamma_{I_2}^3, \tag{6}$$

and the extrapolation function $E_B^{\circ\prime}$ by

$$E_B^{\circ\prime} = E_B - \frac{2.3\,RT}{F} \log m - \frac{2.3\,RT}{F} S_f \mu^{1/2} = [E^\circ_{I_2/I_3^-} - (E_{SCE(w)} + E_j)] + b\mu, \tag{7}$$

where $m_{I_3^-} = m_{I_2} = m$ and other terms are having usual significance. As before, the extrapolation of the observed linear plots of $E_B^{\circ\prime}$ vs. μ to $\mu=0$ yielded $E^\circ_{I_2/I_3^-}$ relative to $[E_{SCE(w)}+E_j]$. The $E^\circ_{I_2/I_3^-}$ relative to $E^\circ_{SHE(w)}$ are

Table 2. Values of $\log K_f(I_3^-)$, $\Delta G_f^\circ(I_3^-)$, $-\log S$, and $\delta[\Delta G_f^\circ(I_3^-)]$ in Pure Solvents PC, DMF, ACN, and Their Binary Mixtures at 25 °C

Wt% cosolvent	$\log K_f(I_3^-)$ (K_f in L mol^{-1})	$\Delta G_f^\circ(I_3^-)$ kJ mol^{-1}	$-\log S$ mol kg^{-1}	$\delta[\Delta G_f^\circ(I_3^-)]$ kJ mol^{-1}
		PC+DMF mixture		
0	7.78(7.8)[a]	−44.1	0.842	0.0
25	6.87	−39.2	−0.392	4.9
50	6.76	−38.6	−0.762	5.5
75	6.70	−38.2	−0.903	5.9
100	6.89(7.0)[b]	−39.3	—	4.8
		PC+ACN mixture		
25	7.15	−40.8	0.639	3.3
50	6.93	−39.6	0.572	4.5
75	6.85	−39.1	0.512	5.0
100	6.76(6.8)[b]	−38.6	0.445	5.5
		ACN+DMF mixture		
0	6.76	−38.6	0.445	0
25	6.18	−35.3	−0.310	3.3
50	6.46	−36.9	−0.636	1.7
75	6.63	−37.8	−0.868	0.8
100	6.89	−39.3	—	−0.7

Values in parentheses are taken from a) J. Courtot-Coupez et M. L'Her, Comptes rendus, 266 series C, 1968, p. 1286; b) B. G. Cox, G. R. Hedwig, A. J. Parker, and D. W. Watts, *Aust. J. Chem.*, **27**, 477 (1979).

then obtained in a similar manner as described earlier.

The value of formation constant (K_f) of I_3^- in these solvents which are identical with the equilibrium constant values of the reaction

$$I_2 + I^- \rightleftharpoons I_3^- \quad (8)$$

were then obtained by the relation

$$\log K_f(I_3^-) = \frac{2}{3} \cdot \frac{F}{2.3RT} [E^\circ_{I_2/I_3^-} - E^\circ_{I^-/I_3^-}]. \quad (9)$$

The standard electrode potential $E^\circ_{I_2/I^-}$ of the redox couple I_2/I^- in these solvents relative to $E^\circ_{SHE(w)}$ were then obtained by proper coupling of the actual standard electrode potentials $E^\circ_{I_3^-/I^-}$ and $E^\circ_{I_2/I_3^-}$ relative to $E^\circ_{SHE(w)}$ with the help of the relation

$$E^\circ_{I_2/I^-} = \frac{1}{3}[2E^\circ_{I_3^-/I^-} + E^\circ_{I_2/I_3^-}] \quad (10)$$

The E° values of the three redox couples thus obtained relative to $[E_{SCE(w)} + E_j]$ and also to $E^\circ_{SHE(w)}$ are listed in Table 1. The estimated uncertainties of the values are about ± 1 mV. In Table 2 are presented the values of $\log K_f(I_3^-)$, $\Delta G_f^\circ(I_3^-)$, and $\delta[\Delta G_f^\circ(I_3^-)]$.

The transfer free energies of I_2 from the chosen reference solvent R (R=PC in PC+DMF and PC+ACN mixtures and R=ACN in ACN+DMF mixtures) to the respective solvent mixtures were computed on mole fraction scale from the measured

Table 3. Various Free Energy Transfer Parameters for I^-, I_2, and I_3^- from PC to (PC+DMF) and (PC+ACN) Mixtures and from ACN to (ACN+DMF) Mixtures at 25°C

Wt% consolvent	mol% consolvent	$\Delta G^\circ_{t,total}$ kJ 1mol^{-1}			$\Delta G^\circ_{t,cav}$ kJ mol^{-1}			$\Delta G^\circ_{t,Born}$ kJ mol^{-1}	
		$I^{-a)}$	I_2	I_3^-	I^-	I_2	I_3^-	I^-	I_3^-
					PC→PC+DMF mixture				
0	0	0	0	0	0	0	0	0	0
25	0.3177	−1.4	−6.8	−3.1	1.2	1.6	3.8	0.3	0.1
50	0.5828	−2.7	−8.7	−5.4	2.3	3.1	7.2	1.0	0.5
75	0.8074	−3.0	−9.3	−5.7	3.3	4.6	10.9	2.1	1.0
100	1.0	−2.9	—	—	4.4	6.2	14.6	3.7	1.9
					PC→PC+ACN mixture				
25	0.4533	0.5	−0.37	4.2	1.0	1.3	2.8	0.7	0.4
50	0.7133	1.6	−0.16	7.4	1.5	1.9	3.9	1.5	0.8
75	0.8819	2.1	−0.02	9.0	1.7	2.1	4.3	2.4	1.2
100	1.0	3.5	0	11.3	1.8	2.3	4.5	3.9	2.0
					ACN→ACN+DMF mixture				
0	0	0	0	0	0	0	0	0	0
25	0.1577	−1.6	−4.6	−3.2	0.5	0.8	2.0	—	—
50	0.3596	−2.8	−6.8	−8.5	1.2	1.7	4.4	—	—
75	0.6275	−5.6	−8.5	−14.3	1.9	2.8	7.2	—	—
100	1.0	−6.0	—	—	2.6	3.9	10.1	—	—

Wt% consolvent	mol% consolvent	$\Delta G^\circ_{t,i-d}$ kJ mol^{-1}		$\Delta G^\circ_{t,i-id}$ kJ mol^{-1}		$\Delta G^\circ_{t,int}$ kJ mol^{-1}		
		I^-	I_3^-	I^-	I_3^-	I^-	I_2	I_3^-
				PC→PC+DMF mixture				
0	0	0	0	0	0	0	0	0
25	0.3177	3.4	1.6	−2.1	−0.5	−4.2	−8.4	−8.1
50	0.5828	6.2	3.1	−3.9	−0.9	−8.2	−11.8	−15.2
75	0.8074	8.6	4.1	−5.4	−1.2	−11.7	−13.9	−20.5
100	1.0	10.6	5.1	−6.7	−1.5	−14.9	—	—
				PC→PC+ACN mixture				
25	0.4533	1.0	1.2	1.0	0.3	−3.2	−1.3	−0.5
50	0.7133	1.6	1.9	1.6	0.4	−4.6	−1.9	0.4
75	0.8819	2.0	2.4	1.9	0.5	−5.9	−2.3	0.6
100	1.0	2.3	2.7	2.2	0.6	−6.7	−2.6	1.5
				ACN→ACN+DMF mixture				
0	0	0	0	0	0	0	0	0
25	0.1577	1.3	0.5	−2.2	−0.6	−1.2	−5.4	−5.1
50	0.3596	3.0	1.1	−5.0	−1.4	−2.0	−8.5	−12.6
75	0.6275	5.3	1.9	−8.7	−2.5	−4.1	−11.3	−20.9
100	1.0	8.4	3.1	−13.8	−3.9	−3.2	—	—

a) These values are taken from Ref. 13.

solubilities (S) (mol kg^{-1} of solvent) of I_2 in the solvents by use of Eq. 11.

$$\Delta G_t^\circ(I_2) = RT \ln {}_RS/{}_SS + RT \ln {}_R\gamma_{I_2}/{}_S\gamma_{I_2} + RT \ln {}_RM/{}_SM = RT \ln {}_RS/{}_SS + RT \ln {}_RM/{}_SM \quad (11)$$

where M=molar and mean molar mass of pure and mixed solvents respectively. The activity coefficients ${}_R\gamma_{I_2}$ and ${}_S\gamma_{I_2}$ being referred to the corresponding states of saturated solution in the respective solvents are likely to be more or less equal and hence the activity coefficient factor $RT\ln {}_R\gamma_{I_2}/{}_S\gamma_{I_2}$ is assumed to be zero. The log S values are presented in Table 2 and the $\Delta G_t^\circ(I_2)$ values in Table 3.

Moreover, recently Kundu and co-workers[13] have also determined the ΔG_t° values of I^- in these solvents [vide Table 3]. So utilizing these values of I^- and those of I_2 as obtained in the present study, the corresponding values of I_3^- were computed by use of the relation (1) and are presented in Table 3.

Discussion

Variation of $\delta[\Delta G_f^\circ(I_3^-)]$ with mole percent cosolvent from PC to PC+DMF and PC+ACN mixtures are shown in Figs. 1 and 2 respectively and those from ACN to ACN+DMF mixtures in Fig. 3. While $\delta[\Delta G_f^\circ(I_3^-)]$ values are found to increase sharply at first but slowly later in PC+ACN mixtures, those for PC+DMF mixtures pass through a broad maximum as the cosolvent concentration increases. Evidently, the formation of I_3^- is less favored in both the cases, as compared to that in pure PC, the extent, however, depends upon the cosolvent composition. On the other hand, $\delta[\Delta G_f^\circ(I_3^-)]$ from ACN to ACN+DMF mixtures (Fig. 3) passes through a slight maximum around 20 mole percent DMF and gradually acquires a negative trend at high DMF content. Thus on addition of DMF to the reference solvent ACN, the equilibrium (Eq. 8) is at first shifted towards left and at higher DMF composition it is shifted towards right compared to that in ACN. Now, $\delta[\Delta G_f^\circ(I_3^-)]$ being a composite parameter, more informative, and meaningful interpretation of these results awaits the dissection of this parameter into less composite individual quantities. For this purpose the solvent effect on the formation equilibrium (Eq. 8) can be expressed as in Eq. 1.

The $\Delta G_t^\circ(i)$-composition curves for PC+ACN and PC+DMF are shown in Figs. 1 and 2 respectively, whereas those from ACN to ACN+DMF mixtures in Fig. 3. Notably, all the three iodine species are stabilized with addition of DMF to either PC or ACN,

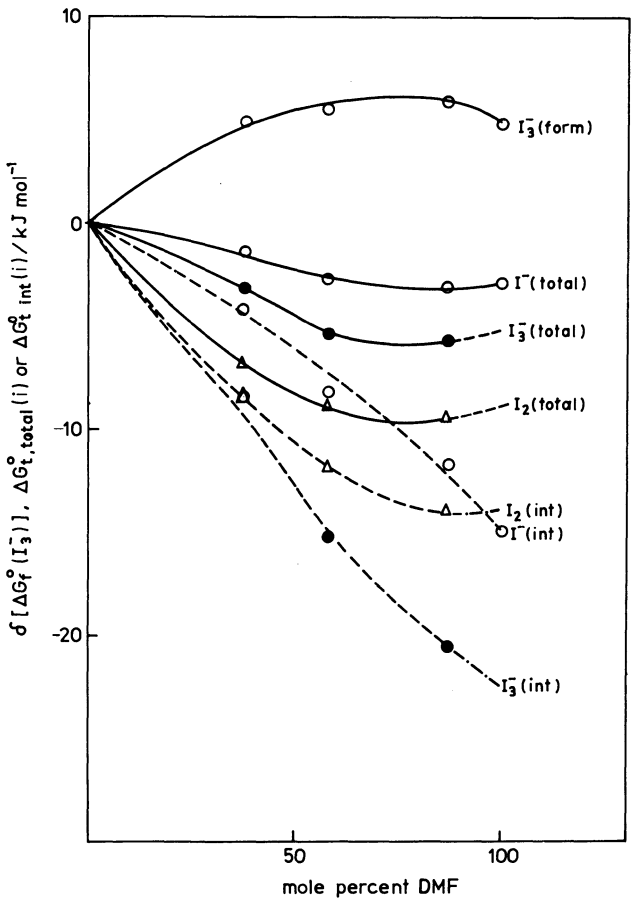

Fig. 1. Variations of $\delta[\Delta G_f^\circ(I_3^-)]$ and $\Delta G_t^\circ(i)$ [i=I^-, I_2, or I_3^-] total (solid lines) and int. (broken lines) with mole percent DMF in PC+DMF mixtures at 25 °C.

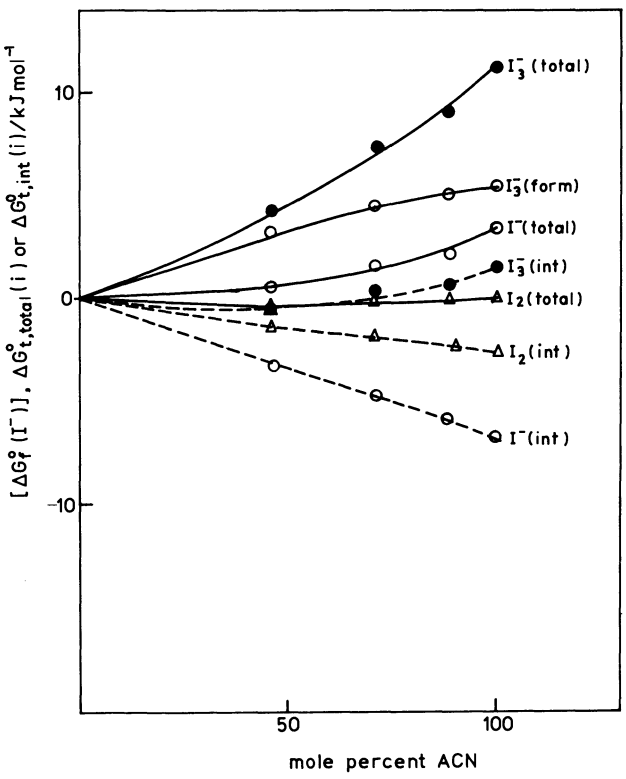

Fig. 2. Variations of $\delta[\Delta G_f^\circ(I_3^-)]$ and $\Delta G_t^\circ(i)$ [i=I^-, I_2, or I_3^-] total (solid lines) and int. (broken lines) with mole percent ACN in PC+ACN mixtures at 25 °C.

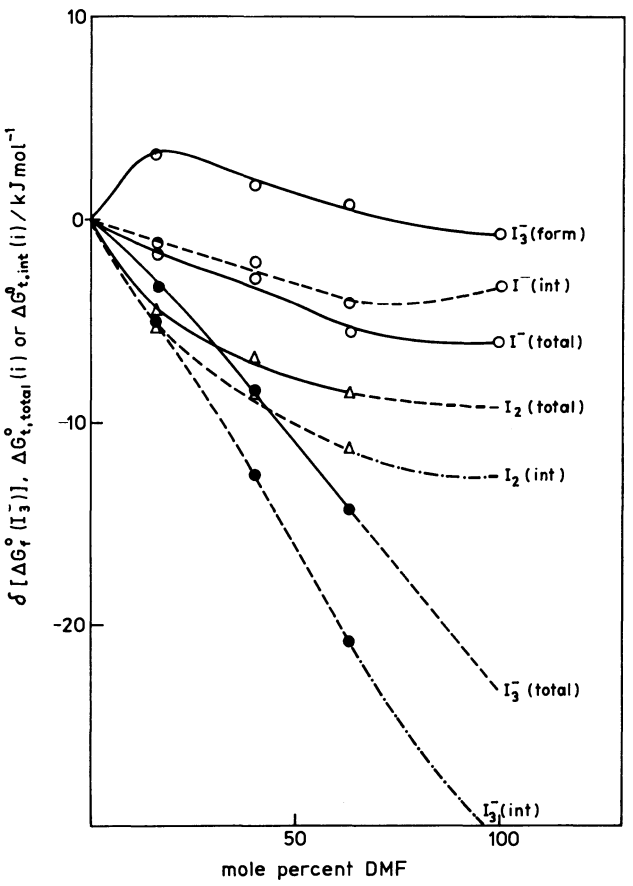

Fig. 3. Variations of $\delta[\Delta G_f^\circ(I_3^-)]$ and $\Delta G_t^\circ(i)$ [i=I^-, I_2, or I_3^-] total (solid lines) and int. (broken lines) with mole percent DMF in ACN+DMF mixtures at 25 °C.

the order of stabilization being $I_2>I_3^->I^-$ in PC+DMF mixtures (Fig. 1) and $I_3^->I_2>I^-$ in ACN+DMF mixtures (Fig. 3). On the other hand in PC+ACN mixtures (Fig. 2) as the ACN content increases, both I^- and I_3^- are increasingly destabilized in the order $I_3^->I^-$, and $\Delta G_t^\circ(I_2)$ passes nearly through the zero line. To rationalize the observed behavior a detailed analysis of the different forces and factors that are likely to be operative to different extents on these iodine species is in order. These are the electrostatic and nonelectrostatic contributions. The electrostatic part consists of a) Born-type electrostatic interaction,[17] corresponding transfer free energy term being designated by $\Delta G_{t,Born}^\circ$, b) ion-dipole interaction[18] [$\Delta G_{t,i\text{-}d}^\circ$], c) ion-quadrupole interaction[18] [$\Delta G_{t,i\text{-}q}^\circ$], and d) ion-induced dipole interaction[18] [$\Delta G_{t,i\text{-}id}^\circ$]. All of these electrostatic contributions would be highest for I^- with highest charge density, followed by I_3^- but absent for I_2. The nonelectrostatic contributions are a) the well-known cavity effect[19] due to the formation of solvent-cage or highly ordered skin-phase inside which solute molecules are caged, b) dispersion or 'soft-soft' interaction[20] dictated by the size and polarizability of both the solute and solvent molecules. In a common solvent, the solvation behavior of the solute species may be expected to be guided by the softness of the solute itself, which is in the order of $I_3^->I_2>I^-$, c) specific complexation effects of charge transfer (CT)[21] or charge transfer to solvent (CTTS)-type.[22] I_2 with a low lying LUMO is known to be a good acceptor of charge and hence often forms stable CT-complex with donor solvents like PC, DMF, and ACN, whereas I^- and I_3^- are expected to form CTTS complexes of the type $(X^-)_{solv}\rightarrow(X+e)_{solv}$ in the order $I^->I_3^-$. These complexation effects are known[21] to depend on the first two nonelectrostatic factors mentioned above, apart from the electrostatic factors for the ions I^- and I_3^-.

It is apparent from the nature of $\Delta G_t^\circ(i)$-composition profiles that none of the above-mentioned factors shows a sole predominance over the others towards the observed behavior. Evidently the evaluation of the individual ΔG_t° terms related to these factors by suitable methods wherever possible may be, at least partially, rewarding in the final analysis.

The widely used simple Born-equation.[17]

$$\Delta G_{t,Born}^\circ = \frac{1}{2} N_A (Z_i e)^2 r_i^{-1}(\varepsilon_S^{-1} - \varepsilon_R^{-1}) \qquad (12)$$

where N_A=Avogadro's number, Z_ie is the charge, r_i=radius of the ion i and ε_S and ε_R the dielectric constant of the solvent and the reference solvent respectively, though somewhat approximate, may be used to evaluate $\Delta G_{t,Born}^\circ$ values. These values in PC+DMF and PC+ACN mixtures are presented in Table 3. ACN and DMF being nearly isodielectric (ε_{ACN}=36.37 and ε_{DMF}=36.71)[16] $\Delta G_{t,Born}^\circ$ values for the transfer from ACN to ACN+DMF mixtures are practically zero. The ion-dipole contribution $\Delta G_{t,i\text{-}d}^\circ$ may be expressed[18] as

$$\Delta G_{t,i\text{-}d}^\circ = -N_A q[\mu_S/\sigma_S^2 - \mu_R/\sigma_R^2] \qquad (13)$$

where q=the charge on the ion, taken as that of electron as no appreciable shielding is presumably possible in the cases under consideration, σ=inter nuclear distance between ion and the solvent molecule, and μ=dipole moment of the solvent. The subscript 'S' stands for the solvent to which transfer is performed from the reference solvent 'R'. For mixed solvents however, $\Delta G_{t,i\text{-}d}^\circ$ values were obtained following Kim[18] by multiplying the quantity obtained above for pure solvent by X_{S_i} where,

$$X_{S_i} = X_S[\mu_S/\sigma_S^2)/(\mu_R/\sigma_R^2)] \qquad (14)$$

and X_s is the mole fraction of the cosolvent in the mixed solvent. The $\Delta G_{t,i\text{-}d}^\circ$ values thus obtained are also given in Table 3. It was not possible to estimate the magnitude of ion-quadrupole interactions due to the absence of quadrupole moment for these solvents though their significance could not be ruled out particularly for single ions. However, $\Delta G_{t,i\text{-}id}^\circ$ values were computed by using[18]

$$\Delta G^{\circ}_{t,i\text{-}id} = \frac{1}{2} Nq^2[(\alpha_S/\sigma_S^4) - (\alpha_R/\sigma_R^4)] \quad (15)$$

where α is the molecular polarizability of the respective solvents. And for the mixed solvents these values were obtained by multiplying the quantity obtained above for pure solvent[18] by X_{S_2} where,

$$X_{S_2} = X_S[(\alpha_S/\sigma_S^4)/(\alpha_R/\sigma_R^4)] \quad (16)$$

These $\Delta G^{\circ}_{t,i\text{-}id}$ values are also given in Table 3. Lastly, $\Delta G^{\circ}_{t,cav}$ values are computed following Triener's formulae[19] and are presented in the same table. The transfer free energies of the iodine species thus free from nearly all the electrostatic contributions barring ion-quadrupole interaction, and the solvent-cage effect as well, is likely to reveal the specific complexation effects along with 'soft-soft' interaction and is denoted by ΔG_t°(int) [vide Table 3]. Variations of ΔG_t°(int) with solvent compositions are depicted in Figs. 1—3 for the respective solvent systems.

From the variation of ΔG_t°(int) in Figs. 1 and 3 it is observed that all the three iodine species are increasingly stabilized with the addition of DMF to either PC or ACN, the order being $I_3^- > I_2 > I^-$ in both the cases. On the other hand, while I_3^- is slightly destabilized with addition of ACN to PC, the other two species are stabilized to some extent in the sequence $I^- > I_2$ (vide Fig. 2).

Now polarizability (α) of the pure solvents when computed from refractive index values[23] assuming monomeric solvent entities, are 4.41, 7.88, and 8.56×10^{-24} cm^3 for ACN, DMF and PC respectively. But the experimental α value of pure DMF is found to be abnormally high (11.02×10^{-24} cm^3).[24] Thus it was suggested[24] that DMF exists as dimers **A** in pure liquid, a part of which however may be converted to monomers in the mixed solvents. Similarly some dimeric species **B** are also found[25] to exist in ACN. No such evidence for dimerization is however found for PC. The dimeric entities obviously make DMF

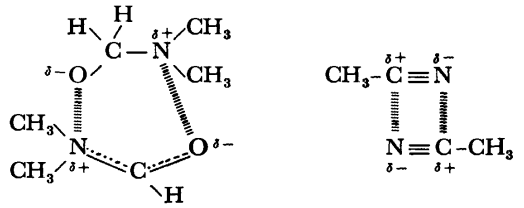

A

B

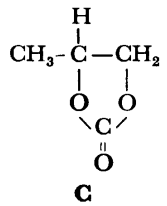

C

the softest among the three solvents. And α values for ACN may rise to some extent but not so as to exceed that of DMF. So on addition of DMF to either PC or ACN, all the iodine species will get stabilized in the order of their relative softness $I_3^- > I_2 > I^-$ as a result of dispersion interaction. The CT or CTTS complexation effect may also be present which will be in the order $I_2 > I^- \gg I_3^-$. The destabilization of I_3^- in PC+ACN mixtures (Fig. 2) is probably due to the difference in dispersion interaction resulting from the difference in effective polarizability between the two solvents concerned. But stabilization of I_2 and I^- though not to a greater extent, may be the result of CT or CTTS complexation or of ion-quadrupole interaction which we have failed to compute.

Notably, while discussions on ΔG_t°(int) are really meaningful in the cases where these values are rather large, as is the case of DMF admixtures, that for low ΔG_t°(int) values will be somewhat less meaningful because of the involved uncertainties in the computation of various ΔG_t° components, the combined effects of which may be as high as[18] ±5 kJ or more. Even then, in a complex situation, where various forces and interactions are at play, the dissection, though very tentative, helps elucidate at least a good qualitative picture of the interactions involved, as is observed in the present paper.

Thanks are due to CSIR, New Delhi for the award of a Research Associateship to J. D.

References

1) R. Jassinski, "High Energy Batteries," Plenum Press, New York (1967).

2) S. Bhattacharya, U. Mandal, J. Datta, K. Das, and K. K. Kundu, Proc. 3rd Int. Conf. on Electrochem. Sc. Tech., held at Madras, India during 10—14 Dec. 1984.

3) R. Memming, *Electrochim. Acta*, **25**, 77 (1980) and the relevant references therein.

4) K. Rajeswar, P. Singh, and J. Du Bow, *Electrochim. Acta*, **23**, 1117 (1978).

5) C. K. Mann "Electroanalytical Chemistry," A series of Advances, Vol. 3, ed by A. J. Bard, Marcell Dekker Inc., New York (1969).

6) L. M. Kuznetsova, V. P. Avdeev, and N. T. Nikurashina, *Russ. J. Phys. Chem.*, **59**, 721 (1985) Eng.

7) R. Alexander, E. C. I. Ko, Y. C. Mac, and A. J. Parker, *J. Am. Chem. Soc.*, **89**, 3703 (1967).

8) J. Datta, S. Bhattacharya, and K. K. Kundu, *Aust. J. Chem.*, **36**, 1779 (1983).

9) C. A. Mann and K. K. Barnes, "Electrochemical Reactions to Nonaqueous Systems," Marcel Dekker, New York (1970); J. N. Butler, *Adv. Electrochem. Eng.*, **7**, 77 (1970); J. N. Kolthoff and J. F. Coetzee, *J. Am. Chem. Soc.*, **79**, 870, 1852 (1957); R. C. Larson and R. T. Iwamoto, *J. Am. Chem. Soc.*, **82**, 3239, 3526 (1960); J. Datta, A. Bhattacharya, and K. K. Kundu, *J. Electroanalchem.*, under publication.

10) R. Alexander, A. J. Parker, J. A. Sharp, and W. E. Waghrone, *J. Am. Chem. Soc.*, **94**, 1148 (1972).

11) A. K. Das and K. K. Kundu, *J. Chem. Soc., Faraday Trans. 1.*, **70**, 1452 (1974); A. K. Das and K. K. Kundu, *J. Soln. Chem.*, **5**, 431 (1976); K. Bose, K. Das, and K. K. Kundu,

Electrochim. Acta, **26**, 479 (1981); A. Bhattacharya, A. K. Das, and K. K. Kundu, *Ind. J. Chem.*, **20A**, 347, 353 (1981).

12) O. Popovych, *Anal. Chem.*, **46**, 2009 (1974); *idem.*, *Crit. Rev. Anal. Chem.*, **1**, 73 (1970).

13) S. Bhattacharya and K. K. Kundu, *Ind. J. Chem.*, submitted.

14) G. Gritzner, *J. Electroanal. Chem.*, **144**, 259 (1983).

15) a) E. Geliadi, E. Kirowa-Eisner, and J. Pencier, "Interfacial Electrochemistry: An experimental Approach," Addison-Wesley Pub. Co. Inc., Massachusetts (1975); b) Jurgen Heinze, *Angew. Chem.*, **23**, 831 (1984) and relevant references therin.

16) A. K. Covington and T. Dickinson, "Physical chemistry of Organic Solvent Systems," Plenum Press, London (1973).

17) M. Born, *Z. Physik.*, **1**, 45 (1920).

18) J. I. Kim., A. Ceacal, H. J. Born, and E. A. Gomaa, *Zeit. fur Physik. Chem. Neue Folge, Bd.*, **110**, 5209 (1978); J. I. Kim, *J. Phys. Chem.*, **82**, 191 (1978).

19) C. Treiner, *Can. J. Chem.*, **55**, 682 (1977); A. Bhattacharya, J. Datta, K. Das, and K. K. Kundu, *Ind. J. Chem.*, **21A**, 9 (1982).

20) R. G. Pearson, *J. Am. Chem. Soc.*, **85**, 3533 (1963).

21) K. M. C. Davis "Molecular Association," ed by R. Forster, Academic Press, London (1975), Vol. 1.

22) M. C. R. Symons and M. J. Blandamer, "Hydrogen Bonded Solvent Systems," ed by A. K. Covington and P. Jones, Taylor and Francis, London (1968).

23) "Handbook of Chemistry and Physics," ed by R. C. Weast, The Chem. Rubber Co. U. S. A. (1971).

24) P. Rohdewald and M. Moldner, *J. Phys. Chem.*, **77**, 373 (1973).

25) E. L. Zukova, *Opt, Spectro.*, **4**, 750 (1958); A. M. Saum, *J. Polym. Sci.*, **42**, 57 (1960).

26) G. Senanayake, Ph. D. Thesis, Murdoch University, Australia, 1986, p. 246.

 © 1988 The Chemical Society of Japan Bull. Chem. Soc. Jpn., 61, 1743—1747 (1988)

Second Virial Coefficients of Axially Symmetric Molecules

Ali BOUSHEHRI* and A. Mohammad ATTARAN
Department of Chemistry, Shiraz University, Shiraz, Iran
(Received March 24, 1987)

The paper presents a contribution to the second virial coefficient due to the asphericity of the molecular charge distribution. This contribution is conveniently divided into terms representing the classical electrostatic interaction between the two charge distributions, the anisotropy of dispersion forces, and the shape of the molecular core. These are considered quantitatively. Results from recalculating the nonspherical contributions to the second virial coefficients with a good spherical core are obtained from statistical mechanics and applied to the CO_2 gas. Explilcit formulas are given for the simple cases of axially symmetric molecules.

The potential energy between two polyatomic molecules is usually assumed to consist of a spherically symmetric component plus a contribution due to the aspherically of the molecular charge distribution. A method of integration for B(T) developed by Pople[1] viewed the orientation-dependent parts of the potential as perturbations on the central-force part. Later the applications to various polar gases were worked out in some detail by Buckingham and Pople.[2] Using Orcutt's method, reasonable values of molecular quadrupole moments could be obtained even by neglecting the effect of the shape component (i.e., the anisotropy of the repulsive part of the potential) on the second virial coefficient.[3]

Spurling and Mason obtained the parameters of the spherical component of the potential from the viscosity data, then, used in conjunction with second virial coefficient data, determined the quadrupole moments and "shape" parameters of the molecules.[4] It was found that one could get rid of the effect of the quadrupole moment on viscosity by simply assigning sligthly different values of ε_0 and σ_0 and using Najafi's correlation curve for the viscosity.[5,6]

The greatest virtue of the virial equation of state lies in the direct relation of the virial coefficients to the intermolecular forces. We provide a quantitative discussion of some of these forces and obtain corresponding expressions for the second virial coefficients. Here, results of recalculating the nonspherial contributions to the second virial coefficients with a spherical core, similar to that used by Boushehri, et al.,[7] are obtained from statistical mechanics and applied to a polyatomic gas.

Calculation

An indirect procedure is usually used to determine intermolecular forces from virial coefficients due to the failure of the direct approach. Many kinetic theory transport properties (viscosity, heat conductivity, ordinary diffusion) depend primarily on the fact that a force exists between molecules, and only secondarily on the nature of the force. But whether the force is one of attraction or repulsion can be an essential point for the virial coefficients, whose very sign depends on the nature of force.

It should be mentioned that while much progress in describing the thermodynamic properties of assemblies of molecules with spherical symmetry has been made, there are many molecules whose force fields depend on relative orientation. The potential model for the calculation of the second virial coefficients may be written as.[7]

$$V(r) = V_0(\text{spherical}) + V(\mu\mu) + V(\mu\theta) + V(\theta\theta) + V(\mu, \text{ind}\mu) + V(\mu\theta, \text{ind}\mu) + V(\theta, \text{ind}\mu) + V(C_6\,\text{anis}) + V(\text{shape}) \quad (1)$$

where

$$V(\mu\mu) = -\frac{\mu^2}{r^3}(2C_1C_2 - S_1S_2C), \quad (2\text{-a})$$

$$V(\mu\theta) = \frac{3\mu\theta}{2r^4}(C_2 - C_1)(3C_1C_2 - 2S_1S_2C + 1), \quad (2\text{-b})$$

$$V(\theta\theta) = \frac{3\theta^2}{4r^5}[1 - 5C_1^2 - 5C_2^2 - 15C_1^2C_2^2 + 2(4C_1C_2 - S_1S_2C)^2], \quad (2\text{-c})$$

$$V(\mu, \text{ind}\mu) = -\frac{\mu^2\bar{\alpha}}{2r^6}(3C_1^2 + 3C_2^2 - 2) - \frac{\mu^2\bar{\alpha}^2}{r^9}(8C_1C_2 - S_1S_2C), \quad (2\text{-d})$$

$$V(\mu\theta, \text{ind}\mu) = -\frac{12\mu\theta\bar{\alpha}}{r^7}(C_1^3 + C_2^3), \quad (2\text{-e})$$

$$V(\theta, \text{ind}\mu) = -\frac{9\theta^2\bar{\alpha}}{8r^8}(4C_1^4 + 4C_2^4 + S_1^4 + S_2^4 - \frac{8}{3}), \quad (2\text{-f})$$

$$V(C_6\,\text{anis}) = \frac{KC_6}{r^6}[1 - \frac{3}{2}(1 - K)(C_1^2 + C_2^2) - \frac{3}{2}K(2C_1C_2 - S_1S_2C)^2]. \quad (2\text{-g})$$

The simplest force field reproducing the orientation effect of the shape of an axially symmetric nonspherical molecule is

$$V(\text{shape}) = \frac{A}{r^n}(3C_1^2 + 3C_2^2 - 2), \quad (2\text{-h})$$

where A is a constant and n is an integer (usually 12). There is no particular theoretical basis for the form of V(shape). The average polarizability $\bar{\alpha}$ is given by $\bar{\alpha}=(\alpha^{11}+2\alpha^{\perp})/3$ and the anisotropy K is defined by $K=(\alpha^{11}-2\alpha^{\perp})/3\bar{\alpha}$, where α^{11} is the polarizability along the axis of symmetry and $\alpha^{\perp}$ that perpendicular to it. The quadrupole moment θ is defined by

$$\theta=\sum_i e_i(Z_i^2-X_i^2)$$

where e_i is the ith element of charge and Z_i and X_i are its coordinates in a system where Z axis is the symmetry axis and the origin is the center of mass. The angle-dependent abbreviations used in Eq. 2 are

$$C_1=\cos\theta_1,\ C_2=\cos\theta_2,\ S_1=\sin\theta_1,\ S_2=\sin\theta_2,$$
$$\text{and } C=\cos\phi.$$

Here θ_1, θ_2, and ϕ are the usual angles describing the mutual orientation of two linear molecules.

The nonspherical contribution to the second virial coefficient, ΔB^*, is obtained using a good spherical core (HFD-I) given in Table 1 of Ref. 8. In conjunction with this model and in terms of the dimensionless quantities $T^*=T/(\varepsilon_o/k)$, $B^*=B/(2\pi N_A\sigma_o^3/3)$, $\mu^*=\mu/(\varepsilon_o\sigma_o^3)^{1/2}$, $\theta^*=\theta/(\varepsilon_o\sigma_o^5)^{1/2}$, $\alpha^*=\bar{\alpha}/\sigma_o^3$, and $C_6^*=C_6/\varepsilon_o\sigma_o^6$

$$\begin{aligned}\Delta B^* = {} & B^*(\mu\mu)+B^*(\mu\theta)+B^*(\theta\theta)+B^*(\mu,\text{ ind}\mu)\\ & +B^*(\mu\theta,\text{ ind}\mu)+B^*(\theta,\text{ ind}\mu)+B^*(C_6\text{ anis})\\ & +B^*(\mu X\theta)+B^*(\mu,\text{ ind}\mu\, X\theta,\text{ ind}\mu)\\ & +B^*(\mu\mu X\mu,\text{ ind}\mu)+B^*(\mu\mu X\theta,\text{ ind}\mu)\\ & +B^*(\theta\theta X\ C_6\text{ anis})+B^*(\mu,\text{ ind}\mu\ X\ C_6\text{ anis})\\ & +B^*(\theta,\text{ ind}\mu\ X\ C_6)\text{ anis}).\end{aligned}\tag{3}$$

Where

$$B^*(\mu\mu)=-\frac{2}{3}\left(\frac{\mu^{*2}}{T^*}\right)^2\left[J_6+\frac{1}{25}\left(\frac{\mu^{*2}}{T^*}\right)^2J_{12}+\cdots\right]\tag{4-a}$$

$$B^*(\mu\theta)=-\frac{6}{5}\left(\frac{\mu^*\theta^*}{T^*}\right)^2\left[J_8+0.22794\left(\frac{\mu^*\theta^*}{T^*}\right)^2J_{16}+\cdots\right]\tag{4-b}$$

$$B^*(\theta\theta)=-\frac{6}{5}\left(\frac{\theta^{*2}}{T^*}\right)^2\left[J_{10}-\frac{6}{49}\left(\frac{\theta^{*2}}{T^*}\right)J_{15}+\cdots\right]\tag{4-c}$$

$$B^*(\mu,\text{ ind}\mu)=-\frac{2}{15}\left(\frac{\mu^{*2}\alpha^*}{T^*}\right)^2\left[J_{12}+11\alpha^{*2}J_{18}+\cdots\right]\tag{4-d}$$

$$B^*(\mu\theta,\text{ ind}\mu)=-\frac{864}{77}\left(\frac{\mu^*\theta^*\alpha^*}{T^*}\right)^2J_{14}+\cdots\tag{4-e}$$

$$B^*(\theta,\text{ ind}\mu)=-\frac{162}{455}\left(\frac{\theta^{*2}\alpha^*}{T^*}\right)^2J_{16}+\cdots\tag{4-f}$$

$$B^*(C_6\text{ anis})=-\frac{2}{15}\left(\frac{K\,C_6^*}{T^*}\right)^2\left(1+\frac{19}{10}K^2\right)J_{12}+\cdots\tag{4-g}$$

$$B^*(\mu X\theta)=\frac{3}{5}\left(\frac{\mu^*\theta^*}{T^*}\right)^2\left[\left(\frac{\mu^{*2}}{T^*}\right)J_{11}+\frac{24}{35}\left(\frac{\theta^{*2}}{T^*}\right)J_{13}+\cdots\right]\tag{4-h}$$

$$B^*(\mu,\text{ ind}\mu X\theta,\text{ ind}\mu)=-\frac{144}{385}\left(\frac{\mu^*\theta^*\alpha^*}{T^{*2}}\right)^2J_{14}+\cdots\tag{4-i}$$

$$B^*(\mu\mu X\mu,\text{ ind}\mu)=-\frac{4}{3}\left(\frac{\mu^{*2}}{T^*}\right)^2\alpha^*J_{12}\left(\alpha^*+\frac{1}{15}\left(\frac{\mu^{*2}}{T^*}\right)\right)+\cdots\tag{4-j}$$

$$B^*(\mu\mu X\theta,\text{ ind}\mu)=-\frac{48}{385}\left(\frac{\mu^{*2}}{T^*}\right)^2\left(\frac{\theta^{*2}}{T^*}\right)\alpha^*J_{14}+\cdots\tag{4-k}$$

$$B^*(\theta\theta X\ C_6\text{ anis})=\frac{27}{25}\left(\frac{\theta^{*2}}{T^*}\right)\left(\frac{C_6^*}{T^*}\right)K^2J_{11}+\cdots\tag{4-l}$$

Table 1. Various Contributions to the Second Virial Coefficient of CO_2 as Calculated by Eq. 3

T^*	$B^*(\theta\theta)$	$B^*(\theta,\text{ ind}\mu)$	$B^*(\theta\theta X C_6\text{anis})$	$B^*(C_6\text{anis})$
0.8969	−0.835640	−0.000653	0.132884	−0.041282
1.1135	−0.490684	−0.000487	0.076886	−0.024025
1.8345	−0.160320	−0.000288	0.024759	−0.007882
2.7313	−0.072695	−0.000217	0.011244	−0.003649
3.5874	−0.043746	−0.000188	0.006810	−0.002245
4.4843	−0.029393	−0.000171	0.004612	−0.001541
T^*	$B^*(\theta,\text{ ind}\mu X C_6\text{anis})$	B_o^*(spherical)	$B_{\text{theo.}}^*$	$B_{\text{expt.}}^{*\,a)}$
0.8969	−0.005654	−2.5329	−3.283245	−3.6755
1.1135	−0.003338	−1.6923	−2.133948	−2.2420
1.8345	−0.001143	−0.5483	−0.693174	−0.6338
2.7313	−0.000552	−0.0664	−0.132269	−0.0578
3.5874	−0.000351	0.1431	0.103380	0.1570
4.4843	−0.000248	0.2668	0.240059	0.2680

$\sigma_o=3.769$ Å, $\varepsilon_o/k=245.3$ K (Ref. 10)
$\bar{\alpha}=2.63$ Å^3 $K=0.2664$ (Ref. 11)
$\theta=4.3\times10^{-26}$ esu (Ref. 12)
$C_6=158.7$ hatree (Bohr)^6 (Ref. 14)
$B_{\text{theo.}}=B_o^*$(spherical)$+\Delta B^*$
a) $B_{\text{expt.}}^*$(smoothed values) (Ref. 13)

Table 2. Functions $J_n(T^*)$ for the Calculation of Nonspherical Contributions to Second Virial Coefficients Obtained by HFD-I Potential

T^*	J_6	J_7	J_8	J_9	J_{10}	J_{11}	J_{12}	J_{13}	J_{14}
0.5	1.7885	1.9875	2.1238	2.2146	2.2721	2.3052	2.3203	2.3222	2.3145
0.6	1.4178	1.5595	1.6577	1.7246	1.7688	1.7966	1.8125	1.8197	1.8208
0.7	1.2115	1.3223	1.4004	1.4550	1.4929	1.5188	1.5361	1.5473	1.5542
0.8	1.0828	1.1750	1.2412	1.2889	1.3237	1.3492	1.3682	1.3827	1.3942
0.9	0.9961	1.0762	1.1349	1.1786	1.2119	1.2378	1.2587	1.2762	1.2916
1.0	0.9344	1.0063	1.0601	1.1014	1.1341	1.1609	1.1837	1.2041	1.2230
1.2	0.8538	0.9156	0.9640	1.0032	1.0364	1.0658	1.0927	1.1185	1.1439
1.4	0.8046	0.8611	0.9071	0.9462	0.9811	1.0135	1.0447	1.0758	1.1074
1.6	0.7724	0.8259	0.8712	0.9113	0.9485	0.9842	1.0198	1.0560	1.0936
1.8	0.7503	0.8024	0.8478	0.8895	0.9292	0.9685	1.0084	1.0498	1.0933
2.0	0.7346	0.7861	0.8324	0.8759	0.9184	0.9613	1.0056	1.0522	1.1017
2.5	0.7118	0.7640	0.8136	0.8626	0.9126	0.9649	1.0203	1.0800	1.1446
3.0	0.7015	0.7561	0.8099	0.8650	0.9228	0.9845	1.0513	1.1242	1.2043
3.5	0.6974	0.7551	0.8137	0.8751	0.9408	1.0121	1.0903	1.1767	1.2727
4.0	0.6969	0.7580	0.8215	0.8893	0.9629	1.0438	1.1336	1.2337	1.3460
4.5	0.6985	0.7632	0.8317	0.9059	0.9874	1.0780	1.1794	1.2935	1.4225
5.0	0.7013	0.7698	0.8433	0.9238	1.0133	1.1135	1.2266	1.3549	1.5010
6.0	0.7093	0.7853	0.8687	0.9618	1.0670	1.1866	1.3235	1.4808	1.6622
7.0	0.7188	0.8022	0.8953	1.0009	1.1217	1.2607	1.4217	1.6088	1.8269
8.0	0.7290	0.8196	0.9223	1.0401	1.1763	1.3349	1.5203	1.7379	1.9942
9.0	0.7394	0.8370	0.9491	1.0789	1.2306	1.4086	1.6187	1.8676	2.1633
10.0	0.7497	0.8543	0.9755	1.1172	1.2841	1.4818	1.7169	1.9977	2.3340

T^*	J_{15}	J_{16}	J_{17}	J_{18}	J_{19}	J_{20}	J_{21}	J_{22}	J_{23}
0.5	2.3001	2.2808	2.2584	2.2340	2.2086	2.1829	2.1574	2.1325	2.1086
0.6	1.8176	1.8114	1.8035	1.7946	1.7853	1.7762	1.7676	1.7598	1.7530
0.7	1.5582	1.5605	1.5618	1.5627	1.5638	1.5653	1.5677	1.5711	1.5758
0.8	1.4037	1.4123	1.4205	1.4288	1.4376	1.4473	1.4581	1.4702	1.4839
0.9	1.3058	1.3195	1.3334	1.3478	1.3631	1.3797	1.3977	1.4174	1.4390
1.0	1.2414	1.2597	1.2787	1.2985	1.3197	1.3425	1.3671	1.3938	1.4227
1.2	1.1697	1.1965	1.2245	1.2544	1.2863	1.3207	1.3577	1.3978	1.4412
1.4	1.1402	1.1747	1.2114	1.2507	1.2930	1.3387	1.3881	1.4417	1.4998
1.6	1.1332	1.1754	1.2206	1.2693	1.3220	1.3792	1.4413	1.5089	1.5825
1.8	1.1397	1.1895	1.2433	1.3016	1.3650	1.4340	1.5094	1.5917	1.6818
2.0	1.1549	1.2125	1.2749	1.3430	1.4173	1.4988	1.5880	1.6860	1.7937
2.5	1.2152	1.2925	1.3775	1.4713	1.5749	1.6896	1.8168	1.9580	2.1150
3.0	1.2928	1.3909	1.4999	1.6214	1.7570	1.9087	2.0786	2.2692	2.4834
3.5	1.3798	1.4996	1.6341	1.7853	1.9557	2.1481	2.3656	2.6120	2.8916
4.0	1.4724	1.6150	1.7764	1.9594	2.1674	2.4042	2.6744	2.9831	3.3366
4.5	1.5688	1.7352	1.9249	2.1418	2.3902	2.6752	3.0030	3.3806	3.8165
5.0	1.6679	1.8590	2.0786	2.3313	2.6228	2.9598	3.3502	3.8035	4.3307
6.0	1.8721	2.1155	2.3988	2.7290	3.1150	3.5672	4.0982	4.7230	5.4599
7.0	2.0822	2.3816	2.7339	3.1494	3.6406	4.2229	4.9148	5.7389	6.7229
8.0	2.2970	2.6559	3.0823	3.5905	4.1977	4.9251	5.7986	6.8504	8.1201
9.0	2.5159	2.9375	3.4432	4.0515	4.7851	5.6725	6.7486	8.0572	9.6526
10.0	2.7384	3.2261	3.8159	4.5315	5.4021	6.4645	7.7644	9.3595	11.3221

T^*	J_{24}	J_{25}	J_{26}	J_{27}	J_{28}	J_{29}	J_{30}
0.5	2.0859	2.0647	2.0449	2.0268	2.0105	1.9959	1.9831
0.6	1.7475	1.7434	1.7407	1.7396	1.7402	1.7426	1.7467
0.7	1.5819	1.5895	1.5988	1.6098	1.6228	1.6377	1.6546
0.8	1.4992	1.5164	1.5356	1.5569	1.5805	1.6064	1.6348
0.9	1.4626	1.4885	1.5168	1.5476	1.5812	1.6177	1.6574
1.0	1.4542	1.4884	1.5255	1.5658	1.6094	1.6567	1.7078
1.2	1.4882	1.5391	1.5942	1.6539	1.7187	1.7888	1.8647

Table 2. (Countinued)

T^*	J_{24}	J_{25}	J_{26}	J_{27}	J_{28}	J_{29}	J_{30}
1.4	1.5628	1.6313	1.7058	1.7867	1.8746	1.9703	2.0745
1.6	1.6627	1.7502	1.8457	1.9500	2.0640	2.1886	2.3249
1.8	1.7805	1.8886	2.0072	2.1374	2.2804	2.4376	2.6107
2.0	1.9122	2.0427	2.1866	2.3454	2.5207	2.7146	2.9291
2.5	2.2898	2.4846	2.7019	2.9448	3.2165	3.5208	3.8621
3.0	2.7244	2.9960	3.3026	3.6490	4.0411	4.4856	4.9902
3.5	3.2094	3.5711	3.9836	4.4546	4.9934	5.6108	6.3192
4.0	3.7419	4.2077	4.7437	5.3617	6.0755	6.9014	7.8586
4.5	4.3207	4.9049	5.5831	6.3719	7.2910	8.3640	9.6190
5.0	4.9452	5.6628	6.5026	7.4873	8.6442	10.0059	11.6120
6.0	6.3309	7.3627	8.5876	10.0449	11.7823	13.8581	16.3434
7.0	7.9004	9.3128	11.0110	13.0575	15.5291	18.5211	22.1508
8.0	9.6565	11.5203	13.7867	16.5495	19.9253	24.0599	29.1355
9.0	11.6028	13.9928	16.9294	20.5464	25.0127	30.5413	37.4012
10.0	13.7434	16.7387	20.4538	25.0738	30.8337	38.0330	47.0540

Table 3. The $B_o^*(T^*)$ for the Calculation of Spherical Contributions to Second Virial Coefficients

T^*	$B_o^*(T^*)$	T^*	$B_o^*(T^*)$	T^*	$B_o^*(T^*)$
0.30	−24.8221	1.50	−0.9123	3.40	0.1078
0.35	−16.5478	1.55	−0.8457	3.50	0.1272
0.40	−12.0793	1.60	−0.7841	3.60	0.1454
0.45	−9.3485	1.65	−0.7270	3.70	0.1624
0.50	−7.5309	1.70	−0.6738	3.80	0.1783
0.55	−6.2440	1.75	−0.6244	3.90	0.1933
0.60	−5.2895	1.80	−0.5781	4.00	0.2075
0.65	−4.5557	1.85	−0.5349	4.10	0.2208
0.70	−3.9752	1.90	−0.4943	4.20	0.2333
0.75	−3.5053	1.95	−0.4562	4.30	0.2452
0.80	−3.1174	2.00	−0.4203	4.40	0.2564
0.85	−2.7922	2.10	−0.3546	4.50	0.2670
0.90	−2.5158	2.20	−0.2958	4.60	0.2771
0.95	−2.2781	2.30	−0.2430	4.70	0.2867
1.00	−2.0716	2.40	−0.1954	4.80	0.2958
1.05	−1.8906	2.50	−0.1521	4.90	0.3044
1.10	−1.7307	2.60	−0.1127	5.00	0.3126
1.15	−1.5885	2.70	−0.0767	6.00	0.3768
1.20	−1.4613	2.80	−0.0437	7.00	0.4188
1.25	−1.3468	2.90	−0.0133	8.00	0.4476
1.30	−1.2432	3.00	0.0147	9.00	0.4679
1.35	−1.1491	3.10	0.0406	10.00	0.4826
1.40	−1.0632	3.20	0.0646	20.00	0.5189
1.45	−0.9846	3.30	0.0870	30.00	0.5084

$$B^*(\mu, \text{ ind}\mu X\ C_6 \text{ anis}) = -\frac{4}{15}\left(\frac{\mu^{*2}}{T^*}\right)\left(\frac{C_6^*}{T^*}\right)\alpha^* K J_{12} + \cdots \quad \text{(4-m)}$$

$$B^*(\theta, \text{ ind}\mu X\ C_6 \text{ anis}) = -\frac{144}{385}\left(\frac{\theta^{*2}}{T^*}\right)\left(\frac{C_6^*}{T^*}\right)\alpha^* K J_{14} + \cdots \quad \text{(4-n)}$$

Here

$$J_n(T^*) \equiv \frac{n-3}{2}\int_0^\infty \frac{dr^*}{(r^*)^{n-2}} \exp\left(-V_o^*/T^*\right)$$

where $V_o^* \equiv V_o/\varepsilon_o$ and $r^* \equiv r/\sigma_o$

The $J_n(T^*)$'s are functions tabulated in Table 2 and B_o^* (spherical) are given in Table 3. Boushehri et al. have tabulated $J_n(T^*)$ using (HFD-C) given by Aziz and Chen[8] for n=6 through 30 and for T^* from 0.5 to 10.0.[7] In Ref. 9 results for molecules with octupole moments have also been discussed.

Results and Discussion

Various contributions to B(T) for CO_2 calculated according to Eq. 3 are given in Table 1. The scaling parameters for CO_2 are taken from Ref. 10. Comparison of present work and experimental value of CO_2 are also shown in Table 1.

It should be mentioned that in Ref. 7 the J_n integrals for the nonspherical contributions were calculated for

the HFD-C potential while in the present paper they are calculated for the HFD-I potential.

In Ref. 7, a set of J_n tables is justified by the argument that the values will be insensitive to the details of the potential. Comparison of the new J_n tables with the earlier J_n tables confirms this observation.

References

1) J. A. Pople, *Proc. R. Soc. London, Ser. A*, **221**, 508 (1954).
2) A. D. Buckingham and J. A. Pople, *Trans. Faraday Soc.*, **51**, 1173 (1955).
3) R. H. Orcutt, *J. Chem. Phys.*, **39**, 605 (1963).
4) T. H. Spurling and E. A. Mason, *J. Chem. Phys.*, **46**, 322 (1967).
5) B. Najafi, E. A. Mason, and J. Kestin, *Physica*, **119A**, 387 (1983).
6) A. Boushehri, *J. Phys. Chem. Ref. Data.*, (Submitted).
7) A. Boushehri, E. A. Mason, and J. Kestin, Intern. *J. Thermophys.*, **7**, 1115 (1986).
8) R. A. Aziz and H. H. Chen, *J. Chem. Phys.*, **67**, 5719 (1977).
9) S. Kielich, *Physica.*, **28**, 511 (1962).
10) J. Kestin and S. T. Ro, *Ber. Bunsenges. Phys. Chem.*, **86**, 948 (1982).
11) N. J. Bridge and A. D. Buckingham, *Proc. R. Soc. London, Ser. A*, **295**, 334 (1966).
12) A. D. Buckingham, R. L. Disch, and D. A. Dummur, *J. Am. Chem. Soc.*, **90**, 3104 (1968).
13) J. H. Dymond and E. B. Smith, "The Virial Coefficients of Pure Gases and Mixtures," Oxford University Press, London (1980).
14) B. L. Jhanwar and W. J. Meath, *Chem. Phys.*, **67**, 185 (1982).

 © 1988 The Chemical Society of Japan Bull. Chem. Soc. Jpn., 61, 1749—1753 (1988)

Theoretical Study of Some Non-Benzenoid Hydrocarbons: Benzo-[3′,4′]cyclobuta[1′,2′:6,7]cycloocta[1,2,3,4-*def*]-biphenylene and Related Compounds

Sukanta K. PAL, Archana DAS GUPTA, and Nanda K. DAS GUPTA*
Department of Chemistry, Visva-Bharati University,
Santiniketan, West Bengal, 731235, India
(Received April 30, 1987)

Benzo[3′,4′]cyclobuta[1′,2′:6,7]cycloocta[1,2,3,4-*def*]biphenylene (**1**), benzo[6,7]cycloocta[1,2,3,4-*def*]biphenylene (**2**), dibenzo[*a*,*c*]benzo[3,4]cyclobuta[1,2-*f*]cyclooctene (**3**), and biphenyleno[8′,1′:4,5,6,7]cycloocta[1,2-*l*]-phenanthrene (**4**) have been studied by semiempirical SCFMO method of Pariser and Parr and Pople. Core resonance intergral values of Lo and Whitehead, Dewar et al. and Yamaguchi et al. have been used. It has been observed that $\pi^*\leftarrow\pi$ spectra predicted by the methods of Lo and Whitehead and Chung and Dewar suitable for the prediction of ground state properties are in good agreement with experimental results and comparable to those predicted by the method of Yamaguchi et al. developed for the prediction of spectral transitions. For comparison values obtained by configuration interaction method has also been included. Resonance stabilization of the molecules has been studied along with other properties such as bond length, ionization potential, electron affinity, and half-wave reduction potential.

The properties of polycyclic hydrocarbons formed by the fusion of $(4n+2)$ π-electron rings have been studied extensively with special reference to six π-electron systems. However, little is known about the properties of hydrocarbons composed of fused $4n$, or of $4n$ and $(4n+2)$, π-electron rings. Few polycyclic compounds have been known with fused $4n$ π-electron rings.[1,2] These molecules are interesting because their properties suggest that it is the nature of the individual $4n$ rings and not the overall number of π-electrons which determine the behavior of such systems. In this paper we report the results of our calculations on benzo[3′,4′]cyclobuta[1′,2′:6,7]cycloocta-[1,2,3,4-*def*]biphenylene (molecules **1**), benzo[6,7]cycloocta[1,2,3,4-*def*]biphenylene (molecules **2**), dibenzo[*a*,*c*]-benzo[3,4]cyclobuta[1,2-*f*]cyclooctene (molecules **3**), and biphenyleno[8,′1′:4,5,6,7]cycloocta[1,2-*l*]phenanthrene (molecules **4**) using the method of Pariser and Parr[3] and Pople.[4] The molecules studied here belong to those class of compounds mentioned above and moreover all of them contain bicyclo[6.2.0]decapentaene (**5**) ring in the moiety. Molecule **5**[5] is isomeric to azulene and naphthalene and obeys Huckel's $(4n+2)$ rule. On these grounds it might be aromatic. But actually it is not. Hence it would be worthwhile to theoretically predict the stability, $\pi^*\leftarrow\pi$ spectra, ionization potential, electron affinity, and half-wave reduction potential of the hydrocarbons **1**—**4**.

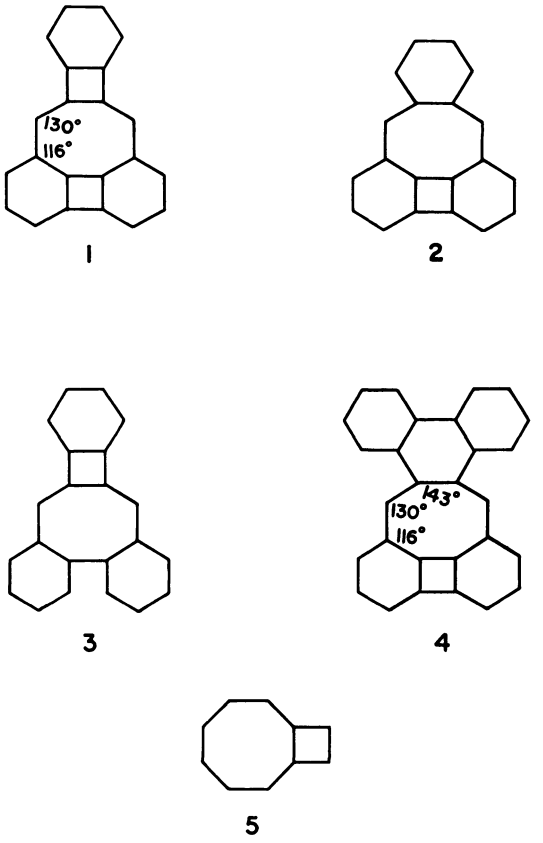

Fig. 1. Molecules studies.
1: Benzo[3′,4′]cyclobuta[1′,2′:6,7]cycloocta[1,2,3,4-*def*]biphenylene (**1**).
2: Benzo[6,7]cycloocta[1,2,3,4-*def*]biphenylene (**2**).
3: Dibenzo[*a*,*c*]benzo[3,4]cyclobuta[1,2-f]cyclooctene (**3**).
4: Biphenyleno[8′,1′:4,5,6,7]cycloocta[1,2-*l*]phenanthrene (**4**).
5: Bicyclo[6.2.0]decapentaene (**5**).

Methods and Parameter

The method has been described elsewhere.[6] Only the salient features are described herein. The resonance integrals, β_{ij} were calculated by the following methods: (I) In the first method, designated as SCF(a), β_{ij} was estimated using the method of Lo and Whitehead;[7] (II) in the second one, designated as SCF(b), β_{ij} was given a value of -1.7901 eV proposed by Chung and Dewar[8] and modified by Birss and Das Gupta.[9] In the SCF(a) and SCF(b) methods the integrals, β_{ij} were not varied at each iteration; (III) the

third method, designated as SCF(c) method was due to Dewar and Harget[10] and (IV) fourth one was due to Yamaguchi et al.[11] In these two methods the integrals, β_{ij}, the bond lengths (r_{ij}) and the two center two electron repulsion integrals (Υ_{ij}) for bonded atoms were adjusted according to the following relations:

In the SCF(c) method[10] the relations used were

$$r_{ij}(\text{Å}) = 1.512 - 0.174\, p_{ij} \quad (1)$$

$$\beta_{ij} = -6.927\, S_{ij} \quad (2)$$

where p_{ij} is the π-bond order and S_{ij} is the overlap integral between $2p_\pi$ Slater-type of orbitals.

In the SCF(d) method[11] the relations used were

$$r_{ij}(\text{Å}) = 1.520 - 0.186\, p_{ij} \quad (3)$$

$$\beta_{ij} = \beta_o \exp[a(r_o - r_{ij})] \quad (4)$$

where r_o=1.397 Å, a=−1.7 Å^{-1} and β_o is the resonance integral of benzene. The value of β_o decreased as the number of ring[12] increased.

For the calculation of bond lengths in the SCF(a) and SCF(b) methods the bond order–bond length relations (Eq. 5), due to Dewar and Gleicher[13] was used.

$$r_{ij}(\text{Å}) = 1.504 - 0.166\, p_{ij} \quad (5)$$

One-center two-electron repulsion integrals Υ_{ii} were calculated using the relation (Eq. 6) of Pariser[14]

$$\Upsilon_{ii} = I_i - A_i \quad (6)$$

where I and A represent the valence state ionization potential and electron affinity of carbon atoms respectively. The values have been taken from the work of Hinze and Jaffe.[15] The values of Υ_{ii} and I for carbon atoms are 11.136 and 11.16 eV respectively.

Except for SCF(d) method the two-center two-electron repulsion integrals, Υ_{ij} were evaluated using the method of Ohno[16] and for SCF(d) method the formula of Mataga and Nishimoto[17] was used. In the SCF(c) and SCF(d) methods the values Υ_{ij} were also not varied for nonbonded centers, but were kept at the values calculated from the initial geometry of the molecules which were assumed to be planar with ideal geometry and bond lengths equal to 1.40 Å.

Spectral transitions have been predicted by both SCF and configuration interaction (CI) methods. The final vectors, resonance integrals and two-center two-electron repulsion integrals obtained at the end of SCF(d) method were transferred in the CI procedure. The value of β_o used in the SCF(d) method was −2.15 eV.[18] In the CI procedure the configurations arising from one-electron excitation has been considered. Except molecule **2** ten highest occupied and ten lowest unoccupied orbitals and for molecule **2** all the occupied and unoccupied orbitals have been considered.

Results and Discussion

Charge Density and Bond Length. All the hydrocarbons **1**—**4** are alternant hydrocarbons. Hence calculated charge densities on each carbon atom is unity. Except molecule **3** all have biphenylene nucleus. The calculated bond lengths of the benzene rings of the biphenylene moiety have aromatic character lying between 1.39 and 1.41 Å. All the hydrocarbons have one eight-membered ring where bond length alternation exists and the bonds have alternately single bond and double bond character. However, the common bonds with the six-membered ring of biphenylene and eight-membered ring have aromatic character. But the common bond between eight-membered ring and six-membered ring other than the biphenylene moiety of molecules **2** and **4** has single-bond character and the predicted bond length is equal to 1.45 and 1.46 Å for these molecules respectively. This suggests that the π-electrons are localized here. In the biphenylene moiety (**1**, **2**, and **4**) the bonds joining the two six-membered rings have single bond character and the length lies between 1.48—1.49 Å same as in the biphenylene itself. The bond length joining the two six-membered rings (molecule **3**) has also single-bond character having length equal to 1.46—1.47 Å. In the molecules **1** and **3** there is a four-membered ring attached in between the eight-membered and six-membered rings. The bond common to the four-membered and six-membered ring has aromatic character with bond length 1.41 Å and the other three bonds of the four-membered ring have single bond character (1.46 Å). Thus π-electrons are not delocalized in this region of the molecules.

$\pi^* \leftarrow \pi$ Spectra. Table 1 presents the theoretical and experimental spectral transitions along with the oscillator strengths (f). The theoretical results have been predicted using the SCF methods and CI procedure. The oscillator strengths were obtained from the relation[19]

$$f = 1.095 \times 10^{-5} \bar{\nu}\, \mu^2 \quad (7)$$

where $\bar{\nu}$ is the transition energy in (cm^{-1}) and μ is the dipole length (in Å) for the corresponding transition.

Literature survey shows that only molecules **1** and **3** have experimental spectral transitions. The experimental spectra of the molecule **1** have a large number of peak maxima many of which are not clearly resolved. Therefore the best one can expect in a comparison of the theoretical and observed transition energies is a general correlation over quite wide spectral regions. Table 1 displays this comparison. In addition to the observed peak maxima included in the table there is a number of observed maxima at low transition energies for which no theoretical counterpart was found. Table 1 also contains the theoretical spectral transitions of molecule **3** along with

Table 1. $\pi^* \leftarrow \pi$ Spectral Transitions [ΔE(eV)] of Molecules **1** and **3**

Symmetry	Exptl. transitions		Present work									
			SCF(a)		SCF(b)		SCF(c)		SCF(d)		CI	
	ΔE	$\log \varepsilon$	ΔE	f	ΔE	f	ΔE	f	ΔE	f	ΔE	f
	Ref. 26						Molecule **1**					
B_2	2.41	3.12	2.20	0.00	2.20	0.00						
	2.79	3.31					2.89	0.01			2.65	0.02
B_2	3.11	4.02									3.06	0.00
	3.30	3.91	3.29	0.29	3.27	0.28	3.69	0.29	3.45	0.18	3.17	0.02
A_1	3.85	4.04	3.86	0.82	3.84	0.82			3.91	0.86	3.95	0.02
B_2	4.27	4.83	4.63	0.00	4.60	0.00	4.27	0.36	4.35	0.39	4.31	0.74
A_1	4.82	4.56	5.13	0.05	5.11	0.05			4.80	0.06	4.82	0.02
B_2	5.56	4.51	5.55	0.47	5.52	0.47	5.41	0.00	5.54	0.51	5.70	1.61
	Ref. 27						Molecule **3**					
A_1	3.52	3.96	3.84	0.99	3.83	0.98			3.88	0.99	3.69	0.002
B_2	4.44	4.66	4.37	0.46	4.36	0.46	4.32	0.41	4.34	0.45	4.42	0.96
B_2	4.71	4.53	5.17	0.09	5.14	0.09	4.66	0.44	4.98	0.08	4.83	0.02

Table 2. $\pi^* \leftarrow \pi$ Spectral Transitions [ΔE(eV)] of Molecules **2** and **4**

Symmetry	SCF(a)		SCF(b)		SCF(c)		SCF(d)		CI	
	ΔE	f	ΔE	f	ΔE	f	ΔE	f	ΔE	f
					Molecule **2**					
B_2	2.86	0.08	2.82	0.08	2.21	0.14			2.68	0.00
B_2	3.10	0.24	3.09	0.24	3.32	0.09	3.11	0.27	2.97	0.13
B_2	3.86	0.09	3.85	0.09	3.76	0.26	3.97	0.11	3.80	0.50
A_1	4.19	0.90	4.18	0.90	4.61	0.81	4.29	0.91	4.50	1.61
A_1	5.25	0.01	5.25	0.01	5.51	0.01	5.07	0.01	5.13	0.04
B_2	5.44	0.36	5.41	0.36	5.59	0.36	5.24	0.35	5.40	1.16
					Molecule **4**					
B_2	2.96	0.11	2.94	0.11	2.60	0.07	3.31	0.26	3.11	0.08
A_1	4.00	0.82	3.99	0.81	4.40	0.77	3.98	0.82	3.95	1.57
B_2	4.82	0.00	4.80	0.00	4.45	0.13	4.65	0.00	4.65	0.11
A_1	5.26	0.15	5.24	0.15	5.48	0.14	5.26	0.10	5.30	0.14
B_2	5.38	0.29	5.35	0.29	5.46	0.27	5.38	0.31	5.39	1.36

experimental ones. In all these molecules (**1** and **3**) the results predicted by the CI method is better than those predicted by the SCF methods. Table 2 contains the theoretical transitions of the molecules **2** and **4** for which no experimental transitions are available in the literature.

Molecular Properties such as Ionization Potentials, Electron Affinities, Half-Wave Reduction Potentials, and Stability. According to Koopmans' theorem[20] ionization potential (IP) could be represented by the highest occuopied orbital energy (HOOE). Electron affinity (EA) could also be represented by the lowest unoccupied orbital energy (LUOE). It has been found[21] that the values obtained by this method are 1 or 2 eV higher than the experimental values of IP and EA. Hence a correction term is to be added to the HOOE and LUOE in order to get the correct value of IP and EA respectively. Correction terms are displayed in Table 3. The half-wave reduction potential ($E_{1/2}$) has been evaluated from the relation[22] (Eq. 8) in the context of SCF(c) method

Table 3. Values of Correction Terms, '*C*' and '*D*'

Method	Value of C[a]	Value of D[a]
SCF(a)	1.29[b]	1.49[c]
SCF(b)	1.28[b]	1.50[c]
SCF(c)	1.88 (Ref. 22)	1.28[c]
SCF(d)[d]	1.06	1.90

a) The values are in eV. b) The values are due to difference between the HOOE and experimental value of IP of some standard molecule. Here it is chrysene the value of which is 8.01 eV (Ref. 29). c) The values are due to difference between the LUOE and experimental value of electron affinity of some standard molecule. Here it is chrysene. The value of which is 0.397 eV (Ref. 30). d) Ref. 31.

$$E_{1/2} = -0.833\, e_j - 3.46 \qquad (8)$$

where e_j is the LUOE. The values of IP, EA, and $E_{1/2}$ are presented in Table 4. For lack of experimental value we can not compare our results with

Table 4. Ionization Potential (IP), Electron Affinity (EA), and Half-Wave Reduction Potential ($E_{1/2}$) of the Hydrocarbons **1**—**4**

Molecule	Method[a]	IP/eV	EA/eV	$-E_{1/2}$/V
1	a	7.68	0.73	
	b	7.68	0.72	
	c	7.41	0.62	1.88
	d	7.53	0.81	
2	a	7.05	1.36	
	b	7.06	1.34	
	c	6.95	1.08	1.49
	d	6.96	1.35	
3	a	7.66	0.74	
	b	7.67	0.74	
	c	7.40	0.63	1.87
	d	7.51	0.80	
4	a	7.31	1.09	
	b	7.32	1.08	
	c	6.09	0.94	1.61
	d	7.17	1.14	

a) a, b, c, and d represent SCF(a), SCF(b), SCF(c), and SCF(d) methods respectively.

Table 5. Heat of Atomization (ΔH_a) and Bond Energies of the Hydrocarbons **1**—**4**

Molecule	Method[a]	ΔH_a/eV	Bond energy/eV	
			π-bond	σ-bond
1	a	184.904	32.738	98.916
	b	185.151	32.226	99.675
	c	185.736	32.002	100.484
2	a	169.955	28.780	87.925
	b	170.173	28.323	88.600
	c	170.759	28.415	89.095
3	a	190.043	32.666	95.253
	b	190.264	32.156	95.983
	c	190.624	31.950	96.549
4	a	237.655	42.094	124.561
	b	237.956	41.440	125.516
	c	238.498	40.963	126.535

a) a, b, and c represent SCF(a), SCF(b), and SCF(c) methods respectively.

experimental ones.

Stability or aromaticity of the molecules has been studied using the criteria of resonance energy (E_R) and resonance energy per carbon-carbon bond (E_R/C-C) or resonance energy per π-electron (RE/PE). The values of E_R of the hydrocarbons have been obtained using the methods of Lo and Whitehead,[7] Chung and Dewar,[8] Dewar and de Llano,[23] Dewar and Harget,[10] and Hess and Schaad.[24]

The values of heat of atomization (ΔH_a) and bond energies of the hydrocarbons have been presented in Tables 5 and 6 contains the values of E_R, E_R/C-C, and

Table 6. Resonance Energy (E_R), Resonance Energy per Carbon-Carbon Bond (E_R/C-C), Resonance Energy per π-Electron (RE/PE) of the Molecules Studied Here

Property[a]	Molecule			
	1	**2**	**3**	**4**
E_R (a)	7.533	6.161	7.610	9.879
E_R (b)	7.497	5.930	7.589	10.025
E_R (c)	2.197	1.457	2.596	3.270
E_R (d)	1.239	0.428	1.754	2.128
E_R (e)	0.2476	0.0607	0.6551	0.6538
E_R/C-C(a)	0.2938	0.2567	0.2927	0.2906
E_R/C-C(b)	0.2776	0.2471	0.2919	0.2948
E_R/C-C(c)	0.0814	0.0607	0.0998	0.0962
E_R/C-C(d)	0.0459	0.0179	0.0675	0.0626
RE/PE(e)	0.0113	0.0028	0.0297	0.0234

a) a, b, c, d, and e represent SCF(a), SCF(b), SCF(c), Dewar-de Llano and Hess, and Schaad method respectively. For a, b, c, and d E_R is in eV and for e it is in β.

Table 7. Criteria of Aromaticity or Stability of Hydrocarbons

Method[a]	Range of E_R/C-C or RE/PE for the hydrocarbons to be aromatic
a	0.26—0.31
b	0.25—0.30
c	0.075—0.112
d	0.041—0.095
e	0.03—0.04

a) a, b, c, d, and e represent the SCF(a), SCF(b), SCF(c), Dewar-de Llano and Hess, and Schaad methods respectively. (Refs. 25 and 32).

RE/PE of the molecules. The hydrocarbons belong to semibenzenoid[25] type of compounds. The criteria for stability of this type of hydrocarbons with respect to E_R/C-C or RE/PE have been discussed by Das Gupta and Das Gupta and are displayed in Table 7.

The molecule **1** is thermally stable[26] and melts without decomposition at 192—193 °C. It exhibits diamagnetic ring current suggesting that it might be aromatic. From Table 6 E_R and E_R/C-C bond calculated by SCF(a), SCF(b), and SCF(c) methods and Dewar-de Llano method[23] suggest also that the molecule might be aromatic. On the other hand resonance energy and RE/PE (0.0113) calculated by Hess and Schaad method predict it to be not aromatic. However, stability[25] predicted by Dewar-de Llano method is better than any other methods.

Resonance energy, E_R/C-C bond calculated by all the SCF methods[7,8,10,23] and RE/PE suggest that the molecule **2** might be unstable one. It predicts paramagnetic ring current[26] which points it out to be not an aromatic compound. Synthesis of **2** has not yet been found in the literature.

Hydrocarbon **3** has been synthesized by Garratt et al.[27,28] They have also studied the properties. According to them the molecule is an aromatic one which is in agreement with the results obtained from the values of E_R, E_R/C-C bond calculated by the SCF methods and E_R and RE/PE calculated by the Hess and Schaad method.

Molecule **4** is an interesting one. It has not yet been synthesized. However, ring current criteria[26] and E_R, E_R/C-C suggest it to be aromatic and stable compound. As in molecule **1**, RE/PE predicts it to be not aromatic.

Biphenylene is an aromatic compound and hydrocarbon **5** is not. The molecules **1**—**4** either contain biphenylene or molecule **5** or both in their nucleus. But aromatic character or not of these molecules is not governed by the presence of biphenylene or molecule **5**. As for example **1** and **3** contain molecule **5** in their nucleus. From the above discussion it is clear that both the molecules **1** and **3** are aromatic. Again **1**, **2**, and **4** contain biphenylene moiety. But as discussed earlier it is clear that the hydrocarbons **1** and **4** are aromatic and **2** is not. Although molecule **4** has not yet been synthesized still we expect that either it or some of its derivatives will be synthesized in near future.

The authors are grateful to the University Grants Commission, New Delhi for the award of offering a Junior Research Fellowship to one of them (SKP).

References

1) W. Tochtermann, *Angew. Chem.*, **75**, 418 (1963).
2) a) R. Breslow, W. Horspoll, H. Sugiyama, and W. Vitale, *J. Am. Chem. Soc.*, **88**, 3677 (1966); b) J. A. Alix, M. V. Sargent, and F. Sondheimer, *Chem. Commun.*, **1966**, 509; *J. Am. Chem. Soc.*, **89**, 180, 5080 (1967).
3) R. Pariser and R. G. Parr, *J. Chem. Phys.*, **21**, 466, 767 (1953).
4) J. A. Pople, *Trans. Faraday Soc.*, **49**, 1375 (1953).
5) S. K. Pal, N. K. Das Gupta, and A. Das Gupta, *Ind. J. Chem.*, **26B**, 243 (1987).
6) R. G. Parr, "Quantum Theory of Molecular Electronic Structure," W. A. Benjamin, New York (1963).
7) D. H. Lo and M. A. Whitehead, *Can. J. Chem.*, **46**, 2027 (1968).
8) A. L. H. Chung and M. J. S. Dewar, *J. Chem. Phys.*, **42**, 756 (1965).
9) F. W. Birss and N. K. Das Gupta, *Can. J. Chem.*, **49**, 2840 (1971).
10) M. J. S. Dewar and A. J. Harget, *Proc. R. Soc. London, Ser. A*, **315**, 443 (1970).
11) H. Yamaguchi, T. Nakajima, and T. L. Kunii, *Theoret. Chim. Acta*, **12**, 349 (1968).
12) K. Nishimoto and R. Fujishiro, *Bull. Chem. Soc. Jpn.*, **37**, 1660 (1964).
13) M. J. S. Dewar and G. J. Gleicher, *J. Am. Chem. Soc.*, **87**, 685, 692 (1965).
14) R. Pariser, *J. Chem. Phys.*, **21**, 568 (1953).
15) J. Hinze and H. H. Jaffe, *J. Am. Chem. Soc.*, **84**, 840 (1962).
16) K. Chno, *Theoret. Chim. Acta*, **2**, 219 (1964).
17) M. Mataga and K. Nishimoto, *Z. Physik. Chim. Frankfurt*, **13**, 140 (1957).
18) N. K. Das Gupta and F. W. Birss, *Bull. Chem. Soc. Jpn.*, **51**, 1211 (1978).
19) L. Salem, "Molecular Orbital theory of Conjugated system," W. A. Benjamin, 358 (1966).
20) T. Koopmans, *Physica*, **1**, 104 (1934).
21) C. Moser, *J. Chim. Phys.*, **52**, 24 (1955).
22) F. W. Birss and N. K. Das Gupta, *Indian J. Chem.*, **17b**, 610 (1979).
23) M. J. S. Dewar and C. de Llano, *J. Am. Chem. Soc.*, **91**, 989 (1979).
24) B. A. Hess, Jr. and L. J. Schaad, *J. Am. Chem. Soc.*, **93**, 305 (1971).
25) A. Das Gupta and N. K. Das Gupta, *Tetrahedron*, **28**, 3587 (1972); *Theoret. Chim. Acta (Berlin).*, **33**, 177 (1974).
26) C. P. Wilcox, Jr. and G. D. Grantham, *Tetrahedron*, **31**, 2889 (1975).
27) F. J. Garratt, K. P. C. Volhardt, and R. H. Mitchell, *J. Chem. Soc. C*, **1970**, 2137.
28) F. J. Garratt and R. H. Mitchell, *Chem. Commun.*, **1968**, 719.
29) M. E. Wacks, *J. Chem. Phys.*, **41**, 1661 (1964).
30) R. S. Becker and E. Chen., *J. Chem. Phys.*, **45**, 2403 (1966).
31) T. L. Kunii and H. Kuroda, *Theoret. Chim. Acta*, **11**, 97 (1968).
32) A. Das Gupta, S. Chatterjee, and N. K. Das Gupta, *Bull. Chem. Soc. Jpn.*, **52**, 3070 (1979).

 © 1988 The Chemical Society of Japan Bull. Chem. Soc. Jpn., 61, 1755—1759 (1988)

Thermochemistry of Cobalt(III) β-Diketonates

Manuel A. V. Ribeiro da Silva* and Maria Luisa C. C. H. Ferrão
Chemistry Department, Faculty of Sciences, University of Oporto, P-4000 PORTO, Portugal
(Received May 25, 1987)

The standard molar enthalpies of formation of the crystalline complexes of cobalt(III) with 1-phenyl-1,3-butanedione (Hbzac), 2,2,6,6-tetramethyl-3,5-heptanedione(Hdpm), and 1,1,1-trifluoro-2,4-pentanedione (Htfac) were determined, at 298.15 K, by solution-reaction calorimetry:

$$\Delta_f H^\circ_m[Co(bzac)_3, cr] = -877.1 \pm 8.7 \text{ kJ} \cdot \text{mol}^{-1}$$

$$\Delta_f H^\circ_m[Co(dpm)_3, cr] = -1708 \pm 12 \text{ kJ} \cdot \text{mol}^{-1}$$

$$\Delta_f H^\circ_m[Co(tfac)_3, cr] = -3191 \pm 15 \text{ kJ} \cdot \text{mol}^{-1}.$$

The enthalpies of sublimation of $Co(dpm)_3$ and $Co(tfac)_3$, at 298.15 K, determined by high-temperature microcalorimetry were 126±3 and 114±2 kJ·mol^{-1}, respectively. From the enthalpies of formation of the gaseous complexes, the average molar bond-dissociation enthalpies, $\langle D \rangle$(Co–O), were derived.

Previous thermochemical studies of cobalt(III) β-diketonates are limited to tris(2,4-pentanedionato)-cobalt(III), made by Wood and Jones,[1] using static-bomb calorimetry. These early combustion results have been shown to be unreliable,[2] probably because insufficient attention was paid to controlling the combustion with auxiliary combustion aids and in defining the completeness of combustion and the nature of the combustion products.

The solution-reaction calorimetric method has proved bo be reliable for determining enthalpies of formation of metal β-diketonates.[3] In this paper, using the solution-reaction calorimetric method, the standard molar enthalpies of formation of three cobalt(III) β-diketonates were determined, to permit consideration of the effect of structural changes in the ligand upon the mean molar (Co–O) bond-dissociation enthalpies.

Experimental

The Solution Calorimeter. The isoperibol LKB 8700 reaction-and-solution precision calorimeter was used. The operation and calculations methods have been reported.[4] The molar enthalpy of reaction was calculated from the relation $\Delta H = \varepsilon \Delta R / n R_m$, where $\Delta R = R_i - R_f$, $R_m = (R_i + R_f)/2$, n=number of moles of reactant, and R_i and R_f are the initial and final thermistor resistances (Ω) as determined by the Dickinson method.[5] The energy constant, ε, of the calorimetric system is given by $\varepsilon = Q_c R_{mc} / \Delta R_c$, where Q_c is an accurately defined quantity of heat supplied electrically via the built-in heater, $Q_c = R_h I^2 t$(R_h is the resistance of the calibrating heater (Ω), I the calibratrion current (A), and t the heating time (s)), and R_{mc} and ΔR_c have the same significance in a calibration experiment as R_m and ΔR have in a reaction. The ratio $\Delta R / R_m$ is directly proportional to the temperature change. The accuracy of the calorimeter was checked by measuring the molar enthalpy of solution of tris(hydroxymethyl)aminomethane (THAM) in aqueous 0.1000 mol·dm^{-3} HCl at 298.15 K: $\Delta_{sol}H_m = -29.769 \pm 0.024$ kJ·mol^{-1}, in agreement with the value of Kilday and Prosen,[6] $\Delta_{sol}H_m = -29.770 \pm 0.032$ kJ·mol^{-1}.

High-Temperature Microcalorimeter. The enthalpies of sublimation of the complexes were measured by the "vacuum sublimation" drop-microcalorimetric method.[7] Samples (about 4 mg) of each complex contained in a small thin-glass capilary tube sealed at one end, were dropped, at room temperature, into the hot reaction vessel in the Calvet High-Temperature Microcalorimeter held at constant temperature, between 407 and 490 K, and then removed from the hot zone by vacuum sublimation. At these temperatures, the complexes showed no signs of decomposition, and sublimed completely in less than 30 min. The observed standard molar enthalpies of sublimation [H°_m(g, T)−H°_m(cr,298.15K)] were corrected to 298.15 K using values of [H°_m(g, T)−H°_m(g, 298.15K)] estimated by group-additivity methods based on data given by Stull et al.[8] The microcalorimeter was calibrated in situ for the measurements by making use of the known molar enthalpies of sublimation of iodine,[9] naphthalene,[8] and benzoic acid.[10,11]

All uncertainty intervals given are twice the standard deviation of the mean.

Materials. 1-Phenyl-1,3-butanedione: Hbzac (Koch-Light Laboratories Ltd.) was purified by repeated recrystallization from ethanol–water; mp 56 °C (lit, 56 °C[12]). Found: C, 73.89; H, 6.25%. Calcd for $C_{10}H_{10}O_2$: C, 74.06; H, 6.22%.

2,2,6,6-Tetramethyl-3,5-heptanedione: Hdpm was prepared by Claisen condensation according to the methods of Adams and Hauser[13] and of Kopecky et al.,[14] was purified by fractional distillation in vacuum and the purity was assessed as better than 99.9 mole per cent by GLC using two different columns.

1,1,1-Trifluoro-2,4-pentanedione: Htfac (Kock-Light Laboratories Ltd.) was purified by fractional distillation and the purity was assessed as greater than 99.9 mole per cent by GLC using two different columns. The purified liquid β-diketones were stored under nitrogen in the dark and were freshly distilled prior to use.

Tris(1-phenyl-1,3-butanedionato)cobalt(III): $Co(bzac)_3$ was prepared as described by Bauer and Drinkard[15] and was purfied by crystallization from acetone–hexane; mp 184—185 °C(lit, 213 °C[15]). Found: C, 66.45; H, 4.89; Co, 10.78%. Calcd for $C_{30}H_{27}O_6Co$: C, 66.42; H, 5.03; Co, 10.87%.

Tris(2,2,6,6-tetramethyl-3,5-heptanedionato)cobalt(III): Co(dpm)$_3$ was prepared as described by Bauer and Drinkard[15] and was purified by vacuum sublimation; mp 244—245 °C (lit, 244—245 °C[16]). Found: C, 65.11; H, 9.38; Co, 9.54%. Calcd for $C_{33}H_{57}O_6Co$: C, 65.11; H, 9.44; Co, 9.68%.

Tris(1,1,1-trifluoro-2,4-pentanedionato)cobalt(III): Co(tfac)$_3$ (Koch-Light Laboratories Ltd.) was crystallized from carbon tetrachloride; mp 152 °C (lit, 156 °C[17]). Found: C, 34.72; H, 2.19; Co, 11.30%. Calcd for $C_{15}H_{12}O_6Co$: C, 34.77; H, 2.33; Co, 11.37%.

Cobalt(II) Sulfate Hexahydrate: Cobalt(II) sulfate heptahydrate (AnalaR BDH) was dried over silica gel; its composition was determined by means of cobalt analyses and found to be $CoSO_4 \cdot 6.00H_2O$.

Iron(II) and Iron(III) Chloride: CERAC samples of $FeCl_2$ and $FeCl_3$(stated minimum purity 99.99%) were used.

Sulfuric Acid: A 1 mol·dm^{-3} H_2SO_4 was made from Merck concentrated volumetric solution; the concentration was checked by titration against $Na_2B_4O_7 \cdot 10H_2O$ and found to be (series of six titrations) 1.000±0.003 mol·dm^{-3}, which corresponds[12] to the composition $H_2SO_4 \cdot 53.54H_2O$.

Hydrochloric Acid: Concentrated HCl (AnalaR BDH) was diluted with distilled water. The concentration was determined by titration against $Na_2B_4O_7 \cdot 10H_2O$ and found to be (series of six titrations) 4.590±0.003 mol·dm^{-3}, which corresponds[12] to the composition $HCl \cdot 10.98H_2O$.

1,4-Dioxane: 1,4-Dioxane (Carl Erba) was purified according to Ref. 18.

Analyses: Carbon and hydrogen analyses were carried out in the Microanalytical Service of the University of Surrey; cobalt was analyzed by the ethylenediaminetetracetic acid method.[19]

For the hydrolysis and oxidation reaction the solvents were degassed and saturated with purified nitrogen prior to each determination.

The relative atomic masses used were the recommended by the IUPAC Commission.[20]

Results and Discussion

Preliminary tests of solubility showed that rapid hydrolyses and oxidation occurred using [0.90(1,4-dioxane)+0.10HCl(aq, 3.0 mol·dm^{-3})] by volume, as the initial calorimetric solvent.

The thermochemical reaction for determining the standard molar enthalpy of formation of Co(bzac)$_3$, Co(dpm)$_3$, and Co(tfac)$_3$ was:

$$CoL_3(cr) + HCl \cdot 10.98H_2O(l) + H_2SO_4 \cdot 53.54H_2O(l) + FeCl_2(cr) = 58.52H_2O(l) + FeCl_3(cr) + 3HL(cr \text{ or } l) + CoSO_4 \cdot 6.00H_2O(cr) \quad (1)$$

The reaction was studied in the presence of an excess of $FeCl_3$: to the calorimetric solvent (100.0 cm^3), 1.00 cm^3 of $FeCl_3$ 0.1 mol·dm^{-3} was added. The same batch of solvent was used for the three cobalt(III) complexes.

The enthalpies of the thermochemical reactions were determined by measuring the enthalpies of reaction and solution of the reactants and products, $\Delta_i H_m$, in succession in the initial calorimetric solvent. The thermochemical cycle and the general procedure for the calorimetric study of the cobalt(III) complexes

$$HCl \cdot 10.98H_2O(l) + H_2SO_4 \cdot 53.54H_2O(l) + FeCl_2(cr) + CoL_3(cr) = 58.52H_2O(l) + FeCl_3(cr) + 3HL(cr \text{ or } l) + CoSO_4 \cdot 6.00H_2O(cr)$$

$$\downarrow \Delta_1 H_m \quad \downarrow \Delta_2 H_m \quad \downarrow \Delta_3 H_m \quad \downarrow \Delta_4 H_m \quad \downarrow \Delta_5 H_m \quad \downarrow \Delta_6 H_m \quad \downarrow \Delta_7 H_m \quad \downarrow \Delta_8 H_m$$

$$\text{Solvent}\{0.90(\text{dioxane}) + 0.10HCl(aq, 3.0 \text{ mol} \cdot \text{dm}^{-3})\} + FeCl_3 \quad \text{Solvent}\{0.90(\text{dioxane}) + 0.10HCl(aq, 3.0 \text{ mol} \cdot \text{dm}^{-3})\} + FeCl_3$$

$$\text{Solution } A_4 \xrightarrow{\Delta_9 H_m = 0} \text{Solution } B_4$$

$$\text{Solvent} + HCl \cdot 10.98H_2O(l) \xrightarrow{\Delta_1 H_m} \text{Solution } A_1$$

$$\text{Solution } A_1 + H_2SO_4 \cdot 53.54H_2O(l) \xrightarrow{\Delta_2 H_m} \text{Solution } A_2$$

$$\text{Solution } A_2 + FeCl_2(cr) \xrightarrow{\Delta_3 H_m} \text{Solution } A_3$$

$$\text{Solution } A_3 + CoL_3(cr) \xrightarrow{\Delta_4 H_m} \text{Solution } A_4$$

$$\text{Solvent} + H_2O(l) \xrightarrow{\Delta_5 H_m} \text{Solution } B_1$$

$$\text{Solution } B_1 + FeCl_3(cr) \xrightarrow{\Delta_6 H_m} \text{Solution } B_2$$

$$\text{Solution } B_2 + HL(cr \text{ or } l) \xrightarrow{\Delta_7 H_m} \text{Solution } B_3$$

$$\text{Solution } B_3 + CoSO_4 \cdot 6.00H_2O(cr) \xrightarrow{\Delta_8 H_m} \text{Solution } B_4$$

$$\Delta_r H_m = \Delta_1 H_m + \Delta_2 H_m + \Delta_3 H_m + \Delta_4 H_m - 58.52\Delta_5 H_m - \Delta_6 H_m - 3\Delta_7 H_m - \Delta_8 H_m$$

Scheme 1.

is given in the Scheme 1. The difference between the molar enthalpies of solution of the products and reactants in the correct stoichiometric ratio gives the enthalpy of the thermochemical reaction, $\Delta_r H^\circ_m$, provided equilibrium is reached from either side within the period of the experiment. The amounts of reactants in a particular series of experiments were determined by the amount of CoL_3(cr), approximately 2.5×10^{-4} mol for Co(bzac)$_3$ and Co(tfac)$_3$ and 1.2×10^{-4} mol for Co(dpm)$_3$. Since the amounts used for the reactants in the study of the Co(dpm)$_3$ complex were different from the other complexes, this made necessary remeasurement of the enthalpies of solution of $HCl\cdot10.98H_2O$(l), $H_2SO_4\cdot53.54H_2O$(l), $FeCl_3$(cr), $FeCl_2$(cr), H_2O(l), and $CoSO_4\cdot6.00H_2O$(cr). These results were found to be the same, within the experimental errors, as determined previously in the study of Co(bzac)$_3$ and Co(tfac)$_3$, hence the previously determined values were used.

The detailed calorimetric results required for determination of the enthalpies of the thermochemical reactions are given in Tables 1—3.

The enthalpies of the thermochemical reactions were derived from the values presented in Tables 1—3

Table 1. Calorimetric Study, at 298.15K, of Co(bzac)$_3$

(a) $HCl\cdot10.98H_2O$(l)+solvent=solution A_1

10^4n/mol	$10^3(\Delta R/R_m)$	ε/J	Δ_1H_m/kJ·mol^{-1}
2.4638	10.101	5380.1	−22.058
2.4933	10.124	5395.3	−21.907
2.5449	10.327	5426.5	−22.020
2.4775	9.9694	5386.5	−21.675
2.4749	9.9983	5405.2	−21.836

Mean: $\Delta_1H_m=-21.90\pm0.14$ kJ·mol^{-1}

(b) $H_2SO_4\cdot53.54H_2O$(l)+solution A_1=solution A_2

10^4n/mol	$10^3(\Delta R/R_m)$	ε/J	Δ_2H_m/kJ·mol^{-1}
2.4648	1.4183	5414.2	−31.155
2.4976	1.4299	5414.1	−30.995
2.5380	1.4631	5439.3	−31.356
2.4493	1.4071	5415.8	−31.112
2.4795	1.4193	5422.7	−31.040

Mean: $\Delta_2H_m=-31.13\pm0.12$ kJ·mol^{-1}

(c) $FeCl_2$(cr)+solution A_2=solution A_3

10^4n/mol	$10^3(\Delta R/R_m)$	ε/J	Δ_3H_m/kJ·mol^{-1}
2.4670	3.3817	5415.4	−72.135
2.5348	3.4255	5429.4	−73.372
2.4709	3.2824	5443.4	−72.310
2.5341	3.3521	5455.8	−72.170
2.4204	3.2131	5459.8	−72.477

Mean: $\Delta_3H_m=-72.69\pm0.47$ kJ·mol^{-1}

(d) Co(bzac)$_3$(cr)+solution A_3+solution A_4

10^4n/mol	$10^3(\Delta R/R_m)$	ε/J	Δ_4H_m/kJ·mol^{-1}
2.4146	3.9881	5430.5	+8.969
2.3051	3.5768	5445.0	+8.449
2.5880	4.3724	5426.7	+9.168
2.4807	4.0486	5419.9	+8.845
2.3510	3.8266	5430.5	+8.839

Mean: $\Delta_4H_m=+8.85\pm0.24$ kJ·mol^{-1}

(e) H_2O(l)+solvent=solution B_1

10^2n/mol	$10^3(\Delta R/R_m)$	ε/J	Δ_5H_m/kJ·mol^{-1}
1.4479	1.3966	5424.5	−0.5232
1.5377	1.4837	5427.3	−0.5236
1.5482	1.4956	5414.5	−0.5230
1.3532	1.3096	5428.7	−0.5254
1.6031	1.5567	5433.5	−0.5276

Mean: $\Delta_5H_m=-0.524\pm0.002$ kJ·mol^{-1}

(f) $FeCl_3$(cr)+solution B_1=solution B_2

10^4n/mol	$10^3(\Delta R/R_m)$	ε/J	Δ_6H_m/kJ·mol^{-1}
2.4802	3.9086	5438.4	−85.705
2.6281	4.0756	5431.3	−84.227
2.3113	3.6221	5439.8	−85.249
2.5005	3.8360	5449.2	−83.594
2.6510	4.1685	5436.0	−85.479
2.7453	4.2115	5446.6	−83.557

Mean: $\Delta_6H_m=-84.64\pm0.79$ kJ·mol^{-1}

(g) Hbzac(cr)+solution B_2=solution B_3

10^4n/mol	$10^3(\Delta R/R_m)$	ε/J	Δ_7H_m/kJ·mol^{-1}
7.5233	3.3298	5450.4	+24.123
7.6306	3.3527	5459.3	+23.987
7.1897	3.1858	5449.8	+24.148
6.8802	3.3739	5459.8	+24.288
7.5073	3.3249	5450.9	+24.141

Mean: $\Delta_7H_m=+24.14\pm0.10$ kJ·mol^{-1}

(h) $CoSO_4\cdot6.00H_2O$(cr)+solution B_3=solution B_4

10^4n/mol	$10^3(\Delta R/R_m)$	ε/J	Δ_8H_m/kJ·mol^{-1}
2.5015	1.4526	5449.3	+31.644
2.6824	1.5772	5424.0	+31.892
2.6390	1.5247	5446.0	+31.466
2.7808	1.6341	5453.5	+32.047
2.6349	1.5457	5456.0	+32.006

Mean: $\Delta_8H_m=+31.81\pm0.22$ kJ·mol^{-1}

Table 2. Calorimetric Study, at 298.15 K, of Co(dpm)$_3$

(a) Co(dpm)$_3$(cr)+solution A_3=solution A_4

10^4n/mol	$10^4(\Delta R/R_m)$	ε/J	Δ_4H_m/kJ·mol^{-1}
1.2442	6.7948	5404.2	+29.513
1.2549	6.9226	5425.6	+29.931
1.2422	6.6561	5467.7	+29.297
1.1284	6.0971	5432.5	+29.354
1.1974	6.5578	5432.5	+29.753

Mean: $\Delta_4H_m=+29.57\pm0.24$ kJ·mol^{-1}

(b) Hdpm(l)+solution B_2=solution B_3

10^4n/mol	$10^4(\Delta R/R_m)$	ε/J	Δ_7H_m/kJ·mol^{-1}
4.0444	4.9170	5377.4	+6.538
4.0265	4.9881	5351.5	+6.630
3.5240	4.3888	5295.6	+6.595
3.3997	4.1227	5365.9	+6.507
4.1860	5.0328	5367.0	+6.453

Mean: $\Delta_7H_m=+6.54\pm0.06$ kJ·mol^{-1}

Table 3. Calorimetric Study, at 298.15 K, of $Co(tfac)_3$

(a) $Co(tfac)_3(cr)$+solution A_3=solution A_4				(b) Htfac(l)+solution B_2=solution B_3			
10^4n/mol	$10^3(\Delta R/R_m)$	ε/J	Δ_4H_m/kJ·mol^{-1}	10^4n/mol	$10^3(\Delta R/R_m)$	ε/J	Δ_7H_m/kJ·mol^{-1}
2.4646	1.1083	5430.4	+24.420	7.5047	3.6182	5444.8	−26.251
2.5277	1.1025	5439.2	+23.724	7.9006	3.7799	5419.2	−25.927
2.4428	1.1046	5420.0	+24.508	7.9824	3.7770	5448.0	−25.778
2.4648	1.1119	5433.5	+24.511	8.2545	3.9619	5441.8	−26.119
2.4793	1.1078	5447.8	+24.344	8.0083	3.8513	5437.1	−26.146
Mean: Δ_4H_m=+24.30±0.30 kJ·mol^{-1}				Mean: Δ_7H_m=−26.04±0.17 kJ·mol^{-1}			

Table 4. Molar Enthalpies of Sublimation of Cobalt(III) Complexes

Complex	No. of exp.	T	$\Delta_{sub}H_m$(obs, T)	$H°_m$(g, T)−$H°_m$(g, 298.15 K)	$\Delta_{sub}H°_m$(298.15 K)
		K	kJ·mol^{-1}	kJ·mol^{-1}	kJ·mol^{-1}
$Co(dpm)_3$	5	490	318±3	192	126±3
$Co(tfac)_3$	3	407	168±2	54	114±2

Table 5. Standard Molar Enthalpies of Formation and Vaporization/Sublimation of β-Diketones

β-Diketone	$\Delta_fH°_m$(cr or l)	$\Delta_{vap/sub}H°_m$	$\Delta_fH°_m$(g)
	kJ·mol^{-1}	kJ·mol^{-1}	kJ·mol^{-1}
Hbzac(cr)	−335.1±2.8[a]	+83.8±0.4[b]	−251.3±2.9
Hdpm(l)	−587.7±3.8[a]	+59.5±0.1[c]	−528.2±3.8
Htfac(l)	−1051.0±5.0	+37.2±0.2[c]	−1013.8±5.0[d]

a) Ref. 24. b) Ref. 25. c) Ref. 26. d) Estimated by using a group scheme.

Table 6. Standard Molar Enthalpies of Formation and Sublimation at 298.15 K

Complex	$\Delta_fH°_m$(cr)	$\Delta_{sub}H°_m$	$\Delta_fH°_m$(g)
	kJ·mol^{-1}	kJ·mol^{-1}	kJ·mol^{-1}
$Co(bzac)_3$	−877.1±8.7	[165±10][a]	−712±13
$Co(dpm)_3$	−1708±12	126±3	−1582±12
$Co(tfac)_3$	−3191±15	114±2	−3077±15

a) Estimated.

and the equation in the Scheme 1, leading to

$$\Delta_rH°_m[Co(bzac)_3] = -105.8\pm1.0 \text{ kJ·mol}^{-1}$$

$$\Delta_rH°_m[Co(dpm)_3] = +32.3\pm1.0 \text{ kJ·mol}^{-1}$$

$$\Delta_rH°_m[Co(tfac)_3] = +60.2\pm1.3 \text{ kJ·mol}^{-1}$$

The experimental results for determination of the standard molar enthalpies of sublimation of $Co(dpm)_3$ and $Co(tfac)_3$ are listed in Table 4. Attempts to measure the enthalpy of sublimation of $Co(bzac)_3$ were unsuccessful because, for temperatures at which vapour pressure was sufficiently high to permit vacuum sublimation, partial thermal decomposition occurred.

To derive the standard molar enthalpies of formation of the crystalline cobalt(III) complexes, the following auxiliary data, at 298.15 K, was used: $\Delta_fH°_m(H_2O, l)$=−285.83±0.04 kJ·mol^{-1};[21] $\Delta_fH°_m$(HCl in 10.98H_2O, l)=−161.77±0.01 kJ·mol^{-1};[22] $\Delta_fH°_m$(H_2SO_4 in 53.54H_2O, l)=−886.87±0.01 kJ·mol^{-1};[22] $\Delta_fH°_m$($FeCl_3$, cr)=−399.49±0.29 kJ·mol^{-1};[22,23] $\Delta_fH°_m$($FeCl_2$, cr)=−341.79±0.21 kJ·mol^{-1};[22,23] $\Delta_fH°_m$($CoSO_4$·6.00H_2O, cr)=−2683.6±2.1 kJ·mol^{-1};[22] as well as the standard enthalpies of formation of the ligands (Table 5), and the above derived molar enthalpies of the thermochemical reactions. Table 6 lists the derived standard molar enthalpies of formation of the crystalline cobalt(III) complexes, their standard molar enthalpies of sublimation and of formation in the gaseous state. The molar enthalpy of sublimation of $Co(bzac)_3$ was estimated on the basis of its structure, molecular weight and other known values for similar complexes, using an estimation scheme.[3]

From the molar enthalpies of the homolytic dissociation of the gaseous molecules into metal atoms and ligand radicals

$$CoL_3(g) = Co(g) + 3L(g) \quad (2)$$

the mean cobalt–oxygen bond-dissociation enthalpies, $\langle D\rangle$(Co–O), were derived. Since the oxygens atoms in metal β-diketonates are equivalent,[27] $\langle D\rangle$(Co–O) may be defined as 1/6 of the molar enthalpy of the disruption Reaction 2.

$$\Delta_{disr}H°_m(2) = \Delta_fH°_m(Co, g) + 3\Delta_fH°_m(HL, g) - 3\Delta_fH°_m(H, g) - \Delta_fH°_m(CoL_3, g) + 3D(O\text{–}H, HL, enol)$$

where D(O–H, HL, enol) is the molar enthalpy of dissociation of the enolic hydrogen in the parent ligand

Table 7. $\langle D \rangle$(Co-O) at 298.15 K

Complex	$\Delta_{disr}H°_m$	$\langle D \rangle$(Co-O)
	kJ·mol^{-1}	kJ·mol^{-1}
Co(bzac)$_3$	984±62	164±10
Co(dpm)$_3$	1023±62	171±10
Co(tfac)$_3$	1060±65	177±10

$$H\text{-}L(g) = L^{\cdot}(g) + H(g) \quad (3)$$

There are no measured values for the molar enthalpy of dissociation of the enolic hydrogen from β-diketones. Different values have been estimated for this parameter, and the situation has been recently reviewed.[3] In this work, for comparison reasons, the value of D(O-H, HL, enol)=418±20 kJ·mol^{-1} [3] is used.

With $\Delta_f H°_m$(H, g)=218.00±0.01 kJ·mol^{-1} [22] and $\Delta_f H°_m$(Co, g)=424.7±4.2 kJ·mol^{-1} [22] the derived values of $\Delta_{disr}H°_m$ and $\langle D \rangle$(Co-O), for the complexes studied are given in Table 7.

As noted previously[28,29] in attempting a rigorous determination of bond-dissociation enthalpies, estimates of some enthalpies of formation were necessary, as well as the enthalpy of dissociation of the enolic hydrogen from the parent β-diketone. The resulting bond-dissociation enthalpies, therefore, have a large uncertainty attached to them, and this makes almost impossible a definite conclusion concerning the magnitude of the bond dissociation enthalpies. Within the uncertainties attached to the mean cobalt(III)-oxygen bond-dissociation enthalpies, there are no significant differences in $\langle D \rangle$(Co-O) for the three cobalt(III) β-diketonates studied in this paper. This shows that there is no effect, or only a very small one, of $-C(CH_3)_3$, $-C_6H_5$, or $-CF_3$ substitution in the ligand, upon $\langle D \rangle$(Co-O). This effect has already been observed for complexes of β-diketones with Be(II),[30] Al(III),[30] Cr(III),[31] Fe(III),[32] and Cu(II).[33]

Thanks, for partial financial support, are due to NATO, Research Grant 1709, and Junta Nacional de Investigação Cientifica e Tecnológica, Lisboa, Research Contract No. 220-80.32. The support given to the research project(L.5) of Centro de Investigação em Quimica, Universidade do Porto, by Instituto Nacional de Investigação Cientifica, Lisboa, is also acknowledged.

References

1) J. L. Wood and M. M. Jones. *Inorg. Chem.*, **3**, 1553 (1964).
2) K. J. Cavell and G. Pilcher, *J. Chem. Soc., Faraday Trans. 1*, **73**, 1590 (1977).
3) "Thermochemistry and its Applications to Chemical and Biochemical Systems," ed by M. A. V. Ribeiro da Silva NATO ASI series, Reidel, Dordrecht (1984), p. 317.
4) M. A. V. Ribeiro da Silva and R. J. Irving, *Bull. Chem. Soc. Jpn.*, **50**, 734 (1977).
5) H. C. Dickinson, *Bull. Nat. Bur. Stand.*, **11**, 189 (1915).
6) M. V. Kilday and E. J. Prosen, *J. Res. Nat. Bur. Stand.*, **A77**, 581, 589 (1973).
7) F. A. Adedeji, D. L. S. Brown, J. A. Connor, M. Leung, M. I. Paz-Andrade, and H. A. Skinner, *J. Organomet. Chem.*, **97**, 221 (1975).
8) D. R. Stull, E. F. Westrum, and G. C. Sinke, "The Chemical Thermodynamics of Organic Compounds," Wiley, New York (1969).
9) JANAF Thermochemical Tables PB 168 370-2. D. R. Stull (Dir.). U. S. National Bureau of Standards, Washington (1969).
10) E. Morawetz, *J. Chem. Thermodynamics*, **4**, 455 (1972).
11) S. Murata, M. Sakiyama, and S. Seki, *J. Chem. Thermodynamics*, **14**, 723 (1982).
12) "Handbook of Chemistry and Physics," 55th ed, ed by R. C. Weast, The Chemical Rubber Co., Cleveland, Ohio (1974).
13) J. T. Adams and C. R. Hauser, *J. Am. Chem. Soc.*, **66**, 1220 (1944).
14) K. R. Kopecky, D. C. Nonhebel, and G. S. Morris, *J. Org. Chem.*, **27**, 1036 (1962).
15) H. F. Bauer and W. C. Drinkard, *J. Am. Chem. Soc.*, **82**, 5031 (1960).
16) E. W. Berg and N. M. Herrera, *Anal. Chim. Acta*, **60**, 117 (1972).
17) H. Veening, W. E. Bachman, and D. M. Wilkinson, *J. Gas. Chromatogr.*, **5**, 248 (1967).
18) D. D. Perrin, W. L. Armarego, and R. D. Perrin, "Purification of Laborary Chemicals," Pergamon Press, Oxford (1966).
19) A. I. Vogel, "Quantitative Inorganic Analysis," 4th ed, Longmans, London (1978).
20) Atomic Weights of the Elements, *Pure Appl. Chem.*, **51**, 409 (1979).
21) CODATA, *J. Chem. Thermodynamics*, **10**, 903 (1978).
22) The N. B. S. Tables of Chemical Thermodynamic Properties, *J. Phys. Chem. Ref. Data*, **11**, (1982). Suplement No. 2.
23) M. F. Koehler and J. P. Coughlin, *J. Phys. Chem.*, **63**, 605 (1959).
24) M. L. C. C. H. Ferrão, M. A. V. Ribeiro da Silva, S. Suradi, G. Pilcher, and H. A. Skinner, *J. Chem. Thermodynamics*, **13**, 567 (1981).
25) A. Aihara, *Bull. Chem. Soc. Jpn.*, **32**, 1242 (1959).
26) R. J. Irving and M. A. V. Ribeiro da Silva, *J. Chem. Soc., Dalton Trans.*, **1975**, 798.
27) E. C. Lingafelter and R. L. Braun, *J. Am. Chem. Soc.*, **88**, 2951 (1966).
28) R. J. Irving and M. A. V. Ribeiro da Silva, *J. Chem. Soc., Dalton Trans.*, **1975**, 1940.
29) R. J. Irving and M. A. V. Ribeiro da Silva, *J. Chem. Soc., Dalton Trans.*, **1975**, 1257.
30) M. A. V. Ribeiro da Silva and A. M. M. Reis, *J. Chem. Thermodynamics*, **15**, 957 (1983).
31) M. A. V. Ribeiro da Silva and M. L. C. C. H. Ferrão, *J. Chem. Thermodynamics*, **19**, 645 (1987).
32) M. A. V. Ribeiro da Silva and M. L. C. C. H. Ferrão, *J. Chem. Thermodynamics*, **20**, 79 (1988).
33) M. A. V. Ribeiro da Silva, M. D. M. C. Ribeiro da Silva, A. P. S. M. Carvalho, M. J. Akello, and G. Pilcher, *J. Chem. Thermodynamics*, **16**, 137 (1984).

 © 1988 The Chemical Society of Japan Bull. Chem. Soc. Jpn., 61, 1761—1765 (1988)

Conductometric Determination of Some Metal Ions Using Oxine as Reagent

Mohamed Tarek Mohamed ZAKI,* Wageh Georgy HANNA, and Mohamed Hossam FAWZY
Department of Chemistry, Faculty of Science, Ain Shams University,
Abbassia, Cairo, Egypt
(Received January 26, 1987)

A simple and sensitive conductometric method for the determination of copper(II), iron(II) and (III), aluminum(III), chromium(III), gold(III), platinum(IV), vanadyl, zirconyl, and uranyl ions with oxine solution in ethanol–water system is described. An average recovery of 100.3% with standard deviation not exceeding 0.4% is observed. The effect of solvent, shape of titration curves and molar ratio of the chelates are studied. The proposed method shows good agreement with the conventional EDTA titration using metallochromic indicators. The advantage over the conventional method is discussed.

Despite the wide application of conductance measurement as a tool for end point detection of acid–base reactions, little attention has been given to complex formation reactions. Conductometric determination of water hardness,[1] divalent metal ions with EDTA[2] or CDTA,[3] silver and mercury ions with cyanide ion[4] and copper(II) chloride with lithium chloride in *N,N*-dimethylformamide[5] have been described.

In the present investigation, oxine (8-hydroxyquinoline) was succesfully used as a chelating agent for the conductometric determination of some metal ions in ethanol–water system (2:1).

Experimental

Reagents. All chemicals used were of analytical grade. The determined metal salts were of the chloride type except for iron (II), vanadyl and zirconyl ions which were of the sulfate type. Bidistilled water of specific conductance, 1.82×10^{-4} S m^{-1} was used throughout. 0.1 M† oxine stock solution in ethanol–water solvent (2:1) was prepared and potentiometrically standardized with a base.[6] 10^{-2} M stock solutions of aqueous metal ions were prepared and standardized using EDTA and metallochromic indicators.[7]

Apparatus. The YSI Model 32M conductance meter [Yellow Spring Co., Inc. (USA)] was used. The measuring range was from 1.0 to 200.0 microsiemens with a maximum error of ±0.2%. Model YSI 3417 cell was used with cell constant K=100/m.

Procedure. 10.0 ml of 10^{-3} M aqueous metal salt solution was transferred to a 50-ml beaker contained 20.0 ml absolute ethanol. The conductance cell was immersed in the solution, which was titrated with 10^{-2} M oxine solution. The conductance was determined after each addiction of the oxine solution. Stirring after each addition was carried out. For an ordinary conductometric titration, a few readings on each side of the anticipated end point are enough. The end point was determined from a graphical plot of conductance vs. milliliters of oxine solution added. All conductance measurements were carried out at 25 °C.

† 1 M=1 mol dm^{-3}.

Results and Discussion

Conductometric titration of metal ions with EDTA in buffer media has been described.[2] However, the presence of high electrolyte concentration affects the end point detection because of the relatively small change in conductance values determined against a relatively high background conductance of the buffer system.[7]

In the present investigation, a conductometric study of the interaction of some metal ions with oxine in absence of buffer has been carried out.

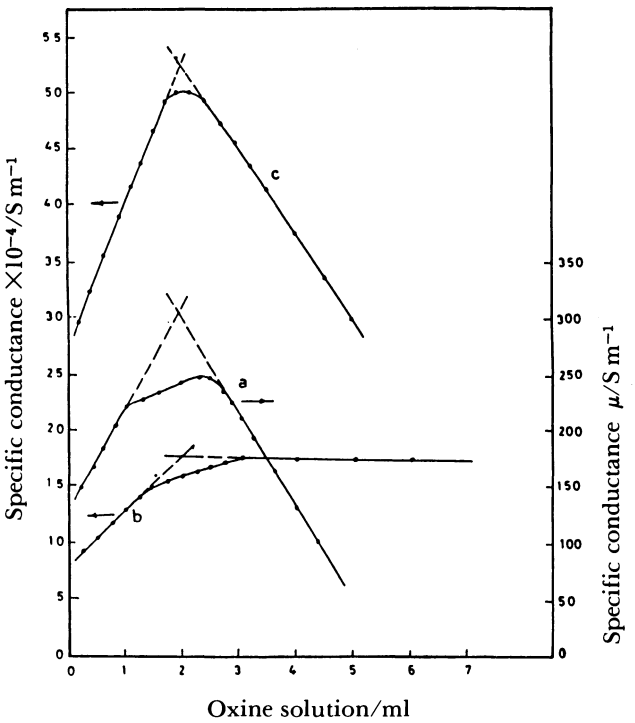

Fig. 1. Conductometic titration curves of (a) 10^{-3} M aqueous copper(II) chloride with 10^{-2} M ethanolic oxine solution, (b) 10^{-3} M ethanolic copper(II) chloride with 10^{-2} M ethanolic oxine solution, and (c) 10^{-3} M copper(II) chloride with 10^{-2} M oxine in ethanol–water system (2:1).

Effect of Solvent. Exploration of the conductometric titration of aqueous copper(II) chloride with ethanolic oxine solution was carried out (Fig. 1-a). However, a wide curvature around the end point was noticed. This is attributed to the formation of a precipitated chelate in aqueous medium. The presence of a precipitate affects conductance value due to the fact that accuracy depends on the speed of precipitation, composition and solubility of the precipitate.

A small curvature around the end point was observed in the titration of ethanolic copper(II) or iron(III) solutions with ethanolic oxine solution (Figs. 1-b and 2-b). However, most of the metal salts studied were insoluble in ethanol.

To overcome the problems of chelate and free metal ion solubility, an ethanol–water system (2:1) was used to prepare the oxine solution and as a medium for the titration.

Shape of Titration Curves. The shape of the titration curve depends on all the species present during the titration. Factors such as viscosity, dielectric constant, solvation, ion-pair association and proton transfer change the shape of the curve.

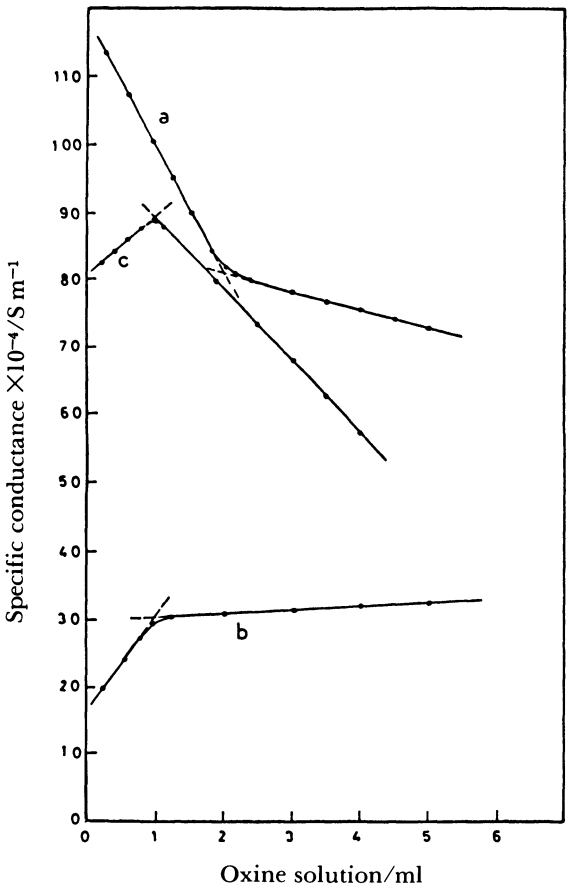

Fig. 2. Conductometric titration curves of (a) 10^{-3} M iron(III) chloride with 10^{-2} M oxine in ethanol–water (2:1), (b) 10^{-3} M ethanolic iron(III) chloride with 10^{-2} M ethanolic oxine solution, and (c) 10^{-2} M iron(III) chloride with 0.1 M oxine in ethanol–water system (2:1).

The conductometric titration of 10^{-3} M copper(II) chloride with 10^{-2} M oxine solution in ethanol–water system (2:1) was performed (Fig. 1-c). The results show an obvious maximum in the conductance curve at a copper(II)–oxine mole ratio of 1:2. The reaction may be represented by the equation:

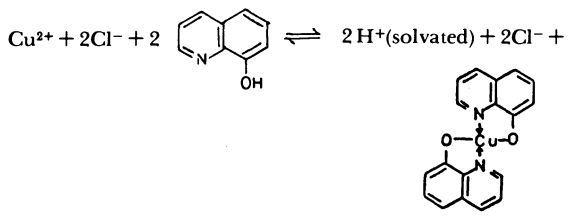

The specific conductance increased at first because each copper(II) ion is replaced by two solvated protons. The interaction of the protons with the solvent depend on the ratio of ethanol–water used.[8]

It was expected that the conductance values would remain constant or slightly increase after the equivalence point, due the the partial dissociation of oxine solution added:

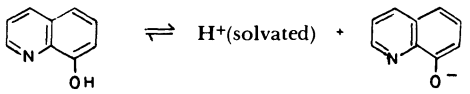

However, after the equivalence point, the conductance of the solution decreased. The decrease may be due to the interaction of the protons available in the titration medium with the added oxine solution:

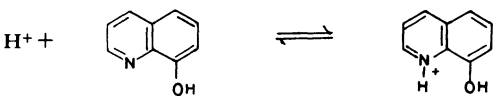

Measurement of the pH before and after the end point shows an increase of about 0.25 pH units indicating the probability of the above reaction. In addition, titration of 10^{-2} M hydrochloric acid in ethanol–water solvent (2:1) with 10^{-2} M oxine solution shows a continuous decrease of specific conductance.

The species which presumably existed before, at, and after the equivalence point are given in Table 1. Similar titration curves were observed for the titration of iron(II), aluminum(III), and vanadyl ions with oxine.

A different behavior in the conductometric titration curve of 10^{-3} M iron(III) chloride with 10^{-2} M oxine solution in ethanol–water solvent was observed (Fig. 2-a). The specific conductance continuously decreased throughout the titration. However, the two rectilinear curves formed gave an easily detected end point. The ions which presumably present through out the titration are given in Table 2. The decrease of conductance before the end point may be attributed to the replacement of the highly mobile iron(III) ions,

Table 1. Species Involved in the Conductometric Titration of Copper(II) Chloride with Oxine Solution in Ethanol-Water (2:1)

Species present before addition of oxine:	Cu^{2+} + 2 Cl^-
	↓ + 2 oxine
Species present at the equivalence point:	2 H^+(solvated) + 2 Cl^- + $[Cu(oxine)_2]$
	↓ + 2 oxine
Species present after the equivalence point:	2 Cl^- + 2 $[H\text{-oxine}]^+$ + $[Cu(oxine)_2]$

Table 2. Ions Involved in the Conductometric Titration of Up to 10^{-3} M Iron(III) Chloride with 10^{-2} M Oxine in Ethanol-Water System (2:1)

Ions present before addition of oxine:	Fe^{3+} + 3 Cl^-
	↓ +2 oxine
Ions present at the equivalence point:	2 H^+(solvated) +3 Cl^- + $[Fe(oxine)_2]^+$
	↓ +2 oxine
Ions present after the equivalence point:	2 $[H\text{-oxine}]^+$ + 3 Cl^- + $[Fe(oxine)_2]^+$

Table 3. Speies Involved in the Conductometric Titration of 10^{-2} M Iron(III) Chloride with 0.1 M Oxine in Ethanol-Water System (2:1)

Species present before addition of oxine:	$FeCl_2^+$ + Cl^+
	↓ + 1 oxine
Species present at the equivalence point:	$[FeCl_2(oxine)]$ + Cl^- + H^+(solvated)
	↓ + 1 oxine
Species present after the equivalence point:	$[FeCl_2(oxine)]$ + Cl^- + $[H\text{-oxine}]^+$

which show abnormally high molar conductance in this medium, by solvated protons and $[Fe(oxine)_2]^+$ ions. The molar conductance of iron(III) chloride in ethanol-water solvent (2:1) is greater than that of hydrochloric acid over the same concentration range of titration. The observed low molar conductance of the formed acid in this solvent is in accordance with that for sulfuric acid in the same solvent.[9] After the end point, the decrease in conductivity is relatively small compared with that noticed in the titration of copper(II)-oxine. This may be attributed to the presence of the charged $[Fe(oxine)_2]^+$ chelate.

However, increasing the concentration of iron(III) chloride ten folds reversed the shape of the titration curve before the end point. Figure 2-c represent the titration of 10^{-2} M iron(III) chloride with 0.1 M oxine solution under identical experimental conditions. This behavior could be explained on the view of incomplete ionization of iron(III) chloride at this relatively higher concentration in the following manner:

$$FeCl_3 \rightleftharpoons FeCl_2^+ + Cl^-$$

Evidence in support of incomplete dissociation as uni-univalent electrolyte in acetone was reported.[10] Also, lanthanum chloride behaves similarly in ethanol.[11] Table 3 shows the expected ions throughout the titration stages. The increase in conductance values before the end point may be attributed to the replacement of $Fe\,Cl_2^+$ ion by H^+(solvated) ion.

A study of the concentration effect for copper(II) chloride solutions was carried out. No change of the shape of the titration curve of 10^{-2}—10^{-3} M copper-(II) chloride with 10^{-1}—10^{-2} M oxine solution were observed. Titration of less than 10^{-3} M copper(II) chloride was not successful.

Similar titration curves to (Fig. 2-a) were observed for the titration of 10^{-3} M chromium(III), gold(III), platinum (IV), zirconyl and uranyl solutions with 10^{-2} M oxine solution using the same experimental conditions.

Metal-Ligand Mole Ratio of the Chelates. The mole ratio of metaloxine chelates were determined from the conductometric titration curves (Table 4-a). It was found that copper(II), platinum(IV), and zirconyl ions form (1:2) chelates with oxine. On the

Table 4-a. Conductometric Determination of Some Metal Ions Using 10^{-3} M Oxine Solution in Ethanol-Water System (2:1)

Metal ion	Weight taken	Weight found	Recovery	Standard deviation	Metal-ligand ratio of chelate
	mg	mg	%	%	
Copper(II)	0.755	0.754	99.9	0.1	1:2
	0.755	0.756	100.0		
	1.511	1.509	99.9		
	1.511	1.510	99.9		
Aluminum(III)	0.284	0.284	100.0	0.4	1:1
	0.284	0.285	100.5		
	0.568	0.569	100.2		
	0.568	0.570	100.3		
Chromium(III)	0.494	0.495	100.2	0.2	1:1
	0.494	0.495	100.2		
	0.988	0.988	100.0		
	0.988	0.989	100.1		
Gold(III)	1.970	1.965	99.7	0.3	1:1
	1.970	1.966	99.8		
	3.940	3.932	99.8		
	3.940	3.933	99.8		
Platinum(IV)	2.262	2.260	99.9	0.1	1:2
	2.262	2.261	100.0		
	4.524	4.525	100.0		
	4.524	4.524	100.0		
Vanadyl	0.510	0.511	100.2	0.4	1:1
	0.510	0.511	100.2		
	1.020	1.021	100.1		
	1.020	1.022	100.2		
Zirconyl	0.910	0.909	99.9	0.3	1:2
	0.910	0.911	100.1		
	1.820	1.822	100.1		
	1.820	1.824	100.2		
Uranyl	2.380	2.377	99.9	0.1	1:1
	2.380	2.381	100.0		
	4.760	4.763	100.1		
	4.760	4.761	100.0		

Table 4-b.

Metal ion	Weight taken	Weight found	Recovery	Standard deviation	Metal-ligand ratio of chelate
	mg	mg	%	%	
Iron(II)	0.532	0.549	103.2	3.7	1:1
	0.532	0.550	103.4		
	1.064	1.097	103.1		
	1.064	1.098	103.2		
Iron(III)	0.588	0.587	99.8	0.2	1:2
	0.588	0.587	99.8		
	1.176	1.175	99.9		
	1.176	1.176	100.0		
Iron(III)[a)]	5.880	5.856	99.6	0.4	1:1
	7.840	7.816	99.7		
	8.820	8.794	99.7		
	11.760	11.740	99.8		

a) 0.1 M oxine soution is used as titrant.

other hand, iron(II), chromium(III), aluminum(III), gold(III), vanadyl, and uranyl ions form (1:1) chelates with the ligand. The mole ration of iron(III)–oxine chelate depends on the original iron(III) concentration (Table 4-b). It was found that up to 10^{-3} M iron (III) forms a (1:2) chelate with oxine while a higher concentration forms a (1:1) chelate. The metal ion octet in the chelate is completed with solvent molecules.

Sensitivity and Precision Down to 0.3 mg of metal ions were successfully determined by conductometric titration with 10^{-2} M oxine solution. The titrant concentration was about ten times that of the metal ion solutions to minimise dilution effect on conductance values throughout the titration. Moreover, dilution correction was carried out using the equation:

$$L_{\text{corrected}} = L_{\text{observed}} \times [(V_1 + V_2)/V_1]$$

where L is the conductance, V_1 the initial volume in the cell and V_2 the volume of added titrant.

Analysis of the data show an average recovery of 100.3% with a standard deviation not exceeding 0.4% (four determinations for each metal ion). However, an average recovery of 103.2% with a standard deviation of 3.7% was observed for the titration of iron(II) sulphate (Table 4-b). The high recovery may be due to the partial oxidation of iron(II) ions. Iron(II) forms (1:1) chelate with oxine whereas low concentrations of iron(III) form (1:2) chelates (Table 4-b).

All experiments have been carried out in a medium of low ionic strength. However, real samples may contain indifferent ions. A study of potassium chloride effect on the conductometric titration curves showed that the method is applicable up to ten fold potassium chloride concentration. Attempts to determine silver(I), thallium(I), nickel(II), palladium-(II), zinc(II), magnesium(II), barium(II), calcium(II), strontium(II), cerium(IV), and molybdenum(VI) were unsuccessful.

Conclusion

The conductometric titration results were in good agreement with the conventional titrimetric method of EDTA using metallochromic indicators. Moreover, the proposed method has the advantage of eliminating the buffer medium and the back titration technique required for some of the measured ions with the conventional method.

We would like to acknowledge the assistance of Dr. W. H. Lee, Department of Chemistry, Surrey University, Guildford, U. K., for his valuable advice.

References

1) G. P. Pasovskaya, *Zh. Anal. Khim.*, **12**, 523 (1957).
2) J. L. Hall, J. A. Gibson, Jr., P. R. Wilkinson, and H. O. Philips, *Anal. Chem.*, **26**, (1954) 1484.
3) F. Vydra and M. Karlik, *Chem. Listy*, **50**, 1749, 1754 (1957).
4) I. M. Kolthoff and P. J. Elving, "Treatise on Analytical Chemistry," Interscience Publishers (1963), Part I, Vol. 4, p. 2618.
5) J. N. Foster, O. C. Hanson, J. F. Hon, and T. S. Muirhead, NASA CR-1425, August (1969) 189.
6) C. F. Richard, R. L. Gustafson, and A. E. Martell, *J. Am. Chem. Soc.*, **81**, 1033 (1959).
7) T. S. West, "Complexometry with EDTA and Related Reagents," 3 rd ed, BDH chemicals Ltd. (1969), p. 83.
8) G. F. Dneprov, Uchenye Zapiski Leningrad. Gosudarst. Univ. im. A. A. Zhdanova No. 169, Ser. Khim. Nauk No. 13 (1953) 56; *Chem. Abst.*, **50**, 5373c (1956).
9) I. Sanghi, D. S. Dater, and S. H. Zaheer, Jr., *J. Chem. Phys.*, **18**, 1415 (1950).
10) L. R. Dawson and R. L. Belcher, *Trans. Kentucky Acad. Sci.*, **13**, 129 (1951).
11) A. M. El-Aggan, D. C. Bradley, and W. Wardlaw, *J. Chem. Soc.*, **1958**, 2092.

 © 1988 The Chemical Society of Japan Bull. Chem. Soc. Jpn., 61, 1767—1771 (1988)

Kinetic Study of the Oxidation of Substituted Benzyl Alcohols by Ethyl Chlorocarbamate

Suman JAIN (nee Mittal) and Kalyan K. BANERJI*
Department of Chemistry, University of Jodhpur, Jodhpur 342001, India
(Received February 23, 1987)

The kinetics of the oxidation of twenty-four monosubstituted benzyl alcohols by ethyl chlorocarbamate (ECC) have been studied in aqueous acetic acid solution, in the presence of perchloric acid. The main product of the oxidation is the corresponding benzaldehyde. The reaction is first order with respect to the alcohol, ECC, and hydrogen ion. The oxidation of [α,α-D_2]benzyl alcohol indicated a primary kinetic isotope effect, k_H/k_D=5.40 at 298 K. The value of solvent isotope effect, $k(H_2O)/k(D_2O)$, is 1.85 at 298 K. Addition of ethyl carbamate does not affect the reaction rate. $[EtOC(OH)NHCl]^+$ has been postulated as the reactive oxidizing species. The rates of oxidation of para- and meta-substituted benzyl alcohols show excellent correlation in Taft's dual substituent parameter equation, with negative reaction constants. The rates of the ortho-substituted compounds correlate well in Charton's equation of inductive, resonance and steric substituent parameters. A mechanism involving simultaneous transfer of a hydride ion from the C–H bond and of a proton from the O–H bond to the oxidant is proposed.

The use of halocarbamates in preparative organic chemistry is well documented.[1] We have been interested in the elucidation of the mechanism of the oxidations by *N*-halogeno reagents for quite some time[2] and have reported the oxidation of aliphatic alcohols by sodium ethyl chlorocarbamate recently.[3] In this article, we report the oxidation of several ortho-, meta-, and para-substituted benzyl alcohols by ethyl chlorocarbamate (ECC) in aqueous acetic acid solution, in the presence of perchloric acid. Attempts have been made to correlate rate and structure in this reaction. The mechanistic aspects are discussed.

Experimental

General. Acetylaminobenzyl alcohols were prepared by the reported methods.[4-6] All other alcohols were commercial products. They were purified by either recrystallization or distillation. [α,α-$^2D_2$]Benzyl alcohol was prepared by the reduction of ethyl benzoate by lithium aluminium deuteride.[7] ECC was prepared by treating ethyl carbamate (Merck) with sodium hypochlorite.[8] Perchloric acid (Merck) was used as a source of hydrogen ions. Deuterium oxide (99.4%) was supplied by BARC, Bombay.

Product Analysis. The product analysis was carried out under kinetic conditions i.e., with an excess of the alcohol over ECC.

In a typical experiment, benzyl alcohol (4.9 g, 0.05 mol) and ECC (1.46 g, 0.01 mol) were made up to 100 ml in 1:1 (v/v) acetic acid–water, in the presence of 0.5 M perchloric acid (1 M=1 mol dm^{-3}). The reaction mixture was allowed to stand in the dark for ca. 12 h to ensure completion of the reaction. It was then treated with an excess of (250 ml) of a saturated solution of 2,4-dinitrophenylhydrazine in 2 M HCl and kept in refrigerator for ca. 10 h. The precipitated 2,4-dinitrophenylhydrazone (DNP) was filtered off, dried, weighed, recrystallized from ethanol, and weighed again. The product was identical (mp and mixture mp) with an authentic sample of DNP of benzaldehyde. The yields of DNP, before and after recrystallization, were 2.75 g (96%) and 2.57 g (90%) respectively. In similar experiments, with other alcohols, the yields of DNP, after recrystallization, were 84 to 93%.

Kinetic Measurements. The pseudo-first-order conditions were attained by keeping a large excess (10-fold or greater) of the alcohol over ECC. The reactions were carried out at constant temperature (±0.1 K) and in flasks blackened from the outside to prevent any photochemical reaction. The reactions were followed iodometrically up to 70% of the reaction. The solvent was 1:1 (v/v) acetic acid–water. The pseudo-first-order rate constant, k_1, was computed from the linear (r>0.98) plots of log[ECC] versus time. The specific rate constant, k, was obtained by the relation $k=k_1/[H^+]\times$[Alcohol]. Preliminary experiments showed that the reaction is not sensitive to ionic strength (0.1—1.0 M) hence no attempt was made to keep it constant. Duplicate kinetic runs showed that the rates were reproducible to within ±3%. The average errors in the values of ΔH^*, ΔS^*, and ΔG^* (at 298 K) are ±3 kJ mol^{-1}, ±5 J mol^{-1} K^{-1}, and ±4 kJ mol^{-1} respectively.

Results

The oxidation of benzyl alcohols by ECC in acid solutions results in the formation of the corresponding benzaldehydes. The overall reaction may be written as follows (Eq. 1).

$$PhCH_2OH + EtOOCNHCl \longrightarrow PhCHO + EtOOCNH_2 + H^+ + Cl^- \quad (1)$$

Rate Laws. The reaction was found to be first order with respect to ECC. Individual kinetic runs were strictly first order with respect to ECC. Further the first-order rate coefficients do not vary with the initial concentration of the oxidant. The effect of variation of the concentration of alcohol on the reaction shows that the reaction is of first order with respect to the alcohol also. The reaction rate increases linearly with an increase in the concentration of hydrogen ion (Table 1).

Isotope Effects. To ascertain the importance of the cleavage of α-C–H bond in the rate-determining step, the oxidation of [α,α-D_2]benzyl alcohol was studied. The results show that the value of primary kinetic isotope effect, k_H/k_D, is 5.40 at 298 K (Table 2).

The oxidation of benzyl alcohol was studied in 95% deuterium oxide. The rate constants for the oxidation in H_2O and D_2O are 10^7k=15.3 and 8.27 $M^{-2}s^{-1}$ respectively at 298 K. The value of solvent isotope effect, $k(H_2O)/k(D_2O)$=1.85. No acetic acid was added in this set of experiments.

Effect of Ethyl Carbamate. Addition of ethyl carbamate has no effect on the rate of oxidation (Table 3).

Induced Polymerization of Acrylonitrile. The oxidation of the alcohols by ECC in an atmosphere of nitrogen, failed to induce polymerization of acrylonitrile. Thus a one-electron oxidation, giving rise to free radicals, is unlikely.

Effect of Substituents. The rates of the oxidation of a series of monosubstituted benzyl alcohols were obtained at different temperatures between 298 and 318 K and the activation parameters were evaluated (Table 4).

Table 1. Rate Constants of the Oxidation of Benzyl Alcohol by ECC at 298 K

10^3[ECC]	[BA]	[H^+]	$k_1\times10^7$
M	M	M	s^{-1}
5.0	0.2	0.5	7.25
10.0	0.2	0.5	7.32
12.5	0.2	0.5	7.47
15.0	0.2	0.5	7.13
20.0	0.2	0.5	7.20
25.0	0.2	0.5	7.25
5.0	0.4	0.5	14.7
5.0	0.6	0.5	22.0
5.0	0.8	0.5	29.0
5.0	1.0	0.5	35.3
5.0	1.5	0.5	54.0
5.0	1.0	0.1	7.30
5.0	1.0	0.2	15.0
5.0	1.0	0.4	28.7
5.0	1.0	0.6	44.0
5.0	1.0	0.8	58.2
5.0	1.0	1.0	75.2

Table 2. Kinetic Isotope Effect in the Oxidation of Benzyl Alcohol by ECC[a)]

[BA]	Type	$k_1\times10^6$
M		s^{-1}
0.4	1,1-H_2	14.7
0.6	1,1-H_2	22.0
0.8	1,1-H_2	29.0
0.2	1,1-D_2	1.35
0.4	1,1-D_2	2.80
0.5	1,1-D_2	3.25
	10^6k_H=7.31 $M^{-2}s^{-1}$	
	10^6k_D=1.35 $M^{-2}s^{-1}$	
	k_H/k_D=5.40	

a) [ECC]=0.005 M, [H]=0.5 M, at 298 K.

Table 3. Effect of Ethyl Carbamate on the Oxidation of Benzyl Alcohol by ECC[a)]

10^3[Ethyl carbamate]/M	0.0	5.0	10.0	20.0
$10^7k_1/s^{-1}$	14.7	14.3	14.5	15.0

a) [ECC]=0.005 M, [Alcohol]=0.4 M, [H^+]=0.5 M, at 298 K.

Table 4. Rate Constants and the Activation Parameters of the Oxidation of Monosubstituted Benzyl Alcohols by ECC

	$10^8k/M^{-2}s^{-1}$			ΔH^*	ΔS^*	ΔG^*
	298 K	308 K	318 K	kJ mol^{-1}	J mol^{-1} K^{-1}	kJ mol^{-1}
H	725	1770	4160	69.0	−105	100
p-NHCOMe	1400	3150	6320	65.1	−105	96.5
p-OMe	4610	7610	14000	44.4	−126	81.8
p-Me	1820	3990	7950	58.1	−113	91.8
p-F	679	1520	4000	69.9	−104	101
p-Cl	247	710	1900	80.8	−97	110
p-NO_2	11.0	63.4	267	126	−56	143
p-COOMe	73.2	157	800	93.4	−87	119
m-NHCOMe	285	675	2460	84.1	−91	111
m-OMe	535	1480	4010	78.9	−93	107
m-OPh	167	500	1320	81.7	−99	107
m-Me	1350	2300	5020	51.5	−125	88.9
m-F	91.4	387	1320	105	−69	126
m-Br	77.7	315	1000	101	−77	124
m-NO_2	8.90	52.6	252	132	−50	147
m-CN	14.6	68.0	310	121	−62	139
o-Me	12600	21300	31700	36.4	−129	74.7
o-F	458	1250	2610	70.0	−107	102
o-Cl	709	1800	5240	78.8	−91	106
o-Br	800	1420	3150	54.3	−126	91.7
o-I	1590	3500	6460	55.4	−118	90.7
o-NO_2	33.3	145	720	121	−54	137
o-NHCOMe	8940	15700	22400	36.4	−132	75.7
o-OMe	6350	12900	19200	43.7	−123	80.6

Discussion

The activation enthalpies and entropies of the oxidation of the alcohols are linearly related (r=0.9864). The correlation was tested and found genuine by applying Exner's criterion.[9] The value of isokinetic temperature determined by Exner's method is 371 K. Current views do not attach much significance to the value of isokinetic temperature.[10] The linear correlation however, is a necessary condition for the validity of linear free energy relationships. It also implies that all the alcohols are oxidized by the same mechanism and the changes in rates are governed by changes in both enthalpy and entropy of activation.

There seems to be no report about the various equilibria and species present in an acidified aqueous solution of ECC. However, based on the reactions of structurally related *N*-haloarenesulfonamides,[11] one can visualize the following equilibria:

$$EtOOCNHCl + H_2O \rightleftharpoons EtOOCNH_2 + HOCl \quad (2)$$

$$2EtOOCNHCl \rightleftharpoons EtOOCNH_2 + EtOOCNCl_2 \quad (3)$$

Hence the probable oxidizing species are ECC, $EtOOCNCl_2$, and HOCl. Ethyl dichlorocarbamate can be ruled out as the oxidizing species in view of the strict first order dependence of the reaction rate on ECC. Moreover, the absence of an effect of ethyl carbamate on the reaction precludes both HOCl and $EtOOCNCl_2$ as the reactive species. Thus, the most likely oxidizing species is EtOOCNHCl. The linear increase in the oxidation rate with acidity suggests that ethyl chlorocarbamate is protonated to give a stronger oxidant and electrophile (Eq. 4).

$$EtOOCNHCl + H_3O^+ \rightleftharpoons \overset{+}{E}tOC(OH)NHCl + H_2O \quad (4)$$

The presence of a primary kinetic isotope effect confirms that the C–H bond is cleaved in the rate-determining step.

The rate of an acid-catalyzed reaction involving the pre-equilibrium proton transfer step[12] is expected to be 2.5—3.0 times faster in D_2O than in H_2O. Labile hydrogens like those present in hydroxyl group undergo rapid exchange in D_2O, and the O–H/O–D isotope effect may neutralize the rate-enhancing effect of D_2O or even result in a slower rate in D_2O. The observed solvent isotope effect ($k(H_2O)/k(D_2O)$=1.85) shows that the k_{OH}/k_{OD} isotope effect is substantially large enough to cancel the effect of D_2O on pre-equilibrium(4). Thus a O–H bond rupture in the rate-determining step is indicated.

Correlation Analysis of Reactivity. (i) Para- and Meta-Substituted Benzyl Alcohols: Since the rates of the oxidation of para- and meta-monosubstituted benzyl alcohols failed to show satisfactory correlation with any single substituent parameter, the rates were subjected to analysis by Taft's[13] and Swain's[14] dual substituent parameter (DSP) equations. The oxidation rates of the *p*- and *m*- substituted compounds were separately correlated with σ_I and four different σ_R substituted constants in Taft's equation[13] and with the field and resonance substituents constants of Swain et al.[14] The results are summarized in Table 5. Both *p*- and *m*-series of substituted benzyl alcohols meet the basic requirements of minimum number of substituents required for the analysis by ESP equation,[15]

The results show that the rates of *p*-substituted benzyl alcohols show excellent correlation with σ_I and σ_R^{BA} values. The correlation with the other σ_R values and in Swain's equation[14] is relatively poor. We have used the standard deviation (SD) and f as the measure of goodness of fit. f has been defined by Dayal, et al.[13] as f=SD/RMS, where RMS is the root mean square of the data points (here $\log k/k_o$). The coefficient of multiple correlation, R, was also determined. The comparison on the f values shows that f is smaller for the σ_R^{BA} scale than those for other scales by the factors of ca. 3 to ca. 7. Therefore, it is apparent that the rates of the oxidation of *p*-substituted benzyl alcohols by ECC correlate best with σ_I and σ_R^{BA} values.

The rates of the oxidation of *m*-substituted compounds show excellent correlation with σ_I and σ_R^o

Table 5. Correlation of the Rates of the Oxidation of Para- and Meta-Substituted Benzyl Alcohols by ECC with Dual Substituent Parameters[a]

σ_R^o		σ_R^{BA}		σ_R^-[b]		σ_R^+		Swain et al.[c]	
SD	f	SD	f	SD	f	SD	f	SD	f
				Para-substituted					
0.09	0.11	0.03	0.04	0.21	0.24	0.21	0.26	0.11	0.13
				Meta-substituted					
0.03	0.03	0.06	0.06	0.09	0.09	0.11	0.11	0.07	0.07

a) Temperature 298 K, SD=standard deviation, f=SD/RMS of $\log k/k_o$, σ_I and σ_R values are from Ref. 13. b) Data for NHCOMe and OPh were not considered, σ_R^- values are not available. c) Field and resonance substituents constants are from Ref. 14.

Table 6. Temperature Dependance of the Reaction Constant[a]

Temp/K	ρ_I	ρ_R[b]	λ	R	SD	f
			Para-substituted			
298	−2.27	−2.35	1.04	0.9996	0.03	0.04
308	−1.87	−2.00	1.07	0.9923	0.10	0.11
318	−1.51	1.58	1.05	0.9986	0.04	0.06
			Meta-substituted			
298	−2.70	−1.28	0.47	0.9995	0.03	0.03
308	−2.06	−1.10	0.53	0.9944	0.07	0.09
318	−1.73	−1.05	0.61	0.9825	0.11	0.16

a) R=Coefficient of multiple correlation, $\lambda=\rho_R/\rho_I$, SD=standard deviation, f=SD/RMS of $\log k/k_o$. b) ρ_R is ρ_R^{BA} and ρ_R^o for para- and meta-substituted compounds respectively.

substituent constants, though the discriminating factor for the precision of fit with the other σ_R scales or in Swain's equation[14] is not as sharp as in the case of *p*-substituted compounds. In fact the correlation with σ_R^{BA}, $\sigma_{\bar{R}}$, and in Swain's equation meet the requirement[16] for a satisfactory fit ($f<0.1$). Even the correlation with σ_R^+ is not very poor. This agrees with the observation of Ehrenson, Brownlee and Taft[16] that the correlation of *m*-substituted compounds is generally best with σ_R^o constants and *m*-substituted compounds are less discriminating.

The reaction constants and statistical data at different temperatures are given in Table 6.

The value of λ^p (1.05) shows that the oxidation of *p*-substituted compounds is almost equally susceptible to localized and delocalized effects. The selectivity of the reaction decreases at higher temperatures and the decrease is of similar order for both the localized and delocalized effects, reflected in the almost constant value of λ^p at different temperatures.

In the oxidation of *m*-substituted compounds, the values of λ are between 0.47 and 0.61, suggesting the greater importance of the localized effect. In this case, at higher temperatures, the decrease is more pronounced in the localized reaction constant, resulting in a gradual increase in the value of λ^m with an increase in the temperature.

(ii) **Ortho-Substituted Benzyl Alcohols:** The rates of the oxidation of *o*-substituted benzyl alcohols were analyzed in the terms of Taft's polar and steric substituent constants separately.[17] The results are given in Eqs. 5 and 6.

$$\log k/k_o = -2.10\,\sigma_o^* \quad (5)$$

$R=0.9324$; SD=0.41; $n=8$

$$\log k/k = -0.33\,E_s \quad (6)$$

$R=0.2783$; SD=0.54; $n=8$

The substituent NHCOMe was not included since the substituent constants are not available. The results show that the observed reactivity is not compatible with either the size of the substituents or with their Taft's polar substituent constant.

Since the single parameter equations did not yield satisfactory correlations, the rates were analyzed using Charton's method.[18] The rate constants were correlated with Eqs. 7 and 8, where σ_I, σ_R, and V are inductive, resonance, and steric substituent constants respectively and the values used were those compiled by Aslam et al.[19]

$$\log k_{ortho} = \alpha\sigma_I + \beta\sigma_R + h \quad (7)$$

$$\log k_{ortho} = \alpha\sigma_I + \beta\sigma_R + \phi V + h \quad (8)$$

In multiple regression analysis using Eq. 7, the correlation coefficient is poor and the standard deviation is high (Eq. 9).

$$\log k_{ortho} = -2.66\sigma_I - 2.21\,\alpha_R - 4.66 \quad (9)$$

$R=0.8714$; SD=0.45; $n=9$

The absence of a significant correlation with Eq. 7 leads to the conclusion that the electrical effects alone are not sufficient to account for the ortho-substituent effect in this reaction.

The correlation with Eq. 8 were performed at temperatures 298, 308, and 318 K. The results are given in Eqs. 10—12 respectively.

$$\log k = -3.01\,\sigma_I - 2.04\sigma_R + 1.58V - 5.10 \quad (10)$$

$R=0.9962$; SD=0.09; $n=9$

$$\log k = -2.57\sigma_I - 1.79\sigma_R + 1.27V = 4.96 \quad (11)$$

$R=0.9877$; SD=0.14; $n=9$

$$\log k = -1.97\sigma_I - 1.25\sigma_R + 0.98V - 4.30 \quad (12)$$

$R=0.9827$; SD=0.15; $n=9$

The effect of *o*-NO_2 group is consistent with the orthogonal conformation.

The significance of the correlation was tested by means of an F-test. The confidence levels for the F-test are greater than 99%. The confidence levels for

the significance of α, β, and ϕ terms were obtained by means of a Student's T-test. The confidence level of the T-test is >99%, indicating the operation of significant inductive, resonance and steric effects. These results show that this reaction belongs to Case 1 of the classification given by Charton.[18]

The contribution of the resonance effect to the polar effect[18] is given by Eq. 13.

$$p_R = \frac{100|\beta|}{|\alpha| + |\beta|} \quad (13)$$

The value of P_R is found to vary between 38.8 and 41.1. This shows that the inductive effect is more pronounced than the resonance effect. The contribution of the steric effect, p_S, was calculated using the Eq. 14.

$$p_S = \frac{|\phi|\ 100}{|\alpha| + |\beta| + |\phi|} \quad (14)$$

The percentage contribution of the steric effect is ca. 23%, pointing to a considerable steric effect in the reaction.

Mechanism. The presence of a primary kinetic isotope effect confirms that in the rate-determining step, α-C–H bond is cleaved. In this respect this reaction resembles the oxidation by chloramine-B and bromamine-B.[2] However, it differs from the other oxidations in the observation of a solvent isotope effect. In the oxidations by chloramine-B and bromamine-B[2] the rate in D_2O is more than that in H_2O. This indicates that the rupture of the O–H bond is also taking place in the rate-determining step. Thus a simultaneous transfer of a hydride ion from the C–H bond and a proton from hydroxyl groups is indicated (15). The negative polar reaction constants points to an electron-deficient carbon center in the transition state. The correlation of the rates of *p*-substituted benzyl alcohols with σ_R^{BA} constants also suggests a weak resonance interaction between a developing positive center and the substituent. Thus it seems that in the transition state the cleavage of the C–H is somewhat ahead of the rupture of the O–H bond. However, it may be mentioned here that the formation of a carbonyl group is also expected to be favored by an electron-releasing substituent.

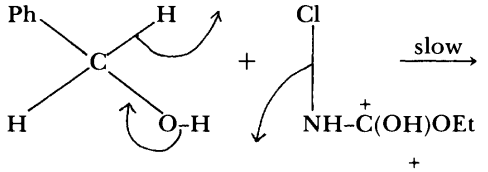

$$PhCHO + HCl + H_2N\overset{+}{C}(OH)OEt \quad (15)$$

$$H_2N\overset{+}{C}(OH)OEt \xrightarrow{fast} H_2NCOOEt + H^+ \quad (16)$$

The positive regression coefficient for the steric term corresponds to a steric acceleration of the reaction by the ortho-substituent. This can be explained on the basis of high ground state energy level of the starting material. Since the crowding is relieved in the product aldehyde as well as in the transition state leading to it, the transition state energy of the crowded (ortho-stbstituted) and uncrowded alcohols do not differ much and steric acceleration, therefore, results.

Thanks are due to the University Grants Commission, India, for the financial support.

References

1) M. M. Campbell and G. Johnson, *Chem. Rev.*, **78**, 65 (1978).
2) J. Mukherjee and K. K. Banerji, *J. Chem. Soc., Perkin Trans. 2*, **1980**, 676; *Indian J. Chem. Sec. A*, **20**, 394 (1981); S. Kothari and K. K. Banerji, *Can. J. Chem.*, **63**, 2726 (1985); S. Kothari, V. Sharma, and K. K. Banerji, *J. Chem. Res. (S)*, **1985**, 234; *J. Chem. Res. (M)*, **1985**, 2371.
3) S. Mittal, V. Sharma, and K. K. Banerji, *Int. J. Chem. Kinet.*, **18**, 689 (1986).
4) *Org. Synth.*, Coll. Vol. III, 60 (1963).
5) R. Grice, *J. Chem. Soc.*, **1963**, 1947.
6) J. E. Bloor, *Tetrahedron*, **20**, 861 (1964).
7) J. F. Bunnett, G. V. Gavies, and H. Tanida, *J. Am. Chem. Soc.*, **84**, 1606 (1962).
8) C. Bachand, D. Hughes, J. M. Paton, T. Daniel, and J. Lessard, *J. Org. Chem.*, **39**, 3137 (1974).
9) O. Exner, *Collect. Czeck. Chem. Commun.*, **29**, 1094 (1964).
10) J. E. Leffler, *J. Org. Chem.*, **31**, 533 (1966).
11) J. C. Morris, J. A. Salazar, and M. A. Wineman, *J. Am. Chem. Soc.*, **70**, 2036 (1948).
12) N. S. Bowman and C. J. Collins, "Isotope Effects in Chemical Reactions," Van Nostrand, New York (1971), p. 267.
13) S. K. Dayal, S. Ehrenson, and R. W. Taft, *J. Am. Chem. Soc.*, **90**, 9113 (1972).
14) C. G. Swain, S. H. Unger, N. R. Rosenquist, and M. S. Swain, *J. Am. Chem. Soc.*, **105**, 492 (1983).
15) J. Shorter, "Correlation Analysis of Organic Reactivity," Research Studies Press, Chichester (1982), p. 50.
16) S. Ehrenson, R. T. C. Brownlee, and R. W. Taft, *Prog. Phys. Org. Chem.*, **10**, 1 (1973).
17) R. W. Taft, "Steric Effects in Organic Chemistry," ed by M. S. Newman, John Wiley, New York (1956), Chap. 13.
18) M. Charton, *J. Org. Chem.*, **40**, 407 (1975).
19) M. H. Aslam, A. G. Burdon, N. B. Chapman, J. Shorter, and M. Charton, *J. Chem. Soc., Perkin Trans. 2*, **1981**, 500.

Liquid Crystalline Catalysis. Kinetics of the Rearrangement of Allyl *p*-(Dimethylamino)benzenesulfonate in a Smectic B-Solvent

Paolo De Maria,* Bruno Samorì,† Anna Tampieri,† and Paolo Zani†
Dipartimento di Chimica Organica, Via Archirafi 20, 90123 Palermo, Italy
†Dipartimento di Chimica Organica, Viale Risorgimento 4, 40136 Bologna, Italy
(Received March 9, 1987)

Allyl *p*-(dimethylamino)benzenesulfonate (ASE) was found to promptly rearrange to the corresponding quaternary zwitterion (AZWI) in a smectic, liquid crystalline solvent (OS 35) 4-pentylcyclohexyl 4-propylcyclohexanecarboxylate. On the contrary, this reaction does not occur in isotropic solvents. In the present study we investigate the effect of temperature and of reactant concentration on the reaction rate. A plot of log k vs. $1/T$ shows a strog upward curvature. In addition, the rate constant, k, strongly depends on ASE concentration: relevant rate depression occurs beyond a threshold value of solute concentration, which in turns depends on temperature. These results are interpreted in terms of reaction mechanism and solute-solvent interaction. From these results we can conclude that smectic B phase has a strong catalytic effect on this particular kind of nucleophilic displacement. Furthermore, catalysis does not depend on solute expulsion from the bulk of the phase; finaly, the detailed mechanism of the catalytic effect may depend on the different location of the solute in distinct solubilization sites existing within the smectic mesophase.

In view of the interest in the field of reactivity within anisotropic media,[1a—e] we have recently exploited the use of smectic (Sm) mesophases in order to prove catalytical effects that the internal organization of these mesomorphic solvents can exert on properly chosen model reactions. Particularly we have reported that smectic B (SmB) solvents (ZLI 1409;[2a,b] ZLI 1544;[2a] ZLI 1756;[2c] OS 44;[2b] OS 53;[2d] OS 35;[2d]) can induce relevant rate variations on the quaternization reaction of *p*-(dimethylamino)benzenesulfonic esters (Scheme 1). The rearrangement of pure solid methyl *p*-(dimethylamino)benzenesulfonate (MSE) to the corresponding quaternary ammonium zwitterion (Scheme 1) was previously described as an example of reaction promoted by appropriate intermolecular orientations in the solid phase.[3] On the contrary allyl *p*-(dimethylamino)benzenesulfonate (ASE) does not rearrange in its crystalline state because of a different kind of molecular orientation within the crystal lattice.[4]

When both esters (MSE and ASE) are dissolved in SmB mesophases a very clean quaternization reaction (Scheme 1) is promoted at a rate higher than that in the melts. On the other hand MSE and ASE do not react at any detectable rate when dissolved in common organic (isotropic) solvents or even in the nematic (N) phases of the investigated liquid crystals. This is the first instance in which Sm solvents are shown to promote a rearrangement which requires a precise orientational control to take place.

Now we report here a more complete kinetic treatment showing the peculiar effects of solute concentration and temperature on the rate of ASE quaternization which are not explainable in the framework of reactivity in common (isotropic) solvents but require a detailed knowledge of the phase equilibria within the SmB liquid crystalline solvent.

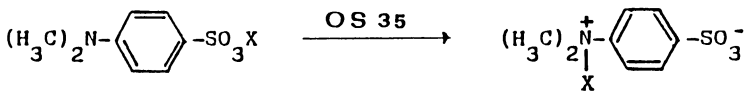

X: CH_3: MSE; MZWI

CH_2-CH=CH_2: ASE; AZWI

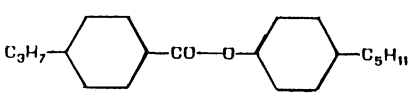

OS 35

Scheme 1.

Results

We have published preliminary results[2] from which it stems that the quaternization reactions of ASE and MSE (Scheme 1) are simple second order processes and that the mechanisms, most likely, are dimeric, S_N2' type pathways. However these are limited results as those concerning MSE were obtained in a liquid-crystalline solvent (ZLI 1409) which is not transparent in the spectral region where reactant and product do absorb. The opacity of the solvent to UV light prevented us from following the reaction course directly. The results concerning ASE were obtained at a single temperature and within a narrow range of solute concentrations. From our previous work it emerged that most kinetic features remained to be clarified. A study of the change of the observed rate constant, k, with temperature was still to be done in order to provide useful information on the activation parameters, and, therefore, on the mechanistic details of the assistance assured by the liquid crystalline solvent to the reaction. In fact, interesting temperature effects have been recently observed by Weiss and collaborators in reactions performed within liquid crystalline phases.[5]

Temperature Effect. Kinetic measurements on ASE conversion to AZWI were carried out in the temperature interval $44>T>28$ °C in the SmB phase of the OS-35 liquid crystalline solvent. Provided that the concentration of ASE was less than that of the threshold value (see below), k is strictly second order at each individual temperature. The values of k at the different temperatures and the investigated concentration ranges where k turned out to be strictly second order are reported in Table 1. An Arrhenius-type plot of log k vs. $1/T$ (Fig. 1) shows a strong upward curvature. Apparently log k tends to infinity when T approaches the transition (SmB→N) temperature of 49 °C. However because of the superimposed concentrations effect (see following section) the temperature interval $44<T<49$ °C is not experimentally accessible to our kinetic technique. For example, even at 44 °C k is rigorously independent of ASE concentration only when [ASE]$<10^{-2}$ mol·dm^{-3}.

Concentration Effect. The observed second order rate constant, k, is by no means independent of total solute concentration at "high" initial ASE concentration. It sharply decreases beyond a definite value of concentration, which, in turn, depends on temper-

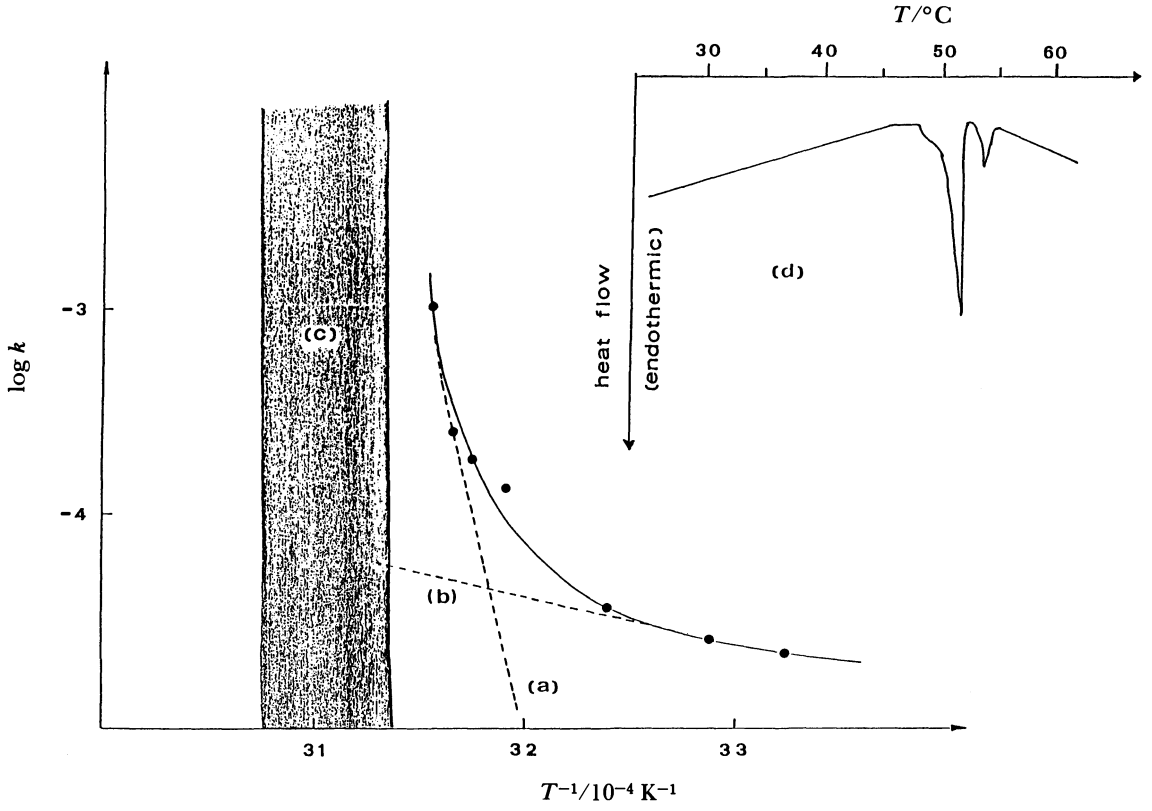

Fig. 1. Arrhenius-type plot for the ASE quaternization in OS 35 SmB phase at ASE concentrations lower than those of the temperature-dependent threshold values (see text and Fig. 2). Lines (a) and (b) are hypothetical straight lines extrapolated from the higher- and lower-temperature data, respectively. The shaded area (c) represents the temperature interval corresponding to the width of the Differential Scan Calorimetry (DSC) peak in (d). Profile (d) is the DSC trace showing the Smectic→Nematic and Nematic→Isotropic transition for the reacting solution at ASE concentration equal to 1.05×10^{-2} mol·dm^{-3}.

ature. The dependence of k on concentration, at one temperature (40 °C), is graphically depicted in Fig. 2. We have evidence that the concentration value at which rate depression starts (threshold concentration), dramatically decreases with increasing temperature. For example, while k is practically coincident with the values determined in more dilute solutions at 36 °C and initial [ASE] 10^{-1} mol·dm^{-3}, at 44 °C and initial [ASE] $2\cdot10^{-2}$ mol·dm^{-3} k is some 20 times lower than the values determined in dilute solutions (Table 1). More dramatically, at 47 °C, where the solvent is still in its smectic phase, disappearance of ASE was not detected after 11 days even at initial [ASE] as low as 5×10^{-4} mol·dm^{-3}

Discussion

The "real" catalytic effect of OS 35 SmB mesophase

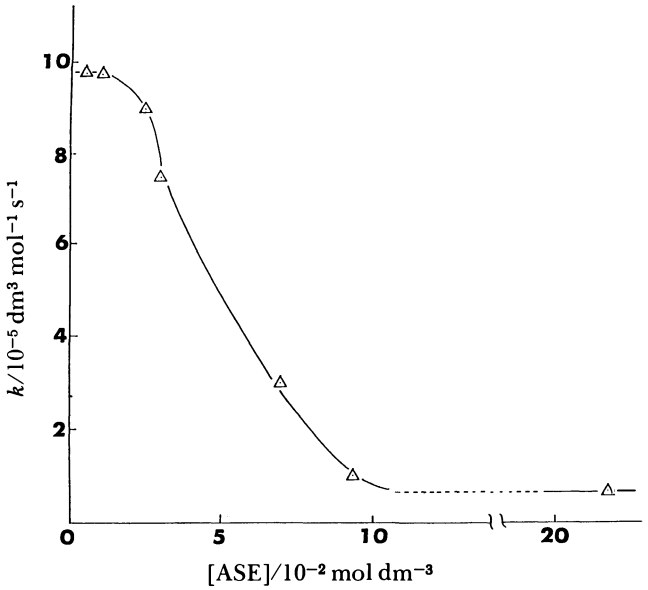

Fig. 2. Dependence of the kinetic constant on the solute concentration at 40 °C. The threshold value of ASE concentration at which rate depression starts and the second-order constant becomes dependent on total solute concentration is clearly displayed.

on the ASE quaternization is clearly displayed by the following data. Whereas 15% conversion to AZWI is achieved in one day at 44 °C in the melt phase, 67% conversion can be obtained in SmB diluted solutions under the same conditions of temperature and time. Moreover we found total conversion of ASE after five days in OS 35 at 44 °C and only after 26 days in the pure melt. From the kinetic data at different temperatures (Fig. 1) it can be seen that the second-order rate constant increases with temperature far more than predicted by a "normal" Arrhenius behavior. To explain this anomalous curvature the most likely reason is that the assistance provided by the SmB solvent is varying with temperature and that this effect is being superimposed upon the "normal" Arrhenius behavior.

The rate breakdown observed with increasing "total" solute concentration also deserves some comments. The sigmoidal shape (Fig. 2) can be explained by a very sudden loss of solvent cooperative effects on the reaction. This discontinuity resembles those observed for thermodynamic parameters in phase transitions.[6] In addition this is further clearcut evidence that the liquid crystalline catalysis cannot be ascribed only to solute bulk aggregation out of the solution. Optical microscopy shows[7] that such solute aggregation occurs only at the highest [ASE] concentrations where the reaction rate becomes very low. Turning again to the temperature effect, one can recall that in general cases the simplest explanation of a curved Arrhenius plot (as in Fig. 1) is the existance of two competitive reaction mechanisms[8] each with its own A and E_a values (sketched by lines (a) and (b) in Fig. 1) and dominating in two different temperature intervals. Therefore a breakdown from linearity occurs at intermediate temperatures when both mechanisms are operating. However this often happens over a temperature interval much wider than the present one. Furthermore two independent mechanisms are hardly conceivable for ASE quaternization. On the contrary our results can be better explained considering that our reaction was not a single-step process due to the occurrence of the reaction in more than one catalytic site provided by

Table 1. Temperature Effect on the Second-Order Rate Constant k in the Quaternization Reaction of ASE in OS 35 SmB-Solvent

Temperature/°C	k/dm^3 mol^{-1} s^{-1}	[ASE]/mol dm^{-3}(intervals)[a]	
28	2.5×10^{-5}	9.8×10^{-3}	2.45×10^{-2}
31	2.7×10^{-5}	9.8×10^{-3}	2.45×10^{-2}
36	3.3×10^{-5}	9.8×10^{-3}	1.00×10^{-1}
40	9.8×10^{-5}	9.8×10^{-3}	1.00×10^{-2}
42	13.0×10^{-5}	4.9×10^{-3}	9.8×10^{-3}
43	15.0×10^{-5}	4.9×10^{-3}	9.8×10^{-3}
44	45.0×10^{-5}	4.9×10^{-3}	9.8×10^{-3}

a) Investigated concentration intervals of ASE where k is strictly second order. At higher values, depending upon temperature, k decreases with [ASE] as discussed in concentration effect.

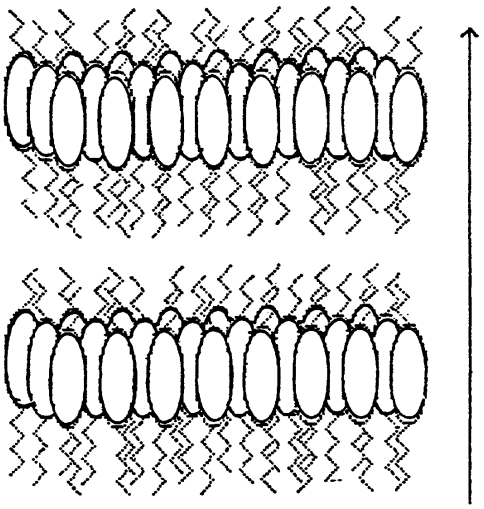

Fig. 3. Layered structure of Sm liquid crystalline media. The rigid-core- and alkyl-chain-sublayers are sketched by ellipsoids and tails respectively.

the solvent. In fact we recently presented evidence[7] arising from linear dichroism (LD) that ASE molecules are located in two different sites within the SmB phase of OS 35.

OS 35 molecules have a fairly rigid core and flexible alkyl chains. This molecular shape leads to a layered structure for the SmB, in which alternating sequencies of sublayers are determined by the alignment in planes of the centers of gravity of adjacent cores or of adjacent tails (Fig. 3). The rigid cores and the more flexible aliphatic tails may therefore provide two distinct solubilization sites for ASE. The LD technique revealed that one site, (characterized by an ASE absorption maximum at 263 nm in the LD spectrum) is more ordered and differently populated than the other (LD maximum at 277 nm). This more ordered site is likely provided by the core. In addition it appears from the same LD data that the partition of ASE between these two sites strongly depends upon temperature. These results may be interpreted in kinetic terms as a sort of pre-equilibrium type situation in which the nature and relative population of the two sites are strongly temperature dependent. Within this framework the concave shape of Fig. 1 should be explained as a positive deviation at lower temperature from the Arrhenius line (a). Similar but far less pronounced effects played by cooperative solvent assistance were recently found even in isotropic solvents such as 2-buthoxyethanol–water and *t*-butyl alcohol–water neutral ester hydrolysis.[9a,b] These effects also led to curvatures in the Arrhenius plots and were attributed to the assistance by aggregates (called "moving units") whose formation depends in a nonlinear manner upon temperature and molar fraction of the solvents.

Experimental

ASE was prepared as previously described.[2b,3] After 2 recrystallizations from petroleum ether (bp 40—60 °C) a material of mp 39—40 °C was obtained. OS 35 was kindly supplied by E. Merck (Darmstädt).

Kinetic Measurements. The general procedure employed can be summarized as follows: ASE was dissolved in the OS 35 solvent (0.1 g. samples) at 50 °C by quick injections of volumes of a diethyl ether solution of known concentration. After complete evaporation of the ether, the homogeneous solution of ASE was rapidly cooled down into its SmB phase by immersion in a bath thermostatted at the desired temperature. Portions (ca. 0.01 g) of the reaction mixture were taken at appropriate intervals and the reaction quenched by dilution with RS-grade ethanol (5 cm^3). The absorbance of these ethanolic solutions of ASE was determined with a Beckmann DU or a Varian spectrophotometer at λ=284 nm. The kinetics were followed[2d] over at least three half lives and were second order according to the equation $-d[ASE]/dt=k[ASE]^2$

Least-squares-slopes of these second order plots gave average rate constants, k, accurate to ±8% at worst.

DSC Measurements. DSC measurements were carried out on a Perkin Elmer Calorimeter Model DSC-2. scan rate was 1 °C min^{-1}. Aluminium containers of 20×10^{-6} dm^3 capacity were used.

We thanks Prof. D. Spinelli (Bologna) and Dr. B. G. Cox (University of Stirling) for helpful discussions. Technical assistance by Dr. Teresa Mutalipassi is also gratefully acknowledged.

References

1) a) R. G. Zimmermann, J. H. Lin, and R. G. Weiss, *J. Am. Chem. Soc.*, **108**, 5264 (1986) and references therein; b) S. Ganaphathy, R. G. Zimmermann, and R. G. Weiss, *J. Org. Chem.*, **51**, 2529, 2535 (1986); c) W. J. Leigh, *Can. J. Chem.*, **64**, 1130 (1986); d) W. J. Leigh, *J. Am. Chem. Soc.*, **107**, 6114 (1985); e) D. A. Hrovat, J. H. Liu, N. J. Turro, and R. G. Weiss, *ibid.*, **106**, 7033 (1984); f) D. A. Hrovat, J. H. Liu, N. J. Turro, and R. G. Weiss, *ibid.*, **106**, 5291 (1984); g) M. J. S. Dewar and B. D. Nahlovsky, *ibid.*, **96**, 460 (1974); h) W. E. Bacon, L. K. Jun, and G. H. Brown, *Mol. Cryst. Liq. Cryst.*, **56**, 13 (1979).

2) a) B. Samorì and L. Fiocco, *J. Am. Chem. Soc.*, **104**, 2634 (1982); b) P. DeMaria, A. Lodi, B. Samorì, F. Rustichelli, and G. Torquati, *ibid.*, **106**, 653 (1984); c) S. Melone, V. Mosini, R. Nicoletti, B. Samorì, and G. Torquati, *Mol. Cryst. Liq. Cryst.*, **98**, 399 (1983); d) P. De Maria, P. Mariani, F. Rustichelli, B. Samorì, *ibid.*, **116**, 115 (1984).

3) C. N. Sukenik, J. A. P. Bonapace, S. H. Mandel, Pin-Yan Lou, G. Wood, and R. G. Bergman, *J. Am. Chem. Soc.*, **99**, 851 (1977).

4) E. Foresti, B. Samorì, and P. Zani, *Mol. Cryst. Liq. Cryst.*, in press.

5) V. C. Anderson and R. G. Weiss, *J. Am. Chem. Soc.*, **106**, 6628 (1984); V. C. Anderson, B. B. Craig, and R. G. Weiss, *ibid.*, **104**, 2972 (1982); J. M. Nerbonne and R. G.

Weiss, *ibid.*, **100**, 5953 (1978).

6) D. E. Martire, "Thermodynamics of phase transitions" in "the Molecular Physics of Liquid Crystals," ed by G. R. Luckhurst and G. W. Gray, Academic Press (1979), Chap. 1.

7) P. De Maria, P. Mariani, F. Rustichelli, B. Samorí, and P. Zani, "Reactivity within Smectic B liquid Crystalline phases," in "Organic Chemistry in anisotropic media," Symposium in print. *Tetrahedron*, **1987**, 1409.

8) J. W. Moore and R. G. Pearson. "Kinetic and Mechanism," J. Wiley & Sons, New York (1981), Chap. 2.

9) a) L. T. Kanerva, *J. Chem. Soc., Perkin Trans. 2*, **1983**, 467. b) L. T. Kanerva, *ibid.*, **1983**, 1573.

 © 1988 The Chemical Society of Japan Bull. Chem. Soc. Jpn., 61, 1779—1783 (1988)

Molecular Rearrangements. XXIX.† Thermolysis of Aromatic Ketoximes

M. Z. A. Badr,* M. M. Aly, S. A. Mahgoub, A. M. Fahmy, and A. A. Atallah
Chemistry Department, Faculty of Science, Assiut University, Assiut, A. R. E.
(Received March 30, 1987)

Thermolysis of benzophenone *O*-benzoyloxime leads to the formation of NH_3, CO_2, benzene, biphenyl, benzophenone, benzanilide, benzonitrile, benzoic acid, 2-phenylbenzoxazole, salicylaldehyde and its *p*-isomer. Analogous results were also obtained on thermolysis of acetophenone *O*-benzoyloxime. Similarly, benzophenone and/or acetophenone *O*-benzyloximes give pyrolysis products of the same nature in addition to others corresponding to the benzyl moiety. Thermolysis of deoxybenzoin oxime gives NH_3, toluene, benzonitrile, bibenzyl, benzil, benzyl alcohol, and 2-phenylindole. Moreover, its *O*-benzoyl ether affords in addition to these products, benzoic acid and benzyl benzoate. The main feature of these pyrolyses is the homolysis of the N–O bond together with either *O*-benzyl or *O*-benzoyl bonds providing free radicals that undergo different reactions involving H-abstraction, dimerization, fragmentation, rearrangement and cyclization to form the identified products.

Benzophenone oxime was reported earlier not to undergo the well-known Beckmann rearrangement on heating between 100 and 150 °C although the oxime salt is characterized by this reaction irreversibly to give mainly benzanilide.[1] However, prolonged heating under these conditions leads to hydrolysis of benzanilide into aniline and benzoic acid. The photo-Beckmann rearrangement of benzaldehyde oximes to the corresponding amides was suggested at one time to proceed through the intermediate oxaziridines.[2] On the other hand, other workers found that *N,O*-diacylhydroxylamines on pyrolysis can act as free-radical initiators for polymerization.[3]

Recently, flash vacuum pyrolysis of acetophenone and/or benzophenone oximes[4] affords nitriles, benzoxazoles, arenes and biaryls which were presumably formed from both iminyl and iminoxyl radicals. Moreover, isomerization of benzophenone oxime into benzanilide was also observed to take place in the ion source of mass spectrophotometer and the process was attributed to a Beckmann-type rearrangement of the corresponding molecular ion via a thermal mechanism.[5] Such results prompted us to reinvestigate the thermal Beckmann rearrangement in order to add more clear mechanistic information. The present work deals with the thermolysis of *O*-benzoyl- and/or *O*-benzyl oximes of acetophenone and benzophenone.

Pyrolysis of benzophenone *O*-benzoyloxime by reflux in air for 30 min leads to the formation of ammonia, carbon dioxide, benzene, biphenyl, benzophenone, benzanilide, benzonitrile, and benzoic acid.

When thermolysis was affected by heating in a sealed tube under nitrogen atmosphere, at 200 °C for 8 h, the previous products were obtained in addition to 2-phenylbenzoxazole, salicylaldehyde and its *p*-isomer; whereas the yield of benzoic acid was greatly suppressed.

Thermolysis of acetophenone *O*-benzoyloxime gives ammonia, carbon dioxide, biphenyl, acetophenone, acetanilide, acetonitrile, 2-methylbenzoxazole, and benzoic acid.

The formation of these products can be assumed to follow the series of reactions shown in Scheme 1, which implies the preliminary homolysis of benzoyl–O bond (route a) forming iminoxyl and benzoyl radicals. The iminoxyl radicals may undergo the Beckmann rearrangement into the corresponding *N*-acylanilide which is rationalized to proceed through a mechanism involving an oxaziridine intermediate **1** and a biradical intermediate **2**.[6]

The formation of acetanilide, in case of acetophenone oximes under the present conditions, rather than its isomer *N*-methylbenzamide provides strong evidence for the selective migration of the phenyl as compared with the methyl group. This result is in agreement with the observed migratory aptitude values of such groups and can be explained in terms of the stability of the bridged intermediate radical **3** as compared with the corresponding intermediate of methyl migration.[7] In other cases alkyl migration has been recorded.[8] The iminoxyl radicals may abstract hydrogen forming the corresponding unsubstituted oxime, which subsequently undergoes homolysis of the N–O bond to form iminyl and hydroxyl free radicals. The iminoxyl radicals can undergo cyclization into benzoxazole derivative.[4]

The iminyl radicals may abstract hydrogen forming the corresponding imine which is considered to be the precursor of ammonia and the corresponding ketone during working-up processes.

The formation of salicylaldehyde and its *p*-isomer may be due to coupling of hydroxyl radicals in the *o*- and/or *p*-positions of the tautomeric benzoyl radicals.

Such a mechanism was further emphasized by the results obtained from the thermolysis of unsubstituted benzophenone oxime where ammonia, benzophen-

† Part (XXVIII), Photolysis and Thermolysis of Aryl Hydroxamic Acids. M. Z. A. Badr, A. M. Fahmy, S. A. Mahgoub, and M. M. Aly; XI IUPAC Symposium on Photochemistry; July 27 (1986); Lisboa; Portugal.

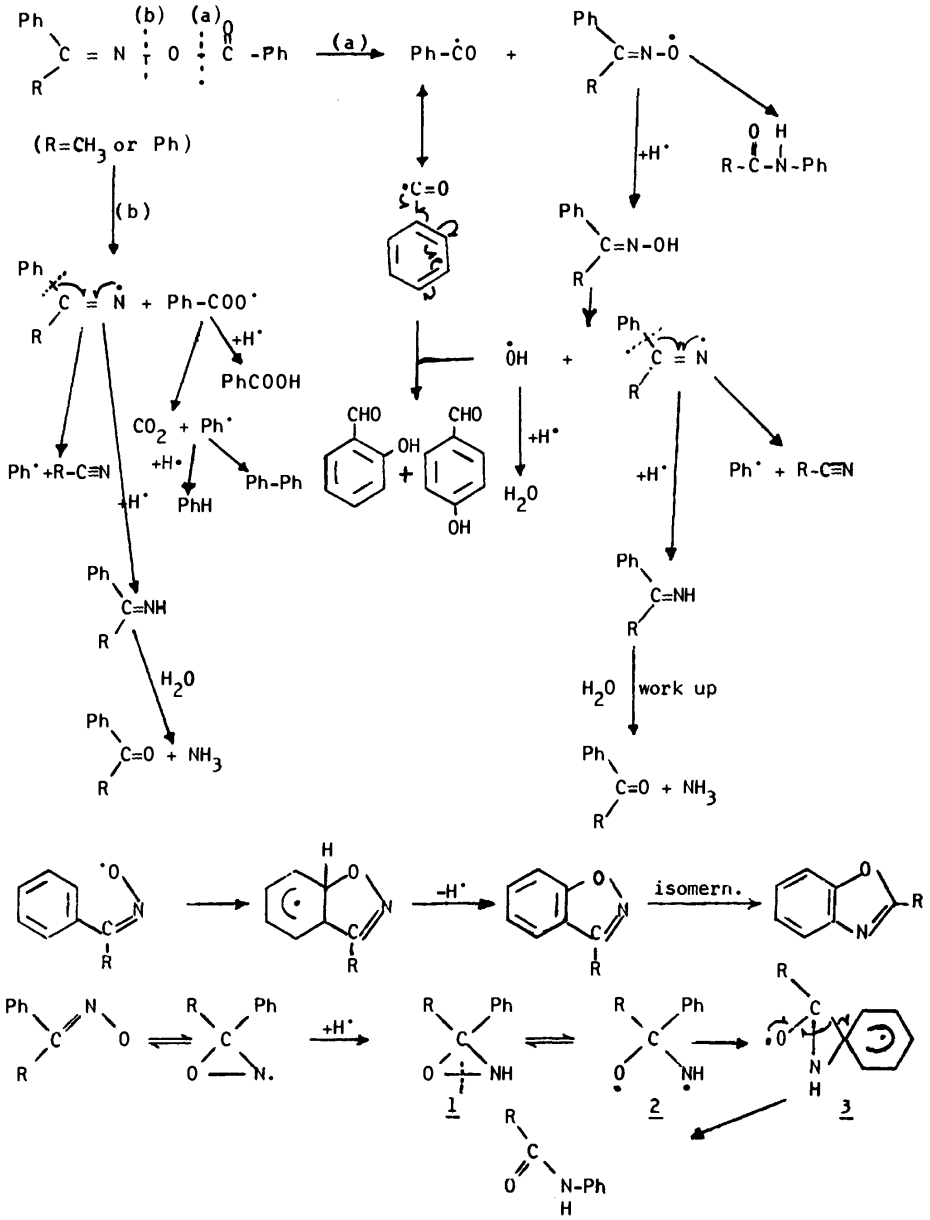

Scheme 1.

one, benzanilide and 2-phenylbenzoxazole were obtained, but no salicylaldehydes were detected among the products. However, such a mechanism cannot correlate for the formation of other products, namely; benzoic acid, biphenyl and carbon dioxide. Consequently, we have to take into consideration an alternative mode for homolysis of the benzophenone *O*-benzoyloxime molecules involving the N–O bond (route b) forming iminyl and benzoyloxyl radicals.

The normal fate of the iminyl radicals has been discussed previously, whereas the benzoyloxyl radicals may undergo decarboxylation into phenyl radicals which are the precursor of benzene and biphenyl through processes of H-abstraction or dimerization respectively. Furthermore, the benzoyloxyl radicals undergo predominantly H-abstraction forming benzoic acid. Although benzoic acid can be suggested to be formed from benzonitrile through hydrolysis, yet attempted hydrolysis of benzonitrile under comparable conditions does not afford benzoic acid.

Thermolysis of benzophenone *O*-benzyloxime on heating in a sealed tube at 200 °C for 8 h. in absence of air gives, ammonia, toluene, benzaldehyde, benzyl alcohol, bibenzyl, biphenyl, benzophenone, and 2-phenylbenzoxazole. The formation of such products can be explained on basis of homolysis of benzyl–O bond (Scheme 2, route a) into iminoxyl and benzyl free radicals to a lesser extent than (route b) as shown by the relative amounts of products formed from both routes (cf. Table 1). Such bond homolysis although unfavorable as compared with the N–O bond as shown from bond energy values which are of the order of 68 and 48 kcal·mol^{-1}, yet the resonance stabilization of the benzyl radical so formed gives a driving

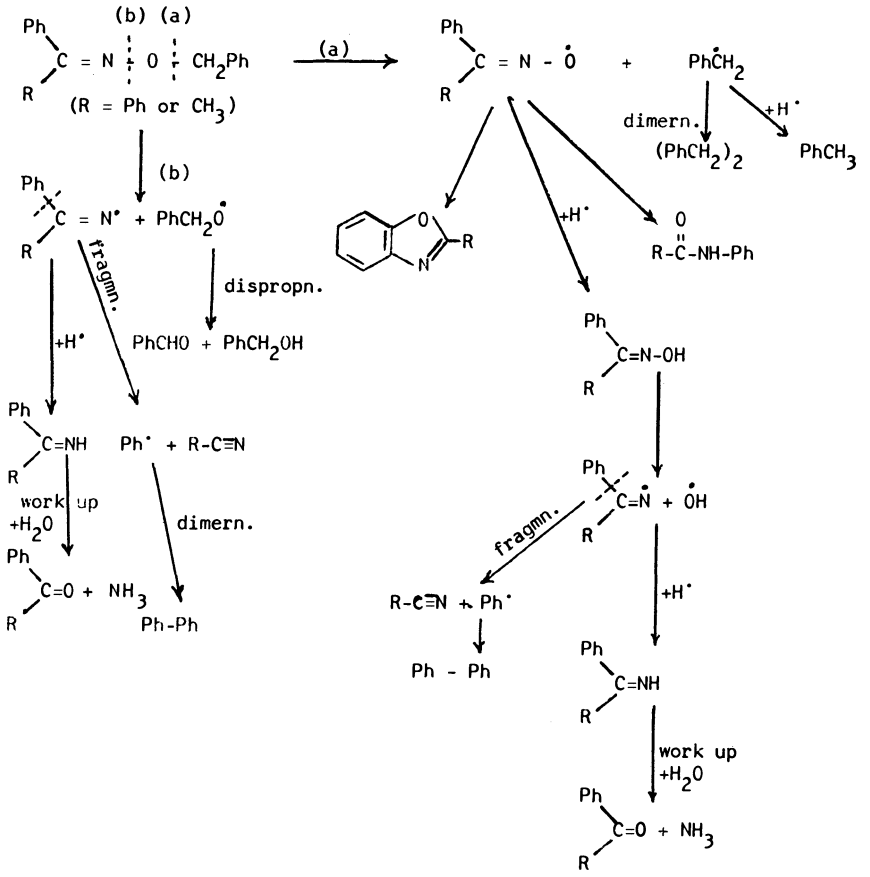

Scheme 2.

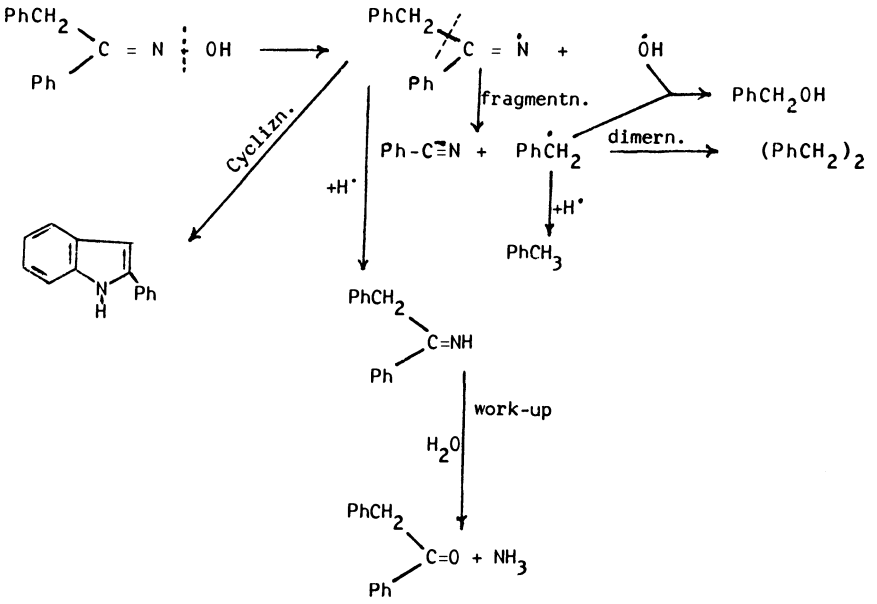

Scheme 3.

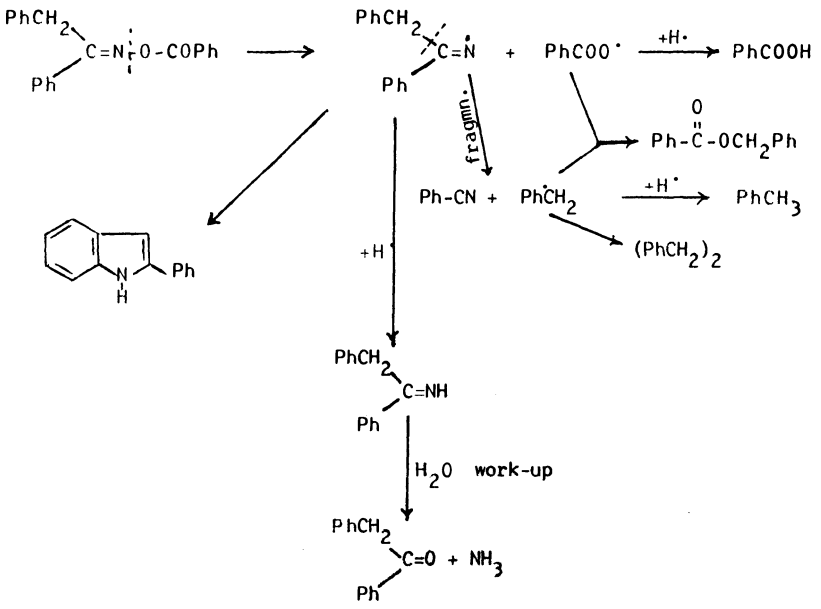

Scheme 4.

force for such process.

The normal fate of the iminoxyl radicals has been discussed previously, whereas the benzyl radicals are the precursor of toluene and bibenzyl through processes of H-abstraction and dimerization respectively. The formation of benzaldehyde and benzyl alcohol can be assumed to proceed through disproportionation of benzyloxyl radicals originating from the suspected homolysis of N–O bond (Scheme 2, route b).

Analoguous results were also obtained in case of acetophenone *O*-benzyloxime. Thermolysis of deoxybenzoin oxime under the same conditions leads to the formation of ammonia, toluene, benzonitrile, bibenzyl, benzil, benzyl alcohol, and 2-phenylindole. Similar results were also obtained in case of deoxybenzoin *O*-benzoyloxime where the previous products were also formed in addition to benzoic acid and benzyl benzoate. The formation of these products can be explained on similar grounds as shown in Schemes 3 and 4.

The main feature of deoxybenzoin oximes pyrolyses is the absence of the Beckmann rearrangement products, namely; α-phenylacetanilide ($PhCH_2-\overset{O}{\overset{\|}{C}}-NHPh$) or *N*-benzylbenzamide ($Ph-\overset{O}{\overset{\|}{C}}-\overset{H}{\overset{|}{N}}-CH_2Ph$), may be attributed to their thermal instabilities or more likely to the absence of the corresponding iminoxyl radical and consequently absence of its cyclization product, 2-benzylbenzoxazole, which implies that homolysis of deoxybenzoin oximes takes place in the N–O rather than the *O*-benzoyl bond.

Experimental

Melting points were measured with a Gallenkamp apparatus and are uncorrected. Thin-layer chromatography was carried out on glass plates covered with silica gel (25—40 mesh) and eluted with benzene–cyclohexane (2:1 v/v). Gas-liquid chromatography was carried out on a Perkin-Elmer Sigma 3B. Columns used are 4 ft.×4 mm. packed with 30% SE 30 on Chromosorb W (35—80 mesh), or 10% SE 30 on Celite (60—80 mesh), using nitrogen as a carrier gas. Molecular weight determination of some reaction products was carried out by Mass spectrophotometer, Model A. E. I. M. S. 902. Oximes were prepared by standard methods in the literature.[9] Acetophenone *O*-benzoyloxime, mp 98—100 °C. Benzophenone *O*-benzoyloxime, mp 101 °C. Acetophenone *O*-benzyloxime, bp 230 °C/20 mmHg (1 mmHg=133.322 Pa); mp 24 °C. Benzophenone *O*-benzyloxime, mp 55—56 °C. Deoxybenzoin oxime, mp 98 °C. Deoxybenzoin *O*-benzoyloxime, mp 75 °C.

Thermolysis of Oximes: The oxime (20 g) was heated either under reflux in air or in a sealed tube under nitrogen atmosphere at 250 °C for 24 h. The gases evolved were detected by standard chemical means (NH_3 detected by Nessler's reagent and CO_2 by baryta solution). The pyrolysate was first distilled under normal pressure up to 120 °C where the voltatile materials such as benzene, toluene are collected and identified. The remaining oil was separated into its constitutents by means of column chromatography over silica gel using gradient elution technique. The separated products were identified by physical constants; bps, mps, TLC, GLC, IR as compared with authentic samples.

The results are shown in Tables 1 and 2.

Preparation of Reference Compounds: α-Phenylacetanilide:[10] crystals from dilute ethanol, mp 117 °C. *N*-Benzylbenzamide:[11] needles from ethanol mp 105—106 °C. *N*-Methylbenzamide:[11] crystals from ethanol mp 82 °C. 2-Phenylindole:[12] crystals from ethanol mp 188—189 °C. 2-Methylbenzoxazole:[13] colorless oil, bp 200—201 °C. 2-Phenylbenzoxazole:[13] crystals from ethanol mp 101—102 °C.

Table 1. Pyrolysis Products of Substituted Ketoximes in g(%)

Product	Expt. No.				
	1	2	3	4	5
NH_3	Evolved	Evolved	Evolved	Evolved	Evolved
CO_2	Evolved	Evolved	Evolved	Evolved	Evolved
Benzene[a]	Trace	Trace	Trace	Trace	Trace
Toluene[b]	—	—	—	1.8(9)	2.5(12.5)
Biphenyl[c]	0.8(4%)	0.7(3.5)	0.7(3.5)	2.4(12)	2.6(13)
Bibenzyl[d]	—	—	—	2.3(11.5)	2.8(14)
Ketones[e]	2.3(11.5)	4.3(21.5)	3.8(19)	2.2(11)	1.8(9)
Aldehydes[f]	—	3.4(17)	3.5(17.5)	1.8(9)	2.1(10.5)
Anilides[g]	4.5(22.5)	3.2(16)	3.1(15.3)	3.1(15.5)	2.3(11.5)
Benzoic acid[h]	2.7(13.5)	1.6(8)	1.8(9)	—	—
Benzoxazoles[i]	—	3.1(15.5)	2.8(14)	1.8(9)	1.5(7.5)
Nitriles[j]	0.5(2.5) k)	0.7(3.5)	0.7(3.5)	0.8(4) l)	0.75(3.75) l)
Other products	1.5(7.5)	—	—	1.3(6.5)	1.7(8.5)
Residue	2.5(15.5)	1.0(5)	1.2(6)	1.2(6)	1.3(6.5)

Expt. (1) Reflux of benzophenone *O*-benzoyloxime in air, (2) heating the same oxime in a sealed tube, (3) acetophenone *O*-benzoyloxime in a sealed tube, (4) benzophenone *O*-benzyloxime in a sealed tube, and (5) acetophenone *O*-benzyloxime in a sealed tube. a) n_n^{20} 1.500; *m*-dinitro deriv. 90 °C, trace amounts less than 1% yield. b) n_D^{20} 1.4970; 2,4-dinitro derivative mp and mixed mp 72—73 °C. c) Mp 70 °C, 4,4′-dinitro derivative mp and mixed mp 234 °C. d) Mp 52 °C, 4,4′-dinitro derivative mp and mixed mp 180 °C. e) Benzophenone in expts. 1, 2, and 4 mp 49 °C, D.N.P. derivative mp 238 °C, and acetophenone in expts. 2 and 5, D.N.P. derivative mp 250 °C. f) Salicyldehydes in expts. 2 and 3 identified by TLC; *o*/*p* ratio as estimated by GLC was 4:1 respectively; and benzaldehyde in expts. 4 and 5, D.N.P. derivative mp and mixed mp 237 °C. g) Benzanilide in expts. 1, 2, and 4, mp and mixed mp 163 °C and acetanilide in expts. 3 and 5, mp and mixed mp 114 °C; IR coincident with that of authentic samples. h) Mp and mixed mp 121 °C. i) 2-Phenylbenzoxazole in expts. 2 and 4 identified by mixed mp 101 °C, *m*/*z* 194 and IR spectrum as compared with an authentic sample, and 2-methylbenzoxazole n_D^{20} 1.550; *m*/*z* 133 in expts. 3 and 5, identified by IR spectroscopy as compared with an authentic sample. j) Benzonitrile from expts. 1, 2, and 4, n_D^{20} 1.5270 and acetonitrile from expts. 3 and 5, n_D^{20} 1.3442, on acid hydrolysis give benzoic and acetic acid respectively. k) Recovered oxime. l) Benzyl alcohol n_D^{20} 1.540; IR spectrum coincident with that of an authentic sample; phenylurethane derivative mp and mixed mp 76 °C.

Table 2. Pyrolysis Products of Deoxybenzoin Oximes in g(%)

Product	Deoxybenzoin oxime	Deoxybenzoin *O*-benzoyloxime
NH_3	Evolved	Evolved
Toluene	1.7(8.5)	1.5(7.5)
Bibenzyl	3.2(16)	2.5(12.5)
Benzil	2.1(10.5)	2.3(11.5)
Benzonitrile	2.0(10)	2.2(11)
Benzyl alcohol	2.2(11)	trace
2-Phenylindole[a]	3.6(18)	3.2(16)
Deoxybenzoin[b]	3.5(17.5)	2.8(14)
Benzoic acid	—	1.5(7.5)
Benzyl benzoate[c]	—	0.7(3.5)
Residue	1.5(7.5)	2.3(11.5)

a) Mp and mixed mp 188 °C and IR coincident with that of an authentic sample. b) Mp and mixed mp 60 °C. c) n_D^{20} 1.5681; IR coincident with that of an authentic sample.

References

1) A. Lachman, *J. Am. Chem. Soc.*, **47**, 260 (1925).

2) J. H. Amin and P. de Mayo, *Tetrahedron Lett.*, **1963**, 1585; Y. Ogata, K. Takagi, and K. Mizuno, *J. Org. Chem.*, **47**, 3684 (1982).

3) C. Walling and A. N. Naglierie, *J. Am. Chem. Soc.*, **82**, 1820 (1960).

4) A. Ohsawa, T. Kawaguchi, and H. Igeta, *Chem. Pharm. Bull.*, **30**, 4352 (1982).

5) J. R. Majer and A. S. Azzouz, *Org. Mass Spectrom.*, **17(8)**, 373 (1982).

6) R. T. Taylor, M. Douek, and C. Just, *Tetrahedron Lett.*, **1966**, 4143.

7) E. S. Gould, "Mechanism and Structure in Organic Chemistry," Holt, Rinchart, and Winston Inc., New York (1959), p. 758.

8) H. Izawa, P. DeMayo, and T. Tabata, *Can. J. Chem.*, **47**, 51 (1969).

9) A. I. Vogel, "Practical Organic Chemistry," Longman, U. K. (1971), p. 721., K. V. Auwers and H. Müller, *J. Prakt. Chem.*, **137**, 81 (1933).

10) H. Staudinger, *Ber.*, **44**, 537 (1911).

11) A. I. Vogel, "Practical Organic Chemistry," Longman, U. K. (1971), p. 424.

12) A. I. Vogel, "Practical Organic Chemistry," Longman, U. K. (1971), p. 886.

13) R. Walther and T. Von Pulawski, *J. Prakt. Chem.*, **59**, 249 (1899).

Magnetism and Electronic Structure of a Cubane-Type Mo_4S_4 Cluster

Tadashi SUGANO, Takashi SHIBAHARA,† Hanako KOBAYASHI,†† Norikiyo URYŪ,††† and Minoru KINOSHITA*

Institute for Solid State Physics, University of Tokyo, Roppongi, Minato-ku, Tokyo 106

†Department of Chemistry, Okayama University of Science, 1-1 Ridai-cho, Okayama 700

††Department of Chemistry, Faculty of Science and Technology, Keio University, Hiyoshi, Kohoku-ku, Yokohama 223

†††Department of Applied Science, Faculty of Engineering, Kyushu University, Higashi-ku, Fukuoka 812

(Received September 30, 1987)

Synopsis. The static magnetic susceptibilities of the stable cubane-type compounds of $[Mo_4S_4]^{m+}$ with a set of consecutive oxidation numbers have been measured in the temperature range from 2 to 300 K at the field strength of 0.5 T. $Na_3[Mo_4S_4(edta)_2]\cdot 10H_2O$ (m=5) has been found to be paramagnetic with S=1/2, whereas $Mg_2[Mo_4S_4(edta)_2]\cdot 22H_2O$ (m=4) and $Mg[Mo_4S_4(edta)_2]\cdot 12H_2O$ (m=6) to be diamagnetic. The electronic structure of the $[Mo_4S_4]^{m+}$ clusters is discussed on the basis of the MO theory from the magnetic properties of these compounds.

The cubane-type $[Mo_4S_4]^{m+}$ clusters have recently been synthesized and found to be stable for a set of consecutive oxidation numbers, m=4, 5, and 6.[1-3] A comparative investigation of $[Mo_4S_4]^{m+}$ clusters will lead to understanding the electronic structure of the clusters. We report herein the temperature dependence of static magnetic susceptibilities of the compounds including $[Mo_4S_4(edta)_2]^{n-}$ anions[4] in the three oxidation states over the range from 2 to 300 K. From the results, we discuss the electronic structure of the clusters.

Experimental

$Mg_2[Mo_4S_4(edta)_2]\cdot 22H_2O$ (m=4), $Na_3[Mo_4S_4(edta)_2]\cdot 10H_2O$ (m=5), and $Mg[Mo_4S_4(edta)_2]\cdot 12H_2O$ (m=6) were prepared by the methods described elsewhere.[1,2] These chemical compositions, particularly the contents of water, were determined by the X-ray crystallographical analyses[1,2] on referring to the results of the elemental analyses.[5] The magnetic susceptibility χ was measured by means of a Faraday-type magnetic balance[6] under the field at 0.5 T. To avoid loss of water of crystallization during the susceptibility measurements, we used the polycrystalline sample in the form of a compressed pellet immersed in liquid paraffin. The spin susceptibilities χ_s of the three compounds were obtained by subtracting the diamagnetic contribution χ_d from χ after correction for liquid paraffin. The diamagnetic susceptibility was determined experimentally from a $\chi-T^{-1}$ plot.

Results and Discussion

The spin susceptibilities of all the compounds, plotted as a function of temperature in Fig. 1, can be fitted to the Curie-Weiss law $\chi=C/(T-\theta)$ over the whole temperature range examined. The Curie constant C and the Weiss constant θ for the $[Mo_4S_4]^{m+}$ clusters are summarized in Table 1 together with the

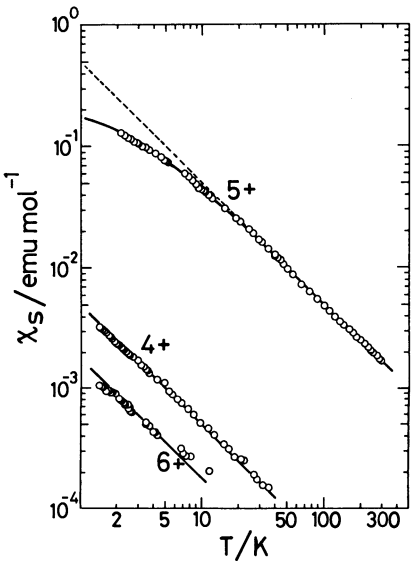

Fig. 1. Temperature dependence of spin susceptibilities of molybdenum compounds consisting of a cubane-type Mo_4S_4 cluster. Open circles represent experimental data. The susceptibilities calculated using Curie-Weiss law are shown by solid lines. The notations 4+, 5+, and 6+ stand for the compounds including $[Mo_4S_4]^{4+}$, $[Mo_4S_4]^{5+}$, and $[Mo_4S_4]^{6+}$ clusters, respectively.

Table 1. Curie Constant C, Weiss Constant θ, and Diamagnetic Susceptibility χ_d for the Molybdenum Compounds Including $[Mo_4S_4]^{m+}$ Clusters[a]

Compound	10^3C / emu K mol^{-1}	θ / K	$10^6\chi_d$ / emu mol^{-1}
$Mg_2[Mo_4S_4(edta)_2]\cdot 22H_2O$ (m=4)	4.9±0.3	0.0±0.2	−1000±20
$Na_3[Mo_4S_4(edta)_2]\cdot 10H_2O$ (m=5)	525±20	−2.0±0.2	−300±20
$Mg[Mo_4S_4(edta)_2]\cdot 12H_2O$ (m=6)	1.7±0.3	0.0±0.2	−410±20

a) 1 emu K mol^{-1}=4π cm^3 K mol^{-1}; 1 emu mol^{-1}=4π cm^3 mol^{-1}.

diamagnetic susceptibility χ_d. The Curie constant for $[Mo_4S_4]^{5+}$ is significantly large and is consistent with the presence of an $S=1/2$ moment per cluster with $g=2.32\pm0.02$; the g-factor being determined by the electron paramagnetic resonance measurements at room temperature. In contrast, the Curie constants for the other compounds are very small. There is a moment with $S=1/2$ per about 100 clusters for $[Mo_4S_4]^{4+}$ and a moment per about 300 clusters for $[Mo_4S_4]^{6+}$. The very small Curie constants observed in $[Mo_4S_4]^{4+}$ and $[Mo_4S_4]^{6+}$ are probably ascribed to extrinsic origin such as chemical impurities. Thus it is concluded that $[Mo_4S_4]^{4+}$ and $[Mo_4S_4]^{6+}$ are essentially diamagnetic, whereas $[Mo_4S_4]^{5+}$ is in the paramagnetic $S=1/2$ ground state.

X-Ray crystal structure analyses of the compounds consisting of $[Mo_4S_4(edta)_2]^{n-}$ ($n=2$, 3, 4) anions have revealed that the structures of the anions are very similar to each other except for a slight difference in the mean Mo–Mo bond distance and the volume of the cubane core.[2] Since the four Mo–Mo distances are almost completely identical in each compound, Mo tetramer can approximately be regarded as belonging to the T_d symmetry. Under this symmetry 4d electrons from the four Mo atoms could occupy six bonding orbitals (a_1+e+t_2) which have mainly Mo 4d character.[7–9] Energy difference between the bonding and antibonding orbitals would be on the order of magnitude of 25000 cm^{-1}, since the lowest energy transition is observed near 400 nm ih $[Mo_4S_4]^{4+}$ as a weak absorption band.[2]

The magnetism of the cubane-type clusters consisting of four transition-metal atoms and four chalcogen atoms has been commonly explained by assuming different values of antiferromagnetic interactions between the magnetic moments localized on the metal atoms.[10,11] This approach seems to be quite natural for those compounds having appreciable difference among the metal–metal distances and among the angles of chalcogen–metal–chalcogen bridges. However, the same approach would not be applicable for the molybdenum cluster compounds, because such appreciable difference in bond length and angle is not observed, although the magnetism changes quite drastically. It seems to be unnatural to assume significantly different values of the antiferromagnetic interactions for the series of compounds having approximately identical mean Mo–Mo distances and quite different magnetic properties.

For the reasons mentioned above, we here adopt the approach based on the MO theory to explain the magnetism of the molybdenum compounds. All the bonding orbitals are fully occupied by the twelve electrons in the case of $m=4$ and hence the Mo_4S_4 cluster has to be diamagnetic as actually observed in $Mg_2[Mo_4S_4(edta)_2]\cdot22H_2O$. Removal of one electron from the orbitals yields an unpaired electron whether HOMO is degenerate or not. Therefore, $[Mo_4S_4]^{5+}$ is expected to be in a paramagnetic ground state with $S=1/2$. This is also consistent with the result observed in $Na_3[Mo_4S_4(edta)_2]\cdot10H_2O$. Removal of two electrons from the orbitals of the $m=4$ state yields different situations depending on the energy sequence of the bonding orbitals. If HOMO of the $[Mo_4S_4]^{4+}$ cluster is not degenerate (i.e., a_1), it becomes empty by removal of two electrons and consequently $[Mo_4S_4]^{6+}$ is diamagnetic. If HOMO is degenerate (i.e., e or t_2), the ground state should be paramagnetic with $S=1$ because of Hund's rule. The experimental result that $Mg[Mo_4S_4(edta)_2]\cdot12H_2O$ is diamagnetic is favorable for the former situation. Although tetragonal distortion from the idealized symmetry ($T_d\rightarrow D_{2d}$) also results in diamagnetic state, there has been no evidence for large distortion in the $[Mo_4S_4]^{6+}$ cluster.[2] Therefore, it is most probable that the HOMO of $[Mo_4S_4]^{4+}$ belongs to the a_1 representation.

References

1) T. Shibahara, H. Kuroya, K. Matsumoto, and S. Ooi, *J. Am. Chem. Soc.*, **106**, 789 (1984).

2) T. Shibahara, H. Kuroya, K. Matsumoto, and S. Ooi, *Inorg. Chim. Acta*, **116**, L25 (1986).

3) J. A. Bandy, C. E. Davis, M. L. H. Green, K. Prout, and D. P. S. Rogers, *J. Chem. Soc., Chem. Commun.*, **1983**, 1395.

4) edta: ethylenediaminetetraacetic acid.

5) Anal. Found: C, 16.02; H, 3.72; N, 3.72. Calcd for $Mg_2Mo_4S_4C_{20}H_{68}N_4O_{38}$: C, 15.66; H, 4.46; N, 3.65; although the results of the analysis were more close to the values calculated for $Mg_2[Mo_4S_4(edta)_2]\cdot20H_2O$, we here calculated for $Mg_2[Mo_4S_4(edta)_2]\cdot22H_2O$, which was given by the crystal structure analysis. Found: C, 17.92; H, 2.97; N, 4.19; Na, 5.00. Calcd for $Na_3Mo_4S_4C_{20}H_{44}N_4O_{26}$: C, 17.95; H, 3.31; N, 4.18; Na, 5.15. Found: C, 17.87; H, 2.97; N, 4.20. Calcd for $MgMo_4S_4C_{20}H_{48}N_4O_{28}$: C, 18.07; H, 3.64; N, 4.21.

6) M. Takahashi, T. Sugano, and M. Kinoshita, *Bull. Chem. Soc. Jpn.*, **57**, 26 (1984).

7) A. S. Foust and L. F. Dahl, *J. Am. Chem. Soc.*, **92**, 7337 (1970).

8) T. Toan, B. K. Teo, J. A. Ferguson, T. J. Meyer, and L. F. Dahl, *J. Am. Chem. Soc.*, **99**, 408 (1977).

9) A. Muller, R. Jostes, W. Eltzner, C.-S. Nie, E. Diemann, H. Bogge, M. Zimmermann, M. Dartmann, U. Reinsch-Vogell, S. Che, S. J. Cyvin, and B. N. Cyvin, *Inorg. Chem.*, **24**, 2872 (1985).

10) L. Merz and W. Haase, *J. Chem. Soc., Dalton Trans.*, **1980**, 875.

11) G. C. Papaefthymiou, E. J. Laskowski, S. Frota-Pessoa, R. B. Frankel, and R. H. Holm, *Inorg. Chem.*, **21**, 1723 (1982).

Phosphorescence Excitation Spectra in the Singlet-Triplet Absorption Region of Pyrazine and Pyrimidine Vapors

Masahisa FUJITA,† Nobuhiro OHTA,* Takeshi TAKEMURA,* and Hiroaki BABA
Division of Chemistry, Research Institute of Applied Electricity,
Hokkaido University, Sapporo 060
(Received December 23, 1987)

Synopsis. Phosphorescence excitation spectra in the $S_0 \rightarrow T_1$ absorption region of pyrazine and pyrimidine have been observed in the vapor phase at room temperature. In pyrimidine vapor, the origin of the $S_0 \rightarrow T_1$ transition has been determined to be at 350.42 nm, and the T_1 state is assigned to the $n\pi^*$ state.

Relaxation dynamics in the triplet states of pyrazine and pyrimidine in the vapor phase seems to be extremely different from the dynamics in rigid media. For example, the phosphorescence quantum yields of these molecules in the vapor phase are much smaller than those in rigid media,[1-3] indicating that a fast nonradiative process occurs in T_1 only in the vapor phase. This suggests that there is a difference in electronic property and/or molecular geometry between the T_1 states of the isolated molecules and the molecules in rigid media. However, these problems remain unsettled.

The purpose of this note is to report the phosphorescence excitation spectra in the $S_0 \rightarrow T_1$ absorption region of pyrazine and pyrimidine in the vapor phase at room temperature. The T_1 states of both compounds are well-known to be of the $n\pi^*$ type in low temperature matrices.[4] In pyrimidine vapor, however, the possibility was suggested that the T_1 state is the $\pi\pi^*$, since the radiative lifetime evaluated from the yield and decay of the phosphorescence in the vapor phase is more than ten times as long as that in a rigid glass.[2] In this note, therefore, the assignment of the T_1 state of pyrimidine vapor is discussed, based on the rotational contour of the absorption band. The excitation spectrum of pyrazine vapor is compared with the absorption spectra.[5,6]

Experimental

The excitation light source is a pulsed dye laser (Lambda Physik FL2002), pumped by a XeCl excimer laser (Lambda Physik EMG 103 MSC). The intensity of phosphorescence dispersed by a monochromator was measured by using a photon counting detection system which is equipped with a circuit for a time-gated high voltage imposed on the photomultiplier (TGHV circuit).[7] With this system, the scattered light is eliminated, and the number of photons which are emitted from the sample in a certain time range after a pulse excitation can be counted. Emission decays were also measured by using the above-mentioned TGHV circuit and a photon counting lifetime apparatus equipped with a time-to-amplitude converter. In the present experiments, the phosphorescence at 390 nm emitted in the time range from 4 μs to 50 μs after pulse excitation was monitored to obtain the excitation spectra and decays of phosphorescence for the two compounds studied.

Results and Discussion

Figure 1 shows the phosphorescence excitation spectrum of pyrazine vapor. The phosphorescence lifetime of pyrazine, which is independent of the excited level, was determined to be ca. 60 μs, in agreement with the result of excitation into S_1.[1] The absorption spectrum of the $S_0 \rightarrow T_1$ transition of pyrazine vapor was observed by Innes and Giddings by using a 70 m absorption path.[5] They reported that the structure of the 0-0 band is predominantly of a parallel type, indicating that the direction of the transition dipole is perpendicular to the molecular plane, i.e., T_1 is the $n\pi^*$ state. Later, the $S_0 \rightarrow T_1$ absorption spectrum of pyrazine vapor was remeasured by Fischer,[6] and recently the $S_0 \rightarrow T_1$ transition in a supersonic jet was detected with a multiphoton ionization technique.[8,9] In the present spectrum, the strong band at 372.77 nm is assigned to the $S_0 \rightarrow T_1$ origin, and the strong bands at 625 and 1140 cm^{-1} above the origin are assigned to the $6a_0^1$ and $9a_0^1$ bands, respectively. Thus, the observed excitation spectrum is essentially the same as the absorption spectrum reported by Fischer, except that the intensity ratios between the 0-0 and the $6a_0^1$ bands in both spectra are different from each other. As is seen in Fig. 2(a), the 0-0 band exhibits a parallel-type rotational contour, in agreement with the report by Innes and Giddings.

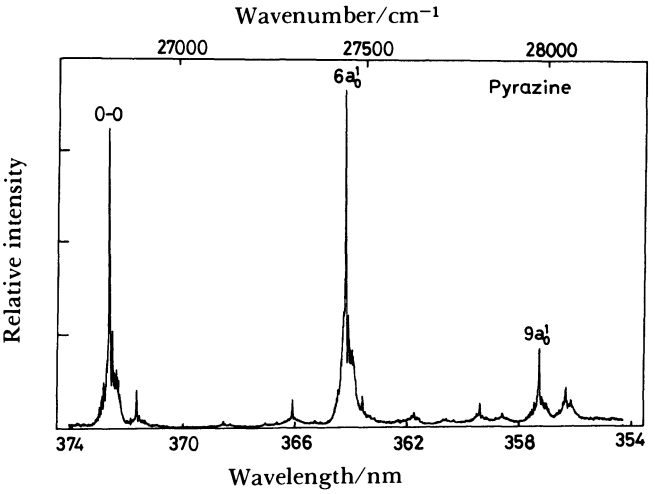

Fig. 1. Phosphorescence excitation spectrum in the $S_0 \rightarrow T_1$ absorption region of pyrazine vapor. The sample pressure is 2 Torr (1 Torr≈133.322 Pa). The 0-0 band is at 372.77 nm.

† Present address: Department of Applied Physics, Faculty of Engineering, Hokkaido University, Sapporo 060.

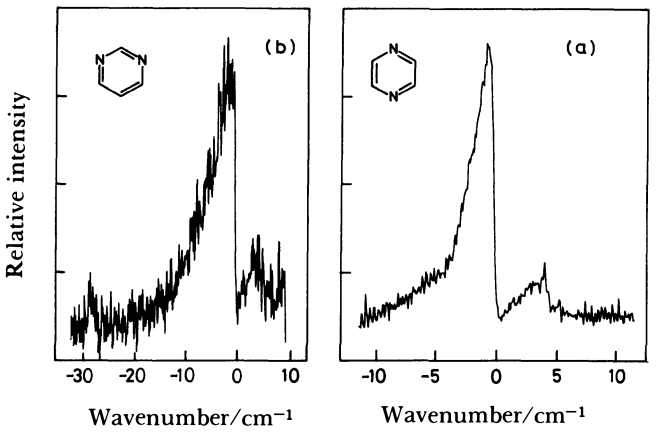

Fig. 2. Rotational contour of the 0-0 band belonging to the $S_0 \rightarrow T_1$ transition of pyrazine (a) and pyrimidine (b) vapors at room temperature.

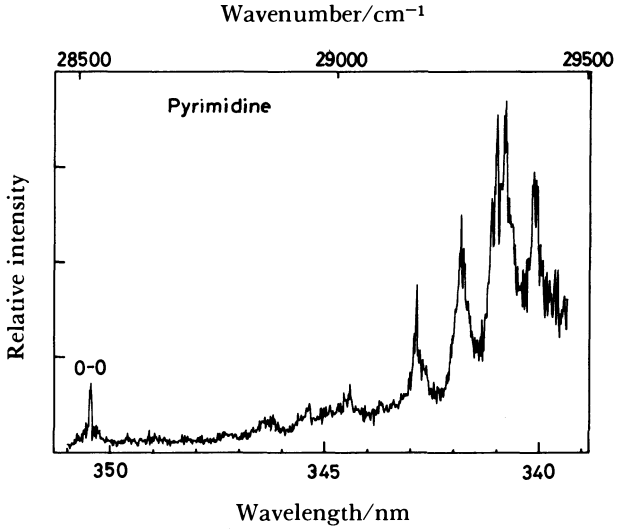

Fig. 3. Phosphorescence excitation spectrum in the $S_0 \rightarrow T_1$ absorption region of pyrimidine vapor at ca. 5 Torr. The 0-0 band is at 350.42 nm.

Figure 3 shows the phosphorescence excitation spectrum in the $S_0 \rightarrow T_1$ absorption region of pyrimidine vapor. The phosphorescence lifetime was determined to be ca. 60 μs, in fair agreement with the previous result of excitation into S_1.[2] In the previous paper,[2] the vibrational structure of the phosphorescence spectrum of pyrimidine vapor observed with excitation into S_1 was analyzed by assuming tentatively that the phosphorescence band at 350.5 nm corresponds to the 0-0 band of the $T_1 \rightarrow S_0$ transition. It is seen in Fig. 3 that in the excitation spectrum a distinct band exists at 350.42 nm, which is in good agreement with 350.5 nm. From these observations we are naturally led to the conclusion that the band at 350.42 nm in the phosphorescence excitation spectrum is the 0-0 band for the $S_0 \rightarrow T_1$ transition of pyrimidine vapor. If the T_1 state of pyrimidine vapor is the $\pi\pi^*$ type, the 0-0 band for the $S_0 \rightarrow T_1$ transition is expected to exhibit a perpendicular-type rotational contour which is similar to the contour observed for the $10a_0^1$ band belonging to the $S_0 \rightarrow S_1$ transition of pyrazine.[10] As is shown in Fig. 2(b), however, the 0-0 band of pyrimidine vapor exhibits a parallel-type rotational contour. Therefore, the T_1 state of pyrimidine vapor is assigned to the $n\pi^*$ state, as in the case of pyrazine.

In pyrazine, the spectral shapes of the $S_0 \rightarrow T_1$ excitation spectra in the vapor phase and in a rigid glass are analogous to each other.[11] However, the excitation spectrum of pyrimidine vapor shown in Fig. 3 is not analogous to the $S_0 \rightarrow T_1$ absorption spectrum of crystal.[12] The excitation (absorption) spectrum of pyrimidine vapor shows more complicated structure for excess energies of more than 600 cm^{-1} above the $S_0 \rightarrow T_1$ origin, as is seen in Fig. 3. The energy separation between S_1 and T_1 of pyrimidine is as small as ca. 2500 cm^{-1}. Then, the intense bands lying above 600 cm^{-1} from the origin may be attributed to the hot bands associated with transitions to S_1 from higher vibronic levels of S_0.

References

1) A. Frad, F. Lahmani, A. Tramer, and C. Tric, *J. Chem. Phys.*, **60**, 4419 (1974).
2) T. Takemura, K. Uchida, M. Fujita, Y. Shindo, N. Suzuki, and H. Baba, *Chem. Phys. Lett.*, **73**, 12 (1980).
3) B. J. Cohen and L. Goodman, *J. Chem. Phys.*, **46**, 713 (1967).
4) D. M. Burland and J. Schmidt, *Mol. Phys.*, **22**, 19 (1971), and references therein.
5) K. K. Innes and L. E. Giddings, Jr., *Disc. Far. Soc.*, **35**, 192 (1963).
6) G. Fischer, *Chem. Phys. Lett.*, **79**, 573 (1981).
7) M. Fujita, T. Takemura, and H. Baba, Technical Report of the Res. Inst. Appl. Electr. Hokkaido Univ., No. 8, 1 (1987).
8) R. E. Turner, V. Vaida, C. A. Molini, J. O. Berg, and D. H. Parker, *Chem. Phys.*, **28**, 47 (1978).
9) E. Villa, M. Terazima, and E. C. Lim, *Chem. Phys. Lett.*, **129**, 336 (1986).
10) S. N. Thakur and K. K. Innes, *J. Mol. Spectrosc.*, **52**, 130 (1974).
11) N. Nishi, M. Kinoshita, T. Nakashima, R. Shimada, and K. Kanda, *Mol. Phys.*, **33**, 31 (1977).
12) R. M. Hochstrasser and C. J. Marzzacco, *J. Mol. Spectrosc.*, **42**, 75 (1972).

Chemistry of Germanium Atoms. III. Reactions of Thermally Evaporated Germanium Vapor with Hydrogermanes[1)]

Kunio MOCHIDA* and Yasuhiro YOSHIDA
Department of Chemistry, Faculty of Science, Gakushuin University,
1-5-1 Mejiro, Tokyo 171
(Received September 19, 1987)

Synopsis. Thermally generated germanium atoms were found to react with hydrogermanes by insertion into germanium-hydrogen bonds. The resulting germylenes were inserted again in a germanium-hydrogen bond to form trigermanes.

We previously reported on the reactions of germanium atoms, thermally generated from a tungsten filament, with organic halides (polyhalomethanes, alkyl halides, and aryl halides), and the characterization of several new organogermanium halides.[1)] We now describe the reactions of germanium atoms with hydrogermanes (R_3GeH, R=Me; Et).

The fact that compounds containing group-4B element-hydrogen bonds like carbon-halogen bonds are good trapping agents for carbon atoms[2)] and silicon atoms[3)] made this class of substrates a logical choice for a germanium atom reaction. The present study is valuable for understanding not only the chemical properties of germanium atoms but also of the reactive intermediates in solutions.

Results and Discussion

Germanium atoms were generated by evaporation from a tungsten filament using essentially the same apparatus as has been described in the literature (ca. 1200—1300 °C and 5×10^{-3} Torr, 1 Torr=133.32 Pa).[4)] Germanium metal was evaporated at a rate of ca. 10 mg min^{-1} for 50 min, while an excess of hydrogermane was co-condensed on the walls of a quartz reaction flask containing the crucible and a perforated inlet tube through which the hydrogermane was introduced. The reaction flask was immersed in liquid nitrogen during germanium evaporation. After the germanium evaporation and introduction of the hydrogermane was completed, the reaction flask was warmed to room temperature and allowed to stand for 1.5 h. After removing the reaction flask from a vacuum line, the products were identified by comparing their GC-MS and retention times on GLC with those of authentic and similar samples. The yields of products were calculated by GLC with an internal-standard method.

The reaction of germanium atoms with trimethylgermane (Me_3GeH) produced 1,1,3,3-tetramethyltrigermane, $(Me_3Ge)_2GeH_2$, (0.2%) and hexamethyldigermane, $Me_3GeGeMe_3$, (1.0%). With triethylgermane (Et_3GeH) as the substrate, germanium atoms produced 1,1,3,3-tetraethyltrigermane, $(Et_3Ge)_2GeH_2$, (0.2%) and hexaethyldigermane, $Et_3GeGeEt_3$, (0.4%). Very small quantities of several unidentified products were formed in both reactions. This is the first observation of the insertion of germanium atoms into germanium-hydrogen bond of hydrogermanes by thermally vaporized germanium atom, so far as we know.

The condensation of hydrogermanes alone was carried out under identical conditions, except for germanium vaporization. As a result, hexamethyldigermane and hexaethyldigermane were formed in 0.1 and 0.2% yields, respectively. No trigermanes were detected.

The mechanism of double insertion is reasonable for the formation of products (Eqs. 1—3):[5)]

$$\dot{G}\dot{e}: + H\text{-}GeR_3 \longrightarrow {}^3[H\text{-}\dot{G}e\text{-}GeR_3] \quad (1)$$

$${}^3[H\text{-}\dot{G}e\text{-}GeR_3] \longrightarrow {}^1[H\text{-}\dot{G}\dot{e}\text{-}GeR_3] \quad (2)$$

$${}^1[H\text{-}\dot{G}\dot{e}\text{-}GeR_3] + H\text{-}GeR_3 \longrightarrow H_2Ge(GeR_3)_2 \quad (3)$$

R = Me; Et

Thus, germanium atoms of the ^3P ground state, thermally evaporated, were inserted into germanium-hydrogen bonds of hydrogermanes (Eq. 1). The initially formed triplet germylenes rapidly relaxed to their singlet states, since the ground states of germylenes have been shown to be singlets by quantum chemical calculations and chemical reactions[6-8)] (Eq. 2). The singlet germylenes insert again into germanium-hydrogen bonds to form trigermanes (Eq. 3).

The digermanes are considered to be derived from the germyl radicals generated by the hydrogen-abstraction of the hydrogermanes with singlet germylenes ($HGeGeR_3$) or germanium atoms. Therefore, the formation of trihydrogermanes (H_3GeGeR_3) or tetrahydrogermane (GeH_4) may be expected. However, these germanium compounds could not be detected. A similar mechanism has been proposed for the co-condensation of thermally vaporized germanium atoms with organic halides.[1)]

Experimental

^1H NMR spectra were recorded on a Varian FT 80A, with tetramethylsilane as an internal standard. GC-MS spectra were obtained on a JEOL JMS-DX 303 mass spectrometer. Infrared spectra were recorded on a Hitachi 260-10 spectrometer. Gas chromatography was performed on a Shimadzu GC-6A and 8A with lm 20% SE30 and 30% Apiezon L columns.

Materials. Me_3GeH and Et_3GeH were prepared by the reduction of the corresponding chlorides with lithium aluminum hydride in ether.[9)] Me_6Ge_2[10)] and Et_6Ge_2[11)] were prepared as described in the cited references.

Reactions of Germanium Atoms with Hydrogermanes. As a typical example, the reaction of germanium atoms with trimethylgermane (Me_3GeH) is described. Germanium

atoms were produced by using essentially the same apparatus and conditions as described in the literature.[1] Germanium metal (0.5 g, 6.9 mmol) was vaporized at a temperature of 1200—1300 °C by using a resistively heated, alumina-coated tungsten spiral crucible, in vacuo (ca. 5×10^{-3} Torr), at a rate of 10 mg min^{-1}. During vaporization of the germanium metal, Me_3GeH (ca. 10 cm^3) was co-condensed on the walls of a quartz reaction flask. The color of the co-condensation product of germanium vapor and Me_3GeH vapor at 77 K is bluish-black. The crucible was maintained at 1200—1300 °C and reaction flask was immersed in liquid nitrogen during germanium the vaporization and the introduction of Me_3GeH. Then, the reaction flask was warmed to room temperature and allowed to stand for 1.5 h. The co-condensation products were characterized by comparing their GC-MS and retention times on GLC with those of authentic and similar compounds. The amounts of products were determined by GLC with an internal standard method. Me_6Ge_2 and $(Me_3Ge)_2GeH_2$ were formed in 1.0 and 0.2% yields, respectively. Small quantites of several unidentified products were also produced. The yields of products were determined on the basis of the germanium metal consumed by supposing that the germanium metal, except for germanium metal that remained in the crucible, completely reacted with Me_3GeH vapor. Therefore, by taking into consideration that the unreacted germanium metal becomes attached to the walls of a reaction flask, the yields of products may be underestimated.

Identification of Products. The known compounds (Me_6Ge_2 and Et_6Ge_2) were identified by comparing their GC-MS and retention times on GLC with those of authentic samples. The unknown compounds were carefully identified by comparing their GC-MS with those of similar samples and parent peaks and cleavage patterns while considering the natural abundance of germanium (ratio, $^{70}Ge/^{72}Ge/^{73}Ge/^{74}Ge/^{76}Ge=56/75/21/100/21$). $(Me_3{}^{74}Ge)_2{}^{74}GeH_2$ (parent ion at peak $m/z=314$); $m/z=309$ (11), 206 (39), 191 (21), and 119 (100). $(Et_3{}^{74}Ge)_2{}^{74}GeH_2$ (parent ion peak at $m/z=394$); $m/z=394$ (28), 365 (3), 312 (4), 223 (17), 161 (100), 133 (82), and 105 (16).

The authors thank Mitsubishi Metal Corporation for a gift of germanium metal. This work was supported in part by Grant-in-Aid for Special Project Research (Nos. 61125004 and 62115003) provided by the Ministry of Education, Science and Culture.

References

1) For paper II see: K. Mochida, K. Tashiro, Y. Yoshida, and Y. Mizuno, *Bull. Chem. Soc. Jpn.*, **61**, 1247 (1988).
2) P. S. Skell, J. J. Havel, and M. J. McGlinchey, *Acc. Chem. Res.*, **6**, 97 (1973).
3) P. S. Skell and P. W. Owen, *J. Am. Chem. Soc.*, **94**, 5434 (1972).
4) K. Mochida and H. Ogawa, *J. Organomet. Chem.*, **243**, 131 (1983).
5) R. T. Conlin, S. H. Lockhart, and P. P. Gasper, *J. Chem. Soc., Chem. Commun.*, **1975**, 825.
6) J. -C. Barthelat, B. S. Roch, G. Trinquir, and J. Satgé, *J. Am. Chem. Soc.*, **102**, 4080 (1980).
7) G. Olbrich, *Chem. Phys. Lett.*, **73**, 110 (1980).
8) M. Schriewer and W. P. Neuman, *J. Am. Chem. Soc.*, **105**, 897 (1983).
9) "Shin Jikken Kagaku Koza," ed by Nippon Kagaku Kai, Maruzen, Tokyo (1976), Vol. 12.
10) M. P. Brown and G. W. A. Fowles, *J. Chem. Soc.*, **1958**, 2811.
11) E. J. Bulten and J. G. Noltes, *J. Organomet. Chem.*, **11**, 22 (1968).

A Convenient Synthesis of 3-Phenacylidenephthalides

Kimihiko HORI and Naotake TAKAISHI*
Tochigi Research Laboratories, Kao Corporation, 2606 Akabane, Ichikaimachi, Tochigi 321-34
(Received December 3, 1987)

Synopsis. 3-Phenacylidenephthalides were prepared by the dehydration of 2-(1,3-dioxo-3-phenylpropyl)benzoic acids, obtained in turn by the condensation of phthalic anhydride with acetophenones.

3-Phenacylidenephthalides (**4**) have attracted wide attention on account of their biological activities as plant growth regulants[1-5] and their reducing effects on the herbicidal injury to plants.[6] Several methods to prepare **4** have been developed.[2,7,8] However, these procedures need complex operations and the yields are often unsatisfactory. The Wittig reaction of phthalidylphosphonium bromide with phenylglyoxal has been reported to give *Z*-**4a** in 40% yield. We now report a convenient procedure for the synthesis of **4** by the dehydration of 2-(1,3-dioxo-3-phenylpropyl)benzoic acids (**3**).

The starting materials, 2-(1,3-dioxo-3-phenylpropyl)benzoic acids (**3**), were prepared in high yields by the reaction of acetophenones (**2**) with phthalic anhydride (**1**) in the presence of sodium methoxide[9] (Table 1). The dehydration was examined by several halogenating or dehydrating reagents (Table 2). Treatment of **3** with thionyl chloride in chloroform at reflux temperature gave **4** in excellent yields as a mixture of *E*- and *Z*-isomers, which was easily separated by silica-gel column chromatography. The stereochemistry of each isomer was determined by a consideration of the ^{1}H NMR spectrum.[8] Similar

Table 1. Preparation of 2-(1,3-Dioxo-3-phenylpropyl)benzoic Acids **3a—e**

Entry	Product	R	Yield [%][a]
1	**3a**	H	85
2	**3b**	CH_3	82
3	**3c**	OCH_3	87
4	**3d**	Cl	81
5	**3e**	CF_3	80

a) Isolated yields.

Table 2. Preparation of 3-Phenacylidenephthalides **4a—e**

Reaction condition				Product	R	Yield [%][a]	*E* : *Z*[b]
Reagent	Solvent	Temp	Time/h				
$SOCl_2$	$CHCl_3$	Reflux	3	**4a**	H	92	50 : 50
$SOCl_2$	$CHCl_3$	Reflux	3	**4b**	CH_3	92	70 : 30
$SOCl_2$	$CHCl_3$	Reflux	3	**4c**	OCH_3	93	70 : 30
$SOCl_2$	$CHCl_3$	Reflux	3	**4d**	Cl	91	54 : 46
$SOCl_2$	$CHCl_3$	Reflux	3	**4e**	CF_3	91	57 : 43
MeCOCl	$CHCl_3$	Reflux	3	**4c**	OCH_3	94	63 : 37
p-TsOH[c]	C_6H_6	Reflux	3	**4c**	OCH_3	96	70 : 30
PPh_3	CCl_4	Reflux	24	**4c**	OCH_3	83	73 : 27
DCC[d]	AcOEt	r.t.	2	**4c**	OCH_3	90	0 : 100

a) Isolated yields. b) Ratios of the stereoisomers (*E* and *Z*) were determined by ^{1}H NMR spectrum. c) *p*-Toluenesulfonic acid. d) Dicyclohexylcarbodiimide.

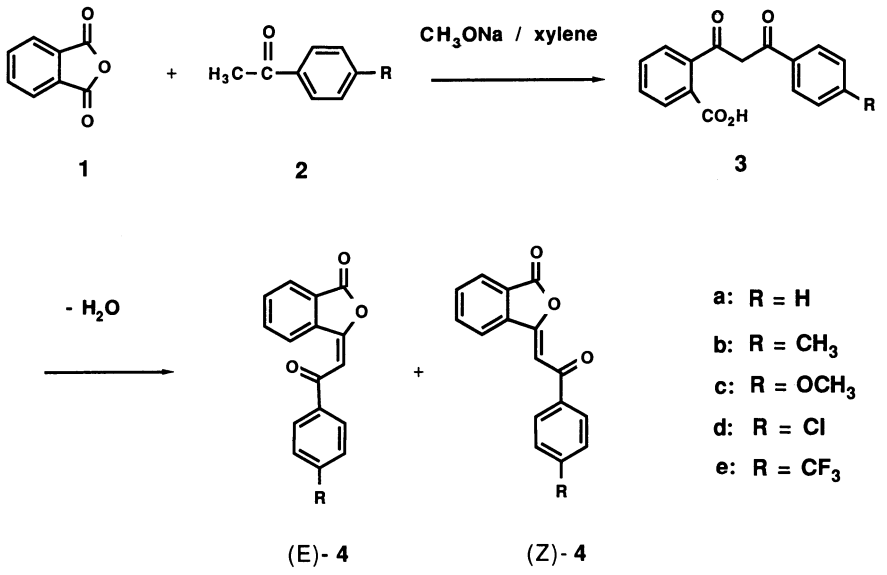

1 2 3

(E)-4 (Z)-4

results were obtained by using acetyl chloride, *p*-toluenesulfonic acid or triphenylphosphine, while the use of dicyclohexylcarbodiimide (DCC) afforded the *Z*-isomer exclusively.

The advantages of this dehydration procedure for the large scale preparation of **4** over existing literature procedures are that the starting materials are readily available, and the procedure is simple, short, and requires only mild conditions.

Experimental

General. All melting points were uncorrected. IR spectra were taken on a Hitachi 270-30 spectrometer. ^{1}H NMR spectra (270 MHz) were taken on a JEOL JNM-GX270 spectrometer.

General Procedure for 2-(1,3-Dioxo-3-phenylpropyl)benzoic Acids (3). A stirred mixture of anhydrous xylene (700 ml) and 28% methanol solution of sodium methoxide (99.2 g, 0.51 mol) was heated at 110 °C until the distillation of methanol had ceased. The mixture was cooled to 60 °C, and then acetophenones (**2**) (0.2 mol) and phthalic anhydride (**1**) (35.0 g, 0.24 mol) were added successively. The reaction mixture was again heated at 110—120 °C for 2 h and cooled to room temperature. The mixture was poured into cooled 12% aqueous hydrochloric acid (160 ml) and extracted with methyl ethyl ketone (350 ml×2). The combined extracts were washed with water (300 ml) and dried over sodium sulfate. The crude product obtained after the evaporation of the solvent was purified by recrystallization from suitable solvents (Table 1).

2-(1,3-Dioxo-3-phenylpropyl)benzoic Acid (3a): Mp 110—112 °C (benzene) (lit,[2] 111—113 °C); IR (KBr) 3046, 1725, 1608, 1575, 1542, 1497, 1461, 1416, 1299, 1245, 1125, 1050, 891, 768 cm^{-1}.

2-[3-(4-Methylphenyl)-1,3-dioxopropyl]benzoic Acid (3b): Mp 154—156 °C (C_2H_5OH/benzene); IR (KBr) 3130, 1713, 1647, 1602, 1575, 1490, 1422, 1311, 1254, 1167, 990, 864, 759 cm^{-1}.

Found: C, 72.20; H, 4.95%. Calcd for $C_{17}H_{14}O_4$: C, 72.33; H, 5.00%.

2-[3-(4-Methoxyphenyl)-1,3-dioxopropyl]benzoic Acid (3c): Mp 152—154 °C (C_2H_5OH); IR (KBr) 3000, 1690, 1595, 1500, 1460, 1440, 1415, 1290, 1260, 1225, 1180, 1020, 930, 850, 805, 775 cm^{-1}.

Found: C, 68.42; H, 4.53%. Calcd for $C_{17}H_{14}O_5$: C, 68.45; H, 4.73%.

2-[3-(4-Chlorophenyl)-1,3-dioxopropyl]benzoic Acid (3d): Mp 150—152 °C (CH_3OH/CCl_4) (lit,[2] 149—153 °C); IR (KBr) 2992, 1713, 1653, 1587, 1575, 1492, 1425, 1407, 1317, 1296, 1254, 1167, 1089, 1010, 990, 870, 822, 768 cm^{-1}.

2-[1,3-Dioxo-3-(4-trifluoromethylphenyl)]benzoic Acid (3e): Mp 151—153 °C (benzene); IR (KBr) 3004, 1698, 1620, 1578, 1458, 1416, 1329, 1284, 1176, 1116, 1071, 1012, 921, 858, 804, 771 cm^{-1}.

Found: C, 60.80; H, 3.27%. Calcd for $C_{17}H_{11}F_3O_4$: C, 60.72; H, 3.30%.

General Procedure for 3-Phenacylidenephthalide (4). A stirred mixture of 2-(1,3-dioxo-3-phenylpropyl)benzoic acids (**3**) (0.34 mol) and thionyl chloride (60.94 g, 0.51 mol) in chloroform (400 ml) was heated under reflux for 3 h. Removal of solvent and excess thionyl chloride in vacuo left the crude product, which was chromatographed on silica-gel column using chloroform as eluent. The pure *E*- and *Z*-isomers of 3-phenacylidenephthalides (**4**) were obtained as slightly yellow crystals (Table 2).

(*E*)-3-Phenacylidenephthalide (*E*-4a): Mp 116—117 °C (lit,[8] 116—118 °C); IR (KBr) 1795, 1665, 1610, 1250, 970 cm^{-1}; ^{1}H NMR ($CDCl_3$) δ=7.21 (s, 1H), 7.48—8.11 (m, 8H), 9.03 (d, 1H, J=8.1 Hz).

(*Z*)-3-Phenacylidenephthalide (*Z*-4a): Mp 165—167 °C (lit,[8] 165—167 °C); IR (KBr) 1795, 1685, 1650, 1225, 1090, 985 cm^{-1}; ^{1}H NMR ($CDCl_3$) δ=6.78 (s, 1H), 7.42—8.08 (m, 9H).

(*E*)-3-(4-Methylphenacylidene)phthalide (*E*-4b): Mp 205—207 °C; IR (KBr) 1795, 1675, 1630, 1235, 1215, 980 cm^{-1}; ^{1}H NMR ($CDCl_3$) δ=2.45 (s, 3H), 7.20 (s, 1H), 7.33 (d, 2H, J=8.1 Hz), 7.66—8.09 (m, 5H), 9.02 (d, 1H, J=7.7 Hz).

Found: C, 77.44; H, 4.61%. Calcd for $C_{17}H_{12}O_3$: C, 77.26; H, 4.58%.

(*Z*)-3-(4-Methylphenacylidene)phthalide (*Z*-4b): Mp 205—207 °C IR (KBr) 1795, 1680, 1630, 1240, 1220, 975 cm^{-1}; ^{1}H NMR ($CDCl_3$) δ=2.43 (s, 3H), 6.76 (s, 1H), 7.29 (d, 2H, J=8.4 Hz), 7.60—8.06 (m, 6H).

Found: C, 77.22; H, 4.60%. Calcd for $C_{17}H_{12}O_3$: C, 77.26; H, 4.58%.

(*E*)-3-(4-Methoxyphenacylidene)phthalide (*E*-4c): Mp 163—164 °C (lit,[6] 145 °C); IR (KBr) 1795, 1660, 1605, 1255, 1180, 975 cm^{-1}; ^{1}H NMR ($CDCl_3$) δ=3.91 (s, 3H), 7.00 (d, 2H, J=8.5 Hz), 7.19 (s, 1H), 7.67—7.88 (m, 2H), 7.95—8.02 (m, 1H), 8.04 (d, 2H, J=8.5 Hz), 9.00 (d, 1H, J=8.1 Hz).

(*Z*)-3-(4-Methoxyphenacylidene)phthalide (*Z*-4c): Mp 172—173 °C (lit,[6] 170 °C); IR (KBr) 1795, 1670, 1615, 1220, 1165, 965 cm^{-1}; ^{1}H NMR ($CDCl_3$) δ=3.89 (s, 3H), 6.72 (s, 1H), 6.93—7.03 (m, 2H), 7.66—7.91 (m, 3H), 7.94—8.05 (m, 3H).

(*E*)-3-(4-Chlorophenacylidene)phthalide (*E*-4d): Mp 165—167 °C (lit,[6] 158—159 °C); IR (KBr) 1800, 1671, 1620, 1251, 1095, 975 cm^{-1}; ^{1}H NMR ($CDCl_3$) δ=7.15 (s, 1H), 7.38—8.05 (m, 7H), 9.04 (d, 1H, J=8.1 Hz).

(*Z*)-3-(4-Chlorophenacylidene)phthalide (*Z*-4d): Mp 202—203 °C (lit,[6] 204 °C); IR (KBr) 1776, 1671, 1626, 1221, 1083, 972 cm^{-1}; ^{1}H NMR ($CDCl_3$) δ=6.69 (s, 1H), 7.42—7.52 (m, 2H), 7.68—8.04 (m, 6H).

(*E*)-3-[4-(Trifluoromethyl)phenacylidene]phthalide (*E*-4e): Mp 156—158 °C; IR (KBr) 1791, 1674, 1620, 1251, 1065, 987 cm^{-1}; ^{1}H NMR ($CDCl_3$) δ=7.18 (s, 1H), 7.70—8.20 (m, 7H), 9.09 (d, 1H, J=8.1 Hz).

Found: C, 64.28; H, 2.84%. Calcd for $C_{17}H_9F_3O_3$: C, 64.16; H, 2.85%.

(*Z*)-3-[4-(Trifluoromethyl)phenacylidene]phthalide (*Z*-4e): Mp 212—214 °C; IR (KBr) 1788, 1677, 1632, 1218, 1065, 969 cm^{-1}; ^{1}H NMR ($CDCl_3$) δ=6.71 (s, 1H), 7.70—8.19 (m, 8H).

Found: C, 64.13; H, 2.81%. Calcd for $C_{17}H_9F_3O_3$: C, 64.16; H, 2.85%.

References

1) B. T. Brown, O. Johansen, and W. H. F. Sasse, *Experientia*, **28**, 1290 (1972).

2) B. T. Brown, O. Johansen, G. F. Katekar, and W. H. F. Sasse, *Pestic. Sci.*, **4**, 473 (1973).

3) G. F. Katekar, *Phytochemistry*, **15**, 1421 (1976).

4) G. F. Katekar, J. F. Nave, and A. E. Geissler, *Plant Physiol.*, **68**, 1460 (1981).

5) J. A. Houbion and M. W. Dayawon, U. S. Patent 4255181 (1981).

6) J. A. Houbion and D. E. Schafer, U. S. Patent 4182622 (1980).

7) D. W. Knight and G. J. Pattenden, *J. Chem. Soc., Perkin Trans. 1*, **1975**, 635.

8) R. L. N. Harris and J. L. Huppatz, *Aust. J. Chem.*, **30**, 2225 (1977).

9) Disodium salt of **3** has been prepared by a similar method: A. L. Johnson and P. B. Sweetser, U. S. Patent 3948937 (1976).

A New Reaction of Tris(alkylthio)cyclopropenium Salt with *m*-Substituted Anilines Affording Quinoline Derivatives

Shigeo YONEDA* and Hideo KOJIMA
Department of Applied Chemistry, University of Osaka Prefecture,
Sakai, Osaka 591
(Received December 17, 1987)

Synopsis. The reaction of tris(alkylthio)cyclopropenium salt with *m*-substituted anilines gave quinoline derivatives.

Owing to its high strain and aromatic character, the tris(alkylthio)cyclopropenium ion (**1**) undergoes a wide range of reactions including substitution,[1] ring opening,[1] and one-electron oxidation reactions.[2] We have recently reported that the reaction of tris(*t*-butylthio)cyclopropenium salt with dialkylamines ($R^1NHCH_2R^2$) resulted in the formation of the corresponding bis(*t*-butylthio)pyrroles.[3] This finding led us to explore a new "one-pot" synthesis of heterocyclic compounds using tris(alkylthio)cyclopropenium salt as a building block.

We now report the successful synthesis of quinolines from **1** and *m*-substituted anilines under mild reaction conditions.

The reactions were carried out in *N*,*N*-dimethylformamide (DMF) at 85 °C for 5—100 h to give 7- and 5-substituted quinolines **2a—d** and **3a—d** in good yields. The results are summarized in Table 1.

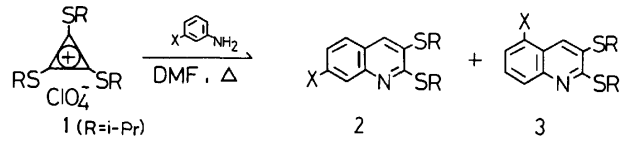

1 (R=i-Pr) 2 3

a. X = OMe
b. X = NH_2
c. X = OH
d. X = Me

Table 1. Reaction of **1** with *m*-Substituted Anilines

	X	Time/h	Yield/%[a]	
			2	**3**
a	OMe	50	68	7
b	NH_2	5	9	25
c	OH	5	85	<1
d	Me	93	52	9

a) Isolated yield except for **2d** and **3d**. The yields of **2d** and **3d** were determined by ^1H NMR.

Scheme 1 outlines a possible pathway for the formation of **2** and **3**. Reversible generation of B from the initially formed ammonium salt A leads to a facile ring opening to C and C′. Protonation of C and C′ would afford D and D′, respectively. Subsequent intramolecular electrophilic aromatic substitution would give the six-membered intermediates E and E′ and result in the formation of **2** and **3** by thiol elimination.

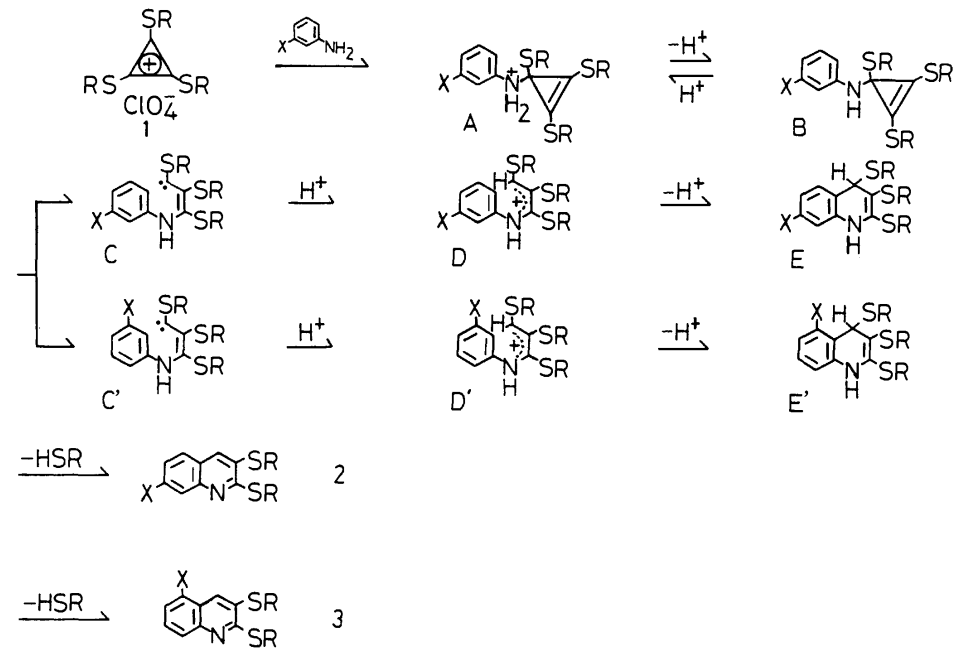

Scheme 1.

Experimental

^1H and ^{13}C NMR spectra were recorded on a JEOL JNM-GX 270 FT NMR spectrometer using chloroform-*d* as a solvent and tetramethylsilane as an internal standard; the chemical shifts are reported in δ values. Mass spectra were recorded on a Shimadzu LKB-9000 spectrometer(70eV). Infrared spectra were recorded on a Hitachi 215 spectrometer. Column chromatography was performed on silica gel (Wakogel C-300). Melting points were determined with a Yanaco MP-S3 melting point apparatus and were uncorrected.

General Synthetic Method of Quinoline Derivatives, 2a—d and 3a—d. All quinoline derivatives were prepared by the reaction of **1** with *m*-substituted anilines in dry DMF. The general procedure will be illustrated below by using the syntheses of **2a** and **3a**.

To a solution of *m*-anisidine (0.5 mmol) in dry DMF (15 ml) was added dropwise a solution of tris(isopropylthio)-cyclopropenium perchlorate (**1**) (0.5 mmol) in dry DMF (15 ml) at 85 °C under nitrogen. The reaction mixture was stirred at 85 °C for 50 h, then poured into water (200 ml), and extracted with ether (200 ml). The organic layer was washed with water (200 ml) and dried (Na_2SO_4). The solvent was evaporated off under reduced pressure, the residual oil was chromatographed on silica gel [hexane–chloroform (3:1) as eluent], and final purification by recrystallization from methanol gave both 7- and 5-methoxyquinolines (**2a** and **3a**) as colorless needles in 68% and 7% yields, respectively.

2a: mp 65.0—65.5 °C; IR (KBr) 1620, 1580, 1495, 1445, 1335, 1225, 1125, 1030, 850, and 825 cm^{-1}; ^1H NMR ($CDCl_3$) δ=7.94 (1H, s, 4-H), 7.55 (1H, d, *J*=9.0 Hz, 5-H), 7.24 (1H, d, *J*=2.6 Hz, 8-H), 7.06 (1H, dd, *J*=9.0 and 2.6 Hz, 6-H), 4.21 (1H, sep, *J*=6.7 Hz, CH of *i*-Pr), 3.94 (3H, s, OMe), 3.47 (1H, sep, *J*=6.7 Hz, CH of *i*-Pr), 1.48 (6H, d, *J*=6.7 Hz, CH_3 of *i*-Pr), and 1.30 (6H, d, *J*=6.7 Hz, CH_3 of *i*-Pr); ^{13}C NMR ($CDCl_3$)δ=163.3, 161.2, 149.0, 140.0, 128.2, 124.8, 120.9, 118.0, 106.6, 55.5, 38.4, 35.4, 23.0$_4$ (2C), and 23.0$_0$ (2C); MS (70 eV) *m/z* 307 (M^+).

3a: mp 66.0—68.0 °C; IR (KBr) 1620, 1575, 1560, 1465, 1335, 1270, 1210, 1130, 1010, and 805 cm^{-1}; ^1H NMR ($CDCl_3$) δ=8.38 (1H, s, 4-H), 7.51—7.49 (2H, m, benzene ring), 6.75 (1H, dd, *J*=5.8 and 2.8 Hz, benzene ring), 4.21 (1H, sep, *J*=6.7 Hz, CH of *i*-Pr), 3.97 (3H, s, OMe), 3.55 (1H, sep, *J*=6.7 Hz, CH of *i*-Pr), 1.47 (6H, d, *J*=6.7 Hz, CH_3 of *i*-Pr), and 1.34 (6H, d, *J*=6.7 Hz, CH_3 of *i*-Pr); ^{13}C NMR ($CDCl_3$) δ=162.6, 154.9, 147.8, 133.6, 129.4, 127.2, 120.1, 118.0, 103.5, 55.7, 38.2, 35.5, 23.0(2C), and 22.9(2C); MS (70 eV) *m/z* 307 (M^+).

Similar reactions of **1** with several *m*-substituted anilines were carried out. The reaction of **1** with *m*-phenylenediamine afforded **2b** as reddish brown solid and **3b** as yellow oil.

2b: mp 89—91 °C; IR (KBr) 3450, 3360, 3225, 1620, 1575, 1495, 1335, 1230, 1120, 1050, 990, 850, and 810 cm^{-1}; ^1H NMR ($CDCl_3$) δ=7.87 (1H, s, 4-H), 7.46 (1H, d, *J*=8.6 Hz, 5-H), 7.05 (1H, d, *J*=2.4 Hz, 8-H), 6.83 (1H, dd, *J*=8.6 and 2.4 Hz, 6-H), 4.16 (1H, sep, *J*=6.7 Hz, CH of *i*-Pr), 4.03 (2H, broad s, NH_2), 3.43 (1H, sep, *J*=6.7 Hz, CH of *i*-Pr), 1.46 (6H, d, *J*=6.7 Hz, CH_3 of *i*-Pr), 1.28 (6H, d, *J*=6.7 Hz, CH_3 of *i*-Pr); ^{13}C NMR ($CDCl_3$) δ=163.5, 149.1, 148.2, 140.9, 128.5, 122.9, 119.7, 116.8, 108.5, 38.6, 35.2, 23.1 (2C), and 23.0 (2C); MS (70 eV) *m/z* 292 (M^+).

3b: IR (neat) 3475, 3375, 3240, 1620, 1580, 1550, 1465, 1370, 1340, 1245, 1150, 1080, 1055, 955, and 805 cm^{-1}; ^1H NMR ($CDCl_3$) δ=8.04 (1H, s, 4-H), 7.45—7.35 (2H, m, benzene ring), 6.69 (1H, dd, *J*=7.0 and 1.5 Hz, benzene ring), 4.20 (1H, sep, *J*=6.9 Hz, CH of *i*-Pr), 4.12 (2H, broad s, NH_2), 3.51 (1H, sep, *J*=6.7 Hz, CH of *i*-Pr), 1.47 (6H, d, *J*=6.9 Hz, CH_3 of *i*-Pr), 1.31 (6H, d, *J*=6.7 Hz, CH_3 of *i*-Pr); ^{13}C NMR ($CDCl_3$) δ=162.8, 148.2, 142.1, 134.4, 130.4, 125.8, 118.7, 116.0, 109.4, 38.6, 35.4, 23.1 (2C), and 23.0 (2C); MS (70 eV) *m/z* 292 (M^+).

The reaction of **1** with *m*-aminophenol afforded **2c** and **3c** as yellow oil.

2c: IR (neat) 3375, 1620, 1580, 1560, 1495 , 1450, 1335, 1200, 1130, 1050, 995, 860, and 810 cm^{-1}; ^1H NMR ($CDCl_3$) δ=7.93 (1H, s, 4-H), 7.56 (1H, d, *J*=8.6 Hz, 5-H), 7.25 (1H, d, *J*=2.7 Hz, 8-H), 7.03 (1H, dd, *J*=8.6 and 2.7 Hz, 6-H), 5.69 (1H, broad s, OH), 4.17 (1H, sep, *J*=6.7 Hz, CH of *i*-Pr), 3.47 (1H, sep, *J*=6.7 Hz, CH of *i*-Pr), 1.45 (6H, d, *J*=6.7 Hz, CH_3 of *i*-Pr), 1.30 (6H, d, *J*=6.7 Hz, CH_3 of *i*-Pr); ^{13}C NMR ($CDCl_3$) δ=163.5, 157.4, 148.4, 140.2, 128.8, 125.0, 120.9, 117.2, 110.0, 38.5, 35.6, 23.0 (2C), and 22.9 (2C); MS (70 eV) *m/z* 293 (M^+).

3c: IR (neat) 3400, 1620, 1580, 1555, 1465, 1335, 1275, 1200, 1130, 1080, 1050, and 805 cm^{-1}; ^1H NMR ($CDCl_3$) δ=8.34 (1H, s, 4-H), 7.51—7.39 (2H, m, benzene ring), 6.73 (1H, dd, 7.3 and 1.2 Hz, benzene ring), 5.44 (1H, broad s, OH), 4.21 (1H, sep, *J*=6.7 Hz, CH of *i*-Pr), 3.56 (1H, sep, *J*=6.7 Hz, CH of *i*-Pr), 1.48 (6 H, d, *J*=6.7 Hz, CH_3 of *i*-Pr), 1.35 (6H, d,*J*=6.7 Hz, CH_3 of *i*-Pr); MS (70 eV) *m/z* 293 (M^+).

The reaction of **1** with *m*-toluidine afforded a mixture of **2d** and **3d** as colorless solid.

2d: ^1H NMR ($CDCl_3$) δ=7.93 (1H, s, 4-H), 7.69 (1H, s, 8-H), 7.54 (1H, d, *J*=8.4 Hz, 5-H), 7.22 (1H, dd, *J*=8.4 and 1.1 Hz, 6-H), 4.21 (1H, sep, *J*=7.0 Hz, CH of *i*-Pr), 3.50 (1H, sep, *J*=6.7 Hz, CH of *i*-Pr), 2.51 (3H, s, Me), 1.48 (6H, d, *J*=7.0 Hz, CH_3 of *i*-Pr), 1.31 (6H, d, *J*=6.7 Hz, CH_3 of *i*-Pr); MS (70 eV) *m/z* 291 (M^+).

3d: ^1H NMR ($CDCl_3$) δ=8.15 (1H, s, 4-H), 7.76 (1H, d, *J*=8.6 Hz, benzene ring), 7.51—7.46 (2H, m, benzene ring), 4.20 (1H, sep, *J*=7.0 Hz, CH of *i*-Pr), 3.54 (1H, sep, *J*=6.7 Hz, CH of *i*-Pr), 2.61 (3H, s, Me), 1.48 (6H, d, *J*=7.0 Hz, CH_3 of *i*-Pr), 1.33 (6H, d, *J*=6.7 Hz, CH_3 of *i*-Pr); MS (70 eV) *m/z* 291 (M^+).

References

1) Z. Yoshida, S. Yoneda, T. Miyamoto, and S. Miki, *Tetrahedron Lett.*, **1974**, 813.
2) R. W. Johnson, *Tetrahedron Lett.*, **1976**, 589.
3) S. Yoneda, H. Hirai, and Z. Yoshida, *Heterocycles*, **15**, 865 (1981).

Novel and Convenient Synthesis of Dioxaphospholes

Maya Shanker SINGH and Kailash Nath MEHROTRA*
Department of Chemistry, Banaras Hindu University, Varanasi 221 005, India
(Received March 9, 1987)

Synopsis. Treatment of 1,2-diketones **1a—d** with sodium in dry THF followed by addition of dry phenyl and ethyl phosphorodichloridate gave 2-phenoxy- and 2-hydroxy-4,5-diaryl-1,3,2-dioxaphosphole 2-oxides, respectively.

The preparation of some heterocyclic compounds containing nitrogen atoms and one four-coordinated phosphorus atom has been reported.[1] The synthesis of spiro-1,3,2-benzooxazaphospholes[2] from the reaction of 2-aminophenols with aryl phosphorodichloridates and 2,4,3-benzodiazaphosphepines[3] from the reaction of *o*-xylene-α,α'-diamines with dichlorophosphinyl carbamates have been described earlier. Five membered N,P and O,N,P-heterocyclic compounds have been obtained from benzil dianils and monoanils.[4] It has been observed that the reaction of phosphorothiodichloridate with benzil in presence of magnesium leads to the formation of 2,4,5-triphenyl-1,3,2-dioxaphosphole 2-sulfide.[5] We now wish to report a new and convenient one pot synthesis of 2-phenoxy- and 2-hydroxy-4,5-diaryl-1,3,2-dioxaphosphole 2-oxides from the dianions of 1,2-diketones. These dioxaphospholes could be used for the phosphorylation of alcohols.[6]

Results and Discussion

Treatment of 1,2-diketones **1a—d** with sodium in dry THF and subsequent addition of dry phenyl or ethyl phosphorodichloridate afforded 2-phenoxy-4,5-diaryl-1,3,2-dioxaphosphole 2-oxides **3a—c** and 2-hydroxy-4,5-diaryl-1,3,2-dioxaphosphole 2-oxides **4d—g** respectively. These products have been characterized by the satisfactory analytical and spectral data. It has been observed that using the reagents in 1:1 mole ratio, the yields of products **3** and **4** are reduced by 7 and 2%, respectively.

The formation of the products **3a—c** and **4d—g** from diketones **1a—d** is depicted in Scheme 1.

This synthesis involves the initial formation of diradical dianion **2**, by the electron teansfer from sodium to diketones, which on radical coupling would give the dianion **2'**;[7] the latter attacks phenyl or ethyl phosphorodichloridate with elimination of chloride ions (detected by the formation of silver chloride with aq. silver nitrate) to give rise to 2-phenoxy- and 2-ethoxy-4,5-diaryl dioxaphole 2-oxides, respectively. In cases of **3d—g**, the 2-ethoxy derivatives, initially formed, are hydrolyzed to 2-

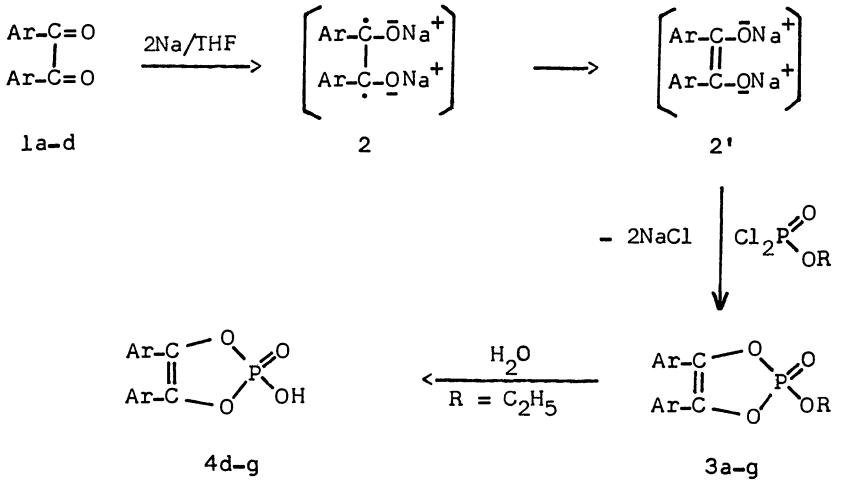

Dioxaphosphole	Ar	R	Yield/%
3a	*p*-CH_3-C_6H_4	C_6H_5	41
3b	*p*-CH_3O-C_6H_4	C_6H_5	30
3c	*p*-Cl-C_6H_4	C_6H_5	36
4d	*p*-CH_3-C_6H_4	C_2H_5	36
4e	*p*-CH_3O-C_6H_4	C_2H_5	45
4f	*p*-Cl-C_6H_4	C_2H_5	44
4g	C_6H_5	C_2H_5	62

Scheme 1.

hydroxy compounds **4d—g** during the work up. A similar hydrolysis of 2-methoxy-4,5-dimethyl-1,3,2-dioxaphosphole 2-oxide at 0 °C has been reported earlier.[8] Although products **3a—c** were stable to alkaline solution for 3 h but were hydrolyzed in 7 h to the corresponding hydroxy derivatives **4a—c**.

Experimental

Measurement. All melting points were uncorrected. The IR spectra were recorded in Nujol mull on a Perkin-Elmer 720 spectrophotometer. The ^{1}H NMR spectra were obtained on a JEOL JNM-FX-90Q NMR spectrometer using $CDCl_3$ as a solvent. The chemical shifts are given in δ, with tetramethylsilane (TMS) as the internal standard. Mass spectra were determined on a CEC 110 double-focussing mass spectrometer, Purdue University, W. Lafayette, U. S. A. Elemental analyses were carried out using Coleman carbon-hydrogen analyzer.

Materials. 4,4′-Dimethylbenzil, 4,4′-dimethoxybenzil, 4,4′-dichlorobenzil, benzil, and phenyl and ethyl phosphorodichloridate were obtained from EGA Chemicals, West Germany. The sodium metal and other solvents were commercially obtained.

Preparation of 4,5-Diaryl-2-phenoxy-1,3,2-dioxaphosphole 2-Oxides 3a—c. Freshly cut sodium pieces (1.0 g, 0.044 g atom) were slowly added to dry THF (65 ml) with stirring under a nitrogen atmosphere and a solution of 1,2-diketone (1.4 g) in dry THF (10 ml) was added dropwise; stirring at reflux temperature was continued for 7 h and the contents were allowed to cool. Unreacted sodium pieces were removed. Dry phenyl phosphorodichloridate (2 ml) was slowly added and the mixture was heated to reflux. The solvent was evaporated under reduced pressure and the residual material was treated with 50 ml of ether. The ethereal suspension was washed 2—3 times with water and dried over anhydrous sodium sulfate. The solvent was removed on a rotary evaporator and the residual material was crystallized from ethanol to afford the products.

Preparation of 4,5-Diaryl-2-hydroxy-1,3,2-dioxaphosphole 2-Oxides 4d—g. In place of phenyl phosphorodichloridate in the above procedure, dry ethyl phosphorodichloridate (2 ml) was slowly added. The products were crystallized from pet. ether.

4,5-Bis(4-methylphenyl)-2-phenoxy-1,3,2-dioxaphosphole 2-Oxide (3a). A yield of 41% was obtained, mp 170—171 °C; IR (Nujol) 1620 (C=C), 1290 (P=O),[9] and 1190 (P-O-C)[9] cm^{-1}; ^{1}H NMR ($CDCl_3$) δ=2.40 (s, 6H, two CH_3) and 7.00—8.10 (m, 13H, aromatic H); MS *m/z* 378 (M^+, 2%) and 119 (100).

Found: C, 69.59; H, 5.16%. Calcd for $C_{22}H_{19}O_4P$: C, 69.84; H, 5.06%.

4,5-Bis(4-methoxyphenyl)-2-phenoxy-1,3,2-dioxaphosphole 2-Oxide (3b). A yield of 30% was obtained, mp 181—182 °C; IR (Nujol) 1610 (C=C), 1260 (P=O),[9] and 1170 (P-O-C)[9] cm^{-1}; ^{1}H NMR ($CDCl_3$) δ=4.00 (s, 6H, two OCH_3) and 6.75—8.20 (m, 13H, aromatic H); MS *m/z* 410 (M^+, 5%) and 135 (100).

Found: C, 64.66; H, 4.73%. Calcd for $C_{22}H_{19}O_6P$: C, 64.39; H, 4.67%.

4,5-Bis(4-chlorophenyl)-2-phenoxy-1,3,2-dioxaphosphole 2-Oxide (3c). A yield of 36% was obtained, mp 215—217 °C; IR (Nujol) 1600 (C=C), 1295 (P=O),[9] and 1200 (P-O-C)[9] cm^{-1}; ^{1}H NMR ($CDCl_3$) δ=7.50—8.00 (m, aromatic H); MS *m/z* 418 (M^+, 7%) and 139 (100).

Found: C, 57.40; H, 3.40%. Calcd for $C_{20}H_{13}O_4Cl_2P$: C, 57.28; H, 3.12%.

4,5-Bis(4-methylphenyl)-2-hydroxy-1,3,2-dioxaphosphole 2-Oxide (4d). A yield of 36% was obtained, mp 198—200 °C; IR (Nujol) 2680—2540 (w, acid, P-OH),[9] 1610 (C=C), 1285 (P=O),[9] and 1190, (P-O-C)[9] cm^{-1}; ^{1}H NMR ($CDCl_3$) δ=2.23 (s, 6H, two CH_3), 6.63 (br, s, 1H, hydroxyl H, which is exchangeable on D_2O shake), and 7.06—8.35 (m, 8H, aromatic H).

Found: C, 63.37; H, 4.98%. Calcd for $C_{16}H_{15}O_4P$: C, 63.58; H, 5.00%.

4,5-Bis(4-methoxyphenyl)-2-hydroxy-1,3,2-dioxaphosphole 2-Oxide (4e). A yield of 45% was obtained, mp 177—179 °C; IR (Nujol) 2660—2550 (w, acid, P-OH), 1610 (C=C), 1270 (P=O),[9] and 1190 (P-O-C)[9] cm^{-1}; ^{1}H NMR ($CDCl_3$) δ=3.40 (s, 6H, two OCH_3), 7.10—8.10 (m, 8H, aromatic H), and 11.10 (br, s, 1H, hydroxyl H, which is exchangeable on D_2O shake).

Found: C, 57.67; H, 4.79%. Calcd for $C_{16}H_{15}O_6P$: C, 57.48; H, 4.52%.

4,5-Bis(4-chlorophenyl)-2-hydroxy-1,3,2-dioxaphosphole 2-Oxide (4f). A yield of 44% was obtained, mp 224—225 °C; IR (Nujol) 2730—2660 (w, acid, P-OH), 1615 (C=C), 1290 (P=O),[9] and 1185 (P-O-C) cm^{-1}; ^{1}H NMR ($CDCl_3$) δ=4.25 (br, s, 1H, hydroxyl H, which is exchangeable on D_2O shake) and 7.20—8.15 (m, 8H, aromatic H).

Found: C, 48.68; H, 2.72%. Calcd for $C_{14}H_9O_4PCl_2$: C, 48.97; H, 2.62%.

4,5-Diphenyl-2-hydroxy-1,3,2-dioxaphosphole 2-Oxide (4g). A yield of 62% was obtained, mp 116—118 °C; IR (Nujol) 2680—2550 (w, acid, P-OH),[9] 1600 (C=C), 1280 (P=O),[9] and 1180 (P-O-C)[9] cm^{-1}; ^{1}H NMR ($CDCl_3$) δ=7.20—8.35 (m, 10H, aromatic H) and 11.05 (br, s, 1H, hydroxyl H, which is exchangeable on D_2O shake).

Found: C, 61.09; H, 3.80%. Calcd for $C_{14}H_{11}O_4P$: C, 61.32; H, 4.04%.

Hydrolysis of 4,5-Bis(4-methylphenyl)-2-phenoxy-1,3,2-dioxaphosphole 2-Oxide (3a). A dilute solution containing 0.50 g of **3a** in 50 ml of ether was treated with 10 ml of a 20% solution of sodium hydroxide at room temperature for 7 h with vigorous shaking. The reaction mixture was extracted with ether and dried over anhydrous sodium sulfate. The solvent was removed on a rotary evaporator and the residual material was crystallized from pet. ether to give 0.29 g (57%) of the product, mp 197—99 °C and mmp 196—199 °C.

We thank the C.S.I.R., New Delhi, for an award of a fellowship to M.S.S.

References

1) M. Bermann and J. R. Van Wazer, *J. Chem. Soc., Dalton Trans.*, **1973**, 813.

2) C. D. Reddy, S. S. Reddy, and M. S. R. Naidu, *Synthesis*, **1980**, 1004.

3) T. L. Lemke and D. Boring, *J. Heterocycl. Chem.*, **17**, 1455 (1980).

4) K. N. Mehrotra, I. S. Singh, and Jalpana Roy, *Synthesis*, **1985**, 81.

5) M. Yoshifuji, S. Nakayama, R. Okazaki, and N. Inamoto, *J. Chem. Soc., Perkin Trans. 1*, **1973**, 2065.

6) T. Koizumi, Y. Arai, and E. Yoshii, *Tetrahedron Lett.*, **1973**, 4763.

7) M. S. Singh and K. N. Mehrotra, *Indian J. Chem., Sect. B*, **23**, 1289 (1984).

8) F. Ramirez, J. F. Marecek, and I. Ugi, *J. Am. Chem. Soc.*, **97**, 3809 (1975).

9) K. Nakanishi, "IR Absorption Spectroscopy," Holden-Day, Inc., San Francisco and Nankodo Co. Ltd., Tokyo (1964), p. 56.

Dielectric Losses of Dehydrated Na_{11}-ZK4 and K_3Na_8-ZK4 Zeolites

Tatsuo OHGUSHI,* Kenji NONAKA, and Tsuyoshi WATANABE
Department of Materials Science, Toyohashi University of Technology, Toyohashi 440
(Received October 28, 1987)

Synopsis. Dielectric properties of completely dehydrated Na_{11}-ZK4 and K_3Na_8-ZK4 zeolites were studied. A relaxation loss peak and a loss in the lower frequency region were observed in both zeolites. The relaxation losses were assigned to the jump of a cation from the 8-ring site to the 4-ring site. The losses in the lower frequency region were attributed to a cation movement beyond the unit cell dimension.

Zeolite ZK4 is isostructural with zeolite A and contains fewer cations than zeolite A,[1] and thus the cation distribution in zeolite ZK4 becomes simpler than that in zeolite A. This simplicity facilitates the determination as to which cation movement an observed dielectric loss is to be assigned. In a previous work,[2] the dielectric properties of the completely dehydrated Rb_3Na_8-ZK4 zeolite were studied, and a relaxation loss peak observed was tentatively assigned to a jump of a Rb^+ ion on the site of an 8-membered oxygen ring (abbreviated as the 8-ring site) to the 4-ring site. The purpose of this study is to confirm this assignment.

Experimental

The apparatus and procedures for dielectric measurements were the same as in the previous paper.[2] The starting material, $Na_{11.0}(AlO_2)_{11.0}(SiO_2)_{13.0}$ ($(AlO_2)_{11.0}(SiO_2)_{13.0}$ is abbreviated as -ZK4), was ion-exchanged with a 0.2 mol dm^{-3} solution of CH_3COOK and the composition of the resultant zeolite was shown by atomic absorption spectrometry to be $K_{3.0}Na_{8.0}$-ZK4 (K_3Na_8-ZK4). Complex dielectric constants ($\varepsilon^*=\varepsilon'-i\varepsilon''$) of Na_{11}-ZK4 and K_3Na_8-ZK4 zeolites were measured as functions of frequency f (10—2×10^6 Hz) and temperature T (room temperature—680 K), and were not corrected for the packing density. A sample placed in a vacuum system was gently heated under pumping and finally baked out at 670 K. The degree of dehydration of the sample was shown to be complete in the same manner as in the previous paper.[2]

Results

Representative spectra of loss tangent and the Cole–Cole plots are shown in Figs. 1 and 2. The figures show the presence of two kinds of dielectric losses, a relaxation loss peak and a loss in the lower frequency region. The frequency of the applied field giving the peak of loss tangent, f_{tan}, is determined on the spectrum of loss tangent and an activation energy of the cation jump, E_{tan}, is determined from Arrhenius plots of ln f_{tan} vs. $1/T$ to be 89±2 kJ mol^{-1} for Na_{11}-ZK4 and 94±3 kJ mol^{-1} for K_3Na_8-ZK4. By the method described in the previous paper,[2] the contribution of the conduction loss, ε''_c, and the apparent specific d.c. conductivity, σ, are estimated and the activation energy of the conduction process is obtained from plots of ln σ vs. $1/T$ to be 86±4 kJ mol^{-1} for Na_{11}-ZK4 and 88±5 kJ mol^{-1} for K_3Na_8-ZK4. A relaxation loss part, ε''_r, is separated from the observed dielectric loss, ε''_{obs}, by the relation of $\varepsilon''_r=\varepsilon''_{obs}-\varepsilon''_c$, as illustrated in Figs. 1(b) and 2(b). Let $f_{\varepsilon''}$ be the frequency at the maximum value of ε''_r, then the activation energy of the cation jump, $E_{\varepsilon''}$, and the frequency factor, ω_0, are determined from Arrhenius plots of ln $f_{\varepsilon''}$ vs. $1/T$, where ω_0 and $E_{\varepsilon''}$ are defined as $\ln f_{\varepsilon''}=\ln \omega_0/2\pi-E_{\varepsilon''}/RT$. The values of log ω_0 for Na_{11}-ZK4 and K_3Na_8-ZK4 are 12.1±0.4 and 11.6±0.3, respectively, and $E_{\varepsilon''}$ is 91±3 kJ mol^{-1} for Na_{11}-ZK4 and 94±4 kJ mol^{-1} for K_3Na_8-ZK4. Plots of E_{tan} vs. r and log ω_0 vs. log M are shown in Figs. 3 and 4, respectively, where r denotes a radius of cation and M a mass of the cation. For comparison, data for Rb_3Na_8-ZK4 zeolite[2] are shown in Figs. 3 and 4.

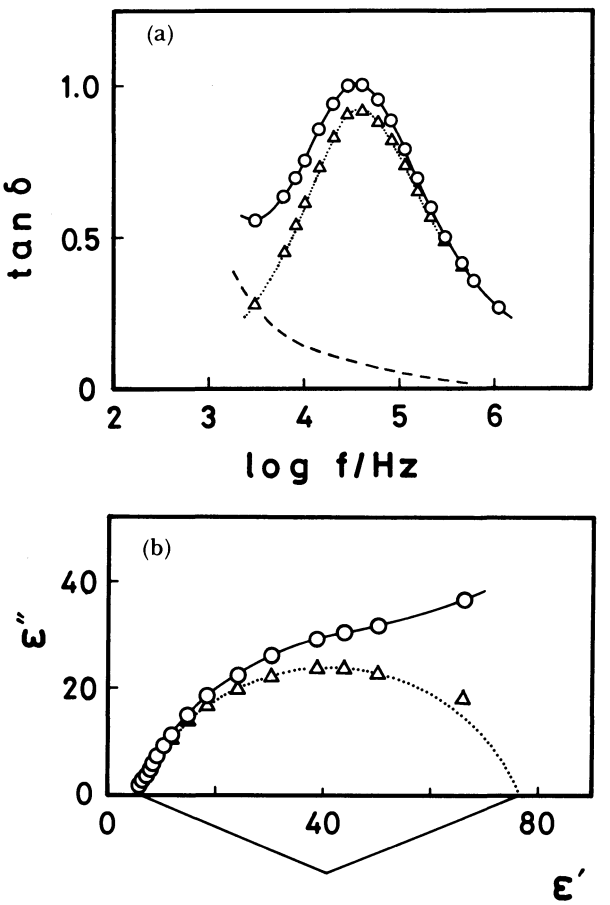

Fig. 1. Dielectric properties of Na_{11}-ZK4 zeolite. (a) Spectrum of loss tangent at 649.0 K. O: observed (tan δ_{obs}), △: loss tangent of relaxation (tan δ_r=tan δ_{obs}−tan δ_c), broken line: loss tangent of conduction (tan $\delta_c=\varepsilon''_c/\varepsilon'_{obs}$). Subscript obs denotes observed value. ε''_c is conduction loss obtained by the method described in Ref. 2. (b) Cole–Cole plots at 649.0 K. O: ε''_{obs} vs. ε'_{obs}, △: ε''_r vs. ε'_{obs}, ($\varepsilon''_r=\varepsilon''_{obs}-\varepsilon''_c$).

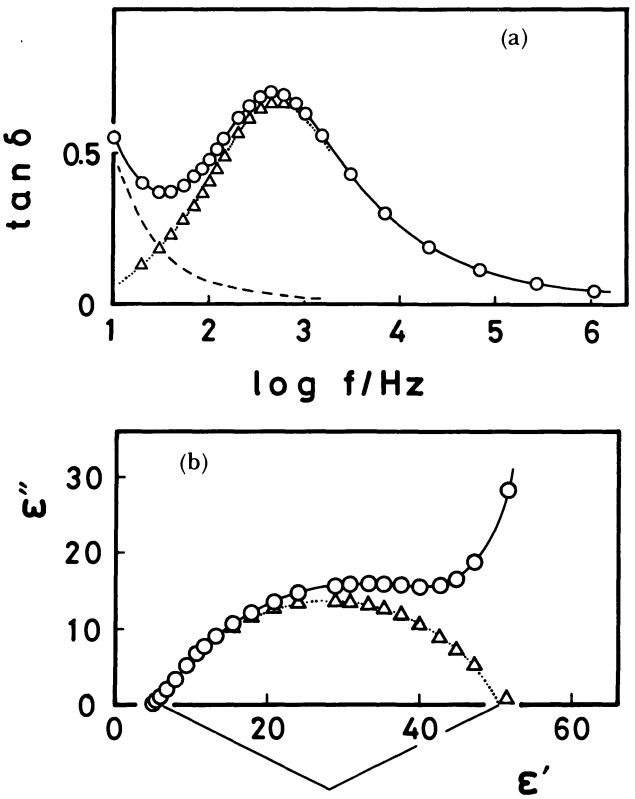

Fig. 2. Dielectric properties of K_3Na_8-ZK4 zeolite. (a) Spectrum of loss tangent at 566.7 K. O: tan δ_{obs}, △: tan δ_r, broken line: loss tangent of conduction. (b) Cole-Cole plots at 566.7 K. O: ε''_{obs} vs. ε'_{obs}, △: ε''_r vs. ε'_{obs}, ($\varepsilon''_r=\varepsilon''_{obs}-\varepsilon''_c$).

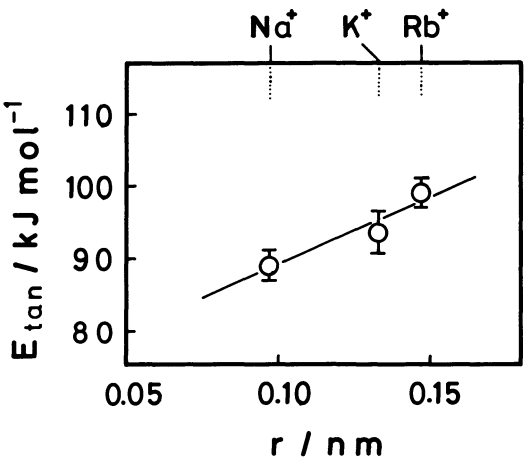

Fig. 3. Plots of activation energy of cation jump against radius of cation. Value concerned with Rb^+ ion is from Ref. 2.

Discussion

Let us consider which cation, the 8-ring cation or the 6-ring cation, causes the relaxation loss. As yet the cation distribution of K_3Na_8-ZK4 zeolite has not been studied. The cation distribution in zeolite A containing Na^+ and/or K^+ ion has been studied in detail,[3-6] and it was shown that the K^+ ion prefers the 8-ring site to the 6-ring site and the Na^+ ion has a reverse site-selectivity. It is presumed that the site-selectivities of K^+ and Na^+ ions do not change in both zeolites A and ZK4 and thus K^+ and Na^+ ions occupy the 8-ring site and the 6-ring site in K_3Na_8-ZK4 zeolite, respectively. In three zeolites, Na_{11}-, K_3Na_8-, and Rb_3Na_8-ZK4,[2] all 6-rings are fully occupied by Na^+ ions. Hence, if the relaxation loss is brought about by the movement of Na^+ ion on the 6-ring site, the activation energy and the frequency factor in the relaxation process must respectively have almost the same values for all three zeolites. These expectations are in contradiction to the observations as shown in Figs. 3 and 4. Thus it is concluded that the relaxation loss is due to the jump of the 8-ring cation.

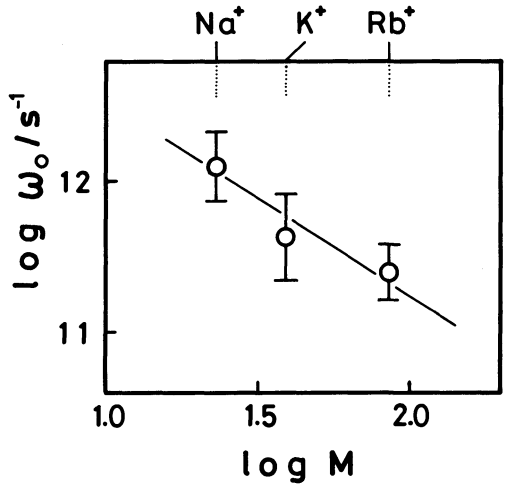

Fig. 4. Plots of frequency factor of jumping cation against mass of cation. Value concerned with Rb^+ ion is from Ref. 2.

In the next place, let us discuss the mechanism of the cation jump. Only two jumps are allowed for the 8-ring cation in the present zeolites, since a cation cannot jump to the sites occupied by the other cations. The 8-ring has four equivalent sites in its plane and can accomodate only one cation. Thus the 8-ring cation can jump to the neighbouring site in the plane. Another possible jump is the jump between the 8-ring site and the 4-ring site (the 4-ring site is vacant in the zeolite ZK4[7]). In these two jumps, the jump in the 8-ring plane is not likely to be the cause of the relaxation loss observed. The jump distance, l, between the sites in the 8-ring plane decreases with the increasing radius of the 8-ring cation and finally converges to zero when Rb^+ ion occupies the 8-ring (l=0.18 nm for Na^+, 0.063 nm for K^+ and 0 nm for Rb^+).[8-10]† Then the jump in the 8-ring plane

† The jump distances were calculated from data of X-ray structural analyses of zeolite A at room temperature. Thus the values may not be valid for zeolite ZK4 at such higher temperatures as the present experimental temperatures. However, it is considered that the dependence of the jump distance upon the ionic radius is valid for the present zeolites.

becomes impossible for the Rb_3Na_8-ZK4 zeolite. Figures 3 and 4 strongly suggest that the same mechanism operates in all three zeolites and the jump in the 8-ring plane is not the cause of the relaxation loss. Therefore, the possible mechanism as the cause of the relaxation loss observed is only the cation jump from the 8-ring site to the 4-ring site. This assignment is supported by the following. In completely dehydrated M_3Na_8-ZK4 zeolite with M= Na, K, or Rb, the allowed conduction mechanism is only the movement of the 8-ring cation through the route of 8-ring→4-ring→another 8-ring.[2] If the mechanisms of the conduction process and the relaxation process are the same, the equation, $E_{\varepsilon'}-E_c=RT$, is valid.[2,11,12] In the present systems, the above relation is satisfied within the experimental error. From the above considerations, it is concluded that the relaxation losses observed in K_3Na_8-ZK4 with M=Na, K, or Rb are caused by the cation jump from the 8-ring site to the 4-ring site.

The present authors sincerely thank Prof. Tetsuo Takaishi of Toyohashi University of Technology, for useful discussions.

References

1) G. T. Kerror, *Inorg. Chem.*, **5**, 1537 (1966).
2) T. Ohgushi, *Bull. Chem. Soc. Jpn.*, **61**, 1109 (1988).
3) L. V. C. Rees and T. Berry, "Proc. Conf. Molecular Sieves," Soc. Chem. Ind., London (1968), p. 149.
4) T. Takaishi, Y. Yatsurugi, A. Yusa, and T. Kuratomi, *J. Chem. Soc., Faraday Trans. 1*, **71**, 97 (1975).
5) A. Yusa, T. Ohgushi, and T. Takaishi, *J. Phys. Chem. Solids*, **38**, 1233 (1977).
6) T. Ohgushi, A. Yusa, and T. Takaishi, *J. Chem. Soc., Faraday Trans. 1*, **74**, 613 (1978).
7) D. W. Breck, "Zeolite Molecular Sieves," John Wiley & Sons, New York (1974), p. 179.
8) J. J. Pluth and J. V. Smith, *J. Am. Chem. Soc.*, **102**, 4704 (1980).
9) J. J. Pluth and J. V. Smith, *J. Phys. Chem.*, **83**, 741 (1979).
10) R. L. Firror and K. Seff, *J. Am. Chem. Soc.*, **99**, 1112 (1977).
11) D. R. Rosseinsky, J. A. Stephan, and J. S. Tonge, *J. Chem. Soc., Faraday Trans. 1*, **77**, 1719 (1981).
12) S. Bone, J. Eden, P. R. C. Gascoyne and P. Pething, *J. Chem. Soc., Faraday Trans. 1*, **77**, 1729 (1981).

Structure Dependence in the Hydrogenation of Acetylene over Columnar Pd Film

Jun TAMAKI and Toshinobu IMANAKA*
Department of Chemical Engineering, Faculty of Engineering Science, Osaka University, Toyonaka, Osaka 560
(Received November 20, 1987)

Synopsis. Pd films prepared by the UHV RF sputtering system had the tapered columnar structure as observed using SEM. The microstructure of the films changed with the film thickness. This affected the hydrogenation of acetylene. The Pd films which showed the strong (220) intensity in XRD exhibited the high ethylene selectivity.

It is known that a preferred orientation of evaporated metal films on glass substrates alters with the film growth.[1] The changes in the microstructure of metal films are expected to influence their catalytic properties. Previously, structure dependence was observed in the hydrogenation of 1,3-butadiene over Ru thin films[2] prepared by an RF sputtering method.[3] The microstructure of the Ru films changed with the film thickness, that is, the (101) peak increased and the (002) peak decreased with increasing film thickness in X-ray diffraction patterns (XRD). The partial hydrogenation of 1,3-butadiene was found to proceed preferably over the (002) face of Ru.

In this investigation, similar structure dependence is examined on Pd films prepared using the new RF sputtering system equipped with a ultra high vacuum (UHV) chamber.

Experimental

A schematic drawing of the experimental apparatus is shown in Fig. 1. The UHV chamber is 200 mm in diameter and 175 mm in height in inside dimensions and evacuated up to 10^{-8} Torr (1 Torr=133.322 Pa) using a turbo molecular pump (Shimadzu TMP-150, 160 l/s). The target (70 mm in diameter) and the substrate (70 mm in diameter) are at floating and at ground potential, respectively, and placed with their distance of 60 mm at the center of the UHV chamber. A high purity gas of Ar (99.9995%) at a pressure of 0.02 Torr was introduced into the chamber through a variable leak valve. The purity of Ar was confirmed using a quadrupole mass filter (ULVAC MSQ-150A) in advance of the glow discharge. RF power (13.56 MHz) of 100 W was supplied to the target on which a Pd plate (99.95%) was mounted. The glow discharge was generated between the target and the substrate because the shield (ground potential) around the target prevented the discharge which occurred at the undesirable place. Sputtered Pd atoms were deposited on a Pyrex glass substrate. The film thickness was simultaneously measured using a film thickness monitor with a quartz oscillator (Inficon XTM) which was set in the neighborhood of the substrate. Under this condition (Ar: 0.02 Torr, RF power: 100 W), the Pd film was deposited at a rate of 13 nm min^{-1}. The target, the substrate, and the sensor head of the film thickness monitor were water-cooled and maintained at room temperature.

The structure of the Pd films with various thickness was investigated by XRD and scanning electron microscopy (SEM). These investigations were performed by using Shimadzu VD-1 X-ray diffractometer and Akashi ALPHA-30A scanning electron microscope.

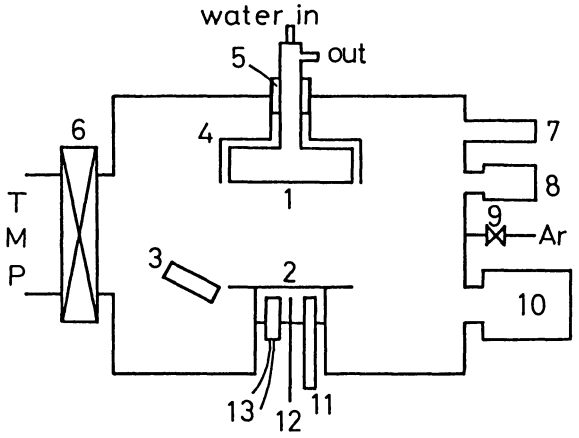

Fig. 1. Schematic drawing of the UHV RF sputtering apparatus. 1: target, 2: substrate, 3: sensor head of film thickness monitor, 4: shield, 5: insulator, 6: bellows stop valve, 7: low vacuum gauge, 8: high vacuum gauge, 9: variable leak valve, 10: mass filter, 11: cooling water tube, 12: thermocouple, 13: heater.

The hydrogenation of acetylene was carried out over the Pd films with various thickness at 273 K using a closed circulation system. A ratio of H_2/acetylene and a total pressure in the system were controlled to 6 and 140 Torr, respectively. The products of the hydrogenation were analysed by the gas chromatograph (Shimadzu GC-8A) with the thermal conductivity detector. A column used was an activated charcoal 3 m column.

Results and Discussion

In the XRD patterns of the Pd films, three peaks due to Miller indices (111), (200), and (220) of Pd fcc structure appeared at 40.3, 46.5, and 68.0 degree of 2θ. Figure 2 shows the changes in the relative intensity of these peaks with the film thickness. The (220) intensity steeply increased and the (111) intensity decreased with increasing film thickness. This indicates that the Pd film above 1 μm in thickness practically has the (220) oriented structure and that the microstructure of the Pd films is obviously changed with the film thickness. The (111) face is the most densely populated face in Pd fcc structure. The (111) face was preferentially oriented in the Pd films at the initial stage of the film growth. Then, the preferred orientation altered from the (111) orientation to the (220) orientation with the film growth. These results are agreed with the previous reports.[1,4]

Figure 3 is the SEM images of the surface view and the fracture cross section of the Pd film with 1 μm in

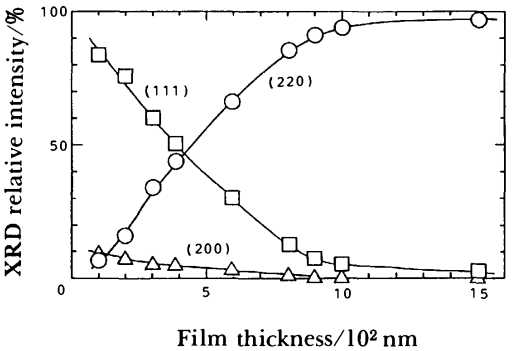

Fig. 2. Dependence of XRD relative intensity for the Pd films on film thickness.

thickness. The Pd film evidently had the tapered columnar structure as observed by Thornton.[5] The surface was not flat and the intercolumn boundaries were obviously voids. At the bottom of the Pd film, the columns were fine (about 40 nm). The diameter of the columns increased toward the top of the film. It was found that both the diameter and the length of the column increased with increasing film thickness. This was also observed in the surface view SEM images of the Pd films with various thickness. The average diameter of the columns was 200 nm in the Pd film with 1 μm in thickness. The column diameter was generally uniform except for some fine columns which had not yet grown. The SEM images elucidated the microstructure of the Pd film prepared by the RF sputtering method. XRD offers the relative composition of the crystal faces which are parallel to the substrate surface. Since the surface of the film is not flat, the (220) face, which is preferentially oriented in the Pd film with 1 μm in thickness, would not be exposed on the column surface in the SEM image. However, it is considered that each column in the SEM image has the same orientation.

The catalytic property of the microstructure of the Pd films with various thickness was evaluated in the hydrogenation of acetylene. Figure 4 shows the dependence of the activity and the initial selectivity for ethylene on the film thickness. The activity was estimated on the basis of the geometrical surface area of the substrate. The activity increased with increasing film thickness. The activity of the 1.5 μm Pd film was 5 times as great as that of the 100 nm Pd film. As observed in the SEM images, the columns grow with the film thickness and the intercolumn boundaries are voids. Therefore, the side of the column is considered to effectively participate in the hydrogenation of acetylene. The increase in the film thickness brings about the enhancement of the true Pd surface area, resulting in the high hydrogenation activity. On the other hand, the selectivity for ethylene in the hydrogenation of acetylene increased with increasing film thickness as well as the activity. The selectivity reached 96% on the Pd films above 800 nm in thickness. The Pd films which showed the stronger (220) intensity in its XRD pattern was found to exhibit the higher selectivity to ethylene. With the

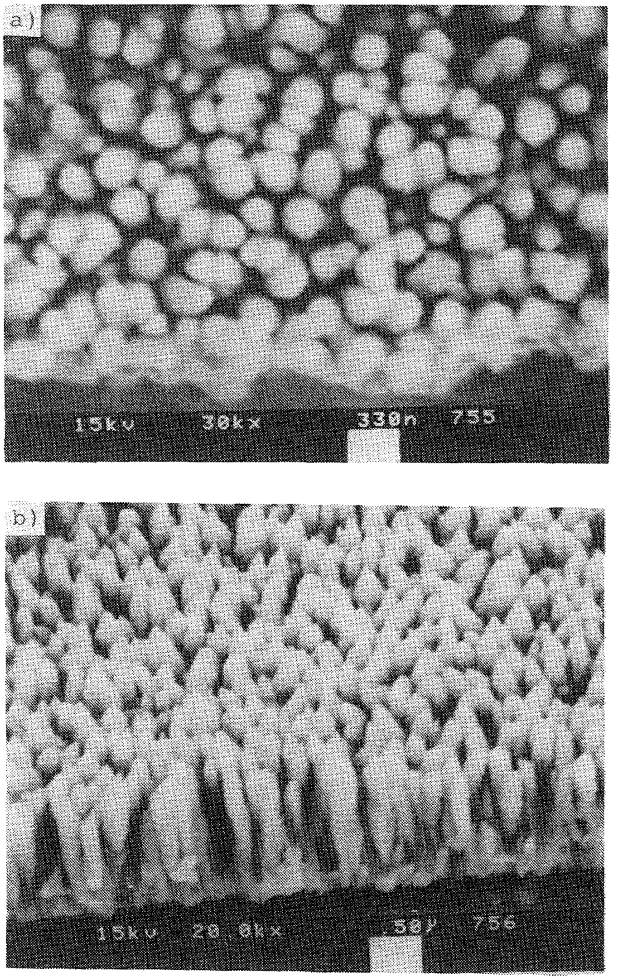

Fig. 3. Scanning electron micrographs of the Pd film with 1 μm in thickness. **a**) surface view, b) fracture cross section.

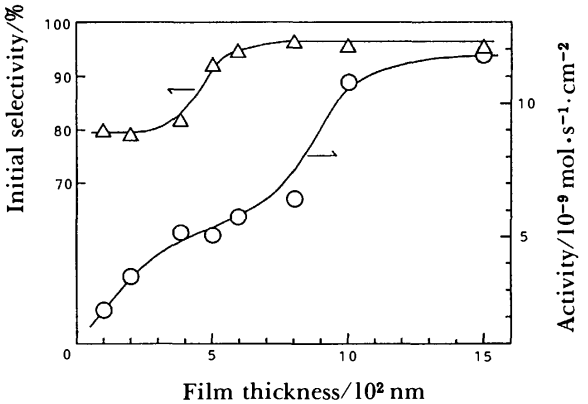

Fig. 4. Dependence of the activity and the initial selectivity for ethylene in the hydrogenation of acetylene on film thickness.

Ru film,[2] the (002) face, which was the most densely populated face of Ru hcp structure, was favorable for the partial hydrogenation of 1,3-butadiene. Although

the (111) face of Pd is the same arrangement of the atom as the (002) face of Ru, the (111) face of Pd does not seem to be suitable for the partial hydrogenation of acetylene.

References

1) D. K. Dutta and H. Wilman, *J. Phys. D, Appl. Phys.*, **3**, 839 (1970).
2) J. Tamaki, T. Miyanaga, T. Imanaka, and T. Yamane, *Chem. Lett.*, **1987**, 1839.
3) T. Imanaka, J. Tamaki, and S. Teranishi, *Chem. Lett.*, **1984**, 449.
4) K. K. Kakati and H. Wilman, *J. Phys. D, Appl. Phys.*, **6**, 1307 (1973).
5) J. A. Thornton, *J. Vac. Sci. Technol.*, **11**, 666 (1974).

Proton Magnetic Relaxation and Molecular Motion in Crystalline Tetramethylsilane

Tooru HASEBE,* Nobuo NAKAMURA,† and Hideaki CHIHARA†
Department of Chemistry, Faculty of Education, Fukushima University, Matsukawa-machi, Fukushima 960-12
†Department of Chemistry, Faculty of Science, Osaka University, Toyonaka 560
(Received November 27, 1987)

Synopsis. The molecular motion in the three modifications of tetramethylsilane was studied by the spin-lattice relaxation time measurements. The activation parameters for the methyl group reorientation, overall molecular tumbling, and the molecular self-diffusion were determined in each phase. A possible correlation between these parameters and the stability of the plastic phase was pointed out.

In our previous NMR and heat capacity measurements we established the phase relation in the crystalline tetramethylsilane, $(CH_3)_4Si$, which is hereafter abbreviated as TMS.[1,2] There are three crystalline modifications in TMS. The α phase is a metastable plastic crystal which melts at 165.9 K and, on cooling down to about 159 K, changes spontaneously into the β phase which melts at 171.0 K. The β phase can be supercooled down to very low temperatures, but transforms, on heating, into another phase, the γ phase, at about 118 K. The γ phase is the most stable phase over the whole temperature range of the crystalline state. It melts at 174.1 K. We also obtained the gross feature of the dynamic structure of the β and the γ phases of TMS by proton magnetic resonance,[1] but were not able to derive the quantitative information about the molecular motional modes in each of the three phases. The present study therefore was undertaken to investigate the characteristics of the molecular motions being excited successively in TMS with extensive measurements of the spin-lattice relaxation times in the laboratory and the rotating frames, T_1 and $T_{1\rho}$. The correlation between the molecular motion and the stability of the unique plastic phase in TMS will also be discussed.

Experimental

TMS from commercial source (Merck) was purified by vacuum distillation, outgassed by the freeze-pump-thaw technique and sealed under vacuum in a glass ampule. The NMR relaxation experiments were done at 15.0 MHz with a Bruker CXP 4-60 MHz pulsed NMR spectrometer. The T_1 was measured by the saturation-90° method. The $T_{1\rho}$ values were measured using the spin-locking method with a rotating r.f. magnetic field, B_1, of 0.7 mT for the β and the γ phases and also of 0.2 and 1.0 mT for the α phase. The estimated error in both relaxation times was less than ±4%. Temperatures were controlled to within ±0.1 K and the accuracy of the temperature measurement was better than ±0.3 K.

Results and Discussion

α Phase. Figure 1 shows the temperature dependence of T_1 and $T_{1\rho}$ in the metastable plastic α phase. The slope in T_1 below about 165 K leads to an activation energy E_a of 5.5±1.3 kJ mol^{-1} which corresponds to the overall molecular tumbling or reorientation. Above about 165 K another motion is excited. This motion shows B_1 independence of $T_{1\rho}$

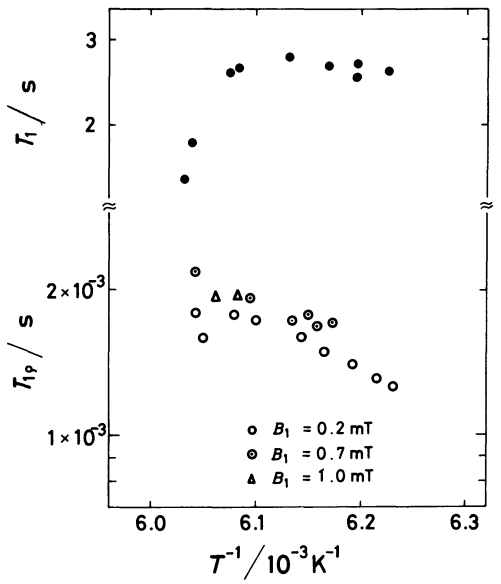

Fig. 1. Temperature dependence of T_1 (●) and $T_{1\rho}$ at B_1=0.2 mT (○), 0.7 mT (◉), and 1.0 mT (△) at the Zeeman frequency, 15.0 MHz for the α phase.

Table 1. Activation Parameters for Overall Molecular Tumbling and Self-Diffusion in Some Plastic Crystals

	$(CH_3)_4C$	$(CH_3)_4Si$	$(CH_3)_3CCl$	$(CH_3)_3CBr$	$(CH_3)_3CNO_2$	CCl_3CF_3
E_a^r/kJ mol^{-1}	3.68	5.5	4.26	13.6	6.8	5.9
E_a^d/kJ mol^{-1}	33.9	20.4	33.5	51.8	46.5	35
E_a^d/E_a^r	9.2	3.7	7.9	3.8	6.8	5.9
Reference	a)	This work	b)	Ref. 4	Ref. 6	c)

a) W. C. Allen, N. Liu, and J. Jonas, *J. Chem. Phys.*, **63**, 3317 (1975). b) D. E. O'Reilly, E. M. Peterson, C. E. Scheie, and E. Seyfarth, *J. Chem. Phys.*, **59**, 3576 (1973). c) T. Tsukamoto, N. Nakamura, and H. Chihara, *J. Mol. Struct.*, **83**, 277 (1982).

Table 2. Activation Energies, E_a, and Inverse Frequency Factors, τ_0, for Molecular Motions in α, β, and γ Phases of Tetramethylsilane

Motion	Parameter	Phase		
		α phase	β phase	γ phase
Methyl reorientation	E_a/kJ mol^{-1}	—	6.44±0.19	6.92±0.09
	τ_0/s	—	(4.72±0.80)×10^{-13}	(3.63±0.31)×10^{-13}
Overall molecular tumbling	E_a^r/kJ mol^{-1}	5.5±1.3	31.9±0.9	43.0±1.6
	τ_0^r/s	—	(5.1±2.6)×10^{-17}	(2.6±1.6)×10^{-19}
Self-diffusion	E_a^d/kJ mol^{-1}	20.4±1.6	—	—

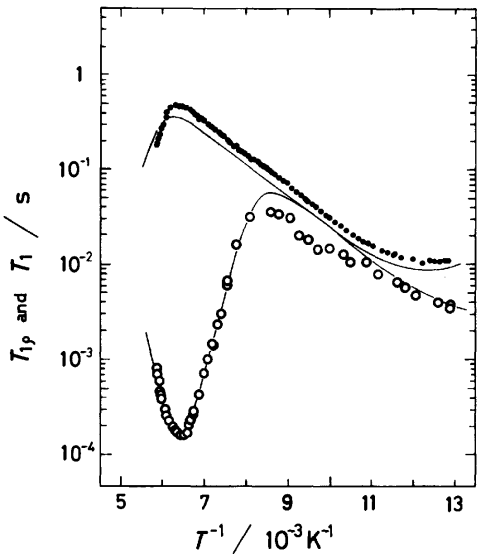

Fig. 2. Temperature dependence of T_1 (●) and $T_{1\rho}$ (○) at B_1=0.7 mT for the β phase; the Zeeman frequency is 15.0 MHz. The solid lines indicate the theoretical relaxation times.

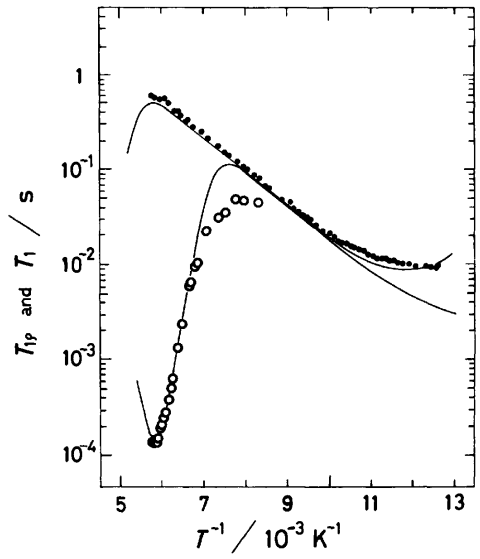

Fig. 3. Temperature dependence of T_1 (●) and T_ρ (○) at B_1=0.7 mT for the γ phase; the Zeeman frequency is 15.0 MHz. The solid lines indicate the theoretical relaxation times.

and causes to increase $T_{1\rho}$ values monotonously on heating. The slope of the $T_{1\rho}$ gives the activation energy, E_a=20.4±1.6 kJ mol^{-1}, which is certainly attributed to molecular self-diffusion.

The activation energies for the overall molecular reorientation, E_a^r, and for molecular self-diffusion, E_a^d, in some typical plastic crystals which were determined by NMR methods are listed in Table 1 together with the ratio E_a^d/E_a^r for each substance. The values of this ratio are in the range between 4 and 12 for usual plastic crystals.[3] However the values of TMS and $(CH_3)_3CBr$ are somewhat small compared with other plastic crystals; they are 3.7 and 3.8, respectively. It is remarked that the α phase of TMS is metastable as mentioned above and $(CH_3)_3CBr$ has two plastic phases.[4] It is also noted that in $(CH_3)_3CCN$ no plastic phase exists and overall molecular tumbling has not been recognized.[5] So we assume to be $E_a^r \gg E_a^d$ at a moment then we get $E_a^d/E_a^r \ll 1$ in the case $(CH_3)_3CCN$. These findings strongly suggest that this ratio is closely related to the stability of plastic phase in globular molecular crystal, giving probably a new criterion for the plastic crystal.

β and γ Phases. The relaxation data in these two phases are shown in Figs. 2 and 3, indication that the gross feature of the dynamics of the molecules is quite similar in both phases. We attributed the minima in T_1 near 80 K to the methyl group reorientation, and the minima in $T_{1\rho}$ at about 155 K (in β phase) and 170 K (in γ phase) to the overall molecular tumbling motion. Analyses of these relaxation data by a usual procedure[6,7] lead to the activation parameters for these two kinds of motions as recorded in Table 2. The solid lines in Figs. 2 and 3 show the theoretical relaxation times reproduced using the parameters in Table 2.

Although we ascribed the minima in T_1 near 80 K in the β and γ phases to the methyl group reorientation, a possibility that an anisotropic molecular rotation or reorientation of "rigid" molecule governs the relaxation at low temperatures cannot be ruled out. Our model calculation predicts, for example, that the axial rotation of $(CH_3)_3C$-group about one C-C bond gives the T_1 minimum which is only 5% shorter than that due to independent reorientation of the individual methyl groups. Therefore, we cannot distinguish these different mechanisms at the present stage without detailed structural data.

This work was partially supported by Grant-in-Aid for Scientific Research No. 61430006 from the Ministry of Education, Science and Culture.

References

1) T. Hasebe, G. Soda, and H. Chihara, *Proc. Jpn. Acad.*, **51**, 168 (1975).
2) M. Harada, T. Atake, and H. Chihara, *J. Chem. Thermodyn.*, **9**, 523 (1977).
3) N. Nakamura, unpublished data.
4) T. Hasebe, J. H. Strange, N. Nakamura, and H. Chihara, *J. Chem. Soc., Faraday Trans. 2*, **81**, 749 (1985).
5) T. Hasebe and J. H. Strange, *J. Chem. Soc., Faraday Trans. 2*, **81**, 735 (1985).
6) T. Hasebe, N. Nakamura, and H. Chihara, *Bull. Chem. Soc. Jpn.*, **57**, 179 (1984).
7) D. E. Woessner, *J. Chem. Phys.*, **36**, 1 (1962).

The Crystal and Molecular Structure of μ-Oxo-bis-[bromotriphenylantimony(V)], $[SbBr(C_6H_5)_3]_2O$

Akira OUCHI* and Shoichi SATO†
Department of Chemistry, College of Arts and Sciences, The University of Tokyo, Komaba, Meguro-ku, Tokyo 153
†The Institute for Solid State Physics, The University of Tokyo, Roppongi-7, Minato-ku, Tokyo 106
(Received October 12, 1987)

Synopsis. The crystal and molecular structure of the title complex was determined by the single-crystal X-ray diffraction method. The crystallographic data are: monoclinic, space group $P2_1/c$, a=19.164(6), b=19.020(9), c=18.649(7) Å, β=95.06(3)°, and Z=8 (16 metal atoms are in a unit cell). There are two crystallographically independent dimeric $[SbBr(C_6H_5)_3]_2O$ molecules, which are almost in the same form. Each antimony atom is bonded with three phenyl carbon atoms equatorially and one bromine as well as one bridging oxygen atoms axially, being in a trigonal-bipyramidal geometry. The Sb–O–Sb′ angles are 170.2(7) and 176.6(8)°, while the Sb–O lengths are in the range of 1.931(13)—1.958(13) Å, which are shorter than the sum of their covalent radii of the atoms: 2.15 Å.

The halogeno derivatives of organoantimony(V) have been one of the best known species since the 19th century.[1a,2] They are hydrolyzed in a solution containing water into their hydroxides or oxides,[1b] and the decomposition is quantitative in a water–acetonitrile mixed solution, even at room temperature.[3]

On the other hand, some intermediate compounds of the type $(SbXR_3)_2O$ (where X^- is a halide or acidate ion, and R is a hydrocarbon group) were obtained and some of their structures were elucidated: the compounds where R=C_6H_5, HX=2-hydroxyethanesulfonic acid[4] or HN_3;[5] R=CH_3, HX=HCl, $HClO_4$ or HN_3,[6] and R=*p*–chlorophenyl, HX=1,1,1-trifluoro-2,4-pentanedione[7] are examples. In addition to them, this time we could obtain the title compound, in spite of the fact that dibromotriphenylantimony is hydrolyzed into $[Sb(C_6H_5)_3]O$ easily and quantitatively in the moistened acetonitrile solution at ambient temperature.

Moreover, the Sb–O–Sb′ bridge of this type dimeric complex is one of the subjects of discussion. In the related compounds such as $[BiClO_4(C_6H_5)_3]_2O$,[8] $[Ge(C_6H_5)_3]_2O$,[9] and $[Sn(C_6H_5)_3]_2O$[10] the M–O–M′ angles are 142.2(7), 135.2(2), and 137.3(1)°, respectively: not 109° of the sp^3 hybridization orbital angle nor 180° to separate both side metal atoms the furthest. Among the $(SbXR_3)_2O$ type dimers, $[SbN_3(C_6H_5)_3]_2O$ has an angle of 139.8(4)°;[5] however, the others were reported to have an angle of 180°, since their oxygen atom is at the center of symmetry. As the Sb–O distances of these bridges are relatively short, the oxygen atom is assumed to be disordered into several positions around it.[6] To discuss this problem more clearly, we need more structural data concerning this type dimers.

From these viewpoints, we have determined the crystal and molecular structures of the title compound using the single crystal X-ray diffraction technique.

Experimental

Synthesis of the μ-Oxo-bis[bromotriphenylantimony(V)]. Dibromotriphenylantimony(V) (1.02 g, 2.0 mmol) was dissolved into 10 cm^3 of benzene, and triethylamine (including trace of water, 0.20 g, 2.0 mmol) was added and stirred. The precipitate (triethylammonium bromide) was filtered off, and the filtrate was dried up by the rotary vacuum evaporator at about 80 °C. The residue was recrystallized from acetonitrile (the title compound is relatively soluble into hot acetonitrile, while $[Sb(C_6H_5)_3]O$ is more insoluble at any temperature). Yield, 0.30 g (34%). Found: C, 48.86; H, 3.39%. Calcd for $Sb_2C_{36}H_{30}OBr_2$: C, 49.03; H, 3.43%.

Single Crystal X-Ray Structure Analysis. The crystal of the title compound (colorless), in the shape of parallelepiped (0.30×0.20×0.30 mm^3) was used for the intensity measurement. Crystallographic data: $Sb_2C_{36}H_{30}OBr_2$, F. W., 881.94, monoclinic, space group $P2_1/c$, a=19.164(6), b=19.020(9), c=18.649(7) Å, β=95.06(3)°, U=6711(5) $Å^3$, Z=8, D_m=1.74(3), D_x=1.74 g cm^{-3}, μ(Mo $K\alpha$)=41.8 cm^{-1}, and the final R value was 0.053.[11] Reflections within a range of $3°<2\theta<36°$ were collected on a Rigaku AFC-6A automated four-circle X-ray diffractometer, using graphite-monochromated Mo $K\alpha$ radiation (λ=0.71073 Å), the ω–2θ scan technique being employed (scan speed, 4° min^{-1} in θ; scan width 1.10+0.5 tan θ). Of the 5155 independent reflections measured, 3553 $|F_o|>3\sigma(|F_o|)$ reflections were used for the structure determination. The intensities were corrected for the Lorentz and polarization factors, but not for the absorption and extinction. The structure was solved by the heavy-atom method. Their positional and thermal parameters were refined by the least-squares method. At the final step, all non-hydrogen atoms were found: all hydrogen atoms were excluded from the structure factor calculations.

All the calculations were carried out on a HITAC M-680H computer at the Computer Center of the University of Tokyo, using the local version of the UNICS program system.[12] The atomic scattering factors were taken from Ref. 13.

Results and Discussion

The selected bond lengths and bond angles are shown in Table 1.[14] A perspective drawings of both dimeric complexes from different visual points, together with their numbering scheme of the atoms in Figs. 1 and 2, and the projection of the unit cell to the ac-plane in Fig. 3.

Although both kinds of the dimers are crystallographically independent, and the bridging oxygen atom is not at the center of symmetry, their general features, as well as the geometries around all anti-

Table 1. Selected Bond Lengths and Bond Angles with Their Standard Deviations in Parentheses

Bond length (l/Å)			
Sb(1)–Br(1)	2.707(4)	Sb(3)–Br(3)	2.716(3)
Sb(1)–O(1)	1.958(13)	Sb(3)–O(2)	1.943(14)
Sb(1)–C(1)	2.09(2)	Sb(3)–C(37)	2.091(19)
Sb(1)–C(7)	2.09(2)	Sb(3)–C(43)	2.08(2)
Sb(1)–C(13)	2.07(2)	Sb(3)–C(49)	2.14(2)
Sb(2)–Br(2)	2.722(3)	Sb(4)–Br(4)	2.693(3)
Sb(2)–O(1)	1.931(13)	Sb(4)–O(2)	1.943(13)
Sb(2)–C(19)	2.107(19)	Sb(4)–C(55)	2.112(19)
Sb(2)–C(25)	2.08(2)	Sb(4)–C(61)	2.06(2)
Sb(2)–C(31)	2.12(2)	Sb(4)–C(67)	2.09(2)
Bond angle (ϕ/°)			
Sb(1)–O(1)–Sb(2)	170.2(7)	Sb(3)–O(2)–Sb(4)	176.6(8)
Br(1)–Sb(1)–O(1)	178.8(4)	Br(3)–Sb(3)–O(2)	178.6(4)
Br(1)–Sb(1)–C(1)	88.3(6)	Br(3)–Sb(3)–C(37)	87.5(5)
O(1)–Sb(1)–C(1)	92.8(7)	O(2)–Sb(3)–C(37)	92.2(7)
C(1)–Sb(1)–C(7)	124.4(8)	C(37)–Sb(3)–C(43)	119.8(8)
C(1)–Sb(1)–C(13)	117.8(8)	C(37)–Sb(3)–C(49)	124.2(8)
C(7)–Sb(1)–C(13)	117.7(8)	C(43)–Sb(3)–C(49)	115.9(8)
Br(2)–Sb(2)–O(1)	178.8(4)	Br(4)–Sb(4)–O(2)	178.5(4)
Br(2)–Sb(2)–C(19)	88.9(5)	Br(4)–Sb(4)–C(55)	90.7(5)
O(1)–Sb(2)–C(19)	90.3(6)	O(2)–Sb(4)–C(55)	90.6(6)
C(19)–Sb(2)–C(25)	118.6(8)	C(55)–Sb(4)–C(61)	122.9(8)
C(19)–Sb(2)–C(31)	121.4(8)	C(55)–Sb(4)–C(67)	117.4(8)
C(25)–Sb(2)–C(31)	120.0(9)	C(61)–Sb(4)–C(67)	119.7(8)

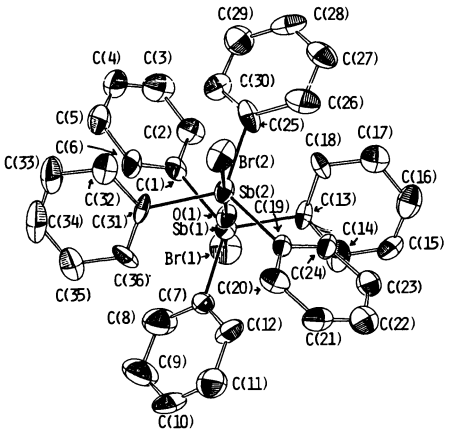

Fig. 1. A perspective drawing of the complex around the Sb(1) and Sb(2) atoms, with the numbering scheme.

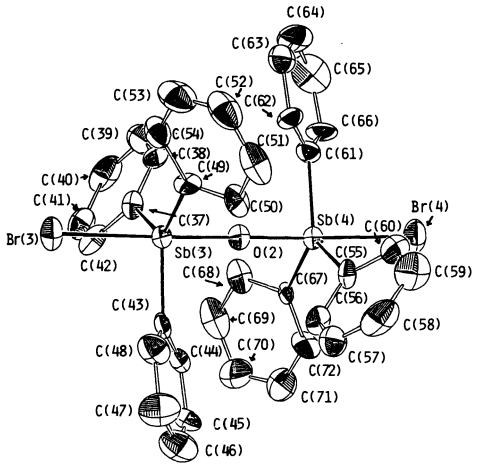

Fig. 2. A perspective drawing of the complex around the Sb(3) and Sb(4) atoms, with the numbering scheme.

mony atoms are approximately the same. Of course, there are some slight differences between them: for example, the angles Sb(1)–O(1)–Sb(2) and Sb(3)–O(2)–Sb(4) are 170.2(7) and 176.6(8)°, respectively, and the mutual dihedral angles between the three benzene ring planes around the Sb(2) atom distribute in the widest range, 49.0—70.6°.

Each antimony atom is coordinated to three phenyl-carbon atoms equatorially, and to one bromine as well as one bridging oxygen atom axially, being in a trigonal-bipyramidal geometry. The lengths of the Sb–C are in the range 2.06(2)—2.14(2) Å, which are not much different from the sum of the Pauling's covalent radii of the atoms C and O: 2.18 Å. On the other hand, the Sb–Br lengths are in the range 2.693(3)—2.722(3) Å, which are longer than the sum of their radii: 2.55 Å.[15] The Sb–O(bridge) lengths are in the range 1.931(13)—1.958(13) Å, which are much shorter than the sum of their radii: 2.15 Å. The common Sb–O bond lengths in the monomeric organoantimony(V) compounds are not so short: for example, in methoxytetraphenylantimony(V) it is 2.061(7) Å, while in dimethoxytriphenylantimony(V) they are 2.039(8) and 2.027(8) Å,[16] while in the other compounds, the bond length is sometimes longer. On the other hand, in cases of this type bridging, the bond is always very short. The Sb–O bond lengths as well as the Sb–O–Sb′ bond angles of some $[SbXR_3]_2O$ type com-

Table 2. Bond Lengths and Angles Around the Bridging Oxygen Atom of the $(SbXR_3)_2O$ (R=C_6H_5, CH_3) Type Compounds

Compound	Sb-O(bridge) (l/Å)	Sb-O-Sb′ (ϕ/°)	Ref.
$[SbBr(C_6H_5)_3]_2O$[a]	1.944 (average)	173.4 (average)	
$[Sb(HOC_2H_4SO_3)(C_6H_5)_3]_2O$	1.936(1)	(180)[b]	4
$[SbN_3(C_6H_5)_3]_2O$	1.985(3)	139.8(4)	5
$[SbCl(CH_3)_3]_2O$	1.907(1)	(180)[b]	6
$[SbN_3(CH_3)_3]_2O$	1.872(3)	(180)[b]	6
$[Sb(ClO_4)(CH_3)_3]_2O$	1.862(2)	(180)[b]	6

a) Respective values with their standard deviations are shown in Table 1. b) The bridging oxygen atom is at the center of symmetry.

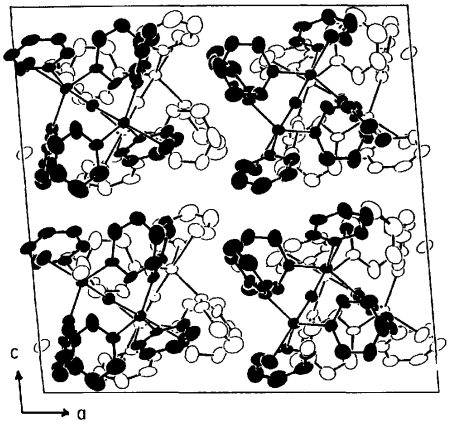

Fig. 3. A projection of the unit cell to the ac-plane. Black atoms belong to the upper, and the white atoms to the lower layers, respectively.

pounds are summarized in Table 2. As shown in this table, of the three triphenylantimony derivatives, the title compound has a bond longer than that of the sulfonato derivative, but shorter than the azido derivative. The polarizability of the bonded anion should not be the sole factor used to determine the length, because in the trimethylantimony derivatives, the Sb-O(bridge) length of the chloro derivative is longer than that of the azido derivative. Moreover, the bond lengths of the azido derivatives of the triphenyl- and trimethylantimony(V) are not the same: the former length is 0.113 Å longer than the latter. Therefore, the massive hydrocarbon groups bonded to the metal atom elongate the bridging bond length. Although the Sb-O-Sb′ angles of the title compound is not much different from 180°, but as the temperature factors of the both bridging oxygen atoms, O(1) and O(2), are not very large, the disorder of the oxygen atoms proposed by Ferguson[6] may not be true in this case. One probable reason is that, although which may not be the sole reason, the mutual steric effect of such large molecules to pack them most closely in the crystal gives the bridging oxygen atom such a large angle, almost 180°, in some of this type dimers.

As shown in Figs. 1 and 2, three benzene rings around each metal atom are situated like the three wing plates of a screw around their shaft. All the mutual dihedral angles between the three benzene ring planes bonded to each metal atom are 59.7°, on the average, and all the angles between the benzene ring planes and the respective Sb-O shafts are 54.6° on the average (in the range of 48.2—66.1°).

There are no bridging ligands nor hydrogen bondings between any dimeric complex molecules: the distances between any non-hydrogen atoms of the different molecules are more than 3.7 Å.

References

1) G. O. Doak and L. D. Freedman, "Organometallic Compounds of Arsenic, Antimony, and Bismuth," Wiley, New York (1970), pp. a) 318, b) 328.
2) A. Michaelis and A. Reese, *Justus Liebigs Ann. Chem.*, **233**, 39 (1886).
3) A. Ouchi, M. Shimoi, S. Hatazawa, and Y. Yoshino, *Bunseki Kagaku*, **29**, 245 (1980).
4) H. Preut, R. Ruther, and F. Huber, *Acta Crystallogr., Sect. C*, **41**, 358 (1985).
5) G. Ferguson and D. R. Ridley, *Acta Crystallogr., Sect. B*, **29**, 2221 (1973).
6) G. Ferguson, F. C. March, and D. R. Ridley, *Acta Crystallogr., Sect. B*, **31**, 1260 (1975).
7) F. Ebina, A. Ouchi, and Y. Yoshino, *Acta Crystallogr., Sect. B*, **34**, 2134 (1978).
8) F. C. March and G. Ferguson, *J. Chem. Soc., Dalton Trans.*, **1975**, 1291.
9) C. Glidewell and D. C. Liles, *Acta Crystallogr., Sect. B*, **34**, 119 (1978).
10) C. Glidewell and D. C. Liles, *Acta Crystallogr., Sect. B*, **34**, 1693 (1978).
11) $R=\sum||F_o|-|F_c||/\sum|F_o|$
12) "The Universal Crystallographic Computation Program System (UNICS)," ed by T. Sakurai, Tokyo (1967).
13) "International Tables for X-Ray Crystallography," Kynoch Press, Birmingham (1974), Vol. IV, pp. 72, 150.
14) The final atomic parameters, their temperature factors, and the final F_o-F_c tables are deposited as Document No. 8787 at the Office of the Editor of Bull. Chem. Soc. Jpn.
15) L. Pauling, "Nature of the Chemical Bonds," 3rd ed., Cornell Univ. Press, N. Y. (1960) pp. 224, 228. Single, double, and triple bond covalent radii of some atoms are as follows (shown in the order, respectively): C, 0.772, 0.667, 0.603; O, 0.74, 0.62, 0.55; Sb, 1.41, 1.31; Br, 1.14, 1.04 Å.
16) K. Shen, W. E. McEvan, S. J. La Placa, W. C. Hamilton, and A. P. Wolf, *J. Am. Chem. Soc.*, **90**, 1718 (1968).

Thermal Cis-Trans Isomerization of Dihalogenobis[trialkyl(or aryl)-phosphine]platinum(II) in the Solid State

Masaki FUSHIMI, Masatatsu SUZUKI, and Akira UEHARA*
Department of Chemistry, Faculty of Science, Kanazawa University, Kanazawa 920
(Received October 17, 1987)

Synopsis. Solid-state thermal cis–trans isomerization of the platinum(II) complexes of the type $[PtX_2(PR_3)_2]$ were investigated by means of DSC methods, where X is Cl, Br, or I; R is CH_3, C_2H_5, n-C_3H_7, n-C_4H_9, or C_6H_5. High isomerization ratios (93—100%) were observed for the cis-complexes of $P(C_2H_5)_3$ (X: Br; I), $P(n$-$C_3H_7)_3$ (X: Br; I), and $P(n$-$C_4H_9)_3$ (X: Cl; Br).

The *cis*-dihalogenobis(phosphine)platinum(II) complexes of the type *cis*-$[PtX_2(PR_3)_2]$, where X is a halide ion and PR_3 is one of trialkyl- or triarylphosphines, have long been known to be useful homogeneous catalysts for the selective hydrogenation of unsaturated organic compounds.[1] The cis complexes can usually be prepared by the following two steps:[2] In the first step, the double complexes having a general formula of $[Pt(PR_3)_4][PtX_4]$ are prepared and then the solid double complexes are heated at appropriate temperatures to produce a mixture of *cis*- and *trans*-$[PtX_2(PR_3)_2]$. In the second step, the mixture is separated into pure *cis*- and *trans*-$[PtX_2(PR_3)_2]$ by the use of the difference in solubilities. In general, trans isomers are much more soluble than cis isomers. The ratios of cis to trans isomers in the mixture are largely dependent on the kinds of phosphines. For example, when tributylphosphine and triarylphosphine are used as the ligands, cis isomers are exclusively formed, whereas trans isomers can be obtained only by the use of the thermal isomerization of the corresponding cis isomers.

The thermal cis–trans isomerization of the platinum(II) complexes $[PtX_2(PR_3)_2]$ in the solid state has been much less thoroughly studied, although the catalyzed isomerization of such complexes in solution has extensively been investigated.[3–8] Jensen first reported the isomerization of $[PtX_2(PR_3)_2]$ in the solid state.[2a] More recently, Mastin,[9] and Lee and Stoufer[10] reported on the thermal behaviors, including cis–trans isomerization of $[PtX_2\{P(C_6H_5)_3\}_2]$. DTA/TG methods were used to investigate the isomerization and volatilization of a number of palladium(II) and platinum(II) complexes of phosphines.[11,12] Unfortunately, any study did not quantitatively determine the isomerization ratios of the phosphine complexes, in spite of the fact that the cis-to-trans isomerization in the solid phase (practically in the melting state) has been used widely as the standard synthetic procedure for trans complexes.[2b]

From the standpoint of the application of the isomerization to synthetic procedure, the present study was undertaken primarily to determine the thermal cis–trans isomerization ratios of $[PtX_2(PR_3)_2]$, where X is Cl, Br, or I, and R is CH_3, C_2H_5, n-C_3H_7, n-C_4H_9, or C_6H_5.

Experimental

Materials. Trimethylphosphine($P(CH_3)_3$), triethylphosphine($P(C_2H_5)_3$), tripropylphosphine ($P(n$-$C_3H_7)_3$), tributylphosphine($P(n$-$C_4H_9)_3$), and triphenylphosphine ($P(C_6H_5)_3$) were commercially available.

Preparation of Complexes. *cis*- and *trans*-$[PtX_2(PR_3)_2]$ were prepared by a method similar to that of literature,[2] where X is Cl, Br, or I, and R is CH_3, C_2H_5, n-C_3H_7, n-C_4H_9, or C_6H_5. The compositions of the complexes obtained were confirmed by elementary analyses; the configurations thereof were characterized by means of electronic, IR, Far-IR, and ^1H and ^{31}P NMR spectroscopies.

Measurements. IR spectra of the samples were measured by a KBr-disk method with a JASCO Model A-3 infrared spectrophotometer. Far-IR spectra were measured by a Nujol-mull method with a JASCO Model IR-F far infrared spectrophotometer. Electronic spectra of the samples were recorded on a JASCO UVIDEC-105 UV/VIS recording digital spectrophotometer. ^1H and ^{31}P NMR spectra were monitored on a JEOL-GX400 spectrometer using $(CH_3)_4Si$ as the internal standard in $CDCl_3$ and 85% H_3PO_4 as the external standard in $CDCl_3/CHCl_3$ (1/6, v/v), respectively.

Differential scanning calorimetries (DSC) were carried out with a RIGAKU DENKI Thermal Analyser. Finely powdered samples were used in each run. The measurements were carried out under a constant flow of nitrogen stream at the heating rate of ca. 1.3 °C min^{-1}. Isothermal measurements were conducted by the use of a Chyo-100-L thermobalance equipped with the heating furnace controlled by SHINYO DIGICON 1200 in static air.

Results and Discussion

Thermal Analyses. Figure 1 shows the DSC curve in the first increasing and decreasing, and the second increasing-temperature processes of *cis*-$[PtCl_2\{P(n$-$C_3H_7)_3\}_2]$. The endothermic peak (A, T_{max}: 149 °C) is

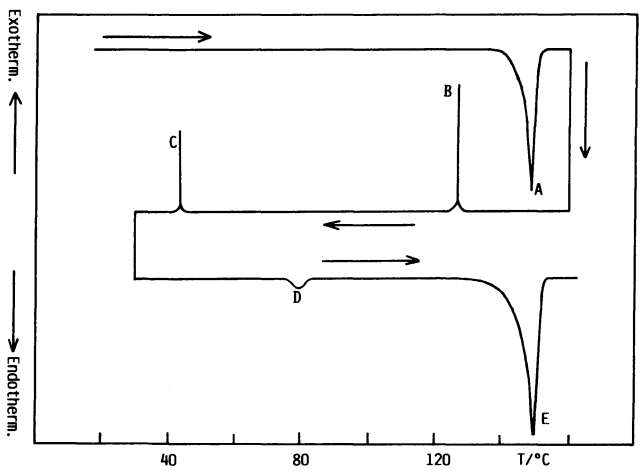

Fig. 1. DSC curve of *cis*-$[PtCl_2\{P(n$-$C_3H_7)_3\}_2]$.

observed in the first increasing-temperature process, which corresponds to the melting point of the cis isomer (mp: 149—150 °C). The product obtained at this stage was confirmed to consist of the mixture of cis and trans isomers (vide infra). The peak is thus ascribable to the melting plus the isomerization of the cis isomer. The exothermic peaks (B, T_{max}: 127 °C) and (C, T_{max}: 44 °C) in the decreasing-temperature process may correspond to the freezing point of the cis isomer and to that of the trans isomer, respectively, because preliminary experiments showed that owing to supercooling the authentic cis and trans complexes are solidified at considerably lower temperatures than their melting points (cis: 149—150 °C; trans: 85—87 °C). Then, the small endothermic peak (D, T_{max}: 80 °C) is found in the second increasing-temperature process, which may come from the melting of the trans isomer (mp: 85—87 °C). The melting point of the trans isomer is thus slightly lowered because of the presence of considerable amount of the cis isomer unchanged. Thus, the appearance of the melting peak of the trans isomer apparently suggests that the cis isomer isomerizes to the corresponding trans isomer to some extent. The endothermic peak (E, T_{max}: 149 °C) in the second increasing-temperature process is the melting point of the cis isomer.

It should be noted that both cis and trans complexes of $P(CH_3)_3$ and $P(C_6H_5)_3$ were decomposed in a complicated fashion with neither melting nor isomerization irrespective of the kind of halide ions. On the other hand, both cis and trans isomers of $P(C_2H_5)_3$, $P(n\text{-}C_3H_7)_3$, and $P(n\text{-}C_4H_9)_3$ were found to have melt to isomerize to the corresponding isomers. It is thus conceivable that the isomerization of the phosphine complexes proceeds in the melting state. This situation is in marked contrast to the case of diamminedihalogenoplatinum(II), isomerization of which takes place easily in the solid state even without melting.[13]

Identification of the Products. The symmetries of the *cis*- and *trans*-$[PtX_2(PR_3)_2]$ are clearly different from each other: the cis isomer possesses local C_{2v} symmetry, while the trans isomer posseses D_{2h} symmetry. For platinum-chloride stretching vibrations, a square planar $PtCl_2P_2$ set should give rise to two bands (A_1 and B_2) for C_{2v} symmetry (cis-configuration) and to one band (B_u) for D_{2v} symmetry (trans configuration).[14] All the cis isomers in the present study exhibit two bands at ca. 270 and 305 cm^{-1}, while the trans isomers, one band at ca. 335 cm^{-1}. On the other hand, the products obtained during heating cis and trans complexes of $P(C_2H_5)_3$, $P(n\text{-}C_3H_7)_3$ and $P(n\text{-}C_4H_9)_3$ show three bands at ca. 270, 305, and 335 cm^{-1}. This evidences that the products are the mixture of cis and trans isomers.

Determination of Isomerization Ratios. The isomerization ratios were estimated spectrophotometrically: in the case of *cis*- and *trans*-$[PtCl_2\{P(n\text{-}C_3H_7)_3\}_2]$, for example, the following simultaneous equation was employed:

$$\begin{cases} 358.5x + 136.7y = D_{330} \\ 396.7x + 821.5y = D_{290} \end{cases}$$

where x and y are the molar concentrations of cis and trans isomers, the numerical factors are the molar extinction coefficients of the pure cis and trans isomers, and the D's represent their absorbances at the wavelengths specified by each subscript. The isomerization ratios are thus given by x(or y)/(x+y).

The isomerization was monitored at varied temperatures and at several time intervals to find suitable conditions for giving maximum isomerization ratios. The results showed that the ratios are considerably altered by the heating temperatures. For example, in the case of *cis*-$[PtCl_2\{P(C_2H_5)_3\}_2]$, the maximum ratio (35%) was detected for one hour at the heating temperature of 196 °C, which is slightly higher than the melting point (191—192 °C). Increasing temperature decreased the ratios: 23 and 2% were found at 205 and 210 °C, respectively. On the other hand, the trans complexes isomerized at

Table 1. Isomerization Ratios of the Complexes $[PtX_2(PR_3)_2]$[a]

$[PtX_2(PR_3)_2]$		Cis complex			Trans complex		
PR_3	X	Isomerizn. ratio(%)	Heating temp/°C	Mp θ_m/°C	Isomerizn. ratio(%)	Heating temp/°C	Mp θ_m/°C
$P(CH_3)_3$	Cl	b)			b)		
	Br	b)			b)		
	I	b)			b)		
$P(C_2H_5)_3$	Cl	35	196	191—192	70	160	133—134
	Br	95	200	197—199	a few %[c]	200	134—135
	I	ca. 100	145	139—140	a few %[c]	145	136—137
$P(n\text{-}C_3H_7)_3$	Cl	25	160	149—150	13	154	85—87
	Br	95	115	105—107	a few %[c]	115	95—96
	I	99	120	116—117	a few %[c]	120	114—116
$P(n\text{-}C_4H_9)_3$	Cl	93	150	143—144	6	150	65—66
	Br	95	103	77—78	a few %[c]	103	69—70
$P(C_6H_5)_3$	Cl	b)			b)		
	Br	b)			b)		
	I	b)			b)		

a) Each sample was heated for one hour at the specified temperatures. Prolonged heating did not increase the ratios. b) The complexes were decomposed with neither melting nor isomerization. c) Partially decomposed just after melting plus isomerization.

considerably higher temperature than the melting points. Table 1 summarizes the isomerization ratios of cis and trans complexes thus estimated together with the melting points of the complexes. The heating time of one hour was selected from the standpoint of the application of the isomerization to synthetic procedure. Prolonged heating did not improve the ratios. Thus, the ratios may be regarded as nearly maximum isomerization ratios. For $P(CH_3)_3$ and $P(C_6H_5)_3$ complexes, both cis and trans isomers were decomposed with neither melting nor isomerization regardless of halide ions. Among the trans isomers, the bromide and iodides of $P(C_2H_5)_3$ and $P(n\text{-}C_3H_7)_3$, and the bromide of $P(n\text{-}C_4H_9)_3$ complexes were partially decomposed just after melting plus isomerization. High isomerization ratios (93—100%) were observed for the cis complexes of $P(C_2H_5)_3$ (X: Br; I), $P(n\text{-}C_3H_7)_3$ (X: Br; I), and $P(n\text{-}C_4H_9)_3$ (X: Cl; Br). The sum of isomerization ratios of cis and trans isomers of the same phosphine is not exactly but approximately close to 100% except for the chloride of $P(n\text{-}C_3H_7)$, implying that the isomerization may reach equilibrium of cis and trans isomers. The sum of the ratios of the chlorides of $P(n\text{-}C_3H_7)_3$ complex amounts to only 38%. The value implys that the isomerization of the complexes incompletely reaches equilibrium under the specified conditions. An indication was detected for the complexes that application of higher heating temperatures than 160 °C for the cis and 154 °C for the trans isomers might improve the isomerization ratios. However, at such high temperatures the complexes in the melting state underwent gradual vaporization and partial decomposition so that the ratios were unable to be estimated in detail.

We expected at the beginning of this study that the bulkiness of the phosphines (steric factor) may play an important role in the isomerization. However, the expectation did not come true: as seen from Table 1, the isomerization ratios do not vary with the phosphines. Marther et al. found that there is a good correlation between NMR coupling constants and the Pt-P bond strengths in the platinum(II) complexes of phosphines.[15] Relationship between the isomerization and the Pt-P bond strengths was investigated by NMR spectroscopy, but no relationship could be found between them.

It has long been known that trans complexes of $[PtX_2(PR_3)_2]$ are isolated with more difficulty in poorer yields than the corresponding cis isomers because the trans isomers are much more soluble than the cis isomers.[2] Thus, the trans isomers have usually been prepared by the use of catalysed isomerization of the cis isomers in solution, but the method requires troublesome steps.[16] On the other hand, the results obtained in the present study declare that the trans complexes of $P(C_2H_5)_3$ (X: Br; I), $P(n\text{-}C_3H_7)_3$ (X: Br; I), and $P(n\text{-}C_4H_9)_3$ (X: Cl; Br) can be easily obtained in good yield by the use of thermal isomerization of the corresponding cis isomers in the solid state (practically in the melting state).

Financial support from the Ministry of Education, Science and Culture Grant-in-Aid for Scientific Research (No. 62470040) is acknowledged.

References

1) J. C. Bailar, Jr. and H. Itatani, *J. Am. Chem. Soc.*, **89**, 1592 (1967).
2) a) K. A. Jensen, *Z. Anorg. Allg. Chem.*, **229**, 225 (1936); b) G. B. Kauffman and L. A. Teter, *Inorg. Synth.*, **7**, 245 (1963); c) F. R. Hartley, *Organomet. Chem. Rev. A*, **6**, 119 (1970).
3) G. K. Anderson and R. J. Cross, *Chem. Soc. Rev.*, **9**, 185 (1980).
4) J. Chatt and R. G. Wilkins, *J. Chem. Soc.*, **1956**, 525.
5) P. Haake and R. M. Pfeiffer, *J. Am. Chem. Soc.*, **92**, 4996; 5243 (1970).
6) D. G. Cooper and J. Powell, *J. Am. Chem. Soc.*, **95**, 1102 (1973).
7) D. A. Redfield and J. H. Nelson, *J. Am. Chem. Soc.*, **96**, 6219 (1974).
8) D. A. Redfield and J. H. Nelson, *Inorg. Chem.*, **12**, 15 (1973).
9) S. H. Mastin, *Inorg. Chem.*, **13**, 1003 (1974).
10) T. W. Lee and R. C. Stoufer, *J. Am. Chem. Soc.*, **97**, 195 (1975).
11) E. A. Allen, J. D. Gaudio, and W. Wilkinson, *Thermochim. Acta*, **11**, 197 (1975).
12) C. E. Scott and S. H. Mastin, *Thermochim. Acta*, **14**, 141 (1976).
13) W. W. Wendlandt and J. P. Smith, "The Thermal Properties of Transition-Metal Ammine Complexes," Elsevier, New York (1967), p. 179.
14) D. A. Duddel, P. L. Goggin, R. J. Goodfellow, M. G. Norton, and J. G. Smith, *J. Chem. Soc. A*, **1970**, 545.
15) G. G. Mather, A. Pidcock, and G. J. N. Rapsey, *J. Chem. Soc., Dalton Trans.*, **1973**, 2095.
16) J. Chatt and R. G. Wilkins, *J. Chem. Soc.*, **1951**, 2532.

The Magnetic Properties of the Copper(II) Alkanoate Adducts with Cyclic Ethers and Tertiary Amines

Shuji EMORI,* Hiroki NONAKA, Noriyasu IKEDA, and Yoneichiro MUTO
Department of Chemistry, Faculty of Science and Engineering, Saga University, Honjo-machi, Saga 840
(Received October 21, 1987)

Synopsis. Various copper(II) alkanoate adducts with cyclic ethers and tertiary amines have been prepared and characterized by means of magnetic susceptibility and IR spectroscopy measurements. The effect on the magnetic moments of the dinuclear copper(II) alkanoates of varying the base strength of the axial ligands is also discussed.

It has often been pointed out that the antiferromagnetic interaction in dinuclear copper(II) carboxylate adducts, $[Cu(RCOO)_2 \cdot L]_2$, is influenced both by the carboxylato substituent R and the axial ligand L.[1,2] As for the latter, Jotham et al. have examined the magnetic properties of the compounds with a series of axial ligands including pyridine and water and have noted that the spin-exchange coupling between the two copper(II) ions tends to increase as the axial ligands become stronger electron donors.[1] However, these magnetic properties may be obscured by other factors, such as the steric hindrance of axial coordination[3] and the intermolecular hydrogen bond between the water molecule and the carboxylato group.[4,5] Actually, the magnetic data of the copper(II) chloroacetate adducts with pyridine analogues[6] rather contradict the remark of Jotham et al.

Thus, we have now prepared various copper(II) alkanoate adducts with 1-azabicyclo[2.2.2]octane (abco), 1,4-diazabicyclo[2.2.2]octane (dabco), 1,3,5,7-tetraazatricyclo[3.3.1.1]decane (tatcd), tetrahydropyran (THP), and tetrahydrofuran (THF), and examined their magnetic moments, together with those of the adducts with 1,4-dioxane (dox). The axial ligands here considered are practically pure sigma donors, containing both oxygen and nitrogen donors. X-Ray analyses[7-9] have shown that the copper(II) propionate adduct with dox and the copper(II) acetate adducts with dabco and tatcd have polymeric structures, in which the carboxylato-bridged dinuclear units are connected by the axial ligands. In spite of this fact, these compounds are appropriate compounds in which to examine the axial-ligand effects on the magnetic properties of dinuclear copper(II) alkanoates, because the interdinuclear interactions are much weaker than the intradinuclear interactions.[10,11]

Various copper(II) alkanoate-abco (1/1), -dabco (2/1), and -tatcd (3/1) compounds were obtained, except for the cyclohexanecarboxylates, in accordance with a method employed by Tennenhouse.[12] The cyclohexanecarboxylates were prepared in a similar way, using dioxane solutions. The 2:1 species of tatcd adducts were obtained according to the procedure of Pickardt.[8] The adducts with the THP and THF were prepared by the use of the procedures reported for the corresponding dox adducts,[13] and their chemical analyses were done and their magnetic susceptibilities were measured within a few hours after preparation to avoid any fluctuations caused by their instabilities.

The effective magnetic moments of these compounds (Table 1) were evaluated from the room-temperature magnetic susceptibilities, which were corrected for the diamagnetic contribution using Pascal constants[14] and for the temperature-independent paramagnetism using the value of 60×10^{-6} emu mol^{-1} (1 emu$=4\pi\times10^{-6}$ m^3). The values determined for the copper(II) acetate adducts with abco and dabco agreed well with those reported previously.[11,15] For the copper(II) propionate-abco (1/1), -dabco (2/1), and -tatcd (3/1) compounds, the temperature dependence of their magnetic susceptibilities was measured in the temperature range of 80—300 K in order to confirm their dinuclear structures. The results agreed well with the Bleaney-Bowers equation[16] when the following parameters were used: $g=2.18$ and $2J=-323$ cm^{-1} for the abco adduct, $g=2.17$ and $2J=-329$ cm^{-1} for the dabco adduct, and $g=2.18$ and $2J=-334$ cm^{-1} for the tatcd adduct. The IR spectra of the solid compounds show characteristic bands in the ranges of 1660—1610 and 1425—1405 cm^{-1} connected with the symmetric and unsymmetric COO stretching vibrations of the carboxyl groups.[17] The magnetic and IR

Table 1. Effective Magnetic Moments (BM) at 20°C for $[Cu(RCOO)_2 \cdot L]_2$ Compounds

R\L	abco	1/2dabco	1/2tatcd	1/3tatcd	THP	THF
CH_3	1.42	1.40	1.38	1.35		
C_2H_5	1.35	1.32		1.30		
C_3H_7	1.37	1.34		1.30		
$ClCH_2CH_2$	1.40	1.35		1.31		1.37
$ClCH_2$		1.42	1.42		1.42	1.40
$(CH_3)_2CH$	1.33	1.31		1.30		
C_6H_{11}	1.35	1.32		1.27		
CH_3CHCl		1.43		1.38	1.42	1.38
CH_3CHBr		1.40		1.39		
Cl_2CH			1.49		1.48	1.48
CH_3CCl_2		1.49			1.46	1.47

spectral data indicate that the present compounds have bridged dinuclear structures similar to that of copper(II) acetate monohydrate.[4,5]

Previously, we have shown that, for the copper(II) (monosubstituted acetate)s and copper(II) (disubstituted acetate)s with coordinated chloride ions in the axial positions, their magnetic moments decrease linearly with the pK_a values of the parent carboxylic acids,[18-20] which may be summarized as follows:

$$\mu_{eff} = -0.052(pK_a - 4.56) + \Delta\mu_\alpha + 1.37_9, \quad (1)$$

where $\Delta\mu_\alpha$ is the correction term for the substitution in the methyl group of acetic acid (−0.06 and −0.07 for the series of mono- and disubstituted acetates respectively), including the corrections for steric strain, field effect, and hyperconjugation. Similarly, the magnetic moments of a series of copper(II) alkanoates with other axial ligands may be expressed as follows.

$$\mu_{eff} = -0.052(pK_a - 4.56) + \Delta\mu_\alpha + A_{ax}, \quad (2)$$

where A_{ax} is a correction term for axial coordination; its value can be evaluated by graphic interpolation (Fig. 1). To plot the points for the 2,2-dichloropropionates, $\Delta\mu_\alpha$=−0.08 BM[21] is used tentatively, since insufficient data are available to evaluate it precisely. The obtained A_{ax} values are 1.42_2, 1.39_3, 1.38_1, and 1.35_9 BM for the abco, 1/2dabco, 1/2tatcd, and 1/3tatcd adducts respectively, and 1.37_2, 1.37_0, and 1.36_3 BM for the THP, THF, and 1/2dox adducts respectively.

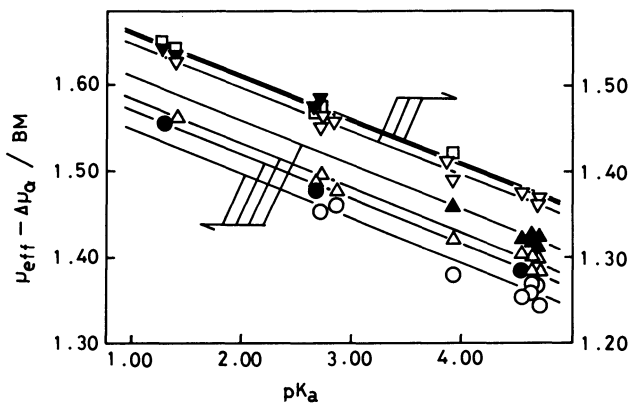

Fig. 1. The corrected magnetic moments at 20°C plotted against the pK_a values of the parent carboxylic acids for the copper(II) alkanoate adducts with abco (▲), 1/2dabco (△), 1/2tatcd (●), 1/3tatcd (○), THP (▼), THF (□), and 1/2dox (▽). The solid lines are the best fit of the data to the Eq. 2.

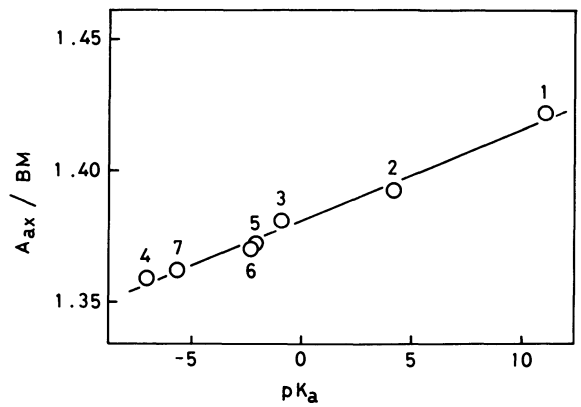

Fig. 2. The axial-coordination correction term plotted against the pK_a value of the conjugate acid of the axial ligand: abco (1), 1/2dabco (2), 1/2tatcd (3), 1/3tatcd (4), THP (5), THF (6), and 1/2dox (7).

Since typical hard bases are involved in this study, it seems likely that the axial-ligation effect of such bases correlates primarily to their donor characters. In order to examine this, the obtained A_{ax}'s are plotted against the pK_a values of the conjugate acids of axial ligands (Fig. 2). To plot the points for dabco and dox ligands, their first dissociation constants are selected, because their second coordination abilities are reduced similarly by H^+- and Cu^{2+}-coordination on the other sites. By similar reasoning, the pK_{a2} and pK_{a3} values (these values are estimated from pK_{a4}[22] by using the Branch-Calvin equation[23]) are selected for the 1/2tatcd and 1/3tatcd adducts respectively. In this series of axial ligands, the pK_a value varies from −7.1 for 1/3tatcd to −5.7, −2.26, −2.10, −1.0, 4.14, and 11.0 for 1/2dox, THP, THF, 1/2tatcd, 1/2dabco, and abco respectively. As can be seen from Fig. 2, there is a linear relation between these quantities. The best line has a slope of +0.0035 BM and the intercept of 1.38_2 BM at pK_a=0. The line in Fig. 2 goes upward to the right, and the variation in singlet-triplet separation values determined for the abco, 1/2dabco, and 1/3tatcd adducts of copper(II) propionate (−2J=323, 329, and 334 cm^{-1} respectively) indicates that the antiferromagnetic interactions decrease as the axial ligands become stronger sigma donors. This fact may be explained on the basis of weak Cu-O covalent bonds on the CuO_4 basal plane resulting from a strong sigma donation of the axial ligand.[24] The observation of the shift in the unsymmetric COO stretching bands (1623, 1620, and 1610 cm^{-1} for the abco, 1/2dabco, and 1/3tatcd adducts of copper(II) propionate) supports this explanation. The magnetic moments of copper(II) tetrahydro-2H-pyran-2-acetate[25] and the copper(II) chloroacetate adducts with 1,3-dioxolane and 2-(diethylamino)ethanol[26] were also found to vary in accord with this trend. In addition, a numerical comparison of the slopes in Figs. 1 and 2 indicates that, in the series of the present compounds, the axial ligand affects the magnetic moment about 15 times less than the bridging carboxylato does. This ratio suggests that the carboxylato substituent R in dinuclear copper(II) carboxylate adducts, $[Cu(RCOO)_2 \cdot L]_2$, affects the covalent Cu-O bonds more strongly than does the apical ligand L, for the spin-exchange coupling between the two copper(II) ions operates predominantly by superexchange interaction through the bridging carboxylato rather than by direct interaction.[27]

References

1) R. W. Jotham, S. F. A. Kettle, and J. A. Marks, *J. Chem. Soc., Dalton Trans.*, **1972**, 428.
2) M. Melnik, *Coord. Chem. Rev.*, **42**, 259 (1982).

3) Y. Muto, N. Hirashima, T. Tokii, M. Kato, and I. Suzuki, *Bull. Chem. Soc. Jpn.*, **59**, 3672 (1986).
4) J. N. van Niekerk and F. R. L. Schoening, *Acta Crystallogr.*, **6**, 227 (1953).
5) G. M. Brown and R. Chidambaram, *Acta Crystallogr., Sect. B*, **29**, 2393 (1973).
6) Y. Muto, T. Tokii, K. Chijiwa, and M. Kato, *Bull. Chem. Soc. Jpn.*, **57**, 1008 (1984).
7) V. M. Rao, D. N. Sathyanarayana, and H. Monohar, *J. Chem. Soc., Dalton Trans.*, **1983**, 2167.
8) Von J. Pickardt, *Acta Crystallogr., Sect. B*, **37**, 1753 (1981).
9) M. M. Borel and A. Leclair, *Acta Crystallogr., Sect. B*, **32**, 1275 (1976).
10) H. W. Richardson, J. R. Wasson, and W. E. Hatfield, *Inorg. Chem.*, **16**, 484 (1977).
11) E. D. Stevens and J. T. Yoke, *Inorg. Chim. Acta*, **4**, 244 (1970).
12) G. T. Tennenhouse and J. C. Bailer, Jr., *J. Inorg. Nucl. Chem.*, **28**, 682 (1966).
13) M. Melnik, R. Nasanen, and I. J. Seppala, *Acta Chem. Scand.*, **25**, 2081 (1971).
14) G. Foex, "Constants Sélectionées, Diamagnétisme et Paramagnétisme," Masson, Paris (1957).
15) V. M. Rao, D. N. Sathyanarayana, and H. Monohar, *Indian J. Chem.*, **24A**, 417 (1985).
16) J. Lewis, Y. C. Lin, L. K. Royston, and R. C. Thomson, *J. Chem. Soc.*, **1965**, 428.
17) S. Yamada, H. Nakamura, and R. Tsuchida, *Bull. Chem. Soc. Jpn.*, **31**, 303 (1958).
18) S. Emori and Y. Muto, *Bull. Chem. Soc. Jpn.*, **57**, 291 (1984).
19) S. Emori, N. Morishita, and Y. Muto, *Bull. Chem. Soc. Jpn.*, **60**, 1913 (1987).
20) S. Emori, Y. Tohyama, and Y. Muto, *Bull. Chem. Soc. Jpn.*, **60**, 4555 (1987).
21) Estimated from the magnetic moment of $Cu[(CH_3)_3CCOO]_2 \cdot CH_3NH_3Cl$ (1.37 BM at 20 °C).
22) F. G. Pavelka, *Z. Electrochem.*, **30**, 180 (1924).
23) G. E. K. Branch and M. Calvin, "The Theory of Organic Chemistry," Prentice-Hall, New York (1941).
24) B. J. Hathaway and P. G. Hodgson, *J. Inorg. Nucl. Chem.*, **35**, 4071 (1973).
25) W. R. Scheidt and P. G. Rasmussen, *Inorg. Chem.*, **8**, 2512 (1969).
26) S. Emori, N. Ikeda, and Y. Muto, unpublished data. The magnetic moments of $Cu(ClCH_2COO)_2 \cdot (C_2H_5)_2NCH_2CH_2OH$ and $Cu(ClCH_2COO)_2 \cdot C_3H_6O_2$ are 1.44 and 1.41 BM respectively at 20 °C.
27) D. M. L. Goodgame, N. J. Hill, D. F. Marsham, A. C. Skapski, M. L. Smart, and P. G. H. Troughton, *J. Chem. Soc., Chem. Commun.*, **1969**, 629.

Improvement in Flash Chromatography

Yoshinori NARUTA,* Hitoshi UEMORI,† Masami FUKUMOTO,† Haruhiko SUGIYAMA,†
Yoshitsugu SAKATA,† and Kazuhiro MARUYAMA
Department of Chemistry, Faculty of Science, Kyoto University,
Sakyo-ku, Kyoto 606
†Osaka Research Laboratory, Wako Pure Chemical Industries,
Ltd., Amagasaki 661
(Received November 24, 1987)

Synopsis. Optimum and higher resolution in flash chromatography (FC) has been realized with 20—40 μm silica gel, which gives 1.4—1.9 times larger theoretical plate numbers, than the reported one, 40—63 μm. A new FC tube is proposed and the combination of quartz-made chromatographic tube and silica gel with fluorescent indicator is conveniently used for the preparative separation of colorless but UV absorbing compounds.

Medium-pressure liquid chromatography (MPLC),[1] flash chromatography (FC),[2,3] and vacuum dry chromatography[4] have been used for rapid and preparative separation of organic compounds as routine methods. These chromatographic techniques overcome the defects encountered in traditional gravity column chromatography, which is characterized by its low resolution, long separation time, inferior recovery of sample, and requisition of large amount of solvent and adsorbent. Among these techniques, FC has been accepted as a substantially reliable one from the respect of its simplicity, acceptable resolution, and speed. Still et al. reported the optimum resolution was obtained when FC column was prepared by simple dry packing of 40—63 μm silica gel.[2] During our practical application of the FC technique, we found silica gel with smaller diameter and a slurry packing method resulted in the better resolution than the reported method; we reexamined the optimization of FC with use of several kinds of silica gel with different physical properties. We also propose the practically useful FC system which allows the convenient treatment.

We systematically prepared and used four kinds of silica gel, Nos. 1—4 shown in Table 1, with different particle distribution. For elimination of the specificity of silica gel prepared, the corresponding silica gel from E. Merck with different specific surface area, average pore size, and pore volume was also examined. Optimization studies were carried out under a set of conditions using a mixed sample of toluene and nitrobenzene (1 : 1) on a 20 mm i.d.×25 cm column. In the previous paper,[2] packing method is shown not to affect the separation efficiency. We, however, found slurry packing method gave higher and reproducible column efficiency at the pressure below 1 kg cm^{-2}.[6] Since the applied pressure on silica gel packing sensitively affected the resultant column efficiency, especially for the silica gel with the diameter below 20 μm, all FC columns examined in this report were packed at the pressure below 1 kg cm^{-2}. Resolution (R_s) and separation factor (α) of aromatic components were determined, and theoretical plate number (N) was evaluated from the peak of nitrobenzene.[5] The results are shown in Fig. 1 and the typical chromatograms are illustrated in Fig. 2. The optimum resolution was obtained with the silica gel (15—40 μm and 20—40 μm) and 1.4—1.9 times larger N values for the gel with narrow particle distribution around $D_{p50}\cong 30$ μm were achieved than the reported one (40—63 μm).[2] This difference is obvious from their chromatograms (Fig. 2). Regardless of the difference in the physical properties, three types of the silica gel (Nos. 1—4, 5—8, and 9—11 in Table 1) exhibited the similar trend and column efficiency. Thus, it is concluded the column effciency is predominantly affected by both the particle size and

Table 1. Physical Properties of Various Silica Gel Used in This Work

No.	Silica gel name	Particle distribution/μm	Mean particle diameter, D_{p50}/μm	Specific surface area, S/m^2 g^{-1}
1	LP-20[a]	10—20	14	462
2	LP-40[a]	20—40	30	462
3	LP-60[a]	40—60	45	456
4	C-300[a]	45—75	55	456
5	E. Merck Si 60H[b]	45	25	486
6	E. Merck Si 60[b]	15—40	29	517
7	E. Merck Si 60[b]	40—63	50	516
8	E. Merck Si 60[b]	63	45	508
9	E. Merck LiChroPrep Si 60[b]	5—20	12	506
10	E. Merck LiChroPrep Si 60[b]	25—40	32	490
11	E. Merck LiChroPrep Si 60[b]	40—63	50	515

a) Average pore size P_d=70 Å, pore volume P_v=0.8 ml g^{-1}. b) P_d=60 Å, P_v=0.75 ml g^{-1}.

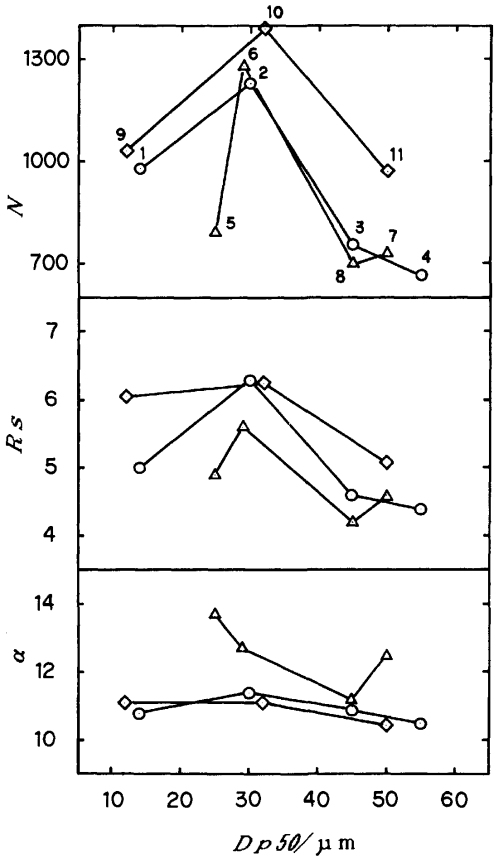

Fig. 1. Mean particle diameter (D_{p50}) vs. parameters of column efficiency, resolution (R_s), theoretical plate number (N), and separation factor (α). Numbers in the figure indicate silica gel employed, see Table 1.

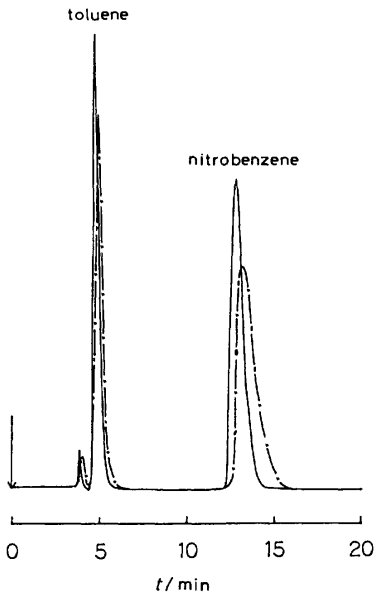

Fig. 2. Chromatograms of toluene-nitrobenzene mixture with the No. 2 silica gel (——) and the No. 3 silica gel (– – –). For chromatographic conditions, see experimental section.

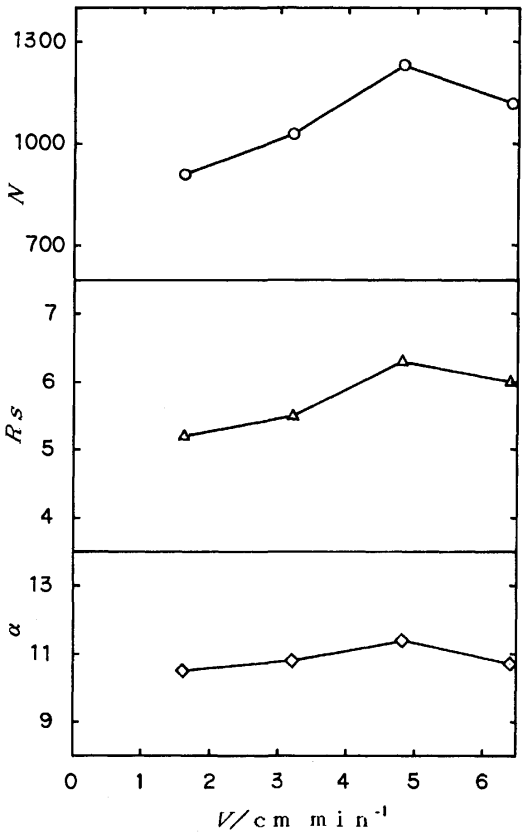

Fig. 3. Flow rate (V) vs. parameters of column efficiency. The No. 2 silica gel (LP-40) was used.

its distribution.

For the No. 2 silica gel in Table 1, effect of eluent flow rate on the resolution was examined (Fig. 3) and its optimum value was about 15 ml min^{-1} (linear velocity ca. 5 cm min^{-1}).

Improvement of FC Column. Since the use of silica gel with finer particles under the optimum separation conditions requires increased gas pressure for elution, the reported FC apparatus[2,3] turned to be not suitable for the present purposes, e.g. compressed gas leakage from the glass joint, leakage of adsorbent from the lower end of column, and difficulty in disposal of used gel. We made a new type of glass column apparatus as shown in Fig. 4. The column head **D** can be installed on the column **G** through fluoro-rubber O-ring **F** with clamp **E**, which makes possible quick installation and removal and holds them without any observable leakage of compressed gas below 2 kg cm^{-2}. The sintered glass filter **H** (G-3) effectively holds the applied adsorbent during the chromatographic operation: as long as No. 2 silica gel was used, the particles did not clog pores of the filter. The combination of the gas-tight O-ring joint and the snap-on clamp makes possible to prepare the larger internal diameter FC columns up to 50 mm and this system has practically and repeatedly been used without any problem.

For convenient monitoring of separation process during chromatography, we used quartz FC chroma-

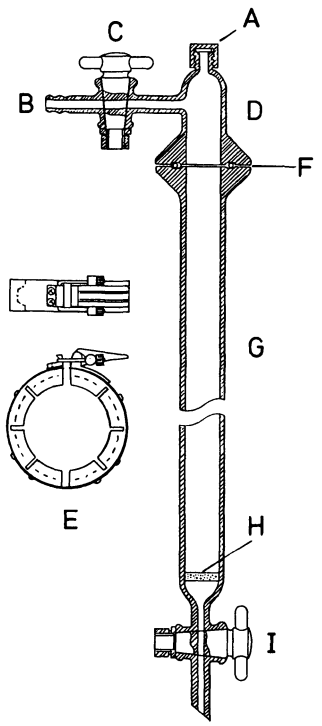

Fig. 4. Improved flash chromatography apparatus and some specifications. **A**, screw cap for pressure release; **B**, compressed gas inlet; **C**, gas stopcock; **D**, column head; **E**, O-ring joint clamp; **F**, fluororubber O-ring; **G**, column; **H**, glass sintered filter; **I**, stop cock.

tographic tubes and silica gel with fluorescent indicator in combination. When the applied solute can be detectable by TLC[7] under the illumination of UV light, this mixed fluorescent material is applicable to most of solvent systems except aromatics.[8] This method is also useful for the optimization of solvent systems during chromatography.

Experimental

Material. Irregular-shaped silica gel (Nos. 1—4 in Table 1) was sorted by pneumatic classifier, Nisshin Eng. Co., Turbo Classifier TC-15N. The particle size distribution and the specific surface area were determined with Coulter Counter, Model ZB and Yuasa Battery Co., Monosorb Surface Area Analyzer, respectively. Three types of silica gel with different distribution of particle size and average particle diameter D_{p50} were prepared (Nos. 1—3 in Table 1). The silica gel used was activated at 110 °C for 2 h. Silica gel with fluorescent indicator was prepared according to the reported method.[8] Three kinds of fluorescent materials, $Sr_2P_2O_7$/Sn, Zn_2SiO_4/Mn, and YVO_4/Eu, were mixed in a 20:5:1 ratio, respectively, and 10 wt% of the mixture was added to silica gel. As one of the silica gel frequently applied for medium pressure chromatography, Wakogel C-300 (No. 4 in Table 1) was used as a reference. For elimination of the specificity of silica gel caused by the difference of its physical properties, Merck silica gel 60 and Merck LiChroPrep (Nos. 5—11 in Table 1) were used. Physical properties of various silica gel used in this work were summerized in Table 1.

Chromatographic tubes made of Pyrex or quartz were assembled as shown in Fig. 4. Solvents for HPLC grade were used in these experiments.

Evaluation of Column Efficiency. Silica gel was charged to 20 mm i.d.×25 cm chromatographic tube by a slurry packing method. Each silica gel (60 g) was suspended in hexane (300 ml) and transferred to the hexane-filled tube at the flow rate of 80—100 ml min^{-1} keeping the pressure below 1 kg cm^{-2}. The net amount of the charged silica gel was 35—40 g. A mixture of toluene (50 g) and nitrobenzene (50 g) was diluted to 100 ml with heptane and used as a stock solution of the samples. After substitution of the column with 1 vol % acetonitril in hexane, the stock solution (250 μl) was loaded to the silica-gel column and eluted with the solvent at the flow rate 15 ml min^{-1} (5 cm min^{-1}). The effect of the flow rate on separation efficiency was examined on the range 5—20 ml min^{-1} (1.6—6.4 cm min^{-1}).

The authors wish to acknowledge to Mr. Yasuyuki Mizui for his technical assistance in the preparation of FC apparatus.

References

1) A. I. Meyers, R. K. Smith, and C. E. Whitten, *J. Org. Chem.*, **44**, 2247 (1979).

2) W. C. Still, M. Kahn, and A. Mitra, *J. Org. Chem.*, **43**, 2923 (1978).

3) L. J. Crane, M. Zief, and J. Horvath; *Am. Lab.*, **13**, 128 (1981); M. Zief, L. J. Crane, and J. Horvath, *ibid.*, **14**, 144 (1982).

4) E. J. Leopold, *J. Org. Chem.*, **47**, 4592 (1982).

5) Parameters of separation efficiency were defined as follows;[6]

$$R_s = \frac{2(t_{R2} - t_{R1})}{W_1 + W_2}, \quad \alpha = \frac{K_2'}{K_1'}$$

$$K' = \frac{t_R - t_0}{t_0}, \quad N = 5.54 \times \left[\frac{t_{R2}}{W_2/2}\right]^2,$$

where t_{Ri} and W_i are the retention time and the peak width of i compornent, respectively.

6) C. Liteanu and S. Gocan, "Gradient Liquid Chromatography," Ellis Horwood, Chichester (1974), pp. 55—90.

7) TLC plates with fluorescent indicator, e.g. silica gel 70 FM Plate-Wako, was applied.

8) Z. Tamura, *Talanta*, **19**, 573 (1972).

Selective Conversion of 2-Mercaptoalkanols to Thiirans with Orthocarbonates

Toshikazu TAKATA and Takeshi ENDO*
Research Laboratory of Resources Utilization, Tokyo Institute of Technology,
Nagatsuta-cho, Midori-ku, Yokohama 227
(Received September 9, 1987)

Synopsis. Tetraalkyl orthocarbonates **1** were demonstrated to serve as potent cyclodehydrating agents for 2-mercaptoalkanols **2** to give the corresponding thiirans in good yields in acid-catalyzed reactions in aprotic solvents. Effects of catalysts, solvents, and alkyl substituents of **1** were examined. Activity of the acid catalysts depended on their acidity (pK_a), and the strong Lewis acid $BF_3 \cdot OEt_2$ also had high catalytic activity. Effects of solvents and alkyl substituents of **1** were little observed.

Tetraalkyl orthocarbonates **1** have extensively been studied as useful reagents capable of reacting with both nucleophiles and electrophiles.[1,2] Especially, the characteristic reactions via carbenium ions under acidic conditions are of interest among the various reactions of **1**. Reactions with protic compounds such as phenols and carboxylic acids gave *O*-alkylation products.[1,3] We have recently utilized the acid-catalyzed alcohol-exchange reaction of **1** with some diols to obtain spiroorthocarbonates in good yields.[4] Although **1** is known to readily react with water to afford dialkyl carbonate and two moles of alcohol,[1,2,5] there is no report on the use of **1** as a dehydrating agent except for only one example of conversion of succinic acid to succinic anhydride.[3a]

In our continuing studies on the chemistry of **1**,[4] we have found that **1** is quite a potent cyclodehydrating agent for 2-mercaptoalkanols to thiirans under acidic conditions. A recent report of Evans et al. on the cyclodehydration of mercaptoalkanols to thiacycloalkanes with 1,3,2-dioxaphospholane derivatives,[6] also prompted us to report our recent results on the dehydration.

Results and Discussion

Orthocarbonate **1**, which is commercially available (R=Me) or easily prepared (R=Et and Bu^n),[7,8] was examined as a dehydrating agent in the acid-catalyzed reaction with 2-mercaptoethanol (**2a**), which often resists dehydration[9] and easily affords polymer of the product thiiran in the presence of a strong acid.[10] When **1** was mixed with an equimolar amount of **2a** in the presence of an acid catalyst such as *p*-toluenesulfonic acid (TsOH), thiiran was formed in more than 95% yield (by NMR) along with a dialkyl carbonate and an alkanol (Eq. 1). Without such an acid no reaction took place. The results examined for catalysts, solvents, and alkyl substituents of **1** are summarized in Table 1.

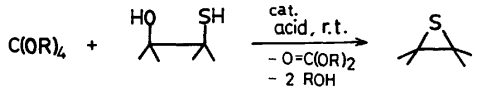

(1)

Using TsOH as the catalyst, the reaction (**1a**, Run 1) was completed within a few minutes, being too fast to monitor the reaction progress, unlike the case of trichloroacetic acid (TCA, Run 4) or acetic acid (AcOH, Run 5). This conversion was very clean, and the reaction gave only thiiran, dimethyl carbonate, and methanol (ratio, 1:1:2) without any by-products. TsOH monohydrate could also be used with slightly excess amount of **1** and similar products were obtained. Catalytic activity of the acids used clearly depended on their acidities: pK_a values were correlated with the effectiveness; accordingly, a strong Lewis acid (boron trifluoride etherate $BF_3 \cdot OEt_2$) was also a highly active one. All aprotic solvents listed could be used as they showed no detectable difference in the reaction progress. No serious difference was confirmed in the reaction efficiency among three orthocabonates **1a—1c** used.

Isolation of thiiran was attempted by distilling the reaction mixture (from **1a**, **2a**, and TsOH), but thiiran (bp 56 °C) was obtained in 67% yield as a mixture with methanol (bp 65 °C) and dimethyl carbonate (bp 90 °C). Part of thiiran still remained in the reaction mixture along with a small amount of white thiiran polymer, which appeared as a

Table 1. Acid-Catalyzed Cyclodehydration of 2-Mercaptoethanol (**2a**) to Thiiran[a] with Tetraalkyl Orthocarbonates (**1**)

Run	Orthocarbonate **1**, C(OR)$_4$		Acid catalyst mol%	pK_a	Solvent	Temp	Time/min
1	R=Me,	**1a**	TsOH[b] (2.0)	−7	$CDCl_3$	RT[c]	<3
2	Et,	**1b**	TsOH (4.6)		Benzene	RT	<5
3		**1b**	TsOH (3.6)		$CDCl_3$	RT	<5
4		**1b**	TCA[d] (11)	0.66	CCl_4	RT	ca. 40
5		**1b**	AcOH (31)	4.56	Benzene	RT	ca. 3 days
6		**1b**	AcOH (31)		$CDCl_3$	60—70 °C	ca. 15
7		**1b**	$BF_3 \cdot OEt_2$ (12)		CCl_4	RT	<3
8	R=Bu^n,	**1c**	TsOH (10)		$CDCl_3$	RT	<3
9		**1b**[e]	TsOH·H_2O (3.0)		$CDCl_3$	RT	<5

a) Yield of thiiran was quantitative (more than 95% by NMR). b) *p*-Toluenesulfonic acid. c) Room temperature. d) Trichloroacetic acid. e) Excess amount of **1b** (1.2 equiv) was used.

Table 2. Acid-Catalyzed Cyclodehydration of 2-Mercaptoalkanols (2) with Tetraalkyl Orthocarbonates (1)

Entry	Substrate 2	Orthocarbonate 1: $C(OR)_4$	Solvent	Product 3	Yield/%
1	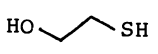 2a	R=Me	$CDCl_3$	3a	95[b]
2		Me	*m*-Xylene		67[b,c]
3		"Bu	None		30[d]
4	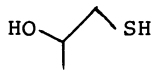 2b	Me	$CDCl_3$	3b	77[b]
5[e]	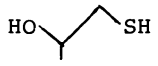 2c	Me	$CDCl_3$	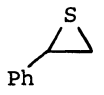 3c	80[b]
6[e]	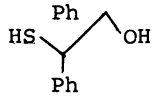 2c′	Me	CH_2Cl_2		63[f]
7	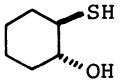 2d	Et	$CDCl_3$	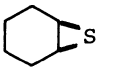 3d	97[g]
8		Me	CH_2Cl_2		78[d]

a) Reaction with 1—3 mol% of TsOH within 10 min. at room temperature. b) NMR yield. c) A mixture of **3a**, methanol and dimethyl carbonate. d) Isolated yield by distillation. e) Mixture of **2c** and **2c′** (ratio=3:2, by ^{1}H NMR) was used. f) The yield was determined by GC and NMR.

broad peak around δ 2.3 in ^{1}H NMR. Thereby, considering the formation of by-products having higher boiling points than 90 °C, use of butyl derivative **1c** instead of **1a** eventually made the isolation of thiiran possible (Table 2, Entry 3), although the yield was low (30%).

Furthermore, a few 2-mercaptoalkanols **2b**, **2c**, and **2d** were examined and in every case it was demonstrated that the corresponding thiirans were obtained in high yields (Table 2). Bicyclic thiiran **3d** was isolated in 78% yield by distillation, while 2-phenylthiiran **3c** was obtained in 63% yield by purification with chromatography (silica gel/hexane).

The rational reaction mechanism does not involve a simple acid-catalyzed dehydration process, because the reaction hardly proceeded without **1**. Therefore, the reaction should be completed via the alcohol-exchange equilibrium[2] followed by intramolecular thiiran cyclization to eliminate a dialkyl carbonate only as a leak process, as shown in Eq. 2. This mechanism can be supported by the following two experimental results: (i) to a mixture of **1b** and methanol is added a catalytic amount of TsOH and the system reaches a certain equilibrium of alcohol-exchange and (ii) **1** does not interact with any sulfhydryl groups, since 1,2-ethanedithiol did not react with **1a** in the presence of TsOH at all under the same conditions (^{1}H NMR study). Therefore, formation of 2,2-dialkoxy-1,3-oxathiolane as an intermediate is unlikely, although monocyclic and spirocyclic orthocarbonates are the main products in the reactions of tetraalkyl orthocarbonates with an equimolar and two equimolar amounts of diols, respectively.[4]

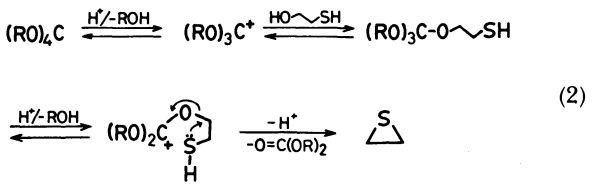

(2)

$$(EtO)_4C + MeOH \underset{}{\overset{H^+}{\rightleftharpoons}} (EtO)_3C(OMe) + (EtO)_2C(OMe)_2 + (EtO)C(OMe)_3 + (MeO)_4C + EtOH \quad (3)$$

(54%) (25%) (13%) (10%) (trace)

Thus, in this paper the orthocarbonate **1** is suggested to be a useful dehydrating agent for 2-mercaptoalkanols to thiirans in the acid-catalyzed reactions. This method is of advantage of its easy procedure and short reaction time under mild conditions.

Experimental

^{1}H NMR spectra were recorded on a JEOL JMN-PMX60 spectrometer using tetramethylsilane (TMS) as the internal standard in deuteriochloroform. Gas chromatography was carried out with a Shimadzu GC 4CPF equipped with FID detector and a data processor (column: PEG-20M, 3 m; carrier: N_2, 30 mL min^{-1}). Catalysts (extra pure grade) were used as received without further purification, except for TsOH which was dehydrated by heating its monohydrate at 100 °C for 6 h under reduced pressure. All solvents were dried before use by usual methods. Preparation of 2-mercaptoalkanols (**2b**, **2c**, and **2d**) was carried out according to the reported method from corresponding oxiranes.[11] Commercial **2a** was available. Orthocarbonates **1b** and **1c** were synthesized according to Sakai's method using tetrachlorostannane ($SnCl_4$),[8] while **1a** was obtained from Aldrich. The products were identified by GC, ^{1}H NMR, and boiling points in comparison with their authentic samples.[12]

Reaction of 2 with 1. (a) NMR Scale Method. An example using **2a** and **1a**. A mixture of **2a** (0.39 g, 0.5 mmol) and slightly excess **1a** (0.70—0.75 g, 0.52—0.55 mmol) in $CDCl_3$ (200 μL) was subjected to measurement of ^{1}H NMR (t=0). Then, to the reaction mixture was added TsOH (ca. 2 mg) at room temperature. After mixing, ^{1}H NMR was recorded promptly (within five min) and further at some intervals in order to monitor the reaction. ^{1}H NMR indicated quantitative conversion of **2a** to thiiran within

three minutes.

(b) Preparative Scale Procedure. An example using **1a** and **2d**. To a mixture of **2d** (800 mg, 6.1 mmol) and **1a** (910 mg, 6.69 mmol) in dichloromethane (5 mL) was added TsOH (monohydrate, 23 mg, 2 mol%) in one portion at room temperature. The mixture was stirred and solid TsOH was soon dissolved. The **2d** smoothly disappeared (by GC) in a few minutes, and then triethylamine (a few drops) was added and evaporated. The resulting residue was carefully distilled using a microdistillation apparatus to give **3d** as colorless oil. Yield 540 mg (78%), bp 100 °C (bath temp)/25 mmHg (1 mmHg=133.322 Pa). Purity ≥95% by GC. Lit,[12] bp 71.5 °C/21 mmHg. ^{1}H NMR ($CDCl_3$) δ=1.45 (4H, m, CH_2), 2.15 (4H, m, CH_2), 3.20 (2H, m, CH). **3a**: bp 50—60 °C (lit,[12] 56 °C); ^{1}H NMR (CCl_4) δ=2.31 (s, CH_2). **3b**: ^{1}H NMR ($CDCl_3$) δ=1.52 (3H, d, J=2.8 Hz, CH_3), 2.12 (1H, d, J=2.7 Hz, H^a or H^b of CH_2), 2.50 (1H, d, J=3.0 Hz, H^b or H^a), 2.93 (1H, m, CH). **3c**: ^{1}H NMR ($CDCl_3$) δ=2.55 (1H, dd, J=0.7 and 2.7 Hz, H^a or H^b of CH_2), 2.74 (1H, dd, J=0.7 and 3.3 Hz, H^b or H^a), 3.79 (1H, t, J=3.0 Hz, CH), 7.17 (5H, s, phenyl).

TsOH-Catalyzed Reaction of 1b with Methanol. To a mixture of **1b** (95 mg, 0.49 mmol) and 20 μL of methanol (0.49 mmol) in 200 μL of dry benzene in a NMR tube was added anhydrous TsOH (6 mg). The resulting mixture was subjected to measurement of ^{1}H NMR and GC. The product structures were estimated by reference to the fast alcohol-exchange equilibrium.[2] The ratio of these products was determined by ^{1}H NMR integration and GC peak area (see Eq. 3).

References

1) R. H. DeWolfe, "Ortho Carboxylic Acid and Derivative, Organic Chemistry Monographs," Academic Press, New York (1970) Vol. 14,; *idem*, *Synthesis*, **1970**, 153.

2) W. Kantlehner, B. Funke, E. Haug, P. Speh, L. Kienitz, and T. Maier, *Synthesis*, **1977**, 73.

3) W. Loffler, Dissertation, Universitat Stuttgart, 1972; quoted in Ref. 2; B. Smith, *Acta Chem. Scand.*, **10**, 1006(1956); G. D. Allen and J. F. Poletto, U. S. Patent 3226397 (1965) (American Cyanamide Co.): *Chem. Abstr.*, **65**, 3836 (1966).

4) T. Endo and M. Okawara, *Synthesis*, **1984**, 837; T. Takata and T. Endo, *Nippon Kagaku Kaishi*, **1987**, 1299.

5) For example, T. H. Fife, *Acc. Chem. Res.*, **5**, 264 (1972).

6) J. W. Kelly, P. L. Robinson, and S. A. Evans, Jr., *J. Org. Chem.* **51**, 4473 (1986).

7) J. D. Roberts and R. E. McMahon, *Org. Synth.*, Coll. Vol. IV, 457 (1963).

8) S. Sakai, M. Kominami, K. Chonan, T. Enomoto, and T. Fujinami, *Synthesis*, **1984**, 233.

9) A. D. B. Sloan, *J. Chem. Soc. D*, **1969**, 1252 and references cited therein. Sloan used a vast amount of potassium hydrogen sulfate as dehydration catalyst for **2a**, but the yield of thiiran was less than 5%.

10) G. M. Bennett, *J. Chem. Soc.*, **121**, 2139(1922). Bennett obtained no thiiran but polymer of thiiran by use of 50% sulfuric acid as the catalyst.

11) E. E. Reid, "Organic Chemistry of Bivalent Sulfur," Chemical Publishing, New York (1958), Vol. I, p. 376.

12) Ref. 11, Vol. III, p. 11.

A Convenient Synthesis of 2-*t*-Alkyldioxy-2-methyl-1-propanols

Yoshiki HIGUCHI,* Kazuo MATSUYAMA, and Takeshi KOMAI
Chemical & Explosives Research Laboratory, Nippon Oil & Fats Co., Ltd.,
Taketoyo-cho, Chita-gun, Aichi-ken 470-23
(Received October 5, 1987)

Synopsis. Several 2-*t*-alkyldioxy-2-methyl-1-propanols have been synthesized conveniently by a ring-opening reaction of 1,2-epoxy-2-methylpropane with *t*-alkyl hydroperoxides in the presence of halogenated acetic acid catalysts.

Hydroxy-substituted dialkyl peroxides and their derivatives have been of interest as a radical source at high temperatures.[1] Some of them have been prepared by the reaction of epoxides with *t*-alkyl hydroperoxides.[2-5] This reaction proceeds via different paths, depending on the type of catalyst. When 1,1-dimethylethyl hydroperoxide was reacted with 1,2-epoxy-2-methylpropane, for instance, *t*-alkyl *n*-alkyl peroxide; 2-(1,1-dimethylethyldioxy)-1,1-dimethylethanol, was obtained in the presence of such base-catalysts as potassium hydroxide[2] and aluminium oxide.[3] On the other hand, *t*-alkyl *t*-alkyl peroxide; 2-(1,1-dimethylethyldioxy)-2-methyl-1-propanol, was formed in the presence of an acid catalyst such as sulfuric acid.[5] This result may be explained by the difference in the stabilization at the transition states (**1** and **2**) involved with the two types of the catalysts, as

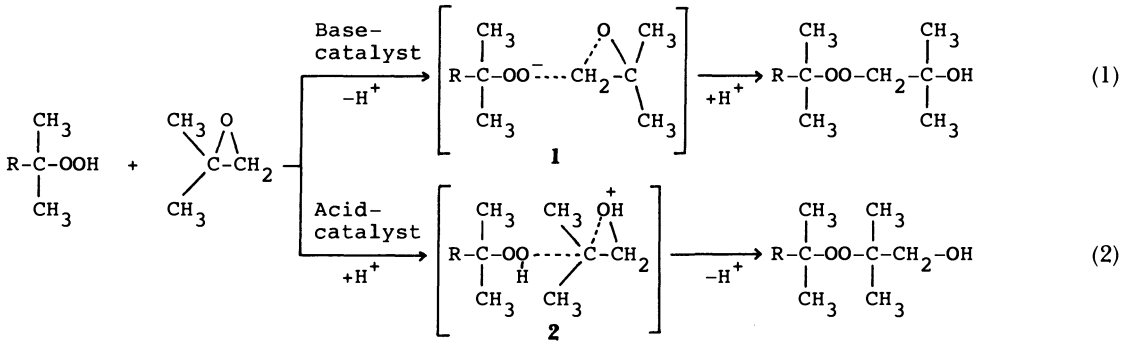

is shown above. Although several studies have been reported on base-catalyzed reactions, there seems to have been only one report concerning an acid-catalyzed reaction, and its yield was very low (20% yield). Therefore, we studied acid-catalyzed reactions in an attempt to prepare *t*-alkyl *t*-alkyl peroxides **3** in good yields, such peroxides are suitable as radical sources at high temperatures and are not liable to undergo a radical-induced decomposition.[1e]

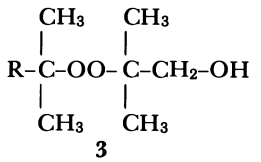

3

3; **a**: R=CH_3
b: R=CH_3CH_2
c: R=$CH_3CH_2CH_2$
d: R=$(CH_3)_3CCH_2$

Results and Discussion

The synthesis of **3a** was carried out by adding 1,2-epoxy-2-methylpropane, drop by drop, to a mixture of 1,1-dimethylethyl hydroperoxide, an acid catalyst and solvent; then the mixture was stirred for 30 min at 35 °C. The yield of **3a** was determined by GC analysis with an internal standard; it is shown in Table 1. The results indicate that the yield depends significantly on the types of acid catalysts and solvents. When dichloro-, trichloro-, and trifluoroacetic acids were used as acid catalysts, **3a** was obtained in a 40—70% yield within 30 min. This reaction is influenced by the amount of the catalyst. The yield of **3a** was only 6% in the presence of trifluoroacetic acid (0.01 mol equivalent) and did not increase even though the reaction mixture was stirred more than 20 h continuously. Similarly, when *p*-toluenesulfonic acid, amberlyst, and such weak acid-catalysts as 30% sulfuric acid and chloroacetic acid were used, the yield was below 23%. The decomposition of the hydroperoxide was observed throughout the reaction in the presence of such strong acid catalysts as sulfuric acid (more than 50%), trifluoromethanesulfonic acid, chlorosulfuric acid, and aluminium chloride. The yield was higher in such nonpolar solvents as hexane, chloroform, carbon tetrachloride, benzene, and nitrobenzene than in the polar solvents. When 1,1-dimethylethyl hydroperoxide was reacted with a reaction mixture containing 2-hydroxy-2-methylpropyl trifluoroacetate,[6] which was formed by the reaction of 1,2-epoxy-2-methylpropane with trifluoroacetic acid in equivalent weights for 30 min at 35 °C, the formation of **3a** was only a trace on GC. These findings indicate that the reaction does not proceed via the addition-elimination of the acid catalyst, but via the nucleophilic attack of 1,1-dimethylethyl hydroperoxide on a protonated epoxide intermediate, such as in the normal acid-catalyzed ring-opening reactions.[7]

Three other 2-*t*-alkyldioxy-2-methyl-1-propanols were synthesized under optimum reaction conditions

Table 1. Influence of Various Acid Catalysts and Solvents on the Yield of **3a**[a]

Acid-catalyst	Mol/mol of 1,2-epoxy-2-methylpropane	Solvent	Yield of **3a**[b] %
Trifluoroacetic acid	1.0	Benzene	54
Trifluoroacetic acid	0.5	Benzene	69
Trifluoroacetic acid	0.1	Benzene	43
Trifluoroacetic acid	0.01	Benzene	6
Trichloroacetic acid	0.5	Benzene	65
Dichloroacetic acid	0.5	Benzene	59
Chloroacetic acid	0.5	Benzene	23
p-Toluenesulfonic acid	0.5	Benzene	20
Amberlyst 15[c]	0.5	Benzene	12
30% H_2SO_4	0.5	Benzene	18
Trifluoroacetic acid	0.5	Hexane	69
Trifluoroacetic acid	0.5	Chloroform	66
Trifluoroacetic acid	0.5	Carbon tetrachloride	66
Trifluoroacetic acid	0.5	1,4-Dioxane	41
Trifluoroacetic acid	0.5	Diethyl ether	52
Trifluoroacetic acid	0.5	Acetonitrile	44
Trifluoroacetic acid	0.5	Nitrobenzene	59
Trifluoroacetic acid	0.5	Isopropyl alcohol	52
Trifluoroacetic acid	0.5	Methanol	31
Trifluoroacetic acid	0.5	*N*,*N*-Dimethylformamide	14

a) 1,2-Epoxy-2-methylpropane of 1.44 g (0.020 mol) was used. b) Based on 1,2-epoxy-2-methylpropane. c) Commercial product from Rohm and Haas company.

Table 2. Synthesis of 2-*t*-Alkyldioxy-2-methyl-1-propanols[b]

Product	Yield[c] %	Bp (°C/mmHg[a])	IR (neat)/cm^{-1}
3a	69	52—53/6[d]	875 (ν_{O-O}), 3450 (ν_{O-H})
3b	72	46—47/3	875 (ν_{O-O}), 3450 (ν_{O-H})
3c	70	57—58/4	875 (ν_{O-O}), 3450 (ν_{O-H})
3d	62	46—48/0.5	875 (ν_{O-O}), 3450 (ν_{O-H})

Product	^1H NMR (δ/ppm) [$CDCl_3$/TMS]	MS (m/z)	n_D^{20}	Anal. (%) Found (Calcd)
3a	1.21 [s, 6H, $-(CH_3)_2C-$], 1.26 [s, 9H, $(CH_3)_3C-$], 2.35 [s, 1H, -OH], 3.59 [s, 2H, $-C\underline{H}_2-OH$]	162 (M^+)	1.4184	C: 58.78 (59.23), H: 10.99 (11.18)
3b	0.89 [t, J=7.5Hz, 3H, $C\underline{H}_3CH_2-$], 1.21 [s, 6H, $-(CH_3)_2C-$]×2, 1.60 [q, J=7.5Hz, 2H, $CH_3C\underline{H}_2-$], 2.33 [s, 1H, -OH], 3.60 [s, 2H, $-C\underline{H}_2-OH$]	176 (M^+)	1.4251	C: 60.94 (61.33), H: 11.52 (11.44)
3c	0.92 [t, J=7.5Hz, 3H, $C\underline{H}_3CH_2-$], 1.19 [s, 6H, $-(CH_3)_2C-$], 1.21 [s, 6H, $-(CH_3)_2C-$], 1.5 [m, 4H, $-(CH_2)_2-$], 2.30 [s, 1H, -OH], 3.60 [s, 2H, $-C\underline{H}_2-OH$]	190 (M^+)	1.4279	C: 62.60 (63.12), H: 11.63 (11.65)
3d	1.02 [s, 9H, $(C\underline{H}_3)_3CCH_2-$], 1.20 [s, 6H, $-(CH_3)_2C-$], 1.33 [s, 6H, $-(CH_3)_2C-$], 1.57 [s, 2H, $-CH_2-$], 2.33 [s, 1H, -OH], 3.60 [s, 2H, $-C\underline{H}_2-OH$]	218 (M^+)	1.4371	C: 65.62 (66.01), H: 12.10 (12.00)

a) 1 mmHg=133.322 Pa. b) 1,2-Epoxy-2-methylpropane of 18.7 g (0.26 mol) was used. c) Based on 1,2-epoxy-2-methylpropane. d) Lit,[5] 38—40 °C/3 mmHg.

of **3a**; the results are listed in Table 2. The peroxides were obtained in 62—72% yields. The crude products were purified by washing with water and an aqueous solution of sodium hydroxide to remove any unreacted materials and by-products and by then distilling them under vacuum pressures. The structures of **3a—d** were identified by means of their boiling points, their refractive indices, and the elemental-analysis, IR, NMR, and mass spectral data, as are shown in Table 2.

Experimental

The reaction products were analyzed by means of gas chromatography (GC) on a Shimadzu Model GC-2D chromatograph using a 1.4 m×2.6 mm glass column of 5% Silicone GE SE-30 on 60—80 mesh Uniport HP, with undecane and dodecane as internal standards. The ^{1}H NMR spectra were obtained, using chloroform-*d* as the solvent, on a JEOL Model JNM-MN-100 spectrometer. The IR spectra were recorded on a JASCO Model A-3 spectrometer.

Purification of Hydroperoxides. The corresponding hydroperoxides of **3a** and **3b** were purified by distillation. The commercial products obtained from the Nippon Oil & Fats Co., Ltd., for the corresponding hydroperoxides of **3c** and **3d** were purified by the isolation of the sodium salts, the regeneration of the hydroperoxides by carbon dioxide, and distillation.

Synthesis of Dialkyl Peroxides. A typical synthesis of **3a** was carried out as follows. 1,2-Epoxy-2-methylpropane (18.7 g, 0.26 mol) was added slowly to a solution of trifluoroacetic acid (14.8 g, 0.13 mol), 1,1-dimethylethyl hydroperoxide (46.5 g, 0.52 mol), and benzene 25 cm^3 below 10 °C, after which the reaction mixure was stirred at 35 °C for 30 min. The yield of **3a** was determined by GC, using undecane as an internal standard; it is shown in Table 2. The reaction mixture was washed with water, an aqueous solution of 5% NaOH, and a saturated solution of NaCl, and then dried over anhydrous $MgSO_4$. After the solvent had been removed, the residue (36.7 g) was distilled to give **3a** (22.4 g). The purity, as checked by GC, was 96.5%.

The syntheses of **3b—d** were carried out by using the corresponding hydroperoxides in place of 1,1-dimethylethyl hydroperoxide by a method similar to that used for **3a**. Crude products were purified by distillation after the residual hydroperoxides in the reaction mixture had been changed into the corresponding alcohols by the use of an aqueous solution of Na_2SO_3. The purities, as checked by GC, were more than 95%.

References

1) N. G. Gayload, Ger. Offen., 2440951 (1975); *Chem. Abstr.*, **83**, 11196h (1975); H. C. Stevens, U. S. Patent, 3640985 (1972); *Chem. Abstr.*, **76**, 142469q (1972); O. L. Mageli and W. A. Swarts, Ger. Offen., 2631911 (1977); *Chem. Abstr.*, **86**, 156821e (1977); A. A. Syrov, S. S. Ivanchev, O. N. Primachenko, V. A. Demidova, B. V. Polosov, I. V. Fionov, and E. N. Barentsevich, Ger. Offen., 2945151 (1980); *Chem. Abstr.*, **93**, 113983m (1980); R. Hiatt, "Organic Peroxides," Vol. III, ed. by D. Swern, John Wiley & Sons, New York (1972), Chap. 1.

2) M. R. Barusch and J. Q. Payne, *J. Am. Chem. Soc.*, **75**, 1987 (1953).

3) H. Kropf, H. M. Amirabadi, M. Mösebach, A. Torkler, and H. von Wallis, *Synthesis*, **1983**, 587.

4) H. Kropf, M. Ball, H. Schroder, and G. Wite, *Tetrahedron*, **30**, 2943 (1974).

5) W. H. Richardson and R. S. Smith, *J. Org. Chem.*, **33**, 3882 (1968).

6) In a separate experiment, 2-hydroxy-2-methylpropyl trifluoroacetate was isolated and confirmed by its IR spectra.

7) K. Ichikawa and M. Inoue, *Yuki Gosei Kagaku Kyokai Shi*, **38**, 61 (1980); R. E. Parker and N. S. Isaacs, *Chem. Rev.*, **59**, 797 (1959); F. A. Long and J. G. Pritchard, *J. Am. Chem. Soc.*, **78**, 2663 (1956).

New Synthesis of Penta-*N,O*-acetyl-DL-validamine and Pseudo-2-amino-2-deoxy-α-DL-mannopyranose, and Their Uronate Analogs[1)]

Seiichiro OGAWA,* Motohiro SUZUKI, and Takeshi TONEGAWA
Department of Applied Chemistry, Faculty of Science and Technology,
Keio University, Hiyoshi, Yokohama 223
(Received October 29, 1987)

Synopsis. Treatment of the hydroxy lactone derived from (±)-*endo*-7-oxabicyclo[2.2.1]hept-5-ene-2-carboxylic acid with hydrogen bromide–acetic acid, followed by esterification, gave 48% of ethyl DL-(1,3,5/2,4)-5-bromo-2,3,4-trihydroxy-1-cyclohexanecarboxylate, from which DL-validamine and pseudo-2-amino-2-deoxy-α-DL-mannopyranose, and their uronate analogs have been synthesized as the totally acetylated derivatives.

Naturally occurring branched-chain aminocyclitols, viz. pseudo-amino sugars such as validamine,[2)] valienamine,[3)] and valiolamine[4)] were isolated from a fermentation broth of *Streptomyces hygroscopicus* sp. *limoneus*. These compounds and their derivatives[5)] show a remarkable inhibitory activity against α-glucosidase, stimulating much interest in their application for a clinical use.

We describe now a preparation of DL-validamine and a pseudo-sugar analog of 2-amino-2-deoxy-α-D-mannopyranose, by a novel sequence from the hydroxy lactone[6,7)] **1** obtained from (±)-*endo*-7-oxabicyclo[2.2.1]hept-5-ene-2-carboxylic acid.[6,7)]

Treatment of the lactone **1** with 20% hydrogen bromide–acetic acid at 95 °C gave after esterification with ethanol 48% of crystalline bromide **2**, which was converted into the methyl ester **3** and its triacetate **4** in the usual way. The ^{1}H NMR spectrum of **4** revealed three coupled triplets (J=10 Hz) at δ 5.35, 5.23, and 5.03, attributable to the axial protons at C-2, C-3, and C-4, being consistent with the structure assigned. The structure of **2** was further confirmed by conversion of **3** into the known epoxide[8)] **5** by treatment with methanolic sodium methoxide followed by acetylation.

Azidolysis of **4** with excess sodium azide in *N,N*-dimethylformamide (DMF) gave a single crystalline azide **6**, the ^{1}H NMR spectrum of which showed a narrow quartet (J=3.5 Hz) at δ 4.18, indicating that the azido group was introduced at C-5 in an axial position. Hydrogenation of **6** in ethanol containing acetic anhydride with Raney nickel gave the *N*-acetyl derivative **7** in 61% yield. On the other hand, **6** was converted, in 56% yield, into DL-penta-*N,O*-acetylvalidamine[7)] (**8**) by reduction with lithium aluminum hydride (LAH) in tetrahydrofuran (THF) followed by acetylation.

When similar azidolysis of **3** was carried out in aqueous 2-methoxyethanol, a single known azido triacetate[8)] **9** was obtained in 65% yield after acetylation. This compound was considered to be obtained through the neighboring group participation of the 4-hydroxyl group, involving a formation of the intermediate 4,5-epoxide, which was successively cleaved by an azide ion via diaxial ring-opening. Catalytic hydrogenation of **9** followed by acetylation gave the *N*-acetyl derivative **10** (84%). Reduction of **9** with LAH and successive acetylation afforded penta-*N,O*-acetyl-pseudo-2-amino-2-deoxy-α-DL-mannopyranose (**11**, 61%). These pseudo-amino sugars are of interest because their corresponding normal sugars occur in biological system.

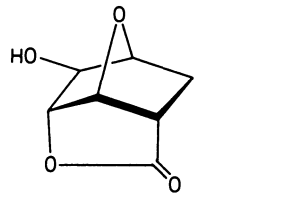

1

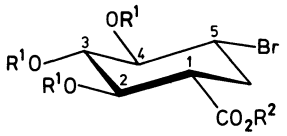

	R^1	R^2
2	H	Et
3	H	Me
4	Ac	Me

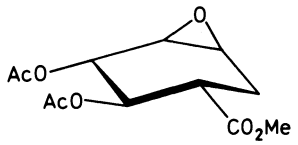

5

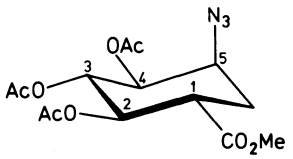

6

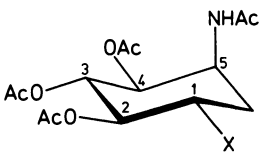

7 X = CO_2Me
8 X = CH_2OAc

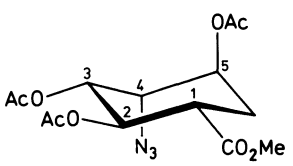

9

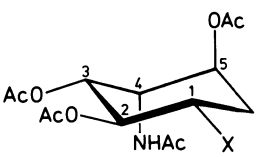

10 X = CO_2Me
11 X = CH_2OAc

Experimental

General Methods. Melting points were determined with a MEL-TEMP capillary melting-point apparatus and are

uncorrected. The ^{1}H NMR spectra were measured with a Varian EM-390 (90 MHz) spectrometer for solution of chloroform-*d* (TMS) or dimethyl-d_6 sulfoxide (DSS). Spectrum at 270 MHz was recorded with a Jeol GX-1 instrument. The silica gel used for column chromatography was Wakogel C-300 (Wako Co., Osaka).

Ethyl (±)-(1,3,5/2,4)-5-Bromo-2,3,4-trihydroxy-1-cyclohexanecarboxylate (2). A mixture of (±)-2-*exo*-hydroxy-4,8-dioxatricyclo[4.2.1.0^{3,7}]nonan-5-one[7] (**1**) (3.0 g, 10.6 mmol) and 20% hydrogen bromide–acetic acid (15 ml) was heated in a sealed tube at 95 °C for 24 h, and poured into ice–water (20 ml). The mixture was refluxed for 9 h and then concentrated. The residue was treated with ethanol (20 ml) at reflux for 5.5 h, and the mixture was concentrated and the residue was crystallized from ethanol to give the bromide **2** (2.6 g, 48%) as prisms: mp 155.5—156 °C.

Found: C, 38.25; H, 5.23%. Calcd for $C_9H_{15}BrO_5$: C, 38.18; H, 5.34%.

Methyl (±)-(1,3,5/2,4)-5-Bromo-2,3,4-trihydroxy-1-cyclohexanecarboxylate (3). To a solution of **2** (5.0 g, 18 mmol) in methanol (100 ml) was added acetyl chloride (1.5 ml, 21 mmol) and it was refluxed for 21 h. The mixture was neutralized with sodium hydrogencarbonate and then concentrated. The residue was crystallized from ethanol to give **3** (3.8 g, 80%) as prisms: mp 137—138 °C.

Found: C, 35.91; H, 4.76%. Calcd for $C_8H_{13}BrO_5$: C, 35.71; H, 4.87%.

Compound **3** (2.3 g, 8.5 mmol) was treated with acetic anhydride (12 ml) and pyridine (12 ml) at room temperature overnight. The mixture was concentrated and the residue was extracted with ethyl acetate. The extract was washed with water, dried, and concentrated. The residue was recrystallized from ethanol to give the triacetate **4** (3.2 g, 96%) as prisms: mp 153—154 °C. ^{1}H NMR ($CDCl_3$, 270 MHz) δ=2.00 (6H, s) and 2.08 (3H, s) (OAc), 2.21 (1H, q, $J_{1,6ax}=J_{5,6ax}=J_{6gem}$=13 Hz, H-6ax), 2.62 (1H, dt, $J_{1,6eq}=J_{5,6eq}$= 4 Hz, H-6eq), 2.69 (1H, ddd, $J_{1,2}$=11 Hz, H-1), 3.72 (3H, s, CO_2Me), 3.92 (1H, m, $J_{4,5}$=10.5 Hz, H-5), 5.03 (1H, t, $J_{2,3}=J_{3,4}$=10 Hz, H-3), 5.23 (1H, dd, H-2).

Found: C, 42.74; H, 4.80%. Calcd for $C_{14}H_{19}BrO_8$: C, 42.55; H, 4.85%.

Methyl (±)-(1,3/2,4,5)-2,3,4-Triacetoxy-5-azido-1-cyclohexanecarboxylate (6). A mixture of **4** (1.7 g, 4.3 mmol), sodium azide (1.3 g, 20 mmol), and aqueous 95% DMF (30 ml) was stirred at 90 °C for 20 h, and then concentrated. The residue was extracted with ethyl acetate, and the extract was washed with water, dried, and concentrated. The residue was recrystallized from ethanol to give **6** (0.72 g, 47%) as needles: mp 110—112 °C. ^{1}H NMR ($CDCl_3$, 90 MHz) δ=1.98 (6H, s) and 2.08 (3H, s) (OAc), 2.91 (1H, td, $J_{1,2}=J_{1,6ax}$=9.5 Hz, $J_{1,6eq}$=3.5 Hz, H-1), 3.67 (3H, s, CO_2Me), 4.18 (1H, q, $J_{4,5}=J_{5,6ax}=J_{5,6eq}$=3.5 Hz, H-5), 5.04 (1H, dd, $J_{3,4}$= 9.5 Hz, H-4), 5.20 (1H, t, $J_{2,3}$=9.5 Hz, H-2), 5.37 (1H, t, H-3).

Found: C, 47.11; H, 5.43; N, 11.57%. Calcd for $C_{14}H_{19}N_3O_8$: C, 47.06; H, 5.36; N, 11.76%.

Methyl (±)-(1,3/2,4,5)-5-Acetamido-2,3,4-triacetoxy-1-cyclohexanecarboxylate (7). A solution of **6** (0.30 g, 0.85 mmol) in ethanol (10 ml) was hydrogenated in the presence of Raney nickel T-4 (1 ml) and acetic anhydride (0.5 ml) in an initial hydrogen pressure of 50 psi at room temperature for 17 h. The catalyst was removed by filtration and the filtrate was concentrated. The residue was crystallized from ethanol to give **7** (0.19 g, 61%) as prisms: mp 231.5—233.5 °C. ^{1}H NMR (DMSO-d_6, 90 MHz) δ=1.90 (6H, s), 1.94 (3H, s), and 1.95 (3H, s) (NAc and OAc), 3.62 (3H, s, CO_2Me), 4.30—4.67 (1H, m, H-5), 4.87 (1H, dd, $J_{3,4}$=9.8 Hz, $J_{4,5}$=4.5 Hz, H-4), 5.17 (1H, t, $J_{2,3}$=9.8 Hz, H-2), 5.33 (1H, H-2), 8.07 (1H, d, $J_{5,NH}$=5 Hz, NH).

Found: C, 51.41; H, 6.06; N, 3.61%. Calcd for $C_{16}H_{23}NO_9$: C, 51.47; H, 6.21; N, 3.75%.

(±)-[(1,3/2,4,5)-5-Acetamido-2,3,4-triacetoxycyclohexyl]-methyl Acetate (8) [(±)-Penta-*N,O*-acetylvalidamine]. Compound **7** (0.30 g, 0.84 mmol) was treated with LAH (0.25 g, 6.6 mmol) in tetrahydrofuran (10 ml) at room temperature for 30 h. To the mixture was added water (1.5 ml), aqueous 15% sodium hydroxide, water (1.5 ml), and aqueous acetone (1:1, 2 ml) in turn, and then it was filtered through a bed of Celite. The filtrate was neutralized with 1 mol dm^{-3} hydrochloric acid and concentrated. The residue was acetylated in the usual way, and the product was crystallized from ethanol to give **8** (0.18 g, 56%) as prisms: mp 197—199 °C (lit,[7] mp 197—198 °C). This compound was identical to an authentic sample[7] in all respects.

Methyl (±)-(1,3,4/2,5)-2,3,5-Triacetoxy-4-azido-1-cyclohexanecarboxylate (9). A mixture of **3** (0.49 g, 1.8 mmol), sodium azide (0.49 g, 7.5 mmol), and 90% aqueous 2-methoxyethanol (20 ml) was refluxed for 3 h, and then concentrated. The residue was refluxed with methanol (50 ml) and acetyl chloride (1 ml), and then the mixture was neutralized with sodium hydrogencarbonate. The mixture was concentrated and the residue was extracted with ethyl acetate. The extract was concentrated and the residue was acetylated in the usual way and the product was crystallized from ethanol to give **9** (0.51 g, 80%) as plates: mp 95.5—96 °C. (lit,[8] mp 92.5—94 °C). This compound was identical with an authentic sample[8] in all respects.

Methyl (±)-(1,3,4/2,5)-4-Acetamido-2,3,5-triacetoxy-1-cyclohexanecarboxylate (10). Into a solution of **9** (0.14 g, 0.38 mmol) in a mixture of pyridine (5 ml) and water (5 ml) was bubbled hydrogen sulfide at room temperature for 4 h. Excess hydrogen sulfide was removed by a stream of nitrogen and the mixture was concentrated. The residue was acetylated in the usual way and the product was crystallized from ethanol to give **10** (0.11 g, 84%) as needles: mp 178.5—180.5 °C. ^{1}H NMR ($CDCl_3$, 90 MHz): δ=1.90 (3H, s), 2.07 (3H, s), 2.26 (3H, s), and 2.30 (3H, s) (NAc and OAc), 2.87 (1H, bq, J=7 Hz, H-1), 3.71 (3H, s, CO_2Me), 4.50 (1H, dt, $J_{3,4}=J_{4,5}$=4 Hz, $J_{4,NH}$=9 Hz, H-4), 5.13 (1H, dd, $J_{2,3}$=7 Hz, H-3), 5.20 (1H, m, H-5), 5.46 (1H, t, $J_{1,2}$=7 Hz, H-2), 6.75 (1H, d, $J_{4,NH}$=9 Hz, NH).

Found: C, 51.40; H, 6.13; N, 3.62%. Calcd for $C_{16}H_{23}NO_9$: C, 51.47; H, 6.21; N, 3.75%.

(±)-[(1,3,4/2,5)-5-Acetamido-2,3,4-triacetoxycyclohexyl]-methyl Acetate (11). Compound **10** (0.30 g, 0.86 mmol) was reduced with LAH in THF as in the preparation of **8**. The product was acetylated in the usual way and the acetate was purified by a silica-gel column with ethanol–toluene (1:10) to give **11** (0.20 g, 61%) as a syrup. ^{1}H NMR (DMSO-d_6, 90 MHz): δ=1.90 (3H, s), 1.91 (3H, s), 2.01 (6H, s), and 2.08 (3H, s) (NAc and OAC), 3.73—4.18 (2 H, m, CH_2OAc), 4.41 (1H, dt, $J_{3,4}=J_{4,5}$=4 Hz, $J_{4,NH}$=9 Hz, H-4), 4.65—4.87 (1H, m, H-5), 4.97 (1H, dd, $J_{2,3}$=9.7 Hz, H-3), 5.22 (1H, t, $J_{1,2}$=9.7 Hz, H-2), 7.92 (1H, d, NH). Mass spectrum, *m/z*; Found: 388.1658 (M^+). Calcd for $C_{17}H_{26}NO_9$: 388.1666 (M^+).

Found: C, 52.06; H, 6.20; N, 3.62%. Calcd for $C_{17}H_{25}NO_9 \cdot 0.25H_2O$: C, 52.10; H, 6.43; N, 3.75%.

The authors thank Mr. Akio Takahashi and Mr. Hisao Arita for elemental analyses, and Mr. Koichi Yokoyama for preparative work.

References

1) Pseudo-Sugars. XX. Presented in part at the 52nd Annual Meeting of the Chemical Society of Japan, Kyoto, April 3, 1986 (Abstract No. 3N 38). The preceding paper of

this series, see S. Ogawa, Y. Uematsu, S. Yoshida, N. Sasaki, and T. Suami, *J. Carbohydr. Chem.*, **6**, 471 (1987).

2) S. Horii, T. Iwasa, E. Mizuta, and Y. Kameda, *J. Antibiot.*, **24**, 59 (1972) and references cited therein.

3) Y. Kameda and S. Horii, *J. Chem. Soc., Chem. Commun.*, **1972**, 746.

4) S. Horii, T. Iwasa, E. Mizuta, and Y. Kameda, *J. Antibiot.*, **24**, 61 (1971).

5) S. Horii, H. Fukase, T. Matsuo, Y. Kameda, N. Asano, and K. Matsui, *J. Med. Chem.*, **29**, 1038 (1986) and references cited therein.

6) M. P. Kunstman, D. S. Tarbell, and R. L. Autrey, *J. Am. Chem. Soc.*, **84**, 4115 (1962).

7) T. Suami, S. Ogawa, K. Nakamoto, and I. Kasahara, *Carbohydr. Res.*, **58**, 240 (1977).

8) S. Ogawa, Y. Yato, K. Nakamura, M. Takata, and T. Takagaki, *Carbohydr. Res.*, **148**, 249 (1986).

Hindered Rotation around Csp^2–Csp^3 Bonds in the Enol Forms of α-(9-Fluorenyl)-β-diketones and in 3,5-Disubstituted 4-(9-Fluorenyl)pyrazoles. An ^1H NMR Study

Marcial MORENO-MAÑAS,* Asensio GONZALEZ, Jorge MARQUET, and Francisco SANCHEZ-FERRANDO
Departamento de Química, Universidad Autónoma de Barcelona, Bellaterra, 08193-Barcelona, Spain
(Received May 16, 1987)

Synopsis. Slow rotation around the Csp^2–Csp^3 bonds of the enol forms of 3-(9-fluorenyl)-2,4-pentanedione, 2-(9-fluorenyl)-1-phenyl-1,3-butanedione, and the corresponding bonds of the derived pyrazoles, was studied by variable temperature ^1H NMR. For the pyrazoles, the values T_c=315—320 K ($\Delta G^{\neq}_{T_c}$=15.1±0.1 kcal mol^{-1}) and T_c=338±5 K (corresponding to $\Delta G^{\neq}_{T_c(sp\rightarrow ap)}$=18.1±0.2 kcal mol^{-1} and $\Delta G^{\neq}_{T_c(ap\rightarrow sp)}$=16.1±0.2 kcal mol^{-1}) were found, respectively.

Hindered rotation around Csp^2–Csp^3 bonds in 9-arylfluorenes is a well-known phenomenon.[1] However, at the best of our knowledge no examples have been reported in which the group accompanying the fluorene moiety is either a five-membered heterocyclic ring (i.e. pyrazole) or a ring held together by hydrogen bonds (i.e. the enol form of a β-diketone). Some of us have reported a synthetic method, based on the use of cobalt(II) complexes of β-dicarbonyl compounds, which enables us to place bulky substituents in the α-positions of β-dicarbonyl compounds,[2-4] among them the fluorenyl radical.

The ^1H NMR spectrum of 3-(9-fluorenyl)-2,4-pentanedione (**1a**) shows in $CDCl_3$ at the ordinary probe temperature two sets of sharp peaks as indicated in Fig. 1. The enol form exhibits hindered rotation since both methyl groups give signals at different chemical shifts. The sharp signal at δ 0.99 is assigned to the methyl group protons placed above the plane of the fluorene moiety.

The major form of 2-(9-fluorenyl)-1-phenyl-1,3-butanedione (**1b**) in solid phase was an enol form (see IR in Experimental). However, in $CDCl_3$ the keto form predominates to an extent of ca. 6:1. The observed enol form exhibits the signal of the methyl group at δ 1.05. Therefore, by comparison with the chemical shift measured for **1a**, we assign the **sp** conformation to the enol form of **1b** (for nomenclature see Ref. 1).

3-(9-Fluorenyl)-5,5-dimethyl-2,4-hexanedione (**1c**) showed only peaks attributed to the keto form, both in KBr (IR) and in $CDCl_3$ (^1H NMR).

Due to the interference of the keto⇄enol equilibria we did not attempt any kinetic study of the rotation in compounds **1a** and **1b**. However, compounds **1** were converted into the pyrazoles **2** by conventional methods and the kinetic behavior at different temperatures of these fluorenyl-substituted heterocycles was studied at 80 MHz in a Bruker WP80SY spectrometer.

In the case of exchange between two equally populated, uncoupled sites, the rotational barrier $\Delta G^{\neq}$ is customarily determined at the coalescence temperature T_c, using the well-known expressions[5] $k=\pi\Delta\nu/\sqrt{2}$ and $k=(k_BT/h)[\exp(-\Delta G^{\neq}/RT)]$, in which $\Delta\nu$ is the frequency separation of the two lines at the slow rotation limit, k_B is the Boltzmann constant, h is the Planck constant, and k is the exchange (interconversion) rate at coalescence. This rather simple approach requires: i) The operation of a single exchange (interconversion) mechanism; ii) the absence of coupling; iii) equal line-widths for both lines; and iv)

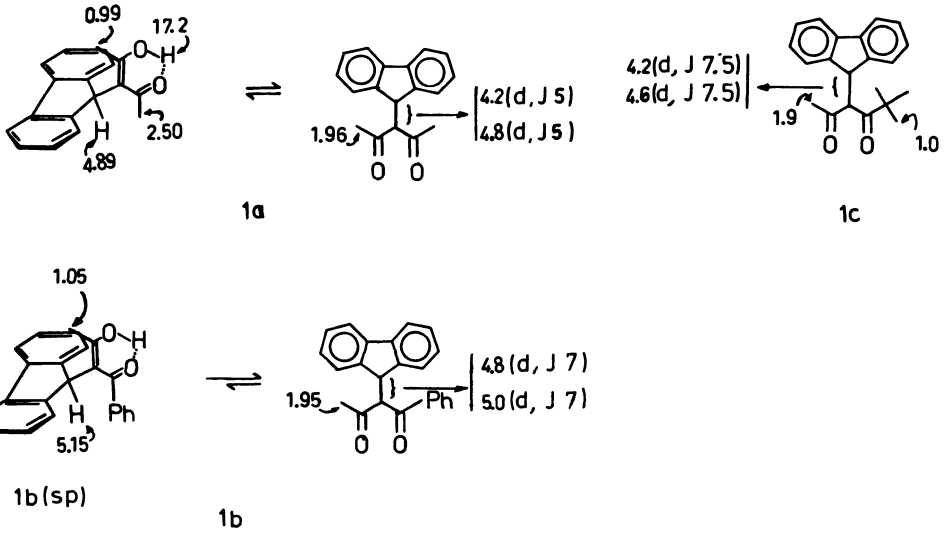

Fig. 1.

linewidths negligible compared with $\Delta\nu$.

The case of exchange between two unequally populated sites has also been solved in much the same simple way.[6] Thus, from the observed coalescence temperature T_c, and the values of $\Delta\nu$ (line separation) and Δp (population difference) obtained at a lower temperature under slow rotation, the mean lifetime at coalescence, $\tau=1/k$ can be obtained using the values tabulated in (Ref. 7), provided conditions i)—iv) above are again met. Of course, validity of this approach depends on the assumption that chemical shift differences and rotamer populations are independent of temperature, assumptions which can often be inadequate. However, if these assumptions are indeed valid, individual rate constants k_A and k_B for the two interconversion processes (A→B and B→A) are derived using the expressions $k_A=2kp_B$ and $k_B=2kp_A$, in which p_A and p_B are the populations of A and B, respectively. Finally, the corresponding barriers at coalescence are calculated in a straightforward manner[8] using the equation $\Delta G_x^{\ddagger}=8.31T[23.76+\ln(T/k_x)]$, with SI units throughout. Thus, these simple cases can be studied without using the more sophisticated methods of line shape analysis.[9]

The ^{1}H NMR spectrum of 3,5-dimethyl-4-(9-fluorenyl)pyrazole (**2a**) in $CDCl_3$ at the probe temperature (305 K) shows very broad signals for the two methyl groups. The two signals sharpen to two singlets at δ 2.59 and 1.17 upon cooling at 250 K, while they coalesce to a singlet upon heating at 365 K (Fig. 2). The T_c was found to be between 315—320 K, while the low temperature frequency separation between the two signals was $\Delta\nu=114.3$ Hz. Ignoring the effect of the N(1)–N(2) prototropic shift which is very rapid in our experimental conditions,[10] and applying the pertinent kinetic equations,[5] the degenerate conversion between the two rotamers at T_c has a rate $k=253.9$ s^{-1}. The rotation barrier at T_c was calculated to be 15.1±0.1 kcal mol^{-1} (63.1±0.4 kJ mol^{-1}).

Three different groups[11–13] have reported a value higher than 25 kcal mol^{-1} (104.5 kJ mol^{-1}) for the rotation barrier in 9-mesitylfluorene. As expected, the smaller angle in the pyrazole ring results in a marked decrease in the rotational barrier.

The ^{1}H NMR spectrum of 4-(9-fluorenyl)-3-methyl-5-phenyl-1*H*-pyrazole (**2b**) in $CDCl_3$ at 305 K shows a single peak for the methyl protons at δ 1.21, but it is not a sharp singlet ($\Delta\nu_{1/2}>5$ Hz). Upon cooling at 263 K, two methyl group signals can be seen at δ 2.58 and 1.13 with a ratio ca. 6:94, attributed respectively to the **ap** and **sp** conformers (Fig. 2). Therefore, the population difference at 263 K is $\Delta p=0.88$, while the measured frequency difference between the two peaks is $\Delta\nu=116.4$ Hz. A series of spectra at increasing temperatures shows that the minor peak at δ 2.58 disappears on heating from 233 to 303 K while both peaks broaden. For $T>303$ K the minor peak is no longer seen, but the major upfield peak continues to broaden. At a temperature between 333 and 343 K this peak reaches maximum broadening (coalescence), and it sharpens at 363 K. Assuming the T_c is 338±5 K and ignoring again the effect of the N(1)–N(2) prototropic shift,[10] we have calculated the barrier to rotation for the unequally populated rotamers by applying the pertinent equations.[6] The individual rates for conversion at T_c of major to minor ($k_{sp\to ap}$) and minor to major ($k_{ap\to sp}$) are 13.38 s^{-1} and 254.2 s^{-1}, and the individual rotation barriers at T_c, $\Delta G^{\ddagger}_{sp\to ap}$ and $\Delta G^{\ddagger}_{ap\to sp}$ are calculated[8] to be 18.1±0.2 kcal mol^{-1} (75.7±0.8 kJ mol^{-1}) and 16.1±0.2 kcal mol^{-1} (67.3±0.8 kJ mol^{-1}).

The ^{1}H NMR spectrum of 3-*t*-butyl-4-(9-fluorenyl)-5-methyl-1*H*-pyrazole (**2c**) shows a single *t*-Bu signal at δ 1.68, both at 308 K and upon cooling at 223 K. Similarly, a single methyl signal is found at δ 1.05 at both temperatures. We conclude that **2c** exists in the **sp** conformation to an extent of more than 99%.

Financial support from **CAICYT** ("Ministerio de Educación y Ciencia" of Spain) through grant 2014/83 is gratefully acknowledged. We are also indebted to "Fundación María Francisca de Roviralta"

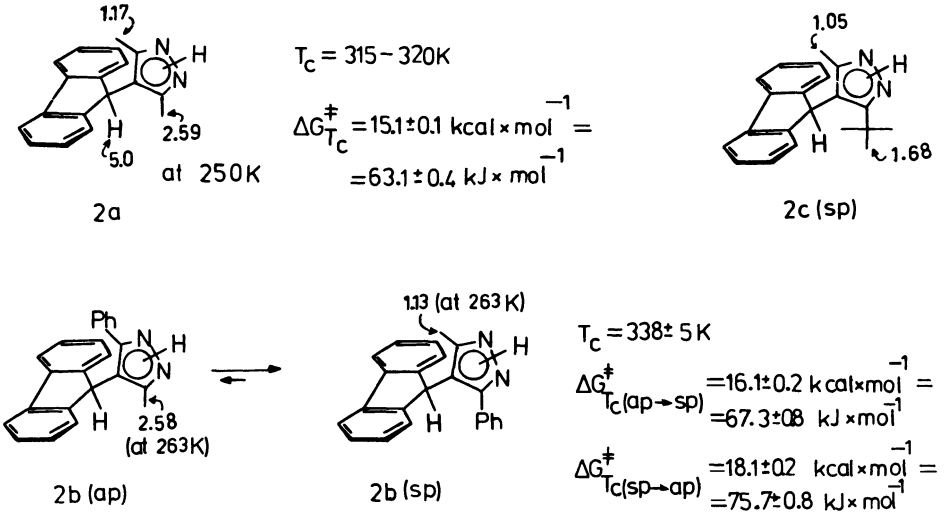

Fig. 2.

for the purchase of the NMR spectrometer, and to "Direcció General d'Ensenyament Universitari (Generalitat de Catalunya)" for the NMR data system.

Experimental

Room temperature 80 MHz ^1H NMR spectra were taken at 32 °C, in the FT mode, using a Bruker WP80SY spectrometer, equipped with a 5 mm switchable $^1H/^{13}C$ dual probe, under Aspect 2000 computer control, and are referenced to internal TMS. Variable temperature spectra were obtained under BVT-1000 control. Temperatures were calibrated against methanol peak separation.[14] Solutions of 2—5 mg of sample in $CDCl_3$ were used in all experiments. The pulse conditions used were: spectral width, 1000 Hz; 8 K data points, with quadrature detection; pulse width, 4 μs (60 deg); acquisition time, 4.1 s, with no relaxation delay; digital resolution, 0.25 Hz per point. FIDs were weighted by exponential multiplication (line broadening 0.25 Hz) prior to Fourier transformation.

Compounds 1. Compounds **1** were prepared by treating the corresponding cobalt(II) complexes of the unsubstituted β-diketones with 9-bromofluorene in refluxing chloroform (for **1a** and **1b**) or in refluxing chlorobenzene (for **1c**), following the procedures described in Ref. 2—4.

1a: Mp 72 °C; IR (KBr) 1720, 1690, 1600—1570 (broad) cm^{-1}; MS *m/z* (rel intensity) 264 (M^+, 40), 221 (100), 203 (48), 178 (26), 176 (21), 165 (59), 43 (91).

1b: Mp 58 °C; IR (KBr) 1600 (broad) cm^{-1}; MS *m/z* (rel intensity) 326 (M^+, 34), 284 (22), 283 (76), 265 (30), 221 (61), 178 (29), 176 (24), 165 (39), 105 (100), 77 (74), 43 (46).

1c: Mp 98—9 °C; IR (KBr) 1710, 1680 cm^{-1}; MS *m/z* (rel intensity) 306 (M^+, 11), 221 (100), 165 (57), 57 (22).

Compounds 2. 2a: Mp 235—6 °C; IR (KBr) 3300—2800 (broad) cm^{-1}; MS *m/z* (rel intensity) 260 (M^+, 100), 259 (44), 245 (28), 218 (38), 176 (23), 165 (26), 42 (63).

2b: Mp 97—9 °C; IR (KBr) 3400—2900 (broad) cm^{-1}; MS *m/z* (rel intensity) 322 (M^+, 100), 321 (38), 280 (25), 176 (21), 165 (27), 77 (48), 42 (29).

2c: Mp 203—4 °C; IR (KBr) 3500—2800 (broad) cm^{-1}; MS *m/z* (rel intensity) 303 (23), 302 (M^+, 100), 287 (78), 245 (22), 165 (62), 57 (23), 42 (30), 41 (37).

References

1) M. Ōki, *Top. Stereochem.*, **14**, 1, (1983).
2) J. Marquet and M. Moreno-Mañas, *Synthesis*, **1979**, 348.
3) A. González, F. Güell, J. Marquet, and M. Moreno-Mañas, *Tetrahedron Lett.*, **26**, 3735 (1985).
4) A. González, J. Marquet, and M. Moreno-Mañas, *Tetrahedron*, **42**, 4253 (1986).
5) M. L. Martin, G. J. Martin, and J.-J. Delpuech, "Practical NMR Spectroscopy," Heyden and Son Ltd., London (1980), pp. 299—300.
6) H. Shanan-Atidi and K. H. Bar-Eli, *J. Phys. Chem.*, **74**, 961 (1970).
7) Ref. 5, p. 297.
8) Ref. 5, p. 340.
9) A. Steigel, *NMR. Basic Principles and Progress*, **15**, 1 (1978).
10) A. N. Nesmeyanov, E. B. Zavelovich, V. N. Babin, N. S. Kochetkova, and E. I. Fedin, *Tetrahedron*, **31**, 1461 (1975).
11) E. A. Chandross and C. F. Sheley, Jr., *J. Am. Chem. Soc.*, **90**, 4345 (1968).
12) T. A. Siddall, III and W. E. Stewart, *J. Org. Chem.*, **34**, 233 (1969).
13) A. Rieker and H. Kessler, *Tetrahedron Lett.*, **1969**, 1227.
14) R. C. Neuman and V. Jonas, *J. Am. Chem. Soc.*, **90**, 1970 (1968).

 © 1988 The Chemical Society of Japan Bull. Chem. Soc. Jpn., 61, 1831—1836 (1988)

Crystal Structures and Electronic Properties of Organic Conductors Based on AzaTCNQ

Hatsumi URAYAMA,*,†† Tamotsu INABE, Takehiko MORI, Yusei MARUYAMA, and Gunzi SAITO†
Institute for Molecular Science, Myodaiji-cho, Okazaki, Aichi 444
†Institute for Solid State Physics, The University of Tokyo, Roppongi, Minato-ku, Tokyo 106
(Received August 7, 1987)

AzaTCNQ ((4-dicyanomethyl-1-pyridinio)dicyanomethanide) is employed as an organic acceptor to form new organic conductors with a TTF family such as TTF,[1] TMTTF, TMTSF, HMTTF, and DBTTF. Among them, TMTTF and TMTSF give 2:1 single crystals and the latter affords the most conductive complex, showing a metallic characteristic down to 150 K. This can be observed by measuring the thermoelectric power and the ESR spectra. A crystal structure analysis indicates that only TMTSF molecules stack to form one-dimensional conduction pathways, while AzaTCNQ molecules are arranged side-by-side and oriented almost perpendicular to the donor molecules. There exists an orientational disorder of the nitrogen atom in the pyridine skeletone of an AzaTCNQ molecule, which may be associated with the weak temperature dependence of the electrical conductivity.

In an attempt to develop new highly conducting organic charge-transfer complexes, a number of novel donors and acceptors have been synthesized. One of the prominent acceptors is AzaTCNQ (Fig. 1). It has a similar geometry to TCNQ. However, the electronic properties of AzaTCNQ are different from those of TCNQ since the AzaTCNQ molecule contains a pyridine skeleton instead of the quinonoid ring of the TCNQ molecule. In the neutral state the spin multiplicity of AzaTCNQ is doublet. AzaTCNQ is, however, more stable as a closed-shell anion than a neutral radical and acts as one of the strongest π-electron acceptors so far obtaind. The reduced acceptor, AzaTCNQ$^-$, can be used as an organic anion instead of inorganic anions, e.g. BF_4^-, ClO_4^-, etc.

Originally, AzaTCNQ was synthesized by Wudl in order to search for conductive neutral radical complexes.[2] He prepared TTF complexes and reported relatively low electrical resistivities of the compacted specimens (1:1 and 2:1 stoichiometries) as 30—100 Ωcm. Later, Matsubayashi et al. regarded it as being an organic anion to form simple salts with cationic species.[3] Relatively high resistivities of more than 10^5 Ωcm were obtained.

We have investigated AzaTCNQ and its complexes for the following two purposes.[4] One was to search for conductive materials based on AzaTCNQ. The other was to elucidate the electronic states of AzaTCNQ in complexes: whether AzaTCNQ could be a neutral radical, a closed-shell anion, or a partially ionized state.

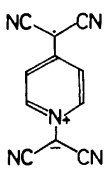

Fig. 1. Molecular structure of AzaTCNQ$^-$.

†† Present address: The Institute for Solid State Physics, The University of Tokyo, Roppongi, Minato-ku, Tokyo 106.

In this report, we discuss the preparation of several AzaTCNQ complexes with TTF derivatives and show detailed physical and structural properties of the metallic complex $(TMTSF)_2$ AzaTCNQ.

Experimental

Microcrystals of *N*-methylpyridinium AzaTCNQ ($NMPy^+$ AzaTCNQ$^-$) were prepared by the method of Tanaka et al.[3] The product was identified by its melting point (232—233 °C, lit, 233—237 °C).[3] Black crystalline complexes with TTF were obtained by direct mixing of 0.062 g of $(TTF)_2(BF_4)_3$ in 22 ml of hot acetonitrile and 0.070 g of $NMPy^+$ AzaTCNQ$^-$ in 13 ml of the same solvent. Black shiny microcrystals of the TMTTF complex were prepared by mixing 0.056 g of $(TMTTF)_{17}(BF_4)_8$ in 40 ml of hot acetonitrile and 0.026 g of $NMPy^+$ AzaTCNQ$^-$ in 10 ml of the same solvent. Complexes with TMTTF, TMTSF, DBTTF, and HMTTF were grown electrochemically in 20 ml of 1,1,2-trichloroethane with 30 mg of $NMPy^+$ AzaTCNQ$^-$ as an electrolyte and 10 mg of donors at a constant current of 1 μA under N_2. TMTTF and TMTSF complexes were obtained as shinny black single crystals in the form of elongated rods and DBTTF and HMTTF complexes had a black polycrystalline form.

For X-ray investigations, the intensity data of the TMTSF complex were measured on a Rigaku automated four-circle diffractometer with graphite monochromated Mo$K\alpha$ radiation up to 2θ=60° by using the ω-2θ scan techniqe. The sample crystal was a black plate with dimensions of 0.08×0.25×0.60 mm^3. Then, 1214 independent reflections ($|F|>3\sigma(|F|)$) were used for a structure analysis. The structure was solved by the Patterson method and refined by the block diagonal least-squares method. Atomic scattering factors were taken from International Tables for X-ray Crystallography.[5] Cell parameters were determined from least-squares applied to 25 reflections with 27°<2θ<31°. The final refinement gave R=0.0548 and R_w=0.0587 for $(TMTSF)_2$ AzaTCNQ. The positional parameters are listed in Table 1. The F_o-F_c table and the anisotropic temperature parameters are deposited as Document No. 8802 at the Office of this Bulletin.

Table 1. Atomic Parameters of $(TMTSF)_2AzaTCNQ$

Atom	$X(\times10^4)$	$Y(\times10^4)$	$Z(\times10^4)$
Se(1)	5890(3)	5426(1)	3152(1)
Se(2)	5903(3)	7074(1)	3174(1)
Se(3)	6007(3)	0434(1)	3172(1)
Se(4)	5707(3)	2015(1)	3196(1)
C(1)	5466(18)	6299(12)	2807(6)
C(2)	6861(24)	6003(11)	3820(7)
C(3)	6443(26)	6594(14)	3841(9)
C(4)	7416(29)	5471(15)	4324(10)
C(5)	7368(47)	7166(23)	4319(13)
C(6)	5220(24)	1206(18)	2726(8)
C(7)	6795(26)	798(12)	3863(9)
C(8)	6422(25)	1571(13)	3876(9)
C(9)	6993(25)	385(13)	4323(8)
C(10)	7052(32)	1925(14)	4387(11)
C(11)	−851(28)	3722(20)	1963(8)
C(12)	945(26)	3747(20)	1995(9)
C(13)	1808(24)	3695(16)	2519(8)
C(14)	−1773(29)	3787(23)	1427(9)
C(15)	−796(34)	3703(19)	921(10)
C(16)	−3557(29)	3724(26)	1399(9)
N(1)	−14(30)	3827(19)	489(9)
N(2)	−5054(28)	3842(13)	1383(10)

Cyclic voltammetry was performed in acetonitrile under a nitrogen atmosphere using 0.1 M tetrabutylammonium tetrafluoroborate (1 M=1 mol dm^{-3}) as a supporting electrolyte using Pt electrodes at a scan speed of 100 mV s^{-1}.

The temperature dependences of electrical resistivities were measured by a standard four-probe d.c. technique. The contacts were applied using gold paint with 20 μm gold wires. Measurements of the thermoelectric power along the a-axis was performed by attaching single crystals with 1 μm thick gold foils to two boron nitride heat sinks.[6] ESR data for a single crystal were obtained by an X-band spectrometer Varian E112 equipped with an Oxford Instruments ESR continuous-flow helium cryostat.

Results and Discussion

A cyclic voltammogram of $NMPy^+$ $AzaTCNQ^-$ in acetonitrile under a nitrogen atmosphere showed a redox wave ($AzaTCNQ^-/AzaTCNQ^{\cdot}$) with $E_{1/2}$=+0.57 V vs. SCE; ΔE^p=90 mV,[7] which is agreeable to that of $K^+AzaTCNQ^-$ ($E_{1/2}$=+0.54 V vs. SCE; ΔE^p=60 mV)[8] in acetonitrile. No second wave corresponding to $AzaTCNQ^{2-}/AzaTCNQ^-$ appeared. Furthermore, the reversible wave of $AzaTCNQ^{\cdot}/AzaTCNQ^+$ could not be obtained, although $AzaTCNQ^+$ has a similar electronic structure to TCNQ. The redox potential is close to those of F_4TCNQ^{-}/F_4TCNQ ($E_{1/2}$=0.53 V vs. SCE; ΔE^p=59 mV) and $HCBD^{-}/HCBD$ ($E_{1/2}$=0.62 V vs. SCE; ΔE^p=68 mV) obtained under the same conditions. From those data the order of acceptor strength is $F_4TCNQ<AzaTCNQ<HCBD$.

Usually, F_4TCNQ gives 1:1 insulating complexes with TTF derivatives in which both component molecules are completely charge-transfered and face-to-face segregated stacks are formed in the TTF, HMTTF, HMTSF, and DBTTF complexes,[9] while HCBD forms not only 1:1 complexes with perylene,[10] TMTTF,[11] and TTMTTF[11] but also 2:1 CT-complexes with pyrene,[12] hexamethylbenzene,[12] TTF,[13] and TMTTF.[11] The AzaTCNQ complexes form both 1:1 and 2:1 systems like the HCBD complexes. Though the chemical structure of AzaTCNQ resembles that of F_4TCNQ, the given complexes have more similar features to those of HCBD complexes.

Table 2. Electrical Properties of the AzaTCNQ Complexes

	ρ_{RT}/Ω cm	E_a/eV
TTF·AzaTCNQ[a]	66	0.20
$(TMTTF)_2AzaTCNQ$	8.1	0.072
$(TMTSF)_2AzaTCNQ$	1.1×10^{-2}	0.015 (at low temp)
DBTTF-AzaTCNQ[b]	19	0.09
HMTTF-AzaTCNQ[b]	1.3×10^6	—

a) A compacted sample. b) The stoichiometries have not been determined.

The electrical resistivities at room temperature and the activation energies of the AzaTCNQ complexes are summarized in Table 2. AzaTCNQ complexes with DBTTF, HMTTF, TMTTF, and TTF are semiconductors and only the TMTSF complex shows a metallic character (vide infra).

It is also noticeable that the electrical resistivity of the TTF complex is rather low, 66 Ω cm, at room temperature for the compacted sample, though it is a complete-charge-transfered salt with 1:1 stoichiometry(vide infra).[14] Our resistivity data agree with those of the Wudl's TTF complex. The appearance of the 1420 cm^{-1} band of C=C stretching and the 508 cm^{-1} band of C-S streching in TTF in the Raman spectrum suggests a complete charge transfer in this complex (cf. TTF^{+1} 1420 cm^{-1} (C=C), 509 cm^{-1} (C-S)).[15] This assignment was further confirmed by the optical absorption spectrum of a complex which does not show any absorption band in the near-infrared region, characteristic of a partial charge-transfer state. Unfortunately, the single crystals have not yet been obtained.

For the TMTSF complex, which shows a metallic character, a crystal structure analysis was performed. Weissenberg photographs and a four-circle diffractometer were employed to determine the crystal data of $(TMTSF)_2AzaTCNQ$: monoclinic, space group $C2/c$, a=7.738(1), b=19.531(2), c=23.146(3) Å, β=90.03(1)°, V=3498.3(8) $Å^3$, and Z=4. The a-axis corresponds to the crystal needle axis. The oscillation photograph along the a-axis displayed strong, even layer lines due to the two-fold periodicity of the donors. All these layer lines were composed of well-defined spots, even at room temperature, and no diffuse track was observed. The crystal structure is illustrated in Figs. 2—4. The planar TMTSF molecules form face-to-face one-dimensional stacks along the a-axis with an interplanar spacing of 3.6 Å, which corresponds to a conduction column (Fig. 4). Within the one-dimensional

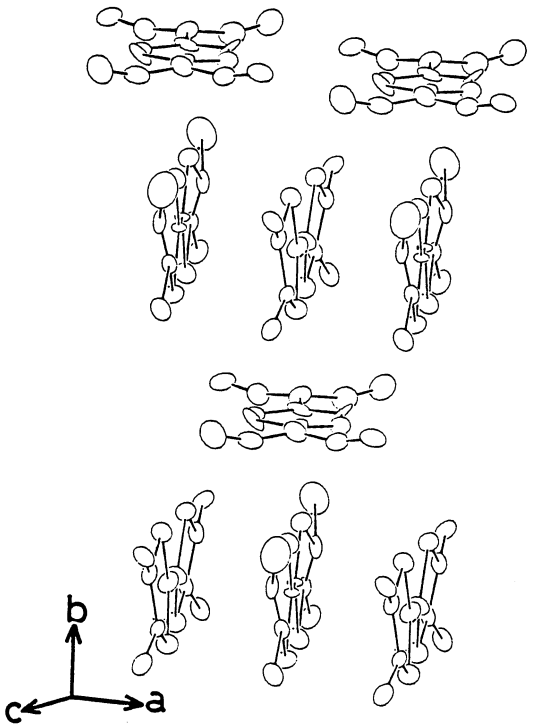

Fig. 2. Molecular arrangement of $(TMTSF)_2$ AzaTCNQ viewed along nearly the long axis of the donor molecule.

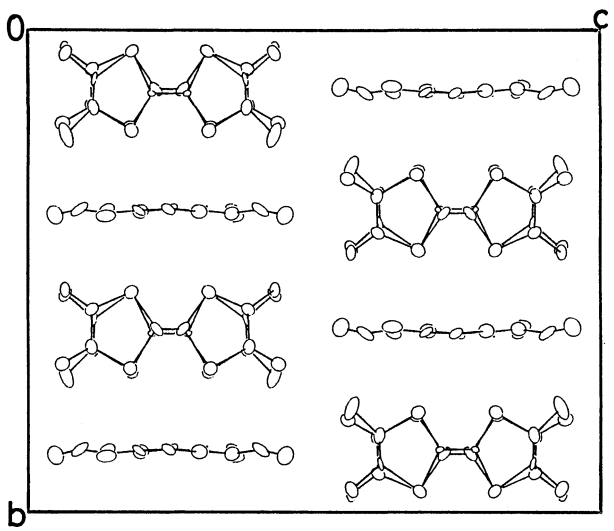

Fig. 3. Crystal structure of $(TMTSF)_2$AzaTCNQ projected along the axis perpendicular to the (100) plane.

stacks the Se···Se distances between the neighboring TMTSF molecules are 3.72—4.02 Å, which are comparable to twice the van der Waals radii of Se···Se, 3.80 Å. On the other hand, the AzaTCNQ molecular planes are arranged side-by-side along the donor stacks and the acceptor molecules surround the TMTSF columns so that the donor stacks are isolated from each other. There are no short atomic contacts between the neighboring donor columns; hence, the molecules form nearly complete one-dimensional stacks, as can

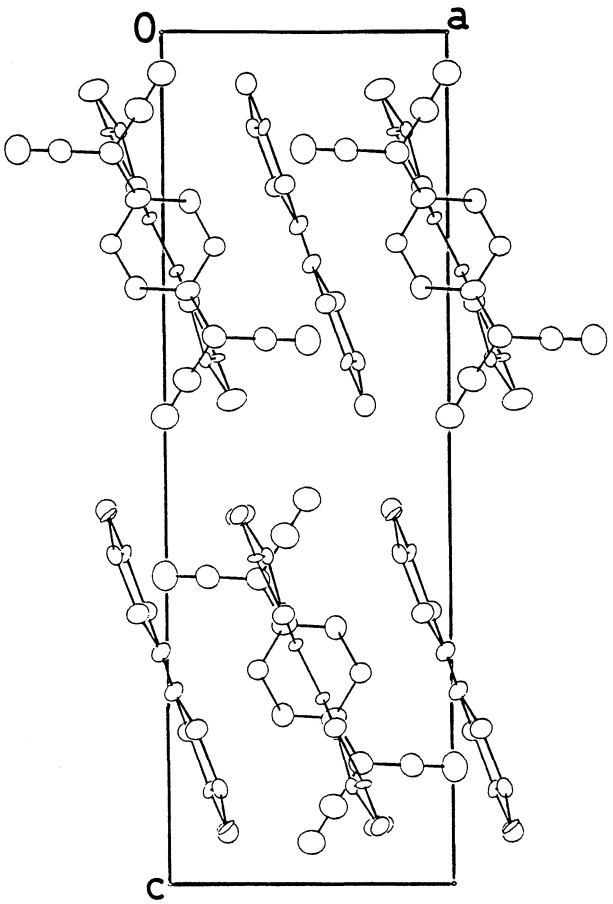

Fig. 4. Crystal structure of $(TMTSF)_2$AzaTCNQ projected along the b axis.

be seen in Fig. 3. The dihedral angle between the least-square planes of donor and acceptor molecules is 93° (Fig. 4). The AzaTCNQ molecules are oriented parallel to the ac plane, while the longitudinal axes of TMTSF molecules are tilted by approximately 20° from the [001] direction (Fig. 4).

Another remarkable feature is that the orientation of AzaTCNQ molecules has a disorder in nature. There appears a two-fold axis through the center of every AzaTCNQ molecule, so that the nitrogen atom in the pyridine skeleton of each AzaTCNQ molecule is randomly located at either position of two equivalent sites.

$(TMTTF)_2$AzaTCNQ is essentially isomorphous with the TMTSF complex. The crystal data are: monoclinic, space group $C2/c$, a=7.670(3), b=19.178(9), c=22.655(3) Å, β=90.25(2)°, V=3332.3(22) Å^3, and Z=4.

These structures have some similarities to that of $(TMTTF)_2$HCBD,[11b] in which the orientationally disordered acceptors lie almost perpendicular to the donor planes and surround the donors, showing one-dimensionality characteristics. A slight difference between $(TMTTF)_2$HCBD and $(TMTTF)_2$AzaTCNQ is that the donors in the HCBD complex stack in a dimerized manner with a molecular separation of ca. 3.5 Å within the dimer and ca. 3.7 Å between the

dimers. The HCBD complex is a semiconductor ($\rho_{RT}=3.3\times10^3$ Ωcm, $E_a=0.16$ eV). As for $(TMTTF)_2$AzaTCNQ, the electrical resistivity and the activation energy are lower than those of $(TMTTF)_2$HCBD. This may be caused by the uniform stacking of donors in $(TMTTF)_2$AzaTCNQ, where the interplanar spacing of 3.5 Å was observed.

A substitution of the selenium for sulfur atoms of donors may cause less on-site Coulomb repulsions and stronger intermolecular interactions between donors and influence the charge transport. As a consequence, $(TMTSF)_2$AzaTCNQ with uniform stackings shows a metallic character down to 200 K, as illustrated in Fig. 5. Upon lowering the temperature to below 150 K the resistivity gradually increases and is activated with a very small activation energy of $E_a=0.015$ eV.

The result of thermoelectric power (S) measurements shows positive values due to the hole conduction, which is consistent with the conducting paths of donors in the crystal (Fig. 6). The thermoelectric power linearly falls with decreasing temperature and the extrapolation tends to approach zero at 0 K, suggesting a metallic state above 150 K. The transition temperature is a little lower than that of the electrical resistivity. The higher transition temperature of the electrical resistivity may be caused by a strong sensitivity to the influence of the random potential originating from the orientational disorder of AzaTCNQ molecules. Assuming a simple one-electron tight-binding band model, the thermoelectric power along the conducting axis can be written as

$$S = \frac{-\pi^2 k_B^2 T}{6|e|t} \cdot \frac{\cos(\pi\rho/2)}{1-\cos^2(\pi\rho/2)},$$

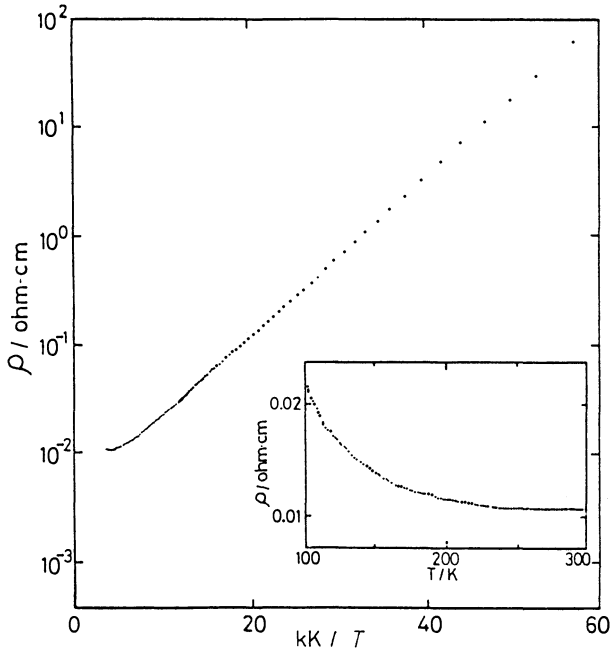

Fig. 5. Temperature dependence of the electrical resistivity of $(TMTSF)_2$AzaTCNQ along the a axis.

where e is the electron charge, k_B is the Boltzmann constant, and ρ is the electron density (in our case $\rho=2-1/2=3/2$).[16] From the slope of S vs. T plots at high temperatures, the transfer integral(t) was obtained as 0.25 eV ($4t=1.0$ eV). Below the metal-semiconductor transition, S gradually increases. For a simple semiconductor, the thermoelectric power can be described as

$$S = \text{constant} - \frac{k_B}{e} \cdot \frac{b-1}{b+1} \cdot \frac{E_g}{2k_B} \cdot \frac{1}{T},$$

where E_g is the energy gap and $b=\mu_e/\mu_h$, i.e., the ratio of an electron to a hole mobility.[16] From the positive values of the thermoelectric power and the one-dimensional conduction pathways composed of the only donor component shown by the crystal structure analysis, $-(b-1/b+1)$ can be regarded as 1. The activation energy was found to be $E_a=0.018$ eV from the slope of S vs. $1/T$ plots below 55 K. This value of the activation energy is in a good agreement with the derived value from the electrical conductivity.

Only one signal of the ESR spectra of $(TMTSF)_2$AzaTCNQ has been observed and the line shape was found to be Lorentzian all the way down to 34 K. The

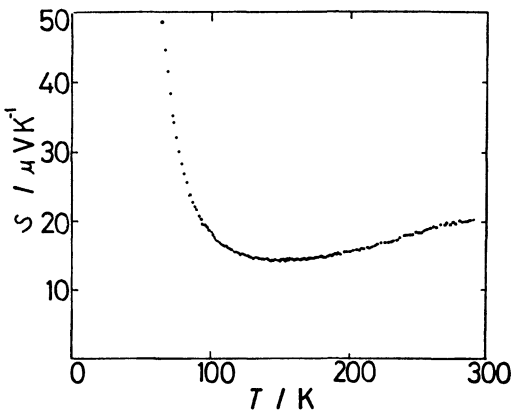

Fig. 6. Temperature dependence of the thermoelectric power S of $(TMTSF)_2$AzaTCNQ along the a axis.

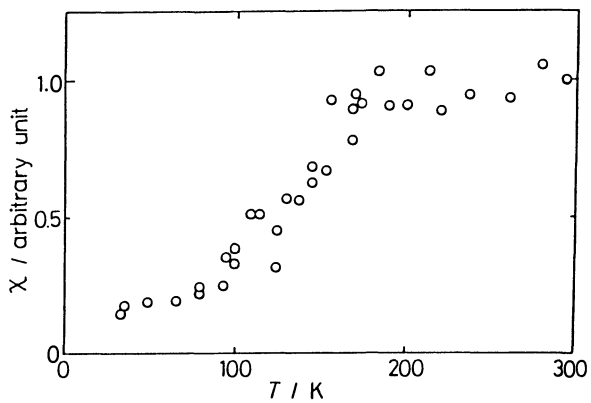

Fig. 7. Temperature dependence of the ESR magnetic susceptibility of $(TMTSF)_2$AzaTCNQ.

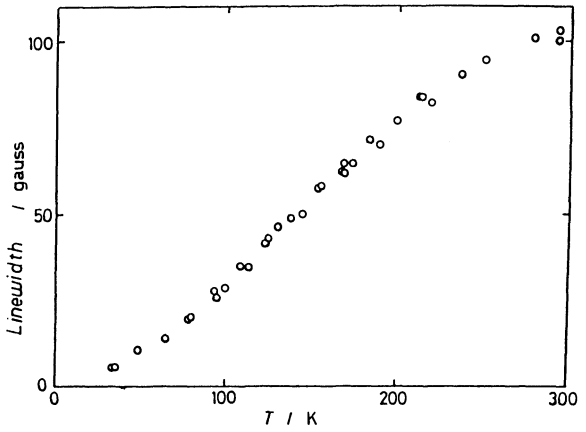

Fig. 8. Temperature dependence of the ESR linewidth of $(TMTSF)_2AzaTCNQ$.

magnetic susceptibility obtained from the ESR intensity of $(TMTSF)_2AzaTCNQ$ is almost constant, indicating a Pauli-like paramagnetism above 150 K (Fig. 7). Below that temperature the susceptibility behaves in an activated manner with E_a=0.03 eV. This value agrees fairly well with those of the electrical resistivity and thermoelectric power. Judging from the charge-transport and magnetic properties, a metal-semiconductor transition is considered to occur at ca. 150 K. It is regarded as being the Peierls transition.

Figure 8 illustrates the temperature dependence of the ESR line width for the applied field H_0 approximately parallel to the a-axis. The line width (ΔH) at 293 K is almost 95 G (1G=10^{-4} T) which is a little narrower than those of $(TMTSF)_2X$ (X=PF_6, BF_4, NO_3, and etc. ΔH>150 G),[17] suggesting a lower dimensionality of the AzaTCNQ complex than those of $(TMTSF)_2X$. Below room temperature the width decrease approximately linearly with the temperature down to about 250 K, below which the temperature dependence becomes stronger and the width decrease linearly to 5 G at 34 K. The temperature dependences are reminiscent of those of single-chain conducting complexes $(TMTSF)_2X$, which show knees at a little bit lower temperature (100—180 K) than that of the AzaTCNQ complex. The anisotoropy in the linewidth becomes smaller as the temperature becomes lower (ΔH=28 G (*//a*), 36 G (*//b*) at 99 K and 95 G (*//a*), 127 G (*//b*) at 293 K). The line width of the AzaTCNQ complex shows no drastic behavior in the temperature region of the metal-semiconductor trasition, which may indicate a gradual transition of this complex due to the orientational disorder of AzaTCNQ molecules.

The angular dependence of the g values is similar to that of the linewidth. The g values are usually different in the direction of the applied H_0 to the donor molecules. The maximum, intermediate, and minimum g values are generally found when H_0 is applied to a long axis, a short axis and perpendicular to a molecular plane, respectively. The observed g-value is

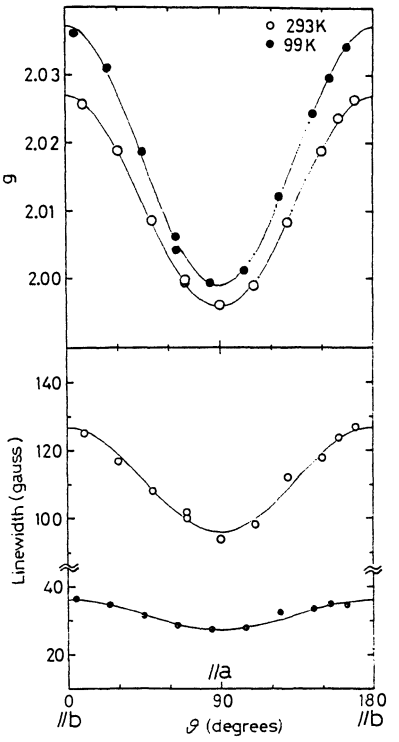

Fig. 9. Angular dependences of the g values and linewidth of $(TMTSF)_2AzaTCNQ$ at 293 and 99 K.

intermediate when H_0 is parallel to the b-axis (g_{int} ca. 2.026), which is approximately parallel to the short axis of the TMTSF molecules in the crystal. However, the minimum g-value is observed for H_0 parallel to the a-axis (g_{min} ca. 1.996), which is nearly normal to the molecular plane of TMTSF and, hence, along the conducting direction. Those values compare well to those of $(TMTSF)_2PF_6$ (g_{int} ca. 2.027, g_{min} ca. 1.989), strongly suggesting that AzaTCNQ behaves as a closed-shell counter anion. The anisotropy of the g-values is in good accordance with those previously reported ones in $(TMTSF)_2X$[18,19] and $(BEDT\text{-}TTF)_2X$[19] in that the intermediate g-value corresponds to the short axis of the donor molecule and the minimum g is perpendicular to the molecular plane. More precise anisotropy studies of the line width and the g-values of the AzaTCNQ complex are presently being carried out.

In summary, AzaTCNQ has been found to form conducting organic compounds with TTF derivatives. Among them $(TMTSF)_2AzaTCNQ$, in which AzaTCNQ most likely acts as a closed-shell counter anion, is the most conductive and the transport properties indicate its metallic character down to 150 K, where the Peierls-type instability takes place.

The authors wish to express their thanks to Professor Gen-etsu Matsubayashi of Osaka University for his valuable advice concerning the synthesis and Mr. Kenichi Imaeda for his helpful advice concerning electrical and ESR measurements.

References

1) Abbreviations for compounds: TTF, tetrathiafulvalene; TMTTF, tetramethyltetrathiafulvalene; TMTSF, tetramethyltetraselenafulvalene; HMTTF, hexamethylenetetrathiafulvalene; DBTTF, dibenzotetrathiafulvalene.

2) F. Wudl, "Chemistry and Physics of One-dimensional Metals," ed. by H. J. Keller, NATO Adv. Study Inst., (1977), p. 249.

3) H. Tanaka, G. Matsubayashi, and T. Tanaka, *Bull. Chem. Soc. Jpn.*, **57**, 2198 (1984).

4) H. Urayama, T. Inabe, T. Mori, Y. Maruyama, G. Saito, *Synth. Metals*, **19**, 469 (1987).

5) "International Tables for X-ray Crystallography," Kynoch Press, Birmingham (1974), Vol. IV.

6) P. M. Chaikin and J .F. Kwak, *Rev. Sci. Instrum*, **46**, 218 (1975).

7) ΔE^p is defined as the difference between the cathodic and anodic peak potentials.

8) G. Matsubayashi, H. Tanaka, T. Tanaka, and K. Nakatsu, *Inorg. Chim. Acta*, **63**, 217 (1982).

9) a) F. M. Wiygul, T. J. Emge, and T. J. Kistenmacher, *Mol. Cryst. Liq. Cryst.*, **90**, 163 (1982); b) J. B. Torrance, J. J. Mayerle, K. Bechgaard, B. D. Silverman, and Y. Tomkiewicz, *Phys. Rev. B*, **22**, 4960 (1980); c) M. E. Hawley, T. O. Poehler, T. F. Carruthers, A. N. Bloch, D. O. Cowan, and T. J. Kistenmacher, *Bull. Am. Phys. Soc.*, **23**, 424 (1978); d) T. J. Emge, W. A. Bryden, F. M. Wiygul, D. O. Cowan, T. J. Kistenmacher, and A. N. Bloch, *J. Chem. Phys.*, **77**, 3188 (1982).

10) H. Yamochi, G. Saito, T. Sugano, M. Kinoshita, C. Katayama, and J. Tanaka, *Chem. Lett.*, **1986**, 1303.

11) a) G. Saito, T. Enoki, H. Inokuchi, H. Kumagai, C. Katayama, and J. Tanaka, *Mol. Cryst. Liq. Cryst.*, **120**, 345 (1985); b) C. Katayama, M. Honda, H. Kumagai, J. Tanaka, G. Saito, and H. Inokuchi, *Bull. Chem. Soc. Jpn.*, **58**, 2272 (1985).

12) O. W. Webster, *J. Am. Chem. Soc.*, **86**, 2898 (1864).

13) F. Wudl and E. W. Southwick, *J. Chem. Soc., Chem. Commun.*, **1974**, 254.

14) Found: S, 30.85; C, 49.02; N, 16.49; H, 1.92%. Calcd for $S_8C_{23}N_5H_{12}$; S, 31.24; C, 49.74; N, 17.06; H, 1.96%.

15) a) Unpublished data by Prof. S. Matsuzaki; b) S. Matsuzaki, T. Moriyama, and K. Toyoda, *Solid State Commun.*, **34**, 857 (1980).

16) P. M. Chaikin, R. L. Greene, S. Etemad, and E. Engler, *Phys. Rev. B*, **13**, 1627 (1976).

17) H. J. Pedersen, J. C. Scott, and K. Bechgaard, *Phys. Rev. B*, **24**, 5014 (1981).

18) N. Kinoshita, M. Tokumoto, H. Anzai, T. Ishiguro, G. Saito, T. Yamabe, and H. Teramae, *J. Phys. Soc. Jpn.*, **53**, 1504 (1984).

19) T. Sugano, G. Saito, and M. Kinoshita, *Phys. Rev. B*, **34**, 117 (1986).

 © 1988 The Chemical Society of Japan Bull. Chem. Soc. Jpn., 61, 1837—1843 (1988)

Basis Set Dependency of Energy Components in Hartree-Fock MO Theories. II.[1] Conservability of Virial Ratio between Different Conformations

Hiroshi ICHIKAWA* and Atsushi SHIGIHARA
Hoshi College of Pharmacy, Ebara, Shinagawa, Tokyo 142
(Received August 8, 1987)

The authors examined 22 different basis sets in order to determine exactly how they reproduce the relative kinetic and potential energies. In an attempt to find the calculation error of such energy components, the virial relationship has been used between two conformations in which all bond lengths are optimized with respect to the total energy: i.e., the relationship, $\Delta V=-2\Delta T$, where ΔV and ΔT are the differences in the potential and kinetic energies. The degree of error was compared in terms of the relative virial error ($(\Delta E+\Delta T)/\Delta E$) to the difference in the total energies (ΔE). STO-*N*G was found to give a large amount of casual error, up to 500% to ΔE. Such an error could be dramatically improved by using a split-valence method. It should be noted that 4-31G and 6-31G methods resulted in a small amount of error and that the inclusion of polarization functions does not always improve the amount of error.

Ruedenberg and co-workers have pointed out that the nature of the chemical bond can be fully understood by only taking into account the kinetic and potential energies.[2-4] The basic energies which govern chemical phenomena are electrostatic potentials and kinetic energies of nuclei and electrons. The kinetic energy of nuclear motion may be considered separately;[5] thus, the major and important energies in a molecule are the potential energy and the kinetic energy of electrons. Therefore, it is possible, in principle, to interpret chemical phenomena in terms of the potential and kinetic energies in a system using MO theories.

Quantum chemists have provided a large number of basis sets for ab initio MO calculation.[6] However, care concerning components of the totel energy has been neglected or considered to be less important. Besides, it has been shown that the kinetic and potential energies are very sensitive to the scaling factor of the wave function, indicating that one must be more careful when analyzing the energy components than when analyzing the total energy.[7,8] The purpose of this paper is to show whether or not the potential energy and the kinetic energy of electrons are meaningful to quote and how they are dependent on the adopted basis set. For this purpose, we have examined 22 different basis sets in the GAUSSIAN 80 program.[9,10]

Theory

Evaluation of the Kinetic and Potential Energies. Since via a Fock matrix three- and four-center integrals out of two-electron integrals can be reduced to two-center terms, the kinetic energy (T) and the electronic potential energy (V) can be expressed in terms of the density (P_{rs}), kinetic energy (T_{rs}), and Fock (F_{rs}) matrices as follows;

$$T=\sum_{r,s} P_{rs}\,T_{rs} \tag{1}$$

and

$$V=1/2\sum_{r,s} P_{rs}\,(F_{rs}-T_{rs})+\sum_{A<B} E_{AB}{}^{N}, \tag{2}$$

where $E_{AB}{}^{N}$ is the internuclear repulsion between atoms A and B, and where r and s run over all atomic orbitals. Details are shown elsewhere.[11]

Since the scaling factor to the wave function applies to the electronic coordinates as well as to the nuclear coordinates, the condition or threshold of geometry optimization is predicted to seriously affect components of the total energy. Therefore, the threshold of geometry optimization was set to be 0.000075 (maximum) and 0.00005 (rms) Hartree/Bohr or radian, which are less than one fifth of the standard geometry optimization.

As Eqs. 1 and 2 show, the convergence on the density matrix may be another important condition. The SCF criterion was set such that every element of the density matrix was to converge within 10^{-10}, 1000-times more severe than the standard SCF criterion. The effects of geometry optimization and the SCF convergence will be discussed in a later section.

Criteria of Energy Components. The first criterion of the adopted basis set is to compare the relative total energy (ΔE) with the experiment (criterion 1). However, this cannot apply to the components of the total energy.

The ratio V/T should be exactly -2 in any *equilibrium* geometry. Nelander has pointed out that the angular coordinates give no contribution to the ratio if all bond lengths are optimized with respect to the total energy.[12] The energy difference between any two sets of geometry-optimized conformations satisfies the relationship $\Delta V=-2\Delta T$, where ΔT and ΔV are the differences of the kinetic energy and the potential energy. Therefore, if the total energy increases when the geometry changes from one conformation to another, the potential energy must increase while the kinetic energy of electrons must decrease (criterion 2)

and the ratio $-\Delta V/\Delta T$ should be exactly 2, as to the appropriate Hartree-Fock wave function. Although the actual wave functions obtained by an SCF MO theory do not always give the required ratio exactly, it could be said that the closer the calculated ratio is to 2, the more the adopted basis set is appropriate for the considered system. This can be another criterion. However, it involves such a difficulty that when ΔT appears to be zero or very close to zero, the ratio becomes infinity or a very large number, overrating the error.

The $\Delta E+\Delta T$ value ($=\Delta V+2\Delta T$) should be zero; the closeness to zero shows exactly how energy components are calculated by the adopted basis set. We call the difference from zero the "virial error" for now. Since the virial error should be compared with respect to ΔE, we adopted the relative value $(\Delta E+\Delta T)/\Delta E$ as a quantitative measure for the error of the energy-component calculation (criterion 3).

Results and Discussion

We have chosen the following compounds: CH_3-CH_3, CH_3-NH_2, CH_2=CH-CH=CH_2, CH_2=CH-NH_2, and CH_2=CH-NO_2. The first and second compounds represent the aliphatic compounds and the others are interesting in that a change in the conformation of the functional group breaks up the conjugation between π systems or between a π system and its substituent.

Ethane. Ethane favors the staggered conformation **1** and the experimental rotational barrier was reported to be 12.3 kJ mol^{-1}.[13] Table 1 shows the results for ethane where the total energies, kinetic energies, and potential energies for the staggered conformation are listed. As for the eclipsed conformation **2**, only the differences from the staggered conformation are shown.

The calculated energy barrier (ΔE) ranges from 11 to 13 kJ mol^{-1}, a good agreement with the experiment,

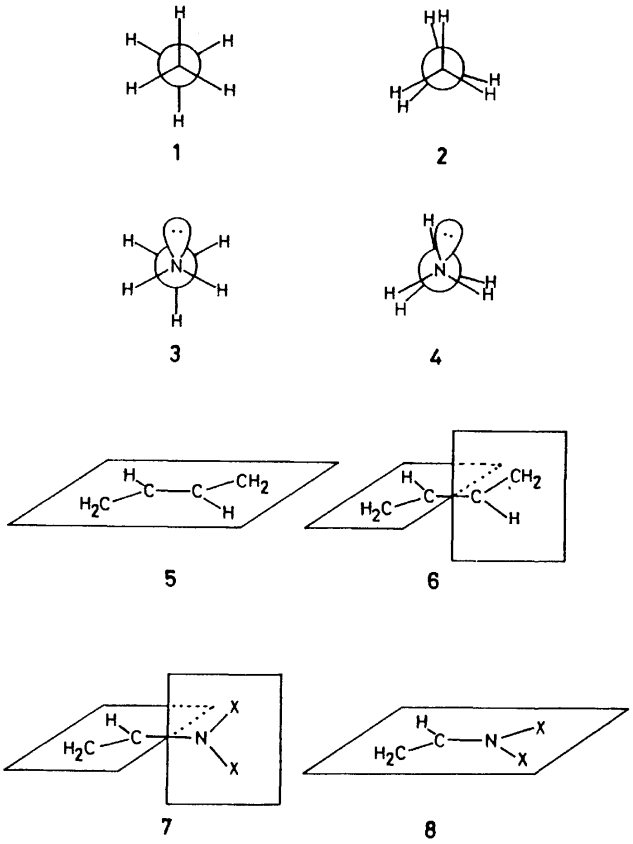

Scheme 1.

Table 1. Total, Kinetic, and Potential Energies in Ethane

	E[a]	T[a]	V[a]	ΔE[b]	ΔT[b]	ΔV[b]
STO-3G	−78.306180	77.672593	−155.978772	12	12	0
STO-4G	−78.863187	78.621105	−157.484292	12	8	4
STO-5G	−79.018148	78.918412	−157.936560	12	10	2
STG-6G	−79.066024	79.021753	−158.087777	12	10	2
3-21G	−78.793948	78.644574	−157.438523	12	−20	32
4-21G	−79.061649	79.093991	−158.155640	11	−20	31
6-21G	−79.138022	79.209755	−158.347777	11	−20	31
3-21G*	−78.824494	78.614277	−157.438771	13	−15	28
4-21G*	−79.091958	79.062910	−158.154868	13	−16	28
6-21G*	−79.168213	79.180491	−158.348704	13	−16	29
3-21G**	−78.844210	78.475882	−157.320092	13	−15	28
4-21G**	−79.109019	78.952629	−158.061647	13	−15	27
6-21G**	−79.184285	79.103225	−158.287510	13	−15	27
4-31G	−79.115933	79.249285	−158.365218	12	−13	25
6-31G	−79.197572	79.340650	−158.538222	12	−12	24
4-31G*	−79.151624	78.671024	−157.822648	13	−15	28
6-31G*	−79.228755	79.199474	−158.428229	12	−16	28
4-31G**	−79.162010	78.678248	−157.840258	13	−16	28
6-31G**	−79.238235	79.199114	−158.437349	13	−16	29
6-311G	−79.211802	79.284061	−158.495863	12	−11	22
6-311G*	−79.242829	79.263740	−158.506569	12	−8	21
6-311G**	−79.251707	79.217743	−158.469450	13	−11	24

a) In terms of au (1 au=2625.5 kJ mol^{-1}). b) kJ mol^{-1}.

regardless of the adopted basis set satisfying criterion 1. In the STO-*N*G methods, however, it is seen that both kinetic and potential energies increase as the geometry changes from the staggered conformation to the eclipsed one. This does not meet criterion 2. All other methods satisfy such a requirement.

Regarding criterion 3, as Fig. 1 shows, only STO-*N*G gave a relative virial error of more than 100% to the difference of the total energies. All other methods gave reasonably correct values where, interestingly, the inclusion of polarization functions did not improve the error. For example, the relative errors by 6-311G, 6-311G*, and 6-311G** were 0.08, 0.33, and 0.15, respectively, where the basis set without polarization functions gave the best result among them. Except for STO-*N*G, the difference of energy components, ΔT

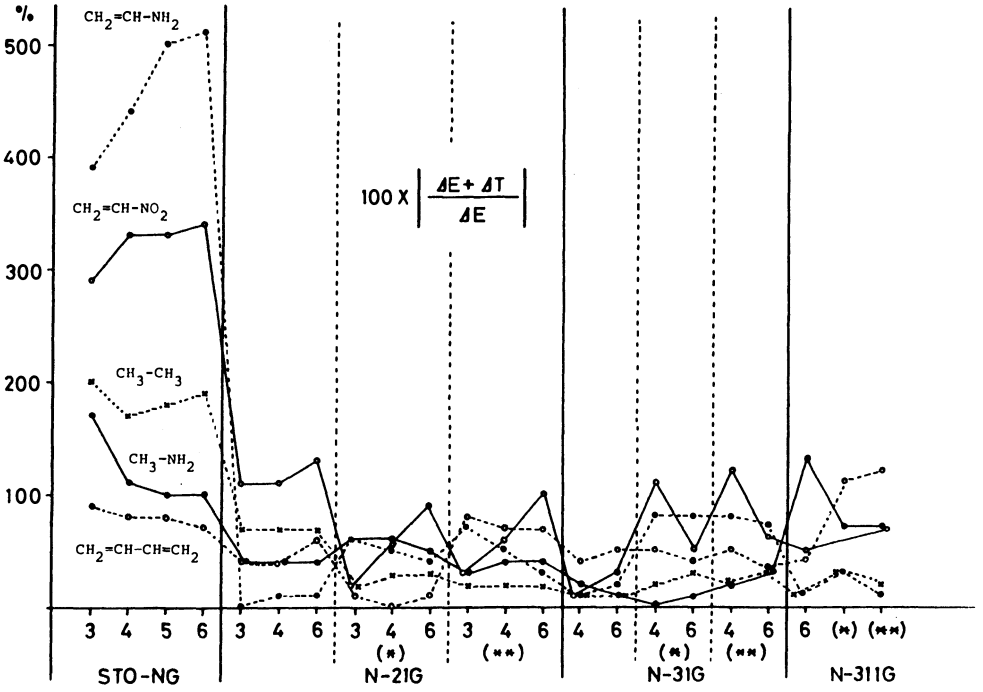

Fig. 1. Relative virial errors.

Table 2. Total, Kinetic, and Potential Energies in Methylamine

	E[a)]	T[a)]	V[a)]	ΔE[b)]	ΔT[b)]	ΔV[b)]
STO-3G	−94.032863	93.218512	−187.251375	12	8	4
STO-4G	−94.704379	94.353756	−189.058136	12	2	10
STO-5G	−94.887253	94.731303	−189.618556	12	0	12
STO-6G	−94.943358	94.862177	−189.805535	12	0	12
3-21G	−94.681656	94.460890	−189.142546	8	−5	13
4-21G	−94.995400	94.990298	−189.985699	8	−5	14
6-21G	−95.084985	95.143410	−190.228395	9	−5	13
3-21G*	−94.721827	94.450702	−189.172528	12	−5	16
4-21G*	−95.035133	94.978065	−190.013198	12	−5	17
6-21G*	−95.124511	95.131635	−190.256145	12	−5	17
3-21G**	−94.744616	94.357714	−189.102330	11	−8	18
4-21G**	−95.055857	94.903976	−189.959833	11	−7	18
6-21G**	−95.144436	95.082366	−190.226802	11	−6	17
4-31G[c)]	−95.071663	95.196402	−190.268065	11	−13	24
6-31G[c)]	−95.170903	95.293703	−190.464606	11	−12	23
4-31G*	−95.117328	94.482331	−189.599659	10	−11	21
6-31G*	−95.209828	95.103524	−190.313353	10	−11	21
4-31G**	−95.130398	94.491786	−189.622183	10	−12	22
6-31G**	−95.221864	95.106854	−190.328718	10	−13	22
6-311G	−95.193323	95.307019	−190.500342	7	2	5
6-311G*	−95.231752	95.305991	−190.537744	10	−3	13
6-311G**	−95.242514	95.255665	−190.498179	10	−3	12

a) In terms of au. b) kJ mol^{-1}. c) HNH was set to be the experimental value (105°52′) since the stationary angle was not obtain.

Table 3. Total, Kinetic, and Potential Energies in Butadiene

	E[a]	T[a]	V[a]	ΔE[b]	ΔT[b]	ΔV[b]
STO-3G	−153.020365	151.994848	−305.015213	23	−2	26
STO-4G	−154.124511	153.827631	−307.952142	23	−4	28
STO-5G	−154.427447	154.412477	−308.839924	23	−5	28
STO-6G	−154.521944	154.616226	−309.138170	23	−6	29
3-21G	−154.059459	153.744461	−307.803920	23	−15	37
4-21G	−154.598599	154.649834	−309.248433	23	−14	37
6-21G	−154.752984	154.892001	−309.644985	23	−9	33
3-21G*	−154.124030	153.624492	−307.748522	47	−43	91
4-21G*	−154.660728	154.548828	−309.209557	49	−47	96
6-21G*	−154.814130	154.813666	−309.627796	51	−48	99
3-21G**	−154.148618	153.468784	−307.617401	41	−8	49
4-21G**	−154.681789	154.427391	−309.109180	43	−12	55
6-21G**	−154.833862	154.731145	−309.565007	46	−13	60
4-31G	−154.699966	154.903200	−309.603166	25	−34	58
6-31G	−154.864579	155.055757	−309.920336	25	−38	63
4-31G*	−154.764143	153.771430	−308.535574	24	−12	37
6-31G*	−154.919656	154.808417	−309.728073	24	−16	40
4-31G**	−154.775600	153.782106	−308.557706	24	−12	37
6-31G**	−154.930326	154.814169	−309.744495	24	−16	41
6-311G	−154.892899	155.018421	−309.911320	24	−33	57
6-311G*	−154.949276	154.966953	−309.916229	45	−96	141
6-311G**	−154.960846	154.939571	−309.900417	45	−100	145

a) In terms of au. b) kJ mol^{-1}.

and ΔV, were calculated to be 10 to 20 and 20 to 30 kJ mol^{-1}, respectively.

Methylamine. We have chosen two conformations: the staggered conformation **3** and the eclipsed conformation **4**. The rotational barrier of methylamine has been reported to be 8.3 kJ mol^{-1}.[14] The calculated rotational barriers shown in Table 2 were from 7 to 12 kJ mol^{-1}, in reasonable agreement with the experiment. However, the components by STO-*N*G appeared to be unsatisfactory, even qualitatively. The split-valence methods gave results which reasonably well satisfy criteria 1, 2, and 3. Very exceptionally, 6-311G gave a large relative virial error in addition to failure of criterion 2, although it was improved by the inclusion of polarization functions. As expected, the contraction number of the primitive Gaussian functions for the inner-shell atomic orbitals did not affect the ratio very much. It is also noted that the inclusion of polarization functions to the first-row atom and to the hydrogen atom seems not always to improve the relative virial error.

Butadiene. The rotational barrier from the trans to cis structures has been observed to be a value ranging between 24 and 32 kJ mol^{-1}.[15-17] We have chosen the planar trans structure with the lowest energy **5** and the orthogonal structure with the highest energy **6.**

As shown in Table 3, the calculated rotational barriers varied from 23 (STO-*N*G) to 51 kJ mol^{-1} (6-21G*), significantly larger than the observed values. This may stem from the difference of the electron-correlation energy between the orthogonal and planar structures: in the orthogonal structure the conjugation between two π systems are broken.

Vinylamine. We consider the orthogonal structure **7** (X=H) and the planar structure **8** (X=H). Vinylamine is the fundamental unit of enamines. The electronic effect of enamine has been explained as being a strong contribution of the structure CH_2^--CH=NH_2^+.[18]

Since vinylamine favors to take the imino form, the experimental rotational barrier may not be obtained, excluding the way to check the difference of total energies. However, the rotational barrier has been calculated to be between 26 and 32 kJ mol^{-1}.[19] Table 4 shows the energies for the planar structure and the differences for the orthogonal structure from the planar structure.

The total energy of the optimized orthogonal structure was calculated to be 25 to 35 kJ mol^{-1} higher than that of the planar structure by all MO methods, perhaps satisfying the first criterion. However, the components were divergent.

A comparison of the relative virial errors by *N*-21G*, *N*-21G**, *N*-31G*, and *N*-31G** leads to the fact that, contrary to the case of methylamine, the number of the primitive Gaussian functions for the inner-shell electrons is slightly concerned with the energy components: as a rule, the larger the number of functions, the better the results.

Nitroethene. Nitroethene has a planar structure with an electric dipole moment of 3.7 d,[20] indicating that a considerable number of electrons move to the nitro group. In an orthogonal structure **7** (X=O) such a conjugation is forced to cease. The conjugation energy is observed to be 20.2 kJ mol^{-1},[21] suggesting a strong contribution of the cannonical structure CH_2^+-CH=NO_2^-.

Table 5 shows that the calculated conjugation

energy ranges between 20 and 40 kJ mol^{-1}. The potential energies calculated by all methods increase in accordance with the corresponding total energies. However, the kinetic energy behaves differently according to the calculation method. This time, STO-*N*G gave the correct signs of ΔT, but ΔT's by *N*-21G, 6-21G**, 4-31G*, and 4-31G** failed to meet the second criterion. Criterion 3 is necessary for a quantitative discussion. Interestingly, such a requirement is satisfied by such rather smaller basis sets as 4-31G and 6-31G; the inclusion of polarization functions does not always improve the relative virial error.

Effect of the Conditions of Geometry Optimization and SCF Convergence. (a) Threshold of Geometry Optimization. It has been known that the kinetic and potential energies change in the first order of the error of the scaling factor to the wave function, while the total energy does only in the second order.[7,22] Since

Table 4. Total, Kinetic, and Potential Energies in Vinylamine

	E[a]	T[a]	V[a]	ΔE[b]	ΔT[b]	ΔV[b]
STO-3G	−131.395801	130.361665	−261.757466	25	73	−48
STO-4G	−132.341207	131.933730	−264.274936	25	85	−60
STO-5G	−132.598103	132.448926	−265.047029	25	99	−74
STO-6G	−132.677501	132.628438	−265.305938	25	104	−79
3-21G	−132.326444	132.018646	−264.345089	33	−33	66
4-21G	−132.775409	132.774694	−265.550103	32	−30	63
6-21G	−132.903865	132.990267	−265.894132	32	−28	61
3-21G*	−132.380162	131.954477	−264.334638	26	−11	37
4-21G*	−132.827356	132.718805	−265.546161	25	−13	38
6-21G*	−132.955071	132.946404	−265.901475	25	−15	40
3-21G**	−132.404789	131.858017	−264.262806	27	−9	36
4-21G**	−132.849484	132.644363	−265.493847	26	−13	40
6-21G**	−132.976248	132.900359	−265.876606	26	−17	43
4-31G	−132.875211	133.031032	−265.906243	35	−31	65
6-31G	−133.015746	133.156180	−266.171926	35	−27	62
4-31G*	−132.930283	132.025368	−264.955651	26	−6	32
6-31G*	−133.061699	132.901443	−265.963142	25	−6	31
4-31G**	−132.944430	132.040734	−264.985164	26	−6	32
6-31G**	−133.074921	132.912700	−265.987621	26	−7	33
6-311G	−133.044367	133.176830	−266.221197	33	−29	62
6-311G*	−133.091500	133.151130	−266.242630	26	−19	45
6-311G**	−133.103747	133.114557	−266.218304	26	−25	51

a) In terms of au. b) kJ mol^{-1}.

Table 5. Total, Kinetic, and Potential Energies in Nitroethene

	E[a]	T[a]	V[a]	ΔE[b]	ΔT[b]	ΔV[b]
STO-3G	−277.781977	275.262008	−553.043984	20	−78	98
STO-4G	−279.784071	278.582771	−558.366843	20	−84	104
STO-5G	−280.313391	279.764341	−560.077732	20	−85	105
STO-6G	−280.475786	280.177739	−560.653525	20	−87	106
3-21G	−279.889056	279.275682	−559.164738	41	3	38
4-21G	−280.811462	280.832774	−561.644236	40	5	35
6-21G	−281.075628	281.294010	−562.369639	40	10	30
3-21G*	−280.070296	279.283942	−559.354238	37	−31	67
4-21G*	−280.984154	280.825887	−561.810042	36	−16	52
6-21G*	−281.245313	281.286143	−562.531456	36	−3	39
3-21G**	−280.082650	279.203616	−559.286266	37	−25	62
4-21G**	−280.994616	280.763170	−561.757785	36	−13	49
6-21G**	−281.255073	281.243522	−562.498595	36	0	36
4-31G	−281.064416	281.333970	−562.398386	34	−37	71
6-31G	−281.356993	281.575193	−562.932185	34	−46	80
4-31G*	−281.232693	279.302221	−560.534914	31	3	28
6-31G*	−281.504092	280.949691	−562.453784	30	−14	45
4-31G**	−281.238623	279.306407	−560.545030	31	5	25
6-31G**	−281.509570	280.951409	−562.460979	30	−12	43
6-311G	−281.435442	281.644113	−563.079554	34	−17	51
6-311G*[c]						
6-311C**	−281.578367	281.659111	−563.237477	30	−10	40

a) In terms of au. b) kJ mol^{-1}. c) Optimized structure was not obtained because of SCF difficulty.

Table 6. Deviation of Energy Components by Incomplete Geometry Optimization (4-31G)

R	r_0(1.4216A)	$r_0-0.0001$	$r_0-0.0002$	$r_0-0.0003$	$r_0-0.0004$
$-\partial E/\partial R$[a)]	0.00000	0.00014	0.00023	0.00031	0.00039
ΔE[b)]	34.45	34.45	34.45	34.46	34.46
ΔT[b)]	−30.56	−28.30	−27.66	−27.01	−26.37
ΔV[b)]	65.02	62.75	62.11	61.47	60.83
$(\Delta E+\Delta T)/\Delta E$	0.11	0.18	0.20	0.22	0.23

a) au/Bohr. b) kJ mol^{-1}.

Table 7. Deviation of Total Energy and Its Components by SCF Threshold (4-31G)

Threshold[a)]	10^{-10}	10^{-7}	10^{-6}	10^{-5}	10^{-4}	10^{-3}
E[b)]	−132.875211	−132.875211	−132.875211	−132.875211	−132.875211	−132.875074
T[b)]	133.031438	133.031441	133.031462	133.031690	133.031002	133.015878
V[b)]	−265.906649	−265.906652	−265.906673	−265.906900	−265.906213	−265.890952

a) Threshold at the density matrix, P_{rs}. b) In terms of au.

the scaling factor applies to the electronic coordinates as well as to the nuclear coordinates, the error of energy components can be grouped into two: the error due to electronic coordinates and that due to nuclear coordinates. The former may be improved by adopting a large basis set which allows a shrinking or expansion of the electronic distribution. The latter may be largely affected by the threshold of geometry optimization.

Table 6 shows how the energy-components are affected by the condition of geometry optimization. As an example, we investigated the case when the orthogonal structure of vinylamine is not properly optimized: namely, the energy difference between the optimized planar structure and the orthogonal structures in which the C-N bond is intentionally shifted from the equilibrium distance (r_0). A decrease of 0.0001A from r_0 makes no difference regarding the total energy. However, the differences of the kinetic or potential energy amount to 2.3 kJ mol^{-1} and the relative virial error increases from 0.11 to 0.18. The force at this point is 0.00014 Hartree/Bohr. Judging from this result, a threshold less than 0.0001 Hartree/Bohr may be absolutely necessary. However, a far more severe optimization than that consumes a large amount of computation time and is likely to go into oscillation. Therefore, a threshold of 0.000075 Hartree/Bohr, which is adopted in the present study, may be a practical compromise.

(b) Concerning the SCF Convergence. As already mentioned, an incomplete convergence of the density matrix, P_{rs}, may create errors in the energy components. Table 7 shows the relationship between the threshold of SCF convergence and the total energy and its components.

The total energy is not very sensitive until a threshold of 10^{-3} at the density matrix. However, the components are susceptible enough, even at 10^{-6} (The deviation from the threshold of 10^{-10} is 0.1 kJ mol^{-1}). Therefore, at least a threshold of 10^{-7} may be desirable.

Concluding Remarks

In the first paper of this series,[23)] we discussed the dependency of the electron density, the kinetic energy, and the potential energy of an atom on the adopted basis set. It was shown that the polarization functions must be added to atoms of the first row and the hydrogen atom in order to obtain well-balanced wave functions. The STO-*N*G method was also shown to give well-balanced wave functions. However, Fig. 1 shows that STO-*N*G gives a large amount of casual error, up to 500%. This error can be dramatically improved by using a split-valence method. This may be because in a split-valence method, the wave function has more spacial freedom for expansion or shrinking than that in the single zeta method, like STO-*N*G. The 4-31G and 6-31G methods resulted in a small amount of error, but the inclusion of polarization functions does not always improve the amount of error. This strongly suggests that the error in the split-valence method is caused by incomplete geometry optimization, rather than an incomplete basis set.

As we stated in the introduction, it may be worth investigating which energy, T or V, plays the major role in chemical phenomena. For such a purpose, we only need qualitative ΔT and ΔV, and any split-valence method seems to be eligible to be adopted. However, care must be taken regarding the calculated energy components, as always, in any kind of MO theoretical calculation.

References

1) Part I: Ref. 23.
2) K. Ruedenberg, *Rev. Mod. Phys.*, **34**, 326 (1962).
3) M. J. Feinberg and K. Ruedenberg, *J. Chem. Phys.*, **54**, 1495 (1971).
4) M. J. Feinberg, K. Ruedenberg, and E. L. Mehler, *Adv. Quantum Chem.*, **5**, 27 (1970).
5) M. Born and J. R. Oppenheimer, *Ann. Physik*, **84**, 457 (1927).

6) R. Poirier, R. Kari, and I. G. Csizmadia, "Handbook of Gaussian Basis Sets," Elsevier, Amsterdam (1985).

7) L. Pedersen and K. Morokuma, *J. Chem. Phys.*, **46**, 3941 (1967).

8) D. E. Magnoli and J. R. Murdoch, *Int. J. Quantum Chem.*, **22**, 1249 (1982).

9) We have used the GAUSSIAN-80H program (a Hitac version of GAUSSIAN-80 program (QCPE 437, 1982)) at the Computer Center of the University of Tokyo.

10) a) STO-3G basis set: J. B. Collins, P. v. R. Schleyer, J. S. Binkley, and J. A. Pople, *J. Chem. Phys.*, **64**, 5142 (1976); b) STO-4G basis set: W. J. Hehre, R. F. Stewart, and J. A. Pople, *ibid.*, **51**, 2657 (1969); c) 3-21G and 6-21G basis sets: J. S. Binkley, J. A. Pople, and W. J. Hehre, *J. Am. Chem. Soc.*, **102**, 939 (1980); M. S. Gordon, J. S. Binkley, J. A. Pople, W. J. Pietro, and W. J. Hehre, *ibid.*, **104**, 2797 (1982); d) 4-21G basis set: P. Pulay, G. Fogarasi, F. Pang, and J. E. Boggs, *ibid.*, **101**, 2550 (1979); e) 3-21* basis set: W. J. Pietro, M. M. Francl, W. J. Hehre, D. J. DeFrees, J. A. Pople, and J. S. Binkley, *J. Am. Chem. Soc.*, **104**, 5039 (1982); f) 4-31G basis set: R. Ditchfield, W. J. Hehre, and J. A. Pople, *J. Chem. Phys.*, **54**, 724 (1971); W. J. Hehre and J. A. Pople, *ibid.*, **56**, 4233 (1972); J. D. Dill and J. A. Pople, *ibid.*, **62**, 2921 (1975); g) 6-31G basis set: W. J. Hehre, R. Ditchfield, and J. A. Pople, *ibid.*, **56**, 2257 (1972); J. S. Binkley and J. A. Pople, *ibid.*, **66**, 879 (1977); J. D. Dill and J. A. Pople, *ibid.*, **62**, 2921 (1975); h) 6-31* and 6-31** basis sets: P. C. Hariharan and J. A. Pople, *Theor. Chim. Acta*, **28**, 213 (1973); J. D. Dill and J. A. Pople, *J. Chem. Phys.*, **62**, 2921 (1975); i) 6-311G and 6-311G** basis sets: R. Krishnan, J. S. Binkley, R. Seeger, and J. A. Pople, *ibid.*, **72**, 650 (1980); The GAUSSIAN-80 program includes other basis sets, whose exponents and contranction coefficients are listed in Ref. 6.

11) a) H. Kollmar, *Theor. Chim. Acta*, **50**, 235 (1978); b) H. Ichikawa and Y. Ebisawa, *J. Am. Chem. Soc.*, **107**, 1161 (1985).

12) B. J. Nelander, *J. Chem. Phys.*, **51**, 469 (1969).

13) S. Weiss and G. E. Leroi, *J. Chem. Phys.*, **48**, 962 (1968).

14) a) T. Itoh, *J. Phys. Soc. Jpn.*, **11**, 264 (1956). b) D. R. Lide, Jr., *J. Chem. Phys.*, **27**, 343 (1957).

15) L. A. Carreira, *J. Chem. Phys.*, **62**, 3851 (1975).

16) J. R. Durig, W. E. Bucy, and A. R. H. Cole, *Can. J. Phys.*, **53**, 1832 (1975).

17) M. E. Squillacote, R. S. Sheridan, O. L. Chapman, and F. A. L. Anet, *J. Am. Chem. Soc.*, **101**, 3657 (1979).

18) Eg. A. G. Cook, "Enamines, Synthesis, Structure, and Reactions," Marcel Dekker, New York (1969).

19) R. A. Eades, D. A. Weil, M. R. Ellenberger, W. E. Farneth, D. A. Dixon, and C. H. Douglass, Jr., *J. Am. Chem. Soc.*, **103**, 5372 (1981).

20) a) A. L. McClellan, "Table of Experimental Dipole Moments," W. H. Freeman, San Francisco (1963); b) B. Starck, "Landolt-Börnstein Tables," New Series, Springer-Verlag, New York (1967).

21) R. Meyer, A. Gammeter, P. Smith, H. Kühne, P. Nösberger, and Hs. Günthard, *J. Mol. Spectrosc.*, **46**, 397 (1973).

22) A similar discussion has been presented by Magnoli and Murdoch (Ref. 8).

23) H. Ichikawa, K. Sameshima, and Y. Ebisawa, *Bull. Chem. Soc. Jpn.*, **59**, 2729 (1986).

 © 1988 The Chemical Society of Japan Bull. Chem. Soc. Jpn., 61, 1845—1851 (1988)

The Electrocapillary Curves of the Phosphatidylcholine Monolayer at the Polarized Oil-Water Interface. I. Measurement of Interfacial Tension Using a Computer-Aided Pendant-Drop Method

Takashi KAKIUCHI, Masatoshi NAKANISHI, and Mitsugi SENDA*
Department of Agricultural Chemistry, Faculty of Agriculture, Kyoto University, Sakyo-ku, Kyoto 606
(Received October 19,1987)

The conditions for obtaining the electrocapillary curves of the dilauroylphosphatidylcholine (DLPC) monolayer formed at the polarized nitrobenzene-water interface have been studied using the pendant drop method. To facilitate the measurement, the system for the interfacial tension measurement, including the computer software for the data handling, has been developed based on digital image processing of the video image of a pendant drop. The 95% confidence interval of the measured interfacial tension value was ± 0.06 mN m^{-1}. The time required to measure an electrocapillary curve with 30 points was 30 min, while the time necessary to convert the image data to the interfacial tension was 1 min. The potential drop across the monolayer has been demonstrated to influence the stability of the monolayer strongly. The DLPC markedly lowered the interfacial tension by forming a stable monolayer when the interface was polarized so that the aqueous phase has a negative potential with respect to the nitrobenzene phase. On the other hand, when the aqueous phase became positively polarized, the adsorbed DLPC molecules started to desorb from the interface, giving rise to the disruption of the monolayer. The electrocapillary curves only in the former potential range were found to be thermodynamically meaningful.

The structure of the electrical double layer in the vicinity of the surface of lipid bilayers, monolayers, and biological membranes is important in understanding various surface phenomena associated with the biological as well as biomimetic membranes and, in general, with oil-water interfaces. The electrically polarizable oil-water interface is a useful means to study the electrical phenomena at the oil-water interface, in that the potential drop across the interface is accurately controlled externally.[1] This type of system has been used successfully to elucidate the double layer structure of ionic surfactant monolayers at oil-water interfaces,[2,3] aside from a wide range of applications to analytical chemistry and the electrochemistry of ion-transfer reactions.[4] If one introduces phospholipids to this type of interface, one may expect to be able to study in detail the interfacial and electrochemical properties of the phospholipid monolayer which are not readily accessible by other methods, e.g., the properties of the electrical double layer and the kinetics of ion-transfer reaction across the monolayer, by using the estahlished method of the analysis of the electrocapillary and electrochemical data.[4,5] Along this line, several groups have reported on the electrochemical characteristics of the phospholipid monolayers at the polarized oil-water interface: a retardation of the ion-transfer reaction from water to oil,[6,7] the differential capacitance of the phospholipid monolayers at the nitrobenzene-water interface[8] and at the dichloroethane-water interface,[9] and the electrocapillarity measurements at the dichloroethane-water interface in the presence of a phospholipid monolayer.[10] To analyse the double layer structure, the basic properties of the monolayer, e.g., the potential of zero charge and the excess charge density, must be evaluated. These quantities can be obtained by measuring the electrocapillary curve of the interface. Since phospholipids are highly surface active, the very dilute concentration of the μmol dm^{-3} order is enough to make up a saturated monolayer at the interface.[8] Such a low concentration of phospholipid requires a long time to reach the adsorption equilibrium. Accordingly, to obtain a thermodynamically meaningful electrocapillary curve, a method that is capable of measuring the equilibrium value of interfacial tension is desirable. For this purpose, the pendant-drop method and the sessil-drop method are the most suitable. Girault and Schiffrin have recently developed a new pendant-drop method by applying a video-image digitizer.[11] They later improved this method by introducing a video-image digitizer with a higher resolution specifically designed for the electrocapillary measurements.[10] In this study, we wish to report a similar apparatus also based on the video-image digitizing technique but with a higher accuracy and faster data handling using a commercially available video image digitizer in combination with computers. By using this new apparatus, the conditions for obtaining the equilibrium electrocapillary curve of the phosphatidylcholine monolayer at the polarized nitrobenzene-water interface have been studied.

Experimental

Reagents. Reagent-grade nitrobenzene was distilied and purified as has been described elsewhere.[1] The nitrobenzene and the nitrobenzene solution were equilibrated with water or an aqueous solution of lithium chloride at 25.0 °C overnight to ensure mutual saturation. Aqueous solutions of lithium chloride and tetrapentylammonium chloride (TPnACl), and a nitrobenzene solution of tetrapentylammonium tetraphenylborate (TPnATPB) were prepared as has been described elsewhere.[13] Reagent grade dichloro-

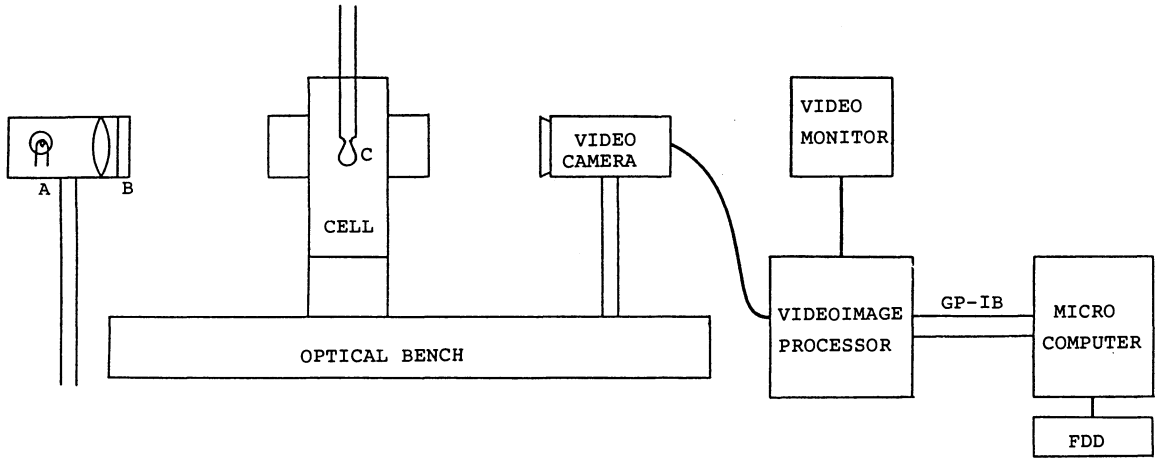

Fig. 1. Block diagram of the apparatus for interfacial tension measurement applying video image processing technique to the pendant drop method. (A) Light source, (B) filter, (C) pendant drop.

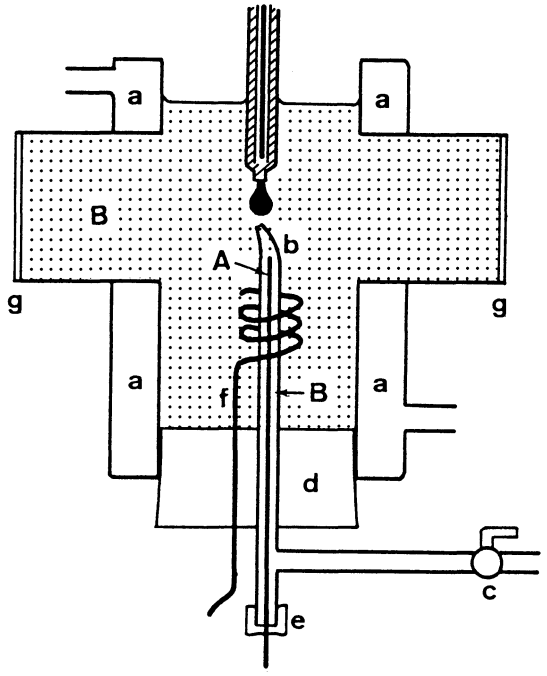

Fig. 2a. Diagram of the cell for the measurement with Configuration I. (a) Water jacket, (b) Luggin capillary, (c) stop cock, (d) silicone rubber stopper, (e) silicone rubber cap, (f) Pt electrode, (g) optically flat Pyrex glass, (A) Ag/AgCl electrode, (B) aqueous solution.

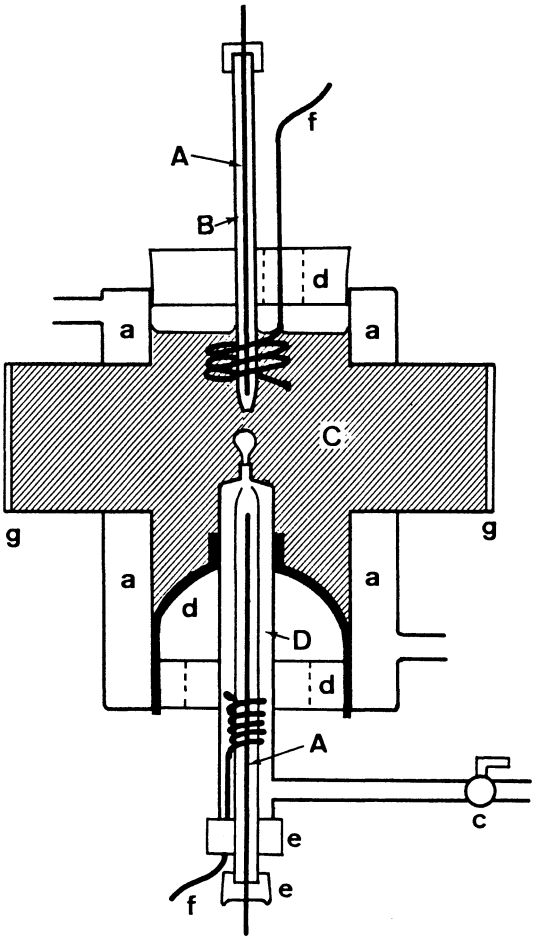

Fig. 2b. Diagram of the cell for the measurement with Configuration II. (a)—(g) and (A) are same to Fig. 2a. (B) Aqueous TPnACl solution, (C) nitrobenzene solution, (D) LiCl aqueous solution.

methane (DCM) and 1,2-dichloroethane (DCE) were purified as follows.[14] These solvents were washed three times with 10% $NaHCO_3$ to remove the HCl. The solvents were then washed with water. After they had then been dried with $CaCl_2$, the solvents were distilled. The fractions of bp 39 °C (DCM) and 83.5 °C (DCE) were collected and stored in the dark. These solvents were equilibrated with water at 25 °C overnight before use in the interfacial-tension measurements. The water used to prepare aqueous solutions for the interfacial tension measurements was first distilled and then redistilled in the presence of potassium permanganate after having been passed through ion-exchange resin and the Organic Removal Filter (Barnstead). The L-α-dilauroylphosphatidylcholine, DLPC, (Sigma) was dissolved in a 3 : 2 toluene-chloroform solution and then stored in a refrigerator until use. All the other chemicals were of a reagent grade.

Interfacial Tension Measurements. The block diagram

of the apparatus used for the interfacial tension measuremts is shown in Fig. 1. A glass cell and a video camera were set on an optical bench (Sigma Koki Co. Σ-06-(3)) 80 cm long and supported by two legs (Σ-02 and Σ-03) on rubber dampers. The cell (Fig. 2) had two windows consisting of optically flat borosilicate glass disks 3 cm in diameter (Fig. 2g), and it was installed in a cell holder mounted on a coarse-fine rotation stage (Σ-401-(2)). Two scale-etched Plexiglas plates mounted on a carrier beneath the rotation stage so that the two plates were parallel with the axis of the optical bench and sandwiched the glass cell were used to locate the position of an object in the cell. Two types of cell configurations were used in the measurement. In Configuration I, the cell (Fig. 2) was filled with an aqueous solution. In Fig. 2a, A is a platinum wire which served as an auxiliary electrode, while b is a reference electrode of a Luggin-capillary type in which an aqueous LiCl solution and an Ag/AgCl electrode were incorporated. A glass tube (Fig. 3) filled with a nitrobenzene solution was inserted into the solution in the cell. In Fig. 3, e and h are the platinum wire and the Luggin capillary used as the counter electrode and the reference electrode respectively in the nitrobenzene phase. The tip of this glass tube (i in Fig. 3) has an outer diameter of 2 mm and an inner diameter of 1 mm. This glass tube was mounted on a tip holder set on an assembly of a X,Y tilt stage (Σ-501), a X,Y precision translation stage (Σ-206), and a rack-pinion type X-block (Narisige, M-6). In Configuration II, a nitrobenzene solution was placed in the cell. In this case, a drop of the aqueous solution was formed in the nitrobenzene solution from the tip of the glass tube (Fig. 2b). The tip for this configuration was made of poly(tetrafluoroethylene) tubing 1 mm in outer diameter and 0.5 mm in inner diameter. Below, the interfacial tension was measured in Configuration I unless otherwise stated. The video camera, a CCD type with a picture element of 381(h)×492(v) (Tokyo Electronic Industry Co., CS3300), was secured with a lens holder (Σ-41-(3)) mounted on a set of a X,Y tilt stage (Σ-501) and a coarse-fine rotation stage (Σ-401-(2)). The television lens (Asahi Precision Co., Cosmicar 50 mm F1.4) was mounted on the CCD camera with an extension tube (Cosmicar, 40 mm). The standard tungsten bulb light source unit (Nikon) with a filter (GIF, Nikon) and a diffuse light mat was used to obtain the green diffuse light, which was shed into the flat window of the glass cell. The video signal from the camera was digitized by means of a video-image processor (Nippon Avionics Co., Image Mate) to 640(h)×482(v) pixels, each of which had 256 gray levels. The conversion can be made every 1/30 s. This image processor was controlled by a micro-computer (Fujitsu Co., FM-11AD2) through the GP-IB interface.

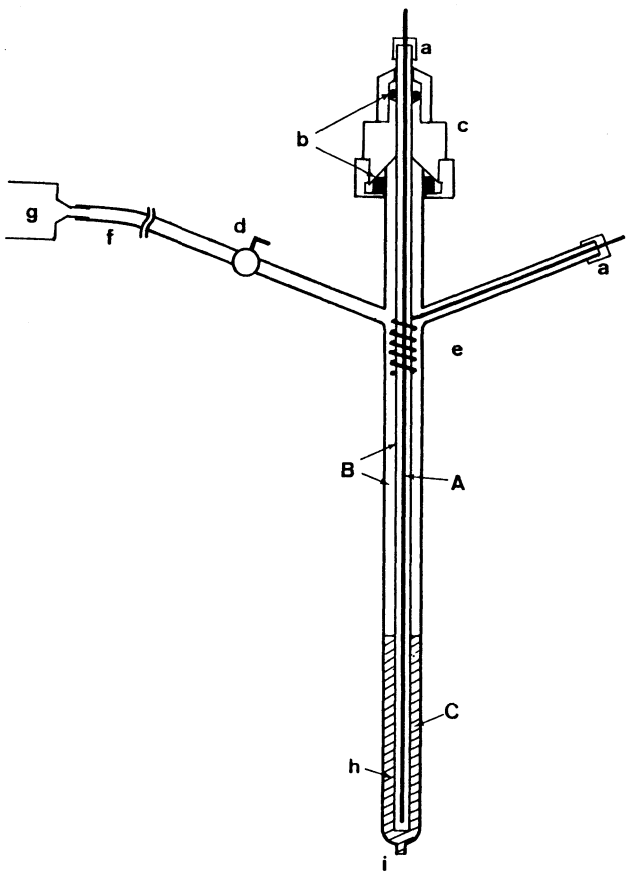

Fig. 3. Diagram of an upper part of the cell for Configuration I. (a) Silicone rubber cap, (b) O-ring, (c) connector, (d) stop cock, (e) Pt electrode, (f) silicone rubber tubing, (g) gas tight syringe, (h) luggin capillary, (i) tip to form a pendant drop, (A) Ag/AgCl electrode, (B) aqueous TPnACl solution, (C) nitrobenzene solution.

Alignment of the Video Camera: First, the rotation angle of the camera was adjusted so that the image of a vertically hanging string was seen horizontally on the screen of a monitor TV (Tokyo Eletronic Industry Co., 9M10A). Then, the position of the focal plane was found as follows. A micrometer with a mesh of 0.5 mm/div. (Kyoto Kogaku) was hung over from the glass tube holder into the position where the glass cell was otherwise located. The position and the angle of the micrometer were adjusted so that the plane of the micrometer was vertical to the axis of the optical bench, which the light beam was introduced in parallel with. The X,Y stage under the glass tube holder was adjusted to bring the micrometer to the focal plane. A high-precision steel ball 5.000±0.001 mm in diameter was hung from the glass tube holder into the focal plane. The number of pixels in the digitized image corresponding to the diameter of the ball in horizontal direction (a pixels) was recorded. The angle of the camera in the vertical direction was adjusted similarly using the micrometer. The number of pixels corresponding to the diameter of the steel ball was again recorded (b pixels). The angle of the camera was adjusted so that the plane of the CCD sensor in the camera was normal to the axis of the optical bench. The micrometer was hung into the position of the focal plane. The camera was turned, step by step, by rotating the rotation stage, and the number of pixels corresponding to the horizontal interval of the micrometer mesh was recorded. The position where the number of pixels was greatest, L_{max}, was found by plotting the number of bits against the rotation angle. The angle of the elevation of the camera was adjusted using the X,Y tilt stage, so that the $L_{max}a/b$ quantity was at its maximum.

Determination of the Conversion Factor and Correction of Distortion: To obtain the coordinates of the edge of the pendant drop from the digitized image, the relation between the true value of the coordinate and its corresponding value in the digitized image was determined by measuring an object having a known shape and dimensions. The possible distortion of the image was corrected by using the microme-

ter described above and a standard image processing technique. As was to be expected from the advantage of a CCD type video camera free from bulge distortion, the distortion of a video image was found to be negligibly small. The vertical and horizontal size factors of the measuring system were determined by measuring the size of a steel ball immersed in the cell (Fig. 2a) filled with 0.05 mol dm^{-3} LiCl.

Measurement of the Shape of a Pendant Drop: The drop was formed at the tip, after the glass tube had been brought to the position of the focal plane. To detect the edge of the drop, the change in the gray level was checked against the transverse distance across the drop image (Fig. 4). The gradient of this plot exhibited maxima at either two (Fig. 4) or four points. The gray level —at these two points in the former case and at the outer two points in the latter case— were used as the threshold level of the thresholding procedure.

Data-Processing: The thresholded data were transferred to the microcomputer through GP-IB and then compressed to generate run-length data before the data storage. The overall data acquisition and transfer required 30 s for 1 image data. The data were further processed by a computer (Fujitsu, FACOM M382) in the Kyoto University Data Processing Center. After the noises on the margin of a plane of the image and those due to dust stuck on the cell surfaces had been removed by a software technique, the coordinate for the circumference of the drop was extracted. The position of the apex was found, assuming that the drop had an axial symmetry.

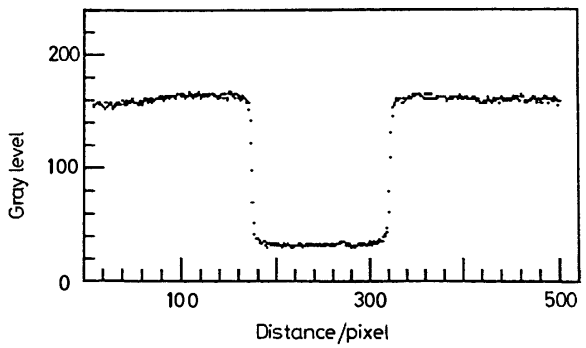

Fig. 4. Change of the gray level on the transverse distance across the drop.

Calculation of Interfacial Tension from the Drop Shape: The theoretical curve was obtained by solving numerically the Bashforth-Adams equation[15] in the following form:

$$\frac{d\theta}{ds} = 2 - \frac{\sin\theta}{x} + \beta y$$

$$\frac{dx}{ds} = \cos\theta$$

$$\frac{dy}{ds} = \sin\theta$$

for the initial conditions, $dx/ds=1$, $dy/ds=0$, and $d\theta/ds=1$ when $s=0$, where

$$\beta = -\frac{\Delta\rho g b^2}{\gamma}$$

In these equations, $x=X/b$, $y=Y/b$, and $s=S/b$. X and Y represent the Cartesian coordinate of a point P on the edge of the drop, S is the distance from the apex to P along the circumference of the drop, and b is the radius of the curvature at the apex. The origin of the coordinate was taken as the apex. θ is the angle between a tangent to the surface at P and the horizontal, $\Delta\rho$ is the density difference, g is the acceleration of gravity, and γ is the interfacial tension. An initial value for b was found from the curvature around the apex obtained by fitting the experimental points around the apex to a third-order polynomial. An initial value for β was set equal to -0.5. The calculated curve obtained using the Runge-Kutta method was fitted into the experimental curve based on the least square principle using the SALS (FORTRAN subroutine for regression analysis).[16] Since the drop shape had an axial symmetry, half of the experimental points were used for the regression

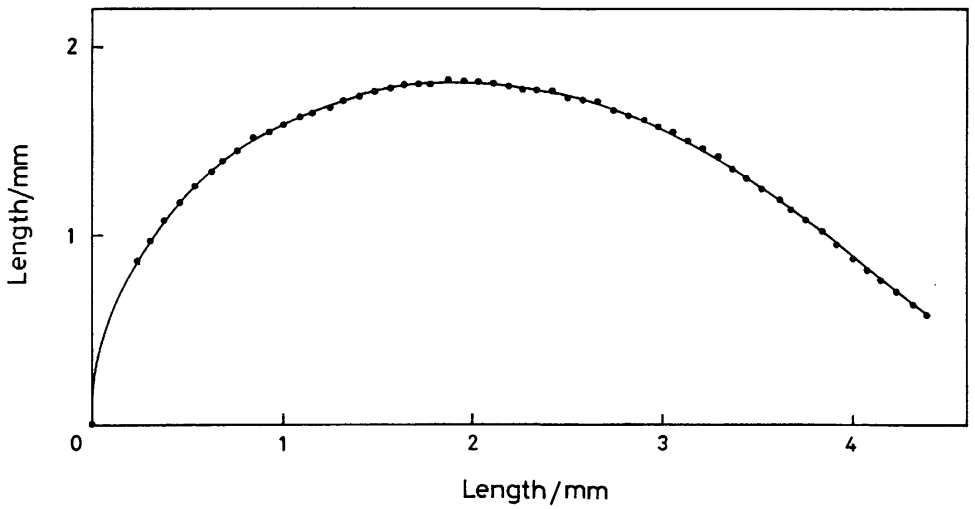

Fig. 5. An example of the result of the least square curve fitting of the numerical solution of the Bashforth-Adams equation to the experimental data; (—●—), experimental; (——), regression curve. The data is for the nitrobenzene-water interface at 25 °C.

Table 1. Values of Interfacial Tension for the 1,2-Dichloroethane-Water, Dichloromethane-Water, and Nitrobenzene-Water Interfaces at 25 °C

Interface	Interfacial tension/mN m^{-1}	
	Present method	Literature data
1,2-Dichloroethane/water	27.93±0.09[a]	28.33[b] (0.19)[d]
Dichloromethane/water	27.93±0.03[a]	28.06[b] (0.22)[d] 28.0[c]
Nitrobenzene/water	25.20±0.07[a]	25.20[c]

a) 95% confidence interval. b) Ref. 10. c) Ref. 18. d) Standard deviation.

Table 2. Comparison of Two Computational Methods for Obtaining an Interfacial Tension Value from a Pendant Drop Image

Method	Interfacial tension[a]
	mN m^{-1}
Curve fitting method	25.34±0.15[b]
Selected plane method	25.03±0.99[b]

a) Interface between a nitrobenzene solution of 0.1 mol dm^{-3} TBATPB and an aqueous solution of 0.05 mol dm^{-3} LiCl at E^{W}_{O+}=0.310 V. b) 95% confidence interval.

analysis. In the calculation with SALS, the Marquardt method and the biweight method were employed for the non-linear regression and the adjustment of the weight attached to each point respectively.[16] The cpu time required to evaluate an interfacial tension value from the run length data for each drop comprised of 250 points for half of the drop image was typically 2 s. Figure 5 shows an example of the curve fitting by the nonlinear regression analysis. The software for the control of the video-image processor and the data processing was written in Basic09 and the machine language on the operating system OS-9.[17] FORTRAN77 was used for data processing on FACOM M-382.

Control of the Pointial Differences. The potential drop across the interface was controlled with a laboratory-made four-electrode potentiostat similar to the type in Ref. 18. The solution resistance was compensated for by using a positive feedback method.[18]

All the measurements were made at 25.00±0.05 °C. The density of the solutions was measured as has been described elsewhere.[1]

Results and Discussion

The Interfacial Tension Measurement for the Pure Organic Solvent-Water Interface. First, the interfacial tensions between water and pure organic solvents were measured. The interfacial tensions for the DCE-water, DCM-water, and nitrobenzene-water interfaces at 25 °C are given in Table 1, with a 95% confidence interval. In general, the present results are in excellent agreement with the literature data given in the second column of Table 1. The 95% confidence interval of the present method is 0.06 on the average, and the precision is better than those obtained by Girault et al.[12] although their video image digitizer had a higher resolution, 1066(h)×575(v). The difference is probably to be ascribed to the method of calculating the interfacial tension from the drop image. They employed the inflection plane method[12] to minimize the computational time. The precision of this method[12] depends greatly on how accurately the point of inflection is determined. The curvature change is not always large enough to determine this point with a high accuracy, even when the curve-fitting technique with a higher polynomial is used. Moreover, the requirement that the inflection point be on the drop shape limits the applicability of this method. The advantage of the direct regression of the data to the Bashforth-Adams equation, which does not require the presence of the inflexion point, seems obvious. This method was first utilized by Girault et al.[11] for the pendant drop data with less resolution.

We have also compared the present method of data-analysis with the selected-plane method, which has been commonly used as a convenient method for calculating the interfacial tension from a drop shape.[19] A comparison of the two methods for the same data is given in Table 2. This table indicates that the selected-plane method gives a comparable interfacial tension value, but with a confidence interval 6 times wider. This result is expected, for the selected-plane method makes use of only a few out of the many experimentally obtained points in the calculation.

Electrocapillary Measurements. Electrocapillary curves in the absence of phospholipid adsorption were first recorded at intervals of 20 mV between 0.1 V and 0.5 V for the system represented by the cell:

I	II	III	IV	V	VI	VII
Ag	AgCl	0.02 M† TPnACl (W)	0.1 M TPnATPB (NB)	0.05M LiCl (W)	AgCl	Ag (I)

The interface between Phases IV and V is the polarized nitrobenzene-water interface. The potential of the right-hand-side of Cell(I) with respect to the left is denoted as E^{W-}_{O+}, where the super- and subscripts indicate that the reference electrodes in the aqueous and nitrobenzene phases are reversible to the anion (Cl^-) and the cation ($TPnA^+$) respectively. The nitrobenzene phase contained a 10% 3:2 toluene-chloroform mixture. The results for the triplicate measurements are shown in Fig. 6 (Curve A), with error bars for standard deviations. The average standard deviation of the interfacial tension was 0.25 mN m^{-1}, larger than the deviation for the pure solvents (Table 1) because of the fluctuation of the potential in the electrocapillarity measurements.

† 1 M=1 mol dm^{-3}.

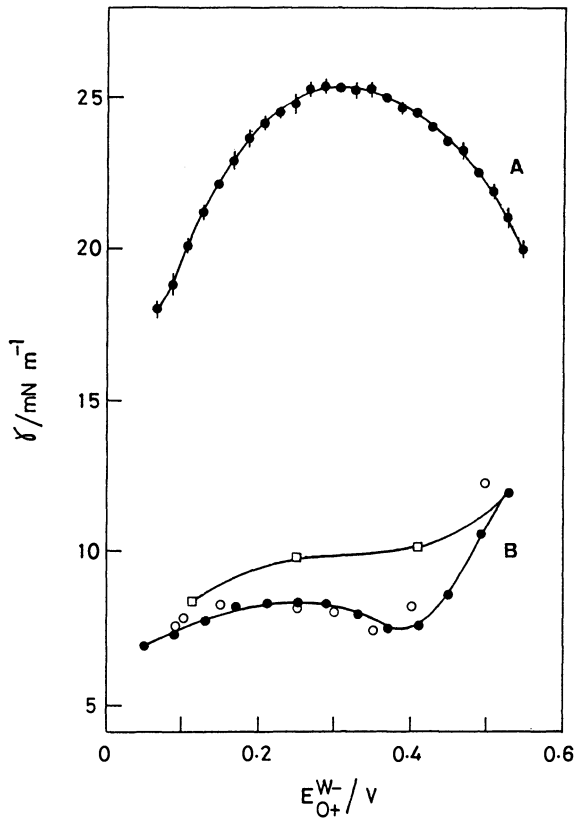

Fig. 6. (A) Electrocapillary curve for the interface between 0.1 mol dm^{-3} TPnATPB and 0.05 mol dm^{-3} LiCl at 25 °C. 20 μmol dm^{-3} DLPC and 0.05 mol dm^{-3} LiCl at 25 °C (—●—). (B) After the adsorption equilibrium was established under open circuit condition, the potential was first scanned from 0.05 to 0.5 V (—●—) and then reversed (—□—). These data are compared with the data obtained through the plot method (—○—).

The electrocapillary curves in the presence of the DLPC monolayer were measured in order to obtain the basic properties of the electrocapillarity of the phospholipid monolayers at the polarized nitrobenzene-water interface. For this measurement, Configuration II of the cell was used to ascertain that the amount of DLPC molecules in the bulk was enough to make up a monolayer at the interface. DLPC was dissolved in the nitrobenzene phase, which contained a 10% 3:2 toluene-chloroform mixture, to facilitate the dissolution of DLPC. The time variation in the interfacial tension was followed after the drop had been squeezed out of the tip at a constant potential. At least one hour was needed for the establishment of adsorption equilibrium, when the concentration of DLPC in the nitrobenzene phase, c_{DLPC}, was 1 μmol dm^{-3}. In the following measurements, the interfacial tension was measured 2 h after the formation of the interface.

The lower curve in Fig. 6 shows the electrocapillary curve recorded at c_{DLPC}=20 μmol dm^{-3} in Cell(I) after the DLPC had been allowed to adsorb 2 h in the open circuit. From the differential capacitance measurements of the same system, the saturated monolayer of DLPC, whose density at the interface was 0.75 nm^2 per DLPC molecule, was found to be formed at this concentration.[8] The measurement was first made at intervals of 40 mV by changing the potential from 0.05 V to 0.55 V (—●— in Curve B in Fig. 6). The interfacial tension was greatly suppressed by the strong adsorption of DLPC. The electrocapillary curve showed a convex shape between E^{W-}_{O+}=0.05 and 0.35 V. Beyond E^{W-}_{O+}=0.35 V, the interfacial tension abruptly increased with the increase in the potential. When the potential was reversed from the positive extreme of the potential to sweep in the negative direction, the interfacial tension gave a much higher value (—□— in Fig. 6) as compared with the value obtained initially at the same E^{W-}_{O+} value. This hysteresis probably reflects the slow diffusion process of DLPC and substantiates the desorption of the DLPC molecules from the interface in the positive extreme range of the potential. The concomitant increase in the differential capacitance in this potential region has also been observed.[8] When the potential was reversed at a potential less than 0.35 V, no such hysteresis was observed.

To check if the applied potential during the monolayer formation influences the properties of the monolayer after the adsorption equilibrium had been established, the monolayer was formed while the applied potential was kept at a constant value during the formation of the monolayer: the plot method. The open circles in Fig. 6 were recorded after the interface had been kept at a given value of E^{W-}_{O+} during the course of adsorption. The agreement of the results in Fig. 6 obtained from the two methods suggests that the electrical potential difference across the interface does not introduce any significant difference to the monolayer formed eventually at the interface, provided that the potential is less than 0.35 V, Region I. The discrepancy between the values obtained by the two methods in the potential range positive to E^{W-}_{O+}=0.35 V, Region II, indicates the slow processes associated with the desorption of DLPC molecules and possibly their reorientation within the monolayer. Correspondingly, the interfacial tension values obtained in Region I were reproducible, whereas the values in Region II were much less reproducible. At this positive extreme of the potential, fine, small, emulsion-like particles were sometimes observed coming spontaneously out of the tip. This is another piece of evidence of complicated non-equilibrium processes occurring in this potential range. Thus, only the data in Region I seem to be thermodynamically meaningful.

Figure 6 shows that the electrocapillary maximum, i.e., the potential of the zero charge was shifted by 100 mV to the negative direction accompanied by the formation of the saturated DLPC monolayer (Curve B). The reduced curvature of Curve B in Fig. 6 compared with the curve without the DLPC monolayer (Curve A in Fig. 6) suggests a decrease in the surface charge

density caused by the DLPC adsorption at a given value of the potential drop across the interface. The curvature, i.e., the second derivative of the interfacial tension with respect to E_{O+}^{W-} in Region I, gave the capacitance value of 11.5 $\mu F\ cm^{-2}$ for the DLPC monolayer. This is in accord with the value of 11 $\mu F\,cm^{-2}$ obtained from the differential capacitance measurements[8] for the same monolayer. This agreement confirms the thermodynamic consistency[1] of the two results in Region I. An electrocapillary curve similar to the curve in Fig. 6 has been obtained by Girault and Schiffrin[10] for an egg-yolk phosphatidylcholine monolayer at the DCE-water interface. They interpreted the positive slope in Region II (Region B in Ref. 10) as showing the positive excess charge density on the aqueous solution side, originating from the positively charged head group of adsorbed phosphatidylcholine molecules due to the protonation of the phosphate group of the phosphatidylcholine. However, the present results indicate that it is difficult to endow the electrocapillary curve in this region with any definite thermodynamic meaning. For the same reason, it is doubtful if we can estimate the surface charge density from the differential capacitance vs. the potential curve in the presence of phosphatidylcholine adsorption by the back-integration of the curve from the far positive potential in Region II, as was claimed by Wandlowski et. al.[9] for the dipalmitoylphosphatidylcholine adsorption at the DCE-water interface. The subsequent paper will treat the electrocapillary curves at different concentrations of DLPC in an attempt to analyze the double-layer structure of the adsorbed DLPC monolayer at the nitrobenzene-water interface.

This work was supported by a Grant-in-Aid for Scientific Research (No. 60211017) and a Grant-in-Aid for Scientific Research on Priority Areas "Macromolecule-Complexes (No. 62612003)" from the Ministry of Education, Science and Culture.

References

1) T. Kakiuchi and M. Senda, *Bull. Chem. Soc. Jpn.*, **56**, 1322, 1753 (1983).

2) T. Kakiuchi. M. Kobayashi, and M. Senda, *Bull. Chem. Soc. Jpn.*, **60**, 3109 (1987).

3) T. Kakiuchi, M. Kobayashi, and M. Senda. *Bull. Chem. Soc. Jpn.*, **61**, 1545 (1988).

4) M. Senda and T. Kakiuchi, *Denki Kagaku*, **54**, 547 (1986).

5) M. Senda, T. Kakiuchi, T. Osakai. and T. Kakutani, "The Interface Structure and Electrochemical Processes at the Boundary between Two Immiscible Liquids," ed by V. E. Kazarinov, Springer-Verlag, Berlin (1987), p. 108.

6) J. Koryta, Le Q. Hung, and A. Hofmanova, *Studia Biophysica*, **90**, 25 (1982).

7) H. H. J. Gilault and D. J. Schiffrin, "Charge and Field Effect in Biosystems," ed by M. J. Allen and P. N. R. Usherwood, Abacus Press, England (1984).

8) T. Kakiuchi, M. Yamane, T. Osakai, and M. Senda, *Bull. Chem. Soc. Jpn.*, **60**, 4223 (1987); M. Yamane, T. Kakiuchi, T. Osakai, and M. Senda, *Rev. Polarg. (Kyoto)*, **29**, 102 (1983).

9) T. Wandlowski, S. Pačinskeý, V. Mareček, and Z. Samec, *J. Electroanal. Interfacial Electrochem.*, **227**, 281 (1987).

10) H. H. J. Girault and D. J. Schiffrin, *J. Electroanal. Interfacial Electrochem.*, **179**, 277 (1984).

11) H. H. J. Girault, D. J. Schiffrin, and B. D. V. Smith, *J. Electroanal. Interfacial Electrochem.*, **137**, 207 (1982).

12) H. H. J. Girault, D. J. Schiffrin, and B. D. V. Smith, *J. Colloid Interface Sci.*, **101**, 257 (1984).

13) T. Kakiuchi and M. Senda, *Bull. Chem. Soc. Jpn.*, **60**, 3099 (1987).

14) J. H. Mathews, *J. Am. Chem. Soc.*, **48**, 562 (1926).

15) F. Bashforth and J. C. Adams, "An Attempt to Test the Theories of Capillary Actions," University Press, Cambridge, England (1883).

16) T. Nakagawa and Y. Oyanagi, "Program System SALS for Nonlinear Least-Square Fitting in Experimental Science," in "Recent Developments in Statistical Inference and Data Analysis," ed by K. Matusita, North-Holland (1980), p. 221.

17) OS-9 Operating System User' Manual, Microware System Co., Iowa (1983).

18) T. Kakutani, T. Osakai, and M. Senda, *Bull. Chem. Soc. Jpn.*, **56**, 991 (1983).

19) J. F. Padday, "Surface and Colloid Science," ed by E. Matijević, Vol. 1, Wiley-Interscience, New York (1969), p. 111.

20) D. Donahue and F. E. Bartell, *J. Phys.*, **56**, 480 (1952).

 © 1988 The Chemical Society of Japan Bull. Chem. Soc. Jpn., 61, 1853—1856 (1988)

The Entropy of Solution of Alkanes Measured by Gas-Liquid Chromatography and Interpreted by Means of Scaled Particle Theory†

Hideaki FUJIWARA,* Ikuji OHTAKU, Tatsuya TAKAGI, Saburo MURATA, and Yoshio SASAKI
Faculty of Pharmaceutical Sciences, Osaka University, 1-6 Yamadaoka, Suita, Osaka 565
(Received November 6, 1987)

The entropy of solution was measured by gas-liquid chromatography for the alkanes from pentane to decane in dibutyl phthalate solution. The results are discussed in relation to the Wertz-type equation, which correlates the entropy of solution with the thermodynamic third-law entropy of the solute, and to the scaled particle theory. A scaled particle treatment assuming non-spheres(spherocylinders) is shown to give improved results and to be promising in reproducing the experimental values of the entropy of solution, whereas the same treatment of spheres failed to explain the trend in the experimental values.

The entropy of reaction in gas phase can be predicted in principle by a molecular statistical theory for thermodynamic functions, since it is equal to the standard entropy of the products minus that of the reactants.[1] However, it is usually not easy to estimate the entropy of a reaction in solution, because each component is solvated more or less in solution and its entropy is considerably affected by the state of solvation. In this sense, the entropy of solution, which represents the difference in entropy between the two phases of gas and solution, becomes important for the understanding of the entropy of reaction in solution.

The authors have previously reported the entropy of reaction in solution in the case of a metal complex formation of organotin compounds[2] and of an inclusion complex formation of α-cyclodextrin with alcohols,[3] where an equation proposed by Wertz[4,5] was utilized to estimate the entropy of solution. In the Wertz-type equaion, molecules are assumed to lose a definite part of their gas phase entropy when transferred from the gas phase to solution. Hence the entropy of solution is expressed as a function of the thermodynamic third-law entropy in the gas phase. In an alternative more theoretical approach, scaled particle theory can give an estimate for the entropy of solution.[6,7] This approach is reported to give reasonable results for nonpolar solutes dissolved in water but not for those dissolved in nonaqueous solvents.[8]

In the present study, the entropy of solution of alkanes in an organic solvent is measured by means of gas-liquid chromatography, and the data are discussed in terms of the scaled particle theory, taking into account the effect of the molecular shape of solute and solvent. As an organic solvent, dibutyl phthalate is chosen. The solutes used are the normal alkanes from pentane to decane.

Experimental

Dibutyl phthalate for the chromatographic stationary phase (solvent) was distilled under reduced pressure, and coated on 60/80 mesh Chromosorb W AW-DMCS (25 wt%). The alkanes from commercial sources were used without further purification. The retention data were measured on a Yanagimoto G1880 gas chromatograph with a TCD cell using a carrier of He gas. The column temperature was measured with a copper-constantan thermocouple. The temperature range studied was from 58 °C to 103 °C. The retention time was measured 5 times at each temperature and averaged. The amount of solute injected was 2 μl. A correction for the vanishing amount of sample injected was not made because it was negligibly small in a preliminary experiment.

Calculations of the above retention data and the entropy of solution described below were all done by using programs written in Basic mode and compiled on personal computers of the NEC 9800 series.

Results

Determination of the Entropy of Solution by Means of Gas-Liquid Chromatography. The partition coefficient (k) is related to the specific retention volume V_g as in Eq. 1 when k, which is defined as the ratio of the concentrations in the gas and liquid phases, is represented as atm (in gas phase)/mol fraction (in liquid).[9] In Eq. 1, M_1 means the molar

$$k=\{M_1/(273.15\mathrm{R})\}V_g \quad (1)$$

weight of solvent and R is the gas constant. The temperature dependence of k affords the enthalpy (ΔH_s^0) and entropy (ΔS_s^0) of solution (Eq. 2).

$$\ln k=-\Delta H_s^0/(RT)+\Delta S_s^0/R \quad (2)$$

The measurement of retention times of solutes (t_s) and air (t_a) on the chromatograph provides the value of the specific retention volume:[10]

$$V_g=\{(t_s-t_a)jF/W\}(273.15/T) \quad (3)$$

where j, F, and W are the correction factor for the pressure, the flow rate of carrier gas, and the weight of solvent in the column, respectively.

A typical plot of $\ln k$ vs. $1/T$ in Eq. 2 is shown in Fig. 1. The values of ΔH_s^0 and ΔS_s^0 thus determined are summaried in Table 1. Errors in these values were

† The Solvation Effect on the Reactions in Solution. III.

Table 1. Enthalpies and Entropies of Solution for Alkanes in Dibutyl Phthalate Determined from Gas-Liquid Chromatography[a)]

Solute	ΔH_s^0/kJ mol^{-1}	ΔS_s^0/JK^{-1} mol^{-1}
Pentane	−22.3±3.0	−80.6±8.6
	(−20.2±3.0)	(−36.0±8.6)
Hexane	−28.2±0.8	−90.2±2.4
	(−26.1±0.9)	(−45.6±2.5)
Heptane	−32.1±0.9	−94.0±2.5
	(−30.1±0.9)	(−49.4±2.5)
Octane	−34.8±0.9	−94.7±2.5
	(−32.7±0.9)	(−50.2±2.6)
Nonane	−38.3±0.8	−97.9±2.2
	(−36.2±0.8)	(−53.4±2.3)
Decane	−41.9±12.7	−101.8±37.0
	(−39.8±12.8)	(−57.3±37.4)

a) The values are given for the standard states of 1 atm in gas phase and 1 mole fraction in liquid phase. Also listed in parentheses are the values for the standard state of 1 mol dm^{-3} in these two phases.

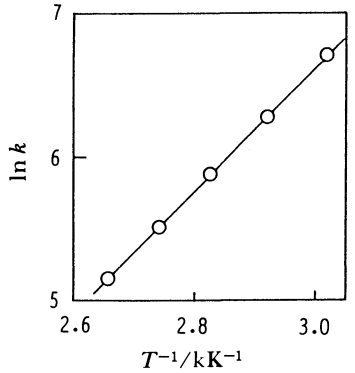

Fig. 1. The Plot of ln k measured by gas-liquid chromatography vs. $1/T$ for nonane in dibutyl phthalate.

estimated as equal to the 95% confidence range in the plot of ln k vs. $1/T$. The values thus determined corresponds to a reference state of 1 atm in the gas phase and 1 mole fraction in the liquid phase. These values are discussed below in terms of the scaled particle theory. Also the values of ΔH_s^0 and ΔS_s^0 can be defined for a reference state of 1 mol dm^{-3} for both the gas and liquid phases. In this case, the partition coefficient (K) is expressed as the ratio of the molar concentration in the gas and liquid phases, and Eq. 1 is replaced by Eq. 4,[9)]

$$K=(T\,\rho_1/273.15)\,V_g \tag{4}$$

where ρ_1 is the density of solvent. The plot of ln K vs. $1/T$ affords the ΔH_s^0 and ΔS_s^0 under a reference state of 1 mol dm^{-3} for both gas and liquid phases. The values thus determined are also listed in Table 1 in parentheses,[11)] where the density of the dibutyl phthalate (ρ_1) was approximated by an equation,

$$\rho_1=-0.000805T+1.0615 \tag{5}$$

from the data between 79.4 and 142.2 °C.[12)]

Discussion

The Wertz-type equation is derived as in Eq. 6 from the values of ΔS_s^0 given under the reference state of 1 mol dm^{-3} and from those of S_{298}^0 (g).[13)]

$$\Delta S_s^0=-0.095\,S_{298}^0\,(g)-6.0 \qquad r=0.952 \tag{6}$$
$$(0.043) \qquad (19.3)$$

In this equation r is the correlation coefficient between the observed and the recalculated values of ΔS_s^0. The standard errors are listed in parentheses. This equation resembles that given for alkylbenzenes dissolved in dimethyl or dioctyl phthalate.[2)] Although the Wertz-type equation can be predicted from the physical constants of the solvent, this was not possible in the present case because of the lack of S_{298}^0 of DBP in the gas and liquid phases. It is reported,[5)] and also observed by the present authors, that the coefficients of the Wertz-type equation vary depending on the series of compounds treated. Therefore, an alternative theoretical approach is attempted below on the basis of a scaled particle theory.

Calculation of the Entropy of Solution under a Sphere Model. According to the scaled particle theory, the entropy of solution is given as in Eq. 7 for the spherical molecules of solute as well as for the solvent, where the terms for cavity formation and for a correction for the different reference states in the gas and liquid phases are included.[5)]

$$\Delta S_s^0=S_{cav}+\alpha_p RT-R-R\ln\,(V_g/V_l) \tag{7}$$

In this equation, α_p is the thermal expansion coefficient of the solvent, and V_g/V_l is equal to RT/V_l under an ideal-gas assumption, V_l being the molar volume of solvent. S_{cav} in Eq. 7 is calculated as in Eq. 8 according to the definition of $S=-(\partial G/\partial T)_P$ and to the equation for G given in Refs. 6 and 7:

$$\begin{aligned}S_{cav}=R[&\{\ln(1-y)-3y/(1-y)\cdot(\sigma_2/\sigma_1)\\&-(3y/2)(2+y)/(1-y)^2\cdot(\sigma_2/\sigma_1)^2\}\\&+\alpha_p yT/(1-y)^3\cdot\{(1-y)^2+3(1-y)(\sigma_2/\sigma_1)\\&+3(1+2y)(\sigma_2/\sigma_1)^2\}]\end{aligned} \tag{8}$$

where σ_1 and σ_2 are the diameter of solvent and solute, respectively, and where y is called a "reduced number density"[7)] or a "compactness factor"[14)] of the solvent which is equal to $\pi\rho_1\sigma_1^3/6$, ρ_1 being the number density of solvent (N_A/V_l). The value of σ_2 is usually estimated by the Stearn-Eyring equation:[8)] $(\sigma_2)^3=V/N_A$ where V is the molar volume and N_A the Avogadro number. The best method of obtaining σ_1 is to utilize the Henry's law constants of rare gases in the relevant solvent. However, these constants are lacking, within the knowledge of the authors, and so σ_1 is also taken from the Stearn-Eyring equation. The values of ΔS_s^0 thus estimated lie between −55.1 J (K·mol)$^{-1}$ for pentane and −56.5 J (K·mol)$^{-1}$ for decane (Table 2): they only amount to around 60% of the experimental values, and the dependency on the carbon number of

the solute is small compared to the experimental results. These estimated values are not improved even if σ_1 is varied near the initial values of 7.74 Å (Fig. 2). Therefore, it is clear that the sphere model fails to explain the experimental values measured in dibutyl phthalate. Similar results are reported[8] for other non-aqueous solvents. In the present study an alternative model which assumes spherocylinderical shapes for the solute and solvent molecules is attempted below.

Calculation of the Entropy of Solution under a Spherocylinder Model. For nonspherical molecules of solute and solvent, a scaled particle treatment has been developed for the spherocylinders in isotropic as well as anisotropic solutions.[15] In this case S_{cav} turns out to be a function of a, l, α, λ, V_1, α_p, and T as in Eq. 9,

$$\begin{aligned} S_{cav} = R[&\ln X + (\alpha_p T/X)(1-X) \\ &+ (\alpha_p T/X - 1)\{\pi a(l+2a)\rho_1/X\}(2\alpha + \lambda/2) \\ &+ (\alpha_p T/X - 1)\{\pi(l+4a)\rho_1/X\}(\alpha\lambda/2 + \alpha^2) \\ &+ (2\alpha_p T/X - 1)\{\pi a(l+2a)\rho_1/X\}^2(\alpha\lambda + 2\alpha^2)] \end{aligned} \quad (9)$$

Table 2. The Entropy of Solution Calculated for the Sphere Model[a]

Solute	$\Delta S^0_{s,\,exptl}$[b]	σ_2[c]	$\Delta S^0_{s,\,calcd}$
Pentane	−80.6	5.78	−55.1
Hexane	−90.2	6.02	−55.3
Heptane	−94.0	6.26	−55.6
Octane	−94.7	6.48	−55.8
Nonane	−97.9	6.83	−56.2
Decane	−101.8	7.08	−56.5

a) Given in a unit of J (K·mol)$^{-1}$. The molar volume and the thermal expansion coefficient are 279.19 ml mol^{-1} and 0.840/1000 K, respectively, for the solvent. b) Experimental values. c) The diameter of the solute in Å.

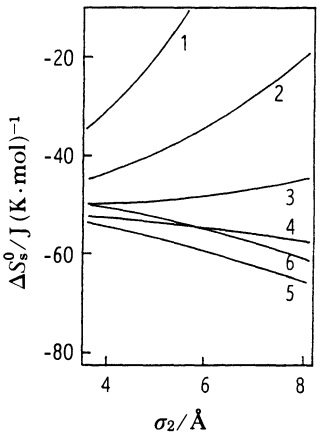

Fig. 2. The dependence of the calculated ΔS^0_s on the values of σ_1 and σ_2. Calculated under the sphere model by the use of Eq. 7. The values of σ_1 are 8.34, 8.14, 7.94, 7.74, 7.34, and 5.74 Å for curves 1 to 6, respectively. Note that the curve shifts upward in the figure on decreasing the values of σ_1 from 7.34 Å, whereas the experimental values ranges from −80 to −101 J (K·mol)$^{-1}$. The value of σ_1 estimated from the Stearn-Eyring equation is 7.74 Å.

where $X = 1 - \pi a^2 l\rho_1 - 4\pi a^2\rho_1/3$, and where α and λ are the radius and length of the solute molecule, respectively, and a and l those of the solvent, respectively (Fig. 3). Equation 9 is derived from Eq. 51 in Ref. 14, assuming that $\ln P_0$ in this reference is equal to $-G_{cav}/RT$ and $S_{cav} = -(\partial G_{cav}/\partial T)_P$. This model is equivalent to the above sphere model when l and λ are both taken as zero.

For the sake of model calculations, the size of the solute and solvent is estimated from the dimension of a single molecule. For solute molecules, a zigzag conformation is assumed and α is taken as the distance from the longer axis of symmetry to the CH_2 protons plus the van der Waals radius of hydrogen, λ being taken as a distance between the two end carbons (Fig. 4). The size of the solvent is not derived straightforwardly, a is set equal to 2.63 Å, a radius of the sphere for benzene derived from the Stearn-Eyring equation, and l is set equal to 7.77 Å to make the reduced number density equivalent to the sphere of radius 3.87 Å derived from the Stearn-Eyring equation for DBP. These values of a and l give the calculated values of ΔS^0_s/J (K·mol)$^{-1}$ amounting from −55.0 for pentane to −59.1 for decane. When the values of a and l are estimated from a molecular model, where the two butyl ester groups extend to the same direction in the same manner, a=2.70 Å and l=4.53 Å are obtained. These values give much improved results as is shown by "spherocylinders" in Fig. 5, i.e., ΔS^0_s/J (K·mol)$^{-1}$= −66.5 for heptane and −76.4 for decane. For these values of a and l, the reduced number density is equal to 0.41 and is well within a reasonable range. Therefore, a proper estimation of the size of the solvent

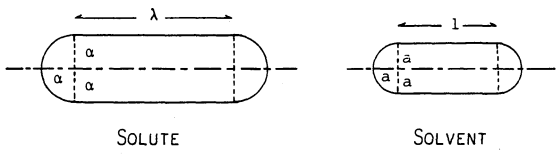

Fig. 3. The spherocylinder model of solute and solvent. -·-·-: the axis of rotation of the rotamer. α and a: the radius of semisphere. λ and l: the length of the part of cylinder.

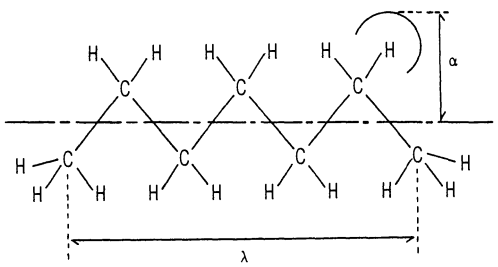

Fig. 4. The size of solute, α and λ, depicted typically for heptane. α is equal to 2.58 Å when the van der Waals radius of 1.2 Å is added. -·-·-: The longer axis of rotation.

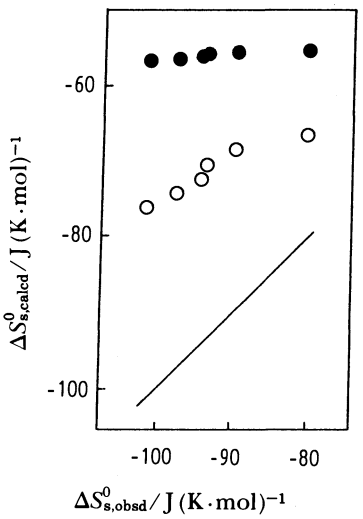

Fig. 5. The plot of ΔS^0_s calculated under the sphere and the spherocylinder models vs. $\Delta S^0_{s,obsd}$. ●: Calculated by means of the sphere model. ○: Calculated by means of the spherocylinder model. ——: The ideal interrelation of $\Delta S^0_{s,calcd}=\Delta S^0_{s,obsd}$.

molecule is expected to give much improved calculations of the entropy of solution. However, more elaborate calculations are not attempted here, because the solvent used in the present study is rather complicated in structure including polar groups. More elaborate calculations are now underway for a few solvents better approximated by simple rotamers such as disks, cylinders, and spherocylinders.

It has been reported,[8] and also confirmed by the authors that the entropy of solution of alkanes in water is well reproduced by calculations based on a sphere model. Contrary to this, the entropy of solution in an organic solvent treated here is better reproduced by a non-sphere model which assumes spherocylinders. Such a contrast may be interpreted as due to the difference in the shape of the solvent and also to the shape of the solute in each solvent. That is, the alkanes are considered to take on a rather spherical form in water as a result of the intramolecular hydrophobic interaction within a single molecule whereas they are considered to acquire a stretched form in organic solvents depending on the solute-solvent interactions in solution.

References

1) G. Herzberg, "Molecular Spectra and Molecular Structure. II. Infrared and Raman Spectra of Polyatomic Molecules," Van Nostrand, New York (1945).

2) H. Fujiwara, H. Arakawa, S. Murata, I. Ohtaku, M. Ishii, and Y. Sasaki, *Bull. Chem. Soc. Jpn.*, **60**, 457 (1987).

3) H. Fujiwara, H. Arakawa, S. Murata, and Y. Sasaki, *Bull. Chem. Soc. Jpn.*, **60**, 3891 (1987).

4) D. H. Wertz, *J. Am. Chem. Soc.*, **102**, 5316 (1980).

5) M. H. Abraham, *J. Am. Chem. Soc.*, **103**, 6742 (1981).

6) H. Reiss, *Adv. Chem. Phys.*, **9**, 1 (1966).

7) R. A. Pierotti, *Chem. Rev.*, **76**, 717 (1976).

8) M. H. Abraham and A. Nasehzadeh, *J. Chem. Soc., Faraday Trans. 1*, **77**, 321 (1981).

9) E. F. Meyer, *J. Chem. Educ.*, **50**, 191 (1973).

10) "Saishin Gas-Chromatography, "(in Japanese) ed by W. Funasaka and N. Ikegawa, Vol. 1, Hirokawa, Tokyo (1965), Chap. 2.

11) The values of ΔH^0_s and ΔH^0_s under the two reference states can be correlated with each other as follows, which are derived from equations given in Ref. 12: ΔH^0_s (atm/mf)$=\Delta H^0_s$ (mol·dm^{-3})$+RT(1+T\cdot d\ln\rho_1/dT)$ and ΔS^0_s (atm/mf)$=\Delta S^0_s$ (mol·dm^{-3})$+R\{1+T\cdot d\ln\rho_1/dT+\ln(\rho_1RT/M_1)\}$, where mf means the molefraction and M_1 the molecular weight of solvent.

12) S. Berman, A. A. Melnychuk, and D. F. Othmer, *Ind. Eng. Chem.*, **40**, 1312 (1948).

13) D. R. Stell, E. F. Westrum, and G. C. Sinke, "The Chemical Thermodynamics of Organic Compounds," Wiley, New York (1969).

14) E. Wilhelm and R. Battino, *J. Chem. Phys.*, **55**, 4012 (1971).

15) M. A. Cotter and D. E. Martire, *J. Chem. Phys.*, **52**, 1909 (1970).

Stress Relaxation of Alginate Gels Crosslinked by Various Divalent Metal Ions

Masakatsu YONESE,* Kazuhiko BABA, and Hiroshi KISHIMOTO
Faculty of Pharmaceutical Sciences, Nagoya City University, Tanabe-dori, Mizuho-ku, Nagoya 467
(Received November 19, 1987)

Rheological properties of Alginate (Alg) gels were studied by measuring tensile stresses under small strains. The Alg gel rods were prepared in $CaCl_2$, $SrCl_2$, $BaCl_2$, and $Pb(NO_3)_2$ solutions in the range of 0.03—1.0 mol dm^{-3}. Their stresses showed long relaxation processes. By curve fitting method, equilibrium elastic moduli G_e, spontaneous elastic moduli G_e+G_r and relaxation times τ were obtained. The results G_e were independent of strains γ, and G_r and τ increased as increasing γ. The effects of Ca ion concentrations C_{Ca} on the elasticities were discussed by taking account of the ratio of Ca ion bindings obtained by dialysis equilibrium and that of junction formation obtained by circular dichroism. The values of G_e were analyzed by the theory of swollen gels. The number of the junctions was found to be constant in the region of $C_{Ca}>0.03$ mol dm^{-3}, and slight increases of G_e to be due to changes of the water content and the density of the Alg gels. The magnitudes of G_e and G_r depended on the kind of counterions, and decreased in the order, Ba-$\gg$Ca-$>$Sr-$>$PbAlg; this was almost the same as that of the ion selectivities.

Alginate (Alg) is a major structural polysaccharide found in intercelluar substances of brown algae. They are gelled by the addition of divalent metal ions except for Mg^{2+} ions. The gelations result from the stackings of alginate chains intermediated by the ions.[1] The interaction of Alg with them and the rheological properties of the gels such as rigidity and elasticity are dominated by the composition of the Alg, i.e., the ratio of β-D-mannulonate and α-L-guluronate, their block compositions and the kind of metal ions added.[2-4]

Alginate and its gels are used widely as food additives and pharmaceutically as hemostats. The gels are examined with respect to their application to matrices of drug delivery systems[5] and to the matrices of immobilized enzymes.[6] These applications of Alg gels take advantage of the characteristics of the lyotropic gels. However, from the basic point of view, the gel properties have not been elucidated sufficiently. In the previous paper,[7] effective charge densities of Alg were studied by a membrane potential method and the effects of sol-gel transition on them were reported. In this report, tensile stress relaxations of Alg gels were studied to elucidate their rheological characteristics, and the effects of the kind of metal ions present.

Experimental

Materials. Purified sodium alginate (NaAlg) was prepared from commercial NaAlg (Tokyo Kasei Kogyo Co., Ltd.) by dialyzing against distilled water for 3 d and by filtrating to remove insoluble substances, as described in the previous paper.[7] The purified NaAlg was stored in a refrigerator after freeze drying. The weight average molar mass of NaAlg was determined to be $\bar{M}_w=1.32\cdot10^5$ g mol^{-1} by using a light scattering photometer LS-8 (Toyo Soda Manufacturing Co., Ltd., Japan). The composition of the NaAlg was analyzed by circular dichroism (CD),[8] and ^{1}H NMR.[9] The guluronate fraction F_G and the consecutive guluronate fraction F_{GG} were determined to be 0.37 and 0.28. All other reagents were of special grade. Distilled and deionized water was used for preparation of aqueous solutions.

Dialysis Equilibrium. NaAlg solutions (0.75 w/v%) were put into dialysis tubes (Seamless Cellulose Tubing, Union Carbide Corp.), which were dipped in $CaCl_2$ and $MgCl_2$ solutions in the range of 0.001—0.1 mol dm^{-3} in dialysis cells. They were shaken in a thermostated bath (25 °C) for 48 h which was long enough to attain equilibrium. The concentrations of Ca, Mg, and Cl ions in the outer solutions were determined by chelate titrations and Mohr method, respectively. From these results, amounts of Ca and Mg ions bound to Alg were determined.

Preparation of Alginate Gel Rods for Measuring Stress Relaxations. NaAlg solutions (1.2 w/v%) in straight Teflon tubes (length: 6.0 cm, diameter: 0.4 cm) were gelled by dipping in $CaCl_2$, $SrCl_2$, $BaCl_2$, $Pb(NO_3)_2$, and HCl solutions in the concentration range of 0.03—1.0 mol dm^{-3}. The gels obtained are denoted as Ca-, Sr-, Ba-, Pb-, and HAlg, respectively. To attain an equilibrium swelling state, the gels had to be matured for 7 d in these solutions, renewed once daily. The Alg gel rods were then dipped for not less than 9 d in these solutions which were kept at 4 °C to prevent rotting. Before the measurements of their tensile stress, the Alg gel rods were reequilibrated for 48 h at the experimental temperature (25 °C).

Preparation of Alginate Gel Membranes for Measuring Circular Dichroism. To obtain Alg gel membranes with flat surfaces, a freezing method was developed. NaAlg solutions (1.2 w/v%) were put into Petri dishes with flat bases and were frozen for 20—30 min in a freezing chamber (−3—−5 °C). The frozen samples thus obtained had smooth surfaces. Then, $CaCl_2$ solutions in the concentration range of 0.001—1.0 mol dm^{-3} cooled to about 4—6 °C were poured gently and slowly down the wall of the petri dishes. To obtain equilibrated Alg gel membranes, the $CaCl_2$ solutions were renewed once daily and held at 25 °C for 7 d. By adding HCl solutions instead of $CaCl_2$ solutions, Alg gel (HAlg) membranes were also prepared.

Measurement of Tensile Stress of Alg Gel Rod. The schematic diagram of the apparatus for measuring the tensile stresses of the gels is shown in Fig. 1. The Alg gel rod G was fixed by clamps A and B made of plastic plates with rough surfaces to prevent them slipping. They were suspended in electrolyte solutions in which the gel was equilibrated. The strains were imposed on the gels in steps and the

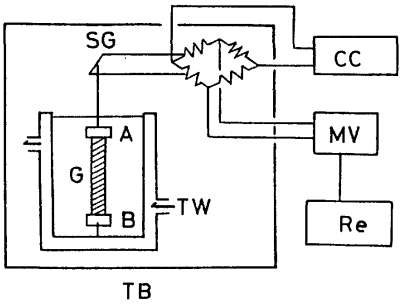

Fig. 1. Apparatus for measurement of gel tensile stress. A and B; clamp, G; Alg gel rod, SG; strain gauge, TW; thermostated water (25 °C), TB; air thermostated bath, CC; constant direct current source, MV; microvolt meter, Re; recorder.

tensile stresses σ were measured at 25 °C by strain gages SG (Shinkoh Communication Industry Co., Ltd.) connected to a constant direct current source CC (Model 691B, Metronix Corp. Tokyo) and a microvolt meter MV (Model AM-1001, Ohkura Electric Co.). The apparatus was set up in an air thermostated bath TB to eliminate temperature effects on the strain gages.

Measurement of Circular Dichroism. Measurements of circular dichroism CD were made on a CD spectropolarimeter (J-40S, NIHON BUNKOU) at 25 °C by using a 1 cm pathlength cell for NaAlg solutions. The CD of the Alg gel membranes were measured by putting them between perforated support film (PARAFILM, AMERICAN CAN COMPANY) and the thermostated 1 cm cell to prevent evaporation of water from the gels as much as possible and to maintain a constant temperature (25 °C).

Measurements of Densities and Water Contents of Alg Gels. The densities of the Alg gels were determined by a floating method, i.e., from the densities of mixed solvents composed of isooctane and carbon tetrachloride in which pieces of Alg gels were floated. The densities of the solvents were measured by densitometer (Anton Paar DMA602). The water content of the Alg gels were measured by the weight change after drying at 70 °C in vacuo for 10 h.

Theory and Method

Determinations of Elastic Modulus. An Alg gel rod elongated under a constant strain γ showes stress relaxation, which is expressed by the following equation as a function of time t,

$$\sigma=(G_e+G_r\exp(-t/\tau))\,\gamma \qquad (1)$$

where G_e and (G_e+G_r) are the equilibrium elastic modulus and the spontaneous elastic modulus respectively and τ is the relaxation time. The time courses of the stress of an Alg gel rod elongated under constant strains γ by steps are shown in Fig. 2 as one example. After a first stress of Alg gel σ_1 resulting from the first strain γ_1 attains an equilibrium value, a second strain γ_2 is imposed at time t_2, and the same process is continued consecutively. Imposing the nth strain, the stress σ_n can be expressed by the following equation according to the superimposal principle,

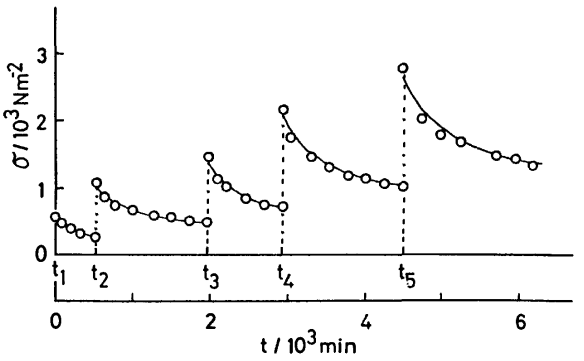

Fig. 2. Stress relaxation curve for CaAlg gel. Solid curves show the values calculated from Eq. 2 by curve fitting method. CaAlg was prepared in 0.3 mol dm^{-3} $CaCl_2$ solution. The value t_k shows time when kth strain is imposed.

$$\sigma_n=\sum_{k=1}^{n}\left\{G_{ek}+G_{rk}\exp\left(-\frac{t-t_k}{\tau_k}\right)\right\}(\gamma_k-\gamma_{k-1}) \qquad (2)$$

where a subscript k denote the values of the gel rod elongated by the kth strain γ_k. The t_1 and γ_0 values are 0. The kth strain γ_k is defined by

$$\gamma_k=(l_k-l_0)/l_0 \qquad (3)$$

where l_0 is the initial length of Alg gel rod and l_k is that of the elongated gel by kth strain.

Determination of Counterion Binding Parameters. Under equilibrium conditions, Donnan equilibrium is maintained between the free ions in an alginate phase in a dialysis tube (α phase) and ions in a bulk solution (β phase).[10] Two kinds of counterions occur in both phases, i.e., one was Na ions resulting from original sample NaAlg and the other was metal ions M from added electrolytes. In this report, bounding characteristics of the latter counterions M are discussed. Approximating the activity coefficients of the free counterions and co-ions are unity, the concentration of the free counterion in α phase $C^f_{M\alpha}$ is obtained by the following equation,

$$C^f_{M\alpha}=C_{M\beta}\,(C_{A\beta}/C_{A\alpha})^{z_M} \qquad (4)$$

where $C_{M\beta}$ is the concentration of the added counterion M in the β phase, $C_{A\alpha}$ and $C_{A\beta}$ are those of the co-ion (Cl^-) in the α and β phases, and z_M is the algebraic charge number of the counterion M. Bounding amounts of the counterions per unit weight of Alg b_M are obtained by

$$b_M=V_\alpha(C^T_{M\alpha}-C^f_{M\alpha})/w \qquad (5)$$

where $C^T_{M\alpha}$ is the total concentration of the counterion in the α phase, and w and V_α are the weight of Alg in the α phase and the volume of the α phase. When the bindings are Langmuir type isotherms, the relation between $1/b_M$ and $1/C^f_{M\alpha}$ is linear as expressed by the following equation

$$1/b_M=1/b^s_M+1/(b^s_M K C^f_{M\alpha}) \qquad (6)$$

and b^s_M and K are the saturated binding amounts and the binding constant.

Results

Counterion Binding Characteristics of Alginate. Binding amounts b_M mol g^{-1} of Ca and Mg ions to Alg at 25 °C were obtained from dialysis equilibria by using Eq. 5 and are shown in Fig. 3 as a function of the free counterion concentrations $C^f_{M\alpha}$. They showed Langmuir type isotherms and linear relations between $1/b_M$ and $1/C^f_{M\alpha}$ held. By Eq. 6, b^s_M/mmol g^{-1} and K/mol dm^{-3} were obtained; for Ca ion, b^s_M=2.25 and K=3.60, and for Mg ion, b^s_M=2.27 and K=0.584, respectively. The binding amounts of the Ca ions were saturated in the region of $C^f_{Ca\alpha}$>0.008 mol dm^{-3}. Since the values $C^f_{Ca\alpha}/C_{Ca\beta}$ were almost 1.0 in the region $C^f_{Ca\alpha}$>0.008 mol dm^{-3}, the saturated binding of Ca ions was attained in the region of the concentration of the bulk solutions $C_{Ca\beta}$>0.008 mol dm^{-3}. Hereinafter, the counterion concentrations in the β phase $C_{M\beta}$ are designated by C_M, as well as the concentrations of the bulk solutions used for the preparation of the Alg gels.

CD Spectrum of Alg Gels Different in Ca Ion Concentrations. The characteristic changes in CD accompanied by the gelation of Alg have been reported in the literature and the magnitudes of the changes have been attributed to the formation of junctions between the guluronate blocks (G block) induced by divalent metal ions such as Ca ion.[11,12] To investigate the effects of Ca ion concentrations on the junction formation by the CD method, attempts were made to prepare CaAlg gel membranes in various Ca ion concentrations (C_{Ca}=0.001—1.0 mol dm^{-3}). In the region of C_{Ca}<0.007 mol dm^{-3}, the gel membranes could not be formed or were too weak to set between the cell and the perforated support film for measuring CD spectrum. The CD spectra of CaAlg gel membranes prepared in the region C_{Ca}>0.007 mol dm^{-3} were measured at 25 °C. Figure 4 shows the ellipticities [θ] of NaAlg (0.6 w/v%) and those of a CaAlg (C_{Ca}=1.0 mol dm^{-3}) and a HAlg (C_H=1.0 mol dm^{-3}) gels. The CD spectrum of NaAlg showed a negative peak at 215 nm, but that of CaAlg gel showed the negative peak at about 219 nm and a positive one at 203 nm. The spectrum of HAlg gel was a negative broad peak and was found to be different from that of CaAlg.

On increasing the binding ratio of Ca ions to the carboxylic groups of Alg, the junctions, i.e., dimers between the G blocks and its aggregations, were reported to increase and the magnitudes of the peaks at 203 nm [θ]$_{203}$ to increase.[12] Morris et al. took the difference values between the values [θ] of NaAlg and Ca-NaAlg as a measures of the formation of the junctions. The relative values of the magnitudes of the peaks at 203 nm and at about 219 nm [θ]$_{203}$/[θ]$_{219}$ can also be taken as this measure. Since the Alg gel mem-

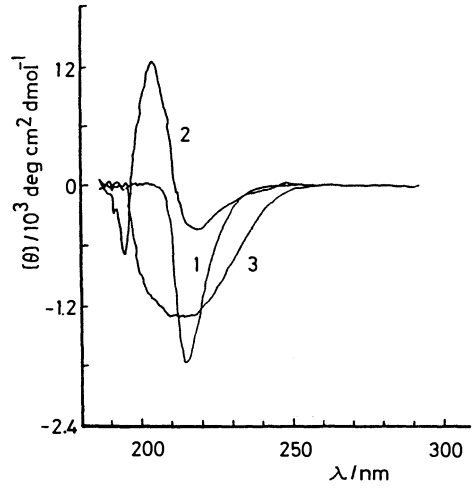

Fig. 4. C.D. spectra of Alg solution (NaAlg) and gels (Ca- and HAlg). 1; NaAlg (0.6 w/v%), 2; CaAlg (C_{Ca}=1.0 mol dm^{-3}, L=0.045 cm, W_{H_2O}=0.87), 3; HAlg (C_H=1.0 mol dm^{-3}, L=0.04 cm, W_{H_2O}=0.96). L is a thickness of a Alg gel membrane.

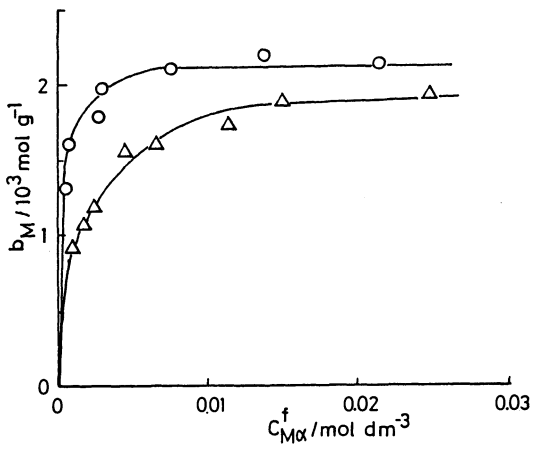

Fig. 3. Counterion binding amounts b_M vs. counterion concentrations $C^f_{M\alpha}$. Ca; O, Mg; △.

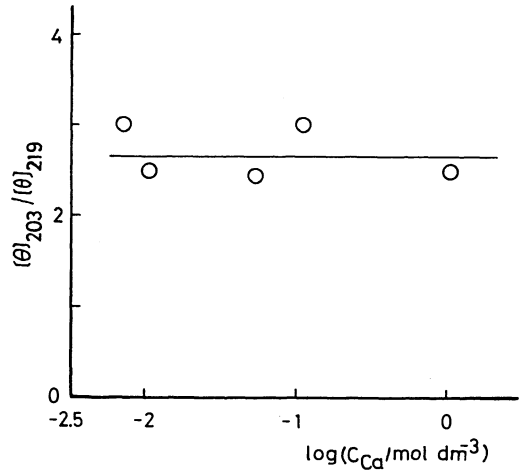

Fig. 5. Relative C.D. values [θ]$_{203}$/[θ]$_{219}$ of CaAlg prepared in various Ca concentrations C_{Ca}.

branes prepared in various Ca concentrations were different in water content and thickness, the relative values are more appropriate values. The values $[\theta]_{203}/[\theta]_{219}$ of CaAlg gel membranes prepared in the region of $0.007<C_{Ca}/\text{mol dm}^{-3}<1.0$ are shown in Fig. 5 as a function of C_{Ca}. They were found to be almost constant above the concentration at which the binding amounts of Ca ions were saturated. Under unsaturated conditions of Ca ion binding, the ratios of the junctions were reported to depend on the binding ratios of the Ca ions.[12] If CD of CaAlg gels prepared in the conditions of the unsaturated Ca ion bindings could be measured, the values $[\theta]_{203}/[\theta]_{219}$ should decrease with decreasing C_{Ca}.

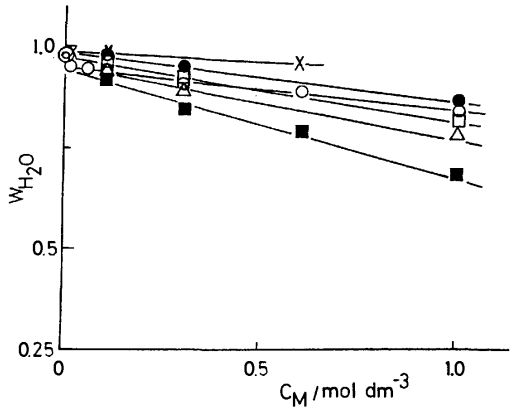

Fig. 6. Effects of counterion concentrations C_M on water contents W_{H_2O} of various Alginate gel and sol. Alginate in sol states: Na; ◎, Mg; ●. Alginate in gel state: Ca; ○, Sr; □, Ba; △, Pb; ■, H; ×.

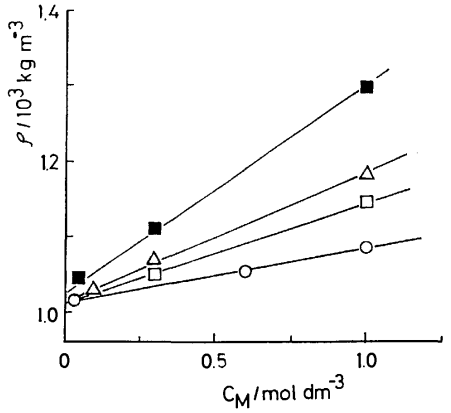

Fig. 7. Effects of counterion concentrations C_M on densities of Alginate gels ρ. Ca; ○, Sr; □, Ba; △, Pb; ■

Water Contents and Densities of Alg Gels. The water contents W_{H_2O} and densities ρ g cm^{-3} of various Alg gels prepared from NaAlg solutions (1.2 w/v%) are shown in Figs. 6 and 7 as a function of the concentration C_M of the solutions. W_{H_2O} decreased and ρ increased linearly with increasing C_M in the experimental range of $C_M<1.0$ mol dm^{-3}, and they depended on the kind of counterions. The order of magnitude of the former was H->Mg->Ca->Sr->Ba->PbAlg, and that of the latter was Pb->Ba->Sr->CaAlg. The smaller the water contents, the bigger became the densities.

Effects of Strains and Ca Ion Concentrations on Stress Relaxation of Alg Gel Rod. The time courses of stress of CaAlg gel rods were measured by imposing strains by steps. Figure 2 shows the results for CaAlg gel prepared in a $CaCl_2$ solution (0.3 mol dm^{-3}). The stress under each strain showed a long relaxation and attained an equilibrium state after above 20 h. From the time courses of the stress under strains, the elastic moduli G_{ek}, G_{rk} and the relaxation time τ_k can be obtained from Eq. 2 by using a curve fitting method. These values obtained by analyzing the time courses of stress measured for more than 20 h were independent of the measuring times. Accordingly we accepted these values as the true ones. The solid curves in Fig. 2 show the results calculated from Eq. 2 by using these elastic parameters. They are in good agreements with the experimental results. The values G_{ek}, G_{rk}, and τ_k obtained under the kth strain γ_k are

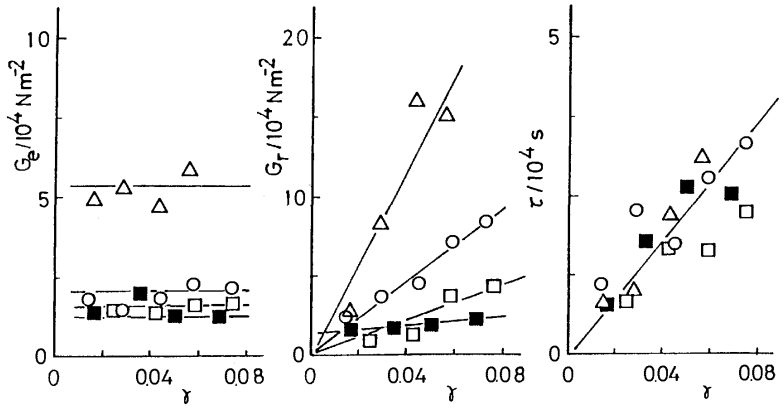

Fig. 8. Effects of strains on elastic moduli G_e, G_r, and relaxation time τ for Alg gels prepared by various divalent counterions. Ca; ○, Sr; □, Ba; △, Pb; ■. Alg gels were prepared in 0.3 mol dm^{-3} solutions.

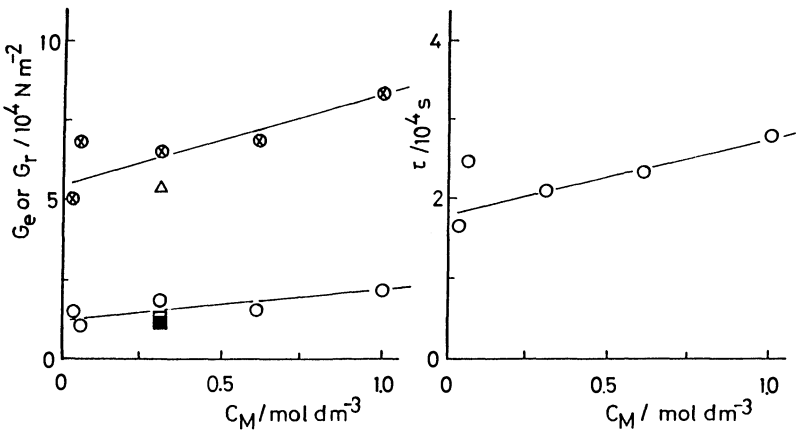

Fig. 9. Effects of counterion concentrations C_M on elastic moduli G_e, G_r, and relaxation time τ at constant strain (γ=0.05). CaAlg: G_e and τ; ○, G_r; ⊗. For Sr-, Ba-, and PbAlg, values G_e (C_M=0.3 mol dm^{-3}) are shown. Sr; □, Ba; △, Pb; ■.

hereinafter designated by G_e, G_r, and τ, i.e., the subscript k is deleted for simplicity. Figure 8 shows the results G_e, G_r, and τ of CaAlg prepared in 0.3 mol dm^{-3} $CaCl_2$ solutions, as a function of strain γ. The values G_e were almost constant in the small strains, but the values G_r and τ increased with increasing γ. The same tendencies were found in the results of CaAlg gels prepared from other $CaCl_2$ solutions at different in concentrations. The diameters and the lengths of the Alg gel rods were measured before and after the stress measurements, and the volume changes were found to be negligible in the experimental region of γ<0.08. Figure 9 shows the values G_e, G_r, and τ of CaAlg gels obtained at γ=0.05 as a function of the concentrations of $CaCl_2$ solutions in which CaAlg gels were prepared. These values were found to increase slightly as increasing C_{Ca} (>0.03 mol dm^{-3}). The increasing rates of G_r and τ were more than those of G_e.

Effects of the Kind of Counterions Used as Crosslinking Agents. The time courses of stress of various Alg gel rods prepared in $BaCl_2$, $SrCl_2$, and $Pb(NO_3)_2$ solutions (C_M=0.3 mol dm^{-3}) were measured. The values G_e, G_r and τ were obtained in the same manner as in the case of CaAlg gels and are shown in Figs. 8 and 9 together with the results for CaAlg. The results G_e of Ba-, Sr-, and PbAlg were independent of γ as well as CaAlg, and their values G_r and τ increased with increasing γ. The values G_e and G_r were found to depend significantly on the kind of counterions, and decreased in the order, Ba-≫Ca->Sr->PbAlg. However, their values for τ did not show significant differences. By adding H ions, Alg was gelled but the gels were too brittle to measure the stress.

Discussion

Estimation of Junction Densities. The stress relaxations of Alg gels are considered to be composed of two components, i.e., (1) a time independent component which is the stress resulting from the permanent junctions, and (2) the time dependent component which is associated with the reorientation of the network from unstable to stable and the rupture of weak junctions. The time independent component in small strains has been reported to be analyzed by the theory of rubber elasticity although the deviations from the ideal rubber elasticity were found at high strains.[13] It is used to give reasonable numbers of junctions per a molecule.[14,15]

Flory developed the theory for the stress of swollen gels by assuming an ideal rubber and a constant volume. The stress σ_e is expressed by the following equation,[16]

$$\sigma_e = RT\, v_p^{-2/3} w_p \left(\frac{1}{\bar{v}_g M_c}\right)\left(1-\frac{2M_c}{\bar{M}}\right)\left(\alpha-\frac{1}{\alpha^2}\right) \qquad (7)$$

where $\bar{M}$ and M_c are number averaged molar mass of polymer and that of the polymer chain interposed by adjacent crosslinks, α is the deformation of the network structure by an elongation ($\alpha=l/l_0=1+\gamma$), v_p and w_p are the volume fraction and the weight fraction of the network polymer in a gel, and $\bar{v}_g$ is a specific volume of the gel. Alg gels showed negligible volume changes due to elongations. The values M_c of Alg gels can be obtained by Eq. 7 from the results σ_e under small strains. The values v_p of Alg gels were obtained by the following equation

$$v_p = 1 - v_w(1-w_p)/\bar{v}_g \qquad (8)$$

where v_w is specific volume of water.

Figure 10 shows the values M_c and the numbers of the junction per alginate molecule $\bar{M}/M_c$ of CaAlg gels as a function of the concentration of Ca ions. They were obtained from the results σ_e of CaAlg gels elongated at γ=0.03 and 0.05, and were found to be independent of the strains (γ<0.05) and the concentrations of Ca ion in the experimental region (0.03<C_{Ca}/

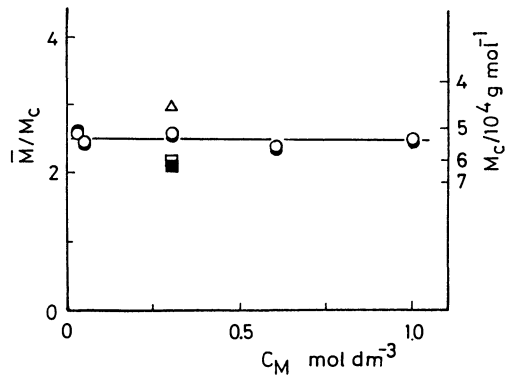

Fig. 10. Effects of counterion concentrations C_M on molar mass per cross-linked unite M_c and number of cross-linked unites per a molecule $\bar{M}/M_c$ under different strains γ=0.03 and 0.05. CaAlg: ●; γ=0.03, ○; γ=0.05. For Sr-, Ba-, and PbAlg, results under γ=0.05 and C_M=0.03 mol dm^{-3} are shown. Sr; □, Ba; △, Pb; ■.

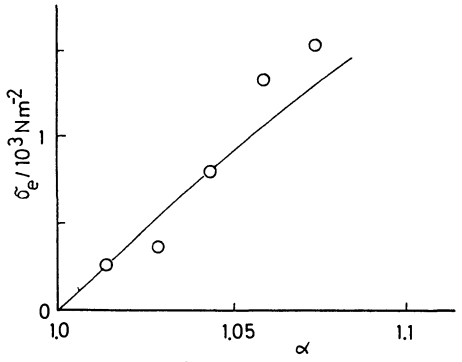

Fig. 11. Equilibrium stress σ_e vs. elongation α for CaAlg (C_M=0.3 mol dm^{-3}). ○; Experimental results. Solid curve shows theoretical values calculated from Eq. 7.

mol dm^{-3}<1.0). In these calculations, the number averaged molar mass of Alg $\bar{M}$ was approximated to be equal to the weight average molar mass obtained by the light scattering method. The mean values M_c and $\bar{M}/M_c$ were $5.2\cdot10^4$ g mol^{-1} and 2.5. From these results, it can be concluded that during stress relaxation, Alg chains deform from unstable elongated network structures to stable ones without altering the numbers of the junctions in small strains. The slight increase of G_e shown in Fig. 9 is not attributable to the change of the numbers of the junction but to that of the water content and the density of the Alg gels shown in Figs. 6 and 7. Figure 11 shows the calculated values σ_e of CaAlg (C_{Ca}=0.3 mol dm^{-3}) from Eq. 7 as a function of α. They are in good agreement with the results in the small α region.

In the concentration region of C_{Ca} ($=C^f_{Ca\alpha}$)>0.008 mol dm^{-3}, the binding of Ca ions to Alg and the junction formation were saturated as shown in Figs. 3 and 5. However, in the region of C_{Ca}<0.03 mol dm^{-3}, the CaAlg gels were so weak that the elasticities could not be measured. From these results, free Ca ions in the region of 0.008<C_{Ca}/mol dm^{-3}<0.03 are considered to strengthen the junctions of the Alg gels, i.e., weaker junctions, such as dimers, aggregate further and grow into strong junctions. The contributions of the former to the elasticities of the gels should be much smaller than those of the latter. The aggregation of the dimers might result from the decrease of electrostatic repulsive force between Alg molecules due to the increase of shielding effects and the decrease of osmotic pressure with the increase of the free Ca ions. These effects also affect the water content W_{H_2O} and the density ρ of CaAlg gels. In the region of C_{Ca}>0.03 mol dm^{-3}, although the number of junctions formed by the aggregation is held constant, the values G_e, G_r, and τ are considered to increase with increasing C_{Ca} due to the effects of the changes of W_{H_2O} and ρ.

Segeren et al.[13] reported the value M_c of CaAlg gel to be $1.22\cdot10^4$ g mol^{-1} which is about 1/4 of our result. Comparing their Alg sample with ours, the molecular weight of theirs is almost equal to ouurs, but the fraction of guluronate in their sample is 0.714 which is more than twice as much as ours. The values M_c were found to depend significantly on the fraction of guluronate.

Effects of Counterion Species on the Stresses of Alg Gels. Figure 10 shows also the values M_c and M/M_c of Ba-, Sr- and PbAlg gels prepared in 0.3 mol dm^{-3} solutions. The results of M_c/g mol^{-1} and $\bar{M}/M_c$ were $4.5\cdot10^4$ and 2.9 for BaAlg, $6.0\cdot10^4$ and 2.2 for SrAlg, and $6.0\cdot10^4$ and 2.2 for PbAlg. The values $\bar{M}/M_c$ of Alg gels were found to vary slightly with the counterion species in the range of 2.2—2.9. As shown in Fig. 8, it is interesting that G_e and G_r of Alg gels are dependent on the kinds of counterions but their τ values are almost the same. The differences in these elastic properties of Alg gels formed by various divalent counterions can be explained by the following two reasons: (1) The junctions intermediated by these counterions differ in their strength, i.e., the contributions to the elastic moduli depend on the kind of divalent counterions. (2) All the guluronate blocks (G-blocks) can not be used for the formations of the crosslinks, and the ratios of the G-blocks used for the junctions differ by the kind of divalent counterions.

O. Smidrod et al. showed that on increasing the fraction of guluronate in Alg the selectivities for divalent ions became clear and decreased in the order, Ba^{2+}> Sr^{2+}>Ca^{2+}≫Mg^{2+}.[4] The magnitudes of G_e of Alg gels decreased in the order, Ba-≫Ca->Sr->PbAlg as shown in Fig. 8. BaAlg showed the maximum values in both properties. Although the orders of Ca and Sr are different between the elasticity and the selectivity, the difference in elasticities of Ca- and SrAlg was slight. MgAlg did not gell and the elasticity should be 0. Then, it can be summarized that the bigger are the selectivities, the bigger are the elasticities.

Guluronic units in the G-blocks take 1C conforma-

tions and form cavities with very hydrophilic inner surface in which the closest distance between the carboxylate groups is 4.7—5.7 A.[17] The junctions of Alg gels are formed by the stackings between the G-blocks intermediated by divalent counterions, which are efficiently coordinated by both carboxylate groups on the inner surface and oxygen atoms of saccharide rings. Taking the hydrophilicity of the cavities in considerations, the stackings between the G-blocks can be intermediated by hydrated counterions. The radii of hydrated ions r_i have been studied by various methods. We discuss qualitatively the relation between G_e of Alg gels and r_i of hydrated ions used for the gelation. The values r_i obtained by Stokes are r_{Mg}=4.4, r_{Ca}=4.2,r_{Sr}=4.2, r_{Ba}=4.1, and r_{Pb}=3.9 Å, respectively.[18] BaAlg possessed the maximum G_e. The size of hydrated Ba ions is considered to be the most suitable for intermediating the stackings of the G blocks and for forming stable junctions. As r_i of counterions are apart from r_{Ba}, weaker junctions are formed. Since r_{Mg} is too large to form stable junctions, Alg can not be gelled by Mg ions.

References

1) A. Haug, B. Larsen, and O. Smidsrod, *Carbohydr. Res.*, **32**, 217 (1974).

2) O. Smidsrod, *Faraday Discuss. Chem. Soc.*, **57**, 263 (1974).

3) O. Smidsrod, A. Haug, and B. Lian, *Acta Chem. Scand.*, **26**, 71 (1972).

4) O. Smidsrod and A. Haug, *Acta Chem. Scand.*, **26**, 79 (1972).

5) Y. F. Leung, G. M. O'Shea, M. F. A. Goosen, and A. M. Sun, *Artif. Organs*, **7**, 208 (1983).

6) H. Tanaka, M. Matsumura, and I. A. Veliky, *Biotechnol. Bioeng.*, **26**, 53 (1984).

7) M. Yonese, K. Baba, and H. Kishimoto, *Bull. Chem. Soc. Jpn.*, **61**, 1077 (1988).

8) E. R. Morris, D. A. Rees, and D. Thom, *Carbohydr. Res.*, **81**, 305 (1980).

9) H. Grasdalen, B. Larsen, and O. Smidsrod, *Carbohydr. Res.*, **68**, 23 (1979).

10) M. Nakagaki, S. Shimabayashi, E. Hayakawa, and T. Kotsuki, *Yakugaku Zasshi*, **99**, 618 (1979).

11) D. Thom, G. T. Grant, E. R. Morris, and D. A. Rees, *Carbohydr. Res.*, **100**, 29 (1982).

12) E. R. Morris, D. A. Rees, and D. Thom, *Carbohydr. Res.*, **66**, 145 (1978).

13) A. J. M. Segeren, J. V. Boskemp, and M. Van Den Temple, *Faraday Discuss. Chem. Soc.*, **57**, 255 (1974).

14) J. R. Mitchell, *J. Texture Studies*, **7**, 313 (1976).

15) J. R. Mitchell, and J. M. V. Blanshard, *J. Texture Studies*, **7**, 219 (1976).

16) P. J. Flory, "Principles of Polymer Chemistry," Cornell University Press, New York (1953), Chap. XI.

17) O. Smidsrod, A. Haug, and S. G. Whittington, *Acta Chem. Scand.*, **26**, 2563 (1972).

18) R. A. Robinson and R. H. Stokes, "Electrolyte Solution," Butterworths, London (1959), p. 126.

 © 1988 The Chemical Society of Japan Bull. Chem. Soc. Jpn., 61, 1865—1872 (1988)

NMR Study of Dynamics of Carboxyl Proton in Crystals of Acetylenedicarboxylic Acid and *p*-Nitrobenzoic Acid

Nobuyoshi IMAOKA,† Sadamu TAKEDA,* and Hideaki CHIHARA
Department of Chemistry, Faculty of Science, Osaka University, Toyonaka, Osaka 560
(Received November 30, 1987)

Two kinds of motions of proton in dimeric carboxyl group were distinguished by the temperature dependence of spin-lattice relaxation times of dipolar system (T_{1d}) and of Zeeman system (T_{1z}) on acethylenedicarboxylic acid (ADCA) and on *p*-nitrobenzoic acid (PNBA) in the *A2/a* form. High temperature motion of ADCA is 180° rotation of the eight-membered ring of dimeric carboxyl group about the axis nearly parallel to the hydrogen bonds. The activation energy of this motion of ADCA is 58 kJ mol^{-1}. The low temperature motion of ADCA and PNBA is the proton translation along the hydrogen bonds in a dimeric carboxyl group, which induces the minima of T_{1z} and T_{1d} at the same temperature. The activation energy derived from the high temperature slope of T_{1z} curve is 6.9 kJ mol^{-1} for ADCA and 2.5 kJ mol^{-1} for PNBA. The low temperature slope gives a small activation energy of 1.9 kJ mol^{-1} for ADCA and 1.0 kJ mol^{-1} for PNBA. The frequency dependence of T_{1z} in the low temperature limit was constant at low Larmor frequency. This result indicates that the translational motion of protons along the hydrogen bonds is not classical but quantum-mechanical.

Coupled motion of atoms, radicals, or molecules in solids is one of very interesting problems of molecular dynamics. We have been interested in the rotational tunneling of methyl groups in solids for some time.[1] In many cases, there are evidences of coupling of such motion between neighboring methyl groups. The strength of this coupling is considered to be determined primarily by the spacial proximity of neighboring methyl groups.

In the case of the eight-membered ring of carboxyl group dimer, two tautometric forms may exist by alternating the chemical bonds (single and double bonds) and the hydrogen bonds as shown in Fig. 1. Two hydrogen atoms in such an eight-membered ring must move in a concerted way along the hydrogen bonds during the alternation, i.e. the motion of the hydrogens must be a coupled transfer. The configurations, I and II, have the same energy in the isolated state (i.e. in gas phase) but in general have different energies in the solid state due to interaction with other molecules. Thus, the configurations can not be distinguished in the gas phase,[2] whereas different populations between I and II are seen in the solid state.[3]

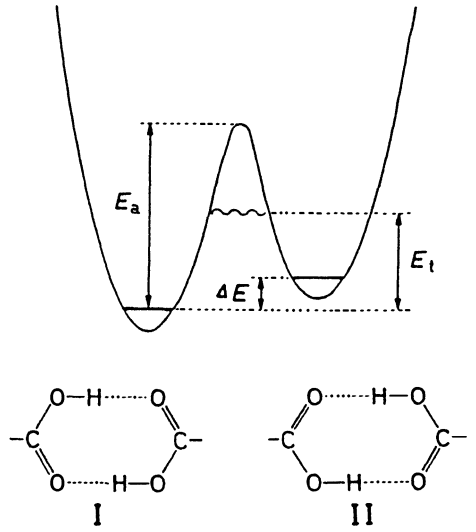

Fig. 1. Schematic view of double minimum potential of proton translation in a dimeric carboxyl groups and two corresponding configurations.

In recent years, the dynamics of protons in the carboxyl group dimers in solids has been investigated by nuclear magnetic resonance[4-6] and neutron scattering methods.[7-9] Meier et al.[4] and Nagaoka et al.[6] found a broad, shallow minimum in the temperature dependence of the proton spin-lattice relaxation time of the Zeeman system T_{1z} for several carboxylic acid dimers. This spin-lattice relaxation behavior can not be interpreted in terms of a classical, simultaneous hopping motion of the two protons between the unequal potential wells which correspond to the states I and II. For example, the activation energy derived from the low temperature side of the T_{1z} minimum is smaller than that from the high temperature side, contrary to the prediction that classical hopping motion of protons must result in a steeper slope of T_{1z} on the low temperature side of the minimum than on the high temperature side. Meier et al. and Nagaoka et al. assigned this T_{1z} minimum to the concerted translational motion of the protons along the hydrogen bonds in the eight-membered ring and also suggested that the quantum-mechanical tunneling effect played an important role in this motion. The temperature dependence of the correlation time of the translational motion of protons was explained by Meyer and Ernst[10] by the pocket state model of the tunneling motion. A preliminary model of the spin-lattice relaxation due to this tunneling mode was proposed by Nagaoka et al.[6] but the detailed nature of the spin relaxation due to tunneling is not known. We are much interested in the tunneling dynamics of the protons in this system and in particular what features will appear in the observables of the

† Present address: Central Laboratry, Asahi Chemical Industry Co., Ltd., 2-1, Samejima, Fuji, Shizuoka 416.

NMR as a result of such proton tunneling. Thus, we report in this paper several remarkable properties of observables of NMR, i.e. spin-lattice relaxation time of the Zeeman system (T_{1z}) and of the dipolar system (T_{1d}) and the shape of the absorption line for acetylenedicarboxylic acid and *p*-nitrobenzoic acid. Nagaoka et al.[6] also measured T_{1z} of *p*-nitrobenzoic acid but they dealt with a polymorphic phase different from the one of the present study.

The conversion between the states I and II in Fig. 1 is also possible by another mechanism, i.e. 180° rotation about the long axis, which is claimed by Furic.[11] There has been some controversy about the mechanism by which the conversion occurs. The initial and final states are the same in both mechanisms for some observables but the nature of the processes and the relevant energy level structure will be very different from each other.

Experimental

Materials. Acetylenedicarboxylic acid (hereafter called ADCA) was purchased from Tokyo Chemical Industry, Co., Ltd. and was further purified. Two kinds of samples were prepared. One was purified by recrystallization from dry diethyl ether solution in an evacuated closed system, keeping the specimen away from humidity. The other was purified by vacuum sublimation from 360 K onto a 273 K tip. Chemical analysis gave the relative masses, C 42.02%, H 1.83%; calculated for $C_4H_2O_4$: C 42.12%, H 1.78%. The differential thermal analysis of this specimen showed no peaks between 77 and 440 K. For the NMR measurements, these specimens were degassed in the glass ampules which were sealed off with helium gas of 2 kPa for heat exchange. Raman scattering experiment was performed on the recrystallized specimen which was sealed into a glass capillary with helium gas at 50 kPa.

p-Nitrobenzoic acid (PNBA) was purchased from Nakarai Chemicals and was recrystallized three times from methanol solution. Small single crystals were obtained. Analysis gave C 50.13%, H 2.97%, N 8.30%; calculated for $C_7H_5NO_4$ were C 50.31%, H 3.02%, N 8.38%.

Two polymorphic forms of PNBA have been known with the space groups, $P2_1/c$ (a=5.043, b=5.153, c=24.692 Å, β=96.89°, Z=4)[12] and $A2/a$ (a=12.918, b=5.042, c=21.298 Å, β=96.66°, Z=8).[13] The specimen we used for the NMR measurements was identified to be the $A2/a$ modification from the lattice parameters, a=12.9, b=5.04, c=21.2 Å and β=95°, from the X-ray Weissenberg photograph. It was confirmed by powder X-ray diffraction that the recrystallized PNBA was clearly different from sublimed PNBA in structure, the latter being used by Nagaoka et al. for their NMR measurements.[6] Here, we note that the differential thermal analysis of sublimed specimen showed a very small exothermic peak at about 100 K in the cooling direction, whereas the recrystallized specimen showed no anomaly between 80 and 510 K.

There was a suspicion that the sublimed specimen was in a metastable phase, which was transformed into a more stable form on cooling. An attempt to detect the thermal anomaly in the heating direction of DTA was not successful because it is the region of large drift in the DTA output. However, the diffraction pattern of a sublimed PNBA that had been anealed at 77 K was the same as that of the virgin sublimed sample. Therefore, the thermal anomaly as seen in the sublimed PNBA at about 100 K must be due to a reversible phase transition. The recrystallized specimen was pulverized and it was treated in the same way as for ADCA for NMR and Raman experiments.

Measurements. The proton spin-lattice relaxation time of the Zeeman system (T_{1z}) was measured by the 90° train-τ-90° pulse sequence; the relaxation times obtained by this method were confermed to be the same as those by the 180°-τ-90° method at several temperatures above 77 K. The length of 90° pulse was typically 1.3 μs. The dependence of T_{1z} on the intensity of external field was measured by the field cycling technique.[1] The spin-lattice relaxation time of the dipolar system (T_{1d}) was measured by the $90°_x$-t-$45°_y$-τ-$45°_y$ pulse sequence. The T_{1z}-process and T_{1d}-process of ADCA and PNBA could be expressed by a single exponential function except in the very low temperature region of ADCA. The absorption line shapes of ADCA and PNBA were recorded by the home-built Robinson type and Pound-Watkins type spectrometers. The width of field modulation was $2H_m$=0.85 G**. The temperature of the specimen was automatically kept constant within ±0.1 K during a measurement and was measured by a Chromel-P-Constantan thermocouple above 15 K and by Au/Fe-Chromel-P thermocouple and a germanium resistance thermometer below 15 K.

Results and Discussion

Identification of Two Types of Molecular Motions and 180° Rotation of Dimeric Carboxyl Group.

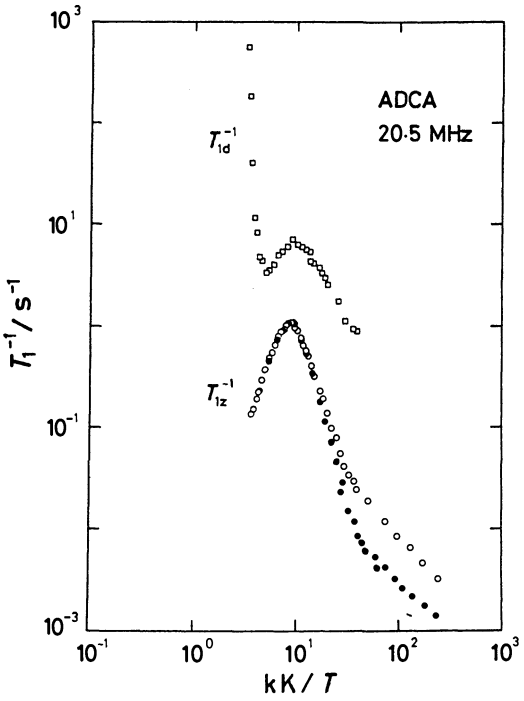

Fig. 2. Log-log plot of the spin-lattice relaxation rates of Zeeman system (O, ●) and of dipolar system (□) of acetylenedicarboxylic acid vs. inverse temperature. O, □ are for recrystallized sample and ● is for sublimed sample.

** 1G=10^{-4}T.

A. Acetylenedicarboxylic Acid. T_{1z}^{-1} and T_{1d}^{-1} curves of ADCA are shown in Fig. 2. Open circles and open squares are, respectively, T_{1z}^{-1} and T_{1d}^{-1} of the recrystallized specimen and closed circles are T_{1z}^{-1} of the sublimed specimen. It was found that the absolute values of T_{1z}^{-1} in the low temperature region ($T<25$ K) depended on the method of preparation. This result suggests that the relaxation process below 25 K is not an intrinsic property of ADCA crystal. We will shortly discuss the low temperature relaxation. The magnetization recovery was described by two exponential functions, i.e. fast relaxing component and slowly relaxing component, rather than by a single exponential function. We derived T_{1z}^{-1} (ex.) from the slowly relaxing component, because the magnetization of fast relaxing component was only about 20% of equilibrium value even at 4.2 K and disappeared at about 15 K. T_{1z}^{-1} (ex.) varied linearly with $H_0^{-1/2}$ (H_0: external magnetic field) and with T. We thus subtracted the extrapolated value of this extrinsic contribution from the observed relaxation rate (T_{1z}^{-1} (obs.)) to obtain the intrinsic relaxation rate (T_{1z}^{-1} (in.)) above 25 K,

$$T_{1z}^{-1}\,(\text{in.}) = T_{1z}^{-1}\,(\text{obs.}) - T_{1z}^{-1}\,(\text{ex.}). \qquad (1)$$

T_{1z}^{-1} (in.) and T_{1d} are shown in Fig. 3. There are two types of molecular motions which are effective on T_{1d} in different temperature regions. We will now consider three types of motions of protons in a dimeric carboxyl groups. These are (i) coupled translation of the two protons along the hydrogen bonds in a dimeric unit, (ii) 180° rotation of this eight-membered ring about the axis nearly parallel to the hydrogen bonds, and (iii) proton diffusion from a dimer to another.

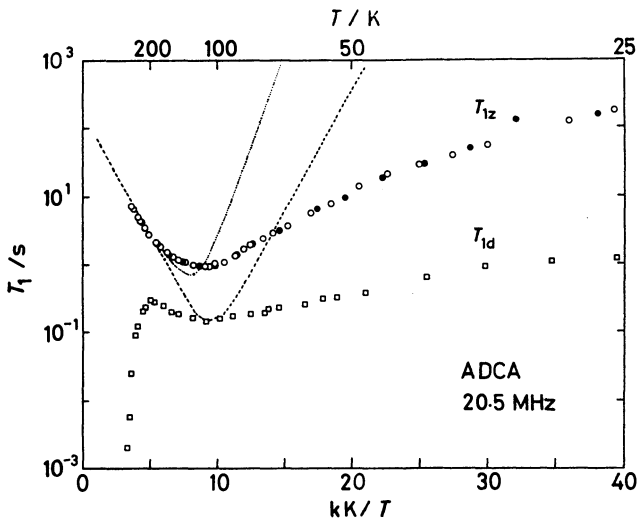

Fig. 3. Temperature dependence of the spin-lattice relaxation times of Zeeman system (O, ●) and of dipolar system (□). The extrinsic contribution to observed T_{1z}, which is seen in the low temperature region ($T<25$ K) in Fig. 2, are subtracted. The broken and dotted curves are the calculated T_{1z} for ΔE=0.2 kJ mol^{-1} and for ΔE=2.9 kJ mol^{-1}, respectively (see in the text).

Only the motion (i) of these three modes has a low enough potential barrier to induce "quantum-mechanical motion." It is noted that the minima of T_{1z} and T_{1d} occur at about the same temperature, 110 K in the case of ADCA (Fig. 3) and 70 K in the case of PNBA, as will be described below. This behavior cannot be expected from any classical random motion. Such a nonclassical behavior of the spin relaxation in the low temperature region will be discussed in detail in the following section (*Quantum mechanical behavior of*···). In contrast, the high temperature behavior of T_{1z} and T_{1d} must arise from slow classical motion because a much larger activation energy is involved. Therefore, it is reasonable to assess that the low temperature motion is of type (i) and high temperature motion is of either type (ii) or (iii); it may be possible to decide on the latter from the line shape measurement.

Typical differential absorption lines of ADCA at several temperatures are reproduced in Fig. 4. The width of the central line, which became observable at a higher temperature, was determined by the width of field modulation even if the modulation width was made as small as possible ($2H_m<0.1$ G). The intensity of this narrow component depended on the method of preparation of the sample, i.e. the intensity of recrystallized specimen was about 30 times larger than that of sublimed specimen. We ignore the contribution of this narrow component to the second moment for the moment and come back to this point in section C. The line shape below 150 K did not depended on the method of preparation.

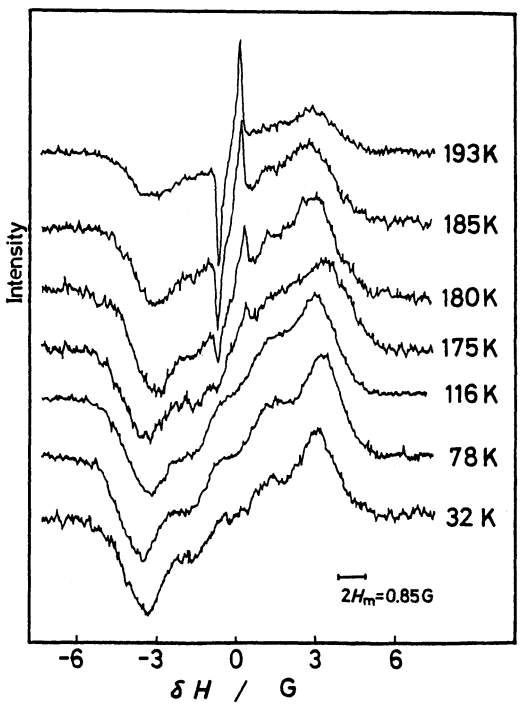

Fig. 4. The typical differential absorption line of recrystallized acetylenedicarboxylic acid at several temperatures.

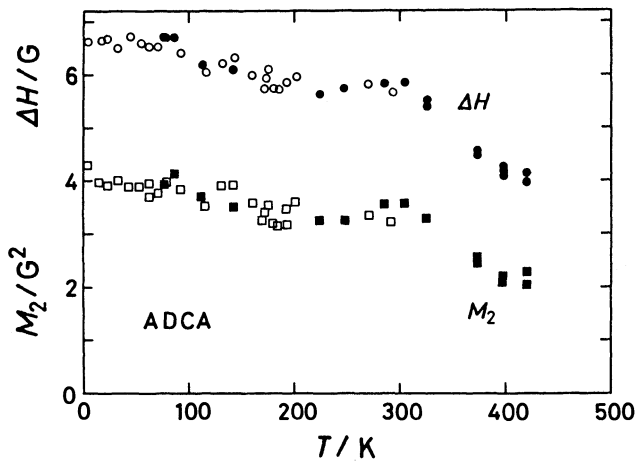

Fig. 5. The temperature dependence of maximum slope width (○, ●) and second moment (□, ■) of acetylenedicarboxylic acid; ○, □ are for the recrystallized sample and ●, ■, are for the sublimed sample.

The temperature dependences of the maximum slope width (ΔH) and the second moment (M_2) are shown in Fig. 5. The reduction of second moment (ΔM_2) due to 180° rotation of the eight-membered ring was estimated as follows. The rigid lattice value of the second moment of ADCA was calculated to be M_2 (rigid)=3.53 G^2 or 2.03 G^2 by using the formula,[14]

$$M_2\,(\text{rigid}) = (3/5)\,\gamma^4\hbar^2\,\mathrm{I}(\mathrm{I}+1)\sum_{j,k} 1/R_{jk}^6. \qquad (2)$$

taking into account only the intradimer contribution. The distance between the two protons within a dimeric unit is known to be R_I=2.37 Å in one configuration and R_II=2.16 Å in the other by the X-ray diffraction experiment[15] as shown in Fig. 6. It was also shown by X-ray diffraction that the configuration with a proton distance of 2.37 Å has somewhat larger population.[15] The angle θ between the two proton vectors (see Fig. 6) is 51.6°.[15] As temperature is increased, the dipolar interaction between the two protons becomes partially averaged by the low temperature motion, fast coupled translation of the two protons along the hydrogen bonds. Therefore, the averaged orientation of the proton-proton vector can be chosen as indicated by the broken line in Fig. 6. The angle ϕ depends on the temperature and on the energy difference ΔE indicated in Fig. 1. The value of ΔE will be discussed in the following section (*Classical picture*). The magnitude of intradimer contribution to ΔM_2 that arises from the 180° rotation was estimated to be less than 0.5 G^2 by assuming that the two potential minima of the rotation have the equal depth. The observed reduction, 1 G^2, which also includes the contribution from the interdimer interaction, is close to the estimate. The diffusion of protons from a dimeric acid unit to another in the crystal should cause a very large decrease in the second moment but there is no such indication in Fig. 5. Thus the high temperature motion of ADCA is the 180° rotation of dimeric carboxyl groups. The activation energy of this motion is 58 kJ mol^{-1} which was obtained from the slope of T_{1d}.

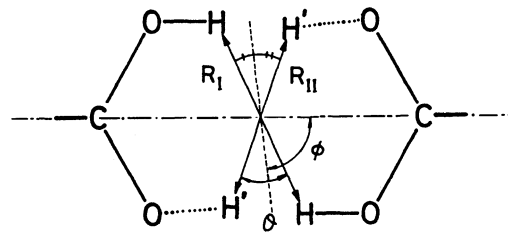

Fig. 6. The configuration of a dimeric carboxyl groups with two possible orientations of a proton-proton vector.

B. *p*-Nitrobenzoic Acid. The spin-lattice relaxation times, T_{1z} and T_{1d}, of PNBA are shown by closed circles and open squares, respectively, in Fig. 7. T_{1z} values measured at 59.53 MHz by Nagaoka et al.,[6] which are for the sublimed $P2_1/c$ modification, are also shown (○). The discrepancy between the T_{1z} values by us (●) and those by Nagaoka et al. (○) is clearly due to different polymorphic forms. It appears that the temperature variation of T_{1z} and $T_{1d}$of PNBA and that of ADCA are similar to each other (compare Figs. 3 and 7). There are also two types of molecular motions which are effective on T_{1d} in different temperature regions as in the case of ADCA and the minima of T_{1z} and T_{1d} at 70 K correspond to the translational motion of proton in a dimeric carboxyl group.

The differential line shape and maximum slope

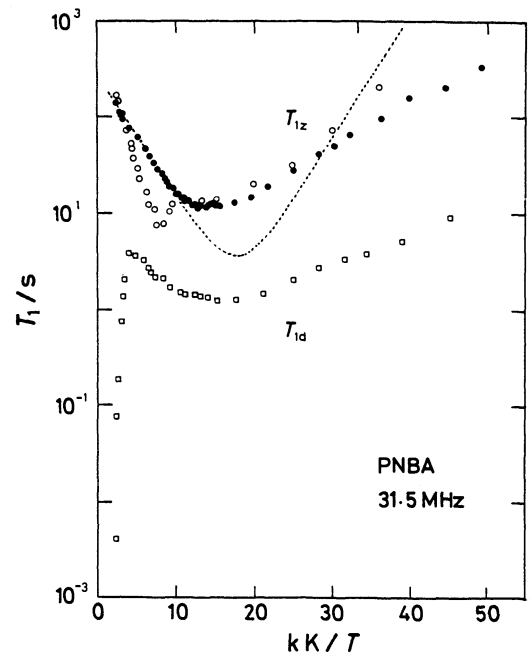

Fig. 7. Temperature dependence of spin-lattice relaxation times of Zeeman system (○, ●) and of dipolar system (□) of *p*-nitrobenzoic acid. ○ is observed at 59.53 MHz by Nagaoka et al.[6] The broken curve is the calculated T_{1z} from the classical formula (see in the text).

width of PNBA are shown in Figs. 8 and 9, respectively. The line shape of PNBA was very different from that reported by Gupta and Saxena.[16] Unlike the case of ADCA, the line width of PNBA stays constant up to 300 K. The apparent activation energy derived from the high temperature slope of T_{1d} of PNBA was 80 kJ mol^{-1}, larger than in the case of ADCA. The steep decrease of T_{1d} at high temperatures was observed for several carboxylic acid dimers and was attributed to the excitation of 180° flip motion of the dimer structure by Chiba for the first time.[17]

C. Narrow Component of Absorption Line of Acetylenedicarboxylic Acid. The narrow component of absorption line was observed at high temperature for sublimed and recrystallized ADCA as described above. It was also observed for α-oxalic acid at high temperature[18] but not for PNBA. The intensity of the narrow component of recrystallized and sublimed ADCA was reproducible during the several cycles of heating and cooling experiments. The narrow component was not due to any gaseous decomposition products because outgassing of the glass ampule did not change its intensity. The molecules of ADCA and oxalic acid have two carboxyl groups on both ends of a molecule (the head and the tail), which makes the exsistence of free carboxyl groups on certain crystal surface very plausible. In contrast, there will be no free carboxyl groups on the crystal surface of PNBA. Assuming that free carboxyl groups adsorb water strongly and, as a result, acid protons can migrate on the surface through hydrogen bonds, the narrow component of differential absorption line may be explained. From the temperature coefficient of the relative peak intensity (height) of this narrow component of the differential absorption line an energy difference of 20 kJ mol^{-1} was derived between the protons in the mobile state and in the static state for the recrystallized ADCA, which is close to the energy of an O-H···O hydrogen bond. The same value was obtained for the sublimed ADCA. Hence, the dependence of the intensity of narrow component on the method of preparation may be attributed to a difference in the water adsorbed area of the surface of the crystals.

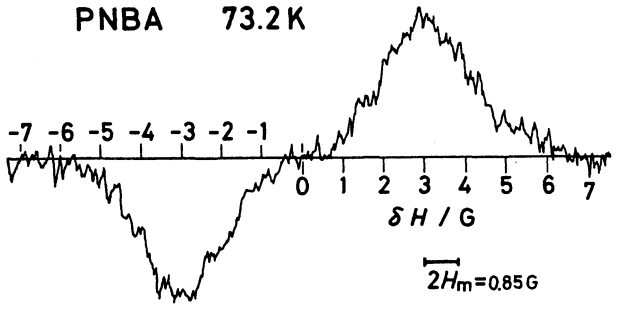

Fig. 8. The typical differential absorption line of *p*-nitrobenzoic acid.

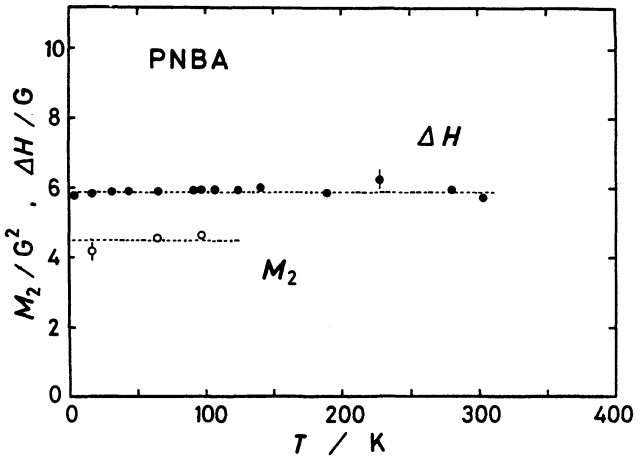

Fig. 9. Temperature dependence of the maximum slope width and second moment of *p*-nitrobenzoic acid.

Proton Translation Along the Hydrogen Bonds in a Dimer of Carboxyl Groups. A. Classical Picture. The translational motion of the two protons within a dimer of carboxyl group is probably the cause of the minimum of T_{1z} and T_{1d} as inferred in the preceding section. The temperature dependence of T_{1z} of PNBA and ADCA is very similar to that of other carboxylic acid dimers.[4-6] We will first attempt to calculate T_{1z} by a classical treatment of proton translation and compare the result of such calculation with the observed T_{1z}.

The spin-lattice relaxation formula due to classical hopping between unequal potential wells was derived[6]*** from a general expression of spin relaxation by Soda.[19] In general, T_{1z}^{-1} is given by

$$T_{1z}^{-1} = mC \sum_l A_l B(\tau_{cl}). \tag{3}$$

The sum is taken over the normal modes l of the molecular motion.[19] The coefficient, $C=(9/4)\gamma^4\hbar^2$, is the spin part of the dipolar interaction between the two protons and A_l is the structure-dependent coefficient for the normal mode l. The coefficient m denotes the fraction of the proton spins which relax directly due to motion among the total proton spins present in the crystal. In the present case of the dimeric carboxyl group, we take into account completely coupled translation of the two protons along the hydrogen bonds. T_{1z}^{-1} is then given by

$$T_{1z}^{-1} = mCAB(\tau_c) \tag{4}$$

where

$$B(\tau_c) = \tau_c/(1+\omega_0^2\tau_c^2) + 4\tau_c/(1+4\omega_0^2\tau_c^2)$$

$$A = (2/15)\,[a/(a+1)^2]\,[R_I^{-6} + R_{II}^{-6} + (1-3\cos^2\theta)R_I^{-3}R_{II}^{-3}]$$

$$a = \exp(\Delta E/RT)$$

$$\tau_c = [\tau_{c0}/(a+1)]\exp(E_a/RT).$$

R_i denotes the distance between the two protons in the i-th configuration and θ is the angle between the proton-proton vector of configurations I and II. Equa-

*** There is an error in the coefficient of Eq. 16 of Ref. 6.

tion 4 is of the same form as that given by Meier et al.[4] in the limit that $R_I=R_{II}$ and $\Delta E \ll E_a$ except for the coefficient A.

The values, ΔE, E_a, R_I, R_{II}, and θ which are necessary for the calculation of T_{1z}^{-1}, were obtained as follows. The energy difference (ΔE) between the two configurations of ADCA was derived from the temperature dependence of the integrated intensity of the Raman bands (O-H stretching vibrations; 2240 and 2280 cm^{-1}). Supposing that these two bands correspond to the different configurations, I and II, the energy difference, ΔE=0.2 kJ mol^{-1}, was derived from the temperature dependence of the relative intensity. The activation energy (E_a) was determined by assuming that on the high temperature side of the T_{1z} minimum the dominating motion is the classical jump over the top of the barrier. For such a classical jump motion, the slope of T_{1z} on the high temperature side of the T_{1z} minimum ($\omega_0\tau_c \ll 1$) is approximately described by $E_a-2\Delta E$ (when $a \gg 1$), and more generally it is described by the relation, ln $(T_{1z}^{-1}(a+1)^3) \propto (E_a+\Delta E)/RT$. The activation energy E_a=6.9 kJ mol^{-1} was thus derived. The values, R_I=2.37 Å, R_{II}=2.16 Å, and θ=51.6°, were calculated from the structural data.[15] T_{1z} calculated by use of these parameters is shown by the broken curve in Fig. 3. Stoeckli et al. recently determined the population difference between the two configurations (I and II) for ADCA from the quasi-elastic neutron scattering experiment.[9] The ratio of the populations was 0.2:0.8 at 250 K, from which energy difference ΔE was calculated to be 2.9 kJ mol^{-1}. T_{1z} was also calculated for ΔE=2.9 kJ mol^{-1} and is shown by the dotted curve in Fig. 3.

Similar calculation of T_{1z} was performed for PNBA (Fig. 7). Because of the absence of knowledge of the structure of configuration II, we assumed $R_I=R_{II}$=2.31 Å and θ=29.5° using the available structural data.[13] The energy difference between the two configurations, ΔE=0.2 kJ mol^{-1}, was obtained from the temperature dependence of the relative intensity of the Raman bands (3080 and 3090 cm^{-1}).

The parameters used in the calculations of T_{1z} of ADCA and PNBA are listed in Table 1.

B. Quantum Mechanical Behavior of Observables of NMR Due to Proton Tunneling. The observed temperature dependences of T_{1z} of ADCA and of PNBA are obviously not explained by the classical motion as shown in Figs. 3 and 7. Especially, the small temperature coefficients of T_{1z} at low temperatures are inexplicable (1.9 kJ mol^{-1} for ADCA and 1.0 kJ mol^{-1} for PNBA). The same behavior has already been pointed out by Nagaoka et al.[6] for several other carboxylic acid dimers.

The validity or failure of the classical model can be tested in another way. Thus, the ratio T_{1z}/T_{1d} is given by[20]

$$T_{1z}/T_{1d}=2+(1/3)\,\omega_0^2\tau_c^2 \qquad (5)$$

in the case that the dipolar field is modulated by random motion and therefore T_{1z}/T_{1d} should become progressively larger as the temperature is decreased ($\omega_0\tau_c \gg 1$). The experimental results, however, showed that T_{1z}/T_{1d} is almost constant even down to such low temperatures.

The frequency dependence of T_{1z} at low temperature limit also shows (Figs. 10 and 11) a large deviation

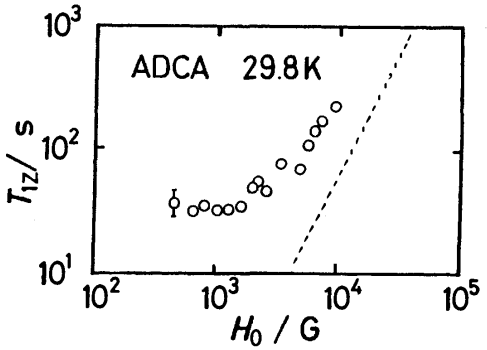

Fig. 10. Frequency (external field) dependence of spin-lattice relaxation time of Zeeman system of sublimed acetylenedicarboxylic acid.

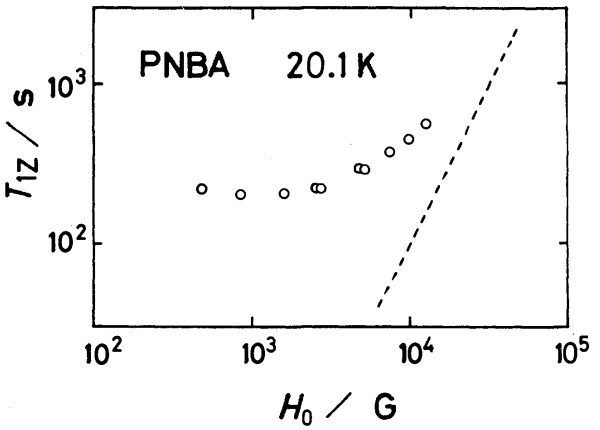

Fig. 11. Frequency (external field) dependence of spin-lattice relaxation time of Zeeman system of *p*-nitrobenzoic acid.

Table 1. Parameters of Proton Translation along the Hydrogen Bonds

	E_a/kJ mol^{-1}	ΔE/kJ mol^{-1}	τ_0/s	mCA'/s^{-2} [a]	R_I/Å	R_{II}/Å	θ/°	E_t/kJ mol^{-1}
ADCA	6.9	0.2	4.3×10^{-12}	2.45×10^{9}	2.16	2.37	51.6	1.9
	10.3	2.9[b]	3.0×10^{-12}	2.45×10^{9}	2.16	2.37	51.6	1.9
PNBA	2.5	0.2	3.7×10^{-12}	1.63×10^{8}	2.31	2.31	29.5	1.0

a) $A'=A/[a/(1+a)^2]$. b) Ref. 9.

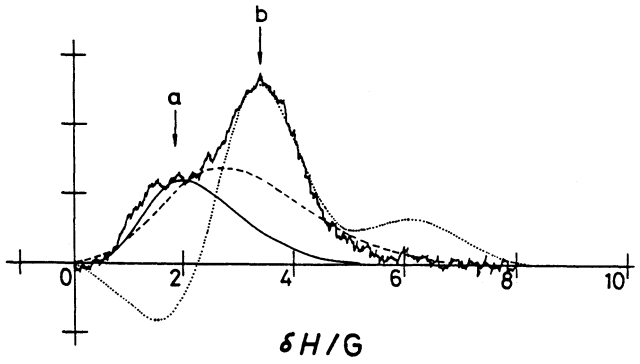

Fig. 12. A half of differential absorption line of ADCA at 4.2 K. Solid curve is the Pake doublet calculated using the parameters, proton distance r=2.37 Å and a Gaussian broadning factor β=0.8 G. Broken and dotted curves are the same calculations using the parameters r=2.16 Å (β=1.2 G) and r=1.9 Å (β=0.8 G), respectively.

from the classical prediction of H_0^2 dependence. It is obvious from this experimental result that some additional frequency terms other than the Larmor frequency must be involved in the spin relaxation formula. We can estimate that the additional frequency terms (ω') are of the order of $10^{7\pm1}$ Hz from Figs. 10 and 11. The value of H_0, at which T_{1z} begins to level off, is larger for PNBA than for ADCA. This means that ω' for PNBA is larger than for ADCA. The frequency, ω', must be connected to the tunneling rate (or tunneling frequency, ω_t) of proton translation along the hydrogen bonds.

Failure of the classical picture is also substantiated by the shape of absorption line at low temperatures (Fig. 12). It is not a simple Pake doublet[14] as one expects for an isolated proton pair like in the case of trichloroacetic acid[21] but there is another component in addition to a Pake doublet as demonstrated in Fig. 12. The peak **a** of Fig. 12 can be reproduced by the solid curve which is the Pake doublet calculated using the parameters, proton distance r=2.37 Å and a Gaussian broadning factor β=0.8 G.[14] The Pake doublet corresponding to the other configuration, r=2.16 Å (broken curve, β=1.2 G) can not explain the peak **b**. If we try to reproduce the peak **b** by a Pake doublet, we should take the parameters, r=1.9 Å and β=0.8 G (dotted curve). But there is no such a short distance between the protons. The shortest distance between the protons of different dimers of carboxyl group is 3.1 Å. Therefore the classical Pake treatment does not apply to ADCA at low temperature. The structure of the line shape disapeared, however, when the temperature was increased up to 190 K.

The more complete analysis of the line shape and its temperature dependence would require more detailed knowledge of the energy levels of the proton spin system.

Conclusion

There are two types of motions of protons in the crystals of ADCA and PNBA. The two motions are successively excited as temperature increases. At low temperatures, the protons jump between double minima along the hydrogen bond through tunneling mechanism. New evidences of proton tunneling were presented. The quantum effects are manifested not only in the temperature dependence of correlation time, τ_c, but also in the transition probability between the spin states, from which the detailed information about "tunneling" will be obtained. As the temperature is increased, the jump occurs also in the classical sense and at the same time the 180° rotation of the dimeric carboxyl group is gradually excited.

The authors would like to express their gratitude to Dr. Yasuhiro Takahashi of Department of Macromolecular Science of Osaka University for help provided in the X-ray diffraction experiment of PNBA. This work was partly supported by the Grant-in-Aid for Scientific Research No. 61430006 from the Ministry of Education, Science and Culture.

References

1) S. Takeda, G. Soda, and H. Chihara, *Solid State Commun.*, **36**, 445 (1980); S. Takeda and H. Chihara, *J. Phys. Soc. Jpn.*, **51**, 642 (1982); S. Takeda and H. Chihara, *J. Phys. Soc. Jpn.*, **54**, 3690 (1985); S. Takeda and H. Chihara *J. Magn. Reson.*, **54**, 285 (1983); S. Takeda and H. Chihara, Springer Proceedings in Physics **17**, "Quantum Aspects of Molecular Motions in Solids" 76 (1987).

2) C. C. Costain and G. P. Srivastava, *J. Chem. Phys.*, **41**, 1620 (1964).

3) S. Hayashi and J. Umemura, *J. Chem. Phys.*, **60**, 2630 (1974). S. Hayashi and J. Umemura, *J. Chem. Phys.*, **63**, 1732 (1975).

4) B. H. Meier, F. Graf, and R. R. Ernst, *J. Chem. Phys.*, **76**, 767 (1982).

5) S. Nagaoka, T. Terao, F. Imashiro, A. Saika, N. Hirota, and S. Hayashi, *Chem. Phys. Lett.*, **80**, 580 (1981).

6) S. Nagaoka, T. Terao, F. Imashiro, A. Saika, and N. Hirota, *J. Chem. Phys.*, **79**, 4694 (1983).

7) B. H. Meier, R. Meyer, R. R. Ernst, P. Zolliker, A. Furrer, and W. Haelg, *Chem. Phys. Lett.*, **103**, 169 (1983).

8) B. H. Meier, R. Meyer, R. R. Ernst, A. Stoeckli, A. Furrer, W. Haelg, and I. Anderson, *Chem. Phys. Lett.*, **108**, 522 (1984).

9) A. Stoeckli, A. Furrer, Ch. Shoenenberger, B. H. Meier, R. R. Ernst, and I. Anderson, *Physica*, **136B**, 161 (1986).

10) R. Meyer and R. R. Ernst, *J. Chem. Phys.*, **86**, 784 (1987).

11) K. Furic, *Chem. Phys. Lett.*, **108**, 518 (1984); K. Furic, *Chem. Phys. Lett.*, **117**, 394 (1985).

12) P. Groth, *Acta Chem. Scand.*, **A34**, 229 (1980).

13) M. Colapietro and A. Domenicano, *Acta Crystallogr.*, **33**, 2240 (1977).

14) A. Abragam, "Principle of Nuclear Magnetism,"

Oxford (1961), Chap. IV and VII.
15) V. Benghiat, L. Leiserowitz, and G. M. J. Schmidt, *J. Chem. Soc., Perkin Trans. 2*, **1972**, 1769.
16) R. C. Gupta and M. Saxena, *Indian J. Pnys.*, **46**, 76 (1972).
17) T. Chiba, to be published.
18) N. Imaoka, S. Takeda, and H. Chihara, unpublished results.
19) G. Soda, *Kagaku no Ryoiki*, **28**, 799 (1974); S. Takeda, G. Soda, and H. Chihara, *Mol. Phys.*, **47**, 501 (1982).
20) M. Goldman, "Spin Temperature and Nuclear Magnetic Resonance in Solids," Oxford (1970), Chap. 3.
21) M. Goldman, *J. Phys. Chem. Solids*, **7**, 165 (1958).

 © 1988 The Chemical Society of Japan Bull. Chem. Soc. Jpn., 61, 1873—1886 (1988)

Excited-State Reactions of Coumarins. VII. The Solvent-Dependent Fluorescence of 7-Hydroxycoumarins

Tetsuo MORIYA
Electrotechnical Laboratory, Umezono, Tsukuba, Ibaraki 305
(Received December 2, 1987)

The excited-state reactions of 7-hydroxycoumarin (7HC) and 7-hydroxy-4-methylcoumarin (7H4MC) have been studied by measuring the absorption and fluorescence spectra in aqueous and organic solvents under acidic and basic conditions. Based on the solvent-dependent fluorescence of the fluorophores, the solvents could be classified into several groups: hydroxylic solvents, nonhydroxylic solvents with low dielectric constants, and those with high dielectric constants. In the hydroxylic solvent, protonation, deprotonation, and tautomerization were the main reactions, while in the nonhydroxylic solvent the formation of hydrogen bonding and ion pairs was essential. The fluorescence in water-ethanol mixtures and in aqueous sodium dodecyl sulfate solutions has also been examined in relation to the solvent-dependent spectra in pure hydroxylic and nonhydroxylic solvents.

The complicated behavior of the fluorescence from 7-hydroxycoumarins has been extensively studied in organic solvents and in neutral, acidic, and basic aqueous solutions.[1-4] Four fluorescent species have typically been observed in the photoexcited state, depending on the pH of the solution; they are identified as neutral, anionic, tautomeric, and protonated forms of the excited molecule. The reactions which generate these excited species are affected by the solvent so strongly that a careful examination of the fluorescence spectra, as well as the absorption spectra, is inevitable if we are to reach a correct conclusion. Basically, the solvents should be classified into two general groups in order to explain reasonably the fluorescent behavior of solvent-sensitive fluorophores; one group consists of "hydroxylic" solvents with hydroxyl substituents (-OH), and the other, of "nonhydroxylic" solvents without -OH. Such a classification is extremely meaningful, because the hydrogen-bonding ability and the ionizing power of the solvent determine in many ways the reaction process in excited states, such as the phototautomerization discussed in Ref. 4. As may readily be supposed, water, alcohols, water-organic mixtures, and aqueous solutions of surfactants belong to the hydroxylic-solvent group. Many of the aliphatic and aromatic solvents without -OH are nonhydroxylic solvents; the fluorescent behavior of the 7-hydroxycoumarins in these solvents is very different from that in the hydroxylic solvent. The purpose of the present study is to find a reasonable explanation of the solvent-dependent fluorescence by means of a unified model, one which includes the tautomerization, the acid-base reaction, and the ion pair formation with various additives.

Experimental

Commercial-grade reagents of 7-hydroxycoumarin (7HC, Wako Pure Chemical) and 7-hydroxy-4-methylcoumarin (7H4MC, Tokyo Kasei) were purified by recrystallization from ethanol and then washed with diethyl ether; 7HC, mp 234 °C; 7H4MC, mp 186 °C. The organic solvents were of a spectroscopic grade from Dojindo Laboratories. The perchloric acid, hydrochloric acid, triethylamine (TEA), and butylamine (BA) were of a pure quality. The sodium dodecyl sulfate (SDS, Wako Pure Chemical) was of a biochemical grade. The water was permeated and distilled. The acidity and basicity of the solution were adjusted by the addition of $HClO_4$ and TEA (or BA) respectively.

The UV absorption spectra were obtained on a Hitachi 323 spectrophotometer, while the fluorescence spectra were measured on a Hitachi MPF 4 spectrofluorometer with an S-5-type photomultiplier. The concentration of fluorescent molecules in the solutions was ca. $4—5\times10^{-5}$ mol dm^{-3}. Spectral measurements were performed at 20 or 25 °C by controlling the temperature of the cell holder.

Results and Discussion

General Scheme for Excited-State Reactions. In a previous study,[4] the complex pH-dependence of the absorption and fluorescence spectra of 7HC and 7H4MC in aqueous solutions has been fully analyzed; the results may be summarized as follows. In the electronic ground state, there exist neutral molecular species (N) or anionic molecular species (A^-), depending on the pH of the solution. If the pH is changed from neutral to basic, the molecule is deprotonated at the 7-hydroxyl group:

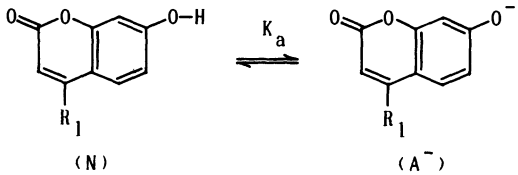

(1)

(N) (A⁻)

R_1=H, 7HC; R_1=CH_3, 7H4MC

The absorption maxima of N and A^- in the aqueous solutions were at 324 and 366 nm (7HC), and at 321 and 361 nm (7H4MC), respectively; 7HC, pK_a=7.75; 7H4MC, pK_a=7.84.[5] Additionally, the absorption band corresponding to the cationic species (C^+), protonated at the 2-carbonyl group, was found at 353 nm (7HC) and 345 nm (7H4MC) in concentrated sulfuric acid ($H_0<-6$).[6] The absorption bands aligned in

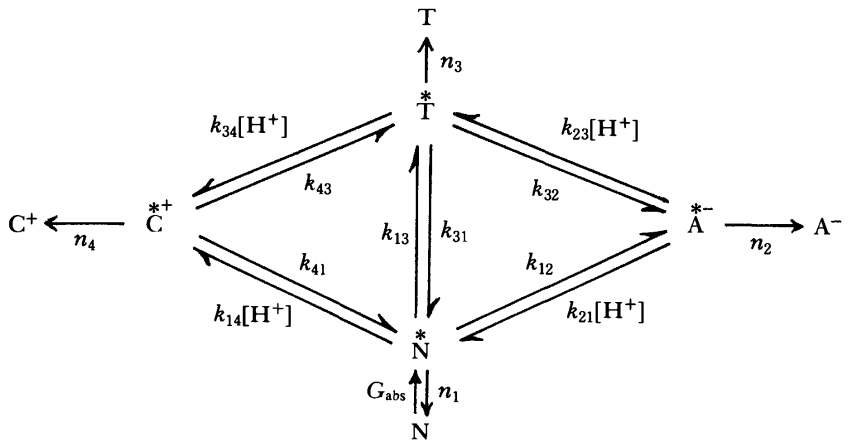

Scheme 1.

wavelength as $N<C^+<A^-$.

When N was optically excited at around its absorption-peak wavelength, the fluorescence from four molecular species in the excited state were observed with the variation in the pH. One was a usual neutral molecule ($\overset{*}{N}$), and another was a tautomeric molecule ($\overset{*}{T}$), in which a hydrogen of the 7-hydroxyl group was transferred to the 2-carbonyl group; contrary to the case of N, A^-, and C^+, the ground state of $\overset{*}{T}$ could never be found by absorption measurements. Analogously to the ground states, an excited cation ($\overset{*+}{C}$) and an excited anion ($\overset{*-}{A}$) were formed in strongly acidic solutions and in basic solutions respectively. A unified scheme for the excited-state reactions may be depicted as Scheme 1.[4] Here, G_{abs} is the generation rate of $\overset{*}{N}$, while the n_j's are the transition rates of the excited species to their ground states. The k_{ij}'s and $k_{ji}[H^+]$'s are the protonation and deprotonation rates of the neutral, anionic, and cationic molecular forms in the excited state. k_{13} and k_{31} represent the reaction rates of the tautomerization that does not involve stepwise protonation or deprotonation processes, i.e., the "nondissociative" reaction rates.[4,7] In aqueous solutions, the fluorescence-peak wavelengths of $\overset{*}{N}$, $\overset{*+}{C}$, $\overset{*-}{A}$, and $\overset{*}{T}$ were 397, 431, 453, and 478 nm for 7HC, and 390, 419, 447, and 474 nm for 7H4MC, respectively. If A^- was selectively excited by choosing the wavelength in a neutral or basic solution, the situation became simple, because the fluorescent species was restricted to the anionic form ($\overset{*-}{A}$) alone; this comes from the fact that $\overset{*-}{A}$ is energetically most stable among the photoexcited states:[4]

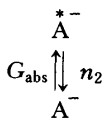

Scheme 2.

Fluorescence Behavior in Hydroxylic Solvents. As hydroxylic solvents, isobutyl alcohol (*i*-BuOH, $D\cong$ 18.3), isopropyl alcohol (*i*-PrOH, 18.6), ethanol (EtOH, 25.0), methanol (MeOH, 32.4), and water (H_2O, 80.4) were employed, where D represents the static dielectric constant of the solvents at 20 °C.[8] The "acidic" and "basic" conditions have been realized by adding 0.29 mol dm^{-3} $HClO_4$ and 0.22 mol dm^{-3} TEA respectively to the solutions of 7HC and 7H4MC. The "strongly acidic" conditions have been attained by adding ca. 6 mol dm^{-3} $HClO_4$, and the "strongly basic" conditions, by adding TEA or BA up to ca. 4 mol dm^{-3}. In order to visualize the fundamental aspect

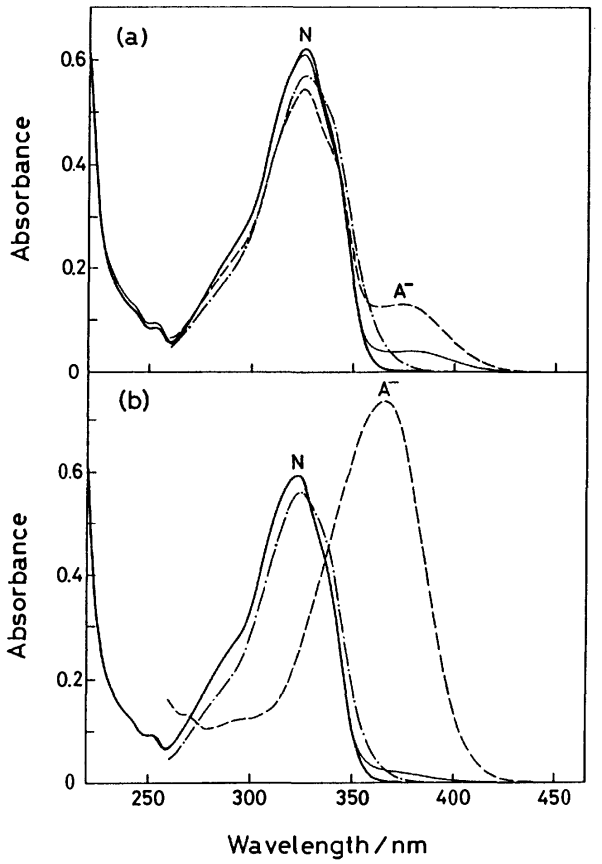

Fig. 1. UV absorption spectra of 7H4MC in *i*-BuOH (a) and in MeOH (b) for the neutral (——), acidic (——), strongly acidic (-·-·-), and basic (– – –) solutions at 20 °C.

of electronically ground states, the absorption spectra of 7H4MC in *i*-BuOH are compared to those in MeOH in Fig. 1. Only the N absorption band is observable in the acidic *i*-BuOH and MeOH solutions, while C^+ coexists with N in the strongly acidic solutions, as is shown by the shoulder on the long-wavelength side of the absorption spectra. The pure C^+ state was ultimately reached in concd. H_2SO_4 ($D \approx 101$ at 25 °C) and was observed at ca. 345 nm. The A^- band is found as a shoulder around 375 nm in the neutral and basic *i*-BuOH and in the neutral MeOH. In the basic MeOH, on the other hand, the pure A^- absorption peaking at 365 nm is observed as a result of the dissociation of 7-OH. When the strongly basic condition was attained by the addition of up to 4 mol dm^{-3} of BA, the 7-OH group was completely dissociated, even in solvents less polar than MeOH. Since the molar extinction coefficients (ε) at the pure A^- absorption peak are thus measurable for all the hydroxylic solvents, the dissociation ratio of the fluorophore, $[A^-]/([A^-]+[N])$, at a given basicity of the solution can be evaluated by $\varepsilon^A/\varepsilon_p^A$, where ε_p^A is the value for the pure A^- state, and ε^A, for the A^- contribution under the present experimental conditions. Figure 2 presents the dependence of $[A^-]/([A^-]+[N])$ on $1/D$ in solutions containing 0.22 mol dm^{-3} of TEA. Based on the dissociation process of 7H4MC, the ionizing power of the hydroxylic solvents can be qualitatively estimated as $H_2O \approx$ MeOH<EtOH<*i*-PrOH$\approx$*i*-BuOH. Irrespective of the drastic change in the ionizing power of the solvents, the spectral shape of each absorption band was similar in the solvents, whereas its peak was gradually blue-shifted with the increase in the D value (see Table 1).

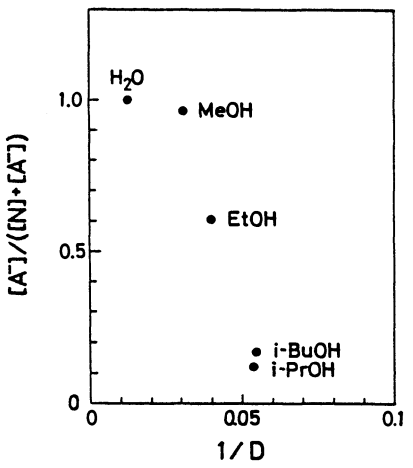

Fig. 2. Plots of the dissociation ratio, $[A^-]/([A^-]+[N])$, vs. $1/D$ in the basic hydroxylic solvents with 0.22 mol dm^{-3} TEA.

Bearing the ground-state behavior in mind, the fluorescence spectra of 7H4MC in the neutral, acidic, strongly acidic, and basic solutions have been studied in detail; some typical spectra in MeOH are shown in Fig. 3. In spite of the complex behavior, the phenomena were common throughout the hydroxylic solvents, and either Scheme 1 or Scheme 2 was again applicable. When the light illumination was actuated at ca. 320 nm in the neutral, acidic, and strongly acidic solutions, Scheme 1 could be applied, for only the neutral excited species $\overset{*}{N}$ was generated by the light absorption; in contrast, when excitation was done at ca. 360 nm in the basic solution, Scheme 2 was applied. The peak wavelengths of the fluorescence bands

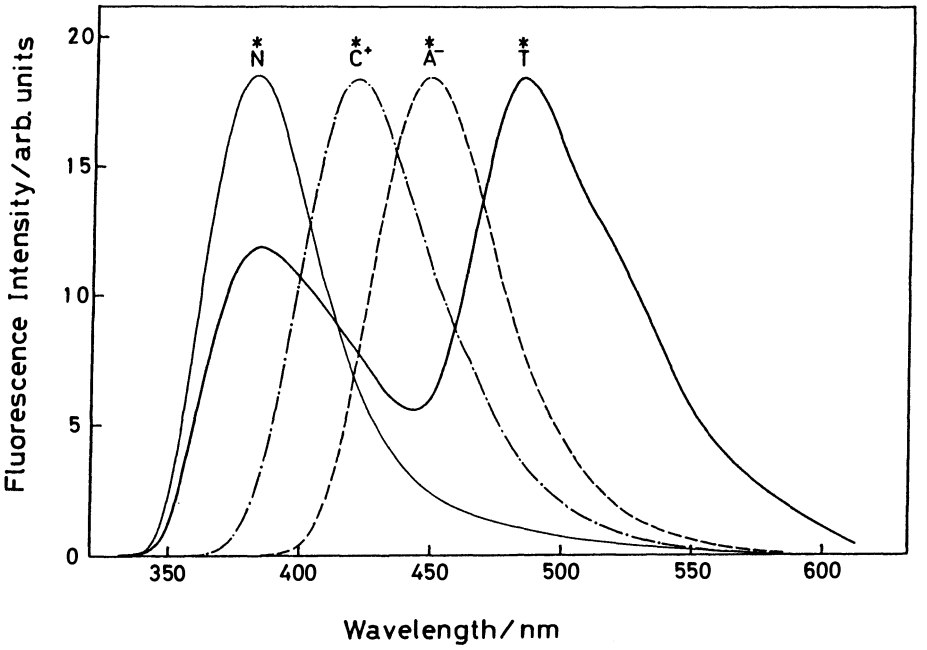

Fig. 3. Fluorescence spectra of 7H4MC in MeOH at 20°C. The excitation wavelength was 320 nm for the neutral (——), acidic (——), and strongly acidic (—·—·—) solutions, and was 380 nm for the basic (----) solution.

Table 1. Peak Positions of the Absorption and Fluorescence Spectra of 7H4MC in the Hydroxylic Solvents under Neutral, Acidic, and Basic Conditions at 20 °C

Solvent	D^{20}	Absorption			Fluorescence			
		N	C^{+} a)	A^{-}	$\overset{*}{N}$ b)	$\overset{*+}{C}$ b)	$\overset{*-}{A}$ c)	$\overset{*}{T}$ b)
i-BuOH	17.1	326	(345)	375	380	419	446	485
i-PrOH	18.3	325	(345)	375	379	419	446	486
EtOH	24.2	324	(345)	373	380	420	448	486
MeOH	32.6	323	(345)	365	382	420	448	484
H_2O	78.5	321	(345)	361	ca. 385 d)	421	446	476

a) The value obtained in concd. H_2SO_4. b) Found by excitation at 320 nm. c) Found by excitation at 380 nm. d) Observed only as a shoulder around 385 nm.

thus obtained were in this order: $\overset{*}{N}<\overset{*+}{C}<\overset{*-}{A}<\overset{*}{T}$; this order is parallel with that in the ground state except for $\overset{*}{T}$. Table 1 gives the peak position of each absorption and fluorescence band observed in the hydroxylic solvents. As D is increased from *i*-BuOH to H_2O, the $\overset{*}{T}$ band obviously bule-shifts, while the other three bands show small shifts without any systematic tendency. The optical transitions of coumarins originate from the π-π^* transition, which induces a very strong absorption ($\varepsilon>10^4$ $cm^{-1}mol^{-1}cm^3$).[9] If there is no other solvent-solute interaciton than the dielectric effect due to the molecular polarization, the dipole moment of the excited π-state (μ_e) is usually larger than that of the ground state (μ_g); then, the fluorescence band is red-shifted with the increase in the solvent polarity, whereas the polarity effect on the absorption band is small.[10] Adopting the qualitative parallelism of solvent polarity with D, the shifts of the absorption and fluorescence bands of the neutral and anionic species contradict the above-mentioned presumption ($\mu_e>\mu_g$) for the π-electron system. Probably, the hydrogen bond between the fluorophore and the solvent molecule as a result of the atomic-level interaction, which originates from the difference in the electronegativity of the heteroatoms, must be appropriately taken into account in the case of 7-hydroxycoumarins. The hydrogen-bonding interaction will stabilize the π-electron system by spreading its distribution towards nearby solvents. If the stabilization is more prominent in the ground state than in the excited state, the data for the neutral and anionic species, which suggest a more polar structure in the ground state ($\mu_e<\mu_g$), are consistently explained. It is hard to conjecture the electronic structures of the cationic and tautomeric species from the data in Table 1, for the pure absorption of the former is not found except in concd. H_2SO_4, while that of the latter cannot be found under any usual conditions. Nevertheless, based on the relative energy position and the small shift of the fluorescence band, $\overset{*+}{C}$ seems to belong in the same groups as $\overset{*}{N}$ and $\overset{*-}{A}$. The tautomeric species, on the other hand, must have a special π-electron distribution compared with the other three, because the increase in the hydrogen-bonding ability or the solvent polarity destabilized the excited state. Since the T absorption does not appear, the energy position of T may be highly pulled up from those of N and A^-. The chemical aspect of the tautomer can be partly presumed from its strained molecular structure, including a quinoid structure of the **b** ring of T in Scheme 3 as the main resonance component.

The $\overset{*+}{C}$ and $\overset{*-}{A}$ bands were singly observed in the strongly acidic and basic solutions respectively, while the $\overset{*}{N}$ and $\overset{*}{T}$ bands are always observed in pairs. An especially interesting situation occurs in the acidic solutions with 0.2—0.5 mol dm^{-3} $HClO_4$, where the rapid equilibration between $\overset{*}{N}$ and $\overset{*}{T}$ seems to be realized after the excitation of N; spectroscopically, the fluorescence of $\overset{*}{N}$ and tautomeric $\overset{*}{T}$ species is clearly measured, but neither that of $\overset{*+}{C}$ nor that of $\overset{*-}{A}$ is (see Fig. 3). It has been shown in Ref. 4 that the tautomerization of $\overset{*}{N}$ to $\overset{*}{T}$ is promoted by dissociative and nondissociative processes. The dissociative process has two possible pathways. The one generates the intermediate protonated species as $\overset{*}{N}\rightarrow\overset{*+}{C}\rightarrow\overset{*}{T}$; the other generates the intermediate deprotonated species as $\overset{*}{N}\rightarrow\overset{*-}{A}\rightarrow\overset{*}{T}$. The absence of $\overset{*+}{C}$ and $\overset{*-}{A}$ in the fluorescence spectra does not mean that $\overset{*+}{C}$ and $\overset{*-}{A}$ are not generated, but that the reactions rapidly proceed toward $\overset{*}{T}$ without enough time to fluoresce in the $\overset{*+}{C}$ or $\overset{*-}{A}$ state, as will be discussed further later. In hydroxylic solvents, there is another posibility: that $\overset{*}{N}$ is directly converted to $\overset{*}{T}$ by means of the concerted transfer of a hydrogen from the hydroxyl site to the carbonyl site with the aid of hydrogen bonds of solvent molecules described as:

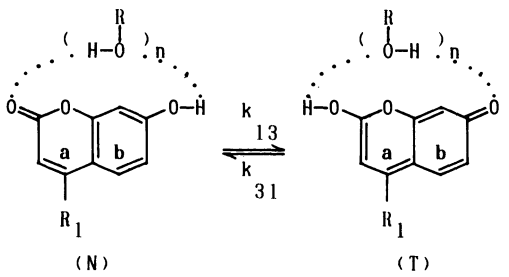

R_1=H, 7HC; R_1=CH_3, 7H4MC

Scheme 3.

The same discussion holds for the three reversed reaction pathways from $\overset{*}{T}$ to $\overset{*}{N}$. Except for the conditions

of $[HClO_4]$=0.2—0.5 mol dm^{-3}, the fluorescence of $\overset{*-}{A}$ or $\overset{*+}{C}$ has been more or less observed in the wavelength region between the $\overset{*}{N}$ and $\overset{*}{T}$ bands. By chance, in the 7HC and 7H4MC solutions with $[HClO_4]$ of 0.29 mol dm^{-3} the fluorescence from $\overset{*-}{A}$ and $\overset{*+}{C}$ is simultaneously negligible; such peculiar conditions were helpful in the detailed study of tautomerization reactions in aqueous solutions.[4,11] Since the $\overset{*}{N}$ and $\overset{*}{T}$ bands are separated enough in wavelength, and since their spectral shapes are almost entirely maintained throughout the solvents, the fluorescent yields of $\overset{*}{N}$ and $\overset{*}{T}$ may be rigorously compared with each other. Although the D value is used as a convenient parameter to describe the macroscopic properties of solvents, it is not an appropriate measure of solvent-solute or solute-solute interactions. Therefore, the ratio of the fluorescence intensity of $\overset{*}{T}$ to that of $\overset{*}{N}$, I^T/I^N, is plotted in Fig. 4 against the polarity factor, $(D-1)/(2D+1)$; the factor was first derived by Kirkwood[12] to estimate the activity coefficient of reacting molecules in solvents and was then discussed extensively by Winstein et al.[13] in treating the linear free-energy relationship for the solvolysis rate of t-butyl chloride. As I^T/I^N is the value that reflects the tautomerization reaction rate in the solvents, the correlation between $\log(I^T/I^N)$ and $(D-1)/(2D+1)$ was examined first; however, the plots showed a marked curvature (Fig. 4). It is frequently seen that $(D-1)/(2D+1)$ does not fully correlate with the log of the reaction rate measured. Böhme et al.[14] plotted, though the theoretical basis was rather poor, the log of the hydrolysis rate of halogenated compounds against "log D"; they thus obtained a quite straight relationship. Therefore, this type of plot has been applied to the present problem, as is shown in Fig. 5; the plots are widely fitted with $I^T/I^N \propto D^{2.0\pm0.05}$ for 7H4MC and with $\propto D^{1.7\pm0.05}$ for 7HC at 20 °C. This empirical relation is exciting, because many reaction rates, either dependent on or independent of D, must be practically concerned in each fluorescence process.

In case that no fluorescence of $\overset{*-}{A}$ and $\overset{*+}{C}$ is detected, the following inequalities are satisfied:[11]

$$k_{12},\ k_{32} \ll k_{21}[H^+],\ k_{23}[H^+],$$

and

$$k_{14}[H^+],\ k_{34}[H^+] \ll k_{41},\ k_{43}. \tag{2}$$

Experimentally, all decay rates of the excited species, n_j's, are of the same order;[4,11] the integrated spectral intensity of each absorption band shows so little change with altering the solvents that the radiative-decay probabilities of the excited species (n_j^r) are nearly constant;[10] the decay rates n_j's are rather insensitive to D, judging from the fluorescence-yield and the lifetime measurements.[4,11] Based on these clues, we obtain the following theoretical prediction by analyzing the rate equations given in Ref. 4:[11]

$$\frac{I^T}{I^N} \propto \frac{n_3{}^r}{n_1{}^r} \cdot \frac{k_{13}+k_{13}^A+k_{13}^C}{n_3+k_{31}+k_{31}^A+k_{31}^C}, \tag{3}$$

where, corresponding to the forth- and back-reaction pathways of $\overset{*}{N} \rightleftarrows \overset{*-}{A} \rightleftarrows \overset{*}{T}$:

$$k_{13}^A = k_{12} \cdot \frac{k_{23}[H^+]}{n_2+k_{21}[H^+]+k_{23}[H^+]},$$

$$k_{31}^A = k_{32} \cdot \frac{k_{21}[H^+]}{n_2+k_{21}[H^+]+k_{23}[H^+]}, \tag{4}$$

and corresponding to the pathways of $\overset{*}{N} \rightleftarrows \overset{*+}{C} \rightleftarrows \overset{*}{T}$:

$$k_{13}^C = k_{14}[H^+] \cdot \frac{k_{43}}{n_4+k_{41}+k_{43}},$$

$$k_{31}^C = k_{34}[H^+] \cdot \frac{k_{41}}{n_4+k_{41}+k_{43}}. \tag{5}$$

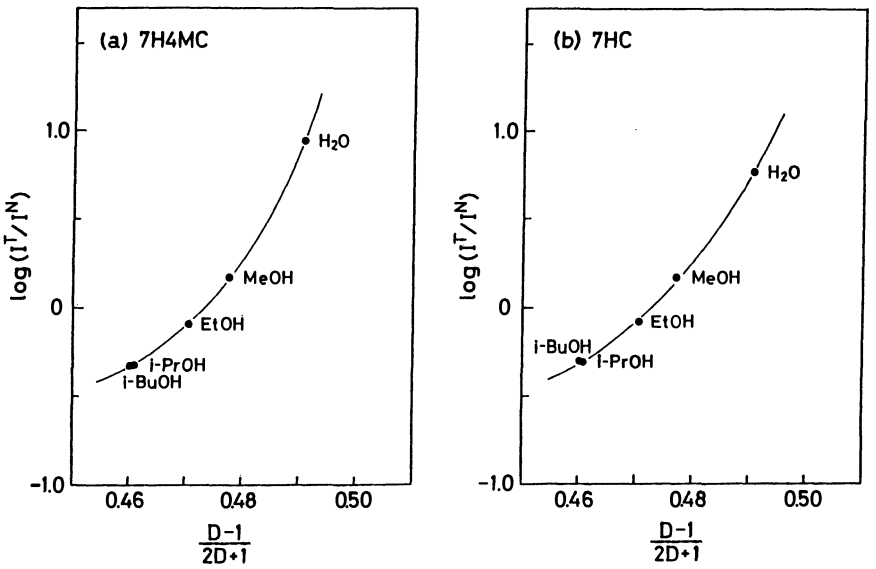

Fig. 4. Plots of $\log(I^T/I^N)$ vs. $(D-1)/(2D+1)$ in the acidic hydroxylic solutions of 7H4MC (a) and of 7HC (b) at 20 °C.

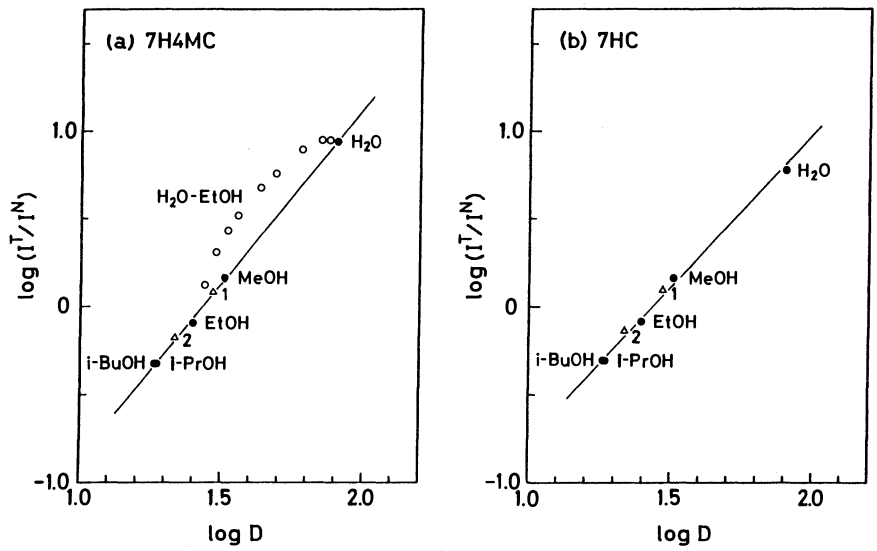

Fig. 5. Plots of $\log(I^T/I^N)$ vs. $\log D$ in the acidic hydroxylic solutions of 7H4MC (a) and of 7HC (b) at 20 °C. The plots for the MeOH–EtOH mixture (1), for the EtOH–*i*-PrOH mixture (2), and for the H_2O–EtOH mixture (○) are also shown.

Although the D dependency of the n_3, k_{13}'s, and k_{31}'s in Eq. 3 has not yet been exactly ascertained, it can be asserted that at least one of the tautomerization rates k_{13}, k_{13}^A, or k_{13}^C, would have a term superlinearly dependent on D if their power expansions of D could be carried out. The reaction pathway described by k_{13} in Scheme 3 is, of course, promoted by the increase in D, for the bridge of hydrogen bonds transferring a hydrogen between the two reactive sites is readily enhanced in polar hydroxylic solvents. This prediction will be confirmed later by an experiment in mixed solvents with various amounts of H_2O.

As for the dissociative tautomerization pathways in an acidic solution, the contribution from k_{13}^C is more important than that k_{13}^A. Equations 4 and 5 show that k_{13}^C linearly increases depending on $[H^+]$, but that k_{13}^A saturates at a large $[H^+]$ value. Furthermore, under the acidic conditions employed, the transiently generated C^{*+} is really evidenced by means of the fluorescence quenching measurement due to halide ions, as will be discussed in a later section. Therefore, $k_{13}^C \gg k_{13}^A$ is reasonable, and the dependence of I^T/I^N on D in Fig. 5 is mainly determined by the competition of k_{13} and k_{13}^C. The back-reaction rates, k_{31} and k_{31}^C, cannot dominate the D dependence of I^T/I^N, because these rates must compete with the large decaying probability, n_3 (ca. 2×10^8 s^{-1}),[4] in the denominator of Eq. 3, which is only slightly dependent on the D value.

Since, at any rate, the straight relationship in Fig. 5 holds very widely from *i*-BuOH to H_2O, log D for various hydroxylic solvents can be employed in order to estimate the chemical properties of microenvironments, such as the microscopic polarity and the hydrogen-bonding ability. It has been further revealed that the data in the mixed solvents of MeOH-EtOH and EtOH-*i*-PrOH follow well the predicted relation; the representative points are plotted in Fig. 5. Therefore, log D is the generally usable parameter that describes the microenvironment and the solvent-solute interaction, even in such mixed solvents.

Fluorescence Behavior in Nonhydroxylic Solvents. As compared with the hydroxylic solvents, nonhydroxylic solvents (also called "inert" or "aprotic" solvents) have so little hydrogen-bonding ability by themselves that the situation for excited-state reactions, as well as for ground-state equilibria, becomes extremely altered. Moreover, the formation of hydrogen bonds and ion pairs between acids and bases in the solution must be taken into account as important phenomena, for the dissociation process of proton liberation is highly suppressed in nonhydroxylic solvents due to the large or immeasurable "autoprotolysis" constant (for acetonitrile, $pK_{HS}\approx28.5$ at 25 °C, while it is immeasurable for the others).[15] As nonhydroxylic solvents, dioxane (D=2.2 at 20 °C), benzene (2.3), chloroform (4.8), ethyl acetate (6.2), dichloromethane (7.4), acetone (21.1), and acetonitrile (36.8) were examined; these solvents were afterwards classified into three groups (**1**, **2a**, and **2b**), as indicated in Table 2, in order to make the subsequent discussion systematic. The "acidic" and "basic" conditions have been realized, as before, by the addition of 0.29 mol dm^{-3} of $HClO_4$ and 0.22 mol dm^{-3} of TEA respectively. Since benzene, $CHCl_3$, and CH_2Cl_2 could not dissolve the indicated amount of $HClO_4$, the data in these solvents under the acidic conditions were taken into account as references.

The typical absorption spectra of 7H4MC in dioxane and in CH_3CN are shown in Fig. 6. In the acidic and basic dioxane, the absorption peak was red-shifted from that in the neutral solution (Fig. 6(a)). The same

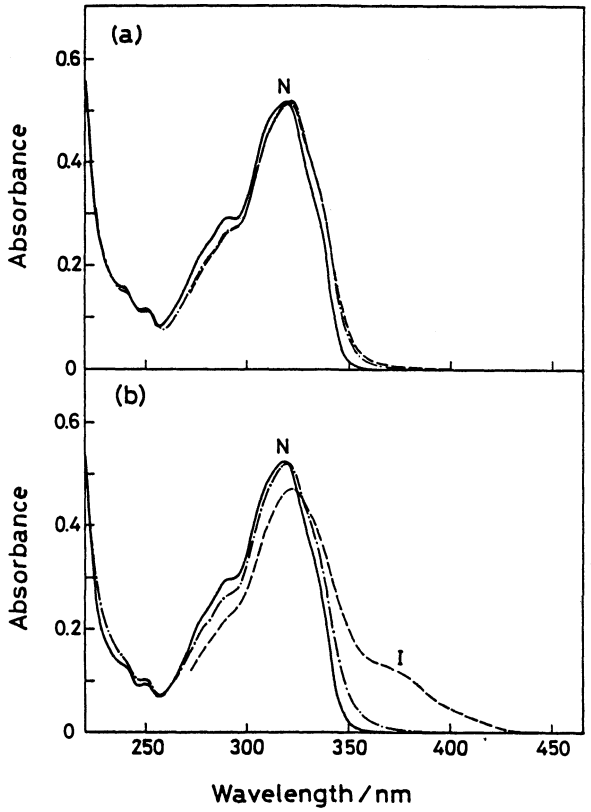

Fig. 6. UV absorption spectra of 7H4MC in dioxane (a) and in CH_3CN (b) for the neutral (——), acidic (–·–·–), and basic (----) solutions at 20°C.

red shift as in dioxane was observed in the acidic CH_3CN (Fig. 6(b)). Because of the very low D of dioxane, it is presumed that the acid-base complexes between the fluorophore and the additives, described as N(>CO)···$HClO_4$ and N(-OH)···NEt_3, are formed, where the substituents in the parentheses are concerned in the association and where the dots represent an attractive interaction such as the hydrogen bond; these ground-state complexes are indicated by NH and NB respectively. The absorption-peak wavelengths measured under various solvent conditions are given in Table 2. Evidently, 7-hydroxycoumarins can work as both acid and base, because they have a proton-donating hydroxyl group and a proton-accepting carbonyl group. Nagakura and Baba[16] found that the absorption spectra of 1 : 1 hydrogen bond complexes of phenols with suitable bases in nonhydroxylic solvents were shifted to longer wavelengths compared with the absorption spectra of the unbonded species; the shift was typically about 500 cm^{-1}, which corresponds to ca. 4 nm in the wavelength region of the present interest. Although a stoichiometric complex has not clearly been affirmed in the case of 7-hydroxycoumarins, it is probable that the hydrogen-bond interaction determines the absorption shift in the nonhydroxylic solvents dissolving $HClO_4$ and dissolving NEt_3 (TEA). The shifts of the NH and NB bands amount to 1—7 nm, as may be seen from Table 2.

In the basic CH_3CN, a long-wavelength side band (350—450 nm) appeared in addition to the main band NB at ca. 322 nm (Fig. 6(b)). This peakless side band, indicated by I, was always accompanied by the NB absorption, and the entire spectral profile was not changed by the further addition of TEA up to 2.4 mol dm^{-3}; this is in contrast with the result in MeOH, which has a D value similar to that of CH_3CN (the "iso-D-value" solvent), where the complete dissociation of 7-OH has been realized. Since the side band is commonly observed in **2a** and **2b**, but not in **1**, the most probable situation is that the ion pair between 7H4MC and TEA described as A^- $(-O^-)\cdots H\overset{+}{N}Et_3$ is generated as a result of the proton transfer in the acid-base complex due to the larger ionizing power of the solvents. If the ion pair is a stabilized molecular complex, and if it contributes to the long-wavelength absorption, the following ground-state equilibria must be taken into account:

$$\underset{(N)}{N}+NEt_3 \rightleftarrows \underset{(NB)}{N(-OH)\cdots NEt_3} \rightleftarrows \underset{(I)}{A^-(-O^-)\cdots H\overset{+}{N}Et_3} \quad (6)$$

Rigorously speaking, the ion pair I is a representative of variously coupled pairs, including such solvent-separated ones as $A^-(-O^-)\cdot\cdot(solvent)_n\cdot\cdot H\overset{+}{N}Et_3$; such a

Table 2. Peak Positions of the Absorption and Fluorescence Spectra of 7H4MC in the Nonhydroxylic Solvents under Neutral, Acidic, and Basic Conditions at 20 °C

	Solvent	D^{20}	Absorption				Fluorescence			
			N	NH	NB	I[b]	$\overset{*}{N}$[c]	$\overset{*}{NH}$[d]	$\overset{*}{NB}$[d]	$\overset{*}{I}$[e]
	Benzene	2.3	319	320	326		372	426	410	
1	Dioxane	2.2	319	321	321		373	422	409	
	$CH_3COOC_2H_5$	6.0	319	321	320		373	418	414	
2a	$CHCl_3$	4.8	321	323	328	ca. 380	376	413	423	459
	CH_2Cl_2	8.9	320	321	327	ca. 380	376	413	427	453
2b	$(CH_3)_2CO$[a]	21.2	<325	<325	<325	ca. 380	374	420	426	447
	CH_3CN	36.1	318	320	322	ca. 380	375	419	449	448

a) Because of the absorption due to the solvent, the absorption peak, possibly < 325 nm, was not precisely decided. b) The absorption tail (360—400 nm) on the longer-wavelength side of the NB band. c) Found by excitation at 320 nm. d) Found by excitation at 360 nm. e) Found by excitation at 410 nm.

dispersed nature in the separation of ions may be reason why the I absorption is broad and peakless. It will be shown later that the ion pair I is intimately correlated with the excited-state ion pair, $\overset{*}{A}^{-}(-O^{-})\cdots H\overset{+}{N}Et_3$, i.e., $\overset{*}{I}$. Since $HClO_4$ usually forms an ion pair by itself, even in considerably inert solvents, it seems proper to state that the acid-base pairing between the fluorophore and $HClO_4$ has the structure described by $N(>CO)\cdots H^{+}\cdot ClO_4^{-}$. However, in contrast to the case of TEA, no distinct sign of the proton transfer from $HClO_4$ to fluorophore could be found by absorption measurements in the nonhydroxylic solvents with $[HClO_4]$ less than 0.3 mol dm^{-3}.

Now that the information on the ground states is fully known, the fluorescent behavior of 7H4MC is to be explored; the typical fluorescence spectra in dioxane and in CH_3CN under the neutral, basic, and acidic conditions are compared to each other in Fig. 7. The light illumination for the neutral solution was carried out at 320 nm, which excited the N state; this yielded the $\overset{*}{N}$ fluorescence. For the acidic and basic solutions, they were illuminated at 360 nm, thus exciting the long-wavelength side of the acid-base-complex absorption (NH and NB) and yielding the $\overset{*}{NH}$ and $\overset{*}{NB}$ fluorescences respectively. Figure 8 schematically depicts the peak positions in **1**, **2a**, and **2b** under various solvent conditions, while Table 2 gives the results. The behavior of these bands can be clearly classified into two types. The fluorescence bands for the one are ordered in wavelengths $\overset{*}{N}<\overset{*}{NB}<\overset{*}{NH}$ (Class 1); for the other, they are ordered $\overset{*}{N}<\overset{*}{NH}<\overset{*}{NB}$ (Class 2). The solutions of benzene, dioxane, and ethyl acetate belong to Class 1 (Solvents **1**), while those of $CHCl_3$, CH_2Cl_2, acetone, and CH_3CN belong to Class 2 (Solvents **2**), the latter being further divided into two groups (Solvents **2a** and **2b**). Here, judging from the energy position and the spectral shape, the $\overset{*}{T}$ band, which was accompanied by the $\overset{*}{N}$ band in the hydroxylic solvents, was not found in any nonhydroxylic solvent. The tautomerization of $\overset{*}{N}$ to $\overset{*}{T}$ may be supposed to be triggered only when the solvent has sufficient hydrogen-bonding ability and ionizing power, as in water and alcohols. This has been proved by the finding that the $\overset{*}{T}$ band appears distinctly in the nonhydroxylic solvents upon the addition of a small amount of H_2O.

From Fig. 8 and Table 2, the following tendencies can, at least, be deduced: 1) The peak shift of the $\overset{*}{N}$ band in each solvent class is small. 2) The $\overset{*}{NH}$ band in **1** and **2a** is blue-shifted with an increase in *D*. 3) The $\overset{*}{NB}$ band in **1** and **2a** is red-shifted with an increase in *D*. 4) By the selective excitation of I, new fluorescence bands ($\overset{*}{I}$) appear around 450 nm in the basic solutins of **2a** and **2b** (dashed curves). Because the peak shift of the $\overset{*}{N}$ fluorescence as well as the N absorption is small, the neutral species in the nonhydroxylic solvents has nonpolar structures in the excited and ground states. Considering that the deprotonation from acids and the protonation to bases in the nonhydroxylic solvents

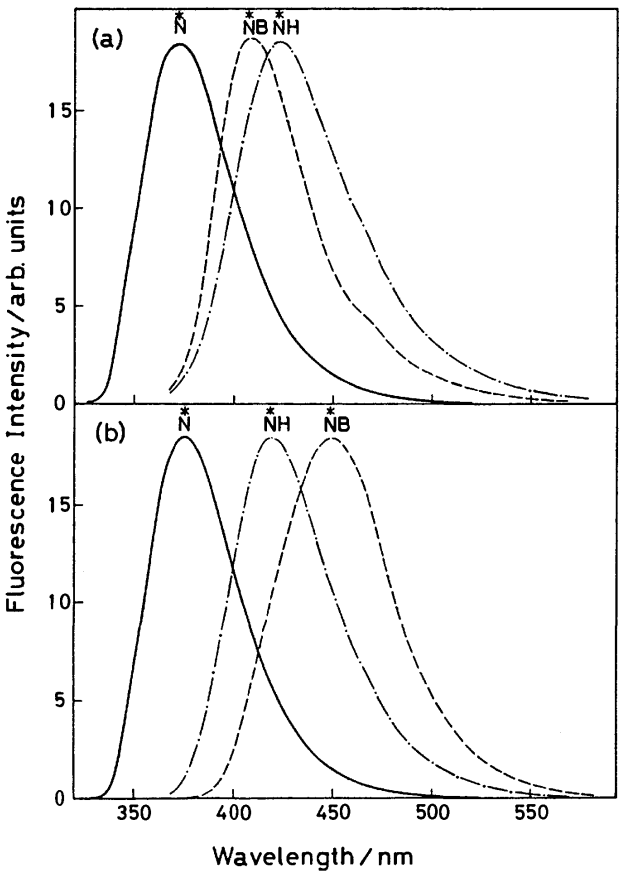

Fig. 7. Fluorescence spectra of 7H4MC in dioxane (a) and in CH_3CN (b) for the neutral (——), acidic (-·-·-), and basic (----) solutions at 20°C.

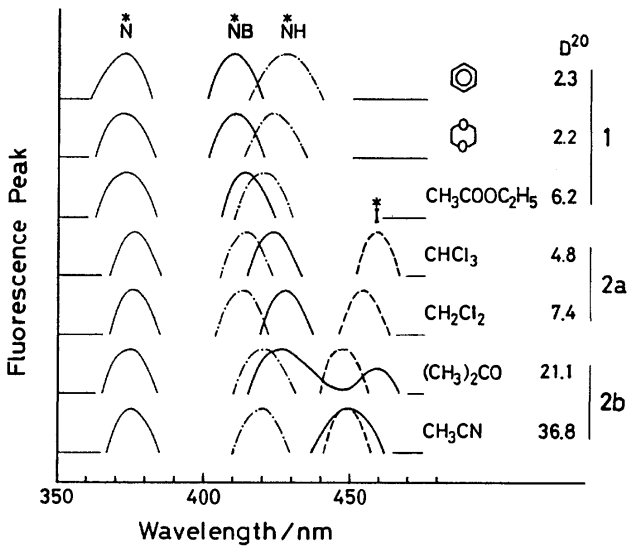

Fig. 8. Schematic drawings of the fluorescence peaks of 7H4MC in the nonhydroxylic solvents for the neutral (——), acidic (-·-·-), and basic (——) solutions excited at the main absorption band. The fluorescence peak shown by (----) was observed in the basic solutions of **2a** and **2b** excited at the long-wavelength absorption tail.

with lower D values are usually improbable, the $\overset{*}{NH}$ and $\overset{*}{NB}$ fluorescence in **1** and **2a** must originate from the excited-state acid-base complexes, analogous to the case in the ground state. Weller et al.[17] showed for several acid-base systems that a stronger hydrogen bond was possible in the excited state than in the ground state. Therefore, the larger red-shifts of the $\overset{*}{NH}$ and $\overset{*}{NB}$ bands from the $\overset{*}{N}$ band, compared with those of the NH and NB bands from the N band, are reasonable (Table 2). As D is increased, the $\overset{*}{NH}$ band systematically blue-shifts, but the $\overset{*}{NB}$ band red-shifts throughout the solutions of **1** and **2a**, in contrast to the small shifts of the NH and NB bands. Confining ourselves to the case in **1** and **2a**, which have D values less than 10, the fluorophore complexed with $HClO_4$ and with TEA is concluded to have a more polar structure in the excited state than in the ground state, although $\overset{*}{NB}$ is stabilized and $\overset{*}{NH}$ is destabilized by the increase in D. Such opposite tendencies result from the difference in the combining strengths of >CO ··· $HClO_4$ and -OH ··· NEt_3; the stabilization of the excited π-electron system due to the former is larger in **1**, while that due to the latter is larger in **2a**.

Several new features appear in the spectra when going from a low-D solvent to a high-D solvent. The most prominent feature is that the fluorescence spectra in the basic solutions of **2a** and **2b** depend complicatedly on the excitation wavelength; some typical examples for $CHCl_3$ and for acetone are shown in Fig. 9. Upon scanning the excitation towards longer wavelengths, the fluorescence spectra changed in shape and finally converged into a simple-shaped band at the excitation wavelength of 410 nm; this band is indicated by $\overset{*}{I}$ in Figs. 8 and 9. Since 410 nm corresponds to the pure I absorption, the $\overset{*}{I}$ fluorescence must result from the excited-state ion pair, $\overset{*-}{A}(-O^-)\cdots H\overset{+}{N}Et_3$. The ion-pair formation in the excited state has been confirmed by Weller et al. for a 2-naphthol-TEA system in methylcyclohexane.[17] Further, they have shown that the wavelength of the fluorescence increases with the promotion of ionization in the complex, in good accordance with the case of 7-hydroxycoumarins. In **2a**, the excitation of NB yields the pure $\overset{*}{NB}$ state, while the excitation of I yields the pure $\overset{*}{I}$ state; the critical transition of the excited state from $\overset{*}{NB}$ to $\overset{*}{I}$ upon a change in the excitation wavelength occurs at 400 nm, as may be seen from Fig. 9(a). This means that the potential barrier of the transformation between $\overset{*}{NB}$ and $\overset{*}{I}$ is large and that the proton transfer in the excited-state complex does not occur within its lifetime in the solutions of **2a**. In **2b**, on the other hand, the excitation of NB yields the long-wavelength component in addition to the $\overset{*}{NB}$ contribution, whereas the excitation of I yields only the pure $\overset{*}{I}$ state, as may be seen from Fig. 9(b). Such a feature comes from the large D values (more than 20) of **2b**. Probably, the potential barrier of the transformation between $\overset{*}{NB}$ and $\overset{*}{I}$ is small in **2b**, and so the following proton-transfer reaction becomes possible:

$$\underset{(\overset{*}{NB})}{\overset{*}{N}(-OH)\cdots NR_3} \rightarrow \underset{(\overset{*}{I})}{\overset{*-}{A}(-O^-)\cdots H\overset{+}{N}R_3} \qquad (7)$$

When $\overset{*}{NB}$ is generated from NB, a mixture of $\overset{*}{NB}$ and $\overset{*}{I}$ is observed by the fluorescence measurements, as may be understood from Eq. 7. The proton-transfer equilibrium in the excited state between species like $\overset{*}{NB}$ and $\overset{*}{I}$ has been extensively studied by Weller et al. for the 2-naphthol-TEA system;[17] the results are analogous to the present case. The stabilization of $\overset{*}{I}$ relative to $\overset{*}{NB}$ depends, of course, on the solvent employed. In this connection, the Class 2 solvents have been divided into two groups at the earlier stage of the analysis; one is comprised of $CHCl_3$ and CH_2Cl_2 (**2a**, halogenated aliphatic solvents), and the other, of acetone and CH_3CN (**2b**, solvents with polar groups such as >CO and -CN). From Table 2, the stabilization of the $\overset{*}{I}$ state from the $\overset{*}{NB}$ state in **2a** is pronounced, while that in **2b** is small or even absent. For the spectral change in **2b** with the excitation wavelength, the longer- and shorter-wavelength parts of the fluorescence band simultaneously decrease, while the center of the spec-

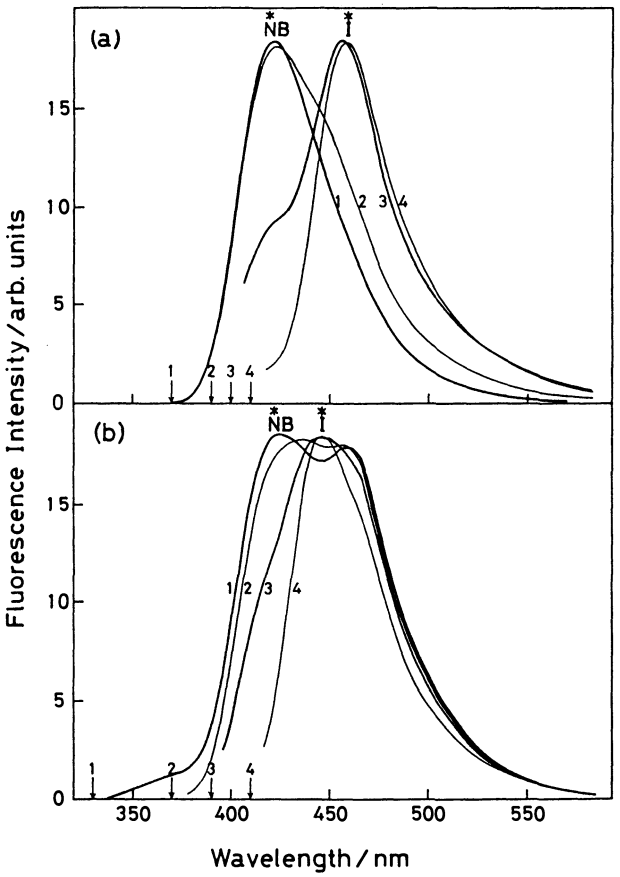

Fig. 9. Dependence of the fluorescence spectra of 7H4MC on the excitation wavelengths in the basic solutions of $CHCl_3$ (a) and of acetone (b). The arrows numbered show the excitation wavelengths for the corresponding fluorescence spectra.

tra is roughly maintained (see Fig. 9(b)). Possibly, the **2a** solvents are suitable for the stabilization of the ion pair, while various types of ion pairs[17] separated by such solvents as $\overset{*}{A}^{-}$ $(-O^{-})\cdots(\text{solvent})_n\cdots H\overset{+}{N}Et_3$ will take part in the fluorescence in **2b**, because **2b** has the hydrogen-bonding ability through the >CO and -CN groups, though it is very small. The hydrogen-bonding ability of the solvents affects the potential barrier for the ion-pair formation, thus making the excited-state reaction of Eq. 7 possible. The complicated behavior of the fluorescence in **2b** is a manifestation of the complex nature of the acid-base complex and the ion pair.

It becomes clear that the hydrogen bond between the fluorophore and TEA persists through the nonhydroxylic solvents. This can be understood from the fact that the only effective hydrogen donor in the basic solution is the 7-OH group of the fluorophore. On the other hand, $HClO_4$, is a rather unstable species as a hydrogen donor, especially in **2b**, due to the probabilities for self-ionization ($H^+ClO_4^-$), proton donation to solvents ($H^+\cdots ClO_4^-$), and protonation of the fluorophore ($\overset{*}{C}^{+}$ $(>COH^+)\cdots ClO_4^-$). Since the systematic blue shift of the $\overset{*}{N}H$ band is interrupted going from **2a** to **2b**, and since the peak position of $\overset{*}{N}H$ in **2b** is very close to that of $\overset{*}{C}^{+}$ in a hydroxylic solvent such as MeOH, a protonated fluorophore may be formed in the acidic solutions, i.e., $\overset{*}{N}H\approx\overset{*}{C}^{+}$ in **2b**. Similarly, the electronic state of $\overset{*}{I}$ in **2b** is thought to resemble that of $\overset{*}{A}^{-}$ of the hydroxylic solutions, judging from the good coincidence of their energy positions.

Fluorescence Behavior in Mixtures of Hydroxylic Solvents. The solvent polarity macroscopically represented by *D* is continuously changeable by using water-organic or organic-organic mixed solvents.[8] Since the excited-state reactions of 7-hydroxycoumarins have been sensitively influenced by the solvent polarity, it seemed fruitful to investigate further the fluorescence change in water-alcohol and alcohol-alcohol mixtures as typical examples. Figure 10 shows the fluorescence spectra of 7HC in a "weakly acidic" solution ($[HClO_4]=2\times10^{-5}$ mol dm^{-3}) and in an "acidic" solution ($[HClO_4]=0.2$—0.5 mol dm^{-3}) of H_2O-EtOH mixtures. Since the absorption was originated from N under these conditions, the optical excitation was fixed at 338 nm, near the absorption peak. In the weakly acidic solution the $\overset{*}{N}$ and $\overset{*}{A}^{-}$ bands, as well as the weak contribution of the $\overset{*}{T}$ band, are observable, while in the acidic solution the $\overset{*}{N}$ and $\overset{*}{T}$ bands, separated considerably in wavelength, are observable. As the ethanol content of the solutions (EtOH wt%) is increased, the polarity and the hydrogen-bond strength decrease continuously; they very much influence the stability of the excited states and the mobility of proton in the solutions.[18] From Fig. 10(a), the $\overset{*}{N}$ band in the wealky acidic solution enormously increases upon the increase in the EtOH wt%, while the $\overset{*}{A}^{-}$ band decreases. The weak $\overset{*}{T}$ contribution, noticed as a shoulder around 500 nm, seems to increase, though the quantitative separation of the overlapping $\overset{*}{A}^{-}$ and $\overset{*}{T}$ bands is difficult. The data can reasonably be explained if $\overset{*}{N}$ in the excited state

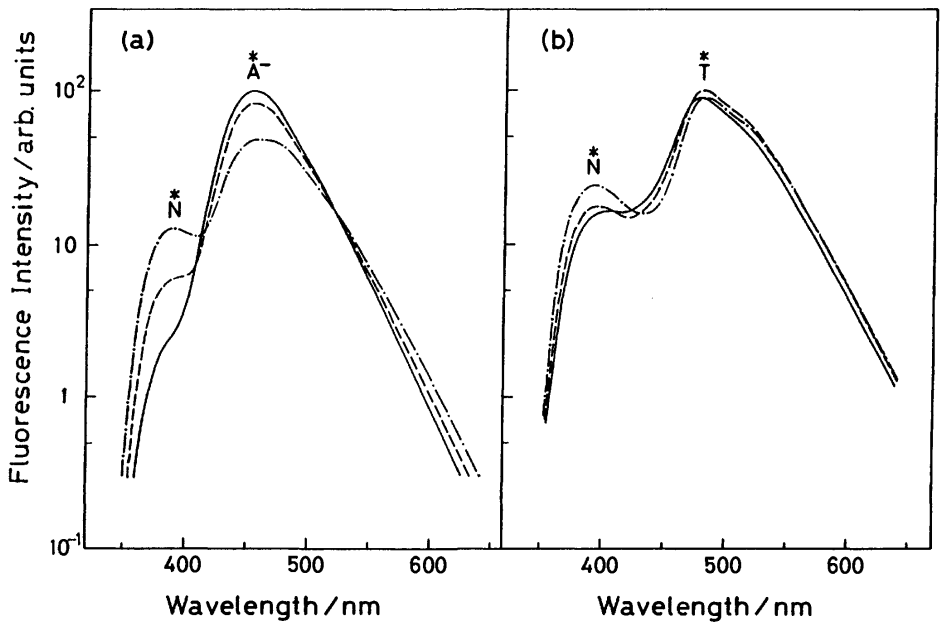

Fig. 10. Fluorescence spectra of 7HC in the H_2O-EtOH mixtures at 25 °C. (a), the weakly acidic solution ($[HClO_4]=2\times10^{-5}$ mol dm^{-3}) with the EtOH content: (——) 0 wt%, (----) 43 wt%, (-·-·-) 74 wt%. (b), the acidic solution ($[HClO_4]=0.5$ mol dm^{-3}) with the EtOH content: (——) 0 wt%, (----) 43 wt%, (-·-·-) 74 wt%.

becomes stabilized relative to $\overset{*}{A}^-$ under lower polarity conditions. It is instructive to note that the ionizing power of EtOH for the N state is much lower than that of H_2O, as has been shown in Fig. 2. Figure 11(a) shows the dependence of I^N/I_0^N on EtOH wt%, where I^N and I_0^N are the fluorescence intensities of the $\overset{*}{N}$ band in the water-ethanol mixtures and in pure water respectively.

As for the acidic solution with 0.5 mol dm^{-3} of $HClO_4$, the change is not straightforward (Fig. 10(b)). As the EtOH wt% is increased, the $\overset{*}{N}$ band increases and its peak position slightly blue-shifts, while the $\overset{*}{T}$ band increases at first and then decreases, with the peak position red-shifted. In Fig 11(b), the dependence of I^N/I_0^N and $(I^T/I_0^T)/(I^N/I_0^N)$ on EtOH wt% is plotted. Since the dependence of the fluorescence yield of each band on the solvent composition is not disregarded, it is difficult to know the precise reason for the curious behavior of the data at a low EtOH wt%. Nevertheless, becuase of the monotonic decrease in $(I^T/I_0{}^T)/(I^N/I_0{}^N)$ at higher EtOH wt% values, the generation rate of the tautomeric form, $\overset{*}{T}$, will be basically determined by the solvent polarity, which is intimately concerned with the promotion of the tautomerization processes from $\overset{*}{N}$ to $\overset{*}{T}$. In Fig. 5(a), log (I^T/I^N) vs. log D is plotted for the H_2O-EtOH system under acidic conditions. The same results for the MeOH-EtOH and EtOH-*i*-PrOH system are shown by the representative points (Δ) in Figs. 5(a) and 5(b). The plots for H_2O-EtOH deviate upwards from the straight dependence obtained earlier, while the plots for MeOH-EtOH and EtOH-*i*-PrOH follow the straight relationship. Obviously, H_2O is in a special position among hydroxylic solvents, because it can contribute a stronger hydrogen bond, even in a mixture, than can the alcoholic mixtures with similar D values. Since the participation of H_2O in the tautomerization of $\overset{*}{N}$ to $\overset{*}{T}$ has been shown to be most effective for the nondissociative pathway,[4] it can naturally be understood that the I^T/I^N of H_2O-EtOH system is larger than that of the alcoholic solvents (e.g., the value at MeOH in Fig. 5(a)). Further, H_2O may form an ordered aggregation of the "iceberg-like" structure around the fluorophore due to its manifold interactions, and the effective mobility of hydrogens may be raised compared with the value in the bulk solvent far from the fluorophore, where random structures of H_2O and EtOH prevail in the thermal equilibrium.

Solubilization into Micelles. It has recently been found that 7-hydroxycoumarins, as well as 7-ethoxycoumarins,[19] are solubilized into micelles formed in aqueous solutions of surfactants. When a surfactant with a concentration higher than the critical micelle concentration (cmc) is dissolved into the aqueous solutions of 7HC and 7H4MC, the fluorescent molecules are distributed between the micellar phase and the bulk-water phase. Such solubilization phenomena of fluorescers are detectable from the change in the fluorescence spectra as a function of the added concentration of surfactants (C_S).[19,20] Figure 12 shows the change in the fluorescence spectra of 7HC upon the addition of sodium dodecyl sulfate (SDS, cmc≈8×10^{-3} mol dm^{-3}); Fig. 12(a) shows the spectra measured under the "weakly acidic" conditions ([$HClO_4$]=3×10^{-4} mol dm^{-3}) at 25 °C, and Fig. 12(b), those measured under the "acidic" conditions ([$HClO_4$]=0.5 mol dm^{-3}).

As for the weakly acidic solution, the $\overset{*}{N}$ fluorescence increases and the $\overset{*}{A}^-$ fluorescence decreases upon the addition of SDS; the $\overset{*}{T}$ band seems to increase, though

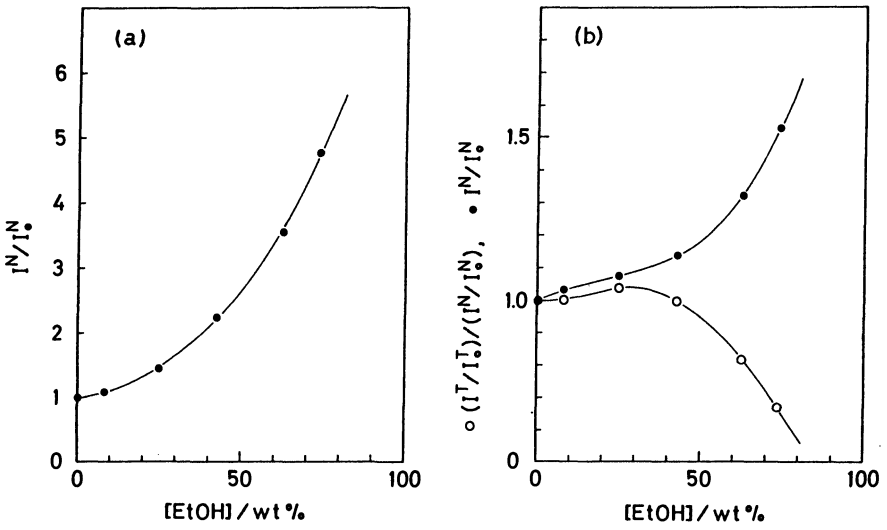

Fig. 11. Dependence of the relative fluorescence intensity of 7HC on the EtOH content of the H_2O-EtOH mixtures at 25 °C. (a), I^N/I_0^N (●) vs. EtOH wt% in the weakly acidic solution; (b), I^N/I_0^N (●) and $(I^T/I_0^T)/(I^N/I_0^N)$ (○) vs. EtOH wt% in the acidic solution.

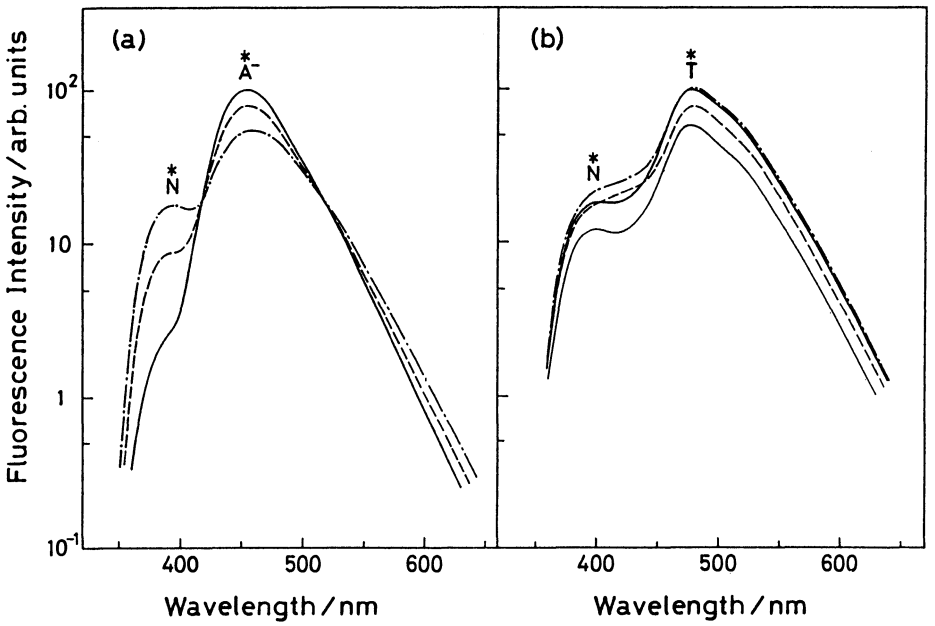

Fig. 12. Fluorescence spectra of 7HC in the aqueous micellar solutions of SDS at 25°C. (a), the weakly acidic solution ($[HClO_4]=3\times10^{-4}$) with the SDS concentration: (——) 0 mol dm^{-3}, (----) 15×10^{-3} mol dm^{-3}, (-·-·-) 50×10^{-3} mol dm^{-3}. (b), the acidic solution ($[HClO_4]=0.5$ mol dm^{-3}) with the SDS concentration: (——) 0 mol dm^{-3}, (-·-·-) 25×10^{-3} mol dm^{-3}, and the acidic solution ([HCl]=0.5 mol dm^{-3}) with the SDS concentration: (——) 0 mol dm^{-3}, (----) 25×10^{-3} mol dm^{-3}.

the quantitative separation of the overlapping $^*A^-$ and $^*T$ bands is difficult (Fig. 12(a)). Just as in the case of the H_2O-EtOH mixtures, the change is caused by the decrease in the microscopic polarity around the fluorophore solubilized into the micelle, for the interior of the micelle is hydrophobic and has a lower polarity than the bulk-water phase; the D value of the solubilized site within the micelle is between the values of aliphatic compounds (ca. 2) and of water (ca. 79).[19] Therefore, the overall spectral change upon the addition of the surfactant is, in effect, similar to that in the case of H_2O-EtOH (Fig. 10(a)). Figure 13 shows that the relative fluorescence intensity I^N/I_0^N begins to increase abruptly when the SDS concentration reaches a value near the cmc. Because the fluorescence change is extremely sensitive to the micelle formation in the solution, even a small-sized pre-micellar aggregation of SDS can be detected as a subtle upward deflection of the plots around 6×10^{-3} mol dm^{-3}. This value should be compared with the value of 8×10^{-3} mol dm^{-3} determined by such macroscopic properties of the solution as the ionic conductance.[21] The SDS concentrations from 6×10^{-3} to 8×10^{-3} mol dm^{-3} are considered to form the transition region from rather unstable pre-micellar formation to stable micellar formation in the equilibrium state. It should be mentioned here that the micellization proceeds as a result of the stepwise-association reaction, $D_{m-1}+S\rightleftarrows D_m$ (S is the surfactant monomer, D_m is the micelle with m surfactants, and $m\leqq n$, where n is the number of S in the stable micelle); strictly speaking, it is not a phase transition with a sharp variation in physical parameters. The change in the absorption spectra of several chromophores has usually been used as microscopic molecular probes for the micellization of surfactants.[21] The fluorescence change which reflects such excited-state reactions as

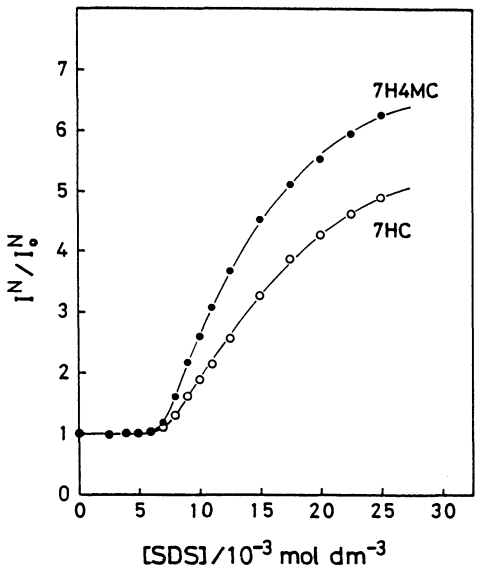

Fig. 13. Plots of the relative fluorescence intensity I^N/I_0^N vs. [SDS], for 7HC and 7H4MC in the weakly acidic solution at 25°C. The fluorescence intensity was monitored at 380 nm for 7HC (○), and at 370 nm for 7H4MC (●), respectively.

$\overset{*}{N} \rightleftarrows \overset{*-}{A}$ is another candidate for an optically sensitive probe of microenvironments being formed in the aqueous micellar system.

As for the acidic solution with 0.5 mol dm^{-3} of $HClO_4$, the fluorescence change is less pronounced than that of the weakly acidic solution. A weak contribution from $\overset{*+}{C}$ appears between the $\overset{*}{N}$ and $\overset{*}{T}$ bands upon the addition of SDS, as can be noticed by the disappearance of the dip between them; the apparent increase in the fluorescence around the $\overset{*}{N}$ band may be due to its contribution (Fig. 12 (b)). Since SDS is an anionic surfactant, cations are readily attached on the micelle surface and the [H^+] near the surface becomes higher than that in the bulk water. If the solubilization site of the fluorophore is not deep within the micelle,[19,20] the $\overset{*}{N}$ state generated from the solubilized N species by the light absorption will be protonated with H^+ concentrated near the surface; consequently, the $\overset{*+}{C}$ fluorescence will appear. It is well-established that halide ions are able to quench the fluorescence from the excited species of coumarins.[22-24] When the acid is altered from $HClO_4$ to HCl in the same concentration, the fluorescence intensity is decreased as a whole (Fig. 12(b)). Because the $\overset{*}{N}$, $\overset{*-}{A}$, and $\overset{*}{T}$ fluorescence were not quenched by Cl^- or ClO_4^- in the aqueous solution,[11] the fluorescence quenching by the addition of HCl instead of $HClO_4$ is attributable to the attractive interaction of $\overset{*+}{C}$ with Cl^-, which effectively induces the quenching. The $\overset{*+}{C}$ state generated by the excited-state reaction contributes, of course, to the tautomerization of $\overset{*}{N}$ to $\overset{*}{T}$ through the dissociative pathway and vice versa, although the $\overset{*+}{C}$ fluorescence is not detected to any extent in the solution without SDS. Therefore, both the $\overset{*}{N}$ and $\overset{*}{T}$ bands are decreased by the addition of Cl^- in the acidic solution. The total decay rate of $\overset{*+}{C}$ is composed of k_{41}, k_{43}, and the fluorescence quenching rate, k_q, corresponding to the $\overset{*+}{C} + Cl^- \rightarrow C^+ + Cl^-$ reaction; usually, their sum is larger than the generation rates of $\overset{*+}{C}$, $k_{14}[H^+]$ and $k_{34}[H^+]$, whereas these are somewhat enhanced for the fluorophore solubilized within the anionic micelle, resulting in the appearance of the $\overset{*+}{C}$ fluorescence. Since anions such as Cl^- are kept away from the surface of the anionic micelle, contrary to the case with H^+,[11] the quenching by Cl^- against the solubilized fluorophore must be weakened by the addition of SDS. The fluorescence intensity of the $\overset{*}{N}$ and $\overset{*}{T}$ bands has been recovered in the presence of the micelle relative to the value in the absence of the micelle, as may be seen from Fig. 12(b). Consequently, the $\overset{*}{N} \rightarrow \overset{*+}{C} \rightarrow \overset{*}{T}$ tautomerization pathway has been clearly confirmed by means of the fluorescence quenching and the solubilization phenomenon.

Conclusion

In order to explore systematically the complicated behavior of the fluorescence from the 7HC and 7H4MC solutions, solvents were divided into the two basic classes of hydroxylic and nonhydroxylic solvents, as popularly used in treating various chemical reactions in solutions. The fluorescence spectra in the hydroxylic solvents could be explained well by using the unified reaction model in the photo-excited states, which had been established by the study of the pH-dependent fluorescence in aqueous solutions. Especially, the fluorescence-intensity ratio between the neutral and tautomeric excited species in an acidic solution showed a remarkably straight relationship when log (I^T/I^N) was plotted against log D. This resulted from the competitive reactions of the tautomerization between the dissociative and nondissociative processes.

The fluorescence spectra in the nonhydroxylic solvents differed greatly from those in the hydroxylic solvents, for the ionizing power and the hydrogen-bonding ability were small. The low polarity of the solvents resulted in the stable formation of hydrogen bond complexes or ion pairs between various acids and bases. From the fluorescent behavior, the nonhydroxylic solvents could be further classified into these three groups; the extremely inert solvents such as dioxane (**1**), the halogenated aliphatic solvents (**2a**), and the solvents with polar groups, such as >CO and -CN (**2b**).

The fluorescence in the water-alcohol and alcohol-alcohol mixtures and that in the aqueous micellar solutions were measured under various conditions. The parameter of log D was well applicable to the alcoholic mixtures, although the aqueous alcohols behaved as stronger hydrogen-bonding solvents than had been expected. The solubilization of the fluorophore into the SDS micelle was detectable by the drastic change in the fluorescence spectra, and the possibility of the use of 7HC and 7H4MC as fluorescent probes of the microenvironment was pointed out.

The author gratefully acknowledges the financial support by the special research program on "Molecular Electronics" of the Ministry of International Trade and Industry, Agency of Industrial Science and Technology.

References

1) O. S. Wolfbeis, E. Lippert, and H. Schwarz, *Ber. Bunsenges. Phys. Chem.*, **84**, 1115 (1980), and the references cited therein.

2) A. Diens, C. V. Shank, and R. L. Kohn, *IEEE J. Quantum Electron.*, **QE-9**, 833 (1973).

3) A. Bergman and J. Jortner, *J. Lumin.*, **6**, 390 (1973).

4) T. Moriya, *Bull. Chem. Soc. Jpn.*, **56**, 6 (1983).

5) T. Moriya and H. Anzai, *Bull. Electrotech. Lab.*, **46**, 431 (1982).

6) M. A. Paul and F. A. Long, *Chem. Rev.*, **57**, 1 (1957).

7) O. Bensaude, M. Dreyfus, G. Dodin, and J. E. Dubois, *J. Am. Chem. Soc.*, **99**, 4438 (1977).

8) Y. Y. Akhadov, "Dielectric Properties of Binary Solutions," Pergamon Press, Oxford (1980).
9) J. Grzywacz and S. Taszner, *Z. Naturforsch.*, **33a**, 1307 (1978).
10) N. Mataga and R. Kubota, "Molecular Interactions and Electronic Spectra," Marcel Dekker, New York (1970).
11) T. Moriya, *Bull. Chem. Soc. Jpn.*, **61**, 753 (1988).
12) J. G. Kirkwood, *J. Chem. Phys.*, **2**, 351 (1934).
13) A. H. Fainberg and S. Winstein, *J. Am. Chem. Soc.*, **78**, 2770 (1956), and the references cited therein.
14) H. Böhme and W. Schürhoff. *Chem. Ber.*, **84**, 28 (1951).
15) R. G. Bates, "Determination of pH," John Wiley and Sons, New York (1973), Chap. 7.
16) S. Nagakura and H. Baba, *J. Am. Chem. Soc.*, **74**, 5693 (1952).
17) H. Beens, K. H. Grellmann, M. Gurr, and A. H. Weller, *Discuss. Faraday Soc.*, **39**, 183 (1965).
18) M. Eigen and L. de Maeyer, "The Structure of Electrolytic Solutions," ed by W. J. Hammer, John Wiley and Sons, London (1959), p. 64.
19) T. Moriya, *Bull. Electrotech. Lab.*, **50**, 1123 (1986).
20) T. Moriya, *Bull. Chem. Soc. Jpn.*, **61**, 585 (1988).
21) P. Mukerjee and K. J. Mysels, "Critical Micelle Concentrations of Aqueous Surfactant Systems," *Nat. Stand. Ref. Data Ser.*, **NBS 36** (1971)
22) T. Moriya, *Bull. Chem. Soc. Jpn.*, **60**, 3855 (1987).
23) T. Moriya, *Bull. Chem. Soc. Jpn.*, **57**, 1723 (1984).
24) T. Moriya, *Bull. Chem. Soc. Jpn.*, **59**, 961 (1986).

 © 1988 The Chemical Society of Japan Bull. Chem. Soc. Jpn., 61, 1887—1892 (1988)

Effect of Attractive Solvent-Solvent and Solvent-Solute Interactions on Partial Molal Quantities

Yosuke YOSHIMURA* and Masaru NAKAHARA
Department of Chemistry, Faculty of Science, Kyoto University, Oiwake-cho, Kitashirakawa, Sakyo-ku, Kyoto 606
(Received December 3, 1987)

The effect of the perturbation due to attractive solute-solvent and solvent-solvent interactions on the partial molal volume (PMV), entropy (PME), and enthalpy in infinitely dilute solution has been formulated on the basis of the first-order perturbation theory which comes from the van der Waals picture of liquid. PMV is found to be composed of the two compensating factors which arise from the solute-solvent and solvent-solvent attractive interactions treated as the perturbation; when the former is larger than the latter PMV becomes smaller. PME is influenced only indirectly by the attractive perturbation through the volume change due to the perturbation interactions. The limitations of the basic expressions derived are discussed in the case of large solute.

Although the perturbation theory of liquid has been developed to a large extent for the past two decades,[1-3] some fundamental problems still remain to be solved for its extensive application to the interpretation of the partial molal volume, entropy, and enthalpy in solution. In this paper we attempt to show how theoretical expressions for the partial molal quantities simply due to repulsive interactions are modified by the attractive interactions between solvent and solvent molecules and between solvent and solute molecules. This kind of study on the partial molal quantities is required for an advance in solution chemistry because it provides a theoretical framework for the molecular interpretation of the accurate experimental data accumulated for a variety of solution systems.

To understand the partial molal quantities, an interesting model was put forward by Sisskind and Kasarnowsky (SK) half a century ago.[4] This may be called "two-step dissolution theory" because a gaseous solute molecule is introduced into solvent in the following two steps: (i) the creation of a cavity in the solvent to accommodate the solute molecule and (ii) the introduction of the solute molecule into the cavity where the attractive interaction between the solute and solvent molecules is switched on. Pierotti used the SK model when he first transferred the fruit of the modern liquid theory to solution chemists.[5,6] He considered the first step in the reference system where no attractive interactions exist, and calculated changes in thermodynamic quantities accompanying the first step by applying the scaled particle theory. This SK picture is instructive but likely to make it ambiguous the role of the solvent-solvent interaction, as pointed out by Neff and McQuarrie (NM) on the basis of the mean field theory (a first-order perturbation theory).[7] Though a perturbation due to attractive interactions between solvent molecules is explicitly taken into account in the NM theory, the role of the solute-solvent and solvent-solvent interactions is not clearly explained. We shall present here simple and meaningful expressions for the partial molal quantities.

The standard form of the perturbation theory comes from the van der Waals (VDW) picture of liquid.[1-3] The VDW picture implies that the liquid structure is determined mainly by repulsive forces between molecules, and that attractive interactions can be regarded as the background mean field; the former forces are treated in the reference system and the latter as a perturbation. Although the VDW picture appears simple and intuitively perceptible, its implication is not so simple when it is applied to the partial molal quantities and their related properties. For example, the isothermal compressibility depends on the presence of attractive interactions as disclosed in this paper. On the other hand, however, the compressibility is directly related through the compressibility equation to the structure factor of liquid which is said to be dominated by repulsive interactions according to the VDW picture. Here we examine in detail how the two different views are related, and present a formulation of the partial molal volume, entropy, and enthalpy at infinite dilution on the basis of the first order perturbation theory. The present work is hoped to provide a perspective for understanding the molecular aspects of each partial molal quantity in solution.

Model of Solution

Our model system is composed of two species S and X; S is the solvent and X is the solute dissolved in S at infinite dilution. For simplicity, all the molecules are assumed to have the spherical symmetry. The molecules are characterized by the pair potentials

$$u_{YZ}(r) = u_{YZ}^{(0)}(r) + u_{YZ}^{(1)}(r), \quad (1)$$

where Y and Z denote S or X, and the superscripts (0) and (1) indicate the reference and the perturbed systems, respectively, and r is the separation. According to the VDW theory, the repulsive part of the intermolecular interaction is taken as the reference interaction and the attractive part as the perturbation. We take the number density of the reference system to be equal to that of the perturbed system.

In general, the repulsive interaction is very large and short-ranged. We assume that the reference potential is due to the hard-sphere interaction:

$$u_{YZ}^{(0)}(r) = +\infty \qquad 0 < r < \sigma_{YZ}$$
$$0 \qquad \sigma_{YZ} \leqq r, \qquad (2)$$

where the hard-core collision diameter σ_{YZ} is assumed to be independent of temperature and density. Since the reference system consists of the hard-sphere molecules, the radial distribution functions in the reference system are independent of temperature, and some restrictions are imposed on the thermodynamic behavior of the perturbed system as well as the reference system; see Appendix.

The attractive perturbation interactions $u_{YZ}^{(0)}(r)$ in Eq. 1 are assumed to vary slowly compared with σ_{SS} which characterizes the short range liquid structure determined by the hard-sphere molecules. This postulate is of great importance for making the mean field theory valid.

The van der Waals Picture for Solution Properties

Mean Field Theory of Solution. According to the present model of solution, the Hamiltonian of the system is described as

$$\mathcal{H} = \mathcal{H}^{(0)} + \mathcal{H}^{(1)}, \qquad (3)$$

where $\mathcal{H}^{(0)}$ is composed of the kinetic energy and the hard-core repulsive interactions between molecules and $\mathcal{H}^{(1)}$ is the perturbation due to the attractive interactions between molecules. According to the Bogoliubov variational theorem,[8] the following equation holds for the Helmholtz free energy A:

$$A \leqq A^{(0)} + \langle \mathcal{H}^{(1)} \rangle_0, \qquad (4)$$

where $A^{(0)}$ is the free energy of the reference system and $\langle \mathcal{H}^{(1)} \rangle_0$ is the ensemoble average of the perturbation in the reference system. In the mean field approximation (a primitive perturbation theory),[8] both sides of Eq. 4 are equal:

$$A = A^{(0)} + \langle \mathcal{H}^{(1)} \rangle_0. \qquad (5)$$

The pertubation term in Eq. 5 can be rewritten in terms of the radial distribution functions as follows:

$$\langle \mathcal{H}^{(1)} \rangle_0 = \frac{N_S^2}{2V} \int u_{SS}^{(1)}(r)\, g_{SS}^{(0)}(r)\, dr$$
$$+ \frac{N_S N_X}{V} \int u_{SX}^{(1)}(r)\, g_{SX}^{(0)}(r)\, dr, \qquad (6)$$

where $g_{YZ}^{(0)}(r)$ denotes the radial distribution function between Y and Z, which are X or S, in the reference system, N_S and N_X are the numbers of the solvent and solute molecules, respectively, and V is the volume of the solution. Though the second term in Eq. 6 disappears in the limit of infinite dilution of solute X, we need to retain it to derive expressions for the partial molal quantities of the solute as shown below.

In the reference system, the molecules occupy only one potential energy state, say 0, because they are hard. Since no changes in the population among the energy states and the probability density in the configurational space take place in the reference system, the entropy of the system is unaffected by the perturbation at the level of the mean field theory; this is easily demonstrated by differentiating Eq. 5 with respect to temperature.

First we examine the effect of the attractive interactions on the chemical potential of the solute because the chemical potential is the fundamental quantity which generates the partial molal quantities. The chemical potential of the solute X is directly obtained by differentiating Eq. 5 with respect to the number of molecules and taking the limit $n_X \to 0$,

$$\mu_X = \mu_X^{(0)} + n_S \int u_{SX}^{(1)}(r)\, g_{SX}^{(0)}(r)\, dr$$
$$+ \frac{n_S^2}{2} \int u_{SS}^{(1)}(r) \frac{\partial g_{SX}^{(0)}(r)}{\partial n_X} dr, \qquad (7)$$

where n_S and n_X are the number densities of the solvent and solute, respectively. Considering that the perturbation interactions $u_{SX}^{(1)}(r)$ and $u_{SS}^{(1)}(r)$ vary slowly compared with the short wavelength of the liquid structure, we can transform Eq. 7 into a more convienient form with a plausible approximation.

Figure 1 shows the solute-solvent radial distribution function $g_{SX}^{(1)}(r)$ and the solute-density derivative of the solvent-solvent radial distribution function, $n_S[\partial g_{SS}^{(1)}(r)/\partial n_X]$ in the hard-sphere system where $\sigma_{SS} = \sigma_{SX}$; the necessary information is available in the literature.[9]

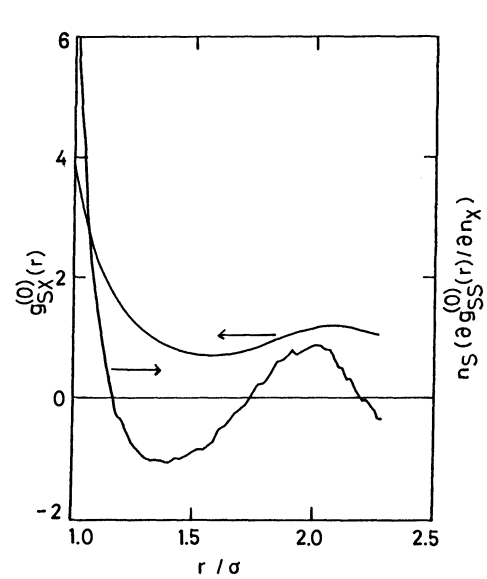

Fig. 1. The solvent(S)–solute(X) radial distribution function in the reference system, $g_{SX}^{(0)}(r)$ and the solute-density (n_X) derivative of the solvent–solvent radial distribution function, $n_S[\partial g_{SS}^{(0)}(r)/\partial n_X]$. $\sigma_{SX} = \sigma_{SS} = \sigma$; $n_S\sigma_{SS}^3 = 0.80$. The density derivative is obtained from the difference in the radial distribution function between $n_S\sigma_{SS}^3 = 0.75$ and 0.85.

The derivative of $g_{SS}^{(1)}(r)$ with respect to the solute density oscillates around zero with a wavelength of the order of σ_{SS}, and fades rapidly with increasing the distance. Since the perturbation pair potential $u_{SS}^{(1)}(r)$ varies slowly, the third term on the right-hand side of Eq. 7 may be ignored. On the other hand, the second term is insensitive to the number density but not negligible because $g_{SX}^{(1)}(r)$ oscillates around unity with a short wavelength. To this approximation, the chemical potential is composed of the following two terms as in the case of the Helmholtz free energy, Eq. 5:

$$\mu_X = \mu_X^{(0)} + n_S \int u_{SX}^{(1)}(r)\, g_{SX}^{(0)}(r)\, d\boldsymbol{r}, \tag{8}$$

$$= \mu_X^{(0)} + a_{SX} n_S , \tag{9}$$

where the integrand in the second term on the right-hand side of Eq. 7 or 8 is taken to be the constant a_{SX} because the integrand is independent of temperature and a dull function of the density as mentioned above. It is to be noted that when the third term on the right-hand side of Eq. 7 is neglected, the chemical potential of the solute becomes independent of the solvent-solvent perturbation interaction. Most of the following discussions are based on this assumption, and its limitations will be referred to later.

Equation of State of Pure Solvent. It is the equation of state of the pure solvent through that the solvent-solvent perturbation interactions affect the partial molal quantities of the solute. The equation of state is easily obtained from the Helmholtz free energy Eq. 5 by putting $N_X=0$. Differentiating the free energy with respect to the volume, we get the expression for pressure P as[1]

$$P = P^{(0)} + \frac{a_{SS}}{2} n_S^2 , \tag{10}$$

where $P^{(0)}$ is the pressure in the reference system. This is a generalized VDW equation of state, and a similar form of equation of state has been used for real system.[10]

Since the reference pressure $P^{(0)}$ is linearly dependent on temperature as shown by Eq. 38 in Appendix, and since a_{SS} is independent of temperature, we get the following equation for the reference pressure by differentiating Eq. 10 with respect to temperature T at constant density:

$$P^{(0)} = T\left(\frac{\partial P}{\partial T}\right)_V \tag{11}$$

It follows from Eqs. 10 and 11 that the "internal pressure" defined by $(\partial U/\partial V)_T$ is equal in magnitude to the attractive perturbation pressure with the sign opposite.

Long-Range Nature of Perturbation. The VDW theory of liquid is valid only for the short-range problem but not for the long-range one. We shall discuss this point according to Eq. 10.

The isothermal compressibility is related to the long-range part of the structure factor of liquid as follows:

$$\kappa kT = \frac{1}{n_S} + \int [g_{SS}(r) - 1] d\boldsymbol{r}. \tag{12}$$

where κ denotes the isothermal compressibility, $-(\partial V/\partial P)_T/V$. Note that the right-hand side of Eq. 12 indicates the Fourier component of the infinitely large wavelength of the total correlation function $g_{SS}(r)-1$. Thus the validity of the VDW picture for the long-range structure may be tested by comparing the isothermal compressibilities of the reference and the perturbed systems.

The VDW equation of state, Eq. 10, can be rewritten as

$$\frac{1}{\kappa} = \frac{1}{\kappa^{(0)}} + a_{SS} n_S^2 , \tag{13}$$

where α is the isobaric expansibility, $(1/V)(\partial V/\partial T)_P$. At 0.1 MPa, the pressure is negligible in comparison with the reciprocal of the compressibility (usually in the order of 1000 MPa). Thus the following equation holds at 0.1 MPa:

$$\frac{1}{\kappa} = \frac{1}{\kappa^{(0)}} + 2\left(-\frac{\alpha}{\kappa} T + P\right) , \tag{14}$$

where $\kappa^{(0)}=-(\partial V/\partial P^{(0)})_T)/V$. Let us show that the second term on the right-hand side of Eq. 13 is not negligible at 0.1 MPa. By inserting Eq. 11 into Eq. 10 and transforming the thermodynamic variables, we have

$$\frac{\kappa}{\kappa^{(0)}} = 1 + 2\alpha T. \tag{15}$$

Since the second term on the right-hand side is usually in the range of 0.6—0.8, it cannot be neglected; e.g., the value is 0.73 for carbon tetrachloride at 25 °C and 0.1 MPa.

The marked effect of the attractive perturbation on the isothermal compressibility tells us that the simple VDW picture is very useful for treating short-range problems but not accurate enough to describe the long-wavelength component of the liquid structure. This feature of the VDW picture has to be taken into account to calculate the thermodynamic quantities in the mean field approximation.

Partial Molal Volume

The partial molal volume is the quantity which reflects a response of the volume of the system to an increase in the number of the molecules of our interest. We can understand the way of the volume response using the following scheme: (i) The introduction of

the solute molecule into the solvent under isochoric conditions causes a pressure change, and (ii) the pressure change is transformed into the partial molal volume which is observed under isobaric conditions. These steps have quite different operational meanings; the second step depends on the compressibility of the whole system which is determined only by the solvent-solvent interaction, whereas the first step is characterized by the solute-solvent interaction. We show below how useful this picture is to understand the effect of perturbative interactions on the partial molal volume.

To make it easy to undestand how the partial molal volume is influenced by the attractive interactions through the pressure change, we may define a "partial molal pressure" P'_X[11] in the following way:

$$P'_X = (N_S+N_X)\left(\frac{\partial P}{\partial N_X}\right)_{T,V,N_S} \tag{16}$$

$$= -(N_S+N_X)\left(\frac{\partial \mu_X}{\partial V}\right)_{T,N_S,N_X}, \tag{17}$$

where the factor (N_S+N_X) is introduced in order to avoid the system size dependence of the "partial molal pressure." Inserting Eq. 9 into Eq. 17, we have

$$P'_X = P'^{(0)}_X + a_{SX}n_S^2, \tag{18}$$

where we take the limit $n_X \to 0$. Thus P'_X decreases with an increase in the perturbation between solute and solvent, without any influence of the solvent-solvent perturbative interaction. The exchange of the subscript S by X in Eq. 18 leads to the following expression for the "partial molal pressure" of solvent:

$$P'_S = P'^{(0)}_S + a_{SS}n_S^2. \tag{19}$$

This equation is consistent with Eq. 13 because the "partial molal pressure" of solvent is equal to the reciprocal of the isothermal compressibility of pure solvent.

The partial molal volume is directly related to the "partial molal pressure" as follows:

$$V_X = \frac{\kappa}{n_S+n_X}P'_X, \tag{20}$$

$$= \frac{\kappa}{\kappa^{(0)}}V_X^{(0)} + a_{SX}\kappa n_S, \tag{21}$$

where the limit of infinite dilution is taken. Using Eq. 13, we rewrite Eq. 21 as

$$V_X = V_X^{(0)} + \kappa n_S^2[a_{SX}V_S^{(0)} - a_{SS}V_X^{(0)}], \tag{22}$$

where we use the relation $V_S^{(0)}=n_S^{-1}$. This equation tells us that in contrast to P'_X, V_X is influenced by the solvent-solvent perturbative interaction through the compressibility. While P'_X decreases with increasing the solute-solvent perturbative interaction, κ increases with increasing the solvent-solvent perturbative interaction. The two factors compete in determining the partial molal volume.

One may expect that the perturbation effect on the partial molal volume will be small because of the presence of the competing factors in Eq. 22. This expectation is rationalized in the system where the solute molecule is identical in size with the solvent molecule in the reference system; $\sigma_{XS}=\sigma_{SS}$ and $g^{(0)}_{SX}(r)=g^{(0)}_{SS}(r)$. In this case the partial molal volume due to the attractive perturbation takes the simple form as

$$V_X^{(1)} = V_X - V_X^{(0)}$$

$$= \kappa n_S^2 V_X^{(0)}\int[u^{(1)}_{SX}(r)-u^{(1)}_{SS}(r)]g^{(0)}_{SX}(r)\,d\boldsymbol{r}. \tag{23}$$

The perturbation part of the partial molal volume arises from the difference in the attractive perturbation between solute-solvent and solvent-solvent pairs of molecules. When the solute-solvent attractive force is larger than the solvent-solvent attractive force, the partial molal volume of the solute is smaller than the reference value and vice versa. Especially when the solute-solvent interaction is identical with the solvent-solvent interaction, of course, the competing perturbations are canceled out.

Partial Molal Enthalpy and Entropy

We have shown in the preceding section that the "partial molal pressure" at constant volume has a simpler form than the partial molal volume at constant pressure. The same thing is said for the partial molal enthalpy and entropy. The partial molal energy $(U_X)_V$ and entropy $(S_X)_V$ at constant volume are given as

$$(U_X)_V = (U_X)_V^{(0)} + a_{SX}n_S, \tag{24}$$

$$(S_X)_V = (S_X)_V^{(0)} \tag{25}$$

The partial molal entropy at constant volume is unaffected by the perturbation interactions because no change in the molecular distribution over the energy states is brought about by the perturbation exerted on the reference system taken here.

As in the case of the partial molal volume discussed above, the conventional partial molal enthalpy and entropy can be derived from the corresponding partial molal quantities at constant volume as follows:

$$H_X = (U_X)_V + \frac{\alpha}{\kappa}TV_X, \tag{26}$$

$$S_X = (S_X)_V + \frac{\alpha}{\kappa}V_X. \tag{27}$$

The second term in Eq. 27 arises from the volume change due to the incorporation of the solute molecule into the solvent at constant pressure. The variation of the volume of the system actually causes a change in the probability density in the configurational phase space. This is the reason why the partial molal entropy is perturbed by the presence of the attractive forces.

Limiting Behavior of Large Solute

It is important to see the limitations of the basic assumptions used so far for deriving the expressions for the partial molal quantities. Only the partial molal volume is discussed below for this purpose.

Let us show that the expression for the partial molal volume, Eq. 21, fails to describe correctly the behavior of a large enough solute molecule. When the solute molecule is much larger than the solvent molecule, the second term in Eq. 21 may be estimated as

$$\kappa a_{SX} n_S = \kappa n_S \int u_{SX}^{(1)}(r) g_{SX}^{(0)}(r)\, dr,$$

$$= \kappa n_S u_{SX}^{(1)}(\sigma_{SX}) g_{SX}^{(0)}(\sigma_{SX}) \cdot \Delta \cdot 4\pi\sigma_{SX}^2, \tag{28}$$

where Δ is the length characteristic of the perturbation interaction; Δ may be as several times as large as σ_{SS}. This indicates that in Eq. 21, the second term of the order of σ_{SX}^2 becomes negligible compared with the first term of the order of σ_{SX}^3. As a result, the partial molal volume of the solute in the perturbed system becomes larger by the factor of $\kappa/\kappa^{(0)}$ than that in the reference system. In the limit of the large solute, on the other hand, the partial molal volume should become identical with the core volume of the solute, i.e., $(\pi/6)\,\sigma_{XX}^3 \simeq (4\pi/3)\sigma_{SX}^3$, both in the reference and the perturbed systems. Thus Eq. 21 cannot describe the true limiting behavior of the large solute.

The limitation of Eq. 21 disclosed above is ascribed to the neglect of the third term on the right-hand side of Eq. 7. The third term is negligible only when the size of the solute molecule is not very different from that of the solvent molecule. In other words, when the solute molecule is large enough, the effect of the solute molecule on the solvent-solvent radial distribution function is really long-ranged because of its large size.

It is difficult to obtain directly the derivative of the solvent-solvent radial distribution function involved in the third term in Eq. 7. However, its asymptotic behavior can be examined using the following relation which holds for the sufficiently large spherical solute:

$$-\frac{\pi}{6}\sigma_{XX}^3 (\delta N_X)_V = (\delta V)_{N_X}, \tag{29}$$

where $(\delta B)_Y$ denotes an infinitesimal change in quantity B at constant Y. Equation 29 shows the fact that the introduction of the macroscopic particle with volume v into the system at the constant volume has the same meaning as the shrinking of the system by the amount of v. Using Eq. 29, we evaluate the derivative involved in the third term in Eq. 7 as follows:

$$\frac{\partial}{\partial N_X}\left[\frac{N_S^2}{2V}\int u_{SS}^{(1)}(r) g_{SS}^{(0)}(r) dr\right] = \frac{\pi}{12}\sigma_{XX}^3 n_S^2$$

$$\times \left[\int u_{SS}^{(1)}(r) g_{SS}^{(0)}(r) dr - V\int u_{SS}^{(1)}(r)\frac{\partial g_{SS}^{(0)}(r)}{\partial V} dr\right], \tag{30}$$

$$= \frac{\pi}{12}\sigma_{XX}^3 n_S^2 a_{SS}, \tag{31}$$

where the second term on the right-hand side of Eq. 30 is neglected; note the relation

$$N_S[\partial g_{SS}^{(0)}(r)/\partial V] = -n_S^2[\partial g_{SS}^{(0)}(r)/\partial n_S]$$

and recall the reason for the neglect of the third term in Eq. 7. Following the abovementioned procedure for the partial molal volume, we have the relation

$$V_X = V_X^{(0)} + a_{SS}\kappa n_S^2\left[\frac{\pi}{6}\sigma_{XX}^3 - V_X^{(0)}\right], \tag{32}$$

where we neglect the term of the order of σ_{XX}^2, $a_{SX}\kappa n_S^2 V_S^{(0)}$. This equation correctly describes the limiting behavior of the large solute molecule; in fact, the second term disappears in the limit of large solute.

Probably because of the presence of the limitation of Eq. 21, Pierotti[5,6] gave a compromising expression for the partial molal volume as

$$V_X = \kappa kT(K_0 + K_1\sigma_{XX} + K_2\sigma_{XX}^2) + \frac{\pi}{6}\sigma_{XX}^3, \tag{33}$$

where K_0, K_1, and K_2 are the parameters which are given by the scaled particle theory as a function of the number density of the solvent, and k is the Boltzmann constant. Equation 33 gives the correct partial molal volume for the reference system where the solvent-solvent perturbation interaction does not exist, and has the correct partial molal volume in the limit of large solute. However, Eq. 33 is no longer valid for the system perturbed by the attractive solvent-solvent interaction, and the last term in Eq. 33 should read as $(\kappa/\kappa^{(0)})\,(\pi/6)\sigma_{XX}^3$ in the case of molecules of the common size, as pointed out by Neff and McQuarrie.[7]

Appendix

Thermodynamics of Hard-Body System. Some restrictions are imposed on the functional form of the thermodynamic quantities of the hard-body system. Such restrictions come simply from the fact that the internal energy of the hard-body system arises only from the kinetic energy of molecules and is independent of the configuration of the molecules. More explicitly, when the molecules have no internal freedom, the internal energy U is expressed by

$$U = \frac{3}{2}NkT, \tag{34}$$

where N and k are the total number of molecules and the Boltzmann constant, respectively. Thus the following equation holds for the hard-body system;

$$\left(\frac{\partial U}{\partial V}\right)_T = 0. \tag{35}$$

Using the thermodynamic relation, the following equations are derived from Eq. 35:

$$T\left(\frac{\partial P}{\partial T}\right)_V - P = 0, \tag{36}$$

$$\frac{P}{T} = \left(\frac{\partial P}{\partial T}\right)_V , \tag{37}$$

$$P = Tf(n), \tag{38}$$

where the $f(n)$ is the function of the number density n and independent of temperature and pressure. Using Eqs. 37 and 38 together with the Maxwell relation, we get the following equation:

$$\left(\frac{\partial S}{\partial V}\right)_T = f(n). \tag{39}$$

Thus the entropy is expressed as

$$S = S^* + \int_{V^*}^{V} f(n)\mathrm{d}V, \tag{40}$$

where the superscript * denotes the low density state of the system in which the system can be regarded as the ideal gas, and V the volume. The temperature dependence of the entropy in the hard-body system is identical with that in the ideal gas state. This equation denotes the fact that the configuration of the molecules are independent of the temperature in the hard-body system. The isothermal compressibility and the isobaric expansibility obey the following relations:

$$\frac{1}{\kappa} = Tn\frac{\mathrm{d}f(n)}{\mathrm{d}n}, \tag{41}$$

$$\frac{1}{\alpha} = \frac{1}{\kappa f(n)}, \tag{42}$$

$$= T\frac{\mathrm{d}\ln f(n)}{\mathrm{d}\ln n}, \tag{43}$$

where $f(n)$ is the function of n and independent of temperature. It can be shown that the behavior of the partial molal quantities in the hard-body system is also restricted; e.g., the partial molal volume is independent of temperature.

References

1) H. C. Andersen, D. Chandler, and J. D. Weeks, *Adv. Chem. Phys.*, **34**, 105 (1976).

2) J. A. Barker and D. Henderson, *Rev. Mod. Phys.*, **48**, 587 (1976).

3) J. P. Hansen and I. R. McDonald, "Theory of Simple Liquids," 2nd ed, Academic, London (1986).

4) B. Sisskind and I. Kasarnowsky, *Z. Anorg. Allgem. Chem.*, **214**, 385 (1933).

5) R. A. Pierotti, *J. Phys. Chem.*, **67**, 1840 (1963).

6) R. A. Pierotti, *Chem. Rev.*, **76**, 718 (1976).

7) R. O. Neff and D. A. McQuarrie, *J. Phys. Chem.*, **77**, 413 (1973).

8) H. B. Callen, "Thermodynamics and an Introduction to Thermostatistics," 2nd ed, John Wiley, New York (1985), Chap. 20.

9) J. A. Barker and D. Henderson, *Annu. Rev. Phys. Chem.*, **23**, 439 (1972); J. A. Barker and D. Henderson, *Mol. Phys.*, **21**, 187 (1971).

10) R. L. Scott, "Physical Chemistry—an Advanced Treatise," ed by D. Henderson, Academic, New York (1971), Vol. 8A; S. Saito, "Heikobussei Suisan no Kiso (Introduction to the Evaluation of Equilibrium Properties)," Baifukan, Tokyo (1983).

11) Note that the commonly used bar over the partial molal quantities are omitted throughout this paper, and instead, pay attention to the presence of the subscript X or S for the partial molal quantities of X or S, respectively.

 © 1988 The Chemical Society of Japan Bull. Chem. Soc. Jpn., 61, 1893—1897 (1988)

On the Reduction of *N*-Alkoxypyridinium Ions

Takashi SUMIYOSHI,* Meiseki KATAYAMA, and Wolfram SCHNABEL†
Department of Atomic Science and Nuclear Engineering, Faculty of Engineering, Hokkaido University, Sapporo 060
(Received December 4, 1987)

The reduction of 1-ethoxy-2-methylpyridinium (EMP^+) ions in aqueous solution at room temperature by e_{aq}^- and $\cdot CO_2^-$ was investigated in a pulse radiolysis study (irradiation with 10 ns pulses of 45 MeV electrons). For comparison, experiments with 1-methylpyridinium (MP^+) and unsubstituted pyridinium (PH^+) ions were carried out. With MP^+ and PH^+ the spectra of pyridinyl radicals were observed at the end of the pulse. In the case of EMP^+ the spectrum of the pyridinyl radical was not detectable. However, a new absorption band at 340 nm was formed with a significant delay after the reduction. Therefore, it was concluded that pyridinyl radicals formed by reduction of EMP^+ decompose very quickly into picoline and ethoxyl radicals. The latter add to EMP^+ with a rate constant $k=6\times10^7$ dm^3 mol^{-1} s^{-1}. The transient absorption band at 340 nm is ascribed to the adduct.

Recently, it was reported[1] that certain *N*-alkoxypyridinium salts of the general structure

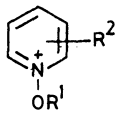

are quite appropriate to act as photoinitiators in free radical polymerizations of compounds possessing ethylenic double bonds. Since these pyridinium salts do not absorb light at $\lambda>300$ nm their utilization as photoinitiators in technical processes is possible only in conjunction with sensitizers. In Ref. 1 amino-substituted 3-ketocoumarins that absorb light at $\lambda>300$ nm were described as highly effective sensitizers. Although the mechanism of the interaction of excited sensitizers with pyridinium ions has not yet been disclosed, it appears probable that pyridinium ions are reduced by electron transfer according to the following mechanism:

$$S \longrightarrow S^* \quad (1)$$

$$S^* + Pyr^+ \longrightarrow S^+ + Pyr\cdot \quad (2)$$

Here, the following denotations are used:
S: sensitizer, S*: electronically excited sensitizer, S^+: sensitizer radical cation, Pyr^+: pyridinium ion, Pyr·: pyridinyl radical.

With respect to the initiation of free radical polymerization the question arises as to whether the pyridinyl radicals formed according to Reaction 2 are capable of reacting effectively with the monomer or Reaction 2 is followed by a rapid decomposition of the pyridinyl radicals yielding highly reactive species. In order to elucidate the reaction mechanism, the reduction of a typical *N*-alkoxypyridinium salt, namely 1-ethoxy-2-methylpyridinium tetrafluoroborate (EMP^+ BF_4^-) and of related compounds have been studied by means of pulse radiolysis. In this connection earlier work devoted to pyridinyl radicals is notable.[2-8] It was found, for instance, that the absorption spectra of pyridinyl radicals are characterized by rather strong maxima around 280 nm.

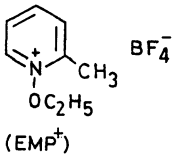

(EMP^+)

Experimental

Materials. 1-Ethoxy-2-methylpyridinium tetrafluoroborate (EMP^+ BF_4^-) was prepared according to a procedure described by Reichardt.[9] 1-Methylpyridinium tetrafluoroborate (MP^+ BF_4^-) was synthesized in the laboratory of Prof. H. Shirahama, Hokkaido University, and pyridinium chloride (PH^+ Cl^-) was a commercially available product (Wako Junyaku).

Irradiation of Sample Solutions. The pyridinium salts were dissolved in triply distilled water and irradiated in rectangular quartz cells with 10 ns pulses of 45 MeV electrons generated by a linear accelerator. As required samples were bubbled with argon or N_2O prior to irradiation. The absorbed dose was determined with the aid of the potassium thiocyanate dosimeter. Absorbed doses ranging from 20 to 130 Gy were applied to the solutions.

Results

(a) Experiments with 1-Ethoxy-2-methylpyridinium Tetrafluoroborate ($EMP^+BF_4^-$). (a-1) Reactions of Hydrated Electrons with EMP^+ Ions. The rate constant of the reaction of EMP^+ ions with hydrated electrons was measured by recording the decay of the optical absorption at 700 nm as a function of time after the pulse. Upon application of pseudo-first-order kinetic treatment $k(e_{aq}^- + EMP^+)=4.2\times10^{10}$ dm^3 mol^{-1} s^{-1} was obtained indicating that EMP^+ ions are reduced in a diffusion controlled reaction by hydrated electrons. In these experiments Ar-saturated aqueous solutions containing t-butyl alcohol (0.1 mol dm^{-3}) were used. The absorbed dose was 24 Gy. The decay of the absorption of the hydrated electrons was not accompanied by the formation of the absorption of the reduction product.

† On leave from Hahn-Meitner-Institut Berlin, Germany.

If pyridinyl radicals having a lifetime longer than the pulse length, were generated according to Reaction 3 a

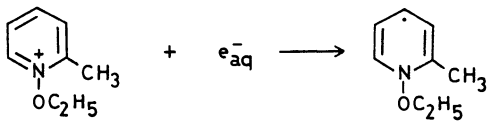

(3)

transient absorption at $\lambda < 300$ nm should be formed simultaneously with the decay of the absorption of hydrated electrons. As can be seen from Fig. 1 a new absorption band was formed, however, with a formation lifetime definitely longer than that of the decay of hydrated electrons. Inset (a) in Fig. 1 shows the decay of the absorption of hydrated electrons at $[EMP^+BF_4^-]=1.12\times10^{-3}$ mol dm^{-3} and inset (b) shows the increase in the absorption at 340 nm at $[EMP^+ BF_4^-]=1.12\times10^{-3}$, 3.37×10^{-3} and 8.92×10^{-3} mol dm^{-3}. Obviously, the build-up rate increased with increasing concentration of pyridinium ions. Application of pseudo-first-order kinetic treatment yielded a bimolecular rate constant $k_2=6\times10^7$ dm^3 mol^{-1} s^{-1}.

(a-2) Reactions of $\cdot CO_2^-$ with EMP^+ Ions. The reduction of EMP^+ ions was also accomplished according to Reaction 4 by formate radical anions which were generated by reaction of hydroxyl radicals with formate ions according to Reaction 5.

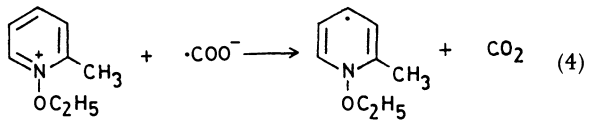

(4)

$$\cdot OH + HCOO^- \longrightarrow H_2O + \cdot COO^- \quad (5)$$

Upon irradiation of N_2O-saturated $EMP^+BF_4^-$ solutions containig 0.05 mol dm^{-3} sodium formate the optical absorption spectrum (a) in Fig. 2 was formed during the pulse. It possesses a rather strong absorption band with a peak below 280 nm. The decay rate of this absorption band was found to be accelerated by increasing the pyridinium salt concentration. Actually, a similar rather strong absorption was also observed in the absence of pyridinium salt. Therefore, it is concluded that the absorption around 280 nm is due to $\cdot CO_2^-$ radical anions which are capable of reacting with pyridinium ions. The absorption peak of $\cdot CO_2^-$ radical anions has been reported to be located at about 250 nm, in aqueous solution.[10] In the present work, the ground state absorption of EMP^+ was very strong at wavelength below about 275 nm, making the solution almost opaque. Therefore, measurements of changes in the optical density below 280 nm were impossible. The decay of the absorption around 280 nm was followed up by the build-up of a new absorption band with a maximum at about 340 nm (spectrum (c) in Fig. 2). The rate of the reduction of EMP^+ ions by $\cdot CO_2^-$ ions was not correlated to the formation of the new absorption band as is demonstrated by typical kinetic traces shown in Fig. 3(a). Notably, the product of the reaction of $\cdot CO_2^-$ with EMP^+ could not be evidenced spectroscopically. Therefore, the reduction product must be very short-lived. In this respect, these findings correspond to results obtained with the reaction of hydrated electrons with EMP^+ (vide ante). In that case, quite similarly, the rate of decay of hydrated electrons did not correspond to the rate of formation of the new absorption band peaked at 340 nm. From the dependence of the lifetime of the absorption at 280 nm on the pyridinium salt concentration $k(\cdot CO_2^- + EMP^+)=2.1\times10^8$ dm^3 mol^{-1} s^{-1} was obtained. The rate of formation of the transient absorbing at 340 nm increased with increasing pyridinium salt concentra-

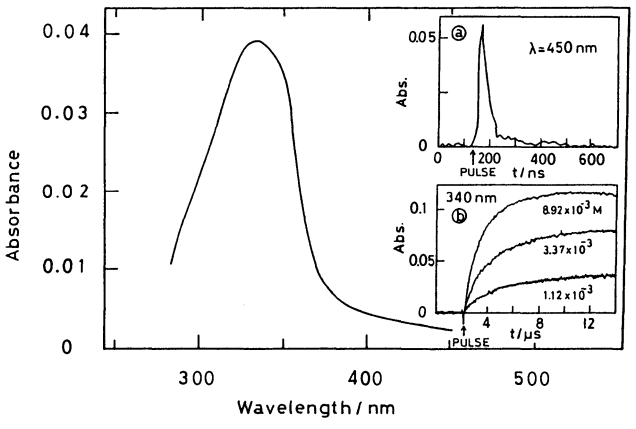

Fig. 1. Irradiation of $EMP^+BF_4^-$ (1.12×10^{-3} mol dm^{-3}) in Ar-saturated aqueous solution containing 0.1 mol dm^{-3} *t*-butyl alcohol with a 10 ns pulse of 45 MeV electrons. D_{abs}=140 Gy. Optical absorption spectrum recorded 20 μs after the pulse. Insets: kinetic traces illustrating the decay of the absorption at 450 nm due to hydrated electrons (a) and the formation of the transient absorption at 340 nm at various concentrations of $EMP^+BF_4^-$ as indicated in the graph (b). D_{abs}=110 Gy.

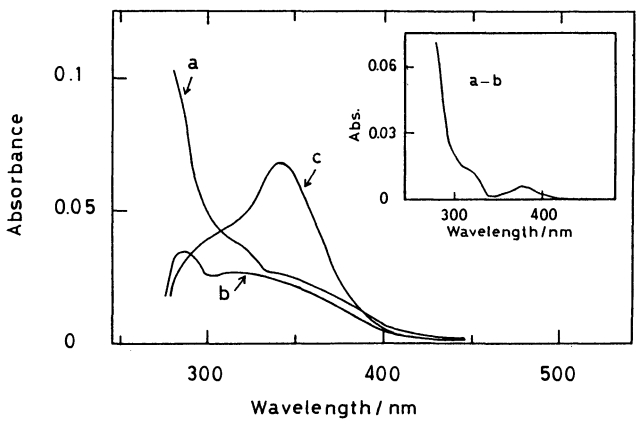

Fig. 2. Irradiation of $EMP^+BF_4^-$ (1.12×10^{-3} mol dm^{-3}) in N_2O-saturated aqueous solution containing 0.05 mol dm^{-3} sodium formate with a 10 ns pulse of 45 MeV electrons. D_{abs}=140 Gy. Optical absorption spectra recorded at the end of the pulse (a) and at 5 μs (b) and 80 μs (c) after the pulse. Inset: difference of spectra (a) and (b).

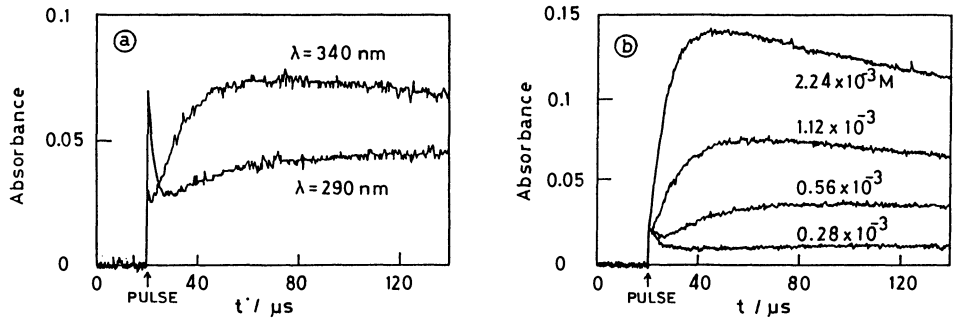

Fig. 3. Kinetic traces illustrating changes in the optical density after the pulse at λ=340 nm and 290 nm at [$EMP^+BF_4^-$]=1.12×10^{-3} mol dm^{-3} (a) and at 340 nm at various concentrations of $EMP^+BF_4^-$ as indicated in the graph (b). For other conditions refer to legend to Fig. 2.

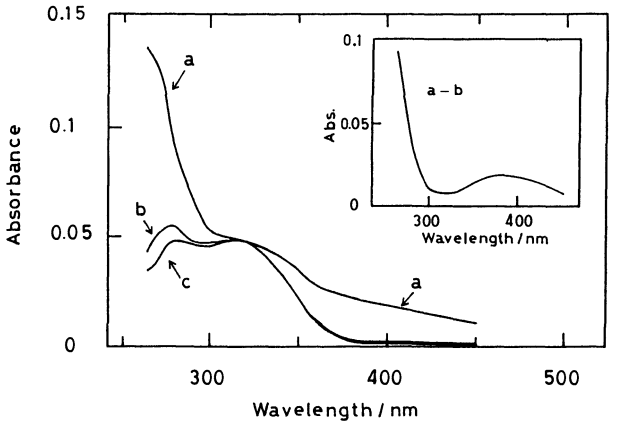

Fig. 4. Irradiation of $MP^+BF_4^-$ (1×10^{-3} mol dm^{-3}) in Ar-saturated aqueous solution containing *t*-butyl alcohol (0.1 mol dm^{-3}) with a 10 ns pulse of 45 MeV electrons. D_{abs}=140 Gy. Optical absorption spectra recorded at the end of the pulse (a) and 80 μs (b) and 160 μs (c) after the pulse. Inset: difference spectrum (a)—(b).

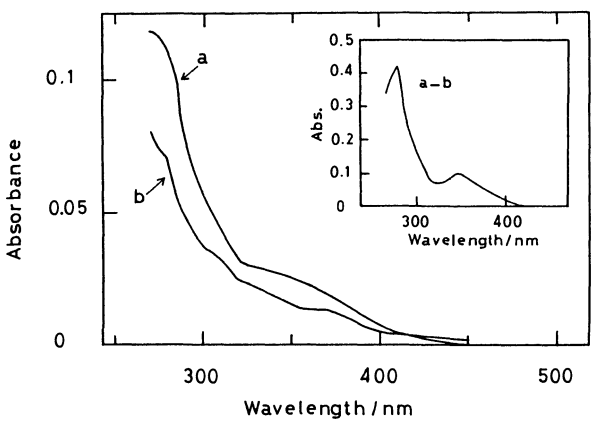

Fig. 5. Irradiation of PH^+Cl^- (6.1×10^{-4} mol dm^{-3}) in N_2O-saturated aqueous solution containing sodium formate (0.025 mol dm^{-3}) with a 10 ns pulse of 45 MeV electrons. D_{abs}=160 Gy. Optical absorption spectra recorded 500 ns (a) and 8 μs (b) after the pulse. Inset: difference spectrum (a)—(b).

tion yielding a bimolecular rate constant $k_2=8.2\times10^7$ dm^3 mol^{-1} s^{-1}.

(b) Experiments with 1-Methylpyridinium Tetrafluoroborate ($MP^+BF_4^-$). Upon reaction of hydrated electrons with MP^+ ions, i.e. upon irradiation of an Ar-saturated $MP^+BF_4^-$ solution containing *t*-butyl alcohol (0.1 mol dm^{-3}) the transient spectrum (a) in Fig. 4 was obtained. It possesses a strong absorption band with a maximum at $\lambda<280$ nm, which could not be disclosed due to the strong absorption of the 1-methylpyridinium salt in this wavelength range, and a weak band peaked at about 310 nm. The low wavelength portion of this spectrum decayed with a rate constant $k=4\times10^4$ s^{-1} leaving a long lasting spectrum with a broad maximum around 300 nm. Quite similar results were obtained with a N_2O-saturated solution containing sodium formate (0.05 mol dm^{-3}), i.e. in the case of the reaction of $\cdot CO_2^-$ with MP^+. Therefore, it is concluded that both hydrated electrons and $\cdot CO_2^-$ radical anions reduce MP^+ ions forming pyridinyl radicals. The rate of decay of hydrated electrons correlated with the rate of formation of the transient spectrum which is, therefore, assigned to the pyridinyl radical.

(c) Experiments with Pyridinium Chloride (PH^+Cl^-). Figure 5 shows a transient absorption spectrum (a) formed upon the reaction of $\cdot CO_2^-$ with PH^+, i.e. upon irradiation of a N_2O-saturated solution of PH^+Cl^- containing sodium formate (0.025 mol dm^{-3}). This spectrum possesses a maximum at about 270 nm. A quite similar spectrum was observed when hydrated electrons reacted with PH^+, i.e. when an Ar-saturated solution containing *t*-butyl alcohol (0.1 mol dm^{-3}) was irradiated. Also in this case, the rate of decay of hydrated electrons correlated with the rate of formation of the transient absorption spectrum as can be seen from Fig. 6, where the decay of the absorption at 450 nm (due to hydrated electrons) and the build-up of the absorption at 265 nm is shown. The latter absorption is, therefore, assigned to the pyridinyl radical. It should pointed out that the transient absorption spec-

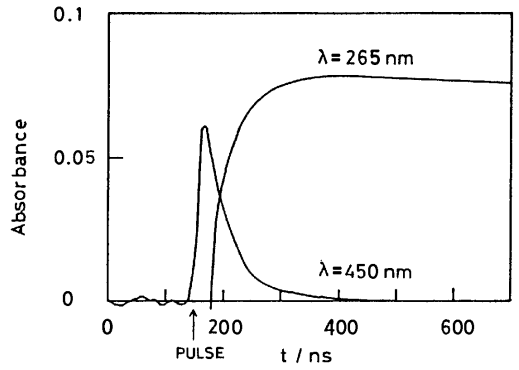

Fig. 6. Irradiation of PH^+Cl^- (8.15×10^{-4} mol dm^{-3}) in Ar-saturated aqueous solution containing *t*-butyl alcohol (0.1 mol dm^{-3}) with a 10 ns pulse of 45 MeV electrons. D_{abs}=140 Gy. Kinetic traces illustrating the decay of the optical absorption at 450 nm due to hydrated electrons and the formation of the optical absorption at 265 nm due to pyridinyl radicals.

trum observed here is quite similar to the spectrum of the pyridinyl radical reported by Cercek and Ebert.[4]

In conclusion, both $\cdot CO_2^-$ and e_{aq}^- were found to react with PH^+ forming the pyridinyl radical

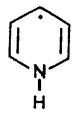

which was detected by its characteristic absorption spectrum.

Discussion

The results show clearly, that, on reduction, the *N*-alkoxypyridinium ion EMP^+ exhibits a behavior quite different from that observed with *N*-methylpyridinium, MP^+, and pyridinium, PH^+. From the transient absorption spectra recorded after the pulse it is inferred that the latter two ions are converted to rather long-lived pyridinyl radicals upon reacting with hydrated electrons or $\cdot CO_2^-$ radical anions. In contrast, in the case of EMP^+ ions, the absorption of the corresponding pyridinyl radical was not observable, although EMP^+ reacts in a diffusion-controlled reaction with e_{aq}^-. From the fact that a new transient absorption band at 340 nm was formed a rather long time after the hydrated electron had reacted with EMP^+, it is concluded that the reduction product decomposes very rapidly, and that the resulting fragments are capable of reacting with EMP^+ ions. Upon studying the reduction of EMP^+ ions by $\cdot CO_2^-$ radical anions the same conclusion was arrived at. Also in this case pyridinyl radicals were not detectable spectroscopically, and the rate of decay of the radical anions did not correspond to the formation rate of a product absorbing at 340 nm. Consequently, it has to be assumed that the lifetime of the reduction product, the pyridinyl radical, is very short, probably shorter than one ns. The decomposition of the pyridinyl radicals leads to products which do not possess absorption bands in the wavelength range inspected (down to 260 nm) differing from that of EMP^+ or do not absorb at all at $\lambda>260$ nm. This conclusion is consistent with a decomposition mechanism according to Reaction 6, a process being comparable to dissociative electron capture processes occurring, e. g., with halogenated hydrocarbons:

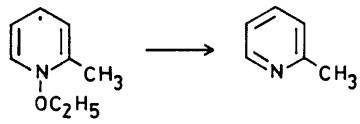

(6)

$$e^- + RCl \longrightarrow R\cdot + Cl^-$$

Ethoxyl radicals are not expected to absorb light markedly above 260 nm and the absorption spectrum of the other reaction product, 2-methylpyridine, is almost identical to that of EMP^+. According to this mechanism ethoxyl radicals are formed as reactive species capable of reacting, e.g., with olefinic compounds when *N*-alkoxypyridinium compounds are used as photoinitiators. In the present case, ethoxyl radicals are expected to undergo a self reaction according to Reaction 7, at sufficiently high $C_2H_5O\cdot$ concentration:

$$2\,C_2H_5O\cdot \longrightarrow \text{Products} \qquad (7)$$

Ethoxyl radicals can also react with EMP^+ ions. They can, for example, add to EMP^+ according to Reaction 8:

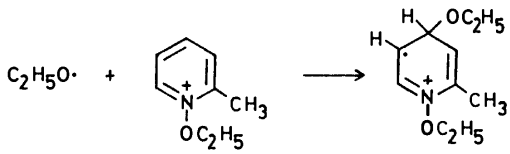

(8)

Reaction 8 is thought to give rise to the formation of the transient absorption peaked at 340 nm which is assigned to the adduct of ethoxyl radical to EMP^+. In accordance with this assignment, the formation rate of the transient absorption at 340 nm increased with inceasing EMP^+ concentration yielding the rate constant $k(C_2H_5O\cdot+EMP^+)=(6—8)\times10^7$ dm^3 mol^{-1} s^{-1}.

The authors are very grateful to Prof. Dr. Haruhisa Shirahama and his co-workers for synthesizing $MP^+BF_4^-$.

References

1) D. P. Specht and S. Y. Farid, U. S. Patent Appl. 185, 854 (1980); *Chem. Abstr.*, **97**, 82722b (1982).

2) E. J. Land and A. J. Swallow, *Biochim. Biophys. Acta*, **162**, 327 (1968).

3) M. Simic and M. Ebert, *Int. J. Radiat. Phys. Chem.*, **3**, 259 (1971).

4) B. Cercek and M. Ebert, *Trans. Faraday Soc.*, **63**, 1687 (1967).

5) E. M. Kosower and E. Pozionek, *J. Am. Chem. Soc.*, **86**, 5515 (1964).
6) M. Itoh and S. Nagakura, *J. Am. Chem. Soc.*, **89**, 3959 (1967).
7) P. Neta and L. K. Patterson, *J. Phys. Chem.*, **78**, 2211 (1974).
8) K. Nakamura, Y. Morita, T. Suzuki, T. Sugiyama, and A. Sugimori, *Bull. Chem. Soc. Jpn.*, **52**, 488 (1979); A. Sugimori, *Hoshasen Kagaku*, **44**, 52 (1987).
9) C. Reichardt, *Chem. Ber.*, **99**, 1769 (1966).
10) J. P. Keene, Y. Raef, and A. J. Swallow, "Pulse Radiolysis," ed by M. Ebert, J.P. Keene, A. J. Swallow, and J. H. Baxendale, Academic Press, London (1965), p. 99.

 © 1988 The Chemical Society of Japan Bull. Chem. Soc. Jpn., 61, 1899—1902 (1988)

Hydrogen Formation from Water Adsorbed on Zeolite during Gamma-Irradiation

Masayoshi Aoki, Chiyoko Nakazato, and Takahiro Masuda*
Department of Chemistry, Faculty of Science, Tokyo Metropolitan University, Fukasawa 2-1-1, Setagaya-ku, Tokyo 158
(Received December 9, 1987)

The γ-radiolysis of water adsorbed on synthetic zeolite, MS 13X (Molecular Sieve 13X), has been investigated by the product analysis method using gas chromatography. One of the main products is molecular hydrogen, the G value of which increases with increasing amount of water adsorbed on MS 13X and reaches a first plateau (0.42) at ca. 4 mmol of water per g of MS 13X. At ca. 6 mmol g^{-1} of water, it resumes the increase and finally approaches a second plateau (1.2) at ca. 9 mmol g^{-1}. The formation of hydrogen is depressed by an electron scavenger, while ammonia, a scavenger of positive hole, enhances the hydrogen formation. The result indicates that hydrogen is produced through a reaction of water with electrons generated in MS 13X. The rate constant for the reaction of electrons with water adsorbed on MS 13X is estimated to be $(2.6\pm0.3)\times10^8$ dm^3 mol^{-1} s^{-1}, on the assumption that rate constants for reactions of electrons with some electron scavengers determined in liquid cyclohexane can be applied to this system.

Enhanced yield in the radiolysis of a substance adsorbed on solid has been explained in terms of the energy transfer from adsorbent to adsorbate. Exciton, electron, and positive hole have been proposed as energy carriers.[1-6] Recently we found that N_2O adsorbed on synthetic zeolite (Molecular Sieve 13X; abbreviated to MS) is radiolyzed to produce N_2 with a G value of 2.8, which is saturated against the adsorbed amount of N_2O.[7] In the presence of a second electron scavenger, $G(N_2)$ decreases with increasing amount of the second scavenger. Relative reactivities of electrons generated in MS toward several kinds of scavengers suggest that these electrons are similar to those produced in liquid 2,2-dimethylpropane with respect to reactivity.[8,9] This implies that electrons generated in MS are possibly in a "quasi-free" state. On the other hand, we found that adsorption of methanol alters relative reactivities to those observed in liquid cyclohexane or hexane.[5] In the system with methanol, molecular hydrogen is produced as a main product and the formation of hydrogen is explained by a mechanism including a reaction of electrons with adsorbed methanol. The estimated rate constant for the reaction of electrons with adsorbed methanol is much higher than that determined in liquid methanol. These suggest that electrons generated in MS adsorbing methanol is "slightly solvated" in a way similar to excess electrons in cyclohexane or hexane.[8-10]

The radiolysis of water adsorbed on MS is of interest in the reactivity and state of electrons generated in the system and their reaction with adsorbed water, because the reaction of "nearly dry" electrons with water can be approximated to a reaction occurring at the initial stage of radiolysis of liquid water.

In this study, an attempt was made to clarify the state of electrons generated in the MS-H_2O system by determining the relative reactivity of the electrons toward some electron scavengers. Molecular hydrogen was found to form from water adsorbed on MS and stepwise increase in $G(H_2)$ was observed with increasing amount of water. The relative reactivity determined by competition kinetics showed that electrons produced in this system are similar to those in the MS-CH_3OH system rather than those in MS-N_2O. The rate constant for the reaction of electrons with water adsorbed on MS was estimated by assuming that rate constants for reactions of electrons with some electron scavengers are the same with those obtained in liquid cyclohexane.

Experimental

Zeolite (Molecular Sieve 13X) was purchased from Nippon Kuromatokogyo K. K. The specific surface area is 1030 m^2 g^{-1}. Dinitrogen monoxide, ammonia, and sulfur hexafluoride were obtained from Takachiho Kagakukogyo K. K. and purified by distillation under vacuum before use. Carbon tetrachloride was obtained from E. Merck, Ltd.

The procedure of pretreatment of MS and introduction of adsorbates were described elsewhere in detail.[7] Molecular hydrogen and nitrogen were analyzed by gas chromatography according to the method employed in a previous work on silica gel.[4] Water was triply distilled after treatment with alkaline permanganate.

Results and Discussion

Molecular hydrogen is produced from water adsorbed on MS during γ-irradiation. The G value for hydrogen formation increases with increasing amount of water stepwise as shown in Fig. 1. G values are calculated on the basis of total energy absorbed by MS and water. At amounts below 6.6×10^{-4} mol g^{-1}, formation of hydrogen was hardly observed. This may be explained by consumption of water due to chemisorption of water by some active site of MS or reaction of hydrogen molecule or atom with the site, as has been discussed with the MS-CH_3OH system.[5] The formation of hydrogen is effectively depressed by electron scavenger. Figure 2 shows the dependence of $G(H_2)$ on the amount of several electron scavengers in the presence of 4 mmol g^{-1} of adsorbed water. At ca. 10^{-4}

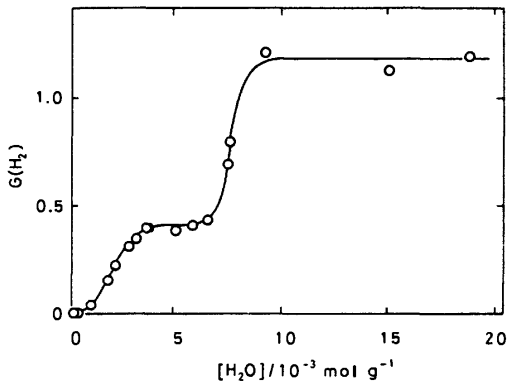

Fig. 1. Dependence of $G(H_2)$ on adsorbed amount of H_2O. Adsorbed amount is expressed as mol of H_2O per g of MS.

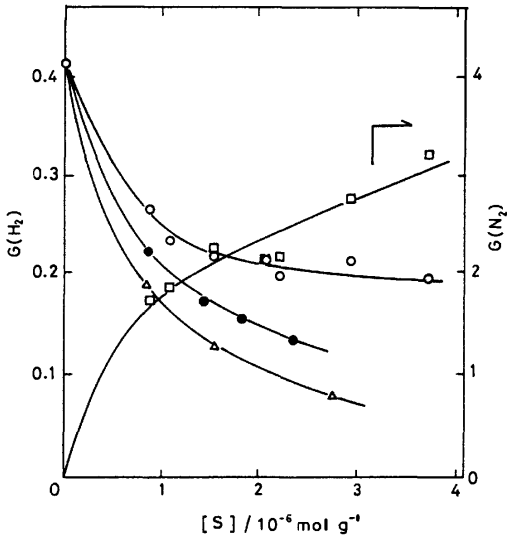

Fig. 2. Dependence of $G(H_2)$ and $G(N_2)$ on adsorbed amounts of scavengers. Adsorbed amount is expressed as mol of scavengers per g of MS. 4×10^{-3} mol g^{-1} of H_2O present. ○; N_2O, ●; CCl_4, △; SF_6, □; $G(N_2)$ produced from N_2O.

mol g^{-1} of scavengers, the formation of hydrogen is completely depressed in every case. Therefore, a precursor of hydrogen is thought to be eliminated by these electron scavengers. On the other hand, addition of ammonia, a positive hole scavenger, results in an enhancement of hydrogen formation. Since the formation of hydrogen from ammonia itself was hardly observed in the absence of water as shown in Fig. 3, the increase in $G(H_2)$ in the presence of water is caused by scavenging of positive hole. Therefore, molecular hydrogen is considered to be produced through a reaction of adsorbed water with electrons generated in MS. The formation of hydrogen is explained by the sequence of reactions

$$MS \longrightarrow MS^+ + e^-, \quad (1)$$

$$e^- + MS^+ \longrightarrow MS^*, \quad (2)$$

$$e^- + H_2O \longrightarrow H + OH^-, \quad (3)$$

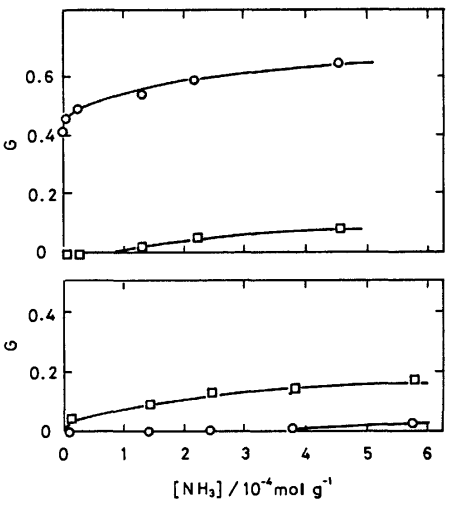

Fig. 3. $G(H_2)$ and $G(N_2)$ vs. $[NH_3]$. ○; $G(H_2)$, □; $G(N_2)$. Upper, 4×10^{-3} mol g^{-1} of H_2O present. Lower, H_2O absent.

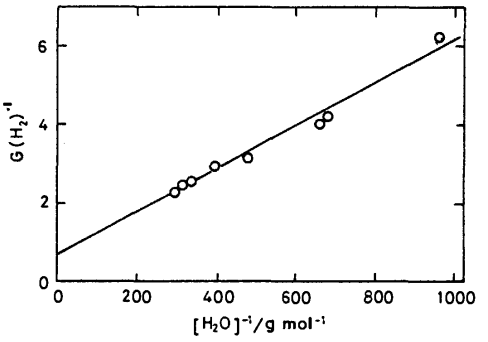

Fig. 4. $1/G(H_2)$ vs. $1/[H_2O_{ad}]$.

$$H + H \longrightarrow H_2. \quad (4)$$

In the presence of an electron scavenger or ammonia, Reaction 5 or 6 takes place:

$$e^- + S \longrightarrow \text{product(s)}, \quad (5)$$

$$MS^+ + NH_3 \longrightarrow \text{product(s)}. \quad (6)$$

From the above reactions, the following equation can be derived:

$$1/G(H_2) = 2(1 + k_2[MS^+]/k_3[H_2O_{ad}])/G_e \quad (I)$$

and

$$1/G(H_2) = 2\{1 + (k_2[MS^+] + k_5[S])/k_3[H_2O_{ad}]\}/G_e \quad (II)$$

where $[H_2O_{ad}]$ represents adsorbed amount of water. By plotting $1/G(H_2)$ against $1/[H_2O_{ad}]$ or $[S]$, G_e and the ratio of rate constants, k_5/k_3, can be estimated. Figures 4 and 5 are examples of the plots, which show a good linear relation. From the intercepts and slopes of these straight lines, G_e and the ratio of rate constants are calculated. In Table 1, the values estimated for various systems are summarized. G-values of electron agree fairly well with each other and the value (3.06 ± 0.07) is obtained as the average. From the ratio

Table 1. Estimated Values of G_e and k_s/k_3 and Comparison of k_s/k_{N_2O}

System	G_e	k_s/k_3	k_s/k_{N_2O}		
			This work	Ref. 9	Ref.10
$MS-H_2O$	3.15				
$MS-H_2O-N_2O$	3.03	8.02×10^3	1	1	1
$MS-H_2O-CCl_4$	2.99	1.04×10^4	1.3	1.1	1.5
$MS-H_2O-SF_6$	3.01	1.71×10^4	2.1	1.7	2

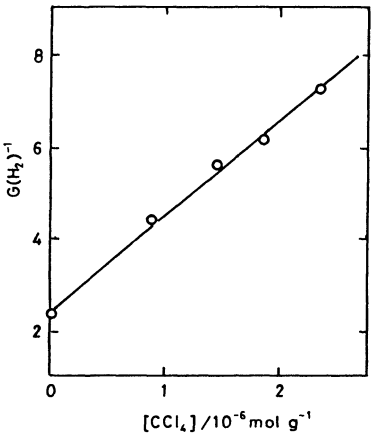

Fig. 5. $1/G(H_2)$ vs. $[CCl_4]$.

of rate constants, k_5/k_3 relative rate constants based on k_{N_2O} can be calculated for CCl_4 and SF_6. In the last three columns, they are compared with those determined in liquid cyclohexane.[9,10] It is indicated that the electrons generated in water-adsorbing MS are similar to those in liquid cyclohexane with respect to the reactivity toward these scavengers. If the rate constants for these scavengers determined in cyclohexane are used as k_5, the rate constant for the reaction of the electrons with water adsorbed on MS is estimated to be $(2.6\pm0.3)\times10^8$ $dm^3\,mol^{-1}\,s^{-1}$ as an average (Table 2). This is quite different from the rate constant for the reaction of hydrated electrons with water in aqueous systems. As mentioned above, $G(H_2)$ increases with increasing amount of water stepwise and the experiments of scavengers were carried out at the amount of water which corresponds to the first plateau. Molecular Sieve 13X includes sodium ion of 6.4 $mmol\,g^{-1}$, which is known as a counterpart of the negative charge located on aluminium atom. Since the sodium ion in the hexagonal prism of MS cannot get into contact with water molecule, the content of the sodium ion effective for the adsorption of water will be less than 6.4 $mmol\,g^{-1}$. It can be considered, therefore, that the amount of the water at the first plateau is approximately equal to the effective amount of sodium ion. Furthermore, it is reported that water is adsorbed predominantly on the Na^+ sites of synthetic zeolite to form $(Na_4)^{3+}$-$(H_2O)_x$ by trapping an electron.[11,12] These suggest that hydrogen atom is formed from water through the reaction with sodium atom. Reaction 3 may be rewritten to

Table 2. Values of k_3 Calculated on the Basis of k_s Determined in Cyclohexane

Scavenger	$k_3/dm^3\,mol^{-1}\,s^{-1}$
N_2O	3.0×10^8
CCl_4	2.6×10^8
SF_6	2.3×10^8
Average	$(2.6\pm0.3)\times10^8$

$$e^- + Na^+ \longrightarrow Na, \quad (7)$$

$$Na + H_2O \longrightarrow Na^+ + OH^- + H. \quad (8)$$

This mechanism is consistent with the observed high reactivity of the electrons generated in the $MS-H_2O$ system toward water molecule.

One of the authors previously found that scavengers of positive hole with ionization potentials below 11.1 eV decolorize a color center of silica gel, which is assigned to a positive hole produced by γ-irradiation.[3] While the color center of silica gel is stable at room temperature, no absorption is observed in the case of irradiated MS. However, the electron affinity of MS^+ is at least above 10.85 eV, because methanol (I_p=10.85) reacts with MS^+ to produce formaldehyde and ethylene glycol.[5] Since the ionization potential of ammonia is 10.2 eV, the proposed mechanism including the scavenging of MS^+ by ammonia is reliable.

As seen in Fig. 2, the G value for nitrogen formation is apparently larger than the decrease in $G(H_2)$, even if $G(N_2)$ is equal to $2G(H_2)$. A similar disagreement in stoichiometry was observed in hexane and cyclohexane when N_2O was used as an electron scavenger.[13,14] As reported in a previous paper, the $G(N_2)$ from N_2O adsorbed on MS is 2.8 at adsorbed amounts of N_2O above 5×10^{-4} $mol\,g^{-1}$. In the presence of CH_3OH, values from 2.6 to 2.8 are estimated as G_e by plotting $1/G(H_2)$ vs. $1/[CH_3OH]$ or [S], whereas $G(N_2)$ is ca. 3.4 and differs from the G value of the electron scavenged by N_2O. Estimated G values for electrons generated in various systems of MS seem to converge in the neighborhood of 2.8. However, the $G(N_2)$ in the $MS-N_2O$ system differs from those in systems $MS-CH_3OH-N_2O$ and $MS-H_2O-N_2O$. The relative reactivity of the electrons produced in these systems toward some electron scavengers can be classified into two types, one observed in liquid 2,2-dimethylpropane and the other in liquid hexane or cyclohexane. These results suggest a resemblance in the energy state of excess electrons between liquid hydrocarbons and MS. The disagree-

ment of stoichiometry between $G(N_2)$ and G value of scavenged electron will, therefore, be related to the energy state of excess electrons generated in the irradiated systems.

References

1) P. K. Wong, *J. Phys. Chem.*, **75**, 201 (1971).
2) K. Sogabe, A. Hasegawa, Y. Yamada, and M. Miura, *Bull. Chem. Soc. Jpn.*, **45**, 3362 (1972).
3) H. Ogura, Y. Tachika, Y. Suzuki, C. Nakazato, M. Kondo, T. Sawai, and T. Sawai, *J. Nucl. Sci. Technol.*, **12**, 167 (1975).
4) H. Ogura, M. Hinata, C. Nakazato, M. Kondo, T. Sawai, and T. Sawai, *J. Nucl. Sci. Technol.*, **15**, 433 (1978).
5) C. Nakazato, R. Murayama, M. Aoki, and T. Masuda, *Bull. Chem. Soc. Jpn.*, **60**, 2775 (1987).
6) J. W. Sutherland and R. Goodrich, *J. Am. Chem. Soc.*, **89**, 6779 (1967).
7) C. Nakazato and T. Masuda, *Bull. Chem. Soc. Jpn.*, **59**, 2237 (1986).
8) A. O. Allen and R. A. Holroyd, *J. Phys. Chem.*, **78**, 796 (1974).
9) A. O. Allen, T. E. Gangwer, and R. A. Holroyd, *J. Phys. Chem.*, **79**, 25 (1975).
10) K. Mori, K. Ito, and Y. Hatano, *J. Phys. Chem.*, **79**, 209 (1975).
11) J. H. Shen, A. C. Zettlemoyer, and K. Kller, *J. Phys. Chem.*, **84**, 1453 (1980).
12) D. N. Stamires, "Molecular Sieves," Soc. Chem. Industry, London (1968), p. 328.
13) Y. Hatano, K. Takeuchi, and S. Takao, *J. Phys. Chem.*, **77**, 586 (1973).
14) Y. Hatano and J. L. Abboud, *Bull. Chem. Soc. Jpn.*, **47**, 236 (1974).

 © 1988 The Chemical Society of Japan Bull. Chem. Soc. Jpn., 61, 1903—1909 (1988)

Optical Absorption by Mn^{2+} Ions in $MnM(edta)\cdot 6H_2O$ (M=Zn, Cu, Ni, and Co)

Hisashi Togashi,*,† Norimichi Kojima, Toshiro Ban, and Ikuji Tsujikawa
Department of Chemistry, Faculty of Science, Kyoto University, Kyoto 606
(Received Decembder 9, 1987)

The optical absorption spectra of the Mn^{2+} ion in $MnM(edta)\cdot 6H_2O$ (M=Zn, Cu, Ni, and Co) were measured at low temperature. Fine structural bands corresponding to the $^6A_{1g}\rightarrow{}^4T_{2g}$ (D) and $^6A_{1g}\rightarrow{}^4A_{1g}$, ^4E_g (G) transitions were found. The fine structure corresponding to the $^6A_{1g}\rightarrow{}^4A_{1g}$, ^4E_g (G) transition in the Zn compound were analyzed with the ligand field theory and the assignment of the absorption peaks was performed. Although the spectra of the Zn, Cu, and Co compounds are similar, those of the Ni compounds show significant broadening, which is possibly due to the energy transfer caused by the overlapping of the absorption bands of the Ni^{2+} and Mn^{2+}ions.

Recently, bimetallic chelate complexes M′M″ (edta)·$6H_2O$ (M′,M″=metal elements in the 4th period, H_4edta= ethylenediaminetetraacetic acid) were synthesized[1,2] and their magnetic properties have been extensively studied.[3-6] It is because they are good models of one-dimensional ferrimagnets.

One can obtain large variety of isomorphous compounds with different magnetic interaction. In these crystals $[M'(H_2O)_4]^{2+}$ and $[M''(edta)]^{2-}$ are alternately bonded by the carboxyl group of the edta, hence bimetallic chains are formed.

The authors think that these compounds are suitable not only for the magnetic studies but also for the study on the interaction between the electronic states in different metal ions. Such studies have been practiced mainly on the crystals doped with foreign metal ions. However the spectra of the electronic transitions in such materials usually suffer inhomogeneous broadening, which is caused by the difference of the energy levels among the impurity sites. On the contrary, the spectra of M′M″ (edta)·$6H_2O$ will be free from inhomogeneous broadening because these compounds are pure crystals. Visible reflectance spectra of M′M″ (edta)·$6H_2O$ at room temperature were already measured by Escrivá et al.[7]

We prepared single crystals of $MnM(edta)\cdot 6H_2O$(M= Zn, Cu, Ni, and Co) and measured optical absorption spectra at low temperatures, for the purpose to observe the effects of the $[M(edta)]^{2-}$ on the electronic transitions in the $[Mn(H_2O)_4]^{2+}$.

First, preparation of the crystals and the measurement procedure are described. Secondly, the absorption spectra and the corresponding energy levels are discussed on the basis of the ligand field theory. Also we discuss the interaction between $[Mn(H_2O)_4]^{2+}$ and $[M(edta)]^{2-}$.

Experimental

$MnM(edta)\cdot 6H_2O$ (M=Zn, Cu, Ni, and Co) were obtained from the aqueous solution of $MnCl_2\cdot 4H_2O$ (1 mol), Na_2H_2 edta (1 mol), and nitrates or sulfates of M (1 mol) by heating on a water bath. The pH of the solution was adjusted between 5 and 6 by the use of Na_2CO_3 and HNO_3. The precipitated products were refined by recrystallization from water solution. The water solution of the recrystallized material was slowly evaporated at a temperature between 50 and 60 °C and yielded single crystals, of which typical dimension was 3×3×3 mm^3. The colors of the crystals were pale pink (M=Zn), blue (Cu), dark purple (Ni), and dark brown (Co).

It had been found[8] that the crystal structures of Cu and Co salts belong to an orthorhombic system C_{2v}^9-$Pn2_1a$ (Fig. 1). The X-ray diffraction pattern for the powder of our crystals of Cu and Co compounds agreed to these structures. From

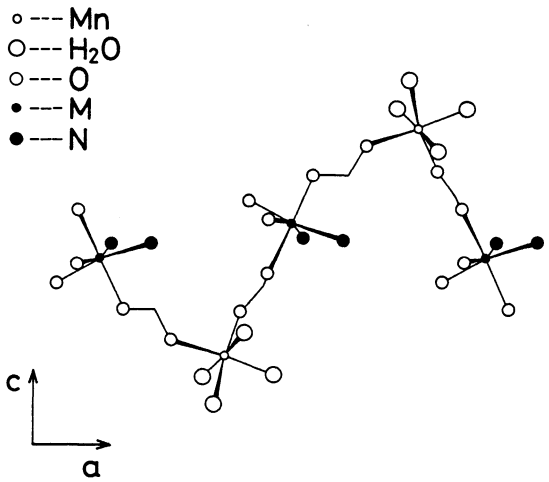

Fig. 1. Schematic view of the structure of MnM(edta)·$6H_2O$ projected on the *ac*-plane. Only metal ions and the atoms which directly coordinate to them are shown.

Table 1. Lattice Constants of $MnM(edta)\cdot 6H_2O$ (M=Zn, Cu, Ni, and Co) with the Space Group of C_{2v}^9-$Pn2_1a$

	a/Å	*b*/Å	*c*/Å
Zn	14.57	13.26	9.84
Cu[a]	14.626	13.068	9.969
Ni	14.40	13.00	9.69
Co[a]	14.584	13.366	9.799

a) Ref. 8.

† Present address: National Chemical Laboratory for Industry, Tsukuba 305.

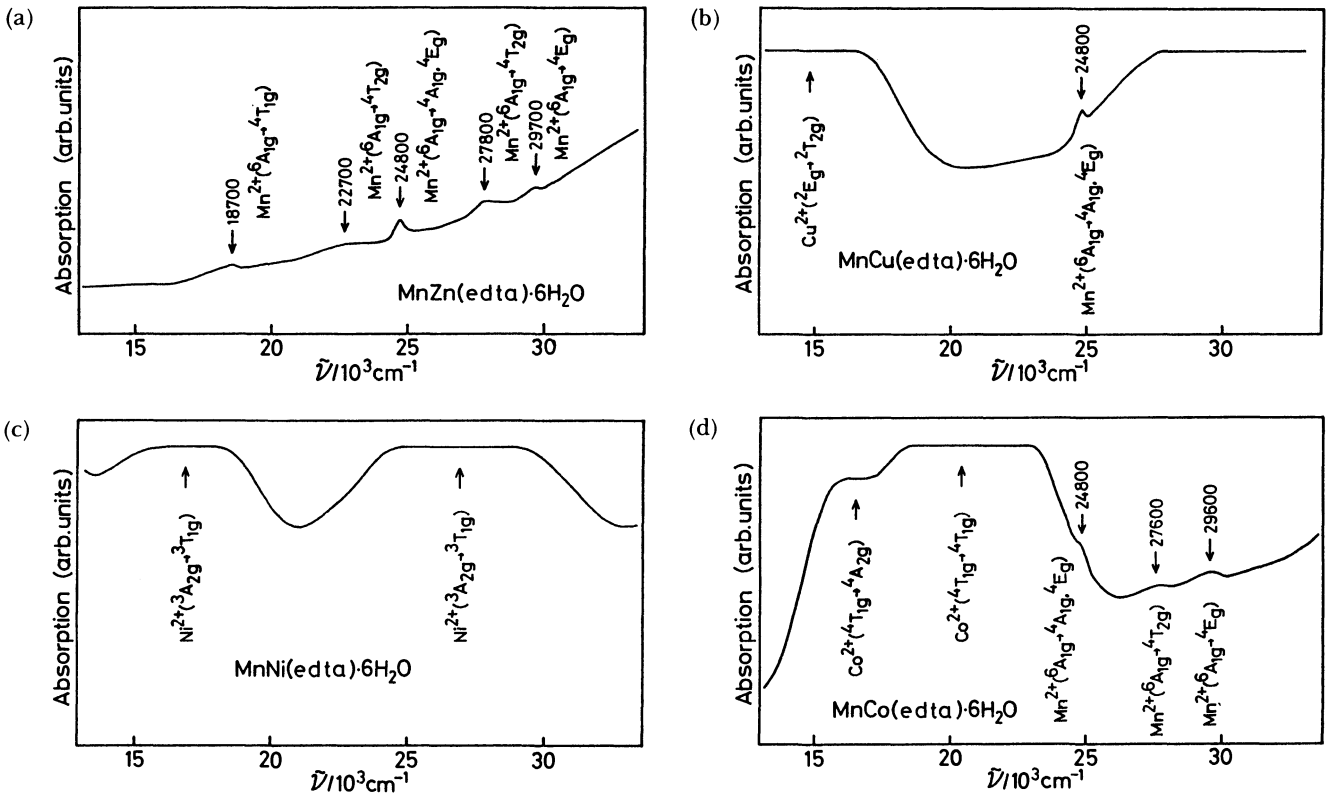

Fig. 2. Unpolarized absorption spectra of MnM(edta)·6H2O at room temperature. a) M=Zn, b) Cu, c) Ni, d) Co.

the diffraction patterns of Ni and Zn compounds, they were found to belong also to the same space group. The lattice constants are shown in Table 1. From the similarity of the crystal parameters and of the spectra, which will be shown in the next section, it is confirmed that, in Ni and Zn compounds, a Mn ion is at the hydrate position and an M ion occupies the chelate position as well as Cu and Co compounds.

In order to measure the absorption spectra, the samples were immersed in liquid helium in a glass dewar. The temperature was lowered by pumping. A spectrometer Jobin-Yvon THR-1500 was used with an iodine lamp, and the electric signal were recorded on chart. When the temperature dependence of the spectra were measured, the samples were hinged to a copper block, with helium gas for heat exchange, sealed in a glass tube immersed in the liquid

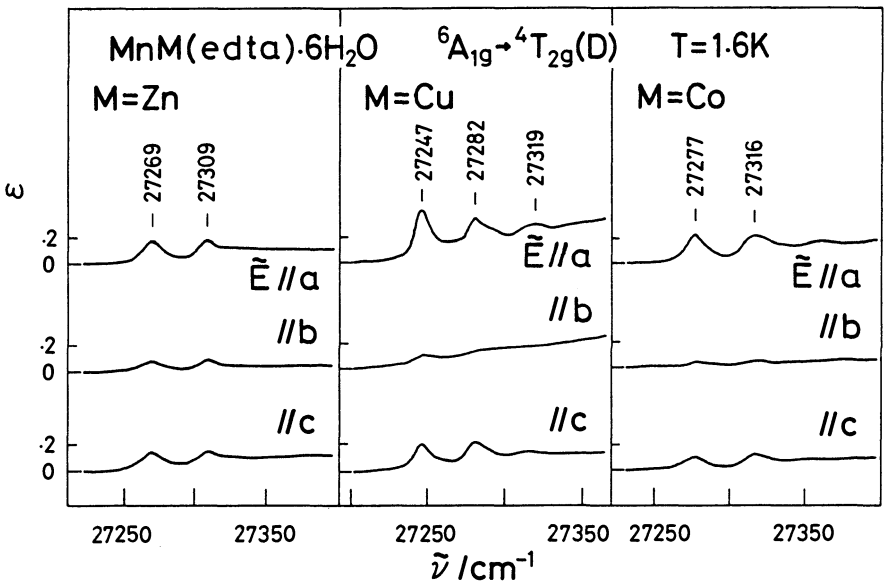

Fig. 3. Absorption spectra corresponding to $^6A_{1g}\rightarrow{}^4T_{2g}(D)$ transition in MnM(edta)·6H2O (M=Zn, Cu, and Co) at 1.6 K.

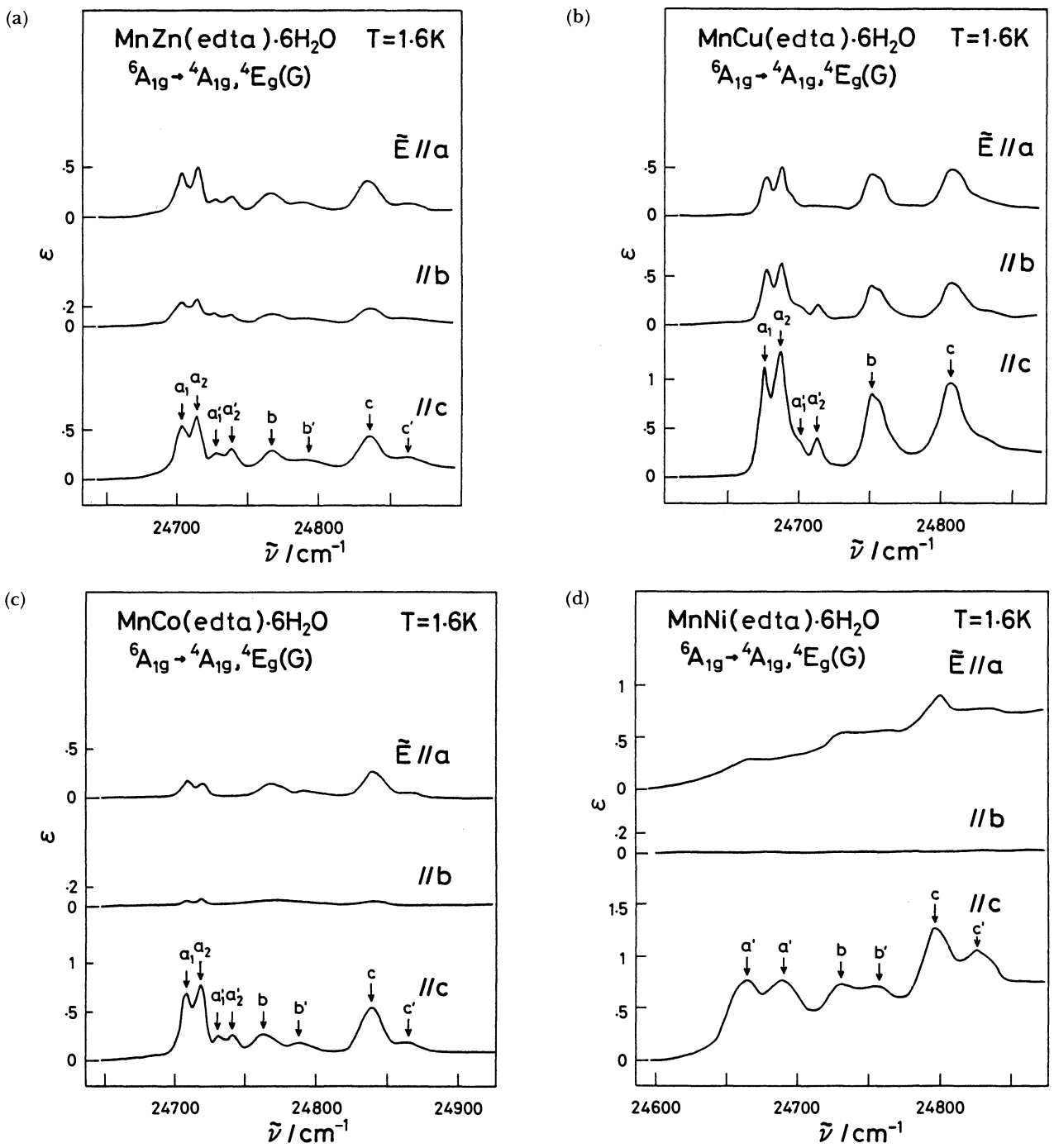

Fig. 4. Absorption spectra corresponding to $^6A_{1g}\rightarrow{}^4A_{1g},{}^4E_g$ (G) transition in MnM(edta)·6H$_2$O at 1.6 K.
a) M=Zn, b) Cu, c) Co, d) Ni.

helium. The copper block was heated by a manganin coil and its temperature was measured by a germanium and a platinum thermometer.

Results and Discussion

Preliminary measurement of absorption spectra was done at room temperature (Fig. 2). The absorption bands due to spin-allowed transitions in $[M(edta)]^{2-}$ (M=Cu, Ni, and Co) are so strong that most of them were saturated. Some absorption bands due to $[Mn(H_2O)_4]^{2+}$ were found. The assignment of the band peaks in Zn compound is shown in Table 2 (the peak energies agree with the results of Escrivá et al.[7]).

In the absorption spectra of Zn, Cu, Co, and Ni compounds at low temperatures, fine-structural bands were found in two energy regions, 27200—27400 cm^{-1} ($^6A_{1g}\rightarrow{}^4T_{2g}$(D)), and 24600—24900 cm^{-1} ($^6A_{1g}\rightarrow{}^4A_{1g}$, ^4E_g(G)), as shown in Figs. 3 and 4, respectively. Theoretically, the $^4T_{2g}$(D) term consists of 6 Kramers doublets, but we observed only two or three peaks which were separated by about 40 cm^{-1}.

As shown in Fig. 4, the absorption spectra of Zn, Cu,

Table 2. Energy Levels of $MnZn(edta)\cdot 6H_2O$ (in cm^{-1})

Calcd.	Obsd.	
18900	18700	$^4T_{1g}(G)$
22370	22700	$^4T_{2g}(G)$
24780	24800	$^4A_{1g}$, $^4E_g(G)$
27920	27800	$^4T_{2g}(D)$
29750	29700	$^4E_g(D)$
34410		$^4T_{1g}(P)$
40370		$^4A_{2g}$
41540		$^4T_{1g}(F)$
44600		$^4T_{2g}(F)$

$10Dq$=8395, B=710, C=3535.

Table 3. Energies of the Transition $^6A_{1g}\rightarrow{}^4A_{1g}$, $^4E_g(G)$ in $\tilde{E}//c$ Spectra of $MnM(edta)\cdot 6H_2O$ (M=Zn, Cu, Co, and Ni) at 1.6 K (in cm^{-1})

	Zn	Cu	Co	Ni		
a_1	24704	24677	24708			
				24664	$^4A_{1g}(G)$	e_1
a_2	24715	24687	24719			
a_1'	24728	24702s)	24733			
				24690		$e_1+h\nu$
a_2'	24740	24713	24744			
b	24769	24752	24764	24731	$^4E_g(G)$	v
b'	24796s)		24790	24757		$v+h\nu$
c	24835	24806	24838	24798	$^4E_g(G)$	u
c'	24862s)		24864	24827		$u+h\nu$

s) Shoulder.

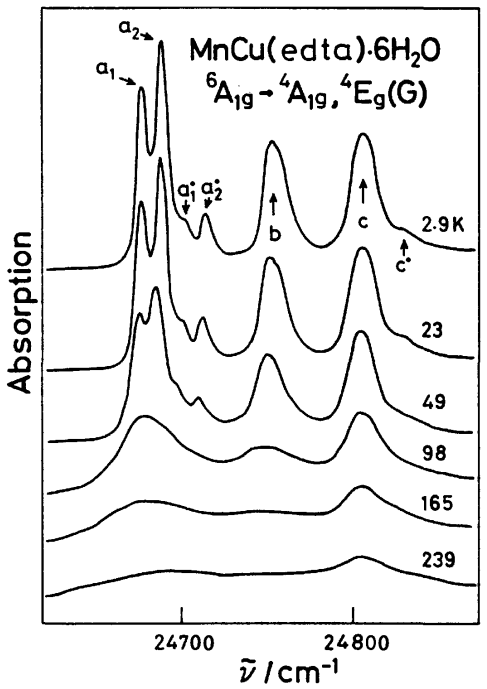

Fig. 5. Absorption spectra corresponding to $^6A_{1g}\rightarrow{}^4A_{1g}$, ^4E_g (G) transition in $MnCu(edta)\cdot 6H_2O$ at various temperatures. The spectra are intentionally shifted to the vertical direction.

and Co compounds in the $^4A_{1g}$, $^4E_g(G)$ region are similar in shape and peak energy. All absorption bands were characterized as due to electric dipole transitions. The absorption spectra can be grouped into three energy regions. We label the peaks and shoulders as shown in the left column of Table 3. The lowest energy region is composed of two peaks (a_1, a_2) associated with weaker peaks at higher energy side (a_1', a_2'); both the middle and the highest energy regions include a rather broad peak (b or c) with a weaker peak lying at higher energy side (b' or c'). For the Co compound the energy differences between a_1 and a_1', a_2 and a_2', b and b', and c and c' are all 25—26 cm^{-1}. Similar tendencies can be seen in the spectra of Zn and Cu compounds. Therefore it is considered that a_1', a_2', b' and c' are the sidebands which originate from a_1, a_2, b and c, respectively and that the elementary excitations corresponding to these sidebands are of the same energy.

In magnetic materials, elementary excitations usually appearing in the optical spectra are phonons and magnons. However, as the present compounds are concerned, the possibility of observing magnon sidebands can be excluded. As Zn^{2+} is not a magnetic ion, it inhibits the interaction between Mn^{2+} ions, then the magnon energy of Zn compound, if any, would be much smaller than the other compounds. Since the phonon energies are expected to be nearly the same because of the similarity in the crystal structure among these compounds, it can be concluded that these sidebands are phonon assisted ones.

The absorption spectra of $^6A_{1g}\rightarrow{}^4A_{1g}$, $^4E_g(G)$ transition in $MnNi(edta)\cdot 6H_2O$ are shown in Fig. 4(d), and the peak energies are listed in Table 3. This energy region is overlapping with the $^3A_{2g}\rightarrow{}^3T_{1g}(P)$ transition band in $[Ni(edta)]^{2-}$ (Ref. 9). In these spectra no splitting was observed for the a band, and the other peaks are also substantially broadened as compared with those in the other compounds. These broadening, of course, is not due to the inhomogeneity of the crystal. Nor does it seem to be due to the significant difference between Ni compound and the other ones in the way that the ligands coordinate to a Mn^{2+} ion, because the crystal parameters seem very similar among these materials (Table 1).

As will be shown later, the absorption hands a, b, and c are due to zero-phonon transitions. The width of a zero-phonon line can be explained[10] by the difference W in curvature between the potential curves for the ground and the excited states. We think that the shape of the potential curves of the $[Mn(H_2O)_4]^{2+}$ is changed, and then the W is increased, because of a resonant transfer of excitons between $^4A_{1g}$ and $^4E_g(G)$ band of $[Mn(H_2O)_4]^{2+}$ and $^3T_{1g}$ band of $[Ni(edta)]^{2-}$. However the elucidation of this phenomenon is the subject for future study.

In order to characterize the excitations corresponding to the absorption lines a_1, a_2, b, and c, we measured the temperature dependence of the absorption spectra of the Cu compound (Fig. 5). Since this compound

has the smallest sideband intensity among the three compounds, we thought that the overall intensity of the absorption in this region can be a good measure for the sum of the intensities of these peaks. The result shows the decrease of the intensity with increasing temperature (Fig. 6). This tendency is characteristic of pure electronic transitions. We analyzed the intensity change quantitatively, using an equation for the intensity of a zero-phonon transition line,[11] with the assumption that the excited state and the ground state have the potential curves of the same shape but the energies at their minima do not necessarily coincide. Also we assume that only one kind of phonon is involved in the temperature change of the zero-phonon transition. The equation is

$$\ln(I(T)/I_0) = -(E_0/\hbar\omega_0)[\coth(\hbar\omega_0/2kT)-1], \quad (1)$$

where $I(T)$ is the intensity at temperature T, I_0 the intensity at absolute zero, $\hbar\omega_0$ the energy of the phonon involved, and E_0 is the Stokes energy loss due to the mutual displacement of the curve minima. Parameters were obtained as E_0=65 cm^{-1}, $\hbar\omega_0$=123 cm^{-1} by the least squares method (Fig. 6).

The value of $\hbar\omega_0$ seems to be overestimated, because the temperature change of absorption intensity due to phonons is usually dominated by the phonon of lowest energy, and, as we already know, the 25 cm^{-1} phonon also exists in MnCu(edta)·6H_2O. This overestimation can be explained from the fact that the values of E_0 and $\hbar\omega_0$ are very sensitive to mixing of other bands (like phonon sidebands) with the intensity I. It is probable that phonon sidebands overlaps the bands of the zero-phonon transition, especially at higher temperatures. Nevertheless, the negative temperature dependence of the intensity of the origin peaks indicates that they are due to zero-phonon transitions.

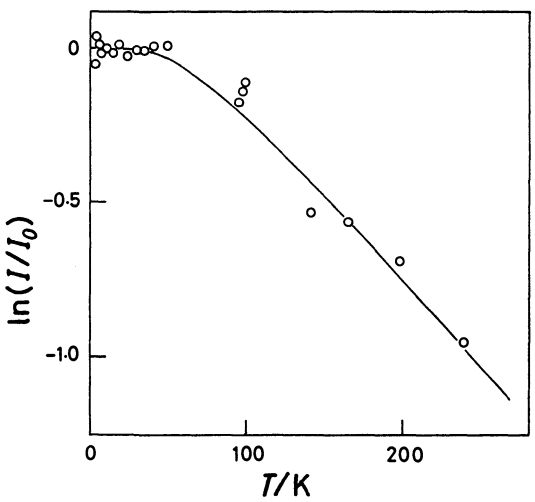

Fig. 6. Temperature dependence of the intensity of the absorption corresponding to the $^6A_{1g} \rightarrow {}^4A_{1g}, {}^4E_g$ (G) transition in MnCu(edta)·6H_2O. The solid line is the best fit one calculated from Eq. 1.

Next, we assign the a_1, a_2, b, and c peaks of MnZn (edta)·6H_2O to the 6 Kramers doublets of the $^4A_{1g}$, ^4E_g(G) terms. In the unit cell all sites of the Mn^{2+} ions are equivalent,[8] therefore all Mn^{2+} ions have the same energy levels.

In order to calculate the energy levels of the components in $^4A_{1g}$(G) and ^4E_g(G), it is necessary to obtain ligand field parameters[12] Dq, B, and C. As described previously a Mn^{2+} ion is coordinated by 4 water molecules and 2 carboxyl groups, forming a distorted octahedron. We calculated the ligand field parameters of this octahedron, using the room temperature data in Table 2, with the least squares method. The calculated energy levels are shown in the same table. These values, $10Dq$=8395, B=710, and C=3535 cm^{-1}, are very close to the parameters for $[Mn(H_2O)_6]^{2+}$, $10Dq$=8480, B=671, and C=3710 cm^{-1} (Ref. 13). This similarity seems to agree with the fact that $C_2O_4^{2-}$ is placed near H_2O in the spectrochemical series.

In coordination compounds of transition metal ions, in general, the most significant factor in lifting the degeneracy of the energy levels of a term ($^{2S+1}\Gamma$) is the ligand field of symmetry lower than cubic. As the site symmetry of Mn^{2+} ion in the MnM(edta)·6H_2O is 1, all kinds of lower symmetry fields, in some degree, contribute to the splitting. It seems that the largest contribution is from the ligand field of C_{2v} symmetry, because it is the highest symmetry a *cis*-MA_4B_2 cluster can have.

We approximate the cluster, $[Mn(H_2O)_4]^{2+}$ with two carboxyl groups, as *cis*-MA_4B_2 with C_{2v} symmetry. For the sake of calculation we define a cartesian coordinate system as follows: The direction of the linearly arranged A-M-A coincide with the z-axis and that the 2-fold axis of C_{2v} coincides with the $x+y$ axis. Also the one-particle wave functions of t_2 and e electrons are defined in the way that, under symmetry operations, wave functions ξ, η, and ζ of t_2 electrons are transformed like yz, zx, and xy, respectively, and u and v of e electrons behave like $3z^2-r^2$ and x^2-y^2, respectively.

When the potential V_0 of C_{2v} symmetry is expanded with r_i, which is the position vector of an i-th electron with its origin at the center of the metal ion, we obtain

$$V_0 = V_{cub} + V_{\alpha+\beta}^{(1)}(T_{1u}) + V_u^{(2)}(E_g) + V_\zeta^{(2)}(T_{2g}) + V_{\alpha+\beta}^{(3)}(T_{1u}) + V_u^{(4)}(E_g) + V_\zeta^{(4)}(T_{2g}) + (\text{higher order terms}), \quad (2)$$

where $V_{cub}=\sum v_{cub}(r_i)$ represents the cubic field potential, $V_\gamma^{(n)}(\Gamma_p)=\sum v_\gamma^{(n)}(\Gamma_p, r_i)$is a nth-order potential operator which is the γ component of an irreducible representation Γ of the cubic point group O_h, and p(=g, u) denotes the parity of the potential.

It is known that all the one-electron matrix elements among the $^4A_{1g}$, ^4E_g(G), and ^4E_g(D) levels are zero, Then, in order to lift the degeneracy of the $^4A_{1g}$ and ^4E_g(G), it is necessary to consider $^4T_{1g}$ and $^4T_{2g}$ terms.

Since the potential operators of odd parity are not important, we can assume that a perturbation Hamiltonian $V_L=V_\zeta^{(2)}$ (T_{2g}), neglecting the higher order terms than the second.

The wave functions of $^4A_{1g}$, $^4E_g(G)$, $^4T_{1g}$'s, and $^4T_{2g}$'s are described as

$$\psi(^4A_{1g}\, e_1\, 3/2)=(30)^{-1/2}\,(3|\xi\eta\zeta u\bar{v}|+3|\xi\eta\zeta\bar{u}v|-2|\bar{\xi}\eta\zeta uv|-2|\xi\bar{\eta}\zeta uv|-2|\xi\eta\bar{\zeta}uv|)$$

$$\psi(^4E_g(G)\, u3/2)=(42)^{-1/2}\,(4|\xi\eta\bar{\zeta}uv|-2|\xi\bar{\eta}\zeta uv|-2|\bar{\xi}\eta\zeta uv|-3|\xi\eta\zeta u\bar{v}|+3|\xi\eta\zeta\bar{u}v|)$$

$$\psi(^4E_g(G)\, v3/2)=(14)^{-1/2}\,(2|\bar{\xi}\eta\zeta uv|-2|\xi\bar{\eta}\zeta uv|-\sqrt{3}|\xi\eta\zeta u\bar{u}|+\sqrt{3}|\xi\eta\zeta v\bar{v}|)$$

$$\psi(^4T_{1g}{}^n\,\gamma\,3/2)=-\lambda_n|\xi\eta\bar{\zeta}\zeta u|-(\mu_n/\sqrt{2})\,(|\zeta\bar{\xi}\xi uv|+|\zeta\eta\bar{\eta}uv|)+\nu_n|\xi\eta uv\bar{v}|$$

$$\psi(^4T_{2g}{}^n\,\zeta\,3/2)=l_n|\xi\eta\bar{\zeta}\zeta v|+(m_n/\sqrt{2})\,(|\zeta\bar{\xi}\xi uv|-|\zeta\eta\bar{\eta}uv|)-n_n|\xi\eta vu\bar{u}|$$

(n=1, 2, and 3),

where superscripts n=1, 2, and 3 of $^4T_{1g}{}^n$ denote G, P, and F terms, respectively, and those of $^4T_{2g}{}^n$ correspond to G, D, and F, respectively, and the parameters λ_n, μ_n, ν_n, l_n, m_n, and n_n were obtained simultaneously with the determination of Dq, B, and C (Table 4).

The matrix elements of the $V_L=V_\zeta^{(2)}$ (T_{2g}) between ($^4A_{1g}$, $^4E_g(G)$) and ($^4T_{1g}$' s, $^4T_{2g}$'s) are expressed as

$$<^4T_{2g}{}^n\,\zeta|V_L|^4E_g(G)\,u>=(1/3\sqrt{14})\,(n_n-l_n)<e||v_\zeta^{(2)}(T_{2g})||t_2>$$

$$<^4T_{1g}{}^n\,\gamma|V_L|^4E_g(G)\,v>=(1/\sqrt{42})\,[\sqrt{3}(\nu_n-\lambda_n)<e||v_\zeta^{(2)}(T_{2g})||t_2>+4\mu_n<t_2||v_\zeta^{(2)}(T_{2g})||t_2>]$$

$$<^4T_{2g}{}^n\,\zeta|V_L|^4A_{1g}\,e_1>=(\sqrt{5/3}\sqrt{2})\,(l_n-n_n)<e||v_\zeta^{(2)}(T_{2g})||t_2>.$$

(n=1, 2, and 3)

The other matrix elements are zero.

The irreducible matrix elements $<t_2||v_\zeta^{(2)}(T_{2g})||t_2>$ and $<e||v_\zeta^{(2)}(T_{2g})||t_2>$ are equal to $\sqrt{6}<\zeta|v_\zeta^{(2)}(T_{2g})|\eta>$ and $\sqrt{3}<u|v_\zeta^{(2)}(T_{2g})|\zeta>$, respectively. For convenience, we approximate that

$$<t_2||v_\zeta^{(2)}(T_{2g})||t_2>=-(3/2)^{1/2}<e||v_\zeta^{(2)}(T_{2g})||t_2>,$$

which exactly holds when the field around the Mn^{2+} ion is spherically symmetric.

Table 4. The Coefficients λ_n,μ_n, and ν_n for $^4T_{1g}{}^n$ and l_n, m_n, and n_n for $^4T_{2g}{}^n$ in MnZn(edta)·6H_2O

	n=1	2	3
λ_n	0.977	−0.053	−0.207
μ_n	−0.125	0.643	−0.755
ν_n	0.173	0.764	0.622
l_n	0.843	−0.437	−0.312
m_n	0.441	0.895	−0.062
n_n	0.307	−0.085	0.948

By Koide and Pryce,[14] it has been shown that the difference in covalency between t_2 and e electrons can separate the $^4A_{1g}$ and $^4E_g(G)$ terms, even if the Mn^{2+} ion is in no lower symmetry field than cubic. Therefore we take into account the effect of the covalency by introducing a parameter Δ, which is defined as

$$\Delta\equiv E_0(^4E_g(G))-E_0(^4A_{1g}),$$

where $E_0(\Gamma)$ is the energy of a Γ term in the cubic field.

The covalency effect (Δ) and the low symmetry field (V_L) combine to separate the $^4A_{1g}$, $^4E_g(G)$ term into three states; $^4A_{1g}e_1$, $^4E_g(G)u$, and v. Furthermore each state is split into two Kramers doublets by spin-orbit interaction V_{so}, which will explain the energy difference between the a_1 and a_2 absorption lines. In the estimation of the magnitude of the spin-orbit interaction for the $^4A_{1g}$ and ^4E_g states, the effect of the α and the β components of the $^4T_{1g}{}^n$ and the ξ and the η components of the $^4T_{2g}{}^n$ can be neglected, because, they contribute, at the most, to the energies of $^4A_{1g}$, $^4E_g(G)$ through terms like

$$|<^4\Gamma e|V_{so}|^4T\delta>|^2/[E_0(^4\Gamma)-E_0(^4T)],$$

where $^4\Gamma e$ is the general expression of the components of the $^4A_{1g}$ and $^4E_g(G)$ terms and $^4T\delta$ represents $^4T_{1g}{}^n\alpha$, β and $^4T_{2g}{}^n\xi$, η. On the other hand, $^4T_{1g}{}^n\gamma$ and $^4T_{2g}{}^n\zeta$ contribute through terms like

$$<^4\Gamma e|V_L|^4T\psi><^4T\psi|V_{so}|^4\Gamma e>/[E_0(^4\Gamma)-E_0(^4T)],$$

where $^4T\psi$ denotes $^4T_{1g}{}^n\gamma$ or $^4T_{2g}{}^n\zeta$.

Therefore, the matrix elements which will significantly contribute to the splitting are calculated as

$$<^4T_{1g}{}^n\,\gamma\,M|V_{so}|^4A_{1g}\,M>=-(i/3\sqrt{15})\,[\sqrt{2}(\lambda_n-\nu_n)\,\zeta'+4\mu_n\zeta]M$$

$$<^4T_{1g}{}^n\,\gamma\,M|V_{so}|^4E_g(G)\,u\,M>=-(i/3\sqrt{21})\,[\sqrt{2}(\lambda_n-\nu_n)\,\zeta'+4\mu_n\zeta]M$$

$$<^4T_{2g}{}^n\,\zeta\,M|V_{so}|^4E_g(G)\,v\,M>=(i\sqrt{2}/\sqrt{21})\,(l_n-n_n)\,\zeta'M$$

(M=3/2, 1/2, −1/2, −3/2),

where $\zeta=(-i/3)<t_2||v_{so}||t_2>$ and $\zeta'=(i/3\sqrt{2})<t_2||v_{so}||e>$. We use the spherical-symmetry approximation also for the spin-orbit interaction parameters, in which $\zeta=\zeta'$.

With the use of the matrix elements obtained above, the energy levels of the $|^4A_{1g}\,e_1\,M>$, $|^4E_g(G)\,u\,M>$, and $|^4E_g(G)\,v\,M>$ ($M=\pm3/2,\ \pm1/2$) can be calculated. Neglecting the non-diagonal matrix elements between different spin states, we can reduce the secular equation of V_L+V_{so} between 36 components of $^4A_{1g}e_1$, ^4E_gu, and v, $^4T_{1g}{}^n\gamma$, $^4T_{2g}{}^n\zeta$ (n=1, 2, and 3) into 4 equations, each one corresponding to each spin state M. Because Kramers degeneracy still remains, we have to consider only two of them, e.g. those for M=3/2 and 1/2. We fixed the parameter ζ at 347 cm^{-1}, which is the value for a free Mn^{2+} ion, and adjusted the $<e||v_\zeta^{(2)}$

$(T_{2g})||t_2>$ and the Δ so as to fit the average energy of each state, $^4A_{1g}e_1$, $^4E_g u$, and v, to the corresponding one observed.

We obtained $<e||v_\zeta^{(2)}(T_{2g})||t_2>=1257$ and $\Delta=125$ cm^{-1}, and found that the (a_1, a_2), b and c bands correspond to the $^4A_{1g}$ e_1, ^4E_g v, and u states, respectively (Table 2). In the theory of Koide and Pryce, the effect of the covalency is taken into account by mixing the σ-orbitals of the ligands with those of the e-orbitals of the metal ion. The observed value of the Δ is a little larger than the theoretical upper limit, $\Delta=114.5$ cm^{-1}, which were estimated from the values of B and C. For the other compounds of Mn^{2+}, it was found[15] that a spin-doublet state situated near this energy region can influence the energy levels of the components of $^4A_{1g}e_1$, $^4E_g(G)u$, and v. Therefore it is possible that the calculated value of the Δ in MnZn (edta)·6H_2O is increased by the effect of a doublet state.

The calculated splittings of the $^4A_{1g}e_1$, $^4E_g(G)v$, and u due to the spin-orbit interaction are 4.6, 1.0, and 0.0 cm^{-1}, respectively. It is also found that the largest contribution to the eigenfunctions of these states is from the ζ components of $^4T_{2g}(G)$ or $^4T_{2g}(D)$ among the $^4T_{1g}$'s and $^4T_{2g}$'s. This result explains the fact that no splitting were observed in the b and c bands. However, for the splitting of the (a_1, a_2), the calculated value is smaller than the observed one. This descrepancy can be explained from the splitting of the $^4T_{2g}(G)$ or $^4T_{2g}(D)$ band due to the low symmetry field V_L; because the energy difference between each of these bands and the $^4A_{1g}$, $^4E_g(G)$ is only about 3000 cm^{-1}, it is possible that the energy shift of the ζ component of the either band toward the $^4A_{1g}$, $^4E_g(G)$ region increase the splitting of the $^4A_{1g}e_1$ state.

Figures 3 and 4 show that the absorption spectra of M=Zn, Cu, and Co compounds are very similar in shape, which implies that the interaction between $[Mn(H_2O)_4]^{2+}$ and $[M(edta)]^{2-}$ is not significant in these spectra.

Conclusion

The absorption spectra corresponding to the electronic transition in Mn^{2+} ion in MnM(edta)·6H_2O (M=Zn, Cu, Ni, and Co) were measured at low temperature.

It was found that the absorption spectra corresponding to the $^6A_{1g}\rightarrow{}^4A_{1g}$, $^4E_g(G)$ transition in Mn^{2+} ions in MnM(edta)·6H_2O (M=Zn, Cu, and Co) are similar to each other; the structure of their energy levels can be explained as caused by the covalency effect and by the interaction from the $^4T_{1g}$'s and $^4T_{2g}$'s through a low symmetry field $V_\zeta(T_{2g})$. The fine structure of the $^4A_{1g}$, $^4E_g(G)$ band in Zn compound was assigned, considering the splitting of the absorption peaks due to the spin-orbit interaction. In MnNi(edta)·6H_2O, although its spectra are similar to those of the other compounds in energy, its line widths are much broader than in the other materials. It seems that this broadening is related to the overlapping of the absorption bands of $[Mn(H_2O)_4]^{2+}$ and $[Ni(edta)]^{2-}$. However, further investigation is needed to solve this problem.

References

1) D. Beltrán and J. Beltrán, *Rev. Acad. Cienc. Exactus, Fis. Quim. Nat. Zaragoza*, **31**, 229 (1976).

2) E. Escrivá, D. Beltrán, and J. Beltrán, *An. R. Soc. Esp. Fis. Quim., Ser. B*, **77**, 330 (1981).

3) D. Beltrán, E. Escrivá, and M. Drillon, *J. Chem. Soc., Faraday Trans. 2*, **78**, 1773 (1982).

4) M. Drillon, E. Coronado, D. Beltrán, and R. Georges, *Chem. Phys.*, **79**, 449 (1983).

5) M. Drillon, E. Coronado, D. Beltrán, J. Curely, R. Georges, P. R. Nugteren, L. J. de Jongh, and J. L. Genicon, *J. Magn. Magn. Mater.*, **54—57**, 1507 (1986).

6) E. Coronado, M. Drillon, A. Fuertes, D. Beltrán, A. Mosset, and J. Galy, *J. Am. Chem. Soc.*, **108**, 900 (1986).

7) E. Escrivá, A. Fuertes, and D. Beltrán, *Transition Met. Chem.*, **9**, 184 (1984).

8) X. Solans, M. Font-Altaba, J. Oliva, and J. Herrera, *Acta Crystallogr., Sect. C*, **39**, 435 (1983).

9) C. K. Jorgensen, *Acta Chem. Scand.*, **9**, 1362 (1955).

10) I. S. Osad'ko, "Spectroscopy and Excitation Dynamics of Condensed Molecular Systems," Chap. 8, ed by V. M. Agranovich and R. M. Hochstrasser, North-Holland, Amsterdam (1983).

11) K. K. Rebane, "Impurity Spectra of Solids," Chap. 2, Plenum Press, New York, (1970).

12) S. Sugano, Y. Tanabe and H. Kamimura, "Multiplets of Transition-Metal Ions in Crystals," Chap. V, Academic Press, New York (1970).

13) L. J. Heidt, G. F. Koster, and A. M. Johnson, *J. Am. Chem. Soc.*, **80**, 6471 (1958).

14) S. Koide and M. H. L. Pryce, *Phil. Mag.*, **3**, 607 (1958).

15) W. van Erk and C. Haas, *Phys. Stat. Sol. (b)*, **70**, 517 (1975).

 © 1988 The Chemical Society of Japan Bull. Chem. Soc. Jpn., 61, 1911—1916 (1988)

Calorimetric and Dielectric Studies of Phase Transitions in Rubidium Nitrite†

Keiichi MORIYA,†† Takasuke MATSUO, and Hiroshi SUGA*
Department of Chemistry and Chemical Thermodynamics Laboratory, Faculty of Science, Osaka University, Toyonaka, Osaka 560
(Received December 11, 1987)

The heat capacities of $RbNO_2$ crystal have been measured between 15 and 330 K. Two phase transitions were found at (264.04±0.06) K and (83.8±0.2) K. The enthalpy and entropy of transition are (9310±450) J mol^{-1} and (35.9±1.8) J K^{-1} mol^{-1} for the former and (48±5) J mol^{-1} and (0.58±0.05) J K^{-1} mol^{-1} for the latter. The entropy of the high temperature transition was interpreted in terms of the orientational disorder of the NO_2^- ion. The dielectric constant increased from 6 to 10 as the transition temperature 264.04 K was traversed from below, indicating the increased motional freedom of the polar anion in the high temperature phase.

A variety of phase transitions arising from orientational disordering of NO_2^- ions has been found in ANO_2 type compounds, where A represents an alkali metal or monovalent thallium.[1-7]

Rubidium nitrite crystallizes in the sodium chloride structure (space group O_h^5-Fm3m).[8] The NO_2^- ions having the C_{2v} symmetry must be orientationally disordered to be compatible with the octahedral symmetry of the anion site in the lattice. Occurrence of a phase transition is expected at a lower temperature because of the disorder. This offers a possibility of studying an order-disorder transition due to ionic orientations in a structurally simple crystal. In fact, Richter and Pistorius reported that $RbNO_2$ transformed to a low-temperature monoclinic phase at (261±2) K.[8] We studied the phase transition by calorimetric and dielectric methods.

Experimental

Sample Preparation. Rubidium nitrite was prepared from $Ba(NO_2)_2 \cdot H_2O$ and Rb_2SO_4(Merck Co., Ltd., suprapur reagent) in aqueous solution. The $Ba(NO_2)_2 \cdot H_2O$ crystal was prepared from extra-pure reagents of $NaNO_2$ and $BaCl_2 \cdot 2H_2O$ (both from Wako Pure Chemicals Co., Ltd.). Colorless crystals of $RbNO_2$ were obtained by slow evaporation of the filtered solution at 298 K. The crystals were purified by recrystallization from aqueous solution and washed with a small amount of ethanol. They were further purified by 30 passages of zone melting in a quartz tube. The crystals were carefully handled in nitrogen gas. Impurity ions found by atomic absorption spectra were Cs; 0.01%, Na; 0.02%, and K; 0.002%. The mass percent of the NO_2^- ion determined by the redox titration was 35% (calcd 35.0%). Nitrate ion impurity was less than 0.1% from the ratio of the Raman intensities of the internal vibrations of NO_3^- and NO_2^- ions.[9]

DTA and DSC. The enthalpy of fusion of $RbNO_2$ was determined by differential scanning calorimetry (Perkin Elmer Model DSC II). The DSC was run at the rate of 5 K min^{-1} from the room temperature to above the melting point. The temperature, enthalpy and the entropy of fusion were (693±3) K, (11.0±1.5) kJ mol^{-1} and (16±2) J K^{-1} mol^{-1}, respectively. The small entropy of fusion indicates that the ions are disordered in the solid phase.

Differential thermal analysis was made as a preliminary to the heat capacity measurement (Fig. 1). On the first cooling (Run 1), an exothermic peak appeared at 250 K. In the first heating run (Run 2), an endothermic and subsequent exothermic peaks appeared around 251 K. A second large endothermic anomaly occurred at 263 K. In the second heating run (Run 4), the two peaks around 251 K disappeared and only the endothermic peak at 263 K occurred. This result was interpreted as follows. In the pressure-temperature phase diagram of $RbNO_2$,[8] a triple point (300 bar, 261 K) was found, at which the high-temperature form I (Fm3m), the low-temperature monoclinic form II and the high-pressure form III (Pm3m) coexist. The temperature 250 K where the first endothermic peak occurred (Run 2) is close to the III-I phase boundary extrapolated to the atmospheric pressure. In the first cooling (Run 1), the sample transformed from the phase I to the metastable high-pressure phase III. It transformed exothermically to the stable monoclinic phase II on the subsequent heating and then endothermically to the stable high temperature phase I (Run 2). The hysteretic behavior thus deduced from DTA was

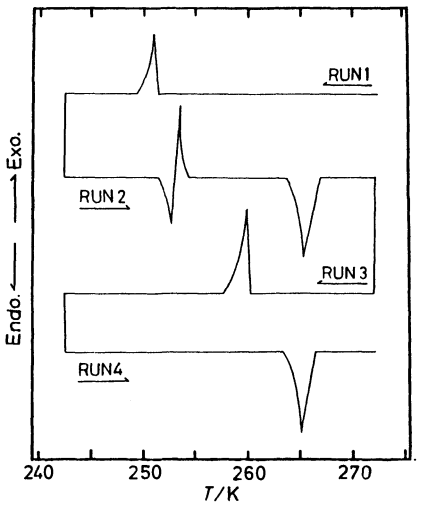

Fig. 1. DTA curves of $RbNO_2$ showing the stable–stable and metastable–stable transitions.

† Contribution No. 125 from the Chemical Thermodynamics Laboratory.

†† Present address: Department of Chemistry, Faculty of Engineering, Gifu University, Yanagido, Gifu 501-11.

Table 1. The Molar Heat Capacity of $RbNO_2$

T_{av} / K	C_p / J K^{-1} mol^{-1}	T_{av} / K	C_p / J K^{-1} mol^{-1}	T_{av} / K	C_p / J K^{-1} mol^{-1}	T_{av} / K	C_p / J K^{-1} mol^{-1}
First series		67.84	49.32	169.64	75.36	265.54	559.5
		70.16	50.55	172.55	75.77	268.14	86.09
13.26	2.691	72.53	51.86	175.45	76.22	270.92	82.91
13.78	3.220	74.92	53.54	178.32	76.63	273.45	82.80
15.26	4.047	77.41	55.03	181.48	77.09	275.98	82.70
16.76	5.145	80.03	57.17	184.02	77.54	278.62	82.77
17.84	6.045	82.66	62.24	186.84	77.93	281.37	82.82
19.01	7.138	85.35	60.30	189.65	78.34	284.19	82.79
20.09	8.153	88.16	59.59	192.52	78.83	286.99	82.83
21.08	9.065	90.99	60.09	195.45	79.23	289.85	82.94
22.03	9.966			198.39	79.66	292.76	83.08
22.91	10.91	Second series		201.28	80.20	293.33	82.93
23.84	11.76			204.16	80.56	296.31	82.94
24.71	12.66	80.64	58.16	207.02	81.08	299.14	82.95
25.58	13.49	83.59	61.36	209.86	81.56	301.96	83.07
26.45	14.40	86.14	59.96	212.69	82.05	304.91	83.04
27.38	15.33	88.72	59.65	215.50	82.61	307.87	83.28
28.44	16.37	91.57	60.30	218.30	82.95	310.86	83.23
29.56	17.51	94.67	61.08	221.15	83.54	313.90	83.37
30.41	18.31	95.15	61.20	224.06	84.02	316.93	83.43
31.14	19.16	97.71	61.80	226.95	84.56	319.94	83.57
32.22	20.31	100.57	62.50	229.82	85.13	322.96	83.72
33.49	21.65	103.46	63.43	232.68	85.58	325.97	83.78
34.75	22.91	106.36	64.09	235.53	86.18	329.96	83.77
35.97	24.19	109.28	64.81	238.35	86.66		
37.11	25.28	112.16	65.49	239.89	86.93	Fourth series	
38.24	26.42	115.07	66.08	242.58	87.71		
39.34	27.55	118.00	66.67	245.25	88.18	70.23	50.74
40.46	28.64	120.91	67.28	247.91	88.69	71.63	51.39
41.74	29.79	123.81	67.67	250.55	89.31	73.01	52.23
43.09	30.83	126.64	68.38	252.76	89.91	74.33	52.98
44.29	32.00	129.44	68.91	254.61	90.22	75.62	53.73
45.68	33.18	132.24	69.43	256.51	90.71	76.89	54.48
47.16	34.40	135.09	70.04	258.41	91.20	78.14	55.18
48.65	35.69	138.00	70.48	260.30	91.69	79.36	56.07
50.11	36.95	140.47	70.97	262.19	92.68	80.57	57.03
51.71	38.19	143.80	71.54			81.72	58.40
53.29	39.46	146.77	71.85	Third series		82.81	62.37
54.93	40.74	149.71	72.40			83.82	75.74
56.57	42.03	152.63	72.84	260.02	91.17	84.83	61.40
58.24	43.27	155.53	73.29	262.14	92.22	85.90	59.55
60.00	44.51	158.40	73.78	263.59	1451	86.97	59.18
61.83	45.72	161.25	74.10	263.99	19300	88.09	59.24
63.74	46.90	164.08	74.58	264.04	93380	89.23	59.62
65.71	48.09	166.89	74.96	264.10	14820	90.47	59.91
				264.28	4804	91.50	59.92

heeded in the following calorimetric experiment to prepare the sample in the stable form.

Heat Capacity Measurement. Heat capacities of $RbNO_2$ crystal were measured with an adiabatic calorimeter between 13 and 330 K. The calorimetric apparatus was described elsewhere.[10-13] The sample crystal was 36.947 g in mass corresponding to 0.28102 mol. The molar heat capacities are plotted in Fig. 2 and the numerical values are given in Table 1. Graphically smoothed heat capacities and derived thermodynamic functions are given in Table 2. A small heat-capacity anomaly occurred at (83.8±0.2) K. The anomaly at (264.04±0.06) K corresponds to the endothermic peak at (261±2) K found by DTA. The anomalous heat capacity appears to start to be significant far below the transition temperature. The disordering proceeded with increasing temperature until it completed discontinuously at the phase transition. No short range effect was found in the heat capacity of the high-temperature phase in contrast to the case of $NaNO_2$[1,14] where such an effect was very significant. The time required for the thermal equilibration in the calorimeter increased near the phase transition to about three days compared with fifteen minutes normally required. Such a behavior is often observed in the first-order phase transition.

Boak and Staveley measured the heat capacity of $RbNO_2$ between 83 and 483 K.[15] General temperature dependence of the present data agrees satisfactorily with theirs where the two sets of data overlap, although the absolute values are somewhat different. The small anomaly at 83.8 K has not been reported previously. However, the hysteretic behavior

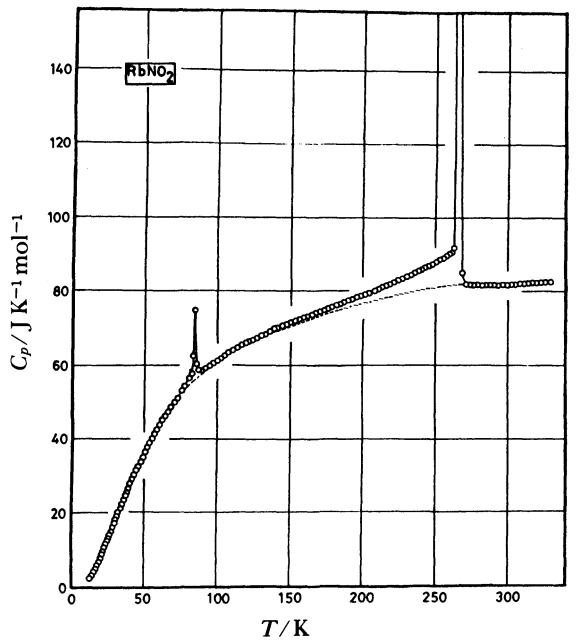

Fig. 2. Heat capacity of $RbNO_2$. The broken line represents the normal heat capacity calculated by the Debye and Einstein approximation optimized for $T \leq 65$ K.

Table 2. Thermodynamic Functions of $RbNO_2$

T	C_p°	$S^\circ - S_0^\circ$	$[H^\circ - H_0^\circ]/T$	$-[G^\circ - H_0^\circ]/T$
K	$J K^{-1} mol^{-1}$	$J K^{-1} mol^{-1}$	$J K^{-1} mol^{-1}$	$J K^{-1} mol^{-1}$
10	(1.41)	(0.45)	(0.34)	(0.11)
20	8.08	3.16	2.31	0.85
30	17.94	8.26	5.84	2.42
40	28.09	14.82	10.15	4.67
50	37.07	22.09	14.66	7.43
60	44.40	29.52	19.03	10.49
70	50.18	36.81	23.08	13.73
80	56.43	44.01	26.95	17.06
90	59.97	51.35	30.90	20.45
100	62.40	57.76	33.93	23.83
110	64.89	63.83	36.63	27.20
120	67.07	69.57	39.08	30.49
130	69.06	75.01	41.31	33.70
140	70.84	80.20	43.36	36.84
150	72.42	85.14	45.24	39.90
160	73.95	89.87	46.99	42.88
170	75.43	94.39	48.62	45.77
180	76.91	98.75	50.15	48.60
190	78.41	102.94	51.65	51.29
200	79.95	107.01	52.98	54.03
210	81.57	110.95	54.30	56.65
220	83.28	114.78	55.58	59.20
230	85.11	118.52	56.82	61.70
240	87.08	122.18	58.04	64.14
250	89.22	125.78	59.25	66.53
260	91.55	129.33	60.44	68.89
270	83.35	165.07	93.04	72.03
280	82.80	168.05	92.67	75.38
290	82.95	170.96	92.33	78.63
298.15	82.96	173.20	92.07	81.13
300	83.01	173.17	92.02	81.75
310	83.24	176.50	91.74	84.76
320	83.50	179.15	91.48	87.67

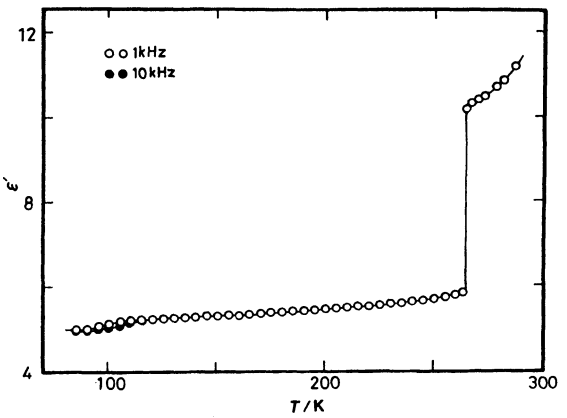

Fig. 3. Dielectric constant of $RbNO_2$ at 1 and 10 kHz.

found by the DTA has its counterpart in Boak and Staveley's calorimetric data that depended on the sample history in the corresponding temperature region. The two sets of data also agree with respect to the extended temperature range of the main anomaly below the transition temperature. The low temperature data ($T<80$ K) obtained in the present study are useful for the computation of the phonon heat capacity because the low frequency part of the entire lattice and molecular vibrational spectra is most significantly represented in the heat capacity of this temperature range.

Dielectric Constant. The dielectric constant was measured on a polycrystalline sample disc with a capacitance bridge, General Radio model 1615A, at 1 and 10 kHz. The sample was placed in a doubly thermostated environment. The temperature was regulated to 0.1 K between 80 and 290 K. As Fig. 3 shows the main transition (from phase II to I) is accompanied by a strong discontinuity of the dielectric constant characteristic of a first order phase transition. There is also a gradual increase of the dielectric constant below the transition point, corresponding to the similar gradual increase in the heat capacity.

A weak frequency dependence was found around 100 K. The magnitude of the dielectric dispersion is much smaller than those found in $TlNO_2$[2] and $CsNO_2$.[6] It is probably related to the residual disorder associated with the main transition. Because of the difference in the temperature, the dielectric dispersion and the subsidiary transition at 83 K cannot be connected with each other.

Results and Discussion

The Vibrational Heat Capacity. It is assumed that the observed heat capacity can be separated into the normal (vibrational) and the anomalous (configurational) parts. In order to evaluate the enthalpy and entropy of the phase transition, the normal heat capacity has to be estimated. $RbNO_2$ has $3 \times 4 = 12$ degrees of freedom, of which 6 degrees of freedom are the translational motion of Rb^+ and NO_2^- ions. The remaining 6 degrees of freedom are rotation (3) and internal vibrations (3) of the NO_2^- ion. The contributions from the acoustic and optical translational modes were calculated using the Debye and Einstein functions with the characteristic temperatures 108.0 and 188.3 K. The rotation vibration of the NO_2^- ion was approximated

with three independent one-dimensional vibrations of the characteristic temperature of 184.7 K. These characteristic temperatures were determined by fitting the Debye and Einstein functions to the heat capacity data between 15 and 65 K by the use of the nonlinear least squares method. There are three internal vibrations, symmetric stretching $\nu_1(A_1)$, antisymmetric stretching $\nu_2(B_2)$, and bending $\nu_3(A_1)$ modes, in the NO_2^- ion. Vibrational heat capacities of the three modes were calculated by the Einstein functions and taken into account in the least squares fitting as the known component of the total heat capacity. The vibrational frequencies, 1240 cm^{-1} (ν_1), 1320 cm^{-1} (ν_2), and 804 cm^{-1} (ν_3), were determined from the Raman and infrared spectra. The temperature dependence of the vibrational frequencies was neglected. The C_p-C_v correction becomes significant at higher temperatures. This term was calculated by the Nernst-Lindemann equation.[15]

$$C_p - C_v = A(T/T_p)C_p^2, \quad (1)$$

where $A=0.00112$ K mol J^{-1}. In this equation, T_p is the triple point temperature (approximated with the fusion temperature). The normal heat capacity was thus calculated as the sum of these five contributions.

$$C_p = C(\text{ac. translation}, 3D) + C(\text{opt. translation}, 3E) + C(\text{rotation}, 3E) + C(\text{internal}, 3E) + C_p - C_v. \quad (2)$$

Here, E and D stand for the Einstein and Debye functions, respectively. The numbers in the parentheses give the numbers of the degrees of freedom included in each term. The normal heat capacity thus calculated is given by the broken lines in Fig. 2.

The lengthy calculations involved in the optimization of the Debye and Einstein temperatures by the nonlinear least squares fitting described above were performed on a personal computer running on the BASIC. The Debye and Einstein parametrization of the vibrational heat capacity and the optimization procedure have been successfully applied to the simpler as well as more complex cases than the present one, including D_2O ice,[17] RbCN,[18] CH_3NH_3I,[19] $(CH_3NH_3)_2(TeBr_6)$,[20] $(CH_3NH_3)_2(TeI_6)$,[20] $NH_3NH_2H(CO_2)_2$,[21] and $(CD_3ND_3)_2(SnCl_6)$.[22]

No enthalpy relaxation was found in the entire temperature range. In $CsNO_2$[3,6] and $TlNO_2$[2,6] enthalpy relaxation related to the ionic reorientation occurred at low temperatures. Strong relaxational effects were also found in the dielectric measurement for these compounds. By contrast, the dielectric constant of $RbNO_2$ as a function of the temperature showed only a minor dispersion (Fig. 3). This agrees with the absence of the enthalpy relaxation in the calorimetric work.

The Enthalpy and Entropy of Transitions. The enthalpies of the transitions were determined by integrating the excess heat capacity and adding the latent heat of the transition to the integrated value. The entropies were determined in a similar way using the excess heat capacity divided by the temperature. They are collected in Table 3.

Table 3. Enthalpies and Entropies of the Phase Transitions of $RbNO_2$

T_t/K	ΔH_t/J mol^{-1}	ΔS_t/J K^{-1} mol^{-1}
83.8±0.2	48±5	0.58±0.05
264.04±0.06	9310±450	35.9±1.8

The entropy of transition determined from the high pressure phase equilibrium is 25.3 J K^{-1} mol^{-1}.[8] The previous calorimetric determination gave 32.3 J K^{-1} mol^{-1},[15] slightly smaller than the present value. The difference between the two calorimetric data may not be significant in view of the probable errors involved. The subsidiary transition at 83 K was found here for the first time and there are no other experimental data to compare with. The small entropy of transition suggests that the subsidiary transition is not an order-disorder change.

Configurational Entropy of the High-Temperature Phase. The phase equilibrium study[8] has shown that the volume change associated with the main transition is negligibly small. Therefore, it is reasonable to assume that the transition entropy is logarithmically related to the change of the number of the orientations available to the ions in the two phases.

$$\Delta S = R\ln(W_h/W_l). \quad (3)$$

Here R is the gas constant and W_h/W_l the ratio of the numbers of accessible ionic orientations in the high- and low-temperature phases, respectively. W_l may be equated to 1, because the NO_2^- ion is most probably ordered in the low-temperature phase in view of the absence of the large scale dielectric dispersion and the glass transition. The ionic disorder in the high-temperature phase is assumed to be orientational rather than positional in the sense that the positions of Rb^+ and NO_2^- ions are fixed on the fcc lattice points. We assumed further that the NO_2^- ions themselves are rigid so that they retain the C_{2v} symmetry in the crystal. Our problem is then to enumerate the allowed ionic orientations compatible with the average face-centered cubic symmetry. There is no configurational entropy for the spherically symmetric Rb^+ ion at the 4a position. The NO_2^- ion having the C_{2v} symmetry on the 4b position in the fcc Bravais lattice is obviously disordered. A nitrite group positioned about (1/2, 1/2, 1/2) is surrounded by the six nearest Rb^+ neighbours situated at the center of six faces of the cubic unit cell. The six cations form a regular octahedron. If we take the origin of the coordinate system at the center of the octahedron, the orientation of an NO_2^- ion can be specified by a set of nine position coordinates of the nitrogen and two oxygen atoms: N(a,b,c), O_I(d,e,f), and O_{II}(g,h,i). Different types of the disorder are generated by assigning one of the special or general positions to

each of the three atoms and then applying the symmetry operations to the first configuration thus specified to produce the rest.

The smallest set of the equivalent orientations has twelve members represented by

$$\begin{matrix} \mathrm{N} & (a,0,0) \\ \mathrm{O_I} & (d,e,0) \\ \mathrm{O_{II}} & (d,\bar{e},0), \end{matrix} \quad (4)$$

and the eleven symmetry-related orientations. An NO_2^- ion in one of these orientations has the nitrogen atom on the 4-fold axis and the ionic plane coincident with the x-y plane or its equivalent. There are two others sets of twelve members each produced from

$$\begin{matrix} \mathrm{N} & (a,a,0) \\ \mathrm{O_I} & (d,e,0) \\ \mathrm{O_{II}} & (e,d,0), \end{matrix} \quad (5)$$

and

$$\begin{matrix} \mathrm{N} & (a,a,0) \\ \mathrm{O_I} & (d,d,f) \\ \mathrm{O_{II}} & (d,d,\bar{f}). \end{matrix} \quad (6)$$

In a similar way three 24-member sets of orientations are obtained from the configurations

$$\begin{matrix} \mathrm{N} & (a,b,0) \\ \mathrm{O_I} & (d,e,0) \\ \mathrm{O_{II}} & (g,h,0), \end{matrix} \quad (7)$$

$$\begin{matrix} \mathrm{N} & (a,a,c) \\ \mathrm{O_I} & (d,e,f) \\ \mathrm{O_{II}} & (e,d,f), \end{matrix} \quad (8)$$

and

$$\begin{matrix} \mathrm{N} & (a,0,c) \\ \mathrm{O_I} & (d,e,f) \\ \mathrm{O_{II}} & (d,\bar{e},f). \end{matrix} \quad (9)$$

The largest set has 48 members generated from the general positions,

$$\begin{matrix} \mathrm{N} & (a,b,c) \\ \mathrm{O_I} & (d,e,f) \\ \mathrm{O_{II}} & (g,h,i). \end{matrix} \quad (10)$$

The entropy of the orientational disorder is $R\ln 12=20.7\ \mathrm{J\,K^{-1}\,mol^{-1}}$ for (4), (5), and (6), $R\ln 24=26.4\ \mathrm{J\,K^{-1}\,mol^{-1}}$ for (7), (8), and (9), and $R\ln 48=32.2\ \mathrm{J\,K^{-1}\,mol^{-1}}$ for (10). The experimental value is close to the last one. Therefore, the nitrite ion is disordered in the most general way in the straightforward interpretation of the experimental data. However, an additional possibility exists that there are two (or more) nonequivalent sets of low-energy configurations being nearly degenerate. If the energy difference between such sets is negligible in comparison with $RT_c\simeq 2\ \mathrm{kJ\,mol^{-1}}$, the orientations belonging to the different sets will be equally occupied in the high-temperature phase. The high-temperature entropy should then be calculated by taking the mixed configurations into account. It is equal to $R\ln(12+24)=29.8\ \mathrm{J\,K^{-1}\,mol^{-1}}$ for the combination of the orientations generated from (4) and (7) as an example. Other combinations are also possible. Therefore, more specific prediction of the disordered structure will be overly speculative at present. The conclusion drawn from the enumeration of the number of configurations is that the orientational entropy as large as $32.2\ \mathrm{J\,K^{-1}\,mol^{-1}}$ can be associated with the single ion.

A set of thirty two orientations has been proposed for a nitrite ion in KNO_2.[23] However, we could not deduce this number by the symmetry argument described here.

The large entropy of transition and the small entropy of melting are complementary with each other as often found in highly disordered molecular crystals.[24] Importance of the orientational disorder was also pointed out by Hirotsu et al. in the ultrasonic study of the cubic phase of $RbNO_2$.[25] Structural determination that may reveal the nature of the ionic disorder at the molecular level will be informative, as it was with the disordered phase of KNO_2.[23]

References

1) M. Sakiyama, A. Kimoto, and S. Seki, *J. Phys. Soc. Jpn.*, **20**, 2180 (1965).
2) K. Moriya, T. Matsuo, H. Suga, and S. Seki, *Chem. Lett.*, **1977**, 1427.
3) K. Moriya, T. Matsuo, and H. Suga, *Chem. Phys. Lett.* **82**, 581 (1981).
4) S. C. Mraw and L. A. K. Staveley, *J. Chem. Thermodyn.*, **8**, 1001 (1976).
5) S. C. Mraw, R. J. Boak, and L. A. K. Staveley, *J. Chem. Thermodyn.*, **10**, 359 (1978).
6) K. Moriya, T. Matsuo, and H. Suga, *J. Phys. Chem. Solids*, **44**, 1103 (1983).
7) K. Moriya and H. Suga, *Kagaku*, **38**, 599 (1983).
8) P. W. Richter and C. W. F. T. Pistorius, *J. Solid State Chem.*, **5**, 276 (1972).
9) B. H. Brooker and D. E. Irish, *Can. J. Chem.*, **46**, 229 (1968).
10) H. Suga and S. Seki, *Bull. Chem. Soc. Jpn.*, **38**, 1000 (1965).
11) T. Matsuo, H. Suga, and S. Seki, *J. Phys. Soc. Jpn.*, **30**, 785 (1971).
12) T. Matsuo, Y. Kume, H. Suga, and S. Seki, *J. Phys. Chem. Solids*, **37**, 499 (1976).
13) M. Oguni, T. Matsuo, H. Suga, and S. Seki, *Bull. Chem. Soc. Jpn.*, **50**, 825 (1977).
14) I. Hatta and A. Ikushima, *J. Phys. Chem. Solids*, **34**, 57 (1973).
15) R. J. Boak and L. A. K. Staveley, *J. Chem. Thermodyn.*, **19**, 661 (1987).
16) V. W. Nernst and F. A. Lindemann, *Z. Electrochem.*, **17**, 817 (1911).
17) T. Matsuo, Y. Tajima, and H. Suga, *J. Phys. Chem. Solids*, **47**, 165 (1986).

18) T. Shimada, T. Matsuo, H. Suga, and F. Luty, *J. Chem. Phys.*, **85**, 3530 (1986).
19) O. Yamamuro, M. Oguni, T. Matsuo, and H. Suga, *J. Chem. Thermodyn.*, **18**, 439 (1986).
20) N. Onoda, T. Matsuo, and H. Suga, *J. Phys. Chem. Solids*, **47**, 211 (1986).
21) T. Matsuo and H. Suga, *Thermochim. Acta*, **109**, 630 (1986).
22) T. Matsuo, H. K. Yan, and H. Suga, *J. Phys. Chem. Solids*, **49**, 85 (1988).
23) J. K. Solbakk and O. K. Strøme, *Acta Chem. Scand.*, **23**, 300 (1969).
24) N. G. Parsonage and L. A. K. Staveley, "Disorder in Crystals," Chap. 9 and 10, Clarendon Press, Oxford (1978).
25) S. Hirotsu, M. Miyamoto, and I. Yamamoto, *Jpn. J. Appl. Phys.*, **20**, L917 (1981).

Polarized Raman and Infrared Spectra of 2,6-Dichloro-, 2,6-Dibromo-, 3,5-Dichloro-, and 3,5-Dibromopyridines

Katsuharu TANAKA, Kinichi KASASAKU, Hiroko SHIMADA,* and Ryoichi SHIMADA†
Department of Chemistry, Faculty of Science, Fukuoka University, Nanakuma, Jonan-ku, Fukuoka 814-01
†Department of Chemistry, Faculty of Science, Kyushu University 33, Hakozaki, Higashi-ku, Fukuoka 812
(Received December 11, 1987)

Assignments of the normal vibrations of 2,6-dichloro-, 2,6-dibromo-, 3,5-dichloro-, and 3,5-dibromopyridines were made based on the polarization behavior of the Raman and infrared spectra in single crystals and the normal coordinate calculations. The effect of halo-substitution on the vibrational frequencies of the normal modes was discussed.

The Raman and infrared spectra of pyridine were studied by many workers.[1-4] Wong and Colson reviewed the previous works and reexamined the assignments of the normal vibrations of pyridine through the analysis of the high resolution FT-IR spectrum.[5] Very recently Ozono et al. reinvestigated the normal vibrations of pyridine based on the polarized Raman spectrum and gave new assignments for the out-of-plane vibrations.[6,7] Few investigations were made on the vibrational spectra of halo-substituted pyridines and reliable assignments of the normal vibrations, which are very important for the analyses of the fluorescence and phosphorescence spectra, have not been made yet.

In this paper, the assignments of the normal vibrations of 2,6- and 3,5-dihalopyridines will be discussed through the analyses of the polarized Raman and infrared spectra and normal coordinate calculations.

Experimental

Material. The samples, 2,6-dichloro- and 3,5-dichloropyridines (Nakarai Chemical Company), 2,6-dibromopyridine (Wako Chemical Company), and 3,5-dibromopyridine synthesized from pyridinium chloride were purified by repeated vacuum distillations.

Optical Measurements. The polarization measurements of the Raman spectrum were made in molten and single crystal phases with a Jeol 400 T Laser Raman Spectrophotometer. The sample was excited with the 514.5 nm line from an Ar^+ ion laser. A well grown single crystal of the sample was obtained by the Bridgman method and a cubic sample of about 5 mm^3 was cut off, where the cleavage plane was selected as one of the planes of the cube. Although the crystallographic analyses for these molecules were not reported yet, the crystal growth direction in the cleavage plane was found to be one of the extinction directions under the polarized light. The crystal growth direction was referred to as u axis and the direction perpendicular to this axis in the cleavage plane was to as v axis and the direction perpendicular to both the u and v axes to as w axis. The polarized Raman spectrum of the single crystal was denoted by two characters such as uv. The first letter refers to the direction of polarization of the excitation light and the latter to that of the scattering light. The method of measurement of the polarized Raman spectrum was exactly the same as that described previously.[8,9]

The infrared spectra were observed in vapor, CCl_4 and CS_2 solutions, and thin film obtained by sublimation, with a Hitachi Infrared Spectrophotometer Model 345. The polarized infrared spectra were observed in the thin film. The spectra measured with the incident lights polarized parallel and perpendicular to the crystal growth direction in the film plane are referred to as // and ⊥ spectra, respectively.

Normal Coordinate Calculation

The normal coordinate calculation was performed

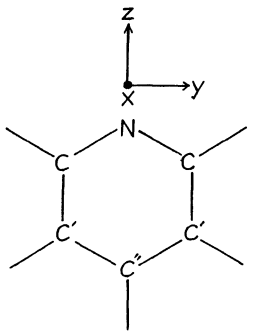

Fig. 1. Symbols for the atoms and internal coordinates.

Table 1. Force Constants for In-Plane Vibrations

K_{N-C}	5.6		$H_{CC'X}$	0.13[b]	0.15[c]
$K_{C-C'}$	4.8		$H_{C'CX}$	0.13[b]	0.15[c]
$K_{C'-C''}$	4.7		$H_{C''C'X}$	0.13[b]	0.15[c]
K_{C-H}	4.6		$F_{C\cdots C}$	0.9	
$K_{C'-H}$	4.6		$F_{N\cdots C'}$	0.5	
$K_{C''-H}$	4.6		$F_{C\cdots C''}$	0.6	
K_{C-X}[a]	2.3[b]	1.7[c]	$F_{C'\cdots C'}$	0.6	
$K_{C'-X}$	2.3[b]	1.7[c]	$F_{N\cdots H}$	0.7	
H_{CNC}	0.2		$F_{C\cdots H}$	0.4	
$H_{NCC'}$	0.25[d]	0.5[e]	$F_{C'\cdots H}$	0.4	
$H_{CC'C''}$	0.45[d]	0.2[e]	$F_{C''\cdots H}$	0.4	
$H_{C'C''C'}$	0.45		$F_{N\cdots X}$	0.8	
H_{NCH}	0.17		$F_{C\cdots X}$	0.8	
$H_{C'CH}$	0.2		$F_{C'\cdots X}$	0.8	
$H_{CC'H}$	0.2		$F_{C''\cdots X}$	0.8	
$H_{C''C'H}$	0.2		ρ	0.38	
$H_{C'C''H}$	0.2		$k^{o}_{H,H}$	0.06	
H_{NCX}	0.13[b]	0.15[c]	$k^{m}_{H,H}$	−0.04	

Force constants are given in hNm^{-1} units. a) X refers to the Cl or Br atom. b) Values for dichloropyridines. c) Values for dibromopyridines. d) Values for 2,6-dihalopyridines. e) Values for 3,5-dihalopyridines.

Table 2. Force Constants for Out-of-Plane Vibrations

Q_{N-C}	0.21	p^{o}	0.02
$Q_{C-C'}$	0.20	$p^{m}_{H,H}$	−0.015
$Q_{C'-C''}$	0.20	$p^{m}_{H,X}$	−0.01
P_H	0.31	$p^{m}_{X,X}$	−0.05
P_X[a]	0.39[b] 0.4[c]	t^{o}_{H}	−0.02
q^{o}	−0.05	t^{m}_{H}	−0.01
q^{m}	0.01		

Force constants are given in aNmrad^{-2} units. a) X refers to the Cl or Br atom. b) Value for the Cl atom. c) Value for the Br atom.

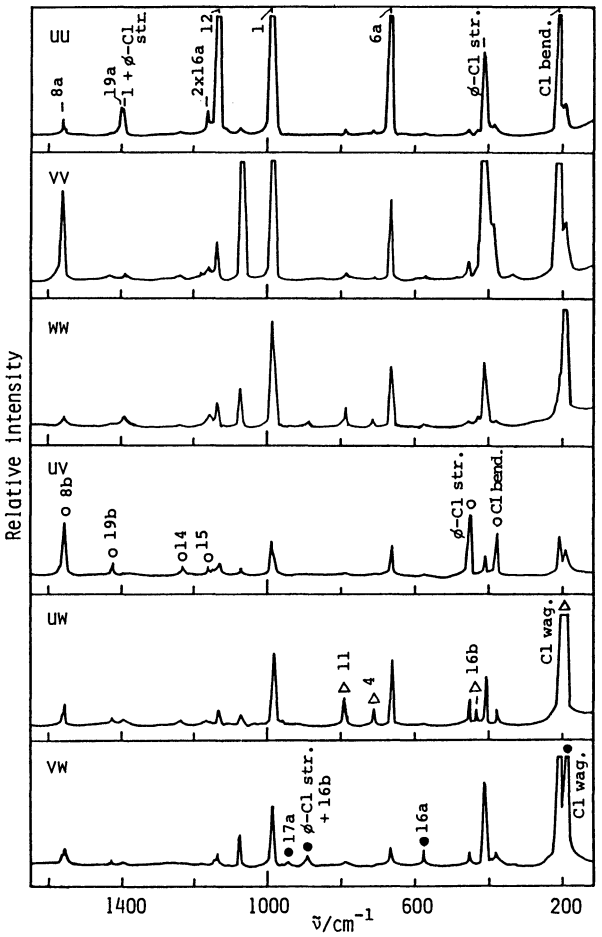

Fig. 2. Polarized Raman spectra of 2,6-dichloropyridine crystal.

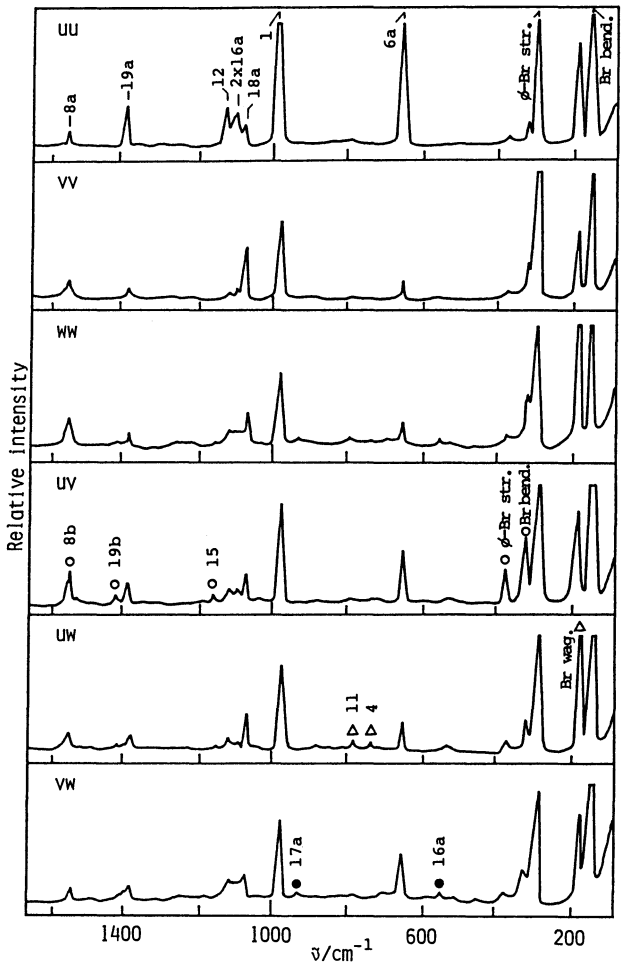

Fig. 3. Polarized Raman spectra of 2,6-dibromopyridine crystal.

through the standard GF matrix method with a FACOM M-380R computer at the Computer Center of Fukuoka University. The geometrical parameters of the molecules were assumed to be the same as those of pyridine except for the C-Cl and C-Br bonds, whose bond lengths were assumed to be 0.180 and 0.185 nm, respectively.

The F matrix elements for the in-plane and out-of-plane vibrations were evaluated with the potential fields of an improved modification of the Urey-Bradley and valence force fields, respectively, described previously.[9,10] The symbols given for the atoms and the molecular axes are illustrated in Fig. 1. The force constants used for the normal coordinate calculations of the in-plane and out-of-plane vibrations are listed in Tables 1 and 2, respectively, and the calculated results of the vibrational modes and frequencies are given in Tables 3 and 4.

Results and Discussion

The relative intensity of the Raman band in the polarized Raman spectra observed in the different orientations of the crystal is governed by the orientation of the molecule in the crystal in the oriented gas model approximation. If the crystal structure is known, the relative intensities of the Raman bands can be calculated from the direction cosines between the crystal and molecular axes and the assignments of the normal vibrations can be quantitatively made from the observed polarization behavior of the Raman bands. Even if the crystal structure is unknown, the polarization behavior of the Raman bands observed along and perpendicular to the crystal growth direction, which is one of the extinction directions, in the cleavage plane gives qualitative information on the classification of the Raman bands into certain symmetry species. This

is because the molecular vibrations belonging to the same symmetry species should show the same polarization behavior. We analyzed the polarized Raman spectra and reasonable assignments of the normal vibrations were made for dichloromaleic anhydride[10] and 2-halosubstituted pyrimidines[11] whose crystal structures were unknown.

The polarized Raman spectra of 2,6-dichloro-, 2,6-dibromo-, 3,5-dichloro-, and 3,5-dibromopyridines are shown in Figs. 2, 3, 4, and 5, respectively. As can be seen in the figures, the depolarized Raman bands observed in a molten phase could be classified into three types of polarization behavior in the polarized Raman spectra observed in the crystal. The intensities of the Raman bands belonging to the first type are the strongest in the uv spectrum and decrease in the uw, vv, and vw spectra in order. The second type bands are strongest in the uw spectrum and their intensities decrease in the ww and uu spectra in order, and the third type bands could be observed clearly only in the vw spectrum. The first, second, and third type polarization behavior will be referred to as the uv, uw, and vw polarization, and the bands showing these types of polarization are marked with ○, △, and ● in the figures, respectively.

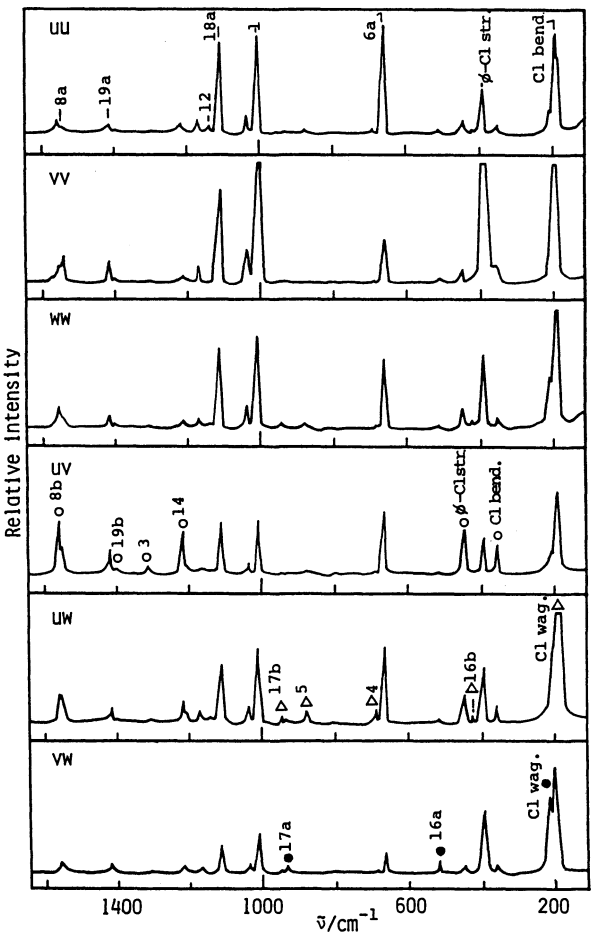

Fig. 4. Polarized Raman spectra of 3,5-dichloropyridine crystal.

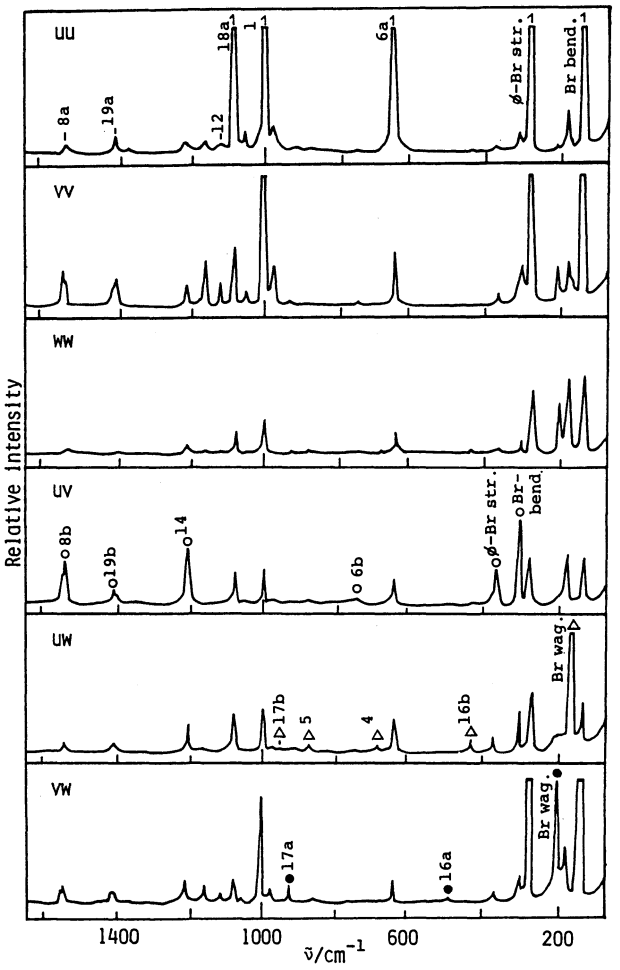

Fig. 5. Polarized Raman spectra of 3,5-dibromopyridine crystal.

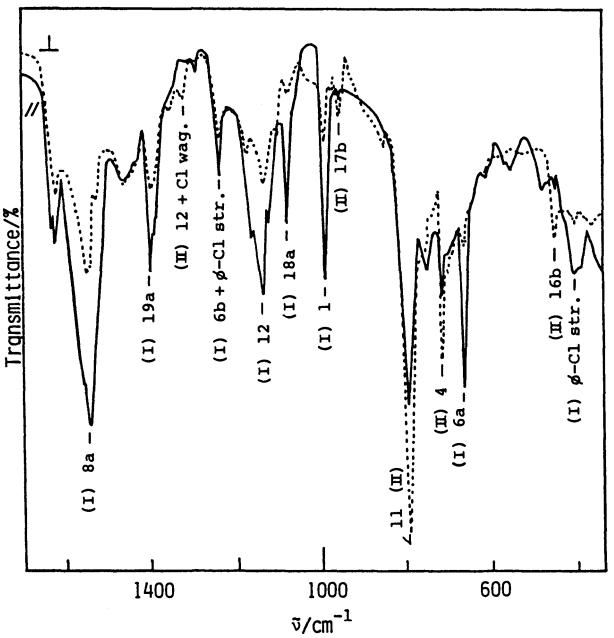

Fig. 6. Polarized infrared spectra of 2,6-dichloropyridine crystal.

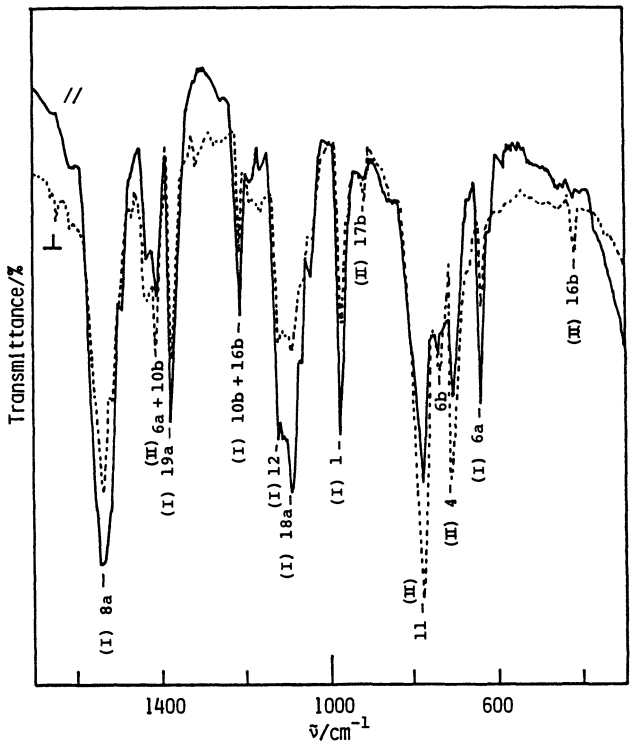

Fig. 7. Polarized infrared spectra of 2,6-dibromopyridine crystal.

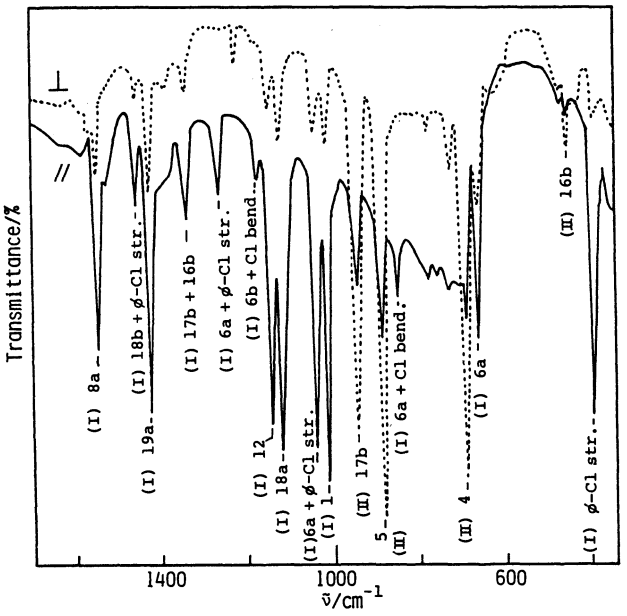

Fig. 8. Polarized infrared spectra of 3,5-dichloropyridine crystal.

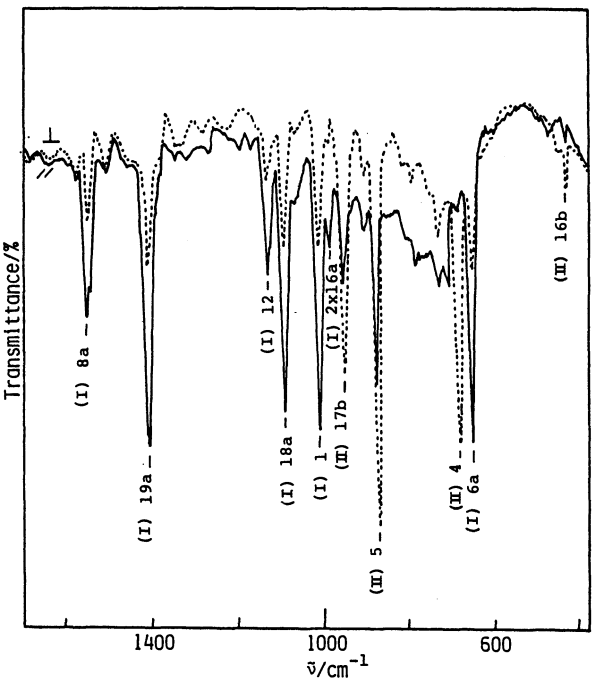

Fig. 9. Polarized infrared spectra of 3,5-dibromopyridine crystal.

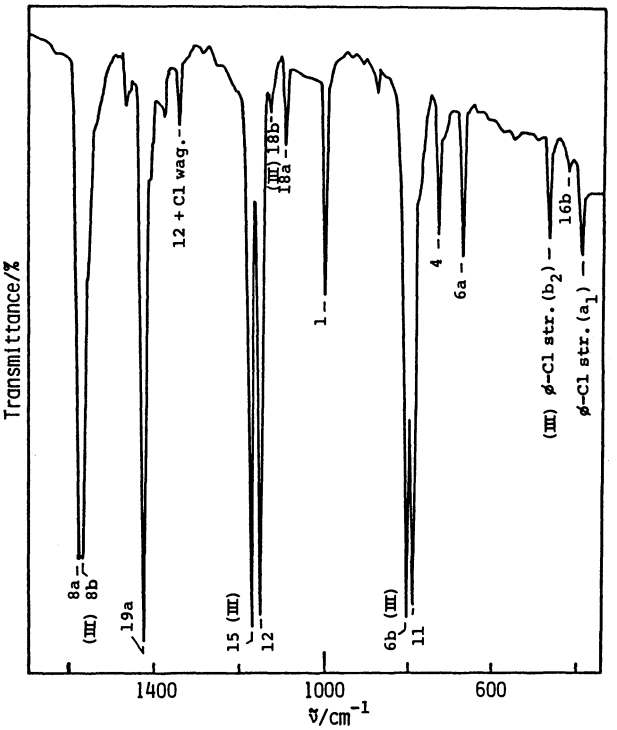

Fig. 10. Infrared spectrum of 2,6-dichloropyridine in solution.

The polarized infrared spectra of 2,6-dichloro-, 2,6-dibromo-, 3,5-dichloro-, and 3,5-dibromopyridines observed in the thin films are shown in Figs. 6, 7, 8, and 9, respectively, where the // and ⊥ spectra are drawn with the solid and dotted lines. The polarization behavior of the infrared bands could be classified into two types. The intensities of the bands belonging to the first type are stronger in the // spectrum than in the ⊥ spectrum while the intensities of the second type bands are weaker in the // spectrum than in the one. These two types of the bands will be referred to as types I and II, respectively as shown in the figures. Some infrared bands were observed strongly or clearly in the

CCl_4 and CS_2 solutions although observed very weakly or hardly in the thin film. This type of the bands will be referred to as type III. As an example, the infrared spectrum of 2,6-dichloropyridine observed in CCl_4 (1700—1000 cm^{-1}) and CS_2 (1000—350 cm^{-1}) is shown in Fig. 10, where these bands are marked with the symbol III. The very weak intensity of the type III bands in the thin film spectrum may be due to the polarization direction being nearly normal to the plane of the thin film.

Calculations of the principal moments of inertia of these molecules suggest that the infrared bands belonging to the a_1, b_2, and b_1 symmetry species show the B, A, and C rotational band contours, respectively. The vibrational modes were determined based on the normal coordinate calculation.

2,6-Dichloropyridine. a_1 Species: The strongly polarized Raman bands observed at 3078, 3030, 1400, 1133, 1072, 985, 664, and 409 cm^{-1} in molten phase could be straightforwardly assigned to the totally symmetric ν_2, ν_{7a}, ν_{19a}, ν_{12}, ν_{18a}, ν_1, ν_{6a}, and ϕ-Cl stretching vibrations, respectively, where ϕ refers to the pyridine ring. The corresponding infrared bands observed in vapor and the thin film showed the B band contour and the type I polarization, respectively. The infrared band observed at 1562 cm^{-1} was assigned to the ν_{8a} vibration because this band showed the type I polarization in the thin film, although the corresponding Raman band was depolarized in molten phase due to overlapping with the band assigned to the ν_{8b} vibration described later. The Raman band at 202 cm^{-1} was assigned to the Cl bending vibration of a_1 species because this band does not show any of the uv, uw, and vw polarization behavior.

b_2 Species: The infrared band observed at 1167 cm^{-1} showed the A band contour in vapor and therefore this band was assigned to the ν_{15} vibration of b_2 species. The corresponding infrared band in the thin film and the Raman bands in the crystal showed the type III and the uv polarization, respectively. The Raman bands observed at 1556, 1423, 1228, 452, and 374 cm^{-1} showed the uv polarization and thus were assigned to the ν_{8b}, ν_{19b}, ν_{14}, ϕ-Cl stretching, and Cl bending vibrations of b_2 species, respectively. The infrared bands observed at 1120 and 800 cm^{-1} showed the type III polarization and were assigned to the ν_{18b} and ν_{6b} vibrations, respectively.

b_1 Species: The infrared bands observed at 790 and

Table 3. Normal Vibrations of 2,6-Dichloro- and 2,6-Dibromopyridines

Sym spec	Mode	2,6-Dichloropyridine						2,6-Dibromopyridine					
		Raman			Infrared		Calcd	Raman			Infrared		Calcd
		$\tilde{\nu}$/cm^{-1}	pol		pol		$\tilde{\nu}$/cm^{-1}	$\tilde{\nu}$/cm^{-1}	pol		pol		$\tilde{\nu}$/cm^{-1}
			liq	cry	vap	cry			liq	cry	cry		
a_1	ν_2	3078	p				3064	3078	p				3064
	ν_{7a}	3030	p				3020	3040	p				3020
	ν_{8a}	1562	dp?			I	1561	1545	dp?		I		1560
	ν_{19a}	1400	p		B	I	1410	1387	p		I		1410
	ν_{12}	1133	p			I	1138	1123	p		I		1105
	ν_{18a}	1072	p			I	1070	1072	p		I		1068
	ν_1	985	p		B	I	998	987	p		I		998
	ν_{6a}	664	p			I	679	650	p		I		651
	ϕ-X str.[a]	409	p			I	400	290	p				297
	X bend.	202	dp				200	140	dp				145
b_2	ν_{7b}	3055	dp				3058						3058
	ν_{8b}	1556	dp	uv			1547	1543	dp	uv			1547
	ν_{19b}	1423	dp	uv			1407	1422	dp	uv			1403
	ν_{14}	1228		uv			1226	1222[b]					1226
	ν_{15}	1167	dp	uv	A	III	1161	1167		uv	III		1159
	ν_{18b}	1120[b]				III	1113	1111[b]			III		1106
	ν_{6b}	800[b]				III	808	747[b]			III		751
	ϕ-X str.	452	dp	uv		III	430	377	dp	uv			392
	X bend.	374	dp	uv			381	316	dp	uv			325
a_2	ν_{17a}	940	dp	vw			934	930		vw			934
	ν_{16a}	577	dp	vw			562	553		vw			562
	X wag.	185	dp	vw			181	190[c]					174
b_1	ν_{17b}	963	dp			II	963	970[b]			II		964
	ν_{11}	790	dp	uw	C	II	805	785		uw	II		808
	ν_4	716	dp	uw	C	II	729	720		uw	II		734
	ν_{16b}	430	dp	uw		II	407	418[b]			II		407
	X wag.	190	dp	uw			172	178	dp	uw			160

a) X refers to the Cl or Br atom. b) Observed in the infrared spectrum. c) Observed as a shoulder of the strong band at 178 cm^{-1}.

Table 4. Normal Vibrations of 3,5-Dichloro- and 3,5-Dibromopyridines

Sym spec	Mode	3,5-Dichloropyridine						3,5-Dibromopyridine					
		Raman			Infrared		Calcd	Raman			Infrared		Calcd
		$\tilde{\nu}$/cm^{-1}	pol		pol		$\tilde{\nu}$/cm^{-1}	$\tilde{\nu}$/cm^{-1}	pol		pol		$\tilde{\nu}$/cm^{-1}
			liq	cry	vap	cry			liq	cry	cry		
	ν_2	3045	p				3041						3041
	ν_{7a}	3077	p				3080						3086
	ν_{8a}	1550	dp?			I	1556	1548	dp?		I		1566
	ν_{19a}	1417	p			I	1404	1407	p		I		1407
a_1	ν_{12}	1141	p			I	1163	1120			I		1157
	ν_{18a}	1109	p			I	1110	1083	p		I		1079
	ν_1	1010	p		B	I	1020	1008	p		I		1021
	ν_{6a}	653	p		B	I	655	635	p		I		642
	ϕ-X str.[a]	393	p			I	395	275	p				289
	X bend.	197	dp				203	155	dp				151
	ν_{7b}						3102						3102
	ν_{8b}	1557	dp	uv			1560	1539	dp	uv			1557
	ν_{19b}	1410	dp	uv			1392	1410	dp	uv			1392
	ν_3	1309		uv		III	1316	1300[b]				III	1316
b_2	ν_{14}	1215	dp	uv		III	1207	1212	dp	uv		III	1208
	ν_{18b}	1103[b]			A	III	1073	1085[b]				III	1066
	ν_{6b}	820[b]				III	811	753	dp	uv		III	752
	ϕ-X str.	447	dp	uv		III	438	365	dp	uv			398
	X bend.	360	dp	uv			381	302	dp	uv			331
	ν_{17a}	935	dp	vw			945	930	dp	vw			945
a_2	ν_{16a}	512	dp	vw			526	492	dp	vw			525
	X wag.	209	dp	vw			199	200	dp	vw			191
	ν_{17b}	945	dp	uw		II	922	950	dp	uw		II	922
	ν_5	878	dp	uw	C	II	870	875	dp	uw		II	870
b_1	ν_4	687	dp	uw	C	II	704	685	dp	uw		II	706
	ν_{16b}	428	dp	uw		II	436	432	dp	uw		II	437
	X wag.	186	dp	uw			155	176	dp	uw			142

a) X refers to the Cl or Br atom. b) Observed in the infrared spectrum.

716 cm^{-1} showed the C band contour in vapor and the type II polarization in the thin film. Hence these bands were assigned to the ν_{11} and ν_4 vibrations of b_1 species, respectively. The corresponding Raman bands showed the uw polarization in crystal. The infrared band observed at 963 cm^{-1} showed the type II polarization and the Raman bands at 430 and 190 cm^{-1} showed the uw polarization. Therefore, these bands were assigned to the ν_{17b}, ν_{16b}, and Cl wagging vibrations of b_1 species, respectively.

a_2 Species: The Raman bands observed at 940, 577, and 185 cm^{-1} showed the vw polarization in crystal and were assigned to the ν_{17a}, ν_{16a}, and Cl wagging vibrations of a_2 species, respectively, because no corresponding bands could be observed in the infrared spectrum.

The polarization behavior of the Raman and the infrared bands of 2,6-dibromo-, 3,5-dichloro- and 3,5-dibromopyridines was exactly the same as that of 2,6-dichloropyridine except for the fact that the rotational band contours of the infrared bands were not resolved in the dibromopyridines. Assignments of the normal vibrations of these molecules were made based on the following polarization behavior.

a_1 Species: The polarized Raman bands in molten phase could be definitely assigned to the a_1 vibrations. The corresponding infrared bands showed the type I polarization in the thin films and some bands clearly showed the B band contour in vapor.

b_2 Species: The infrared bands showing the A band contour in vapor showed the type III polarization in the thin film and the corresponding Raman bands showed the uv polarization in crystal.

b_1 Species: The infrared bands showing the C band contour in vapor showed the type II polarization in the thin film and the corresponding Raman bands showed the uw polarization in crystal.

a_2 Species: The Raman bands showing the vw polarization were assigned to the a_2 vibration, because no corresponding infrared bands were observed.

The normal vibrations thus determined are given in Tables 3 and 4 and also shown in Figs. 2—10. The normal vibrations of the dihalopyridines show the following characteristic features. (1) The vibrational frequencies of the ν_{6a}, ν_{12}, ν_{6b}, ν_{18b}, ν_{16a}, and ν_{16b} vibrations increase markedly compared with those of pyridine. (2) The frequencies of the ϕ-Cl and ϕ-Br stretching vibrations decrease remarkably compared with the frequencies of the C-Cl and C-Br stretching vibrations of aliphatic compounds. These observations are well

explained in terms of the normal coordinate calculation.

The normal coordinate calculation gave the following results. (1) The ν_{6a} vibration mixes with the ϕ-X (X=Cl or Br) stretching vibration of a_1 species in the dihalopyridines and its frequency increases compared with the corresponding frequency of pyridine (602 cm^{-1}). The ν_{6a} vibration also interacts with the ν_{12} vibration and the frequency of the ν_{12} vibration increases compared with the corresponding frequency of pyridine (1030 cm^{-1}). The mixing of the ϕ-X stretching, ν_{6a}, and ν_{12} vibrations is larger in the dichloropyridines than in the dibromopyridines and thus the frequencies of the ν_{6a} and ν_{12} vibrations increase more largely in the dichloropyridines than in the dibromopyridines. The difference of the mixing may be due to the fact that the energy separation between the C-Cl stretching and ν_{6a} vibrations is smaller than that between the C-Br stretching and ν_{6a} ones. (2) The ν_{6b} vibration interacts with the ϕ-X stretching vibration of b_2 species and the frequency of the ν_{6b} vibration increases compared with the corresponding frequency of pyridine (650 cm^{-1}). The ν_{6b} vibration also interacts with the ν_{18b} vibration and the frequency of the ν_{18b} vibration increases compared with the corresponding frequency of pyridine (1045 cm^{-1}). The mixing of the ϕ-X stretching, ν_{6b}, and ν_{18b} vibration is larger in the dichloropyridines than in the dibromopyridines and thus the frequencies of the ν_{16b} and ν_{18b} vibrations increase more largely in the dichloropyridines than in the dibromopyridines. This may be due to the smaller energy separation between the ν_{6b} and C-Cl stretching vibrations compared with that between the ν_{6b} and C-Br stretching vibrations. (3) The ν_{16b} and ν_{16a} vibrations mix with the Cl or Br wagging vibrations. Thus the frequencies of the ν_{16b} and ν_{16a} vibrations of dihalopyridines increase compared with those of pyridine (408 and 377 cm^{-1}) but the frequency increase of the ν_{16a} vibration is larger than that of the ν_{16b} vibration. This may be due to the difference of the energy separation between the two interacting vibrations as described above.

References

1) L. Corrsin, B. J. Fax, and R. C. Lord, *J. Chem. Phys.*, **21**, 117 (1953).

2) J. K. Wilmshurst and H. J. Bernstein, *Canad. J. Chem.*, **35**, 1184 (1957).

3) E. Castellucci, G. Sbrana, and F. D Verderame, *J. Chem. Phys.*, **51**, 3762 (1969).

4) H. D. Stidham and D. P. DiLella, *J. Raman Spectrosc.*, **9**, 90, 247 (1980).

5) K. N. Wong and S. D. Colson, *J. Mol. Spestrosc.*, **104**, 129 (1984).

6) Y. Ozono, M. Maehara, Y. Nibu, H. Shimada, and R. Shimada, *Bull. Chem. Soc. Jpn.*, **59**, 1617 (1986).

7) H. Shimada, Y. Ozono, and M. Maehara, *Fukuoka Univ. Sci. Reports*, **16 (2)**, 113 (1986).

8) Y. Ishibashi, R. Shimada, and H. Shimada, *Bull. Chem. Soc. Jpn.*, **55**, 2765 (1982).

9) S. Nakama, H. Shimada, and R. Shimada, *Bull. Chem. Soc. Jpn.*, **57**, 2584 (1984).

10) S. Kizuki, Y. Ishibashi, H. Shimada, and R. Shimada, *Mem. Fac. of Sci. Kyushu Univ., Ser. C*, **13**, 7 (1981).

11) Y. Ishibashi, R. Shimada, and H. Shimada, *Bull. Chem. Soc. Jpn.*, **56**, 1362 (1983).

Long-Lived Triplet Radical Ion Pair State of Porphyrin-Methylviologen Combined Systems as Revealed by a Large Magnetic Field Effect on Its Lifetime

Toshiro SAITO, Yoshinori HIRATA,* Hisashi SATO, Toshikatsu YOSHIDA,† and Noboru MATAGA*
Department of Chemistry, Faculty of Engineering Science, Osaka University, Toyonaka, Osaka 560
(Received December 28, 1987)

The external magnetic field effect on the lifetime of the ion pair state has been examined for the porphyrin-methylviologen combined systems in polar solvents by using nanosecond laser flash photolysis techniques. Applying the external magnetic field, a drastic increase in the lifetime has been observed. For PIIMV^{2+} in DMSO under the magnetic field of 50 mT, the ion pair lifetime was almost three times longer than the zero field value, which can be deemed the ideal case of the external magnetic field effect due to the hyperfine interaction mechanism. The results clearly showed that the long-lived ion pair was formed by the intramolecular electron transfer from the triplet state of porphyrin.

Studies of external magnetic field effects upon photochemical reactions in solution provide important information concerning the microscopic reaction mechanisms. The external magnetic field effect on the behavior of radical ion pairs of electron acceptor/donor (A/D) systems such as pyrene/*N*,*N*-dimethylaniline (DMA) in polar solvents was observed already more than ten years ago.[1] The effect saturates at a rather low magnetic field (less than 20 mT) and, accordingly, is due to the hyperfine interaction (hfi) mechanism, by which singlet (S) and triplet (T) radical ion pairs can interconvert. Under the influence of an external magnetic field greater than the hyperfine coupling energy (ΔE_{hfc}), the triplet sublevels split due to the Zeeman effect into T_+, T_0, and T_- and the degeneracy of T_+, T_-, and S is lifted. Then such a strong external magnetic field inhibits the spin interconversion between singlet and triplet sublevels of the radical ion pair except for that between S and T_0. Although the effect is usually not large for the intermolecular (unlinked) systems, it can provide important informations about an interaction and separation distance between cation and anion radicals.

For the A/D systems linked by a polymethylene chain, both the mutual motion and distance of the individual radical ions are restricted compared with the unlinked systems. If the separation distance of the individual radical ions is so short that the spin exchange interaction, which splits the singlet and triplet levels of the radical ion pairs by the amount of twice of the exchange integral, 2J, is larger than the hyperfine interaction, the magnetic field effect of the hfi mechanism should not be observed. On the other hand, if the radical ions are kept at a proper distance where the hfi can play the dominant role, we can expect that the magnetic field effect is larger than that in the unlinked systems.

The external magnetic field effect of the pyrene-$(CH_2)_n$-DMA systems in acetonitrile solution was studied by Staerk et al.[2] They measured the exciplex fluorescence yield and lifetime for the molecules of n=8—16. The magnetic field effect increased with increasing chain length, while the larger influence of the exchange interaction, which appears as an effect inverse to the hfi, was observed for the shorter chain compounds. In their system the singlet radical ion pair, which is formed by photoinduced electron transfer from DMA to the excited pyrene and associates to form the fluorescent exciplex, changes its spin state by the hyperfine induced conversion to the triplet radical ion pair. For the longest chain molecule (n=16), the yield of the exciplex fluorescence at high magnetic field was 147% of the zero field value. Similar effect was observed for the fluorescence lifetimes (31 and 22 ns for 35 and 0 mT, respectively).

Tanimoto et al.[3] measured the external magnetic field effect on the fluorescence of phenanthrene-$(CH_2)_n$-DMA (n=3, 6, 8, 10). No magnetic field effect on the intramolecular exciplex fluorescence was observed for the molecules with n=3 and 6, while for the system of n=10 the fluorescence lifetime of the exciplex was 50 and 92 ns at the magnetic field of 0 and 810 mT, respectively. The dip, which seems to be an indication of the spin exchange effect, was clearly observed for the system of n=8.

In a previous paper we reported that the extremely long-lived radical ion pair was formed in the porphyrin (P)-methylviologen (MV^{2+}) system combined with flexible chains in highly polar solvents, such as dimethyl sulfoxide (DMSO) and methanol-acetone (1 : 1 by volume) mixture.[4] Such a long-lived intramolecular radical ion pair was not observed for the porphyrin (P)-quinone (Q) combined systems.[5] These results seemed to suggest that the coulomb interaction between the ionic species formed by the intramolecular photoinduced electron transfer may cause the quite different dynamic behavior between these two kinds of combined systems. Contrary to the latter case where the attraction force between P^+ and Q^- groups is expected, the repulsion between the P^+ and MV^+

† Present address: College of Integrated Arts and Science, University of Osaka Prefecture, Sakai, Osaka 591.

groups may prevent the ionic recombination and prolong the lifetime of the radical ion pair in the former case.

In order to elucidate the details of the dynamic behavior and structure of the radical ion pair, we have studied extensively the external magnetic field effect on the lifetime of the radical ion pair for P-MV^{2+} systems in DMSO and in a methanol-acetone (1 : 1) mixture. Applying an external magnetic field of less than 50 mT, the lifetime has increased extremely. The effect seems to saturate at about 30 mT, which suggests that the hfi mechanism is important for the observed effect. We propose here the mechanism that the long-lived radical ion pair of the P-MV^{2+} combined system observed in polar solvents is produced by the intramolecular electron transfer between triplet P and ground state MV^{2+}.

Experimental

A microcomputer-controlled excimer laser (XeF, 15 ns fwhm) photolysis system[6] was used for the transient absorption measurements in the nanosecond to microsecond time region. An excitation laser beam and a monitor light from a pulsed Xe lamp were crossed in a sample cell at the right angles. The monitor light was detected by a photomultiplier tube after passing through a monochromator. The signal, which was digitized by a digital storage scope (100 MHz, 8 bit), was accumulated and then the transient absorbance was calculated by a microcomputer. A Helmholtz coil with a gap width of 200 mm was used to apply an external magnetic field of up to 54 mT. The sample cell was placed at the center of the electro magnet and the field strength was monitored with a gaussmeter.

The porphyrin-methylviologen combined systems, P*n*MV^{2+} were synthesized by the method as given in the Appendix, and the synthesis of the reference compound PII by the similar method was described elsewhere.[9] Methylviologen was purified by repeated recrystallization from ethanol. All the solvents (Spectro Grade) were used without further purification.

Sample solutions were deaerated by several freeze-pump-thaw cycles and sealed in quartz cells with 1-cm optical path length. All the measurements were performed at room temperature.

Results and Discussion

Unlinked System. The fluorescence lifetime of the reference compound of porphyrin, PII, which has two long chains with an *N*-methylpyrolidine group instead of MV^{2+}, was 2 ns. Although we did not measure the triplet yield, it was reasonable to expect the high triplet yield, because the molecular structure and the fluorescence lifetime are similar to those of Zn etioporphyrin I (ϕ_T=0.94, τ_f=2.3 ns).[7] The triplet energy of etioporphyrin I is about 0.4 eV higher than that of the porphyrin cation-methylviologen monocation (MV^+) pair, which was estimated from the redox potential.[8] Therefore the electron transfer between the triplet state of PII and the ground state of MV^{2+} should

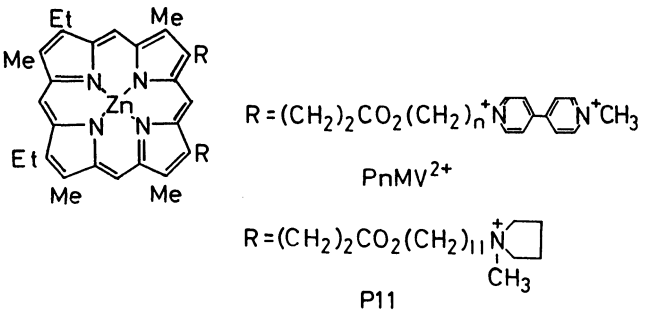

Fig. 1. Molecular structure of the samples.

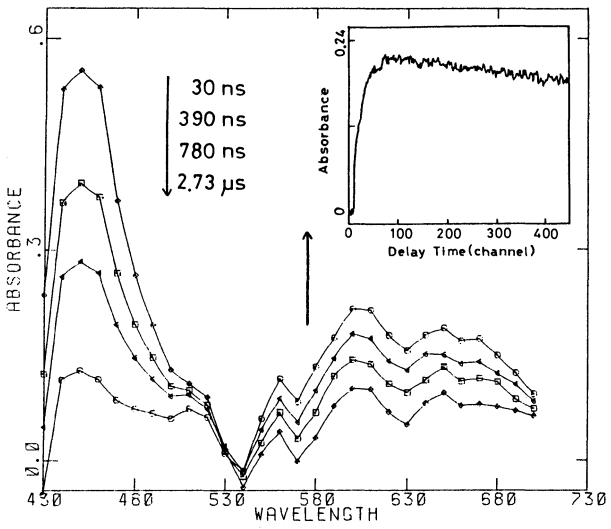

Fig. 2. Nanosecond time resolved absorption spectra of PII/MV^{2+} in DMSO. The decay time after the laser pulse excitation was indicated in the Figure. The rise and decay curve measured at 600 nm was also shown (insert, 39 ns/channel).

be a rapid process.

Figure 2 shows transient absorption spectra of PII/MV^{2+} in DMSO system. The absorption band in the short wavelength region (ca. 430 nm) can be ascribed to the triplet state of PII, the decay of which followed the exponential kinetics and the lifetime depended on the concentration of MV^{2+}. Increasing the delay time after the nanosecond laser pulse excitation, the $T_n \leftarrow T_1$ absorption of PII disappeared and a new absorption band in the 540—700 nm region built up. The latter should be assigned to the superposition of the absorption bands of PII cation and MV^+, the recombination of which seemed to be a quite slow process. The decay time of the PII triplet and the rise time of the ion radicals showed a quite good agreement. Therefore, it was concluded that the ion radicals were formed by the electron transfer from the triplet state of PII to MV^{2+}. Similar behavior was observed also in the methanol-acetone mixed solvent. Even at a high concentration of MV^{2+} (0.1 M), although the stable MV^+ formation disturbed the transient absorption measurements, the time dependence of the concentration of the ion radi-

cals could be explained by a homogeneous recombination kinetics, except at very short delay time (≦30 ns), where the porphyrin fluorescence was observed. We could not find any evidence for the presence of the long lived ion pair, which was observed for the linked system.[5] By the application of the external magnetic field less than 54 mT, no effect on the free ion yield was observed either in DMSO or methanol-acetone. In the case of the Py/DMA in acetonitrile system, the triplet yield decreased about 10% by the application of a magnetic field of 20 mT. little magnetic field effect on th Pll/MV^{2+} system may suggest that the lifetime of the geminate ion pair was too short because of the repulsive force between the radical cations.

Linked System. As described in Introduction, P6MV^{2+} and P11MV^{2+} in DMSO and methanol-acetone solutions form the long-lived ion pairs, of which the lifetimes are longer than 100 ns, through a photoinduced electron transfer reaction. The time dependence of the transient absorbance measured at 600 nm was shown in Fig. 3. The yield of the long lived

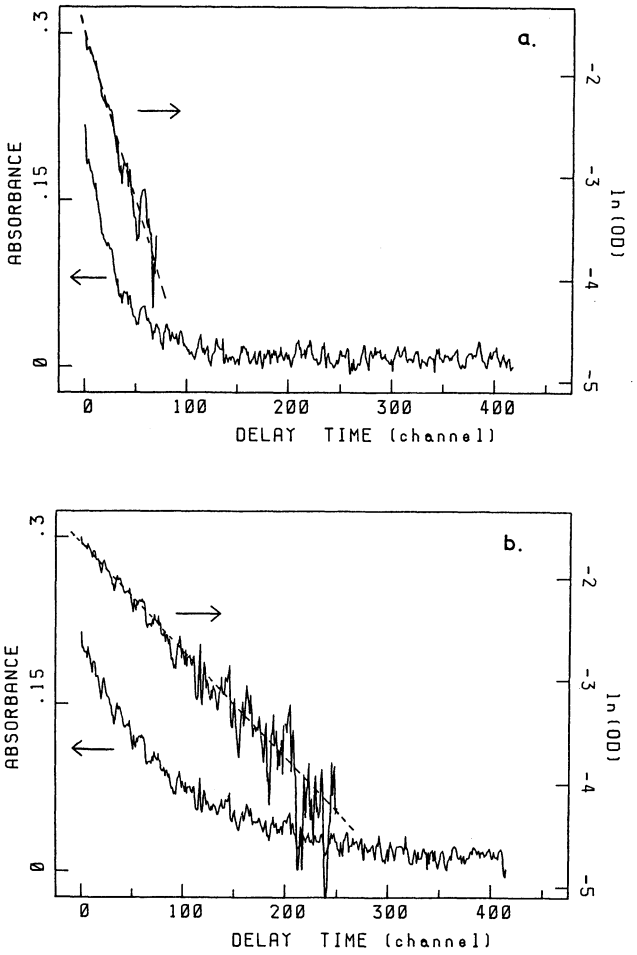

Fig. 3. Time dependence of the transient absorbance of P11MV^{2+} in DMSO (3.9 ns/channel): (a) in the absence of a magnetic field and (b) in the presence of maganetic field (50 mT). Semilogarithmic plot were also shown in the figure (right axis).

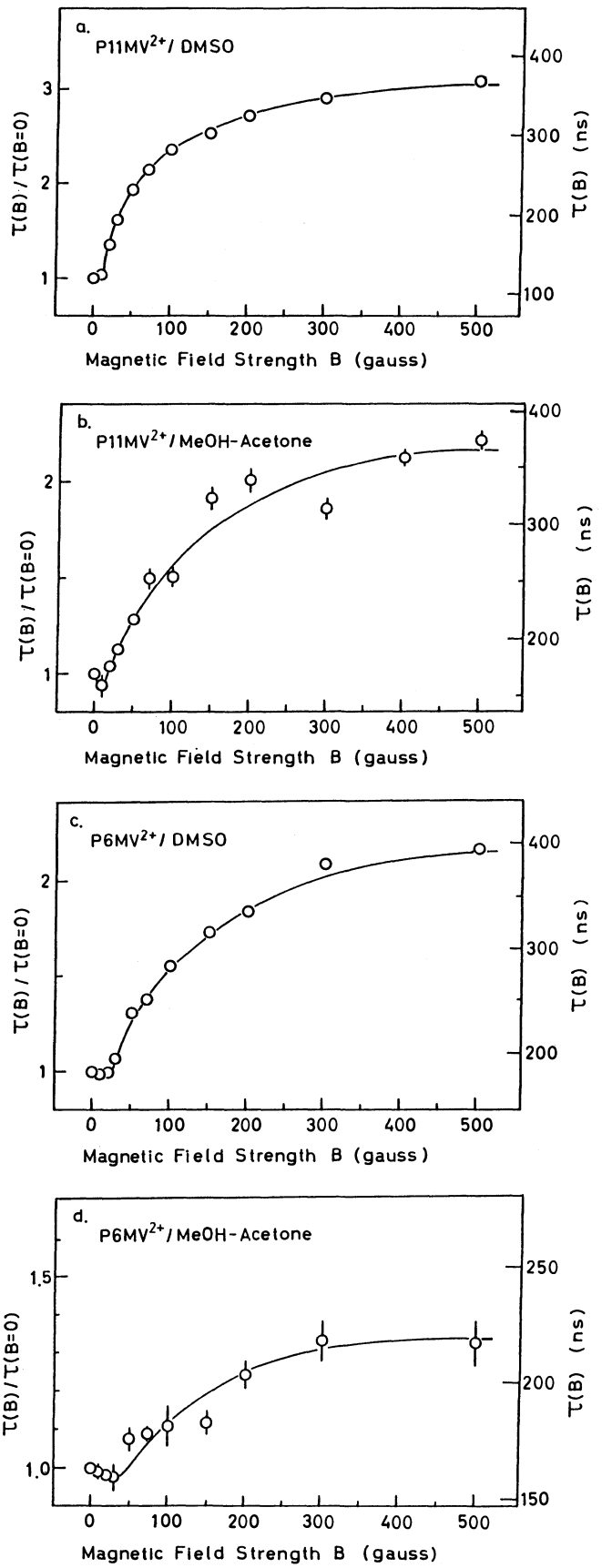

Fig. 4. Magnetic field dependence of the lifetime of $P^{+}nMV^{+}$: (a) n=11 in DMSO, (b) n=11 in methanol-acetone, (c) n=6 in DMSO, and (d) n=6 in methanol-acetone.

component depended on the excitation laser intensity, which should be due to the porphyrin radical cation produced via the two photon ionization. by subtracting this component decaying slowly via the homogeneous ionic recombination, the decay followed an exponential kinetics, as shown in the figure (semilogarithmic plot). In this way the lifetime of the short lived component of PllMV^{2+} in DMSO was determined to be 120 and 360 ns at 0 and 50 mT, respectively.

As shown in Fig. 4, by applying the external magnetic field, the lifetime of the ion pair increased drastically. The effect was prominent for the longer chain molecule and the larger effect was observed for the DMSO solution. For P6MV^{2+} the external magnetic field did not affect the ion pair lifetime up to 4 and 5 mT in DMSO and methanol-acetone solutions, respectively. Such threshold seemed to be lower for PllMV^{2+} in both solvents. The magnetic field effect was almost saturated at about 30 mT and under the influence of the external magnetic field of 50 mT, the lifetime of the ion pair of PllMV^{2+} in DMSO was three fold of that at zero field. This is a quite large effect compared with the results reported for other intramolecular exciplex systems.[2,3]

The magnetic field effect observed here should be due to the hfi mechanism since the effect saturates at a rather low external field of about 30 mT. Hyperfine interaction causes the interconversion between the almost degenerate singlet and triplet ion pair states and the degeneracy is lifted by the external magnetic field. The relaxation mechanism of this system can be shown as in Scheme 1. ^{1}P, ^{3}P, and P represent the first excited singlet, triplet, and ground states of the porphyrin moiety, respectively; k_{ISC} is the $S_1 \rightarrow T_1$ intersystem crossing rate constant of the porphyrin moiety; k^1_{et} and k^1_r are charge transfer and charge recombination rate constants in the singlet excited state, respectively, and k^3_{et} and k^3_r are those in the triplet state, respectively; $k_{T\text{-}S}(B)$ and $k_{S\text{-}T}(B)$ are the magnetic field dependent rate constants of interconversion between the triplet and singlet ion pairs. A singlet state and

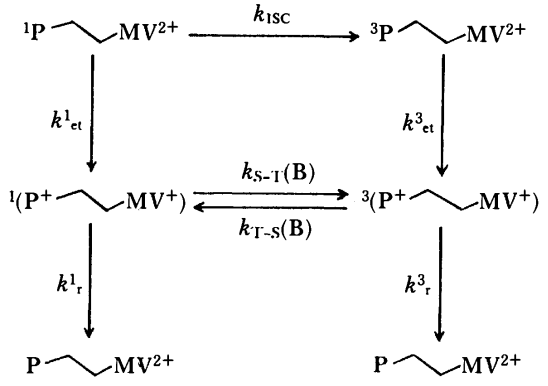

Scheme 1.

three sublevels of a triplet state of the ion pairs are almost degenerate at zero-field. Under the influence of the external magnetic field only the degeneracy between S and T_0 remains. Therefore if the relaxation between the triplet sublevels are rapid compared with the S-T interconversion, it is quite reasonable to assume that $k_{T\text{-}S}(B)=k_{T\text{-}S}(0)/3$ and $k_{S\text{-}T}(B)=k_{S\text{-}T}(0)/3$ at the high external magnetic field limit.

In the previous paper,[4] by using the picosencond laser photolysis techniques we observed the formation of the singlet ion pair in the picosecond to nanosecond time regime. If we assume that the long-lived ion pair was originally formed in the singlet spin alignment, the magnetic field effect as observed in the present work requires that the rate constant of the recombination in the singlet phase is at most the same magnitude as the S-T interconversion rate, $k^1_r \leqq k_{S\text{-}T}$. Moreover, k^1_r should be much smaller than k^3_r. However, this is highly improbable. If k^1_r is larger than k^3_r, the observed magnetic field effect should be opposite to the actually observed, i.e. the ion pair lifetime should decrease with increase of the magnetic field strength. In the present system the energy level of the triplet state of porphyrin is higher than that of the triplet ion pair state estimated from the redox potentials ($E(A^-/A)=-0.216$ and -0.319 V NHE for $n=6$ and 11, and $E(D/D^+)=0.95$ V NHE).[9] Therefore the triplet ion pair should have a longer lifetime than that of the singlet ion pair, because the latter can recombine to form the ground state of the components, while the recombination process of the former is spin forbidden.

The above results strongly suggest that the long-lived ion pair is born in the triplet spin alignment. It is known that the rate constant of the $S_1 \rightarrow T_1$ intersystem crossing (k_{ISC}) of etioporphyrin I is about 4×10^8 s^{-1} [7] and a similar value can be expected for the present combined molecules. Although the $T_n \leftarrow T_1$ absorption was not observed clearly by our picosecond time resolved absorption measurements, the triplet yield of PllMV^{2+} in DMSO can be estimated to be about 0.4 (by using the value of τ_f=980 ps). This triplet yield seems to be high enough for the observed long-lived ion pair to be formed from the triplet porphyrin.

In tens of nanosecond regime, the yield of the long-lived ion pair for PllMV^{2+} in methanol-acetone was almost 30% of that in DMSO, which was consistent with the results of fluorescence lifetime measurements.[4] Namely the decay of the fluorescence in methanol-acetone did not follow the single exponential kinetics and the lifetime of the main component was shorter than that in DMSO, which seems to be consistent with the results of ion pair yield measurements. The conformation of PllMV^{2+} in methanol-acetone, which shows shorter fluorescence lifetime than in DMSO, seems to be more shrank. We could not observe the decay of the singlet ion pair in the previous work[4] because it was difficult to measure the time dependences of the transient absorption spectra of

the relevant species (triplet porphyrin, singlet ion pair, and triplet ion pair) in the 5—20 ns region; the singlet ion pair should decay in this time regime.

Assuming that k^3_r and k^1_r was 0 and in the order of 10^8—10^9 s^{-1}, respectively, the lifetime of the ion pair should be $1/k_{T\text{-}S}(B)$. The system of PllMV^{2+} in DMSO seems to be such an ideal case, because the rate of the T-S interconversion at the high magnetic field was one third of the zero-field value ($1/k_{T\text{-}S}(0)$=120 ns and $1/k_{T\text{-}S}(H_{sat})$=370 ns). This should be due to the large separation distance of the present radical ion pair linked by flexible chain, which makes the hyperfine interaction a dominant mechanism of the S-T interconversion. Similar large magnetic field effect was observed previously for k_{T-S} of the intermediate ion pair for the hydrogen abstraction of xanthone- xanthene in micellar solution.[1] In the case of the PllMV^{2+} in methanol-acetone mixed solvent, although the lifetime at high field limit was similar to that in DMSO, the magnetic field effect was about 250%. This result suggests that the spin-exchange effect is stronger in methanol-acetone than in DMSO, which should reduce $k_{T\text{-}S}$ even at zero-field. This reasoning is in accord with the possibility described above that PllMV^{2+} in methanol-acetone will have a more shrank conformation than in DMSO and also with the fact that the megnetic field effect starts at slightly higher field in methanol-acetone than in DMSO, although the difference is very small.

The threshold observed for the $\tau(B)/\tau(0)$ vs. B relation of P6MV^{2+} should be due to the spin exchange interaction. Even at zero-field, the singlet and triplet sublevels have slightly different energies bacause of the spin-exchange interaction. Since the exchange interaction decreases exponentially with increasing separation distance between radical ions, the effect is not significant for PllMV^{2+} in DMSO but seems to affect slightly the extent of the lifetime increase in methanol-acetone. Because of the shorter average distance between P$^+$ and MV$^+$ in P6MV^{2+} than in PllMV^{2+}, the exchange interaction will be stronger in the former. This stronger exchange interaction may bring about a smaller magnetic field effect on the lifetime of the radical ion pair of P6MV^{2+} in DMSO as well as methanol-acetone. It should be noted, however, that, in the case of P6MV^{2+} in methanol-acetone solution, the lifetime at the high field limit was much shorter than in the case of the other systems, which may suggest that k^3_r was not negligible compared with the T-S interconversion rate. This might be partially due to the chemical reaction from the triplet ion pair because we can recognize a slight degradation of P6MV^{2+} in the solvent after prolonged irradiation.

Although the threshold B value for the $\tau(B)/\tau(0)$ vs. B relation of P6MV^{2+} in methanol-acetone solution appears to be slightly greater than that in DMSO, the difference was not so large. It was confirmed[4] that P6MV^{2+} in methanol-acetone showed a large fraction of rapid decay component ($\tau \approx 330$ ps) of fluorescence, which could be ascribed to P6MV^{2+} with a little shrank conformation. Nevertheless, the singlet ion pair state produced by the rapid electron transfer corresponding to this fluorescence decay component will be rapidly deactivate to the ground state by back electron transfer and the long-lived triplet ion pair produced by electron transfer from triplet porphyrin which is formed by intersystem crossing competing with the slow fluorescence decay component ($\tau \approx 1$ ns) will be mainly responsible with the present study of the external magnetic field effect. On the other hand, the results of the previous study[4] on the fluorescence decay of P6MV^{2+} in DMSO indicate that the long-lived triplet ion pair in this solvent is produced also by electron transfer from the triplet porphyrin which is formed by intersystem crossing competing with electron transfer in the singlet state in the same time region (ca. 1 ns). Although the final configuration of the triplet ion pair state may be affected to some extent by a slight conformation change in the course of the electron transfer or immediately after the electron transfer from the triplet state, the above reasoning will interpret the fact that the exchange interaction in the long-lived ion pair of P6MV^{2+} in methanol-acetone is not much different from that in DMSO.

Appendix

Preparation of Covalently Linked Zn Mesoporphyrin IX-Viologen Complexes: Two Zn mesoporphyrins covalently linked with two viologen molecules through two long side chains of $-(CH_2)_2CO_2(CH_2)_n-$ (n=6 and 11), Zn mesoporphyrin IX bis[6-(1′-methyl-4,4′-bipyridinio)hexyl ester] tetrabromide (**1**) and bis[11-[4-(1-methyl-4-bipyridinio)-1-pyridino]undecyl ester] tetrabromide (**2**), were prepared by modification of the propionate groups in mesoporphyrin IX (Scheme 2). Thus, mesoporphyrin IX was converted into the 6-bromohexyl ester and 11-bromoundecyl ester by treating the corresponding bromohydrins with mesoporphyrin IX bis(acid chloride) in CH_2Cl_2 in the presence of Et_3N at room temperature. The acid chloride was prepared in situ from triethylammonium salt of mesoporphyrin IX with oxalyl dichloride. After removing an excess of bromohydrin by chromatography on Al_2O_3, the crude ω-bromoalkyl esters thus obtained were heated with $Zn(OAc)_2$ in $CHCl_3$ to give the Zn mesoporphyrin IX bromoalkyl esters **3** and **4** as reddish purple crystals. Treatment of **3** and **4** with a large excess of 4,4′-bripyridyl in DMF under reflux gave the respective monoalkylated 4,4′-bipyridinediim dibromides, **5** and **6**. On bubbling MeBr through a DMF solution of **5** and **6** at ambient temperature the expected Zn mesoporphyrin IX-methylviologen complexes **1** and **2** were precipitated as reddish brown crystals. The overall yield of **1** and **2** from mesoporphyrin IX was 23 and 25%, respectively. The formation of **1** and **2** as well as the intermediary compounds **3**—**6** were confirmed by elemental analyses, IR and ^{1}H NMR spectral data (see Experimental).

Experimental. ^{1}H NMR spectra were recorded on JEOL 4H-100 spectrometer. IR and UV-visible spectra were measured on a Hitachi Model 295 and Hitachi EPS-3T spec-

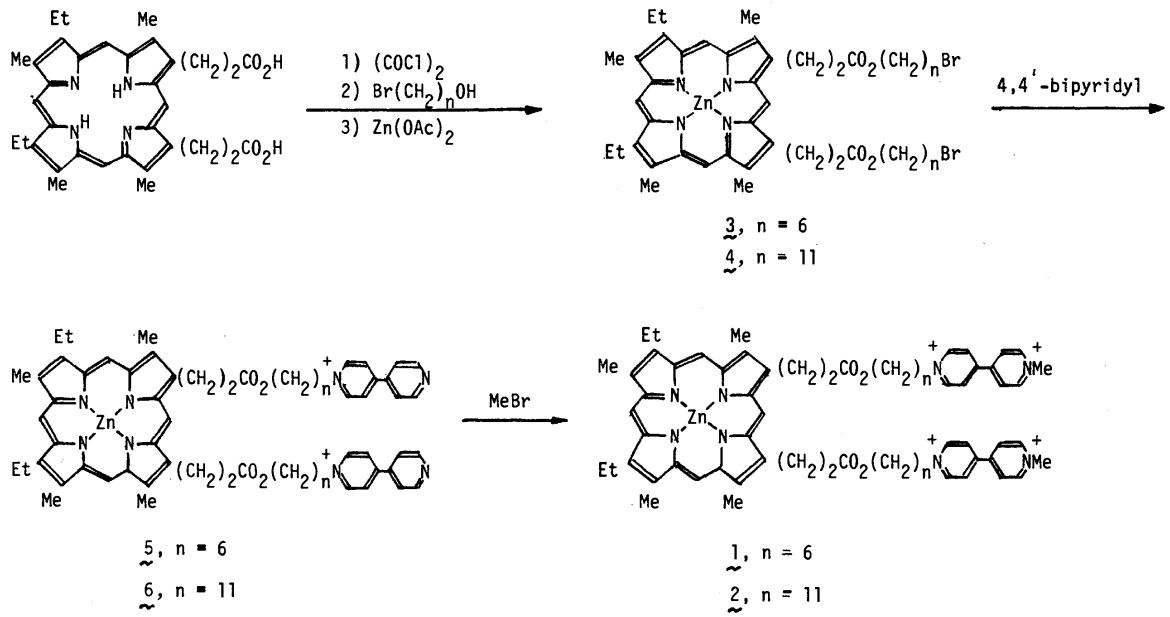

Scheme 2.

trometers, respectively. All reactions were carried out under N_2 atmosphere and all solvents used were dried by the conventional methods.

Zn Mesoporphyrin IX Bis(6-bromohexyl ester) (3) and Bis(11-bromoundecyl ester) (4): To a suspension of mesoporphyrin IX hydrochloride (0.25 g, 0.39 mmol) in CH_2Cl_2 (20 ml) was added Et_3N (0.9 ml, 6.5 mmol) and the mixture was stirred at room temperature for 1 h. The red solid residue obtained by concentration was treated with $(COCl)_2$, (0.25 ml, 3 mmol) in CH_2Cl_2 (30 ml) at ambient temperature for 1 h. Concentration of the reaction mixture in vacuo to dryness gave the diacid chloride as purple solids. A mixture of the bis(acid chloride) thus obtained, $Br(CH_2)_6OH$ (1.8 g, 10 mmol), and Et_3N (1 ml, 7.2 mmol) in CH_2Cl_2 (20 ml) was heated under reflux for 6 h. The concentrated residue was washed with H_2O and was chromatographed on Al_2O_3. Elution with $CHCl_3$ and subsequent evaporation gave mesoporphyrin IX bis(6-bromohexyl ester) as purple crystals (0.14 g, 40%). IR(nujol), ν (CO) 1730 cm^{-1}. A saturated solution of $Zn(OAc)_2$, (0.27 mmol) in MeOH (1.5 ml) was added to the bromo ester (0.14 g, 0.16 mmol) in $CHCl_3$ (15 ml) and the mixture was heated under reflux for 10 min. The concentrated mixture was purified by chromatography (Al_2O_3, benzene-$CHCl_3$ (1 : 1)). Recrystallization from $CHCl_3$-hexane gave **3** (0.13 g, 90%) as reddish purple crystals, mp 135—139 °C. Calcd for $C_{46}H_{58}N_4O_4Br_2Zn$: C, 58.16; H, 6.15; N, 5.90. Found: C, 58.52; H, 6.10; N, 5.92. IR (Nujol), ν (CO) 1730 cm^{-1}. ^1H NMR ($CDCl_3$); δ=9.00 (s, 1H, meso), 8.90 (s, 1H, meso), 8.72 (s, 2H, meso), 3.60 (s, 3H, ring CH_3), 3.56 (s, 3H, ring CH_3), 3.12 (s, 6H, ring CH_3), 1.66 (t, 3H, CH_3C), 1.58 (t, 3H, CH_3C), 0.5—1.5 (b, 16H, $C(CH_2)_4C$), 2.7—4.3 (m, 20H, other CH_2).

The compound **4** was also prepared as reddish-purple crystals by a similar procedure employed for the preparation of **3**, but using $Br(CH_2)_{11}OH$. The yield based on mesoporphyrin IX hydrochloride was 29%, mp 101—103.5 °C. Calcd for $C_{56}H_{78}N_4O_4Br_2Zn$: C, 61.37; H, 7.17; N, 5.11%. Found; C, 60.85; H, 7.34; N, 5.21%. IR (Nujol), ν (CO) 1730 cm^{-1}. ^1H NMR($CDCl_3$); δ=9.11 (s, 1H, meso), 8.95 (s, 1H, meso), 8.92 (s, 1H, meso), 8.84 (s, 1H, meso), 3.32 (s, 3H, ring CH_3), 3.26 (s, 3H, ring CH_3), 3.19 (s, 3H, ring CH_3), 3.11 (s, 3H, ring CH_3), 1.68 (t, 3H, CH_3C), 1.60 (t, 3H, CH_3C), 0.6—1.4 (b, 36H, $C(CH_2)_9C$), 3.0—4.2 (m, 20H, other CH_2).

Zn Mesoporphyrin IX Bis[6-(4,4'-bipyridinio)hexyl ester] Dibromide (5) and Bis[11-(4,4'-bipyridinio)undecyl ester] Dibromide (6): A mixture of **3** (0.086 g, 0.09 mmol) and 4,4'-bipyridyl (0.28 g, 1.8 mmol) in DMF (10 ml) was heated at 100 °C for 24 h. The concentrated reddish purple solids were washed with benzene (5×20 ml) to remove an excess of 4,4'-bipyridyl. On addition of benzene the solids became oil, which could be crystallized on treatment with hexane to give reddish-purple crystals (0.10 g, 90%), mp 177 °C. Calcd for $C_{66}H_{74}N_8O_4Br_2Zn \cdot 2H_2O$: C, 61.59; H, 6.11; N, 8.71%. Found: C, 61.25; H, 5.85; N, 8.45%. IR (Nujol); ν (CO) 1730, ν (C=C+C=N) 1540 and 1640 cm^{-1}. ^1H NMR (DMSO-d_6); δ=10.08 (s, 1H, meso), 10.05 (s, 2H, meso), 9.99 (s, 1H, meso), 8.40 (d, 4H, bpy), 8.10 (d, 2H, bpy), 8.02 (d, 2H, bpy), 7.88 (d, 2H, bpy), 7.72 (d, 4H, bpy), 7.40 (d, 2H, bpy), 3.62 (s, 6H, ring CH_3), 3.56 (s, 6H, ring CH_3), 1.80 (t, 6H, CH_3C), 1.28 (b, 8H, $C(CH_2)_4C$), 0.86 (b, 8H, $C(CH_2)_4C$), 3.10—4.38 (m, 20H, other CH_2).

The compounds **6** was prepared similarly from **4** as described above in 98% yield, mp 150—158 °C. Calcd for $C_{76}H_{94}N_8O_4Br_2Zn \cdot 2H_2O$: C, 63.17; H, 6.56; N, 7.75%. Found: C, 62.90; H, 6.72; N, 7.63%. IR (Nujol); ν (CO) 1730, ν (C=C+C=N) 1540 and 1640 cm^{-1}. ^1H NMR (DMSO-d_6); δ=10.04 (s, 1H, meso), 10.02 (s, 2H, meso), 9.98 (s, 1H, meso), 8.82 (d, 4H, bpy), 8.44 (d, 4H, bpy), 8.22 (d, 4H, bpy), 7.78 (d, 4H, bpy), 3.60 (s, ring CH_3), 3.58 (s, 6H, ring CH_3), 1.80 (t, 6H, CH_3C), 0.8—1.5 (b, 36H, $C(CH_2)_9C$), 3.2—4.6 (m, 20H, other CH_2).

Zn Mesoporphyrin IX Bis[6-(1'-methyl-4,4'-bipyridinio)-hexyl ester] Tetrabromide (1) and Bis[11-[4-(1-methyl-4-pyridinio))-1-pyridino]undecyl ester] Tetrabromide (2): A large excess of CH_3Br was bubbled through a solution of **5** (0.10 g, 0.08 mmol) at ambient conditions for 1 h. Reddish brown solids precipitated was filtered and washed with acetone. Recrystalization from MeOH-acetone gave **1** (0.08 g,

70%), mp 251 °C. Calcd for $C_{68}H_{80}N_8O_4Br_4Zn \cdot 2H_2O$: C, 54.65; H, 5.66; N, 7.49%. Found: C, 54.83; H, 5.86; N, 7.23%. IR (Nujol); ν (CO) 1730, ν (C=C+C=N) 1560 and 1640 cm^{-1}. ^1H NMR (MeOH-d_4); δ=9.96 (s, 1H, meso), 9.90 (s, 3H, meso), 8.49 (d, 2H, bpy), 8.35 (d, 2H, bpy), 8.03 (d, 2H, bpy), 7.89 (d, 2H, bpy), 7.56 (d, 4H, bpy), 7.43 (d, 2H, bpy), 7.24 (d, 2H, bpy), 4.11 (s, 6H, CH_3N^+), 3.61 (s, 6H, ring CH_3), 3.57 (s, 6H, ring CH_3), 1.85 (t, 6H, CH_3C), 0.97 (b, 8H, $C(CH_2)_4C$), 1.35 (b, 8H, $C(CH_2)_4C$), 3.3—4.5 (bm, 20H, other CH_2).

The compound **2** was prepared similarly from **6** as reddish brown crystals (87%), mp 269 °C. Calcd for $C_{78}H_{100}N_8O_4Zn \cdot 2H_2O$: C, 57.30; H, 6.41; N, 6.99. Found C, 57.08; H, 6.33; N, 6.99. IR (Nujol); (CO) 1730, ν (C=C+C=N) 1550 and 1640 cm^{-1}. ^1H NMR (MeOH-d_4); δ=9.96 (s, 1H,, meso), 9.94 (s, 2H, meso), 9.89 (s, 1H, meso), 8.70 (d, 2H, bpy), 8.41 (d, 2H, bpy), 8.10 (d, 2H, bpy), 7.90 (d, 2H, bpy), 7.42 (d, 4H, bpy), 7.26 (d, 4H, bpy), 4.29 (s, 3H, CH_3N^+), 4.12 (s, 3H, CH_3N^+), 3.56 (s, 6H, ring CH_3), 3.60 (s, 6H, ring CH_3), 1.85 (t, 6H, CH_3C), 1.0—1.7 (b, 36H, $C(CH_2)_9C$), 3.2—4.5 (bm, 20H, other CH_2).

The present work was partly supported by Grant-in-Aid (Nos. 60040059, 61123008, 61540327, 62065006) from the Japanese Ministry of Education, Science and Culture.

References

1) K. Schulten, H. Staerk, A. Weller, H.-J. Werner, and B. Nickel, *Z. Physik. Chem. NF*, **101**, 371 (1976); M. E. Michel-Beyerle, R. Haberkorn, W. Bube, E. Steffens, H. Schroder, E. W. Schlag, and H. Seidlitz, *Chem. Phys.*, **17**, 139 (1976), H.-J. Werner, H. Staerk, and A. Weller, *J. Chem. Phys.*, **66**, 2419 (1977).

2) H. Staerk, W. Kuhnle, R. Treichel, and A. Weller, *Chem. Phys. Lett.*, **117**, 19 (1985).

3) Y. Tanimoto, N. Okada, M. Itoh, K. Iwai, K. Sugioka, F. Takemura, R. Nakagaki, and S. Nagakura, *Chem. Phys. Lett.*, **136**, 42 (1987).

4) Y. Kanda, H. Sato, T. Okada, and N. Mataga, *Chem. Phys. Lett.*, **129**, 306 (1986).

5) N. Mataga, A. Karen, T. Okada, S. Nishitani, N. Kurata, Y. Sakata, and S. Misumi, *J. Phys. Chem.*, **88**, 5138 (1984).

6) Y. Hirata and N. Mataga, *J. Spectrosc. Soc. Jpn.*, **34**, 104 (1985).

7) F. Wilkinson, "Organic Molecular Photophysics," ed by J. B. Birks, Wiley, London (1975) Vol. 2, pp. 150—151.

8) D. G. Davis, "The Porphyrins," ed by D. Dolphin, Academic Press, New York (1978) Vol. 5, pp. 137—150.

9) H. Sato, Master's Thesis; Osaka University, (1983).

10) Y. Tanimoto, M. Takashima, and M. Itoh, *J. Phys. Chem.*, **88**, 6053 (1984).

 © 1988 The Chemical Society of Japan Bull. Chem. Soc. Jpn., 61, 1933—1937 (1988)

The Micellar Properties of Dodecyltrimethylammonium Chloride as Studied by Ion-Selective Electrodes and Fluorescence Probe Technique

Tamaki MAEDA* and Iwao SATAKE
Department of Chemistry, Faculty of Science, Kagoshima University, Korimoto, Kagoshima 890
(Received January 9, 1988)

The activities of the surfactant ion, counter ion, and co-ion in micellar solutions of dodecyltrimethylammonium chloride (DTAC) in the presence of NaCl were determined by using ion-selective electrodes. An application of the charged phase separation model gave an apparent degree of counter ion association to the micelle of 0.68 regardless of the salt concentration. A tentative estimation of the intermicellar concentrations of surfactant ion and counter ion was made on the basis of an assumption that the activity coefficients of the monomeric surfactant ion and co-ion were identical with each other. In the concentration range above the critical micelle concentration (cmc), the intermicellar concentration of the surfactant ion decreased gradually with increasing surfactant concentration, whereas the reverse was found for that of counter ion. Similar behaviors were also found for the activity coefficients of these ions. However, an increase in salt concentration caused a successive decrease in the concentration dependences of intermicellar concentrations as well as activity coefficients. Measurements were also made with the fluorescence decay curves of micelle-solubilized pyrene. An analysis based on the knowledge of the intermicellar concentration of surfactant ion estimated above revealed that the micelle aggregation number of DTAC remained virtually constant over wide concentration range above the cmc.

The use of the ion-selective electrodes gives valuable informations about the micellar properties of ionic surfactant solutions such as an apparent degree (β) of counter ion association to the micelle and the intermicellar concentrations of surfactant ion (C_1) and counter ion (C_2). In the concentration range above the critical micelle concentration (cmc), an increase in surfactant concentration has been found to accompany always a monotonous decrease in surfactant ion activity (a_1)[1-11] while a linear increase in counter ion activity (a_2).[2-4,6,7,9-17] It has also been noted by Sasaki et al.[2] and Koshinuma[3] that $a_1a_2^{\beta}$ remains constant in accordance with a charged phase separation model. This fact provides a simple method for the determination of β. However the estimations of C_1 and C_2 require a knowledge of the activity coefficients of surfactant ion and counter ion in the presence of polyvalent micellar ions. In this connection, Sasaki et al.[2] and Cutler et al.[4] have ignored the effect of micellar ions on the activity coefficients of monomeric ions in their calculations of C_1 and C_2 in sodium dodecyl sulfate solution. The same procedure was also applied for the potentiometric study of 1-dodecylpyridinium chloride solution with and without added salt.[11]

In this paper is described an attempt to estimate C_1 and C_2 from activity data of surfactant ion, counter ion, and co-ion in solution of dodecyltrimethylammonium chloride with added salt. On the basis of a knowledge of C_1, we also determined the concentration dependence of the micelle aggregation number from the fluorescence decay curves of micelle-solubilized pyrene.

Experimental

Materials. Dodecyltrimethylammonium chloride (DTAC) was prepared by passing the aqueous solution of the corresponding bromide (purity>99%, Tokyo Kasei Kogyo Co., Ltd.) through an anion-exchange column (Organo, IRA-400) in the Cl^- state. The concentration of DTAC was determined by drying aliquots of the stock solution over phosphorus pentaoxide in vacuo at 110 °C. Pyrene (purity> 98%, Wako Pure Chemical Industries Co., Ltd.) was passed through silica gel in cyclohexane solution and recovered as white crystals. The purified pyrene gave the value of 1.8—1.9 for the ratio I_1/I_3 of the intensities of the first and the third vibronic peaks of the fluorescence spectrum in aqueous solution.

Electromotive Force Measurements. The counter ion and co-ion activities in DTAC solutions were measured potentiometrically by using a National chloride ion selective ceramic electrode IE-510103 and a HORIBA sodium ion selective glass electrode 1512A-06T, respectively. The following cell was constructed for the measurement of the surfactant ion activity.

> Reference electrode (Ag-AgCl)| Reference solution (DTAC, 1 mmol dm^{-3})|PVC membrane|Sample solution (DTAC; C, NaCl; C_S)| 1 mol dm^{-3} NH_4NO_3 agar bridge|Reference electrode (Ag-AgCl)

The preparation of the PVC membrane electrode is described elsewhere.[18] The electromotive forces (emf) of these cells were measured at 25 °C to a precision of ±0.1 mV with a Yokogawa Universal Digital Meter Model 2502 connected to a voltage follower amplifier (input impedance=10^{15} Ω). Prior to the measurements with DTAC solutions, the chloride ion and sodium ion electrodes were calibrated with a sodium chloride solution of known activity.[19] The semilogarithmic plot of emf vs. NaCl concentration gave a straight line down to ca. 5×10^{-4} mol dm^{-3} with a slope of 59.2 mV for the chloride ion electrode and 57.5 mV for the sodium ion electrode, respectively.

Fluorescence Decay Measurements. Fluorescence decay curves were measured by using the time-resolved fluorescence spectrophotometer (NAES-1100, HORIBA,Ltd.) at

25 °C. Pyrene was solubilized in DTAC stock solution (0.22 mol dm^{-3}) by sonicating the mixture for 30 min. All of the sample solutions were thoroughly deoxygenated before measurements by repeated freeze-pump-thaw cycles. Pyrene was excited at 337 nm and its emission was monitored through the filters (TOSHIBA, V-V40 monochrofilter and UV-35 cut-off filter). After fluorescence decay measurements, the concentration of pyrene was determined spectrophotometrically at 337 nm.

All measurements were conducted at constant salt concentrations (C_S).

Results and Discussion

The electromotive forces of the foregoing cells can be described as

$$E_i = E_i^{\ominus} + S_i \log a_i, \quad i = 1, 2, \text{ and } 3 \qquad (1)$$

where $E_i^{\ominus}$ refers to the standard electromotive force, a_i to the ion activity of component i, S_i to the observed slope of E_i vs. log a_i plot, and subscript 1, 2, and 3 to the surfactant ion, counter ion, and co-ion, respectively. If we denote the values at the cmc by superscript °, we immediately have

$$a_i/a_i^{\circ} = \exp\,[2.303(E_i - E_i^{\circ})/S_i]. \qquad (2)$$

In Figs. 1, 2, and 3 are shown the plots of E_1, E_2, and E_3 vs. the logarithm of DTAC concentration (C) at various NaCl concentrations (C_S), respectively. In consistent with previous results for 1-dodecylpyridinium chloride solutions,[11] an increase in DTAC concentration causes a monotonous decrease in a_1 but an increase in a_2 in the concentration range above the cmc. It should also be noted that the concentration dependences of a_1 and a_2 tend to decrease regularly with increasing salt concentrations. Similar salt effects are also noted for surfactant ion[5] and counter ion[16] activities in anionic surfactant solutions. The values of cmc (C_o) determined from the break points in Figs. 1 and 2 are summarized in Table 1. At higher surfactant concentrations, the value of E_3 is seen to decrease slightly but regularly with increasing concentrations, though the rate of decrease becomes progressively smaller as the salt concentration increases. The observed decrease in E_3 can reasonably be ascribed to the decrease in the activity coefficient (γ_3) of Na^+ ion, since the concentration of which is kept constant under our experimental conditions. These results allow us to estimate not only the degree (β) of counter ion association to the micelle but the activity coefficients and intermicellar concentrations of surfactant ion and counter ion respectively.

According to the charged phase separation model which has been confirmed to hold both in anionic[2-4,6,9,10] and cationic[9,11] surfactant solutions, $a_1 a_2^{\beta}$ should be constant in the concentration range above

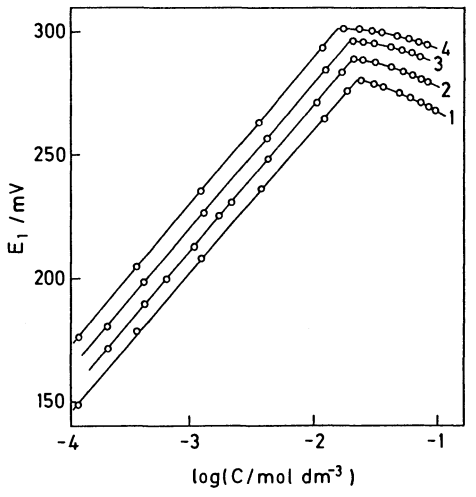

Fig. 1. The semilogarithmic plots of E_1 vs. C at 25 °C. The curves 2, 3, and 4 are displaced upward by 10, 20, and 30 mV, respectively. C_S/mmol dm^{-3}: 1; 0.5, 2; 5, 3; 10, 4; 20. The data for C_S=0 and 0.5 mmol dm^{-3} agree with each other within an experimental error.

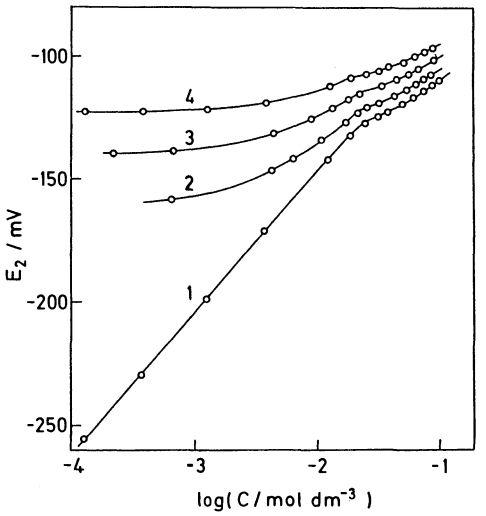

Fig. 2. The semilogarithmic plots of E_2 vs. C at 25 °C. C_S/mmol dm^{-3}: 1; 0, 2; 5, 3; 10, 4; 20.

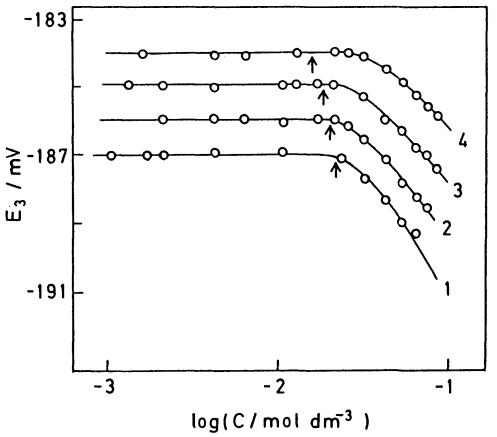

Fig. 3. The semilogarithmic plots of E_3 vs. C at 25 °C. The curves 2, 3, and 4 are displaced upward by 59, 72, and 92 mV, respectively. The arrow indicates the cmc determined from the break points in Figs. 1 and 2. C_S/mmol dm^{-3}: 1; 0.5, 2; 5, 3; 10, 4; 20.

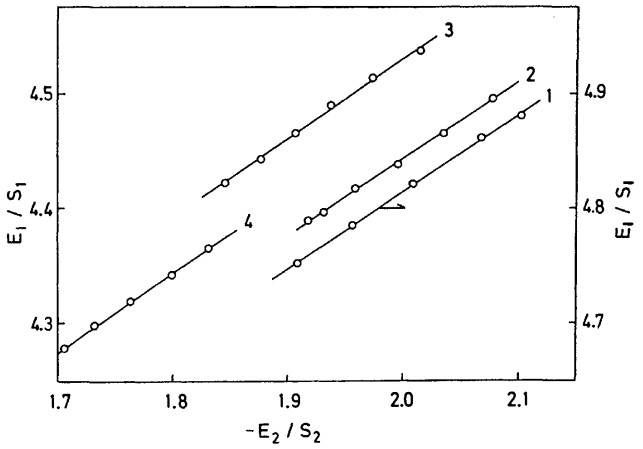

Fig. 4. Plots of E_1/S_1 vs. E_2/S_2 at varying salt concentrations. C_S/mmol dm^{-3}: 1; 0, 2; 5, 3; 10, 4; 20.

the cmc. It follows immediately from Eq. 1 that

$$E_1/S_1 = \text{const.} - \beta \cdot E_2/S_2. \quad (3)$$

As is shown in Fig. 4, a plot of E_1/S_1 against E_2/S_2 gives in fact a straight line regardless of the salt concentration. It should be noted that the value of β summarized in Table 1 is little affected by the salt concentration. A similar constancy in β was also found for 1-dodecylpyridinium chloride solutions with added salt.[11]

The estimation of the intermicellar concentration (C_1) of surfactant ion from a_1 data requires a knowledge of the activity coefficient (γ_1) which is experimentally rather difficult to determine. In this connection, it seems reasonable to assume that the activity coefficients of surfactant ion and co-ion in the bulk phase are nearly identical with each other, since the only difference between them lies in their ionic sizes. At a constant salt concentration, which is the case for the present experiment, this assumption leads immediately to

$$\gamma_1/\gamma_1^\circ \simeq \gamma_3/\gamma_3^\circ = a_3/a_3^\circ \quad (4)$$

$$C_1/C_1^\circ = C_1/C_o \simeq a_1 a_3^\circ/a_1^\circ a_3. \quad (5)$$

These equations enable us to estimate the concentration dependences of γ_1 and C_1 from the electromotive force data. The knowledge of the intermicellar concentration (C_2) and the activity coefficient (γ_2) of the counter ion can then be obtained by substituting the values of β and C_1 estimated above into the following relations.

$$C_2/C_2^\circ = C_2/(C_S + C_o) = [C_1 + C_S + (1-\beta)(C - C_1)]/(C_S + C_o) \quad (6)$$

$$\gamma_2/\gamma_2^\circ = a_2 C_2^\circ/a_2^\circ C_2 \quad (7)$$

The estimated values of γ_1, C_1, γ_2, and C_2 relative to those at the cmc are plotted in Figs. 5 and 6 as a function of $C-C_o$. At a given salt concentration, γ_1 and C_1 decrease monotonously with increasing surfactant concentrations, whereas the reverse change is found for γ_2 and C_2. An increase in salt concentration tends to depress the variations in γ_1, C_1, and γ_2 with surfactant concentration.

Table 1. The Values of C_o and β at Varying Salt Concentrations

C_S/mmol dm^{-3}	C_o/mmol dm^{-3}	β
0	22.4	0.68
5	20.4	0.67
10	18.8	0.69
20	16.2	0.68

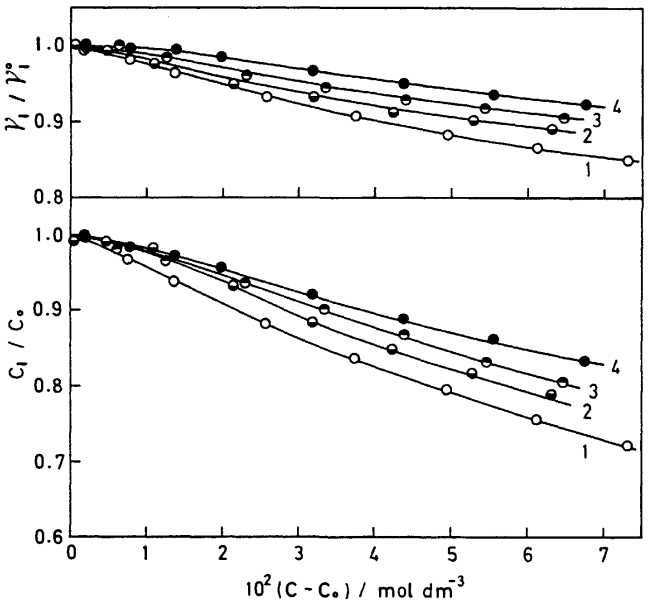

Fig. 5. The concentration dependences of γ_1/γ_1° and C_1/C_o estimated from Eqs.4 and 5. C_S/mmol dm^{-3}: 1; 0.5, 2; 5, 3; 10, 4; 20.

An attempt to estimate these parameters was made by Sasaki et al.,[2] Cutler et al.,[4] and Koshinuma[6,10] on the basis of the assumption that the mean ionic molarity of surfactant ion and counter ion in a micellar solution is identical with that in a hypothetical solution composing only of monomeric ions at a given mean activity. In solution of sodium dodecyl sulfate,[2,4] the value of C_1 thus calculated was found to have a tendency to decrease monotonously with surfactant concentration. According to the same assumption, we[11] also estimated the concentration dependences of γ_1, C_1, and γ_2 in solutions of 1-dodecylpyridinium chloride with and without added salt, and obtained the similar curves to those shown in Figs. 5 and 6. Unfortunately, however, an application of the above treatment to the present system leads to somewhat larger variations in these parameters with surfactant concentration. In their electrostatic approach based on the cell model, Gunnarsson et al.[20] made the numerical calculations of not only surfactant ion and counter ion activities but the intermicellar concentration of surfactant ion. It should be noted that their result for C_1 in sodium

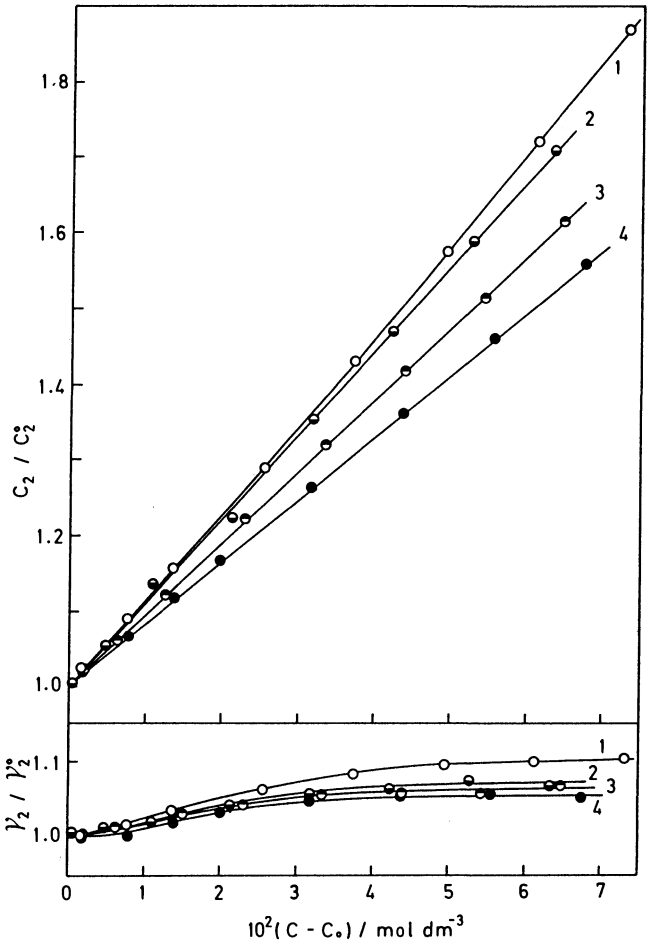

Fig. 6. The concentration dependences of C_2/C_2° and γ_2/γ_2° estimated from Eqs. 6 and 7. C_S/mmol dm^{-3}: 1; 0, 2; 5, 3; 10, 4; 20.

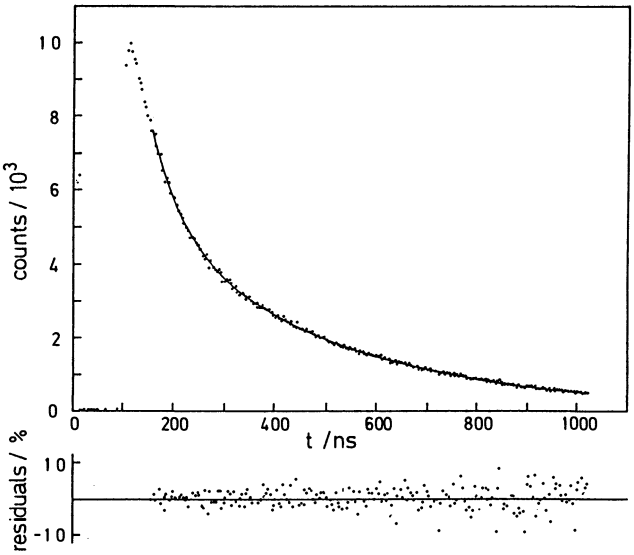

Fig. 7. The typical fluorescence decay curve and residuals at 25 °C. C=41.8 mmol dm^{-3}, C_S= 0.5 mmol dm^{-3}, [pyrene]=0.252 mmol dm^{-3}. Solid line: nonlinear least-squares fit.

Table 2. The Micelle Aggregation Number of DTAC at C_S=0.5 mmol dm^{-3}

C/mmol dm^{-3}	n	n'
35.2	62	56
41.8	61	55
48.4	63	57
52.8	61	55
59.4	62	56
72.6	63	57
220.0	—	63

dodecyl sulfate solution without added salt agree qualitatively well with the present results given in Fig. 5.

In order to demonstrate the utility of C_1 data, we determined the micelle aggregation number (n) of DTAC by fluorescence probe technique under the same experimental conditions as those for the activity measurements. Figure 7 shows the typical fluorescence decay curve of the micelle-solubilized pyrene at C_S=0.5 mmol dm^{-3} and C=41.8 mmol dm^{-3}. It has been well-known that this type of decay curve is described by the following equation based on the Poisson distribution of the pyrene molecules in micelles.[21]

$$I = I_0 \exp[R\{\exp(-k_E t) - 1\} - k_1 t] \quad (8)$$

where, I and I_0 are the fluorescence intensities at time t and zero, k_E and k_1 are the first-order rate constants for the intramicellar excimer formation and decay processes, and R is the number of fluorescence probe per micelle, i.e., R=[Pyrene]/[micelle], respectively. The values of I_0, R, k_E, and k_1 were evaluated from the observed decay curves by using the nonlinear least squares treatment based on modified Marquardt method.[22] According to the definition of R, we immediately have

$$n = R(C - C_1)/[\text{Pyrene}]. \quad (9)$$

The use of Eq. 9 together with C_1 data shown in Fig. 5 permits the precise determination of the micelle aggregation number. The values of n thus determined at C_S=0.5 mmol dm^{-3} are summarized in the second column of Table 2. It is worth noting that the value of n remains essentially constant over wide concentration range above the cmc. In conventional estimations of n based on the fluorescence probe technique,[23-28] C_1 in Eq. 9 has always been replaced by the cmc, C_o. Such a calculation is valid only at higher surfactant concentrations where C_1 can safely be ignored as compared to C. In the concentration range near the cmc, however, it must be kept in mind that the use of C_o instead of C_1 tends to underestimate the value of n. For the sake of comparison, the micelle aggregation number, n', calculated from Eq. 9 with C_1=C_o is also given in Table 2. As would be anticipated, an appreciable difference is found between n and n' in the concentration range up to ca. 7×10^{-2} mol dm^{-3}. At sufficiently high surfactant concentrations, however, the value of n' agrees

well with the constant value of n at lower concentrations. These observations seem not only to reveal the importance of the knowledge of C_1 in the determination of micelle aggregation number by fluorescence probe technique, but to support the validity of the potentiometric method for estimating C_1 in ionic surfactant solution.

The authors wish to express their thanks to Professor Yoshihumi Kusumoto and Dr. Junichi Kurawaki of Chemical Institute, College of Liberal Art, Kagoshima University, for fluorescence decay measurements on a HORIBA NAES-1100 time-resolved fluorescence spectrophotometer.

References

1) K. Kaibara, T. Nakahara, I. Satake, and R. Matuura, *Mem. Fac. Sci. Kyushu Univ. Ser. C.*, **7**, 1 (1970).
2) T. Sasaki, M. Hattori, J. Sasaki, and K. Nukina, *Bull. Chem. Soc. Jpn.*, **48**, 1397 (1975).
3) M. Koshinuma and T. Sasaki, *Bull. Chem. Soc. Jpn.*, **48**, 2755 (1975).
4) S. G. Cutler, P. Meares, and D. G. Hall, *J. Chem. Soc., Faraday Trans. 1*, **74**, 1758 (1978).
5) A. Yamauchi, T. Kunisaki, T. Minematsu, Y. Tomokiyo, T. Yamaguchi, and H. Kimizuka, *Bull. Chem. Soc. Jpn.*, **51**, 2791 (1978).
6) M. Koshinuma, *Bull. Chem. Soc. Jpn.*, **52**, 1790 (1979).
7) E. Vikingstad, *J. Colloid Interface Sci.*, **72**, 68 (1979).
8) J. E. Newbery, *J. Colloid Interface Sci.*, **74**, 483 (1980).
9) K. M. Kale, E. L. Cussler, and D. F. Evans, *J. Phys. Chem.*, **84**, 593 (1980).
10) M. Koshinuma, *Bull. Chem. Soc. Jpn.*, **54**, 3128 (1981).
11) T. Maeda and I. Satake, *Bull. Chem. Soc. Jpn.*, **57**, 2396 (1984).
12) C. Botré, V. L. Crescenzi, and A. Mele, *J. Phys. Chem.*, **63**, 650 (1959).
13) L. Shedlovsky, C. W. Jakob, and M. B. Epstein, *J. Phys. Chem.*, **67**, 2075 (1963).
14) M. E. Feinstein and H. L. Rosano, *J. Colloid Interface Sci.*, **24**, 73 (1967).
15) P. Stennius and P. Ekwall, *Acta Chem. Scand.*, **21**, 1643 (1967).
16) I. Satake, T. Tahara, and R. Matuura, *Bull. Chem. Soc. Jpn.*, **42**, 319 (1969).
17) J. T. Pearson and K. J. Humphreys, *J. Pharm. Pharmacol.*, **22**, 126S (1970)
18) T. Maeda, M. Ikeda, M. Shibahara, T. Haruta, and I. Satake, *Bull. Chem. Soc. Jpn.*, **54**, 94 (1981).
19) J. Kielland, *J. Am. Chem. Soc.*, **59**, 1675 (1937).
20) G. Gunnarsson, B. Jönsson, and H. Wennerström, *J. Phys. Chem.*, **84**, 3114 (1980).
21) S. S. Atik, M. Nam, and L. A. Singer, *Chem. Phys. Lett.*, **67**, 75 (1979).
22) T. Awaya, "Deta Kaiseki," Gakukai Shuppan Senta, Tokyo (1983).
23) N. J. Turro and A. Yekta, *J. Am. Chem. Soc.*, **100**, 5951 (1978).
24) P. Lianos and R. Zana, *J. Phys. Chem.*, **84**, 3339 (1980).
25) P. Lianos and R. Zana, *J. Colloid Interface Sci.*, **84**, 100 (1981).
26) A. Malliaris, J. L. Moigne, J. Sturm, and R. Zana, *J. Phys. Chem.*, **89**, 2709 (1985).
27) A. Malliaris, J. Lang, and R. Zana, *J. Colloid Interface Sci.*, **110**, 237 (1986).
28) W. Binana-Limbele and R. Zana, *Colloid and Surfaces*, **21**, 483 (1986).

The Structure of the Cyclodextrin Complex. XXI. Crystal Structures of Heptakis(2,6-di-*O*-methyl)-β-cyclodextrin Complexes with *p*-Iodophenol and *p*-Nitrophenol

Kazuaki HARATA
Research Institute for Polymers and Textiles, 1-1-4 Higashi, Tsukuba, Ibaraki 305
(Received January 9, 1988)

Crystal structures of heptakis(2,6-di-*O*-methyl)-β-cyclodextrin complexes with *p*-iodophenol and *p*-nitrophenol were determined by the X-ray analysis. These two crystals were isomorphous with the space group $P2_12_12_1$ and cell dimensions: a=14.796(3), b=18.853(5), and c=28.989(6) Å for the *p*-iodophenol complex, and a=14.779(2), b=18.965(3), and c=28.741(4) Å for the *p*-nitrophenol complex. The structures were solved by the heavy atom method combined with the phase refinement by the tangent formula and refined by the block-diagonal least-squares method to the R-values of 0.12 (*p*-iodophenol complex) and 0.10 (*p*-nitrophenol complex). The host molecule has a round shape, which is maintained by the intramolecular hydrogen bonds between the O(3)H hydroxyl group and O(2)CH_3 methoxyl group of the adjacent residue. The guest molecules in the both complexes are not included within the host cavity but located in the intermolecular space between host molecules. The host cavity includes water molecules and a methoxyl group of the adjacent host. Hydrogen bonds are formed only within the host cavity.

Cyclodextrins form a number of host-guest complexes with a variety of guest molecules.[1] In the crystalline state, guest molecules are usually included within the cavity of the host macrocycle.[2] Methylated cyclodextrins also form inclusion complexes with many guests, although the geometry of the host-guest interaction differs from that of corresponding cyclodextrin complexes because of the change in size and shape of the host cavity.[3] Therefore, it has been believed that the guest molecule should be fit into the host cavity to form the complex, even if only partially. Recently we have found that some disubstituted benzenes form 1 : 1 crystalline complexes with heptakis(2,6-di-*O*-methyl)-β-cyclodextrin (DM-β-CDx) but are not included within the host cavity. The short communication on the structure of the DM-β-CDx complexes with *p*-iodophenol (*p*-IP) and *p*-nitrophenol (*p*-NP) has been published.[4] In this paper, we destribe details of these crystal structures and discuss the host-guest interaction in comparison with cyclodextrin and other methylated cyclodextrin complexes.

Experimental

The DM-β-CDx complex with *p*-IP was crystallized at 50 °C by standing an aqueous solution of DM-β-CDx saturated with *p*-IP. Crystals of the *p*-NP complex were obtained at room temperature by the slow evaporation of an aqueous solution containing DM-β-CDx and *p*-NP in ca. 1 : 1 molar ratio. Lattice parameters of the crystals and diffraction intensity data were measured at room temperature on a Nicolet P3/F diffractometer with graphite-monochromated Cu $K\alpha$ radiation. By using θ-2θ scan mode, 4045 (*p*-IP complex) and 4670 (*p*-NP complex) independent reflections with $|F_o| \geqq 3\sigma(F)$ were obtained up to 118° in 2θ.

The structure of the *p*-IP complex was solved by the combination of the heavy atom method and the phase-refinement by the tangent-formula. On the electron-density map calculated by using the iodine phases, light atoms could

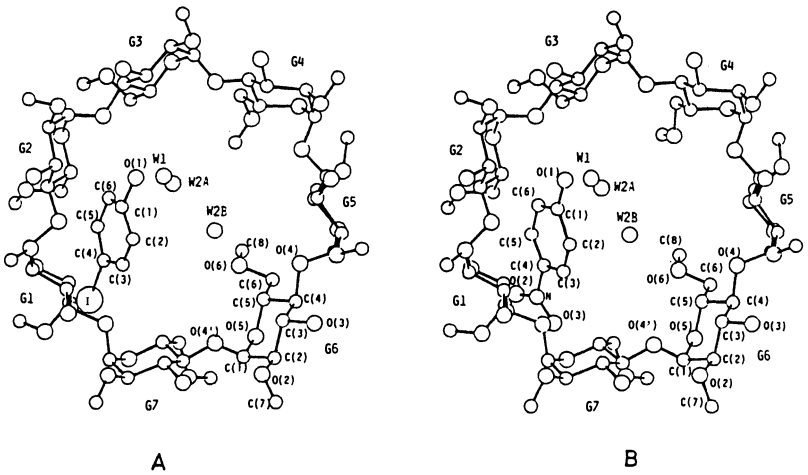

Fig. 1. Structures and numbering scheme of the DM-β-CDx complexes with *p*-IP (A) and *p*-NP (B).

Table 1. Atomic Coordinates ($\times 10^4$) and B_{eq} Values (Å^2) of the DM-β-CDx Complex with p-IP

	x	y	z	B_{eq}		x	y	z	B_{eq}
C(1,G1)	4631(16)	3475(13)	4276(7)	6.8	O(6,G4)	−323(25)	6682(25)	5938(14)	26.6
C(2,G1)	5382(16)	3808(12)	3991(7)	5.7	C(1,G5)	1320(17)	9159(11)	4299(9)	8.0
C(3,G1)	5040(14)	4471(15)	3751(7)	6.6	C(2,G5)	2046(21)	9548(13)	4593(9)	8.8
C(4,G1)	4185(16)	4295(12)	3457(8)	6.6	C(3,G5)	2289(18)	9076(13)	5022(8)	7.3
C(5,G1)	3503(15)	4005(13)	3781(7)	6.2	C(4,G5)	1434(16)	8941(12)	5273(7)	6.2
C(6,G1)	2658(18)	3709(12)	3474(10)	8.2	C(5,G5)	763(17)	8472(14)	4964(8)	7.1
C(7,G1)	6990(15)	3863(15)	4152(10)	8.4	C(6,G5)	−214(35)	8382(18)	5155(20)	20.9
C(8,G1)	2623(66)	2592(30)	3177(16)	40.2	C(7,G5)	3253(24)	10419(13)	4424(12)	11.9
O(2,G1)	6120(12)	4012(9)	4298(5)	7.7	C(8,G5)	−1303(29)	8678(29)	5729(19)	22.1
O(3,G1)	5737(9)	5754(8)	3461(5)	6.4	O(2,G5)	2781(14)	9704(9)	4311(6)	9.2
O(4,G1)	3869(10)	4976(7)	3279(4)	5.9	O(3,G5)	2863(13)	9547(10)	5305(6)	9.0
O(5,G1)	3852(12)	3366(8)	3987(5)	6.9	O(4,G5)	1690(11)	8474(8)	5656(6)	7.1
O(6,G1)	2890(18)	3298(12)	3083(6)	12.9	O(5,G5)	569(11)	8971(10)	4573(7)	9.1
C(1,G2)	3840(15)	3969(9)	6036(7)	5.2	O(6,G5)	−545(18)	8891(19)	5415(10)	19.2
C(2,G2)	4793(15)	3868(10)	5887(6)	4.9	C(1,G6)	2089(17)	7460(12)	2866(7)	6.4
C(3,G2)	4951(13)	4100(10)	5376(7)	4.6	C(2,G6)	2398(20)	8237(13)	2873(7)	7.7
C(4,G2)	4238(14)	3715(11)	5083(7)	5.2	C(3,G6)	2561(18)	8469(11)	3376(8)	7.4
C(5,G2)	3303(12)	3890(12)	5247(6)	5.0	C(4,G6)	1593(20)	8422(11)	3621(8)	7.8
C(6,G2)	2569(16)	3449(13)	4964(9)	7.1	C(5,G6)	1268(19)	7570(12)	3614(8)	7.2
C(7,G2)	6189(20)	3865(16)	6312(9)	9.8	C(6,G6)	319(14)	7468(15)	3838(9)	7.5
C(8,G2)	2128(21)	2318(17)	4744(10)	11.8	C(7,G6)	3550(42)	8641(21)	2355(12)	22.1
O(2,G2)	5376(11)	4228(8)	6195(4)	6.3	C(8,G6)	−427(23)	6507(21)	4184(14)	14.9
O(3,G2)	5850(9)	3920(7)	5254(4)	4.9	O(2,G6)	3200(16)	8256(12)	2682(6)	12.1
O(4,G2)	4362(9)	4013(7)	4629(5)	5.3	O(3,G6)	2701(13)	9230(8)	3378(6)	8.7
O(5,G2)	3237(11)	3643(7)	5732(5)	6.6	O(4,G6)	1754(10)	8548(7)	4129(5)	5.6
O(6,G2)	2791(12)	2742(9)	4963(6)	8.2	O(5,G6)	1244(11)	7441(7)	3110(5)	6.5
C(1,G3)	2348(16)	6236(11)	6840(8)	6.5	O(6,G6)	376(14)	6721(10)	4015(7)	10.2
C(2,G3)	3306(17)	6013(10)	6984(7)	5.8	C(1,G7)	3560(19)	4981(13)	2799(6)	7.2
C(3,G3)	3791(12)	5659(11)	6598(7)	5.4	C(2,G7)	4143(17)	5624(13)	2587(6)	6.4
C(4,G3)	3205(14)	4975(12)	6456(7)	5.5	C(3,G7)	3922(18)	6323(13)	2785(7)	6.9
C(5,G3)	2263(15)	5254(11)	6337(7)	5.3	C(4,G7)	2831(16)	6372(11)	2805(7)	5.6
C(6,G3)	1623(18)	4621(11)	6191(8)	6.9	C(5,G7)	2396(14)	5780(11)	3014(6)	5.0
C(7,G3)	4435(21)	6642(14)	7471(9)	9.6	C(6,G7)	1367(17)	5770(15)	2986(8)	7.8
C(8,G3)	1278(18)	3431(14)	6362(8)	8.1	C(7,G7)	5680(28)	5440(28)	2253(10)	18.3
O(2,G3)	3764(12)	6651(8)	7090(4)	6.9	C(8,G7)	112(19)	6064(12)	2497(9)	11.3
O(3,G3)	4696(11)	5419(9)	6709(6)	7.7	O(2,G7)	5064(11)	5457(11)	2625(5)	8.4
O(4,G3)	3651(9)	4695(7)	6039(5)	5.5	O(3,G7)	4311(13)	6876(10)	2550(5)	9.2
O(5,G3)	1890(10)	5584(8)	6725(4)	5.5	O(4,G7)	2677(10)	7018(8)	3046(4)	6.3
O(6,G3)	1717(11)	4093(9)	6489(5)	7.1	O(5,G7)	2637(10)	5129(8)	2786(5)	6.2
C(1,G4)	1222(18)	8585(12)	6091(8)	7.1	O(6,G7)	1096(13)	5933(10)	2532(6)	8.9
C(2,G4)	2039(18)	8615(13)	6454(9)	8.1	C(1,IP)	283(19)	4129(21)	4672(16)	16.5
C(3,G4)	2506(16)	7912(11)	6498(8)	6.7	C(2,IP)	−336(23)	3581(17)	4810(11)	12.8
C(4,G4)	1880(15)	7300(10)	6556(8)	5.8	C(3,IP)	−686(21)	3253(16)	4418(10)	10.0
C(5,G4)	1126(22)	7291(14)	6177(9)	9.4	C(4,IP)	−406(18)	3501(15)	3950(10)	8.9
C(6,G4)	471(24)	6648(18)	6193(12)	12.9	C(5,IP)	−20(26)	4068(18)	3906(12)	13.0
C(7,G4)	2941(23)	9654(16)	6661(10)	10.9	C(6,IP)	516(26)	4391(24)	4248(19)	19.5
C(8,G4)	69(36)	6462(23)	5656(16)	22.2	O(1,IP)	576(22)	4505(18)	5095(10)	22.2
O(2,G4)	2611(14)	9171(10)	6316(6)	9.0	I(1,IP)	−1050(2)	2978(1)	3417(1)	11.3
O(3,G4)	3123(11)	7968(9)	6876(5)	7.5	O(W1)	3306(27)	5966(29)	5258(10)	28.8
O(4,G4)	2358(11)	6722(7)	6514(5)	6.4	O(W2A)	1447(21)	5580(21)	5038(14)	13.3
O(5,G4)	707(11)	8039(10)	6197(5)	7.9	O(W2B)	1679(31)	6119(38)	4539(24)	16.9

The occupancy factor of W2A and W2B is 0.6 and 0.4, respectively.

not be located because of the low resolution. Then, phases of 803 reflections with $|E| \geqq 1.4$ were refined by the tangent-formula. Most of light atoms were found on the E-map. The structure was refined by the block-diagonal least-squares method to the R-value of 0.12. A set of the coordinates of DM-β-CDx of the p-IP complex was used to determine the isomorphous structure of the p-NP complex, which was refined to the R-value of 0.10. The quantity minimized was $\sum w(|F_o|-|F_c|)^2$ with $w=1.0$ for all the reflections used. Final atomic coordinates are given in Tables 1 and 2. Tables of observed and calculated structure factors and anisotropic temperature factors are deposited to the Chemical Society of Japan (Document No. 8798). The computations were carried out on a FACOM M380 computer at the Research Information Processing System (RIPS) Center, Agency of Industrial Science and Technology, Tsukuba.

Crystal Data: (1) p-Iodophenol complex, $C_{56}H_{98}O_{35}\cdot C_6H_5OI\cdot 2H_2O$, F.W.=1587.4, orthorhombic, space group $P2_12_12_1$, $Z=4$, $a=14.796(3)$, $b=18.853(5)$, $c=28.989(6)$ Å, $V=8086(3)$ Å^3, $D_X=1.304$ g·cm^{-3}, (2) p-nitrophenol complex,

Table 2. Atomic Coordinates ($\times 10^4$) and B_{eq} Values (Å^2) of the DM-β-CDx Complex with *p*-NP

	x	y	z	B_{eq}		x	y	z	B_{eq}
C(1,G1)	4601(10)	3525(7)	4280(5)	6.6	C(1,G5)	1314(11)	9197(7)	4300(5)	7.4
C(2,G1)	5364(9)	3854(8)	3995(5)	6.4	C(2,G5)	2013(12)	9561(7)	4608(5)	8.0
C(3,G1)	5036(9)	4521(5)	3763(4)	5.8	C(3,G5)	2243(10)	9133(8)	5028(5)	6.8
C(4,G1)	4191(9)	4352(7)	3474(4)	6.0	C(4,G5)	1381(10)	8937(8)	5280(5)	7.1
C(5,G1)	3471(10)	4007(8)	3802(5)	7.3	C(5,G5)	705(11)	8467(9)	4955(5)	7.7
C(6,G1)	2629(11)	3756(11)	3492(6)	10.8	C(6,G5)	−239(20)	8364(12)	5144(8)	18.4
C(7,G1)	6965(10)	3879(10)	4129(5)	8.2	C(7,G5)	3203(15)	10380(9)	4465(7)	11.8
C(8,G1)	2722(44)	2595(18)	3116(12)	47.1	C(8,G5)	−1341(18)	8618(19)	5725(10)	20.0
O(2,G1)	6105(6)	3994(5)	4311(3)	7.3	O(2,G5)	2764(8)	9727(6)	4329(4)	9.2
O(3,G1)	5744(6)	4772(5)	3464(3)	6.7	O(3,G5)	2811(7)	9527(5)	5340(4)	8.4
O(4,G1)	3888(6)	5018(5)	3297(3)	6.3	O(4,G5)	1636(7)	8442(5)	5656(3)	7.0
O(5,G1)	3831(7)	3392(5)	3984(3)	7.8	O(5,G5)	547(7)	9010(6)	4568(3)	8.2
O(6,G1)	2871(11)	3334(10)	3096(4)	16.6	O(6,G5)	−594(10)	8855(11)	5420(6)	16.7
C(1,G2)	3810(11)	3940(6)	6061(4)	6.3	C(1,G6)	2023(11)	7514(7)	2841(5)	6.9
C(2,G2)	4814(9)	3836(7)	5923(5)	6.2	C(2,G6)	2353(12)	8282(9)	2874(5)	8.2
C(3,G2)	4937(9)	4094(7)	5408(4)	5.6	C(3,G6)	2524(13)	8516(8)	3394(5)	8.2
C(4,G2)	4254(9)	3689(7)	5114(4)	5.6	C(4,G6)	1549(12)	8433(8)	3625(5)	8.1
C(5,G2)	3289(9)	3836(7)	5262(4)	5.7	C(5,G6)	1251(11)	7647(7)	3604(5)	6.6
C(6,G2)	2562(11)	3431(8)	4988(5)	7.5	C(5,G6)	319(11)	7529(7)	3797(5)	7.2
C(7,G2)	6209(12)	3835(13)	6367(6)	11.4	C(7,G6)	3413(23)	8605(14)	2281(8)	19.9
C(8,G2)	2140(15)	2318(10)	4730(6)	11.9	C(8,G6)	−468(15)	6580(13)	4145(9)	14.9
O(2,G2)	5386(7)	4208(5)	6233(3)	7.5	O(2,G6)	3237(10)	8285(7)	2679(3)	10.9
O(3,G2)	5847(6)	3902(5)	5272(3)	6.4	O(3,G6)	2719(9)	9252(5)	3380(4)	9.7
O(4,G2)	4368(6)	3992(4)	4650(3)	5.8	O(4,G6)	1733(7)	8567(4)	4116(3)	6.3
O(5,G2)	3222(7)	3603(4)	5747(3)	6.7	O(5,G6)	1191(7)	7483(5)	3102(3)	7.0
O(6,G2)	2819(8)	2729(5)	4967(4)	8.3	O(6,G6)	298(8)	6809(7)	3965(5)	10.5
C(1,G3)	2351(10)	6169(8)	6888(5)	7.4	C(1,G7)	3643(10)	5067(8)	2809(4)	6.7
C(2,G3)	3323(10)	5966(7)	7011(4)	6.3	C(2,G7)	4157(10)	5644(9)	2593(5)	7.3
C(3,G3)	3779(10)	5623(7)	6611(4)	6.1	C(3,G7)	3882(11)	6362(8)	2816(5)	7.3
C(4,G3)	3227(10)	4965(7)	6471(4)	5.7	C(4,G7)	2843(9)	6441(7)	2794(5)	6.0
C(5,G3)	2261(9)	5207(7)	6347(4)	5.9	C(5,G7)	2371(9)	5790(7)	3021(5)	6.2
C(6,G3)	1611(12)	4599(8)	6211(4)	7.9	C(6,G7)	1379(11)	5756(10)	2998(5)	9.2
C(7,G3)	4454(12)	6602(10)	7490(5)	9.2	C(7,G7)	5613(14)	5367(19)	2248(6)	18.0
C(8,G3)	1266(14)	3390(8)	6378(6)	10.0	C(8,G7)	107(12)	6071(14)	2512(8)	13.8
O(2,G3)	3771(7)	6632(5)	7123(3)	7.3	O(2,G7)	5102(7)	5515(6)	2646(3)	7.9
O(3,G3)	4682(7)	5396(5)	6741(3)	7.5	O(3,G7)	4318(8)	6927(6)	2570(4)	8.8
O(4,G3)	3658(6)	4678(4)	6069(3)	5.9	O(4,G7)	2667(6)	7067(5)	3047(3)	6.3
O(5,G3)	1854(6)	5538(5)	6752(3)	6.3	O(5,G7)	2674(7)	5169(5)	2798(3)	6.6
O(6,G3)	1697(8)	4052(5)	6527(3)	8.5	O(6,G7)	1114(8)	5958(7)	2554(4)	10.5
C(1,G4)	1194(11)	8520(8)	6100(5)	7.4	C(1,NP)	165(12)	4081(10)	4725(7)	10.8
C(2,G4)	1954(11)	8596(8)	6476(6)	8.1	C(2,NP)	−398(14)	3467(11)	4738(7)	11.4
C(3,G4)	2448(11)	7876(7)	6496(5)	7.4	C(3,NP)	−787(13)	3210(9)	4331(6)	9.5
C(4,G4)	1821(11)	7273(7)	6560(5)	6.7	C(4,NP)	−526(14)	3585(10)	3925(6)	10.7
C(5,G4)	1107(12)	7264(8)	6171(6)	8.4	C(5,NP)	−17(16)	4180(12)	3876(10)	15.4
C(6,G4)	398(14)	6701(10)	6235(7)	11.0	C(6,NP)	399(16)	4453(11)	4263(9)	14.5
C(7,G4)	2906(15)	9593(10)	6691(7)	11.7	O(1,NP)	554(13)	4356(9)	5113(5)	17.1
C(8,G4)	−498(20)	6170(20)	5660(15)	31.4	N(1,NP)	−966(13)	3306(9)	3493(6)	13.1
O(2,G4)	2548(8)	9121(5)	6329(4)	9.2	O(2,NP)	−987(14)	3687(9)	3149(5)	16.6
O(3,G4)	3032(8)	7946(5)	6908(4)	8.3	O(3,NP)	−1364(18)	2714(7)	3501(5)	19.8
O(4,G4)	2343(7)	6663(5)	6528(3)	6.7	O(W1)	3337(19)	5867(19)	5256(8)	33.7
O(5,G4)	634(7)	7939(6)	6191(3)	8.0	O(W2A)	1428(18)	5476(11)	5080(9)	14.5
O(6,G4)	−19(15)	6562(9)	5786(7)	20.9	O(W2B)	1683(22)	6107(22)	4434(17)	18.6

The occupancy factor of W2A and W2B is 0.6 and 0.4, respectively.

$C_{56}H_{98}O_{35} \cdot C_6H_6O_3N \cdot 2H_2O$, F.W.=1506.5, orthorhombic, space group $P2_12_12_1$, Z=4, a=14.779(2), b=18.965(3), c=28.741(4) Å, V=8056(2) Å^3, D_X=1.242 g·cm^{-3}.

Description of the Structure and Discussion

As shown in Figs. 1 and 2, DM-β-CDx molecule has a round and rather symmetrical structure. The radius of the heptagon composed of seven glycosidic oxygen atoms is 4.84—5.21 Å in the *p*-IP complex and 4.92—5.16 Å in the *p*-NP complex. The average values of 5.05 and 5.07 Å is in good agreement with the radius of parent β-CDx.[5,6] The side lengths of the heptagon are in the range 4.25—4.49 Å (*p*-IP complex) and 4.33—4.44 Å (*p*-NP complex). Each 2,6-di-*O*-methylglucose residue inclines with the O(6) side turning to the inside of the macrocycle. The tilt-angles are in the range 5.6—24.4° in the *p*-IP complex and 2.2—24.7° in

the *p*-NP complex. Among the seven residues, the G6 residue is most tilted in both complexes. The distances between O(2) and O(3) of the adjacent residue, 2.72—3.10 Å in the *p*-IP complex and 2.79—3.05 Å in the *p*-NP complex, indicate that the O(3)H hydroxyl group is hydrogen-bonded to the O(2) atom of the adjacent

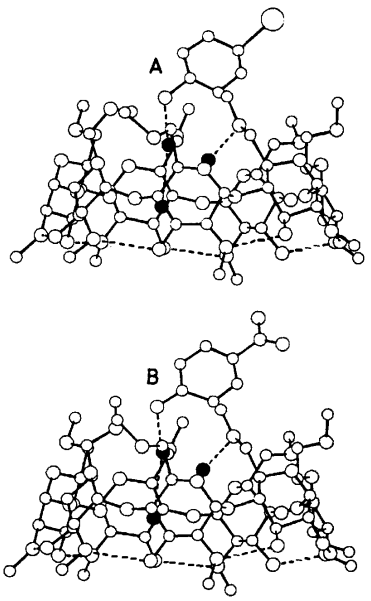

Fig. 2. Side-view of the DM-β-CDx complexes with *p*-IP (A) and *p*-NP (B). Water molecules are shown by full circles. Dashed lines indicate possible hydrogen-bonding contacts.

Table 3. Geometrical Data for Describing the Macrocyclic Conformation of DM-β-CDx

I. Distance from the center of gravity of seven O(4) atoms to each O(4) atom[a)]

Residue	Distance (*l*/Å)		Residue	Distance (*l*/Å)	
	p-IP	*p*-NP		*p*-IP	*p*-NP
G1	5.20	5.13	G5	5.11	5.08
G2	4.92	4.84	G6	4.98	4.92
G3	4.98	5.13	G7	5.13	5.14
G4	5.21	5.16	Average	5.05	5.07

a) Estimated standard deviations are 0.03 (*p*-IP complex) and 0.03 Å (*p*-NP complex).

II. Distance between O(4) and O(4′) of the adjacent residue[a)]

	Distance (*l*/Å)	
	p-IP	*p*-NP
O(4,G1)···O(4,G2)	4.38	4.41
O(4,G2)···O(4,G3)	4.41	4.41
O(4,G3)···O(4,G4)	4.49	4.44
O(4,G4)···O(4,G5)	4.25	4.33
O(4,G5)···O(4,G6)	4.43	4.44
O(4,G6)···O(4,G7)	4.48	4.41
O(4,G7)···O(4,G1)	4.29	4.34
Average	4.39	4.40

a) Estimated standaed deviations are 0.03 (*p*-IP complex) and 0.02 Å (*p*-NP complex).

III. Distance between O(2) and O(3′) of the adjacent residue[a)]

	Distance (*l*/Å)	
	p-IP	*p*-NP
O(2,G1)...O(3,G2)	2.81	2.79
O(2,G2)...O(3,G3)	2.88	2.88
O(2,G3)...O(3,G4)	2.73	2.79
O(2,G4)...O(3,G5)	3.04	2.97
O(2,G5)...O(3,G6)	2.85	2.87
O(2,G6)...O(3,G7)	3.10	3.05
O(2,G7)...O(3,G1)	2.94	2.90
Average	2.91	2.89

a) Estimated standard deviations are 0.03 (*p*-IP complex) and 0.02 Å (*p*-NP complex).

IV. Torsion-angle index[a)] and tilt-angle[b)] of each residue

Residue	Torsion-angle index (ϕ/°)		Tilt-angle (ϕ/°)	
	p-IP	*p*-NP	*p*-IP	*p*-NP
G1	112	124	5.8	5.5
G2	106	107	15.5	17.0
G3	138	122	16.1	14.2
G4	121	117	17.8	18.1
G5	107	112	5.6	2.2
G6	138	123	24.4	24.7
G7	106	113	19.7	17.6
Average	118	117	15.0	14.2

a) The torsion-angle index is defined as: $\phi=|\phi(C(1)-C(2))|+|\phi(C(2)-C(3))|+|\phi(C(5)-O(5))|+|\phi(O(5)-C(1))|-|\phi(C(3)-C(4))|-|\phi(C(4)-C(5))|$, where $\phi(C(1)-C(2))$ indicates the conformation angle of O(5)-C(1)-C(2)-C(3). b) The tilt-angle is defined as an angle made between the plane through seven O(4) atoms and the plane through C(1), C(4), O(4), and O(4′) of each residue.

V. Deviation of each O(4) atoms from the least-squares plane through seven O(4) atoms

Residue	Deviation (*d*/Å)		Residue	Deviation (*d*/Å)	
	p-IP	*p*-NP		*p*-IP	*p*-NP
G1	−0.01	−0.01	G5	0.17	0.13
G2	0.13	0.11	G6	0.01	0.03
G3	−0.04	−0.02	G7	−0.11	−0.10
G4	−0.16	−0.14	r.m.s. deviation	0.11	0.09

residue. All methyl groups point away from the center of the host macrocycle, thus the host cavity of DM-β-CDx is deeper than the cavity of parent β-CDx. The comparison of the O(4)···O(4′) distance (the side length of the O(4) heptagon) with the torsion-angle index gives no obvious correlation between them, although in parent β-CDx the strong correlation has been observed between the O(4)···O(4′) distance and the torsion-angle index. The methyl group may affect the conformation of the pyranose ring to break such linear correlation.

Except for methyl groups, the macrocyclic conformation of DM-β-CDx does not significantly differ from the conformation of parent β-CDx, as shown in

Table 4. Comparison of Geometrical parameters among β-Cyclodextrin and Methylated β-Cyclodextrins

Average values are given with standard deviations.

	β-CDx[a]	DM-β-CDx	TM-β-CDx[b]
Radius of the O(4) heptagon (l/Å)	5.0(0.2)	5.1(0.1)	5.0(0.3)
O(4)...O(4′) distance (l/Å)	4.3(0.1)	4.4(0.1)	4.3(0.1)
O(2)...O(3′) distance (l/Å)	2.9(0.1)	2.9(0.1)	3.5(0.2)
Glycosidic O(4) angle (ϕ/°)	118(1)	117(2)	117(3)
Planarity of the O(4) heptagon (d/Å)[c]	0.18	0.09	0.44
Torsion-angle index (ϕ/°)	120(7)	117(6)	123(13)
Tilt-angle (ϕ/°)	12(10)	14(8)	20(25)

a) See Ref. 5. b) Heptakis(2,3,6-tri-*O*-methyl)-β-cyclodextrin (Ref. 7). c) The root-mean-square deviation of the seven O(4) atoms.

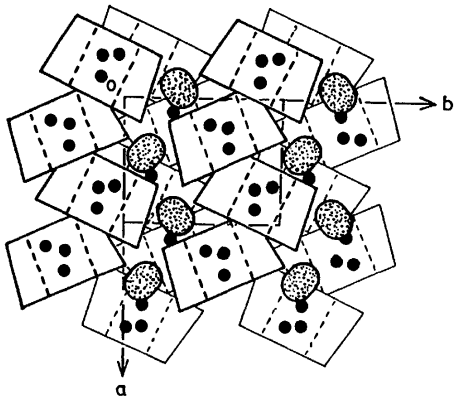

Fig. 3. A schematic drawing of the crystal structure. Water molecules are shown by full circles. Shaded ellipses indicate guest molecules.

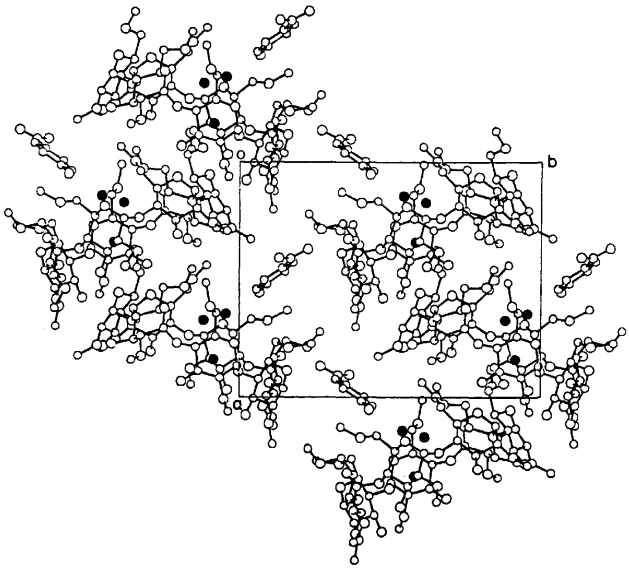

Fig. 4. The crystal structure of the DM-β-CDx complex with *p*-NP viewed along the c axis. Water molecules are shown by full circles. Symmetry-related molecules by the two-fold screw axis along the c axis are not shown because of the clarity of representation.

Table 4. By the methylation of O(3)H hydroxyl groups, the distance between O(2) and O(3) of the adjacent residue is increased from 2.9 Å to 3.5 Å. Moreover, each residue much more inclines with the tilt-angle in the range from −16.3° to 43.0°.[7] This indicates that the round shape of the macrocycle is maintained by the intramolecular O(2)···O(3′) hydrogen bonds in β-CDx and DM-β-CDx. The methylation of the O(2)H hydroxyl group does not affect the formation of intramolecular hydrogen bonds because the O(2)C(7)H_3 methoxyl group points away from the adjacent O(3)H hydroxyl group. The further methylation at the O(3) position blocks the formation of O(2)···O(3′) hydrogen bonds, and as the result, the macrocycle can no more retain the round structure.

Figure 3 shows the packing feature in the crystal. The DM-β-CDx molecules are stacked along the a axis. Since the DM-β-CDx molecule inclines by an angle of 25° against the a axis, the stacked molecules do not form a column structure but show a zigzag pattern. The O(2), O(3) side of the DM-β-CDx cavity is blocked by the O(6) side of the adjacent DM-β-CDx molecule which is related by the two-fold screw axis along the a axis. The O(6) side of the cavity is open to the intermolecular space, where the guest molecule is located. It is noteworthy that the guest *p*-IP and *p*-NP mole-

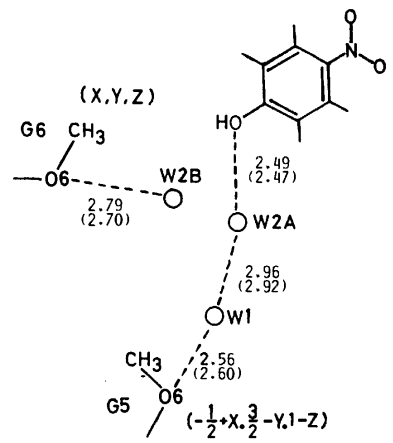

Fig. 5. A possible hydrogen bond scheme in the DM-β-CDx complex with *p*-NP. Corresponding hydrogen bond distances of the *p*-IP complex are given in parentheses.

cules are not included within the DM-β-CDx cavity but located in the crevice running zigzag along the a axis. Such geometrical relationship between host and guest is not observed in other cyclodextrin or methylated cyclodextrin complexes, except for the α-CDx-*m*-nitrophenol (1:2) complex, in which one guest is included within the host cavity and the other being located in the intermolecular space.[8] It is not easy to explain fully why the guest molecule is excluded from the host cavity, since the inclusion of the guest molecule by DM-β-CDx has been observed in the crystalline complex with 2-adamantanol.[9] One possible reason is that the intermolecular space has highly hydrophobic property because of many methyl groups. The guest molecule could be located in the intermolecular space rather than in the host cavity when the size and shape of the intermolecular space are more suitable for the guest molecule. On the other hand, in the crystal of native cyclodextrins, the intermolecular space is usually filled with water molecules which form a hydrogen bond network with many hydroxyl groups of the host molecule.

The DM-β-CDx cavity includes water molecules and one methoxyl group, O(6,G5)C(8,G5)H_3, which is inserted from the O(2), O(3) side. A possible hydrogen-bond scheme inside the host cavity is shown in Fig. 5. The W2 water molecule is disordered and occupies two sites, W2A and W2B. W2B is hydrogen-bonded to O(6,G6), while W2A forms hydrogen bonds with the hydroxyl group of the guest and W1 water molecule which is also hydrogen-bonded to O(6,G5) of the adjacent DM-β-CDx molecule related by the two-fold screw axis. Although the host cavity is extended and deepened by the methylation, the effective space of the cavity to include the guest molecule is reduced by the insertion of one methoxyl group of adjacent DM-β-CDx. Such close contact between host molecules may play an important role to exclude the guest molecule from the host cavity. It has been considered that the guest molecule should be included within the host cavity in the crystalline state. The present study, however, shows that the guest molecule is not necessarily included by the host molecule even if the complex has a 1:1 host-guest stoichiometry.

References

1) J. Szejtli, "Cyclodextrins and their Inclusion Complexes," Academiai Kiado, Budapest (1982).

2) W. Saenger, "Inclusion Compounds," ed by J. L. Atwood, J. E. D. Davies, and D. D. MacNicol, Academic press, London (1984), Vol. 2, pp. 231—259.

3) K. Harata, K. Uekama, M. Otagiri, and F. Hirayama, *J. Inclusion Phenom.*, **1**, 279 (1984).

4) K. Harata, *Chem. Lett.*, **1984**, 1644.

5) K. Lindner and W. Saenger, *Carbohydr. Res.*, **99**, 103 (1982).

6) K. Harata, *Bull. Chem. Soc. Jpn.*, **55**, 2315 (1982).

7) K. Harata, K. Uekama, M. Otagiri, and F. Hirayama, *Bull. Chem. Soc. Jpn.*, **56**, 1732 (1983).

8) K. Harata, H. Uedaira, and J. Tanaka, *Bull. Chem. Soc. Jpn.*, **51**, 1267 (1978).

9) M. Czugler, E. Eckle, and J. J. Stezowski, *J. Chem. Soc., Chem. Commun.*, **1981**, 1291.

 © 1988 The Chemical Society of Japan Bull. Chem. Soc. Jpn., 61, 1945—1951 (1988)

Role of Ti-O-Zr Bonding in TiO_2-ZrO_2 Catalyst for Dehydrogenation of Ethylbenzene

Yutaka HIRASHIMA, Katsuhiko NISHIWAKI, Akihiko MIYAKOSHI, Hideyasu TSUIKI, Akifumi UENO,* and Hirotoshi NAKABAYASHI†

Department of Materials Science, Toyohashi University of Technology, Tempaku-cho, Toyohashi, Aichi 440

†Department of Chemistry, Kochi Technical College, Monobe, Nangoku, Kochi 783

(Received May 29, 1987)

A relationship between acid amounts over TiO_2-ZrO_2 catalysts and their activities for nonoxidative dehydrogenation of ethyl benzene to styrene was examined. The catalysts were prepared by two different methods; one is simultaneous hydrolysis of Ti and Zr mixed alkoxides solution and the other is physical mixing of pure TiO_2 and ZrO_2. The former consists of fine TiO_2 and ZrO_2 particles and is expected a lot of Ti-O-Zr bonding between the fine particles, while the latter is composed of large particles and less amounts of Ti-O-Zr bonding might be expected. Although the Ti-O-Zr bonding has been considered to generate a new acid site and to enhance the rate of dehydrogenation of ethylbenzene, the acid amounts and the rates observed on unit surface areas of both catalysts were not significantly different. On the basis of these results, the role of Ti-O-Zr bondig in TiO_2-ZrO_2 catalyst for dehydrogenation of ethylbenzene is discussed.

Catalysis by metal oxides often depends upon their surface acidities originated from surface OH groups and structural deficiencies. It has been well-accepted that the surface acidity of a metal oxide can be improved by mixing it with another metal oxide to form a binary oxide.[1] The binary oxide should be prepared by coprecipitation method so as to be composed of fine respective oxide particles, resulting in a lot of metal(1)-O-metal(2) bonding at the fringe of particles. New and strong acid sites generated on the binary oxide have been believed due to the formation of this kind of bonding.[2]

Recently, TiO_2-ZrO_2 binary oxide has been reported to exhibit a high potential for nonoxidative dehydrogenation of ethylbenzene to styrene and this high activity has been explained by a concerted two-center mechanism based on the generation of Ti-O-Zr bonding on the binary oxide catalyst, where Zr ions act as acid sites and Ti as basic sites.[3] Since the catalyst was prepared by coprecipitation of a mixed solution of Ti and Zr tetra chlorides in alcohol with aqueous ammonia, a small amount of chloride ions might remain in the powder as contamination. Considering that the surface acidity is too sensitive to contamination, the catalyst examined should be free from any impurities. In this experiment the TiO_2-ZrO_2 binary catalyst was prepared by simultaneous hydrolytic decomposition of a mixed solution of Ti tetraisopropoxide and Zr tetrapropoxides, which will be one of the best method to prepare oxide powders free from impurities.

The purpose of the present work is to examine the acidity and the rate of dehydrogenation of ethylbenzene on the catalyst thus prepared and to discuss the role of surface Ti-O-Zr bondings during the catalysis.

Experimental

Preparation of TiO_2-ZrO_2 Binary Oxide. The binary oxide composed of TiO_2 and ZrO_2 was prepared by two different methods described in Table 1. In one method, the binary oxide A was prepared by a simultaneous hydrolytic decomposition of titanium tetraisopropoxide (Kishida Chemical Co.) and zirconium tetrapropoxide (Alpha Products Co.) dissolved in benzene. The hydrolysis was carried out at room temperature using an excess amount of distilled water in flowing dry nitrogen. The precipitates thus obtained were dried at 110 °C in an oven, followed by calcination at 500—800 °C in air for 2 h. The weight ratio of TiO_2/ZrO_2 in the binary oxide was varied from 10/90 to 90/10 by changing the amounts of respective alkoxides in an appropriate ratio. In the other method, which will be designated as P, pure TiO_2 and ZrO_2 (total amount being ca. 2 g) were physically mixed and ground in an agate mortar for ca. 30 min, and subse-

Table 1. Preparation Procedures of the Binary Oxides A and P

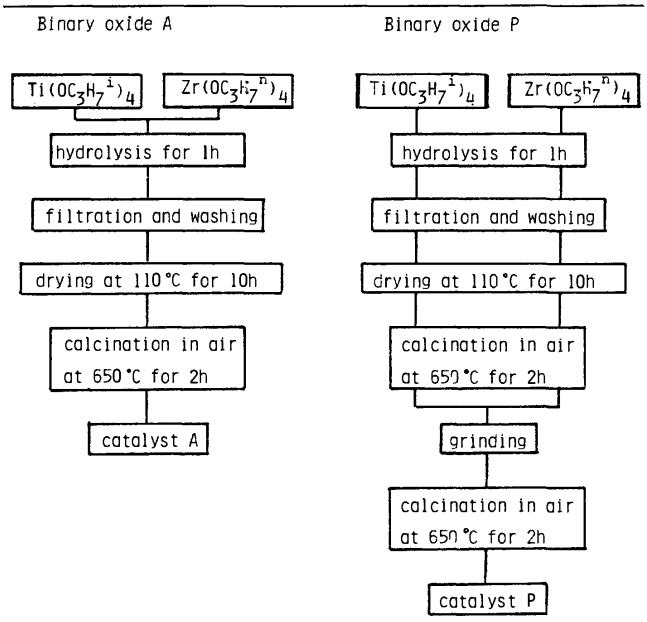

Preparation procedures of TiO_2-ZrO_2 catalysts.

quently calcined at 650 °C in a similar manner as A. Pure TiO_2 and ZrO_2 were prepared by the hydrolysis of respective alkoxides, followed by drying at 110 °C in an oven and calcination at 650 °C in air. The specific surface areas of these oxides were measured by BET method using nitrogen at its liquid temperature. The structural differences in these binary oxides were studied by X-ray diffraction (Rigaku Denki Co., Geigerflex), operated at 30 kV with a filament current of 15 mA using Ni filter for Cu $K\alpha$ radiation. The distributions of metal ions in the TiO_2-ZrO_2 binary oxide powders were measured by means of EPMA (electron probe X-ray micro analyser, Hitachi Co., X-650), operated at an accelerating voltage of 20 kV. For EPMA measurements the sample powder was covered with thin Pt film to avoid a charge-up phenomenon.

Measurements of Acidity and Catalytic Activity. The surface acidity of the binary oxide was decided by butylamine titration using 1-phenylazo-2-naphthylamine (H_0=+4.0), *p*-dimethylaminoazobenzene (+3.3), benzeneazodiphenylamine (+1.5) and dicinnamal acetone (−3.0), dissolved in benzene, as indicators.[4] The sample powder was first calcined at 650 °C in air and prior to the acidity test the sample was recalcined at 300 °C in O_2 atmosphere, followed by evacuation at the same temperature. The sample thus treated was pored into benzene without exposure to air and a few drops of indicator were added to the sample. The sample was left for 24 h and then submitted to the titration test with butylamine. Several times of the titration tests were made for one sample to decide its surface acidity. The acid amount thus measured has an error larger than +0.1 mmol·g^{-1} because of the difficulty to find out the end point of titration.

The binary oxide powders were employed as catalysts for nonoxidative dehydrogenation of ethylbenzene to styrene. The catalyst powder was calcined at 650 °C for 4 h and the reaction was carried out at 620 °C with a continuous flow reaction system. A mixture of ethylbenzene and water was supplied into the reactor with N_2 stream. The flow rate of N_2 was 25 ml·min^{-1} and the feed rates of ethylbenzene and water were 25 and 43 ml·min^{-1}, respectively. This corresponds to the weight ratio of ethylbenzene/water being 2.

Table 2. Conversions of Ethylbenzene and Selectivities to Styrene, Toluene, and Benzene over the Binary Oxides A and P at 620 °C

Composition (Ti/Zr)	Surface area	EB conversion	Selectivity/%		
	$m^2 g^{-1}$	%	Sty	Tol	Ben
Binary oxide A					
10/90	56	6.7	93.2	2.0	4.8
25/75	92	9.0	94.6	1.7	3.7
50/50	141	11.6	95.5	1.4	3.1
75/25	128	13.6	96.4	1.2	2.4
90/10	113	14.5	96.8	1.1	2.1
Binary oxide P					
10/90	54	7.6	92.4	2.0	5.6
25/75	60	6.5	91.3	2.1	6.6
50/50	40	4.7	91.4	2.7	5.9
75/25	40	6.7	91.0	2.1	6.9
90/10	47	7.1	92.2	3.4	5.8
TiO	50	5.8	92.5	2.4	5.1
ZrO_2	56	3.7	89.0	3.4	7.6

The catalyst powder (2.5 g) was pelleted and placed over the catalyst bed located just below the preheater, containing rashig rings. A cooling trap was equipped at the outlet of the reactor to collect ethylbenzene, water and liquid products such as styrene, benzene and toluene. These liquids were analysed by gas chromatography using a column packed with SP-1200 and Bentone 34 coated Chromosorb W.

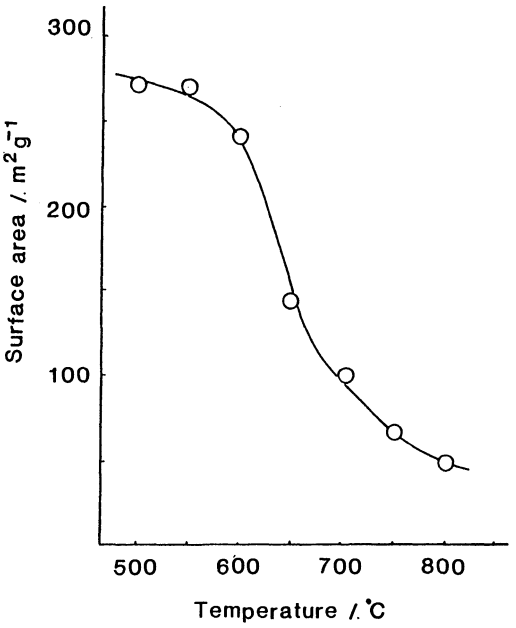

Fig. 1. Change in the surface area of binary oxide A (TiO_2/ZrO_2=50/50) with the calcination temperature.

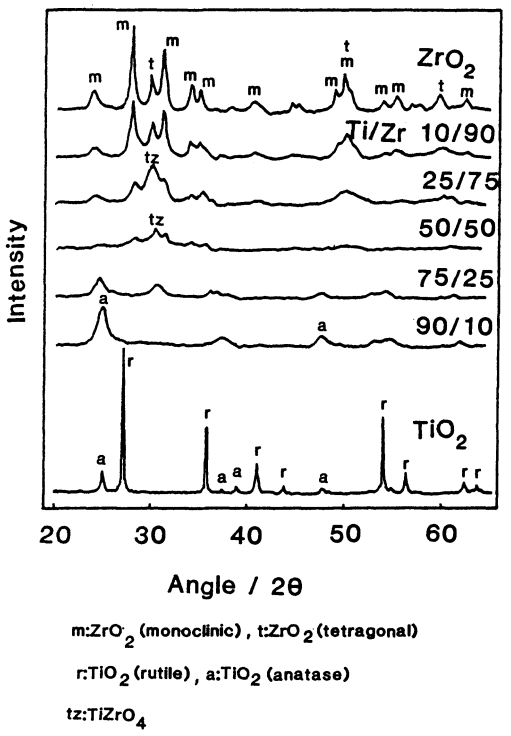

Fig. 2. X-Ray diffraction spectra of the binary oxides A with various TiO_2/ZrO_2 ratios.

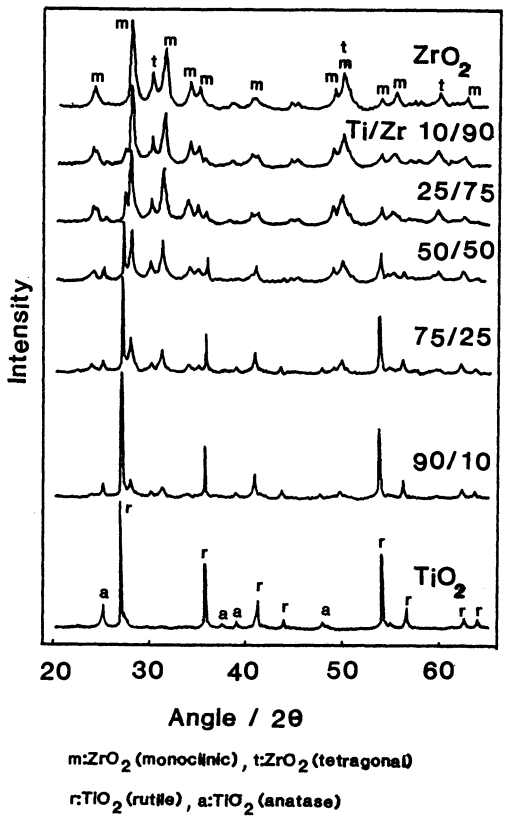

Fig. 3. X-Ray diffraction spectra of the binary oxides P with various TiO_2/ZrO_2 ratios.

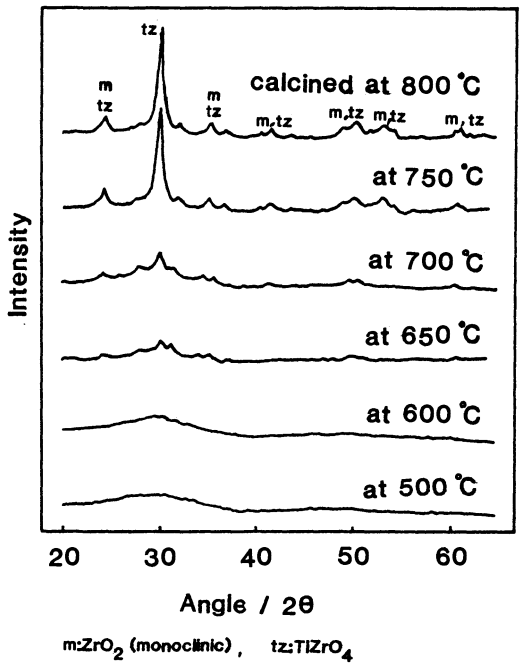

Fig. 4. Change in the X-ray diffraction spectrum of binary oxide A (TiO_2/ZrO_2=50/50) with calcination temperature.

Results

BET Surface Area and X-Ray Diffraction. The BET surface areas of TiO_2, ZrO_2, and the binary oxide powders calcined at 650 °C are listed in Table 2 with other results. The surface area of the binary oxide A (TiO_2/ZrO_2=50/50) decreased with increasing the calcination temperature and reached constant above 750 °C (Fig. 1). The X-ray diffraction spectra of pure TiO_2 and ZrO_2 and the binary oxides are depicted in Figs. 2 and 3. The crystallographic structures of TiO_2 and ZrO_2 are determined to be rutile and monoclinic with a small amount of tetragonal, respectively, when calcined at 650 °C. The binary oxide P calcined at 650 °C showed sharp diffraction peaks assigned to TiO_2 (rutile) and ZrO_2 (monoclinic and tetragonal) with rational intensities according to the respective concentration. On the other hand the binary oxide A calcined at 650 °C showed rather broad diffraction peaks assigned to TiO_2 (anatase), ZrO_2 (monoclinic and tetragonal) and probably to the complex oxide, $TiZrO_4$, when the TiO_2/ZrO_2 ratio of the oxide A is in the range between 25/75 and 75/25. In Fig. 4 are shown the changes in X-ray diffraction pattern of the oxide A (TiO_2/ZrO_2=50/50) with the calcination temperature, indicating that a small amount of $TiZrO_4$ seems to be formed at 650 °C. In the case of binary oxide P, no formation of $TiZrO_4$ was observed even when the powder was calcined at 1100 °C in air for 12 h.

EPMA Measurements. The homogeneous distributions of Ti and Zr ions on the surface of the binary oxide A calcined at 650 °C are demonstrated by X-ray images with EPMA measurements (Fig. 5). While on the surface of the binary oxide P calcined at 650 °C, Ti and Zr ions were found to be localized, forming relatively large TiO_2 and ZrO_2 particles (also in Fig. 5).

Acidity and Catalytic Activity. The total acid amounts on TiO_2, ZrO_2 and the binary oxides calcined at 650 °C were measured by butylamine titration using 1-phenylazo-2-naphthylamine (H_0=+4.0) as an indicator and the results obtained are given in Figs. 6a and b. In Fig. 6a, the acid amount was expressed in terms of $mmol \cdot g^{-1}$, while in Fig. 6b in terms of $\mu mol \cdot m^{-2}$. The strong acid sites with $H_0 \leq +3.3$ were observed on the binary oxide A, while those strong acid sites were never observed on the binary oxide P. The acid amounts with various strengths measured on the binary oxide A are depicted in Fig. 7.

The catalytic activities of TiO_2, ZrO_2, and the binary oxide A and P for dehydrogenation of ethylbenzene at the stationary state are listed in Table 2 and depicted in Figs. 8a and b, where the activities were expressed in terms of $molecules \cdot g^{-1} \cdot s^{-1}$ and $molecules \cdot m^{-2} \cdot s^{-1}$, respectively, assuming first order reaction with respect to ethylbenzene.

Dscussion

The initial stage of the preparation of the binary

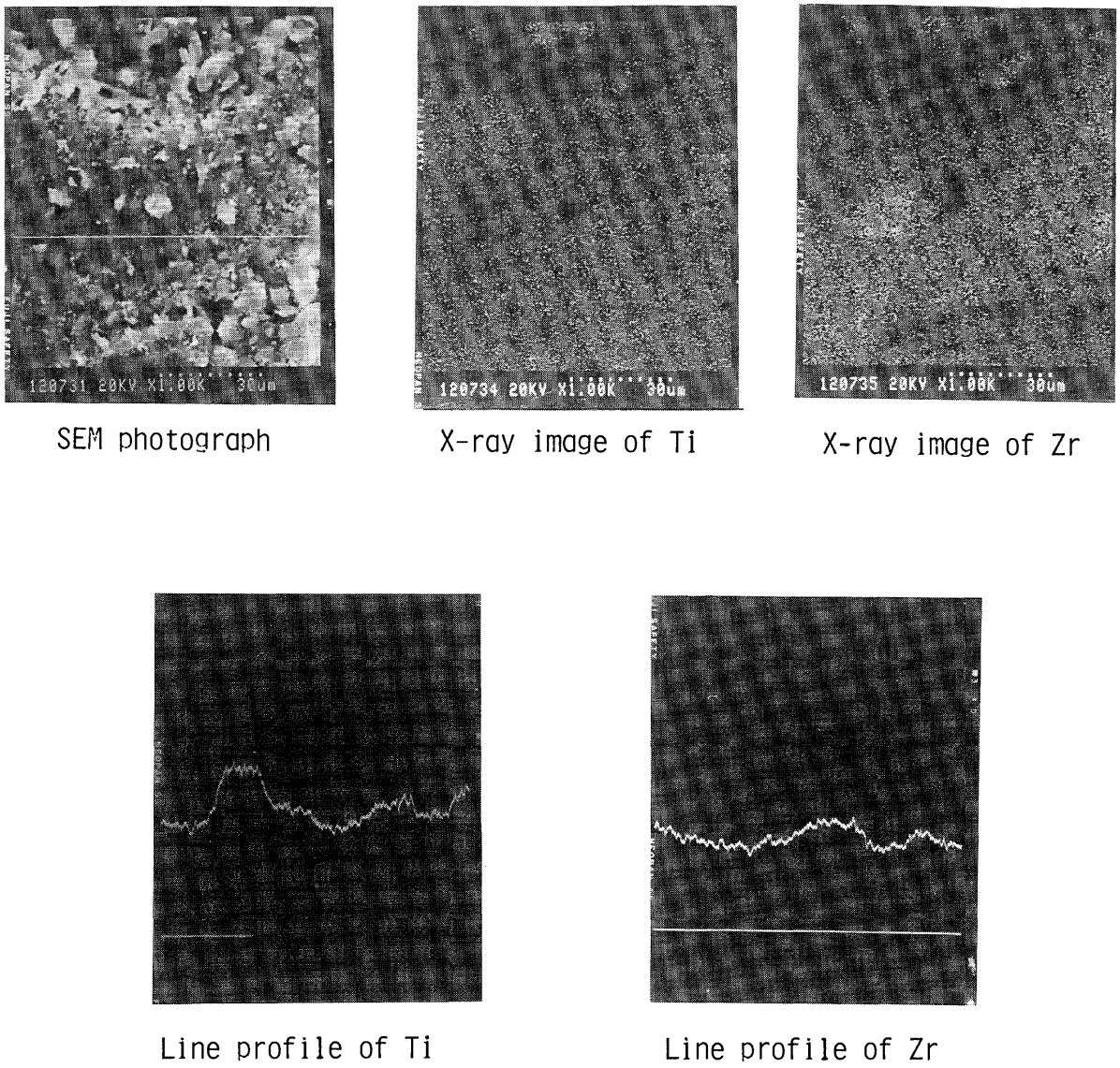

Fig. 5a. Distributions of Ti and Zr ions in the binary oxide A (TiO_2/ZrO_2=50/50) calcined at 650°C, measured by EPMA.

oxide A is the simultaneous hydrolytic decomposition of Ti and Zr alkoxides. Before the hydrolysis, the alkoxides solution was vigorously stirred at 60 °C for 2 h in flowing dry N_2, expecting that the rearrangements of metal ions will take place according to the following reaction;

$$n\ Ti(OC_3H_7)_4 + n\ Zr(OC_3H_7)_4 \longrightarrow [Ti(OC_3H_7)_m\text{-}O\text{-}Zr(OC_3H_7)_m] \quad (1)$$

By adding water the $(OC_3H_7)_m$ groups in the species above were substituted with $(OH)_m$ groups producing propyl alcohol, C_3H_7OH, due to the following reaction;

$$[Ti(OC_3H_7)_m\text{-}O\text{-}Zr(OC_3H_7)_m] + 2m\ H_2O \longrightarrow [Ti(OH)_m\text{-}O\text{-}Zr(OH)_m] + 2m\ C_3H_7OH \quad (2)$$

The hydrogen bonding between (OH) groups in the $[Ti(OH)_m\text{-}O\text{-}Zr(OH)_m]$ species might result in the formation of a gel-like precipitate, where Ti and Zr ions are highly dispersed forming a chemical bonding of Ti-O-Zr. This idea has been already adopted for the preparation of glassy materials such as SiO_2-ZrO_2[5] and SiO_2-TiO_2-ZrO_2[6] systems and of oxide powders such as $BaTiO_3$[7] and $SrTiO_3$.[8] Although the atomic dispersions of Ti and Zr ions are desired, considerable amounts of $[Ti(OC_3H_7)_m\text{-}O\text{-}Ti(OC_3H_7)_m]$ and $[Zr(OC_3H_7)_m\text{-}O\text{-}Zr(OC_3H_7)_m]$ species may be formed in spite of vigorous stirring of the alkoxides solution, and Ti-O-Ti and Zr-O-Zr bondings may also remain in the precipitate produced by hydrolysis. The Ti-O-Ti and Zr-O-Zr structures thus prepared may turn out to be fine TiO_2 and ZrO_2 crystallites, respectively, when the precipitate was dried and calcined in air.

In order to examine the structures of the products, X-ray diffraction patterns of the binary oxide A with various TiO_2/ZrO_2 ratios were obtained (see Figs. 2

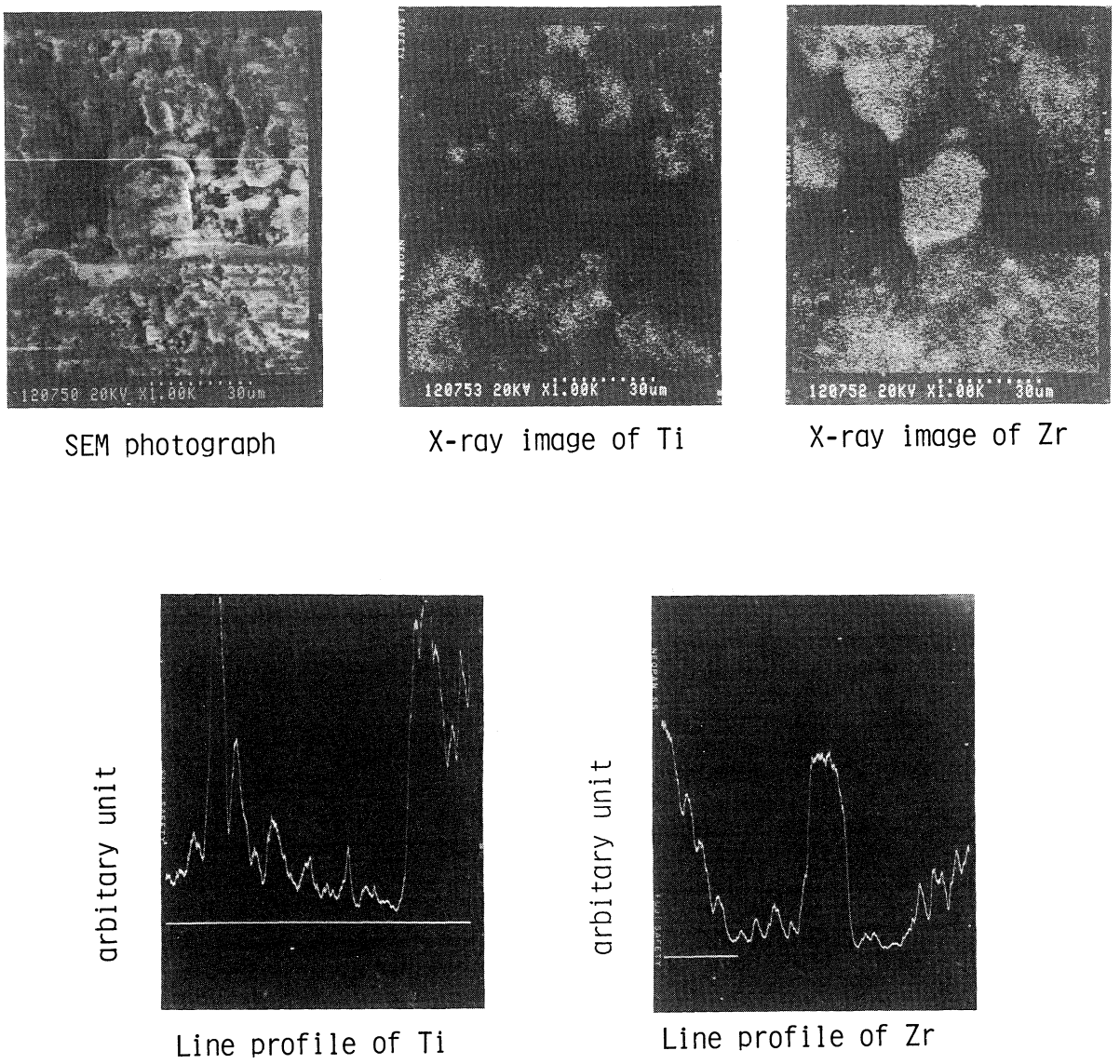

Fig. 5b. Distributions of Ti and Zr ions in the binary oxide P (TiO_2/ZrO_2=50/50) calcined at 650°C, measured by EPMA.

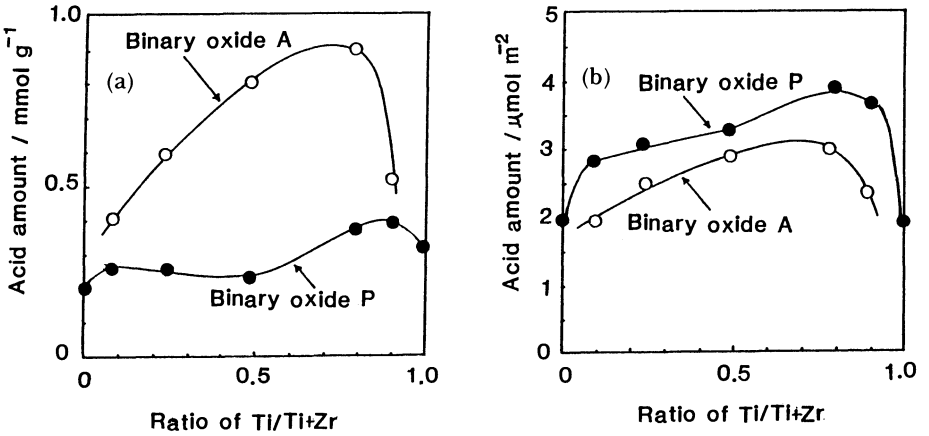

Fig. 6. a) Acid amounts on the binary oxides A and P with varaious TiO_2/ZrO_2 ratios expressed in terms of mmol·g^{-1}; the oxides were calcined at 650°C. b) Acid amounts on the binary oxides A and P with various TiO_2/ZrO_2 ratios expressed in terms of μmol·m^{-2}; the oxides were calcined at 650°C.

and 3). Several broad peaks were observed for the binary oxide A calcined at 650 °C with TiO_2/ZrO_2 ranging from 25/75, while for pure TiO_2 and ZrO_2 sharp diffraction peaks assigned to rutile and monoclinic with a small amount of tetragonal form, respectively, were observed. This indicates that the coexistence of Ti and Zr ions in the precipitate prevents the fine TiO_2 and ZrO_2 crystallites from their crystalline growth during calcination. It might be possible to say that the suppressions of the crystalline growth are attributed to formation of Ti-O-Zr network structure. As could be seen in Fig. 4, the formation of a small amount of $TiZrO_4$ was first observed when the binary oxide A was calcined at 650 °C for 4 h, which resulted in the reduction of the surface area of the oxide A (see Fig. 1). On the contrary, no peaks assigned to $TiZrO_4$ were observed in the binary oxide P even when calcined at the temperature as high as 1100 °C for 12 h. This means that the dispersions of Ti and Zr ions in the binary oxide A are extremely higher than those in the binary oxide P. The high dispersions of Ti and Zr ions in the binary oxide A were evidenced by EPMA measurements (see Fig. 5). It has been already proved by EXAFS (extended X-ray absorption fine structure) study[9] that the binary oxide A is predominantly composed of fine TiO_2 and ZrO_2 crystallites and that the binary oxide P mainly consists of large TiO_2 and ZrO_2 ones.

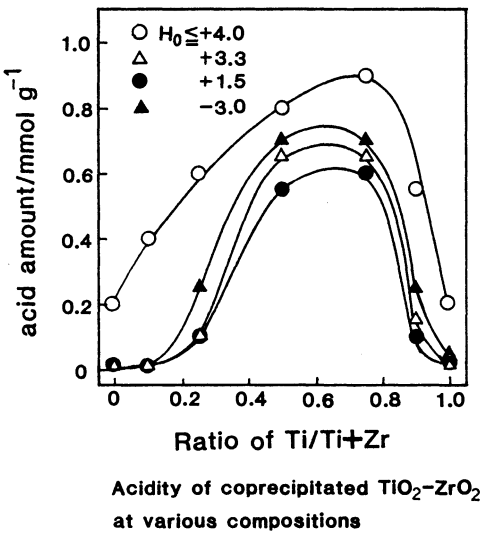

Fig. 7. Acid amounts with various acid strengths on the binary oxide A calcined at 650 °C.

Thus, a lot of Ti-O-Zr structures are expected at the interface between fine TiO_2 and ZrO_2 crystallites in the binary oxide A. It has been widely accepted that mixed oxide powders consisting of fine respective oxide crystallites often showed new acid sites originated from the generation of new bonding, M(1)-O-M(2), where M(1) and M(2) represent metal ions in the mixed oxide powders.[2] TiO_2-ZrO_2 system has been reported a typical case to generate new acid sites when the respective oxide crystallites are so small.[10] Indeed, the acid amount over 1 g of the binary oxide A was higher than that of the oxide P at any TiO_2/ZrO_2 ratios employed. (see Fig. 6a) While, as shown in Fig. 6b, the acid amounts over unit surface area of the binary oxide P is observed rather higher than those of the binary oxide A. Although the results might not be favorable for the opinion above, it is difficult to obtain rigid conclusions concerning the difference in the acid properties of the binary oxide A and P because of the ambiguity of the acid amounts measured in this work. No acid sites with $H_0 \leq +3.3$ were observed over the surface of binary oxide P, while considerable amounts of the acid sites with $H_0 \leq +3.3$ were generated on the surface of

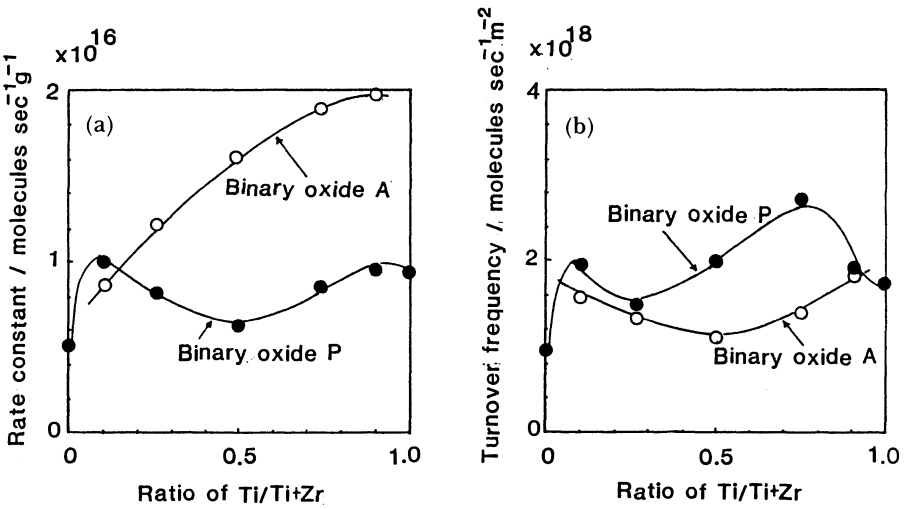

Fig. 8. a) Catalytic activities of binary oxides A and P expressed in terms of molecules·g^{-1}·s^{-1}; the catalysts were calcined at 650 °C before the reaction. b) Catalytic activities of binary oxidea A and P expressed in terms of molecules·m^{-2}·s^{-1}; the catalysts were calcined at 650 °C before the reaction.

binary oxide A, as shown in Fig. 7. Consequently, the total amounts of acid sites with $H_0 \leq +4.0$ over the binary oxide A might be the same as that on the binary oxide P, but the acid sites generated on the binary oxide A are much stronger than those on the binary oxide P. This probably due to the formation of Ti-O-Zr bonding over the binary oxide A[2] with a timid suspect whether the Ti-O-Zr bondings are merely required to generate a new and strong acid site. It must be mentioned that the acid amount, containing strong acid sites with $H_0 < +3.3$, on the binary oxide prepared by coprecipitation of a mixed solution of Ti and Zr tetrachlorides were observed almost the same as that on the binary oxide A. No significant effects of chlorine ions contaminated upon the acid property were recognized.

Recently, it has been reported that the binary oxide composed of fine TiO_2 and ZrO_2 particles is a potential catalyst for nonoxidative dehydrogenation of ethylbenzene to styrene.[3] It has been proposed that the reaction requires bifunctional sites, where one acts as an acid and the other acts as a basic site.[3] The high potential of the binary oxide for the dehydrogenation of ethylbenzene has been explained in terms of the generation of Ti-O-Zr bonding in the binary oxide, Ti ions being proposed to act as base and Zr ions as acid.

The nonoxidative dehydrogenation of ethylbenzene on the binary oxides A and P prepared in the present work was carried out at 620 °C to examine the role of Ti-O-Zr bonding during the reaction. The conversions of ethylbenzene and the selectivities to styrene over various catalysts are summarized in Table 2. From these results the rate constants and turnover frequencies were estimated assuming the first order with respect to ethylbenzene. As could be seen in Fig. 8a the rate constants over the binary oxide A expressed in terms of molecules $\cdot g^{-1} \cdot s^{-1}$ are observed to be higher than those over the binary oxide P. While the turnover frequency, given in Fig. 8b, showed the opposite results; turnover frequencies over the oxide A are rather smaller than those over the oxide P. If the dehydrogenation of ethylbenzene would take place on the bifunctional sites originated from Ti-O-Zr bonding over the catalyst surface, the results above means that almost the same or rather less amounts of Ti-O-Zr bonding are present over the unit surface area of the binary oxide A than on the binary oxide P. This is inconsistent with the idea that a lot of Ti-O-Zr bonding are on the surface of binary oxide A. In order to interpret this problem it might be favorable to deduce the conclusion that dehydrogenation of ethylbenzene would occur on the sites exposed on the surface of TiO_2 and ZrO_2 particles as well as on the sites composed of Ti-O-Zr bonding and that the reaction rate might not be so different in these active sites.

Thus, Ti-O-Zr bonding in TiO_2-ZrO_2 may not play an important role for nonoxidative dehydrogenation of ethylbenzene, being opposited to the previous opinion.[3]

References

1) K. Tanabe, C. Ishiya, I. Matsuzaki, I. Ichikawa, and H. Hattori, *Bull. Chem. Soc. Jpn.*, **45**, 47 (1972); K. H. Steinberg, and H. Bremer, 4th Intern. Congr. Catalysis, Moscow, Preprint of Papers, No.76 (1968); K. Arata, S. Akutagawa, and K. Tanabe, *Bull. Chem. Sco. Jpn.*, **49**, 390 (1976).

2) C. L. Thomas, *Ind. Eng. Chem.*, **41**, 2569 (1949); K. Shibata, T. Kiyoura, J. Kitagawa, T. Sumiyoshi, and K. Tanabe, *Bull. Chem. Soc. Jpn.*, **46**, 2985 (1973); K. Tanabe, T. Sumiyoshi, K. Shibata, and J. Kitagawa, *Bull. Chem. Soc. Jpn.*, **47**, 1064 (1974).

3) Ikai wang, Wun-Fu Chung, Ru-Jen Shiau, Jung-Chung Wu, and Chung-Sun Chung, *J. Catal.*, **83**, 428 (1983); Jung-Chung Wu, Chung-Sun Chung, Ching-Lan Ay, and Ikai Wang, *J. Catal.*, **87**, 98 (1984).

4) K. Tanabe, "Solid Acids and Bases," Kodansha, Tokyo, Academic Press, New York, London (1970).

5) M. Nogami and Y. Moriya, *Yogyo Kyokaishi*, **85**, 448 (1977).

6) C. Zhu, L. Hou, F. Can, and Z. Jiang, *J. Non-Cryst. Solids*, **63**, 105 (1984).

7) K. S. Mazdiyasni, C. T. Lynch, and J. S. Smith II, *J. Am. Ceram. Soc.*, **50**, 532 (1967).

8) J. S. Smith II, R. T. Dolloff, and K. S. Mazdiyasni, *J. Am. Ceram. Soc.*, **53**, 91 (1970).

9) Y. Hirashima, H. Tsuiki, A. Ueno, K. Tohji, and Y. Udagawa, *J. Catal.*, **102**, 249 (1986).

10) K. Shibata and T. Kiyoura, *J. Res. Inst. Catalysis, Hokkaido Univ.*, **19**, 35 (1971).

 © 1988 The Chemical Society of Japan Bull. Chem. Soc. Jpn., 61, 1953—1958 (1988)

Magnetic Behavior of Spin-Crossover Iron(III) Complexes Adsorbed on the Surface of Silicon Dioxide and Metal Dilution Effects on Magnetism

Yonezo MAEDA,* Masahiro TOMOKIYO, Kenji KITAZAKI, and Yoshimasa TAKASHIMA
Department of Chemistry, Faculty of Science, Kyushu University, Hakozaki, Higashi-ku, Fukuoka 812
(Received October 2, 1987)

The effects of metal dilution and adsorption on the surface of silicon dioxide on the spin-crossover behavior of $[Fe(acpa)_2]PF_6$, $[Fe(acpa)_2]BPh_4$, and $[Fe(bzpa)_2]PF_6$, which undergo fast spin-state interexchange on the ^{57}Fe Mössbauer timescale have been studied by using ^{57}Fe Mössbauer and EPR spectroscopies, powder X-ray diffraction and magnetic susceptibility, where Hacpa is *N*-(1-acetyl-2-propylidene)-2-pyridylmethylamine and Hbzpa *N*-(1-benzoyl-2-propylidene)-2-pyridylmethylamine. Solid solution compounds, $[Fe_xCo_{1-x}(acpa)_2]BPh_4$($x$=0.035 and 0.074) and $[Fe_{0.05}Co_{0.95}(bzpa)_2]PF_6$ exhibit spin-crossover phenomena. No difference in the spin-state interexchange rate is observed between the diluted compound and the corresponding undiluted one as far as the rates are evaluated by Mössbauer spectroscopy. Mössbauer spectra for $[Fe_{0.074}Co_{0.926}(acpa)_2]PF_6$ exhibit only a pair of quadrupole doublets assigned to the low-spin state in the temperature range from 78 to 298 K. The spin-state interexchange rates for $[Fe(acpa)_2]BPh_4$ and $[Fe(bzpa)_2]PF_6$ adsorbed on the surface of silicon dioxide become slow compared to those for the corresponding pure complexes and the narrowing of the spin-state transition temperature range is observed. On the contrary no detectable differences in the spin-state interexchange rates are observed between the Mössbauer spectra for $[Fe(acpa)_2]PF_6$ adsorbed on the surface of silicon dioxide and that for the pure complexes. These observations are interpreted in terms of a spin-state transition behavior in these complexes which is affected by the packing state in the solid state, which is dependent on the characteristic structure of the respective complex.

The study of thermally induced spin-state transition-(SST) phenomena has recently become an interesting research field.[1,2] Dynamical behavior in spin-state interexchange is caused by a cooperative solid state effect[3] and/or an intramolecular reorganization. It is important to gain some understanding about the mechanisms by which intermolecular interactions inhibit or enhance the rate of intramolecular spin-state interexchanges and to separate the intermolecular interaction from the intramolecular interaction. To solve the above problem, it is most effective to study the SST behavior in a system free from intermolecular interaction.

To study the nature of the interaction responsible for the spin-crossover behavior in "gradual transition type" complexes where SST takes place across a broad temperature range, the complexes $[Fe_xCo_{1-x}(acpa)_2]$-BPh_4(x=0.035 and 0.074), $[Fe_{0.074}Co_{0.926}(acpa)_2]PF_6$, $[Fe_{0.05}Co_{0.95}(bzpa)_2]PF_6$, and the complexes adsorbed on the surface of silicon dioxide(SD) were prepared.

Mössbauer spectroscopy is a useful tool for observing spin-state interexchange rates because the lifetime of the excited state of ^{57}Fe is critical. For a system of a very rapid interexchange rate ($>10^7$ s^{-1}) iron nuclei "see" an average of the properties of the low-spin and the high-spin states in the Mössbauer spectrum which depends on the proportion of each state. For a slow system ($<10^7$ s^{-1}) the Mössbauer spectrum shows a superposition of the two electronic states. The magnetic, ^{57}Fe Mössbauer and EPR spectroscopic properties of the complexes have been examined by Maeda et al.[4-6] The spin-state interexchange rates of $[Fe(acpa)_2]PF_6$ are comparable to the reciprocal of the ^{57}Fe Mössbauer timescale (0.98×10^{-7}s) and those of $[Fe(acpa)_2]BPh_4$ and $[Fe(bzpa)_2]PF_6$ are fast on the ^{57}Fe Mössbauer timescale.

Gütlich et al. and Seki and Sorai studied the spin-crossover propersies of diluted solid solutions $[Fe_xM_{1-x}$ $(phen)_2(NCS)_2]$ (x=0.01—1 and M=Mn, Co, Ni, and Zn),[7] $[Fe_xZn_{1-x}(2\text{-pic})_3]Cl_2\cdot C_2H_5OH$,[8,9] $[Fe_{0.01}Co_{0.99}(2$-$CH_3phen)_3](ClO_4)_2$[10] and $[Fe_xZn_{1-x}(ptz)_6](BF_4)_2$,[11] and suggested that for some systems the sizes of the low-spin domains decreased as the concentration of the host complexes increased.

Effects of counter ion sizes, solvation, grinding, and metal dilution on SST for $[Fe_xM_{1-x}(3\text{-}OCH_3\text{-}SalEen)_2]$-$PF_6$(M=Co, Cr)[12] and $[Fe_xCo_{1-x}(SalAPA)_2]ClO_4$[13] were studied by Hendrickson et al. They explained the various observations in terms of the nucleation and growth mechanism of phase.

All of these complexes except for $[Fe_xCo_{1-x}(Sal$-$APA)_2]ClO_4$ are spin-crossover complexes of "abrupt transition type" (SST which takes place in narrow temperature range, i.e., 2 K) with large cooperativity. The metal dilution sometimes influences the spin-state interexchange rate (R), transition temperature range (ΔT) and the transition temperature (T_c) defined as the temperature at which equal amounts of the high-spin and low-spin states coexist.

Experimental

Iron complexes were prepared using enriched ^{57}Fe by the same method as described elsewhere.[15]

$[Co(acpa)_2]BPh_4$: An ethanol solution of $Co(CH_3$-$COO)_2\cdot4H_2O$ is added to a solution containing a Schiff base prepared by mixing acetylacetone and 2-(aminomethyl)-pyridine in ethanol. Oxidation to give Co(III) complexes was carried out by adding 30% H_2O_2 solution. After the oxidant

was added, the solution was boiled for 5 min and an ethanol solution of $K[BPh_4]$ was added to the solution. The precipitation was separated, washed with ethanol and recrystallized twice from CH_2Cl_2-methanol.

Other cobalt complexes were prepared with the same procedure as described above except that the $[Co(bzpa)_2]BPh_4$ was recrystallized from acetone.

The ^{57}Fe-doped cobalt complexes were prepared by dissolving the corresponding cobalt complexes together with the appropriate weight of ^{57}Fe enriched iron(III) complexes in the solvent used for recrystallization and then by evaporation to dryness. X-Ray powder diffraction patterns for $[Fe(acpa)_2]BPh_4$ and $[Fe(bzpa)_2]PF_6$ were similar to that for the corresponding cobalt complexes, respectively. The diffraction positions for the solid solutions $[Fe_xCo_{1-x}(acpa)_2]BPh_4$ and $[Fe_{0.05}Co_{0.95}(bzpa)_2]PF_6$ were situated near those for the corresponding cobalt complexes, respectively. The diffraction pattern for $[Fe(acpa)_2]PF_6$ did not agree with that of the corresponding cobalt complex. The diffraction pattern for $[Fe_{0.074}Co_{0.926}(acpa)_2]PF_6$ was the same as that for the corresponding cobalt complex.

Two types of silicon dioxide(SD) were used; SD(A) and SD(AB)(Fuji Davison Co.). They are characterized by pores of average diameter 2.2 and 4 nm and of specific surface 650 and 590 $m^2 g^{-1}$, respectively. Finely powdered SD was dried in vacuo at 120 °C before use. The iron complexes were adsorbed on the surface of the SD at room temperature.

SD(A) of 200 mg was introduced into a CH_2Cl_2 solution containing $[Fe(acpa)_2]PF_6$ of 15 mg. The solution was shaken for a few minutes. It turned pale in color and the SD was separated by using a glass filter. The iron content adsorbed on the SD was determined by an atomic absorption technique. The SD adsorbing the complexes was coated with cellulose adhesive (alcohol-free collodion solution diluted with ether) to avoid decomposition of the complexes. The saturated amounts of the complexes adsorbed on the SD were $(10.9\pm3.3)\times10^{-4}$ mol g^{-1}.

$[Fe(acpa)_2]PF_6$ of 7.7 mg was adsorbed on the surface of SD of 200 mg. This volume corresponds to the area occupation of 1.6×10^{-13} cm^2 (a spuare of 4 nm) per one molecule. The size of the molecule is about 0.85 nm in diameter, which is calculated from the data of the crystal structure.[5]

$[Fe(acpa)_2]BPh_4$ and $[Fe(bzpa)_2]PF_6$ adsorbed on SD were prepared with the same procedure as that for $[Fe(acpa)_2]PF_6$, except that SD(AB) was used for the former complex because the former complexes were adsorbed much more on SD(AB) than on SD(A). The saturated amounts of the complexes adsorbed on SD were $(1.1\pm0.1)\times10^{-4}$ mol g^{-1} for the tetraphenylborate and $(3.0\pm0.4)\times10^{-4}$ mol g^{-1} for the hexafluorophosphate.

Mössbauer spectra and magnetic susceptibilities were measured by using an apparatus described elsewhere.[6] EPR spectra were obtained with a FES-FEX(JEOL, Ltd.) X-band spectrometer. The Mössbauer spectra were fitted to Lorentzian lines by using a least squares method. The isomer shift, δ was calibrated relative to the center of a spectrum of iron foil enriched with ^{57}Fe at 296 K, which was also used as a standard material for the velocity calibration.

Results and Discussion

The purities of the iron and cobalt complexes were checked by elemental analysis for C, H, and N, and the magnetic behavior vs. temperature for the enriched iron complexes was similar to that reported before.[4,5]

Spin-Crossover Properties of the Iron Complexes Diluted with Cobalt Complexes. Figure 1 illustrates the temperature dependence of the Mössbauer spectra for $[Fe_{0.074}Co_{0.926}(acpa)_2]BPh_4$. The temperature dependences of the isomer shift and quadrupole splitting QS for $[Fe_xCo_{1-x}(acpa)_2]BPh_4$ are shown in Fig. 2. The decrease of the quadrupole splitting and the increase in the isomer shift for the diluted complexes

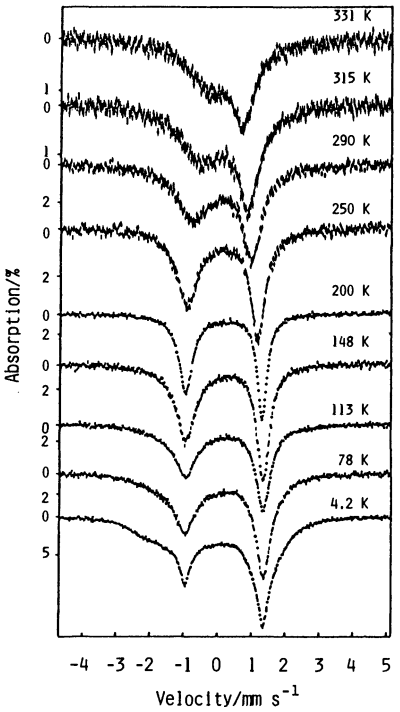

Fig. 1. Temperature dependence of Mössbauer spectra for $[Fe_{0.074}Co_{0.926}(acpa)_2]BPh_4$.

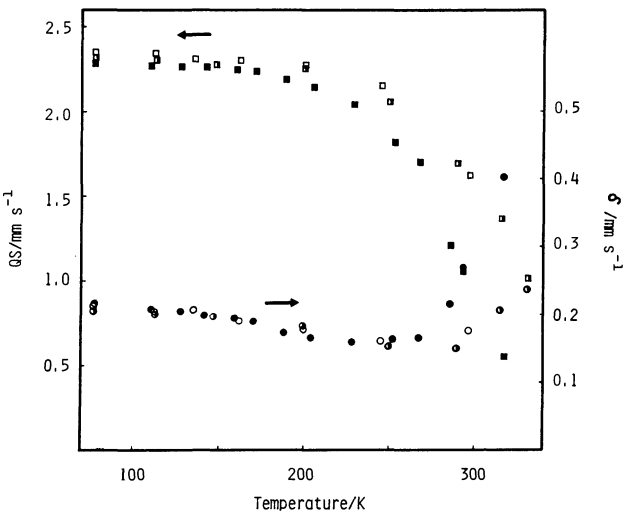

Fig. 2. Temperature dependences of the isomer shift and quadrupole splitting for $[Fe_xCo_{1-x}(acpa)_2]BPh_4$. QS; (■) for x=1, (◨) for x=0.074, (□) for x=0.035. δ; (●) for x=1, (◑) for x=0.074, (○) for x=0.035.

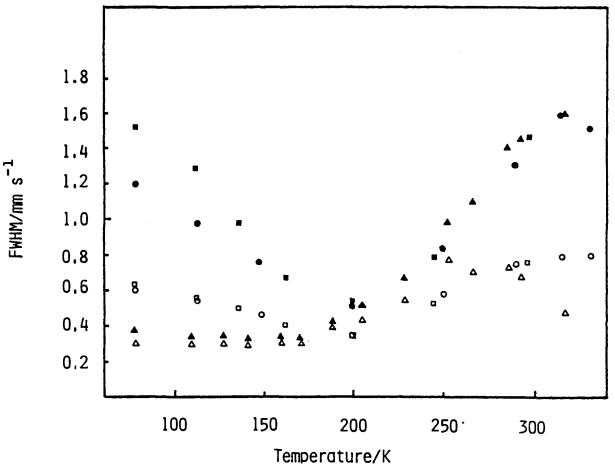

Fig. 3. Temperature dependences of fwhm for $[Fe_xCo_{1-x}(acpa)_2]BPh_4$. (△, ▲) for x=1, (○, ●) for x=0.074, (□, ■) for x=0.035. Open signs are for low energy line, closed ones for high energy line.

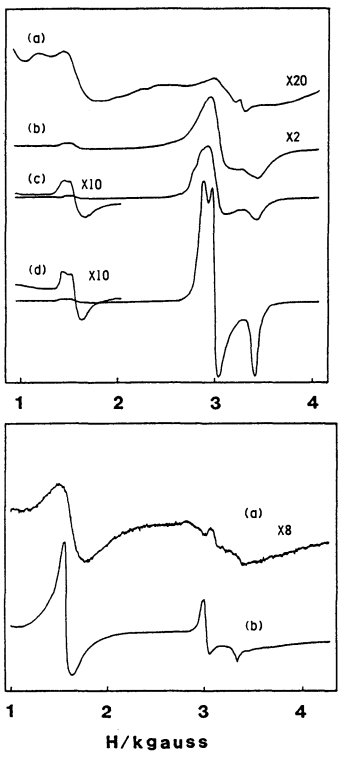

Fig. 4. Temperature dependences of EPR spectra for $[Fe_{0.035}Co_{0.965}(acpa)_2]BPh_4$ (in upper figure, a: 295 K, b: 193 K, c: 173 K, d: 130 K) and $[Fe_{0.05}Co_{0.95}(bzpa)_2]PF_6$ (in lower figure, a: 293 K, b: 78 K).

begin at higher temperature (about 20 K) than those for the undiluted complexes; the temperature range of SST for the diluted complexes shifts to higher temperature than that for the undiluted ones. Iron ions doped in cobalt complexes feel "positive pressure" by the lattice of the cobalt complexes because the radius of a cobalt(III) ion(0.075 nm in the high-spin state) is 0.004 nm smaller than that of an iron(III) ion(0.079 nm in the high-spin state). Therefore the ligand field at the position of an iron(III) ion becomes slightly stronger and thus the low-spin state is more stable. This "pressure effect/size effect" has been observed for some spin-crossover complexes.[7] The large shifts of T_c have been reported for $[(Fe_x, M_{1-x})(phen)_2(NCS)_2]$(M=Co, Cr, Zn) and $[Fe_xCo_{1-x}(3\text{-}OCH_3\text{-}SalEen)_2]PF_6$, which undergo "abrupt transition type" spin-crossover behavior. The complex $[Fe(acpa)_2]BPh_4$ belongs to the "gradual transition type" complexes, in which the coupling between SST and the lattice is supposed to be weak, and thus the small shift of T_c is reasonable. No difference in the spin-state interexchange rate between the diluted compound and the undiluted one is observed as far as the rates are evaluated by a Mössbauer spectroscopy.

The iron complexes doped in the cobalt complexes show broad spectra above or below 200 K. Figure 3 shows the temperature variation of full width at half maximum (fwhm) for $[Fe_xCo_{1-x}(acpa)_2]BPh_4$. The observation that the line broadening increases with rising temperature above 200 K shows that the decrease in mixing of the ^2T state with increase in temperature weakens the spin-spin interaction, because the interaction is significant in the high-spin iron(III) complexes ($^6A_{1g}$). The fraction of the low-spin isomers to the total isomers is estimated to be 0.77 at 200 K on the basis of the magnetic susceptibility data. The line broadening at temperatures below 200 K may result from the spin-lattice relaxation dependent on temperature and spin-spin relaxation. The reasons for the line broadening below 200 K are complex due to the magnetic effects and the spectral shape at 4.2 K is not similar to that for $K_3[Fe(CN)_6]$ doping $K_3[Co(CN)_6]$[14] This problem was not examined further, but the observation of the line broadening supports the view that the iron complexes are isolated.

EPR spectra for the complexes were measured at various temperatures. The representative spectra are illustrated in Fig. 4 and the low-spin signals were observed at g=1.965, 2.219, and 2.291 for the diluted complexes. This observation suggests that an iron atom in the diluted complex is situated in a more distorted environment than that in the pure complex. The g=4 signal is characteristic of a high-spin ferric ion in a rhombically distorted environment.

The Mössbauer spectra for $[Fe_{0.05}Co_{0.95}(bzpa)_2]PF_6$ were measured at various temperatures and the temperature variations of the Mössbauer parameters are plotted in Figs. 5 and 6. In this case the effect of metal dilution on the magnetism is not clear except that slight line broadenings are observed. No observation of "pressure effect/size effect" for this complex shows that this effect does not have a dominant role in the stabilization of a low-spin state and that the effect of intermolecular interaction on spin-state transition may be weak for these complexes. SST properties T_c

and ΔT may be influenced by the lattice energy or elastic property of the complexes. The Mössbauer spectrum at 4.2 K is similar in the shape to that for $[Fe_{0.074}Co_{0.926}(acpa)_2]BPh_4$ except for the smaller quadrupole splitting observed. EPR signals for pure $[Fe(bzpa)_2]PF_6$ were very broad at 78 K,[4] but that for the diluted complexes are observed at $g_{//}=1.961$ and $g_{\perp}=2.166$ and the values are similar to that observed for pure $[Fe(acpa)_2]PF_6$. The observation of EPR spectra for the diluted complexes supports the view that the iron species are isolated satisfactorily in accordance with the results of the Mössbauer spectra measurements.

The Mössbauer spectra for $[Fe_{0.074}Co_{0.926}(acpa)_2]PF_6$ are shown in Fig. 7. From the Mössbauer spectrum for $[Fe_{0.074}Co_{0.926}(acpa)_2]PF_6$ at 298 K the ground state of the complexes is in a low-spin state. The iron complexes are not isomorphous with the cobalt complexes as seen from the powder X-ray diffraction patterns. The local geometric structure around an iron atom in $[Fe_{0.074}Co_{0.926}(acpa)_2]PF_6$ is assumed to be different from that in $[Fe(acpa)_2]PF_6$. This is reflected in the value of the quadrupole splitting; the diluted and pure complexes show QS=2.506 and QS=2.235 mm s^{-1} at 78 K, respectively. At 298 K the Mössbauer parameters for the former complex are QS=1.960 mm s^{-1} and δ=0.169 mm s^{-1}, and the decrease in the QS value for the diluted complexes is due to the increase in the population of the high-spin isomer or the temperature dependence of the quadrupole splitting. But the latter reason can be excluded because EPR analysis indicates that the first excited electronic state($^4T_2$) is at least 3000 cm^{-1} higher in energy than the ground state. The EPR signals for the low-spin isomer in the diluted com-

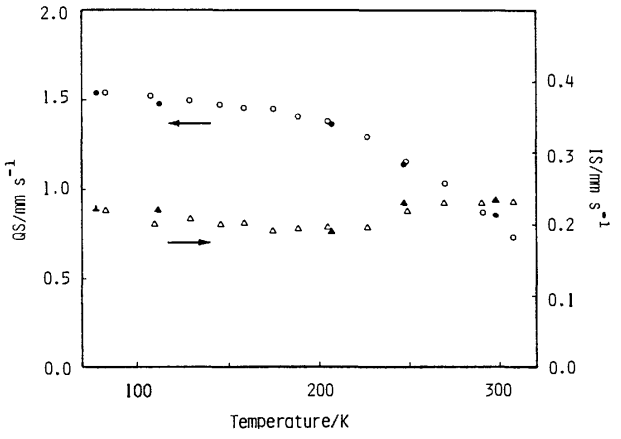

Fig. 5. Temperature dependences of the isomer shift and quadrupole splitting for $[Fe_{0.05}Co_{0.95}(bzpa)_2]PF_6$ (closed signs) and $[Fe(bzpa)_2]PF_6$ (open signs).

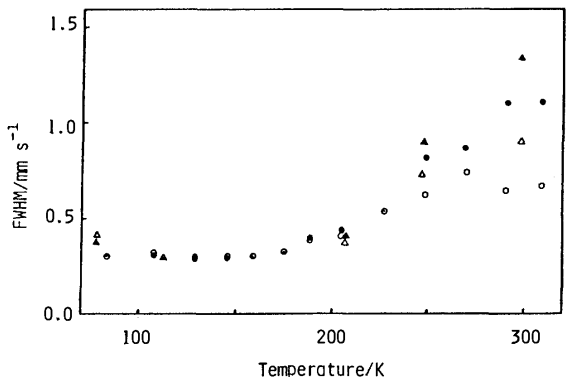

Fig. 6. Temperature dependences of fwhm for $[Fe_{0.05}Co_{0.95}(bzpa)_2]PF_6$ (○, ●) and $[Fe(bzpa)_2]PF_6$ (△, ▲). Open signs are for low energy peaks and closed ones for high energy peaks.

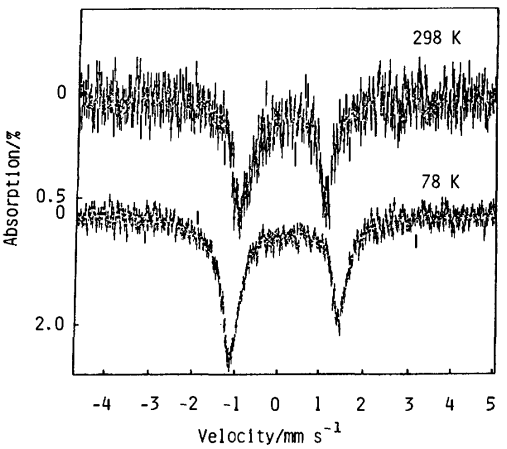

Fig. 7. Mössbauer spectra for $[Fe_{0.074}Co_{0.926}(acpa)_2]PF_6$ at 78 and 298 K.

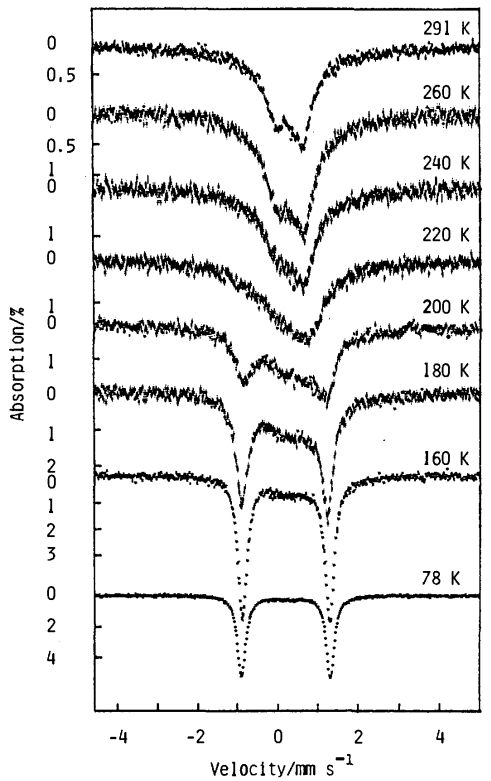

Fig. 8. Temperature dependence of the Mössbauer spectra for $[Fe(acpa)_2]PF_6$ absorbed on SD(A).

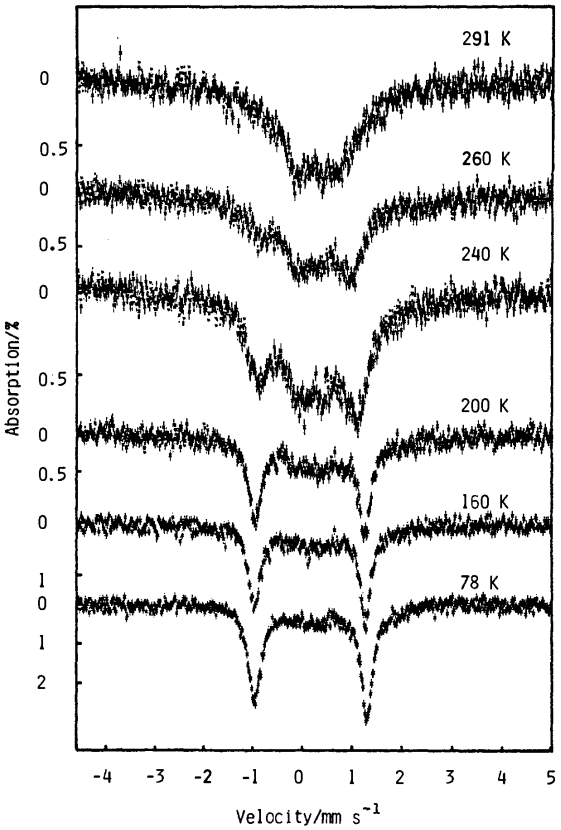

Fig. 9. Temperature dependence of the Mössbauer spectra for $[Fe(acpa)_2]BPh_4$ adsorbed on SD(AB).

plexes are observed at g=1.948, 2.207, and 2.287 at 130 K.

Spin-Crossover Properties of the Complexes Adsorbed on the Surface of SD. Figure 8 shows the temperature dependence of the Mössbauer spectra for $[Fe(acpa)_2]PF_6$ adsorbed on SD(A). These spectra apparently exhibit two pairs of quadrupole doublets; the inner doublet is assigned to the high-spin isomer and the outer doublet to the low-spin isomer. However it is assumed from the spectral shapes that the spin-state interexchange rate is comparable to the inverse of the Mössbauer lifetime. The apparent SST behavior—R, ΔT, and T_c— is estimated to be similar to that for the undiluted complexes. From the Mössbauer parameters for the low-spin isomers at 78 K, QS=2.187 mm s^{-1} and δ=0.198 mm s^{-1}, the geometric structure of the molecule on SD(A) is estimated not to be influenced by physical adsorption on SD in contrast to that of the diluted complexes.

It is curious that no line broadening is observed for the Mössbauer spectra of the complexes supported on SD and as one of the reasons it may be that the complexes are not isolated satisfactorily but adsorbed linearly in the pores. The EPR spectra for the complexes supported on SD are in accord with that for the pure complexes except that the former material shows a signal at g=4.

The Mössbauer spectra for $[Fe(acpa)_2]BPh_4$ and

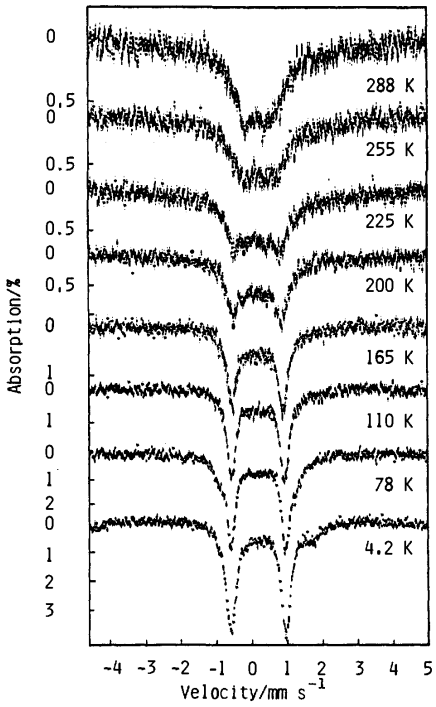

Fig. 10. Temperature dependence of the Mössbauer spectra for $[Fe(bzpa)_2]PF_6$ adsorbed on SD(A).

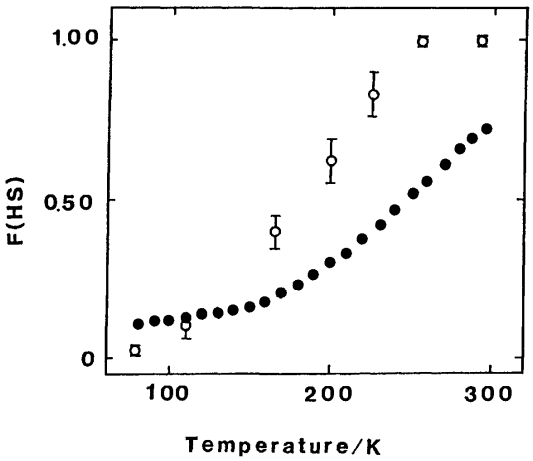

Fig. 11. Temperature dependences of the high-spin population F(HS) for $[Fe(bzpa)_2]PF_6$ adsorbed on SD(A) (○) and the pure complexes (●).

$[Fe(bzpa)_2]PF_6$ adsorbed on SD are illustrated in Figs. 9 and 10, respectively, in which the spectra show a superposition of the quadrupole doublets for the high-spin and low-spin isomers; The Mössbauer spectra at 78 K for both of the complexes show the existence of some impurity due to decomposed paramagnetic products and/or remaining high-spin species. In the spectra at 78 K (Fig. 9) the paramagnetic species and/or the high-spin isomers are observed in 0.4% absorption. They are observed in 0.7% absorption at 240 and 260 K. This illustrates that the absorptions in the center of the spectra are composed of that of the paramagnetic species and the high-spin isomers. That

is, the spectra have a superposition of the spectra for the high-spin isomers and that for the low-spin isomers. This supports a fact that the packing effect enhances the spin-state interexchange rate because it is likely that the complexes feel "free" in the adsorbed state than in the solid state.

At 78 K the quadrupole splitting for the outer doublet(QS=2.254 mm s^{-1}) of the adsorbed $[Fe(acpa)_2]BPh_4$ is almost equal to that(QS=2.288 mm s^{-1}) of the pure complexes, and the quadrupole splitting(QS=1.539 mm s^{-1}) for the adsorbed $[Fe(bzpa)_2]PF_6$ is equal to that (QS=1.542 mm s^{-1}) for the pure complexes. This supports the view that the geometric structures of the adsorbed complexes are consistent with that of the corresponding pure complexes, respectively.

As a representative example the temperature dependence of population of the high-spin isomers F(HS) for $[Fe(bzpa)_2]PF_6$ is plotted in Fig. 11, where the values for the adsorbed complexes were estimated from the Mössbauer spectra and that for the pure complexes from the effective magnetic moments. For the adsorbed complexes corrected values were used because the paramagnetic species are observed in the Mössbauer spectrum at 78 K. The T_c for the adsorbed complexes is estimated to be about 60 K lower than that for the pure complexes, but this large shift is unreliable because the temperature dependence of recoilless fraction of the paramagnetic species is not taken into account. It is unfortunate not to be able to prepare pure samples free from the paramagnetic species. However it is likely that T_c for the adsorbed complexes shifts to lower temperature and that the complexes are essentially in a high-spin state at 300 K. Similar transition behavior is observed for the adsorbed $[Fe(acpa)_2]$-BPh_4.

The EPR spectra of $[Fe(bzpa)_2]PF_6$ adsorbed on SD were measured at 293 and 78 K. The EPR signals for the low-spin isomer are observed at $g_{//}=1.960$ and $g_{\perp}=2.166$. These values are in accordance with that reported by Hendrickson et al. for the complexes dissolved in toluene and with that for the diluted complexes. This fact shows that the adsorbed complexes are satisfactorily isolated.

Finally the Mössbauer spectrum at 4.2 K for $[Fe(bzpa)_2]PF_6$ adsorbed on SD was measured. The high-spin species are not observed in the spectrum, but a shoulder which occurs at the Doppler velocity of 1.5 mm s^{-1} could have originated from decomposition products. The Mössbauer spectrum for $[Fe(bzpa)_2]PF_6$ decomposed by being kept in air on the surface of SD was measured. The relaxation spectrum of the magnetic hyperfine splitting observed will prove that the complexes are isolated from each other on the surface of SD.

The packing effects observed here are weaker than that for "spin transition type" complexes. The values of V and ΔV(V: volume per single molecule for the high-spin isomer, ΔV:volume difference between high-spin and low-spin isomers for single molecule) for $[Fe(acpa)_2]PF_6$ are $V=655.7$ Å^3, $\Delta V=23$ Å^3 and $\Delta V/V=3.5\%$. On the other hand for $[Fe(acpa)_2]BPh_4$ $V=1003.1$ Å^3. $\Delta V=34$ Å^3 and $\Delta V/V=3.4\%$ are observed.[15] Generally the ΔV values of from 23 to 98 Å^3, and $\Delta V/V$ values of from 3.4 to 6.2% are reported. These values for the complexes examined here seem to be in the same range as that reported for the abrupt transition type complexes. Hendrickson et al. have reported an example that the spin-state interexchange rate of diluted complexes is slower than that for the pure complexes.[13] Threfore, it is positive at the present time that spin-state interexchange rates are effected by crystal packing and that intramolecular SST takes place more or less under the co-oparativities with intermolecular interaction.

We wish to thank Dr. Hiroki Oshio of Institute for Molecular Science, Okazaki for the EPR measurement and Dr. Yoichi Sakai of Tokyo University for making available to us silicon dioxide.

References

1) P. Gütlich, *Struct. Bonding(Berlin)*, **44**, 83 (1981).
2) W. R. Scheidt and C. A. Reed, *Chem. Rev.*, **81**, 543 (1981).
3) M. Sorai and S. Seki, *J. Phys. Chem. Solids*, **35**, 555 (1974).
4) Y. Maeda, N. Tsutsumi, and Y. Takashima, *Inorg. Chem.*, **23**, 2440 (1984).
5) Y. Maeda, H. Ohshio, Y. Takashima, M. Mikuriya, and M. Hidaka, *Inorg. Chem.*, **25**, 2958 (1986).
6) H. Ohshio, Y. Maeda, and Y. Takashima, *Inorg. Chem.*, **22**, 2684 (1983).
7) P. Ganguli, P. Gütlich, and E. W. Müller, *Inorg. Chem.*, **21**, 3429 (1982).
8) P. Gütlich, R. Link, and H. G. Steinhäuser, *Inorg. Chem.*, **17**, 2509 (1978); H. Spiering, E. Meissner, H. Köppen, E. W. Müller, and P. Gütlich, *Chem. Phys.*, **68**, 65 (1982).
9) K. Kaji and M. Sorai, *Thermochimica Acta*, **88**, 185 (1985).
10) J. Ensling, P. Gütlich, and K. M. Hasselbach, *Chem. Phys. Lett.*, **42**, 232 (1976).
11) E. W. Müller, J. Ensling, H. Spiering, and P. Gütlich, *Inorg. Chem.*, **22**, 2074 (1983); A. Hauser, P. Gütlich, and H. Spiering, *Inorg. Chem.*, **25**, 4245 (1986).
12) M. S. Haddad, M. W. Lynch, W. D. Federer, and D. N. Hendrickson, *Inorg. Chem.*, **20**, 123 (1981); M. S. Haddad, W. D. Federer, M. W. Lynch, and D. N. Hendrickson, *Inorg. Chem.*, **20**, 131 (1981).
13) W. D. Federer and D. N. Hendrickson, *Inorg. Chem.*, **23**, 3861, 3870 (1984); M. D. Timken, A. M. Abdel-Mawgoud, and D. N. Hendrickson, *Inorg. Chem.*, **25**, 160 (1986).
14) W. T. Oosterhuis and G. Lang, *Phys. Rev.*, **178**, 439 (1969).
15) H. Oshio, K. Toriumi, Y. Maeda, and Y. Takashima, being in preparation.

 © 1988 The Chemical Society of Japan Bull. Chem. Soc. Jpn., 61, 1959—1965 (1988)

Coordination Selectivity in Aluminum(III) Complex with 8-Hydroxy-7-[(2-hydroxy-5-carboxyphenyl)azo]-5-quinolinesulfonic Acid: Evidence for Linkage Isomerism

Zhi-Ping Bai, Hisahiko Einaga,*,† and Jinsai Hidaka
Department of Chemistry, University of Tsukuba, Ibaraki 305
†Institute of Materials Science, University of Tsukuba, Ibaraki 305
(Received October 12, 1987)

The coordination reaction of 8-hydroxy-7-[(2-hydroxy-5-carboxyphenyl)azo]-5-quinolinesulfonic acid (hcqs) to aluminum(III) has been investigated spectrophotometrically in a weakly acidic aqueous solution (pH 2—5) with 0.1 mol dm^{-3} NaCl at 22.0 °C; the thermodynamic stability, kinetics, and mechanism of the formation of the aluminum(III) complex were deduced. The ligand rapidly coordinates to aluminum(III), with its 8-quinolinol (*O-N*) moiety, to form a yellow complex (metal : ligand=1 : 1), and then the complex slowly changes, via an intramolecular rearrangement, to a red complex with its dihydroxyazo (*O-N-O*) moiety, thus showing a linkage isomerism. In the first coordination process, the complex is formed mainly via a pathway of the reaction of $AlOH^{2+}$ with $Hhcqs^{3-}$. The coordination reaction mechanism of aluminum(III) with related ligands, 4-hydroxy-3-[(2-hydroxy-5-carboxyphenyl)azo]-1-naphthalenesulfonic and 7-[(4-carboxyphenyl)azo]-8-hydroxy-5-quinolinesulfonic acid, is also discussed.

The selectivity of coordination modes[1] in metal complexes is one of the fundamental functions of multidentate ligands because of their steric restrictions. In our previous papers,[1-4] the reactions of aluminum(III) with such multidentate ligands as 8-hydroxy-7-[(6-sulfo-2-naphthyl)azo]-5-quinolinesulfonic acid (nqs),[1,2] 7-[(3,6-disulfo-8-hydroxy-1-naphthyl)azo]-8-hydroxy-5-quinolinesulfonic acid (hns),[3] and 7-[(2-carboxyphenyl)azo]-8-hydroxy-5-quinolinesulfonic acid (pqs),[4] have been investigated. The selective coordination sites of these ligands were found to be the 8-quinolinol moiety for nqs, the dihydroxyazo moiety for hns, and the carboxyhydroxyazo moiety for pqs. These findings mean that the coordination ability of the azo nitrogen atom is lower than that of the quinoline nitrogen atom, but that the fused chelate ring structure facilitates the coordination of the azo nitrogen atom in the aluminum(III) complex. Furthermore, it has been found that these ligands react with aluminum(III) with a single rate-determining step to form mono-ligand complexes, which involve a five-membered chelate ring with the *O-N* coordination mode for nqs[1,2] and two six-membered fused chelate rings with the *O-N-O* coordination mode for hns[3] and pqs.[4]

In this work, 8-hydroxy-7-[(2-hydroxy-5-carboxyphenyl)azo]-5-quinolinesulfonic acid (hcqs, **1**), which potentially coordinates to aluminum(III) either with the dihydroxyazo (*O-N-O*) moiety to form five- and six-membered fused chelate rings or with the 8-quinolinol (*O-N*) moiety to form a five-membered chelate ring, was synthesized for the first time in order to investigate its coordination behavior to aluminum(III). It was found that hcqs initially reacts with aluminum(III) to form a yellow complex with the *O-N* coordination mode, but finally forms a red complex with the *O-N-O* mode; the complex shows a linkage isomerism. This paper will be concerned with a detailed investigation of the equilibrium, kinetics, and mechanism of the aluminum(III) complex with hcqs.

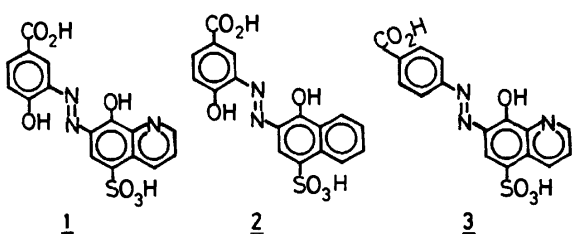

1 2 3

Experimental

Reagents. The ligand, hcqs, was synthesized by the diazotization of 3-amino-4-hydroxybenzoic acid and by coupling to 8-hydroxy-5-quinolinesulfonic acid in a conventional way. The crude product was purified by a repeated salting-out of the aqueous solution with NaCl at pH 7—8. Found: C, 31.77; H, 3.18; N, 6.80%. Calcd for $C_{16}H_{10}N_3O_7SNa \cdot 2NaCl \cdot 4.5H_2O$: C,31.54; H, 3.14; N, 6.90%.

In order to compare them, the ligands, 4-hydroxy-3-[(2-hydroxy-5-carboxyphenyl)azo]-1-naphthalenesulfonic acid (hcns, **2**) and 7-[(4-carboxyphenyl)azo]-8-hydroxy-5-quinolinesulfonic acid (cqs, **3**), were synthesized by the diazotization of 3-amino-4-hydroxybenzoic acid and coupling to 1-naphthol-4-sulfonic acid, and by the diazotization of 4-aminobenzoic acid and coupling to 8-hydroxy-5-quinolinesulfonic acid, respectively. These ligands were then purified by repeated precipitations from an alkaline aqueous solution by means of acidification with HCl. Found: C, 38.44; H, 3.68; N, 5.34%. Calcd for $C_{17}H_{11}N_2O_7SNa \cdot NaCl \cdot 3.5H_2O$: C,38.38; H, 3.41; N, 5.27%. Found: C, 43.89; H, 3.43; N, 9.54%. Calcd for $C_{16}H_{10}N_3O_6SNa \cdot 2.5H_2O$: C,43.64; H, 3.43; N, 9.54%.

An aqueous aluminum(III) solution was prepared by precipitating $Al(OH)_3$ from an aqueous solution of $AlK(SO_4)_2 \cdot 12H_2O$ with alkali, after which the hydroxide was dissolved in water with a minimum amount of HCl. The solution was acidified slightly to prevent the hydrolysis of

aluminum(III) ions. It was then standardized by the EDTA titration method. All the other chemicals used were of an analytical or equivalent grade.

Measurements. Electronic absorption spectral measurements were made on JASCO spectrophotometers, models UVIDEC-505 and -601C. The rapid kinetic measurements were done on a JASCO spectrophotometer, model SS-25, to which a stopped flow apparatus, model SFC-5, a data processor, model DP-500, and a RIKADENKI X-Y recorder, model RW-11, were attached. The slow kinetic runs were monitored on a JASCO spectrophotometer, model UVIDEC-1. All the kinetic runs were carried out in an aqueous solution of 0.1 mol dm^{-3} NaCl at 22.0±0.1 °C under pseudo-first-order kinetic conditions with respect to the aluminum(III) concentration (ligand concentration: (1—7)×10^{-5} mol dm^{-3}). The absorbance changes with time were followed at 495 nm for the aluminum(III) complex with hcqs, at 375 nm for that with hcns, and at 490 nm for that with cqs. The complex formation can be clearly recognized at these wavelengths, which correspond to the maxima or shoulders in the spectra of the ligands. The observed rate constant, k_{obsd}, was calculated from the slope of the linear relation $-\ln(A_i-A_f)$ vs. t on the basis of Eq. 1:

$$\ln[(A_i-A_f)/(A_t-A_f)]=k_{obsd}\cdot t \quad (1)$$

where A_i, A_t, and A_f stand for the absorbances at the initial state, at time t, and at the equilibrium state of the kinetic process respectively. The $k_{obsd(1)}$ and $k_{obsd(2)}$ values for the first and second steps in the case of hcqs were calculated separately on the basis of Eq. 1, because the two steps take place according to different time scales. The A_t vs. t data were separately simulated on an NEC personal computer, model PC-9801E.

The pH value, pH_{meas}, was measured with a HORIBA pH meter, model F7-SS, equipped with glass and 3.33 mol dm^{-3} KCl calomel electrodes. The hydrogen ion concentration, $-\log[H^+]$, was calculated from pH_{meas} according to Eq. 2:

$$-\log[H^+]=pH_{meas}+\log f_{H^+} \quad (2)$$

The activity coefficient of the hydrogen ion, f_{H^+} (0.923), was estimated by defining a solution containing 0.0100 mol dm^{-3} HCl and 0.0900 mol dm^{-3} NaCl at 22 °C as $-\log[H^+]\equiv 2.00$. An acetic acid-sodium acetate buffer solution of less than 0.01 mol dm^{-3} was used to adjust the hydrogen ion concentration.

Results

Electronic Absorption Spectra. Figures 1 and 2 show the absorption spectra of hcqs and its aluminum-(III) complexes, together with those of aluminum(III) complexes of hcns and cqs for comparison. The fully deprotonated species, hcqs^{4-}, gives its dominant peaks corresponding to $\pi^*\leftarrow\pi$ transitions in the 20.0×10^3 cm^{-1} region due to the azo group and at 33.0×10^3 cm^{-1} due to the quinoline and benzene rings. The same spectral features were observed in cqs^{3-} and hcns^{4-}. Protonations at the coordination sites in hcqs^{4-} cause characteristic spectral shifts, which were used for the estimation of the protonation constants.

In the hcqs-aluminum(III) system, the absorbance at 495 nm, which corresponds to an absorption maximum wavelength of H_2hcqs^{2-} (at pH 4.5), decreased rapidly to attain a constant value within 10 s; afterwards, the absorbance began to increase slowly with the time to reach a limiting value after 10 min. The rate of the slow process was independent of the aluminum(III) concentration. Curve (1) in Fig. 2 shows the absorption spectrum when the absorbance at 495 nm is at its minimum. Upon standing, the absorption spectrum changes gradually with the time to Curve (2), but thereafter it does not change. Figure 3 depicts the absorption spectral change with the time in the slow process. The four isosbestic points at 457, 357, 323, and 292 nm indicate that the yellow complex corresponding to Curve (1) changes quantitatively to the red complex corresponding to Curve (2) in Fig. 2. Furthermore, Fig. 2 clearly demonstrates that Curve (1) conforms well to the absorption spectrum (Curve(3)) of the aluminum(III) complex with cqs, which coordi-

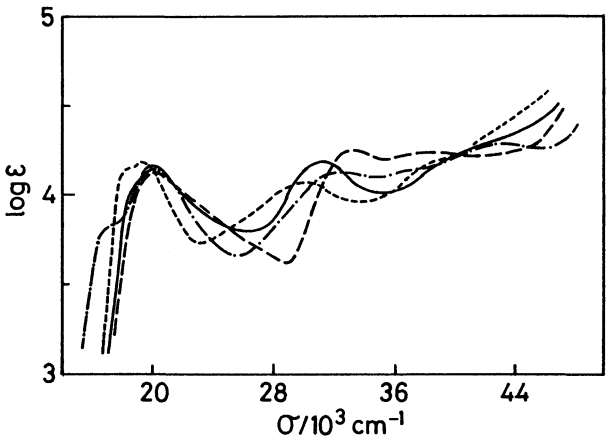

Fig. 1. Absorption spectra of hcqs: (----), H_3hcqs^- (pH 2.4); (——), H_2hcqs^{2-} (pH 5.0); (-·-·-), $Hhcqs^{3-}$ (pH 8.0); and (— — —), $hcqs^{4-}$ (pH 12.0). 0.1 mol dm^{-3} NaCl, 22 °C (cf. Table 1).

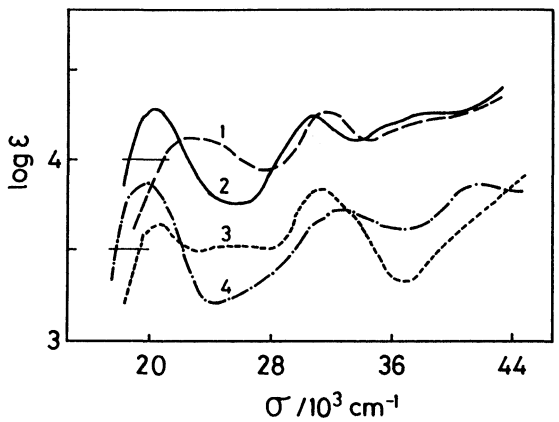

Fig. 2. Absorption spectra of aluminum(III) complexes with hcqs, hcns, and cqs at pH 4.5: 1, (— — —), Al(Hhcqs-*O*,*N*); 2, (——), Al(hcqs-*O*,*N*,*O*)$^-$; 3, (----), Al(cqs)$^-$; and 4, (-·-·-), Al(hcns)$^-$. Curves 3 and 4 are shifted 0.5 unit downward for clarity. 0.1 mol dm^{-3} NaCl, 22 °C.

nates solely with the 8-quinolinol moiety, and that Curve (2) conforms well to that (Curve(4)) of the aluminum(III) complex with hcns, which coordinates solely with the dihydroxyazo moiety.

Hence, it can be inferred that hcqs rapidly coordinates to aluminum(III) to give the yellow complex as a bidentate ligand with the *O-N* moiety and that it then rearranges to the red complex as a terdentate ligand with the *O-N-O* moiety:

$$\underset{\text{red}}{H_2hcqs^{2-}} + Al^{3+} \xrightarrow[\text{fast}]{k_{obsd(1)}} \underset{\text{yellow}}{Al(Hhcqs\text{-}O,N)} \xrightarrow[\text{slow}]{k_{obsd(2)}} \underset{\text{red}}{Al(hcqs\text{-}O,N,O)^-}$$

Protonations of Ligands and Stabilities of Complexes

Protonation. The protonation constants, K_{ai} (i= 1—4), of hcqs:

$$K_{ai}=[H_ihcqs^{(4-i)-}]/[H_{i-1}hcqs^{(5-i)-}][H^+] \quad (3)$$

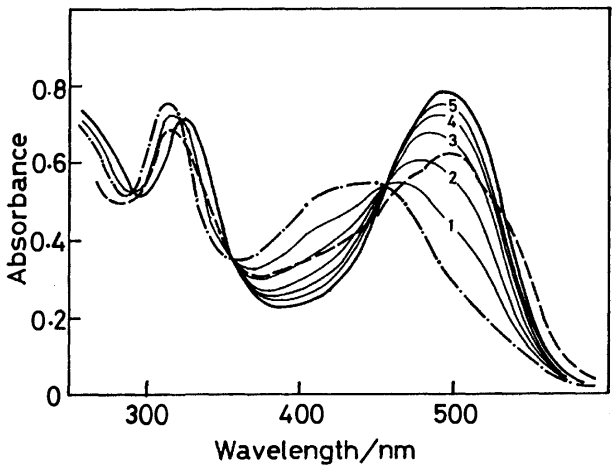

Fig. 3. Absorption spectral change with time of aluminum(III) complex with hcqs. (———), H_2hcqs^{2-}; (-·-·-), spectrum corresponding to yellow complex; (——), spectrum corresponding to red complex; (——), intermediate spectra from yellow to red complex recorded at 1, 1.5 min; 2, 3.5 min; 3, 6 min; 4, 9 min; and 5, 12 min. C_{Al}, 4.7×10^{-4} mol dm^{-3}; C_{hcqs}, 2.16×10^{-5} mol dm^{-3}, pH 4.5, 0.1 mol dm^{-3} NaCl, 22°C.

were determined spectrophotometrically[4] with the aid of Eq. 4:

$$\log\{(A_{(i-1)hcqs}-A_X)/(A_X-A_{(i)hcqs})\} = \log K_{ai}+\log[H^+] \quad (4)$$

where $A_{(i-1)hcqs}$, $A_{(i)hcqs}$, and A_X refer to the absorbances of solutions containing the ligand species $H_{i-1}hcqs^{(5-i)-}$ alone, $H_ihcqs^{(4-i)-}$ alone, and both of them respectively. Absorbance measurements were made at the following wavelengths: hcqs, 585, 345, and 295 nm (K_{a1}), 585 nm (K_{a2}), 550 and 360 nm (K_{a3}), and 360 nm (K_{a4}); hcns, 580 and 335 nm (K_{a1}), 508 and 265 nm (K_{a2}), and 527 nm (K_{a3}); cqs, 525 and 435 nm (K_{a1}), 530 nm (K_{a2}), and 510 nm (K_{a3}). The protonation constants of hcqs, together with those of hcns and cqs, are summarized in Table 1. A mutual comparison of these protonation constants and a comparison with those of the related ligands[1-4] indicate that, in the case of hcqs, K_{a1} corresponds to the protonation at the phenolate oxygen; K_{a2}, to that at the quinolinolate oxygen; K_{a3}, to that at the heterocyclic nitrogen; and K_{a4}, to that at the carboxylate oxygen atoms.

The compositions of the hcqs complexes were estimated by the method of continuous variation.[5] A sharp and single maximum at the ligand mole fraction of 0.5 was obtained for both the yellow and red complexes at 400, 497, and 270 nm, indicating that complexes with a 1 : 1 (Al : hcqs) composition are formed. The formation of the 1 : 1 complexes was also confirmed in the aluminum(III) complex with hcns (at 380 and 325 nm) and in that with cqs (at 519.5 and 320 nm).

Determination of Stability Constants. On the basis of the characteristic spectral features of the hcqs complexes, the protonation constants of hcqs, and the hydrolysis constant[6] of aluminum(III), K_{OH}(=$10^{-4.49}$ defined as $K_{OH}=[AlOH^{2+}][H^+]/[Al^{3+}]$), the 1 : 1 red complex formation equilibrium related to the H_2hcqs^{2-} species at pH 2.69 can be defined as follows:

$$Al^{3+}+H_2hcqs^{2-} \rightleftharpoons Al(hcqs)^-+2H^+ \quad (5)$$

The following materials balance relations hold for the present system:

$$C_{Al}=[Al^{3+}]+[AlOH^{2+}]+[Al(hcqs)^-] \quad (6)$$

Table 1. Protonations of Ligands and Stabilities of Complexes (0.10 mol dm^{-3} NaCl, 22°C)

Ligand	hcqs	hcns	cqs	Remark
I	10.26±0.04	10.84±0.06	—	Phenolate
II	6.36±0.05	6.74±0.05	7.40±0.08	Quinolinolate, naphtholate
III	2.98±0.05	—	2.43±0.05	Quinoline
IV	3.60±0.10	4.25±0.05	2.90±0.05	Carboxylate
Complex	$Al(hcqs\text{-}O,N,O)^-$	$Al(hcns)^-$	Al(cqs)	
$\log\beta_{11}$	14.15±0.10	15.27±0.10	7.49±0.10	

I) $\log(K_{a1}/\text{mol}^{-1}\text{ dm}^3)$ for hcqs, hcns; II) $\log(K_{a2}/\text{mol}^{-1}\text{ dm}^3)$ for hcqs, hcns, $\log(K_{a1}/\text{mol}^{-1}\text{ dm}^3)$ for cqs; III) $\log(K_{a3}/\text{mol}^{-1}\text{ dm}^3)$ for hcqs, $\log(K_{a2}/\text{mol}^{-1}\text{ dm}^3)$ for cqs; IV) $\log(K_{a4}/\text{mol}^{-1}\text{ dm}^3)$ for hcqs, $\log(K_{a3}/\text{mol}^{-1}\text{ dm}^3)$ for hcns, cqs.

$$C_{hcqs}=[H_2hcqs^{2-}]+[Hhcqs^{3-}]+[hcqs^{4-}]+[Al(hcqs)^{-}] \quad (7)$$

Equation 8 can be derived thus from Eqs. 5—7:

$$\log \alpha/r(1-\alpha)=\log \beta_{11}-\log K_{a1}K_{a2}-2\log[H^+]+\log[Al^{3+}] \quad (8)$$

$$\alpha \equiv [Al(hcqs)^-]/C_{hcqs}$$
$$r \equiv K_{a1}K_{a2}[H^+]^2/(1+K_{a1}[H^+]+K_{a1}K_{a2}[H^+]^2)$$
$$[Al^{3+}] \equiv (C_{Al}-\alpha C_{hcqs})/(1+K_{OH}/[H^+])$$

The experimental data are given in Fig. 4; the plot of $\log \alpha/r(1-\alpha)$ vs. $\log[Al^{3+}]$ is linear, with a unit slope. The $\log \beta_{11}$ ($\beta_{11}=[Al(hcqs)^-]/[Al^{3+}][hcqs^{4-}]$) value was determined to be 14.15±0.10 from the intercept; the stability constants are shown in Table 1.

Likewise, the 1 : 1 complex formation equilibrium related to $Hcqs^{2-}$ at pH 3.56 and to H_2hcns^{2-} at pH 2.83 can be defined as follows:

$$Al^{3+}+Hcqs^{2-} \rightleftharpoons Al(cqs)^-+H^+ \quad (9)$$

$$Al^{3+}+H_2hcns^{2-} \rightleftharpoons Al(hcns)^-+2H^+ \quad (10)$$

For cqs:

$$\log \alpha/r(1-\alpha)=\log \beta_{11}-\log K_{a1}-\log[H^+]+\log[Al^{3+}] \quad (11)$$
$$r \equiv K_{a1}[H^+]/(1+K_{a1}[H^+]+K_{a1}K_{a2}[H^+]^2)$$

For hcns:

$$\log \alpha/r(1-\alpha)=\log \beta_{11}-\log K_{a1}K_{a2}-2\log[H^+]+\log[Al^{3+}] \quad (12)$$
$$r \equiv K_{a1}K_{a2}[H^+]^2/(1+K_{a1}[H^+]+K_{a1}K_{a2}[H^+]^2)$$

The experimental data are plotted in Fig. 4 to obtain a $\log \beta_{11}$ value of 7.49±0.12 for the 1 : 1 cqs complex and a $\log \beta_{11}$ value of 15.27±0.10 for the 1 : 1 hcns complex; the stability constants are shown in Table 1.

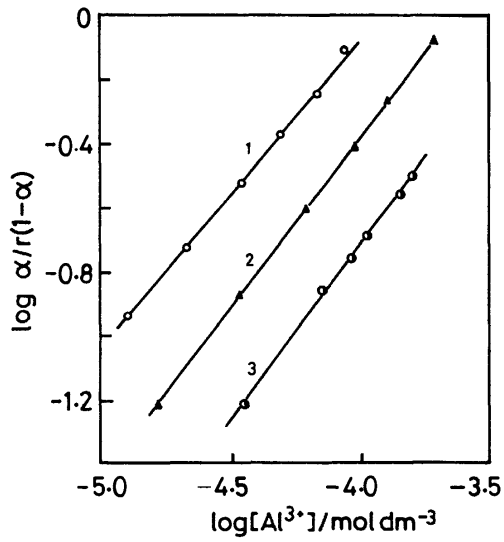

Fig. 4. Relations between $\log \alpha/r(1-\alpha)$ and $\log[Al^{3+}]$. 0.1 mol dm^{-3} NaCl, 22 °C. 1, for 1:1 hcqs complex(red), pH 2.69 (formate buffer), at 550 nm; 2, for 1:1 cqs complex, pH 3.56 (acetate buffer), at 405 nm; and 3, for 1:1 hcns complex, pH 2.83 (formate buffer), at 520 nm.

Kinetics and Mechanism. The formation of the hcqs complex can be treated in term of two consecutive reactions with different time scales: The rapid coordination of hcqs to aluminum(III) to form the yellow complex, Al(Hhcqs-*O*,*N*), followed by a slow intramolecular change to the red complex, $Al(hcqs\text{-}O,N,O)^-$. Each reaction step obeyed the first-order kinetics. A linear relation was obtained between the logarithmic absorbance change with time for more than 3.5 half-life periods for each step at 495 nm.

Rapid Process. By taking into consideration[7] the protonation constants of hcqs, the hydrolysis constant of aluminum(III), the stability constant of the 1 : 1 complexes, and the more rapid attainment of equilibria for the protolytic process[8] as compared with the complex formation process, which proceeds at pH 2—5, the rapid formation of Al(Hhcqs-*O*,*N*) can be considered to proceed as is shown in Scheme 1. Six possible

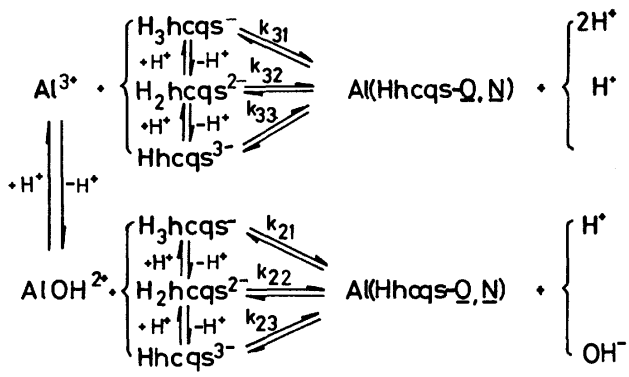

Scheme 1.

reaction pathways are proposed here, with their rate equations:

$$d[Al(Hhcqs\text{-}O,N)]/dt = \{k_{31}[H_3hcqs^-]+k_{32}[H_2hcqs^{2-}]+k_{33}[Hhcqs^{3-}]\}[Al^{3+}] + \{k_{21}[H_3hcqs^-]+k_{22}[H_2hcqs^{2-}]+k_{23}[Hhcqs^{3-}]\}[Al\,OH^{2+}] - \{k_{-31}[H^+]^2+(k_{-32}+k_{-21})[H^+]+(k_{-33}+k_{-22})+k_{-23}[OH^-]\}[Al(Hhcqs\text{-}O,N)] \quad (13)$$

Here, k_{ij} refers to the rate constant for the forward reaction pathway of $AlOH_{3-i}^{i+}$ (i=2 and 3) with $H_{4-j}hcqs^{j-}$, while k_{-ij} refers to the rate constant for the corresponding backward reaction pathway. Under the pseudo-first-order kinetic conditions with respect to the aluminum(III) concentration, the relation 14 between the modified rate constant, $k'_{obsd(1)}$, which can be defined by Eq. 15 from the $k_{obsd(1)}$ determined experimentally by using Eq. 1, while $[H^+]$ can be derived thus from Eq. 13:

$$k'_{obsd(1)}=k_{31}K_{a3}K_{a2}[H^+]^2+(k_{32}+k_{21}K_{a3}K_{OH})K_{a2}[H^+]+(k_{33}+k_{22}K_{a2}K_{OH})+k_{23}K_{OH}[H^+]^{-1} \quad (14)$$

Table 2. Kinetic Parameters (0.10 mol dm^{-3} NaCl, 22 °C)

Pathway	Rate constant/mol^{-1} dm^3 s^{-1}	Remark
$AlOH^{2+}+Hhcqs^{3-}$ (k_{23})	k_{23}: (1.37±0.35)×10^5	First step
Al(hcqs-*O*,*N*)(OH)→	k_{IV}: (3.43±0.45)×10^3	k_{IV}/s^{-1}, second step
$Al^{3+}+cqs^{3-}$(k_{33}) and $AlOH^{2+}+Hcqs^{2-}$(k_{22})	$k_{33}+k_{22}K_{a1}K_{OH}$: (1.34±0.40)×10^5	$K_{a1}=K_{a1(cqs)}$
$AlOH^{2+}+cqs^{3-}$(k_{23})	k_{23}: (7.20±0.30)×10^5	$K_{OH}=K_{OH(Al)}$
$Al^{3+}+Hhcns^{3-}$(k_{33}) and $AlOH^{2+}+H_2hcns^{2-}$(k_{22})	$k_{33}+k_{22}K_{a2}K_{OH}$: (4.44±0.46)×10^2	$K_{a2}=K_{a2(hcns)}$
$AlOH^{2+}+Hhcns^{3-}$(k_{23})	k_{23}: (3.91±0.35)×10^3	

$$k'_{obsd(1)} \equiv k_{obsd(1)}/\{1/\beta'_{11} + C_{Al}/[(K_{a3}K_{a2}[H^+]^2 + K_{a2}[H^+] + 1)(1 + K_{OH}/[H^+])]\} \quad (15)$$

where C_{Al} refers to the total concentration of aluminum(III) and β'_{11}, to the stability constant of Al(Hhcqs-*O*,*N*), which was tentatively estimated to be the same as that of Al(cqs). Figure 5 shows the experimental data plotted on the relation of $k'_{obsd(1)}$ vs. $[H^+]$; a linear relation with an intercept of zero, which indicates that Al(Hhcqs-*O*,*N*) is formed through the reaction pathway of $AlOH^{2+}$ with $Hhcqs^{3-}$. The rate constant, k_{23}, is given in Table 2.

Slow Process. In the slow process, the observed rate constant, $k_{obsd(2)}$, does not depend on C_{Al} at a constant hydrogen ion concentration; this is in contrast to the rapid process, in which $k_{obsd(1)}$ is linearly dependent on C_{Al}. This fact indicates that the slow process (the second reaction step) corresponds to an intramolecular rearrangement of the hcqs complex between two possible coordination modes of the ligand.

Scheme 2 shows the equilibria among possible complex species of Al(Hhcqs-*O*,*N*). Hence, the formation of the red complex, Al(hcqs-*O*,*N*,*O*)$^-$, can be expected via four possible reaction pathways, with the rate equations given as follows:

$$\begin{aligned} &d[Al(hcqs\text{-}O,N,O)]/dt \\ &\quad = -d[Al(Hhcqs\text{-}O,N)]/dt \\ &\quad = k_I[I] + k_{II}[II] + k_{III}[III] + k_{IV}[IV] \\ &\quad - \{k_{-I}[H^+] + (k_{-II} + k_{-III}) \\ &\quad + k_{-IV}[OH^-]\}[Al(hcqs\text{-}O,N,O)] \end{aligned} \quad (16)$$

By defining the modified rate constant, $k'_{obsd(2)}$, which can be defined by the use of Eq. 17 from the $k_{obsd(2)}$ value determined experimentally by using Eq. 1:

$$k'_{obsd(2)} \equiv k_{obsd(2)}/\{1/\beta''_{11} + 1/[(1 + K_{a1}[H^+])(1 + K_{OH}/[H^+])]\} \quad (17)$$

Eq. 18 can then be derived:

$$k'_{obsd(2)} = k_I K^{II}_{a1}[H^+] + (k_{II} + k_{III}K^{IV}_{a1}K^{I}_{OH}) + k_{IV}K^{I}_{OH}[H^+]^{-1} \quad (18)$$

Here, k_I, k_{II}, k_{III}, and k_{IV} are the rate constants for the forward pathways of the second reaction step related to the complex species of I, II, III, and IV; k_{-I}, k_{-II}, k_{-III}, and k_{-IV} are those for the reverse pathways corresponding to each species; β''_{11} is the stability constant of Al(hcqs-*O*,*N*,*O*)$^-$ with reference to Al(Hhcqs-*O*,*N*,); K^{II}_{a1} and K^{IV}_{a1} are the protonation constants of the complex species II and IV corresponding to the K_{a1} values of hcqs, and K^{I}_{OH} and K^{II}_{OH} are the hydrolysis constants of aluminum(III) in the complex species I and II respectively. In the following treatments, for convenience, K^{II}_{a1} and K^{IV}_{a1} were approximated to K_{a1}, and K^{I}_{OH} and K^{II}_{OH}, to K_{OH}. Figure 5 shows a linear relation with a zero intercept between $k'_{obsd(2)}$ and $[H^+]^{-1}$. That is, the intramolecular rearrangement

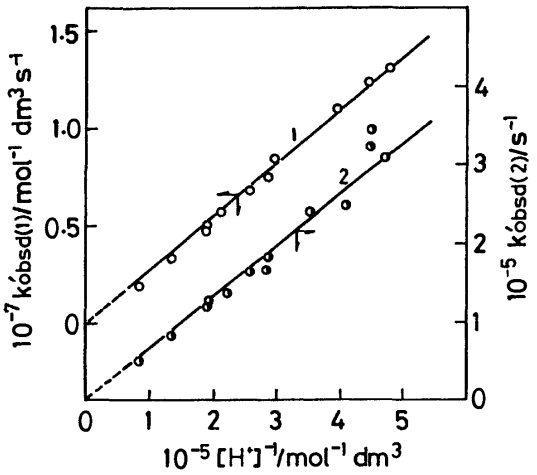

Fig. 5. Relation between $k'_{obsd(1)}$ and $1/[H^+]$ in the first step (1), and between $k'_{obsd(2)}$ and $1/[H^+]$ in the second step (2): C_{Al}, 4.7×10^{-4} mol dm^{-3}; C_{hcqs}, 2.16×10^{-5} mol dm^{-3}; 0.1 mol dm^{-3} NaCl, 22 °C; absorbance at 495 nm.

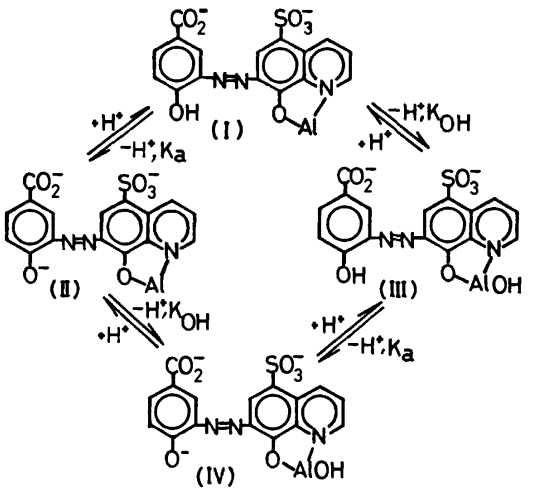

Scheme 2.

takes place through the pathway of the complex species IV. The rate constant, k_{IV}, is given in Table 2.

Formation of the cqs and the hcns Complexes. The kinetics of the formation of aluminum(III) complexes with cqs and hcns were also studied under pseudo-first-order kinetic conditions with respect to the aluminum(III) concentration. The coordination reaction of cqs to aluminum(III) was rapid, just as in the case of the first step of that of hcqs to aluminum(III); a linear relation was found between the logarithmic absorbance change with time for more than 3.5 half-life periods at 316, 400, and 495 nm. On the contrary, the coordination reaction of hcns to aluminum(III) was rather slow as compared with that of cqs, and the reaction rate was of the same order as that of the second step of the hcqs complex; a linear relation was obtained between the logarithmic absorbance change with time for more than 3.5 half-life periods at 495 nm.

The same mathematical treatments as in the case of the rapid process of the hcqs complex were carried out for the cqs and the hcns complexes in order to deduce the reaction pathways; similar relations between the modefied rate constant, k'_{obsd}, and $[H^+]$ were derived as follows:

For the cqs complex:

$$K'_{obsd} = k_{31}K_{a1}K_{a2}[H^+]^2 + (k_{32} + k_{21}K_{a2}K_{OH})K_{a1}[H^+] + (k_{33} + k_{22}K_{a1}K_{OH}) + k_{23}K_{OH}[H^+]^{-1} \quad (17)$$

For the hcns complex:

$$K'_{obsd} = k_{32}K_{a1}K_{a2}[H^+]^2 + (k_{33} + k_{22}K_{a2}K_{OH})K_{a1}[H^+] + (k_{34} + k_{23}K_{a1}K_{OH}) + k_{24}K_{OH}[H^+]^{-1} \quad (18)$$

Here, k_{ij} have the usual meanings. The plots of the experimental data in Fig. 6 indicate a linear relation between k'_{obsd} and $1/[H^+]$ for the cqs complex and a linear relation between k'_{obsd} and $[H^+]$ for the hcns complex. The kinetic parameters are summarized in Table 2.

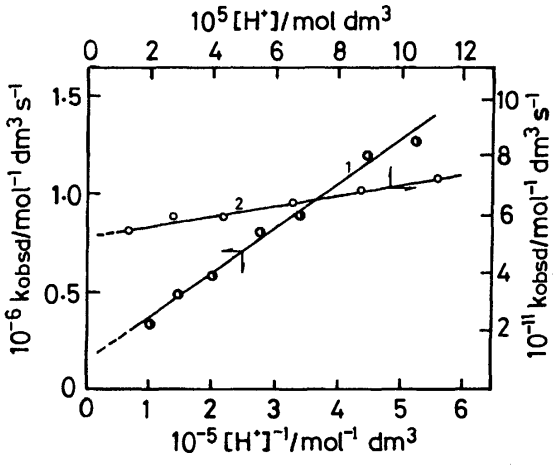

Fig. 6. Relation between k'_{obsd} and $1/[H^+]$ for 1:1 cqs complex at 490 nm (1); and between k'_{obsd} and $[H^+]$ for 1:1 hcns complex at 375, 330, and 265 nm (2). C_{Al}, 4.7×10^{-4} mol dm^{-3}; C_{cqs} or C_{hcns}, 2.4×10^{-5} mol dm^{-3}; 0.1 mol dm^{-3} NaCl, 22°C.

Discussion

The ligand hcqs shows coordination behavior unique to aluminum(III); namely, it forms two types of complexes, Al(Hhcqs-*O,N*) (yellow) and Al(hcqs-*O,N,O*)$^-$ (red),[9] which are in the linkage isomerism. This is unlike hns and pqs, which coordinate selectively to aluminum(III) only with one of the two coordination modes, although the linkage isomerism is possible for hns and pqs as well as for hcqs. The molecular models of the ligand species suggest that hcqs is stabilized more to a *trans-O,O* form (phenolate and quinolinolate oxygen atoms) with regard to the azo group by the intramolecular hydrogen bonds, whereas hns is less stabilized to the *trans-O,O* form with the intramolecular hydrogen bonds, while pqs has no such hydrogen bonds for the stabilization of the *trans-O,O* form. Hence, it can tentatively be inferred that the hydroxyl group ortho to the azo group on the aromatic ring opposite the 8-quinolinol moiety is prerequisite for the linkage isomerism.

The ligand hcqs first coordinates to aluminum(III) with the 8-quinolinol moiety to form the yellow complex. The absorption spectral and kinetic evidence indicates that the coordination behavior of hcqs to aluminum(III) was superposable on that of cqs, which functions as the *O-N* bidentate ligand, but was quite different from that of hcns, which functions as the *O-N-O* terdentate ligand. Taking the differences in molecular structure of these ligands into consideration,[10] Table 2 clearly indicates that the rate constants for each of the reaction pathways of hcqs and of cqs are of the same magnitude as those for the corresponding pathways of hns, nqs, pqs, and hqs.[1-4] Therefore, the rate-determining steps of hcqs and cqs for their coordination to aluminum(III) must be the same as those of hns, nqs, pqs, and hqs; donation via the 8-quinolinolate oxygen atom to aluminum(III). Chelate ring closure as the rate-determining step can probably be ruled out because the rate constants for cqs, hcqs, nqs, and hqs, all having the *O-N* bidentate ring, are intrinsically of the same magnitude, and they agree with those of hns and pqs. Incidentally, the considerably small rate constant for hcns compared with the rate constants for hns and pqs indicates that the chelate ring closure is the rate-determining step in the coordination of hcns to aluminum(III). Hence, it is inferred that the formation of Al(Hhcqs-*O,N*) proceeds through the coordination of the 8-quinolinolate oxygen atom to aluminum(III) as the rate-determining step,[1-4] followed by a rapid chelate ring closure to form a five-membered chelate ring.

The formation of the red hcqs complex shows a unique kinetic feature: The rate constant for the formation of the red complex is considerably smaller than

that of the cqs complex; rather, it is in line with that of the hcns complex. The molecular models of hcqs and hcns indicate that the coordination of these ligands with the *O-N-O* terdentate moieties requires transformation from the *trans-O,O* to the *cis-O,O* form with regard to the azo group by breaking the intramolecular hydrogen bond(s) after the coordination through the 8-quinolinolate oxygen atom as unidentate ligands. The small rate constants for the formation of the red hcqs complex and of the hcns complex reflect some contribution of this transformation; therefore, it may be concluded that the linkage isomerization of the yellow hcqs complex to the red one and the formation of the hcns complex proceed with the chelate ring closure as the rate-determining step.

Finally, it should be noted that hcqs and the related ligands can be classified into two groups with respect to the experimental relation of the modified rate constant, k'_{obsd} vs. $[H^+]$; linear relations between k'_{obsd} and $[H^+]$ hold for hcns, hns, pqs, and hqs, whereas linear relations between k'_{obsd} and $[H^+]^{-1}$ hold for hcqs, cqs, and nqs. The classification can be explained in terms of the basicity (protonation constant) of the oxygen donor atom on the quinoline ring; those ligands having a higher basicity conform to the former relation, while those having a lower basicity conform to the latter relation. This evidence also supports the important role of the oxygen atom in the 8-quinolinol moiety on the reaction kinetics with aluminum(III), especially the rate-determining step, of hcqs and the related multidentate ligands.

References

1) K. Hayashi, K. Okamoto, J. Hidaka, and H. Einaga, *J. Chem. Soc., Dalton Trans.*, **1982**, 1377.

2) K. Hayashi, K. Okamoto, J. Hidaka, and H. Einaga, *J. Coord. Chem.*, **12**, 243 (1983).

3) H. Iwasaki, K. Okamoto, J. Hidaka, and H. Einaga, *J. Coord. Chem.*, **12**, 219 (1983).

4) I. Ohkura, K. Fujiwara, K. Okamoto, J. Hidaka, and H. Einaga, *J. Coord. Chem.*, **13**, 221 (1984).

5) H. L. Schläfer, "Komplexbilbung in Lösung," Springer, Berlin (1961), Chap. 8.

6) L. P. Holmes, D. L. Cole, and E. M. Eyring, *J. Phys. Chem.*, **72**, 301 (1968).

7) Y. Hara, K. Okamoto, J. Hidaka, and H. Einaga, *Bull. Chem. Soc. Jpn.*, **57**, 1211 (1984).

8) M. Eigen, *Pure Appl. Chem.*, **6**, 97 (1963).

9) In this type, hcqs is able to form two kinds of chelate ring arrangements, depending upon which nitrogen atom in the azo group serves as a donor atom. They can be considered to be in equilibrium because of the high lability of the aluminum(III) complex and the lack of any difference in steric restrictions between these arrangements.

10) There are several pairs of reaction pathways proceeding in a parallel way and indistinguishable by a kinetic investigation because of proton ambiguity. The highest probable rate constant for each reaction pathway was tentatively estimated for the discussion.

 © 1988 The Chemical Society of Japan Bull. Chem. Soc. Jpn., 61, 1967—1973 (1988)

Accelerating Effect of Donor Solvents on Racemization of the Tris(1,10-phenanthroline)iron(II) Cation

Terufumi FUJIWARA,* Yoshiharu OKAMOTO, and Yuroku YAMAMOTO†
Department of Chemistry, Faculty of Science, Hiroshima University, Higashisenda, Naka-ku, Hiroshima 730
†Environmental and Safety Engineering Department, Fukui Institute of Technology, Gakuen, Fukui 910
(Received October 24, 1987)

Rates of racemization of the tris(1,10-phenanthroline)iron(II) cation, $[Fe(phen)_3]^{2+}$, have been measured at 7.5 °C to 17.5 °C in 1,2-dichloroethane, *o*-dichlorobenzene, nitrobenzene, and nitromethane, and in 1,2-dichloroethane solutions containing dimethyl sulfoxide (DMSO), *N*,*N*-dimethylformamide (DMF), methanol (MeOH), acetone (Ac), and acetonitrile (AN). In the four pure solvents, the observed racemization rates are markedly smaller than those calculated by the Van Meter and Neumann equation, which relates the racemization rate to the solvation energy of the phen ligands and viscous resistance. Addition of donor solvents to 1,2-dichloroethane solutions of the iron complex enhances the racemization rates. The degree of enhancement increases in the order AN < Ac < MeOH < DMF < DMSO and the activation energy decreases in the same order. This sequence lies in the order of increasing Gutmann donor number of the solvents, indicating a nucleophilic interaction of the solvents with the iron metal in the transition state. These obsevations may be interpreted in terms of Kepert's model for solvent-assisted racemization of tris-chelated complexes and the molecular structure of a solvate complex determined previously, and allow us to modify the Van Meter and Neumann equation.

The kinetics of racemization of the tris-chelated complexes of 1,10-phenanthroline (phen) with iron(II), nickel(II), and cobalt(III), $[Fe(phen)_3]^{2+}$, $[Ni(phen)_3]^{2+}$, and $[Co(phen)_3]^{3+}$, have been studied extensively,[1] and it was concluded that these three complexes racemize through different mechanisms: twist,[2] dissociative,[3,4] and electron exchange,[5] respectively. Solvent effects on the racemization reactions have been examined in organic solvents or in aqueous-organic solvent mixtures during recent decades.[6] In aqueous solutions, we have shown that a different solvent effect appears to reflect a difference between their racemization mechanisms.[7]

In our previous studies of racemization of the nickel complex in several solvents[8] and in 1,2-dichloroethane solutions containing various amounts of donor solvents,[9] the racemization rates were found to decrease with decreasing donicity of the solvents (Gutmann donor number[10]), indicating that attack of the donor on the central metal may be important for the racemization.[11] On the other hand, the racemization reaction of the iron complex has been thought to provide one of interesting examples of unimolecular reactions involving no formal separation of charge but the role of solvent in the racemization has not been obvious and is still a matter for discussion, especially with respect to the mechanism. In a study of the rates of dissociation and racemization of $[Fe(phen)_3]^{2+}$ in various solvents,[12] Van Meter and Neumann reported that solvent variation affects the rates of racemimization k_r, and derived empirically the equation,

$$\log k_r = c_i - (0.26\Delta G_L/2.303RT) - 0.48\log(\eta V_m), \quad (1)$$

where c_i, ΔG_L, η, and V_m are a constant, the free energy of solvation of the phen ligand, the solvent viscosity, and the molar volume of the solvent, respectively. Recently, the polarizability of solvents and added salts in aqueous solutions was suggested to be one of important factors which facilitate the racemization of the iron complex.[13] On the other hand, we noted that the racemization rates in aprotic solvents decrease with the solvent in the order, *N*,*N*-dimethylformamide > acetonitrile > nitrobenzene, despite the fact that the three solvents are very similar in ΔG_L; this sequence lies in the order of decreasing donicity of the solvents, implying that the donicity play a significant role on the racemization even in the case of the $[Fe(phen)_3]^{2+}$ complex,[14] as well as in the case of the $[Ni(phen)_3]^{2+}$ complex.[8,9]

In order to explore this possibility, first, we present further examples of solvents such as nitrobenzene in which the observed rate of the racemization is markedly smaller than that calculated by Eq. 1. Here, the contribution to the solvation energy, ΔG_L, for the $[Fe(phen)_3]^{2+}$ cations arising from ligand-solvent interactions was calculated from the solubility data for naphthalene by the method of Van Meter and Neumann.[15] Second, measurements of the racemization rates in 1,2-dichloroethane solutions with varying concentration of the donor solvents, dimethyl sulfoxide, *N*,*N*-dimethylformamide, methanol, acetone, and acetonitrile, were made over a temperature range. The results may be interpreted based on Kepert's model for solvent-assisted racemization of tris-chelated complexes.[16] Support for this is furnished by the X-ray structure of the nitrobenzene solvate, $[Fe(phen)_3]I_2 \cdot NB \cdot 2H_2O$, reported already.[17]

Experimental

Materials. The preparation of the optically active complex, (+)-$[Fe(phen)_3](ClO_4)_2 \cdot 3H_2O$, was performed according to the method of Dwyer and Gyarfas involving diastereoisomer resolution with antimonyl (+)-tartrate.[18]

Reagent-grade non-aqueous solvents were further purified before experimental use as follows. Nitrobenzene (NB), *o*-

dichlorobenzene (DCB), and 1,2-dichloroethane (DCE) were purified according to the procedures described in our previous papers[7,19,20] and nitromethane (NM) according to the method of Unni et al.[21]

Dimethyl sulfoxide (DMSO) was refluxed with potassium hydroxide for 3 h at 125 °C, and then fractionally distilled twice at 95 °C under reduced pressure with a nitrogen bleed. The middle fraction was collected each time. *N,N*-Dimethylformamide (DMF) was distilled fractionally under a pressure of a few millimeters. The middle cut was taken and, after being dried over 4-A Molecular Sieves for one week, distilled once more under vacuum at 65 °C with a nitrogen bleed. The middle fraction was collected. Methanol (MeOH), to which 6 M (1 M=1 mol dm^{-3}) sulfuric acid (25 cm^3 per liter) was added, was refluxed for several hours and distilled. The product was treated with 20 g of potassium hydroxide and 10 g of silver nitrate per liter, the mixture being refluxed and distilled. The distillate was dried over 3-A Molecular Sieves for 1 d, and then distilled fractionally from magnesium over nitrogen. Acetone (Ac) was dried over 4-A Molecular Sieves, filtered, and distilled. Acetonitrile (AN) was intermittently shaken or stirred (magnetic stirrer) with calcium hydride (10 g per liter) for 2 d, decanted, and then fractionally distilled from phosphorus pentaoxide (5 g per liter). The product was refluxed over calcium hydride (5 g per liter) for several hours, then fractionally distilled very slowly. The middle fraction was collected. All solvents have densities identical with or close to literature values: Observed densities for DCE, DCB, NB, and NM are given in Table 1; DMSO, 1.09525 (1.0958); DMF, 0.94401 (0.94397); MeOH, 0.78653 (0.78664); Ac, 0.78447 (0.78440); AN, 0.77662 (0.7766). Values in parentheses are from the literature.[22] Water contents in the solvents were measured coulometrically by using a Hiranuma AQ-3 aquacounter to be less than 0.01 M. Naphthalene was recrystallized three times from methanol. The melting point was 80.7 °C (lit,[23] 80.5 °C).

Rates of Racemization. The rates of racemization of (+)-$[Fe(phen)_3](ClO_4)_2$ in various solutions were determined over a temperature range by the method described in our previous work.[7] The optical rotations of the chelate were measured at 365 nm in DCE and DCB solutions and at 589 nm in NB and NM solutions by using a Perkin-Elmer Model 141 polarimeter with Hg and Na lamps, respectively. About 10^{-4} M solutions of the chelate were prepared by its dissolution in the appropriate solution. This solution was immediatedly poured into a 1-dm, water-jacketed, polarimeter tube and maintained at constant temperature (±0.1° C) by circulating water.

The values of the observed rotation, α, were plotted in the usual fashion, log α vs. time, and the slope of the straight line obtained is equal to $-k_r/2.303$ where k_r is the rate constant in s^{-1} for the racemization.

Solubility of Naphthalene. The procedure of solubility measurement was similar to that for $[Fe(phen)_3](ClO_4)_2$[24] except that the solubility of naphthalene, S_{naphth}, was determined from density measurements by using the equation,

$$S_{naphth} = 1000(d_0 - d)/(V_m d_0 - M_w), \quad (2)$$

where d_0 and d are the densities of a pure solvent and its solution containing naphthalene, respectively, and M_w is the molecular weight of naphthalene (M_w=128.175). The apparent molar volumes, V_m, of naphthalene, which are given in Table 1, were determined from density measurements by using the Eq. 2 for DCE, DCB, NB, and NM solutions with varying concentration of naphthalene prior to the solubility measurements. The densities of the sample solutions were measured by using a digital densimeter (Anton Paar Precision Density Meter, Model DMA 02D) with an internal measuring cell which is water jacketed with a water-circulating thermostat at 25.00±0.005 °C.

Table 1. Solubilities and Apparent Molar Volumes of Naphthalene and Densities of Solvents at 25 °C

Solvent	S_{naphth}	V_m	d_0	
	M	cm^3 mol^{-1}	obsd.	lit.
DCE	3.418±0.002	125.528±0.003	1.24574	1.2458[a]
DCB	2.724±0.004	125.70 ±0.01	1.30036	1.30033[a]
NB	2.747±0.002	125.75 ±0.03	1.19820	1.1983[b]
NM	1.400±0.002	126.77 ±0.06	1.13111	1.13124[c]

a) Data from Ref. 22. b) Data from Ref. 19. c) Data from Ref. 21.

Results

Rates of Racemization. The rate constants in the various pure solvents are given in Tables 2 and 3. The errors are the standard derivations estimated from the residuals of the least-squares line for each run. The reproducibility of the measurements can be evaluated from the data obtained in duplicate under the same reaction conditions. There is no dependence of the racemization rate on the complex concentration in each solvent as given in Table 2. The activation parameters, E_a and log A for the rates were calculated from the Arrhenius plot of log k_r vs. $1/T$. The rate constants for DCE, DCB, NB, and NM at 25 °C were extrapolated from the Arrhenius plots. Table 4 gives the results and includes the data for AN, MeOH, Ac, and DMF[12] for comparison, indicating that the racem-

Table 2. Concentration Dependence of the Rate Constant for Racemization on $[Fe(phen)_3](ClO_4)_2$ in Various Pure Solvents at 15.0 °C

Solvent	$10^4 C_c$[a]	$10^4 k_r$
	M	s^{-1}
DCE	0.128	7.56±0.07
	0.580	7.65±0.03
	1.18	7.75±0.01
	1.44	7.63±0.05
DCB	0.45	8.15±0.11
	0.51	8.38±0.16
	0.56	7.72±0.17
NB	0.554	6.99±0.11
	0.817	6.70±0.06
	1.38	7.02±0.23
	2.52	6.69±0.06
NM	1.17	5.45±0.06
	2.31	5.53±0.07
	2.32	5.48±0.10
	3.21	5.51±0.13

a) C_c is the concentration of $[Fe(phen)_3](ClO_4)_2$.

Table 3. Rate Constants for Racemization of $[Fe(phen)_3](ClO_4)_2$ in Various Pure Solvents

Solvent	$10^4 k_r/s^{-1}$				
	7.5 °C	10.0 °C	12.5 °C	17.5 °C	
DCE	2.20±0.02	3.35±0.01	5.00±0.02	11.54±0.05	
	2.02±0.02	3.40±0.01	5.08±0.02	11.59±0.05	
DCB	—	3.87±0.06	5.55±0.04	13.93±0.06	
		4.06±0.02	5.45±0.04	13.81±0.12	
NB	2.03±0.02	3.03±0.01	4.78±0.08	10.06±0.13	
	2.14±0.02	3.06±0.02	4.85±0.04	9.90±0.10	
NM	1.66±0.01	2.54±0.02	3.90±0.02	8.17±0.04	13.0[a]
	1.68±0.01	2.58±0.03	3.86±0.02	8.50±0.08	

a) Data (at 20.1 °C) from Ref. 13.

Table 4. Arrhenius Parameters and Rate Constants for Racemization and Dissociation of $[Fe(phen)_3](ClO_4)_2$ in Various Pure Solvents at 25 °C

Solvent	Racemization			Dissociation
	E_a	log A	log k_r	log k_d
	kJ mol^{-1}	s^{-1}	s^{-1}	s^{-1}
DCE	114±2	17.6±0.3	−2.42	−6.84
DCB	112±7	17.2±1.2	−2.39	−5.61
NB	107±2	16.3±0.3	−2.51 −2.73[a]	−7.57
NM	109±2	16.5±0.3	−2.59	−8.58
AN[b]	—	—	−1.83	−5.69
MeOH[b]	90	13.93	−1.73	−4.40
DMF[b]	97	15.8	−1.16	−3.62
Ac[b]	90	15.6	−0.70	−5.22

a) Data from Ref. 2. b) Data from Ref. 12.

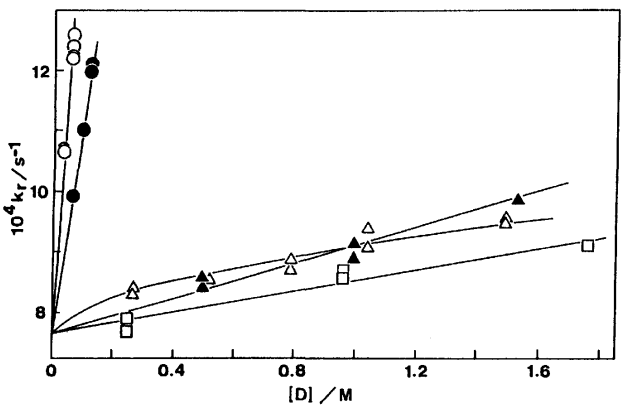

Fig. 1. Dependence of rate constant (k_r) for racemization of $[Fe(phen)_3]^{2+}$ on the concentration of donor solvent, [D], in DCE solution at 15.0 °C: (○), DMSO; (●), DMF; (△), MeOH; (▲), Ac; (□), AN.

ization occurs more slowly in DCE, DCB, NB, and NM.

Table 5 gives the rate constants in the DCE solutions with varying concentration of the various donor solvents and the typical results are illustrated in Fig. 1, where the data are plotted as k_r vs. donor solvent concentration, [D]. Figure 1 shows that the plots were good straight lines, except for MeOH. By a weighted least-squares procedure, the results were fitted to the equation,

$$k_r = k_0 + k_s[D], \quad (3)$$

where k_0 and k_s are the intercept and the slope of the plot, respectively. The values of k_0 were in agreement with the corresponding rate constants in the pure DCE solvent within error. Table 6 gives the k_s values with the activation parameters determined by the Arrhenius plots for k_s.

For MeOH, on the other hand, the plot shows a curve (Fig. 1). Similar rate behavior was observed for the racemization of $[Ni(phen)_3]^{2+}$ in the analogus solvent system.[9] The decrease of the accelerating effect is due to loss of MeOH activity[25] which is caused by self association of MeOH in DCE as reported for water and alcohols in relatively inert solvents.[26] Assuming dimerization of MeOH, we estimated an equilibrium constant of 0.49±0.20 M^{-1} for the formation of a dimer of MeOH and a k_s value of (2.28±0.43)×10^4 s^{-1} M^{-1} (Table 6).

In our previous study of the racemization of $[Ni(phen)_3]^{2+}$ in DCE solutions containing various amount of water,[8] it was found that the rate increases dramatically with increasing water content. However, the analogous increase in rate for $[Fe(phen)_3]^{2+}$ is very small: The k_r value at 15.0 °C is (8.19±0.06)×10^{-4} s^{-1}

Table 5. Observed Rate Constants for Racemization of $[Fe(phen)_3](ClO_4)_2$ in DCE Solutions Containing Various Donor Solvents

		$10^4k_r/s^{-1}$						
Temp	[DMSO]		[DMF]		[Ac]		[AN]	
°C	M		M		M		M	
7.5	0.0813	4.56±0.03						
		4.54±0.01						
	0.1240	5.75±0.02						
		5.70±0.03						
	0.1647	6.69±0.03						
		6.69±0.02						
	0.1965	7.46±0.04						
10.0	0.0186	4.13±0.02	0.0319	4.10±0.01	0.385	3.79±0.01	0.982	3.72±0.02
		4.17±0.01		4.03±0.01		3.70±0.01		3.68±0.01
	0.0275	4.71±0.04	0.0682	4.77±0.01	0.789	4.13±0.02	1.373	3.86±0.01
		4.72±0.02		4.88±0.01		4.03±0.01		3.94±0.01
	0.0537	5.56±0.02	0.1017	5.52±0.04	1.171	4.23±0.01	1.945	3.95±0.01
		5.54±0.01		5.36±0.02		4.27±0.01		4.01±0.01
	0.0736	6.48±0.04	0.1418	6.23±0.04	1.625	4.58±0.02	2.230	4.14±0.02
		6.23±0.01		6.08±0.02		4.57±0.01		4.18±0.01
	0.1060	8.04±0.06	0.1768	6.54±0.03				
		7.86±0.03		6.80±0.02				
	0.1371	8.97±0.06						
		8.78±0.02						
	0.1496	9.47±0.01						
		9.73±0.03						
12.5	0.0488	8.30±0.10	0.0268	6.04±0.04	0.394	5.67±0.03	0.475	5.49±0.03
		8.05±0.04		5.96±0.04		5.56±0.03		5.52±0.03
	0.0732	8.88±0.03	0.0586	6.67±0.03	0.808	6.01±0.03	0.972	5.56±0.03
		9.10±0.03		6.64±0.03		6.01±0.03		5.61±0.02
	0.0983	10.78±0.03	0.0885	7.40±0.04	1.630	7.14±0.02	1.482	5.84±0.03
		10.56±0.07		7.32±0.04				5.84±0.03
	0.1208	11.73±0.10	0.1203	8.48±0.06	1.985	7.55±0.04	1.957	6.01±0.02
		11.71±0.05		8.17±0.03				6.04±0.02
			0.1478	8.83±0.05			2.435	6.34±0.04
				8.74±0.05				6.10±0.03
15.0	0.0316	10.65±0.04	0.0617	9.91±0.04	0.493	8.60±0.06	0.251	7.87±0.03
		10.71±0.04		9.91±0.03		8.46±0.02		7.68±0.03
	0.0594	12.17±0.04	0.0940	10.99±0.09	0.994	8.89±0.03	0.960	8.71±0.04
		12.26±0.13				9.15±0.04		8.57±0.03
	0.0612	12.61±0.06	0.1215	11.94±0.03	1.530	9.81±0.02	1.760	9.12±0.05
		12.39±0.14		12.10±0.03		9.87±0.03		9.13±0.03
	0.0832	14.59±0.06	0.1575	13.51±0.06	2.010	10.95±0.04	2.470	9.20±0.03
		14.41±0.11		13.61±0.04		10.69±0.02		9.24±0.02
	0.0994	15.44±0.08	0.1835	15.01±0.05	2.530	11.48±0.04	5.003	11.44±0.07
		14.97±0.09		14.59±0.10		11.78±0.04		11.66±0.09
					3.010	12.30±0.04		
						12.30±0.04		

		$10^4k_r/s^{-1}$					
Temp	[MeOH]		Temp	[Ac]		[AN]	
°C	M		°C	M		M	
15.0	0.27	8.40±0.03	17.5	0.207	11.99±0.07	0.408	11.71±0.03
		8.27±0.02			12.17±0.08		11.96±0.04
	0.52	8.54±0.02		0.412	12.35±0.06	0.806	12.37±0.06
		8.51±0.03			12.39±0.11		12.31±0.06
	0.79	8.86±0.04		0.532	12.89±0.06	1.243	12.76±0.10
		8.68±0.03			12.87±0.07		13.00±0.04
	1.04	9.40±0.02		0.621	13.49±0.06	2.031	13.53±0.05
		9.12±0.02			12.97±0.07		
	1.49	9.59±0.04		0.732	13.30±0.07		
		9.50±0.03			13.15±0.06		
	1.94	9.73±0.02		0.927	13.63±0.07		
		9.83±0.02			13.79±0.10		
	2.93	10.76±0.04					
		10.45±0.04					

Table 6. Derived Rate Constants k_s and Arrhenius Parameters for the Racemization of $[Fe(phen)_3](ClO_4)_2$ in DCE Solutions Containing Various Donor Solvents

Temp	$10^4 k_s/s^{-1} M^{-1}$				
°C	DMSO	DMF	MeOH	Ac	AN
7.5	27.5±0.6	—	—	—	—
10.0	41.0±0.7	18.7±0.5	—	0.717±0.038	0.339±0.021
12.5	55.0±1.8	25.2±0.8	—	1.25±0.03	0.449±0.035
15.0	77.3±2.2	38.2±0.7	2.28±0.43	1.55±0.03	0.761±0.032
17.5	—	—	—	2.38±0.15	1.026±0.052
			E_a/kJ mol^{-1}		
	91±4	96±8	—	104±12	106±9
			log A (in s^{-1} M^{-1})		
	14.4±0.7	14.9±1.4	—	15.1±2.2	15.0±1.6

Table 7. Solvent Parameters and the c_i Values Calculated from Eq. 1[a] at 25 °C

Solvent	ΔG_L / kJ mol^{-1}	log (ηV_m)[b] / P cm^3 mol^{-1} [c]	DN[d]	c_i/s^{-1}
DCE	−68.9	−0.207	0	−5.65
DCB	−67.9	0.175	(2.3)[e]	−5.40
NB	−67.9	0.270	4.4	−5.47
NM	−64.5	−0.483	2.7	−5.76
AN	−65.0[f]	−0.743	14.1	−5.15[g]
Water	−19.4[f]	−0.794	18.0	−4.45[g]
MeOH	−53.6[f]	−0.654	19.0	−4.48[g]
FA	−49.5[f]	0.120	24.7[h]	−4.42[g]
DMF	−68.6[f]	−0.207	26.6	−4.38[g]
Ac	−67.5[f]	−0.648	17.0	−4.09[g]

a) Values calculated by the equation, $c_i = \log k_r + (0.26\Delta G_L/2.303RT) + 0.48 \log(\eta V_m)$. b) Data of η from Ref. 22. c) 1P=0.1 Pa s. d) Data from Ref. 10. e) See Ref. 36. f) Data from Ref. 15. g) Data of k_r from Ref. 12. h) Data from M. S. Greenberg, R. L. Bodner, and A. I. Popov, *J. Phys. Chem.*, **77**, 2449 (1973).

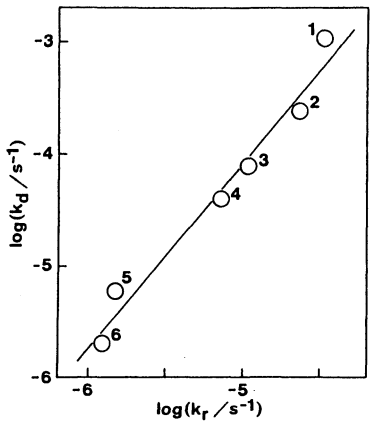

Fig. 2. Plot of log k_d[a] for dissociation of $[Fe(phen)_3]^{2+}$ vs. log k_r[b] for racemization of $[Ni(phen)_3]^{2+}$ at 25 °C in various solvents: (1), DMSO[c]; (2), DMF; (3), water; (4), MeOH; (5), Ac; (6), AN. a) Data from Ref. 12. b) Data from Ref. 8. c) Data of k_d from D. J. Farrington, J. G. Jones, and M. V. Twigg, *J. Chem. Soc., Dalton Trans.*, **1979**, 221.

in water-saturated DCE ($[H_2O]$=0.094 M) and is 7.65×10^{-4} s^{-1} in pure DCE (Table 2).

Solubility of Naphthalene. Table 1 gives the solubilities of naphthalene in the various solvents. Each value of the solubilities is the mean of data obtained in triplicate and the error is a mean deviation. Van Meter and Neumann showed that the solvation energy is related to the solubility or the free energy of solvation of naphthalene, ΔG_{naphth}, by the equation,[15]

$$\Delta G_L = 2.053\, \Delta G_{naphth}, \quad (4)$$

for which $\Delta G_{naphth} = -RT \ln S_{naphth} - \Delta G_{subl}$, where the free energy change, ΔG_{subl}, for the sublimation of naphthalene, is calculated, from the vaper pressure[27] of naphthalene at 25 °C, to be 30.57 kJ mol^{-1}. The Eq. 4 is valid especially for aprotic solvents, althouth some steric factors may become important in such a tris complex. The ΔG_L values calculated for DCE, DCB, NB, and NM are comparable to those for other aprotic solvents such as AN, Ac, DMF, etc. as given in Table 7.

Discussion

Since the racemization of $[Ni(phen)_3]^{2+}$ complex occurs mainly by a dissociative process,[4,28] measurements of the racemization rate, k_r, of the nickel complex allow us to estimate the dissociation rate, k_d, of the $[Fe(phen)_3]^{2+}$ complex as follows.[29] Figure 2 shows that a linear free-energy relationships[30] exists: A plot of log k_d for the iron complex against log k_r for the nickel complex in various solvents is linear, with slope 1.66±0.15 and intercept 4.21±0.77. The k_d values for DCE, DCB, NB, and NM can be extrapolated from this plot as the k_r values for the solvents are available from our data.[31] Table 4 gives the estimated k_d values with the values of k_r for the iron complex, indicating that racemization of the iron complex is extremely faster than dissociation in these solvents where the complex favors an intramolecular racemization process, as well as that in the other organic solvents, AN, Ac, DMF, etc. (more than 99.5% of the time).[1,12,32]

When the Van Meter and Neumann Eq. 1 is valid for a given solvent, the value of the constant, c_i, of an intrinsic part in the Eq. 1 should be -4.56.[33] Table 7 shows that this is the case for DMF and MeOH while the solvents, DCE, DCB, and NM, as well as NB,[14] have significantly lower c_i values: Despite similarities of ΔG_L and $\log(\eta V_m)$ between DMF and DCE, for example, the rate in DCE is smaller than that in DMF (Table 4). Furthermore, DCE or DCB is a solvent of lower dielectric constant compared to NM or NB and thus substantially all the complex cations are associated with the ClO_4^- ion into ion-pairs in the former solvent (about 10^{-4} M solutions of the complex used here)[34] while they are dissociated to a great extent in the latter.[35] However, the racemization rate or the c_i value in DCE or DCB is comparable to that in NM or NB. In addition, the racemization rates are independent of the complex concentrations in the solvents (Table 2). These results indicate that the ion pairing effect is negligibly small. DCE, DCB, NB, and NM have extremely low donicities[36] and so the c_i value appears to increase predominantly with increasing donor number of the solvents (Table 7). This implies that the c_i constant for the racemization should contain not only an intrinsic part but also a part due to a nucleophilic interaction with the iron metal.

In order to clarify the role of donor solvents in the racemization of the iron complex, the dependence of the rate on the concentration of added solvents was investigated in DCE solutions.[37] Figure 1 shows that addition of donor solvents to DCE solutions enhances the racemization rates and the correlation between them is linear. As presented for the $[Ni(phen)_3]^{2+}$ complex,[9] the rate behavior can be understood on the basis of the scheme,

$$(+)\text{-}[Fe(phen)_3]^{2+} + D \rightleftarrows (+)\text{-}[Fe(phen)_3]^{2+}\cdot D \rightarrow (-)\text{-}[Fe(phen)_3]^{2+} + D, \quad (13)$$

which, provided that an outer-sphere complex in a rapid preequilibrium is weak, leads to a second-order rate law.[38] Since the sizes of the added solvents do not greatly differ or the solvents are similar in ΔG_L, it is reasonable that equilibrium constants for the formation of the outer-sphere complexes for the solvents are approximately equal. Thus it is quite likely that the kinetics are controlled by the interaction of the complex cation with the added donor solvent molecule in the process concerned in the rate-determining step.

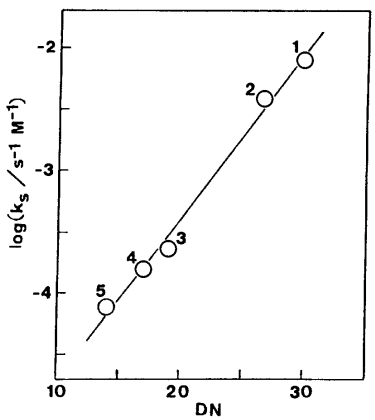

Fig. 3. Correlation of $\log k_s$ in DCE solutions containing donor solvents at 15 °C with Gutmann donor number DN of the solvents: (1), DMSO; (2), DMF; (3), MeOH; (4), Ac, (5), AN.

The k_s values derived by using Eq. 3 increase with added solvent in the order AN < Ac < MeOH < DMF < DMSO. This sequence lies in the order of increasing donicity of the solvents. A plot of $\log k_s$ against donor number shows a good linear correlation between them as shown in Fig. 3. Futher, Table 6 shows that a decrease in the activation energy, E_a, for the system, AN > Ac > DMF > DMSO, is consistent with the trend in $\log k_s$ as donor number of the solvent increases. This can be rationalized in terms of a mechanism involving expansion of a complex cation to a 7-coordinate transition state with one donor solvent as proposed for racemization of the $[Ni(phen)_3]^{2+}$ complex.[8,9,11] The trends in $\log k_s$ and E_a may be attributable to the ability of the solvents to stabilize the transition state by donation, which thus leads to a lower energy of activation for racemization.

Recently, we have reported the detailed structure of the nitrobenzene solvate, $[Fe(phen)_3]I_2 \cdot NB \cdot 2H_2O$, as a result of the X-ray structure determination.[17] In the structure, the nitrobenzene molecule occupies one of the three major V-shaped pockets between the phen ligands. Thus, the above solvent-assisted racemization of the tris-chelated complexes can be explained by a double-opposed-initiated twist proposed by Kepert[39] if it is assumed that a donor solvent molecule is placed instead of the nitrobenzene molecule in the solvate (Fig. 1 of Ref. 17), although differences in coordination to the metal center may be also involved, as well as differences in solvation energy in the transition state. Moreover, it has been reported that for ion-pair formation of the iron complex and arenesulfonate ions the above major pockets are also important.[40]

In summary, it is concluded that the donor number of the solvent is one of the important factors in solvent effects on the racemization of $[Fe(phen)_3]^{2+}$. From this point of view, we can relate the c_i constant to donor number (Table 7)[41] and derive the equation,

$$c_i = -5.66 + 0.057DN,$$

which may allow us to modify the Van Meter and Neumann Eq. 1. On the other hand, it is surprising that the racemization of the iron complex in Ac is extremely rapid (Table 4) while the accelerating effect of Ac on the racemization in DCE solutions is lower (Table 6). Langford and Tong have pointed out that changes in the bulk properties of the solvent beyond the contact solvation shell may influence reaction rates.[42] Further investigation is undertaken for clari-

fying bulk solvent effects on the racemization.

The present work was partially supported by a Grant-in-Aid for Scientific Research No. 57740317 from the Ministry of Education, Science and Culture.

References

1) F. Basolo and R. G. Pearson, "Mechanisms of Inorganic Reactions," 2nd ed, John Wiley & Sons, New York (1967), pp. 300—334.

2) N. R. Davies and F. P. Dwyer, *Trans. Faraday Soc.*, **50**, 1325 (1954); F. Basolo, J. C. Hayes, and H. M. Neumann, *J. Am. Chem. Soc.*, **76**, 3807 (1954); P. Dowley, K. Garbett, and R. D. Gillard, *Inorg. Chim. Acta*, **1**, 278 (1967).

3) F. Basolo, J. C. Hayes, and H. M. Neumann, *J. Am. Chem. Soc.*, **75**, 5102 (1953).

4) R. G. Wilkins and M. J. G. Williams, *J. Chem. Soc.* **1957**, 1763.

5) C. S. Lee, E. M. Gorton, H. M. Neumann, and H. R. Hunt, Jr., *Inorg. Chem.*, **5**, 1397 (1966); M. Yamamoto and Y. Yamamoto, *Inorg. Nucl. Chem. Lett.*, **11**, 691 (1975); M. Yamamoto, Y. Uwate and Y. Yamamoto, *ibid.*, **12**, 713 (1976); R. J. Mureinik, *ibid.*, **12**, 319 (1976).

6) See, for example, J. Burgess, *Inorg. React. Mech.*, **5**, 260 (1977); **6**, 278 (1979); **7**, 287 (1981).

7) E. Iwamoto, T. Fujiwara, and Y. Yamamoto, *Inorg. Chim. Acta*, **43**, 95 (1980).

8) T. Fujiwara and Y. Yamamoto, *Inorg. Nucl. Chem. Lett.*, **11**, 635 (1975).

9) M. Yamamoto, T. Fujiwara, and Y. Yamamoto, *Inorg. Nucl. Chem. Lett.*, **15**, 37 (1979).

10) V. Gutmann and R. Schmid, *Coord. Chem. Rev.*, **12**, 263 (1974); V. Gutmann, "The Donoor-Acceptor Approach to Molecular Interactions," Plenum Press, New York (1978).

11) T. Fujiwara and Y. Yamamoto, *Inorg. Chem.*, **19**, 1903 (1980).

12) F. M. Van Meter and H. M. Neumann, *J. Am. Chem. Soc.*, **98**, 1388 (1976).

13) S. Tachiyashiki and H. Yamatera, *Bull. Chem. Soc. Jpn.*, **54**, 3340 (1981); **55**, 1014 (1982).

14) Y. Yamamoto, M. Yamamoto, and T. Fujiwara, Proc. 4th Int. Symp. Solute-Solute-Solvent Interactions, Vienna, 1978, Abstr., 59.

15) F. M. Van Meter and H. M. Neumann, *J. Am. Chem. Soc.*, **98**, 1382 (1976).

16) D. L. Kepert, *Inorg. Chem.*, **13**, 2758 (1974).

17) T. Fujiwara, E. Iwamoto, and Y. Yamamoto, *Inorg. Chem.* **23**, 115 (1984).

18) F. P. Dwyer and E. C. Gyarfas, *J. Proc. Roy. Soc. N. S. Wales*, **83**, 263 (1949).

19) E. Iwamato, K. Ito, and Y. Yamamoto, *J. Phys. Chem.*, **85**, 894 (1981).

20) T. Fujiwara, K. Matsuda, and Y. Yamamoto, *Inorg. Nucl. Chem. Lett.*, **16**, 301 (1980).

21) A. K. R. Unni, L. Ellas, and H. I. Schiff, *J. Phys. Chem.*, **67**, 1216 (1963).

22) J. A. Riddick and W. B. Bunger, "Organic Solvent," in "Techniques of Chemistry," 3rd ed, ed by A. Weissberger, John Wiley & Sons, New York (1970), Vol. 2.

23) R. C. Weast, "CRC Handbook of Chemistry and Physics," 64th ed, CRC Press, Florida (1983).

24) Y. Yamamoto, T. Tarui, E. Iwamoto, and T. Tarumoto, *Anal. Chim. Acta*, **84**, 217 (1976).

25) T. Tarumoto and Y. Yamamoto, *Chem. Lett.*, **1973**, 7.

26) S. D. Christian, A. A. Taha, and B. W. Gash, *Quart. Rev. Chem.*, **24**, 20 (1970); R. Mecke, *Discuss. Faraday Soc.*, **9**, 161 (1950); W. A. P. Luck, "The Hydrogen Bond," ed by P. Schuster, North Holland, Amsterdam (1976); M. C. R. Symons and V. K. Thomas, *J. Chem. Soc., Faraday Trans. 1*, **77**, 1883 (1981).

27) G. C. Sinke, *J. Chem. Thermodyn.*, **6**, 311 (1974).

28) Aqueous acids or nickel salts are required for the measurements of dissociation rate of the complex but almost insoluble in the solvents, DCE, DCB, and NB and the use needs some justification.

29) J. A. Broomhead, *Aust. J. Chem.*, **16**, 186 (1963).

30) R. G. Wilkins, "The Study of Kinetics and Mechanism of Reactions of Transition Metal Complexes," Allyn and Bacon, Boston (1974), pp. 88—96.

31) The value for DCE (containing 0.009 M water at 25 °C) from Ref. 8 is used and the values for NB (at 25 °C), DCB (at 30 °C) and NM (at 25 °C) are unpublished.

32) L. Seiden, F. Basolo, and H. M. Neumann, *J. Am. Chem. Soc.*, **81**, 3809 (1959).

33) See Fig. 5 of Ref. 12.

34) The ionic association was shown by our measurements of conductivity, although the data are unpublished.

35) Y. Yamamoto, E. Sumimura, K. Miyoshi, and T. Tominaga, *Anal. Chim. Acta*, **64**, 225 (1973); E. Iwamoto, S. Monya, and Y. Yamamoto, *J. Chem. Soc., Faraday Trans. 1*, **79**, 625 (1983).

36) Although the donor number of DCB has not been reported, it is presumed to be comparable to that of benzoyl chloride (2.3) from data of Ref. 10.

37) On the definition of Gutmann donor number, the solvent, DCE, was used as an inert medium: V. Gutmann and E. Wychera, *Inorg. Nucl. Chem. Lett.*, **2**, 257 (1966). Further, the ΔG_L value of DCE is comparable to those of other aprotic solvents as given in Table 7. For these reasons, we also used DCE here as an inert medium.

38) H. P. Bennetto, R. Bulmer, and E. F. Caldin, "Hydrogen-bonded Solvent Systems," ed by A. K. Covington and P. Jones, Taylor and Francis Ltd., London (1968), p. 335.

39) D. L. Kepert, *Inorg. Chem.*, **13**, 2754 (1974) and also in Ref. 6. Kepert calculated repulsive energy around a seven-coordinate metal atom without taking account of all possible electronic structures of the 7-coordinate complex, for example, spin excitation to high-spin state discussed by: G. A. Lawrance and D. R. Stranks, *Inorg. Chem.*, **17**, 1804 (1978).

40) S. Tachiyashiki and H. Yamatera, *Inorg. Chem.*, **25**, 3209 (1986).

41) Table 7 includes the c_i values calculated from data of Ref. 12 for water and formamide (FA) by using Eq. 1.

42) C. H. Langford and J. P. K. Tong, *Acc. Chem. Res.*, **10**, 258 (1977); *Pure Appl. Chem.*, **49**, 93 (1977).

New Synthesis, Properties, and the Formation of the Hexamer of Nickel(II) Ethanethiolate, $[Ni(SEt)_2]_6$

Takeshi YAMAMURA
Department of Chemistry, Faculty of Science, Science University of Tokyo, Kagurazaka 1-3, Shinjuku-ku, Tokyo 162
(Received November 12, 1987)

$[Ni_3(SEt)_8]^{2-}$ reacted with water in acetone to give the known hexameric ring compound, $[Ni(SEt)_2]_6$, where SEt means $CH_3CH_2S^-$. The $[Ni(SEt)_2]_6$ was oxidized electrochemically in a quasi-reversible manner at +0.60 V (vs. SCE) in CH_2Cl_2. ^1H and ^{13}C NMR revealed that this compound has two types of -SEt (low- and high- field types; the chemical shift discrepancy is ca. 0.4 ppm for ^1H NMR), probably corresponding to the axial-equatorial configurations of the thiolate. The formation of the cyclic hexamer in CH_3CN and $CHCl_3$ in the presence of protic reagents was studied.

Metal complexes of simple thiolates (alkanethiolates or arenethiolates) are now substances that are of topochemical interest as potential sources of a variety of multi-nuclear compounds because of the bridging disposition of thiolate ligands.[1] The hexagonal molecular cycles, $[Ni(SEt)_2]_6$,[2] (Fig. 1),[3] $[Ni(SCH_2CH_2OH)_2]_6$,[4] $[Pd(SCH_2CH_2OH)_2]_6$,[5] the tetragonal analogue, tetrakis[bis-(*N*-methylpiperidine-4-thiolato) nickel],[6] and the octagonal analogue, $[Ni(SCH_2CH_2COOEt)_2]_8$,[7] form a novel topochemical group by their ring crown structure, with linked square planar units of M(II) (M=Ni and Pd) and bridging thiolates. The M-S frameworks of these compounds hold inside cylindrical vacancies surrounded by arrays of coplanar metal centers. This salient structural feature, the so called "tiara",[2] involves the possibility of developing new types of inclusion complexes. In practice, $[Ni(SCH_2CH_2COOEt)_2]_8$ takes one of the substituent pendant groups (-OEt) in a solid into its own hole by anchoring the ester oxygen to nickel atoms.[7]

In spite of its central situation in the tiara group, almost no efforts have been made to elucidate its basic character of the hexamer, $[Ni(SEt)_2]_6$, since the detouring[2a,c] synthesis and a structural short communication.[2b] In the course of our study of nickel-thiolate systems,[8] we have found a simple way to obtain the hexamer. This paper will present a description of the new synthetic method, aspects of the formation in aprotic media, and the result of the usual physicochemical measurements (NMR and electrochemistry).

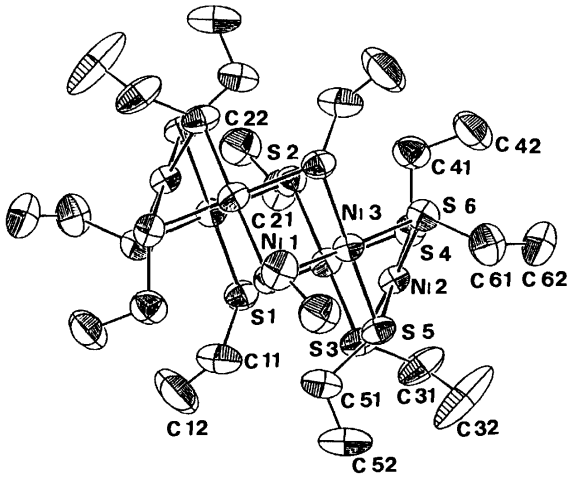

Fig. 1. ORTEP plot of the non-hydrogen atoms of $[Ni(SEt)_2]_6$ (triclinic) with 50% probability thermal elipsoids and the atom numberlings.[3]

Experimental

Every synthetic procedure was performed under a nitrogen or argon atmosphere. The solvents were refluxed over appropriate drying agents and distilled under argon. Sodium ethanethiolate was prepared from sodium and excess ethanethiol in methanol and dried completely (120 °C, in vacuo) before use.

Preparation of the Materials. $(NEt_4)_2[Ni_3(SEt)_8]$ was prepared according to A. D. Watson's method.[9]

$[Ni(SEt)_2]_6$: To a greenish brown solution of 0.50 g (0.37 mmol) of $(NEt_4)_2[Ni_3(SEt)_8]$ in 450 ml of acetone was added 0.2 g of commercial $[NMe_3Ph]^+Cl^- \cdot nH_2O$ (in acetone). The solution was then refluxed for 30 min, cooled to room temperature, and passed through a sintered glass to remove any insoluble impurities (red brown powder and an extra amount of $[NMe_3Ph]^+Cl^- \cdot nH_2O$). The filtrate, wine red in color, was placed in a refrigerator at −20 °C for 2 weeks. The black crystals which slowly grew in the flask were collected and dried in vacuo. Stable in air. Yield, 0.21 g (72%). Found: C, 26.65; H, 5.45; N, 0%. Calcd for $C_{24}H_{60}Ni_6S_{12}$: C, 26.55; H, 5.57; N, 0%. Absorption spectrum (in chloroform): 335 nm (ε=55600), 407 (20100), 515 (7030), 570 (sh, 5430). Soluble in benzene, toluene, xylene, chloroform, and dichloromethane. Slightly soluble in ethyl acetate. Insoluble in acetone, acetonitrile, dimethyl sulfoxide, ethanol, and water.

Physicochemical Measurements. The electronic spectra were recorded on a Hitachi Recording Spectrometer 340. The ^1H NMR spectra were obtained by the use of JEOL FX-90Q spectrometer. Electrochemical measurements were carried out by using a Yanaco Polarographic Analyzer, model P-1100, or a Hokuto Potentiostat/Galvanostat HA-201 in connection with a Fuso function generator, model 321. the molecular weight of the hexamer in solution was decided by the use of a Knauer Vapor Pressure Osmometer No. 01.00.

Results

The molecular weight of the "tiara" in benzene was

decided as 1100 (accuracy 10%) by means of vapor pressure osmometry with benzyl (molecular weight=210.3) as the standard. This result agrees with the theoretical value for $[Ni(SEt)_2]_6$, 1080. Therefore, the hexameric aggregation is maintained also in solution, at least in benzene.

Figure 2-a depicts the absorption spectrum of $[Ni(SEt)_2]_6$ in chloroform. This is composed of an intense LMCT band at 335 nm (ε=9270 $M^{-1}cm^{-1}$/Ni (1 M=1 mol dm^{-3})) and much weaker ones at 407 nm (ε=3350 $M^{-1}cm^{-1}$/Ni), 515 nm (ε=1170 $M^{-1}cm^{-1}$/Ni, deconvoluted), and 570 nm (ε=905 $M^{-1}cm^{-1}$/Ni, deconvoluted). No absorption was observed in NIR region. The spectrum differs in its intensity from that of $[Ni_3(SEt)_8]^{2-}$ [3d] (Fig. 2-b) at ca. 400 nm and in the 500—600 nm region.[10] According to Maki,[11] the bands at 407, 515, and 600 nm of the hexamer are to be assigned to the d-d transitions, $^1A_{1g} \rightarrow {}^1A_{2g}$, $^1B_{2g}$, and $^1A_{1g} \rightarrow {}^1E_g$ respectively, of a square planar Ni(II), judging from their wavelength regions and intensities.[12]

The ^1H NMR spectrum of the hexamer (in chloroform, at room temperature) is shown in Fig. 3-a. The spectrum reveals that two types of ethanethiolate, different in the strength of their diamagnetic shielding, exist in the solution. The correlation between the methylene and methyl protons of each EtS^- was decided by means of proton-proton decoupling technique (depicted in the figure). The observed chemical shifts of the methyl and methylene protons of the high-magnetic-field -SEt (CH_2; δ=1.76, CH_3; δ=1.08) agree well with those of $[Ni_2(SEt)_6]^{2-}$ (CH_2; δ=1.79—1.87, CH_3; δ=1.05 and 1.20) and $[Ni_3(SEt)_8]^{2-}$ (CH_2; δ=1.85—1.88, CH_3; δ=1.04—1.08).[13] Compared with these, the values of the low-magnetic-field -SEt are shifted ca. 0.4 ppm downward. The result of ^{13}C NMR indicates the same situation, showing that 4 kinds of carbon atoms exist in the solution (Fig. 3-b). The peaks were assigned by means of selective decoupling technique. (Low field -SEt: CH_2; δ=26.367, CH_3; δ=19.446. High field -SEt: CH_2; δ=20.177, CH_3; δ=16.229.)

The electrochemical behavior of $[Ni(SEt)_2]_6$ in dichloromethane (0.2 M $NBu^n_4PF_6$, vs. SCE, glassy carbon electrode) was studied over the potential range from −1.8 to +1.8 V by means of cyclic voltammetry (CV) at various scan rates (10—200 mV s^{-1}) and by means of differential pulse polarography (DPP) with a modulation amplitude 10 mV. No evidence for the reduction of the hexamer corresponding to the formation of the monoanion $[Ni(SEt)_2]_6^-$ was obtained in the region observed. The CV chart exhibited three oxidation peaks at +0.655, +1.05, and +1.61 V, within which the higher two were irreversible. Cyclic scans limited within 0.8 to 0 V revealed that the +0.655 V anodic peak was followed by a cathodic peak at +0.55 V (see Fig. 4). No scan rate dependence was observed for either anodic or cathodic peaks. That is, we obtained the relationship $(\partial E/\partial \log v)_T$=0,[17] which is applicable to reversible and quasireversible cases, while the cathodic anodic current ratio, i_{pc}/i_{pa},[18] calculated for the case of a 100 mV s^{-1} scan rate, was 0.92. Consequently, the oxidation process was quasireversible. This was also confirmed by DPP measurements. The

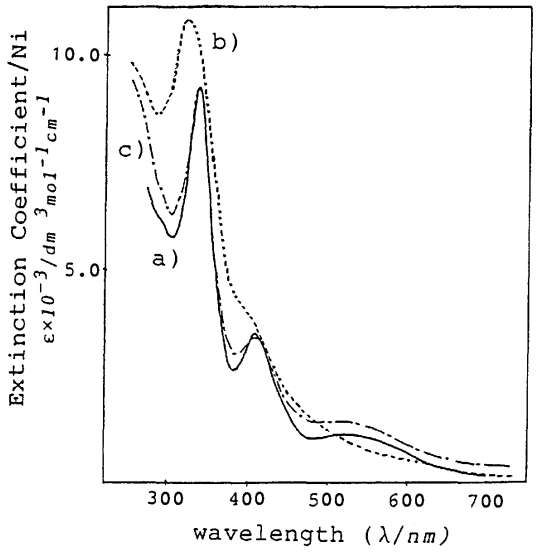

Fig. 2. Absorption spectra converted for extinction coeffient/Ni. a) $[Ni(SEt)_2]_6$ in $CHCl_3$ (commercial), b) $[Ni_3(SEt)_8]^{2-}$ in CH_3CN (dried over CaH_2), c) $[Ni_3(SEt)_8]^{2-}$ in $CHCl_3$ (commercial) or in CH_3CN (dried over CaH_2) with exess amount of $NEt_3H \cdot BF_4$.

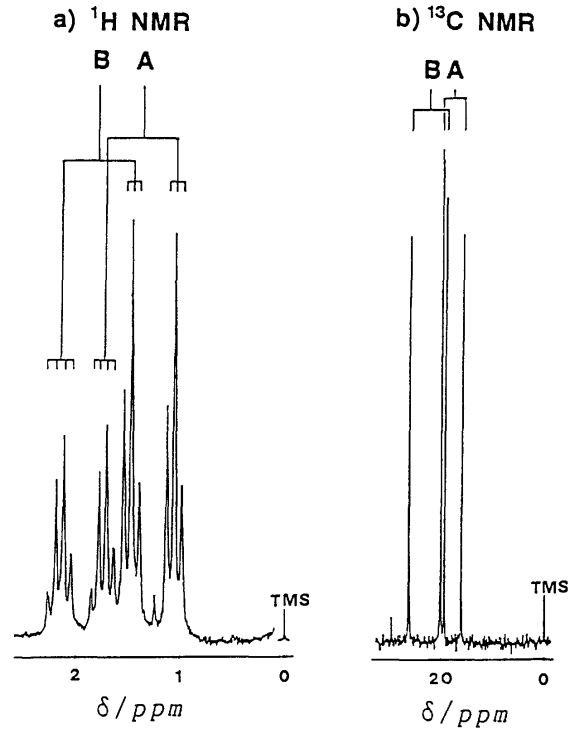

Fig. 3. NMR spectra of $[Ni(SEt)_2]_6$ in $CDCl_3$: a) ^1H NMR; A; high field EtS^-, B; low field EtS^-. b) ^{13}C NMR; A; high field EtS^-, B; low field EtS^-. TMS internal standard.

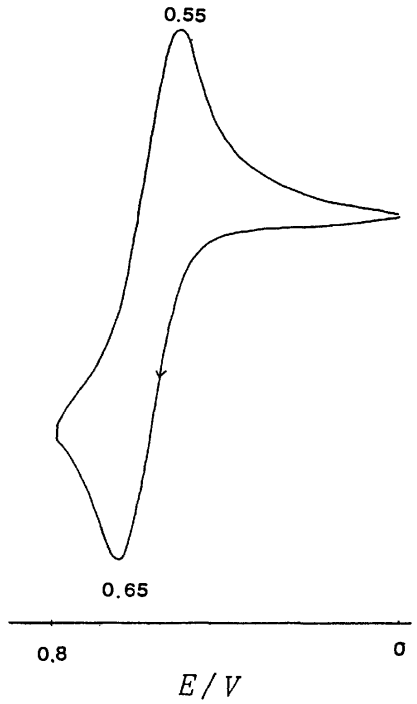

Fig. 4. The cyclic voltammogram of $[Ni(SEt)_2]_6$ in CH_2Cl_2 (scan range +0.8—0 V, vs. SCE, 0.2 M $NBu^n_4PF_6$, glassy carbon electrode).

half height width, 100 mV, was slightly larger than the ideal reversible case (91 mV).[19]

The effects of ethanol, water, and H^+ itself on the hexamer generation were also examined. The absorption spectra of (a) $[Ni(SEt)_2]_6$ in $CHCl_3$ (b) $[Ni_3(SEt)_8]^{2-}$ in CH_3CN, and (c) $[Ni_3(SEt)_8]^-$ in commercial $CHCl_3$ including 1% EtOH are depicted in Fig. 2, with the extinction coefficient *per* Ni on the ordinate. As may be seen in Fig. 2, the major species in the $[Ni_3(SEt)_8]^{2-}/CHCl_3$ (commercial) solution was not $[Ni_3(SEt)_8]^{2-}$ itself, but $[Ni(SEt)_2]_6$, while the amount of the hexamer generated in commercial $CHCl_3$ was the same as in (b). Consequently, almost all of the $[Ni_3(SEt)_8]^{2-}$ was converted to the hexamer in commercial $CHCl_3$. On the other hand, in a purified $CHCl_3$ (dried with H_2SO_4, hence including almost no alcohol for stabilization) the original absorption spectrum of $[Ni_3(SEt)_8]^{2-}$, which was observed in dried acetonitrile, changed in a different way. In this case the spectrum changed inconspicuously in the 500—600 nm region both in spectral shift and in intensity. On the other hand, in the 300—400 nm region, the original peaks at 316 nm and 400 nm (sh) shifted to 330 nm and 416 nm respectively. Especially the latter peak grew remarkably. The reaction which accompanied this incomplete absorption change was also studied by ^1H NMR in dried $CDCl_3$. However, the results were not unequivocal except that the signals characteristic of the hexamer appeared only slightly. This means that the significant step generating the hexamer proceeds in the presence of EtOH. The addition of EtOH afforded the hexamer's spectrum also in acetonitrile. $[Ni(SEt)_2]_6$ was also generated in acetone by the addition of an almost equimolar amount of water to the trimer, as has been described above in discussing the synthesis.

The effect of water was more rigorous, and the use of excess water yielded an insoluble polymer, $[Ni(SEt)_2]_\infty$, in acetone or acetonitrile. For example, when 0.454 mM of $[Ni_3(SEt)_8]^{2-}$ in acetonitrile (dried 3 days over CaH_2; 1g/200 ml) was treated with water (5.0 equiv), the absorption pattern changed to one which resembled the hexamer's, but more gentle, and the intensity diminished to ca. 1/2 of the theoretical value within 4 h. However, 25 equiv of water led to a pseudo-exponential decomposition of $[Ni_3(SEt)_8]^{2-}$ with a decay constant of $k=1.29\times10^{-4}$ s^{-1} and yielded insoluble polymers. Eventually, the formation reaction of the hexamer from $[Ni_3(SEt)_8]^{2-}$ and water competed with polymerization processes. These results led us to the idea that the H^+ originating from EtOH or water play an important role in the hexamer formation or at least in the elongation of an open chain $[Ni(SEt)_2]_n(SEt)_2^{2-}$. The effect of H^+ was examined in a more direct manner by using $[NHEt_3]^+[BF_4]^-$ to $[Ni_3(SEt)_8]^{2-}$ in acetonitrile. The result was satisfactory. Immediately after mixing, the absorption spectrum changed from that of $[Ni_3(SEt)_8]^{2-}$ to one similar to the hexamer's spectrum, just as is observed in the $[Ni_3(SEt)_8]^{2-}/CHCl_3$(commercial) system.

Consequently, the reaction described as Eq. 1 proceeds in commercial $CHCl_3$, wet acetonitrile, or wet acetone:

$$2(NEt_4)_2[Ni_3(SEt)_8] \xrightarrow{(H^+)} [Ni(SEt)_2]_6 + 4(NEt_4)(EtS) \quad (1)$$

It should be added that the isolation of the crystalline hexamer from a chloroform solution was impossible, probably due to contamination by other oligomeric species.

Discussion

The synthesis of $[Ni(SEt)_2]_6$ was first achieved by the reaction of bis(alkylthio)dialkyltin with nickel chloride in cold ethanol.[2a] The hexamer was also synthesized from tetracarbonylnickel and dialkyldisulfides in benzene by the same authors.[2c] A simple synthesis of this compound from commercial nickel salts and ethanethiol in protic media has not yet been published. The condition of such synthesis in aprotic media (chloroform, acetonitrile) is, as has been studied in this work, not straightforward; it is suggestive of the necessity of mild protic conditions. The mixing of an excess amount of water promotes the formation of uncharacterizable polymer. However, as for the other thiols, the aspect is not so tedious. In practice, $[Ni(SCH_2CH_2OH)_2]_6$, and $[Ni(SCH_2CH_2COOEt)_2]_8$, are readily prepared from simple nickel salts and the corresponding thiols in an alkaline aqueous solution[4]

and 1-propanol[7] respectively. Dance and his coworkers referred briefly to an aqueous system in relation to the chain elongation of multinuclear Ni-SR.[7] According to them, in $Ni^{2+}/^{-}SCH(CH_3)CH_2OH$ in water, $[Ni(SR)_2]_6$ predominates at 25 °C, but a series of open chain complexes, $Ni[Ni(SR)_2]_n$ ($n<30$), appear at 75 °C in an appropriate pH region. This is a result which somewhat agrees with those of our study, suggesting the participation of H^+ in chain elongation. The cyclization process might be promoted by the presence of an oxygen atom. The structure of the upper tiara, $[Ni(SCH_2CH_2COOEt)_2]_8$, in the solid state would remain the actual field where the tiara is cyclized from its open-chain precursor by anchoring to an oxygen atom and is then stabilized.

To account for the appearance of geminal EtS- signals in ^1H and ^{13}C NMR experiments, two mechanisms can be proposed: 1) the ring-current mechanism and 2) the $d\pi(Ni)$-$d\pi(S)$ interaction mechanism. The most important orbitals in the ring-current mechanism are those composed of d_z2 orbitals on Ni atoms. If we assume ca. 2 Å as the radius and six electrons for this ring orbital, the shifts calculated for the equatorial and axial methylene protons are −0.27 and +0.26 ppm respectively at the position of the methylene protons.[20] This result agrees well with the experimental result obtained by ^1H NMR, but not with the ^{13}C measurement, which afforded about 10 times as large. Consequently, it is necessary to assume for any of axial or equatorial EtS^- a $d\pi(Ni)$-$d\pi(S)$ overlap, which promotes the magnetic shielding at the ethyl groups. However, it is impossible to decide which is the low field case, axial or equatorial.

The "tiara" structure is attractive from the point of view of developing a new type of inclusion catalyst. The quasireversible oxidation of the hexamer suggests the potentiality of "tiara" compounds for inclusive oxidation catalysts.

The present work was partially supported by a Grant-in-Aid for Scientific Research (No. 62540475) from the Ministry of Education, Science and Culture. The author gratefully acknowledges to the kind support of Professor Yukiyoshi Sasaki of Tokyo University, and wishes also to thank Dr. Toshio Kamata of the National Chemical Laboratory for Industry for the measurement of the molecular weight of $[Ni(SEt)_2]_6$.

References

1) T. Costa, J. R. Dorfman, K. S. Hagen, and R. H. Holm, *Ionorg. Chem.*, **22**, 4091 (1983).

2) a) E. W. Abel, D. G. Brady, and B. C. Crosse, *J. Organomet. Chem.*, **5**, 260 (1966); b) P. Woodward, L. C. Dahl, E. W. Abel, and B. C. Crosse, *J. Am. Chem. Soc.*, **87**, 5251 (1965); c) E. W. Abel, and B. C. Crosse, *J. Chem. Soc. A*, **1966**, 1379.

3) The hexamer was found to crystallize in two forms, monoclinic and triclinic. The details of the X-ray structural analyses of both crystal forms of $[Ni(SEt)_2]_6$ are to be published in Acta Crystallogr.

4) R. O. Gould and M. M. Harding, *J. Chem. Soc. A*, **1970**, 875.

5) N. R. Kunchur, *Acta Crystallogr., Sect. B*, **27**, 2293 (1971).

6) W. Gaete, J. Ros, X. Solans, M. Font-Altaba, and J. L. Brianso, *Inorg. Chem.*, **23**, 39 (1984).

7) I. G. Dance, M. L. Scudder, and R. Secomb, *Inorg. Chem.*, **24**, 1201 (1985).

8) a) T. Yamamura, H. Miyamae, Y. Katayama, and Y. Sasaki, *Chem. Lett.*, **1985**, 269; b) T. Yamamura, *Chem. Lett.*, **1986**, 801.

9) A. D. Watson, Ch. Pulla Rao, J. R. Dorfman, and R. H. Holm, *Inorg. Chem.*, **24**, 2820 (1985).

10) The electronic structure of $[Ni_3(SEt)_8]^{2-}$ is presumed to be complicated, reflecting its unusual structure,[9] which contains one square planar unit (central $Ni(S_b)_4$ moiety) and two strongly distorted end units ($Ni(S_b)_2(S_t)_2$). The reported dihedral angle between $Ni(S_b)_2$ and $Ni(S_t)_2$ planes is 53°.

11) G. Maki, *J. Chem. Pyes.*, **28**, 651 (1958); **29**, 1129 (1958).

12) Thiolate anions are intrinsically weak ligands ranked between chloride and azide, with an usual nephelausetic effect as is manifested for the Co^{2+} and Fe^{2+} complexes.[13,14] This fact, however, does not lead to the expectation that the local geometry of $Ni(SR)_4$ is limited to Td, because LMCT is also dominant in stabilizing the "tiara" framework as well as the ligand-field stabilization. The A_{2u} array of the Ni($3d_{xz}$, $3d_{yz}$)-S(2p) orbitals in the D_{3d} symmetry is the most plausible for such stabilization. Thus, the d-d transitions of $[Ni(SEt)_2]_6$ may be said to be characterized by a square planar local symmetry perturbed with the exchange interaction due to the thiolato bridging. At any rate, an assignment based on a simple crystal field calculation is not neccesarily reliable in a square planar case because it fails to estimate the π-bonding effect.[16]

13) R. W. Lane, J. A. Ibers, R. B. Frankel, G. C. Papaefthymiou, and R. H. Holm, *J. Am. Chem. Soc.*, **99**, 84 (1977).

14) Our crystal-field calculation based on Liehr and Ballhausen's method[15] for a series of $[Ni(SR)_4]^{2-}$ (RS^-=*m*- or *p*-substituted benzenethiolate) has shown that thiolates are situated at I^-~Br^- in both spectrochemical series and nephelausetic series (to be published elsewhere).

15) A. D. Liehr and C. J. Ballhausen, *Ann. Phys.*, **2**, 134 (1959).

16) C. J. Ballhausen, "Introduction to Ligand Field Theory," McGraw-Hill, New York (1962).

17) R. S. Nicholson and I. Shain, *Anal. Chem.*, **36**, 706 (1964).

18) R. S. Nicholson, *Anal. Chem.*, **37**, 1351 (1965).

19) E. P. Parry and R. A. Osteryoung, *Anal. Chem.*, **37**, 1634 (1964).

20) J. A. Pople, *J. Chem. Phys.*, **24**, 1111 (1956).

Simultaneous Measurement of Electrical Conductivity and the Amount of Adsorbed Oxygen in Porous ZnO

Satoru FUJITSU,* Hiroshi TOYODA, Kunihito KOUMOTO, Hiroaki YANAGIDA,†
Masatoshi CHIKAZAWA,†† and Takafumi KANAZAWA††
Department of Industrial Chemistry, Faculty of Engineering, University of Tokyo, 7-3-1 Hongo, Bunkyo-ku, Tokyo 113
†Research Center for Advanced Science and Technology, University of Tokyo, 4-6-1 Komaba, Meguro-ku, Tokyo 153
††Department of Industrial Chemistry, Faculty of Technology, Tokyo Metropolitan University, 2-1-1 Fukasawa, Setagaya-ku, Tokyo 156
(Received January 11, 1988)

Changes in electrical conductivity and the amount of adsorbed oxygen in porous ZnO were measured simultaneously in the temperature range of 200—600 °C. The saturated amount of adsorbed oxygen increased initially, went through a maximum at 500 °C, and then decreased with increasing temperature. The conductivity decreased exponentially with increase in the amount of adsorbed oxygen, which indicates that the energy barrier formed due to the chemisorbed oxygen controls the total conductivity. In a high temperature region, not only the chemisorbed oxygen, but also the oxygen diffused into the grain boundaries played important roles in changing the electrical conductivity. The diffused oxygen was examined by means of a depth profile of tracer ^{18}O measured by SIMS. The formation of the energy barrier at the grain boundary was confirmed by current-voltage characteristic measurements.

Zinc oxide is an n-type semiconductor with extrinsic defects, $V_O^{\cdot}$, $V_O^{\cdot\cdot}$, $Zn_i^{\cdot}$ and/or $Zn_i^{\cdot\cdot}$.[1-4] Based on the non-stoichiometry of ZnO, the logarithm of the electrical conductivity of pure ZnO is linear with respect to that of the oxygen partial pressure with a slope of $-1/4$ or $-1/6$ depending on the ionization state of donor defects. The rate of change in electrical conductivity is determined by slow diffusion of ionic species, and so the change is too slow to be observed at low temperatures in ZnO single crystal or polycrystals with high density.

On the other hand, the change in electrical conductivity of porous ZnO is rapid and large at low temperatures (<600 °C). It is well known that the electrical conductivity of the porous ZnO depends strongly on the amount and nature of the chemisorbed oxygen.[5-10] Negatively charged chemisorbed oxygen is attained by trapping conduction electrons from the bulk of ZnO. Then, the carrier concentration decreases and the electron depletion layer to compensate the negative charge on the surface is generated, simultaneously. This depletion layer acts as the conduction barrier. In a polycrystalline sample with high density or in a single crystal, the thickness of such a layer is thin enough and its effect as the barrier can be neglected. However, considering porous ZnO in which the average neck radius to connect the grains with each other is supposed to be very small, the thickness of a depletion layer could not be neglected as shown in Fig. 1.[6] Therefore, the electrical conductivity of a porous ZnO is affected not only by the additives but also by the microstructure associated with its processing. Various electrical conductivities for porous ZnO have been reported by many researchers.[7,11-14] The decrease in the electrical conductivity caused by chemisorbed oxygen has been explained either by carrier concentration decrease due to electron trapping by chemisorbed oxygen or by surface energy barrier formation.

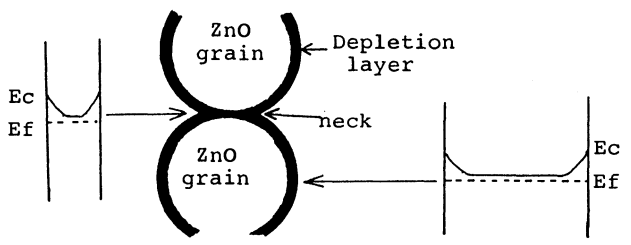

Fig. 1. Cross section of a connecting neck in a porous ZnO and energy band.

In this study, to determine the dominant mechanism for the electrical conductivity change of porous ZnO, the electrical conductivity of porous ZnO was measured as a function of the amount of adsorbed oxygen. The effect of oxygen diffused into grain boundaries was also examined by means of the depth profile of tracer (^{18}O) and the current-voltage characteristic measurements.

Experimental

(1) Sample Preparation. Nominally pure ZnO powder (99.99%, from Kojundo Chemical Lab. Co., Ltd.) was dispersed in an aqueous solution of $Al(NO_3)_3$ (99.9%, from Kanto Chemical Co., Ltd.) and dried. The resulting powder containing 0.5 mol% Al_2O_3 was calcined at 600 °C to decompose nitrate into oxide. The powder was shaped into a rectangular bar (5 by 5 by 15 mm) in a steel die (under 100 MPa pressure) and sintered at 900 °C for 1 min (S-1) or 800 °C for 1 h (S-2) in air. Aluminum oxide addition was to maintain the ZnO body porous. Of course, a trace amount of Al_2O_3 must have dissolved into the bulk ZnO promoting donor genera-

tion. To obtain a dense sample (S-3), the pressed powder was also sintered at 1300 °C for 4 h in air. The samples with the surface area of 2.1 $m^2 g^{-1}$ and 50% relative density (S-1), 3.2 $m^2 g^{-1}$ and 50% (S-2) and 95% (S-3), respectively, were obtained. SEM observation showed partial progress of sintering having occurred in the surface area of S-1 body.

(2) Electrical Conductivity and Adsorption of Oxygen. Surface area of the sample was determined by BET method at 77 K. The sample (S-1 or S-2) was enclosed in the holder illustrated in Fig. 2(b). The electrical conductivity was measured by a dc four probe method.

As the starting condition, the sample was heated at 600 °C in vacuum (10^{-4} Pa) until the conductivity reached 0.04 to 0.05 $S m^{-1}$ (about 20—25 h). At prescribed temperatures, oxygen was introduced into the holder, and the changes in the pressure and the electrical conductivity were measured simultaneously for 1 h. Change in the pressure by adsorption of oxygen was measured by using a fine vacuum gauge (BARATORON 222BA-0010 from MKS Co. Ltd.).

(3) The *I–V* Characteristic. After evacuation by the same method mentioned in (2), oxygen gas (400 Pa) was introduced into the sample holder at a fixed temperature, and after a prescribed oxidizing time the sample was quenched in liquid nitrogen. The relation between applied voltage and current was measured by a curve tracer (No. 5802 Kikusui Electronics Corp.) at room temperature.

(4) Depth Profile of Tracer ^{18}O. The enclosed sample (S-3) whose surface had been polished by diamond paste was heated at 600 °C in vacuum for 3 h, and ^{18}O (50 vol%) enriched oxygen was introduced into the sample holder at prescribed temperatures and annealed for 3 h. After annealing, the holder was quenched in liquid nitrogen.

The depth profile of tracer ^{18}O was measured by SIMS (Hitachi IMA-2A) under the so-called static SIMS condition; primary ion $^{40}Ar^+$, primary ion energy 1 keV, primary ion current 10^{-10} A, probe size 1 mm, secondary ion accelerating voltage 3 kV and residual gas pressure $<10^{-5}$ Pa.

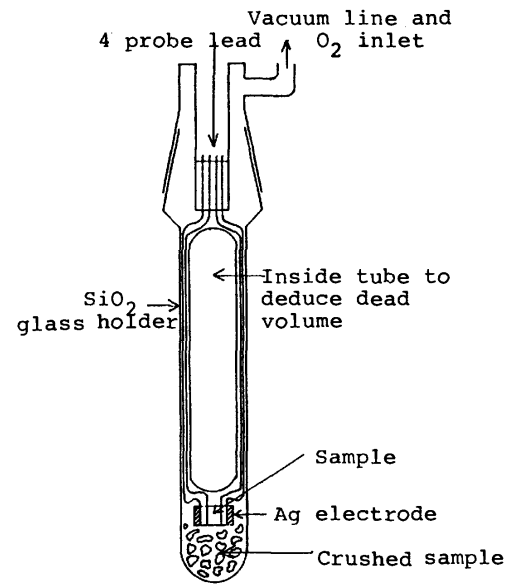

Fig. 2. Sample holder to measure the amount of adsorbed oxygen and the electrical conductivity, simultaneously.

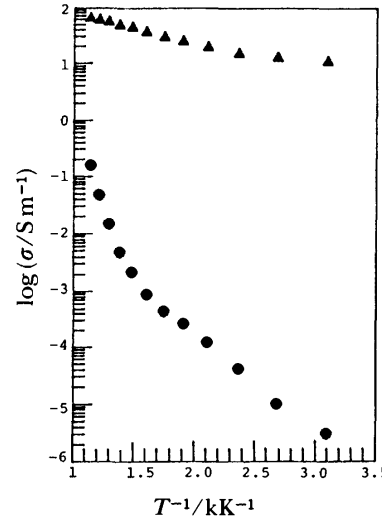

Fig. 3. Temperature dependences for a porous ZnO(S-2) in air (●) and under vacuum (▲). The electrical conductivity was measured on cooling process.

Results and Discussion

(1) Effect of Oxygen on the Electrical Conductivity of Porous ZnO. Figure 3 shows the temperature dependencies of electrical conductivity for S-2 in vacuum and in air. After annealing at 600 °C for 20 h in the respective atmosphere, the electrical conductivity was measured in the cooling process. Though the temperature dependence of electrical conductivity in vacuum was very small with an activation energy of 0.07 eV, that in air was large with an activation energy to be 2 to 3 eV.

The resulting adsorption isotherms coincided with the Langmuir type[15] in the whole temperature range from 200 to 600 °C in both samples. The saturated amount of adsorbed oxygen increased initially, went through a maximum at 500 °C and then decreased with increasing temperature in S-2. This pattern was similar to that measured by TDS (thermal desorption spectroscopy) in which the kind of chemisorbed oxygen was assumed as O^{2-},[8] while the saturated amount of adsorption decreased by repetition of the adsorption and desorption of oxygen and this effect was remarkable in S-1. This effect was explained in the following manner:[5] If high oxygen pressure causes some adsorption during sintering at high pretreatment temperature, the coulombic attraction between the adsorbed oxygen and the positively ionized defects§ may draw such defects toward the surface. Conversely, if the oxygen has been desorbed at high temperature, the adsorption centers, the defects, may diffuse away from the surface, and the number of sites for the low temperature adsorption would decrease slowly with

§ In this system, zinc atoms at interstitial sites, oxygen vacancies and substituted Al are the candidates for these defects.

time. Though the saturated amount of adsorption slightly depended on the order of measurement, the tendency of the temperature dependence of the saturated amount for S-1 with a low surface area corresponded to that measured by TDS.

Electrical conductivity decreased with increase in the amount of adsorbed oxygen in the whole temperature range as shown in Fig. 4. If the decrease in electrical conductivity resulted from the decrease in the total carrier concentration, the conductivity should have decreased linearly with increase in the amount of adsorbed oxygen which behaves as the electron trap. So, this model could not account for the change in the conductivity.

The effect of oxidation and reduction in the bulk should be also considered. The dependence of electrical conductivity on oxygen partial pressure was larger than expected from the change in nonstoichiometric composition by atmosphere. And the conductivity did not change above the pressure to attain saturation of adsorption which is approximately 1000 Pa at 600 °C. From these experimental results it is judged that oxidation and reduction in the bulk would have a the minor effect on changing the electrical conductivity in the present temperature and pressure regions.

The assumption that the energy barrier whose height increases with increase in the amount of adsorbed oxygen controls the total conductivity, could explain this result. Considering that the carrier mobility is constant throughout the sample, the electrical conductivity of a semiconductive material depends on the energy difference between the bottom of the conduction band (E_c) and the Fermi level (E_f) as $\sigma \propto \exp(-(E_c-E_f)/kT)$. The difference ($E_c-E_f$) is very small, about several hundredths of an electron volt as appeared in the temperature dependence measured in vacuum (Fig. 3). The presence of energy barrier makes this energy difference to be large as shown in Fig. 1. If

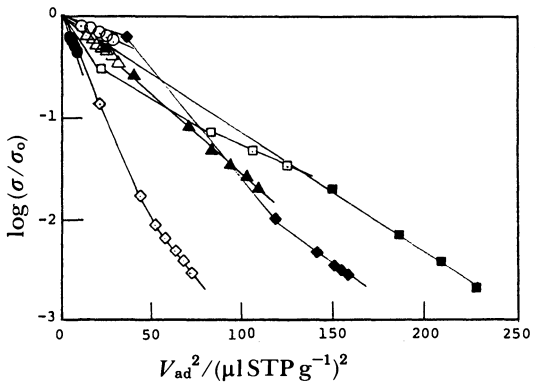

Fig. 4. The change of electrical conductivity against the amount of adsorbed oxygen: $\log(\sigma/\sigma_o)-V_{ad}^2$ where σ_o is the electrical conductivity in vacuum. Sample S-1; ●: 300°C, ▲: 400°C, ■: 500°C, ◆: 600°C. Sample S-2; ○: 300°C, △: 400°C, □: 500°C, ◇: 600°C.

the chemisorbed oxygen makes an acceptor type trap level on the surface of ZnO, the resulting energy barrier to compensate the excess charge is generated. The height of such a surface energy barrier (ϕ_s) is estimated as[5,16]

$$\phi_s = \frac{2eN_{ss}^2}{\varepsilon\varepsilon_o N_d} \quad (1)$$

where N_{ss} the trap state density which is proportional to the amount of adsorbed oxygen, N_d the donor density and the other symbols have their usual meanings. When N_{ss} is large, the change in the height, $\Delta\phi_s$, is approximated to be proportional to the change in N_{ss}. The effective thickness of such a barrier is so small that this effect is negligible in single crystal or polycrystal with high density. While this barrier plays an important role to decrease the conductivity in the case of porous body where a narrow neck connects the grains with each other. When this barrier is formed into an interior of the narrow neck region, the total conductivity should be controlled by such necks as $\sigma \propto \exp(-(E_{cv}-E_f+\phi)/kT)$ where E_{cv} is the bottom of the conduction band in vacuum and ϕ is the effective barrier height. Though the height of energy barrier at the surface is estimated by Eq. 1., the effective height is determined by the lowest energy barrier at the center of the cross section of the neck.

If the conductivity measured in this experiment was controlled by the mechanism discussed above, $\log(\sigma/\sigma_o)$ in Fig. 4 equals to ϕ/kT and the decrease in conductivity by two orders of magnitude corresponds to the generation of the energy barrier with an effective height to be 0.3 eV at 500 °C. The ϕ/kT increased linearly with increase in the amount of adsorbed oxygen at 600 °C or its square at 300—500 °C. This dependence agrees with the rule of generation of the surface energy barrier by the surface state of acceptor type. The effective height of the energy barrier might reflect the height of the surface energy barrier. The right end plot of each measurement almost agreed with the saturation of the change in the electrical conductivity and the adsorption of oxygen. Though the change in electrical conductivity depended on the amount of adsorbed oxygen in S-2 with a large surface area, that in S-1 with a smaller surface area showed a larger change in electrical conductivity at 600 °C where the amount of adsorption is smaller than at 500 °C. It is peculiar that a similar change in the electrical conductivity was observed in S-1 and S-2 at 600 °C. These results suggest that another mechanism is operative to change the electrical conductivity. When the surface energy barrier controls the total conductivity, the grains should be connected with each other by a small neck with the width to be comparable to the thickness of the depletion layer. The thickness of this layer is approximately by the Debye length.[7] The samples of this experiment contain Al_2O_3 as a promoter of donor

generation. Though the exact solubility limit of Al_2O_3 into ZnO has not been determined, the thickness is estimated to be below 10 nm by the assumption that 100 ppm of Al_2O_3 could dissolve into ZnO.

Because of the complicated microstructure, the precise neck radius could not be determined. Two kinds of samples, S-1 and S-2, have almost the same relative density of 50% and the average grain size of 0.5 μm. From the viewpoint of surface area, it is supposed that the neck radius of S-2 might be larger than that of S-1. Since the current flows through the wide neck which is difficult to form the barrier in its interior, the effective neck radius might have been enhanced by the partial progress of sintering in S-1. Considering that the neck radius of S-1 is larger than the thickness of the surface energy barrier, the smaller change in the electrical conductivity in S-1 by the oxygen chemisorption could be explained, i.e., the formation of the energy barrier is imperfect in S-1.

On the other hand, the anomalous change in the conductivity at 600 °C has not been clarified yet. Recognizing the neck as the grain boundary and assuming that the selective oxidation of the grain boundary by the rapid oxygen diffusion into such an area occurs, the energy barrier should be generated at the grain boundary and considerably change the electrical conductivity even in a sample with wide neck. Though the definite model to explain the formation of the barrier by the selective oxidation of the grain boundary could not be determined by this experiment, two models have been proposed for ZnO varistor: one is the formation of stoichiometric ZnO near the grain boundary regions,[17] and the other is the generation of acceptor states due to oxygen chemisorption along the grain boundaries.[18]

(2) The Energy Barrier along the Grain Boundary. If the energy barrier along the grain boundary is formed in ZnO, the non-ohmic behavior of resistivity should be observed like a varistor.[19,20] As reported in our previous paper, the non-ohmic property was observed in the porous ZnO.[21] From the proposed tunnel theory,[20] the non-ohmic coefficient, α, in the expression $I=(V/C)^{\alpha}$, where I is the current, V the applied voltage and C a constant, can be written as

$$\alpha = \frac{4}{3}(m\varepsilon_s)^{1/2}\frac{V}{hN_d^{1/2}(1+V/\phi)^{3/2}} \qquad (2)$$

where ϕ is the barrier height, N_d the donor density, V the applied voltage, and the other symbols have their usual meanings. Though it is not yet recognized which mechanism controls the non-ohmic characteristic in this experiment, the higher the barrier is, the larger α becomes in any model if the donor density is constant. As shown in Fig. 5,[18] the non-ohmic coefficient, α, increased with an increase in the oxidizing period, and α larger at 600 °C where the oxygen diffusion might be effective to generate the energy barrier than at 500 °C where the amount of adsorption was larger than that at 600 °C in S-1, while in the case of S-2 the maximum non-ohmic coefficient, α, was attained by the oxidation within several minutes. Therefore, the high energy barrier along the grain boundary is also formed by oxygen diffusion at 600 °C in even a wide neck. The deterioration of the characteristic for the sample oxidized for 24 h is explained by the diffusion into the bulk; i.e., the difference in chemical potential between the bulk and grain boundary might decrease.

(3) Oxygen on the Surface and in the Bulk. In the previous sections, the phenomena which could not be explained by the adsorption of oxygen were discussed on the assumption that the energy barrier along the grain boundary was formed by the rapid diffusion of oxygen into the grain boundary. To confirm the

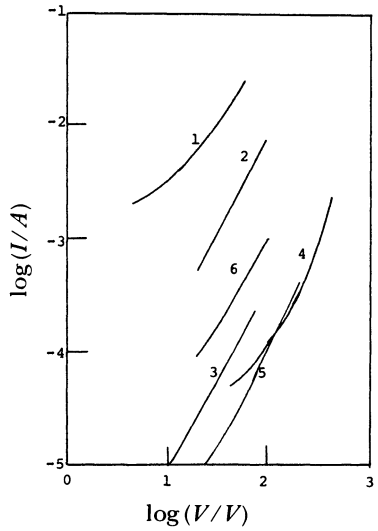

Fig. 5. I–V relation for porous ZnO under various oxidation conditions; (1) 1 min at 600 °C (α=1.31), (2) 3 min at 600 °C (1.68), (3) 10 min at 600 °C (2.28), (4) 1 h at 600 °C (2.93), (5) 24 h at 600 °C (2.44), and (6) 1 h at 500 °C (1.91).

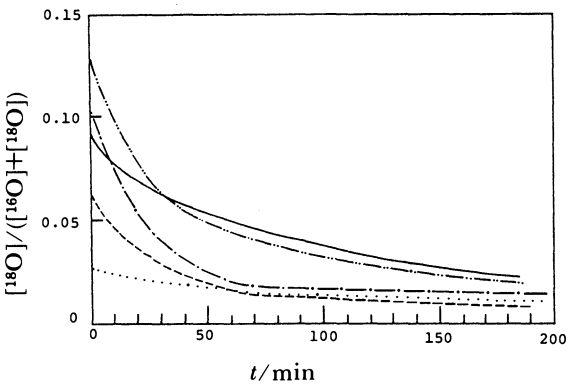

Fig. 6. The depth profile of tracer (^{18}O) in dense ZnO. --------: 200 °C, ----: 300 °C, -·-·-: 400 °C, -··-··-: 500 °C. ——: 600 °C.

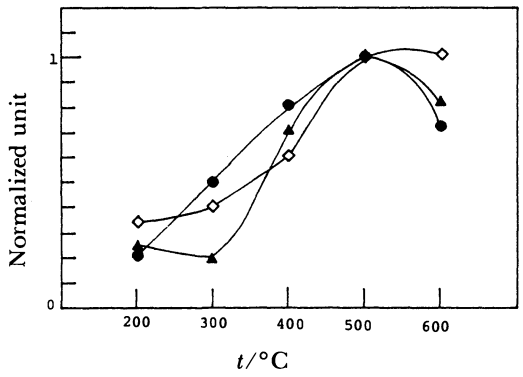

Fig. 7. The saturated amount of adsorbed oxygen, the tracer concentration at surface and the integrated concentration calculated from Fig. 5. The values were normalized under the condition as $V/V_{500°C}$. ●: from Langmuir's method ($V_a/V_{a500°C}$), ▲: Surface concentration ($V_s/V_{s500°C}$), ◇: Integrated concentration ($V_i/V_{i500°C}$).

validity of this assumption, the oxygen diffusion into the grain boundary should be examined.

The depth profiles of tracer ^{18}O in ZnO annealed at prescribed temperatures are shown in Fig. 6. In all measurements, the strengths of the primary beam of SIMS were weak and constant. Figure 6 shows the atomic fraction of ^{18}O against the measuring period. The measured fraction at the beginning might be strongly affected by the chemisorbed oxygen and that after long measuring period might indicate the effect of the penetration of oxygen into the interior of the sample. Though this time corresponds to the depth of etched crater, the depth was too small to be measured precisely. Hence, the correct diffusion coefficient could be not estimated.

In the temperature region 200—500 °C, the concentration of tracer increased with increasing temperature. At 600 °C, the concentration of tracer at the surface was smaller than that at 500 °C, but on the other hand, that in the interior was larger than that at 500 °C. The saturated amount of adsorption measured by Langmuir's method (V_a) for S-1, the tracer concentration at the surface (V_s) and the integrated concentration calculated from Fig. 6 in the time range 0 to 3 h (V_i) are shown in Fig. 7. Each plot was normalized to the values obtained at 500 °C as $V/V_{500°C}$. Though the temperature dependencies of V_a and V_s were similar in the whole temperature range, the V_i at 600 °C was larger than that at 500 °C. From Fig. 7, V_s reflects the amount of adsorbed oxygen. The integrated value (V_i) involved not only the enrichment of the tracer at the surface but also that in the interior.

The observation of the enrichment of the tracer in the interior of the sample indicated that the diffusion of oxygen effectively occurred at 600 °C. It is well known that the oxygen diffusion is accelerated along grain boundaries. The oxygen transport by diffusion is higher at higher temperatures and the difference in the diffusion rate between the grain and grain boundary is large at low temperatures due to the difference in its activation energy. The rapid diffusion along the grain boundary was observed even at 1000 °C.[22,23] Therefore, it would be reasonable to consider that the grain boundary is oxidized selectively at 600 °C by the rapid grain boundary diffusion, and this area might become the energy barrier for electron transport.

The authors wish to thank Dr.Shunichi Hishita of National Institute for Research in Inorganic Materials for analysis of the depth profile by using SIMS and helpful discussion. They also wish to thank Mr. Shigeru Ando of Ando Glass Blowing Technology Ltd. for his excellent technique for glass blowing. This work was partially supported by a Grant-in-Aid for Scientific Research from the Japanese Ministry of Education, Science and Culture (No. 60550543).

References

1) M. H. Sukkar and H. L. Tuller, "Additives and Interface in Electronic Ceramics," ed by M. F. Yan and A. H. Heuer, The American Ceramics Society, Columbus (1983), pp. 71—90.
2) K. I. Hagemark and L. C. Chocka, *J. Solid State Chem.*, **15**, 261 (1975).
3) K. I. Hagemark, *J. Solid State Chem.*, **16**, 292 (1976).
4) K. Koumoto and H. Yanagida, *Ceram. Jpn.*, **18**, 927 (1983).
5) S. R. Morrison, *Adv. Catal.*, **7**, 259 (1955).
6) N. M. Beekmans, *J. Chem. Soc., Faraday Trans. 1*, **74**, 31 (1978).
7) M. Takata and H. Yanagida, *Yogyo Kyokaishi*, **87**, 19 (1979).
8) W. Gopel, *J. Vac. Sci. Technol.*, **15**, 1298 (1978).
9) N. Miura, O. Nakagawa, N. Yamazoe, and T. Seiyama, *Denki Kagaku*, **49**, 367 (1981).
10) H. Chon and J. Pajares, *J. Catal.*, **14**, 257 (1969).
11) P. H. Miller, *Phys. Rev.*, **60**, 890 (1941).
12) M. Takata, D. Tsubone, and H. Ynagida, *J. Am. Ceram. Soc.*, **59**, 4 (1976).
13) K. Intemann and F. Stockmenn, *Z. Physic*, **131**, 10 (1950).
14) P. Chandra, V. B. Tare, and A. P. B. Sinha, *Indian J. Pure Appl. Phys.*, **5**, 313 (1967).
15) I. Langmuir, *J. Am. Chem. Soc.*, **40**, 1361 (1918).
16) R. H. Kingston and S. F. Neustadter, *J. Appl. Phys.*, **26**, 718 (1955).
17) R. Einginger, *Appl. Surf. Sci.*, **3**, 390 (1979).
18) K. Tsuda and K. Mukae, "High Tech Ceramics," ed by P. Vincentini, Elsevier (1987), p. 1781.
19) M. Matsuoka, *Jpn. J. Appl. Phys.*, **10**, 736 (1971).
20) K. Mukae, K. Tsuda, and I. Nagasawa, *Jpn. J. Appl. Phys.*, **16**, 1361 (1977).
21) S. Fujitsu, H. Toyoda, and H. Yanagida, *J. Am. Ceram. Soc.*, **70**, C71 (1987).
22) S. Shirasaki, Y. Moriyoshi, H. Yamamura, H. Haneda, K. kakegawa, K. Manabe, and M. Ogawa, *Zairyo*, **31**, 850 (1982).
23) W. J. Moore and E. L. William, *Disc. Faraday Soc.*, **28**, 86 (1959).

 © 1988 The Chemical Society of Japan Bull. Chem. Soc. Jpn., 61, 1985—1990 (1988)

The Cyanation of Aromatic Halides Catalyzed by Nickel(0) Complexes Generated In Situ. I. General Scope and Limitations

Yasumasa SAKAKIBARA,* Fumio OKUDA, Akira SHIMOBAYASHI, Kunihiko KIRINO, Mutsuji SAKAI, Norito UCHINO, and Kentaro TAKAGI†

Department of Polymer Science and Engineering, Kyoto Institute of Technology, Matsugasaki, Sakyo-ku, Kyoto 606
†College of Liberal Arts and Science, Okayama University, Tsushima, Okayama 700

(Received July 30, 1987)

The cyanation of chlorobenzene catalyzed by $Ni(PPh_3)_n$, which was generated in situ from $NiBr_2(PPh_3)_2$-Zn-PPh_3(Ni : Zn : P=1 : 3 : 2 molar ratio), was at first examined with various MCN (M=K, Na)-solvent systems by three procedures in order to clarify the conditions under which the reaction occurs. The effects of the systems and the procedures on the reaction were remarkable. It was observed that the cyanide ion has an inhibitory action on both the reduction of Ni(II) and the oxidative addition of the halide to Ni(0). However, when such MCN-dipolar aprotic solvent systems as KCN-HMPA, KCN or NaCN-MeCN, which give low cyanide concentrations, were used, the reaction readily took place at 50—60 °C without reducing Ni(II) prior to the addition of MCN and adding MCN slowly. Various Y-substituted chlorobenzenes, except for those with Y=*o*-Cl, *o*-CN, and *m*-NO_2, were cyanated to give the corresponding nitriles in fair to good yields. $NiBr_2$-PPh_3 can be used in place of $NiBr_2(PPh_3)_2$ if MCN is added after reduction. In addition, less reactive halides, such as *o*-dichlorobenzene and *o*-chlorobenzonitrile, were fairly smoothly cyanated by the use of $NiBr_2$-1,1′-bis(diphenylphosphino)-ferrocene.

It was first reported by the present authors[1] and by Cassar[2] that non-activated aryl halides can react with the cyanide ion under moderate conditions in the presence of Pd and Ni catalysts to afford the corresponding nitriles. Pd(II) salts,[3,4] $Pd(PPh_3)_4$,[5] $Ni(PPh_3)_3$ (isolated or generated in situ from $NiCl_2(PPh_3)_2$-Mn·Fe alloy-PPh_3),[6,7] and $NiClAr(PPh_3)_2$[6] are known to be homogeneous transition metal catalysts for the cyanation. Recently, $K_3[Co(CN)_4]$, which is formed in situ from $CoCl_2$-KCN-KOH(aq)-H_2 has also been found to be effective.[8]

Previously, the present authors pointed out that the Pd(II)-catalyzed cyanation proceeds smoothly when KCN-HMPA is used as the MCN(M=K, Na)-solvent system, but fails to proceed in the NaCN-HMPA system, in which cyanide is more soluble.[3] This suggests that the cyanide ion itself has also an inhibitory action on the catalytic reaction. Hence, the selection of MCN-solvent systems is important for keeping the catalyst active. In the case of the nickel catalysts, however, little has been reported about the utility of dipolar aprotic solvents and the selection of MCN-solvent systems. Cassar et al. mainly used the NaCN-EtOH[2,6] and MCN-benzene-crown ether systems.[7] Concerning the use of dipolar aprotic solvents, it has been reported by them that, in DMF, the Ni(0)-catalyzed cyanation occurs only if NaCN is added slowly.[6]

In this paper, we investigate, under various conditions, the cyanation of aromatic halides catalyzed by Ni(0) phosphine complexes, which were generated in situ from the $NiBr_2(PPh_3)_2$-Zn-PPh_3 and $NiBr_2$-Zn-phosphorus ligand, and define the scope and limitations of the reaction more clearly.

Experimental

Materials. All the solvents were purified by the ordinary methods. The KCN (Merck), NaCN, zinc powder, triphenylphosphine, anhydrous $NiBr_2$ (Nakarai), 1,2-bis(diphenylphosphino)ethane, and 1,1′-bis(diphenylphosphino)ferrocene(Strem) were commercially available. All the aromatic halides were commercially available and were used without further purification. The tri-*o*-tolylphosphine,[9] dibromobis(triphenylphosphine)nickel,[10] and dicyanobis(triphenylphosphine)nickel[11] were prepared according to the literature methods.

Procedures. Four procedures were examined and compared. A typical example of each is described below.

Procedure A: A 30-ml flask was charged with $NiBr_2(PPh_3)_2$ (740 mg, 1.0 mmol), Zn powder (200 mg, 3.0 mmol), PPh_3 (520 mg, 2.0 mmol), and KCN (2.15 g, 33 mmol). This mixture was degassed by evacuation and flushed with nitrogen, and a solution of chlorobenzene (3.38 g, 30 mmol) and naphthalene (about 0.2 g, internal standard) in HMPA (8 ml) was added by the use of a syringe. The mixture was then heated at 60 °C for 6 h with vigorous stirring and, after cooling, shaken with aq NaCl-CH_2Cl_2. The organic layer was subjected to GC analysis.

Procedure B: The catalyst components, $NiBr_2(PPh_3)_2$, Zn, and PPh_3 (1 : 3 : 2 molar ratio), were placed in a flask whose side arm was connected, by means of a ground-glass joint, to a KCN container. After replcing the air with nitrogen, HMPA was added by the use of a syringe. The mixture was heated at 60 °C for 30 min with stirring, and then chlorobenzene was added. After continued heating for 30 min, KCN was added from the KCN container, and the reaction mixture was further heated at 60 °C for 6 h.

Procedure C: This procedure was the same as Procedure B except that the order of the addition of chlorobenzene and KCN was reversed.

Procedure D: Anhydrous $NiBr_2$, Zn powder, and phosphorus ligand (1 : 3 : 4 molar ratio; 1 : 3 : 2 for the bidentate ligand) were placed in a flask fitted with a KCN container. After replacing the air with nitrogen, HMPA was added by the use of a syringe. The mixture was heated at 60 °C for 1 h with stirring, and then KCN was added from the KCN container, followed by the addition of chlorobenzene without

delay. The reaction mixture was subsequently further heated at 60 °C for 6 h.

Analysis. The gas-chromatographic analyses were made by the use of a Shimadzu-GC-7A apparatus with He carrier gas, using a 3-m PEG-20M column for the analysis of the *p*-bromo-*N*,*N*-dimethylaniline, *m*-chlorofluorobenzene, methyl *p*-chlorobenzoate, *p*-chloroacetophenone, and 3-bromopyridine and a 3-m EGS column for the analysis of the other halides. The products were identified by comparison with authentic samples, and the yields were determined by using internal standards.

Preparation of Nitriles. Three isolated examples will be described here for illustration.

Benzonitrile: Chlorobenzene (3.38 g, 30 mmol) was cyanated by Procedure A described above. The resulting mixture was poured into water (20 ml), which was then extracted twice with ether (20 ml). The combined extracts were washed with water (10 ml), dried (Na_2SO_4), and concentrated. The residue was distilled to give 2.39 g (77%) of benzonitrile: bp 81—83 °C (20 mmHg (1 mmHg=133.322 Pa)); n_D^{20} 1.5279.

Methyl *p*-Cyanobenzoate: A mixture of methyl *p*-chlorobenzoate (5.12 g, 30 mmol), KCN (2.15 g, 33 mmol), $NiBr_2(PPh_3)_2$ (740 mg, 1.0 mmol), Zn powder (200 mg, 3.0 mmol), PPh_3 (520 mg, 2.0 mmol), and acetonitrile (12 ml) was kept at 50 °C for 6 h while being stirred under nitrogen (Procedure A). The resulting mixture was chromatographed on a silica-gel column, using hexane-ethyl acetate (29/1) as the eluent, to give 3.87 g (80%) of methyl *p*-cyanobenzoate: mp 66—67 °C; ^{1}H NMR ($CDCl_3$) δ=4.0 (3H, s), 7.7 (2H, d, J=8.8 Hz), and 8.1 (2H, d, J=8.8 Hz).

***p*-Acetylbenzonitrile:** *p*-Chloroacetophenone (4.64 g, 30 mmol) was cyanated in the same manner as methyl *p*-chlorobenzoate. The resulting mixture was chromatographed on a silica-gel column, using hexane-ethyl acetate (9/1) as the eluent, to give 3.58 g (82%) of *p*-acetylbenzonitrile: mp 57—58 °C; ^{1}H NMR ($CDCl_3$) δ=2.6 (3H, s), 7.7 (2H, d, J=8.7 Hz), and 8.1 (2H, d, J=8.7 Hz).

Solubilities of KCN and NaCN. Saturated solutions were generated by stirring the respective solvents (30 ml) with a large excess of cyanide at 60±1 °C under a nitrogen atmosphere. One-milliliter aliquots were withdrawn at intervals for analysis until it was evident that equilibrium had been attained. Samples were diluted to 100 ml with 0.1 mol l^{-1} NaOH and analyzed for the cyanide ion using a cyanide ion electrode-F-7 pH meter (Horiba).

Results and Discussion

In the Ni(0)-catalyzed cyanation of aromatic halides, the use of $Ni(PPh_3)_3$ generated in situ as a catalyst is convenient and practical because $Ni(PPh_3)_n$(n=3 or 4) and $NiXAr(PPh_3)_2$ are troublesome to prepare and handle. Thus, as the first attempt, the cyanation of bromobenzene with KCN-DMF as the MCN-solvent system was examined according to Procedure A, using four kinds of metals (powder) as reducing agents of Ni(II) (Table 1). The cyanation proceeded catalytically together with the coupling reaction. It is noteworthy that the catalytic cyanation occurred by only heating the reaction mixture, without reducing Ni(II) previously and adding KCN slowly. When NaCN-DMF was used instead of KCN-DMF, however, the reaction did not occur. Of the four metals, Zn was found to be most favorable. In what follows, $NiBr_2(PPh_3)_2$-Zn-PPh_3 (Ni : Zn : P=1 : 3 : 2 molar ratio) and $NiBr_2$-Zn-phosphorus ligand (Ni : Zn : P=1 : 3 : 4; 1 : 3 : 2 for bidentate ligand) will be used as the catalyst

Table 1. Catalytic Activity of $NiBr_2(PPh_3)_2$-Metal-PPh_3 for the Cyanation of Bromobenzene with KCN[a]

Metal(powder)	Conversion	Selectivity/%[b]	
	%	PhCN	Ph-Ph
Zn	100	68	28
Zn	100[c]	55	40
Mn	91	55	28
Mn-Fe(77-23)[d]	63	61	23
Mg[e]	70	77	14

a) Carried out according to Procedure A as described in Experimental Section. $NiBr_2(PPh_3)_2$, 1 mmol (Ni : Metal : P=1 : 3 : 2 molar ratio); PhBr, 10 mmol; KCN, 11 mmol; DMF, 10 ml; temp, 60 °C; time, 4 h. b) Yield based on the halide consumed. c) Chlorobenzene was used as halide. d) Calculated for Mn on the basis of the ratio. e) The reproducibility of the reaction was poor.

$$\mathrm{ArX} + \mathrm{MCN} \xrightarrow[\text{or } NiBr_2\text{-Zn-P ligand}]{NiBr_2(PPh_3)_2\text{-Zn-}PPh_3} \mathrm{ArCN} + \mathrm{MX}$$

M : K, Na

systems to generate Ni(0) phosphine complexes in situ.

Comparison of MCN-Solvent Systems and Reaction Procedures. The cyanation of chlorobenzene catalyzed by $Ni(PPh_3)_3$, which was generated in situ from $NiBr_2(PPh_3)_2$-Zn-PPh_3, was examined with various MCN(M=K, Na)-solvent systems by means of three procedures: A(catalyst-reactant mixing without pretreatment), B(catalyst reduction-halide addition-cyanide addition), and C(catalyst reduction-cyanide addition-halide addition) (see Experimental section for further details). The results are shown, together with the solubilities of MCN, in Table 2. The effect of MCN-solvent systems is remarkable and appears to be closely related to the solubilities of MCN.

With Procedure A, which is the most convenient of the three procedures, the cyanation proceeded smoothly by the use of certain MCN-dipolar aprotic solvent systems with lower cyanide solubilities than about 15 mmol l^{-1}. Of the systems tested, the KCN-HMPA and KCN-MeCN systems gave especially good results: benzonitrile was obtained in high selectivities (92—95%) at high conversions (99%), together with biphenyl in very low selectivities (2—6%). The KCN-TMU and NaCN-MeCN systems also gave good results. With the KCN-DMF and KCN-THF systems, biphenyl was produced in somewhat high selectivities compared with the above four systems. On the other hand, the KCN-EtOH system (solubility, 51.8 mmol l^{-1}) was not especially useful, though it caused the cyanation to

Table 2. Cyanation of Chlorobenzene with Various MCN-Solvent Systems by Three Procedures

KCN system		Procedure[a]	Conversion/%	Selectivity/%	
Solvent	Solubility[b]/mmol l^{-1}			PhCN	Ph-Ph
Acetone[c]	0.5	A	58	82	10
HMPA	1.5	A	99	95	2
		B	100	88	4
		C	85	88	8
MeCN	1.9	A	99	92	6
		B	21	57	35
		C	74	87	8
TMU[d]	2.1	A	95	91	9
THF	2.4	A	88	86	12
Sulfolane	8.1	A	54	59	28
DMAC[e]	10.8	A	58	91	9
DMF	15.0	A	83	80	19
		B	67	83	20
		C	94	88	13
EtOH	51.8	A	49	47	8
		B	59	63	4
		C	0		
DMSO	131	A	3	—	—
Diglyme	—	A	18	59	26
Monoglyme	—	A	42	73	24
Benzene	—	A	13	7	86

NaCN system		Procedure[a]	Conversion/%	Selectivity/%	
Solvent	Solubility[b]/mmol l^{-1}			PhCN	Ph-Ph
Acetone[c]	0.9	A	76	89	6
MeCN	4.4	A	84	97	2
		B	20	55	37
		C	93	97	3
THF	10.4	A	65	92	8
TMU[d]	10.8	A	78	84	14
Sulfolane	15.0	A	62	65	23
DMAC[e]	123	A	0		
DMF	127	A	0		
		B	89	86	14
		C	0		
EtOH	227	A	0		
		B	33	93	1
HMPA	461	A	0		
		B	95	88	2
		C	0		

a) $NiBr_2(PPh_3)_2$, 1 mmol(Ni : Zn : P=1 : 3 : 2); KCN, 33 mmol; PhCl, 30 mmol; solvent, 8 ml. Procedure A: Ni-Zn-P+KCN+solvent+PhCl, 60 °C-6 h. Procedure B: Ni-Zn-P+solvent, 60 °C-0.5 h, +PhCl, 60 °C-0.5 h, +MCN, 60 °C-6 h. Procedure C: Ni-Zn-P+solvent, 60 °C-0.5 h, +MCN, 60 °C-0.5 h, +PhCl, 60 °C-6 h (see Experimental section). b) Values at 60 °C except for acetone (50 °C). c) Reaction temp, 50 °C. d) *N,N,N′,N′*-Tetramethylurea. e) *N,N*-Dimethylacetamide.

proceed, in contrast with the NaCN-EtOH system (solubility, 227 mmol l^{-1}).

With Procedure B, the catalytic cyanation proceeded even when the NaCN-EtOH (solubility, 227 mmol l^{-1}) and NaCN-HMPA (solubility, 461 mmol l^{-1}) systems were used, giving high cyanide concentrations. The KCN-HMPA and NaCN-HMPA systems gave particularly good results (95—100% conversions, 88% selectivity), near to those obtained using the KCN-HMPA and KCN-MeCN systems by Procedure A. However, the MeCN solvent gave less favorable results than did HMPA: in both KCN-MeCN and NaCN-MeCN systems, the reaction stopped at a conversion of about 20%, and the formation of biphenyl, accompanied by the oxidation of Ni(0) to Ni(II), was remarkable (35—37% selectivities). With the MCN-EtOH systems, the reproducibility of the results was fairly poor, especially with the NaCN-EtOH system, and good results were not obtained.[12]

With Procedure C, it was found that the inhibitory effect of the cyanide ion was remarkable and that the cyanation was accomplished by the use of MCN-dipolar aprotic solvent systems with cyanide solubilities lower than about 15 mmol l^{-1}. With the MCN-MeCN

systems, Procedure C gave better results than did Procedure B. In the NaCN-DMF system (solubility, 127 mmol l^{-1}), the cyanation was also attempted by adding chlorobenzene 5 min after the addition of NaCN, but the reaction was not initiated, such as when it was added 30 min later. This suggests that the cyanide ion coordinates to $Ni(PPh_3)_3$ rapidly under the conditions used (vide infra).

Distinct differences in the occurrence and progress of the cyanation between these three procedures, A—C, were thus observed. Here, the inhibition by the cyanide ion for the catalytic cyanation will be discussed mainly. With Procedure A, the reduction of $NiBr_2(PPh_3)_2$ by Zn powder appears to compete with the replacement of its bromine atom by a cyano group (Scheme 1). With good systems such as KCN-HMPA and KCN-MeCN, the solution turned reddish from green at an initial stage of the reaction to reveal the formation of $Ni(PPh_3)_3$ by reduction, while with poor systems, such as KCN-DMSO and NaCN-DMF, the solution turned pale yellow, suggesting that no reducible cyanonickel(II) complexes, $NiBr_{2-m}(CN)_m(PPh_3)_2$, were formed. In fact, the cyanation did not occur when $Ni(CN)_2(PPh_3)_2$(yellow) was used instead of $NiBr_2(PPh_3)_2$ in Procedure A. It was observed, however, that the dicyanonickel(II) complex served as a cyanation reagent instead of MCN in the Ni(0)-catalyzed cyanation.[13] Accordingly, even if $NiBr_{2-m}(CN)_m(PPh_3)_2$ is formed in part, it is advantageously converted into reducible $NiBr_{2-m}Cl_m(PPh_3)_2$ when the cyanation of chlorobenzene proceeds.

The results obtained by Procedure C, in which MCN is introduced prior to chlorobenzene, suggest that the cyanide ion also inhibits the oxidative addition of chlorobenzene to $Ni(PPh_3)_3$. Probably, a cyanide ion would coordinate to $Ni(PPh_3)_3$ to form $[Ni(CN)(PPh_3)_3]^-$,[14] for which it is difficult to undergo the oxidative addition of chlorobenzene. Therefore, the systems with low solubilities of MCN may be required also for the cyanation by Procedure C. On the other hand, Procedure B, in which chlorobenzene is introduced prior to MCN, made the cyanation possible even in the systems with relatively high solubilities of MCN, in contrast to Procedure C. This implies that the cyanation is smoothly initiated by a rapid reaction of CN^- with $NiClPh(PPh_3)_2$, which is formed prior to the addition of MCN, and that the concentration of the cyanide ion stays low, thus suppressing the formation of inactive $[Ni(CN)(PPh_3)_3]^-$ as a catalyst and permitting the catalytic cycle.

Biphenyl, the main by-product, is formed by the Ni(0)-catalyzed coupling of aryl halides: 2PhCl+Ni(0)→Ph-Ph+$NiCl_2$.[15] This reaction lowers the catalyst turnover of the cyanation because the Ni(0) is oxidized to ineffective Ni(II). This was remarkable in Procedure B in the MeCN solvent (vide supra).

Effect of Temperature and Time. The cyanation of PhCl by KCN was made by means of Procedure A at

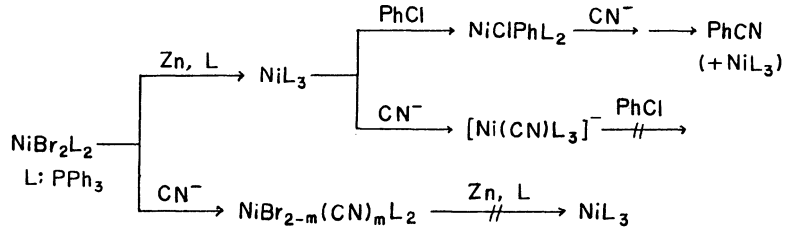

Scheme 1.

Table 3. Effects of Temperature and Time[a]

Solvent	Temp	Time	Conversion	Selectivity/%		PhCN
	°C	h	%	PhCN	Ph-Ph	Ph-Ph
HMPA	40	6	56	80	19	4.2
	60	1	16	85	11	7.7
	60	3	70	93	3	31
	60	6	99	95	2	48
	70	6	100	87	12	7.3
	80	6	35	53	46	1.2
MeCN	40	6	81	97	1	97
	60	6	99	92	6	15
	70	6	26	56	31	1.8
	80	6	18	52	46	1.1
DMF	40	6	2	70	—	—
	60	6	83	80	19	4.2
	80	6	51	66	34	1.9

a) Made by Procedure A. $NiBr_2(PPh_3)_2$, 1 mmol (Ni : Zn : P=1 : 3 : 2); PhCl, 30 mmol; KCN, 33 mmol; solvent, 8 ml.

Table 4. Cyanation of Various Aromatic Halides[a)]

Y-C_6H_4X(mmol) Y	X	Solvent (ml)	Temp °C	Time h	Conversion %	Selectivity %
H	Cl (100)	HMPA (20)	60	16	67	99
H	Cl (100)	CH_3CN (20)	50	16	76	95
H	Br (100)	HMPA (20)	60	16	100	94
p-NMe_2	Br (30)	HMPA (12)	60	16	89	54
p-OMe	Cl (30)	HMPA (8)	60	6	98	94
m-OMe	Cl (30)	HMPA (8)	60	6	100	97
o-OMe	Cl (30)	HMPA (12)	60	16	98	98
m-Me	Cl (30)	HMPA (8)	60	6	100	95
o-Me	Cl (30)	HMPA (12)	60	6	69	97
o-Me	Cl (30)	HMPA (12)	60	16	91	95
m-F	Cl (30)	HMPA (8)	60	6	100	99[d)]
o-Cl	Cl (30)[b)]	HMPA (12)	60	16	11	Mono 28 Di 67
p-CO_2Me	Cl (30)	CH_3CN (12)	50	6	99	97
m-CF_3	Cl (30)	HMPA (8)	60	6	98	27
m-CF_3	Cl (30)	CH_3CN (12)	50	6	64	72
p-CF_3	Cl (30)	HMPA (8)	60	6	99	82
p-COMe	Cl (30)	CH_3CN (12)	50	6	96	96
m-CN	Cl (30)	CH_3CN (8)	50	6	76	91
m-CN	Cl (30)	HMPA (8)	60	6	27	11
p-CN	Cl (30)	CH_3CN (12)	50	6	96	99
o-CN	Cl (30)	CH_3CN (12)	60	16	20	70
o-CN	Cl (30)	HMPA (12)	60	16	29	71
m-NO_2	Cl (30)	HMPA (12)	60	6	≈0	
3-Br-Py[c)]	(30)	HMPA (8)	60	8	19	12
3-Br-Py[c)]	(30)	CH_3CN (8)	60	8	77	74

a) Made by Procedure A. $NiBr_2(PPh_3)_2$, 1 mmol (Ni : Zn : P=1 : 3 : 2); KCN/halide=1.1 molar ratio. b) KCN/*o*-$C_6H_4Cl_2$=2.2 molar ratio. c) 3-Br-Py=3-bromopyridine. d) For *m*-fluorobenzonitrile.

Table 5. Cyanation of Aromatic Halides with the $NiBr_2$-Zn-Phosphorus Ligand Catalyst

Y-C_6H_4Cl(mmol) Y	$NiBr_2$ mmol	L[a)]	HMPA ml	Procedure[b)]	Time h	Conversion %	Selectivity %
H (30)	1	PPh_3	8	A	6	59	84
H (30)	1	PPh_3	12	D	6	95	94
H (15)	0.5	DPPF	6	D	6	47	72
o-Cl (15)	0.5	PPh_3	6	D	24	10	Mono 39 Di 51
o-Cl (15)	0.5	DPPF	6	D	6	33	31 37
					24	68	9 75
o-CN (15)	0.5	DPPF	6	D	24	94	87

a) Phosphorus ligand, DPPF=1,1′-bis(diphenylphosphino)ferrocene. b) $NiBr_2$: Zn : L=1 : 3 : 4 molar ratio for PPh_3 and 1 : 3 : 2 for DPPF; KCN/halide=1.1 molar ratio for monohalide and 2.2 for dihalide. Procedure D: Ni-Zn-L+HMPA, 60 °C-1 h, +KCN+halide, 60 °C-6 or 24 h (see Experimental section).

temperatures ranging from 40 to 80 °C in three solvents: HMPA, MeCN, and DMF. The results are shown in Table 3. In all cases, the best results were obtained at about 60 °C. It is noteworthy that the reaction always proceeded fairly smoothly, even at the low temperature of 40 °C (conversion: 81% at 6 h), in MeCN. Generally, at 80 °C the coupling reaction became much more rapid, thus deactivating the catalyst. In the case, for example, of HMPA at 80 °C, the reaction stopped at the low conversion of 35%; the solution turned from reddish brown to black (colloidal nickel), thus revealing the decomposition of the catalyst. Furthermore, the selectivity of biphenyl varied also with the reaction time(conversion), as exemplified by the results obtained with HMPA. The PhCN/Ph-Ph ratio increased with the increase in the conversion, ranging from 7.7 at 16% conversion to 48 at 99% conversion. This suggests that most of the biphenyl is fomed at an initial stage of the reaction.

Cyanation of Various Aromatic Halides. The cyanation of various aromatic halides was examined with the KCN-HMPA and KCN-MeCN systems by means of Procedure A, which is the most convenient of the three (Table 4). At first, the cyanation of chloroben-

zene and bromobenzene was attempted at a high halide/Ni ratio of 100 (KCN/Ni=110) in 20 ml of HMPA and MeCN. With the above two systems, good results were obtained even at such a high ratio, whereas with the KCN-DMF system, with a higher cyanide solubility, the cyanation was not initiated under similar conditions. Furthermore, with 20 ml of DMF, the halides were not cyanated even at a halide/Ni ratio of 30 (KCN/Ni=33), which is allowable with 8 ml of DMF.

All the Y-substituted chlorobenzenes were reactive for cyanation except those with Y=*o*-Cl, *o*-CN, and *m*-NO_2; they all gave fair to good yields, regardless of the Hammett σ values for the Y-substituents. In general, *o*-Y-substituted chlorobenzenes, especially those with Y=Cl and CN, were less reactive. However, *o*-chloroanisole and *o*-chlorotoluene were cyanated almost completely during a long reaction time. With *m*-chlorobenzylidyne trifluoride, the MeCN solvent gave a much higher selectivity than that obtained in HMPA. The former solvent was also a better one for *m*- and *p*-chlorobenzonitrile. *m*-Chlorofluorobenzene gave only *m*-fluorobenzonitrile selectively. Further, *p*-bromo-*N*,*N*-dimethylaniline and 3-bromopyridine also reacted to give fair yields of the nitriles.

Cyanation of Aromatic Halides with $NiBr_2$-Zn-Phosphorus Ligand Catalyst. The use of $NiBr_2$-PPh_3 in place of $NiBr_2(PPh_3)_2$, if it were allowable, would provide a more convenient procedure because it would then be unnecessary to prepare the nickel complex prior to the catalytic cyanation. Therefore, first the cyanation of chlorobenzene was attempted using $NiBr_2$-PPh_3 in place of $NiBr_2(PPh_3)_2$ in Procedure A (Table 5). As a result, the conversion was low (59%) compared with that with $NiBr_2(PPh_3)_2$. The good result of a 94% selectivity at a 95% conversion was, however, obtained by adopting Procedure D, in which a mixture of $NiBr_2$, Zn, and PPh_3 in HMPA was heated at 60 °C for 1 h prior to the addition of KCN and chlorobenzene.

Next, combinations of $NiBr_2$ and three phosphorus ligands (tri-*o*-tolylphosphine, 1,2-bis(diphenylphosphino)ethane, and 1,1′-bis(diphenylphosphino)ferrocene(DPPF)) were used for the cyanation of chlorobenzene and much less reactive halides, such as *o*-dichlorobenzene and *o*-chlorobenzonitrile. The former two ligands were ineffective for the cyanation of chlorobenzene. DPPF was effective, but not so good as PPh_3 (47% conversion, 72% selectivity). DPPF was, however, found to be a good ligand for *o*-dichlorobenzene and *o*-chlorobenzonitrile; the former halide gave *o*-chlorobenzonitrile and phthalonitrile in a total yield of 57% (68% conversion, 84% total selectivity), in contrast to a yield of 9% with PPh_3, while the latter halide gave phthalonitrile in the good yield of 82%. On the other hand, tri-*o*-tolylphosphine and 1,2-bis(diphenylphosphino)ethane were also ineffective for the cyanation of *o*-dichlorobenzene and *o*-chlorobenzonitrile.

The present work was partially supported by a Grant-in-Aid for Scientific Research (No. 254158) from the Ministry of Education, Science and Culture.

References

1) K. Takagi, T. Okamoto, Y. Sakakibara, and S. Oka, *Chem. Lett.*, **1973**, 471.

2) L. Cassar, *J. Organomet. Chem.*, **54**, C57 (1973).

3) K. Takagi, T. Okamoto, Y. Sakakibara, A. Ohno, S. Oka, and N. Hayama, *Bull. Chem. Soc. Jpn.*, **48**, 3298 (1975).

4) K. Takagi, T. Okamoto, Y. Sakakibara, A. Ohno, S. Oka, and N. Hayama, *Bull. Chem. Soc. Jpn.*, **49**, 3177 (1976).

5) A. Sekiya and N. Ishikawa, *Chem. Lett.*, **1975**, 277.

6) L. Cassar, S. Ferrara, and M. Foa′, "Homogeneous Catalysis II," Adv. Chem. Ser. 132, Am. Chem. Soc. (1974), p. 252.

7) L. Cassar, M. Foá, F. Montanari, and G. P. Marinelli, *J. Organomet. Chem.*, **173**, 335 (1979).

8) T. Funabiki, H. Nakamura, and S. Yoshida, *J. Organomet. Chem.*, **243**, 95 (1983).

9) F. G. Mann and E. J. Chaplin, *J. Chem. Soc.*, **1937**, 527.

10) K. Yamamoto, *Bull. Chem. Soc. Jpn.*, **27**, 501 (1954).

11) B. B. Chastain, E. A. Rick, R. L. Pruett, and H. B. Gray, *J. Am. Chem. Soc.*, **90**, 3994 (1968).

12) Cassar et al. have obtained good results by the use of the NaCN-EtOH system in the in-situ generated $Ni(PPh_3)_3$-catalyzed cyanation of aromatic halides (Ref. 6). However, the results we obtained following their procedure exactly were not so good as those reported by them and moreover, were poorly reproducible.

13) The reaction of PhCl (4.8 mmol) with $Ni(CN)_2(PPh_3)_2$ (2.4 mmol) for 6 h at 60 °C in HMPA (8 ml) in the presence of a nickel catalyst ($NiBr_2(PPh_3)_2$, 1 mmol; Ni : Zn : P=1 : 3 : 2) gave benzonitrile in a 78% yield.

14) The equilibrium between $Ni(PPh_3)_4$ and $Ni(PPh_3)_3$ in toluene is found to lie well to the latter side at room temperature (R. Mynott, A. Mollbach, and G. Wilke, *J. Organomet. Chem.*, **199**, 107 (1980)). Cyanonickel(0)-complex ions $[Ni(CN)_n(PPh_3)_{4-n}]^{n-}$ (n=1—4) are not obtained by the action of CN^- on $Ni(PPh_3)_4$, while it is known that $K_4[Ni(CN)_4]$ undergoes a complete triphenylphosphine displacement of cyanide to give $Ni(PPh_3)_4$ without any intermediate substitution products (H. Behrens and A. Müller, *Z. Anorg. Allg. Chem.*, **341**, 124 (1965); R. del Rosario and L. S. Stuhl, *J. Am. Chem. Soc.*, **106**, 1160 (1984)). Cassar et al. have, however, reported that the IR bands assigned to coordinate cyanide are observed when NaCN is added to a *N*,*N*-dimethylformamide solution of $Ni(PPh_3)_3$ (Ref. 6). Recently, it has been reported that a related nickel complex anion $[Ni(CN)(P(OMe)_3)_3]^-$ is formed by the reaction of (K · 18-crown-6)$_2$[$Ni(CN)_2\{\eta^2$-PhC≡CPh$\}$] with $P(OMe)_3$ (R. del Rosario and L. S. Stuhl, *Organometallics*, **5**, 1260 (1986)).

15) a) A. S. Kende, L. S. Liebeskind, and D. M. Braitsch, *Tetrahedron Lett.*, **1975**, 3375; b) M. Zembayashi, K. Tamao, J. Yoshida, and M. Kumada, *Tetrahedron Lett.*, **1977**, 4089; c) T. T. Tsou and J. K. Kochi, *J. Am. Chem. Soc.*, **101**, 7547 (1979); d) M. F. Semmelhack, P. Helquist, L. D. Jones, L. Keller, L. Mendelson, L. S. Ryono, J. G. Smith, and R. D. Stauffer, *J. Am. Chem. Soc.*, **103**, 6460 (1981).

A Search for New Synthetic Routes toward Siccanin

Michiharu KATO, Yukio MATSUMURA, Kiyoshi HEIMA, and Akira YOSHIKOSHI*
Chemical Research Institute of Non-Aqueous Solutions, Tohoku University, Sendai 980
(Received August 24, 1987)

11-Acetoxy-12bα-methoxymethyl-4,4,6aα,9-tetramethyl-1,2,3,4,4aα,5,6,6a,12aβ,12b-decahydro-12*H*-benzo[*a*]xanthene (**34**), which has been expected as a promising key intermediate for the synthesis of siccanin (**1**), was synthesized via acid-catalyzed cyclization of 1α-(2-hydroxy-6-methoxy-4-methylbenzyl)-8aα-methoxymethyl-2,5,5-trimethyl-1,4,4aα,5,6,7,8,8aα-octahydronaphthalene (**13**) and isomeric exo olefin **21**. The phenol acetate **34**, however, was so resistant to oxidation that no corresponding 12-oxo derivative, which was expected to provide 11-acetoxy-12bα-acetoxymethyl-12-oxo-4,4,6aα,9-tetramethyl-1,2,3,4,4aα,5,6,6a,12aα,12b-decahydro-12*H*-benzo[*a*]xanthene (**4**) on epimerization at its C(12a) position as well as hydrofuran ring formation at the C(12) position with its angular methoxymethyl substituent, was obtained.

Siccanin (**1**) is a mold metabolite produced by *Helminthosporium siccans*[1] and exhibits a remarkable antifungal activity against a variety of fungi. In particular, its high activity in low concentrations against *Trichophyton interdigitale* and *T. asteroids*, which cause fungal infection in skin, has been demonstrated to be clinically useful.[2]

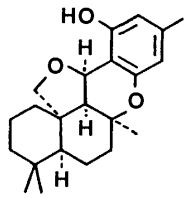

1

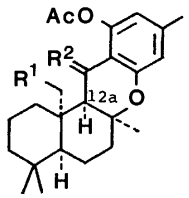

2, R^1=H, R^2=H_2
3, R^1=H, R^2=O
4, R^1=OAc, R^2=O
5, R^1=OAc, R^2=H_2

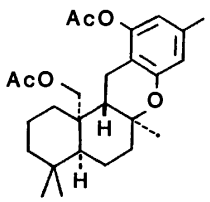

6

In the course of structural elucidation of **1**, Ishibashi et al.[2] have found that chromium trioxide oxidation of tetracyclic compound **2**, a derivative of **1**, gave dihydro-4*H*-1-benzopyran-4-one derivative **3** in moderate yield. They also demonstrated the cis, cisoid, cis ring system of **2** to be thermodynamically more stable than the corresponding 12aβ-H isomer as indicated by treatment of **3** with various bases giving unchanged material. Oida et al.[3] also reported that lithium aluminium hydride reduction converted tetracyclic ketone **4**, obtained on benzylic oxidation of diacetate **5**, to **1** as a result of concomitant tetrahydrofuran ring formation by internal nucleophilic displacement.

The above Sankyo group's work implies that a compound **6** epimeric with **5** at the C(12a) position would also serve as a synthetic intermediate for **1**, i.e. oxidation of **6** with chromium trioxide at its benzylic position followed by epimerization can be expected to produce **4**. Model syntheses of **1** based on the above presumption were thus reported by the Sankyo group.[3,4]

In preceding papers,[5] we reported the first total synthesis of racemic siccanin (*dl*-**1**), which was achieved from readily available octalone **7** via tetrahydrofuran derivative **8**. Our continuing effort for the synthesis of **1** was then directed to finding an alternative route based on the above presumption in combination with the olefin-phenol cyclization protocol, which seemed to be a more efficacious approach to the characteristic 1-benzopyran-4-one structure of **1** than that reported earlier.[5] We report here our findings in the investigation on this line.

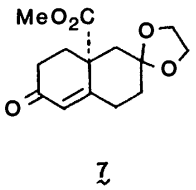

7

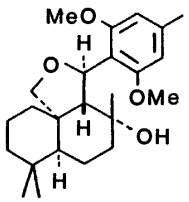

8

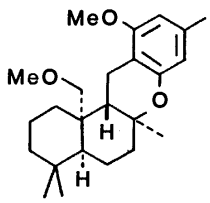

9

We planned to synthesize tetracyclic compound **9**, a synthetic equivalent of the proposed compound **6**, from two olefinic phenols **13** and **21** by the olefin-phenol cyclization. For derivation to the former phenol, benzylic alcohol **10**,[5] epimeric mixture regarding the benzylic hydroxyl, was submitted to hydrogenolysis to give alcohol **11** smoothly (Scheme 1). Sub-

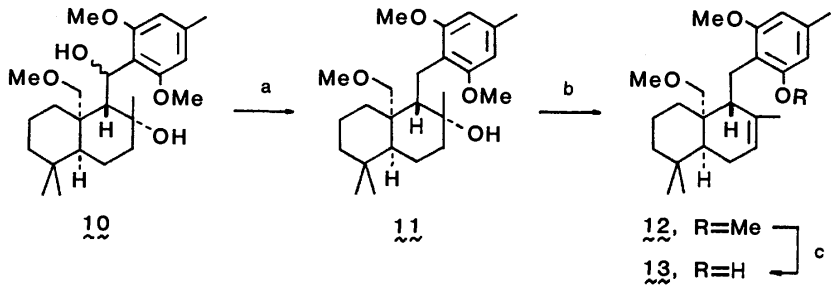

(a) H_2, 10% Pd-C, EtOH: (b) $SOCl_2$, Py: (c) NaSEt, DMF

Scheme 1.

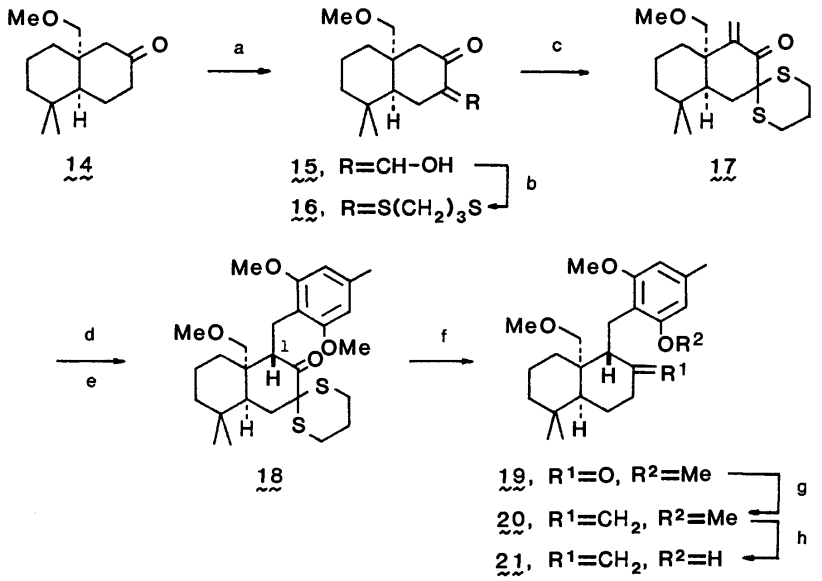

(a) NaH, HCO_2Et, PhH: (b) $CH_2(CH_2STs)_2$, KOAc, MeOH, (c) NaH, DMSO, CH_2O(g): (d) BuLi, orcinol dimethyl ether: (e) H_3O^+: (f) Raney-Ni(W-4), EtOH: (g) NaH, DMSO, Ph_3PCH_3Br: (h) NaSEt, DMF

Scheme 2.

sequent dehydration of **11** with thionyl chloride in pyridine provided trisubstituted olefin **12** as the sole product in good yield. The phenol **13** was obtained from **12** by demethylation on heating with sodium ethanethiolate in *N,N*-dimethylformamide,[6] and its structure was confirmed by its physical data (IR and ^1H NMR) as well as regeneration of **12** on methylation with dimethyl sulfate under alkaline conditions.

Preparation of the latter phenol **21** was conducted from cis decalone **14**[5] on the application of the reported method.[4] According to our experience,[5] the C(3) position of **14** was protected to prevent preferential alkylation at this position under basic conditions (Scheme 2). Formylation of the sodium enolate of **14** with ethyl formate and subsequent thioacetalization of the resulting hydroxymethylene ketone **15** with 1,3-propanedithiol ditosylate afforded crystalline ketone **16** in 80% overall yield. The enolate anion of the product generated with methylsulfinylmethanide anion was then treated with formaldehyde at −10 °C to give exo-methylene ketone **17** in moderate yield. The ketone **17** was submitted to the Michael addition with the lithium salt of orcinol dimethyl ether[7] and gave oily diastereomeric mixture, from which single epimer **18**[8] was obtained by acid epimerization in high yield. After removal of the thioacetal group in **18** by desulfurization with Raney nickel, methylenation of the resulting ketone **19** by the Wittig reaction with methylenetriphenylphosphorane afforded exo olefin **20** in high overall yield. The desired phenol **21** was derived by demethylation of **20** with sodium ethanethiolate.[6]

Having the olefinic phenols **13** and **21** in hand, we focused our attention on their acid-catalyzed olefin-phenol cyclizations. The cyclization of **13** proceeded smoothly upon heating with *p*-toluenesulfonic acid in benzene to provide two isomeric tetracyclic compounds **9** and **22** in 51 and 16% yields, while **21** similarly produced the same products in 54 and 26% yields, respectively (Scheme 3).

As no informative data were obtained from their

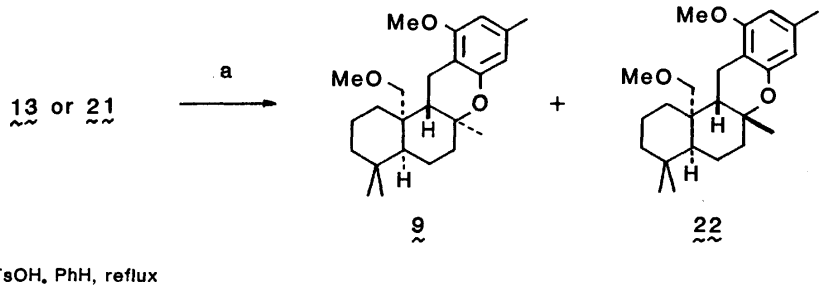

Scheme 3.

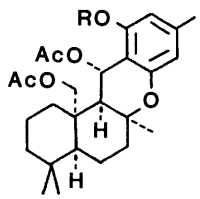

23, R=Ac
24, R=Me

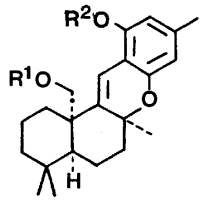

25, R^1=R^2=Ac
26, R^1=H, R^2=Me
27, R^1=Ac, R^2=Me

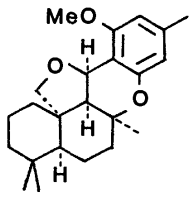

28

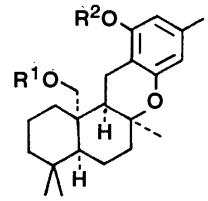

29, R^1=H, R^2=Me
30, R^1=R^2=Me
31, R^1=R^2=H
32, R^1=Me, R^2=H

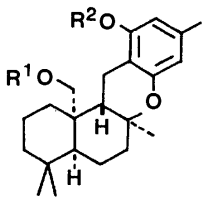

33, R^1=H, R^2=Me
34, R^1=Me, R^2=Ac
35 R^1=Me, R^2=H

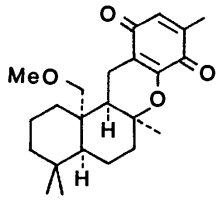

36

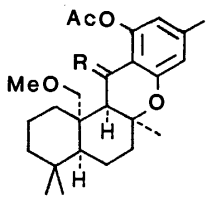

37, R=H_2
38, R=O

^{1}H NMR spectra to distinguish between **9** and **22**, we attempted to define their structures by derivation of the authentic compound from natural siccanin (*l*-**1**).

Nozoe et al. reported that siccanin (**1**), on treatment with boron trifluoride etherate in acetic anhydride, underwent cleavage of the C-O bond at the benzylic position to give triacetate **23** and siccanochromene E diacetate (**25**) as major and minor products, respectively.[9] With a view to obtaining siccanochromene E methyl ether (**26**), siccanin methyl ether (**28**)[9] was treated with the above Lewis acid under similar conditions, thus providing diacetoxy methyl ether **24** and acetoxy siccanochromene E methyl ether (**27**) in 80 and 19% yields, respectively. Subsequent reduction of the latter with lithium aluminium hydride afforded **26** quantitatively.

The methyl ether **26** was then submitted to catalytic hydrogenation over Pd-$SrCO_3$, affording two products, oily **29** and crystalline **33**, in a ratio of 81 : 19, and these products were presumed to be isomeric with respect to B/C ring juncture. Anticipation of the stereoselective hydrogenation at the convex face of molecule allowed us to assign the structure **29** to the major product. This surmise was chemically supported; dimethyl ether **30** obtained by methylation of **29** with methyl iodide was identical in all respects, except for optical rotations, with the exhaustive methylation product of the known diol **31**.[9]

Consequently, the structure **33** could be assigned to the minor hydrogenation product, whose methyl ether was identical with the major cyclization product in comparison of their spectra.[1] This result also indicated that the structure **22** should be assigned to the minor cyclization product.

^{1}H NMR study of these cyclization products were highly suggestive of their conformations. Irradiation at methylene protons at δ 3.24 (CH_3OCH_2) in the spectrum of **9** in C_6D_6 resulted in a 4% NOE of the methyl protons (δ 1.39) on the carbon bearing an oxygen atom, whereas any ^{1}H NOE was not detectable between the methylene and gem. dimethyl protons. This finding seemed to indicate the steroid conformation **9a**[11]

with respect to the A/B rings for this compound. On the other hand, in the spectrum of **22** in $CDCl_3$, irradiation at one (δ 0.98) of methyl signals due to the gem. dimethyl grouping showed a 10% NOE in one of methylene proton signals at δ 2.63 (CH_3OCH_2), whereas no effect was observed between the methylene and the methyl protons (δ 1.20) on the carbon bearing an oxygen atom. In addition, the observed chemical shift (δ 2.63) of a methylene proton in methoxymethyl group of **22** is unusually high in comparison with other related compounds **9** (δ 3.27), **19** (δ 3.22), and **20** (δ 3.4), and this upfield shift would be ascribable to the shielding effect of aromatic ring. Such a stereochemical disposition seems to be allowed by a distorted conformation of its B ring by which one of methylene hydrogen atoms is disposed above the plane of aromatic ring. (cf. **22a**[11]), although we have no other evidence supporting this conformation.

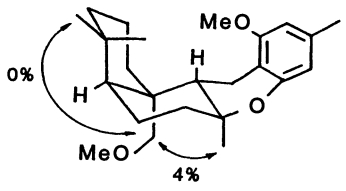

9a

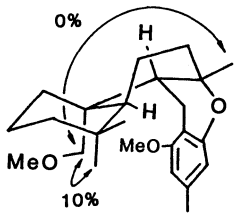

22a

The subsequent step in this synthesis was oxidation of the benzylic position of **9**. In expectation of preliminary information regarding this oxidation, we first submitted **30** to oxidation with chromium trioxide in aqueous acetic acid at 0 °C according to the literature.[1] The product, however, was *p*-quinone **36** formed in 40% yield.[12] Since this result indicated that methoxy was inadequate as a protective group in this oxidation, **9** was then transformed into acetylated phenol **34** by demethylation with sodium ethanethiolate[6] followed by acetylation of the resulting phenol **35**.

The acetylated phenol **34**, unfortunately, was extremely resistant to oxidation under similar conditions and gave rise to recovery of the unchanged substrate. On long duration of the oxidation at room temperature, some unidentified polar products[13] were formed, while no desired 1-benzopyran-4-one derivative was detectable despite of careful inspection of the reaction mixture. Attempted oxidation of **34** with other oxidants (cerium(IV) ammonium nitrate, lead(IV) acetate selenium dioxide, etc.) were also all fruitless. On the other hand, acetylated phenol **37** derived from **30** by demethylation with sodium ethanethiolate followed by acetylation of the resulting phenol **32** was submitted, for comparison, to chromium trioxide oxidation, yielding 1-benzopyran-4-one derivative **38**, albeit in low yield, in harmony with the previous observation.[3] Obviously **34** is suffered from a severe steric hindrance at the benzylic position.

In conclusion, the tetracyclic compound **34**, an equivalent of **6** that has been proposed as a promising synthetic intermediate[3,4] for *dl*-**1**, was synthesized via acid-catalyzed cyclization of the olefinic phenols **13** and **21**. This approach toward **1**, however, seems not to be feasible due to unsuccessful oxidation of **34** to the corresponding 12-oxo derivative.

Experimental

Melting points are uncorrected. IR spectra were obtained with a JASCO A-3 infrared spectrometer. ^{1}H NMR spectra were recorded on a JEOL FX90Q spectrometer using tetramethylsilane as an internal standard, and chemical shift values are given in δ and coupling constants (J) in hertz. Mass spectra were obtained on a Shimadzu LKB gas chromatograph-mass spectrometer equipped with a column (1 m) packed with OV-1 (1%). Ultraviolet spectra were recorded on a Cary model 14 spectrophotometer. Dry tetrahydrofuran (THF) and ethylene glycol dimethyl ether (DME) were obtained by distillation over lithium aluminium hydride. Other organic solvents, *N*,*N*-dimethylformamide (DMF), dimethyl sulfoxide (DMSO), and benzene were dried according to the standard procedure. All reactions, except for those in aqueous solutions, were carried out under dry N_2 or Ar atmosphere with use of standard procedures for the exclusion of moisture. Extracts obtained on workup of reaction mixtures were washed successively with water and brine, and then dried over $MgSO_4$, unless otherwise stated. Column chromatography was performed on silica gel (Merck, kieselgel 60, 70—230 mesh), and kieselgel GF_{254} was employed for preparative thin-layer chromatography (TLC) as absorbent. Solvents used for elution are shown in parentheses.

1α-(2,6-Dimethoxy-4-methylbenzyl)-8aα-methoxymethyl-2,5,5-trimethyl-1,4,4aα,5,6,7,8,8a-octahydronaphthalene (12). A mixture of **10**[5] (403 mg, 0.96 mmol), 10% Pd-C (80 mg) and ethanol (8 ml) was stirred at room temperature for 2 d under hydrogen. Filtration and subsequent concentration of the filtrate left an oil (395 mg), whose purification by TLC (1 : 1 ether-hexane) gave **11** (330 mg, 85%) as colorless crystals; mp 149—151 °C (from ether). IR (KBr) 3500, 1610, 1590, 1110, 970, 820 cm^{-1}. ^{1}H NMR ($CDCl_3$) δ=0.92 and 0.98 (3H, s each, $C(CH_3)_2$), 1.08 (3H, s, O-CCH_3), 1.1—2.1 (12H, m), 2.35 (3H, s, $ArCH_3$), 2.47 (1H, t, J=9 Hz, $CHCH_2Ar$), 2.85 (2H, d, J=9 Hz, $ArCH_2$), 3.15 and 4.05 (1H, d, J=10 Hz each, CH_2O), 3.39 (3H, s, OCH_3), 3.85 (6H, s, $ArOCH_3$), 6.40 (2H, s, ArH), and a small amount of **10**.

To a stirred solution of **11** (110 mg, 0.27 mmol) in pyridine (1 ml) was added thionyl chloride (36 μl, ca. 0.5 mmol) at 0 °C, and stirring was continued for 5 h at this temperature and then at room temperature for an additional 5 h. Ether was added and the solution was washed successively with water, aqueous $CuSO_4$, water, and brine, and then dried. The oily residue obtained by evaporation was purified by TLC (4 : 1 hexane-ether) to give **12** (69 mg, 66%) as colorless needles; mp 137—138 °C (from hexane-ether). IR (KBr) 1610, 1590, 1120, 975, 810 cm^{-1}. ^{1}H NMR ($CDCl_3$) δ=0.85 and 0.93 (3H, s each, $C(CH_3)_2$), 1.2—2.2 (10H, m), 1.48 (3H, br s, =C-CH_3), 2.35 (3H, s, $ArCH_3$), 2.67 (2H, d, J=7.2 Hz, CH_2Ar), 3.35 (3H, s, OCH_3), 3.24 and 3.52 (1H, d, J=9 Hz each, CH_2O), 3.81 (6H, s, $ArOCH_3$), 5.38 (1H, br s, =CH), 6.36 (2H, s, ArH).

Found: C, 77.40; H, 9.90%. Calcd for $C_{25}H_{38}O_3$: C, 77.67; H, 9.91%.

1α-(2-Hydroxy-6-methoxy-4-methylbenzyl)-8aα-methoxymethyl-2,5,5-trimethyl-1,4,4aα,5,6,7,8,8a-octahydronaphthalene (13). A mixture of **12** (176 mg, 0.46 mmol), sodium ethanethiolate (370 mg, 4.4 mmol) and DMF (5 ml) was heated at 110 °C for 4.5 h. After cooling to room temperature, water was added and the resultant solution was extracted with ether. Concentration of the extract and purification of the oily residue by TLC (1 : 1 hexane-ether) gave **13** (164 mg, quantitaive) as a viscous oil. IR ($CHCl_3$) 3300, 1620, 1580, 1110, 815 cm^{-1}. ^1H NMR ($CDCl_3$) δ=0.88 and 0.92 (3H, s each, $C(CH_3)_2$), 1.0—2.2 (9H, m), 1.55 (3H, s, $=CCH_3$), 2.24 (3H, s, $ArCH_3$), 2.4—3.05 (3H, m), 3.42 (3H, s, OCH_3), 3.56 and 3.70 (1H, d, J=10 Hz each, CH_2O), 3.77 (3H, s, $ArOCH_3$), 5.35 (1H, br s, =CH), 6.21 and 6.33 (1H, s each, ArH), 7.75 (1H, s, OH). MS (70 eV) m/z 372 (M^+).

Methylation of 13 with Dimethyl Sulfate. To a stirred solution of **13** (10 mg) in ethanol (0.5 ml) was added aqueous NaOH (38%, 0.1 ml) and then dimethyl sulfate (0.1 ml) at room temperature. After stirring for 1 h, the same amounts of dimethyl sulfate and the alkali solution were added and stirring was continued for an additional 1 h. The mixture was diluted with water and extracted with CH_2Cl_2. Concentration of the extract left crystals (10 mg, quantitative), whose IR and ^1H NMR were identical with those of **12**.

5,5-Dimethyl-3-hydroxymethylene-8aα-methoxymethyl-3,4,4aα,-5,6,7,8,8a-octahydro-2(1*H*)-naphthalenone (15). A 50% sodium hydride dispersion in mineral oil (1.453 g, 15.14 mmol) was washed with pentane, and benzene (20 ml) was added. A solution of **14**[5] (3.390 g, 15.14 mmol) in benzene (20 ml) was added to the above suspension, and the mixture was stirred at 0 °C for 30 min. A solution of ethyl formate (4.486 g, 60.5 mmol) in benzene (5 ml) was added, and stirring was continued at 0 °C for 1.5 h and then at room temperature for 10 h. The mixture was poured into ice water, and the benzene layer was extracted with aqueous NaOH. The extract was acidified with dilute HCl at 0 °C and extracted with CH_2Cl_2. Concentration of the extract left a semisolid, which was filtered through a short silica gel-column with the aid of hexane-ether (1 : 3) to give **15** (3.550 g, 93%) as colorless needles; mp 76—77 °C (from hexane-ether). IR (KBr) 3300—2500, 1650, 1600, 1120, 890 cm^{-1}. ^1H NMR ($CDCl_3$) δ=0.81 and 0.98 (3H, s each, $C(CH_3)_2$), 1.1—1.8 (8H, m), 2.05 (1H, m), 2.3—2.6 (2H, m), 3.00 and 3.10 (1H, d, J=10.0 Hz each, CH_2O), 3.30 (3H, s, OCH_3), 8.27 (1H, s, =CHOH), 13.9—14.4 (1H, br, =CHOH).

Found: C, 71.11; H, 9.19%. Calcd for $C_{15}H_{24}O_3$: C, 71.39; H, 9.59%

5,5-Dimethyl-8aα-methoxymethyl-3-(trimethylenedithio)-3,4,4aα,5,6,7,8,8a-octahydro-2(1*H*)-naphthalenone (16). A mixture of **15** (137 mg, 0.54 mmol), 1,3-propanedithiol ditosylate (225 mg, 0.54 mmol), potassium acetate (180 mg, 1.8 mmol), and methanol (5 ml) was gently refluxed for 15 h. The solvent was mostly removed under reduced pressure, and the residual oil was dissolved in CH_2Cl_2. The solution was washed successively with aqueous $NaHCO_3$, water and brine, and dried. The oily residue obtained on concentration was purified by TLC (1 : 1 ether-hexane) to provide **16** (152 mg, 85%) as colorless needles; mp 95—96 °C (from hexane-ether). IR (KBr) 1700, 1100, 620 cm^{-1}. ^1H NMR ($CDCl_3$) δ=0.95 and 1.13 (3H, s each, $C(CH_3)_2$), 1.1—2.6 (16H, m), 2.7—3.7 (1H, m), 3.03 and 3.53 (1H, d, J=10 Hz each, CH_2O), 3.30 (3H, OCH_3).

Found: C, 62.44; H, 8.45; S, 19.17%. Calcd for $C_{17}H_{28}O_2S_2$: C, 62.17; H, 8.59; S, 19.14%.

1α-(2,6-Dimethoxy-4-methylbenzyl)-5,5-dimethyl-8aα-methoxymethyl-3-(trimethylenedithio)-3,4,4aα,5,6,7,8,8a-octahydro-2(1*H*)-naphthalenone (18). A 50% sodium hydride dispersion in mineral oil (983 mg, 9.75 mmol) was washed with pentane, and DMSO (20 ml) was added. The mixture was warmed at 65 °C with stirring for 1.5 h and then cooled to 0 °C. To the resulting solution, a solution of **16** (3.20 g, 9.75 mmol) in THF (30 ml) was added dropwise, and the whole was stirred for an additional 30 min. Formaldehyde vapor generated by heating paraformaldehyde (ca. 3 g) at 160—170 °C was passed through the well-stirred, above mixture at −10 °C with the aid of a dry N_2 stream over 40 min. The reaction was then quenched with aqueous NH_4Cl, and the mixture was extracted with benzene. Concentration of the extract left a semisolid, which was chromatographed over 50 g of silica gel (1 : 3 hexane-ether) to give **17** (1.94 g, 58%) as colorless crystals; mp 80—82 °C (from hexane-ether). IR (KBr) 1680, 1595, 1100, 950 cm^{-1}. ^1H NMR ($CDCl_3$) δ=0.97 and 1.00 (6H in total, s, $C(CH_3)_2$), 1.1—2.75 (15H, m), 3.25 and 3.60 (1H, d, J=10 Hz each, CH_2-O), 3.30 (3H, OCH_3), 5.42 and 6.13 (1H, finely splitted s each, $=CH_2$). MS (70 eV) m/z 340 (M^+).

1.5 M butyllithium in hexane (5.1 ml, 7.63 mmol) was added to a stirred solution of orcinol dimethyl ether (1.48 g, 9.72 mmol) in THF (20 ml) at 0 °C and the resulting mixture was stirred at room temperature for an additional 30 min. The mixture was cooled at −40—−50 °C and a solution of **17** (1.18 g, 3.47 mmol) in THF (10 ml) was added dropwise. Stirring was continued for an additional 2 h, and the reaction was quenched with ice water. The product was extracted with ether, and the oily residue obtained by concentration of the extract was dissolved in $CHCl_3$ (30 ml). A $CHCl_3$ solution (0.1 ml) saturated with dry HCl was added to the above solution, and the mixture was stirred at room temperature for 30 min. Removal of the solvent under reduced pressure gave a semisolid, which was then chromatographed over 50 g of silica gel (1 : 3 ether-hexane) to give **18** (1.52 g, 89%) as colorless crystals; mp 148—149 °C (from ether). IR (KBr) 1710, 1610, 1580, 1110, 810, 580 cm^{-1}. ^1H NMR ($CDCl_3$) δ=0.93 and 1.03 (3H, s each, $C(CH_3)_2$), 1.1—4.0 (18H, m), 2.30 (3H, s, $ArCH_3$), 3.35 (3H, s, OCH_3), 3.43 (2H, s, CH_2O), 3.80 (6H, s, $ArOCH_3$), 6.28 (2H, s, ArH). MS (70 eV) m/z 492 (M^+).

Found: C, 65.63; H, 8.40; S, 12.74%. Calcd for $C_{27}H_{40}O_4S_2$: C, 65.83; H, 8.19; S, 13.00%.

1α-(2,6-Dimethoxy-4-methylbenzyl)-5,5-dimethyl-8aα-methoxymethyl-3,4,4aα,5,6,7,8,8a-octahydro-2(1*H*)-naphthalenone (19). A mixture of W-4 Raney-Ni (ca. 4 g) and a solution of **18** (320 mg, 0.64 mmol) in ethanol (10 ml) was gently refluxed for 2.5 h with stirring. After cooling to room temperature, precipitates were filtered and washed with ethanol. The combined filtrates were evaporated and the residue was dissolved in CH_2Cl_2. Concentration of the solution left a solid, which was purified by TLC (3 : 1 hexane-ether) to give **19** (230 mg, 91%) as colorless needles; mp 130—131 °C (from ether). IR (KBr) 1710, 1605, 1590, 810 cm^{-1} ^1H NMR ($CDCl_3$) δ=1.02 and 1.15 (3H, s each, $C(CH_3)_2$), 1.0—2.9 (14H, m), 2.28 (3H, s, $ArCH_3$), 3.28 (3H, s, OCH_3), 3.22 and 3.33 (1H, d, J=10 Hz each, CH_2O), 3.78 (6H, s, $ArOCH_3$), 6.30 (2H, s, ArH).

Found: C, 74.16; H, 9.40%. Calcd for $C_{24}H_{36}O_4$: C, 74.19; H, 9.34%.

1α-(2,6-Dimethoxy-4-methylbenzyl)-5,5-dimethyl-8aα-methoxymethyl-2-methylene-1,2,3,4,4aα,5,6,7,8,8a-decahydronaphthalene (20). A 50% sodium hydride dispersion in mineral oil (65 mg, 1.36 mmol) was washed with pentane, and DMSO (2 ml) was added. The resulting suspension was warmed at 60 °C for 1.5 h with stirring. A solution of methyltriphenylphosphonium bromide (480 mg, 1.36 mmol) in DMSO (1.5 ml) was added to the above solution at 0 °C, and stirring was continued at the same temperature for 30 min and then at room temperature for 30 min. A solution of **19** (250 mg, 0.64 mmol) in THF (1.5 ml) was added to the above ylide solution, and the mixture was stirred for an additional 15 h. The reaction was quenched with aqueous NH_4Cl, and the product was extracted with ether. Concentration of the extract gave an oil, which was purified by TLC (4 : 1 hexane-ether) to give **20** (199 mg, 80%) and recovered **19** (20 mg). **20**: colorless needles; mp 79—81 °C (from hexane-ether). IR (KBr) 1650, 1600, 1120, 980, 870, 820 cm^{-1}. ^1H NMR ($CDCl_3$) δ=0.97 and 1.05 (3H, s each, $C(CH_3)_2$), 1.1—2.3 (12H, m), 2.30 (3H, s, $ArCH_3$), 2.6—2.9 (2H, m), 3.28 (3H, s, OCH_3), 3.40—3.43 (2H, m, CH_2-O), 3.77 (6H, s, $ArOCH_3$), 4.26 and 4.45 (1H, br d, J=3 Hz each, $=CH_2$), 6.27 (2H, s, ArH).

Found: C, 77.60; H, 9.89%. Calcd for $C_{25}H_{38}O_3$: C, 77.67; H, 9.91%.

5,5-Dimethyl-1α-(2-hydroxy-6-methoxy-4-methylbenzyl)-8aα-methoxymethyl-2-methylene-1,2,3,4,4aα,5,6,7,8,8a-decahydronaphthalene (21). A mixture of **20** (120 mg, 0.31 mmol), sodium ethanethiolate (250 mg, 2.97 mmol) and DMF (3 ml) was gently refluxed for 1.5 h. After cooling to room temperature, water was added and the solution was extracted with ether. Concentration of the extract gave a semisolid, which was purified by TLC (3 : 1 hexane-ether) to afford **21** (95 mg, 82%) and recovered **20** (5 mg). **21:** mp 145—146 °C (from ether). IR (KBr) 3300, 1650, 1620, 1595, 1110, 925, 880, 820 cm^{-1}. ^1H NMR ($CDCl_3$) δ=0.91 and 1.07 (3H, s each, $C(CH_3)_2$), 1.1—2.6 (14H, m), 2.27 (3H, s, $ArCH_3$), ca. 3.5 (2H, m, CH_2O), 3.50 and 3.60 (3H, s each, OCH_3 and $ArOCH_3$), 4.0 and 4.45 (1H, finely splitted s each, $=CH_2$), 6.15 and 6.35 (1H s each, ArH), 7.63 (1H, s, ArOH). MS (70 eV) m/z 372 (M^+).

Found: C, 77.56; H, 10.07%. Calcd for $C_{24}H_{36}O_3$: C, 77.38; H, 9.74%.

11-Methoxy-12bα-methoxymethyl-4,4,6aα,9-tetramethyl-1,2,3,4,4aα,5,6,6a,12aβ,12b-decahydro-12*H*-benzo[*a*]xanthene (9) and 11-Methoxy-12bα-methoxymethyl-4,4,6aβ,9-tetramethyl-1,2,3,4,4aα,5,6,6a,12aα,12b-decahydro-12*H*-benzo[*a*]-xanthene (22). a) A solution of **21** (46 mg, 0.12 mmol) and *p*-toluenesulfonic acid (2 mg) in benzene (2 ml) was gently refluxed for 2 h. After cooling to room temperature, the mixture was diluted with benzene and washed successively with aqueous $NaHCO_3$, water and brine, and then dried. The oily residue obtained by concentration was purified by TLC (14 : 1 hexane-ether) to provide **9** (25 mg, 54%) as crystals, mp 111—112 °C (from hexane-ether). IR (KBr) 1615, 1585, 1130, 1105, 810 cm^{-1}. ^1H NMR ($CDCl_3$) δ=0.98 and 1.10 (3H, s each, $C(CH_3)_2$), 1.2—2.8 (14H, m), 1.28 (3H, s, O-CCH_3), 2.25 (3H, s, $ArCH_3$), 3.27 (5H, s, CH_2OCH_3), 3.78 (3H, s, $ArOCH_3$), 6.20 (2H, br s, ArH); ^1H NMR (C_6D_6) δ= 0.97 and 1.09 (3H, s each, $C(CH_3)_2$), 1.2—3.0 (14H, m), 1.39 (3H, s, O-CCH_3), 2.28 (3H, s, $ArCH_3$), 3.09 (3H, s, OCH_3), 3.24 (2H, s, CH_2O), 3.53 (3H, s, $ArOCH_3$), 6.24 and 6.72 (1H, s each, ArH). MS (70 eV) m/z 372 (M^+), and **22** (12 mg, 26%) as crystals, mp 175—176 °C (from ether). IR (KBr) 1615, 1590, 1115, 810 cm^{-1}. ^1H NMR ($CDCl_3$) δ=0.98 and 1.10 (3H, s each, $C(CH_3)_2$), 1.20 (3H, s, O-CCH_3), 1.27—2.8 (14H, m), 2.23 (3H, s, $ArCH_3$), 2.63 and 3.50 (1H, d, J=10 Hz each, CH_2O), 2.92 (3H, s, OCH_3), 3.77 (3H, s, $ArOCH_3$), 6.17 and 6.20 (1H, br s each, ArH). MS (70 eV) m/z 372 (M^+).

Found for **9:** C, 77.16; H, 10.04%. Found for **22:** C, 76.94; H, 9.50%. Calcd for $C_{24}H_{36}O_3$: C, 77.37; H, 9.74%.

b) A solution of **13** (172 mg, 0.46 mmol) and *p*-toluenesulfonic acid (5 mg) in benzene (4 ml) was gently refluxed for 2 h. Workup and subsequent purification of the oily residue obtained by the same procodure as described in a) gave **9** (86 mg, 51%) and **22** (28 mg, 16%).

Siccanochromene E Methyl Ether (26). A solution of 640 mg (1.80 mmol) of siccanin methyl ether (**28**)[9] in acetic anhydride (4 ml) was treated with a catalytic amount of boron trifluoride etherate at 0 °C. After stirring for 10 min, the mixture was poured into ice water and extracted with ether. The extract was successively washed with aqueous $NaHCO_3$, water, and brine, and then dried. Concentration left a semisolid, which was chromatographed over 15 g of silica gel (1 : 4 ether-hexane) to provide **27** (135 mg, 19%), mp 137—138 °C (from hexane-ether). IR (KBr) 1735, 1625, 1610, 1580, 1240, 1140, 1050, 830 cm^{-1}. ^1H NMR ($CDCl_3$) δ=0.90 and 1.03 (3H, s, $C(CH_3)_2$), 1.35 (3H, s, O-CCH_3), 1.9—2.2 (11H, m), 2.02 (3H, s, CH_3C=O), 2.28 (3H, s, $ArCH_3$), 3.81 (3H, s, OCH_3), 3.87 and 4.10 (1H, d, J=10 Hz each, CH_2O), 6.24 and 6.28 (2H in total, s each, ArH), 6.62 (1H, s, =CH), and **24** (646 mg, 80%) as colorless needels, mp 208—209 °C (from ether). IR (KBr) 1735, 1620, 1600, 1500, 1250, 1120, 1050, 820 cm^{-1}. ^1H NMR ($CDCl_3$) δ=0.90 and 1.20 (3H, s each, $C(CH_3)_2$), 1.32 (3H, s, O-CCH_3), 1.0—1.9 (12H, m), 1.98 and 2.07 (6H in total, s each, CH_3C=O), 2.26 (3H, s, $ArCH_3$), 3.75 (3H, s, OCH_3), 4.57 (2H, s, CH_2O), 6.00 (1H, s, ArCH-O), 6.22 and 6.29 (2H in total, s each, ArH).

Found for **27**: C, 75.60; H, 8.69%. Calcd for $C_{25}H_{34}O_4$: C, 75.34; H, 8.60%. Found for **24:** C, 70.40; H, 8.53%. Calcd for $C_{27}H_{38}O_6$: C, 70.71; H, 8.35%.

A mixture of **27** (282 mg, 0.71 mmol) and lithium aluminium hydride (54 mg) in THF (4 ml) was stirred at room temperature for 10 h, and the reaction was quenched with wet ether. Precipitates were filtered and washed with ether. Concentration of the combined filtrates left a semisolid, which was filtered through a short silica-gel column with the aid of ether-hexane (1 : 1) to afford **26** (247 mg, 98%) as colorless needles. The IR and ^1H NMR spectra of the product was identical with those of an authentic sample.

12bα-Hydroxymethyl-11-methoxy-4,4,6aα,9-tetramethyl-1,2,3,4,4aα,5,6,6a,12aα,12b-decahydro-12*H*-benzo[*a*]xanthene (29) and 12bα-Hydroxymethyl-11-methoxy-4,4,6aα,9-tetramethyl-1,2,3,4,4aα,5,6,6a,12aβ,12b-decahydro-12*H*-benzo[*a*]-xanthene (33). A mixture of **26** (85 mg, 0.24 mmol), Pd-$SrCO_3$ (20 mg) and ethanol (5 ml) was stirred at room temperature for 20 h under hydrogen. The catalyst was filtered and washed with a small amount of ethanol, and the combined filtrates were concentrated under reduced pressure to give an oil. The oil was purified by TLC (1 : 1 ether-hexane) to provide **29** (R_f 0.57, 64 mg, 75%), **33** (R_f 0.5, 15 mg, 18%), and unchanged **26** (R_f 0.43, 5 mg). **29** (viscous oil): IR (neat) 3400, 1620, 1590, 1110, 1030, 810 cm^{-1}. ^1H NMR ($CDCl_3$) δ=1.0 and 1.22 (9H in total, s each, $C(CH_3)_2$ and

O-CCH$_3$), 1.1—2.1 (13H, m), 2.31 (3H, s, ArCH$_3$), 2.73 (2H, d, J=7 Hz, CH$_2$Ar), 3.83 (3H, s, ArOCH$_3$), 3.67 and 4.10 (1H, d, J=10 Hz each, CH$_2$O), 6.20 and 6.25 (2H in total, s each, ArH). MS (70 eV) m/z 358 (M$^+$). **33** (colorless crystals): mp 155—156 °C (from hexane-ether). IR (KBr) 3500, 1620, 1590, 1120, 1100, 810 cm^{-1}. ^{1}H NMR (CDCl$_3$) δ=1.04, 1.12, and 1.30 (9H in total, s each, C(CH$_3$)$_2$ and O-CCH$_3$), 1.0—2.9 (15H, m), 2.25 (3H, s, ArCH$_3$), 3.52 and 3.72 (1H, d, J=10 Hz each, CH$_2$O), 3.83 (3H, s, ArOCH$_3$), 6.25 and 6.29 (2H in total, s each, ArH). MS (70 eV) m/z 358 (M$^+$).

Found for **29:** C, 77.39; H, 9.36%. Calcd for $C_{23}H_{34}O_3$: C, 77.05; H, 9.56%.

11-Methoxy-12bα-methoxymethyl-4,4,6aα,9-tetramethyl-1,2,3,4,4aα,5,6,6a,12aα,12b-decahydro-12*H*-benzo[*a*]xanthene (30). a) To a stirred mixture of 50% sodium hydride in mineral oil (14 mg, 0.3 mmol) and DME (0.5 ml) was added a solution of **29** (57 mg, 0.16 mmol) in DME (0.5 ml) at room temperature. After stirring for 20 min, a solution of methyl iodide (50 mg, 0.35 mmol) in DME (0.5 ml) was added and stirring was continued for an additional 10 h. Ether was added, and the oily residue obtained by workup the solution was purified by TLC (2 : 1 hexane-ether) to give **30** (45 mg, 77%) as colorless crystals; mp 157—158 °C (from hexane-ether). IR (KBr) 1620, 1590, 1115, 820 cm^{-1}. ^{1}H NMR (CDCl$_3$) δ=0.90 and 1.12 (3H, s each, C(CH$_3$)$_2$), 1,18 (3H, s, O-CCH$_3$), 1.1—2.1 (12H, m), 2.27 (3H, s, ArCH$_3$), 2.68 (2H, d, J=6 Hz, CH$_2$Ar), 3.30 and 3.72 (1H, d, J=10.5 Hz each, CH$_2$O), 3.29 (3H, s, OCH$_3$), 3.80 (3H, s, ArOCH$_3$), 6.2 and 6.24 (2H in total, s each, ArH); MS (70 eV) m/z 372 (M$^+$).

Found: C, 77.64; H, 9.62%. Calcd for $C_{24}H_{36}O_3$: C, 77.37; H, 9.74%.

b) To a stirred mixture of 50% sodium hydride in mineral oil (30 mg, 0.6 mmol) and DME (1 ml) was added a solution of **31**[9] (69 mg, 0.2 mmol) in DME (0.5 ml), and stirring was continued for 30 min at room temperature. A solution of methyl iodide (92 mg, 0.64 mmol) in DME (0.5 ml) was added, and the mixture was stirred for an additional 10 h. Workup and subsequent purification by the same procedure as described in a) gave **30** (59 mg, 80%).

Conversion of 33 to 9. A mixture of **33** (35 mg, 0.09 mmol), 50% sodium hydride in mineral oil (10 mg, 0.18 mmol), methyl iodide (29 mg, 0.18 mmol) and DME (1.5 ml) was stirred at room temperature for 12 h. Purification of the resulting oily residue, obtained by workup, by TLC (5 : 1 hexane-ether) gave crystals (31 mg, 86%), whose IR and ^{1}H NMR were identical with those of authentic **9** derived by acid-catalyzed cyclization of **13** or **21**.

Chromium Trioxide Oxidation of 30. To a stirred solution of **30** (25 mg, 67.1 mol) in acetic acid (0.4 ml) was added a 25% chromium trioxide solution in 80% aqueous acetic acid (92 µl) at 0 °C, and the mixture was stired at 0 °C for 15 h. After dilution with brine, the product was extracted with ether, and the extract was washed successively with aqueous NaHCO$_3$, water and brine, and dried. The oily residue obtained by evaporation was purified by TLC (10 : 1 hexane-ether) to afford, along with unreacted **30** (4 mg), **36** (10 mg, 40%) as pale yellow needles; mp 159—160 °C (from hexane-ether). IR (KBr) 1672, 1650, 1634, 1612, 1120, 980 cm^{-1}. ^{1}H NMR (CDCl$_3$) δ=1.00 and 1.08 (6H in total, s each, C(CH$_3$)$_2$), 1.2—2.3 (14H, m), 1.27 (3H, s, O-CCH$_3$), 2.03 (3H, d, J=1.4 Hz, CH=C-C<u>H</u>$_3$), 3.05 (3H, s, OCH$_3$), 3.1—3.3 (2H, m, OCH$_2$), 6.47 (1H, q, J=1.4 Hz, =CH). UV (EtOH) 262 (ε 11,400), 405 (ε 760) nm. MS (70 eV) m/z 372 (M$^+$).

Found: C. 74.12; H. 8.45%. Calcd for $C_{23}H_{32}O_4$: C, 74.16; H, 8.66%.

11-Acetoxy-12bα-methoxymethyl-4,4,6aα,9-tetramethyl-1,2,3,4,4aα,5,6,6a,12aβ,12b-decahydro-12*H*-benzo[*a*]xanthene (34). A solution of **9** (39 mg, 0.10 mmol), sodium ethanethiolate (66 mg, 0.78 mmol) and DMF (2 ml) was gently refluxed for 6 h. After cooling to room temperature, water was added and the product was extracted with benzene. The oily residue obtained by concentration was purified by TLC (7 : 1 hexane-ether) to give **35** (31 mg, 83%) as a colorless oil. IR (neat) 3350, 1623, 1590, 1100, 1050, 820 cm^{-1}. ^{1}H NMR (CDCl$_3$) δ=0.97 and 1.10 (6H in total, s each, C(CH$_3$)$_2$), 1.27 (3H, s, O-CCH$_3$), 1.3—2.9 (14H, m), 2.18 (3H, s, ArCH$_3$), 3.28 (3H, s, OCH$_3$), 3.31 (2H, s, CH$_2$O), 4.98 (1H, s, OH), 6.17 and 6.20 (2H in total, br s each, ArH).

A solution of **35** (30 mg, 0.08 mmol), acetic anhydride (0.5 ml) and pyridine (0.5 ml) was stirred at room temperature for 5 h. The mixture was poured into ice water and extracted with ether. A semisolid obtained by concentration was purified by TLC to give **34** (24 mg, 72%) as colorless crystals; mp 160—162 °C (from hexane-ether). IR (KBr) 1760, 1625, 1585, 1205, 1100, 1050 cm^{-1}. ^{1}H NMR (CDCl$_3$) δ=0.97 and 1.08 (3H, s each, C(CH$_3$)$_2$), 1.27 (3H, s, O-CCH$_3$), 1.3—2.8 (14H, m), 2.23 and 2.28 (3H, s each, ArCH$_3$ and CH$_3$C=O), 3.29 (5H, m, CH$_2$OCH$_3$), 6.43 and 6.50 (2H in total, br s each, ArH).

Found: C, 74.81; H, 9.15%. Calcd for $C_{25}H_{36}O_4$: C, 74.96; H, 9.09%.

Attempted Oxidation of 34 with Chromium Trioxide. a) To a solution of **34** (24 mg, 0.06 mmol) in acetic acid (1 ml) was added a 25% chromium trioxide solution in 80% aqueous acetic acid (82 µl) at 0 °C, and the mixture was stirred at 0 °C for 20 h. After dilution with brine, the product was extracted with ether, and the extract was washed successively with aqueous NaHCO$_3$, water and brine, and dried. The oily residue obtained by concentration was purified by TLC (10 : 1 hexane-ether) to provide unchanged **34** (18 mg).

b) A 25% chromium trioxide solution in 80% aqueous acetic acid (90 µl) was added to a solution of **34** (25 mg, 0.06 mmol) in acetic acid (1 ml), and the mixture was stirred at room temperature for 20 h. Workup followed by purification in a similar manner provided unchanged **34** (4 mg) and unidentified polar oily products.

11-Acetoxy-12bα-methoxymethyl-4,4,6aα,9-tetramethyl-1,2,3,4,4aα,5,6,12aα,12b-decahydro-12*H*-benzo[*a*]xanthene (37). A mixture of **30** (116 mg, 0.31 mmol), sodium ethanethiolate (235 mg, 2.8 mmol) and DMF (3 ml) was heated at 110 °C for 7 h. After cooling to room temperature, water was added and the resulting solution was extracted with ether. Evaporation followed by purification of the oily residue by TLC (2 : 1 hexane-ether) provided phenol **32** (97 mg, 87%) as an amorphous powder. IR (KBr) 3500, 1630, 1595, 1110, 1080, 1060 cm^{-1}. ^{1}H NMR (CDCl$_3$) δ=0.90, 1.10 and 1.15 (3H, s each, C(CH$_3$)$_2$ and O-CCH$_3$), 1.1—2.0 (m, 12H), 2.20 (3H, s, ArCH$_3$), 2.68 (2H, d, J=6 Hz, CH$_2$Ar), 3.32 (3H, s, OCH$_3$), 3.35 and 3.70 (1H, d, J=10.0 Hz each, CH$_2$O), 5.0 (1H, s, OH), 6.15 and 6.20 (1H, s each, ArH).

A solution of **32** (66 mg, 0.18 mmol), acetic anhydride (0.5 ml), and pyridine (0.5 ml) was stirred at room temperatutre for 15 h. The mixture was poured into water and extracted with ether. Concentration of the extract afforded an oil, which was purified by TLC (2 : 1 hexane-ether) to give **37** (70 mg, 96%) as an amorphous powder. IR (KBr) 1760, 1630,

1580 cm^{-1}. ^1H NMR ($CDCl_3$) δ=0.90, 1.10 and 1.18 (3H, s each, $C(CH_3)_2$ and $O\text{-}CCH_3$), 1.0—2.2 (m, 12H), 2.25 (3H, s, $ArCH_3$), 2.32 (3H, s, $CH_3C{=}O$), 2.60 (2H, d, J=3.6 Hz, CH_2Ar), 3.18 and 3.68 (1H, d, J=10.0 Hz each, CH_2O), 3.30 (3H, s, OCH_3), 6.38 and 6.47 (1H, s each, ArH).

Found; C, 74.70; H, 9.03%. Calcd for $C_{25}H_{36}O_4$: C, 74.96; H, 9.06%.

Oxidation of 37. A 25% chromium trioxide solution in 80% aqueous acetic acid (0.3 ml) was added to a solution of **37** (88 mg, 0.23 mmol) in acetic acid (1 ml), and the mixture was stirred at 0 °C for 15 h. After dilution with water, the product was extracted with ether, and the combined extracts were washed successively with aqueous $NaHCO_3$, water, and brine, and dried. Removal of the solvent left an oil, which was purified by TLC (1 : 1 hexane-ether) to give **38** (19 mg, 23%) as a viscous oil. IR (neat) 1765, 1675, 1620, 1560 cm^{-1}. ^1H NMR ($CDCl_3$) δ=0.92, 1.13, and 1.22 (3H, s each, $C(CH_3)_2$ and $O\text{-}CCH_3$), 1.0—2.1 (m, 11H), 2.30 (3H, s, $ArCH_3$), 2.39 (3H, s, $CH_3C{=}O$), 2.54 (1H, s, $CHC{=}O$), 3.22 and 3.63 (1H, d, J=10.0 Hz each, CH_2O), 3.35 (3H, s, OCH_3), 6.40 and 6.61 (1H, s each, ArH). MS (70 eV) m/z 414 (M^+).

This work was supported by a Grant-in-Aid for Scientific Research (354, 187). We acknowledge Sankyo Co. for a generous gift of natural siccanin.

References

1) K. Ishibashi, *J. Antibiot. Ser. A.*, **15**, 161 (1962).

2) K. Ishibashi, K. Hirai, M. Arai, S. Sugasawa, A. Endo, A. Yasumura, H. Masuda, and T. Muramatsu, *Ann. Sankyo Res. Lab.*, **22**, 1 (1970).

3) S. Oida, Y. Ohashi, A. Yoshida, and E. Ohki, *Chem. Pharm. Bull.*, **20**, 2634 (1972).

4) A. Yoshida, S. Oida, Y. Ohashi, C. Tamura, and E. Ohki, *Chem. Pharm. Bull.*, **20**, 2642 (1972).

5) M. Kato, K. Heima, Y. Matsumura, and A. Yoshikoshi, *J. Am. Chem. Soc.*, **103**, 2434 (1981); M. Kato, Y. Matsumura, K. Heima, N. Fukamiya, C. Kabuto, and A. Yoshikoshi, *Tetrahedron*, **43**, 711 (1987).

6) G. I. Feutrill and R. N. Mirrington, *Tetrahedron Lett.*, **1970**, 1312; *idem*, *Org. Synth.*, **53**, 90 (1978).

7) R. Adam, H. Wolff, C. K. Cain, and J. H. Clark, *J. Am. Chem. Soc.*, **62**, 1779 (1940).

8) The depicted stereochemistry at C(1) in this compound was deduced from that of **9** which could unambiguously be assigned (vide post).

9) K. Hirai, K. T. Suzuki, and S. Nozoe, *Tetrahedron*, **27**, 6057 (1971).

10) It is noteworthy that the observed diastereomeric distribution was in contrast with that previously reported for a simpler olefinic phenol (Ref. 4).

11) Although all six-membered rings of this compound were formally drawn with chair conformations, a distorted conformation has discussed for the A ring in some 4,4,10-trimethyldecalin systems. For example, see Y. Tsuda, K. Yoshimoto, T. Yamashita and K. Kaneda, *Chem. Pharm. Bull.*, **29**, 3228 (1981).

12) The quinone **36** would have been formed via a phenol formate. Cf. I. T. Harrison and S. Harrison, *Chem. Commun.*, **1966**, 752.

13) Although structural elucidation of these products were not attempted, they seemd to be degradation products resulting from an aromatic ring cleavage. The oxidative fission of an aromatic ring has been reported for **5** (Ref. 3).

Asymmetric Diels-Alder Reactions of Some Chiral Dienophiles Derived from Cinchona Alkaloids

Hideo SUZUKI,* Koichi MOCHIZUKI, Tatsuya HATTORI, Noriyuki TAKAHASHI, Osamu TAJIMA, and Toshio TAKIGUCHI
Department of Synthetic Chemistry, Faculty of Technology, Gunma University, Kiryu, Gunma 376
(Received September 11, 1987)

Acrylates, crotonate, and fumarates derived from cinchona alkaloids were easily prepared. The highly *re*-facial selective additions of the dienophiles derived from cinchonidine or quinine to some dienes were achieved in the presence of $SnCl_4$. Similarly, *si*-facial selective additions were also achieved by the use of cinchonine instead of cinchonidine or quinine as a chiral auxiliary alcohol with equal ease. The inverse diastereofacial selectivity was observed by the use of $TiCl_4$ instead of $SnCl_4$ as a Lewis acid in the case of the reaction of the acrylates cited above with cyclopentadiene. It was suggested by the infrared spectra of the dienophile-$SnCl_4$ complexes and by some circumstantial evidence that in the complexes, $SnCl_4$ coordinates with the oxygen atom of the C-O bond (not C=O bond) and probably also with the nitrogen atom of the quinuclidine framework to form a rigid five-membered ring structure.

The Diels-Alder reactions have been of considerable interest in organic syntheses. Recently, extensive efforts have been made concerning the asymmetric Diels-Alder reaction; cycloadducts with high stereoselectivity have been obtained by a variety of reactions.[1,2] Many kinds of auxiliary groups have been used.

Unfortunately, though, because of the limited availability of the auxiliary, only one of enantiomers of an auxiliary or one of the alternative topological counterparts has often been used as a chiral auxiliary, and only products enriched in one enantiomer have been synthesized. We aimed at the use of chiral auxiliary alcohols which 1) are readily available in both antipodal forms, 2) give their crystalline dienophiles, and 3) are removed easily from the final products without chromatography.

Thus, we made use of cinchona alkaloids as an auxiliary alcohol which seem to have the following merits: a) Several diastereomers are commercially available

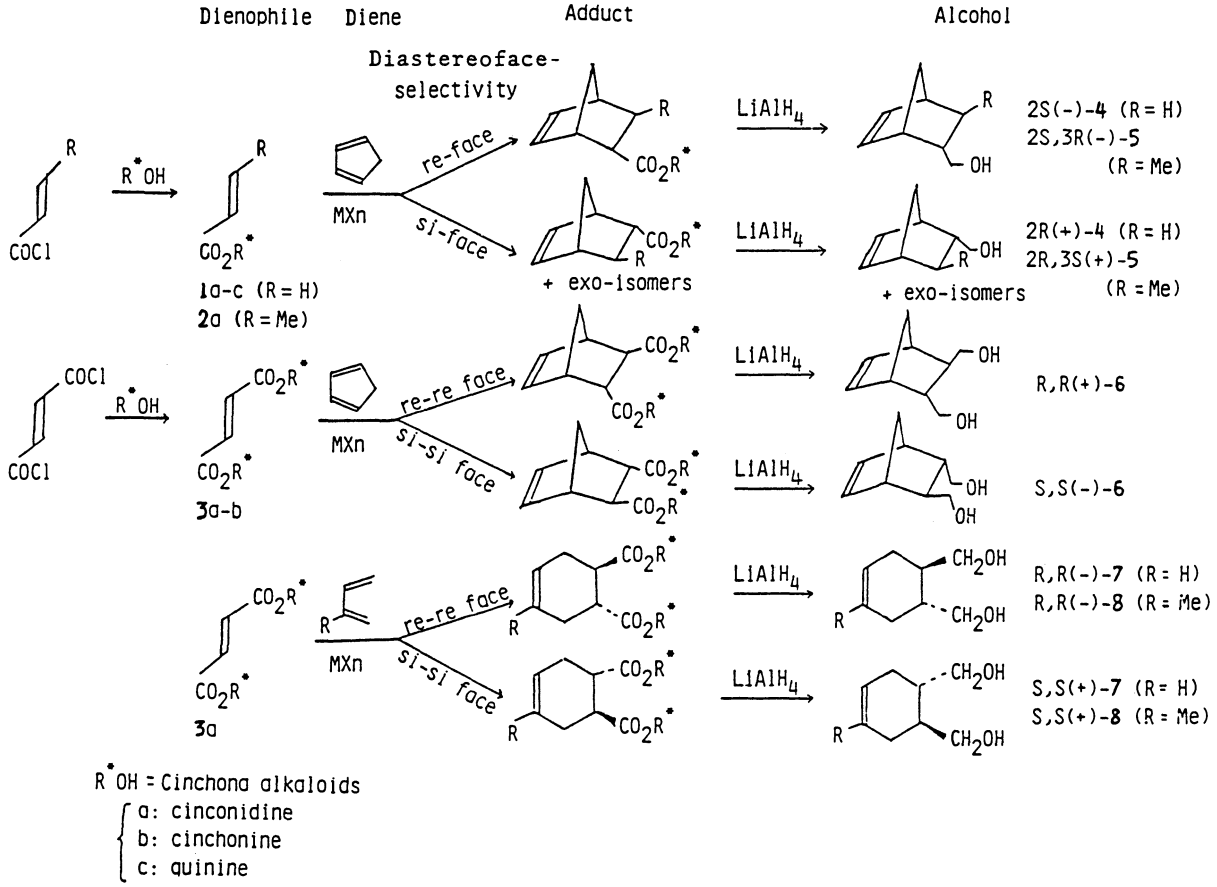

Scheme 1.

in optically pure forms and can be directly treated with acids or acid chlorides to give the corresponding esters as dienophiles. b) The rigid structure containing the quinuclidine framework is capable of forming stable complexes with a suitable Lewis acid. In this paper we describe the highly diastereofacial selective Diels-Alder reactions of the dienophiles derived from cinchona alkaloids with some dienes.

Results and Discussion

The acrylic, crotonic, and fumarylic esters of cinchona alkaloids were prepared as dienophiles in high yields by reactions of the corresponding acid chlorides with cinchona alkaloids in THF followed by treatment with Et_3N in $CHCl_3$. The Diels-Alder reaction of the dienophiles with various dienes is shown in the Scheme 1 and Tables 1, 2. The reaction of cinchonidine acrylate (**1a**) with cyclopentadiene followed by a reduction of the adduct with $LiAlH_4$ (Table 1) was undertaken so as to determine the effects of the characteristics of the Lewis acid, solvents, and cinchona alkaloids used as auxiliary alcohol, as well as the reaction temperature on the chemical yield and the diastereofacial selectivity.

Lewis Acid. The extent and direction of the diastereoface-selection and the rate in the reaction of **1a** with cyclopentadiene varied greatly with the nature and quantity of the Lewis acid used. A low chemical yield and low diastereofacial selectivity were observed for a reaction using $BF_3 \cdot Et_2O$, $AlCl_3$, and $ZrCl_4$ as the Lewis acid, and upon a thermal reaction at −20 °C (entries 2 and 4—6). The use of $SnCl_4$ (entry 3) was found to greatly increase not only the chemical yield but also the diastereofacial selectivity, giving 2*S*(−)-2-hydroxymethyl bicyclo[2.2.1]hept-5-ene (**4**) with 93% *re*-facial selection of **1a** after a reduction of the adduct with $LiAlH_4$. The use of $TiCl_4$ or $BF_3 \cdot Et_2O$ (entries 6 and 7) instead of $SnCl_4$ caused a decrease in the endo as well as the diastereofacial selectivity to give **4**, which is unexpectedly enriched in the 2*R*(+)-enantiomer with *si*-facial selection, in low chemical yield. A reversal in the diastereoface-selection of dienophile by the different Lewis acids used is very unique in an asymmetric Diels-Alder reaction, and only one has been reported (T. Poll et al.[8] in 1984). A similar reversal was further observed in reactions using cinchonine acrylate (**1b**) and quinine acrylate (**1c**) as dienophiles (entries 18, 19, 21, and 22). The quantiy of $SnCl_4$ was found to strongly affect the diastereofacial selectivity. Generally, the selectivity was enhanced by increasing the mole equivalent of $SnCl_4$ toward **1a**; the highest value,

Table 1. Asymmetric Diels-Alder Reactions of **1a—c**[a] and **2a**[b] with Cyclopentadiene (5 mol equiv)

Entry	Dienophile	Lewis acid (mol equiv)	Reaction temp/°C (time/h)	Solvent	Yield/%[c]	endo/exo	Endo-isomer	
							%ee[d]	Abs. config.[e]
1	**1a**	None	+20(24)	CH_2Cl_2	95	87/13	20	2*S*(−)
2	**1a**	None	−20(7)	CH_2Cl_2	3	92/8	—	—
3	**1a**	$SnCl_4$(1.5)	−20(5)	CH_2Cl_2	70	96/4	93	2*S*(−)
4	**1a**	$AlCl_3$(1.5)	−20(6)	CH_2Cl_2	11	94/6	20	2*S*(−)
5	**1a**	$ZrCl_4$(1.5)	−20(6)	CH_2Cl_2	21	97/3	6	2*S*(−)
6	**1a**	$BF_3 \cdot Et_2O$(1.5)	−20(6)	CH_2Cl_2	18	92/8	13	2*R*(+)
7	**1a**	$TiCl_4$(1.5)	−20(6)	CH_2Cl_2	35	88/12	33	2*R*(+)
8	**1a**	$SnCl_4$(0.5)	−20(6)	CH_2Cl_2	45	96/4	42	2*S*(−)
9	**1a**	$SnCl_4$(1.0)	−20(6)	CH_2Cl_2	64	95/5	80	2*S*(−)
10	**1a**	$SnCl_4$(2.0)	−20(6)	CH_2Cl_2	65	95/5	90	2*S*(−)
11	**1a**	$SnCl_4$(1.5)	0(4)	CH_2Cl_2	64	95/5	91	2*S*(−)
12	**1a**	$SnCl_4$(1.5)	−45(6)	CH_2Cl_2	82	96/4	93	2*S*(−)
13	**1a**	$SnCl_4$(1.5)	−70(6)	CH_2Cl_2	58	97/3	92	2*S*(−)
14	**1a**	$SnCl_4$(1.5)	−20(5)	PhCl	72	96/4	90	2*S*(−)
15	**1a**	$SnCl_4$(1.5)	−20(5)	PhMe	66	96/4	86	2*S*(−)
16	**1a**	$SnCl_4$(1.5)	−20(5)	Xylene	45	96/4	82	2*S*(−)
17	**1b**	None	+20(24)	CH_2Cl_2	90	87/13	13	2*R*(+)
18	**1b**	$SnCl_4$(1.5)	−20(5)	CH_2Cl_2	79	96/4	88	2*R*(+)
19	**1b**	$TiCl_4$(1.5)	−20(6)	CH_2Cl_2	37	84/16	49	2*S*(−)
20	**1c**	None	+20(24)	CH_2Cl_2	90	87/13	13	2*S*(−)
21	**1c**	$SnCl_4$(1.5)	−20(5)	CH_2Cl_2	69	96/4	82	2*S*(−)
22	**1c**	$TiCl_4$(1.5)	−20(6)	CH_2Cl_2	44	86/14	34	2*R*(+)
23	**2a**	$SnCl_4$(1.6)	0(3)	CH_2Cl_2	38	93/7	70	2*S*,3*R*(−)
24	**2a**	$SnCl_4$(1.6)	−20(3)	CH_2Cl_2	67	93/7	93	2*S*,3*R*(−)
25	**2a**	$SnCl_4$(1.6)	−40(3)	CH_2Cl_2	27	93/7	85	2*S*,3*R*(−)

a) **1a**: cinchonidine acrylate; **1b**: cinchonine acrylate; **1c**: quinine acrylate. b) **2a**: cinchonidine crotonate. c) Combined yield (by GLC) of endo and exo alcohols. d) HPLC analysis of the corresponding chiral Pirkle's carbamate.[3] e) Assigned by means of chiroptic measurements of endo alcohols (2-hydroxymethyl bicyclo[2.2.1]hept-5-ene (**4**)[4] for entries 1—22 and 2-hydroxymethyl-3-methylbicyclo[2.2.1]hept-5-ene (**5**)[5] for entries 23—25.

Table 2. Asymmetric Diels-Alder Reactions of **3a** and **b**[a] with Some Dienes in CH_2Cl_2

Entry	Dienophile	Diene (mol equiv)	Lewis acid (mol equiv)	Reaction temp/°C (time/h)	Yield/%[b]	%ee[c]	Abs. config.[d]
26	**3a**	(5)	$SnCl_4$(1.5)	−20(4)	62	25	*R,R*(+)
27	**3a**	(5)	$SnCl_4$(3.0)	−20(4)	61	67	*R,R*(+)
28	**3a**	(5)	$SnCl_4$(3.0)	0(4)	63	38	*R,R*(+)
29	**3a**	(5)	$SnCl_4$(3.0)	−45(4)	96	95	*R,R*(+)
30	**3a**	(5)	$SnCl_4$(3.0)	−70(8)	62	90	*R,R*(+)
31	**3b**	(5)	$SnCl_4$(3.0)	−45(4)	74	93	*S,S*(−)
32	**3a**	(30)	$SnCl_4$(3.0)	0(4)	44	94	*R,R*(−)
33	**3a**	(30)	$SnCl_4$(3.0)	−20(4)	46	92	*R,R*(−)
34	**3a**	(20)	$SnCl_4$(3.0)	0(4)	71	98	*R,R*(−)
35	**3a**	(20)	$SnCl_4$(3.0)	−20(4)	70	99	*R,R*(−)
36	**3a**	(20)	$SnCl_4$(3.0)	−40(4)	30	99	*R,R*(−)

a) **3a**: cinchonidine fumarate; **3b**: cinchonine fumarate. b) GLC yields. c) HPLC analysis of the corresponding chiral Pirkle's carbamates.[3] d) Assigned by means of chiroptic measurements of alcohols (2,3-bis(hydroxymethyl)bicyclo[2.2.1]hept-5-ene (**6**)[6] for Entries 26—31, 1,2-bis(hydroxymethyl)-4-cyclohexene (**7**)[7] for Entries 32 and 33, and 1,2-bis(hydroxymethyl)-4-methyl-4-cyclohexene (**8**)[7] for Entries 34—36).

up to 93%, was recorded by carring out the reaction in the presence of 1.5 mol equiv of $SnCl_4$ (entry 3). On the other hand, in a reaction of cyclopentadiene with cinchonidine fumarate (**3a**), containing two pieces of the cinchonidine group, the highest value, up to 95% (entry 29 in Table 2), was recorded by carring out the reaction in the presence of 3 mol equiv of $SnCl_4$ toward **3a**. Thus, the use of 1.5 mol equiv mol of $SnCl_4$ toward per cinchona alkaloid group was found to be most efficient regarding asymmetric Diels-Alder reactions of the dienophile derived from cinchona alkaloids with diene.

Reaction Temperature. No evident temperature dependency in $SnCl_4$-promoted reactions (Tables 1 and 2), excluding the reaction of cinchonidine fumarate (**3a**) with cyclopentadiene, was observed between 0 and −45 °C, mainly because of its heterogeneity in the reaction media.

Solvent Effect. As can be seen in entries 14—16, increasing the density of π-electrons in the aromatic solvents (chlorobenzene, toluene, and xylene) caused a stepwise decrease, mainly in the chemical yield. This decrease may be attributable to the increased donating ability of these solvents to the acryloyl group in cinchonidine acrylate (**1a**) coordinated by $SnCl_4$.[9]

Cinchona Alkaloids as Chiral Auxiliary and the Diastereofacial Selectivities of Their Dienophiles. Three commercially available cinchona alkaloids (cinchonidine, cinchonine, and quinine) were selected as auxiliary alcohols. The dienophiles, **1a** and **1c**, derived from cinchonidine and quinine, respectively, containing the same configuration (8α ,9*R*), gave 2*S*(−)-**4** with a high *re*-facial selection upon reacting with cyclopentadiene in the presence of $SnCl_4$, followed by a reduction with $LiAlH_4$.

As expected, **1b** (antipode of **1a**) derived from cinchonine (8α, 9*S*) gave 2*R*(+)-**4** with a *si*-facial selection

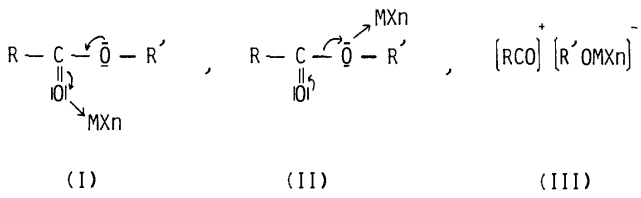

Fig. 1. Ester-Lewis acid complexes.

with equal ease (entry 18). Similarly, a highly *re-re* facial selective addition was achieved upon the reaction of cinchonidine fumarate (**3a**) with cyclopentadiene in the presence of $SnCl_4$ to yield 2*R*,3*R*(+)-2,3-bis(hydroxymethyl)bicyclo[2.2.1]hept-5-ene (**6**) followed by a reduction with $LiAlH_4$ (entry 29 in Table 2). A *si-si* facial selective addition was also achieved by the use of cinchonine fumarate (**3b**) instead of **3a** as a dienophile (entry 30 in Table 2). In the other reactions (entries 23—25 in Table 1 and 32—36 in Table 2), it was further confirmed that when cinchonidine was used as a chiral auxiliary alcohol, a high *re* (or *re-re*)-facial selection of the dienophiles used could be achieved in reactions with various dienes in the presence of $SnCl_4$.

Therefore, both diastereoface-differential Diels-Alder reactions were achieved by the use of the dienophiles derived from (8α, 9*R*) and (8α, 9*S*)-cinchona alkaloids in the presence of $SnCl_4$.

Structure of the Dienophile-$SnCl_4$ Complexes. Regarding the structures and infrared spectra of the ester-Lewis acid complexes, three structures (**I—III**) shown in Fig. 1 have been considered.[10]

A lengthening of the C=O bond (shift of the $\nu_{C=O}$ band to lower frequency), and a shortening of the C(O)-O bond (shift of the $\nu_{C(O)-O}$ band to higher frequency) are anticipated by a coordination of the Lewis acid with acyl-oxygen (structure **I**),[10] which has been

found in most cases of the ester-Lewis acid complexes.

On the other hand, the reverse is anticipated by a coordination with the alkyl-oxygen (structure **II**), which has been postulated in various reports.[11-13] However, it is apparently unprecedented in an identified form, with the exception of some cases that are somewhat different from structure **II** (i.e., the intramolecular hydrogen bonding to alkyl-oxygen in certain steroid hydroxy-esters,[14] the infrared spectra of which shows the $\nu_{C=O}$ band raised by 8—13 cm^{-1} and the $\nu_{C(O)-O}$ band lowered by 10—14 cm^{-1}, compared with the bands in esters with no hydrogen bonding to the alkyl-oxygen, were reported; also, the coordination of Cu with the nitrogen atom of amide in *N,N*-di(2-pyridylmethyl)amide-Cu(II) complexes,[15] the infrared spectrum of which shows the $\nu_{C=O}$ band raised by 26 cm^{-1} compared with that in free amide, was reported).

The acylinium ion in structure **III** would require the presence of the $\nu_{C\equiv O}$ band near 2190 cm^{-1}, which was observed in $[MeCO]^+[BF_4]^-$.[16]

Now, the addition of $SnCl_4$ to **1a** in CH_2Cl_2 gave insoluble solids, the **1a**-$SnCl_4$ complex; the infrared spectrum (Nujol mulls) showed the $\nu_{C=O}$ band at 1738 cm^{-1}, raised by 20 cm^{-1}, and the $\nu_{C(O)-O}$ band at 1155 cm^{-1}, lowered by 25 cm^{-1}, compared with the bands in **1a**. The direction and extent of the shifts of these bands caused by adding $SnCl_4$ to **1a** agreed with that in the reports[14,15] cited regarding structure **II** (mentioned above), suggesting that $SnCl_4$ coordinates with the oxygen atom of the C-O bond (not C=O bond) in the **1a**-$SnCl_4$ complex.

On the other hand, the addition of $SnCl_4$ to a simple acrylate, methyl acrylate, in CH_2Cl_2 gave a homogeneous solution; the infrared spectrum showed the $\nu_{C=O}$ band at 1658 cm^{-1}, lowered by 67 cm^{-1}, and the $\nu_{C(O)-O}$ band at 1340 cm^{-1}, raised by 135 cm^{-1}, compared with the bands in free methyl acrylate, showing that $SnCl_4$ coordinates with the carbonyl-oxygen in the methyl acrylate-$SnCl_4$ complex.

The difference of the **1a**-$SnCl_4$ complex from the methyl acrylate-$SnCl_4$ complex in the infrared spectrum mentioned above may be caused by the presence of a quinuclidine framework in **1a**, suggesting that $SnCl_4$ coordinates not only with the oxygen atom in the C-O bond, but also with the nitrogen atom of the framework in the **1a**-$SnCl_4$ complex to form a rigid five-membered ring.

Assuming that $SnCl_4$ ordinarily coordinates with the carbonyl-oxygen and also with nitrogen atom, it is anticipated that a seven-membered ring structure is formed, resulting in the synthesis of **4** rich in the 2*R*(+)-enantiomer with a *si*-facial selection upon the reaction of **1a** with cyclopentadiene in the presence of $SnCl_4$ followed by reduction with $LiAlH_4$. However, our result (entry 3) showed a synthesis of 2*S*(−)-enantiomer with *re*-facial selection. Therefore, the coordination of $SnCl_4$ with the carbonyl-oxygen in the **1a**-$SnCl_4$ complex could be contradicted by the configuration of product **4**, and also the absence of the $\nu_{C=O}$ band near 1658 cm^{-1}, which was observed in the methyl acrylate-$SnCl_4$ complex mentioned above.

Similarly, the coordination of $SnCl_4$ with only the nitrogen atom in the **1a**-$SnCl_4$ complex could also be contradicted by the fact that $SnCl_4$ significantly promotes the rate in the reaction of **1a** with cyclopentadiene (entries 2 and 3), suggesting that $SnCl_4$ coordinates with the cabonyl-oxygen or the oxygen atom of the C-O bond.

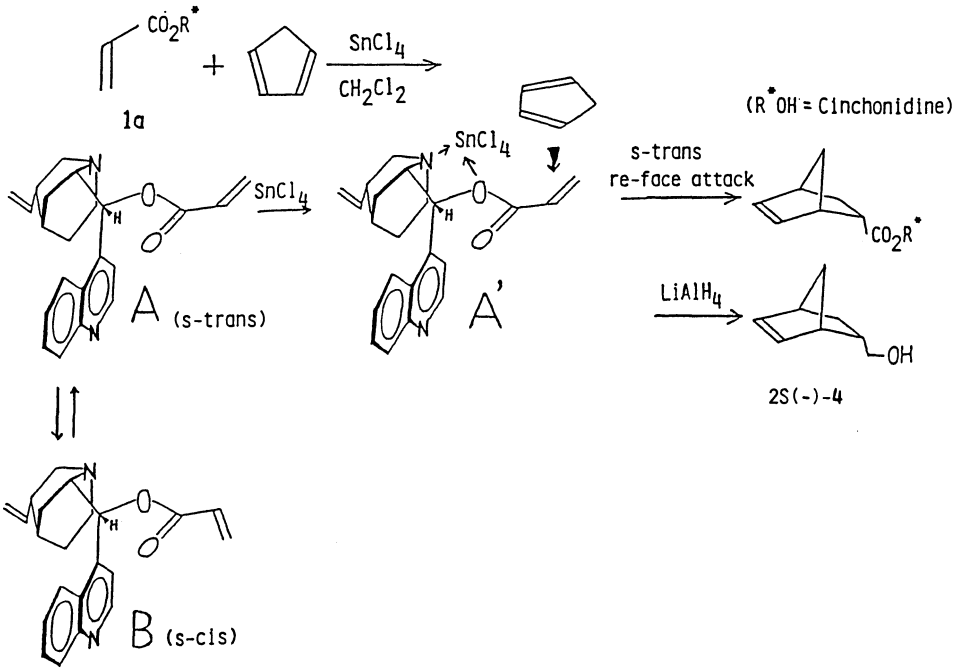

Scheme 2.

Therefore, according to the infrared spectrum of the **1a**-$SnCl_4$ complex and the circumstantial evidence described above, it was suggested that $SnCl_4$ in the complex probably coordinates with the nitrogen atom of the quinuclidine framework and also with the oxygen atom, which is situated at the δ-position, counted from the nitrogen atom of the framework, of the C-O bond (not C=O bond), to form a rigid five-membered ring structure.

Reaction Models. For the purpose of illustrating the $SnCl_4$-promoted high diastereofacial selectivity descrived above, we referred to several models regarding the reaction of **1a** or **3a** with cyclopentadiene in the presence of $SnCl_4$.

Concerning the structures of the esters in solution or in solids, it has been widely accepted as a result of a spectral study[17] that the ester exists in solution as an equilibrium mixture of s-trans and s-cis conformations, in which the former is thermodynamically more stable, and by an X-ray analysis[18] that the ester exists in solids as s-trans conformation.

Now, cinchonidine acrylate (**1a**) dissolves in CH_2Cl_2 and seems to exists as an equilibrium mixture of the s-trans conformation **A** and the s-cis conformation **B** in Scheme 2, where the former is more stable (as mentioned above). Therefore, cyclopentadiene attacks **1a** more from the less-hindered *re*-face of conformation **A** than from the less-hindered *si*-face of conformation **B**, to yield **4** enriched in 2*S*(−)-enantiomer in the thermal reaction (entry 1), followed by reduction with $LiAlH_4$.

On the other hand, the addition of $SnCl_4$ to **1a** in CH_2Cl_2 gave solids that were insoluble in CH_2Cl_2. In solids composed of the **1a**-$SnCl_4$ complex, **1a** exists mainly as a s-trans conformation (as mentioned above) to yield conformation **A′**.

Therefore, cyclopentadiene selectively attacks **1a** in the presence of $SnCl_4$ from the less-hindered *re*-face of conformation **A′** to yield 2*S*(−)-**4** with a high diastereofacial selectivity, followed by a reduction with $LiAlH_4$.

Similarly, cyclopentadiene attacks cinchonidine fumarate (**3a**), in which two pieces of the cinchonidine group cover the *si-si* face by a cooperative blocking effect,[19] selectively from the less-hindered *re-re* face of conformation **C**, according to Scheme 3, to yield *R,R*(+)-**6** followed by a reduction with $LiAlH_4$.

Experimental

General. The preparation of dienophiles, the Diels-Alder reaction and reduction of the adduct with $LiAlH_4$ were carried out under an atmosphere of argon.

Materials. Solvents and dienes were dried in the usual manner and distilled just before use. $SnCl_4$, $TiCl_4$, $BF_3 \cdot Et_2O$, acryloyl chloride, crotonyl chloride, and fumaroyl dichloride were also distilled under argon just before use. $AlCl_3$ and $ZrCl_4$ were purified by sublimation. Chiral 1-(1-naphthyl)ethyl isocyanate was obtained from the Aldrich Chemical Company and used without further purification.

Measurements. The melting point (uncorrected) were determined in a sealed tube with a Yamato melting-point apparatus. The IR spectra and the optical rotations were recorded with a Hitachi infrared spectrophotometer (EPI-G3) and a Union 101 polarimeter, respectively. The gas chromatographs were recorded with a Shimadzu gas chromatograph (GC-8A) using a column packed with 10% PEG-20M on Chromosorb W AW. The high-performance liquid chromatography (HPLC) was recorded with a Kyowa Seimitsu liquid chromatograph (column packed with SiO_2; eluents: hexane-ethyl acetate for entries 1—25 in Table 1 or hexane-ethanol for entries 26—36 in Table 2).

Dienophiles. Preparation of Cinchonidine Acrylate (1a) as a Typical Procedure. To a stirred solution of cinchonidine (25 g, 85 mmol) in THF (600 ml) was slowly added a solution of acryloyl chloride (5.8 ml, 71 mmol) in THF (50

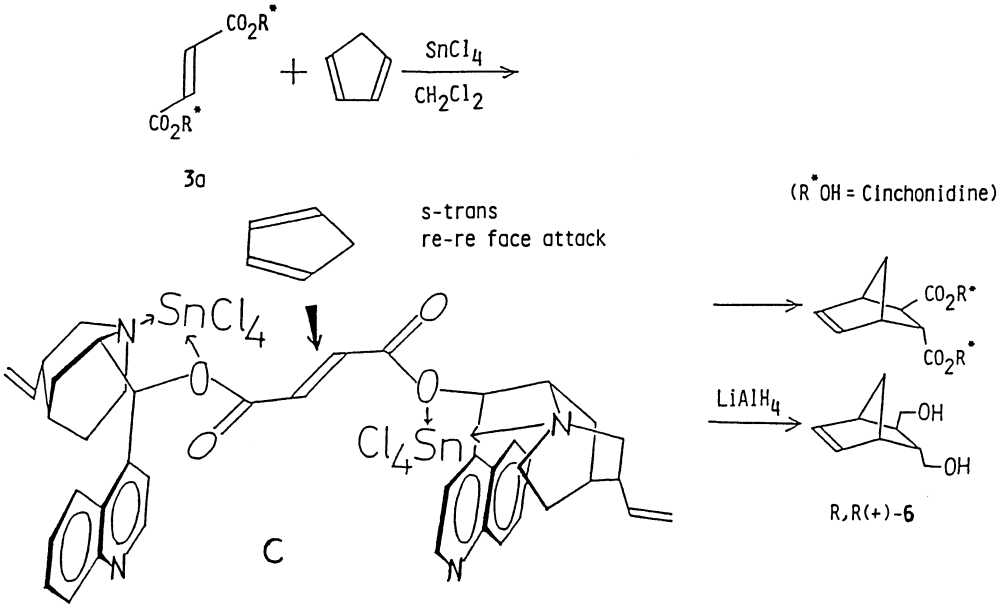

Scheme 3.

ml) at 0 °C in the dark. The mixture was stirred for 24 h at 0 °C—r.t. in a dark room. After concentration under reduced pressure and a subsequent addition of $CHCl_3$ (50 ml) to the residual mass, Et_3N (19.8 ml, 142 mmol) was added dropwise under stirring at 0 °C. Stirring was continued for 2 h at r.t. and then acetone (500 ml) was added to the mixture. After cooling in a refrigerator overnight, precipitates composed of Et_3NHCl and excess cinchonidine were filtered off. The filtrate was evaporated and the pale-yellow residual mass was twice recrystallized from hexane-isopropyl alcohol to give white crystals **1a**; yield: 20 g (80%); mp 113—114 °C; $[\alpha]_D^{25}$ +10.5° (*c* 1.5, $CHCl_3$); IR(Nujol mulls); 1718 ($\nu_{C=O}$) and 1180 cm^{-1} ($\nu_{C(O)-O}$); Found: C, 75.64; H, 7.11; N, 7.98%. Calcd for $C_{22}H_{24}N_2O_2$: C, 75.86; H, 6.90; N, 8.05%. The other dienophiles: cinchonidine crotonate (**2a**); yield: 82%; mp 152—153 °C; $[\alpha]_D^{25}$ +38.0 (*c* 1.5, $CHCl_3$; IR(Nujol mulls) 1720 ($\nu_{C=O}$) and 1177 cm^{-1} ($\nu_{C(O)-O}$); Found: C, 75.91; H, 7.41; N, 7.53%. Calcd for $C_{23}H_{26}N_2O_2$: C, 76.21; H, 7.23; N, 7.73%. Cinchonidine fumarate (**3a**); yield: 78%; mp 221—223 °C; $[\alpha]_D^{25}$ +81.2° (*c* 1.5, $CHCl_3$); IR (Nujol mulls) 1718 ($\nu_{C=O}$) and 1167 cm^{-1} ($\nu_{C(O)-O}$); Found: C, 75.50; H, 6.70; N, 8.43%. Calcd for $C_{42}H_{44}N_4O_4$: C, 75.42; H, 6.63; N, 8.38%. Cinchonine fumarate (**3b**); yield: 86%; mp 104—107 °C; $[\alpha]_D^{25}$ +40.5° (*c* 1.5, $CHCl_3$); IR (Nujol mulls) 1720 ($\nu_{C=O}$) and 1164 cm^{-1} ($\nu_{C(O)-O}$); Found: C, 75.25; H, 7.10; N, 7.90%. Calcd for $C_{42}H_{44}N_4O_4$: C, 75.42; H, 6.63; N, 8.38%. Cinchonine acrylate[20] (**1b**); mp 63—64 °C; $[\alpha]_D^{25}$ +81.6° (*c* 1.5, $CHCl_3$), which was reported to be an oily material, $[\alpha]_D^{20}$ +80° (*c* 2, $CHCl_3$), and quinine acrylate[21] (**1c**) were also prepared by a similar procedure.

Asymmetric Diels-Alder Reaction. $SnCl_4$-Promoted Addition of 1a to Cyclopentadiene (Entry 3) as a Typical Procedure. To a stirred solution of **1a** (1.04 g, 3 mmol) in CH_2Cl_2 (18 ml) was added cyclopentadiene (1.2 ml, 15 mmol) at −70 °C. Subsequently, a solution of $SnCl_4$ (0.52 ml, 4.5 mmol) in CH_2Cl_2 (6 ml) was added dropwise to the mixture at −20 °C. The increase in the temperature of the mixture and the appearance of pale-yellow precipitates were noted as the addition of $SnCl_4$ proceeded.

After stirring for 5 h at −20 °C, Et_3N (2.5 ml, 18 mmol) and H_2O (1 ml) were added to the mixture. Excess cyclopentadiene was then removed in vacuo. To the resulting mass were added CH_2Cl_2 (200 ml), Et_3N (2.5 ml, 18 mmol), and saturated aq. NH_4Cl (20 ml), and stirred for 1 h. The two layers were separated and the aqueous layer was extracted with CH_2Cl_2. The combined organic phases were washed (H_2O), dried (Na_2SO_4), and evaporated to dryness. After the residue was treated with $LiAlH_4$ (1.5 g, 40 mmol) in ether for 20 h, the excess $LiAlH_4$ was decomposed by saturated aq. NH_4Cl, then acidified to pH 2—3. The two layers were separated and the aqueous layer was extracted with ether. The combined organic phases were washed (H_2O), dried (Na_2SO_4), concentrated, and distilled under reduced pressure to give the alcohol **4**, containing some of its exo isomer, as shown by GLC analysis. After removing the exo isomer by preparative GLC, the endo alcohol was treated with chiral 1-(1-naphthyl)ethyl isocyanate in benzene at 80 °C to give chiral carbamate for an HPLC analysis.[3] The other reactions were carried out in a similar way according to Scheme 1 and are shown in Tables 1 and 2 together with the results.

Dienophile-Lewis Acid Complexes. Preparation of 1a-$SnCl_4$ Complex as a Typical Procedure. To a stirred solution of **1a** (0.52 g, 1.5 mmol) in CH_2Cl_2 (10 ml) was added $SnCl_4$ (0.26 ml, 2.25 mmol). The mixture was stirred for 1 h at r.t. A cream-colored complex was filtered, washed (CH_2Cl_2), and dried in vacuo. Yield 1.03 g (93%); Decomp: 183 °C; IR(Nujol mulls) 1738 ($\nu_{C=O}$) and 1155 cm^{-1} ($\nu_{C(O)-O}$); Found: Cl, 28.6%. Calcd for $C_{44}H_{48}N_4O_4Cl_8Sn_3$ (**1a**-1.5 $SnCl_4$): Cl, 28.8%

The other complexes of some dienophiles with $SnCl_4$ or $TiCl_4$ were prepared in a similar way, and the infrared spectra showed similarly the $\nu_{C=O}$ band shifted to a higher frequency and the $\nu_{C(O)-O}$ band shifted to a lower frequency, compared with the bands in the corresponding free dienophiles.

References

1) For recent reviews see: Y. Mori, *Yuki Gosei Kagaku Kyokai Shi*, **40**, 321 (1982); L. A. Paquette, "Asymmetric Cycloaddition Reactions," in "Asymmetric Synthesis," ed by J. D. Morrison, Academic Press, Orland (1984), Vol 3, part B, Chap. 7; W. Oppolzer, *Angew. Chem., Int. Ed. Engl.*, **23**, 876 (1984).

2) R. Gleiter and M. C. Böhn, *Pure Appl. Chem.*, **55**, 237 (1983); T. Koizumi, I. Hakamada, and H. Toshii, *Tetrahedron Lett.*, **25**, 87 (1984); J. Mulzer and M. Kappert, *ibid.*, **26**, 1631 (1985); J. Jurczak, T. Bauer, and S. Jarosz, *Tetrahedron*, **42**, 5045 (1986); **42**, 6477 (1986); C. Chapuis and J. Jurczak, *Helv. Chim. Acta*, **70**, 436 (1987); K. Narasaka, M. Inoue, and N. Okada, *Chem. Lett.*, **1986**, 1109; K. Narasaka, M. Inoue, and T. Yamada, *ibid.*, **1986**, 1967; K. Maruoka, M. Sakurai, J. Fujiwara, and H. Yamamoto, *Tetrahedron Lett.*, **27**, 4895 (1986); G. H. Posner and D. G. Wettlaufer, *ibid.*, **27**, 667 (1986); R. M. Ortuno, J. Corbera, and J. Font, *ibid.*, **27**, 1081 (1986); S. W. Remiszewski, J. Yang, and S. M. Weinreb, *ibid.*, **27**, 1853 (1986); G. Helmchen, K. Ihrig, and H. Shindler, *ibid.*, **28**, 183 (1987); S. G. Davies and J. C. Walker, *J. Chem. Soc., Chem. Commun.*, **1986**, 609; T. K. M. Shing and P. L. Williams, *ibid.*, **1987**, 423; M. Quimpepre and K. Jankowski, *ibid.*, **1987**, 676; T. R. Kelley, A. Whiting, and N. S. Chandrakumar, *J. Am. Chem. Soc.*, **108**, 3510 (1986).

3) W. H. Pirkle and M. S. Hoekstra, *J. Org. Chem.*, **39**, 3904 (1974); W. H. Pirkle and J. R. Hauske, *ibid.*, **42**, 1839 (1977).

4) J. A. Berson, A. Remanic, S. Suzuki, P. R. Warnhoff, and D. Willner, *J. Am. Chem. Soc.*, **83**, 3986 (1961).

5) W. Oppolzer, C. Chapuis, and G. Bernardinelli, *Helv. Chim. Acta*, **67**, 1397 (1984).

6) D. Horton and T. Machinami, *J. Chem. Soc., Chem. Commun.*, **1981**, 33.

7) H. M. Walborsky, L. Barash, and T. C. Davis, *Tetrahedron*, **19**, 2333 (1963).

8) T. Poll, G. Helmchen, and B. Bauer, *Tetrahedron Lett.*, **25**, 2191 (1984).

9) A. Kemura and B. T. Iwamoto, *J. Phys. Chem.*, **72**, 2764 (1968); J. Furukawa, Y. Iseda, and E. Kobayashi, *J. Polym. Sci., Polym. Lett. Ed.*, **8**, 631 (1970).

10) M. F. Lappert, *J. Chem. Soc.*, **1961**, 817.

11) R. Baltzly, W. S. Ide, and A. P. Phillips, *J. Am. Chem. Soc.*, **77**, 2522 (1955).

12) H. C. Brown, H. I. Schlesinger, and A. B. Burg, *J. Am. Chem. Soc.*, **61**, 673 (1939).

13) C. R. Wasmuth and H. Freiser, *Talanta*, **9**, 1061 (1962).

14) H. B. Henbest and B. J. Lovell, *J. Chem. Soc.*, **1957**, 1965.

15) R. P. Houghton and R. R. Puttner, *J. Chem. Soc., Chem. Commun.*, **1970**, 1270.
16) B. P. Susz and J. J. Wuhrmann, *Helv. Chim. Acta*, **40**, 971 (1957).
17) W. O. Geoge, D. V. Hassid, and W. F. Maddams, *J. Chem. Soc., Perkin Trans. 2*, **1972**, 400; J. Brunn, M. Dethloff, and H. Ribenstahl, *Z. Phys. Chem.*, **258**, 209 (1977).
18) A. M. Mathieson, *Tetrahedron Lett.*, **1965**, 4137; W. B. Schweizer and J. D. Dunitz, *Helv. Chim. Acta*, **65**, 1547 (1982).
19) K. Furuta, K. Iwanaga, and H. Yamamoto, *Tetrahedron Lett.*, **27**, 4507 (1986).
20) T. Yamashita, H. Yasueda, Y. Miyauchi, and N. Nakamura, *Bull. Chem. Soc. Jpn.*, **50**, 1532 (1977).
21) T. Yamashita, H. Yasueda, and N. Nakamura, *Chem. Lett.*, **1974**, 585.

 © 1988 The Chemical Society of Japan Bull. Chem. Soc. Jpn., 61, 2007—2012 (1988)

Polymerization of Diene-Containing Lipids as Liposomes by Radical Initiators. 6:[1] Polymerization of 1,3-Bis(2,4-octadecadienoyl)-*rac*-glycero-2-phosphorylcholine

Shinji TAKEOKA, Etsuo HASEGAWA, Hiroyuki OHNO, and Eishun TSUCHIDA*
Department of Applied Chemistry, Waseda University, Tokyo 160
(Received September 26, 1987)

1,3-Bis(2,4-octadecadienoyl)-*rac*-glycero-2-phosphorylcholine (1,3-DPC), polymerizable lipid which contains diene groups in both 1- and 3-acyl chains, was polymerized as liposomes in an aqueous medium. Polymerization was initiated by water-insoluble azobis(isobutyronitrile) (AIBN) or water-soluble azobis(2-amidinopropane) dihydrochloride (AAPD). AIBN was mixed with the monomeric lipids and the mixture was dispersed in an aqueous medium by sonication to facilitate transfer of AIBN into monomeric lipid liposomes. On the other hand, AAPD was simply added to the liposome suspension. The 1,3-DPC liposomes were easily polymerized by the addition of either water-soluble AAPD or water-insoluble AIBN to give polymerization conversion of over 80% in both cases. No selective polymerization of diene groups in the different acyl chains was found in 1,3-DPC liposomes whereas the selective polymerization was clearly seen in 1,2-bis(2,4-octadecadienoyl)-*sn*-glycero-3-phosphorylcholine (DODPC). Polymerized 1,3-DPC liposomes were not soluble in organic solvent suggesting the formation of crosslinked bilayer structure. The obtained results suggested that the diene groups in both 1- and 3-acyl chains were almost equivalent and located in the interface between an aqueous phase and hydrophobic region. Polymerized liposomes thus prepared were stable against heating, detergent attack and even methanol washing. Copolymerization of mixed liposomes composed of 1,3-DPC and DODPC (5 : 1) revealed that the AIBN or AAPD initiated polymerization conversion of DODPC reached about 68%. 1,3-DPC is considered to be radical propagation transfer between diene groups in 1- and 2-acyl chains of DODPC during polymerization.

Liposomes and the lipid assemblies have attracted attention as one of potent candidates for the basic materials for the coming molecular devices. However, they are generally not so stable and usually cause aggregation and fusion.[2,3] Polymerizable amphiphiles have been synthesized as major components to construct stable bilayer membrane.[4-13] In our previous paper,[14] small unilamellar liposomes composed of 1,2-bis(2,4-octadecadienoyl)-*sn*-glycero-3-phosphorylcholine (DODPC), which contains one diene group in each acyl chain, were polymerized by radical initiators. It was revealed that the polymerization profile was significantly dependent on the characteristics of the applied radical initiators.[1] However this monomeric lipid had polymerizable groups in the same position (2,4-diene) in two acyl chains, polymerization of diene groups bound to the 1-acyl chains was selectively initiated by AIBN which was incorporated into a hydrophobic region of the bilayer membrane. On the contrary, the diene groups in the 2-acyl chains were polymerized by the addition of water-soluble radical initiators suggesting that the diene groups in 2-acyl chains faced an aqueous phase. Selective initiation of diene groups bound to 2-acyl chains by AAPD was clearly demonstrated by the model reaction using 1-palmitoyl-2-(2,4-octadecadienoyl)-*sn*-glycero-3-phosphorylcholine (POPC).[15] The polymerization of this POPC was initiated only by the addition of AAPD and no effect was found when AIBN was added to them.[15] We reported the unique method to evaluate the chemical environment of polymerizable groups in the lipid liposomes with their polymerization manner initiated by different radical initiators.[14,16] In the present paper, polymerizable lipid containing one diene group in 1- and 3-acyl chains was polymerized as liposomes by two different radical initiators to clarify the chemical environment of diene groups and the effects of the molecular packing of polymerizable lipids on the polymerization profile as liposomes.

Experimental

1,3-Bis(2,4-octadecadienoyl)-*rac*-glycero-2-phosphorylcholine (1,3-DPC) was synthesized according to the method as reported previously.[17] The purity was confirmed by thin layer chromatography (Merck, silica gel). TLC plates were developed with chloroform/methanol/water (65:35:5 by vol) to show a single spot with R_f value of 0.3.

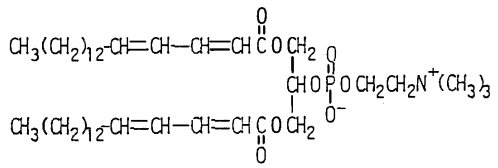

1,3-DPC

Azobis(isobutyronitrile) (AIBN) and azobis(2-amidinopropane) dihydrochloride (AAPD) were purchased from Tokyo Kasei Co. AIBN and AAPD were purified twice by recrystallization from methanol and water, respectively. Triton X-100, polyethylene glycol mono-*p*-octylphenyl ether, was purchased from Tokyo Kasei Co. Ltd. and used without further purification. Fluorescent grade 5(6)-carboxyfluorescein (CF) was purchased from Kodak Co. and used

without further purification. Chloroform, methanol, and water were distilled twice before use.

Preparation of Liposomes. A total of 0.200 g of monomeric amphiphiles was dissolved in dehydrated chloroform and was slowly evaporated in a rotated sample tube to prepare thin lipid film on the inner surface of the tube.[14,18] Distilled water was then added to the tube to set the lipid concentration 1.0 wt%. Small unilamellar liposome suspension was prepared by sonication (Tip-type Tomy Seiko UR-200P) at 60 W for 20 min under nitrogen atmosphere. The freshly prepared liposomes were incubated in a refrigerator to prepare larger unilamellar liposomes with an average diameter of 75 nm. This process minimizes the structural defects and irregular molecular packing.[19]

Polymerization of Liposomes Initiated by Organic Free Radicals. Free radical initiated polymerization of 1,3-DPC was carried out by a similar manner as mentioned previously.[14] A total of 0.200 g of 1,3-DPC was dissolved with 2.1 mg of AIBN (5.0 mol% to the monomeric lipids) in chloroform and slowly evaporated in a rotated sample tube. Degassed distilled water (20.0 ml) was added to the tube. Liposome suspension was prepared by sonication method as mentioned above. These liposomes were polymerized at 60 °C under nitrogen atmosphere. The polymerization conversion was successively analyzed by the decrease in the absorption intensity at 243 nm for diene groups.

On the other hand, AAPD was added to the liposome suspension to avoid the decomposition of AAPD by sonication.[15] Liposomes were polymerized at 60 °C for several hours under nitrogen atmosphere. AAPD was added to the liposomes which had already been polymerized by AIBN. These were then re-polymerized to check the possibility of selective polymerization.[14]

UV Spectroscopic Analysis of the Polymerization. A small amount of the liposome suspension was periodically withdrawn with a pipette from the sample tube during polymerization. Accurately diluted sample solution was analyzed by UV spectrometry to quantitatively determine the polymerization conversion. Spectral change at 243 nm corresponding to the diene groups of 1,3-DPC as liposomes in an aqueous solution was analyzed to determine the polymerization conversion of 1,3-DPC.

Transmission Electron Microscopy. Polymerized liposome suspension was dropped on copper grids, and they were stained with uranyl acetate. The dried sample grids were analyzed to confirm their bilayer structure by TEM (JEOL-100CX).

Light-Scattering Measurement. A liposome suspension (concentration; 0.100 g/100 cm^3) was placed in a round cell of 10 mm diameter. Methanol was added to the suspension and the scattered-light intensities (90°) were subsequently recorded with apparatus (Union Giken LS-601) at 25 °C to evaluate stability of the polymerized liposomes upon addition of organic solvent. He-Ne laser with wavelength of 632.8 nm was used as the light source.

Fluorescein Leakage. 0.100 mol·l^{-1} of CF was incorporated into an inner aqueous phase of the polymerized liposomes at 60 °C for 100 h.[20] Then CF-containing liposome suspension was passed through gel permeation chromatography column (Sepharose CL-4B 30 mm ϕ, 600 mm h) to expel an excess CF dissolved in an outer aqueous phase. The leakage of CF was determined as the increase of fluorescence intensity at 520 nm by fluorescence spectrometer (JASCO FP-550) with excitation beam at 330 nm. A 100% CF leakage was carried out by the sonication of CF containing liposomes with the existence of Triton X-100.

Results and Discussion

Polymerization and Stability of 1,3-DPC Liposomes. 1,3-Bis(2,4-octadecadienoyl)-*rac*-glycero-2-phosphorylcholine (1,3-DPC) was dispersed in an aqueous medium, and small unilamellar liposomes were prepared by sonication under N_2 atmosphere. Preparation of closed small liposomes was confirmed by TEM and ^{1}H NMR measurements.[21] A DSC measurement revealed that the 1,3-DPC formed liposomes with gel-to-liquid crystalline phase transition temperature(T_c) of 28 °C. The T_c was also determined with ^{1}H NMR spectrometry. Proton signals attributed to hydrophobic methylene and terminal methyl groups appeared at temperatures higher than 28 °C, suggesting the formation of liposome structure. Figure 1 shows the ^{1}H NMR spectra for 1,3-DPC liposomes in deuterium oxide at 50 °C in the absence and presence of Eu^{3+}, a shift reagent. The proton signals attributed to hydrophilic choline methyl groups were split by the addition of 3.8 m mol·l^{-1} $Eu(NO_3)_3$. This is the proof of the closed liposome structure because Eu^{3+} interacted with polar head groups of lipids facing outer aqueous phase to shift its signal to higher magnetic field as shown in Fig. 1 (b). The ratio of the split signal intensities showed no change for over 60 min suggesting no Eu^{3+} leakage through the membrane. The average radius of the liposomes can be estimated from the intensity ratio of the split choline methyl proton signals.[20] The average radius of the liposomes analyzed in this experiment was calculated to be about

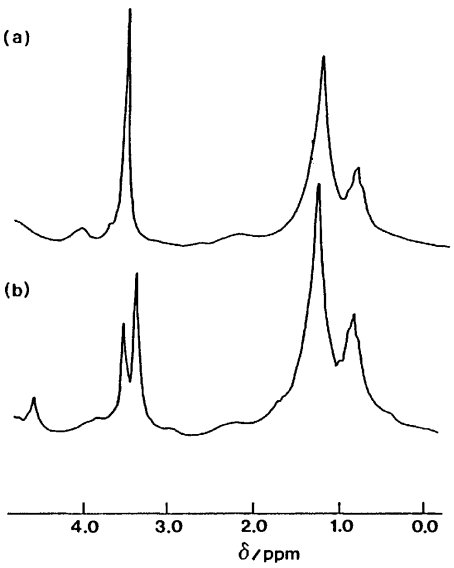

Fig. 1. ^{1}H NMR spectra of 1,3-DPC liposomes in D_2O at 50 °C in (a) absence or (b) presence of Eu^{3+}. [1,3-DPC]=10.0 g lipids dm^{-3} D_2O, [Eu^{3+}]=3.8 mmol·l^{-1}.

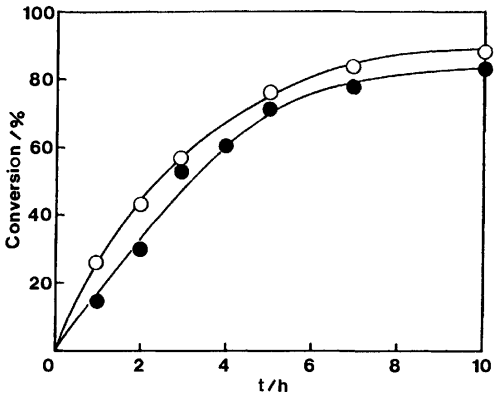

Fig. 2. Polymerization conversion of 1,3-DPC as liposomes at 60°C. 1,3-DPC liposomes (10.0 g lipids dm^{-3} H_2O) were polymerized by AIBN (●) or AAPD (○).

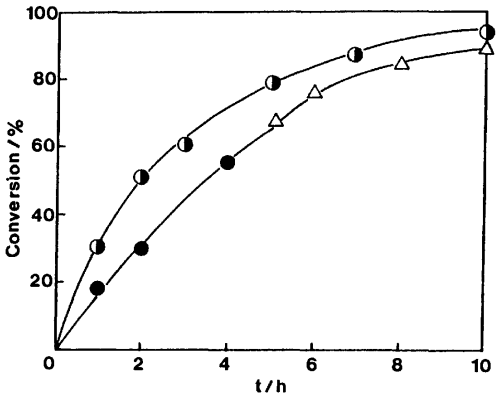

Fig. 3. Polymerization conversion of 1,3-DPC as liposomes. 1,3-DPC liposomes were polymerized by AIBN and AAPD simultaneously (◑), or by the addition of AAPD (△) to the DODPC liposomes which were pre-polymerized by AIBN (●) at 60°C for 5 h.

210 nm.

The AIBN and AAPD are potential azo compounds to initiate radical polymerization of lipids as liposomes.[9,10] AIBN and AAPD generate free radicals in hydrophobic region and aqueous region of lipid liposomes, respectively. It is known that polymerization profile reflects the acyl chain packing and chemical environment of diene group.[16] The 1,3-DPC liposomes were also polymerized by either one or both of these radical initiators to analyze chemical environment of diene groups. Figure 2 shows the results on the polymerization of 1,3-DPC as liposomes initiated by either AIBN or AAPD. Both AIBN and AAPD initiated radical polymerization of diene groups in 1,3-DPC liposomes and the polymerization conversion reached about 80% in both cases. It is previously reported that AIBN (5 mol% to the monomeric lipids) initiates radical polymerization of 1,2-bis(2,4-octadecadienoyl)-*sn*-glycero-3-phosphorylcholine (DODPC) for only 50%.[14,16] A simultaneous use of both AIBN and AAPD provided polymerization of DODPC in almost 100%. For DODPC liposomes, the diene groups bound in 1-acyl chains and those in 2-acyl chains were selectively polymerized by AIBN and AAPD radicals because of their non-equivalent chemical environment[16] Namely, diene groups in 2-acyl chains are considered to face the aqueous phase and they are polymerized by water-soluble radical initiators. And those in 1-acyl chains are located in the hydrophobic region and therefore polymerization should be initiated by the radical attack from hydrophobic region. 1,3-DPC however showed high polymerization conversion regardless the solubility of radical initiators, suggested that the chemical environment of diene groups in 1- and 3-acyl chains was almost equivalent. Furthermore they are located in the interface between the aqueous phase and hydrophobic region. One could also explain the result by assuming incomplete lipid packing which enabled the attack of radical initiators from both region. This was however denied by the ^1H NMR data as shown in Fig. 1, in which no leakage of Eu^{3+} was found.

We must note the following results for spectroscopic analysis of the polymerizable lipids as liposomes. Both 1,3-DPC and DODPC show the maximum UV absorbance at 265 nm attributed to diene groups in chloroform solution. The maximum UV absorbance of 1,3-DPC shifted to 243 nm when they formed liposomes in an aqueous phase. Against this, DODPC liposome suspension showed the maximum UV absorbance at 255 nm.[18] These different λ_{max} can be discussed in terms of different acyl chain packing. The maximum absorbance was found at 243 nm for both 1,3-DPC and DODPC below the phase transition temperature and it shifted to 255 nm beyond it. In the present work, polymerization conversion was carried out by UV spectrometry. The solution temperature for measurement was about 20°C and it was therefore lower than the T_c of 1,3-DPC. Anyway, spectral shift is strongly suggested to reflect the molecular packing of the polymerizable lipid as liposomes. Detailed results will be published elsewhere.

A simultaneous use of AIBN and AAPD did not improve the polymerization conversion of 1,3-DPC liposomes as shown in Fig. 3. There is little contribution of AAPD addition to the 1,3-DPC liposomes which has been previously initiated by AIBN radicals (Fig. 3 ●→△). This is considerably different from the polymerization profile for DODPC liposomes. These data also support equivalent chemical environment of the diene groups in 1- and 3-acyl chains for 1,3-DPC and their radical polymerization can be initiated by radical attack from both hydrophobic and hydrophilic phases. It can be concluded that 1,3-DPC packed more symmetrically than DODPC. No difference was found in the polymerization profile of 1,3-DPC with radical initiators employed in the present experiments. How-

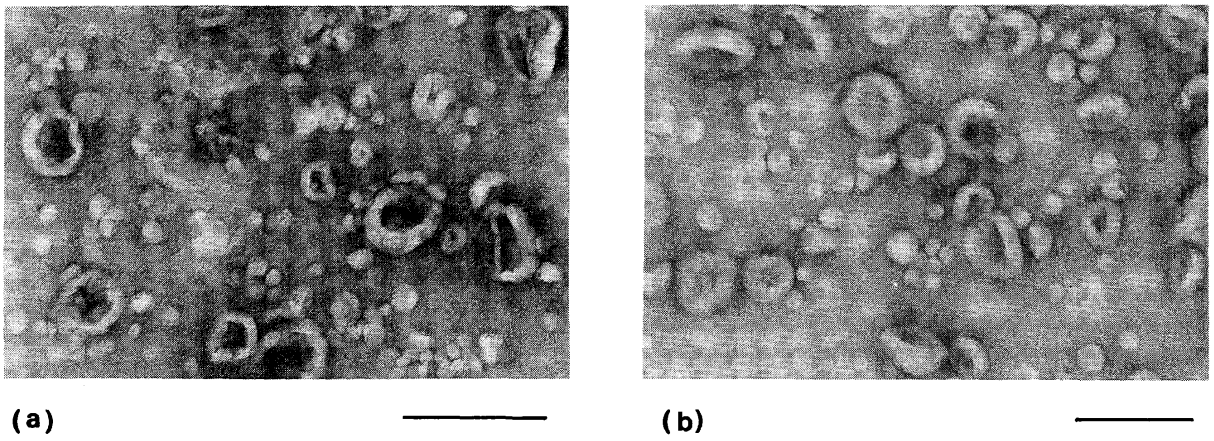

Fig. 4. Transmission electron micrographs of 1,3-DPC as liposomes (a) before and (b) after polymerization initiated with AIBN and AAPD simultaneously. Space bar indicates 0.2 μm.

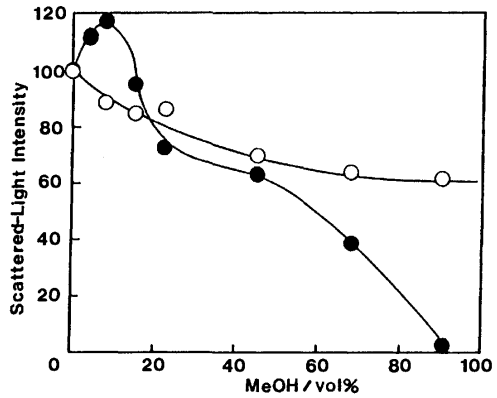

Fig. 5. Effect of methanol on scattered-light intensity for 1,3-DPC liposomes at 25°C. Liposomes were monomeric (●), or polymerized by AIBN and AAPD simultaneously (○).

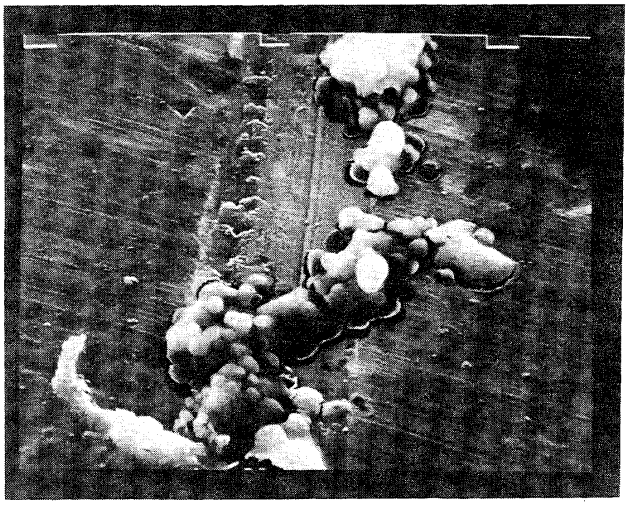

Fig. 6. Scanning electron micrograph of 1,3-DPC liposomes polymerized by AIBN and AAPD. Space bar indicates 5 μm. Sample was dried after washing with methanol.

ever, 1,3-DPC cannot be packed completely symmetrically but slight difference should be detected by other techniques such as small angle X-ray scattering.

The liposome structures of 1,3-DPC before and after polymerization were analyzed with TEM measurements. Figure 4 shows the TEM picture for the polymerized 1,3-DPC liposomes. Bilayer liposome structure is clearly seen in the micrographs for both monomeric and polymerized ones. The outlines of polymerized liposomes are more smooth than those of monomeric ones. It indicates that polymeric liposomes are more stable and maintain their spherical structures perfectly after dryness. This structure is found to be kept even after methanol washing. The effect of added methanol content on the scattered-light intensity from 1,3-DPC liposome suspension is depicted in Fig. 5. Monomeric liposomes showed decrease in the scattered light intensity, which may be attributed to the structural change such as destruction of liposomes structure with the addition of methanol. Nevertheless only a little intensity change was found for the polymerized one suggesting a stable membrane structure. Liposome structure was also observed with SEM even after washing large polymerized 1,3-DPC liposomes with pure methanol. In this experiment, giant 1,3-DPC liposomes were prepared by hydration method.[13] Polymerized 1,3-DPC liposomes with average diameter of about 1 μm were filtered on a Millipore membrane filter with average pore size of 0.05 μm. They were washed with pure methanol for several times, and their liposome structure was directly monitored with SEM after Au sputtering as shown in Fig. 6. Although they were aggregated, it was found that liposome structure was clearly maintained almost completely. This stable membrane structure was also confirmed by solubility test. The 1,3-DPC liposomes, polymerized with appropriate radical initiators, were insoluble in any organic solvents. This insolubility also supported the formation of crosslinking between

polymer chains, i.e., their polymerization underwent intermolecularly and no intramolecular polymerization occurred. In other words, diene group in 1-acyl chain does not form covalent bonding with that in 3-acyl chain of the same lipid monomer, but it may attack diene groups in not only 1-acyl chains but also 3-acyl chains of the neighboring lipid monomers. Related discussions on this polymerization manner will be mentioned later.

The leakage measurement of carboxyfluorescein (CF) was commonly used to evaluate the membrane structure or stability of the liposomes.[8,20] Figure 7 shows the leakage of CF from polymerized 1,3-DPC liposomes. Those from DODPC liposomes before and after polymerization were also plotted as references. Preparation of the polymerized liposomes containing CF molecules in their inner aqueous phase has already been mentioned elsewhere.[20] The CF leakage data for monomeric 1,3-DPC was not measured consistently because their liposomes were unstable and easily aggregated in solution under the conditions for this experiment. There was a certain temperature dependence of CF leakage from liposomes. No CF leakage was found from these polymerized liposomes at room temperature, and these measurements were therefore made at 50 °C to accelerate CF leakage. The CF leakage rate from an inner aqueous phase of the DODPC liposomes was considerably decreased by the polymerization, and almost the same CF leakage rate was found for the polymerized 1,3-DPC liposomes. It was demonstrated that radical polymerization of 1,3-DPC provided very stable membrane structure which was almost equivalent for that of polymerized DODPC liposomes.

Copolymerization of 1,3-DPC with DODPC in Mixed Liposomes. From the results obtained in the previous section, it was expected that the existence of 1,3-DPC might disturb selective polymerization manner and might induce further polymerization of DODPC as liposomes. Chloroform solution of 1,3-DPC was mixed with that of DODPC, and their mixed liposomes were prepared through the same procedure as mentioned above. Polymerization of the mixed liposomes was also analyzed by UV spectroscopy. Figure 8 shows the polymerization conversion for the DODPC/1,3-DPC (5/1 by mol) mixed liposomes initiated by AIBN (5.0 mol% to the total lipid monomers) at 60 °C. If 1,3-DPC and DODPC did not affect the polymerization manner with each other in the mixed liposome, theoretical polymerization conversion could be calculated from the results of their individual polymerization manner. For liposomes with average radius of 30 nm or more, AIBN initiated the polymerization of 1,3-DPC and DODPC liposomes to reach the polymerization conversion of about 80% (see Fig. 2) and 50%,[14] respectively at 60 °C for 12 h. Since we have collected kinetic data on the polymerization conversion of those lipid liposomes, the average polymerization conversion for the mixed liposome system can be calculated as a simple summation of the individual polymerization conversion at every stage of the polymerization. The calculated polymerization conversion was depicted in Fig. 8. The experimental data on the polymerization conversion (open circles in Fig. 8) was always higher than the calculated one. For example, the polymerization conversion reached 68% was actually found for the mixed liposomes after 12 h. heating at 60 °C in the presence of AIBN whereas the calculated value was only 55%. When the increase in the polymerization conversion was assumed to be due to the newly polymerized diene groups in 2-acyl chains of DODPC lipids, 31% of the diene groups in the 2-acyl chains of DODPC were calculated to be polymerized. The polymerized mixed liposomes obtained were stable against organic solvent washing and no channel or hole was formed by the skeletonization.[13] These results strongly suggest the following points: Firstly,

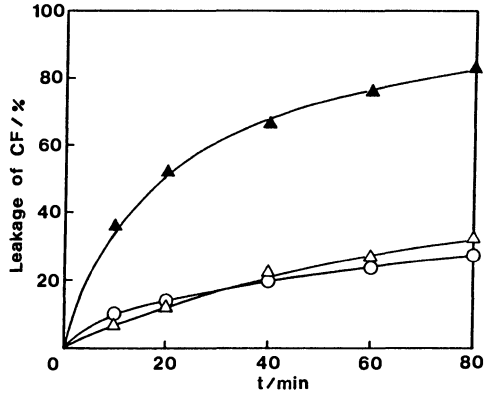

Fig. 7. Leakage of CF from inner aqueous phase of 1,3-DPC liposomes polymerized by both AIBN and AAPD simultaneously (○) at 50 °C. Monomeric (▲) and polymerized (△) DODPC liposomes were also analyzed under the same condition as references. No CF leakage was found at 30 °C.

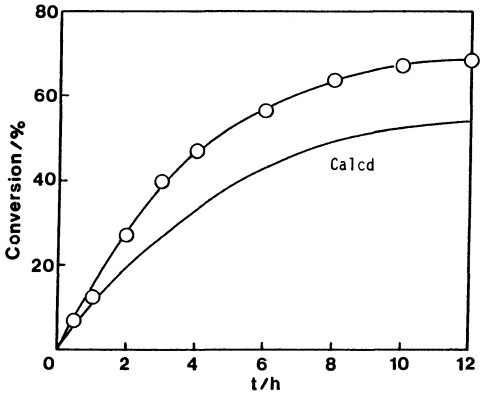

Fig. 8. Polymerization conversion of DODPC/1,3-DPC (5/1 by mol) mixed liposomes. Liposomes were polymerized by AIBN. Solid curve was obtained by calculation from polymerization conversions of DODPC[14] and 1,3-DPC liposomes.

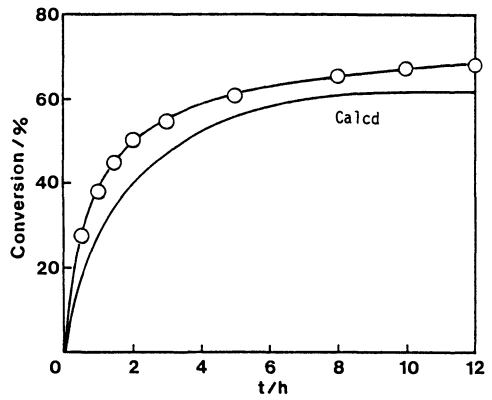

Fig. 9. Polymerization conversion of DODPC/1,3-DPC (5/1 by mol) mixed liposomes. Liposomes were polymerized by AAPD. Solid curve was obtained by calculation from polymerization conversions of DODPC[14] and 1,3-DPC liposomes.

1,3-DPC and DODPC were miscible with each other in the mixed liposomes and no phase-separated structure might be formed at 60 °C. Secondly, 1,3-DPC and DODPC lipids were copolymerized to form highly crosslinked ultrathin polymer membrane. And finally, terminal radicals on the 1,3-DPC in the copolymers might attack the diene groups in 2-acyl chains of DODPC which were never attacked by AIBN radicals in liposome systems.[14] Especially, the final point is very interesting and important. The diene groups in 2-acyl chains of DODPC lipids can be polymerized by the addition of AIBN in the presence of 1,3-DPC. The detailed study on the relationship between the improved polymerization conversion and composition of the mixed liposomes is now in progress.

It was previously reported that AAPD, a water-soluble radical initiator, was able to initiate radical polymerization of diene groups in 2-acyl chains of DODPC as liposomes.[14] The effect of 1,3-DPC on the polymerization of DODPC initiated by AAPD was also analyzed. A slight improvement was also found as shown in Fig. 9. About 16% of the diene groups in 1-acyl chains of DODPC were polymerized by AAPD under coexistence of 1,3-DPC. It is important that the polymerization conversion of 1,3-DPC/DODPC mixed liposomes reached a constant value, 68% regardless the employed radical initiators. This suggests that 1,3-DPC lipids certainly play a significant role to improve polymerization conversion as crosslinking agents.

This work was partially supported by the Grant-in-Aid for Scientific Research on Priority Area "Macromolecular Complexes" from the Ministry of Education, Science and Culture.

References

1) Part 5: H. Ohno, S. Takeoka, H. Iwai, and E. Tsuchida, *Makromol. Chem., Rapid Commun.*, in contribution.

2) J. H. Fendler, "Membrane Mimetic Chemistry," Wiley-Interscience, New York (1982), and references therein.

3) B. Bader, K. Dorn, B. Hupfer, and H. Ringsdorf, *Adv. in Polym. Sci.*, **64**, 1 (1985) and references therein.

4) S. L. Regen, B Czech, and A. Singh, *J. Am. Chem. Soc.*, **102**, 6638 (1980).

5) D. S. Johnson, S. Sanghera, M. Pons, and D. Chapman, *Biochim. Biophys. Acta*, **602**, 57 (1980).

6) H. H. Hub, B. Hupfer, H. Koch, and H. Ringsdorf, *Angew. Chem., Int. Ed. Engl.*, **19**, 938 (1980).

7) D. F. O'Brien, T. H. Whitesides, and R. T. Klingbiel, *J Polym. Sci., Polym. Lett. Ed.*, **19**, 95 (1981).

8) L. Gros, H. Ringsdorf, and H. Schupp, *Angew. Chem., Int. Ed. Engl.*, **20**, 305 (1981).

9) P. Tundo, D. J. Kippenberger, P. L. Klahn, N. E. Prieto, T. C. Jao, and J. H. Fendler, *J. Am. Chem. Soc.*, **104**, 456 (1982).

10) K. Dorn, R. T. Klingbiel, D. P. Specht, P. N. Tyminsky, H. Ringsdorf, and D. F. O'Brien, *J. Am. Chem. Soc.*, **106**, 1627 (1984).

11) R. Buschl, T. Folda, and H. Ringsdorf, *Makromol. Chem., Suppl.*, **6**, 245 (1984).

12) S. L. Regen and J.-S. Shin, *J. Am. Chem. Soc.*, **106**, 5756 (1984).

13) H. Ohno, S. Takeoka, and E. Tsuchida, *Polym. Bull.*, **14**, 487 (1985).

14) H. Ohno, Y. Ogata, and E. Tsuchida, *Macromolecules*, **20**, 929 (1987).

15) H. Ohno, S. Takeoka, H. Iwai, and E. Tsuchida, *J. Polym. Sci., Polym. Chem. Ed.*, **25**, 2737 (1987).

16) H. Ohno, S. Takeoka, and E. Tsuchida, *Bull. Chem. Soc. Jpn.*, **60**, 2945 (1987).

17) E. Hasegawa, K. Eshima, Y. Matsushita, H. Ohno, and E. Tsuchida, *Polym. Bull.*, **18**, 65 (1987).

18) H. Ohno, Y. Ogata, and E. Tsuchida, *J. Polym. Sci., Polym. Chem. Ed.*, **24**, 2959 (1986).

19) H. Ohno, S. Takeoka, H. Iwai, and E. Tsuchida, *Macromolecules*, **21**, (1988) in press.

20) H. Ohno, S. Takeoka, N. Hayashi, and E. Tsuchida, *Macromol. Chem., Rapid Commun.*, **8**, 215 (1987).

21) H. Ohno, Y. Maeda, and E. Tsuchida, *Biochim. Biophys. Acta*, **642**, 27 (1981).

 © 1988 The Chemical Society of Japan Bull. Chem. Soc. Jpn., 61, 2013—2018 (1988)

Dichalcogen-Bridged Acenaphthenes as New Electron Donors

Yoshio Aso, Koji Yui, Takanori Miyoshi, Tetsuo Otsubo,
Fumio Ogura,* and Jiro Tanaka†
Department of Applied Chemistry, Faculty of Engineering, Hiroshima University, Saijo, Higashi-Hiroshima 724
†Department of Chemistry, Faculty of Science, Nagoya University, Chikusa-ku, Nagoya 464
(Received October 7, 1987)

Three new electron donors, 5,6-dihydroacenaphtho[5,6-*cd*]-1,2-dithiole (**1a**), -diselenole (**1b**), and -ditellurole (**1c**) have been prepared with a view to developing new electron donors for low-dimensional molecular complexes. Their donor characters are markedly enhanced as compared with the corresponding dichalcogen-bridged naphthalenes. They formed charge-transfer complexes with tetracyanoquinodimethane (TCNQ). Their electrical conductivities increase in the order of polarizable chalcogen. The crystal structures of **1a**–TCNQ complex and neutral **1c** were determined by X-ray analyses. In the crystal, **1a** and TCNQ form a unique mixed stack, that is, a pair of donors and a pair of acceptors make an alternately stacking column. Neutral **1c** takes an almost planar conformation and molecules are connected to each other with strong Te–Te interactions.

Polycyclic aromatic compounds bearing peri-dichalcogen bridges, as represented by tetrathiotetracene (TTT), have been recognized as good electron donors for the formation of low-dimensional molecular complexes.[1] Although a number of tetrathiafulvalene (TTF) derivatives possessing alkyl or heteroatom substituents have been synthesized and have attracted much attention, there have been known few examples of chemical modifications of TTT-type donors. Meinwald et al. reported that even simple 1,8-dichalcogen-bridged naphthalenes **2a—c**, when the chalcogen was replaced by heavy element such as tellurium, could form a conducting charge-transfer (CT) complex with tetracyanoquinodimethane (TCNQ),[2] and they and we extended its study to acenaphthylene[3] and fluoranthene[4] system, respectively. In both cases, a donor character of peri-dichalcogenonaphthalene was rather reduced by the expansion of the π-system at another peri-position. We have recently reported the syntheses and some physical properties of 1,8:4,5-bis(dichalcogeno)-2,3,6,7-tetramethylnaphthalenes as the first example of alkyl-substituted TTT-type donors.[5] However, a marked enhancement of their donor characters, predicted by an electron-releasing effect of the methyl groups, was not observed for the sulfur nor selenium derivatives.[6] This is presumably a result of a lowering of the molecular planarity caused by steric repulsion.

Now we wish to report the syntheses of 5,6-dichalcogen-bridged acenaphthenes **1a—c** and their properties as electron donors. The introduced methylene groups are not only located in opposite peri-positions of dichalcogen bridge but also bound together so as not to bring about steric repulsion, therefore being capable of increasing the donor character.

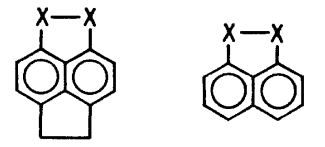

1a, X = S **2a**. X = S
1b, X = Se **2b**. X = Se
1c, X = Te **2c**. X = Te

Results and Discussion

Syntheses and Properties. 5,6-Dichalcogen-bridged acenaphthenes **1a—c** were synthesized starting from acenaphthene (**3**) (Scheme 1). 5,6-Dibromoacenaphthene (**4**) was prepared by bromination of **3** according to a reported method.[3] A reaction of 5,6-dilithioacenaphthene, generated from **4** and 2 equiv of butyllithium, with elemental chalcogen gave a complex mixture. However, the sequential reactions of **4** with 1 equiv of butyllithium, 1 equiv of elemental chalcogen, second 1 equiv of butyllithium, and 1 equiv of elemental chalcogen and subsequent air-oxidation resulted in the formation of **1a** (17%) or **1b** (6%). The tellurium analogue **1c** could not be obtained by the same series of reactions. On the other hand, 5,6-dichloroacenaphthene (**5**), prepared by the chlorination of **3** with sulfuryl chloride in the presence of aluminium chloride,[7] was submitted to a reaction with Na_2Te_2 in hexamethylphosphoric triamide (HMPA) to yield **1c** (5%). Furthermore, treatment of **5** with Na_2Se_2 gave **1b** in an improved yield (16%).

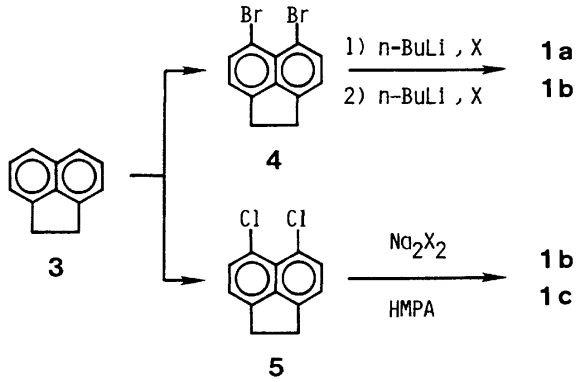

Scheme 1.

In the electronic spectra of compounds **1a—c**, marked bathochromic shifts of the longest wavelength absorptions, which were assigned to π-σ^* transition,[8] were observed in the order of polarizable chalcogens, indicating an increased electronic interaction between the naphthalene chromophore and the heavy chalcogen, λ_{max} in tetrahydrofuran (THF); **1a:** 422; **1b:** 550; **1c:** 691 nm. This phenomenon is common to the dichalcogen-bridged arenes.[4,5] More interestingly, the corresponding absorptions of naphthalene series, λ_{max} (THF); **2a:** concealed behind a strong shorter wavelength absorption at 368 nm; **2b:** 512; **2c:** 685 nm,[9] are shifted to longer wavelength by introduction of the ethylene bridge, reflecting an elevated π-HOMO level due to its electron-releasing effect. Its magnitude, however, decreases with increasing polarizability of chalcogen. In the wavelength region of π-π^* transition, the absorptions of **1b** are quite similar to those of **1a** except for slight bathochromic shifts whereas those of **1c** are considerably different in shape (cf. experimental section). This specificity of the tellurium derivative, also observed in naphthalene series, may be attributed to geometrical as well as electronic perturbation of very large and polarizable ditelluro bridge on the π-system of naphthalene.

The cyclic voltammograms of compounds **1a—c** exhibited one reversible wave corresponding to apparent one-electron oxidation,[8] and the second one was not observed in the measurable region. Their half-wave potentials $E_{1/2}$ are given in Table 1, together with those of peri-dichalcogenonaphthalenes **2a—c**. The donor strength of **1a—c** increases with introduction of the heavy chalcogen. Moreover, the ethylene bridges evidently exert an electron-donating perturbation on the π-system. These results are consistent with the electronic interactions stated above. Once again the effect of ethylene bridge decreases in the order of chalcogen triad and, in other words, is proportional to the oxidation potential of the naphthalene derivative. This is understandable as follows: The π-HOMO level of dichalcogen-bridged naphthalenes is raised in the order of polarizable chalcogen, and accordingly the interaction of the HOMO with ethylene bridge (hyperconjugation) decreases in the same order due to an increasing energy gap between the two interactive orbitals. It is worth noting that the oxidation potential of tellurium compound **1c** is the quite same as the first one of TTF (+0.33 V under the same conditions listed in Table 1) which forms a metallic complex with TCNQ.

Table 1. Half Wave Oxidation Potentials of **1** and **2** (V vs. Ag/AgCl)[a]

X	S	Se	Te
1	0.68	0.57	0.32
2	0.94	0.77	0.43

a) Measured by cyclic voltammetry in 0.1 mol dm^{-3} Bu_4NClO_4/CH_2Cl_2 at a glassy-carbon working electrode.

Table 2. Physical Properties of CT Complexes

CT complex	**1a**-TCNQ	**1b**-TCNQ	**1c**-TCNQ
Crystal form	black needles	black needles	black powder
Composition[a]	1 : 1	1 : 1	1 : 1
ΔE[b]	0.43	0.32	0.07
ν_{CN}/cm^{-1}	2211	2216	2172
σ/S cm^{-1}	1.0×10^{-8} c)	1.0×10^{-5} c)	1.8×10^{-1} d)

a) Determined by elemental analysis. b) See text. c) Measured on a single crystal by two-probe method. d) Measured on a compressed pellet by four-probe method.

Compounds **1a** and **1b** readily formed black crystalline 1 : 1 CT complexes with TCNQ in THF. Tellurium compound **1c** was resistant to complexation with TCNQ (in THF or dichloromethane), and even if the complex was formed (in chloroform), its stoichiometry was rich in donor and lack of reproducibility. From chlorobenzene solution the 1 : 1 complex was eventually obtained under an atmosphere of nitrogen. Their physical properties are listed in Table 2. The difference between the half-wave potentials of donor and acceptor (TCNQ: +0.25 V under the same conditions listed in Table 1), ΔE, is known to be a measure to predict electrical properties of the complex.[10] From the ΔE value for each complex, therefore, it is predictable that **1a**-TCNQ and **1b**-TCNQ are non- or slightly ionic and **1c**-TCNQ is in incomplete CT state. Complexation with **1a** and **1b** caused slightly lower shifts in the nitrile stretching frequency of TCNQ, but with **1c** led to a great shift, supporting a large charge transfer in **1c**-TCNQ.[11] Electrical conductivities of **1a**-, **1b**-, and **1c**-TCNQ complexes increase in that order, reflecting the estimated degree of CT.

Crystal Structure. The crystal structures of **1a**-TCNQ complex and neutral **1c** were determined by X-ray analysis.

Complex 1a-TCNQ: The crystal composition is one donor and one acceptor, and both molecules take quite planar conformations. As shown in Fig. 1, they form unusual modified mixed stacking columns along [111] direction. A pair of donors and a pair of acceptors make an alternately stacking column.[12] A mixed stacking is often observed in low conductive CT complexes and, in such cases, the overlapping pattern is usually "direct" overlap or slightly "shifted" form so as to facilitate CT interaction.[13] As shown in Fig. 2, the donor and the acceptor overlapping of this complex is not of such type. The long molecular axis of TCNQ and **1a** are twisted to ca. 40°. The donors are overlapped head to tail, and there exist no short intrastack interactions of the S-S nor S-N type. On the other hand, there exist somewhat short interstack contacts; the shortest S-N distance of 3.39 Å is approximately equal to the van der Waals distance of S-N

(3.35 Å).[14] Applying the method of Kistenmacher et al.[15] to estimating the degree of CT based on TCNQ geometry, we calculated it at 0.12, a value which indicates a small CT.

Neutral 1c: In the crystal, **1c** maintains the almost planar molecular structure though substitution of very large and long (2.748 Å) ditelluro bridge considerably distorts bond length and angles of acenaphthene skeleton in its molecular plane, and this is consistent with the inference from the electronic spectrum. As shown in Fig. 3, the molecules are stacked along c axis, forming the tellurium columns, and also arranged side by side along a axis forming linear chains of tellurium atoms. Moreover, each column is arranged along b axis alternately with opposite orientation of ditelluro bridge, and hence there exist the tellurium layers in the ac plane. Intrastack Te-Te distances of 4.15 and 4.37 Å are somewhat longer than the sum of the corresponding van der Waals distance (4.12 Å).[14] A more interesting feature in the crystal is the strong interactions between adjacent columns caused by shorter Te-Te contacts; the shortest one goes down to 3.57 Å (Fig. 4). In adjacent columns along b axis, the positions of ditelluro bridges are shifted one another to c axis by one half of unit (Fig. 3, left). Therefore, each molecule is connected with other four molecules by strong Te-Te interactions (Fig. 4), that is, molecule A is connected with two molecules B and B′ by Te(2)-Te(2) (3.75 Å) and Te(2)-Te(1) (3.93 Å) interactions and also connected with two molecules C and C′ by Te(1)-Te(1) (3.57 Å) interaction. These situations result in the formation of a two-dimensional sheet-like tight network in the ac plane.

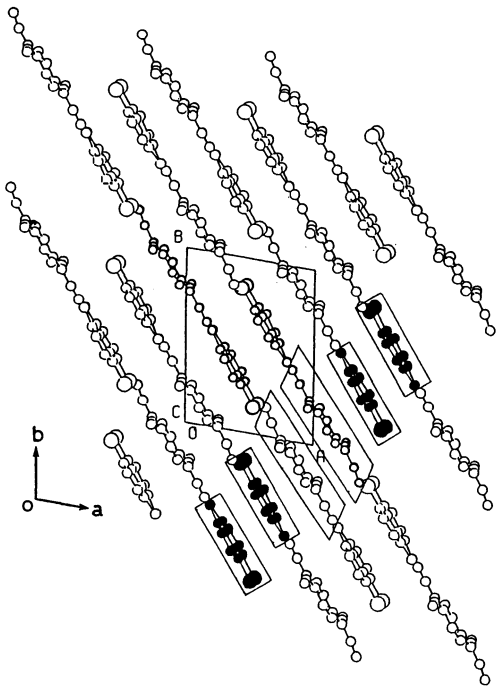

Fig. 1. Crystal structure of **1a**-TCNQ projected along c axis.

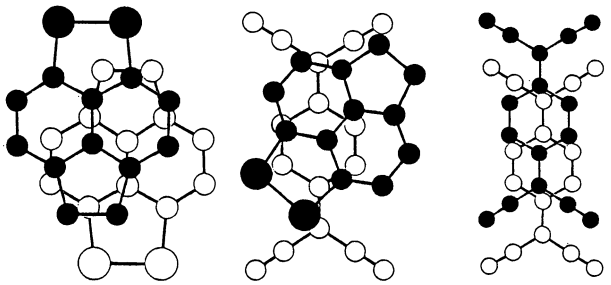

Fig. 2. Molecular overlapping patterns viewed perpendicular to the molecular plane.

Conclusion

The electron-donating character of dichalcogen-bridged naphthalene could be markedly enhanced by introduction of alkyl group without lowering the molecular planarity. Neither that of dithio- nor diseleno-bridged acenaphthene, however, was high enough to bring about an incomplete charge transfer in the TCNQ complex. Moreover, the result of X-ray analysis of **1a**-TCNQ indicated that the donor and the acceptor formed unusual mixed-staking columns probably due to the strong electronic and/or structural disorder of **1a**, and that this complex was characterized by a small CT, weak intrastack interactions, and tight interstack S-N interactions. The oxidation potential

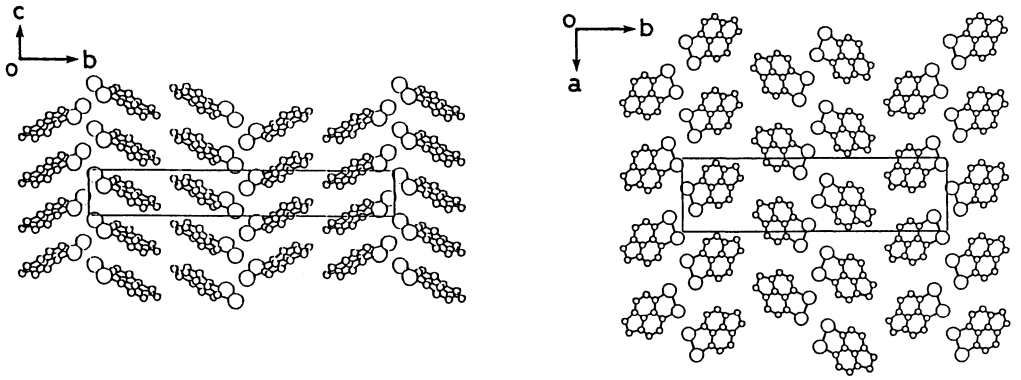

Fig. 3. Crystal structure of neutral **1c** projected along a axis (left) and c axis (right).

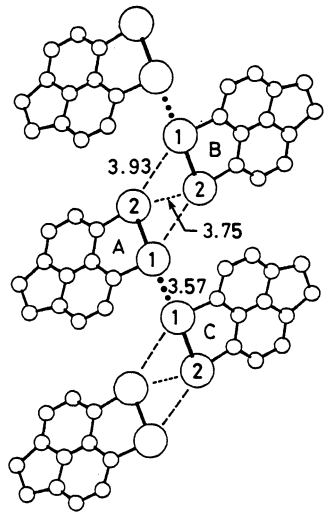

Fig. 4. The network of **1c** molecules projected along c axis. Close intermolecular Te-Te distances are illustrated. The symmetry operations are A (x,y,z), B ($-0.5-x,2.0-y,0.5+z$), B′ ($-0.5-x,2.0-y,-0.5+z$), C ($0.5-x,2.0-y,0.5+z$), and C′ ($0.5-x,2.0-y,-0.5+z$).

of **1c** was low enough, so that it formed a highly conducting TCNQ complex. In the crystal the molecules of **1c** associated to form densely packed tellurium layers resulting from the very strong Te-Te interactions. This marked tendency to aggregate seems to be reflected in low crystallinity of the CT complex and in its composition rich in donor. Such intermolecular strong interactions, however, are preferable for the enhancement of dimensionality of molecular complexes, especially for radical cation salts.[16] Finally, this study suggests that an enhancement of dimensionality of the CT complex as well as an increase in the donor strength may be achieved by the introduction of alkyl groups to a highly symmetrical doubly ditelluro-bridged arene without steric repulsion and a lowering of the symmetry. This is our target for future studies.

Experimental

General. All the melting points were uncorrected. Mass spectra were determined with a JEOL JMS-DX300 mass spectrometer. Proton NMR spectra were recorded with a JEOL JNM-PMX-60 spectrometer. Electronic spectra were measured with a JASCO UVIDEC-610A double beam spectrophotometer. Infrared spectra were recorded on a Hitachi infrared spectrophotometer, Model 260-30. The cyclic voltammetry was carried out at room temperature under nitrogen using a Hokuto Denko potentiostat/galvanostat HA-301 and a function generator HB-104. Gel-permeation liquid chromatography was carried out using a Japan Analytical Industry LC-08 liquid chromatograph, equipped with JAIGEL 1H and 2H columns, with chloroform as eluent.

Preparation of the Donors. 5,6-Dihydroacenaphtho[5,6-*cd*]-1,2-dithiole (1a): To a stirred solution of 5,6-dibromoacenaphthene (**4**)[3] (312 mg, 1.00 mmol) and *N,N,N′,N′*-tetramethylethylenediamine (232 mg, 2.00 mmol) in THF (30 cm^3) was slowly added a 1.6 mol dm^{-3} hexane solution of butyllithium (0.64 cm^3, 1.0 mmol) at −78 °C under argon. After the mixture was stirred for 15 min at −78 °C, sulfur (32 mg, 1.0 mmol) was added, and stirring was continued at −40—−30 °C for 2 h. After the mixture was cooled again to −78 °C, it was treated with butyllithium (0.64 cm^3, 1.0 mmol) and then sulfur (32 mg, 1.0 mmol) in the same way as described above. The mixture was quenched with acetic acid (0.2 cm^3), followed by exposure to air stream for oxidation. The resulting solution was concentrated under reduced pressure. After water was added, the mixture was extracted with dichloromethane. The extract was dried over anhydrous magnesium sulfate. After the solvent was removed under reduced pressure, the residue was purified by gel-permeation liquid chromatography and recrystallized from hexane to give 37 mg (17%) of **1a** as reddish brown prisms: mp 190.3 °C; MS (70 eV) m/z 216 (M^+); ^{1}H NMR (CCl_4) δ=3.25 (4H, s) and 6.90 (4H, s); UV (THF) 250 (ε 19600), 351 (11500), 369 (14000), and 422 nm (99.1); Anal. ($C_{12}H_8S_2$) C, H.

5,6-Dihydroacenaphtho[5,6-*cd*]-1,2-diselenole (1b): The title compound was prepared as described for **1a** (6%), and also as follows. To a solution of sodium diselenide, which was in situ prepared by heating sodium (308 mg, 13.4 mmol) and selenium (1.06 g, 13.4 mmol) at 120 °C for 2 h in HMPA (30 cm^3) under an argon atmosphere, was added a solution of 5,6-dichloroacenaphthene (**5**)[7] (1.00 g, 4.47 mmol) in HMPA (15 cm^3), and the mixture was stirred at 140 °C for 30 h. To the resulting solution were added brine (30 cm^3) and acetic acid (15 cm^3) with vigorous stirring. The resulting suspension was extracted with CS_2, and the extract was washed with water, dried over anhydrous magnesium sulfate, and then concentrated under reduced pressure. The residual solid was recrystallized from CS_2-hexane (3/1 volume ratio), purified with gel-permeation liquid chromatography, and again recrystallized from benzene to give 220 mg (16%) of **1b** as deep violet prisms: mp 208—213 °C; MS (70 eV) m/z 312 (M^+); ^{1}H NMR (CS_2) δ=3.22 (4H, s), 6.90 (2H, d, J=7 Hz), and 7.12 (2H, d, J=7 Hz); UV (THF) 259 (ε 10000), 379 (15000), and 550 nm (73.1); Anal. ($C_{12}H_8Se_2$) C, H.

5,6-Dihydroacenaphtho[5,6-*cd*]-1,2-ditellurole (1c): To a solution of sodium ditelluride, which was in situ prepared by heating sodium (154 mg, 6.71 mmol) and tellurium (856 mg, 6.71 mmol) at 125 °C in HMPA (20 cm^3) for 2 h under an argon atmosphere, was added a solution of **5** (500 mg, 2.24 mmol) in HMPA (15 cm^3), and the mixture was stirred at 150 °C for 31 h. The mixture was poured into water and extracted with CS_2. The extract was washed with water, dried over anhydrous magnesium sulfate, and then concentrated under reduced pressure. To the residual oil was added water, and the precipitated solid was filtered off, washed with acetone-water (1/1 volume ratio), and recrystallized from CS_2-hexane (3/1 volume ratio) to give 46 mg (5%) of **1c** as greenish black needles: mp 231 °C (decomp); MS (70 eV) m/z 408 (M^+); ^{1}H NMR (CS_2) δ=3.29 (4H, s), 6.92 (2H, d, J=7 Hz), and 7.15 (2H, d, J=7 Hz); UV (THF under argon) 223 (ε 3920), 258 (sh, 4830), 302 (1570), 404 (10400), 498 (2500), and 691 nm (134); Anal. ($C_{12}H_8Te_2$) C, H.

Preparation of Charge-Transfer Complexes. Both **1a**-TCNQ and **1b**-TCNQ complexes were prepared by mixing THF solutions of the donor and the acceptor in the same flask and standing for a few days. In the case of **1c**-TCNQ, hot chlorobenzene solutions of **1c** and TCNQ were mixed

Table 3. Crystallographic Data

	1a-TCNQ	**1c**
Chemical formula	$C_{24}H_{12}S_2N_4$	$C_{12}H_8Te_2$
FW	420.15	407.40
Crystal system	Triclinic	Orthorhombic
Space group	$P\bar{1}$	$P2_12_12_1$
a/Å	9.647(1)	8.137(3)
b/Å	12.181(1)	29.241(12)
c/Å	8.797(2)	4.364(4)
α/°	93.96(1)	
β/°	109.32(1)	
γ/°	97.65(1)	
V/Å^3	959.7(2)	1038.4(10)
Z	2	4
D_m/g cm^{-3}	1.439	2.572
D_c/g cm^{-3}	1.456	2.606
R	0.038	0.065
$2\theta_{max}$/°	126	126
No. of non-zero unique data	3037	1003
Crystal size/mm	0.21×0.10×0.50	0.06×0.04×0.60

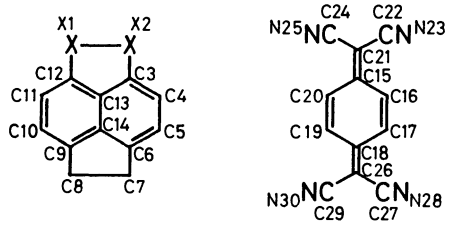

Fig. 5. Atomic numbering scheme of dichalcogen-bridged acenaphthene (left) and TCNQ (right).

under an atmosphere of nitrogen and stood at 0 °C for 15 min to give a black fine solid. The 1 : 1 stoichiometry of donor and acceptor was determined by elemental analyses which agreed with calculated values within ±0.3% for C, H, and N. Their properties are summarized in Table 2.

Crystal Structure Analysis. The X-ray diffraction data were collected by use of an automated four-circle diffractometer, Rigaku AFC-5, set on a rotating anode X-ray generator, Rigaku RU-200, with a graphite monochromated Cu radiation (Cu $K\alpha$=1.5418 Å). Crystallographic data are listed in Table 3. Crystal structures were solved by the Monte-Carlo direct method[17] using MULTAN 78 program system[18] and were refined on F^2 by the full-matrix least-squares program with the analytical absorption correction.[19] Atomic scattering factors were taken from International Tables for X-ray Crystallography.[20] Anisotropic temperature factors were used for the refinement of the non-H atoms. The hydrogen atoms of **1a**-TCNQ complex were located from difference Fourier maps and were refined with the isotropic temperature factors equivalent to that of the bonded carbon atoms. In the case of neutral **1c**, the H atoms were not included in the refinement. The atomic numbering scheme and the final atomic parameters are listed in Fig. 5 and Table 4, respectively. All estimated standard deviations for intermolecular atomic distances mentioned in the text were 0.00, and that for the Te-Te bond length of **1c** was 0.002. All computations were carried out at the Computation Center of Nagoya University using the library program of CRYSTAN system. Tables of structure factors, anisotropic thermal parameters, coordinates of hydrogen atoms, bond lengths, and bond angles are deposited as Document No. 8797 at the Office of the Editor of Bull. Chem. Soc. Jpn.

Table 4. Positional Parameters (×10^4) and Equivalent Isotropic Thermal Parameters

1a-TCNQ	x	y	z	B_{eq}/10^2 Å^2 a)
S1	5663(1)	1784(0)	7706(1)	380(1)
S2	5296(1)	1560(0)	9899(1)	420(1)
C3	4321(2)	2684(1)	9888(2)	311(4)
C4	3760(2)	3056(2)	11060(2)	376(4)
C5	2997(2)	3978(2)	10863(2)	378(4)
C6	2778(2)	4517(1)	9487(2)	322(4)
C7	2060(2)	5520(2)	8895(3)	380(5)
C8	2166(2)	5591(2)	7173(3)	419(5)
C9	3042(2)	4684(1)	6933(2)	334(4)
C10	3564(2)	4345(2)	5725(2)	397(5)
C11	4376(2)	3447(2)	5888(2)	388(5)
C12	4645(2)	2891(1)	7259(2)	317(4)
C13	4104(2)	3227(1)	8483(2)	290(4)
C14	3332(2)	4112(1)	8310(2)	295(4)
C15	10400(2)	1885(1)	7481(2)	292(4)
C16	11092(2)	958(2)	8136(2)	320(4)
C17	11767(2)	371(1)	7318(2)	313(4)
C18	11837(2)	658(1)	5777(2)	287(4)
C19	11138(2)	1581(1)	5116(2)	304(4)
C20	10454(2)	2160(1)	5930(2)	303(4)
C21	9699(2)	2475(2)	8315(2)	328(4)
C22	9639(2)	2220(2)	9863(3)	399(5)
N23	9594(3)	2018(2)	11102(3)	585(6)
C24	8980(2)	3378(2)	7669(2)	360(4)
N25	8422(2)	4107(2)	7141(2)	499(5)
C26	12538(2)	66(1)	4946(2)	313(4)
C27	13210(2)	−871(2)	5536(2)	359(4)
N28	13731(2)	−1637(2)	5964(3)	523(5)
C29	12583(2)	311(2)	3389(2)	366(4)
N30	12606(3)	477(2)	2129(2)	536(6)

1c	x	y	z	B_{eq}/10^2 Å^2 a)
Te1	907(2)	9810(1)	3914(6)	291(10)
Te2	−1992(2)	9499(1)	1446(6)	300(10)
C3	−697(27)	8946(7)	−121(66)	201(56)
C4	−1422(39)	8619(10)	−2142(75)	303(76)
C5	−582(38)	8220(11)	−3339(91)	376(80)
C6	1059(38)	8162(9)	−2360(90)	327(80)
C7	2326(38)	7785(19)	−3069(105)	404(95)
C8	3911(50)	7944(11)	−1450(154)	570(127)
C9	3509(36)	8396(10)	4(108)	440(107)
C10	4348(28)	8690(11)	1806(97)	383(89)
C11	3615(32)	9093(11)	2985(119)	410(107)
C12	1955(28)	9212(7)	2505(65)	223(55)
C13	1050(29)	8886(8)	602(79)	246(69)
C14	1834(37)	8502(10)	−568(83)	324(77)

a) $B_{eq}=(4/3)\sum_{ij}\beta_{ij}(a_i\cdot a_j)$.

This work was partially supported by Grants-in-Aid for the Scientific Research No. 62550635 and the Special Research Project on Properties of Molecular Assemblies No. 60104002 from the Ministry of Education, Science and Culture, and Mazda Foundation's Research Grant.

References

1) R. C. Wheland and J. L. Gillson, *J. Am. Chem. Soc.*,

98, 3916 (1976); H. Tanaka, T. Nogami, and H. Mikawa, *Chem. Lett.*, **1982**, 727 and references cited therein.

2) J. Meinwald, D. Dauplaise, F. Wudl, and J. J. Hauser, *J. Am. Chem. Soc.*, **99**, 255 (1977); J. Meinwald, D. Dauplaise, and J. Clardy, *ibid.*, **99**, 7743 (1977); D. Dauplaise, J. Meinwald, J. C. Scott, H. Temkin, and J. Clardy, *Ann. N. Y. Acad. Sci.*, **313**, 382, (1978).

3) L. Chiang and J. Meinwald, *Tetrahedron Lett.*, **21**, 4565 (1980).

4) H. Miyamoto, K. Yui, Y. Aso, T. Otsubo, and F. Ogura, *Tetrahedron Lett.*, **27**, 2011 (1986); T. Otsubo, H. Miyamoto, Y. Aso, and F. Ogura, *Synthetic Metals*, **19**, 595 (1987).

5) T. Otsubo, N. Sukenobe, Y. Aso, and F. Ogura, *Chem. Lett.*, **1987**, 315.

6) F. Wudl, D. E. Schafer, and B. Miller, *J. Am. Chem. Soc.*, **98**, 252 (1976); A. Yamahira, T. Nogami, and H. Mikawa, *J. Chem. Soc., Chem. Commun.*, **1983**, 904; J. C. Stark, R. Reed, L. A. Acampora, D. J. Sandman, S. Jansen, M. T. Jones, and B. M. Foxman, *Organometallics*, **3**, 732 (1984).

7) H. Okada, Y. Sato, Y. Kimura, and M. Kaneko, Japan Patent **77** 08307 (1977); *Chem. Abstr.*, **87**, 134828f (1977).

8) A. Zweig and A. K. Hoffmann, *J. Org. Chem.*, **30**, 3997 (1965).

9) 1,8-Dichalcogenonaphthalenes **2a—c** were prepared from 1,8-dihalonaphthalene with Na_2X_2 in 46%, 59%, and 5.6% yields, respectively; K. Yui, Y. Aso, T. Otsubo, and F. Ogura, *Chem. Lett.*, **1986**, 551, and their electronic spectra and cyclic voltammograms were recorded under the same conditions as in the case of acenaphthene series.

10) G. Saito and J. P. Ferraris, *Bull. Chem. Soc. Jpn.*, **53**, 2141 (1980) and references cited therein.

11) The exact degree of CT is estimated on the basis of infrared analysis; J. S. Chappell, A. N. Bloch, W. A. Bryden, M. Maxfield, T. O. Poehler, and D. O. Cowan, *J. Am. Chem. Soc.*, **103**, 2442 (1981). It is, however, difficult to analyze in detail the infrared spectra of complexes with a mixed stacking mode; M. Meneghetti, A. Girlando, and C. Pecile, *J. Chem. Phys.*, **83**, 3134 (1985).

12) A. Singhabhandhu, P. D. Robinson, J. H. Fang, W. E. Geiger, Jr., *Inorg. Chem.*, **14**, 318 (1975); T. Otsubo, Y. Shiomi, Y. Aso, F. Ogura, and J. Tanaka, *Nippon Kagaku Kaishi*, **1987**, 1288.

13) K. Nakasuji, M. Nakatsuka, H. Yamochi, I. Murata, S. Harada, N. Kasai, K. Yamamura, J. Tanaka, G. Saito, T. Enoki, and H. Inokuchi, *Bull. Chem. Soc. Jpn.*, **59**, 207 (1986) and references cited therein.

14) A. Bondi, *J. Phys. Chem.*, **68**, 441 (1964).

15) T. J. Kistenmacher, T. J. Emge, A. N. Bloch, and D. O. Cowan, *Acta Crystallogr., Sect. B*, **38**, 1193 (1982).

16) The electrical conductivity of the single crystal of **1c** by two-probe method was 1.6×10^{-7} S cm^{-1}, a value which was comparatively high as a neutral molecule, and increased to 7.6×10^{-5} S cm^{-1} when the crystal was exposed to vapor of iodine. However, its radical cation salt was not obtained by an electrochemical technique due to the lability of **1c** in solution.

17) A. Furusaki, *Acta Crystallogr., Sect. A*, **35**, 220 (1979).

18) P. Main, S. E. Hull, L. Lessinger, G. Germain, J. P. Declercq, and M. M. Woolfson, MULTAN 78, (1978). Univ. of York, England, and Louvain, Belgium.

19) C. Katayama, N. Sakabe, and K. Sakabe, *Acta Crystallogr., Sect. A*, **28**, S207 (1972).

20) "International Tables for X-ray Crystallography," Kynoch Press, Birmingham (1974), Vol. IV.

Synthesis of Naphthoquinone Derivatives. XIII. Reaction of 2,3-Dihydro-2-thioxo-1*H*-naphth[2,3-*d*]imidazole-4,9-dione with Dimethyl Acetylenedicarboxylate[1)]

Tateo NAKAMORI,* Toshiyuki SAITO, and Toshiyasu KASAI
Faculty of Engineering, Tokyo Institute of Technology, Ookayama, Meguro-ku, Tokyo 152
(Received October 14, 1987)

Tetracyclic compounds with a thiazolidinone or thiazinone ring fused to 1*H*-naphth[2,3-*d*]imidazole-4,9-dione were synthesized. Dimethyl 2-(4,9-dioxo-4,9-dihydronaphth[2,3-*d*]imidazol-2-ylthio)fumarate (**3**) was obtained by a reaction of 2,3-dihydro-2-thioxo-1*H*-naphth[2,3-*d*]imidazole-4,9-dione with dimethyl acetylenedicarboxylate in methanol. A ring-closure reaction of **3** in acetic anhydride was found to give selectively methyl (3,5,10-trioxo-2,3,5,10-tetrahydronaphth[2′,3′:4,5]imidazo[2,1-*b*]thiazol-2-ylidene)acetate, while, the cyclization of **3** in polyphosphoric acid afforded methyl 4,6,11-trioxo-6,11-dihydro-4*H*-naphth[2′,3′:4,5]imidazo[2,1-*b*]-thiazine-2-carboxylate.

1,4-Naphthoquinone derivatives fused with the azole ring have attracted much attention because of their physiological and coloring properties. However, a few reports[2)] have appeared in the literature which have described the synthesis of tetracyclic azole compounds. In our previous papers, we reported on the syntheses of imidazo[2,1-*b*]naphtho[2,3-*d*]thiazole-5,10-diones[3a)] and naphth[2′,3′:4,5]imidazo[2,1-*b*]thiazole-5,10-diones,[3b,c)] showing physiological activities. We then developed a convenient method for the synthesis of 2,3-dihydro-2-thioxo-1*H*-naphth[2,3-*d*]imidazole-4,9-dione (**1**). We were also interested in the syntheses of tetracyclic azole compounds, which may be easily available from compound **1**. This paper describes the preparation of tetracyclic azole compounds, fused thiazolidione or thiazinone ring from dimethyl 2-(4,9-dioxo-4,9-dihydronaphth[2,3-*d*]imidazol-2-ylthio)-fumarate (**3**), which was obtained by a Michael-type reaction of **1** with dimethyl acetylenedicarboxylate (DMAD). Furthermore, the effects of the quinone carbonyl groups on the cyclization reactions will be discussed.

Results and Discussion

A few reports[4)] concerning reactions of 2*H*-benzimidazole-2-thione (**2**) with DMAD have already appeared. A recent report by Wade[4a)] indicated that a reaction in methanol yields methyl 4-oxo-4*H*-[1,3]-thiazino[3,2-*a*]benzimidazole-2-carboxlate in one step. We first investigated the reaction of the thione **1** with DMAD by the method of Wade. When a solution of **1** with DMAD in methanol was stirred at room temperature for 3 h, the adduct **3** was isolated in 74% yield. A structural assignment for the product **3**, depending on the sulfur atom participates in the addition reaction, was accomplished through its ^{1}H NMR and IR spectra. The (*Z*)-geometry of **3**, which results from a trans addition, is assumed on the basis of the results of Hendrickson[5a)] and Truce[5b)] (Scheme 1). On the other hand, a reaction of **1** with DMAD at reflux temperature for 24 h gave yellow crystals **4a** (mp 171.0—172.0 °C, 11%) and **4b** (mp 131.0—132.0 °C, 15%). Also, compounds **4a** and **4b** were obtained from adduct **3** under the same conditions. The structures of diastereoisomers **4a** and **4b** formed by the addition of methanol to **3** were established on the basis of IR, ^{1}H NMR, and elemental analysis data. The structure of diastereoisomer **4b** was supported, rather than structure **5**, since there was little variation in the yield between **4a** and **4b**, and the proton coupling constant of **4a** and **4b** showed 3.5 and 5 Hz, respectively.

The reaction was carried out in the presence of sodium methoxide as a base in methanol, in order to

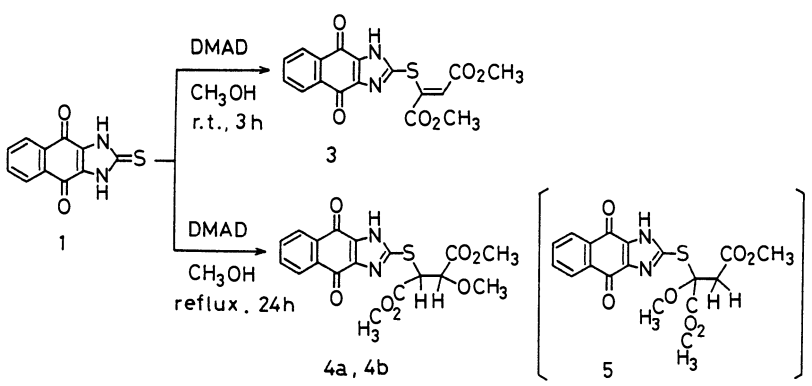

Scheme 1.

obtain cyclized compounds, i.e., methyl (3,5,10-trioxo-2,3,5,10-tetrahydronaphth[2′,3′ : 4,5]imidazo[2,1-*b*]thiazol-2-ylidene)acetate (**6**), methyl 4,6,11-trioxo-6,11-dihydro-4*H*-naphth[2′,3′ : 4,5]imidazo[2,1-*b*]thiazine-2-carboxylate (**7**). Compound **1** gave adduct **3** at room temperature for 30 min, but for prolonged reaction times compound **6** or **7** was not isolated but compound **1** formed by the methanolysis of **3** was recovered. These results could be explained in terms of the nucleophilicity of nitrogen in the imidazole ring being diminished by means of the electron-withdrawing character of the quinonoid moiety.

However, a mixture of **1** and DMAD in acetic acid was refluxed for 3 h to give the two isomers (**6** and **7**) in 22% yield, which could not be separated by column chromatography. The ^{1}H NMR analysis showed that **6** and **7** were produced in the ratio of 7 : 4. (Pure **6** and **7** were prepared from the adduct **3** individually as mentioned later.) In addition, when the reaction was carried out for 24 h, compound **8** (mp 209.0—210.0 °C) was unexpectedly obtained in 31% yield without the formation of **6** and **7**. The formation of **8** may involve the addition of methanol eliminated to the thiazinone ring of **7**. The position of the methoxyl group in compound **8** was determined by the ^{1}H NMR spectrum, which shows *vicinal* H_2 and H_3 protons at δ 5.98 and 5.07 ($J_{2,3}$=2 Hz), respectively. Furthermore, the H_7 proton of compound **8** appears at a lower field, compared with the other protons in the aromatic ring.[6] This downfield shift may be explained on the basis that the 4-oxo function is held in a rigid position, coplanar with and oriented toward the aromatic ring, thus exerting a deshielding effect on the H_7 proton. Secondly, the cyclization of adduct **3** using condensing agents[7,8] was investigated.

The solution of **3** in acetic anhydride was heated at 100 °C for 20 min to afford compound **6** in 42% yield. A prolonged reaction time did not show any increase in the yield of compound **6** nor in the formation of compound **7**. The formation of **6** might involve an attack of the nitrogen situated closely to the ester moiety (Scheme 3, route A). Under these conditions, using acetic anhydride acetylation on the nitrogen atom is postulated to be an initial reaction. It seems, however, that the acetylation does not occur because ethyl 3-(4,9-dioxo-4,9-dihydronaphth[2,3-*d*]imidazol-2-ylthio)acrylate (**9**) reacted unchanged in acetic anhydride, as will be mentioned later. On the other hand, the reaction of **3** in polyphosphoric acid (PPA) at 140—150 °C for 30 min gave compound **7** in 66% yield as the sole product. One possible mechanistic pathway to **7** is shown in route B of Scheme 3. Of particular interest is the selective formation into **6** and **7**. The structures of **6** and **7** were determined by the ^{1}H NMR spectra. In addition, to make this analysis more complete, we wanted to prepare a compound with a thiazinone ring like that of the structure of **7** by employing the alternative procedure shown in Scheme 4.

A suspension of **1** and ethyl propiolate in ethanol was refluxed for 5 h to afford a yellow compound **9a** (mp 260.5—262.0 °C) and an orange compound **9b** (mp 233.0—234.0 °C) in 29 and 48% yield, respectively. The

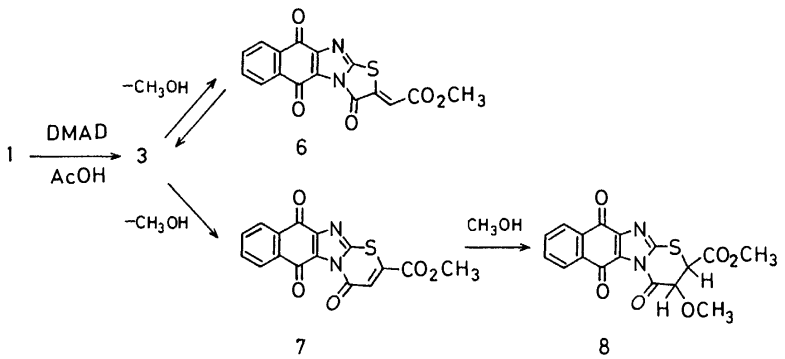

Scheme 2.

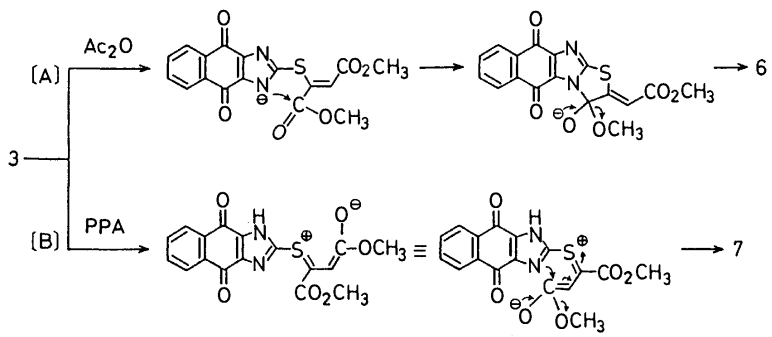

Scheme 3.

^{1}H NMR spectra of **9a** (*Z* form /trans addition product) and **9b** (*E* form /cis addition product) showed two doublets for the olefinic protons at δ 6.31 and 8.23 (J=10 Hz) and at 6.46 and 8.32 (J=16 Hz), respectively. The coupling constants were consistent with these geometorical assignments. The formation of the two isomers is of interest since the reaction of **1** with DMAD gave a single isomer (as mentioned above). No isomerization of **9a** to **9b** was observed under reflux in ethanol.

A cyclization of **9** is expected to produce compound **10** with a fused thiazinone ring. A suspension of **9a** or **9b** in PPA was heated to afford **10**: mp 265 °C (decomp); no reaction occurred in acetic anhydride. This result is in accord with the above-mentioned expectation. The synthesis of compound **10** via **12** from **7**, obtained by a reaction of **1** with DMAD, was tried. However, the hydrolysis of **7** with sodium hydroxide did not give compound **12** but, rather, compound **13** via a cleavage of the thiazinone ring; also, a reaction with hydrochloric acid or sulfuric acid did not give any isolable compound. The hydrolysis of **6**, as well as **7**, gave the monomethyl ester of fumaric acid (**14**). It is thus thought that the amide bond in the thiazolidinone or thiazinone ring was easily cleavaged since the quinone-carbonyl groups result in a decrease in the nucleophilicity of the nitrogen atom. Attempts to obtain compound **12** by the hydrolysis of **7** were unsucessful.

Compound **12** was finally obtained in PPA from adduct **11**, prepared by a reaction of **1** with acetylenedicarboxylic acid. A decarboxylation of **12** by thermolysis in biphenyl-diphenyl ether (1 : 3) at 250 °C afforded compound **10**, while the cyclization of **11** in acetic anhydride gave compound **15**. Furthermore, the $\nu_{C=O}$ of **12** and **15** were similar to those of **7** and **6**, respectively. These results suggest that compound **7** or **6** has a fused thiazinone or thiazolidinone ring, respectively.

The cyclization of the other related adducts in PPA and acetic anhydride are summarized in Table 1. It is of interest that the cyclization of **13** in acetic anhydride and of **14** in PPA gave the methyl esters, **6** and **7**, respectively, which might be formed via a further reac-

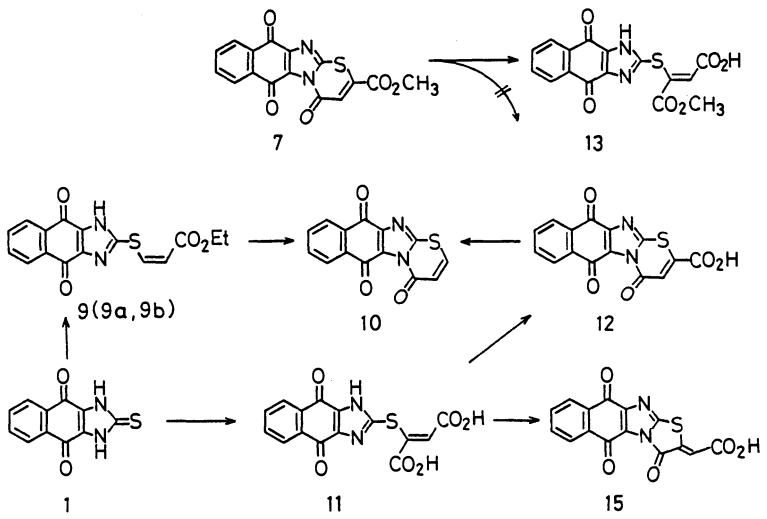

Scheme 4.

Table 1. Cyclization of the Adducts in Acetic anhydride or Polyphosphoric Acid (PPA)

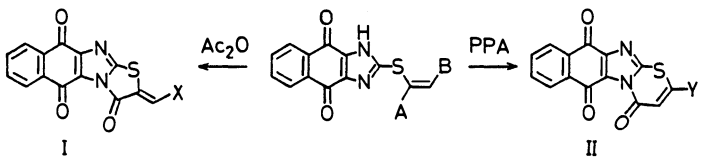

Substrate			Product			
			[I]		[II]	
Compd No.	A	B	Compd No.	X	Compd No.	Y
3	COOMe	COOMe	**6**	COOMe	**7**	COOMe
13	COOMe	COOH	**6**	COOMe	**7**	COOMe
14	COOH	COOMe	**6**	COOMe	**7**	COOMe
11	COOH	COOH	**15**	COOH	**12**	COOH
9	H	COOEt	No reaction		**10**	H

tion of **12** with methanol eliminated during the reaction.

In summary, tetracyclic azole compounds with a fused thiazolidinone or thiazinone ring were obtained from adduct **3**, prepared by the reaction of **1** with DMAD. It was found that the cyclization of **3** gave compound **6** or **7** by the use of acetic anhydride or PPA as an effective condensing agent, respectively.

Physiological evaluations of the synthesized compounds are currently under way and the results will be reported elesewhere.

Experimental

Measurements. The melting points were determined with a Yamato MP-1 apparatus and are uncorrected. IR spectra were taken on a JASCO IRA-1 spectrophotometer using KBr pressed discs. ^{1}H NMR spectra were recorded on a JEOL PS-100 (100MHz) spectrometer. Chemical shifts are given in ppm relative to tetramethylsilane as an internal standard. Mass specra were taken on a Hitachi RMU-7M mass spectrometer at an ion-source temperature of 200 °C and an ionizing potential of 75 eV.

Dimethyl 2-(4,9-Dioxo-4,9-dihydronaphth[2,3-*d*]imidazol-2-ylthio)fumarate (3). DMAD (0.65 g, 4.57 mmol) in 5 cm^3 of methanol was added dropwise with stirring to a suspension of the thione **1** (1.0 g, 4.35 mmol) in 15 cm^3 of methanol. After being stirred for 3 h at room temperature, the solid was collected by filtration, washed with ether, and dried to give 1.20 g (74%) of **3** (mp 204.0—206.0 °C). Recrystallization from ethyl acetate-hexane gave 0.74 g (46%) of pure **3** as yellow plates: mp 207.0—209.0 °C; IR 3215 (NH), 1715 and 1675 (C=O), 1600, 1418, 1337, 1275, 1220, 1065, and 980 cm^{-1}; ^{1}H NMR (DMSO-d_6) δ=3.57 (3H, s), 3.78 (3H, s), 6.86 (1H, s), 7.78—7.96 (2H, m), 7.98—8.18 (2H, m); MS *m/z* (rel intensity) 372 (M$^+$; 3), 342 (13), 341 (30), 340 (35), 283 (8), 282 (12), 281 (55), 260 (12), 259 (55), 258 (100), 255 (13), and 254 (50). Found: C, 54.91; H, 3.11; N, 7.58; S, 8.67%. Calcd for $C_{17}H_{12}N_2O_6S$: C, 54.84; H, 3.25; N, 7.52; S, 8.61%.

Methanol Addition to 3. A suspension of **3** (0.50 g, 1.34 mmol) in 20 cm^3 of methanol was heated at refluxing temperature for 24 h. After the mixture was allowed to stand overnight, the solid was collected by filtration, washed with ether, and dried to give 0.13 g of crude **4b** (mp 104.0—106.0 °C). Recrystallization from benzene gave 0.08 g (15%) of pure **4b** as a yellow powder: mp 131.0—132.0 °C; IR 3190 (NH), 2940 (CH), 1725 and 1670 cm^{-1} (C=O); ^{1}H NMR ($CDCl_3$) δ=3.52 (3H, s), 3.82 (3H, s), 3.85 (3H, s), 4.39 (1H, d, *J*=5 Hz), 4.85 (1H, d, *J*=5 Hz), 7.63—7.81 (2H, m), 8.05—8.30 (2H, m). Found: C, 53.60; H, 4.34; N, 6.41; S, 7.48%. Calcd for $C_{18}H_{16}N_2O_7S$: C, 53.47; H, 3.96; N, 6.93; S, 7.92%. To the mother liquor was added 100 cm^3 of water and was extracted with chloroform. The solution was evaporated under reduced pressure, giving 0.06 g (11%) of a yellow powder (mp 171.0—172.0 °C). Recrystallization from benzene-hexane gave 0.05 g of pure **4a**: mp 172.0—173.0 °C; IR 3300 (NH), 2920 (CH), 1740 and 1665 cm^{-1} (C=O); ^{1}H NMR ($CDCl_3$) δ=3.58 (3H, s), 3.80 (6H, s), 4.61 (1H, d, *J*=3.5 Hz), 5.02 (1H, d, *J*=3.5 Hz), 7.56—7.73 (2H, m), 8.00—8.18 (2H, m). Found: C, 53.49; H, 3.81; N, 6.93; S, 7.78%. Calcd for $C_{18}H_{16}N_2O_7S$: C, 53.47; H, 3.96; N, 6.93; S, 7.92%.

Methyl (3,5,10-Trioxo-2,3,5,10-tetrahydronaphth[2′,3′:4,5]-imidazo[2,1-*b*]thiazol-2-ylidene)acetate (6). A suspension of **3** (1.00 g, 2.69 mmol) in 20 cm^3 of acetic anhydride was heated at 100 °C for 20 min. After the mixture was allowed to come to room temperature, the solid was filtered off, washed with ether, and dried to give 0.38 g (42%) of **6** as yellowish green crystals. Recrystallization from chlorobenzene gave 0.23 g (25%) of pure **6**: mp 248.0 °C (decomp); IR 3050 (CH), 1770, 1725, 1680, and 1665 cm^{-1} (C=O); ^{1}H NMR ($CDCl_3$) δ=3.93 (3H, s), 7.32 (1H, s), 7.70—7.88 (2H, m), 8.12—8.32 (2H, m); MS *m/z* (rel intensity) 342 (M$^+$+2; 10), 341 (M$^+$+1; 9), 340 (M$^+$; 100), 312 (10), 309 (10), 283 (13), 282 (12), 281 (37), 258 (13), 255 (21), 254 (67). Found: C, 56.40; H, 2.34; N, 7.90; S, 9.24%. Calcd for $C_{16}H_8N_2O_5S$: C, 56.47; H, 2.35; N, 8.24; S, 9.42%.

Methyl 4,6,11-Trioxo-6,11-dihydro-4*H*-naphth[2′,3′:4,5]-imidazo[2,1-*b*]thiazine-2-carboxylate (7). A suspension of **3** (1.35 g, 3.63 mmol) in ca. 60 g of PPA was heated at 140—150 °C for 30 min. The reaction mixture was allowed to cool and then suspended in 300 cm^3 of water. The solid was collected by filtration, washed with acetone, and dried to yield 0.81 g (66%) of crude **7**: mp 245.0 °C (decomp). Recrystallization from 1-butanol gave 0.57 g (46%) of pure **7** as yellow needles: mp 255.0 °C (decomp); IR 3060 (CH), 1727, and 1680 cm^{-1} (C=O): ^{1}H NMR ($CDCl_3$) δ=4.06 (3H, s), 7.56 (1H, s), 7.68—7.84 (2H, m), 8.14—8.30 (2H, m); MS *m/z* (rel intensity) 342 (M$^+$+2; 30), 341 (M$^+$+1; 21), 340 (M$^+$; 100), 312 (10), 284 (16), 282 (10), 281 (20), 255 (12), 254 (24). Found: C, 56.26; H, 2.21; N, 8.21; S, 9.32%. Cacld for $C_{16}H_8N_2O_5S$: C, 56.47; H, 2.35; N, 8.24; S, 9.42%.

Methyl 3-Methoxy-4,6,11-trioxo-3,4,6,11-tetrahydro-2*H*-naphth[2′,3′:4,5]imidazo[2,1-*b*]thiazine-2-carboxylate (8). A suspension of DMAD (0.13 g, 0.91 mmol) in 3 cm^3 of acetic acid was added with stirring to a suspension of **1** (0.20 g, 0.87 mmol) in **2** cm^3 of acetic acid. After refluxing for 24 h, an insoluble solid was filtered off and the filtrate was left standing overnight in an ice box. The solid was collected by filtration, dried to give 0.18 g of yellow crystals and chromatographed on a Wakogel C-200 column using chloroform as an eluant. The evaporation residue from the second fraction gave 0.10 g (31%) of **8** as yellow needles: mp 209.0—211.0 °C; IR 2965 (CH), 1740, 1683, and 1660 cm^{-1} (C=O); ^{1}H NMR ($CDCl_3$) δ=3.86 (6H, s), 5.07 (1H, d, *J*=2 Hz), 5.98 (1H, d, *J*=2 Hz), 7.64—7.80 (2H, m), 8.04—8.17 (1H, m), 8.19—8.32 (1H, m). Found: C, 54.73; H, 3.10; N, 7.30; S, 8.13%. Calcd for $C_{17}H_{12}N_2O_6S$: C, 54.83; H, 3.25; N, 7.52; S, 8.61%.

Ethyl 3-(4,9-Dioxo-2-naphth[2,3-*d*]imidazolylthio)acrylate (9). Ethyl propiolate (0.24 g, 2.39 mmol) in 5 cm^3 of ethanol was added with stirring to a suspension of **1** (0.50 g, 2.17 mmol) in 10 cm^3 of ethanol and refluxed for 5 h. The solid was filtered off, washed with ether and dried to yield 0.68 g (95%) of **9**. Recrystallization from acetone gave 0.21 g (29%) of **9a** (*Z* form: mp 260.5—262.0 °C) as yellow needles. Crude **9a** was recrystallized from ethyl acetate-hexane to give pure **9a**: mp 263.0—264.0 °C; IR 3180 (NH), 3090, 3060, 2985 (CH), 1700, and 1680 cm^{-1} (C=O); ^{1}H NMR (DMSO-d_6) δ=1.24 (3H, t, *J*=7 Hz), 4.18 (2H, q, *J*=7 Hz), 6.31 (1H, d, *J*=10 Hz), 7.76—7.92 (2H, m), 8.01—8.15 (2H, m), 8.23 (1H, d, *J*=10 Hz); MS *m/z* (rel intensity) 329 (M$^+$+1, 1), 328 (M$^+$, 1), 285 (1), 284 (2), 283 (7), 282 (2), 267 (1), 258 (2), 257 (7), 256 (17), 255 (100), 254 (2), 231 (5), 230 (17). Found: C, 58.47; H, 3.55; N, 8.44; S, 9.82%. Calcd for $C_{16}H_{12}N_2O_4S$: C, 58.54; H, 3.66; N, 8.54; S, 9.77%. The filtrate of acetone recrystallization was evaporated and the residue was recrystallized from

chloroform and ethanol to give 0.34 g (48%) of **9b** (*E* form: mp 233.0—234.0 °C) as orange needles: IR 3125 (NH), 3085, 3035, 2985 (CH), 1695, 1685, and 1662 cm^{-1} (C=O); ^1H NMR (DMSO-d_6) δ=1.26 (3H, t, J=7 Hz), 4.24 (2H, q, J=7 Hz), 6.46 (1H, d, J=16 Hz), 7.84—8.05 (2H, m), 8.08—8.30 (2H, m), 8.32 (1H, d, J=16 Hz). Found: C, 59.32; H, 3.58; N, 8.58; S, 9.87%. Calcd for $C_{16}H_{12}N_2O_4S$: C, 58.54; H, 3.66; N, 8.54; S, 9.77%.

***4H*-Naphth[2′,3′:4,5]imidazo[2,1-*b*]thiazine-4,6,11-trione (10).** This compound as yellow needles: mp 265.0 °C (decomp) was obtained in 66% yield from **9a** using conditions similar to those described for **7**. IR 3030, 3000 (CH), 1715, and 1663 cm^{-1} (C=O); ^1H NMR (DMSO-d_6) δ=6.93 (1H, d, J=10 Hz), 7.81—7.95 (2H, m), 8.04—8.16 (2H, m), 8.35 (1H, d, J=10 Hz); MS m/z (rel intensity) 284 (M^++2, 12), 283 (M^++1, 21), 282 (M^+, 100), 255 (6), 254 (26), 238 (12), 230 (6). Found: C, 59.99; H, 1.98; N, 9.94; S, 11.34%. Calcd for $C_{14}H_6N_2O_3S$: C, 59.57; H, 2.13; N, 9.93; S, 11.35%.

2-(4,9-Dioxo-4,9-dihydronaphth[2,3-*d*]imidazol-2-ylthio)-fumaric Acid (11). Acetylenedicarboxylic acid (0.28 g, 2.45 mmol) in 5 cm^3 of acetonitrile was added to a suspension of **1** (0.50 g, 2.17 mmol) in 5 cm^3 of acetonitrile. After being stirred for 10 h at room temperature, the solid was collected by filtration, washed with ether, and dried to give 0.66 g (88%) of **11** as yellow crystals: mp 218.0 °C (decomp): IR 3300 (NH), 3050 (CH), and 1710—1670 cm^{-1} (C=O); ^1H NMR (DMSO-d_6) δ=6.90 (1H, s), 7.83—8.07 (2H, m), 8.08—8.27 (2H, m). Found: C, 52.56; H, 2.60; N, 7.61; S, 9.03%. Calcd for $C_{15}H_8N_2O_6S$: C, 52.33; H, 2.33; N, 8.14; S, 9.30%.

4,6,11-Trioxo-6,11-dihydro-4*H*-naphth[2′,3′:4,5]imidazo-[2,1-*b*]thiazine-2-carboxylic Acid (12). This compound as yellow plates: mp 252.0 °C (decomp) was obtained in 42% yield from **11** using conditions similar to those described for **7**. IR 3400 (OH), 1730 and 1673 cm^{-1} (C=O); MS m/z (rel intensity) 326 (M^+, 2), 285 (3), 284 (17), 283 (24), 282 (100), 256 (3), 255 (6), 254 (25), 239 (3), 238 (12), 232 (2), 231 (6), 230 (26). Found: C, 55.76; H, 1.61; N, 8.67; S, 10.12%. Calcd for $C_{15}H_6N_2O_5S$: C, 55.22; H, 1.84; N, 8.59; S, 9.82%.

(3,5,10-Trioxo-2,3,5,10-tetrahydronaphth[2′,3′:4,5]imidazo-[2,1-*b*]thiazol-2-ylidene)acetic Acid (15). A suspension of **11** (0.50 g, 1.45 mmol) in 5 cm^3 of acetic anhydride was heated at 100—110 °C for 10 min. The solid was collected by filtration, washed with ether, and dried to yield 0.36 g (76%) of **15** as yellow crystals: mp 255.0 °C (decomp): IR 3250—2800 (broad, OH), 1855, 1840, 1773, and 1670 cm^{-1} (C=O); MS m/z (rel intensity) 326 (M^+, 19), 284 (4), 283 (9), 282 (23), 256 (4), 255 (14), 254 (55), 238 (4), 232 (7), 231 (23), 230 (100).

Decarboxylation of 12. A suspension of **12** (0.10 g, 0.31 mmol) in 8.0 g of biphenyl-diphenyl ether (1 : 3) was heated at 250 °C for 10 min. The solid was collected by filtration, washed with hexane and ether, and dried to yield 0.07 g (80%) of **10**. This compound was identical as **10** on the basis of IR spectrum and mixed melting point.

References

1) Part XII: T. Nakamori and T. Kasai, *Nippon Kagaku Kaishi*, **1986**, 1091.

2) a) A. M. Simonov and B. H. Komissalov, *Khim. Geterotsikl. Soedin.*, **1976**, 783; b) I. M. Issa, A. A. EL-Samahy, R. M. Issa, G. EL-Naggar, and H. S. EL-Kashef, *Indian J. Chem.*, **15B**, 356 (1977).

3) a) T. Nakamori, Y. Sato, and T. Kasai, *Nippon Kagaku Kaishi*, **1982**, 98, 105; b) T. Nakamori, I. Osaki, and T. Kasai, *ibid.*, **1982**, 450; c) T. Nakamori, Y. Kogure, and T. Kasai, *ibid.*, **1982**, 456.

4) a) J. J. Wade, *J. Org. Chem.*, **44**, 1816 (1979); b) A. Mckillop, G. C. A. Bellinger, P. N. Preston, and A. Davidson, *Tetrahedron Lett.*, **1978**, 2621; c) E. I. Grinblat and I. Y. Postvskii, *Zh. Obshch. Khim.*, **31**, 394 (1961); *J. Gen. Chem. USSR*, **31**, 357 (1961).

5) a) J. B. Hendrickson, R. Rees, and J. F. Tmpleton, *J. Am. Chem. Soc.*, **86**, 107 (1964); b) W. E. Truce, G. H. Klein, and R. B. Kruse, *ibid.*, **83**, 4636 (1961).

6) R. J. Alaimo, *J. Heterocycl. Chem.*, **10**, 769 (1973).

7) D. H. Kim, *J. Heterocycl. Chem.*, **13**, 179 (1976).

8) F. D. Popp and W. E. McEen, *Chem. Rev.*, **58**, 321 (1958).

Synthesis of (*S*)- and (*R*)-3-Hydroxy-4-butanolide and (2*S*,4*S*)-, (2*R*,4*S*)-, (2*S*,4*R*)-, and (2*R*,4*R*)-2-Hydroxy-4-hydroxymethyl-4-butanolide and Their Satiety and Hunger Modulating Activities

Osamu UCHIKAWA,† Nobuhisa OKUKADO,* Toshiie SAKATA,†† Koichi ARASE,†† and Kenji TERADA††
Department of Chemistry, Faculty of Science, Kyushu University, Hakozaki, Higashi-ku, Fukuoka 812
††Department of Internal Medicine 1, Faculty of Medicine, Kyushu University, Maidashi, Higashi-ku, Fukuoka 812
(Received October 23, 1987)

Two endogenous γ-lactones, 3-hydroxy-4-butanolide (**1**) and 2-hydroxy-4-hydroxymethyl-4-butanolide (**2**) have been identified as substances that enhance, respectively, satiety and hunger by their effects on the feeding behavior and the central neurons of rats. To determine the stereochemistry of the physiologically active isomers, all the stereoisomers of these two lactones were synthesized and their effects on the feeding behavior and humoral factors were assessed by infusion into the rat third cerebroventricle. Among four isomers, (2*S*,4*S*)-2-hydroxy-4-hydroxymethyl-4-butanolide (**2a**) was most effective in elicitating the feeding and caused potent hypoglycemia with hyperinsulinemia. (*S*)-3-Hydroxy-4-butanolide (**1a**) suppressed the food intake more potently than the antipode and caused humoral responses reciprocal to those of **2a**. From these facts, it was concluded that **1a** and **2a** are physiologically active forms for conveying intrinsic signals of satiety and hunger to neurons in the hypothalamus.

Sufficient evidence has been accumulated to show that some endogenous blood factors such as glucose, free fatty acids, insulin, glucagon, and some peptides contribute to the induction of hunger and satiety.[1] In search of humoral factors that might be related to hunger and satiety, Oomura and coworkers analyzed human and rat blood serum, identified many organic acid derivatives in a gas chromatography-mass spectrometry system and investigated the effect of starvation on their blood serum levels.[2] From the observed patterns of changes of their serum levels at various stages of hunger, they postulated that two of them, structurally simple γ-lactones, 3-hydroxy-4-butanolide (**1**) and 2-hydroxy-4-hydroxymethyl-4-butanolide (**2**), might modulate food intake.[3] To confirm this assumption, they injected the synthesized lactones into the third cerebral ventricle of rats. Interestingly, the injection of 2.5 μmol of **1** suppressed both food intake and single neuron activity in the lateral hypothalamic area (LHA). The same treatment with **2** elicited feeding and increased LHA single neuron activity. From the high correlation between the feeding behavior and changes in LHA neuron activity, Oomura concluded that 3-hydroxy-4-butanolide (**1**) acts as an endogenous satiety substance and that 2-hydroxy-4-hydroxymethyl-4-butanolide (**2**) acts as a hunger substance.[4,5] The question arose as to which stereoisomers of the two possible isomers of **1** and the four isomers of **2** were really responsible for the suppression or elicitation of food intake. The question had been left unsolved since the materials used for the infusion tests were the racemate of **1** and the mixture of two pairs of diastereomers of **2**. Though the report that (*S*)-3,4-dihydroxybutanoic acid exists in human blood and urine suggests the possibility of (*S*)-3-hydroxy-4-butanolide (**1a**) to be the active isomer,[6] no report had been published about the natural occurrence of **2**.[7] It seemed to be impractical to isolate these two lactones from rat blood serum to decide their stereochemistry because of their paucity.[8] We decided to synthesize all the stereoisomers of these two lactones, **1a**, **b** and **2a**—**d**, in order to examine the effects on feeding activities and humoral factors of each isomer by direct infusion into rats. In this paper, we wish to report on the synthesis of these lactones and give a brief summary of the results of infusion test which led to the conclusion that (*S*)-3-hydroxy-4-butanolide (**1a**) and (2*S*,4*S*)-2-hydroxy-4-hydroxymethyl-4-butanolide (**2a**) are the physiologically active isomers.

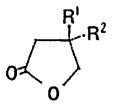

1

a: R^1=H, R^2=OH
b: R^1=OH, R^2=H

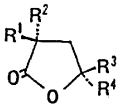

2

a: R^1=OH, R^2=H, R^3=CH_2OH, R^4=H
b: R^1=H, R^2=OH, R^3=CH_2OH, R^4=H
c: R^1=OH, R^2=H, R^3=H, R^4=CH_2OH
d: R^1=H, R^2=OH, R^3=H, R^4=CH_2OH

Results and Discussion

Both optically active forms of **1** had been prepared by several methods.[9] Though a few reports had been published concerning the preparation of optically

† Present address: Takeda Chemical Industries, Ltd. 2-17-85 Jusohonmachi, Yodogawa-ku, Osaka 532.

active isomers of **2** from some sugars, these preparation methods did not necessarily seem to be suitable for obtaining all the stereoisomers.[10] We adopted a different approach. As common starting materials for the preparation of both lactones, we selected (*S*)-[11] and (*R*)-3,4-*O*-isopropylidene-3,4-dihydroxybutanal,[9b] (**3** and **3'**) which had been derived from (*S*)- and (*R*)-malic acid, respectively. For the preparation of **1a**, the method reported by Mori et al.[9b] was modified. (*S*)-

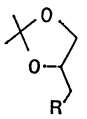

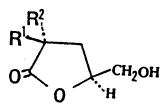

3: R=CHO
4: R=COOH
5: R=CH(OH)CH=CH_2
6: R=CH(OBz)CH=CH_2
7: R=CH(OBz)COOH

8a: R^1=OBz, R^2=H
b: R^1=H, R^2=OBz

Aldehyde (**3**) was oxidized to a carboxylic acid (**4**) in 65% yield with $RuCl_3$ and $NaIO_4$ according to the method reported by Sharpless et al.[12] This made the very water-soluble product (**4**) isolation much easier compared with Mori's method which used Jones' reagent. Deprotection and lactonization with *p*-TsOH gave **1a** with $[\alpha]_D^{20}$ −75.7° in 94% yield. The same treatment of (*R*)-aldehyde (**3'**) gave **1b** with $[\alpha]_D^{20}$ +78.2°.

The preparation of **2a** and **2b** was carried out as follows. After some unsuccessful attempts to incorporate one carbon atom into (*S*)-aldehyde (**3**) by some reactions such as cyanosilylation,[13] vinylmagnesium bromide was treated with **3** to give a mixture consisting of two diastereomeric vinyl alcohols (**5**) in 95% yield. No essential diastereoselectivity was observed. No effort to increase the selectivity was carried out in this study. After benzoylation, the mixture (**6**) was subjected to double-bond cleavage with $RuCl_3$ and $NaIO_4$ by the method of Sharpless[12] to afford a mixture of two carboxylic acids (**7**) in high yield. All attempts to separate the two diastereomeric mixtures at stages **5**, **6**, and **7** were unsuccessful. However, the treatment of **7** with *p*-TsOH also gave a mixture of two diastereomeric benzoylated lactones in quantitative yield, which could be separated by preparative thin-layer chromatography (TLC) to obtain two benzoylated lactones, **8a** with $[\alpha]_D^{20}$ +21.1° and **8b** with $[\alpha]_D^{20}$ +41.9° in a ratio of 6 : 5. The hydrolysis and lactonization of **8a** and **8b** gave the desired optically active lactones, **2a** and **2b**, respectively, which showed $[\alpha]_D^{20}$ +23.2° and $[\alpha]_D^{20}$ +50.3°.

The stereochemistry of the benzoylated lactones, **8a** and **8b**, and the lactones, **2a** and **2b**, must be either (2*S*,4*S*) or (2*R*,4*S*), since the starting aldehyde (**3**) had the (*S*)-configuration. The nuclear magnetic resonance (NMR) signal of the proton at the 4-position of the benzoylated lactone, **8b**, appeared at 0.16 ppm down-field, compared with that of **8a**, while no significant difference of chemical shifts was observed between 4-positioned protons of **2a** and **2b**. This observation means that the 4-positioned proton of **8b** is apparently in the deshielding region of the benzoyloxyl group at the 2-position, and strongly suggests that the benzoyloxyl group and the proton at the 4-position locate at the same side of the lactone ring in **8b**. This means that **8b**, and then **2b**, have the (2*R*,4*S*)-configuration and that **8a** and **2a** have the (2*S*,4*S*)-configuration. This assignment was confirmed by reducing both lactones. As expected,[14] the lithium aluminum hydride reduction of **2a** gave an optically active tetrol (**9a**) with a (2*S*,4*S*)-configuration, which showed $[\alpha]_D^{20}$ −44.8° after benzoylation.[15] However, an optically inactive meso product (**9b**) was obtained by the reduction of **2b**, which did not show any essential optical rotation after benzoylation.[16] According to the same procedure started with (*R*)-aldehyde (**3'**), we obtained two lactones, **2d**, with a (2*R*,4*R*)-configuration and $[\alpha]_D^{20}$ −22.0° and **2c**, with a (2*S*,4*R*)-configuration and $[\alpha]_D^{20}$ −45.6°.

A preliminary comparison of 2-hydroxy-4-hydroxymethyl-4-butanolide in rat and human sera with the four lactone isomers of **2** was carried out after trimethylsilylation by gas chromatography. The retention time of the lactone from a natural source coincided with that of one pair of diastereomer, **2a** and **2d**, but no signal corresponding to that of **2b** and **2c** was observed in rat or human sera. This excluded the possibility of the stereochemistry of the natural lactone to be (2*R*,4*S*) or (2*S*,4*R*).

The effects of each isomer (**1a**, **1b**, **2a**, **2b**, **2c**, and **2d**) on feeding behavior and humoral factors were assessed by infusion into the rat third cerebroventricle in a laboratory of internal medicine I, faculty of medicine, Kyushu University. Details regarding the experiments and results are published elsewhere, but a brief summary of the results is given here. Adult male Wister King A rats were implanted with a cannula aimed at the third cerebroventricle[17] and used for tests after food and water intake, body weight and ambulatory activity returned to normal following surgery. Ten μl of a 0.25

Table 1. Ingestive and Ambulatory Behavior in a One-Hour Test Period Following Infusion of Each Stereoisomer of 2-Hydroxy-4-hydroxymethyl-4-butanolide (**2**) at Doses of 2.5 μmol or Phosphate Buffered Saline (PBS)

	2a	**2b**	**2c**	**2d**	PBS
Feeding incidence (%)	75[a)]	17	0	0	0
Drinking incidence (%)	0	0	0	0	0
Ambulation	+++	+			

a) $p<0.05$, compared to PBS.

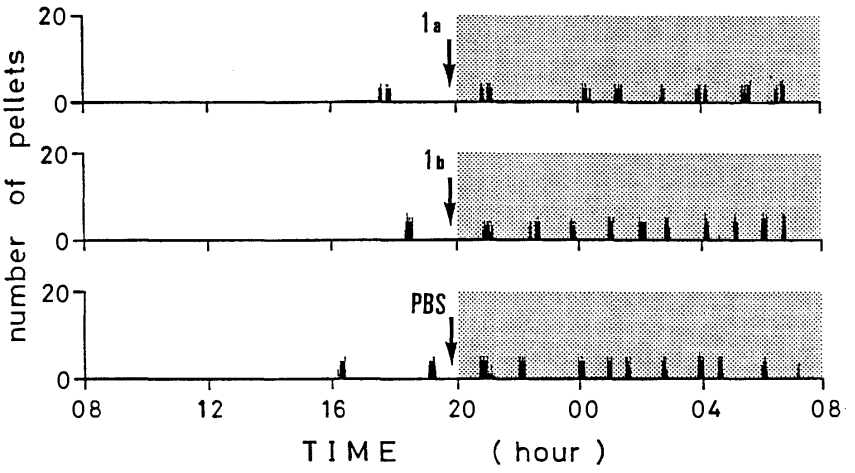

Fig. 1. Typical feeding patterns for rats after infusion of 2.5 μmol of **1a**, **1b**, and PBS solution into the third cerebro-ventricle. Shaded, dark time.

M solution (1 M=1 mol dm^{-3}) of each isomer in phosphate buffered saline (PBS. pH 7.3) was infused at a rate of 1 μl/1 min. The incidence and duration of eating and drinking, meal size, postprandial intermeal interval, and number of pellets and water-droplets ingested during meals[18,19] were recorded with a pellet-sensing eatometer and photoresistor drinkometer.[20] The ambulatory activity was measured by counting the crossings of 3×4 arrays of photobeams.[21] A statistical evaluation was carried out by either Fisher's exact probability test,[22] or by an analysis of the variance with replication. Typical feeding patterns after injection of **1a**, **1b**, and PBS are shown in Fig. 1. Compared with **1b** and PBS control groups which did not show any significant feeding suppression, the injection of **1a** potently suppressed food intake ($p<0.01$). In addition, **1a** prolonged the postprandial intermeal intervals and decreased the ambulatory bursts. The injection of **1a** raised the serum glucose level and decreased the serum insulin level over a 30-min testing period, while **1b** and PBS did not change these values.[23]

The injection of **2a** induced feeding more (75%) (Table 1), with a shorter latency to eat and a longer duration of meals than any other. Among the remaining isomers, **2b** elicited feeding (17%), but **2c**, **2d**, and PBS did not affect feeding. The intensity and frequency of ambulation were parallel to feeding. The effect to humoral factors was examined with **2a** and **2b**. In contrast to **1a**, injection of **2a** decreased the serum glucose level and raised the serum insulin level over a 30 min-testing period, but **2b** and PBS had no effect.[24]

From the facts described above, it seems quite reasonable to conclude that (*S*)-3-hydroxy-4-butanolide (**1a**) and (2*S*, 4*S*)-2-hydroxy-4-hydroxymethyl-4-butanolide (**2a**) are compounds that exist in human and rat sera and physiolosically active forms for conveying intrinsic signals to the LHA in feeding modulation.

Experimental

The ^{1}H NMR and ^{13}C NMR spectra were recorded at 90 and 25 MHz with a JEOL JNM-FX90Q spectrometer using Me_4Si as an internal standard. The IR spectra were taken with a Hitachi R-215 spectrometer. The MS spectra were taken with a JEOL-OISG-2 spectrometer. Optical rotations were measured on a Yanagimoto OR-50 polarimeter. Kieselgel F-254 (Merck) was used for column chromatography and glass plates precoated with silica gel 60F-254 (0.25 mm, Merck) were used for TLC and preparative TLC.

(*S*)-3-Hydroxy-4-butanolide (1a). A solution of $RuCl_3(H_2O)_n$ (4.8 mg) in water (0.5 ml) was added to a mixture of (*S*)-3,4-*O*-isopropylidene-3,4-dihydroxybutanal[11] (**3**, 150 mg, 1.04 mmol), $NaIO_4$ (912 mg, 4.27 mmol), CCl_4 (2 ml), CH_3CN (2 ml), and water (3 ml). The brown color of the solution changed to deep green immediately. The solution was stirred for 2 h at room temperature and the product was extracted with CH_2Cl_2. After drying and evaporation of the solvent, the residue was chromatographed on a short column of silica gel (AcOEt) to give a crude acid (**4**) as an oil (108 mg, 65%). This was used for the next step without further purification. *p*-TsOH (8.3 mg) was added to a solution of **4** (69.5 mg, 0.434 mmol) in CH_2Cl_2 (5 ml) and the solution was stirred at room temperature overnight. Triethylamine (7 μl) was added to the solution and the solvent was evaporated in vacuo. The residue was subjected to silica-gel chromatography (AcOEt) to give **1a** (42 mg, 94.8%). Colorless oil, $[\alpha]_D^{20}$ −75.7° (*c* 0.806, MeOH). (lit,[9d] $[\alpha]_D^9$ −85.9° (*c* 2.2, EtOH)). IR (neat) 3350, 1760, 1180, 1085, 1050, 992, and 965 cm^{-1}. ^{1}H NMR (CD_3OD) δ=2.45 and 2.68 (2H, H-2, and H-2′, dd and dd, $J_{2,2'}$=18 Hz, $J_{2,3}$=2.5 Hz, $J_{2',3}$=5.5 Hz), 4.2—4.8 (3H, H-3, H-4, and H-4′, m). ^{13}C NMR ($CDCl_3$) δ=37.45, 66.96, 76.14, and 177.03. Found: *m/z* 102.0311. Calcd for $C_4H_6O_3$: M, 102.0317. Found: C, 46.83; H, 6.01%. Calcd for $C_4H_6O_3$: C, 47.06; H, 5.92%.

(*R*)-3-Hydroxy-4-butanolide (1b) was prepared according to the same procedure starting with (*R*)-3,4-*O*-isopropylidene-3,4-dihydroxybutanal (**3′**).[9b] Colorless oil, $[\alpha]_D^{20}$ +78.2° (*c* 0.972, MeOH). (lit,[9b] $[\alpha]_D^{23}$ +77.3° (*c* 2.0, EtOH). Found: *m/z* 102.0317. Calcd for $C_4H_6O_3$: M, 102.0317. Found: C, 46.62;

H, 6.06%. Calcd for $C_4H_6O_3$: C, 47.06; H, 5.92%. The other spectroscopic properties are same as those of **1a**.

A Mixture of (3*S*,5*S*)- and (3*R*,5*S*)-5,6-*O*-Isopropylidene-1-hexene-3,5,6-triol (5). A solution of vinylmagnesium bromide which was prepared from vinyl bromide (1.11 ml, 15.8 mmol) and Mg (486 mg, 20 mmol) in THF (5 ml) was added dropwise to a cold solution (ice bath) of **3** (760 mg, 5.27 mmol) in THF (5 ml). The solution was stirred for 2 h at room temperature and quenched with an aqueous NH_4Cl solution. After extraction with ether and drying with $MgSO_4$, the evaporation of the solvent gave crude products. Purification by silica-gel chromatography (hexane : AcOEt =5 : 2) gave a mixture of (3*S*,5*S*)- and (3*R*,5*R*)-products (**5**, 865 mg, 95.3%). Colorless oil.[25] Found: C, 62.43; H, 9.11%. Calcd for $C_9H_{16}O_3$: C, 62.77; H, 9.36%.

A Mixture of (3*S*,5*S*)- and (3*R*,5*S*)-3-Benzoyloxy-5,6-*O*-isopropylidene-1-hexene-5,6-diol (6). Benzoyl chloride (507 μl, 4.35 mmol) was added to a solution of **5** (500 mg, 2.9 mmol) in pyridine (2.5 ml) at room temperature. After stirring overnight, the mixture was treated with an aqueous $NaHCO_3$ solution and the products were extracted with ether. After washing with an aqueous $NaHCO_3$ solution and water, the evaporation of the solvent gave a mixture of the benzoates (**6**) in a quantitative yield. The purification by silica-gel chromatography (CH_2Cl_2 : hexane=3 : 1) gave **6** as a colorless oil (788 mg, 98.2%).[25] Found: C, 69.72; H, 7.29%. Calcd for $C_{16}H_{20}O_4$: C, 69.55; H, 7.29%.

A Mixture of (2*S*,4*S*)- and (2*R*,4*S*)-2-Benzoyloxy-4-hydroxymethyl-4-butanolide (8a and 8b). A solution of $RuCl_3(H_2O)_n$ (3.1 mg) in water (1 ml) was added to a mixture of **6** (186 mg, 0.673 mmol), $NaIO_4$ (590 mg, 2.76 mmol), CCl_4 (2 ml), CH_3CN (2 ml), and water (2 ml). The solution was vigorously stirred at room temperature. The color of the solution changed to deep green immediately and to yellowish green after 2 h; the products were extracted with CH_2Cl_2. After drying with $MgSO_4$ and filtration through a short column of celite, evaporation of the solvent gave a mixture of acids (**7**, 187 mg, 95.4%). This was employed for the next step without further purification. *p*-TsOH (9.2 mg, 0.048 mmol) was added to a solution of **7** (141.8 mg, 0.482 mmol) in CH_2Cl_2 (3 ml) and stirred at room temperature overnight. After adding triethylamine (8 μl, 0.058 mmol), the solution was concentrated in vacuo and the residue was chromatographed on a short column of silica-gel (AcOEt) to give a mixture of lactones (120 mg, 75.5%). For the separation of **8a** and **8b**, the lactone mixture (400 mg) was subjected to preparative thin-layer chromatography (hexane : AcOEt=3 : 2). Since the difference of R_f-values was small (R_f-values, 0.1 and 0.15), development was repeated four times. From the lower zone, **8a** was obtained as colorless solids (120 mg). Mp 50—51 °C. $[\alpha]_D^{20}$ +21.1° (*c* 0.9, MeOH). IR (neat) 3490, 2950, 1790, 1721, 1278, 1200, 1130, and 718 cm^{-1}. ^1H NMR ($CDCl_3$) δ=2.38 and 2.68 (2H, H-3, and H-3′, dt and ddd, $J_{3,3'}$=14.0 Hz, $J_{2,3}$=$J_{3,4}$=11.2 Hz, $J_{2,3'}$=9.8 Hz, $J_{3',4}$=6.8 Hz), 2.95 (1H, s, -OH), 3.72 and 3.96 (2H, H-5, and H-5′, ddd, $J_{5,5'}$=12.5 Hz, $J_{4,5}$=2.6 Hz, $J_{4,5'}$=4.8 Hz), 4.65 (1H, H-4, m), 5.78 (1H, H-2, dd, $J_{2,3}$=9.0 Hz, $J_{2,3'}$=10.5 Hz), 7.30—8.60 (5H, aromatic, m). Found: *m/z* 236.0819. Calcd for $C_{12}H_{12}O_5$: M, 236.0684. Found: C, 60.58; H, 5.22%. Calcd for $C_{12}H_{12}O_5$: C, 61.01; H, 5.12%. **8b** was obtained from the upper zone as colorless solids (100 mg). Mp 84—86 °C. $[\alpha]_D^{20}$ +41.9° (*c* 1.0, MeOH). IR (neat) 3450, 1785, 1765, 1610, 1460, 1390, 1365, 1292, 1235, 1000, 725, and 720 cm^{-1}. ^1H NMR ($CDCl_3$) δ=2.48 and 2.78 (2H, H-3, and H-3′, dt and ddd, $J_{3,3'}$=14.0 Hz, $J_{2,3}$=$J_{3,4}$=8.9 Hz, $J_{2,3'}$=10.0 Hz, $J_{3',4}$=9.8 Hz), 2.90 (1H, s, -OH), 3.70 and 3.98 (2H, H-5 and H-5′, ddd, $J_{5,5'}$=12.5 Hz, $J_{4,5}$=2.9 Hz, $J_{4,5'}$=2.4 Hz), 4.81 (1H, H-4, m). Found: *m/z* 236.0717. Calcd for $C_{12}H_{12}O_5$: M, 236.0684. Found: C, 60.64; H, 5.21%. Calcd for $C_{12}H_{12}O_5$: C, 61.01; H, 5.12%.

(2*S*,4*R*)- and (2*R*,4*R*)-Isomers (8c and 8d) were prepared starting with (*R*)-aldehyde (**3′**) according to the same method described above. **8c**, Colorless solides. Mp 82—85 °C. $[\alpha]_D^{20}$ −42.1° (*c* 1.12, MeOH). Found: *m/z* 236.0647. Calcd for $C_{12}H_{12}O_5$: M, 236.0684. Found: C, 60.88; H, 5.22%. Calcd for $C_{12}H_{12}O_5$: C, 61.01, H, 5.12%. **8d**, colorless solids. Mp 49—50 °C. $[\alpha]_D^{20}$ −20.3° (*c* 0.87, MeOH). Found: *m/z* 236.0685. Calcd for $C_{12}H_{12}O_5$: M, 236.0685. Found: C, 60.91; H, 5.03%. Calcd for $C_{12}H_{12}O_5$: C, 61.01; H, 5.12%. The other spectroscopic properties of these lactones are same as those of **8b** and **8a**, respectively.

(2*S*,4*S*)-2-Hydroxy-4-hydroxymethyl-4-butanolide (2a). A mixture of **8a** (98.9 mg, 0.49 mmol), an aqueous NaOH solution (10%, 0.5 ml), and MeOH (0.5 ml) was stirred overnight at room temperature. The mixture was acidified with a diluted HCl solution and the solvents were evaporated in vacuo as much as possible. The product was extracted with AcOEt. After evaporation of the solvent, the residue was subjected to silica-gel chromatography (AcOEt) to give **2a** (40 mg, 72.2%) as a colorless oil. $[\alpha]_D^{20}$ +23.2° (*c* 3.61, MeOH). IR (neat) 3450, 2930, 1760, 1325, 1200, 1130, 995, 960, 900, and 803 cm^{-1}. ^1H NMR (CD_3OD) δ=1.93 and 2.53 (2H, H-3, and H-3′, dt and ddd, $J_{3,3'}$=12.3 Hz, $J_{2,3}$=$J_{3,4}$=10.6 Hz, $J_{2,3'}$=8.5 Hz, $J_{3',4}$=5.7 Hz), 3.59 and 3.81 (2H, H-5, and H-5′, ddd, $J_{5,5'}$=12.7 Hz, $J_{4,5}$=3.1 Hz, $J_{4,5'}$=4.8 Hz), 4.34—4.67 (2H, H-2, and H-4, m.). ^{13}C NMR (CD_3OD) δ=33.48, 63.76, 69.04, 78.48, and 178.59. Found: C, 44.92; H, 6.03%. Calcd for $C_5H_8O_4$: C, 45.46; H, 6.10%.[25]

(2*R*,4*S*)-, (2*S*,4*R*)-, and (2*R*,4*R*)-Isomers (2b, 2c, and 2d) were prepared by the same procedure described above from **8b**, **8c**, and **8d**, respectively. **2b**, colorless oil. $[\alpha]_D^{20}$ +50.3° (*c* 1.75, MeOH). IR (neat) 3400, 2950, 1775, 1640, 1460, 1357, 1205, 1115, 980, and 803 cm^{-1}. ^1H NMR (CD_3OD) δ=2.12 and 2.48 (2H, H-3, and H-3′, dt and ddd, $J_{3,3'}$=13.1 Hz, $J_{2,3}$=$J_{3,4}$=8.3 Hz, $J_{2,3'}$=8.5 Hz, $J_{3',4}$=3.2 Hz), 3.58 and 3.76 (2H, H-5, and H-5′, ddd, $J_{5,5'}$=13.1 Hz, $J_{4,5}$=2.6 Hz, $J_{4,5'}$=3.4 Hz), 4.47—4.73 (2H, H-2, and H-4, m). ^{13}C NMR (CD_3OD) δ=33.93, 64.35, 68.19, 79.59, and 179.17. Found: C, 45.56; H, 6.19%. Calcd for $C_5H_8O_4$: C, 45.46; H, 6.10%.[25] **2c**, colorless oil. $[\alpha]_D^{20}$ −45.6° (*c* 1.60, MeOH). Found: C, 44.99; H, 6.21%. Calcd for $C_5H_8O_4$: C, 45.46; H, 6.10%.[25] **2d**, colorless oil. $[\alpha]_D^{20}$ −22.2° (*c* 1.26, MeOH). Found: C, 44.96; H, 6.33%. Calcd for $C_5H_8O_4$: C, 45.46; H, 6.10%.[25] The other spectroscopic properties of **2c** and **2d** are the same as those of **2b** and **2a**, respectively.

(2*S*,4*S*)-1,2,4,5-Tetrakis(benzoyloxy)pentane (10a). A solution of **2a** (20 mg, 0.15 mmol) in THF (2 ml) was added to a solution of LAH (30 mg, 0.79 mmol) in THF (2 ml) and the mixture was stirred for 2 h at room temperature. The mixture was decomposed by the addition of a few drops of water and filtered and the residue was extracted thoroughly with a 2 : 1 mixture of THF and water. The concentration of the combined filtrate and extracts gave the residue which was dissolved in pyridine (1 ml) and treated with benzoyl chloride (120 mg, 0.85 mmol) overnight at room temperature. The mixture was treated with water, extracted with ether, and washed with diluted HCl and Na_2CO_3 solutions. After

drying over Na_2SO_4, removing the solvent gave a residue which was purified by silica-gel chromatography to give **10a** as a gum (59 mg, 76%). (lit,[26] a gum.) $[\alpha]_D^{20}$ −44.8° (*c* 1.12, AcOEt). ^{1}H NMR ($CDCl_3$) δ=2.39 (2H, H-3, and H-3′, dd, $J_{2,3}=J_{3,4}$=6.1 Hz, $J_{2,3'}=J_{3',4}$=7.0 Hz), 4.60 (4H, OCH_2×2, m), 5.70 (2H, H-2, and H-4, m), 7.20—8.10 (20H, aromatic).

***(meso)*-1,2,4,5-Tetrakis(benzoyloxy)pentane (10b)** was prepared according to the same procedure. Colorless solids. Mp 98—101 °C. (lit,[16] mp 104—105 °C). $[\alpha]_D^{20}$ ±0°. ^{1}H NMR ($CDCl_3$) δ=2.41 (2H, H-3, and H-3′, m), 4.60 (4H, OCH_2×2, m), 5.70 (2H, H-2, and H-4, m), 7.20—8.10 (20H, aromatic).

The authors wish to express their sincere thanks to Professor Yutaka Oomura, Faculty of Medicine, Kyushu University, for giving them the opportunity to carry out this study. We are indebted to Center of Advanced Instrumental Analysis Kyushu University for the measurement of mass spectroscopy.

References

1) Y. Oomura and H. Nishimura, *Kagaku*, **42**, 440 (1987); Y. Oomura and N. Shimizu, *Kagaku to Seibutsu*, **22**, 228 (1984); Y. Oomura and K. Hattori, *Gendai-Kagaku*, 140, (1982); W. J. Freed, M. J. Perlow, and R. J. Wyatt, *Science*, **206**, 850 (1979); J. R. Martin and D. Novin, *Physiol. Behab.*, **19**, 850 (1977); Y. Oomura, "Hunger" ed by D. Novin, W. Wyrwicka, and G. A. Bray, Raven, New York (1976), p. 145; S. C. Woods, E. C. Lotter, L. D. Mckay, and D. Porte, Jr., *Nature (London)*, **282**, 503 (1979); J. Knoll, *Physiol. Behav.*, **25**, 519 (1982).

2) T. Kuhara, I. Matsumoto, Y. Oomura, T. Sakata, M. Fukushima, and K. Hashimoto, "Recent Developments in Mass Spectrometry in Biochemistry and Medicine," ed by A. Frigerio and M. McCamish, Elsevier, Amsterdam (1980), p. 121.

3) T. Sakata, Y. Oomura, M. Fukushima, K. Tsutsui, and K. Hashimoto, *Brain Res. Bull.*, (*Suppl.* 4), **5**, 23 (1980).

4) N. Shimizu, Y. Oomura, and T. Sakata, *Am. J. Physiol.*, **246**, 542 (1984).

5) In the early stage of the studies, the active substances were thought to be free acids and named as 2-deoxytetronic acid (erroneously) and 3-deoxypentonic acid. However, it was clarified that these acids were converted to lactones in vivo following administration into the blood or the cerebrospinal fluid: T. Sakata, K. Fujimoto, K. Terada, and K. Arase. *Physiol. Behav.*, **34**, 969 (1985).

6) V. Fall, C. R. Lee, and R. J. Pollit, *Biochem. Med.*, **13**, 40 (1975).

7) 3-Deoxyxylonic acid γ-lactone was reported to exist in Tobacco smoke. However, it is not certain whether this is a natural product or an artifact: S. Ishiguro and S. Sugawara, *Agric. Biol. Chem.*, **42**, 407 (1978).

8) The concentration of **1** and **2** in blood is estimated to be in the range of 110—170 μM and 220—370 μM, respectively. The values vary depending on the starvation time: 1a.

9) From (±)-3,4-dihydroxybutanoic acid by resolution: a) J. W. Glattfeld and G. E. Miller, *J. Am. Chem. Soc.*, **42**, 2310 (1920). From (*S*)- or (*R*)-malic acid: b) K. Mori, T. Takigawa, and T. Matsuo, *Tetrahedron*, **35**, 933 (1979). c) H. M. Shieh and G. D. Prestwich, *Tetrahedron Lett.*, **23**, 4643 (1982). d) S. Saito, T. Hasegawa, M. Inaba, R. Nishida, T. Fujii, S. Nomizu, and Moriwake, *Chem. Lett.*, 1389 (1984).

10) a) Four optically active isomers were prepared by the alkali treatment of sugars such as D-xylose or D-arabinose and the repeated recrystallization of their crystalline derivatives: I. U. Nef, *Ann.*, **376**, 1 (1910). b) (2*R*,4*S*)-Isomer by degradation of 3-*O*-methyl-D-xylose with lime water: W. M. Corbett, G. N. Richard, and R. L. Whistler, *J. Chem. Soc.*, **1957**, 11. c) (2*S*,4*S*)-Isomer from acetylated aldonolactones such as triacetyl-D-arabono-1,4-lactone, D-ribono-1,4-lactone, D-xylono-1,4-lactone, and D-lyxono-1,4-lactone by hydrogenolysis: K. Bock, I. Lundt, and C. Pedersen, *Acta Chem. Scand. B*, **35**, 155 (1981).

11) a) H. Hayashi, K. Nakanishi, C. Brandon, and J. Marmur, *J. Am. Chem. Soc.*, **95**, 8749 (1973); b) E. J. Corey, H. Niwa, and J. Knoll, *J. Am. Chem. Soc.*, **100**, 1942 (1978).

12) P. H. Carlson, T. Katsuki, V. S. Martin, and K. B. Sharpless, *J. Org. Chem.*, **46**, 3936 (1981).

13) D. A. Evans, L. K. Truesdale, and G. L. Caroll, *J. Chem. Soc., Chem. Commun.*, **1973**, 55.

14) It is well-known that carbonyl compounds containing an asymmetric group in the α-position are reduced by LAH without racemization of the compounds: S. S. Pizey, "Synthetic Reagents," Vol. 1, Halsted Press, New York (1974), p. 151.

15) The specific rotation of (2*S*,4*S*)-1,2,4,5-tetrakis(benzoyloxy)pentane is not known, but those of (2*S*,4*S*)-1,2,4,5-pentanetetrol and its tetraacetate are known to be +25° (*c* 12.7, EtOH) and +12° (*c* 3.45, $CHCl_3$), respectively; R. G. S. Ritchie, D. M. Vyas, and W. A. Szarek, *Can. J. Chem.*, **56**, 794 (1978).

16) P. W. Kent, M. Stacey, and L. F. Wiggins, *J. Chem. Soc.*, **1949**, 1232.

17) K. Arase, T. Sakata, Y. Oomura, M. Fukushima, K. Fujimoto, and K. Terada, *Physiol. Behav.*, **33**, 1596 (1984).

18) Meal parameters were defined as follows. Meal: Consumption of at least 10 pellets separated from any other eating by at least 20 min. Meal size: the number of pellets eaten during a meal. Postprandial intermeal interval: the time from the last pellet in one meal to the first pellet in the next: T. Sakata, K. Fujimoto, K. Terada, K. Arase, and M. Fukushima, *Arch. Intern. Pharmacodyn. Ther.*, **270**, 11 (1984).

19) Rats were allowed free access to standard pelleted rat chow (pellet weight, 48.5±0.2 mg) and tap water (droplet volume, 63.4±0.8 μl).

20) T. Sakata, M. Fukushima, K. Tsutsui, K. Arase, and K. Fujimoto, *Physiol. Behav.*, **28**, 641 (1982).

21) T. Sakata, K. Fujimoto, M. Fukushima, K. Terada, and K. Arase, *Physiol. Behav.*, **34**, 969 (1985).

22) S. Siegel, "Nonparametric Statistics for the Behavioral Sciences," McGraw-Hill, New York (1956).

23) **1a** raised the glucose level (maximum 9%) compared to **1b** ($p<0.05$) and PBS levels ($p<0.01$). Serum insulin in **1a** group was lower (maximum 30%) than that of **1b** group ($p<0.01$) or PBS control ($p<0.05$) over the 30-min testing period.

24) Maximal decrease of 8% of glucose level ($p<0.05$) and increase of 37% of the insulin level ($p<0.05$) were observed in the **2a** group over the 30-min testing period.

25) The molecular ion peak was not observed.

26) Y. Tsuda, T. Nunokawa, K. Nitta, and Y. Yamamoto, *Chem. Pharm. Bull.*,**28**, 920 (1980).

 © 1988 The Chemical Society of Japan Bull. Chem. Soc. Jpn., 61, 2031—2037 (1988)

NMR Spectroscopic Study of the Conformational Preference of Methoxycarbonyl and Methyl Substituted Thiophenecarbaldehydes. Possibility of a Hydrogen-Bond-Like Interaction between Formyl C-H and the Ester Carbonyl Group

Hajime SATONAKA,* Kazuhisa ABE,† and Minoru HIROTA*,†

Industrial Research Institute of Kanagawa Prefecture, 3173, Showa-machi, Kanazawa-ku, Yokohama 236

†Department of Synthetic Chemistry, Faculty of Engineering, Yokohama National University, Hodogaya-ku, Yokohama 240

(Received October 23, 1987)

The predominance of planar C-H/O=C approached conformations in methyl 3-formyl-2-, 2-formyl-3-, and 4-formyl-3-thiophenecarboxylates was shown experimentally by the chemical shifts of the formyl protons, the unusually large $^1J_{CH}$ values of the formyl groups, and their infrared C-H and C=O absorptions. The stability of the C-H/O=C approached conformation was attributed to the hydrogen-bond-like interaction between the two groups. The considerably large positive bond population between non-bonded H/O and the additional charge separation indicated by the MNDO calculations supported the presence of the intramolecular hydrogen bond.

In the course of our investigations of thiophene derivatives, we have synthesized a variety of thiophenecarbaldehydes and studied their NMR spectroscopic behaviors. The ^1H and ^{13}C chemical shifts, as well as the coupling constants ($^1J_{CH}$ and $^3J_{HH}$), of several series of substituted 2- and 3-thiophenecarboxylic[1,2] and β-(2- and 3-thienyl)acrylic esters[3,4] were measured and correlated with each other and with the substituent electronic parameters. Some formyl esters were included in these series of thiophene derivatives. As they are capable of taking a C-H/O=C approached conformation in which an intramolecular C-H/O hydrogen bond may be persistent, the possibility of such intramolecular interaction was further examined.

The existence of intramolecular CH/O hydrogen bonds has been suggested by several investigations. Pinchas insisted on the existence of intramolecular C-H/O hydrogen bonds in *o*-nitrobenzaldehyde and related compounds on the basis of their unusually high formyl C-H frequencies.[5] On the other hand, hydrogen bonds involving C-H groups have been studied theoretically[6] and the important role of the electrostatic factor has been pointed out.[7] The formyl group is expected to be a strong C-H donor because the hydrogen is linked to a very electronegative carbonyl carbon atom; therefore, the C-H bond is expected to have some ionic character. Thus, the possibility of an intramolecular hydrogen bonding of this sort in these and related formyl esters will be discussed in this paper on the basis of NMR and infrared spectroscopic evidence and also on the basis of the theoretical consequences from molecular orbital calculations.

Experimental

Spectral Measurements. The thiophenecarbaldehydes were prepared according to the methods reported previously.[1,2,8-12]

The NMR spectra were recorded on a JEOL FX-90Q spectrometer. The samples were dissolved in chloroform-*d*, the concentrations of the solutions being adjusted to approximately 0.6 mol dm^{-3}. The chemical shifts were measured from the internal TMS reference at the probe temperature. The ^{13}C spectra were collected by using a 30° pulse, 16k data points, and a 4.5 or 5.0 kHz sweep width. The ^{13}C-^1H coupling constants were obtained by measurements using a pulse sequence which allowed us to observe the non-decoupled spectra while maintaining a full NOE. (Pulse conditions: 45° pulse, 3 repetition rates, 16k data points, and 450 Hz sweep width.)

The infrared spectra were recorded on a Perkin-Elmer 257 spectophotometer in CCl_4.

MNDO Calculation.[13,14] The calculations were carried out by the use of the MOPAC program package[15] on a HITAC M-280H computer at the Computer Center of the University of Tokyo. A routine calculation gave the electronic energy, the density matrix (electron densities and bond orders), the eigen values and eigenvectors of MO's, and the other necessary quantities. The geometrical parameters of the stable conformations for MNDO calculations were cited from the Cambridge XDC Data Base whenever available. The s characters of the C-H bonds were computed from appropriate MO coefficients.

Results and Discussion

The ^{13}C NMR chemical shifts of substituted thiophenecarbaldehydes (**1a—4a**) were assigned on the basis of (i) the difference in the line intensities of the protonated and quarternary carbons, (ii) the substituent effect on the chemical shifts,[16,17] and (iii) the characteristics of the ^{13}C-^1H coupling constants, as reported previously.[18] The results are given in Tables 1—3.

A glance of the tables will show that the formyl $^1J_{CH}$ values of methyl *o*-formylthiophenecarboxylates are considerably larger than those of the other thiophenecarbaldehydes which have no neighboring methoxycarbonyl groups. Thus, the ^1J values of methyl 2-formyl-3-, 3-formyl-2-, and 4-formyl-3-thiophenecarboxylates (**1a**, **3a**, and **3b**) are 191.5, 188.9, and 187.5 Hz, respectively, larger than those of methyl 5-formyl-3-, 5-formyl-2-, and 4-formyl-2-thiophenecarboxylates (**1b**,

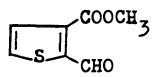

1a

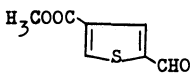

1b

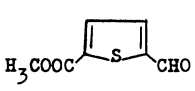

1c

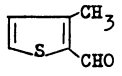

2a

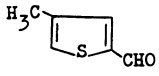

2b

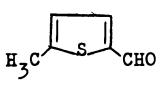

2c

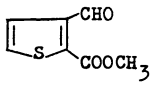

3a

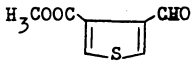

3b

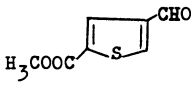

3c

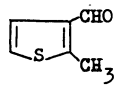

4a

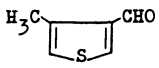

4b

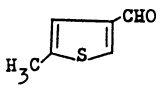

4c

1c, and **3c**) by ca. 10 Hz. We compared the ring $^1J_{CH}$'s in order to examine the effects of substituents. All the other one-bond spin-coupling constants, $^1J_{C(2)\text{-}H(2)}$, $^1J_{C(3)\text{-}H(3)}$, $^1J_{C(4)\text{-}H(4)}$, and $^1J_{C(5)\text{-}H(5)}$, are affected by the position and the nature of ring substituents to a considerably less extent than in the cases of the formyl $^1J_{CH}$'s of the *o*-formylesters **1a**, **3a**, and **3b**. The very remarkable fact about the $^1J_{CH}$ values of other aldehydes is that the $^1J_{CH}$'s of vicinally methyl-substituted thiophenecarbaldehydes **2a**, **4a**, and **4b** have almost the same values as those of other methyl-substituted thiophenecarbaldehydes void of a vicinal methyl group in spite of the fact that the formyl C-H group is located in the proximity of the methyl group on the neighboring carbon atom and is susceptible to the effect of steric compression. After all, the $^1J_{CH}$ values larger than normal were observed only with formylthiophenecarboxylates carrying formyl and alkoxycarbonyl groups on adjacent carbon atoms. This fact apparently contradicts the hypothesis that the larger $^1J_{CH}$ value is

Table 1. ^{13}C-H Coupling Constants of Substituted 2-Thiophenecarbaldehydes

Compound	$^1J_{CH}$/Hz				$^2J_{CH}$/Hz				$^3J_{CH}$/Hz				$^4J_{CH}$/Hz		
	$J_{CHO\text{-}CHO}$	$J_{C_3H_3}$	$J_{C_4H_4}$	$J_{C_5H_5}$	$J_{C_3H_4}$	$J_{C_4H_3}$	$J_{C_4H_5}$	$J_{C_5H_4}$	$J_{CHO\text{-}H_3}$	$J_{C_3\text{-}CHO}$	$J_{C_3H_5}$	$J_{C_5H_3}$	$J_{CHO\text{-}H_4}$	$J_{CHO\text{-}H_5}$	$J_{C_4\text{-}CHO}$
1a	191.5	—	174.4	188.0	—	—	4.2	6.6	—	—	—	—	1.0	1.0	0.5
1b	180.7	172.6	—	189.0	—	—	—	—	4.1	—	7.6	9.1	—	1.1	—
1c	181.2	170.7	173.8	—	4.6	4.6	—	—	3.2	—	—	—	0.8	—	—
2a	175.8	—	168.6	185.7	—	—	3.8	6.9	—	—	—	—	1.0	1.0	—
2b	177.2	165.8	—	182.9	—	—	—	—	3.7	0.6	8.6	9.9	—	1.3	—
2c	176.8	167.7	168.4	—	5.2	4.3	—	—	3.8	0.9	—	—	0.6	—	—

Table 2. ^{13}C-H Coupling Constants of Substituted 3-Thiophenecarbaldehydes

Compound	$^1J_{CH}$/Hz				$^2J_{CH}$/Hz		$^3J_{CH}$/Hz							
	$J_{CHO\text{-}CHO}$	$J_{C_2H_2}$	$J_{C_4H_4}$	$J_{C_5H_5}$	$J_{C_4H_5}$	$J_{C_5H_4}$	$J_{C_2\text{-}CHO}$	$J_{C_2H_4}$	$J_{C_2H_5}$	$J_{CHO\text{-}H_2}$	$J_{CHO\text{-}H_4}$	$J_{C_4H_2}$	$J_{C_5H_2}$	$J_{C_4\text{-}CHO}$
3a	188.8	—	173.9	187.8	4.0	6.8	—	—	—	—	1.5	—	—	3.7
3b	187.5	190.7	—	190.2	—	—	1.7	—	5.5	2.0	—	—	5.6	—
3c	177.5	186.5	174.1	—	—	—	1.5	9.5	—	1.7	3.3	7.9	—	3.0
4a	172.9	—	170.1	188.2	4.0	6.5	—	—	—	—	1.9	—	—	3.0
4b	173.8	184.9	—	184.5	—	—	1.5	—	5.6	3.8	—	—	5.5	—
4c	174.4	186.0	168.7	—	—	—	1.1	9.0	—	1.5	3.8	7.4	—	3.5

Table 3. ^{13}C NMR Chemical Shifts of Substituted Thiophenecarbaldehydes

Compound	δ_{CHO}	δ_{C_2}	δ_{C_3}	δ_{C_4}	δ_{C_5}	Others
1a	184.4	147.6	136.5	130.0	132.7	162.4($COOCH_3$) 52.4($COOCH_3$)
1b	182.5	144.5	136.1	134.7	140.2	162.1($COOCH_3$) 52.1($COOCH_3$)
1c	183.2	148.0	135.0	133.4	141.0	161.9($COOCH_3$) 52.7($COOCH_3$)
2a	182.1	137.6	147.3	131.8	134.2	14.0(CH_3)
2b	182.8	139.2	138.0	143.7	131.0	15.4(CH_3)
2c	182.5	142.0	137.3	127.2	151.6	16.1(CH_3)
3a	186.3	138.5	144.6	127.7	130.6	161.5($COOCH_3$) 52.7($COOCH_3$)
3b	186.5	133.2	140.7	132.2	135.2	162.6($COOCH_3$) 52.1($COOCH_3$)
3c	184.3	140.4	142.9	131.2	135.8	161.7($COOCH_3$) 52.5($COOCH_3$)
4a	184.5	151.6	137.1	127.4	122.6	13.5(CH_3)
4b	185.7	139.1	140.6	137.7	123.5	15.1(CH_3)
4c	184.8	135.5	143.2	122.8	142.0	15.1(CH_3)

Table 4. The Stable Conformers of Substituted Thiophenecarbaldehydes and Their Abundances (%)

Conformer	Abundance %	Conformer	Abundance %	Conformer	Abundance %	Conformer	Abundance %
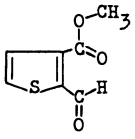	96	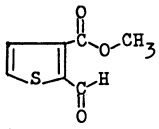	4				
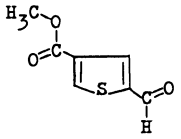	45	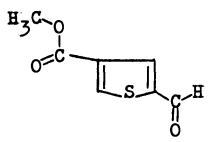	21	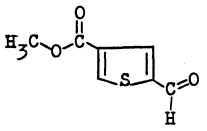	19	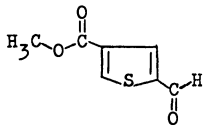	15
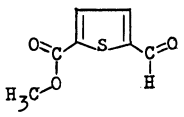	65	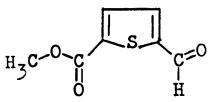	27	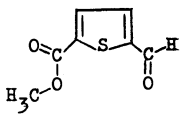	8		
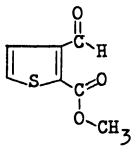	95	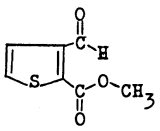	5				
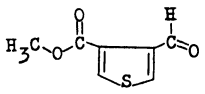	91	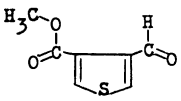	9				
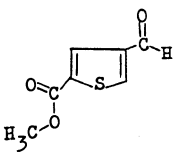	52	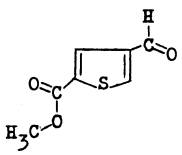	20	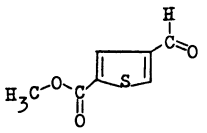	18	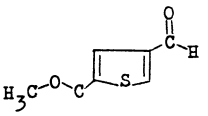	10
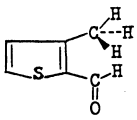	76	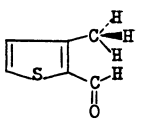	19	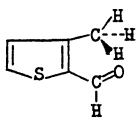	5		
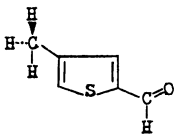	39	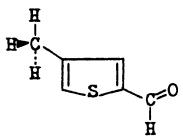	36	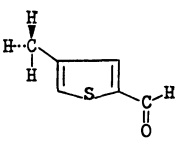	13	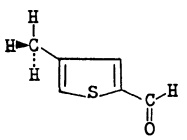	12
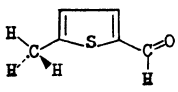	38	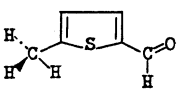	36	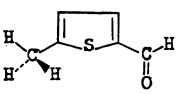	13	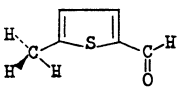	13
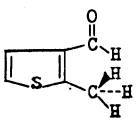	77	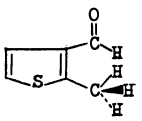	21	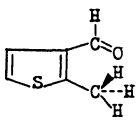	2		
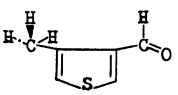	80	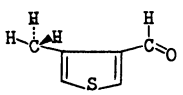	18	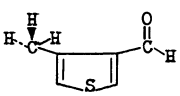	2		
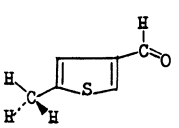	33	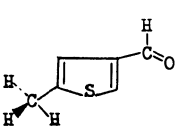	30	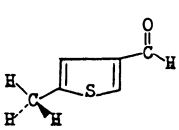	19	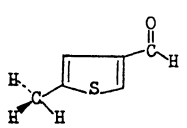	18

ascribable to the steric compression, though it may be relieved partly in the methylaldehydes (**2a**, **4a**, and **4b**) by taking the D conformer, in which the formyl hydrogen is located just in-between the two syn-clinal methyl hydrogens, in order to avoid the very large effect of steric hindrance; the reason for this anomaly might be found in the preferred C-H/O approached conformation of these aldehydes. Thus, an alternative interpretation which ascribes the larger $^1J_{CH}$ value to a specific interaction became necessary in order to account for the phenomenon. By analogy with the cases of other hydrogen atoms attached to electronegative carbon atoms such as those in chloroform and in hydrogen cyanide, a hydrogen-bond-like interaction is suspected to be operating in these circumstances where the C-H group is opposed to the carbonyl oxygen and is capable of forming a planar six-membered chelate ring by the interaction.

Thus, MNDO calculations were carried out on these aldehydes in order to gain some insight into the nature of the interaction involved and the bonds concerned and in order to reproduce the stability of the C-H/O=C approached conformations. The stable conformations and their populations, as estimated by means of MNDO calculations are given in Table 4 for a series of methoxycarbonyl- and methyl-substituted thiophenecarbaldehydes. The populations of the C-H/O approached conformers (A—C) were calcu' lated to be 96, 95, and 91% for **1a**, **3a**, and **3b**, respectively; they were expected to be privileged with the aldehydes carrying a vicinal methoxycarbonyl group.

In contrast, the calculated energies of all the possible planar conformers of the other methyl formylthiophenecarboxylates which have no formyl group in the neighborhood of the ester group were nearly equal at the ambient temperature (i.e., the variation was less than, or comparable to, the kinetic energy for thermal motion, kT, at that temperature). Thus, the aldehydes can be expected to exist as a mixture of several

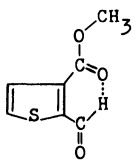

A

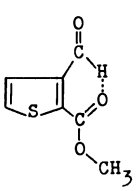

B

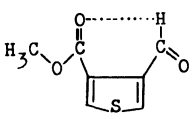

C

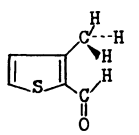

D

Table 5. Comparison of Observed and Calculated Percent *s* Characters of C-H Bonds for Substituted Thiophenecarbaldehydes

Compound	ρ_{CHO}/%	
	Obs	Calcd
1a	38.3	39.0
1b	36.1	38.0
1c	36.2	38.0
2a	35.2	37.8
2b	35.4	37.8
2c	35.4	37.8
3a	37.8	38.5
3b	37.5	38.5
3c	35.5	37.6
4a	34.6	37.4
4b	34.8	37.4
4c	34.9	37.4

conformers.

The percent s-character of the bonding orbital of the carbon atom which forms the formyl C-H bond (ρ_{CHO}) was estimated from the observed one-bond C-H coupling constants by the equation of Muller and Pritchard;[19] it is shown in Table 5, together with the values obtained from the MNDO calculations. The MNDO calculations gave a higher s-character of the carbon orbital for the C-H/O approached conformations of the *o*-formyl esters (**1a**, **3a**, and **3b**) than the others, accounting for the unusually large ^1J values observed with these aldehydes. Because of the high s-character of its bonding orbital, the formyl carbon becomes more electronegative, increasing the polarity of the formyl C-H bond. This should favor the attractive and hydrogen-bond-like interaction between the formyl C-H bond and carbonyl oxygen to a considerable extent. In turn, the attractive C-H/O interaction can be the driving force to force the *o*-formyl esters to take the C-H/O approached conformations (A—C).

The chemical shifts in Table 3 also suggest the predominance of the C-H/O approached conformations in the *o*-formyl esters. The ^{1}H chemical shifts of the formyl protons of **1a**, **3a**, and **3b** were observed at δ 10.65, 10.62, and 10.50, respectively.[1,2] These chemical shifts are about 0.7 ppm downfield from those of the non-adjacently functionalized formylthiophenecarboxylates. The downfield shift was observed also with the formyl ^{13}C chemical shifts of these aldehydes; it is ascribable to the strong magnetic anisotropy effect on the nucleus placed opposite to the robe of lone pair electrons of the carbonyl group.[20] In this way, the theoretically predicted predominance of the C-H···O approached conformers is supported experimentally by the unusually low ^{1}H NMR chemical shifts of the formyl protons of these aldehydes. The situation is very favorable to the hydrogen-bond-like interaction between the formyl C-H and the carbonyl groups. In fact, the downfield shifts are usually observed with both intra- and intermolecularly hydrogen-bonded

hydroxyl and amino protons and are used frequently as a criterion to prove the presence of hydrogen bonds.

Hydrogen bonds involving OH and NH groups as proton donors have been studied most frequently and most extensively by means of infrared spectroscopy.[21] Hvdrogen bond formation causes a significant low frequency shift of the OH or NH stretching absorption. The hydrogen bond shift of the X-H stretching band is very often accompanied with a considerable broadening and an increase in the intensity of the band, which can be another clue to detect the presence of a hydrogen bond.[22] Thus the infrared spectra of these formyl esters were measured with the aim of proving the presence of C-H/O hydrogen bonds.

Many aldehydes have been shown by the extensive study by Pozefsky and Coggeshall[23] to have two CH stretching absorption bands near 2720 and 2820 cm^{-1}. The doubling of the absorption band has been

Table 6. Frequencies of C-H and C=O Stretching Vibrations of (Methoxycarbonyl)thiophenecarbaldehydes

Compound	CHO						$COOCH_3$	
	ν_{C-H}/cm^{-1}				$\nu_{C=H}/cm^{-1}$		$\nu_{C=H}/cm^{-1}$	
1a	2896				1673		1729	
1b	2825				1688		1731	
1c	2845	2806			1688		1731	1725[a]
3a	2904	2881			1687		1725	
3b	2891	2827			1689		1729	
3c	2845	2827	2804	2789	1704	1698[a]	1725	1735[a]

a) Shoulder peak.

Table 7. Atomic and Bond Populations of the CH···O=C Hydrogen-Bonded (Most Stable) and the Next Most Stable Conformers of Methyl *o*-Formylthiophenecarboxylates

Compound	Confermer	Atom	Formal charge	Bond	Bond population
1a	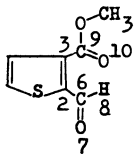	C(2)	−0.1769	C(6)=O(7)	1.9697
		C(3)	−0.0785	C(9)=O(10)	1.7750
		C(6)	0.3032	C(6)-H(8)	0.8995
		O(7)	−0.2715	C(8)···O(10)	0.0049
		H(8)	0.0711		
		C(9)	0.3901		
		O(10)	−0.3873		
1a	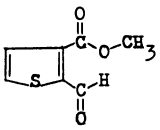	C(2)	−0.1957	C(6)=O(7)	1.9708
		C(3)	−0.0684	C(9)=O(10)	1.7989
		C(6)	0.3077	C(6)-H(8)	0.8983
		O(7)	−0.2690	H(8)···O(10)	0.0000
		H(8)	0.0547		
		C(9)	0.3796		
		O(10)	−0.3652		
3a	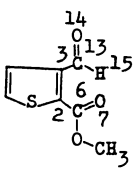	C(2)	−0.1636	C(6)=O(7)	1.7752
		C(3)	−0.0951	C(13)=C(14)	1.9670
		C(6)	0.3967	C(13)-H(15)	0.9020
		O(7)	−0.3797	H(15)···O(7)	0.0047
		C(13)	0.2982		
		O(14)	−0.2791		
		H(15)	0.0624		
3a	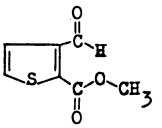	C(2)	−0.1612	C(6)=O(7)	1.7998
		C(3)	−0.1108	C(13)=C(14)	1.9679
		C(6)	0.3863	C(13)-H(15)	0.9006
		O(7)	−0.3582	H(15)···O(7)	0.0000
		C(13)	0.3029		
		O(14)	−0.2773		
		H(15)	0.0468		
3b	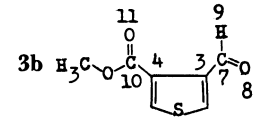	C(3)	−0.1603	C(7)=O(8)	1.9550
		C(4)	−0.1113	C(10)=O(11)	1.7798
		C(7)	0.3055	C(7)-H(9)	0.9009
		O(8)	−0.2949	H(9)···O(11)	0.0067
		H(9)	0.0669		
		C(10)	0.3923		
		O(11)	−0.3833		
3b	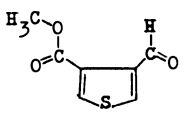	C(3)	−0.1711	C(7)=O(8)	1.9565
		C(4)	−0.1151	C(10)=O(11)	1.7890
		C(7)	0.3099	C(7)-H(9)	0.8995
		O(8)	−0.2916	H(9)···O(11)	0.0000
		H(9)	0.0508		
		C(10)	0.3887		
		O(11)	−0.3769		

ascribed to a Fermi resonance between the CH-stretching vibration and the first overtone of the CH-deformation vibration. The higher-frequency band has been shown to have the main CH-stretching character.[24] For this reason, our attention was focused on the CH bands above 2800 cm^{-1}. In contrast to the cases of the O-H/X and N-H/X hydrogen bonds, high frequency shifts of CH-stretching absorptions have been reported with some intramolecularly hydrogen bonded CH groups. For instance, the formyl CH group of *o*-nitrobenzaldehyde has been shown to absorb at 2860 cm^{-1}, about 50 cm^{-1} higher than unsubstituted benzaldehyde (2807 cm^{-1}).[5] Similar high-frequency shifts have been observed with the formyl esters **1a**, **3a**, and **3b**, which absorb at 2896, 2904, and 2891 cm^{-1}, respectively (Table 6). The frequencies are more than 50 cm^{-1} higher than those of the other aldehydes in Table 6.

The high-frequency shift is plausible if a C-H bond can interact attractively with an electronegative group (X) without weakening itself, i.e., without a decrease in its stretching force constant (k_{CH}), because the vibrational frequency of a linear (or, when the C-H···X angle is larger than 90°) C-H/X system can be expected to become higher than the isolated C-H bond when k_{CH} remains constant.[25] The effect of the steric compression of the CH bond may also operate. However, it cannot be very significant, since the steric crowdedness around the formyl hydrogen can easily be relaxed by tilting itself towards outside the plane of the thiophene ring. 3-Methyl-2-thiophenecarbaldehyde absorbs at 2819 cm^{-1}, and the effect of possible steric compression is not reflected significantly in the frequency of its formyl absorption band, even if the steric crowdedness of a same magnitude as in the formyl esters **1a**, **3a**, and **3b** can be expected from their molecular models.

The MNDO calculations[13-15] (Table 7) helped us to gain an insight into this apparently contradictory shift of the CH-stretching bands of the *o*-formyl esters. The nonbonded H···O bond populations in the C-H/O approached conformations of the formyl esters **1a**, **3a**, and **3b** range from 4.7×10^{-3} to 6.7×10^{-3}. These populations are comparable to the total CH_3···Ph bond population (4.79×10^{-3}) in the CH_3/pi interacted conformation of 1-phenyl-2-propanol and to about half of the OH···Ph bond population (1.62×10^{-2}) of the OH/π interacted conformation of the same molecule.[26] As both the OH/π and CH/π interactions have been well characterized and supported by experimental evidence, the hydrogen-bond-like C-H/O interaction in the *o*-formyl esters becomes more realistic.

The C-H and C=O bond populations of the formyl group seemed unperturbed by the C-H/O=C interaction. In the cases of all three *o*-formyl esters, the C-H bond populations tend to increase when compared with those of the corresponding next stable conformers. However, the increase is very slight and is assumed to be negligible when the reference is extended to all the formyl esters investigated. At any rate, there is no evidence for the decrease in the C-H bond population such as is often observed with the OH and NH bonds under similar circumstances. This gave a very clear explanation for the high frequency shift of the C-H stretching vibration in the C-H/O interacted system. On the other hand, the bond population of the hydrogen-accepting carbonyl group in the methoxycarbonyl moiety was shown to decrease considerably. The decrease was not very large, but it was meaningful when the populations were compared with those of other conformations and of other isomeric formyl esters. As to the hydrogen-accepting carbonyl group of the methoxycarbonyl moiety, the atomic populations of both carbon and oxygen vary in the direction of increasing their polarity, i.e., decreasing at the originally positive carbon atom and increasing at the negative oxygen atom in the C-H/O hydrogen-bonded conformer, when compared with the other less favorable conformer. In cooperation with the change in the charge distribution in the ester carbonyl group, the hydrogen-donating C-H bond becomes more polarized without perturbing the formyl carbonyl group appreciably. Thus, the attractive interaction was shown to originate both from the delocalizative contribution revealed as the positive bond population of nonbonded H···O and from the electrostatic contribution caused by the enhanced polarization of the originally dipolar C=O and C-H groups. Both the delocalizative and electrostatic stabilzations have been known as theoretical criteria for hydrogen bonding. In conclusion, the C-H/O attractive interaction involved have been shown to be hydrogen-bond-like in their nature both by the experimental evidence and by the theoretical consequences.

We wish to thank Mr. Hitoshi Shimazaki for his assistance in the MNDO calculations. Part of this work was supported by a Grant-in-Aid for Scientific Research from the Ministry of Education, Science, and Culture, to which the authors are also grateful.

References

1) H. Satonaka, *Bull. Chem. Soc. Jpn.*, **56**, 2463 (1983).
2) H. Satonaka, *Bull. Chem. Soc. Jpn.*, **56**, 3337 (1983).
3) M. Hirota, S. Yoshida, Y. Nagawa, M. Ono, H. Endo, and H. Satonaka, *Bull. Chem. Soc. Jpn.*, **49**, 3200 (1976).
4) H. Satonaka, *Bull. Chem. Soc. Jpn.*, **57**, 473 (1983).
5) S. Pinchas, *Anal. Chem.*, **29**, 334 (1957); *J. Phys. Chem.*, **67**, 1862 (1963).
6) A. Goel and C. N. R. Rao, *Trans. Farad. Soc.*, **67**, 2828 (1971).
7) P. L. Olympia, Jr., *Chem. Phys. Lett.*, **5**, 593 (1970).
8) S. Gronowitz, A. Biezais, and B. Mathiasson, *Ark. Kemi.*, **21**, 265 (1963).
9) E. Campaigne and W. L. Archers, *J. Am. Chem. Soc.*,

75, 989 (1953).

10) S. Gronowitz, P. Moss, A. Hornfeldt, and R. Hakansson, *Ark. Kemi.*, **17**, 165 (1961).

11) R. Guilard, P. Fournari, and M. Person, *Bull. Soc. Chim. Fr.*, **1967**, 421.

12) S. Gronowitz, B. Gestblem, and B. Mathiasson, *Ark. Kemi.*, **20**, 407 (1962).

13) M. J. S. Dewar and W. Thiel, *J. Am. Chem. Soc.*, **99**, 4899 (1977).

14) M. J. S. Dewar and E. Healey, *J. Comput. Chem.*, **4**, 542 (1983).

15) M. J. S. Dewar, QCPE Program #464.

16) K. Takahashi, T. Sone, and K. Fujieda, *J. Phys. Chem.*, **74**, 2765 (1970).

17) S. Gronowitz, I. Johnson, and A. B. Hornfeldt, *Chem. Scr.*, **7**, 76 (1978).

18) H. Satonaka and M. Watanabe, *Bull. Chem. Soc. Jpn.*, **58**, 3651 (1983).

19) N. Muller and D. E. Pritchard, *J. Chem. Phys.*, **31**, 1471 (1959).

20) J. W. ApSimmon, P. V. Demarco, D. W. Mathieson, W. G. Craig, A. Karim, L. Saunders, and W. B. Whalley, *Tetrahedron*, **26**, 119 (1970).

21) J. W. ApSimmon and H. Beierbeck, *Can. J. Chem.*, **49**, 1328 (1971).

22) N. S. Shepard, "Hydrogen Bonding," ed by D. Hadzi, Pergamon Press, London (1959), p. 85.

23) A. Pozefsky and N. D. Coggeshall, *Anal. Chem.*, **23**, 1611 (1951).

24) L. J. Bellamy, "Infra-red Spectra of Complex Molecules," 3rd ed., Chapman and Hall, London (1975), Vol. 1, p. 176.

25) If we assume that the C-H group, absorbing at 2800 cm^{-1} when free, forms a linear C-H···X hydrogen bond keeping its stretching force constant (k_{CH}, 4.26×10^5 dyn cm) unchanged, and that the stretching force constant of the newly formed H···X is as large as the 1/22.4 of k_{CH}, the high frequency shift of 50 cm^{-1} could be reproduced by a simple calculation using the valence force field approximation. The authors wish to thank Mr. Tamiki Komatsuzaki for this calculation.

26) K. Abe, M. Hirota, and K. Morokuma, *Bull. Chem. Soc. Jpn.*, **58**, 2713 (1985).

The 2- or 6-(α-Hydroxyalkyl- and α-Oxoalkyl)-5,8-dimethoxy-1,4-naphthoquinones from the Oxidative Demethylation of 2-(α-Hydroxyalkyl- and α-Oxoalkyl)-1,4,5,8-tetramethoxynaphthalenes with Cerium(IV) Ammonium Nitrate, and the Further Demethylations to Naphthazarins[1)]

Yasuhiro TANOUE and Akira TERADA*
Department of Chemistry, Kyushu Institute of Technology, Tobata, Kitakyushu, Fukuoka 804
(Received October 28, 1987)

Oxidative demethylation of 2-(α-hydroxyalkyl- and α-oxoalkyl)-1,4,5,8-tetramethoxynaphthalene with $(NH_4)_2Ce(NO_3)_6$ gave two isomeric dimethoxynaphthoquinones: 2-substituted and 6-substituted 5,8-dimethoxy-1,4-naphthoquinones. Further demethylations of the former isomers to the corresponding dihydroxynaphthoquinones required an AgO-40%HNO_3 reagent, while the latter isomers needed $AlCl_3$ as the demethylation reagent. Some comments regarding the mechanism of these oxidative demethylations with $(NH_4)_2Ce(NO_3)_6$ are given.

Naphthoquinones occur widely in nature among microorganisms and fungi,[2)] and have been studied regarding their colors and structures[3)] by many investigators. These days, many people are placing their hopes on such physiological activities[4)] as antitumor and antibiotic actions. Recently, Isayama et al.[5)] have applied for many patents for 5,8-dihydroxy-1,4-naphthoquinones as drugs for thrombosis, delayed hypersensitivity, and the healing of wounds.

Since our synthetic studies of naphthoquinone derivatives started, many problems have often occurred concerning the demethylation process of polymethoxynaphthalenes to hydroxynaphthoquinones. Therefore, the purpose of the present investigation was to search for a suitable reagent for a complete methoxyl cleavage of polymethoxynaphthalene intermediates. Although many reports[6)] have already appeared concerning demethylation, for example, on simple methyl ethers such as anisole, *p*-dimethoxybenzene, and monomethoxynaphthalene, no information in the literature has been found concerning the tetramethoxynaphthalenes, which we will report here.

It has been found by us that the demethylation of 1,4,5,8-tetramethoxynaphthalene with boron tribromide easily give naphthazarin.[7)] However, the treatment of the 2-substituted 1,4,5,8-tetramethoxynaphthalenes with boron tribromide or trimethylsilyl iodide gave no any desirable product, but, rather, only unidentified polymeric colored materials.

Demethylations of them with cerium(IV) ammonium nitrate[8)] (CAN) were successful and gave two isomeric dimethoxynaphthoquinones.

Further demethylation of them to the corresponding naphthazarins required AgO-40%HNO_3 or $AlCl_3$.

Fusarubin,[9)] Erythrostominone,[9)] Purpuromycin,[10)] and Fredericamycin A[11)] are new series of naphthazarin antibiotics.

Knowledge and information concerning demethylation, and the products obtained here, will generally be applicable for the synthesis of the above-mentioned naphthazarin antibiotics.[12)]

Results and Discussion

The demethylation of 2-substituted 1,4,5,8-tetramethoxynaphthalene (**1—9**) with 2.5 equiv of CAN usually gave two isomeric products, 2-substituted and 6-substituted 5,8-dimethoxy-1,4-naphthoquinones (former is named as type A and latter as type B) (Scheme 1, Table 1). The product mixture of A and B could be separated by silica gel or alumina column chromatography, and eluted by chloroform in the order of B and A.

Identifications of these naphthoquinone isomers were easy by ^1H NMR. The signals of their quinone ring protons were always observed more upfield than those of the benzene ring protons (Chart 1).[3a)] For example, in 5,8-dimethoxy-1,4-naphthoquinone (**1a**), the proton signals due to the quinone ring were observed at δ 6.77 (lit,[3a)] 6.75) and the benzene ring protons were at δ 7.32 (lit,[3a)] 7.31). A quinone ring proton of type A showed an allylic coupling with the

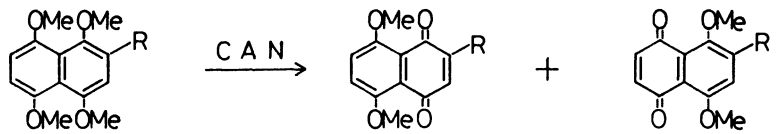

1 - 9 Type A 1a - 9a Type B 2b - 9b

Scheme 1.

protons at the α-positions of the side chain. For instance, the C_3-proton in 2-hydroxymethyl-5,8-dimethoxy-1,4-naphthoquinone (**2a**) showed a sharp triplet (J=1.6 Hz), clearly showing a coupling with two methylene protons of the hydroxymethyl side chain (Chart 2).

From Table 1, it can be seen that upon the demethylation of 2-substituted 1,4,5,8-tetramethoxynaphthalenes with CAN, substrates having electron-donating α-hydroxyalkyls gave, principally, type-A quinones; the minors were type-B. On the other hand, a substrate having electron-withdrawing an acetyl or a formyl group resulted in the formation of type-B, preferentially. These results suggested that CAN chose its target and attacked at the carbon atom having the highest electron density among the C_1, C_4, C_5, and C_8 (Table 2).

The ^{13}C chemical shifts of the ring carbon atoms of 2-substituted 1,4,5,8-tetramethoxynaphthalenes (**2—7**)

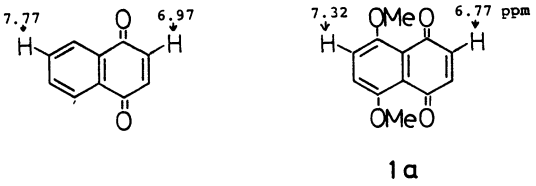

Chart 1.

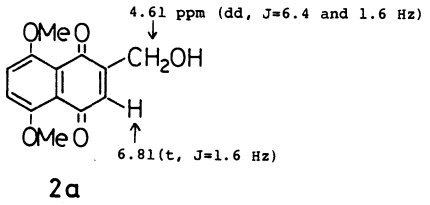

Chart 2.

Table 1. Demethylation of 2-Substituted 1,4,5,8-Tetramethoxynaphthalene with CAN

Substrate	Product (yield %)	
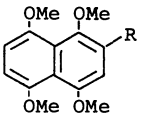	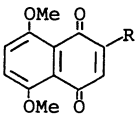	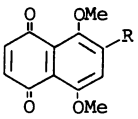
R	Type A	Type B
1:[a] H	**1a** (70)	—
2: CH_2OH	**2a** (75)	**2b** (13)
3: $CH(OH)CH_3$	**3a** (61)	**3b** (13)
4: $CH(OH)(CH_2)_3CH_3$	**4a** (42)	**4b** (16)
5:[a] $CH(OH)(CH_2)_2CH(CH_3)_2$	**5a**[a] (52)	**5b**[a] (17)
6:[a] $CH(OH)(CH_2)_2C(OH)(CH_3)_2$	**6a**[a] (70)	**6b**[a] (15)
7:[a] $CH(OH)(CH_2)_2COCH_3$	**7a** (33)	**7b** (33)
8: $COCH_3$	**8a** (3)	**8b** (77)
9:[a] CHO	**9a** (0)	**9b**[b] (85)

a) See Ref. 7. b) See Ref. 12.

Table 2. ^{13}C NMR Chemical Shifts (ppm) of the Ring Carbon Atoms of 2-Substituted 1,4,5,8-Tetramethoxynaphthalene and 2-Substituted or 6-Substituted 5,8-Dimethoxy-1,4-naphthoquinone

Substrate 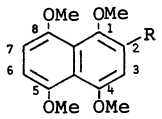

R	C_1	C_2	C_3	C_4	C_5	C_6	C_7	C_8
1: H	151.27	108.84	108.84	151.27	151.27	108.84	108.84	151.27
2: CH_2OH	146.82	131.17	107.45	153.03	151.12	107.61	108.05	150.00
3: $CH(OH)CH_3$	145.84	135.58	105.51	153.27	151.22	107.61	108.25	150.10
4: $CH(OH)(CH_2)_3CH_3$	146.09	134.69	105.95	153.13	151.18	107.61	108.20	150.10
5: $CH(OH)(CH_2)_2CH(CH_3)_2$	146.23	134.65	106.00	153.18	151.22	107.71	108.30	150.14
6: $CH(OH)(CH_2)_2C(OH)(CH_3)_2$	145.70	134.75	106.05	153.03	151.03	107.37	108.15	149.95
7: $CH(OH)(CH_2)_2COCH_3$	145.96	134.02	105.71	153.11	151.09	107.59	108.24	149.99
8: $COCH_3$	153.11	129.66	105.71	151.22	151.22	111.16	108.11	151.48
9: CHO	156.81	125.84	101.29	151.29	151.29	112.72	108.37	153.43
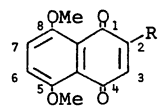								
1a: H	184.59	138.17	138.17	184.59	153.56	120.38	120.38	153.56
2a: CH_2OH	184.92	148.36	133.69	185.44	153.95	120.25	120.77	153.76
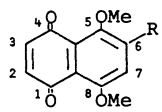								
9b: CHO	183.81	138.88	137.96	183.81	156.09	135.12	116.88	155.83

are shown in Table 2. In the compounds **2—7** of the electron-donating groups, the C_1s were shielded to an extent of about 5 ppm; inversely in **8** and **9** of the electron-withdrawing groups, the C_1s were deshielded to 1.8 and 5.5 ppm, respectively.

Our study on the correlation between Tables 1 and 2 resulted in the following conclusions. The carbon atom having the highest electron density among the C_1, C_4, C_5, and C_8 (namely, the carbon atom which was observed[13] at the most upfield), will receive the CAN-attack, and the para positional methoxyl group will immediately suffer the next oxidative demethylation to form dimethoxynaphthoquinones. The obtained dimethoxynaphthoquinones should not be affected by CAN any more because of their two carbonyls (as described later in this text). This conclusion will be supported by the fact that the demethylation of tetramethoxynaphthalene to dimethoxynaphthoquinone required 2 molar equiv of CAN (Table 3), and the use of any excess amount of CAN resulted only in the formation of dimethoxynaphthoquinone, with no other possible product such as mono-, tri-, and tetrahydroxylated naphthalenes.

Castagnoli et al.[8] studied the demethylation of 1,4-dimethoxy-2,3,5,6-tetramethylbenzene (**10**) with CAN in $H_2{}^{18}O$ and proved the fact that the product, quinone **12**, received two heavy oxygen atoms in their carbonyls from the heavy water medium. They proposed a demethylation mechanism (Scheme 2) in which a pathway through intermediate **11** is shown. However, they did not discuss the more detailed reaction mechanism.

Table 3. Demethylation of 2-Formyl-1,4,5,8-tetramethoxynaphthalene **9** with Various Amounts of CAN

CAN(molar equiv. amount)	Yield of **9b** (%)
1.0	38+47[a]
1.5	68+16[a]
2.0	81
2.5	85
3.0	80
5.0	79
10.0	73

a) The recovery of **9**.

In our case, we also suppose two kinds of intermediates: one is **16** when the substituent R is electron-donating, and the other is **20** when R is electron-withdrawing (Chart 3).

The mechanism of the side-chain oxidation of alkylated aromatic hydrocarbons with CAN has been well established by Baciocchi et al.[14] There is no doubt that the first step of the reactions on toluene, for example, is a formation of the radical cation:

$$ArCH_3 + Ce^{IV}NO_3 \rightarrow ArCH_3^{\ddagger} + Ce^{III}NO_3$$

By analogy with their result, we supposed that the compounds **2—7** will form a radical cation intermediate **13**, which will be attacked by water to form the next radical **14**. Accordingly, as CAN in an aqueous solution is dissociated into $[Ce(NO_3)_6]^{2-}$ and $NH_4{}^+$ ions,[15] one-electron oxidation in the case of **2—7** with $[Ce(NO_3)_6]^{2-}$ gives a radical cation[16] **13** and an electron-donating group R will help in its formation and stabilization. Next, water attacks **13** to form radical **14** and the subsequent oxidation of the para positional methoxyl by another $[Ce(NO_3)_6]^{2-}$ ion affords **16** and the final products **2a—7a**, through **15**.

On the other hand, when R is an electron-withdrawing group, substrates **8** and **9** gave **8b** and **9b**,

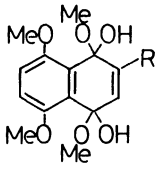

16

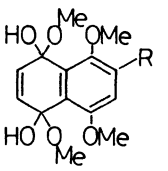

20

Chart 3.

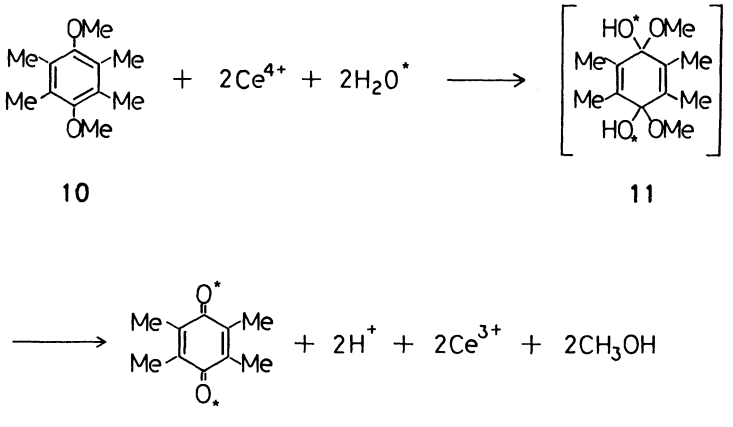

10 11 12

Scheme 2.

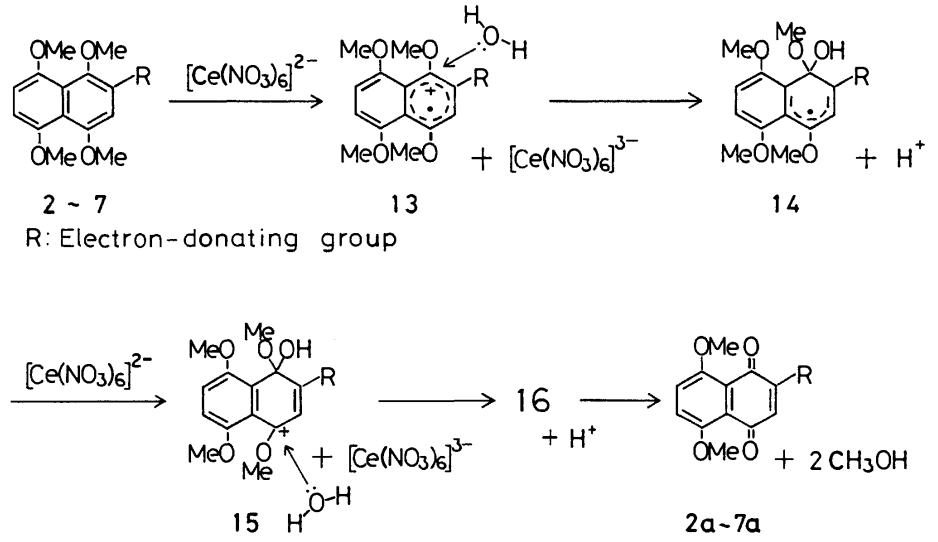

Scheme 3.

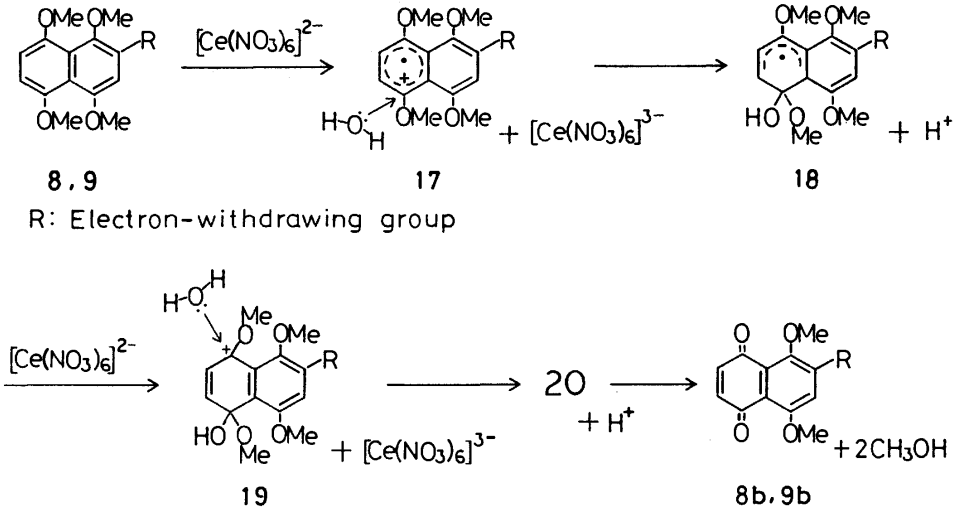

Scheme 4.

respectively, via intermediates **17**, **18**, **19**, and **20**.

A further treatment of these dimethoxynaphthoquinones **1a—6a**, **8a**, and **9b** with CAN resulted in no reaction; only the starting materials were recovered.

The ^{13}C chemical shifts of the ring carbon atoms of **1a**, **2a**, and **9b** are shown in Table 2, where the C_5 and C_8 carbons are more deshielded than those of **1**, **2**, and **9** within a range of 2—5 ppm. These downfield shifts are attributable to a decrease in the electron density of the carbon atoms (C_5 and C_8 of **1a**, **2a**, and **9b**) by near $C_{1,4}$-quinone-dicarbonyls. The decrease of the electron density at C_5 or C_8 prohibits a further CAN-attack either at C_5 or C_8.

Our subsequent studies concerning further demethylation of the 5,8-dimethoxy-1,4-naphthoquinones have yielded some other interesting results, as follows. The demethylation of the dimethoxynaphthoquinones (**1a—6a**) having electron-donating substituents with AgO-40% HNO_3[17] reagent gave 5,8-dihydroxy-1,4-naphthoquinones (**1c—6c**) (Table 4).

Table 4. Demethylation of 2-Substituted or 6-Substituted 5,8-Dimethoxy-1,4-naphthoquinone

Substrate	Product (%)
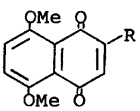 AgO-40%HNO_3 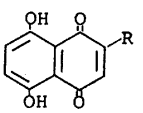	
R	
1a: H	**1c** (53)
2a: CH_2OH	**2c** (52)
3a: $CH(OH)CH_3$	**3c** (22)
4a: $CH(OH)(CH_2)_3CH_3$	**4c** (22)
5a: $CH(OH)(CH_2)_2CH(CH_3)_2$	**5c** (28)
6a: $CH(OH)(CH_2)_2C(OH)(CH_3)_2$	**6c** (27)
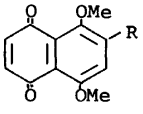 $AlCl_3$ 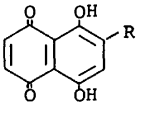	
8b: $COCH_3$	**8c** (71)
9b: CHO	**9c** (43)

However, the demethylation of the dimethoxynaphthoquinones **8b** and **9b**, having electron-withdrawing substitutents, required $AlCl_3$ instead of the above AgO-40%HNO_3 as the demethylation agent (Table 4). The AgO-40%HNO_3 system was quite unsuitable in these cases because of no reaction.

Experimental

^1H and ^{13}C NMR spectra were taken on a JEOL JNM-60 in $CDCl_3$ using Me_4Si and $CDCl_3$ as internal standards, respectively. Mass spectra and IR spectra were obtained with a JEOL DX-300 spectrometer, and a Hitachi 260-30 spectrometer, respectively. Column chromatography was carried out on silica gel (Wakogel C-200) or on alumina (Sumitomo, KCG-30) eluting with chloroform. Melting points were determined with a Yanagimoto micromelting point apparatus and were uncorrected.

2-Hydroxymethyl-1,4,5,8-tetramethoxynaphthalene (2). A sample of 2-formyl-1,4,5,8-tetramethoxynaphthalene (**9**)[7] (2.0 g, 7.24 mmol) in THF (40 ml) was reduced with $LiAlH_4$ (1.37 g, 36 mmol) under ice cooling. After stirring at room temperature for 3 h, the reaction mixture was decomposed by an addition of 1M HCl (1M=1 mol dm^{-3}), and extracted with chloroform (100 ml×3). The chloroform solution was washed with brine, dried over Na_2SO_4, and the solvent was evaporated. The crude product was chromatographed on silica gel to give 1.92 g (99%) of a sample of **2**, mp 99—100 °C. IR (KBr) 3520 (OH) and 1060 cm^{-1} (OCH_3, OH); ^1H NMR δ=2.42 (s, 1H, OH), 3.76, 3.88, 3.90, 3.92 (each s, 3H, OCH_3), 4.84 (s, 2H, CH_2), 6.80 (s, 2H, ArH), and 6.91 (s, 1H, ArH); MS, m/z 278 (M^+), 263, and 245. Calcd for $C_{15}H_{18}O_5$: C, 64.74; H, 6.52%. Found: C, 64.39; H, 6.57%.

2-(1-Hydroxyethyl)-1,4,5,8-tetramethoxynaphthalene (3). The aldehyde **9** (2.76 g, 10 mmol) in THF (40 ml) was added to methylmagnesium iodide (30 mmol) in ether (30 ml), and the mixture was stirred at room temperature for 1 h, decomposed with aq. NH_4Cl, and extracted with chloroform (100 ml×3). The usual work up and purification of the crude product by alumina chromatography gave 2.9 g (99%) of a sample of **3**. Recrystallization from hexane gave an analytical sample, mp 84—85 °C. IR (KBr) 3450 (OH), 1600, and 1070 cm^{-1}; ^1H NMR δ=1.50 (d, J=6.5 Hz, 3H, CH_3), 2.23 (broad, 1H, OH), 3.76, 3.89 (each s, 3H, OCH_3), 3.93 (s, 6H, OCH_3), 5.43 (q, J=6.5 Hz, 1H, CH), 6.81 (s, 2H, ArH), and 7.00 (s, 1H, ArH); MS, m/z 292 (M^+), 274 (M^+-H_2O), and 220. Calcd for $C_{16}H_{20}O_5$: C, 65.73; H, 6.91%. Found: C, 65.62; H, 7.00%.

2-(1-Hydroxypentyl)-1,4,5,8-tetramethoxynaphthalene (4). Treatment of the aldehyde **9** (1.66 g, 6 mmol) with butylmagnesium bromide (18 mmol) gave a crude product. Chromatographic purification on silica gel gave 1.99 g (99%) of a sample of **4** as an oil. IR (neat) 3450 (OH), 1600, and 1070 cm^{-1}; ^1H NMR δ=0.89 (t, J=6.6 Hz, 3H, CH_3), 1.1—1.9 (m, 6H, CH_2), 2.42 (broad, 1H, OH), 3.74, 3.88 (each s, 3H, OCH_3), 3.92 (s, 6H, OCH_3), 5.22 (t, J=6.0 Hz, 1H, CH), 6.80 (s, 2H, ArH), and 6.97 (s, 1H, ArH); MS, m/z 334 (M^+), 316 (M^+-H_2O), 301, 270, 231, and 137; HRMS m/z Calcd for $C_{19}H_{26}O_5$ 334.1781. Found 334.1784.

2-Acetyl-1,4,5,8-tetramethoxynaphthalene (8). A mixture of the alcohol **3** (610 mg, 2.09 mmol) and an activated manganese dioxide[18] (6 g) in benzene (20 ml) was refluxed for 15 h. Filtration, concentration, and chromatography on silica gel gave 382 mg (63%) of a sample of **8**. Recrystallization from hexane gave yellow crystals, mp 68—68.5 °C. IR (KBr) 1665 (C=O), 1600, 1370, 1070, and 1050 cm^{-1}; ^1H NMR δ=2.77 (s, 1H, $COCH_3$), 3.79, 3.90, 3.96, 3.98 (each s, 3H, OCH_3), 6.92 (s, 2H, ArH), and 7.09 (s, 1H, ArH); MS, m/z 290 (M^+), 275 (M^+-CH_3), 260, 232, and 218. Calcd for $C_{16}H_{18}O_5$: C, 66.20; H, 6.25%. Found: C, 66.11; H, 6.30%.

General Procedure for Oxidative Demethylation of 2-Substituted 1,4,5,8-Tetramethoxynaphthalenes (1—9) with CAN. A solution of CAN (2.5—3 mmol, 2.5—3 equiv) in water (5 ml) was added dropwise to a solution of 2-substituted 1,4,5,8-tetramethoxynaphthalene (1 mmol) in acetonitrile (10 ml), or in a mixture of acetonitrile-chloroform (5 : 1 v/v), at room temperature for 30 min, the reaction mixture was diluted with water, extracted with chloroform, washed with brine, dried over Na_2SO_4, and concentrated. The residue was purified by chromatography on silica gel with chloroform as eluent and recrystallized.

1a: reddish-orange crystals from ligroine (bp 75—120 °C)-benzene; mp 160—161 °C (lit,[19] 157 °C); IR (KBr) 1650 (C=O), 1582, 1565, 1045, and 1020 cm^{-1}; ^1H NMR δ=3.96 (s, 6H, OCH_3), 6.77 (s, 2H, quinone ring H), and 7.32 (s, 2H, benzene ring H); MS, m/z 218 (M^+), 189, 172, 161, 131, and 76.

2a and 2b. 2b: the first fraction from silica gel chromatography; mp 135—136 °C; ^1H NMR δ=2.49 (t, J=6.1 Hz, 1H, OH), 3.83, 3.40 (each s, 3H, OCH_3), 4.87 (d, J=6.1 Hz, 2H, CH_2), 6.78 (s, 2H, quinone ring H), and 7.51 (s, 1H, benzene ring H). **2a:** the second fraction; orange crystals (from ethanol); mp 176—176.5 °C; IR (KBr) 3480, 3350, 1640 (C=O), 1585, 1565, 1075, 1045, and 965 cm^{-1}; ^1H NMR δ=2.41 (t, J=6.1 Hz, 1H, OH), 3.96 (s, 6H, OCH_3), 4.61 (dd, J=6.1 and 1.6 Hz, 2H, CH_2), 6.81 (t, 1H, J=1.6 Hz, quinone ring H), and 7.32 (s, 2H, benzene ring H); MS, m/z 248 (M^+), 233, 218, and 201. Calcd for $C_{13}H_{12}O_5$: C, 62.90; H, 4.87%. Found: C, 62.56; H, 4.88%.

3a and 3b. 3b: the first fraction from silica-gel chromatography; an orange semisolid; ^1H NMR δ=1.56 (d, J=6.5 Hz, 3H, CH_3), 2.2 (broad, 1H, OH), 3.83, 3.99 (each s, 3H, OCH_3), 5.30 (q, J=6.5 Hz, 1H, CH), 6.76 (s, 2H, quinone ring H), and 7.55 (s, 1H, benzene ring H). **3a:** the second fraction; orange crystals (from ligroine-benzene); mp 144—145 °C; IR (KBr) 3480 (OH), 1650 (C=O), 1050, and 1020 cm^{-1}; ^1H NMR δ=1.48 (J=6.6 Hz, 3H, CH_3), 2.70 (d, J=5.2 Hz, 1H, OH), 3.96, 3.97 (each s, 3H, OCH_3), 4.94 (m, 1H, CH), 6.78 (d, J=1.3 Hz, 1H, quinone ring H), and 7.32 (s, 2H, benzene ring H); MS, m/z 262 (M^+), 247 (M^+-CH_3), 231, 219, and 205. Calcd for $C_{14}H_{14}O_5$: C, 64.12; H, 5.38%. Found: C, 64.33; H, 5.43%.

4a and 4b. 4b: the first fraction from alumina chromatography; an orange oil; ^1H NMR δ=0.90 (t, J=6.0 Hz, 3H, CH_3), 1.1—1.9 (m, 6H, CH_2), 2.55 (broad, 1H, OH), 3.83, 3.99 (each s, 3H, OCH_3), 5.12 (m, 1H, CH), 6.77 (s, 2H, quinone ring H), and 7.51 (s, 1H, benzene ring H). **4a:** the second fraction; an orange oil; IR (neat) 3480 (OH), 1655, 1590, 1570, and 1060 cm^{-1}; ^1H NMR δ=0.90 (t, J=6.0 Hz, 3H, CH_3), 1.1—1.9 (m, 6H, CH_2), 2.55 (broad, 1H, OH), 3.96 (s, 6H, OCH_3), 4.74 (m, 1H, CH), 6.76 (d, J=1.4 Hz, 1H, quinone ring H), and 7.31 (s, 2H, benzene ring H); MS, m/z 304 (M^+), 289 (M^+-CH_3), and 247; HRMS, m/z Calcd for $C_{17}H_{20}O_5$ 304.1311. Found 304.1314.

7a and 7b. 7b: the first fraction from silica-gel chromatography; an orange oil; ^1H NMR δ=2.18 (s, 3H, $COCH_3$), 1.5—

2.9 (m, 5H, CH_2 and OH), 3.81, 3.94 (each s, 3H, OCH_3), 5.10 (m, 1H, CH), 6.77 (s, 2H, quinone ring H), and 7.55 (s, 1H, benzene ring H). **7a:** the second fraction; an orange oil; IR (KBr) 3470 (OH), 1710 (ketone C=O), 1655 (quinone C=O), 1590, 1570, and 1055 cm^{-1}; ^1H NMR δ=2.18 (s, 3H, $COCH_3$), 1.5—2.9 (m, 5H, CH_2 and OH), 3.94 (s, 6H, OCH_3), 4.78 (m, 1H, CH), 6.83 (s, 1H, quinone ring H), and 7.30 (s, 2H, benzene ring H); MS, *m/z* 318 (M^+), 300, and 247; HRMS, *m/z* Calcd for $C_{17}H_{18}O_6$ 318.1104. Found 318.1129.

8a and 8b. 8b: the first fraction from silica-gel chromatography; orange crystals (from ligroine-benzene); mp 155—155.5 °C; IR (KBr) 1685 (ketone C=O), 1655 (quinone C=O), 1620, 1580, and 1040 cm^{-1}; ^1H NMR δ=2.69 (s, 3H, $COCH_3$), 3.85, 4.00 (each s, 3H, OCH_3), 6.84 (s, 2H, quinone ring H), and 7.48 (s, 1H, benzene ring H); MS, *m/z* 260 (M^+), 245 (M^+-CH_3), 231, and 131. Calcd for $C_{14}H_{12}O_5$: C, 64.61; H, 4.65%. Found: C, 64.17; H, 4.72%. **8a:** the second fraction; an orange semisolid; ^1H NMR δ=2.60 (s, 3H, OCH_3), 3.85, 3.97 (each s, 3H, OCH_3), 6.98 (s, 1H, quinone ring H), and 7.35 (s, 2H, benzene ring H).

General Procedure for Oxidative Demethylation of 2-Substituted 5,8-Dimethoxy-1,4-naphthoquinones (1a—6a) with AgO-40%HNO_3. 40% HNO_3 (12 ml) was added dropwise to a mixture of AgO (10 mmol, 10 equiv), acetone (24 ml), and 2-substituted 5,8-dimethoxy-1,4-naphthoquinone (1 mmol) at 15—25 °C for 5 min. After stirring at room temperature for 30 min, the mixture was diluted with water, extracted with dichloromethane (50 ml×3) washed with brine, dried over Na_2SO_4, and concentrated. The residue was purified by silica-gel chromatography and recrystallized.

1c: reddish brown crystals; mp 202—205 °C (lit,[20] 201—202 °C); IR (KBr) 1610 (C=O), 1565, and 1225 cm^{-1}; ^1H NMR δ=7.14 (s, 4H, ArH) and 12.39 (s, 2H, ArOH); MS, *m/z* 190 (M^+), 136, 134, and 108.

2c: brown crystals (from hexane-ethanol); mp 180—183 °C; IR (KBr) 3430 (sharp, OH), 1610 (C=O), 1560, 1205, and 1080 cm^{-1}; ^1H NMR δ=2.11 (t, *J*=6.1 Hz, 1H, OH), 4.76 (dd, *J*=6.1 and 1.7 Hz, 2H, CH_2), 7.16 (t, *J*=1.5 Hz, 1H, quinone ring H), 7.21 (s, 2H, benzene ring H), 12.46 and 12.48 (each s, 1H, ArOH); MS, *m/z* 220 (M^+), 202 (M^+-H_2O), 191, 174, and 149. Calcd for $C_{11}H_8O_5$: C, 60.01; H, 3.66%. Found: C, 59.98; H, 3.77%.

3c: brown crystals (from hexane); mp 128—129.5 °C; IR (KBr) 3350 (broad, OH), 1610, 1570, 1200, 1105, and 1045 cm^{-1}; ^1H NMR δ=1.54 (d, *J*=6.6 Hz, 3H, CH_3), 1.96 (broad, 1H, OH), 5.08 (qd, *J*=6.6 and 1.3 Hz, 1H, CH), 7.17 (d, *J*=1.3 Hz, quinone ring H), 7.21 (s, 2H, benzene ring H), 12.46 and 12.58 (each s, 1H, ArOH); MS, *m/z* 234 (M^+), 216 (M^+-H_2O), 168, and 139. Calcd for $C_{12}H_{10}O_5$: C, 61.54; H, 4.30%. Found: C, 60.80; H, 4.30%.

4c: brown crystals (from hexane-ethanol); mp 95.5—96.5 °C; IR (KBr) 3250 (broad, 1H, OH), 1615, 1575, 1200, 1115, and 1060 cm^{-1}; ^1H NMR δ=0.92 (t, *J*=5 Hz, 3H, CH_3), 1.1—1.9 (m, 6H, CH_2), 2.20 (broad, 1H, OH), 4.89 (td, *J*=5.1 and 1.0 Hz, 1H, CH), 7.12 (d, *J*=1.0 Hz, 1H, quinone ring H), 7.19 (s, 2H, benzene ring H), 12.46 and 12.58 (each s, 1H, ArOH); MS, *m/z* 276 (M^+), 258 (M^+-H_2O), 229, 220, and 219. Calcd for $C_{15}H_{16}O_5$: C, 65.21; H, 5.84%. Found: C, 64.45; H, 5.91%.

General Procedure for Demethylation of 6-Substituted 5,8-Dimethoxy-1,4-naphthoquinones (8b and 9b) with $AlCl_3$. $AlCl_3$ (10 mmol, 10 equiv) was added to a solution of 6-substituted 5,8-dimethoxy-1,4-naphthoquinone (1 mmol) in dichloromethane (10 ml) cooled in an ice bath. After stirring at room temperature for 2 h, the reaction mixture was decomposed with 5 wt% aqueous oxalic acid (100 ml), extracted with chloroform, washed with brine, dried over Na_2SO_4, and concentrated. The residue was purified by silica-gel chromatography and recrystallized from hexane. **8c:** brown crystals; mp 120—121.5 °C; IR (KBr) 1678 (ketone C=O), 1610 (quinone C=O), 1550, and 1215 cm^{-1}; ^1H NMR δ=2.71 (s, 3H, CH_3), 7.11 (s, 2H, quinone ring H), 7.60 (s, 1H, benzene ring H), 12.13 and 13.08 (each s, 1H, ArOH); MS, *m/z* 232 (M^+), 217, 189, and 161. Calcd for $C_{12}H_8O_5$: C, 62.07; H, 3.47%. Found: C, 61.73; H, 3.51%.

9c: brown crystals; mp 172—174 °C (decomp); IR (KBr) 1690 (ketone C=O), 1610 (quinone C=O), 1555, and 1190 cm^{-1}; ^1H NMR δ=7.10 (s, 2H, quinone ring H), 7.79 (s, 1H, benzene ring H), 10.54 (s, 1H, CHO), 12.03 and 12.77 (each s, 1H, ArOH); MS, *m/z* 218 (M^+), 190 (M^+-CO), 172, and 134. Calcd for $C_{11}H_6O_5$: C, 60.56; H, 2.77%. Found: C, 60.42; H, 3.00%.

We are grateful to Professor Otohiko Tsuge of Kyushu University for valuable suggestions. We also thank Mr. Yoshiyuki Kitajima, Mr. Iwao Seto, Mr. Toshiyuki Tsuboi, and Mr. Takayuki Hayashida for their technical assistances, Mr. Yoshiharu Okada for the elemental analyses, Mrs. Eriko Furukawa for the NMR spectra, and Mrs. Keiko Yamaguchi for MS spectra.

References

1) Synthesis on Naphthoquinone Derivatives. 7. For 6, Y. Tanoue, A. Terada, I. Seto, Y. Umezu, and O. Tsuge, *Bull. Chem. Soc. Jpn.*, **61**, 1221 (1988).

2) For example, R. H. Thomson, "Naturally Occurring Quinones," 2nd ed., Academic Press, London (1971).

3) a) R. E. Moore and P. J. Scheuer, *J. Org. Chem.*, **31**, 3272 (1966); b) F. Farina, R. M. Utrilla, and M. C. Paredes, *Tetrahedron*, **38**, 1531 (1982).

4) For example, J. S. Driscoll, G. F. Hazard, Jr., H. B. Wood, Jr., and A. Goldin, *Cancer Chemotherapy Reports Part 2*, **4**, 1 (1974).

5) S. Isayama, H. Ohno, T. Ishinori, and H. Nakamura, *Open Patent Journal* (A), Japan, 61-145144; T. Ishinori, S. Isayama, and H. Ohno, *Open Patent Journal* (A), Japan, 61-143334.

6) For example, M. V. Bhatt and S. U. Kulkarni, *Synthesis*, **1983**, 249.

7) A. Terada, Y. Tanoue, A. Hatada, and H. Sakamoto, *Bull. Chem. Soc. Jpn.*, **60**, 205 (1987).

8) P. Jacob, III; P. S. Callery, A. T. Shulgin, and N. Castagnoli, Jr., *J. Org. Chem.*, **41**, 3627 (1976).

9) See Ref. 2, pp. 291 and 297, respectively.

10) C. Coronell, H. Pagani, M. R. Bardone, and G. C. Lancini, *J. Antibiot.*, **27**, 161 (1974).

11) R. C. Pandey, M. W. Toussaint, R. M. Stroshane, C. C. Kalita, A. A. Aszalos, A. L. Garretson, T. T. Wei, K. M. Byrne, R. F. Geoghegan, Jr., and R. J. White, *J. Antibiot.*, **34**, 1389 (1981); R. Misra, R. C. Pandey, and J. V. Silverton, *J. Am. Chem. Soc.*, **104**, 4478 (1982).

12) Y. Tanoue, A. Terada, T. Tsuboi, T. Hayashida, and O. Tsuge, *Bull. Chem. Soc. Jpn.*, **60**, 2927 (1987).

13) For example, G. L. Nelson, G. C. Levy, and J. D. Cargioli, *J. Am. Chem. Soc.*, **94**, 3089 (1972); E. Breitmaier and W. Voelter, "^{13}C NMR Spectroscopy," 2nd ed., Verlag Chemie, New York (1978), p. 68.

14) E. Baciocchi, D. Bartoli, C. Rol, R. Ruzziconi, and G. V. Selastiani, *J. Org. Chem.*, **51**, 3587 (1986); E. Baciocchi, C. Rol, and L. Mandolini, *J. Am. Chem. Soc.*, **102**, 7597 (1980).

15) T. A. Beineke and J. Delgaudio, *Inorg. Chem.*, **7**, 715 (1968).

16) Torii reported that one-electron oxidation of *p*-methoxytoluene with CAN gave a corresponding radical-cation. S. Torii, "Yūki Denkai Gōsei," Kōdansha, Tokyo (1981), Chap. 11; S. Torii, H. Tanaka, T. Inokuchi, S. Nakane, M. Akada, N. Saito, and T. Sirakawa, *J. Org. Chem.*, **47**, 1647 (1982).

17) C. D. Snyder and H. Rapoport, *J. Am. Chem. Soc.*, **94**, 227 (1972).

18) J. Attenburrow, A. F. B. Cameron, J. H. Chapman, R. M. Evans, B. A. Hems, A. B. A. Jansen, and T. Walker, *J. Chem. Soc.*, **1952**, 1094.

19) D. B. Bruce and R. H. Thomson, *J. Chem. Soc.*, **1955**, 1089.

20) The Chemical Society of Japan, "Handbook of Chemistry," 2nd ed., Maruzen, Tokyo (1975), p. 213.

Studies on Synthetic Ionophores. VI.[1] Synthesis of Polyether Carboxylic Acids and Their Use as Carriers for Alkali Metal Ion Transport through Liquid Membrane

Kazuo YAMAGUCHI, Shigeto NEGI, Shohei KOZAKAI, Roichi NAGANO, Hitoshi KUBONIWA, Akira HIRAO, Seiichi NAKAHAMA,* and Noboru YAMAZAKI†

Department of Polymer Chemistry, Tokyo Institute of Technology, 2-12-1 Ohokayama, Meguro-ku, Tokyo 152
†Department of Chemistry, Kanagawa Dental College, Inaokacho, Yokosuka, Kanagawa 238

(Received November 12, 1987)

ω-Hydroxy carboxylic acids (**3**, **5**, **6**, **7**, **10**, **12**, **14**, **17**, **18**, **20**, and **22**) bearing 2—6 ether oxygens and aromatic rings with or without a tetrahydrofuran ring and the ω-methoxy and ω-benzyloxy derivatives of **5** (**8** and **9**) were synthesized. These were employed as carriers for active and competitive transport of alkali metal ions through liquid membrane as well as for extraction of alkali metal ions to organic layers. Effect of hydrophobic group of aromatic and tetrahydrofuran rings, number of ether oxygens, and terminal hydroxyl group of the ionophores on the ion transport ability and selectivity were investigated. The hydrophobic groups increased total amount of transported ions as well as partition coefficients. The ionophore, **5**, which contains five ether oxygens, two aromatic rings, and *o*-toluic acid moiety transported K^+ selectively over Na^+ and Li^+ through 1,2-dichloroethane being consistent with the extraction experiments. The *m*- and *p*-substituted isomers, **6** and **7**, exhibited no transport ability through 1,2-dichloroethane. The ω-alkoxy derivatives of **5** (**8** and **9**) exhibited less selectivity for K^+ through 1,2-dichloroethane than **5** did. Through 1-hexanol, the ionophores, **5**—**9**, including linoleic acid with no ether linkage transported alkali metal ions. The ionophores (**3**, **12**, **20**, and **22**) containing 2—4 ether oxygens did not exhibit high transport ability.

Among naturally occurring compounds, there is a class of ionophores which form stable, lipophilic complexes with ions and are able to transport them across membranes.[2] The ionophores are classified based on their structures into two types. One is neutral ionophore which is cyclic and contains no ionizable functional group.[2a] Another is charged ionophore characterized by a carboxylic acid head group and a tail of a hydroxyl or an amino group capable of hydrogen-bonding interactions. The backbones are linear, containing heterocyclic rings with a variety of oxygen-containing functional groups. The carboxylic group is ionized at physiological pH and the complex with cation is neutral. Their complex formation and physiological activity have been investigated extensively.[3] A number of synthetic models for neutral ionophores, such as crown ethers, were reported in order to understand the mechanism of action of the naturally occurring ionophores as well as to dissolve reactive inorganic salts in organic solvents for organic synthesis.[4] However, synthetic analogues of natural carboxylic ionophores remain relatively unexplored.[5]

We have already reported transport of alkali metal ions across an organic liquid membrane mediated by synthetic carboxylic acid ionophores.[1] It was found that an ion was pumped against its concentration gradient by a coupled counterflow of proton and that formation of a pseudocyclic structure of the ionophore, with or without hydrogen bonding of the head and tail, was essential for lipophilization and transport of the cation similar to the case of natural ionophores.[1c,e]

We describe here synthetic procedures for new carboxylic acid ionophores together with already reported ones and systematic studies on transport of alkali metal ions by these ionophores.

Results and Discussion

Synthesis of Polyether Carboxylic Acids. As ionophore, eleven carboxylic acids containing 2—6 ether oxygens and one terminal hydroxyl group were synthesized. Aromatic and tetrahydrofuran rings were employed as hydrophobic groups and acetic or toluic acid moieties serving as the carboxyl group. Two derivatives with terminal ether groups were also prepared to clarify a role of head-to-tail hydrogen bonding. The synthetic procedures are based mainly on the Williamson ether synthesis.

2-(2-Hydroxyethoxy)phenol (**1**) was obtained by conventional means using the reaction of sodium catecholate with ethylene chlorohydrin.[6] A better yield was obtained using the previously reported reaction of phenol with ethylene carbonate.[7] Heating a mixture of catechol and ethylene carbonate at 160 °C in the presence of tetrabutylammonium iodide gave a 77% yield of **1**.

Coupling of ethylene glycol ditosylate with **1** gave the best result for synthesis of **4**.[8] Williamson coupling of **4** with methyl 2-(bromomethyl)benzoate and subsequent hydrolysis provided **5**. Similarly, *m*- and *p*-substituted isomers, **6** and **7** were afforded. ω-Alkoxy derivatives, **8** and **9**, were obtained by reaction of **5** with methyl iodide and benzyl chloride respectively and successive hydrolysis. Instead of methyl 2-(bromomethyl)benzoate, chloroacetic acid was employed for synthesis of **10**. Methyl 2-(bromomethyl)-benzoate was allowed to react with **1** directly followed

by hydrolysis to synthesize **3**. Treatment of **1** with tosyl chloride formed the ditosylate, **2**. Reaction of **2** with **1** and subsequent hydrolysis yielded **11**. Compound **12** was derived from **11**. Compound **14** was obtained similarly from **13** which was prepared by reaction of two equivalents of the sodium salt of **1** with bis(2-chloroethyl) ether. Coupling of tetrahydro-2,5-furandimethanol ditosylate (**15**)[9] with two equivalents of **1** afforded **16**. The reaction of **16** with methyl 2-(bromomethyl)benzoate formed **17**. The acetic acid derivative **18** was obtained from **16** and ethyl bromoacetate. Two equivalents of catechol and bis(2-hydroxyethyl) ether were employed to synthesize **19**[10] which was converted into **20** using methyl 2-(bromomethyl)benzoate. Compound **21**[11] obtained from catechol and two equivalents of ethylene chlorohydrin was allowed to react with methyl 2-(bromomethyl)benzoate to form lactone which was hydrolyzed to **22**.

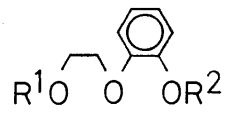

1; $R^1=R^2=H$
2; $R^1=R^2=Ts$
3; $R^1=H$, $R^2=o\text{-}CH_2\text{-}C_6H_4\text{-}COOH$

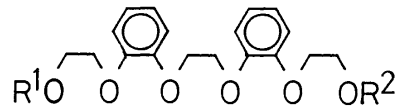

4; $R^1=R^2=H$
5; $R^1=H$, $R^2=o\text{-}CH_2\text{-}C_6H_4\text{-}COOH$
6; $R^1=H$, $R^2=m\text{-}CH_2\text{-}C_6H_4\text{-}COOH$
7; $R^1=H$, $R^2=p\text{-}CH_2\text{-}C_6H_4\text{-}COOH$
8; $R^1=CH_3$, $R^2=o\text{-}CH_2\text{-}C_6H_4\text{-}COOH$
9; $R^1=PhCH_2$, $R^2=o\text{-}CH_2\text{-}C_6H_4\text{-}COOH$
10; $R^1=H$, $R^2=CH_2COOH$

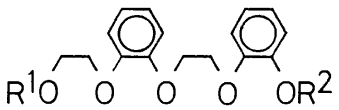

11; $R^1=R^2=H$
12; $R^1=H$, $R^2=o\text{-}CH_2\text{-}C_6H_4\text{-}COOH$

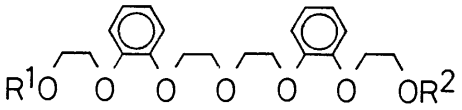

13; $R^1=R^2=H$
14; $R^1=H$, $R^2=o\text{-}CH_2\text{-}C_6H_4\text{-}COOH$

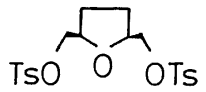

15

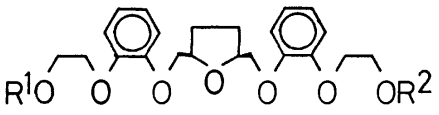

16; $R^1=R^2=H$
17; $R^1=H$, $R^2=o\text{-}CH_2\text{-}C_6H_4\text{-}COOH$
18; $R^1=H$, $R^2=CH_2COOH$

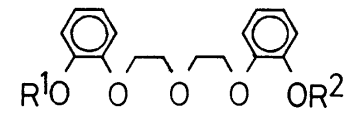

19; $R^1=R^2=H$
20; $R^1=H$, $R^2=o\text{-}CH_2\text{-}C_6H_4\text{-}COOH$

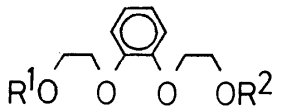

21; $R^1=R^2=H$
22; $R^1=H$, $R^2=o\text{-}CH_2\text{-}C_6H_4\text{-}COOH$

These ionophores are classified by the number of ether oxygens in Table 1. Cavity sizes of the pseudocyclic conformers which are formed by head-to-tail hydrogen bonding between carboxyl and hydroxyl groups were measured in their CPK models. The cavity size increases as the number of ether oxygens increases. Hydrophobicity parameters (log *P*) are also shown in Table 1 where *P* is calculated value of partition coefficient to octanol obtained by the literature method.[12] Tetrahydrofuran compounds (**17**, **18**) have higher log *P* than the analogues containing oxyethylene residue (**5**, **10**) do. Toluic acid derivatives (**5**, **17**) are more hydrophobic than the corresponding acetic acid ones (**10**, **18**). Ionophores become more lipophilic by alkylation of terminal hydroxyl group (**5** to **8** or **9**). The cavity sizes and log *P*'s will be correlated with the

Table 1. Synthetic Ionophores

Compound	Cavity size/Å	Numbers of ethereal and hydroxyl oxygens	log *P*
3	1.4	3	4.4
22	1.6	4	4.4
12	2.1	5	7.5
20	2.2	5	7.1
10	2.5	6	5.0
5	2.5	6	7.6
6	—	6	7.6
7	—	6	7.6
8	2.5	6	8.2
9	2.5	6	10.4
18	2.8	7	5.8
17	3.0	7	8.4
14	3.2	7	7.6

Diameter of alkali metal ions(Å): Li^+; 1.56, Na^+; 1.96, K^+; 2.66, Rb^+; 2.98, Cs^+; 3.30.

Table 2. Partition Coefficient of Alkali Metal Salts of **5** to Organic Solvents

Solvent	μ	ε	Na^+	K^+	Rb^+	Cs^+
1-Hexanol	1.9	13.3	1.9	5.3	4.9	4.0
1-Hexanol/toluene						
(5/5)	1.13	7.84	0.79	4.0	4.0	3.8
(3/7)	0.82	5.66	0.43	2.8	—	—
(2/8)	0.67	4.56	0.22	1.6	—	—
(1/9)	0.51	3.47	0.064	0.52	—	—
Toluene	0.36	2.38	0	0	—	—
1,2-Dichloroethane	1.44	10.65	0.042	0.54	0.27	0.11

Table 3. Partition Coefficient of Alkali Metal Salts of Synthetic Ionophores to Organic Solvents

Compound	Solvent	Na^+	K^+	Rb^+	Cs^+
10	1-Hexanol	0.064	0.22	0.47	0.33
14		1.7	8.1	4.9	3.5
17		5.3	16.0	6.1	6.1
10	1-Hexanol-toluene	0.10	0.18	0.30	0.35
14	(1/1)	0.82	4.0	3.3	2.8
17		1.9	6.1	5.7	6.1
10	1,2-Dichloroethane	0.14	0.12	0.042	0.053
14		0.087	0.33	0.33	0.37
17		0.18	1.2	1.4	1.7

ion transport ability and ion selectivity.

Partition Coefficient of Alkali Metal Salts of Synthetic Ionophores. In order to investigate the hydrophobicity of alkali metal salts of synthetic carboxylic ionophores the salts in water were extracted with organic solvents. Partition coefficients of alkali metal salts of **5** to organic solvents (such as 1-hexanol, toluene, 1-hexanol-toluene, and 1,2-dichloroethane) together with dipole moment (μ) and dielectric constant (ε) are shown in Table 2. 1-Hexanol extracted more of the salts than 1,2-dichloroethane and none of the salts was extracted by toluene. With increased ratio of toluene in 1-hexanol-toluene (decrease in polarity), the amount of extracted salts decreased. The potassium salt was more extracted than the sodium salt. There was not much difference among the partition coefficients of the potassium, rubidium, and cesium salts.

Partition coefficients of alkali metal salts of synthetic ionophores **10**, **14**, **17** to organic solvents are shown in Table 3. The salts of **14** and **17** with toluic acid moiety as well as **5** (Table 2) have larger partition coefficients than that of **10** with acetic acid moiety. As can be seen in log *P*, the toluic acid derivatives are more hydrophobic, so that these salts are more soluble in organic solvents. K, Rb, and Cs salts of **14** and **17** were more extracted than that of the sodium salts in most cases.

Table 4. Active Ion Transport through Various Liquid Membrane by **5**

Liquid membrane	Transported ion (%)				
	5			None	
	Na^+	K^+	total	Na^+	K^+
1-Hexanol	31	54	85	13	10
1-Hexanol/toluene					
5/5	22	66	88	8	5
3/7	22	69	91	5	9
2/8	20	70	90	2	4
1/9	15	68	83	1	4
1,2-Dichloroethane	13	62	75	0	0

Table 5. Active Ion Transport through 1-Hexanol by Ionophores Containing 5—6 Ether Oxygens

Compound	Transported ion (%)				
	Na^+	K^+	Rb^+	Cs^+	Total
5	31	54	—	—	85
17	34	52	—	—	86
18	31	51	—	—	82
None	13	10	—	—	23
5	—	41	44	—	85
17	—	47	48	—	95
18	—	30	31	—	61
None	—	17	10	—	27
5	26	42	—	21	89
10	20	25	—	18	63
14	24	41	—	25	90
17	25	42	—	22	89
18	29	42	—	17	88
None	12	11	—	9	32

Active Transport of Alkali Metal Ions by Ionophores Containing 5—6 Ether Oxygens. Competitive transport of Na^+ and K^+ through various liquid membranes was carried out by using **5** which was expected to exhibit high selectivity from partition coefficient experiments. The results are shown in Table 4. The ionophore exhibited high transport ability and K^+-selectivity through all the liquid membranes. 1,2-Dichloroethane gave the highest selectivity. Total transport was comparable at all ratios of 1-hexanol-toluene mixtures, and increase in toluene content enhanced K^+-selectivity. The ratio of 1/9 gave the highest selectivity comparable to that in 1,2-dichloroethane. Transport of Na^+ and K^+, by **5** exhibited preference for K^+ in all the liquid membranes consistent with the results of extraction experiments.

Competitive transport of alkali metal ions using **10**, **14**, **17**, and **18** as well as **5** was carried out. 1-Hexanol and 1,2-dichloroethane were employed as the liquid membrane and ion combinations of Na^+-K^+, Na^+-K^+-Cs^+, and K^+-Rb^+ were used. These results are shown in Tables 5 and 6.

Table 5 shows competitive ion transport through 1-hexanol. All the ionophores were K^+-selective in the transport of Na^+ and K^+. Although **17** and **18** with tetrahydrofuran ring have one more ether oxygen and the cavity sizes are larger than that of **5**, both had similar transport ability and selectivity to those of **5**. Results of competitive transport of Na^+, K^+, and Cs^+ by **5**. **10**, **14**, **17**, and **18** show that all the ionophores preferred K^+. The cavity size of **14** with six ether oxygens seems to fit diameter of Cs^+ better than that of K^+, whereas **14** had selectivity for K^+. No ionophore distinguished between K^+ and Rb^+ with similar diameter.

Table 6 shows the results of ion transport through 1,2-dichloroethane instead of 1-hexanol. In the transport of Na^+ and K^+, not only **5** but also **17** and **18** exhibited higher selectivity for K^+ than seen in 1-hexanol. Acetic acid derivative, **18** transported only 25% of the total salt. In the transport of Na^+, K^+, and Cs^+, the ionophores except for **10** displayed K^+-preference. Selective transport of Cs^+ was not achieved even by the compounds with six ether oxygens such as **14**, **17**, and **18**. Ionophores containing seven or more ether oxygens might fit for Cs^+. Poor transport ability of compounds bearing acetic acid moiety (**10** and **18**) is consistent with their partition coefficient experiments. Compounds **5** and **18** showed no preference between K^+ and Rb^+, but **17** exhibited a slight selectivity for Rb^+.

As mentioned above, it was found that the ionophores having five or six ether oxygens transported K^+ and Rb^+ in preference to the smaller Na^+ and the larger Cs^+. Since the cavity size of these ionophores in a pseudocyclic conformation formed by head-to-tail hydrogen bonding meets diameter of K^+ and Rb^+ rather than Na^+ and Cs^+, the hydrophobic conformations of the potassium and rubidium salts are more stable to diffuse into organic phase than those of the sodium and cesium salts resulting in the K^+- and Rb^+-preference.

Table 6. Active Ion Transport through 1,2-Dichloroethane by Ionophores Containing 5—6 Ether Oxygens

Compound	Transported ion (%)				
	Na^+	K^+	Rb^+	Cs^+	Total
5	13	62	—	—	75
17	20	71	—	—	91
18	5	20	—	—	25
None	0	0	—	—	0
5	—	42	45	—	87
17	—	36	49	—	85
18	—	10	11	—	21
None	—	0	0	—	0
5	11	56	—	13	80
10	7	4	—	3	14
14	11	53	—	21	85
17	12	69	—	12	93
18	8	15	—	8	31
None	0	0	—	0	0

Active Transport of Alkali Metal Ions by Derivatives of 5. Table 7 illustrates competitive active transport of alkali metal ions by **5** and its analogues including linoleic acid through 1,2-dichloroethane liquid membrane. Compound **5** and its methyl and benzyl ethers (**8** and **9**) were able to transport alkali metal ions whereas *m*- and *p*-substituted isomers of **9** (**6** and **7**) and linoleic acid had almost no transport ability. Compound **5** exhibited high specificity for K^+ over Na^+ and Li^+, but the methyl ether was less selective and the benzyl ether had no selectivity. Compounds **5** and **8** showed less selectivity for K^+ over Rb^+ and Cs^+ than over Na^+ and Li^+ in 1,2-dichloroethane.

All the compounds react with cations to form the salts at water/1,2-dichloroethane interface. In the case of **5** and its derivatives subsequent replacement of water molecules out of the hydration sphere by ether oxygens affords a lipophilic complex soluble in the liquid membrane. On the contrary, the ether oxygens of *m*- and *p*-isomers of **5** are too far away to interact with from hydrated metal ions and linoleic acid had no ether oxygen to coordinate metal ion, so the salts stayed at the interface. Ion selectivity of **5** could be accounted for in a similar manner to naturally occurring carboxylic ionophores.[2] A metal ion is entrapped in a hydrophilic cavity made by head-to-tail hydrogen bonding between carboxylato and hydroxyl groups of ionophore. The diameter of a potassium ion (2.66 Å) meets the cavity size of **5** (2.6 Å by CPK model) result-

Table 7. Active Transport of Alkali Metal Ions through 1,2-Dichloroethane by **5** and Its Derivatives

Compound	Transported ion (%)					
	Li^+	Na^+	K^+	Rb^+	Cs^+	Total
5	0	11	—	—	—	11
	—	13	62	—	—	75
	—	—	40	36	24	100
8	11	28	—	—	—	39
	—	28	41	—	—	69
	—	—	42	32	26	100
9	40	33	—	—	—	73
	—	35	35	—	—	70
	—	—	42	30	28	100
6	0	0	—	—	—	0
	—	0	0	—	—	0
	—	—	1	5	1	7
7	0	0	—	—	—	0
	—	0	0	—	—	0
	—	—	1	2	1	4
Linoleic acid	0	0	—	—	—	0
	—	0	0	—	—	0
None	0	0	—	—	—	0
	—	0	0	—	—	0
	—	—	0	0	0	0

Table 8. Active Ion Transport through 1-Hexanol by **5** and Its Derivatives

Compound	Transported ion (%)					
	Li^+	Na^+	K^+	Rb^+	Cs^+	Total
5	44	26	—	—	—	70
	—	31	54	—	—	85
	—	—	34	30	26	89
8	56	28	—	—	—	84
	—	35	47	—	—	82
	—	—	26	26	21	73
9	36	13	—	—	—	49
	—	13	20	—	—	33
6	56	27	—	—	—	83
	—	34	41	—	—	75
	—	—	33	30	36	99
7	54	23	—	—	—	77
	—	32	32	—	—	64
	—	—	31	27	32	90
Linoleic acid	70	30	—	—	—	100
	—	47	43	—	—	90
None	15	13	—	—	—	28
	—	13	10	—	—	23
	—	—	17	16	15	48

Table 9. Active Ion Transport by Ionophores Containing 2—4 Ether Oxygens

Compound	Liquid membrane	Transported ion (%)			
		Li^+	Na^+	K^+	Total
3[a]	1-Hexanol	24	15	14	53
12		36	24	—	60
20		20	15	—	35
22		29	24	—	53
None		15	13	—	28
None[a]		20	17	19	56
3[a]	1,2-Dichloroethane	2	0	3	5
12		4	16	—	20
20		0	2	—	2
None		0	0	0	0

a) Donor phase I contains an aqueous solution of 0.1 M Li^+ (1 M=1 mol dm^{-3}), 0.1 M Na^+, 0.1 M K^+, and 0.3 M OH^-. The other conditions are described in experimental section.

ing in the potassium selectivity. Since Na^+ and Li^+ are too small to fit in the cavity, these complexes are less stable than that of potassium salt of **5**. Smaller difference between the diameters of K^+ and Rb^+ (Cs^+) leads to less selectivity for K^+ over Rb^+ (Cs^+) by **5**. The methyl and benzyl ethers of **5**, **8**, and **9**, where the head-to-tail hydrogen bonding is impossible, could still adopt a pseudocyclic conformation fitting the size of K^+. However, the other conformations with smaller cavity sizes to meet Na^+ or Li^+ diameter would be also possible because of the enhanced hydrophobicities of **8** and **9**. This is responsible for less selectivity and increase in transported amount of Na^+ and Li^+. All the salts of the ionophores where cations are coordinated by all or some ether oxygens depending on the sizes of cations were hydrophobic enough to be extracted into organic membrane. There is not much difference between the stability of the complexes.

Behavior of these ionophores in 1-hexanol membrane is quite different from that in 1,2-dichloroethane as shown in Table 8. Not only *o*-substituted compounds **5**, **8**, and **9** but also *m*- and *p*-isomers **6** and **7** and linoleic acid served as a carrier. Compound **5** had still specificity for K^+ over Li^+ and Na^+, but Li^+ was more transported than Na^+. The other ionophores preferred Li^+. Any ionophore did not exhibit remarkable selectivity for K^+ over Rb^+ and Cs^+ regardless of the position of terminal carboxyl group or the structure of the other end.

Selectivity in the ion transport through 1-hexanol might be explained as follows: Water molecules of hydrated cations of linoleic acid salts formed at the interface were replaced by 1-hexanol molecules to solubilize in the organic membrane. The transport selectivity for Li^+ suggests that 1-hexanol can dehydrate more easily out of Li^+ with higher charge density. In the case of the synthetic ionophores containing ether oxygens, metal ions were coordinated by the ether oxygens of the ionophores and alcohol oxygens of the liquid membrane competitively. Compound **5** whose ether oxygens may be stronger ligands toward K^+ than 1-hexanol exhibited K^+ selectivity, but the complex coordinated by 1-hexanol oxygens was also produced resulting in lowering K^+-selectivity.

Active Transport of Alkali Metal Ions by Ionophores Containing 2—4 Ether Oxygens. The ionophores containing two to four ether oxygens were employed for ion transport as shown in Table 9. In 1-hexanol, the ionophores transported Li^+ more than Na^+ similar to the case of **5** and its derivatives as mentioned above. However, the total amount of transported ions was small. This could be accounted for by the small stability constant of the salt complexes solvated by 1-hexanol resulting from the low lipophilicity of these ionophores. Although the ionophores were expected to exhibit Li^+- or Na^+-selectivity through 1,2-dichloroethane from the cavity sizes, almost no ion was transported.[13]

Experimental

Methods. IR spectra were run with a Jasco IR-G spectrophotometer. ^1H NMR specta were recorded with a JEOL JNM-PMX 60 instrument using tetramethylsilane as internal standard. UV spectra were recorded on a Hitachi 124 spectrophotometer. Mass spectra were obtained on a Hitachi M-80 mass spectrometer operating at 30 eV. Elemental analyses were performed on a Yanaco Model MT-3. Flame spectrochemical analyses were performed with Hitachi 170-30 Atomic Absorption Spectrophotometer.

Materials. Unless stated otherwise reagent grade reactants and solvents were obtained from commercial suppliers and used without further purification. Dry ethanol and dry methanol were distilled in the presence of sodium alkoxides.

Dry *N*,*N*-dimethylformamide (DMF) and dry pyridine were distilled over NaH. Methyl 2-(bromomethyl)benzoate was prepared by photobromination of methyl 2-methylbenzoate with bromine according to the literature method[14] and the *m*- and *p*-isomers, methyl 3-(bromomethyl)benzoate and methyl 4-(bromomethyl)benzoate, were obtained similarly. Bis[2-(2-hydroxyphenoxy)ethyl] ether (**19**),[10] and 1,2-bis(2-hydroxyethoxy)benzene (**21**)[11] were prepared by Williamson synthesis from catechol and the appropriate halides according to the literatures. Ethylene glycol ditosylate[15] and tetrahydro-2,5-furandimethanol ditosylate (**15**)[9] were obtained according to the literature methods.

2-(2-Hydroxyethoxy)phenol (1). A mixture of catechol (22 g, 0.2 mol), ethylene carbonate (17.6 g, 0.2 mol), and tetrabutylammonium iodide (2.4 g, 6.5 mmol) was heated at 160 °C for about 1 h until evolution of CO_2 ceased. The mixture was distilled under reduced pressure (ca. 115 °C/0.1 mmHg(1 mmHg=133.322 Pa)) to get a solid. Recrystallization of this from water gave pure product (23.1 g, 77%). Mp 99—101 °C (lit,[6] mp 100—101 °C).

1,2-Bis[2-(2-hydroxyethoxy)phenoxy]ethane (4). A mixture of **1** (2 g, 13 mmol) and NaH (13 mmol) in dry DMF (8 ml) was stirred at room temperature for 30 min. To this was added dropwise ethylene glycol ditosylate[13] (2.4 g, 6.4 mmol) in dry DMF (25 ml) and the mixture was stirred at room temperature for 24 h. After removal of DMF in vacuo, water (40 ml) was added to the residue followed by reflux. After cooling, the precipitate was collected by suction. It was recrystallized from ethanol-water (1/1) to get **4** (1.71 g, 81%). Mp 88—89 °C (lit,[8] mp 99 °C). ^{1}H NMR ($CDCl_3$) δ=3.6—4.3 (8H, m, $OC\underline{H}_2C\underline{H}_2OH$), 4.3 (4H, s, $OC\underline{H}_2C\underline{H}_2$), 6.9 (8H, s, aromatic).

2,5-Bis[[2-(2-hydroxyethoxy)phenoxy]methyl]tetrahydrofuran (16). NaOH (2.1 g, 52 mmol) was dissolved in 1-butanol (100 ml) under reflux. After addition of **1** (8 g, 52 mmol) the mixture was refluxed for 1 h. To this was added dropwise a solution of **15**[14] (11 g, 25 mmol) in dry DMF (100 ml) and the mixture was heated under reflux for 16 h. After distillation of the solvents under reduced pressure the residue was dissolved in water (50 ml) with heating followed by acidification with 1 M HCl (1 M=1 mol dm^{-3}). The formed precipitate was collected by suction and was recrystallized from ethanol-water (1/1) to give **16** (4 g, 40%). Mp 99—101 °C. ^{1}H NMR (DMSO-d_6) δ=1.9 (4H, m, CH_2 of tetrahydrofuran), 3.1—4.7 (14H, m, OCH= and OCH_2), 6.9 (8H, s, aromatic). Found: C, 62.11; H, 7.31%. Calcd for $C_{22}H_{28}O_7 \cdot H_2O$: C, 62.54; H, 7.16%.

Bis[2-[2-(2-hydroxyethoxy)phenoxy]ethyl] Ether (13). From **1** (10 g), NaOH (2.6 g), and bis(2-chloroethyl) ether (4.65 g), **13** was synthesized similar to **4**. Yield (11 g, 90%). Mp 84—86 °C (50% ethanol). ^{1}H NMR ($CDCl_3$) δ=3.7—4.3 (16H, m, CH_2), 6.9 (8H, s, aromatic). Found: C, 57.72; H, 7.38%. Calcd for $C_{20}H_{26}O_7 \cdot 2H_2O$: C, 57.96; H, 7.30%.

2-(2-Hydroxyethoxy)phenol Ditosylate (2). To **1** (3.0 g, 20 mmol) in dry pyridine (20 ml) at 0 °C was added portionwise tosyl chloride (8.4 g, 44 mmol). The mixture was stirred at room temperature for 40 h and poured into ice water. The precipitate was filtered and washed with water. The solid dried in vacuo was recrystallized from ethanol-ethyl acetate to give white crystal of **2** (5.6 g, 61%); mp 125.5—126 °C. ^{1}H NMR ($CDCl_3$) δ=2.4 (6H, s, CH_3), 3.8—4.3 (4H, m, CH_2), 6.6—7.9 (12H, m, aromatic). Found: C, 57.23; H, 4.67; S, 13.96%. Calcd for $C_{22}H_{22}O_7S_2$: C, 57.13; H, 4.79; S, 13.87%.

2-[2-[2-(2-Hydroxyethoxy)phenoxy]ethoxy]phenol (11). A mixture of **1** (1.5 g, 10 mmol) and NaH (10 mmol) in dry DMF (70 ml) was stirred at 80—90 °C to form alkoxide. To this was added dropwise **2** (4.6 g, 10 mmol) in dry DMF (40 ml) at room temperature and the mixture was stirred at 80—90 °C for 18 h. DMF was removed in vacuo and the residue dissolved in chloroform was washed with water. The organic layer dried over sodium sulfate was evaporated and chromatographed over silica gel (chloroform/methanol=100/5) to separate the monotosylate roughly. To this was added KOH (8.4 g), H_2O (14 ml), and ethanol (14 ml) followed by reflux for 1 h. This was acidified with HCl followed by extraction with chloroform. The organic layer dried over sodium sulfate was evaporated and applied to a silica-gel column (chloroform) to separate **11** (1.8 g, 62%). ^{1}H NMR ($CDCl_3$) δ=3.8—4.1 (4H, m, $OC\underline{H}_2C\underline{H}_2OH$), 4.2 (4H, s, $OC\underline{H}_2C\underline{H}_2$), 6.9 (8H, s, phenylene). Found: C, 66.16; H, 6.33%. Calcd for $C_{16}H_{18}O_5$: C, 66.20; H, 6.25%.

[2-[2-[2-[2-(2-Hydroxyethoxy)phenoxy]ethoxy]phenoxy]-ethoxy]acetic Acid (10). To **4** (2.6 g, 7.4 mmol) dissolved in dry THF (80 ml) under gentle reflux was added portionwise small pieces of K (0.59 g, 15 mmol) and the mixture was stirred for 1 h to form precipitate of the alkoxide. Chloroacetic acid (0.7 g, 7.4 mmol) in dry DMF (20 ml) was added dropwise to the suspension and the mixture was refluxed for 9 h. After cooling, THF was removed in vacuo and to the residue was added appropriate amount of dil NaOH, then H_2O was removed in vacuo. The residual oil was washed with dioxane to remove the starting material of **4**. To the resulting solid was added 2 M HCl and chloroform and it was shaken. The organic layer was separated, dried over magnesium sulfate, and evaporated. The solid was recrystallized from 50% ethanol to give **10** (1.8 g, 60%). Mp 73—76 °C. IR (KBr) 1740 cm^{-1} (C=O); ^{1}H NMR ($CDCl_3$) δ=3.7—4.2 (10H, m, CH_2O), 4.3 (4H, s, OCH_2CH_2O), 6.9 (8H, s, aromatic). Found: C, 60.72; H, 6.34%. Calcd for $C_{20}H_{24}O_8$: C, 61.22; H, 6.17%.

2-[[2-[2-[2-[2-(2-Hydroxyethoxy)phenoxy]ethoxy]phenoxy]-ethoxy]methyl]benzoic Acid (5). A mixture of **4** (3.34 g, 10 mmol) and NaH (10 mmol) in dry DMF (70 ml) was stirred at room temperature for 4 h. To the alkoxide was added dropwise methyl 2-(bromomethyl)benzoate (2.17 g, 10 mmol) in dry DMF (40 ml) and the mixture was stirred at room temperature for 4 h and at 80—90 °C for 24 h. DMF was removed in vacuo and to the residue was added 1 M NaOH followed by reflux for 2 h. It was acidified with dil HCl and the precipitate was collected by suction and washed with water thoroughly. To the solid dissolved in methanol was added anion-exchange resin (Amberlyst, OH^-, 5 g) and the mixture was stirred for 1 h. The resin was filtered, washed with methanol, and was poured into 1 M HCl. The resin was filtered off and washed with methanol. The combined filtrate and washing were evaporated in vacuo. The residue was recrystallized from 50% ethanol to give **5** (2.8 g, 59%). Mp 112—113 °C. IR (KBr) 1690 cm^{-1} (C=O); ^{1}H NMR ($CDCl_3$) δ=3.8—4.4 (8H, m, OCH_2), 4.4 (4H, s, OCH_2), 4.9 (2H, s, benzyl), 6.9 (8H, s, aromatic), 7.3—8.1 (4H, m, aromatic). Found: C, 66.03; H, 6.02%. Calcd for $C_{26}H_{28}O_8$: C, 66.66; H, 6.02%.

Compounds **18**, **14**, and **17** were prepared from **16** and ethyl bromoacetate, **13** and methyl 2-(bromomethyl)benzoate and **16** and methyl 2-(bromomethyl)benzoate respectively by

Williamson synthesis similar to that for **5**.

[2-[2-[[Tetrahydro-5-[[2-(2-hydroxyethoxy)phenoxy]methyl]-2-furanyl]methoxy]phenoxy]ethoxy]acetic Acid (18). Yield (0.9 g, 20%). Mp 115—118 °C (50% ethanol). IR (KBr) 1730 cm^{-1} (C=O); ^1H NMR (DMSO-d_6) δ=1.9—2.1 (4H, m, tetrahydrofuranyl CH_2), 3.5—4.5 (16H, m, all other CH_2 and tetrahydrofuranyl CH), 6.9 (8H, s, aromatic). Found: *m/z* 462.1901. Calcd for $C_{24}H_{30}O_9$: M, 462.1890.

2-[[2-[2-[2-[2-[2-(2-Hydroxyethoxy)phenoxy]ethoxy]ethoxy]-phenoxy]ethoxy]methyl]benzoic Acid (14). Yield (0.51 g, 10%). Mp 82—84 °C (50% ethanol). IR (KBr) 1690 cm^{-1} (C=O); ^1H NMR (DMSO-d_6) δ=3.5—4.3 (16H, m, CH_2O), 4.85 (2H, s, benzyl), 6.9 (8H, s, phenylene), 7.3—7.9 (4H, m, aromatic of toluic acid). Found: *m/z* 512.2081. Calcd for $C_{28}H_{32}O_9$: M, 512.2046.

2-[[2-[2-[[Tetrahydro-5-[[2-(2-hydroxyethoxy)phenoxy]methyl]-2-furanyl]methoxy]phenoxy]ethoxy]methyl]benzoic Acid (17). Yield (1.35 g, 30%). The crystal from 50% ethanol became oil on drying under vacuum. IR (neat) 1710 cm^{-1} (C=O); ^1H NMR ($CDCl_3$) δ=1.9—2.2 (4H, m, tetrahydrofuranyl CH_2), 3.6—4.5 (14H, m, all other CH_2 and tetrahydrofuranyl CH), 6.9 (8H, s, aromatic), 7.3—8.1 (4H, m, aromatic of toluic acid). Found: *m/z* 538.2148. Calcd for $C_{30}H_{34}O_9$: M, 538.2203.

2-[[2-(2-Hydroxyethoxy)phenoxy]methyl]benzoic Acid (3). To sodium alkoxide prepared from **1** (0.87 g, 5.65 mmol) and NaH (5.68 mmol) in dry DMF (10 ml) was added dropwise methyl 2-(bromomethyl)benzoate (1.3 g, 5.68 mmol) in dry DMF (10 ml) and the reaction mixture was stirred at room temperature for 3 h and at 80 °C for 24 h. DMF was removed in vacuo and to the residue was added 1 M NaOH followed by reflux. It was acidified with 1 M HCl and extracted with chloroform. The organic layer was washed with water, dried over magnesium sulfate, and evaporated. The solid was recrystallized from CCl_4-$CHCl_3$-acetone (5/1/2) to give white crystals of **3** (0.42 g, 25%). Mp 138—139 °C. IR (KBr) 1690 cm^{-1} (C=O); ^1H NMR (acetone-d_6) δ=3.7—4.3 (4H, m, CH_2), 5.5 (2H, s, benzyl), 6.9 (4H, s, aromatic), 7.3—8.1 (4H, m, aromatic). Found: C, 66.08; H, 5.61%. Calcd for $C_{16}H_{16}O_5$: C, 66.66; H, 5.59%.

2-[[2-[2-(2-Hydroxyethoxy)phenoxy]ethoxy]methyl]benzoic Acid (22). A mixture of **21**[11] (1.98 g, 10 mmol) and NaH (10 mmol) in dry DMF (30 ml) was stirred at 80—90 °C until evolution of hydrogen ceased. Methyl 2-(bromomethyl)benzoate (2.3 g, 10 mmol) in dry DMF (80 ml) was added dropwise and the mixture was stirred at 80—90 °C for 48 h. DMF was removed in vacuo and the residue dissolved in methanol was neutralized by addition of cation-exchange resin. The resin was filtered and the filtrate was evaporated. The residue was dissolved in hexane with heating and it was allowed to stand at room temperature to separate crystals of lactone (0.2 g, 6.4%). Mp 89—90 °C. IR (KBr) 1720 cm^{-1} (C=O); ^1H NMR ($CDCl_3$) δ=3.7—4.0 (2H, m, CH_2O), 4.0—4.3 (4H, m, CH_2O), 4.5—4.7 (2H, m, CH_2O), 5.1 (2H, s, benzyl), 6.8 (4H, s, phenylene), 7.0—7.8 (4H, m, aromatic of toluic acid). Found: C, 68.46; H, 5.88%. Calcd for $C_{18}H_{18}O_5$: C, 68.77; H, 5.77%. The lactone (0.13 g, 0.4 mmol) in 1 M NaOH (25 ml) was refluxed for 1 h. It was neutralized with 1 M HCl and extracted with $CHCl_3$. The organic layer dried over sodium sulfate was evaporated to give **22** (0.13 g, 98%). Mp 105—107 °C. IR (KBr) 1690 cm^{-1} (C=O); ^1H NMR ($CDCl_3$) δ=3.6—4.3 (8H, m, CH_2O), 4.9 (2H, s, benzyl), 6.8 (4H, s, phenylene), 7.0—7.9 (4H, m, aromatic of toluic acid). Found: C, 64.46; H, 6.26%. Calcd for $C_{18}H_{20}O_6$: C, 65.05; H, 6.07%.

2-[[2-[2-[2-(2-Hydroxyethoxy)phenoxy]ethoxy]phenoxy]-methyl]benzoic Acid (12). A mixture of **11** (0.8 g, 2.8 mmol) and NaH (2.8 mmol) in dry DMF (30 ml) was stirred at room temperature to form alkoxide. To this was added dropwise methyl 2-(bromomethyl)benzoate (0.64 g, 2.8 mmol) in dry DMF (10 ml) and the mixture was stirred at room temperature for 18 h. DMF was removed in vacuo and to the residue was added 2 M NaOH followed by reflux for 2 h. It was acidified with 2 M HCl followed by extraction with chloroform. The organic layer dried over sodium sulfate was evaporated and applied to a silica-gel column (chloroform/methanol=100/1) to obtain **12** (0.34 g, 29%). IR (KBr) 1710 cm^{-1} (C=O); ^1H NMR ($CDCl_3$) δ=3.3—4.4 (8H, m, CH_2O), 5.4 (2H, s, benzyl), 6.9 (8H, s, phenylene), 7.2—8.0 (4H, m, aromatic of toluic acid). Found: *m/z* 424.1457. Calcd for $C_{24}H_{24}O_7$: M, 424.1522.

Compound **20** was synthesized from **19** and methyl 2-(bromomethyl)benzoate similar to synthesis of **12**.

2-[[2-[2-[2-(2-Hydroxyphenoxy)ethoxy]ethoxy]phenoxy]-methyl]benzoic Acid (20). Yield (0.5 g, 12%). Mp 111—114 °C. IR (KBr) 1710 cm^{-1} (C=O); ^1H NMR (acetone-d_6) δ=3.5—4.3 (8H, m, CH_2), 5.5 (2H, s, benzyl), 6.7—7.0 (8H, m, phenylene), 7.2—8.1 (4H, m, aromatic of toluic acid). Found: *m/z* 424.1438. Calcd for $C_{24}H_{24}O_7$: M, 424.1522.

4-[[2-[2-[2-[2-(2-Hydroxyethoxy)phenoxy]ethoxy]phenoxy]-ethoxy]methyl]benzoic Acid (7). A mixture of **4** (3.3 g, 10 mmol) and NaH (10 mmol) in dry DMF (70 ml) was stirred at 80—90 °C to form alkoxide. To this was added dropwise methyl 4-(bromomethyl)benzoate (2.3 g, 10 mmol) in dry DMF (40 ml) and the mixture was stirred at 80—90 °C for 18 h. DMF was removed in vacuo and to the residue was added 2 M NaOH followed by reflux for 2 h. It was acidified with 2 M HCl followed by extraction with chloroform. The organic layer dried over sodium sulfate was evaporated and was applied to a silica-gel column (chloroform/methanol=100/1) to obtain **7** (0.70 g, 15%). IR (KBr) 1690 cm^{-1} (C=O); ^1H NMR (DMSO-d_6) δ=3.5—4.4 (12H, m, CH_2), 4.6 (2H, s, benzyl), 6.9 (8H, s, aromatic), 7.3—8.0 (4H, m, aromatic of toluic acid). Found: C, 66.18; H, 5.82%. Calcd for $C_{26}H_{28}O_8$: C, 66.02; H, 6.07%.

3-[[2-[2-[2-[2-(2-Hydroxyethoxy)phenoxy]ethoxy]phenoxy]-ethoxy]methyl]benzoic Acid (6). Compound **6** was synthesized by the same procedure as that for **7** using methyl 3-(bromomethyl)benzoate instead of *p*-isomer. Yield (1.2 g, 26 %). IR (KBr) 1690 cm^{-1} (C=O); ^1H NMR ($CDCl_3$) δ=3.6—4.4 (12H, m, CH_2), 4.6 (2H, s, benzyl), 7.0 (8H, s, aromatic), 7.4—8.1 (4H, m, aromatic of toluic acid). Found: C, 66.51; H, 5.96%. Calcd for $C_{26}H_{28}O_8$: C, 66.66; H, 6.02%.

2-[[2-[2-[2-[2-(2-Methoxyethoxy)phenoxy]ethoxy]phenoxy]-ethoxy]methyl]benzoic Acid (8). A mixture of **5** (0.5 g, 1.1 mmol) and NaH (4 mmol) in dry DMF (10 ml) was stirred at room temperature to form alkoxide. To this was added dropwise methyl iodide (0.71 g, 5 mmol) in dry DMF (5 ml) and the mixture was stirred at room temperature for 48 h. DMF was removed in vacuo and to the residue was added a mixture of KOH (0.84 g, 5 mmol), H_2O (5 ml), and ethanol (5 ml) followed by reflux for 2 h. It was acidified with HCl followed by extraction with chloroform. The organic layer dried over sodium sulfate was evaporated. The residue was applied to a silica-gel column (chloroform/methanol=100/1) to obtain **8** (0.38 g, 73%). IR (KBr) 1690 cm^{-1} (C=O);

^{1}H NMR ($CDCl_3$) δ=3.4 (3H, s, OCH_3), 3.6—4.4 (12H, m, CH_2O), 5.0 (2H, s, benzyl), 6.9 (8H, s, phenylene), 7.3—8.1 (4H, m, aromatic of toluic acid). Found: C, 67.28; H, 6.40%. Calcd for $C_{27}H_{30}O_8$: C, 67.21; H, 6.27%.

Compound **9** was prepared from **5** and benzyl chloride instead of methyl iodide by the same procedure as that for **8**.

2-[[2-[2-[2-[2-(2-Benzyloxyethoxy)phenoxy]ethoxy]phenoxy]ethoxy]methyl]benzoic Acid (9). Yield (0.54 g, 89%). IR (KBr) 1690 cm^{-1} (C=O); ^{1}H NMR ($CDCl_3$) δ=3.6—4.4 (12H, m, CH_2O), 4.6 (2H, s, benzyl), 4.9 (2H, s, toluic benzyl), 6.9 (8H, s, phenylene), 7.3 (5H, s, aromatic of benzyl), 7.3—8.1 (4H, m, aromatic of toluic acid). Found: C, 71.07; H, 6.29%. Calcd for $C_{33}H_{34}O_8$: C, 70.95; H, 6.14%.

Extraction of Alkali Metal Salts of Ionophores. Ionophore (10^{-4} mol) was dissolved in 0.1 M alkali metal hydroxide (10 ml) in 50 ml vial. To 10 ml was diluted 0.1 ml of the aqueous solution and the optical density of the diluted solution (OD_0) was measured at 273 nm. To the native aqueous solution was added an organic solvent (20 ml) and the mixture was vigorously shaken 60 times by hand. The vial was allowed to stand for 2 d to separate the aqueous layer from the organic layer. The aqueous solution (0.1 ml) was diluted to 10 ml and optical density of the diluted solution (OD_1) was measured at 273 nm. Partition coefficient of a salt of a carboxylic ionophore was calculated as follows: Partition coefficient=$(OD_0-OD_1)/2OD_1$.

Ion Transport Experiment. Ion transport was carried out in U-type or H-type cells[1b] at 35±1 °C for 5 d with stirring at 200 rpm. Donor phase I contains 10 ml aqueous solution of an alkali metal hydroxide (0.1 M) and other alkali metal chlorides (0.1 M). Acceptor phase II contains 10 ml aqueous solution of HCl (0.1 M) and all alkali metal cations with chloride anion (0.1 M). Organic phase III contains an organic solution of a 10^{-4} mol ionophore. An aqueous solution at acceptor phase was diluted to an appropriate volume. The concentration of alkali metal ions (10—100 ppm) was determined to be c_0 and c_1 before and after transport experiment by flame spectrochemical analysis. Transported ion (%) was calculated by $[(c_1-c_0)/c_0]\times100$.

References

1) This series are as follows: a) N. Yamazaki, S. Nakahama, A. Hirao, and S. Negi, *Tetrahedron Lett.*, **1978**, 2429; b) N. Yamazaki, A. Hirao, and S. Nakahama, *J. Macromol. Sci., Chem.*, **A13**, 321 (1979); c) H. Kuboniwa, K. Yamaguchi, A. Hirao, S. Nakahama, and N. Yamazaki, *Chem. Lett.*, **1982**, 1937; d) H. Kuboniwa, S. Nagami, K. Yamaguchi, A. Hirao, S. Nakahama, and N. Yamazaki, *J. Chem. Soc., Chem. Commun.*, **1985**, 1468; e) H. Kuboniwa, K. Yamaguchi, A. Hirao, and S. Nakahama, *Mag. Res. Chem.*, **24**, 961 (1986).

2) a) Y. A. Ovchinnikov, V. T. Ivanov, and A. M. Shkrob, "Membrane Active Complexes, B. B. A. Library Vol. 12," Elsevier, New York (1974); b) B. C. Pressman, *Ann. Rev. Biochem.*, **45**, 501 (1976).

3) B. C. Pressman, *Fed. Proc.*, **27**, 1283 (1968).

4) a) C. J. Pedersen, *J. Am. Chem. Soc.*, **89**, 7017 (1967); b) D. J. Sam and H. E. Simmons, *J. Am. Chem. Soc.*, **94**, 4024 (1972).

5) K. Okahara and Y. Nakatsuji, "Topics in Current Chemistry 128. Biomimetic and Bioorganic Chemistry," ed by F. L. Boschke, Springer-Verlag, Berlin (1985), p. 37; and references cited therein.

6) K. Ziegler, A. Lüttringhaus, and K. Wöhlgemuth, *Ann. Chem.*, **162**, 528, (1937).

7) T. Yoshino, S. Inaba, and Y. Ishido, *Bull. Chem. Soc. Jpn.*, **46**, 553 (1973).

8) D. L. Hughes and J. N. Wingfield, *J. Chem. Soc., Chem. Commun.*, **1978**, 1001.

9) J. M. Timko, S. S. Moore, D. M. Walba, P. C. Hiberty, and D. J. Cram, *J. Am. Chem. Soc.*, **99**, 4207 (1977).

10) E. P. Kyba, R. C. Helgeson, K. Madan, G. W. Gokel, T. L. Tarnowski, S. S. Moore, and D. J. Cram, *J. Am. Chem. Soc.*, **99**, 2564 (1977).

11) D. Landini, F. Montanari, and F. Rolla, *Synthesis*, **1978**, 223.

12) a) T. Fujita, J. Iwasa, and C. Hansch, *J. Am. Chem. Soc.*, **86**, 5175 (1964); b) A. Leo, C. Hansch, and D. Elkins, *Chem. Rev.*, **71**, 525 (1971).

13) Through chloroform membrane, a carboxylic ionophore containing four ether oxygens based on oxypropylene moieties was reported to be selective for lithium ion. See K. Hiratani, *Chem. Lett.*, **1982**, 1021.

14) E. L. Eliel and D. E. Rivard, *J. Org. Chem.*, **17**, 1252 (1952).

15) E. J. Sakellarios, *Helv. Chim. Acta*, **29**, 1675 (1946).

Preparation of New Nitrogen-Bridged Heterocycles. 18.[1] Facile Formations of 3-Arylpyrazolo[1,5-*a*]pyridines and 1-Arylindolizines

Akikazu KAKEHI,* Suketaka ITO, Naosumi KINOSHITA, and Yukio ABAKA
Department of Industrial Chemistry, Faculty of Engineering, Shinshu University, Wakasato, Nagano 380
(Received November 14, 1987)

The alkaline treatment of 1-[(substituted benzylthio)methyleneamino]pyridinium and 1-[2-(substituted benzylthio)vinyl]pyridinium bromides possessing an electron-withdrawing substituent such as a nitro or cyano group in the presence or absence of a dehydrogenating agent afforded the corresponding 3-arylpyrazolo[1,5-*a*]-pyridines and 1-arylindolizines in moderate to good yields, while the reactions of the parent pyridinium salts and those having an electron-releasing group did not produce any significant products. The mode of the reaction, a ring contraction-desulfurization, is the same as that observed in related monocyclic species.

In a series of papers,[1,2] we have described convenient syntheses of various indolizines and pyrazolo[1,5-*a*]pyridines from the reactions of 1-[2-(substituted methylthio)vinyl]pyridinium and 1-[(substituted methylthio)methyleneamino]pyridinium halides with base in the presence or absence of a dehydrogenating agent. In addition, we stated that transient bicyclic intermediates such as **A** having a 12π system (see Fig. 1) are involved in these reactions and that their rearrangement and desulfurization aptitudes to give the corresponding heteroarmatics depend predominantly on the class of the substituent (R′). On the other hand, it is well-documented that the monocyclic 1,3,4-thiadiazinyl anion and related compounds such as **B** afforded only the desulfurized pyrazoles or pyrroles unless the substituent (R′) is hydrogen.[3] Since their substituents (R′) in both species **A** and **B** are not the same and there are some differences between their reactivities, however, it is still doubtful to conclude their mechanistic similarity. Therefore, it is worthwhile to introduce the same type of groups (R′=aryl group) in our bicyclic system **A** and to compare their reactivity with that of the monocyclic system **B**. In this paper we wish to report the generation of 4-arylpyrido[1,2-*d*]-1,3,4-thiadiazine and 1-arylpyrido[2,1-*c*]-1,4-thiazine intermediates and their transformations to desulfurized 3-arylpyrazolo[1,5-*a*]pyridines and 1-arylindolizines.

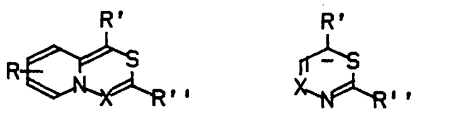

Fig. 1.

Results and Discussion

Preparations of 3-Arylpyrazolo[1,5-*a*]pyridines and 1-Arylindolizines. According to the procedure described in the syntheses of 3-cyano-, 3-ethoxycarbonyl-, and 3-aroylthiopyrazolo[1,5-*a*]pyridines,[2a,c,d] we examined first the reactions of 1-[(benzylthio)methyleneamino]pyridinium (**3a**) and 1-[(4-methylbenzylthio)-methyleneamino]pyridinium bromide (**3b**), readily obtainable from the *S*-alkylation of *N*-(1-pyridinio)-[(methylthio)thiocarbonyl]aminide (**1a**) with benzyl bromide (**2a**) and 4-methylbenzyl bromide (**2b**), in the presence of potassium carbonate in chloroform at room temperature. However, the expected heterocyclic products, 2-methylthio-3-phenyl- (**4a**) and 2-methylthio-3-(4-methylphenyl)pyrazolo[1,5-*a*]pyridine (**4b**), could not be detected. Similarly, the uses of other bases such as 1,8-diazabicyclo[5.4.0]undec-7-ene (DBU) or sodium hydride instead of potassium carbonate and of a dehydrogenating agent such as 2,3-dichloro-5,6-dicyano-*p*-benzoquinone (DDQ), chloranil, or lead tetraacetate in these reactions afforded always intractable tarry materials and no significant product could be isolated from them.[4] Since the inaccessibility of these heterocycles **4a, b** was ascribed to the lack of the acidity of the benzyl proton, we focused our attention on the reactions of pyridinium salts possessing a benzyl group activated with an electron-withdrawing group. As expected, the treatment of 1-[(2-nitrobenzylthio)-methyleneamino]pyridinium bromides (**3c—h**) with DBU followed by the addition of chloranil or DDQ to the resulting reaction solutions at 0 °C gave the corresponding 3-(2-nitrophenyl)pyrazolo[1,5-*a*]pyridine derivatives (**4c—h**) in 46—89% yields, respectively. Similar reactions of 1-[(4-nitrobenzylthio)-(**3i—n**), 1-[(2-cyanobenzylthio)- (**3o—t**), and 1-[(4-cyanobenzylthio)-methyleneamino]pyridinium bromides (**3u—z**) in the presence or absence of a dehydrogenating agent afforded 3-arylpyrazolo[1,5-*a*]pyridines derivatives (**4i—z**) in considerable yields. In all cases, the possible alternatives, 3-(arylthio)pyrazolo[1,5-*a*]pyridines such as **6**, were not formed. In the reactions of the salts **3s**, y, *N*-(1-pyridinio)-[1-(2-cyanobenzylthio)-(**5s**) and 1-[1-(4-cyanobenzylthio)carbonyl]aminide (**5y**) were also formed in 14 and 24% yields together with pyrazolopyridines **4s** (34%) and **4y** (29%) (Scheme 1).

On the other hand, similar treatment of 1-[2-(benzylthio)-(**8a**) and 1-[2-(4-methylbenzylthio)vinyl]-pyridinium bromide (**8b**) prepared from 1-(1-pyridinio)-

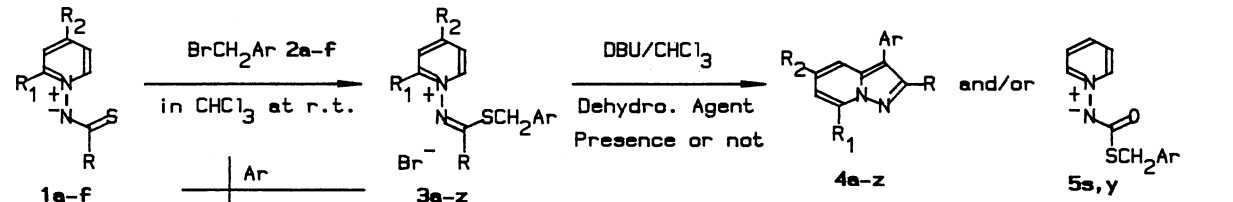

1a-f

	R_1	R_2	R
1a	H	H	SMe
1b	Me	H	SMe
1c	H	Me	SMe
1d	H	H	Ph
1e	H	H	OEt
1f	H	H	NMe_2

	Ar
2a	Ph
2b	C_6H_4Me-*p*
2c	$C_6H_4NO_2$-*o*
2d	$C_6H_4NO_2$-*p*
2e	C_6H_4CN-*o*
2f	C_6H_4CN-*p*

3a-z

Prod.	Salt	R_1	R_2	R	Ar
(4a)	3a	H	H	SMe	Ph
(4b)	3b	H	H	SMe	C_6H_4Me-*p*
4c	3c	H	H	SMe	$C_6H_4NO_2$-*o*
4d	3d	Me	H	SMe	$C_6H_4NO_2$-*o*
4e	3e	H	Me	SMe	$C_6H_4NO_2$-*o*
4f	3f	H	H	Ph	$C_6H_4NO_2$-*o*
4g	3g	H	H	OEt	$C_6H_4NO_2$-*o*
4h	3h	H	H	NMe_2	$C_6H_4NO_2$-*o*
4i	3i	H	H	SMe	$C_6H_4NO_2$-*p*
4j	3j	Me	H	SMe	$C_6H_4NO_2$-*p*
4k	3k	H	Me	SMe	$C_6H_4NO_2$-*p*
4l	3l	H	H	Ph	$C_6H_4NO_2$-*p*
4m	3m	H	H	OEt	$C_6H_4NO_2$-*p*
4n	3n	H	H	NMe_2	$C_6H_4NO_2$-*p*
4o	3o	H	H	SMe	C_6H_4CN-*o*
4p	3p	Me	H	SMe	C_6H_4CN-*o*
4q	3q	H	Me	SMe	C_6H_4CN-*o*
4r	3r	H	H	Ph	C_6H_4CN-*o*
4s(+5s)	3s	H	H	OEt	C_6H_4CN-*o*
4t	3t	H	H	NMe_2	C_6H_4CN-*o*
4u	3u	H	H	SMe	C_6H_4CN-*p*
4v	3v	Me	H	SMe	C_6H_4CN-*p*
4w	3w	H	Me	SMe	C_6H_4CN-*p*
4x	3x	H	H	Ph	C_6H_4CN-*p*
4y(+5y)	3y	H	H	OEt	C_6H_4CN-*p*
4z	3z	H	H	NMe_2	C_6H_4CN-*p*

	Ar
5s	C_6H_4CN-*o*
5y	C_6H_4CN-*p*

6

Scheme 1.

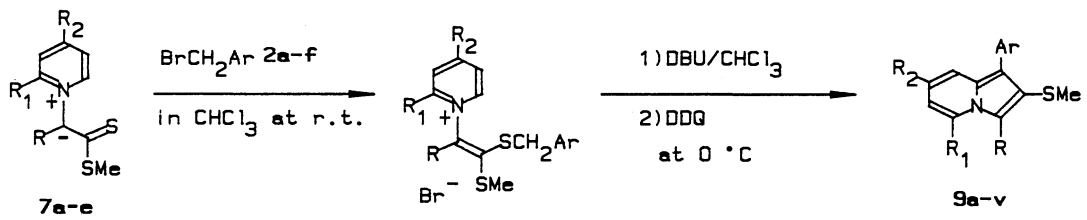

7a-e

	R_1	R_2	R
7a	H	H	COOEt
7b	Me	H	COOEt
7c	H	Me	COOEt
7d	H	H	CN
7e	H	H	COPh

8a-v

Prod.	Salt	R_1	R_2	R	Ar
(9a)	8a	H	H	COOEt	Ph
(9b)	8b	H	H	COOEt	C_6H_4Me-*p*
9c	8c	H	H	COOEt	$C_6H_4NO_2$-*o*
9d	8d	Me	H	COOEt	$C_6H_4NO_2$-*o*
9e	8e	H	Me	COOEt	$C_6H_4NO_2$-*o*
9f	8f	H	H	CN	$C_6H_4NO_2$-*o*
9g	8g	H	H	COPh	$C_6H_4NO_2$-*o*
9h	8h	H	H	COOEt	$C_6H_4NO_2$-*p*
9i	8i	Me	H	COOEt	$C_6H_4NO_2$-*p*
9j	8j	H	Me	COOEt	$C_6H_4NO_2$-*p*
9k	8k	H	H	CN	$C_6H_4NO_2$-*p*
9l	8l	H	H	COPh	$C_6H_4NO_2$-*p*
9m	8m	H	H	COOEt	C_6H_4CN-*o*
9n	8n	Me	H	COOEt	C_6H_4CN-*o*
9o	8o	H	Me	COOEt	C_6H_4CN-*o*
9p	8p	H	H	CN	C_6H_4CN-*o*
9q	8q	H	H	COPh	C_6H_4CN-*o*
9r	8r	H	H	COOEt	C_6H_4CN-*p*
9s	8s	Me	H	COOEt	C_6H_4CN-*p*
9t	8t	H	Me	COOEt	C_6H_4CN-*p*
9u	8u	H	H	CN	C_6H_4CN-*p*
9v	8v	H	H	COPh	C_6H_4CN-*p*

9a-v

Scheme 2.

[(methylthio)thiocarbonyl]methylide (**7a**) and benzyl bromides (**2a, b**) did not afford any products, but those of pyridinium salts **8c—v** obtained from methylides **7a—e** and bromides **2c—f** gave the corresponding 1-aryl-2-(methylthio)indolizine dervatives (**9c—v**) in moderate yields, respectively (Scheme 2).

The structures of 3-arylpyrazolo[1,5-*a*]pyridines (**4c—z**), and 1-arylindolizines (**9c—v**) were determined mainly by their elemental analyses and their IR and ^1H NMR spectral inspections. For example, the elemental analyses of pyrazolopyridines **4c—z** and indolizines **9c, e—m, o—v** were in good accord with the proposed compositions but not with their arylthio analogs such as **6**. The chemical shifts and signal

patterns of the pyridine moiety in the ^{1}H NMR spectra (see Tables 1 and 2) of compounds **4c—z** and **9c—v** were similar to those of various pyrazolo[1,5-*a*]pyridine and indolizine derivatives previously reported.[1,2,5] The IR spectra of products **4c—n** and **9c—l** showed two characteristic nitro absorption bands at near 1510 and 1340 cm^{-1} and compounds **4o—z** and **9m—v** exhibited a cyano absorption band at near 2220 cm^{-1}. The structures of *N*-(1-pyridinio) [1-(substituted benzylthio)carbonyl]aminides (**5s**, y) were established by their spectral inspection and their independent syntheses. In particular, the elemental analyses and the ^{1}H NMR spectra of **5s**, y clearly showed the absence of the ethoxy moiety in these molecules, and the thermolyses of pyridinium salts **3s**, y in chloroform at the reflux temperature gave the same *N*-ylides **5s**, y in 88 and 90% yields. From these results and our previous observation of the smooth dealkylation of 1-(2-alkoxyvinyl)pyridinium halides[2b] we concluded compounds **5s**, y are *N*-(1-pyridinio) aminides.

Reductions of the Nitro Group. Since the versatility of a nitro group to various functional groups is well-known, the transformations of some 4-nitrophenyl derivatives to 4-aminophenyl compounds were investigated. The hydrogenation of 2-methylthio-3-(4-nitrophenyl)pyrazolo[1,5-*a*]pyridines (**4i—k**) and ethyl 2-methylthio-1-(4-nitrophenyl)indolizine-3-carboxylates (**9h—j**) over palladium on charcoal (10%) in THF proceeded smoothly to give the corresponding 4-aminophenyl derivatives **10a—f** in good yields, respectively. These transformations complement our present method in which an aryl group having an electron-donating group can not be introduced to the corresponding heteroaromatics.

The structures of these compounds **10a—f** were determined mainly by the presence of the primary amino absorption bands appeared in the range of 3321—3620 cm^{-1} and by the absence of the nitro bands in their IR spectra.

Reaction Mechanism. A possible mechanism for these reactions is shown in Scheme 4. The corresponding 3-arylpyrazolo[1,5-*a*]pyridines (**4c—z**) and 1-aryl-

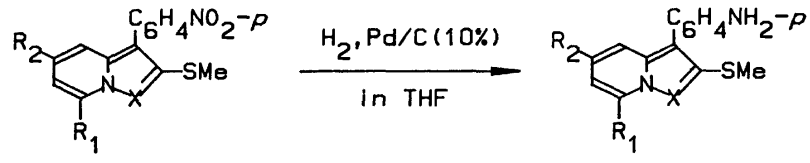

Prod.	React.	R_1	R_2	X
10a	4i	H	H	N
10b	4j	Me	H	N
10c	4k	H	Me	N
10d	9h	H	H	CCOOEt
10e	9i	Me	H	CCOOEt
10f	9j	H	Me	CCOOEt

Scheme 3.

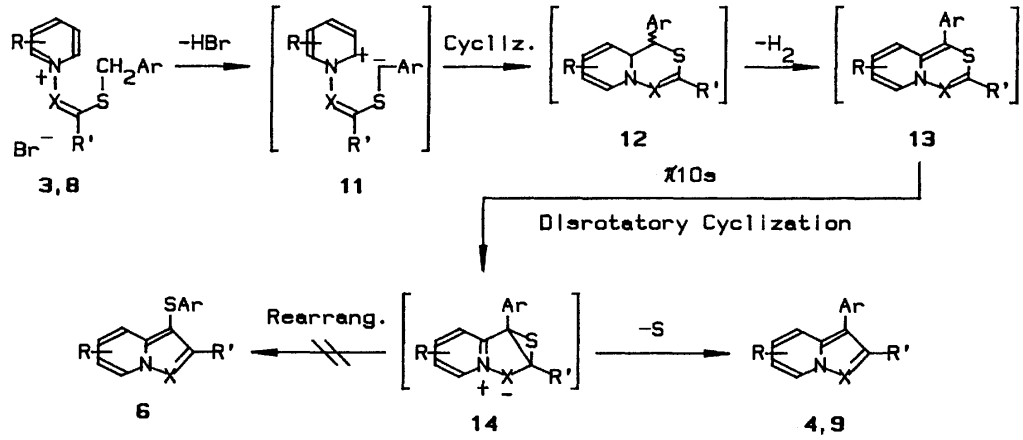

Scheme 4.

indolizines (**9c—v**) were formed only from pyridinium salts **3c—z** and **8c—v** having a benzyl substituent activated by an electron-withdrawing group but not from those **3a, b** and **8a, b** possessing a parent or methyl-substituted benzyl group; accordingly it can be presumed that the benzyl proton must be acidic for the generation of the zwitterionic intermediate **11**. Furthermore, it is noted that these reactions proceeded via the ring contraction-desulfurization of transient 1-arylpyrido[2,1-*c*]-1,4-thiazine and its 4-aza-analog such as **13** but not via their ring contraction-rearrangement leading to arylthio derivatives such as **6**. This behavior is the same as that in related monocyclic species, since Schmidt and Huth reported already the smooth transformations of monocyclic 2,6-diphenyl-1,3-thiazinyl and 6-phenyl-1,3,4-thiadiazinyl anions to the desulfurized 2,3-diphenylpyrrole and 4-phenylpyrazole.[3]

Our method for the preparation of 3-arylpyrazolopyridines and 1-arylindolizines, even if a parent phenyl and electron-rich aryl groups could not be introduced into them, has still a high value because of the cheapness and ready availability of the starting materials, and the wide versatility of the heterocycles formed.

Table 1. ^{1}H NMR Spectral Data of Pyrazolopyridines in $CDCl_3$

Compd[a]	C-4	C-5	C-6	C-7	R	Ar
4c	b)	b)	6.76 dt	8.49 br d	2.58 s	7.4—8.3 m
4d	b)	b)	6.65 m	2.76 s	2.59 s	7.4—8.3 m
4e	7.00 br s	2.33 s	6.60 dd	8.37 d	2.58 s	7.4—8.3 m
4f	c)	c)	6.83 dt	8.58 br d	7.1—8.2 m	7.1—8.2 m
4g	c)	7.18 br t	6.71 dt	8.35 br d	1.41 t, 4.41 q	7.3—8.2 m
4h	d)	d)	6.65 m	8.33 br d	2.82 s	7.3—8.2 m
4i	7.66 br d	7.29 br t	6.81 dt	8.51 br d	2.69 s	7.6—8.5 m
4j	7.59 br d	7.21 q	6.69 br d	2.78 s	2.71 s	7.6—8.5 m
4k	7.41 br s	2.40 s	6.65 dd	8.41 d	2.68 s	7.6—8.5 m
4l	c)	c)	6.85 dt	8.55 br d	7.0—8.4 m	7.0—8.4 m
4m	7.68 br d	7.23 br t	6.71 dt	8.29 br d	1.48 t, 4.48 q	7.6—8.4 m
4n	7.58 br d	7.22 br t	6.73 dt	8.41 br d	2.90 s	7.7—8.6 m
4o	c)	c)	6.77 dt	8.48 br d	2.64 s	7.0—8.0 m
4p	c)	c)	6.66 br d	2.75 s	2.66 s	7.0—8.0 m
4q	7.17 br s	2.38 s	6.66 dd	8.42 d	2.63 s	7.3—8.0 m
4r	c)	c)	6.85 dt	8.59 br d	7.0—8.0 m	7.0—8.0 m
4s	c)	c)	6.70 dt	8.33 br d	1.47 t, 4.50 q	7.0—8.0 m
4t	c)	c)	6.63 m	8.32 br d	2.81 s	6.9—8.0 m
4u	7.64 br d	7.26 br t	6.81 dt	8.52 br d	2.69 s	7.5—8.0 m
4v	7.58 br d	7.20 q	6.68 br d	2.78 s	2.70 s	7.5—8.0 m
4w	7.38 br s	2.41 s	6.64 dd	8.39 d	2.67 s	7.5—8.0 m
4x	c)	c)	6.85 dt	8.58 br d	7.0—7.9 m	7.0—7.9 m
4y	7.52 br d	7.22 br t	6.72 dt	8.34 br d	1.49 t, 4.49 q	7.5—8.0 m
4z	7.48 br d	7.11 br t	6.65 dt	8.34 br d	2.87 s	7.76 s

a) The coupling constants are as follows: $J_{4,5}$=9.0, $J_{5,6}$=$J_{6,7}$=7.0, $J_{4,6}$=2.0, J_{Et}=7.0. b) Overlapped with each other at δ 6.9—7.4. c) Overlapped with the phenyl proton signals. d) Overlapped with each other at δ 6.8—7.3.

Table 2. ^{1}H NMR Spectral Data of Indolizines in $CDCl_3$

Compd[a]	C-5	C-6	C-7	C-8	SMe	R	Ar
9c	9.57 br d	6.81 dt	7.03 br t	7.25 br d	2.23 s	1.46 t, 4.47 q	7.4—8.3 m
9d	2.57 s	6.60 br d	6.92 q	7.17 br d	2.24 s	1.46 t, 4.48 q	7.4—8.3 m
9e	9.48 d	6.72 dd	2.31 s	6.98 br s	2.25 s	1.47 t, 4.49 q	7.4—8.3 m
9f	8.28 br d	6.88 dt	7.09 br t	7.28 br d	2.40 s	—	7.4—8.3 m
9g	9.55 br d	6.92 dt	7.18 br t	7.40 br d	1.74 s	7.0—8.3 m	7.4—8.3 m
9h	9.55 br d	6.91 dt	7.15 br t	7.55 br d	2.28 s	1.50 t, 4.52 q	7.6—8.6 m
9i	2.57 s	6.60 br d	6.98 q	7.47 br d	2.20 s	1.47 t, 4.50 q	7.6—8.5 m
9j	9.51 d	6.77 dd	2.31 s	7.34 br s	2.26 s	1.47 t, 4.51 q	7.6—8.6 m
9k	b)	6.98 dt	7.23 br t	7.67 br d	2.49 s	—	7.7—8.6 m
9l	9.52 br d	6.93 dt	7.23 br t	b)	1.78 s	7.5—8.6 m	7.5—8.6 m
9m	9.59 br d	6.85 dt	7.08 br t	7.28 br d	2.32 s	1.49 t, 4.51 q	7.3—8.0 m
9n	2.56 s	6.59 br d	6.93 q	7.15 br d	2.29 s	1.44 t, 4.47 q	7.3—8.0 m
9o	9.49 d	6.73 dd	2.35 s	7.00 br s	2.35 s	1.48 t, 4.50 q	7.2—8.0 m
9p	8.33 br d	6.90 dt	7.12 br t	7.35 br d	2.49 s	—	7.4—8.0 m
9q	9.60 br d	6.94 dt	b)	b)	1.77 s	7.1—8.1 m	7.1—8.1 m
9r	9.55 br d	6.87 dt	7.11 br t	7.51 br d	2.26 s	1.49 t, 4.51 q	7.5—8.0 m
9s	2.58 s	6.62 br d	6.98 q	7.46 br d	2.21 s	1.48 t, 4.51 q	7.5—8.0 m
9t	9.45 d	6.73 dd	2.34 s	7.27 br s	2.23 s	1.48 t, 4.50 q	7.5—8.0 m
9u	8.31 br d	6.91 dt	7.16 br t	7.37 br d	2.46 s	—	7.4—8.0 m
9v	9.49 br d	6.90 dt	7.20 br t	b)	1.77 s	7.4—8.0 m	7.4—8.0 m

a) The coupling constants are as follows: $J_{5,6}$=$J_{6,7}$=7.0, $J_{7,8}$=9.0, $J_{6,8}$=2.0, and J_{Et}=7.0 Hz. b) Overlapped with the phenyl proton signals.

Experimental

Melting points were measured with a Yanagimoto micro-melting point apparatus and are uncorrected. The microanalyses were carried out on a Perkin-Elmer elemental analyzer. The ^{1}H NMR spectra were determined with a Varian EM360A spectrometer in deuteriochloroform with tetramethylsilane as an internal standard; the chemical shifts are expressed in δ values. The IR spectra were taken with a Hitachi 260-10 infrared spectrophotometer.

Materials. *N*-(1-Pyridinio) aminides (**1a—f**) and 1-(1-pyridinio) methylides (**7a—e**) employed in the above reactions were prepared according to the procedures described in the literatures.[2,6]

Preparations of 3-Arylpyrazolo[1,5-*a*]pyridines and 1-Arylindolizines. General Method A. A solution of pyridinum *N*-ylide (2 mmol) and benzyl bromide (2.2 mmol) in chloroform (20 ml) was kept at room temperature until the spot of the *N*-ylide completely disappeared (1—4 d, by TLC monitoring). The resulting solution was concentrated under reduced pressure and the residue was washed three times with ether to remove unaltered benzyl bromide. To the chloroform solution (30 ml) of the pyridinium salt, DBU (0.38g, 2.5 mmol) was added dropwise and the resulting mixture was stirred at room temperature for 1 d. The solution was concentrated at reduced pressure, and the residual oil was separated by column chromatography (alumina) using chloroform as eluent. The removal of the solvent and recrystallization from chloroform-hexane gave the corresponding pyrazolo[1,5-*a*]pyridines.

Method B. To the chloroform solution of pyridinium bromide (2 mmol) prepared in Method A, DBU (0.38g, 2.5 mmol) was added dropwise in an ice bath. After 10 min, chloranil (0.49 g, 2 mmol) was added and the resulting mixture was allowed to react for a further 12 h at that temperature (0 °C). The solution was filtered to remove insoluble substances and the filtrate was concentrated under reduced pressure. The same work-up as described above afforded pyrazolo[1,5-*a*]pyridines.

Method C. In the procedure described in Method B, DDQ (0.45g, 2 mmol) instead of chloranil was used as a dehydrogenating agent.

Only 3-(4-nitrophenyl)pyrazolo[1,5-*a*]pyridine derivatives **4i—n** were formed without a dehydrogenating agent (Method A), but none of the other pyrazolo[1,5-*a*]pyridines **4c—h, o—z** and indolizines **9c—v** could be obtained by this method because 4,4a-dihydropyrido[1,2-*d*]-1,3,4-thiadiazine[2c] and 1,9a-dihydropyrido[2,1-*c*]-1,4-thiazine derivatives[2a,e] such as **12** generated in situ from the corresponding pyridinium salts **3c—h, o—z** were not oxidized under the conditions employed here.

The reactions of pyridinium salts such as **3a, b** and **8a, b**, prepared from pyridinium *N*-ylides **1a** and **7a** and benzyl bromide (**2a**), 4-methylbenzyl bromide (**2b**), 4-chlorobenzyl bromide, and 4-bromobenzyl bromide, were carried out under several reaction conditions, but no significant products could be isolated.

Compounds **4c, e, g, k, m, n** and **9c, g** were obtained as orange prisms, **4d** and **9e, j** as orange needles, **4f, l** and **9f, h, i, k, l, v** as yellow needles, **4h** as violet needles, **4i, j** and **9q** as

Table 3. Some Physical and Analytical Data of 3-Arylpyrazolo[1,5-*a*]pyridines

Compd No.	Salt (SM[a])	Method (%)			Mp	$\nu^{KBr}_{NO_2 \text{ or } CN}$/cm^{-1}		Formula[b]
		A	B	C	θ_m/°C			
4a	**3a(1a,2a)**	0	0	0				
4b	**3b(1a,2b)**	0	0	0				
4c	**3c(1a,2c)**	0	75	83	125—127	1521	1352	$C_{14}H_{11}N_3O_2S$
4d	**3d(1b,2c)**		70	80	111—113	1514	1346	$C_{15}H_{13}N_3O_2S$
4e	**3e(1c,2c)**		88	89	109—111	1516	1347	$C_{15}H_{13}N_3O_2S$
4f	**3f(1d,2c)**		46	58	111—114	1512	1346	$C_{19}H_{13}N_3O_2$
4g	**3g(1e,2c)**		60	65	133—135	1504	1349	$C_{15}H_{13}N_3O_3$
4h	**3h(1f,2c)**		88		122—124	1513	1348	$C_{15}H_{14}N_4O_2$
4i	**3i(1a,2d)**	89			180—182	1508	1343	$C_{14}H_{11}N_3O_2S$
4j	**3j(1b,2d)**	79			169—172	1501	1344	$C_{15}H_{13}N_3O_2S$
4k	**3k(1c,2d)**	91			202—205	1503	1340	$C_{15}H_{13}N_3O_2S$
4l	**3l(1d,2d)**	74			188—190	1502	1336	$C_{19}H_{13}N_3O_2$
4m	**3m(1e,2d)**	54			168—170	1490	1309	$C_{15}H_{13}N_3O_3$
4n	**3n(1f,2d)**	89			121—123	1496	1341	$C_{15}H_{14}N_4O_2$[c]
4o	**3o(1a,2e)**		42		116—117	2219		$C_{15}H_{11}N_3S$
4p	**3p(1b,2e)**		38	54	117—119	2218		$C_{16}H_{13}N_3S$
4q	**3q(1c,2e)**		41	48	147—149	2218		$C_{16}H_{13}N_3S$
4r	**3r(1d,2e)**		34		144—146	2220		$C_{20}H_{13}N_3$
4s[d]	**3s(1e,2e)**			34	135—137	2216		$C_{16}H_{13}N_3O$
4t	**3t(1f,2e)**		37		122—123	2218		$C_{16}H_{14}N_4$
4u	**3u(1a,2f)**		51		207—209	2220		$C_{15}H_{11}N_3S$
4v	**3v(1b,2f)**		49		157—158	2218		$C_{16}H_{13}N_3S$
4w	**3w(1c,2f)**		55		217—219	2220		$C_{16}H_{13}N_3S$
4x	**3x(1d,2f)**		34		166—169	2218		$C_{20}H_{13}N_3$
4y[e]	**3y(1e,2f)**			29	157—159	2220		$C_{16}H_{13}N_3O$
4z	**3z(1f,2f)**		30		154—156	2220		$C_{16}H_{14}N_4$

a) Starting materials. b) Satisfactory analytical data (within 0.3% for C, H, and N) were obtained for all new compounds except **4n**. c) Found: C, 63.49; H, 5.03; N, 20.15%. Calcd for $C_{15}H_{14}N_4O_2$: C, 63.82; H, 5.00; N, 19.85%. d) Plus **5s**, 14%. e) Plus **5y**, 24%.

Table 4. Some Physical and Analytical Data of 1-Arylindolizines

Compd No.	Salt (SM[a])	Yield[b] %	Mp θ_m/°C	ν^{KBr}/cm^{-1}			Formula[c]
9a	**8a**(**7a**,**2a**)	0					
9b	**8b**(**7a**,**2b**)	0					
9c	**8c**(**7a**,**2c**)	56	98—100	1654	1513	1348	$C_{18}H_{16}N_2O_4S$
9d	**8d**(**7b**,**2c**)	18	[d]	1695	1520	1348[e]	[f]
9e	**8e**(**7c**,**2c**)	33	134—136	1660	1519	1343	$C_{19}H_{18}N_2O_4S$
9f	**8f**(**7d**,**2c**)	20	179—181	2198	1515	1346	$C_{16}H_{11}N_3O_2S$
9g	**8g**(**7e**,**2c**)	28	127—128	1592	1513	1348	$C_{22}H_{16}N_2O_3S$
9h	**8h**(**7a**,**2d**)	68	128—129	1662	1507	1344	$C_{18}H_{16}N_2O_4S$
9i	**8i**(**7b**,**2d**)	10	122—124	1709	1506	1334	$C_{19}H_{18}N_2O_4S$
9j	**8j**(**7c**,**2d**)	64	171—172	1672	1504	1329	$C_{19}H_{18}N_2O_4S$
9k	**8k**(**7d**,**2d**)	25	180—182	2201	1507	1340	$C_{16}H_{11}N_3O_2S$
9l	**8l**(**7e**,**2d**)	37	141—143	1590	1508	1336	$C_{22}H_{16}N_2O_3S$
9m	**8m**(**7a**,**2e**)	37	130—131	2221	1673		$C_{19}H_{16}N_2O_2S$
9n	**8n**(**7b**,**2e**)	21	[d]	2221	1699[e]		[f]
9o	**8o**(**7c**,**2e**)	28	144—145	2221	1660		$C_{20}H_{18}N_2O_2S$
9p	**8p**(**7d**,**2e**)	22	162—163	2220	2200		$C_{17}H_{11}N_3S$
9q	**8q**(**7e**,**2e**)	14	149—150	2223	1591		$C_{23}H_{16}N_2OS$
9r	**8r**(**7a**,**2f**)	53	110—111	2225	1665		$C_{19}H_{16}N_2O_2S$
9s	**8s**(**7b**,**2f**)	10	130—132	2224	1690		$C_{20}H_{18}N_2O_2S$
9t	**8t**(**7c**,**2f**)	21	157—159	2221	1664		$C_{20}H_{18}N_2O_2S$
9u	**8u**(**7d**,**2f**)	13	209—210	2221	2200		$C_{17}H_{11}N_3S$
9v	**8v**(**7e**,**2f**)	11	168—169	2225	1591		$C_{23}H_{16}N_2OS$

a) Starting materials. b) All of these yields were obtained by Method C. c) Satisfactory analytical data (within 0.3% for C, H, and N) were obtained for all new compounds except **9d**, **n**. d) Viscous oil. e) Neat. f) The preparation of a pure sample for analysis was unsuccessful.

yellow prisms, **4o—r**, **t**, **x** as colorless prisms, **4s**, **u—w** and **9m**, **p**, **s** as colorless needles, **4y**, **z** and **9o**, **r**, **t**, **u** as pale yellow needles, **9d** as orange viscous oil, and **9n** as yellow viscous oil.

These results together with some physical and analytical data are summarized in Tables 1—4.

Thermolyses of 1-[(2- or 4-Cyanobenzylthio)ethoxymethyleneanimo]pyridinium Bromides. General Method. Pyridinium bromide (**3s** or **3y**, 2 mmol) prepared as above was heated under reflux in chloroform (30 ml) on a water bath for 12 h. The usual work-up of the resulting solution and recrystallization from chloroform-ether gave *N*-(1-pyridinio)-[1-(2- or 4-cyanobenzylthio)carbonyl]aminides: **5s**, 88%, colorless needles, mp 119—121 °C, IR ν (KBr) 2218 (CN) and 1598 cm^{-1} (CO). ^{1}H NMR ($CDCl_3$) δ=4.33 (2H, s, SCH_2), 7.1—8.2 (7H, m, phenyl protons and 3-, 4-, and 5-protons), and 8.7—9.0 (2H, m, 2- and 6-protons). Anal. ($C_{14}H_{11}N_3OS$) C, H, N. **5y**, 90%, colorless needles, mp 135—136 °C, IR ν (KBr) 2221 (CN) and 1588 cm^{-1} (CO). ^{1}H NMR ($CDCl_3$) δ=4.14 (2H, s, SCH_2), 7.3—8.3 (7H, m, phenyl protons and 3-, 4-, and 5-protons), and 8.7—9.0 (2H, m, 2- and 6-protons). Anal. ($C_{14}H_{11}N_3OS$) C, H, N. These compounds **5s**, y were completely in accord with those obtained from the alkaline treatement of the salts **3s**, y.

Reduction of the Nitro Group. General Method. A mixture of 4-nitrophenyl derivatives (0.5 mmol), palladium on carbon (10%, 0.5 g), and THF (50 ml) was stirred at room temperature under hydrogen (1 atmosphere) for 1 d. The resulting mixture was filtered to remove the catalyst, and the filtrate was concentrated under reduced pressure. The residue was separated by column chromatography on alumina using chloroform as eluent. The removal of the solvent and the recrystallizations from chloroform-hexane afforded the corresponding 4-aminophenyl compounds **10c—f**. On the other hand, 3-(4-aminophenyl)-2-(methylthio)pyrazolo-[1,5-*a*]pyridines **10a**, **b** were converted to the *N*-acetyl derivatives by the action of acetic anhydride/pyridine because they were unstable and the preparation of pure samples for analyses was unsuccessful.

Some physical and analytical data of these 4-aminophenyl derivatives are shown below: **10a**, 96%, unstable colorless crystals, IR ν (KBr) 3330 and 3420 cm^{-1} (NH_2), ^{1}H NMR ($CDCl_3$) δ=2.62 (3H, s, SMe), 3.62 (2H, br s, NH_2), 6.5—7.7 (7H, m, 4-, 5-, 6-H, and phenyl protons), and 8.48 (1H, br d, J=7.0 Hz, 7-H). Its *N*-acetyl derivative, pale yellow prisms, mp 140—143 °C. Anal. ($C_{16}H_{15}N_3OS+H_2O$) C, H, N. **10b**, 86%, unstable colorless crystals, IR ν (KBr) 3321 and 3419 cm^{-1} (NH_2), ^{1}H NMR ($CDCl_3$) δ=2.62 (3H, s, SMe), 2.73 (3H, s, 7-Me), 3.61 (2H, br s, NH_2), 6.88 (1H, br d, 6-H), and 6.7—7.6 (6H, m, 4-, 5-H, and phenyl protons). Its *N*-acetyl derivatives, pale yellow prisms, mp 77—79 °C. Anal. ($C_{17}H_{17}N_3OS+H_2O$) C, H, N. **10c**, 92%, colorless prisms, mp 115—118 °C, IR ν (KBr) 3325 and 3392 cm^{-1} (NH_2), ^{1}H NMR ($CDCl_3$) δ=2.33 (3H, s, 5-Me), 2.61 (3H, s, SMe), 3.24 (2H, br s, NH_2), 6.50 (1H, dd, J=7.0 and 2.0 Hz, 6-H), 6.7—7.6 (5H, m, 4-H and phenyl protons), and 8.32 (1H, d, J=7.0 Hz, 7-H). Anal. ($C_{15}H_{15}N_3S$) C, H, N. **10d**, 99%, pale yellow prisms, mp 104—107 °C, IR ν (KBr) 1670 (CO), 3341 and 3420 cm^{-1} (NH_2), ^{1}H NMR ($CDCl_3$) δ=1.46 (3H, t, J=7.0 Hz, $OCH_2C\underline{H}_3$), 2.21 (3H, s, SMe), 3.33 (2H, br s, NH_2), 4.48 (2H, q, J=7.0 Hz, $OC\underline{H}_2CH_3$), 6.6—7.6 (7-H, m, 6-, 7-, 8-H, and phenyl protons), 9.47 (1H, br d, J=7.0 Hz, 5-H). Anal. ($C_{18}H_{18}N_2O_2S$) C, H, N. **10e**, 57%, pale yellow prisms, mp 144—146 °C, IR ν (KBr) 1665 (CO), 3377 and 3462 cm^{-1} (NH_2), ^{1}H NMR ($CDCl_3$) δ=1.45 (3H, t, J=7.0 Hz, $OCH_2C\underline{H}_3$), 2.19 (3H, s, SMe), 2.53 (3H, s, 5-Me), 3.51 (2H, br s, NH_2), 4.47 (2H, q, J=7.0 Hz, $OC\underline{H}_2CH_3$), 6.51 (1H, br d, J=7.0 Hz, 6-H), and 6.6—7.6 (6H, 7-, 8-H, and phenyl pro-

tons). Anal. ($C_{19}H_{20}N_2O_2S$) C, H, N. **10f**, 99%, pale yellow prisms, mp 164—167 °C, IR ν (KBr) 1650 (CO), 3370 and 3456 cm^{-1} (NH_2), ^1H NMR ($CDCl_3$) δ=1.45 (3H, t, J=7.0 Hz, $OCH_2\underline{CH_3}$), 2.19 (3H, s, SMe), 2.28 (3H, s, 7-Me), 3.41 (2H, br s, NH_2), 4.46 (2H, q, J=7.0 Hz, $OC\underline{H_2}CH_3$), 6.59 (1H, dd, J=7.0 and 2.0 Hz, 6-H), 6.6—7.4 (5H, m, 8-H and phenyl protons), and 9.35 (1H, d, J=7.0 Hz, 5-H). Anal. ($C_{19}H_{20}N_2O_2S$) C, H, N.

References

1) For part 17 of this series, see A. Kakehi, S. Ito, S. Matsumoto, and Y. Morimoto, *Chem. Lett.*, **1987**, 2043.

2) a) A. Kakehi, S. Ito, M. Ito, and T. Yotsuya, *Heterocycles*, **22**, 2337 (1984); b) A. Kakehi, S. Ito, S. Yonezu, K. Maruta, and K. Yuito, *ibid*, **23**, 33 (1985); c) A. Kakehi, S. Ito, M. Ito, T. Yotsuya, and K. Nagata, *Bull. Chem. Soc. Jpn.*, **58**, 1432 (1985); d) A. Kakehi, S. Ito, K. Nagata, N. Kinoshita, and N. Kakinuma, *Chem. Pharm. Bull.*, **35**, 156 (1987); e) A. Kakehi, S. Ito, S. Yonezu, K. Maruta, K. Yuito, M. Shiohara, and K. Adachi, *Bull. Chem. Soc. Jpn.*, **60**, 1867 (1987); f) A. Kakehi, S. Ito, Y. Ohno, S. Shiba, and S. Kamata, *Bull. Chem. Soc. Jpn.*, **60**, 3713 (1987).

3) R. R. Schmidt, *Angew. Chem., Int. Ed. Engl.*, **14**, 581 (1975); R. R. Schmidt and H. Huth, *Tetrahedron Lett.*, **1975**, 33.

4) Similar reactions of the pyridinium salts, prepared from pyridinium *N*-ylides **1a** and **7a** and 4-chlorobenzyl bromide and 4-bromobenzyl bromide, did not provide any significant products.

5) C. Maseda, M. Sone, Y. Tominaga, R. Natsuki, Y. Matsuda, and G. Kobayashi, *Yakugaku Zasshi*, **94**, 839 (1974); Y. Tominaga, H. Fujito, K. Mizuyama, Y. Matsuda, and G. Kobayashi, *Chem. Pharm. Bull.*, **25**, 1519 (1977); H. Pauls and F. Krohnke, *Chem. Ber.*, **110**, 1294 (1977); A. Kakehi , S. Ito, T. Maeda, R. Takeda, M. Nishimura, M. Tamashima, and T. Yamauchi, *J. Org. Chem.*, **43**, 4837 (1978); E. K. Pohjara, *J. Heterocycl. Chem.*, **15**, 955 (1978); K. Matsumoto, T. Uchida, Y. Ikemi, T. Tanaka, M. Asahi, T. Kato, and H. Konishi, *Bull. Chem. Soc. Jpn.*, **60**, 3645 (1987).

6) Y. Tominaga, Y. Miyake, H. Fujito, Y. Matsuda, and G. Kobayashi, *Yakugaku Zasshi*, **97**, 927 (1977); A. Kakehi, S. Ito, and K. Watanabe, *Bull. Chem. Soc. Jpn.*, **53**, 1775 (1980); H. Yoshida, K. Urushibata, and T. Ogata, *ibid.*, **56**, 1561 (1983).

 © 1988 The Chemical Society of Japan Bull. Chem. Soc. Jpn., 61, 2063—2066 (1988)

An Observation on Carboxylation of 4*H*-Cyclopenta[*def*]phenanthrene

Masahiro MINABE,* Keisuke ISOZUMI, Ken-ichi KAWAI, and Masaaki YOSHIDA
Department of Industrial Chemistry, Faculty of Engineering, Utsunomiya University, Ishiicho, Utsunomiya 321
(Received November 18, 1987)

Photocarboxylation of 4*H*-cyclopenta[*def*]phenanthrene by carbon dioxide in the presence of *N*,*N*-dimethylaniline in dimethyl sulfoxide afforded 8,9-dihydro-4*H*-cyclopenta[*def*]phenanthrene-8- and 2-carboxylic acid, and 4*H*-cyclopenta[*def*]phenanthrene-8-carboxylic acid. These acids were derived into methyl-4*H*-cyclopenta[*def*]phenanthrenes.

The synthesis of arenecarboxylic acids was achieved by various methods, such as the hydrolysis of carboxylic acid derivatives, the oxidation of aralkyl reactants, the carbonylation of organometallic compounds, a direct carboxylation of arenes by carbonyl compounds, and a Kolbe-Schmidt reaction of phenols.[1] One recent advance in this field is the reductive carboxylation of arenes by photoirradiation in the presence of amine and carbon dioxide (CO_2), developed by Tazuke and colaboratorians: irradiation upon a mixture of phenanthrene and *N*,*N*-dimethylaniline (DMA) in dimethyl sulfoxide (DMSO) in the presence of CO_2 afforded 9,10-dihydro-9-phenanthrenecarboxylic acid.[2,3] Similar reactions have been applied to anthracene,[3] pyrene,[3] naphthalene,[2] and biphenyl,[2] giving the corresponding dihydro carboxylic acids.

During the course of studies on the reactivities of 4*H*-cyclopenta[*def*]phenanthrene (**1**),[4] 4*H*-cyclopenta[*def*]phenanthrene-8-carboxylic acid (**2a**)[5] has been required as a synthetic intermediate, in spite of the 8-derivatives being fairly hard to form by a direct acylation of **1**. The present paper deals with the photocarboxylation of **1** and with the conduction of carboxylic acid isomers of **1** to the corresponding methyl derivatives. This would suggest that the procedure has the possibility to promote a substitutional carboxylation of an aryl compound, in addition to reductive carboxylation.

Photoirradiation upon **1** and DMA in DMSO with bubbling of CO_2 afforded three kinds of monocarboxylic acid **2a**,[5] **3a**,[5] and **4a**, dimeric dibasic acid isomers **5a** and **6a**, and reductive hydrocarbon **7** as the derivatives of **1**, accompanied by bis(*p*-dimethylaminophenyl)methane (**8**)[6] and *p*-(dimethylamino)benzyl methyl sulfone (**9**) (Scheme 1).[7] The formations of **8** and **9** are ascribed to a reaction between DMA and DMSO under the conditions: *p*-(dimethylamino)benzyl methyl sulfoxide is temporarily assumed to be formed by the interaction of a radical cation of DMA with the carbanion of DMSO followed by the abstraction of

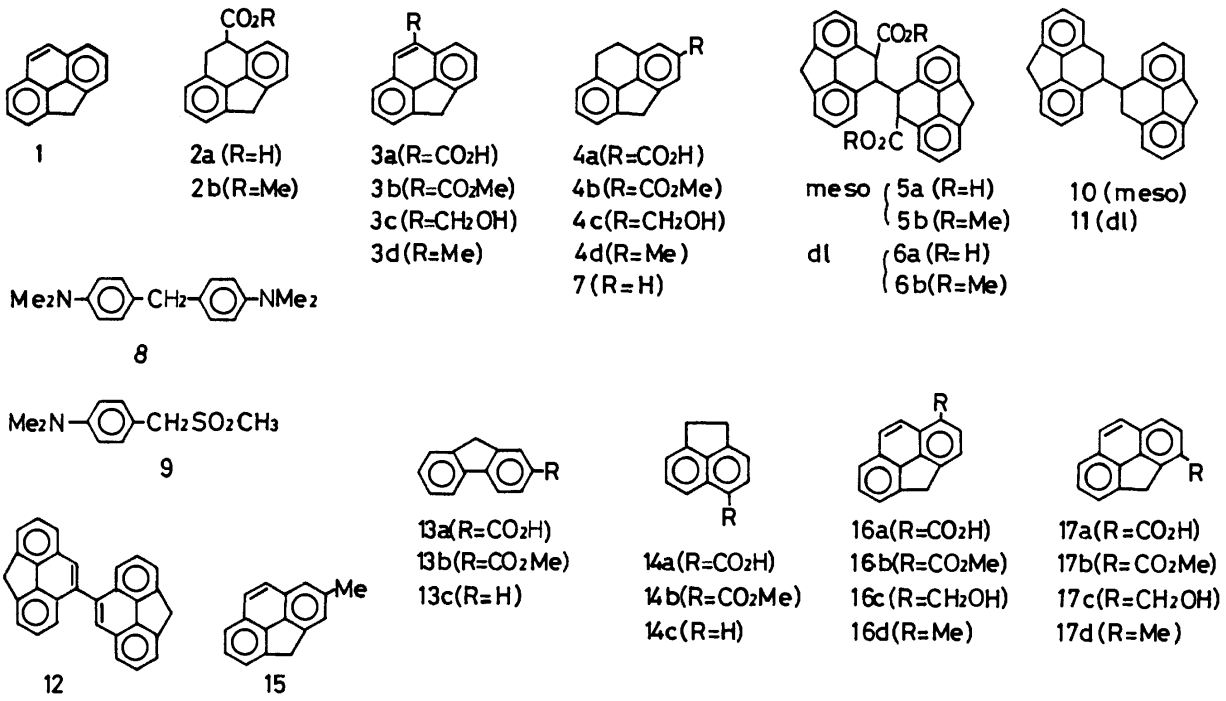

Scheme 1.

hydrogen. Reaction of the sulfoxide with the second radical cation should give **8** by elimination of methyl sulfoxide. Oxidation of *p*-(dimethylamino)benzyl methyl sulfoxide affords **9**.

The photoirradiation of **1** and DMA in DMSO was carried out under an atmosphere of nitrogen in order to clarify the effect of CO_2. The reaction gave *meso*- (**10**) and *dl*-8,8′-bi(8,9-dihydro-4*H*-cyclopenta[*def*]-phenanthrene) (**11**), **7**, and **9**. Dehydrogenations of **10** and **11** afforded 8,8′-bi(4*H*-cyclopenta[*def*]phenanthrene) (**12**): this supports that **10** and **11** are mutually steric isomers. These findings could be agreeably explained in a similar manner as the photoreaction of anthracene.[8]

One significant difference regarding the results with those of prior photocarboxylations[2,3] is the formation of **4a**: the reactions of phenanthrene, anthracene, and pyrene afforded the corresponding dihydro carboxylic acids by an interaction of the radical anion with CO_2 followed by a hydrogen transfer from the donor.[3] A part of **3a** can be regarded to be formed by the dehydrogenation of **2a** during the reaction. However, **4a** and the other part of **3a** should be assumed to be formed from **7** and **1**, respectively, as by-products by the substitutional sequence, different from reductive carboxylation.

In order to confirm the substitutional carboxylation, similar reactions of **7**, 9*H*-fluorene (**13c**), and acenaphthene (**14c**) were examined, giving **4a**, 9*H*-fluorene-2-carboxylic acid (**13a**),[9] and 5-acenaphthenecarboxylic acid (**14a**),[10] respectively. The isolated yields of these acids were very low due to the difficulty of the isolation procedure; only these acids were detected by gas-chromatographic analyses of the crude mixtures. The carboxylation could not proceed in the absence of light under similar conditions of DMA-DMSO. In the formations of **4a**, **13a**, and **14a**, therefore, it is postulated that the photoexcited hydrocarbons react with weak electrophile, CO_2, through an electrophilic sequence[11] under the conditions of DMA-DMSO with photoirradiation. In other words, there is a possibility that the system gives a reductive carboxylation product and an electrophilic-substituted product in the case of polycyclic aromatic hydrocarbons possessing a located double-bond character.

These carboxylic acids were isolated as the corresponding methyl esters. The esters, **3b** and **4b**, were converted into methanols, **3c** and **4c**; these were derived to the corresponding methyl derivatives, **3d** and **4d**. Dihydro compound, **4d**, was aromatized to give **15**. Isomeric 4*H*-cyclopenta[*def*]phenanthrene-1- (**16a**) and 3-carboxylic acid (**17a**)[12,13] were obtained by haloform reactions of the corresponding acetyl derivatives.[5] Compounds, **16a** and **17a**, gave 1-methyl- (**16d**)[14] and 3-methyl-4*H*-cyclopenta[*def*]phenanthrene (**17d**)[13] through the corresponding esters **16b** and **17b** and methanols **16c** and **17c**.

Experimental

All melting points are uncorrected. The NMR spectra were recorded on a Varian VXR-300 spectrometer in $CDCl_3$. The IR data (KBr-pellet) were obtained with a Jasco IR-G apparatus.

Photocarboxylation of 4*H*-Cyclopenta[*def*]phenanthrene (1). A mixture of **1** (2.85 g, 15 mmol) and DMA (18.2 g, 150 mmol) in DMSO (460 ml) was stirred at room temperature for 200 h with bubbling (ca. 12 l h^{-1}) of CO_2 under irradiation of a high-pressure mercury lamp (100 W) through a quartz tube. The reaction mixture was evaporated in vacuo and the residue was dissolved in dichloromethane (150 ml) and extracted with 5% HCl (3×50 ml).

The inorganic layer was neutralized with 5% aq. NaOH and extracted with PhH. The benzene layer was evaporated in vacuo to give a mixture of DMA and *N*-methylaniline (total 0.81 g). The residue was chromatographed on silica gel with PhH-AcOEt (3 : 1) to give **8** (70 mg, 0.4%, mp 88.0—88.5 °C) and **9** (40 mg, 0.1%). **9:** mp 156—157 °C; IR, 2940, 1618, 1533, 1300, and 1127 cm^{-1}; ^1H NMR, δ=2.72 (3H, s), 2.98 (6H, s), 4.16 (2H, s), 6.72 (2H, d, J=8.7 Hz), and 7.25 (2H, d, J=8.7 Hz); ^{13}C NMR, δ=38.53, 40.29, 60.95, 112.48, 114.99, 131.22, and 150.83; MS, m/z 213 (M^+) and 134.

The dichloromethane layer was extracted with 5% aq. NaOH (3×50 ml) and the organic layer was submitted to GLPC (5% sp-1000, 1 m, 200 °C); it (640 mg) contained **1** (347 mg, 12%) and **7** (64 mg, 2%). The residual part was chromatographed on silica gel with hexane to give **7** (20 mg, mp 139—141 °C) and **1** (231 mg).

The base extract was neutralized with aq HCl, extracted with dichloromethane, evaporated, and followed by esterification with MeOH (150 ml)-concd H_2SO_4 (0.5 ml) under refluxing for overnight. GLPC (sp-1000, 250 °C) data indicated the presence of **2b**[5] (1.15 g, 31%), **3b**[5] (0.94 g, 25%), and **4b** (0.11 g, 3%). Upon chromatography on SiO_2 with PhH, the residue gave **2b** (520 mg), **3b** (333 mg), **4b** (31 mg), **5b** (6 mg, 0.3%), and **6b** (7 mg, 0.4%). **2b:** mp 52.0—52.5 °C; ^1H NMR, δ=3.34 (1H, dd, J=16.8, 7.2 Hz), 3.54 (1H, dd, J=16.8, 7.2 Hz), 3.73 (3H, s), 3.91 (2H, s), 4.26 (1H, t, J=7.2 Hz), 7.16 (1H, d, J=7.5 Hz), 7.20—7.29 (3H, m), 7.36 (1H, d, J=7.5 Hz), and 7.41 (1H, d, J=7.5 Hz). **3b:** mp 82.0—82.5 °C; ^1H NMR, δ=4.08 (3H, s), 4.37 (2H, s), 7.66—7.81 (4H, s), 7.92 (1H, d, J=7.9 Hz), 8.71—8.74 (1H, m), and 8.78 (1H, s, H_9).

4b: mp 77.5—78.5 °C; IR, 1705 and 1300 cm^{-1}; ^1H NMR, δ=3.18 (4H, s), 3.93 (5H, s), 7.15 (1H, d, J=7.5 Hz, H_7), 7.26 (1H, t, J=7.5 Hz, H_6), 7.38 (1H, d, J=7.5 Hz, H_5), 7.87 (1H, s, H_1), and 8.06 (1H, s, H_3); ^{13}C NMR, δ=26.01, 26.03, 37.34, 52.01, 122.91 (C_5), 124.56 (C_3), 124.92 (C_7), 126.94 (C_1), 128.60 (C_6), 129.00, 130.00, 131.53, 138.35, 139.99, 141.68, 143.91, and 167.95. Found: C, 81.68; H, 5.67%. Calcd for $C_{17}H_{14}O_2$: C, 81.58; H, 5.64%.

4a: mp 273—274 °C; IR, 2930, 1688, and 1298 cm^{-1}; ^1H NMR ($CDCl_3$-DMSO-d_6, 60 MHz), δ=3.19 (4H, s), 3.93 (2H, s), 7.13—7.37 (3H, m), 7.87 (1H, s), and 8.06 (1H, s); MS (70 eV), m/z 236 (M^+), 219, and 189. Found: C, 81.16; H, 4.89%. Calcd for $C_{16}H_{12}O_2$: C, 81.34; H, 5.12%.

5b: mp 272.5—273.5 °C; IR, 2950, 1711, and 1185 cm^{-1}; ^1H NMR, δ=3.32 (6H, s), 3.58 (2H, bs), 3.97 (4H, bs), 4.36 (2H, bs), 6.56 (2H, d, J=7.5 Hz), 7.01 (2H, t, J=7.5 Hz), 7.29—7.37 (6H, m), and 7.44 (2H, dd, J=6.8, 0.9 Hz); ^{13}C NMR, δ=37.58, 44.42, 46.95, 52.03, 123.57, 123.80, 125.21,

125.58, 126.20, 127.49, 128.17, 129.76, 138.08, 139.05, 140.12, 140.37, and 173.58; MS, *m/z* 498 (M^+), 374, 250, and 190. Found: C, 81.73; H, 5.40%. Calcd for $C_{34}H_{26}O_4$: C, 81.91; H, 5.26%.

6b: mp 249.0—250.5 °C; IR, 2960, 1726, and 1150 cm^{-1}; ^1H NMR, δ=3.45 (6H, s), 3.72 (2H, s), 3.75 (2H, s), 3.88 (2H, s), 4.12 (2H, s), 6.59 (2H, d, J=7.5 Hz), 6.92—6.97 (4H, m), 7.12 (2H, t, J=7.5 Hz), 7.17 (2H, d, J=6.9 Hz), and 7.30 (2H, d, J=7.5 Hz); ^{13}C NMR, δ=37.36, 47.13, 47.22, 52.20, 123.45, 123.82, 125.30, 125.46, 126.20, 126.80, 127.30, 129.43, 138.87, 140.09, and 173.08; MS, *m/z* 498 (M^+), 377, 250, and 189. Found: C, 81.71; H, 5.18%.

Reaction of DMA in DMSO under Photoirradiation. A solution of DMA (13.4 g, 111 mmol) in DMSO (200 ml) was irradiated for 90 h with bubbling of CO_2. Upon evaporation of DMSO, the residue was chromatographed on Al_2O_3 with PhH giving 1.14 g (9%) of **8:** mp 88—89 °C (lit,[6] mp 88—89 °C); IR, 2920, 2820, 1613, 1522, and 1342 cm^{-1}; ^1H NMR, δ=2.90 (12H, s), 3.81 (2H, s), 6.69 (4H, d, J=8.7 Hz), and 7.06 (4H, d, J=8.7 Hz); ^{13}C NMR, δ=40.05, 41.12, 113.22, 129.58, 130.51, and 149.23; MS, *m/z* 254 (M^+), 210, 189, and 134.

Photoirradiation of 7 with CO_2. A mixture of **7** (960 mg, 5 mmol) and DMA (13.4 g, 111 mmol) in DMSO (200 ml) was stirred for 90 h with bubbling of CO_2 under irradiation of ultraviolet ray. Upon evaporation of solvent, 0.22 g (crude, ca. 19%) of **4a** and 0.43 g (45%) of **7** were isolated from the reaction mixture. The crude acid **4a** was treated with thionyl chloride (10 ml) in the presence of one drop of pyridine in ether (40 ml) with a gentle reflux, followed by refluxing of crude acid chloride in methanol (50 ml). Ester **4b** was given in a yield of 0.22 g (17%).

Reaction of 13c. A mixture of **13c** (1.66 g, 10 mmol) and DMA (13.4 g, 111 mmol) in DMSO (200 ml) was stirred for 90 h with bubbling of CO_2 under photoirradiation. Upon treatment similar to the above, 0.62 g (37%) of **13c** and 0.22 g (crude, ca. 10%, IR, 1688 cm^{-1}) of **13a** were obtained. Esterification of **13a** gave 110 mg (5%) of **13b**; mp 112—113 °C (lit,[9] mp 122 °C); ^1H NMR, δ=3.94 (5H, s), 7.36—7.41 (2H, m), 7.58 (1H, m), 7.81—7.85 (2H, m), 8.09 (1H, d, H_3), and 8.21 (1H, s, H_1); ^{13}C NMR, δ=36.81, 52.08, 119.53, 120.76, 125.21, 126.22, 126.99, 127.89, 128.25, 128.66, 140.56, 143.05, 144.32, 146.24, and 167.42.

Reaction of 14c. Hydrocarbon **14c** (1.54 g, 10 mmol) was treated by the similar procedure as the case of **13c**; 0.44 g (crude, ca. 22%, IR, 1662 cm^{-1}) of **14a**, 0.18 g (1.1%) of **8**, and 0.20 g (13%) of **14c** were obtained. Esterification of **14a** afforded 89 mg (4%) of **14b**; mp 71—73 °C (lit,[10] mp 73—74 °C); ^1H NMR, δ=3.41 (4H, s), 3.99 (3H, s), 7.29 (1H, d, J=7.2 Hz, H_3), 7.34 (1H, d, J=6.9 Hz, H_8), 7.58 (1H, t, J=6.9 Hz, H_7), 8.28 (1H, d, J=7.2 Hz, H_4), and 8.63 (1H, d, J=6.9 Hz, H_6); ^{13}C NMR, δ=30.32, 30.41, 51.77, 118.36, 119.92, 121.91, 122.01, 129.79, 130.16, 133.09, 139.54, 146.21, 152.92, and 167.85.

Photoirradiation of 1 in the Presence of DMA. A mixture of **1** (3.80 g, 20 mmol) and DMA (24 g, 0.2 mol) in DMSO (400 ml) was irradiated for 60 h at room temperature. After addition of PhH (200 ml), the reaction mixture was extracted with 5% aq HCl (300 ml), and the extract was neutralized with aq. $NaHCO_3$, extracted with PhH and distilled under reduced pressure to give 5.7 g of DMA. The residue was chromatographed on SiO_2 with cyclohexane-AcOEt (10 : 1) giving 43 mg (0.2%) of **9** (mp 156—157 °C).

The benzene solution was chromatographed on SiO_2 with cyclohexane. The first eluate afforded 981 mg (26%) of **7** (mp 138—140 °C). The second eluate was fractionally recrystallized from cyclohexane to yield **10** (186 mg, 5%) and **11** (706 mg, 19%). **10:** mp 189.5—191.5 °C; IR, 2930 and 1420 cm^{-1}; ^1H NMR, δ=3.13 (4H, d, J=5.4 Hz), 3.69 (2H, t, J=5.4 Hz), 3.83 (4H, s), 6.90 (2H, d, J=7.4 Hz), 6.95 (2H, d, J=7.4 Hz), 7.04 (2H, t, J=7.4 Hz), 7.14 (2H, t, J=7.4 Hz), 7.26 (2H, d, J=7.4 Hz), and 7.29 (2H, d, J=7.4 Hz); ^{13}C NMR, δ=30.75, 37.46, 42.26, 122.41, 122.94, 124.23, 125.35, 126.62, 127.23, 130.35, 132.08, 139.42, 140.01, and 140.42; MS, *m/z* 382 (M^+) and 191. Found: C, 94.27; H, 5.91%. Calcd for $C_{30}H_{22}$: C, 94.20; H, 5.80%.

11: mp 150.0—151.5 °C; IR, 2940 and 1455 cm^{-1}; ^1H NMR, δ=3.00 (4H, d, J=7.0 Hz), 3.95 (4H, s), 4.12 (2H, t, J=7.0 Hz), 6.80 (2H, d, J=7.4 Hz), 7.01—7.17 (2H, m), 7.25—7.33 (6H, m), and 7.41—7.45 (2H, m); ^{13}C NMR, δ=27.39, 37.57, 41.47, 122.46, 123.06, 123.78, 124.63, 127.30, 127.51, 130.26, 132.58, 139.08, 139.99, 140.32, and 140.53; MS, *m/z* 382 (M^+), 333, and 191. Found: C, 94.42; H, 5.74%. Calcd for $C_{30}H_{22}$: C, 94.20; H, 5.80%.

Dehydrogenations of 10 and 11. A mixture of **10** (19.1 mg, 0.05 mmol) and DDQ (42 mg, 0.18 mmol) in PhH (20 ml) was refluxed for 10 h, followed by chromatography on Al_2O_3 giving **12** (13.5 mg, 71%): mp 269—270 °C; IR, 1420 cm^{-1}; ^1H NMR, δ=4.67 (4H, s), 7.49—7.57 (4H, m), 7.69—7.79 (6H, m), 7.89 (2H, dd, J=7.6, 0.8 Hz), and 8.02 (2H, s); ^{13}C NMR, δ=37.70, 121.30, 121.42, 122.36, 122.69, 126.38, 127.19, 127.53, 127.84, 128.31, 137.09, 138.31, 138.51, 141.59, and 141.90; MS, *m/z* 378 (M^+), 189, and 187. Found: C, 95.17; H, 4.76%. Calcd for $C_{30}H_{18}$: C, 95.21; H, 4.79%.

The similar reaction of **11** (19.1 mg, 0.05 mmol) afforded 13.1 mg (69%) of **12**.

4*H*-Cyclopenta[*def*]phenanthrene-1-carboxylic Acid (16a). To a mixture of Br_2 (0.46 ml, 8.7 mmol) in aq. NaOH (1.44 g in H_2O, 6.5 ml) there was added 1-acetyl-4*H*-cyclopenta[*def*]-phenanthrene[5] (116 mg, 0.5 mmol) in dioxane (20 ml) at 0—5 °C. Upon refluxing for 30 min, the resulting mixture gave 71 mg (57%) of **16a**; mp>320 °C (decomp); IR, 3000, 1668, and 1265 cm^{-1}. The acid **16a** was converted into **16b** by refluxing in MeOH-H_2SO_4; yield 43%; mp 84—85 °C; IR, 1710 and 1242 cm^{-1}; ^1H NMR, δ=4.06 (3H, s), 4.39 (2H, s), 7.67—7.76 (3H, m), 7.88 (1H, d, J=7.6 Hz), 8.00 (1H, d, J=9.2 Hz, H_8), 8.46 (1H, d, δ=7.5 Hz, H_2), and 8.81 (1H, d, J=9.2 Hz, H_9); ^{13}C NMR, δ=37.53, 51.98, 120.65, 121.50, 122.74, 124.83, 125.91, 127.17, 127.43, 127.71, 127.82, 131.42, 137.85, 138.88, 141.36, 147.66, and 168.00. Found: C, 82.35; H, 4.91%. Calcd for $C_{17}H_{12}O_2$: C, 82.24; H, 4.87%.

17a;[12] yield 58%; mp>290 °C (lit,[12] mp 286—287 °C). **17b;**[12,13] yield 74%; mp 114—115 °C (lit,[12] mp 114—115 °C); ^1H NMR, δ=4.06 (3H, s), 4.67 (2H, s), 7.70 (1H, t, J=7.4 Hz), 7.78 (1H, d, J=6.4 Hz), 7.85—7.90 (3H, m), 7.97 (1H, d, J=8.5 Hz), and 8.28 (1H, d, J=8.5 Hz).

4*H*-Cyclopenta[*def*]phenanthrene-1-methanol (16c). A solution of **16b** (280 mg, 1.1 mmol) in ether (20 ml) was refluxed for 3 h with $LiAlH_4$ (209 mg, 5.5 mmol) to give 217 mg (87%) of **16c**; mp 105—106 °C; IR, 3350 and 1006 cm^{-1}; ^1H NMR, δ=1.75 (1H, t, J=5.1 Hz), 4.36 (2H, s), 5.23 (2H, d, J=5.1 Hz), 7.64—7.74 (4H, m), 7.86 (1H, d, J=7.6 Hz), 7.91 (1H, d, J=9.0 Hz), and 8.08 (1H, d, J=9.0 Hz). Found: C, 86.98; H, 5.60%. Calcd for $C_{16}H_{12}O$: C, 87.24; H, 5.49%.

17c;[13] yield 32%; mp 181—182 °C (lit,[13] mp 177—178.5 °C); ^1H NMR, δ=1.79 (1H, t, J=5.1 Hz), 4.40 (2H, s), 5.06 (2H, d, J=5.1 Hz), 7.63—7.74 (3H, m), and 7.83—7.87 (4H, m).

3c; yield 68%; mp 154—155 °C; IR, 3360, 1029, and 1000 cm^{-1}; ^1H NMR, δ=1.85 (1H, t, J=5.9 Hz), 4.38 (2H, s), 5.27 (2H, d, J=5.9 Hz), 7.65—7.74 (4H, m), 7.83 (1H, d, J=7.7 Hz), 7.88 (1H, s, H_9), and 8.02 (1H, d, J=7.7 Hz, H_7); MS, m/z 220 (M^+), 202, 191, and 189.

4c; yield 68%; mp 121—122 °C; IR, 3350 and 1010 cm^{-1}; ^1H NMR, δ=1.55 (1H, bs), 3.15 (4H, s), 3.89 (2H, s), 4.72 (2H, s), and 7.10—7.15 (2H, m), 7.20 (1H, t, J=7.4 Hz), and 7.33—7.38 (2H, m); MS, m/z 222 (M^+), 205, 193, 192, 191, and 189.

1-Methyl-4*H*-cyclopenta[*def*]phenanthrene (16d).[14] A solution of **16c** (206 mg, 1.0 mmol) in AcOH (10 ml) was added into a mixture of HI (57%, 1.0 ml) and red phosphorus (1.0 g) in AcOH (10 ml), and the resulting mixture was refluxed for 10 h to yield **16d** (138 mg, 72%); mp 80—81 °C (lit.[14] mp 83.5—84.5 °C); ^1H NMR, δ=2.76 (3H, s), 4.31 (2H, s), 7.45 (1H, dd, J=7.2, 0.9 Hz), 7.59 (1H, d, J=6.7 Hz), 7.63 (1H, t, J=7.2 Hz), 7.69 (1H, dd, J=7.2, 0.9 Hz), 7.82 (1H, d, J=6.7 Hz), 7.85 (1H, d, J=9.0 Hz), and 7.92 (1H, d, J=9.0 Hz).

17d;[13] yield 60%; mp 73—74 °C; ^1H NMR, δ=2.61 (3H, s), 4.21 (2H, s), 7.45 (1H, d, J=8.0 Hz), and 7.59—7.81 (6H, m).

3d; yield 57%; mp 83—84 °C; IR, 2960, 2900, and 1420 cm^{-1}; ^1H NMR, δ=2.79 (3H, s), 4.35 (2H, s), 7.58—7.75 (6H, m), and 7.88 (1H, d, J=7.5 Hz). Found: C, 93.86; H, 5.94%. Calcd for $C_{16}H_{12}$: C, 94.08; H, 5.92%.

4d; yield 44%; mp 78—79 °C; IR, 2950 and 1440 cm^{-1}; ^1H NMR, δ=2.41 (3H, s), 3.11 (4H, s), 3.84 (2H, s), 6.94 (1H, s, H_1), 7.08 (1H, d, J=7.3 Hz, H_7), 7.15 (1H, t, J=7.3 Hz, H_6), 7.16 (1H, s, H_3), and 7.31 (1H, d, J=7.3 Hz, H_5); MS, m/z 206 (M^+), 191, and 189.

15; obtained by aromatization of **4d** with DDQ in 75% yield; mp 90.0—90.5 °C; IR, 2940, 2850, and 1390 cm^{-1}; ^1H NMR, δ=2.66 (3H, s), 4.31 (2H, s), and 7.54—7.84 (7H, m); MS, m/z 204 (M^+) and 189.

We greatly thank Professor Takashi Toda, Utsunomiya University for his continuing interest.

References

1) R. B. Wagner and H. D. Zook, "Synthetic Organic Chemistry," John Wiley and Sons, New York (1953), pp. 411—478.

2) S. Tazuke and H. Ozawa, *J. Chem. Soc., Chem. Commun.*, **1975**, 237.

3) S. Tazuke, S. Kazama, and N. Kitamura, *J. Org. Chem.*, **51**, 4548 (1986).

4) M. Minabe and K. Suzuki, *Yuki Gosei Kagaku Kyokai Shi*, **44**, 421 (1986).

5) M. Yoshida, K. Hishida, M. Minabe, and K. Suzuki, *J. Org. Chem.*, **45**, 1783 (1980).

6) J. R. Feldman and E. C. Wagner, *J. Org. Chem.*, **7**, 31 (1942).

7) A. Mangini, L. Ruzzier, and A. Tundo, *Bull. Sci. fac. chim. ind. Bologna*, **14**, 81 (1956); *Chem. Abstr.*, **52**, 19446 (1958).

8) M. Yoshida, C. Pac, and H. Sakurai, *Bull. Chem. Soc. Jpn.*, **54**, 2352 (1981).

9) F. E. Ray and G. Riveschl, *J. Am. Chem. Soc.*, **65**, 836 (1943).

10) F. R. Lorriman, *J. Am. Chem. Soc.*, **47**, 211 (1925).

11) M. Yoshida, H. Kaneko, A. Kitamura, T. Ito, K. Oohashi, N. Morikawa, H. Sakuragi, and K. Tokumaru, *Bull. Chem. Soc. Jpn.*, **49**, 1697 (1976).

12) A. Sieglitz and W. Schidlo, *Chem. Ber.*, **96**, 1098 (1963).

13) W. E. Barth and R. G. Lawton, *J. Am. Chem. Soc.*, **93**, 1730 (1971).

14) W. E. Bachmann and J. C. Sheehan, *J. Am. Chem. Soc.*, **63**, 2598 (1941).

 © 1988 The Chemical Society of Japan Bull. Chem. Soc. Jpn., 61, 2067—2070 (1988)

Reinvestigation on Thermal Cycloaddition of 1-Aryl-2-(9-fluorenylidene)-1-haloethylenes[1)]

Masahiro MINABE, Masaaki YOSHIDA, Seiji SAITO, Keisuke TOBITA, and Takashi TODA*
Department of Industrial Chemistry, Faculty of Engineering, Utsunomiya University, Ishiicho, Utsunomiya 321
(Received December 10, 1987)

The thermal treatment of 1-bromo-2-(9-fluorenylidene)-1-phenylethylene afforded three different types of [2+2]cycloaddition products. The 1-tolyl homolog showed similar trends, but the chloro analog gave only two types. These results suggest that reactions of the rigid and bulky allenes take place through a 2,2′-biradical giving head-to-head, head-to-tail, and tail-to-tail adducts through the expected processes.

The chemistry of allenes has widely been investigated owing to the unique reactivities, important as synthetic intermediates, as well as the unique structures.[2)] The thermal [2+2]cycloaddition of haloallenes has suggested that it proceeds nonconcertedly via 2,2′-biradical and gives head-to-head and tail-to-tail adducts as the major products.[2,3)] The reaction of 1-chloro-2-(9-fluorenylidene)ethylene has been reported to yield a head-to-head dimer, 3,4-dichloro-1,2-bis(9-fluorenylidene)cyclobutane.[4,5)] However, a detailed study of the reaction showed that the above cycloaddition product was confirmed as a head-to-tail compound, 2-chloro-4-chloromethylene-3-(9-fluorenylidene)spiro[cyclobutane-1,9′-[9*H*]fluorene], with evidence of a similar product of bromo analog.[6,7)] The thermal treatment of 1-bromo-2-(9-fluorenylidene)-1-phenylethylene (**1a**),[5)] which was derived from 9-(phenylethynyl)-9-fluorenol (**2a**), also afforded a head-to-tail adduct **3a**[6,8)] (Scheme 1).

The present paper deals with a reinvestigation of the thermal cycloaddition of 1-bromo- and 1-chloroallenes **1**. This suggests that the reaction takes place to give all three possible dimers: head-to-head, head-to-tail, and tail-to-tail adducts.

By refluxing in benzene, **1a** afforded **3a** as the major product, accompanied by the formation of several other products: **4a**, **6a**, **7a**, **8a**, **9a**, and **10a** (Scheme 1). The reaction of 9-fluorenone with (*p*-tolylethynyl)-

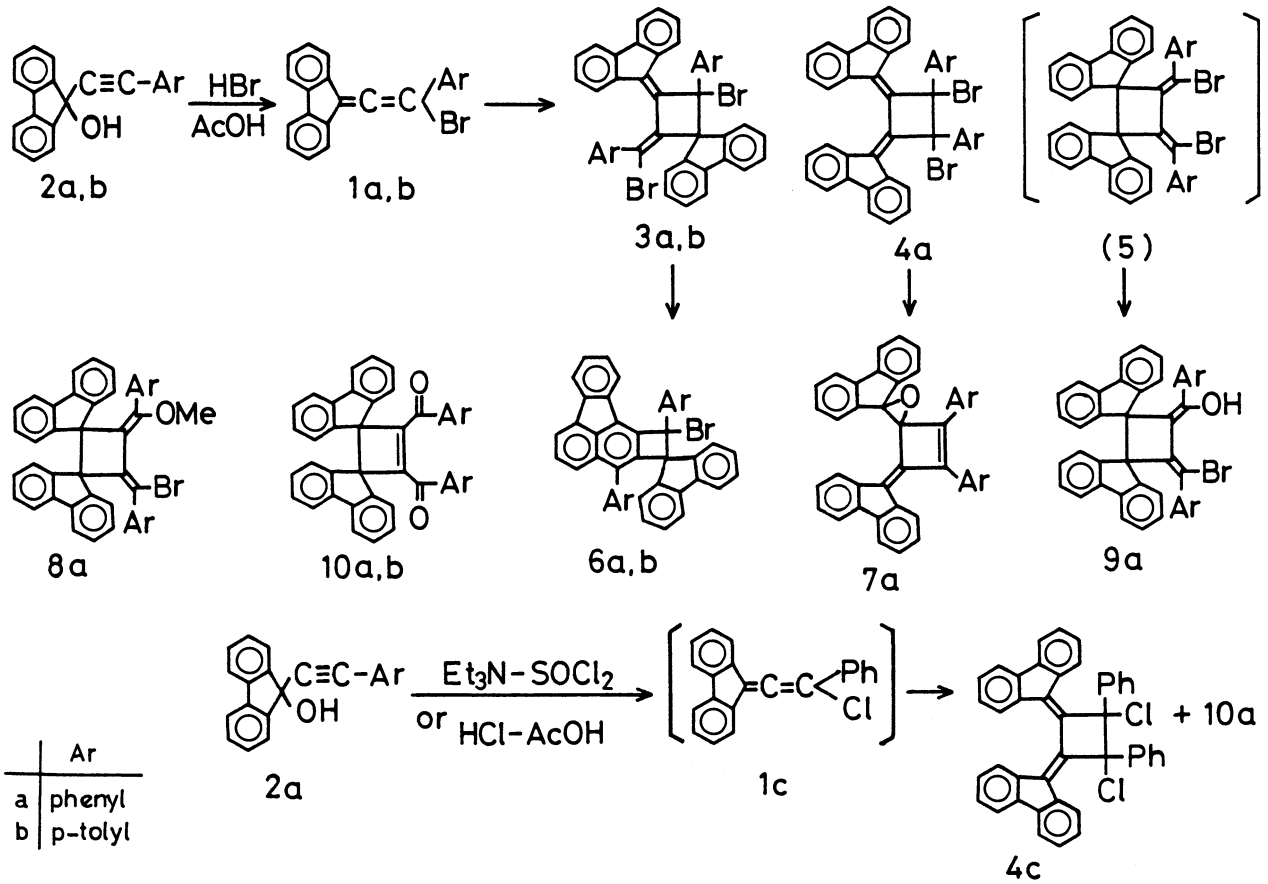

Scheme 1.

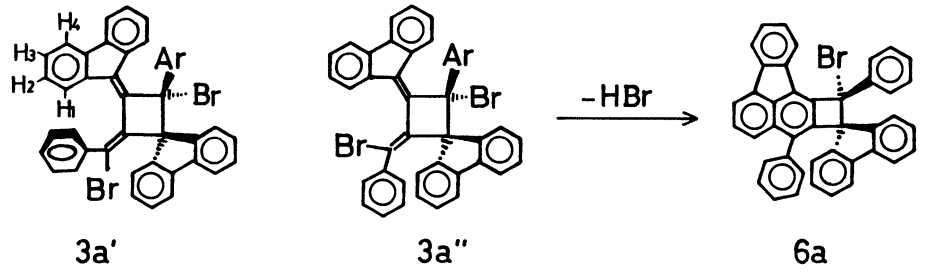

Scheme 2.

magnesium bromide, which was derived from *p*-tolylacetylene,[9] gave 9-(*p*-tolylethynyl)-9-fluorenol (**2b**); the alcohol was converted into another allene, **1b**. The reaction of **1b** gave **6b** as the major product and **3b** and **10b** as the minor products. Several attempts to obtain chloroallene **1c** failed as the result of reactions of **2a** with thionyl chloride in the presence of amine and with hydrochloric acid in acetic acid, though small amounts of **4c** and **10a** were isolated.

The orange needles, **3a**, were concluded to be the head-to-tail compound previously described in the literature[6,8] through a comparison with their UV data. The UV spectrum of **3b** is similar to that of **3a**. Characteristic peaks of the NMR spectra of **3a** and **3b** are high-field one-proton doublets, at δ 5.13 for **3a** and δ 5.18 for **3b**. The *J*-coupling and COSY data show that the doublets connect vicinally triplet at δ 6.29, successively triplet at δ 6.97, and doublet at δ 7.48 for **3a**, and triplet at δ 6.29, triplet at δ 6.97, and doublet at δ 7.53 for **3b**. These four-proton sets were reasonably assigned to H_1, H_2, H_3, and H_4, respectively, of the 9-fluorenylidene moiety, which is located in the same plane as the cyclobutane ring, as shown as **3a'** (Scheme 2). The high-field shift of H_1 is due to the ring current of the adjacent phenyl moiety of the arylbromomethylene group.

Compound **3a'** was stable under refluxing in cyclohexane. The geometrical isomer of **3a'** (**3a"**) should form by cycloaddition, but convert easily into a fluoranthene derivative **6a** by dehydrobromination during a reaction and/or separation. The UV spectra of **6a** and **6b** are very similar to that of fluoranthene, showing a red shift (about 40 nm). The molecular model of **6a** indicates that the aryl group attached to the fluoranthene moiety can rotate freely, but that the aryl group situated on the cyclobutane ring is restricted from free rotation. The two phenyl groups of **6a** are distinguishable by COSY spectra: the two-proton doublet at δ 5.95 is correlated to the two-proton triplet (δ 6.65), successively a one-proton triplet (δ 6.79); these were assigned to be attached to the free-rotating phenyl group connected to the fluoranthene. The other phenyl protons appear separately at δ 6.38 (d), 6.89 (t), 7.15 (t), 7.59 (t), and 7.36(d); this suggests that the ring is fixed sterically. The NMR spectra of **6b** show similar trends; the methyl-proton singlet (δ 1.96) and a

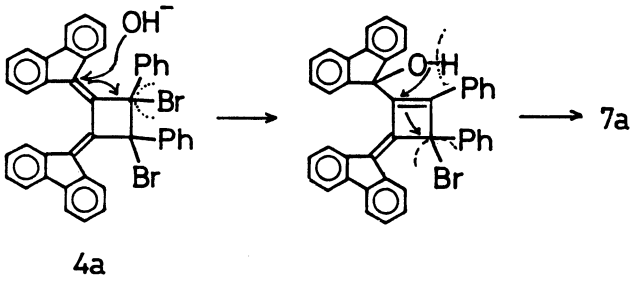

Scheme 3.

couple of two-proton doublets at δ 5.81 and 6.47 are due to the tolyl protons attached to the fluoranthene moiety. Also, the methyl protons (δ 2.02), the one-proton singlet (δ 6.16), and the one-proton doublet (δ 6.94) belong to the restricted-rotating tolyl group of the cyclobutane moiety.[10]

The absorption maxima (480—490 nm) of reddish **4a** and **4c** are similar to those of the head-to-head cycloadducts[7] obtained from 2,3-dibromo-1,4-bis(9-fluorenylidene)-1,3-butadiene. A molecular model of **4** shows that a part of the two 9-fluorenylidene plane accumulates each other. The NMR spectrum of **4c** is relatively simple and shows slightly broad signals, because of the symmetrical molecule and of the mutual interaction of the two fluorenylidene moieties.

The UV spectrum of **7a** is similar to that of **3a** and supports the conjugating system being 9-(4-phenyl-1,3-butadienyl)fluorene. However, **3a** may not be easy to give a compound having a molecular formula of $C_{42}H_{26}O$: **7a** is postulated to form by the hydrolysis of **4a** during the reaction and/or its separation, since **7a** does not show any carbonyl or hydroxyl absorption band in its IR spectrum (Scheme 3). The NMR signals of **7a** indicate an intramolecular mutual interaction that is similar to **4c**.

The UV spectra of the other cycloadducts, **8a**, **9a**, **10a**, and **10b**, significantly differ from those of head-to-tail and head-to-head addition products, and have absorption maxima between 300 and 310 nm. These compounds should be derived from tail-to-tail adduct **5**, which could not be isolated. The methoxy compound **8a** (OCH_3, ^1H NMR, δ=2.67) may be a tail-to-tail adduct formed from **1a**, **2a**, or **5a**. A small amount of methoxyallene could be formed from **2a** with contam-

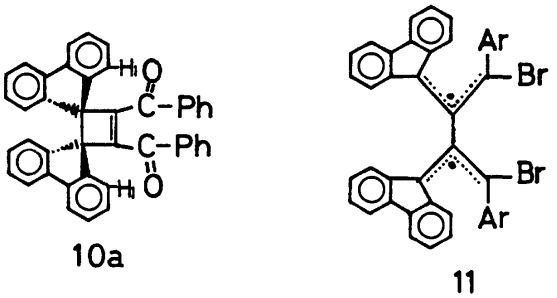

Scheme 4.

inating methanol which was used for the recrystallization of **2a**; the methanol should be contained in **2a** since it is difficult to remove the methanol from **2a** due to the inclusion complex of **2a** with methanol, as in the case of 9-(1-propynyl)-9-fluorenol.[11]

The molecular formula ($C_{42}H_{27}OBr$) and the IR spectrum (3500 cm^{-1}) of **9a** indicate that one bromine of the primary product **5a** was hydrolyzed during the reaction and/or separation process.

Analytical data and strong absorptions (ca. 1650—1655 cm^{-1}) in the IR spectra of **10a** and **10b** suggest that **10a**, **b** possess two carbonyl groups which were formed by removing two halogen atoms of **5** by hydrolyses and a following oxidation. Phenyl protons of **10a** appear at δ 7.11 as a four-proton triplet, at δ 7.30 as a two-proton triplet, and at δ 7.74 as a four-proton doublet. The two-proton doublet at δ 8.36 is assigned to H_1 (Scheme 4, **10a**), which is sterically deshielded by the carbonyl group. Similarly, the tolyl groups of **10b** are a singlet at δ 2.22 and doublets at δ 6.90 and 7.62; the doublet at δ 8.35 is H_1.

The small amounts of these minor products did not allow for any further investigation. The [2+2]cycloaddition of **1** afforded mainly head-to-tail product **3** accompanied by the formation of head-to-head **4** and tail-to-tail **5**, in spite of the fact that the material balance of the reaction products was not good. These results could reasonably explained why the thermal [2+2]cycloaddition proceeds via 2,2′-biradical **11** from the 1-haloallene **1**, and **11** cyclizes by three possible ways, giving cyclobutanes.

Experimental

All melting points are uncorrected. The ^1H NMR spectra were measured on a Varian VXR 300 or (a part) a Jeol C-60 HL spectrometer in $CDCl_3$ (0.62 ml for 2—10 mg samples in 5 mm tube). The UV data were recorded using a Shimadzu UV-180 or a Hitachi U-3400 apparatus in CH_2Cl_2.

1-Bromo-2-(9-fluorenylidene)-1-phenylethylene (1a). According to the method described in literature,[6] to a cooled solution of **2a** (0.50 g, 1.77 mmol) in AcOH (15 ml) was added dropwise a solution of hydrobromic acid (47%, 1.5 g, 8.71 mmol) in H_2O (5 ml). Upon stirring for 1 h with cooling, the precipitate was filtered, washed with water in order to be neutralized, dried, and recrystallized from hexane giving yellow needles, **1a**: 0.546 g (89%); mp 117—119 °C (decomp); IR (KBr), 1936 cm^{-1} (C=C=C) (lit,[6] 1940 cm^{-1}); UV, λ_{max} 319 (log ε 4.28), 284 (4.27), 260 (4.74), and 253 nm (4.63); MS (70 eV), m/z 346, 344 (M^+), 265, and 187; ^1H NMR, δ=7.27—7.42 (7H, m), 7.61—7.67 (4H, m), and 7.72 (2H, dt, J=7.5, 0.9 Hz).

The allene **1a** (100 mg, 0.29 mmol) was percolated through silica-gel column (1 cm i.d. 10 cm) with benzene and 72 mg (72%) of **1a** was recovered. When alumina was used instead of silica, only 15 mg (18%) of 2-(9-fluorenylidene)-1-phenylethanone was isolated; mp 137—139 °C (lit,[12] 137 °C); IR (KBr), 1650 (C=O) and 1591 cm^{-1} (C=C).

9-(*p*-Tolylethynyl)-9-fluorenol (2b). To a ethylmagnesium bromide (obtained from ethyl bromide (13.10 g, 120 mmol) and magnesium (2.92 g, 120 mmol) in ether (100 ml) under an argon atmosphere) was added dropwise *p*-tolylacetylene (12.76 g, 110 mmol) with ice-cooling; the resulting mixture was refluxed for an additional 16 h. A solution of 9-fluorenone (18.0 g, 100 mmol) in benzene (150 ml) was added dropwise to the Grignard solution and the mixture was refluxed for an additional 26 h. Upon the usual treatment, 26.5 g (90%) of **1b** was isolated by means of column chromatography on silica gel: mp 44.5—46.5 °C; IR, 3530 cm^{-1} (OH); MS (70 eV), m/z 296 (M^+), 281, and 181; ^1H NMR (CCl_4), δ=2.24 (3H, s), 3.07 (1H, bs), and 6.88—7.77 (12H, m).

9-Methoxy-9-(*p*-tolylethynyl)fluorene was obtained as colorless oil by percolation of **2b** on silica gel with methanol: MS (70 eV), m/z 310 (M^+) and 279; ^1H NMR (CCl_4), δ=2.28 (3H, s), 3.01 (3H, s), and 6.78—7.68 (12H, m).

1-Bromo-2-(9-fluorenylidene)-1-(*p*-tolyl)ethylene (1b). The foregoing alcohol **2b** was treated in a manner similar to the case of **2a** to give **1b**: yield 84%; mp 125—127 °C (decomp); IR (KBr), 1920 cm^{-1} (C=C=C); UV, λ_{max} 321 (log ε 4.38), 285 (4.34), 261 (4.80), and 253 nm (4.68); MS (70 eV), m/z 360, 358 (M^+), and 279; ^1H NMR, δ=2.35 (3H, s), 7.14 (2H, d, J=8.1 Hz), 7.28 (2H, t, J=7.5 Hz), 7.38 (2H, t, J=7.5 Hz), 7.52 (2H, d, J=8.1 Hz), 7.61 (2H, d, J=7.5 Hz), and 7.71 (2H, d, J=7.5 Hz). Found: C, 74.09; H, 4.33%. Calcd for $C_{22}H_{15}Br$: C, 73.55; H, 4.21%.

Thermal Treatment of 1a. A solution of **1a** (1.99 g, 5.8 mmol) in benzene (40 ml) was refluxed in the dark under an atmosphere of argon for 4 h. Upon evaporation of the solvent, the residue was fractionally recrystallized from ethyl acetate to give **3a** (590 mg, 30%), **6a** (158 mg, 9%), and **4a** (75 mg, 3.8%). The separation of the mother liquor by silica-gel column chromatography with dichloromethane-cyclohexane (1 : 3) successively afforded **7a** (25 mg, 1.6%) and **8a** (65 mg, 3.5%). The eluent was exchanged into ethyl acetate and afforded **10a** (33 mg, 2%) and **9a** (54 mg, 3%). These compounds were recrystallized from dichloromethane-hexane. **3a**: mp 206—208 °C (decomp) (lit,[6] 203—204 °C), orange needles; UV, λ_{max} 412 (log ε 4.35), 276 (4.59), and 237 nm (4.75); MS (19 eV), m/z 692, 690, 688 (M^+), 611, 609, 529, 452, 365, and 265; ^1H NMR, δ=5.13 (1H, d, J=7.6 Hz), 6.29 (1H, dt, J=7.6, 1.0 Hz), 6.68 (2H, t, J=7.1 Hz), 6,78—6.88 (3H, m), 6.97 (1H, dt, J=7.6, 1.0 Hz), 7.03—7.10 (2H, m), 7.13—7.20 (1H, m), 7.22—7.47 (7H, m), 7.48 (1H, d, J=7.6 Hz), 7.57 (1H, d, J=7.8 Hz), and 7.63—7.83 (6H, m). Found: C, 72.53; H, 4.03%. Calcd for $C_{42}H_{26}Br_2$: C, 73.06; H, 3.80%.

4a: mp 169—171 °C (decomp), red needles; UV, λ_{max} 490 (log ε 5.30), 330 (4.97), 275 (5.58), and 244 nm (5.73); MS (70 eV), m/z 692, 690, 688 (M^+), 611, 609, 530, and 453.

6a: mp 317—319 °C (decomp), yellow crystals; UV, λ_{max} 398

(log ε 4.28), 378 (4.55), 359 (4.48), 343 (4.27), 307 (4.15), 295 (4.12), and 264 nm (4.96); MS (19 eV), *m/z* 610, 608 (M^+), 529, 452, 375, and 224; ^{1}H NMR, δ=5.95 (2H, d, *J*=7.5 Hz), 6.38 (1H, dd, *J*=7.5, 1.2 Hz), 6.65 (2H, t, *J*=7.5 Hz), 6.79 (1H, t, *J*=7.5 Hz), 6.89 (1H, dd, *J*=7.5, 1.2 Hz), 7.15 (1H, dt, *J*=7.5, 1.2 Hz), 7.22—7.26 (3H, m), 7.36 (1H, dd, *J*=7.5, 1.2 Hz), 7.40—7.45 (6H, m), 7.55 (2H, d, *J*=8.6 Hz), 7.59 (1H, dd, *J*=7.8, 1.3 Hz), 7.88 (2H, d, *J*=7.5 Hz), and 7.94 (2H, d, *J*=7.5 Hz). (Found: C, 81.68; H, 3.77%. Calcd for $C_{42}H_{25}Br$: C, 82.76; H, 4.13%.)

7a: mp 291—292 °C (decomp), orange-red needles; no halogen; IR (KBr), 1085 cm^{-1}; UV, λ_{max} 378 (log ε 4.55), 266 (4.61), and 246 nm (4.80); MS (20 eV), *m/z* 546 (M^+), 529, 453, 365, and 265; ^{1}H NMR, δ=6.76—6.90 (6H, m), 7.13 (2H, dt, *J*=7.4, 1.0 Hz), 7.23—7.39 (12H, m), 7.56 (2H, d, *J*=7.9 Hz), 7.69 (2H, d, *J*=7.0 Hz), and 7.75 (2H, d, *J*=7.3 Hz). Found: C, 92.07; H, 5.13%. Calcd for $C_{42}H_{26}O$: C, 92.28; H, 4.79%.

8a: mp 242—244 °C (decomp), colorless crystals; IR (KBr), 1085 cm^{-1} (C-O-C); UV, λ_{max} 309 (log ε 4.31) and 267 nm (4.50); MS (19 eV), *m/z* 642, 640 (M^+), 611, 609, 561, 529, 365, and 195; ^{1}H NMR, δ=2.67 (3H, s), 6.30 (2H, bs), 6.68 (2H, bs), 6.88—7.44 (16H, m), 7.58 (2H, d, *J*=6.6 Hz), 7.68 (2H, d, *J*=6.6 Hz), and 7.80 (2H, d, *J*=6.8 Hz). Found: C, 80.27; H, 4.55%. Calcd for $C_{43}H_{29}OBr$: C, 80.50; H, 4.56%.

9a: mp 214—216 °C (decomp), colorless crystals; IR (KBr), 3500 cm^{-1} (OH); UV, λ_{max} 311 (log ε 4.30) and 266 nm (4.52); MS (19 eV), *m/z* 628, 626 (M^+), 547, 546, 447, 445, and 181; ^{1}H NMR, δ=4.52 (1H, bs), 6.0—7.8 (24H, m), and 7.94 (2H, d, *J*=8.1 Hz). Found: C, 80.43; H, 4.44%. Calcd for $C_{42}H_{27}OBr$: C, 80.38; H, 4.34%.

10a: mp 290—292 °C (decomp), yellow crystals; IR (KBr), 1653 (C=O), 1593, and 1578 cm^{-1}; UV, λ_{max} 302 (log ε 4.24) and 264 nm (4.90); MS (20 eV), *m/z* 562 (M^+), 456, and 351; ^{1}H NMR, δ=6.96 (2H, dt, *J*=7.5, 1.2 Hz), 7.05 (2H, dt, *J*=7.5, 1.2 Hz), 7.11 (4H, t, *J*=7.6 Hz), 7.25—7.31 (8H, m), 7.63 (4H, dt, *J*=8.5, 1.0 Hz), 7.74 (4H, dd, *J*=7.6, 1.2 Hz), and 8.36 (2H, dd, *J*=7.8, 0.9 Hz). Found: C, 89.60; H, 4.57%. Calcd for $C_{42}H_{26}O_2$: C, 89.66; H, 4.66%.

Thermal Reaction of 1b. A solution of **1b** (1.436 g, 4 mmol) in benzene (50 ml) was refluxed for 5 h. Upon evaporation of the solvent, the residue was recrystallized from ether, yielding yellow needles, **6b** (244 mg, 19.2%). The mother solution was chromatographed on silica gel with hexane and **10b** (37 mg, 1.6%) was isolated as yellow crystals (from dichloromethane-hexane).

Another experiment using **1b** (718 mg, 2 mmol) in cyclohexane (7.5 ml) was carried out by refluxing for 4 h and concentrating into a small volume; yellow needles, **3b** was obtained in yield of 143 mg (19.9%). **3b**: mp 195.5—197.0 °C (decomp); UV, λ_{max} 413 (log ε 4.30), 277 (4.62), and 271 nm (s, 4.60); MS (70 eV), *m/z* 720, 718, 716 (M^+), 639, 637, and 558; ^{1}H NMR, δ=2.02 (3H, s), 2.34 (3H, s), 5.18 (1H, d, *J*=7.5 Hz), 6.29 (1H, dt, *J*=7.5, 1.2 Hz), 6.46 (2H, d, *J*=7.8 Hz), 6.66 (2H, d, *J*=8.4 Hz), 6.93 (1H, dt, *J*=8.1, 1.9 Hz), 6.97 (1H, dt, *J*=7.5, 1.2 Hz), 7.04—7.14 (2H, m), 7.19—7.50 (7H, m), 7.53 (1H, dd, *J*=7.5, 1.4 Hz), 7.55—7.64 (2H, m), and 7.69—7.82 (4H, m). Found: C, 73.47; H, 4.13%. Calcd for $C_{44}H_{30}Br_2$: C, 73.55; H, 4.21%.

6b: mp 314—316 °C (decomp); UV, λ_{max} 404 (log ε 4.37), 383 (4.57), 364 (4.50), 350 (s, 4.31), 306 (4.23), 295 (4.23), and 265 nm (4.70); MS (70 eV), *m/z* 638, 636 (M^+), 557, 449, and 277; ^{1}H NMR, δ=1.96 (3H, s), 2.02 (3H, s), 5.81 (2H, d, *J*=8.3 Hz), 6.16 (1H, s), 6.47 (2H, d, *J*=8.3 Hz), 6.94 (1H, d, *J*=8.0 Hz), 7.23—7.49 (11H, m), 7.54 (2H, d, *J*=8.0 Hz), 7.86 (2H, d, *J*=7.5 Hz), and 7.93 (2H, d, *J*=6.9 Hz). Found: C, 82.34; H, 4.73%. Calcd for $C_{44}H_{29}Br$: C, 82.88; H, 4.58%.

10b: mp 298.5—299.5 °C (decomp); IR (KBr), 1654 (C=O) and 1602 cm^{-1} (C=C); UV, λ_{max} 301 (log ε 4.38), 264 (4.86), and 258 nm (4.58); MS (70 eV), *m/z* 590 (M^+), 471, 352, and 119; ^{1}H NMR, δ=2.22 (6H, s), 6.90 (4H, d, *J*=7.8 Hz), 6.96 (2H, dt, *J*=7.8, 1.2 Hz), 7.03 (2H, dt, *J*=7.5, 1.5 Hz), 7.22—7.31 (6H, m), 7.60 (4H, d, *J*=7.5 Hz), 7.62 (4H, d, *J*=7.8 Hz), and 8.35 (2H, d, *J*=7.8 Hz). Found: C, 89.78; H, 4.95%. Calcd for $C_{44}H_{30}O_2$: C, 89.46; H, 5.12%.

Reaction of 2a with Thionyl Chloride. A cooled (0 °C) mixture of **2a** (282 mg, 1.0 mmol) and triethylamine (0.3 g, 3 mmol) in dry ether (5 ml) was added dropwise to thionyl chloride (0.3 g, 2.5 mmol). Upon stirring for 1 h, the reaction mixture was filtered; the filtrate was evaporated and chromatographed on silica gel with dichloromethane-cyclohexane (1 : 3) to yield **4c** (8 mg, 4%) and **10a** (2 mg, 1%, mp 290—292 °C, decomp). **4c**: mp 247.5—249.5 °C (decomp), red crystals; UV (EtOH), λ_{max} 481 (log ε 4.41), 330 (3.75), 272 (4.64), and 247 nm (4.75); MS (70 eV), *m/z* 604, 602, 600 (M^+), 567, 565, 530, 453, 365, and 265; ^{1}H NMR, δ=6.93 (2H, dt, *J*=7.7, 1.1 Hz), 6.98 (2H, dt, *J*=7.6, 1.1 Hz), 7.18 (2H, t, *J*=7.7 Hz), 7.23—7.30 (4H, m), 7.34—7.39 (4H, m), 7.45—7.49 (4H, m), 7.57—7.65 (6H, m), and 8.40 (2H, d). Found: C, 83.72; H, 4.51%. Calcd for $C_{42}H_{26}Cl_2$: C, 83.86; H, 4.36%.

The present work was partially supported by a Grant-in-Aid for Scientific Research (No. 61470022) from the Ministry of Education, Science and Culture.

References

1) Presented at 53rd Annual Meeting of the Chemical Society of Japan, Nagoya, Oct. 1986, Abstr., No. 1D25.

2) D. R. Taylor, *Chem. Rev.*, **67**, 317 (1967); W. Swadja, *ibid.*, **83**, 263 (1983); "The Chemistry of the Allenes," ed by S. R. Landor Vol. I—III, Academic Press, London (1982).

3) N. D. Epiotis, *J. Am. Chem. Soc.*, **95**, 5624 (1973); D. J. Pasto, *ibid.*, **101**, 37 (1979).

4) G. F. Hennion and B. R. Fleck, *J. Am. Chem. Soc.*, **77**, 3253 (1955); T. Nagase, *Bull. Chem. Soc. Jpn.*, **34**, 139 (1961); H. Kollmar and H. Fischer, *Tetrahedron Lett.*, **1968**, 4291.

5) R. Kuhn and D. Rewicki, *Chem. Ber.*, **98**, 2611 (1965).

6) Y. Takehira, M. Ohoi, and F. Toda, The 30th Spring Meeting of Chemical Society of Japan, preprint, p. 1800 (1974).

7) F. Toda, H. Motomura, and H. Oshima, *Bull. Chem. Soc. Jpn.*, **47**, 467 (1974).

8) K. Ueda and F. Toda, *Chem. Lett.*, **1975**, 257.

9) L. I. Smith and H. H. Hoehn, *J. Am. Chem. Soc.*, **63**, 1175 (1941).

10) Unexpected singlet at δ 6.16 is correlated to the peaks at δ 2.02 and 6.94 by normal and long-range COSY technique and is concluded to be the tolyl protons on the cyclobutane. However, the other two protons of the tolyl group are failed to confirm on the spectra due to overlap of peaks.

11) F. Toda, K. Tanaka, G. U. Daumas, and M. C. Sanchez, *Chem. Lett.*, **1983**, 1521.

12) C. Dufrraisse and A. P. de Carvalho, *Bull. Soc. Chim. Fr. [5]*, **3**, 882 (1936); *Chem. Abstr.*, **30**, 358 (1936).

Conformational Analysis of Methacrylates by IR and ^{1}H NMR Spectroscopies

Eiji YASHIMA,*,§ Yoshio OKAMOTO,* Koichi HATADA, Hiroyuki KAGEYAMA,†,§§ and Nobutami KASAI†
Department of Chemistry, Faculty of Engineering Science, Osaka University, Toyonaka, Osaka 560
†Department of Applied Chemistry, Faculty of Engineering, Osaka University, Suita, Osaka 565
(Received November 21, 1987)

The molecular structures of α-methylbenzyl methacrylate, 1,2-diphenylethyl methacrylate, α-*t*-butylbenzyl methacrylate, 1,2,2,2-tetraphenylethyl methacrylate, diphenylmethyl methacrylate, and 1,1-diphenylethyl methacrylate in solution were investigated by means of IR spectroscopy and ^{1}H NMR spectroscopy using a lanthanoid-induced chemical shift (LIS) reagent [Eu(fod)$_3$] by reference to X-ray analysis data. The preferred conformation between the C=C double bond and the C=O group was estimated to be s-cis in solution. The conformation of ester groups of α-substituted benzyl methacrylates in toluene depended upon the α-substituent and the temperature. On the basis of structural data, the mechanism of the highly enantiomer-selective polymerization of racemic methacrylates with a (−)-sparteine-Grignard reagent complex is discussed.

(−)-Sparteine (Sp)-Grignard reagent complexes are effective initiators in the enantiomer-selective (asymmetric-selective or stereoelective) polymerization of racemic α-monosubstituted benzyl methacrylates such as α-methylbenzyl methacrylate (MBMA),[1,2] α-ethylbenzyl methacrylate (EBMA),[3] α-isopropylbenzyl methacrylate (iPrBMA),[3] 1,2-diphenylethyl methacrylate (DPEMA-1,2),[4] and α-*t*-butylbenzyl methacrylate (*t*-BBMA).[3] For example, in the polymerization of racemic MBMA with a cyclohexylmagnesium bromide (*c*-HexMgBr)-Sp complex in toluene at −78 °C, the polymer obtained in the early stage of the polymerization was rich in (*S*)-antipode whose optical purity was as high as 93%; the monomer recovered at about 65% conversion was almost optically pure.[2] (S)-Selective polymerization was also achieved for EBMA, iPrBMA, and DPEMA-1,2. However, for *t*-BBMA (*R*)-enantiomer was polymerized preferentially over (*S*)-enantiomer.[3] It has been pointed out that this reverse enantiomer selection of *t*-BBMA and other methacrylates may be caused by the difference in conformation of the monomers.[3] Recently, we also found that (*S*)-antipode of 1,2,2,2-tetraphenylethyl methacrylate (TrBMA) was polymerized preferentially with rather low enantiomer selectivity.[5] Among these monomers, DPEMA-1,2, *t*-BBMA, and TrBMA gave crystals suitable for X-ray diffraction study. The results of X-ray analyses have already been reported and the mechanism of the enantiomer-selective polymerization has been discussed on the basis of the determined molecular structures.[6] X-Ray structure analyses were also achieved on some achiral methacrylates, diphenylmethyl methacrylate (DPMMA),[7] 1,1-diphenylethyl methacrylate (DPEMA-1,1),[8] triphenylmethyl methacrylate (TrMA),[8] and diphenyl-2-pyridylmethyl methacrylate (D2PyMA)[9] which show interesting phenomena in the stereospecific polymerization with anionic and radical initiators.[10-12]

One of the problems concerning the molecular structures of methacrylates is the conformation between the C=C double bond and the C=O group: that is, whether it is s-trans or s-cis. This, especially on

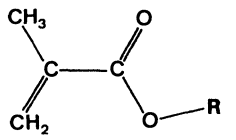

s-trans

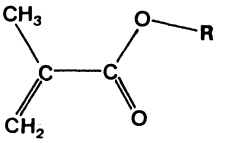

s-cis

methyl methacrylate (MMA), has been studied by several methods. However, the results obtained are not always consistent with one another. It has been found that the molecules of DPMMA, DPEMA-1,2, and D2PyMA have the s-trans form in crystal.[6,7,9] This is consistent with the results of an electron diffraction study,[13] molecular polarizability measurements[14] and an ab initio MO calculation of MMA.[15] On the other hand, DPEMA-1,1, TrMA, and TrBMA exist as the s-cis form in crystal.[6,8] This agrees with the results of the ^{1}H NMR study of molecular complexes of MMA and Lewis acids,[16] and the conformational analysis of MMA by a lanthanoid-induced chemical shift (LIS) reagent.[17]

The present work was undertaken in order to obtain more detailed information on the conformation of DPMMA, MBMA, DPEMA-1,2, DPEMA-1,1, TrMA, and TrBMA, in solution by IR spectroscopy and ^{1}H NMR spectroscopy with an LIS reagent. The results helped us to understand the mechanism of the

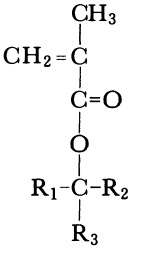

	R_1	R_2	R_3
MBMA	H	CH_3	Ph
DPEMA-1,2	H	CH_2-Ph	Ph
t-BBMA	H	*t*-Bu	Ph
TrBMA	H	$C(Ph)_3$	Ph
DPMMA	H	Ph	Ph
DPEMA-1,1	CH_3	Ph	Ph
TrMA	Ph	Ph	Ph

§ Present address: Department of Applied Chemistry, Faculty of Engineering, Kagoshima University, Korimoto, Kagoshima 890.
§§ Present address: Government Industrial Research Institute, Ikeda, Osaka 563.

enantiomer-selective polymerization of the racemic methacrylates with the (−)-Sp-Grignard reagent system in toluene.

Experimental

Materials. All methacrylates used in this study were synthesized and characterized according to our previous work.

An NMR shift reagent Eu(fod)$_3$ (Nakarai Chemical Co.) was used without further purification.

Measurements. IR spectra of the methacrylates were measured with a JASCO IR-810 spectrophotometer in KBr pellets and in CCl_4 or toluene with a 50-μm NaCl cell at room temperature. The wavenumbers were calibrated using a polystyrene film. The ^1H NMR spectra were recorded on a JNM MH-100 or JNM FX-100 (100 MHz) instrument in toluene-d_8; tetramethylsilane (TMS) was used as an internal standard.

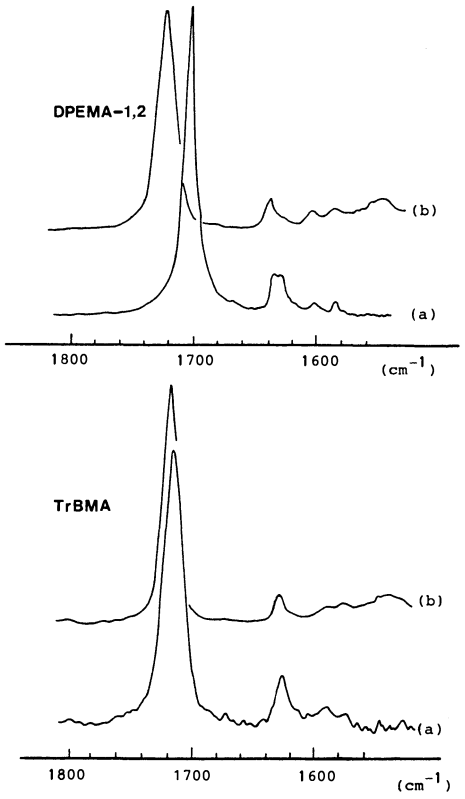

Fig. 1. IR spectra of C=O and C=C bands of DPEMA-1,2 and TrBMA in KBr (a) and in CCl_4 (b).

LIS Measurements. The lanthanoid-induced chemical shifts were measured with Eu(fod)$_3$ in toluene-d_8 at 35 and −40 °C. The concentration of the methacrylates was 0.5 mol l^{-1} and the molar ratio of [Eu(fod)$_3$]/[Methacrylate]([Ld]/[M]) was changed in a range of 0—0.30.

Results and Discussion

IR Spectra of Methacrylates. It has been well-known that IR spectroscopy differentiates the s-cis and s-trans conformations of α,β-unsaturated ketones and there exist some relatively simple rules in the relationship between the conformation (s-cis or s-trans) and the C=O and C=C bands of α,β-unsaturated ketones;[18,19] (1) there is a greater frequency separation between the C=O and C=C stretching bands of the s-cis form than the s-trans form, (2) the ratio of the band intensities of the C=O to the C=C stretching vibrations is considerably larger for the s-trans than the s-cis. However, so far, no such rules have been reported for α,β-unsaturated esters. The molecular structures of the methacrylates used in this study have already been determined by X-ray analysis. This promoted us to investigate the relationships between the conformation and the C=O and C=C bands of methacrylates in both crystal and solution by IR spectroscopy.

Figure 1 shows the IR spectra of DPEMA-1,2 and TrBMA in KBr pellets (a) and in CCl_4 solutions (b). The former methacrylate has the s-trans form and the latter the s-cis form in crystal according to X-ray diffraction studies. DPEMA-1,2 had a C=O band of 1702.5 cm^{-1} in KBr and its frequency moved by 20.2 cm^{-1} to 1722.7 cm^{-1} in a CCl_4 solution. TrBMA showed a C=O band at 1714.2 cm^{-1} in KBr and it only slightly shifted to 1719.0 cm^{-1} that was similar to the frequency of the C=O band of DPEMA-1,2 in a CCl_4 solution. The C=C bands appeared at ca. 1635 cm^{-1} in both KBr and CCl_4. These results strongly suggest that the conformation of DPEMA-1,2 changes from the s-trans in a crystalline solid to the s-cis in solution and TrBMA exists as the s-cis form both in a solid state and in a CCl_4 solution. Similar results were also obtained for other methacrylates (Table 1). The C=O band of

Table 1. Frequencies of C=O and C=C Bands of α-Substituted Benzyl Methacrylates

Monomer	R_1	R_2	Crystal structure[a]	ν(KBr)/cm^{-1}		ν(CCl_4)/cm^{-1}		$\Delta\nu_{C=O}$[b]	$\Delta\nu_{C=C}$[b]
				C=O	C=C	C=O	C=C	cm^{-1}	cm^{-1}
DPMMA	Ph	H	s-trans	1707.8	1636.0	1722.8	1637.8	15.0	1.8
DPEMA-1,2	Bz	H	s-trans	1702.5	1635.0	1722.7	1637.4	20.2	2.4
						(1721.4	1636.4	18.9	1.4)[c]
DPEMA-1,1	Ph	CH_3	s-cis	1721.4	1635.3	1724.0	1636.3	2.6	1.0
TrMA	Ph	Ph	s-cis	1725.9 (1718.8)[d]	1635.3	1727.6	1637.6	1.7	2.3
TrBMA	$C(Ph)_3$	Ph	s-cis	1714.2	1634.7	1719.0	1636.7	4.8	2.0

a) Conformation between C=O and C=C in crystal determined by X-ray diffraction study. b) Frequency difference in CCl_4 and KBr. c) In parenthesis are shown the frequencies in toluene solution. d) Shoulder.

Table 2. Chemical Shifts and $Eu(fod)_3$ Induced Shifts of Methacrylates in Toluene-d_8[a)]

		DPMMA		MBMA		DPEMA-1,2		*t*-BBMA		TrBMA	
		35 °C	−40 °C	35 °C	−40 °C	35 °C	−40 °C	35 °C	−40 °C	35 °C	−40 °C
Ha	δ[b)]	5.20	5.13	5.20	5.13	5.25	5.11	5.30	5.11	5.08	5.09
	$\Delta\delta$[c)]	4.00	6.44	3.64	6.44	3.25	5.34	2.47	4.80	2.78	4.55
	$\Delta\delta_{rel}$[d)]	0.64	0.66	0.72	0.59	0.64	0.57	0.62	0.61	0.58	0.58
	$\Delta\delta_{cal}$[e)]	3.49	6.43	3.29	6.27	2.88	5.16	2.18	4.86	2.37	4.32
Hb	δ[b)]	6.18	6.19	6.09	6.15	6.14	6.12	6.22	6.11	5.95	6.10
	$\Delta\delta$[c)]	8.30	16.07	7.69	14.97	7.25	13.33	5.58	10.71	6.50	9.30
	$\Delta\delta_{rel}$[d)]	1.32	1.66	1.53	1.37	1.44	1.43	1.40	1.32	1.35	1.19
	$\Delta\delta_{cal}$[e)]	8.29	16.01	7.78	14.98	7.45	13.35	5.82	10.69	6.37	9.47
Hc	δ[b)]	7.10	7.10	5.93	5.91	6.16	6.06	5.72	5.61	7.66	7.88
	$\Delta\delta$[c)]	16.40	22.04	12.10	19.00	14.07	17.09	12.03	15.30	14.17	12.50
	$\Delta\delta_{rel}$[d)]	2.61	2.27	2.40	1.74	2.79	1.83	3.62	1.83	2.94	1.60
	$\Delta\delta_{cal}$[e)]	16.35	22.06	12.05	19.04	13.91	17.09	11.79	15.28	14.13	12.60
CH_3	δ[b)]	1.80	1.75	1.80	1.77	1.79	1.70	1.85	1.76	1.68	1.67
	$\Delta\delta$[c)]	6.28	9.71	5.05	10.91	5.05	9.32	3.99	8.30	4.82	7.80
	$\Delta\delta_{rel}$[d)]	1.00	1.00	1.00	1.00	1.00	1.00	1.00	1.00	1.00	1.00
	$\Delta\delta_{cal}$[e)]	6.67	9.76	5.29	10.92	5.37	9.40	4.45	8.32	5.26	7.56
Δ(Hb−Ha)		0.98	1.06	0.89	1.02	0.89	1.01	0.92	1.00	0.87	1.01

a) Concentration of methacrylates=0.5 (mol l^{-1}). b) Chemical shift in toluene-d_8. c) Molar induced shift by $Eu(fod)_3$. d) Relative induced shift based on CH_3 resonance. e) Molar induced shift calculated for the structure giving the minimum AF value.

another s-trans methacrylate, DPMMA also shifted to a higher frequency in solution (from 1707.8 to 1722.8 cm^{-1}) but those of other s-cis methacrylates were little changed in a CCl_4 solution. The higher frequency shift of the C=O band of DPEMA-1,2 was also observed in a toluene solution (Table 1). These results are quite consistent with those of α,β-unsaturated ketones as mentioned above. However, the C=C band frequency and the ratio of the band intensities of the C=O to C=C stretching vibrations do not seem to be closely related to the conformation.

Conformational Analysis with LIS Reagent. The observed molar LISs were obtained from the line slopes of the plots of induced chemical shifts versus [Ld]/[M] ratios. The plots for DPEMA-1,2 is shown in Fig. 2 as an example. In all cases, good straight lines were obtained in the plots. The chemical shifts (δ) and molar LISs ($\Delta\delta$) are summarized in Table 2.

The molar LIS is the change in chemical shift caused by complexation with an equimolar lanthanoid shift reagent, being expressed by the McConnell and Robertson equation (Eq. 1):[20)]

$$\mathrm{LIS}(\Delta\delta) = K(3\cos^2 X - 1)/r^3, \quad (1)$$

where X is the O(2)-Ld-H internuclear angle (O(2) is the carbonyl oxygen in an ester group, see Fig. 3), r is the corresponding Ld-H distance and K is the pseudo-contact constant which refers to the magnitude of the induced magnetic dipole of a lanthanide ion. The most probable conformation of a methacrylate can be chosen by comparing the observed $\Delta\delta$ with the calculated molar LIS for a set of conformers.

The LIS simulation processes were worked-up according to the method reported by Montaudo et al.[21)] The structure of the complex of a methacrylate and $Eu(fod)_3$ in solution is shown in Fig. 3, where R is the Eu-O(2) distance (2.0—3.0 Å at 0.1 Å intervals), ϕ the Eu-O(2)-C(1) angle (120—180° at 5° intervals), ω the torsion angle of Eu-O(2)-C(1)-C(2) about the O(2)-C(1) bond (0—360° at 10° intervals) and θ the torsion angle of Hc-C(5)-O(1)-C(1) about the C(5)-O(1) (0—360° at 10° intervals). The conformation between the C=C and the C=O group was fixed to be

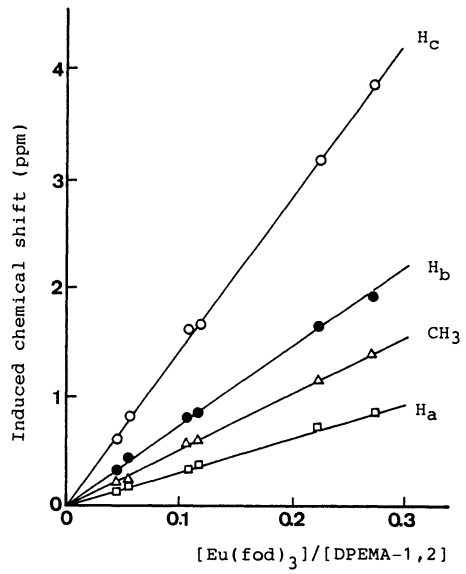

Fig. 2. The plots of induced shifts vs. molar ratio [$Eu(fod)_3$]/[DPEMA-1,2] in toluene-d_8 at 35 °C; assignment of protons are shown in Fig. 2.

s-cis or s-trans. It has been confirmed that esters coordinate to a Eu ion at the carbonyl rather than the ether oxygen.[22] The structural data of a methacrylate are also shown in Fig. 3 which is depicted according to the molecular structures of methacrylates determined by X-ray analysis. However, two assumptions are involved; (1) methacrylate (CH_2=C(CH_3)-COOC) has a planar structure, (2) all bond angles in the methacryloyl group are 120°. These two assumptions seem reasonable for the LIS simulation process since the differences from the actual molecular structures determined by X-ray analysis are very little.

A computer simulation was performed according to the method reported by Montaudo et al.[21] The calculated LISs for a given set of R, ϕ, ω, θ values (i.e., for each Eu and Hc spatial location) were obtained. Evaluation of the difference between the observed and calculated LISs was carried out by using the agreement factor (AF) which is defined by the following equation (Eq. 2):[23]

$$AF = \sqrt{\frac{(LIS_{obsd} - LIS_{calcd})^2}{(LIS_{obsd})^2}} \qquad (2)$$

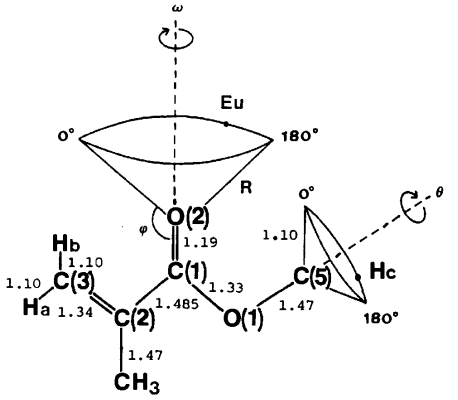

Fig. 3. Structure of the Eu(fod)$_3$-methacrylate complex.

The conformer giving the minimum value of AF is assumed the most likely molecular geometry of a complex (Tables 2 and 3).

It has been pointed out that in the NMR of α,β-unsaturated ketones or esters, the C=O group causes the deshielding of β-methylene protons when the C=O and C=C are in s-cis position.[19,24] This deshielding effect of the C=O is considered to induce a significant difference of chemical shifts of the two methylene protons on β-carbon atom due to much closer position of one of methylene protons to the other (see Fig. 3). This effect is amplified by employing aromatic solvents. The differences of chemical shifts δ (Hb—Ha) observed for the β-methylene of all the methacrylates used in this study were in a range of 0.87—0.98 ppm at 35 °C and 1.00—1.06 ppm at −40 °C in toluene-d_8 (Table 2). These values are much greater than that of 0.19 ppm of s-trans alkyl vinyl ketone calculated by Naito et al.[25] and rather similar to 0.80 ppm for the s-cis form. The δ (Hb—Ha) value (0.83 ppm) of α-methylene-δ-valerolactone (MVL),[26] which exists only

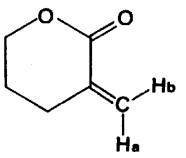

MVL

in s-cis form, is nearly equal to those of the methacrylates. These results also indicate that the C=C and C=O groups of the methacrylates are likely to be in the s-cis position in toluene, although DPMMA and DPEMA-1,2 take the s-trans position in crystals.

The results of conformational analyses of the methacrylates by LIS are collected in Tables 2 and 3. The observed and calculated LISs at 35 and −40 °C are shown in Table 2, and the molecular geometry of the Eu(fod)$_3$ complexes giving the minimum AF values are listed in Table 3. The best agreement between experimental and calculated LISs i.e., the minimum agree-

Table 3. Summary of the Conformation of Methacrylates

Monomer	Temp	R	ϕ	ω	θ	K	AF	C(1)-C(2)		O(1)-C(5)[b]
	°C	Å	°	°	°		%	I[a]	II[b]	A or B
DPMMA	35	2.3	170	−30, 30	0	866	3.3	s-trans	s-cis	A
	−40	2.4	175	−30, 30	−20, 20	1295	0.3		s-cis	A
MBMA	35	2.3	175	−30, 30	0	672	2.8	—	s-cis	A
	−40	2.3	170	−50, 50	−40, 50	1405	0.6	—	s-cis	B
DPEMA-1,2	35	2.4	170	0	0	730	3.3	s-trans	s-cis	A
	−40	2.4	170	−20, 20	−50, 50	1274	0.8		s-cis	B
t-BBMA	35	2.4	165	−40, 40	0	614	4.5	s-trans	s-cis	A
	−40	2.2	175	−30, 30	−30, 30	1010	0.3	and s-cis	s-cis	B
TrBMA	35	2.4	165	−30, 30	0	730	3.7	s-cis	s-cis	A
	−40	2.2	175	−10, 10	−40, 40	921	2.1		s-cis	B

a) Conformation in crystal determined by X-ray analysis. b) Conformation in toluene-d_8, see Fig. 4.

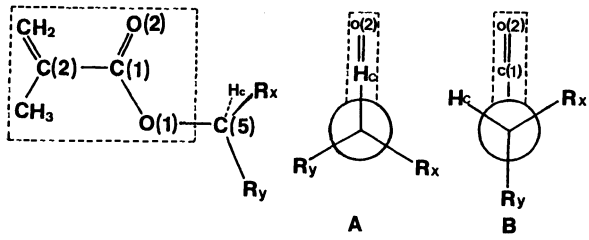

Fig. 4. Conformers of methacrylate.

Table 4. Molar Induced Shifts ($\Delta\delta$, ppm) of Two Groups (R and Ph) on the Asymmetric Carbon of Methacrylates[a]

	MBMA		DPEMA-1,2		*t*-BBMA	
	35 °C	−40 °C	35 °C	−40 °C	35 °C	−40 °C
R[b]	3.95	7.69	4.13	5.79	2.20	2.70
Ph[c]	2.91	4.99	1.88 3.55	2.20[d] 4.42[d]	3.98	4.80

a) In toluene-d_8, concentration of methacrylates=0.5 (mol l^{-1}). b) R are methyl, methylene, and *t*-butyl groups on the asymmetric carbon atoms of MBMA, DPEMA-1,2, and *t*-BBMA, respectively. c) Ortho proton of phenyl group. d) Two phenyl groups were observed separately.

ment factor, was always observed in the s-cis form. The s-trans form gave much greater agreement factors. The results in Tables 2 and 3 also indicates that the hydrogen atom (Hc) attached to the asymmetric carbon atom of the all methacrylates exists on the methacryloyl plane containing the C=C double bond and C=O group at 35 °C as shown in Fig. 4(A) and its position is rather similar to that determined by X-ray analysis. However, at −40 °C, the minimum agreement factor (AF) values for most methacrylates were obtained for the conformer in which Hc was at the gauche position to the methacryloyl plane as depicted in Fig. 4(B). DPMMA showed little conformational change at −40 °C, probably because of the symmetrical structure of the ester group.

We also presumed the positions of the other two groups attached to the asymmetric carbon atom by comparing the LISs at 35 and −40 °C (Table 4). In MBMA, the difference of LISs of the methyl group at two temperatures was larger than that of the ortho protons of the phenyl group. The same was true in DPEMA-1,2; the LIS change of the methylene group in benzyl group is also larger than those of the ortho protons of the phenyl groups, which seem to indicate that at −40 °C, the largest phenyl group attached to the asymmetric carbon atom occupy the position remote from the carbonyl group and the other groups are in staggered positions on either side of the ester carbonyl (see Fig. 5(a)). This was also supported by the fact that the Hc resonances of MBMA and DPEMA-1,2 did not shift downfield at −40 °C as large as Ha and Hb. On the other hand, in *t*-BBMA, the difference of LISs of the largest *t*-butyl group at 35 and −40 °C was nearly equal to that of the phenyl group and the LIS values of the *t*-butyl group were smaller than those of the ortho protons of the phenyl group. These results indicate that in *t*-BBMA the largest *t*-butyl group may occupy a position remote from the carbonyl group; the other groups, hydrogen and phenyl, may be in a staggered position as illustrated in Fig. 5(b). However, the deviation of Hc from the methacryloyl plane in *t*-BBMA at −40 °C seems to be smaller than that of MBMA and DPEMA-1,2, and the conformation may be analogous to that determined by X-ray analysis. It seemed to be difficult to estimate the positions of the two groups attached to the asymmetric carbon atom of TrBMA in a similar manner. Therefore, we assumed that the bulkyl triphenylmethyl group occupies a position remote from the carbonyl and other two, hydrogen and phenyl, groups were in a staggered position as in *t*-BBMA (Fig. 5(c)). This conformation has been observed in crystal although the deviation of Hc is smaller in crystal.

Mechanism of the Enantiomer-Selective Polymerization. Previously, we demonstrated that the enantiomer-selective polymerization of racemic methacrylates with Grignard reagent-Sp complexes in toluene at −78 °C proceeded in a coordination mechanism; that is, a monomer always coordinates to an active center before being incorporated into a polymer chain end.[2,3] The enantiomer selection may be controlled by two main interations. One is the interation between the ester group of a monomer and Sp, and the other is the interaction between the ester group of a monomer and the growing chain end. The hydrogen on the asymmetric carbon atom of the ester group is important in order to avoid any steric hindrance when the monomer, probably, its carbonyl group coordinates to the magnesium (Mg) counterion in the active center because the Sp-Grignard reagent complexes can not polymerize α,α-dimethylbenzyl methacrylate which has no hydrogen atom on the asymmetric carbon.[2] Figure 5 shows the schematical structures of active centers in the enantiomer-selective polymerization of MBMA (a), *t*-BBMA (b), and TrBMA (c) which have (*S*), (*R*), and (*S*) configurations, respectively. Their molecular structures are illustrated on the basis of the results obtained in this study.

In the case of (*S*)-MBMA, the large phenyl group occupies a position remote from the carbonyl group and other two smaller hydrogen and methyl group are in a staggered position. This conformation is analogous to those proposed for α-keto esters by Prelog.[27] The close position of the hydrogen on asymmetric carbon to (−)-sparteine makes it easy for the monomer to coordinate to Mg and to add to the growing end. However, in (*R*)-MBMA, the position of the hydrogen and methyl group is reversed, and the methyl group appears to hit (−)-sparteine moiety upon the coordination to Mg in the same way as shown in Fig. 5(a).

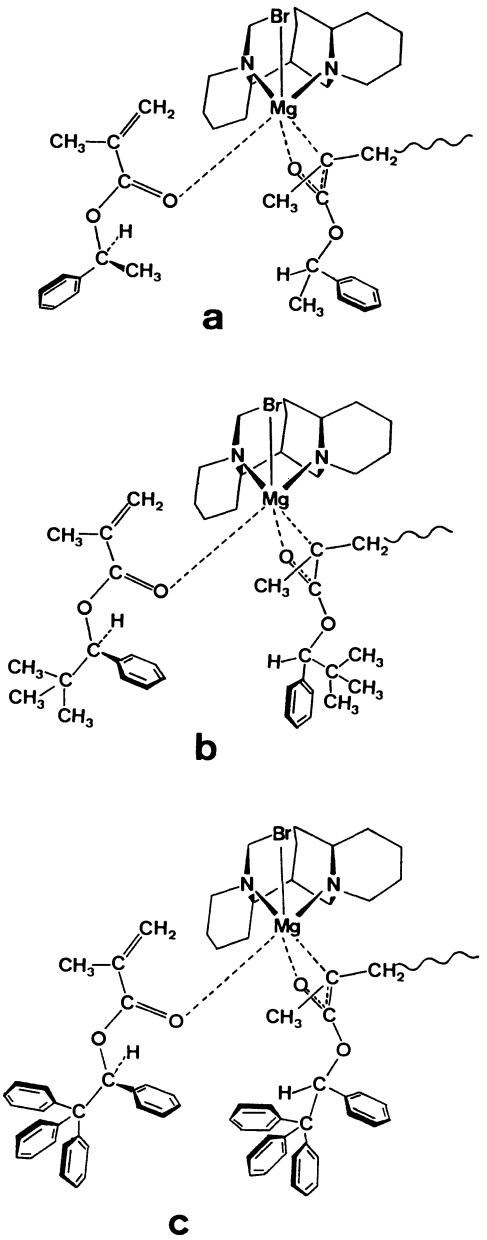

Fig. 5. Schematical structures of active centers in the enantiomer-selective polymerization of MBMA (a), *t*-BBMA (b), and TrBMA (c).

Hence, (*S*)-MBMA may be more reactive than (*R*)-MBMA. The structure of the active center, where the positions of the growing chain end and monomer are those in Fig. 5, may be favorable because the left-hand side of (−)-sparteine in Fig. 5 is more sterically hindered than the right-hand side of (−)-sparteine according to the molecular structure of Sp-ethylmagnesium bromide complex obtained by X-ray analysis, then the bulky growing chain end appears to occupy the right-hand side.[28]

In other monomers having smaller alkyl groups than phenyl on asymmetric carbon atom like EBMA, iPrBMA, and DPEMA-1,2, their conformation is probably similar to that as shown in Fig. 5(a) and (*S*) enantiomers are expected more reactive for the same reason discussed regarding MBMA.

However, when the alkyl group is larger than the phenyl group, like a *t*-butyl group, an enantiomer with the conformation shown in Fig. 5(b) must be preferable. Again, the hydrogen on the asymmetric carbon plays an important role to avoid any steric hindrance in the coordination process of the monomer to the Mg cation. Therefore, the reactive enantiomer must be the (*R*) isomer as observed in the polymerization of *t*-BBMA. In the case of TrBMA, we can also rationally explain that the preferable enantiomer is the (*S*) isomer, as shown in Fig. 5(c), where the phenyl group and hydrogen occupy staggered positions, as in *t*-BBMA and the bulky triphenylmethyl group exists at trans position to carbonyl group. Since the relative positions of the phenyl group to the triphenylmethyl group in the Cahn-Ingold-Prelog system is reversed to that of phenyl to the *t*-butyl group in *t*-BBMA, the (*S*)-isomer is favored for the enantiomer-selective polymerization of TrBMA.

The authors thank Mr. Kenji Wada for his help in the study using the LIS reagent.

References

1) Y. Okamoto, K. Ohta, and H. Yuki, *Chem. Lett.*, **1977**, 617.

2) Y. Okamoto, K. Urakawa, K. Ohta, and H. Yuki, *Macromolecules*, **11**, 719 (1978); **11**, 724 (1978).

3) Y. Okamoto, K. Urakawa, and H. Yuki, *J. Polym. Sci., Polym. Chem. Ed.*, **19**, 1385 (1981).

4) Y. Okamoto, E. Yashima, K. Hatada, H. Yuki, H. Kageyama, K. Miki, and N. Kasai, *J. Polym. Sci., Polym. Chem. Ed.*, **22**, 1831 (1984).

5) Y. Okamoto, E. Yashima, K. Hatada, H. Kageyama, and N. Kasai, unpublished data.

6) H. Kageyama, K. Miki, N. Kasai, Y. Okamoto, E. Yashima, and K. Hatada, *Makromol. Chem.*, **185**, 913 (1984); H. Kageyama, Y. Yanagisawa, N. Kasai, Y. Okamoto, E. Yashima, T. Takeda, and H. Yuki, *ibid*, **185**, 933 (1984).

7) H. Kageyama, K. Miki, N. Tanaka, N. Kasai, Y. Okamoto, K. Hatada, and H. Yuki, *Makromol. Chem.*, **183**, 2863 (1982).

8) H. Kageyama, Y. Hayashi, S. Harada, Y. Kai, N. Kasai, Y. Okamoto, and K. Hatada, *Makromol. Chem.*, **186**, 203 (1985).

9) H. Kageyama, K. Miki, N. Kasai, H. Mohri, Y. Okamoto, and K. Hatada, *Bull. Chem. Soc. Jpn.*, **59**, 2707 (1986).

10) H. Yuki, K. Hatada, T. Niinomi, and Y. Kikuchi, *Polym. J.*, **1**, 36 (1970).

11) H. Yuki, Y. Okamoto, Y. Shimada, K. Ohta, and K. Hatada, *Polym. J.*, **7**, 618 (1976).

12) Y. Okamoto, M. Ishikura, K. Hatada, and H. Yuki, *Polym. J.*, **15**, 851 (1983).

13) T. Ukaji, *Bull. Chem. Soc. Jpn.*, **32**, 1266 (1959); **32**, 1270 (1959); **32**, 1275 (1959).

14) R. J. W. Le Fevre and K. M. S. Sundaram, *J. Chem. Soc.*, **1963**, 1880.

15) T. Fueno, *Production and Technique (Jpn.)*, **35**, 44 (1983).
16) P. E. M. Allen and B. O. Bateup, *Eur. Polym. J.*, **9**, 1283 (1973); J. Furukawa, E. Kobayashi, and S. Nagata, *J. Polym. Sci., Polym. Chem. Ed.*, **13**, 237 (1976); M. Komiyama and H. Hirai, *ibid*, **14**, 627 (1976); **14**, 2009 (1976).
17) J. Furukawa, E. Kobayashi, and S. Nagata, *J. Polym. Sci., Polym. Chem. Ed.*, **13**, 237 (1976).
18) L. J. Bellamy, "Advances in Infrared Group Frequencies," Methuen & Co. Ltd., (1958), Chap. 2, p. 34.
19) D. D. Faulk and A. Fry, *J. Org. Chem.*, **35**, 364 (1970).
20) H. M. McConnell and R. E. Robertson, *J. Chem. Phys.*, **29**, 1361 (1958).
21) G. Montaudo, V. Librando, S. Caccamese, and P. Maravigna, *J. Am. Chem. Soc.*, **95**, 6365 (1973).
22) S. Amiya, I. Ando, S. Watanabe, and R. Chujo, *Polym. J.*, **6**, 194 (1974).
23) W. C. Hamilton, *Acta Crystallogr.*, **18**, 502 (1965).
24) F. A. Bovey, "Nuclear Magnetic Resonance Spectroscopy," Academic Press, New York (1969), p. 76.
25) I. Naito, A. Kinoshita, and T. Yonemitsu, *Bull. Chem. Soc. Jpn.*, **49**, 339 (1976).
26) A. D. Harmon and C. R. Hutchinson, *Tetrahedron Lett.*, **1973**, 1293.
27) V. Prelog, *Helv. Chim. Acta*, **36**, 308 (1953); V. Prelog, *Bull. Soc. Chim. Fr.*, **1956**, 987.
28) Y. Okamoto, K. Suzuki, T. Kitayama, H. Yuki, H. Kageyama, K. Miki, N. Tanaka, and N. Kasai, *J. Am. Chem. Soc.*, **104**, 4618 (1982).

 © 1988 The Chemical Society of Japan Bull. Chem. Soc. Jpn., 61, 2079—2082 (1988)

Determining Factors for the Product Para/Ortho Ratio and Reaction Rate in the Formation of (Hydroxymethyl)phenols from Phenol and Formaldehyde

Makoto KOMIYAMA
Institute of Materials Science, University of Tsukuba, Tsukuba, Ibaraki 305
(Received November 26, 1987)

Formations of 2- and 4-(hydroxymethyl)phenols from phenol and formaldehyde in aqueous alkaline solutions were kinetically investigated by the use of HPLC. The para/ortho ratio for the products sigmoidally increased with increasing concentration of sodium hydroxide, whereas the total yield of the (hydroxymethyl)-phenols showed a steep maximum at the charged molar ratio unity of sodium hydroxide to phenol. Use of lithium hydroxide and potassium hydroxide, in place of sodium hydroxide, as alkaline catalysts results in almost the same para/ortho ratios. The addition of potassium chloride and magnesium sulfate decreased both the para/ortho ratio and the yield. These results indicate that the reactions proceed via an electrophilic attack of formaldehyde, which is free from the adduct formation with hydroxide ion, at phenolate ion. Electrostatic interactions between the phenoxide oxygen atom of the phenol and the incoming hydroxymethyl residues in the transition state exhibit a predominant role in the determination of the para/ortho ratio.

Preparations of (hydroxymethyl)phenols by the reactions of phenol and formaldehyde in alkaline solutions (Eq. 1) are important in industry, since both of the products, 2- and 4-(hydroxymethyl)phenols, are valuable intermediates for the syntheses of various fine chemicals.

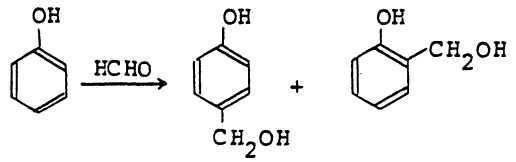

(1)

Previously, these reactions were kinetically examined by several authors.[1-7] However, the reported results are not necessarily consistent with each other. For example, the para/ortho ratios in the products for the sodium hydroxide-catalyzed reactions were 0.61, 1.0, and 1.4, according to Freeman,[1] Minami,[2] and Peer,[5] respectively. For all the reactions, the molar ratio of sodium hydroxide to phenol was unity. These discrepancies are, at least partly, associated with the fact that the reactions were followed by paper chromatography; thus, quantitative analyses were rather difficult. The reaction mechanism has not been sufficiently clarified yet.

Quite recently, the present author found that 4-(hydroxymethyl)phenol can be selectively prepared by the use of cyclodextrin as a catalyst for the reaction of Eq. 1.[8] This finding has prompted the author to study in more detail the effects of the reaction conditions on the selectivity and the rate for the reaction in the absence of cyclodextrin. The reactions have been precisely followed by HPLC.

This paper reports on the effects of kinds and concentrations of alkaline catalysts on the para/ortho ratio in the products and the rate for the formation of (hydroxymethyl)phenols from phenol and formaldehyde in water. Furthermore, results for the reactions in various organic solvents are described. Factors determining the para/ortho ratio and the reaction rate are shown.

Experimental

The reactions between phenol and formaldehyde were carried out at 30 °C under nitrogen. The product analyses were made by HPLC (JASCO $C_{18}S$ column, 10 cm; eluent, 2:1 water-ethanol mixture). All the reactions in the present study satisfactorily followed pseudo-first-order kinetics, and the reaction rates were expressed in terms of the yields with respect to the charged phenol in 1 h or 1 day. The formation of phenols having two or more hydroxymethyl groups was not detected.

Results

Effect of Concentration of Sodium Hydroxide on the Para/Ortho Ratio and the Reaction Rate. Figure 1 shows plots of the para/ortho ratio (4-(hydroxymeth-

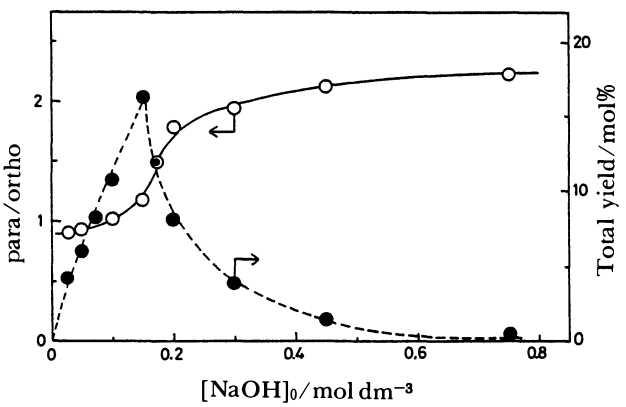

Fig. 1. Plots of the para/ortho ratio (○) and the total yield of 2- and 4-(hydroxymethyl)phenols (●) vs. the charged concentration of sodium hydroxide for the reactions of phenol and formaldehyde in water: $[phenol]_0=0.15$ and $[HCHO]_0=0.58\,mol\,dm^{-3}$; at 30 °C for 1 h.

yl)phenol/2-(hydroxymethyl)phenol) and the total yield of 2- and 4-(hydroxymethyl)phenols as functions of the charged concentration of sodium hydroxide for reactions in water. The initial concentrations of phenol and formaldehyde were kept constant at 0.15 and 0.58 mol dm^{-3}, respectively.

As shown by the open circles, the para/ortho ratio sigmoidally increases with an increase in the charged concentration of sodium hydroxide, showing a gradual saturation at large concentrations of sodium hydroxide.

The total yield (the closed circles) significantly increases with increasing concentration of sodium hydroxide up to the concentration 0.15 mol dm^{-3}, and then rapidly decreases. Thus, it shows a steep maximum at the charged molar ratio unity of sodium hydroxide to phenol.

Effects of Kinds of Alkaline Catalysts on the Para/Ortho Ratio and the Reaction Rate. Table 1 shows the para/ortho ratios and the yields for the reactions using various alkali metal hydroxides as catalysts. The concentrations of the catalysts are 0.75 mol dm^{-3}. The yields for the reaction with sodium hydroxide are larger than the values for the reactions with lithium hydroxide and potassium hydroxide. However, the para/ortho ratio is not significantly affected by the kinds of alkali metal hydroxide.

Table 1. Yields and Para/Ortho Ratios for the Reactions of Phenol and Formaldehyde Using Various Alkali Metal Hydroxides as Catalysts[a)]

Catalyst	Yield/mol%		para/ortho
	p	*o*	
LiOH	0.33	0.15	2.2
NaOH	0.44	0.20	2.2
KOH	0.24	0.11	2.2
NaOH+LiOH[b)]	0.35	0.15	2.3
NaOH+KOH[c)]	0.38	0.17	2.2

a) $[phenol]_0$=0.15 mol dm^{-3}; [alkali metal hydroxide]$_0$=0.75 mol dm^{-3}; $[HCHO]_0$=0.58 mol dm^{-3}; at 30 °C for 1 d. b) $[NaOH]_0$=0.15 and $[LiOH]_0$=0.60 mol dm^{-3}. c) $[NaOH]_0$=0.15 and $[KOH]_0$=0.60 mol dm^{-3}.

Table 2. Effects of Additive Salts on the Yields and the Para/Ortho Ratios for the Reactions of Phenol and Formaldehyde Using Sodium Hydroxide as Catalyst[a)]

Additive salt	Concentration of NaOH/mol dm^{-3}	Yield/mol%		para/ortho
		p	*o*	
KCl	0.75[b)]	0.23	0.12	1.9
KCl[c)]		0.22	0.13	1.7
None		0.44	0.20	2.2
KCl	0.15[b)]	5.0	4.4	1.1
$CaCl_2$		5.9	5.4	1.1
$MgSO_4$		5.0	5.3	0.94
None		8.8	7.7	1.1

a) $[phenol]_0$=0.15 mol dm^{-3}; $[HCHO]_0$=0.58 mol dm^{-3}; a) [Additive Salt]$_0$=0.6 mol dm^{-3} unless otherwise noted; at 30 °C. b) Reaction time, 1 d. c) $[KCl]_0$=2.0 mol dm^{-3}. d) Reaction time, 1 h.

The reaction involving mixture of sodium hydroxide and either lithium hydroxide or potassium hydroxide at the total concentration 0.75 mol dm^{-3} gives a similar para/ortho ratio.

Effects of Additive Salts. The effects of the addition of neutral salts on the para/ortho ratio and the yields for the formation of (hydroxymethyl)phenols are listed in Table 2. The charged concentration of phenol is 0.15 mol dm^{-3}.

When the charged concentration of sodium hydroxide is 0.75 mol dm^{-3}, the addition of potassium chloride exhibits a small but definite decrease in the para/ortho ratio. At a concentration 0.15 mol dm^{-3} of sodium hydroxide, magnesium sulfate also decreases the para/ortho ratio. However, potassium chloride and calcium chloride show no significant effects at concentration 0.6 mol dm^{-3}.

All the metal salts examined decreased the yields of both 2- and 4-(hydroxymethyl)phenols.

Reactions in Various Organic Solvents. The para/ortho ratios and the yields for the reactions in various organic solvents are presented in Table 3. The para/ortho ratio decreases in the following order:

ethanol > 2-propanol ≫ water ≈ methanol ≈ *N*,*N*-dimethylformamide ≫ 1,4-dioxane.

Discussion

Factors Determining the Reaction Rate. A plot of the yield vs. the concentration of sodium hydroxide (the closed circles in Fig. 1) satisfactorily fits the theoretical line (the dotted line) calculated in terms of the following scheme:

$$C_6H_5OH \underset{}{\overset{K_a}{\rightleftharpoons}} C_6H_5O^- + H^+ \quad (2)$$

$$HCHO + OH^- \overset{K}{\rightleftharpoons} H-\underset{\displaystyle OH}{\overset{\displaystyle O^-}{\underset{|}{\overset{|}{C}}}}-H \quad (3)$$

$$\text{Rate} = k[C_6H_5O^-]\,[HCHO_{free}] \quad (4)$$

Here, the activation of phenol for the reaction by deprotonation (Eq. 2) and the deactivation of formaldehyde by the addition of hydroxide ion (Eq. 3) are taken into consideration. The reaction rate is proportional to the product of the concentrations of phenolate ion and free formaldehyde, as shown by Eq. 4. The equilibrium constant K_a for Eq. 2 is taken as $10^{-9.998}$,[9)] and the value K for Eq. 3 has been determined as 13 mol^{-1} dm^3 by best-fitting method.

The concentration of phenolate ion significantly increases with an increase in the charged concentra-

tion of sodium hydroxide, when the charged molar ratio of sodium hydroxide to phenol is smaller than unity. Here, the concentration of free formaldehyde is almost identical with the charged concentration, since the equilibrium concentration of hydroxide ion is minimal. When the charged molar ratio of sodium hydroxide to phenol is larger than unity, however, the concentration of phenolate ion shows a gradual saturation, and the concentration of free formaldehyde decreases in a hyperbolic manner with increase in the equilibrium concentration of hydroxide ion. Thus the rate shows a steep maximum at a charged molar ratio unity of sodium hydroxide to phenol, as clearly shown in Fig. 1.

Similar kinetic analysis was attempted by Peer.[5] However, the analysis was qualitative due to insufficient accuracy of the data, especially at the large concentration of sodium hydroxide, as described by the author.

Factors Determining the Para/Ortho Ratio. The sigmoidal increase of the para/ortho ratio with increase in the charged concentration of sodium hydroxide, depicted by the open circles in Fig. 1, indicates that the electrostatic interactions between the incoming hydroxymethyl residues and the phenoxide oxygen atoms of phenol in the transition states predominantly determine the para/ortho ratio. In the highly alkaline media containing sufficient amounts of sodium hydroxide, the protonation of the hydroxymethyl groups prior to the transition state can not proceed efficiently; these groups are present mostly in anionic forms in the transition state. As a result, the electrophilic attack by formaldehyde at the ortho positions of phenolate is suppressed with respect to the reaction at the para position, since the magnitude of the electrostatic repulsion between the negative charge at the phenoxide oxygen atom and the negative charge at the hydroxymethyl residue is larger for the ortho-reaction.

On the other hand, the hydroxymethyl groups are effectively protonated to neutral species prior to the transition state, when the charged molar ratio of sodium hydroxide to phenol is smaller than unity and, thus, the media are less alkaline. The electrostatic repulsion is less important, and a reaction at the ortho positions takes place rather smoothly.

These arguments are definitely confirmed by the fact that the para/ortho ratio largely changes around the charged concentration 0.15 mol dm^{-3} of sodium hydroxide, where the equilibrium concentration of hydroxide ion significantly increases with increase in the charged concentration of sodium hydroxide (see Fig. 1). The charged concentration of phenol is 0.15 mol dm^{-3}.

The significance of the electrostatic interaction between the phenoxide oxygen atom and the incoming hydroxymethyl residues in the determination of the para/ortho ratio is further supported by the results for the reactions in organic solvents, shown in Table 3. The para/ortho ratios (2.1 and 1.7) for the reactions in ethanol and 2-propanol are larger than the values (1.1, 1.0, and 0.96) in water, methanol, and *N,N*-dimethylformamide, since the electrostatic interaction is stronger due to smaller dielectric constants (24.55 and 19.92); the dielectric constants for water, methanol, and *N,N*-dimethylformamide are 80.2, 32.7, and 36.71.[10] Quite a small para/ortho ratio (0.43) in 1,4-dioxane is ascribed to the fact that sodium phenoxide is present as an intimate ion pair, rather than as dissociated ions, in the solvent of small dielectric constant (2.209).[10]

Table 3. Yields and Para/Ortho Ratios for the Reactions of Phenol and Formaldehyde Using Sodium Hydroxide as Catalyst in Various Solvents[a]

Solvent	Yield/mol%		para/ortho
	p	*o*	
Ethanol	0.30	0.14	2.1
2-Propanol	1.4	0.81	1.7
Water	8.8	7.7	1.1
Methanol	0.05	0.05	1.0
N,N-Dimethylformamide	0.26	0.27	0.96
1,4-Dioxane	1.2	2.8	0.43

a) $[phenol]_0=[NaOH]_0=0.15$ mol dm^{-3}; $[HCHO]_0=0.58$ mol dm^{-3}; at 30 °C for 1 h.

A decrease of the para/ortho ratio upon the addition of potassium chloride (Table 2) is also consistent with the above arguments. The electrostatic repulsion is reduced by the increase in the ionic strength, promoting the ortho-reaction more than the para-reaction. The smaller effect of potassium chloride on the para/ortho ratio at the concentration 0.15 mol dm^{-3} of sodium hydroxide than that at the concentration 0.75 mol dm^{-3} is associated with the minor importance of the electrostatic repulsion here due to a smaller magnitude of the ionization of the hydroxymethyl residues.

The decrease in the para/ortho ratio by the addition of magnesium sulfate is consistent with the previous results[3,5] that the ratio for the magnesium hydroxide-catalyzed reaction is smaller than the value for the sodium hydroxide-catalyzed reaction.

Of the previously reported para/ortho ratios at the charged molar ratio unity of sodium hydroxide to phenol, Minami's value (1.0)[2] is close to the value (1.1) determined in the present study. Freeman's value (0.61)[1] is considerably smaller than the present one, whereas Peer's one (1.4)[5] is larger.

In conclusion, the present kinetic study shows that the rate of the formation of (hydroxymethyl)phenols from phenol and formaldehyde is governed by the concentration of hydroxide ion. The para/ortho ratio in the products is determined by factors affecting the magnitude of the electrostatic interaction between the phenoxide oxygen atom and the incoming hydrox-

ymethyl residue in the transition state.

This work was partially supported by the Mitsubishi Foundation.

References

1) J. H. Freeman and C. W. Lewis, *J. Am. Chem. Soc.*, **76**, 2080 (1954).
2) T. Minami and T. Ando, *Kogyo Kagaku Zasshi*, **59**, 79 (1956).
3) S. Seto and H. Horiuchi, *Kogyo Kagaku Zasshi*, **60**, 653 (1957).
4) H. G. Peer, *Rec. Trav. Chim.*, **78**, 631 (1959).
5) H. G. Peer, *Rec. Trav. Chim.*, **78**, 851 (1959).
6) H. G. Peer, *Rec. Trav. Chim.*, **79**, 825 (1960).
7) K. C. Eapen and L. M. Yeddanapalli, *Makromol. Chem.*, **119**, 4 (1968).
8) M. Komiyama, *Polym. J.*, **20**, 439 (1988).
9) "Kagaku Binran, Kiso-hen Vol. II," ed by Chemical Society of Japan, Maruzen (1975), p. 996.
10) J. A. Riddick and W. B. Bunger, "Technologies of Chemistry Vol. II. Organic Solvents," 3rd ed., Wiley-Interscience, New York (1970).

 © 1988 The Chemical Society of Japan Bull. Chem. Soc. Jpn., 61, 2083—2087 (1988)

Diastereomers of Methionine *S*-Oxide in the Hinge-Ligament Proteins of Molluscan Bivalve Species

Yasuo KIKUCHI,* Kiyoshi HIGASHI, and Nobuo TAMIYA
Department of Chemistry, Faculty of Science, Tohoku University, Aobayama, Sendai, Miyagi 980
(Received December 5, 1987)

The diastereomer ratio was analyzed on methionine *S*-oxide residues formed by in vivo posttranslational oxidation of methionine residues in a protein. The hinge-ligament protein of molluscan bivalves is distinct from usual proteins in containing a large amount of methionine *S*-oxide. The methionine *S*-oxide was released from the protein by proteolytic digestions and was found to be a mixture of approximately equall amounts of two diastereomers, (5*S*)- and (5*R*)-L-methionine *S*-oxide.

Molluscan bivalve species have ligaments at their hinges. The hinge-ligaments are elastic and function to open the shells: When the shells are closed by the contraction of adductor muscles, the hinge-ligaments are strained, and when the adductor muscles relax, the shells are opened by the elastic properties of the ligaments.

The hinge-ligaments are composed of proteins and aragonite crystals of calcium carbonate,[1,2] of which the protein may be primarily important for the elastic property. The hinge-ligament proteins contain cross-linking components, desmosine and isodesmosine,[3] and are insoluble unless hydrolyzed.[1] In the previous papers[1,4] we reported unusual amino acid compositions of hinge-ligament proteins from various bivalve species, such as surf clams (superfamily Mactracea), pearl oysters (superfamily Pteriacea) and a mussel (superfamily Mytilacea). They contain methionine (Met) at extremely high levels (20—40 mol% of the total amino acids) as compared to the Met contents of usual proteins, and almost all of the Met is found in an oxidized form, methionine *S*-oxide (MetO).[5] Since free MetO cannot be utilized as such in protein synthesis,[6] the MetO residues must have been derived from Met residues incorporated in the precursor form of the hinge-ligament proteins. It is known that the Met residues in proteins are oxidized slowly into MetO in various biochemical treatments. In the case of bivalves hinge-ligament proteins, however, the possibility of the artefactual oxidation is excluded by the observation that the intact hinge-ligaments are resistant to BrCN treatment[1] and by the non-destructive analyses of the hinge-ligament in solid-state ^{13}C NMR[7] and IR[2] spectrometries. The hinge-ligament protein is the first and the only instance of the MetO-containing proteins normally functioning in animals. The other instances of MetO-containing proteins are associated with some pathologically defective symptoms such as cataract[8] or rheumatoid arthritis.[9] Moreover, the in vitro oxidation of Met residues resulted in the loss of biological activities of various proteins.[10]

The conversion of Met into MetO introduces another asymmetric center into the amino acid molecule, namely *S*-oxide group of *S*- and *R*-configurations; they are designated as (5*S*)-MetO and (5*R*)-MetO, respectively.[5] Only one of the diastereomers can be expected when the Met-oxidation is catalyzed by enzymes, and even when the oxidation is non-enzymatic, the molecular size of the oxidant and the three-dimensional environments of the target Met residues may affect the stereochemical specificities in the Met oxidation. But the absolute configurations of MetO residues formed in vivo or in vitro have not been examined. The information on the composition of MetO diastereomers is essential for the understanding of the mechanism of Met-oxidation reaction and the roles of MetO residues in the elastic properties of hinge-ligaments. In the present paper we describe the analyses of MetO diastereomers released from the intact hinge-ligament proteins and those from the chemically reduced and reoxidized preparations.

Experimental

Bivalve Species and Their Hinge-Ligaments. Table 1 shows the bivalve species and their hinge-ligament layers subjected to the present study. The classification and the common names of the species are given according to Habe[11] and Abbott and Dance.[12] The hinge-ligaments of the species in superfamilies Mactracea and Limacea are a big rubber-like mass called 'resilium' (internal hinge-ligament). The ligaments of Veneracea species are composed of two histologically distinct layers, outer and inner layers. The ligaments of species in superfamilies Pteriacea and Ostracea are also composed of two layers, fibrous layer and lamellar layer. The resiliums, inner layers and fibrous layers were employed in the present study. They are ontogenetically homologous to one another.[13]

Methionine *S*-Oxide. An authentic MetO was prepared from Met (Wako Pure Chem. Ind. Co. Ltd., Osaka, Japan) and hydrogen peroxide as described by Toennies and Kolb.[14] Two diastereomers were resolved by fractional crystallization of the picrates as described by Lavine.[15] Their absolute configurations were determined by Christensen and Kjær.[16] Found (5*S*-diastereomer): C, 36.23; H, 6.89; N, 8.35%. Found (5*R*-diastereomer): C, 36.10; H, 6.91; N, 8.40%. Calcd for $C_5H_{11}NO_3S$: C, 36.35; H, 6.71; N, 8.48%.

Amino Acid Analyses. The amino acid compositions of the hinge-ligament proteins were determined on the HCl-hydrolysates prepared from ligament pieces (2—3 mg) in 6 M

Table 1. Bivalve Species and Their Hinge-Ligament Layers Subjected to the Present Work

Sample No.	Bivalve species	Ligament layer
	Mactracea species	
1	*Pseudocardium sachalinensis* (Sakhalin surf clam)[a]	Resilium
2	*Spisula (Hemimactra) solidissima* (Atlantic surf clam)[b]	Resilium
3	*Spisula solidia* (Solid mactra)[c]	Resilium
4	*Mactra chinensis* (Chinese mactra)[d]	Resilium
5	*Tresus keenae* (Keen's graper)[a]	Resilium
6	*Coecella chinensis* (Chinese anapella clam)[c]	Resilium
	Veneracea species	
7	*Saxidomus purpuratus* (Purplish Washington clam)[c]	Inner layer
	Pteriacea species	
8	*Malleus (Malleus) albus* (White hammer oyster)[c]	Fibrous layer
	Limacea species	
9	*Acesta (Acesta) goliath* (Giant lima)[d]	Resilium
	Ostracea species	
10	*Crassostrea gigas* (Giant pacific oyster)[d]	Fibrous layer

a) From Fukushima, Jpn.; b) from Woods Hole, MA. U. S. A.; c) provided by Dr. T. Habe (National Scientific Museum, Tokyo, Jpn.); d) from Miyagi, Jpn.; e) from Mie, Jpn.

(1 M=1 mol dm^{-3}) HCl (0.3 ml) at 105 °C for 24 h in vacuo. The amino acid analyses were carried out with JLC 200A amino acid analyzer (JEOL Co. Ltd., Tokyo, Japan). The contents of MetO, Met and homocysteic acid, the latter two of which were derived from MetO during the HCl-hydrolysis,[17,18] were combined and taken as Met content. The MetO contents were determined on NaOH-hydrolysates prepared from ligament pieces (2—3 mg) in 2.5 M NaOH (0.3 ml) at 105 °C for 15 h in vacuo. No correction was made for hydrolytic losses.

Decalcification of the Hing-Ligaments. The dried hinge-ligament pieces (about 50 mg) were swollen in H_2O (5 ml) at 4 °C for 18 h and powdered in an agate mortar with a pestle. The ligament powder was collected by centrifugation at 3000 *g* for 10 min and stirred in 2% (v/v) acetic acid (3 times, 2 ml each for 2, 4, and 18 h, at 4 °C). The decalcified ligament powder was washed with H_2O thoroughly and freeze-dried.

Proteolytic Solubilization of the Hinge-Ligament Protein. A suspension of decalcified ligament powder (4 mg) in 0.1 M sodium borate buffer solution (pH 8.8) (1 ml) and one drop of chloroform as preservative was added with 0.1 ml aliquots of crystalline bacterial alkaline protease (Katayama Chem. Ind. Co. Ltd., Osaka, Japan) (4 mg ml^{-1} in the same buffer solution) at the time intervals of 24 h and the mixture stirred at 25 °C for 120 h. The extent of the solubilization was monitored by the combined contents of Met, MetO and homocysteic acid in the HCl-hydrolysates of the supernatant aliquots (30 μl) taken out from the mixture at every 24 h.

Proteolytic Liberation of MetO. The above mixture was stirred at 25 °C and added with 0.1 ml aliquots of leucine amino peptidase (cytosole) (Sigma) (2 mg ml^{-1}) at the incubation times of 0, 27, 50, and 90 h. The contents of free MetO in the supernatant aliquots (30 μl) were determined with amino acid analyzer at the incubation times of 27, 50, 90, and 120 h.

Analyses of MetO Diastereomers. Two columns (0.8 cm×70 cm each) of sulfonated polystyrene resine (JLC-R-2, JEOL Co. Ltd. Tokyo, Japan) were tandemly connected and equipped on an amino acid analyzer, JLC 8AH (JEOL Co. Ltd.). The analysis was carried out at 54 °C with 0.067 M sodium citrate-NaCl buffer solution (pH 2.85, I[5]=0.2) at a flow rate of 0.5 ml min^{-1}. Under these conditions the diastereomers, (5*S*)- and (5*R*)-MetO, were equally sensitive to ninhydrin and eluted at 4.4 and 4.6 h, respectively. The peak areas were proportional to the amounts of materials up to 230 nmol and the routine analyses were carried out with 50—80 nmol each of the diastereomers.

Chemical Reduction of MetO Residues in the Hinge-Ligament Proteins. The decalcified ligament protein powder (about 150 mg) was stirred in 50% (w/v) aqueous *N*-methylmercaptoacetamide[19] (10 ml) at room temperature for 11 days. The protein powder was washed with H_2O by centrifugation and freeze-dried.

Chemical Reoxidation of Met Residues in the Reduced Hinge-Ligament Protein. Oxidation with Hydrogen Peroxide: A suspension of reduced ligament protein (8 mg) in H_2O (5 ml) was adjusted to pH 2 with 0.1 M HCl, added with 30% (w/v) hydrogen peroxide (0.5 ml) and stirred at room temperature for 18 h. The protein powder was washed thoroughly with H_2O and freeze-dried. The reduced ligament protein (8 mg) was also reoxidized in 0.1 M sodium borate (pH 8.8) (5 ml) in the same procedures as described above.

Oxidation with Chloramine T or *N*-Chlorosuccinimide: The Met residues in the reduced protein (12 mg) were oxidized with chloramine T or *N*-chlorosuccinimide (5 mol/mol of Met residues) in 0.033 M sodium citrate-NaCl buffer solution (pH 2.2, I=0.1) or 0.1 M Tris-HCl (pH 8.5) (40 ml) for 1 h at room temperature as described by Shechter et al.[20] The protein powder was washed with H_2O and freeze-dried.

Chemical Oxidation of Free Methionine. Oxidation with *N*-Chlorosuccinimide: A solution containing L-Met (75 mg) and *N*-chlorosuccinimide (80 mg) in 0.033 M sodium citrate-NaCl buffer solution (pH 2.2, I=0.1) (2 ml) was stirred for 1 h at room temperature, adjusted to pH 7 with 1-butylamine and added with methanol (4 ml) and acetone (40 ml). The precipitated amino acid was collected by centrifugation (3000 *g* for 10 min), washed with acetone (3 times, 30 ml each) and dried in vacuo (83 mg, 100%). The product agreed with the authentic MetO on TLC analysis using 0.1 mm precoated cellulose plates (Merck) and 1-butanol/water/acetic acid (5/2/1, by vol) as developing solvent.

Oxidation with Chloramine T: A solution containing L-Met (75 mg) and Chloramine T (170 mg) in 0.1 M Tris-HCl buffer solution (pH 8.5) (4 ml) was stirred for 1 h at room temperature and added with methanol (4 ml) and acetone (100 ml). The precipitated MetO was collected and characterized as described above (45 mg, 54%).

Results and Discussion

The compounds containing *S*-oxide moieties are

widely distributed in the natural products. Since their S-oxide groups are not racemic as reviewed by Kjær,[21] the enzymatic sulfide oxidation may be common in their biosynthetic pathways. On the other hand, the non-enzymatic mechanism was suggested for the in vivo oxidation of Met residues in the proteins from pathologically defective tissues, although the absolute configuration of the MetO residues was not analyzed.[22] In contrast to the above proteins, the ligament proteins are from non-defective and normally functioning hinge-ligaments of the bivalve species. They contain Met in extremely high contents and the extent of Met-oxidation in them is almost complete.

The amino acid compositions of the hinge-ligament proteins are shown in Fig. 1. The resilium proteins of the Mactracea species (1—6) are similar to one another in containing Gly and Met to the extents of 50 and 20 mol%, respectively, and almost all of their Met residues are present in the S-oxide form, MetO (Table 2, column 2). The ligament proteins from other species (7—10) also contain Met as predominant constituents and their Met residues are mostly in S-oxide form.

Since the hinge-ligament proteins are insoluble in usual protein solvents, they were solubilized by the proteolysis with crystalline bacterial alkaline protease (Fig. 2). The extents of solubilization were 80% or more in most cases examined. Amino acids were released from the solubilized peptides by the action of an exopeptidase, leucine amino peptidase (Fig. 3). About 80% of MetO was detected as a free amino acid in the digests of the ligament proteins from Sakhalin surf clam (*Ps. sachalinensis*) and Giant pacific oyster (*C. gigas*) (Fig. 3, A and E, respectively), but only 30—

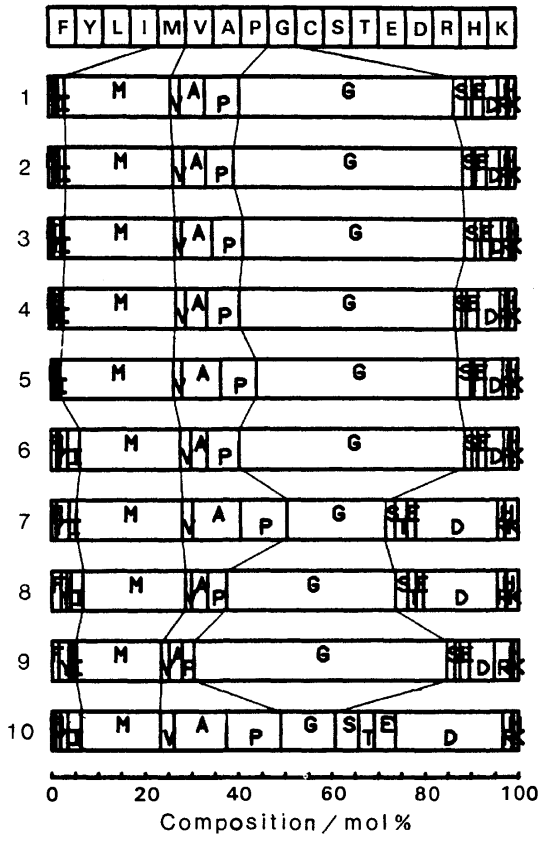

Fig. 1. Amino acid compositions of the hinge-ligament proteins of bivalve species.[5] The numbers for species and ligament layers are the same as those in Table 1.

Table 2. Methionine S-Oxide in the Hinge-Ligament Protein of Various Bivalve Species

Species and ligament layer[a]	Content: MetO/(Met+MetO) ratio in the NaOH-hydrolysate/%	Diastereomer ratio: (5S)-MetO/(5R)-MetO
Mactracea species		
1	100	1.1
2	100	1.2
3	100	1.2
4	100	1.2
5	100	1.2
6	92	1.2
Veneracea species		
7	100	1.1
Pteriacea species		
8	100	1.1
Limacea species		
9	100	1.5
Ostracea species		
10	100	1.1

a) Numbers for the bivalve species and the ligament layers are the same as those in Table 1.

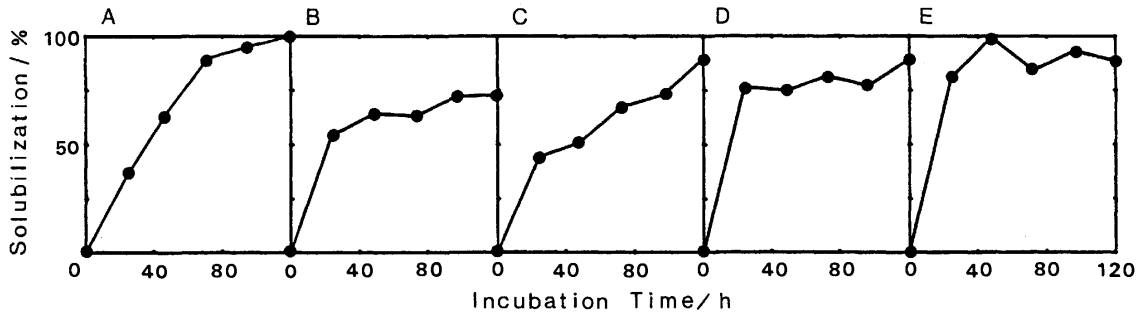

Fig. 2. Time-courses of the proteolytic solubilization of the hinge-ligament proteins. The samples in A, B, C, D, and E are those introduced as 1, 7, 8, 9, and 10 , respectively, in Table 1.

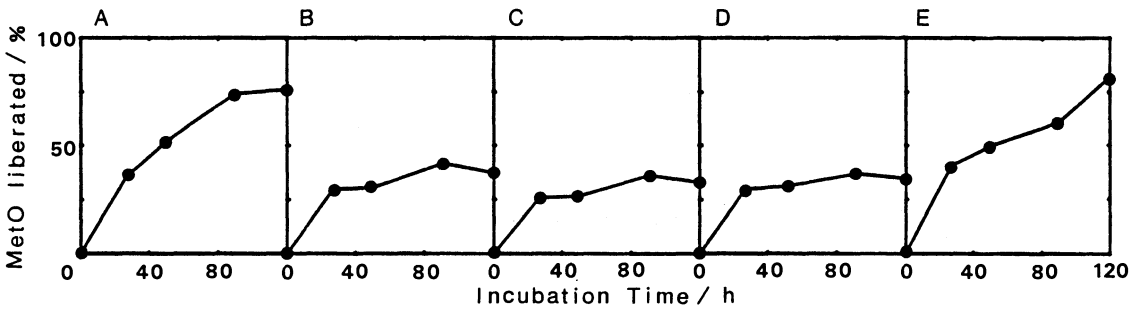

Fig. 3. Time-courses of proteolytic liberation of methionine *S*-oxide from the solubilized fragment-peptides of the hinge-ligament proteins. The samples in A, B, C, D, and E are those introduced as 1, 7, 8, 9, and 10, respectively, in Table 1.

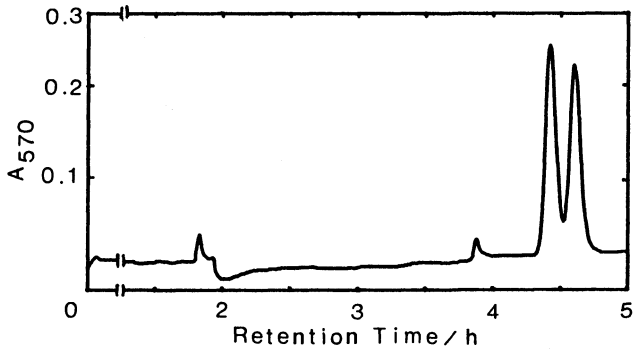

Fig. 4. Separation of MetO diastereomers on amino acid analyzer. For detailed chromatographic conditions see ex_erimental section.

Table 3. The Ratio of MetO Diastereomers Prepared by Chemical Oxidation of Met Residues in Reduced Resilium Protein of Sakhalin Surf Clam

Oxidant	(5*S*)-MetO/(5*R*)-MetO ratio	
	pH 2.2	pH 8.8
Hydrogen peroxide	1.1	1.1
N-Chlorosuccinimide	1.1	1.1
Chloramine T	n.d.[a)]	1.2

a) n.d.: not determined because of the low yield due to low solubility of the reagent in the buffer solution.

40% of MetO was liberated from the peptides in the other cases (Fig. 3, B, C, and D). The difference in the extent of the MetO liberation might be due to the difference in amino acid sequence of the protein.

The ratio of MetO diastereomers was determined by amino acid analysis. Figure 4 shows the results for the MetO from the resilium protein of Sakhalin surf clam (*Ps. sachalinensis*). The peaks at 4.4 and 4.6 h were assigned to (5*S*)- and (5*R*)-MetO, respectively. From their peak areas, the (5*S*)-MetO/(5*R*)-MetO ratio was determined as 1.1. Table 2 (column 3) shows the ratios of MetO diastereomers in the ligament proteins from various bivalve species. The values are 1.1—1.2 in most cases and 1.5 for the MetO from the resilium protein of Giant lima, *A. (A). goliath.* Since no interconversion was observed between the two diastereomers during the above proteolytic treatments (data not shown), the values show the ratios of MetO diastereomers in the ligament proteins. The results show that the two diastereomers are present in approximately equal amounts in the hinge-ligament proteins from bivalve species of a wide variety of the taxonomic classes.

The MetO residues in the resilium protein of Sakhalin surf clam (*Ps. sachalinensis*) were reduced into Met with *N*-methylmercaptoacetamide,[19] and the Met residues in the reduced protein were reoxidized with various reagents. The MetO/(Met+MetO) ratios were less than 0.03 in the reduced protein and more than 0.95 in the reoxidized preparations. The ratios of MetO diastereomers in the reoxidized preparations are shown in Table 3. The chemical reoxidations of Met residues with various reagents in either acidic or alkaline solutions resulted in the formation of the two MetO diastereomers in approximately equal amounts. The results may suggest that the in vivo Met oxidation is a nonenzymatic reaction, although the active oxidizing species, which is not identified yet, can be produced by some enzymes as suggested by Wong and Travis,[23] Fliss et al.[24] and Kühn et al.[25] The participation of enzymes in Met oxidation was examined as follows. The soft body of Sakhalin surf clam (*Ps. sachalinensis*) was dissected into eight tissues; adductor muscles, gills, mantle, labial palp, viceral mass, siphon, crystalline style and body wall (foot). The tissues were homogenized in phosphate buffer saline and the homogenates centrifuged at 15000 *g* for 30 min. The supernatant fractions were taken and incubated with reduced resilium protein of Sakhalin surf clam at 25 °C for 20 h. But no significant and reproducible increase in MetO/(Met+MetO) ratio was observed in any protein preparations incubated with the tissue extracts. Since the addition of D-glucose and L-leucine (50 mM each) into the medium did not affect the results, the possibilities of participation of glucose oxidase or amino acid oxidase, which would release hydrogen peroxide into the medium, were also

Table 4. The Ratio of MetO Diastereomers Prepared by Chemical Oxidation of Free L-Methionine

Oxidant	pH	(5S)-MetO/(5R)-MetO ratio
Hydrogen peroxide	2	1.4
N-Chlorosuccinimide	2.2	1.7
Chloramine T	8.5	1.6

excluded. When free Met was incubated with freshly prepared resilium powder, a small portion of it was converted into MetO. The results can, however, be explained by chemical exchange of oxygen atom between free Met and MetO residues in the protein.[26] Although these results indicate no enzyme participation in the in vivo oxidation of Met residues, the examination might be too preliminary to exclude the possibilities of enzymatic formation of active oxidizing species.

The chemical oxidation of free Met was not highly stereospecific: The (5S)-MetO/(5R)-MetO ratios were 1.4—1.7 in the MetO preparations obtained from free L-Met and various oxidizing reagents under conditions similar to those described above (Table 4). On the other hand, in the oxidation of Met residues in proteins, the stereospecificity of the reaction can be largely affected by the three-dimensional protein structures. Since the MetO in the hinge-ligament proteins was found to be a mixture of two diastereomers in approximately equal amounts, the conformation of the hinge-ligament proteins might be random and the two MetO diastereomers might be formed with equal probabilities. Alternatively, the protein conformation might determine the stereospecificities at every Met-oxidation sites in the protein to form the two MetO diastereomers in equal amounts.

As the MetO is a predominant constituent of the hinge-ligament proteins of some bivalve species, and as the conversion of Met into MetO is almost complete in these proteins, the MetO residues are supposed to play some essential roles in the properties of the hinge-ligaments. The MetO side chains make the protein highly hydrophilic and promote the swelling of the hinge-ligaments (Y. Kikuchi et al., unpublished data). The relationship between the MetO residues and the elastic properties of the ligaments will be discussed elsewhere.

The authors are grateful to professor Tadashige Habe (National Scientific Museum, Tokyo, Japan) for providing hinge-ligaments of some bivalve species, and to Mr. Hisaku Abe of this laboratory for amino acid analysis.

References

1) Y. Kikuchi and N. Tamiya, *J. Biochem.*, **89**, 1975 (1981).
2) Y. Kikuchi and N. Tamiya, *Bull. Chem. Soc. Jpn.*, **57**, 122 (1984).
3) Y. Kikuchi, O. Tsuchikura, M. Hirama, and N. Tamiya, *Eur. J. Biochem.*, **164**, 397 (1987).
4) Y. Kikuchi and N. Tamiya, *Biochem. J.*, **242**, 505 (1987).
5) Abbreviations for amino acids are used according to the recomendation of IUPAC-IUB Joint Commission on Biological Nomenclature: *Eur. J. Biochem.*, **138**, 9 (1984). All amino acids except for glycine are of L-configuration. The sulfur in methionine *S*-oxide was treated as carbon in the numbering. Other abbreviations: *I*, ionic strength; Tris, 2-amino-2-hydroxymethylpropane-1,3-diol.
6) E. Lemoine, *Eur. J. Biochem.*, **4**, 213 (1968).
7) Y. Kikuchi, N. Tamiya, T. Nozawa, and M. Hatano, *Eur. J. Biochem.*, **125**, 575 (1982).
8) R. J. W. Truscott and R. C. Augusteyn, *Biochim. Biophys. Acta*, **492**, 43 (1977).
9) P. S. Wong and J. Travis, *Biochem. Biophys. Res. Commun.*, **96**, 1449 (1980).
10) N. Brot and H. Weissbach, *Trends. Biochem. Sci.*, **7**, 137 (1982).
11) T. Habe, "Systematics of Mollusca in Japan: Bivalvia and Scaphopoda," Hokuryukan, Tokyo (1977).
12) R. T. Abbott and S. P. Dance, "Compendium of Seashells," E. P. Dutton, New York (1982); Japanese edition by T. Habe and T. Okutani, Heibonsha Publishers, Tokyo (1985).
13) E. R. Trueman, "Ligament" in "Treatise on Invertebrate Paleontology," ed by R. C. Moore, Geological Society of America, Boulder, and University of Kansas, Lawrence (1969), Part N, Vol. 1, pp. N58—N64.
14) G. Toennies and J. J. Kolb, *J. Biol. Chem.*, **128**, 399 (1939).
15) T. F. Lavine, *J. Biol. Chem.*, **169**, 477 (1947).
16) B. W. Christensen and A. Kjær, *Chem. Commun.*, **1965**, 225.
17) N. F. Floyd, M. S. Cammaroti, and T. F. Lavine, *Arch. Biochem. Biophys.*, **102**, 343 (1963).
18) K. Morihara, *Bull. Chem. Soc. Jpn.*, **37**, 1781 (1964).
19) R. A. Houghten and C. H. Li, *Anal. Biochem.*, **98**, 34 (1979).
20) Y. Shechter, Y. Burstein, and A. Patchornik, *Biochemistry*, **14**, 4497 (1975).
21) A. Kjær, *Tetrahedron*, **30**, 1551 (1974).
22) J. J. Harding, *Advances in Protein Chemistry*, **37**, 247 (1985).
23) P. S. Wong and J. Travis, *Biochem. Biophys. Res. Commun.*, **96**, 1449 (1980).
24) H. Fliss, H. Weissbach, and N. Brot, *Proc. Natl. Acad. Sci. U.S.A.*, **80**, 7160 (1983).
25) H. Kühn, H. Holzhütter, T. Schewe, C. Hiebsch, and S. M. Rapoport, *Eur. J. Biochem.*, **139**, 577 (1984).
26) Y. Shechter, *J. Biol. Chem.*, **261**, 66 (1986).

Enantioselective Reduction of 2-Methyl-3-oxopropionate by Bakers' Yeast[1)]

Kaoru NAKAMURA,* Takehiko MIYAI, Kazutoshi USHIO, Shinzaburo OKA, and Atsuyoshi OHNO
Institute for Chemical Research, Kyoto University, Uji, Kyoto 611
(Received December 18, 1987)

Various esters of 2-methyl-3-oxopropionic acid were subjected to the reduction with bakers' yeast. Effects of size and bulkiness as well as hydrophobicity of alcohol moieties of the substrates on the enantioselectivity of the reduction were investigated. The substrates having bulky ester groups gave the (*R*)-hydroxy esters with high enantioselectivities. A mechanism to alter the stereoselectivity of the reduction is proposed.

Optically active 3-hydroxy-2-methylpropionic acid derivatives (**1**) have been used widely as versatile chiral building blocks.[2)] Although the use of a microbe in hydroxylation of isobutyric acid to obtain **1** of high optical purity has been reported,[3,4)] the handling of special microbes such as those reported is not so easy in laboratories of organic chemistry. However, bakers' yeast (BY), which is also a microbe, has advantages as a reagent in organic chemistry. BY is easily available and cheap. Special caution, such as sterilization or careful operation, is not necessary. Because of its simplicity of handling, BY has been used as a convenient pack of various enzymes to convert achiral organic compounds into chiral products.[5)] In this paper, we would like to report an enantioselective reduction of 2-methyl-3-oxopropionate (**2**) with BY to obtain chiral **1**. Although the reduction of **2** with BY was attempted by Seebach et al., the enantiomer excess (e.e.) observed was not satisfactory for practical use (54%).[6)] It should be noted that in the process of reduction, chirality is introduced at the position different from the reaction center. That is, the chirality arises on the C-2 position, whereas the reduction takes place at the C-3 position. Therefore, there is no doubt that the introduced chirality stems from difference in the rate of reduction of both enantiomers of the starting material (*R*-2 and *S*-2) by an enzyme or a set of enzymes that are operating simultaneously in bakers' yeast. In other words, the present reaction is a reductive resolution of racemic material. Since the starting material **2** is composed of a mixture of an aldehyde and its enol form, which was confirmed by ^{1}H NMR spectroscopy, interconversion between the two enantiomers (of the aldehyde form) is expected to be fast enough to keep the starting material as a racemic mixture during the whole reduction period even though one enantiomer is reduced faster than the other. Therefore, in principle, a particular enantiomer of the product can be obtained quantitatively, although the process itself is a kinetic resolution.

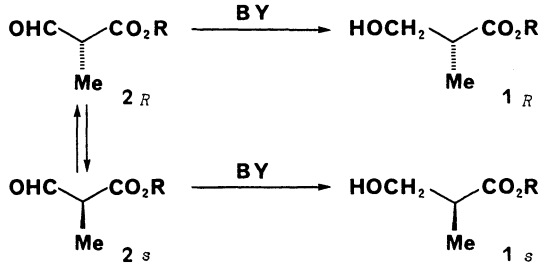

Scheme 1.

It seems that relatively low selectivity reported by Seebach et al. was due to a small difference in the reaction rates of both enantiomers of the aldehyde. One may therefore be able to obtain chiral **1** in high e.e. if one can modify the substrate so that the enantiomers exhibit a large difference in the reaction rate. According to the concept mentioned above, we investigated the reduction of **2** by BY.

Usually, the microbial reduction of a carbonyl compound does not necessarily afford the alcohol of desired configuration with satisfied e.e., and several methods to control the stereochemistry of reduction have been developed. Screening of microbes[7)] has been the method employed most widely but this is troublesome for organic chemists. Immobilization of microbes can also control the stereochemistry of the product.[8)] Modification of substrates has been used for stereochemical control.[9-11)] Since the latter two methods are familiar techniques for organic chemists, we have investigated the application of these two techniques for the reduction of **2**. The present report will discuss the results obtained from the modification of a substrate.

Results

In the ^{1}H NMR spectrum of **2a** ($CDCl_3$-TMS), the aldehydic proton appears at δ 9.77 and the olefinic proton appears at δ 6.98, which indicates that **2a** exists as a mixture of the aldehyde and its enol form.

Various esters of 2-methyl-3-oxopropionic acid were reduced with BY in water in the presence of glucose. Results are summarized in Table 1. The reduction of **2a** (ethyl ester) was resulted in low enantioselectivity (e.e.=45%). The e.e. of the reduction was slightly improved in the reduction of octyl ester (**2c**, e.e.=60%). Better results were obtained, however, in the reduction of substrates with bulky alcohol moieties such as 3-methylbutyl (**2f**, e.e.=84%), cyclohexylethyl (**2p**, e.e.=74%), and 2-(trimethylsilyl)ethyl (**2n**, e.e.=79%) groups.

Table 1. Reduction of **2** by Bakers' Yeast

Substrate	R	$[\alpha]_D^{20}$	e.e./%	Isolated yield/%
2a	$-C_2H_5$	−8.459	45	94
2b	$-(CH_2)_3CH_3$	−4.167	53	73
2c	$-(CH_2)_7CH_3$	−6.103	60	41
2d	$-CH(CH_3)_2$	−8.736	19	49
2e	$-CH_2CH(CH_3)_2$	−7.195	64	84
2f	$-(CH_2)_2CH(CH_3)_2$	−8.000	84	66
2g	$-(CH_2)_3CH(CH_3)_2$	−8.889	81	83
2h	$-CH_2CH(CH_2CH_3)_2$	−8.210	71	76
2i	$-CH_2CH{=}CH_2$	−8.587	48	58
2j	$-(CH_2)_2OCH_2CH_3$	−4.789	29	73
2k	$-(CH_2)_2OCH_3$	−10.047	47	59
2l	$-CH_2C(CH_3)_3$	−13.471	90	78
2m	$-(CH_2)_2C(CH_3)_3$	−9.923	81	66
2n	$-(CH_2)_2Si(CH_3)_3$	−6.344	79	70
2o	$-CH_2$-*c*-C_6H_{11}	−7.778	74	70
2p	$-(CH_2)_2$-*c*-C_6H_{11}	− 6.799	74	71

The substrate having the 2,2-dimethylpropyl group **2l** gave the highest value (e.e.=90%).

3-Hydroxy-2-methylpropionates thus obtained by the reduction with BY were converted into the corresponding ethyl ester and the absolute configuration of this ethyl ester was determined by comparing the sign of optical rotation with that reported.[6]

Discussion

Recently two reports described the effect of length in alcohol moeity on yeast reduction. The reduction of 3-oxo-6-heptenoic acid and its esters afforded (*R*)-3-hydroxy-6-heptenoic acid and its esters, respectively. The e.e. increased as the length in the alcohol moiety decreased and the best result was observed with the free acid.[9] The reduction of 4-chloro-3-oxobutanoate gave the corresponding (*R*)-hydroxy ester of higher e.e. with the substrate which had the alcohol moiety of longer alkyl chain.[10] Since the configuration of (*R*)-4-chloro-3-hydroxybutanoic acid is opposite to that of (*R*)-3-hydroxy-6-heptenoic acid,[11] these two reports show that the length of alkyl chain in alcohol moiety exerts the same stereochemical effect on different substrate.

We reported that the length of alkyl chain in the alcohol moiety affects the diastereoselectivity of reduction of 2-methyl-3-oxobutanoate (**3**), an analog of **2**.[12] Thus although methyl, ethyl, and other short alkyl esters did not give satisfactory results, the octyl ester yielded (2*R*, 3*S*)-3-hydroxy-2-methylbutanoate in excellent diastereoselectivity. Since 2-substituted 3-oxobutanoates are known to afford the (3*S*)-hydroxy esters in higher e.e. than the corresponding unsubstituted substrates,[13] the high diastereoselectivity in the reduction of **3** directly means that the reduction is highly enantioselective with respect to the 2-position, or the reduction affords only one stereoisomer almost exclusively out of four possible isomers (2*R*,3*S*: 2*R*, 3*R*: 2*S*,3*R*: 2*S*,3*S*=95 : < 1 : < 1 : 5).

Since **2** and **3** have quite similar molecular structures (aldehyde vs. ketone) each other, it is reasonably expected that the BY reduction of the octyl or higher alkyl esters of **2** might exert satisfactory enantioselectivity.

However, contrary to the expectation, the reduction of **2c** (the octyl ester) did not give the hydroxy ester in a high e.e. Thus, although the e.e. increased in the order; ethyl (45%), butyl (53%), and octyl (60%), the increase in the selectivity was not remarkable. It should be noted that the reduction of **2** is catalyzed by a primary alcohol dehydrogenase(s), but the secondary alcohol dehydrogenase(s) must be involved for the reduction of **3**. The same phenomenon was also observed in the BY reduction of 5-methoxy-3-oxopentanoate where the e.e. of the product increases from the ethyl (60%) to the butyl (82%) ester, then decreases in the hexyl ester (71%).[14] The substrate with a long alkyl chain in the ester part did not give the highest value. These results suggests that the structural similarity in substrates does not necessarily result in similar results in multi-enzyme systems. It is unfortunate that complex structure of microbe does not allow to predict a simple relationship between the structure of a substrate and the stereoselectivity of the reduction.

Since an attempt to control the stereochemistry in yeast reduction by changing the length of alkyl chain in the ester group appeared unsatisfactory, we intended to look for another method which affected stereochemical course of the reduction. In order to change the electronic property in the alcohol moiety, an oxygen function was introduced and the substrate was subjected to the BY reduction. It was expected that the difference in affinities to enzyme(s) along with changing a hydrocarbon unit to an oxygen might affect the stereochemistry of the reduction. However, this modification was found to shift the specificity toward the *S*-configuration, if any. Thus the e.e. of products from the 2-ethoxyethyl derivative was 29% and that of the 2-methoxyethyl derivative was 47%. Both of these substrates are not suitable in order to produce the (2*R*)-hydroxy esters in high enantioselectivities.

In order to achieve the third way of our challenge to increase the e.e. of yeast reduction, we focused attention on the bulkiness of the alcohol moiety of the substrate. In contrast to the length, the bulkiness of the alcohol moiety was found to play an important factor to change the e.e. of the products. That is, the substitution of a methyl group at the 3-position of the butyl ester resulted in the hydroxy ester in 81% e.e. whereas the e.e. of the corresponding butyl ester was 53%. Encouraged by these observations, we prepared several substrates from bulky alcohols. Neither 3,3-dimethylbutyl ester (81% e.e.) nor 2-(trimethylsilyl)ethylester (79% e.e.) improved the stereoselectivity. In other words, bulkiness of isopropyl group is enough as a single substituent at the 2-position of the ester to shift

the e.e. to an asymptotic value of about 80%. However, on the other hand, double substitution at the 2-position increases the e.e. value further; the reduction of the 2,2-dimethylpropyl ester proceeded with 90% e.e.

The reason why the bulkiness at the 2-position of the ester shifts the stereospecificity of the reaction toward the *R*-configuration is not clear at present. One plausible mechanism is that more than two dehydrogenases are involved in the reduction and each of them reduces a substrate in high e.e. but in opposite configuration. When both (*R*)- and (*S*)-hydroxy ester-producing enzymes contribute to the reduction in comparable extents, the e.e. of the product becomes low. On the contrary, if a bulky ester is not reduced by the (*S*)-hydroxy ester-producing enzyme, only the (*R*)-hydroxy ester-producing enzyme opperates and consequently the (*R*)-hydroxy ester will be produced exclusively. Although several dehydrogenases contribute to the reduction in the BY reduction of ethyl 4-chloro-3-oxobutanoate, it was pointed out that the octyl ester is reduced only by the (*R*)-hydroxy ester-producing enzyme and thus produced (*R*)-hydroxy ester has high e.e. We believe that the same recognition is operating here in the reduction of 2,2-dimethylpropyl 2-methyl-3-oxopropionate as that seen in the reduction of octyl 4-chloro-3-oxobutanoate. To confirm our suggestion, further investigation is necessary.

Experimental

^{1}H NMR spectra were recorded on a JEOL FX-100 (100 MHz), a Varian VXR-200 (200 MHz), and a JEOL GX-400 (400 MHz) spectrometer in $CDCl_3$ with Me_4Si as an internal reference. Gas chromatography was recorded on a Yanaco G-2800 gas chromatograph. HPLC was performed with a Hitachi 655 Liquid Chromatography (pump) and IRICA 852-III spectrophotometer, using a Cosmosil 5SL (4.6×250) column. IR spectra were recorded on a Hitachi EPI-S2 infrared spectrometer. Optical rotations were measured with a Perkin-Elmer 241 polarimeter.

Organic reagents were purchased from Nakarai Chemical Co., Tokyo Kasei Co., and Aldrich Chemical Co. unless otherwise indicated. Solvents and commercially available starting materials were generally used without additional purification unless otherwise indicated. Pyridine and benzene were refluxed on calcium hydride for 1 day and distilled before the use. Satisfactory results were obtained from elemental analyses of all of the products.

Preparation of Esters of 2-Methyl-3-oxopropionate. The corresponding ethyl ester was prepared according to the reference.[6] The other esters were prepared by transesterification with the ethyl ester. Two methods were used.

Method A. Ethyl 2-methyl-3-oxopropionate (10 mmol) and alcohol (50 mmol) were heated for an appropriate time and distilled under reduced pressure.

Method B. Ethyl 2-methyl-3-oxopropionate (10 mmol) was added to 15 mmol of alcohol in 20 ml of benzene and the solution was refluxed for an appropriate time, then distilled under reduced pressure, affording the desired ester.

Ethyl 2-Methyl-3-oxopropionate (2a): bp 60 °C/20 mmHg (1 mmHg=133.322 Pa); ^{1}H NMR ($CDCl_3$-TMS) δ=1.29 (aldehyde form, a), 1.32 (enol form, e) (3H, t, J=3.4 Hz (a), 3.4 Hz (e)), 1.34 (a), 1.66 (e) (3H, d, J=7.2Hz (a), 1.6Hz (e)), 3.37 (a), 6.98 (e) (1H, qd, J=7.2 Hz, 1.5Hz (a), dq, J=12.5Hz, 1.5Hz (e)), 4.23 (2H, q, J=7.3Hz (a,e)), 9.77 (a), 11.31 (e) (1H, d, J=1.5Hz (a), 12.5Hz (e)); IR (neat), 1727, 1673 cm^{-1}.

Butyl 2-Methyl-3-oxopropionate (2b): Method A; bp 85 °C/26 mmHg; ^{1}H NMR ($CDCl_3$-TMS) δ=0.93 (a), 0.94 (e) (3H, t, J=7.3 Hz (a), 6.9 Hz (e)) 1.30—1.77 (4H, m), 1.34 (a), 1.66 (e) (3H, d, J=7.2 Hz (a), 1.2 Hz (e)), 3.38 (a), 6.98 (e) (1H, qd, J=7.2 Hz, 1.4 Hz (a), dq, J=12.4 Hz, 1.2 Hz (e)), 4.17 (2H, t, J=6.5 Hz (a,e)), 9.77 (a), 11.31 (e) (1H, d, J=1.4 Hz (a), 12.4 Hz (e)); IR (neat), 1730, 1673 cm^{-1}.

Octyl 2-Methyl-3-oxopropionate (2c): Method A; bp 135—140 °C/20 mmHg; ^{1}H NMR ($CDCl_3$-TMS) δ=0.86 (3H, b (a,e)), 1.12—1.40 (12H, m (a,e)), 1.34 (a), 1.66 (e) (3H, d, J=7.3 Hz (a), 1.2 Hz (e)), 3.38 (a), 6.98 (e) (1H, qd, J=7.3 Hz, 1.5 Hz (a), dq, J=12.5 Hz, 1.2 Hz (e)), 4.15 (2H, t, J=6.6 Hz (a,e)), 9.77 (a), 11.31 (e) (1H, d, J=1.5 Hz (a), 12.5 Hz (e)); IR (near), 1735, 1674 cm^{-1}.

1-Methylethyl 2-Methyl-3-oxopropionate (2d): Prepared from 1-methylethyl propionate and 1-methylethyl formate according to the reference:[6] bp 60 °C/20 mmHg; ^{1}H NMR ($CDCl_3$-TMS) δ=1.27 (a), 1.28 (e) (6H, dd, J=1.1 Hz, 6.2 Hz (a), d, J=6.4 Hz (e)), 1.33 (a), 1.65 (e) (3H, d, J=7.2 Hz (a), 1.2 Hz (e)), 3.34 (a), 6.97 (e) (1H, qd, J=7.2 Hz, 1.6 Hz (a), dq, J=12.4 Hz, 1.2 Hz (e)), 5.02—5.18 (1H, m (a,e)), 9.77 (a), 11.38 (e) (1H, d, J=1.6 Hz (a), 12.4 Hz (e)); IR (neat), 1735, 1675 cm^{-1}.

2-Methylpropyl 2-Methyl-3-oxopropionate (2e): Method A; bp 75 °C/27 mmHg; ^{1}H NMR ($CDCl_3$-TMS) δ=0.93 (a), 0.95 (e) (6H, d, J=6.7 Hz (a), 6.7 Hz (e)), 1.36 (a), 1.68 (e) (3H, d, J=7.2 Hz (a), 1.2Hz (e)), 1.80—2.00 (1H, m (a,e)), 3.39 (a), 6.98 (e) (1H, qd, J=7.2 Hz, 1.5 Hz (a), dq, J=12.5 Hz, 1.2 Hz (e)), 3.95 (2H, d, J=6.6 Hz (a,e)), 9.78 (a), 11.30 (e) (1H, d, J=1.5 Hz (a), 12.5 Hz (e)); IR (neat), 1732, 1677 cm^{-1}.

3-Methylbutyl 2-Methyl-3-oxopropionate (2f): Method A; bp 97—99 °C/20 mmHg; ^{1}H NMR ($CDCl_3$-TMS) δ=0.91 (a), 0.92 (e) (6H, d, J= 4.0 Hz (a), 4.9 Hz (e)), 1.12—1.78 (3H, m (a,e)), 1.36 (a), 1.68 (e) (3H, d, J=7.5 Hz (a), 1.0Hz (e)), 3.37 (a), 6.98 (e) (1H, qd, J=7.2 Hz, 1.5 Hz (a), dq, J=12.5 Hz, 1.0 Hz (e)), 4.05—4.33 (2H, m (a,e)), 9.78 (a), 11.31 (e) (1H, d, J=1.5 Hz (a), 12.5 Hz (e)); IR (neat), 1733, 1677 cm^{-1}.

4-Methylpentyl 2-Methyl-3-oxopropionate (2g): Method A; bp 119 °C/20 mmHg: ^{1}H NMR ($CDCl_3$-TMS) δ=0.88 (a), 0.89 (e) (6H, d, J=6.6 Hz (a), 6.6 Hz (e)), 1.15—1.77 (5H, m (a,e)), 1.34 (a), 1.67 (e) (3H, d, J=7.3 Hz (a), 1.1 Hz (e)), 3.38 (a), 6.98 (e) (1H, qd, J=7.3 Hz, 1.5 Hz (a), dq, J=12.5 Hz, 1.1 Hz (e)), 4.05—4.26 (2H, m (a,e)), 9.78 (a), 11.31 (e) (1H, d, J=1.5 Hz (a), 12.5 Hz (e)); IR (neat), 1728, 1672 cm^{-1}.

2-Ethylbutyl 2-Methyl-3-oxopropionate (2h): Method A; bp 115.5 °C/20 mmHg; ^{1}H NMR ($CDCl_3$-TMS) δ=0.85—0.94 (6H, m (a,e)), 1.12—1.58 (4H, m (a,e)) 1.36 (a), 1.67 (e) (3H, d, J=7.3 Hz (a), 1.3 Hz (e)) 3.37 (a), 6.98 (e) (1H, qd, J=7.2 Hz, 1.5 Hz (a), dq, J=12.4 Hz, 1.3 Hz (e)), 3.98—4.18 (1H, m (a,e)), 4.10 (2H, q, J=5.6 Hz (a,e)), 9.77 (a), 11.31(e) (1H, d, J=1.5 Hz (a), 12.4 Hz (e)); IR (neat), 1735, 1677 cm^{-1}.

Allyl 2-Methyl-3-oxopropionate (2i): Method A; bp 70 °C/15 mmHg; ^{1}H NMR ($CDCl_3$-TMS) δ=1.36 (a), 1.69 (e) (3H, d, J=7.2 Hz (a), 1.2 Hz (e)), 3.42 (a), 7.00 (e) (1H, qd, J=7.2 Hz, 1.4 Hz (a), dq, J=11.4 Hz, 1.2 Hz (e)), 4.56—4.70 (2H, m (a,e)), 5.26—5.39 (2H, m (a,e)), 5.83—6.05 (1H, m (a,e)), 9.78 (a), 11.22 (e) (1H, d, J=1.4 Hz (a), 11.4 Hz (e)); IR

(neat), 1727, 1674 cm^{-1}.

2-Ethoxyethyl 2-Methyl-3-oxopropionate (2j): Method A; bp 107—109 °C/15 mmHg; ^1H NMR ($CDCl_3$-TMS) δ=1.15—1.24 (3H, m (a,e)), 1.35 (a), 1.69 (e) (3H, d, J=7.3 Hz (a), 1.0 Hz (e)), 3.43—3.73 (m, (a,e)), 6.99 (dq, J=12.6, 1.0 (e)) (5H), 4.24—4.41 (2H, m (a,e)), 9.79 (a), 11.18 (e) (1H, d, J=1.4 Hz (a), 12.6 Hz (e)); IR (neat), 1743, 1675 cm^{-1}.

2-Methoxyethyl 2-Methyl-3-oxopropionate (2k): Method A; bp 134 °C/20 mmHg; ^1H NMR ($CDCl_3$-TMS) δ=1.34 (a), 1.68 (e) (3H, d, J=7.3 Hz (a), 1.0 Hz (e)), 3.36 (3H, d, J=1.5 Hz (a,e)), 3.52—3.76 (m (a,e)), 6.92 (dq, J=12.5, 1.0 (e)) (3H), 4.27—4.36 (2H, m (a,e)), 9.74 (a), 11.18 (e) (1H, d, J=1.5 Hz (a), 12.5 Hz (e)); IR (neat), 1729, 1673 cm^{-1}.

2,2-Dimethylpropyl 2-Methyl-3-oxopropionate (2l): Method A; bp 90 °C/20 mmHg; ^1H NMR ($CDCl_3$-TMS) δ=0.95 (9H, d, J=4.1 Hz (a,e)), 1.36 (a), 1.70 (e) (3H, d, J=7.2 Hz (a), 1.2 Hz (e)), 3.42 (a), 7.05 (e) (1H, qd, J=7.2 Hz, 1.5 Hz (a), dq, J=12.6 Hz, 1.2 Hz (e)), 3.77—3.96 (2H, m (a,e)), 9.81 (a), 11.29 (e) (1H, d, J=1.5 Hz (a), 12.6 Hz (e)); IR (neat), 1732, 1678 cm^{-1}.

3,3-Dimethylbutyl 2-Methyl-3-oxopropionate (2m): Method B; Kugelrohr distillation; bp 75 °C/20 mmHg; ^1H NMR ($CDCl_3$-TMS) δ=0.97 (9H, s (a,e)), 1.14—1.18 (2H, m (a,e)) 1.35 (a), 1.67 (e) (3H, d, J=7.3 Hz (a), 1.5 Hz (e)), 3.38 (a), 6.99 (e) (1H, qd, J=7.3 Hz, 1.5 Hz (a), dq, J=12.2 Hz, 1.5 Hz (e)), 4.25 (2H, t, J=7.3 Hz (a,e)), 9.78 (a), 11.33 (e) (1H, d, J=1.5 Hz (a), 12.2 Hz (e)); IR (neat), 1745, 1677 cm^{-1}.

2-(Trimethylsilyl)ethyl 2-Methyl-3-oxopropionate (2n): Method A; bp 113.5—114 °C/20 mmHg; ^1H NMR ($CDCl_3$-TMS) δ=0.06 (9H, d, J=1.0 Hz (a,e)), 0.95—1.14 (2H, m (a,e)), 1.35 (a), 1.67 (e) (3H, d, J=7.3 Hz (a), 1.5 Hz (e)), 3.37 (a), 6.99 (e) (1H, qd, J=7.3 Hz, 1.5 Hz (a), dq, J=12.2 Hz, 1.5 Hz (e)), 4.29 (2H, m (a,e)), 9.78 (a), 11.37 (e) (1H, d, J=1.5 Hz (a), 12.2 Hz (e)); IR (neat) 1728, 1673 cm^{-1}.

Cyclohexylmethyl 2-Methyl-3-oxopropionate (2o): Method B; bp 139 °C/20 mmHg; ^1H NMR ($CDCl_3$-TMS) δ=0.90—1.78 (11H, m (a,e)), 1.36 (a), 1.69 (e) (3H, d, J=7.3 Hz (a), 1.0 Hz (e)), 3.40 (a), 6.99 (e) (1H, qd, J=7.3 Hz, 1.5 Hz (a), dq, J=12.7 Hz, 1.0 Hz (e)), 3.99 (2H, d, J=6.3 Hz (a,e)), 9.80 (a), 11.31 (e) (1H, d, J=1.5 Hz (a), 12.7 Hz (e)); IR (neat), 1727, 1675 cm^{-1}.

2-Cyclohexylethyl 2-Methyl-3-oxopropionate (2p): Method B; bp 150 °C/20 mmHg; ^1H NMR ($CDCl_3$-TMS) δ=0.97—1.77 (13H, m (a,e)), 1.36 (a), 1.68 (e) (3H, d, J=7.3 Hz (a), 1.0 Hz (e)), 3.39 (a), 6.99 (e) (1H, qd, J=7.2 Hz, 1.5Hz (a), dq, J=12.7 Hz, 1.0 Hz (e)), 4.22 (2H, t, J=6.6 Hz (a,e)), 9.79 (a), 11.33 (e) (1H, d, J=1.5 Hz (a), 12.7 Hz (e)); IR (neat) 1730, 1675 cm^{-1}.

Preparation of Racemic 3-Hydroxy-2-methylpropionate. Sodium borohydride (9.5 mg, 0.25 mmol) was added to a stirred and cooled solution of one mmol of 2-methyl-3-oxopropionate and 10 ml of ethanol in an ice bath. The resulted solution was stirred at room temperature for 1 h and the ethanol was removed under reduced pressure, then the residual solution was acidified with dilute hydrochloric acid. The organic portion was extracted with ether (30 ml), and the ether layer was washed with water, aqueous sodium hydrogencarbonate, and water (10 ml each) respectively. After dried over anhydrous sodium sulfate, the solvent was evaporated from the ether solution. Esters of 3-hydroxy-2-methylpropionate were obtained by Kugelrohr distillation.

Ethyl 2-Methyl-3-hydroxypropionate (1a): Kugelrohr distillation; bp 90 °C/21 mmHg; ^1H NMR ($CDCl_3$-TMS) δ=1.26 (3H, t, J=7.1 Hz), 1.17 (3H, d, J=7.4 Hz), 2.41 (1H, m), 2.64 (1H, m), 4.15 (2H, q, J=7.1 Hz); IR (neat), 1739, 3470 cm^{-1}.

Butyl 2-Methyl-3-hydroxypropionate (1b): Kugelrohr distillation; bp 120 °C/21 mmHg; ^1H NMR ($CDCl_3$-TMS) δ=0.93 (3H, t, J=7.2 Hz), 1.17 (3H, d, J=7.3 Hz), 1.29—1.70 (4H, m), 2.28—2.34 (1H, m), 2.57—2.74 (1H, m), 3.67—3.74 (2H, m), 4.11 (2H, t, J=6.6 Hz); IR (neat), 1737, 3480 cm^{-1}.

Octyl 2-Methyl-3-hydroxypropionate (1c): Kugelrohr distillation; bp 150 °C/21 mmHg; ^1H NMR ($CDCl_3$-TMS) δ=0.88 (3H, t, J=5.9 Hz), 1.18 (3H, d, J=6.8 Hz), 1.28 (12H, m), 2.34 (1H, m), 2.70 (1H, m), 3.71 (2H, d, J=6.1 Hz), 4.11 (2H, t, J=6.8 Hz); IR (neat), 1738, 3460 cm^{-1}.

1-Methylethyl 2-Methyl-3-hydroxypropionate (1d): Kugelrohr distillation: bp 95 °C/24 mmHg; ^1H NMR ($CDCl_3$-TMS) δ=1.24 (6H, m), 1.15 (3H, d, J=7.3 Hz), 2.37 (1H, m), 2.52—2.68 (1H, m), 3.64—3.72 (2H, m), 4.94—5.12 (1H, m); IR (neat), 1733, 3490 cm^{-1}.

2-Methylpropyl 2-Methyl-3-hydroxypropionate (1e): Kugelrohr distillation; bp 120 °C/25 mmHg; ^1H NMR ($CDCl_3$-TMS) δ=0.93 (6H, d, J=6.7 Hz), 1.185 (3H, d, J=7.3 Hz), 1.65—2.05 (1H, m), 2.34 (1H, t, J=5.7 Hz), 2.58—2.75 (1H, m), 3.70 (2H, t, J=5.1 Hz), 3.89 (2H, m); IR (neat), 1737, 3480 cm^{-1}.

3-Methylbutyl 2-Methyl-3-hydroxypropionate (1f): Kugelrohr distillation; bp 130 °C/27 mmHg; ^1H NMR ($CDCl_3$-TMS) δ=0.92 (6H, d, J=6.4 Hz), 1.17 (3H, d, J=7.3 Hz), 1.48—1.75 (3H, m), 2.28 (1H, m), 2.58—2.74 (1H, m), 3.65—3.77 (2H, m), 4.14 (2H, t, J=6.8 Hz); IR (neat), 1738, 3480 cm^{-1}.

4-Methylpentyl 2-Methyl-3-hydroxypropionate (1g): Kugelrohr distillation; bp 140 °C/27 mmHg; ^1H NMR ($CDCl_3$-TMS) δ=0.88 (6H, d, J=6.6 Hz), 1.17 (3H, d, J=7.3 Hz), 1.22—1.28 (1H, m), 1.46—1.71 (4H, m), 2.31 (1H, m), 2.57—2.74 (1H, m), 4.09 (2H, t, J=6.8 Hz); IR (neat), 1738, 3490 cm^{-1}.

2-Ethylbutyl 2-Methyl-3-hydroxypropionate (1h): Kugelrohr distillation; bp 125 °C/22 mmHg; ^1H NMR ($CDCl_3$-TMS) δ=0.89 (6H, t, J=7.6 Hz), 1.18 (3H, d, J=7.3 Hz), 1.28—1.43 (4H, m), 1.47—1.59 (1H, m), 2.32 (1H, m), 2.58—3.76 (1H, m), 3.68 (2H, m), 4.02—4.06 (2H, m); IR (neat), 1739, 3490 cm^{-1}.

Allyl 2-Methyl-3-hydroxypropionate (1i): Kugelrohr distillation; bp 105 °C/23 mmHg; ^1H NMR ($CDCl_3$-TMS) δ=1.19 (3H, d, J=7.2 Hz), 2.27 (1H, m), 2.60—2.80 (1H, m), 3.70 (2H, m), 4.60 (2H, m), 5.20—5.40 (2H, m), 5.80—6.00 (1H, m); IR (neat), 1738, 3470 cm^{-1}.

2-Ethoxyethyl 2-Methyl-3-hydroxypropionate (1j): Kugelrohr distillation; bp 140 °C/23 mmHg; ^1H NMR ($CDCl_3$-TMS) δ=1.18 (3H, d, J=7.3 Hz), 1.20 (3H, d, J=7.0 Hz), 2.35—2.55 (1H, m), 2.55—2.88 (1H, m), 3.53 (2H, q, J=7.0 Hz), 3.61—3.74 (4H, m), 4.25—4.33 (2H, m); IR (neat), 1738, 3480 cm^{-1}.

2-Methoxyethyl 2-Methyl-3-hydroxypropionate (1k): Kugelrohr distillation; bp 130 °C/26 mmHg; ^1H NMR ($CDCl_3$-TMS) δ=1.58 (3H, d, J=7.2 Hz), 2.44 (1H, m), 3.38 (3H, s), 3.60 (2H, t, J=4.7 Hz), 3.71 (2H, m), 4.24—4.35 (2H, m); IR (neat), 1740, 3480 cm^{-1}.

2,2-Dimethylpropyl 2-Methyl-3-hydroxypropionate (1l): Kugelrohr distillation; bp 120 °C/25 mmHg; ^1H NMR ($CDCl_3$-TMS) δ=0.95 (9H, d, J=4.1 Hz), 1.21 (3H, d, J=7.3 Hz), 2.36 (1H, m), 2.60—2.80 (1H, m), 3.73 (2H, m), 3.82 (2H,

d, J=1.5 Hz); IR (neat), 1737, 3490 cm^{-1}.

3,3-Dimethylbutyl 2-Methyl-3-hydroxypropionate (1m): Kugelrohr distillation; bp 130 °C/23 mmHg; ^1H NMR ($CDCl_3$-TMS) δ=0.95 (9H, s), 1.17 (3H, d, J=7.3 Hz), 1.57 (2H, t, J=7.3 Hz), 2.33 (1H, m), 2.55—2.75 (1H, m), 3.71 (2H, m), 4.18 (2H, t, J=7.3 Hz); IR (neat) 1740, 3490 cm^{-1}.

2-(Trimethylsilyl)ethyl 2-Methyl-3-hydroxypropionate (1n): Kugelrohr distillation; bp 135 °C/24 mmHg; ^1H NMR ($CDCl_3$-TMS) δ=0.05 (9H, s), 1.01 (2H, m), 1.17 (3H, d, J=7.3 Hz), 2.35 (1H, m), 2.54—2.74 (1H, m), 3.71 (2H, d, J=5.9Hz), 4.21 (2H, m); IR (neat), 1738, 3500 cm^{-1}.

Cyclohexylmethyl 2-Methyl-3-hydroxypropionate (1o): Kugelrohr distillation; bp 145 °C/22 mmHg; ^1H NMR ($CDCl_3$-TMS) δ=0.70—1.90 (11H, m), 1.18 (3H, d, J=7.3 Hz), 2.40 (1H, t, J=6.1Hz), 2.58—2.77 (1H, m), 3.71 (2H, dd, J=5.4Hz, 6.4Hz), 3.93 (2H, d, J=6.4 Hz); IR (neat), 1739, 3480 cm^{-1}.

2-Cyclohexylethyl 2-Methyl-3-hydroxypropionate (1p): Kugelrohr distillation; bp 160 °C/23 mmHg; ^1H NMR ($CDCl_3$-TMS) δ=0.62—1.82 (13H, m), 1.18 (3H, d, J=7.3 Hz), 2.38 (1H, t, J=5.9 Hz), 2.56—2.76 (1H, m), 3.71 (2H, t, J=5.9 Hz), 4.15 (2H, t, J=6.8 Hz); IR (neat), 1736, 3480 cm^{-1}.

Reduction of 2 with Bakers' Yeast. One millimole of **2** was added to a suspension of 5 g of BY in 15 ml of water and the mixture was stirred at room temperature until no starting material was detected on gas chromatography (PEG, 1 m, 80 °C). Then Hiflo-Super-Cell (10 g) and ethyl acetate (30 ml) was added to the mixture and the resulted suspension was filtered. The organic portion was concentrated under reduced pressure and the residue was subjected to column chromatography (silica gel, eluent; hexane-ethyl acetate=9 : 1) to give the corresponding alcohol. The NMR and IR spectra were the same with the corresponding hydroxy ester obtained by sodium borohydride reduction. The optical rotational values, e.e.s, and chemical yields of each hydroxy ester are listed in the Table.

Reduction of 2a with Immobilized Bakers' Yeast. One millimole of **2a** in 50 ml of water was reacted for two days with immobilized BY prepared from 10 g of polyurethane prepolymer, 10 g of BY, and 10 g of water.[8] After filtration and extraction from the aqueous phase with ethyl acetate, **1a** was obtained in 45% chemical yield with 55% e.e. The e.e. was slightly improved from the reduction of **2a** by free BY (45% e.e.).

Determination of e.e. of the Reduced Product. The reduced product (**1a—p**) was converted into the corresponding (*R*)-(+)-α-methoxy-α-(trifluoromethyl)phenylacetic acid (MTPA) ester by the reaction of **1** and MTPA-chloride in the presence of pyridine in benzene. The e.e. was determined by HPLC analysis of the MTPA ester.

Determination of Absolute Configuration. The absolute configuration of the reduction product was determined by converting **1** into the corresponding ethyl ester and comparing its rotational value with that reported.

A mixture of 1 mmol of **1l**, ethanol (10 ml) and catalytic amount of *p*-toluenesulfonic acid was heated at reflux temperature for 4 days. Ethanol was distilled off under reduced pressure and the residue was subjected to column chromatography (silica gel, eluent; hexane-ethyl acetate=9 : 1), giving ethyl 3-hydroxy-2-methylpropionate. The hydroxy ester obtained from the yeast reduction of 2,2-dimethylpropyl 2-methyl-3-oxopropionate (**1l**) afforded the corresponding ethyl ester in 56% yield; $[\alpha]_D^{20}$ −20.26 (*c* 3.41, MeOH). Since the optical rotational value of (*R*)-ethyl 3-hydroxy-2-methylpropionate is −21.6, the absolute configuration of **1l** was determined to be *R*.

References

1) Stereochemical control in microbial reduction. Part 7.

2) A. Fishli, "Chiral Building Blocks in Enantiomer Synthesis Using Enzymatic Transformations" in "Modern Synthetic Methods," ed. by R. Schefold, Otto Salle Verlag, Frankfurt am Main (1980), pp. 314—319.

3) C. T. Goodhue and J. R. Schaeffer, *Biotech. Bioeng.*, **13**, 203 (1971).

4) J. Hasegawa, M. Ogura, S. Hamaguchi, M. Shimazaki, H. Kawaharada, and K. Watanabe, *J. Ferment. Technol.*, **59**, 203 (1981); J. Hasegawa, M. Ogura, H. Kanema, N. Noda, H. Kawaharada, and K. Watanabe, *ibid.*, **60**, 501 (1982).

5) C. J. Sih and C-S. Chen, *Angew. Chem., Int. Ed. Engl.* **23**, 570 (1984).

6) M. F. Zücker, F. Giovannini, and D. Seebach, *Angew. Chem., Int. Ed. Engl.*, **22**, 1012 (1983).

7) J. P. Rosazza, "Application of Biochemical Systems in Organic Chemistry," ed. by J. B. Jones, C. J. Sih, and D. Perlman, John Wiley & Sons, New York (1976), pp. 69—106.

8) K. Nakamura, M. Higaki, K. Ushio, S. Oka, and A. Ohno, *Tetrahedron Lett.*, **26**, 4213 (1985).

9) M. Hirama, M. Shimizu, and M. Iwashita, *J. Chem. Soc., Chem. Commun.*, **1983**, 559.

10) B. N. Zhou, A. S. Gopalan, F. Van Middlesworth, W. R. Shieh, and C. J. Sih, *J. Am. Chem. Soc.*, **105**, 3958 (1983).

11) Because the CH_2Cl group has priority in order of notation over the CO_2R group.

12) K. Nakamura, T. Miyai, K. Nozaki, K. Ushio, S. Oka, and A. Ohno, *Tetrahedron Lett.*, **27**, 3155 (1986).

13) T. Fujisawa, T. Itoh, and T. Sato, *Tetrahedron Lett.*, **25**, 5083 (1984); H. Akita, H. Matsukura, and T. Oishi, *Tetrahedron Lett.*, **27**, 5397 (1986).

14) M. Hirama, T. Nakamine, and S. Ito, *Chem. Lett.*, **1986**, 1381.

Flavin Activation by Intramolecular Acid Catalysis at N(1) Position†

Seiji SHINKAI,* Sayuri KAWANABE, Akito KAWASE, Toshiro YAMAGUCHI, Osamu MANABE, Shigeharu HARADA,†† Hideki NAKAMURA,†† and Nobutami KASAI*,††

Department of Industrial Chemistry, Faculty of Engineering, Nagasaki University, Nagasaki 852
††Department of Applied Chemistry, Faculty of Engineering, Osaka University, Yamadaoka, Suita, Osaka 565

(Received December 19, 1987)

In order to assess the effect of intramolecular acid catalysis on the specific flavin reactivities, 3-methyl-10-(2-hydroxyphenyl)isoalloxazine (**1**(2OH)) and 3-methyl-10-(2-hydroxy-1-naphthyl)isoalloxazine (**2**(2OH)) were synthesized and the redox properties were compared with those of reference flavins such as 3-methyl-10-(2-methoxyphenyl)isoalloxazine (**1**(2OMe)) and 3-methyl-10-(2-methoxy-1-naphthyl)isoalloxazine (**2**(2OMe)). The pK_a values for **1**(2OH) and **2**(2OH) were determined to be 7.7 and 7.0, respectively, which were lower than that of 3-methyl-10-(4-hydroxyphenyl)isoalloxazine (**1**(4OH): pK_a 8.6). It is thus unlikely that 2′-OH and N(1) form a hydrogen bond at the initial state of the reaction (i.e., at the oxidized state). The X-ray crystallographic studies indicated that the phenyl ring makes an angle of 79.7° with the isoalloxazine ring and the 2′-OH group forms a hydrogen bond with methanol included in the crystal lattice. In acetonitrile at 30 °C 1-benzyl-1,4-dihydronicotinamide was not oxidized by **1**(2OMe), **1**(4OH), and **2**(2OMe). On the other hand, the oxidation took place with **1**(2OH) and **2**(2OH) which have an acidic OH group at the 2′-position of the 10-aryl substituent. The presence of the intramolecular acid catalysis suggests that 2′-OH and N(1) can interact at least at the transition state or at the final state of the reaction (i.e., at the reduced state). In general, the oxidized flavin adopts a "planar" structure which is sterically tense while the reduced flavin adopts a "bent" structure which is sterically relaxed. As the structure of the transition state is more or less similar to the reduced form, the hydrogen-bonding interaction could increase on going from the tense initial state to the relaxed transition state. This is a novel example for acid catalysis in flavin-mediated reactions.

Flavin coenzymes act as versatile redox catalysts in many biological systems, and it is now known that more than 100 proteins called flavoproteins require flavin coenzymes as their prosthetic groups.[1-3] In 1980, Massey and Hemmerich[4] proposed a stimulative hypothesis that a large number of flavoproteins may be classified into two groups from a viewpoint of their regiospecific reactivities: the first group is characterized by red semiquinone, high sulfite affinity, and bent structure of the reduced form, whereas the second group is characterized by blue semiquinone, low sulfite affinity, and almost planar structure of the reduced form. They explained that the most essential difference between these two groups is caused by regiospecific hydrogen bonding between flavin coenzymes and apoproteins:[4] that is, the first group has a hydrogen bond with N(1) leading to activation of the N(5) position while the second group has a hydrogen bond with the N(5) leading to activation of the C(4a) position. The situation reminds us of the role of 3-OH in pyridoxal coenzymes.

In order to obtain an insight into the latent capability of the hydrogen bond, we previously synthesized a flavin with hydrogen-bonded N(5) (OHFl: sodium 1-hydroxy-7-methyl-9,10-dioxo-7,9,10,11-tetrahydronaphtho-[1,2-g]pteridine-3-sulfonate).[5,6] We found that OHFl is "regioselectively" activated toward reactions involving 4a intermediates, for example, oxidation of thiols.[5,6] On the basis of several lines of evidence, the specific reactivity was ascribed to activation of the C(4a) position through hydrogen bonding with N(5).[5,6] Thus, the half of the hypothesis has been proved with OHFl, but the another half of the hypothesis (i.e., activation of the N(5) position through hydrogen bonding with N(1)) has been left equivocal. Based on our experience, it is extremely difficult to design a flavin derivative which involves hydrogen-bonded N(1).[7] Unlike OHFl, it is almost impossible to attach a fused aromatic ring to N(10) because of steric crowding. Also, $CH_2CH_2NH_3^+$ and CH_2COOH groups on N(10) were ineffective.[7] These examples of past failure suggest that the proximity effect plays a crucial role in the intramolecular acid catalysis.[5-7] Here, we wish to report the redox properties of 3-methyl-10-(2-hydrophenyl)isoalloxazine (**1**(2OH)) and 3-methyl-10-(2-hydroxy-1-naphthyl)isoalloxazine (**2**(2OH)). Examination of space-filling molecular models suggests that although it seems difficult for 2′-OH and N(1) to form a direct hydrogen bond at the oxidized state, the interaction is latently

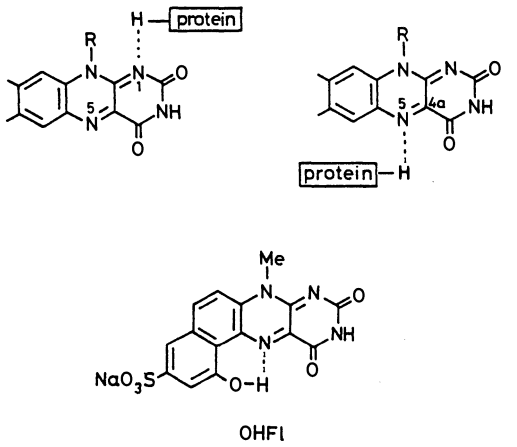

OHFl

† Coenzyme Models 50.

possible at the sterically-relaxed reduced state. We have found that the acid catalysis arising from the hydrogen-bonding interaction (probably at the transition state) is observable in acetonitrile.

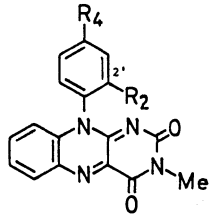

1

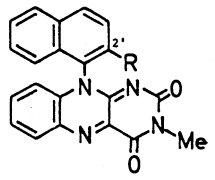

2

1(H): R_2=R_4=H
1(2OH): R_2=OH, R_4=H
1(2OMe): R_2=OMe, R_4=H
1(4OH): R_2=H, R_4=OH
1(4OMe): R_2=H, R_4=OMe

2(H): R=H
2(2OH): R=OH
2(2OMe): R=OMe

Experimental

Materials. Preparations of 3-methyl-10-phenylisoalloxazine (**1**(H)), 3-methyl-10-(1-naphthyl)isoalloxazine (**2**(H)), and 3-methyl-10-(2-methoxy-1-naphthyl)isoalloxazine (**2**(2OMe)) were described previously.[8]

3-Methyl-10-(2-hydroxy-1-naphthyl)isoalloxazine (2(2OH)). **2**(2OMe) (0.80 g; 2.08 mmol) was treated with 47% HBr (20 ml) at 130 °C. The progress of the reaction was followed by a TLC method. After 3 h the reaction mixture was diluted with water (100 ml) and neutralized by $NaHCO_3$. The precipitate was collected by filtration, washed with water, and then dried in vacuo. The yellow solid was recrystallized from acetic acid; mp >300 °C, yield 51%. Found: C, 63.90; H, 4.18; N, 12.99%. Calcd for $C_{21}H_{14}N_4O_3 \cdot CH_3CO_2H$: C, 64.18; H, 4.22; N, 13.02%. The elemental analysis indicates that the crystals contain one mol of acetic acid per one mol of **2**(2OH). We thus repeated recrystallization from ethanol; mp >300 °C, yield 49%. Found: C, 66.06; H, 4.76; N, 13.45%. Calcd for $C_{21}H_{14}N_4O_3 \cdot C_2H_5OH$: C, 66.33; H, 4.84; N, 13.46%. The result suggests that one mol of ethanol is included in the crystals. Toda et al.[9] demonstrated that molecules having crossed planes and the hydroxyl group(s) at the suitable position(s) easily form host-guest complexes in the solid state. Probably, **2**(2OH) satisfies this structural prerequisite to act as host molecules. Since the inclusion of acetic acid is very unfavorable for the titration experiments, we used the sample containing ethanol all through the present study.

Compounds **1** were synthesized according to the following scheme. The synthetic method was originally exploited by Yoneda et al.[10]

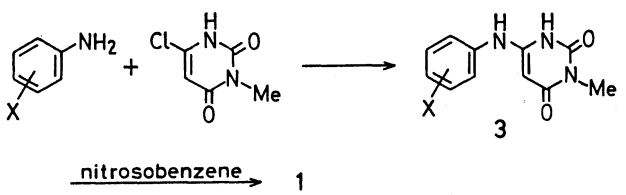

Scheme 1.

3-Methyl-6-(2-hydroxyanilino)uracil (3(2OH)). 3-Methyl-6-chlorouracil (1.00 g; 6.23 mmol) and *o*-aminophenol (2.71 g; 24.8 mmol) were stirred at 180—190 °C under a nitrogen stream. After 10 min the precipitate was formed from the melted reaction mixture. The product was well washed with 4 M[§] HCl; mp 273—275 °C, yield 68%; IR(KBr) ν_{OH}3400 cm^{-1} $\nu_{C=O}$ 1700, 1740 cm^{-1}. Found: C, 56.36; H, 4.76; N, 17.95%. Calcd for $C_{11}H_{11}N_3O_3$: C, 56.65; H, 4.75; N, 18.02%.

3-Methyl-6-(2-methoxyanilino)uracil (3(2OMe)). 3-Methyl-6-chlorouracil (1.00 g; 6.23 mmol) and *o*-methoxyaniline (3.06 g; 24.8 mmol) were stirred at 150—160 °C under a nitrogen stream. After 20 min the precipitate was formed from the melted reaction mixture. The product was well dispersed in ethanol and the precipitate was recovered by filtration. This operation was repeated once again; mp 261—263 °C, yield 85%; IR(KBr) ν_{NH} 3240 cm^{-1}, $\nu_{C=O}$ 1700, 1715 cm^{-1}. Found: C, 58.30; H, 5.18; N, 17.26%. Calcd for $C_{12}H_{13}N_3O_3$: C, 58.29; H, 5.30; N, 17.00%.

3(4OH) and **3**(4OMe) were prepared from *p*-aminophenol and *p*-methoxyaniline in manners similar to those described for **3**(2OH) and **3**(2OMe), respectively. We thus omit the detailed description of the experimental methods and recorded their analytical data.

3-Methyl-6-(4-hydroxyanilino)uracil (3(4OH)). Mp >300 °C, yield 82%; IR(KBr) ν_{OH} 3300 cm^{-1}, $\nu_{C=O}$ 1700, 1720 cm^{-1}. Found: C, 56.22; H, 4.77; N, 17.94%. Calcd for $C_{11}H_{11}N_3O_3$: C, 56.65; H, 4.75; N, 18.02%.

3-Methyl-6-(4-methoxyanilino)uracil (3(4OMe)). Mp 290—292 °C, yield 88%; IR(KBr) ν_{NH} 3250 cm^{-1}, $\nu_{C=O}$ 1720 cm^{-1}. Found: C, 58.26; H, 5.26; N, 17.17%. Calcd for $C_{12}H_{13}N_3O_3$: C, 58.29; H, 5.30; N, 17.00%.

3-Methyl-10-(2-hydroxyphenyl)isoalloxazine (1(2OH)). **3**(2OH) (1.90 g; 8.15 mmol) and nitrosobenzene (2.62 g; 24.5 mmol) were refluxed in 40 ml of acetic acid-acetic anhydride (1 : 4 v/v) under a nitrogen stream. The progress of the reaction was followed by a TLC method. After 30 min the reaction mixture was cooled and concentrated in vacuo. The residual oil was subjected to preparative TLC (silica gel, chloroform-methanol 30 : 1 v/v). There were two yellow spots on the TLC plate, which were identified to be **1**(2OH) (R_f=0.5) and 3-methyl-10-(2-acetoxyphenyl)isoalloxazine (R_f=0.7). We thus collected two isoalloxazines together and the mixture was refluxed for 1 h in 16 ml of 4 M HCl to hydrolyze the ester. The solution was neutralized by $NaHCO_3$ and the precipitate was recrystallized from acetic acid; mp >300 °C, yield 12%; IR(KBr) ν_{OH} 3350 cm^{-1}, $\nu_{C=O}$ 1660, 1710 cm^{-1}. ^1H NMR (Me_2SO-d_6): δ=3.27 (3H, NCH_3), 6.88 (1H, 9-H), 7.11 (1H, 5′-H), 7.16 (1H, 3′-H), 7.28 (1H, 6′-H), 7.49 (1H, 7-H), 7.65 (1H, 4′-H), 7.81 (1H, 8-H), 8.25 (1H, 6-H), 9.96 (1H, OH). Found: C, 63.90; H, 3.83; N, 17.38%. Calcd for $C_{17}H_{12}N_4O_3$: C, 63.75; H, 3.78; N, 17.49%.

3-Methyl-10-(4-hydroxyphenyl)isoalloxazine (1(4OH)). This compound was synthesized in a manner similar to that described for **1**(2OH). Mp >300 °C, yield 14%; IR (KBr) ν_{OH} 3370 cm^{-1}, $\nu_{C=O}$ 1660, 1720 cm^{-1}. Found: C, 63.59; H, 3.74; N, 17.30%. Calcd for $C_{17}H_{12}N_4O_3$: C, 63.75; H, 3.78; N, 17.49%.

3-Methyl-10-(4-methoxyphenyl)isoalloxazine (1(2OH)). This compound was synthesized from **3**(2OMe) (1.50 g; 6.07 mmol) and nitrosobenzene (1.95 g; 18.2 mmol) in 40 ml of acetic acid-acetic anhydride (1 : 1 v/v) at the reflux temperature under a nitrogen stream. After 30 min the reaction

§ 1 M=1 mol dm^{-3}.

mixture was cooled and concentrated in vacuo. The residual solid was recrystallized from acetic acid in the presence of activated charcoal: mp >300 °C, yield 47%; IR(KBr) $\nu_{C=O}$ 1660, 1710 cm^{-1}, ν_{C-O-C} 1270 cm^{-1}. Found: C, 64.52; H, 4.21; N, 16.67%. Calcd for $C_{18}H_{14}N_4O_3$: C, 64.66; H, 4.22; N, 16.76%.

3-Methyl-10-(4-methoxyphenyl)isoalloxazine (1(4OMe)). This compound was synthesized in a manner similar to that described for **1**(2OMe). Mp >300 °C, yield 45%: IR(KBr) $\nu_{C=O}$ 1655, 1710 cm^{-1}, ν_{C-O-C} 1270 cm^{-1}. Found: C, 64.66; H, 4.19; N, 16.64%. Calcd for $C_{18}H_{14}N_4O_3$: C, 64.66; H, 4.22; N, 16.76%.

Kinetic Measurements. The aqueous reaction with 1-benzyl-1,4-dihydronicotinamide was carried out aerobically at 30 °C and μ=0.1 with KCl. Under the aerobic conditions flavins are recycled automatically, so that the decrease in the absorption band of 1-benzyl-1,4-dihydronicotinamide (360 nm) satisfies the first-order equation. The medium pH was maintained by 0.01 M phosphate (pH<7.0), 0.01 M *N*-ethylmorpholine (7.0<pH<8.0), 0.01 M borate (8.0<pH<9.5), and 0.01 M carbonate (pH>9.5).

The reaction with 1-benzyl-1,4-dihydronicotinamide in acetonitrile was carried out anaerobically at 30 °C. The decrease in the absorption band of flavins (440 nm) satisfied the first-order equation in the presence of excess 1-benzyl-1,4-dihydronicotinamide (2.09×10^{-3} M; [flavin]=5.00×10^{-5} M). Since the pseudo-first-order rate constants (k_1') were first-order in 1-benzyl-1,4-dihydronicotinamide, the results were discussed with the second-order rate constants ($k_2=k_1'$/[1-benzyl-1,4-dihydronicotinamide]).

X-Ray Crystal Structure Analysis. Crystal data. $C_{17}H_{12}N_4O_3$, CH_3OH, *F.W.* 352.3, monoclinic, space group *C*2/*c*, *a*=23.853(3), *b*=10.342(1), *c*=13.894(1) Å, β=100.16(1)°, *V*=373.9(5) Å^3, D_c=1.387 g cm^{-3} for *Z*=8.

Orange colored, prismatic crystals were obtained by the recrystallization from a methanol-benzene mixed solvent. The crystal used had approximate dimensions of 0.45×0.23×0.18 mm.

Integrated intensities were collected on a Rigaku rotating anode, four-circle diffractometer using nickel-filtered Cu $K\alpha$ radiation(λ=1.5418 Å) by the θ-2θ scan technique up to 2θ=120°. The 2θ scan rate was 8° min^{-1}, and the scan width $\Delta2\theta=(2.4+0.3\tan\theta)°$. Backgrounds were counted for 4 s at both ends of a scan. Three standard reflections measured after every 100 reflections to monitor the stability and orientation of the crystal showed no significant decay through the experiment. Of the 2885 reflections measured, number of reflections observed was 2114 ($|F_o|>2\sigma(F_o)$, where σ is the standard deviation obtained from the counting statistics). Usual Lorentz and polarization corrections were applied but absorption correction was ignored [μ(Cu $K\alpha$)=8.50 cm^{-1}].

The structure was solved by the direct method (MULTAN 78).[11] All the non-hydrogen atoms could be located on successive Fourier syntheses. The hydrogen atoms except those of methanol, the crystalline solvent, were located on the calculated positions, which were confirmed on the difference Fourier map. The structure was refined by the block-diagonal least-squares procedure (HBLS V)[12] with anisotropic thermal parameters for nonhydrogen atoms and isotropic ones for hydrogen atoms. During the course of the refinement, the only remaining peak on the difference Fourier map was found to be assigned as the alternative position of the disordered methanol oxygen atom, O(5), which was included in the refinement with 20% occupancy. The final *R* value was 0.056. The weighting schemes used at the final cycle of the refinement were $w=(\sigma^2+0.01886|F_o|+0.00254|F_o|^2)^{-1}$ for $|F_o|>0$ and $w=0$ for $|F_o|=0$. The final atomic parameters are given in Table 1.[§§] Atomic scattering factors were taken from those of International Tables for X-Ray Crystallography, Vol. IV.[13] Computations were done on an ACOS S850 computer at the Crystallographic Research Center, Institute for Protein Research, Osaka University.

Table 1. Final Atomic Parameters with Estimated Standard Deviations in Parentheses

Nonhydrogen atoms with equivalent isotropic temperature factors.[27]

Atom	*x*	*y*	*z*	B_{eq}/Å^2
C(1)	0.18654(15)	−0.0146(4)	0.0355(3)	5.27
C(2)	0.16813(17)	−0.1074(5)	−0.0318(4)	7.09
C(3)	0.20136(18)	−0.1410(5)	−0.0996(4)	6.95
C(4)	0.25281(15)	−0.0821(4)	−0.1036(3)	5.20
C(5)	0.27215(11)	0.0138(3)	−0.0342(2)	3.47
C(6)	0.23899(12)	0.0474(3)	0.0362(3)	3.64
C(7)	0.30620(11)	0.1907(3)	0.10837(19)	3.25
C(8)	0.34319(11)	0.1652(3)	0.03753(19)	3.11
C(9)	0.41213(12)	0.3052(3)	0.1110(3)	4.28
C(10)	0.32745(12)	0.2836(3)	0.1876(3)	3.92
C(11)	0.40526(16)	0.4235(5)	0.2627(3)	6.78
C(12)	0.35763(11)	0.0485(3)	−0.10735(19)	3.18
C(13)	0.34356(13)	0.1033(4)	−0.1984(3)	4.09
C(14)	0.37549(13)	0.0739(4)	−0.2698(3)	4.38
C(15)	0.42118(13)	−0.0102(4)	−0.2473(3)	4.13
C(16)	0.43502(13)	−0.0657(3)	−0.1562(3)	4.16
C(17)	0.40277(12)	−0.0367(3)	−0.0841(2)	3.53
C(18)	0.50905(10)	−0.3136(3)	0.11610(16)	7.90
N(1)	0.25703(9)	0.1377(3)	0.10721(15)	3.59
N(2)	0.32338(10)	0.0769(3)	−0.03314(18)	3.14
N(3)	0.38039(9)	0.3354(3)	0.18365(17)	4.45
N(4)	0.39222(10)	0.2207(3)	0.03773(16)	3.63
O(1)	0.30078(10)	0.3112(3)	0.25191(19)	5.42
O(2)	0.45882(10)	0.3564(3)	0.11613(15)	6.19
O(3)	0.41308(12)	−0.0874(4)	0.0071(3)	5.04
O(4)	0.47930(18)	−0.2888(6)	0.0222(4)	5.81
O(5)	0.5111(4)	−0.2108(8)	0.0609(7)	3.3

Hydrogen atoms with isotropic temperature factors

Atom	*x*	*y*	*z*	B_{eq}/Å^2
H(1)	0.1644(13)	0.004(4)	0.086(3)	3.0(7)
H(2)	0.1327(17)	−0.149(5)	−0.038(3)	6.0(11)
H(3)	0.1841(18)	−0.203(4)	−0.155(3)	5.7(11)
H(4)	0.2781(16)	−0.102(4)	−0.149(3)	4.8(9)
H(5)	0.3789(14)	0.496(4)	0.251(3)	4.4(9)
H(6)	0.493(3)	0.450(6)	0.258(4)	8.4(14)
H(7)	0.401(3)	0.379(6)	0.321(4)	9.3(15)
H(8)	0.3062(14)	0.166(4)	−0.212(3)	3.4(8)
H(9)	0.3663(13)	0.117(4)	−0.340(3)	2.7(7)
H(10)	0.4434(13)	−0.032(3)	−0.297(3)	2.9(7)
H(11)	0.4684(11)	−0.122(3)	−0.134(2)	1.5(6)
H(12)	0.4473(16)	−0.154(4)	0.020(3)	5.1(10)

Results and Discussion

Crystal Structure of 1(2OH). The molecular struc-

§§ Tables of anisotropic thermal parameters of nonhydrogen atoms, coordinates of hydrogen atoms, and observed and calculated structure factors are kept at the Chemical Society of Japan, Document No. 8803.

ture is shown in Fig. 1.[14] The atom numbers in Fig. 1 are used only for the crystal structure. Selected bond lengths and bond angles are given in Table 2. The remarkable feature of the structure is that three six-membered hetero rings in the isoalloxazine ring is not coplanar: the dihedral angle between the rings I and II is 2.2(1)° and that between II and III also 2.2(1)°. The ring IV attached to the N(2) atom of the ring II makes an angle of 79.7° with the ring II. The *o*-hydroxyl group of the ring IV is, therefore, located too far from the N(4) atom of the ring III to form the hydrogen bond [O(3)···N(4)=3.265(3) and H(12)···N(4)=4.11(5) Å].

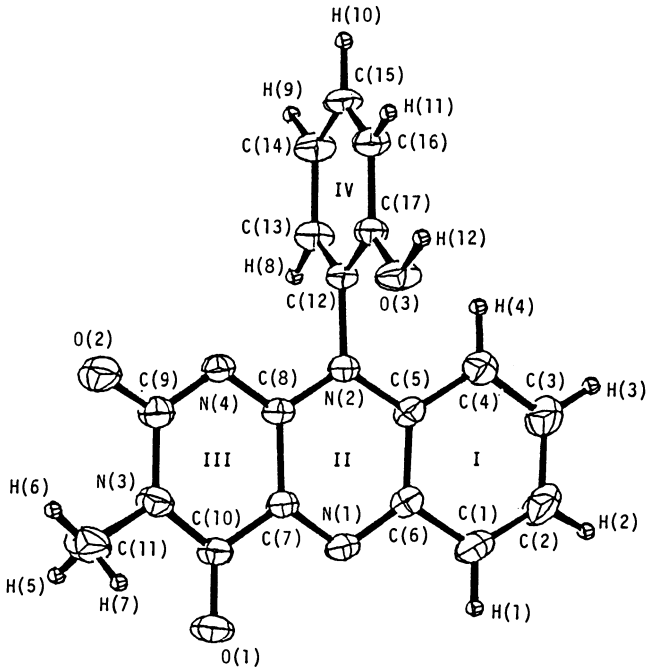

Fig. 1. A perspective view[14] of **1**(2OH). Nonhydrogen atoms are expressed as thermal ellipsoids with 20% probability level, and hydrogen atoms as spheres with B=1.0 Å^2.

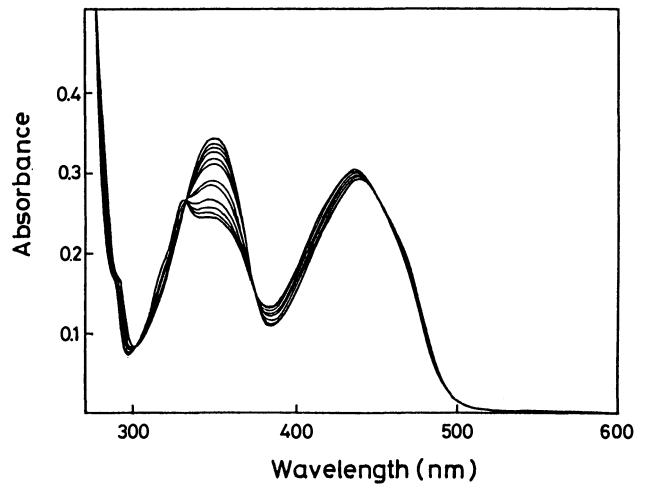

Fig. 2. pH Dependent spectral change in **2**(2OH) (4.00×10^{-5} M).

Instead, the hydroxyl group is bound by the hydrogen bond with the methanol molecule, the solvent of crystallization. However, the methanol showed a positional disorder: the major component, C(18)H_3O(4)H with 80% occupancy and the minor, C(18)H_3O(5)H with 20% occupancy [O(3)···O(4)=2.599(4), O(3)-H(12)=1.06(5), H(12)···O(4)=1.59(4) Å, and O(3)-H(12)-O(4)=158(4)°, and O(3)···O(5)=2.652(10), H(12)···O(5)=1.64(4) Å, and O(3)-H(12)-O(5)=159(4)°].

Phototitration of 1(2OH), 1(4OH), and 2(2OH). The pK_a values of the 2′-OH in three isoalloxazines were estimated by phototitration. As shown in Fig. 2, the absorption spectra of **2**(2OH) changed as a function of pH. This change is attributed to the dissociation of the 2′-OH because this group is the sole dissociable group in **2**(2OH) at pH 4—10. In Fig. 3 we

Table 2. Bond Lengths (l/Å) and Bond Angles (ϕ/°) with Estimated Standard Deviations in Parentheses

Bond lengths			
C(1)-C(2)	1.358(6)	C(1)-C(6)	1.405(5)
C(2)-C(3)	1.379(4)	C(3)-C(4)	1.380(6)
C(4)-C(5)	1.403(5)	C(5)-C(6)	1.406(4)
C(7)-C(8)	1.457(4)	C(7)-C(10)	1.482(4)
N(1)-C(6)	1.371(4)	N(1)-C(7)	1.292(4)
N(2)-C(5)	1.383(4)	N(2)-C(8)	1.363(4)
N(2)-C(12)	1.454(4)	N(3)-C(9)	1.400(5)
N(3)-C(10)	1.382(5)	N(3)-C(11)	1.469(6)
N(4)-C(8)	1.302(4)	N(4)-C(9)	1.362(4)
O(1)-C(10)	1.218(4)	O(2)-C(9)	1.224(5)
C(12)-C(13)	1.373(5)	C(12)-C(17)	1.385(4)
C(13)-C(14)	1.387(7)	C(14)-C(15)	1.386(5)
C(15)-C(16)	1.376(5)	C(16)-C(17)	1.399(5)
O(3)-C(17)	1.354(4)		
C(18)-O(4)[a]	1.395(7)	C(18)-O(5)[b]	1.32(2)
Bond angles			
C(2)-C(1)-C(6)	120.4(4)	C(1)-C(2)-C(3)	119.6(4)
C(2)-C(3)-C(4)	122.5(4)	C(3)-C(4)-C(5)	118.2(4)
C(4)-C(5)-C(6)	119.7(3)	C(3)-C(5)-N(2)	121.6(3)
C(6)-C(5)-N(2)	118.7(3)	C(1)-C(6)-C(5)	119.5(3)
C(1)-C(6)-N(1)	118.8(3)	C(5)-C(6)-N(1)	121.7(3)
C(8)-C(7)-C(10)	116.8(3)	C(8)-C(7)-N(1)	124.8(3)
C(10)-C(7)-N(1)	118.4(3)	C(7)-C(8)-N(2)	115.7(3)
C(7)-C(8)-N(4)	124.7(3)	N(2)-C(8)-N(4)	119.6(3)
N(3)-C(9)-N(4)	121.4(3)	N(3)-C(9)-O(2)	117.6(3)
N(4)-C(9)-O(2)	121.0(3)	C(7)-C(10)-N(3)	114.6(3)
C(7)-C(10)-O(1)	122.8(3)	N(3)-C(10)-O(1)	122.6(3)
C(6)-N(1)-C(7)	117.8(3)	C(5)-N(2)-C(8)	121.2(3)
C(5)-N(2)-C(12)	120.2(3)	C(8)-N(2)-C(12)	118.7(3)
C(9)-N(3)-C(10)	123.8(3)	C(9)-N(3)-C(11)	117.5(3)
C(10)-N(3)-C(11)	118.6(3)	C(8)-N(4)-C(9)	118.6(3)
C(13)-C(12)-C(17)	122.1(3)	C(13)-C(12)-N(2)	119.6(3)
C(17)-C(12)-N(2)	118.3(3)	C(12)-C(13)-C(14)	119.5(3)
C(13)-C(14)-C(15)	119.0(3)	C(14)-C(15)-C(16)	121.4(3)
C(15)-C(16)-C(17)	119.7(3)	C(12)-C(17)-C(16)	118.2(3)
C(12)-C(17)-O(3)	118.0(3)	C(16)-C(17)-O(3)	123.7(3)
C(17)-O(3)-H(12)	115(3)		
Hydrogen bonds			
O(3)···O(4)[a]	2.599(4)	O(3)···O(5)[b]	2.652(10)
O(3)-O(12)	1.06(5)		
H(12)···O(4)[a]	1.59(4)	H(12)···O(5)[b]	1.64(4)
O(3)-H(12)···O(4)	158(4)	O(3)-H(12)···O(5)[b]	159(4)

a) Occupancy 0.8. b) Occupancy 0.2.

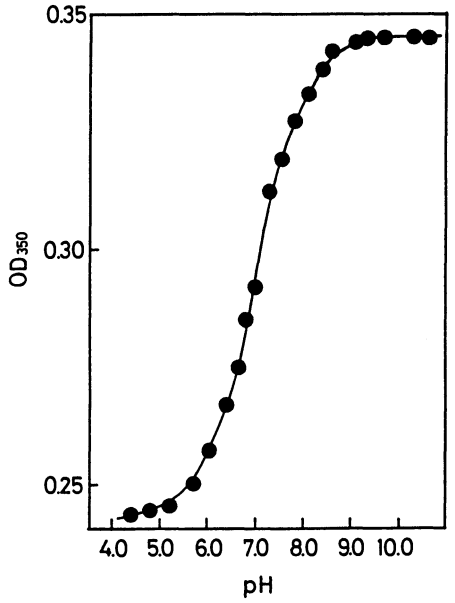

Fig. 3. Plot of OD_{350} vs. pH for **2**(2OH).

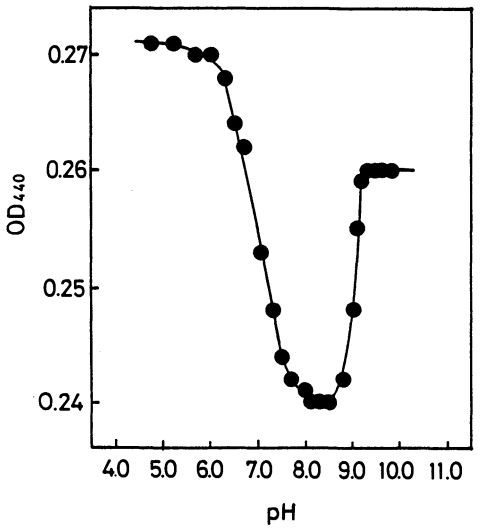

Fig. 4. Plot of OD_{440} vs. pH for **1**(2OH) (4.00×10^{-5} M).

plotted OD_{350} against medium pH. The analysis of this plot by a titration equation afforded pK_a=7.0 for **2**(2OH). Similarly, the pK_a of the 2′-OH in **1**(4OH) was estimated to be 8.6. On the other hand, **1**(2OH) showed a spectral change different from others: with increasing medium pH the absorbance at 320—470 nm region first decreases with isosbestic points (314 and 478 nm) and then increases with different isosbestic points (275 and 490 nm). The plot of OD_{440} vs. pH gave a minimum absorbance at pH 8.3 (Fig. 4). We carefully examined the correlation between the spectral change and the consumed NaOH. It was found that 0.5 mol of NaOH is consumed per one mol of **1**(2OH) at pH 5.0—8.3 and another 0.5 mol of NaOH is consumed at pH 8.3—9.3. The finding supports that the biphasic spectral change is caused by the specific interaction between neutral **1**(2OH) and dissociated **1**($2O^-$). It is known that flavins easily form stacked aggregates in aqueous solution.[15,16] This is due to the poor solubility of flavins in water and also due to the large dipole moment across flavin molecules.[17] If this is the case in **1**(2OH), the flavin-flavin interaction would become maximum at the half-titrated pH, for example, owing to intermolecular hydrogen bonding between neutral **1**(2OH) and dissociated **1**($2O^-$) (Eq. 1). Anyway, we estimated the pK_a of **1**(2OH) to be the half-titrated pH 7.7.

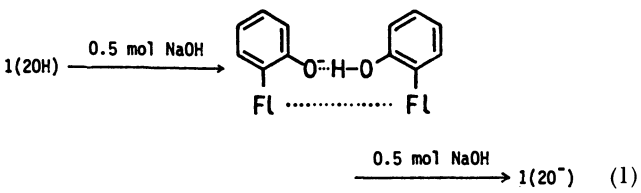

(1)

It is not clear yet why such a biphasic spectral

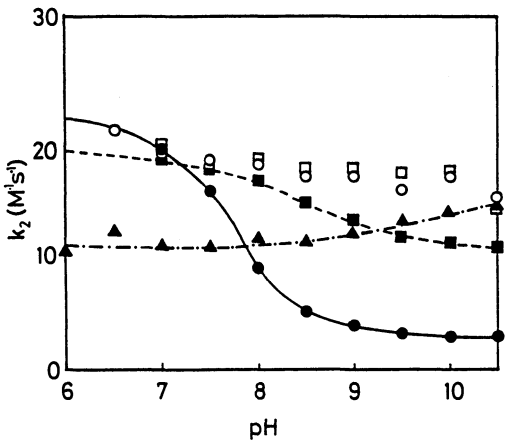

Fig. 5. pH Dependence of the k_2 for the reaction of **1**(2.75×10^{-5} M) and BNAH (7.91×10^{-5} M): ▲ **1**(H), ● **1**(2OH), ○ **1**(2OMe), ■ **1**(4OH), □ **1**(4OMe).

change is observed for **1**(2OH) but not for **2**(2OH). We have found that the rotation of the aryl group at the N(10) position of flavins is considerably restricted because of the steric effect and the rotation of the naphthyl group is much more difficult than the phenyl group.[8,18] Probably, the two isoalloxazines in **2**(2OH) cannot come closer enough to interact electronically because of steric hindrance arising from the 10-naphthyl group.

The pK_a values determined above are generally lower than those for analogous compounds (e.g., 9.71 for *o*-aminophenol and 10.30 for *p*-aminophenol).[19] Furthermore, **1**(2OH) has the pK_a lower than **1**(4OH). When the OH group forms the stable intramolecular hydrogen bond, the pK_a should be raised. Hence, these pK_a data suggest that **1**(2OH) and **2**(2OH) do not form the stable hydrogen bond at least at the initial state (i.e., oxidized state). The conclusion obtained in solution is in line with that obtained from the X-ray crys-

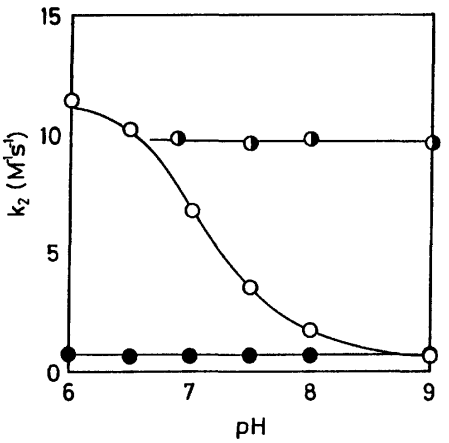

Fig. 6. pH Dependence of the k_2 for the reaction of **2**(2.75×10^{-5} M) and BNAH (7.91×10^{-5} M): ○ **2**(H), ○ **2**(2OH), ● **2**(2OMe).

tallographic analysis.

pH Dependence for the Reaction with 1-Benzyl-1,4-dihydronicotinamide. The hydrogen-transfer reaction from 1-benzyl-1,4-dihydronicotinamide (BNAH) to five flavins was carried out at pH 7.0—10.4. As a prelude to kinetic studies, we confirmed that this reaction is not catalyzed by buffers (10^{-3}—10^{-1} M) in water. In Figs. 5 and 6 the second-order rate constants (k_2) are plotted against medium pH. It is seen from these figures that the k_2 values for **1**(H), **1**(2OMe), **1**(4OMe), **2**(H), and **2**(2OMe) which have no dissociable group at this pH range are almost constant. On the other hand, **1**(2OH), **1**(4OH), and **2**(2OH) gave the sigmoid curves which could be expressed by Scheme 2 (**1**(2OH) is taken as an example). Thus, the k_2 is expressed by Eq. 2 including the true second-order rate constants for each species, $k_{2,OH}$ and k_{2,O^-}.

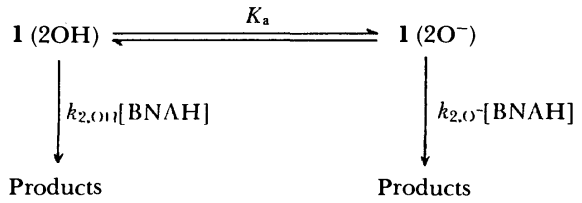

Scheme 2.

$$k_2 = \frac{k_{2,OH}[H^+] + k_{2,O^-}K_a}{[H^+] + K_a} \quad (2)$$

The $k_{2,OH}$ and k_{2,O^-} determined by computer-assisted curve-fitting with Eq. 2 are summarized in Table 3. Examination of Table 3 reveals that (i) in **1**(2OH) and **2**(2OH) the $k_{2,OH}$ values are greater by 8.1—27 fold than the k_{2,O^-} values but in **1**(4OH) the $k_{2,OH}$ is greater only by 1.8 fold than the k_{2,O^-} and (ii) the $k_{2,OH}$ for **2**(2OH) is greater by 2 fold than that for the 2′-methoxy counterpart but the $k_{2,OH}$ values for **1**(2OH) and **1**(4OH) are almost equal to those for the 2′-methoxy counterparts (less than 1.3). As described above, the aryl group at the N(10) position cannot enjoy the coplanarity with the isoalloxazine ring.[8,18] Therefore, the resonance effect of the 10-substituent should be relatively small. In fact, the dissociation of the 2′-OH group in **1**(4OH) decreased the rate constant only by a factor of 1.8. In contrast, the large rate decrease was observed for **1**(2OH) and **2**(2OH). The difference observed between the 2′-substituent and the 4′-substituent would be explained by the spatial electrostatic effect but not by the resonance effect: that is, reduction of these flavins develops an anionic charge on the N(1) position which is very close to the 2′-oxide anion (Eq. 3). Therefore, the progress of this reaction would induce an energetically-unfavorable electrostatic repulsion. Probably, this is why the large diffence was observed for **1**(2OH) and **2**(2OH).

Table 3. pK_a of the 2′-OH Group and the Second-Order Rate Constants (k_2) in an Aqueous System (30 °C)

Flavin	pK_a	$k_2/M^{-1}s^{-1}$	
		Neutral ($k_{2,OH}$)	Dissociated (k_{2,O^-})
1(H)	—	11.6	—
1(2OH)	7.7	22.0	2.70
1(2OMe)	—	16.6	—
1(4OH)	8.6	18.0	9.94
1(4OMe)	—	16.8	—
2(H)	—	9.71	—
2(2OH)	7.0	13.3	0.50
2(2OMe)	—	0.66	—

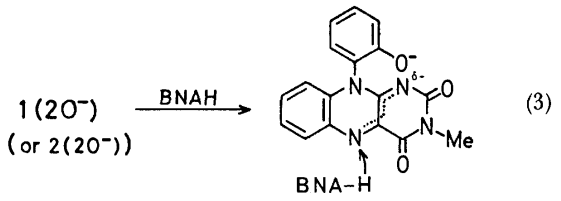

(3)

More important is the finding (ii). The rate difference between **2**(2OH) and **2**(2OMe) may be rationalized in terms of hydrogen bonding. On the other hand, the absence of the rate difference between **1**(2OH) and **1**(2OMe) may be due to the aggregate formation discovered through the phototitration. Subsequently, we carried out the reaction in acetonitrile where the effect of hydrogen bonding would be more strengthened.

Reaction with BNAH in Acetonitrile. It is known that the electrostatic and the hydrogen-bonding effect appear more clearly in organic solvents (especially, in aprotic solvents). For example, the influence of hydrogen bonding with trichloroacetic acid or trifluoroacetic acid on the absorption spectra of flavins was studied in detail in CCl_4.[20] Similarly, Sigman et al.[21,22] demonstrated that an anionic charge placed in the vicinity of N(1) in 1,4-dihydronicotinamide effectively

enhances the reducing ability in acetonitrile but not in an aqueous system. Yagi et al.[20] also found that the photoreduction of riboflavin tetrabutyrate by *N*-benzyl-*N*,*N*′-dimethylethylenediamine in CCl_4 is weakly catalyzed (1.2—1.4 fold) by strong proton acids such as trichloroacetic acid and trifluoroacetic acid. This suggests that the reduction of flavins may be general-acid-catalyzed in aprotic solvents such as CCl_4 although the position of the acid catalysis cannot be specified. We thus chose acetonitrile to obtain a further insight into the hydrogen bonding effect.

In the anaerobic reaction with BNAH (2.09×10^{-3} M) we found that only **1**(2OH) and **2**(2OH) (5.00×10^{-5} M) can oxidize BNAH with $k_2=2.06\times10^{-2}$ $M^{-1}s^{-1}$ and 7.31×10^{-2} $M^{-1}s^{-1}$, respecticely. The reaction with other six flavins was not detected at all ($k_2<10^{-5}$ $M^{-1}s^{-1}$). It is particularly worthy mentioning that **1**(2OH) is reactive but **1**(4OH) is totally unreactive in acetonitrile. The essential difference in the reactivity indicates that the reaction with **1**(2OH) (and also with **2**(2OH)) is acid catalyzed intramolecularly. It is known that oxidized flavins employ the planar structure with sp^2-hybridized N(5) and N(10) while reduced flavins employ the bent structure folded through sp^3-hybridized N(5) and N(10).[23-25] Thus, the steric crowding in oxidized flavins is significantly relaxed in folded reduced flavins.[8,18] Examination of Corey-Pauling-Koltun models suggests that it is not impossible to form a hydrogen bond in reduced **1**(2OH) (and also **2**(2OH)) (Eq. 4).

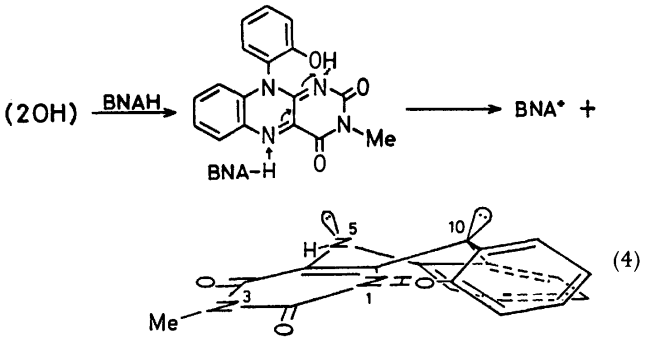

Presumably, intramolecular general-acid catalysis by the 2′-OH begins when the anionic charge is partially developed on N(1) and the isoalloxazine ring is partially folded. This implies that the transition state of this reaction lies more or less close to the final state.

We also found that the reaction with BNAH is general-acid-catalyzed by added acidic species in acetonitrile. As shown in Fig. 7, the k_2 increased linearly with increasing *p*-cyanophenol concentration: k_{ga} and 1.8×10^{-2} $M^{-2}s^{-1}$ for **2**(2OMe). If the acidity difference between 2′-OH and *p*-cyanophenol (pK_a 7.95)[19] is neglected, the effective concentration (k_2/k_{ga}) of the 2′-OH group in general-acid catalysis amounts to 0.71 M for **1**(2OH) and 4.1 M for **2**(2OH). These values are relatively small and are classified as a less effective contribution of general-acid catalysis.[26] It is concluded, therefore, that flavin activation through hydrogen bonding with N(1) does exist but is not so effective in these model compounds, **1**(2OH) and **2**(OH).

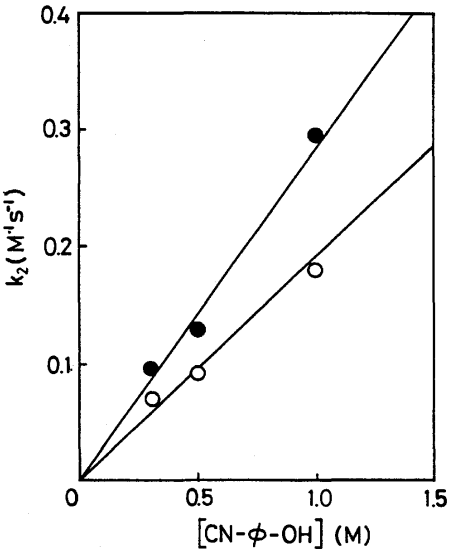

Fig. 7. General-acid catalysis by *p*-cyanophenol for the reaction of **1**(2OMe) (●) or **2**(2OMe) (○) (5.00×10^{-5} M) with BNAH (2.09×10^{-3} M) in acetonitrile.

We are currently devoting our research efforts on the development of more effective model systmes to prove the flavin activation through hydrogen bonding with N(1).

This research was supported by the Grant-in-Aid from the Ministry of Education, Science and Culture. We thank Professor Fumio Yoneda for helpful discussion.

References

1) P. Hemmerich, G. Nagelschneider, and C. Veeger, *FEBS Lett.*, **8**, 69 (1970).
2) T. C. Bruice, *Acc. Chem. Res.*, **13**, 256 (1980).
3) C. Walsh, *Acc. Chem. Res.*, **13**, 148 (1980).
4) V. Massey and P. Hemmerich, *Biochem. Soc. Trans.*, **8**, 246 (1980).
5) S. Shinkai, N. Honda, Y. Ishikawa, and O. Manabe, *Chem. Lett.*, **1984**, 327.
6) S. Shinkai, N. Honda, Y. Ishikawa, and O. Manabe, *J. Am. Chem. Soc.*, **107**, 6286 (1985).
7) N. Honda, S. Shinkai, and O. Manabe, *Rep. Fac. Eng. Nagasaki Univ.*, **15**, 73 (1985) and related unpublished results.
8) S. Shinkai, H. Nakao, I. Kuwahara, M. Miyamoto, T. Yamaguchi, and O. Manabe, *J. Chem. Soc., Perkin Trans. 1*, **1988**, 313.
9) F. Toda, *Kagaku To Kogyo*, **40**, 300 (1987).
10) F. Yoneda, Y. Sakuma, M. Ichiba, and K. Shinomura, *J. Am. Chem. Soc.*, **98**, 830 (1976).
11) P. Main, S. E. Hull, L. Lessinger, G. Germain, J. P. Declerq, and M. M. Woolfson, *MULTAN 78*, "A System

Computer Programs for the Automatic Solution of Crystal Structures from X-Ray Diffraction Data," Univs. of York, England and Louvain, Belgium (1978).
12) T. Ashida, HBLS V, "The Universal Crystallographic Computing System-Osaka," The Computation Center, Osaka University, (1979).
13) "International Tables for X-Ray Crystallography," Kynoch Press, Birmingham, England 1974, Vol. IV, p. 71.
14) C. K. Johnson, ORTEP II, Report ORNL-5138, Oak Ridge National Laboratory, Tennessee (1976).
15) S. Shinkai, A. Harada, Y. Ishikawa, and O. Manabe, *J. Chem. Soc., Perkin Trans. 2*, **1982**, 125.
16) S. Shinkai, A. Harada, O. Manabe, and F. Yoneda, *Bull. Chem. Soc. Jpn.*, **55**, 928 (1982).
17) P.-S. Song, *J. Phys. Chem.*, **72**, 536, 4724 (1968).
18) S. Shinkai, H. Nakao, and O. Manabe, *Tetrahedron Lett.*, **26**, 5183 (1985).
19) W. P. Jencks and J. Regenstein, "Handbook of Biochemistry and Molecular Biology," ed by G. D. Fasman, CRC Press, Cleveland (1976), p. 314.
20) K. Yagi, N. Ohishi, K. Nishimoto, J. D. Choi, and P.-S. Song, *Biochemistry*, **19**, 1553 (1980).
21) J. Hajdu and D. S. Sigman, *J. Am. Chem. Soc.*, **97**, 3524 (1975).
22) J. Hajdu and D. S. Sigman, *Biochemistry*, **16**, 2841 (1977).
23) L. Tauscher, S. Ghisla, and P. Hemmerich, *Helv. Chim. Acta*, **56**, 630 (1973) and references cited therein.
24) P. Kierkegaard, R. Norrestam, P. Werner, I. Csoregh, M. Glehn, R. Karlsson, M. Leijonmarch, O. Ronnquist, B. Sternland, O. Tillberg, and L. Torbjornsson, "Flavins and Flavoproteins," University Park Press, Baltimore (1971), p. 1.
25) C. T. Moonen, J. Vervoort, and F. Müller, *Biochemistry*, **23**, 4859, 4868 (1984).
26) T. C. Bruice and S. J. Benkovic, "Bioorganic Mechanisms," Vol. I, New York, N.Y., W. A. Benjamin (1966).
27) W. C. Hamilton, *Acta Crystallogr.*, **12**, 609 (1959).

The Reaction of Lupane and Friedo-Oleanane Type Triterpenes with *m*-Chloroperbenzoic Acid[1)]

Motoo Tori, Reiko Matsuda, Masakazu Sono, Yoshihiro Kohama, and Yoshinori Asakawa*
Faculty of Pharmaceutical Sciences, Tokushima Bunri University, Yamashiro cho, Tokushima 770
(Received December 23, 1987)

Lupane-3β,28-diol, lupan-3β-ol, and friedelan-3β-ol were treated with *m*-chloroperbenzoic acid (*m*CPBA) in refluxing chloroform to afford corresponding lactones in one step, while lupane-3β,28-diyl diacetate, lupan-3β-yl acetate, and friedelan-3β-yl acetate to give hydroxylated or keto derivatives. Similar reaction of dendropanoxide with *m*CPBA yielded 6β-, 7β-, 21α-, and 22β-hydroxylated compounds.

Recently, we reported the reaction of natural products, monoterpenes,[2)] sesquiterpenes,[3)] triterpenes,[4)] and other class of compounds,[5)] with *m*CPBA in chloroform under reflux to afford hydroxylated or carbonyl compounds as a result of functionalization at unactivated carbon atoms. These reactions are very similar to dry ozonization[6)] of natural products. Takahashi et al., in 1977, reported dry ozonization of friedelane and friedelin to yield the corresponding 15, 16, 19, and 21-keto derivatives as well as the 18,19-epoxide.[7)] In these cases ozone attacked the rings D and E, which were protruding. We expect that the reactions of this class of compounds with *m*CPBA might occur at these positions. In order to compare dry ozonization with *m*CPBA oxidation, lupane-3β,28-diol (**1**), lupan-3β-ol (**2**), friedelan-3β-ol (**3**), lupane-3β,28-diyl diacetate (**4**), lupan-3β-yl acetate (**5**), friedelan-3β-yl acetate (**6**), and dendropanoxide (**7**) were allowed to react with *m*CPBA in chloroform under reflux. We now report the details of these reactions.

Triterpene Alcohols. Dihydrobetulin (**1**) was allowed to react with *m*CPBA (2.2 equiv) in chloroform for 6 h under reflux. After the removal of acidic fractions of the product by means of chromatography over Sephadex LH-20 ($CHCl_3$-MeOH=1 : 1), the product was subjected to silica-gel column chromatography (PhH-EtOAc, gradient) [work up procedure A] to afford 28-hydroxylupan-3-one (**8**, 50.2%), methyl 4,28-dihydroxy-3,4-seco-lupan-3-oate (**9**, 4.7%), and methyl 28-hydroxy-3,4-seco-lup-4(23)-en-3-oate (**10**, 7.9%). The structure of **8** was easily assigned by the spectral data [*m/z* 442; 3450 and 1700 cm^{-1}; δ 3.32 and 3.78 (each d, *J*=11 Hz, H-28)]. The MS and IR spectra of compound **9** showed the peaks at *m/z* 472 $(M-H_2O)^+$, 385, and 373 and the absorptions at 3450 and 1730 cm^{-1}, respectively. The ^1H NMR spectrum indicated the presence of a methoxycarbonyl group [δ 3.67 (3H, s)] and the protons at C-28 (δ 3.31 and 3.77, each d, *J*=11 Hz). As the signals of the two methyl groups shifted downfield (δ 1.23 and 1.28, each 3H, s), this compound was found to be a 4-hydroxy-3,4-seco derivative. Compound **10** showed similar spectral data to those of **9**, including the methoxycarbonyl group [1730 cm^{-1}, δ 3.66 (3H, s)] and the C-28 hydroxyl group [3450 cm^{-1}, δ 3.31 and 3.77 (each d, *J*=11 Hz)], except for the exo-methylene group (890 cm^{-1}, δ 4.65 and 4.85) and the vinyl methyl group (δ 1.73). Thus, this compound was found to be derived from compound **9** by dehydration. These two compounds, **9** and **10**, were presumably formed by methanolysis of the initially produced lactone **11** catalyzed by *m*-chlorobenzoic acid present in the reaction mixture during column chromatography over Sephadex LH-20 ($CHCl_3$-MeOH=1 : 1). Indeed, when lactone **11** was exposed to similar conditions (*m*-chlorobenzoic acid/$CHCl_3$-MeOH), **9** and **10** were formed. Therefore, the reaction of **1** with *m*CPBA was worked up by washing with aq Na_2SO_3, aq. $NaHCO_3$, and brine, successively [work up procedure B] to afford **8** (50.2%) and **11** (20%). These results were presumably explained as follows: **1** was oxidized to ketone **8** which underwent Baeyer-Villiger oxidation to give **11**, the lactone ring of which opened by methanolysis to afford the hydroxy methyl ester **9**. **9** underwent dehydration to give the unsaturated methyl ester **10** under the conditions employed.

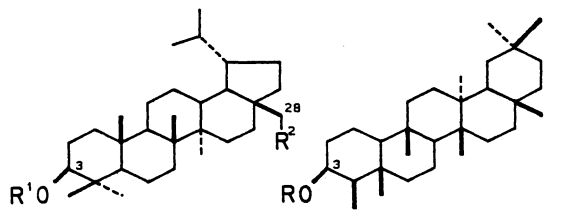

1 R¹=H, R²=OH
2 R¹=H, R²=H
4 R¹=Ac, R²=OAc
5 R¹=Ac, R²=H

3 R=H
6 R=Ac

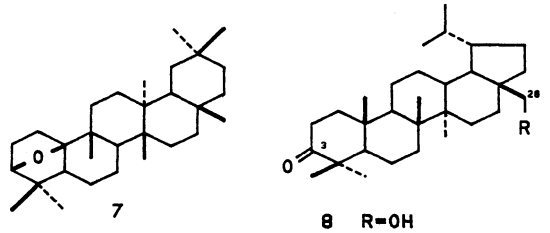

7

8 R=OH
12 R=H

Lupan-3β-ol (**2**) was treated with *m*CPBA in refluxing chloroform for 6 h. The reaction mixture was

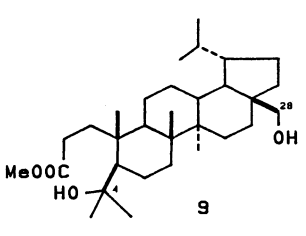

9

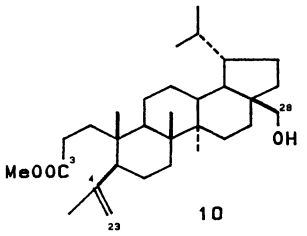

10

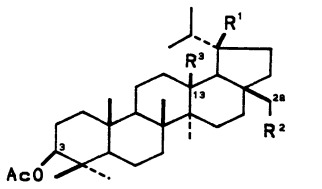

17 R^1=OH, R^2=OAc, R^3=H

18 R^1=R^2=H, R^3=OH

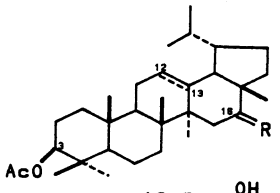

19 R=<OH/H

20 R=H_2, Δ^{12}

21 R=O

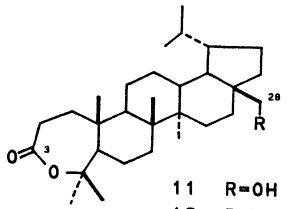

11 R=OH

13 R=H

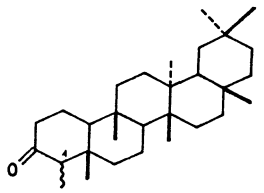

14 4β-Me

15 4α-Me

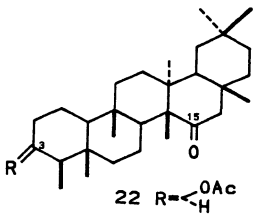

22 R=<OAc/H

23 R=O

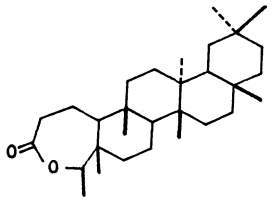

16

worked up [procedure B] and purified by column chromatography over silica gel to give lupan-3-one (**12**, 33.5%),[8] and 3,4-seco-lupan-4,3-olide (**13**, 4.3%). The IR spectrum of lactone **13** showed the absorption at 1710 cm^{-1} and the molecular ion peak at m/z 442 was observed in its mass spectrum. The ^1H NMR spectrum was very similar to those of **11**. It showed the signals of two tertiary methyl groups (δ 1.40 and 1.47), two secondary methyl groups (δ 0.75 and 0.84) and four tertiary methyl groups (δ 0.76, 0.93, 1.08, and 1.09). These data clearly indicated that compound **13** is a lactone.

Similar treatment of friedelan-3β-ol (**3**) with *m*CPBA gave friedelin (**14**, 42.7%),[9] 4-epi-friedelin (**15**, 9.5%),[9] and 3,4-seco-friedelan-4,3-olide (**16**, 20.3%)[10] after work up procedure B. The structure of compound **15** was determined to be 4-epi-friedelin, since the base treatment (KOH/EtOH) of **15** yielded **14** very easily. Compound **16** was identical with that of the Baeyer-Villiger oxidation product of **14**. 4-Epi-friedelin was presumably derived from the 3α,4α-epoxide by acid-catalyzed opening under the conditions employed. The epoxide was formed through friedel-3-ene, which was derived from **3** by acid-catalyzed dehydration.

The hydroxyl groups at C-3 position of these triterpenes were susceptible to this oxidation to give ketones and/or followed by further oxidation to afford lactones, but the hydroxyl groups at C-28 of the lupane triterpenes were not attacked under these conditions presumably due to the steric hindrance.

Triterpene Acetates. Lupane-3β,28-diyl diacetate (**4**) was subjected to the reaction with *m*CPBA. In this case only one compound was produced (83.2%) and its spectral data were identical with those of 19β-hydroxylupane-3β,28-diyl diacetate (**17**) reported in the literature.[11] It is interesting to note that **17** was the sole product of both dry ozonization and *m*CPBA oxidation. It is probably owing to the assistance of the acetoxyl group located at C-28.

Lupan-3β-yl acetate (**5**) was next treated with *m*CPBA in $CHCl_3$ under reflux for 12 h to afford 13β-hydroxylupan-3β-yl acetate (**18**, 20.4%) and 16β-hydroxylupan-3β-yl acetate (**19**, 5.1%). Compound **18** showed molecular ion peak at m/z 486 and absorptions at 3500 and 1720 cm^{-1} in its MS and IR spectra, respectively, suggesting that a tertiary hydroxyl group was introduced in the skeleton. When **18** was subjected to dehydration with $POCl_3$ in pyridine, olefin **20** [δ 5.16, t, J=8 Hz; m/z 468 (M^+)] was formed. Since the MS spectrum of **20** indicated a fragment peak at m/z 218 due to retro-Diels-Alder fragmentation of the ring C, **20** must be formulated as lup-12-en-3β-yl acetate.[12] Hence, **18** was determined to be 13β-hydroxylupan-3β-yl acetate, providing that hydroxylation occurred with retention of configuration. The spectroscopic data of product **19** were identical with the literature data of 16β-hydroxylupan-3β-yl acetate.[12,13] The structure **19** was reconfirmed by Jones oxidation into known 16-oxolupan-3β-yl acetate (**21**)[13] and by measuring the solvent shift of the ^1H NMR data of **21**.

In the case of friedelan-3β-yl acetate (**6**), 15-oxofriedelan-3β-yl acetate (**22**, 12.9%) [m/z 484 (M^+), 1730 and 1695 cm^{-1}] was produced under similar conditions. The ^1H NMR spectrum of **22** showed the signals of two protons resonating at δ 2.16 and 2.50 (each d, J=18 Hz), suggesting the protons α to the carbonyl group. When compound **22** was hydrolyzed (KOH/EtOH) followed by Jones oxidation to afford diketone

23, it was found that the spectral data of **23** were identical with those of authentic friedelane-3,15-dione.[7] Hence, product **22** should be formulated to be 15-oxofriedelan-3β-yl acetate.

When the hydroxyl groups were protected as acetates, unactivated carbon atoms at relatively unhindered positions were attacked to give a hydroxylated and/or a carbonyl compound. In these cases, the reaction products are quite similar to those of dry ozonization.

Triterpene Ether. Dendropanoxide (**7**) is a hexacyclic triterpene oxide isolated from *Dendropanax trifidus*.[14] Dendropanoxide (**7**) was treated with *m*CPBA in $CHCl_3$ under reflux to afford four alcoholic products **24—27** and ketone **28** after purification by column chromatography, prep. TLC, and HPLC. The first product **24**, $C_{30}H_{50}O_2$ (by HRMS), showed a signal at δ 4.10 (dt, J=11.8 and 7 Hz) due to the proton attached to the carbon bearing the hydroxyl group (3400 cm^{-1}) as well as a signal at δ 3.77 (d, J=7 Hz) due to H-3. These data indicated that **24** is a secondary alcohol and that the position of the hydroxyl group is at either C-6 or C-7, because there were three protons in the neighbor of the hydroxyl group judging from the coupling pattern. Irradiation of the proton at δ 4.10 (H-6β) induced NOE's into two methyl groups (δ 1.09 and 1.10). Since the 24-Me (δ 1.10) was assigned by observing NOE between the H-3 and the 24-Me and NOE's between the 24-Me (δ 1.10) and H-6β, and the 25-Me (δ 1.09) and the H-6β were expected, **24** should be formulated to be 6α-hydroxydendropanoxide. The ^{1}H NMR spectrum of the second compound **25** showed pattern of signals (δ 4.20, brt, J=5 Hz) very similar to that of **24**, indicating the presence of a secondary hydroxyl group probably at C-7. As actually only one methyl (δ 1.19, 25-Me) was observed in the NOE difference spectrum, when the proton at δ 4.20 (H-7β) was irradiated, **25** was determined to be 7α-hydroxydendropanoxide. These structures were in good agreement with the assignment of the ^{13}C NMR data (vide infra).

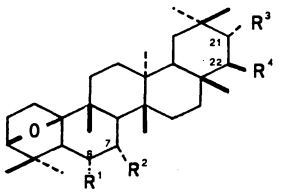

24 R^1=OH, R^2=R^3=R^4=H
25 R^2=OH, R^1=R^3=R^4=H
26 R^3=OH, R^1=R^2=R^4=H
27 R^4=OH, R^1=R^2=R^3=H

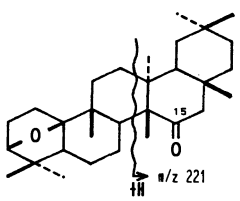

28

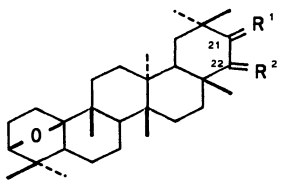

29 R^1=O, R^2=H_2
30 R^1=H_2, R^2=O

The spectral data of **26** (δ 3.70, dd, J=12 and 4 Hz) and **27** (δ 3.67, dd, J=12 and 5.6 Hz) only showed that these compounds had secondary hydroxyl groups having two protons in the neighbor. They would be located at C-11, 12, 15, 16, 21, or 22 position. It is difficult to assign by analysis of the ^{1}H NMR data or NOE experiments unless the ^{13}C NMR data of **7** are fully assigned. The ^{13}C NMR data of **7** were analyzed by the use of 2D NMR spectroscopy (COSY, ^{13}C-^{1}H correlation, long-range ^{13}C-^{1}H correlation, and H-H-C relayed correlation) and the results were shown in Table 1.[15] As the carbons of rings A—C of both compounds, **26** and **27**, have very similar chemical shifts to those of **7**, the positions of the hydroxyl groups are deduced to be at either C-21 or C-22. When **26** and **27** were subjected to Jones oxidation, they were converted to different ketones, namely, 21-oxodendropanoxide (**29**) and 22-oxodendropanoxide (**30**), respectively. Thus, **26** was determined to be 21α-hydroxydendropanoxide, because the irradiation of the proton at δ 3.70 (H-21β) induced NOE's into two methyl groups (28-Me and 29-Me). Only this position can give rise to

Table 1. ^{13}C NMR Data of Derivatives of Dendropanoxide (**7**)

Carbon	7	24	25	26	27	28
1	31.9	32.1	31.9	31.9	31.9	31.7
2	24.7	24.5	24.8	24.8	24.7	24.7
3	84.4	84.6	84.0	84.4	84.4	84.6
4	43.3	44.0	43.5	43.4	43.4	43.4
5	53.1	60.3	51.8	53.2	53.1	52.7
6	19.8*	67.5	31.5	19.8*	19.8*	19.8*
7	20.0*	32.5	68.4	20.3*	20.0*	21.7*
8	41.9	42.9	48.0	40.3	42.3	44.1
9	36.7	36.6	36.9	36.7	36.6	36.6
10	93.6	93.6	93.3	93.7	93.5	93.2
11	30.6	29.9	31.1*	29.7†	30.3†	30.1
12	30.0	29.9	30.0*	29.8†	30.9†	28.9
13	39.2	39.1*	39.3†	38.7#	38.9#	42.6
14	39.3	39.3*	40.4†	39.9#	39.4#	54.8
15	31.8	31.8	31.8	30.3	31.2	214.4
16	35.9	35.8	36.0	36.0	32.0	53.5
17	30.1	30.2	29.8	33.0	41.6	33.1
18	43.6	43.6	44.2	45.2	45.2	35.2
19	35.0	35.0	34.6	36.3	34.5	35.4
20	28.3	28.3	28.3	34.5	34.7	28.0
21	33.4	33.4	33.9	74.8	41.5	33.5
22	38.7	38.6	38.1	46.0	75.4	38.8
23	24.4	25.6	23.9	24.4	24.4	24.5
24	23.0	22.5	22.8	23.0	23.0	23.1
25	20.5	20.9	21.7	20.9	20.4	19.9
26	19.3	19.3	19.8	19.1	20.0	15.6
27	18.5	18.5	18.8	16.9	18.7	18.7
28	31.9	32.0	33.5	32.5	23.3	32.4†
29	32.8	32.9	32.4	33.0	31.9	32.7†
30	34.1	34.1	34.0	24.6	34.9	33.9

*,†,# Singles may be interchanged in each vertical column.

Table 2. Yields of the Products from **1**—**7**

Substrate	Work-up	Product (yield/%)[a]
1	A	**8** (50.2), **9** (4.7), **10** (7.9)
	B	**8** (50.2), **11** (20)
2	B	**12** (33.5),[8] **13** (4.3)
3	B	**14** (42.7),[9] **15** (9.5),[9] **16** (20.3)[10]
4	B	**17** (83.2)[11]
5	B	**18** (20.4), **19** (5.1)[12,13]
6	B	**22** (12.9)
7	B	**24** (1.6), **25** (1), **26** (0.4) **27** (0.2), **28** (0.3)

a) Yields shown indicate isolation yields based on consumed starting material.

NOE's into two methyl groups. However, the irradiation of the methine at δ 3.67 (H-22α) of **27** did not give any NOE into the methyl groups. If the hydroxyl group is located at 22α position, NOE into the 28-Me is expected upon irradiation of H-22β. Therefore, **27** was determined to be 22β-hydroxydendropanoxide.

The spectral data of **28** [1690 cm^{-1}; m/z 440 (M^+) and 221], which were not identical with those of **29** or **30**, showed the presence of the ketone instead of the alcohol. The protons which showed absorptions at δ 2.17 and 2.44 (each d, J=17 Hz) indicated the partial structure ■-CO-CH_2-■, in the molecule. The predominant fragment ion (m/z 221) shown by the wave line in the structure **28** suggests that the position of the carbonyl group is at C-15. This ion has been proved to possess the composition of $C_{15}H_{25}O$ by HRMS. The ^{13}C NMR data supported this result (Table 1). Thus, ketone **28** was determined to be 15-oxodendropanoxide. As a result, dendropanoxide was attacked at methylene carbons in rings B, D, and E, which were protruded and unhindered.

The results obtained in this work (Table 2) clearly show that when the compound has a hydroxyl group in the ring A, oxidation to the corresponding ketone predominates. Sometimes further oxidation, Baeyer-Villiger oxidation, occurs. While in the case of the acetate, oxidation by this method occurs at an unactivated carbon atom of the sterically unhindered position to afford a secondary or tertiary alcohol or a ketone. Dendropanoxide has been attacked in its rings B, D, and E, which are unhindered. Although the reaction site is not easy to predict, it is quite interesting to note that the sites of the reaction are similar to those of dry ozonization. These reactions would be convenient for introduction of the oxygen functions at unactivated carbon atoms of various bioactive natural products.

Experimental

General Procedures. See Ref. 4b.

Reaction of Lupane-3β,28-diol (1) with *m*CPBA. Method A: The diol **1** (600 mg) was dissolved in chloroform (36 ml) and *m*CPBA (800 mg, 2.3 equiv) was added. The mixture was refluxed for 6 h. After removal of the solvent, the residue was chromatographed over Sephadex LH-20 using $CHCl_3$-MeOH (1 : 1) for elution. The mixture was further purified by silica-gel column chromatography (PhH-AcOEt) to give 28-hydroxylupan-3-one (**8**, 200 mg), **9** (35 mg), **10** (20 mg), and **1** (200 mg).

28-Hydroxylupan-3-one (8): mp 210 °C; IR ($CHCl_3$): 3450, and 1700 cm^{-1}; ^1H NMR: δ=0.77 (3H, d, J=7 Hz), 0.84 (3H, d, J=7 Hz), 0.94, 0.97, 1.03, 1.07, 1.08 (each 3H, s), 2.55 (2H, m, H-2), 3.32 and 3.78 (each 1H, d, J=11 Hz, H-28); MS m/z: 442 (M^+), 411 (base), 205, and 191; HRMS, Found: m/z 442.3807, Calcd for $C_{30}H_{50}O_2$: M, 442.3811.

Methyl 3,28-Dihydroxy-3,4-seco-lupan-3-oate (9): mp 155—158 °C; IR ($CHCl_3$): 3450 and 1730 cm^{-1}; ^1H NMR: δ=0.77 (3H, d, J=7 Hz), 0.84 (3H, d, J=7 Hz), 0.95, 1.00, 1.05, 1.23, 1.28 (each 3H, s), 2.21 (1H, m, H-2), 2.45 (1H, m, H-2), 3.31 (1H, d, J=11 Hz, H-28), 3.67 (3H, s, -OMe), and 3.77 (1H, d, J=11 Hz, H-28); MS m/z: 472 ($M-H_2O$)$^+$, 441, 385, 373, 361, 191, and 109 (base); HRMS, Found: m/z 472.3902, Calcd for $C_{31}H_{52}O_2$: $M-H_2O$, 472.3916.

Methyl 28-Hydroxy-3,4-seco-lup-4(23)-en-3-oate (10): mp 122 °C (EtOAc); IR ($CHCl_3$): 3450, 1730, and 890 cm^{-1}; ^1H NMR: δ=0.77 (3H, d, J=7 Hz), 0.84 (3H, s), 0.87 (3H, d, J=7 Hz), 0.97 (3H, s), 1.07 (3H, s), 1.73 (3H, s, vinyl Me), 2.18 (1H, m, H-2), 2.33 (1H, m, H-2), 3.31 (1H, d, J=11 Hz, H-28), 3.66 (3H, s, -OMe), 3.77 (1H, d, J=11 Hz, H-28), and 4.65 and 4.85 (each 1H, s, C=CH_2); MS m/z: 472 (M^+), 441, 373, and 81 (base); HRMS, Found: m/z 472.3902, Calcd for $C_{31}H_{52}O_3$: M, 472.3916.

Method B: To a stirred solution of **1** (200 mg) in chloroform (12 ml) was added *m*CPBA (270 mg, 2.3 equiv). The mixture was refluxed for 6 h. More chloroform was added and the solution was washed successively with 5% Na_2SO_3 aq, 5% $NaHCO_3$ aq, and brine. The dried solution was evaporated in vacuo to give a residue (198 mg), which was separated by silica-gel column chromatography (PhH-EtOAc and PhH-Et_2O) to give **8** (60 mg), **1** (80 mg), and **11** (25 mg).

28-Hydroxy-3,4-seco-lupan-4,3-olide (11); mp 142 °C; IR ($CHCl_3$): 3450 and 1715 cm^{-1}; ^1H NMR: δ=0.77 (3H, d, J=7 Hz), 0.84 (3H, d, J=7 Hz), 0.96, 1.07, 1.08, 1.40, 1.48 (each 3H, s), 2.49 (1H, ddd, J=13, 6, and 3.5 Hz, H-2), 2.63 (1H, td, J=13 and 4 Hz, H-2), 3.32 and 3.77 (each 1H, d, J=11 Hz, H-28); MS m/z: 458 (M^+), 427, 369, 191, and 81 (base); HRMS, Found: m/z 458.3775, Calcd for $C_{30}H_{50}O_3$: M, 458.3760.

Methanolysis of Lactone 11. *m*-Chlorobenzoic acid (0.3 mg) was added to a solution of the lactone **11** (0.3 mg) in methanol (0.1 ml) and chloroform (2 drops) and the mixture stirred at rt for 1 h. TLC examination showed that there were three spots, one of which was **11**. Two new spots had the same R_f values (0.47 and 0.25: solvent system PhH-EtOAc (4:1)) as those of **10** and **9**, respectively.

Reaction of Lupan-3β-ol (2) with *m*CPBA. Lupan-3β-ol (**2**) (470 mg) was treated with *m*CPBA (250 mg, 2.2 equiv) in $CHCl_3$ (14 ml) under reflux for 6 h. After work up by method B, the solvent was evaporated to give a residue (253 mg), which was chromatographed over silica gel (EtOAc-PhH gradient as eluant) to give lupan-3-one **12** (30 mg),[8] **2** (110 mg) and **13** (4 mg). **3,4-Seco-lupan-4,3-olide (13);** mp 190 °C (EtOAc); IR: 1710 cm^{-1}; ^1H NMR: δ=0.75 (3H, d, J=7 Hz), 0.76 (3H, s), 0.84 (3H, d, J=7 Hz), 0.93, 1.08, 1.09, 1.40, 1.47 (each 3H, s), 2.49 (1H, ddd, J=14, 6.5, and 3.5 Hz, H-2),

2.63 (1H, td, J=14 and 4.5 Hz, H-2); MS m/z: 442 (M^+), 399, 369, 341, 291, 206, 191, and 81 (base); HRMS, Found: m/z 442.3792, Calcd for $C_{30}H_{50}O_2$: M, 442.3809.

Reaction of Friedelan-3β-ol (3) with *m*CPBA. Friedelan-3β-ol (**3**, 200 mg) was dissolved in $CHCl_3$ (20 ml) and *m*CPBA (260 mg, 2.2 equiv) was added. The mixture was refluxed for 12 h and worked up [procedure B] to give a residue (203 mg), which was chromatographed over silica gel using PhH-EtOAc and PhH-Et_2O solvent systems for elution to afford friedelin (**14**, 85 mg), 4-epi-friedelin (**15**, 8 mg), and lactone (**16**, 35 mg).

3,4-Seco-friedelan-4,3-olide (16); mp 273 °C (EtOAc); IR ($CHCl_3$): 1720 cm^{-1}; ^1H NMR: δ=0.83 (3H, s), 0.89 (3H, s), 0.95 (3H, s), 0.98 (3H, s), 0.99 (3H, s), 1.00 (3H, s), 1.17 (3H, s), 1.20 (3H, d, J=7 Hz), 2.52 (1H, t, J=13 Hz, H-2), 2.64 (1H, dd, J=13 and 6 Hz, H-2), and 4.21 (1H, q, J=7 Hz, H-4); MS m/z: 442 (M^+), 398, 205, and 95 (base); HRMS, Found: m/z 442.3815, Calcd for $C_{30}H_{50}O_2$: M, 442.3810.

Isomerization of 4-Epi-friedelin (15). 4-Epi-friedelin (**15**, 1.5 mg) was dissolved in 5% KOH-MeOH (5 ml) and the mixture was stirred at rt for 5 h. Work up as usual yielded friedelin (**14**, 1.0 mg).

Baeyer-Villiger Reaction of Friedelin (14). Friedelin (**14**, 50 mg) was treated with *m*CPBA (35 mg, 1.2 equiv) in $CHCl_3$ (60 ml) at rt for 2 days to afford the lactone **16** (40 mg) after chromatographic purification.

Acetylation of Diol 1. A solution of diol **1** (350 mg) in pyridine (15 ml) and acetic anhydride (2 ml) was stirred at 50° overnight. The mixture was worked up as usual to yield diacetate **4** (365 mg).

Reaction of Lupane-3β,28-diyl Diacetate (4) with *m*CPBA. *m*CPBA (168 mg, 1.2 equiv) was added to a solution of diacetate **4** (270 mg) in $CHCl_3$ (16 ml) in one portion and the mixture was refluxed for 6 h. The reaction mixture was worked up by method A to give a residue (273 mg). The mixture was purified by silica-gel column chromatography (PhH-Et_2O) to give **4** (235 mg) and 19β-hydroxylupane-3β,28-diyl diacetate (**17**) (30 mg).[11]

Reaction of Lupan-3β-yl Acetate (5) with *m*CPBA. Lupan-3β-yl acetate (**5**, 470 mg) was treated with *m*CPBA (280 mg, 1.2 equiv) in $CHCl_3$ (25 ml) under reflux for 12 h to afford a residue (490 mg) after work up by method A. The residue was subjected to column chromatography over silica gel. Elution with hexane-EtOAc solvent system afforded **5** (375 mg), **18** (20 mg), and **19** (5 mg).[12,13]

13β-Hydroxylupan-3β-yl Acetate (18); mp 250 °C; IR ($CHCl_3$): 3500 and 1720 cm^{-1}; ^1H NMR: δ=0.84 (3H, s), 0.85 (3H, s), 0.86 (3H, d, J=7 Hz), 0.87 (3H, s), 0.93 (3H, d, J=7 Hz), 0.96 (3H, s), 1.02 (3H, s), 1.07 (3H, s), 2.04 (3H, s, Ac), 4.48 (1H, dd, J=12 and 4.5 Hz, H-3α); ^{13}C NMR: δ=14.6 (q), 16.1 (q×2), 16.5 (q), 17.4 (q), 18.3 (t), 18.7 (q), 19.2 (q), 20.8 (t), 21.3 (q), 23.7 (t), 25.8 (t), 27.3 (t), 28.0 (q), 34.1 (t), 34.4 (t), 34.5 (d), 37.1 (t), 37.1 (d), 37.1 (s), 37.8 (s), 38.4 (t), 40.4 (t), 41.1 (s), 42.9 (s), 43.3 (s), 49.5 (d), 50.1 (d), 55.4 (d), 81.0 (d, H-3), 85.8 (s, H-13), and 171.0 (s, Ac); MS m/z: 486 (M^+), 426, 383, 365, 189, and 43 (base); HRMS, Found: m/z 486.4051, Calcd for $C_{32}H_{54}O_3$: M, 486.4073.

Dehydration of 18. The alcohol **18** (10 mg) was treated with $POCl_3$ (4 drops) in pyridine (3 ml) at 90 ° for 1 h. The usual work up and prep. TLC gave lup-12-en-3β-yl acetate (**20**, 6 mg).[12,13]

Oxidation of the Alcohol 19. To a stirred solution of **19** (3 mg) in acetone (1.5 ml) was added Jones reagent (3 drops) at rt. The mixture was stirred for 1 h and usual work up afforded 16-oxolupan-3β-yl acetate (**21**, 1.5 mg).[13]

Reaction of Friedelan-3β-yl Acetate (6) with *m*CPBA. Friedelan-3β-yl acetate (**6**, 100 mg) was treated with *m*CPBA (60 mg, 1.2 equiv) in $CHCl_3$ (10 ml) under reflux for 12 h. Work up by method B afforded a residue (104 mg), which was subjected to column chromatography over silica gel (hexane-Et_2O as eluant) and HPLC (μ-PORASIL, hexane-Et_2O 9:1, 2 ml min^{-1}) to give **6** (85 mg) and the ketone **22** (2 mg).

15-Oxofriedelan-3β-yl Acetate (22); mp 245 °C; IR ($CHCl_3$): 1730 and 1695 cm^{-1}; ^1H NMR: δ=0.82 (3H, d, J=7 Hz), 0.88, 0.89, 0.95, 1.01, 1.21, 1.32 (each 3H, s), 2.04 (3H, s, Ac), 2.16 and 2.50 (each 1H, d, J=18 Hz, H-16), and 4.89 (1H, m, H-3α).

Friedelane-3,15-dione (23). To a solution of 15-oxofriedelan-3β-yl acetate (**22**, 1 mg) in MeOH (0.5 ml) was added 5% KOH-MeOH (5 drops) and the mixture was stirred at 75 °C for 10 h. The reaction mixture was worked up as usual and chromatographed on silica gel (hexane-EtOAc) to give 3β-hydroxyfriedelan-15-one (0.5 mg). The alcohol in acetone (0.2 ml) was oxidized with Jones reagent (2 drops) at rt for 1 h to afford friedelane-3,15-dione (**23**, 0.3 mg).[7]

Reaction of Dendropanoxide (7) with *m*CPBA. To a stirred solution of dendropanoxide (**7**) (1.6 g) in chloroform (70 ml) was added *m*CPBA (0.98 g) and the mixture was refluxed for 12 h. More chloroform was added and the mixture was worked up by method B to give a residue (2.5 g), which was purified by silica-gel column chromatography (PhH-EtOAc, gradient), prep. TLC, and HPLC (Finepak SIL, hexane-EtOAc, gradient) to afford **24** (27 mg, 1.6%), **25** (17 mg, 1%), **26** (7 mg, 0.4%), **27** (3 mg, 0.2%), and **28** (4 mg, 0.3%) as well as **7**.

6α-Hydroxydendropanoxide (24); IR ($CHCl_3$): 3400 cm^{-1}; ^1H NMR: δ=0.95, 0.97, 0.99, 1.09, 1.10, 1.14, 1.14, and 1.17 (each 3H, s, Me), 3.76 (1H, d, J=5.8 Hz, H-3α), and 4.10 (1H, dt, J=11.8 and 7 Hz, H-6β); MS m/z: 442 (M^+), 427; HRMS, Found: m/z 442.3794, Calcd for $C_{30}H_{50}O_2$: M, 442.3811.

7α-Hydroxydendropanoxide (25); IR ($CHCl_3$): 3400 cm^{-1}; ^1H NMR: δ=0.90, 0.96, 0.96, 1.05, 1.05, 1.14, 1.19, and 1.19 (each 3H, s, Me), 3.77 (1H, d, J=5.6 Hz, H-3α), and 4.19 (1H, brt, J=5 Hz, H-7β); MS m/z: 442 (M^+), 427; HRMS, Found: m/z 442.3803, Calcd for $C_{30}H_{50}O_2$: M, 442.3811.

21α-Hydroxydendropanoxide (26); IR ($CHCl_3$): 3400 cm^{-1}; ^1H NMR: δ=0.90, 0.98, 1.01, 1.04, 1.04, 1.06, 1.15, and 1.19 (each 3H, s), 3.70 (1H, dd, J=12 and 4 Hz, H-21β), and 3.76 (1H, d, J=5.6 Hz, H-3α); MS m/z: 442 (M^+), 427; HRMS, Found: m/z 442.3794, Calcd for $C_{30}H_{50}O_2$: M, 442.3810.

22β-Hydroxydendropanoxide (27); IR ($CHCl_3$): 3400 cm^{-1}; ^1H NMR: δ= 0.90, 0.99, 1.01, 1.01, 1.03, 1.13, 1.18, and 1.21 (each 3H, s), 3.67 (1H, dd, J=12 and 5.6 Hz, H-22α), and 3.75 (1H, d, J=5.7 Hz, H-3α); MS m/z: 442 (M^+), 427; HRMS: Found: m/z 442.3816, Calcd for $C_{30}H_{50}O_2$: M, 442.3811.

15-Oxodendropanoxide (28); IR ($CHCl_3$): 1690 cm^{-1}; ^1H NMR: δ=0.86, 0.91, 0.96, 1.02, 1.02, 1.19, 1.31, and 1.38 (each 3H, s, Me), 2.17 and 2.44 (each 1H, d, J=17 Hz, H_2-16), and 3.76 (1H, d, J=5 Hz, H-3α); MS m/z 440 (M^+) and 221; HRMS, Found: m/z 440.3644, Calcd for $C_{30}H_{48}O_2$: M, 440.3655, Found: m/z 221.1893, Calcd for $C_{15}H_{25}O$: M, 221.1905.

Oxidation of 21α-Hydroxydendropanoxide (26). 21α-Hydroxydendropanoxide (**26**, 2 mg) was treated with Jones reagent (1 drop) in acetone (2 ml) at rt for 15 min. Work up as usual gave 21-oxodendropanoxide (**29**, 1.5 mg); ^1H NMR:

δ=3.77 (1H, d, J=5.6 Hz), 1.80 and 2.62 (each 1H, d, J=12.4 Hz); MS m/z: 440 (M^+); HRMS, Found: m/z 440.3649, Calcd for $C_{30}H_{48}O_2$: M, 440.3654.

Oxidation of 22β-Hydroxydendropanoxide (27). 22β-Hydroxydendropanoxide (**27**, 2 mg) was oxidized with Jones reagent (1 drop) in acetone (2 ml) at rt for 15 min. Work up as usual afforded 22-oxodendropanoxide (**30**, 1 mg); ^{1}H NMR: δ=3.75 (1H, d, J=5.4 Hz), 2.55 and 2.16 (each 1H, d, J=17 HZ); MS m/z: 440 (M^+); HRMS, Found: m/z 440.3659, Calcd for $C_{30}H_{48}O_2$: M, 440.3654.

We thank Professors Takeyoshi Takahashi and Takahiko Tsuyuki, The University of Tokyo, for their generous gift of betulin and friedelin used in this work and the spectra of authentic friedelane-3,15-dione. This work was supported in part by a Grant-in-Aid for Cancer Research from the Ministry of Health and Welfare.

References

1) A part of this work was published in a preliminary form: M. Tori, R. Matsuda, and Y. Asakawa, *Chem. Lett.*, **1985**, 167.

2) Y. Asakawa, R. Matsuda, and M. Tori, *Experientia*, **42**, 201 (1986).

3) M. Tori, R. Matsuda, and Y. Asakawa, *Bull. Chem. Soc. Jpn.*, **58**, 2523 (1985).

4) a) M. Tori, R. Matsuda, and Y. Asakawa, *Tetrahedron Lett.*, **26**, 227 (1985); b) *idem*, *Tetrahedron*, **42**, 1275 (1986).

5) M. Tori, M. Sono, and Y. Asakawa, *Bull. Chem. Soc. Jpn.*, **58**, 2669 (1985).

6) Y. Mazur, *Pure Appl. Chem.*, **41**, 145 (1975).

7) E. Akiyama, M. Tada, T. Tsuyuki, and T. Takahashi, *Chem. Lett.*, **1978**, 305; *idem*, *Bull. Chem. Soc. Jpn.*, **52**, 164 (1979).

8) I. M. Heilbron, T. Kennedy, and F. S. Spring, *J. Chem. Soc.*, **1938**, 329.

9) R. Aoyagi, S. Yamada, T. Tsuyuki, and T. Takahashi, *Bull. Chem. Soc. Jpn.*, **46**, 959 (1973).

10) S. K. Talapatra, S. Bhattacharya, and B. Palapatra, *J. Indian Chem. Soc.*, **47**, 600 (1970).

11) E. Suokas and T. Hase, *Acta Chem. Scand., Ser. B*, **32**, 623 (1978).

12) J. Protiva, F. Tureček, and Vystrčil, *Collect. Czech. Chem. Commun.*, **42**, 140 (1977).

13) G. V. Baddeley, A. J. Bealing, P. R. Jefferies, and R. W. Retallack, *Aust. J. Chem.*, **17**, 908 (1964).

14) K. Kimura, Y. Hashimoto, and I. Agata, *Chem. Pharm. Bull.*, **8**, 1145 (1960); J. H. Block and G. H. Constantine, Jr., *Phytochemistry*, **11**, 3279 (1972) and references cited therein.

15) M. Tori, R. Matsuda, M. Sono, and Y. Asakawa, *Magn. Reson. Chem.*, **26** (1988) in press.

A Novel Synthesis of 2-Acyl Cyclic Ethers and 3-Keto Cyclic Ethers Including Spiro Cyclic Ethers via Intramolecular Ring-Opening of α,β-Epoxy Sulfoxides with Hydroxyl Group[1)]

Tsuyoshi SATOH, Ken-ichi IWAMOTO, Atsushi SUGIMOTO, and Koji YAMAKAWA*
Faculty of Pharmaceutical Sciences, Science University of Tokyo, Ichigaya-funagawara-machi, Shinjuku-ku, Tokyo 162
(Received December 26, 1987)

The α,β-epoxy sulfoxides **1** and **2** bearing a ω-oxyalkyl group were synthesized from ω-oxyalkyl carbonyl compounds and 1-chloroalkyl phenyl sulfoxide. The intramolecular ring opening of the oxirane ring of these α,β-epoxy sulfoxides, through an attack of the terminal hydroxyl group, gave 2-acyl cyclic ethers or 3-keto cyclic ethers, including spiro-type cyclic ethers. This procedure is applicable to the preparation of five- and six-membered cyclic ethers.

The intramolecular ring opening of an oxirane ring[2)] with a hydroxyl group is a quite useful method for constructing cyclic ether systems which are found in many natural products having remarkable biological activity, e.g., polyether antibiotics.[3)] However, the compounds containing an epoxy group is usually synthesized from olefins by an epoxidation with several oxidizing agents. In other words, in the step of constructing epoxy groups, carbon-carbon bond formation reactions were rarely used.

Recently, we have reported a new synthetic method for the preparation of α-substituted carbonyl compounds from carbonyl compounds with carbon homologation through α,β-epoxy sulfoxides.[4)] In our papers we reported that the β-position of α,β-epoxy sulfoxides was quite reactive toward many kinds of nucleophiles, such as selenolate,[4a)] thiolates[4b)] and amines,[4c)] giving α-substituted carbonyl compounds in very good yields. With these results in hand, it was anticipated that the intramolecular version of this reaction would be quite promising for constructing heterocyclic compounds having a carbonyl group. In this paper, as a continuation of our studies on the development of new synthetic methods using α,β-epoxy sulfoxides, we report a novel method for the synthesis of 2-acyl cyclic ethers **3** and 3-keto cyclic ethers including spirocyclic 3-keto ethers **4**, both from carbonyl compounds and 1-chloroalkyl phenyl sulfoxides via α,β-epoxy sulfoxides. The whole sequence is shown in Scheme 1.

Results and Discussion

A Synthesis of 2-Acyl Cyclic Ethers. In a previous paper[4d)] we reported that the intermolecular reaction of the α,β-epoxy sulfoxides with alcohols did not work well; however, an intramolecular version of this reaction was thought to be possible since the rate of the intramolecular reaction was usually much faster than that of intermolecular reaction.

First, the α,β-epoxy sulfoxide **1d** was synthesized from 1-chloro-2-phenylethyl phenyl sulfoxide and aldehyde **6** (n=4)[6)] via chlorohydrins[4)] in over 85% yield. The treatment of **1d** with 0.2 equivalents of pyridinium p-toluenesulfonate (PPTS)[7)] in refluxing ethanol afforded deprotected alcohol within ten minutes; then an intramolecular ring opening of the epoxide group by the resulting alcohol took place slowly with a liberation of benzenesulfenic acid to give 2-acyltetrahydropyran **13** in 86% yield after heating for 6 h. The reaction time could be shortened to 2.5 h in refluxing 1-propanol. In this reaction PPTS was essential; upon heating the isolated intermediate alcohol in refluxing ethanol without PPTS, only a very

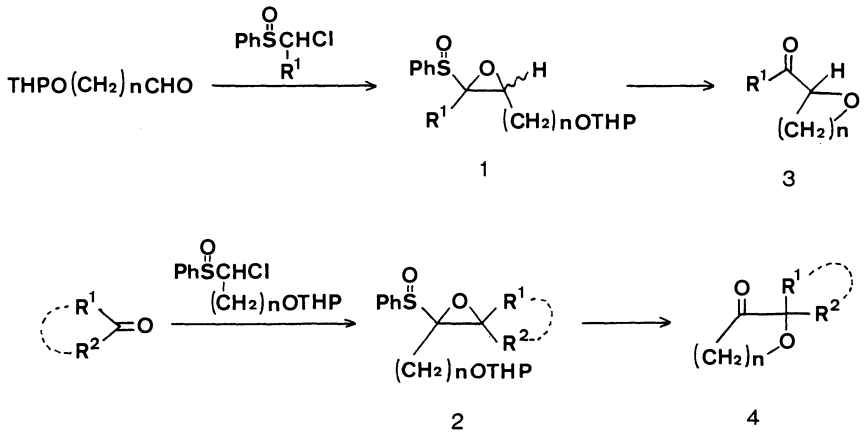

Scheme 1.

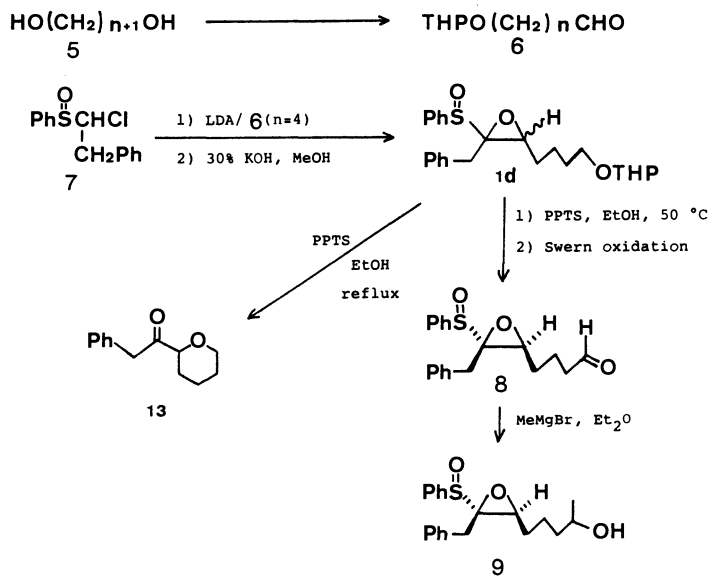

Scheme 2.

Table 1. Preparation of 2-Acyl Cyclic Ethers from α,β-Epoxy Sulfoxides

Entry	α,β-Epoxy sulfoxide			Condition[a]		Product		Yield[b]
	R^1	n		Solvent	Time			%
1	$PhCH_2$	1	**1a**	*n*-PrOH	5 h	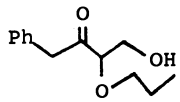	**10**	70
2	$PhCH_2$	3	**1b**	EtOH (50 °C)	30 min	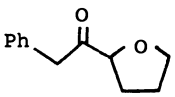	**11**	90
3		3	**1c**	EtOH	5 h	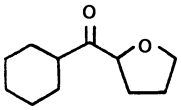	**12**	87
4	$PhCH_2$	4	**1d**	EtOH *n*-PrOH	6 h 2.5 h	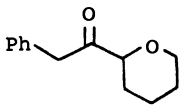	**13**	86 85
5	$PhCH_2$	4	**9**	*n*-PrOH	4.5 h	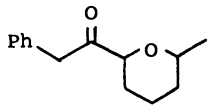	**14**[c]	81
6		4	**1e**	*n*-PrOH	5 h	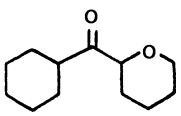	**15**	85
7	$PhCH_2$	5	**1f**	*n*-PrOH	2 d	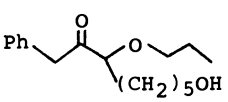	**16**	46
8	$PhCH_2$	11	**1g**	*n*-PrOH	2 d	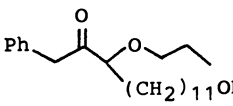	**17**[8]	77

a) Unless otherwise noted the reaction was carried out in refluxing solvent. b) Isolated yield after silica-gel column chromatography. c) Single isomer.

slow reaction was observed. Encouraged by this result, some kinds of α,β-epoxy sulfoxides **1** were allowed to react under the conditions described above. The results are summarized in Table 1. These α,β-epoxy sulfoxides **1** were synthesized from **7** or 1-chloro-1-cyclohexylmethyl phenyl sulfoxide and the aldehyde **6**. The α,β-epoxy sulfoxide **9** was conveniently synthesized from **1d** through the aldehyde **8**, as shown in

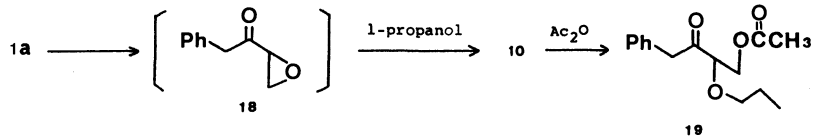

Scheme 3.

Table 2. Preparation of 3-Keto Cyclic Ethers from α,β-Epoxy Sulfoxides

Entry	α,β-Epoxy sulfoxide **2**		Additive (equiv)	Condition[a]		Product		Yield[b]
				Solvent	Time			%
1	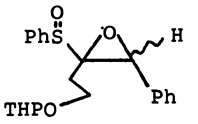	**2a**	PPTS (0.1)	EtOH	2 d	—[c]		—
				n-PrOH	11 h	—[c]		—
2	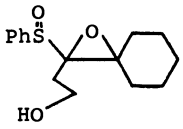	**2b**	$MgCl_2$ (1)	*i*-PrOH	29 h	—[c]		—
3	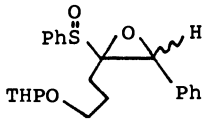	**2c**	PPTS (0.1)	EtOH	17 h	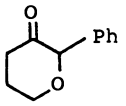	**20**	60
				n-PrOH	4 h			57
4	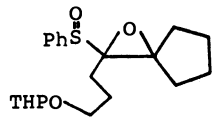	**2d**	PPTS (0.1)	MeOH	1 h	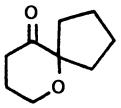	**21**	77
5	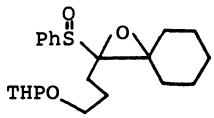	**2e**	PPTS (0.1)	*n*-PrOH	1 h	—[c]		—
6	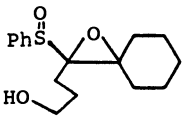	**2f**	$MgCl_2$ (1)	*i*-PrOH	13 h	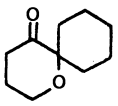	**22**	74
7	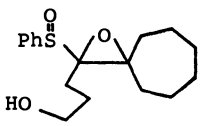	**2g**	$MgCl_2$ (1)	*i*-PrOH	4 h	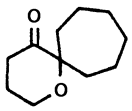	**23**	73
8	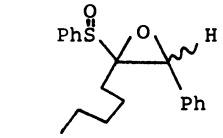	**2h**	PPTS (0.1)	*n*-PrOH	3 d	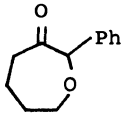	**24**	11
9	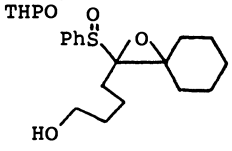	**2i**	$MgCl_2$ (1)	*i*-PrOH	29 h	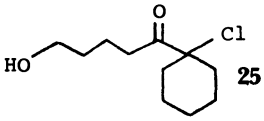	**25**	26

a) All reactions were carried out in refluxing solvent. b) Isolated yield after silica-gel column chromatography. c) A complex mixture.

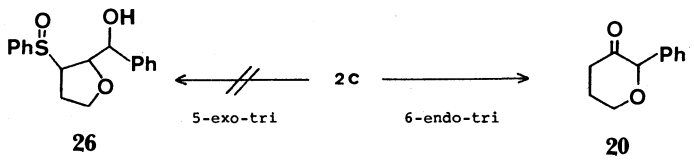

26 20

Scheme 4.

Scheme 2.

The product **10** of the reaction in entry 1 was thought to be produced from the expected cyclic ether **18** with 1-propanol. The structure of **10** was determined by the NMR spectrum of the corresponding acetate **19**. Entries 2—6 show that this method is quite promising for constructing five- and six-membered cyclic ethers. Even secondary alcohol **9** reacted well to afford cyclic ether **14**. Entries 7 and 8 show that the limitation of this procedure lies between the formation of six- and seven-membered cyclic ether. The α,β-epoxy sulfoxides **1f** and **1g** upon heating in refluxing 1-propanol with PPTS gave the products quite slowly; however, the products were not the desired cyclic ethers but, rather, alcohols **16** and **17**.[8] In these cases, **1f** and **1g** gave only deprotected alcohols and no trace of cyclic ethers, even though 2-butanol (the secondary alcohol having higher boiling point than 2-propanol) was used as the solvent.

A Synthesis of 3-Keto Cyclic Ethers. Next, endo-type ring opening of the oxirane ring of the α,β-epoxy sulfoxides **2** was investigated. First of all the α,β-epoxy sulfoxides **2c** and **2e** (see Table 2) were synthesized from 1-chloro-4-(tetrahydropyranyloxy)butyl phenyl sulfoxide[9] and benzaldehyde or cyclohexanone according to the procedure shown in Scheme 1. Heating of this α,β-epoxy sulfoxide **2c** in refluxing ethanol in the presence of 0.1 equivalents of PPTS quickly gave the deprotected alcohol; however, the cyclization was quite sluggish, giving the desired 3-oxo-2-phenyltetrahydropyran in 60% yield after 17 h. It is interesting to note that this endo-type reaction was much slower than that of exo-type (compare with entry 4 in Table 1). Another important characteristic of this reaction was that **2c** only gave a 6-endo-trigonal[10] type product **20** and no trace of the 5-exo-trigonal[10] type product **26**. This result is inconsistent with our finding that the β-position of α,β-epoxy sulfoxides is much more reactive than the α-position.

In contrast to this result, heating the α,β-epoxy sulfoxide **2e** in ethanol or 1-propanol with PPTS gave a complex mixture very quickly. Recently, we reported[11] that magnesium in primary alcohol was quite effective in promoting the ring opening of α,β-epoxy sulfoxides giving α-alkoxy ketones. The result was applied to this intramolecular ring opening of the epoxy group of **2e**. The tetrahydropyranyl group of **2e** was deprotected to afford the alcohol **2f**. Heating of **2f** in refluxing 2-propanol in the presence of one equivalent of magnesium chloride for 13 h gave the desired spirocyclic β-keto ether **22** in 74% yield. The results of this reaction are summarized in Table 2.

Entries 1 and 2 indicate that the 5-endo-trigonal ring closure is quite difficult, as reported by Baldwin.[10] The result in entry 4 is notable. The α,β-epoxy sulfoxide **2d** gave spirocyclic ether **21** in 77% yield in refluxing methanol for 1 h. This remarkable reactivity of **2d** may be attributable to the highly strained nature of the spiro-cyclic structure of **2d**. Entries 8 and 9 indicate that the limitation of this procedure again lies between the formation of six- and seven-membered cyclic ethers.

In conclusion, because of the total simplicity of the reaction this procedure contributes to the synthesis of five- and six-membered cyclic ethers having ketone group.

Experimental

All melting points are uncorrected. The IR spectra were measured directly on a NaCl plate or KBr disks with a Hitachi 215 spectrometer. ^{1}H NMR spectra were measured in a $CDCl_3$ solution with a JEOL FX-100 spectrometer or Hitachi R-24B spectrometer using Me_4Si as an internal standard. Electron-impact mass spectra (MS) were obtained on a Hitachi M-80 double-focusing spectrometer at 70 eV by direct insertion. Silica gel BW-127 ZH (Fuji-Devison) containing a 2% fluoresence reagent (254) and a quartz column were used for column chromatography; products showing ultraviolet (UV) absorption were detected by UV irradiation.

α,β-Epoxy Sulfoxides. All α,β-epoxy sulfoxides, **1** and **2**, except **8** and **9** used in this study were prepared from carbonyl compounds and 1-chloroalkyl phenyl sulfoxides through chlorohydrins in nearly quantitative yields, which were reported previously.[4]

α,β-Epoxy Sulfoxide 1a: *Z*-Isomer, colorless oil, IR (neat) 1090, 1050, 1035, and 1025 (SO) cm^{-1}; ^{1}H NMR δ=1.3—1.8 (6H, m), 2.61, 3.51 (each 1H, d, J=16 Hz), 2.91 (1H, dd, J=4, 5 Hz), 3.4—4.3 (4H, m), 4.61 (1H, bs), and 6.8—7.8 (10H, m). *E*-Isomer, colorless oil, IR (neat) 1090, 1080, 1060, and 1035 (SO) cm^{-1}; ^{1}H NMR δ=1.3—1.8 (6H, m), 3.0—4.1 (7H, m), 4.55 (1H, bs), and 7.0—7.7 (10H, m).

α,β-Epoxy Sulfoxide 1b: *E*-Isomer, colorless oil, IR (neat) 1095, 1080, 1060, and 1040 (SO) cm^{-1}; ^{1}H NMR δ=1.1—2.0 (10H, m), 3.07 (2H, s), 3.1—4.0 (5H, m), 4.50 (1H, bs), 7.18, and 7.53 (each 5H, m). *Z*-Isomer, colorless oil, IR (neat) 1090, 1055, 1040, and 1030 (SO) cm^{-1}; ^{1}H NMR δ=1.2—2.2 (10H, m), 2.54 (1H, d, J=15 Hz), 2.73 (1H, t, J=5 Hz), 3.1—4.1 (4H, m), 3.58 (1H, d, J=15 Hz), 4.56 (1H, bs), and 6.8—7.9 (10H, m).

α,β-Epoxy Sulfoxide 1c: Less polar isomer, colorless oil, IR (neat) 1090, 1055, 1040, and 1030 (SO) cm^{-1}; ^{1}H NMR δ=0.3—2.4 (21H, m), 3.2—4.0 (5H, m), 4.62 (1H, bs), and

7.3—7.8 (10H, m). More polar isomer, colorless oil, IR (neat) 1090, 1080, 1060, 1040, and 1030 (SO) cm^{-1}; ^1H NMR δ=0.6—2.1 (21H, m), 3.2—4.0 (5H, m), 4.55 (1H, bs), and 7.4—7.8 (10H, m).

α,β-Epoxy Sulfoxide 1d: *E*-Isomer, colorless oil, IR (neat) 1095, 1080, 1060, 1040, and 1030 (SO) cm^{-1}; ^1H NMR δ=1.1—2.0 (12H, m), 3.01, 3.05 (each 1H, d, J=16 Hz), 3.1—4.0 (5H, m), 4.52 (1H, bs), and 6.9—7.7 (10H, m). *Z*-Isomer, colorless oil, IR (neat) 1090, 1060, 1040, and 1030 (SO) cm^{-1}; ^1H NMR δ=1.2—1.8 (10H, m), 2.01 (2H, m), 2.53, 3.54 (each 1H, d, J=15 Hz), 2.64 (1H, t, J=7 Hz), 3.2—4.0 (4H, m), 4.53 (1H, bs), and 6.8—7.8 (10H, m).

α,β-Epoxy Sulfoxide 9: A solution of 389 mg of **1d** (*E*-isomer) and PPTS (24 mg) in 20 ml of EtOH was heated at 50 °C for 4 h. The EtOH was evaporated to give a residue, which was dissolved in ether-benzene. The solution was washed once with half-saturated brine and dried over Na_2SO_4. The product was purified by silica-gel column chromatography to give 276 mg (90%) of deprotected alcohol as a colorless oil. IR (neat) 3430 (OH), 1095, and 1060 (SO) cm^{-1}; ^1H NMR δ=1.3—1.7 (6H, m), 3.01, 3.08 (each 1H, d, J=16 Hz), 3.4—3.8 (3H, m), and 6.9—7.7 (10H, m).

A solution of oxalyl dichloride (80 μl) in 3 ml of dry CH_2Cl_2 in a dry flask was cooled to −50 °C. DMSO (142 mg in 0.5 ml of CH_2Cl_2) was added to the solution dropwise with stirring and the mixture was stirred at −50 °C for 2 min. To this was added the alcohol (250 mg in 1 ml of CH_2Cl_2). The reaction mixture was stirred at −50 °C for 15 min; then, triethylamine (0.53 ml) was added. The reaction mixture was stirred and allowed to warm to 0 °C. The reaction was quenched by adding 10 ml of water and the whole was extracted with CH_2Cl_2. The product was purified by silica-gel column chromatography to afford 190 mg (77%) of the aldehyde **8** as a colorless oil. IR (neat) 2750 (CHO), 1730 (CO), 1095, and 1060 (SO) cm^{-1}; ^1H NMR δ=1.4—2.1 (4H, m), 2.2—2.6 (2H, m), 2.99, 3.08 (each 1H, d, J=16 Hz), 3.69 (1H, t, J=6 Hz), 7.0—7.8 (10H, m), and 9.66 (1H, t, J=1.5 Hz).

MeMgBr (1.1 equiv) was added dropwide to a solution of the aldehyde (**8**; 156 mg) in 7 ml of dry ether at −60 °C. The reaction mixture was stirred for 10 min; then, the reaction was quenched by satd. aq. NH_4Cl. The whole mixture was extracted with ether-benzene and the product was purified by silica-gel column chromatography to afford 142 mg (87%) of the alcohol **9** as a colorless oil. IR (neat) 3440 (OH), 1090, and 1060 (SO) cm^{-1}; ^1H NMR δ=1.14 (3H, d, J=6 Hz), 1.2—1.8 (6H, m), 2.97, 3.03 (each 1H, d, J=16 Hz), 3.4—3.9 (2H, m), and 6.9—7.7 (10H, m).

α,β-Epoxy Sulfoxide 1e: Less polar isomer, colorless oil, IR (neat) 1090, 1055, 1040, and 1030 (SO) cm^{-1}; ^1H NMR δ=0.5—2.5 (23H, m), 3.26 (1H, t, J=6 Hz), 3.2—4.0 (4H, m), 4.57 (1H, bs), and 7.3—7.8 (5H, m). More polar isomer, colorless oil, IR (neat) 1090, 1055, 1040, and 1030 (SO) cm^{-1}; ^1H NMR δ=0.6—2.0 (23H, m), 3.2—4.0 (5H, m), 4.54 (1H, bs), and 7.3—7.8 (5H, m).

α,β-Epoxy Sulfoxide 1f: *E*-Isomer, colorless oil, IR (neat) 1095, 1085, 1065, 1040, and 1030 (SO) cm^{-1}; ^1H NMR δ=1.0—1.9 (14H, m), 3.00, 3.06 (each 1H, d, J=16 Hz), 3.1—4.0 (5H, m), 4.53 (1H, bs), and 7.0—7.7 (10H, m). *Z*-Isomer, colorless oil, IR (neat) 1090, 1060, 1045, and 1030 (SO) cm^{-1}; ^1H NMR δ=1.1—2.1 (14H, m), 2.52 (1H, d, J=16 Hz), 2.63 (1H, t, J=6 Hz), 3.55 (1H, d, J=16 Hz), 3.2—4.0 (4H, m), 4.54 (1H, bs), and 6.8—7.8 (10H, m).

α,β-Epoxy Sulfoxide 1g: *E*-Isomer, colorless oil, IR (neat) 1090, 1080, 1055, 1045, and 1025 (SO) cm^{-1}; ^1H NMR δ=1.0—1.9 (26H, m), 3.00, 3.05 (each 1H, d, J=16 Hz), 3.1—4.0 (5H, m), 4.55 (1H, bs), and 6.9—7.7 (10H, m). *Z*-Isomer, colorless oil, IR (neat) 1090, 1085, 1055, 1040, and 1030 (SO) cm^{-1}; ^1H NMR δ=1.0—2.1 (26H, m), 2.52 (1H, d, J=15 Hz), 2.61 (1H, t, J=6 Hz), 3.53 (1H, d, J=15 Hz), 3.2—4.0 (4H, m), 4.54 (1H, bs), and 6.8—7.8 (10H, m).

α,β-Epoxy Sulfoxide 2a: *E*-Isomer, colorless oil, IR (neat) 1090, 1060, 1040, and 1030 (SO) cm^{-1}; ^1H NMR δ=1.2—2.1 (8H, m), 3.2—4.0 (4H, m), 4.54 (1H, bs), 4.97 (1H, s), and 7.0—7.9 (10H, m). *Z*-Isomer, colorless oil, IR (neat) 1090, 1080, 1055, and 1040 (SO) cm^{-1}; ^1H NMR δ=1.3—2.0 (7H, m), 2.4—2.9 (1H, m), 3.2—4.0 (4H, m), 4.64, 4.71 (each singlet), and 7.2—7.8 (10H, m).

α,β-Epoxy Sulfoxide 2b: Colorless crystals, mp 59—61 °C (AcOEt-hexane), IR (KBr) 3410 (OH), 1090, 1050, and 1035 (SO) cm^{-1}; ^1H NMR δ=1.3—2.4 (12H, m), 3.2—4.0 (3H, m), and 7.4—7.8 (5H, m); Found: C, 64.25; H, 7.29; S, 11.50%. Calcd for $C_{15}H_{20}O_3S$: C, 64.26; H, 7.19; S, 11.44%.

α,β-Epoxy Sulfoxide 2c: *E*-Isomer, colorless oil, IR (neat) 1095, 1085, 1065, 1045, and 1030 (SO) cm^{-1}; ^1H NMR δ=1.1—1.9 (10H, m), 2.9—3.9 (5H, m), 4.39 (1H, bs), 4.81 (1H, s), and 7.0—7.9 (10H, m). *Z*-Isomer, colorless oil, IR (neat) 1095, 1080, 1055, 1040, and 1030 (SO) cm^{-1}; ^1H NMR δ=1.1—2.0 (9H, m), 2.1—2.5 (1H, m), 3.0—3.9 (4H, m), 4.25 (1H, s), 4.28 (1H, bs), and 7.2—7.8 (10H, m).

α,β-Epoxy Sulfoxide 2d: Colorless oil, IR (neat) 1090, 1080, 1055, 1040, and 1030 (SO) cm^{-1}; ^1H NMR δ=0.6—1.2 (1H, m), 1.2—2.2 (16H, m), 2.3—2.8 (1H, m), 2.9—3.24 (1H, m), 3.24—3.56 (2H, m), 3.56—3.90 (1H, m), 4.40 (1H, bs), and 7.3—7.8 (5H, m).

α,β-Epoxy Sulfoxide 2e: Colorless oil, IR (neat) 1095, 1055, 1040, and 1030 (SO) cm^{-1}; ^1H NMR δ=0.5—1.1 (1H, m), 1.1—2.3 (19H, m), 2.8—4.0 (4H, m), 4.35 (1H, bs), and 7.3—7.9 (5H, m).

α,β-Epoxy Sulfoxide 2f: Colorless crystals, mp 90.5—92 °C (AcOEt-hexane), IR (KBr) 3460 (OH), 1090, 1050, 1040, and 1030 (SO) cm^{-1}; ^1H NMR δ=0.7—1.2 (1H, m), 1.2—2.3 (13H, m), 3.37 (2H, t, J=6 Hz), and 7.3—7.8 (5H, m); Found: C, 65.20; H, 7.59; S, 11.08%. Calcd for $C_{16}H_{22}O_3S$: C, 65.27; H, 7.53; S, 10.89%.

α,β-Epoxy Sulfoxide 2g: Colorless crystals, mp 80.5—82.5 °C (AcOEt-hexane), IR (KBr) 3470 (OH), 1085, 1070, 1035, and 1025 (SO) cm^{-1}; ^1H NMR δ=1.0—2.1 (14H, m), 2.1—2.5 (2H, m), 3.35 (2H, t, J=6 Hz), and 7.3—7.8 (5H, m); Found: C, 66.11; H, 7.77; S, 10.48%. Calcd for $C_{17}H_{24}O_3S$: C, 66.20; H, 7.84; S, 10.40%.

α,β-Epoxy Sulfoxide 2h: *E*-Isomer, colorless oil, IR (neat) 1090, 1080, 1060, 1040, and 1030 (SO) cm^{-1}; ^1H NMR δ=1.0—2.0 (11H, m), 2.1—2.7 (1H, m), 3.0—3.9 (4H, m), 4.44 (1H, bs), 4.78 (1H, s), and 7.0—7.8 (10H, m). *Z*-Isomer, colorless oil, IR (neat) 1090, 1080, 1055, 1040, and 1030 (SO) cm^{-1}; ^1H NMR δ=1.1—1.9 (11H, m), 2.0—2.5 (1H, m), 3.0—4.0 (4H, m), 4.44 (1H, s), 4.48 (1H, bs), and 7.2—7.8 (10H, m).

α,β-Epoxy Sulfoxide 2i: Colorless oil, IR (neat) 3450 (OH), 1085, and 1050 (SO) cm^{-1}; ^1H NMR δ=0.4—0.8 (1H, m), 1.0—2.3 (15H, m), 3.41 (2H, t, J=6 Hz), and 7.4—7.8 (5H, m).

General Procedure for the Preparation of 2-Acyl Cyclic Ethers and 3-Keto Cyclic Ethers from α,β-Epoxy Sulfoxides by PPTS-Induced Opening of the Oxiran Ring: The synthesis of 2-(1-oxo-2-phenylethyl)tetrahydrofuran (**11**) from

1b is described. To a solution of **1b** (96 mg) in 2 ml of EtOH was added PPTS (0.1 equiv) and the reaction mixture was stirred and heated at 50 °C for 30 min. The EtOH was evaporated under vacuum and the residue was dissolved in benzene. The solution was washed with satd. brine and dried over Na_2SO_4. The solvent was evaporated and the residue was purified by silica-gel column chromatography to afford 43 mg (90%) of **11** as a colorless oil. IR (neat) 1730 (CO) cm^{-1}; ^1H NMR δ=1.5—2.5 (4H, m), 3.83 (2H, s), 3.8—4.0 (2H, m), 4.20—4.45 (1H, m), and 7.0—7.4 (5H, m); MS *m/z* (%) 190 (M^+, 5), 136 ([M−C_4H_6]$^+$, 34), 91 ([M−$C_5H_7O_2$]$^+$, 100), and 71 ([M−C_8H_7O]$^+$, 42); Found: *m/z* 190.0985. Calcd for $C_{12}H_{14}O_2$: M, 190.0993.

4-Hydroxy-3-propoxy-1-phenyl-2-butanone (10) and Its Acetate (19). **10**: Colorless oil, IR (neat) 3450 (OH), 1730 (CO) cm^{-1}; ^1H NMR δ=0.93 (3H, t, *J*=6 Hz), 1.60 (2H, sextet, *J*=6 Hz), 2.12 (1H, t, *J*=6 Hz, OH), 3.38 (2H, t, *J*=6 Hz), 3.55—3.80 (2H, m), 3.80 (2H, s), and 7.12 (5H, bs). Acetate **19**: Colorless oil, IR (neat) 1740 (CO), 1250 (COC) cm^{-1}; ^1H NMR δ=0.95 (3H, t, *J*=7 Hz), 1.65 (2H, sextet, *J*=7 Hz), 2.02 (3H, s), 3.44 (2H, m), 3.91 (2H, s), 3.95 (1H, dd, *J*=5, 4 Hz), 4.32 (2H, dq, *J*=12, 4 Hz), and 7.24 (5H, m); MS *m/z* (%) 264 (M^+, 0.4), 204 ([M−$C_2H_4O_2$]$^+$, 0.3), 145 ([M−C_8H_7O]$^+$, 42), 103 (45), and 43 (100); Found: *m/z* 264.1374. Calcd for $C_{15}H_{20}O_4$: M, 264.1360.

2-(Cyclohexylcarbonyl)tetrahydrofuran (12). Colorless oil, IR (neat) 1720 (CO) cm^{-1}; ^1H NMR δ=0.6—2.4 (14H, m), 2.70 (1H, m), 3.90 (2H, m), and 4.41 (1H, m); MS *m/z* (%) 182 (M^+, 4), 111 ([M−C_4H_7O]$^+$, 7), and 71 (100).

2-(1-Oxo-2-phenylethyl)tetrahydropyran (13). Colorless oil, IR (neat) 1730 (CO) cm^{-1}; ^1H NMR δ=1.2—2.0 (6H, m), 3.28—3.60 (1H, m), 3.68—4.20 (2H, m), 3.86 (2H, s), and 7.21 (5H, m); MS *m/z* (%) 204 (M^+, 6), 136 ([M−C_5H_8]$^+$, 2), 91 ([M−$C_6H_9O_2$]$^+$, 25), and 85 ([M−C_8H_7O]$^+$, 100); Found: *m/z* 204.1128. Calcd for $C_{13}H_{16}O_2$: M, 204.1149.

2-Methyl-5-(1-oxo-2-phenylethyl)tetrahydropyran (14). Colorless oil, IR (neat) 1730 (CO) cm^{-1}; ^1H NMR δ=1.1—2.0 (6H, m), 1.26 (3H, d, *J*=6 Hz), 3.3—3.6 (1H, m), 3.76—3.95 (1H, m), 3.87, and 3.90 (each 1H, d, *J*=15 Hz); MS *m/z* (%) 218 (M^+, 9), and 99 ([M−C_8H_7O]$^+$, 100); Found: *m/z* 218.1320. Calcd for $C_{14}H_{18}O_2$: M, 218.1306.

2-(Cyclohexylcarbonyl)tetrahydropyran (15). Colorless oil, IR (neat) 1720 (CO) cm^{-1}; ^1H NMR δ=0.8—2.1 (16H, m), 2.80 (1H, m), 3.28—3.64 (1H, m), and 3.86—4.24 (2H, m); MS *m/z* (%) 196 (M^+, 2), and 85 ([M−$C_7H_{11}O$]$^+$, 100); Found: *m/z* 196.1463. Calcd for $C_{12}H_{20}O_2$: M, 196.1462.

8-Hydroxy-3-propoxy-1-phenyl-2-octanone (16). Colorlsss oil, IR (neat) 3400 (OH), 1730 (CO) cm^{-1}; ^1H NMR δ=0.93 (3H, t, *J*=7 Hz), 1.0—1.8 (10H, m), 3.32 (2H, m), 3.4—3.8 (3H, m), 3.82 (2H, s), and 7.23 (5H, m); MS *m/z* (%) 278 (M^+, 0.4), 218 ([M−C_3H_8O]$^+$, 1), 159 ([M−C_8H_7O]$^+$, 70), 99 (88), and 81 (100); Found: *m/z* 278.1876. Calcd for $C_{17}H_{26}O_3$: M, 278.1880.

14-Hydroxy-3-propoxy-1-phenyl-2-tetradecanone (17). Colorless oil, IR (neat) 3420 (OH), 1730 (CO) cm^{-1}; ^1H NMR δ=0.94 (3H, t, *J*=7 Hz), 1.0—1.9 (22H, m), 3.31 (2H, m), 3.5—3.8 (3H, m), 3.81 (2H, s), and 7.22 (5H, m); MS *m/z* (%) 362 (M^+, 0.3), 332 [M−CH_2O]$^+$, 0.3), 302 ([M−C_3H_8O]$^+$, 0.3), 243 ([M−C_8H_7O]$^+$, 88), and 43 (100); Found: *m/z* 362.2802. Calcd for $C_{23}H_{38}O_3$: M, 362.2818.

2-Phenyl-5,6-dihydro-2*H*-pyran-3(4*H*)-one (20). Colorless oil, IR (neat) 1730 (CO) cm^{-1}; ^1H NMR δ=1.96—2.32 (2H, m), 2.45—2.70 (2H, m), 3.68—4.22 (2H, m), 4.91 (1H, s), and 7.30 (5H, s); MS *m/z* (%) 176 (M^+, 25), 146 ([M−CO]$^+$, 84), 147 ([M−CHO]$^+$, 87), and 105 (100); Found: *m/z* 176.0823. Calcd for $C_{11}H_{12}O_2$: M, 176.0835.

6-Oxaspiro[4.5]decan-10-one (21). Colorless oil, IR (neat) 1710 (CO) cm^{-1}; ^1H NMR δ=1.4—2.2 (10H, m), 2.32 (2H, t, *J*=6 Hz), and 3.82 (2H, t, *J*=6 Hz).

2-Phenyl-3-oxepanone (24). Colorless oil, IR (neat) 1720 (CO) cm^{-1}; ^1H NMR δ=1.8—2.4 (4H, m), 2.4—2.6 (2H, m), 3.6—4.2 (2H, m), 4.87 (1H, s), and 7.35 (5H, s); MS *m/z* (%) 190 (M^+, 12), 162 ([M−CO]$^+$, 39), 161 ([M−CHO]$^+$, 45), and 105 ([M−C_5H_9O]$^+$, 100); Found: *m/z* 190.0994. Calcd for $C_{12}H_{14}O_2$: M, 190.0933.

General Procedure for the Preparation of Spirocyclic β-Keto Ethers from α,β-Epoxy Sulfoxides by $MgCl_2$-Induced Opening of the Oxirane Ring: The synthesis of 1-oxaspiro[5.5]undecan-5-one (**22**) from **2f** is described. $MgCl_2$ (33 mg; 0.34 mmol) was added to a solution of **2f** (100 mg; 0.34 mmol) in 7 ml of 2-propanol. The mixture was stirred and heated at reflux temperature under N_2 for 13 h. To the reaction mixture was added excess NH_4Cl and the 2-propanol was evaporated. The residue was extracted with benzene–ether and the organic layer was washed with satd. aq. NH_4Cl and dried over Na_2SO_4. The product was purified by silica-gel column chromatography to afford 45 mg (74%) of **22** as a colorless oil. IR (neat) 1720 (CO) cm^{-1}; ^1H NMR δ=0.8—2.0 (10H, m), 2.10 (2H, q, J=6 Hz), 2.49 (2H, t, *J*=6 Hz), and 3.84 (2H, t, *J*=6 Hz).

1-Oxaspiro[5.6]dodecan-5-one (23). Colorless oil, IR (neat) 1720 (CO) cm^{-1}; ^1H NMR δ=1.0—2.0 (12H, m), 2.10 (2H, q, *J*=6 Hz), 2.51 (2H, t, *J*=6 Hz), and 3.81 (2H, t, *J*=6 Hz); MS *m/z* (%) 182 (M^+, 16), 154 ([M−CO]$^+$, 28), and 112 (100); Found: *m/z* 182.1303. Calcd for $C_{11}H_{18}O_2$: M, 182.1305.

1-Chloro-1-(5-hydroxy-1-oxoheptyl)cyclohexane (25). Colorless oil, IR (neat) 3400 (OH), 1720 (CO) cm^{-1}; ^1H NMR δ=1.0—2.2 (14H, m), 2.77 (2H, t, *J*=6 Hz), and 3.64 (2H, t, *J*=6 Hz); MS *m/z* (%) 218 (M^+, 3), 157 (4), and 101 ([M−$C_6H_{10}Cl$]$^+$, 100).

The authors are grateful to Dr. Sei-ichi Saito, Tanabe Seiyaku Co., Ltd., for elemental analysis and Miss Noriko Sawabe and Miss Tomoko Fujimori of this laboratory for NMR and MS measurements.

References

1) α,β-Epoxy sulfoxides as useful intermediates in organic synthesis. XVI. Part XV: T. Satoh, S. Motohashi, and K. Yamakawa, *Chem. Pharm. Bull.*, **36**, 1169 (1988).

2) For review see: A. S. Rao, S. K. Paknikar, and J. G. Kirtane, *Tetrahedron*, **39**, 2323 (1983); J. G. Smith, *Synthesis*, **1984**, 629.

3) Structure: D. E. Cane, W. D. Celmer, and J. W. Westley, *J. Am. Chem. Soc.*, **105**, 3594 (1983) and the references cited therein. Synthesis: Y. Kishi, *Aldrichimica Acta*, **13**, 23 (1980); P-T. Ho, *Can. J. Chem.*, **60**, 90 (1982); R. E. Ireland, L. Courtney, and B. J. Fitzsimmons, *J. Org. Chem.*, **48**, 5186 (1983); M. Isobe, Y. Ichikawa, and T. Goto, *Tetrahedron Lett.*, **26**, 5199 (1985); M. Isobe, Y. Ichikawa, D-lu. Bai, and T. Goto, *ibid.*, **26**, 5203 (1985); T. L. B. Boivin, *Tetrahedron*, **43**, 3309 (1987).

4) a) T. Satoh, Y. Kaneko, T. Izawa, K. Sakata, and K. Yamakawa, *Bull. Chem. Soc. Jpn.*, **58**, 1983 (1985); b) T.

Satoh, T. Kumagawa, and K. Yamakawa, *ibid.*, **58**, 2849 (1985); c) T. Satoh, Y. Kaneko, K. Sakata, and K. Yamakawa, *ibid.*, **59**, 457 (1986); d) T. Satoh, S. Motohashi, and K. Yamakawa, *ibid.*, **59**, 946 (1986); e) T. Satoh, T. Kumagawa, and K. Yamakawa, *Tetrahedron Lett.*, **27**, 2471 (1986); f) T. Satoh, S. Motohashi, and K. Yamakawa, *ibid.*, **27**, 2889 (1986); g) T. Satoh, T. Kumagawa, A. Sugimoto, and K. Yamakawa, *Bull. Chem. Soc. Jpn.*, **60**, 301 (1987); h) T. Satoh, M. Itoh, T. Ohara, and K. Yamakawa, *ibid.*, **60**, 1839 (1987).

5) A part of the results of this reaction was reported as a communication: T. Satoh, K. Iwamoto, and K. Yamakawa, *Tetrahedron Lett.*, **28**, 2603 (1987).

6) The desired aldehydes **6** used in this study were synthesized from α,ω-diol **5** by a half protection of the hydroxyl groups with dihydropyran followed by Swern oxidation of the remaining hydroxyl group.

7) M. Miyashita, A. Yoshikoshi, and P. A. Grieco, *J. Org. Chem.*, **42**, 3772 (1977).

8) In the previous communication[5] we reported the wrong structure of this product **17**.

9) The synthesis of these chloroalkyl phenyl sulfoxides, see Ref. 4g.

10) J. E. Baldwin, *J. Chem. Soc., Chem. Commun.*, **1976**, 734; J. E. Baldwin, J. Cutting, W. Dupont, L. Kruse, L. Silberman, and R. C. Thomas, *ibid.*, **1976**, 736.

11) T. Satoh, A. Sugimoto, and K. Yamakawa, *Chem. Pharm. Bull.*, **35**, 4632 (1987).

Indirect Electrolytic Oxidation of Thioamides Using Organotellurium as a Mediator

Toshiaki MATSUKI, Nan Xing HU, Yoshio ASO, Tetsuo OTSUBO, and Fumio OGURA*
Department of Applied Chemistry, Faculty of Engineering, Hiroshima University, Saijo, Higashi-Hiroshima 724
(Received December 26, 1987)

Bis(*p*-methoxyphenyl) telluride (**1**) electrochemically reacted with supporting electrolytes such as tetrabutylammonium acetate and tetraethylammonium tosylate under anhydrous conditions to give tellurium(IV) diacetate **2a** and ditosylate **2b**, respectively. On the other hand, **1** was electrolyzed in the presence of water to give telluroxide **3**. It has turned out that the tellurium compounds **2a** and **2b** like telluroxide **3** are mild oxidizing agents, but **2b** behaves differently in a reaction towards thioamide. Thus **2a** and **3** converted it into nitrile, while **2b** did it into 1,2,4-thiadiazole. An indirect electrolytic oxidation of thioamides with **1** as a mediator was examined under various conditions. As a result, nitriles or 1,2,4-thiadiazoles could be chemoselectively formed, depending on the intermediacy of **2a** or **3** as an active species for the former and **2b** for the latter.

There are few publications concerning the electrochemistry of organotellurium compounds. Recently Liftman and Albeck have reported that diaryl telluride electrochemically reacted with tetrabutylammonium perchlorate or lithium perchlorate as a supporting electrolyte under anhydrous conditions, giving diaryltellurium(IV) diperchlorate.[1] One might expect that the electrochemical oxidation of telluride in aqueous solution leads to the formation of telluroxide like the known conversion of sulfide into sulfoxide.[2] Diaryl telluroxide has been recently accepted as a versatile, mild oxidizing agent, which is reduced to the corresponding telluride in the oxidation reactions.[3,4] Taking into consideration that tellurium has the advantage of a lower oxidation potential than the other lighter chalcogens such as sulfur and selenium,[5] it looks promising to constitute a tellurium-mediated electrolytic oxidation. Such scope and limitation have been evaluated in this investigation. Here we like to report the electrochemical behavior of bis(*p*-methoxyphenyl) telluride (**1**) as well as an indirect electrolytic oxidation of thioamides using it as a mediator.

Results and Discussion

The electrochemical behavior of telluride **1** in the presence of tetrabutylammonium acetate or tetraethylammonium tosylate as an electrolyte is shown in Table 1. The electrolysis in water-free acetonitrile gave tellurium(IV) compound **2a** or **2b** (Scheme 1). On the other hand, the electrolysis in the presence of water gave a mixture of **2** and telluroxide **3**. Tellurium(IV) compound **2** is considered to be formed via a mechanism of a one-electron oxidation followed by a dispropotionation or a second one-electron oxidative reaction of the radical intermediate **4** as shown in Scheme 2.[1] The formation of telluroxide **3** must take a similar pathway (Scheme 3). From additional experiments, **2** and **3** have turned out to be in an equilibrium state

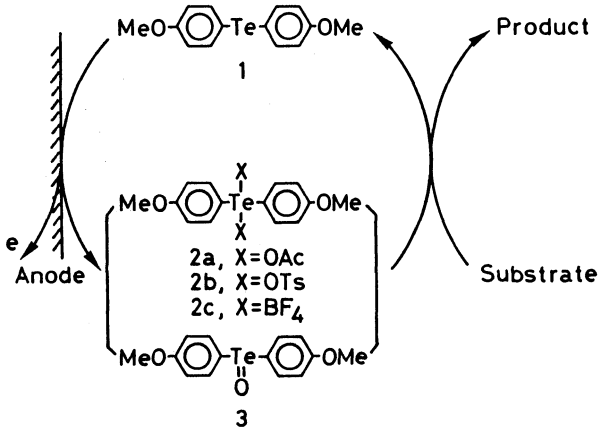

Scheme 1.

Table 1. Electrolysis of Bis(*p*-methoxyphenyl) Telluride (**1**) Leading to Tellurium(IV) Compound (**2**)[a] or Telluroxide (**3**)

Run	Electrolyte	Solvent	Current density / mA cm^{-2}	Electricity / F mol^{-1}	Yield/% **2**	Yield/% **3**
1	Bu_4NOAc	Anhyd MeCN	8	2.2	95	0
2	Bu_4NOAc	2% aq MeCN	8	2.2	40	53
3	Bu_4NOAc	10% aq MeCN	8	2.2	42	56
4	Et_4NOTs	Anhyd MeCN	8	2.4	93	0
5	Et_4NOTs	2% aq MeCN	8	2.4	85	7
6	Et_4NOTs	10% aq MeCN	8	2.3	39	58

a) Bis(*p*-methoxyphenyl)tellurium diacetate (**2a**) for Runs 1—3 and ditosylate (**2b**) for Runs 4—6.

under electrolysis. These results suggest that it is possible to effect a chemoselective electrochemical reaction with **1** as a mediator, whose selectivity depends on the intermediacy of either **2** or **3** (Scheme 1).

An indirect electrolytic oxidation with 5 mol% of telluride **1** as a mediator was examined for thiobenzamide (**5**) as a model substrate, since thioamide resists a direct electrochemical oxidation,[6] but is more reactive to telluroxide **3**. The electrolysis resulted in the formation of benzonitrile (**6**) and 3,5-diphenyl-1,2,4-thiadiazole (**7**) (Scheme 4). The selectivity evidently depended on the adopted electrolytic conditions as

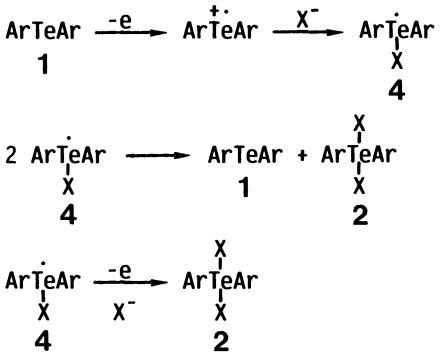

Scheme 2.

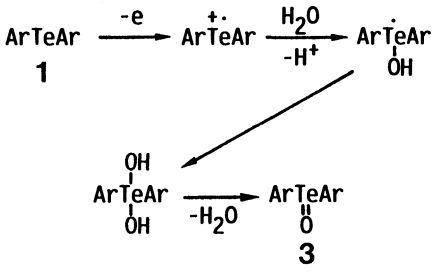

Scheme 3.

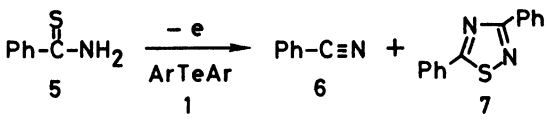

Scheme 4.

Table 2. Indirect Electrolytic Oxidations of Thiobenzamide (**5**) to Benzonitrile (**6**) and 3,5-Diphenyl-1,2,4-thiadiazole (**7**) Using 5 mol% of Bis(*p*-methoxyphenyl) Telluride (**1**)

Run	Electrolyte	Solvent	Current density	Electricity	Yield/%	
			mA cm^{-2}	F mol^{-1}	**6**	**7**
1	Bu_4NOAc	Anhyd MeCN	4	3.0	89	Trace
2	Bu_4NOAc	2% aq MeCN	4	2.7	95	Trace
3	Bu_4NOAc	2% aq EtOH	4	2.2	86	Trace
4	Bu_4NOAc	2% aq EtOH	3	2.1	90	Trace
5	Et_4NOTs	Anhyd MeCN	4	3.6	5	90
6	Et_4NOTs	0.5% aq MeCN	8	2.4	72	11
7	Et_4NOTs	10% aq MeCN	4	2.7	Trace	92
8	Et_4NOTs	Anhyd EtOH	4	2.4	0	95
9	Et_4NOTs	0.5% aq EtOH	4	3.6	0	90
10	Et_4NOTs	2% aq EtOH	4	2.7	0	98
11	Bu_4NBF_4	Anhyd MeCN	8	3.0	0	72
12	Bu_4NBF_4	0.5% aq MeCN	8	2.4	44	32
13	Bu_4NBF_4	1% aq MeCN	8	2.4	70	11
14	Bu_4NBF_4	2% aq MeCN	8	2.4	Trace	74
15	Bu_4NBF_4	Anhyd EtOH	4	2.4	0	79
16	Bu_4NBF_4	2% aq EtOH	4	2.4	0	82

a) Determined by HPLC analysis.

Table 3. Reactions of Thiobenzamide (**5**) with Tellurium(IV) Compound (**2**) or Telluroxide (**3**) to Benzonitrile (**6**) and 3,5-Diphenyl-1,2,4-thiadiazole (**7**)[a]

Run	Reagent	Solvent	Time	Yield/%[b]			Rate constant
			h	**5**	**6**	**7**	dm^3 mol^{-1} h^{-1}
1	**2a**	Anhyd MeCN	12	0	80	18	151
2	**2a**	10% aq MeCN	14	0	82	15	143
3	**2b**	Anhyd MeCN	16	0	Trace	90	137
4	**2b**	10% aq MeCN	17	0	Trace	89	121
5	**3**	Anhyd MeCN	0.5	0	93	Trace	1913
6	**3**	2% aq MeCN	1.5	0	91	Trace	876
7	**3**	10% aq MeCN	20	11	81	Trace	50
8	**3**	Anhyd EtOH	24	60	31	Trace	4
9	**3**	2% aq EtOH	23	49	43	5	5

a) Reaction temperature 25 °C. b) Determined by HPLC analysis.

summarized in Table 2. In order to elucidate these results, the reactivities of bis(*p*-methoxyphenyl)tellurium diacetate (**2a**), tellurium ditosylate (**2b**), and telluroxide (**3**) towards thiobenzamide (**5**) were investigated in detail. Thiobenzamide was treated with one molar equivalent reagent **2** or **3** under conditions specified in Table 3. The reaction was monitored by HPLC analysis and followed good second-order kinetics with 1:1 stoichiometry, a typical example being demonstrated in Fig. 1. As shown in Table 3, the reaction with telluroxide proceeded very fast in water-free acetonitrile, giving benzonitrile (**6**) in an excellent yield. However, the rate dropped drastically in acetonitrile containing some water or in ethanol with water or not. This less reactivity may be rationalized as due to the fact that telluroxide **3** with water or ethanol forms tellurium(IV) adducts **8a** or **8b**.[7] Both tellurium(IV) diacetate **2a** and ditosylate **2b** were also not so reactive as telluroxide **3**, but the reactivities were little affected by the presence of water and, as a result, surpassed that of telluroxide **3** in the presence of water. Furthermore, it should be noted that the reaction with **2a** gave rise to benzonitrile (**6**) and with **2b** to thiadiazole (**7**) as the main product.

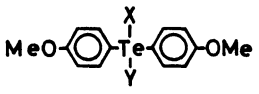

8a, X=Y=OH
8b, X=OH, Y=OEt

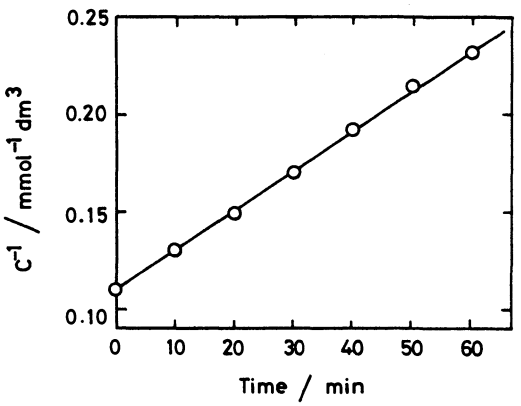

Fig. 1. Time dependence of the reciprocal of the concentration of **2b** in the equimolar reaction towards thiobenzamide in 10% aqueous acetonitrile at 25 °C.

As already indicated from Table 1, an active species in the electrolysis with tetrabutylammonium acetate as a supporting electrolyte is tellurium diacetate **2a** under water-free conditions and either **2a** or telluroxide **3** under water-containing conditions. Either species can give benzonitrile as the main product, being consistent with the indirect electrolyses of Table 2. On the other hand, the electrolysis with tetraethylammonium tosylate as electrolyte behaves differently. Tellurium ditosylate **2b** acted as an active species in anhydrous acetonitrile to give thiadiazole (**7**) in a high yield. The addition of a slight amount of water resulted in the formation of benzonitrile (**6**), indicating the intermediacy of telluroxide **3** as an active species. Further addition of water again gave thiadiazole (**7**). Telluroxide **3** with additional water can be understood to change to adduct **8a** which is less reactive than tellurium ditosylate **2b**. Such water dependence was not found in ethanol solution because the resulting telluroxide **3** with ethanol immediately forms a less reactive adduct **8b**. The electrolysis with tetrabutylammonium tetrafluoroborate as an electrolyte demonstrates a similar tendency. That is to say, tellurium bis(tetrafluo-

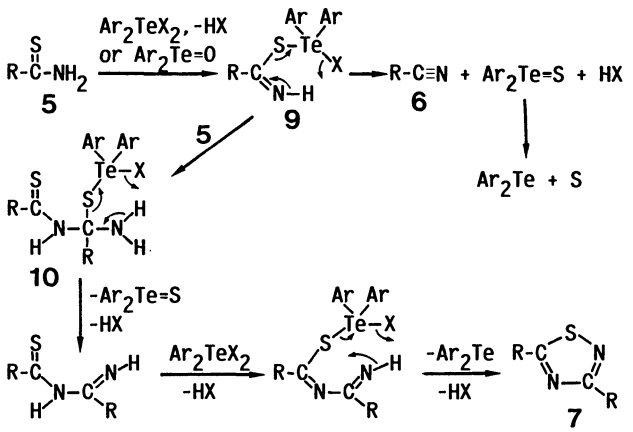

Scheme 5.

Table 4. Indirect Electrolytic Oxidations of Some Thioamides to Nitriles and 1,2,4-Thiadiazoles

Run	Substrate	Method[a]	Isolated yield/%	
			Nitrile	Thiadiazole
1	*p*-Methoxythiobenzamide	A	71	0
2	*p*-Methoxythiobenzamide	B	0	73
3	*p*-Chlorothiobenzamide	A	63	18
4	*p*-Chlorothiobenzamide	B	0	71
5	*N,N'*-Diphenylthiourea	A	80	6
6	*N,N'*-Diphenylthiourea	B	4	77

a) Method A: Current density 4mA cm^{-2}, Electricity 2.4 F mol^{-1}, Solvent 2% aq MeCN, Supporting electrolyte Bu_4NOAc. Method B: Current density 4 mA cm^{-2}, Electricity 2.4 F mol^{-1}, Solvent 2% aq EtOH, Supporting electrolyte Et_4NOTs.

roborate) **2c** is considered to be generated in the electrolysis and behaves like tellurium tosylate **2b** as an oxidizing agent, though it was not isolated.

Scheme 5 proposes a reasonable mechanism for the transformations of thioamide **5** into nitrile **6** and thiadiazole **7**.[4] A selection of both paths seems to depend on facility in eliminating an acid H-X in the initial common adduct **9**, in other words, basicity of the conjugated base X. Therefore, the elimination is favorable for X=OH and OAc, leading to nitrile **6**. On the other hand, it is hard for X=OTs and BF_4, so that the dimerization to **10** occurs, finally leading to thiadiazole **7**.

In conclusion, bis(*p*-methoxyphenyl) telluride (**1**) can be electrochemically oxidized to tellurium(IV) compound **2** or telluroxide **3**, enabling a chemoselective reaction using it as exemplified for the transformation of thiobenzamide to benzonitrile or diphenylthiadiazole. Table 4 demonstrates some other examples in which thioamides can be arbitarily transformed into either nitriles or thiadiazoles, depending on the two typical electrolytic conditions.

Experimental

Materials. Bis(*p*-methoxyphenyl) telluride (**1**)[8] and telluroxide (**3**)[3] were prepared according to the literatures.

Electrolytic Apparatus. A 20 ml of H-type glass cell with a fine frit diving the anolyte and catholyte compartments was used for electrolyses. It was equipped with platinum plates (1 cm^2) as the working and counter electrodes. All electrolyses with carefully purified reagent, solvent, and supporting electrolyte were conducted at room temperature in a nitrogen atmosphere.

General Procedure for Electrolyses of Bis(*p*-methoxyphenyl) Telluride (1). A solution of dry acetonitrile (10 ml) containing tetrabutylammonium acetate (360 mg) was placed in the electrolytic cell. Bis(*p*-methoxyphenyl) telluride (**1**) (100 mg, 0.3 mmol) was added in the anolyte compartment and electrolyzed under a constant current density of 8 mA cm^{-2}. After 2.2 F (1 F=96485 C) mol^{-1} of electricity had been passed, the mixture was thoroughly extracted with chloroform. The extract was washed with water, dried ($MgSO_4$), and concentrated in vacuo. Recrystallization of the residue from benzene gave colorless crystals of bis(*p*-methoxyphenyl)tellurium diacetate (**2a**); 131 mg (95%), mp 134.5—135.5 °C (lit,[9] mp 135—136 °C). ^1H NMR ($CDCl_3$) δ=7.69 (d, J=9 Hz, 4H, ArH), 6.90 (d, J=9 Hz, 4H, ArH), 3.77 (s, 6H, OMe), and 1.93 (s, 6H, OCOMe); IR (KBr) 1630 (C=O), 1585, 1490 (Ar ring), 1290, 1255, and 1175 (C-O) cm^{-1}. Found: C, 47.02; H, 4.39%. Calcd for $C_{18}H_{20}O_6Te$: C, 47.03; H, 4.39%.

When the electrolysis was carried out in aqueous acetonitrile, the isolated product was a mixture of **2a** and telluroxide **3** as shown in Table 1.

A similar electrolysis with tetraethylammonium tosylate electrolyte in dry acetonitrile deposited white crystals of bis(*p*-methoxyphenyl)tellurium ditosylate (**2b**) in the anolyte compartment, which was collected by filtration and washed with acetonitrile; 180 mg (93%), mp 257—260 °C. ^1H NMR ($CDCl_3$) δ=7.67 (d, J=9 Hz, 4H, ArH), 7.37 (d, J=8 Hz, 4H, ArH), 6.96 (d, J=8 Hz, 4H, ArH), 6.80 (d, J=9 Hz, 4H, ArH), 3.72 (s, 6H, OMe), and 2.30 (s, 6H, Me); IR (KBr) 1585, 1495 (Ar ring), 1295, 1250, 1220, 1180, 1130, and 1015 (SO_2O and C-O) cm^{-1}. Found: 49.09; H, 4.01%. Calcd for $C_{28}H_{28}O_8S_2Te$: C, 49.15; H, 4.12%.

General Procedure for Indirect Electrooxidations of Thioamides to Nitriles or Thiadiazoles. A mixture of thiobenzamide (**5**) (68.6 mg, 0.5 mmol) and bis(*p*-methoxyphenyl) telluride (**1**) (8.6 mg, 0.025 mmol) in 16 ml of dry acetonitrile containing tetrabutylammonium acetate (602 mg) was electrolyzed under a constant current density of 4 mA cm^{-2}. The reaction was monitored by HPLC (Microsorb C18 standard column, methanol eluent). After passage of 3.0 F mol^{-1} of electricity (10 h), the starting material **5** was consumed, forming benzonitrile (**6**) (89%) and 3,5-diphenyl-1,2,4-thiadiazole (**7**) (trace). Both products **6** and **7** were isolated as colorless oil and as colorless crystals with mp 89.5—90.5 °C (lit,[10] mp 89—90 °C), respectively, from column chromatography of the concentrate of the reaction mixture on silica gel with 1 : 1 benzene-hexane eluent. All the products from the electrolyses shown in Table 4 were similarly isolated as colorless crystals and characterized: *p*-methoxybenzonitrile, mp 56—57 °C (lit,[11] mp 59.5—60.5 °C); *p*-chlorobenzonitrile, mp 94—94.5 °C (lit,[12] mp 92 °C); diphenylcyanamide, mp 73.5—74 °C (lit,[13] mp 73 °C); 3,5-bis(*p*-methoxyphenyl)-1,2,4-thiadiazole, mp 137—138 °C (lit,[10] mp 139—140 °C); 3,5-bis(*p*-chlorophenyl)-1,2,4-thiadiazole, mp 161.5—162 °C (lit,[10] mp 161—162 °C; 3,5-bis(diphenylamino)-1,2,4-thiadiazole, mp 154—154.5 °C (lit,[10] mp 155 °C).

General Procedure for Reactions of Thiobenzamide (5) with Bis(*p*-methoxyphenyl)tellurium(IV) Compound 2 or Telluroxide 3. A 15 ml solution of thiobenzamide (**5**) (18.7 mg) was treated with one molar equivalent reagent **2** or **3** under conditions specified in Table 3. The reaction was monitored by HPLC analysis (Microsorb C18 standard column, methanol eluent). The rate constant k at 25 °C was evaluated by use of a second-order rate equation: $kt=(1/c)-(1/c_0)$ where c is the time-dependent concentration of thiobenzamide and c_0 is the initial one. A plot of $1/c$ against time is linear with less than 7.4% standard deviation.

The authors thank Dr. A. Kunai of Hiroshima University for helpful discussions. This work was partially supported by a Grant-in-Aid of Scientific Research No. 62470023 from the Ministry of Education, Science and Culture.

References

1) Y. Liftman and M. Albeck, *Electrochim. Acta*, **28**, 1835, 1841 (1983).

2) A. A. Humffray and D. S. Houghton, *Electrochim. Acta*, **17**, 1435 (1972); D. S. Houghton and A. A. Humffray, *ibid.*, **17**, 1421 (1972); K. Uneyama and S. Torii, *J. Org. Chem.*, **37**, 367 (1972).

3) D. H. R. Barton, S. V. Ley, and C. A. Meerholz, *J. Chem. Soc., Chem. Commun.*, **1979**, 755; S. V. Ley, C. A. Meerholz, and D. H. R. Barton, *Tetrahedron Lett.*, **21**, 1785 (1980); *Tetrahedron*, **37**, 213 (1981).

4) N. X. Hu, Y. Aso, T. Otsubo, and F. Ogura, *Bull. Chem. Soc. Jpn.*, **59**, 879 (1986).

5) The cyclic voltammogram of bis(*p*-methoxyphenyl)

telluride (**1**) showed an irreversible oxidation peak E_p^{ox} at 0.80 V vs. Ag/AgCl while the corresponding sulfide at 1.35 V and selenide at 1.21 V (5 mol m^{-3} acetonitrile solution, glassy carbon working electrode, 0.1 mol dm^{-3} tetrabutylammonium perchlorate electrolyte, 100 mV s^{-1} sweep rate).

6) Thiobenzamide (**5**) was sluggishly electrolyzed in a blank galvanostatic experiment, giving 3,5-diphenyl-1,2,4-thiadiazole (**7**) in ca. 20% yield.

7) K. J. Irgolic, "The Organic Chemistry of Tellurium," Gorden and Breach, New York (1974), p. 192.

8) J. Bergman, *Tetrahedron*, **28**, 3323 (1972).

9) I. D. Sadekov and A. A. Maksimenko, *Zhur. Obshch. Khim.*, **47**, 2536 (1977).

10) G. Kresze, A. Horn, R. Philippson, and A. Trede, *Chem. Ber.*, **98**, 3401 (1965).

11) E. Bamberger and W. Pemsel, *Ber.*, **36**, 359 (1903).

12) A. Hantzsch and O. W. Schulze, *Ber.*, **28**, 666 (1895).

13) J. V. Braun, *Ber.*, **33**, 1438 (1900).

Syntheses and Cytotoxicity of the AB-, C-, and BC-Ring Systems of Sesbanimides

Fuyuhiko MATSUDA, Masako OHSAKI, Kaoru YAMADA, and Shiro TERASHIMA*
Sagami Chemical Research Center, Nishi-Ohnuma, Sagamihara, Kanagawa 229
(Received December 26, 1987)

Preparation of some AB-ring systems **5** and **8** of sesbanimides **1** and **2**, potent antitumor alkaloids, were performed starting from the synthetic intermediates of our first total synthesis of **1** and **2**. The C-ring systems **14a—d** were synthesized by applying the previously explored novel Reformatsky reaction to various aldehydes. The optically active BC-ring systems **20** and **21** having the same absolute configurations as those of **1** and **2**, were derived from (−)-2,4-*O*-methylene-D-sorbitol (**15**) as the B-ring synthon. Since all of these compounds **5**, **8**, **14a—d**, **20**, and **21** and the previously synthesized AB-ring system **3** showed no significant in vitro cytotoxicity against P388 murine leukemia, its appeared evident that **1** and **2** exhibit their notable antitumor activity owing to cooperation of the A- and C-rings.

Sesbanimide A (**1**) and sesbanimide B (**2**), isolated as alkaloids from the seeds of the leguminous plants,[1,2] have been reported to exhibit notable cytotoxicity against KB cells in vitro and potent inhibitory activity against P388 murine leukemia in vivo. These compounds have unique tricyclic structures in which the three characteristic rings, glutarimide (A-ring), 1,3-dioxane (B-ring), and tetrahydrofuran (C-ring), are linked by two single bonds. Although the structure of **1** including its relative stereochemistry had been established by X-ray crystallographic analysis,[1a] its absolute configuration had not been determined.

Previously, we reported the first total synthesis of natural (+)-sesbanimide A (**1**) and (−)-sesbanimide B (**2**) from readily available D-(+)-xylose by way of the AB-ring system **3**.[3-5] Our total synthesis of these alkaloids obviously confirmed their absolute configurations.[3] With an aim to explore which parts of the structures of **1** and **2** are most responsible for their pronounced antitumor activity, the structure-activity relationships were next studied using various partial structures of **1** and **2**.

This report concerns with the syntheses of the AB-, C-, and BC-ring systems of sesbanimides achieved by employing the synthetic scheme explored in the course of our total synthesis,[3] and evaluation of cytotoxicity of these sesbanimide congeners produced in this and the previous studies.[3]

Results and Discussion

Syntheses and In Vitro Cytotoxicity of the Sesbanimide AB-Ring Systems. It was reported that **1** and **2** exhibits IC_{50} values of 7.7×10^{-3} μg ml^{-1} and 6.8×10^{-2} μg ml^{-1} against KB cells in vitro[1c] and T/C values of 140—181% in 8—12 μg kg^{-1}and 157—161% in 1.87—3.75 μg kg^{-1} dose levels against P388 murine leukemia in vivo,[1c] respectively. When the total synthesis of **1** and **2** were completed,[3] the synthetic samples of **1** and **2** were subjected to P388 murine leukemia in vitro cytotoxicity assay along with natural **1** provided by Powell. As shown in Table 1, synthetic and natural **1** were found to show the same magnitudes of cytotoxicity. Moreover, fairly intense cytotoxicity was also

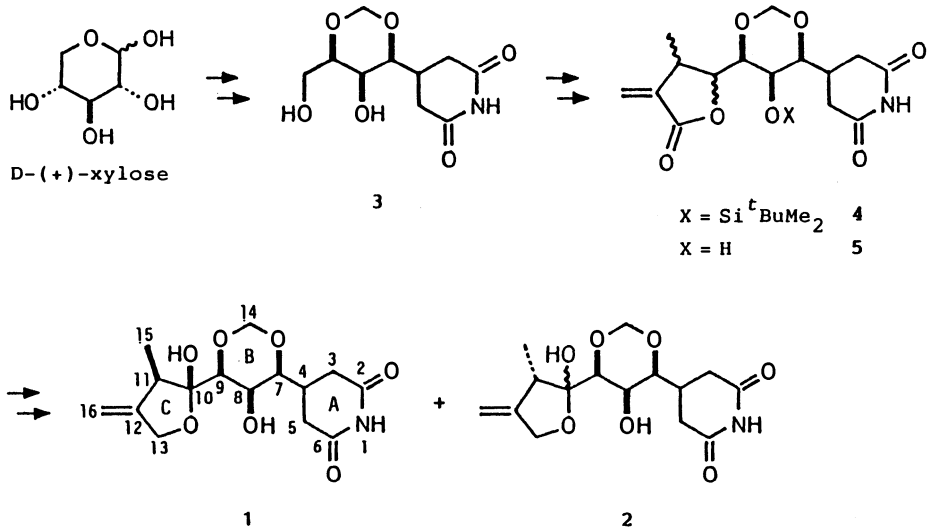

Scheme 1.

observed for synthetic **2**. These results were quite useful for identifying the synthetic samples with natural **1** and **2**, respectively.

With completion of the total synthesis of **1** and **2**, the sesbanimide congeners **3**, **5**, and **8** were first subjected to in vitro cytotoxicity assay to evaluate the roles of the AB-ring systems in prominent antitumor activity of **1** and **2**. The diol **3** had already been obtained during the course of our total synthesis. The *exo*-methylene-γ-lactone (**5**) was prepared from the synthetic intermediate **4** of **1** and **2** by simple deprotection. As shown in Scheme 2, the preparation of **8** was carried out by introducing an allyl group into the aldehyde **6** obtainable from **3**, followed by desilylation of the siloxy ketone **7**. The overall process proceeded in a moderate overall yield. Results summarized in Table 1 cleanly disclose that the AB-ring systems except for **5** carrying an *exo*-methylene-γ-lactone moiety which is well-known as a cytotoxic functionality, show no in vitro cytotoxicity against P388 murine leukemia. Although considerable in vitro cytotoxicity was recorded on **5**, it showed no significant antitumor activity against P388 murine leukemia in vivo (T/C 95% in 10 mg kg^{-1} dose level).

Table 1. In Vitro Cytotoxicity of Sesbanimides and Their AB-Ring Systems against P388 Murine Leukemia

Compound	$IC_{50}/\mu g\,ml^{-1}$ [a]
1	4.6×10^{-5} (3.3×10^{-5})[b]
2	3.1×10^{-2}
3	>25
5	9.0×10^{-3}
8	>30

a) Cell growth inhibition (percent) after incubation for 48 h at 37 °C. b) In vitro cytotoxicity observed on natural **1**.

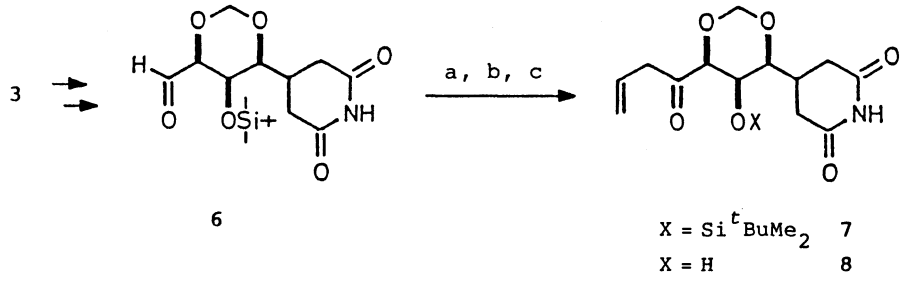

Scheme 2. a) CH_2=$CHCH_2MgCl$, ether, −78 °C, 1 h. b) CrO_3·2Py, CH_2Cl_2, rt, 20 min, 42% (2 steps). c) AcOH, MeOH, rt, 5 min, 86%.

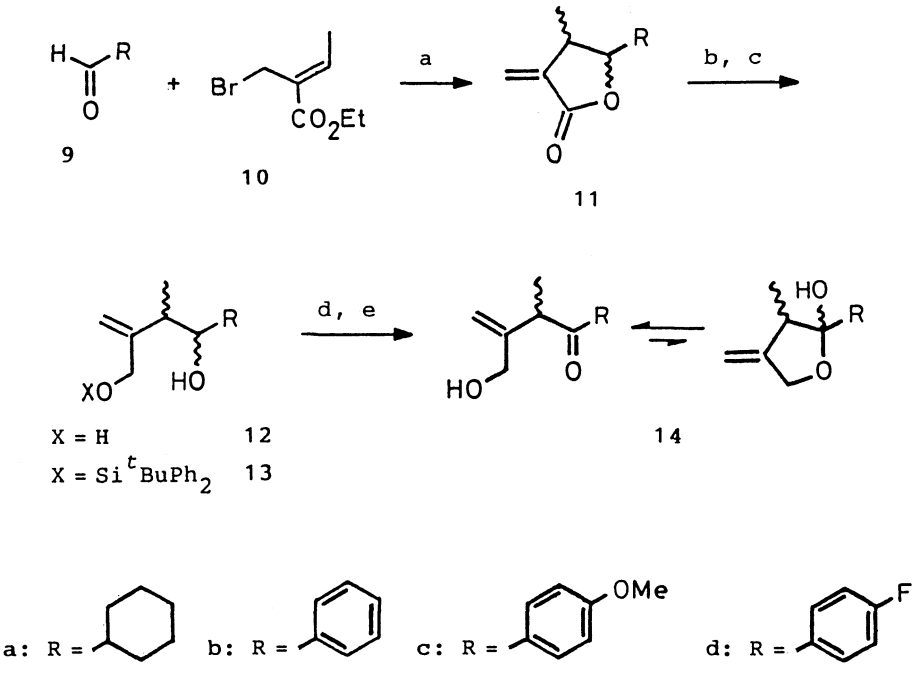

Scheme 3. a) Zn, THF, 0 °C, 2 h (for **9a**), reflux, 20 min (for **9b**), reflux, 8 min (for **9c**), reflux, 50 min (for **9d**). b) 1) ^{i}Bu$_2$AlH, CH_2Cl_2, 0 °C, 20 min; 2) $NaBH_4$, $CeCl_3$·7H_2O, MeOH, 0 °C, 30 min. c) ^{t}BuPh$_2$SiCl, imidazole, DMF, rt, 30 min, 65% (**13a**, 3 steps). d) CrO_3·2Py, CH_2Cl_2, rt, 10 min. e) Bu_4NF, THF, rt, 1 h, 49% (**14a**, 2 steps), 30% (**14b**, 5 steps), 39% (**14c**, 5 steps), 49% (**14d**, 5 steps).

Based on these results, it was anticipated that, in place of the AB-ring systems, the C-ring systems play an important role for **1** and **2** to exhibit their antitumor activity.

Syntheses and In Vitro Cytotoxicity of the C-Ring Systems. The compounds **14a—d** were selected as representative examples of the C-ring systems of **1** and **2**. Preparation of **14a—d** were examined employing the synthetic method explored in the course of the total synthesis, to cyclohexanecarbaldehyde (**9a**) and three sorts of the aromatic aldehydes **9b—d**. As shown in Scheme 3, the regioselective Reformatsky reaction[6] of **9a** with ethyl (*E*)-2-(bromomethyl)crotonate (**10**)[7] proceeded smoothly at 0 °C to afford the *exo*-methylene-γ-lactone (**11a**) as a 1 : 1.3 mixture of the two diastereomers. The Reformatsky reaction of **9b—d** carried out in refluxing tetrahydrofuran similarly gave **11b—d** as mixtures of the two diastereomers in good yields (the ratio of diastereomers: **11b**, 1 : 6; **11c**, 1 : 5; **11d**, 1 : 6). When **9a** was subjected to the Reformatsky reaction in refluxing tetrahydrofuran, extensive decomposition of **11a** was observed. The diastereomeric mixtures of **9a—d** were immediately used for the next step without separation of the isomers. Reduction of **11a—d** to the diol **12a—d** were attempted in a similar stepwise manner to that previously reported.[3] Thus, treatments of **11a—d** with diisobutylaluminum hydride yielded the corresponding lactols, which without isolation were further reduced with sodium borohydride in the presence of cerium(III) chloride,[8] giving **12a—d**. After selective protections of the primary hydroxyl groups of **12a—d** in forms of *t*-butyldiphenylsilyl ether, Collins oxidations of the remaining secondary hydroxyl groups of the siloxy alcohols **13a—d**, followed by removal of the silyl groups with tetrabutylammonium fluoride, afforded **14a—d** in fairly good overall yields (5 steps, 30—49%). The ^{1}H NMR spectra of **14a—d** revealed that these compounds consist of equilibrated mixtures of the ketonic and hemiacetal forms in which the formers predominate (**14a**, 4 : 1; **14b**, 3 : 1; **14c**, 10 : 1; **14d**, 3 : 1). It was uncovered by the ^{1}H NMR spectra that the hemiacetal forms of **14a—d** also involve the two epimeric isomers.

With completion of the synthesis, in vitro cytotoxicity assay was carried out on **14a—d** along with the corresponding *exo*-methylene-γ-lactones (**11a—d**). Disappointingly, **14a—d** showed no significant cytotoxicity despite slight activity was observed for **11a—d**. These results are summarized in Table 2. Accordingly, it appeared that the pronounced antitumor activity of **1** and **2** do not depend merely upon their C-ring systems.

Syntheses and In Vitro Cytotoxicity of the Sesbanimide BC-Ring Systems. Since it turned out obvious that both the AB- and C-ring systems are not the origin of antitumor activity of **1** and **2**, cytotoxicity of the BC-ring systems **20** and **21** was finally studied.

The synthetic route to optically active **20** and **21** in which (−)-2,4-*O*-methylene-D-sorbitol (**15**) is employed as the B-ring synthon, are shown in Scheme 4. Thus, after oxidative cleavage of the 1,2-glycol moiety of **15** prepared from D-(−)-sorbitol according to the reported method,[9] the resulting lactol was subjected to the Reformatsky reaction with **10**, affording the *exo*-methylene-γ-lactone (**16**) in a good overall yield. Similarly to the case of previous total synthesis of **1** and **2**,[3] **16** was found to consist of a mixture of the three diastereomers concerning the C-10 and C-11 positions (sesbanimide numbering). Determination of the stereostructures of these isomers was not attempted.

Table 2. In Vitro Cytotoxicity of the Sesbanimide C- and BC-Ring Systems and Their Corresponding *exo*-Methylene-γ-lactones against P388 Murine Leukemia

Sesbanimide C- and BC-ring system		*exo*-Methylene-γ-lactone	
Compound	IC_{50}/μg ml^{-1} [a]	Compound	IC_{50}/μg ml^{-1} [a]
14a	1.6	**11a**	0.39
14b	19	**11b**	2.6
14c	22	**11c**	1.1
14d	5.8	**11d**	0.49
20	>25	**16**	0.95
21	>25		

a) Cell growth inhibition (percent) after incubation for 48 h at 37 °C.

At the next stage, protection of the two hydroxyl groups of **16** was required for constructing the C-ring system according to the explored synthetic route.[3] After various protective groups were examined,[10] *p*-methoxybenzylidene group was found to be most suitable for this purpose. Benzylidenation of **16** under the usual conditions yielded the benzylidene γ-lactone (**17**) as a mixture of the three diastereomers. Separation of the mixture with column chromatography afforded a 1 : 1 mixture of the two isomers **17a** (66%) along with a small amount of the other isomer **17b** (6%). Each of the three diastereomers turned out to consist of a single isomer with regard to the benzylic position. Taking into account the difference of thermodynamic stability between the two possible isomers, the *p*-methoxyphenyl group was anticipated to take an equatorial position. Based on this speculation, stereochemistry of the benzylic position was tentatively assigned as shown in Scheme 4. Simply from practical reasons, only the main product **17a** was converted into the BC-ring systems **20** and **21**.

After reduction of the lactone part of **17a**, successive protection of the primary alcohol and Collins oxidation of the remaining secondary alcohol in a similar manner to that previously reported, gave the ketones as a mixture of the two diastereomers **18** and **19**. This mixture could be easily separated by TLC. Stepwise deprotections of the benzylidene and *t*-butyldiphenylsilyl groups transformed **18** and **19** into the optically active BC-ring systems of **1** and **2** (**20** and **21**), respec-

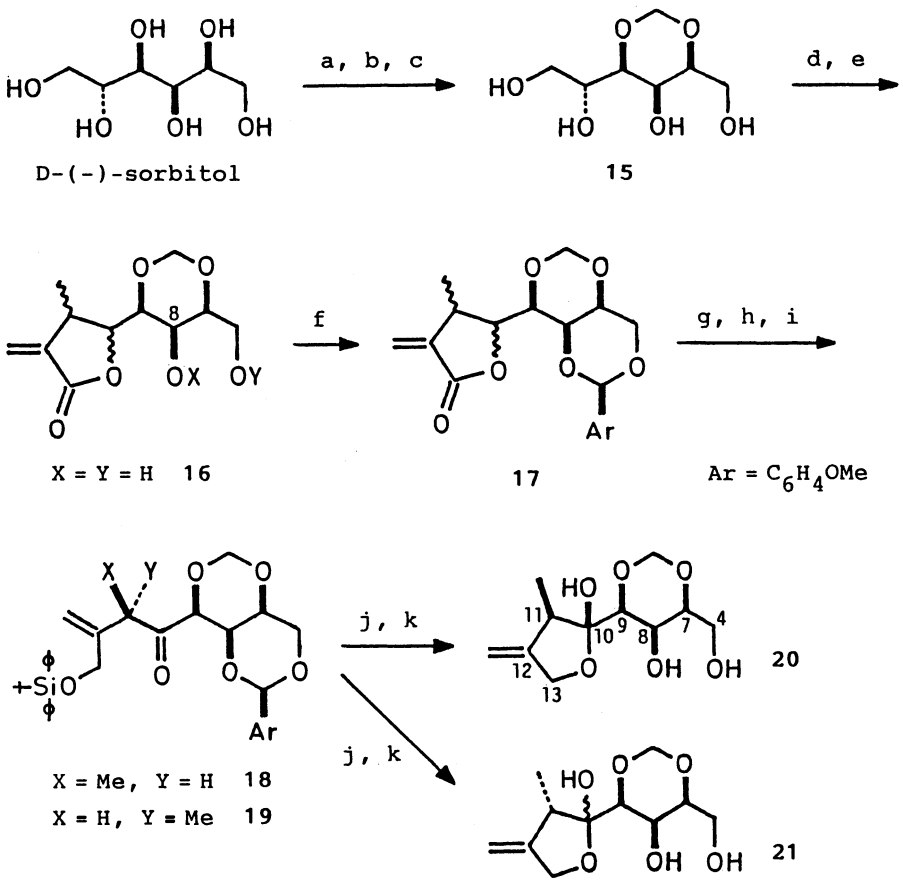

Scheme 4. a) 40% aq H_2CO–12M HCl, 60°C, 2 days, 52%. b) 18M H_2SO_4, AcOH–Ac_2O, 0°C, 10 min, 57%. c) NH_3 gas, MeOH, 0°C→rt, 5 h, 88%. d) $NaIO_4$, H_2O, rt, 5 min. e) **10**, Zn, THF–DMF, reflux, 1 h, 60% (2 steps). f) $MeOC_6H_4CHO$, *p*-TsOH·H_2O, PhH–CH_2Cl_2, reflux, 2 h, 66% (**17a**), 6% (**17b**). g) 1) $^iBu_2AlH$, CH_2Cl_2, −78°C, 1 h; 2) $NaBH_4$, $CeCl_3 \cdot 7H_2O$, MeOH, 0°C, 10 min, 89% (2 steps). h) $^tBuPh_2SiCl$, imidazole, DMF, rt, 5 min, 89%. i) CrO_3·2Py, CH_2Cl_2, rt, 10 min, 36% (**18**), 34% (**19**). j) 80% aq AcOH, rt, 1 h. k) Bu_4NF, THF, rt, 5 min, 70% (**20**, 2 steps), 68% (**21**, 2 steps).

tively. The 400 MHz ^1H NMR spectra of **20** and **21** showed that, similarly to **1** and **2**, these compounds completely adopt the hemiacetal structures. These phenomena may be rationalized by the formation of two intramolecular hydrogen bonds between the B- and C-rings which efficiently stabilized the hemiacetal structure.[11] Furthermore, **20** and **21** were found to consist of a single C-10 epimer and a 1 : 1.3 mixture of two equilibrated C-10 epimers, respectively. Detailed comparisons of coupling patterns of **20** and **21** with those of **1** and **2** revealed that the B- and C-rings of **20** and **21** take the same conformations as those of **1** and **2**, respectively. Based on these results, stereochemistries of the C-11 methyl groups of **18**—**21**, and that of the C-10 hydroxyl group of **20** were assigned as shown in Scheme 4.

In vitro cytotoxicity of **20** and **21** are shown in Table 2 along with that of **16**. Contrary to our expectation, no cytotoxicity was again observed for **20** and **21** although **16** showed marginal activity. These results are almost the same as those obtained for the C-ring systems **14a**—**d**. Accordingly, it became evident that the antitumor activity of **1** and **2** did not originate merely from their BC-ring systems.

Conclusion

Summing up the results accumulated by the structure-activity relationships, it appears evident that the marked antitumor activity of **1** and **2** does not originate solely from their AB-, C-, and BC-ring systems since these partial structures exhibited no significant cytotoxicity against P388 murine leukemia in vitro. Accordingly, it is anticipated that **1** and **2** show antitumor activity owing to delicate cooperation of their A- and C-rings probably including their B-rings.

Experimental

General. All melting points were determined with a Yamato MP-21 melting point apparatus and are uncorrected. Measurements of optical rotations were carried out using a Horiba SEPA-200 automatic digital polarimeter. IR

spectra measurements were performed with a JASCO A-200 IR spectrometer. ^{1}H NMR spectra were measured with a Hitachi R-90H spectrometer (90 MHz) and a Bruker AM-400 spectrometer (400 MHz). All signals are expressed as ppm down field from tetramethylsilane used as an internal standard (δ value). The following abbreviations are used: singlet (s), doublet (d), triplet (t), quartet (q), multiplet (m), broad (br). Assignments of signals are indicated according to the numbering of IUPAC nomenclature to avoid confusion. Mass spectra were taken with a Hitachi RMV-6MG mass spectrometer. Unless otherwise noted, all reactions were carried out using anhydrous solvents. Especially, tetrahydrofuran and ether freshly distilled from benzophenone ketyl were used. Wako Gel C-200 and Merck Silica Gel 60F$_{254}$ were used as an adsorbent for column chromatography and preparative thin-layer chromatography (PTLC), respectively. The following abbreviations are used for solvents and reagents: acetic acid (AcOH), chloroform ($CHCl_3$), dichloromethane (CH_2Cl_2), diisobutylaluminum hydride (DIBAL), *N*,*N*-dimethylformamide (DMF), ethanol (EtOH), ethyl acetate (AcOEt), methanol (MeOH), tetrabutylammonium fluoride (Bu_4NF), tetrahydrofuran (THF).

Syntheses of the AB-Ring Systems (5 and 8). 4-[(4*S*,5*R*,6*R*)-5-Hydroxy-6-(3-methyl-4-methylene-5-oxotetrahydrofuran-2-yl)-1,3-dioxan-4-yl]-2,6-piperidinedione (5). A solution of **4** (21 mg, 48 μmol)[3] and 10-camphorsulfonic acid (1.0 mg, 4.0 μmol) in wet CH_2Cl_2 (2.0 ml) was stirred at room temperature for 3 h. The mixture was diluted with AcOEt, washed successively with saturated aqueous $NaHCO_3$ and brine, dried ($MgSO_4$), filtered, and concentrated in vacuo. The crude product was chromatographed (SiO_2, 50% AcOEt in $CHCl_3$) to give pure **5** (a mixture of the three diastereomers by NMR) as a colorless caramel (12 mg, 77%). ^{1}H NMR (90MHz, $CDCl_3$-D_2O) δ=1.13, 1.30, 1.32 (total 3H, each d, J=7 Hz, $C_{3''}$-Me), 2.1—3.2 (6H, m, C_3-H_2, C_4-H, C_5-H_2, $C_{3''}$-H), 3.2—4.0 (3H, m, $C_{4'}$-H, $C_{5'}$-H, $C_{6'}$-H), 4.1—4.5 (1H, m, $C_{2''}$-H), 4.74, 4.77 (total 1H, each d, J=6 Hz, $C_{2'\text{-ax}}$-H), 5.16, 5.18 (total 1H, each d, J=6 Hz, $C_{2'\text{-eq}}$-H), 5.69 (1H, m, olefinic proton), 6.32 (1H, m, olefinic proton); IR (film) 3490, 3250, 1770, 1705 cm^{-1}; MS *m*/*z* 326 (M^+H), 325 (M^+), 307 (M^+-H_2O); High-resolution MS, 325.1196, Calcd for $C_{15}H_{19}O_7N$: M, 325.1161.

(−)-4-[(4*S*,5*R*,6*R*)-6-(3-Butenoyl)-5-(*t*-butyldimethylsiloxy)-1,3-dioxan-4-yl]-2,6-piperidinedione (7). The aldehyde **6** (26 mg, 73 μmol) produced from the corresponding siloxy alcohol (30 mg, 84 μmol) in 87% yield by the same Collins oxidation as that reported,[3] was dissolved in ether (2.2 ml). Allylmagnesium chloride (1.0 ml, 0.8 M (1M=1 mol dm^{-3}) ethereal solution, 0.80 mmol) was added to the ethereal solution cooled at −78 °C under an argon atmosphere. After stirring for 1 h, the mixture was diluted with saturated aqueous $NaHCO_3$, allowed to warm up to room temperature, and extracted with AcOEt. The combined extracts were washed with brine, dried ($MgSO_4$), filtered, and concentrated in vacuo. The residue was dissolved in CH_2Cl_2 (3.0 ml). The dichloromethane solution was added to a stirred mixture of Collins reagent, prepared from anhydrous CrO_3 (0.26 g, 2.6 mmol) and pyridine (0.59 g, 7.5 mmol), and dry celite (0.52 g) in CH_2Cl_2 (3.8 ml) at room temperature under an argon atmosphere. After being stirred for 20 min, the mixture was diluted with ether and filtered through a pad of celite. The filtrate was concentrated in vacuo. The residue was dissolved in AcOEt, and the ethyl acetate solution was washed with brine, dried ($MgSO_4$), filtered, concentrated in vacuo. The residue was chromatographed (SiO_2, $CHCl_3$) to give pure **7** as a colorless caramel (12 mg, 42%), $[\alpha]_D^{20}$ −24.4° (*c* 0.50, $CHCl_3$). ^{1}H NMR (400 MHz, $CDCl_3$) δ=0.10 (3H, s, SiMe), 0.22 (3H, s, SiMe), 0.86 (9H, d, Si^{t}Bu), 1.73 (1H, dd, J=2.9 and 12.5 Hz, $C_{3\text{-ax}}$-H), 2.35 (1H, brd, J=18.6 Hz, $C_{5\text{-eq}}$-H), 2.40 (1H, ddt, J=3.6, 12.5, and 1.8 Hz, $C_{3\text{-eq}}$-H), 2.52 (1H, brdq, J=7.2 and 3.6 Hz, C_4-H), 2.67 (1H, dd, J=7.2 and 18.6 Hz, $C_{5\text{-ax}}$-H), 3.34 (1H, ddt, J=6.8, 18.2, and 1.5 Hz, $C_{2''}$-H), 3.48 (1H, ddt, J=6.8, 18.2, and 1.5 Hz, $C_{2''}$-H), 3.48 (1H, brs, $C_{4'}$-H), 4.06 (1H, brs, $C_{5'}$-H), 4.14 (1H, d, J=2.2 Hz, $C_{6'}$-H), 4.78 (1H, d, J=6.3 Hz, $C_{2'\text{-ax}}$-H), 5.12 (1H, dq, J=17.2 and 1.5 Hz, $C_{4''\text{-cis}}$-H), 5.20 (1H, dq, J=10.3 and 1.5 Hz, $C_{4''\text{-trans}}$-H), 5.23 (1H, d, J=6.3 Hz, $C_{2''\text{-eq}}$-H), 5.29 (1H, ddt, J=10.3, 17.2, and 6.8 Hz, $C_{3''}$-H), 6.01 (1H, brs, NH); IR (film) 3310, 3275, 1670 cm^{-1}; MS *m*/*z* 397 (M^+), 340 ($M^+-{}^t$Bu); High-resolution MS, Found: *m*/*z* 397.1910, Calcd for $C_{19}H_{31}O_6NSi$: M, 397.1921.

4-[(4*S*,5*R*,6*R*)-6-(3-Butenoyl)-5-hydroxyl-1,3-dioxan-4-yl]-2,6-piperidinedione (8). AcOH (1.0 ml) was added to a solution of **7** (12 mg, 30 μmol) in MeOH (1.0 ml) at room temperature. After stirring for 5 min, the mixture was concentrated in vacuo. The residue was chromatographed (SiO_2, 70% AcOEt in $CHCl_3$) to afford **8** as a colorless caramel (7.5 mg, 88%). ^{1}H NMR (90 MHz, $CDCl_3$-D_2O) δ=2.0—3.2 (5H, m, C_3-H_2, C_4-H, C_5-H_2), 3.42 (2H, dq, J=7 and 1 Hz, $C_{2''}$-H_2), 3.43 (1H, d, J=9 Hz, $C_{4'}$-H), 4.02 (1H, brs, $C_{5'}$-H), 4.11 (1H, d, J=1 Hz, $C_{6'}$-H), 4.80 (1H, d, J=6 Hz, $C_{2'\text{-ax}}$-H), 5.21 (1H, dq, J=17 and 1 Hz, $C_{4''\text{-cis}}$-H), 5.23 (1H, dq, J=10 and 1 Hz, $C_{4''\text{-trans}}$-H), 5.25 (1H, d, J=6 Hz, $C_{2'\text{-eq}}$-H), 5.95 (1H, ddt, J=10, 17, and 7 Hz, $C_{3''}$-H); IR (film) 3480, 3260, 1705 cm^{-1}; MS *m*/*z* 284 (M^+H), 214 ($M^+-COCH_2CH{=}CH_2$). This sample was found to readily undergo migration of the double bond on chromatographic purification. Since **8** was sufficiently pure (ca. 90% by NMR), it was directly subjected to in vitro cytotoxicity assay.

Syntheses of the C-Ring Systems 14a—d. Syntheses of the γ-Lactone 11a—d. Cyclohexanecarbaldehyde (**9a**) and three sorts of the aromatic aldehydes **9b—d** were found to show considerably different reactivity in the Reformatsky reaction. Therefore, typical experimental procedures are given for syntheses of the lactones **11a, b**. Other γ-lactones **11c, d** were prepared in a similar manner to that described for **11b**.

4-Cyclohexyl-3-methyl-2-methylene-4-butanolide (11a). A solution of **10** (0.11 g, 0.53 mmol)[7] in THF (1.5 ml) was added to a mixture of **9a** (39 mg, 0.35 mmol) and powdered Zn (0.23 g, 3.5 mmol) in THF (5.0 ml) cooled in an ice bath with stirring. After stirring for 2 h, water was added and the mixture was filtered through a pad of celite. The filtrate was extracted with ether and the combined extracts were washed with brine, dried ($MgSO_4$), filtered, and concentrated in vacuo. Column chromatography (SiO_2, 5% AcOEt in hexane) of the crude product afforded pure **11a** (a 1 : 1.3 mixture of the two diastereomers by NMR) as a colorless caramel (62 mg, 92%). ^{1}H NMR (90 MHz, $CDCl_3$) δ=0.6—2.1 (11H, m, C_6H_{11}), 1.16 (1.7H, d, J=7 Hz, C_3-Me, major isomer), 1.25 (1.3H, d, J=7 Hz, C_3-Me, minor isomer), 2.87 (0.43H, m, C_3-H, minor isomer), 3.14 (0.57H, m, C_3-H, major isomer), 3.85 (0.43H, t, J=5 Hz, C_4-H, minor isomer), 4.15 (0.57H, t, J=5 Hz, C_4-H, major isomer), 5.55 (0.57H, d, J=2 Hz, olefinic proton, major isomer), 5.58 (0.43H, J=3 Hz, olefinic proton, minor isomer), 6.17 (0.57H, d, J=2 Hz, olefinic

proton, major isomer), 6.26 (0.43H, d, J=3 Hz, olefinic proton, minor isomer); IR (film) 1770, 1670 cm^{-1} MS m/z 194 (M^+), 111 ($M^+-C_6H_{11}$); High-resolution MS, Found: m/z 194.1303, Calcd for $C_{12}H_{18}O_2$: M, 194.1307.

3-Methyl-2-methylene-4-phenyl-4-butanoilde (11b). A mixture of **9b** (0.14 g, 1.3 mmol), powdered Zn (0.88 g, 13 mmol), and **10** (0.42 g, 2.0 mmol)[7] in THF (10 ml) was heated at reflux for 20 min and cooled to room temperature. The same work-up as that described for **11a**, followed by purification with column chromatography (SiO_2, 50% $CHCl_3$ in hexane), gave pure **11b** (a 1 : 6 mixture of the two diastereomers by NMR) as a colorless caramel (0.20 g, 81%). ^1H NMR (90 MHz, $CDCl_3$) δ=0.87 (2.58H, d, J=7 Hz, C_3-Me, major isomer), 1.46 (0.42H, d, J=7 Hz, C_3-Me, minor isomer), 3.25 (0.14H, m, C_3-H, minor isomer), 3.80 (0.86H, m, C_3-H, major isomer), 5.43 (0.14H, d, J=8 Hz, C_4-H, minor isomer), 6.15 (0.86H, d, J=3 Hz, olefinic proton, major isomer), 6.17 (0.14H, d, J=3 Hz, olefinic proton, minor isomer), 6.21 (0.86H, d, J=9 Hz, C_4-H, major isomer), 6.96 (0.14H, d, J=3 Hz, olefinic proton, minor isomer), 6.98 (0.86H, d, J=3 Hz, olefinic proton, major isomer), 7.7—8.2 (5H, m, aromtic protons); IR (film) 1770, 1670, 1610, 1500 cm^{-1}; MS m/z 188 (M^+); High-resolution MS, Found: m/z 188.0812, Calcd for $C_{12}H_{12}O_2$: M, 188.0837.

4-(*p*-Methoxyphenyl)-3-methyl-2-methylene-4-butanolide (11c). The butanolide **11c** (a 1 : 6 mixture of the two diastereomers by NMR) was obtained as white crystals after purification with column chromatography. ^1H NMR (90 MHz, $CDCl_3$) δ=0.84 (2.58H, d, J=7 Hz, C_3-Me, major isomer), 1.30 (0.42H, d, J=7 Hz, C_3-Me, minor isomer), 2.29 (0.14H, m, C_3-H, minor isomer), 3.43 (0.86H, m, C_3-H, major isomer), 3.80 (3H, s, ArOMe), 4.87 (0.14H, d, J=8 Hz, C_4-H, minor isomer), 5.58 (0.86H, d, J=3 Hz, olefinic proton, major isomer), 5.60 (0.14H, J=3 Hz, olefinic proton, minor isomer), 5.61 (0.86H, J=9 Hz, C_4-H, major isomer), 6.31 (0.14H, d, J=3 Hz, olefinic proton, minor isomer), 6.33 (0.86H, d, J=3 Hz, olefinic proton, major isomer), 6.91 (2H, d, J=9 Hz, aromatic protons), 7.10 (2H, d, J=9 Hz, aromatic protons); IR (film) 1740, 1670, 1615, 1520 cm^{-1}; MS m/z 218 (M^+); High-resolution MS, Found: m/z 218.0939, Calcd for $C_{13}H_{14}O_3$: M, 218.0943.

4-(*p*-Fluorophenyl)-3-methyl-2-methylene-4-butanolide (11d). The butanolide **11d** (a 1 : 5 mixture of the two diastereomers by NMR) was obtained as a colorless caramel after purification with column chromatography. ^1H NMR (90 MHz, $CDCl_3$) δ=0.83 (2.5H, d, J=7 Hz, C_3-Me, major isomer), 1.34 (0.5H, d, J=7 Hz, C_3-Me, minor isomer), 2.98 (0.17H, m, C_3-H, minor isomer), 3.48 (0.83H, m, C_3-H, major isomer), 4.93 (0.17H, d, J=8 Hz, C_4-H, minor isomer), 5.64 (0.83H, d, J=3 Hz, olefinic proton, major isomer), 5.65 (0.83H, d, J=9 Hz, C_4-H, major isomer), 5.66 (0.17H, d, J=3 Hz, olefinic proton, minor isomer), 6.36 (0.17H, d, J=3 Hz, olefinic proton, minor isomer), 6.38 (0.83H, d, J=3 Hz, olefinic proton, major isomer), 6.9—7.5 (4H, m, aromatic protons); IR (film) 1770, 1670, 1610, 1510 cm^{-1}; MS m/z 206 (M^+); High-resolution MS, Found: m/z 206.0742, Calcd for $C_{12}H_{11}O_2F$: M, 206.0743.

Syntheses of the C-Ring Systems 14a—d from the γ-Lactones 11a—d. A typical experimental procedure is given for the synthesis of **14a**. Other C-ring systems were prepared according to the same procedure as that described for **14a**.

1-Cyclohexyl-4-hydroxy-2-methyl-3-methylene-1-butanone and 2-Cyclohexyl-2-hydroxy-3-methyl-4-methylenetetrahydrofuran (14a). DIBAL (0.56 ml, 1.0 M hexane solution, 0.56 mmol) was added to a stirred solution of **11a** (54 mg, 0.28 mmol) in CH_2Cl_2 (1.5 ml) cooled at 0 °C under an argon atmosphere. After stirring was continued for 20 min, MeOH (1.5 ml) was added, and the mixture was allowed to warm up to room temperature and concentrated in vacuo. The residue was dissolved in MeOH (3.5 ml) and the methanolic solution was cooled at 0°C. $CeCl_3 \cdot 7H_2O$ (0.11 g, 0.29 mmol) and $NaBH_4$ (11 mg, 0.29 mmol) was successively added, and the mixture was stirred for 30 min. After acidified to pH 3 with 1M HCl, the mixture was extracted with ether. The combined ethereal extracts were washed with brine, dried ($MgSO_4$), filtered, and concentrated in vacuo, to give crude **12a** as a colorless caramel. ^1H NMR (90 MHz, $CDCl_3$-D_2O) δ=0.9—2.0 (11H, m, C_6H_{11}), 1.05, 1.15 (total 3H, each d, J=7 Hz, C_2-Me), 2.3—2.8 (1H, m, C_2-H), 3.1—3.4 (1H, m, C_1-H), 4.11 (2H, brs, C_4-H_2), 5.00 (1H, brs, olefinic proton), 5.17 (1H, brs, olefinic proton). *t*-Butyldiphenylsilyl chloride (0.11 g, 0.40 mmol) was added to a stirred solution of **12a** and imidazole (59 mg, 0.87 mmol) in DMF (0.20 ml) at room temperature under an argon atmosphere. After stirred for 30 min, the mixture was diluted with AcOEt, washed with brine, and dried ($MgSO_4$). Filtration and concentration in vacuo, followed by separation with column chromatography (SiO_2, 10% AcOEt in hexane), afforded pure **13a** as a colorless caramel (79 mg, 65%). ^1H NMR (90 MHz, $CDCl_3$-D_2O) δ=0.9—1.8 (11H, m, C_6H_{11}), 0.98, 1.01 (total 3H, each d, J=7 Hz, C_2-Me), 1.07 (9H, s, Si^{t}Bu), 2.1—2.6 (1H, m, C_2-H), 3.0—3.3 (1H, m, C_1-H), 4.16 (2H, brs, C_4-H_2), 5.03, 5.10 (total 1H, each brs, olefinic proton), 5.32 (1H, brs, olefinic proton), 7.3—7.6 (6H, m, aromatic protons), 7.6—8.6 (4H, m, aromatic protons); IR (film) 3480, 1740, 1650, 1595 cm^{-1}; MS m/z 379 ($M^+-{}^t$Bu).

Pyridine (0.35 g, 4.4 mmol) was added to a stirred suspension of anhydrous CrO_3 (0.18 g, 1.8 mmol) in CH_2Cl_2 (4.5 ml) at room temperature under an argon atmosphere. After stirring was continued for 20 min, dry celite (0.36 g) and a solution of **13a** (79 mg, 0.18 mmol) in CH_2Cl_2 (1.0 ml) were successively added. After being stirred for 10 min, the mixture was diluted with ether and filtered through a pad of celite. The filtrate was washed successively with saturated aqueous $CuSO_4$ and brine, dried ($MgSO_4$), filtered, and concentrated in vacuo. The residue was dissolved in THF (2.7 ml) and Bu_4NF (0.27 ml, 1.0 M THF solution, 0.27 mmol) was added at room temperature under an argon atmosphere. After stirring for 1 h, the mixture was diluted with ether. The ethereal solution was washed with brine, dried ($MgSO_4$), filtered, and concentrated in vacuo. The residue was chromatographed (SiO_2, 10% AcOEt in hexane) to afford pure **14a** [a 4 : 1 mixture of the equilibrated ketonic and the hemiacetal (a 4 : 1 mixture of the two diastereomeric hemiacetals) forms by NMR] as a colorless caramel (17 mg, 48%). ^1H NMR (90 MHz, $CDCl_3$-D_2O) δ=1.0—2.9 (11H, m, C_6H_{11}), 1.05, 1.12 (total 0.6 H, each d, J=7 Hz, C_3-Me, hemiacetals), 1.22 (2.4H, d, J=7 Hz, C_2-Me, ketone), 3.52 (0.8H, q, J=7 Hz, C_2-H, ketone), 4.12 (1.6H, brs, C_4-H_2, ketone), 4.43 (0.4H, m, C_5-H_2, hemiacetals), 4.9—5.1 (0.4H, m, olefinic protons, hemiacetals), 5.00 (0.8H, brs, olefinic proton, ketone), 5.20 (0.8H, brs, olefinic proton, ketone); IR (film) 3480, 1710, 1650 cm^{-1}; MS m/z 196 (M^+), 129 ($M^+-C_3H_5O$); High-resolution MS, Found: m/z 196.1469, Calcd for $C_{12}H_{20}O_2$: M, 196.1463.

4-Hydroxy-2-methyl-3-methylene-1-phenyl-1-butanone and 2-Hydroxyl-3-methyl-4-methylene-2-phenyltetrahydrofuran (14b): Prepared as a colorless caramel [a 3 : 1 mixture of the equilibrated ketonic and the hemiacetal (a 4:1 mixture of the two diastereomeric hemiacetals) forms by NMR]. ^{1}H NMR (90 MHz, $CDCl_3$-D_2O) δ=0.61, 1.10 (total 0.75H, each d, J=7 Hz, C_3-Me, hemiacetals), 1.40 (2.25H, d, J=7 Hz, C_2-Me, ketone), 2.5—2.8 (0.25H, m, C_3-H, hemiacetals), 4.18 (1.5H, brs, C_4-H_2, ketone), 4.32 (0.75H, q, J=7Hz, C_2-H, ketone), 4.70 (0.5H, m, C_5-H_2, hemiacetals), 4.9—5.1 (0.5H, m, olefinic protons, hemiacetals), 5.06 (0.75H, brs, olefinic proton, ketone), 5.22 (0.75H, brs, olefinic proton, ketone), 7.3—8.1 (5H, m, aromatic protons); IR (film) 3450, 1680, 1600, 1580 cm^{-1}; MS m/z 190 (M^+), 123 ($M^+-C_3H_5O$); High-resolution MS, Found: m/z 190.0969, Calcd for $C_{12}H_{14}O_2$: M, 190.0994.

4-Hydroxy-1-(*p*-methoxyphenyl)-2-methyl-3-methylene-1-butanone and 2-Hydroxy-3-methyl-4-methylene-2-(*p*-methoxyphenyl)tetrahydrofuran (14c): Prepared as a colorless caramel (a 10 : 1 mixture of the equilibrated ketonic and hemiacetal forms by NMR). The ^{1}H NMR spectrum of the ketonic form is as follows. ^{1}H NMR (90 MHz, $CDCl_3$-D_2O) δ=1.40 (3H, d, J=7 Hz, C_2-Me), 3.89 (3H, s, ArOMe), 4.22 (2H, brs, C_4-H_2), 4.32 (1H, q, J=7 Hz, C_2-H), 5.06 (1H, brs, olefinic proton), 5.22 (1H, brs, olefinic proton), 7.66 (2H, d, J=9 Hz, aromatic protons), 8.02 (2H, d, J=9 Hz, aromtic protons); IR (film) 3460, 1675, 1600, 1575, 1510 cm^{-1}; MS m/z 220 (M^+), 153 ($M^+-C_3H_5O$); High-resolution MS, Found: m/z 220.1080, Calcd for $C_{13}H_{16}O_3$: M, 220.1099. The ratio of the two diasteromeric hemiacetals could not be determined.

1-(*p*-Fluorophenyl)-4-hydroxy-2-methyl-3-methylene-1-butanone and 2-(*p*-Fluorophenyl)-2-hydroxy-3-methyl-4-methylenetetrahydrofuran (14d): Prepared as a colorless caramel [a 3 : 1 mixture of the eqilibrated ketonic and the hemiacetal (a 1 : 4 mixture of the two diastereomeric hemiacetals) forms by NMR]. ^{1}H NMR (90 MHz, $CDCl_3$-D_2O) δ=0.67, 1.10 (total 0.75H, each d, J=7 Hz, C_3-Me, hemiacetals), 1.37 (2.25H, d, J=7 Hz, C_2-Me, ketone), 2.4—2.7 (0.25H, m, C_3-H, hemiacetals), 4.19 (1.5H, brs, C_4-H_2, ketone), 4.28 (0.75H, q, J=7 Hz, C_2-H, ketone), 4.66 (0.5H, m, C_5-H_2, hemiacetals), 4.9—5.1 (0.5H, m, olefinic protons, hemiacetals), 5.02 (0.75H, brs, olefinic proton, ketone), 5.22 (0.75H, brs, olefinic proton, ketone), 7.06 (0.5H, t, J=9 Hz, aromatic protons, hemiacetals), 7.13 (1.5H, t, J=9 Hz, aromatic protons, ketone), 7.61 (0.5H, dd, J=6 and 9 Hz, aromatic protons, hemiacetals), 8.05 (1.5H, dd, J=6 and 9 Hz, aromatic protons, ketone); IR (film) 1685, 1600, 1510 cm^{-1}; MS m/z 208 (M^+), 141 ($M^+-C_3H_5O$); High-resolution MS, Found: m/z 208.0885, Calcd for $C_{12}H_{13}O_2F$: M, 208.0899.

Syntheses of the BC-Ring Systems (20 and 21). (−)-2,4-*O*-Methylene-D-sorbitol (15). Methylene acetalization of D-(−)-sorbitol, mp 92—95°C $[\alpha]_D^{20}$ −2.2° (*c* 10.0, H_2O), with 40% aqueous formaldehyde and 12 M HCl (52%),[9] followed by sequential selective acetolysis with AcOH and Ac_2O (57%),[9] and deacetylation with NH_3 gas in MeOH (89%), afforded **15** via (−)-1,3 : 2,4 : 5,6-tri-*O*-methylene-D-sorbitol, mp 214—216°C (recrystallized from EtOH) [lit, 212—216°C (recrystallized from EtOH)[9]], $[\alpha]_D^{20}$ −31.3° (*c* 1.20, $CHCl_3$) [lit, $[\alpha]_D^{20}$ −30.8° (*c* 1.20, $CHCl_3$)[9]] and (+)-3,5-bis(*O*-acetoxymethyl)-1,6-di-*O*-acetyl-2,4-*O*-methylene-D-sorbitol, mp 110—112°C (recrystallized from EtOH) [lit, mp 111—112°C (recrystallized from EtOH)[9]], $[\alpha]_D^{20}$ +29.5° (*c* 1.20, $CHCl_3$) [lit, $[\alpha]_D^{20}$ +29.8° (*c* 1.20, $CHCl_3$)[9]]. The product **15** showed mp 165—166°C (recrystallized from EtOH) [lit, mp 163—164°C (recrystallized from EtOH)[9]] and $[\alpha]_D^{20}$ −9.8° (*c* 1.30, H_2O) [lit, $[\alpha]_D^{20}$ −9.8° (*c* 1.30, H_2O)[9]].

4-[(4*R*,5*R*,6*S*)-5-Hydroxy-6-hydroxymethyl-1,3-dioxan-4-yl]-3-methyl-2-methylene-4-butanolide (16). $NaIO_4$ (2.2 g, 10 mmol) was added to a solution of **15** (2.0 g, 10 mmol) in water (40 ml) at room temperature. After stirring for 5 min, the mixture was concentrated in vacuo. The residue was diluted with MeOH, and filtered through a pad of celite. The filtrate was concentrated in vacuo. A mixture of the residual oil, **10** (3.2 g, 15 mmol),[7] and powdered Zn (6.8 g, 0.10 mol) in a mixture of THF (80 ml) and DMF (5.0 ml) was heated at reflux for 1 h. After cooling to ambient temperature, the mixture was concentrated in vacuo. The residue was diluted with AcOEt, washed with brine, dried ($MgSO_4$), filtered, and concentrated in vacuo. The residue was chromatographed (SiO_2, AcOEt) to give pure **16** (a mixture of the three diastereomers by NMR) as a colorless caramel (1.5 g, 60%). ^{1}H NMR (90 MHz, $CDCl_3$-D_2O) δ=1.13, 1.32, 1.38 (total 3H, each d, J=7 Hz, C_3-Me), 2.7—3.4 (1H, m, C_3-H), 3.5—4.1 (5H, m, $C_{4'}$-H, $C_{5'}$-H, $C_{6'}$-H, $C_{4'}$-CH_2OH), 4.2—4.8 (1H, m, C_4-H), 4.82, 4.83, 4.85 (total 1H, each d, J=6 Hz, $C_{2'\text{-ax}}$-H), 5.18, 5.20, 5.35 (total 1H, each d, J=6 Hz, $C_{2'\text{-eq}}$-H), 5.68 (1H, m, olefinic proton), 6.29 (1H, m, olefinic proton); IR (film) 3450, 1765, 1665 cm^{-1}; MS m/z 245 (M^+H), 244 (M^+); High-resolution MS, Found: m/z 244.0956, Calcd for $C_{11}H_{16}O_6$: M, 244.0947.

4-[(1*R*,2*R*,6*S*,9*R*)-9-(*p*-Methoxyphenyl)-3,5,8,10-tetraoxabicyclo[4.4.0]dec-2-yl]-3-methyl-2-methylene-4-butanolide (17). A solution of **16** (0.82 g, 3.4 mmol), *p*-anisaldehyde (2.3 g, 17 mmol), and *p*-toluenesulfonic acid monohydrate (0.20 g, 1.1 mmol) in a mixture of benzene (100 ml) and CH_2Cl_2 (20 ml) was heated at reflux for 3 h. After being cooled to room temperature, the mixture was concentrated in vacuo. The residue was diluted with AcOEt and the ethyl acetate solution was washed successively with saturated aqueous $NaHCO_3$ and brine, dried, filtered, and concentrated in vacuo. The crude product was separated with column chromatography (SiO_2, 30% AcOEt in hexane) to yield pure **17a** (a 1 : 1 mixture of the two diastereomers by NMR) as a colorless caramel (0.80 g, 66%) and pure **17b** as a colorless caramel (68 mg, 6%).

17a (the mixture of two less polar diastereomers): ^{1}H NMR (90 MHz, $CDCl_3$) δ=1.25 (1.5H, d, J=7 Hz, C_3-Me), 1.28 (1.5H, d, J=7 Hz, C_3-Me), 3.20 (1H, m, C_3-H), 3.63 (1H, brs, $C_{6'}$-H), 3.77 (1H, dd, J=2 and 9 Hz, $C_{2'}$-H), 3.82 (1.5H, s, ArOMe), 3.84 (1.5H, s, ArOMe), 4.11 (1H, brs, $C_{1'}$-H), 4.15 (1H, dd, J=2 and 12 Hz, $C_{7'}$-H), 4.35 (1H, dd, J=1 and 12 Hz, $C_{7'}$-H), 4.45 (0.5H, dd, J=5 and 9 Hz, C_4-H), 4.84 (0.5H, d, J=6 Hz, $C_{4'\text{-ax}}$-H), 4.85 (0.5H, d, J=6 Hz, $C_{4'\text{-ax}}$-H), 4.87 (0.5H, dd, J=7 and 9 Hz, C_4-H), 5.29 (1H, d, J=6 Hz, $C_{4'\text{-ax}}$-H), 5.65 (2H, m, $C_{9'}$-H, olefinic proton), 6.29 (0.5H, d, J=2 Hz, olefinic proton), 6.32 (0.5H, d, J=3 Hz, olefinic proton), 6.95 (2H, d, J=9 Hz, aromatic protons), 7.50 (2H, d, J=9 Hz, aromatic protons); IR (film) 1760, 1665, 1615, 1590, 1515 cm^{-1}; MS m/z 362 (M^+), 361 (M^+−H); High-resolution MS, Found: m/z 362.1359, Calcd for $C_{19}H_{22}O_7$: M, 362.1365.

17b (the more polar diastereomer): ^{1}H NMR (90 MHz, $CDCl_3$) δ=1.24 (3H, d, J=7 Hz, C_3-Me), 3.25 (1H, m, C_3-H), 3.60 (1H, brs, $C_{6'}$-H), 3.82 (3H, s, ArOMe), 3.88 (1H, dd, J=1 and 13 Hz, $C_{7'}$-H), 4.23 (1H, dd, J=1 and 13 Hz, $C_{7'}$-H), 4.48 (1H, dd, J=5 and 8 Hz, C_4-H), 4.85 (1H, d, J=6 Hz, $C_{4'\text{-ax}}$-H), 5.32 (1H, d, J=6 Hz, $C_{4'\text{-eq}}$-H), 5.48 (1H, d, J=3 Hz, olefinic proton), 5.50 (1H, s, C9′-H), 6.19 (1H, d, J=3 Hz, olefinic

proton), 6.90 (2H, d, J=9 Hz, aromatic protons), 7.40 (2H, d, J=9 Hz, aromatic protons); IR (film) 1770, 1670, 1615, 1590, 1515 cm^{-1}; MS m/z 362 (M^+), 361 (M^+−H); High-resolution MS, Found: m/z 362.1354, Calcd for $C_{19}H_{22}O_7$: M, 362.1365.

(−)-(2*R*)-4-(*t*-Butyldiphenylsiloxy)-1-[(1*R*,2*S*,6*R*,9*R*)-9-(*p*-methoxyphenyl)-3,5,8,10-tetraoxabicyclo[4.4.0]dec-2-yl]-2-methyl-3-methylene-1-butanone (18) and (−)-(2*S*)-4-(*t*-Butyldiphenylsiloxy)-1-[(1*R*,2*S*,6*R*,9*R*)-9-(*p*-methoxyphenyl)-3,5,8,10-tetraoxabicyclo[4.4.0]dec-2-yl]-2-methyl-3-methylene-1-butanone (19). DIBAL (6.7 ml, 1.0 M hexane solution, 6.7 mmol) was added to a solution of **17a** (0.78 g, 2.2 mmol) in CH_2Cl_2 (40 ml) cooled at −78°C under an argon atmosphere. After stirring for 1 h, the reaction was quenched by the addition of MeOH (40 ml). The mixture was allowed to warm up to room temperature, and concentrated in vacuo. The residue was diluted with MeOH. $CeCl_3 \cdot 7H_2O$ (2.0 g, 5.4 mmol) and $NaBH_4$ (90 mg, 2.4 mmol) were successively added to the methanolic solution cooled at 0°C. After stirring for 10 min, AcOH was added to the mixture to destroy excess $NaBH_4$. The mixture was concentrated in vacuo. The residue was diluted with AcOEt, washed with brine, dried ($MgSO_4$), and concentrated in vacuo. Purification of the residue with column chromatography (SiO_2, 10% AcOEt in $CHCl_3$) afforded the corresponding diol (a 1 : 1 mixture of the two diastereomers by NMR) as a colorless caramel (0.60 g, 86%). ^1H NMR (90 MHz, $CDCl_3$–D_2O) δ=1.11, 1.21 (total 3H, each d, J=7 Hz, $C_{2''}$-Me), 2.5—3.2 (1H, m, $C_{2'}$-H), 3.5—4.5 (6H, C_1-H, C_2-H, C_6-H, C_7-H_2, $C_{1'}$-H), 3.83 (3H, s, ArOMe), 4.15 (2H, brs, $C_{4'}$-H_2), 4.75, 4.83 (total 1H, each d, J=6 Hz, $C_{4\text{-ax}}$-H), 5.09 (1H, brs, olefinic proton), 5.20 (1H, brs, olefinic proton), 5.26, 5.29 (total 1H, each d, J=6 Hz, $C_{4\text{-eq}}$-H), 5.60 (1H, s, C_9-H), 6.94 (2H, d, J=9 Hz, aromatic protons), 7.51 (2H, d, J=9 Hz, aromatic protons).

t-Butyldiphenylsilyl chloride (1.6 g, 5.8 mmol) was added to a solution of the resulting diol (0.68 g, 1.9 mmol) and imidazole (0.89 g, 13 mmol) in DMF (1.5 ml) at room temperature under an argon atmosphere. After stirring for 5 min, the mixture was diluted with AcOEt. The ethyl acetate solution was washed successively with saturated aqueous $NaHCO_3$ and brine, dried ($MgSO_4$), filtered, and concentrated in vacuo. The crude product was chromatographed (SiO_2, 20% AcOEt in hexane) to give the siloxy alcohol (a 1 : 1 mixture of the two diastereomers by NMR) as a colorless caramel (1.0 g, 89%). ^1H NMR (90 MHz, $CDCl_3$–D_2O) δ=1.04, 1.08 (total 9H, each s, Si^{t}Bu), 1.09, 1.18 (total 3H, each d, J=7 Hz, $C_{2''}$-Me), 2.5—2.9 (1H, m, $C_{2'}$-H), 3.2—4.5 (8H, m, C_1-H, C_2-H, C_6-H, C_7-H_2, $C_{1'}$-H, $C_{4'}$-H_2), 4.50, 4.80 (total 1H, each d, J=6 Hz, $C_{4\text{-ax}}$-H), 5.0—5.2 (2H, m, olefinic protons), 5.25 (1H, d, J=6 Hz, $C_{4\text{-eq}}$-H), 5.58 (1H, s, C_9-H), 6.86, 6.90 (total 2H, each d, J=9 Hz, C_9-aromatic protons), 7.2—7.9 (12H, C_9-aromatic protons, $SiPh_2$).

Pyridine (2.5 g, 32 mmol) was added to a stirred suspension of anhydrous CrO_3 (1.1 g, 11 mmol) in CH_2Cl_2 (20 ml) at room temperature under an argon atmosphere. After stirring for 20 min, dry celite (4.4 g) and a solution of the obtained siloxy alcohol (0.21 g, 0.35 mmol) in CH_2Cl_2 (5.0 ml) were successively added, and the mixture was stirred for 10 min. The mixture was diluted with ether and filtered through a pad of celite. The filtrate was washed successively with water, saturated aqueous $CuSO_4$, and brine, and dried ($MgSO_4$). Filtration and concentration in vacuo followed by separation with PTLC (SiO_2, 20% AcOEt in hexane), yielded pure **18** as a colorless caramel (76 mg, 36%) and pure **19** as colorless solid (72 mg, 34%). The latter solid (**19**) was recrystallized from ether–hexane to give colorless crystals.

18 (the less polar diastereomer): $[\alpha]_D^{20}$ −104° (c 1.00, $CHCl_3$). ^1H NMR (90 MHz, $CDCl_3$) δ=1.07 (9H, s, Si^{t}Bu), 1.10 (3H, d, J=7 Hz, C_2-Me), 3.57 (1H, brs, $C_{6'}$-H), 3.62 (1H, q, J=7 Hz, C_2-H), 3.79 (3H, s, ArOMe), 4.06 (1H, dd, J=2 and 12 Hz, $C_{7'}$-H), 4.15 (1H, d, J=2 Hz, $C_{2'}$-H), 4.26 (3H, m, C_4-H_2, $C_{1'}$-H), 4.32 (1H, dd, J=1 and 12 Hz, $C_{7'}$-H), 4.63 (1H, d, J=6 Hz, $C_{4'\text{-ax}}$-H), 4.88 (1H, brs, olefinic proton), 5.05 (1H, d, J=6 Hz, $C_{4'\text{-eq}}$-H), 5.36 (1H, brs, olefinic proton), 5.50 (1H, s, $C_{9'}$-H), 6.85 (2H, d, J=9 Hz, $C_{9'}$-aromatic protons), 7.3—7.8 (10H, m, $SiPh_2$), 7.35 (2H, d, J=9 Hz, $C_{9'}$-aromatic protons); IR (film) 1725, 1650, 1620, 1590, 1520 cm^{-1}; MS m/z 545 (M^+−^{t}Bu). Found: C, 69.46; 7.14%. Calcd for $C_{35}H_{42}O_7Si$: C, 69.74; H, 7.02%.

19 (the more polar diastereomer): mp 210—211°C, $[\alpha]_D^{20}$ −5.4° (c 1.00, $CHCl_3$). ^1H NMR (90 MHz, $CDCl_3$) δ=1.06 (9H, s, Si^{t}Bu), 1.18 (3H, d, J=7 Hz, C_2-Me), 3.50 (1H, brs, $C_{6'}$-H), 3.60 (1H, q, J=7 Hz, C_2-H), 3.75 (3H, s, ArOMe), 4.00 (1H, dd, J=2 and 12 Hz, $C_{7'}$-H), 4.21 (2H, m, $C_{1'}$-H, $C_{2'}$-H), 4.26 (1H, dd, J=1 and 12 Hz, $C_{7'}$-H), 4.28 (2H, s, C_4-H_2), 4.72 (1H, d, J=6 Hz, $C_{4'\text{-ax}}$-H), 4.95 (1H, brs, olefinic proton), 5.24 (1H, d, J=6 Hz, $C_{4'\text{-eq}}$-H), 5.28 (1H, brs, olefinic proton), 5.52 (1H, s, $C_{9'}$-H), 6.80 (2H, d, J=9 Hz, $C_{9'}$-aromatic protons), 7.34 (2H, d, J=9 Hz, $C_{9'}$-aromatic protons), 7.3—7.8 (10H, m, $SiPh_2$); IR (Nujol) 1725, 1650, 1615, 1590, 1520 cm^{-1}; MS m/z 524 (M^+−^{t}Bu). Found: C, 69.73; H, 7.10%. Calcd for $C_{35}H_{42}O_7Si$: C, 69.74; H, 7.20%.

(+)-(4*S*,5*R*,6*S*)-5-Hydroxy-6-hydroxymethyl-4-[(2*R*,3*R*)-2-hydroxy-3-methyl-4-methylenetetrahydrofuran-2-yl]-1,3-dioxane (20). A solution of **18** (73 mg, 0.12 mmol) in 80% aqueous AcOH (6.0 ml) was stirred at room temperature for 1 h and concentrated in vacuo. Bu_4NF (0.25 ml, 1.0 M THF solution, 0.25 mmol) was added to a solution of the concentration residue in THF (1.5 ml) at room temperature under an argon atmosphere. After being stirred for 5 min, the mixture was concentrated in vacuo. The residue was diluted with AcOEt, washed with brine, dried ($MgSO_2$), and filtered. Concentration of the filtrate in vacuo followed by purification with column chromatography (SiO_2, 10% AcOEt in $CHCl_3$), gave pure **20** as a colorless caramel (21 mg, 70%), $[\alpha]_D^{20}$ +68.2° (c 1.00, $CHCl_3$). ^1H NMR (400 MHz, $CDCl_3$–D_2O) δ=1.22 (3H, d, J=6.8 Hz, $C_{3'}$-Me), 2.61 (1H, m, $C_{3'}$-H), 3.61 (1H, d, J=1.1 Hz, C_4-H), 3.70 (1H, ddd, 1.3, 4.4, and 5.7 Hz, C_6-H), 3.85 (1H, dd, J=4.4 and 12.0 Hz, C_6-C*H*OH), 3.91 (1H, dd, J=5.7 and 12.0 Hz, C_6-C*H*OH), 4.17 (1H, brs, C_5-H), 4.47 (1H, dq, J=13.0 and 2.2 Hz, $C_{5'}$-H), 4.57 (1H, dq, J=13.0 and 2.2 Hz, $C_{5'}$-H), 4.87 (1H, d, J=6.2 Hz, $C_{2\text{-ax}}$-H), 4.95 (1H, q, J=2.2 Hz, olefinic proton), 5.01 (1H, dt, J=3.0 and 2.2 Hz, olefinic proton), 5.27 (1H, d, J=6.2 Hz, $C_{2\text{-eq}}$-H); IR (film) 3420, 1720 cm^{-1}; MS m/z 246 (M^+), 228 (M^++H_2O); High-resolution MS, Found: m/z 246.1079, Calcd for $C_{11}H_{18}O_6$: M, 246.1103.

(−)-(4*R*,5*R*,6*S*)-5-Hydroxy-6-hydroxymethyl-4-[(3*S*)-2-hydroxy-3-methyl-4-methylenetetrahydrofuran-2-yl]-1,3-dioxane (21). The same sequential deprotections of **19** (72 mg, 0.12 mmol) as that described for **20**, followed by purification with column chromatography (SiO_2, 30% AcOEt in $CHCl_3$) yielded pure **21** (a 1 : 1.3 mixture of the two equilibrated epimers at the $C_{2'}$-position by NMR) as a colorless caramel (20 mg, 68%), $[\alpha]_D^{20}$ −21.2° (c 1.00, $CHCl_3$). ^1H NMR (400 MHz, $CDCl_3$–D_2O) δ=1.09 (1.3H, d, J=7.3 Hz, $C_{3'}$-Me, minor epimer), 1.17 (1.7H, d, J=6.8 Hz, $C_{3'}$-Me, major epi-

mer), 2.76 (0.43H, brq, J=7.3 Hz, $C_{3'}$-H, minor epimer), 2.92 (0.57H, m, $C_{3'}$-H, major epimer), 3.60 (0.43H, d, J=1.2 Hz, C_4-H, minor epimer), 3.66 (0.57H, d, J=1.2 Hz, C_4-H, major epimer), 3.69 (0.57H, ddd, J=1.2, 4.6, and 6.2 Hz, C_6-H, major epimer), 3.72 (0.43H, ddd, J=1.0, 4.4, and 5.4 Hz, C_6-H, minor epimer), 3.83 (0.57H, dd, 4.6 and 11.9 Hz, C_6-C*H*OH, major epimer), 3.87 (0.43H, dd, J=4.4 and 12.0 Hz, C_6-C*H*OH, minor epimer), 3.90 (0.43H, dd, J=5.4 and 12.0 Hz, C_6-C*H*OH, minor epimer), 3.95 (0.57H, dd, J=6.2 and 11.9 Hz, C_6-C*H*OH, major epimer), 4.05 (0.57H, brs, C_5-H, major epimer), 4.22 (0.43H, brs, C_5-H, minor epimer), 4.46 (0.43H, dq, J=12.9 and 2.2 Hz, $C_{5'}$-H, minor epimer), 4.52 (0.57H, dq, J=12.8 and 2.2 Hz, $C_{5'}$-H, major epimer), 4.56 (0.57H, dq, J=12.8 and 2.2 Hz, $C_{5'}$-H, major epimer), 4.59 (0.43H, ddt, J=1.2, 12.9, and 2.2 Hz, $C_{5'}$-H, minor epimer), 4.85 (0.43H, d, J=6.2 Hz, $C_{2'\text{-ax}}$-H, minor epimer), 4.87 (0.57H, d, J=6.2 Hz, $C_{2'\text{-ax}}$-H, major epimer), 4.96 (0.43H, q, J=2.2 Hz, olefinic proton, minor epimer), 5.00 (0.57H, q, J=2.2 Hz, olefinic proton, major epimer), 5.04 (0.43H, dt, J=1.5 and 2.2 Hz, olefinic proton, minor epimer), 5.07 (0.57H, dt, J=3.0 and 2.2 Hz, olefinic proton, major epimer), 5.24 (0.43H, J=6.2 Hz, $C_{2\text{-eq}}$-H, minor epimer), 5.26 (0.57H, J=6.2 Hz, $C_{2\text{-eq}}$-H, major epimer); IR (film) 3420, 1725 cm^{-1}; MS m/z 246 (M^+), 228 (M^+-H_2O); High-resolution MS, Found: m/z 246.1089, Calcd for $C_{11}H_{18}O_6$: M, 246.1103.

We are grateful to Dr. Kunikazu Sakai and Miss Nobuko Hida, Sagami Chemical Research Center, Drs. Shigeru Tsukagoshi and Tazuko Tashiro, Cancer Chemotherapy Center, Japanese Foundation for Cancer Research, for evaluation of in vitro cytotoxicity and in vivo antitumor activity against P388 murine leukemia.

References

1) a) R. G. Powell, C. R. Smith, Jr., D. Weisleder, G. K. Matsumoto, J. Clardy, and J. Kozlowski, *J. Am. Chem. Soc.*, **105**, 3739 (1983); b) R. G. Powell, C. R. Smith, Jr., and D. Weisleder, *Phytochemistry*, **23**, 2789 (1984); c) R. G. Powell and C. R. Smith, Jr., U. S. Patent 4534327 (1985).

2) C. P. Gorst-Allman, P. S. Steyn, and R. Vleggaar, *J. Chem. Soc., Perkin Trans. 1*, **1984**, 1311.

3) a) F. Matsuda, M. Kawasaki, and S. Terashima, *Tetrahedron Lett.*, **26**, 4639 (1985); b) F. Matsuda and S. Terashima, *ibid.*, **27**, 3407 (1986); c) F. Matsuda and S. Terashima, *Yuki Gosei Kagaku Kyokai Shi*, **45**, 983 (1987); d) F. Matsuda and S. Terashima, *Tetrahedron*, in press.

4) For other two independent total syntheses of the antipodes of sesbanimides, see, M. J. Wanner, G.-J. Koomen, and U. K. Pandit, *Heterocycles*, **22**, 1483 (1984); M. J. Wanner, N. P. Willard, G.-J. Koomen, and U. K. Pandit, *J. Chem. Soc., Chem. Commun.*, **1986**, 396; M. J. Wanner, N. P. Willard, G.-J. Koomen, and U. K. Pandit, *Tetrahedron*, **43**, 2549 (1987); R. H. Schlessinger and J. L. Wood, *J. Org. Chem.*, **51**, 2621 (1986).

5) A number of synthetic studies on sesbanimides were also reported: K. Tomioka and K. Koga, *Tetrahedron Lett.*, **25**, 1599 (1984); G. W. J. Fleet and T. K. M. Sing, *J. Chem. Soc., Chem. Commun.*, **1984**, 835; M. Shibuya, *Heterocycles*, **23**, 61 (1985); T. Kinoshita, K. Okamoto, and J. Clardy, *Synthesis*, **1985**, 402; G. Sacripante, C. Tan, and G. Just, *Tetrahedron Lett.*, **26**, 5643 (1985); A. V. Rama Rao, J. S. Yadav, A. N. Naik, and A. G. Chaudhary, *ibid.*, **27**, 993 (1986); W. R. Roush and M. R. Michaelides, *ibid.*, **27**, 3353 (1986).

6) A. Löffler, R. D. Pratt, J. Pucknat, G. Gelbard, and A. S. Dreiding, *Chimia*, **23**, 413 (1969).

7) Prepared from ethyl acrylate and acetaldehyde according to the known procedure: H. M. R. Hoffmann and J. Rabe, *Angew. Chem., Int. Ed. Engl.*, **22**, 795 (1983).

8) J.-L. Luche, *J. Am. Chem. Soc.*, **100**, 2226 (1978); A. L. Gemal and J.-L. Luche, *ibid.*, **103**, 5454 (1981).

9) A. T. Ness, R. M. Hann, and C. S. Hudson, *J. Am. Chem. Soc.*, **66**, 665 (1944).

10) Initially, protection of **16** in a form of the bis(*t*-butyldimethylsilyl) ether was examined by treating with *t*-butyldimethylsilyl trifluoromethanesulfonate in the presence of 2,6-lutidine as a base. However, the C-8 silyl group (sesbanimide numbering) of the produced bissilyl ether (**16**: X=Y=Si^{t}BuMe$_2$) was found to be so labile that most of this silyl ether cleaved during purification with silica-gel column chromatography to give the monosilyl ether (**16**: X=H, Y=Si^{t}BuMe$_2$) as the main product. Comparisons of the ^{1}H NMR spectra of **16** and its bis- and monosilyl ethers made it clear that unexpected lability of the C-8 silyl group can be explained by remote distortion of the γ-lactone moiety brought about by the C-8 bulky silyl group. Thus, in the NMR spectrum of **16** (X=Y=Si^{t}BuMe$_2$), the signals of olefinic protons appeared at δ 5.07 and 5.33. In contrast, the olefinic protons of **16** (X=Y=H) and **16** (X=H, Y=Si^{t}BuMe$_2$) show the ordinary chemical shifts at δ 5.68 and 6.29 and δ 5.65 and 6.28, respectively. Similar remote distortion of the glutarimide ring by the C-8 bulky silyl group has been observed in the course of the total synthesis of **1** and **2**.[3)]

11) The similar two intramolecular hydrogen bonds may stabilize the structures of **1** and **2** which solely take the hemiacetal forms.

Synthesis of 2-(1-Phosphorylalkyl)- and 2-(1-Alkenyl)furans through Nitrile Oxide Cycloaddition Route

Otohiko TSUGE,* Shuji KANEMASA, and Hiroyuki SUGA
Institute of Advanced Material Study, and Department of Molecular Science and Technology, Interdisciplinary Graduate School of Engineering Sciences, Kyushu University, Kasugakoen, Kasuga 816
(Received January 11, 1988)

A new synthetic method of 2-(1-phosphorylalkyl)furans with a variety of substituents on the ring is presented. Cycloaddition of (diethoxyphosphoryl)acetonitrile oxide to *O*-protected allyl alcohols is followed by a simple sequential procedure including Raney Ni reduction and acid treatment to give 2-(1-phosphorylmethyl)-furans. The phosphorus-stabilized carbanions derived from the phosphorus-functionalized furans are applied to alkylation, oxidation with oxygen, or olefination to provide 2-(1-phosphorylalkyl)furans, 2-acylfurans, or 2-(1-alkenyl)furans, respectively. Some other synthetic applications are also described.

We have already reported some synthetic applications of a phosphorus-functionalized nitrile oxide, (diethoxyphosphoryl)acetonitrile oxide.[1] It undergoes regioselective 1,3-dipolar cycloadditions to olefins or acetylenes to furnish good yields of 2-isoxazolines[1a,b] or isoxazoles[1c] bearing a phosphorylmethyl moiety at the 3-position. Reductive N-O bond cleavage provides 4-hydroxy-2-oxo- or 2,4-dioxoalkylphosphonates which can be further converted into 1,4-alkadien-3-ones,[1b] 1-hydroxy-4-alken-3-ones,[1d] and 5-(1-alkenyl)-3(2*H*)-furanones.[1c]

Regioselective cycloadditions of nitrile oxides to allyl alcohols will produce 2-isoxazoline-5-methanols. They are then hydrogenated leading to β,γ-dihydroxy ketones whose acid-catalyzed cyclization would give rise to furans (Eq. 1). Although the last cyclization step has not been well documented before,[2] similar acid-catalyzed furan syntheses from β,γ-epoxy ketones are known.[3] Substitution patterns of the furans depend upon those of the 2-isoxazolines, hence the nitrile oxides and allyl alcohols.

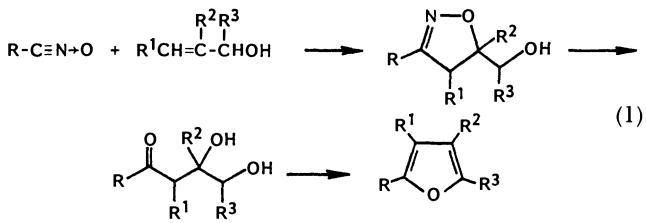

(1)

4-Substituted 2-(1-alkenyl)furan structures often occur in the important family of furanosesquiterpenoids, some of which are illustrated below.[4-8] As a phosphorylmethyl moiety may be introduced at the 2-position of furan rings by the cycloaddition route shown in Eq. 1 using a phosphorylacetonitrile oxide (RCNO, R=$(EtO)_2POCH_2$), this route will find useful synthetic applications in the construction of 2-(1-alkenyl) substituent of these furanosesquiterpenoids, especially the olefin substituent bearing *E*-configuration.

The present article describes a new synthesis of 2-(1-phosphorylmethyl)furans through cycloadditions of a phosphorus-functionalized nitrile oxide to *O*-protected allyl alcohols and a subsequent sequence of reductive N-O bond fission and acid treatment. These furans are further converted into 2-(1-phosphorylalkyl)furans, 2-(1-alkenyl)furans, 2-acylfurans, and 2,5-dioxoalkylphosphonates.

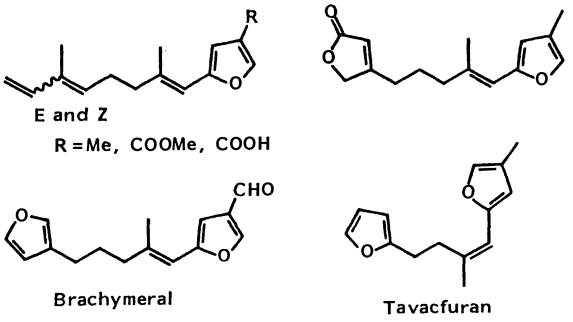

Results and Discussion

Cycloadditions of a Phosphorylacetonitrile Oxide to *O*-Protected Allyl Alcohols Leading to 2-Isoxazolines. The cycloaddition of (diethoxyphosphoryl)acetonitrile oxide (**2**) to allyl alcohol itself was first tried under the reaction conditions previously employed in the successful cycloadditions to olefins.[1a,b] Thus oxime **1** and 2-propen-1-ol (5 equiv) were treated with *N*-bromosuccinimide (NBS, 2 equiv) and triethylamine (1 equiv) in *N*,*N*-dimethylformamide (DMF)-diethyl ether (1 : 1 v/v) at room temperature for 18 h to give only 6% yield of the expected cycloadduct, 3-(diethoxyphosphoryl)methyl-2-isoxazoline-5-methanol, indicating the need of *O*-protection.

Therefore the tetrahydropyranyl (THP, **3a**) and trimethylsilyl ethers of 2-propen-1-ol were employed in the reaction with **2**. Under the same reaction conditions (5 equiv of the ether, rt, 18 h), the THP ether **3a** gave a better yield of cycloadduct **4a** (62%) than the trimethylsilyl ether (32%). When the former reaction was carried out under reflux in a mixed solvent, DMF-diethyl ether-hexane (1 : 1 : 1 v/v), the yield of **4a** was not improved (58%).[9]

Cycloadditions of **2** to a variety of allyl THP ethers

3a—f were performed at room temperature for 18 h by using excess amounts of the ethers **3** (5 equiv). Nitrile oxide **2** was generated in advance from *N*-[2-(diethoxyphosphoryl)ethylidene]hydroxylamine (**1**) according to the reported method (NBS in DMF, −20 °C, 1 h then 0 °C, 0.5 h, NEt_3 in diethyl ether).[1b]

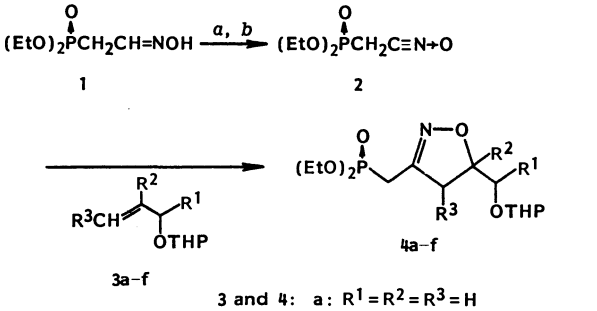

3 and 4: a: $R^1=R^2=R^3=H$
b: $R^1=Me$, $R^2=R^3=H$
c: $R^1=Et$, $R^2=R^3=H$
d: $R^1=R^2=H$, $R^3=Me$
e: $R^1=R^2=H$, $R^3=CH_2OTHP$
f: $R^1=H$, $R^2R^3=(CH_2)_3$

a: NBS (2 equiv) in DMF, −20 °C (1 h) → 0 °C (0.5 h).
b: NEt_3 (1 equiv)

Scheme 1.

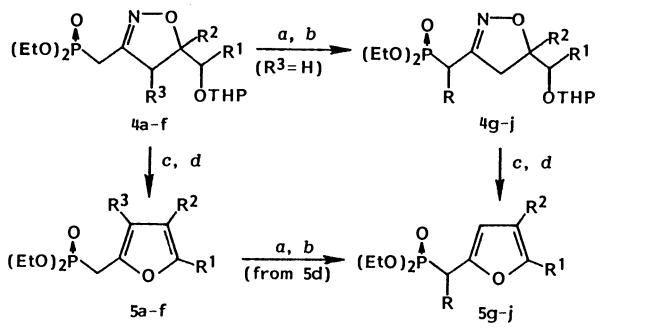

4 and 5: a: $R^1=R^2=R^3=H$
b: $R^1=Me$, $R^2=R^3=H$
c: $R^1=Et$, $R^2=R^3=H$
d: $R^1=R^3=H$, $R^2=Me$
e: $R^1=R^2=H$, $R^3=CH_2OTHP$ (5e: $R^3=CH_2OH$)
f: $R^1=H$, $R^2R^3=(CH_2)_3$
g: $R^1=Et$, $R^2=H$, $R=n\text{-}C_8H_{17}$
h: $R^1=Et$, $R^2=H$, $R=n\text{-}C_5H_{11}$
i: $R^1=H$, $R^2=Me$, $R=n\text{-}C_5H_{11}$
j: $R^1=H$, $R^2=Me$, $R=PhCH_2$

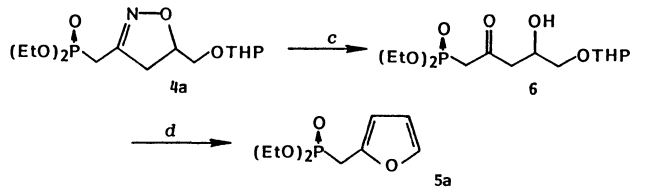

a: n-BuLi in THF, −78 °C. *b*: RX, rt. *c*: Raney Ni, $B(OH)_3$, in aq AcOH. *d*: AcONa in AcOH, 100 °C

Scheme 2.

Unsymmetrically mono- and disubstituted olefins provided satisfactory yields of regioselective cycloadducts **4a—d** (62—76% based on the oxime **1**), while a symmetrically disubstituted olefin and a trisubstituted olefin gave **4e** and **4f** only in fair yields (**4e**: 46%. **4f**: 29%. Scheme 1 and Table 1). These cycloadducts **4** were obtained all as mixtures of more than two diastereomers (^1H and ^{13}C NMR), however their separation was not attempted.

Conversion of 3-(1-Phosphorylalkyl)-2-isoxazolines into 2-(1-Phosphorylalkyl)furans. Conversion of the above cycloadducts, 3-(phosphorylmethyl)-2-isoxazolines **4**, into furans **5** was initially examined by using **4a** as an example (Scheme 2): Hydrogenation of **4a** on Raney Ni (W-2) in aq EtOH in the presence of $B(OH)_3$ gave β-hydroxy ketone **6** with the THP protecting group intact in 87% yield. Heating **6** with AcONa in AcOH at 100—110 °C for 3 h furnished the desired product, 2-[(diethoxyphosphoryl)methyl]furan (**5a**) in 77% yield. Since about a half of **6** is consumed by decomposition in a single operation on silica-gel chromatography, the purification step of **6** was omitted.

Thus the crude reaction mixtures separated in the Raney Ni reduction of isoxazolines **4a—f** were immediately treated with AcONa in AcOH at 90—100 °C for 0.5 h to give the expected furans **5a—f** in satisfactory yields (Scheme 2 and Table 1). As the isoxazoline **4e** affords a mixture of **5e**, its THP ether, and its *O*-acetate when cyclized in acetic acid, the cyclization was carried out in aq tetrahydrofuran (THF) in the presence of *p*-toluenesulfonic acid to give **5e** as a sole product. Yields of **5e** and **5f** are lower than the other cases.

An alkyl group can be introduced at the side chain of 2-isoxazolines **4c** and **4d** via the phosphorus-stabilized carbanions generated by the action of butyllithium to produce 3-(1-phosphorylalkyl)-2-isoxazolines **4g—j** in 59—65% yields. These alkylated 2-isoxazolines **4g—j** can be also converted into the corresponding furans **5g—j** through a sequence of reductive ring opening and acid-catalyzed cyclization (Scheme 2 and Table 2). The furans **5i** and **5j** bearing a methyl substituent at the 4-position were obtained only in fair yields. An alternative and more effective route leading to the furans **5i** and **5j** consists of alkylation after construction of the furan rings as shown in two examples of alkylation of **5d** (87—88%, Scheme 2 and Table 2).

Horner-Emmons Olefinations of 2-(1-Phosphorylalkyl)furans Leading to 2-(1-Alkenyl)furans. Two 2-[(diethoxyphosphoryl)methyl]furans **5b** and **5d** were employed in the Horner-Emmons olefinations using aldehydes: 4-Methylfuran **5d** was deprotonated with butyllithium in THF at −78 °C and then treated with benzaldehyde at room temperature to furnish 61% of (*E*)-4-methyl-2-(2-phenylethenyl)furan (**8b**). On the other hand, only 33% of (*E*)-5-methyl-2-(1-pentenyl)-furan (**8a**) and recovered **5b** (26%) were obtained from 5-methylfuran **5b** and butanal (2 equiv). In this case

Table 1. Cycloaddition of **2** to Allyl Ethers **3** and Subsequent Furan Synthesis

Cycloaddition to allyl ethers 3[a]			Furan synthesis[b,c]			
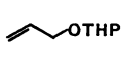	**3a**	A[d]	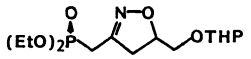	**4a** B (62%)	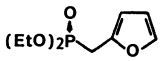	**5a** (60%)
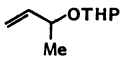	**3b**	A	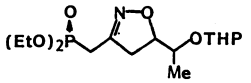	**4b** B (76%)	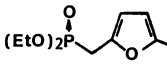	**5b** (54%)
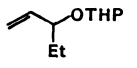	**3c**	A	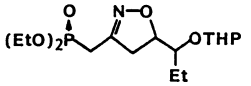	**4c** B (73%)	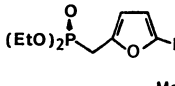	**5c** (60%)
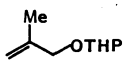	**3d**	A	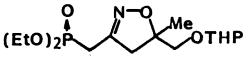	**4d** B (67%)	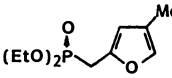	**5d** (61%)
	3e	A	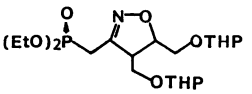	**4e** C (46%)	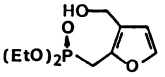	**5e** (41%)
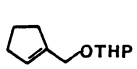	**3f**	A	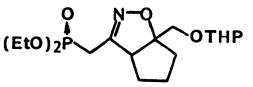	**4f** D (29%)	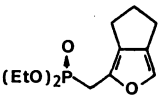	**5f** (25%)

a) Excess of **3** was used (5 equiv). b) Raney Ni, $B(OH)_3$ in aq EtOH, rt. c) Cyclization to furans **5** was performed under either of the following conditions: B: AcONa in AcOH, 100 °C, 0.5 h. C: *p*-TsOH in aq THF, 70 °C, 8 h. D: AcONa in AcOH, 90 °C, 0.5 h. d) A: rt, 18 h.

Table 2. Synthesis of 2-(1-Phosphorylalkyl)furans **5**

Alkylation of 2-isoxazolines 4[a]		Synthesis of 2-(1-phosphorylalkyl)furans 5[b,c]		
4c	n-$C_8H_{17}I$, 14 h, 64%[d]	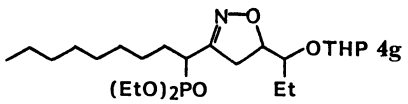 **4g**	64%	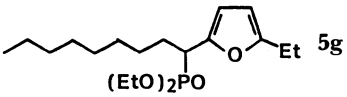 **5g**
4c	n-$C_5H_{11}I$, 14 h, 65%[e]	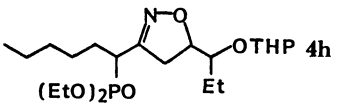 **4h**	64%	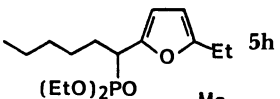 **5h**
4d	n-$C_5H_{11}I$, 16 h, 59%[f]	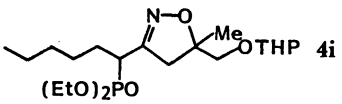 **4i**	26%	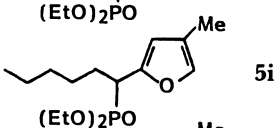 **5i**
4d	$PhCH_2Br$, 16 h, 65%[g]	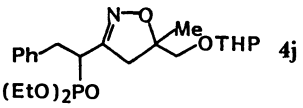 **4j**	16%	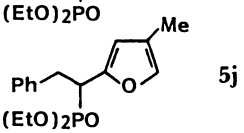 **5j**

Alkylation of furan **5d**[h]

5d → n-$C_5H_{11}I$, 5 h, 88% → **5i**

5d → $PhCH_2Br$, 2.5 h, 87% → **5j**

a) Lithiation: *n*-BuLi, −78 °C, 1 h. Alkylation: −78 °C (1 h)→0 °C (1 h)→rt. b) Raney Ni, $B(OH)_3$ in aq EtOH, rt. c) AcONa in AcOH, 100 °C, 0.5 h. d) Recovered **4c**: 8%. e) −78 °C, 1 h. Alkylation: −78 °C.

condensation of butanal itself was the major reaction. Use of sodium hydride instead of butyllithium did not improve the yield of **8a** (29%).

It is known that, in olefination reactions between carbanions derived from alkylphosphonates and aldehydes, the addition step of aldehydes occurs rapidly in high yields but the rate-determining elimination step competes with the retro addition step, resulting in low yield formation of olefins.[10] Recently an example of the effective elimination of a phosphorus moiety from

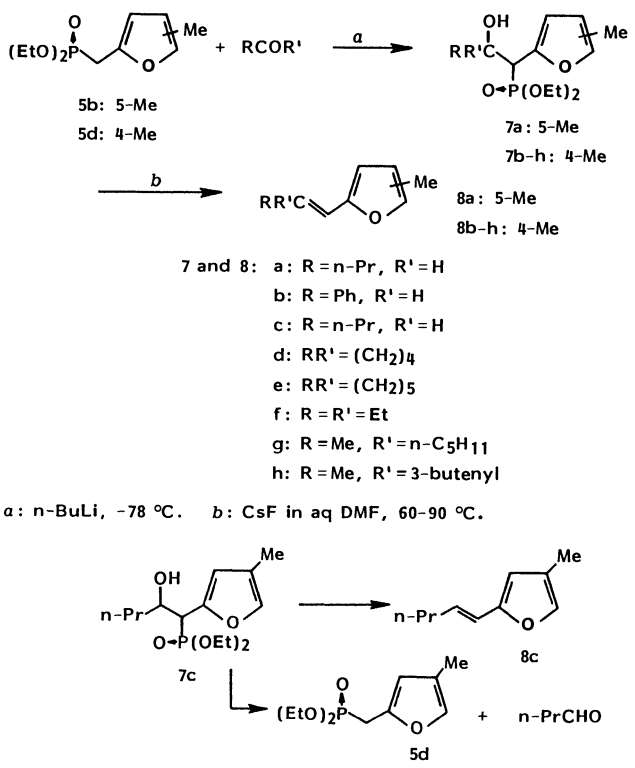

Scheme 3.

carbonyl adducts has been reported.[11]

The reaction of the carbanion derived from 4-methylfuran **5d** and butyllithium with butanal at −78 °C for 30 min afforded an adduct **7c** as a mixture of two diastereomers (7:3) in 93% yield. The adduct **7c** was then subjected to an olefination by treatment with cesium fluoride and water (each 3.8 equiv) in DMF at 60 °C for 36 h to give 4-methyl-2-(1-pentenyl)furan (**8c**) (*E*:*Z*=96:4) in 64% yield together with the recovered **7c** (18%) and 4-methyl-2-(phosphorylmethyl)furan (**5d**) (4%) (Scheme 3). The latter compound **5d** corresponds to a retro-addition product of **7c**.

This two-step olefination procedure of 4-methyl-2-(phosphorylmethyl)furan **5d** was applied to some other carbonyl compounds. Like aldehydes, cyclic and acyclic ketones undergo smooth additions to furnish adducts **7d—h** whose elimination reactions are even cleaner than those of the aldehyde adducts **7b** and **7c** to produce 2-(1-alkenyl)-4-methylfurans **8d—h** (Scheme 3 and Table 3). Total yields of **8** are 49—71% based on **5** except for **8a** which was obtained by the one-pot procedure without isolation of **7a**. Compared to the almost exclusive formation of (*E*)-olefins (**8b** and **8c**) from the aldehyde adducts **7b** and **7c**, *E*-selectivities are only higher than 80% in olefinations from the adducts (**7g** and **7h**) to unsymmetrical ketones.

Table 3. Olefination of 2-(Phosphorylmethyl)furans **5**

Addition of **5** to aldehydes or ketones[a]		Synthesis of 2-(1-alkenyl)furans **8**[b]									
			Yield/%[c]					Yield/%[c]			*E*:*Z*[d]
5b+butanal	A	**7a**[e]						**8a**	33[f]	26*	— 98:2
5d+benzaldehyde	B	**7b**	93	7:3[g]	C			**8b**	53	—	20** 99:1
5d+butanal	B	**7c**	89	4:1[g]	C			**8c**	64	18*	4** 96:4
5d+cyclopentanone	B	**7d**	91	4*	C	51 h		**8d**	78	3*	6** —
5d+cyclohexanone	B	**7e**	80	6*	C	33 h		**8e**	85	5*	— —
5d+3-pentanone	B	**7f**	80	9*	C	30 h		**8f**	75	3*	8** —
5d+2-heptanone	B	**7g**	88	3*	4:1[g]	C	30 h	**8g**	73	6*	10** 80:20
5d+5-hexen-2-one	B	**7h**	90	2*	4:1[g]	C	30 h	**8h**	67	4*	12** 82:18

a) A: NaH (1.2 equiv), rt, 2h; butanal (2 equiv), rt, 2h. B: *n*-BuLi, −78 °C, 1 h; a carbonyl compound (1.5 equiv), −78 °C, 0.5 h. b) C: CsF (3.8 equiv) in aq DMF, 60 °C. c) Yield of isolated products. Yield with an asterisk: recovered **5** or **7**; two asterisks: retro aldol product **5**. d) Determined by GLC. e) Not isolated. f) Yield based on **5b**. g) Diastereomer ratio (^{1}H NMR).

Though the adduct **7b** was a 7:3 mixture of two diastereomers, *E*-selectivity in the olefination leading to **8b** is as high as 99% (Table 3). Under our elimination conditions (CsF in aqueous DMF at 60 °C), it is unlikely to happen that the anion of adduct **7b** is equilibrating with benzaldehyde and the anion of **5d**, a retro addition. Accordingly the high *E*-selectivity must be a kinetical result: Based on steric hindrance in the transition states, the major isomer **B** whose cis elimination leads to the *E*-isomer (*E*)-**8b** should undergo much more ready elimination than the other diastereomer **C** (Fig. 1, R=Ph). As a result, the retro addition product **5d** (20%) presumably arises mainly from the unreacted diastereomer **C** (R=Ph).

Similar kinetical resolution is observed in the olefination of **7c** (4:1) producing **8c** (64%, *E*:*Z*=96:4). In this case the unreacted **7c** recovered in 18% yield consists of almost pure diastereomer **C** (R=*n*-Pr), indicating the rapid olefin formation from the major diastereomer **B** (R=*n*-Pr).

Predominant formation of the diastereomers **B** over the other **C** in the addition reactions of lithiated **5d** with aldehydes can be well-interpreted with a six-membered chelation model (Fig. 1). The chair transition state **A** with two bulky substituents (4-methyl-2-furyl and R) at equatorial positions gives the major diastereomers **B**.

Two diastereomers of the adduct **7g** or **7h** to unsymmetrical ketones do not show such different reactivity in the elimination leading to **8g** or **8h**. Thus the isomer ratios between the two diastereomers of **7g** or **7h** (both 4:1) are nearly equal to those between the *E*- and *Z*-isomers of **8g** (80:20) or **8h** (82:18) (Table 3).

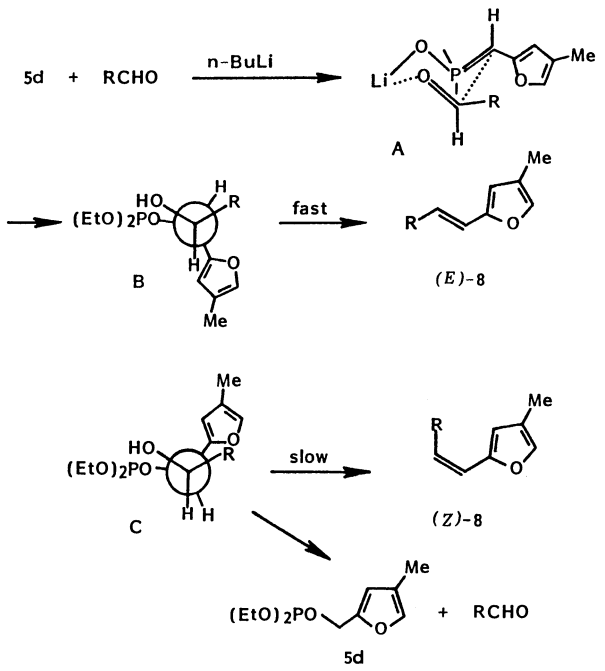

Fig. 1. Stereochemistry of Horner-Emmons olefinations of **5d** with aldehydes.

Conversion of 2-(1-Phosphorylalkyl)furans into 2-Acylfurans and 2,5-Dioxoalkylphosphonates. Air-oxidation of phosphorus-stabilized carbanions offers a simple preparation of ketones.[12] According to our previous procedure[1a,b] by which 3-acyl-2-isoxazolines have been prepared from 3-(1-phosphorylalkyl)-2-isoxazolines, the carbanion generated from 4-methyl-2-(1-phosphorylalkyl)furans **5i** and butyllithium was oxidized by dry oxygen at −78 °C to give 2-acylfuran **9a** in 30% yield (Scheme 4). Monitoring this reaction by thin-layer chromatography (TLC) showed the formation of complex mixture. Presumably the ketone **9a** as a product further reacted with the starting carbanion. So the carbanion of **5j** was oxidized at −100 °C in order to avoid the further condensation, but again only a low yield (20%) of **9b** was afforded.

On the other hand 5-substituted 2-(1-phosphorylalkyl)-furans **5** can be converted into 2,5-dioxoalkylphosphonates **10** through the usual hydrolysis method of furan rings.[13] Thus **5b**, **5c**, and **5g** were heated at 120 °C together with a catalytic amount of sulfuric acid in aqueous acetic acid to furnish moderate yields of 1,4-diketones **10a—c**, respectively, with the phosphoryl moiety intact (Scheme 4).

Though intramolecular cyclization of 1,4-diketones is one of the most important accesses to cyclopentenones, its regiochemical control has been a serious problem.[14] As the use of 2,5-dioxoalkylphosphonates will enable regioselective cyclization,[15] **10c** was treated with triethylamine (1.1 equiv) in the presence of lithium bromide (1.5 equiv) in refluxing THF to give 31% of 3-ethyl-2-octyl-2-cyclopenten-1-one (**11**) (Scheme 4).

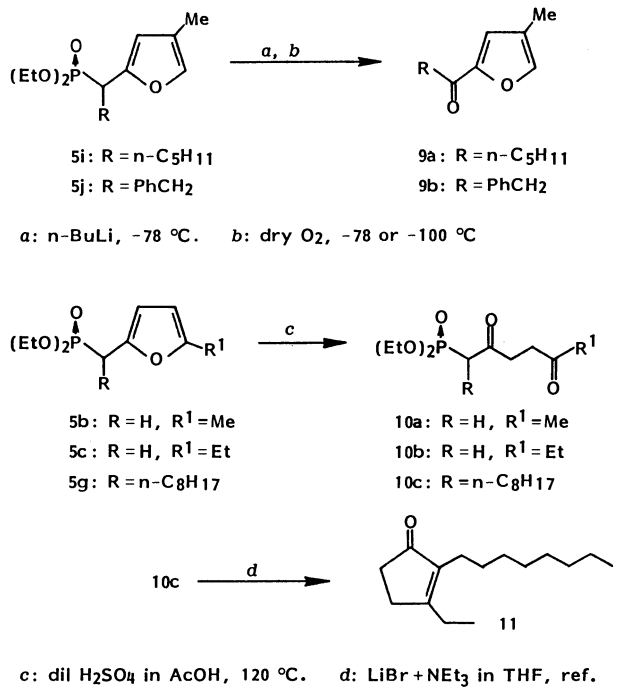

Scheme 4.

Table 4. ^{13}C NMR Chemical Shifts of **12a—d**

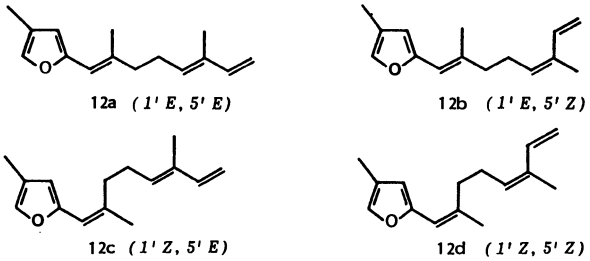

	2'-Me	3'-C	5'-C	6'-C	6'-Me	7'-C	8'-C
12a	18.52	40.36	132.13	134.38	11.68	141.49	110.64
12b	19.74	40.75	130.15	133.63	19.74	133.63	113.57
12c	24.71	33.38	132.65	134.31	11.63	141.56	110.89
12d	25.74	33.78	130.58	133.74	19.74	133.74	113.42

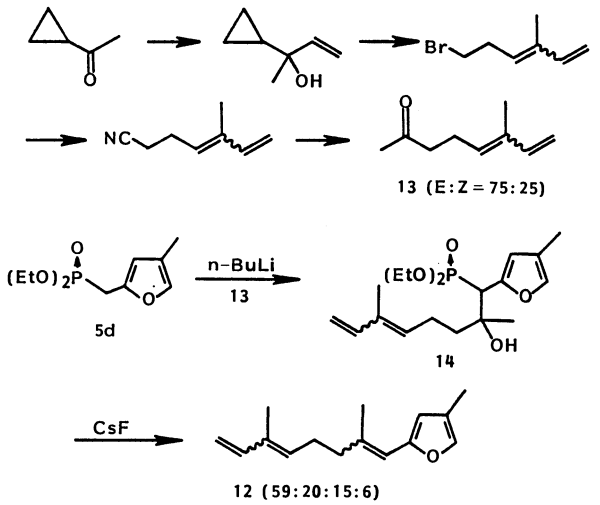

Scheme 5.

Synthesis of a Furanosesquiterpene. As briefly shown in the introduction, there are several furanosesquiterpenoids which bear a general structure of (*E*)-4-methyl-2-(2-methyl-1-alkenyl)furans. They would be readily accessible by the Horner-Emmons olefination of 4-methyl-2-[(diethoxyphosphoryl)methyl]furan (**5d**) with methyl ketones. Furanosesquiterpene **12**,[4] isolated from an Australian soft coral, also belongs to this family. And two isomers, (1'*E*, 5'*E*)-isomer **12a** and (1'*E*, 5'*Z*)-isomer **12b**, of 4-methyl-2-(2,6-dimethyl-1,5,7-octatrienyl)furan are naturally occurring. *E*-Geometry at the 1-position of the alkatrienyl substituent of **12** will be conveniently constructed by use of the Horner-Emmons olefination of **5d**.

6-Methyl-5,7-octadien-2-one (**13**) is the requisite ketone, and a mixture of *E*- and *Z*-isomers of **13** has been previously prepared.[16,17] A 75:25 inseparable mixture (GLC in a capillary column) of *E*- and *Z*-isomers of **13** was prepared according to this method (Scheme 5).

After 4-methyl-2-(phosphorylmethyl)furan **5d** was lithiated with butyllithium in THF, the resulting anion was allowed to react with the ketone **13** (1.5 equiv) at −78 °C for 30 min to give 79% of the adduct **14**. Though *E*:*Z* ratio of **14** was found to be 3:1 (by ^{1}H NMR), its diastereomer ratio could not be determined. The crude **14** was therefore treated with cesium fluoride (3.8 equiv) in aq DMF at 60 °C for 38 h to produce a mixture of four isomers of the desired furanosesquiterpene **12** in 60% yield.

The product **12** contains four isomers in a 59:20:15:6 isomer ratio (GLC in a capillary column). The two major products were identified to be (1'*E*, 5'*E*)-**12a** and (1'*E*, 5'*Z*)-isomer **12b** by comparison of the ^{1}H and ^{13}C NMR spectra with those of natural products.[4] The ratio **12a**/**12b** (59/20) is almost equal to the *E*/*Z* ratio (3/1) of the starting ketone **13**, confirming the 1'*E*, 5'*E* and 1'*E*, 5'*Z* structures of **12a** and **12b**. The remaining two minor products should have 1'*Z* geometry, and were determined to be (1'*Z*, 5'*E*)- **12c** and (1'*Z*, 5'*Z*)-isomer **12d** on the basis of the isomer ratio (15/6) as well as the NMR data, especially the ^{13}C NMR chemical shifts of 2'-Me, 3'-C, 5'-C, 6'-Me, and 8'-C (Table 4). *E*-Selectivity of the Horner-Emmons olefination is estimated to be 79:21 which is comparable to the selectivities obtained in similar olefinations using other methyl ketones (Table 3).

Separation of each isomer from the mixture was attempted by column chromatography on silica gel, thin-layer chromatography on silica gel containing 2% of silver nitrate, or high performance liquid chromatography (HPLC), but not even one of them could be isolated. Though gas-liquid chromatography (GLC) in a capillary column separates the four isomers, no separation was made on a preparative scale by GLC.

Experimental

General. Melting points were determined on a Yanagimoto melting point apparatus and are uncorrected. IR spectra were taken with a JASCO IRA-1 or a JASCO A-702 spectrometer. ^{1}H NMR spectra were recorded on a Hitachi R-40 (90 MHz), a JEOL FX-100 (100 MHz), or a JEOL GSX-270

(270 MHz) instrument and ^{13}C NMR on a JEOL FX-100 (25.05 MHz) or a GSX-270 spectrometer (67.94 MHz). Chemical shifts are expressed in parts per million downfield from tetramethylsilane as an internal standard. Mass spectra were measured with a JEOL-OlSG-2 spectrometer at 70 eV of ionization energy. High-resolution mass spectra were obtained on the same instrument. Elemental analyses were performed on a Hitachi 026 CHN analyzer. Thin-layer chromatography (TLC) was accomplished on 0.2 mm precoated plates of silica gel 60 F-254 (Merck). Visualization was made with ultraviolet light (254 and 365 nm), iodine, molybdophosphoric acid (5% in ethanol), or *p*-anisaldehyde (5% in ethanol containing 5% of sulfuric acid). For preparative column chromatography, Wakogel C-200, C-300 (Wako), and Silicagel 60 (Merck) were employed. preparative high-performance liquid chromatography (HPLC) was performed on a Kusano KHLC-201 apparatus with a UV-detector Uvilog-III using a column (22×300 mm) packed with silica gel (Wakogel LC-50H). Gas liquid chromatography (GLC) was accomplished on a Yanaco G-2800 gas chromatograph (Yanagimoto) with an ionization flame detector using a glass column (SE-30, 3×2000 mm) or a glass capillary column (Silicone GE, SE-30, 0.25×50000 mm). Micro vacuum distillation was carried out on a Sibata GTO-250R Kugelrohr distilling apparatus. Solvents were evaporated with a Tokyo Rikakikai rotary evaporator type-V at about 50 °C unless otherwise stated.

Materials. Tetrahydrofuran (THF) was distilled over lithium aluminum hydride in prior to its use. 2-(Diethoxyphosphoryl)acetaldehyde oxime (**1**) was prepared by the reaction with hydroxylamine hydrochloride according to the reported method.[1b] Allyl tetrahydropyranyl ethers **3a—f** were synthesized from the corresponding allyl alcohols and 3,4-dihydro-2*H*-pyran.[18] The boiling points and ^{1}H NMR spectra are given as follows: **3a**: Bp 80—83 °C/5187 Pa; ^{1}H NMR ($CDCl_3$) δ=1.4—2.0 (6H, m, THP), 3.3—4.4 (4H, m, CH_2OTHP and THP), 4.56 (1H, m, THP), 5.0—5.4 (2H, m, $=CH_2$), and 5.7—6.1 (1H, m, =CH). **3b**: Bp 87—90 °C/4522 Pa; ^{1}H NMR ($CDCl_3$) δ=1.4—2.0 (6H, m, THP), 1.72 (3H, s, Me), 3.3—4.3 (4H, m, CH_2OTHP and THP), 4.53 (1H, m, THP), and 4.7—5.0 (2H, m, $=CH_2$). **3c** (a mixture of two diastereomers): Bp 83—85 °C/4655 Pa; ^{1}H NMR ($CDCl_3$) δ=1.19, 1.27 (3H, each d, J=7.0 Hz, Me), 1.4—2.1 (6H, m, THP), 3.3—4.0 (2H, m, THP), 4.15, 4.23 (1H, each dq, CHOTHP), 4.60 (1H, m, THP), 4.9—5.3 (2H, m, $=CH_2$), and 5.4—6.1 (1H, m, =CH). **3d** (a mixture of two diastereomers): Bp 97—100 °C/4655 Pa; ^{1}H NMR ($CDCl_3$) δ=0.87, 0.93 (3H, each t, J=7.0 Hz, Et), 1.3—2.0 (8H, m, Et and THP), 3.3—4.1 (3H, m, CHOTHP and THP), 4.60 (1H, m, THP), 4.9—5.3 (2H, m, $=CH_2$), and 5.4—6.0 (1H, m, =CH). **3e**: Bp 125—127 °C/200 Pa; ^{1}H NMR ($CDCl_3$) δ=1.4—2.2 (12H, m, THP), 3.3—4.4 (8H, m, CH_2OTHP and THP), 4.55 (2H, m, THP), and 5.66 (2H, m, =CH). **3f**: Bp 150—155 °C/3325 Pa (bulb-to-bulb); ^{1}H NMR ($CDCl_3$) δ=1.1—2.1 (8H, m, THP and cyclopentenyl), 2.31 (4H, t, J=7.0 Hz, cyclopentenyl), 3.3—4.4 (4H, m, CH_2OTHP and THP), 4.59 (1H, m, THP), and 5.61 (1H, m, =CH). 6-Methyl-5,7-octadien-2-one (**13**) was prepared as a 75:25 mixture of *E*- and *Z*-isomers (GLC) from the commercially available 3-acetyltetrahydrofuran-2-one according to the known methods.[16,17]

Cycloadditions of Nitrile Oxide 2 to Allyl Ethers 3a—f Leading to 2-Isoxazolines 4a—f. As a standard procedure the reaction of **2** with **3a** is described below: To a solution of oxime **1** (0.39 g, 2 mmol) in DMF (4 ml) was added dropwise, at −20 °C in a period of 5 min, a solution of NBS (0.712 g, 4 mmol) in DMF (4 ml). The mixture was stirred at −20 °C for 1 h and then at 0 °C for 30 min. After cooled to −20 °C again, a solution of triethylamine (0.202 g, 0.28 ml, 2 mmol) in dry diethyl ether (4 ml) and then a solution of allyl ether **3a** (1.422 g, 10 mmol) in diethyl ether (4 ml) were added. The resulting mixture was stirred at room temperature for 18 h and then diluted with dichloromethane (250 ml). This solution was washed with water (200 ml×3), dried over magnesium sulfate, and evaporated in vacuo. The residue was chromatographed over silica gel by using ethyl acetate to give **4a** (0.419 g, 62%) as a mixture of two diastereomers. These 3-phosphorylmethyl-2-isoxazolines **4** except for **4e** are too hygroscopic to provide authentic samples for analyses. They were used in subsequent reactions without further purification.

4a: Pale yellow liquid; IR (neat) 1620, 1250, 1025, and 810 cm^{-1}; ^{1}H NMR ($CDCl_3$) δ=1.32 (6H, t, J=7.0 Hz, OEt), 1.4—1.9 (2H, m, THP), 2.93 (2H, d, $J_{H\text{-}P}$=22.0 Hz, CH_2P), 2.7—3.4 (2H, m, 4-H), 3.4—3.9 (4H, THP and CH_2OTHP), 4.12 (4H, dq, $J_{H\text{-}P}$=7.5 and J=7.0 Hz, OEt), 4.62 (1H, m, THP), and 4.77 (1H, m, 5-H); ^{13}C NMR ($CDCl_3$) δ=16.18 (dq, $J_{C\text{-}P}$=5.9 Hz, OEt), 19.00, 19.12, 25.18 (each t, THP), 26.06 (dt, $J_{C\text{-}P}$=141.2 Hz, CH_2P), 30.24 (t, THP), 39.30, 39.59 (each t, 4-C), 61.89, 62.06 (each t, CH_2OTHP), 62.42 (dt, $J_{C\text{-}P}$=5.9 Hz, OEt), 67.71, 68.24 (each t, THP), 79.54 (d, 5-C), 98.83, 99.01 (each d, THP), and 151.27 (d, $J_{C\text{-}P}$=7.4 Hz, 3-C); MS *m/z* (rel intensity, %) 252 (5), 251 (16), 220 (M^+-CH_2THP, base peak), 164 (24), 153 (30), and 83 (73).

4b: A similar procedure using oxime **1** (0.39 g, 2 mmol), NBS (0.712 g, 4 mmol), triethylamine (0.202 g, 0.28 ml, 2 mmol), and allyl ether **3b** (1.562 g, 10 mmol) gave **4b** (0.533 g, 76%) as a mixture of four diastereomers after column chromatography over silica gel with ethyl acetate. Pale yellow liquid; IR (neat) 1620, 1255, 1025, and 810 cm^{-1}; ^{1}H NMR ($CDCl_3$) δ=1.15, 1.18 (3H, each d, J=6.5 Hz, Me), 1.32 (6H, t, J=7.0 Hz, OEt), 1.3—1.9 (6H, m, THP), 2.9—3.2 (2H, m, 4-H), 2.93 (2H, d, $J_{H\text{-}P}$=22.0 Hz, CH_2P), 3.3—4.1 (3H, m, THP and CHOTHP), 4.13 (4H, dq, $J_{H\text{-}P}$=7.5 and J=7.0 Hz, OEt), 4.50 (1H, m, 5-H), and 4.68 (1H, m, THP), ^{13}C NMR ($CDCl_3$) δ=13.88, 15.24, 17.00, 18.06 (each q, Me), 16.35 (dq, $J_{C\text{-}P}$=5.9 Hz, OEt), 19.35, 19.82, 25.47 (each t, THP), 26.24 (dt, $J_{C\text{-}P}$=141.2 Hz, CH_2P), 30.94 (t, THP), 37.65, 38.30, 39.18 (each t, 4-C), 62.59 (dt, $J_{C\text{-}P}$=5.9 Hz, OEt), 69.06, 71.42, 73.71, 74.12 (each d, CHOTHP), 82.95, 83.83, 84.06, 84.42 (each d, 5-C), 95.31, 96.42, 99.83, 100.24 (each d, THP), and 151.51 (d, $J_{C\text{-}P}$=7.4 Hz, 3-C); MS *m/z* (rel intensity, %) 304 (1), 220 (M^+−MeCHOTHP, 43), 193 (31), 178 (26), 164 (20), 153 (77), 125 (28), and 85 (base peak).

4c: A similar procedure using oxime **1** (0.39 g, 2 mmol), NBS (0.712 g, 4 mmol), triethylamine (0.202 g, 0.28 ml, 2 mmol), and allyl ether **3c** (1.682 g, 10 mmol) gave **4c** (0.529 g, 73%) as a mixture of three diastereomers after column chromatography over silica gel with ethyl acetate. Pale yellow liquid; IR (neat) 1620, 1255, 1025, and 810 cm^{-1}, ^{1}H NMR ($CDCl_3$) δ=0.92, 0.99 (3H, each t, J=6.5 Hz, Et), 1.32 (6H, t, J=7.0 Hz, OEt), 1.3—1.9 (6H, m, THP), 2.93 (2H, d, $J_{H\text{-}P}$=22.0 Hz, CH_2P), 2.9—3.3 (2H, m, 4-H), 3.3—4.0 (5H, m, THP, CHOTHP, and Et), 4.13 (4H, dq, $J_{H\text{-}P}$=7.0 Hz, OEt), and 4.4—4.9 (2H, m, 5-H and THP), ^{13}C NMR ($CDCl_3$) δ=9.06, 10.12 (each q, Et), 16.41 (dq, $J_{C\text{-}P}$=5.9 Hz, OEt),

19.71, 20.12 (each t, THP), 22.06, 23.30 (each t, Et), 25.53 (t, THP), 26.35 (dd, J_{C-P}=141.2 Hz, CH_2P), 31.06 (t, THP), 37.36 (t, 4-C), 38.41, 39.47 (each t, 4-C), 62.45 (dt, J_{C-P}=4.4 Hz, OEt), 62.59 (dt, J_{C-P}=2.9 Hz, OEt), 63.18, 63.36 (each t, THP), 77.65, 78.12 (each d, CHOTHP), 81.71, 82.01, 83.54 (each d, 5-C), 97.54, 99.65, 100.30 (each d, THP), and 151.75 (d, J_{C-P}=10.3 Hz, 3-C); MS *m/z* (rel intensity, %) 280 (1), 279 (1), 220 (M^+−EtCHOTHP, 37), 193 (37), 178 (27), 164 (25), 153 (78), 125 (26), and 85 (base peak).

4d: A similar procedure using oxime **1** (0.39 g, 2 mmol), NBS (0.712 g, 4 mmol), triethylamine (0.202 g, 0.28 ml, 2 mmol), and allyl ether **3d** (1.562 g, 10 mmol) gave **4d** (0.467 g, 67%) as a mixture of two diastereomers after column chromatography over silica gel with ethyl acetate. Pale yellow liquid; IR (neat) 1620, 1250, 1020, and 810 cm^{-1}; ^1H NMR ($CDCl_3$) δ=1.32 (6H, t, J=7.0 Hz, OEt), 1.36 (3H, s, Me), 1.4—1.9 (6H, m, THP), 2.6—3.2 (2H, m, 4-H), 2.81 (2H, d, J_{H-P}=21.5 Hz, CH_2P), 3.3—3.9 (4H, m, THP and CH_2OTHP), 4.13 (4H, dq, J_{H-P}=7.5 and J=7.0 Hz, OEt), and 4.63 (1H, m, THP); ^{13}C NMR ($CDCl_3$) δ=16.41 (dq, J_{C-P}=5.9 Hz, OEt), 19.18, 19.35 (each t, THP), 23.06, 23.18 (each q, Me), 26.59 (dt, J_{C-P}=141.2 Hz, CH_2P), 30.47 (t, THP), 45.00, 45.47 (each t, 4-C), 61.89, 62.18 (each t, THP), 62.53 (dt, J_{C-P}=5.9 Hz, OEt), 71.06, 71.36 (each t, CH_2OTHP), 86.18, 86.42 (each s, 5-C), 98.83, 99.18 (each d, THP), and 151.42 (d, J_{C-P}=8.8 Hz, 3-C); MS *m/z* (rel intensity, %) 234 (M^+−CH_2OTHP, base peak), 206 (24), 178 (58), 152 (35), and 85 (49).

4e: To a solution of oxime **1** (0.585 g, 3 mmol) in dry DMF (6 ml) was added NBS (1.068 g, 6 mmol) in DMF (6 ml) at −20 °C in a period of 5 min. The mixture was stirred at −20 °C for 1 h and then at 0 °C for 30 min. After diluted with dry diethyl ether (6 ml), triethylamine (0.304 g, 0.42 ml, 3 mmol) and then allyl ether **3e** (3.845 g, 15 mmol in diethyl ether (6 ml)) were added. The mixture was stirred at room temperature for 18 h and diluted with dichloromethane (200 ml). The dichloromethane was washed with water (200 ml×3), dried over magnesium sulfate, and finally evaporated in vacuo. The residue was chromatographed over silica gel by using ethyl acetate to give **4e** (0.618 g, 46%) as a mixture of four diastereomers. Colorless viscous liquid; IR (neat) 1620, 1250, 1025, and 810 cm^{-1}; ^1H NMR ($CDCl_3$) δ=1.2—2.0 (12H, m, THP), 1.32 (6H, t, J=7.0 Hz, OEt), 2.6—3.2 (2H, m, CH_2P), 3.3—4.0 (5H, m, THP and 4-H), 4.13 (4H, dq, J_{H-P}=7.5 and J=7.0 Hz, OEt), and 4.32 (3H, m, THP and 5-H); ^{13}C NMR ($CDCl_3$) δ=16.41 (dq, J_{C-P}=5.9 Hz, OEt), 19.18, 19.41 (each t, THP), 25.44 (dt, J_{C-P}=145.6 Hz, CH_2P), 25.47, 30.53 (each t, THP), 50.36 (d, 4-C), 61.89, 62.30 (each t, CH_2OTHP), 65.30, 65.56 (each d, THP), 81.18, 81.36, 81.71, 81.95 (each d, 5-C), 98.99, 99.18 (each d, THP), 153.75 (d, J_{C-P}=10.3 Hz, 3-C), and 153.83 (d, J_{C-P}=5.9 Hz, 3-C); MS *m/z* (rel intensity, %) 366 (4), 281 (51), 264 (22), 251 (32), 250 (42), 234 (20), 233 (72), 232 (28), 220 (base peak), 178 (21), 152 (37), and 85 (92).

Found: C, 53.28; H, 8.14; N, 3.31%. Calcd for $C_{20}H_{36}O_8NP$: C, 53.44; H, 8.07; N, 3.12%.

4f: A similar procedure as employed for **4e** was applied to oxime **1** (0.39 g, 2 mmol), NBS (0.712 g, 4 mmol), triethylamine (0.202 g, 0.28 ml, 2 mmol), and allyl ether **3f** (1.823 g, 10 mmol) to give **4f** (0.2 g, 29%) as a mixture of two diastereomers. Yellow liquid; IR (neat) 1260, 1025, and 810 cm^{-1}; ^1H NMR ($CDCl_3$) δ=1.32 (6H, t, J=7.0 Hz, OEt), 1.0—2.1 (12H, m, THP and CH_2), 2.5—3.2 (3H, CH_2P and 4-H), 3.3—3.8 (4H, m, THP and CH_2OTHP), 4.14 (4H, dq, J_{H-P}=7.5 and J=7.0 Hz, OEt), and 4.65 (1H, m, THP); ^{13}C NMR ($CDCl_3$) J=16.43 (dq, J_{C-P}=6.1 Hz, OEt), 19.14, 19.34 (t, THP), 24.27 (t, 5-C), 25.12 (dt, J_{C-P}=140.4 Hz, CH_2P), 25.49, 30.47 (each t, THP), 37.21 (t, 4- and 6-C), 55.71, 56.05 (each d, 3a-C), 61.74, 62.43 (each dt, J_{C-P}=6.1 Hz, OEt), 62.74, 63.33 (each t, CH_2OTHP), 69.48, 69.68 (each t, THP), 97.31, 97.51 (each s, 6a-C), 98.78, 99.32 (each d, THP), and 153.17 (d, J_{C-P}=9.8 Hz, 3-C); MS *m/z* (rel intensity, %) 292 (10), 291 (18), 261 (16), 260 (base peak), 178 (45), 152 (34), 125 (30), 122 (26), and 85 (65).

Alkylation of 2-Isoxazolines 4c—d Leading to 4g—j. As a typical procedure the alkylation of **4c** with 1-iodooctane is presented as follows: To a solution of **4c** (0.321 g, 0.883 mmol) in dry THF (3 ml) was added at −78 °C butyllithium (15% in hexane, 0.55 ml, 0.883 mmol). After the mixture was stirred for 1 h at the same temperature, octyl iodide (0.424 g, 0.32 ml, 1.766 mmol) was added. The resulting mixture was stirred at 0 °C for 1 h and then at room temperature for 14 h. Saturated aqueous sodium chloride (30 ml) was added to the mixture and then extracted with dichloromethane (30 ml×3). The combined extracts were dried over magnesium sulfate and then chromatographed over silica gel by using hexane–ethyl acetate (1 : 1 v/v) to afford **4g** (0.267 g, 64%). The elution with ethyl acetate gave the starting **4c** (0.026 g, 8%).

4g (a mixture of four diastereomers): Colorless liquid; IR (neat) 1615, 1250, and 810 cm^{-1}; ^1H NMR ($CDCl_3$) δ=0.7—1.1 (6H, m, Et and n-C_8H_{17}), 1.1—2.0 (22H, m, Et, n-C_8H_{17}, and THP), 1.31 (6H, t, J=7.0 Hz, Et), 2.7—4.0 (6H, m, CH_2P, CHOTHP, THP, and 4-H), 4.11 (4H, dq, J_{H-P}=7.5 and J=7.0 Hz, OEt), and 4.4—4.9 (2H, m, THP and 5-H), ^{13}C NMR ($CDCl_3$) δ=9.06, 10.06 (each q, Et), 14.12 (q, n-C_8H_{17}), 16.47 (dq, J_{C-P}=5.9 Hz, OEt), 20.18, 22.71, 23.64, 25.53, 26.46, 27.65, 28.18, 29.30, 31.06, 31.88 (each t, CH_2 and THP), 34.53, 35.88, 36.59, 38.00 (each t, 4-C), 37.80 (dd, J_{C-P}=139.7 Hz, CHP), 62.59 (t, OEt), 63.24, 63.83 (each t, THP), 76.89, 78.01 (each d, EtCHOTHP), 81.59, 82.89, 83.36 (each d, 5-C), 97.42, 99.83, 100.18, 100.65 (each d, THP), and 155.77 (s, 3-C); MS *m/z* (rel intensity, %) 475 (M^+, 3), 391 (83), 332 (23), 331 (base peak), 263 (77), 165 (31), 152 (39), and 85 (66). HRMS Found: *m/z* 475.3049. Calcd for $C_{24}H_{46}NO_6P$: M, 475.3060.

4h: A similar procedure using **4c** (0.396 g, 1.09 mmol), butyllithium (15% in hexane, 0.68 ml, 1.09 mmol), and pentyl iodide (0.432 g, 0.28 ml, 2.18 mmol) gave **4h** (0.307 g, 65%) after silica-gel chromatography with hexane–ethyl acetate (1:1 v/v) and the starting **4c** (0.049 g, 12%) from the elution with ethyl acetate. **4h** (a mixture of five diastereomers): Colorless liquid; IR (neat) 1610, 1250, 1025, and 810 cm^{-1}; ^1H NMR ($CDCl_3$) δ=0.7—1.2 (6H, m, OEt), 1.2—2.0 (16H, m, n-C_5H_{11}, Et, and THP), 1.31 (6H, t, J=7.0 Hz, OEt), 2.8—4.0 (6H, m, PCH, CHOTHP, THP, and 4-H), 4.11 (dq, J_{H-P}=7.5 and J=7.0 Hz, OEt), and 4.4—4.9 (2H, m, THP and 5-H); ^{13}C NMR ($CDCl_3$) δ=9.03, 10.01, 10.16 (each q, Et), 13.96 (q, n-C_5H_{11}), 16.43 (qd, J_{C-P}=6.1 Hz, OEt), 19.72, 19.87, 20.12, 22.12, 22.41, 23.14, 23.63, 25.54, 26.46, 26.61, 27.29, 27.88, 31.02, 31.30 (each t, CH_2 and THP), 34.52, 36.57 (each t, 4-C), 37.79 (dt, J_{C-P}=139.2 Hz, CHP), 62.57 (dt, J_{C-P}=6.1 Hz, OEt), 63.04, 63.82 (each t, THP), 76.86, 77.68, 77.98 (each d, CHOTHP), 81.54, 83.15, 83.35 (each d, 5-C), 97.41, 97.51, 99.80, 100.14, 100.59 (each d, THP), and 155.46 (s, 3-C); MS *m/z* (rel intensity, %) 349 (4), 331 (7), 290 (24), 289 (base peak), 222 (85), 165 (42), and 85 (79).

Found: C, 57.90; H, 9.17; N, 3.27%. Calcd for $C_{21}H_{40}NO_6P$: C, 58.18; H, 9.39; N, 3.23%.

4i: A similar perocedure using **4d** (0.5 g, 1.43 mmol), butyllithium (15% in hexane, 0.89 ml, 1.43 mmol), and pentyl iodide (0.567 g, 0.37 ml, 2.862 mmol) afforded **4i** (0.352 g, 59%) after silica-gel column chromatography with hexane-ethyl acetate (1 : 1 v/v) together with the starting **4d** (0.054 g, 11%) from the fraction eluted with ethyl acetate. **4i** (a mixture of four diastereomers): Pale yellow viscous liquid; IR (neat) 1615, 1250, 1035, and 800 cm^{-1}; ^1H NMR ($CDCl_3$) δ=0.88 (3H, t, J=6.0 Hz, n-C_5H_{11}), 1.0—2.0 (14H, m, THP and n-C_5H_{11}), 1.32 (6H, t, J=7.0 Hz, OEt), 1.37 (3H, s, 5-Me), 2.5—3.9 (7H, m, THP, CH_2OTHP, CHP), 4.12 (4H, dq, J_{H-P}=7.5 and J=7.0 Hz, OEt), and 4.64 (1H, br s, THP); ^{13}C NMR ($CDCl_3$) δ=14.00 (q, n-C_5H_{11}), 16.47, (dq, J_{C-P}=5.9 Hz, OEt), 19.12, 19.35, 19.53, 22.41, 26.47, 27.24, 27.83 (each t, CH_2 and THP), 23.35 (q, 5-Me), 25.53, 30.36, 31.30 (each t, THP), 37.91 (dd, J_{C-P}=139.7 Hz, CHP), 42.36, 42.89, 43.24, 43.77 (each t, 4-C), 61.95 (dt, J_{C-P}=5.9 Hz, OEt), 62.45 (dt, J_{C-P}=7.4 Hz, OEt), 70.83, 71.24 (each t, CH_2OTHP), 85.77, 85.95, 86.06 (each s, 5-C), 98.60, 98.83, 99.12, 99.42 (each d, THP), and 155.12 (d, J_{C-P}=4.4 Hz, 3-C); MS m/z (rel intensity, %) 304 (M^+-CH_2OTHP, base peak) and 85 (21). Found: 56.97; H, 9.01; N, 3.36%. Calcd for $C_{20}H_{38}NO_6P$: C, 57.26; H, 9.13; N, 3.34%.

4j: A similar procedure using **4d** (0.5 g, 1.43 mmol), butyllithium (15% in hexane, 0.89 ml, 1.43 ml), and benzyl bromide (0.49 g, 0.34 ml, 2.86 mmol) gave **4j** (0.41 g, 65%) after silica-gel column chromatography with hexane-ethyl acetate (1 : 1 v/v) together with the starting **4d** (0.043 g, 9%) from the fraction eluted with ethyl acetate. As **4j** was hygroscopic, it was used for subsequent reactions without further purification. **4j** (a mixture of four diastereomers): Pale yellow viscous liquid; IR (neat) 1610, 1250, 1030, and 800 cm^{-1}; ^1H NMR ($CDCl_3$) δ=1.11, 1.16, 1.26, 1.29 (3H, each s, 5-Me), 1.32 (6H, t, J=7.0 Hz, OEt), 1.3—1.9 (6H, m, THP), 2.3—3.9 (6H, m, CHP, CH_2OTHP, THP, and 4-H), 4.13 (4H, dq, J_{H-P}=7.5 and J=7.0 Hz, OEt), 4.4—4.7 (1H, m, THP), and 7.29 (5H, br s, Ph); ^{13}C NMR ($CDCl_3$) δ=16.47 (dq, J_{C-P}=5.9 Hz, OEt), 19.30 (t, THP), 23.00 (q, 5-Me), 25.47, 30.41 (t, THP), 32.71 (t, CH_2Ph), 39.36 (dd, J_{C-P}=138.2 Hz, CHP), 43.18, 43.47, 43.94, 44.06 (each t, 4-C), 61.95 (t, THP), 62.68 (dt, J_{C-P}=7.4 Hz, OEt), 70.24, 70.48, 71.01 (each t, CH_2OTHP), 85.89, 86.12 (each s, 5-C), 98.95 (d, THP), 126.95, 128.72, 128.89 (each d), 137.89, 138.54 (each s), 154.51, and 154.80 (d, J_{C-P}=7.4 Hz, 3-C); MS m/z (rel intensity, %) 325 (15), 324 (M^+-CH_2OTHP, 87), 296 (22), 268 (30), 242 (21), 186 (25), 185 (21), 144 (31), 138 (24), 109 (26), 105 (21), 104 (40), 103 (35), 91 (base peak), 85 (98), 81 (36), and 77 (24).

Conversion of 2-Isoxazolines 4a—j to 2-(1-Phosphorylalkyl)-furans 5a—j. As a typical procedure the conversion of **4a** into **5a** is described: A mixture of 2-isoxazoline **4a** (0.173 g, 0.516 mmol), Raney Ni W-2 (suspension in ethanol, 0.5 ml), and boric acid (0.066 g, 1.06 mmol) in aqueous ethanol (17%, 3 ml) was stirred under hydrogen atmosphere at room temperature for 13.5 h. Insoluble material was filtered through Celite and washed with water and then dichloromethane. The combined filtrate and washings were extracted with dichloromethane (30 ml×3). The dichloromethane was dried over magnesium sulfate and evaporated in vacuo. The residue was heated with sodium acetate (0.179 g, 2.185 mmol) in acetic acid (1 ml) at 100 °C for 2 h. The reaction mixture was cooled to room temperature, diluted with dichloromethane (90 ml), washed with water (50 ml) and then saturated sodium hydrogencarbonate (50 ml), and finally dried over magnesium sulfate. The solvent was evaporated in vacuo and the residue was chromatographed over silica gel by using hexane-ethyl acetate (1 : 5 v/v) to give **5a** (0.067 g, 60%).

The same product **5a** was obtained in 77% yield (0.039 g) by a similar procedure (100 °C for 3 h) using purified **6** (0.079 g, 0.233 mmol), sodium acetate (0.095 g, 1.165 mmol), and acetic acid (0.5 ml). The preparation of **6** is described later.

5a: Pale yellow liquid; IR (neat) 3000, 1595, 1250, 1025, and 790 cm^{-1}; ^1H NMR ($CDCl_3$) δ=1.26 (6H, t, J=7.0 Hz, OEt), 3.21 (2H, d, J_{H-P}=21.5 Hz, CH_2P), 4.04 (4H, dq, J_{H-P}=8.0 and J=7.0 Hz, OEt), 6.1—6.4 (2H, m, 3- and 4-H), and 7.31 (1H, m, 5-H); ^{13}C NMR ($CDCl_3$) δ=16.41 (dq J_{C-P}=4.9 Hz, OEt), 26.78 (dt, J_{C-P}=142.8 Hz, CH_2P), 62.45 (dt, J_{C-P}=7.3 Hz, OEt), 108.45 (dd, J_{C-P}=7.3 Hz, 3-C), 111.01 (dd, J_{C-P}=3.7 Hz, 4-C), 142.16 (dd, J_{C-P}=3.7 Hz, 5-C), and 145.95 (d, J_{C-P}=9.8 Hz, 2-C); MS m/z (rel intensity, %) 218 (M^+, 15), 162 (21), 109 (19), and 81 (base peak). HRMS Found: m/z 218.0704. Calcd for $C_9H_{15}O_4P$: M, 218.0707.

5b: A similar procedure using 1) **4b** (0.215 g, 0.615 mmol), Raney Ni W-2 in ethanol (0.6 ml), boric acid (0.078 g, 1.261 mmol), and aqueous ethanol (17%, 3.6 ml) at room temperature for 13 h, 2) sodium acetate (0.252 g, 3.075 mmol) and acetic acid (1.3 ml) at 100 °C for 30 min, and silica-gel column chromatography with hexane-ethyl acetate (1 : 3 v/v) gave **5b** (0.077 g, 54%): Pale yellow liquid; IR (neat) 3000, 1565, 1250, and 790 cm^{-1}; ^1H NMR ($CDCl_3$) δ=1.27 (6H, t, J=7.0 Hz, OEt), 2.24 (3H, d, J=1.7 Hz, 5-Me), 3.17 (2H, d, J_{H-P}=20.5 Hz, CH_2P), 4.06 (4H, dq, J_{H-P}=8.0 and J=7.0 Hz, OEt), 5.88 (1H, m, 4-H), and 6.08 (1H, t, J_{H-P}=J=3.4 Hz, 3-H), ^{13}C NMR ($CDCl_3$) δ=13.41 (q, 5-Me), 16.27 (dq, J_{C-P}=7.4 Hz, OEt), 26.65 (dt, J_{C-P}=144.1 Hz, CH_2P), 62.27 (dt, J_{C-P}=7.4 Hz, OEt), 106.71 (dd, J_{C-P}=2.9 Hz, 4-C), 109.01 (dd, J_{C-P}=8.8 Hz, 3-C), 143.66 (d, J_{C-P}=8.8 Hz, 2-C), and 151.54 (d, J_{C-P}=2.9 Hz, 5-C); MS m/z (rel intensity, %) 232 (M^+, 4) and 95 (base peak). HRMS Found: m/z 232.0887. Calcd for $C_{10}H_{17}O_4P$: M, 232.0863.

5c: A similar procedure using 1) **4c** (0.215 g, 0.615 mmol), Raney Ni W-2 in ethanol (0.6 ml), boric acid (0.075 g, 1.207 mmol), and aqueous ethanol (17%, 3.6 ml) at room temperature for 13 h, 2) sodium acetate (0.252 g, 2.945 mmol) and acetic acid (1.3 ml) at 100 °C for 30 min, and silica-gel column chromatography with hexane-ethyl acetate (1 : 3 v/v) gave **5c** (0.084 g, 60%): pale yellow liquid; IR (neat) 3000, 1560, 1250, 1025, and 800 cm^{-1}; ^1H NMR ($CDCl_3$) δ=1.18 (3H, t, J=8.0 Hz, Et), 1.27 (6H, t, J=7.0 Hz, OEt), 2.60 (2H, q, J=8.0 Hz, Et), 3.16 (2H, d, J_{H-P}=21.0 Hz, CH_2P), 4.05 (4H, dq, J_{C-P}=8.0 and 7.0 Hz, OEt), 5.88 (1H, d, J=3.5 Hz, 4-H), and 6.09 (1H, t, J_{H-P}=J= 3.5 Hz, 3-H); ^{13}C NMR ($CDCl_3$) δ=12.24 (q, Et), 16.35 (dp, J_{C-P}=5.9 Hz, OEt), 21.35 (t, Et), 26.74 (dt, J_{C-P}=142.7 Hz, CH_2P), 62.33 (dt, J_{C-P}=7.4 Hz, OEt), 105.24 (dd, J_{C-P}=2.9 Hz, 4-C), 108.86 (dd, J_{C-P}=7.4 Hz, 3-C), 143.69 (d, J_{C-P}=10.3 Hz, 2-C), and 157.30 (s, 5-C); MS m/z (rel intensity, %), 246 (M^+, 4), 109 (base peak), 94 (12), and 81 (11). HRMS Found: m/z 246.1017. Calcd for $C_{11}H_{19}O_4P$: M, 246.1020.

5d: A similar procedure using 1) **4d** (2.48 g, 7.1 mmol), Raney Ni W-2 in ethanol (6 ml), boric acid (4.35 g, 71 mmol), and aqueous ethanol (17%, 41 ml) at room temperature for 13.5 h, 2) sodium acetate (2.91 g, 35.5 mmol) and acetic acid (16 ml) at 100 °C for 30 min, and silica-gel column chromatography with hexane-ethyl acetate (1 : 1 v/v) afforded **5d**

(1.16 g, 70%): Pale yellow liquid; IR (neat) 3000, 1620, 1240, 1020, and 790 cm^{-1}; ^1H NMR ($CDCl_3$) δ=1.27 (6H, t, J=7.0 Hz, OEt), 1.96 (3H, d, J=1.0 Hz, Me), 3.14 (2H, d, J_{H-P}=21.5 Hz, CH_2P), 4.05 (4H, dq, J_{H-P}=8.0 and J=7.0 Hz, OEt), 6.08 (1H, d, J_{H-P}=3.5 Hz, 3-H), and 7.06 (1H, m, 5-H); ^{13}C NMR ($CDCl_3$) δ=9.77 (q, Me), 16.41 (dq, J_{C-P}=5.9 Hz, OEt), 26.83 (dd, J_{C-P}=144.1 Hz, CH_2P), 62.42 (dt, J_{C-P}=5.9 Hz, OEt), 111.15 (dd, J_{C-P}=7.4 Hz, 3-C), 121.30 (d, J_{C-P}=2.9 Hz, 4-C), 138.78 (dd, J_{C-P}=2.9 Hz, 5-C), and 145.77 (d, J_{C-P}=8.8 Hz, 2-C); MS m/z (rel intensity, %) 232 (M^+, 10), 176 (10), 96 (12), 95 (base peak), and 80 (11). HRMS Found: m/z 232.0867. Calcd for $C_{10}H_{17}O_4P$: M, 232.0863.

5e: A similar procedure using **4e** (0.134 g, 0.298 mmol), Raney Ni W-2 in ethanol (0.3 ml), boric acid (0.038 g, 0.611 mmol), and aqueous ethanol (17%, 1.8 ml) at room temperature for 14 h gave a hydrogenated product (0.11 g). This crude product was added to aqueous THF (50%, 1 ml) containing *p*-toluenesulfonic acid (0.028 g, 0.149 mmol) and the mixture was heated at 70 °C for 6.5 h. After an additional *p*-toluenesulfonic acid (0.028 g, 0.149 mmol) was added, heating was continued at the same temperature for 1.5 h. To the cooled mixture was added saturated aqueous sodium hydrogencarbonate (20 ml), and extracted with ethyl acetate (30 ml×3). The combined extracts were similarly treated and chromatographed over silica gel with hexane-ethyl acetate (1 : 1 v/v) to give **5e** (0.03 g, 41%): Colorless liquid; IR (neat) 3400, 3000, 1510, 1240, 1025, 970, and 800 cm^{-1}. ^1H NMR ($CDCl_3$) δ=1.26 (6H, t, 7.0 Hz, OEt), 3.28 (2H, d, J_{H-P}=20.8 Hz, CH_2P), 4.00 (4H, dq, J_{H-P}=8.0 and J=7.0 Hz, OEt), 4.30 (1H, br s, OH), 4.44 (2H, s, CH_2OH), 6.38 (1H, d, J=1.8 Hz, 4-H), and 7.28 (1H, dd, J_{H-P}=3.5 and J=1.8 Hz, 5-H); ^{13}C NMR ($CDCl_3$) δ=16.35 (dq, J_{C-P}=5.9 Hz, OEt), 25.62 (dt, J_{C-P}=142.7 Hz, CH_2P), 56.06 (t, CH_2OH), 62.95 (dt, J_{C-P}=5.9 Hz, OEt), 112.39 (dd, J_{C-P}=4.4 Hz, 4-C), 141.75 (dd, J_{C-P}= 4.4 Hz, 5-C), and 142.04 (d, J_{C-P}=10.3 Hz, 2-C); MS m/z (rel intensity, %) 248 (M^+, 6), 153 (21), 112 (52), 111 (52), 109 (75), 94 (34), 83 (69), 81 (70), 65 (25), and 56 (base peak). HRMS Found: m/z 248.0808. Calcd for $C_{10}H_{17}O_5P$: M, 248.0813.

5f: A procedure similar to that employed for **5a** using 1) **4f** (0.17 g, 0.494 mmol), Raney Ni W-2 in ethanol (0.5 ml), boric acid (0.063 g, 1.013 mmol), and aqueous ethanol (17%, 2.4 ml) at room temperature for 15 h, 2) sodium acetate (0.203 g, 2.47 mmol) and acetic acid (1 ml) at 90 °C for 30 min, and silica-gel column chromatography with hexane-ethyl acetate (1 : 3 v/v) gave **5f** (0.032 g, 25%): Pale yellow liquid; IR (neat) 2900, 1650, 1250, 1025, and 830 cm^{-1}; ^1H NMR ($CDCl_3$) δ=1.27 (6H, t, J=7.0 Hz, OEt), 2.1—2.7 (6H, m, CH_2), 3.14 (2H, d, J_{H-P}=20.5 Hz, CH_2P), 4.05 (4H, dq, J_{H-P}=8.0 and J=7.0 Hz, OEt), and 6.94 (1H, m, 5-H); MS m/z (rel intensity, %) 258 (M^+, 33), 121 (63), 120 (base peak), and 91 (25). HRMS Found: m/z 258.1019. Calcd for $C_{12}H_{19}O_4P$: M, 258.1020.

5g: A similar procedure using 1) **4g** (0.188 g, 0.395 mmol), Raney Ni W-2 in ethanol (0.4 ml), boric acid (0.05 g, 0.81 mmol), and aqueous ethanol (17%, 3 ml) at room temperature for 14 h, 2) sodium acetate (0.162 g, 1.975 mmol) and acetic acid (1 ml) at 100 °C for 30 min, and silica-gel column chromatography with hexane-ethyl acetate (1 : 5 v/v) gave **5g** (0.09 g, 64%): Pale yellow liquid; IR (neat) 2920, 1555, 1250, 1025, and 790 cm^{-1}; ^1H NMR ($CDCl_3$) δ=0.86 (3H, t, J=7.0 Hz, Et), 1.0—1.4 (21H, m, n-C_8H_{17} and OEt), 1.7—2.1 (2H, m, CH_2CHP), 2.60 (2H, q, Et), 3.11 (1H, ddd, J_{H-P}=23.0, J=9.0, and 6.0 Hz, CHP), 3.7—4.2 (4H, m, OEt), 5.88 (1H, d, J=3.2 Hz, 4-H), and 6.08 (1H, t, J_{H-P}=J=3.2 Hz, 3-H); ^{13}C NMR ($CDCl_3$) δ=12.29 (q, Et), 14.06 (q, n-C_8H_{17}), 16.41 (dq, J_{C-P}=5.9 Hz, OEt), 21.47, 22.70, 27.53, 28.18, 28.53, 28.65, 29.24 (each t, n-C_8H_{17}), 31.88 (t, Et), 38.59 (dd, J_{C-P}=141.2 Hz, CHP), 62.45, 62.93 (each dt, J_{C-P}=7.4 Hz, OEt), 105.13 (dd, J_{C-P}=2.9 Hz, 4-C), 108.45 (dd, J_{C-P}=7.4 Hz, 3-C), 148.48 (d, J_{C-P}=8.8 Hz, 2-C), and 157.07 (d, J_{C-P}=2.9 Hz, 5-C); MS m/z (rel intensity, %) 358 (M^+, 34), 221 (base peak), 155 (66), 127 (41), 110 (41), 99 (57), 85 (28), and 81 (21). Found: m/z 358.2288. Calcd for $C_{19}H_{35}O_4P$: M, 358.2271.

5h: A similar procedure using 1) **4h** (0.198 g, 0.457 mmol), Raney Ni W-2 in ethanol (0.5 ml), boric acid (0.283 g, 4.57 mmol), and aqueous ethanol (17%, 2.4 ml) at room temperature for 20 h, 2) sodium acetate (0.187 g, 2.285 mmol) and acetic acid (1 ml) at 100 °C for 30 min, and silica-gel column chromatography with hexane-ethyl acetate (1 : 1 v/v) gave **5h** (0.092 g, 64%): Pale yellow liquid; IR (neat) 2940, 1555, 1250, 1025, and 790 cm^{-1}; ^1H NMR ($CDCl_3$) δ=0.85 (3H, t, J=7.0 Hz, Et), 1.0—1.4 (15H, m, OEt and n-C_5H_{11}), 1.7—2.1 (2H, m, CH_2CHP), 2.60 (2H, q, J=7.0 Hz, Et), 3.11 (1H, ddd, J_{H-P}=23.0, J=9.0, and 6.0 Hz, CHP), 3.7—4.3 (4H, m, OEt), 5.89 (1H, d, J=3.2 Hz, 4-H), and 6.08 (1H, t, J_{H-P}=3.2 Hz, 3-H); ^{13}C NMR ($CDCl_3$) δ=12.24 (q, Et), 13.94 (q, n-C_5H_{11}), 16.38 (dq, J_{C-P}=4.4 Hz, OEt), 21.41, 22.35 (each t, n-C_5H_{11}), 27.44 (dt, J_{C-P}=13.2 Hz, n-C_5H_{11}), 28.53 (dt, J_{C-P}=2.9 Hz, n-C_5H_{11}), 31.36 (t, Et), 38.53 (dd, J_{C-P}=141.2 Hz, CHP), 62.03 (dt, J_{C-P}=7.4 Hz, OEt), 62.36 (dt, J_{C-P}=8.8 Hz, OEt), 105.06 (dd, J_{C-P}=2.9 Hz, 4-C), 108.39 (dd, J_{C-P}=7.4 Hz, 3-C), 148.42 (d, J_{C-P}=8.8 Hz, 2-C), and 157.07 (d, J_{C-P}=2.9 Hz, 5-C); MS m/z (rel intensity, %) 316 (M^+, 13), 179 (base peak), and 110 (66). HRMS Found: m/z 316.1806. Calcd for $C_{16}H_{29}O_4P$: M, 316.1802.

5i: A similar procedure using 1) **4i** (0.33 g, 0.787 mmol), Raney Ni W-2 (0.8 ml), boric acid (0.1 g, 1.613 mmol), and aqueous ethanol (17%, 4.8 ml) at room temperature for 15 h, 2) sodium acetate (0.323 g, 3.935 mmol) and acetic acid (1.7 ml) at 100 °C for 0.3 h, and silica-gel column chromatography with hexane-ethyl acetate (1 : 1 v/v) afforded **5i** (0.062 g, 26%): Colorless liquid; IR (neat) 1610, 1250, 1025, and 790 cm^{-1}; ^1H NMR ($CDCl_3$) δ=0.85 (3H, t, J=6.0 Hz, n-C_5H_{11}), 1.1—2.1 (8H, m, n-C_5H_{11}), 1.22, 1.28 (6H, m, OEt), 1.99 (3H, s, 4-Me), 2.10 (1H, ddd, J_{H-P}=23.0, J=9.0, and 6.0 Hz, CHP), 3.7—4.2 (4H, m, OEt), 6.09 (1H, d, J_{H-P}=4.0 Hz, 3-H), and 7.09 (1H, m, 5-H); ^{13}C NMR ($CDCl_3$) δ=9.82 (q, 4-Me), 14.00 (q, n-C_5H_{11}), 16.41 (dq, J_{C-P}=5.9 Hz, OEt), 22.41 (t, n-C_5H_{11}), 27.53 (dt, J_{C-P}=14.7 Hz, n-C_5H_{11}), 28.15 (dt, J_{C-P}=16.2 Hz, n-C_5H_{11}), 31.41 (t, n-C_5H_{11}), 38.68 (dd, J_{C-P}=139.7 Hz, CHP), 62.09 (dt, J_{C-P}=7.4 Hz, OEt), 62.50 (dt, J_{C-P}=7.4 Hz, n-C_5H_{11}), 110.74 (dd, J_{C-P}=7.4 Hz, 3-C), 121.19 (s, 4-C), 138.54 (dd, J_{C-P}=2.9 Hz, 5-C), and 150.48 (d, J_{C-P}=8.8 Hz, 2-C); MS m/z (rel intensity, %) 302 (M^+, 32), 232 (27), 165 (base peak), 164 (21), and 95 (92). HRMS Found: m/z 302.1656. Calcd for $C_{15}H_{27}O_4P$: M, 302.1645.

5j: A similar procedure using 1) **4j** (0.395 g, 0.899 mmol), Raney Ni W-2 (0.9 ml), boric acid (0.114 g, 1.843 mmol), and aqueous ethanol (17%, 5.4 ml) at room temperature for 15 h, 2) sodium acetate (0.369 g, 4.495 mmol) and acetic acid (2 ml) at 100 °C for 30 min, and silica-gel column chromatography with hexane-ethyl acetate (1 : 1 v/v) gave **5j** (0.045 g, 16%): Colorless liquid; IR (neat) 3000, 1610, 1250, 1025, and 790 cm^{-1}; ^1H NMR ($CDCl_3$) δ=1.22, 1.28 (6H, m,

OEt), 1.92 (3H, s, 4-Me), 3.0—3.6 (3H, m, $PhCH_2$ and CHP), 3.7—4.2 (4H, m, OEt), 6.01 (1H, d, J_{H-P}=3.5 Hz, 3-H), and 6.9—7.3 (6H, m, 5-H and Ph); ^{13}C NMR ($CDCl_3$) δ=9.29 (q, 4-Me), 15.94 (dq, J_{C-P}=5.9 Hz, OEt), 34.18 (t, CH_2), 40.24 (dd, J_{C-P}=141.2 Hz, CHP), 61.74 (dt, J_{C-P}=7.4 Hz, OEt), 111.15 (dd, J_{C-P}=7.4 Hz, 3-C), 120.57 (d, J_{C-P}=4.4 Hz, 4-C), 126.07, 127.95, 128.36 (each d), 138.24 (dd, J_{C-P}=2.9 Hz, 5-C), 139.07 (s), and 148.83 (d, J_{C-P}=8.8 Hz, 2-C); MS *m/z* (rel intensity, %) 322 (M^+, 50), 231 (96), 185 (60), 184 (99), 155 (21), 141 (34), 129 (25), 128 (23), 121 (47), 116 (23), 110 (46), 95 (74), 91 (base peak), and 81 (51). HRMS Found: *m/z* 322.1339. Calcd for $C_{17}H_{23}O_4P$: M, 322.1333.

Alkylation of 2-(Phosphorylmethyl)furan 5d Leading to 2-(1-Phosphorylalkyl)furans 5i, j. To a solution of **5d** (0.241 g, 1.033 mmol) in dry THF (3 ml) was added at −78 °C butyllithium (15% in hexane, 0.65 ml, 1.033 mmol). After 1 h at −78 °C under nitrogen, pentyl iodide (0.205 g, 0.13 ml, 1.033 mmol) was added and the mixture was stirred for 5 h at the same temperature. Aqueous THF (1 : 1 v/v, 50 ml) was added slowly and the product was extracted with dichloromethane (30 ml×3). The combined extracts were dried over magnesium sulfate and evaporated in vacuo. The residue was chromatographed over silica gel by using hexane–ethyl acetate (2 : 1 v/v) to give **5i** (0.274 g, 88%) and a later fraction afforded the starting **5d** (0.013 g, 5%). Spectral data of **5i** is presented above.

A similar procedure using **5d** (0.197 g, 0.848 mmol), butyllithium (15% in hexane, 0.53 ml, 0.848 mmol), and benzyl bromide (0.145 g, 0.1 ml, 0.848 mmol) in THF (3 ml) was followed by silica-gel column chromatography with hexane–ethyl acetate (1 : 1 v/v) to give **5j** (0.239 g, 87%).

Reductive Ring-Opening of 4a into 6. A mixture of **4a** (0.202 g, 0.614 mmol), Raney Ni W-2 (0.5 ml), and boric acid (0.078 g, 1.259 mmol) in aqueous ethanol (17%, 17.5 ml) was stirred under hydrogen atmosphere at room temperature for 19 h. After another portion of Raney Ni (0.5 ml) was added, stirring was continued also under hydrogen for additional 19.5 h. All the insoluble material was filtered through Celite and washed with water and then dichloromethane. The combined filtrate and washings were extracted with dichloromethane (50 ml×3). The extract was dried over magnesium sulfate and evaporated in vacuo. The residue (0.181 g, 87%) was chromatographed over silica gel by using ethyl acetate to give **6** (0.095 g) as a mixture of two diastereomers. Colorless liquid; IR (neat) 3400, 1710, 1250, 1025, and 810 cm^{-1}; ^1H NMR ($CDCl_3$) δ=1.32 (6H, t, *J*=7.0 Hz, OEt), 1.4—1.96 (6H, m, THP), 2.80 (2H, d, *J*=6.5 Hz, 3-H), 3.14 (2H, d, J_{H-P}=22.5 Hz, CH_2P), 3.3—4.2 (6H, m, THP, CH_2OTHP, OH, and CHOH), 4.12 (4H, dq, J_{H-P}=8.0 and *J*=7.0 Hz, OEt), 4.54 (1H, m, THP), ^{13}C NMR ($CDCl_3$) δ=16.32 (dq, J_{C-P}=7.4 Hz, OEt), 19.82, 25.35, 30.65 (each t, THP), 43.12 (dt, J_{C-P}=126.5 Hz, CH_2P), 47.71, 47.94 (each t, 3-C), 60.83 (t, CH_2OTHP), 62.77 (dt, J_{C-P}=5.9 Hz, OEt), 67.01 (d, CHOH), 71.71, 72.01 (each t, THP), 99.89, 100.01 (each d, THP), and 201.71 (d, J_{C-P}=5.9 Hz, CO); MS *m/z* (rel intensity, %) 266 (1), 226 (12), 224 (39), 223 (M^+-CH_2OTHP, base peak), 219 (43), 195 (20), 152 (27), and 85 (42).

As this compound **6** is too hygroscopic to be submitted for analysis, it was converted into *O*-silyl derivative according to the following procedure: To a solution of **6** (0.16 g, 0.47 mmol) in dry DMF (1 ml) were added *t*-butyldimethylsilyl chloride (0.086 g, 0.568 mmol) and imidazole (0.081 g, 1.183 mmol). The mixture was stirred at room temperature for 15.5 h. Diethyl ether (100 ml) was added, the resulting mixture was washed with aqueous sodium chloride (50 ml×3), dried over magnesium sulfate, and then evaporated in vacuo. The residue was chromatographed over silica gel by using hexane–ethyl acetate (1 : 2 v/v) to give ethyl 4-(*t*-butyldimethylsilyloxy)-2-oxo-5-(2-tetrahydropyranyloxy)pentylphosphonate (0.171 g, 80%). Colorless liquid; IR (neat) 1720, 1250, 1030, 830, and 780 cm^{-1}; ^1H NMR ($CDCl_3$) δ=0.09 (6H, s, Me_2Si), 0.84 (6H, s, *t*-BuSi), 1.33 (6H, t, *J*=7.0 Hz, OEt), 1.4—1.7 (6H, THP), 2.7—2.9 (2H, m, 3-H), 3.11 (2H, d, J_{H-P}=22.5 Hz, CH_2P), 3.6—3.9 (4H, m, THP and CH_2OTHP), 4.12 (4H, dq, J_{H-P}=8.0, and 7.0 Hz, OEt), 4.22 (1H, m, 4-H), and 4.55 (1H, m, THP); ^{13}C NMR ($CDCl_3$) δ=−4.59, −4.88 (each q, Me_2Si), 16.35 (dq, J_{C-P}=5.9 Hz, OEt), 18.06 (s, *t*-BuSi), 19.24, 19.41, 25.47 (each t, THP), 25.88 (q, *t*-BuSi), 30.53 (t, THP), 43.77 (dt, J_{C-P}=126.5 Hz CH_2P), 49.24 (t, 3-C), 62.06, 62.59 (each dt, J_{C-P}=5.9 Hz, OEt), 62.48, 62.71 (each t, CH_2OTHP), 68.18, 68.36 (each d, 4-C), 71.24 (t, THP), 98.83 (d, THP), 200.72, and 200.83 (each d, J_{C-P}=2.9 Hz, CO); MS *m/z* (rel intensity, %) 395 (M^+-t-Bu, 10), 337 (14), 311 (56), 220 (11), 219 (base peak), 191 (15), 163 (12), 84 (20), and 75 (13). Found: C, 53.11; H, 9.15%. Calcd for $C_{20}H_{41}O_7PSi$: C, 53.08; H, 9.13%.

Reactions of 2-(Phosphorylmethyl)furan with Carbonyl Compounds Leading to 7b—h. To a solution of **5d** (0.232 g, 1 mmol) in dry THF (3 ml) was added butyllithium (15% in hexane, 0.63 ml, 1 mmol) at −78 °C. The mixture was stirred at the same temperature under nitrogen for 1 h and a carbonyl compound (1 to 1.5 mmol) was added. After 30 min at −78 °C, saturated ammonium chloride (20 ml) was added and extraction with dichloromethane (30 ml×3) followed. The combined extracts were dried over magnesium sulfate and evaporated in vacuo. The residue was chromatographed over silica gel with hexane–ethyl acetate (2 : 1 v/v) as an eluent to give **7**. Further elution with hexane–ethyl acetate (1 : 1 v/v) recovered the unreacted **5d**. Amounts of the carbonyl compounds are as follows: benzaldehyde (1.5 mmol), butanal (1 mmol), cyclopentanone (1.5 mmol), cyclohexanone (1.2 mmol, reaction time: 2 h), 3-pentanone (1.5 mmol), 2-heptanone (1.5 mmol), 5-hexen-2-one (1.5 mmol).

These adducts **7** are too hygroscopic to be submitted for analyses except for **7e** and **7g**. Accordingly they were used in the subsequent olefination without further purification.

7b: (a 7 : 3 mixture of two diastereomers): Pale yellow viscous liquid; ^1H NMR ($CDCl_3$) δ=1.0—1.4 (6H, m, OEt), 1.86 (7/10×3H, s, 4-Me), 1.95 (3/10×3H, s, 4-Me), 3.4—3.8 (1H, m, CHP), 3.8—4.3 (4H, m, OEt), 4.83 (1H, m, OH), 5.1—5.5 (1H, m, CHOH), 5.94 (7/10H, d, J_{H-P}=3.0 Hz, 3-H), 6.26 (3/10H, d, J_{H-P}=3.0 Hz, 3-H), 6.96 (1H, m, 5-H), and 7.20 (5H, s, Ph).

7c: (a 4 : 1 mixture of two diastereomers): Colorless viscous liquid; IR (neat) 3400, 2970, 1615, 1230, 1025, and 800 cm^{-1}; ^1H NMR ($CDCl_3$) δ=0.87 (3H, m, *n*-Pr), 1.1—1.7 (10H, m, OEt and *n*-Pr), 2.02 (3H, s, 4-Me), 3.1—3.5 (1H, m, CHP), 3.8—4.4 (6H, m, OEt and CHOH), 6.14 (4/5H, d, *J*=3.0 Hz, 3-H), 6.34 (1H, d, *J*=3.0 Hz, 3-H), and 7.13 (1H, m, 5-H); MS *m/z* (rel intensity, %) 232 (M^+−PrCHO, base peak), 204 (22), 176 (33), and 95 (30).

7d: Colorless viscous liquid; IR (neat) 3440, 2980, 1610, 1225, 1025, and 800 cm^{-1}; ^1H NMR ($CDCl_3$) δ=1.16, 1.31 (each 3H, t, *J*=7.0 Hz, OEt), 1.4—2.1 (8H, m, CH_2), 1.90 (3H, s, 4-Me), 3.39 (1H, d, J_{H-P}=24.0 Hz, CHP), 3.6—4.3 (4H, m, OEt), 6.30 (1H, d, J_{H-P}=3.0 Hz, 3-H), and 7.10 (1H, br s,

5-H); MS *m/z* (rel intensity, %) 316 (M^+, 7), 232 (M^+−cyclopentanone, base peak), and 95 (23).

7e: Colorless viscous liquid; IR (neat) 3440, 2940, 1630, 1225, 1025, and 800 cm^{-1}; ^1H NMR ($CDCl_3$) δ=1.16, 1.29 (each 6H, t, J=7.0 Hz, OEt), 1.0—1.9 (10H, m, CH_2), 1.99 (3H, d, J=1.2 Hz, 4-Me), 3.40 (1H, d, J_{H-P}=24.0 Hz, CHP), 3.6—4.3 (5H, m, OEt), 6.27 (1H, d, J_{H-P}=3.0 Hz, 3-H), and 7.22 (1H, q, J=1.2 Hz, 5-H); MS *m/z* (rel intensity, %) 330 (M^+, 3), 232 (M^+−cyclohexanone), 159 (base peak), 129 (31), 126 (68), 117 (81), and 91 (73). HRMS Found: *m/z* 330.1592. Calcd for $C_{16}H_{27}O_5P$: M, 330.1595.

7f: Colorless viscous liquid; IR (neat) 3440, 2990, 1610, 1225, 1025, and 790 cm^{-1}; ^1H NMR ($CDCl_3$) δ=0.82, 0.90 (each 3H, t, J=7.5 Hz, Et), 1.14, 1.32 (each 3H, t, J=7.0 Hz, OEt), 1.5—1.9 (4H, m, Et), 2.00 (3H, s, 4-Me), 3.48 (1H, d, J_{H-P}=24.0 Hz, CHP), 3.6—4.3 (5H, m, OEt), 6.30 (1H, d, J_{H-P}=3.0 Hz, 3-H), and 7.12 (1H, m, 5-H); MS *m/z* (rel intensity, %) 318 (M^+, 1), 232 (M^+−3-pentanone, base peak), 176 (29), and 95 (32).

7g: (a 4 : 1 mixture of two diastereomers): Colorless viscous liquid; IR (neat) 3440, 2940, 1610, 1225, 1025, and 790 cm^{-1}; ^1H NMR ($CDCl_3$) δ=0.89 (3H, t, J=7.0 Hz, *n*-C_5H_{11}), 1.0—1.7 (17H, m, OEt, Me, and *n*-C_5H_{11}), 2.02 (3H, s, 4-Me), 3.40 (1/5H, d, J_{H-P}=24.0 Hz, CHP), 3.45 (4/5H, J_{H-P}=24.0 Hz, CHP), 3.7—4.3 (4H, m, OEt), 4.38 (1H, s, OH), 6.23 (4/5H, d, J_{H-P}=3.0 /Hz, 3-H), 6.28 (1/5H, d, J_{H-P}=3.0 Hz, 3-H), and 7.12 (1H, m, 5-H); MS *m/z* (rel intensity, %) 346 (M^+, 0.1) and 232 (M^+−2-heptanone, base peak). Found: C, 58.70; H, 8.98%. Calcd for $C_{17}H_{31}O_5P$: C, 58.94; H, 9.02%.

7h: (a 4 : 1 mixture of two diastereomers): Colorless viscous liquid; IR (neat) 3430, 3000, 1640, 1610, 1225, 1025, and 790 cm^{-1}; ^1H NMR ($CDCl_3$) δ=1.1—1.4 (9H, m, OEt and Me), 1.4—1.9 (2H, m, CH_2), 1.9—2.4 (2H, m, $CHCH_2$), 2.00 (3H, s, 4-Me), 3.42 (1/5×2H, d, J_{H-P}=24.0 Hz, CHP), 3.45 (4/5×2H, d, J_{H-P}=24.0 Hz, CHP), 3.7—4.3 (4H, m, OEt), 4.44 (1H, br s, OH), 4.8—5.1 (2H, m, $=CH_2$), 5.80 (1H, m, CH), 6.23 (4/5H, d, J_{H-P}=3.0 Hz 3-H), 6.28 (1/5H, d, J_{H-P}=3.0 Hz, 3-H), and 7.12 (1H, br s, 5-H); MS *m/z* (rel intensity, %) 232 (M^+−5-hexen-2-one, 15), 176 (25), 95 (26), 81 (20), 55 (22), and 43 (base peak).

Condensation of 5b with Butanal Leading to 8a. At −78 °C butyllithium (15% in hexane, 0.29 ml, 0.469 mmol) was added to a solution of **5b** (0.109 g, 0.469 mmol) in dry THF (3 ml). The mixture was stirred under nitrogen for 30 min. After butanal (0.068 g, 0.08 ml, 0.938 mmol) was added, the resulting mixture was stirred at −78 °C for 1 h, at −15 °C for 1 h, at 0 °C for 3 h, and at room temperature for 16 h. Saturated aqueous ammonium chloride (20 ml) was added and the extraction with diethyl ether (30 ml×3) followed. The combined extracts were dried over magnesium sulfate and evaporated in vacuo. The residue was chromatographed over silica gel by using hexane to give **8a** (0.023 g, 33%). From the fraction with hexane-ethyl acetate (1 : 3 v/v) the unreacted **5b** (0.028 g, 26%) was recovered. **8a** (*E* : *Z*=98 : 2 by GLC): Colorless liquid; IR (neat) 2900, 1600, and 960 cm^{-1}; ^1H NMR ($CDCl_3$) δ=0.92 (3H, t, *n*-Pr), 1.2—1.7 (2H, m, *n*-Pr), 2.0—2.3 (2H, m, $=CHCH_2$), 2.25 (3H, s, 5-Me), and 5.8—6.3 (4H, m, 3-, 4-H, and CH=CH); MS *m/z* (rel intensity, %) 150 (M^+, 55), 122 (11), 121 (base peak), 91 (13), and 77 (14). Elemental analysis by HRMS was not attempted because of its easy polymerization.

Dehydration of Adducts 7b—h Leading to 8b—h. A mixture of adduct **7** (1 mmol) and cesium fluoride (0.578 g, 3.8 mmol) in wet DMF (2 ml containing water (0.07 ml)) was heated at 60 °C for 33—36 h. Diethyl ether (80 ml) was added, the ether solution was washed with water (50 ml×5), dried over magnesium sulfate, and evaporated in vacuo. The residue was chromatographed over silica gel with hexane to give **8** as rather unstable products. Further elution with the eluents shown below gave unreacted **7** and/or **5d** as a retro addition product.

8b: (*E* : *Z*=99 : 1 by GLC): Pale yellow prisms (hexane); mp 60—62 °C; IR (KBr) 1600 and 960 cm^{-1}; ^1H NMR ($CDCl_3$) δ=1.98 (3H, d, J=1.0 Hz, Me), 6.17 (1H, s, 3-H), 6.76 (1H, J=16.0 Hz, furylCH=), 6.91 (1H, s, 5-C), and 7.0—7.5 (6H, m, PhCH=); ^{13}C NMR ($CDCl_3$) δ=111.48 (d, 3-C), 116.89 (d, furylCH=), 122.13 (s, 4-C), 126.48, 127.01, 127.66, 128.83 (each d), 137.36 (s), 139.19 (d, 5-C), and 153.48 (s, 2-C); MS *m/z* (rel intensity, %) 184 (M^+, base peak), 155 (31), 141 (41), and 116 (25). Found: C, 84.18; H, 6.52%. Calcd for $C_{13}H_{12}O$: C, 84.75; H, 6.56%. The elution with hexane-ethyl acetate (1 : 2 v/v) afforded **5d** (20%).

8c: (*E* : *Z*=96:4 by GLC): Colorless liquid; IR (neat) 2940, 1600, and 960 cm^{-1}; ^1H NMR ($CDCl_3$) δ=0.92 (3H, t, J=7.0 Hz, *n*-Pr), 1.3—1.7 (2H, m, *n*-Pr), 1.96 (3H, s, 4-Me), 2.0—2.3 (2H, m, CH_2CH=), 6.06 (1H, d, J=15.5 Hz, furylCH=), 6.0—6.2 (1H, m, *n*-PrCH=), 6.10 (1H, s, 3-H), and 7.06 (1H, br s, 5-H); MS *m/z* (rel intensity, %) 150 (M^+, 19), 121 (28), 64 (21), 57 (29), 55 (27), and 43 (base peak). HRMS Found: *m/z* 150.1035. Calcd for $C_{10}H_{14}O$: M, 150.1044. The elution with hexane-ethyl acetate (1 : 2 v/v) gave a mixture of **7c** and **5d** (**7c**: 18%, **5d**: 4%).

8d: The reaction of **7d** (0.17 g, 0.537 mmol) with cesium fluoride (0.31 g, 2.041 mmol) in wet DMF (6.1 ml containing 0.04 ml of water) was heated at 60 °C for 30 h. Another portions of cesium fluoride (0.31 g, 2.041 mmol) and water (0.04 ml) were added and the heating was continued at 60 °C for 15 h and then at 80 °C for 5.5 h. A similar work-up gave **8d** (0.086 g, 78%). **8d**: Colorless liquid; IR (neat) 2960, 1660 and 1600 cm^{-1}; ^1H NMR ($CDCl_3$) δ=1.4—2.0 (4H, m, CH_2), 2.00 (3H, s, 4-Me), 2.3—2.6 (4H, m, CH_2), 5.99 (1H, s, 3-H), 6.18 (1H, tt, J=2.1 and 2.1 Hz, CH), and 7.08 (1H, s, 5-H); MS *m/z* (rel intensity, %) 162 (M^+, base peak), 121 (49), 105 (20), 91 (36), and 77 (20). HRMS Found: *m/z* 162.1048. Calcd for $C_{11}H_{14}O$: M, 162.1044. The fraction eluted with hexane-ethyl acetate (1 : 2 v/v) gave **7d** (0.005 g, 3%) and then **5d** (0.008 g, 6%).

8e: Colorless liquid; IR (neat) 2930, 1655, and 1600 cm^{-1}; ^1H NMR ($CDCl_3$) δ=1.4—1.8 (6H, m, CH_2), 1.99 (3H, d, J=1.2 Hz, 4-Me), 2.22 (2H, m, CH_2CH=), 2.58 (2H, m, CH_2), 5.89 (1H, s, CH=), 6.02 (1H, s, 3-H), and 7.06 (1H, t, J=1.2 Hz, 5-H); MS *m/z* (rel intensity, %) 176 (M^+, base peak), 108 (55), and 95 (21). HRMS Found: *m/z* 176.1186. Calcd for $C_{12}H_{16}O$: M, 176.1200. The fraction eluted with hexane-ethyl acetate (2 : 1 v/v) gave **7e** (5%).

8f: Colorless liquid; IR (neat) 2960, 1655, and 1600 cm^{-1}; ^1H NMR ($CDCl_3$) δ=1.06 (6H, t, J=7.0 Hz, Et), 2.00 (3H, s, 4-Me), 2.18, 2.40 (each 2H, q, J=7.0 Hz, Et), 5.94 (1H, s, CH=), 6.04 (1H, s, 3-H), and 7.09 (1H, m, 5-H); MS *m/z* (rel intensity, %) 164 (M^+, base peak), 149 (22), 135 (91), 107 (26), 93 (22), and 91 (28). HRMS Found: *m/z* 164.1209. Calcd for $C_{11}H_{16}O$: M, 164.1200. The fraction eluted with hexane-ethyl acetate (1 : 1 v/v) provided **7f** (3%) and with eluent of 1 : 2 v/v gave **5d** (8%).

8g: (*E* : *Z*=80 : 20 by GLC): Colorless liquid; IR (neat) 2940, 1655, and 1600 cm^{-1}; ^1H NMR ($CDCl_3$) δ=0.87 (3H, t, J=7.0

Hz, n-C_5H_{11}), 1.1—1.6 (6H, m, n-C_5H_{11}), 1.83 (20/100×3H, d, 1.0 Hz, =CMe, *Z*), 1.90 (80/100×3H, d, *J*=1.0 Hz, =CMe, *E*), 1.95 (3H, s, 4-Me), 2.0—2.5 (2H, m, =CCH_2), 5.98 (2H, s, 3-H and =CH), and 7.03 (s, 5-H); ^{13}C NMR ($CDCl_3$) δ=9.76 (q, 4-Me, *Z*), 9.81 (q, 4-Me, *E*), 14.07 (q, n-C_5H_{11}), 18.46 (q, =CMe, *E*), 22.63 (t, CH_2), 24.66 (q, =CMe, *Z*), 27.54 (t, CH_2, *Z*), 27.73 (t, CH_2, *E*), 31.53 (t, CH_2, *E*), 32.08 (t, CH_2, *Z*), 33.62 (t, =CCH_2, *Z*), 40.79 (t, =CCH_2, *E*), 109.76 (d, 3-C, *Z*), 110.10 (d, 3-C, *E*), 114.16 (d, =CH, *E*), 114.41 (d, =CH, *Z*), 121.18 (s, 4-C, *Z*), 121.29 (s, 4-C, *E*), 137.19 (d, 5-C, *Z*), 137.25 (d, 5-C, *E*), 138.66 (s, =C, *E*), 139.39 (s, =C, *Z*), 153.50 (s, 2-C, *Z*), and 153.85 (s, 2-C, *E*); MS *m/z* (rel intensity, %) 192 (M^+, 84), 135 (base peak), 122 (20), 107 (34), and 91 (38). HRMS Found: *m/z* 192.1528. Calcd for $C_{13}H_{20}O$: M, 192.1513. The fraction eluted with hexane-ethyl acetate (1 : 1 v/v) gave **7g** (0.019 g, 6%) and with eluent of 1 : 2 v/v afforded **5d** (0.01 g, 10%).

8h: (*E* : *Z*=82 : 18 by GLC): Colorless liquid; IR (neat) 2940, 1660, 1640, and 1600 cm^{-1}; ^{1}H NMR ($CDCl_3$) δ=1.87 (18/100×3H, d, *J*=1.2 Hz, =CMe), 1.94 (82/100×3H, d, *J*=1.2 Hz, =CMe), 2.00 (3H, *J*=1.2 Hz, 4-Me), 2.1—2.6 (4H, m, CH_2), 4.9—5.2 (2H, m, =CH_2), 5.6—6.0 (1H, m, CH=), 6.01 (1H, s, 3-H), and 7.08 (1H, t, *J*=1.2 Hz, 5-H); ^{13}C NMR ($CDCl_3$) δ=9.76 (q, 4-Me), 18.50 (q, =CMe, *E*), 24.62 (q, =CMe, *Z*), 31.98 (t, CH_2, *Z*), 32.32 (t, CH_2, *E*), 32.94 (t, =CCH_2, *Z*), 40.16 (t, =CCH_2, *E*), 109.96 (d, 3-C, *Z*), 110.29 (d, 3-C, *E*), 114.76 (t, =CH_2), 121.28 (s, 4-C), 137.32 (d, CH=), 137.49 (d, 5-C), 138.17 (s, =CMe, *E*), 138.51 (s, =CMe, *Z*), 153.26 (s, 2-C, *Z*), and 153.62 (s, 2-C, *E*); MS *m/z* (rel intensity, %) 176 (M^+, 38), 135 (base peak), 107 (46), 91 (49), and 79 (25). HRMS Found: *m/z* 176.1197. Calcd for $C_{12}H_{11}O$: M, 176.1200. The fraction eluted with hexane-ethyl acetate (1 : 1 v/v) gave **7h** (0.008 g, 4%) and with eluent of 1 : 2 v/v afforded **5d** (0.019 g, 12%).

4-Methyl-2-(1-oxohexyl)furan (9a): To a solution of **5i** (0.265 g, 0.876 mmol) in dry THF (4 ml) was added butyllithium (15% in hexane, 0.55 ml, 0.876 mmol) at −78 °C and stirred for 1 h. After dry oxygen gas was bubbled at −100 °C for 15 min, aqueous THF (50%, 20 ml) was slowly added. The products were extracted with diethyl ether (30 ml×3). The combined extracts were dried over magnesium sulfate and evaporated in vacuo. The residue was chromatographed over silica gel with hexane-ethyl acetate (10 : 1 v/v) to give **9a** (0.047 g, 30%): Colorless liquid; IR (neat) 2930, 1675, and 1600 cm^{-1}; ^{1}H NMR ($CDCl_3$) δ=0.90 (3H, t, *J*=6.0 Hz, n-C_5H_{11}), 1.2—2.0 (6H, m, n-C_5H_{11}), 2.08 (3H, s. 4-Me), 2.77 (2H, t, *J*=6.0 Hz, $COCH_2$), 7.03 (1H, s, 3-H), and 7.33 (1H, t, *J*=1.0 Hz, 2-H); MS *m/z* (rel intensity, %) 180 (M^+, 9), 124 (base peak), 110 (63), 53 (22), 43 (24), and 41 (30). Found: C, 73.38; H, 8.94%. Calcd for $C_{11}H_{16}O$: C, 73.30; H, 8.95%.

4-Methyl-2-(1-oxo-2-phenylethyl)furan (9b): Dry oxygen gas was bubbled at −78 °C for 1 h through the anion solution generated by a similar method using **5j** (0.21 g, 0.65 mmol) and butyllithium (15% in hexane, 0.45 ml, 0.65 mmol) in dry THF (3 m]). Usual hydrolytic work-up and silica-gel column chromatography with hexane-ethyl acetate (5 : 1 v/v) afforded **9b** (0.026 g, 20%): Colorless needles (hexane); mp 60.5—61 °C; IR (KBr) 3100, 1650, and 1600 cm^{-1}; ^{1}H NMR ($CDCl_3$) δ=2.04 (3H, dd, *J*=1.0 and 0.5 Hz, Me), 3.04 (2H, s, CH_2), 7.03 (1H, t, *J*=0.5 Hz, 3-H), 7.26 (5H, br s, Ph), and 7.32 (1H, t, *J*=1.0 Hz, 5-H); MS *m/z* (rel intensity, %) 200 (M^+, 9), 110 (base peak), 91 (55), and 65 (44). Found: C, 77.79; H, 5.86%. Calcd for $C_{13}H_{12}O_2$: C, 77.98; H, 6.04%.

Hydrolysis of 2-(1-Phosphorylalkyl)furans 5b, c and 5g Leading to 2,5-Dioxoalkylphosphonates 10a—c. A furan **5** (1 mmol) in aqueous acetic acid (67%, 2—3 ml) containing a catalytic amount of concd sulfuric acid was heated at 120 °C for 5 h. The reaction mixture was diluted with water (40 ml), neutralized with saturated aqueous sodium hydrogencarbonate, and then extracted with ethyl acetate (50 ml×3). The combined extracts were dried over magnesium sulfate and evaporated in vacuo. The residue was chromatographed over silica gel to give **10** (**10a**: from ethyl acetate, 62%. **10b**: from ethyl acetate, 52%. **10c**: from hexane-ethyl acetate (3 : 2 v/v), 53%).

10a: Pale yellow liquid; IR (neat) 1710, 1250, 1020, and 800 cm^{-1}; ^{1}H NMR ($CDCl_3$) δ=1.33 (6H, t, *J*=7.0 Hz, OEt), 2.17 (3H, s, Me), 2.6—3.0 (4H, m, CH_2), 3.12 (2H, d, J_{H-P}=22.5 Hz, PCH_2), and 4.13 (4H, dq, J_{H-P}=7.8 and *J*=7.0 Hz, OEt); MS *m/z* (rel intensity, %) 250 (M^+, 7), 232 (34), 208 (31), 207 (70), 179 (98), 153 (56), 152 (76), 125 (53), 123 (52), 109 (42), 97 (28), 95 (51), 81 (34), and 43 (base peak). HRMS Found: *m/z* 250.0969. Calcd for $C_{10}H_{19}O_5P$: M, 250.0969.

10b: Pale yellow liquid; IR (neat) 1710, 1250, 1020, and 815 cm^{-1}; ^{1}H NMR ($CDCl_3$) δ=1.05 (3H, t, *J*=7.0 Hz, Et), 1.33 (6H, t, *J*=7.0 Hz, OEt), 2.47 (2H, q, *J*=7.0 Hz, Et), 2.6—3.0 (4H, m, CH_2), 3.12 (2H, d, J_{H-P}=22.5 Hz, PCH_2), and 4.13 (4H, dq, J_{H-P}=8.0 and *J*=7.0 Hz, OEt); ^{13}C NMR ($CDCl_3$) δ=7.77 (q, Et), 16.29 (dq, J_{C-P}=5.9 Hz, OEt), 35.77, 37.65 (each t, $COCH_2$), 42.50 (dt, J_{C-P}=128.0 Hz, PCH_2), 62.65 (dt, J_{C-P}=5.9 Hz, OEt), 201.01 (d, J_{C-P}=5.9 Hz, CO), and 209.72 (s, CO); MS *m/z* (rel intensity, %) 264 (M^+, 19), 246 (36), 235 (41), 208 (44), 207 (95), 179 (base peak), 153 (46), 152 (60), 125 (30), 123 (30), and 109 (32). HRMS Found: *m/z* 264.1116. Calcd for $C_{11}H_{21}O_5P$: M, 264.1125.

10c: Pale yellow liquid; IR (neat) 1710, 1250, 1025, and 790 cm^{-1}; ^{1}H NMR ($CDCl_3$) δ=0.87 (3H, t, *J*=6.0 Hz, n-C_8H_{17}), 1.05 (3H, t, *J*=7.0 Hz, Et), 1.1—1.4 (12H, m, n-C_8H_{17}), 1.32 (6H, t, *J*=7.0 Hz, OEt), 1.5—2.1 (2H, m, n-C_8H_{17}), 2.49 (2H, q, *J*=7.0 Hz, Et), 2.5—3.4 (5H, m, PCH and $COCH_2$), and 4.11 (4H, dq, J_{H-P}=8.0 and *J*=7.0 Hz, OEt); ^{13}C NMR ($CDCl_3$) δ=7.88 (q, Et), 14.12 (q, n-C_8H_{17}). 16.41 (dq, J_{C-P}=5.9 Hz, OEt), 22.71 (t, n-C_8H_{17}), 26.68 (dt, J_{C-P}=4.4 Hz, n-C_8H_{17}), 28.41 (dt, J_{C-P}=14.7 Hz, n-C_8H_{17}), 29.24, 29.41, 31.88 (each t, n-C_8H_{17}), 35.71, 35.94, 38.06 (each t, CH_2CO), 52.97 (dd, J_{C-P}=125.0 Hz, PCH), 62.56 (dt, J_{C-P}=4.4 Hz, OEt), 62.77 (dt, J_{C-P}=5.90 Hz, OEt), 205.04 (d, J_{C-P}=4.4 Hz, CO), and 209.71 (s, CO); MS *m/z* (rel intensity, %) 376 (M^+, 15), 347 (28), 319 (48), 291 (29), 264 (base peak), 263 (36), 221 (26), 207 (41), 179 (27), 165 (48), 153 (46), and 110 (26). HRMS Found: *m/z* 376.2365. Calcd for $C_{19}H_{37}O_5P$: M, 376.2377.

3-Ethyl-2-octyl-2-cyclopenten-1-one (11). A mixture of lithium bromide (0.029 g, 0.33 mmol) and **10c** (0.083 g, 0.22 mmol) in dry THF (3.5 ml) was stirred at room temperature for 10 min. After cooled to 0 °C triethylamine (0.027 g, 0.04 ml, 0.246 mmol) was added. The resulting mixture was stirred for 1.5 h at room temperature, heated under reflux for 24 h, diluted with water (20 ml), and then extracted with diethyl ether (30 ml×3). The combined extracts were dried (magnesium sulfate) and evaporated in vacuo. The residue was chromatographed over silica gel by using hexane-ethyl acetate (3 : 1 v/v) as an eluent to give **11** (0.015 g, 31%). The starting **10c** (0.01 g, 12%) was recovered from a fraction eluted with hexane-ethyl acetate (1 : 1 v/v): Pale yellow liquid; IR (neat) 1700 and 1640 cm^{-1}; ^{1}H NMR ($CDCl_3$) δ=0.86 (3H, t, *J*=6.0 Hz, n-C_8H_{17}), 1.12 (3H, t, *J*=7.5 Hz, Et), 1.0—1.5 (12H, m, n-C_8H_{17}), and 2.0—2.6 (8H, m, CH_2C=, 4- and

5-H); MS *m/z* (rel intensity, %) 222 (M^+, 16), 193 (base peak), 124 (60), 123 (24), and 79 (23). HRMS Found: *m/z* 222.1982. Calcd for $C_{15}H_{26}O$: M, 222.1982.

Synthesis of Furanosesquiterpene 12. To a solution of **5d** (0.188 g, 0.81 mmol) in dry THF (2 ml) was added butyllithum (15% in hexane, 0.51 ml, 0.81 mmol) at −78 °C under nitrogen. After the mixture was stirred for 1 h, **13** (*E*:*Z*=75:25, 0.168 g, 1.215 mmol) was added and the stirring was continued for 30 min. The mixture was treated with saturated ammonium chloride solution (20 ml) and extracted with dichloromethane (30 ml×3). The combined extracts were dried over magnesium sulfate and evaporated in vacuo. The residue was chromatographed over silica gel with hexane-ethyl acetate (3:1 v/v) to give **14** (0.237 g, 79%). The fraction eluted with hexane-ethyl acetate (1:1 v/v) afforded the starting **5d** (0.022 g, 12%). **14** (a mixture of diastereomers, *E*:*Z*=3:1 by ^{1}H NMR): Colorless viscous liquid; IR (neat) 3440, 3000, 1640, 1610, 1225, and 1025 cm^{-1}; ^{1}H NMR ($CDCl_3$) δ=1.2—1.8 (14H, m, OEt, CH_2, MeC(OH), and MeCH=), 2.01 (3H, 4-Me), 2.1—2.3 (2H, m, CH_2CH), 3.41 (1/4H, d, J_{H-P}=23.8 Hz, PCH, *Z*), 3.47 (3/4H, d, J_{H-P}=23.5 Hz, PCH, *E*), 3.8—4.3 (4H, m, OEt), 4.46 (1H, s, OH), 4.9—5.4 (2H, m, CH_2), 6.23, 6.28 (1H, each d, J_{H-P}=3.3 Hz, 3-H), 6.33 (3/4H, dd, *J*=17.2 and 10.6 Hz, CH=, *E*), 6.7—6.8 (1/4H, m, CH=, *Z*), and 7.13 (1H, s, 5-H); MS *m/z* (rel intensity, %) 370 (M^+, 3), 232 (base peak), and 95 (23). HRMS Found: *m/z* 370.1906. Calcd for $C_{19}H_{31}O_5P$: M, 370.1907. A mixture of **14** (0.21 g, 0.567 mmol), cesium fluoride (0.327 g, 2.155 mmol), and water (0.04 ml, 2.155 mmol) in DMF (6.5 ml) was heated at 60 °C for 38 h. Diethyl ether (100 ml) was added to the mixture, the organic layer was washed with water (100 ml×4), dried over magnesium sulfate, and evaporated in vacuo. The residue was chromatographed over silica gel by using hexane as an eluent to give **12** (0.074 g, 53%). The fraction eluted with hexane-ethyl acetate (1:2 v/v) gave **5d** (0.017 g, 13%). **12** (a 59:20:15:6-mixture of **12a**:**12b**:**12c**:**12d** by GLC): Colorless liquid; IR (neat) 2940, 1640, and 1610 cm^{-1}; ^{1}H NMR ($CDCl_3$) δ=1.56, 1.75, 1.81, 1.87, 1.96, 2.00, 2.02 (9H, each s, Me), 2.2—2.4 (4H, m, CH_2), 4.9—5.2 (2H, m, $=CH_2$), 5.4—5.6 (1H, m, 5′-H), 6.04 (2H, m, 3- and 1′-H), 6.36 (59/100H, dd, *J*=17.1 and 10.8 Hz, 7′-H of **12a**), 6.37 (15/100H, dd, *J*=17.1 and 10.8 Hz, 7′-H of **12c**), 6.78 (20/100H, dd, *J*=17.1 and 10.8 Hz, 7′-H of **12b**), 6.80 (6/100H, dd, *J*=17.1 and 10.8 Hz, 7′-H of **12d**), and 7.10 (1H, s, 5-H); ^{13}C NMR ($CDCl_3$) δ=9.76 (q, 4-Me), 11.63 (q, 6′-Me of **12c**), 11.68 (q, 6′-Me of **12a**), 18.52 (q, 2′-Me of **12a**), 19.74 (q, 2′-Me of **12b**, 6′-Me of **12b**, and 6′-Me of **12d**), 24.71 (q, 2′-Me of **12c**), 25.74 (q, 2′-Me of **12d**), 25.85 (t, 4′-C, **12d**), 26.00 (t, 4′-C of **12b**), 26.75 (t, 4′-C of **12c**), 26.91 (t, 4′-C of **12a**), 33.38 (t, 3′-C of **12c**), 33.78 (t, 3′-C of **12d**), 40.36 (t, 3′-C of **12a**), 40.75 (t, 3′-C of **12b**), 110.05 (d, 3-C of **12d**), 110.08 (d, 3-C of **12c**), 110.36 (d, 3-C of **12a** and 3-C of **12b**), 110.64 (t, 8′-C of **12a**), 110.87 (t, 8′-C of **12c**), 113.42 (t, 8′-C of **12d**), 113.57 (t, 8′-C of **12b**), 114.57 (d, 1′-C of **12a** and 1′-C of **12b**), 114.91 (d, 1′-C of **12d**), 115.09 (d, 1′-C of **12c**), 121.19 (s, 4-C of **12c** and 4-C of **12d**), 121.29 (s, 4-C of **12a** and 4-C of **12b**), 130.15 (d, 5′-C of **12b**), 130.58 (d, 5′-C of **12d**), 132.13 (d, 5′-C of **12a**), 132.65 (d, 5′-C of **12c**), 133.63 (6′- and 7′-C of **12b**), 133.74 (6′- and 7′-C of **12d**), 134.31 (s, 6′-C of **12c**), 134.38 (s, 6′-C of **12a**), 137.00, 137.46, 137.52, 137.85, 138.11, 141.49 (d, 7′-C of **12a**), 141.56 (d, 7′-C of **12c**), 153.26 (s, 2-C of **12c** and 2-C of **12d**), and 153.59 (s, 2-C of **12a** and 2-C of **12b**); MS *m/z* (rel intensity, %) 216 (M^+, 27), 135 (base peak), 107 (38), 91 (31), 78 (15), and 41 (12). HRMS Found: *m/z* 216.1515. Calcd for $C_{15}H_{20}O$: M, 216.1513.

The present work was partially supported by a Grant-in-Aid for Scientific Research No. 61470095 from the Ministry of Education, Science and Culture.

References

1) a) O. Tsuge, S. Kanemasa, and H. Suga, *Chem. Lett.*, **1986**, 183. b) O. Tsuge, S. Kanemasa, H. Suga, and N. Nakagawa, *Bull. Chem. Soc. Jpn.*, **60**, 2463 (1987). c) O. Tsuge, S. Kanemasa, and H. Suga, *Chem. Lett.*, **1987**, 323. d) O. Tsuge, S. Kanemasa, N. Nakagawa, and H. Suga, *Bull. Chem. Soc. Jpn.*, **60**, 4091 (1987).

2) H. Hagiwara, H. Uda, and T. Kodama, *J. Chem. Soc., Perkin Trans. 1*, **1980**, 963.

3) K. Inomata, S. Aoyama, and H. Kotake, *Bull. Chem. Soc. Jpn.*, **51**, 930 (1970); K. Inomata, M. Sumita, and H. Kotake, *Chem. Lett.*, **1979**, 709; D. W. Knight and D. C. Rustidge, *J. Chem. Soc., Perkin Trans. 1*, **1981**, 679.

4) B. F. Bowden, J. C. Coll, E. D. de Silva, M. S. L. de Costa, P. J. Djura, M. Mahendran, and D. M. Tapiolas, *Aust. J. Chem.*, **36**, 371 (1983).

5) F. Bohlmann and M. Grenz, *Chem. Ber.*, **108**, 357 (1975).

6) F. Bohlmann and C. Zdero, *Phytochemistry*, **21**, 1989 (1982).

7) G. Guella, I. Manchini, A. Guerriero, and F. Pietr, *Helv. Chim. Acta*, **68**, 1276 (1985).

8) F. Bohlmann and C. Zdero, *Phytochemistry*, **17**, 1155 (1978).

9) Cycloadditions of nitrile oxide **2** with 2-alkyn-1-ol was successfully performed under reflux in the same combination of the solvents (see Ref. 1c).

10) E. J. Corey and G. T. Kwiatowski, *J. Am. Chem. Soc.*, **88**, 5652 (1966).

11) T. Kawashima, T. Ishii, and N. Inamoto, *Chem. Lett.*, **1983**, 1375.

12) M. Mikolajiczyk, W. Midura, and S. Grzejszczak, *Tetrahedron Lett.*, **25**, 2489 (1984).

13) G. Buchi and H. Wuest, *J. Org. Chem.*, **31**, 977 (1966).

14) R. A. Ellison, *Synthesis*, **1973**, 397; N. Finch, J. J. Fitt, and I. H. C. Hsu, *J. Org. Chem.*, **36**, 3191 (1971).

15) R. D. Clark, L. G. Kozar, and C. H. Heathcock, *Synth. Commun.*, **5**, 1 (1975).

16) G. W. Cannon, R. C. Ellis, and J. R. Leal, *Org. Synth.*, Coll. Vol. **4**, 597 (1963).

17) M. Julia, S. Julia, B. S.-Bourdillon, and C. Descoins, *Bull. Soc. Chim. Fr.*, **10**, 2533 (1964).

18) N. Miyashita, A. Yoshikoshi, and P. A. Grieco, *J. Org. Chem.*, **42**, 3772 (1977).

Synthetic Studies of Amphotericin B. III.[1] An Enantiospecific Synthesis of the C-1—C-19 Segment of the Amphotericin B Aglycon†

Mitsuhiro KINOSHITA,* Masato TANIGUCHI, Masahiko MORIOKA, Hitoshi TAKAMI, and Yasuhiro MIZUSAWA
Department of Applied Chemistry, Faculty of Science and Technology, Keio University, Hiyoshi, Kohoku-ku, Yokohama 223
(Received January 14, 1988)

The title compound, (3*S*,4*S*,5*S*,9*S*,11*R*,12*R*,15*R*,17*S*)-4-[(*t*-butyldimethylsilyloxy)methyl]-1,3,5,9,11,12,15,17,19-nonahydroxy-3,5 : 11,12 : 15,17-tri-*O*-isopropylidene-19-*O*-(4-methoxybenzyl)-9-*O*-[(2-methoxyethoxy)methyl]-7-nonadecanone (**1**) was effectively synthesized through the coupling of (3*S*,5*R*,8*R*,9*R*,11*S*)-12-iodo-3,5 : 8,9-di-*O*-isopropylidene-1-*O*-(4-methoxybenzyl)-11-*O*-[(2-methoxyethoxy)methyl]-1,3,5,8,9,11-dodecanehexol (**2**) and (3*S*,4*R*,5*S*)-4-[(*t*-butyldimethylsilyloxy)methyl]-3,5-*O*-isopropylidene-1,1-bis(methylthio)-1-trimethylstannyl-6-heptene-3,5-diol (**36**). The C-13—C-19 segment **36** was enantiospecifically synthesized from 1,2 : 5,6-di-*O*-isopropylidene-α-D-*threo*-D-*glycero*-3-hexofuranosulose (**7**) via (2*S*,4*R*,5*S*)-5,6-epoxy-3-[(*t*-butyldimethylsilyloxy)-methyl]-1-hexen-3-ol (**6a**) in 11.6% overall yield.

Recently, the total syntheses of amphotericin B and its aglycon have been first achieved by Nicolaou et al.[2] The synthesis of key intermediate **A** corresponding to the C-1—C-19 portion of the aglycon has also been announced by Abiko et al.[3] In connection with our synthetic efforts[1] toward the aglycon of amphotericin B, we required access to the compound **1** which was considered to be practically useful as a C-1—C-19 synthetic segment for the construction of the aglycon. In this paper, we wish to describe an enantiospecific synthesis of **1**.

The synthetic plan is outlined in Scheme 1. The synthetic route to **1** through the intermediate **B** which is expected to be formed by the coupling of **2** and the dithioacetal compound **C** seems to be conventional and simple, whereas it may be rather interesting as a synthetic challenge because success of the coupling of **2** and **C** probably depends on the chemical stability of a lithiation derivative of **C**, which is now never precisely predictable (see Ref. 18). The C-1—C-12 segment **2** would be obtainable via **4** from **5**[1] which was previously prepared in our laboratory. The key intermediate **6a** useful for the preparation of various dithioacetal compounds **C** would be enantiospecifically synthesized via the compound **9** (see Scheme 2)

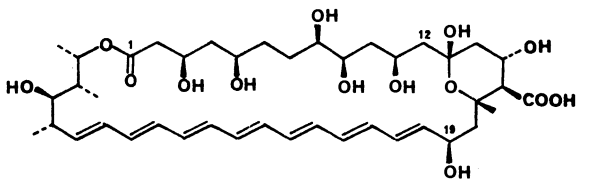

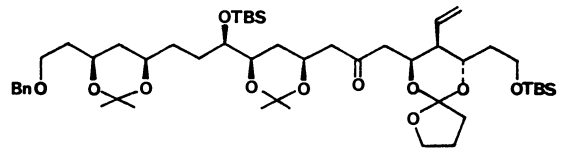

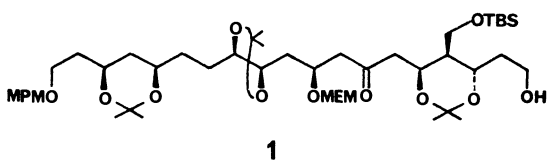

† A part of this paper was read at the 54th National Meeting of the Chemical Society of Japan, Tokyo, April 1987, Abstract papers No. 3III L 26.

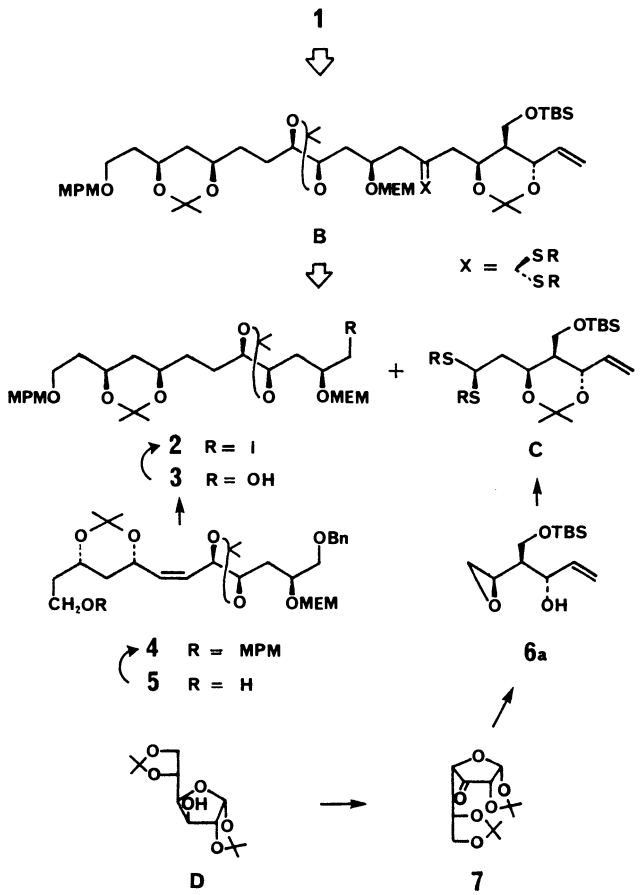

Scheme 1.

which will be stereoselectively prepared from the known compound **7**.[4] This plan was devised by considering that the absolute stereochemistry at C-2, C-3, and C-4 of **9** correlates to that of C-3, C-4, and C-5, respectively, of **6a**. The successful pursuit of the basic elements of this synthetic plan forms the topic of this report.

Preparation of 2. The alcohol **5**[1] was treated with 4-methoxybenzyl chloride (MPM-Cl) and NaH in THF to afford the O-MPM derivative **4** in 88% yield. Simultaneous catalytic reduction of the double bond and benzyloxy group in **4** proceeded effectively with Raney Ni W-4 (1 atm H_2, EtOH, 20 °C, 6 h) to give **3** in 86% yield. In this reduction, no cleavage of the O-MPM bond occurred.[5] In the last step, the iodination of the hydroxyl group at C-1 was carried out by treatment of **3** with triphenylphosphine, imidazole, and iodine in benzene to provide the segment **2** in 99% yield.

Synthesis of 6a. The synthesis of the key intermediate **6a** started with the known **7**[4] which was obtainable in 5 steps from commercially supplied 1,2:5,6-di-*O*-isopropylidene-α-D-glucofuranose (**D**). Wittig methylenation of **7** with methylenetriphenylphosphorane[7] in benzene at 25 °C afforded an 84% yield of **8** and a 7% yield of the α-D-erythro epimer 8'.[8] Hydroboration of **8** with dicyclohexylborane followed by oxidation with alkaline H_2O_2 gave the alcohol **9** in 94% yield, which was *O*-pivaloylated to afford **10** in quantitative yield. Partial hydrolysis of **10** with 75% aqueous acetic acid yielded **11** (67% yield) and unchanged **10** (31% yield). Periodate-oxidation of **11** followed by sodium borohydride reduction of the aldehyde **12** afforded the alcohol **13** in 85% yield. Dithioacetalization of **13** with ethanethiol and boron trifluoride etherate gave **14** in 74% yield from **11**. Regioselective 1,2-*O*-isopropylidenation of **14** with 2,2-dimethoxypropane (DMP) in acetone containing a catalytic amount of H_2SO_4 gave **15** in 95% yield. *t*-Butyldimethylsilylation (TBSOTf, 2,6-lutidine) of **15** followed by dedithioacetalization of the silyl ether **16** (83% yield) with 1:1 $HgCl_2$–HgO (red) in 80% aqueous acetone afforded the aldehyde **17** which was immediately methylenated with methylenetriphenylphosphorane[7] in ether at 23 °C to give **18** in 80% yield from **16**. Treatment of **18** with 75% aqueous acetic acid at 50 °C afforded the triol **19** in 95% yield, which was directly subjected to the one stage epoxidation[9] of vicinal diol with triphenylphosphine, diethyl azodicarboxylate (DEAD), and 3A Molecular Sieves in refluxed benzene to give the epoxide **20** in 72% yield. One step conversion of **20** into **6a** was well-achieved in 81% yield by the treatment of **20** in THF with *n*-BuLi (3.5 equiv) at −50 °C and then with TBS-Cl (2.5 equiv) at −8 °C for 12 h. The overall yield of **6a** from **7** in 14 steps was 11.6%.

The direct conversion of **20** to the *O*-[2-(trimethylsilylethoxy)methyl] (O-SEM) derivative **6b** using *n*-BuLi and SEM-Cl was not practicable (42% yield) because of low regioselectivity of SEM-Cl. However, **6b** was obtainable in 84% yield by the sequence of reactions involving *O*-*t*-butyldimethylsilylation, one-stage exchange of pivaloyl and SEM groups, and selective de-*O*-*t*-butyldimethylsilylation. It is noteworthy that a sample of **6b** which was prepared via **23** from **14** through the alternative reaction sequence as shown in Scheme 3 was revealed to be a ca. 3:1 4-epimeric mixture by the ^{1}H NMR (400 MHz) examination. The

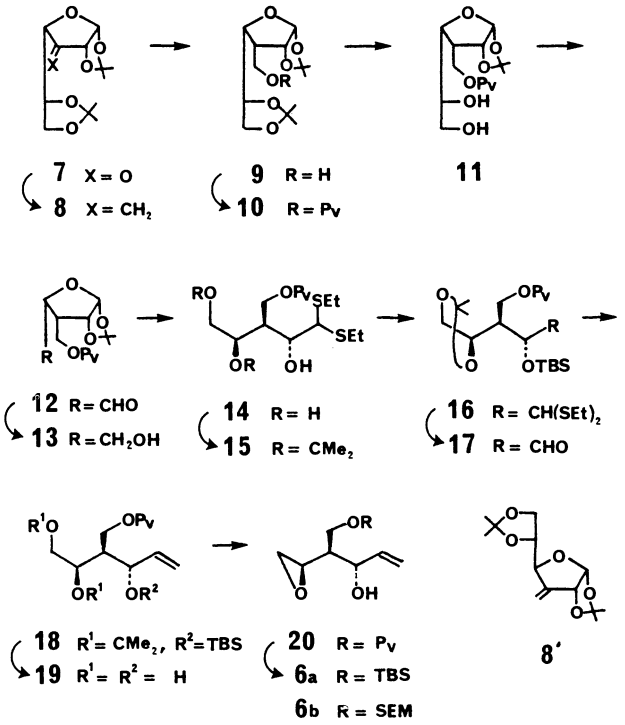

Scheme 2.

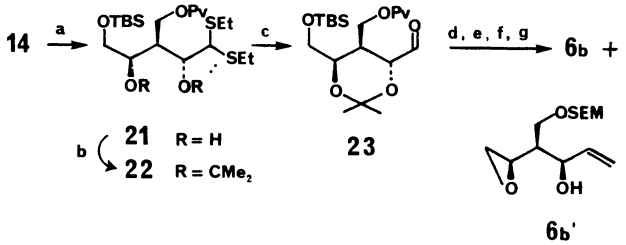

Scheme 3. (a) TBS-Cl, imidazole, DMF, 24°C; (b) DMP, Me_2CO, cat. H_2SO_4, 25°C; (c) $HgCl_2$, HgO, 80% Me_2CO–H_2O, 24°C; (d) $(Ph_3PCH_3)Br$, $NaCH_2SOMe$, Et_2O; (e) 75% AcOH–H_2O, 50°C; (f) Ph_3P, DEAD, PhH, MS 3A, 80°C; (g) 1. TBS-Cl, imidazole, DMF, 25°C, 3 h; 2. *n*-BuLi, THF (−60°C, 15 min); SEM-Cl, THF, 0°C, 16 h; 3. TBAF, THF, 0°C, 4 h.

major and minor epimers proved to be **6b** and **6b'**, respectively, by the following fashions (Scheme 4): (a) The sample (**6b**+**6b'**) was converted into **24** (as an anomeric mixture) in 5 steps. The ^{1}H NMR spectrum of **24** showed signals in line with the depicted structure

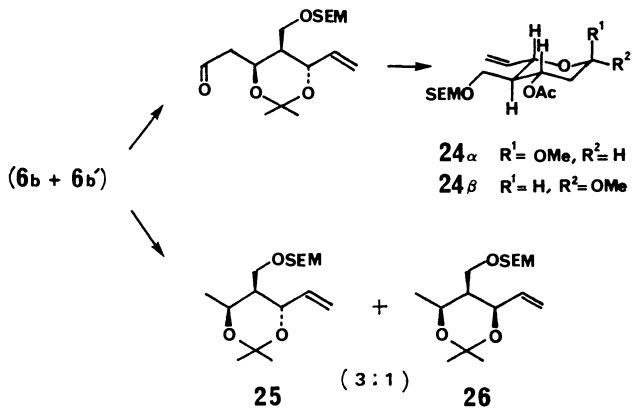

Scheme 4.

(see Experimental). (b) The sample (**6b**+**6b'**) was converted in two steps into a 3:1 mixture of **25** and **26**, whose structures were confirmed by ^{1}H NMR analysis (see Experimental). The formation of the epimer **6b'** in the route to **6b** via **23** from **14** may be ascribed to the epimerization that occurred at the C-4 carbon of the thermodynamically unstable 1,3-dioxane-4-carbaldehyde **23** during its Wittig methylenation using the ylide prepared from methyltriphenylphosphonium bromide by the Corey's method.[10]

Synthesis of C. For the construction of the target compound **1**, we first took account of the coupling of a dithiane derivative **28** (the segment **C**) with a model compound **32** or **33** which was obtained from the

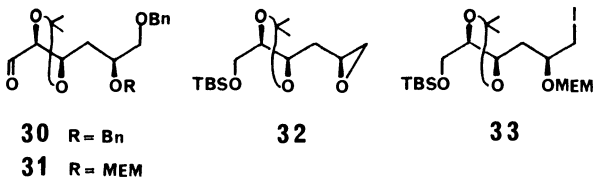

known **30** or **31**,[1] respectively. The treatment of the epoxide **6a** with 5 equivalents of 2-lithio-1,3-dithiane afforded the dithiane derivative **27** in 81% yield, which was subsequently isopropylidenated to give **28** in 92% yield. However, the attempted coupling of **28** with heptanal by the usual dithiane lithiation procedure[11] (*n*-BuLi, THF, −25 °C, 3 h) afforded no coupling product **29a**, recovering the reactants, **28** and heptanal. Even though the reaction mixture of lithiation was treated with D_2O instead of heptanal, no deuterio derivative **29b** could be detected. These facts suggested to us that the desired lithium derivative **29c** is very short-lived probably due to its unusually increased kinetic basicity[12] and it is practically impossible to generate **29c** from its conjugate acid **28**, which is far less acidic than 1,3-dithiane, by the lithiation using *n*-BuLi.[13] This suggestion prompted us to use the trimethylstannylated dimethyl dithioacetal compound **36** for the dithiane derivative **28**. The trimethylstannyl group in **36** would be instantaneously substituted by

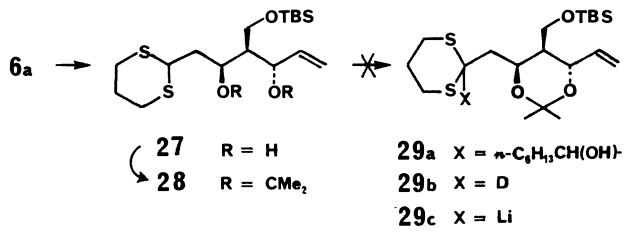

Scheme 5.

lithium on treatment with *n*-BuLi.[14] Moreover, it pleased us very much that in contrast to the H/Li-exchange, the Sn/Li-transmetallation should easily be detected by TLC. The validity of our choice was proved by the following sequence of reactions (Scheme 6). Lithiation of [bis(methylthio)methyl]trimethylstannane[15] (**34**) with lithium diisopropylamide (LDA)

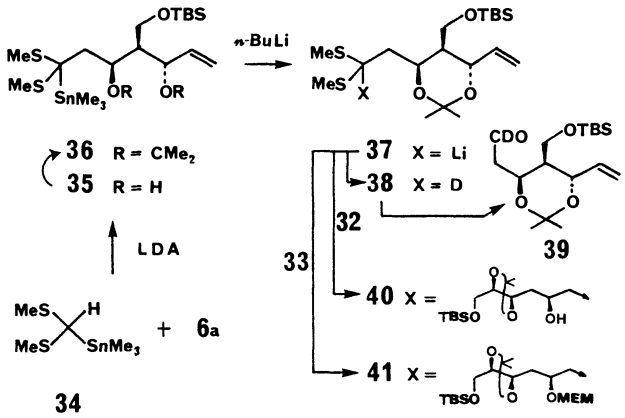

Scheme 6.

in THF-HMPA followed by treatment with the epoxide **6a** afforded **35** in a ca. 70% yield, which was isopropylidenated with 2-methoxy-1-propene and pyridinium *p*-toluenesulfonate (PPTS) in dichloromethane to yield **36** in 62% yield from **6a**. Immediately the addition of *n*-BuLi (2 equiv) to a solution of **36** in THF-HMPA at −30 °C was complete, the reaction mixture was treated with D_2O to give the product **38** in 85% yield, which was carefully hydrolyzed to the deuterio aldehyde **39** in moderate yield (44%) by using *N*-bromosuccinimide (NBS) and $AgNO_3$ in 85% aqueous acetonitlile containing 2,4,6-trimethylpyridine.[16] Thus obtained sample of **39** showed a ca. 75—80% aldehydic deuterium content by ^{1}H NMR analysis. The reaction of the epoxide **32** with the lithium compound **37** generated from **36** (1.5 equiv) and *n*-BuLi (1.8 equiv) afforded a ca. 5:7 mixture of the coupling product **40** and the starting epoxide **32**. Whereas the iodo derivative **33** reacted more smoothly with **37** generated from **36** (1.43 equiv) and *n*-BuLi (1.71 equiv) to yield the coupling product **41** in 76% yield.

Synthesis of 1. In keeping with the successful results in the similar model coupling reactions using **36**, the coupling of the C-1—C-12 segment **2** with **36** was carried out to afford in 84% yield the desired prod-

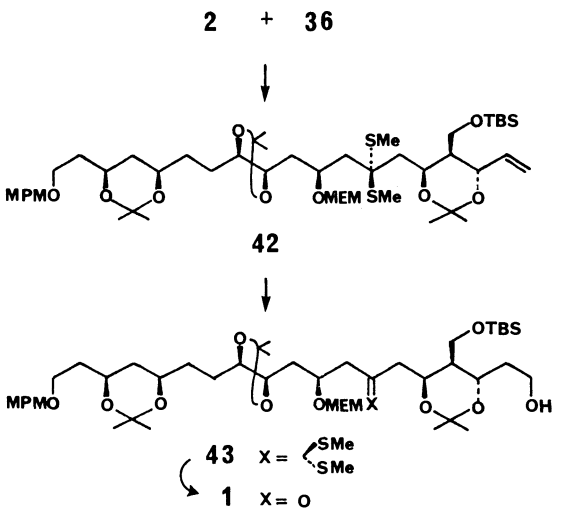

Scheme 7.

uct **42** corresponding to the intermediate **B** (Scheme 7).[17] Hydroboration of **42** using dicyclohexylborane followed by treatment with alkaline H_2O_2 gave the alcohol **43** in 92% yield. Dedithioacetalization of **43** with 1 : 1 $HgCl_2$–HgO provided the target compound **1** in 82% yield.

Experimental

Melting points were determined on a micro hot stage Yanaco MP-S3 and were uncorrected. Optical rotations were measured on a JASCO DIP-360 photoelectric polarimeter in chloroform, and ^{1}H NMR spectra were recorded on a Varian EM-390 or a JEOL GX-400 spectrometer in $CDCl_3$ using TMS as internal standard unless stated otherwise. Mass spectra were measured on a Hitachi M-80 mass spectrometer. TLC was performed on Merck TLC plate (60F-254, 0.25 mm), and column chromatography on silica gel, Wakogel C-200 and Merck Kieselgel 60 (230—400 mesh) for "Flash Chromatography." In general, organic solvents were purified and dried by appropriate procedure, and evaporation and concentration were carried out under reduced pressure below 30°C, unless otherwise noted.

(2*S*,4*R*,5*R*,8*S*,10*S*)-(6*Z*)-1-*O*-Benzyl-4,5:8,10-di-*O*-isopropylidene-12-*O*-(4-methoxybenzyl)-2-*O*-[(2-methoxyethoxy)methyl]-6-dodecene-1,2,4,5,8,10,12-heptol (4). To an ice-cold solution of **5**[1] (321 mg, 0.597 mmol) in dry DMF (3.2 ml) was added 55% NaH suspension (65 mg, 1.49 mmol). After being stirred at 25 °C for 0.5 h, to this reaction mixture was added 4-methoxybenzyl chloride (130 µl, 0.90 mmol) at 0 °C. After being stirred at 25 °C for 15 h, the reaction mixture was poured into saturated aqueous $NaHCO_3$, which was extracted with benzene (3×5.0 ml). The extracts were washed with saturated aqueous NaCl, dried, and evaporated. The residue was chromatographed on silica gel (20 g) with 2 : 1 hexane-ethyl acetate to afford **4** (346 mg, 88%) as a colorless syrup: R_f=0.74 (1 : 1 hexane-ethyl acetate); $[\alpha]_D^{32}$ −12.7° (*c* 1.32); ^{1}H NMR (90 MHz) δ=1.34, 1.40, 1.43 (6H, 3H, 3H, each s, 2×CMe_2), 1.17—2.20 (6H, m, 2×H-3, 2×H-9, 2×H-11), 3.33 (3H, s, OMe of MEM), 3.30—4.63 (13H, m, OCH_2-CH_2O, 2×H-1, H-2, 4, 5, 8, 10, 2×H-12), 3.80 (3H, s, OMe of MPM), 4.43 (2H, s, OCH_2(MPM)), 4.53 (2H, s, OCH_2(Bn)), 4.80 (2H, s, OCH_2O), 5.30—5.77 (2H, m, H-6,7), 6.80—7.00 (2H, m, MPM), and 7.20—7.50 (7H, m, MPM, Ph).

Found: C, 67.77; H, 8.26%. Calcd for $C_{37}H_{54}O_{10}$: C, 67.45; H, 8.26%.

(2*S*,4*R*,5*R*,8*S*,10*S*)-4,5:8,10-Di-*O*-isopropylidene-12-*O*-(4-methoxybenzyl)-2-*O*-[(2-methoxyethoxy)methyl]-1,2,4,5,8,10,12-dodecaneheptol (3). A solution of **4** (346 mg) in ethanol (6.9 ml) was stirred with a catalytic amount of Raney Ni W-4 under bubbling with H_2 gas at 20 °C for 6 h. The reaction mixture was filtered and concentrated to a syrup which was chromatographed on silica gel (15 g) with 1 : 2 benzene-ethyl acetate to afford **3** (257 mg, 86%): colorless syrup; R_f=0.20 (1 : 1 hexane-ethyl acetate); $[\alpha]_D^{32}$ +31.4° (*c* 1.02); ^{1}H NMR (90 MHz) δ=1.37, 1.43 (12H, each s, 2×CMe_2), 1.10—2.00 (10H, m, 2×H-3, 2×H-6, 2×H-7, 2×H-9, 2×H-11), 3.40 (3H, s, OMe (MEM)), 3.40—4.20 (10H, m, OH, 2×H-1, H-2, 4, 5, 8, 10, 2×H-12), 4.43 (2H, s, OCH_2(MPM)), 4.80 (2H, s, OCH_2O), 6.80—7.00 and 7.20—7.40 (each 2H, each m, MPM).

Found: C, 62.95; H, 8.74%. Calcd for $C_{30}H_{50}O_{10}$: C, 63.14; H, 8.83%.

(3*S*,5*R*,8*R*,9*R*,11*S*)-12-Iodo-3,5:8,9-di-*O*-isopropylidene-1-*O*-(4-methoxybenzyl)-11-*O*-[(2-methoxyethoxy)methyl]-1,3,5,8,9,11-dodecanehexol (2). A mixture of **3** (42.3 mg, 0.0741 mmol), benzene (0.846 ml), imidazole (10.1 mg, 0.148 mmol), triphenylphosphine (38.9 mg, 0.148 mmol), and iodine (28.2 mg, 0.111 mmol) was stirred at 25 °C for 0.5 h and then cooled at 0 °C. To this mixture were added saturated aqueous $Na_2S_2O_3$ and $NaHCO_3$ in sequence under vigorous stirring. The mixture was then extracted with benzene (3×3 ml) and the extracts were washed with saturated aqueous NaCl, dried, and evaporated. The residue was chromatographed on silica gel (2.5 g) with 3 : 1 hexane-ethyl acetate to afford **2** (50.1 mg, 99.4%) as a colorless syrup: R_f=0.76 (1 : 1 hexane-ethyl acetate); $[\alpha]_D^{32}$ +11.7° (*c* 0.92); ^{1}H NMR (400 MHz) δ=1.16 (1H, ddd, H-4, $J_{4,3}\fallingdotseq J_{4,5}\fallingdotseq J_{gem}\fallingdotseq$12.5 Hz), 1.35, 1.36, 1.41 (3H, 6H, 3H, each s, 2×CMe_2), 1.43—1.90 (9H, m, 2×H-2, H-4, 2×H-6, 2×H-7, 2×H-10), 3.39 (3H, s, OMe (MEM)), 3.39 (1H, dd, *J*=4.8, 9.6 Hz), 3.46—3.59 (5H, m), 3.60—3.67 (3H, m), 3.72 (1H, ddd, *J*=3.5, 5.1, 11.2 Hz), 3.81 (3H, s, OMe(MPM)), 3.79—3.88 (2H, m), 3.94—4.05 (1H, m), 4.41 and 4.43 (2H, ABq, CH_2Ph, *J*=11.2 Hz), 4.80 (2H, s, OCH_2O), 6.88 and 7.25 (each 2H, ddd-like, MPM).

Found: C, 52.91; H, 7.17%. Calcd for $C_{30}H_{49}O_9I$; C, 52.94; H, 7.26%.

3-Deoxy-1,2:5,6-di-*O*-isopropylidene-3-*C*-methylene-α-D-*threo*-D-*glycero*-hexofuranose (8) and α-D-*erythro* Epimer (8′). To a suspension of freshly prepared methylenetriphenylphosphorane[7] (140 g, 507 mmol) in dry benzene (291 ml) was added a solution of **7**[4] (29.1 g, 113 mmol) in benzene (582 ml) dropwise at 25 °C in a 20-min period. After being stirred for 1.7 h, the reaction mixture was concentrated and diluted with ether (873 ml). The mixture was poured into cold water (800 ml), which was extracted with ether (3×700 ml). The extracts were washed with saturated aqueous NaCl, dried, and evaporated. The residue was chromatographed on silica gel (1450 g) with 5 : 2 hexane-ethyl acetate to afford **8** (24.1 g, 84%) and **8′** (2.02 g, 7%). **8**: R_f=0.68 (1 : 1 hexane-ethyl acetate); mp 49 °C; $[\alpha]_D^{34}$ −0.32°, $[\alpha]_{365}^{34}$ +1.94° (*c* 1.23); ^{1}H NMR (90 MHz) δ=1.32, 1.38, 1.44, 1.56 (each 3H, each s, 2×CMe_2), 3.7—4.1, 4.3—4.6 (each 2H, each m, H-4,5, 2×H-6), 4.83 (1H, dd-like, H-2, $J_{2,1}$=4.2, $J_{2,C=CH_2}\fallingdotseq$1.0 Hz), 5.28 5.48 (each 1H,

each dd-like, C=C$\underline{H}_2$, J_{gem}≒1.5 Hz), 5.81 (1H, d, H-1).

Found: C, 60.88; H, 7.81%. Calcd for $C_{13}H_{20}O_5$: C, 60.93; H, 7.87%.

8′: Colorless syrup; R_f=0.89 (1 : 1 hexane-ethyl acetate); $[\alpha]_D^{30}$ +99° (*c* 1.30) [lit, $[\alpha]_D$ +75° (*c* 1.0);[8a]) $[\alpha]_D^{22}$ +104° (*c* 2)[8b]]; ^{1}H NMR (90 MHz) δ=1.38, 1.45, 1.52 (6H, 3H, 3H, each s, 2×CMe_2), 3.85—4.40 (4H, m, H-4,5, 2×H-6), 4.70—5.70 (1H, m, H-2), 5.40—5.60 (2H, m, C=C$\underline{H}_2$), 5.80 (1H, d, H-1, $J_{1,2}$=4.2 Hz).

3-Deoxy-3-*C*-hydroxymethyl-1,2:5,6-di-*O*-isopropylidne-α-D-gulofuranose (9). To a solution of dicyclohexylborane (55.2 mmol) in THF (50.0 ml) was added a solution of **8** (7.00 g, 27.3 mmol) in THF (21.0 ml) at 0 °C under Ar, and the mixture was stirred at 25 °C for 100 min. The reaction was quenched by addition of water (70.9 ml). To the mixture was added 3M†† aqueous NaOH (18.4 ml) and 30% H_2O_2 (16.6 ml) at 0 °C. After being stirred at 50 °C for 1 h, the reaction mixture was extracted with ethyl acetate (5×100 ml). The extracts were evaporated and the residue was chromatographed on silica gel (400 g) with 1 : 4 hexane-ethyl acetate to afford **9** (7.14 g, 94%) as colorless crystals. Recrystallization from hexane-ethyl acetate gave a pure sample of **9**: mp 145 °C; R_f=0.41 (1 : 4 hexane-ethyl acetate); $[\alpha]_D^{31}$ −20.4° (*c* 1.08); ^{1}H NMR (90 MHz) δ=1.34, 1.38, 1.46, 1.59 (each 3H, each s, 2×CMe_2), 2.5—2.7 (1H, m, H-3), 3.0—3.2 (1H, m, OH), 3.4—4.3 (5H, m, H-5, 2×H-6, $C\underline{H}_2OH$), 4.4—4.6 (1H, m, H-4), 4.76 (1H, dd, H-2, $J_{2,1}$=4.8, $J_{2,3}$=5.7 Hz), 5.82 (1H, d, H-1).

Found: C, 56.98; H, 8.01%. Calcd for $C_{13}H_{22}O_6$: C, 56.92; H, 8.08%.

3-Deoxy-1,2 : 5,6-di-*O*-isopropylidene-3-*C*-[(pivaloyloxy)methyl]-α-D-gulofuranose (10). To a solution of **9** (7.14 g, 26.0 mmol) in dry CH_2Cl_2 (71.4 ml) were added 4-(dimethylamino)pyridine (DMAP) (6.36 g, 52.1 mmol) and pivaloyl chloride (4.76 ml, 39.1 mmol) in sequence at 0 °C. The mixture was stirred at 25 °C for 40 min and then diluted with ethanol (7.14 ml). After being stirred at 25 °C for 0.5 h, the mixture was evaporated. The residue was dissolved in ethyl acetate and the solution was washed with water and saturated aqueous NaCl, dried, and evaporated to give a crude sample of **10** (9.3 g, 100%). Recrystallization from ethyl acetate-hexane afforded an analytical sample: mp 127°C, R_f=0.60 (1 : 2 hexane-ethyl acetate; IR (KBr) 1720 cm^{-1}; $[\alpha]_D^{31}$ −23.9° (*c* 1.08); ^{1}H NMR (90 MHz) δ=1.23 (9H, s, *t*-Bu), 1.31, 1.37, 1.46, 1.57 (each 3H, each s, 2×CMe_2), 2.5—2.9 (1H, m, H-3), 3.4—4.8 (7H, m, H-2, 4, 5, 2×H-6, PvOC$\underline{H}_2$), 5.83 (1H, d, H-1).

Found: C, 60.18; H, 8.15%. Calcd for $C_{18}H_{30}O_7$: C, 60.32; H, 8.44%.

3-Deoxy-1,2-*O*-isopropylidene-3-*C*-[(pivaloyloxy)methyl]-α-D-gulofuranose (11). A solution of **10** (7.63 g) in 75% aqueous acetic acid (76.3 ml) was stirred at 30 °C for 4.5 h. The mixture was evaporated at 40 °C in a 2-h period. The residue was then chromatographed on silica gel (350 g) with 2 : 1 hexane-ethyl acetate to afford unchanged **10** (2.34 g, 30.7%) and **11** (4.54 g, 67% from **9**) as colorless crystals. **11**: R_f=0.37 (1 : 1 hexane-ethyl acetate); mp 63 °C; $[\alpha]_D^{31}$ −14.8° (*c* 1.03), ^{1}H NMR (90 MHz) δ=1.20 (9H, s, *t*-Bu), 1.30, 1.55 (each 3H, each s, CMe_2), 2.4—3.3 (3H, m, H-3, 2×OH), 3.4—4.7 (6H, m, H-4,5, 2×H-6, PvOC$\underline{H}_2$), 4.65 (1H, dd, H-2, $J_{2,1}$=4.2, $J_{2,3}$=5.7 Hz), 5.83 (1H, d, H-1).

†† 1M=1 mol dm^{-3}.

Found: C, 56.81; H, 8.19%. Calcd for $C_{15}H_{26}O_7$: C, 56.59; H, 8.23%.

3-Deoxy-1,2-*O*-isopropylidene-3-*C*-[(pivaloyloxy)methyl]-α-L-lyxofuranose (13). To a solution of **11** (11.5 g, 36.2 mmol) in 80% aqueous acetone (115 ml) was added a solution of $NaIO_4$ (11.6 g, 53.5 mmol) in water (116 ml) at 0 °C in a 15-min period. After being stirred at 25 °C for 35 min, the reaction mixture was evaporated. Ethyl acetate was added to the residue and the mixture was washed with water and saturated aqueous NaCl, dried, and evaporated to afford crystalline aldehyde **12** (11.6 g). To an ice cold solution of the aldehyde **12** (11.6 g) in methanol (116 ml) was added $NaBH_4$ (2.74 g, 72.4 mmol) and was stirred at 25 °C for 15 min. The reaction mixture was neutralized (pH=7) with CO_2 and evaporated. Ethyl acetate (550 ml) was added to the residue and the mixture was washed with water and saturated aqueous NaCl, dried, and evaporated to give crude **13** (8.92 g, 85% yield from **11**). An analytical sample was obtained after silica-gel column chromatography with 1 : 1 hexane-ethyl acetate: colorless crystals; R_f=0.54 (1 : 1 hexane-ethyl acetate); mp 81°C; $[\alpha]_D^{30}$ −14.1° (*c* 1.02); ^{1}H NMR (90 MHz) δ=1.21 (9H, s, *t*-Bu), 1.30, 1.55 (each 3H, each s, CMe_2), 2.42 (1H, br-s, OH), 2.5—2.9 (1H, m, H-3), 3.3—4.6 (5H, m, H-4, 2×H-5. PvOC$\underline{H}_2$), 4.68 (1H, dd, H-2, $J_{2,1}$=$J_{2,3}$=4.5 Hz), 5.84 (1H, d, H-1).

Found: C, 58.46; H, 8.28%. Calcd for $C_{14}H_{24}O_6$: C, 58.32; H, 8.39%.

(2*S*,3*R*,4*R*)-5,5-Bis(ethylthio)-3-[(pivaloyloxy)methyl]-1,2,4-heptanetriol (14). To a solution of the crude **13** (8.92 g, 30.9 mmol) in EtSH (268 ml) was added $BF_3 \cdot Et_2O$ (2.6 ml) at 0 °C. After being stirred at 25 °C for 0.5 h, the reaction mixture was neutralized with triethylamine (pH=7) at 0 °C, and was diluted with ethyl acetate (250 ml). The mixture was washed with water and saturated aqueous NaCl, dried, and evaporated. The residue was chromatographed on silica gel (550 g) with 2 : 3 hexane-ethyl acetate to afford **14** (8.09 g, 74% from **11**). **14**: Colorless syrup; R_f=0.29 (1 : 1 hexane-ethyl acetate); $[\alpha]_D^{30}$ +64.5° (*c* 1.01); ^{1}H NMR (90 MHz) δ=1.21 (9H, s, *t*-Bu), 1.26, 1.29 (each 3H, each t, 2×$SCH_2\underline{Me}$), 2.2—2.9 (6H, m, 2×$SC\underline{H}_2$, H-3, OH), 3.4—4.6 (9H, m, H-1, 2,4, 2×H-5, PvOC$\underline{H}_2$, 2×OH).

Found: C, 50.68; H, 8.35%. Calcd for $C_{15}H_{30}O_5S_2$: C, 50.82; H, 8.53%.

(2*S*,3*R*,4*R*)-5,5-Bis(ethylthio)-1,2-*O*-isopropylidene-3-[(pivaloyloxy)methyl]-1,2,4-heptanetriol (15). To a solution of **14** (1.82 g, 5.14 mmol), 2,2-dimethoxypropane (DMP) (1.26 ml, 10.3 mmol) in dry acetone (36.4 ml) was added 1% H_2SO_4-acetone (0.188 ml) at 0 °C. After being kept at 25 °C for 25 min, the mixture was neutralized with $NaHCO_3$ (pH=7) under ice-cooling, and evaporated. The residue was partitioned between ethyl acetate and water. The organic layer was separated and washed with saturated aqueous NaCl, dried, and evaporated to afford an essentially pure sample of **15** (1.93 g, 95%) as colorless crystals. An analytical sample of **15** was obtained after silica-gel column chromatograpy with 8 : 1 hexane-ethyl acetate: R_f=0.24 (8 : 1 hexane-ethyl acetate; mp 65°C; $[\alpha]_D^{37}$ −0.47°, $[\alpha]_{365}^{37}$ +7.49° (*c* 1.28); ^{1}H NMR (90 MHz) δ=1.20 (9H, s, Pv), 1.15—1.50 (6H, m, 2×$SCH_2\underline{Me}$), 1.33, 1.39 (each 3H, each s, CMe_2), 2.30—2.65 (2H, m, H-3, OH), 2.62, 2.73 (4H, q, 2×$SC\underline{H}_2$, *J*=6.3 Hz), 3.70—4.50 (7H, m, 2×H-1, H-2, 4, 5, $C\underline{H}_2OPv$).

Found: C, 54.86; H, 8.56%. Calcd for $C_{18}H_{34}O_5S_2$: C, 54.79; H, 8.68%.

(2*S*,3*R*,4*R*)-4-*O*-(*t*-Butyldimethylsilyl)-1,2-*O*-isopropylidene-3-[(pivaloyloxy)methyl]-1,2,4-heptanetriol (16). To a solution of **15** (1.93 g, 4.88 mmol) in dry CH_2Cl_2 (4.88 ml) were added 2,6-lutidine (1.71 ml, 14.6 mmol), TBSOTf (2.24 ml, 9.76 mmol) at 0 °C. After being stirred at 0 °C for 70 min, the reaction mixture was poured into ice-water, which was extracted with ethyl acetate (3×20 ml). The extracts were washed with saturated aqueous NaCl, dried, and evaporated. The residue was chromatographed on silica gel (250 g) with 12 : 1 hexane-ethyl acetate to afford **16** (2.06 g, 83%) as colorless syrup: R_f=0.54 (8 : 1 hexane-ethyl acetate); $[\alpha]_D^{35}$ −0.70°, $[\alpha]_{365}^{35}$ +7.72° (*c* 1.14); ^{1}H NMR (90 MHz) δ=0.90 (9H, s, *t*-BuSi), 1.20 (9H, s, Pv), 1.13—1.43 (12H, m, CMe_2, 2×$SCH_2\underline{Me}$), 2.1—2.48 (1H, m, H-3), 2.60, 2.68 (4H, 2×$SC\underline{H}_2$, *J*=4.5 Hz), 3.70—4.50 (7H, m, 2×H-1, H-2, 4, 5, $C\underline{H}_2OPv$).

Found: C, 56.89; H, 9.47%. Calcd for $C_{24}H_{28}O_5SiS_2$: C, 56.65; H, 9.51%.

(2*S*,3*R*,4*S*)-4-*O*-(*t*-Butyldimethylsilyl)-1,2-*O*-isopropylidene-3-[(pivaloyloxy)methyl]-5-hexene-1,2,4-triol (18). To a solution of **16** (2.06 g, 4.05 mmol) in 80% aqueous acetone (72.1 ml) were added in sequence HgO (3.86g, 17.8 mmol) and $HgCl_2$ (4.84 g, 17.8 mmol) at 25 °C with efficient stirring. After the addition, stirring was continued at 25 °C for 20 min. The reaction mixture was filtered through a Celite, and the filter cake was washed with acetone (5×5 ml). The filtrate and washings were evaporated, and to the residue was added chloroform. The mixture was washed with 10% aqueous KI and saturated aqueous NaCl, dried, and evaporated to give the aldehyde **17** (1.72 g). A solution of the crude aldehyde (1.72 g) in dry benzene (32.6 ml) was added to a solution of $Ph_3P{=}CH_2$ (5.03 g, 18.2 mmol) in dry benzene (16.3 ml) at 25 °C in a 5-min period. After being stirred at 25 °C for 20 min, the reaction mixture was evaporated. The residue was taken up in ether (40 ml) which was washed with water and then saturated aqueous NaCl, dried, and evaporated. The residual syrup was chromatographed on silica gel (130 g) with 15 : 1 hexane-ethyl acetate to afford **18** (1.30 g, 80% from **16**) as a colorless syrup: R_f=0.60 (8 : 1 hexane-ethyl acetate); $[\alpha]_D^{34}$ −1.20° $[\alpha]_{365}^{34}$ −11.3° (*c* 1.51); ^{1}H NMR (400 MHz, $CHCl_3$, δ=7.26) δ=0.02, 0.05 (each 3H, each s, $SiMe_2$), 0.89 (9H, s, *t*-BuSi), 1.19 (9H, s, Pv), 1.31 ,1.36 (each 3H, each s, CMe_2), 1.86 (1H, ddd, H-3), 3.70 (1H, dd, *J*=7.8, 7.8 Hz), 4.05 (1H, dd, *J*=5.9, 7.8 Hz), 4.13 (1H, dd, *J*=5.9, 11.2 Hz), 4.18—4.24 (2H, m), 4.26 (1H, dd, *J*=3.9, 11.2 Hz), 5.11 (1H, ddd, H-6, $J_{6,5}$=10.1 Hz), 5.15 (1H, ddd, H-6, $J_{6,5}$=17.3 Hz), 5.75 (1H, ddd, H-5, $J_{5,4}$=6.8 Hz).

Found: C, 63.32; H, 10.01%. Calcd for $C_{21}H_{40}O_5Si$: C, 62.96; H, 10.06%.

(2*S*,4*R*,5*S*)-5,6-Epoxy-3-[(pivaloyloxy)methyl]-1-hexen-3-ol (20). A solution of **18** (2.92 g, 7.29 mmol) in 75% aqueous acetic acid (58.4 ml) was stirred at 50 °C for 5 h. The reaction mixture was concentrated to give a syrup, which was chromatographed on silica gel (50 g) with 1 : 2 hexane-ethyl acetate to afford **19** (1.72 g, 95%). A mixture of **19** (1.71 g, 6.95 mmol), triphenylphosphine (2.19 g, 8.34 mmol), Molecular Sieves 3A powder (17.1 g), and dry benzene (85.6 ml) was vigorously stirred at 80 °C for 10 min, and DEAD (1.29 ml, 8.34 mmol) was added dropwise to the mixture. After being stirred at 80 °C for 14 h, the cold reaction mixture was filtered through a Celite, and the filter cake was washed with benzene (5×40 ml). The filtrate and washings were evaporated, and the residue was chromatographed on silica gel (170 g) with 2 : 1 hexane-ethyl acetate to give **20** (1.15 g, 72%) as a colorless syrup: R_f=0.56 (1 : 1 hexane-ethyl acetate); $[\alpha]_D^{32}$ −11.2° (*c* 1.39); ^{1}H NMR (90 MHz) δ=1.23 (9H, s, *t*-Bu), 1.50—2.00 (1H, m, H-3), 2.57 (1H, d, OH, *J*=2.7 Hz), 2.67 (1H, dd, H-1, $J_{1,2}$=2.7, J_{gem}=4.5 Hz), 2.85 (1H, dd, H-1, $J_{1,2}$=4.5 Hz), 3.10 (1H, ddd, H-2, $J_{2,3}$=8.7 Hz), 4.1—4.5 (3H, m, H-4, PvO$C\underline{H}_2$), 5.40 (1H, ddd-like, H-6, $J_{6,5}$=10.5 Hz), 5.50 (1H, ddd-like, H-6, $J_{6,5}$=17.4 Hz), 5.95 (1H, ddd, H-5, $J_{5,4}$=6.6 Hz).

Found: *m/z* 211.1336. Calcd for $C_{12}H_9O_3(M^+-OH)$: 211.1333.

(2*S*,4*R*,5*S*)-5,6-Epoxy-3-[(*t*-butyldimethylsilyloxy)methyl]-1-hexen-3-ol (6a). To a cold (−50°C) solution of **20** (153 mg, 0.67 mmol) in dry THF (1.53 ml) was added a 1.64 M solution of *n*-BuLi in hexane (1.43 ml, 2.35 mmol) under stirring, and stirring was continued at −50 °C for 1 h. To this mixture was added a solution of TBS-Cl (252 mg, 1.68 mmol) in dry THF (0.504 ml). After being stirred at 8 °C for 12 h, the mixture was neutralized (pH=7) with 0.12 M HCl under ice-cooling, and then extracted with ethyl acetate (3× 4.0 ml). The extracts were washed with saturated aqueous NaCl, dried, and evaporated. The residue was flushchromatographed on silica gel (10 g) with 30:1 chloroform-acetone to afford **6a** (140.4 mg, 81%) as a colorless syrup: R_f=0.43 (15 : 1 chloroform-acetone); $[\alpha]_D^{31}$ −2.7°, $[\alpha]_{365}^{31}$ −12.5° (*c* 0.83); ^{1}H NMR (90 MHz) δ=0.83 (9H, s, *t*-Bu), 1.20—1.50 (1H, m, H-3), 2.53 (1H, dd, H-1, J_{gem}=4.8, $J_{1,2}$=2.7 Hz), 2.77 (1H, dd, H-1, $J_{1,2}$=4.8 Hz), 2.90—3.20 (1H, m, H-2), 3.37 (1H, d-like, OH, *J*=3.6 Hz), 3.80—4.29 (2H, m, $SiOCH_2$), 4.30—4.60 (1H, m, H-4), 5.18 (1H, ddd, H-6, $J_{6,5}$=10.5 Hz), 5.28 (1H, ddd, H-6, $J_{6,5}$=18.0 Hz), 5.93 (1H, ddd, H-5, $J_{5,4}$=4.8 Hz).

Found: *m/z* 259.1733. Calcd for $C_{13}H_{27}O_3Si$: M^++1, 259.1728.

(2*S*,3*R*,4*R*)-1-*O*-*t*-Butyldimethylsilyl-5,5-bis(ethylthio)-3-[(pivaloyloxy)methyl]-1,2,4-pentanetriol (21). To a solution of **14** (8.09 g, 22.8 mmol) in dry DMF (80.9 ml) were added imidazole (3.73 g, 54.7 mmol) and TBS-Cl (6.88 g, 45.6 mmol) at 0 °C. After being stirred at 25 ° for 20 min, the mixture was poured into cold water, which was extracted with benzene (3×100 ml). The extracts were washed with saturated aqueous NaCl, dried, and evaporated. The residue was chromatographed on silica gel (540 g) with 5 : 1 hexane-ethyl acetate to afford **21** (8.71 g, 81.5%) as a colorless syrup: R_f=0.18 (8 : 1 hexane-ethyl acetate); $[\alpha]_D^{30}$ +33.1° (*c* 1.25); ^{1}H NMR(90 MHz) δ=0.93 (9H, s, *t*-BuSi), 1.22 (9H, s, Pv), 1.27, 1.30 (6H, each t, 2×$SCH_2\underline{Me}$, *J*=6.3 Hz), 2.4—2.6 (1H, m, H-3), 2.66, 2.70 (4H, each q, 2×$SC\underline{H}_2$), 3.09 (1H, d, OH, *J*=2.1 Hz), 3.56 (1H, d, OH, *J*=2.7 Hz), 3.6—4.4 (7H, m, 2×H-1, H-2,4,5, $C\underline{H}_2OPv$).

Found: C, 54.10; H, 9.11%. Calcd for $C_{21}H_{44}O_5SiS_2$: C, 53.81; H, 9.46%.

(2*S*,3*R*,4*R*)-1-*O*-*t*-Butyldimethylsilyl-5,5-bis(ethylthio)-2,4-*O*-isopropylidene-3-[(pivaloyloxy)methyl]-1,2,4-pentanetriol (22). To a solution of **21** (8.71 g, 18.6 mmol) and DMP (9.14 ml, 73.3 mmol) in dry acetone (174 ml) was added 1% H_2SO_4-acetone(0.87 ml) at 25 °C. After being kept at 25 °C for 21 min, the mixture was neutralized with $NaHCO_3$ (pH=7) at 0 °C, and evaporated. The residue was taken up in ethyl acetate (250 ml) which was washed with water and saturated aqueous NaCl, dried, and evaporated to crude **22** (9.36 g, 99%). An analytical sample was obtained after silica-gel chromatography with 10:1 hexane-ethyl acetate: R_f=0.73 (8 : 1 hexane-ethyl acetate); $[\alpha]_D^{30}$ −3.3°, $[\alpha]_{365}^{30}$ −11.3° (*c* 1.20); ^{1}H NMR (90 MHz) δ=0.93 (9H, s, *t*-BuSi), 1.25 (9H,

s, Pv), 1.2—1.5 (12H, m, 2×$SCH_2\underline{Me}$, CMe_2), 2.4—2.9 (5H, m, 2×$SC\underline{H}_2$, H-3), 3.6—4.3 (7H, m, 2×H-1, H-2, 4,5, $C\underline{H}_2OPv$).

Found: C, 56.66; H, 9.33%. Calcd for $C_{24}H_{48}O_5SiS_2$: C, 56.65; H, 9.51%.

Preparation of (6b+6b′) via 23 from 22. By the procedure described in the preparation of **17**, the aldehyde **23** (6.86 g, 91.7% from **21**) was obtained from **22** (9.36 g, 18.5 mmol) after silica-gel chromatography with 6:1 hexane-ethyl acetate ($[\alpha]_D^{30}$ +21.8° (*c* 1.24)). A 4 M solution of methylsulfinylmethanide anion in DMSO (17.0 ml, 68.2 mmol) prepared from NaH and DMSO[10] was added to a stirred suspension of methyltriphenylphosphonium bromide (24.4 g, 68.2 mmol) in dry ether (274 ml) under Ar at 25 °C. The mixture was stirred at 25 °C for 15 min, and to the resulting yellow suspension of ylide, a solution of **23** (6.86 g, 17.0 mmol) in dry ether (137 ml) was added dropwise in a 20-min period. After being stirred at 25 °C for 20 min, the reaction mixture was poured into ice-water (500 ml), and the mixture was extracted with ether (3×500 ml). The extracts were washed with saturated aqueous NaCl, dried, and evaporated. The residue was chromatographed on silica gel (340 g) with 12 : 1 hexane-ethyl acetate to afford the vinylic compound (5.51 g, 80.7%) as a colorless syrup which was treated with 75% aqueous acetic acid at 50 °C for 5 h to give a sample of **19** (3.39 g, 100%) after silica-gel chromatography with 1 : 2 hexane-ethyl acetate. By the procedure described in the preparation of **20**, the sample of **19** (349 mg) was epoxidated to afford a sample of **20** (230 mg, 71%) after silica-gel chromatography with 2 : 1 hexane-ethyl acetate. To a solution of the sample of **20** (42.7 mg, 0.187 mmol) in dry DMF (427 μl) were added imidazole (63.7 mg, 0.935 mmol) and TBS-Cl (113 mg, 0.748 mmol) at 0 °C. After being kept at 25 °C for 3 h, the reaction mixture was poured into ice-water which was extracted with ethyl acetate (3×1 ml). The extracts were washed with saturated aqueous NaCl, dried, and evaporated. The residue was chromatographed on silica gel (3.2 g) with 6 : 1 hexane-ethyl acetate to give a colorless syrup (70.2 mg). To a solution of this syrup (64.1 mg, 0.187 mmol) in dry THF (641 μl) was added 1.07 M *n*-BuLi in hexane (437 μl, 0.468 mmol) at −60 °C. After being stirred at −60 °C for 15 min, a solution of SEM-Cl (99.3 μl, 0.561 mmol) in dry THF (497 μl) was added to the reaction mixture, which was stored at 0 °C for 16 h. Saturated aqueous NH_4Cl (2.0 ml) was added to the reaction mixture, and was extracted with ethyl acetate (3×2.0 ml). The extracts were washed with saturated aqueous NaCl, dried, and evaporated. A mixture of the residual syrup (104 mg), dry THF (727 μl), and *n*-Bu_4NF (374 μl, 0.374 mmol) was stored at 0 °C for 4 h. The reaction mixture was poured into ice-water which was extracted with ethyl acetate (3×2.0 ml). The extracts were washed with saturated aqueous NaCl, dried, and evaporated. The residue was chromatographed on silica gel (1.5 g) with 5 : 2 hexane-ethyl acetate to afford an inseparable 3 : 1 mixture of **6b** and **6b′** (43.1 mg, 84% from **20**) as a colorless syrup: R_f=0.20 (3 : 1 hexane-ethyl acetate); ^1H NMR (400 MHz, $CHCl_3$, δ=7.26) δ=0.88—0.93 (2H, m, $SiCH_2$), 1.42—1.48 (0.25H, m, H-3), 1.53—1.61 (0,75H, m, H-3), 2.62 and 2.59—2.63 (1H, dd and m, H-1, $J_{1,2}$=3.0, J_{gem}=4.0 Hz), 2.81 (1H, dd, H-1, $J_{1,2}$=4.0 Hz), 2.87—2.94 and 2.97—3.02 (0.75H and 0.25H, br-s, OH), 3.05—3.39 (1H, m, H-2), 3.57—3.63 (2H, m, $SiCH_2C\underline{H}_2O$), 3.72 and 3.78 (1.5H, ABX , $SEMOC\underline{H}_2$, J_{AB}=9.6, J_{AX}=J_{BX}=4.5 Hz), 3.77 and 3.84 (0.5H, ABX, $SEMOC\underline{H}_2$, J_{AB}=9.6, J_{AX}=J_{BX}=4.5 Hz), 4.30—4.35 (0.25H, m, H-4), 4.37—4.42 (0.75H, m, H-4), 4.66 (2H, s, OCH_2O), 5.15—5.20 (1H, m, H-6), 5.28—5.35 (1H, m, H-6), 5.88 (0.25H, ddd, H-5, $J_{5,4}$=5.9, $J_{5,6}$=10.7, 16.6 Hz), 5.90 (0.75H, ddd, H-5, $J_{5,4}$=5.9, $J_{5,6}$=10.7, 16.6 Hz).

Conversion of (6b+6b′) into 24. To a solution of bis(methylthio)methane (173 μl, 1.73 mmol) in dry THF (1.73 ml) was added 1.53 M *n*-BuLi in hexane (1.13 ml, 1.73 mmol) at −40 °C. The mixture was stirred at −20 °C for 2 h, and a solution of (**6b+6b′**) (95.1 mg, 0.346 mmol) in dry THF (285 μl) was added to the mixture at −20 °C under stirring. After the mixture was stirred at −20 °C for 0.5 h, to this was added saturated aqueous NH_4Cl, and the mixture was extracted with ethyl acetate (3×4.0 ml). The extracts were washed with saturated aqueous NaCl, dried, and evaporated. The residue was chromatographed on silica gel with 3 : 1 hexane-ethyl acetate to give the dimethyl dithioacetal compound [122 mg, 93%, R_f=0.58 (2 : 1 hexane-ethyl acetate]. By the procedure described in the preparation of **36** from **35**, the dithioacetal (122 mg) was isopropylidenated to afford a sample of acetonide [123 mg, 91.4%, R_f=0.37 (10 : 1 hexane-ethyl acetate)] after chromatography. The acetonide (21.2 mg) was dedithioacetalized by the procedure described in the preparation of **39** from **36** to give a crude sample of aldehyde which was purified by silica-gel chromatography to afford pure aldehyde [7.2 mg, 42%, R_f=0.40 (5 : 1 hexane-ethyl acetate)] as a main product. A solution of the aldehyde (3.4 mg) in 0.02% methanolic HCl (60 μl, pH=4) was kept at 25 °C for 50 min. The mixture was neutralized (pH 7) with $NaHCO_3$ and filtered. The filtrate was evaporated and the residue was chromatographed on silica gel (0.5 g) with 2 : 1 hexane-ethyl acetate to give a cyclic methyl acetal derivative (2.6 mg, 83%) as a mixture of anomers [R_f=0.62, 0.56 (15 : 1 chloroform-methanol)]. Acetylation of this sample of acetal (2.6 mg) with Ac_2O (1.6 μl) and DMAP (3.0 mg) in CH_2Cl_2 (78 μl) at 25 °C for 17 min afforded the acetate **24** (2.9 mg) after chromatography (R_f=0.63, 8 : 1 benzene-acetone). This sample revealed to be a 6 : 4 mixture of **24α** and **24β** by its 400 MHz ^1H NMR spectrum ($CHCl_3$, δ=7.26): δ=0.017 (5.4H, s, Me_3Si of **24α**), 0.021 (3.6H, s, Me_3Si of **24β**), 0.86—0.94 (4H, m, $SiCH_2$), 1.45—1.68 (1.4H, m, H-4 and H-2 of **24β**), 0.66 (0.6H, dd, H-2 of **24α**, J_{gem}=12.8, $J_{2,1}$=3.4, $J_{2,3}$=11.5 Hz), 2.03 (1.8H, s, Ac of **24α**), 2.05 (1.2H, s, Ac of **24β**), 2.25 (0.6H, dd, H-2 of **24α**, $J_{2,1}$=ca. 1, $J_{2,3}$=4.8 Hz), 2.34 (0.4H, dd, H-2 of **24β**, $J_{2,1}$=2.0, $J_{2,3}$=5.8 Hz), 3.34 (1.8H, s, MeO of **24α**), 3.50 (1.2H, s, MeO of **24β**), 3.46—3.59 (4H, m, $SiCH_2$-$C\underline{H}_2OCH_2OC\underline{H}_2$), 3.98 (0.4H, dd, H-5 of **24β**, $J_{5,4}$=10.0, $J_{5,6}$=6.7 Hz), 4.28 (0.6H, dd, H-5 of **24α**, $J_{5,4}$=10.0, $J_{5,6}$=6.4 Hz), 4.43 (0.4H, H-1 of **24β**, $J_{1,2}$=10.0 Hz), 4.52 and 4.58 (0.8H, ABq, OCH_2O of **24β**, J_{gem}=6.4 Hz), 4.53 and 4.60 (1.2H, ABq, OCH_2O of **24α**, J_{gem}=6.4 Hz), 4.83 (0.6H, dd, H-1 of **24α**), 5.14 (0.4H, ddd, H-3 of **24β**, $J_{3,2}$=4.8, $J_{3,4}$=11.5 Hz), 5.28 (1H, ddd, H-7, $J_{7,6}$=9.6, J_{gem}=1.6, $J_{7,5}$=1.6 Hz), 5.35 (0.6H, ddd, H-3 of **24α**, $J_{3,4}$=11.5 Hz), 5.37 (1H, dd, H-7, $J_{7,6}$=17.9, $J_{7,5}$=0 Hz), 5.85 (0.4H, ddd, H-6 of **24β**, $J_{6,5}$=9.9 Hz), 5.88 (0.6H, ddd, H-6 of **24α**, $J_{6,5}$=9.9 Hz).

Conversion of (6b+6b′) into 25 and 26. To an ice-cooled solution of (**6b+6b′**) (140 mg, 0.51 mmol) in dry ether (4.2 ml) was added $LiAlH_4$ (29.1 mg, 0.765 mmol) and the mixture was stirred at 25 °C for 35 min. After water (0.1 ml), 3 M NaOH (0.1 ml), water (0.3 ml), and 3 M NaOH (0.3 ml) were added in sequence with vigorous stirring at 0 °C, the mixture was filtered through a Celite, and the filter cake was washed with ether (3×10 ml). The filtrate and washings were evapo-

rated and the residue was taken up in ethyl acetate (10 ml), which was washed with water and saturated aqueous NaCl, dried, and evaporated. The residue was chromatographed on silica gel (7.0 g) with 2:1 hexane-ethyl acetate to afford the diol (109 mg, 78%); R_f=0.32 (2:1 hexane-ethyl acetate). By the procedure described in the preparation of **36** from **35**, the diol (83.4 mg) was isopropylidenated to give an inseparable 3:1 mixture of **25** and **26** (78.5 mg, 82%) after silica-gel chromatography with 10:1 hexane-ethyl acetate: colorless syrup; ^{1}H NMR (400 MHz, $CHCl_3$, δ=7.26) δ=0.02 (9H, s, Me_3Si), 0.90—0.97 (2H, m, $SiCH_2$), 1.21 (2.25H, d, H-1 of **25**, $J_{1,2}$=6.8 Hz), 1.24 (0.75H, d, H-1 of **26**, $J_{1,2}$=6.8 Hz), 1.38 (4.5H, s, CMe_2 of **25**), 1.39 and 1.46 (1.5H, each s, CMe_2 of **26**), 1.54—1.58 (0.25H, m, H-3 of **26**), 1.88—1.96 (0.75, m, H-3 of **25**), 3.49 and 3.58 (1.5H, ABX, SEMOC$\underline{H}_2$ of **25**, J_{AX}=J_{BX}=5.1, J_{AB}=9.3 Hz), 3.57—3.64 (1.5H, OC$\underline{H}_2$CH$_2$Si of **25**), 3.65—3.72 (0.5H, m, OC$\underline{H}_2$CH$_2$Si of **26**), 3.66 and 3.75 (0.5H, ABX, SEMOC$\underline{H}_2$ of **26**, J_{AX}=J_{BX}=5.1, J_{AB}=9.3 Hz), 4.03 (0.75H, dddd, H-4 of **25**, $J_{3,4}$=$J_{4,5}$=6.7 Hz), 4.17 (1H, dq, H-2, $J_{2,3}$=6.7 Hz), 4.48 (0.25H, dddd, H-4 of **26**, $J_{4,3}$=2.2, $J_{4,5}$=4.8 Hz), 4.59—4.67 (2H, m, OCH_2O), 5.16 (0.25H, ddd, H-6 of **26**, $J_{6,5}$=11.2, $J_{6,4}$=J_{gem}=ca. 0.8 Hz), 5.17 (0.75H, ddd, H-6 of **25**, $J_{6,5}$=11.2, $J_{6,4}$=J_{gem}=ca. 0.8 Hz), 5.26 (0.25 H, ddd, H-6 of **26**, $J_{6,5}$=17.6, $J_{6,4}$=ca. 0.8 Hz), 5.28 (0.75H, ddd, H-6 of **25**, $J_{6,5}$=17.6, $J_{6,4}$=ca. 0.8 Hz), 5.87 (0.75H, ddd, H-5 of **25**), 5.94 (0.25H, ddd, H-5 of **26**).

(2*S*,3*R*,4*S*)-3-[(*t*-Butyldimethylsilyloxy)methyl]-1-(1,3-dithian-2-yl)-2,4-*O*-isopropylidene-5-hexene-2,4-diol (28). To a solution of 1,3-dithiane (47.3 mg, 0.390 mmol) in dry THF (473 ml) was added 1.64 M *n*-BuLi in hexane (237 µl, 0.390 mmol) at −40 °C. After being stirred at −20 °C for 2 h, to this mixture was added a solution of **6a** (20.2 mg, 0.078 mmol) in dry THF (60.6 µl) at −40 °C. After being stirred at −20 °C for 0.5 h, the reaction mixture was poured into cold water which was extracted with ethyl acetate (3×1 ml). The extracts were washed with saturated aqueous NaCl, dried, and evaporated. The residue was chromatographed on silica gel 30:1 chloroform-acetone to give **27** (23.9 mg, 81%). A sample of **27** (22 mg) was isopropylidenated by the procedure described in the preparation of **15** from **14** to afford **28** (22.4 mg, 92%) after silica-gel chromatography with 10:1 hexane-ethyl acetate: R_f=0.75 (3:1 hexane-ethyl acetate), $[\alpha]_D^{32}$ −1.22°, $[\alpha]_{546}^{32}$ −1.71° (*c* 0.82); ^{1}H NMR (90 MHz) δ=0.86 (9H, s, *t*-Bu), 1.32 and 1.36 (each 3H, each s, CMe_2), 1.6—2.1 (5H, m, 2×H-1,3, $SCH_2C\underline{H}_2$), 2.6—2.9 (4H, m, 2×SCH_2), 3.57 and 3.69 (2H, ABX, TBSOC$\underline{H}_2$, J_{AX}=J_{BX}=6.6, J_{AB}=9.9 Hz), 3.8—4.4 (3H, m, S-C$\underline{H}$-S, H-2,4), 5.0—5.4 (2H, m, 2×H-6), 5.95 (1H, ddd, H-5, $J_{5,4}$=5.7, $J_{5,6}$=9.9, 17.4 Hz).

Found: C, 57.20; H, 8.79%. Calcd for $C_{20}H_{38}O_3Si$: C, 57.37; H, 9.15%.

(3*S*,4*R*,5*S*)-4-[(*t*-Butyldimethylsilyloxy)methyl]-3,5-*O*-isopropylidene-1-trimethylstannyl-1,1-bis(methylthio)-6-heptene-3,5-diol (36). To a solution of diisopropylamine (0.931 ml, 6.64 mmol) in a 4:1 mixture of THF-HMPA (16.5 ml) was added 1.64 M *n*-BuLi in hexane (4.05 ml, 6.64 mmol) at 0 °C. After being stirred at 0 °C for 15 min, to this mixture was added rapidly with stirring under Ar a solution of [bis(methylthio)methyl]trimethylstannane (1.64 g, 6.04 mmol) in dry THF (3.3 ml) at −65 °C and stirring was continued at −40 °C for 0.5 h. A solution of **6a** (130 mg, 0.503 mmol) in dry THF (390 µl) was then introduced and the mixture was stirred at −40 °C for 23 min. Then saturated aqueous NH_4Cl was added to the mixture which was extracted with ethyl acetate (3×20 ml). The extracts were washed with saturated aqueous NaCl, dried, and evaporated. The oily residue was chromatographed on silica gel (40 g) with 8:1 hexane-ethyl acetate to afford **35** (190 mg, 71%) as a colorless syrup. To a solution of **35** (190 mg, 0.349 mmol) in dry CH_2Cl_2 (1.9 ml) was added 2-methoxy-1-propene (0.20 ml, 2.10 mmol) and PPTS (13.2 mg, 0.0524 mmol) at 0°C. After being stirred at 24 °C for 3 h, the reaction mixture was diluted with ethyl acetate (7.0 ml) and was washed with water and saturated aqueous NaCl, dried, and evaporated. The residue was chromatographed on silica gel (18.5 g) with 15:1 hexane-ethyl acetate to give **36** (173 mg, 87%) as a colorless syrup: R_f=0.70 (10:1 hexane-ethyl acetate); $[\alpha]_D^{30}$ +8.8°, $[\alpha]_{435}^{30}$ +11.0° (*c* 0.82); ^{1}H NMR (400 MHz, δ ($CHCl_3$)=7.26) δ=0.055, 0.063 (each 3H, each s, $SiMe_2$), 0.24 (9H, s, Me_3Sn), 0.90 (9H, s, *t*-BuSi), 1.33, 1.46 (each 3H, each s, CMe_2), 1.80 (1H, dddd-like, H-4), 1.99, 2.03 (each 3H, each s, 2×SMe), 2.26 (1H, dd, H-2, $J_{2,3}$=2,4, J_{gem}=15.1 Hz), 2.39 (1H, dd, H-2, $J_{2,3}$=10.3 Hz), 3.62 and 3.78 (2H, ABX, C$\underline{H}_2$OTBS, J_{AX}=J_{BX}=5.4, J_{AB}=10.3 Hz), 4.10 (1H, dddd-like, H-5, $J_{5,4}$=$J_{5,6}$=6.4 Hz), 4.22 (1H, ddd, H-3, $J_{3,4}$=3.9 Hz), 5.16 (1H, ddd, H-7, J_{gem}≒$J_{7,5}$≒1.5, $J_{7,6}$=10.7Hz), 5.23 (1H, ddd, H-7, $J_{7,5}$≒1.0, $J_{7,6}$=17.6 Hz), 5.99 (1H, ddd, H-6).

Found: C, 46.64; H, 7.92%. Calcd for $C_{22}H_{46}O_3SiS_2Sn$: C, 46.40; H, 8.14%.

Preparation of Deuterio Product 38. To a solution of **36** (29.2 mg, 0.0495 mmol) in a 3:1 mixture of dry THF-HMPA (117 µl) were added a 1.5 M solution of *n*-BuLi in hexane (66.0 µl, 0.0991 mmol) and immediately D_2O (1.0 ml) at −20 °C. The reaction mixture was warmed up to room temperature and extracted with ethyl acetate (3×1 ml). The extracts were washed with saturated aqueous NaCl, dried and evaporated. The residue was chromatographed on silica gel (1.6 g) with 12:1 hexane-ethyl acetate to afford **38** (17.1 mg, 84.7%) as a colorless syrup: R_f=0.67 (5:1 hexane-ethyl acetate).

Preparation of Deuterio Aldehyde 39. To a mixture of NBS (40.6 mg, 0.228 mmol), $AgNO_3$ (40.8 mg, 0.240 mmol), 2,4,6-trimethylpyridine (60.3 µl, 0.456 mmol), and 85% aqueous acetonitrile (0.62 ml) was added a solution of **38** (15.5 mg, 0.380 mmol) in acetonitrile (46.5 µl) at room temperature. After being stirred at room temperature for 20 min, to the stirred mixture were added in sequence saturated aqueous Na_2SO_3 (0.11 ml), saturated aqueous $NaHCO_3$ (0.11 ml), and saturated aqueous NaCl (0.11 ml) in each 1-min period. Then, this mixture was filtered and the filter cake was washed with acetonitrile (3×2.0 ml). The filtrate and washings were extracted with ethyl acetate (3×2.0 ml), and the extracts were washed with water, saturated aqueous K_2SO_4, $NaHCO_3$, and NaCl, dried, and evaporated. The residue was chromatographed on silica gel (1.7 g) with 5:1 hexane-ethyl acetate to afford **39** (5.0 mg, 43.6%) as a colorless syrup.

Formation of 40 by Coupling of 36 and 32. To a solution of **36** (18.4 mg, 0.0312 mmol) in dry 3:1 THF-HMPA (98.8 µl) was added 1.5 M *n*-BuLi in hexane (25.0 µl, 0.0375 mmol) at −30 °C, and immediately a solution of **32** (6.3 mg, 0.0208 mmol) in dry THF (18.9 µl) was added. After being stirred at 0 °C for 5 h, saturated aqueous NH_4Cl (1.0 ml) was added to the reaction mixture which was extracted with ethyl acetate (3×1.0 ml). The extracts were washed with saturated aqueous NaCl, dried, and evaporated. The residue was chromatographed on silica gel (1.5 g) with 8:1 hexane-ethyl acetate to afford a mixture of **40** and **32** (8.4 mg) as a colorless syrup

(R_f=0.44, 20 : 1 benzene-ethyl acetate). The ratio of **40** and **32** was determined to be 5 : 7 by ^{1}H NMR (90 MHz).

Preparation of 41 by Coupling of 36 and 33. To a solution of **36** (15.0 mg, 0.0254 mmol) in dry 3 : 1 THF-HMPA (60.0 μl) was added 1.5 M *n*-BuLi in hexane (20.3 μl, 0.0305 mmol) at −30 °C, and immediately a solution of **33** (9.2 mg, 0.0177 mmol) in dry THF (27.6 μl) was added. After being stirred at 25 °C for 40 min, saturated aqueous NH_4Cl (1.0 ml) was added to the reaction mixture which was extracted with ethyl acetate (3×1 ml). The extracts were washed with saturated aqueous NaCl, dried, and evaporated. The residue was chromatographed on silica gel (1.4 g) with 10 : 1 hexane-ethyl acetate to afford **41** (10.1 mg, 76%) as colorless syrup: R_f=0.44 (5 : 1 hexane-ethyl acetate); ^{1}H NMR (90 MHz) δ=0.92 (18H, s-like, 2×*t*-Bu), 1.33, 1.38, and 1.47 (total 12H, each s, 2×CMe_2), 1.4—2.3 (7H, m, H-10, 2×H-8, 2×H-6, 2×H-4), 1.97 and 2.03 (each 3H, each s, 2×SMe), 3.38 (3H, s, OMe), 3.4—4.3 and 4.4—4.6 (total 13H, each m, H-2,3,5,9,11, 2×H-1, CH_2OTBS, OCH_2CH_2O), 4.74 and 4.88 (2H, ABq, OCH_2O, *J*=6.9 Hz), 5.0—5.4 (2H, m, 2×H-13), 5.8—6.3 (1H, m, H-12).

(3*S*,5*R*,8*R*,9*S*,11*S*,15*S*,16*R*,17*S*)-16-*O*-[(*t*-Butyldimethylsilyloxy)methyl]-3,5 : 8,9 : 15,17-tri-*O*-isopropylidene-1-*O*-(4-methoxybenzyl)-11-*O*-[(2-methoxyethoxy)methyl]-13,13-bis(methylthio)-18-nonadecene-1,3,5,8,9,11,15,17-octol (42). To a stirred solution of **36** (24.7 mg, 0.0434 mmol) in a 3 : 1 mixture of dry THF and HMPA (91.4 μl) was added rapidly 1.64 M *n*-BuLi in hexane (32.0 μl, 0.0521 mmol) at −29 °C. Immediately, to the resulting brown colored mixture was added a solution of **2** (20.6 mg, 0.0304 mmol) in dry THF (61.8 μl) rapidly. Then, saturated aqueous NH_4Cl was added to the yellow reaction mixture which was extracted with ethyl acetate (5×1.0 ml). The extracts were washed with saturated aqueous NaCl, dried, and evaporated to a syrup, which was chromatographed on silica gel (2.9 g) with 3 : 1 hexane-ethyl acetate to afford **42** (24.3 mg, 84%) as a colorless syrup: R_f=0.55 (3 : 1 hexane-thyl acetate); $[\alpha]_D^{32}$ +11.1° (*c* 0.90); ^{1}H NMR (400 MHz, δ($CHCl_3$)=7.26) δ=0.055, 0.061 (each 3H, each s, $SiMe_2$), 0.90 (9H, s, *t*-BuSi), 1.15 (1H, ddd, H-4, $J_{4,3}\fallingdotseq J_{4,5}\fallingdotseq J_{gem}\fallingdotseq$11.5 Hz), 1.32, 1.33, 1.347, 1.355, 1.40, 1.47 (each 3H, each s, 3×CMe_2), 1.97, 2.03 (each 3H, each s, 2×SMe), 1.25—2.15 (14H, m, 2×H-2, H-4, 2×H-6, 2×H-7, 2×H-10, 2×H-12, 2×H-14, H-16), 3.37 (3H, s, MeO of MEM), 3.45—3.67 (7H, m), 3.80 (3H, s, MeO of MPM), 3.73—3.88 (4H, m), 3.97—4.10 (3H, m), 4.41 and 4.43 (2H, ABq, OCH_2Ar, *J*=14.4 Hz), 4.45—4.51 (1H, m), 4.73 and 4.93 (2H, ABq, OCH_2O of OMEM, *J*=7.3 Hz), 5.16 (1H, ddd, H-19, $J_{19,18}$=10.7, $J_{gem}\fallingdotseq J_{19,17}\fallingdotseq$1.5 Hz), 5.25 (1H, ddd, H-19, $J_{19,18}$=17.6, $J_{19,17}\fallingdotseq$1.5 Hz), 5.97 (1H, ddd, H-18, $J_{18,17}$=5.9 Hz), 6.87, 7.25 (each 2H, each ddd-like, Ar).

Found: C, 61.26; H, 8.82%. Calcd for $C_{49}H_{86}O_{12}SiS_2$: C, 61.34; H, 9.03%.

(3*S*,4*S*,5*S*,9*S*,11*R*,12*R*,15*R*,17*S*)-4-[(*t*-Butyldimethylsilyloxy)methyl]-1,3,5,9,11,12,15,17,19-nonahydroxy-3,5 : 11,12 : 15,17-tri-*O*-isopropylidene-19-*O*-(4-methoxybenzyl)-9-*O*-[(2-methoxyethoxy)methyl]-7-nonadecanone (1). To a solution of dicyclohexylborane (0.406 mmol) in dry THF (0.228 ml) was added a solution of **42** (77.9 mg, 0.0812 mmol) in dry THF (0.234 ml) at 0 °C under Ar. After being stirred at 23 °C for 45 min, the reaction mixture was diluted with water (0.463 ml), and added in sequence 3 M aqueous NaOH (0.135 ml, 0.406 mmol) and 30% H_2O_2 (0.122 ml, 1.22 mmol) at 0 °C. After being stirred at 23 °C for 1 h, the reaction mixture was extracted with chloroform (3×1.0 ml). The extracts were washed with saturated aqueoud NaCl, dried, and evaporated. The residue was chromatographed on silica gel (7.9 g) with 2 : 1 hexane-ethyl acetate to afford **43** (73.2 mg, 92%) as a colorless syrup. To a solution of **43** (73.2 mg, 0.0749 mmol) in 80% aqueous acetone (2.6 ml) was added HgO (71.4 mg, 0.330 mmol) and $HgCl_2$ (89.5 mg, 0.330 mmol) at 23 °C. After being stirred at 23 °C for 25 min, the reaction mixture was filtered through a Celite and the filter cake was washed with acetone. The combined filtrate and washings were concentrated to remove acetone. The aqueous residue was extracted with chloroform (3×4.0 ml) and extracts were washed with aqueous 10% KI (2×5.0 ml), saturated aqueous NaCl, dried, and evaporated. The residue was chromatographed on silica gel (6.7 g) with 1 : 1 hexane-ethyl acetate to afford **1** (54.9 mg, 81.6%) as a colorless syrup: R_f=0.42 (1 : 1 hexane-ethyl acetate); $[\alpha]_D^{31}$ +6.5°, $[\alpha]_{435}^{31}$ +11.2° (*c* 0.68); IR($CHCl_3$) 1710 cm^{-1} (C=O); ^{1}H NMR 400 MHz, δ($CHCl_3$)=7.26) δ=0.05, 0.055 (each 3H, each s, $SiMe_2$), 0.89 (9H, s, *t*-Bu), 1.15 (1H, ddd, H-16, $J_{16,17}\fallingdotseq J_{16,15}\fallingdotseq J_{gem}\fallingdotseq$11.0 Hz), 1.318, 1.324, 1.33, 1.34, 1.35, 1.40 (each 3H, each s, 3×CMe_2), 1.42—1.95 (12H, m, 2×H-2, H-4, 2×H-10, 2×H-13, 2×H-14, H-16, 2×H-18), 2.53 (1H, br-t-like, OH), 2.54 (1H, dd, *J*=3.8, 16.8 Hz), 2.68 (1H, dd, *J*=9.6, 16.8 Hz), 2.72 and 2.80 (each 1H, each dd, *J*=6.4 and 16.8 Hz), 3.38 (3H, s, MeO of MEM), 3.46—3.87 (10H, m), 3.80 (3H, s, MeO of MPM), 3.97—4.05 (1H, m), 4.24—4.31 (1H, m), 4.41 and 4.44 (2H, ABq, OCH_2Ar, *J*=12.8 Hz), 4.43—4.49 (1H, m), 4.71 and 4.74 (2H, ABq, OCH_2O of MEM, *J*=6.4 Hz), 6.88 and 7.25 (each 2H, each ddd-like, Ar).

Found: C, 62.75; H, 8.79%. Calcd for $C_{47}H_{82}O_{14}Si$: C, 62.78; H, 9.19%.

We are grateful to the Institute of Microbial Chemistry for the generous support of our program. The present work was partially supported by a Grant-in Aid for Scientific Research No. 60470091 from the Ministry of Education, Science and Culture and by the Japan Antibiotics Research Association (Japan) Research Grant. We would like to thank Dr. Masaya Nakata for 400 MHz ^{1}H NMR spectral analyses, and Mr. Hisao Arita for elemental analyses.

References

1) Part II: M. Kinoshita, M. Morioka, M. Taniguchi, and J. Shimizu, *Bull. Chem. Soc. Jpn.*, **60**, 4005 (1987).

2) K. C. Nicolaou, R. A. Daines, J. Uenishi, W. S. Li, D. P. Papahatjis, and T. K. Chakraborty, *J. Am. Chem. Soc.*, **109**, 2205 (1987); K. C. Nicolaou, R. A. Daines, and T. K. Chakraborty, *ibid.*, **109**, 2208 (1987); K. C. Nicolaou, R. A. Daines, T. K. Chakraborty, and Y. Ogawa, *ibid.*, **109**, 2821 (1987).

3) J. Abiko, T. Takemasa, and S. Masamune, 54th National Meeting of the Chemical Society of Japan, Tokyo, April, 1987, Abstr. No. 3IIIL28.

4) K. N. Slessor and A. S. Tracey, *Can. J. Chem.*, **47**, 1989 (1969); W. M. Reckendorf, *Method in Carbohdr. Chem.*, **6**, 129 (1972).

5) Y. Oikawa, T. Tanaka, K. Horita, and O. Yonemitsu, *Tetrahedron Lett.*, **25**, 5397 (1984).

6) P. J. Garegg and B. Samuelson, *J. Chem. Soc., Chem.*

Commun., **1979**, 978.

7) P. Köster, D. Simić, and M. A. Grassberger, *Liebigs Ann. Chem.*, **739**, 211 (1970).

8) a) J. S. Jewell and W. A. Szarek, *Tetrahedron Lett.*, **1969**, 43; b) A. Rosenthal and M. Sprinzl, *Can. J. Chem.*, **47**, 3941 (1969).

9) S. Achab and B. C. Das, *Synth. Commun.*, **12**, 931 (1982); K. Toshima, K. Tatsuta, and M. Kinoshita, *Tetrahedron Lett.*, **27**, 4741 (1986).

10) E. J. Corey and M. Chaykovsky, *J. Am. Chem. Soc.*, **84**, 866 (1962).

11) D. Seebach and E. J. Corey, *J. Org. Chem.*, **40**, 231 (1975).

12) The short-lived characteristic of **29c** was confirmed by the fact that a sample of the lithium derivative **37** generated in a moment from **36** with *n*-BuLi in THF (see text) changed rapidly at −25 °C into the protonated dithioacetal compound by the proton-abstraction probably from the solvent (THF). The unusually increased kinetic basicity as seen in the lithium compounds, **29c** and **37**, may be attributed to their extremely destabilized carbanion structures which may inherently exist in some complex polyoxygenated d^3-anions.[18,19]

13) The coupling of heptanal and **28** using *t*-BuLi instead of *n*-BuLi was also unsuccessful, affording only a complex mixture of side products formed by the reaction of **28** and *t*-BuLi.

14) B.-T. Gröbel and D. Seebach, *Synthesis*, **1977**, 371,

15) R. Bürstinghaus and D. Seebach, *Chem. Ber.*, **110**, 841 (1977).

16) E. J. Corey and B. W. Erickson, *J. Org. Chem.*, **36**, 3553 (1971).

17) Unfortunately, for the present, this procedure can not be adapted for large scale preparation of **42**. When the amount of **36** was greater than 25 mg, the yield of **42** sharply lowerd probably due to the short-lived characteristic of **37**.

18) I. Oppong, H. W. Pauls, D. Lang, and B. Fraser-Reid, *J. Chem. Soc., Chem. Commun.*, **1986**, 1241.

19) D. Seebach, *Angew. Chem., Int. Ed. Engl.*, **18**, 239 (1979).

Clay Montmorillonite: An Efficient, Heterogeneous Catalyst for Michael Reactions of Silyl Ketene Acetals and Silyl Enol Ethers with α,β-Unsaturated Carbonyl Compounds

Motomitsu KAWAI, Makoto ONAKA,* and Yusuke IZUMI*
Department of Synthetic Chemistry, Faculty of Engineering, Nagoya University, Furo-cho, Chikusa-ku, Nagoya 464
(Received December 28, 1987)

The Michael addition of silyl ketene acetals to α,β-unsaturated esters (enoates) is investigated. The reaction is catalyzed by clay montmorillonite (solid acid) most effectively among various, homogeneous and heterogeneous acid promoters. The montmorillonite-catalyzed reaction has several prominent features: (1) Not only α- or β-monosubstituted acrylates but also α,β- or β,β-disubstituted acrylates are applicable. (2) The highly regioselective 1,4-addition to a polyenoate is achievable. (3) The Michael adduct can be obtained in the form of a labile silyl ketene acetal owing to a simple work-up procedure. The Michael reaction of a silyl enol ether and silyl ketene acetals with α,β-unsaturated ketones (enones) is also described.

The Michael addition of an enolate to an α,β-unsaturated carbonyl system is one of the most important reactions for carbon-carbon bond formation.[1] However, its use in organic syntheses is occasionally restricted owing to a concurrent 1,2-addition reaction and polymerization of α,β-unsaturated carbonyl compounds. A new methodology to overcome these problems has been devised by the use of lithium enolates.[2,3] Another approach is to use silyl enol ethers and silyl ketene acetals as enolates. The Michael reaction of the silyl enol ethers with α,β-unsaturated ketones (enones) is generally performed with the aid of a stoichiometric amount of Lewis acid to afford 1,5-dicarbonyl compounds.[4,5] When the reaction is conducted thermally in acetonitrile,[6] under high pressure,[7] or by the use of $(Me_2N)_3S^+Me_3SiF_2^-$ [8] or $Ph_3C^+ClO_4^-$,[9] the intermediate adducts are isolable in the form of synthetically valuable silyl enol ethers.

Concerning the Michael reaction of a silyl enol ether with an α,β-unsaturated ester (enoate), the reaction with acrylate was the only example with the yield being not so high.[4] The reaction of fumarate or crotonate with a cyclic silyl enol ether gave a [2+2]cycloaddition product.[10] The single example of Michael reaction of a silyl ketene acetal with an enoate was reported in the study of "Group Transfer Polymerization (GTP)" by the use of $(Me_2N)_3S^+Me_3SiF_2^-$ [11] or Lewis acids.[12] One-to-one addition of a silyl ketene acetal to an enoate has not been reported.

Recently we have shown that clay montmorillonite (sheet silicate) is an efficient, heterogeneous acid catalyst for the aldol reaction of silyl enol ethers[13] or silyl ketene acetals[14] with aldehydes or acetals. We have also demonstrated that the Michael reaction of silyl ketene acetals with enoates can be effectively accomplished by the use of clay montmorillonite.[15,16] In this paper, we provide a detailed description of the Michael reaction catalyzed by montmorillonite, and show its scope and limitations.

Results and Discussion

In the presence of aluminium ion-exchanged montmorillonite (Al-Mont),[17] the reactions of silyl ketene acetals derived from propionates with croton-

Table 1. The Al-Mont-Catalyzed Michael Reactions of Silyl Ketene Acetals Derived from Propionates with Enoates

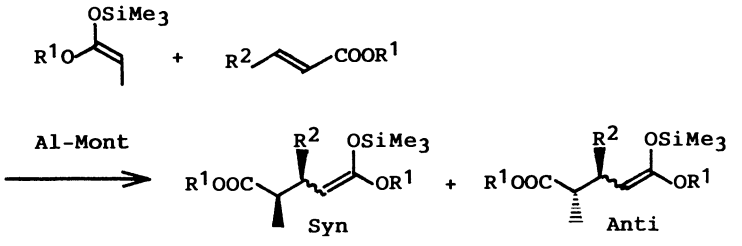

Entry	R^1	R^2	Temp/°C (Time/h)	Product	Yield/%	Syn : Anti
1	Me	Me	−78(0.5)	**23a**	84	27 : 73
2	Pr^i	Me	−60(0.5)	**24a**	90	55 : 45
3	Me	Ph	−50(0.5)	**25a**	91	61 : 39
4	Me	$CH_3CH=CH$	−50(0.5)	**26a**	96	39 : 61
5	Et	EtOOC	−78(0.5)	**27a**	85	42 : 58

Reaction conditions: Nucleophile (1 mmol), Acceptor (1 mmol), Al-Mont (0.2 g), CH_2Cl_2 (4 ml).

1: 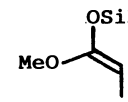

2: 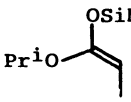

3: 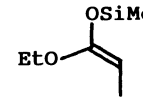

4: 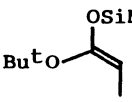

5: 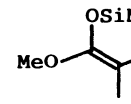

6: 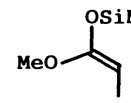

7: 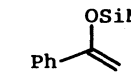

8: 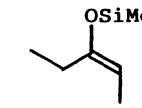

9: 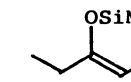

10: 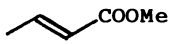

11: 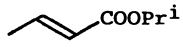

12:

13:

14:

15: 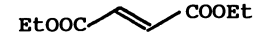

16:

17: 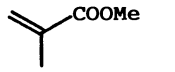

18: 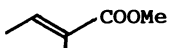

19: 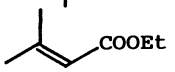

20: 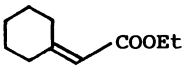

21: 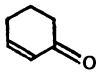

22: 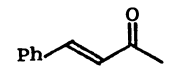

ate, cinnamate, sorbate, or fumarate were examined and the results are listed in Table 1. The reactions proceeded at low temperatures. After the reactions were complete, the solid catalyst of Al-Mont was easily removed through a Celite pad. Thereby the Michael products were isolated by simple distillation in the form of a trimethylsilyl ketene acetal. These products showed strong IR absorption around 1670 cm^{-1} ($\nu_{C=C}$), which is characteristic of the silyl ketene acetal structure.[18]

After the hydrolysis of the products with dilute HCl, the stereochemical assignment was made in comparison with authentic samples prepared via the conjugate addition of the corresponding lithium enolates.[3] Unfortunately the diastereoselectivities were low to moderate (1 : 1—3 : 1).

It is noteworthy that the present Michael addition to a polyenoate occurred regioselectively in the 1,4-fashion. In the case of methyl sorbate (Entry 4), the preferential 1,4-addition (98%) over 1,6-addition (2%) is notable because the addition of a lithium enolate gave a mixture (70 : 30) of 1,4- and 1,6-adducts in low yield (total yield 37%).[19]

For demonstrating the utility of the Al-Mont catalyst, representative, homogeneous acid promoters were employed for the same reaction (Table 2, Entries 2—6).[20] Compared with Al-Mont (Table 2, Entry 1), these promoters gave lower yield of the Michael product (**23a** or **23b**) due to deactivation during the reaction. For example, when Ph_3CClO_4 was added to the mixture of a silyl ketene acetal and an enoate in CH_2Cl_2, the yellow color of the trityl cation (Ph_3C^+) immediately disappeared at −78 °C, showing that Ph_3CClO_4 was destroyed.[21] In the case of CF_3SO_3H and $CF_3SO_3SiMe_3$, the Michael product was also isolable in the form of a silyl ketene acetal after the reaction mixture was

Table 2. The Michael Reaction of **1** with **10**[a]

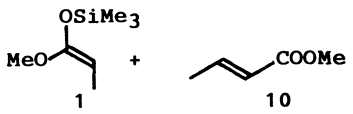

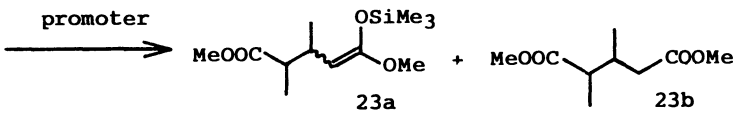

Entry	Promoter (mol%)	Temp/°C (Time/h)	Product[b]	Yield/%	Syn : Anti
1	Al-Mont[c]	−78(0.5)	**23a**	84	27 : 73
2	CF_3SO_3H (5+5)[d]	−30(2)	**23a**	47	37 : 63
3	$CF_3SO_3SiMe_3$ (5+5)[d]	−30(2)	**23a**	46	39 : 61
4	Ph_3CClO_4 (5)	−50(2)	**23b**	38	35 : 65
5	$ZnBr_2$ (100)	−78(2)	**23b**	47	40 : 60
6	$BF_3 \cdot OEt_2$ (100)	−50(1)	—	0	—

a) **1** (1 mmol), **10** (1 mmol), CH_2Cl_2 (4 ml). b) Procedure for the isolation of products is described in the experimental section. c) Al-Mont (0.2 g) was used. d) The promoter was added in two portions.

quenched with organic amine (Entries 2 and 3).

In order to investigate the scope and limitations of the montmorillonite-catalyzed Michael reactions, we employed variously substituted silyl ketene acetals and enoates (Table 3). Concerning enoates, α- or β-monosubstituted and α,β- or β,β-disubstituted acrylates are applicable. Acrylate is the only case giving a Michael adduct in low yield and polymeric by-products (Entry 1). It should be noted that α,β- and β,β-disubstituted acrylates are reactive by the present method (Entries 3—5), while a lithium enolate of an ester is reported to have no reactivity to these disubstituted acrylates.[3a] In contrast to a silyl ketene acetal, a silyl enol ether is not reactive to enoates in the presence of Al-Mont (Entry 8).

Even though the Al-Mont catalyst was dried at 120 °C/0.5 Torr (1 Torr=133.322 Pa) prior to use,[22] a small amount of water remained in the interlayer of the catalyst. When the Michael reaction was carried out at low temperature, the product could be obtained in the form of a labile silyl ketene acetal without being hydrolyzed. However, in some cases of a sterically hindered substrate a higher reaction temperature was required, and the product was partly hydrolyzed with the water in Al-Mont (Table 3, Entries 4 and 6).

The tandem reaction[23] of the Michael addition of a silyl ketene acetal to an enoate followed by the aldol reaction with an aldehyde was also successful to give a corresponding product in good yield without isolation of an intermediate, the silyl ketene acetal (Scheme 1).

The Michael addition to enones was also achieved by the use of Al-Mont (Table 4). It is well-known that enones are more reactive than enoates in the 1,4-addition of alkylcopper reagents.[24] A similar trend was observed in the present Al-Mont-catalyzed reaction since enones reacted not only with silyl ketene acetals but also with a silyl enol ether in the 1,4-fashion.[25] The products were obtained in the form of a silyl enol ether. The behavior of diastereoselection of the reaction was similar to that of the reactions promoted by $TiCl_4$[5] and Ph_3CClO_4.[9b]

In conclusion, in spite of under heterogeneous con-

Table 3. The Michael Reactions of Enol Silanes with Enoates Catalyzed by Al-Mont[a]

Entry	Nucleophile	Acceptor	Temp/°C (Time/h)	Product	Yield/%
1	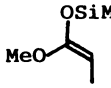	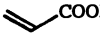	−78(0.5)	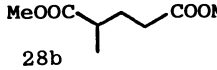 28b	31
2	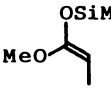	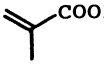	−50(1)	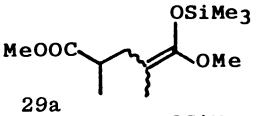 29a	79
3	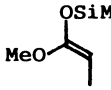	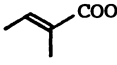	−30(1)	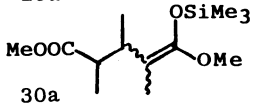 30a	56
4	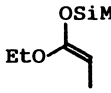	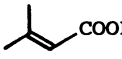	25(2)	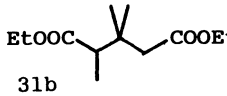 31b	71
5	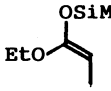	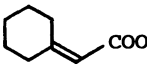	15(9)	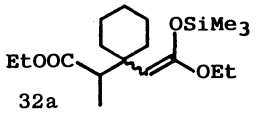 32a	87
6	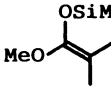		−10(1)	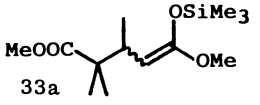 33a	52[d,e]
7	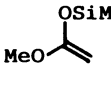		−50(1)	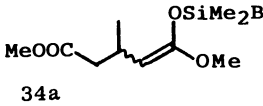 34a	86
8	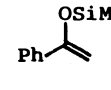		0(1)	———	0

a) Reaction conditions: Nucleophile (1 mmol), Acceptor (1 mmol), Al-Mont (0.2 g), CH_2Cl_2 (4 ml). b) The product was isolated after the hydrolysis treatment. c) Silyl ketene acetal (1.5 mmol) was used. d) Al-Mont (0.5 g) was used. e) A hydrolyzed product (dimethyl 2,2,3-trimethylglutarate) was also obtained in 18% yield.

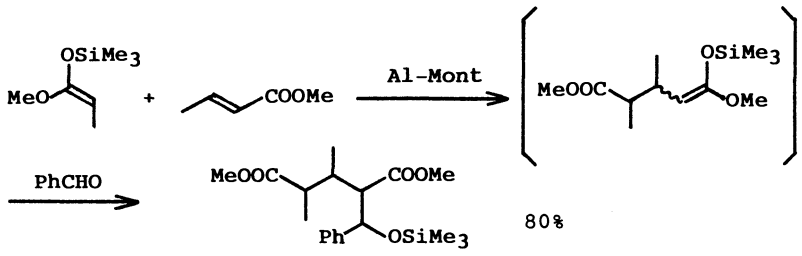

35a

Scheme 1.

Table 4. The Michael Reactions of Enol Silanes with Enones Catalyzed by Al-Mont[a)]

Entry	Nucleophile	Acceptor	Temp/°C (Time/h)	Product	Yield/%	Syn : Anti
1	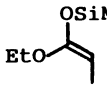		−78(0.5)	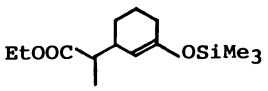 36a	87	57 : 43
2	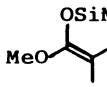		−20(1)	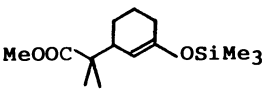 37a	86	—
3	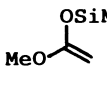		−78(0.5)	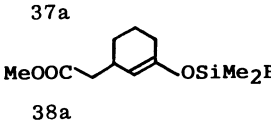 38a	95	—
4	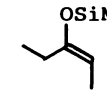		−78(1)	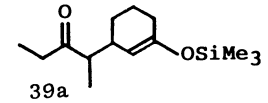 39a	83	38 : 62
5	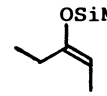	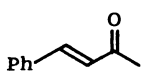	−78(1)	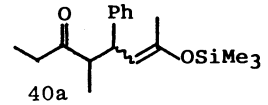 40a	98	29 : 71
6	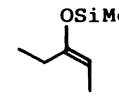	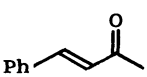	−30(1)	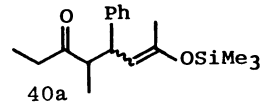 40a	81	21 : 79[b)]

a) Reaction conditions: Nucleophile (1 mmol), Acceptor (1 mmol), Al-Mont (0.2 g), CH_2Cl_2 (4 ml). b) 1,2-Dimethoxyethane was used as a solvent.

ditions, solid montmorillonite can facilitate the Michael additions of silyl ketene acetals and silyl enol ethers to enoates and enones. The montmorillonite proved to be an alternative to conventional, moisture-sensitive homogeneous acids which are frequently troublesome in manipulation and work-up.

Experimental

Measurement. ^1H NMR spectra were recorded in $CDCl_3$ with a Hitachi R-600 (60 MHz) spectrometer. ^{13}C NMR spectra were recorded in C_6D_6 with a JEOL JNM GX-500 (125 MHz) spectrometer. Infrared spectra were recorded in CCl_4 on a JASCO IRA-2 spectrometer. Analytical gas-liquid chromatography (GC) was done with a Shimadzu GC-8A instrument with a flame ionization detector and nitrogen carrier gas. The following capillary columns were used for analysis: OV-1 Bonded, 25 m×0.25 mm; PEG-HT Bonded, 25 m×0.25 mm. The flow rate of carrier gas was 2 ml min^{-1} (1.0 kg cm^{-2}). The following packed column was also used for monitoring the reaction: Silicone SE-30 on Uniport B, 1 m×3 mm.

Solvents and Reagents. Preparation of Aluminium ion-exchanged montmorillonite (Al-Mont) was previously described.[13)] Dichloromethane was distilled from P_2O_5 and stored over Molecular Sieves 3A. 1,2-Dimethoxyethane (DME) and diethyl ether were distilled from $LiAlH_4$ prior to use. $CF_3SO_3SiMe_3$ was distilled from CaH_2. $ZnBr_2$ was dried over flames at ca. 350 °C/0.5 Torr for 10 min. α,β-Unsaturated carbonyl compounds **10,13,15—18,21**, benzaldehyde, and CF_3SO_3H were purified by distillation. $BF_3 \cdot OEt_2$, **12**, and **22** were used without purification. Silyl enol ethers **7**,[26a)] **8** ($E:Z$=83 : 17)[26b)] and **9**[27)] were prepared according to the literatures. Enoates **11**[28a)] and **14,19,20**[28b)] were prepared by means of the known methods.

Silyl Ketene Acetals. These compounds should be free from amine for the present Michael reaction. They were prepared according to a minor modification of the standard procedure reported earlier.[18a,27)] The preparation of **3** is illustrative. To a stirred solution of 50 ml of hexane and 27

ml (0.19 mol) of diisopropylamine at 0 °C was added 100 ml (0.16 mol) of a 15% solution of butyllithium in hexane under nitrogen atmosphere. Hexane and excess amine were removed under reduced pressure at 0 °C. The flask was refilled with N_2 and residual white solids were redissolved in 50 ml of THF at 0 °C. The solution was cooled to −78 °C and a solution of 18 ml (0.16 mol) of ethyl propionate in 20 ml of THF was added over 10 min. After the mixture was stirred for 10 min, a solution of 20 ml (0.16 mol) of chlorotrimethylsilane in 20 ml of THF was added over 10 min. The reaction mixture was warmed to 0 °C over 1 h, diluted with 300 ml of cold pentane. The mixture was washed 15 times with 300 ml of ice-cold water and then with a 1 M (1 M=1 mol dm^{-3}) $Cu(OAc)_2$ solution until the aqueous layer became neutral. The organic layer was then washed with saturated brine and dried over Na_2SO_4. The solvent was removed with a rotary evaporator and the resulting crude product was purified by distillation to give 14 g (0.08 mol) of **3** (50%): bp 76—78 °C/55 Torr; *E*:*Z*=80:20 (isomeric ratio was determined by GC). **1** (*E*:*Z*=60:40) and **2** (*E*:*Z*=89:11) were similarly prepared. **4** (*E*:*Z*=32:68),[27] **5**,[18a] and **6**,[27] were prepared according to the known methods.

General Procedure for Al-Mont-Catalyzed Michael Additions of Silyl Ketene Acetals and Silyl Enol Ethers to α,β-Unsaturated Carbonyl Compounds. Al-Mont (0.2 g) in a 20 ml round-bottomed flask was dried at 120 °C and 0.5 Torr for 3 h in an oil bath, and cooled to −78 °C under nitrogen. A solution of an α,β-unsaturated carbonyl compound (1 mmol) in CH_2Cl_2 (4 ml) was added. After the mixture being stirred for 1 min, a solution of a silyl ketene acetal or a silyl enol ether (1 mmol) in CH_2Cl_2 (1 ml) was added at −78 °C. Then the mixture was stirred under the conditions listed in tables. The reaction was monitored by GC (SE-30, 1 m). As work-up, cold ether (−50 °C, 5 ml) was added, the montmorillonite was filtered off through a Celite pad and washed with ether. The organic layer was evaporated and distilled on a Kugelrohr apparatus to yield the Michael product.

If necessary, the Michael products in the form of silyl ketene acetals or silyl enol ethers were hydrolyzed as follows. One drop of 1 M HCl was added to a solution of the Michael product in methanol, ethanol, or THF at room temperature. The mixture was stirred for 0.5 h and quenched with aqueous $NaHCO_3$. Organic product was extracted with CH_2Cl_2. The extract was washed with brine, dried over Na_2SO_4, and the product was isolated by distillation in quantitative yield.

General Procedure for Homogeneous Acid Promoter-Mediated Reactions (Table 2, Entries 2—6). To a stirred solution of **1** (1 mmol) and **10** (1 mmol) in CH_2Cl_2 (4 ml) was added an appropriate amount of an acid promoter in CH_2Cl_2 (1 ml) under a nitrogen atmosphere at −78 °C. When the reaction was slow, the temperature was raised and/or the acid promoter was supplemented. The mixture was quenched with a few drops of triethylamine, diluted with ether, and poured into an aqueous $NaHCO_3$ solution. Organic products were extracted with ether. The extract was washed with water and with brine, and dried over Na_2SO_4. The products were purified by distillation.

Stereochemistry of Products. In comparison with the authentic samples (**23b**,[3b] **25b**,[3b] **26c**,[3b] **27b**,[3b] **36b**,[5] and **40b**,[9b]) prepared according to the known procedures, the relative configuration (syn or anti)[29] of the Michael products in the hydrolyzed form (1,5-dicarbonyl compounds) was assigned. Diastereomer ratios were determined by GC. The geometrical isomers (*E* or *Z*) of the Michael products in the form of a silyl ketene acetal or a silyl enol ether were not assigned.

Methyl 5-Methoxy-2,3-dimethyl-5-trimethylsiloxy-4-pentenoate (23a). Bp 110 °C (bath temp)/0.5 Torr; ^{1}H NMR ($CDCl_3$) δ=0.19 and 0.24 (two s, 3:7 ratio, 9H, CH_3Si), 0.96 (d, *J*=6.4 Hz, 3H, $C\underline{H}_3CHCH{=}C$), 1.10 (d, *J*=6.4 Hz, 3H, $C\underline{H}_3CHC{=}O$), 2.1—3.0 (m, 2H, $C\underline{H}C\underline{H}C{=}O$), 3.3—3.6 (m, 1H, CH=C), 3.51 (s, 3H, $CH_3OC{=}C$), and 3.68 (s, 3H, $CH_3OC{=}O$); IR (CCl_4) 1670 (C=C) and 1732 (C=O) cm^{-1}.

Dimethyl 2,3-Dimethylglutarate (23b). Obtained from **23a** by hydrolysis. A mixture of diastereomers (syn:anti=27:73): ^{1}H NMR ($CDCl_3$) δ=0.9—1.0 (m, 3H, $C\underline{H}_3CHCH_2$), 1.15 (d, *J*=6.4 Hz, 3H, $C\underline{H}_3CHC{=}O$), 2.2—2.6 (m, 4H, $C\underline{H}_2C\underline{H}C\underline{H}$), and 3.70 (s, 6H, CH_3O); IR (CCl_4) 1735 (C=O) cm^{-1}; GC (PEG-HT, 100 °C) t_R 10.8 min (anti), 11.3 min (syn).

Isopropyl 5-Isopropoxy-2,3-dimethyl-5-trimethylsiloxy-4-pentenoate (24a). Bp 130 °C (bath temp)/0.3 Torr; ^{1}H NMR ($CDCl_3$) δ=0.20 and 0.22 (two s, 9H, CH_3Si), 0.95 (d, *J*=6.4 Hz, 3H, $C\underline{H}_3CHCH{=}C$), 1.19 (d, *J*=6.0 Hz, 3H, $C\underline{H}_3CH{=}O$), 1.22 (d, *J*=6.0 Hz, 12H, $(C\underline{H}_3)_2CH$), 2.0—2.9 (m, 2H, $C\underline{H}C\underline{H}C{=}O$), 3.31, 3.44, 3.55, and 3.71 (four d, *J*=9.2, 9.3, 9.4, and 9.3 Hz, 1H, CH=C), 4.0—4.5 (m, 1H, $(CH_3)_2C\underline{H}OC{=}C$), and 4.98 (septet, *J*=6.0 Hz, 6H, $(CH_3)_2C\underline{H}OC{=}O$); IR ($CCl_4$) 1672 (C=C) and 1732 (C=O) cm^{-1}.

Diisopropyl 2,3-Dimethylglutarate (24b). Obtained from **24a** by hydrolysis. A mixture of diastereomers (syn:anti=55:45). ^{1}H NMR ($CDCl_3$) δ=0.9—1.1 (m, 6H, $C\underline{H}_3CH$), 1.23 (d, *J*=6.0 Hz, 12H, $(C\underline{H}_3)_2CH$), 2.1—2.6 (m, 4H, $C\underline{H}_2C\underline{H}C\underline{H}$), and 5.01 (septet, *J*=6.0 Hz, 2H, $(CH_3)_2C\underline{H}$); IR (CCl_4) 1732 (C=O) cm^{-1}. Diastereomer ratio was determined in the form of **23b** after transesterification.

Methyl 5-Methoxy-2-methyl-3-phenyl-5-trimethylsiloxy-4-pentenoate (25a). Bp 150 °C (bath temp)/0.5 Torr; ^{1}H NMR ($CDCl_3$) δ=0.10, 0.13, 0.20, and 0.22 (four s, 9H, CH_3Si), 0.98, 1.00, 1.17, and 1.19 (four d, *J*=7.0, 7.0, 7.0, and 7.0 Hz, 3H, $C\underline{H}_3CH$), 2.4—3.1 (m, 1H, $CH_3C\underline{H}$), 3.4—4.1 (m, 8H, $C\underline{H}C{=}C$, $PhC\underline{H}$, and $C\underline{H}_3O$), and 7.24 (s, 5H, C_6H_5); IR (CCl_4) 1670 (C=C) and 1732 (C=O) cm^{-1}.

Dimethyl 2-Methyl-3-phenylglutarate (25b). Obtained from **25a** by hydrolysis. A mixture of diastereomers (syn:anti=61:39). ^{1}H NMR ($CDCl_3$) δ=0.96 and 1.18 (two d, 3:2 ratio, *J*=6.4, 7.0 Hz, 3H, $C\underline{H}_3CH$), 2.6—3.1 (m, 3H, $C\underline{H}_2CHPhC\underline{H}$), 3.2—3.6 (m, 1H, $PhC\underline{H}$), 3.51, 3.56, and 3.72 (three s, 6H, CH_3O), and 7.26 (s, 5H, C_6H_5); IR (CCl_4) 1735 (C=O) cm^{-1}; GC (PEG-HT, 150 °C) t_R 24.0 min (syn), 24.5 min (anti).

Methyl 5-Methoxy-2-methyl-3-(1-propenyl)-5-trimethylsiloxy-4-pentenoate (26a). Bp 135 °C (bath temp)/0.8 Torr; ^{1}H NMR ($CDCl_3$) δ=0.19 (s, 9H, CH_3Si), 1.10 (d, *J*=6.6 Hz, 3H, $C\underline{H}_3CHC{=}O$), 1.66 (d, *J*=4.2 Hz, 3H, $C\underline{H}_3CH{=}CH$), 2.2—2.7 (m, 1H, $CHC{=}O$), 2.9—3.2 (m, 1H, $C\underline{H}CHC{=}O$), 3.2—3.7 (m, $CH{=}COSi$), 3.51 and 3.53 (two s, 3H, $CH_3OC{=}C$), 3.66 and 3.68 (two s, 3H, $CH_3OC{=}O$), and 5.3—5.5 (m, 2H, $C\underline{H}{=}C\underline{H}$); IR ($CCl_4$) 1670 (C=C) and 1730 (C=O) cm^{-1}.

Dimethyl 2-Methyl-3-(1-propenyl)glutarate (26b). Obtained from **26a** by hydrolysis. A mixture of diastereomers (syn:anti=39:61): ^{1}H NMR ($CDCl_3$) δ=1.11 and 1.13 (two d, *J*=6.6 and 6.6 Hz, 3H, $C\underline{H}_3CHC{=}O$), 1.66 (d, *J*=5.0 Hz, 3H, $C\underline{H}_3CH{=}CH$), 2.3—2.8 (m, 4H, $C\underline{H}_2C\underline{H}C\underline{H}C{=}O$), 3.68 and 3.70 (two s, 6H, CH_3O), and 5.3—5.7 (m, $C\underline{H}{=}C\underline{H}$, 2H); IR

(CCl_4) 1730 (C=O) cm^{-1}; GC (PEG HT, 120 °C) t_R 10.6 min (anti), 10.9 min (syn).

Dimethyl 2-Methyl-3-propylglutarate (26c). Obtained from **26** by hydrogenation on Pd/C in methanol. A mixture of diastereomers: ^1H NMR ($CDCl_3$) δ=0.90 (t, J=6.0 Hz, 3H, $C\underline{H}_3CH_2$), 1.10 and 1.13 (two d, 3:2 ratio, J=7.0 and 7.0 Hz, 3H, $C\underline{H}_3CH$), 1.3 (br, 4H, $CH_2C\underline{H}_2$), 2.2—2.9 (br, 4H, $CH_3C\underline{H}C\underline{H}C\underline{H}_2C$=O), and 3.69 (s, 6H, CH_3O); IR (CCl_4) 1735 (C=O) cm^{-1}.

The Michael Addition of Lithium Enolate of Methyl Propionate to 13.[3b] A solution of methyl propionate (2 mmol) in THF (5 ml) was added to a stirred solution of lithium diisopropylamide (2 mmol) in THF-HMPA (2 and 1 ml, respectively) at −78 °C. Then a solution of **13** (1.5 mmol) in THF (1.5 ml) was added and the mixture was stirred for 1 h at −78 °C. The reaction was quenched by adding saturated aqueous ammonium chloride. The organic layer was extracted with ether, washed with water and with brine, and dried over Na_2SO_4. The solvent was evaporated and the resulting crude product was distilled on a Kugelrohr apparatus to yield a mixture of 1,4-product **26b** (syn:anti=5:95) and 1,6-product **26d** in 37% yield (total yield). The ratio of **26b** to **26d** was 70:30 determined by GC. **26b** and **26d** were separated by column chromathography on silica gel using hexane-ether (4:1) as eluent.

Dimethyl 5,6-Dimethyl-3-heptenedioate (26d; 1,6-adduct). ^1H NMR ($CDCl_3$) δ=1.01 (d, J=7.0 Hz, 3H, $C\underline{H}_3CHCH$=C), 1.11 (d, J=7.0 Hz, 3H, $C\underline{H}_3CHC$=O), 2.2—2.6 (m, 2H, $CH_3C\underline{H}C\underline{H}CH_3$), 3.05 (d, J=5.6 Hz, 2H, CH_2C=O), 3.67 and 3.69 (two s, 6H, CH_3O), and 5.4—5.7 (m, 2H, $C\underline{H}$=$C\underline{H}$); IR (CCl_4) 1738 (C=O) cm^{-1}; GC (PEG-HT, 120 °C) t_R 16.5 and 17.1 min.

Diethyl 2-[2-Ethoxy-2-(trimethylsiloxy)ethenyl]-3-methylsuccinate (27a). Bp 145 °C (bath temp)/0.5 Torr; ^1H NMR ($CDCl_3$) δ=0.22 (s, 9H, CH_3Si), 1.17 (d, J=7.0 Hz, 3H, $C\underline{H}_3CH$), 1.23 (t, J=7.0 Hz, 9H, $C\underline{H}_3CH_2O$), 2.5—3.1 (m, 1H, $CH_3C\underline{H}$), 3.5—3.8 (m, 2H, $C\underline{H}C\underline{H}$=C), and 3.8—4.3 (m, 6H, $CH_3C\underline{H}_2O$); IR (CCl_4) 1668 (C=C) and 1725 (C=O) cm^{-1}.

Diethyl 3-Ethoxycarbonyl-2-methylglutarate (27b). Obtained from **27a** by hydrolysis. A mixture of diastereomers (syn:anti=42:58): ^1H NMR ($CDCl_3$) δ=1.19 (d, J=7.0 Hz, 3H, $C\underline{H}_3CH$), 1.27 (t, J=7.0 Hz, 9H, $C\underline{H}_3CH_2O$), 2.5—3.5 (m, 4H, $C\underline{H}C\underline{H}C\underline{H}_2$), and 4.18 (q, J=7.0 Hz, 6H, $CH_3C\underline{H}_2O$); IR (CCl_4) 1730 (C=O) cm^{-1}; GC (PEG-HT, 120 °C) t_R 14.2 min (syn), 14.9 min (anti).

Dimethyl 2-Methylglutarate (28b). Bp 105 °C (bath temp)/0.5 torr; ^1H NMR ($CDCl_3$) δ=1.17 (d, J=7.0 Hz, 3H, $C\underline{H}_3CH$), 1.8—2.1 (m, 2H, $C\underline{H}_2CHCH_3$), 2.3—2.7 (m, 3H, $CH_3C\underline{H}CH_2C\underline{H}_2$), and 3.67 (s, 6H, CH_3O); IR (CCl_4) 1742 (C=O) cm^{-1}.

Methyl 5-Methoxy-2,4-dimethyl-5-trimethylsiloxy-4-pentenoate (29a). Bp 115 °C (bath temp)/0.6 Torr; ^1H NMR ($CDCl_3$) δ=0.19 (s, 9H, CH_3Si), 1.10 (d, J=6.8 Hz, 3H, $C\underline{H}_3CH$), 1.49 and 1.53 (two s, 1:2 ratio, 3H, CH_3C=C), 2.1—2.7 (m, 3H, $C\underline{H}_2C\underline{H}$), 3.48 and 3.52 (two s, 1:2 ratio, 3H, CH_3OC=C), and 3.67 (s, 3H, CH_3OC=O); IR (CCl_4) 1690 (C=C) and 1732 (C=O) cm^{-1}; ^{13}C NMR (C_6D_6) δ=0.0, 0.1, 14.2, 15.0, 16.7, 35.4, 35.7, 38.4, 38.6, 51.0, 56.1, 56.8, 92.0, 92.3, 151.6, 152.3, and 176.5; GC (OV-1, 150 °C) t_R 4.0 and 4.6 min (67:33).

Dimethyl 2,4-Dimethylglutarate (29b). Obtained from **29a** by hydrolysis. ^1H NMR ($CDCl_3$) δ=1.15 and 1.17 (two d, J=6.7 and 6.7 Hz, 6H, $C\underline{H}_3CH$), 1.5—2.2 (m, 2H, CH_2), 2.2—2.8 (m, 2H, $CH_3C\underline{H}$), and 3.67 (s, 6H, CH_3O); IR (CCl_4) 1741 (C=O) cm^{-1}; GC (OV-1, 120 °C) t_R 3.8 and 4.2 min (42:58). Found: C, 57.18; H, 8.72%. Calcd for $C_9H_{16}O_4$: C, 57.43; H, 8.56%.

Methyl 5-Methoxy-2,3,4-trimethyl-5-trimethylsiloxy-4-pentenoate (30a). Bp 120 °C (bath temp)/0.4 Torr; ^1H NMR ($CDCl_3$) δ=0.19 and 0.21 (two s, 9H, CH_3Si), 0.9—1.2 (m, 6H, $C\underline{H}_3CH$), 1.38 and 1.43 (two s, 2:1 ratio, 3H, CH_3C=C), 2.3—2.9 (m, 2H, CH), 3.47, 3.49 and 3.61 (three s, 3H, CH_3OC=C), and 3.67 (s, 3H, CH_3OC=O); IR (CCl_4) 1682 (C=C) and 1732 (C=O) cm^{-1}.

Dimethyl 2,3,4-Trimethylglutarate (30b). Obtained from **31a** by hydrolysis. ^1H NMR ($CDCl_3$) δ=0.8—1.0 (m, 3H, $C\underline{H}_3CHCHC$=O), 1.18 (d, J=7.0 Hz, 6H, $C\underline{H}_3CHC$=O), 1.7—2.0 (m, 1H, $C\underline{H}CHC$=O), 2.2—2.9 (m, 2H, CHC=O), and 3.67 (s, 6H, CH_3O); IR (CCl_4) 1732 (C=O) cm^{-1}.

Diethyl 2,3,3-Trimethylglutarate (31b). Bp 115 °C (bath temp)/0.5 Torr; ^1H NMR ($CDCl_3$) δ=1.07 (s, 6H, $(CH_3)_2C$), 1.12 (d, J=7.0 Hz, 3H, $C\underline{H}_3CH$), 1.25 (t, J=7.0 Hz, 6H, $C\underline{H}_3CH_2$), 2.32 (s, 2H, CH_2C=O), 2.55 (q, J=7.0 Hz, 1H, $CH_3C\underline{H}$), and 4.12 (q, J=7.0 Hz, 4H, $CH_3C\underline{H}_2O$); IR (CCl_4) 1725 (C=O) cm^{-1}. Found: C, 62.29; H, 9.69%. Calcd for $C_{12}H_{22}O_4$: C, 62.58; H, 9.63%.

1-(1-Ethoxycarbonylethyl)-1-[2-ethoxy-2-(trimethylsiloxy)-ethenyl]cyclohexane (32a). Bp 150 °C (bath temp)/0.4 Torr; ^1H NMR ($CDCl_3$) δ=0.20 and 0.25 (two s, 5:1 ratio, 9H, CH_3Si), 1.07 (d, J=7.0 Hz, 3H, $C\underline{H}_3CH$), 1.25 (t, J=7.0 Hz, 3H, $C\underline{H}_3CH_2OC$=O), 1.28 (t, J=7.0 Hz, 3H, $C\underline{H}_3CH_2OC$=C), 1.2—1.8 (br, 10H, $(CH_2)_5$), 2.58 (q, J=7.0 Hz, 1H, $CH_3C\underline{H}$), 3.07 (s, 1H, CH=C), 3.74 (q, J=7.0 Hz, 2H, $CH_3C\underline{H}_2OC$=C), and 4.08 (q, J=7.0 Hz, 2H, $CH_3C\underline{H}_2OC$=O); IR (CCl_4) 1670 (C=C) and 1722 (C=O) cm^{-1}.

1-(1-Ethoxycarbonylethyl)-1-(ethoxycarbonylmethyl)cyclohexane (32b). Obtained from **32a** by hydrolysis. ^1H NMR ($CDCl_3$) δ=1.10 (d, J=7.0 Hz, 3H, $C\underline{H}_3CH$), 1.25 (t, J=7.0 Hz, 6H, $C\underline{H}_3CH_2O$), 1.5 (br, 10H, $(CH_2)_5$), 2.44 and 2.48 (two s, 2H, CH_2C=O), 2.85 (q, J=7.0 Hz, 1H, $CH_3C\underline{H}$), and 4.12 (q, J=7.0 Hz, 4H, $CH_3C\underline{H}_2O$); IR (CCl_4) 1735 (C=O) cm^{-1}. Found: C, 66.71; H, 9.77%. Calcd for $C_{15}H_{26}O_4$: C, 66.64; H, 9.77%.

Methyl 5-Methoxy-2,2,3-trimethyl-5-trimethylsiloxy-4-pentenoate (33a). Bp 120 °C (bath temp)/0.5 Torr; ^1H NMR ($CDCl_3$) δ=0.21 and 0.26 (two s, 5:1 ratio, 9H, CH_3Si), 0.89 (d, J=6.8 Hz, 3H, $C\underline{H}_3CH$), 1.09 and 1.14 (two s, 6H, $(CH_3)_2C$), 2.5—2.9 (m, 1H, $C\underline{H}CH_3$), 3.34 and 3.57 (two d, 5:1 ratio, J=10.0 and 10.0 Hz, CH=C), 3.51 (s, 3H, CH_3OC=C), and 3.67 (s, 3H, CH_3OC=O); IR (CCl_4) 1668 (C=C) and 1725 (C=O) cm^{-1}.

Dimethyl 2,2,3-Trimethylglutarate (33b). Obtained from **33a** by hydrolysis. ^1H NMR ($CDCl_3$) δ=0.91 (d, J=6.7 Hz, 3H, $C\underline{H}_3CH$), 1.13 (s, 6H, $(CH_3)_2C$), 1.7—2.1 (m, 1H, CH), 2.2—2.6 (m, 2H, CH_2), and 3.67 (s, 3H, CH_3O); IR (CCl_4) 1740 (C=O) cm^{-1}. Found: C, 57.18; H, 8.72%. Calcd for $C_9H_{16}O_4$: C, 57.43; H, 8.56%.

Methyl 5-(*t*-Butyldimethylsiloxy)-5-methoxy-3-methyl-4-pentenoate (34a). Bp 135 °C (bath temp)/0.8 Torr; ^1H NMR ($CDCl_3$) δ=0.16 (s, 6H, CH_3Si), 0.96 (s, 9H, $(CH_3)_3CSi$), 1.01 (d, J=6.0 Hz, 3H, $C\underline{H}_3CH$), 2.27 and 2.30 (two d, J=7.8 and 5.8 Hz, 2H, $CHC\underline{H}_2CO$), 2.7—3.2 (m, 1H, $C\underline{H}CH_3$), 3.38 and 3.63 (two d, J=8.6 and 8.6 Hz, CH=C), 3.48 (s, 3H, CH_3C=C), and 3.67 (s, 3H, CH_3C=O); ^{13}C NMR (C_6D_6) δ=−4.1, 22.0, 22.1, 25.1, 27.9, 42.8, 43.1, 50.7, 54.2, 54.6, 80.9, 86.9, 154.1, 156.9, and 172.4; IR (CCl_4) 1668 (C=C) and 1735 (C=O) cm^{-1}.

Found: C, 58.07; H, 9.94%. Calcd for $C_{14}H_{28}O_4Si$: C, 58.29; H, 9.78%.

Dimethyl 3-Methylglutarate (34b). Obtained from **34a** by hydrolysis. ^{1}H NMR ($CDCl_3$) δ=1.03 (d, J=6.0 Hz, 3H, $C\underline{H}_3CH$), 2.37 (br, 5H, $CH_2C\underline{H}C\underline{H}_2$), and 3.70 (s, 6H, CH_3O); IR (CCl_4) 1732 (C=O) cm^{-1}. Found: C, 54.88; H, 8.25%. Calcd for $C_8H_{14}O_4$: C, 55.16; H, 8.10%.

The Tandem Michael-Aldol Reaction of 1, 10, and Benzaldehyde. Al-Mont (0.2 g) in a 20 ml round-bottomed flask was dried at 120 °C and 0.5 Torr for 3 h in an oil bath, and cooled to −78 °C under nitrogen. A solution of **10** (1 mmol) in CH_2Cl_2 (4 ml) was added. After the mixture being stirred for 1 min, a solution of **1** (1 mmol) in CH_2Cl_2 (1 ml) was added at −78 °C. After stirring for 30 min, a solution of benzaldehyde (1 mmol) in CH_2Cl_2 (1 ml) was added at −78 °C. The temperature was raised to 0 °C, and the mixture was stirred for 1 h. After the addition of cold ether (−50 °C, 5 ml), the montmorillonite was filtered off through a Celite pad and washed with ether. The organic layer was evaporated and distilled on a Kugelrohr apparatus to yield the product of **35a** in 80% yield.

Dimethyl 2,3-Dimethyl-4-[α-(trimethylsiloxy)benzyl]-glutarate (35a). Bp 170 °C (bath temp)/0.5 Torr; ^{1}H NMR ($CDCl_3$) δ=−0.08 and −0.05 (two s, 9H, CH_3Si), 0.7—1.3 (m, 6H, $C\underline{H}_3CH$), 1.8—3.1 (m, 3H, $CH_3C\underline{H}C\underline{H}(CH_3)C\underline{H}C{=}O$), 3.3—3.8 (m, 6H, CH_3O), 4.8—5.1 (m, 1H, PhCH), and 7.30 and 7.33 (two s, 5H, C_6H_5); IR (CCl_4) 1732 (C=O) cm^{-1}.

Dimethyl 2,3-Dimethyl-4-(α-hydroxybenzyl)glutarate (35b). Obtained from **35a** by hydrolysis. ^{1}H NMR ($CDCl_3$) δ=0.8—1.5 (m, 6H, $C\underline{H}_3CH$), 1.8—3.2 (m, 4H, $CH_3C\underline{H}C\underline{H}$-$(CH_3)C\underline{H}C{=}O$ and OH), 3.45 and 3.68 (br s, 6H, CH_3O), 4.80—5.25 (m, 1H, PhC$\underline{H}$), and 7.35 (br s, 5H, C_6H_5); IR (CCl_4) 1740 (C=O) and 3520 (OH) cm^{-1}.

Ethyl 2-(3-Trimethylsiloxy-2-cyclohexenyl)propanoate (36a). Bp 135 °C (bath temp)/0.4 Torr; ^{1}H NMR ($CDCl_3$) δ=0.17 (s, 9H, CH_3Si), 1.09 (d, J=6.4 Hz, 3H, $C\underline{H}_3CH$), 1.24 (t, J=7.0 Hz, 3H, $C\underline{H}_3CH_2$), 1.5—2.6 (m, 8H, aliphatic CH), 4.15 (q, J=7.0 Hz, 2H, $CH_3C\underline{H}_2O$), and 4.71 and 4.85 (two br, 1:1 ratio, 1H, CH=C); IR (CCl_4) 1660 (C=C) and 1725 (C=O) cm^{-1}.

Ethyl 2-(3-Oxocyclohexyl)propanoate (36b). Obtained from **36a** by hydrolysis. A mixture of diastereomers (syn: anti=57:43): ^{1}H NMR ($CDCl_3$) δ=1.15 and 1.18 (two d, J=6.4 Hz and 6.4 Hz, 3H, $C\underline{H}_3CH$), 1.28 (t, J=7.0 Hz, 3H, $C\underline{H}_3CH_2$), 1.6—2.6 (m, 10H, aliphatic CH), and 4.16 (q, J=7.0 Hz, 3H, $CH_3C\underline{H}_2O$); IR (CCl_4) 1710 (C=O) and 1730 (C=O) cm^{-1}; GC (PEG-HT, 120 °C) t_R 14.2 min (syn), 14.9 min (anti). The authentic sample of **36b** was prepared by means of $TiCl_4$-mediated reaction[5] of **4** with **21** followed by transesterification.

Methyl 2-Methyl-2-(3-trimethylsiloxy-2-cyclohexenyl)propanoate (37a). Bp 130 °C (bath temp)/0.2 Torr; ^{1}H NMR ($CDCl_3$) δ=0.18 (s, 9H, CH_3Si), 1.11 (s, 6H, CH_3C), 1.4—2.8 (m, 7H, aliphatic CH), 3.68 (s, 3H, CH_3O), and 4.71 (br, 1H, CH=C); IR (CCl_4) 1658 (C=C) and 1725 (C=O) cm^{-1}.

Methyl 2-[3-(*t*-Butyldimethylsiloxy)-2-cyclohexenyl]acetate (38a). Bp 140°C (bath temp)/0.5 Torr); ^{1}H NMR ($CDCl_3$) δ=0.11 (s, 6H, CH_3Si), 0.91 (s, 9H, $(CH_3)_3CSi$), 1.5—2.1 (m, 6H, $C\underline{H}_2C\underline{H}_2C\underline{H}_2$); 2.27 and 2.29 (two d, J=7.8 and 6.2 Hz, 2H, $CH_2C{=}O$), 2.4—2.8 (m, 1H, C$\underline{H}$CH=C), 3.69 (s, 3H, CH_3O), and 4.80 (br, 1H, CH=C); IR (CCl_4) 1662 (C=C) and 1735 (C=O) cm^{-1}.

2-(3-Trimethylsiloxy-2-cyclohexenyl)-3-pentanone (39a). Bp 130 °C (bath temp)/0.2 Torr; ^{1}H NMR ($CDCl_3$) δ=0.16 and 0.18 (s, 9H, CH_3Si), 1.01 (d, J=6.3 Hz, 3H, $C\underline{H}_3CH$), 1.04 (t, J=7.0 Hz, 3H, $C\underline{H}_3CH_2$), 1.4—2.6 (m, 6H, aliphatic CH), 2.44 (q, J=7.0 Hz, 2H, CH_2CH_3), 2.5 (m, 2H, C$\underline{H}$C$\underline{H}$CO), and 4.60 and 4.79 (two br, 62:38 ratio, 1H, C=CH); IR (CCl_4) 1657 (C=C) and 1706 (C=O) cm^{-1}.

4-Methyl-5-phenyl-7-trimethylsiloxy-6-octen-3-one (40a) (Table 4, Entry 5). Bp 155 °C (bath temp)/0.6 Torr; ^{1}H NMR ($CDCl_3$) δ=0.11 and 0.13 (two s, 1:2 ratio, 9H, CH_3Si), 0.78 (t, J=7.3 Hz, 3H, $C\underline{H}_3CH_2$), 0.88 and 1.08 (two d, 1:2 ratio, J=6.7 and 6.7 Hz, 3H, $C\underline{H}_3CH$), 1.73 and 1.79 (two s, 1:2 ratio, 3H, $C\underline{H}_3C{=}CH$), 2.0—2.5 (m, 2H, $CH_3C\underline{H}_2$), 2.7—3.1 (m, 1H, $CH_3C\underline{H}$), 3.92 (t, J=9.3 Hz, 1H, PhCH), 4.55—4.80 (m ,1H, CH=C), and 7.17 (s, 5H, C_6H_5); IR (CCl_4) 1665 (C=C) and 1708 (C=O) cm^{-1}.

5-Methyl-4-phenyl-2,6-octanedione (40b). Obtained from **40a** by hydrolysis. A mixture of diastereomers (syn: anti=31:69). ^{1}H NMR ($CDCl_3$) δ=0.82 (t, J=7.0 Hz, 3H, $C\underline{H}_3CH_2$), 1.09 (d, J=7.0 Hz, 3H, $C\underline{H}_3CH$), 1.97 and 2.00 (two s, 1:2.2 ratio, 3H, CH_3CO), 2.1—2.4 (m, 2H, $CH_3C\underline{H}_2$), 2.4—3.1 (m, 3H, $C\underline{H}_2CHC\underline{H}CH_3$), 3.3—3.8 (m, 1H, PhC$\underline{H}$), and 7.20 (s, 5H, C_6H_5); IR (CCl_4) 1710 (C=O) cm^{-1}; GC (OV-1, 160 °C) t_R 9.1 min (syn), 9.6 min (anti). The authentic sample of **39b** was prepared by means of the $Ph_3C^+ClO_4^-$-mediated reaction of **9** with **22**.[9b]

References

1) Review: E. D. Bergmann, D. Ginsburg, and R. Pappo, *Org. React. (N.Y.)*, **10**, 179 (1959); H. O. House, "Modern Synthetic Reactions," 2nd ed, W. A. Benjamin, Inc., Menlo Park, Ca. (1972), p. 595.

2) a) A. G. Shults and Y. K. Yee, *J. Org. Chem.*, **41**, 4044 (1976); b) C. H. Heathcock, M. A. Henderson, D. A. Oare, and M. A. Sanner, *J. Org. Chem.*, **50**, 3019 (1985); C. H. Heathcock and D. A. Oare, *J. Org. Chem.*, **50**, 3022 (1985) and references cited therein.

3) a) M. Yamaguchi, M. Tsukamoto, and I. Hirao, *Chem. Lett.*, **1984**, 375; b) M. Yamaguchi, M. Tsukamoto, S. Tanaka, and I. Hirao, *Tetrahedron Lett.*, **25**, 5661 (1984).

4) K. Narasaka, K. Soai, Y. Aikawa, and T. Mukaiyama, *Bull. Chem. Soc. Jpn.*, **49**, 779 (1976).

5) C. H. Heathcock, M. H. Norman, and D. E. Uehling, *J. Am. Chem. Soc.*, **107**, 2797 (1985).

6) Y. Kita, J. Segawa, J. Haruta, T. Fujii, and Y. Tamura, *Tetrahedron Lett.*, **21**, 3779 (1980).

7) R. A. Bunce, M. F. Schlecht, W. G. Dauben, and C. H. Heathcock, *Tetrahedron Lett.*, **24**, 4943 (1983); Y. Yamamoto, K. Maruyama, and K. Matsumoto, *Tetrahedron Lett.*, **25**, 1075 (1984); K. Matsumoto, A. Sera, and T. Uchida, *Synthesis*, **1985**, 1.

8) T. V. RajanBabu, *J. Org. Chem.*, **49**, 2083 (1984).

9) a) S. Kobayashi, M. Murakami, and T. Mukaiyama, *Chem. Lett.*, **1985**, 953; b) T. Mukaiyama, M. Tamura, and S. Kobayashi, *Chem. Lett.*, **1986**, 1017.

10) R. D. Clark and K. G. Untch, *J. Org. Chem.*, **44**, 248 (1979).

11) O. W. Webster, W. R. Hertler, D. Y. Sogah, W. B. Farnham, and T. V. RajanBabu, *J. Am. Chem. Soc*, **105**, 5706 (1983).

12) W. R. Hertler, D. Y. Sogah, O. W. Webster, and B. M. Trost, *Macromolecules*, **17**, 1415 (1984).

13) M. Kawai, M. Onaka, and Y. Izumi, *Chem. Lett.*, **1986**, 1581; *idem*, *Bull. Chem. Soc. Jpn.*, **61**, 1237 (1988).

14) M. Onaka, R. Ohno, M. Kawai, and Y. Izumi, *Bull. Chem. Soc. Jpn.*, **60**, 2689 (1987).

15) A preliminary communication: M. Kawai, M. Onaka, and Y. Izumi, *J. Chem. Soc., Chem. Commun.*, **1987**, 1203.

16) At the same time that we reported our preliminary results,[15] a homogeneous catalyst of $Al(OTf)_3$ was successfully applied: N. Minowa and T. Mukaiyama, *Chem. Lett.*, **1987**, 1719.

17) According to our previous investigation on the aldol reaction,[13] Al-Mont showed higher catalytic activity than titanium ion- or proton-exchanged montmorillonite.

18) a) C. Ainsworth, F. Chen, and Y. Kuo, *J. Organomet. Chem.*, **46**, 59 (1972); b) I. F. Lutsenko, Y. I. Baukov, G. S. Burlachenko, and B. N. Khasapov, *J. Organomet. Chem.*, **5**, 20 (1966).

19) As another example of selective 1,4-addition of a silicon-containing nucleophile, the $Bu_4N^+F^-$-mediated reaction of allyltrimethylsilane with ethyl sorbate was reported: G. Majetich, A. M. Casares, D. Chapman, and M. Behnke, *Tetrahedron Lett.*, **24**, 1909 (1983).

20) Entry 2 in Table 2 is the first example of the Michael reaction of a silyl ketene acetal with α,β-unsaturated carbonyl compounds by use of a protic strong acid such as CF_3SO_3H. We also showed that CF_3SO_3H catalyzed the aldol reactions such as silyl enol ethers with aldehydes or acetals.[13]

21) When the Michael reaction of an enone with a silyl enol ether was conducted by use of Ph_3CClO_4, the yellow color of the trityl cation remained during the reaction, and the Michael product was obtained in good yield.

22) The catalytic activity of Al-Mont is dependent on the drying conditions. On heat treatment at higher temperature, the structure of montmorillonite irreversibly changes and the cation-exchange capacity decreases: a) R. E. Grim, "Clay Mineralogy," ed by R. R. Shrock, McGraw-Hill, New York (1953), p. 139; b) A. C. Mathers, S. B. Weed, and N. T. Coleman, "Clays and Clay Minerals," ed by W. O. Milligan, Natl. Acad. Sci., Natl. Research Council, Washington, (1955), Publ. 395, p. 403.

23) A tandem Michael-aldol reaction of an enone was reported by the use of Ph_3CClO_4: S. Kobayashi and T. Mukaiyama, *Chem. Lett.*, **1986**, 221, 1805.

24) G. H. Posner, *Org. React.*, **19**, 1 (1972).

25) No 1,2-adduct was obtained in the reaction between an enone and silyl enol ethers or silyl ketene acetals.[4-9] On the contrary, a competitive 1,2-addition is a serious problem in the Michael reaction of enones with lithium enolates under basic conditions.[1,2]

26) a) H. O. House, L. T. Czuba, M. Gall, and H. D. Olmstead, *J. Org. Chem.*, **34**, 2324 (1969); b) C. H. Heathcock, C. T. Buse, W. A. Kleshick, M. C. Pirrung, J. E. Sohn, and J. Lampe, *J. Org. Chem.*, **45**, 1066 (1980).

27) R. E. Ireland, R. H. Mueller, and A. K. Willard, *J. Am. Chem. Soc.*, **98**, 2868 (1976).

28) a) C. R. Hauser, B.E. Hudson, B. Abramoyitch, and J. C. Shivers, *Org. Synth.*, Coll. Vol. **3**, 143 (1955); b) W. S. Wadsworth, Jr. and W. D. Emmons, *Org. Synth.*, Coll. Vol. **5**, 547 (1973).

29) For a definition of the syn/anti convention, see: S. Masamune, S. A. Ali, D. L. Snitman, and D. S. Garvey, *Angew. Chem., Int. Ed. Engl.*, **19**, 557 (1980).

 © 1988 The Chemical Society of Japan Bull. Chem. Soc. Jpn., 61, 2165—2170 (1988)

Conductance of Electrolytes in Dipolar Aprotic Solvent Mixtures. II. Conductance of Lithium Perchlorate in Mixtures of Ethyl Methyl Ketone and Acetone with *N,N*-Dimethylformamide at 25 °C

M. S. K. Niazi
Department of Chemistry, Quaid-i-Azam University, Islamabad, Pakistan
(Received May 22, 1987)

The electrolytic conductance of $LiClO_4$ has been determined in *N,N*-dimethylformamide (DMF) and its binary mixtures with acetone (Ac) and ethyl methyl ketone (MEK) at 25 °C. Ion association constants (K_A) and limiting molar conductance (Λ_0) were calculated from these data using Fuoss equation with modifications. The K_A values of $LiClO_4$ in these binary mixtures are interpreted in terms of solvent separated ion pairs while in pure Ac and MEK almost contact ion pairs are expected. A comparison is made for Λ_0 and K_A values of this salt in Ac and Ac-DMF mixtures with those obtained by Gill et al. Further, a comparison is made between these results and spectroscopically derived results by others in analogous media. $LiClO_4$ has been found more associated in Ac-DMF solvent system than in the MEK-DMF mixed solvent system.

A large number of conductometric and spectroscopic studies of concentrated solutions of $LiClO_4$ have been carried out in an aprotic solvent systems in various laboratories.[1-4,14] But very few number of precise conductance measurements on dilute solution of this salt in acetone (Ac), *N,N*-dimethylformamide (DMF), and Ac-DMF mixed solvent system are available in literature.[5-7] No literature data have been found about conductance of $LiClO_4$ in ethyl methyl ketone (MEK) and its binary mixtures with DMF at 25 °C.

As a continuation of conductance measurements of electrolytes in dipolar aprotic solvent mixtures,[8] present paper reports conductance of $LiClO_4$ in Ac, MEK, DMF, Ac-DMF, and MEK-DMF binary mixtures in a concentration range 10^{-4}—10^{-2} mol dm^{-3} at 25 °C. The limiting molar conductance (Λ_0) and ion association constant (K_A) were evaluated from the conductance data using the Fuoss equation[10] with modifications. The Bjerrum ion association theory as modified by Fernandez-Prini and Pure[11,12] was also used for derivation of K_A (as K_A^{BFPP}) and ion pair distance parameter *a*. The derived parameters are compared with those obtained by Gill et al. for this salt in Ac-DMF binary mixtures. Further, results of spectroscopic studies of $LiClO_4$ in pure solvents (in Ac and DMF) which are available from literatures[4b,5,13] are discussed for comparison purpose with the present results.

Experimental

Chemicals. Acetone, DMF, and MEK were products of Merck (for synthesis). The procedure for purification of these solvents together with densities ρ, viscosities η, and dielectric constants ε are given in detail in previous papers.[8,9] All solution preparation was carried out in the presence of dry nitrogen gas. The purified solvents contained no more than 0.01% (w/w) water. The mixtures were prepared by weight and are given in Table 1. $LiClO_4$ and KCl were of analytical grade (pure p. a Fluka). They were twice recrystallized from conductivity water, dried in an oven at 170 °C for several days and then dried in vaccum at 70 °C over P_2O_5 and were kept in a desiccator over P_2O_5.

Conductance Measurements. Conductance measurements were carried out using ORION Research Conductivity Meter, Model 101 at 1 kHz. Two 1 dm^3 Kraus-type conductance cells were used, whose cell constants were 1.1538 and 0.1932 cm^{-1} calibrated with aqueous KCl solutions at 25±0.005 °C. The platinized Pt electrodes were used. Further procedure was the same as described earlier.[8] Measurements were carried out in a water bath at 25±0.005 °C and the reproducibility of the conductance measurement was better than ±0.01%. The conductance data are listed in Tables 2 and 3 and are presented in Figs. 1 and 2.

Results

The molar conductance of the salt solutions (listed in Tables 2 and 3) were corrected for the solvent conductances. The Fuoss conductance equation,[10] with modifications was used to evaluate the limiting molar conductance (Λ_0) and the conductometric association constant (K_A) from conductance data using his scan

Table 1. Physical Properties of AC-DMF and MEK-DMF Binary Mixtures at 25 °C

S.No.	DMF/wt%	ε	η/cp[a]	ρ/g cm^{-3}
		Ac-DMF mixture		
1	0.00	20.14	0.300	0.7838
2	3.45	20.62	0.310	0.7890
3	11.50	21.85	0.334	0.8000
4	28.00	24.26	0.383	0.8238
5	36.00	25.44	0.405	0.8363
6	45.00	27.16	0.457	0.8503
7	62.00	29.74	0.514	0.8815
8	82.00	33.47	0.649	0.9141
9	100.00	36.71	0.796	0.9439
		MEK-DMF mixture		
1′	0.00	18.01	0.379	0.7998
2′	5.00	18.80	0.396	0.8045
3′	11.00	19.78	0.411	0.8128
4′	17.00	20.70	0.430	0.8237
5′	28.00	22.49	0.471	0.8445
6′	54.00	27.29	0.560	0.8748
7′	77.00	31.85	0.669	0.9199
8′	86.00	33.77	0.713	0.9235

a) 1cp=10^{-3} Pa s.

Table 2. Molar Concentrations and Conductances of $LiClO_4$ Solutions in AC-DMF Mixtures at 25 °C

Acetone		3.45% DMF		11.50% DMF		28.00% DMF		36.00% DMF	
10^4c	Λ	10^4c	Λ	10^4c	Λ	10^4c	Λ	10^4c	Λ
mol dm^{-3}	S cm^2 mol^{-1}	mol dm^{-3}	S cm^2 mol^{-1}	mol dm^{-3}	S cm^2 mol^{-1}	mol dm^{-3}	S cm^2 mol^{-1}	mol dm^{-3}	S cm^2 mol^{-1}
1.1822	168.836	2.1862	170.354	1.8623	158.888	1.2243	149.666	1.3785	134.908
2.3248	152.629	4.2994	165.122	3.6624	154.585	2.4076	146.624	3.6943	132.133
3.4299	142.372	6.3430	161.283	5.4033	151.485	3.554	144.886	5.4503	130.042
4.4990	134.587	8.3205	158.075	7.0875	148.777	4.6595	142.258	7.1495	128.321
5.5345	128.613	10.3250	155.221	8.7187	146.678	5.7316	140.642	8.7945	126.870
6.5345	123.656	12.0895	153.128	10.2985	144.702	6.7702	139.021	10.3881	125.591
7.5092	119.473	13.8868	150.111	11.8295	143.021	7.7702	138.859	11.9324	124.454
8.4515	115.905	15.6295	149.428	13.3140	141.598	8.7525	136.503	13.4298	123.442
9.3656	112.706	17.3200	147.888	14.7541	140.228	9.6992	135.425	14.8824	122.504
10.2528	110.081	18.9607	146.445	16.1517	139.025	10.6179	134.501	16.2921	121.666
11.2528	107.390	20.5536	145.227	17.5086	137.887	11.6179	133.522	17.9213	120.753
11.9909	105.393	22.1009	143.933	18.8267	136.854	12.3765	132.649	18.9905	120.176
12.7639	103.636	23.6046	142.708	20.1076	135.892	13.2186	132.000	20.2824	119.503
13.5544	101.759	25.0663	141.758	21.3528	135.128	14.0371	131.205	21.5385	118.882
14.3231	100.137	27.8709	140.855	22.5637	134.354	14.8332	130.642	22.7598	118.222
15.0709	98.648	29.2171	139.999	23.7419	133.588	15.6077	130.001	23.9484	117.735
16.5075	96.006	30.5276	139.125	24.8886	132.001	16.3676	129.432	25.1050	117.224
17.1977	95.628	31.8041	138.656	26.3526	131.628	17.0955	128.844		

45% DMF		62% DMF		Pure DMF		82% DMF	
10^4c	Λ	10^4c	Λ	10^4c	Λ	10^4c	Λ
mol dm^{-3}	S cm^2 mol^{-1}	mol dm^{-3}	S cm^2 mol^{-1}	mol dm^{-3}	S cm^2 mol^{-1}	mol dm^{-3}	S cm^2 mol^{-1}
1.7127	129.032	0.9717	107.638	1.9044	75.004	1.5158	86.655
3.3625	126.499	1.9108	106.808	3.7454	73.898	2.9809	85.400
4.9527	124.488	2.8191	104.888	5.5255	73.053	4.5778	84.528
6.4865	122.955	3.6980	104.003	7.2481	72.246	5.7688	83.787
7.9668	121.563	4.5489	103.344	8.9158	71.722	8.3821	82.613
9.3964	120.446	5.3731	102.846	10.5313	71.156	9.6282	82.006
10.7778	119.404	6.1719	102.272	12.0970	70.721	10.8365	81.642
12.1195	118.465	6.9464	101.844	13.6150	70.266	12.0086	81.058
13.4057	117.642	7.6978	101.415	15.0877	69.788	13.1461	80.522
14.6567	116.801	8.4269	101.002	16.5168	69.342	14.2505	80.012
15.8678	116.200	9.1349	100.623	17.9045	69.001	15.3233	79.488
17.0666	115.535	9.8226	99.988	19.2524	68.653	16.3658	78.900
		10.4909	99.333	20.5622	68.349	17.3793	78.384
		11.1405	98.489	21.8355	68.001	18.3649	77.867
		11.6129	97.788	23.0739	67.752	19.3231	77.244
		12.3871	97.212	24.2787	67.482	20.2572	76.849

program[10a] in which R (Gurney cosphere distance) was varied from 3 to 30 Å with increment of 0.2 Å.

K_A for ion pair formation of the type $M^+ + X^- = M^+X^-$ is given by

$$K_A = (1-\gamma)/C\gamma^2 f_{\pm}^2, \quad (1)$$

where $f_{\pm}$ was given by $\exp[-\tau/(1+kR)]$ with $\tau=\beta k/2$ where k^{-1} is the Debye distance, $\beta=e^2/\varepsilon RT$, and other symbols have their usual meanings. The scan program also evaluated σ (standard deviation expressed as a percentage of Λ_0). Plots of σ vs. R showed minima for each solvent mixtures and the derived values of Λ_0 and K_A along with σ and R are given in Tables 4 and 5.

The association constant K^{BFPP} from the Bjerrum ion association theory[11] as modified by Fernandez-Prini and Prue[12] was also evaluated from the following expression

$$K_A^{BFPP} = 4\pi NA \int_{r=a}^{q} \exp[-U(r)/K_BT]r^2 dr, \quad (2)$$

and

$$U(r) = \int_{\infty}^{r} e^2 \cdot dr/\varepsilon' r^2 = e^2 \int_{\infty}^{r_1} dr/\varepsilon r^2 + e^2 \int_{r_1}^{r} dr/\varepsilon' r^2, \quad (3)$$

where q is Bjerrum distance parameter.

In this modification, the association is corrected by introduction of a distance dependent dielectric coefficient ε' replacing the static dielectric constant (ε) of the medium. Booth[23] derived the following expression for the variation of ε' with intensity of electric field

$$\varepsilon' = (3/y)(\varepsilon - n^2)L(y) + n^2, \quad (4)$$

where $y=\beta' Ze/\varepsilon' r^2$, $L(y)$ is the Langevin function, $L(y) = \mathrm{Cot}\ h(y) - 1/y$, and $Ze/\varepsilon' r^2$ is the intensity of electric

Table 3. Molar Concentrations and Conductances of $LiClO_4$ Solutions in MEK-DMF Mixtures at 25°C

Pure MEK		5% DMF		11% DMF		17% DMF	
10^4c	Λ	10^4c	Λ	10^4c	Λ	10^4c	Λ
mol dm^{-3}	S cm^2 mol^{-1}	mol dm^{-3}	S cm^2 mol^{-1}	mol dm^{-3}	S cm^2 mol^{-1}	mol dm^{-3}	S cm^2 mol^{-1}
0.9878	165.078	1.9608	150.136	1.9608	139.312	1.9608	129.022
1.9427	158.053	3.8461	144.062	3.8461	134.754	3.3461	125.441
2.8661	152.736	5.6604	139.582	5.6604	131.342	5.6604	122.694
3.7596	148.422	7.4074	136.030	7.4074	128.600	7.4074	120.457
4.6247	144.804	9.0909	133.075	9.0909	126.301	9.0909	118.668
5.4627	141.688	10.7143	130.568	10.7143	124.316	10.7143	116.987
6.2748	139.001	12.2807	128.477	12.2807	122.602	12.2807	115.502
7.0622	136.564	13.7931	126.456	13.7931	121.043	13.7931	114.232
7.8261	134.408	15.2542	124.753	15.2542	119.882	15.2542	113.0178
8.5674	132.460	16.6666	123.220	16.6666	118.430	16.6666	112.043
9.2872	130.587	18.0328	121.905	18.0328	117.300	18.0328	111.098
9.9863	129.081	19.3548	120.588	19.3548	116.270	19.3548	110.220
10.6658	127.600	20.6349	119.425	20.6348	115.321	20.6349	109.410
11.3262	126.232	21.3750	118.781	21.3750	114.445	21.3750	108.676
11.9686	125.000	23.0769	117.457	23.0769	113.610	23.0769	107.999
12.5935	123.886	24.2424	116.482	24.2424	112.903	24.2424	107.345
13.2018	122.700	25.3731	115.555	25.3731	112.128	25.3731	106.745
		26.2706	114.849	26.2706	111.506	26.2706	106.193
		27.5314	113.222	27.5314	110.905	27.5314	105.657

28% DMF		54% DMF		77% DMF		86% DMF	
10^4c	Λ	10^4c	Λ	10^4c	Λ	10^4c	Λ
mol dm^{-3}	S cm^2 mol^{-1}	mol dm^{-3}	S cm^2 mol^{-1}	mol dm^{-3}	S cm^2 mol^{-1}	mol dm^{-3}	S cm^2 mol^{-1}
1.9608	123.854	1.9608	118.8521	1.9608	96.859	1.9608	85.500
3.8461	120.137	3.8461	114.2111	3.8461	93.284	3.8461	82.715
5.6604	117.586	5.6604	111.568	5.6604	91.036	5.6604	80.585
7.4074	115.241	7.4074	109.555	7.4074	89.285	7.4074	79.238
9.0909	113.006	9.0909	107.121	9.0909	88.176	9.0909	77.956
10.7143	111.586	10.7143	106.103	10.7143	87.034	10.7143	76.834
12.2807	110.132	12.2807	104.889	12.2807	86.003	12.2807	75.723
13.7931	109.211	13.7931	103.522	13.7842	85.135	13.7842	74.688
15.2592	107.867	15.2542	102.285	15.2542	84.276	15.2542	73.601
16.6666	106.999	16.6666	101.200	16.6666	83.358	16.6666	72.702
18.0328	105.878	18.0328	100.285	18.0328	82.488	18.0328	71.811
19.3548	105.003	19.3548	99.376	19.3548	81.693	19.3548	70.928
20.6349	104.355	20.6349	98.433	20.6349	80.888	20.6349	70.037
21.8769	103.853	21.8769	97.621	21.8750	80.001	21.8750	69.254
23.0760	103.021	23.0760	96.831	23.0769	79.205	23.0769	68.600
24.2424	102.285	24.2424	96.100	24.2424	78.531	24.2424	68.000
25.3731	101.573	25.3731	95.452	25.3731	77.866	25.3731	67.418
26.5362	101.003	26.4706	94.833	26.4704	77.214	26.4704	66.805
27.5362	99.582	27.5362	94.304	27.5314	76.666	27.5314	66.233

field in the region r from the charge (Ze). The β' is given by the expression

$$\beta' = (n^2+2)\mu/2K_BT, \quad (5)$$

where n, μ are the refractive index and dipole moment of the medium respectively. The values of n and μ for pure solvents were taken from the literature[24] and for mixture it was supposed that $n_{mix.}=x_1n_1+x_2n_2$ and $\mu_{mix.}=(x_1\mu_1+x_2\mu_2)$ as found in case of other physical properties of these solvent mixtures.[9] Integrals Eqs. 2 and 3 were solved numerically and derived parameters are listed in Tables 6 and 7. In Eq. 2, a is the contact ion-pair distance. All the symbols in Eqs. 2 and 3 are described in detail in original papers.[12a] The values of K_A^{BFPP} were found almost the same as K_A. The values of $U(r)/K_BT$ and a derived from Eqs. 2 and 3 are given in Tables 6 and 7.

The thermodynamic ion pair association constant K_a for the reaction $M^+ + X^- \rightleftarrows M^+X^-$ was calculated from the K_A values using a relationship

$$K_a = (1000\,\rho/M)K_A, \quad (6)$$

where $M/1000\rho$ (dm^3 mol^{-1}) is the molecular volume of the solvent and M is its molecular weight.[10] The free energy of ion pair formation is related with K_a through a relationship

$$\Delta G = -RT \ln K_a. \quad (7)$$

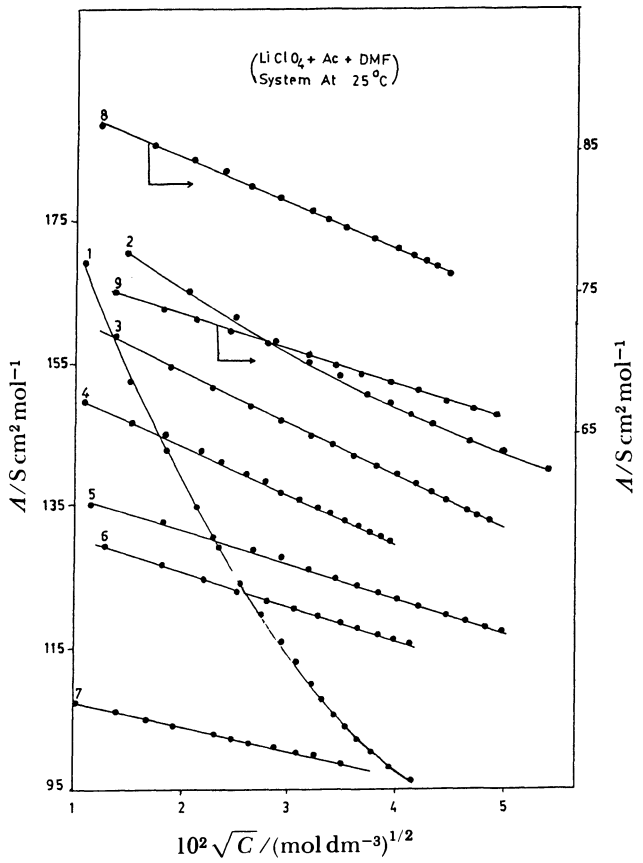

Fig. 1. Dependence of molar conductances of $LiClO_4$ on square root of its concentration in Ac-DMF binary mixtures at 25°C.

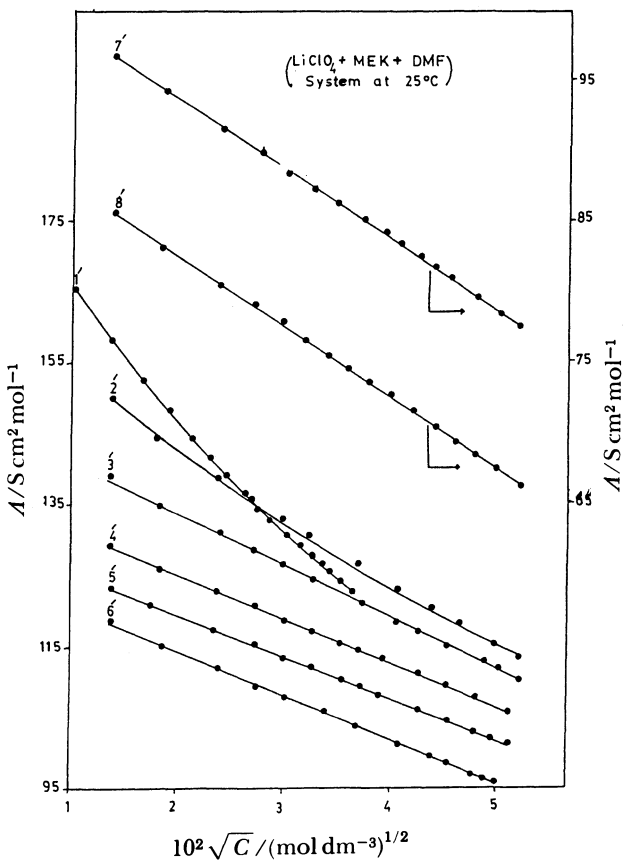

Fig. 2. Dependence of molar conductances of $LiClO_4$ on square root of its concentration in MEK-DMF binary mixtures at 25°C.

Table 4. Conductance Parameters for $LiClO_4$ in Ac-DMF Binary Mixtures at 25°C

DMF	Λ_0	K_A	σ	10^8R
wt%	S cm² mol⁻¹		%	cm
0.00	197.24 ±2.42	1550±255	0.032	15—18
3.45	182.36 ±0.14	540±20	0.021	10—12
11.50	168.32 ±0.16	198±9	0.060	8.6
28.00	155.81 ±0.12	93±4	0.103	8.2
36.00	143.23 ±0.03	55±3	0.033	7.8
45.00	134.00 ±0.04	41±7	0.012	7.4
62.00	110.79 ±0.03	26±4	0.011	6.8
82.00	90.40 ±0.02	17±3	0.005	6.6
100.00	77.24 ±0.18	9±2	0.003	6.00

Table 5. Conductance Parameters for $LiClO_4$ in MEK-DMF Binary Mixture at 25°C

DMF	Λ_0	K_A	σ	10^8R
wt%	S cm² mol⁻¹		%	cm
0.00	178.86±0.63	785±25	0.037	13—15
5.00	163.45±0.55	231±8	0.014	10.8
11.00	155.92±0.13	126±6	0.011	9.4
17.00	149.38±0.39	89±3	0.005	8.6
28.00	137.3 ±0.28	63±5	0.033	7.8
54.00	125.75±0.06	28±4	0.027	7.6
77.00	96.85±0.03	18±3	0.041	6.8
86.00	86.63±0.02	12±2	0.007	6.6

The values of $-\Delta G/RT$ for $Li^+ClO_4^-$-ion-pair formation in the Ac, MEK, DMF, Ac-DMF, and MEK-DMF solvent systems are included in Tables 6 and 7.

Discussion

Limiting Molar Conductances. The Λ_0 ($LiClO_4$) values found for pure Ac, DMF, and MEK in the present work are 197.24, 77.24, and 178.86 $S \cdot cm^2 \cdot mol^{-1}$, respectively, in agreement with values reported in literature.[5-7] No values of Λ_0 for $LiClO_4$ in MEK were available in literature. Comparing with the values of Λ_0 for $LiClO_4$ in Ac and LiBr and LiI in MEK (154 and 147 $S \cdot cm^2 \cdot mol^{-1}$) respectively,[12b] the present value seems to be reasonable. This can be confirmed further by comparing viscosities of Ac and MEK which are 0.300 and 0.379 cp respectively. Addition of DMF either to Ac or to MEK decreased the values of Λ_0 for $LiClO_4$ in the Ac-DMF and MEK-DMF mixed solvent systems (Tables 4 and 5) due to the corresponding increase of viscosities of the mixtures.

The Association Constants. The association constants K_A and K_A^{BFPP} for $LiClO_4$ in Ac-DMF as well as in MEK-DMF showed no significant difference and consequently, only K_A are reported in Tables 4 and 5. These values for $LiClO_4$ in pure Ac, MEK, and DMF derived from conductance data in present work are

Table 6. Parameters Derived for $LiClO_4$ Using Eqs. 2 and 3 and Values of Free Energy Change of Ion-Pair Formation in Ac-DMF Binary Mixtures at 25°C

DMF wt%	K_A^{BFPP}	ε	ε'	$10^8 q$ cm	$10^8 a$ cm	$-U^{(r)}/K_BT$	$-\Delta G/RT$
0.00	1650	20.14	7.42	13.91	3.00	11.26	9.91
3.45	580	20.64	9.69	13.57	3.25	9.68	8.89
11.50	212	21.80	15.38	12.85	3.73	7.35	7.88
28.00	99	24.12	19.77	11.61	4.11	5.86	7.13
36.00	62	25.28	23.21	11.08	4.92	4.58	6.59
45.00	48	26.77	24.83	10.46	5.03	4.21	6.29
62.00	31	29.58	27.55	9.47	5.03	3.81	5.81
82.00	21	33.23	30.35	8.43	4.69	3.65	5.40
100.00	9	36.71	34.87	7.63	5.33	2.90	4.63

Table 7. Parameters Derived for $LiClO_4$ Using Eqs. 2 and 3 and Values of Free Energy Change of Ion-Pair Formation in MEK-DMF Mixture at 25°C

DMF wt%	K_A^{BFPP}	ε	ε'	$10^8 q$ cm	$10^8 a$ cm	$-U/K_BT$	$-\Delta G/RT$
0.00	790	18.01	10.03	15.56	3.66	9.51	9.04
5.00	235	18.95	16.17	14.78	4.72	6.46	7.82
11.00	128	20.07	18.77	13.96	5.66	4.99	7.23
17.00	92	21.19	20.04	13.22	6.04	4.42	6.89
28.00	68	23.25	22.04	12.05	5.76	4.22	6.58
54.00	31	28.11	26.66	9.97	5.54	3.64	5.80
77.00	18	32.41	31.28	8.65	5.93	2.94	5.41
86.00	14	34.00	33.37	8.22	6.12	2.48	5.01

1.5×10^3, 7.9×10^2, and 9 mol^{-1} dm^3, respectively, in agreement with the literature.[5,7,18] But literature survey shows that $LiClO_4$ is almost dissociated in pure DMF. These results have been derived both from spectroscopic as well as conductimetric studies of $LiClO_4$ in DMF. Gill et al. have recently reported the value of K_A for $LiClO_4$ in Ac and DMF, but not reported K_A values in Ac-DMF binary mixtures.[7] Justice[18] has reported the K_A value of 8 mol^{-1} dm^3 for $LiClO_4$ in pure DMF, which is in good agreement with the value 9 ± 2 $mol^{-1}dm^3$ derived in the present work. Tables 4 and 5 show that, as the proportion of DMF increased, the corresponding association constant decreased in both Ac-DMF and MEK-DMF binary solvent systems. This is mainly due to the increase in dielectric constant of the medium with addition of DMF to Ac or MEK.

Comparing the K_A values for $LiClO_4$ in the Ac-DMF and MEK-DMF binary solvent system, it is observed that, despite higher dielectric constant values of the Ac-DMF binary mixtures, $LiClO_4$ is more associated in these mixtures than in the MEK-DMF binary mixtures. Thus, the isodielectric rule is again not valid in the present case. The present results also do not agree with the K_A values of $LiClO_4$ in MEK reported by Milaev.[15] Similar results were found in a previous study on LiCl in these mixed solvent systems.[8] Though MEK has lower dielectric constant, it has a greater polarizability volume than Ac. As pointed out by others[19] the solute-solvent interaction is specific. Both solute and solvent nature (shape, size, polarizability, dipole moment, and refractive index, etc.) are determinative factors for evaluation of the extent of association constant of electrolytes.

Further, the values of the contact ion-pair distance a for $Li^+ClO_4^-$ in pure Ac and DMF have been found to be 3 ± 0.2 and 5.33 ± 0.15 Å, respectively, which are in good agreement with values cited in literature.[5-7] The values of K_A and a in pure Ac, indicate that $LiClO_4$ exists as contact ion pairs; in MEK partial solvent-separated and in DMF almost solvent-separated ion pairs are expected (Tables 6 and 7). But small values of K_A and large values of a of $LiClO_4$ in the Ac-DMF binary solvent system clearly indicate that $LiClO_4$ is almost dissociated in these solvent systems. The value of K_a of $LiClO_4$ in MEK-DMF are smaller than those found in the Ac-DMF solvent system. Also, the values of a of $LiClO_4$ are larger in the MEK-DMF system than those found in the Ac-DMF solvent system. It shows that, the nature of the solvent is an important factor for determining an extent of ionic association. The order of preferential solvation of the Li^+ ion by these solvents is found to be DMF > MEK > Ac. Comparing the present results with those observed by others spectroscopically, in pure Ac[4b] and DMF,[13] an agreement with Popov's results of complete dissociation of $LiClO_4$ in DMF and disagreement with James et al.'s results—postulating no association of $LiClO_4$ in Ac upto 1 mol dm^{-3} concentration were found.

Free Energy Changes of Ion-Pair Formation and Potential Energy Function of Interionic Interaction. The values of ΔG, calculated from $\Delta G^\circ = -RT \ln K_a$

for ($Li^+ClO_4^-$) ion pair formation, become less negative as ε increases or the contents of DMF increase in Ac-DMF and MEK-DMF binary mixtures (Tables 6 and 7). This is because the enthalpic term ΔH in ΔG contains the work done in constituting a contact pair from free ions. The ΔH also contains a positive term due to replacement of nearest neighbor solvent molecule by the partner ion and hence causing a decrease in entropy. Tables 6 and 7 show that for $LiClO_4$—$|\Delta G(MEK)| < |\Delta G(Ac)|$, which is mainly due to larger polarizability volume of MEK than that of Ac and consequently major role of entropy term and decrease of ΔG value of ion-pair formation.

Tables 6 and 7 include the value of ε' —a parameter from dielectric saturation modification, and potential energy function ($U(r)/K_BT$) of interionic interactions. It is observed that the effect of dielectric saturation plays effective role in pure Ac, MEK and in mixtures of Ac-DMF; MEK-DMF, rich in Ac or MEK contents, respectively, for evaluation of K_A and a parameters for $LiClO_4$ in these solvent systems. As the contents of DMF increase in these two mixed solvent systems, the difference of (ε—ε') became less. The same trend is found for potential energy function (P.E.F) of Li^+ ion and ClO_4^- ion interactions. Both, ε' and P.E.F. are interionic distance dependent. Therefore, it can be postulated that Li^+ and ClO_4^- ions are separated by solvent molecules in Ac-DMF and MEK-DMF mixtures.

Gilkerson et al.[20] have recently studied conductimetrically some lithium salts in MEK and 2-proponal respectively. They have discussed their results in terms of the square-mound potential model[21] modification of Bjerrum's theory for ion association. Similarly, Salomon et al.[17] have also studied some lithium salts in dimethylsulfite (DMSI). They have discussed their results on the basis of Barthel's model[22] modification of the Bjerrum theory for ion association. In both above models, non-coulombic interaction term in P.E.F has been introduced. It has been found that in present case of Ac-$LiClO_4$-DMF and MEK-$LiClO_4$-DMF systems, all the three modifications of Bjerrum ion association theory, (i.e. those by Fernandez-Prini and Prue, Justice and Justice's squaremound potential model, and that of Barthel), give almost the same result which indicates that $LiClO_4$ ion pair is solvent-separated. Since it has been found previously a preferential solvation of Li^+ ion by DMF molecules,[7,8] it can be concluded that solvation of Li^+ ion by these solvents is of the order DMF > MEK > Ac.

Finally, it can be concluded that though Ac-DMF and MEK-DMF constitute almost ideal systems,[9,16] the binary mixtures do not act as a single solvent towards an electrolyte. The previous[8] as well as the present studies show that the ion association process depends upon both solvent and solute.

A comparison of above mentioned modifications of the Bjerrum ion association theory, for the systems Ac-LiCl-DMF, MEK-LiCl-DMF, Ac-$LiClO_4$-DMF, and MEK-$LiClO_4$-DMF will be published later on in a near future.

Author is thankful to Prof. O. Fischer of J. E. Purkyne University, BRNO for his useful discussion and guidance.

References

1) Y. Matsuda, M. Morita, and F. Tachihara, *Bull. Chem. Soc. Jpn.*, **59**, 1967 (1986).

2 a) J. Barthel and R. Buchner, *Pure Appl. Chem.*, **58**, 1077 (1986); b) H. J. Gores and J. Barthel, *Nature Wiss. Schaften*, **70**, 495 (1983).

3) a) I. S. Perelygin and V. S. Osipov, *Russ. J. Phys. Chem.*, **53**, 1036 (1979); b) I. S. Perelygin, V. S. Osipov, and S. I. Gryazonv, *Russ. J. Phys. Chem.*, **59**, 1462 (1985).

4) a) R. L. Frost, D. W. James, R. Appleby, and R. E. Mayes, *J. Phys. Chem.*, **86**, 3840 (1982); b) D. W. James and R. E. Mayes, *Aust. J. Chem.*, **35**, 1775 (1982).

5) a) H. C. Brookes, M. C. B. Hotz, and A. H. Spong, *J. Chem. Soc. A*, **1971**, 2410; b) D. F. Evans, J. Thomas, J. A. Nadas, and S. M. A. Mateish, *J. Phys. Chem.*, **75**, 1714 (1971).

6) J. E. Prue and P. J. Sherrington, *Trans. Faraday Soc.*, **57**, 1795 (1961).

7) D. S. Gill and A. N. Sharma, *J. Chem. Soc., Faraday Trans. 1*, **78**, 465 (1982).

8) M. S. K. Niazi, O. Fischer, and E. Fischerova, *J. Solution Chem.*, **15**, 957 (1986).

9) O. Fischer, M. S. K. Niazi, and E. Fischerova, *Electrochimica Acta*, **27**, 791 (1982).

10) a) R. M. Fuoss, *Proc. Natl. Acad. Sci., U.S.A.*, **75**, 16 (1978); **77**, 34 (1980); b) *idem*, *J. Am. Chem. Soc.*, **100**, 5876 (1978); c) *idem*, *J. Solution Chem.*, **15**, 231 (1986).

11) N. Bjerrum and K. Dan Vidensk, *Selsk*, **7**, 1 (1926).

12) a) R. Fernandez-Prini and J. E. Prue, *Trans. Faraday Soc.*, **62**, 1257 (1966); b) R. Fernandez-Prini, "Physical Chemistry of Organic Solvent Systems," ed by A. K. Covington and T. Dickinson, Plenum Press, London (1973), Chap. 5.

13) A. I. Popov, *Pure Apple Chem.*, **47**, 275 (1975).

14) H. A. Berman and T. R. Stengle, *J. Phys. Chem.*, **79**, 1001 (1975).

15) S. M. Milaev, *Russ. J. Phys. Chem.*, **56**, 1816 (1982).

16) P. P. S. Saluja, L. A. Peacock, and R. Fuchs, *J. Am. Chem. Soc.*, **101**, 1958 (1979).

17) E. Plichta, M. Salomon, S. Slane, and M. Uchiyamn, *J. Solution Chem.*, **15**, 663 (1986).

18) J. C. Justice, *Electrochimica Acta*, **16**, 708 (1971).

19) A. D. Aprano and R. M. Fuoss, *J. Solution Chem.*, **3**, 45 (1974); **3**, 363 (1974); **4**, 175 (1975).

20) W. R. Gilkerson and K. L. Kendrick, *J. Phys. Chem.*, **88**, 5352 (1984); H. F. Chun and W. R. Gilkerson, *J. Solution Chem.*, **12**, 161 (1983).

21) J.-C. Justice and M.-C. Justice, *Faraday Disc. Chem. Soc.*, **64**, 265 (1977).

22) J. Barthel, H.-J. Gores, G. Schemeer, and R. Wachter, "Topics in Current Chemistry," Vol. 3, Springer-Verlag Heidelberg (1982), pp. 33—144.

23) F. Booth, *J. Chem. Phys.*, **19**, 391 (1951).

24) "Techniques of Chemistry Vol. II, Organic Solvents," 3rd ed, ed by J. A. Riddick and W. B. Bunger, Wiley-Interscience, New York (1970).

 © 1988 The Chemical Society of Japan Bull. Chem. Soc. Jpn., 61, 2171—2173 (1988)

Ultrasonic Investigation on the Structure of Aqueous Solution of 2-Butanone

T. RAMANJAPPA* and E. RAJAGOPAL
Department of Physics, Sri Krishnadevaraya University, Anantapur-515003, India
(Received June 1, 1987)

The effect of 2-butanone on the temperature corresponding to adiabatic compressibility minimum (TACM), sound velocity maximum (TSVM) and specific acoustic impedance maximum (TSAIM) of pure water has been studied by experimentally determining the sound velocity and density of aqueous solution at different concentrations over a temperature range 34—70.5 °C. The structural contribution to the shift in TACM, TSVM, and TSAIM has been evaluated. The shift is positive throughout the concentration range studied and indicates that 2-butanone is hydrophobic in nature.

The hydrogen-bonded structure of water plays an important role in the nonideal thermodynamic behavior exhibited by aqueous nonelectrolytes. The solution structure of aqueous nonelectrolytes can be understood from the studies on the effect of these solutions on the anomalous behavior exhibited by water such as density maximum at 3.98 °C[1-3] adiabatic compressibility minimum at 64 °C,[4,5,16] sound velocity maximum at 74 °C[6,7,16] and impedance maximum[8] at 56.4 °C etc.

The physicochemical properties of water-2-butanone system has been studied extensively by various workers.[9-11] Roux et al.[9] have studied the concentration dependence of ϕ_C and ϕ_V for this system in the temperature range 4 to 40 °C. The studies on apparant molal volumes ϕ_V of various hydrophobic solutes indicate that ϕ_V decreases with concentration in the water rich region. In general, the more the hydrophobic nature of solute is the more negative would be the initial slope A_V. The apparant molal heat capacities ϕ_C decrease as a function of concentration and the decrease is more important for hydrophobic solutes. The apparant molal expansibilities ϕ_E are positive for such systems.

For water-2-butanone system, Roux et al.[9] observed a slight deviation from the typical behavior at 40 °C. Therefore an attempt has been made in the present investigation to study the temperature effect on the behavior of the solute.

The present paper deals with the studies carried out on the effect of 2-butanone on the temperature corresponding to adiabatic compressibility minimum (TACM), sound velocity maximum (TSVM), and specific impedance maximum (TSAIM) of water in order to see how the hydrophobic character of 2-butanone would change with temperature.

Experimental

Analar grade 2-butanone was used after necessary purification. The purity of the sample was checked by determining the density at 25 °C using a bicapillary pycnometer with an accuracy of 2 in 10^5. The density value, 800.44 kg m^{-3}, is in good agreement with the data available in the literature.[14] Ultrasonic velocity in pure liquid and aqueous solution was determined using a single crystal variable path interferometer working at 3 MHz with an accuracy of ±0.003%. The details of experimental technique were published elsewhere.[12] Ultrasonic velocities and densities were determined at an interval of ca. 2 °C over a temperature range of 34—70.5 °C.

Results and Discussion

The measurements of ultrasonic velocity in and density of aqueous 2-butanone solution as a function of temperature are presented in Table 1. Adiabatic compressibility ($\beta=1/u^2\rho$) and specific acoustic impedance ($z=u\rho$) are evaluated from the experimental data. The template method[12] has been employed to fix TACM, TSVM, and TSAIM with an accuracy of ±0.4 °C, ±0.2 °C, and ±0.3 °C respectively. The ultrasonic

Table 1. u and ρ at Different Temperatures for the System: Water-2-Butanone

t / °C	u / m s^{-1}	ρ / 10^3 kg m^{-3}	t / °C	u / m s^{-1}	ρ / 10^3 kg m^{-3}
	X_2=0.0082			X_2=0.0144	
45.29	1549.18	0.98754	37.83	1551.14	0.98827
47.86	1551.38	0.98640	40.05	1553.21	0.98734
50.07	1553.02	0.98540	42.01	1554.70	0.98650
52.34	1554.46	0.98433	44.13	1556.27	0.98557
54.71	1555.78	0.98319	46.40	1557.57	0.98455
56.97	1556.75	0.98208	48.44	1558.55	0.98362
59.09	1557.39	0.98100	50.78	1559.65	0.98253
61.31	1557.92	0.97985	53.04	1560.33	0.98146
63.93	1558.35	0.97846	55.16	1560.75	0.98043
66.09	1558.37	0.97728	57.58	1561.03	0.97924
68.51	1558.27	0.97593	59.85	1561.07	0.97810
70.53	1558.07	0.97478	61.96	1560.91	0.97700
	X_2=0.0108			X_2=0.0194	
42.97	1550.76	0.98590	34.05	1554.38	0.98636
45.49	1552.72	0.98482	36.72	1556.83	0.98523
48.26	1554.86	0.98358	39.29	1558.69	0.98412
50.43	1556.07	0.98258	41.86	1560.15	0.98298
52.59	1557.21	0.98156	44.23	1561.35	0.98190
54.81	1558.05	0.98049	46.40	1562.07	0.98089
57.23	1558.81	0.97923	48.66	1562.59	0.97982
59.59	1559.25	0.97808	50.78	1562.99	0.97879
61.91	1559.47	0.97687	52.89	1563.11	0.97775
64.18	1559.47	0.97565	55.01	1563.13	0.97669
66.58	1559.38	0.97433	57.33	1562.91	0.97550
68.71	1558.85	0.97314	59.24	1562.55	0.97451

velocity data have been corrected for diffraction effects.[13]

The adiabatic compressibility minimum (T_β) of the solution is given[5,12] by

$$T_\beta = \left[64 - \frac{\phi_2}{\phi_1}\frac{\alpha_\beta}{0.0032}\right]\left[1 + \frac{\phi_2}{\phi_1}\frac{\alpha_\beta^1}{0.0016}\right]^{-1} - \left[\frac{d\beta^E}{dt}\right]\left[1 + \frac{\phi_2}{\phi_1}\frac{\alpha_\beta^1}{0.0016}\right]^{-1}[\phi_1 \times 0.0032]^{-1}, \quad (1)$$

where ϕ_1 and ϕ_2 represent the volume fractions of pure water and organic solute respectively in the solution. α_β and α_β^1 are the constants of organic solute involved in adiabatic compressibility versus temperature relation given by

$$\beta_2 = \beta_2^\circ + \alpha_\beta t + \alpha_\beta^1 t^2. \quad (2)$$

The sound velocity maximum (T_u) of the solution is given[5,15] by

$$T_u = 74 - \left[\frac{\phi_2}{\phi_1}\right]^2 \frac{w_1}{w_2}\frac{\alpha_u}{0.049}\left[\frac{u_1}{u_2}\right]^3 - \frac{w_1}{\phi_1^2}\frac{u_1^3}{0.098}\left[\rho\frac{d\beta^E}{dt} + \beta^E\frac{d\rho}{dt}\right], \quad (3)$$

where w_1 and w_2 represent weight fractions of pure water and organic solute respectively in the solution. α_u is the temperature coefficient of sound velocity in the relation

$$u_2 = u_2^\circ - \alpha_u t. \quad (4)$$

The specific acoustic impedance maximum (T_z) of the solution is given[8] by

$$T_z = -\frac{\frac{7.5603\ w_1}{z_1^3} + \frac{2\alpha_z w_2}{z_2^3}}{\frac{-0.13404\ w_1}{z_1^3} + \frac{4\alpha_z^1 w_2}{z_2^3}} + \frac{\frac{1}{\rho}\left[\frac{d\beta^E}{dt} - \frac{\beta^E}{\rho}\frac{d\rho}{dt}\right]}{\frac{-0.13404\ w_1}{z_1^3} + \frac{4\alpha_z^1 w_2}{z_2^3}}, \quad (5)$$

where α_z and α_z^1 are the temperature coefficients of specific acoustic impedance in the relation

$$z_2 = z_2^\circ + \alpha_z t + \alpha_z^1 t^2 \quad (6)$$

The values of β_2°, α_β, α_β^1, u_2°, α_u, z_2°, α_z, and α_z^1 for 2-butanone are evaluated using the experimentally determined ultrasonic velocity and density data at different temperatures and the values are presented in Table 2.

In Eqs. 1, 3, and 5, first term ($T_{\beta\ \text{or u or z id}}$) represents the dilution effect and second term ($\Delta T_{\beta\ \text{or u or z str}}$) represents the structural contribution. ($\Delta T_{\beta\ \text{or u or z str}}$) can be evaluated experimentally from the relation

$$(\Delta T_{\beta\ \text{or u or z str}})_{\text{exp}} = T_{\beta\ \text{or u or z exp}} - T_{\beta\ \text{or u or z id}}. \quad (7)$$

The results of $(\Delta T_{\beta\ \text{str}})_{\text{exp}}$, $(\Delta T_{\text{u str}})_{\text{exp}}$, and $(\Delta T_{\text{z str}})_{\text{exp}}$ are presented in Table 3.

The variation of $[\Delta T_{\beta\ \text{str}}]_{\text{exp}}$ with mole fraction x_2 of 2-butanone is shown in Fig. 1. From this figure it is clear that the structural shifts are positive throughout the concentration range, indicating that the solute behaves as structure maker.

The concentration dependence of ϕ_C and ϕ_V of 2-butanone have been studied by Roux et al.[9] over a temperature range of 4 to 40 °C. The initial slopes are negative and become less negative as the temperature increases. The initial slopes exhibit a flat minimum around 40 °C. The slight change in the initial slopes

Table 2. Pure Liquid Parameters of 2-Butanone

$\beta_2^\circ/(10^{-11}\,m^2N^{-1})$	74.367
$\alpha_\beta/(10^{-11}\,m^2N^{-1}\,°C^{-1})$	0.3759
$\alpha_\beta^1/(10^{-14}\,m^2N^{-1}\,°C^{-2})$	6.2850
$u_2^\circ/(m\,s^{-1})$	1299.94
$\alpha_u/(m\,s^{-1}\,°C^{-1})$	4.2117
$z_2^\circ/(10^3\,kg\,m^{-2}\,s^{-1})$	1076.90
$\alpha_z/(10^3\,kg\,m^{-2}\,s^{-1}\,°C^{-1})$	−4.9216
$\alpha_z^1/(kg\,m^{-2}\,s^{-1}\,°C^{-2})$	4.916

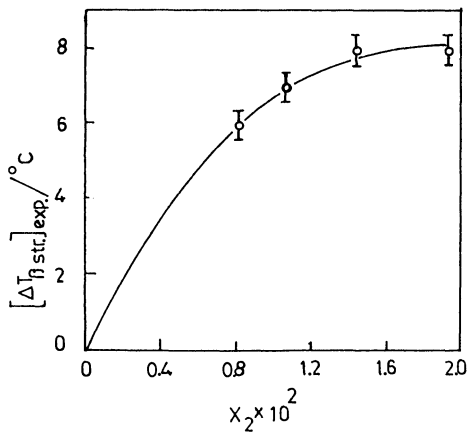

Fig. 1. Variation of $[\Delta T_{\beta\ \text{str}}]_{\text{exp}}$ with mole fraction (X_2) of 2-butanone.

Table 3. Experimental and Theoretical Values of ($\Delta T_{\beta\text{str}}$), ($\Delta T_{\text{u str}}$) and ($\Delta T_{\text{z str}}$) at Different Mole Fractions for the System: Water-2-Butanone

X_2	$(\Delta T_{\beta\ \text{str}})_{\text{exp}}$ °C	$(\Delta T_{\beta\ \text{str}})_{\text{th}}$ °C	$(\Delta T_{\text{u str}})_{\text{exp}}$ °C	$(\Delta T_{\text{u str}})_{\text{th}}$ °C	$(\Delta T_{\text{z str}})_{\text{exp}}$ °C	$(\Delta T_{\text{z str}})_{\text{th}}$ °C
0.0082	5.9±0.4	5.4	7.2±0.2	9.8	5.0±0.3	4.2
0.0108	6.9±0.4	6.1	8.2±0.2	11.5	5.6±0.3	5.2
0.0144	7.9±0.4	6.7	8.9±0.2	13.3	5.9±0.3	6.2
0.0194	7.9±0.4	7.0	9.2±0.2	14.5	6.2±0.3	7.2

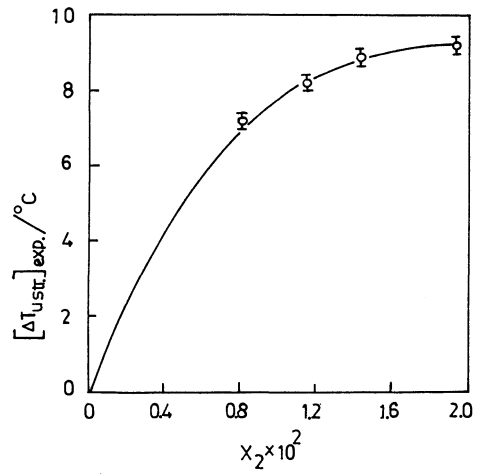

Fig. 2. Variation of $[\Delta T_{u\ str}]_{exp}$ with mole fraction (X_2) of 2-butanone.

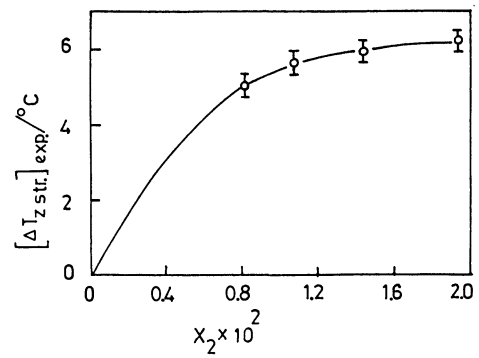

Fig. 3. Variation of $[\Delta T_{z\ str}]_{exp}$ with mole fraction (X_2) of 2-butanone.

as a function of temperature still indicate the hydrophobic character of 2-butanone (the initial slope A_V at 40 °C is -0.11 cm^3 mol^{-2} kg).

$[\Delta T_{u\ str}]_{exp}$ (Fig. 2) is positive for 2-butanone and the magnitude is found to increase with increase in the concentration, indicating structural promoting nature of solution.

The variation of $[\Delta T_{z\ str}]_{exp}$ with mole fraction x_2 is shown in Fig. 3. $[\Delta T_{z\ str}]_{exp}$ is positive and increases with increase in concentration. This trend also confirms hydrophobic character of 2-butanone. From these studies, one can infer that 2-butanone is hydrophobic throughout the temperature range of the present study.

References

1) G. Wada and S. Umeda, *Bull. Chem. Soc. Jpn.*, **35**, 646 (1962).
2) G. Wada and S. Umeda, *Bull. Chem. Soc. Jpn.*, **35**, 1979 (1962).
3) M. Sakurai, T. Komatsu, and T. Nakagama, *Bull. Chem. Soc. Jpn.*, **45**, 1038 (1972).
4) S. V. Subrahmanyam and N. Manohara Murthy, *J. Solution Chem.*, **5**, 405 (1976).
5) N. Manohara Murthy and S. V. Subrahmanyam, *Can. J. Chem.*, **56**, 2412 (1978).
6) S. V. Subrahmanyam and N. Manohara Murthy, *Z. Phys. Chem. (Neue Folge)*, **88**, 116 (1974).
7) N. Manohara Murthy and S. V. Subrahmanyam, *J. Acoust. Soc. India*, **7**, 79 (1979).
8) T. Ramanjappa, "Ultrasonic Studies in Liquids and Solutions" Ph. D. Thesis submitted to Sri Krishnadevaraya University, Anantapur, India (1985).
9) G. Roux, G. Perron, and J. E. Desnoyers, *Can. J. Chem.*, **56**, 2808 (1978).
10) L. Bφje and A. Hvidt, *J. Chem. Thermodyn.*, **3**, 663 (1971).
11) J. T. Edwards, P. G. Farrell, and F. Shahidi, *J. Chem. Soc., Faraday Trans. 1*, **73**, 705 (1977).
12) S. V. Subrahmanyam and N. Manohara Murthy, *J. Solution Chem.*, **4**, 347 (1975).
13) S. V. Subrahmanyam, V. Hyderkhan, and C. V. Raghavan, *J. Acoust. Soc. Am.*, **46**, 272 (1969).
14) O. Kiyohara and G. C. Benson, *J. Chem. Thermodyn.*, **9**, 315 (1977).
15) N. Manohara Murthy and S. V. Subrahmanyam, *Bull. Chem. Soc. Jpn.*, **50**, 2589 (1977).
16) K. Subbarangaiah, N. Manohara Murthy, and S. V. Subrahmanyam, *Bull. Chem. Soc. Jpn.*, **54**, 2200 (1981).

 © 1988 The Chemical Society of Japan Bull. Chem. Soc. Jpn., 61, 2175—2179 (1988)

Electrophoresis of Progesterone Particles Dispersed in Aqueous Solutions of D-Glucose and Urea

M. L. SRIVASTAVA* and Bali RAM†
Department of Chemistry, University of Gorakhpur, Gorakhpur-273001, India
†Department of Chemistry, College of Basic Sciences and Humanities, G. B. Pant University of Agriculture and Technology, Pantanagar-263145, Nainital, India
(Received June 15, 1987)

Electrophoretic mobilities of progesterone particles dispersed in aqueous solutions of D-glucose and urea, in the concentration range 10^{-3}—10^{4} mol l^{-1} have been measured to investigate electrical properties of the interface. Zeta potentials have been determined for this purpose. The dependence of zeta potentials on concentration has also been examined. Theory of the electrical double layer has been used to explain the results.

Electrophoresis is a subject of interest in many branches of pure and applied science, playing an important role in matters as diverse as clinical diagnosis and study of colloid stability. It plays significant roles in clay technology, water purification, detergency, ore floatation, electrodeposition and is extensively used for the fractionation and analysis of proteins, nucleic acids, polysaccharides and other complex substances of biological interest and activity.[1-3] In our earlier papers[4-6] we have reported results on the electrophoresis of testosterone (a male sex hormone) particles dispersed in aqueous solutions of electrolytes (e.g. NaCl, KCl, and $MgCl_2$), nonelectrolyte (e.g. urea) and carbohydrate (e.g. D-glucose) to characterize the electrified testosterone-permeant interface. Such studies with other hormones are highly desirable. Progesterone, a female sex hormone, responsible for normal development of female sex organs and for the maintenance of secondary sex characteristics[7] has been chosen for this purpose. The characteristic biochemical and physiological effects of this hormone depends to a large extent on the properties of hormone/solution interface. A comprehensive physicochemical study with respect to progesterone interface in different type of nonelectrolytic solutions is thus needed for an understanding of the various facets of its functions.

Electroosmotic studies on progesterone-carbohydrate and progesterone-urea systems have been reported quite recently.[8] In order to supplement these studies, the electrophoresis of progesterone particles dispersed in aqueous solutions of D-glucose and urea which are of great metabolic relevane and medicinal utility[9] is being reported in the present communication

Experimental

(a) Materials and Suspensions. Progesterone obtained from Sigma Chemical Company (Saint Louis, U.S.A.) was used. AR grade samples of D-glucose and urea obtained from BDH (India) were employed as such without further purification.

Solutions of D-glucose and urea were prepared in doubly distilled water, redistilled over $KMnO_4$, having specific conductance of the order of 10^{-6} mho cm^{-1}. Suspensions were prepared by homogenizing finely grounded particles of progesterone in these solutions.

(b) Measurement of Electrophoretic Velocity. Measurements of electrophoretic velocities were made using an experimental cell shown in Fig. 1. Progesterone particles were pulverized and suspensions of these particles were prepared in the various solutions. Care was taken to obtain a fairly stable suspension. The experimental cell was fixed in a vertical position. The suspension was introduced into the experimental cell through K by opening the stopcock S, till half of the tube was filled. The stopcock S was then closed and the pure solvent/solution was gently filled in the remainder of the tube PQ so that a distinctly sharp boundary B, was formed. The diameter of the tube PQ was 0.35

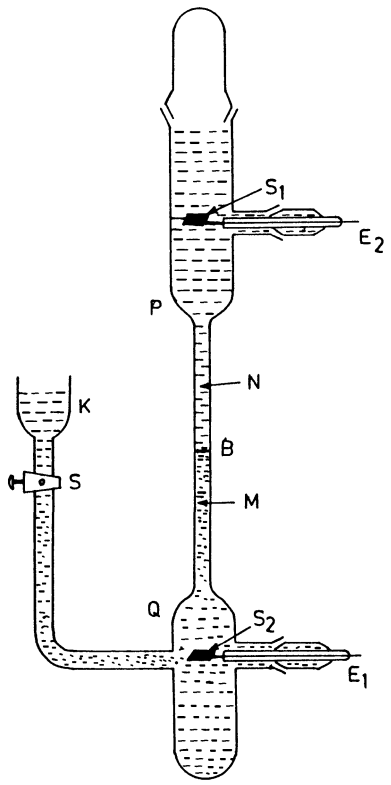

Fig. 1. Apparatus for measurement of electrophoretic velocity, S_1 and S_2 are silver plates coated with silver chloride; E_1 and E_2 are the silver wires attached with S_1 and S_2. S is the stopcock, B; boundary, K; wide mouth side tube for introducing the suspension. M; suspension, N; solvent/solution.

cm. Potential differences up to 50 volts were applied through silver-silver chloride electrodes E_1 and E_2, 15.1 cm apart, with an electronically operated power supply (HIL, India) in such a way that the movement of boundary occurred in the downward direction. The downward displacement of boundary was observed with a cathetometer reading up to ±0.001 cm. The position of boundary at various time intervals was noted and the rate of movement of boundary/electrophoretic velocity was thus determined. Corrections were made for downward movement due to the action of gravitational force. This was done by plotting the observed electrophoretic velocity against applied potential difference. The intercept on the ordinate gives the rate of suspended progesterone particles due to gravity alone. The movement of the boundary was found to occur from anode to cathode. All measurements were made in an air thermostat maintained at 25±0.5 °C.

Results and Discussion

The data on electrophoretic velocities, presented in Figs. 2 and 3, have been corrected by taking sedimentation velocities into account.

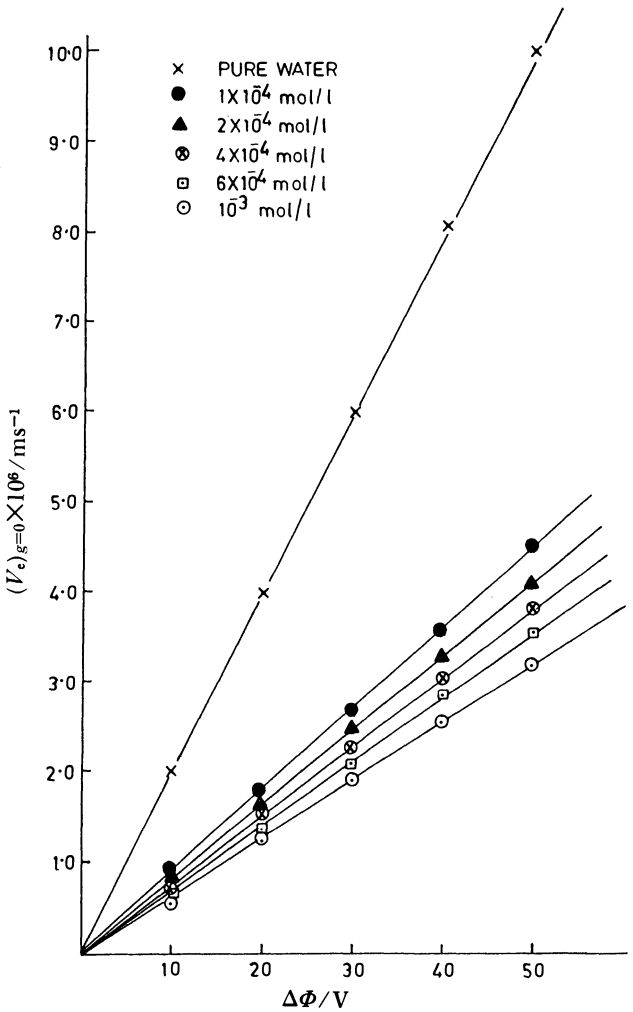

Fig. 2. Dependence of electrophoretic velocity $(V_e)_{g=0}$ on the applied potential difference, $\Delta\Phi$; for progesterone particles dispersed in aqueous solutions of D-glucose of different concentrations. (—×—) Pure water; (—●—) 1×10⁻⁴, (—▲—) 2×10⁻⁴, (—⊗—) 4×10⁻⁴, (—⊡—) 6×10⁻⁴, (—⊙—) 10⁻³ mol l⁻¹.

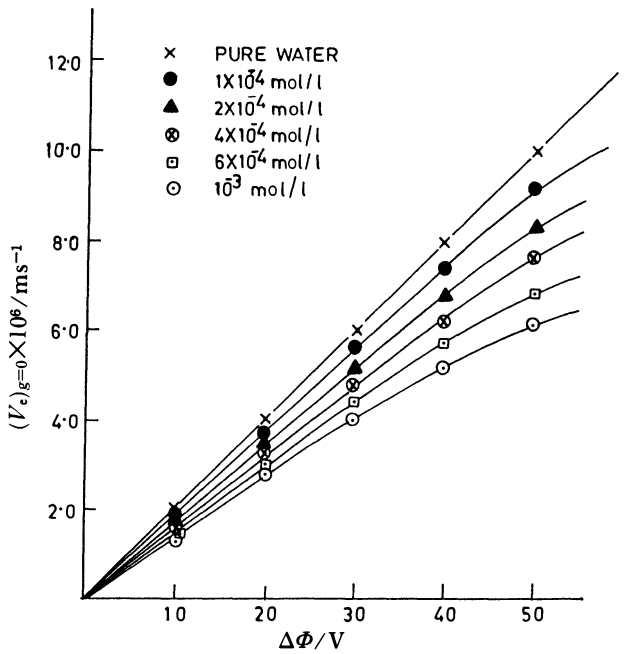

Fig. 3. Dependence of electrophoretic velocity $(V_e)_{g=0}$ on the applied potential difference, $\Delta\Phi$; for progesterone particles dispersed in aqueous solutions of urea at of different concentrations. (—×—) Pure water; (—●—) 1×10⁻⁴, (—▲—) 2×10⁻⁴, (—⊗—) 4×10⁻⁴, (—⊡—) 6×10⁻⁴, (—⊙—) 10⁻³ mol l⁻¹.

The following nonlinear second-order phenomenological equation has been found to satisfy the experimental data in case of progesterone-urea systems

$$(V_e)_{g=0} = L_{12}^* \left(\frac{\Delta\Phi}{T}\right) + \frac{1}{2} L_{122}^* \left(\frac{\Delta\Phi}{T}\right)^2, \quad (1)$$

However, in the case of progesterone-D-glucose systems, $(V_e)_{g=0}$ is found to be linearlity dependent on $\Delta\Phi$ (cf. Fig. 2) satisfying the euqation

$$(V_e)_{g=0} = L_{12}^* \quad (2)$$

with

$$\frac{L_{12}}{T} = \frac{\varepsilon\zeta_{e.p.}}{4\pi\eta l'} . \quad (3)$$

Here L_{12}^* and L_{122}^* are the first and second order electrophoretic transport coefficients respectively, ε is the dielectric constant of the medium, $\zeta_{e.p.}$ is the electrokinetic potential (or zeta potential), η is the coefficient of the viscosity of medium, and l' is the distance between the two electrodes in the electrophoretic cell.

According to Eq. 1 a plot of $(V_e/\Delta\Phi)$ against $\Delta\Phi$ yields a straight line as shown in Fig. 4.

The slope gives L_{122}^* and the intercept L_{12}^* for progesterone-urea systems. The value of L_{12}^* for progesterone-D-glucose system was obtained from the slope of linear plots of Eq. 2. The values of L_{12}^* and L_{122}^* evaluated in this way are recorded in Table 1.

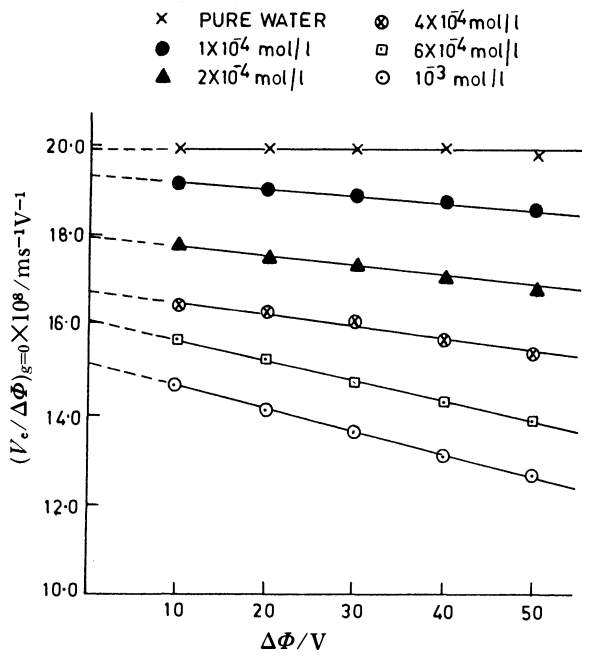

Fig. 4. Test of the applicability of the second order phenomenological equation (Eq. 1) for progesterone/aqueous urea solution systems.
(—×—) Pure water; (—●—) 1×10⁻⁴, (—▲—) 2×10⁻⁴, (—⊗—) 4×10⁻⁴, (—⊡—) 6×10⁻⁴, (—⊙—) 10⁻³ mol l⁻¹.

Evaluation of Zeta Potential. Electrophoresis, an electrokinetic phenomenon, is directly related to the nature of the mobile part of the electrical double layer, and may, therefore, only be interpreted in terms of zeta potential or the charge density at the surface of shear. Since no direct information is given about the charge density at the surface of the particles, only the zeta potential can give better information regarding the electrical nature of progesterone particles. Hence zeta potential was evaluated from the electrophoretic flux data by using the following equation.[5]

$$\zeta_{e.p.} = \frac{4\pi\eta l'}{\varepsilon} \times \left(\frac{L_{12}^*}{T}\right) \times 9 \times 10^4 \quad \text{volts} \qquad (4)$$

The occurrence of electrophoretic movement towards the cathode is an indication that an electrical double layer is formed at the surface of progesterone particles dispersed in these solutions due to adsorption of ions

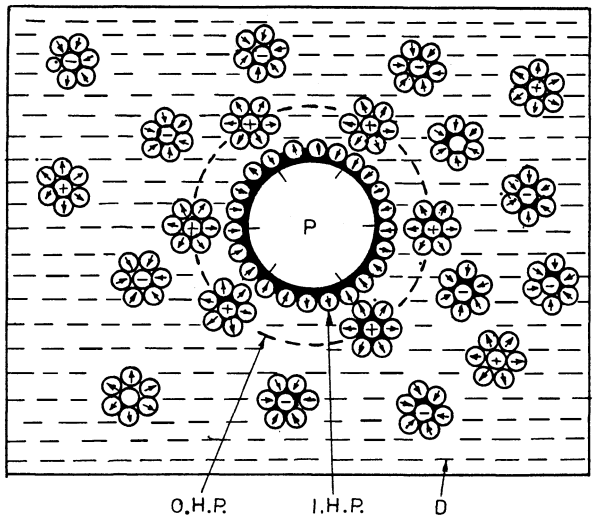

Fig. 5. Postulated picture of the electrical double layer at the progesterone/solution interface:
P=progesterone particle
D=diffused part of the electrical double layer

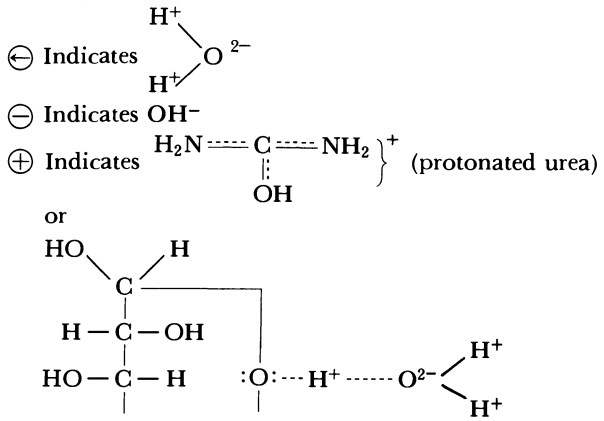

Glucose molecule surrounded with water molecules.

particularly cations (protonated urea and glucose) as shown in Fig. 5. From the schematic representation of the electrical double layer it is evident that all the progesterone particles bear a net positive charge facilitating their movement towards cathode when potential differences, $\Delta\Phi$, are imposed.

Origin of Nonlinearity. The nonlinear dependence of electrophoretic velocity, $(V_e)_{g=0}$ on applied electrical potential difference $\Delta\Phi$, for progesterone-urea system indicates that significant polarization of the electrical

Table 1. Phenological Coefficients and Zeta Potentials

$C\times10^4$ / mol l⁻¹	$\frac{L_{12}^*}{T}\times10^8$ / ms⁻¹V⁻¹K⁻¹		$\frac{1}{2}\frac{L_{122}^*}{T^2}\times10^{10}$ / ms⁻¹V⁻²K⁻²	$\zeta\times10^3$ / V	
	D-Glucose	Urea	Urea	D-Glucose	Urea
0.0	19.98	19.92	0.00	39.5	39.4
1.0	8.96	19.28	−1.67	15.98	34.3
2.0	8.31	17.93	−2.12	14.88	32.2
4.0	7.56	16.74	−2.67	13.86	30.0
6.0	7.16	16.10	−4.41	13.27	28.9
10.0	6.44	15.18	−5.00	12.48	27.3

double layer has occurred during electrophoresis, since water and urea both have permanent dipole moments (μ_{urea}=4.56D, μ_{H_2O}=1.85D). The polarizability α, may be represented as Ref. 10a

$$\alpha = \alpha_o + \alpha_\mu, \tag{5}$$

where α_o is the distortion polarizability and α_μ is the orientation-polarizability. The orientation-polarizability defined by[10b]

$$\alpha_\mu = \frac{\mu^2}{3kT}, \tag{6}$$

arises from the tendency of the permanent dipole moments to be oriented in the direction of the applied field.

Further, the polarizability α, is also dependent on the dipole moment that water and urea molecules acquire in an electric field $\Delta\Phi$, by the relation.[11]

$$\alpha = \frac{\mu}{\Delta\Phi} \tag{7}$$

Rastogi and Shabd[12] used Bockris[13] model of the electrical double layer for explaining the nonlinearity in electroosmotic measurements. According to them the zeta potential is regarded to be made up of two terms, $\Delta\psi$ the charge contribution potential and $\Delta\chi$, the dipolar contribution potential i.e.

$$\zeta = \Delta\psi + \Delta\chi_{eff} \tag{8}$$

with

$$\Delta\chi_{eff} = \Delta\chi_{H_2O} + \Delta\chi_{urea}. \tag{9}$$

The applied electrical potential may affect either of these contributions.

Similar considerations apply even in the case of electrophoresis. The electrical double layer around the particle is considered to be formed on account of —(i) uneven distribution of ions produced by the partial ionization of the dissociable groups of the particle itself, (ii) self dissociation of the solvent molecules, and (iii) preferential orientation of the adsorbed solvent dipoles at the particle surface.

However, the possibility of dissociation of progesterone particles under the influence of applied electrical potential does not exist.

Bockris, Devanathan, and Muller have taken into account the competition between the molecules of water and an organic substance for a site in the double layer and have emphasized the role of charge dependent orientation of water dipoles at the interface.[14] The charge on the particle will stimulate the water molecules to orient themselves (charge implies fields and dipoles tend to align with fields), resulting a water layer of oriented water dipoles at the surface. However, it must not be imagined that the water molecules are unaffected by the presence of their neighbors (urea molecule in this case). After all dipoles interact with dipoles; hence, the oriented water molecules experience lateral interaction — a phenomenon which

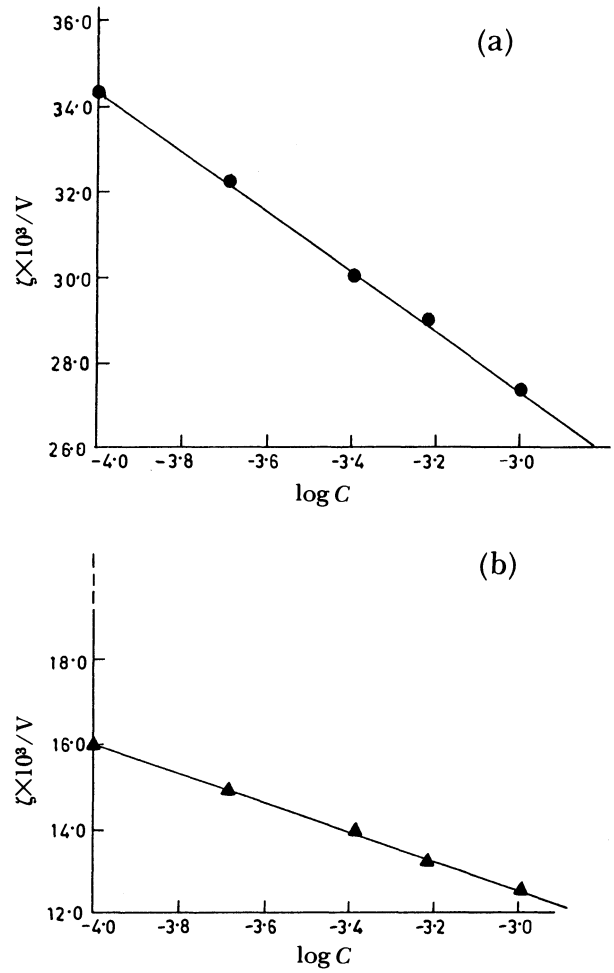

Fig. 6. Dependence of zeta potential (ζ) on log C for progesterone/aqueous solutions of urea (a); D-glucose (b).

affects the number of water molecules oriented in one direction and therefore the value of dipole potential $\Delta\chi$. Through, $\Delta\chi$, the potential difference across the interface and the structure of the interface will be affected. Thus the observed nonlinear variation of electrophoretic velocity and hence the ζ potential may be attributed to the enhanced dipolar contribution when $\Delta\Phi$ is varied. In addition, pronounced nonlinearity is observed at higher concentrations owing to strong interactions.

Zeta potential varies nonlinearly with concentration. However, the following linear equation[5,6] satisfies the dependence of zeta potential on log C.

$$\zeta = A - B \log C \tag{10}$$

where A may be taken as approximately constant for the conditions under which the charge on the membrance surface does not change sign and B is another constant which depends on topography of the surface. The results are shown in Fig. 6.

The authors are grateful to Prof. S. C. Tripathi, Head, Chemistry Department, University of Gorakhpur

for provoiding laboratory facilities, One of us (Bali Ram) is also grateful to CSIR, New-Delhi (India) for the award of a Senior Research Fellowship

References

1) M. W. Lisse, "Biocolloids," Edwards Brothers, Inc. Ann. Arbor, Michigan (1930).

2) M. Bier, "Electrophoresis (Theory, Methods and Applications)," Academic Press, New York (1959).

3) D. J. Shaw, "Electrophoresis," Academic Press, London (1969).

4) M. L. Srivastava and R. Bali, *J. Memb. Sci.*, **19**, 137 (1984).

5) M. L. Srivastava and R. Bali, *J. Carbohydr. Res.* **132**, 209 (1984).

6) M. L. Srivastava and R. Bali, *J. Non-Equilib. Thermodyn.*, **10**, 52 (1985).

7) J. M. Orten and O. W. Neuheus, "Biochemistry," The C. V. Mozby Company, Saint Louis (1970), pp. 500—501.

8) M. L. Srivastava and R. Bali, *J. Memb. Sci.*, (Communicated).

9) C. O. Wilson, O. R. Gisvold, "F. Text Book of Organic Medicinal and Pharmaceutical Chemistry," 6th ed, J. B. Lippincott Company Phildelphia, Toronto, pp. 190, 602, 856—858.

10) a) G. W. Castelian, "Physical Chemistry," 2nd ed, Addison Wesley Publishing Company, Amsterdam (1980), p. 612; b) *ibid.*, p. 613.

11) A. Levy Robert "Principles of Solid State Physics," Academic Press, Inc., New York (1968), p. 151.

12) R. P. Rastogi and S. Ram, *J. Phys. Chem.*, **81**, 1953 (1977).

13) J. O'M. Bockris and A. K. Reddy, "Modern Electrochemistry," Vol. 2, Plenum Press, New York (1970), p. 781.

14) L. T. Antropov, "Theoretical Electrochemistry," Mir Publishers, Moscow (1972), p. 263.

Ion-Exchange Properties of Niobium(V) Materials. II. Synthesis and Characterization of Crystalline Niobium(V) Phosphate

Mohsin QURESHI,* Jai Prakash GUPTA,†† Hina KHAN, and Anees AHMAD†
Chemistry Section, Z. H. College of Engg. and Technology, Aligarh Muslim University, Aligarh 202002, India
†Analytical Laboratory, Chemistry Department, A.M.U. Aligarh 202002, India
(Received February 9, 1987)

An attempt has been made to synthesize and characterize the crystalline niobium(V) phosphate. The characterization was done on the basis of pH titration, X-ray, XPS, TGA, DSC, and IR studies. It is an ion exchange material which shows about 20% higher chemical stability over the amorphous niobium(V) phosphate. It was found to have a pseudocubical unit cell structure with a_0(H)=10.244 Å and a stiff three dimensional zeolytic structure. The empirical formula of the compound was obtained as $Nb_2O_5 \cdot 1.5\ P_2O_5 \cdot 7.5\ H_2O$. The proposed chemical formula is $(NbO)_2(HPO_4)_3 \cdot 6H_2O$ (d_{110}=7.23 Å). The exchanger is monofunctional in nature having the maximum exchange capacity of 4.6 meq g^{-1} for potassium ion at pH 8.5

During the last few years some niobium and tantalum based inorganic ion exchangers have been systhesized and their ion-exchange properties and analytical applications have been explored.[1-8] The exchangers were mostly amorphous or poorly crystalline. These studies suffer from the fact that the gels used were poorly characterized and/or the correct exchange capacity was not determined. In order to obtain thermodynamically meaningful results, the gel has to be well characterized.[9] Qureshi et al.[3] showed for the first time that when niobium antimonate is refluxed with mother liquor, its ion exchange behavior becomes more reproducible. Clearfield et al.[9] refluxed a precipitated gel of zirconium phosphate for 48 h in 0.5 M (M=mol dm^{-3}) phosphoric acid. These refluxed gels were more resistent to hydrolysis and their behavior was more reproducible than that of unrefluxed gels.

It is worthwhile to study the crystalline materials in detail as these materials show a more reproducible behavior and hence they can be used for the mechanistic studies. It is rather difficult to locate the exact exchange sites in amorphous materials and very little information exists regarding the structural aspects of amorphous inorganic ion exchangers. Further the amorphous materials show a greater tendency towards hydrolysis than the corresponding crystalline materials.

In this paper the results on the preparation and characterization of the crystalline niobium(V) phosphate are presented. Its structural properties have been elucidated on the basis of TGA, DSC, IR, XPS, and X-ray diffraction studies. An attempt has also been made to investigate the mechanism of ion exchange of alkali metal ions on this material and to locate the possible exchange sites.

Experimental

Reagents and Synthesis. Diniobium pentaoxide was obtained from BDH (Poole, England). All other reagents of analytical reagent grade were used.

Niobium solution (0.1M)[12] was prepared by dissolving calculated amount of Nb_2O_5 in concd H_2SO_4 in presence of sufficient amount of $(NH_4)_2SO_4$. The crystalline niobium(V) phosphate has been synthesized by mixing niobium solution (0.1M) and phosphoric acid (0.5M) in the volume ratio of 1:4. The pH of this mixture was adjusted to 1 with concentrated ammonia solution. The precipitate so obtained was left with mother liquor for 24 h. Then it was filtered and washed with dimineralized water until the filtrate was neutral to litmus and free from SO_4^{2-} ions. The gel was dried at 45 °C in an oven and then refluxed with 1M H_3PO_4 for 10 h. The exchanger was again washed and dried and stored over saturated solution of $BaCl_2$. It is partially in H^+-form and hence designated as C-NbPx. For ion-exchange studies, C-NbPx was converted completely into H^+-form by the batch method of Townsend[23] using 1M HNO_3. The sample will hereafter be referred to as C-NbP-H^+ in the H^+-form and C-NbP-M^+ (M^+=Li^+, Na^+, K^+ etc.) in the metal form.

Ion-Exchange Capacity. The breakthrough capacity measurements for Li^+, Na^+, Rb^+, and Cs^+ were done by the column elution method[13] using a column of 0.5 cm (i.d.). The feed (0.5 M) was passed until its pH became equal to that of the effluent collected. The hydrogen ions so eluted were titrated against standarized 0.1 M NaOH.

Composition and Chemical Stability. The exchanger was analyzed for the presence of niobium and phosphorus gravimetrically while its chemical stability in different solvents was checked spectrophotometrically using Bausch and Lomb Spectronic-710 spectrophotometer by the methods described earlier.[12]

Thermal Analysis. The TGA was performed by using 0.1 g sample. The heating was done in the atmosphere of air at the rate of 10 °C min^{-1}. The DSC was recorded in the atmosphere of helium at a flow rate of 200 ml min^{-1} and a heating rate of 10 °C min^{-1}. The results are given in Figs. 2(a) and 2(b). DuPont Thermal Analysers Model 950 and 900 were used for TGA and DSC studies respectively.

Water Absorption. The sample in H^+-form (0.5 g) was heated at 120 °C for 24 h in a covered silica crucible. It was then stored in a desiccator over a saturated solution of ammonium nitrate. The weight of the sample along with the crucible was recorded at different intervals.

pH Titration. The pH titrations were carried out by Topp and Pepper method.[10] Each sample of dry C-NbP-H^+ (200 mg) was equilibrated with 20 ml portions of

†† Present address: FOSROC Technology Ltd., Bourne Road, Aston, Birmingham, England.

0.1 M (MCl-MOH) solutions at 25±0.5 °C (M^+=Li^+, Na^+, K^+, and Cs^+). The molar ratio of MCl/MOH was varied to maintain a constant ionic strength (μ=0.1) of the equilibrating mixture. After 24 h the pH of the supernatant solutions were recorded and plotted against the milli equivalents of OH^- added per gram of dry exchanger (Fig. 1). Orion Research Microprocessor Ionalyzer/901 having combination glass electrode was used for the pH measurements.

X-Ray Diffraction and XPS Studies. Powder X-ray diffractograms of the exchanger in H^+, Li^+, Na^+, and K^+-forms were taken using nickel filtered Cu $K\alpha$ radiations. On the other hand only two samples of the exchanger, namely, C-NbPx and C-NbP-K^+ were used for XPS (or ESCA) studies (see Table 1).

IR Studies. The infrared spectra of niobium phosphate in H^+, Li^+, Na^+, and K^+-forms along with that of niobium hydroxide, synthesized in the laboratory, were taken using the KBr disc technique and recorded on a Perkin Elmer Spectrophotometer-621. The results are shown in Fig. 3.

Results and Discussion

The crystalline phase of niobium(V) phosphate, C-NbP, shows reproducibility in its ion-exchange capacity, composition and other characteristics. The chemical dissolution data of C-NbP-H^+ (Table 2) show an overall ca. 20% higher chemical stability over the amorphous niobium(V) phosphate[12] probably due to its crystalline nature. The trend of its stability, in different media, is similar to that of the amorphous material, i.e., HNO_3>HCl>CH_3COOH≫tartaric acid>H_2SO_4>NH_4OH>KOH. The same trend of stability of the two materials may be due to their similar chemical nature. They are less stable in sulfuric and tartaric acids due to the formation of sulfate and tartarate of niobium. On the other hand they are more soluble in ammonium and potassium hydroxides because of high pH.

The breakthrough capacities (meq g^{-1}) of C-NbP for the alkali metal ions decreas in the order K^+ (1.37)>Na^+(1.06) >Rb^+(0.86) >Cs^+(0.84) >Li^+ (0.70) showing a preferential uptake for potassium ions and the least uptake for lithium ions. The pH titration curves (Fig. 1) shows a similar trend. Furthermore, this order of uptake is only possible when the exchanger has an inelastic matrix. If the matrix were elastic, it would have resulted in a different order of exchange, probably parallel to the Hofmeister's lyotropic series i.e., Li^+<Na^+<$K^+$$Rb^+$<$Cs^+$. This adsorption sequence has been observed in zirconium phosphate and organic cation-exchange resins, which possess the elastic structure.[8] As we do not find this order of uptake in the crystalline niobium(V) phosphate, we can say that it may have a stiff three dimensional structure having a fixed pore size.

The results of X-ray diffraction (XRD) studies of C-NbP-H^+ show a large number of d-values of which the important $d(I/I_0)_{hkl}$ are 7.23 $(85)_{110}$, 4.55 $(41)_{210}$, 3.23 $(100)_{310}$, 2.28 $(43)_{420}$, and 1.42 $(29)_{551,711}$. The XRD of the different cationic forms (H^+, Li^+, Na^+, and K^+-forms) of the exchanger show that their d values are very close to each other and hence one can say that the exchanger possesses an appreciably stiff structure. The analysis of the X-ray data reveals its pseudocubical unit cell structure with $a_0(H^+)$=10.224 Å.

Since the exchanger is precipitated in presence of large amounts of SO_4^{2-} and NH_4^+ ions with the help of concentrated ammonia solution, it is reasonable to assume the possible contamination of the exchanger with these ions. XPS (or ESCA) studies were conducted to check this possibility. It is worth noting from Table 1 that only initially some NH_4^+ ions are present (as shown by a peak of nitrogen) in the exchanger which are later replaced by the potassium ions when the exchanger is converted into K^+-form. The XPS studies show no sign for the presence of sulfur and this rules out the possibility of sulfate contami-

Table 1. Binding Energies and Percent Atomic Compositions of Niobium(V) Phosphate Obtained by XPS

Element	BE	C-NbPx	C-NbP(K^+-form)
	eV	At. comp./%	At. comp./%
Phosphorus	150	13.6	14.4
Niobium	230	8.8	10.1
Potassium	320	—	2.1
Nitrogen	416	2.9	—
Oxygen	545	49.3	52.8
Carbon	300	25.4	20.6

Table 2. Solubility of Crystalline Niobium(V) Phosphate in Different Solvents

Solvent	C-NbP		NbP3	
	Nb/mg L^{-1}	P/mg L^{-1}	Nb/mg L^{-1}	P/mg L^{-1}
4M Sulfuric acid	841.5	20.9	1051.5	26.2
4M Nitric acid	0.0	0.9	0.0	1.2
4M Hydrochloric acid	0.0	1.4	0.0	1.8
1M Tartaric acid	292.1	1.4	343.7	1.8
1M Acetic acid	0.0	53.3	0.0	65.0
4M Ammonia	145.8	71.2	180.0	91.7
0.1M Potassium hydroxide	1651.0	553.0	2000.0	675.0
1M Sodium chloride	0.0	23.1	0.0	62.5
1M Ammonium nitrate	0.0	18.7	0.0	43.7
Demineralized water	0.0	5.2	0.0	10.4

NbP3 = Amorphous niobium phosphate [12]

nation of the exchanger. Hence we can say that initially the exchanger (C-NbPx) contains some ammonium ions in exchanged form only and not due to entrapped ammonia/ammonium salt. The binding energies also confirm the presence of Nb and P in their pentavalent state. The ESCA of the sample shows surface contamination of niobium(V) phosphate due to carbon (Table 1). This contamination may be due to (i) rotary pump oil vapours adsorbed on the surface of the pellet during the pressing, (ii) the presence of niobium carbide as an impurity in Nb_2O_5, (iii) the adsorption of atmospheric CO_2 by the exchanger leading to the formation of carbonate on the surface of the material. Similar results were obtained by Alberti in the ESCA spectra of $ZrPO_4$.[10,11] The percent atomic composition of the surface obtained by XPS shows the Nb/P mole ratio between 1.42—1.54 (Table 1) which is very close to the 1.5 obtained by chemical analysis of the sample. This shows that the surface and the bulk composition is the same. On the basis of these findings one can assign the following formula to the H^+-form of C-NbP.

$$(NbO)_2(HPO_4)_3 \cdot nH_2O \quad (1)$$

The infrared spectra of C-NbP-H^+ (Fig. 3,b) shows a band between 3600—3100 cm^{-1} having two strong maxima at 3150 and 3450 cm^{-1}. They are characteristic of stretching vibrations of coordinated water molecules and this implies that hydrogen bonding exists between OH groups and water molecules surrounding them.[18] A sharp peak at 1630 cm^{-1} corresponds to the deformation vibration of interstitial water molecules and the hydroxyl group [$\delta(H_2O)$ and (OH)]. The sharp peak at 1400 cm^{-1} and a broad and strong peak at 1010 cm^{-1} may be assigned to the deformation vibration of P-OH groups [δ_2(P-OH)]. The peak at 690 cm^{-1} corresponds to the P-O stretching while those at 510 and 380 cm^{-1} may correspond to M-O interatomic vibrations [ν_1(Nb-O, P-O)]. The small peaks appearing between 260—200 cm^{-1} are due to the lattice vibrations.

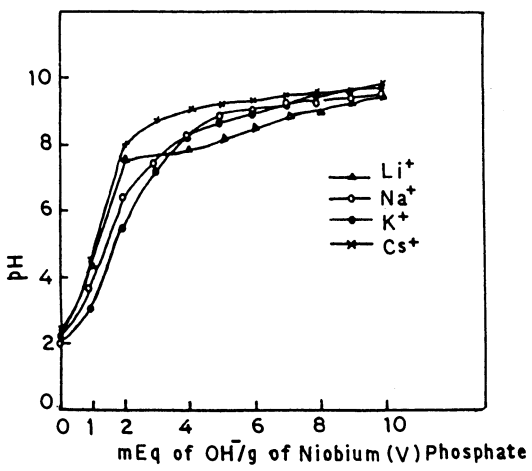

Fig. 1. pH-titration curves of Li^+, Na^+, K^+, and Cs^+, ions on the crystalline niobium(V) phosphate.

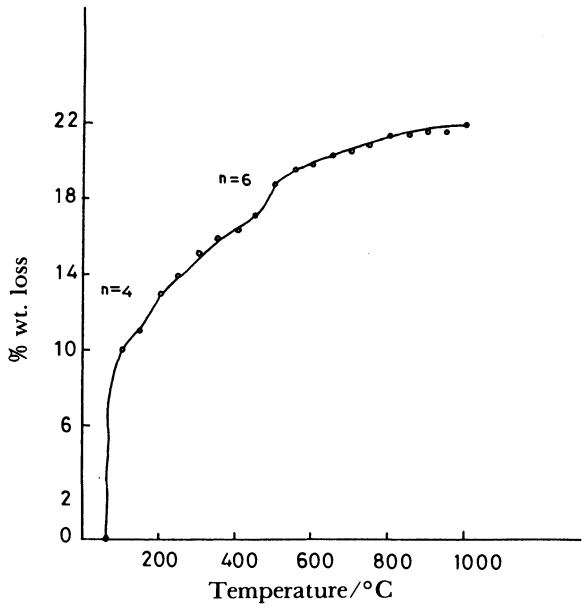

Fig. 2(a). TGA curve of crystalline niobium(V) phosphate(C-NbP-H^+).

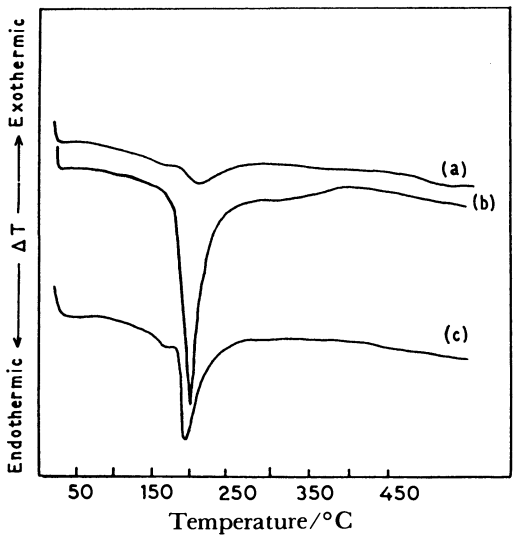

Fig. 2(b). DSC curves of crystalline niobium(V) phosphate; a=C-NbP-H^+, b=C-NbP-Na^+, c= C-NbP-K^+.

On comparing the IR spectroscopic behavior of niobium phosphate in the H^+-form with those in the Na^+ and K^+-forms (Fig. 3), it is found that all the three have a similar type of lattice structure. In the spectra of these three samples, bands relating to acidic HPO_4^{2-} groups (3150, 2320, 1400, and 510 cm^{-1}) are found.[18] If the alkali metal content approaches the total capacity value, these frequencies virtually disappear and only bands relating to water of crystallization are visible. Such a change suggests that the material was composed of strongly hydrogen bonded three dimensional aggregate,[19,20] having HPO_4^{2-} groups as the cation exchange sites. Here the proton of HPO_4^{2-} group is exchanged by M^+.

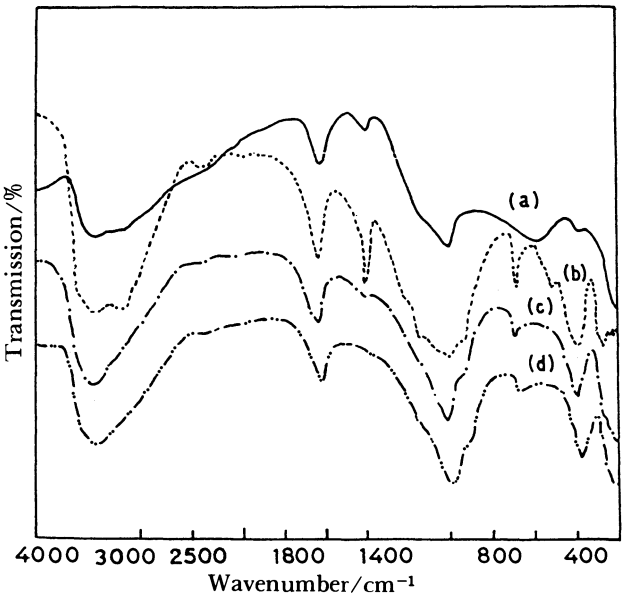

Fig. 3. IR spectra of niobium hydroxide and crystalline niobium(V) phosphate;
a=Nb-OH, b=C-NbP-H^+, c=C-NbP-Na^+, d=C-NbP-K^+.

$$HPO_4^{2-} + M^+ \rightleftarrows MPO_4^{2-} + H^+$$

Further the thermoanalytical investigations of C-NbP-H^+ indicate a weight loss of 22% up to 1000 °C (Fig. 2a). Assuming that at this temperature the composition of the sample is $Nb_2O_5 \cdot 1.5\ P_2O_5$, the number of moles of water lost per formula weight of the exchanger was calculated as 7.5.[21] It is the total number of moles of water present, a part of these are present as water of crystallization (6 mol) and the rest as water of constitution (1.5 mol). The later split up to form the OH species of the anionic part (HPO_4^{2-}) of which H^+ seems to give hydrogen exchange capacity in the H^+-form of the exchanger.[22] The DTA curves of the sample in H^+, Na^+, and K^+-forms are shown in Fig. 2b. It is evident that most of the water of crystallization is removed up to 200 °C after which there is a continuous energy consumption and loss in weight. It may be due to the removal of the remaining water of crystallization which are probably coordinated to niobium.

The weight loss at a higher temperature in C-NbP-H^+ may be owing to the condensation of HPO_4^{2-} species to $P_2O_7^{4-}$. This process of dehydration is an irreversible process above 200 °C and the water lost is not regained even after immersing the treated sample in water. But at 150 °C, 3.32 moles of water per formula weight are reversibly lost by the exchanger. The exchanger reabsorbs the lost water when left in atmosphere and results in the cracking of the former.

Further there is only one inflection point in the pH titration of C-NbP-H^+ corresponding to the monofunctional behavior of this material (see Fig. 1). Its ion-exchange capacity as determined by the titration curve, is 4.6 meq g^{-1} for K^+ at pH 8.5.

On the basis of these findings we can write the empirical formula as follows

$$(NbO)_2(HPO_4)_3 \cdot 6H_2O \quad (d_{110} = 7.231\ Å) \quad (2)$$
[Theoretical Exchange Capacity = 4.88 meq g^{-1}]

This formula agrees well with the experimental findings. The uptake of K^+ ions (46 meq g^{-1}) is very close to the theoretical exchange capacity of the proposed formula.

The CSIR (INDIA) is thanked for financial assistance.

References

1) M. Qureshi, J. P. Rawat, and A. P. Gupta, *J. Chromatog.*, **118**, 167 (1976).
2) M. Qureshi, J. P. Rawat, and A. P. Gupta, *J. Chromatographia*, **11**, 202 (1978).
3) M. Qureshi, J. P. Gupta, A. P. Gupta, and T. Gupta, *J. Chromatog.*, **144**, 231 (1977).
4) M. Qureshi, A. P. Gupta, D. V. Nowell, and J. P. Gupta, *J. Inorg. Nucl. Chem.*, **40**, 545, (1978).
5) M. Qureshi, A. P. Gupta, I. S. Thakur, and V. P. Singh, *Sep. Sci. Tech.*, **15**, 1255 (1980).
6) J. P. Rawat and S. Q. Mujtaba, *Can. J. Chem.*, **53**, 5286 (1975).
7) J. P. Rawat and P. S. Thind, *J. Phys. Chem.*, **80**, 1387 (1976).
8) M. Qureshi, J. P. Gupta, and V. Sharma, *Anal. Chem.*, **45**, 1901 (1973).
9) A. Clearfield, "Inorg. Ion Exch. Mater. I. CRC: Boca Raton," Florida, U.S.A. (1982), Chap. I, p. 16.
10) G. Alberti, U. Constantino, G. Marletta, O. Puglisi, and S. Pignataro, *J. Inorg. Nucl. Chem.*, **43**, 3329 (1981).
11) G. Marletta, O. Puglisi, S. Pignataro, G. Alberti, and U. Constantino, *Polyhedron*, **2**(3), 157 (1983).
12) M. Qureshi, A. Ahmad, N. A. Shakeel, and A. P. Gupta, *Bull. Chem. Soc. Jpn.*, **59**, 3247 (1986).
13) O. Samuelson, "Ion Exchange Separations in Analytical Chemistry," Stockholm (1944).
14) G. E. F. Lundell and J. I. Hoffman, "Outlines of Methods of Chemical Analysis," Wiley, New York (1958), p. 117.
15) N. H. Furman, "Standard Methods of Chemical Analysis," Van Nostrand, New York (1971), 6th ed., p. 812.
16) D. Alan Westland and Jerome Bezaire, *Anal. Chim. Acta*, **66**, 187 (1973).
17) APHA-AWWA-WPCF, Standard Methods for the examination of water and waste water, 14th ed., 1975, p. 479.
18) J. A. Marinsky and Y. Marcus, "Ion Exchange and Solvent Extraction Series," Marcel Dekker, Inc., New York (1973), Vol. 5, p. 19.
19) W. Feitknecht, R. Giovanoli, W. Michaelis, and M. Muller, *Z. Anorg. Allgen, Chem.*, **417**, 114 (1975).
20) J. Burgess, "Metal Ions in Solution," Ellis Hawood, London (1978), Chap. 10.
21) G. Alberti, U. Costantino, and L. Zsinka, *J. Inorg. Nucl. Chem.*, **36**, 3549 (1972).
22) J. S. Gill and S. N. Tandan, *J. Radioanal. Chem.*, **36**, 345 (1977).
23) R. M. Bairer, R. R. Townsend, *J. Chem. Soc., Faraday Trans., 1*, **72**, 661 (1976).

 © 1988 The Chemical Society of Japan Bull. Chem. Soc. Jpn., 61, 2185—2189 (1988)

Barium Ferrate Monohydrate $BaFeO_4 \cdot H_2O$, a Useful Oxidant for the Oxidation of Organic Compounds under Aprotic Conditions

Habib FIROUZABADI,* Daryoush MOHAJER, and Mohsen ENTEZARI-MOGHADAM
Chemistry Department, Shiraz University, Shiraz, Iran
(Received April 20, 1987)

Preparation of barium ferrate monohydrate with a slight modification is described. It is shown that this reagent is capable of oxidizing different organic compounds and could be used as a versatile reagent in organic synthesis. Primary and secondary alcohols are converted to their carbonyl compounds, α-hydroxy ketones to their diketones, and hydroquinones to their quinones. Aromatic amines are converted to their azo compounds, benzylamine to benzaldehyde, phenylhydrazones and oximes to their carbonyl compounds. Thiols are also converted to their disulfides in high yields. This reagent seems to be a non-toxic and a non-pollutant compound.

Oxidations of organic substrates have long been performed by manganese dioxide, potassium permanganate, chromium trioxide, and pottasium dichromate in organic synthesis.[1-3] The reaction conditions, special treatment for the activation of the reagent, and the lack of selectivity have restricted their use as oxidizing reagents in modern organic synthesis. Recently several chromium(VI) and manganese based oxidants have been prepared and reported in the literature,[4-35] in order to minimize the limitations encountered with mentioned reagents.

Reports are available which discuss manganese and chromium(VI) based oxidants and indicate that these reagents are toxic, pollutant, and are also corrosive and irritant to skin and mucous membrane.[26] Very recently it is reported that Cr(III), the product of the reduction of Cr(VI) is an animal carcinogen.[37]

Manganate, chromate, and ferrate anions are structurally similar species and as an oxidizing agent, organic chemists have long been familiar with potassium chromate. Recently attention has been paid to manganates as oxidizing agents and a few reports are also available in the literature.[30-32] Reports also exist which indicate that potassium ferrate has been used as an oxidizing reagent,[38-40] but the results reported are contradictory. Moreover, the reactions are performed in strongly basic aqueous media (pH 11.5—13.5) which limits drastically the use of this reagent as a versatile oxidizing agent in organic synthesis.

Ferrate anion decomposes in the presence of water according to the following equation;

$$2H_2O + 2FeO_4^{2-} \rightarrow Fe_2O_3 + 3/2O_2 + 4OH^-$$

The products obtained are unlikely to be toxic and pollutant. It is also reported that ferrate anion is a strong oxidant.[41] Unfortunately very little attention has been paid to these properties in preparative organic chemistry.

Very recently we have reported that silver ferrate[42] could be a good substitute for the potassium ferrate phase-transfer catalysis oxidation,[40] where a neutral, nonaqueous, and aprotic medium is of importance. However, silver ferrate is an expensive and a moderately stable reagent, therefore, these findings limit the use of this compound as a versatile agent.

The purpose of this investigation was to find a ferrate compound which would be stable and cheap, and could be used as a versatile oxidant in organic synthesis. The preparation of Co^{2+}, Pb^{2+}, Hg^{2+}, Fe^{3+}, and Zn^{2+} ferrate have been examined. Unfortunately it was found that all of these compounds were highly unstable and liberate their oxygen immediately after their formation in the reaction media.

Lately in a communication we introduced barium ferrate monohydrate[43] as an oxidizing agent for the oxidation of alcohols, and its advantages over potassium ferrate and manganese dioxide were indicated. Here we discuss with a slight modification, the preparation of pure barium ferrate monohydrate. We have extended our studies upon the oxidation of different classes of organic compounds with this reagent. Most of the results obtained are also extensively compared with barium manganate, a new and commercially available reagent.[31,32]

Results and Discussion

First sodium ferrate was prepared according to the procedure described by Thompson et al.[44]

In the previous report, barium ferrate monohydrate[45] has been prepared from potassium ferrate which in turn was made from sodium ferrate. In the present report we have used directly the solution of sodium ferrate as the precurser for the preparation of the barium salt, which improves drastically the yield of the desired product. By the addition of saturated solution of barium nitrate to the solution of sodium ferrate, barium ferrate monohydrate was precipitated immediately. In this preparation carbon dioxide-free distilled water was important, in order to avoid the formation of the corresponding carbonate. The precipitated barium ferrate monohydrate was washed with a weakly acidic solution (pH=5) until the filtrates pH reached 7, and was dried overnight in a vacuum desiccator under a dynamic vacuum.

Oxidation of organic substrates with barium ferrate monohydrate gives reproducible results and activation

of the reagent is not necessary. In contrast, oxidation with manganese dioxide usually does not give reproducible results.[20] Barium ferrate monohydrate is a very stable compound and could be stored for months without losing its oxidizing potential. This compound is a dark purple powder, which is very slightly soluble in water. Barium ferrate monohydrate does not irritate mucous membrane and skin, whereas barium manganate seriously does irritate mucous membrane. According to our findings, barium ferrate monohydrate is a good oxidizing reagent in organic synthesis and may replace toxic and pollutant reagents. This reagent is a good substitute for manganese dioxide in many respects; 1) it does not need special treatment for its activation, 2) the ratio of substrate to manganese dioxide can range from 1 : 5 to 1 : 50, this ratio for barium ferrate monohydrate in this study ranged from 1 : 1 to 1 : 10, which makes the isolation of the oxidation product from the reaction mixture easier and more practical, 3) the rate of the reaction and 4)

Table 1. Comparison of Oxidation of Some Organic Compounds with $BaFeO_4 \cdot H_2O$ and $BaMnO_4$, MnO_2

No.	Substrate	Product	Mp θ_m/ °C[32,49] (n_D^{20})	$BaFeO_4 \cdot H_2O$ Reaction time/h	$BaFeO_4 \cdot H_2O$ Yield %	$BaFeO_4 \cdot H_2O$ Oxidant Reactant	$BaMnO_4$[32] Reaction time/h	$BaMnO_4$[32] Yield %	MnO_2 Reaction time/h	MnO_2 Yield %
1	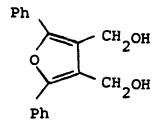	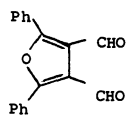	126—128	4	80—85	10	4	90	17	20—40[50]
2	Benzhydrol	Benzophenone	58	0.5	100	2	0.5	100	2	87[45]
3	Benzyl alcohol	Benzaldehyde	(1.5455)	0.8	95—100	1	1.5	90	3	26.7[45]
4	Hydroquinone	*p*-Benzoquinone	—	0.25	100	2	0.3	75	0.5	38[45]
5	Aniline	Azobenzene	66—68	0.25	>95	3	0.5	90	6	87[45]
6	*p*-Toluidine	4,4′-Dimethyl-azobenzene	67	2	40	5	1.5	67	6	87[45]
7	*m*-Nitroaniline	3,3′-Dinitro-azobenzene	148—150	4.5	25	5	2.5	55	24	04[45]
8	*o*-Nitroaniline	2,2′-Dinitro-azobenzene	—	4.5	0	5	24	0	24	0[45]
9	*p*-Nitroaniline	4,4′-Dinitro-azobenzene	220—222	4.5	27	5	2.5	30	24	0[45]
10	Benzylamine	Benzaldehyde	(1.5454)	1	100	2	1	95	24	34[45]
11	1-Naphthyl-amine	1,1′-Azona-phthalene	187—189	4.5	15	5	4.5	25	24	0[45]
12	*p*-Chloroaniline	4,4′-Dichloro-azobenzene	220—221	2	50	5	1.5	80	6	87[45]
13	2,4-Dinitro-phenylhydrazine	*m*-Dinitro-benzene	86—88	1	60	5	1.5	50	5	50[45]
14	Cinnamyl alcohol	Cinnamaldehyde	(1.6220)	1	100	4	0.75	100		
15	Cyclohexanol	Cyclohexanone	(1.4500)	24	70	2	24	56—60		
16	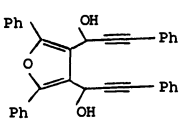	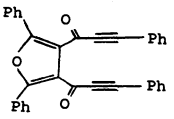	165	4	70	10	4	70		
17			170—173	24	80	5	15	90		
18	Furfuryl alcohol	Furfural	(1.5244)	0.15	40	2	0.15	75		
19	Citronellol	Citronellal	(1.5490)	24	40	10	24	85—90		
20	*p*-Nitrobenzyl alcohol	*p*-Nitro-benzaldehyde	106	2	85	2	4.5	60		
21	1-Phenylethanol	Acetoplenone	(1.5352)	1	100	3				
22	Benzoin	Benzil	43—45	6	95	6				
23	Furoin	Furil	162—163	1.5	100	6				
24	Catechol	*o*-Benzoquinone	113—115	0.7	100	6				
25	Alizarin	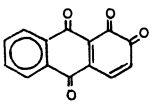	—	5	0	6				
26	1-Heptanol	Heptanal	(1.4217)	48	60	10				

the yields are usually higher with barium ferrate monohydrate than those reported for active manganese dioxide (Table 1). The results obtained with this reagent are also very comparable with those obtained with barium manganate (Table 1). Barium ferrate monohydrate is a mild oxidizing agent and oxidizes different organic substrates in benzene, heptane, and toluene under reflux conditions.

Benzylic alcohols were converted to the corresponding carbonyl compounds in high yields. Cinnamyl alcohol was converted to cinnamaldehyde almost quantitatively. Saturated primary and secondary alcohols were also converted to their carbonyl compounds in good yields. α-Hydroxyketones, such as benzoin and furoin were converted to benzil and furil in excellent yields (Table 1).

The mildness of this reagent is demonstrated by the oxidation of different thiols to their corresponding disulfides in excellent yields (Table 2).

Coupling reaction of aromatic amines to their corresponding azo compounds were also investigated. 1-Naphthylamine and aromatic amines with nitro groups substituted on the aromatic ring gave low yields of their corresponding azo compounds. The same oxidations with manganese dioxide is reported to be quite unreactive.[46] Other amines such as benzylamine were converted to benzaldehyde quantitatively. Aniline, *m*- and *p*-chloroanilines, and *m*-toluidines were converted to their azo compounds in moderate yields (Table 3). Phenylhydrazine was converted to biphenyl in good yield. Oxidation of *p*-nitrophenylhydrazine and 2,4-dinitrophenylhydrazine produced nitrobenzene and *m*-dinitrobenzene respectively in good yields (Table 3). Oxidation of several oximes were also investigated. Benzophenone oxime, benzaldehyde oxime, and 2-naphthaldehyde oxime produced their corresponding carbonyl compounds from low to good yield. Anisaldehyde phenylhydrazone produced anisaldehyde in good yield. Benzophenone phenylhydrazone produced benzophenone in high yields and also biphenyl as a by-product (Table 3).

Catechol and hydroquinone were converted their

Table 2. Oxidation of Thiols with $BaFeO_4 \cdot H_2O$

No.	Substrate	Product	Mp θ_m/°C[32,49] (n_D^{20})	$BaFeO_4 \cdot H_2O$		Oxidant
				Reaction time/h	Yield/%	Reactant
1	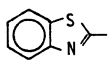	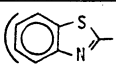	182—183.5	0.33	100	2
2	Thiophenol	Diphenyl disulfide	60—61	0.25	100	2
3	α-Toluenethiol	Dibenzyl disulfide	70—71	1	100	2
4	1-Butanethiol	Dibutyl disulfide	116—118/20	0.5	85—90	2
5	Cyclohexanethiol	Dicyclohexyl disulfide	—	0.5	85—90	2
6	*m*-Thiocresol	Di-*m*-tolyl disulfide	—	1	90	2

Table 3. Oxidation of Nitrogen-Containing Organic Compounds with $BaFeO_4 \cdot H_2O$

No.	Substrate	Product	Mp θ_m/°C[32,49] (n_D^{20})	$BaFeO_4 \cdot H_2O$		Oxidant
				Reaction time/h	Yield/%	Reactant
1	Benzylamine	Benzaldehyde	1.5454	1	100	2
2	1-Naphthylamine	1,1′-Azonaphthalene	187—188	4.5	15	2
3	Aniline	Azobenzene	66—68	0.25	100	3
4	*m*-Nitroaniline	3,3′-Dinitroazobenzene	146—149	4.5	23	5
5	*p*-Nitroaniline	4,4′-Dinitroazobenzene	138—140	4.5	27	5
6	o-Nitroaniline	2,2′-Dinitroazobenzene	—	4.5	0	5
7	*m*-Chloroaniline	3,3′-Dichloroazobenzene	98—100	2	40	5
8	*p*-Chloroaniline	4,4′-Dichloroazobenzene	219—221	2	50	5
9	Phenylhydrazine	Biphenyl	70—72	0.1	70	5
10	p-Nitrophenylhydrazine	Nitrobenzene	1.5511	0.25	94	5
11	2,4-Dinitrophenylhydrazine	*m*-Dinitrobenzene	86—88	1	60	5
12	Benzophenone phenylhydrazone	Benzophenone + Biphenyl	58 70—72	6	85 + 10	6
13	*p*-Anisaldehyde phenylhydrazone	*p*-Anistaldehyde	1.5715	6	70	6
14	Benzophenone oxime	Benzophenone	58	0.5	90	5
15	*p*-Chlorobenzaldehyde oxime	*p*-Chlorobenzaldehyde	42—43	0.5	30	5
16	2-Naphthaldehyde oxime	2-Naphthaldehyde	59—62	1	18	6

quinones in excellent yields. Alizarin was quite resistant towards oxidation with this oxidant (Table 1).

Experimental

General. All yields refer to isolated products. Products were characterized by comparison with authentic sample (IR spectrum, thin-layer and gas chromatography, melting point, and refractive index). Most reaction proceeded in dry benzene, unless otherwise indicated.

Preparation of Barium Ferrate Monohydrate. Sodium hydroxide (30 g) was dissolved in 75 ml of carbon dioxide-free distilled water and the solution was cooled to 20 °C. Chlorine gas was slowly bubbled through this solution, while being stirred vigorously, until a total weight gain of 20 g was achieved. The resulting hypochlorite solution was made strongly basic with the slow addition of 70 g of sodium hydroxide while the solution was being stirred vigorously and the temperature was permitted to rise to 30 °C. The resulting reaction mixture was cooled to 20 °C and the precipitated sodium chloride was removed by filtration. To the stirred solution of the resulting sodium hypochlorite at 25—30 °C, 25 g of iron(III) nitrate was added slowly, and this solution was saturated with sodium hydroxide at 30 °C with stirring. The reaction mixture was filtered with suction and to the resulting filtrate a sufficient amount of saturated solution of barium nitrate was added with stirring. The precipitated barium ferrate monohydrate was filtered rapidly and washed with a weakly acidic solution (pH=5) until the filtrates pH reached 7. The precipitate was dried overnight in a vacuum desiccator under a dynamic vacuum. The yield, based on sodium ferrate was almost quantitative. The analytical data were consistent with the proposed structure.

Oxidation of Benzhydrol to Benzophenone, Typical Procedure. To a solution of benzhydrol (194 mg, 0.001 mol) in dry benzene (30 ml), in a 100 ml round-bottomed flask, equipped with a condenser and magnetic stirrer, barium ferrate (1188 mg, 0.003 mol) was added and refluxed for 50 min. The reaction mixture was filtered with suction and the solid material was washed with benzene for several times. The filtrates were added together and evaporated. The resulting material was chromatographed on a silica-gel column eluted with benzene. Evaporation of the solvent afforded benzophenone (176 mg, 97%) (Table 1).

Oxidation of *p*-Chloroaniline to Its Corresponding Azo Compound, Typical Procedure. In a round-bottomed flask (100 ml), equipped with a condenser and a magnetic stirrer, *p*-chloroaniline (101 mg, 0.01 mol) in dry benzene (30 ml) was mixed with barium ferrate (1375 mg, 0.005 mol) and refluxed for 1.5 h. The reaction mixture was filtered with suction. The solid material was washed with acetone (15 ml). The filtrates were added together and evaporated. The resulting material was chromatographed on a silica-gel column eluted with benzene. Evaporation of the solvent afforded the desired azo compound (22.5 mg, 50% yield) (Table 3).

Conversion of Cyclohexanethiol to Dicyclohexyl Disulfide, Typical Procedure. To a solution of cyclohexanethiol (116 mg, 0.001 mol) in dry benzene (20 ml) in a 50 ml round-bottomed flask, equipped with a condenser and a magnetic stirrer, the oxidant (550 mg, 0.002 mol) was added. The resulting mixture was refluxed for 30 min. The reaction mixture was filtered, the solid material was washed with acetone (10 ml). The filtrates were added together and evaporated. The resulting material was chromatographed on a silica-gel column eluted with benzene. Evaporation of the solvent afforded the desired disulfide quantitatively (Table 2).

Conversion of Phenylhydrazine to Biphenyl, Typical Procedure. In a round-bottomed flask (50 ml), equipped with a condenser, and a magnetic stirrer, the oxidant (1375 mg, 0.005 mol) was added to a solution of phenylhydrazine (108 mg, 0.001 mol) in dry benzene (30 ml). The resulting mixture was refluxed for 6 min. The reaction mixture was filtered and the filter cake was washed with acetone (10 ml). The filtrates were added together and evaporated. The resulting material was chromatographed on a silica-gel column eluted with benzene. Evaporation of the solvent afforded biphenyl (54 mg, 70%) (Table 3).

Oxidation of Benzophenone Phenylhydrazone, Typical Procedure. In a round-bottomed flask (50 ml), equipped with a condenser and a magnetic stirrer, benzophenone phenylhydrazone (81 mg, 0.0003 mol) in dry benzene (30 ml) was mixed with the oxidant (495 mg, 0.00018 mol) and refluxed for 6 h. The reaction mixture was filtered with suction. The solid material was washed with acetone (10 ml). The filtrates were added together and evaporated. The resulting material was chromatographed on a silica-gel column eluted with benzene. Two fractions were isolated; benzophenone (47 mg, 85%) and biphenyl (4.5 mg, 10%) (Table 3).

Deoximation of Benzophenone Oxime, Typical Procedure. Barium ferrate monohydrate (171 mg, 0.0006 mol) was added to a solution of benzophenone oxime (24 mg, 0.00012 mol) in dry benzene (31 ml) in a round-bottomed flask (50 ml) equipped with a condenser and a magnetic stirrer. The resulting mixture was refluxed for 30 min. The reaction mixture was filtered and the filter-cake was washed with benzene (10 ml). The filtrates were added together and evaporated. The resulting material was chromatographed on a silica-gel column eluted with benzene. Evaporation of the solvent afforded benzophenone (20 mg, 91%) (Table 3).

References

1) L. F. Fieser and M. Fieser, "Reagents for Organic Synthesis," Wiley, New York (1967), Vol. 1.
2) H. O. House, "Modern Synthetic Reactions" 2nd ed., W. A. Benjamin (1972).
3) R. B. Augustine, "Oxidation," Marcel Dekker, New York (1969).
4) J. C. Collins, W. W. Hess, and F. J. Frank, *Tetrahedron Lett.*, **1968**, 3363.
5) E. J. Corey and J. W. Suggs, *Tetrahedron Lett.*, **1975**, 2647.
6) E. J. Corey and G. Schmidt, *Tetrahedron Lett.*, **1979**, 399.
7) S. J. Flatt, G. W. J. Fleet, and B. J. Taylor, *Synthesis*, **1979**, 815.
8) E. Santaniello and P. Ferraboschi, *Synth. Commun.*, **10**, 75 (1980).
9) J. Drowbowicz, *Synthesis*, **1980**, 125.
10) F. S. Guziec and F. A. Luzzio, *Synthesis*, **1980**, 691.
11) J. M. J. Frechet, P. Barling, and M. J. Farrel, *J. Org. Chem.*, **46**, 1728 (1981).
12) M. N. Bhattacharjee, M. K. Chaudhuri, H. S. Dasgupta, and N. Roy, *Synthesis*, **1982**, 588.
13) X. Huang and C. C. Chan, *Synthesis*, **1982**, 1091.

14) F. S. Guziec and F. A. Luzzio, *J. Org. Chem.*, **47**, 1787 (1982).
15) C. Lopez. A. Gonzalez, F. P. Cassto, and C. Palmo, *Synth. Commun.*, **15**, 1197 (1985).
16) J. E. Baldwin, J. C. Swallow, and H. W. S. Chan, *Chem. Commun.*, **1971**, 1407.
17) G. W. J. Fleet and W. Little, *Tetrahedron Lett.*, **1977**, 3749.
18) H. Firouzabadi, N. Iranpoor, F. Kiaeezadeh, and J. Toofan, *Tetrahedron*, **42**, 719 (1986).
19) D. F. Evans, *J. Chem. Soc.*, **1957**, 4013.
20) D. F. Evans, *J. Chem. Soc.*, **1976**, 133.
21) A. W. Herriott and D. Picker, *Tetrahedron Lett.*, **1974**, 1511.
22) D. J. Sam and H. E. Simmons, *J. Am. Chem. Soc.*, **94**, 4024 (1972).
23) H. J. Schmidt and H. J. Schafer, *Angew. Chem., Int. Ed. Engl.*, **18**, 68 (1979).
24) T. Sala and M. V. Sargent, *J. Chem. Soc., Chem. Commun.*, **1978**, 253.
25) W. Reischl and E. Zbiral, *Tetrahedron Lett.*, **1979**, 1109.
26) H. Firouzabadi, B. Vessal, and M. Naderi, *Tetrahedron Lett.*, **23**, 1847 (1982).
27) H. Firouzabadi and A. Sardarian, *Synth. Commun.*, **13**, 863 (1983).
28) H. Firouzabadi, M. Naderi, A. Sardarian, and B. Vessal, *Synth. Commun.*, **13**, 611 (1983).
29) R. Stewart, *J. Am. Chem. Soc.*, **79**, 3057 (1957).
30) W. Rigby, *J. Chem. Soc.*, **1956**, 2452.
31) H. Firouzabadi and E. Ghaderi, *Tetrahedron Lett.*, **1978**, 839.
32) H.Firouzabadi and Z. Mostafavipoor, *Bull. Chem. Soc., Jpn.*, **56**, 914 (1983).
33) H.Firouzabadi, A. R. Sardarian, M. Naderi, and B. Vessal, *Tetrahedron*, **40**, 5001 (1984).
34) H. Firouzabadi, A. R. Sardarian, and H. Gharibi, *Synth. Commun.*, **14**, 89 (1984).
35) H. Firouzabadi, A. R. Sardarian, H. Moosavipour, and G. M. Afshari, *Synthesis*, **1986**, 285.
36) Kirk-Othmer, "Encyclopedia of Chemical Technology," Wiley, New York (1964), Vol. 5, p. 505 and (1967), Vol. 13, p. 46.
37) Chemical and Engineering News, Jan. **14**, 47 (1985).
38) R. J. Audette, J. W. Quail, and P. J. Smith, *Tetrahedron Lett.*, **1971**, 279.
39) Y. Tsuda and S. Nakazima, *Chem. Lett.*, **1978**, 1397.
40) K. S. Kim, Y. K. Chang, S. K. Bae, and C. S. Halai, *Synthesis*, **1984**, 866.
41) F. A. Cotton, G. Wilkinson, "Advanced Inorganic Chemistry," 4th ed., Wily, New York (1980), p. 765.
42) H. Firouzabadi, D. Mohajer, and M. Entezari-Moghaddam, *Synth. Commun.*, **16**, 211 (1986).
43) H. Firouzabadi, D. Mohajer, and M. Entezari-Moghaddam, *Synth. Commun.*, **16**, 723 (1986).
44) G. W. Thompson, L. T. Ockerman, and J. M. Schreyer, *J. Am. Chem. Soc.*, **73**, 1379 (1951).
45) L. Losana, *Gazz. Chim. Ital.*, **55**, 468 (1925); *Chem. Abstr.*, **20**, 156 (1926).
46) M. Z. Barakat, M. F. Abdel-Wahab, and M. M. Elsadr, *J. Chem. Soc.*, **1956**, 4685.
47) K. Nakagawa, R. Konaka, and T. Nakata, *Chem. Pharm. Bull. Jpn.*, **11**, 296 (1963).
48) R. G. Srivastava and P. S. Venkataramani, *Indian J. Chem.*, **20B**, 996 (1981).
49) Aldrich Catalog handbook of Fine Chemicals, 1986—87.
50) A. Verine and Y. Lepage, *Bull. Soc. Chim. Fr.*, **1973**, 1154.

The Preparation and the Crystal Structure of 1,3,5,7-Tetramethyltetrahydro-1,3,5,7-tetrazocine-2,6(1*H*,3*H*)-dione

Toichi EBISUNO,*,† Michiaki TAKIMOTO,† Miyuki TAKAHASHI, †† and Ryuichi SHIBA††
†Department of Chemistry, Faculty of Science, Toho University, Miyama 2-2-1, Funabashi, Chiba 274
††Department of Applied Science, Faculty of Technology, Tokyo Denki University, Kanda, Chiyoda-ku, Tokyo 101
(Received October 15, 1987)

Synopsis. 1,3,5,7-Tetramethyltetrahydro-1,3,5,7-tetrazocine-2,6-(1*H*,3*H*)-dione was prepared in a good yield, and its crystal structure was determined by means of X-ray analysis. The molecule is centrometric. It has practically a planar structure except for four methyl groups and two methylene linkages and a hole of 0.5—1.6 Å in the interior of the ring structure.

Many investigators[1-5] have reported on the condensation products of urea and urea derivatives with formaldehyde since Tollens.[6] Although most of these products are soluble crystalline compounds, however, no report on their crystal structures has been published.

1,3,5,7-Tetramethyltetrahydro-1,3,5,7-tetrazocine-2,6-(1*H*,3*H*)-dione (tetramethyldimethylenediurea: TMDMU) was prepared as needle crystals by Kadowaki in 1936.[7] *N,N'*-Dimethylurea was hydroxymethylated with formalin in the presence of barium hydroxide. Without the isolation of the hydroxymethylated products, they were methylenized in MeOH and concd HCl using the procedure of Kadowaki.[7] The yield of TMDMU from *N,N'*-dimethylurea was found to be 13%. It was supposed to have an eight-membered ring structure.

In order to confirm the cyclic nature of this compound and to elucidate its structural characteristics, TMDMU was prepared in a good yield and its crystal structure was determined by means of X-ray analysis.

Experimental

Preparation of TMDMU. Ten grams of *N,N'*-dimethylurea and 23.5 g of formalin were mixed, and the pH of the reaction solution was adjusted to 8.8 by the successive addition of a 0.1M NaOH solution (1 M=1 mol dm^{-3}). While its temperature was kept at 50 °C, the solution was stirred for 30 min. These hydroxymethylation conditions were milder than those adopted by Kadowaki.[7] The reaction mixture was then evaporated to dryness under reduced pressure at a low temperature. A large excess of MeOH was added to the desiccated products. Keeping the temperature of the solution at 0—5 °C by using an ice bath, the hydroxymethylated products were methoxymethylated in the presence of concd HCl. After 30 min, the reaction solution was neutralized with a 20% NaOH solution below −15 °C and then concentrated under reduced pressure. The resulting viscous solution was distilled at 1—2 Torr (1 Torr=133.322 Pa), and a distillate of 95—99 °C containing *N*-methoxymethyl-*N,N'*-dimethylurea was collected (71% yield). As an acid catalyst, 100 mg of *p*-toluenesulfonic acid was added to 5 g of *N*-methoxymethyl-*N,N'*-dimethylurea. The reaction mixture was heated in an oil bath at 110 °C for 30 min. On cooling, white crystals were deposited; they were subsequently recrystallized from EtOH. The yield of TMDMU from *N*-methoxymethyl-*N,N'*-dimethylurea was 86%. The overall yield of TMDMU from *N,N'*-dimethylurea was ca. 60%. Possibly this good yield is due to the mild hydroxymethylation and the use of isolated *N*-methoxymethyl-*N,N'*-dimethylurea and *p*-toluenesulfonic acid. The use of concd HCl or sulfonic acid slightly decreased the yield of TMDMU and increased the amount of bis(*N,N'*-dimethylureido)-methane. TMDMU was identified by means of elemental analysis, FD-MS, and ^{1}H NMR spectrometry. Mp 258 °C: Found: C, 47.98; H, 8.14; N, 27.99%: ^{1}H NMR (DMSO-d_6): δ=2.99 (12H, s, -C$\underline{H}_3$), 4.33 (4H, q, J_{ab}=15 Hz, -C$\underline{H}_2$-): MS (FD): m/z=200 (M^+).

X-Ray Analysis. A white crystal with dimensions of ca. 0.2×0.2×0.3 mm^3 was used. The intensity data were measured on a Rigaku AFC-6S automated four-circle X-ray diffractometer, with graphite-monochromated Mo $K\alpha$ radiation (λ=0.7107 Å), by means of the ω-2θ scan technique up to 2θ of 60° (scan speed=4° min^{-1}). The absence of systematic ($0k0$) reflections for $k=2n+1$ and ($h0l$) for $l=2n+1$ indicates that the space group is $P2_1/c$.

Crystal Data: $C_8H_{16}N_4O_2$, M.W.=200.24, monoclinic, space group $P2_1/c$: a=4.095(2), b=11.262(2), c=11.134(2) Å, β=103.68(4)°, V=498.9(5) Å^3, Z=2, D_c=1.33 g·cm^{-3}, μ(Mo $K\alpha$)=0.9 cm^{-1}. Among the 1462 reflections measured, 1119 reflections with $|F_o|>3\sigma(|F_o|)$ were used for the structure determinations. The measured intensities were corrected for the Lorentz-polarization factors, but no absorption correction was applied. All the calculations were carried out on a HITAC M-680H computer at the Computer Center of The University of Tokyo, using the local version of UNICS.[8] All the scattering factors were taken from the International Tables for X-Ray Crystallography.[9] The structure of TMDMU was solved by the direct method and refined by the block-diagonal least-squares procedure to a final R value of 0.047. The final atomic parameters are listed in Table 1. The complete table of observed and calculated structure factors is kept as Document No. 8800 at the Editor of the Bulletin of the Chemical Society of Japan.

Table 1. Final Atomic Parameters (Positional ×10^4, for H×10^3) and Thermal Parameters (B_{eq} for non H×10, B_{iso} for H×10), with Their Estimated Standard Deviations in Parentheses

Atom	x	y	z	B_{eq} (B_{iso})/Å^2
O	−1513(4)	2981(1)	2924(1)	37(1)
N_1	814(4)	3533(1)	4910(1)	25(1)
N_2	−1997(4)	4907(1)	3483(1)	25(1)
C_1	−940(5)	3750(2)	3713(2)	24(1)
C_2	201(5)	5871(2)	4073(2)	23(1)
C_3	2332(6)	2358(2)	5153(2)	34(1)
C_4	−4199(6)	5139(2)	2270(2)	32(1)
H_{21}	256(6)	557(2)	436(2)	6(5)
H_{22}	19(6)	646(2)	339(2)	17(6)
H_{31}	362(7)	215(2)	456(2)	25(6)
H_{32}	70(7)	179(2)	516(3)	25(6)
H_{33}	394(4)	234(2)	595(2)	22(6)
H_{41}	−513(7)	594(2)	223(2)	21(6)
H_{42}	−618(6)	461(2)	215(2)	18(6)
H_{43}	−308(6)	506(2)	165(2)	16(5)

Results and Discussion

A perspective drawing of the molecular structure of TMDMU is shown in Fig. 1. This figure is a view perpendicular to the plane which is composed of O, C_1, N_1, and N_2. The four atoms of O′, C_1', N_1', and N_2' are placed on practically the same plane. The structure agrees with that deduced from the spectroscopic data. The selected interatomic distances and angles are given in Table 2. The observed interatomic distance for the carbonyl group in TMDMU (1.216 Å(C_1-O)) is in fair agreement with 1.207 Å (C=O),[10] but differs from that of 1.262 Å in urea.[11] The C-N bonds of the ureido moiety in TMDMU (C_1-N_1: 1.377 and C_1-N_2: 1.378 Å) are longer than that of 1.335 Å in urea. These differences are correlated to the extent to which resonance occurs in TMDMU and urea. Furthermore, the difference in the C-O bond is probably due to the absence and presence of hydrogen bonds in TMDMU and urea respectively. All the hydrogen atoms of the two amino groups have been substituted in TMDMU, while four hydrogen atoms in urea form hydrogen bonds with oxygen atoms in the adjacent three molecules.[11]

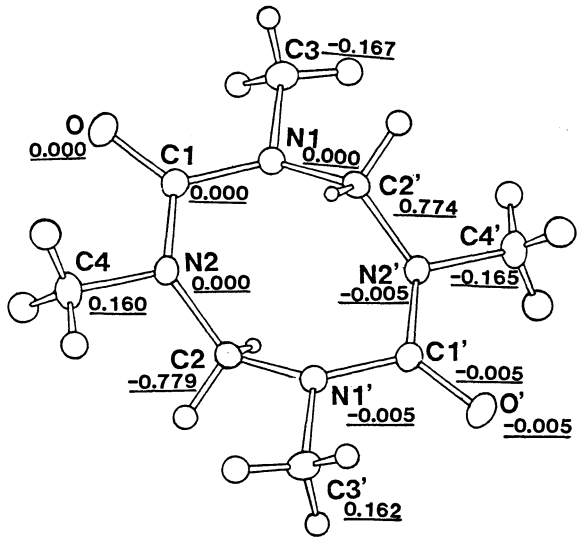

Fig. 1. The structure of 1,3,5,7-tetramethyltetrahydro-1,3,5,7-tetrazocine-2,6(1*H*,3*H*)-dione projected on the plane composed of O, C_1, N_1, and N_2. Underscored numbers are heights in Å of the atoms above or below the plane.

Table 2. Selected Interatomic Distances and Bond Angles for 1,3,5,7-Tetramethyltetrahydro-1,3,5,7-tetrazocine-2,6(1*H*,3*H*)-dione
N'_1 is the nitrogen atom opposite to N_1.

Bond distance	l/Å	Bond angle	ϕ/°
O-C_1	1.216(7)	C_1-N_1-C_3	116.2(7)
N_1-C_1	1.377(3)	C_1-N_2-C_2	119.0(11)
N_1-C_3	1.461(5)	C_1-N_2-C_4	116.1(4)
N_2-C_1	1.378(4)	C_2-N_2-C_4	117.5(12)
N_2-C_2	1.464(7)	O-C_1-N_1	122.7(6)
N_2-C_4	1.459(9)	O-C_1-N_2	122.7(10)
C_1-N_1'	1.458(9)	N_1-C_1-N_2	114.6(5)
		N_1-C_2-N_2	115.6(8)
		N_2-C_2-N_1	115.6(8)

In TMDMU, the interatomic distances between C_1-C_1', C_2-C_2', N_1-N_1', and N_2-N_2' are 4.09, 2.88, 3.38, and 3.76 Å respectively. The molecule has a hole which is surrounded by four electronegative nitrogen atoms, four hydrophobic methyl groups, and two methylene linkages. The size of the hole is estimated to be 0.5—1.6 Å by considering the radius of van der Waals. When the addition of TMDMU to the solution of phenol alkaline metal salts, the characteristic shoulder at 225 nm disappears and the absorption spectrum in UV region changes to that of phenol. This spectral change is observed in the solution of Li or Na salt, but not in that of K salt. The addition of *N,N′*-dimethylurea or *N*-methoxymethyl-*N,N′*-dimethylurea causes no spectral change in the solution of phenol alkaline metal salts. Although the details remain to be elucidated, these may be a specific interaction between TMDMU and Li^+ or Na^+.

The authors wish to express their hearty thanks to Prof. Hayao Kobayashi of Toho University for his kind support in the data collection on the Rigaku AFC-6S and the computation.

References

1) A. Einhorn and A. Hamburger, *Chem. Ber.*, **41**, 24 (1908).
2) J. I. de Jong and J. de Jonge, *Rec. Trav. Chim.*, **71**, 890 (1952).
3) J. I. de Jong and J. de Jonge, *Rec. Trav. Chim.*, **72**, 213 (1953).
4) Y. Ito, *Kogyo Kagaku Zasshi*, **64**, 382 (1961).
5) Y. Ito, *Kogyo Kagaku Zasshi*, **64**, 742 (1961).
6) B. Tollens, *Chem. Ber.*, **17**, 657 (1884).
7) H. Kadowaki, *Bull. Chem. Soc. Jpn.*, **11**, 248 (1936).
8) "The Universal Crystallographic Computation Program System (UNICS)," ed by T. Sakurai, Crystallographic Society of Japan, Tokyo (1967).
9) "International Tables for X-Ray Crystallography," The Kynoch Press, Birmingham (1974), Vol. IV.
10) V. Schomaker and D. P. Stevenson, *J. Am. Chem. Soc.*, **63**, 37 (1941).
11) P. Vaughan and J. Donohue, *Acta Crystallogr.*, **5**, 530 (1952).

The Refractive Index of Molten $CaCl_2$-NaCl Mixtures

Kazuo IGARASHI* and Junichi MOCHINAGA
Department of Synthetic Chemistry, Faculty of Engineering, Chiba University, Chiba-shi, Chiba 260
(Received December 21, 1987)

Synopsis. The refractive indices of molten $CaCl_2$-NaCl mixtures were measured goniometrically with visible light at nine wavelengths and represented as a function of both the temperature and the wavelength using a modified Cauchy relation. Information on electronic polarization is also reported.

The knowledge of the refractive index of a melt is very useful for obtaining the hypersonic velocity which characterizes the high-temperature relaxation process.[1] Moreover the temperature derivatives of the indices are necessary for measuring the thermal conductivity of the liquids by means of wave-front shearing interferometry.[2] Furthermore the indices can be used to estimate the molar refractivity and the electronic polarizability in terms of the Lorentz-Lorenz equation and the Clausius-Mossotti equation, based on the evaluation of the effective local field around the species. We have measured the refractive indices for several binary chloride melts[3-7] and have evaluated the electronic polarizabilities of the ions in the mixture melts. The molten $CaCl_2$-NaCl mixture is of interest because the Ca^{2+} (0.100 nm) and Na^+ (0.102 nm) cations have nearly equal ionic radii.[8] For this molten system, we have already measured the molar volume[9] and the surface tension.[10] In the present study, the refractive indexes of this melt were measured, and the electronic polarizabilities of the ions were evaluated.

Experimental

A hollow prismatic cell made of fused silica was used for the goniometric measurement of the refractive index. The apparatus has been described in detail previously.[11] The angle of minimum deflection was read with a precision of 1 minute. The relation between the refractive index, n_λ, and the angle of minimum deflection, σ_λ is:

$$n_\lambda = \sin((\sigma_\lambda + A)/2)/\sin(A/2), \quad (1)$$

where A is the apex angle of the prismatic cell and the subscript λ refers to the wavelength. The apex angle A has been calibrated beforehand by the use of a reference material whose refractive index has been accurately measured by Gustafsson and Karawacki.[12] The temperature of the melt was automatically controlled and recorded with a precision of 0.1 °C using a sheathed chromel-alumel thermocouple inserted into the melt. The light of nine wavelengths, from 434.1 to 680 nm, was used. The chemicals, $CaCl_2$ and NaCl, are of an analytical reagent grade and were dried by means of a conventional technique.[7]

Results and Discussion

The refractive indices at 560 nm of the binary melts measured are shown in Fig. 1, together with those of molten pure $CaCl_2$ and NaCl reported previously.[3,7] They decreased linearly with the increase in the temperature at fixed wavelengths over the whole range of $CaCl_2$ composition. Such behavior is the same as that reported previously.[3-7] The accuracy attained for an aqueous electrolyte solution has usually been $\pm 1\times10^{-5}$ in the refractive index,[13] but for the molten $CaCl_2$-NaCl mixture $\pm 1\times10^{-4}$ was estimated because of the experimental difficulty at elevated temperatures.

The refractive indices decreased non-linearly with the increase in the wavelength at a given temperature, as is shown in Fig. 2. For the refractive index of molten salt with a normal dispersion, we have already proposed the following modification of Cauchy's equation:

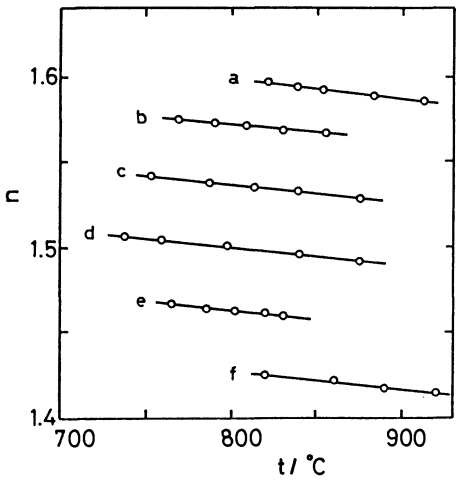

Fig. 1. Refractive indices of molten $CaCl_2$-NaCl at 560 nm. $CaCl_2$ mol%, a: 100.0, b: 79.2, c: 58.6, d: 39.1, e: 19.3, f: 0.0.

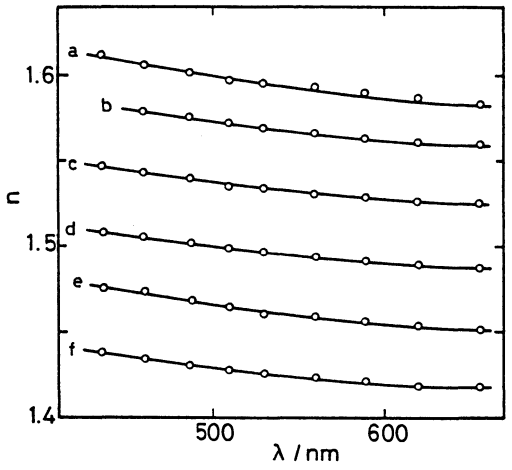

Fig. 2. Dispersions in refractive index of molten $CaCl_2$-NaCl at 850 °C. Symbols are the same as those in Fig. 1.

Table 1. Parameters of the Modified Cauchy Equation

$CaCl_2$ mol%	19.3	39.1	58.6	79.2
P_0	1.5718	1.5597	1.6003	1.6635
$P_1\times10^{-4}$	−2.1053	1.3311	8.6674	−1.0233
$P_2\times10^{-9}$	4.0838	−0.8439	−0.2582	2.0819
$Q_0\times10^{4}$	−1.6480	−1.0960	−1.0693	−1.4336
$Q_1\times10^{-1}$	3.5653	−0.4482	−0.3261	2.0814
$Q_2\times10^{-6}$	−5.1769	0.6514	0.5773	−2.3498
$\varepsilon\times10^{4}$	4.49	3.05	3.25	3.41
Temp range/°C	765—830	738—875	753—875	769—855

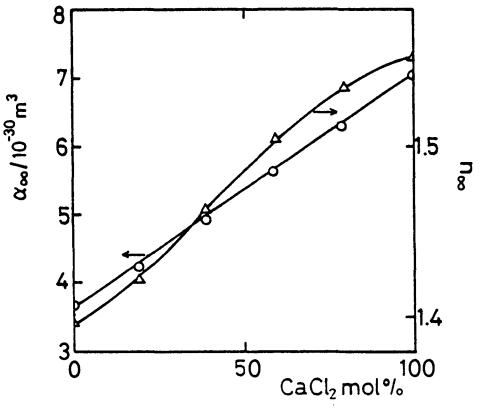

Fig. 3. Refractive index at infinite wavelength and electronic polarizability of molten $CaCl_2$-NaCl at 900 °C.

$$n(\lambda, t)=(\sum_{0}^{2} P_i\lambda^{-2i})+(\sum_{0}^{2} Q_i\lambda^{-2i})\,t, \qquad (2)$$

where t is the temperature in °C and λ is the wavelength in nm. The physical interpretation of the P_i and Q_i parameters was outlined previously.[6] The parameters determined by the least-squares fit are listed in Table 1, in which ε is the standard error of estimation.

The molar refractivity, R_λ, is one of the best parameters for the polarization phenomenon; it is calculated from the refractive index, n_λ, and the molar volume, V_m, by the use of the Lorentz-Lorenz equation:

$$R_\lambda=(n_\lambda^2-1)/(n_\lambda^2+2)V_m. \qquad (3)$$

It is generally known in binary systems that R_λ possesses a linear dependence on the composition. For the molten $CaCl_2$-NaCl mixture, a strong linear dependende was also observed. The molar volume used in the calculation was taken from a previous report.[9]

The polarizability discussed here is the electronic one,[14] which is reduced to a scalar in the case of a dense ionic melt. The electronic polarizability of a molecule is defined by the Clausius-Mossotti equation, in which an optical dielectric constant is substituted for the static one:

$$\alpha_\infty=(3/4\,\pi N_A)[(n_\infty^2-1)/(n_\infty^2+2)]V_m, \qquad (4)$$

where the subscript ∞ indicates an infinite wavelength and N_A is Avogadro's number. The electronic polarizabilities of the Ca^{2+}, Na^+, and Cl^- ions in the pure $CaCl_2$ and NaCl melts at 900 °C are known to 0.61, 0.43, and 3.24×10^{-30} m^3 respectively.[3,7] The isotherm of the electronic polarizability for the molten mixture is shown in Fig. 3, together with that of the refractive index at an infinite wavelength, as calculated from Eq. 2 by interpolating λ to ∞. The refractive indices at an infinite wavelength deviate from additivity, while the electronic polarizabilities increase linearly, with an increase in the mole fraction of $CaCl_2$, and their values seem to lie on the additive line. This indicates that the electronic polarizability is approximately inherent in the ion, even in the case of condensed systems such as molten salt.

The authors would like to express their gratitude to Mr. Junji Tominaga for assistance in measuring the refractive index.

References

1) L. M. Torell, *J. Chem. Phys.*, **76**, 3467 (1982).
2) S. E. Gustafsson, *Z. Naturforsch.*, **22a**, 1005 (1967).
3) Y. Iwadate, K. Igarashi, and J. Mochinaga, *Denki Kagaku*, **48**, 97 (1980).
4) Y. Sasaki, K. Igarashi, and J. Mochinaga, *Denki Kagaku*, **50**, 226 (1982).
5) Y. Iwadate, K. Kikuchi, K. Igarashi, and J. Mochinaga, *Z. Naturforsch.*, **37a**, 1284 (1982).
6) Y. Iwadate, J. Tominaga, K. Igarashi, and J. Mochinaga, *Chem. Phys. Lett.*, **110**, 643 (1984).
7) K. Igarashi, Y. Iwadate, J. Mochinaga, and K. Kawamura, *Z. Naturforsch.*, **39a**, 754 (1984).
8) R. D. Shannon, *Acta Crystallgr., Sect. A*, **32**, 751 (1976).
9) K. Igarashi, Y. Iwadate, H. Ohno, and J. Mochinaga, *Z. Naturforsch.*, **40a**, 520 (1985).
10) K. Igarashi, Y. Iwadate, and J. Mochinaga, *Z. Naturforsch.*, **42a**, 853 (1987).
11) J. Mochinaga and Y. Iwadate, *J. Fac. Eng. Chiba Univ.*, **30**, 213 (1979).
12) S. E. Gustafsson and E. Karawacki, *Appl. Opt.*, **14**, 1105 (1975).
13) Y. Marcus and N. Soffer, *J. Solution Chem.*, **10**, 549 (1981).

A Green Complex from the Reaction of a Binuclear Copper(II) Complex of 2-Hydroxy-1,4-butanediamine-*N,N,N',N'*-tetraacetic Acid and H_2O_2

Satoshi KAWATA, Masamoto IWAIZUMI, Hiroshi KOSUGI, and Hiroshi YOKOI*,†
Chemical Research Institute of Non-aqueous Solutions, Tohoku University, Sendai 980
†Department of Applied Chemistry, Faculty of Engineering, Shizuoka University, Hamamatsu 432
(Received December 26, 1987)

Synopsis. Spectrophotometric studies have revealed that a green complex is formed by the reaction of a blue binuclear copper(II) complex of 2-hydroxy-1,4-butanediamine-*N,N,N',N'*-tetraacetic acid and H_2O_2, although analogous binuclear complexes of 2-hydroxy-1,3-propanediamine- and 3-hydroxy-1,5-pentanediamine-*N,N,N',N'*-tetraacetic acids are unreactive to H_2O_2.

New binuclear copper complexes which can interact with O_2 and related small compounds are of great interest as models for the active sites of Type III copper-containing proteins and as candidates for catalysts in oxidative synthetic reactions.[1,2] We recently reported the preparation of three analogous binuclear copper(II) complexes of amine-*N*-polycarboxylic acids with μ-alkoxide bridges at pH<6 as model complexes for Type III copper with respect to bridging ligands.[3] In this study, the reactivity of these three complexes with H_2O_2 has been investigated spectrophotometrically.

Experimental

Materials. The binucleating ligands used here are 2-hydroxy-1,3-propanediamine-, 2-hydroxy-1,4-butanediamine-, and 3-hydroxy-1,5-pentanediamine-*N,N,N',N'*-tetraacetic acids, which will be hereafter abbreviated as AC_3OH, AC_4OH, and AC_5OH, respectively. AC_3OH is commercially available. AC_4OH and AC_5OH were synthesized and purified by our own method which will be reported elsewhere in detail. The concentration of H_2O_2 in a commercial 30 wt% solution was determined precisely by redox titration with a standardized $KMnO_4$ solution. The sample solutions for spectral measurements were prepared by dissolving 2.5 mM AC_nOH (n=3, 4, or 5), 5.0 mM $Cu(ClO_4)_2$, 0.50 M $NaClO_4$, 0.05 M $Na_2B_4O_7$, and the desired amount of H_2O_2 in water and then by adjusting the solutions to pH 10.1 (1 M=1 mol dm^{-3}).

Measurements. UV and visible absorption spectra were recorded at 5.0±0.1 °C with a Shimadzu Model UV-240 spectrophotometer using 10 and 1-mm quartz cells.

Results and Discussion

In this study, it has been found that, when H_2O_2 is added to the blue aqueous solutions of the binuclear copper(II) complexes of AC_3OH, AC_4OH, and AC_5OH[3] at pH>7, only the solution of the second complex produces an intense green color. UV and visible absorption spectra for this complex system at varying H_2O_2 concentrations were measured at 5.0 °C in order to depress the formation of by-products as efficiently as possible (Fig. 1). In these spectra at $[H_2O_2]/[\text{the } Cu_2\text{-}AC_4OH \text{ complex}]<20$, there are two isosbestic points at 288 and 790 nm, indicating that there exists a reaction equilibrium. We analyzed these spectral changes at a constant pH of 10.1 on the assumption of the following equilibrium:

$$\text{Complex } \mathbf{1} + H_2O_2 \rightleftharpoons \text{Complex } \mathbf{2} + H^+ \quad (1)$$

where Complexes **1** and **2** are $[Cu_2(AC_4O)(OH)]^{2-}$ and $[Cu_2(AC_4O)(O_2)]^{3-}$ respectively and where K'=[Complex **2**][Complex **1**]$^{-1}$[H_2O_2]$^{-1}$. The analyses could be done at three wavelengths of 350, 600, and 650 nm, as exemplified by Fig. 2. The results thus analysed are summarized in Table 1.

Now, it seems probable that Complex **2** contains a peroxide ion, as shown in Eq. 1, because the absorption spectra of Fig. 1 have been satisfactorily analyzed

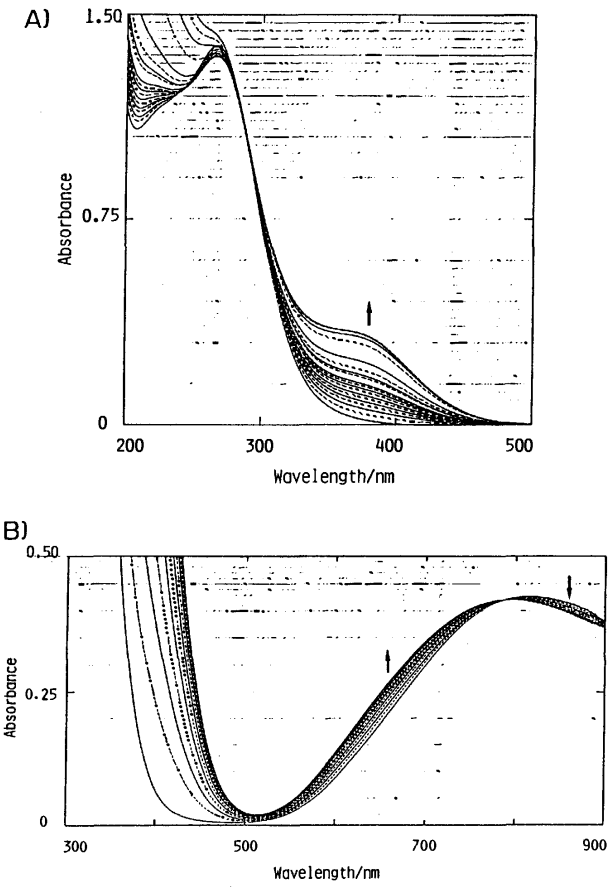

Fig. 1. UV (A) and visible (B) absorption spectra for the system of the Cu_2-AC_4OH complex (Complex **1**) and H_2O_2 in aqueous solutions at pH 10.1 at 5.0 °C (0.05 M $Na_2B_4O_7$ buffer; [$NaClO_4$]= 0.50 M; [$Cu(ClO_4)_2$]=5.114 mM; [AC_4OH]=2.557 mM; A), 1-mm quartz cells; B), 10-mm quartz cells). The spectra changed along the direction of arrows with increasing concentrations of H_2O_2, the concentrations being varied from 0 to 0.127 M for A and to 1.02 mM for B.

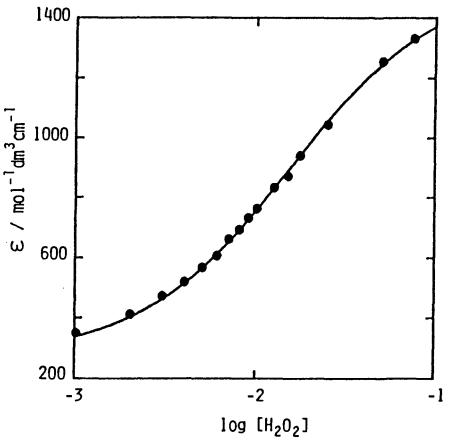

Fig. 2. Plots of molar extinction coefficients (ε) at 350 nm in Fig. 1(A) against the concentration of H_2O_2: darked circle, experimental; solid line, calculated with the parameter values listed in Table 1.

Table 1. Results[a] of Absorption Spectral Measurements for the Reaction System of Complex **1** and H_2O_2

Wavelength / nm	ε_1	ε_2	log K'
350	264.9	1533	1.84
600	35.35	88.8	1.83
650	75.83	140.6	1.84

a) ε_1 and ε_2 are the molar extinction coefficients (mol^{-1} dm^{-3} cm^{-1}) of Complexes **1** and **2**, respectively (see text as to Complexes **1** and **2** and K').

on the assumption of Eq. 1. Furthermore, it is obvious that Complex **2** shows two spectral pesks around 370 nm ($\varepsilon \approx 2000$) and 650 nm ($\varepsilon \approx 150$). Interestingly, this complex is quite similar to oxyhemocyanin and its analogues in the spectral band positions and in their intensity ratio.[4] However these bands of the present complex are too weak in intensity compared with those of oxyhemocyanin and its analogues. It is an interesting fact that H_2O_2 does not react with the binuclear copper(II) complexes of AC_3OH and AC_5OH, but only with that of AC_4OH, suggesting that the reactivity is severely dependent upon small structural variations of the binuclear complexes, for instance, the relative positions and asymmetrical environments of the two cupric ions. This study also shows that model complexes for the active sites of oxyhemocyanin and its analogues may be stably produced even in aqueous solutions at room temperature, contrary to the general belief that a hydrophobic environment is desirable for the dioxygen binding center in the biological systems and their model complexes.[1]

References

1) H. Gampp and A. D. Zuberbuhler, *Metal Ions in Biological Systems*, **12**, 133 (1981); K. D. Karlin and Y. Gultneh, *J. Chem. Educ.*, **62**, 983 (1985); *Progr. Inorg. Chem.*, **35**, 219 (1987).

2) R. A. Sheldon and J. K. Kochi, "Metal-Catalyzed Oxidations of Organic Compounds," Academic Press, New York (1981); P. Zanello, S. Tamburini, P. A. Vigato, and G. A. Mazzocchin, *Coord. Chem. Rev.*, **77**, 165 (1987).

3) S. Kawata, M. Iwaizumi, H. Kosugi, and H. Yokoi, *Chem. Lett.*, **1987**, 2321.

4) N. C. Eickman, R. S. Himmelwright, and E. I. Solomon, *Proc. Natl. Acad. Sci. U.S.A.*, **76**, 2094 (1979); E. I. Solomon, K. W. Penfield, and D. E. Wilcox, *Struct. Bond. (Berlin)*, **53**, 1 (1983).

The Reaction of *N''*-Cyanoguanidine with Formaldehyde. II. Bis-(*N''*-carbamoylguanidino)methane or *N,N'*-Methylenebis-[*N'*-(diaminomethylene)urea]

Ryuichi SHIBA,* Miyuki TAKAHASHI, Toichi EBISUNO,† and Michiaki TAKIMOTO†
Department of Applied Science, Faculty of Technology, Tokyo Denki University, Kanda, Chiyoda-ku, Tokyo 101
†Department of Chemistry, Faculty of Science, Toho University, Miyama 2-2-1, Funabashi, Chiba 274
(Received August 6, 1987)

Synopsis. The condensation product in the reaction of *N''*-cyanoguanidine with paraformaldehyde under strongly acidic conditions was identified as *N,N'*-methylenebis[*N'*-(diaminomethylene)urea] by X-ray analysis. This structure agreed with that estimated from the ^{1}H NMR data.

The resinous products from *N''*-cyanoguanidine (CG) and formaldehyde are useful as modifiers for urea- and melamine-formaldehyde resins,[1] sticking agents for dyes,[2] and commercial flocculants.[3] The reaction of CG with formaldehyde is, however, complicated under acidic conditions because of the simultanious structural conversion of CG into diaminomethyleneaminourea (DU).[4]

Spiethoff[5] has prepared a condensate of CG with paraformaldehyde in the presence of 30% hydrochloric acid and identified it as bis(*N''*-carbamoylguanidino)-methane (**1**) on the basis of the infrared absorption bands at 1680 and 1740 cm^{-1}, which have been considered to be characteristic of the primary carbamoyl group:

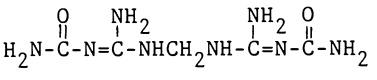

(1)

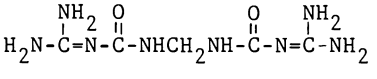

(2)

The hydrochloride of the condensate was prepared according to the procedure of Spiethoff.[5] Elemental analysis: Found, C, 20.68; H, 4.92; N, 38.88; Cl, 24.22%: Calcd for $C_5H_{12}N_8O_2 \cdot 2HCl$, C, 20.77; H, 4.88; N, 38.76; Cl, 24.52%. It showed the same melting point (230—232 °C) as has previously reported. Its infrared spectrum in the KBr pellet exhibited the same absorption bands at 1680 and 1740 cm^{-1}. The ^{1}H NMR spectrum of the free base of the condensate was measured in a DMSO-d_6 solution, with TMS as the internal standard, at 90 MHz on a JEOL FX90Q instrument. In addition to the signal of methylene protons (δ=4.30, t, 2H), two signals (δ=6.57, s, 8H, -N<u>H</u>$_2$; 6.18, t, 2H, -N<u>H</u>-) were observed. This observation was conflict with Spiethoff's identification and suggested that the condensate was not **1** but *N,N'*-methylenebis[*N'*-(diaminomethylene)urea] (**2**).

X-Ray analysis was employed in order to confirm the structure of **2**. As crystals of dihydrochloride of **2** were twinned, a crystal of the free base was prepared by passing it through a Dowex SBR column, followed by extraction with acetone and the cooling of the acetone solution.

The unit-cell parameters and intensity data for a single crystal (ca. 0.1×0.2×0.2 mm^3) were measured on a Rigaku four-circle diffractometer AFC-6S with graphite-monochromatized Mo $K\alpha$ radiation (λ=0.7107 Å). Systematic absences led to the space group $P2_1/c$.

Crystal Data: $C_5H_{12}N_8O_2$, M.W.=216.21, monoclinic, space group $P2_1/c$, a=7.954(3), b=9.553(6), c=14.963(7) Å, β=123.76(3)°, V=945.2(9) Å^3, D_c=1.52 g·cm^{-3}, Z=4 and μ(Mo $K\alpha$)=1.1 cm^{-1}.

The intensity data were collected by the ω-2θ scan technique up to 2θ=60° with a scan rate of 4° min^{-1}. The intensity data were corrected to the F_o data in the usual manner. Absorption corrections were not applied. Reflections with $|F_o| > 3\sigma(|F_o|)$ were used for the structure determination. The structure was solved by the direct method and refined by a block-diagonal least-squares procedure. All the calculations were carried out on a HITAC M-680H computer at the Computer Center of The University of Tokyo, using the local version of UNICS III.[6] All the scattering factors were taken from the International Tables for X-Ray Crystallography.[7] The final residual values for 1862 reflections were R=0.068 and R_w=0.075.

The final atomic parameters are listed in Table 1. The equivalent isotropic temperature parameters were defined by Hamilton.[8] The coordinate and isotropic temperature factors of hydrogen atoms, the anisotropic thermal parameters of the non-hydrogen atoms, and

Table 1. Final Atomatic Parameters (Positional ×10^4) and Equivalent Isotropic Temperature Parameters (B_{eq}×10), with Their Estimated Standard Deviations in Parentheses

Atom	x	y	z	B_{eq}/Å^2
O(1)	7204(4)	9549(3)	5855(2)	32(1)
O(2)	6661(4)	5605(3)	4907(2)	27(1)
N(1)	10222(4)	9014(3)	6141(2)	26(1)
N(2)	8699(5)	7186(4)	4853(3)	32(1)
N(3)	9685(4)	11271(3)	6354(2)	24(1)
N(4)	6688(5)	5921(4)	3365(3)	28(1)
N(5)	4675(6)	4815(4)	1754(3)	41(1)
N(6)	4376(7)	4151(5)	3136(3)	36(1)
N(7)	6442(5)	12304(4)	5611(3)	36(1)
N(8)	9451(3)	13603(3)	6531(3)	30(1)
C(1)	9793(6)	7540(4)	5985(3)	28(1)
C(2)	7306(5)	6175(4)	4400(3)	23(1)
C(3)	8902(5)	9948(4)	6097(3)	23(1)
C(4)	5279(5)	4949(4)	2795(3)	30(1)
C(5)	8465(5)	12356(4)	6163(3)	23(1)

Table 2. Selected Intermolecular Bond Lengths and Bond Angles, with Their Estimated Standard Deviations in Parentheses

Bond length	l/Å	Bond angle	ϕ/°
O(1)-C(3)	1.247(6)	C(1)-N(1)-C(3)	122.1(5)
O(2)-C(2)	1.253(6)	C(1)-N(2)-C(2)	123.4(14)
N(1)-C(1)	1.437(5)	C(3)-N(3)-C(5)	119.5(9)
N(1)-C(3)	1.352(5)	C(2)-N(4)-C(4)	119.6(15)
N(2)-C(1)	1.450(6)	N(1)-C(1)-N(2)	110.6(4)
N(2)-C(2)	1.336(6)	O(2)-C(2)-N(2)	120.9(9)
N(3)-C(3)	1.366(6)	O(2)-C(2)-N(4)	127.0(8)
N(3)-C(5)	1.338(8)	N(2)-C(2)-N(4)	112.3(16)
N(4)-C(2)	1.361(5)	O(1)-C(3)-N(1)	119.9(4)
N(4)-C(4)	1.335(5)	O(1)-C(3)-N(3)	128.0(5)
N(5)-C(4)	1.358(5)	N(1)-C(3)-N(3)	112.1(7)
N(6)-C(4)	1.328(8)	N(4)-C(4)-N(5)	115.7(16)
N(7)-C(5)	1.339(7)	N(4)-C(4)-N(6)	126.5(6)
N(8)-C(5)	1.338(5)	N(5)-C(4)-N(6)	117.7(12)
		N(3)-C(5)-N(7)	125.7(5)
		N(3)-C(5)-N(8)	116.5(12)
		N(7)-C(5)-N(8)	117.7(8)

the F_o—F_c tables have been deposited as Document No. 8799 at the Office of the Editor of the Bulletin of the Chemical Society of Japan. Selected bond lengths and bond angles are listed in Table 2, while a perspective drawing of the molecular structure of the condensate is shown in Fig. 1. The structure agrees with that estimated from the ^{1}H NMR data. These results clearly show that the structure of the condensate is not **1** but **2**.

Although dihydrochloride of **2** has absorption bands at 1680 and 1740 cm^{-1} in the infrared region, these are not necessarily assigned to the primary carbamoyl group, but perhaps to the stretching of the C=N and C=O of **2**. Under strongly acidic conditions, CG can be expected to be converted into DU by the hydration of the cyano group, and the resulting DU can be estimated to be hydroxymethylated with formaldehyde selectively on the amino group in the carbamoyl group, but not on the amino group in the diaminomethyleneamino group probably because of the protonated amino group in the diaminomethyleneamino group is less active with the protonated formaldehyde ($^+CH_2OH$) than that in the carbamoyl group.

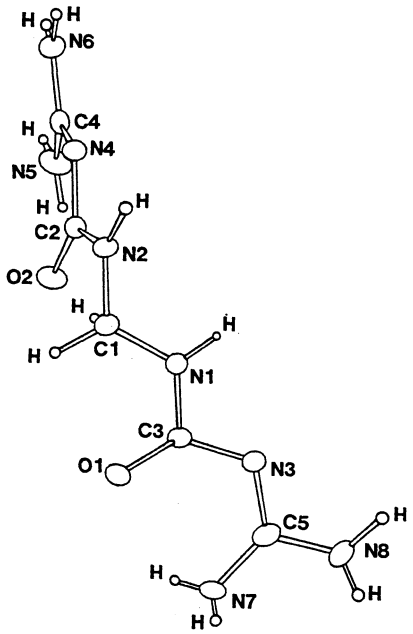

Fig. 1. A perspective drawing of the molecular structure of the condensate from *N*″-cyanoguanidine and paraformaldehyde projected on the plane at right angles to bc plane.

The authors wish to express their deep gratitude to Professor Hayao Kobayashi of Toho University for his kind support in the data collection and the computation.

References

1) K. Ripper, U. S. Patent 2286228 (1942); *Chem. Abstr.*, **36**, 7189^5 (1942).
2) L. Sellet and W. O. Dawson, U. S. Patent 2690434 (1954); *Chem. Abstr.*, **49**, 1370a (1955).
3) S. Sakai, *Kobunshi*, **8**, 612 (1959).
4) E. Yamada, *Kogyo Kagaku Zasshi*, **62**, 1161 (1959).
5) W.-D. Spiethoff, *Chem. Ber.*, **100**, 4050 (1967).
6) T. Sakurai and K. Kobayashi, *Rikagaku Kenkyusho Hokoku*, **55**, 69 (1979).
7) "International Tables for X-Ray Crystallography," Kynoch Press, Birmingham (1974), Vol. IV.
8) W. C. Hamilton, *Acta Crystallogr.*, **12**, 609 (1959).

A Convenient Synthesis of 3-Cyano-2-methylpyridines under Ultrasonic Irradiation

Katsuyoshi SHIBATA,* Katsuyoshi URANO, and Masaki MATSUI
Department of Chemistry, Faculty of Engineering, Gifu University, 1-1 Yanagido, Gifu 501-11
(Received September 18, 1987)

Synopsis. Ultrasonic irradiation of α,β-unsaturated carbonyl compounds **1a**—**i** with acetonitrile in the presence of potassium *t*-butoxide gave 3-cyano-2-methylpyridines **2a**—**i** in moderate to good yields. The pyridines are produced by a Michael reaction of 3-iminobutanonitrile, an acetonitrile dimer, to the substrates **1a**—**i**.

Ultrasonic irradiation has gained rapidly growing recognition as an effective method for increased reaction rates and yields in organic chemistry.[1-3] Meyer and Chatterjea have prepared 3-cyanopyridines from α,β-unsaturated carbonyl compounds and 3-aminocrotononitrile in low yields.[4,5] We report here a successful synthesis of 3-cyano-2-methylpyridines from α,β-unsaturated carbonyl compounds and acetonitrile in the presence of potassium *t*-butoxide under ultrasonic irradiation.

The results of ultrasonic irradiation of α,β-unsaturated carbonyl compounds are summarized in Table 1. In order to examine the effects of ultrasonic irradiation, a few experiments were conducted. Ultrasonic irradiation and mechanical agitation of **1a** with potassium *t*-butoxide in acetonitrile afforded **2a** in 70 and 30% yields, respectively (Runs 1 and 2). Reflux and ultrasonic irradiation of **1a** with 3-aminocrotononitrile in acetonitrile gave **2a** in 72 and 34% yields, respectively (Runs 3 and 4). The results clearly show that the advantages of ultrasonic irradiation include the shorter reaction time and the higher yield for the synthesis of 3-cyano-2-methylpyridines. Other pyridines **2b**—**i** were also obtained in moderate to good yields (Runs 5—12). In the case of **1f**, 4-cyano-1,2,3-triphenyl-1-butanone was produced by a Michael addition of acetonitrile to **1f** (Run 9). In the case of **1g**, 2-methyl-6-phenylbenzophenone was produced by a Michael reaction of 4-oxo-4-phenyl-2-buten-1-ide to **1g** followed by protonation, intramolecular aldol condensation, and aromatization (Run 10).

A reasonable mechanism in these pyridine formations is shown in Scheme 1. A key compound produced during the ultrasonic irradiation was identified as 3-aminocrotononitrile (**3**), the dimer of acetonitrile. No remarkable difference in the yield of **2a** was observed (Runs 1 and 3, in Table 1), suggesting that ultrasonic irradiation is effective for the formation of 3-aminocrotononitrile (**3**) in the solution. The nitrile exists as enamino and imino tautomers (**3** and **3'**, respectively) in the acetonitrile solution. On the basis of the ^{1}H NMR spectrum, the proportionality ratio of the imino isomer **3'** was calculated to be ca. 30% in acetonitrile. The imino isomer **3'** is easily converted into the carbanion **4** with potassium *t*-butoxide.

Table 1. Synthesis of 3-Cyano-2-methylpyridines **2a**—**i** from α,β-Unsaturated Carbonyl Compounds **1a**—**i** with Acetonitrile in the Presence of Potassium *t*-Butoxide under Ultrasonic Irradiation

Run	Compd	Substituent			Time	Yield[a]/%
		R^1	R^2	R^3	min	**2**
1	**1a**	Ph	H	*p*-ClC_6H_4	15	70
2	**1a**	Ph	H	*p*-ClC_6H_4	60	30[b]
3	**1a**	Ph	H	*p*-ClC_6H_4	15	72[c]
4	**1a**	Ph	H	*p*-ClC_6H_4	30	34[d], (lit[e] 35)
5	**1b**	Ph	H	Ph	15	93
6	**1c**	*p*-$MeOC_6H_4$	H	Ph	15	93
7	**1d**	*t*-Bu	H	Ph	30	97
8	**1e**	Me	H	Ph	45	66
9	**1f**	Ph	Ph	Ph	30	59[f]
10	**1g**	Ph	H	Me	5	29[g]
11	**1h**	Ph	Me	Ph	30	32
12	**1i**	H	H	Ph	30	40

a) Isolated yield. b) Mechanical agitation at room temperature. c) **1a** was irradiated with 3-aminocrotononitrile (**3**, 0.04 mmol) in the presence of potassium *t*-butoxide in acetonitrile. d) Refluxed with 3-aminocrotononitrile (**3**, 0.04 mmol) in acetonitrile. e) Reference 2. f) 4-Cyano-1,2,3-triphenyl-1-butanone and *trans*-stilbene were obtained in 10 and 13% yields, respectively. g) 2-Methyl-6-phenylbenzophenone was also obtained in a 9% yield.

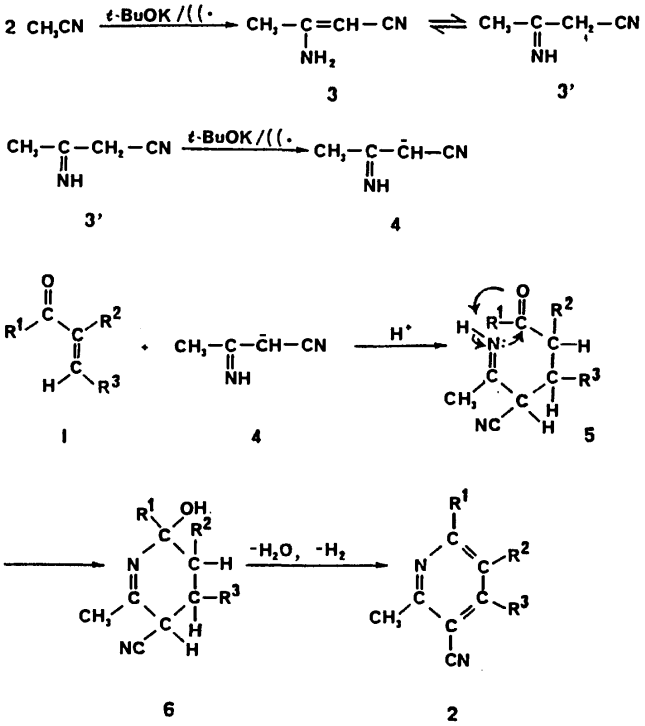

Scheme 1.

There are two possibilities for the formation of pyridines. One is the condensation reaction of the carbonyl group of **1** with the amino group of **3** followed by dehydrocyclization. Another is a Michael reaction of carbanion **4**. The ultrasonic irradiation of 4-oxo-2,4-diphenyl-2-butene did not give the corresponding pyridines, because of the steric hindrance of the methyl group at the β-position. This result suggests that a Michael addition of the imino isomer **3'** plays an important role in this reaction. α,β-Unsaturated carbonyl compounds react with the carbanion **4** followed by protonation to give the adduct **5**. Since the imino group is located close to the carbonyl group in the most stable conformation, the adduct **5** is easily cyclized to give the pyridine precursor **6**. Unfortunately, these compounds were not isolated. The precursor **6** is dehydrated, and dehydrogenated to give pyridine **2**.

Experimental

General. Melting points were measured with a Yanagimoto micro melting point apparatus and uncorrected. IR and NMR spectra were recorded with Jasco A302 and JEOL GX-270 spectrometers, respectively. Mass spectra were obtained with a Shimadzu GCMS 9020-DF spectrometer. Ultrasonic irradiation was carried out with a Branson ultrasonic laboratory cleaner (45 kHz, 100W).

Materials. α,β-Unsaturated carbonyl compounds **1e**, **1g**, and **1i** were available from Nakarai Chemicals Ltd. and used without further purification. The other compounds, **1a**, **1b**, **1c**, **1d**, **1f**, and **1h**, were prepared as described in the literature and their purity was checked by GLC. The melting or boiling points were as follows: **1a**: mp 114.5—115.0 °C (lit[6] 114.0—115.0 °C). **1b**: mp 56.0—57.0 °C (lit[7] 55.0—57.0 °C). **1c**: mp 106.5—108.0 (lit[8] 105—106 °C). **1d**: mp 42.0 °C (lit[9] 45.0 °C). **1f**: mp 99.0—100.0 °C (lit[10] 100 °C). **1h**: bp 180 °C (267 Pa) (lit[11] 167 °C (80 Pa)).

Preparation of 3-Cyano-2-methylpyridines. A dry acetonitrile suspension (50 cm^3) of potassium *t*-butoxide (100 mg) was irradiated on a water bath for 15 minutes at room temperature. α,β-Unsaturated carbonyl compounds (**1**, 0.48 mmol) was then added to the suspension, which was further irradiated. The end point of the reaction was checked by TLC. After the addition of water (50 cm^3) saturated with sodium chloride, the reaction mixture was extracted with ether (20 cm^3×2). The extract was dried over anhydrous sodium sulfate. The solvent was then evaporated under reduced pressure. In the cases of **1a—d**, the residue was recrystallized from ethanol. In the cases of **1e—i**, the residue was chromatographed on a silica-gel column (Wakogel C-200, hexane : chloroform=1 : 5). **2a**: Mp 178.0—178.5 °C (lit[5] 173 °C); IR (KBr) 2215 cm^{-1}; ^1H NMR ($CDCl_3$) δ=2.92 (3H, s) and 7.4—8.1 (10H, m). **2b**: Mp 121.5—122.5 °C (lit[5] 115—116 °C); IR (KBr) 2240 cm^{-1}; ^1H NMR ($CDCl_3$) δ=2.92 (3H, s) and 7.5—8.0 (11H, m). **2c**: Mp 138.5—139.0 °C; IR (KBr) 2220 cm^{-1}; ^1H NMR ($CDCl_3$) δ=2.89 (3H, s), 3.92 (3H, s), and 7.0—8.1 (10H, m). Found: *m/z* 300.1290. Calcd for $C_{20}H_{16}N_2O$: M, 300.1264. **2d**: Mp 89.0—90.5 °C; IR (KBr) 2220 cm^{-1}; ^1H NMR ($CDCl_3$) δ=1.38 (9H, s), 2.82 (3H, s), and 7.3—7.6 (6H, m). Found: *m/z* 250.1407. Calcd for $C_{17}H_{18}N_2$: M, 250.1471. **2e**: Mp 109.0—110.0 °C (lit[5] 105—106 °C); IR (KBr) 2220 cm^{-1}; ^1H NMR ($CDCl_3$) δ=2.63 (3H, s), 2.82 (3H, s), and 7.1—7.6 (6H, m). **2f**: Mp 180.0—181.5 °C; IR (KBr) 2220 cm^{-1}; ^1H NMR ($CDCl_3$) δ=2.93 (3H, s) and 6.8—7.3 (15H, m). Found: *m/z* 346.1550. Calcd for $C_{25}H_{18}N_2$: M, 346.1471. **2g**: Mp 74.0—76.5 °C; IR (KBr) 2220 cm^{-1}; ^1H NMR ($CDCl_3$) δ=2.53 (3H, s), 2.78 (3H, s), and 7.5—8.0 (10H, m). Found: *m/z* 208.1058. Calcd for $C_{14}H_{12}N_2$: M, 208.1002. **2h**: Mp 116.0—116.5 °C; IR (KBr) 2240 cm^{-1}; ^1H NMR ($CDCl_3$) δ=2.08 (3H, s), 2.83 (3H, s), and 7.2—7.8 (10H, m). Found: *m/z* 284.1296. Calcd for $C_{20}H_{16}N_2$: M, 284.1315. **2i**: Mp 98.5—99.5 °C; IR (KBr) 2240 cm^{-1}; ^1H NMR ($CDCl_3$) δ=2.87 (3H, s), 7.29 (1H, d, *J*=5.2 Hz), 7.5—8.6 (5H, m), and 8.68 (1H, d, *J*=5.2 Hz). Found: *m/z* 194.0825. Calcd for $C_{13}H_{10}N_2$: H, M, 194.0845.

The authors wish to express their thanks to Messrs. Katsuaki Shiratsuchi and Shozo Onishi of Shimadzu Corporation for the measurement of the mass spectra.

References

1) S. Raucher and P. Klein, *J. Org. Chem.*, **46**, 3558 (1981).
2) J. Yamawaki,S. Sumi, T. Ando, and T. Hanafusa, *Chem. Lett.*, **1983**, 379.
3) J. Einhorn and J. L. Luche, *J. Org. Chem.*, **52**, 4124, (1987).
4) E. V. Meyer, *J. Prakt. Chem.*, **78**, 497 (1908).
5) J. N. Chatterjea, *J. Indian Chem. Soc.*, **29**, 323 (1952); J. N. Chatterjea and K. Prasad, *J. Sci. Industr. Res.*, **14B**, 383 (1955).
6) H. H. Szmant and A. J. Basso, *J. Am. Chem. Soc.*, **74**, 4397 (1952).
7) E. P. Kohler and H. M. Chadwell, *Org. Synth.*, Coll. Vol. I, 78 (1941).
8) H Staudinger and N. Kon, *Justus Liebigs Ann. Chem.*, **384**, 123 (1911).
9) G. A. Hill and G. M. Bramann, *Org. Synth.*, Coll. Vol. I, 81 (1941).
10) E. Knoevenagel and R. Weissgerber, *Chem. Ber.*, **26**, 441 (1893).
11) C. A. Kingsbury, D. Draney, A. Sopchik, W. Rissler, and D. Durham, *J. Org. Chem.*, **41**, 3863 (1976).

Photoresponsive Peptide and Polypeptide Systems. VI.[1] Reversible Solubility Change of Azo Aromatic Lysine

Hiroyuki YAMAMOTO* and Ayako NISHIDA
Institute of High Polymer Research, Faculty of Textile Science and Technology, Shinshu University, Ueda 386
(Received December 12, 1987)

Synopsis. The reversible solubility change of azo aromatic lysines due to the trans-cis photoconversion of azo moieties was studied. On irradiation at different wavelengths, azo aromatic lysines are soluble under ultraviolet light (cis) and precipitate under visible light (trans). The dipole moments of the solvents used are considered to play a role in the solubility change.

The two conformers of azobenzene are known to have two different dipole moments (μ); that is, the μ values are 0.5D for the trans conformer and 3.1D for the cis conformer.[2] Recently, Irie et al.[3-5] reported on the photostimulated reversible solubility change of aggregated polystyrene and poly(glutamic acid) containing azobenzene. Our group has previously investigated the photoresponsive systems using cationic peptides and polypeptides[1,6-9] because of their relevance to the molecular mechanism of photoregulation in biological materials and process. One difficulty in studying such photoresponsive systems is, however, the subject of their solubilities, since azo aromatic peptides with high azo moieties are sparingly soluble in common solvents. This series of studies raises the question of whether or not azo aromatic amino acids undergo a rapid change in their solubilities upon the irradiation of light.

In this note azo aromatic lysine (compound **1**) will be described in order to increase knowledge regarding the photoresponsive change in azo aromatic peptide systems, giving a clue to its improved solubility.

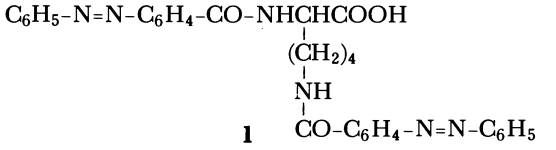

1

Experimental

Bis[*p*-(phenylazo)benzoyl]-L-lysine (BPAZ-L-Lys, **1**) was prepared according to the usual Schotten-Baumann procedure using L-lysine hydrochloride and *p*-(phenylazo)benzoyl chloride in a mixed NaOH-1,4-dioxane solvent; yield, 72%; mp 229 °C, $[\alpha]_D^{23}=-128°$ (*c* 0.25, 1,4-dioxane). Found: C, 68.45; H, 5.32; N, 14.94%. Calcd for $C_{32}H_{30}N_6O_4$: C, 68.31; H, 5.37; N, 14.94%. D-Antipode was prepared by the same procedure; yield, 64%; mp 229°C, $[\alpha]_D^{23}=132°$ (*c* 0.25, 1,4-dioxane). The absorbance spectra were measured with a Jasco UVIDEC-1 spectrometer. The critical solubilities of trans BPAZ-L-Lys at 25 °C are 3.8×10^{-4} mol dm^{-3} in a 1,4-dioxane-water mixture (1 : 1.1 v/v) and 2.3×10^{-4} mol dm^{-3} in acetonitrile, while those of the cis isomer are 1.6×10^{-3} mol dm^{-3} in a 1,4-dioxane-water mixture (1 : 1.1 v/v) and 9.8×10^{-4} mol dm^{-3} in acetonitrile. The cis isomer is 4.3 times more soluble in solvents than is its trans isomer. The turbid solutions were prepared by adding water to a clear trans BPAZ-L-Lys solution in 1,4-dioxane (ca. 1 : 1 v/v) until the precipitated solute could be observed or by using solvents with a poor solubility to BPAZ-L-Lys. The concentrations of BPAZ-L- and D-Lys in solutions were in the 4.8×10^{-4}—1.5×10^{-3} mol dm^{-3} range.

The irradiation of the sample solutions was carried out at 25 °C with a mercury lamp (400W) filtered with narrow-band interference filters from Toshiba, Ltd. The light intensities, as determined by chemical actinometry, were 1.8×10^{19} photon cm^{-2} s^{-1} at 360 nm and 1.3×10^{19} photons cm^{-2} s^{-1} at 460 nm.

Results and Discussion

Figure 1 shows the changes in the absorption spectra of BPAZ-L-Lys in 1,4-dioxane on irradiation. Before irradiation (trans, in the dark), the BPAZ-L-Lys exhibits its absorption bands at 217, 232, 258, 327, and 440 nm. The absorption bands exhibit photochromism when the trans conformer is converted to cis on irradiation at

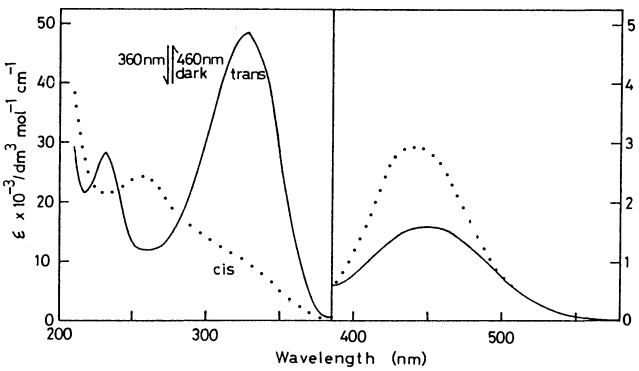

Fig. 1. Absorption spectra of BPAZ-L-Lys in 1,4-dioxane at 25 °C: —— trans, before irradiation and after reirradiation at 460 nm for 10 min; ····· cis, after irradiation at 360 nm for 10 min.

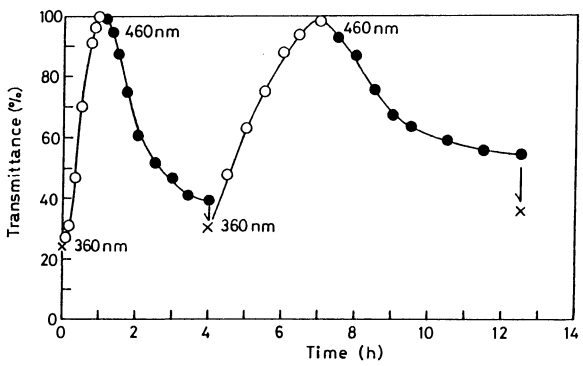

Fig. 2. Time dependence of the solubility change of BPAZ-L-Lys on irradiation at different wavelengths in 1,4-dioxane-water (1:1.1, v/v) at 25 °C: × dark adaptation. Transmittance at 650 nm; concentration 4.8×10^{-4} mol dm^{-3}.

360 nm (ultraviolet), whereas on the reirradiation of the irradiated solution at 460 nm (visible) the cis conformer returns to trans. The photoconversion from trans to cis on irradiation at ultraviolet and visible wavelengths is reversible.

Since the two conformers of azobenzene have the two different dipole moments of 0.5D (trans) and 3.1D (cis),[2] before irradiation we made turbid BPAZ-L-Lys solutions by mixing low- and high-dipole moment solvents or by cooling the heated solution to under the critical solubility. To a solution of trans BPAZ-L-Lys in 1 ml of 1,4-dioxane (μ, 0D), 1—1.1 ml of water (μ, 1.9D) was added to make it turbid. The turbid mixture becomes clear on irradiation at 360 nm for 1 h, accompanied by photoconversion to cis. On reirradiation at 460 nm, the clear solution becomes turbid again, as is shown in Fig. 2. Although this photoinduced solubility change due to the trans-cis isomerization of azo aromatic moieties is reversible, the time course to complete the first cycle (4 h) was much longer than is the case with the azo aromatic poly(glutamic acid) system.[5] Moreover, the second reversible cycle took 8 h, and bigger particles of the precipitated crystals were observed. Though not so marked, the dark adaptation (overnight) after irradiation at 460 nm further decreased the transmittance of the system. The reason for the rapid reversible change of the solubility on irradiation in the azo aromatic polymer system may be attributed to the solubilizing effect among azo aromatic moieties in the backbone chain, i.e., the polymeric effect.

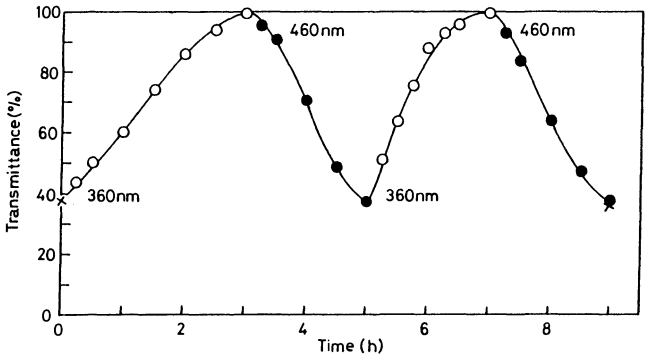

Fig. 3. Time dependence of the solubility change of BPAZ-L-Lys on irradiation at different wavelengths in acetonitrile at 25 °C: × dark adaptation. Transmittance at 650 nm; concentration 5×10^{-4} mol dm^{-3}.

Figure 3 shows the reversible solubility change of BPAZ-L-Lys in acetonitrile (μ, 3.8D). In the acetone (μ, 2.9D) and acetone-hexane (μ, 0.09D) mixed solvent the BPAZ-L-Lys photoresponded as in acetonitrile. D-Antipode, BPAZ-D-Lys, exhibited the same behavior as BPAZ-L-Lys. Thus, when their response times are improved, azo aromatic amino acids might be promising as physicochemical detective and sensory systems under controlled light conditions.

The present work was supported by a Grant-in-Aid for Scientific Research (No. 61490014) from the Ministry of Education, Science and Culture.

Reference

1) Part V: H. Yamamoto and A. Nishida, *J. Photochem. Photobiol., A. Chem.*, **42**, 149 (1988).
2) D. W. Bullock, C. N. Cumper, and I. Vogel, *J. Chem. Soc.*, **1965**, 5316.
3) M. Irie and H. Tanaka, *Macromolecules*, **16**, 210 (1983).
4) M. Irie and W. Schnabel, *Macromolecules*, **18**, 394 (1985).
5) M. Irie and O. Pieroni, *Polymer Preprints Jpn.*, **36**, 2814 (1987).
6) H. Yamamoto, *Bull. Chem. Soc. Jpn.*, **58**, 2439 (1985).
7) H. Yamamoto and A. Nishida, *Macromolecules*, **19**, 943 (1986).
8) H. Yamamoto, *Macromolecules*, **19**, 2472 (1986).
9) H. Yamamoto, Y. Miyagi, A. Nishida, T. Takagishi, and S. Shima, *J. Photochem.*, **39**, 343 (1987).

A New Synthetic Route to Aliphatic and Alicyclic Nitriles via Homolytic Desulfurization of α-(Dithiocarbamoylthio) Nitriles

Makoto YANAGAWA, Osamu MORIYA, Yoshihiko WATANABE, Yoshio UENO,† and Takeshi ENDO*
Research Laboratory of Resources Utilization, Tokyo Institute of Technology, Nagatsuta, Midori-ku, Yokohama 227
(Received December 26, 1987)

Synopsis. Chloroacetonitrile was transformed into aliphatic and alicyclic nitriles through (dimethyldithiocarbamoylthio)acetonitrile. The key steps in the synthetic route consisted of mono- and dialkylation via sulfur-stabilized carbanion and homolytic desulfurization using tributyltin hydride.

Recently, synthetic applications of homolytic processes by use of organotin hydrides have been intensively exploited in synthetic methodology.[1] One of the fundamental value of organotin hydrides lies in the selective reduction of carbon-sulfur bond via radical intermediates.[2] With regard to reductive desulfurization, several methods using reagents such as Raney nickel,[3] alkali metal in ammonia solution,[4] copper(II) chloride-zinc chloride-lithium aluminium hydride,[5] hydrazine,[6] and nickel boride[7] have been reported. Although these procedures are effective for the purpose of complete desulfurization, they lack the selectivity for the reduction of one carbon-sulful bond in polyfunctional-sulfur compounds.[8] In comparison with such procedures, the homolytic desulfurization using organotin hydrides enables an effective and a chemoselective reduction of sulfur containing moiety. On the other hand, the technique for carbon-carbon bond formation via sulfur-stabilized carbanion has been utilized for syntheses of various nitrile compounds, in which organosulfur derivatives are employed as the useful intermediates.[9] The combination of this technique and the homolytic desulfurization has the possibility to provide a convenient process for the preparation of nitriles. In this report, we wish to present a new synthetic route to aliphatic and alicyclic nitriles from chloroacetonitrile, which is derived from the strategy involving alkylation via sulfur-stabilized carbanion and reductive desulfurization via the homolytic process by use of tributyltin hydride (Bu_3SnH).

Results and Discussion

The choice of organosulfur intermediate was (dimethyldithiocarbamoylthio)acetonitrile (**1**), since the carbanion derived from **1** has been shown to possess suitable stability and reactivity towards electrophiles in the preceeding paper.[10] In addition, dithiocarbamoyl moiety is preferable to alkylthio one in view of facility of the desulfurization using organotin hydrides.[11]

The intermediate **1** was readily prepared by the reaction of chloroacetonitrile with sodium dimethyldithiocarbamate. The alkylation of **1** using alkyl halides with tetrabutylammonium iodide ($Bu_4N^+I^-$) in alkaline aqueous medium gave various α-cyano dithioesters **2** and **3**.[10] The reductive desulfurization using

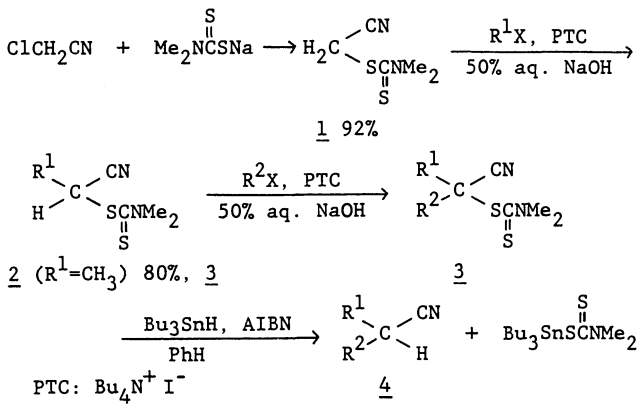

Table 1. Preparation of α-Cyano Dithioesters **3** and Nitriles **4**

Entry	α-Cyano dithioester **3**			Nitrile **4**, Yield/%	
	R^1	R^2	Yield/%		
a	$PhCH_2$	H	79	$PhCH_2CH_2CN$	95
b	$PhCH{=}CHCH_2$	H	45	$PhCH{=}CHCH_2CH_2CN$	82
c	$PhCH_2$	CH_3	85	$PhCH_2CH(CH_3)CN$	88
d	$PhCH{=}CHCH_2$	CH_3	40	$PhCH{=}CHCH_2CH(CH_3)CN$	90
e	$PhCH_2$	$PhCH_2$	65	$(PhCH_2)_2CHCN$	71
f	$-(CH_2)_3-$		93	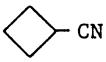	71
g	$-(CH_2)_4-$		81	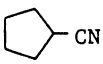	85
h	$-(CH_2)_5-$		90	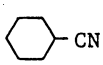	93

† Deceased February 27, 1985.

Bu_3SnH was performed under the usual conditions. Thus, a solution of **3**, Bu_3SnH, and a catalytic amount of azobisisobutyronitrile (AIBN) in dry benzene was refluxed under a nitrogen atmosphere for 5—6 h. The results of these reactions are listed in Table 1.

The process employing appropriate 1, ω-dibromoalkanes enabled the preparations of various carbocyclic cyanides such as cyclohexyl (**4f**), cyclopentyl (**4g**), and cyclobutyl cyanide (**4h**). The potential utility of the homolytic desulfurization was demonstrated by the preparations of functionalized nitriles **4b** and **4d**, which contained unsaturated carbon-carbon bond. Those results demonstrated that both primary and secondary cyanides could be prepared in high yields by the process starting from simple nitrile compound. The effectiveness of this procedure for desulfurization may be explained by the favorable influence of cyano group, which stabilizes the carbon-centered radical generated at the α-position.

Experimental

Preparation of α-Cyano Dithioesters 2 and 3. The α-cyano dithioesters **2**, **3a**, **3c**, and **3e—h** were prepared by the procedure reported before.[10] In the same manner, **3b** and **3d** were prepared as follows: 2-dimethyldithiocarbamoylthio-5-phenyl-4-pentenonitrile (**3b**). The mixture of (dimethyldithiocarbamoylthio)acetonitrile (**1**) (0.56 g, 3.5 mmol), cinnamyl bromide (0.45 g, 2.3 mmol) and tetrabutylammonium iodide (0.08 g) in benzene (5 ml) and 50% aqueous sodium hydroxide solution (10 ml) was stirred vigorously at room temperature. After 17 h, the mixture was diluted with water and extracted with ether. The ethereal extracts were dried over sodium sulfate and then evaporated. The residue was chromatographed on alumina with hexane and dichloromethane as eluant. The pure **3b** was obtained as viscous oil (0.30 g, 45%), IR (neat) 3040, 2920, 2240 (νC≡N), 1490, 1375, 1245 970, 745 cm^{-1}; ^1H NMR δ=2.86 (t, 1H, *J*=6.0 Hz), 3.28, 3.49 (ss, 6H), 5.23 (t, 1H, *J*=7.0 Hz), 5.99—6.86 (m, 2H), 7.35 (s, 5H). Found: C, 60.50; H, 5.73; N, 10.19; S, 23.39%. Calcd for $C_{14}H_{16}N_2S_2$: C, 60.84; H, 5.83; N, 10.19; S, 23.20%.

2-Methyl-2-dimethyldithiocarbamoylthio-5-phenyl-4-pentenonitrile (3d). Colorless prisms (methanol), mp 124—127 °C. IR (KBr) 3040, 2930, 2240 (νC≡N), 1490, 1380, 1250, 970, 750 cm^{-1}; ^1H NMR δ=1.87 (s, 3H), 2.75—3.62 (m, 8H), 5.85—6.85 (m, 2H), 7.38 (s, 5H). Found: C, 62.35; H, 6.19; N, 9.41; S, 21.8%. Calcd for $C_{15}H_{18}N_2S_2$: C, 62.04; H, 6.24; N, 9.64; S, 22.1%.

Reductive Desulfurization of α-Cyano Dithioesters (3). The solution of **3a** (0.76 g, 3.3 mmol), Bu_3SnH (0.96 g, 3.3 mmol), and AIBN (0.03 g, 5.5 mol%) in benzene (4 ml) was stirred at 80 °C for 5 h. The resulting solution was concentrated by a rotary evaporator and then distilled with a Kugelrohr apparatus to give hydrocinnamonitrile (**4a**) (0.18 g, 91%): bp 164—166 °C/6 mmHg (1 mmHg≈133.322Pa) (Kugelrohr). In the same manner, the nitriles **4b—h** were obtained in the yields shown in Table 1 and identified by comparison of spectral data with those of authentic samples.[12]

References

1) J.-M. Surzur, "Reactive Intermediates," ed by R. A. Abramovitch, Plenum, New York (1979), Vol. 2, p. 204; B. Giese, "Radicals in Organic Synthesis: Formation of Carbon-Carbon Bonds," ed by J. E. Baldwin, Pergamon, Oxford (1986).

2) H. G. Kuivila, *Synthesis*, **1970**, 499.

3) See, for review: H. Hauptman and W. F. Walter, *Chem. Rev.*, **62**, 347 (1962).

4) R. E. Ireland, T. I. Wringley, and W. G. Young, *J. Am. Chem. Soc.*, **80**, 4606 (1958).

5) T. Mukaiyama, *Int. J. Sufur Chem.*, **7**, 173 (1972).

6) E. J. Corey, M. Ohno, R. B. Mitra, and P. A. Vatakenchery, *J. Am. Chem. Soc.*, **86**, 478 (1964).

7) R. B. Boar, D. W. Hawkins, J. F. MchGie, and D. H. R. Barton, *J. Chem. Soc., Perkin Trans. 1*, **1979**, 654.

8) C. G. Gutierrez, R. A. Stringham, T. Nitasaka, and K. G. Glasscock, *J. Org. Chem.*, **45**, 3393 (1980) and references cited therein.

9) S. Arseniyadis, K. S. Kyler, and D. S. Watt, *Org. React.*, **31**, 298 (1984).

10) Y. Masuyama, Y. Ueno, and M. Okawara, *Chem. Lett.*, **1976**, 2967.

11) J. C. Scaiano, P. Schmid, and K. U. Ingold, *J. Organomet. Chem.*, **124**, C4 (1976).

12) H. Kameoka and S. Hashimoto, *Nippon Nogei Kagaku Kaishi*, **54**, 865 (1980); I. Hashimoto, M. Ryang, and S. Tsutsumi, *Tetrahedron Lett.*, **1970**, 4567; D. S. Watt, *ibid.*, **1974**, 707; D. D. Tanner and N. J. Bunce, *J. Am. Chem. Soc.*, **91**, 3028 (1969); M. T. Rogers and J. D. Roberts, *ibid.*, **68**, 843 (1946); M. Larcheveque, P. Mulot, and T. Cuvigny, *J. Organomet. Chem.*, **57**, C33 (1973).

Radical Reactions of Alkenylstannanes with *S*-Benzoyl *Se*-Phenyl Selenosulfide

Takeshi Toru,* Yoshio Yamada, Eturô Maekawa, and Yoshio Ueno
Department of Applied Chemistry, Faculty of Engineering, Nagoya Institute of Technology, Gokiso, Showa-ku, Nagoya 466
(Received December 2, 1987)

Synopsis. Free radical reactions of allyltributylstannane or 2-butenyltributylstannane with *S*-benzoyl *Se*-phenyl selenosulfide (**1**) gave *S*-allyl benzenecarbothioate or a mixture of *S*-2-butenyl and *S*-1-methyl-2-propenyl benzenecarbothioates, respectively. The reaction of tributylvinylstannane with **1** gave an addition product, whereas the reaction of tributylstyrylstannane gave an addition-elimination product.

Alkyl radicals generated from alkyl halides or other radical precursors such as selenides or sulfides react with allylstannane in S_H2' manner to give allylated compounds.[1] The reaction of alkyl radicals with vinylstannanes affords addition-elimination products only when vinylstannanes bear an electron-withdrawing group.[2] Heteroatom-centered radicals such as seleno or thio radicals also react with allylstannane to give allyl selenide or sulfide.[3] Recently we have shown that *S*-benzoyl *Se*-phenyl selenosulfide [*SSe*-phenyl benzenecarbo(selenothioperoxoate)] (**1**) is a useful reagent for introducing both seleno and thioester groups by virtue of the free radical reaction with various olefins,[4] and is also useful for substitution of mercurials with a seleno group.[5] In order to extend the scope and limitations of reactions with selenosulfide **1** as a synthetic reagent we have examined the photo and thermal reactions of allylic and vinylic stannanes with **1**.

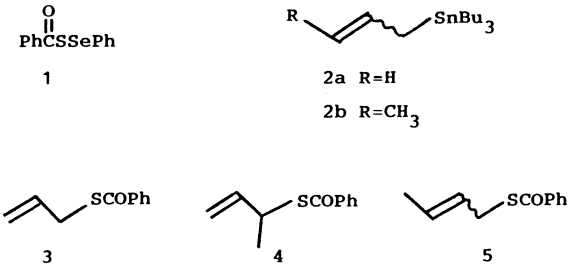

Table 1. Reaction of Alkenylstannanes with Selenosulfide **1**

Alkenyl-stannane	Method[a]	Reaction Time	Product (Yield,[b] %)
2a	A	2	**3** (86)
2a	B	1.5	**3** (84)
2b[c]	A	2	**4** and **5** (89)[d]
2b[c]	B	0.6	**4** and **5** (79)[e]
6	A	7.5	**7** (92)
6	B	1	**7** (95)
8	A	3	**9** (60)
8	B	2.5	**9** (60)

a) A: Thermal reaction in the presence of AIBN. B: Photoreaction. See Experimental Section. b) Isolated yields. c) A 1:3 mixture of *Z*/*E* isomers was used. d) The product was obtained as a 79:14:7 mixture of **4**/(*E*)-**5**/(*Z*)-**5**. e) The product was obtained as a 77:17:6 mixture of **4**/(*E*)-**5**/(*Z*)-**5**.

Results and Discussion

Ultraviolet irradiation of tributyl(2-propenyl)stannane[6] (**2a**) (referred to as allyltributylstannane) and 1.8 fold excess of selenosulfide **1** in benzene for 1.5 h resulted in the formation of *S*-2-propenyl benzenecarbothioate (**3**) in 84% yield. Thermal reaction of allylstannane **2** with selenosulfide **1** in benzene in the presence of AIBN (10 mol%) also afforded benzenecarbothioate **3** in high yield. These results together with others described below are summarized in Table 1. In the above reactions we encountered some difficulty in purifying **3** by silica-gel column chromatography because of contamination of tributyl(phenylseleno)-stannane formed during the reaction. Mercury(II) acetate was found to be most superior among several salts tested, including potassium fluoride that is effective to remove stannyl bromide,[7] to separate the stannane from benzenecarbothioate **3** in the reaction mixture. Thus, isolation of **3** could be achieved by addition of a small amount of mercury(II) acetate to the reaction mixture and subsequent filtration of the resultant precipitates followed by column chromatography.

The photo and thermal reactions of 2-butenyltributylstannane[6] (**2b**) (a 1:3 mixture of *Z*/*E* isomers) with selenosulfide **1** gave *S*-1-methyl-2-propenyl benzenecarbothioate[8] (**4**) and *S*-2-butenyl benzenecarbothioate[8] (**5**), the latter compound consisting of a mixture of the *Z*- and *E*-isomers whose ratio was 1:3 in the photostimulated reaction and 1:2 in the thermal reaction. The ratio of **4** to **5** was found to decrease as the reaction proceeded. In the photolysis monitored by the ^{1}H NMR spectroscopy it was shown that the first formed benzenecarbothioate **4** rearranged to **5** during the irradiation and reached to a mixture of **4** and **5** in the ratio 1:1 after about 80 min in carbon tetrachloride or in the ratio 2:1 after 110 min in deuterated benzene (see Table 2 in Experimental Section). This rearrangement was further verified by the irradiation of isolated benzenecarbothioate **4** which resulted in rapid and complete conversion to benzenecarbothioate **5** within 10 min. The complete conversion of **4** to **5** is probably due to the conditions without selenosulfide **1** or tributyl(phenylseleno)stannane in the reaction mixture. Similar facile rearrangement from 1-methyl-2-propenyl selenide to 2-butenyl selenide have been reported by Russell et al. in the reaction of 2-butenylstannane with diphenyl diselenide.[3] The above overall reactions can be rationalized by the S_H2' mechanism and subsequent interconversion of **4** to **5** as shown in Scheme 1, i.e., benzenecarbothioate **3** or **4** is

formed by β-elimination of the stannyl radical from the carbon radical generated at the vicinal position to the stannyl group by the reaction of stannane **2a** or **2b** with the thiyl radical and then resulting benzenecarbothioate **4** rearranges to benzenecarbothioate **5**.

Another example of facile β-elimination of the stannyl radical was encountered in the reaction of tributyl[(*E*)-styryl]stannane[9] (**6**) with selenosulfide **1**, affording *S*-styryl benzenecarbothioate (**7**) which is apparently formed via addition of the thiyl radical to the β-olefinic carbon and subsequent β-elimination of the stannyl radical. The photoinduced reaction proceeded much faster than the thermal reaction in this case (see Table 2).

On the other hand, tributylvinylstannane[10] (**8**) reacted with selenosulfide **1** to give the addition product **9** in moderate yield after 3 h in thermal reaction and 2.5 h on irradiation. Longer reaction time in both reactions did not improve the yield but caused the decomposition of the addition product **9**. The structure of **9** was assigned by the spectral data. The ^{13}C NMR spectrum showed the signals of butyl carbons at δ 12.77, 26.53 ($^3J_{Sn-C}$=58.5 Hz), 28.22 ($^2J_{Sn-C}$=19.5 Hz), 9.67 ($^1J_{Sn-C}$=312.7 and 327.7 Hz) assigned to the methyl carbon, γ-carbon, β-carbon, and α-carbon to the stannane, respectively, by their coupling constants between ^{13}C and $^{117,119}Sn$.[11] The methylene carbon appeared at δ 35.03 without any significant couplings, while the signal assigned to the methine carbon was observed at δ 22.70 with two sets of definitive couplings, J_{Sn-C}=217.6 and 227.8 Hz, and J_{Se-C}=90.8 Hz),[12] confirming the regiochemistry of the addition product **9**. The ^1H NMR spectrum showed three sets of a doublet of doublet at 3.28 (J=8.8 and 6.8 Hz), 3.47 (J=13.2 and 8.8 Hz), and 3.76 (J=13.2 and 6.8 Hz) ppm. The double resonance study of the ^{13}C NMR spectroscopy irradiated at δ 3.28, 3.47 and 3.76 confirmed the signal at δ 3.28 to correspond to the methine proton CH(Seph)$SnBu_3$ and the other two to the methylene protons attached to the thioester group. In addition, ^{77}Se appeared at δ 358 relative to dimethyl selenide. We have already shown that the thiyl radical generated from selenosulfide **1** adds selectively to the terminal carbon of monosubstituted olefins.[4] This high regioselectivity is derived from that the electron-deficient thiyl radical (PhCOS·) adds to the electron-rich terminal carbon.[13] It should be noted that alkyl radicals generated from alkyl halides does not react with unsubstituted and alkyl-substituted vinylstannanes.[2c] Vinylstannanes should be substituted with an electron-withdrawing group probably due to the nucleophilic nature of alkyl radicals. On the other hand, in our case the thiyl radical (PhCOS·) bearing an electron-withdrawing benzoyl group reacted readily with vinylstannane **8** as well as styrylstannane **6** because of its electrophilic nature.

The present reactions may serve a new synthetic method for the synthesis of thioates providing further scope of reactions with *S*-benzoyl *Se*-phenyl selenosulfide (**1**) as a synthetic reagent.[14]

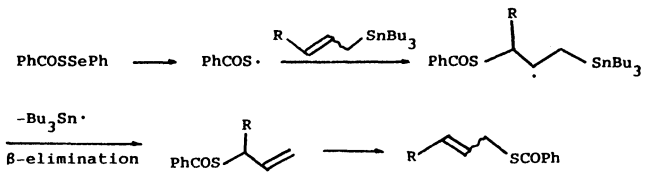

Scheme 1.

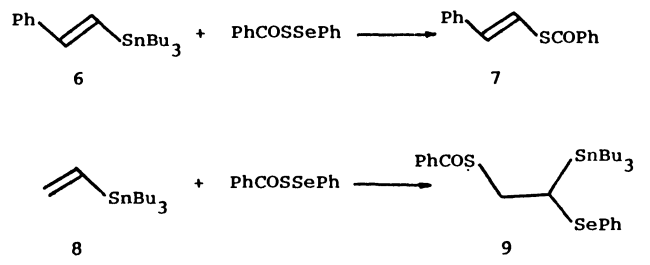

Scheme 2.

Table 2. Photostimulated Reaction of **2b** with **1**

Reaction time	Ratio of **4** to **5**, **4**/**5**	
min	In CCl_4	In C_6D_6
10	2.5	9
20	2	4
30	1.5	3
80	1	2
100	1	2

Experimental

Apparatus. IR spectra were taken with a JASCO A-102 spectrometer. ^1H NMR spectra were recorded on a Varian XL-200 (200 MHz) or JEOL JNM-PMx60si (60 MHz) instruments. Chemical shifts are reported on the δ scale relative to Me_4Si as the internal standard. ^{13}C and ^{77}Se NMR spectra were obtained on a Varian XL-200 spectrometer for solutions in deuterochloroform. Microanalyses were performed by the Institute of Microanalyses, Kyoto University. All reactions were carried out under an argon atmosphere. Flash chromatography was performed using a Michael Miler column packed with Fuji Davison silica gel BW-200, equipped with FMI LAB Pump RP-G150 and FMI Pulse Damper PD-60LF, normally at a pressure of 1—2 kg cm^{-2}.

Reaction of Tributyl(2-propenyl)stannane (2a) with Selenosulfide 1. Thermal Reaction (Method A). A mixture of tributyl(2-propenyl)stannane (**2a**) (34 mg, 0.10 mmol), selenosulfide **1** (54 mg, 0.18 mmol) and AIBN (3 mg, 0.018 mmol) in degassed benzene (0.2 ml) was heated under reflux for 2 h. To the resulting yellow clear solution was added mercury(II) acetate (20 mg, 0.063 mmol) at room temperature and the mixture was stirred for 5 min when white precipitates appeared. The precipitates were filtered and the filtrate was concentrated in vacuo to leave an oil which was purified by flash column chromatography with hexane-benzene (98:2 to 8:2) to give 16 mg (86%) of *S*-2-propenyl benzenecarbothioate[8] (**3**): ^1H NMR (CCl_4) δ=3.73 (d, 2H, J=8 Hz), 5.00—5.40 (m, 2H), 5.50—6.10 (m, 1H), 7.26—8.00 (m, 5H); IR (film) 1660 cm^{-1}; MS (70 eV) m/z (rel intensity) 192 (M^+; 2), 137 (1), 105 (100), 77 (45), 56 (22), and 51 (30).

Photostimulated Reaction (Method B). A solution of tributyl(2-propenyl)stannane (**2a**) (36 mg, 0.11 mmol) and selenosulfide **1** (57 mg, 0.19 mmol) in degassed benzene (0.2 ml) was externally irradiated in a glass tube at a distance of 15 cm with an Toshiba H-400F high-pressure Hg lamp for 1.5 h. Similar treatment of the reaction mixture to Method A

and purification afforded 16 mg (84%) of *S*-2-propenyl benzenecarbothioate (**3**).

Reaction of 2-Butenyltributylstannane (2b) with Selenosulfide 1. Thermal reaction of 2-butenyltributylstannane (**2b**) (37 mg, 0.11 mmol) with selenosulfide **1** (66 mg, 0.23 mmol) in the presence of AIBN (4 mg) in benzene (0.2 ml) for 2 h and subsequent purification described above afforded a 79:14:7 mixture of **4**/(*E*)-**5**/(*Z*)-**5** (18 mg, 89%), whose ratio was determined by the ^{1}H NMR (200 MHz) spectrum.

Irradiation of a mixture of **2b** (32 mg, 0.093 mmol) and **1** (49 mg, 0.17 mmol) for 40 min afforded a 77:17:6 mixture of **4**/(*E*)-**5**/(*Z*)-**5** (14 mg, 79%).

The signals of the ^{1}H NMR spectrum were assigned as follows; for *S*-1-methyl-2-propenyl benzenecarbothioate[8] (**4**): δ=1.52 (d, 3H, J=8.0 Hz), 4.36 (ddq, 1H, J=5.0, 1.5, and 8.0 Hz), 5.08 (ddd, 1H, J=10.0, 1.5, and 1.5 Hz), 5.30 (ddd, 1H, J=17.0, 1.5, and 1.5 Hz), 5.94 (ddd, 1H, J=17.0, 10.0, and 1.5 Hz), 7.36—8.22 (m, 5H); for *S*-(*E*)-2-butenyl benzenecarbothioate[8] (*E*)-(**5**): δ=1.72 (d, 3H, J=7.2 Hz), 3.64 (d, 2H, J=5.0 Hz), 5.48 (dt, 1H, J=15.4 and 7.2 Hz), 5.70 (dq, 1H, J=15.4 and 5.0 Hz), and 7.40—8.20 (m, 5H); for *S*-(*Z*)-2-butenyl benzenecarbothioate[8] (*Z*)-(**5**): δ=1.78 (d, 3H, J=7.2 Hz), 3.71 (d, 2H, J=5.0 Hz), 5.40—5.80 (m, 2H), 7.40—8.20 (m, 5H).

Irradiation of 2-Butenyltributylstannane (2b) and 1 in a NMR Tube. The ^{1}H NMR signals (60 MHz) were monitored by the integration of a C-2 methine proton of *S*-1-methyl-2-propenyl benzenecarbothioate (**4**) at δ 4.00—4.63 and of a C-1 methylene proton of *S*-2-butenyl benzenecarbothioate (**5**) at δ 3.47—3.76. The results are shown in Table 2. The rearrangement in benzene proceeded slower than in CCl_4.

Irradiation of Benzenecarbothioate 4. The complete rearrangement of **4** to **5** in deuterated benzene was observed by the irradiation of **4**, obtained as a ca. 20:1 mixture of **4**/**5** by the short time thermal reaction, for 10 min as monitored by the ^{1}H NMR spectroscopy.

***S*-Styryl Benzenecarbothioate (7).** ^{1}H NMR (CCl_4) δ=6.67 (d, 1H, J=16 Hz), 7.10—8.10 (m, 11H); IR (KBr) 1665 cm^{-1}; MS (70 eV) m/z (rel intensity) 240 (M^+, 4), 105 (100). Found: C, 74.89; H, 5.10%. Calcd for $C_{15}H_{12}OS$: C, 74.97; H, 5.08%.

***S*-(2-Tributylstannyl-2-phenylselenoethyl) Benzenecarbothioate (9).** ^{1}H NMR (CCl_4) δ=0.80—1.70 (m, 27H), 3.28 (dd, 1H, J=8.8 and 6.8 Hz), 3.42 (dd, 1H, J=13.2 and 8.8 Hz), 3.76 (dd, 1H, J=13.2 and 6.8 Hz), 7.12—8.00 (m, 10H); ^{13}C NMR ($CDCl_3$) δ=9.67 (J_{Sn-C}=312.7 and 327.7 Hz, Sn$\underline{C}$H$_2$), 12.77 (SnCH$_2$CH$_2$CH$_2\underline{C}$H$_3$), 22.70 (J_{Sn-C}=217.6 and 227.8 Hz, J_{Se-C}=90.8 Hz, Sn-$\underline{C}$H-Se), 26.53 (J_{Sn-C}=58.5 Hz, SnCH$_2$CH$_2\underline{C}$H$_2$), 28.22 (J_{Sn-C}=19.7 Hz, SnCH$_2\underline{C}$H$_2$), 35.03 (PhCOS$\underline{C}$H$_2$), 125.91, 126.26, 127.33, 127.54, 128.06, 130.64, 131.65, 132.26, 136.21 (2Ph), 190.05 (C=O): ^{77}Se NMR ($CDCl_3$) δ=358 (m) (dimethyl selenide: ν=0 ($CDCl_3$)); IR (film) 1650 cm^{-1}; MS (20 eV) m/z (rel intensity) 473 (M^+—PhCOS, 6), 370 (100), 290 (14), 157 (5), 105 (50), 77 (13), 51 (3). Found: C, 53.34; H, 6.61%. Calcd for $C_{27}H_{40}OSSeSn$: C, 53.13; H, 6.62%.

The present work was partially supported by a Grant-in-Aid for Science Research No. 61470086 from the Ministry of Education, Science and Culture.

References

1) a) M. Kosugi, K. Kurino, K. Takayama, and T. Migita, *J. Organometal. Chem.*, **56**, C11 (1973); b) J. Grignon and M. Pereyre, *ibid.*, **61**, C33 (1973); c) J. Grignon, C. Servens, and M. Pereyre, *ibid.*, **96**, 225 (1975); d) G. E. Keck and J. B. Yates, *J. Am. Chem. Soc.*, **104**, 5829 (1982); *J. Organomet. Chem.*, **248**, C21 (1983); e) S. Chandrasekhar, S. Latour, J. D. Wuerst, and B. Zacharie, *J. Org. Chem.*, **48**, 3810 (1983); for the review, see f) B. Giese, "Radicals in Organic Synthesis: Formation of Carbon-Carbon Bonds," Pergamon Press, Oxford (1986).

2) a) G. A. Russell, H. Tashtoush, and P. Ngoviwatchai, *J. Am. Chem. Soc.*, **106**, 4622 (1984); b) G. A. Russell and P. Ngoviwatchai, *Tetrahedron Lett.*, **26**, 4975 (1985); c) J. E. Baldwin and D. R. Kelly, *J. Chem. Soc., Chem. Commun.*, **1985**, 682.

3) G. A. Russell and L. L. Herold, *J. Org. Chem.*, **50**, 1037 (1985) and ref. cited therein.

4) T. Toru, T. Seko, and E. Maekawa, *Tetrahedron Lett.*, **26**, 3263 (1985).

5) T. Toru, Y. Yamada, E. Maekawa, and Y. Ueno, *Chem. Lett.*, **1987**, 1827.

6) F. A. Abel, *J. Organomet. Chem.*, **84**, 199 (1975).

7) J. E. Liebner and J. Jacobus, *J. Org. Chem.*, **44**, 449 (1979).

8) S. G. Smith, *J. Am. Chem. Soc.*, **83**, 4285 (1961).

9) J. W. Cabodie, *J. Am. Chem. Soc.*, **105**, 6129 (1983).

10) D. Seyferth and F. G. A. Stone, *J. Am. Chem. Soc.*, **79**, 515 (1957).

11) T. N. Mitchell, *J. Organometal. Chem.*, **59**, 189 (1973); V. S. Petrosyan, *Progress in NMR Spectroscopy*, **11**, 115 (1977); W. Kitching, H. A. Olszowy, and K. Harvey, *J. Org. Chem.*, **47**, 1893 (1982).

12) For the review: C. Paulmier, *"Selenium Reagents and Intermediates in Organic Synthesis,"* in *"Organic Chemistry Series,"* ed by J. E. Baldwin, Pergamon Press, Oxford (1986), Vol. 4, Chap. 1, p 17; N. P. Lutha and J. D. Odom, *"The Chemistry of Organic Selenium and Tellurium Compounds,"* ed by S. Patai and Z. Rappoport, John Wiley & Sons, Chichester (1986), Vol. 1, Chap. 6.

13) For the excellent reviews: A. L. J. Beckwith, *Tetrahedron*, **37**, 3073 (1981); B. Giese, *Angew, Chem., Int. Ed. Engl.*, **22**, 753 (1983); and see also Ref. 1f.

14) **1** can be also used as an acylating agent of amines; T. Toru, Y. Yamada, T. Oshima, S. Imao, and E. Maekawa, *Nippon Kagaku Kaishi*, **1987**, 1442.

The Electronic Spectra of 6,6′-Diamino-2,2′-bipyridine

Masaki YAMADA, Koji ARAKI,* and Shinsaku SHIRAISHI*
Institute of Industrial Science, The University of Tokyo, 7-22-1 Roppongi, Minato-ku, Tokyo 106
(Received December 9, 1987)

Synopsis. The lowest-energy π–π^* band of 6,6′-diamino-2,2′-bipyridine (dabp) appeared at near-UV region, and was found to suffer a characteristic solvent effect. The results were discussed in terms of its electronic structure calculated by ab initio method using a STO-3G basis set.

Electronic structures of polyazabiphenyls and their derivatives, particularly 2,2′-bipyridine (bpy) and its derivatives, have been studied in relation to their physical, chemical, and physiological importances.[1,2] However, the effect of substituent(s), especially at 6,6′-positions, on the electronic structures and photochemical properties of bpy have not been so well understood though ligands of the bpy family are familiar in inorganic chemistry. We previously reported the synthesis, properties, and complexability of 6,6′-diamino-2,2′-bipyridine (dabp)[3] and its derivatives.[4] Introduction of the amino groups at 6,6′-positions of bpy causes a large red shift of the π–π^*-transition band, appearing in the near-UV region (320—340 nm) with a strong intensity ($\log\varepsilon>4$).[3] Furthermore, the absorption band has been found to suffer a characteristic solvent effect. In this report, a detailed study on the electronic spectra of dabp has been carried out, and the photometric and some related properties of dabp has been discussed in terms of the effect of amino substituents at 6,6′-positions.

Experimental

6,6′-Diamino-2,2′-bipyridine (dabp) was prepared and purified according to the method previously reported.[3] For spectral measurements, dabp was further purified by reprecipitation with a KOH–methanol/water system to remove a trace amount of acid salt and subsequent sublimation under reduced pressure. 2,2′-Bipyridine (bpy), 6,6′-dimethyl-2,2′-bipyridine (dmbp), and 2-aminopyridine (amp) were obtained from Wako Pure Chem. Ind., Ltd, and purified by usual procedures. 6,6′-Dibromo-2,2′-bipyridine (dbbp) were prepared according to the literature's method.[5] The electronic spectra were recorded on a JASCO UVIDEC-505 spectrophotometer at 20 °C. ^{13}C and ^{1}H NMR spectra were measured with a JEOL JNM-GX270 Spectrometer (67.8 and 270 MHz, respectively) at 27 °C.

Ab initio calculation with a STO-3G basis set was carried out at The Computer Center of The University of Tokyo, using GAUSSIAN 80 HITAC Version. To avoid prohibitive geometry optimizations, the reported geometries of the bpy ring having s-trans planar structure in the Ref. 6 and of the amino group of 2-aminopyridine (amp) in Ref. 7 were used in the calculation.

Results and Discussion

The measured absorption maxima at the longest wavelength of bpy and some of its 6,6′-disubstituted derivatives in methanol appear in the order of bpy (λ_{max}=281 nm, $\log\varepsilon$=4.13), dmbp (289 nm, 4.18), dbbp (303 nm, 4.19), and dabp (334 nm, 4.08). Dabp has a strong absorption band ($\log\varepsilon>4$) at around 330 nm, at much longer wavelength than other compounds. These absorption bands of bpy derivatives undergo a large red shift without decrease in the intensity upon protonation to the ring nitrogens in an acidic medium, i.e., the absorption maxima at the longest wavelength appear in the order of bpy (λ_{max}=302 nm, $\log\varepsilon$=4.21), dmbp (311 nm, 4.20), and dabp (358 nm, 4.19) in acidic methanol.[8] These results indicate that the bands are not due to a n–π^* but to a π–π^* transition band.[9,10]

Table 1. The absorption Maxima at the Longest Wavelength in Various Solvents

Solvent	λ_{max}/nm				
	dabp	bpy	dmbp	dbbp	amp
Cyclohexane	326	281	290	306	288
Chloroform	329	282	291	305	291
Acetone	334	—	—	—	—
Dioxane	334	281	291	306	295
DMF[a]	339	281	291	305	297
DMSO[b]	341	282	292	305	300
Ethanol	335	281	289	304	296
Methanol	334	280	289	303	296
Water[c]	325	279	287	—[d]	287

a) Dimethyl formamide. b) Dimethyl sulfoxide. c) pH 9.3 buffer solution (0.2 mol dm^{-3} of pottasium borate). d) Insoluble.

Table 2. Chemical Shifts in NMR Spectra of dabp in Various Solvents

Solvent	^{13}C[a]					^{1}H[a]
	2,2′	3,3′	4,4′	5,5′	6,6′	$\delta_{3,3'}-\delta_{5,5'}$[b]
Chloroform-d	155.1	111.6	138.4	108.6	157.9	1.04
Acetone-d_6	155.7	110.5	138.4	108.9	159.9	1.09
DMSO-d_6[c]	154.1	108.6	137.4	107.9	158.9	1.00
Methanol-d_4	156.1	111.9	139.5	110.0	160.8	0.72
Methanol-d_4+D_2O (1 : 3 v/v)	155.1	113.1	140.4	111.0	159.9	0.55

a) Chemical shift δ/ppm from TMS. b) Differences of chemical shifts between 3,3′-positions and 5,5′-positions. c) Dimethyl-d_6 sulfoxide.

Relatively few has been known as to the solvent effect on the electronic spectra of 6,6′-disubstituted bpy derivatives, and that of bpy has been reported to be little.[10,11] Those of dmbp and dbbp also suffered only a small solvent effect (Table 1). On the contrary, a larger and characteristic solvent effect was observed in the spectrum of dabp, i.e., an aprotic solvent of higher polarity caused a larger red shift to the π-π^* transition band of dabp, while water caused a blue shift. As the absorption maximum of this band suffered no change over the wide range of dabp concentration (10^{-4}—10^{-5} mol dm^{-3}) in any solvent, the solvent-dependent shifts were not due to a solute-solute interaction.[7] The imino-type tautomer of dabp is unlikely to contribute to the solvent-induced shifts, since the ^{13}C NMR spectra of dabp suffered only a small solvent effect in several different solvents (Table 2), indicating that dabp was presumably in the amino-form in these solvents.[3] The change in the conformation of two pyridine rings as a possible origin of the shifts[11] can be also ruled out from the ^{1}H NMR studies in several different solvents. The extent of the lower-field shift of the 3,3′-protons compared with the 5,5′-protons is known to be a good measure of the ring conformation of bpy moiety, and that of dabp was essentially the same as that of bpy in all solvents studied (Table 2),[11] confirming that dabp was in s-trans planar conformation.[3,4,12] Therefore, the solvent-induced shift of the absorption band may be attributed to the direct electronic effect of the amino substituents. Almost similar solvent-induced shift was observed for amp (Table 1).[7,13]

In order to understand the electronic structure of dabp, ab initio calculation with a STO-3G basis set was carried out. Bpy has six higher-lying occupied MO's, four π-MO's (π_3—π_6) and two n-MO's (n+ and n-), and four unoccupied π-MO's (π_1^*—π_4^*), which play essential role in the photochemical properties and complexability of bpy.[1,2,6] Dabp had also the same set of the corresponding MO's (Fig. 1). The MO levels of dabp were generally higher than the corresponding MO levels of bpy. In particular π_5 and π_6 levels of dabp were higher than the corresponding MO levels of bpy presumably due to an antibonding character between the amino-nitrogens and the 6,6′-carbons (Fig. 1, Table 3). However, the π_1^*-MO of dabp has small coefficients at the amino-nitrogens, affecting little to the energy level of this MO, thus lowering the energy gap between occupied π_5 or π_6-MO's and unoccupied π_1^*-MO (Fig. 1, Table 3). As the strong absorption band at the longest wavelengths are thought to have large weight on the allowed transition from the π_6 (B_g, HOMO) to the π_1^* (A_u, LUMO),[1,14] it is not surprising that the large red shift of this band was observed for dabp by introduction of amino substituents.

The solvent effect on the absorption band can be interpreted in terms of the calculated MO coefficients of π_6 (Fig. 1, Table 3). Hydrogen-bond formation by the amino-hydrogen of dabp to aprotic polar solvents may cause an increase in the electron density on the amino-nitrogens, raising the energy-level of π_6 and resulting in the red shift of the absorption band. While, the opposite effect may be resulted from hydrogen bonding of the amino-nitrogen of dabp with protons of the protic solvents (Fig. 2),[13] explaining the observed blue shift in water.

Introduction of amino substituents also affected the

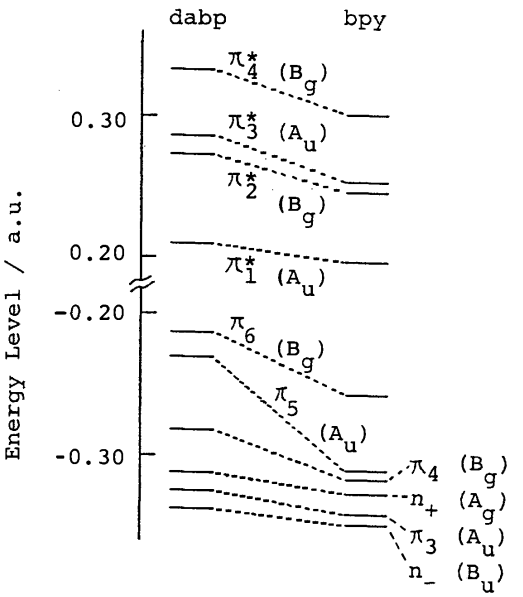

Fig. 1. The energy diagram of calculated MO of dabp and bpy.

Table 3. Energy Levels and Coefficients of the Calculated π_5, π_6, and π_1^* of dabp and bpy

Material	Orbital	Energy level/a.u.	Coefficient						
			N_1	C_2	C_3	C_4	C_5	C_6	N_{amino}
dabp	$\pi_1^*(A_u)$[a]	0.209	−0.38	0.42	−0.22	−0.27	0.40	−0.07	0.04
	$\pi_6(B_g)$[b]	−0.214	−0.07	−0.22	−0.37	−0.03	0.36	0.22	−0.35
	$\pi_5(A_u)$[c]	−0.230	−0.29	0.12	0.31	0.10	−0.23	−0.24	0.43
dpy	$\pi_1^*(A_u)$	0.197	−0.35	0.42	−0.26	−0.24	0.43	−0.10	—
	$\pi_6(B_g)$	−0.257	−0.18	−0.35	−0.31	0.07	0.37	0.23	—
	$\pi_5(A_u)$	−0.311	0.30	−0.10	−0.35	−0.28	0.05	0.34	—

a) 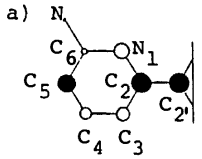

b) 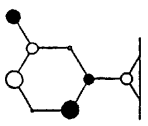
c) 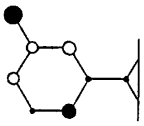

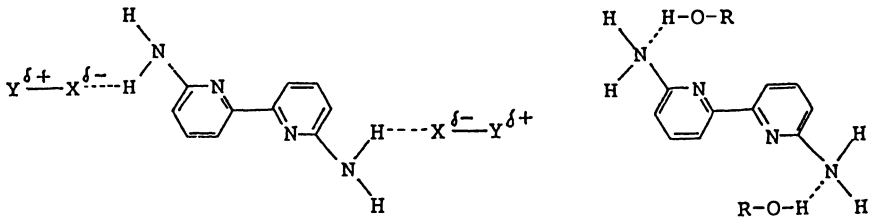

Fig. 2. The solute-solvent interactions of dabp.

basicities (proton affinities) of the nitrogen atoms of dabp, which were estimated from their ls-electron levels according to the method of Catalán et al.[15,16] The calculated proton affinities for dabp and bpy in this work[17] showed that the proton affinity of the ring-nitrogens of dabp (9.80×10^2 kJ mol^{-1}) were much higher than either those of bpy (9.22×10^2 kJ mol^{-1}) or the amino-nitrogens of dabp (8.67×10^2 kJ mol^{-1}), being in agreement with the results reported in Ref. 3.

Thus, the amino substituents at 6,6′-positions increased the σ-donating ability of the ring-nitrogens though they affected little to the lowest π^*-level (π_1^*). Since the σ-donor and π-acceptor capacities of the ligand interact synergistically in the transition-metal complexes,[18] the results described above explain the high stability of 1 : 1 complexes of dabp with divalent transition-metal ions.[3]

References

1) V. Barone, F. Lelj, C. Cauletti, M. N. Piancastelli, and N. Russo, *Mol. Phys.*, **49**, 559 (1983), and references therein.

2) D. E. Morris, K. W. Hanck, and M. K. DeArmond, *J. Am. Chem. Soc.*, **105**, 3032 (1983); Y. Ohsawa, M. Whangbo, K. W. Hanck, and M. K. DeArmond, *Inorg. Chem.*, **23**, 3426 (1984).

3) N. Kishii, K. Araki, and S. Shiraishi, *Bull. Chem. Soc. Jpn.*, **57**, 2121 (1984).

4) N. Kishii, K. Araki, and S. Shiraishi, *J. Chem. Soc., Chem. Commun.*, **1984**, 103; N. Kishii, K. Araki, and S. Shiraishi, *J. Chem. Soc., Dalton Trans.*, **1985**, 373; M. Yamada, K. Araki, and S. Shiraishi, *Bull. Chem. Soc. Jpn.*, **60**, 3149 (1987).

5) J. E. Parks, B. E. Wagner, and R. H. Holm, *J. Organomet. Chem.*, **56**, 53 (1973).

6) M. Yagi, K. Makiguchi, A. Ohnuki, K. Suzuki, J. Higuchi, and S. Nagase, *Bull. Chem. Soc. Jpn.*, **58**, 252 (1985).

7) K. Inuzuka and A. Fujimoto, *Spectrochim. Acta*, **42A**, 929 (1986).

8) In the case of dbbp, spectral change by protonation was not observed even in methanol containing 1% of sulfuric acid.

9) M. S. Henry and M. Z. Hoffman, *J. Phys. Chem.*, **83**, 618 (1979).

10) C. C. Deb, D. K. Hazra, and S. C. Lahiri, *Indian J. Chem.*, **21A**, 26 (1982).

11) T. Mcl. Spotswood and C. I. Tanzer, *Aust. J. Chem.*, **20**, 1227 (1967).

12) For more detailed discussion, see Refs. 3 and 11.

13) S. F. Mason, *J. Chem. Soc.*, **1960**, 219; C. W. N. Cumper and A. Singleton, *J. Chem. Soc. B*, **1968**, 649.

14) G. Favini, A. Gamba, and I. R. Bellobono, *Spectrochim. Acta*, **23A**, 89 (1967).

15) J. Catalán, O. Mó, P. Pérez, and M. Yáñez, *J. Am. Chem. Soc.*, **101**, 6520 (1979).

16) J. Catalán and M. Yáñez, *J. Chem. Soc., Perkin Trans. 2*, **1979**, 1627.

17) Calculation was performed applying the equation in Ref. 16 (ring-nitrogens of pyridine derivatives) for ring-nirogens and that in Ref. 15 (amino-nitrogens of aniline derivatives) for amino-nitrogens.

18) S. Ernst and W. Kaim, *J. Am. Chem. Soc.*, **108**, 3578 (1986)

Band Structure of DEBP(TCNQ)$_4$

Martin R. WILLIS,† Takehiko MORI,* and Hiroo INOKUCHI
Institute for Molecular Science, Okazaki, 444
†Chemistry Department, Nottingham University, England
(Received January 21, 1988)

Synopsis. Band structure calculations are reported for the intermediate conducting complex salt, DEBP(TCNQ)$_4$ (DEBP: *N,N'*-diethyl-4,4'-bipyridinium, TCNQ: tetracyanoquinodimethane). They show that the array of TCNQs forms a two-dimensional band structure with conduction and valence band widths 0.1 and 0.03 eV respectively. Conduction in the third direction is likely to be by hopping or tunnelling. The results are consistent with the experimental observations of electrical conductivity, magnetic susceptibility and thermoelectric power.

TCNQ complex salts have been extensively studied to explore the relationship between structure and properties. The series of general formula R^{2+}-$(TCNQ)_n^{2-}$, where $2<n<5$ and R^{2+} is an organic dication, has been investigated in some detail and a wide range of electrical and magnetic behaviour reported.[1-4] The complex salt DEBP(TCNQ)$_4$ displays intermediate conductivity and is typical of this group of materials (Table 1). It is a semiconductor with a band gap of 0.5 eV, and the anisotropy of conductivity is qualitatively consistent with the crystal structure. Assuming the application of band theory, the mobilities of electrons and holes have been deduced from an analysis of thermoelectric power measurements.[2] Alternating current conductivity studies reveal a significant concentration of localized states resulting from crystal imperfections.[4] Magnetic measurements are consistent with a thermally accessible localized triplet state, and also indicate the presence of a significant concentration of imperfections.[3]

In this paper, band structure calculations are reported in an attempt to provide a more quantitative relationship between structure and properties.

Table 1. Summary of Electrical and Magnetic Properties

(A) Single crystal conductivity

Axis	Conductivity/ S cm^{-1}	E_A (260 K)/eV
a	1.2×10^{-4}	0.25
b	2.5×10^{-3}	0.28
c	3.2×10^{-3}	0.27

(B) Carrier mobility
Seebeck effect shows,
μ_e=10—25 cm^{2}V^{-1}s^{-1}, μ_h=4—8 cm^{2}V^{-1}s^{-1}
in intrinsic region, assuming 3-D band theory and $m^*=m$,

(C) E.S.R. intensity varies as

$$I \propto \frac{1}{T(3+\exp(J/k_BT))}$$

with J=0.075 eV.

(D) Indications of defect concentration
(i) Curie component of magnetic susceptivility gives
1.6×10^{22} spins per mole
(ii) Alternating current conductivity gives density of localized states at Fermi level as
1.3×10^{25} m^{-3}

Band Calculation

X-Ray crystallography shows that the TCNQ molecules are stacked plane to plane in groups of four along the b-axis (Fig. 1),[2] giving rise to a two-dimensional molecular lattice in the bc plane. The tetrad carries two negative charges which are evenly distributed over the four molecules. The dications lie between the conduction planes of the TCNQ molecules (Fig. 2).

The band structure calculation uses the tight-binding approximation based on the extended Hückel method and is similar to that of Whangbo and Hoffmann.[5] The programming details are described elsewhere.[6] Firstly the molecular wave functions for

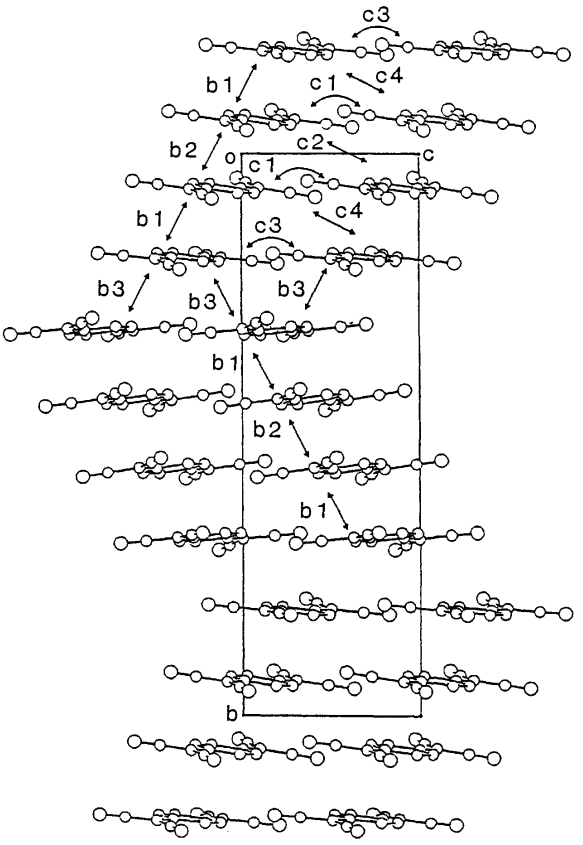

Fig. 1. The crystal structure of DEBP(TCNQ)$_4$ showing the interactions in the bc plane.

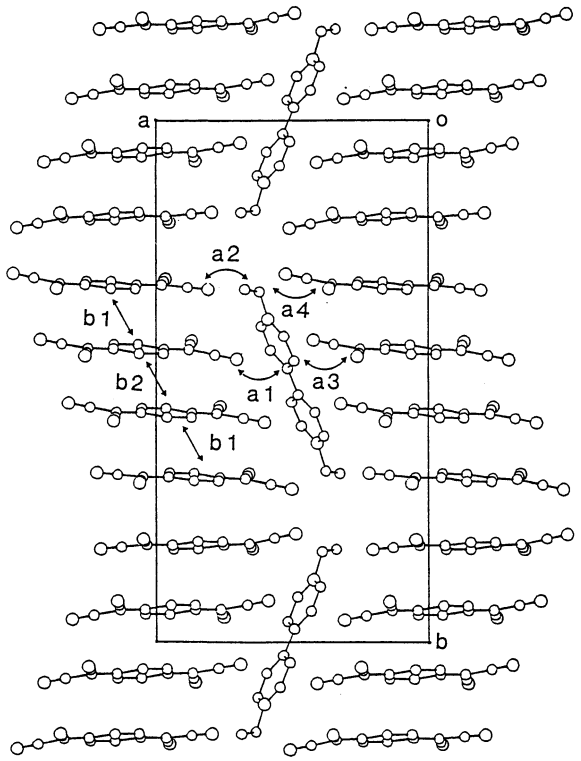

Fig. 2. The crystal structure of DEBP(TCNQ)$_4$ showing the interactions between the cation and the TCNQ tetrad, as well as within the tetrad.

Table 2. Transfer Integrals t/eV

(a) Within the TCNQ sheet			
b1	0.176	c1	0.1×10^{-3}
b2	0.194	c2	1.4×10^{-3}
b3	0.038	c3	0.2×10^{-3}
		c4	1.4×10^{-3}
(b) Between cation and TCNQ sheet			
a1, a2, a3, a4	$<10^{-4}$		

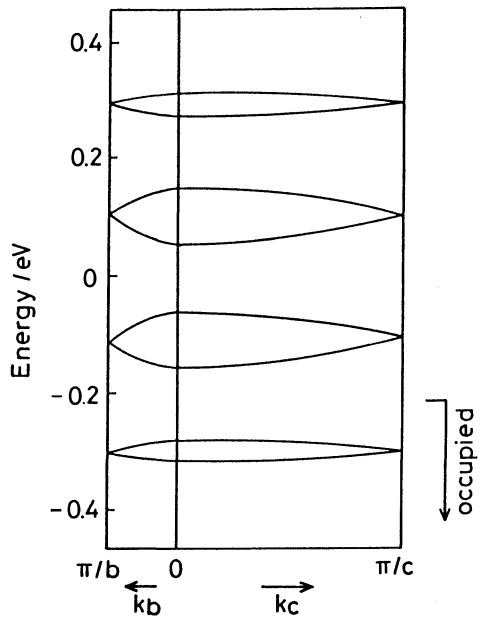

Fig. 3. The band structure of DEBP(TCNQ)$_4$.

the TCNQ molecules were calculated using the experimentally determined atomic positions. The various nearest neighbours overlap integrals (S) relevant to conduction, shown in Fig. 1 as b1, b2, b3, c1, c2, c3, and c4, were then calculated and the transfer integrals were obtained assuming proportionality to overlap integrals,

$$t = KS \tag{1}$$

where K is taken as -10 eV.[7]

Similarly, the molecular orbitals of the cation were calculated and the transfer integrals between cation and the nearest TCNQ molecules were estimated using second order perturbation theory because of the large energy difference.

The absolute values of the transfer integrals are listed in Table 2. Knowing the transfer integrals the band structure was calculated (Fig. 3). The interactions split the LUMO of TCNQ (or the HOMO of $TCNQ^-$) into four bands, the lowest of which is filled and the others empty at 0 K.

Results and Discussion

Dimensionality. From the values of the transfer integrals it is clear that interaction within the tetrad is nearly uniform (b1=b2), and that the most significant interaction between tetrads which determines the conduction path , is b3. By comparison, the transfer integrals between any of the TCNQ s in the tetrads and the cation (a1—a4) are negligible. The material can therefore be represented, to a good approximation, by a two-dimensional band structure. Furthermore, since the band width is determined by the transfer integral corresponding to b3, the conductivity in the b and c directions should be equivalent, which is in good agreement with the experimental observations (Table 1).

Band Conduction. The band calculation shows the material to be a semiconductor. The one-electron calculation gives a separation between the bands of 0.1 eV but allowance must be made for Coulomb interaction between the electrons to obtain the true band gap (E_g). It has been suggested that for a two-dimensional system,[3] the band gap is given by

$$2E_A = E_g = (U - 8t), \tag{2}$$

where t is identified with the average interaction. By taking U to be 1.5 eV, as proposed by Tanaka,[8] then E_g=0.5 eV, in good agreement with experiment.

The band widths calculated for the conduction band of 0.1 eV and for the valence band of 0.03 eV are well within the criterion for band conduction and since the band widths are both greater than k_BT (0.025 eV at room temperature), just satisfy the criterion for broad band conduction.[9] The greater width of the conduction band indicates that the electron has the higher mobility, in agreement with experiment (Table 1).

Conduction in the a Direction. Conduction in the direction normal to the two-dimensional array of TCNQs is clearly not band conduction, as the small

transfer integral would lead to far too narrow a band. A likely mechanism is hopping or tunnelling of the carriers via the cation. This is supported by the observation that the conductivity is lower in this direction by an order of magnitude, whilst the activation energy is isotropic within experimental error, indicating a low hopping barrier. When the carrier is an electron, the intermediate species formed is the resonance stabilized monocation, which corresponds to the violet species readily formed in solution.[10] In contrast, for methyltriphenylphosphonium$(TCNQ)_4$, which does not form such a stabilized intermediate, the anisotropy is two orders of magnitude greater.[11]

Thermoelectric Power. The band calculations give some insight into the validity of the assumptions made earlier in the analysis of the thermoelectric power measurements to derive electron and hole mobilities and their temperature dependencies.[2] The assumption of band conduction is clearly valid, but a two-dimensional density of states with allowance for the number of TCNQ sheets per unit cross section, might have been more appropriate. However, the significant concentration of imperfections tends to shift the density of states towards the three-dimensional value, so the error is likely to be small. No information was available on electron and hole effective masses so they were assumed to be approximately equal to the free electron mass. The calculated band widths enable the effective masses to be estimated from,[9]

$$m = \frac{\hbar}{Wa^2}, \tag{3}$$

where W is the band width and a the lattice constant. The value of m is clearly strongly dependent on the value of a which is not obvious for such a complex structure. If we regard the TCNQ tetrad, over which the electronic charges are fully delocalized, as the basic structural unit, then the repeat distance is 7—13 Å depending on the direction chosen. This gives m_e/m=0.5 to 1.6 and m_h/m=1.5 to 5, suggesting that equating the carrier masses with the free electron mass is a fair approximation.

Magnetic Properties. Since the intra-tetrad transfer integrals are much greater than those between tetrads, temperature dependent paramagnetism associated with the thermal population of a low lying triplet state is to be expected. The singlet triplet splitting is given by[8]

$$J = \frac{4t^2}{U}. \tag{4}$$

Taking the average transfer integral within the tetrad and U=1.5 eV, then J=0.088 eV, in reasonable agreement with the experimental value (Table 1).

Conclusion

The satisfactory agreement between theory and experiment provides strong support for the two-dimensional band model adopted for this group of compounds.

The authors are grateful to the Japan Society for the Promotion of Science for the award of a Fellowship to M. R. W.

References

1) A. Rembaum, A. M. Hermann, F. E. Stewart, and F. Gutmann, *J. Phys. Chem.*, **73**, 513 (1969).
2) G. J. Ashwell, D. D. Eley, S. C. Wallwork, and M. R. Willis, *Proc. R. Soc. London, Ser. A*, **343**, 461 (1975).
3) G. S. Ashwell, D. D. Eley, S. C. Wallwork, M. R. Willis, and J. Woodward, *Ann. N.Y. Acad. Sci.*, **313**, 417 (1978).
4) I. Diaconu, D. D. Eley, and M. R. Willis, *Phys. Status Solidi A*, **85**, 283 (1984).
5) M.-H. Whangbo and R. Hoffmann, *J. Am. Chem. Soc.*, **100**, 6083 (1978).
6) T. Mori, Dr. Thesis, University of Tokyo (1985).
7) T. Mori, A. Kobayashi, Y. Sasaki, H. Kobayashi, G. Saito, and H. Inokuchi, *Bull. Chem. Soc. Jpn.*, **57**, 627 (1984).
8) J. Tanaka, M. Tanaka, T. Kawai, T. Takabe, and O. Maki, *Bull. Chem. Soc. Jpn.*, **49**, 2358 (1976).
9) H. Meier, "Organic Semiconductors," Verlag Chemie, 1974.
10) L. Michaelis and E. S. Hill, *J. Am. Chem. Soc.*, **55**, 1481 (1933).
11) D. Zosel, H. Ritschel, and H. Hansel, *Phys. Status Solidi*, **32**, K75 (1975).

The Crystal and Molecular Structure of Diaquadihydroxotetrakis-(*m*-nitrobenzenesulfonato)discandium(III) in a Linear Polymeric Form, $[Sc_2(OH)_2(O_2NC_6H_4SO_3)_4(H_2O)_2]_n$

Yoshikuni TATEYAMA,† Yoshiyuki OHKI,† Yasuo SUZUKI,† and Akira OUCHI*
Department of Chemistry, College of Arts and Sciences, The University of Tokyo, Komaba, Meguro-ku, Tokyo 153
†Department of Industrial Chemistry, Faculty of Engineering, Meiji University, Higashi-Mita, Tama-ku, Kawasaki-shi, Kanagawa 214
(Received November 27, 1987)

Synopsis. The crystal and molecular structures of the title complex has been determined by the single-crystal X-ray diffraction method. It is monoclinic, with the space group *Pn*, *Z*=2 (including 4 metal atoms), *a*=28.90(2), *b*=10.251(4), *c*=5.981(1) Å, and *β*=94.68(3)°. Both of the metal atoms, Sc(1) and Sc(2), have the hexa-coordinated octahedral geometry, being coordinated to four sulfonato oxygen atoms as well as to two water oxygen (Sc(1)) or to two hydroxide oxygen atoms (Sc(2)). Any pair of the neighboring metal atoms along the b-axis are bridged by two sulfonato ions, forming an infinite chain structure; however, the Sc(2)-O bond lengths (2.307(10)—2.556(19) Å; average, Sc(2)-O (sulfonate), 2.422; Sc(2)-O(OH^-), 2.394 Å) are much longer than the Sc(1)-O lengths (2.031(7)—2.150(8) Å; average, Sc(1)-O(sulfonate), 2.055; Sc(1)-O(H_2O), 2.122 Å).

Many scandium(III) salts are known to have a hexa-coordinated octahedral geometry around their metal atoms;[1-3] they are not in high coordination number like yttrium(III) or lanthanoid(III) complexes.[4,5] However, some scandium(III) salts, especially its carboxylates, have a chain structure like the other rare earth complexes.[6,7]

On the other hand, it was reported that arenesulfonate ions act as a unidentate in many rare earth(III) complexes;[8,9] moreover, alkyl sulfate ligands are not coordinated to the metal atoms in their salts,[10] although both of them are also oxo acidate anions.

Therefore, it is interesting to examine whether such sulfonate ligands can act as multidentates in some rare earth complexes, and whether or not the scandium(III) atom keeps the hexa-coordination geometry in such salts.

This time, since we could synthesize the title complex, its crystal and molecular structure was determined by the single-crystal X-ray diffraction technique.

Experimental

Synthesis of Deaquadihydroxotetrakis(*m*-nitrobenzenesulfonato)discandium(II) Scandium oxide (Sc_2O_3 0.14 g, including 2 mmol of Sc) was dissolved into hydrochloric acid (6 mol dm^{-3}, 20 cm^3), and the solution was evaporated off on a water bath. The residue was dissolved into 15 cm^3 of water together with sodium *m*-nitrobenzenesulfonate (1.36 g, 6.0 mmol). The solution was kept in a silica-gel desiccator until about one third of the solvent was evaporated off. The crystals deposited. Yield: 0.75 g (0.77 mmol (as a dimer), 77%). Found, C, 30.11; H, 2.48; N, 5.86%. Calcd for $Sc_2C_{24}H_{22}O_{24}N_4S_4$ (F.W., 968.62): C, 29.76; H, 2.29; N, 5.78%.

X-Ray Structure Analysis. The used crystal was colorless, approximately parallelepiped in shape (0.35×0.35×0.20 mm^3), monoclinic, space group *Pn*, *Z*=2 (including four Sc atoms in a unit cell), *a*=28.90(2), *b*=10.251(4), *c*=5.981(1) Å, *β*=94.68(3)°, *U*=1776(1) $Å^3$, D_m=1.79(3), D_x=1.82 g cm^{-3}, *μ*(Mo *Kα*)=7.25 cm^{-1}. The intensities were measured on a Rigaku AFC-6A automated 4-circle X-ray diffractometer with graphite monochromated Mo *Kα* radiation (*λ*=0.71073 A), an *ω*-scan technique being employed (the scanspeed was 4° min^{-1} (*θ*), scan width 1.03° (*θ*), and the scanned range was 3—65° (2*θ*)). Of the 6721 independent reflections measured, 4507 (reflections of $|F_o|>3\sigma(|F_o|)$) were used for a structure determination. The intensities were corrected for the Lorentz and polarization factors, but not for absorption and extinction. The structure was solved by the heavy-atom method. The positional and thermal parameters of the atoms were refined repeatedly by the block-diagonal least-squares method. At the final step, all non-hydrogen atoms were found and included in the refinement with the anisotropic temperature factors: all the hydrogen atoms were excluded from the structure factor calculations. The final *R* value was 0.074 (the *R* value for the structure assuming an inversed chirality was also 0.074).

All of the calculations were carried out on a HITAC M-682H computer at the Computer Center of the University of Tokyo using a local version of the UNICS program system.[11] The atomic scattering factors were taken from Ref. 12.

Table 1. Bond Lengths and Bond Angles of the Complex with the Standard Deviations in Parentheses

Bond length	(*l*/Å)	Bond length	(*l*/Å)
Sc(1)-O(1)	2.150(8)	Sc(1)-O(2)	2.094(7)
Sc(1)-O(11)	2.035(7)	Sc(1)-O(21)	2.059(8)
Sc(1)-O(32^{ii})	2.031(7)	Sc(1)-O(42^{ii})	2.095(8)
Sc(2)-O(3)	2.367(12)	Sc(2)-O(4)	2.420(11)
Sc(2)-O(12)	2.460(11)	Sc(2)-O(22)	2.364(9)
Sc(2)-O(31)	2.307(10)	Sc(2)-O(41)	2.556(10)
S(1)-O(11)	1.517(8)	S(1)-O(12)	1.390(8)
S(1)-O(13)	1.467(10)	S(2)-O(21)	1.484(8)
S(2)-O(22)	1.409(7)	S(2)-O(23)	1.436(9)
S(3)-O(31)	1.434(8)	S(3)-O(32)	1.484(8)
S(3)-O(33)	1.448(9)	S(4)-O(41)	1.427(8)
S(4)-O(42)	1.438(8)	S(4)-O(43)	1.414(9)
Sc(1)···Sc(2)	5.102(6)	Sc(2)···Sc(1^{i})	5.149(6)
O(1)···O(23^{iii})	2.670(11)	O(1)···O(43^{iv})	2.656(11)
O(2)···O(13^{v})	2.736(11)	O(2)···O(33^{vi})	2.652(10)
O(3)···O(12^{v})	3.086(15)	O(4)···O(41^{iii})	3.064(13)
Bond angle	**(*φ*/°)**	**Bond angle**	**(*φ*/°)**
Sc(1)-O(11)-S(1)	142.8(4)	Sc(2)-O(12)-S(1)	141.1(6)
Sc(1)-O(21)-S(2)	164.2(5)	Sc(2)-O(22)-S(2)	135.6(5)
Sc(2)-O(31)-S(3)	139.4(6)	Sc(1^{i})-O(32)-S(3)	160.5(5)
Sc(2)-O(41)-S(4)	140.7(5)	Sc(1^{i})-O(42)-S(4)	143.6(5)

Key to the symmetry operations: i, *x*, 1+*y*, *z*; ii, *x*, −1+*y*, *z*; iii, *x*, *y*, −1+*z*; iv, *x*, 1+*y*, −1+*z*; v, *x*, *y*, 1+*z*; vi, *x*, 1+*y*, 1+*z*.

Results and Discussion

The selected bond lengths and bond angles are shown in Table 1. The perspective drawing of the complex, together with the numbering scheme of the atoms is shown in Fig. 1, and the projection of the unit cell to the ab-plane in Fig. 2.[13]

Both of the scandium(III) atoms, Sc(1) and Sc(2), are in an octahedral geometry, being coordinated with six oxygen atoms: in addition to four sulfonate oxygen atoms, two water oxygen (Sc(1)), or two hydroxide oxygen atoms (Sc(2)), are ligated to the respective metal atoms in a trans-configuration.

Each pair of the neighboring metal atoms along the b-axis are apparently bridged with two sulfonate ions,

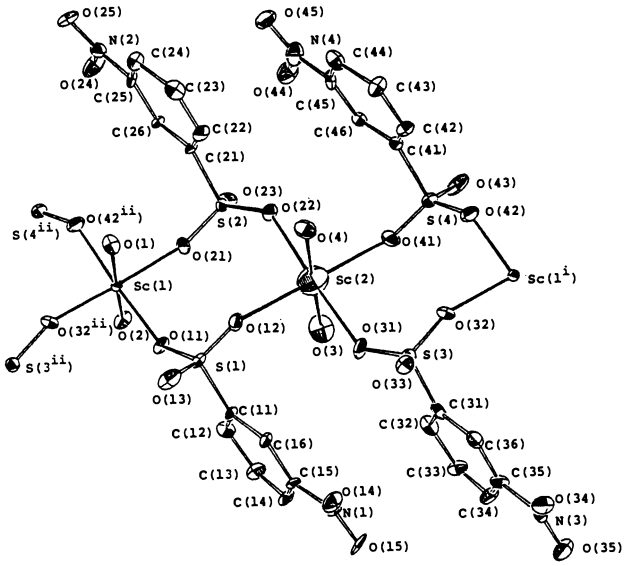

Fig. 1. A perspective drawing of the structure of the complex in a chain form, with the numbering scheme of the atoms. Key to the symmetry operations: i, x, $1+y$, z; ii, x, $-1+y$, z.

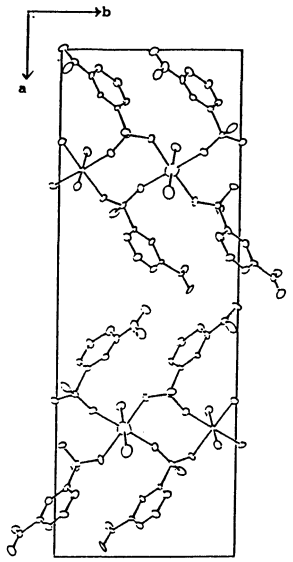

Fig. 2. A projection of the unit cell to the ab-plane.

where the anions act as a bidentate being coordinated to the both side metal atoms with their sulfonato oxygen atoms.

However, it is an interesting fact that the Sc-O bond lengths around the Sc(1) and Sc(2) atoms are much different from each other.

The Sc(1)-O(1,2) bond lengths (2.150(8) and 2.094(7) Å) are shorter than the Sc(2)-O(3,4) lengths (2.367(12) and 2.420(11) Å). From the spectrochemical study, it was proposed that a hydroxide ion is coordinated to a metal atom more weakly than a water molecule.[14] Therefore, the O(1) and O(2) atoms are assigned to be the water oxygen atoms, while the O(3) and O(4) atoms the hydroxide ones. This is also supported by the fact that, as shown in Table 1, the former two oxygen atoms have two hydrogen bondings to the sulfonate oxygen atoms of the neighboring complexes, while the latter two oxygen atoms have only one such hydrogen bonding, respectively.

Moreover, not only the Sc-O (H_2O, or OH^-) bond lengths, but also the Sc-O (sulfonato) bond lengths around the Sc(1) and Sc(2) atoms are different from each other: the average bond lengths around the Sc(1) atom is 2.055 Å (2.031(7)—2.095(8) Å), while that around the Sc(2) atom is 2.422 Å (2.307(10)—2.556(10) Å). The average of the all six Sc-O coordination bond lengths around the Sc(1) atom is 2.077 Å, while that around the Sc(2) atom is 2.412 Å: the former is approximately the same as the sum of the Shannon's ionic radii, 2.10 Å,[15] while the latter is much longer than the value.

Therefore, the circumstances around the Sc(1) and Sc(2) atoms are much different from each other. The Sc(1) atom is normally coordinated with the ligands, while the Sc(2) atoms is apparently only trapped in a cage of the negatively charged six oxygen atoms around it, because not only all the Sc(2)-O bond lengths are abnormally long, but also the thermal parameter of the latter metal atom is very large (B_{eq}=8.1$_9$ Å^2). Along the linear polymeric chain, which is formed parallel to the b-axis, these two types of the metal atoms are arranged alternately.

The inter-metal-atomic distances of Sc(1)$\cdots$Sc(2) and Sc(2)$\cdots$Sc(1^i) (key to the symmetry operation; i, x, $1+y$, z) are 5.102(6) and 5.149(6) A, respectively. Each linear complex chain along the b-axis is connected with the neighboring complex chains on both sides along the c-axis with some hydrogen bondings, but no such bondings are found in the a-axis direction. The nitro-group oxygen and nitrogen atoms are not ligated to any metal atoms.

Of the bridging ligands, the couples of the Sc-O-S angles on both sides of the S(1) and S(4) atoms are not much different from each other: the four angles are in the range of 140.7(5)—143.6(5)°. On the other hand, couples of the bond angles on both sides of the S(2) and S(3) atoms are much different from each other: 135.6(5)° and 164.2(5)° for the couple around the S(2), and 139.4(6)° and 160.5(5)° for those around the S(3) atoms, respectively. Therefore, the latter two bridgings are found to be deformed; however, no clear relation has yet been obtained between the angles and the corresponding Sc-O bond lengths.

References

1) T. J. Anderson, M. A. Neuman, and G. A. Melson, *Inorg. Chem.*, **12**, 927 (1973).
2) E. Hansson, *Acta Chem. Scand.*, **26**, 1337 (1972).
3) J. L. Atwood and K. D. Smith, *J. Chem. Soc., Dalton Trans.*, **1974**, 921.
4) T. Moeller, "Comprehensive Inorganic Chemistry," ed by J. C. Bailar, H. J. Emeleus, Sir R. Nyholm, and A. F. Trotman-Dickenson, Pergamon Press, New York (1973), Vol. 4, p. 22.
5) E. L. Muetterties and C. M. Wright, *Quart. Rev.*, **21**, 109 (1967).
6) E. R. Birnbaum, "Gmelin Handbook of Inorganic Chemistry," 8th ed, ed by T. Moeller, Syst. No. 39, Part D5, Springer Verlag, New York (1984), pp. 2, 21.
7) Y. Sugita, Y. Ohki, Y. Suzuki, and A. Ouchi, *Bull. Chem. Soc. Jpn.*, **60**, 3441 (1987).
8) Y. Ohki, Y. Suzuki, M. Nakamura, M. Shimoi, and A. Ouchi, *Bull. Chem. Soc. Jpn.*, **58**, 2968 (1985).
9) Y. Ohki, Y. Suzuki, T. Takeuchi, and A. Ouchi, *Bull. Chem. Soc. Jpn.*, **61**, 393 (1988).
10) J. Albertsson and I. Elding, *Acta Crystallogr., Sect. B*, **33**, 1460 (1977).
11) "Universal Crystallographic Computation Program System (UNICS)," ed by T. Sakurai, Crystallographic Society of Japan, Tokyo (1967).
12) "International Tables for X-Ray Crystallography," Kynoch Press, Birmingham, U. K. (1974), Vol. IV, pp. 72, 150.
13) The final atomic positional and thermal parameters, the final F_o—F_c table, and some additional data of bond lengths and bond angles are deposited as Document No. 8796 at the Office of the Editor of Bull. Chem. Soc. Japan.
14) B. N. Figgis, "Introduction to Ligand Fields," Interscience, New York (1966), p. 242.
15) R. D. Shannon, *Acta Crystallogr., Sect. A*, **32**, 751 (1976). (Sc(coordination number, 6; valence, 3+): 0.745 Å. O(coordination number, 2; valence, 2−): 1.35 Å).

X-Ray Structure Determination and NMR Characterization of Some Fused Heterocycles with a 1,3,5-Triazine-2,4(1*H*,3*H*)-dione Ring. Reaction of 2-Amino-4(3*H*)-pyrimidinone with Chloroformyl Isocyanate

Masami SAWADA,* Takanori TANAKA, Yoshiro FURUKAWA, Tomoki TODA, Yoshio TAKAI, and Terukiyo HANAFUSA
Material Analysis Center, the Institute of Scientific and Industrial Research, Osaka University, 8-1, Mihogaoka, Ibaraki, Osaka 567
(Received August 26, 1987)

Synopsis. The reaction product **a** of 2-amino-4(3*H*)-pyrimidinone with chloroformyl isocyanate was methylated and the two resulting products were determined as **4** (for the major product) and **5** (for the minor one) by X-ray crystal structure analyses. In a DMSO solution of **a**, the **2a** tautomer was shown to be predominant by ^{13}C NMR analysis.

The reactions and reactivities of heterocyclic compounds have been extensively studied in view of synthetic, mechanistic, and biological interest.[1,2] We have reported on the formation of fused 1,3,5-triazine-2,4(1*H*,3*H*)-diones by a reaction of 4(1*H*)-pyridinone with alkyl isocyanates.[3,4]

Recently, Kamal et al.[5] communicated the reaction of 2-aminopyrimidine with chloroformyl isocyanate (CFI)[6] to give 2*H*-pyrimido[1,2-*a*][1,3,5]triazine-2,4-(3*H*)-dione. As an extension of our synthetic studies using 4-pyridinone families,[3] we carried out a reaction of 2-amino-4(3*H*)-pyrimidinone (**1**) with CFI in acetonitrile under heterogeneous conditions. Here, we describe the structures of the reaction product and the dialkylated derivatives which have been determined by means of X-ray and ^{13}C NMR analyses.

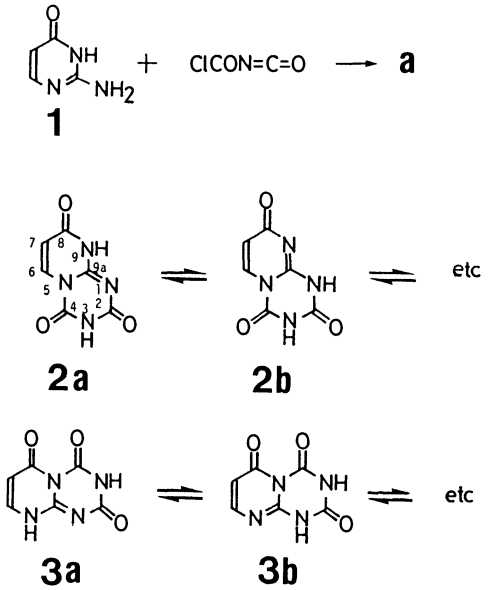

Experimental

Materials. 2-Amino-4(3*H*)-pyrimidinone (mp 273—275 °C; 4.0 g; 36 mmol), which was synthesized by following the literature method,[7] was suspended in acetonitrile and triethylamine (4.0 g; 40 mmol). An acetonitrile solution (10 ml) of chloroformyl isocyanate (3.2 ml; 40 mmol) was added dropwise with cooling to the above solution under nitrogen atmosphere. The mixture was stirred overnight at room temperature. After removal of the solvent, water (40 ml) was added. The precipitated product was collected, washed twice with water (20 ml), and dried in vacuo (5.9 g; 91% yield, **a**); mp 279—281 °C (decomp); ^{1}H NMR (DMSO-d_6) δ=12.38 (1H, br, NH), 11.88 (1H, br, NH), 8.16 (1H, d, J=8.1 Hz, =CH-N), 6.05 (1H, d, J=8.1 Hz, =CH-CO); ^{13}C NMR (DMSO-d_6) δ=162.47 (C7), 152.55 and 151.24 (C2, C4), 146.35 (C8a), 134.25 (C5), 108.32 (C6); IR (Nujol) 1770, 1710, 1650 (CO) cm^{-1}; MS (70 eV) m/z 180 (M^+); pK_{a_1}=5.47±0.01, pK_{a_2}=9.71±0.03 (20 °C, H_2O); Anal. ($C_6H_4N_4O_3$) C, H, N.

Methylation of **a** was performed in DMF by excess methyl iodide in the presence of potassium carbonate. After the usual workup by medium-pressure column chromatography (silica gel), two kinds of dimethyl derivatives, **b** (mp 253—256 °C, 64% yield) and **c** (mp 218—219 °C, 13% yield) were obtained. Similarly, after benzylation of **a** by excess benzyl bromide, **d** (mp 122—123 °C, 72% yield) and **e** (mp 253—255 °C, 24% yield) were obtained(: for ^{13}C NMR data, see Table 2).

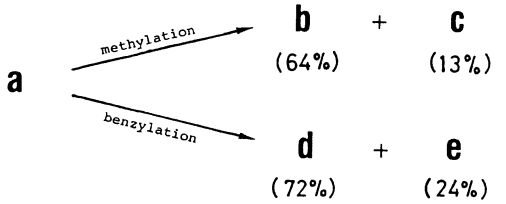

X-Ray Analysis. Colorless crystals of **b** and **c** were obtained by recrystallizations from ethanol and **d** from acetonitrile. Crystal data and analytical conditions are summarized in Table 1.[4a] Three dimensional intensity data were collected on a Rigaku AFC-5FOS automated four-circle diffractometer at room temperature. Mo$K\alpha$ (λ 0.710679 Å) radiation with a graphite crystal monochromator in the incident beam was used. Unit cell constants were determined by a least-squares fit of 15—25 reflections in the range of $15° < 2\theta < 35°$ for all cases. Intensity data were reduced to structure factors without any absorption corrections. Structures were reduced by MULTAN direct methods, refined by block-diagonal least-squares methods. Non-hydrogen atoms were assigned with anisotropic temperature factors. Hydrogen atoms were found from difference Fourier calculations and refined with isotropic thermal parameters. In the case of **c**, hydrogens were not included in the computation. The function minimized was $\sum\omega\,(|F_o|-|F_c|)^2$ with the same equation as described before.[4a]

Computations were carried out on a FACOM S3500 superminicomputer at Material Analysis Center, ISIR, Osaka Univ. or an ACOS-850 computer at Crystallographic Research Center, IPR, Osaka Univ.[8] In the former case, RASA and ANCHOR software were employed for structure analyses and a 3-dimensional graphic display, respectively.[9] From the results, it was determined that the structure of **b** is

Table 1. Crystal and Experimental Data for **b**, **c**, **d**

Compound	**4** (**b**)	**5** (**c**)	**8** (**d**)
Formula	$C_8H_8N_4O_3$	$C_8H_8N_4O_3$	$C_{20}H_{16}N_4O_3$
Molecular weight	208.18	208.18	360.24
Crystal system	triclinic	tetragonal	orthorhombic
Space group	$P\bar{1}$	$P42bc$	$Fdd2$
a/Å	10.1187(7)	17.228(5)	39.083(9)
b/Å	10.4462(13)	17.228(5)	16.794(4)
c/Å	4.3015(10)	6.4446(25)	10.714(3)
a/deg	89.181(15)		
b/deg	95.687(11)		
c/deg	106.220(8)		
V/Å^3	434.39(12)	1912.78(14)	7031.82(26)
Z	2	8	16
D_c/g cm^{-3}	1.5922	1.4463	1.3620
μ(Mo $K\alpha$), cm^{-1}	1.232	1.356	1.022
Crystal size/mm^3	0.4×0.3×0.2	0.2×0.08×0.1	0.4×0.3×0.15
Scan method	θ-2θ	θ-2θ	θ-2θ
Scan range $\Delta(2\theta)$/deg	1.4+0.5tanθ	1.40+0.7tanθ	1.20+0.6tanθ
Scan speed in 2θ/deg min^{-1}	4	4	12
$2\theta_{max}$/deg	55	55	60
Background/s	2×5.0	2×5.0	2×5.0
Refl. measd	2270	1549	2845
Refl. independ.	2003	1366	2640
Direct method	MULTAN84	MULTAN84	MULTAN(78),84
Refl. used[a)]	1694	800	1568
Final R	0.048	0.083	0.046
Final R_w	0.040	0.076	0.041

a) $F_o > \sigma(F_o)$.

4, that of **c** is **5**, and that of **d** is **8**. Tables of the final atomic positional and thermal parameters, and anisotropic thermal parameters of the non-hydrogen atoms, F_o and F_c, and figures of bond lengths for **b**, **c**, **d** are deposited as Document No. 8794 at the Office of the Editor of Bull. Chem. Soc. Jpn.

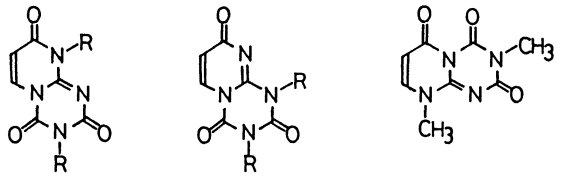

4 (R = CH_3-) **5** (R = CH_3-) **6**

8 (R=$C_6H_5CH_2$-) **9** (R=$C_6H_5CH_2$-)

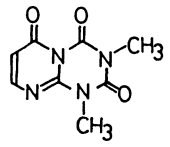

7

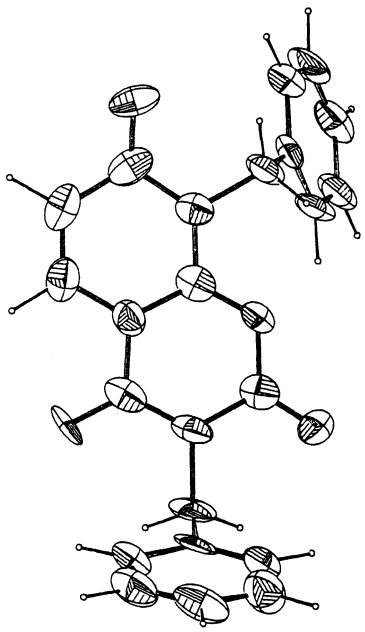

Fig. 1. ORTEP view of **d**. The non-hydrogen atoms were drawn at the 50% probability level and the hydrogen atoms at an arbitrary diameter.

Results and Discussion

By using elemental analysis, mass, ^{1}H, and ^{13}C NMR spectroscopic data of **a**, we could not identify one of four possible structures among **2a**, **2b**, **3a**, and **3b**. Since it was difficult to obtain a single crystal, **a** was converted into dimethyl (**b**,**c**) and dibenzyl derivatives (**d**, **e**). By X-ray crystal analyses, the structures of **b**, **c**, and **d** were confirmed to be **4**, **5**, and **8** (Fig. 1), respectively. Neither abnormal bond lengths nor bond angles were found in these structures.[4a)] These results suggest that the reaction of 2-amino-4(3*H*)-pyrimidinone with CFI gives 2*H*-pyrimido[1,2-*a*][1,3,5]-triazine-2,4,8(3*H*,9*H*)-trione in high yield.

^{13}C NMR data of alkyl-substituted derivatives of **2a** or **2b** are summarized in Table 2. There exist clear

Table 2. ^{13}C NMR Data (δ, ppm from TMS)[a]

Compd	*N*-Subst[b] of **2a** or **2b**	Solvent[c]	C8	C4, C2	C9a	C6	C7
4(b)	3,9-Me_2 (**2a**)	C	159.29	152.60, 150.32	146.99	132.74	107.95
5(c)	1,3-Me_2 (**2b**)	C	168.05	147.82, 146.54	144.67	132.83	112.40
8(d)	3,9-Bz_2 (**2a**)	C	159.25	152.13, 150.00	146.87	132.86	108.01
9(e)	1,3-Bz_2 (**2b**)	C	167.90	147.76, 146.18	144.52	132.93	112.72
10	9-Bz[d] (**2a**)	D	159.77	153.11, 151.87	146.72	134.01	106.28
11	1-Bz[d] (**2b**)	D	167.92	148.08, 148.02	144.47	133.74	110.53
12	3-Bz[d] (**2a**/**2b**)	D	161.30	152.43, 150.66	147.13	135.00	108.32
2	None (**2a**/**2b**)	D	162.47	152.55, 151.24	146.35	134.25	108.32

a) Bruker AM360 (90 MHz). b) Bz: $C_6H_5CH_2$–. c) C: $CDCl_3$, D: DMSO-d_6. d) Ref. 2a.

differences in ^{13}C NMR chemical shifts. We can classify them into two types of derivatives: compounds with an alkyl substituent at the N-9 position and those at the N-1 position. For example, compared with N-1 substitutions (**5**, **9**, **11**), N-9 substitutions (**4**, **8**, **10**) show upfield-shifts in C8 (ca. 8 ppm), C7 (ca. 4 ppm), and downfield-shifts in C2, C4 (ca. 4 ppm), C9a (ca. 2 ppm): on the other hand, there are no clear differences in the ^1H NMR chemical shifts (C6-H, C7-H) between the two classes.

The ^{13}C NMR data of the parent compound (**2**) and the monobenzyl derivative at N-3 position (**12**)[2a] resemble each other. Furthermore, both compounds show a very similar ^{13}C NMR pattern to the former (N-9) substitution class. These observations indicate that the tautomer structure **2a** is much more favorable than **2b** in a DMSO solution.

References

1) a) "Advances in Heterocyclic Chemistry," ed by A. R. Katritzky, Vol. 39, Academic Press (1986); b) *ibid.*, Vol. 40, (1986).

2) a) Y. Furukawa, Ph. D. Thesis, ISIR, Osaka University, 1987; b) M. Sawada, M. Ichihara, Y. Yukawa, T. Nakachi, and Y. Tsuno, *Bull. Chem. Soc. Jpn.*, **53**, 2055 (1980); c) M. Sawada, Y. Takai, S. Yamano, S. Misumi, T. Hanafusa, and Y. Tsuno, *J. Org. Chem.*, **53**, 191 (1988).

3) a) M. Sawada, M. Ichihara, Y. Furukawa, Y. Takai, T. Ando, and T. Hanafusa, *Tetrahedron Lett.*, **23**, 3181 (1982); b) M. Sawada, Y. Furukawa, Y. Takai, and T. Hanafusa, *Synthesis*, **1983**, 593. c) M. Sawada, Y. Furukawa, Y. Takai, and T. Hanafusa, *Heterocycles*, **22**, 501 (1984).

4) a) M. Sawada, T. Tanaka, Y. Takai, Y. Furukawa, T. Hanafusa, and S. Misumi, *Bull. Chem. Soc. Jpn.*, **59**, 949 (1986); b) M. Sawada, H. Yamada, Y. Furukawa, C. Chong, F. Fukuda, T. Tanaka, Y. Takai, T. Hanafusa, and S. Misumi, *Nippon Kagaku Kaishi*, **1986**, 560.

5) A. Kamal and P. B. Sattur, *Synthesis*, **1985**, 892.

6) H. Hagemann, *Angew. Chem., Int. Ed. Engl.*, **16**, 743 (1977).

7) W. T. Caldwell and H. B. Kime, *J. Am. Chem. Soc.*, **62**, 2365 (1940).

8) a) P. Main, S. E. Hull, L. Lessinger, G. Germain, J-P. Declercq, and M. M. Woolfson, "A System of Computer Programs for the Automatic Solution of the Crystal Structures from X-Ray Diffraction Data, MULTAN 78," University of York (1978); b) T. Ashida, "The Universal Crystallographic Computing System-Osaka, HBLS-V," the Computation Center, Osaka University (1979), p. 53. c) "International Tables for X-Ray Crystallography," Kynoch Press, Birmingham (1974), Vol. 4, p. 71; d) C. K. Johnson, "ORTEP-II: A FORTRAN Thermal Ellipsoid Plot Program for Crystal-structure Illustrations, ORNL-5138," March, 1976, Oak Ridge National Laboratory.

9) a) M. Sawada, Y. Takai, H. Yamada, F. Fukuda, T. Tanaka, T. Ishimaru, S. Misumi, and T. Hanafusa, to be submitted; b) M. Sawada, *Chemistry*, **1987**, 300; c) P. Main, G. Germain, and M. M. Woolfson, MULTAN 84, "A Computer Program for the Automatic Solution of Crystal Structures from X-Ray Diffraction Data," University of York (1984).

The Synthesis of a Heavy-Atom Derivative of Gramicidin S (GS), [D-Phe(4-Br)$^{4,4'}$]-GS, by a Novel Method

Saburo AIMOTO
Institute for Protein Research, Osaka University, Yamadaoka, Suita, Osaka 565
(Received September 7, 1987)

Synopsis. A new approach for the preparation of cyclic peptides was successfully applied to the synthesis of *cyclo*(-Val-Orn-Leu-D-Phe(4-Br)-Pro-Val-Orn-Leu-D-Phe (4-Br)-Pro-) ([D-Phe(4-Br)$^{4,4'}$]-GS). [D-Phe(4-Br)$^{4,4'}$]-GS showing antibacterial activity was obtained as crystals.

Cyclic peptides show interesting functions, such as acting as ionophores or antibiotics, and also serve as good model compounds for the basic study of peptide and protein conformation. Thus, many cyclic peptides have been synthesized, but mostly by the solution method which takes much time and effort. To overcome these difficulties, a new, simple, and time-saving method was developed. The present paper describes how it was used to prepare [D-Phe(4-Br)$^{4,4'}$]-GS and also reports some characteristics of the compound.

Results and Discussion

Synthesis of [D-Phe(4-Br)$^{4,4'}$]-GS (7). [D-Phe(4-Br)$^{4,4'}$]-GS was synthesized according to the scheme shown in Fig. 1. The chain assembly of the peptide was carried out by the standard Merrifield solid-phase method[1] using Boc-amino acid derivatives of Val, Orn(Z), Leu, D-Phe(4-Br) and Pro for the chain elongation and Troc-Val for the introduction of N-terminal Troc-Val. The Troc group was used to block the α-amino group of the peptide because it is stable under acid-treatment conditions.[2-4] The weight increase in the protected-peptide resin **2** was 0.48 g, based on 1.54 g of Boc-Pro-$OCH_2C_6H_4$-resin (**1**). The HF treatment[5] of 1.05 g of Compound **2** gave 275 mg of a crude product **3**. This peptide was very soluble in aq acetonitrile and could be easily purified by reversed-phase high-performance liquid chromatography (HPLC), for it had no extra-protecting groups except for the Troc group. The purified Compound **3** (261 mg) was confirmed by fast-atom-bombardment (FAB) mass measurement. The Boc group was introduced to 200 mg of Compound **3** with the aid of *N*-(*t*-butoxycarbonyloxy)succinimide (Boc-ONSu) in the presence of triethylamine (TEA). The resultant material was purified by crystallization and gave 175 mg of Compound **4**. The Troc group on Compound **4** (84.5 mg) was cleaved by zinc-dust treatment in 90% aq acetic

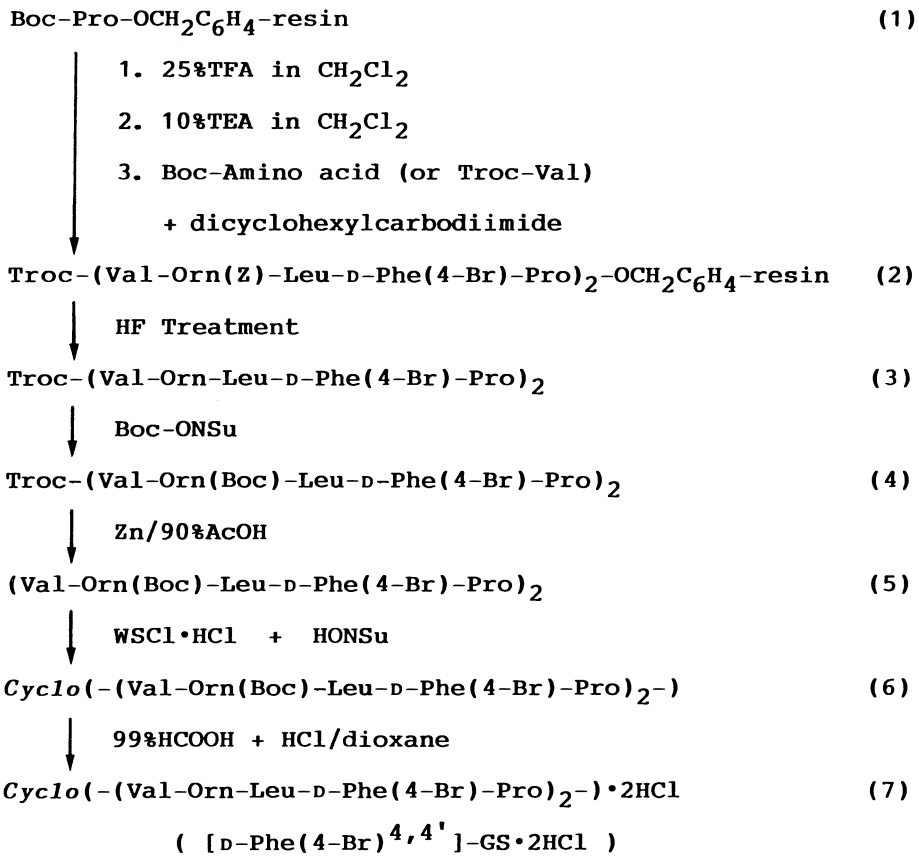

Fig. 1. Synthetic scheme of [D-Phe(4-Br)$^{4,4'}$]-GS.

acid.[2] After the removal of the zinc dust and zinc ions, the peptide solution was freeze-dried to a powder. Compound **5** (64.1 mg) was cyclized by adding about a twofold excess of 1-ethyl-3-(3-dimethylaminopropyl)-carbodiimide hydrochloride (WSCI·HCl) and *N*-hydroxysuccinimide (HONSu) in a mixture of *N*,*N*-dimethylformamide (DMF)-CH_2Cl_2 at about 2.5 mM (1 M=1 mol dm^{-3}). One-pot cyclization proceeded, with a yield of about 80%, judging from the elution profile of the reaction mixture on HPLC. This yield was almost equal to those described by two other research groups.[6,7] No cyclic dimer was detected in the reaction mixture by FAB mass measurements. Compound **6** was purified by crystallization to give 36 mg of crystals in a 50% yield, based on Compound **4**. Compound **6** was treated with a mixture of 99% formic acid and HCl in dioxane to remove the Boc groups. After the separation of minor impurities from the main product by means of HPLC, the final product **7** was obtained in an 80% yield, based on Compound **6**. Each of the steps gave good yields, and the purities of the intermediates and the final products were satisfactory. This new approach was successfully applied to the synthesis of [D-Phe(4-Br)$^{4,4'}$]-GS. Starting from Boc-Pro-$OCH_2C_6H_4$-resin (**1**), the final product **7** was obtained as crystals in 2 weeks.

Biological Activity. The minimum concentration of [D-Phe(4-Br)$^{4,4'}$]-GS needed to completely inhibit the growth of several microorganisms was determined by a dilution method using nutrient agar. [D-Phe(4-Br)$^{4,4'}$]-GS showed antibacterial activity. The bromine atom on the phenyl group of D-Phe affected the biological activity of GS, but not seriously.

Crystallization. We attempted to prepare crystals of [D-Phe(4-Br)$^{4,4'}$]-GS under several conditions. The trifluoroacetate or hydrochloride gave fine needle crystals in aq EtOH, aq MeOH, or aq DMF. The perchlorate gave thick needle crystals in dimethyl sulfoxide. These crystals will be analyzed in a subsequent X-ray crystallographic study.

Experimental

The melting points were determined by the capillary method and are given as uncorrected values. The Pro, Val, Orn, and Leu used were of the L-configuration. High-performance liquid chromatography (HPLC) was carried out on a handmade column of the YMC-GEL ODS S5 100 Å Type (8×300 mm) (Yamamura Chemical Laboratory Co., Ltd., Kyoto, Japan), with the acetonitrile concentration increasing from 40 to 80% in 0.05% aq trifluoroacetic acid (TFA) at a flow rate of 2 ml min^{-1}.

Troc-Val-Orn-Leu-D-Phe(4-Br)-Pro-Val-Orn-Leu-D-Phe(4-Br)-Pro (3). The chain elongation of a peptide was carried out on a Beckman Model 990E synthesizer (Palo Alto, Ca, USA) according to the standard Merrifield solid-phase method. Boc-Pro-$OCH_2C_6H_4$-resin (**1**) (1.54 g), containing 0.4 mmol of Boc-Pro was used as the starting material. For the deprotection of the Boc group, the resin was treated twice with 25% TFA in CH_2Cl_2, for 1 min and then for 30 min. The resin was treated twice with 10% TEA in CH_2Cl_2, for 2 min and then for 5 min, to neutralize the resin. In each coupling reaction, 1.2 mmol of Boc-amino acid or Troc-Val was mixed with a peptide resin in the presence of dicyclohexylcarbodiimide (250 mg, 1.2 mmol) for 2 h. The Boc-amino acids used were Boc-Val, Boc-Orn(Z), Boc-Leu, Boc-D-Phe(4-Br), and Boc-Pro. Weight increase, 480 mg. The protected peptide resin **2** (1.05 g) was treated with anhydrous hydrogen fluoride (10 ml) containing anisole (1 ml) at 0 °C for 70 min. After the evaporation of the hydrogen fluoride, a peptide was extracted with 50% aq acetonitrile. The solution was passed through a column of Amberlite IR-45 (acetate form) (3.5×8 cm). All of the eluent was then collected and freeze-dried. The crude material was purified on HPLC. Lyophilization of the main fractions gave 261 mg of Compound **3**. Found: *m/z* 1489.2 $(M+H)^+$. Calcd for $C_{63}H_{94}O_{13}N_{12}Br_2Cl_3$: *m/z* 1489.5 $(M+H)^+$.

Troc-Val-Orn(Boc)-Leu-D-Phe(4-Br)-Pro-Val-Orn(Boc)-Leu-D-Phe(4-Br)-Pro (4). Compound **3** (200 mg, ca. 130 μmol) was dissolved in DMF (1.7 ml) containing 85 μl (ca. 600 μmol) of TEA. Boc-ONSu (110 mg, 512 μmol) was added to the solution, which was then stirred at room temperature for 1 h. The reaction mixture was poured into a dilute aqueous solution of citric acid. The precipitate thus formed was collected, dried over diphosphorus pentaoxide in vacuo, and crystallized from MeOH-EtOAc to give 175 mg of crystals **4** (ca. 79%): mp 228—229 °C, $[\alpha]_D^{24}$ −108° (*c* 0.5, EtOH). Found: *m/z* 1690.1 $(M+H)^+$. Calcd for $C_{73}H_{110}O_{17}N_{12}Br_2Cl_3$: *m/z* 1689.7 $(M+H)^+$. Found: C, 51.33; H, 6.56; N, 9.69; Br, 9.42; Cl, 6.27%. Calcd for $C_{73}H_{109}O_{17}N_{12}Br_2Cl_3 \cdot H_2O$: C, 51.24; H, 6.54; N, 9.82; Br, 9.34; Cl, 6.22%.

Val-Orn(Boc)-Leu-D-Phe(4-Br)-Pro-Val-Orn(Boc)-Leu-D-Phe(4-Br)-Pro (5). Compound **4** (84.5 mg, 49.4 μmol) in 90% acetic acid (5 ml) was treated with zinc dust (100 mg) while being stirred at room temperature for 5 h. After the removal of the remaining zinc dust and zinc ions, the peptide solution was freeze-dried to give 64.1 mg of Compound **5** (ca. 85%). Found: *m/z* 1515.4 $(M+H)^+$. Calcd for $C_{70}H_{109}O_{15}N_{12}Br_2$: *m/z* 1515.7 $(M+H)^+$.

***cyclo*(-Val-Orn(Boc)-Leu-D-Phe(4-Br)-Pro-Val-Orn (Boc)-Leu-D-Phe(4-Br)-Pro-) (6).** Compound **5** (64 mg, ca. 42 μmol) was dissolved in DMF (10 ml) containing 11.5 mg (100 μmol) of HONSu. Into the solution, 19.2 mg (100 μmol) of WSCI·HCl in CH_2Cl_2 (10 ml) was added at 0 °C. The solution was stirred at 0 °C for 1 h and at room temperature for 24 h. After the concentration of the reaction mixture in vacuo, the residual mass was solidified with water, collected by centrifugation, and dried over diphosphorus pentaoxide in vacuo. The solid material was crystallized from EtOAc-MeOH; yield, 36 mg (ca. 57%); mp 231—232 °C; $[\alpha]_D^{21}$ −277° (*c* 0.5, AcOEt). Found: *m/z* 1497.5 $(M+H)^+$. Calcd for $C_{70}H_{107}O_{14}N_{12}Br_2$: *m/z* 1497.7 $(M+H)^+$. Found: C, 54.70; H, 7.12; N, 10.91; Br, 10.46%. Calcd for $C_{70}H_{106}O_{14}N_{12}Br_2 \cdot 2H_2O$: C, 54.75; H, 7.22; N, 10.91; Br, 10.41%.

***cyclo*(-Val-Orn-Leu-D-Phe(4-Br)-Pro-Val-Orn-Leu-D-Phe(4-Br)-Pro-)·HCl·3H$_2$O (7).** Compound **6** (76 mg, 50 μmol) in 99% formic acid (2 ml) and 6.72 M HCl in dioxane (0.2 ml) was stirred for 20 min at room temperature. After the evaporation of the solvent, the crude product was purified on HPLC and lyophilized from dilute hydrochloric acid. The powder thus obtained was crystallized from MeOH-ether; yield, 57.8 mg (81%); mp 266—270 °C (decomp), $[\alpha]_D^{20}$ −284° (*c* 0.15, MeOH). Found: *m/z* 1297.3 $(M+H)^+$. Calcd for $C_{60}H_{91}O_{10}N_{12}Br_2$: *m/z* 1297.6 $(M+H)^+$. Found: C, 50.94; H, 6.80; N, 11.54%. Calcd for $C_{60}H_{90}O_{10}N_{12}Br_2 \cdot 2HCl \cdot 3H_2O$: C,50.52; H, 6.93; N, 11.79%.

Crystallization of [D-Phe(4-Br)$^{4,4'}$]-GS Perchlorate. [D-Phe(4-Br)$^{4,4'}$]-GS trifluoroacetate or hydrochloride was dissolved in a small amount of methanol. To the solution, dilute perchloric acid was added until a precipitate formed. This precipitate was collected by centrifugation, washed with distilled water, and dried; then a minimum amount of dimethyl sulfoxide was added until the precipitate had dissolved completely. The solution in the uncovered test tube

was left standing. Crystals appeared after 3 d and were allowed to grow for one week. The crystal dimensions were 0.1×0.1×1.0 mm.

Microbiological Assays. The minimum inhibitory concentrations of [D-Phe(4-Br)$^{4,4'}$]-GS·2HCl·3H_2O for several microorganisms were determined by a dilution method using nutrient agar. The minimum inhibitory concentrations of the compound were 12.5 μg ml^{-1} on *Staphylococcus aureus* FDA 209P and *Staphylococcus aureus* 1840, 25 μg ml^{-1} on *Staphylococcus aureus* 308A-1, and 6.25 μg ml^{-1} on *Bacillus subtilis* PCI 219.

This paper is dedicated to the late Dr. Gopinath Kartha of the Roswell Park Memorial Institute, Buffalo, New York, who planned the synthesis of a heavy-atom derivative of GS. The author wishes thank Dr. Jake Bello of the Roswell Park Memorial Institute for his helpful discussions; he is also indebted to the members of the Analytical Laboratories of Takeda Chemical Industries, Ltd., for their assays of the activity and to Dr. Toshifumi Takao and Dr. Yasutsugu Shimonishi for the mass-spectral measurements.

References

1) R. B. Merrifield, *J. Am. Chem. Soc.*, **85**, 2149 (1963).
2) R. B. Woodward, K. Heusler, J. Gosteli, P. Naegeli, W. Oppolzer, R. Ramage, S. Ranganathan, and H. Vorbruggen, *J. Am. Chem. Soc.*, **88**, 852 (1966).
3) T. B. Windholz and D. B. R. Johnston, *Tetrahedron Lett.*, **1967**, 2555.
4) H. Yajima, H. Watanabe, and M. Okamoto, *Chem. Pharm. Bull.*, **19**, 2185 (1971).
5) S. Sakakibara, Y. Shimonishi, Y. Kishida, M. Okada, and H. Sugihara, *Bull. Chem. Soc. Jpn.*, **40**, 2164 (1967).
6) T. Mukaiyama, K. Kamekawa, and Y. Watanabe, *Chem. Lett.*, **1981**, 1367.
7) S. Nozaki and I. Muramatsu, *Bull. Chem. Soc. Jpn.*, **58**, 331 (1985).

Syntheses and NMR Spectroscopic Studies on the Conformations of 1-[1-(2-Aralkyloxy- and 2-Acyloxyphenyl)vinyl]-1*H*-Imidazoles[1)]

Kazuko YAMAMOTO, Yoshiki HAMADA, Isao TAKEUCHI, Hiroko SUEZAWA, and Minoru HIROTA*,†
Department of Pharmacy, Meijo University, Yagoto-Urayama, Tempaku-ku, Nagoya 468
†Department of Applied Chemistry, Faculty of Engineering, Yokohama National University, Hodogaya-ku, Yokohama 240
(Received September 25, 1987)

Synopsis. The title compounds were synthesized from 2-[1-(1-imidazolyl)vinyl]phenol and their conformations were discussed on the basis of their ^{1}H and ^{13}C NMR spectra.

In recent decades, antifungal substaces have attracted considerable interests from pharmaceutical and agricultural points of view, and many investigations concerning their syntheses, structural elucidations, and biological activities have been reported.[2-4)] The present authors have also been studying a series of antifungal imidazole derivatives.[5,6)] One of our recent research includes the syntheses, NMR spectra, and antifungal activities of 4-(substituted aryl)-2-(1-imidazolyl, 1-pyrazolyl, and 1,2,4-triazol-1-yl)-1,3-dioxolanes.[7,8)]

In this connection, we synthesized several heterocyclic analogs of the above imidazole derivative and acyl derivatives of 2-[1-(1-imidazolyl)vinyl]phenol (**19**).[4)] Their syntheses, NMR spectroscopic studies, and antifungal activities are reported in this paper.

Experimental

The (imidazolylvinyl)phenol **19** was obtained by the reaction of *o*-hydroxyacetophenone and *N*,*N*′-sulfinyldiimidazole, prepared by adding thionyl chloride to a suspension of imidazole in dichloromethane.[4)] Then, acyl chloride (0.0176 mol) was added gradually to an ice-cooled pyridine solution (30 ml) of the phenol **19** (0.016 mol). The reaction mixture was kept standing for additional 10 min. The whole was poured into water and extracted with dichloromethane. Thus obtained crude products **1**—**14** were recrystallized or distilled in vacuo, and purified further by column chromatography on silica gel. Similarly ethers **15**—**18** were prepared by treating potassium phenolate of **19** with the corresponding arylmethyl chlorides in *N*,*N*-dimethylformamide.

^{1}H and ^{13}C NMR spectra were recorded on a JEOL FX-90Q spectrometer.

Results and Discussion

Various 1-[1-(2-aralkyloxy- and 2-acyloxyphenyl)-vinyl]-1*H*-imidazoles **1**—**18** were prepared starting form known 2-[1-(1-imidazolyl)vinyl]phenol (**19**). Most of them were prepared newly by the present authors and characterized by their physical properties, NMR spectra, and elemental analyses.

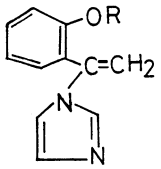

1; R=CH_3CO **2**; R=C_2H_5CO
3; R=C_3H_7CO **4**; R=C_4H_9CO
5; R=$C_5H_{11}CO$ **6**; R=4-FC_6H_4CO
7; R=4-ClC_6H_4CO **8**; R=4-BrC_6H_4CO
9; R=4-$CH_3C_6H_4CO$ **10**; R=4-$CH_3OC_6H_4CO$
11; R=3-ClC_6H_4CO **12**; R=3-BrC_6H_4CO
13; R=3-$CH_3C_6H_4CO$ **14**; R=2,4-$Cl_2C_6H_3CO$
15; R=4-Pyridylmethyl **16**; R=2-Pyridylmethyl
17; R=2-Thienylmethyl **18**; R=5-Cl-2-thienylmethyl
19; R=H

These *N*-(1-arylvinyl)imidazoles are structurally similar to cloconazole[4)] and potential antibacterial and antifungal agents.[7,8)] Since the biological activity is closely related with the shape of the active molecule, the conformations of the *N*-(1-arylvinyl)imidazoles **1**—**19** were elucidated by ^{1}H and ^{13}C NMR spectroscopy. The ^{13}C NMR chemical shifts are given in Table 1.

As the shapes of the *N*-(1-vinylaryl)imidazole molecules are expected to be altered most significantly by the conformational change caused by the rotations about the C-C bond connecting vinyl and *o*-R-oxyaryl groups, the C-N bond connecting vinyl and imidazolyl groups, and the C-O bond connecting the aryl and R-oxy groups, the substituent effect on the spectra of vinylidene groups were examined most carefully. Overviewing Tables 1 and 2, chemical shifts of vinyli-

Table 1. ^{13}C NMR Chemical Shifts

Compd	Vinylidene		Aromatic						Imidazolyl			CO/CH_2
	C_{alpha}	C_{beta}	1	2	3	4	5	6	2′	4′	5′	
1	139.3	107.2	128.6	148.2	123.3	130.6	126.6	130.6	118.2	129.6	136.2	168.5
2	139.4	107.2	128.7	148.4	123.3	130.8	126.2	130.8	118.2	129.7	136.2	172.1
7	139.2	107.4	128.4	148.4	123.4	131.0	126.7	131.0	118.3	129.7	136.2	163.6
9	139.3	107.4	128.9	148.9	123.7	130.9	126.4	130.9	118.3	129.7	136.3	164.6
14	138.2	106.7	128.1	147.4	122.2	130.2	126.0	130.3	117.4	128.7	135.3	161.2
15	140.7	105.9	121.5	155.5	112.1	131.2	124.9	131.4	117.8	129.3	135.9	68.2
16	140.9	105.9	121.2	156.3	112.5	131.3	125.0	131.4	117.8	129.6	136.2	70.9
17	140.4	106.6	121.4	156.0	113.0	130.9	125.5	131.2	117.9	129.3	136.2	65.5
18	140.2	106.6	121.6	155.6	112.8	130.5	125.3	131.2	117.9	131.0	137.2	65.4

dene carbons (C_α and C_β), as well as those of protons (H_a and H_b), were rather insensitive to the modifications in the acyl side chain.

The vinylidene ^{13}C chemical shifts were dependent on whether the side chain is acyloxyl or aralkyloxyl. The effect might be induced by a through-bond perturbation since the α-carbon connected directly to the aromatic carbon ortho to the RO group is affected more significantly. The through-bond effect of the RO group should be transmitted in an alternate manner causing high and low field shifts alternately and decaying gradually due to the pi-electron releasing mesomeric effect by RO group.[9,10] The observed ^{13}C chemical shifts are in accord with the above reasoning and can be rationalized if we assume that the original perturbation by an aralkyloxyl group is larger than that by an acyloxyl group.[11]

The vinylidene proton signals appeared as AX quartets. The signals at lower fields are assigned to the proton cis to the aryl group (hereafter designated as H_a) and the one at the higher fields to the proton cis to the imidazolyl group (hereafter designate as H_b) (Table 2). Geminal coupling constants J_{ab} are small, ranging from 1.0 to 1.2 Hz, and insensitive to the substituent and solvent effects. Modification of the side chain from aliphatic acyl group to aroyl causes a small but discernible high field shift of H_a signal in chloroform solutions. The shift might be ascribed to the anisotropy effect due to the aroyl aromatic ring. However the effect is obscured in other solvents.

As revealed by the chemical shifts of H_a and H_b in various solvents (in Table 2), their chemical shifts are susceptible to the solvent effect. Especially H_a is very sensitive to the nature of solvents and shows general tendency to shift considerably towards upfield in benzene-d_6 and, in contrast, to shift towards downfields in pyridine-d_5 and DMSO-d_6. With a very minor exception which shows the reversal of the order within an experimental error, the H_a signals are subjected to the solvent effect which aligns the chemical shifts in the order (from the high field); benzene>chloroform>pyridine>dimethyl sulfoxide. The upfield shifts in benzene is rather larger than the usual aromatic solvent induced shifts (ASIS) expected for this sort of proton. The larger shift might be caused by the acidic character of H_a, since ASIS is supposed to be originated from weak C-H···pi hydrogen bonding,[13] The acidity seems plausible if we consider the fact that the vinylidene protons occupy the positions vinylogous to acidic imidazole NH. As a large ASIS was not observed with the beta-protons of *o*-methoxy styrene (**20**), the importance of acidity in ASIS becomes more evident. Benzene induced shifts including the protons and carbons of other parts of the molecule were also examined with several of the *N*-(1-arylvinyl)imidazoles. Generally speaking, positively charged hydogen (and carbon) atoms orienting themselves toward outside the molecule showed the positive ASIS in accord with the reported trend of ASIS[12] and theoretical consequences. Besides those given in Table 2, the ^1H ASIS of arylmethoxyl CH_2 groups of **15—18** comes to be +0.75, +0.23, +0.55, and 0.57,

Table 2. Chemical Shifts of Vinylidene Protons H_a and H_b and T_1 Values in $CDCl_3$

Compd	^1H-Chemical shift δ/ppm (from TMS)								T_1/s		
	In $CDCl_3$		In C_6D_6		In C_5D_5N		In $(CD_3)_2SO$				
	H_a	H_b	H_a	H_b	H_a	H_b	H_a	H_b	H_a	H_b	CH_2
1	5.43	5.15	4.89	4.68	5.50	5.10	5.63	5.12	0.55	0.87	
2	5.43	5.10	4.84	4.64	5.51	5.09	5.63	5.11			
4	5.43	5.10	4.84	4.64	5.53	5.09	5.57	5.10	0.53	0.83	
7	5.38	5.07	4.82	4.68	5.46	5.11	5.56	5.14	0.60	0.76	
9	5.35	5.13	4.84	4.77	5.46	5.13	5.61	5.15	0.60	0.76	
14	5.44	5.15	4.85	4.67	5.55	5.14	5.68	5.18			
15	5.44	5.11	4.93	4.22	5.55	5.08	5.63	5.10	0.34	0.68	0.83
16	5.45	5.12	4.94	4.69	5.54	5.09	5.59	5.05	0.93	1.09	1.11
17	5.40	5.13	4.92	4.74	—	—	5.59	5.04	1.13	1.30	1.30
18	5.41	5.11	4.95	4.74	5.51	5.06	5.61	5.03	0.97	1.02	1.03
19	5.43	5.14	4.83	4.71	5.57	5.25	5.55	5.08	0.50	0.53	
20	5.73	5.24	5.74	5.20	5.83	5.27	5.79	5.25	2.79	2.70	

Table 3. Antibacterial and Antifungal Activities (MIC, mg l^{-1})

Organism	Compound						
	1,2,5,7,9,14	**3,8**	**4**	**15**	**16**	**17**	**18**
Staphylococcus aureus FDA209P	*	*	*	50	50	*	100
Escherichia coli NIHJ	*	*	*	*	*	*	*
Candida albicans YU-1200	*	*	*	50	50	25	3.12
Aspergillus melleus IFO4339	*	100	50	50	50	50	50
Aspergillus orizeae	*	*	*	50	50	12.5	12.5
Trychophyton mentagrophytes IFO833	*	*	*	12.5	25	3.12	12.5
Trychophyton asteroides 429	*	*	*	12.5	25	1.56	3.12
Penicillium chrisogenum ATCC10002	*	*	*	25	50	1.56	1.56

respectively, and that of the terminal methyl group of acyloxyl side chain in the series of compounds **1**—**5** is shown to decrease as the alkyl chain of the acyl group elongates (i. e., +0.39 for **1**, +0.20 for **2**, +0.17 for **3**, +0.13 for **4**, and +0.08 for **5**). As expected, relatively positive ^1H ASIS were observed with the CH_2 groups bonded to oxygen and the CH_3 in acetyl group of **1** which are expected to be considerably acidic owing to the inductive effect of adjacent electronegative groups.

In order to estimate the preferred conformation about the C_{vinyl}-C_{aryl} and C_{vinyl}-$N_{imidazoyl}$ bonds qualitatively, several NOE experiments were carried out. The irradiation of hetarylmethoxyl CH_2 protons in **15**—**17** enhanced the intensities of H_a in 4—10% (**15**, 5%; **16**, 4%; **17**, 10%; and **18**, 10%) in reference to other unirradiated protons. Similarly the irradiation of acetoxyl CH_3 protons in **1** caused the 3% enhancement of H_a signal. As the enhancement was rather small, the increase in intensity was ascertained by several repetitions of the measurements. The NOE experiments showed unambiguously that the acyloxyl or arylmethoxyl group is located syn to the vinylidene group with respect to the C_{vinyl}-C_{aryl} bond, taking a nearly coplanar conformation judging from the observed enhancement. In contrast, the imidazolyl ring should be nearly perpendicular to the plane of vinylidene moiety, keeping the 2′- and 5′-hydrogens farther than 3.4 Å away from both H_b and H_a of vinylidene moiety, since no enhancement of the H_a signal was observed by the irradiation of 2′-H and 5′-H. If we assume that the carbonyl group is exactly coplanar to the aryloxyl moiety, methyl group in **1** is located too far from H_a to observe NOE enhancement. However, the carbonyl group is expected to be twisted to a certain extent around $C_{carbonyl}$-$O_{aryoxyl}$ bond and pushed away from the aryloxyl plane in order to reduce the steric hindrance by 3-hydrogen atom on the benzene ring. In this conformation, methyl group should approach nearer to H_a, which enables us to observe the small enhancement. Judging from their chemical shifts of H_a higher than those of **1**—**5**, similar conformations in which H_a approaches from above the plane of aroyl aromatic ring might be realized. Analogously the pyridine and thiophene rings are assumed to occupy a position considerably deviated from the plane of vinylidenearyloxyl part of the molecule.

If the vinylidenearyloxyl moiety is nearly coplanar as stated above, one of the vinylidene hydrogen H_a should lie very close (as close as 1.63 Å, if completely coplanar) to the aryloxyl oxygen atom. When an acidic hydrogen is in the proximity of electronegative oxygen atom, C-H ··· O hydrogen bond is expected to be formed. T_1 measurements showed that the H_a has somewhat shorter T_1 than H_b and other hydrogens in the molecule. When the T_1 values were compared with those in *o*-methoxystyrene (**20**), T_1 values of H_a and H_b are generally short. The results imply the fact that the motion of H_a is significantly restricted in these molecules. Intramolecular C-H ··· O hydrogen bond may persist under such sterically favored circumstances, which, in turn, contributes to stabilize the planar vinylidenearyloxyl moiety.

In conclusion, following sketches for the steric structures of the title compound 1-(1-arylvinyl)-imidazoles can be drawn. This is in accord with the X-ray result recently reported by Ogata and coworkers,[14] and the solution structure was shown to be similar to that in crystal.

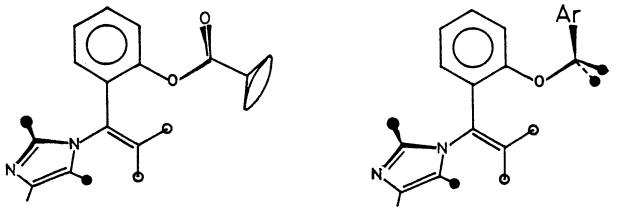

Antifungal and antibacterial activities of the 1-(1-arylvinyl)imidazoles are given in Table 3. The hetarylmethoxyl derivatives **15**—**18** are shown to have broad spectrum fungicidal and bacteriocidal activities, while the acyloxyl derivatives **1**—**14** are seldom active. The NMR spectroscopic studies showed that the difference in conformations between the hetarylmethoxyl derivatives and the acyloxyl derivatives is very slight in contrast to the remarkable difference in biological activities.

Since the acyloxyl derivatives are rather susceptible to hydrolysis and some of them are sensitive to atmospheric moisture, the instability might be the reason for the discrepancy. However, further investigation is necessary before ascribing the inactivity of the acyloxyl derivative to the hydrolytic degradation.

References

1) See H. Suezawa, M. Hirota, and Y. Hamada, Preprints of the 53rd National Meeting of the Chemical Society of Japan, Nagoya, 1986, II, p. 592 (No. 1F08).

2) a) K. H. Buchel, W. Draber, E. Regel, and M. Plempel, *Arzeim. Forsch.*, **22**, 1260 (1972); b) C. Metzger, W. Meiser, K. H. Buchel, and M. Plempel, U. S. Patent, 3796704 (1974).

3) J. Heeres, L. J. Backx, J. H. Mostmans, and T. Van Cutsem, *J. Med. Chem.*, **22**, 1003 (1979).

4) M. Ogata, H. Matsumoto, Y. Hamada, M. Takehara, and K. Tawara, *J. Med. Chem.*, **26**, 768 (1983).

5) H. Suezawa, M. Hirota, K. Yamamoto, I. Takeuchi, and Y. Hamada, *Bull. Chem. Soc. Jpn.*, **57**, 883 (1984).

6) Y. Hamada, I. Takeuchi, K. Yamamoto, M. Hirota, and H. Suezawa, *Chem. Pharm. Bull.*, **32**, 302 (1984).

7) I. Takeuchi, M. Sugiura, K. Yamamoto, T. Ito, and Y. Hamada, *Yakugaku Zasshi*, **105**, 554 (1984).

8) I. Takeuchi, K. Yamamoto, T. Ito, and Y. Hamada, *Yakugaku Zasshi*, **106**, 567 (1986).

9) A. C. Rojas and J. K. Crandall, *J. Org. Chem.*, **40**, 2225 (1975).

10) E. Taskinen, *J. Org. Chem.*, **43**, 2776 (1978).

11) This assumption is justified from the values of the substituent increments for these substituents given in the following book: G. C. Levy, R. L. Lichter, and G. L. Nelson, "Carbon-13 Nuclear Magnetic Resonance Spectroscopy," 2nd ed., John Wiley & Sons, N. Y. (1980), pp. 109—112.

12) T. Ledaal, *Tetrahedron Lett.*, **1968**, 1683.

13) R. W. Reeves and W. G. Schneider, *Can. J. Chem.*, **35**, 251 (1957).

14) M. Ogata, H. Matsumoto, S. Shimizu, S. Kida, S. Motoo, and K. Tawara, *J. Med. Chem.*, **30**, 1348 (1987).

Regioselective Para Halogenation of Substituted Benzenes with Benzeneseleninyl Chloride and Aluminum Halide

Nobumasa KAMIGATA,* Takeshi SATOH, Masato YOSHIDA, Haruo MATSUYAMA, and Masayuki KAMEYAMA
Department of Chemistry, Faculty of Science, Tokyo Metropolitan University, Fukazawa, Setagaya-ku, Tokyo 158
(Received September 26, 1987)

Synopsis. In the presence of aluminum halide, benzeneseleninyl chloride is an efficient regioselective halogenating reagent for activated aromatics such as toluene, phenol, anisole, phenetole, diphenyl ether, and *N,N*-dimethylaniline. Benzene and chlorobenzene are not halogenated under similar conditions.

Extensive studies on the halogenation of aromatic compounds have been reported.[1] Electron-donating substituents in a benzenoid compound generally give ortho- and para-substituted compounds, with the ortho-isomer frequently exceeding the para. Since the ortho- and para-isomers have similar physical properties, their separation is tedious. Many studies on the bromination of anilines and phenols have been reported in order to obtain a high para-regioselectivity.[2] However, these methods tend to give lower yields and also lead to di- or tri-substitution. The following three papers reportred recently are excellent methods for para-halogenation. Osa et al. found a high para-chlorination of anisole (para/ortho ratio= 25/1) by an electrochemical anodic reaction in the presence of α-CD.[3] Watson found a high para chlorination of phenols (para/ortho ratio=10.5/1) by use of sulfuryl chloride catalyzed by diphenyl disulfide and aluminum chloride.[4] Olah et al. found that phenols and anilines gave more than 97% para-halogenated products by a reaction with bromodimethylsulfonium bromide or chlorodimethylsulfonium chloride.[5]

Recently, we reported that benzeneseleninyl chloride in the presence of aluminum chloride or bromide is an excellent vinylic chlorinating or brominating reagent of olefins, respectively, in one step under mild reaction conditions, and the reaction mechanism involving positive halogen (chloronium or bromonium ion) intermediate is proposed.[6] If such a positive halogen intermediate is formed under the reaction conditions, the electrophilic halogenation of aromatic compounds would also be expected by this method. We have investigated the halogenation of aromatic compounds with benzeneseleninyl chloride (**1**) in the presence of aluminum halide and found that aromatic compounds possessing electron donating-group are halogenated regioselectively at para-position in high yield. We report herein the results of these novel para-halogenations of aromatic compounds.

Benzeneseleninyl chloride (**1**), prepared from benzeneselenenyl chloride treated with ozone in dichloromethane, was allowed to react with anisole in the presence of aluminum chloride. *p*-Chloroanisole (**2a**) was formed in quantitative yield, and no formation of *o*-chloroanisole was detected by gas chromatography. Similarly, compound **1** was allowed to react with phenetole, diphenyl ether, and *N,N*-dimethylaniline in the presence of aluminum chloride in dichloromethane at room temperature to give *p*-chlorophenetole (**2b**), *p*-chlorodiphenyl ether (**2c**), and *p*-chloro-*N,N*-dimethylaniline (**2d**), respectively, in quantitative yield; and no corresponding ortho-isomer was detected by gas chromatography. These observations show that the chlorination of activated aromatics with **1** cata-

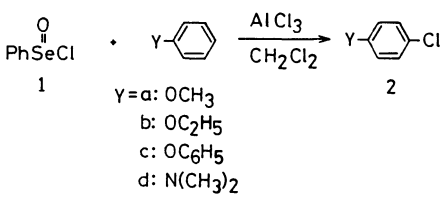

Table 1. Halogenation of Aromatic Compounds with Benzeneseleninyl Chloride and Aluminum Halide

Aromatic compound	Aluminum halide	Reaction temp/°C	Reaction time/h	Product	Yield[a] /%	Isomer ratio para/ortho
Anisole	$AlCl_3$	Room temp	2	**2a** *p*-Chloroanisole	100(84)	100/0
Phenetole	$AlCl_3$	Room temp	3	**2b** *p*-Chlorophenetole	100(89)	100/0
Diphenyl ether	$AlCl_3$	Room temp	10	**2c** *p*-Chlorodiphenyl ether	100	100/0
N,N-Dimethylaniline	$AlCl_3$	Room temp	10	**2d** *p*-Chloro-*N,N*-dimethylaniline	95	100/0
Phenol	$AlCl_3$	40	2	**2e** *o*-Chlorophenol **2f** *p*-Chlorophenol	34 61	64/36
Toluene	$AlCl_3$	40	14	**2g** *o*-Chlorotoluene **2h** *p*-Chlorotoluene	30 35	54/46
Benzene	$AlCl_3$	40	24	—	0	—
Chlorobenzene	$AlCl_3$	40	48	—	0	—
Anisole	$AlBr_3$	Room temp	6	**5a** *p*-Bromoanisole	90(83)	100/0
Phenetole	$AlBr_3$	Room temp	8	**5b** *p*-Bromophenetole	94(86)	100/0
Diphenyl ether	$AlBr_3$	−10	6	**5c** *p*-Bromodiphenyl ether	92	100/0
N,N-Dimethylaniline	$AlBr_3$	−10	3	**5d** *p*-Bromo-*N,N*-dimethylaniline	99	100/0

a) Determined by GLC using an internal standard. Isolated yields are given in parentheses.

lyzed by aluminum chloride is regiospecific, and that the method is quite efficient for the synthesis of para-chlorinated aromatic compounds.

On the other hand, the reaction of **1** with phenol in the presence of aluminum chloride in dichloromethane at 40 °C gave a mixture of *o*- and *p*-chlorophenol (para/ortho ratio=64/36) in high yield. Similarly, the reaction of **1** with toluene under similar conditions afforded *o*- and *p*-chlorotoluene in 30 and 35% yield, respectively. The results show that both the yield and regioselectivity are lowered when the substituents on the benzene ring are OH or CH_3. Moreover, benzene and chlorobenzene were not chlorinated by **1** under similar reaction conditions. The results are summarized in the Table 1. These observations suggest that chlorination by this method is an electrophilic substitution on the activated aromatic nucleus.

The reaction mechanism is accounted for by Scheme 1, which involves a chloronium ion intermediate.[6] The aluminum chloride interacts with the oxygen atom of **1** to give chloronium trichloro(phenylselenooxy)aluminum intermediate (**3**). The following electrophilic reaction of the chloronium ion toward aromatic nucleus affords para-chlorinated products via carbocation intermediate (**4**). The observed high para-selectivity is a consequence of the transfer chlorinations going through a "late" arenium ion like transition state and of the bulky nature of the halogenating reagent (**3**).

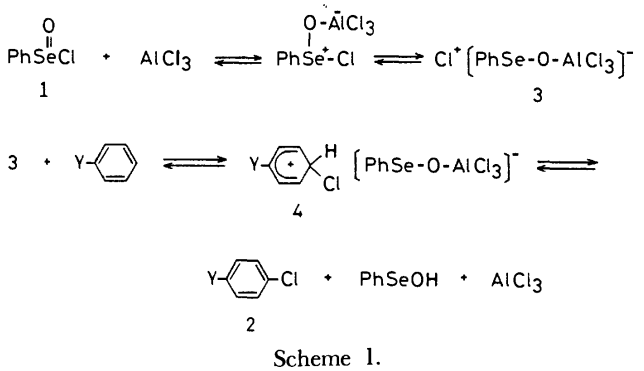

Scheme 1.

When a reaction of **1** with anisole was carried out in the presence of aluminum bromide instead of aluminum chloride in dichloromethane at room temperature, *p*-bromoanisole (**5a**) was obtained in 90% yield and no formation of the ortho-isomer was observed. Similarly, compound **1** was allowed to react with phenetole, diphenyl ether, and *N*,*N*-dimethylaniline in the presence of aluminum bromide to give *p*-bromophenetole (**5b**), *p*-bromodiphenyl ether (**5c**), and *p*-bromo-*N*,*N*-dimethylaniline (**5d**) in high yield, respectively. The results show that benzeneseleninyl chloride in the presence of aluminum bromide is a quite efficient para-brominating reagent of activated aromatics. The results indicate that a bromonium ion is involved in this reaction as a reactive intermediate, as shown in Scheme 2.

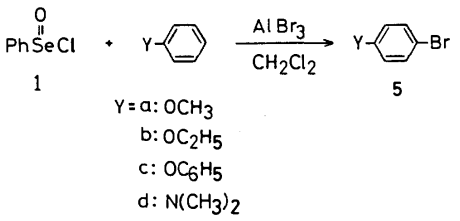

Y=a: OCH_3
b: OC_2H_5
c: OC_6H_5
d: $N(CH_3)_2$

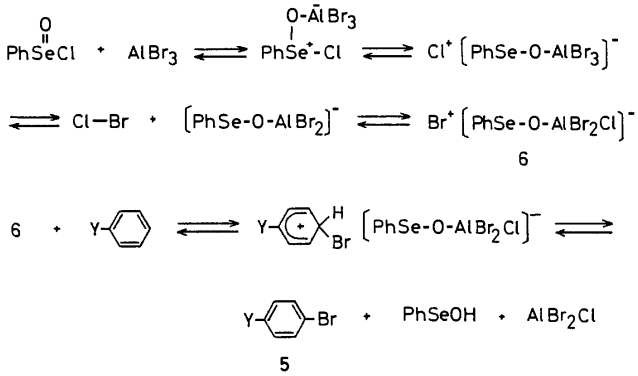

Scheme 2.

In conclusion, benzeneseleninyl chloride in the presence of aluminum chloride and aluminum bromide is a versatile chlorinating and brominating reagent at the para-position of activated benzenes.

Experimental

Measurement. Gas chromatography was performed by using a Hitachi 163 and 263-10 gas chromatograph using SE 30 (10 %), 1 m column. Mass spectra were determined with a JEOL JMX-DX 300 mass spectrometer with JEOL JMA 5000 Mass Data System at an ionizing voltage of 20—70 eV.

Materials. Benzeneselenenyl chloride of Nakarai Chemicals was distilled prior to use; bp 82 °C/3 mmHg (120 °C/20 mmHg) (1 mmHg=133.322 Pa).[7] Benzeneseleninyl chloride (**1**) was prepared by ozonization of benzeneselenenyl chloride with stirring in dry dichloromethane at −70 °C until the orange-red color has faded to a light yellow[8] by introducing ozone prepared by a Nippon Ozone Model O-3-2 ozonizer. The benzeneseleninyl chloride prepared was used to the reaction with aromatic compounds in situ since the compound is extremely hygroscopic and care must be taken to avoid moisture. Toluene, chlorobenzene, phenol, anisole, phenetole, diphenyl ether, and *N*,*N*-dimethylaniline used were obtained from Tokyo Kasei Co.

General Procedure for the Reaction of Benzeneseleninyl Chloride (1) with Aromatic Compound. To a stirred solution of benzeneseleninyl chloride, prepared from benzeneselenenyl chloride (192 mg, 1 mmol) by ozonization at −70 °C in dichloromethane (20 cm^3), was added corresponding aromatic compound (1 mmol) and aluminum halide (1 mmol) under nitrogen-gas bubbling. The mixture was allowed to raise the temperature at 40 °C or room temperature and was stirred for an appropriate time (see Table 1). Water (30 cm^3) was added to the reaction mixture, which was then extracted with dichloromethane (20 cm^3×2). The combined organic extracts were washed with saturated solution of sodium carbonate (20 cm^3) and water (30 cm^3), and dried over magnesium sulfate. The halogenated aromatic products were analyzed by GLC and GC-MS comparing with their authentic samples, and the yields were determined by using acetophenone as the internal standard.

General Procedure for the Isolation of Para-Halogenated Benzenes. The halogenation of substituted benzene (30

mmol) by benzeneseleninyl chloride (10 mmol) in the presence of aluminum halide (10 mmol) in dichloromethane (300 cm^3) was carried out in a similar procedure shown above. The reaction mixture was quenched by water (50 cm^3); then dichloromethane was evaporated. The organic layer was extracted with ether (300 cm^3), dried over magnesium sulfate; the solvent was evaporated, and the residue was subjected to the silica-gel chromatography by using hexane as an eluent to give *p*-halogenated benzene. The product was further purified (if necessary) by gel-permeation chromatography on a JAI LC-08 liquid chromatograph with a JAIGEL-1m column (20ϕ×600 mm×2) using chloroform as an eluent.

References

1) H. O. House, "Modern Synthetic Reactions," 2 nd ed., W. A. Benjamin, Menlo Park, California, 1972.

2) R. Adams and C. S. Marvel, *Org. Synth.*, Coll. Vol. I, 128 (1944); G. M. Kosolapoff, *J. Am. Chem. Soc.*, **75**, 3596 (1953); H. E. Podall and W. E. Foster, *J. Org. Chem.*, **23**, 280 (1958); E. M. Kosower, W. J. Cole, G. S. Wu, D. E. Cardy, and G. Meisters, *ibid.*, **28**, 630 (1963); V. Colo, F. Ciminale, L. Lopez, and P. E. Todesco, *J. Chem. Soc. C*, **1971**, 3652; V. Calo, F. Ciminale, L. Lopez, G. Pesce, and P. E. Todesco, *Chim. Ind. (Milan)*, **53**, 467 (1971); P. A. Zoretic, *J. Org. Chem.*, **40**, 1867 (1975).

3) T. Matsue, M. Fujihira, and T. Osa, *J. Electrochem. Soc.*, **126**, 500 (1979); T. Matsue, M. Fujihira, and T. Osa, *Bull. Chem. Soc. Jpn.*, **52**, 3692 (1979).

4) W. D. Watson, *J. Org. Chem.*, **50**, 2145 (1985).

5) G. A. Olah, L. Ohanneesian, and M. Arvanaghi, *Synthesis*, **1986**, 868.

6) N. Kamigata, T. Satoh, and M. Yoshida, *Bull. Chem. Soc. Jpn.*, **61**, 449 (1988).

7) O. Behaghel and H. Seibert, *Ber.*, **66**, 708 (1933).

8) G. Ayrey, D. Barnard, and D. T. Woodbridge, *J. Chem. Soc.*, **1962**, 2089; H. J. Reich, J. M. Renga, and I. L. Reich, *J. Am. Chem. Soc.*, **97**, 5434 (1975).

Hydroxyalkylation and Lactone Formation from Dialkyl Malonate by Means of a Eu^{III}/Eu^{II} Photoredox System

Akito ISHIDA,* Shinya YAMASHITA,† and Setsuo TAKAMUKU
The Institute of Scientific and Industrial Research, Osaka University, Ibaraki, Osaka 567
(Received October 7, 1987)

Synopsis. A Eu^{III}/Eu^{II} photoredox system in alcohol induced an effective hydroxyalkylation at an α-position of a dialkyl malonate. The alcohol adduct was then converted to the lactone. A step-by-step hydroxyalkylation mechanism was suggested in which the Eu ion is used as a photocatalyst and also as a condensation catalyst for the reaction of dialkyl malonates and aldehydes.

We have investigated a series of photo-hydroxyalkylations of various unsaturated compounds induced by a Eu^{III}/Eu^{II} photoredox system in alcohols. The reaction of aromatic and aliphatic alkenes provided dihydrodimers and alcohol adducts as main products via a radical mechanism.[1,2] On the other hand, 1,3-dimethyluracil and its derivatives provided a hydroxyalkylation product at the C-6 position in a very high yield; a one-electron reduction mechanism has been suggested.[3,4] In this paper, we present an effective hydroxyalkylation and lactone formation of dialkyl malonates by the use of a Eu^{III}/Eu^{II} photoredox system in which the Eu ion is used as a photocatalyst and also catalyzes the condensation of dialkyl malonates and aldehydes.

Results and Discussion

A 180 mL methanol solution of dimethyl malonate (**1**: 85 mmol dm^{-3}) and $EuCl_3$ (2.2 mmol dm^{-3}) was saturated with Ar and irradiated in a Pyrex cell with a 350-W high-pressure mercury lamp at the temperature of running water. During the irradiation, the evolution of hydrogen gas was observed much as in substrate-free solution.[1,2] After a 22-h irradiation, all the substrate has been consumed; the reaction mixture was then worked up. The crude product was a mixture of a hydroxyethylated product **2** and its lactone **3**, which were confirmed by the NMR spectra. By distillation, **3** was isolated as a sole product in a yield of 76%. Without $EuCl_3$, no reaction was observed, and **1** was recovered. The absorption spectra suggested that $EuCl_3$ was the main light-absorbing agent. The reaction of diethyl malonate (**4**) in ethanol was carried out under similar reaction conditions, but the reaction rate was rather lower than that of **1** and the conversion was 77% at an 84-h irradiation.[5] In addition to a 1:2 alcohol adduct **5** (31%, based on conversion) and its lactone **6** (27%), a 1:1 adduct **7** (19%) and its dehydrated product **8** (8%) were obtained. They were presumed to be the primary products. The NMR spectra of **6** suggested the presence of two diastereomers **6a** and **6b**.[6].

The time course observation of the reaction of **4** was carried out to get an insight into the initial step of the reaction. The conversion of **4** and the product-formation were monitored by means of GLC(FID), so that **5** and **7** were determined to be **6** and **8** respectively. The reaction of dialkyl malonates needed a very long risetime compared with that of other olefinic substrates reported previously.[1,2] In the initial 20 h, hydrogen gas and acetaldehyde were obtained as the photolytic products of ethanol by means of a Eu^{III}/Eu^{II} photoredox stem.[1,2] After the 20-h irradiation, the products derived from **4** were barely observed. After a 75-h irradiation, **6** (and/or **5**) was determined in a yield of 24% (absolute yield). Furthermore, **8** (and/or **7**) which had been slightly observed during the irradiation, increased and became the main product (26%) upon standing for 45 h in the dark after a 75-h irradiation. These facts suggest that **8** might be a product of the dark reaction of **4** with acetaldehyde, which is a photolytic product of ethanol.[7] Indeed, the intentional addition of acetaldehyde (0.5 mol dm^{-3}) to this system obviously shortened the risetime of the photoproducts (**6** and/or **5**). In order to confirm this process, the reac-

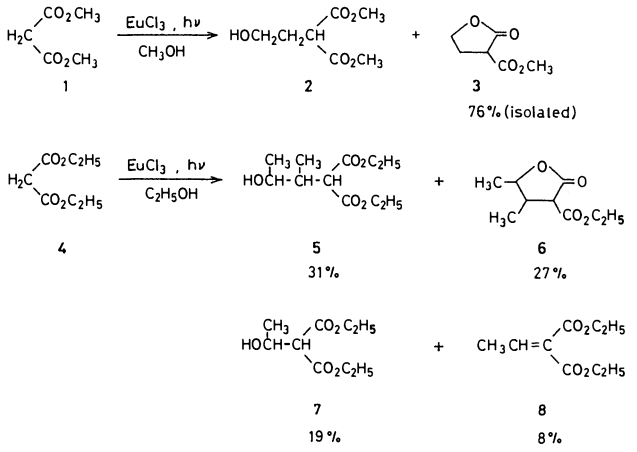

Table 1. Reaction of Dialkyl Malonate and Aldehydes in the Dark in the presence of $EuCl_3$[a]

Ester	Aldehyde	Solvent	Reaction time/h	Conv. %	Product yield/%[b]
1	HCHO	MeOH	24	100	**9**+**10**[c] 0[d]
4	CH_3CHO	EtOH	72	70	**7**+ **8**[c] 100

a) [ester]=100 mmol dm^{-3}, [$EuCl_3$]=10 mmol dm^{-3}, [aldehyde]=1.2 mmol dm^{-3}; at room temp.,in the dark. b) Yields are based on the amounts of esters consumed. c) **9** and **7** were determined by GLC(FID) as **10** and **8** respectively. d) Oligomerization products were observed.

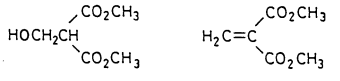

† Present address: Fuji Oil Co., Ltd., Izumisano, Osaka 598.

tion of dialkyl malonates with aldehydes were carried out in the dark.

The monitoring of reactions was carried out by means of GLC(FID). Thus, the alcohol adducts were determined to be the dehydrated esters. In the presence of $EuCl_3$, an ethanol solution of **4** and acetaldehyde provided an ethanol adduct **7** and/or **8** quantitatively, while no product was observed when there was no $EuCl_3$ (Table 1). In the reaction of **1** with formaldehyde, **1** disappeared. However, only oligomeric products were obtained instead of **9** (and/or **10**). This is consistent with the fact that **9** is easily dehydrated to provide **10**, which is very unstable and polymerizable under these conditions.[7] These observations suggest that the present reaction proceeds by the two steps shown in Scheme 1:

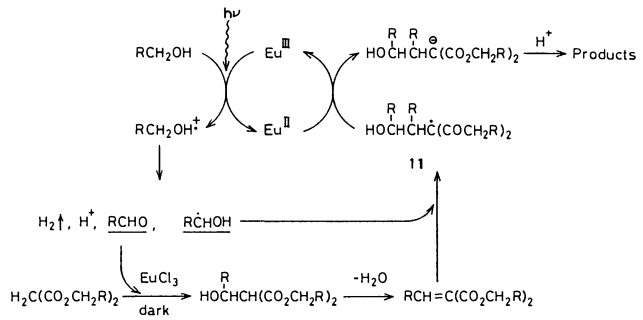

Scheme 1.

The first step is a reaction in the dark of dialkyl malonate with aldehyde, which is a primary photoproduct. This type of reaction, known as Knoevenagel reaction, was catalyzed by a Lewis acid, and the product was easily dehydrated to provide an unsaturated ester.[8] In this stem, $EuCl_3$ may act as a Lewis acid for the condensation. In the photoreaction of **1**, **9** may be supplied in a very low concentration; thus, the further reaction of **9** to produce **3** is preferred to the oligomerization.

The second step of the reaction, the photo-addition of alcohol to unsaturated esters **8** and **10**, is presumed to be induced by a hydroxyalkyl radical. The radical **11** produced by the addition of the hydroxyalkyl radical has two methoxycarbonyl group and is supposed to be easily reduced by Eu^{II}, thus generating the carbanion, which then, gives the product by protonation (Scheme 1).

Dimethyl maleate (**12**), another α,β-unsaturated ester, was irradiated in the presence of $EuCl_3$ in methanol. An alcohol adduct **13** and its lactone **14** were thus obtained in high yields. There, the Eu^{III}/Eu^{II} photoredox reaction is an efficient system for the hydroxyalkylation and successive lactone formation of unsaturated esters. The photo-reaction of dimethyl maleate in CH_3OD resulted in the incorporation of the D atom at the α-carbon of the product **13**,[9] which was consistent with the mechanism via a carbanion.

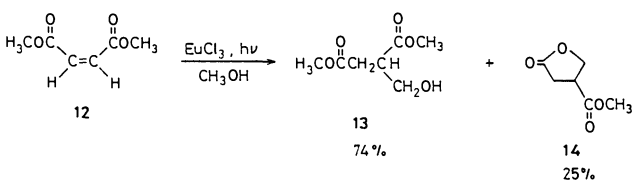

Experimental

The ^1H and ^{13}C NMR spectra were recorded on a Bruker WM-360 instrument using tetramethylsilane as the internal standard. The gas chromatography was carried out on a Shimadzu GC-7A apparatus with FID using OV-17 or Porapak Type QS. The mass spectra were recorded on a JEOL DX-300 apparatus with a JEOL JMA-3100 data processor.

Reaction of 1. A 180 mL methanol solution of **1** (2.0 g, 15.2 mmol) and $EuCl_3$ (150 mg, 0.4 mmol) was irradiated in a Pyrex cell with a high-pressure mercury lamp for 22 h under an Ar atmosphere. After the irradiation, the methanol was removed in vacuo. The residue was extracted with $CHCl_3$, after which, the solution was washed with water two times and dried with $MgSO_4$, and the $CHCl_3$ was removed in vacuo. The crude product, a colorless oil (1.96 g), was distilled (bath temp 80—100 °C/4 mmHg††) with a "One-Pot Still" after the NMR analyses. As the sole product, **3** was obtained (1.66 g).

2: Not isolated, but identified as a mixture with **3** by ^1H NMR and ^{13}C NMR; ^1H NMR ($CDCl_3$ δ=2.15 [d (J=6.1 Hz) and t (J=6.6 Hz), 2H], 3.17 (bs, 1H), 3.68 (t, J=6.1 Hz, 1H), and 3.75 (s, 6H). The 2H of -$C\underline{H}_2OH$ was not identified, because it was in the multiplet of 4.52—4.32 ; ^{13}C NMR ($CDCl_3$) δ=29.5, 48.1, 52.8, 63.4, and 174.3.

3: Colorless oil; ^1H NMR ($CDCl_3$) δ=2.54 (dddd, J=5.3, 7.5, 9.3, and 13.1 Hz, 1H), 2.68 (dddd, J=7.4, 7.9, 8.2, and 13.1 Hz, 1H), 3.59 (dd, J=7.9 and 8.9 Hz, 1H), 3.81 (s, 3H), 4.35 (ddd, J=7.4, 7.5, and 8.9 Hz, 1H), and 4.48 (ddd, J=5.3, 8.2, and 8.9 Hz, 1H); ^{13}C NMR ($CDCl_3$) δ=26.5 (t), 45.8 (d), 53.0 (q), 67.4 (t), 168.3 (s), and 172.3 (s); EIMS, m/z (relative intensity) 145 (M^++1, 2), 144 (4, M^+), 113 (29), 100 (32), 69 (100), 59 (22), 55 (39), and 41 (51); Found C, 49.74; H, 5.62%. Calcd for $C_6H_8O_4$: C, 50.00; H, 5.60%.

Reaction of 4. The crude product, which had been obtained much as in the photoreaction of **1**, was a colorless oil (22.29 g); and when it was separated by column chromatography on silica gel (eluent; a mixture of Et_2O and hexane, 2 : 1 v/v), and the three fractions were obtained: a mixture of **4** and **7**: 0.57 g; a mixture of **7** and **8**: 0.29 g; and a mixture of **5** and **6**: 0.91 g. The product yields were calculated by the use of the product ratio obtained by means of the ^1H NMR data.

5: Not isolated but identified by NMR analyses as a mixture with **6**; ^1H NMR ($CDCl_3$) δ=0.98 (d, J=7.0 Hz, 3H), 1.28 (t, J=7.1 Hz, 6H), 1.29 (d, J=6.4 Hz, 3H), 2.31 [d (J=2.5 Hz), t (J=7.0 Hz), and t (J=8.5 Hz), 1H], 2.47 (bs, 1H), 3.49 (d, J=8.5 Hz, 1H), 3.93 [d (J=2.5 Hz) and q (J=6.4 Hz), 1H], and 4.21 (q, J=7.1 Hz, 4H); ^{13}C NMR ($CDCl_3$) δ=10.7 (q), 14.1 (q), 20.7 (q), 39.5 (d), 55.7 (d), 61.5 (t), 68.3 (d), 169.1 (s), and 169.5 (s); m/z 204.

6a: Colorless oil. ^1H NMR ($CDCl_3$) δ=1.18 (d, J=6.6 Hz, 3H), 1.32 (t, J=7.1 Hz, 3H), 1.46 (d, J=6.2 Hz, 3H), 2.56 (m, 1H), 3.25 (d, J=11.6 Hz, 1H), 4.13 [d (J=9.4 Hz) and q (J=6.1 Hz), 1H], and 4.27 (q, J=7.1 Hz 2H); ^{13}C NMR ($CDCl_3$) δ=14.1 (q), 15.1 (q), 18.4 (q), 42.8 (d), 55.1 (d), 61.9 (t), 81.6 (d), 167.6 (s), and 171.1 (s).

6b: Colorless oil; ^1H NMR ($CDCl_3$) δ=1.11 (d, J=7.1 Hz, 3H), 1.29 (d, J=6.7 Hz, 3H), 1.32 (t, J=7.1 Hz, 3H), 3.00 (m, 1H), 3.26 (d, J=8.3 Hz, 1H), 4.26 (q, J=7.1 Hz, 2H), and 4.82 (quintet, J=6.7 Hz, 1H); ^{13}C NMR ($CDCl_3$) δ=13.3 (q), 14.1 (q), 15.5 (q), 38.0 (d), 53.6 (d), 61.9 (t), 78.7 (d), 167. 1 (s), and 171.5 (s); Found: m/z (mixture of **6a** and **6b**) 186.08935. Calcd

†† 1 mmHg=133.322 Pa.

for $C_9H_{14}O_4$: M, 186.08912.

7: Not isolated but identified by NMR analyses as a mixture with **8**; ^{1}H NMR ($CDCl_3$) δ=1.25 (d, J=7.0 Hz, 3H), 1.27 (t, J=7.0 Hz, 3H), 1.28 (t, J=7.0 Hz, 3H), 3.46 (d, J=9.2 Hz, 1H), 3.62 [d (J=9.1 Hz) and q (J=7.0 Hz), 1H], 4.19 (q, J=7.1 Hz, 2H), and 4.21 (q, J=7.1 Hz, 2H); ^{13}C NMR ($CDCl_3$) δ=14.1 (q), 18.0 (d), 59.0 (d), 61.4 (t), 73.9 (d), 167.3 (s), and 167.7 (s).

8: Colorless oil; ^{1}H NMR ($CDCl_3$) δ=1.29 (t, J=7.1 Hz, 3H), 1.34 (t, J=7.1 Hz, 3H), 1.96 (d, J=7.2 Hz, 3H), 4.25 (q, J=7.1 Hz, 2H), 4.31 (q, J=7.1 Hz 2H), and 7.09 (q, J=7.3 Hz, 1H); ^{13}C NMR ($CDCl_3$) δ=14.2 (q), 15.4 (q), 61.2 (t), 130.1 (s), 144.6 (d), 163.4 (s), 165.4 (s).

Reaction of 4 for the Quantitative Analysis. A 5-mL ethanol solution of **4** (100 mmol dm^{-3}) and $EuCl_3$ (5 mmol dm^{-3}) was saturated with Ar and irradiated in a Pyrex cell this with a 350-W high-pressure mercury lamp for 75 h. After this irradiation, the reaction mixture was left in the dark for 45 h. The reaction was followed by GLC every 5 h.

Reaction of 4 in the Dark. A 5-mL ethanol solution of **4** (800 mg, 5.0 mmol), $EuCl_3$ (180 mg, 0.5 mmol), and acetaldehyde (7 mL, 60 mmol) was stirred for the 72 h at room temperature in the dark, and then the EtOH was removed in vacuo. The mixture was extracted with $CHCl_3$, washed with water two times, and dried with $MgSO_4$; and $CHCl_3$ was then removed in vacuo. The products were distilled under reduced pressure (110 °C/4 mmHg). The NMR data were identical with those of photogenerated **10**.

Reaction of 12. A 180-mL methanol solution of **12** (123 mmol dm^{-3}) and $EuCl_3$ (2.2 mmol dm^{-3}) was saturated with Ar and irradiated in a Pyrex cell with a 350-W high-pressure mercury lamp for 24 h (conv. 100%). After the irradiation, the methanol was removed in vacuo, and the residue was extracted with a large amount of ether. The ether solution was filtered through Hyflosuper-cel to remove the $EuCl_3$; and a colorless oil was then obtained by removing the ether. The crude product was separated by column chromatography on silica gel (eluent: $CHCl_3$).

13: Colorless oil; ^{1}H NMR ($CDCl_3$) δ=2.63 (dd, J=6.2 Hz and 16.8 Hz, 1H), 2.78 (dd, J=7.5 Hz and 16.8 Hz, 1H), 2.87 (bs, 1H), 3.04 (dist. quintet, 1H), 3.70 (s, 3H), 3.73 (s, 3H), and 3.82 (d, J=5.4 Hz, 2H); ^{13}C NMR δ=32.7 (t), 44.1 (q), 50.3 (q), 52.0 (q), 62.6 (t), 172.7 (s), and 173.9 (s); Found: C, 47.77, H, 6.86%. Calcd for $C_7H_{12}O_5$: C, 47.72; H, 6.87%.

14: Colorless oil; ^{1}H NMR ($CDCl_3$) δ=2.76 (dd, J=9.6 Hz and 17.9 Hz, 1H), 2.88 (dd, J=7.3 Hz and 18.0 Hz, 1H), 3.48 (dist. quintet, 1H), 3.78 (s, 3H), 4.46 (dd, J=6.6 Hz and 9.4 Hz, 1H), and 4.52 (dd, J=8.4 Hz and 9.3 Hz, 1H); ^{13}C NMR ($CDCl_3$) δ=39.9 (d), 52.7 (q), 69.2 (t), 171.9 (s), and 175.3 (s); Found: C, 49.74; H, 5.46%. Calcd for $C_6H_8O_4$: C, 50.00; H, 5.60%.

This work was supported by a Grant-in-Aid for Developmental Scientific Research from the Ministry of Education, Science and Culture of Japan (Nos. 61223019 and 62750785). We wish to thank the Material Analysis Center of the Institute of Scientific and Industrial Research of Osaka University for the spectral analyses and elemental analyses.

References

1) A. Ishida, S. Toki, and S. Takamuku, *Chem. Lett.*, **1985**, 893.

2) A. Ishida, S. Toki, and S. Takamuku, *Bull. Chem. Soc. Jpn.*, **59**, 1195 (1986).

3) A. Ishida, S. Toki, and S. Takamuku, *J. Chem. Soc., Chem. Commun.*, **1985**, 1481.

4) A. Ishida, S. Toki, and S. Takamuku, *Chem. Lett.*, **1986**, 117.

5) In the presence of $EuCl_3$, a rapid transesterification was observed in the dark at room temperature; we used the alcohol corresponding to the ester as the solvent.

6) P. Kolsaker and A. Berg, *Acta Chem. Scand. B*, **33**, 10 (1979); Y. Yamamoto, T. Komatsu, and K. Maruyama, *J. Chem. Soc., Chem. Commun.*, **1983**, 191; T. Shono and S. Fujita, *Chem. Lett.*, **1981**, 1217; L. Bassi and W. K. Schierlein, *Helv. Chim. Acta*, **66**, 92 (1983).

7) A. A. Vanscheidt, *J. Gen. Chem., USSR*, **15**, 574 (1945).

8) B. Wojcik and H. Adkins, *J. Am. Chem. Soc.*, **56**, 2424 (1934); W. Lehnert, *Tetrahedron*, **1970**, 4723.

9) The product **14** incorporated a deuterium (ca. 100% d_1) which was confirmed by NMR.

Formation of 1,4,2,5-Dithiadiazines as a Heterocyclic System by Reaction of 1,4,2-Dithiazolium Salts with Sulfenamides

Katsumi YONEMOTO,* Isao SHIBUYA,* and Kazumasa HONDA
National Chemical Laboratory for Industry, Tsukuba, Ibaraki 305
(Received December 5, 1987)

Synopsis. The first example of application of sulfenamides for ring expansion on nitrogen atom has been reported to give 1,4,2,5-dithiadiazines (**3**) from 1,4,2-dithiazolium salts (**1**). The structure of **3** was confirmed by X-ray crystallographic analysis. The similar ring expansion reaction occurred on 1,3-dithiolium salts (**5**) to afford 1,4,2-dithiazines (**6**).

The chemistry of 1,4-dithiins, an interesting 8π-electron ring system containing heteroatoms, has been extensively studied[1] and reviewed.[2] Their aza-analogues, 1,4,2-dithiazines, which were conveniently accessible by the reaction of 1,3-dithiolium salts with sodium azide,[3] have also been known and studied; much attention has been focused on their thermal decomposition reactions.[3,4] In contrast, the chemistry of 1,4,2,5-dithiadiazines, a higher aza-analogue, remains virtually unexplored, mainly because they were prepared for the first time only a few years ago by the reaction between thiobenzamide *S*-oxide and $Et_3O^+BF_4^-$.[5] Generally, 6-membered ring systems with four heteroatoms are much less known. As an extension of our studies on the reactivity of 1,4,2-dithiazolium salts (**1**) toward various kinds of amino compounds, we will report an alternative method for the preparation of unsymmetrically substituted 1,4,2,5-dithiadiazines (**3**) by the reaction of **1** with *S*-dimethylthiocarbamoyl-substituted sulfenamides (**2**).

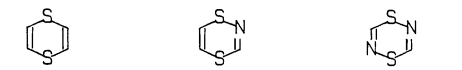

Results and Discussion

1,4,2-Dithiazolium perchlorates **1** were allowed to react with 2 molar amount of sulfenamide **2a** in MeCN at room temperature to give 1,4,2,5-dithiadiazines **3** in good yields, whereupon tetramethylthiuram disulfide (**4**) and ammonium perchlorate were also formed.[6] The results are presented in Table 1. The products **3** were identified with spectral data and elemental analysis. However, we cannot unequivocally distinguish the spectral data between 1,4,2,5- and 1,4,2,6-dithiadiazine isomers; the structure, on the other hand, was determined by X-ray crystallographic analysis of **3f**. This analysis showed that the molecule is a 1,4,2,5-isomer and has a boat conformation similar to that of dithiins (Fig. 1).

In order to investigate the versatility of other sulfenamides for this reaction, the reaction of **1a** with sulfenamides **2b—g** was examined under the same conditions as used for **2a**. The results are presented in Table 2. The yield of **3a** was remarkably dependent on the kind of sulfenamides, ranging from 95 to 0%. From the present results, *S*-dimethylthiocarbamoyl-substituted

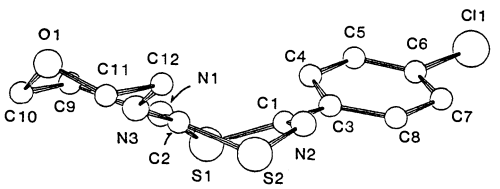

Fig. 1. The molecular structure of 3f.

Table 1. Synthesis of 1,4,2,5-Dithiadiazines (**3a—f**)

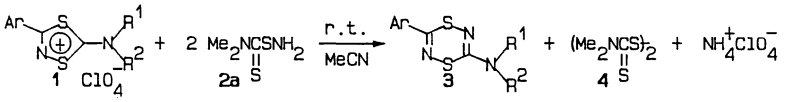

Compd	Ar	R^1R^2N	Time	Yield[a]	Mp	Found(Calcd)/%[b]			
			d	%	θ_m/°C	C	H	N	S
3a	Ph	Et_2N	2	89	71.0—71.5	54.13 (54.31)	5.67 (5.70)	15.83 (15.83)	24.07 (24.16)
3b	Ph	Me_2N	2	83	59.0—59.5				
3c	Ph	*i*-Pr_2N	3	41	125.0—125.5	57.37 (57.30)	6.54 (6.53)	14.29 (14.32)	21.79 (21.85)
3d	Ph	PhMeN	1	88	74.0—74.5	59.97 (60.17)	4.39 (4.38)	13.94 (14.03)	21.37 (21.42)
3e	4-MeC_6H_4	Et_2N	2	90	49.5—50.0				
3f	4-ClC_6H_4		3	60	157.0—158.0	45.79 (45.93)	3.84 (3.85)	13.31 (13.39)	20.34 (20.43)

a) Isolated yield. b) Elemental analyses of **3b** and **3e** were difficult due to instability in crystal form.

Table 2. Formation of **3a** by Reaction of **1a** with Various Kinds of Sulfenamides **2a**—g

	Sulfenamide	Time d	Yield of **3a**[a] %
2a	$Me_2NCSSNH_2$	2	89
2b	$i\text{-}Pr_2NCSSNH_2$	2	60
2c		2	87
2d		3	10
2e	$PhN{=}C(Ph)SNH_2$	1	95
2f	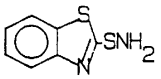	4	0[b]
2g	$PhCOSNH_2$	3	0[c]

a)Isolated yield. b) No reaction. c) 5-Benzoylimino-3-phenyl-1,4,2-dithiazole **8** was formed; see Ref. 13.

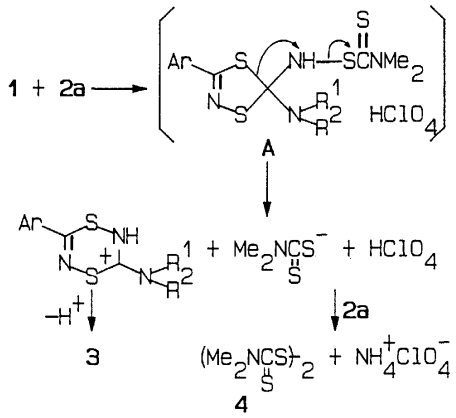

Scheme 1.

sulfenamides **2a**—**c** were most favorable for this reaction in terms of availability, stability, and high yields of **3**.

A mechanistic interpretation for the formation of **3** is shown in Scheme 1. Nucleophilic attack of the terminal amino group of sulfenamide **2a** on the C-5 carbon atom of dithiazolium cation leads to an intermediate **A** (Scheme 1), which is then converted into dithiadiazine **3** with liberation of dimethyldithiocarbamate followed by S-4 migration and deprotonation, although the exact timing of each step is indefinite. This mechanism is similar to that of the reaction of *N*-methylacridinium salts with hydroxylamine-*O*-sulfonic acid which gives 4-methyldibenzo-[*b*,*e*][1,4]-diazepine.[7] Furthermore, the observation in a separate experiment that disulfide **4** is formed by reaction of **2a** with sodium dimethyldithiocarbamate in the presence of *p*-toluenesulfonic acid is consistent with the proposed reaction mechanism.

Other attempts to convert **1b** into the target molecule **3b** by a ring expansion reaction using standard "*N*-expansion" reagents, such as sodium azide and *S*,*S*-diphenylsulfilimine ($Ph_2S{=}NH$), were unsuccessful. But 5-phenyl-1,2,3,4-tetrazole[8] and *N*-(dimethylthiocarbamoyl)-*S*,*S*-diphenylsulfilimine,[9] respectively, were obtained instead. It is therefore likely that the attack of nitrogen of these nucleophiles on the C-5 position in dithiazolium cation induces further ring cleavage in preference to the formation of nitrene.

In order to check the possibility of application of this reaction to other cation compounds, the reaction of 2-dialkylamino-4,5-diphenyl-1,3-dithiolium perchlorates (**5a**, **b**) with sulfenamide **2a** was carried out under the same conditions, from which 3-dialkylamino-5,6-diphenyl-1,4,2-dithiazines (**6a**, **b**) were obtained in good yields. On the other hand, treatment of **5a** with NaN_3 in refluxing toluene for 30 min did not give the expected **6a**. Furthermore, 2,4,5-triphenyl-1,3-dithiolium perchlorate (**5c**) was allowed to react with **2a** to give 3,5,6-triphenyl-1,4,2-dithiazine (**6c**) (20%) together with 3,4,5-triphenylisothiazole (**7**) (30%, mp 209 °C, lit,[3a] mp 211.5—212.5 °C), while Nakayama et al. reported that **5c** was subjected to react with NaN_3 in refluxing toluene to afford only a product **7**, which arose from **6c** by thermal elimination of sulfur.[3a]

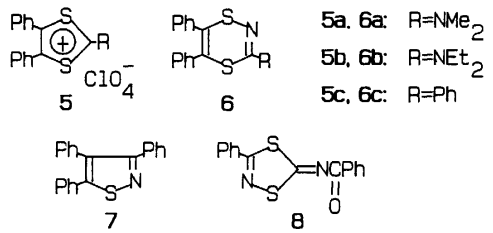

In summary, we believe that this is the first example of the ring expansion on nitrogen atom with sulfenamides **2**. It belongs to important class of ring expansion reactions, especially because it can be smoothly carried out under mild conditions, i.e., at ambient temperature, without irradiation, and in the absence of a base. The application of this reaction to a wide range of cation compounds is currently under way.

Experimental

All the melting points were uncorrected. The ^1H NMR and ^{13}C NMR spectra were recorded on a Hitachi R-40 and a JEOL FX-90A spectrometers, respectively, in $CDCl_3$, using TMS as an internal standard. The IR spectra were measured on a JASCO A-302 spectrometer using KBr disks. The low-resolution mass spectra were taken on Hewlett Packard 5995A spectrometer by electron impact ionizing technique at 70 eV.

1,4,2-Dithiazolium salts **1** were readily prepared from disubstituted dithiocarbamate in three steps, utilizing our reported procedure.[10] 1,3-Dithiolium salts **5** were prepared from the reaction of dithiocarbamate (or dithiobenzoate) and 2-bromo-2-phenylacetophenone in a manner similar to that described in Ref. 11. Sulfenamides **2a**—**g** were prepared from the reaction of thiolates (RS^-) with hydroxylamine-*O*-sulfonic acid by the same method as described in literatures.[10,12]

Preparation of 1,4,2,5-Dithiadiazines 3a—f; General Procedure. 1,4,2-Dithiazolium perchlorate **1a—f** (1 mmol) was added to stirred solution (MeCN, 4 ml) of sulfenamide **2a** (2 mmol). The reaction mixture was stirred for a few days at room temperature, during which time disulfide **4** and/or ammonium perchlorate were crystallized out and filtered off.

The crude product was extracted with dichloromethane after addition of water. The residual solid was purified by column chromatography on silica gel and recrystallization from appropriate solvents (MeCN–ether, dichloromethane–hexane, etc.) to give **3a**—**f** as yellow powder.

3a: ^{1}H NMR δ=1.21 (6H, t, J=7.5 Hz), 3.53 (4H, q, J=7.5 Hz), 7.4—7.6 (3H, m), 7.9—8.1 (2H, m). ^{13}C NMR δ=13.65, 44.48, 127.74, 128.64, 131.67, 134.81, 162.50, 176.96. IR ν 1535, 939, 695 cm^{-1}. MS m/z (rel intensity) 265 (M^+; 20), 232 (M^+−SH; 62), 121 ($PhCS^+$; 100).

3b: ^{1}H NMR δ=3.12 (6H, s), 7.4—7.6 (3H, m), 7.9—8.1 (2H, m). ^{13}C NMR δ=39.17, 127.72, 128.64, 131.70, 134.68, 163.55, 175.96. IR ν 1546, 936, 695 cm^{-1}. MS m/z (rel intensity) 237 (M^+; 34), 204 (M^+−SH; 84), 121 ($PhCS^+$; 100), 88 (Me_2NCS^+; 97).

3c: ^{1}H NMR δ=1.32 (12H, d, J=6.9Hz), 4.07 (2H, m, J=6.9Hz), 7.4—7.6 (3H, m), 7.9—8.1 (2H, m). ^{13}C NMR δ=20.80, 49.46, 127.72, 128.61, 131.59, 134.95, 161.60, 177.45. IR ν 1527, 1286, 1030, 939, 689 cm^{-1}. MS m/z (rel intensity) 293 (M^+; 16), 260 (M^+−SH; 41), 218 (82), 121 ($PhCS^+$; 82), 103 ($PhCN^+$; 80), 69 (100).

3d: ^{1}H NMR δ=3.43 (3H, s), 7.1—7.6 (8H, m), 7.8—8.0 (2H, m). ^{13}C NMR δ=40.41, 126.09, 127.53, 127.64, 128.56, 129.53, 131.54, 134.60, 143.48, 161.06, 173.44. IR ν 1536, 1268, 935, 689 cm^{-1}. MS m/z (rel intensity) 299 (M^+; 24), 266 (M^+−SH; 12), 150 ($PhMeNCS^+$; 24), 132 ($PhMeNCN^+$; 100), 121 ($PhCS^+$; 61), 103 ($PhCN^+$; 31).

3e: ^{1}H NMR δ=1.19 (6H, t, J=7.0 Hz), 2.36 (3H, s), 3.49 (4H, q, J=7.0 Hz), 7.22 (2H, d, J=9.0 Hz), 7.85 (2H, d, J=9.0 Hz). ^{13}C NMR δ=13.65, 21.43, 44.42, 127.64, 129.34, 132.21, 142.15, 162.60, 176.66. IR ν 1531, 1251. 931, 825, 761 cm^{-1}. MS m/z (rel intensity) 279 (M^+; 29), 246 (M^+−SH; 74), 135 ($MeC_6H_4CS^+$; 82), 117 ($MeC_6H_4CN^+$; 100).

3f: ^{1}H NMR δ=3.5—3.9 (8H, m), 7.43 (2H, d, J=9.0 Hz), 7.90 (2H, d, J=9.0 Hz). ^{13}C NMR δ=47.57, 66.28, 129.04, 129.10, 133.08, 138.28, 163.39, 175.01. IR ν 1541, 1206, 1115, 949, 825 cm^{-1}. MS m/z (rel intensity) 315 (M^++2; 15), 313 (M^+; 36), 280 (M^+−SH; 76), 155 ($ClC_6H_4CS^+$; 100), 137 ($ClC_6H_4CN^+$; 69).

Preparation of 1,4,2-Dithiazines 6a—c. The similar treatment of **5a**—c (1 mmol) with **2a** (2 mmol) gave crude products **6a**—c which were purified by the same procedure as mentioned above.

6a: Yield 81%. Mp 164.0—164.5 °C. ^{1}H NMR δ=3.18 (6H, s) 7.1—7.5 (10H, m). ^{13}C NMR δ=40.58, 123.14, 127.26, 127.96, 128.10, 128.18, 129.40, 130.32, 135.79, 138.63, 147.79, 164.47. IR ν 1553, 1358, 1243, 1117, 907, 693 cm^{-1}. MS m/z (rel intensity) 312 (M^+; 22), 242 ($(PhCS)_2^+$; 32), 178 ($PhCCPh^+$; 69), 121 ($PhCS^+$; 100). Found: C, 65.36; H, 5.16; N, 8.91; S, 20.39%. Calcd for $C_{17}H_{16}N_2S_2$: C, 65.35; H, 5.16; N, 8.97; S, 20.52%.

6b: Yield 80%. Mp 123.0—124.5 °C. ^{1}H NMR δ=1.18 (6H, t, J=7.2 Hz), 3.55 (4H, q, J=7.2 Hz), 7.1—7.5 (10H, m). ^{13}C NMR δ=13.71, 45.70, 123.14, 127.20, 127.96, 128.10, 128.69, 129.42, 130.37, 135.95, 138.82, 148.68, 163.12. IR ν 1540, 1259, 1123, 692 cm^{-1}. MS m/z (rel intensity) 340 (M^+; 13), 242 ($(PhCS)_2^+$; 36), 178 ($PhCCPh^+$; 50), 121 ($PhCS^+$; 100). Found: C, 67.00; H, 5.95; N, 8.23; S, 18.65%. Calcd for $C_{19}H_{20}N_2S_2$: C, 67.02; H, 5.92; N, 8.23; S, 18.83%.

6c: Yield 20%. Yellow oil. ^{1}H NMR δ=7.1—7.5 (13H, m) 8.0—8.2 (2H, m). ^{13}C NMR δ=123.65, 127.80, 128.12, 128.34, 128.58, 128.77, 129.64, 130.18, 131.51, 135.54, 135.65, 137.74, 140.93, 164.47. IR ν 1498, 1439, 1210, 898, 689 cm^{-1}. MS m/z (rel intensity) 345 (M^+; 13), 313 (M^+−S; 10), 242 ($(PhCS)_2^+$; 29), 178 ($PhCCPh^+$; 50), 121 ($PhCS^+$; 100). **6c** tends to decompose slowly on standing in air, so elemental analysis of **6c** has been unsuccessful.

X-Ray Analysis of 3f. Crystal data: $C_{12}H_{12}ClN_3OS_2$; MW 313.83; orthorhombic; space group $Pca2_1$; a=15.408(4), b=4.064(2), and c=42.855(9) Å; U=2686(2) Å^3; D_c=1.55 g cm^{-3} for Z=8; μ(Cu $K\alpha$)=52.6 cm^{-1}. Intensity data were collected on a Rigaku AFC-4 four-circle diffractometer by using graphite monochromated Cu $K\alpha$ radiation (λ=1.5418 Å) in the 2θ–ω scan mode with a scan width of $\Delta\omega$=(1.0+0.5 tanθ) and a scan speed of 4.0° min^{-1} over the range of 2θ values of 3 to 120°. Intensities of 2240 reflections were measured and 1310 independent reflections ($|F_o|>3.0\sigma(|F_o|)$) were used for the analysis. The structure was solved by *MULTAN* 78 program. The structural parameters were refined by a full-matrix least-squares method to the final R value of 0.130 and the R_w=0.141 in conjunction with the weighting scheme of $w=(-0.002|F_o|^2+|F_o|-1)^{-1}$. The unit cell contains two crystallographically independent molecules and they have almost similar configurations. The difficulty in convergence may be attributable to some disorders and a pseudo symmetry of the crystal. All the computations were carried out on a FACOM M-380 computer using the *UNICS* III system.[14] Lists of the atomic coordinates and other structural parameters are deposited as Document No. 8801 at the Office of the Editor of Bull. Chem. Soc. Jpn.

References

1) a) K. Kobayashi, K. Mutai, and H. Kobayashi, *Tetrahedron Lett.*, **1979**, 5003; b) P. A. Howell, R. M. Curtis, and W. N. Lipscomb, *Acta Crystallogr.*, **7**, 498 (1954).

2) K. Kobayashi, *Yuki Gosei Kagaku Kyokai Shi*, **40**, 642 (1982).

3) a) J. Nakayama, A. Sakai, A. Tokiyama, and M. Hoshino, *Tetrahedron Lett.*, **24**, 3729 (1983); b) E. Fanghänel, K. H. Kühnemund, and A. M. Richter, *Synthesis*, **1983**, 50.

4) a) J. Nakayama, A. Sakai, S. Tokita, and M. Hoshino, *Heterocycles*, **22**, 27 (1984); b) J. Nakayama, H. Fukushima, R. Hashimoto, and M. Hoshino, *J. Chem. Soc., Chem. Commun.*, **1982**, 612; c) E. Fanghänel and H. Poleschner, *J. Prakt. Chem.*, **323**, 1 (1981).

5) a) B. G. Lenz and B. Zwanenburg, *J. Chem. Soc., Chem. Commun.*, **1984**, 1386; b) J. M. M. Smits, P. T. Beurskens, B. G. Lenz, and B. Zwanenburg, *Acta Crystallogr., Sect. C*, **41**, 1086 (1985). Recently, 3,5-diphenyl-1,4,2,6-dithiadiazine, a new ring system, was also prepared from the reaction of S_4N_4 with diphenylacetylene, see; c) S. T. A. K. Daley, C. W. Rees, and D. J. Williams, *J. Chem. Soc., Chem. Commun.*, **1984**, 57.

6) **4** was identified by direct comparison with an authentic sample.

7) M. Hirobe and T. Ozawa, *Tetrahedron Lett.*, **1971**, 4493.

8) W. G. Finnegan, R. A. Henry, and R. Lofquist, *J. Am. Chem. Soc.*, **80**, 3908 (1958).

9) H. Yoshida, H. Taketani, T. Ogata, and S. Inokawa, *Bull. Chem. Soc. Jpn.*, **49**, 3124 (1976).

10) I. Shibuya and K. Yonemoto, *Bull. Chem. Soc. Jpn.*, **59**, 2017 (1986).

11) K. Hirai and T. Ishiba, *Chem. Pharm. Bull.*, **20**, 304 (1972).

12) a) M. S. Raasch, *J. Org. Chem.*, **37**, 3820 (1972). b) F. A. Davis, W. A. R. Slegeir, S. Evans, A. Schwartz, D. L. Goff, and R. Palmer, *J. Org. Chem.*, **38**, 2809 (1973).

13) **8** was obtained as colorless solid in 29% yield. IR(KBr) 1619, 1491, and 1281 cm^{-1}. MS m/z 298 (M^+), 195 (M^+ −PhCN), and 135 ($PhCNS^+$). Found: C, 60.18; H, 3.32; N, 9.37; S, 21.49%. Calcd for $C_{15}H_{10}N_2OS_2$: C, 60.38; H, 3.38; N, 9.39; S, 21.49%.

14) T. Sakurai and K. Kobayashi, *Rep. Inst. Phys. Chem. Res.*, **55**, 69 (1978).

Preparation of Novel *N*-Vinyl-, *N*-(1-Butylvinyl)-, and *N*-(1-Methyl-1-pentenyl)iminotriphenylphosphoranes and Their Reactions with α,β-Unsaturated Ketones[1)]

Yukio IINO and Makoto NITTA*
Department of Chemistry, School of Science and Engineering, Waseda University, Shinjuku-ku, Tokyo 160
(Received December 11, 1987)

Synopsis. The novel *N*-vinyl- (**2a**) and a mixture of *N*-(1-butylvinyl)- (**2b**) and *N*-(1-methyl-1-pentenyl) iminotriphenylphosphoranes (**2c**) were prepared by the reaction of azidoethylene and 2-azido-1-hexene with triphenylphosphine, respectively. The thermal reaction of **2a**, **2b**, and **2c** with α,β-unsaturated ketones undergoes an enamine-type alkylation and the subsequent aza-Wittig reaction to give pyridine derivatives in modest yields.

Previously, we have accomplished the preparation of novel *N*-(1-phenylvinyl)iminophosphoranes by the Staudinger reaction[2)] of α-azidostyrene with trimethyl phosphite, triphenylphosphine, or tributylphosphine. These *N*-(1-phenylvinyl)iminophosphoranes seemed to provide convenient routes to 1,2-λ^5-azaphosphorines,[3)] 2-phenyl-1-azaazulenes,[4)] phenyl-substituted pyrroles,[1,5)] and phenyl-substituted pyridines.[1,6)] However, the potential value of *N*-vinyliminophosphorane bearing no substituent and alkyl substituent on vinyl groups remains unexplored. We describe here the first preparation of *N*-vinyliminotriphenylphosphorane (**2a**) and a mixture of *N*-(1-butylvinyl)- (**2b**) and *N*-(1-methyl-1-pentenyl) iminotriphenylphosphoranes (**2c**), and their reactions with α,β-unsaturated ketones to give pyridine derivatives.

The reaction of azidoethylene (**1a**)[7)] with triphenylphosphine in anhydrous ether at 0 °C for 2 h gave crystalline *N*-vinyliminotriphenylphosphorane (**2a**) in 84% yield. The compound **2a** is unstable in moist solvent and hydrolyzed to acetaldehyde in quantitative yield (Scheme 1). Similarly, 2-azido-1-hexene (**1b**)[8)] was made to react with triphenylphosphine at room temperature for 2 h to give iminophosphoranes, which were inferred to be a mixture of *N*-(1-butylvinyl)-iminotriphenylphosphorane (**2b**) and *N*-(1-methyl-1-pentenyl)iminotriphenylphosphorane (**2c**) in a ratio of 1/2 (see Experimental). Since unstable **2b** and **2c** were not separable in pure form, no distinct physical data were obtained. However, the preparation of a mixture of **2b** and **2c** in CD_3CN and its ^1H NMR spectral study suggested several features of **2b** and **2c** (see Experimental). The initial ratio of **2b**/**2c** (1/2) changed to 1/4 after heating the mixture at 80 °C for 10 min. The ratio was fixed at 1/6 after 30 min or even after a prolonged heating at 80 °C. Thus, the thermal isomerization was suggested to occur, and the equilibrium between **2b** and **2c** is considered to lie on the side of **2c**. The tautomer **2b**, which is derived from **1b** directly, seems to be less stable than **2c**. Furthermore, the mixture of **2b** and **2c** (1/2) was hydrolyzed in moist benzene under refluxing for 10 h to give 2-hexanone in quantitative yield. Thus, the formation of **2b** and **2c** from **1b** and triphenylphosphine was assessed.

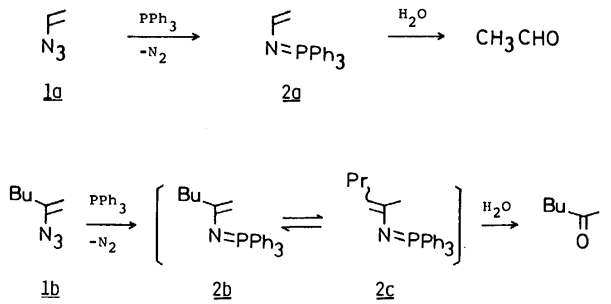

Scheme 1.

The reaction of **2a** with α,β-unsaturated ketones **3a—f** in anhydrous benzene was carried out under reflux to give pyridine derivatives **7a—f** in addition to **8a—d**. The reaction conditions and the yields of the products are summarized in Table 1. The structure of **7a—f** was unequivocally deduced from physical data (see Experimental). As previously reported,[1,6)] the results are very similar to those of *N*-(1-phenylvinyl)-iminophosphoranes with α,β-unsaturated ketones. The postulated reaction pathway for the present reaction is shown in Scheme 2. The enamine alkylation of **2a** to the β-carbon atom of **3a—f** initially occurs to give **4a—f**, followed by proton transfer to regenerate iminophosphoranes **5a—f**, which then undergo an intramolecular aza-Wittig reaction to give dihydropyridines **6a—f**. The compounds **6a—f** are dehydrogenated to give pyridines **7a—f** under the reaction conditions. The compounds **3a—d** seem also to act as a hydrogen acceptor of **6a—d** to result in the formation of **8a—d**.[6,9)]

Similarly, the reaction of a mixture of **2b** and **2c** with **3a** or **3e** in anhydrous benzene under refluxing, gave pyridines **10** and/or **11** in low yields (Scheme 3). When the reactions were carried out in toluene under refluxing, the yields of the pyridines were improved.

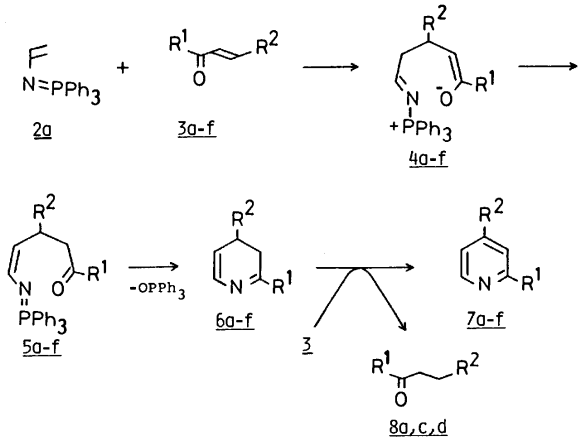

Scheme 2.

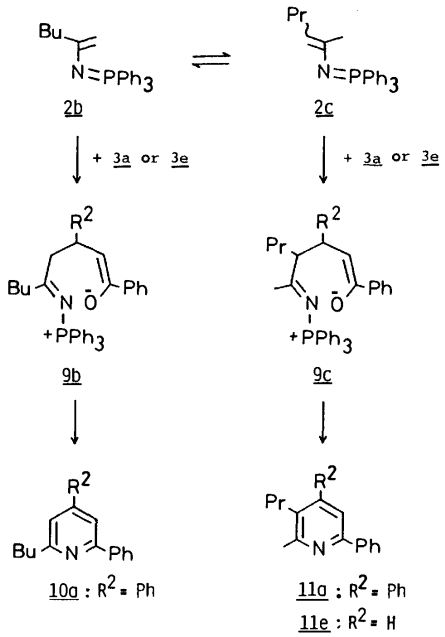

Scheme 3.

Table 1. Results Obtained in the Reaction of **2a** with **3a**—**f**[a]

3	R^1	R^2	Reaction time/h	Product yield/%		Recovery of 3/%
				7	**8**	
a	Ph	Ph	48	56	15	17
b	4-Cl-C_6H_4		12	50	8	—
c	4-MeO-C_6H_4		42	28	6	57
d	Ph	Me	24	31	8	35
e	Ph	H	24	27	—	—
f	Me	H	24	25	—	—

a) The reactions were carried out in anhydrous benzene under refluxing.

Table 2. Results Obtained in the Reaction of **2b** and **2c** with **3a**, **e**

3	R^1	R^2	Reaction time/h	Solvent	Product yield/%		Recovery of 3/%
					10	**11**	
a	Ph	Ph	28	PhH	15	Trace	65
a			24	PhMe	28	8	21
e	Ph	H	28	PhH	0	30	0
e			24	PhMe	0	52	0

The structural proofs for the pyridines were obtained from their physical data (see Experimental). The results are summarized in Table 2. In the case of **3a**, the addition of both **2b** and **2c** occurs on the β-carbon atom of **3a** to give **9b** and **9c**, and the following reaction sequences (cf. Scheme 2) give pyridines **10a** and **11a**, respectively.

In conclusion, the preparations of novel *N*-vinyl- (**2a**) and *N*-(1-butylvinyl)- (**2b**), and *N*-(1-methyl-1-pentenyl) iminotriphenylphosphorane (**2c**), and their reaction with α,β-unsaturated ketones were clarified. Although preparations, properties, and synthetic applications of pyridines have also been studied,[10,11] the present results will serve as a convenient method for preparating pyridine derivatives.

Experimental

The IR spectra were recorded on a Shimadzu IR-400 spectrometer. The ^1H NMR spectra and ^{13}C NMR spectra were recorded on a Hitachi R-24 and a R-90H spectrometer and the chemical shifts are given in ppm (δ) relative to the internal $SiMe_4$ standard. The mass spectral and high-resolution mass spectral studies were conducted using Shimadzu GCMS-QP1000 and JEOL DX-300 spectrometer. All of the melting points are uncorrected.

Preparation of *N*-Vinyliminotriphenylphosphorane (2a). A solution of azidoethylene (**1a**)[7] (480 mg, 7.0 mmol) and triphenylphosphine (1.31 g, 5.0 mmol) in dry ether (20 cm^3) was stirred for 2 h at 0 °C. The precipitated crystalline solids were filtered to give **2a** (1.27 g, 84%, based on triphenylphosphine used): mp 90 °C (decomp); ^1H NMR ($CDCl_3$) δ=3.97 (1H, ddd, J=7.4, 5.7, 1.4 Hz), 4.52 (1H, ddd, J=14.2, 1.4, 1.4 Hz), 6.69 (1H, ddd, J=14.2, 7.4, 23.2 Hz), 7.25—7.90 (15H, m); ^{13}C NMR ($CDCl_3$) δ=93.92, 129.98, 131.59, 132.43, 138.38, 142.36; IR ($CHCl_3$), 2985, 2916, 1591, 1487, 1437, 1405, 1311, 1106 cm^{-1}; HRMS Found: m/z 303.1194. Calcd for $C_{20}H_{18}NP$: M, 303.1178.

Reaction of 2a with Water. A solution of **2a** (91 mg, 0.3 mmol) in moist methanol (2 cm^3) was stirred at room temperature for 1 h. To this reaction mixture was added 2,4-dinitrophenylhydrazine (99 mg, 0.5 mmol) and a catalytic ammount of HCl, and the mixture was stirred for further 3 h. After the solvent was evaporated, the residue was separated by TLC on silica gel using benzene-AcOEt (1/1) as a developer to give 64 mg (95%) of acetaldehyde 2,4-dinitrophenylhydrazone, the structure of which was identical with that of the authentic specimen.

Preparation of *N*-(1-Butylvinyl)- (2b) and *N*-(1-Methyl-1-pentenyl)iminotriphenylphosphorane (2c). A solution of 2-azido-1-hexene (**1b**)[8] (63 mg, 0.5 mmol) and triphenylphosphine (131 mg, 0.5 mmol) in CD_3CN (0.2 cm^3) was made to react for 2 h. The ^1H NMR spectrum of the reaction mixture exhibited δ=0.7—2.4 (m), 3.39 (t, J=1.2 Hz), 3.67 (broad s), 4.08—4.54 (m), 7.1—7.8 (m). The signals at 3.39 and 3.67 are assigned to the vinyl protons of **2b**, and the signal at 4.08—4.54 is also assigned to the vinyl proton of **2c**. The ratio of **2b**/**2c** was estimated to be ca. 1/2 by the ^1H NMR spectrum. The ratio of **2b**/**2c** changed to 1/4 after heating the mixture at 80 °C for 10 min. Furthermore, by heating the mixture for 30 min, the ratio of **2b**/**2c** (1/4) changed to 1/6 and any further change was not observed after a prolonged heating.

Reaction of 2b and 2c with Water. A mixture of **2b** and **2c**, which were prepared by the reaction of **1b** (63 mg, 0.5 mmol) and triphenylphosphine (131 mg, 0.5 mmol) in benzene (2 cm^3), was made to react with water (30 mg) under refluxing for 10 h. To this reaction mixture was added 2,4-dinitrophenylhydrazine (119 mg, 0.6 mmol) in methanol (2 cm^3) containing a catalytic ammount of HCl and stirred for 5 h. The reaction mixture was then concentrated and separated by TLC on silica gel using AcOEt-hexane (1/1) as a developer to give 2-hexanone 2,4-dinitrophenylhydrazone (135 mg, 96%), which was identical with the authentic specimen.

General Procedure for the Reaction of 2a with 3a—f. A solution of **2a** (152 mg, 0.5 mmol) and **3** (0.5 mmol) in dry benzene (2 cm^3) was refluxed for a period indicated in Table 1 under nitrogen atmosphere. The reaction mixture was concentrated and the resulting residue was separated by TLC on silica gel using benzene-hexane (1/1) as a developer to give pyridine derivatives **7**, along with **3**, **8**, and triphenylphosphine oxide (60—90% based on **2a** used). The results are summarized in Table 1. The structural proofs for the pyridine derivatives **7a**—**f** were based on the following physical

data.

2,4-Diphenylpyridine (**7a**): mp 186—187 °C (from ethanol) (lit,[12] 190.5—192.5 °C); ^{1}H NMR (CCl_4) δ=7.20—7.90 (9H, m), 7.83 (1H, m), 7.95—8.20 (2H, m), 8.65 (1H, d, J=5.0 Hz).

2,4-Bis(4-chlorophenyl)pyridine (**7b**): mp 105—106 °C (from hexane); ^{1}H NMR ($CDCl_3$) δ=7.22—7.65 (7H, m), 7.75 (1H, broad s), 7.83 (2H, d, J=8.2 Hz), 8.66 (1H, d, J=4.8 Hz); IR ($CHCl_3$), 2977, 1603, 1545, 1497, 1469, 1382, 1093, 1015, 820 cm^{-1}; MS, m/z (rel intensity), 303 (M^+, 10), 301 (M^+, 69), 299 (M^+, 100). Found: C, 67.86; H, 3.77; N, 4.57%. Calcd for $C_{17}H_{11}NCl_2$: C, 68.02; H, 3.69; N, 4.67%.

2,4-Bis(4-methoxyphenyl)pyridine (**7c**): mp 152—153 °C (from benzene-hexane); ^{1}H NMR ($CDCl_3$) δ=3.81 (6H, s), 7.01 (2H, d, J=9.3 Hz), 7.02 (2H, d, J=10.7 Hz), 7.34 (1H, dd, J=5.2, 1.7 Hz), 7.63 (2H, d, J=9.3 Hz), 7.80—7.90 (1H, m), 8.05 (2H, d, J=10.7 Hz), 8.67 (1H, d, J=5.2 Hz); IR ($CHCl_3$), 2964, 2846, 1614, 1586, 1514, 1469, 1286, 1254, 1242, 1176, 1034, 824 cm^{-1}; MS, m/z (rel intensity), 293 (M^++2, 5), 292 (M^++1, 23), 291 (M^+, 100). Found: C, 78.69; H, 5.89; N, 4.78%. Calcd for $C_{19}H_{17}NO_2$: C, 78.33; H, 5.88; N, 4.81%.

4-Methyl-2-phenylpyridine (**7d**): mp 183—184 °C (picrate) (lit,[13] 185—187 °C); ^{1}H NMR (CCl_4) δ=1.41 (3H, s), 7.02 (1H, broad d, J=5.5 Hz), 7.33—7.60 (4H, m), 7.85—8.15 (2H, m), 8.55 (1H, d, J=5.5 Hz).

2-Phenylpyridine (**7e**): mp 174—175 °C (picrate) (lit,[14] 176—177 °C); ^{1}H NMR ($CDCl_3$) δ=7.03—7.30 (1H, m), 7.32—7.52 (3H, m), 7.60—7.72 (2H, m), 7.84—8.04 (2H, m), 8.67—8.70 (1H, m).

2-Methylpyridine (**7f**): 1,2-dimethylpyridinium iodide: mp 221—222 °C (from ethanol) (lit,[15] 229—231 °C). The hydrogenated compounds **8a**, **8b**, **8c**, and **8d** are known, and were confirmed by comparison of the physical data.

General Procedure for the Reaction of 2b and 2c with 3a,e. A solution of **2b** and **2c** was prepared in situ by the reaction of **1b** (75 mg, 0.6 mmol) and triphenylphosphine (131 mg, 0.5 mmol) at room temperature for 2 h. To this solution was added **3** (0.5 mmol), and the mixture was refluxed for a period indicated in Table 1 under nitrogen atmosphere. The reaction mixture was then concentrated and the resulting residue was separated by TLC on silica gel using benzene-hexane (1/1) as a developer to give pyridine derivatives and triphenylphosphine oxide (60—90%). The results are summarized in Table 2. The structural proof for the pyridine derivatives was based on the following physical data.

2-Butyl-4,6-diphenylpyridine (**10a**): mp 163—164 °C (picrate); ^{1}H NMR (CCl_4) δ=0.98 (3H, t, J=6.0 Hz), 1.17—2.17 (4H,m), 2.87 (2H, t, J=7.0 Hz), 7.12 (2H, s), 7.24—7.69 (8H, m), 7.90—8.15 (2H, m); IR ($CHCl_3$), 2963, 2938, 2868, 1596, 1584, 1549, 1496, 1452, 1402 cm^{-1}; MS, m/z (rel intensity) 287 (M^+, 1), 245 (100). HRMS Found: m/z 287.1657. Calcd for $C_{21}H_{21}N$: M, 287.1675.

2-Methyl-4,6-diphenyl-3-propylpyridine (**11a**): mp 145—146 °C (picrate); ^{1}H NMR (CCl_4) δ=0.80 (3H, t, J=6.4 Hz), 1.10—1.70 (2H, m), 2.40—2.70 (2H, m), 2.60 (3H, s), 7.10—7.45 (9H, m), 7.80—8.00 (2H, m); IR ($CHCl_3$), 2961, 2878, 1591, 1581, 1546, 1496, 1445, 1383 cm^{-1}; MS, m/z (rel intensity), 287 (M^+, 35), 258 (100). HRMS Found: m/z287.1657. Calcd for $C_{21}H_{21}N$: M, 287.1675.

2-Methyl-6-phenyl-3-propylpyridine (**11e**): mp 108—110 °C (picrate); ^{1}H NMR (CCl_4) δ=1.00 (3H, t, J=6.6 Hz), 1.23—1.87 (2H, m), 2.57 (2H, t, J=7.6 Hz), 2.57 (3H, s),7.25—7.50 (5H, m), 7.80—8.20 (2H, m); IR ($CHCl_3$), 2959, 2934, 2874, 1587, 1565, 1461, 1447, 1385 cm^{-1}; MS, m/z (rel intensity), 211 (M^+, 25), 182 (100). HRMS Found: m/z 211.1365. Calcd for $C_{15}H_{17}N$: M, 211.1362.

References

1) Part 6 of the reaction of *N*-vinyliminophosphoranes. Part 5: T. Kobayashi, Y. Iino, and M. Nitta, *Nippon Kagaku Kaishi*, **1987**, 1237.

2) Yu. G. Gololobov, I. N. Zhmurova, and L. F. Kasukhin, *Tetrahedron*, **37**, 437 (1981); and references cited therein.

3) T. Kobayashi and M. Nitta, *Chem. Lett.*, **1985**, 1459.

4) M. Nitta and T. Kobayashi, *Chem. Lett.*, **1986**, 463.

5) Y. Iino, T. Kobayashi, and M. Nitta, *Heterocycles*, **24**, 2437 (1986).

6) T. Kobayashi and M. Nitta, *Chem. Lett.*, **1986**, 1549.

7) R. H. Wiley and J. Moffat, *J. Org. Chem.*, **22**, 995 (1957).

8) F. W. Fowler, A. Hassner, and L. A. Levy, *J. Am. Chem. Soc.*, **89**, 2077 (1967).

9) J. A. VanAllan and G. A. Reynolds, *J. Org. Chem.*, **33**, 1102 (1968).

10) "Comprehensive Heterocyclic Chemistry", ed by A. R. Katritzky, and C. W. Rees, Pergamon Press, **2** (1984).

11) H. B. Degussa, *Aldrichimica Acta*, **11**, 13 (1978); **14**, 13 (1981).

12) A. R. Katritzky, A. V. Chapman, M. J. Cook, and G. H. Millet, *J. Chem. Soc., Perkin Trans. 1*, **1980**, 2743.

13) G. J. Jang and W. J. H. McCulloch, *J. Am. Chem. Soc.*, **77**, 3143 (1955).

14) R. Forsyth and F. L. Pyman, *J. Chem. Soc.*, **1926**, 2917.

15) E. M. Kosower and P. E. Klinedinst Jr., *J. Am. Chem. Soc.*, **78**, 3483 (1956).

New and Convenient Synthesis of 2-Substituted 2,3-Dihydro-1*H*-benz[*de*]isoquinolin-1-ones

Ryu SATO,* Katsuyuki OIKAWA, Takehiko GOTO, and Minoru SAITO
Department of Resource Chemistry, Faculty of Engineering, Iwate University, Morioka 020
(Received December 24, 1987)

Synopsis. Various 2-substituted 2,3-dihydro-1*H*-benz[*de*]isoquinolin-1-ones were obtained in high yields by chemoselective reduction of 2-substituted 1*H*-benz[*de*]isoquinoline-1,3(2*H*)-diones with sodium or zinc borohydride at room temperature.

Although there have been many reports on the synthesis of isoindoles such as 2,3-dihydro-1*H*-isoindol-1-one,[1] the synthesis of 2,3-dihydro-1*H*-benz[*de*]isoquinolin-1-ones (**2**) have little been studied. Thus, only two papers have been reported on the troublesome synthesis of isoquinoline **2** by electrolytic[2] and catalytic[3] reduction of 2-substituted 1*H*-benz[*de*]isoquinoline-1,3(2*H*)-diones (**1**). In the course of our investigations on the chemistry of isoindoles,[4] we have been looking for new and convenient method for synthesis of isoquinolines **2**, which were novel heterocycles and considered to be versatile for synthesis of biologically active isoquinoline derivatives in connection with alkaloids.[5] It is well-known that carbonyl group of acid anhydride can be reduced to methylene group by sodium borohydride[6] but that of dicarboximides can not be reduced.[1] We could not find actually any example of such reduction in literatures. Therefore, our attempts to synthesize **2** were initially directed to the reactions of 1,8-naphthalenedicarbaldehydes with amines based on the previous results.[7] We could not, however, obtain 2-substituted isoquinolines **2** except for parent isoquinoline **2a**. Meanwhile, a successful example of the demethoxylation of 2,3-dihydro-3-methoxy-1*H*-benz[*de*]isoquinolin-1-one to **2a** with sodium borohydride by Warashawsky[8] was reported to stimulated us to examine selective reduction of 2-substituted 1*H*-benz[*de*]isoquinoline-1,3(2*H*)-diones (**1**), which were readily prepared by treating 1*H*,3*H*-naphtho[1,8-*cd*]pyran-1,3-dione with various amines,[9] to **2** using sodium or zinc borohydride.[10] In this paper, we wish to report a new and convenient chemoselective synthesis of **2** (Scheme 1).

As shown in Table 1, nine isoquinolines **2a—f** and **2o—q** having alkyl substituents were readily formed via intermediate **A** (Scheme 1) in high yields on treatment with sodium borohydride. When desired **2** could not be obtained from **1** with sodium borohydride, zinc borohydride was employed as a reductant to give **2** in moderate yields (Runs 7—11, 13, and 16) together with by-products, 2,3-dihydro-2-alkyl-1*H*-benz[*de*]isoquinoline (**4h—k**). It is noteworthy that the present reduction was compatible with hydroxyl, chloro, and carboxyl groups (Runs 13, 16, and 20—22). Interestingly, three new heterocycles **3l—n** were obtained by treating **1l—n** with sodium borohydride in moderate yields together with desired **2l—n**, as shown in Table 1. Moreover, an addition of magnesium perchlorate to the reaction system using sodium borohydride increased exceedingly the yields of cyclized products **3l—n** (Runs 14, 17, and 19). Although the role of magnesium ion is not necessarily obvious, **3l—n** seem to be formed by intramolecular migration of alkoxyl group of intermediate **B**, in which boron coordinated[11] with two oxygen atom of two hydroxyl groups, in basic conditions as shown in Scheme 2.

3n was obtained as a mixture of two diastereomers. The results of Table 1 show that a bulky substituent **1n** prevented the cyclization and **1o** having five methylene chains did not give the corresponding cyclic compounds (Runs 18 and 20). In the reactions of **1l** and **1m**, the use of zinc borohydride afforded desired **2l** and **2m** preferentially (Runs 13 and 16). Although various solvents such as methanol or tetrahydrofuran were

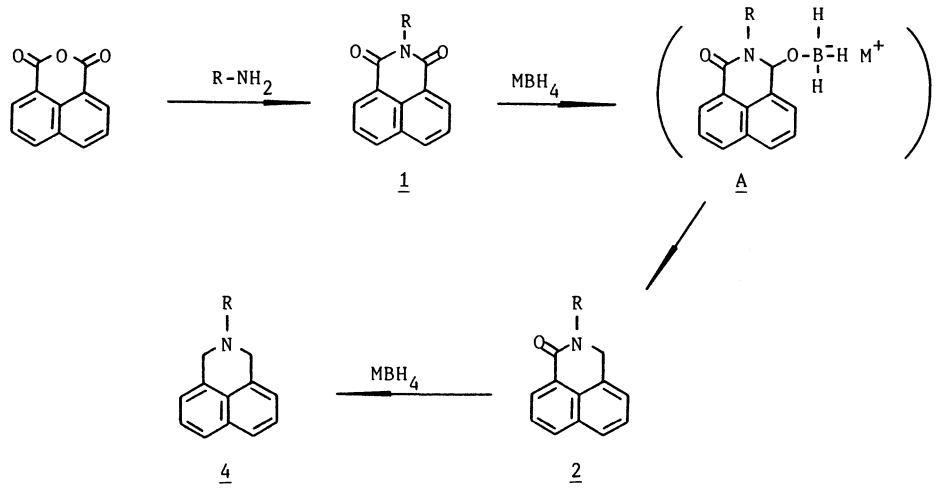

Scheme 1.

Table 1. The Chemoselective Reduction of Benzisoquinoline-1,3-diones **1**

Run[a]	Substrate R	1	React. time/h	Boro-hydride	Yield of product/%[b] 2	3	4
1	H-	**1a**	24	$NaBH_4$	97 **2a**[8]	—	—
2	CH_3-	**1b**	24	$NaBH_4$	94 **2b**	—	—
3	$CH_3CH_2CH_2$-	**1c**	24	$NaBH_4$	98 **2c**	—	—
4	$(CH_3)_2CH$-	**1d**	8	$NaBH_4$	79 **2d**	—	—
5	CH_2=CH-CH_2-	**1e**	14	$NaBH_4$	79 **2e**	—	—
6	$CH_3CH_2CH_2CH_2$-	**1f**	5	$NaBH_4$	82 **2f**	—	—
7	C_6H_{11}-	**1g**	24	$Zn(BH_4)_2$	53 **2g**	—	—
8	C_6H_5-	**1h**	25	$Zn(BH_4)_2$	49 **2h**	—	13 **4h**[12]
9	C_6H_5-CH_2-	**1i**	25	$Zn(BH_4)_2$	50 **2i**	—	20 **4i**[13]
10	4-CH_3-C_6H_4-	**1j**	29	$Zn(BH_4)_2$	41 **2j**	—	24 **4j**[12]
11	4-Cl-C_6H_4-	**1k**	23	$Zn(BH_4)_2$	40 **2k**	—	43 **4k**[12]
12	HO-$(CH_2)_2$-	**1l**	4	$NaBH_4$	55 **2l**	22 **3l**	—
13	HO-$(CH_2)_2$-	**1l**	27	$Zn(BH_4)_2$	32 **2l**	—	—
14[c]	HO-$(CH_2)_2$-	**1l**	10	$NaBH_4$	—	81 **3l**	—
15	HO-$(CH_2)_3$-	**1m**	4	$NaBH_4$	34 **2m**	55 **3m**	—
16	HO-$(CH_2)_3$-	**1m**	28	$Zn(BH_4)_2$	36 **2m**	—	—
17[c]	HO-$(CH_2)_3$-	**1m**	10	$NaBH_4$	—	78 **3m**	—
18	HO-$CH(CH_3)CH_2$-	**1n**	4	$NaBH_4$	81 2n	9 **3n**[d]	—
19[c]	HO-$CH(CH_3)CH_2$-	**1n**	12	$NaBH_4$	36 2n	55 **3n**[d]	—
20	HO-$(CH_2)_5$-	**1o**	4	$NaBH_4$	68 **2o**	—	—
21	Cl-CH_2CH_2-	**1p**	4	$NaBH_4$	73 **2p**	—	—
22	HOCO-$(CH_2)_2$-	**1q**	4	$NaBH_4$	83 **2q**	—	—

a) Reaction conditions: **1**, 0.5 mmol, $NaBH_4$, 5 mmol, $Zn(BH_4)_2$, 10 mmol, r.t. b) Isolated yields based on the substrate. c) $Mg(ClO_4)_2$(5 mmol) was added to the reaction system. d) A mixture of two diastereomer was obtained.

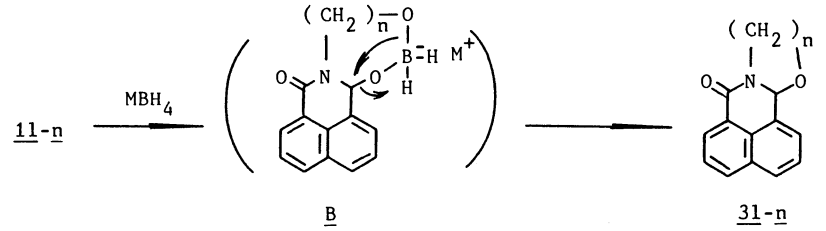

Scheme 2.

examined in all cases, only ethanol-water gave preferable results.

Experimental

Measurements. All the melting points were uncorrected. IR spectra were obtained on a Hitachi 295 spectrophotometer and ^1H NMR spectra were obtained on a Hitachi R-22 spectrometer using tetramethylsilane as an internal standard. Mass spectra were taken with a Hitachi RMU-6M mass spectrometer. Elemental analyses were performed with a Yanagimoto MT-3. All the reactions were carried out under a nitrogen atmosphere and monitered by TLC (Merck Kieselgel 60-GF).

Materials. All the reagents were obtained from Wako Pure Chemical Industries Ltd., Tokyo Kasei Co. Ltd., or Aldrich Chemical Co. The reagents used were further purified by usual methods such as recrystallization or distillation. Wako gel C-200 was used as a silica gel for column chromatography.

General Procedure. To a solution of sodium borohydride (5 mmol) in EtOH/H_2O (20 ml, v/v: 10/1) was added **1** (0.5 mmol) and then the mixture was stirred for 4 h at 25 °C. After quenching with aq. HCl, the reaction mixture was extracted with CH_2Cl_2 (20 ml×3). The combined organic layer was dried over $MgSO_4$ and evaporation of the solvent followed by chromatography on silica gel gave colorless crystals, 2-substituted 2,3-dihydro-1*H*-benz[*de*]isoquinolin-1-one (**2**). Elemental analyses for **2d**, **2e**, and **2f** were not available because of the lability and the difficulty of further purifications of these compounds.

2a,[8] **4h**,[12] **4i**,[13] **4j**,[12] and **4k**[12] was identified by comparison of the spectral and physical data with those of authentic sample.

2b: Mp 76 °C (from hexane-AcOEt); IR (KBr) 1610 and 1640 cm^{-1}; ^1H NMR ($CDCl_3$) δ=3.23 (s, 3H, CH_3), 4.93 (s, 2H, CH_2), and 7.20—8.36 (m, 6H, arom); MS (20 eV) *m/z* 195 (M^+). Found: C, 79.17; H, 5.67; N, 7.02%. Calcd for $C_{13}H_{11}NO$: C, 79.17; H, 5.62; N, 7.10%.

2c: Mp 84 °C (from AcOEt); IR (KBr) 1620 and 1645 cm^{-1}; ^1H NMR ($CDCl_3$) δ=1.00 (t, 3H, *J*=7 Hz, CH_3), 1.76 (sex, 2H, *J*=7 Hz, CH_2), 3.64 (t, 2H, *J*=7 Hz, CH_2), 4.94 (s, 2H, CH_2), and 7.15—8.42 (m, 6H, arom); MS (20 eV) *m/z* 225 (M^+). Found: C, 79.64; H, 6.78; N, 6.21%. Calcd for $C_{15}H_{15}NO$: C, 79.97; H, 6.71; N, 6.22%.

2d: Oil; IR (neat) 1620 and 1640 cm^{-1}; ^1H NMR ($CDCl_3$) δ=1.34 (d, 6H, *J*=8 Hz, CH_3), 4.86 (s, 2H, CH_2), 5.24 (sept, 1H, *J*=8 Hz, CH), and 7.27—8.44 (m, 6H, arom); MS (20 eV) *m/z* 225 (M^+).

2e: Oil; IR (neat) 1610 and 1635 cm^{-1}; ^1H NMR ($CDCl_3$) δ=4.23—4.38 (m, 2H, CH_2), 4.88 (s, 2H, CH_2), 5.15—5.43 (m, 2H, =CH_2), 5.68—6.23 (m, 1H, -CH=), and 7.17—8.40 (m,

6H, arom); MS (20 eV) m/z 223 (M^+).

2f: Oil; IR (neat) 1610 and 1635 cm^{-1}; ^1H NMR ($CDCl_3$) δ=1.00 (t, 3H, J=7 Hz, CH_3), 1.24—1.93 (m, 4H, CH_2), 3.71 (t, 2H, J=7 Hz, CH_2), 4.97 (s, 2H, CH_2), and 7.27—8.46 (m, 6H, arom); MS (20 eV) m/z 239 (M^+).

2g: Mp 127 °C (from AcOEt); IR (KBr) 1610 and 1630 cm^{-1}; ^1H NMR ($CDCl_3$) δ=0.90—2.30 (m, 1H, cyclohexyl), 4.80 (s, 2H, CH_2), and 7.10—8.27 (m, 6H, arom); MS (70 eV) m/z 265 (M^+). Found: C, 81.67; H, 7.27; N, 5.35%. Calcd for $C_{18}H_{19}NO$: C, 81.48; H, 7.22; N, 5.28%.

2h: Mp 164 °C (from AcOEt); IR (KBr) 1615 and 1640 cm^{-1}; ^1H NMR ($CDCl_3$) δ=5.33 (s, 2H, CH_2) and 7.24—8.54 (m, 11H, arom); MS (70 eV) m/z 259 (M^+). Found: C, 83.36; H, 4.96; N, 5.31%. Calcd for $C_{18}H_{13}NO$: C, 83.38; H, 5.05; N, 5.40%.

2i: Mp 102 °C (from AcOEt); IR (KBr) 1615 and 1640 cm^{-1}; ^1H NMR ($CDCl_3$) δ=4.87 (s, 2H, CH_2), 4.93 (s, 2H, CH_2), and 7.15—8.55 (m, 11H, arom); MS (70 eV) m/z 273 (M^+). Found: C, 83.25; H, 5.47; N, 5.09%. Calcd for $C_{19}H_{15}NO$: C, 83.49; H, 5.53; N, 5.13%.

2j: Mp 153 °C (from AcOEt); IR (KBr) 1615 and 1640 cm^{-1}; ^1H NMR ($CDCl_3$) δ=2.40 (s, 3H, CH_3), 5.30 (s, 2H, CH_2), and 7.11—8.50 (m, 10H, arom); MS (70 eV) m/z 273 (M^+). Found: C, 83.64; H, 5.47; N, 5.05%. Calcd for $C_{19}H_{15}NO$: C, 83.49;H, 5.53; N, 5.13%.

2k: Mp 232 °C (from AcOEt); IR (KBr) 1620 and 1645 cm^{-1}; ^1H NMR ($CDCl_3$) δ=5.26 (s, 2H, CH_2) and 7.18—8.42 (m, 10H, arom); MS (70 eV) m/z 293 (M^+). Found: C, 73.53; H, 4.06; N, 4.88%. Calcd for $C_{18}H_{12}NOCl$: C, 73.60; H, 4.12; N, 4.77%.

2l: Mp 125 °C (from AcOEt); IR (KBr) 1610, 1635, and 3380 cm^{-1}; ^1H NMR ($CDCl_3$) δ=3.64—4.14 (m, 5H, CH_2×2 and OH), 4.96 (s, 2H, CH_2), and 7.09—8.25 (m, 6H, arom); MS (70 eV) m/z 227 (M^+). Found: C, 73.73; H, 5.77; N, 5.98%. Calcd for $C_{14}H_{13}NO_2$: C, 73.99; H, 5.77; N, 6.16%.

2m: Mp 86 °C (from AcOEt); IR (KBr) 1640 and 3375 cm^{-1}; ^1H NMR ($CDCl_3$) δ=1.89 (quint, 2H, J=7 Hz, CH_2), 3.55 (q, 2H, J=7 Hz, CH_2), 3.78 (t, 2H, J=7 Hz, CH_2), 4.01 (t, 1H, J=7 Hz, OH), 4.90 (s, 2H, CH_2), and 7.13—8.27 (m, 6H, arom); MS (70 eV) m/z 241 (M^+). Found: 74.50; H, 6.31; N, 5.73%. Calcd for $C_{15}H_{15}NO_2$: C, 74.67; H, 6.27; N, 5.80%.

2n: Mp 102 °C (from AcOEt); IR (KBr) 1610, 1635, and 3300 cm^{-1} ; ^1H NMR ($CDCl_3$) δ=1.22 (d, 3H, J=7 Hz, CH_3), 3.51 (d, 2H, J=7 Hz, CH_2), 3.91 (bs, 1H, OH), 4.14 (sext,1H, J=7 Hz, CH), 4.90 (s, 2H, CH_2), and 6.96—8.12 (m, 6H, arom); MS (70 eV) m/z 241 (M^+). Found: C, 74.27; H, 6.34; N, 5.67%. Calcd for $C_{15}H_{15}NO_2$: C, 74.67; H, 6.27; N, 5.80%.

2o: Mp 103 °C (from AcOEt); IR (KBr) 1615, 1640, and 3390 cm^{-1}; ^1H NMR ($CDCl_3$) δ=0.95—1.97 (m, 6H, CH_3), 2.24 (s, 1H, OH), 3.53—3.83 (m, 4H, CH_2), 4.95 (s, 2H, CH_2), and 7.23—8.42 (m, 6H, arom); MS (70 eV) m/z 269 (M^+). Found: C, 75.48; H, 7.05; N, 4.92%. Calcd for $C_{17}H_{19}NO_2$: C, 75.81; H, 7.11; N, 5.20%.

2p: Mp 64 °C (from AcOEt); IR (KBr) 1610 and 1640 cm^{-1}; ^1H NMR ($CDCl_3$) δ=2.20 (quint, 2H, J=7 Hz, CH_2), 3.62 (t, 2H, J=7 Hz, CH_2), 3.75 (t, 2H, J=7 Hz, CH_2), 4.94 (s, 2H, CH_2), and 7.16—8.38 (m, 6H, arom); MS (20 eV) m/z 259 (M^+). Found: C, 69.10; H, 5.47; N, 5.53%. Calcd for $C_{15}H_{14}NOCl$: C, 69.37; H, 5.43; N, 5.39%.

2q: Mp 149 °C (from AcOEt); IR (KBr) 1605, 1630, 1720, and 3000 cm^{-1}; ^1H NMR (DMSO-d_6) δ=2.76 (t, 2H, J=7 Hz, CH_2), 3.87 (t, 2H, J=7 Hz, CH_2), 5.17 (s, 2H, CH_2), and 7.47—8.52 (m, 7H, arom and COOH); MS (70 eV) m/z 182 (M^+−CH_2CH_2COOH). Found: C, 70.00; H, 5.12; N, 5.43%. Calcd for $C_{15}H_{13}NO_3$: C, 70.58; H, 5.13; N, 5.49%.

3l: Mp 142 °C (from AcOEt); IR (KBr) 1620 and 1640 cm^{-1}; ^1H NMR (DMSO-d_6) δ=3.48—4.35 (m, 4H, CH_2), 6.14 (s, 1H, CH), and 7.60—8.35 (m, 6H, arom); MS (70 eV) m/z 225 (M^+). Found: C, 74.59; H, 4.85; N, 6.15%. Calcd for $C_{15}H_{13}NO_2$: C, 74.65; H, 4.92; N, 6.22%.

3m: Mp 126 °C (from AcOEt); IR (KBr) 1660 cm^{-1}; ^1H NMR ($CDCl_3$) δ=1.52—2.41 (m, 2H, CH_2), 2.90—3.26 (m, 1H, CH), 3.93—4.42 (m, 2H, CH_2), 4.97—5.26 (m, 1H, CH), 6.04 (s, 1H, CH), and 7.44—8.52 (m, 6H, arom); MS (70 eV) m/z 239 (M^+). Found: C, 75.64; H, 5.52; N, 5.94%. Calcd for $C_{15}H_{13}NO_2$: C, 75.30; H, 5.48; N, 5.85%.

3n: Mp 111 °C (from AcOEt); IR (KBr) 1670 cm^{-1}; ^1H NMR ($CDCl_3$) δ=1.43 (d, 3H, J=7 Hz, CH_3), 3.37 (d, 2H, J=7 Hz, CH_2), 3.01—3.25 (m, 0.09H, CH), 4.18—4.75 (m, 0.91H, CH), 6.05 (s, 0.82H, CH), 6.15 (s, 0.18H, CH), and 7.43—8.30 (m, 6H, arom); MS (70 eV) m/z 239 (M^+). Found: C, 75.47; H, 5.48; N, 5.86%. Calcd for $C_{15}H_{13}NO_2$: C, 75.30; H, 5.48; N, 5.85%.

References

1) For example: Z. Horii, C. Iwata, and Y. Tamura, *J. Org. Chem.*, **26**, 2273 (1961); R. T. Major and R. T. Hendrick, *J. Org. Chem.*, **30**, 1270 (1965); D. Bailey and R. Johnson, *J. Org. Chem.*, **35**, 3574 (1970); Y. Maki, K. Kikuchi, H. Sugiyama, and S. Seto, *Chem. Ind.*, **1976**, 322; A. J. McAlees, R. McCrindle, and D. W. Sneddon, *J. Chem. Soc., Perkin. Trans. 1*, **1977**, 2037; T. Watanabe, F. Hamaguchi, and S. Ohki, *Chem. Pharm. Bull.*, **26**, 530 (1978); C. S. D. Favreau and M. M. Kayser, *J. Org. Chem.*, **52**, 129 (1987).

2) B. Sakurai, *Bull. Chem. Soc. Jpn.*, **14**, 173 (1939).

3) T. Misono, T. Fukuda, and Y. Nagao, *Nippon Kagaku Kaishi*, **1979**, 799.

4) R. Sato, T. Senzaki, Y. Shikazaki, T. Goto, and M. Saito, *Chem. Lett.*, **1984**, 1423; R. Sato, T. Senzaki, T. Goto, and M. Saito, *ibid.*, **1984**, 1599; R. Sato, M. Nakayama, Y. Yuzawa, T. Goto, and M. Saito, *ibid.*, **1985**, 1887; R. Sato, T. Senzaki, T. Goto, and M. Saito, *Bull. Chem. Soc. Jpn.*, **59**, 2950 (1986).

5) A. R. Katritzky and A. J. Boulton, "Advances in Heterocyclic Chemistry," Academic Press, New York (1981), Vol. 29, p. 341, R. H. Thomson, D. Sc, "The Chemistry of Natural Products," Blackie, New York (1985), p. 298.

6) A. Nose snd T. Kudo, *Yakugaku Zasshi*, **95**, 1390 (1975) and see Ref. 1.

7) I. Yamamoto, Y. Tabe, and H. Gotoh, *Tetrahedron Lett.*, **25**, 2295 (1971); T. DoMinnh, A. L. Johnson, and P. P. Senise, Jr., *J. Org. Chem.*, **42**, 4217 (1977).

8) A. Warshawsky and D. Ben-Ishai, *Tetrahedron Lett.*, **1968**, 541.

9) C. F. Allen and G. A. Reynolds, *J. Am. Chem. Soc.*, **74**, 5801 (1952).

10) W. J. Gensler, F. Johnson, and A. D. B. Sloan, *J. Am. Chem. Soc.*, **82**, 6074 (1960).

11) S. Yamada, *Yuki Gosei Kagaku Kyokaishi*, **28**, 1083 (1970).

12) H. Eugen, R. Alfred, and S. Hartmut, *Justus Liebigs Ann. Chem.*, **697**, 181 (1966).

13) R. Walter and G. Jaochim, *Chem. Ber.*, **91**, 2485 (1958).

Conjugate Reduction of α,β-Unsaturated Ketones with Amphiphilic Reaction System

Katsumasa NONOSHITA, Keiji MARUOKA, and Hisashi YAMAMOTO*
Department of Applied Chemistry, Faculty of Engineering, Nagoya University, Chikusa, Nagoya 464
(Received January 16, 1988)

Synopsis. The conjugate reduction of α,β-unsaturated ketones has been effected with amphiphilic reaction system consisting of methylaluminum bis(2,6-di-*t*-butyl-4-alkylphenoxide) and certain complex aluminum hydride reagent.

Conjugate reduction of α,β-unsaturated carbonyl compounds is an important synthetic operation and a variety of promising approaches have been developed for this purpose.[1] Those include (1) catalytic hydrogenation of various noble metals;[2] (2) electrochemical reductions including dissolving metal reductions;[3] (3) biochemical reductions using microbioorganisms;[4] (4) reduction with several transition-metal hydride reagents including those produced in situ from transition-metal compounds and conventional reducing agents;[5] and (5) reduction with certain aluminum hydride and borohydride type reagents such as L-Selectride.[6] Here we wish to disclose a conceptually new approach to this transformation based on the amphiphilic reduction, i.e. nucleophilic reduction of electrophilically activated substrate by combining use of exceptionally bulky methylaluminum bis(2,6-di-*t*-

Table 1. Conjugate Reduction of α,β-Unsaturated Ketones[a]

Entry	Substrate	Reagent[b]	1,4-Reduction % yield[c]	1,2-Reduction % yield[c]
1		A	68	0
2	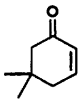	A	76	0
3	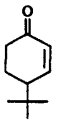	A	0	74
4	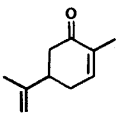	A	93	2
5		A[d]	6	87
6		A[e]	71	15
7		A[f]	52	11
8		A	45	49
9	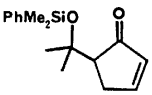	A	83	0
10	(*E*)-PhCH=CHC(=O)CH_3	A	0	99
11	(*E*)-PhCH=CHC(=O)Ph	A	60	28
12		B	57	12
13		C	51	43
14		D	2	97
15		E	37	61
16	(*E*)-PhCH=CHC(=O)(*o*-Tolyl)	A	76	11
17	(*E*)-PhCH=CHC(=O)(Mesityl)	A	84	0

a) Unless otherwise noted, reduction was carried out at −78 °C by adding complex aluminum hydride reagent (2 equiv) in ether to the carbonyl compound (1 equiv)–MAD (2 equiv) complex in toluene. b) Reagent **A**: MAD/Li(*n*-Bu)(*i*-Bu)$_2$AlH; **B**: MAD/Li(*t*-Bu)(*i*-Bu)$_2$AlH; **C**: MAD/Li(Me)(*i*-Bu)$_2$AlH; **D**: MAD/$LiAlH_4$; **E**: MAT/Li(*n*-Bu)(*i*-Bu)$_2$AlH. c) Isolated yield. d) Use of a toluene solution of Li(*n*-Bu)(*i*-Bu)$_2$AlH. e) Use of a THF solution of Li(*n*-Bu)(*i*-Bu)$_2$AlH. f) Each 1 equiv of MAD and Li(*n*-Bu)(*i*-Bu)$_2$AlH was utilized.

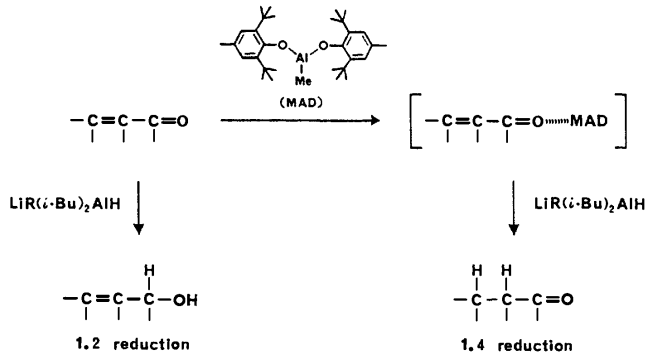

Scheme 1.

butyl-4-alkylphenoxide) (as Lewis acid) and certain complex aluminum hydride reagent (as nucleophile) as illustrated in Scheme 1.[7]

Reaction of carvone with lithium butyl(diisobutyl)-aluminum hydride (Li(n-Bu)(i-Bu)$_2$AlH) was reported to give 1,2-reduction product solely.[8] However, initial complexation of carvone with methylaluminum bis(2,6-di-t-butyl-4-methylphenoxide) (abbreviated to MAD) in toluene and subsequent treatment with Li(n-Bu)(i-Bu)$_2$AlH in ether at −78 °C resulted in total reversal of selectivity, producing 1,4-reduction product almost exclusively in 93% yield. The initial hydride transfer from Li(n-Bu)(i-Bu)$_2$AlH to MAD followed by reduction of the resulting bulky hydride with the enone seems to be unlikely, since treatment of carvone with a pre-mixture of MAD and Li(n-Bu)(i-Bu)$_2$AlH at −78 °C gave result (88% of 1,2 adduct and 8% of 1,4 adduct) close to that in the sole addition of Li(n-Bu)(i-Bu)$_2$AlH. Some other examples are listed in Table 1, which revealed the following characteristic features. The α,β-unsaturated ketone possessing the sterically less demanding carbonyl moiety, even when combined with MAD, is readily susceptible toward the 1,2-hydride attack (Entries 3 and 10). The similar tendency was observed in the conjugate addition of RLi to the enone in the presence of MAD,[7d] although the present conjugate reduction exhibited better 1,4-selectivity. Among various nucleophilic aluminum hydride reagents examined, Li(n-Bu)(i-Bu)$_2$AlH would be most suitable in view of selectivity (Entries 11—14) and the ready availability.[3] The choice of solvents profoundly affects the selectivity. For example, in the MAD-mediated reduction of carvone, ether as solvent was found to be satisfactory, but use of toluene resulted in the predominant 1,2-reduction (Entry 5). Methylaluminum bis(2,4,6-tri-t-butylphenoxide) (MAT) lowered 1,4 selectivity (Entry 15).

Experimental

The IR spectra were determined on a Hitachi 260-10 spectrometer. The ^{1}H NMR spectra were recorded on a JNM-PMX 60 spectrometer, using TMS (tetramethylsilane) as an internal standard. Splitting patterns are indicated as s, singlet; d, doublet; m, multiplet; br, broad. The microanalyses were performed at the Institute of Applied Organic Chemistry, Faculty of Engineering, Nagoya University. Analytical gas-liquid phase chromatography (GLC) was performed on Gasukuro Kogyo Model 370 instruments with a flame-ionization detector and a capillary column of PEG-HT (0.25×25,000 mm) using nitrogen as carrier gas. Ether and tetrahydrofuran (THF) were distilled from benzophenone ketyl. Toluene was dried over sodium metal. Dichloromethane (CH_2Cl_2) was stored over 4-A Molecular Sieves. All experiments were carried out under an argon atmosphere. Purification of the product was carried out by column chromatography on silica gel Fuji-Davison BW-300.

Preparation of α,β-Unsaturated Ketones. 6-Methyl-2-cyclohexen-1-one and 4-t-butyl-2-cyclohexen-1-one were prepared by selenenylation-selenoxide elimination sequence according to Reich's method.[9] 5,5-Dimethyl-2-cyclohexen-1-one was prepared by reduction of enol ether of 5,5-dimethyl-1,3-cyclohexanedione with $LiAlH_4$ and subsequent acid hydrolysis. 5-(1-Dimethylphenylsiloxy-1-methylethyl)-2-cyclopenten-1-one was derived from aldol reaction of 2-cyclopenten-1-one lithium enolate (generated with LDA) with acetone followed by silylation with $Me_2PhSiCl$ and NEt_3. 1-(2-Methylphenyl)-3-phenyl-2-propen-1-one and 3-phenyl-1-(2,4,6-trimethylphenyl)-2-propen-1-one were prepared by aldol condensation according to the literature procedure.[10]

General Procedure. To a solution of 2,6-di-t-butyl-4-methylphenol (441 mg, 2 mmol) in toluene (5 ml) was added a 2 mol cm^{-3} hexane solution of Me_3Al (0.5 ml, 1 mmol) and the resulting colorless solution was stirred at room temperature for 1 h. After cooling to −78 °C, enone (0.5 mmol) was added at −78 °C, and after 5 min, Li(R)(i-Bu)$_2$AlH (1 mmol) in ether (2 ml) (prepared in another flask from DIBAH and RLi (R =n-Bu, t-Bu, and Me) at 0 °C for 10 min) was transferred to the enone-MAD complex by cannula. The mixture was stirred at −78 °C for 15 min, poured into 10% HCl, extracted with ether, and dried over Na_2SO_4. Evaporation of solvents and purification of the residue by column chromatography on silica gel (ether/hexane as eluant) gave the saturated ketone and/or the unsaturated alcohol depending on the enone substrates, hydride reagents, and reaction conditions.

2-Methylcyclohexanone: IR (neat) 2940, 2870, 1715, 1450 cm^{-1}; ^{1}H NMR (CCl_4) δ=0.97 (d, J=7 Hz, 3H), 1.03—2.70 (m, 9H).

3,3-Dimethylcyclohexanone: IR (neat) 2950, 2875, 1705, 1450 cm^{-1}; ^{1}H NMR (CCl_4) δ=0.96 (s, 6H), 1.17—2.40 (m, 6H), 2.05 (s, 2H).

4-t-Butyl-2-cyclohexen-1-ol: IR (neat) 3325, 3010, 2950, 2850, 1645, 1060, 735 cm^{-1}; ^{1}H NMR (CCl_4) δ=0.87 (s, 9H), 1.01—2.20 (m, 5H), 3.16 (br s, 1H), 3.78—4.25 (m, 1H), 4.60 (s, 2H).

5-Isopropenyl-2-methylcyclohexanone: IR (neat) 3100, 2925, 2850, 1720, 1640, 1450, 890 cm^{-1}; ^{1}H NMR (CCl_4) δ=0.92—2.85 (m, 11H), 0.97 (d, J=6 Hz, trans CHC$\underline{H}_3$), 1.02 (d, J=6 Hz, cis CHC$\underline{H}_3$), 1.75 (s, 3H, CH_3-C=C), 4.70 (s, 2H). GLC analysis showed the cis/trans ratio to be 14:86. t_R (trans)=14.2 min, t_R (cis)=15.2 min at 90 °C.

5-Isopropenyl-2-methyl-2-cyclohexen-1-ol: Bp 90—95 °C (Kugelrohr bath temp, 5 Torr (1 Torr≈133.322 Pa)); IR (neat) 3325, 3090, 2925, 1650, 1450, 1040, 895, 815 cm^{-1}; ^{1}H NMR (CCl_4) δ=1.13—2.60 (m, 8H), 1.70 (s, 3H, CH_3-C=C), 2.94 (br s, 1H), 3.70—4.30 (m, 1H), 4.65 (s, 2H), 5.36 (br s, 1H). Anal. ($C_{10}H_{16}O$) C, H.

3,5-Dimethylcyclohexanone: IR (neat) 2965, 2885, 1720, 1455 cm^{-1}; ^{1}H NMR (CCl_4) δ=0.66-2.50 (m, 8H), 1.03 (br d, 6H). GLC analysis indicated the cis/trans ratio to be 1:99. t_R (trans)=8.6 min, t_R (cis)=9.7 min at 70 °C.

3,5-Dimethyl-2-cyclohexen-1-ol: IR (neat) 3360, 2930, 1675, 1455, 1380, 1035 cm^{-1}; ^{1}H NMR (CCl_4) δ=0.50—2.73 (m, 9H), 1.67 (s, 3H), 4.03 (br s, 1H), 5.16—5.73 (m, 1H).

2-(1-Dimethylphenylsiloxy-1-methylethyl)cyclopentanone:

IR (neat) 2970, 1715, 1635, 1445, 1415, 1370, 1265, 1190, 1005, 815 cm^{-1}; ^1H NMR (CCl_4) δ=0.28 (s, 6H), 1.25 (s, 6H), 1.48—2.41 (m, 7H), 6.98—7.61 (m, 5H). This product was spectroscopically identical with authentic sample which was prepared by aldol reaction of cyclopentanone lithium enolate (generated with LDA) with acetone followed by silylation with $Me_2PhSiCl$ and NEt_3.

(*E*)-4-Phenyl-3-buten-2-ol: IR (neat) 3325, 3020, 2975, 1650, 1490, 1455, 1060, 965, 745, 690 cm^{-1}; ^1H NMR (CCl_4) δ=1.27 (d, J=6 Hz, 3H), 3.53 (s, 1H), 4.33 (quintet, J=6 Hz, 1H), 5.86—6.66 (m, 2H), 7.13 (s, 5H).

1,3-Diphenyl-1-propanone: IR (neat) 3040, 2945, 1690, 1595, 1580, 1490, 1450, 1205, 750, 690 cm^{-1}; ^1H NMR (CCl_4) δ=2.54—3.55 (m, 4H), 6.83—8.04 (m, 5H), 7.11 (s, 5H).

(*E*)-1,3-Diphenyl-2-propen-1-ol: Bp 200—205 °C (Bath temp, 7 Torr); IR (neat) 3350, 3035, 2870, 1600, 1580, 1495, 1450, 1070, 1030, 965, 745, 695 cm^{-1}; ^1H NMR (CCl_4) δ=3.12 (br s, 1H), 5.11 (d, J=6 Hz, 1H), 5.87—6.68 (m, 2H), 6.94—7.72 (m, 10H). Anal. ($C_{15}H_{14}O$) C, H.

1-(2-Methylphenyl)-3-phenyl-1-propanone: Bp 170—175 °C (Bath temp, 4 Torr); IR (neat) 3060, 3025, 2930, 1685, 1600, 1575, 1490, 1450, 745, 695 cm^{-1}; ^1H NMR (CCl_4) δ=2.34 (d, J=7 Hz, 3H), 2.70—3.53 (m, 4H), 6.53—8.06 (m, 4H), 7.12 (s, 5H). Anal. ($C_{16}H_{16}O$) C, H.

(*E*)-1-(2-Methylphenyl)-3-phenyl-2-propen-1-ol: IR (neat) 3325, 3030, 2935, 2870, 1600, 1585, 1495, 1460, 1450, 1075, 1015, 970, 755, 695 cm^{-1}; ^1H NMR (CCl_4) δ=2.16 (s, 3H), 3.73 (br s, 1H), 5.25 (m, 1H), 5.86—6.70 (m, 2H), 6.83—7.60 (m, 9H).

3-Phenyl-1-(2,4,6-trimethylphenyl)-1-propanone: Bp 185—190 °C (Bath temp., 4 Torr); IR (neat) 3045, 2935, 1705, 1615, 1500, 1455, 1235, 855, 755, 700 cm^{-1}; ^1H NMR (CCl_4) δ=2.03 (s, 6H), 2.20 (s, 3H), 2.90 (s, 4H), 6.63 (s, 2H), 7.08 (s, 5H). Anal ($C_{18}H_{20}O$) C, H.

References

1) Reviews: a) C. Sc. A. Hajós, "Complex Hydrides and Related Reducing Agents in Organic Synthesis," Elsevier, New York (1979); b) M. Hudlický, "Reductions in Organic Chemistry," John Wiley & Sons, New York (1984).

2) a) M. Freifelder, "Catalytic Hydrogenation in Organic Synthesis. Procedures and Commentary," John Wiley & Sons, New York (1978); b) P. N. Rylander, "Hydrogenation Methods", Academic Press, New York (1985).

3) a) H. O. House, "Modern Synthetic Reactions," Benjamin, Menlo Park (1965); b) M. M. Baiser, "Organic Electrochemistry," Dekker, New York (1973).

4) a) A. Kergomard, M. F. Renaud, and H. Veschambre, *J. Org. Chem.*, **47**, 792 (1982); b) J. C. Gramain, A. Kergomard, M. F. Renard, and H. Veschambre, *ibid.*, **50**, 120 (1985).

5) a) E. Keinen and N. Greenspoon, *Tetrahedron Lett.*, **26**, 1353 (1985); b) T. Tsuda, T. Hayashi, H. Satomi, T. Kawamoto, and T. Saegusa, *J. Org. Chem.*, **51**, 537 (1986) and references cited therein.

6) J. M. Fortunato and B. Ganem, *J. Org. Chem.*, **41**, 2194 (1976).

7) Amphiphilic Reactions in Organic Synthesis: a) Y. Matsumura, K. Maruoka, and H. Yamamoto, *Tetrahedron Lett.*, **23**, 929 (1982); b) K. Maruoka, T. Itoh, and H. Yamamoto, *J. Am. Chem. Soc.*, **107**, 4573 (1985); c) K. Maruoka, M. Sakurai, and H. Yamamoto, *Tetrahedron Lett.*, **26**, 3853 (1985); d) K. Maruoka, K. Nonoshita, and H. Yamamoto, *ibid.*, **28**, 5723 (1987); e) K. Maruoka, T. Itoh, M. Sakurai, K. Nonoshita, and H. Yamamoto, *J. Am. Chem. Soc.*, in press.

8) S. Kim and K. H. Ahn, *J. Org. Chem.*, **49**, 1717 (1984).

9) H. J. Reich, J. M. Renga, and I. L. Reich, *J. Am. Chem. Soc.*, **97**, 5434 (1975).

10) E. P. Kohler and H. M. Chadwell, *Org. Synth.*, Coll. Vol. **1**, 78 (1932).

Asymmetric Carbonyl Addition and Asymmetric Polymerization Assisted by Axially Chiral Diamines Give Disparate Ligand/Product Configurational Correlations

Shigeyoshi KANOH, Hiroki MURAMOTO, Kazunobu MAEDA, Naotaka KAWAGUCHI, Masatoshi MOTOI, and Hiroshi SUDA*

Department of Chemistry and Chemical Engineering, Faculty of Technology, Kanazawa University, 2-40-20 Kodatsuno, Kanazawa 920

(Received January 16, 1988)

Synopsis. Organolithium reagents complexed with axially chiral biphenyl-substituted *N,N,N′,N′*-tetramethylethylenediamines (**1** and **2**) add to aldehydes in good enantioface selectivity. The pattern of the stereoselection, however, disagrees with that of the helical choice observed for the asymmetric polymerization of triphenylmethyl methacrylate with the same complexes.

Recently, Cram and co-workers[1,2] have been reported that *N,N,N′,N′*-tetramethylethylenediamine (TMEDA) derivatives having an atropisomeric 1,1′-binaphthyl unit (**3** and **4**) can be utilized as highly effective chirality-inducing ligands for organolithium compounds. They have successfully achieved the highly asymmetric alkylation of aldehydes by using the above complexes.[1] There is another interesting report, in which the asymmetric polymerization of methyl methacrylate (MMA) has been also studied with butyllithium (BuLi) complexed with **4**.[2] We almost concurrently presented reports that similar complexes between organolithiums and axially chiral biphenyl-substituted TMEDAs, such as **1** and **2**, serve as effective initiators in the asymmetric polymerization of related triphenylmethyl methacrylate (TrMA).[3,4] We directed our special attention to Cram's consideration:[2] a single stereoelectronic feature can explain consistently a variety of the ligand/product configurational correlations in the above two asymmetric reactions.

Herein, we report the asymmetric carbonyl addition of organolithium reagents to aldehydes assisted by **1** or **2**, and discuss the stereochemistry in connection with the mechanistic consideration on our asymmetric polymerization.

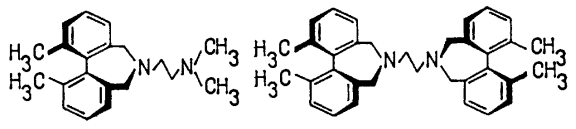

(S)-(1) (S,S)-(2)

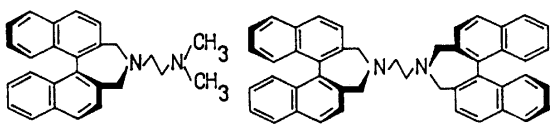

(S)-(3) (S,S)-(4)

Experimental

Materials. Optically pure diamines, **1** and **2**, were prepared from the resolved 6,6′-dimethylbiphenyl-2,2′-dicarboxylic acid,[5] according to the method reported previously.[3] (*R*)-**1**: Bp 140 °C (0.05 Torr (1 Torr=133.322 Pa)) $[\alpha]_D^{25}$ +43.0° (*c* 1.0, tetrahydrofuran); (*S*)-**1**: $[\alpha]_D^{25}$ −42.9°. (*R,R*)-**2**: Mp 156.5—158 °C (from hexane), $[\alpha]_D^{25}$ +115.1° (*c* 1.0, ethanol); (*S,S*)-**2**, mp 155—157 °C, $[\alpha]_D^{25}$ −114.0°. These diamines gave satisfactory analytical data and the expected ^{1}H NMR and mass spectra.

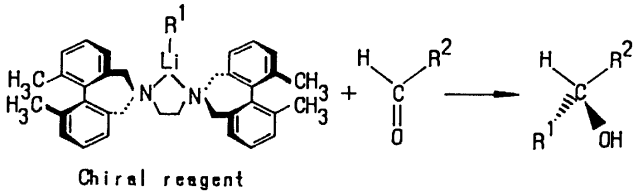

Chiral reagent

Asymmetric Carbonyl Additions. According to the procedure of Mazaleyrat and Cram,[1] a typical chiral organolithium (R^1Li) complex was prepared by mixing 4.6 cm^3 (3.0 mmol) of BuLi (0.65 mol l^{-1}) in hexane with a solution of (*S,S*)-**2** (1.56 g, 3.3 mmol) in 50 cm^3 of dry Et_2O under a nitrogen atmosphere at −50 °C. The solution was cooled to −78 °C, and a solution (1.0 cm^3; 1.2 mol l^{-1}) of benzaldehyde (1.2 mmol) in Et_2O was added. The homogeneous mixture was stirred for 3 h at −78 °C, and then rapidly quenched with 1 mol l^{-1} HCl. Extractive work-up gave an oil, which was purified by preparative TLC (silica gel, benzene) followed by bulb-to-bulb distillation to give (*S*)-(−)-1-phenyl-1-pentanol (0.17 g, 87%) pure by GLPC and ^{1}H NMR. Similarly, routine runs were carried out in various combinations among aldehydes, R^1Li, and the chiral diamines under different reaction conditions. The dominant configurations and enantiomeric excesses (ee's) of the produced alcohols were determined from their optical rotations based on the reported maximum values. The used bases were recovered in more than 90% yields without any noticeable loss in optical purity.

Results and Discussion

The results are summarized in Table 1. As can be seen from the ee's of produced alcohols, the both-side substituted TMEDA (**2**) exhibited a more preferable enantioface selectivity than **1** did. Both the temperature and the solvent of the reaction were important in order to achieve high optical yields. The highest ee. value of 99% was recorded in the reaction by using **2** in Et_2O at −120 °C. An addition way that R^2CHO was treated with an R^1Li reagent having a more bulky R^1 than R^2 resulted in a substantial decrease of the optical yield compared with that of the same product obtained in the reversed way. These results were quite analogous to those observed previously with similar chiral ligands of a 1,1′-binaphthyl analogue, **3** and **4** by Mazaleyrat and Cram.[1] Under the same reaction con-

Table 1. Asymmetric Carbonyl Addition of Organolithium Complexes of **1** or **2** to Aldehydes.[a]

Chiral reagent		R^2 in R^2CHO	Solvent	Alcohol produced		
Diamine	R^1			Isolated yield/%	$[\alpha]_D^{25}$ [b] /°	%Ee.[c] (configuration)
(*S*)-**1**	Bu	Ph	Et_2O	95	−20.1	53 (*S*)
(*S*)-**1**	Bu	Ph	PhMe	93	−12.4	33 (*S*)
(*S,S*)-**2**	Bu	Ph	Et_2O	88	−32.2	86 (*S*)
(*R,R*)-**2**	Bu	Ph	Et_2O	75	+32.2	86 (*R*)
(*R,R*)-**2**	Bu	Ph	Et_2O[d]	62	+37.1	99 (*R*)
(*S,S*)-**2**	Bu	Ph	PhMe	74	−10.2	27 (*S*)
(*R*)-**1**	Ph	Bu	Et_2O	59	−6.7	18 (*S*)
(*S,S*)-**2**	Ph	Bu	Et_2O	53	+6.8	18 (*R*)
(*S*)-**1**	$PhCH_2$[e]	Ph	PhMe	64	0[f]	0
(*S,S*)-**2**	$PhCH_2$[e]	Ph	PhMe	48	0[f]	0

a) Reaction conditions: R^2CHO/R^1Li/diamine=1.2/3.0/3.3 mmol; solvent, 50 cm^3; reaction temperature, −78 °C; reaction time, 3 h. b) The optical rotations were taken in benzene solutions. c) Based on $[\alpha]_D$ 37.6° (*c* 3, benzene) (Refs. 1 and 5). d) Temperature, −120 °C, at which the reaction system became heterogeneous. e) When the BuLi complexes were prepared in toluene at room temperature, the anion was smoothly replaced by $PhCH_2Li$ (Ref. 6). f) In ethanol (Ref. 7).

ditions, **1** and **2** were found to provide almost equal levels of enantioface selection to those of **3** and **4**, respectively, as expected from the structural similarity of each couple of the ligands. The stereochemical consequences gained or reported in various combinations among the four axially chiral ligands, R^1Li, and R^2CHO can be predicted consistently in terms of the axial chirality of the biaryl substituents; that is, when the ligands have (*R*)-configuration, the chiral R^1Li complexes always prefer the *re*-facial approach onto aldehydes.

Previously, we reported that **1** and **2** recognized the helicity in high levels in the asymmetric polymerization of TrMA by using several organolithium complexes of these diamines in toluene at −78 °C.[3,4] The chiral catalysts generated successively asymmetric carbons of a single configuration through the polymerization in an isotactic manner, though after growing up, the polymer became pseudoasymmetric as the whole polymer chain. Okamoto et al. have reported that when poly(TrMA) is composed of the (*S*)-configurated monomer units in the initiating side, the polymer adopts (*P*)-helical conformation because of the isotactic sequence (more than 9-mer) of the bulky ester groups.[8] Accordingly, it was obvious that the chiral consequences of both the present carbonyl addition and the previous polymerization were dominated by carbon-carbon bond-forming processes.

Thus, we compared the ligand/product correlations in the two reactions. One of the most suitable anionic initiators was the benzyllithium (BzLi) complex of **1**.[4] On the contrary, no asymmetric induction occurred in the addition of this complex to benzaldehyde in toluene, which was the same solvent as that used for the polymerization. The result suggested that the initiation reaction between TrMA and the chiral complex took place with no or a very poor stereoselectivity. The stereoselection in the following addition steps might be considered to be primarily important to form the monomer sequence of single configuration, as pointed out by Okamoto et al.[8]

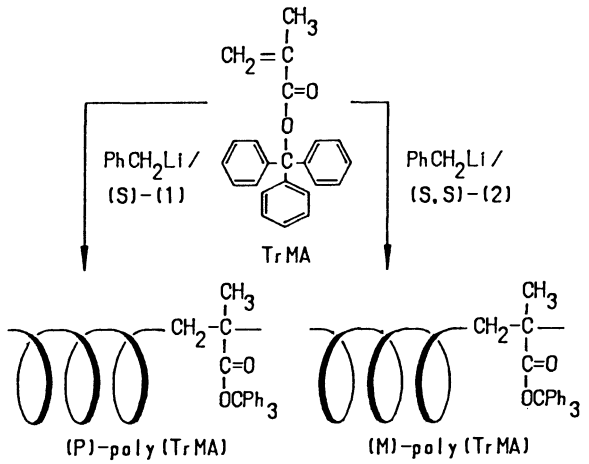

Most interestingly, even if **1** and **2** had the same configuration their BzLi complexes showed the opposed helical preferences in the asymmetric polymerization,[4] as shown in the scheme. The polymerization with (*S*)-**1** gave the (*P*)-helical polymer composed of the (*R*)-configurated monomeric units, while (*S,S*)-**2** induced (*S*)-configuration to the monomeric units leading to (*M*)-helicity. This pattern of the ligand/product stereochemical outcomes was contrary to that observed for the above asymmetric addition. It has been found that the BuLi complexes are not suitable initiators for the asymmetric polymerization.[9] This however does not mean a poor stereoselectivity toward the helical conformation, but does a problem on the poor solubility of the produced polymer in organic solvents because of its high molecular weight.[4] In the polymerization of TrMA by using the various complexes of **1** or **2**,[4] the pattern of the helical choice was not altered at all by changing organolithium compounds including BuLi. The disagreement in the stereoselection between the asymmetric carbonyl addition and the asymmetric polymerization of TrMA strongly suggests that different stereoelectronic interactions

operate in the chiral discrimination of the two reactions by using **1** or **2**.

On the other hand, Cram et al. have proposed an explanation that the stereochemistry of the asymmetric carbonyl addition of the BuLi/**4** complex may be applicable to that of the asymmetric polymerization of MMA with the same complex.[2] However this is contrary to our present results, although the monomers differ in the bulkiness of their ester groups. We may conclude at least that a transition state for the asymmetric polymerization of TrMA can't be compatibly depicted by Cram's model.

The asymmetric polymerization of less bulky MMA is very interesting for us and now under studying.

This work was partly supported by a Grant-in-Aid for Scientific Research No. 61470105 from the Ministry of Education, Science and Culture.

References

1) J.-P. Mazaleyrat and D. J. Cram, *J. Am. Chem. Soc.*, **103**, 4585 (1981).
2) D. J. Cram and D.Y. Sogah, *J. Am. Chem. Soc.*, **107**, 8301 (1985).
3) S. Kanoh, H. Suda, N. Kawaguchi, and M. Motoi, *Makromol. Chem.*, **187**, 53 (1986).
4) S. Kanoh, N. Kawaguchi, T. Sumino, Y. Hongoh, and H. Suda, *J. Polym. Sci., Part A, Polym. Chem.*, **25**, 1603 (1987).
5) S. Kanoh, H. Muramoto, N. Kobayashi, M. Motoi, and H. Suda, *Bull. Chem. Soc. Jpn.*, **60**, 3661 (1987).
6) A. Horeau, J. P. Guetté, and R. Weidmann, *Bull. Soc. Chim. Fr.*, **1966**, 3513.
7) B. T. Golding, D. R. Hall, and S. Sakrikar, *J. Chem. Soc., Perkin Trans. 1*, **1973**, 1214.
8) Y. Okamoto, E. Yashima, T. Nakano, and K. Hatada, *Chem. Lett.*, **1987**, 759.
9) H. Suda, S. Kanoh, and T. Sumino, unpublished data.

Vacuum Sublimation Behavior of Molybdenum(VI) and Tungsten(VI) Chelates with 8-Quinolinol

Takaharu HONJO* and Sumiko KAWASAKI
Department of Chemistry, Faculty of Science, Kanazawa University, Kanazawa 920
(Received September 3, 1987)

Synopsis. A vacuum sublimation apparatus with a continuous-temperature gradient (30—280 °C) along the glass tube (60—0 cm) at 10^{-2} and 10^{-1} Torr (1 Torr=133.322 Pa) was used. 8-Quinolinol (Oxine, ox) and its Mo^{6+} and W^{6+} chelates ($MoO_2(ox)_2$ and $WO_2(ox)_2$) in milligram amounts were sublimed without any thermal decomposition. The Mo^{6+} chelate (orange yellow) forms large, rectangular crystals in the crossed state, while the W^{6+} chelate (pale yellow) forms small, rectangular crystals in the scattered states after vacuum sublimation.

8-Quinolinol (Oxine, ox) forms extractable chelates with at least 50 metals.[1-3] Of these chelates, Al^{3+}, Fe^{3+}, $Co^{2+,3+}$, Ni^{2+}, Cu^{2+}, Zn^{2+}, and In^{3+} oxinates have been found to be useful for the purification and separation of metals by means of the vacuum sublimation method.[4] Now, the present authors have found that the Mo^{6+} and W^{6+} oxinates ($MoO_2(ox)_2$ and $WO_2(ox)_2$) in milligram amounts sublime without any thermal decomposition; their vacuum-sublimation behavior has been studied in detail with a continuous-temperature gradient under low pressure.

Experimental

Apparatus. A model PD-51 Yamato Vacuum Pump; a model PM-12 Shimadzu Pirani Gauge; a model CL Yamato Denki Mantle Heater; a model 105-A Tokyo Shibaura Electric Voltage Stabilizer; a model FPW-4 Hitachi Voltage Stabilizer; a model MP-S2 Yanagimoto Melting Point Measuring Apparatus; a model M-7II Hitachi-Horiba pH meter, and a model BH Olympus System Microscope were used.

Materials. The 8-quinolinol (Oxine, ox), purchased from the Wako Junyaku Kogyo Co., was a guaranteed-grade material. The metal oxinates were generally prepared by the addition of an acetic-acid solution of oxine to an aqueous solution of an excess of both metal salts, $Na_2MoO_4 \cdot 2H_2O$ and $Na_2WO_4 \cdot 2H_2O$, adjusted to pH 3—5 by adding 6M (1M=1 mol dm^{-3}) hydrochloric acid or 6M ammonia. After aging overnight on a water bath, the products were filtered off with a glass filter (1G4), washed with hot distilled water, and finally dried in a desiccator under low pressure or on heating at 100—120 °C.[2] The Mo^{6+} and W^{6+} oxinates ($MoO_2(ox)_2$ and $WO_2(ox)_2$) were decomposed at 291—295 °C and about

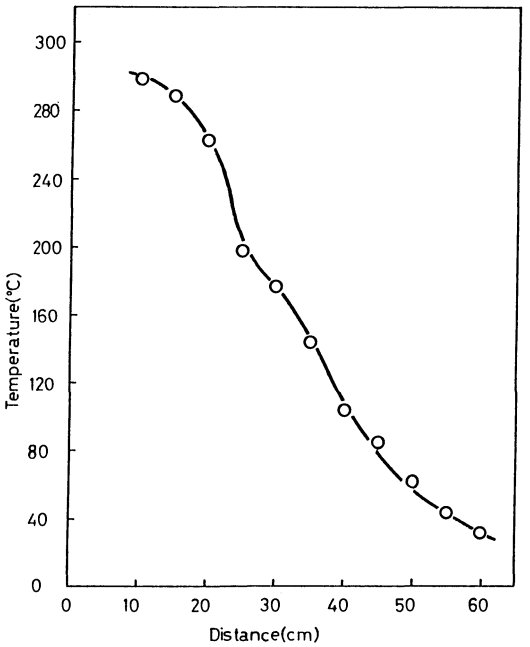

Fig. 1. Continuous temperature gradient along vacuum sublimator.

Table 1. Sublimation-Recrystallization-Zone Temperatures, Amounts Remaining, and Colors of Mo^{6+} and W^{6+} Oxinates after Sublimation at 10^{-2} and 10^{-1} Torr

Metal chelate	Sublimation pressure/Torr	Recrystallization-zone temperature /°C	Color	Chelate taken /mg	Metal compound remained[a]
Oxine(ox)	10^{-1}	<31	White	9.60	—
	10^{-2}	<31	White	9.60	—
$MoO_2(ox)_2$	10^{-1}	222—185	Orange yellow	6.18	A little
	10^{-2}	221—136	Orange yellow	6.30	A little
$WO_2(ox)_2$	10^{-1}	232—204	Pale yellow	3.43	Much
	10^{-2}	224—187	Pale yellow	3.85	Much

a) A little, 10—30%; much, <30%.
All the chelates taken were sublimed a few times without thermal decomposition. The examination of the metal compounds remaining in the sample tubes after every sublimation gave different values, depending on the state of their packing in the sample glass tube.

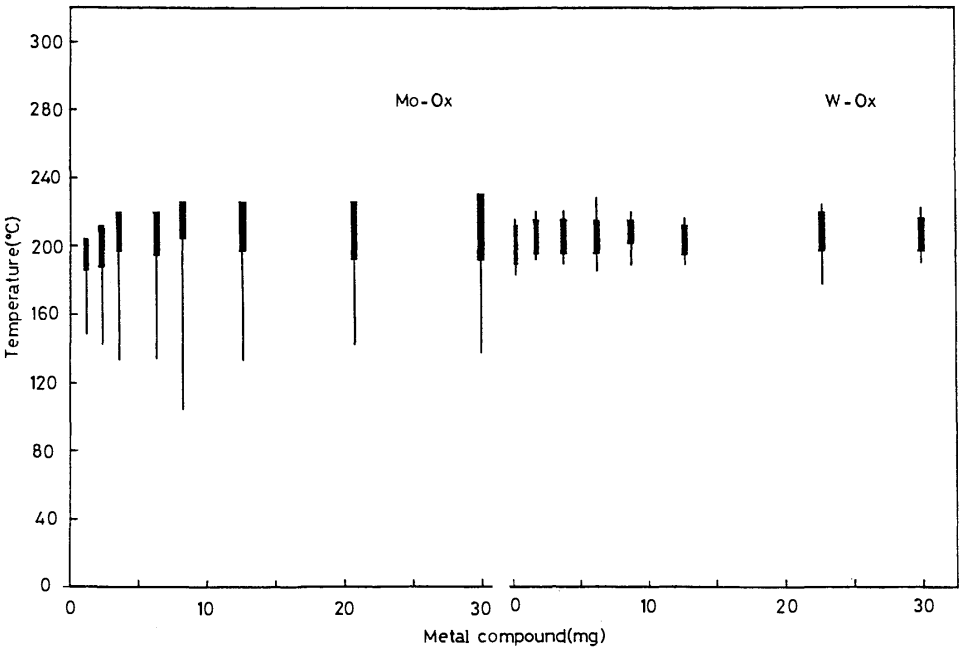

Fig. 2. Sublimation-recrystallization zone of Mo^{6+} and W^{6+} oxinates in various quantities.

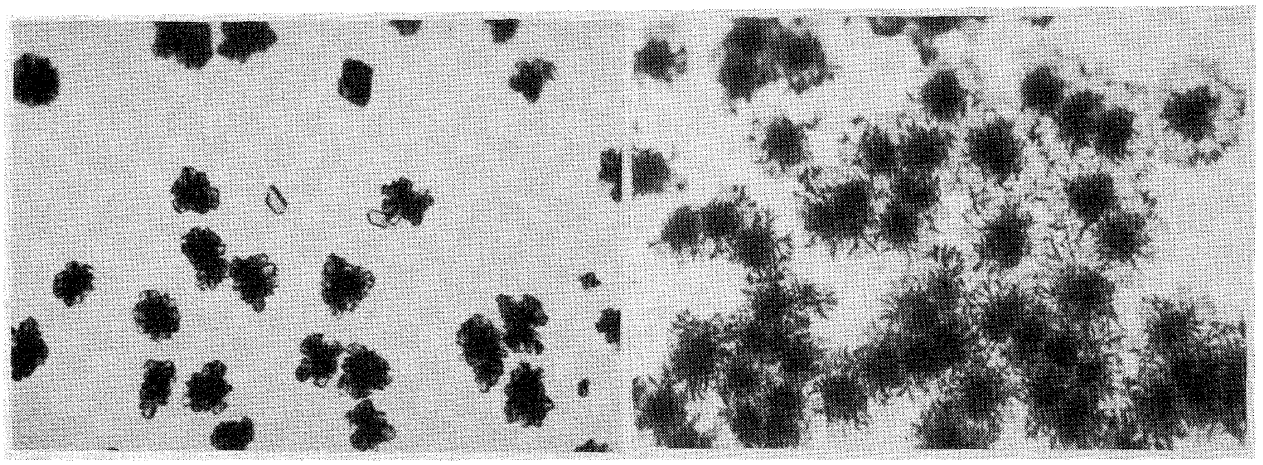

$MoO_2(ox)_2$ $WO_2(ox)_2$

Fig. 3. Microphotographs of metal chelates. Hox: Oxine, Magnification: ×32.

300 °C respectively under normal pressure; the materials were purified by vacuum sublimation before use, and were identified by means of spectrophotometry (λ_{max}=373 nm for $MoO_2(ox)_2$ and 367.5 nm for $WO_2(ox)_2$ in chloroform[2]).

Sublimation Procedure. A vacuum-sublimation apparatus which provided a continuous-temperature gradient (30—280 °C) along the tube (70—0 cm) at 10^{-2} and 10^{-1} Torr (1 Torr=133.322 Pa) was used, as has previously been described.[4-7] The temperature gradient along the sublimator, which consists of a Pyrex glass tube (3 cm in outer diameter; 100 cm in length) covered with a heating mantle, is shown in Fig. 1; it was obtained after the thermal equilibrium had been kept for 4 h. These patterns were obtained by supplying the following electric power through the heating mantle; 20, 10, and 4 V at 1.30 A. A small glass sample tube (0.6 cm in inner diameter; 5 cm in length) containing an individual chelate (0.5—30 mg) and an attached long glass tube (0.5 cm in outer diameter; 55 cm in length), wrapped tightly with Teflon tape, were inserted into the higher-temperature end of the sublimator. Metal chelates were placed inside of the apparatus for 5 h after the thermal equilibrium had been established. The sublimate zone along the sublimation tube was decided from the color of the chelate and its position. The thermal conditions of the sublimator were always checked from the sublimation zone of a definite amount of copper(II) acetylacetonate after sublimating it by the use of another sublimation tube with the metal chelates to be investigated, as has previously been described.[7] The sublimation-recrystallization-zone temperatures of copper(II) acetylacetonate (in 12 mg amounts) were about 89—60 °C at 10^{-2} Torr and 120—66 °C at 10^{-1} Torr (bluish rectangular crystal).

Results and Discussion

The temperature range of the deposited zones, the recovery, and the colors of the Mo^{6+} and W^{6+} oxinates

($MoO_2(ox)_2$ and $WO_2(ox)_2$) after sublimation at 10^{-2} and 10^{-1} Torr are summarized in Table 1. The Mo^{6+} chelate was almost sublimed without any thermal decomposition, while the W^{6+} chelate was thermally stable, but did not sublime completely. The sublimation-recrystallization temperatures of these chelates gave lower values under low pressures. This may have been caused by the rate of the sublimation of the chelate compounds, which depends upon the temperature established at the high-temperature end of the sublimator.[3-7] The sublimation-recrystallization zones for Mo^{6+} and W^{6+} oxinates in varying quantities (0.5—30 mg) at 10^{-2} Torr are graphically presented in Fig. 2. In general, the sublimation-recrystallization temperature of the Mo^{6+} chelate (0.5—6 mg) and the W^{6+} chelate (0.5—2 mg) gave higher values with an increase in the quantity of the chelates, while that of the Mo^{6+} chelate (6—30 mg) and the W^{6+} chelate (2—30 mg) gave almost invariable values. In cases where the recrystallization-zone pattern was not uniform, the deposition zones (where more than 90% of the chelates were found) are indicated by thicker lines.

Representative photomicrographs of metal oxinates deposited on the glass wall inside the sublimation tube are given in Fig. 3. The Mo^{6+} chelate forms large rectangular crystals in the crossed states, while the W^{6+} chelate forms small, rectangular crystals in the scattered states. Both of the metal chelates generally form large crystals under higher pressures. Therefore, it is evident that sublimation is useful for the purification of milligram amounts of both the Mo^{6+} and W^{6+} oxinates because of the sublimation of only mg amounts of metal compounds. The oxinates can be obtained as uniform and beautiful crystals by the use of the present experimental apparatus.

The authors wish to thank Professor Kikuo Terada of Kanazawa University for his helpful advice.

References

1) J. Stary, "The Solvent Extraction of Metal Chelates," Pergamon Press, New York (1964).
2) K. Motojima, H. Hayakawa, T, Kitagawa, and Y. Yamamoto, "Separation Analysis Method by Organic Reagents," Kyoritsu Shuppan, Tokyo (1959).
3) T. Honjo, K. Ameno, M. Horiuchi, and T. Kiba, *Bull. Chem. Soc. Jpn.*, **47**, 1799 (1974).
4) T. Honjo, H. Imura, S. Shima, and T. Kiba, *Anal. Chem.*, **50**, 1545 (1978).
5) T. Honjo and S. Shima, *DOJIN News*, **1980**, 1.
6) T. Honjo and S. Shima, *Bull. Chem. Soc. Jpn.*, **57**, 293 (1984).
7) T. Honjo and K. Nukui, *Bull. Chem. Soc. Jpn.*, **59**, 2645 (1986).

Crystal Structure of [Chloro[tris[(1-ethyl-1*H*-benzimidazol-2-yl)-methyl]amine]zinc(II)] Tetraphenylborate Acetone

Naohide MATSUMOTO,* Toshifumi AKUI, Akira OHYOSHI,*,† and Hisashi ŌKAWA†
Department of Applied Chemistry, Faculty of Engineering, Kumamoto University, Kurokami 2-39-1, Kumamoto 860
†Department of Chemistry, Faculty of Science, Kyushu University, Hakozaki, Higashi-ku, Fukuoka 812
(Received November 21, 1987)

Synopsis. The crystal structure of the title complex has been determined by the single-crystal X-ray diffraction method. The zinc complex has approximately a trigonal bipyramidal coordination geometry, which is different from the copper(II) complex with the same tripod ligand.

The X-ray crystal structure of bovine erythrocyte superoxide dismutase(BESOD) has elucidated the specific binuclear structure of the active site, in which a zinc ion with a tetrahedral coordination sphere is linked to a cooper(II) ion with a square planar geometry through an imidazolate group.[1] In order to obtain the physical properties, the zinc ion has been substituted by copper(II) or cobalt(II) ion and the magnetic parameters have been obtained.[2,3] It is questionable whether the metal replaced compound has the same structure as the original complex. In a series of our studies on imidazolate-bridged binuclear complexes, we have shown an effective synthetic method which can mimic the structural characteristics of the active site of BESOD.[4-6] By applying the synthetic method, an imidazolate-bridged binuclear copper(II)-copper-(II) complex, **1**, has been prepared and its crystal structure has been determined.[4] In this study, we report on the crystal structure of the title zinc complex with the same tripod ligand, **2**.

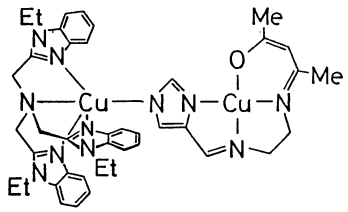

1

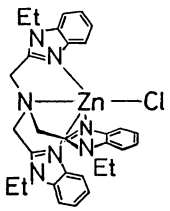

2

Experimental

Synthesis. The tripod ligand tris[(1-ethyl-1*H*-benzimidazol-2-yl)methyl]amine (abbreviated as NTBEt) was prepared by a method described in the literature.[7]

[Zn(Cl⁻)(NTBEt)][BPh₄]·Acetone. To a solution of NTBEt (2 mmol) in 20 cm³ of acetone was added a solution of zinc(II) chloride (2 mmol) in 10 cm³ of methanol. The solution was warmed in a water bath for 10 min and then filtered. To the filtrate was added a solution of sodium tetraphenylborate (2 mmol) in 10 cm³ of methanol. After several hours, colorless prisms precipitated and were collected by suction filtration. Found: C, 70.34; H, 6.11; N, 10.04%. Calcd for $ZnClC_{54}H_{53}N_7B\cdot(CH_3)_2C{=}O$: C, 70.60; H, 6.13; N, 10.11%. Λ_M 144 S mol^{-1} cm^2 (in acetonitrile).

Physical Measurements. The elemental analysis was performed by Mr. Shinichi Miyazaki at The Technical Service Center of Kumamoto University. The molar electrical conductance was measured on a Denki Kagaku Keiki AOC-10 digital conductometer in 10^{-3} mol dm^{-3} solutions. The magnetic susceptibility was measured by the Faraday method at room temperature.

X-Ray Diffraction Study. Diffraction data were obtained on a Rigaku AFC-5 four-circle diffractometer at the Faculty of Science, Kyushu University, using graphite monochromatized Mo $K\alpha$ radiation at 20 °C. Information concerning conditions for crystallographic data collection and structure refinement is summarized below. [Zn(Cl⁻)(NTBEt)][BPh₄]·Acetone, Formula=$ZnClON_7C_{57}BH_{59}$ F.W.=969.7, triclinic, space group $P\bar{1}$, a=14.009(2) Å, b=17.372(2) Å, c=11.607(1) Å, α=95.52(1)°, β=113.08(1)°, γ=76.75(1)°, V=2529.4 Å^3, D_{calcd}=1.273 g cm^{-3} (Z=2), D_{obsd}=1.25 g cm^{-3} (by floatation method in aqueous KI solution), μ(Mo $K\alpha$)=5.94 cm^{-1}, crystal dimension 0.5×0.4×0.3 mm, scan mode θ-2θ, scan width (1.0+0.5tanθ), 2θ range 2.5°—48°, octant collected +h, ±k, ±l, no. of unique data used 5852.

The reflection data were corrected for Lorentz-polarization effects, but not for absorption. The structure was solved by a standard heavy-atom method and refined by a block-diagonal least-squares method. The final discrepancy indices, R and R_w, are 5.79 an 5.46%, where equal weight w=1 was adopted. The calculation was carried out by a FACOM M 386 computer at thc Computer Center of Kyushu University using the UNICS III computer program system.[8] The final positional parameters of non hydrogen atoms with their estimated standard deviations in parentheses are given in Table 1.[9]

Results and Discussion

The molar electrical conductance measured in acetonitrile is 144 S mol^{-1} cm^2, consistent with 1 : 1 electrolyte.[10] This indicates that the Cl⁻ ion is coordinated to the zinc ion. The complex is diamagnetism, being consistent with the d^{10} electronic configuration of Zn(II).

A perspective drawing of the cation [Zn(Cl⁻)-(NTBEt)]$^+$ with the atom numbering scheme is shown in Fig. 1. The zinc ion is coordinated by three imidazolyl nitrogen atoms of the tripod ligand NTBEt, forming a basal plane and a tertiary amine nitrogen atom N(7) and a Cl⁻ ion occupying two axial positions. The bond distances of Zn-axial ligand (Zn-Cl 2.236(1) and Zn-N(7) 2.274(4) Å) are elongated compared with those of Zn-basal plane ligand (Zn-N(1) 2.031(3), Zn-N(3) 2.056(4), and Zn-N(5) 2.046(4) Å). The geometry of the penta-coordinate metal complex can be analyzed and described by using an approach developed by Muetterties and Guggenberger.[11] In this method, the important dihedral angles (known as the shape determining angles (e_1, e_2, e_3)) can be calculated in order to describe the complex geometry. The two

Table 1. Fractional Atomic Coordinates ($\times 10^4$) of [Zn(Cl)(NTBEt)][BPh_4]·Acetone with Their Estimated Standard Deviations in Parentheses

Atom	X	Y	Z	B_{eqv}	Atom	X	Y	Z	B_{eqv}
Zn	8255(0)	−839(0)	6330(1)	4.27(1)	C26	8735(4)	271(3)	3501(5)	4.51(16)
Cl	8495(1)	119(1)	7783(1)	5.97(4)	C27	9047(4)	−904(3)	2107(5)	5.35(19)
N1	9246(3)	−1817(2)	7293(3)	3.74(11)	C28	8098(5)	−777(4)	904(6)	7.72(26)
N2	9844(3)	−3116(2)	7376(3)	3.77(11)	C29	8651(3)	−873(3)	4066(4)	3.97(14)
N3	6722(3)	−938(2)	5930(3)	3.85(11)	C30	8636(4)	−1730(3)	4101(4)	4.15(15)
N4	5226(3)	−1268(2)	4607(3)	4.10(12)	B	−2781(4)	6003(3)	11515(5)	4.21(18)
N5	8510(3)	−374(2)	4946(3)	4.10(12)	C31	−1589(4)	6205(3)	12177(4)	4.33(16)
N6	8799(3)	−524(2)	3175(4)	4.41(13)	C32	−883(4)	5967(3)	13389(4)	4.33(15)
N7	7976(3)	−1782(2)	4802(3)	3.73(11)	C33	135(4)	6114(3)	13925(5)	5.60(18)
C1	10047(3)	−1999(2)	8461(4)	3.68(14)	C34	496(4)	6509(3)	13268(6)	6.16(20)
C2	10488(4)	−1526(3)	9489(4)	4.52(16)	C35	−163(4)	6767(3)	12079(6)	6.13(22)
C3	11289(4)	−1898(3)	10524(4)	5.11(17)	C36	−1199(4)	6620(3)	11522(5)	5.34(19)
C4	11667(4)	−2717(3)	10568(5)	5.18(17)	C37	−2932(4)	5527(3)	10163(4)	4.21(15)
C5	11249(4)	−3192(3)	9557(5)	4.71(16)	C38	−2142(4)	5266(3)	9698(5)	5.07(18)
C6	10438(3)	−2816(2)	8519(4)	3.78(14)	C39	−2311(5)	4845(3)	8565(5)	6.33(23)
C7	9876(4)	−3962(2)	7087(4)	4.40(16)	C40	−3289(5)	4685(3)	7880(5)	6.70(23)
C8	9254(5)	−4285(3)	7647(6)	6.32(23)	C41	−4089(5)	4915(4)	8309(5)	6.80(22)
C9	9143(3)	−2498(2)	6681(4)	3.53(13)	C42	−3902(4)	5326(3)	9429(5)	6.07(20)
C10	8294(3)	−2551(2)	5430(4)	3.87(14)	C43	−2949(3)	5448(3)	12457(4)	4.14(15)
C11	5963(3)	−717(2)	6458(4)	3.87(14)	C44	−3142(4)	5761(3)	13519(5)	5.49(19)
C12	6046(4)	−365(3)	7618(4)	4.43(15)	C45	−3226(5)	5305(4)	14373(5)	6.78(23)
C13	5161(4)	−248(3)	7910(5)	5.35(18)	C46	−3136(5)	4511(4)	14189(5)	7.00(23)
C14	4225(4)	−463(3)	7082(5)	5.91(20)	C47	−2953(5)	4165(3)	13161(6)	6.50(22)
C15	4130(4)	−798(3)	5925(5)	5.48(18)	C48	−2860(4)	4631(3)	12314(5)	5.07(17)
C16	5026(3)	−921(3)	5645(4)	4.06(15)	C49	−3736(4)	6818(3)	11176(4)	4.46(16)
C17	4451(4)	−1552(3)	3472(4)	5.21(17)	C50	−3594(4)	7556(3)	10983(4)	4.72(16)
C18	4228(5)	−2330(4)	3656(6)	7.25(24)	C51	−4420(5)	8204(3)	10541(5)	5.95(20)
C19	6245(3)	−1271(2)	4843(4)	3.70(13)	C52	−5433(5)	8141(4)	10275(6)	7.37(24)
C20	6828(4)	−1597(3)	4009(4)	4.09(14)	C53	−5619(5)	7432(4)	10488(6)	7.59(25)
C21	8564(3)	361(3)	4610(5)	4.35(15)	C54	−4775(4)	6794(3)	10948(6)	6.35(22)
C22	8436(4)	1106(3)	5167(5)	5.23(17)	CA3	3741(5)	2834(3)	12910(6)	7.29(25)
C23	8473(4)	1737(3)	4559(6)	6.18(21)	CA1	2952(7)	2532(4)	11791(6)	9.66(34)
C24	8623(4)	1638(3)	3441(6)	6.67(23)	CA2	4637(8)	3000(6)	12761(9)	12.46(47)
C25	8776(4)	907(3)	2889(5)	5.76(20)	OA	3590(4)	2923(3)	13869(4)	7.91(17)

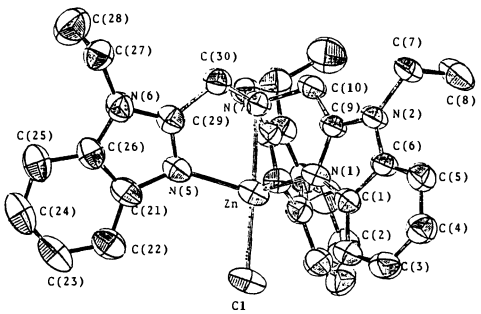

Fig. 1(a). Perspective drawing of [Zn(Cl^-)(NTBEt)]$^+$ with the atom numbering scheme.

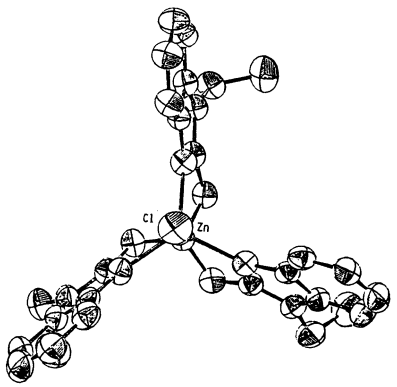

Fig. 1(b). Perspective drawing of [Zn(Cl^-)(NTBEt)]$^+$ projected along Zn-axial ligand direction.

possible limiting geometries for a penta-coordinate metal center are square-base pyramid(SP) and trigonal bipyramid(TBP) geometries. The shape-determining parameters are (e_1, e_2, e_3)=(75.7°, 75.7°, 0°) for an SP complex and (e_1, e_2, e_3)=(53.1°, 53.1°, 53.1°) for a TBP complex. As applied to the present complex **2**, the analysis yields parameters (44.9°, 46.9°, 54.9°), indicating that the coordination geometry is described as a trigonal bipyramid. On the other hand, the copper(II) sphere with the same tripod ligand NTBEt in the complex **1** has the shape determining parameters (72.0°, 63.7°, 18.5°),[4] indicating that the coordination geometry of the copper(II) sphere is an intermediate geometry between a square-base pyramid and a trigonal bipyramid. The structural difference between the zinc (II) and copper(II) sphere with the same ligand is probably attributable to their electronic configurations. The present result suggests that the molecular

structure of the metal-replaced compound of the hetero-metal polynuclear complex may be different from that the original complex.

This work was in part supported by a Grant-in-Aid from the Ministry of Education, Science and Culture.

References

1) J. A. Tainer, E. D. Getzoff, K. M. Beem, J. S. Richardson, and D. C. Richardson, *J. Mol. Biol.*, **160**, 181 (1982).

2) G. Kolks, S. J. Lippard, J. V. Wasczak, and H. R. Lilienthal, *J. Am. Chem. Soc.*, **104**, 717 (1982).

3) L. Banci, I. Bertini, C. Luchinat, R. Monnanni, and A. Scozzafava, *Inorg. Chem.*, **26**, 153 (1987).

4) N. Matsumoto, T. Akui, H. Murakami, J. Kanesaka, A. Ohyoshi, and H. Ōkawa, *J. Chem. Soc., Dalton Trans.*, **1988**, 1021.

5) N. Matsumoto, H. Murakami, T. Akui, J. Honbo, H. Ōkawa, and A. Ohyoshi, *Bull. Chem. Soc. Jpn.*, **59**, 1609 (1986).

6) N. Matsumoto, J. Kanesaka, A. Ohyoshi, M. Nakamura, S. Kohata, and H. Ōkawa, *Bull. Chem. Soc. Jpn.*, **60**, 3056 (1987).

7) L. K. Thompson, B. S. Ramaswamy, and E. A. Seymour, *Can. J. Chem.*, **55**, 878 (1977); V. McKee, M. Zvagulis, J. V. Dagdigian, M. G. Patch, and C. A. Reed, *J. Am. Chem. Soc.*, **106**, 4765 (1984).

8) T. Sakurai and K. Kobayashi, Rikagaku Kenkyusho Houkoku, **55**, 69 (1978); S. Kawano, Rep. Compt. Cent. Kyushu Univ., **13**, 39 (1980).

9) H-atoms coordinates (calculated), thermal parameters, F_o-F_c tables, and complete lists of bond distances and angles are deposited as Document No. 8795 at the office of the Editor of the Bull. Chem. Soc. Jpn.

10) W. J. Geary, *Coord. Chem. Rev.*, **7**, 81 (1971).

11) E. L. Muetterties and L. J. Guggenberger, *J. Am. Chem. Soc.*, **96**, 1748 (1974).

A Simple and Convenient Synthesis of Aryl-Substituted Push-Pull Butadienes from 1,1-Diaryl-2-propyn-1-ols[1)]

Shin'ichi NAKATSUJI,* Kenichiro NAKASHIMA, Masahiko IYODA, † and Shuzo AKIYAMA*
Faculty of Pharmaceutical Sciences, Nagasaki University, 1-14 Bunkyo-machi, Nagasaki 852
†Department of Chemistry, Faculty of Science, Osaka University, Toyonaka, Osaka 560
(Received December 14, 1987)

Synopsis. 1,1-Diaryl-2-propyn-1-ol derivatives reacted with several nucleophiles to afford novel 1,1-diarylbutadiene systems. An efficient one-step synthesis of aryl-substituted push-pull butadiene systems was achieved by this reaction.

Push-pull butadienes bearing an electron-donor on one end and an electron-acceptor on the other end of the molecule are one of the fundamental π-electron systems in merocyanine dyes.[2)] Recently, special interest regarding such π-electron systems is focused on their potential applicability to non-linear optics.[3)] Moreover, the systems are useful building blocks for the formation of cyclic systems by a Diels-Alder reaction.[4)]

In this paper, we wish to report on a new method for the synthesis of such butadienes, which have been found in the course of our studies on the new xanthenylium dye ethynologs **2**, possible near infrared dyes for the optical and laser data-storage technology.[5)]

Treatment of acetylenic alcohol **1** at room temperature with inorganic acids (e.g., $HClO_4$, HBF_4, etc.) or various organic acids (e.g., picric acid, *p*-TsOH, etc.) gave the mono-cationic salt **2**, as shown in Scheme 1.[5)] On the contrary, the reaction of **1** with thiobarbituric acid gave no cationic salt and resulted in the formation of reddish crystals (80%) with an absorption maximum at 588 nm (CH_2Cl_2). The spectroscopic investigations (IR, ^1H NMR, and MS), as well as elemental analyses, showed that the compound obtained was a new 1,3-butadiene derivative (**3b**).[6)] It was apparent from the result that the acidity of thiobarbituric acid was sufficiently strong to remove the hydroxyl group of **1** and the nucleophilicity of the conjugated base was sufficient to attack the terminal carbon (i.e., C_3) of the triple bond. Analogous reactions of **1** with barbituric acid, malononitrile, and 2,4-dinitrophenylhydrazine[7)]

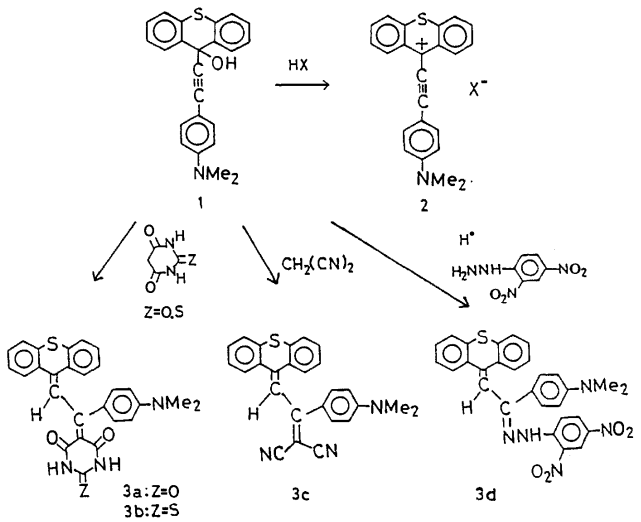

Scheme 1.

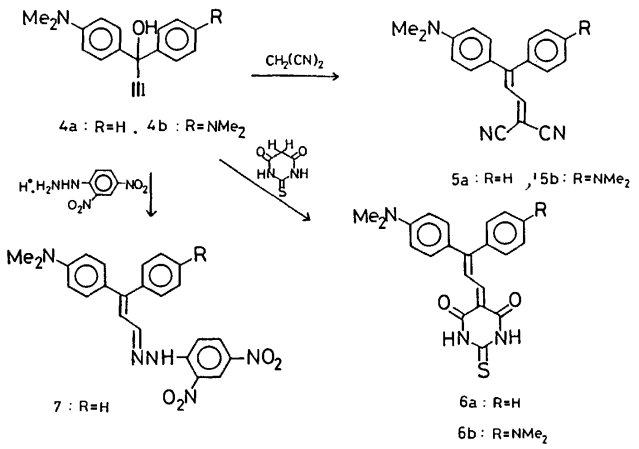

Scheme 2.

Table 1. Yields, Melting Points, Analytical Data, and Electronic Spectra of **3**, **5**, **6**, and **7**

Compound	Yield[a)] %	Mp θ_m/°C	Molecular formula	Found (Calcd) C(%)	H(%)	N(%)	UV[d)] λ_{max}/nm ($\varepsilon\times10^{-4}$)
3a	81	>300	$C_{27}H_{21}N_3O_3$	69.17(69.36)	4.75(4.53)	8.81(8.99)	557(1.53)
3b	80	>300	$C_{27}H_{21}N_3O_2S_2$	67.06(67.06)	4.55(4.38)	8.54(8.69)	588(1.19)
3c	62	214—216	$C_{26}H_{19}N_3S$	76.89(77.01)	4.93(4.72)	10.21(10.36)	447(2.22)
3d	79	ca. 230[b)]	$C_{29}H_{23}N_5O_4S$	64.62(64.80)	4.45(4.31)	12.91(13.03)	446(2.28)
5a	83	79—80	$C_{20}H_{17}N_3$	80.45(80.24)	5.83(5.72)	14.00(14.04)	496(3.69)
5b	85	136—137	$C_{22}H_{22}N_4$	76.72(77.16)	6.66(6.48)	16.13(16.36)	498(3.32)
6a	92	ca. 279[b)]	$C_{21}H_{19}N_3O_2S$	66.55(66.82)	4.85(5.07)	10.90(11.13)	595(7.88)
6b	86	ca. 250[b)]	$C_{23}H_{24}N_4O_2S$	63.22(62.99)	5.84(5.98)	12.64(12.78)[c)]	595(8.06)
7	82	ca. 215[b)]	$C_{23}H_{21}N_5O_4$	63.82(64.03)	4.99(4.91)	16.09(16.23)	496(3.96)

a) Yield of isolated product. b) Decomposition point. c) $C_{23}H_{24}N_4O_2S\cdot H_2O$. d) The longest wavelength band (solvent CH_2Cl_2).

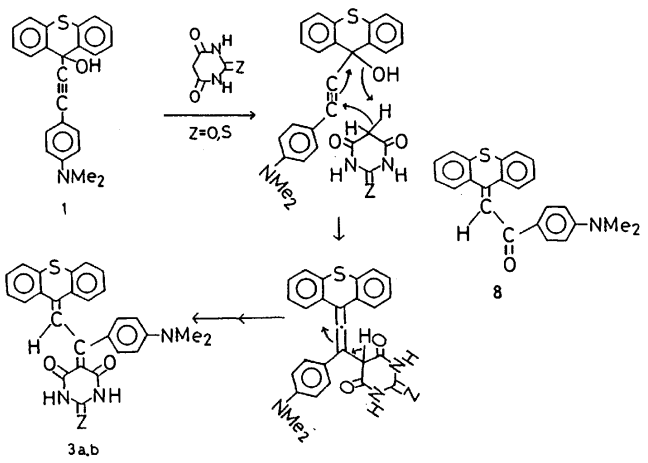

Scheme 3.

afforded **3a**, **3c**, and **3d** in 81, 62, and 79%, respectively (Scheme 1, Table 1).

As an extension of the reaction using acetylenic alcohol **1**, we have tried such reactions as shown in Scheme 2, using acetylenic alcohols **4a**, **4b** prepared by the ethynylation of the corresponding ketones.

The reaction with barbituric acid or thiobarbituric acid (**4**→**6**) could proceed readily, even at room temperature, in good yields. In the case of malononitrile (**4**→**5**), however, appropriate heating was necessary. The acid-catalyzed reaction with 2,4-dinitrophenylhydrazine (**4**→**7**) occurred readily in good yield.

A sort of acid-catalyzed propargylic rearrangement[8] would participate in the reactions and a plausible process of the formation of **3** is shown above (Scheme 3). No reaction of thiobarbituric acid with the ketone **8**[9] occurred under the same conditions and the starting materials were recovered. Therefore, the formation of the ketone as an intermediate in the reaction might be ruled out.

In conclusion, this simple, efficient method provides a new practical way to obtain push-pull type diene systems having potential applicability to dye chemistry and to synthetic chemistry as well.

Experimental

Melting points were uncorrected. IR spectra were obtained on Shimadzu IR 408 and JASCO IRA 810 spectrophotometers. ^{1}H NMR spectra were measured on a JEOL JNM-FX 90Q instrument and the chemical shifts are given in δ-values with respect to TMS used as an internal standard. UV spectra were obtained on a Hitachi 200-10 spectrophotometer. MS spectra were taken using a JEOL JMS-DX303 mass spectrometer.

The syntheses and some physical properties of acetylenic alcohol **1** and cationic salts **2** were partly reported in Ref. 5.

The Syntheses of Acetylenic Alcohol 4a and 4b: To a chilled solution (−10 °C) of 4-dimethylaminobenzophenone (2.0 g, 8.8 mmol) in abs. tetrahydrofuran (100 ml) was bubbled acetylene gas to be saturated. After 10 min, a lithium acetylide-ethylenediamine complex (6.1 g, 67 mmol) was added. The reaction mixture was stirred for 1.5 h at the same temperature and then for 1.5 h at ambient temperature, and poured into H_2O (100 ml). After separation and extraction of the water layer with benzene (100 ml, and then 50 ml), the combined organic layer was washed with brine (150 ml), dried over $MgSO_4$, and evaporated in vacuo. The crude solid obtained was recrystallized with ether to give 1.8 g (78%) of pure **4a** as colorless crystals: mp 121—122 °C; IR (Nujol) ca. 3300 (OH), 3270 (C≡CH), 2110 (C≡C), and 1610 cm^{-1} (C=C); ^{1}H NMR ($CDCl_3$) δ=2.75 (1H, s, OH), 2.82 (1H, s, C≡CH), 2.92 (6H, s, NMe_2), 6.62 (2H, d, J=9 Hz), 7.22—7.75 (5H, m, aromatic H); EI-MS m/z 251 (M^+). Found: C, 81.31; H, 6.77; N, 5.47%. Calcd for $C_{17}H_{17}NO$: C, 81.24; H, 6.82; N, 5.57%. By the same method as above, **4b** was prepared in 95% yield; mp 154—155 °C: IR (Nujol) ca. 3300 (OH), 3250 (C≡CH), 2110 (C≡C), and 1610 cm^{-1} (C=C); ^{1}H NMR ($CDCl_3$) δ=2.80 (1H, s, C≡CH), 2.93 (12H, s, NMe_2), 3.05 (1H, s, OH), 6.63 (4H, d, J=9 Hz, aromatic H), 7.40 (4H, d, J=9 Hz, aromatic H); EI-MS m/z 294 (M^+). Found: C, 77.18; H, 7.64; N, 9.41%. Calcd for $C_{19}H_{22}N_2O$: C, 77.52; H, 7.53; N, 9.52%.

Reactions of Acetylenic Alcohols 1, 4a, and 4b with Barbituric or Thiobarbituric Acid; General Procedure: Acetylenic alcohol **1** (80 mg, 0.22 mmol) in MeOH (20 ml) was mixed with thiobarbituric acid (32 mg, 0.22 mmol) in MeOH (20 ml) at room temperature. The color of the solution turned immediately from pale yellow to deep bluish-violet. After stirring for 1 h, the mixture was concentrated to give precipitates, which were filtered and then washed with ether. The resulting dark-red crystals (82 mg, 80%) were recrystallized with CH_2Cl_2-ether for an analytical sample: mp>300 °C; IR (Nujol) 3175 (NH), 1690, 1650 (C=O), and 1600 cm^{-1} (C=C); ^{1}H NMR (DMSO-d_6) δ=2.88 (6H, s, NMe_2), 6.29 (2H, J=9 Hz, aromatic H), 7.18 (2H, d, J=9 Hz, aromatic H), 7.14—7.42 (9H, m, aromatic and olefinic H), 11.83 (1H, s, NH); FAB-MS m/z 484 (M+1). By the same method as above **3a**, **6a**, **6b** were prepared from **1**, **4a** or **4b**; **3a**: dark-reddish violet crystals; IR (Nujol) 3200 (NH), 1720, 1690, 1665 (C=O), and 1600 cm^{-1} (C=C); ^{1}H NMR (DMSO-d_6) δ=2.88 (6H, s, NMe_2), 6.27 (2H, d, J=9 Hz, aromatic H), 7.12 (2H, d, J=9 Hz, aromatic H), 7.08—7.43 (9H, m, aromatic and olefinic H), 10.74 (1H, s, NH); FAB-MS m/z 468 (M+1). **6a**: yellowish green crystals; IR (Nujol) 3150 (NH), 1690, 1640 (C=O), and 1610 cm^{-1} (C=C); ^{1}H NMR (DMSO-d_6) δ=3.05 (6H, s, NMe_2), 6.77 (2H, d, J=9 Hz, aromatic H), 7.05—7.58 (7H, m, aromatic H), 7.65 (1H, d, J=13 Hz, olefinic H), 8.55 (1H, d, J=13 Hz, olefinic H), 12.02 (1H, s, NH); FAB-MS m/z 378 (M^+). **6b**: blue crystals; IR (Nujol) 3150 (NH), 1695, 1635 (C=O), and 1595 cm^{-1} (C=C); ^{1}H NMR (DMSO-d_6) δ=3.06 (12H, s, NMe_2), 6.79 (2H, d, J=9 Hz, aromatic H), 6.83 (2H, d, J=9 Hz, aromatic H), 7.13 (2H, d, J=9 Hz, aromatic H), 7.32 (2H, d, J=9 Hz, aromatic H), 7.82 (1H, d, J=13 Hz, olefinic H), 8.24 (1H, d, J=13 Hz, olefinic H), 11.32 (1H, s, NH), 11.93 (1H, s, NH); FAB-MS m/z 421 (M^+).

Reaction of 4b with Malononitrile: **4b** (0.11 g, 0.37 mmol) in EtOH (20 ml) was mixed with malononitrile (0.11 ml, 5 equiv) in EtOH (20 ml). The color of the solution gradually turned from pale yellow to slightly red. The solution was successively heated to reflux for 2 h. After cooling the solution to room temperature, the resulting wine-red solution was concentration in vacuo and the red residual oil obtained was purified by column chromatography (silica gel 10 g) using chroloform-ether as eluent to give **5a** as dark red crystals (0.11 g, 85%): mp 136—137 °C; IR (Nujol) 2240 (C≡N) and 1600 cm^{-1} (C=C); ^{1}H NMR ($CDCl_3$) δ=3.06 (6H, s, NMe_2), 3.07 (6H, s, NMe_2), 6.63 (2H, d, J=9 Hz, aromatic H), 6.71 (2H, d, J=9 Hz, aromatic H), 6.94 (1H, d, J=12 Hz, olefinic H), 7.10 (2H, d, J=9 Hz, aromatic H), 7.34 (2H, d, J=9 Hz, aromatic H), 7.47 (1H, d, J=12 Hz, olefinic H); EI-MS m/z 342 (M^+). By the similar manner **3c** and **5a** were prepared from **1** or **4a**; **3c**: dark red crystals; IR (Nujol) 2210 (C≡N) and 1605 cm^{-1} (C=C); ^{1}H NMR ($CDCl_3$) δ=2.97 (6H, s, NMe_2), 6.42 (2H, d, J=9 Hz, aromatic H), 6.78—7.55 (8H, m,

aromatic and olefinic H), 7.46 (2H, d, J=9 Hz, aromatic H), 7.55—7.88 (1H, m, aromatic H); EI-MS m/z 405 (M^+). **5a**: dark red crystals; IR (Nujol) 2220 (C≡N) and 1605 cm^{-1} (C=C); ^1H NMR ($CDCl_3$) δ=3.06 (6H, s, NMe_2), 6.62 (2H, d, J=9 Hz, aromatic H), 7.31 (2H, d, J=9 Hz, aromatic H), 7.06—7.51 (7H, m, aromatic and olefinic H); EI-MS m/z 299 (M^+).

Reaction of 1 with 2,4-Dinitrophenylhydrazine: **1** (80 mg, 0.22 mmol) and 2,4-dinitrophenylhydrazine (44 mg, 0.22 mmol) in EtOH (5 ml) containing 1 drop of concd HCl was warmed on a steam bath for 1 h. The resulting deep-red solution was concentrated to give precipitates, which were filtered and then washed with ether to give dark-red crystals (93 mg, 79%): mp ca. 231 °C (decomp); IR (Nujol) ca. 3500 (NH), 1605 (C=C and C=N), and 1585 cm^{-1} (NH); ^1H NMR ($CDCl_3$) δ=2.99 (6H, s, NMe_2), 5.46 (1H, d, J=9.5 Hz, aromatic H), 6.63 (2H, d, J=9 Hz, aromatic H), 7.51—7.79, 8.01—8.14 (12H, m, aromatic and olefinic H), 8.49 (1H, d, J=2.5 Hz, aromatic H); EI-MS m/z 537 (M^+). **7** was prepared by the similar manner: dark red crystals; IR (Nujol) ca. 3300 (NH), 1615 (C=C and C=N), and 1590 cm^{-1} (NH); ^1H NMR δ=3.00 (6H, s, NMe_2), 6.63 (2H, d, J=9 Hz, aromatic H), 6.88 (1H, d, J=10 Hz, olefinic H), 7.14—7.49 (7H, m, aromatic H), 7.63 (1H, d, J=9 Hz, aromatic H), 7.95 (1H, d, J=10 Hz, olefinic H), 8.27 (1H, dd, J=2, 9 Hz, aromatic H), 9.07 (1H, d, J=2 Hz, aromatic H), 10.97 (1H, s, NH); EI-MS m/z 430 (M^+).

The authors wish to thank Professor Emeritus Masazumi Nakagawa (Osaka University) for valuable discussions and Misses M. Kawakami and K. Takeshita for technical assistance. This work has been supported in part by a Grant-in-Aid for Scientific Research (No. 62470035) from the Ministry of Education, Science and Culture of Japan, which is gratefully acknowledged.

References

1) Ethynologs of Triphenylmethane Dyes Part 6. Part 5 of the series, S. Akiyama, S. Nakatsuji, K. Nakashima, and S. Yamasaki, *Dyes and Pigments*, **9**, in press.

2) Cf., "Colour and Constitution of Organic Molecules," ed by J. Griffith, Academic Press, London (1976); "Light Absorption of Organic Colorants," ed by J. Fabian and H. Hartmann, Springer-Verlag, Berlin (1980); J. Griffith, *Rev. Prog. Coloration*, **14**, 21 (1984); for our precedent study on merocyanine dyes, see, S. Akiyama, K. Nakashima, S. Nakatsuji, M. Suzuki, and C. Umekawa, *Dyes and Pigments*, **8**, 459 (1987).

3) Cf., D. J. Williams, *Angew. Chem.*, **96**, 637 (1984); *Angew. Chem., Int. Ed. Engl.*, **23**, 690 (1984); K. Yamaguchi, M. Nakano, and T. Fueno, *Kagaku*, **42**, 757 (1987).

4) Cf., V. Nair and T. S. Jahnke, *Tetrahedron Lett.*, **25**, 3547 (1984) and references cited therein.

5) S. Akiyama, S. Nakatsuji, K. Nakashima, and M. Watanabe, *J. Chem. Soc., Chem. Commun.*, **1987**, 710.

6) The diene systems have predominantly *s*-trans, i.e., (1*E*, 3*E*)-diene configurations suggested from ^1H NMR data.

7) H^+-source is necessary in this case.

8) Cf., F. Theron, M. Verny, and R. Vessiere, "Chemistry of Carbon-Carbon Triple Bond. Part 1," ed by S. Patai, John Wiley & Sohns, New York (1978), Chap. 10.

9) The ketone **8** was easily obtained by chromatography of alcohol **1** on alumina (Merck II—III); mp 132—137 °C; IR (Nujol) 1620 (C=O) and 1590 cm^{-1} (C=C); ^1H NMR ($CDCl_3$) δ=2.99 (6H, s, NMe_2), 6.49 (2H, d, J=9 Hz, aromatic H), 6.67 (1H, s, olefinic H), 6.96—7.46 (8H, m, aromatic H), 7.77 (2H, d, J=9 Hz, aromatic H); EI-MS m/z 357 (M^+).

Regioselective Alkylation in the Course of Aldol Condensation under Phase-Transfer Catalytic Conditions

Xue-Ping GU, Isao IKEDA, and Mitsuo OKAHARA*
Department of Applied Chemistry, Faculty of Engineering, Osaka University, Yamadaoka 2-1, Suita, Osaka 565
(Received December 18, 1987)

Synopsis. Regio- and stereoselective alkylation in the course of aldol condensation under liquid-solid phase-transfer catalytic conditions, affording conjugated dienyl ether (**5**) or α-substituted β,γ-olefinic aldehyde (**7**) depending on the starting halides, both in good yields, was disclosed. The reaction mechanism is also discussed.

Aldol condensation is a basic and useful reaction of aldehydes, and plays an important role in organic synthesis.[1-3] Recently, direct alkylation of aldehyde has also attracted attention. The aldehydes having one α-hydrogen atom[4] or an α,β-unsaturated group[5] have been directly alkylated to afford alkylated aldehydes such as α-,γ-, or *O*-alkyl products.

During the course of investigations regarding the reactivity of epichlorohydrin under phase transfer (PT) catalytic conditions, we have recently found a simple synthetic method for the preparation of oligoethylene glycol diglycidyl ethers in good yields,[6] and also the regioselective addition of organic chlorides to epoxides under mild conditions.[7] Now we wish to report a regio- and stereoselective alkylation of aliphatic aldehydes with epichlorohydrin or other organic halides during the course of aldol condensation in the presence of PT catalyst and solid sodium hydroxide.

The reaction of octanal with epichlorohydrin was carried out at 55 °C for 2 h in the presence of solid sodium hydroxide and tetrabutylammonium hydrogensulfate in dioxane. The reaction was very clean judging from inspection by GLC. Only two peaks were observed. The main peak was characterized as (5*Z*, 7*E*)-1,2-epoxy-6-hexyl-4-oxatetradeca-5,7-diene (**5**) by spectral analyses: absorptions due to conjugated carbon-carbon double bonds and an ether linkage were observed in the infrared spectra (1660, 1640, 1120 cm^{-1}). The presence of an epoxide ring and two kinds of olefinic moieties in *E* and *Z* forms respectively were deduced from chemical shift values and coupling constants in ^1H NMR. Especially H_h was characterized by Pascual's empirical equation[8] to support the structure of **5** (δ=2.52—2.70 (m, H_a), 2.70—2.90 (m, H_b), 3.04—3.28 (m, H_c), 3.40—4.08 (m, $H_{d,e}$), 5.30—5.70 (m, *J*=17.2 Hz, H_f), 5.70—5.95 (d, *J*=17.2 Hz, H_g), 6.10 (s, H_h)). A conspicuous component of short retention time was identified as *trans*-3-chloroallyl glycidyl ether, which was formed by the isomerization of epichlorohydrin under PT catalytic conditions followed by the condensation with another molecule of epichlorohydrin.[9]

In the absence of PT catalyst, the reaction mentioned above is different. The main product isolated is 2-hexyl-2-decenal (**8**) resulting from the aldol condensation. The alkylated product, **5**, formed only in a small amount in this case.

The stereospecific formation of product **5** under PT catalytic conditions can be explained reasonably by the postulation shown in Scheme 1: the intermediate **1** formed by aldol condensation of two aldehyde molecules rearranges to the intermediate **2**, which further changes to the enolate **3** forming a six-membered ring stabilized by the intramolecular hydrogen bonding. This structure of enolate **3** may cause the formation of a *Z* conformation at one of the two double bonds in **5**. Finally, the enolate **3** attacks epichlorohydrin to produce compound **4**, which is then dehydrated under alkaline conditions to form the conjugated dienyl glycidyl ether **5** with the thermodynamically stable *E*

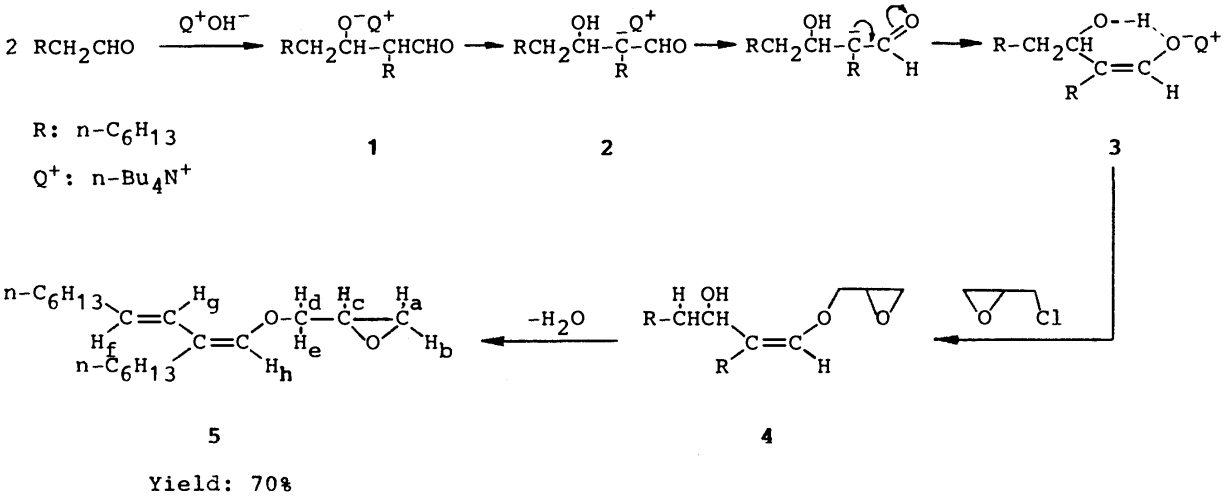

5 **4**

Scheme 1.

Table 1. Results of Alkylation during the Course of Aldol Condensation under PT Catalytic Conditions[a)]

Alkylating reagent	Product (R: n-C_6H_{13})		Yield %	Bp θ_m[b)] °C/Torr
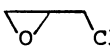	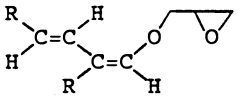	(**5**)	70	130/0.05
$PhCH_2Cl$	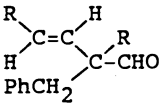	(**7a**)	66	130/0.02
$CH_2=C(CH_3)-CH_2Cl$	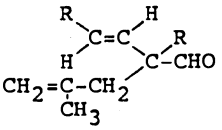	(**7b**)	68	120/0.02
n-$C_8H_{17}Cl$	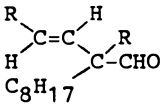	(**7c**)	31	135/0.02
$ClCH_2C(=CH_2)-OCH_2OCH_3$	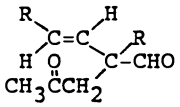	(**7d**)	72	125/0.05
(without PT catalyst)	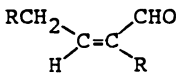	(**8**)	30	115/0.05

a) Octanal was used in all cases, and the reaction was carried out at 55 °C for 2 h in the presence of PT catalyst and solid sodium hydroxide. b) By Kugelrohr distillation.

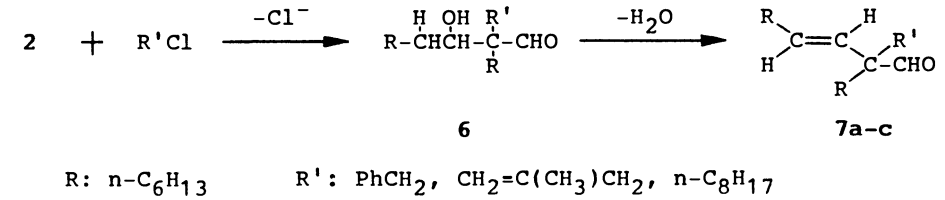

Scheme 2.

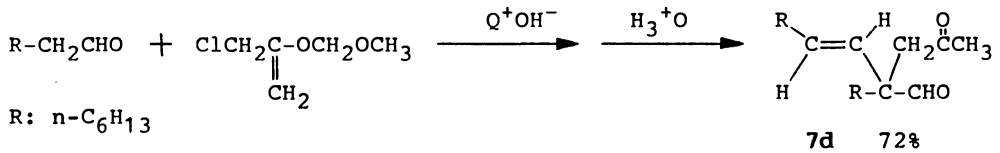

Scheme 3.

conformation.

However, the reaction of octanal with benzyl, methallyl, or octyl chlorides afforded different products even under the same PT catalytic conditions, as reported by Suyama and Shimizu.[10)] The sole product isolated was an α-substituted β,γ-olefinic aldehyde **7a—c** (Scheme 2). The distinguishing spectral feature of products **7** are the following: no infrared absorption due to conjugated carbon-carbon double bonds nor ether linkage appeared, while absorption due to isolated double bond and carbonyl group was observed in the IR spectra (1460, 1720 cm^{-1}, respectively). The signal of the aldehyde proton was clearly seen in the ^1H NMR spectra (δ 9.30). In these cases, the following reaction route is indicated. The intermediate **2** attacks organic chloride directly to afford compound **6** before rearrangement to the intermediate **3** (or even if **2** exists in equilibrium with **3**), **6** is then further dehydrated to **7a—c** (Scheme 2). Judging from the GLC, this reaction was also selective, and the yields of these products were 66, 68, and 31% for benzyl (**7a**), methallyl (**7b**), and octyl (**7c**) derivatives, respectively. Without PT catalyst, the main product in these cases was also an aldol condensation product **8** instead of **7**. The results of alkylation during the course of the aldol condensation are summarized in Table 1.

The reaction of octanal with 2-(chloromethyl)-3,5-dioxahex-1-ene, which was developed recently as an effective acetonylating reagent,[11] afforded γ-keto aldehyde **7d** in yield of 72% after hydrolysis in acidic medium (Scheme 3). It has been reported that γ-keto aldehydes are an important class of compounds especially as intermediates for the preparation of cyclopentenones.[12]

It is well-known that PT catalyst often modifies the mode of chemical reaction or changes the selectivity of the reaction.[13] The title alkylation during the course of aldol condensation under PT catalytic conditions provided additional highly selective examples. It is difficult properly to account for the different selectivities depending on the organic chloride observed in this study. The results of this alkylation reaction, however, agree with those for alkylation of ambident anions reported in the references.[4,14]

In the case of 2-octanone, the reaction with epichlorohydrin did not proceed under the same reaction conditions as those for octanal even at 80 °C for 2 h. The raw material, 2-octanone, was recovered almost quantitatively, except for the formation of a small amount of 3-chloroallyl glycidyl ether.

Experimental

^{1}H NMR spectra were recorded on a JEOL-PS-100 instrument in $CDCl_3$ with Me_4Si as an internal standard. Mass spectra were measured on a Hitachi RMU-6E spectrometer. HRMS were measured on a JMS-DX300 spectrometer. All the reagents were of reagent grade and were used without further purification. Evaporative distillation was performed from bulb to bulb distillation by a glass tube oven model GTO-250RS (Kugelrohr distillation).

Typical Procedure: Synthesis of (5*Z*, 7*E*)-1,2-Epoxy-6-hexyl-4-oxatetradeca-5,7-diene (5). A mixture of octanal (12.8 g, 0.1 mol), epichlorohydrin (9.2 g, 0.1 mol), sodium hydroxide (8 g, 0.2 mol, pellet), tetrabutylammonium hydrogensulfate (1.7 g, 0.005 mol) and dioxane (30 ml) was stirred with a magnetic stirrer at 55 °C for 2 h. After removing the solid materials by filtration through a short column filled with silica gel, and evaporating off the solvent, product **5** was obtained by Kugelrohr distillation under reduced pressure in 70% yield as a colorless oil; bp 130 °C/0.05 Torr (1 Torr≈133.322 Pa). ^{1}H NMR ($CDCl_3$) δ=0.72—1.10 (t, 6H), 1.30 (s, 16H), 1.90—2.36 (m, 4H), 2.52—2.70 (m, 1H), 2.70—2.90 (m, 1H), 3.04—3.28 (m, 1H), 3.40—4.08 (m, 2H), 5.30—5.70 (m, *J*=17.2 Hz, 1H), 5.70—5.95 (d, *J*=17.2 Hz, 1H), and 6.10 (s, 1H); MS *m/z* (relative intensity) 294 (M^+, 80), 223 (50), and 57 (100); IR (neat) 2950, 1660, 1480, 1640, 1180, 1120, 970, and 860 cm^{-1}; Found: *m/z* 294.2549. Calcd for $C_{19}H_{34}O_2$: M, 294.2557.

2-Benzyl-2-hexyl-3-decenal (7a). With the general procedure described above, **7a** was isolated as a colorless liquid in yield of 66%; bp 130 °C/0.02 Torr. ^{1}H NMR ($CDCl_3$) δ= 0.76—1.08 (t, 6H), 1.28 (s, 18H), 1.90—2.24 (m, 2H), 2.94 (s, 2H), 5.28—5.50 (m, *J*=17 Hz, 2H), 7.00—7.40 (m, 5H), and 9.45 (s, 1H); MS *m/z* (relative intensity) 328 (M^+), 237 (50), and 91 (100); IR (neat) 2950, 1735, 1460, 980, and 705 cm^{-1}; Found: *m/z* 328.2760. Calcd for $C_{23}H_{36}O$: M, 328.2764.

2-(2-Methylallyl)-2-hexyl-3-decenal (7b). With the general procedure described above, **7b** was obtained as a colorless oil in yield of 68%; bp 120 °C/0.02 Torr. ^{1}H NMR ($CDCl_3$) δ= 0.72—1.04 (t, 6H), 1.25 (s, 18H), 1.64 (s, 3H), 1.92—2.24 (m, 2H), 2.37 (s, 2H), 4.62—5.00 (d, 2H), 5.20—5.60 (m, *J*=17 Hz, 2H), and 9.34 (s, 1H); MS *m/z* (relative intensity) 292 (M^+), 237 (50), 179 (80), 55 (100), and 43 (90); IR (neat) 2950, 1720, 1460, 980, and 900 cm^{-1}. Found: C, 82.19; H, 12.70%. Calcd for $C_{20}H_{36}O$: C, 82.13; H, 12.41%.

2-Octyl-2-hexyl-3-decenal (7c). With the general procedure described above, **7c** was isolated in yield of 31% as a colorless liquid; bp 132 °C/0.02 Torr. ^{1}H NMR ($CDCl_3$) δ=0.76—1.04 (t, 9H), 1.10—1.80 (m, 32H), 1.96—2.25 (m, 2H), 5.20—5.60 (m, 2H), and 9.30 (s, 1H); MS *m/z* (relative intensity) 350 (M^+), 321 (83), 69 (100), 55 (100), and 43 (100); IR (neat) 2900, 1720, 1460, and 970 cm^{-1}; Found: *m/z* 350.3577. Calcd for $C_{24}H_{46}O$: M, 350.3546.

2-Acetonyl-2-hexyl-3-decenal (7d). A mixture of octanal (12.8 g, 0.1 mol), 2-(chloromethyl)-3,5-dioxahex-1-ene[11] (9.5 g, 0.075 mol), sodium hydroxide (8 g, 0.2 mol, pellet), tetrabutylammonium hydrogensulfate (1.7 g, 0.005 mol) and dioxane (30 ml) was stirred with a magnetic stirrer at 55 °C for 2 h. After removing the solid material by filtration through a short column filled with silica gel, the solvent was evaporated off. Then, 1% aqueous sulfuric acid 10 ml and dioxane 10 ml were added to the residue, and the mixture was stirred at 60 °C for 1 h. The organic components were extracted with ether and dried over anhydrous magnesium sulfate, then the solid material was removed by filtration and the solvent evaporated off. By Kugelrohr distillation of the resulting oil under reduced pressure, **7d** was isolated in yield of 72% (10.6 g) as a colorless liquid; bp 125 °C/0.05 Torr. ^{1}H NMR ($CDCl_3$) δ=0.76—1.00 (t, 6H), 1.24 (s, 20H), 1.90—2.20 (m, 5H), 2.84 (s, 2H), and 5.38—5.50 (m, 2H); MS *m/z* (relative intensity) 294 (M^+), 208 (25), and 43 (100); IR (neat) 2950, 1730, 1470, 1370, 1180, and 900 cm^{-1}; Found: *m/z* 294.2539. Calcd for $C_{19}H_{34}O_2$: M, 294.2557.

2-Hexyl-2-decenal (8): With the procedure similar to the preparation of **5** but in the absence of PT catalyst, **8** was obtained in yield of 30% as a colorless liquid; bp 115 °C/0.05 Torr. ^{1}H NMR ($CDCl_3$) δ=0.80—1.00 (t, 6H), 1.30 (s, 18H), 2.20—2.50 (m, 4H), 6.40—6.60 (t, 1H), and 9.40 (s, 1H); MS *m/z* (relative intensity) 238 (M^+), 55 (100), and 43 (100); IR (neat) 2950, 1700, and 1480 cm^{-1}.

References

1) L. C. Gruen and P. T. McTigue, *Aust. J. Chem.*, **17**, 953 (1964).
2) A. T. Nielsen and W. J. Houlihan, *Org. React.*, **16**, 1 (1968).
3) T. Mukaiyama, *Org. React.*, **28**, 203 (1982).
4) S. A. G. De Graaf, P. E. R. Oosterhoff, and A. Van Der Den, *Tetrahedron Lett.*, **1974**, 1653.
5) H. K. Dietl and K. C. Brannock, *Tetrahedron Lett.*, **1973**, 1273.
6) X.-P. Gu, I. Ikeda, and M. Okahara, *Synthesis*, **1985**, 649.
7) X.-P. Gu, I. Ikeda, and M. Okahara, *Bull. Chem. Soc. Jpn.*, **60**, 397 (1987).
8) C. Pascual, J. Meier, and W. Simon, *Helv. Chim. Acta*, **49**, 164 (1966).
9) X.-P. Gu, I. Ikeda, and M. Okahara, *Bull. Chem. Soc. Jpn.*, **60**, 667 (1987).
10) S. Suyama and M. Shimizu, Japan Kokai Tokkyo Koho 78141210 (17. 5. 1977).
11) X.-P. Gu, I. Ikeda, and M. Okahara, *J. Org. Chem.*, **52**, 3192 (1987).
12) R. A. Ellison, *Synthesis*, **1973**, 397.
13) E. V. Dehmlow and S. S. Dehmlow, "Phase Transfer Catalysis," Verlag Chemie GmbH, D-6940, Weinheim (1980), p. 1.
14) G. J. Heiszwolf and H. Kloosterziel, *Rec. Trav. Chim.*, **89**, 1153 (1970).

Synthetic Photochemistry. XLI.[1] Photorearrangement of 5-Alkyl-1-hydroxy-8-oxabicyclo[3.2.1]octa-3,6-dien-2-ones to 2-Alkyl-3-oxatricyclo[3.3.0.0^{2,8}]octane-4,6-diones

Akira MORI,* Seishi KASAI,† and Hitoshi TAKESHITA*
Institute of Advanced Material Study, 86, Kyushu University, Kasuga-koen, Kasuga, Fukuoka 816
†Graduate School of Engineering Sciences, 39, Kyushu University, Kasuga-koen, Kasuga, Fukuoka 816
(Received December 21, 1987)

Synopsis. The irradiations of 5-alkyl-1-hydroxy-8-oxabicyclo[3.2.1]octa-3,6-dien-2-ones, either in benzene or methanol by means of a high-pressure mercury lamp produced 2-alkyl-3-oxatricyclo[3.3.0.0^{2,8}]octane-4,6-diones. Although the intermediate ketenes could be detected by low-temperature NMR, no adduct was formed in protic solvents.

In the late 1960s, Kende[2] and Chapman[3] respectively studied photorearrangements of bicyclic dienones and trienones via ketene intermediates, which were detected and characterized by low-temperature IR and ^{1}H NMR spectroscopies. Many related works have been reported. Among them particularly interesting was a facile formation of a potential precursor of prostanoids by photolysing 1-hydroxytricyclo[3.3.2.0^{2,4}]deca-6,9-dien-8-one (**A**) to a methoxycarbonyl derivative (**B**) in methanol and a tetracyclic β-diketone (**C**) and a cyclopentenone (**D**) in a mixed solution of methanol and acetic acid via a ketene (**E**).[4]

The photolysis of 5-alkyl-1-hydroxy-8-oxabicyclo-[3.2.1]octa-3,6-dien-2-ones (**1a**, R=CH_3; **1b**, R=CH=CH_2, and **1c**, R=C_4H_9) revealed a facile rearrangement to 2-alkyl-3-oxatricyclo[3.3.0.0^{2,8}]octa-4,6-diones (**2a**, **2b**, and **2c**), but no solvolysis occurred. The results will be briefly described herein.

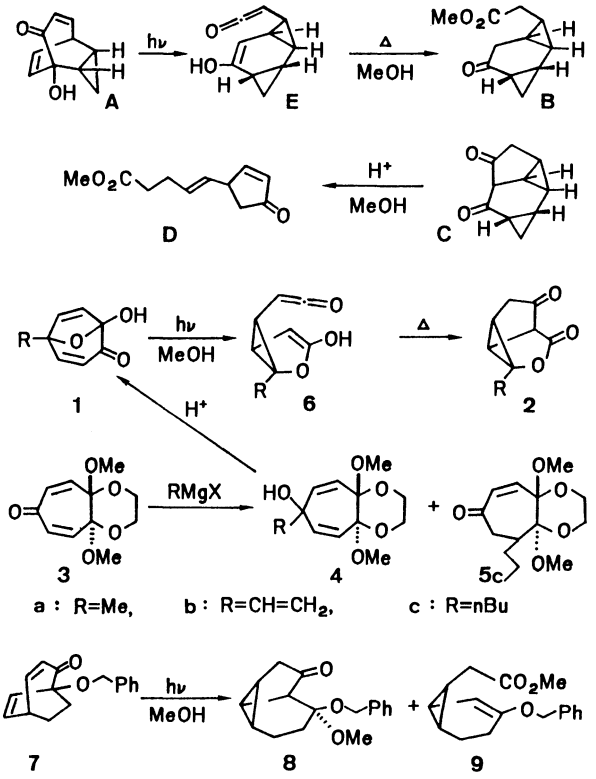

Scheme 1.

The substrates, **1**, were prepared by Grignard reaction of *p*-tropoquinone bisacetal (**3**)[5] followed by an acid hydrolysis of alcohols (**4a**, **4b**, and **4c**) to spontaneously give bicyclic acetals, **1**. In a preparation of **4c**, a by-product, conjugate addition product **5c**, was isolated.

Structural evidence for **1** was obtained from the ^{1}H and ^{13}C NMR spectra; e.g., four vinylic proton signals appeared as two AB-type doublets with J=9.5 and J=5.5 Hz, respectively. Accordingly, **1** can only be explained as the 8-oxabicyclo[3.2.1]octadienone derivative.

When **1a** was irradiated with a 400-W high-pressure mercury lamp in benzene, a single product (**2a**, 57%) was obtained. Its NMR spectrum showed no C=C bond, and its IR spectrum [1790 and 1740 cm^{-1}] showed $\nu_{C=O}$ bands due to γ-lactone and cyclopentanone, but the former was ca. 20 cm^{-1} higher than those of ordinary γ-lactones, suggesting a partial enol lactone character by the π-like cyclopropyl linkage. These allowed us to assign the structure as shown in Scheme 1. In addition, the irradiation of **1a** in methanol only gave **2a** in 49% yield.

Similar irradiations of **1b** and **1c** derivatives in methanol formed corresponding γ-lactones (**2b**, 55%, and **2c**, 81%), but no methanol adduct.

Although adducts were undetectable, the intermediary of the ketene was certain: When the photoreaction of **1a** was carried out in methanol-d_4 at −80 °C, its low-temperature ^{1}H NMR revealed a formation of a new compound **6a** as showing an olefinic proton signal ascribable to a ketene. Warming up the solution to room temperature confirmed the formation of **2a**-d_1, whose yield from **1a** was 93% according to the NMR, which diminished the signal (δ=2.72) of *exo*-H-7 as shown in Fig. 1. Therefore, **6a** must be the ketene.

An apparent contrast to the photolysis of **A**, which gave **C** only in a mixed solution of methanol and acetic acid, is noteworthy. Since we obtained **2** by irradiating **1** in methanol without acetic acid, the Uyehara's proposal, an involvement of acetic acid to form **C**, should not be operative in **1** to **2**. In view of a facile formation of tricyclic compounds, **2**, reinvestigations of the bicyclo[3.2.n]dienones is desirable to understand the generality of the process.

Indeed, an irradiation of 1-benzyloxybicyclo[3.2.2]-nona-3,6-dien-2-one (**7**) in methanol gave 5-benzyloxy-5-methoxytricyclo[4.3.0.0^{2,9}]nonan-7-one (**8**), in 64% yield, together with methyl [3-benzyloxybicyclo[4.1.0]-hept-2-en-7-yl]acetate (**9**), in 9% yield.

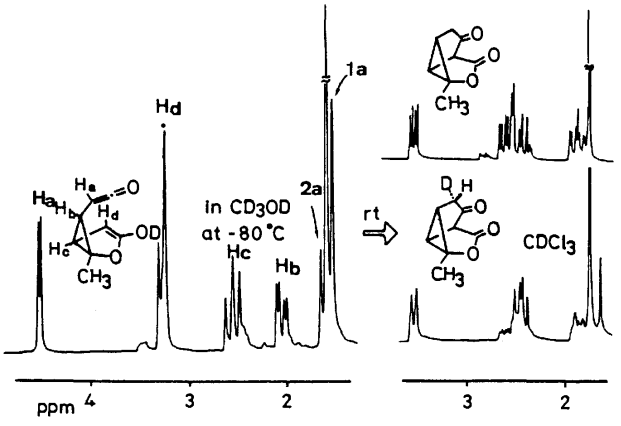

Fig. 1. Low-temperature NMR identification of ketene **6a**. A part of the doublet signal, Hd, overlapped with the solvent signal.

Nevertheless, a replacement of the carbon chain to the oxygen bridge in the vicinity of the hydroxyl group dramatically altered the course of the rearrangement to form cyclopropanes exclusively. The tricyclic derivatives, **2**, will be a good starting material for certain functionalized carbocycles since its rigid carbon skeleton will allow the introduction of various substituents via stereocontrolled reactions.

Experimental

Preparation of 4 (General Method). The starting materials, **4a**, **4b** and **4c**, were prepared from **3** by Grignard reaction. After the ordinary workup by hydrolysis and extraction with ether, the organic extracts were chromatographed on a silica-gel column to give **4** along with **5**.

4a [a colorless oil, 98%. Found: *m/z*, 242.1136. Calcd for $C_{12}H_{18}O_5$: M, 242.1152. ^{1}H NMR $\delta^{6)}$=1.37 (3H, s), 2.28 (1H, br s), 3.24 (3H, s), 3.28 (3H, s), 3.3—3.4 (4H, m), 5.40 (1H, d, J=12.5 Hz), 5.43 (1H, d, J=12.5 Hz), 5.73 (1H, dd, J=12.5, 2 Hz), and 5.83 (1H, dd, J=12.5, 2 Hz). ^{13}C NMR δ=28.5, 49.1, 49.2, 58.6 (2C), 71.5, 96.4, 97.1, 126.8, 127.2, 137.2, and 139.0. IR ν: 3550, 1450, 1400, 1215, 1150, 1090, 1065, and 1000 cm^{-1}].

4b [a pale yellow oil, 69%. Found: *m/z*, 254.1149. Calcd for $C_{13}H_{18}O_5$: M, 254.1151. ^{1}H NMR δ=2.40 (1H, br s), 3.18 (3H, s), 3.27 (3H, s), 3.4—4.2 (4H, m), 5.12 (1H, dd, J=10.2, 1.5 Hz), 5.36 (1H, dd, J=17, 1.5 Hz), 5.22 (1H, d, J=12.5 Hz), 5.47 (1H, d, J=12.5 Hz), 5.65 (1H, dd, J=12.5, 2 Hz), 5.73 (1H, dd, J=12.5, 2 Hz), and 5.83 (1H, dd, J=17, 10.2 Hz). ^{13}C NMR δ=49.1, 49.3, 58.5 (2C), 74.7, 97.4, 96.2, 113.8, 127.7, 127.9, 134.8, 136.7, and 139.8].

4c [a yellow oil, 48%. Found: C, 63.12; H, 8.46%. Calcd for $C_{15}H_{24}O_5$: C, 63.36; H, 8.51%. ^{1}H NMR δ=0.89 (3H, t, J=6 Hz), 1.1—1.5 (4H, m), 1.5—1.8 (2H, m), 2.18 (1H, br s), 3.22 (3H, s), 3.25 (3H, s), 3.3—4.2 (4H, m), 5.45 (1H, d, J=12.5 Hz), 5.47 (1H, d, J=12.5 Hz), 5.72 (1H, dd, J=12.5, 1.5 Hz), and 5.75 (1H, dd, J=12.5, 1.5 Hz). ^{13}C NMR δ=14.0, 23.1, 25.8 (2C), 42.2, 49.2, 58.7 (2C), 73.5, 96.8 (2C), 127.8, 128.9, 136.7, and 138.1. IR ν: 3450, 1450, 1400, 1210, 1145, 1100, 1060, and 1000 cm^{-1}].

5c [a pale yellow oil, 23%. Found: C, 63.30; H, 8.60%. Calcd for $C_{15}H_{24}O_5$: C, 63.36; H, 8.51%. ^{1}H NMR δ=0.90 (3H, t, J=6 Hz), 1.1—1.6 (4H, m), 1.7—2.0 (2H, m), 2.1 (1H, br m), 2.62 (2H, d, J=8 Hz), 3.15 (3H, s), 3.29 (3H, s), 3.4—4.2 (4H, m), and 6.07 (2H, s). ^{13}C NMR δ=14.2, 22.9, 30.9 (2C), 40.1, 45.3, 47.2, 49.2, 58.7, 59.1, 98.8, 100.4, 133.5, 141.2, and 202.7. IR ν: 1680, 1460, 1380, 1215, 1135, and 1090 cm^{-1}].

Hydrolysis of 4 to 1. An acetone solution containing 5% HCl (7 cm^3) of **4** (100 mg) was stirred at room temperature for 30 min. After evaporation of the volatile material in vacuo, the residue was diluted with water and extracted with $CHCl_3$. Silica-gel column chromatography of the extract gave **1**.

1a [a pale yellow oil, 59%. Found: *m/z*, 152.0479. Calcd for $C_8H_8O_3$: M, 152.0474. ^{1}H NMR δ=1.63 (3H, s), 4.49 (1H, br s), 5.61 (1H, d, J=9.6 Hz), 6.16 (1H, d, J=5.4 Hz), 6.74 (1H, d, J=5.4 Hz), and 7.19 (1H, d, J=9.6 Hz). ^{13}C NMR δ=21.4, 85.9, 107.4, 120.7, 133.7, 145.7, 158.1, and 193.2. IR ν: 3400, 1700, 1445, and 1305 cm^{-1}].

1b [a pale yellow oil, 20%. Found: *m/z*, 164.0468. Calcd for $C_9H_8O_3$: M, 164.0471. ^{1}H NMR δ=4.54 (1H, br s), 5.39 (1H, dd, J=10.5, 1 Hz), 5.50 (1H, dd, J=17.5, 1 Hz), 6.12 (1H, dd, J=17.5, 10.5 Hz), 5.64 (1H, d, J=9.6 Hz), 6.27 (1H, d, J=5.9 Hz), 6.76 (1H, d, J=5.9 Hz), and 7.26 (1H, d, J=9.6 Hz). IR ν: 3400, 1700, 1300, and 1180 cm^{-1}].

1c [a yellow oil, 82%. Found: *m/z*, 194.0939. Calcd for $C_{11}H_{14}O_3$: M, 194.0940. ^{1}H NMR δ=0.91 (3H, t, J=6 Hz), 2.1—2.7 (4H, m), 2.7—3.1 (2H, m), 4.65 (1H, br s), 5.60 (1H, d, J=9.5 Hz), 6.14 (1H, d, J=5.8 Hz), 6.70 (1H, d, J=5.8 Hz), and 7.19 (1H, d, J=9.5 Hz). ^{13}C NMR δ=13.9, 22.9, 26.1, 34.5, 89.1, 107.4, 121.0, 133.7, 145.0, 157.7, and 193.5. IR ν: 3400, 1700, 1460, and 1370 cm^{-1}. UV λ_{max}^{MeOH}: 224 nm (ε=2800), 267 (630), and 376 (70)].

Photorearrangement of 1a. a) A benzene solution (2 cm^3) of **1a** (65 mg) was irradiated with a high-pressure mercury lamp for 2 h under an N_2 atmosphere with cooling by water. After evaporation of the solvent, the residue was chromatographed on a silica-gel column to give **2a** [a colorless oil, 37.1 mg; 57%. Found: *m/z*, 152.0468. Calcd for $C_8H_8O_3$: M, 152.0471. ^{1}H NMR δ=1.72 (3H, s), 1.89 (1H, ddd, J=7.5, 6, 1.5 Hz), 2.40 (1H, dd, J=7.5, 5 Hz), 2.43 (1H, dd, J=19.5, 1.5 Hz), 2.72 (1H, ddd, J=19.5, 6, 2.5 Hz), and 3.54 (1H, dd, J=5, 2.5 Hz). ^{13}C NMR δ=18.4, 25.3, 26.6, 32.9, 58.7, 69.9, 172.1, and 206.5. IR ν: 1790, 1740, 1440, 1410, and 1330 cm^{-1}].

b) An MeOH solution (2 cm^3) of **1a** (44 mg) was irradiated under the similar conditions as above. Silica-gel column chromatography of the product gave **2a** [22 mg; 49%].

Photorearrangement of 1b. An MeOH solution (2 cm^3) of **1b** (36.7 mg) was similarly irradiated to give **2b** [a pale yellow oil, 20.1 mg; 55%. Found: *m/z*, 164.0476. Calcd for $C_9H_8O_3$: M, 164.0471. ^{1}H NMR δ=2.15 (1H, ddd, J=7, 6, 2 Hz), 2.34 (1H, dd, J=7, 5 Hz), 2.50 (1H, dd, J=19.5, 2 Hz), 2.78 (1H, ddd, J=19.5, 6, 2.5 Hz), 3.58 (1H, dd, J=5, 2.5 Hz), 6.25 (1H, dd, J=10.5, 1.5 Hz), 6.44 (1H, dd, J=17, 1.5 Hz), and 6.83 (1H, dd, J=17, 10.5 Hz). IR ν: 1800, 1750, 1410, and 1215 cm^{-1}].

Photorearrangement of 1c. Similarly, an MeOH solution (2 cm^3) of **1c** (36 mg) was irradiated to give **2c** [a pale yellow oil, 29.1 mg; 81%. Found: C, 67.75; H, 7.41%. Calcd for $C_{11}H_{14}O_3$: C, 68.02; H, 7.27%. ^{1}H NMR δ=0.92 (3H, t, J=6 Hz), 1.1—1.8 (4H, m), 1.8—2.1 (3H, m), 2.42 (1H, dd, J=19.5, 2 Hz), 2.43 (1H, dd, J=8, 5 Hz), 2.70 (1H, ddd, J=19.5, 6, 2.7 Hz), and 3.52 (1H, dd, J=5, 2.5 Hz). ^{13}C NMR δ=13.9, 22.4, 24.4, 25.6, 27.9, 32.2, 32.8, 58.4, 73.4, 172.2, and 206.4. IR ν: 1800, 1740, 1460, 1410, 1195, 1140, and 1075 cm^{-1}].

Photorearrangement of 1a in Methanol-*d*$_4$. A CD_3OD solution (0.3 cm^3) of **1a** (32 mg) was irradiated at −80 °C for 2 h to observe **6a** [^{1}H NMR (CD_3OD) at −80 °C δ=1.60 (3H, s), 2.05 (1H, dd, J=7.5, 3 Hz), 2.58 (1H, dd, J=7.5, 6.5 Hz), 3.30 (1H, d, J=6.5 Hz), and 4.56 (1H, d, J=3 Hz)]. An ordinary workup of the mixture via silica-gel column chromatography gave **2a**-d_1 [30 mg; 93%].

Diels-Alder Reaction of 2-Benzyloxytropone with Ethylene. A toluene solution (10 cm^3) of 2-benzyloxytropone (1.80 g) saturated with ethylene at 40 bar was placed in an autoclave and heated at 160 °C for 24 h. The mixture was chro-

matographed to give **7** [colorless crystals, mp 67—68 °C, 890 mg; 44%. Found: C, 80.40; H, 6.79%. Calcd for $C_{16}H_{16}O_2$: C, 79.97; H, 6.71%. ^{1}H NMR δ=1.6—2.3 (4H, m), 3.30 (1H, m), 4.75 (2H, s), 5.82 (1H, dd, J=11.5, 0.5 Hz), 6.06 (1H, d, J=9 Hz), 6.48 (1H, dd, J=9, 7 Hz), 7.01 (1H, dd, J=11.5, 8.5 Hz), and 7.2—7.5 (5H, m), ^{13}C NMR δ=24.4, 27.8, 36.5, 66.9, 87.4, 127.4, 127.7 (2C), 128.4 (2C), 128.7, 130.8, 136.7, 139.4, 152.2, and 195.9. IR ν: 1675, 1660, 1630, 1215, 995, and 740 cm^{-1}].

Photolysis of 7 to 8 and 9. An MeOH solution (5 cm^3) of **7** (370 mg) was irradiated with a high-pressure Hg lamp through a Pyrex-glass filter for 6 h. The mixture was then chromatographed on silica-gel column to give **8** [colorless crystals, mp 45—48 °C, 268 mg; 64%. Found: C, 74.74; H, 7.53%. Calcd for $C_{17}H_{20}O_3$: C, 74.97; H, 7.40%. ^{1}H NMR δ=0.7—2.2 (7H, m), 2.28 (1H, dd, J=20, 2 Hz), 2.60 (1H, ddd, J=20, 6, 2 Hz), 3.02 (1H, dt, J=7, 2 Hz), 3.29 (3H, s), 4.48 (2H, s), and 7.2—7.5 (5H, m). ^{13}C NMR δ=14.3, 14.9, 17.0, 18.1, 27.8, 37.7, 48.7, 49.8, 62.6, 65.4, 100.1, 127.6 (2C), 128.6 (2C), 138.8, and 217.9. IR ν: 1740 and 1110 cm^{-1}] and **9** [a colorless oil, 36.9 mg; 9%. Found: C, 74.94; H, 7.42%. ^{1}H NMR δ=1.0—2.4 (9H, m,), 3.64 (3H, s), 4.70 (1H, d, J=4 Hz), 4.73 (2H, s), and 7.29 (5H, m). ^{13}C NMR δ=12.2, 13.9, 18.6, 20.1, 26.3, 29.3, 51.6, 68.7, 91.2, 127.6 (2C), 127.8, 128.6 (2C), 137.6, 157.2, and 174.6. IR ν: 1730, 1710, 1419, and 1170 cm^{-1}].

The authors thank The Ministry of Education, Science, and Culture for a Grant-in-Aid for Scientific Research to H. T. (No. 61540401).

References

1) Part XL. A. Mori, S. Kasai, Y. Isayama, and H. Takeshita, *Kyushu Daigaku Sogo Rikogaku Kenkyuka Hokoku*, **9**, 197 (1987).

2) J. Ciabattoni, J. E. Crowley, and A. S. Kende, *J. Am. Chem. Soc.*, **89**, 2778 (1967); A. S. Kende, Z. Goldschmidt, and P. T. Izzo, *ibid.*, **91**, 6858 (1969).

3) O. L. Chapman, M. Kane, J. D. Lassila, R. L. Loeschen, and H. E. Wright, *J. Am. Chem. Soc.*, **91**, 6856 (1969).

4) T. Uyehara, Y. Kayama, M. Taniguchi, C. Kabuto, and Y. Kitahara, *Chem. Lett.*, **1977**, 569.

5) H. Takeshita, A. Mori, and Y. Isayama, *Bull. Chem. Soc. Jpn.*, **58**, 1678 (1985).

6) The NMR spectra were measured with an FX 100 Spectrometer, JEOL, in $CDCl_3$ solutions. The mass spectra were measured with an OlSG-2 Spectrometer, JEOL.

Volume of Mixing in the Liquid Bismuth-Lead System

Walid Ahmad BADAWI
Department of Chemistry, Faculty of Science, Al-Fateh University, Tripoli, Libya
(Received October 1, 1986)

Synopsis. The results obtained in determining the volume of mixing v^m in the liquid Bi-Pb system at 660 K using the pycnometer method indicate the compound Pb_3Bi_2 at the composition 0.6. The shifting of the slight positive v^m_{max} to the composition 0.4 is attributed to a nonlinear Wagner effect.

The behavior of liquid metallic systems has not yet been thoroughly explored. The theoretical relationships between the thermodynamic functions of metallic mixtures were derived for simple models e.g, the theory by Prigogine[1] which gives the relation of the volume of mixing to the enthalpy of mixing but could not illustrate the behavior of mixing in the liquid bismuth-lead system[2] or other of complicated behaviors.

In the present investigation we report the results obtained in determining the volume of mixing in the liquid Bi-Pb system at 660 K by using the pycnometer method since these results could shed light on the behavior of mixing in the Bi-Pb system and other related binary ones.

Experimental

The metal used were of extra purity grade (E. Merck Company). The experimental procedures adopted were similar to those used earlier.[3] The apparatus employed was a slightly modified version of the type used by Wittig and Huber.[3] Argon gas was used as a protector in order to avoid oxidation.

Theory and Procedure. The additional behavior y^{ad} is given by

$$y^{ad}=y_1^\circ+(y_2^\circ-y_1^\circ)x_2 \tag{1}$$

where y_1° and y_2° are the values of the molar quantities of the components 1 and 2, respectively and x_2 the mole fraction of the component 2. The form function of the excess function, X^y is given through the equation

$$X^y(x_2)=\frac{y^e}{x_2(1-x_2)} \tag{2}$$

y^e refers to the excess quantity. The excess volume and partial excess volumes can be expressed as polynomial functions:

$$v^e(x_2)=\sum_{k,l} a_{kl}\,x_2^k=\sum_{k,l} a_{kl}\,x_2^k(1-x_2)^l \tag{3}$$

$$v_1^e(x_2)=\sum_{k,l}(1-k)\,a_{kl}\,x_2^k \tag{4}$$

$$v_2^e(x_2)=\sum_{k,l}(1-k)\,a_{kl}\,x_2^k+\sum_{k,l} k\,a_{kl}\,x_2^{k-l}. \tag{5}$$

The density d has been computed at the temperature of measurement ϑ from the mass m and the volume of the pycnometer V_{py} as follows:

$$d=m/V^{22.9}\cdot[1+3a(\vartheta-22.9)], \tag{6}$$

where 22.9 °C is the calibration temperature of the pycnometer and a the thermal coefficient of silica glass which is given by

$$a_{SiO_2}=0.59\times10^{-6}\,K^{-1}. \tag{7}$$

Results and Discussion

Results of the density determinations are presented in Table 1. The results have been least squares fitted by the following polynomial expression:

$$d(x_2)=9.9297+0.5003\,x_2+0.2332\,x_2^2-0.0769\,x_3^3. \tag{8}$$

The standard deviation is 0.02% for a single measurement.

In Table 2 are collected the values of the average molar volume of the mixture of Bi-Pb as found in the present study. The results have been least squares fitted by a polynomial expression with a standard deviation of 0.012% for a single measurement. The polynomial expression is given by

$$v(x_2)=21.0458-1.2445\,x_2-0.4103\,x_2^2+0.1805\,x_3^3 \tag{9}$$

Table 3 represents the values of the integral and partial molar volume of mixing as determined in the present study. The volume of mixing can be calculated according to the following equation:

$$v^m=v-v^{ad}=v-v_1^\circ+x_2(v_2^\circ-v_1^\circ) \tag{10}$$

Table 1. Experimentally Determined Densities ($\times10^{-3}$) for Liquid Lead-Bismuth at 660K in kg m^{-3}. Estimated Standard Deviations in Parenthesis

x_2	d	x_2	d
0	9.9318(21)	0.6	10.2994(15)
0.1	9.9839(20)	0.7	10.3656(21)
0.2	10.0404(20)	0.8	10.4417(20)
0.3	10.0967(20)	0.9	10.5148(21)
0.4	10.1643(21)	1.0	10.5882(20)
0.5	10.2305(20)		

Table 2. Average Molar Volumes ($\times10^6$) for the Mixture Bi-Pb in m^3 mol^{-1}. Estimated Standard Deviations in Parenthesis

x_2	v	x_2	v
0	21.0483(25)	0.6	20.1929(26)
0.1	20.9200(26)	0.7	20.0378(23)
0.2	20.7844(25)	0.8	19.8774(25)
0.3	20.6429(26)	0.9	19.7229(25)
0.4	20.4913(26)	1.0	19.5737(23)
0.5	20.3410(25)		

Table 3. Integral and Partial Molar Volume of Mixing ($\times 10^6$) for the Liquid Bi-Pb System at 660 K in $m^3 mol^{-1}$. Estimated Standard Deviations in Parenthesis

x_2	v^m	v_1^m	v_2^m
0	0.0022(22)	0.0000	0.2297
0.1	0.0213(24)	0.0037	0.1569
0.2	0.0285(23)	0.0135	0.1009
0.3	0.0348(24)	0.0272	0.0595
0.4	0.0353(24)	0.0425	0.0308
0.5	0.0325(23)	0.0575	0.0123
0.6	0.0267(23)	0.0697	0.0021
0.7	0.0240(24)	0.0772	−0.0019
0.8	0.0112(23)	0.0778	−0.0022
0.9	0.0035(24)	0.0692	−0.0008
1.0	0.0024(24)	0.0493	0.0000

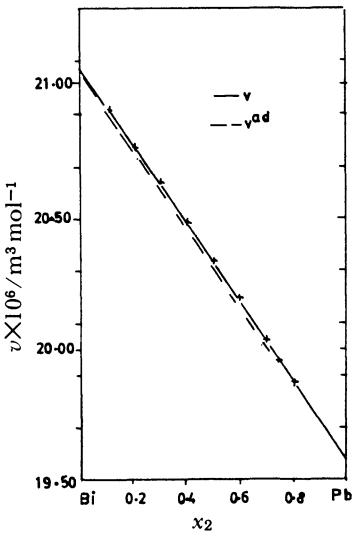

Fig. 1. Average molar volume, v, and additional volume, v^{ad}, for the mixture Bi-Pb.

where v_1° and v_2° are the molar volumes of the pure components 1 and 2, respectively. Figure 1 shows the average molar volume of the mixture, v and the additional volume v^{ad}. For the volume of mixing, the following polynomial expression is derived:

$$v^m = 0.2298\, x_2 - 0.4103\, x_2^2 + 0.1805\, x_2^3 \quad (11)$$

The partial molar volume of mixing of bismuth and lead are given through the following equations:

$$v_1^m = 0.04103\, x_2^2 - 0.3610\, x_2^3 \quad (12)$$

$$v_2^m = 0.2298 - 0.8206\, x_2 + 0.9518\, x_2^2 - 0.3610\, x_2^3 \quad (13)$$

As illustrated in Table 3, the estimated standard deviation (esd.) is not larger than expected from the pycnometer measurement uncertainties, 2.2×10^{-9}, 2.4×10^{-9} $m^3 mol^{-1}$. The plot of v^m versus the mole fraction x_2 is shown in Fig. 2. It is clearly observable that v^m takes slight positive values. The curve of v^m against x_2 and those of v_{Bi}^m and v_{Pb}^m point out to the existence of a compound. This was also recognized from the behavior of the enthalpy and free enthalpy in this system.[4]

According to the Wagner effect,[5] the compound will

Table 4. The Form Function of the Volume of Mixing ($\times 10^6$) for the Liquid Bi-Pb System at 660 K in $m^3 mol^{-1}$. Estimated Standred Deviations in Parenthesis

x_2	X^v	x_2	X^v
0	0.2323(26)	0.6	0.1194(20)
0.1	0.2137(20)	0.7	0.1059(25)
0.2	0.1912(20)	0.8	0.0833(20)
0.3	0.1781(25)	0.9	0.0698(25)
0.4	0.1597(22)	1.0	0.0492[a]
0.5	0.1372(23)		

a) Calculated value.

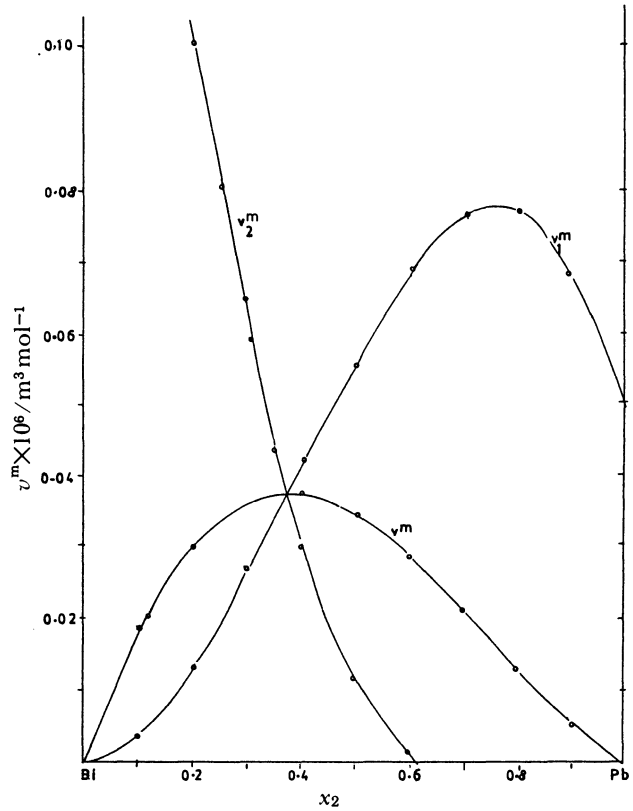

Fig. 2. Integral and partial molar volume of mixing for the liquid Bi-Pb system at 660 K.

be formed as follows: 3 Pb+2 Bi=Pb_3Bi_2. The composition of the compound and also that of the maximum of the volume of mixing, v_{max}^m, will be: 1−2/(2+3)=0.6. However, the Wagner effect requires sufficiently large difference in electronegativity between the acceptor (Bi) and the donor (Pb). In fact, the electronegativity difference between Bi and Pb (0.1—0.12) is not large enough. This could be a reason for the shifting of the maximum of the volume of mixing from the composition 0.6 to 0.4 (Fig. 2). This means that we have here to deal with a nonlinear Wagner effect as found in the systems Zn-Sb[7] and Cd-Bi.[8] A second possibility of the existence of a compound at the composition 0.4 (the composition of v_{max}^m) still remains under investigation.

In Table 4 are listed the values of the form function of the volume of mixing which is given by the follow-

ing linear function:

$$X^{v} = 0.2298 - 0.1805\, x_2 \qquad (14)$$

As given in Table 4, the esd. ranged from 2.0×10^{-9} to 2.6×10^{-9} $m^3\,mol^{-1}$.

References

1) I. Prigogine, A. Belleman, and V. Mathot, "The Molecular Theory of Solutions," Longmans Green, London (1957).
2) B. Predel and W. Schwermann, *Z. Metalk.*, **58**, 553 (1967).
3) F. E. Wittig and F. Z. Huber, *Phys. Chem.*, **18**, 330 (1958).
4) R. Hultgren, P. D. Desai, D. T. Hawkins, M. Gleiser, and K. K. Kelley, "Selected Values of Thermodynamic Properties of Metals and Alloys," Amer. Soc. Metals, Ohio (1973).
5) C. Wagner, "Thermodynamics of Alloys, Reading, Mass.," Addison-Wesley (1952).
6) A. Crawley, *F. Met. Trans.*, **3**, 971 (1972).
7) O. Kleppa, *J. Phys. Chem.*, **64**, 1542 (1960).

One Pot Synthesis of Dinuclear Tungsten(V) Compounds Containing $[W_2XY(\mu\text{-}S)_2]^{2+}$ (X=O, S; Y=O, S) Cores by Thermally Induced Internal Electron-Transfer Processes

Mohammad A. ANSARI, Jayanthi CHANDRASEKARAN, and Sabyasachi SARKAR*
Department of Chemistry, Indian Institute of Technology, Kanpur 208016, India
(Received March 30, 1987)

Synopsis. New synthetic methods for the preparation of dimeric tungsten(V) complexes are described containing the core $[W_2XY(\mu\text{-}S)_2]^{2+}$ (X=O,S; Y=O,S). The synthesized complexes have been characterized by a variety of spectroscopic techniques. $[W_2OS(\mu\text{-}S)_2(S_2CNEt_2)_2]$ has been found to react with cyanide to give $[W_2O_2(\mu\text{-}S)_2(S_2CNEt_2)_2]$.

The tungsten-sulfur chemistry has received far less attention contrary to molybdenum-sulfur systems, partly due to the importance of molybdenum-sulfur systems in biology[1,2] and in catalysis[3,4] and partly due to the facile reactivity of molybdenum systems in terms of synthetic methodology. Recent observations place tungsten parallel to molybdenum in its biological aspects[5] as well as in its catalytic role.[6,7] Thus, there is a surge of new synthetic strategies to explore tungsten-sulfur chemistry.[8-10] But the synthesis of dinuclear tungsten(V)-sulfur complexes invariably involve multistep procedures.[8,10,11] Our present approach to form $[W_2O_2(\mu\text{-}S)_2]^{2+}$ core using externally induced, internal electron transfer reaction,[12] prompted us to search for a one-pot synthetic strategy for this type of complexes. In this paper we report the synthesis of a series of complexes containing $[W_2O_2(\mu\text{-}S)_2]^{2+}$, $[W_2OS(\mu\text{-}S)_2]^{2+}$ and $[W_2S_2(\mu\text{-}S)_2]^{2+}$ core with diethyl dithiocarbamate as ligand invoking intramolecular electron transfer.

Experimental

All the reactions were carried out under dry nitrogen atmosphere and in the absence of light unless otherwise specified. Solvents used were of analytical grade and were distilled before use but not degassed. Pyridine-d_5 (Aldrich) was used as received. Ammonium tetrathiotungstate, oxotrithiotungstate and dioxodithiotungstate were prepared by literature procedure.[13] Diethylammonium tetrathiotungstate and oxotrithiotungstate were prepared by our own method described below.

Infrared spectra were recorded on Perkin Elmer-580 spectrometer as KBr or CsI pressed pellets and referenced to polystyrene bands. Electronic spectra were recorded on Shimadzu UV-190 double beam spectrometer. NMR spectra were taken on Varian EM-390, 90 MHz spectrometer. XPS measurements were done on ESCALAB 510 photoelectron spectrometer using Al$K\alpha$ X-ray line (1486.6 eV) radiation. Binding energies were computed taking C ($1s_{1/2}$) binding energy (285.0 eV) as standard. Carbon, hydrogen, and nitrogen analyses were carried out at Microanalytical Laboratory, I.I.T, Kanpur (India) and sulfur was estimated as $BaSO_4$.

Synthesis of $(Et_2NH_2)_2WS_4$. Tungstic acid (5 g) was dissolved in a mixture of H_2O (10 ml) and Et_2NH (15 ml) by refluxing for 1 h. The solution was filtered and H_2S was passed rapidly for 4 h at 60 °C. The reaction mixture was cooled to obtain yellow crystals, which were washed with 2-propanol and ether. Found: C, 20.71; H, 5.42; N, 6.25%. Calcd for $C_8H_{24}N_2S_4W$: C, 20.86; H, 5.21; N, 6.08%. IR(KBr): ν(W-S) 460 cm^{-1}. Electronic spectrum: λ_{max} (in water) 387 (ε 7400 $dm^3\ mol^{-1}cm^{-1}$) and 277 nm (8100).[13] Yield: 7.36 g (80%).

Synthesis of $(Et_2NH_2)_2WOS_3$. Tungstic acid (5 g) was refluxed in a mixture of H_2O (10 ml) and Et_2NH (10 ml) for 1.5 h, filtered, into which H_2S was passed rapidly for 30 min. at 60 °C. The solution was cooled and to this 2-propanol (50 ml) and ether (20 ml) were added. The yellow orange oily mass obtained was recrystallized from methanol/ether. Found: C, 20.71; H, 5.32; N, 6.28%. Calcd for $C_8H_{24}N_2OS_3W$: C, 21.62; H 5.40; N, 6.30%. IR(KBr) ν(W=O) s, 880, ν(W-S) 450 cm^{-1}. Electronic spectrum λ_{max} (in water) 375 (ε 1400 $dm^3\ mol^{-1}cm^{-1}$), 332 (6150), and 270 nm (6200).[13] Yield: 6.48 g (73%).

Synthesis of $[W_2O_2(\mu\text{-}S)_2(S_2CNEt_2)_2]$ (1): Method A. To a solution of $(Et_2NH_2)_2WOS_3$ (888 mg, 2 mmol) in DMF (10 ml), CS_2 (2 ml) was added and the mixture was refluxed for 4 h. Addition of 2-propanol (10 ml) and ether (100 ml) to the cold solution, precipitated a small amount of green brown product, which was filtered off and the filtrate was kept overnight at room temperature to yield **1** as yellow needle shaped crystals which were washed with water, ethanol and finally with ether. The compound was recrystallized from dichloromethane/petroleum ether. Found: C, 15.90; H, 2.81; N, 3.48; S, 25.31%. Calcd for $C_{10}H_{20}N_2O_2S_6W_2$: C, 15.78; H, 2.63; N, 3.68; S, 25.26%. IR(KBr): ν(C=N) 1550, ν(W=O) 985, 970, ν(WS_2W) 470, 338. Electronic spectrum: λ_{max} (in CH_2Cl_2) 415 (ε 200 $dm^3\ mol^{-1}cm^{-1}$), 332 (1500), and 296 nm (7600), ^1H NMR ($CDCl_3$): δ=3.54 (CH_2, q), 0.95 (CH_3, t). Yield: 290 mg (38%).

Method B. To a hot solution (130 °C) of $(NH_4)_2WO_2S_2$[13] (632 mg, 2 mmol) in DMF (10 ml), tetraethylthiuram disulfide (296 mg, 1 mmol) dissolved in DMF (5 ml) was added and the solution was cooled to 25 °C immediately. Addition of 2-propanol (20 ml) and ether (100 ml) yielded 340 mg (45%) of **1**, which was recrystallized as in method A.

Synthesis of $[W_2S_2(\mu\text{-}S)_2(S_2CNEt_2)_2]$ (2): Method A. A solution of $(Et_2NH_2)_2WS_4$ (920 mg, 2 mmol) in DMF (10 ml) and CS_2 (2 ml) was refluxed for 4 h under nitrogen atmosphere and in the absence of light. To the cold solution (ca. 25 °C), 2-propanol (10 ml) and ether (100 ml) were added. A small amount of dark brown product precipitated. This was filtered off and the filtrate was left at room temperature for 24 h to yield compound **2** as dark red needle shaped crystals, which were washed with water, ethanol, and ether. The crude product was recrystallized from dichloromethane/petroleum ether and further purified by chromatography.[14] Found: C, 15.43; H, 2.40; N, 3.68; S, 28.43%. Calcd for $C_{10}H_{20}N_2S_8W_2$: C, 15.15; H, 2.52; N, 3.53; S, 28.28%. IR (KBr): ν(C=N) 1545, ν(W=S) 535, 525, ν(WS_2W) 460, 332. Electronic spectrum: λ_{max} (in CH_2Cl_2) 420 (ε 2200 $dm^3\ mol^{-1}cm^{-1}$), 382 (6500), and 292 nm (30100), ^1H NMR ($CDCl_3$): δ=3.74 (CH_2, q), 1.08 (CH_3, t). Yield: 220 mg (ca. 28%).

Method B. Tetraethylthiuram disulfide (296 mg, 1 mmol) dissolved in DMF (5 ml) was added to a solution of $(NH_4)_2WS_4$ (696 mg; 2 mmol) in DMF (10 ml) at 130 °C under nitrogen atmosphere. The reaction mixture was cooled immediately to room temperature and 2-propanol (10 ml) and ether (250 ml) were added and kept in the refrigera-

Table 1. Binding Energy (eV) Observed by XPS

Compound	W($4f_{7/2}$)	W($4f_{5/2}$)	S(2p)	S($2s_{1/2}$)	W($4d_{5/2}$)	W($4d_{3/2}$)
$[W_2O_2(\mu\text{-}S)_2(S_2CNEt_2)_2]$	33.9	36.1	163.3	227.0	245.7	259.4
$[W_2S_2(\mu\text{-}S)_2(S_2CNEt_2)_2]$	33.6	35.7	162.8	227.0	245.2	258.0

tor overnight. The crude product thus obtained was purified by chromatography as described in method A. The analytical results and spectral data are in agreement with those shown in method A. Yield: 96 mg (12%).

Synthesis of $[W_2OS(\mu\text{-}S)_2(S_2CNEt_2)_2]$ (3). The same procedure for the preparation of **2** (method A) was followed except that the reaction was carried out in the presence of air. The major product **3** (234 mg, 30%) was obtained after chromatographic purification.[15] However, if method B for synthesis of **2** is followed in the presence of air, **3** is obtained in low yield (90 mg, 12%).[16] Found: C, 15.78; H, 2.50; N, 3.72; S, 26.68%. Calcd for $C_{10}H_{20}N_2OS_3W_2$: C, 15.46; H, 2.57; N, 3.60; S, 26.80%. IR(KBr): ν(C=N) 1555, ν(W=O) 980, ν(W=S) 540, ν(WS_2W) 465, 335. Electronic spectrum: λ_{max} (in CH_2Cl_2) 418 (ε 700 $dm^3\ mol^{-1}\ cm^{-1}$), 352 (4400), and 294 nm (27400). ^1H NMR ($CDCl_3$): δ=3.62 (CH_2, q), 0.98 (CH_3, t). Yield: 90 mg (12%).

Reaction of 3 with KCN. A suspension of **3** (776 mg, 1 mmol); KCN (65 mg, 1 mmol) and Et_4NBr (210 mg, 1 mmol) in chloroform (50 ml), ethanol (15 ml) and water (5 ml) was refluxed for 96 h. The solvents were evaporated under vacuum and the residue was washed with water, methanol and diethyl ether. The bright yellow residue was dried in vacuo and recrystallized from dichloromethane/petroleum ether (yield: 544 mg, 73%). The compound showed identical results to that of **1** in elemental and spectral analysis. The washings gave positive test for thiocyanate.

Results and Discussion

Tungsten(V)-sulfur complexes have generally been prepared by multi-step synthesis.[8,10] Here we report new synthetic methods for their efficient one step preparation. Gradual heating of diethylammonium thiotungstates (WOS_3^{2-}, WS_4^{2-}) with excess CS_2 in DMF affords desired compounds with the overall reaction as shown in Eq. 1:

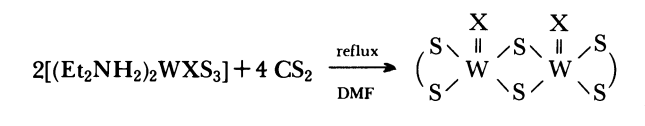

$$2[(Et_2NH_2)_2WXS_3] + 4\,CS_2 \xrightarrow[DMF]{reflux} \left(\begin{array}{ccc} S & X & S \\ \diagdown & \| & \diagup \\ & W & \\ \diagup & & \diagdown \\ S & X & S \end{array}\right) + (Et_2NCS_2)_2 + 4\,H_2S \quad (1)$$

X=O, S; $\left(\begin{array}{c} S \\ \\ S \end{array}\right)$ $= S_2CNEt_2^-$

The formation of H_2S and tetraethylthiuram disulfide (TLC comparison with an authentic sample) as by-products of the reaction suggests the above stoichiometry of the reaction.

In the synthesis of $[W_2S_2(\mu\text{-}S)_2(S_2CNEt_2)_2]$ (**2**), $[W_2OS(\mu\text{-}S)_2(S_2CNEt_2)_2]$ (**3**) is formed as by-product of the reaction, probably as a result of **2** hydrolyzing with traces of moisture present in the reaction medium. The characterization of tetraethylthiuram disulfide as by-product shows that the reaction is a thermally induced redox reaction.

Spectral Studies. The IR, NMR, and electronic spectral studies of these complexes demonstrate the following important points. The strength of tungsten-oxygen bond is greater than that of molybdenum analogues[17] but the reverse has been observed for metal-sulfur bonds. Similar down field shifts of both methyl and methylene protons are observed by the replacement of oxygen by sulfur in the NMR studies. In the electronic spectral studies as expected, the intraligand transitions[18] and ligand to metal charge-transfer transitions[19] are observed. However the intensities of some of these transitions are not as high compared to similar tungsten(V) dimeric complexes.[10,11] Even using other substituted dithiocarbamates, the relative intensities of these transitions differ.[10,11] We do not have any explanations to offer for this discrepancy. The mixing of the orbitals especially between the metal and oxygen/sulfur might control the components of the electric dipolemoment. In the present case, especially with the oxo species probably there is not considerable charge redistribution during the transition for which the intensity of the band is weak.

XPS results have been tabulated in Table 1. In the spectra of $[W_2O_2(\mu\text{-}S)_2(S_2CNEt_2)_2]$ and $[W_2S_2(\mu\text{-}S)_2(S_2CNEt_2)_2]$ a broad band around 163 eV is observed. In the first case, a resolution of the broad band (FWHM 2.87 eV) gives two sets of S(2p) binding energies at 163.1 and 163.5 eV. Thus a distinction can be made between the sulfur attached to two tungstens (163.5 eV) and the sulfur attached to one tungsten and one carbon atom (163.1 eV).[20] For the all sulfur compound **2**, S(2p) band is broader (FWHM 3.1 eV). This extra broadness for this compound compared to **1** suggests the presence of three different types of sulfur, S_{term}, S_{bri}, and S_{dtc}. For tungsten, the XPS shows considerable difference between the binding energies of W($4d_{5/2}$) as well as W($4d_{3/2}$) in $[W_2O_2(\mu\text{-}S)_2(S_2CNEt_2)_2]$ and $[W_2S_2(\mu\text{-}S)_2(S_2CNEt_2)_2]$. The former compound **1** shows more formal positive charge on the metal than the all sulfur compound **2**. This difference may be attributed to the difference in electron population across W=O and W=S bonds. The oxygen being more electronegative withdraws more electron from the metal compared to its sulfur analogue.

Comparison of X-ray powder diffractogram of **1** with its molybdenum analogue $[Mo_2O_2(\mu\text{-}S)_2(S_2CNEt_2)_2]$ suggests that both the compounds are isostructural.[21]

The treatment of **3** with one equivalent of cyanide results in the substitution of terminal sulfur with oxygen affording **1** in high yield, as shown in Eq. 2.

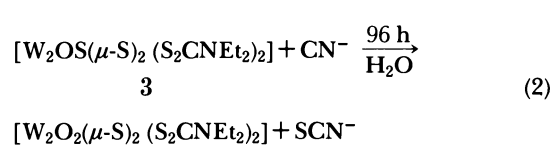

$$[W_2OS(\mu\text{-}S)_2(S_2CNEt_2)_2] + CN^- \xrightarrow[H_2O]{96\ h} [W_2O_2(\mu\text{-}S)_2(S_2CNEt_2)_2] + SCN^- \quad (2)$$

3 1

After extracting **1** from the reaction mixture, the residue was acidified and treated with iron(III) chloride solution. It gave red color, thus confirming the formation of SCN^-. Attempt to replace the bridging sulfur was not successful, by increasing the quantity of CN^- and the reaction time. This suggests that bridging sulfur atoms are more strongly bound with the metal centers than the terminal ones.

We are deeply indebted to Professor Achim Müller, University of Bielefeld, W. Germany for XPS measurements. This work has been supported by Department of Science and Technology, Government of India. M.A.A. thanks CSIR (India) for the award of a senior research fellowship.

References

1) "Molybdenum Chemistry of Biological Significance," ed by W. E. Newton and S. Otsuka, Plenum Press, New York and London (1980).
2) "Current Perspectives in Nitrogen Fixation," ed by A. H. Gibson and W. E. Newton, Elsevier/North-Holland Biomedical Press, Amsterdam, New York, Oxford (1981).
3) "Proceedings of the Second International Conference on the Chemistry and Uses of Molybdenum," ed by P. C. H. Mitchell and A. Seaman, Climax Molybdenum Co., London, England (1977).
4) W. Eltzner, M. Breysse, M. Lacroix, and M. Vrinat, "Proceedings of the Fifth International Conference on the Chemistry and Uses of Molybdenum," P. C. H. Mitchell and A. G. Sykes, *Polyhedron*, **5**, 203 (1986).
5) I. Yamamoto, T. Saiki, S. M. Liu, and L. G. Ljungbahl, *J. Biol. Chem.*, **258**, 1826 (1983), and references therein.
6) "Proceedings of the Climax Fourth International Conference on the Chemistry and Uses of Molybdenum," ed by H. F. Barry and P. C. H. Mitchell, Climax Molybdenum Co., Ann. Arbor, MI (1982).
7) E. I. Stiefel and R. R. Chianelli, "Nitrogen Fixation," ed by A. Müller and W. E. Newton, Plenum Press, New York (1983), pp. 341—369 and references therein.
8) S. S. Cohen and E. I. Stiefel, *Inorg. Chem.*, **24**, 4657 (1985).
9) W.-H. Pan, M. E. Leonowicz, and E. I. Stiefel, *Inorg. Chem.*, **22**, 672 (1983).
10) R. Lozano, E. Alarcon, A. L. Doadrio, and A. Doadrio, *Polyhedron*, **2**, 435 (1983).
11) R. Lozano, E. Alarcon, J. Roman, and A. Doadrio, *Polyhedron*, **8**, 1021 (1984).
12) S. Sarkar and M. A. Ansari, *J. Chem. Soc., Chem. Commun.*, **1986**, 324.
13) J. W. McDonald, G. D. Friesen, L. D. Rosenhein, and W. E. Newton, *Inorg. Chim. Acta*, **72**, 205 (1982).
14) Chromatography on silica gel (dichloromethane-petroleum ether mixture, 75 : 25) yielded **1** as the major product and further elution afforded **2** (4%) as a minor product.
15) Chromatography on silica gel (dichloromethane pet. ether mixture 75 : 25) yielded first the minor product, **1** (50 mg, 6%) and then the desired compound as major product and then a third compound **3** (15 mg, 2%).
16) This method also gives **3** and **1** by chromatographic separation, with yields 60 mg (8%) and 75 mg (10%), respectively.
17) W. E. Newton, J. W. McDonald, K. Yamanouchi, and J. H. Enemark, *Inorg. Chem.*, **18**, 1621 (1979).
18) Electronic spectrum of sodium diethyl dithiocarbamate in EtOH shows three bands in the UV region at 257, 290, and 340 nm.
19) W. Jaegermann, Ph. D. Thesis, University of Bielefeld, W. Germany (1981).
20) K. Siegbahn, C. Nordling, G. Johanson, J. Hedman, P. F. Heden, K. Hamrin, U. Gelius, T. Bergmark, L. O. Werme, R. Manne, and Y. Baer, "ESCA Applied to Free Molecules," North-Holland Publishing Company, Amsterdam-London (1969).
21) R. Winograd, B. Spivack, and Z. Dori, *Cryst. Struct. Commun.*, **5**, 373 (1976).

Ion-Exchange Rate of Chromate and Dichromate Ions on Bis(triethylamine)zirconium

J. P. RAWAT* and CHITRA
Department of Chemistry, Aligarh Muslim University, Aligarh-202001, India
(Received May 6, 1987)

Synopsis. Kinetic studies of $K_2Cr_2O_7$ and K_2CrO_4 have been performed on an inorganic anion exchanger, bis(triethylamine)zirconium in Cl^- form. *F* values have been determined at four different temperatures 30, 40, 50, and 60 °C with ±1 °C variation and corresponding *Bt* values are evaluated and plotted as a function of temperature. The mechanism is found to be particle diffusion control. Various parameters viz. effective diffusion coefficient (D_i), diffusion coefficient (D_o), energy of activation (E_a), and entropy of activation (ΔS^*) have been evaluated.

Some studies on kinetics of ion exchange on inorganic ion exchangers have been reported.[1-9] The present report summarizes the kinetic studies for ion-exchange rate of chromate and dichromate ions on bis-(triethylamine)zirconium. Experimental and theoretical approaches have been used to show that the rate determining step is the diffusion through the particles. The energy of activation and other parameters are calculated.

Experimental

Synthesis of Ion-Exchange Material. Bis(triethylamine)-zirconium was prepared by mixing 0.1 M† zirconium dichloride oxide and 0.1 M triethylamine solution in the volume ratio of 1:2. After 24 h it was filtered, washed and dried in an incubator at 40±1 °C. The product was then broken down into small particles by immersing in water. Exchanger was kept in 1.0 M NaCl solution to convert it in chloride form. It was then washed and dried again at 40±1 °C.

Kinetic Measurements. Limited bath technique was applied to perform the kinetic measurements. The exchanger was finely ground and sieved into particles of different mesh sizes (30—50, 50—100, and 100—150) by using the U.S. standard mesh sieves. In all the cases studied, particles of 50—100 mesh were used, unless otherwise stated. In stoppered conical flasks 4 ml of standard anionic solutions of 0.02 M were shaken with exchanger (0.2 g) in a temperature controlled shaker (Sew India) at various temperatures at a frequency of 120 RPM. The pH of 0.02 M $K_2Cr_2O_7$ solution was 4.6 and that of K_2CrO_4, 8.2. After appropriate intervals of time, the solutions were filtered through Whatman No. 42 filter paper. The amount of $Cr_2O_7^{2-}$ and CrO_4^{2-} ions were determined iodometrically.[10] Kinetic experiments were performed at 30, 40, 50, and 60 °C with ±1 °C variation. Interruption test was performed in the similar way at 30 °C. After 20 min the solutions were separated from the exchanger and reimmersed after 10 min. The metal ion contents were determined at different intervals of time.

Results and Discussion

Interruption test for $Cr_2O_7^{2-}$ ion was used as an experimental test to decide whether the kinetics is controlled by film diffusion or particle diffusion. The results of interruption test (Fig. 1) show that rate of exchange increases after 10 min interruption. This indicates that mechanism should be particle diffusion. This is because the concentration gradients disappear in the particle during the interruption and are much greater than before at the surface.

Equations developed by Boyd et al.[11] and improved by Reichenberg[12] were used to obtain kinetic parameters. *F* values at different time intervals and temperatures were obtained for $Cr_2O_7^{2-}$-Cl^- exchange and plotted in Fig. 2. These results show that the rate of exchange increases with temperature. The uptake of ion is rapid initially but it decreases with the elapse of time. Similar behavior was shown by CrO_4^{2-} ion.

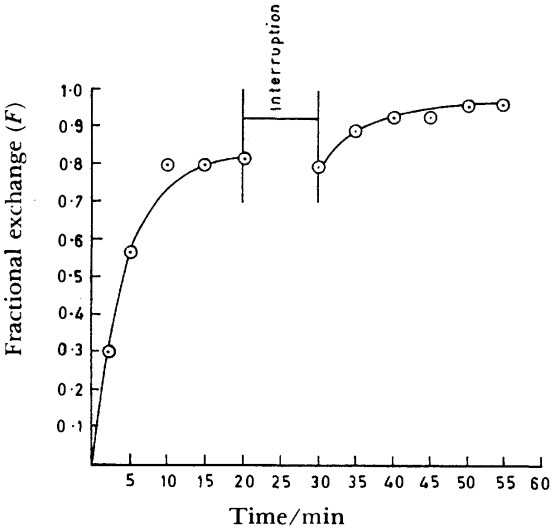

Fig. 1. Effect of an interruption test on the rate of $Cr_2O_7^{2-}$-Cl^- exchange on zirconium bis(triethylamine) at 30 °C.

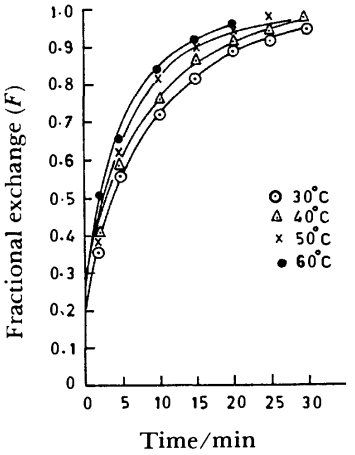

Fig. 2. Rate of exchange of $Cr_2O_7^{2-}$ at different temperatures on zirconium bis(triethylamine).

† 1M=1 mol dm^{-3}.

$$F = \frac{\text{amount of exchange after time } t}{\text{amount of exchange after infinite time (equil.)}}$$

For the limited bath technique the equations developed by Boyd et al.[11] can be used here

$$F = 1 - \frac{6}{\pi^2} \sum_{n=1}^{\infty} \frac{1}{n^2} \exp(-n^2 Bt), \quad (1)$$

where $$B = \frac{\pi^2 D_i}{\gamma^2}. \quad (2)$$

D_i is the effective diffusion coefficient, γ is the radius of the particle. Bt values were evaluated from the F values from the table of Reichenberg.[12] A typical Bt vs. t plot for $Cr_2O_7^{2-}$ ion (Fig. 3) at four different temperatures indicates that the plots are straight lines passing through the origin. The results confirm that the rate determining step is diffusion through the particle.

The particle size also has a marked influence on the rate of exchange which can be shown by the Bt vs. t plot for $Cr_2O_7^{2-}$ ion for three different particle radii at 40±1 °C (Fig. 4). The rate of exchange is inversely proportional to the square of the particle radius (Fig 5). The radius of the particles was calculated by the mesh size using the conversion table.[13] For this purpose the lower limit mesh corresponding to higher limit radius was taken instead of taking a mean radius. The higher limit radius was considered by keeping the view of slight swelling of the exchanger particles.

Equation 2 was used for the calculation of D_i. A linear relationship was obtained on plotting log D_o against T^{-1}/K (Fig. 6) assuming the Arrhenius equation

$$D_i = D_o \exp(-E_a/RT). \quad (3)$$

On extrapolating the plot of log D_i against T^{-1}/K, log

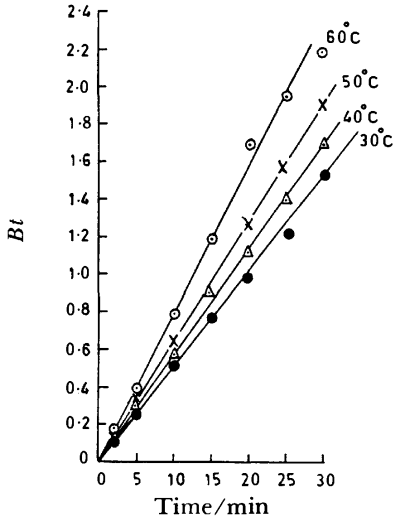

Fig. 3. Influence of temperature on the rate of exchange for $Cr_2O_7^{2-}$ ion using zirconium bis(triethylamine) r=0.015 cm.

Table 1. Diffusion Coefficient, D_o, Energy of Activation, E_a and Entropy of Activation, ΔS^*, of $Cr_2O_7^{2-}$ Ions on Bis(triethylamine)zirconium in Cl^- Form

Migrating ion	D_o	E_a	ΔS^*
	$m^2\,s^{-1}$	$kJ^{-1}mol^{-1}$	$JK^{-1}mol^{-1}$
$Cr_2O_7^{2-}$	5.01×10^{-7}	25.42	−25.72
CrO_4^{2-}	5.01×10^{-7}	23.89	−25.72

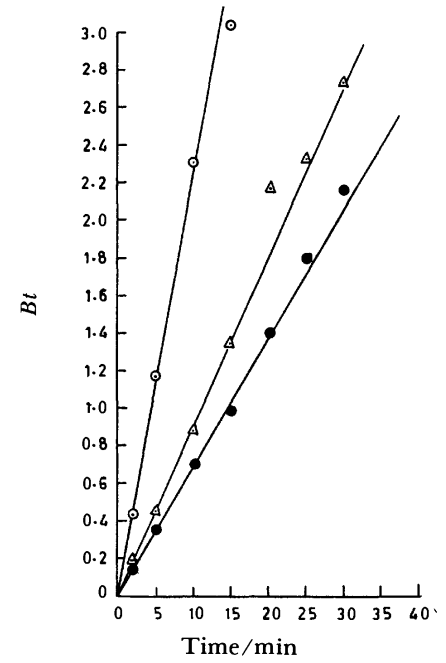

Fig. 4. Effect of particle size on the rate of exchange for $Cr_2O_7^{2-}$-Cl^- on zirconium bis(triethylamine). △ 0.015 cm, ● 0.030 cm, ⊙ 0.0075 cm.

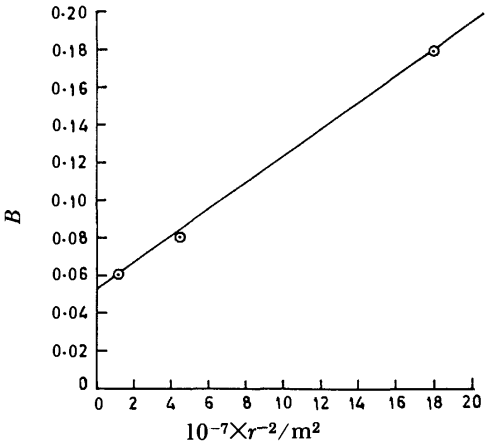

Fig. 5. Plots of B vs. r^{-2} for $Cr_2O_7^{2-}$ at 40 °C.

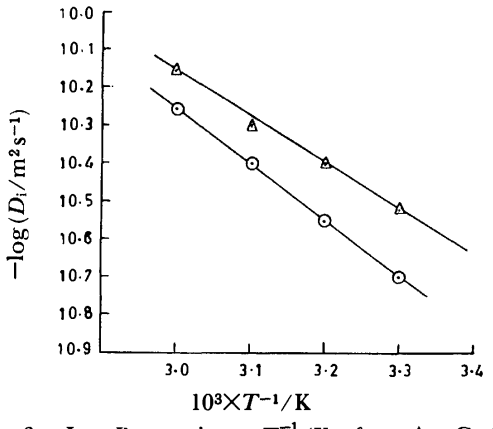

Fig. 6. Log D_i against T^{-1}/K for △ $Cr_2O_7^{2-}$, ⊙ CrO_4^{2-}.

D_o values are calculated. Substitution of these values in the following equation gives entropy of activation, ΔS^*

$$D_o = 2.72\, d^2\, KT/h \exp(\Delta S^*/R) \quad (4)$$

where d is the ionic jump distance assumed equal to 5×10^{-10} m (1), K the Boltzman constant, h Planck's constant, and R the gas constant. The values of E_a, D_o, and ΔS^* are given in Table 1.

References

1) S. J. Harvie and G. H. Nancollas, *J. Inorg. Nucl. Chem.*, **30**, 272 (1968).
2) A. Dyer and F. T. Ocon, *J. Inorg. Nucl. Chem.*, **33**, 3153 (1971).
3) A. Dyer and J. S. Gill, *J. Inorg. Nucl. Chem.*, **39**, 665 (1977).
4) K. Bunzyl, *J. Inorg. Nucl. Chem.*, **39**, 1045 (1977).
5) J. P. Rawat and P. S. Thind, *J. Phys. Chem.*, **80**, 1384 (1976).
6) J. P. Rawat and D. K. Singh, *J. Inorg. Nucl. Chem.*, **40**, 897 (1978).
7) J. P. Rawat and M. A. Khan, *J. Inorg. Nucl. Chem.*, **42**, 905 (1979).
8) K. G. Varshney, A. A. Khan, K. Varshney, and S. Agrawal, *Solvent Extraction and Ion Exchange*, **2**, 923 (1984).
9) Y. Baba, S. Doi, K. Inoue, and I. Nakamori, *Solvent Extraction and Ion Exchange*, **3**, 741 (1985).
10) I. M. Kolthoff and Philip J. Elving, "Treatise on Analytical Chemistry," Part II, John Wiley and Sons, Inc., New York—London, Vol. 8, p. 330.
11) G. E. Boyd, A. W. Adamson, and L. S. Myers, *J. Am. Chem. Soc.*, **69**, 2836 (1947).
12) D. Reichenberg, *J. Am. Chem. Soc.*, **75**, 589 (1953).
13) F. G. Helfferich, "Ion Exchange," McGraw-Hill Book Co., New York (1962), p. 513.

Carbon-13 NMR of *N*-Substituted 2,4,6-Trimethylpyridinium Salts

Salman R. SALMAN,* A. H. HASSAN, and M. A. R. KHAYAT†
Chemistry Department, College of Science, University of Baghdad, Baghdad, Iraq
†Chemistry Department, College of Science, Al-Mustansiriyah University, Baghdad, Iraq
(Received June 9, 1987)

Synopsis. Carbon-13 chemical shifts of twelve *N*-substituted, 2,4,6-trimethylpyridinium (TMP) salts were determined. The data have been used to estimate the relative ring current (RRC) of the *N*-substituents on the pyridinium ring.

Verhoeven et al.[1-5] studying the UV spectra of some substituted pyridinium salts has pointed out that when R=phenyl, their UV spectra display a charge transfer band. Balaban et al.[6,7] utilized the proton NMR spectral data of some *N*-substituted TMP salts to estimate the relative ring current (RRC) of these systems.

Carbon-13 chemical shift, recieved little attention in this respect.[8,9] In this paper twelve new *N*-substituted TMP perchlorates (Scheme 1) were prepared[10] and their carbon-13 chemical shifts have been determined. Equation 2 is suggested for calculating RRC of the R group, using carbon-13 chemical shift of carbons 2 and 4.

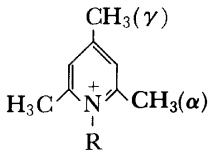

Results and Discussion

Proton decoupled, as well as proton-coupled, carbon-13 spectra of the compounds **1—12** were recorded. Assignment of the chemical shift of these compounds (Tables 1 and 2) are based on; (i) the application of carbon-13 chemical shift of amines (RNH_2),[11] (ii) by applying the additivity rule, and substitution parameters, for the phenyl,[12,13] and the pyridinium rings,[14] and (iii) using off-resonance spectra of those compounds to determine the quaternary and protonated carbons.

Table 1 shows the trend of carbon-13 chemical shift of carbon 2,6, and the methyl carbons. It demonstrates the pronounced ring current effect of the N-aza aromatic ring on the chemical shift of those carbons.

It is accepted that analogous compounds are not coplanar.[15] Thus the α-methyl and carbons 2 and 6 are exposed to the ring current of the R substituent.

Equation 1[6] has been applied to calculate RRC using ^{1}H-chemical shift of compounds **6—12** (Table 3). The results are given in Table 3.

$$\mathrm{RRC} = 200\,(D + 0.25) - T \qquad (1)$$

where $T = 71.7\,x/(1+2.26\,x)$, x=the number of ortho substituents in R.

$$D = \delta_{(\gamma\text{-methyl})} - \delta_{(\alpha\text{-methyl})}$$

Furthermore Eq. 2 is suggested by us, as an extention, to calculate (RRC) using carbon-13 chemical shift of carbons 2 and 4.

Equation 1 was used as a basis to derive Eq. 2 which use carbon-13 chemical shift of carbon 2 and 4 for calculating the RRC. In Eq. 2 T have the same definition as in Eq. 1, and D is given as

$$\delta_{4,2} = D = \delta\,(\text{carbon 4}) - \delta\,(\text{carbon 2}). \qquad (1a)$$

When R=H, there is no ring current affecting carbons 2 and 4. The value of δ_4 and δ_2 in 2,4,6-trimethylpyridinium salt is 147.4 and 157.4 ppm,[16] therefore $\delta_{4,2}$ (−10 ppm) in this compound represents a correction factor for the D values in compounds **5—12**. Equation 1 could be modified as Eq. 1b by taking into account the above $\delta_{4,2}$ value.

$$\mathrm{RRC} = a\,(D + 10) - T. \qquad (1b)$$

Using compound **5** as a reference (compound) where RRC=100, and D=5.22 ppm (Table 2), applying those values to Eq. 1b, one obtain a value for a=6.57. Thus Eq. 2 could be written as

$$\mathrm{RRC} = 6.57\,(D + 10) - T. \qquad (2)$$

The calculated RRC values for compounds **6—12** are given in Table 3.

As it is expected $\delta_{C\text{-}2}$ and $\delta_{C\text{-}4}$ are affected by the nature of R. The difference between $\delta_{C\text{-}2}$ and $\delta_{C\text{-}4}$ increases in compounds **7—9** (Table 1). This increase might be due to a slight change in ring current of R, which shields C-2 in compounds **5—12** relative to compounds **1—4** (Table 1). These results are consistent with available data, emphasizing the leterature reports that the α-methyl, C-2 and C-6 are oriented in the shielding region of the aromatic ring.[17] It is obvious that the RRC effect decreases when there is one ortho substituent on R (compound **6**), or when there is a bulky substituent (compounds **10—12**, Table 1). This might suggest a change of the dihedral angle between the two rings relative to that in compound **5**. It seems that RRC calculated from carbon-13 chemical shift for compounds **6—12** is more realistic than that obtained from ^{1}H chemical shift because the steric crowdening will change the dihedral angle thus decrease the RRC. On this basis one expects that the RRC will have a maximum value when R=phenyl (Table 3). This may be explained on the basis that as ortho substituent on R ring increases, the methyl group, carbons 2 and 4 become less exposed to the ring current of R, thus RRC decreases for those compounds relative to compound **5**. A rather interesting case is that of compound **2** whose $\Delta\delta_{4,2}$=0.71 ppm. This value is appreciably different from those of compounds **1**, **3**, and **4** (Table 1). Such apparent inconsistency may be interpreted in terms of the deshielding

Table 1. Chemical Shifts (ppm) of 2,4,6-Trimethylpyridinium

	R	δ_2	δ_3	δ_4	$\delta_{CH_3(\alpha)}$	$\delta_{CH_3(\gamma)}$	$\Delta\delta_{4,2}$	$\Delta\delta_{\gamma,\alpha}$	$\Delta\delta_2^*$	$\Delta\delta_4^*$	$\Delta\delta_\alpha^*$	$\Delta\delta_\gamma^*$
1		154.79	127.42	156.83	20.85	21.05	2.04	0.20	0.0	0.0	0.0	0.0
2		156.89	127.91	157.60	20.99	21.53	0.71	0.54	2.10	0.77	−0.14	0.48
3		154.18	129.57	156.90	20.51	22.04	2.72	1.53	−0.61	0.07	0.34	0.99
4	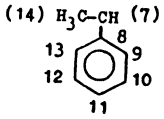	154.67	129.45	158.63	21.16	22.29	3.96	1.14	−0.12	1.80	−0.31	1.24
5	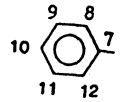	154.03	127.34	159.25	21.34	21.59	5.22	0.25	−0.76	2.42	−0.49	0.54
6	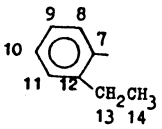	153.85	127.78	159.69	20.86	21.98	5.84	1.12	−0.94	2.86	0.01	0.93
7	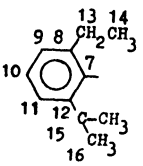	153.75	128.32	160.15	20.40	21.27	6.40	0.87	−1.04	3.32	0.45	0.22
8	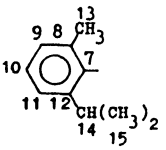	153.54	128.34	160.12	20.19	21.26	6.58	1.07	−1.25	3.29	0.66	0.21
9	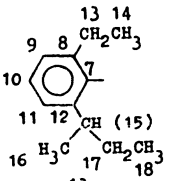	153.86	128.32	160.28	20.51	21.36	6.42	0.85	−0.93	3.45	0.34	0.31
10	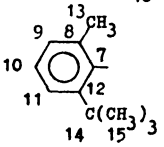	154.77	128.44	160.78	20.50	21.59	6.02	1.09	−0.02	3.95	0.35	0.54
11	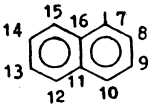	154.98	127.90	159.98	20.50	21.47	5.00	0.97	0.19	3.15	0.35	0.42
12	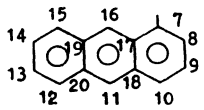	154.94	127.98	159.71	20.39	21.44	4.77	1.05	0.15	2.88	0.46	0.39

$\Delta\delta_x=\delta_x$ (compound **1**)$-\delta_x$(other compounds).

Table 2. Carbon-13 Chemical Shift (ppm) of the R Substituents

Compd.	δ_7	δ_8	δ_9	δ_{10}	δ_{11}	δ_{12}	δ_{13}	δ_{14}	δ_{15}	δ_{16}	δ_{17}	δ_{18}	δ_{19}	δ_{20}
1	39.59													
2	36.00	10.95	10.95											
3	64.86	29.85	24.74	24.74	29.85									
4	62.58	136.32	130.30	125.12	128.42	125.12	130.30	17.04						
5	137.71	124.96	130.58	130.73	130.58	124.96								
6	136.81	136.17	131.21	128.27	129.85	125.00	21.98	12.42						
7	141.90	133.81	131.46	125.71	127.19	136.46	23.20	12.35	27.37	22.25				
8	142.04	131.07	131.28	125.78	129.59	134.37	27.19	23.19	16.50					
9	141.41	134.16	131.43	127.22	128.46	136.81	22.37	12.42	34.42	20.25	29.83	11.44		
10	142.72	132.26	130.94	129.79	130.44	134.06	36.45	31.47						
11														
12														

Table 3. Proton Chemical Shifts (ppm) of α and γ Methyl Protons and Relative Ring Current

Compd.	$\delta_{CH_3(\alpha)}$	$\delta_{CH_3(\gamma)}$	$\Delta\delta_{\gamma\cdot\alpha}$	T	RRC Eq. 1	RRC Eq. 2
1						
2						
3						
4						
5	2.31	2.56	0.25	0	100	100
6	2.25	2.62	0.63	22	84	82
7	2.30	2.64	0.34	26	96	82
8	2.24	2.65	0.41	26	106	83
9	2.28	2.64	0.36	26	96	81
10	2.34	2.63	0.29	26	82	79
11	2.37	2.76	0.39	22	106	99
12	2.41	2.80	0.39	22	104	97

effect of the σ-ring current of the strained cyclopropyl ring on carbon 2.

Experimental

2,4,6-Trimethylpyrylium salts were prepared by reported procedures.[18,19] They were reacted with aliphatic primary amines to produce compounds **1—4**,[10] and with aromatic amines to yield compounds **5—12**. Carbon-13 spectra were recorded as 20 mol% solution in DMSO-d_6 in 5 mm NMR tubes. Optimum amount of TMS was added to the samples to act as internal reference. The proton-decoupled and proton-coupled carbon-13 NMR spectra were recorded on Varian FT 80 A operating at 20 MHz. The spectral width was 4 KHz, pulse width, 8 μs (θ=45°); aquisition time 1 s, pulse delay 2 s. Chemical shift were accurate to better than 0.06 ppm. The proton spectra were recorded for 5 mol% solution in $CDCl_3$ in 5 mm NMR tubes. TMS was added as internal reference. Varian FT 80 A operating at 80 MHz used to record the proton spectra.

References

1) J. W. Verhoeven, I.P. Dirkx, and T. J. Deboer, *Tetrahedron Lett.*, **1966**, 4399.

2) J. W. Verhoeven, I. P. Dirkx, and T. J. Deboer, *Tetrahedron*, **25**, 3395 (1969).

3) A. J. Degee, J. W. Verhoeven, I. P. Dirkx, and T. J. Deboer, *Tetrahedron*, **25**, 3407 (1969).

4) J. W. Verhoeven, I. P. Dirkx, and T. J. Deboer, *Tetrahedron*, **25**, 4037 (1969).

5) J. W. Verhoeven, I. P. Dirkx, and T. J. Deboer, *J. Mol. Specty.*, **36**, 284 (1970).

6) A. T. Balaban, A. Dinculescu, H. N. Koutrakis, and F. Chiraleu, *Tetrahedron Lett.*, **1979**, 437.

7) A. T. Balaban and J. Pure, *Appl. Chem.*, **54**, 1075, 1085 (1982).

8) R. Maria and J. Elguero, *Collect. Czech. Chem. Commun.*, **46**, 584 (1981).

9) A. T. Balaban, A. Dinculescu, J. Elguero, and R. Faure, *Mag. Reson in Chem.*, **23**, 553 (1985).

10) A. H. Hassan, M. Sc. Thesis, Chemistry Department, College of Science, University of Baghdad, 1983.

11) F. W. Wehrli, "Interpretation of Carbon-13 Spectra," Heyden, London (1976); G. C. Levy, R. L. Lichter, and G. L. Nelson, "Carbon-13 NMR Spectroscopy," John Wiley & Son, New York (1980); P. E. Hansen, *Org. Mag. Reson.*, **12**, 109 (1979).

12) D. F. Ewing, *Org. Mag. Reson.*, **12**, 499 (1979).

13) J. W. Stothers, "Carbon-13 NMR Spectroscopy," Academic Press, New York (1972), pp. 111, 250.

14) M. Shamma and D. M. Hindelang, "Carbon-13 NMR Shift Assignment of Amines and Alkaloides," Plenum Press, New York (1979).

15) A. Camerman, L. H. Jensen, and A. T. Balaban, *Acta Crystallogr., Sect. B*, **25**, 2623 (1969).

16) M. Shamma and D. M. Hindenlang, "Carbon-13 NMR Shift Assignments of Amines and Alkaloids," Plenum Press, New York (1979).

17) L. M. Jackman and S. Sternhell, "Application of NMR Spectroscopy in Organic Chemistry," 2nd ed, Pergamon Press, London (1969), pp. 95—98.

18) A. R. Katritzky and S. S. Thind, *J. Chem. Soc., Perkin Trans. 1*, **1980**, 1895.

19) A. T. Balaban, A. Dinculescu, J. N. Dorofeenko, J. W. Fischer, A. V. Koblik, V. V. Mezheritskii, and V. Schrotr, "Pyrylium Salts, Syntheses, Reactions, and Physical Properties," Advances in Heterocyclic Chemistry, Supplements 2 ed. A. R. Katritzky, Academic Press, London (1982).

Synthesis and Properties of Three Sulfur-Containing Porphyrins, One Water-Soluble

Nirmalendu DATTA-GUPTA,* Debasis MALAKAR, Celestine JENKINS, and Cynthia STRANGE
Department of Natural Sciences, South Carolina State College Orangeburg, South Carolina 29117, U.S.A.
(Received February 7, 1987)

Synopsis. Three new porphyrins with sulfur functional groups, one of which is water-soluble, have been prepared. Their UV-visible absorption, fluorescence emission, and ^{1}H NMR spectra as well as their copper(2+) insertion kinetics, pK_3 values and first and second reduction potentials determined. For the water soluble porphyrin, its binding with human serum albumin (HSA) determined.

In recent years several water-soluble synthetic porphyrins and metalloporphyrins have been studied as photosensitizers and radiation modifiers,[1-3] as DNA intercalators,[4-6] as binder with protein macromolecules,[7,8] and as tumor localizers.[9,10] Widely studied among these porphyrins are 5,10,15,20-tetrakis(4-sulfonatophenyl)porphyrin (4TSPP), 5,10,15,20-tetrakis(4-carboxyphenyl)porphyrin (4TCPP), 5,10,15,20-tetrakis(1-methyl-4-pyridinio)porphyrin (4TMPyP) and 5,10,15,20-tetrakis[4-(trimethylammonio)phenyl]porphyrin (4TAPP) and some of their metal complexes. The same porphyrins are also under study as sensitizers in photochemical systems for solar energy conversion.[11,12] In addition to the above, other water soluble porphyrins, namely, 5,10,15,20-tetrakis(2-carboxyphenyl)porphyrin (2TCPP), 5,10,15,20-tetrakis(3-carboxyphenyl)-porphyrin (3TCPP), 5,10,15,20-tetrakis(1-methyl-2-pyridinio)porphyrin (2TMPyP) and 5,10,15,20-tetrakis(1-methyl-3-pyridinio)porphyrin (3TMPyP) are known. Some of these are difficult to synthesize and purify. Besides, porphyrins with four negative charges usually remain as dimer in solution.[13] Therefore, it was felt that new water-soluble prophyrins with four positive charges should be prepared for studying the earlier mentioned important biological, biochemical, and photochemical properties. We report here the synthesis of three sulfur containing porphyrins and their physicochemical properties. They are 5,10,15,20-tetrakis[*p*-(methylthio)phenyl]porphyrin (**3**), 5,10,15,20-tetrakis[*p*-(methylsulfonyl)phenyl]-porphyrin (**4**), and 5,10,15,20-tetrakis[(*p*-ethylmethylsulfonio)phenyl]porphyrin perchlorate (**5**). Porphyrin **5** is water-soluble.

Experimental

The porphyrin **3** was obtained by refluxing equimolar amounts of pyrrole (**1**) and *p*-(methylthio)benzaldehyde (**2**). Upon reacting **3** with excess *m*-chloroperbenzoic acid in dichloromethane, porphyrin **4** was obtained. Porphyrin **5** was obtained by refluxing **3** with excess triethyloxonium tetrafluoroborate in DMF, followed by removal of DMF, dissolving the residue in water and saturating with solid $NaClO_4$.

UV-visible absorption and fluorescence emission spectra were measured on a SLM/AMINCO DW2C and SLM 4800S

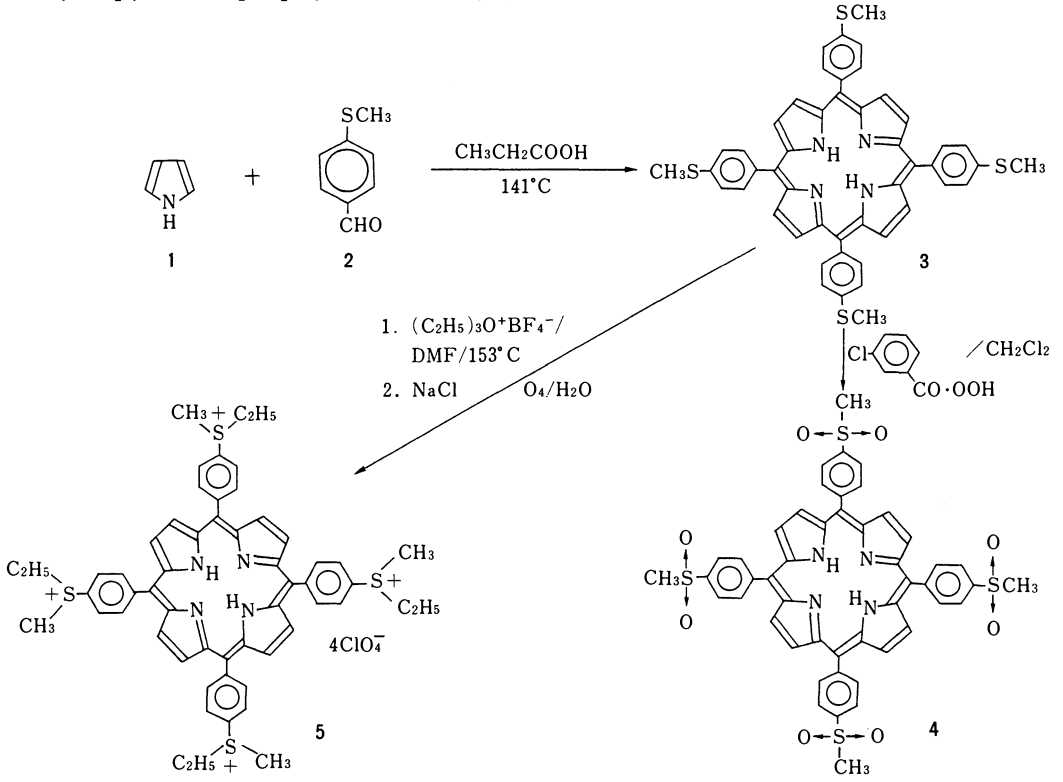

Table 1. UV-Visible Absorption Spectral Data in DMF

Porphyrin	λ_{max}/nm ($\varepsilon\times10^{-3}$)					
3	424(434)	490(9.9)	519(23)	556(18)	594(11)	631(12)
4	424(475)	484(14)	515(32)	549(20)	590(18)	646(13)
5	422(315)	—	516(25)	552(18)	591(16)	646(13)

recording spectrophotometers respectively. ^{1}H NMR spectra were recorded on a Bruker Spectrospin 250 MHz spectrometer. The pK_3[14] values and kinetics of Cu^{2+} insertion[15] are determined by methods described elsewhere. The first and second reduction potentials for the porphyrins were measured by square wave voltammetry (SWV), and verified by cyclic voltammetry. SWV were measured with an EG&G PARC Model 173 Potentiostat/Galvanostat attached to a Model 276 Interface and a Model 178 Electrometer connected to an ACC 178/41 Noise Filter. In addition, an Apple IIe computer with a monitor, an EPSON printer and a software, Model 276 Interface Demonstration Program, Volume II, were used. The Model 276 Interface allowed the potentiostat/galvanostat to be controlled by the Apple IIe computer which incorporates an IEEE-488 Interface. The cyclic voltammograms were measured with an EG&G Model 264A Polarographic Analyzer, an RE 0089 X-Y Recorder and a Model 303A SMDE. A glassy carbon electrode (EG&G PARC Part #G0197) was used as the working electrode throughout. A 10^{-4} M porphyrin solution (1 M=1 mol dm^{-3}) in DMF containing 0.1M TBAP was used for all electrochemical studies. As reference electrode, an aqueous saturated calomel electrode (SCE) was used. The SCE was placed in a bridge tube with vycor tip and was filled with 0.1 M TBAP in DMF. The tip of the bridge tube was placed in the porphyrin solution. A platinum wire was as a counter electrode. Deaeration of the porphyrin solution was achieved by bubbling oxygen-free-argon-saturated with DMF. The binding of porphyrin **5** with HSA was measured by fluorescence quenching of the single tryptophan residue in the protein as it was titrated with the porphyrin solution.[16]

Nitrobenzene and DMF were purified by standard methods and distilled under nitrogen before use. TBAP was recrystallized from ethanol and dried in vacuum at room temperature. All other chemicals were used as purchased.

5,10,15,20-Tetrakis[*p*-(methylthio)phenyl]porphyrin (3) was prepared by refluxing equimolar amounts of distilled pyrrole (**1**) and *p*-(methylthio)benzaldehyde (**2**) (0.1 mol each) in propionic acid, (500 ml), for 0.5 h; the solvent was removed under reduced pressure, the residue was dissolved in methanol, cooled and filtered to obtain the porphyrin. Yield: 8—10%. Found: C, 72.31; H, 5.00; N, 7.08%. Calcd for $C_{48}H_{38}N_4S_4$: C, 72.18; H, 4.76; N, 7.02%. ^{1}H NMR ($CDCl_3$): δ=−2.78 (s, 2H from NH), 2.75 (s, 12H from S-CH_3), 7.62 (d, 8H, phenyl protons ortho to porphyrin ring, J=8.23 Hz), 8.11 (d, 8H, phenyl protons meta to porphyrin ring, J=8.25 Hz), 8.85 (s, 8H, pyrrolic).

5,10,15,20-Tetrakis[*p*-(methylsulfonyl)phenyl]porphyrin (4) was prepared by refluxing **3**, (0.01 mol) in dichloromethane (500 ml) solution with *m*-chloroperbenzoic acid (0.16 mol) for 1 h. and subsequent removal of the solvent as well as excess *m*-chloroperbenzoic acid. Yield: 90%. Found: C, 61.80; H, 4.16; N, 5.77; S, 13.69%. Calcd for $C_{48}H_{38}N_4S_4O_8$: C, 62.00; H, 4.10; N, 6.04; S, 13.82%. ^{1}H NMR ($CDCl_3$) δ=2.85 (s, 2H from NH), 3.09 (s, 12H, S-CH_3), 8.09 (d, 8H phenyl protons ortho to porphyrin ring, J=7.26 Hz), 8.44 (d, 8H, phenyl protons meta to porphyrin ring, J=7.94 Hz), 8.85 (s, 8H, pyrrolic).

5,10,15,20-Tetrakis[*p*-(ethylmethylsulfonio)phenyl]porphyrin Perchlorate (5) was prepared by refluxing **3** (0.01 mol) in DMF (250 ml) with triethyloxonium tetrafluoroborate (0.08 mol) for 2 h. The solvent was removed under reduced pressure. The residue was dissolved in boiling water and solid $NaClO_4$ was added to obtain a precipitate of **5**. It was recrystallized from water and dried. Yield: 85%. Found: C, 51.47; H, 4.64; N, 4.32%. Calcd for $C_{56}H_{58}N_4O_{16}Cl_4S_4$: C, 51.22; H, 4.42; N, 4.27%. ^{1}H NMR (D_2O) δ=−2.79 (s, 2H, from NH), 1.72 (t, 12H, methyl protons of S-CH_2CH_3), 2.06 (q, 8H, methylene protons), 2.76 (S, 12H, S-CH_3), 7.64 (d, 8H, phenyl protons ortho to porphyrin ring, J=6.9 Hz), 8.12 (d, 8H, phenyl protons meta to porphyrin ring J=7.5 Hz), 8.83 (S, 8H, pyrrolic).

Table 2. Corrected Fluorescence Emission Spectral Data in DMF

Porphyrin	$\lambda_{ex\ max}$ /nm	$\lambda_{em\ max}$ /nm	Intensity ratio
3	423	663, 728	10:5.8
4	418	665, 719	10:9.9
5	421	659, 722	10:8.9
TPP[a]	420	655, 720	10:8.0

a) TPP is tetraphenylporphyrin. Included for comparison.

Results and Discussion

In the UV-visible absorption spectrum of porphyrin **5**, a shoulder at around 490 nm, observed in **3** and **4**, is missing (see Table 1). Compared to porphyrin **3**, porphyrin **4** and **5** show a blue shift in most of the absorption bands. In 0.05 M NaOH solution, **5** obeyed Beer's law over concentration range of 2×10^{-4} and 2×10^{-7} M. Therefore it does not dimerize or aggregate in aqueous solution, a property observed with 4TMPyP, 3TMPyP, and 2TMPyP. Unlike **3** and TPP, the two corrected emission maxima for porphyrins **4** and **5** are found to be almost equal in intensity (see Table 2). The pK_3 values (see Table 3) show that porphyrin **5** is more acidic than **3** and **4** as well as other water-soluble porphyrins. A good correlation between the rate of Cu^{2+} ion insertion in TPP and porphyrins **3**, **4**, and **5** is observed with their corresponding pK_3 values as well as their first and second reduction potentials (see Table 3). The lower the basicity and the negative first and second reduction potentials of the porphyrin, the

Table 3. pK_3 Values and Kinetics of Cu^{2+} Insertion, and Reduction Potentials

Porphyrin	pK_3±0.01	$\frac{10^{-3}\times k}{\text{min}^{-1}}$	$-E_{1/2}(1)$[b]	$-E_{1/2}(2)$[c]
TPP	3.99[a]	9.7	1.15	1.57
3	3.99[a]	9.4	1.06	1.54
4	3.20[a]	3.3	0.96	1.44
5	2.81[b]	1.2	0.80	1.13

a) In nitrobenzene, b) in water, c) in DMF, d) volts (±0.005) vs. SCE for the reaction (H_2 porphyrin)$^\circ$ $+e^- \rightarrow$ (H_2 porphyrin)$^-$, e) volts (±0.005) vs. SCE for the reaction (H_2 Porphyrin)$^-+e^- \rightarrow$ (H_2 porphyrin)$^{2-}$.

lower is the rate of Cu^{2+} insertion in it.

The binding of the water-soluble porphyrin **5** was studied with HSA in 0.1 M phosphate buffer, pH 7.2, and compared to the results obtained with other monomeric water soluble porphyrins,. Each of these porphyrins bound 1 : 1 with HSA. The dissociation constants for the porphyrin-HSA complex to HSA and the corresponding porphyrins, **5**, 4TMPyP, 3TMPyP, and 2TMPyP are found to 3.26, 2.20, 2.08, and 2.22 M respectively.

This research has been supported by 1890 Research, South Carolian State College, CSRS-USDA Project #SCX-120-03-81 and NIH MBRS Grant #RR08060.

References

1) "Methods of Porphyrin Photosensitization," ed by D. Kessel, Plenum Publishing Corporation, New York (1985).
2) R. J. Fiel, N. Datta-Gupta, E. H. Mark, and J. C. Howard, *Cancer Research*, **41**, 3543 (1981).
3) D. A. Musser and N. Datta-Gupta, *JNCI, J. Natl. Cancer Inst.*, **72**, 427 (1984).
4) M. J. Carvlin, N. Datta-Gupta, and R. J. Fiel, *Biochem. Biophs. Res. Commun.*, **108**, 66 (1984).
5) R. J. Fiel, J. C. Howard, E. H. Mark, and N. Datta-Gupta, *Nucleic Acids Res.*, **6**, 3093 (1979).
6) R. R. Pasternack, D. Sidney, P. A. Hunt, E. A. Snowden, and E. J. Gibbs, *Nucleic Acids Res.*, **14**, 3927 (1986).
7) N. Datta-Gupta, L. K. Thomas, R. Hodges, S. Lawton, and D. Malakar, *Res. Commun. Clin. Pathol. Pharmacol.*, **27**, 199 (1980).
8) D. A. Musser, J. M. Wagner, and N. Datta-Gupta, *Res. Commun. Clin. Pathol. Pharcacol.*, **36**, 251 (1982).
9) N. Foster, D. V. Woo, F. Kaltovich, J. Emrich, and C. Ljungquist, *J. Nucl. Med.*, **26**, 756 (1985).
10) J. Moan, *Photochem. Photobiol.*, **43**, 681 (1986).
11) J. Darwent, P. Douglas, A. Harriman, G. Porter, and M.-C. Richoux, *Coord. Chem. Rev.*, **44**, 83 (1982).
12) K. Kalyanasundaram, *J. Chem. Soc., Fraraday Trans. 2*, **79**, 1365 (1983).
13) T. Turray, P. Hambright, and N. Datta-Gupta, *J. Inorg. Nucl. Chem.*, **40**, 1687 (1978).
14) N. Datta-Gupta, D. Malakar, V. O. Jones, and T. Wright, *Chem. Lett.*, **1986**, 1659.
15) N. Datta-Gupta, D. Malakar, S. Datta-Gupta, and R. Gibson, *Bull. Chem. Soc. Jpn.*, **57**, 2339 (1984).
16) Detailed method is described in a forthcoming publication.

Synthesis of New Naturally Occurring 4-Phenyl-2*H*-1-benzopyran-2-ones

Virinder S. PARMAR,* Rajni JAIN, and Suddham SINGH
Department of Chemistry, University of Delhi, Delhi-110007, India
(Received February 9, 1987)

Synopsis. 5,7-Dimethoxy-4-(4-hydroxyphenyl)-2*H*-1-benzopyran-2-one and 5,7-dimethoxy-4-(4-methoxyphenyl)-2*H*-1-benzopyran-2-one, two new neoflavonoids occurring in *Courtarea hexandra* have been synthesized via Pechmann condensation. Attempts made to synthesize another 4-arylcoumarin, 5-hydroxy-7-methoxy-4-(2,5-dihydroxyphenyl)-2*H*-1-benzopyran-2-one, constituent of the same plant, led to the formation of the hitherto unknown 2-ethoxy-6-hydroxy-4*H*-1-benzopyran-4-one.

A few 4-phenylcoumarins having rare type of oxygenation pattern have recently been isolated[1,2] from the caulis of *Courtarea hexandra,* a folk medicinal plant used in Brazil as an antimalarial and antidiabetic agent. The structures to these compounds were assigned on the basis of their spectral data alone. In order to provide confirmation to the proposed structures of the natural products, we have attempted the syntheses of three of them (**1** and **2**,[1] and **3**[2]) and those of their dihydroxy analogues via Pechmann condensation of phloroglucinol and corresponding suitably substituted ethyl benzoylacetate.

Results and Discussion

Ethyl 4-(benzyloxy)benzoylacetate (**4**) and ethyl 4-methoxybenzoylacetate (**6**) were prepared by treating 4-(benzyloxy)acetophenone[3] and 4-methoxyacetophenone,[4] respectively with diethyl carbonate in the presence of sodium hydride; **4** and **6** were fully characterized from their spectral data. Pechmann condensation of **4** with phloroglucine yielded 5,7-dihydroxy-4-(4-hydroxyphenyl)-2*H*-1-benzopyran-2-one (**5**), which on methylation with diazomethane yielded mainly the coumarin **1** along with a small amount of the coumarin **2**. The IR, UV, and ^{1}H NMR spectral data of **1** and **5** supported their structures. Similarly, the ester **6** on condensation with phloroglucine yielded the 4-phenylcoumarin **7**, which on methylation with dimethyl sulfate gave 5,7-dimethoxy-4-(4-methoxyphenyl)-2*H*-1-benzopyran-2-one (**2**); **2** and **7** were fully characterized from their spectral data. The mp behavior, and UV, IR, and ^{1}H NMR spectral data of our synthetic **1** and **2** were in agreement with those of the corresponding natural samples,[1] thus confirming the structures of the natural products occurring in *Courtarea hexandra.* However, a direct comparison of our synthetic samples with the natural samples could not be done because of the non-availability of the latter with us.

For the preparation of 5-hydroxy-7-methoxy-4-(2,5-dihydroxyphenyl)-2*H*-1-benzopyran-2-one (**3**),[2] ethyl 2,5-bis(benzyloxy)benzoylacetate (**8**), prepared by the reaction of 2,5-bis(benzyloxy)acetophenone[5] with diethyl carbonate in the presence of NaH was condensed with phloroglucine, as well as with mono-*O*-methylphloroglucine[6] under four different experimental conditions. The condensations in the presence of H_3PO_4, $POCl_3$, and concd H_2SO_4 led to the formation of only tarry materials, from which no crystalline substance could be isolated. Condensation in the presence of ethanolic HCl, in both the cases yielded the compound **9**, quite different from the required coumarin **3**; structure of **9** was established from a detailed study of its UV, IR, ^{1}H NMR, and mass spectra.

The UV absorption maxima of **9** at 202, 218, 258 (sh), 267, 280 (sh), and 326 nm suggested it to be a

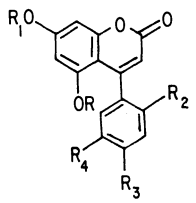

(1) $R=R_1=CH_3$, $R_2=R_4=H$, $R_3=OH$
(2) $R=R_1=CH_3$, $R_2=R_4=H$, $R_3=OCH_3$
(3) $R=R_3=H$, $R_1=CH_3$, $R_2=R_4=OH$
(5) $R=R_1=R_2=R_4=H$, $R_3=OH$
(7) $R=R_1=R_2=R_4=H$, $R_3=OCH_3$

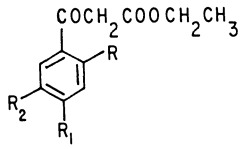

(4) $R=R_2=H$, $R_1=OCH_2C_6H_5$
(6) $R=R_2=H$, $R_1=OCH_3$
(8) $R=R_2=OCH_2C_6H_5$, $R_1=H$

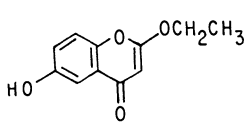

(9)

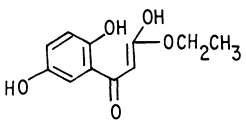

(10)

chromone; the IR spectra supported this and further indicated **9** to be an alkoxy- and hydroxy-substituted chromone as it exhibited strong absorptions at 3200, 1660, 1623, and 1280 cm^{-1}. A bathochromic shift of 38 nm in its λ_{max} in the presence of NaOMe and the presence of a D_2O exchangeable singlet (1H) at δ 9.80, a triplet (for 3H) at δ 1.40, and a quartet (for 2H) at δ 4.15 in its ^1H NMR spectrum confirmed **9** to be monohydroxy-monoethoxy-substituted. As there was no change in the λ_{max} of **9** on addition of NaOAc, the position of -OH group was indicated to be either C-6 or C-8; the location of -OH at C-6 was substantiated by the chemical shift values of the three protons in the aromatic ring in the ^1H NMR spectrum (a multiplet for 2H at δ 7.15 and an ortho-coupled doublet for 1H at δ 7.26). These data suggested **9** to be the hitherto unknown 2-ethoxy-6-hydroxy-4*H*-1-benzopyran-4-one; this structure was fully confirmed by its mass spectrum, which exhibited prominent peaks at *m/z* 207 $(M+1)^+$, 206 (M^+), 178 $(M-CO)^+$, 150 $(M-CO-C_2H_4)^+$, 137 (A_1+H), 136 $(A_1)^+$, 108 (A_1-CO) and 80 $(A_1-CO-CO)$. We believe that **9** is formed via the intermediate **10**, derived from the ester **8** under strongly acidic conditions of the experiment.

Experimental

All melting points were taken on a Nalge micro melting point apparatus and are uncorrected. Silica gel was used for all thin-layer and column chromatographic separations. UV spectra were recorded in methanol on a Perkin Elmer 554 spectrophotometer. IR spectra were recorded on Shimadzu model 535 spectrophotometer and ^1H NMR spectra on 90 MHz Perkin Elmer R-32 and 200 MHz Jeol JNM FX-200 FT NMR spectrometers using TMS as the internal standard. The mass spectra were recorded on a Varian Mat 311A instrument.

Ethyl 4-(Benzyloxy)benzoylacetate (4). To a vigorously stirred suspension of sodium hydride (4g) in dry ether (100 ml) containing diethyl carbonate (5.48 ml), a solution of 4-(benzyloxy)acetophenone[3] (5 g) in dry benzene (100 ml) was added dropwise during the course of 6 h. The mixture was then refluxed for 30 h, cooled, treated with ice and acidified with dilute hydrochloric acid; the organic layer that separated was washed with sodium hydrogen carbonate solution and dried. Residue obtained on removal of benzene and ether was macerated with petrol to remove unreacted diethyl carbonate; ethyl 4-(benzyloxy)benzoylacetate was obtained as an oil (**4**, 4 g); IR (Nujol) ν_{max}: 1735, 1660, 1260, 1105, 1030, and 830 cm^{-1}; UV λ_{max}: 210, 274 nm; ^1H NMR (90 MHz, $CDCl_3$): δ=1.25 (3H, t, *J*=7 Hz, $-COOCH_2C\underline{H}_3$), 3.90 (2H, s, $-COC\underline{H}_2COOC_2H_5$), 4.20 (2H, q, *J*=7 Hz, $-COOC\underline{H}_2CH_3$), 5.10 (2H, s, $-OC\underline{H}_2C_6H_5$), 7.00 (2H, d, *J*=8.5 Hz, H-3 and H-5), 7.35 (5H, s, $-OCH_2C_6\underline{H}_5$), and 7.85 (2H, d, *J*=8.5 Hz, H-2 and H-6). Found: C, 72.80; H, 6.40%; Calcd for $C_{18}H_{18}O_4$: C, 72.48; H, 6.04%.

5,7-Dihydroxy-4-(4-hydroxyphenyl)-2*H*-1-benzopyran-2-one (5). A cooled suspension of ethey 4-(benzyloxy)benzoylacetate (**4**, 1.5 g) and phloroglucine (0.71 g) in absolute ethanol (50 ml) was saturated with dry HCl gas (5.5 h). The reaction mixture was left at 28 °C for 2 d, water was added and the solution was concentrated in vacuo and cooled, when a yellowish-orange solid precipitated. It was filtered and crystallized from methanol as yellow crystals (**5**, 500 mg), mp 293—294 °C; IR (KBr) ν_{max}: 3530, 3235, 1660, 1550, 1480, 1360, 1020, and 830 cm^{-1}; UV λ_{max} (log ε): 260 (3.95), 322 (3.98); +NaOMe: 272, 304, 368 nm; ^1H NMR (90 MHz, CD_3COCD_3): δ=5.70 (1H, s, H-3), 6.25 (1H, s, H-6), 6.30 (1H, s, H-8), 6.80 (2H, d, *J*=8.5 Hz, H-3′ and H-5′), 7.23 (2H, d, *J*=8.5 Hz, H-2′ and H-6′), 8.50 (1H, s, -OH), 8.60 (1H, s, -OH).

5,7-Dimethoxy-4-(4-hydroxyphenyl)-2*H*-1-benzopyran-2-one (1). To a solution of (**5**, 100 mg) in methanol (8 ml), a saturated solution of diazomethane in ether (7 ml) was added under stirring. After 45 min, the reaction mixture was evaporated in vacuo and the residue was column-chromatographed using benzene–ethyl acetate (4 : 1) as eluent to give **1** (40 mg); mp 214—216 °C (mp of the natural product[1] 214—215 °C); IR (KBr) ν_{max}: 3300, 1706, 1612, 1159, 1048, 962, and 835 cm^{-1}; UV λ_{max} (log ε): 254 (4.09), 322 (4.05); +NaOMe: 254, 328, 372 nm; ^1H NMR (200 MHz, CD_3COCD_3): δ=3.56 (3H, s, C-5-OMe), 3.96 (3H, s, C-7-OMe), 5.84 (1H, s, H-3), 6.40 (1H, d, *J*=2.5 Hz, H-6), 6.56 (1H, d, *J*=2.5 Hz, H-8), 6.92 (2H, d, *J*=8.5 Hz, H-3′ and H-5′), 7.16 (2H, d, *J*=8.5 Hz, H-2′ and H-6′), 8.56 (1H, s, C-4′-OH). Fuund: C, 68.20; H, 5.00%; Calcd for $C_{17}H_{14}O_5$: C, 68.46; H, 4.70%.

Ethyl 4-Methoxybenzoylacetate (6). To a vigorously stirred suspension of sodium hydride (5.8 g) in dry ether (100 ml), diethyl carbonate (15 ml) was added in one lot and to this mixture, a solution of 4-methoxyacetophenone (9 g)[4] in dry ether (100 ml) was added dropwise during 6 h. The mixture was then refluxed for 30 h, cooled, treated with ice and acidified with dil HCl. The organic layer was separated, washed with sodium hydrogencarbonate solution, dried, concentrated and treated with dry hexane when **6** was obtained as an oil (8 g); IR (Nujol) ν_{max}: 1730, 1670, 1600, 1360, 1250, 1160, 1100, 1020, and 830 cm^{-1}; UV λ_{max}: 216, 276 nm; ^1H NMR (90 MHz, $CDCl_3$): δ=1.25 (3H, t, *J*=7 Hz, $-COOCH_2C\underline{H}_3$), 3.80 (3H, s, $-OCH_3$), 3.90 (2H, s, $-OC\underline{H}_2-COOCH_2CH_3$), 4.20 (2H, q, *J*=7 Hz, $-COOC\underline{H}_2CH_3$), 6.85 (2H, d, *J*=8.5 Hz, H-3 and H-5), and 7.85 (2H, d, *J*=8.5 Hz, H-2 and H-6). Found: C, 65.10%; H, 5.90%; Calcd for $C_{12}H_{14}O_4$: C, 64.86%; H, 6.31%.

5,7-Dihydroxy-4-(4-methoxyphenyl)-2*H*-1-benzopyran-2-one (7). Through a cooled solution of **6** (4 g) and phloroglucine (2.25 g) in absolute ethanol (100 ml), a stream of dry HCl gas was passed for 6 h and the reaction mixture was left at 30 °C for 3 d. Water was added and the solution was concentrated in vacuo. The solid obtained was filtered, washed with water and crystallized from methanol as yellowish brown solid (2.5 g); mp 256—258 °C; IR (Nujol) ν_{max}: 3300, 3190, 1688, 1620, 1595, 1510, 1170, 820, and 700 cm^{-1}; UV λ_{max} (log ε): 260 (4.07), 315 (4.05); +NaOMe: 262, 315, 380 nm; ^1H NMR (90 MHz, DMSO-d_6): δ=3.82 (3H, s, C-4′-OCH_3), 5.76 (1H, s, H-3), 6.28 (1H, d, *J*=2.5 Hz, H-6), 6.35 (1H, d, *J*=2.5 Hz, H-8), 6.93 (2H, d, *J*=8.5 Hz, H-3′ and H-5′), 7.32 (2H, d, *J*=8.5 Hz, H-2′ and H-6′), and 9.7 (1H, s, -OH). Found: C, 68.00; H, 4.60%; Calcd for $C_{16}H_{12}O_5$: C, 67.60; H, 4.23%.

5,7-Dimethoxy-4-(4-methoxyphenyl)-2*H*-1-benzopyran-2-one (2). A solution of **7** (0.5 g) in acetone (50 ml) was refluxed with potassium carbonate (1 g) and dimethyl sulfate (0.23 ml) for 3 h. Potassium salts were filtered off and washed with hot acetone. The combined filtrate and washings were concentrated and treated with ice. The solid obtained was filtered, washed with water and dried. It crystallized from methanol as yellowish-brown crystals **2** (0.4 g), mp 151—152 °C (mp of the natural product[1] 151—152 °C); IR (Nujol) ν_{max}: 1710, 1620, 1595, 1158, 1100, 1050, 940, 860, and 830 cm^{-1}; UV λ_{max} (log ε): 255 (4.04), 315 (4.00); ^1H NMR (90 MHz, $CDCl_3$): δ=3.50 (3H, s, C-5-OCH_3), 3.86 (6H, s, C-7 and C-4′-OCH_3), 5.96 (1H, s, H-3), 6.22 (1H, d, *J*=2.5 Hz, H-6), 6.50 (1H, d, *J*=2.5 Hz, H-8), 6.87 (2H, d, *J*=8.5 Hz, H-3′ and H-5′), and 7.20 (2H, d, *J*=8.5 Hz, H-2′ and H-6′).

Ethyl 2,5-Bis(benzyloxy)benzoylacetate (8). To a vigorously stirred suspension of NaH (10 g) in dry ether (100 ml) containing diethyl carbonate (6.2 ml), a solution of 2,5-bis(benzyloxy)acetophenone[5] (10 g) in dry benzene (100 ml)

was added dropwise during the course of 6 h. The mixture was refluxed for 36 h. Usual work-up gave the ester **8** as an oil (8 g); IR (KBr) ν_{max}: 2910, 2850, 1730, 1660, 1600, 1460, 1380, 1200, 1020, 810, and 740 cm^{-1}; UV λ_{max}: 210, 286, 334 nm; ^1H NMR (90 MHz, $CDCl_3$): δ=1.23 (t, J=7H, 3H, $-COOCH_2C\underline{H}_3$), 4.00 (s, 2H, $-COC\underline{H}_2COOCH_2CH_3$), 4.10 (q, J=7 Hz, 2H, $-COOC\underline{H}_2CH_3$), 5.03 (s, 2H, $-OC\underline{H}_2C_6H_5$), 5.11 (s, 2H, $-OC\underline{H}_2C_6H_5$), 7.05 (m, 2H, H-3, and H-4), 7.42 (m, 10H, $2\times-OCH_2C_6\underline{H}_5$), and 7.50 (d, 1H, J=2.5 Hz, H-6). Found: C, 73.90; H, 6.20%; Calcd for $C_{25}H_{24}O_5$: C, 74.26; H, 5.94%.

2-Ethoxy-6-hydroxy-4*H*-1-benzopyran-4-one (9). Through a cooled suspension of the ester **8** (2 g) and phloroglucine (0.75 g) in absolute ethanol (100 ml), a stream of dry HCl gas was passed for 6 h. The reaction mixture was left at 30 °C for 4 d. After usual work up, only one solid compound could be isolated which crystallized from methanol as yellow crystals **9** (100 mg), mp 228—230 °C; IR (Nujol) ν_{max}: 3200, 1660, 1623, 1615, 1560, 1500, 1460, 1410, 1380, 1280, 1230, 1190, 1082, 970, 830, 807, and 710 cm^{-1}; UV λ_{max} (log ε): 202 (4.25), 218 (4.29), 258 (sh) (3.85), 267 (3.89), 280 (sh) (3.76), 326 (3.57); +$AlCl_3$: 202, 218, 258 (sh), 267, 280 (sh), 326; +NaOAc: 205, 210, 258 (sh), 267, 280 (sh), 326; +NaOAc/Boric Acid: 210, 258 (sh), 267, 280 (sh), 326; +NaOMe: 202, 237, 274, 288, 364 nm; ^1H NMR (200 MHz, DMSO-d_6): δ=1.40 (t, J=7 Hz, 3H, $-OCH_2C\underline{H}_3$), 4.15 (q, J=7 Hz, 2H, $-OC\underline{H}_2CH_3$), 5.80 (s, 1H, H-3), 7.15 (m, 2H, H-5 and H-7), 7.26 (d, J=8 Hz, 1H, H-8), and 9.80 (s, 1H, -OH); EIMS m/z (%): 207 (9), 206 (M^+) (64), 178 $(M-CO)^+$ (10.5), 150 $(M-CO-C_2H_2)^+$ (5), 149 $(M-CO-C_2H_2-H)^+$ (3.5), 137 $(A_1+H)^+$ (12.8), 136 $(A_1)^+$ (100), 134 $(178-CH_2{=}CHOH)^+$ (10.5), 121 (149—CO) (3.5), 108 $(A_1-CO)^+$ (12.8), 80 $(A_1-CO-CO)$ (7). Found: C, 64.00; H, 4.50%; Calcd for $C_{11}H_{10}O_4$; C, 64.08; H, 4.85%.

The condensation of the ester **8** with monomethyl ether of phloroglucine[6] by the procedure given above yielded only **9**.

Two of us (RJ and SS) thank the CSIR, New Delhi for the award of Senior Research Fellowships.

References

1) G. D. Monache, B. Botta, A. S. Neto, and R. A. Delima, *Phytochemistry*, **22**, 1657 (1983).
2) G. Reher, L. Kraus, V. Sinnwell, and W. A. Konig, *Phytochemistry*, **22**, 1524 (1983).
3) H. M. Priestley and E. Monness, *J. Org. Chem.*, **5**, 355 (1940).
4) A. I. Vogel, "A text book of practical organic chemistry," Longmans, Green and Co., London (1956), p. 733.
5) S. G. Morris, *J. Am. Chem. Soc.*, **71**, 2056 (1949).
6) H. Bredereck, I. Hennig, and W. Rau, *Ber.*, **86**, 1085 (1953).

Mixed Colloidal Dispersions of Silica and Hematite

Kunio ESUMI,* Hiroyuki IDOGAWA, and Kenjiro MEGURO
Department of Applied Chemistry, Institute of Colloid and Interface Science,
Science University of Tokyo, Kagurazaka, Shinjuku-ku, Tokyo 162
(Received November 4, 1987)

The colloidal behavior of mixed dispersions containing hematite (diameter=138.9 nm) and silica (diameter=7.0 nm) has been studied by measuring the stability ratio, zeta potential, and particle size. When various particle numbers of silica were added to a constant particle number of hematite, different colloidal behavior was observed, depending on the pH. In a pH region where the two solids were oppositely charged, hematite particles showed a dispersion-coagulation-redispersion process with increasing particle number of silica, resulting in a coating layer of silica particles on the hematite surface. On the other hand, in a region where both solids were negative, the addition of silica enhanced the stability of the hematite.

When an aqueous colloidal dispersion contains solid particles of more than one kind, it is expected that the various solids will have different surface charges in the solution and complicate interactions between their solids occur. Under these conditions, hetero coagulation due to the interaction of opposite charges can take place. The experimental testing of the theories of hetero coagulation proposed by Derjaguin,[1] Hogg et al.,[2] and Wiese and Healy[3] has been attempted by several workers.[4-6]

The phenomenon of hetero coagulation can be applied in the preparation of oxide supported metal catalysts. An oxide and an ultra fine particle of catalyst are mixed in aqueous solution. By adjusting the pH so that the oxide and the particle of catalyst are oppositely charged, it is possible to produce a well-spaced layer of catalyst particles on the oxide particle. However, many hetero coagulation studies have been limited to solid particles having similar particle size.

The aim of this work is to study the colloidal dispersion behavior of mixed silica and hematite spherical particles with narrow size distribution and a considerable difference in particle size. The mixed colloidal properties were characterized by measurement of the zeta potential, the stability ratio and the particle size.

Experimental

Materials. As solid particles, hematite, and silica were used.

Spherical hematite particles with a narrow size distribution were prepared by essentially the same procedure as Matijević and Scheiner[7] described. The 2×10^{-2} mol dm^{-3} of $FeCl_3$ aqueous solution was adjusted to pH 3.1 with HCl. The solution was then aged for 24 h at 100 °C. After cooling to room temperature, the collected particles were washed several times with aqueous $HClO_4$ solution (pH 3.1) to remove chloride and iron(III) ions. The particles were then redispersed in ion-exchanged water to be used as a stock sol. The final stock sol had a concentration of 3.20 mg cm^{-3}, as determined directly by dry-weight measurement. The particle diameter was determined to 138.9 nm by transmission electron microscopy.

Well monodispersed spherical silica was obtained from Japan Aerosil Co. The particle diameter was determined to 7.0 nm.

Procedure. Zeta potentials were measured using a Laser-Zee meter Model 500(Pen Kem Inc.).

The particle size of the mixed dispersion was measured using an Autosizer Model 700(Malvern Co., Ltd.).

Coagulation kinetics were followed using a standard turbidimetric technique,[8] in which the change of absorbance at 540 nm as a function of time was recorded continuously on a 220A Hitachi Spectrophotometer. As soon as the hematite sols had been mixed with the silica sols, the absorbance of the mixed dispersions was recorded and the initial slope of the absorbance vs. time curve was obtained. The stability ratio (W) was calculated from the ratio of the rapid-coagulation (k_0) to the slow-coagulation rate (k) of the sols:

$$W = k_0/k$$

The stability of the mixed dispersions was also evaluated from the magnitude of the absorbance after 12 h standing of the mixed dispersions, where the absorbance was also taken at 540 nm.

All measurements were carried out in 1×10^{-2} mol dm^{-3} sodium nitrate to keep the ionic strength constant. Nitric acid and sodium hydroxide were used to adjust the pH of these dispersions.

Results and Discussion

Figure 1 shows the zeta potentials of hematite and silica as a function of the pH and indicates that their isoelectric points are 7.9 for hematite and 3.1 for silica. To elucidate the behavior of colloidal mixed dispersions of hematite and silica, four different pH values were selected: pH 3.0, 4.0, 5.5, and 10.0. At pH 3.0, the zeta potential of the silica was almost zero, while that of the hematite was positive. At pH 4.0 and 5.5, the hematite and silica had opposite zeta potential values and at pH 10.0, they both showed negative zeta potentials. By using mixtures of these monodispersed particles with different isoelectric points, it is possible to study the interactions of dissimilar electrical double layers around spherical particles with different particle size.

The stability ratio (W) and absorbance of the mixed dispersions are shown in Fig. 2 in which the various

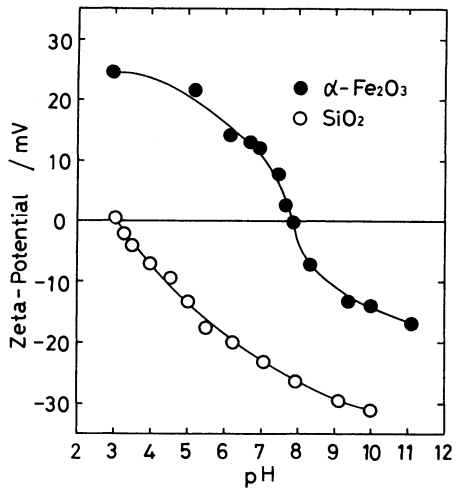

Fig. 1. Zeta potentials of hematite and silica as a function of pH.

particle numbers of silica are added to a constant particle number of hematite at four different pH. Here, the turbidity was mainly attributed to hematite particles because the particle size of the silica was too small to provide an appropriate turbidity value. Further, the silica particles were very stable over the entire pH region. In the case of hematite alone, the stability ratio was almost one at pH 3.0 and 10.0, whereas that at pH 4.0 and 5.5 was more than eight. When silica particles were added to the hematite dispersion system, the stability ratio varied, depending on the pH. At pH 3.0, the stability ratio was almost constant, i.e., one, against various particle numbers of silica. On the other hand, at pH 4.0 and 5.5, the stability ratio decreased upon addition of the silica particles. Further addition of silica considerably increased the stability ratio and a maximum stability ratio at pH 5.5 was greater than that at pH 4.0. At pH 10.0, the stability ratio upon addition of the silica increased gradually up to a certain amount of added silica (ca. 180). Thus, hematite particles exhibited the

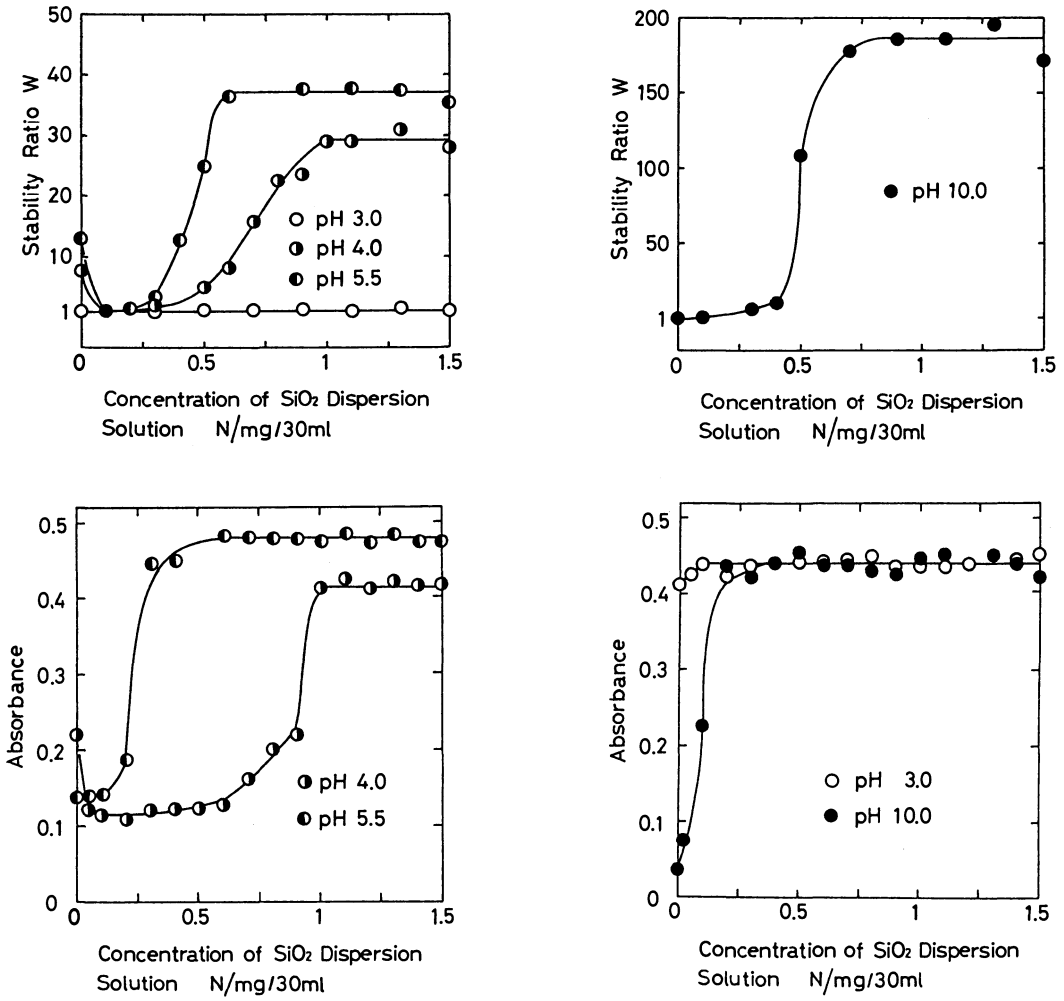

Fig. 2. Variations of stability ratio and optical density in mixed dispersion of hematite and silica with increasing amounts of silica: amount of hematite, 0.64 mg/30 ml.

dispersion–coagulation–redispersion process on addition of silica at pH 4.0 and 5.5. The optical density of the mixed dispersion after 12 h standing was also measured to evaluate the colloidal stability of mixed dispersion. The result is also shown in Fig. 2 which indicates that the behavior of the optical density upon addition of silica almost coincides with the stability ratio except at pH 3.0. At pH 3.0, the optical density of the mixed dispersions was high upon addition of silica although the stability ratio was almost unity. In order to clarify the relationship between the pH and the zeta potential in the mixed dispersion, the zeta potential of the mixed dispersion was plotted as a function of pH (Fig. 3). It can be seen that the zeta potential is significantly altered upon addition of silica at different pH. Further, it is noteworthy that the zeta potential values of the mixed dispersion upon addition of more than 0.5 mg/30 ml of silica at each pH coincide with that of silica alone at the corresponding pH. This implies that a coating layer of silica particles is formed on the hematite particle.

The change in mean particle size of the mixed dispersions is shown in Fig. 4. Here, the mean particle size is mainly considered to be due to hematite or silica coated hematite. At pH 4.0, 5.5, and 10.0, the behaviors in mean particle size of mixed dispersions are in fair agreement with the stability ratio and optical density. However, at pH 3.0, the mean particle size hardly changed upon addition of silica. This can be interpreted as follows: since the silica particles form a three-dimentional chain structure throughout the volume of the aqueous solution, this structure can generate a well dispersion state of hematite. The rate of structure formation will be remarkedly influenced by the time which the silica particles exist in aqueous solution. That is, during the measurement of the

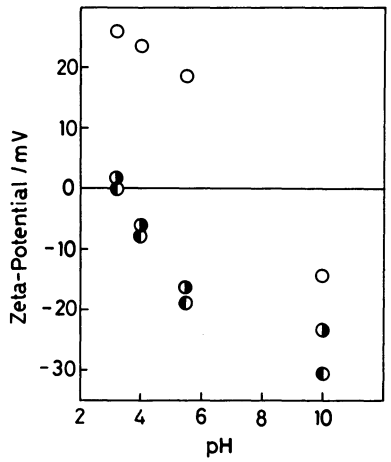

Fig. 3. Variation of zeta potential of mixed dispersion of hematite and silica with different additive amounts of silica at pH 3.0, 4.0, 5.5, and 10.0: concentration of silica; (○) 0, (◑) 0.1, (◐) 0.5 mg/30 ml.

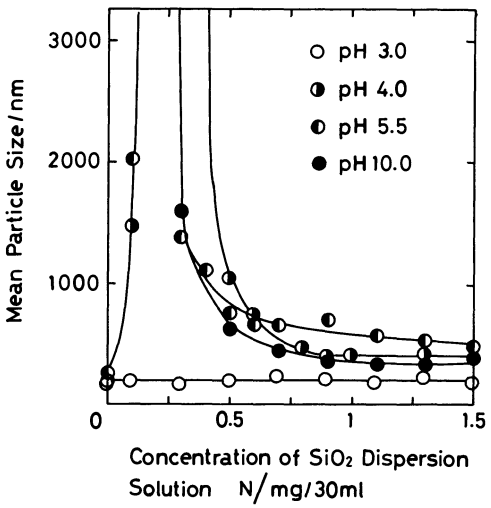

Fig. 4. Mean particle size of mixed dispersion of hematite and silica as a function of the concentration of silica: amount of hematite, 0.64 mg/30 ml.

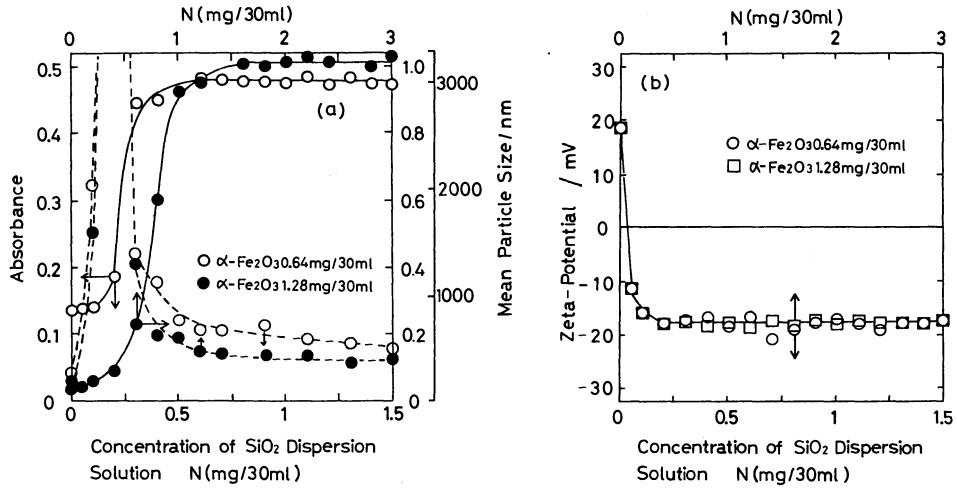

Fig. 5. Effect of amount of hematite on mixed dispersion of hematite and silica: (a) absorbance; solid line, mean particle size; dotted line (b) zeta potential.

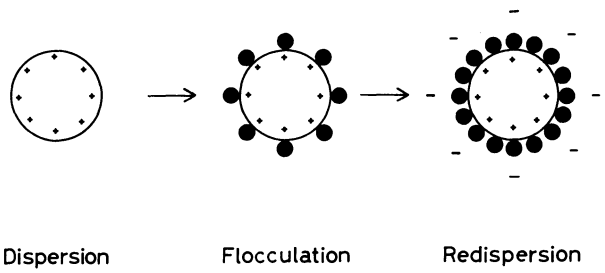

Fig. 6. A model for mechanism of coagulation and dispersion of mixed hematite and silica.

stability ratio, the structure formation is not fully established so that the stability ratio remains unity. On the other hand, during the measurement of the mean particle size and absorbance, sufficient time will be provided for the structure formation to stabilize the hematite particles.

Further, the amounts of hematite was varied and its effect on the mixed dispersion was studied. The result is shown at pH 5.5 in Fig. 5. Even using different amounts of hematite, the behavior in zeta potential, particle size and absorbance at pH 5.5 was similar to the result described before. Similar trends were observed for the other pH.

From the above results, the following mechanisms of mixed dispersions are proposed: at pH 4.0 and 5.5, silica particles are adsorbed on hematite particle due to electrical attraction forces since silica and hematite particles are oppositely charged. In the region where the zeta potential of the mixed dispersion becomes zero and the mean particle size becomes significantly large, the mixed dispersion leads to a coagulated state. On further addition of silica, a significant amount of silica particles are adsorbed on to the hematite particle and both the zeta potential and the mean particle size decrease appreciably, resulting in redispersion of the mixed coagulate. This model is presented in Fig. 6. Similar behavior was reported with latex and silica mixtures where the much smaller silica particles also adsorbed on the latex to form a monolayer and caused the latex to behave like a silica sol.[9]

In conclusion, when hematite and silica are oppositely charged, silica particles with a small particle size are adsorbed on hematite particles, resulting in coagulation of the hematite particles. Upon further addition of silica the coagulated hematite particles are redispersed due to considerable adsorption of silica particles on hematite. This mechanism is demonstrated by measurements of the stability ratio, the zeta potential and the particle size.

References

1) B. V. Derjaguin, *Disc. Faraday Soc.*, **18**, 85 (1954).
2) R. Hogg, T. W. Healy, and D. W. Fuerstenau, *Trans, Faraday Soc.*, **62**, 1638 (1966).
3) G. R. Wiese and T. W. Healy, *Trans. Faraday Soc.*, **66**, 490 (1970).
4) G. R. Wiese and T. W. Healy, *J. Colloid Interface Sci.*, **52**, 458 (1975).
5) R. J. Pugh and J. A. Kitchener, *J. Colloid Interface Sci.*, **38**, 656 (1972).
6) R. O. James, A. Homola, and T. W. Healy, *J. Chem. Soc., Faraday Trans. 1*, **73**, 1436 (1977).
7) E. Matijević and R. Scheiner, *J. Colloid Interface Sci.*, **63**, 509 (1978).
8) R. H. Ottewill and J. N. Shaw, *Disc. Faraday Soc.*, **42**, 154 (1966).
9) A. Bleier and E. Matijević, *J. Chem. Soc., Faraday Trans. 1*, **74**, 1346 (1978).

 © 1988 The Chemical Society of Japan Bull. Chem. Soc. Jpn., 61, 2291—2294 (1988)

Liquid-Phase Dehydrogenation of Methanol with Homogeneous Ruthenium Complex Catalysts

Hiroaki ITAGAKI, Sumio SHINODA,† and Yasukazu SAITO*
Institute of Industrial Science, University of Tokyo,
22-1 Roppongi 7 Chome, Minato-ku, Tokyo 106
(Received November 17, 1987)

Catalytic dehydrogenation of methanol proceeded with homogeneous ruthenium(II) complexes, yielding formaldehyde and dihydrogen as primary products under refluxing conditions of the solution. The effects of additives on the initial reaction rate were examined for lithium chloride, lithium acetate, acetic acid and ethyldiphenylphosphine. A catalyst complex, $[Ru(OAc)Cl(PEtPh_2)_3]$, was deactivated gradually by the displacement of the bidentate OAc ligand with H and CO ligands during the reaction. These cis-disposed sites would be used for splitting the C-H bonds. A catalytic reaction cycle is proposed, in which such processes are included as solvolysis of the catalyst complex, β-H elimination from the OCH_3 ligand and attack of acetic acid on the hydride intermediate to generate dihydrogen.

Dehydrogenation of methanol, yielding formaldehyde and dihydrogen, is thermodynamically less favorable ($\Delta G°=64.0$ kJ mol^{-1}) than oxidative dehydrogenation ($\Delta G°=-173.2$ kJ mol^{-1}). The endothermic reaction ($\Delta H°=130.4$ kJ mol^{-1}) of Eq. 1 proceeds, however, in the liquid phase under very mild conditions, since most of the product dihydrogen is removed from the reaction medium owing to its limited solubility.[1]

$$CH_3OH \longrightarrow HCHO + H_2 \quad (1)$$

Homogeneous catalysts for alcohol dehydrogenation evolving dihydrogen have been extensively studied both thermally[2] and photochemically[3] except for methanol. Dobson and Robinson proposed a reaction mechanism for (trifluoroacetato)ruthenium(II) complexes, $[Ru(OAc_F)_2CO(PPh_3)_2]$,[2c] the catalytic activity of which was compared later among a series of (trifluoroacetato)ruthenium(II) complexes.[2e]

As for the methanol photocatalytic dehydrogenation was explored to give not only carbon monoxide[3d] but also ethylene glycol,[4a-c] dimethoxymethane,[4b,c] and products related to its reaction counterpart. Homogeneous catalytic dehydrogenation of methanol to yield organic products without photoirradiation has never been reported until some ruthenium(II) complexes were revealed to be active. Formaldehyde was formed under refluxing conditions (65 °C) with $[Ru_2(OAc)_4Cl]$ mixed with tertiary phosphine, or with $[Ru(OAc)Cl(PEtPh_2)_3]$.[5] Independently, the catalytic activity of $[RuCl_2(PPh_3)_3]$ was shown by Smith et al. to form methyl formate as the main product together with dimethoxymethane at 150 °C in good stoichiometric correlation with dihydrogen.[6]

In the present work, a reaction scheme is given for the acetato and phosphine-coordinated ruthenium(II) complexes based on the experimental details concerning the time course of the product distribution, the effect of additives on the initial rates and the structural change of a catalyst complex during deactivation.

Experimental

Procedure. All the operations of catalyst syntheses and dehydrogenation reactions were conducted under argon or nitrogen atmosphere. Degassing by repeated freeze-pump-thaw cycles was necessary for methanol, as the catalyst complexes were air sensitive in solution. The gas evolution reaction from the solution of $[Ru_2(OAc)_4Cl]$ (0.0474 g, 0.1 mmol) admixed with triphenylphosphine (0.1836 g, 0.7 mmol) (designated as 'composite-type' hereafter) or of $[Ru(OAc)Cl(PEtPh_2)_3]$ (0.1677 g, 0.2 mmol) in methanol (200 ml) was performed under refluxing conditions in a flask (500 ml) connected to a gas buret (50 ml) through a condenser. All the products, other than dihydrogen, were condensed by using an ethylene glycol/water mixture cooled to −15—−20 °C with a circulating cooler (Taiyo Kagaku Kogyo Ltd., Type CML-III). The volume increase due to the gas evolution was started to plot against the elapsed time after thermal equilibrium had been attained in the closed reaction system at atmospheric pressure. After the reaction, the solution was chilled with ice in order to perform GC analysis of the liquid components without loss by evaporation of dehydrogenated products.

Spectra. Infared spectra using pressed potassium bromide pellets were taken on a Hitachi 260-10 spectrophotometer from 650 to 4000 cm^{-1} with polystyrene reference. Proton, $^{31}P\{^1H\}$ and $^{13}C\{^1H\}$NMR spectra were recorded on a Jeol JNM-FX60Q spectrometer operating in the FT mode at 59.80, 24.21, and 15.04 MHz, respectively. ^{31}P chemical shifts were referenced to an external standard of 85% H_3PO_4, with the downfield chemical shifts taken to be positive, whereas ^1H and ^{13}C NMR spectra were referenced internally to the CH_2Cl_2 solvent and converted to the TMS scale by using the CH_2Cl_2 chemical shifts of +5.3 and +54.2 ppm, respectively. GC analysis was performed on a Yanagimoto G-3800 gas chromatograph using GP-54 and active carbon culumns. The sensitivity of formaldehyde detection was enhanced by adopting a methane converter with the Ru/Al_2O_3 catalyst, which was added to a Porapak-T column in the Ohkura Rikagaku GC 103 gas chromatograph.

† Present address: Department of Industrial Chemistry, Faculty of Engineering, Seikei University, 3-1 Kichijyoji-Kitamachi 3 Chome, Musashino-Shi, Tokyo 180.

Syntheses. $[Ru_2(OAc)_4Cl]$ was prepared by the literature method.[7] Ruthenium(III) trichloride trihydrate and tertiary phosphine from commercial sources were used without further purification.

$[Ru(OAc)Cl(PPh_3)_3]$ was synthesized from $[Ru_2(OAc)_4Cl]$ and PPh_3. A methanol (500 ml) solution of $[Ru_2(OAc)_4Cl]$ (0.437 g, 1.00 mmol) and PPh_3 (1.836 g, 7.00 mmol) was refluxed for 1 h, after which part of the solvent methanol was removed by evacuation. When the solution was allowed to stand at −20 °C overnight, an orange crystal was precipitated. Its isolation was performed by decantation, washing with methanol, and drying in vacuo. Yield 0.81 g, 82%. Found: C, 70.61; H, 4.94; P, 9.20%. Calcd for $C_{56}H_{48}P_3O_2ClRu$: C, 68.46; H, 4.92; P, 9.46%. ^{31}P NMR: δ=43.8(2P) and 77.7(1P), J(PP) 27.3 Hz; ^{13}C(OAc): δ=182.2 and 24.3.

$[Ru(OAc)Cl(PEtPh_2)_3]$ was synthesized in a similar manner. Yield 0.58 g, 69%. Found: C, 63.03; H, 5.62; P, 10.81%. Calcd for $C_{44}H_{48}P_3O_2ClRu$: C, 63.04; H, 5.77; P, 10.84%. ^{31}P NMR: δ=40.0; ^{13}C(OAc): δ=187.1 and 25.8.

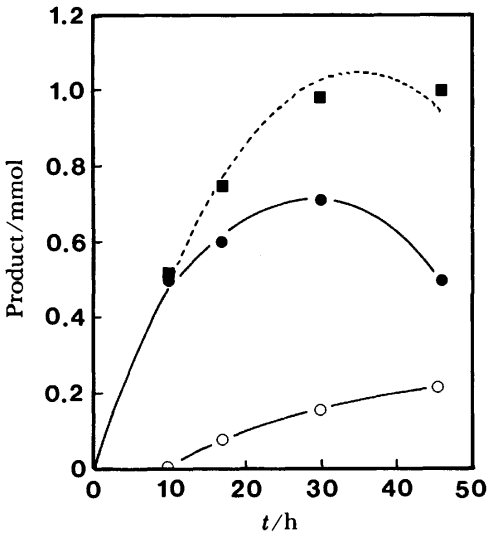

Fig. 1. Time-course plot of product distribution for methanol dehydrogenation with $[Ru_2(OAc)_4Cl]$/PPh_3 catalyst. $[Ru_2(OAc)_4Cl]$ 0.5 mmol dm^{-3}, $[PPh_3]$ 3.5 mmol dm^{-3}, methanol 200 ml, 65 °C (refluxing), (●) HCHO, (○) $HCOOCH_3$, (■) H_2. (------) amount of H_2 equivalence calculated from the dehydrogenated products ([HCHO]+[$HCOOCH_3$]×2).

Results and Discussion

Product Distribution. The change of product distribution in the composite-type ($[Ru_2(OAc)_4Cl]$-PPh_3; $[PPh_3]/[Ru_2]$=7.0) catalyst solution during the reaction was shown in Fig. 1. The reaction product in the initial 10 h period was only formaldehyde (5.2 turnovers), whereas methyl formate was formed as the secondary product, without accompanying dimethoxymethane in this catalyst solution. Neither carbon monoxide nor methane was detected in the evolved gas.

Excellent stoichiometry between dihydrogen and the sum of the dehydrogenated products was ascertained throughout the reaction.

Products during the 17 h reaction in the catalyst solutions of both the composite-type, $[Ru_2(OAc)_4Cl]$-PR_3(PR_3=PPh_3, $PEtPh_2$, and PEt_2Ph; $[PR_3]/[Ru_2]$= 7.0), and the mononuclear type, $[Ru(OAc)Cl(PEtPh_2)_3]$ are summarized in Table 1. Formaldehyde was found for all the catalysts. Methyl formate was found as the main product for the ruthenium complex coordinated with $PEtPh_2$ or PEt_2Ph. Some dimethoxymethane was detected in these catalyst solutions after the 17 h reaction.

Excellent stoichiometric coincidence of dihydrogen toward the sum of the dehydrogenated products was observed throughout the catalysts.

Initial Reaction Rate Dependence on Catalyst Concentration. The reaction rates at the refluxing temperature (65 °C) for the methanol solution of $[Ru(OAc)Cl(PEtPh_2)_3]$ were almost time-independent over a concentration range from 0.5 mmol dm^{-3} to 5.0 mmol dm^{-3} during the initial 17 h period (Fig. 2).

The dependence of the initial rate on catalyst concentration was linear below 0.5 mmol dm^{-3} and deviated to decrease from linearity at higher concentration (>1.0 mmol dm^{-3}). A similar rate dependence on the catalyst concentration was noted for the $[RuCl_2(PPh_3)_3]$ complex previously in the dehydrogenation of alcohol to evolve dihydrogen[8] and hydrogen transfer processes.[9]

Catalyst Deactivation Due to Structural Change. The catalytic activity of $[Ru(OAc)Cl(PEtPh_2)_3]$ for

Table 1. Product Distribution in Catalytic Methanol Dehydrogenation with Ruthenium Complexes

Catalyst	Gas phase	Product/mmol Liquid phase			
	H_2	HCHO 1	$CH_2(OCH_3)_2$ 2	$HCOOCH_3$ 3	1+2+3×2
$[Ru_2(OAc)_4Cl]/PPh_3$[a]	0.75	0.60	Trace	0.08	0.76
$[Ru_2(OAc)_4Cl]/PEtPh_2$[b]	3.65	0.40	0.04	1.67	3.78
$[Ru(OAc)Cl(PEtPh_2)_3]$[c]	2.49	0.26	0.18	0.99	2.42
$[Ru_2(OAc)_4Cl]/PEt_2Ph$[d]	3.20	0.24	0.09	1.56	3.45

a) $[Ru_2(OAc)_4Cl]$ 0.5 mmol dm^{-3}, PPh_3 3.5 mmol dm^{-3}. b) $[Ru_2(OAc)_4Cl]$ 2.5 mmol dm^{-3}, $PEtPh_2$ 17.5 mmol dm^{-3}. c) $[Ru(OAc)Cl(PEtPh_2)_3]$ 2.5 mmol dm^{-3}. d) $[Ru_2(OAc)_4Cl]$ 2.5 mmol dm^{-3}, PEt_2Ph 17.5 mmol dm^{-3}. Methanol 200 ml, reaction period 17 h, 65 °C (refluxing).

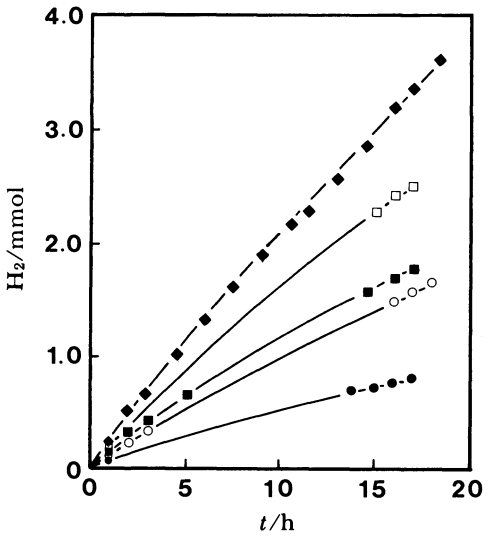

Fig. 2. Time-course plot of dihydrogen evolution from methanol with [Ru(OAc)Cl($PEtPh_2$)$_3$] catalyst. [Ru(OAc)Cl($PEtPh_2$)$_3$]: (●) 0.50 mmol dm^{-3}, (○) 1.0 mmol dm^{-3}, (■) 1.5 mmol dm^{-3}, (□) 2.5 mmol dm^{-3}, (◆) 5.0 mmol dm^{-3}. Methanol 200 ml, 65 °C (refluxing).

methanol dehydrogenation decreased gradually and disappeared finally (88 h). From the deactivated solution, a white complex was isolated and identified as [RuClH(CO)($PEtPh_2$)$_3$] on the basis of NMR, IR and elemental analyses. Found: C, 63.92; H, 5.79%. Calcd for $C_{43}H_{46}P_3OClRu$: C, 63.90; H, 5.74%. ^{31}P NMR: δ=36.9(2P) and 12.8(1P). ^2J(PP)=15.1 Hz, $^2J(PH)_{cis}$=22.9 Hz, and $^2J(PH)_{trans}$=103.9 Hz. ^{1}H NMR: δ=−7.1. IR (KBr): ν (CO) at 1924 (s), ν (RuH) at 1819 (w) cm^{-1}. Since one of the phosphine and hydride ligands are trans-disposed to each other ($^2J(PH)_{trans}$=103.9 Hz) and the other two and hydride are cis-disposed ($^2J(PH)_{cis}$=22.9 Hz), the remaining two ligands of Cl and CO are required to be coaxial. Based on these chemical analyses and spectroscopic characteristics, the coordination structure of the hydride carbonyl complex **1** in the solution is described as shown below.

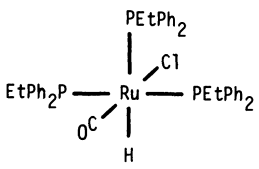

1

After the 20 h reaction, the ^{31}P NMR spectrum of the catalyst solution (5.0 mmol dm^{-3}) consisted of only the hydride carbonyl complex **1** besides the original complex, suggesting its exclusive change into **1** during the reaction. The addition of paraformaldehyde accelerated the rate decrease, supporting the view that the product formaldehyde supplied the H and CO ligands of this deactivated complex **1**. Provided that these ligands replaced the bidentate OAc ligand of the original complex, these cis-disposed sites were usable for splitting the methoxyl C–H bond to give a hydride complex.[10]

Table 2. Effect of Additives on the Initial Rate of Dihydrogen Evolution from Methanol with [Ru(OAc)Cl($PEtPh_2$)$_3$] Catalyst[a]

Additive	Amount/mmol dm^{-3}	H_2/mmol
None	—	0.54
LiCl	1.0	0.58
$LiOAc\cdot 2H_2O$	1.0	0.55
$PEtPh_2$	3.0	0.55

a) [Ru(OAc)Cl($PEtPh_2$)$_3$] 1.0 mmol dm^{-3}, methanol 200 ml, reaction period 5 h, 65 °C (refluxing).

Table 3. Effect of Added CH_3COOH on the Rate of Dihydrogen Evolution from Methanol with [Ru(OAc)Cl($PEtPh_2$)$_3$] Catalyst[a]

[CH_3COOH]/[Ru] ratio	Turnover number 17 h	42 h
0.0	10.20	18.59
0.5	14.11	21.81
1.0	16.15	24.52
2.0	16.32	26.87
5.1	15.30	26.97
20.0	14.28	29.67

a) [Ru(OAc)Cl($PEtPh_2$)$_3$] 0.25 mmol dm^{-3}, methanol 400 ml, 65 °C (refluxing).

Effect of Additives on Reaction Rate. As shown in Table 2, initial reaction rate of the [Ru(OAc)Cl($PEtPh_2$)$_3$] complex was unchanged by adding either an equimolar amount of lithium acetate or lithium chloride. Even at a three-fold excess, free $PEtPh_2$ gave a negligible effect. Consequently, spontaneous dissociation of the acetato, chlorido and phosphine ligands would be unlikely in the methanol solution.

Rate enhancement was observed, however, on the addition of acetic acid (Table 3). During the initial reaction period (17 h), the rate increased up to an optimum ratio of catalyst to acid of 2.0 mol mol^{-1}, accompanied by progressive inhibition at higher concentrations. Monotonous rate enhancement was observed after the reaction period of 42 h. As is well-known, some kinds of hydride complexes react with protonic compounds, yielding dihydrogen.[11] It is therefore reasonable that acetic acid accelerates the dihydrogen evolution, as far as a hydride complex is incorporated as the reaction intermediate in the catalytic dehydrogenation cycle. In the presence of excess free acid, this accelerating effect would be depressed by another reaction process such as solvolysis of the catalyst.[2c]

Postulated Reaction Scheme for Dehydrogenation of Methanol. A reaction mechanism of alcohol de-

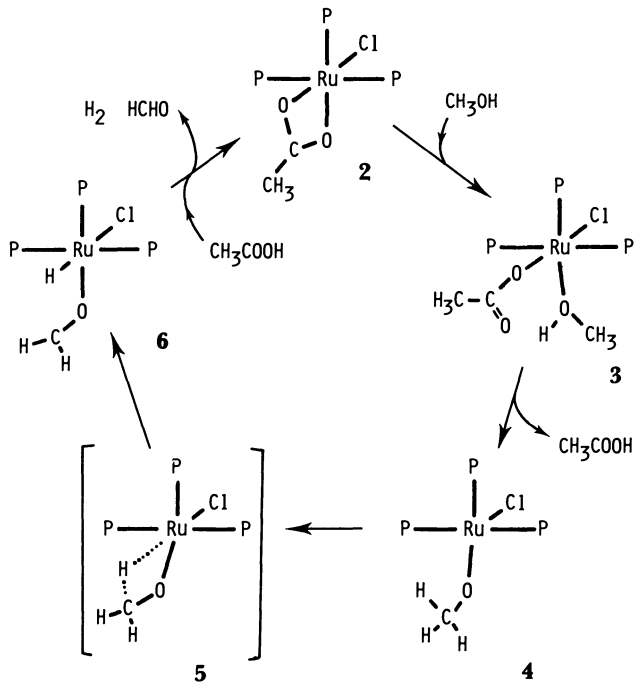

Scheme 1. Reaction scheme postulated for methanol dehydrogenation.

hydrogenation was proposed previously by Dobson and Robinson. This consisted of three essential processes: (1) substitution of a bidentate carboxylato ligand (Ac_FO) with alcohol (ROH) to generate free acid (Ac_FOH), an alkoxyl ligand (RO) and a vacant site, (2) splitting of the C–H bond at the β position of the alkoxyl ligand to give an intermediate coordinated with a hydride ligand, leaving the dehydrogenated product, and (3) dihydrogen evolution by protonating this hydride ligand with free acid (Ac_FOH) to regenerate the carboxylato ligand (Ac_FO).[2c] On the basis of this reaction mechanism in addition to our experimental results concerning the structure of deactivated complex **1** and the effect of additives on the initial reaction rate, the following reaction scheme is postulated for the catalytic methanol dehydrogenation with $[Ru(OAc)Cl(PEtPh_2)_3]$ (Scheme 1).

The bidentate acetato ligand of the original complex **2** is changed into a monodentate one by methanol coordination **3**. By a proton transfer from the coordinated methanol to the monodentate acetato ligand, acetic acid is liberated from the complex, leaving a vacant site cis-disposed to the methoxyl ligand **4**. The C–H splitting at the β-position of the methoxyl ligand would be facilitated by an agostic interaction[12,13] between the ruthenium and hydrogen atoms **5**.[10] The hydride intermediate complex **6** thus formed is attacked by free acetic acid to yield the products H_2 and HCHO, regenerating the original complex **2**.

References

1) A. Seidell, "Solubilities of Inorganic and Metal Organic Compounds," 3rd ed., Vol. 1, D. Van Nostrand, New York (1940), p. 567.

2) a) H. B. Charman, *J. Chem. Soc. B*, **1970**, 584; b) W. Strohmeier, E. Hitzel, and B. Kraft, *J. Mol. Catal.*, **3**, 61 (1977); c) A. Dobson and S. D. Robinson, *Inorg. Chem.*, **16**, 137 (1977); d) C. Fragale, M. Gargano, and M. Rossi, *J. Mol. Catal.*, **5**, 65 (1979); e) C. W. Jung and P. E. Garrou, *Organometallics*, **1**, 658 (1982); f) S. Shinoda, T. Kojima, and Y. Saito, *J. Mol. Catal.*, **18**, 99 (1983).

3) a) S. Shinoda, H. Moriyama, Y. Kise, and Y. Saito, *J. Chem. Soc., Chem. Commun.*, **1978**, 348; b) H. Arakawa and Y. Sugi, *Chem. Lett.*, **1981**, 1323; c) H. Moriyama, T. Aoki, S. Shinoda, and Y. Saito, *J. Chem. Soc., Perkin Trans. 2*, **1982**, 369; d) E. Delgalo-Lieta, M. A. Luke, R. F. Jones, and D. J. Cole-Hamilton, *Polyhedron*, **1**, 839 (1982); e) R. Irie, X. Li and Y. Saito, *J. Mol. Catal.*, **18**, 263 (1983); f) C. G. Griggs and D. J. H. Smith, *J. Organomet. Chem.*, **273**, 105 (1984); g) D. M. Roundhill, *J. Am. Chem. Soc.*, **107**, 4354 (1985); h) T. Yamakawa, H. Miyake, H. Moriyama, S. Shinoda, and Y. Saito, *J. Chem. Soc., Chem. Commun.*, **1986**, 326.

4) a) H. Arakawa, Y. Sugi, K. Takeuchi, K. Bando, and Y. Takami, *Shokubai (Catalyst)*, **25**, 392 (1983); b) H. Yamamoto, S. Shinoda, and Y. Saito, *J. Mol. Catal.*, **30**, 259 (1985); c) T. Takahashi, S. Shinoda, and Y. Saito, *J. Mol. Catal.*, **31**, 301 (1985).

5) S. Shinoda, H. Itagaki, and Y. Saito, *J. Chem. Soc., Chem. Commun.*, **1985**, 860.

6) T. A. Smith, R. P. Aplin, and P. M. Maitlis, *J. Organomet. Chem.*, **291**, C13 (1985).

7) R. W. Mitchell, A. Spencer, and G. Wilkinson, *J. Chem. Soc., Dalton Trans.*, **1973**, 846.

8) I. Pri-Bar and O. Buchman, H. Schumann, and H. J. Kroth, J. Blum, *J. Org. Chem.*, **45**, 4418 (1980).

9) Y. Sasson and J. Blum, *J. Org. Chem.*, **40**, 1887 (1975).

10) H. Itagaki, Y. Saito, and S. Shinoda, *J. Mol. Catal.*, **41**, 209 (1987).

11) R. A. Schunn, "Transition Metal Hydrides," ed by E. L. Muetterties, Marcel Dekker, New York (1971), pp. 203—269.

12) Z. Dawoodi, M. L. H. Green, V. S. B. Mtetwa, and K. Prout, *J. Chem. Soc., Chem. Commun.*, **1982**, 802.

13) N. Koga, S. Obara, and K. Morokuma, *J. Am. Chem. Soc.*, **106**, 4625 (1984).

Characterization of Active Sites in Sulfided Molybdenum/Alumina Hydrodesulfurization Catalysts

Akinori MAEZAWA, Masaru KITAMURA, Yasuaki OKAMOTO,* and Toshinobu IMANAKA
Department of Chemical Engineering, Faculty of Engineering Science, Osaka University, Toyonaka, Osaka 560
(Received December 4, 1987)

The site configuration of Al_2O_3-supported molybdenum sulfides catalytically active for hydrodesulfurization (HDS) of thiophene has been investigated as a function of pretreatment conditions (H_2S/H_2=0—0.2) by using X-ray photoelectron, laser Raman and IR spectroscopies and temperature-programmed desorption of adsorbed NO. It has been found that when MoO_3/Al_2O_3 catalysts are presulfided with H_2S/H_2, MoS_2-like species are formed, whereas when prereduced and subsequently sulfided during the HDS reaction, molybdenum oxide sulfides or highly dispersed amorphous molybdenum sulfides are initially produced. The turnover frequency of the HDS reaction calculated on the basis of the NO adsorption was shown to increase with decreasing dispersion degree of sulfided molybdenum. It is proposed that two kinds of NO adsorption sites are present; triply and doubly coordinatively unsaturated (cus) molybdenum sites. It is considered that both sites are catalytically active, possibly, the triply cus species being more active. It is concluded that the HDS activity of sulfided MoO_3/Al_2O_3 catalysts is determined by the structure, dispersion and coordinative unsaturation of sulfided molybdenum.

Supported molybdenum catalysts are widely used in industry for hydrodesulfurization (HDS). Cobalt and/or nickel are employed to promote the molybdenum catalysts. The synergic effects of the promoters have been studied by many workers[1-6] and reviewed by several authors.[7-12] Recently, Topsøe et al. have shown by using Mössbauer emission spectroscopy that a Co-Mo-S phase on promoted sulfide catalysts is responsible for HDS reactions.[12-15] In this model, it is considered that molybdenum is described as a MoS_2-like structure. EXAFS studies indicated the presence of such structures on sulfided Mo/Al_2O_3 and $Co\text{-}Mo/Al_2O_3$ catalysts.[16-18] However, the configurations of active sites on these dispersed molybdenum sulfides have not been unveiled yet. They are functions of the degree of the molybdenum sulfidation[19] and support.[20]

In order to characterize the catalytically active Mo-sites, several molecules are used as a probe; NO,[21-27] O_2,[14,28-35] CO,[36,37] H_2S,[38,39] and pyridine.[19,40,41] The amount of NO,[15,42] O_2,[43] or H_2S[38] chemisorption is relatively well correlated to HDS activities. However, it has not been established yet which is the most appropriate probe molecule. Nitric oxide is considered to be one of the most convenient molecule for the IR studies due to its high extinction coefficient and for differentiating adsorption sites.[21-27] In addition, it is well-established that NO adsorbs on multiply cus (coordinatively unsaturated) molybdenum sites as a dinitrosyl[21] or dimeric[23] complex. Valyon and Hall[22] have suggested that cus Mo-sites in reduced catalysts are Mo^{2+} from the IR study of the coadsorption of NO and O_2.

In order to reveal the configuration of the active sites on molybdenum sulfides responsible for the thiophene HDS reaction, an NO adsorption study was carried out herein for MoO_3/Al_2O_3 catalysts sulfided under various conditions, coupled with X-ray photoelectron (XPS), laser Raman (LRS) and IR spectroscopies and temperature-programmed desorption techniques.

Experimental

γ-Al_2O_3 was supplied by the Catalysis Society of Japan as a reference catalyst (JRC-ALO-4).[39] The B.E.T. surface area of the support was 163 m^2g^{-1}.

Supported molybdenum catalysts were prepared by an incipient impregnation method.[39] The loading level of MoO_3 was adjusted to be 2.5—30 wt% with respect to the support. An aqueous solution of the appropriate concentration of ammonium heptamolybdate (Nakarai Chemicals) was added to the Al_2O_3 (1.2 $cm^3g\text{-}(Al_2O_3)^{-1}$) and kneaded for 10 min at room temperature. Subsequently, the catalyst slurry was dried at 383 K for 18 h, followed by calcination in air at 823 K for 5 h.

The presulfidation of the catalyst was carried out at 673 K for 1.5 h in a stream of an atmospheric pressure of H_2S/H_2 (H_2S/H_2; 0—0.20, 500 mL STP min^{-1}). Subsequently, the HDS reaction of thiophene was carried out at the same temperature in an atmospheric pressure of a thiophene/H_2 stream (1.6% thiophene, 1 L STP min^{-1}), followed by measurements of catalytic activity at the reaction time of 1—1.5 h. The reaction gas was analyzed by GLC. The catalyst was, then, treated with an atmospheric pressure of a deoxygenated and dehydrated H_2-stream at 673 K for 1 h and evacuated for 1 h at the same temperature. After being cooled to room temperature under a dynamic vacuum, the amount of NO chemisorption was measured at room temperature (exposed to NO for 0.5 h and evacuated for 1 h, accompanied by NO physisorption experiments). After that, the XP spectra of the catalyst was measured without exposing the catalyst to air. The XPS measurements were made on a Hitachi 507 photoelectron spectrometer using Al $K\alpha_{1,2}$ radiation (1486.6 eV). The anode was operated at 9 kV and 50 mA. Assuming linear backgrounds, the intensity ratios were determined by using the integrated

areas of the Mo3d, S2p, S2s, and A12p levels. The binding energies were referenced to the A12p level at 74.5 eV.

The measurements of IR, temperature-programmed desorption (TPD) of NO and LR spectra were made in situ for the activated catalyst samples. The samples were exposed to NO and/or H_2S at room temperature for the IR and TPD studies. The IR spectra of the catalyst were recorded in a transmittance mode at room temperature on a Hitachi EPl-G double beam spectrophotometer by employing self-supporting wafers. The TPD study of NO adsorbed on the sulfided catalyst was conducted in a dynamic vacuum at a rate of 1.8 K min^{-1} from room temperature to ca. 570 K and evolved gases were continuously and repeatedly analyzed by a mass filter (ULVAC, MSQ-150A). The LR spectra were obtained by using an in situ cell at room temperature with a JASCO R-800 spectrometer equipped with a double monochromater. The 514.5 nm line of a NEC GLS-3200 Ar^+ laser was used for excitation at the intensity of 150—200 mW at the source. A spectral resolution was 5 cm^{-1}.

Results and Discussion

The HDS activities of the MoO_3/Al_2O_3 catalysts for thiophene are shown in Fig. 1 as a function of the H_2S/H_2 ratio in the presulfidation and the loading level of MoO_3. It is apparent that when the catalyst (5–30 wt% MoO_3) is presulfided at an increasing H_2S/H_2 ratio, the activity decreases steeply at a low H_2S/H_2 ratio (< 0.02) and then diminishes gradually at a futher increase in the ratio. At $H_2S/H_2=0$, the MoO_3/Al_2O_3 catalyst was reduced with H_2 and then sulfided with thiophene and/or resultant H_2S during the HDS reaction. At 2.5 wt% MoO_3 content, on the other hand, the HDS activity increases as the H_2S/H_2 ratio increases. It has been previously found that the activation mode of the catalyst affects the activity of the sulfided catalyst.[19]

In addition, the duration of the sulfiding treatment is an important factor determing the HDS activity when the H_2S/H_2 ratio is very low. On the sulfidation by thiophene/H_2 ($H_2S/H_2=0$ in Fig. 1), the catalytic activity of the 15 wt% MoO_3/Al_2O_3 catalyst decreased gradually to a conversion of 35% after a 12 h-treatment. During this treatment, the H_2S/H_2 ratio caused by the conversion of thiophene was calculated to be ca. 0.008. Therefore, the H_2S/H_2 ratio is considered to determine the rate of the sulfidation of molybdena under our experimental conditions. A direct sulfidation of the catalyst without the prereduction has been found to provide a sulfided catalyst similar to the one obtained at $H_2S/H_2=0$.[19] Accordingly, it is considered that the dependence of the HDS activity on both the sulfidation conditions and the loading level of MoO_3 is correlated to the differences in the structure (including a transient one) and dispersion degree of molybdenum sulfides formed on the catalyst surface.

As shown in Fig. 1 the HDS activity increases up to a loading level of 15 wt% MoO_3 and becomes independent of the MoO_3 loading level regardless of the sulfidation conditions. This is attributable to a formation of well-dispersed molybdenum species up to 15 wt% MoO_3 and in accord with the XRD and XPS results; no detection of crystalline MoS_2 by XRD and a linear correlation between the Mo3d/A12p XPS intensity ratio and the surface concentration of molybdenum at <15 wt% MoO_3 as observed previously.[19] No significant change in the Mo3d/A12p ratio was observed on the sulfidation of the catalyst with H_2S/H_2. The previous observations[19] of a considerable variation in the XPS intensity ratio on sulfidation may be attributed to the use of CS_2/H_2 for sulfiding instead of H_2S/H_2 and/or to different levels of impurities on Al_2O_3 surfaces which greatly modify the surface properties of Al_2O_3 as shown previously for the H_2S adsorption.[39]

The degree of sulfidation of molybdenum, S/Mo atomic ratio, is depicted in Fig. 2 as a function of the

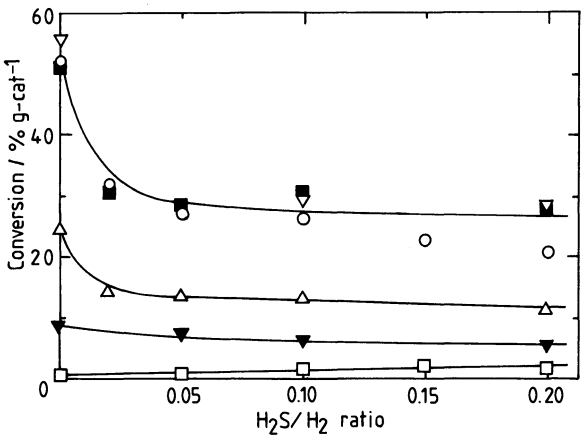

Fig. 1. Dependence of the thiophene HDS activity of sulfided MoO_3/Al_2O_3 catalyst on the H_2S/H_2 ratio in sulfiding.
□, 2.5 wt%; ▼, 5 wt%; △, 10 wt%; ○, 15 wt%; ▽, 20 wt%; ■, 30 wt%.

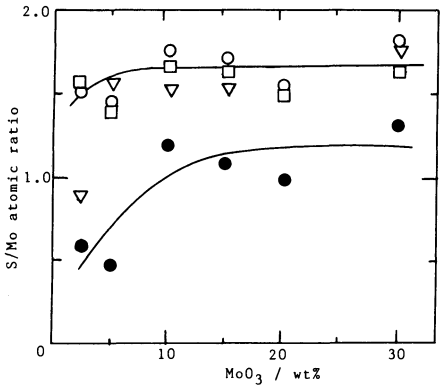

Fig. 2. S/Mo atomic ratio as a function of the MoO_3 content for the sulfided catalyst after the HDS of thiophene at 673 K.
●, $H_2S/H_2=0$; ▽, 0.05; ○, 0.1; □, 0.2.

MoO_3 content. The S/Mo ratio was calculated from the S2p/Mo3d XPS intensity ratio.[19] Apparently, the S/Mo ratio is increased by the H_2S/H_2-presulfidation and almost independent of the H_2S/H_2 ratio at>0.05. The S/Mo ratio gradually increases with the MoO_3 content up to 10 wt% (except a considerably low S/Mo ratio for the 2.5 wt% MoO_3 catalyst activated at 0.05) and becomes constant (S/Mo=1.6—1.7). It is evident that the S/Mo ratio is lower than two, this suggesting an incomplete transformation of supported molybdenum to MoS_2. As shown in Fig. 2, under the conditions of H_2S/H_2=0, however, the S/Mo atomic ratio increases with increasing the MoO_3 content up to 15 wt% and levels off at a lower S/Mo ratio (1.0—1.2) compared with that attained when presulfided. This suggests that the structures of sulfided molybdenum species formed on the catalyst surface are significantly different between the presulfidation and prereduction conditions. It is noted that the molybdenum sulfide species produced at a very low H_2S/H_2 ratio are gradually transformed to the stable molybdenum sulfide species produced at H_2S/H_2> 0.1 (vide infra).

These findings suggest that a considerable portion of molybdenum species which resists sulfiding exists in the low MoO_3 content catalysts, especially, at 2.5 wt% MoO_3. Zingg et al.[44] have reported with MoO_3/Al_2O_3 catalysts that the molybdenum occupies mainly tetrahedral sites at a low MoO_3 content and that two types of tetrahedral molybdenum species are present on the oxidic catalyst. These are monomeric and dimeric species. The monomeric species resists sulfiding, while the dimeric species are easily sulfided to MoS_2. Our results are in line with their model.

It is well-established that NO adsorbs on cus Mo-sites in a pair.[21] The amount of NO adsorption is relatively well correlated to the HDS activity.[15,42] Therefore, the dispersion degree of molybdenum was assessed by the amount of NO chemisorption. The fraction of cus Mo-sites thus obtained is shown in Fig. 3 against the MoO_3 content. The fraction varied with the H_2S/H_2 ratio, too. At H_2S/H_2 ratio of >0.1, the proportion of the adsorption site decreases as the MoO_3 content increases. As for the 2.5 wt% MoO_3 catalyst, 25–30% of molybdenum adsorb two NO molecules when properly activated. While, at the low H_2S/H_2 ratios, the fraction of NO-adsorption sites shows a maximum (at 10 and 20 wt% MoO_3 for H_2S/H_2=0.05 and 0, respectively). The proportion of cus Mo-sites in the low MoO_3 content catalysts (2.5 and 5 wt%) increases with increasing H_2S/H_2 ratio, while the fraction decreases for the catalysts containing 10—30 wt% MoO_3.

The turnover frequency (TOF) of the thiophene HDS reaction on the sulfided molybdenum catalyst was obtained on the basis of the amount of NO chemisorption. The TOF is shown in Fig. 4 as a function of the MoO_3 content. When the catalyst was presulfided with H_2S/H_2, the TOF increased with the MoO_3 content almost irrespective of the sulfidation conditions. At H_2S/H_2=0, however, a plateau is seen above 15 wt% MoO_3. It is considered that the dependence of TOF on the MoO_3 content results from the changes of the structure and dispersion of active molybdenum species.

In an analogy with the estimation of the dispersion degree of metal by using CO or H_2 adsorption for supported metal catalysts,it is proposed that the extent of dispersion of molybdenum sulfides (D_{Mo-S}) is evaluated from the amount of NO adsorption and the degree of sulfidation of molybdenum as in Eq. 1.

$$D_{Mo-S} = \text{(Fraction of Mo which adsorbs } (NO)_2\text{)/ (Fraction of molybdenum sulfides)} \quad (1)$$

On the basis of the XPS results of Li and Hercules,[45] it is assumed here that the stoichiometry of sulfided

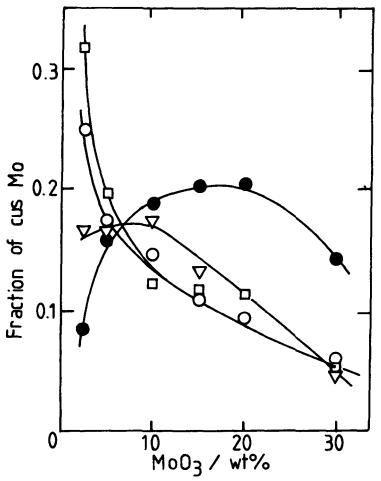

Fig. 3. Fraction of cus Mo (a half of the NO/Mo molecular ratio) vs. MoO_3 content measured after the HDS of thiophene at 673 K.
●, H_2S/H_2=0; ▽, 0.05; ○, 0.1; □, 0.2.

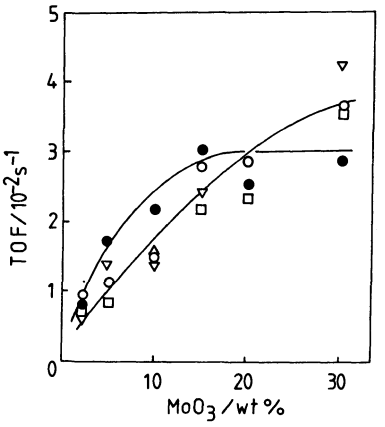

Fig. 4. Dependence of the TOF of thiophene HDS reaction over the sulfided catalyst upon the MoO_3 content.
●, H_2S/H_2=0; ▽, 0.05; ○, 0.1; □, 0.2.

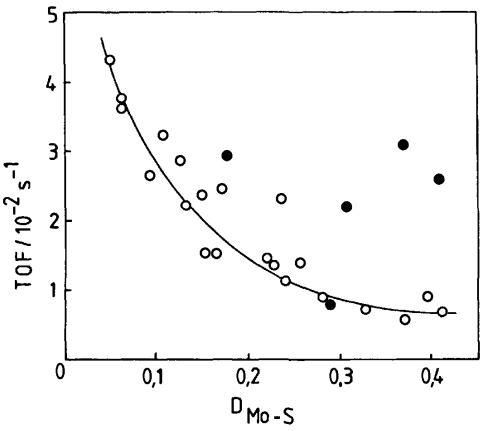

Fig. 5. Dependence of the TOF of thiophene HDS reaction on the dispersion degree of molybdenum sulfide.
●, $H_2S/H_2=0$; ○, >0.1.

molybdenum species is two. The incomplete sulfiding of Mo in Fig. 2 indicates a partial transformation of Mo oxides to the sulfide species. The TOF of the thiophene HDS reaction is depicted in Fig. 5 against the dispersion degree of molybdenum sulfides. When the catalyst was presulfided ($H_2S/H_2 > 0$),the TOF is evidently correlated to the dispersion degree of molybdenum sulfides; the TOF increases, as the degree of MoS_2 dispersion decreases. The decreased dispersion degree is considered to correspond to an increased size of molybdenum sulfides, although no crystalline MoS_2 was detected by XRD except the catalyst with the lowest dispersion (30 wt% MoO_3). However, the TOF at $H_2S/H_2=0$ is higher than that for the presulfided catalysts and seems independent of the dispersion degree of molybdenum sulfides. It is suggested that the structure of sulfided molybdenum species formed at $H_2S/H_2=0$ are different from those produced by presulfiding with H_2S/H_2.

In order to characterize the molybdenum sulfides, in situ LRS techniques were used. Typical spectra are shown in Fig. 6. Regardless of the H_2S/H_2 ratio and loading levels, the peak at ca. 960 cm^{-1} in the oxidic state, which is characteristic of well-dispersed polymolybdate phases,[46-48] completely disappeared after sulfidation. The LR spectra indicated that molybdenum oxides with Mo=O bonds were completely sulfided by H_2S/H_2 or the thiophene HDS reaction. When the catalyst was presulfided, a strong peak at 405 cm^{-1} accompanied by broad peaks at ca. 450 and 380 cm^{-1} was observed. These pair peaks are assigned to a MoS_2 phase.[49] The above findings indicate that the molybdenum sulfides formed on sulfided catalyst have a MoS_2-like structure. Clausen et al.[16,17] and Huntly et al.[18] recently observed the presence of microcrystalline MoS_2 in sulfided catalysts by using EXAFS. On the other hand, when the catalyst was prereduced and subsequently sulfided during the

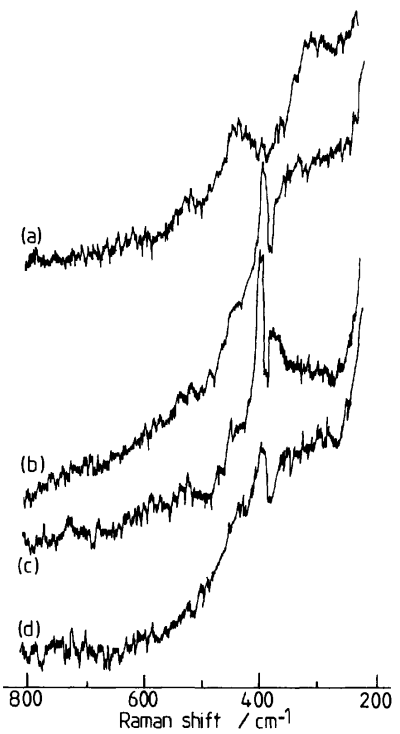

Fig. 6. In situ laser Raman spectra for MoO_3/Al_2O_3 catalysts sulfided at 673 K in an atmospheric H_2S/H_2 stream, followed by the HDS of thiophene at the same temperature.
(a) 15 wt%, $H_2S/H_2=0$; (b) 15 wt%, 0.02; (c) 15 wt%, 0.1; (d) 2.5 wt%, 0.1.

reaction, the peaks at 380 and 405 cm^{-1} were not observed and only broadened peaks at 450 and 350 cm^{-1} due to a Mo-S stretching bands[49] were detected as shown in Fig. 6. It is considered that the structure of the active molybdenum species is not a MoS_2-like structure, suggesting the formation of molybdenum oxide sulfides or highly dispersed amorphous molybdenum sulfides. However, after a prolonged sulfiding by the thiophene/H_2(12 h), the LR spectra showed a transformation of the above sulfides to MoS_2-like species. This is consistent with the variation in the catalytic activity.

The IR spectra of NO adsorbed on the sulfided catalysts are illustrated in Fig. 7. Irrespective of the pretreatment conditions, the spectra consist of two adsorption peaks at 1795 and 1715—1690 cm^{-1}. They are assigned to symmetric and asymmetric stretching bands of dinitrosyl species, respectively.[50] The band positions indicate that two NO molecules adsorb on sulfided Mo-sites.[22,25] It is considered that even under the pretreatment conditions of $H_2S/H_2=0$, cus Mo-sites are actually sulfided during the HDS reaction of thiophene. However, the spectroscopic features at $H_2S/H_2=0$ and those at 0.1 are significantly different; the symmetric/asymmetric intensity ratios are 1.02 and 1.36 at $H_2S/H_2=0$ and 0.1, respectively. The ON-Mo-NO angle (θ) is suggested to be different in

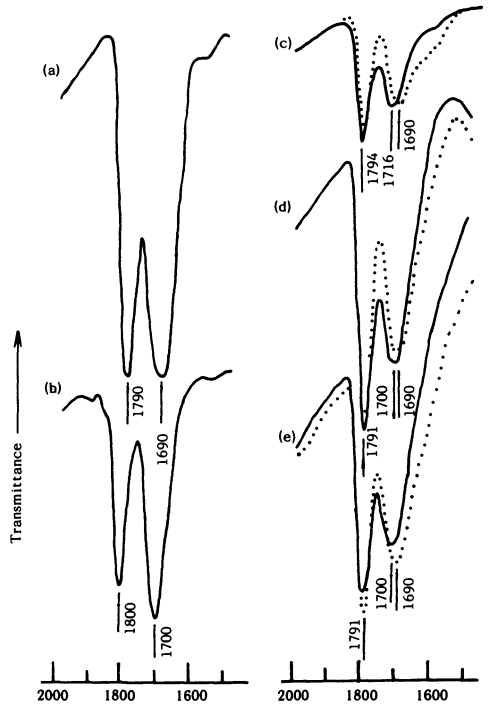

Fig. 7. IR spectra of NO adsorbed on the MoO_3/Al_2O_3 catalysts reduced or sulfided at 673 K in an atmospheric H_2 or H_2S/H_2 stream, followed by the HDS of thiophene at the same temperature.
(a) 10 wt%, only reduced; (b) 10 wt%, $H_2S/H_2=0$; (c) 2.5 wt%, 0.1; (d) 10 wt%, 0.1; (e) 20 wt%, 0.1. The dotted line shows the change of the IR spectrum of preadsorbed NO when the sample was exposed to H_2S (5.3 kPa) and evacuated at room temperature for 30 min.

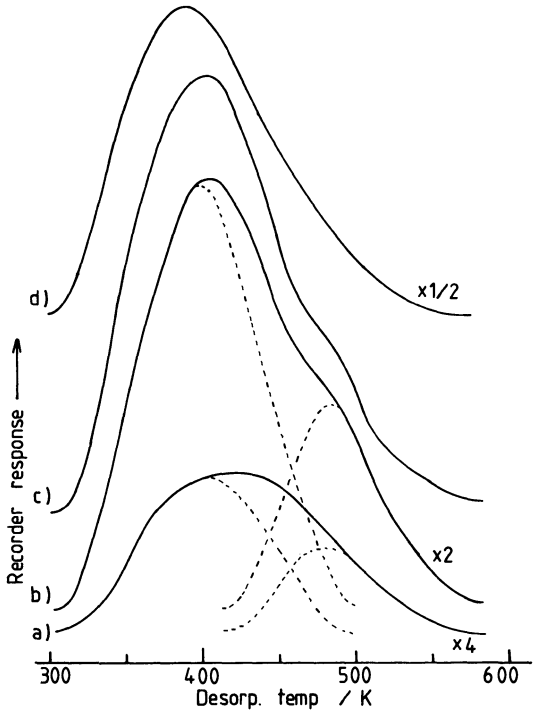

Fig. 8. TPD profiles ($m/z=30$) of NO adsorbed on the sulfided MoO_3/Al_2O_3 catalyst ($H_2S/H_2=0.1$).
(a) 2.5 wt%, (b) 5 wt%, (c) 10 wt%, (d) 20 wt%. The broken lines show the resolved peaks.

these two sulfides and calculated to be 90 and 81°, when prereduced and presulfided, respectively, on the basis of a theoretical equation;[50] $I_{sym}/I_{asym}=\cot^2(\theta/2)$. In conjunction with the results of LRS measurements, the IR spectrum observed at $H_2S/H_2=0.1$ is assigned to NO molecules adsorb on a MoS_2-like structure, whereas the spectrum at $H_2S/H_2=0$ to dinitrosyls adsorbed on molybdenum oxide sulfides or highly dispersed amorphous molybdenum sulfides. The IR spectroscopic features for NO adsorbed on the catalyst at $H_2S/H_2=0$ is very close to those for NO held on a reduced MoO_3/Al_2O_3 catalyst as shown in Fig. 7. This suggests that the structure of the sulfides formed under mild sulfidation conditions is similar to the structure of molybdenum oxide precursor phase. Taking into consideration the observations[51] that part of polymolybdate species are reduced at a relatively low temperature such as 673 K employed here, it is considered that initial sulfidations occur with polymolybdate species irrespective of the prereduction and keep these original structures almost intact to produce molybdenum oxide sulfides or amorphous molybdenum sulfides. A formation of oxide sulfides from polymolybdates has been proposed by Schrader and Chang using LRS.[49]

The dependence of the TOF of thiophene HDS reaction on the dispersion degree of sulfided molybdenum in Fig. 5 suggests the presence of several kinds of molybdenum sites. In order to characterize further the NO adsorption sites, the TPD study of NO adsorbed on sulfided catalyst was conducted. The TPD profiles of NO ($m/z=30$) are shown in Fig. 8. The main peak is observed at a desorption temperature of ca. 400 K, accompanying a weak shoulder at a higher temperature side (ca. 480 K). It seems that the relative intensity of the main peak at ca. 400 K increases with increasing MoO_3 content in the catalyst. It is revealed that two kinds of NO adsorption sites are differentiated by the TPD techniques. According to the IR measurements in Fig. 7, the TPD peaks are likely to be attributed to the signals due to distinct sulfided Mo-sites but not to composite peaks of sulfided and reduced Mo-sites. The presence of two desorption peaks in the TPD study was confirmed for molybdenum sulfides supported on TiO_2 in a more conclusive manner.[52] Segawa et al.[53] reported two NO desorption peaks for reduced MoO_3/TiO_2 systems. The thermal desorption of NO accompanied a production of N_2O; the desorption temperature of N_2O was ca. 400 K and the peak area intensity ratio of N_2O/NO did not vary significantly with MoO_3 content.

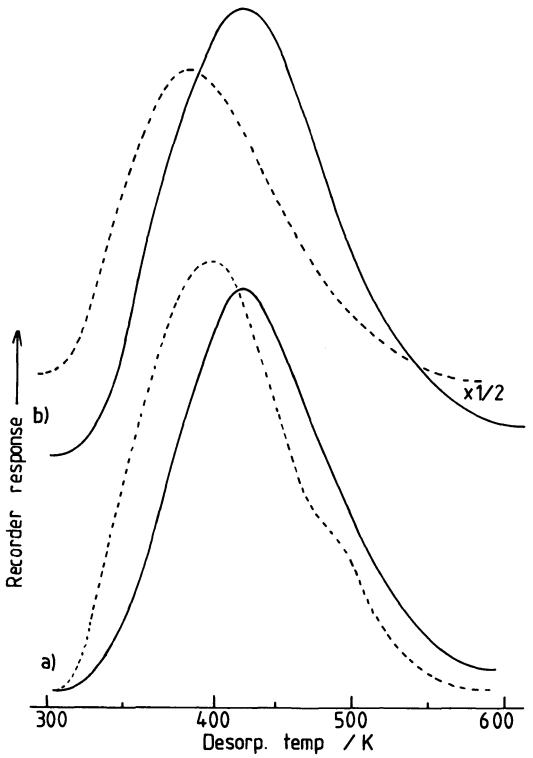

Fig. 9. TPD profiles (m/z=30) of NO on the sulfied MoO_3/Al_2O_3 catalyst (H_2S/H_2=0.1) coadsorbed with H_2S.
(a) 10 wt%, (b) 20 wt%. The broken lines show the TPD profile of adsorbed NO alone.

In order to determine the configuration of the sulfided Mo-sites, a coadsorption of NO and H_2S was examined. Figure 7 shows the changes in the IR spectra of NO when H_2S was introduced. No NO molecules were desorbed by the exposure of the sample to H_2S and by a subsequent evacuation at room temperature. On a contact of the NO-adsorption system with H_2S, the symmetric and asymmetric bands became considerably well separated, since the wavenumber of the latter peak was red-shifted by ca. 10 cm^{-1}. A pre-adsorption of H_2S considerably reduced the IR intensity of adsorbed NO. However, a similar red-shift of the lower-wavenumber peak of NO band was also observed. Accordingly, the spectral changes are considered to result from the interactions between adsorbed NO and H_2S molecules.

The TPD profiles of NO coadsorbed with H_2S are shown in Fig. 9. The desorption peak of H_2S (m/z=34) was observed at ca. 360 K. This is attributed to α-H_2S adsorbed on bare Al_2O_3 surface.[39] Hydrogen sulfide adsorbed on sulfided molybdenum sites is expected to desorb at higher temperature than 600 K.[39] It is noteworthy that the temperature of NO desorption at ca. 400 K is increased by 30 K on the exposure of the sample to H_2S. The peak area intensity ratio of N_2O/NO significantly decreased by the H_2S adsorption. These findings also suggest the presence of direct interactions between adsorbed NO and H_2S molecules. On the basis of the IR and TPD results, we propose here that sulfided Mo-sites for NO adsorption consist of triply and doubly cus molybdenum species and that NO molecules adsorbed on the triply cus sites desorb at ca. 400 K, while those on the doubly cus sites at ca. 480 K. Both NO species adsorb to form dinitrosyl or dimeric complex. Hydrogen sulfide molecule adsorbs on the triply cus Mo-sites preadsorbed with two NO molecules, affecting the IR and TPD of NO. The TPD peak at 430 K is assigned to the desorption of NO adsorbed on the triply cus Mo-sites coadsorbed with H_2S or SH. With increasing MoO_3 content in the MoO_3/Al_2O_3 catalyst, the size of MoS_2 particles increases as deduced from the decrease in the NO/Mo ratio, accompanying an increase in the fraction of the triply cus Mo-sites. This may be rationalized by a stabilization of multiply cus Mo-sites by electronically compensating properties of bulky semiconducting MoS_2 phases.

Combining the results on the TOF of sulfided MoO_3/Al_2O_3 catalysts for the HDS reaction with the configuration of the NO adsorption sites, it is suggested that both the triply and doubly cus molybdenum species are active for the HDS of thiophene, probably the triply cus Mo-sites showing higher activity. The activity of the sulfided MoO_3/Al_2O_3 catalyst is determined by two adverse factors; the number of active sites (NO adsorption sites) and the relative proportion of the triply and doubly cus Mo-sites. These adverse factors are considered to cause a volcano type correlation between the intrinsic activity (activity/unit weight of Mo) and sulfidation degree of molybdenum (S/Mo) as observed previously.[19]

Conclusion

On the basis of the results of XPS, LRS, and IR of NO absorbed on the catalyst, it is revealed that the structure of molybdenum sulfides formed on MoO_3/Al_2O_3 catalysts varies with the H_2S/H_2 ratio in the presulfiding atmosphere. It is demonstrated that MoS_2-like structure is formed when presulfided (H_2S/H_2>0.02), while molybdenum oxide sulfides or highly dispersed amorphous molybdenum sulfides are initially formed when prereduced (H_2S/H_2=0). The difference in the structure causes the difference in the thiophene HDS activity.

From the results of IR and TPD of NO adsorbed on sulfided catalysts, it is suggested that the NO adsorption sites consist of multiply cus molybdenum species, triply and doubly cus Mo-sites. The fraction of the triply cus Mo-sites increases with increasing molybdenum content or with increasing size of

molybdenum sulfide clusters. Taking into account the thiophene HDS activity, it is considered that both sites are active for the reaction, the triply cus sulfided molybdenum species being more active than the doubly cus sulfided molybdenum species.

References

1) J. M. J. Lipsch and G. C. A. Schuit, *J. Catal.*, **15**, 179 (1969).

2) G. C. A. Schuit, P. Courty, and B. Delmon, *AIChE J.*, **19**, 417 (1973).

3) G. Hagenbach, P. Courty, and B. Delmon, *J. Catal.*, **31**, 264 (1973).

4) B. Delmon "Proc. Climax 3rd Int. Conf. Chemistry and Uses of Molybdenum," ed by H. F. Barry and P. C. H. Mitchell, Climax Molybdenum Co. Ann Arbor, Michigan (1979), p. 73.

5) R. J. H. Voorhoeve and J. C. M. Stuiver, *J. Catal.*, **23**, 288, 243 (1971).

6) A. L. Farragher and P. Cosses, "Proc. 5th Int. Congr. Catal.," ed by J. W. Hightower, (1973), p. 1301.

7) F. E. Massoth, *Adv. Catal.*, **27**, 265 (1978).

8) V. H. J. de Beer and G.C.A.Schuit "Preparation of Catalysts" ed by B. Delmon, P. A. Jacobs, and G. Poncelet, Elsevier, Amsterdam (1976), p. 343.

9) P. Ratnasamy and S. Sivasanker, *Catal. Rev.-Sci. Eng.*, **22**, 401 (1980).

10) P. Grange, *Catal. Rev.-Sci. Eng.*, **21**, 135, (1980).

11) P. C. H. Mitchell, "Catalysis," ed by C.Kemball and D. A. Dowden, Specialist Periodic Report, Royal Society of Chemistry, London (1980), Vol. 4, p. 175.

12) H.Topsøe and B. S. Clausen, *Catal. Rev.-Sci. Eng.*, **26**, 395 (1984).

13) H. Topsøe, B. S.Clausen, R. Candia, C. Wievel, and S. Mørup, *J. Catal.* , **68**, 433 (1981).

14) C. Wivel, R. Candia, B. S. Clausen, S. Mørup, and H. Topsøe, *J. Catal.*, **68**, 453 (1981).

15) Nan-Yu Topsøe and H. Topsøe, *J. Catal.*, **84**, 386 (1983).

16) B. S. Clausen, H. Topsøe, R. Candia, J. Villdsen, B. Lengeler, J. Als-Nielsen, and F. Christenen, *J. Phys. Chem.*, **85**, 3868, (1981).

17) R. Candia, B. S. Clausen, J. Bartholdy, Nan-Yu Topsøe, B. Lengeler, and H.Topsøe, Proc. 8th Int. Congr. Catal., Verlag Chemie, Weinheim, 1984 Vol. 2 p. 375.

18) R. D. Huntley, T. J. Parham, R.P.Merrill, and M. J. Sienlco, *Inorg. Chem.*, **22**, 4144 (1983).

19) a) Y. Okamoto, H. Tomioka, Y. Katoh, T. Imanaka, and S. Teranishi, *J. Phys. Chem.*, **84**, 1833 (1980); b) Y. Okamoto, H. Tomioka, T. Imanaka, and S. Teranishi, *J. Catal.*, **66**, 93, (1980).

20) a) Y. Okamoto, T. Imanaka, and S. Teranishi, *J. Phys. Chem.*, **85**, 3798 (1981); b) H. Topsøe, B. S. Clausen, N. Burriesci, R. Candia, and S. Mørup, "Proc. Preparation of Catalysts II," ed by B. Delmon, P. A. Jacobs, and G. Poncelet, Elsevier, Amsterdam (1979), p.479; c) J. C. Dushet, E. M. van Oers, V. H. J. de Beer, and R. Prins, *J. Catal.*, **80**, 386 (1983); d) G. Muralidhar,F. E. Massoth, and J. Shabtai, *J. Catal.*, **85**, 44 (1984); e) F. E. Massoth, G. Muralidhar, and J. Shabtai, *J. Catal.*, **85**, 53 (1984).

21) W. S. Millman and W. K. Hall, *J. Phys. Chem.*, **83**, 427 (1979).

22) J. Valyon and W. K. Hall, *J. Catal.*, **84**, 216 (1983).

23) J. B. Peri, *Amer. Chem. Soc. Div. Petrol. Chem. Prepr.*, **23**, 1281 (1978).

24) Nan-Yu Topsøe and H. Topsøe, *J. Catal.*, **75**, 354 (1982).

25) Y. Okamoto, Y. Katoh, Y. Mori, T. Imanaka, and S. Teranishi, *J.Catal.*, **70**, 445 (1981).

26) K. Segawa and W. K. Hall, *J. Catal.*, **77**, 221 (1982).

27) W. S. Millman and W. K. Hall, *J. Catal.*, **59**, 311 (1979).

28) S. J. Tauster, T. A. Pecoraro, and R. R. Chianelli, *J. Catal.*, **63**, 515 (1980).

29) S. J. Tauster and L. J. Riley, *J. Catal.*, **67**, 250 (1981); **70**, 230 (1981).

30) B. S. Parekh and S. W. Weller, *J. Catal.*, **47**, 100 (1977); **55**, 58 (1978).

31) C. H. Lui, L. Yuan, and S. W. Weller, *J. Catal.*, **61**, 282 (1980); **66**, 65 (1980).

32) J. L. G. Fierro, S. Mendioroz, J. A. Pajares, and S. W. Weller, *J. Catal.*, **65**, 263 (1980).

33) S. W. Weller, *Acc. Chem. Res.*, **16**, 101 (1983).

34) G. Muraslidhar, B. E. Concha, G. L. Bartholomew, and C. H. Bartholomew, *J. Catal.*, **89**, 274 (1984).

35) J. L. G. Fierro, L. Gonzalez, A. Lopez, and S. W. Weller, *J. Catal.*, **89**, 111 (1984).

36) M. I. Zaki, B. Vielhaber, and H. Knözinger, *J. Phys. Chem.*, **90**, 3176 (1986).

37) E. Delgado, G. A. Fuentes, C. Hermann, and H. Knözinger, *Bull. Soc. Chim. Belg.*, **93**, 735 (1984).

38) R. Burch and A. Collins, *Appl. Catal.*, **18**, 373 (1985).

39) Y. Okamoto, M. Oh-Hara, A. Maezawa, T. Imanaka, and S. Teranishi, *J. Phys. Chem.*, **90**, 2396 (1986).

40) K. Segawa and W. K. Hall, *J. Catal.*, **94**, 133 (1982).

41) W. Suarez, J. A. Dumesic, and C. G. Hill, *J. Catal.*, **94** 408 (1985).

42) A. Lopez Agudo, F. J. Gil Llambias, J. M. D. Tascon, and J. L. G. Fierro, *Bull. Soc. Chim. Belg.*, **93**, 719 (1984).

43) W. Zierczak, G. Muralidhar, and F. E. Massoth, *J. Catal.*, **77**, 432 (1983).

44) D. S. Zingg, L. E. Makovsky, R. E. Tischer, F. R. Brown, and D. M. Hercules, *J. Phys. Chem.*, **84**, 2898 (1980).

45) C. P. Li and D. M. Hercules, *J. Phys. Chem.*, **88**, 456 (1984).

46) C. P. Chang and G. L. Schrader, *J. Catal.*, **60**, 276 (1979).

47) F. R. Brown, L. E. Makovsky, and K. H. Rhee, *J. Catal.*, **50**, 162 (1977).

48) H. Jeziorowski and H. Knozinger, *J. Phys. Chem.*, **83**, 1166 (1979).

49) G. L. Schrader and C. P. Chang, *J. Catal.*, **80**, 369 (1983).

50) H. C. Yao and W. G. Rothschild, "Proc. 4th Intern. Conf. Chemistry and Uses of Molybdenum," ed by H. F. Barry and P. C. H. Mitchell, 1982, p. 31.

51) W. K. Hall, "Proc. 4th Intern. Conf. Chemistry and Uses of Molybdenum," ed by H. F. Barry and P. C. H. Mitchell, 1982, p. 224.

52) Y. Okamoto, A. Maezawa, and T. Imanaka, unpublished results.

53) K. Segawa, D. S. Kim, and Y. Kurusu, Proc. 8th Japan-USSR Catalysis Seminar, Tokyo, Japan, 1986, p. 131.

 © 1988 The Chemical Society of Japan Bull. Chem. Soc. Jpn., 61, 2303—2308 (1988)

Synthesis, Crystal Structure, and Physical Properties of the Charge-Transfer Complex Bis[benzo[1,2-*c*:3,4-*c'*:5,6-*c''*]trithiophene]-tetrafluorotetracyanoquinodimethan, $(BTT)_2(TCNQF_4)$

Tadashi SUGANO, Takashi HASHIDA,§ Akiko KOBAYASHI,† Hayao KOBAYASHI,†† and Minoru KINOSHITA*

The Institute for Solid State Physics, The University of Tokyo, Roppongi, Minato-ku, Tokyo 106

†Department of Chemistry, Faculty of Science, The University of Tokyo, Hongo, Bunkyo-ku, Tokyo 113

††Department of Chemistry, Faculty of Science, Toho University, Funabashi, Chiba 274

(Received December 11, 1987)

The semiconductive 2:1 charge-transfer complex between benzo[1,2-*c*:3,4-*c'*:5,6-*c''*]trithiophene and 2,2'-(2,3,5,6-tetrafluoro-2,5-cyclohexadiene-1,4-diylidene)bis[propanedinitrile], $(BTT)_2(TCNQF_4)$, crystallizes in the monoclinic system, space group $P2_1/c$, with the following cell constants: a=8.893(2) Å, b=10.589(2) Å, c=18.528(4) Å, β=114.52(1)°, V=1587.5(10) Å^3, D_x=1.61 g cm^{-3}, and Z=2. The crystal structure of $(BTT)_2(TCNQF_4)$ consists of stacking columns of alternating donor dyads and acceptor monads (DAD units) along the crystallographic b axis. Side-by-side sulfur-sulfur contacts shorter than the sum of the van der Waals radii were found along the axis between BTT molecules on the neighboring columns. Polarized reflectance spectra were measured with the single crystal of $(BTT)_2(TCNQF_4)$ at room temperature, showing a charge-transfer band polarized parallel to the stacking direction. The degree of charge transfer was estimated to be 0.21 from the oscillator strength and the transition energy of the charge-transfer band. From this, as well as the electric and magnetic properties of the complexes and the atomic distances for $TCNQF_4$, it was concluded that $(BTT)_2(TCNQF_4)$ is a weakly ionized charge-transfer complex.

Benzo[1,2-*c*:3,4-*c'*:5,6-*c''*]trithiophene (BTT) is one of aromatic molecules with heteroatoms at the periphery, which may act to increase transverse interchain interactions in the solid consisting of molecular stacking columns. BTT was first synthesized by Hart and Sasaoka[1] as a model chalcogen-bridged hexaradiarene, a molecule of considerable theoretical interest. However it was also shown by them that BTT forms air- and moisture-stable crystalline 1:1 charge-transfer (CT) complexes with the electron acceptors TCNE, TCNQ, DDQ, and chloranil.[1,2]

Recently, bis(ethylenedithio)tetrathiafulvalene (BEDT-TTF), which is an electron-donating aromatic molecule with heteroatoms at the periphery, was found to form side-by-side contacts shorter than the sum of the van der Waals radii between the heteroatoms.[3] This fact prompts us to investigate CT complexes based on BTT in order to find another electron donor which could form side-by-side contacts between molecules, since BTT gives CT complexes with some electron acceptors. 2,2'-(2,3,5,6-tetrafluoro-2,5-cyclohexadiene-1,4-diylidene)bis[propanedinitrile] (commonly abbreviated to tetrafluorotetracyanoquinodimethan $TCNQF_4$) is an electron acceptor having a redox potential higher than that of chloranil, TCNE, TNCQ, and DDQ. $TCNQF_4$ was therefore chosen as an electron acceptor to find ionic CT complexes, which might exhibit interesting electric and magnetic properties.

The present paper describes the synthesis and crystal structure of 2:1 CT complex of BTT with $TCNQF_4$, $(BTT)_2(TCNQF_4)$.[4] The polarized reflectance spectra observed for $(BTT)_2(TCNQF_4)$ are discussed on the basis of the crystal structure. The degree of charge transfer in $(BTT)_2(TCNQF_4)$ is estimated from the molecular geometry of $TCNQF_4$ and also from the oscillator strength and the transition energy of the CT band observed in the reflectance spectra. The electric and magnetic properties are discussed in relation to the degree of charge transfer.

Experimental

BTT was prepared according to the procedures described by Hart and Sasaoka.[1] $TCNQF_4$ was kindly provided by Professor Gunzi Saito of the Institute for Solid State Physics. $(BTT)_2(TCNQF_4)$ was obtained by the following way: 41.8 mg (0.170 mmol) of BTT and 46.0 mg (0.166 mmol) of $TCNQF_4$ were dissolved into a hot acetonitrile solution under an argon atmosphere and then the solution was allowed to stand until it cooled to room temperature. The precipitate was filtered off and washed with small amount of acetonitrile to give 47.4 mg (73%) of dark-green long-needle crystals of $(BTT)_2(TCNQF_4)$. Found: C, 56.22; H, 1.51; N, 7.08%; Calcd for $(C_{12}H_6S_3)_2C_{12}N_4F_4$: C, 56.24; H, 1.57; N, 7.29%. A 1:2 mixture of chlorobenzene and acetonitrile was also used as the solvent.[5] The crystals of the same composition with larger width were obtained from the mixture.

X-Ray diffraction intensities were measured at room temperature with the θ–2θ scan technique on a Rigaku automated four-circle diffractometer employing Mo $K\alpha$ radiation ($2\theta \leqq 60°$) and were corrected for Lorentz and polarization effects, but not for the absorption. The dimensions of the crystal used were 0.10×0.25×0.40 mm.

§ Present address: Matsushita Electric Industrial Co., Ltd., Kadoma, Osaka 571.

The structure was solved by the direct method and refined by the block-diagonal least-squares procedure to an R value of 0.063 with unit weight, using 2581 independent reflections ($|F_o|>3\sigma(|F_o|)$). Anisotropic thermal parameters were adopted for all non-hydrogen atoms, and the hydrogen atoms were refined isotropically. Atomic scattering factors and anomalous scattering corrections were taken from International Tables for X-ray Crystallography.[6] Observed and calculated structure factors, anisotropic thermal factors, and positional parameters for H atoms are deposited as Document No. 8809 at the Office of the Chemical Society of Japan. Calculations were carried out on a FACOM-U1300 computer at Toho University and a HITAC M680H computer at the Computer Centre of the University of Tokyo with a local version of UNICS.[7]

The polarized reflectance spectra at normal incidence on the ab and ac planes were measured at room temperature over the spectral range from 8000 to 28000 cm^{-1} using a microspectrophotometer described briefly in a previous paper.[8]

The dc conductivity along the needle (crystallographic b) axis of the single crystal was measured in the temperature range between 240 and 300 K by means of the two probe method.

The static magnetic susceptibility for 37 mg of the tiny crystals oriented randomly was measured with a Faraday-type susceptometer over the temperature range from 2 to 300 K at 3 T. The details of the apparatus were described previously.[9]

Crystal Structure

$(BTT)_2(TCNQF_4)$ crystallizes in the monoclinic system, space group $P2_1/c$, with the following cell constants: a=8.893(2) Å, b=10.589(2) Å, c=18.528(4) Å, β=114.52(1)°, V=1587.5(10) Å^3, Z=2, D_x=1.61 g cm^{-3}, and μ(Mo $K\alpha$)=47.1 mm^{-1}. The positional parameters for the atoms are given in Table 1. The atomic numbering schemes and the molecular geometries within the BTT donor and the $TCNQF_4$ acceptor are shown in Fig. 1. The $TCNQF_4$ molecule is located on a center of symmetry. The BTT and $TCNQF_4$ molecules are nearly planar with maximum diviations from their least-squares planes by 0.06 Å [S(1)] and 0.13 Å [F(2)], respectively. No anomalous bond distances and angles are found for both molecules.

The crystal structure of $(BTT)_2(TCNQF_4)$, as illustrated in Fig. 2, consists of stacks of alternating donor dyads and acceptor monads, extending along the crystallographic b axis. Within these stacking columns, the interplanar separations between two donors and between donor and acceptor are 3.42 Å and 3.29 Å respectively. The latter separation is an average value because of the slightly unparallel overlap with the dihedral angle of 5.5° between the planes. Crystallographic symmetry requires that the components

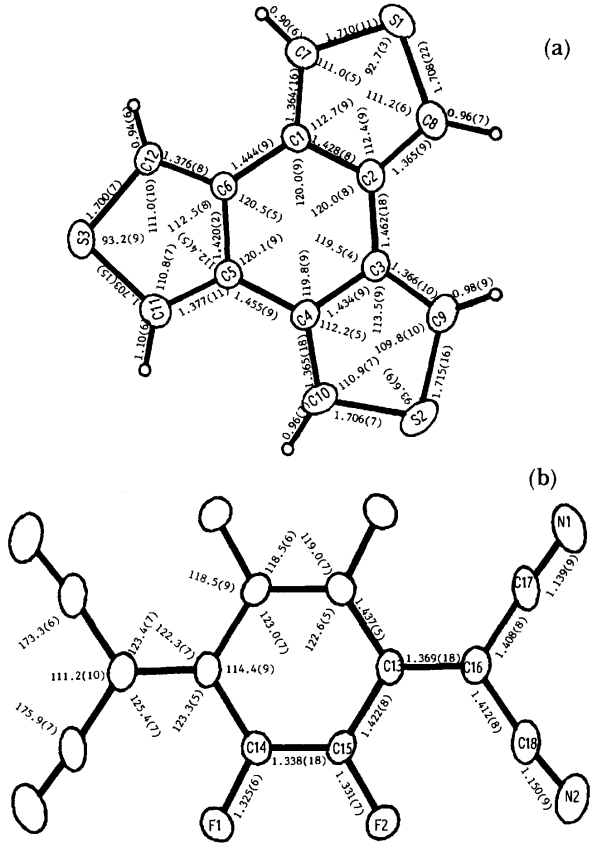

Fig. 1. Atomic numbering schemes and molecular geometries of the BTT donor (a) and the $TCNQF_4$ acceptor (b).

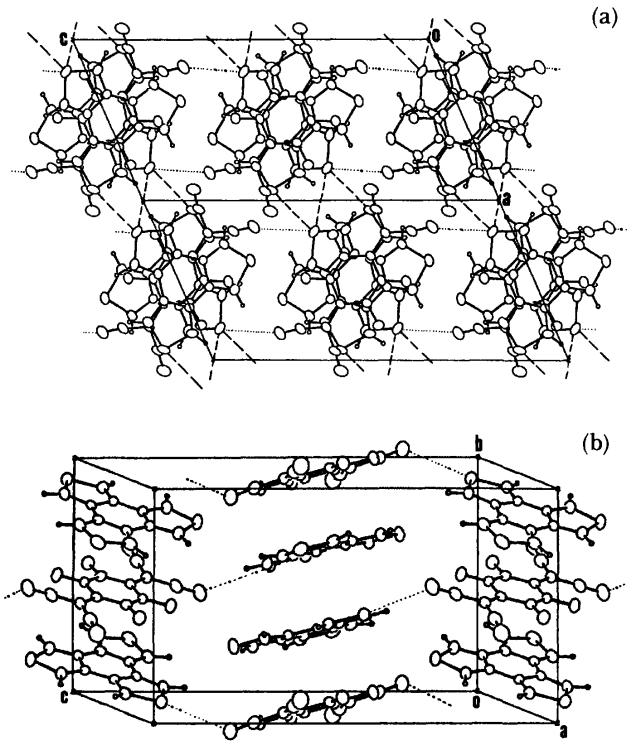

Fig. 2. Projection of the structure on the ac (a) and bc (b) planes. Broken lines represent S–S contacts shorter than the sum of vdW radii 3.70 Å between BTT molecules. Dotted lines represent S–N contacts between BTT and $TCNQF_4$ molecules.

of the donor dyads be parallel. The donor-acceptor interplanar separation is unusually short for a sulfur containing donor and rather close to that observed in the TCNQ complexes with donors containing no sulfur atoms, (perylene)$_3$(TCNQ) (3.37 Å)[10] and (benzidine)(TCNQ) (3.24 Å)[11] which exhibit a strong CT band.[12,13]

Table 1. Positional Parameters ($\times 10^4$) and Equivalent Isotropic Thermal Parameters (Å^2) for $(BTT)_2(TCNQF_4)$ with Esd's in Parantheses. $B_{eq}=(3/4)(B_{11}a^2+B_{22}b^2+B_{33}c^2+B_{12}ab\cos\gamma+B_{13}ac\cos\beta+B_{23}bc\cos\alpha)$

	x	y	z	$B_{eq}(\times 10^2)$/Å^2
S(1)	6191(2)	2771(2)	7283(1)	237(2)
S(2)	630(2)	2661(2)	3728(1)	236(2)
S(3)	8011(2)	4347(2)	4423(1)	217(2)
C(1)	6192(5)	3240(4)	5939(3)	133(6)
C(2)	4555(5)	2836(4)	5786(3)	139(6)
C(3)	3282(5)	2806(4)	4973(3)	143(7)
C(4)	3683(6)	3208(4)	4334(3)	143(7)
C(5)	5362(6)	3597(4)	4497(3)	144(3)
C(6)	6597(6)	3593(4)	5287(3)	133(7)
C(7)	7215(6)	3249(5)	6727(3)	187(8)
C(8)	6384(7)	2541(6)	6465(3)	205(9)
C(9)	1667(6)	2461(6)	4734(3)	202(8)
C(10)	2345(7)	3170(5)	3619(3)	203(9)
C(11)	5958(7)	4003(5)	3959(3)	199(9)
C(12)	8115(7)	3968(5)	5334(3)	184(9)
F(1)	4897(4)	−658(3)	6387(2)	213(5)
F(2)	2182(4)	−789(3)	5083(2)	218(5)
N(1)	−673(7)	−1074(7)	3469(4)	340(11)
N(2)	1693(7)	562(6)	2218(3)	301(10)
C(13)	3503(6)	−81(4)	4281(3)	143(6)
C(14)	4952(6)	−347(4)	5706(3)	148(7)
C(15)	3568(6)	−417(5)	5036(3)	151(7)
C(16)	2081(6)	−169(5)	3600(3)	174(8)
C(17)	564(6)	−649(6)	3550(3)	225(9)
C(18)	1957(7)	232(6)	2850(3)	213(9)

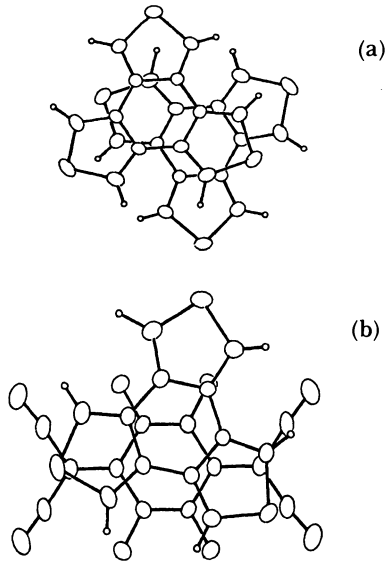

Fig. 3. Molecular overlapping modes of the donor-donor (a) and donor-acceptor (b) pairs.

The donor-donor and donor-acceptor molecular overlapping modes are shown in Fig. 3. Within the donor dyad the BTT molecule is rotated by approximately 60° with respect to the neighboring molecule so that the sulfur atoms at the periphery of the neighboring molecules keep away from each other. The central benzene rings of BTT are stacked in a ring-over-bond motif found commonly in planar aromatic hydrocarbons. One of the in-plane twofold rotation axes of BTT is rotated by 18° with respect to the molecular long-axis of $TCNQF_4$.

A significant feature of the crystal structure of $(BTT)_2(TCNQF_4)$ is that the interchain side-by-side sulfur-sulfur contacts shorter than the sum of the van der Waals radii (vdW) are found along the a axis. Short contacts between S(2)-S(3^i) at 3.572(4) Å and S(3)-S(3^i) at 3.567(2) Å (2×vdW(S)=3.70 Å), where i represents the key to symmetry code $1+x$, y, z, are indicated by the broken lines in Fig. 2(a). No sulfur-sulfur contacts shorter than the sum of vdW is found along the c axis. However close contact between S(3) and N(2^{ii}) at 3.41(6) Å (vdW(S)+vdW(N)=3.35 Å; ii represents the key to symmetry code $1-x$, $1/2+y$, $1/2-z$) is found along the c axis as shown in Fig. 2(b). The S-N contacts along the c axis are restricted within a DAD unit, whereas the S-S contacts along the a axis extend over an infinite chain. These findings demonstrate that BTT is capable of forming multi-dimensional molecular networks as expected from its molecular structure.

Polarized Reflectance Spectra

Figure 4 shows the reflectance spectra of $(BTT)_2(TCNQF_4)$ for light polarizations parallel to the crystallographic a, b, and c axes. Figure 5 shows the frequency dependent conductivity $\sigma(\tilde{\nu})$ of $(BTT)_2(TCNQF_4)$ calculated from the reflectance spectra

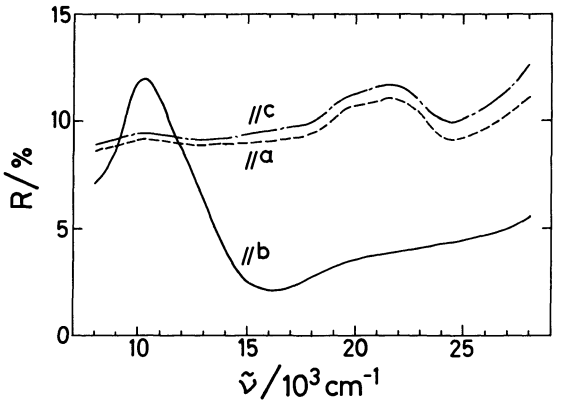

Fig. 4. Reflectance spectra of $(BTT)_2(TCNQF_4)$ with the polarization parallel to the crystallographic a, b, and c axes.

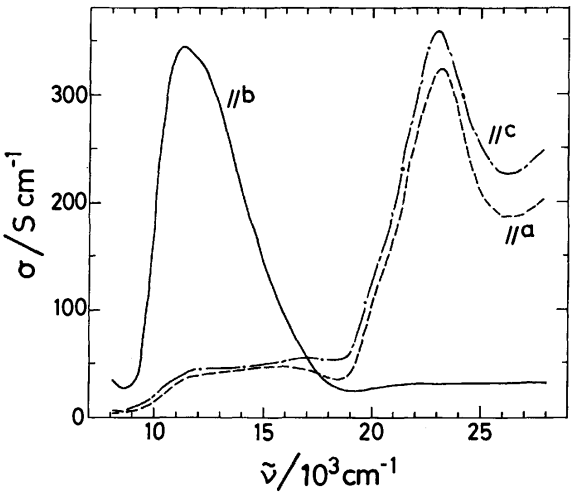

Fig. 5. Frequency dependent conductivity $\sigma(\tilde{\nu})$ of $(BTT)_2(TCNQF_4)$ with the polarizations parallel to the a, b, and c axes obtained by a Kramers-Kronig analysis of the reflectance spectra.

using the modified Kramers-Kronig transformation technique.[14] A conductivity peak appears in the near infrared region of the //b spectrum, whereas another peak appears in the visible region of the //a and //c spectra.

The conductivity peak located at 11200 cm^{-1} is almost completely polarized in the b axis which is parallel to the stacking direction and nearly perpendicular to the molecular planes of BTT and $TCNQF_4$. Since the lowest intramolecular excitations in BTT, $TCNQF_4$, and $TCNQF_4^-$ are expected to be polarized parallel to the planes, this peak would not be attributable to such intramolecular excitations, even if the low-lying excitation in $TCNQF_4^-$ appears in the region between 11000 and 15000 cm^{-1}.[15] The polarization direction of excitation corresponding to the conductivity peak is approximately parallel to the direction passing through the molecular centers of the donor and the acceptor. Therefore the conductivity peak at 11200 cm^{-1} can safely be attributed to the CT excitation between BTT and $TCNQF_4$,. The CT excitation band is asymmetric and tails to the high frequency side. A possible interpretation of the asymmetric band shape is superimposing of the progressional vibronic bands, since a more clear superimposed shoulder is sometimes observed for the CT band of the mixed-stack CT complexes such as $(perylene)_3(TCNQ)$.[12]

The conductivity peak appearing at 23100 cm^{-1} in the //a and //c spectra would be attributed to the intramolecular excitation in $TCNQF_4$. Absorption spectrum of $TCNQF_4$ exhibits an intense peak at 22900 cm^{-1} in a solid and at 26000 cm^{-1} in a solution,[16] while BTT shows absorption peaks at positions higher than 30000 cm^{-1}.[1] Thus it is unlikely to attribute the conductivity peak to the intramolecular excitation in BTT. It is clear from the //a, //b, and //c spectra that the conductivity peak is almost polarized along the ac plane in which the molecular planes of $TCNQF_4$ lie. The conductivity peak located at 23100 cm^{-1} is therefore most likely assigned to the low-lying intramolecular excitation in $TCNQF_4$.

Degree of Charge Transfer

It is of great importance to know the degree of charge transfer from the donor to the acceptor in order to discuss the physical properties of $(BTT)_2(TCNQF_4)$. The value of the degree of CT ρ from donor D to acceptor A may be related to the oscillator strength f by[17]

$$f = \frac{4\pi mc}{\hbar}\tilde{\nu}_{CT}|R_{DA}|^2\rho = 3.254\times10^{-5}\tilde{\nu}_{CT}|R_{DA}|^2\rho, \quad (1)$$

where R_{DA} is the distance (Å) between the molecular centers of D and A and $\tilde{\nu}_{CT}$ is the excitation energy of CT band in the cm^{-1} scale. The oscillator strength is given by[18]

$$f = \frac{4mc}{Ne^2}\int_{\tilde{\nu}_1}^{\tilde{\nu}_2}\sigma(\tilde{\nu})d\tilde{\nu}\cos^2\theta, \quad (2)$$

where N is the number of D-A pair per unit volume and θ is the angle between the light polarization and the transition dipole moment. By a numerical integration of the CT band in the conductivity spectrum, f is found to be 0.89. Thus ρ is estimated to be 0.21 from f using $\tilde{\nu}_{CT}$=11200 cm^{-1} and R_{DA}=3.43 Å.

The degree of CT obtained is 0.21. This value strongly suggests that $(BTT)_2(TCNQF_4)$ is not an ionic CT complex but a non-ionic (weakly ionized) CT complex. This finding is further checked by the comparison of bond distances of $TCNQF_4$ in $(BTT)_2(TCNQF_4)$ with those of neutral $TCNQF_4$[19] and ionic complexes of $TCNQF_4$[20-22] summarized in Table 2. The bond distance c is most sensitive to the ionicity of $TCNQF_4$. As seen in Table 2, c of $(BTT)_2(TCNQF_4)$ is close to that of neutral $TCNQF_4$. In general, however, bond distances are influenced by the molecular packing even if the molecule has the same ionicity. Kistenmacher et al.[23] proposed a way to determine the degree of CT for the crystal of TCNQ derivatives that consists of mixed stacks of alternating donors and the acceptors. The degree of CT ρ may be related to the ratio $\alpha=c/(b+d)$ by

$$\rho = \frac{\alpha_x - \alpha_0}{\alpha_1 - \alpha_0}, \quad (3)$$

where α_0, α_1, and α_x are the ratios for $TCNQ^0$, $TCNQ^-$, and $TCNQ^{x-}$ ($0<x<1$), respectively. We applied the relation to the $TCNQF_4$ complexes to estimate the degree of CT because the ratios obtained for $TCNQF_4$ and TCNQ are very close to each other (0.477 for $TCNQF_4^0$ and 0.476 for $TCNQ^0$; 0.498 for

Table 2. Comparison of Specific Bond Distances (Å) for the $TCNQF_4$ Molecules

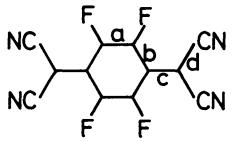

	a/Å	b/Å	c/Å	d/Å	$\alpha=c/(b+d)$	Ref.
$(BTT)_2(TCNQF_4)$	1.338(18)	1.430(10)	1.369(18)	1.411(12)	0.482	This work
$TCNQF_4$	1.334(2)	1.437(4)	1.372(2)	1.437(4)	0.477	17
M_2P-$TCNQF_4$[a]	1.354(6)	1.414(4)	1.415(4)	1.430(6)	0.498	18
DBTTF-$TCNQF_4$[b]	1.351(7)	1.421(7)	1.412(7)	1.425(7)	0.496	19
NBP-$TCNQF_4$[c]	1.350(4)	1.410(4)	1.413(4)	1.419(5)	0.499	20

a) M_2P: *N,N'*-dimethylphenazinium. b) DBTTF: dibenzotetrathiafulvalene. c) NBP: *N*-butylphenazinium.

$TCNQF_4^-$ and 0.500 for $TCNQ^-$). By using Eq.3 and the ratio 0.482 obtained for $(BTT)_2(TCNQF_4)$, ρ is found to be 0.24. This value agrees reasonably with that estimated from the conductivity spectra.

Electric and Magnetic Properties

Although BTT and $TCNQF_4$ molecules are essentially in non-ionic states as shown in the preceding section, charge transport may occur passing through the crystal. We examined the temperature dependence of electrical conductivity of the single crystal. The conductivity at room temperature along the stacking direction is found to be 1.0×10^{-8} S cm^{-1} and the activation energy 0.27 eV (1 eV=1.602×10^{-19} J). The conductivity is smaller than that (6×10^{-8} S cm^{-1}) reported for the 1:1 complex by Cowan et al., for which the degree of CT is estimated to be 0.60 from the CN stretching frequency.[4]

The activation energy is small for non-ionic CT complexes. The energy gap E_g (i.e., the energy required for the intrinsic carrier formation) for a CT complex can be estimated by the following relation;

$$E_g = I(D) - A(A) - \{P(D^+) + P(A^-)\} \quad (4)$$

where I(D) is the ionization potential of the donor D and A(A) is the electron affinity of the acceptor A. $P(D^+)$ and $P(A^-)$ are the polarization energies associated with the formations of D^+ and A^- ions in the crystal, respectively. The ionization potential of BTT in the solid state is determined experimentally to be 4.9 eV.[24] This value corresponds to $I(D)-P(D^+)$. At present, the electron affinity and the polarization energy of $TCNQF_4$ have not been experimentally determined. The electron affinity A(A) of TCNQ is, however, estimated to be 2.8 eV.[25] $P(A^-)$ of TCNQ could reasonably be assumed to be 1.5—2 eV. If we put these figures into Eq.4, the energy gap is estimated to be in the range of 0.1—0.6 eV, into which the twice the activation energy (i.e., energy gap) actually observed for $(BTT)_2(TCNQF_4)$ falls. The agreement between estimated and observed values would be further improved by using the parameters proper to $TCNQF_4$. It is therefore suggested that the observed conductivity in $(BTT)_2(TCNQF_4)$ is due to the intrinsic carrier formation.

The suggestion mentioned above is further supported by the results of static magnetic susceptibility measurements. The paramagnetic susceptibility was evaluated by subtracting the diamagnetic contribution $\chi_d=-418\times10^{-6}$ emu mol^{-1} (1 emu mol^{-1}=4π cm^3 mol^{-1}) which is the sum of the diamagnetic susceptibilities of the components $\chi_d=-134\times10^{-6}$ emu mol^{-1} for $TCNQF_4$ and -142×10^{-6} emu mol^{-1} for BTT). The paramagnetic susceptibility follows the Curie-Weiss law over the entire temperature range with a small Weiss constant -2.9 K. The Curie constant 4.7×10^{-4} emu K mol^{-1} is very small and corresponds to only 0.05% of unpaired electrons per formula unit. Therefore, there are essentially no unpaired electrons carrying charges and spins in the ground state, while the degree of CT is estimated to be 0.21—0.24. Thus the charge carriers are produced intrinsically by the excitation across the energy gap.

Conclusion

Benzo[1,2-*c*:3,4-*c'*:5,6-*c''*]trithiophene (BTT) gives a weakly ionized 2:1 charge-transfer (CT) complex with tetrafluorotetracyanoquinodimethan ($TCNQF_4$). The crystal structure of $(BTT)_2(TCNQF_4)$ consists of stacking columns of alternating donor dyads and acceptor monads, extending along the b axis. The degree of CT from BTT to $TCNQF_4$ is estimated to be 0.21 from the conductivity spectra and 0.24 from the molecular geometry of $TCNQF_4$. Semiconducting charge transport passing through the crystal occurs with intrinsic carrier formation due to the CT interaction between BTT and $TCNQF_4$. Side-by-side sulfur-sulfur contacts shorter than the sum of the van der Waals radii are found between the BTT molecules as expected from its molecular structure. However, the effects of the contacts on the physical properties of the crystal remains unclear because of the non-ionic ground state. It is therefore of interest to search ionic complexes and salts of BTT in order to elucidate the

transverse interchain interaction through the side-by-side contacts provided by the sulfur atoms at the periphery of the BTT molecule.

This work was partly supported by a Grant-in-Aid for Scientific Research from the Minitry of Education, Science and Culture.

References

1) H. Hart and M. Sasaoka, *J. Am. Chem. Soc.*, **100**, 4326 (1978).

2) TCNE: tetracyanoethylene. TCNQ: tetracyanoquinodimethan; 2.2′-(2,5-cyclohexadiene-1,4-diylidene)bis[propanedinitrile]. DDQ: 2,3-dichloro-5,6-dicyano-*p*-benzoquinone. Chloranil: 2,3,5,6-tetrachloro-*p*-benzoquinone.

3) H. Kobayashi, A. Kobayashi, Y. Sasaki, G. Saito, T. Enoki, and H. Inokuchi, *J. Am. Chem. Soc.*, **105**, 297 (1983).

4) CT complex between BTT and $TCNQF_4$ was first reported as a 1:1 complex in the paper appeared in D. O. Cowan, A. Kini, L.-Y. Chiang, K. Lerstrup, T. O. Poehler, and A. N. Bloch, *Mol. Cryst. Liq. Cryst.*, **86**, 1 (1982).

5) The 1:1 complex was obtained using this solvent in Ref. 4.

6) "International Tables for X-ray Crystallography", Vol. IV, Kynoch Press, Birmingham (1974), p. 152.

7) T. Sakurai, "UNICS, Universal Crystallographic Computation Program System", The Crystallographic Society of Japan, Tokyo, Japan (1967).

8) T. Sugano, K. Yamada, G. Saito, and M. Kinoshita, *Solid State Commun.*, **55**, 137 (1985).

9) M. Takahashi, T. Sugano, and M. Kinoshita, *Bull. Chem. Soc. Jpn.*, **57**, 26 (1984).

10) A. W. Hanson, *Acta Crystallogr., Sect. B*, **34**, 2339 (1978).

11) K. Yakushi, I. Ikemoto, and H. Kuroda, *Acta Crystallogr., Sect. B*, **30**, 835 (1974).

12) K. Ishii, K. Yakushi, H. Kuroda, and H. Inokuchi, *Bull. Chem. Soc. Jpn.*, **57**, 3043 (1984).

13) K. Yakushi, M. Iguchi, and H Kuroda., *Bull. Chem. Soc. Jpn.*, **52**, 3180 (1979).

14) R. K. Ahrenkiel, *J. Opt. Soc. Am.*, **61**, 1651 (1971).

15) G. Saito, H. Kumagai, J. Tanaka, T. Enoki, and H. Inokuchi, *Mol. Cryst. Liq. Cryst.*, **120**, 337 (1985).

16) M. T. Jones, T. Maruo, S. Jansen, J. Roble, and R. D. Rataiczek, *Physica*, **143B**, 518 (1986).

17) C. S. Jacobsen and J. B. Torrance, *J. Chem, Phys.*, **78**, 112 (1983).

18) F. Wooten, "Optical Properties of Solids", Academic Press, New York (1972), p. 72.

19) T. J. Emge, M. Maxfield, D. O. Cowan, and T. J. Kistenmacher, *Mol. Cryst. Liq. Cryst.*, **65**, 161 (1981).

20) Z. G. Soos. H. J. Keller, K. Ludolf, J. Queckborner, D. Wehe, and S. Flandrois, *J. Chem. Phys.*, **74**, 5287 (1981).

21) T. J. Emge, W. A. Bryden, F. M. Wiygul, D. O. Cowan, and T. J. Kistenmacher, *J. Chem. Phys.*, **77**, 3188 (1982).

22) R. M. Metzger, N. E. Heimer, D. Gundel, H. Sixl, R. H. Harms, H. J. Keller, D. Nothe, and D. Wehe, *J. Chem. Phys.*, **77**, 6203 (1982).

23) T. J. Kistenmacher, T. J. Emge, A. N. Bloch, and D. O. Cowan, *Acta Crystallogr., Sect. B*, **38**, 1193 (1982).

24) N. Sato, private communication.

25) E. C. M. Chen and W. E. Wentworth, *J. Chem. Phys.*, **63**, 3183 (1975)

Prebiotic Synthesis Obeys the Rule of Topological Charge Stabilization

Jun-ichi AIHARA
Department of Chemistry, Faculty of Science, Shizuoka University,
Oya, Shizuoka 422
(Received December 18, 1987)

Most organic molecules synthesized in primitive-Earth-simulation experiments conform to the rule of topological charge stabilization. Heteroatoms in these molecules are all located at the best sites to stabilize the conjugated systems. The situation must be the same for organic molecules formed under prebiotic conditions on primitive Earth.

Chemical evolution may be defined as prebiotic chemical processes leading to the origin of life on Earth.[1-7] It must have occurred in the presence of water and minerals, utilizing the components of the primitive atmosphere, such as carbon dioxide, carbon monoxide, methane, and hydrogen.[1-7] Small amounts of ammonia, hydrogen cyanide (HCN), and hydrogen sulfide were presumably dissolved in the primitive lakes and oceans. Chemical processes must have been driven principally by solar energy in the form of light, lightning, and heat. Some thermal energy was provided by volcanoes, meteoritic impact and radioactive decay.

Many laboratory experiments have been designed to model the prebiotic formation of amino acids, nucleoside bases, and many other biologically important molecules.[1-7] A variety of organic molecules can indeed be synthesized in primitive-Earth-simulation (PES) experiments. Most organic molecules synthesized in PES experiments have one or more heteroatoms in their π-electron systems. It might be a very important matter to seek for the reason why these molecules are produced under prebiotic conditions. Of course, it is never easy to answer this question. Even a partial answer will mark an important progress in the study of chemical evolution and the origin of life.

In 1983 Gimarc pointed out that the pattern of charge densities in a molecule is determined primarily by the connectivity or the topology of the molecule.[8-11] Many examples indicate that nature prefers to place heteroatoms of great electronegativity in those positions where the isostructural, iso-π-eleccronic hydrocarbon has large charge densities. Gimarc called the effect the rule of topological charge stabilization or the TCS rule.[8] This paper aims at explaining the stability of organic molecules formed in PES experiments in terms of Gimarc's TCS rule. We will show below that all these molecules are thermodynamically stable owing to the heteroatoms located at the right sites.

Theory

Charge densities calculated for a molecule containing heteroatoms depend on the choice of semiempirical parameters, but in the isostructural, iso-π-electronic hydrocarbon charge densities are determined only by the topology of the molecule and the number of π electrons. Gimarc referred to the isostructural, iso-π-electronic hydrocarbon as the uniform reference frame (URF).[8-10] The URF is nothing other than a conjugated hydrocarbon obtained by replacing all heteroatoms in a given molecule by sp^2 carbons and then by donating the same number of π electrons to the resulting system. The TCS rule utilizes such URF's to estimate the stability of organic molecules of abiotic origin. First-order perturbation theory has given a justification for the rule.[8]

All charge densities given below will be those calculated for the π-electron systems of the URF's. We used the Hückel molecular orbital (HMO) model in its simplest form. The HMO model is best suited for the present purpose which requires only a qualitative pattern of charge distributions.[8,11] All alkyl substituents will be disregarded for simplicity because they are scarcely conjugated with the parent π-electron framework.

Results and Discussion

Amino acids are crucial building blocks of life. Since the Miller-Urey experiment reported in 1953,[12] a great number of amino acid syntheses have been accomplished using a variety of gas mixtures subjcted to different energy sources.[1-4,7] Various amino acids can also be obtained by heating solutions of hydrogen cyanide.[1-6] All amino acids have one or more isolated carboxylic π-electron systems. A general formula for amino acids is shown in **1**. Here and hereafter, R, R_1, and R_2 represent the substituents not conjugated with a π-electron system in question. Not only amino acids but also carboxylic acids have been detected in many PES experiments.[1,4,6] Carboxylic acids can also be

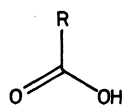

1

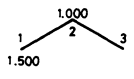

2

expressed as **1**.

The allyl anion $C_3H_5^-$ (**2**, four π electrons) represents the URF of a carboxyl group **1** not conjugated with the remainder of the molecule (R in **1**). The calculated charge densities in the URF are greater at the edge carbons than at the central carbon. Topological charge stabilization says that electronegative heteroatoms prefer to occupy the sites where electron density is already very great in the iso-π-electronic URF.[8-11] Oxygen is much more electronegative than carbon.[13] Stability of amino acids and carboxylic acids is attributable to the two constituent oxygens. These atoms occupy the two sites of greatest charge density in the URF. Oxalic acid (**3**) has also been formed in some PES experiments.[6] This acid again conforms to the TCS rule. Four oxygens in oxalic acid or oxalates occupy the sites of high charge density in the URF (**4**).

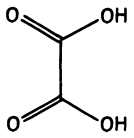

3

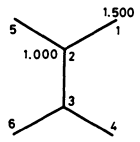

4

Urea (**5**) was produced in many PES experiments.[1-4,6] The trimethylenemethane dianion (**6**, six π electrons) constitutes the URF of urea. The calculated charge densities are greater at the peripheral carbons than at the central carbon. Nature puts electronegative atoms, oxygen and nitrogen, in the peripheral positions of the URF.[8] A molecule which is iso-π-electronic with **6** has been referred to as a Y-aromatic species, i.e., an exceptionally Y-shaped aromatic molecule, since it is of great stability.[14] Urea is a stable aromatic species in this sense, conforming to the TCS rule.

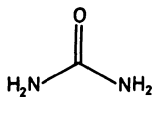

5

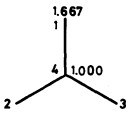

6

The purine and pyrimidine bases are key components of nucleic acids. Adenime (**7**), guanine (**8**) cytosine (**9**), thymine (**10**), and uracil (**11**) are formed under various prebiotic conditions.[1-7] These bases can be synthesized all at once in the electric-discharge experiment with methane-nitrogen-water mixtures.[15] Senarios can be developed for the prebiotic synthesis of aino acids, purines, and pyrimidines, using HCN as the sole source of carbon.[6] The occurrence of HCN on primitive Earth is supported by its facile formation under a variety of conditions.[6] HCN oligomerizes easily in laboratory experiments. HCN oligomers then hydrolyze to amino acids, purines, and pyrimidines. This synthetic scheme is very attractive, in that all three types may have been produced at the same time and place on primitive Earth.[6]

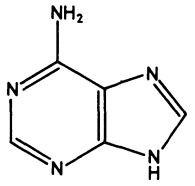

7

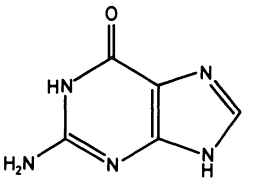

8

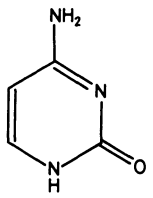

9

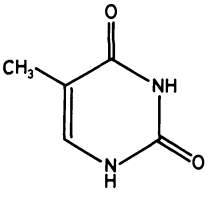

10

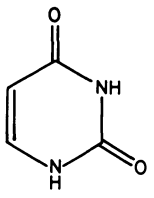

11

The URF's of two purine bases **7** and **8** are shown in **12** and **13**, respectively. Heteroatoms in these bases, without exception, are situated at the sites of large charge density in their respective URF's. All positions of high charge density in the URF's are occupied by heteroatoms in the corresponding purine bases. Three pyrimdine bases **9**, **10**, and **11** happen to have the same URF (**14**) with ten π electrons. Heteroatoms in these bases occupy the sites of high charge density in their common URF. Thus, nucleoside bases are not only stable but also easy to form on primordial Earth.

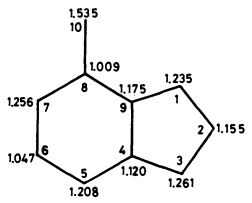

12

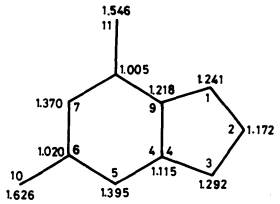

13

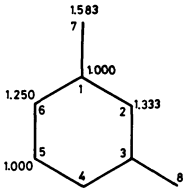

14

Similar PES experiments yield some more molecules which have either a purine or pyrimidine nucleus.[5,6] Among them are hypoxanthine (**15**),

xanthine (**16**), 4,5-dihydroxypyrimidine (**17**), 5-hydroxyuracil (**18**), and orotic acid (**19**). The URF's of hypoxanthine and xanthine are the same as those of adenine (**12**) and guanine (**13**), respectively. The URF's of 4,5-dihydroxypyrimidine, 5-hydroxyuracil, and orotic acid are shown in **20**, **21**, and **22**, respectively. All these molecules conform to the TCS rule.

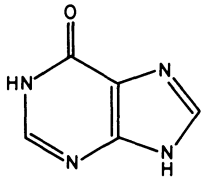

15

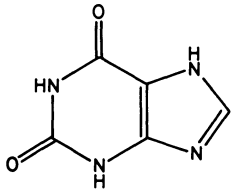

16

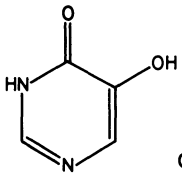

17

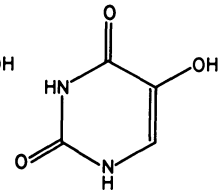

18

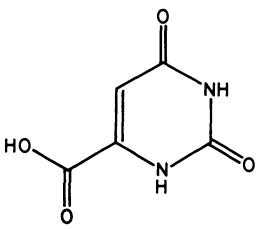

19

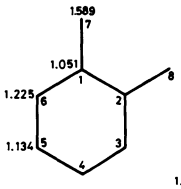

20

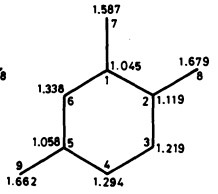

21

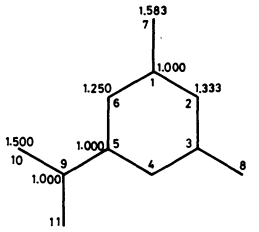

22

According to the original TCS rule,[8] one does not need to place heteroatoms at all sites of high charge density in the URF to construct a stable molecule. Position 6 in the URF of pyrimidine bases (**14**) has high charge density, but these bases has no heteroatom there. In contrast, heteroatoms in **2**, **3**, **5**, **7**, **8**, **15**, and **16** occupy all sites of high charge density in their respective URF's. We might say that these molecules are extremely faithful to the TCS rule.

The tetramerization of HCN to form diaminomaleonitrile (DAMN, **23**) is a key step for the synthesis of nucleoside bases from HCN.[2-6] 5-Amino-4-imidazolecarbonitrile (AICN, **24**), 5-amino-4-imidazolecarboxamide (AICA, **25**), and 5-amino-4-imidazolecarboxamidine (AICAI, **26**) are formed during the origomerization of HCN. These molecules are plausibly prebiotic since they are produced by the reaction of DAMN with some appropriate simple molecules.[2-6] Then, purine bases are synthesized from AICA and AICAI. Therefore, it is instructive to

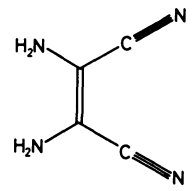

23

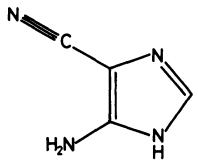

24

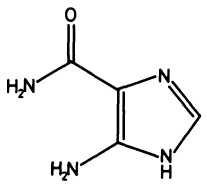

25

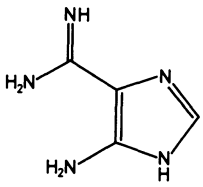

26

see if these three molecules conform to the TCS rule. The URF's of **23**, **24**, and **25** are shown in **27**, **28**, and **29**, respectively. The URF of **26** is identical with that of **25**. It is clear from these URF's that **23**–**26** obey the TCS rule. This implies that the TCS rule operates in almost every step of prebiotic chemistry.

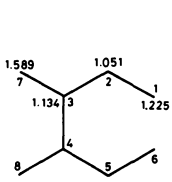

27

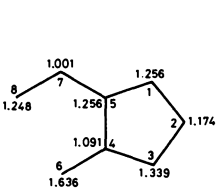

28

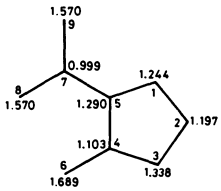

29

Cyanamide (**30**) can be formed under prebiotic conditions from ammonium cyanide by a photochemical reaction.[1,2,6] This molecule undergoes self-addition to form a dimer, cyanoguanidine (**31**).[2,6]

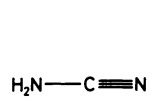

30

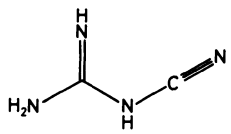

31

These two compounds may funtion as condensing agents in phosphorylation and peptide formation. The URF of cyanamide is identical with that of carboxylic acid **2**. The URF of cyanoguanidine is shown in **32**, which may be regarded as a cyano derivative of a Y-aromatic compound (guanidine). Heteroatoms in both molecules are placed at the sites of high charge density in the URF's. Individual peptide bonds **33** in polypeptide are iso-π-electronic with the allyl anion **1**. Peptide bonds also confrom to the TCS rule.

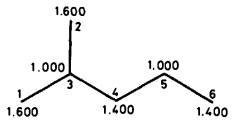

32

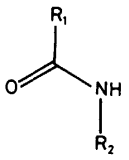

33

Concluding Remarks

Gimarc pointed out that the TCS rule has potential value as a guide for synthetic efforts to be made by organic chemists.[8] We have shown above that many candidates for prebiotic organic molecules conform to the TCS rule. All heteroatoms in every molecule investigated are placed at the sites of large charge density in its URF. Amino acids, nucleoside bases, and related molecules are fully consistent with the TCS rule. This may imply that a chemical reaction with simple molecules, driven by a primitive energy source, yields molecules conforming to the TCS rule.

It seems very likely that real prebiotic chemical evolution[1,2] occurred in harmony with the TCS rule on primitive Earth. Then, nature presumably picked up these molecules to construct living organisms. Some of the molecules must have exerted important functions incidentally in cellular systems. Conversely, nature has been so skillful as to choose biologically important molecules from the products of chemical evolution on primitive Earth.

As noted by Gimarc,[8] a molecule conforming to the TCS rule is relatively stable in a thermodynamic sense. In general, a stable molecule is associated with low activation energy of formation.[16] Thus, nature has utilized energetically very accessible ways of organic synthesis. Living organisms must have chosen useful molecules from organic molecules readily available on primitive Earth. These molecules necessarily conform to the TCS rule. Thus, topological charge stabilization[8,11] serves as a unifying principle for the systematization of chemical evolution.

We thank Prof. Kensei Kobayashi (Yokohama National University) for familializing us with the concept of chemical evolution.

References

1) M. Calvin, "Chemical Evolution," Oxford University Press, Oxford (1969).
2) S. L. Miller and L. E. Orgel, "The Origins of Life on Earth," Prentice-Hall, Englewood Cliffs, N. J. (1974).
3) R. M. Lemmon, *Chem. Rev.*, **70**, 95 (1970).
4) K. Harada, *Kagaku Sosetsu*, **30**, 109 (1980).
5) J. P. Ferris, *Chem. Eng. News*, **62** (35), 22 (1984).
6) J. P. Ferris and W. J. Hagan, Jr., *Tetrahedron*, **40**, 1093 (1984).
7) K. Kobayashi and C. Ponnamperuma, *Viva Origino* **14**, 42 (1986).
8) B. M. Gimarc, *J. Am. Chem. Soc.*, **105**, 1979 (1983).
9) B. M. Gimarc and J. J. Ott, *J. Am. Chem. Soc.*, **108**, 4298 (1986).
10) J. J. Ott and B. M. Gimarc, *J. Am. Chem. Soc.*, **108**, 4303 (1986).
11) J. Aihara, *Bull. Chem. Soc. Jpn.*, **60**, 2268 (1987).
12) S. L. Miller and H. C. Urey, *Science*, **117**, 528 (1953).
13) L. Pauling, "The Nature of the Chemical Bond," Cornell University Press, Ithaca, N. Y. (1960), pp. 64–107.
14) P. Gund, *J. Chem. Educ.*, **49**, 100 (1972).
15) K. Kobayashi, L.-L. Hua, C. W. Gehrke, K. O. Gerhardt, and C. Ponnamperuma, *Origins of Life*, **16**, 299 (1986).
16) W. J. le Noble, A. R. Miller, and S. D. Hamann, *J. Org. Chem.*, **42**, 338 (1977).

 © 1988 The Chemical Society of Japan Bull. Chem. Soc. Jpn., 61, 2313—2320 (1988)

Characterization of Monomeric and Polymeric (Octacyanophthalocyaninato)metals in Thin Films

Hisao YANAGI, Yasukiyo UEDA, and Michio ASHIDA*
Department of Industrial Chemistry, Faculty of Engineering, Kobe University, Rokkodai, Nada-ku, Kobe 657
(Received January 5, 1988)

Thin films were prepared by the reaction of 1,2,4,5-tetracyanobenzene with Ni, Co, Fe, Zn films at various temperatures. The films were characterized by infrared, UV/visible and photoelectron spectroscopy and analytical electron microscopy in comparison with films prepared on substrates of a KCl single crystal and a Cu film. The films produced on the metal films below 400 °C were composed of tentacle-like crystals growing from the surface and an amorphous layer condensed over the metal substrate. The tentacle-like crystals were soluble in concentrated sulfuric acid and were identified as intercalation compounds of (octacyanophthalocyaninato)metal with the respective metal atoms. The amorphous layers contained polymerization products with a polynitrile structure, which were insoluble in concentrated sulfuric acid. The films produced on the metal films at 450 °C were composed of a thick layer and had a very limited solubility in concentrated sulfuric acid. They were ascribed to metal complexes of polyphthalocyanines(poly-M(Pc)) and cross-linked polymers with structure elements such as polynitrile and triazine.

(Phthalocyaninato)metals(M(Pc))[1-7] (**1**) and their polymeric derivatives[8-11] have recently attracted a good deal of attention as new functional materials because of their interesting electronic and optical properties. According to Wöhrle et al.[12,13] phthalocyanine polymers were synthesized by a reaction of 1,2,4,5-tetracyanobenzene(TCNB) (**2**) with metal salts or metals, and (octacyanophthalocyaninato)metals (M[Pc(CN)$_8$]) (**3**) were produced as precursors of polymeric (phthalocyaninato)metals (poly-M(Pc)). The structure of polymeric phthalocyanines has been considered that phthalocyanine units link each other by the peripheral benzene ring to form either a ribbon or a sheet of parquet pattern (**4**).

In order to prepare thin films of these phthalocyanine derivertives, the synthesis has been proceeded by a reaction of TCNB vapor with substrates such as a KCl crystal and a Cu plate in an evacuated tube.[14] The films produced on these substrates at temperatures between 250 and 400 °C were composed of tentacle-like crystals which were characterized as M[Pc(CN)$_8$] (M=K$_2$,Cu). The films included extra metals, more than would be required for coordination in phthalocyanine rings; the metals were distributed uniformly in the film. High-resolution electron microscopic observation of the thin crystal produced on KCl[15] has elucidated that the film is composed of an intercalation compound of K$_2$[Pc(CN)$_8$] with potassium atoms coordinated to the peripheral cyano groups of the Pc molecules. The reaction of TCNB with KCl or a Cu plate above 450 °C produced amorphous and continuous films of poly-M(Pc) (M=K$_2$, Cu). The ratio of polymeric phthalocyanine to monomeric one increased with elevating reaction temperature. However, their structure and molecular weights have not been examined in detail, owing to the poor solubility of the polymers. Wöhrle et al.[13] has pointed out that the structure of polymer is affected by the condition of the reaction and polymeric phthalocyanines with uniform structure are obtained only in a reaction with specific metals.

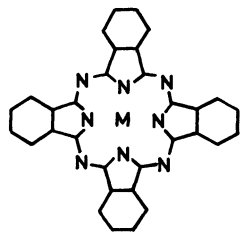

1 : M(Pc)

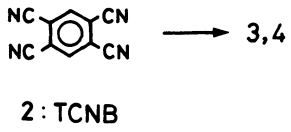

2 : TCNB

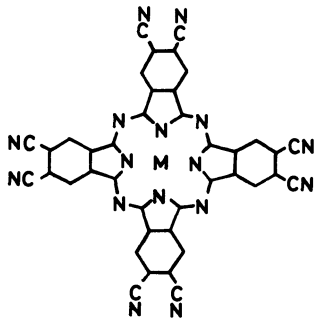

3 : M[Pc(CN)$_8$]

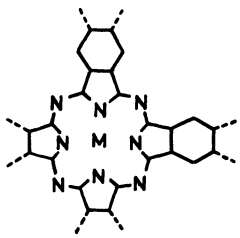

4 : poly-M(Pc)

In the present work, thin films were prepared by the reaction of TCNB vapor with various metal substrates of Ni, Co, Fe, and Zn films as well as KCl and a Cu film. The products were characterized by infrared(IR) and UV/visible(UV/VIS) spectroscopy and morphologies of the films were observed by scanning electron microscopy(SEM). The compositions of the films produced on the substrates were examined by photoelectron spectroscopy and X-ray microanalysis. The structures of the products are discussed in comparison with those of films produced on KCl and Cu.

Experimental

Synthesis. TCNB was synthesized from pyromellitic dianhydride by the method of Bailey et al.[16] The crude TCNB was purified by recrystallization from acetic acid. The substrate materials used were a cleavage surface of a KCl single crystal and metallic films. As metallic films, Cu, Ni, Co, Fe, and Zn were evaporated on a cleavage surface of KCl which had been preheated at 150 °C and then kept at room temperature in a vacuum of 1×10^{-4} Pa. Thickness of the metallic films was estimated to be about 100 nm by a quarts crystal microbalance. The refined TCNB and the substrate material were sealed in an evacuated Pyrex glass tube at 10 Pa after flushing with argon gas. The tube was heated at temperatures between 250 and 450 °C for 10 h in a hot air oven. After the reaction the tube was opened in air at room temperature.

IR and UV/VIS Spectra. IR spectra were recorded on a Shimazu 20 DXB spectrometer. The produced films were milled and pressed together with the substrates and examined by the KCl tablet method. The films were dissolved in concentrated sulfuric acid and UV/VIS spectra of the solutions were recorded by a Shimadzu UV-240 spectrometer.

Photoelectron Spectroscopy. X-Ray photoelectron spectra (XPS) were taken on a KRATOS EXAM800, using Mg $K\alpha$ radiation ($h\nu$=1254 eV). A produced film on a substrate was directly attached to a sample holder. All measurements were performed at a pressure of 1×10^{-7} Pa in the analyzing chamber. Surface cleanliness was checked by scanning through the region of binding energy from 0 to 1150 eV. The binding energy was calibrated by a thin gold film vacuum-deposited on the sample, taking the Au($4f_{7/2}$) peak as a reference at 83.8 eV. The C(1s) spectra were deconvoluted with Gaussian curves after subtraction of the background. The spectra of the films were compared with those of metal-free octacyanophthalocyanine (H_2[Pc(CN)$_8$]) synthesized by Wöhrle et al.[12] and copper phthalocyanine (Cu(Pc)) evaporated on a cleavage surface of KCl. The sample of powdered H_2[Pc(CN)$_8$] was examined on an indium plate.

Scanning Electron Microscopy and X-Ray Microanalysis. The morphology of the films produced on substrates was observed by the SEM mode of a JEM-200CX electron microscope. The metal distribution in the films was analyzed by a Kevex-7000 energy dispersive X-ray spectrometer(EDS).

Results and Discussion

UV/VIS Spectra. Films with green or dark blue color were formed on the substrates of Ni, Co, Fe, and Zn films by reaction of TCNB at temperatures between 250 and 400 °C. The films produced below 300 °C were completely soluble in concentrated sulfuric acid. Figure 1 shows the UV/VIS absorption spectra of solutions of the films produced at 300 °C. The films produced on Ni, Co, Fe, and Zn films showed identical absorption bands as those of M[Pc(CN)$_8$] reported by Wöhrle and Hündorf.[12] The intense bands in the 600—750 and 200—400 nm regions are assigned,

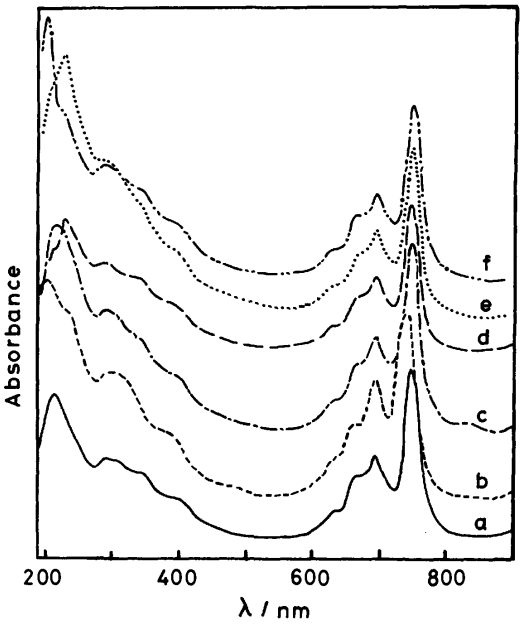

Fig. 1. UV/VIS spectra (in concd sulfuric acid) of films produced on KCl(a), Cu(b), Ni(c), Co(d), Fe(e), and Zn(f) at 300°C.

respectively, as the Q-band and the Soret band caused by π-π^* transitions in phthalocyanine macrocycles. The maximum peaks in the Q-band of those products appear at a shorter wavelength than those of M(Pc).[17] This shift of the Q-band peaks is caused by an electron-withdrawing effect of the peripheral cyano groups in M[Pc(CN)$_8$] molecules. Because the electronegative cyano groups attract a certain amount of electrons from the conjugated π electron system of the Pc macrocycle, the ground state of the π electrons becomes a lower energy level, giving rise to an increase in the π-π^* transition energy. Therefore, the Q-band peaks of M[Pc(CN)$_8$] shift to shorter wavelengths. The films became less soluble in concentrated sulfuric acid upon elevating the reaction temperature. The films produced at 350 °C contained a small amount of insoluble portion in concentrated sulfuric acid, and those at 400 °C contained a considerable amount of the insoluble one. The soluble portions of the films produced on the substrates at 350 and 400 °C, except the film produced on Zn at 400 °C, showed the same spectra as those produced at 300 °C. The films produced on the substrates at 450 °C were gray and black color with a metallic gloss and had a very limited solubility in concentrated sulfuric acid. Figure 2 shows the UV/VIS absorption spectra of the soluble portions of the films produced at 450 °C. The film produced on Zn at 400 °C showed the same spectrum as that at 450 °C. The absorption bands became broader and the maximum peaks in the Q-band shifted to shorter wavelengths by 15 to 21 nm than those of the films produced at 300 °C . The blue shifts of the Q-bands have been observed for associated

Table 1. IR Spectra of $K_2[Pc(CN)_8]$, $Cu[Pc(CN)_8]$, and Synthesized Films[a)]

Assignment	Compound					
	$K_2[Pc(CN)_8]$[14)]	$Cu[Pc(CN)_8]$[14)]	Film on Ni	Film on Co	Film on Fe	Film on Zn
	716w	720m	710w	712w	715w	715w
def.(C-H)	787s	800m	765m	765m	765m	766m
					795w	
	924m	870w	915w	910m	910m	915m
			995m	996m	995w	995m
	1022m	1020m	1025w	1025w	1020w	1020w
	1082s		1075m	1080m		1080s
	1105s	1095s	1100s	1100s	1100s	1100s
str.(C-C)	1165w	1165w	1165w	1164w	1168m	1160w
str.(C-N)	1231m	1230s	1220w	1225w	1220m	1225w
str.(C=N)	1318s	1310s	1310s	1310s	1310s	1305s
	1449w	1460m	1410w		1400w	1440w
	1498m	1500w	1500m	1510m	1510s	1500m
	1555w	1550w	1540m		1560m	1550m
	1610w	1615w	1620m	1610s	1620m	1620m
str.(C≡N)	2231s	2230s	2225s	2230s	2220s	2240s
$\frac{I_{2220-2240}}{I_{1095-1105}}$	0.51	0.78	1.01	1.32	1.33	1.04

a) Frequencies in cm^{-1}; intensity: s=strong, m=medium, w=weak.

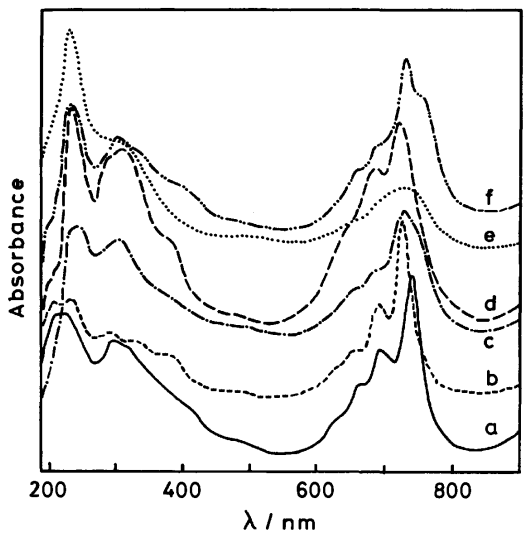

Fig. 2. UV/VIS spectra (in concd sulfuric acid) of films produced on KCl(a), Cu(b), Ni(c), Co(d), Fe(e), and Zn(f) at 450°C.

porphyrins[18)] and Pc's,[19,20)] dimeric Pc's,[21,22)] and cofacially polymerized Pc's.[9)] These shifts have been discussed in terms of exciton coupling,[23)] which is based on the interaction between the excited states of Pc molecules. On the other hand, Wörhle et al.[13)] have found a red shift of the maximum peak in Q-band for polymerized M(Pc), and concluded that the red shift was caused by an intramolecular π electron delocalization in the Pc polymer. In the present case, it is considered that the soluble portion of the films produced at 450°C is associated or oligomeric $M[Pc(CN)_8]$ and that the insoluble portion of the films produced above 350°C is polymerization products of TCNB.

Infrared Spectra. The IR absorption spectra of the films produced on metal substrates at 350°C are listed in Table 1. The spectra of the films produced on Ni, Co, Fe, and Zn showed similar absorption bands to those of $K_2[Pc(CN)_8]$ and $Cu[Pc(CN)_8]$,[14)] though slight changes in the wave number occurred. The absorption bands in a range from 1000 to 1600 cm^{-1} are characteristic ones of Pc's, which are assigned to C-C and C-N stretching in a Pc skeleton. The absorption bands with high intensity at 2220—2240 cm^{-1} are ascribed to a C≡N stretching of peripheral cyano groups of $M[Pc(CN)_8]$ molecules. In the case of $M[Pc(CN)_8]$ the band appears at 2220 cm^{-1} being independent of metals.[13)] In the present case, however, the bands are of higher wave number than 2220 cm^{-1}, depending on the kinds of metal. In a previous study,[15)] we found that the product formed on KCl could be identified as an intercalation compound of $K_2[Pc(CN)_8]$ with potassium atoms coordinated to the peripheral cyano groups of the Pc molecules. It is assumed that a certain amount of charge is transferred from the potassium atom to the cyano groups by this coordination. The band of C≡N may be affected by this charge transfer, which depends on the electronic configuration of metal atoms. Therefore, the shift suggests that the films produced on the metal substrates form similar complexes between the cyano groups and the respective metals. The formations of these complexes have been confirmed by direct imaging of the thin films with high-resolution electron microscopy.[24)] The ratio of the absorption intensity of the cyano group at 2220—2240 cm^{-1} to the characteristic band of M(Pc) at 1095—1105 cm^{-1}, listed in Table 1, reveals the quantitative value of the cyano groups per Pc unit.[25)] Those ratios of the films

produced on Ni, Co, Fe, and Zn are larger than those of $K_2[Pc(CN)_8]$ and $Cu[Pc(CN)_8]$.[14] This suggests that Pc skeletons are less produced and other products having cyano groups, such as polynitrile, are yielded in reactions with Ni, Co, Fe, and Zn, in comparison with the reaction with KCl and Cu. It is also noted that the films on Ni, Co, Fe, and Zn show absorption bands at 1610—1620cm^{-1} which are stronger than those of the films on KCl and Cu. Lin et al.[26] have observed this band for polymeric Cu(Pc) and Wöhrle et al.[13] have reported that this absorption band is attributed to a -C=N-C=N- linkage in the polynitrile structure **5** produced by the polymerization of the cyano groups. Therefore, it is considered that the films produced on Ni, Co, Fe, Zn contain a certain amount of polynitrile, and the products on these substrates are not so structurally uniform in comparison with those on KCl and Cu. Figure 3 shows the IR spectra of the films produced on Ni at various reaction temperatures. The films produced at 300 and 350 °C showed almost same absorption bands. The spectrum of the film produced at 400 °C showed some signs of structural change. The absorption of C≡N stretching at 2225 cm^{-1} decreased significantly and other absorption bands became broader than those of the fimls produced below 350 °C. The spectrum of the film produced at 450 °C showed a very weak absorption at 2225 cm^{-1} and a broad band without fine structure between 1600 and 1000 cm^{-1}. The ratio, I_{2225}/I_{1100}, decreases with elevating reaction temperature. The films produced on Co, Fe, and Zn showed a similar spectral change upon elevating the reaction temperature. It seems that Pc units polymelize by their residual peripheral cyano groups to form poly-M(Pc) and polynitriles, and that extensive reaction causes a cross linkage such as triazine structure[13] **6** at high temperature. These polymeric products are considered to correspond to the insoluble portions of the films in concentrated sulfuric acid, as mentiond in the previous section.

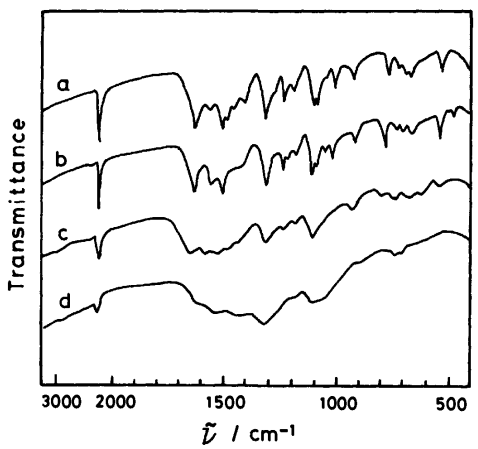

Fig. 3. Infrared spectra of films produced on Ni at 300 °C (a), 350 °C(b), 400 °C(c), and 450 °C(d).

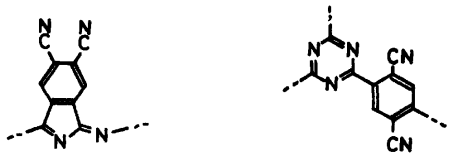

5 6

Photoelectron Spectroscopy. Figure 4 shows the C(1s) XPS spectra of Cu(Pc), $H_2[Pc(CN)_8]$, and the films produced on KCl and Cu at 350 °C. The spectra were deconvoluted to the bands shown with dashed

Table 2. C1s Spectra of Cu(Pc), $H_2[Pc(Cn)_8]$, and Synthesized Films

Compound	BE/eV	FWHM/eV[a]	Integrated area/%[b]
Cu(Pc)	284.8	1.2	72.5
	286.1	1.2	25.9
$H_2[Pc(CN)_8]$	284.7	2.0	66.5
	286.4	1.8	20.7
	288.6	2.5	11.6
Film on KCl	284.6	1.7	59.7
	286.3	1.8	42.3
Film on Cu	284.5	2.2	51.2
	286.5	2.5	46.2

a) Full width at half maximum. b) The areas evaluated from deconvoluted bands are considered accurate to ±5%.

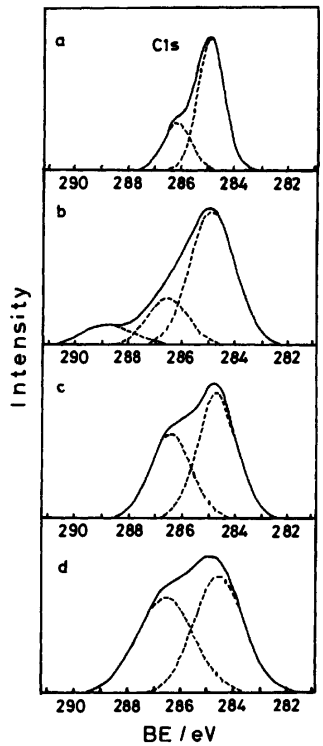

Fig. 4. Carbon 1s photoelectron spectra of Cu(Pc)(a), $H_2[Pc(CN)_8]$(b), and films produced on KCl(c) and Cu(d) at 350 °C.

lines; the data are summarized in Table 2. The spectrum of Cu(Pc) consists of two C(1s) bands with an intensity ratio of 1:3. The band with high energy is attributed to eight carbon atoms bonding with two meso-position nitrogens, and the band with low energy is attributed to 24 carbon atoms in benzene rings of a Cu(Pc) molecule.[27,28] The spectrum of $H_2[Pc(CN)_8]$ shows three C(1s) bands in relative intensity of about 1:2:6. The lowest-energy band is attributed to the carbons of the benzene rings and the intermediate band to the carbons bonding with the two meso-position nitrogen atoms. The third band with a FWHM of 2.5 eV is observed at 288.6 eV. It is well known that a satellite band accompanied with the C(1s) band is observed at about 288 eV for $H_2(Pc)$ and M(Pc).[28,29] However, the third band indicates a considerably strong intensity and a large FWHM for $H_2[Pc(CN)_8]$, as compared with that of the satellite band. Chemical shifts in the photoelectron spectrum of the core electrons are caused by a variation of the valence electron state. Cyano groups polarize to draw the valence electrons from the carbon atom to the nitrogen atom, and the core electrons in the carbon atom are attracted to the nucleus more tightly than those in an isolated carbon atom. Therefore, the binding energy of the C(1s) electron in the cyano groups is higher than that of the normal carbon atoms. Thus, the third band of $H_2[Pc(CN)_8]$ may be assigned to the carbon of the peripheral cyano groups. However, the intensity ratio of the cyano group is smaller than that estimated from the molecular structure of $H_2[Pc(CN)_8]$, which would give an intensity ratio of 1:1:3. This finding suggests that a sample of $H_2[Pc(CN)_8]$ would include a certain amount of polymeric products, such as poly-M(Pc) and triazine structure, since the contents of the cyano groups in these compounds are lower than that of $H_2[Pc(CN)_8]$. The C(1s) spectrum of the film produced on KCl showed two bands with an intensity ratio of 2:3; however, the third band, ascribed to the cyano groups, was not observed in the spectrum and the intensity of high energy band was twice of that of Cu(Pc). The film produced on KCl is composed of an intercalation compound of $K_2[Pc(CN)_8]$ with potassium atoms, in which half of cyano groups coordinate to the intercalated potassium atom and other ones overlap in antiparallel between the adjacent $K_2[Pc(CN)_8]$ molecules, owing to counterbalance of the opposite polarity of $-\overset{\delta+}{C}\equiv\overset{\delta-}{N}$.[30] Because the polarization in -C≡N is relaxed by the coordination and antiparallel overlap, the C(1s) spectrum from cyano groups in the complex crystal would shift to an energy lower than that of the cyano groups in $H_2[Pc(CN)_8]$. Consequently, the band of high energy in the film produced on KCl is ascribed to eight carbons in the cyano groups and eight carbons bonding with meso-position nitrogen atoms in a Pc ring, and the band of low energy to 24 carbons in the benzene rings of a $K_2[Pc(CN)_8]$ molecule. The C(1s) spectrum of the film produced on Cu showed two bands similar to that of the film produced on KCl and did not show the third band ascribed to isolated cyano groups. It suggests that the film on Cu is composed of an intercalation compound of $Cu[Pc(CN)_8]$ with copper atoms isomorphous to that of $K_2[Pc(CN)_8]$ with potassium atoms.

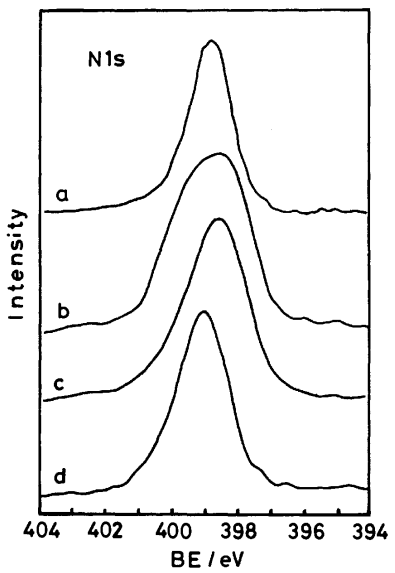

Fig. 5. Nitrogen 1s photoelectron spectra of Cu(Pc)(a), $H_2[Pc(CN)_8]$(b), and films produced on KCl(c) and Cu(d) at 350°C.

Figure 5 shows the N(1s) spectra of Cu(Pc), $H_2[Pc(CN)_8]$, and the films produced on KCl and Cu at 350 °C. The N(1s) band of $H_2[Pc(CN)_8]$ is broad because a $H_2[Pc(CN)_8]$ molecule has four kinds of nitrogen atoms, that is, four pyrrole nitrogens(two -NH- and two -N=), four meso-position nitrogens, and eight nitrogens of the peripheral cyano groups. On the other hand, the N(1s) spectrum of Cu(Pc) showed a narrow band, since the energy separation between the four equivalent pyrrole-ring nitrogens and the four meso-position nitrogens is estimated to be small.[29] The N(1s) spectra of the films produced on KCl and Cu also showed relatively narrow bands. The nitrogen atoms of the peripheral cyano groups seem to have a binding energy close to those of the other nitrogens in $K_2[Pc(CN)_8]$ and $Cu[Pc(CN)_8]$ molecules, owing to formation of the complex crystals. The films produced on Ni, Co, Fe, and Zn at 350 °C showed similar N(1s) spectra to those of films produced on KCl and Cu.

Figure 6 shows C(1s) and K(2p) spectra of the films produced on KCl at various temperatures. The film produced at 300°C shows one broad C(1s) band, which can not be separated into two bands by deconvolution. This suggests that $M[Pc(CN)_8]$ is not completely

formed at 300 °C, and that the films contain a certain amount of products with low molecular weights. In a film produced at 400 °C, the high-energy band of the C(1s) spectrum shows a large intensity and the K(2p) spectrum emerges clearly. The film produced at 450 °C shows a C(1s) shoulder of low energy at about 283 eV. Such a low-energy C(1s) band is well-known for graphite, which consists of a planar conjugated system of π electrons. It seems that the film produced at 450 °C is composed of poly-M(Pc) and cross-linked planar polymers with structure elements such as polynitrile and triazine. The intensity of the K(2p) band increased with elevating the reaction temperature. This indicates that more potassium atoms diffuse from the substrate to the surface of the produced film as temperature increases.

Figure 7 shows the valence band spectra of the films produced on various substrates at 350 °C. The spectrum of a film produced on KCl is in good agreement in binding energy from 8 to 30 eV with that of phthalocyanines reported by Höchst et al.[28] The valence band spectra in this region of M(Pc) could be explained as the spectra of benzene and pyrrole; the spectra were not interfered with by the bond between the central metals and the Pc ligands.[28,29] The spectrum of the film produced on Cu shows similar bands to those of the film produced on KCl, although their relative intensities are different. The spectral features of the films produced on Ni, Co, Fe, and Zn deviate from that of the film produced on KCl and the relative intensities in their spectra are different from that of M(Pc). It seems that the spectral deviation is ascribed to a smaller yield of M[Pc(CN)$_8$] in these films, as compared with the films produced on KCl and Cu.

Scanning Electron Microscopy and X-Ray Microanalysis. Figure 8 shows scanning electron micro-

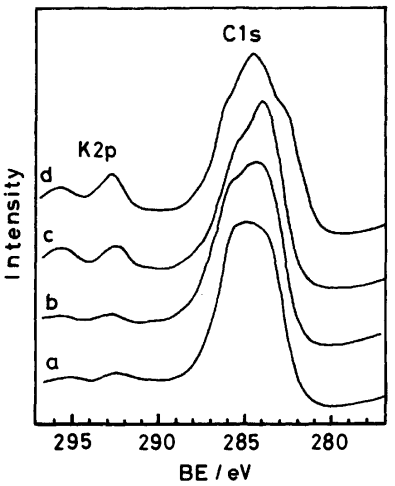

Fig. 6. Carbon 1s and potassium 2p photoelectron spectra of films produced on KCl at 300°C(a), 350°C(b), 400°C(c), and 450°C(d).

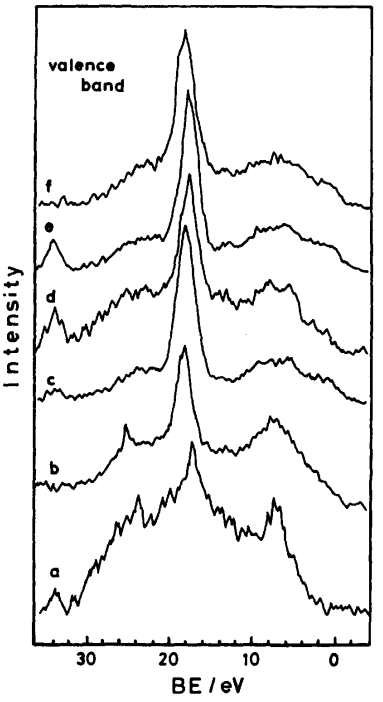

Fig. 7. Valence-band photoelectron spectra of films produced on KCl(a), Cu(b), Ni(c), Co(d), Fe(e), and Zn(f) at 350°C.

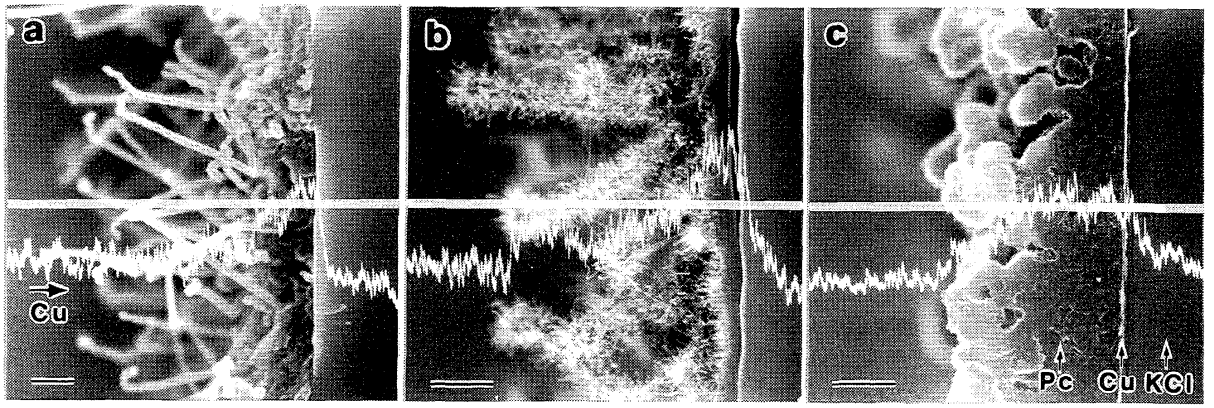

Fig. 8. Scanning electron micrographs and X-ray microanalyses of copper in the films produced on Cu at 250°C(a), 350°C(b), and 450°C(c). Bar=5 μm.

graphs of sections of the films produced on Cu at various temperatures and the distribution of Cu measured by EDS in which the electron beam was scanned from the surface to the bottom of the film along the center line of the figure. The film produced at 250 °C is composed of long and slender crystals of the intercalation compound of Cu[Pc(CN)$_8$] with Cu atoms. At 350 °C, the crystals grow thin and are a fine tentacle-like type which branch from each thick crystal. The EDS signal shows that Cu atoms are distributed from the bottom to the surface of the film and that the tentacle-like crystals contain Cu atoms. At 450 °C, the film is composed of an amorphous thick layer with bulb-like crystals on the surface. The thick layer is considered to be highly polymerized products of poly-M(Pc) and cross-linked polymers with structure elements, such as polynitrile and triazine, which are insoluble in concentrated sulfuric acid.

Figure 9 shows the morphology of films produced on various substrates at 350 °C and the distribution of the respective metal atoms. The film on KCl is composed of long tentacle-like crystals of the intercalation compound of K_2[Pc(CN)$_8$] with potassium atoms, as observed previously.[14] These crystals grow directly on the surface of the KCl substrate. On the other hand, the films on Ni, Co, Fe, and Zn consist of three layers: that is, a thin metal layer evaporated on KCl, a thick amorphous layer, and tentacle-like crystals in the top layer. The EDS signals show that the respective metals are distributed from the substrates to the surfaces of the films. The tentacle-like crystals are considered to be intercalation compound of M[Pc(CN)$_8$] (M=Ni, Co, Fe, and Zn) with the respective metal atoms, because their morphology resembles that of the K_2[Pc(CN)$_8$] complex. It seems that the amorphous layer contains polynitriles which condense among the tentacle-like crystals. Furthermore, this layer may correspond to the insoluble portion in concentrated sulfuric acid, because the film on Cu (Fig. 8(b)) which has only a thin amorphous layer shows a higher solubility than the others.

In conclusion, the products in the films are summarized in Table 3. The films produced on Cu, Ni, Co, Fe, and Zn below 400 °C contained M[Pc(CN)$_8$] (M=Cu, Ni, Co, Fe, and Zn) and polymerized products such as polynitrile. The M[Pc(CN)$_8$] molecules formed tentacle-like crystals of the intercalation compound with the respective metals and were soluble in concentrated sulfuric acid. The intercalation compounds were produced less in these films compared with that in a film produced on KCl. The polymerized products formed amorphous layers, which were insoluble in concentrated sulfuric acid. These polymerized products increased in the films

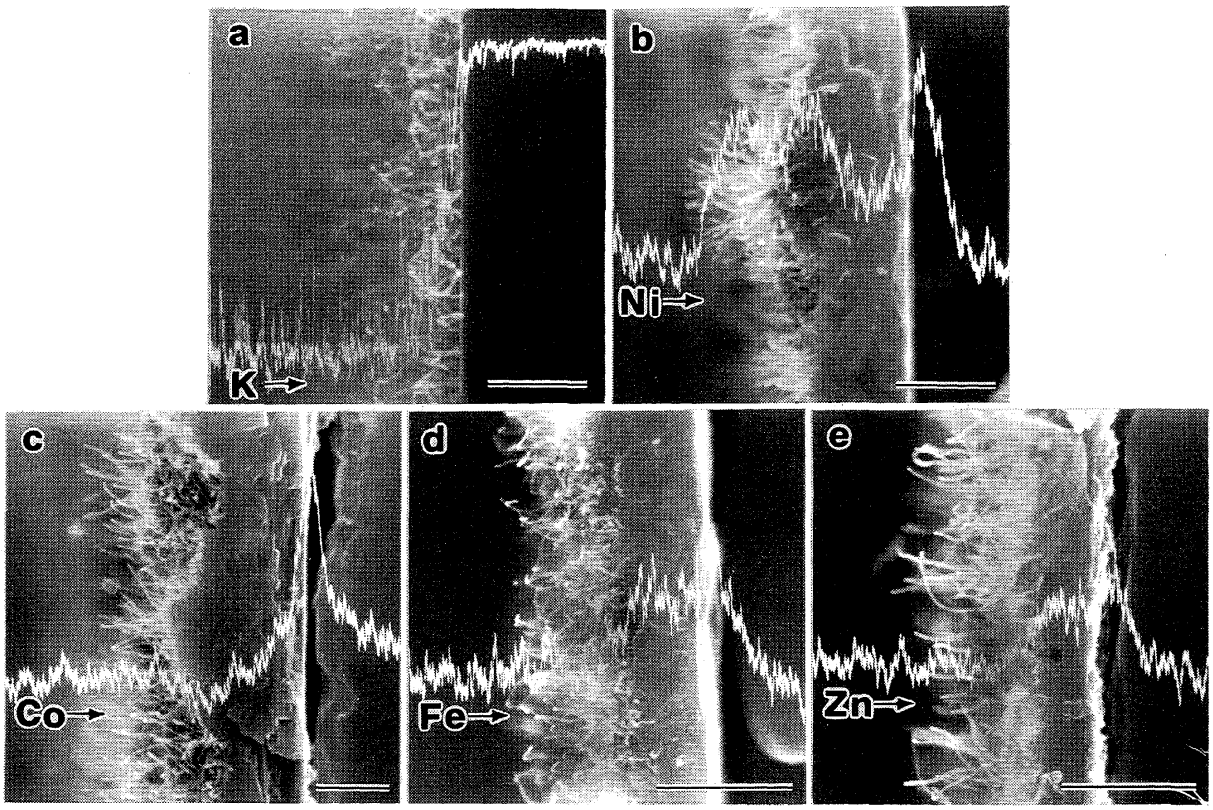

Fig. 9. Scanning electron micrographs and X-ray microanalyses of films produced on KCl(a), Ni(b), Co(c), Fe(d), and Zn(e) at 350 °C. Bar=5 μm.

Table 3. Products[a] of the Reactions of TCNB with Different Substrates

T/°C	Substrate					
	KCl	Cu	Ni	Co	Fe	Zn
300	3'[b]	3'	3,3'	3,3'	3,3'	3,3'
350	3'	3',5	3',5	3',5	3',5	3',5
400	3',4	3',4	3',4,5	3',4,5	3',4,5	3'',4
450	3'',4	3'',4	3'',4	3'',4	3'',4	3'',4

a) Products; 3:M[Pc(CN)$_8$] (M=K$_2$, Cu, Ni, Co, Fe, Zn), 3': intercalation compounds of M[Pc(CN)$_8$], 3'': associated or oligomeric M[Pc(CN)$_8$], 4: poly-M(Pc) containing structure elements of 5 and 6, 5: polynitrile, 6: triazine. b) K$_2$[Pc(CN)$_8$] is not completely formed and a certain amount of products with low molecular weight is contained.

with elevating reaction temperature. The film produced at 450 °C contained highly polymerized products of poly-M(Pc) and cross-linked polymers with such structural elements as polynitrile and triazine. A small amount of the soluble portion in concentrated sulfuric acid was identified as associated or oligomeric M[Pc(CN)$_8$].

The authors are grateful to Professor Dieter Wöhrle of Bremen University for supplying the sample of H$_2$[Pc(CN)$_8$] and helpful discussions. Thanks are also due to Mr. Satoru Nishiyama for access to the photoelectron spectroscopy and for his helpful advice.

References

1) A. Giraudeau, F. R. F. Fan, and A. J. Bard. *J. Am. Chem. Soc.*, **102**, 5137 (1980).
2) C. J. Schramm, R. P. Scaringe, D. R. Stojakovic, B. M. Hoffman, J. A. Ibers, and T. J. Marks, *J. Am. Chem. Soc.*, **102**, 6702 (1980).
3) B. N. Diel, T. Inabe, J. W. Lyding, K. F. Schoch,Jr., C. R. Kannewurf, and T. J. Marks, *J. Am. Chem. Soc.*, **105**, 1551 (1983).
4) Z. D. Popovic and J. H. Sharp, *J. Chem. Phys.*, **66**, 5076 (1977).
5) E. R. Menzel and R. O. Loufty, *Chem. Phys. Lett.*, **72**, 522 (1980).
6) R. O. Loufty, J. H. Sharp, and C. K. Hsiao and R. Ho, *J. Appl. Phys.*, **52**, 5218 (1981).
7) R. O. Loufty and L. F. McIntyre, *Can. J. Chem.*, **61**, 73 (1983).
8) R. S. Nohr, P. M. Kuznesof, K. J. Wynne, M. E. Kenny, and P. G. Siebenman, *J. Am. Chem. Soc.*, **103**, 4371 (1981).
9) C. W. Dirk, T. Inabe, K. F. Schoch, Jr., and T. J. Marks, *J. Am. Chem. Soc.*, **105**, 1539 (1983).
10) B. N. Diel, T. Inabe, N. K. Jaggi, J. W. Lyding, O. Schneider, M. Hanack, C. R. Kannewurf, T. J. Marks, and L. H. Schwartz, *J. Am. Chem. Soc.*, **106**, 3207 (1984).
11) E. Ciliberto, K. A. Doris, W. J. Pietro, G .M . Reinser, D. E. Ellis, I. F. Fragala, F. H. Herbstein, M. A. Ratner, and T. J. Marks, *J. Am. Chem. Soc.*, **106**, 7748 (1984).
12) D. Wöhrle and U. Hündorf, *Makromol. Chem.*, **186**, 2177 (1985).
13) D. Wöhrle, U. Marose, and R. Knoop, *Makromol. Chem.*, **186**, 2209 (1985).
14) M. Ashida, Y. Ueda, H. Yanagi, and K. Sayo, *J. Polym. Sci., Polym. Chem. Ed.*, in press.
15) M. Ashida, Y. Ueda, H. Yanagi, Y. Fujiyoshi, N. Uyeda, and J. R. Fryer, *Acta Crystallogr.*, in press.
16) A. S. Bailey, R. B. Henn, and J. M. Langdon, *Tetrahedron*, **19**, 161 (1963).
17)D. Wöhrle, G. Meyer, and B. Wahl, *Makromol. Chem.*, **181**, 2127 (1980).
18) S. Konishi, M. Hoshino, and M. Imamura, *J. Phys. Chem.*, **86**, 4888 (1982).
19) M. Abkowitz and A. R. Monahan, *J. Chem. Phys.*, **58**, 2281 (1973).
20) A. T. Davidson, *J. Chem. Phys.*, **77**, 168 (1982).
21) A. R. Kane, J. F. Sullivan, D. H. Kenny, and M. E. Kenny, *Inorg. Chem.*, **9**, 1445 (1970).
22) W. A. Nevin, M. R. Hempstead, W. Liu, C. C. Leznoff, and A. B. P. Lever, *Inorg. Chem.*, **26**, 570 (1987).
23) M. Gouterman, D. Holten, and E. Lieberman, *Chem. Phys.*, **25**, 139 (1977).
24) H. Yanagi, S. Maeda, Y. Ueda, and M. Ashida, *J. Electron Microsc.*, in press.
25) R. Bannehr, N. Jaeger, G. Meyer, and D.Wöhrle, *Makromol. Chem.*, **182**, 2683 (1981).
26) J. W. P. Lin and L. P. Dudek, *J. Polym. Sci., Polym. Chem. Ed.*, **23**, 1579 (1985).
27) M. V. Zeller and R. G. Hayes, *J. Am. Chem. Soc.*, **95**, 3855 (1973).
28) M. Höchst, A.Goldmann, S.Hüfner, and H. Malter, *Phys. Status Solidi B*, **76**, 559 (1976).
29) Y. Niwa, H. Kobayashi, and T. Tsuchiya, *J. Chem. Phys.*, **60**, 799 (1974).
30) Detailed structure will be published in Ultramicroscopy, in press.

Photoinduced Extraction and Active Transport of Anions by a Triphenyl Methane Derivative

Hiroshi SASAKI, Akihiko UENO, and Tetsuo OSA*
Pharmaceutical Institute, Tohoku University, Aobayama, Sendai 980
(Received January 26, 1988)

Triphenylmethane derivative leukobase (**1**) was converted to its cation form **2** by UV irradiation. This lipophilic cation form was stable in dichloromethane with green color (λ_{max}=634 nm), and returns to the original colorless form of **1** when shaked with an alkaline solution. Compound **2** exhibited excellent anion extraction ability (from aqueous solution into dichloromethane) under the conditions of appropriate pH, but **1** has no anion extraction ability. Photoinduced active transport of anions across a liquid (dichloromethane) membrane was achieved by using the difference in the extraction ability between **1** and **2** together with the difference in pH between the source and receiving phases.

Many photoresponsive systems are widely studied for the purposes of developing excellent photosensors, photomemories, and molecular devices for efficient energy conversion. Among many chromophores, which can be used as photoswitches of these systems,[1,2] azobenzene and spirobenzopyran have most frequently been employed. We have already shown that photoinduced changes of ion permeability[3,4] and of membrane potential,[5-15] can be attained with poly(vinyl chloride) (PVC) membranes containing azobenzene or spirobenzopyran derivatives. The photoresponsiveness of triphenylmethane derivatives is very different from that of azobenzene and spirobenzopyran since it is dissociated into two species, one is an organic cation and another is a hydroxide anion, and consequently triphenylmethane derivatives have been used to change solution properties[16-18] or ionic features of materials[19,20] by light. The present study deals with the use of a triphenylmethane derivative leukobase (**1**) as a photocontrollable anion carrier, and the active transport performed here may be compared with the similar phenomena achieved in the systems where spirobenzopyran[21] and azobenzene[22] derivatives act as photoresponsive carrier.

Experimental

Materials. Sodium picrate was prepared according to the Fuoss method.[23] Methyl Orange purchased as extra pure reagent grade was purified by recrystallization. The pH values of the aqueous solutions used in liquid-liquid extraction and active transport experiments were adjusted by using NaOH and HCl solutions. Dichloromethane was of spectral grade.

Bis[4-(dibutylamino)phenyl]phenylmethanol (1). *N,N*-Dibutylaniline (6 g, 29.2 mmol) and benzaldehyde (1 g, 9.4 mmol) were dissolved in a mixture of ethanol (8 ml) and 35% HCl (3 ml). The mixture was refluxed for 48 h, and cooled and alkalized with 2 mol dm^{-3} NaOH. The solution was extracted with dichloromethane, and the organic layer was dried over K_2CO_3 and evaporated. Purification by silica-gel column chromatography (eluted by hexane until *N,N*-dibutylaniline was completely removed and subsequently by a mixed solvent of hexane and ether (50:1 by volume)) afforded 3 g (62%) of **1** as pale yellow oil. Found: C, 81.83; H, 10.01; N, 5.15%. Calcd for $C_{35}H_{50}N_2O$: C, 81.66; H, 9.79; N, 5.44%. ^{1}H NMR ($CDCl_3$) δ=0.7—1.7 (28H, m, $N(CH_2C_3\underline{H}_7)_2$), 3.1—3.6 (8H, m, $N(C\underline{H}_2C_3H_7)_2$), 5.3 (1H, s, OH), 6.4—7.4 (13H, m, aromatic ring).

Liquid-Liquid Extraction. At 25 °C, a 2 ml of aqueous solution containing sodium picrate or Methyl Orange (1.0×10^{-5} mol dm^{-3}) and sodium hydroxide (various concentrations) was vigorously shaken with an equal volume of dichloromethane solution containing **1** or **2** (1.0×10^{-5} mol dm^{-3}). After sufficient agitation, the picrate concentration in aqueous layer was determined by absorbance change at 354 nm. The Methyl Orange concentration was also determined in a similar manner at 462 nm.

Method of Anion Transport across a Liquid Membrane. All measurements were carried out at 25 °C with a cylindrical U-tube (diameter: 17 mm) having a plain area (2.0 cm^2) in the center of the tube, which allows effective UV irradiation. The composition of the system is as follows: phase A: Methyl Orange (1.0×10^{-5} mol dm^{-3}) solution (5 ml of water); phase B: dichloromethane solution (20 ml) containing 5.0×10^{-6} mol dm^{-3} of **1**; phase C: Methyl Orange (1.0×10^{-5} mol dm^{-3}) solution containing various concentrations of NaOH (5 ml of water). During transport experiments the phase B (liquid membrane) was stirred gently.

Photoirradiation Conditions. Photoirradiation was performed with a 500 W xenon lamp (Ushio Electric Inc.) using a Toshiba cut-off filter UV D-35 for isolating UV light (320 nm$<\lambda<$400 nm).

Results and Discussion

Photochemical and pH-Dependent Interconversion between 1 and 2. Absorption spectra of **1** before and after UV irradiation in dichloromethane are shown in Fig. 1. Compound **1** before UV irradiation showed an absorption band at 270 nm (ε=35000) and the solution was colorless. After UV irradiation (ca. 6 min), the absorption band at 270 nm was decreased and a new absorption band was observed at 634 nm (ε=55000), the color of the solution being green. This spectral change indicates that **1** was converted to **2**.[16] The time course of the reaction monitored by the absorbance change at 634 nm is shown in Fig. 2. The reaction was completed within 6 min. The cation form **2** was very stable as shown by no change in the

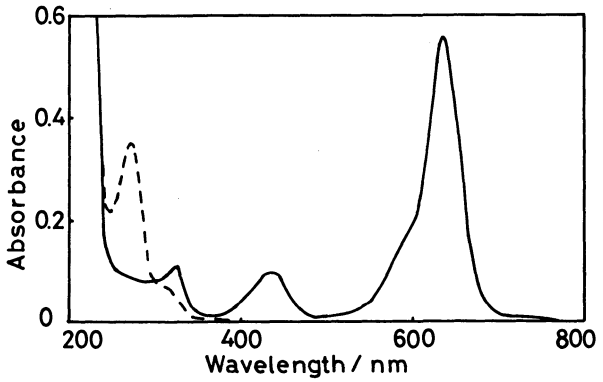

Fig. 1. Absorption spectra of **1** in dichloromethane (1.0×10^{-5} mol dm^{-3}) before (---) and after (——) UV irradiation.

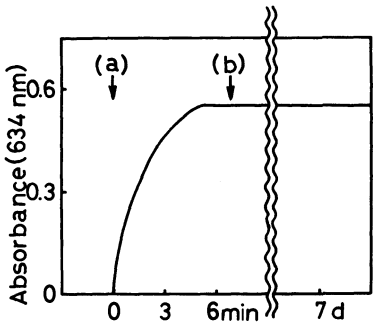

Fig. 2. The change of the absorbance at 634 nm of **1** (1.0×10^{-5} mol dm^{-3}) in dichloromethane induced by UV irradiation.
(a) On the set of UV irradiation. (b) End of UV irradiation.

absorbance at 634 nm even after 7 d. The extent of the reversal of **2** to **1** was examined at 25 °C by shaking a 2 ml of dichloromethane solution of **2** (1.0×10^{-5} mol dm^{-3}) with the equal volume of the aqueous solutions of different pHs. The concentration of **2** depended upon the pH of the aqueous solutions (line (a) in Fig. 3); the cation form **2** was transformed into the original form of **1** by the addition reaction of hydroxide ions to the tertiary carbon in **2** when shaked with alkaline solutions. On the contrary, **2** was not transformed to **1** when shaked with acidic solutions of pH>1.

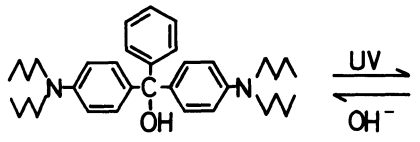

1

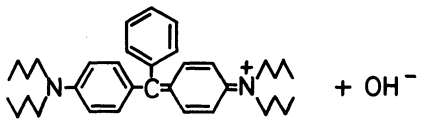

2

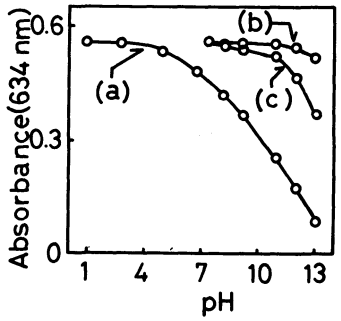

Fig. 3. The change of the absorbance at 634 nm of **2** (1.0×10^{-5} mol dm^{-3}) in dichloromethane induced by shaking with aqueous solutions with different pHs. (a) Shaked with aqueous solution without organic anions. (b) Shaked with aqueous solution containing sodium picrate (1.0×10^{-5} mol dm^{-3}). (c) Shaked with aqueous solution containing Methyl Orange (1.0×10^{-5} mol dm^{-3}).

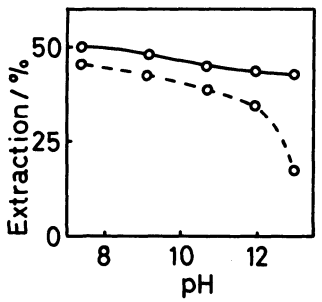

Fig. 4. Effect of pH on extraction by **2**.
——; Sodium picrate. ---; Methyl Orange. The conditions are same as those in Fig. 3.

Liquid-Liquid Extraction. The results of liquid-liquid extraction with **1** and **2** are shown in Fig. 4. The extraction ability of **2** decreased with increasing pH value. In the case of Methyl Orange, an abrupt drop of the extraction ability was observed around pH 12. The absorbances of the dichloromethane solutions measured after the extraction are shown as lines (b) and (c) in Fig. 3. The results indicate that electrostatic interaction of **2** with picrate or Methyl Orange enables **2** to be hardly affected by hydroxide ion. This effect has not been seen with benzoate anion or 1- or 2-naphthaleneacetate anion, the pH profiles being the same as shown in Fig. 3-(a). It is interesting that there are significant differences between picrate and Methyl Orange anions in extraction facility and in the ability of stabilizing the cation form **2** against the attack of hydroxide ion. These results also imply that various anions may be selectively extracted by **2** under appropriate conditions (the selectivity for the picrate anion is most remarkable around pH 13 in this study).

Photoinduced Active Transport. Based on the anion extraction ability of **2**, photoinduced active transport has been attempted. Figure 5 illustrates time response of the concentration of Methyl Orange in phases A and C. The pHs of phases A (without

NaOH) and C (containing 0.10 mol dm^{-3} of NaOH) were initially set to be 7.3 and 13.0, respectively. In the dark the concentration changes of Methyl Orange in both phases A and C were negligible. After UV irradiation for 10 min onto phase B,[24] the concentration of Methyl Orange began to decrease in phase A, and increase in phase C with time. After 10 h, the concentrations of Methyl Orange in phases A and C became ca. 30% and ca. 150%, respectively, of the initial concentration.[25] After 72 h, the concentrations in phases A and C became ca. 1% and ca. 196%, respectively, and at this point 90% of compound **2** was found to be changed to **1**. The result also indicates that the system can be used for transporting various organic salts against the gradient of hydroxide ion. When the pH of phase C is 11.9, active transport still proceeds, but the rate of the Methyl Orange transportation is smaller than the case of pH 13.0. When the pH in phase C was 10.6, active transport was not attained, the concentration of Methyl Orange in phase C decreasing as in phase A (Fig. 6). When the pH in phase C was 8.8, the rate of Methyl Orange diminution in phase C was almost equal to in phase A. Table 1 lists the concentrations of Methyl Orange in phases A and C, at the time of 8 and 72 h after UV irradiation in the above mentioned pH runs. In any case the concentration in phase A decreases with time. On the contrary, the profile of concentration change of Methyl Orange in phase C is affected by the pH in the phase.

The mechanism of the active transport is shown in

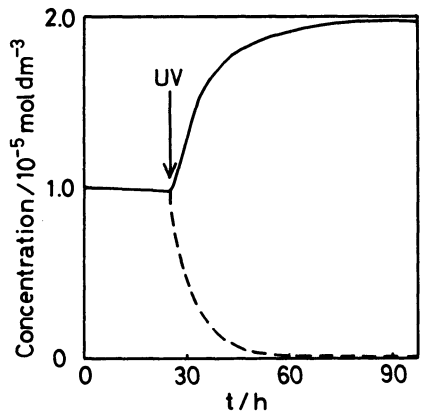

Fig. 5. Time response of the concentration of Methyl Orange in phases A (---) and C (——).
pH values in phases A and C were 7.3 and 13.0, respectively. The concentration of **1** in phases A and C was 1.0×10^{-5} mol dm^{-3}. UV means UV irradiation for 10 min.

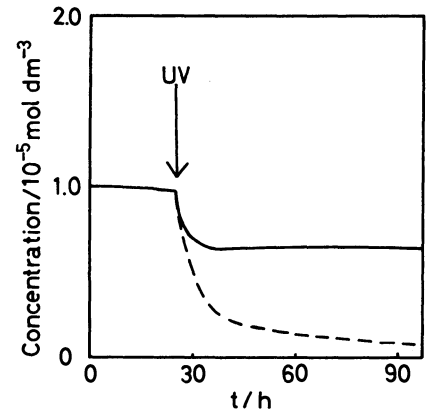

Fig. 6. Time response of the concentration of Methyl Orange in phases A (---) and C (——).
pH values in phases A and C were 7.3 and 10.6, respectively. The concentration of **1** in phases A and C was 1.0×10^{-5} mol dm^{-3}. UV means UV irradiation for 10 min.

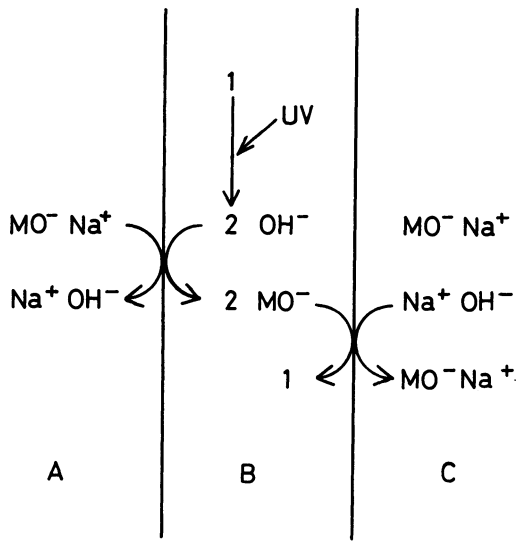

Scheme 1. Schematic sketch of the photoinduced active transport mechanism (the pH in phase C was higher than 11). MO$^-$; Methyl Orange anion.

Table 1. Methyl Orange Concentrations in Phases A and C after UV Irradiation for 10 min

pH in phase C	Methyl Orange concentration/10^{-5} mol dm^{-3}			
	a)		b)	
	Phase A	Phase C	Phase A	Phase C
13.0	0.39	1.40	0.01	1.96
11.9	0.39	1.29	0.04	1.49
10.6	0.36	0.65	0.08	0.64
8.8	0.56	0.55	0.53	0.59

pH in phase A was 7.3. Initial concentration of Methyl Orange in phases A and C was 1.0×10^{-5} mol dm^{-3}. a) 8 h after UV irradiation. b) 72 h after UV irradiation.

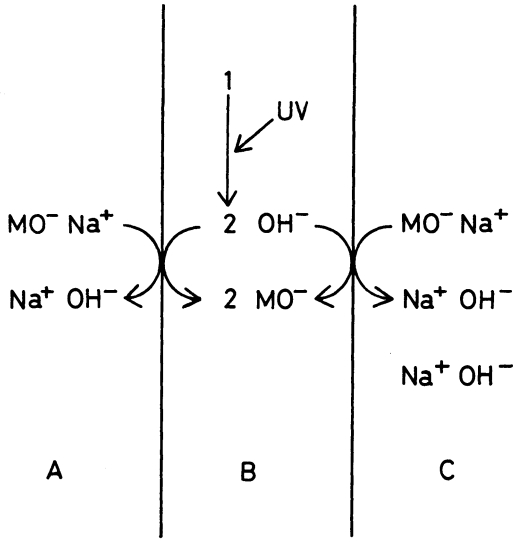

Scheme 2. Schematic sketch of the photoinduced transport mechanism (the pH in phase C was lower than 11). MO^-; Methyl Orange anion.

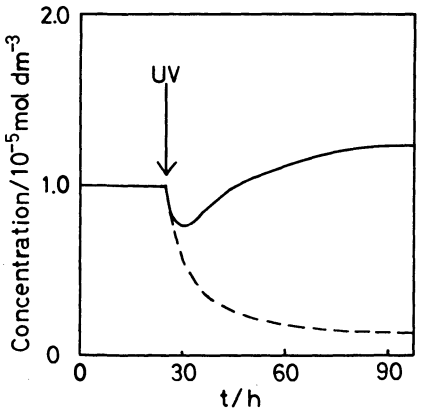

Fig. 7. Time response of the concentration of sodium picrate in phases A (---) and C (——).
pH values in phases A and C were 7.0 and 12.9, respectively. The concentration of **1** in phases A and C was 1.0×10^{-5} mol dm^{-3}. UV means UV irradiation for 10 min.

Scheme 1. At first compound **1** is converted to **2** by UV irradiation, and then **2** binds Methyl Orange at the interface between A and B, releasing hydroxide ion toward phase A. The complex of Methyl Orange anion and **2** is attacked by excess hydroxide ion at the interface between phases B and C, and **2** is converted to **1** releasing Methyl Orange anion toward phase C. When the pH in phase C was less than 11, the concentration of Methyl Orange in phase C decreased as in phase A. The proposed mechanism of the phenomenon is shown in Scheme 2. In this case, the conversion from **2** to **1** does not occur and Methyl Orange is extracted into phase B from both phases of A and C.

We also examined active transport of sodium picrate. The result is shown in Fig. 7. According to the extraction data (Figs. 3 and 4), the anion binding ability of **2** for sodium picrate was stronger than for Methyl Orange, and the ability for sodium picrate was depended upon the pH value to a lesser extent than for Methyl Orange. Therefore, the concentration in phase C (cf. Fig. 5) decreased at an early stage of UV irradiation as in phase A. After 72 h the concentration in phase C slightly increased as the subsequent phenomenon of efficient extraction of picrate anion from phase A to phase B.

Conclusion

The results of extraction data indicate that compound **2** has excellent anion binding ability which depends upon pH value and anion species. Photoinduced active transport of anions through a liquid membrane was achieved on this basis. This photochromic compound works without host–guest complexation and may be regarded as a new system for photoregulated transportation.

This work was supported by a Grant-in-Aid for Encouragement of Young Scientist (No. 61790179) from the Ministry of Education, Science and Culture.

References

1) A. Ueno and T. Osa, *Yuki Gosei Kagaku Kyokai Shi*, **38**, 207 (1980).
2) "Molecular Models of Photoresponsiveness," ed by G. Monatagnoli and B. F. Erlanger, Plenum Press, New York (1983).
3) J. Anzai, A. Ueno, H. Sasaki, K. Shimokawa, and T. Osa, *Makromol. Chem., Rapid Commun.*, **4**, 731 (1983).
4) J. Anzai, H. Sasaki, A. Ueno, K. Shimokawa, and T. Osa, *Nippon Kagaku Kaishi*, **1984**, 338.
5) J. Anzai, H. Sasaki, A. Ueno, and T. Osa, *J. Chem. Soc., Chem. Commun.*, **1983**, 1045.
6) J. Anzai, H. Sasaki, A. Ueno, and T. Osa, *Chem. Lett.*, **1984**, 1205.
7) J. Anzai, H. Sasaki, A. Ueno, and T. Osa, *Membrane*, **9**, 277 (1984).
8) J. Anzai, H. Sasaki, A. Ueno, and T. Osa, *Bull. Chem. Soc. Jpn.*, **57**, 3331 (1984).
9) J. Anzai, H. Sasaki, A. Ueno, and T. Osa, *J. Chem. Soc., Perkin Trans. 2*, **1985**, 903.
10) H. Sasaki, J. Anzai, A. Ueno, and T. Osa, *Nippon Kagaku Kaishi*, **1985**, 1194.
11) J. Anzai, H. Sasaki, A. Ueno, and T. Osa, *J. Polym. Sci., Polym. Chem. Ed.*, **24**, 681 (1986).
12) J. Anzai, H. Sasaki, A. Ueno, and T. Osa, *Chem. Lett.*, **1985**, 1443.
13) J. Anzai, H. Sasaki, A. Ueno, and T. Osa, *Chem. Pharm. Bull.*, **33**, 5589 (1985).
14) J. Anzai, H. Sasaki, A. Ueno, and T. Osa, *Makromol. Chem., Rapid Commun.*, **7**, 133 (1986).
15) H. Sasaki, A. Ueno, J. Anzai, and T. Osa, *Bull. Chem. Soc. Jpn.*, **59**, 1953 (1986).
16) R. N. Macnair, *Photochem. Photobiol.*, **6**, 779 (1967).

(1967).
17) M. L. Herz, *J. Am. Chem. Soc.*, **97**, 6777 (1975).
18) M. Irie, *J. Am. Chem. Soc.*, **105**, 2078 (1983).
19) M. Irie and D. Kunwatchakun, *Macromolecules*, **19**, 2476 (1986).
20) T. Kinoshita, M. Sato, A. Takizawa, and Y. Tsujita, *J. Am. Chem. Soc.*, **108**, 6399 (1986).
21) T. Shimidzu and M. Yoshikawa, *J. Membr. Sci.*, **13**, 1 (1983).
22) P. Haberfield, *J. Am. Chem. Soc.*, **109**, 6177 (1987).
23) M. A. Coplan and R. M. Fuoss, *J. Phys. Chem.*, **68**, 1177 (1964).
24) After UV light irradiation for 10 min, **1** in phase B was converted to **2** perfectly in this condition.
25) The remained Methyl Orange is present in phase B.

Thermodynamic Studies on Order-Disorder Phase Transitions of *p*-Terphenyl and *p*-Terphenyl-d_{14}†

Kazuya SAITO,†† Tooru ATAKE,††† and Hideaki CHIHARA*
Department of Chemistry and Chemical Thermodynamics Laboratory, Faculty of Science, Osaka University, Toyonaka, Osaka 560
††Department of Chemistry, Faculty of Science, Tokyo Metropolitan University, Fukazawa, Setagaya-ku, Tokyo 158
†††Research Laboratory of Engineering Materials, Tokyo Institute of Technology, 4259 Nagatsuta-cho, Midori-ku, Yokohama 227
(Received January 30, 1988)

The heat capacities of *p*-terphenyl and *p*-terphenyl-d_{14} were measured by adiabatic calorimetry between 3 and 300 K. The phase transition associated with a molecular conformation change was observed as a λ-shaped anomaly at (193.5±0.1) K and at (180.3±0.1) K. The enthalpies of transition are (304±20) J mol^{-1} and (288±20) J mol^{-1} and the entropies of transition are (1.63±0.10) J K^{-1} mol^{-1} and (1.63±0.10) J K^{-1} mol^{-1}, respectively. The anisotropy of the intermolecular interaction is discussed and the anomalous portion of the heat capacities in the transition region was compared favorably with a two-dimensional Ising model.

The molecule of *p*-terphenyl (1,1′:4′,1″-terphenyl) is twisted in the gaseous and in the liquid states.[1-4] However, it is seemingly planar in the crystal at room temperature.[5-8] The crystal belongs to the space group $P2_1/a$ and the molecule occupies the center of inversion. On cooling, however, the crystal undergoes a phase transition at about 194 K, below which the molecule is twisted though it still occupies the inversion center.[9] The space group of the low temperature phase is $P\bar{1}$. Similar phase transitions (twist transitions) have been observed in the related substances, so-called poly(*p*-phenylene)s, i.e. in biphenyl[10-17] at 40.4 K[18-20] and in *p*-quaterphenyl[21,22] at 233.0 K.[23]

Many experimental works which made use of optical[24-31] and other techniques[32-40] have revealed that the transition of *p*-terphenyl is continuous or very-nearly continuous under the normal pressure. Under high pressures ($\gtrsim 10^8$ Pa), the transition has been reported discontinuous.[19,31] Critical exponents for some physical properties under the normal pressure have been reported as β=0.15[41] and ν=0.12.[42] These values can be related to a two-dimensional Ising model. The two-dimensionality of the interaction has been supported by neutron[43,44] and NMR[45] experiments.

Baudour et al.[7] refined the crystal structure at room temperature on the assumption that the room temperature phase was a disordered one. They have obtained a doubly peaked electron density diagram for the central phenyl ring, which strongly suggests an order-disorder nature of the transition and is consistent with the failure in search for soft-modes.[25,26] Dynamical aspects of the transition have been investigated by using neutron scattering[41,43,44,46,47] and NMR,[45,48-51] and thereby the critical phenomenon, the critical slowing down of the order parameter fluctuation, was found, which also implied an order-disorder nature of the transition.

It is interesting to note that the pressure dependence of the transition temperature is negative,[29,31] which fact also suggests that the transition is related to a subtle balance between intra- and intermolecular interactions because the intermolecular interaction, which prefers a planar conformation, is more affected by compression than the intramolecular interaction.

A theoretical work by Ramdas and Thomas[52] predicted the existence of another unknown phase on the basis of calculation of static lattice energies. Raich and Bernstein[53] theoretically confirmed an order-disorder nature of the transition through calculation of generalized susceptibility of twisting motion within one-particle scheme.

Although extensive investigations have been carried out on the twist transitions of poly(*p*-phenylene)s and many interesting features were revealed, no systematic study had been reported on thermodynamics of the transitions when we began thermodynamic investigations on biphenyl and related substances[18-20,23,54-60] in an attempt toward a unified understanding of the twist transitions of poly(*p*-phenylene)s. After completion of the study presented here, the results of precision heat capacity measurements on nonlabelled *p*-terphenyl were reported by Chang.[40] Because we measured also on *p*-terphenyl-d_{14} for which there had been no precision thermodynamic data reported, we thought it deserves publication. To provide a consistent set of data from the same calorimeter, we will record the heat capacity values of nonlabelled *p*-terphenyl as well as those of *p*-terphenyl-d_{14}.

Experimental

p-Terphenyl was purchased from Nakarai Chemicals, Ltd. and purified by the method of fractional sublimation in vacuum at about 400 K. The purity of the sublimed specimen was better than 99.9 moles per cent as confirmed by gas chromatography. A part of the sublimed specimen

† Contribution No. 143 from Chemical Thermodynamics Laboratory, Faculty of Science, Osaka University.

was used for adiabatic calorimetry without any further treatment; it weighed 21.0701 g (0.091488 mol) in vacuum. The rest of the sublimed specimen was melted under a helium atmosphere (10^5 Pa), gradually cooled down to room temperature for recrystallization, and pulverized gently. The heat capacity of the melt-pulverized sample was also measured; its mass was 15.2290 g (0.066124 mol). Each sample was loaded into a gold-plated copper calorimeter vessel, which was sealed after adding some helium gas (7 kPa at room temperature) to aid thermal uniformity of the vessel. The contribution of the helium gas was negligibly small in comparison with both the sample and the total heat capacities. The as-sublimed sample contributed 64 per cent at 10 K to the total heat capacity including that of the calorimeter vessel; the contribution decreased to 40 per cent at 100 K and then increased to 54 per cent at 300 K as temperature rose.

p-Terphenyl-d_{14} (nominal isotope purity of 98 per cent, Merck Sharp & Dohme Canada, Ltd.) was purified by fractional sublimation in vacuum at about 400 K. The sublimed specimen was melted under a helium atmosphere (10^5 Pa) and cooled gradually down to room temperature for recrystallization. The specimen was then pulverized gently for the ease of loading it into the calorimeter vessel. The chemical and the isotope purities of the specimen were better than 99.9 moles per cent as confirmed by gas chromatography and 98 per cent by high-resolution NMR, respectively. The powdered specimen (8.7131 g, 0.035652 mol) was loaded into the same calorimeter vessel and treated in the same way as for *p*-terphenyl. The contribution of the sample to the total heat capacity was 51 per cent at 10 K, 27 per cent at 100 K and 42 per cent at 300 K.

The working thermometers attached to the calorimeter vessel were a platinum (model 8164, Leeds & Northrup Co.) and a germanium (model CR-1000, CryoCal Inc.) resistance thermometers. Their temperature scales are based on the IPTS-68, helium gas thermometry and the 1958 ^{4}He vapor pressure scale. The apparatus and the operation of the adiabatic calorimetry were the same as described elsewhere.[58]

Results and Discussion

Heat Capacities and Thermodynamic Functions.

The heat capacity measurements were made between 3 and 300 K. The primary data are tabulated in Table 1 for *p*-terphenyl and Table 2 for *p*-terphenyl-d_{14} in chronological sequence and both are plotted in Fig. 1, where data of the *p*-terphenyl specimen that was sublimed and melted are not included. Curvature corrections were not made. After each energy input was over, thermal equilibrium within the calorimeter vessel was attained in 2 min below 20 K. As temperature rose, the time needed for equilibration gradually increased to 10 min at 80 K and 20 min just below the transition temperature, and it abruptly decreased to 10 min above the transition.

As the difference in sample preparation might cause differences in thermodynamic properties especially at the phase transition, the heat capacities of the as-sublimed *p*-terphenyl sample was compared with

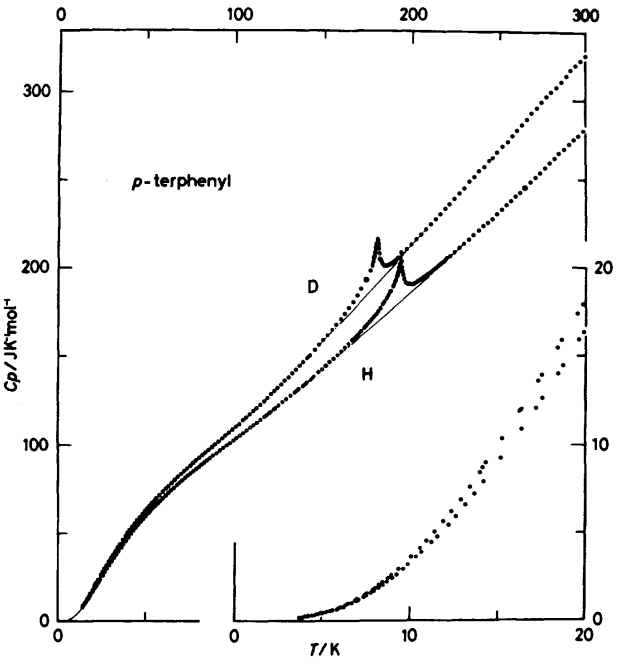

Fig. 1. Measured molar heat capacities of *p*-terphenyl (○) and *p*-terphenyl-d_{14} (●).

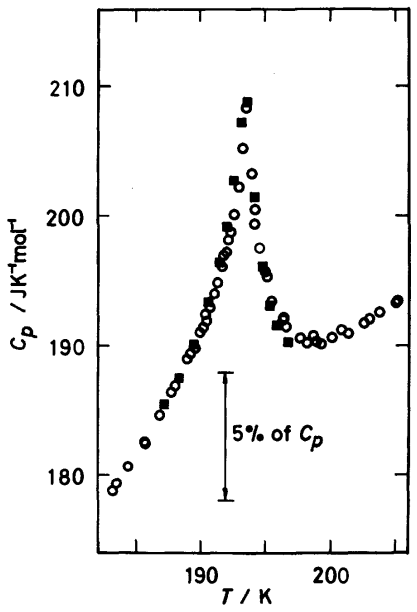

Fig. 2. Comparison of the anomalies due to the twist transition of the as-sublimed (○) and the sublimed-melted (■) *p*-terphenyl samples.

those of the melt-pulverized sample as shown in Fig. 2. The fact that there is no apparent difference rules out any possibilities of the formation of metastable phases and/or difference in crystallinity.

Figure 3 shows deviations of the present and Chang's[40] data from the smooth heat capacities determined from the present *p*-terphenyl results. The present results are systematically smaller by ca. 0.2 per cent than Chang's data in other than the transition region above 20 K.

Table 1. Measured Molar Heat Capacities of *p*-Terphenyl

T	$C_{p,m}$	T	$C_{p,m}$	T	$C_{p,m}$	T	$C_{p,m}$	T	$C_{p,m}$
K	$J K^{-1} mol^{-1}$	K	$J K^{-1} mol^{-1}$	K	$J K^{-1} mol^{-1}$	K	$J K^{-1} mol^{-1}$	K	$J K^{-1} mol^{-1}$
as-sublimed sample		248.401	230.28	192.042	197.26	5.164	0.449	Series 25	
Series 1		251.110	233.11	192.358	198.77	5.549	0.549	56.689	67.044
118.932	117.87	253.820	235.56	192.677	200.09	5.928	0.673	58.033	68.438
120.626	119.82	256.511	238.22	192.996	202.20	6.293	0.809	Series 26	
122.532	120.82	259.160	240.71	193.313	205.17	6.650	0.946	189.034	188.97
124.595	122.44	261.845	242.95	193.628	208.36	7.014	1.109	190.434	192.46
126.794	124.29	264.277	245.37	193.943	203.25	7.397	1.301	191.770	196.96
129.081	126.00	Series 7		194.259	199.35	7.811	1.548	192.414	200.65
Series 2		265.118	246.09	194.575	197.55	8.258	1.840	192.478	200.89
129.181	125.88	267.871	248.87	194.892	195.77	8.741	2.181	192.562	201.15
131.472	127.80	270.598	251.68	Series 13		9.279	2.619	192.671	201.04
133.763	129.71	273.358	254.20	195.549	193.55	9.897	3.168	192.805	201.83
136.027	131.62	276.152	256.83	196.588	191.55	10.646	3.870	192.962	203.13
138.259	133.43	278.924	259.69	197.719	190.65	11.555	4.794	193.144	204.02
140.461	135.17	281.670	262.39	198.921	190.32	12.590	5.928	193.342	206.54
142.655	136.94	284.395	264.95	200.148	190.59	13.663	7.239	193.521	209.80
144.841	138.86	287.157	267.44	201.373	190.94	Series 19		193.672	210.71
146.986	140.98	289.959	270.62	202.595	191.68	6.720	0.989	193.810	207.64
149.059	142.65	292.736	273.02	203.813	192.58	7.111	1.174	193.935	205.46
151.056	144.76	295.492	275.42	205.026	193.29	7.528	1.391	194.051	203.97
152.989	145.90	298.228	278.16	206.237	194.11	7.983	1.669	194.163	202.47
Series 3		Series 8		207.456	194.99	8.478	2.003	194.279	201.77
132.987	128.86	84.253	90.983	208.685	195.91	9.019	2.419	194.405	200.39
135.299	130.88	86.121	92.552	209.909	196.80	9.631	2.941	Series 27	
137.593	132.92	87.982	94.001	211.129	197.80	10.358	3.622	195.123	195.31
139.847	134.66	89.838	95.456	212.344	198.78	11.218	4.456	196.436	192.09
142.087	136.67	91.722	96.907	213.555	199.73	12.184	5.471	Series 28	
144.356	138.52	93.632	98.347	214.776	200.78	13.175	6.623	188.569	187.35
146.611	140.57	95.562	99.842	216.005	201.78	Series 20		189.662	189.94
148.884	142.43	97.461	101.15	217.224	202.87	17.163	12.094	198.214	190.15
151.173	144.51	99.337	102.73	218.437	203.77	18.440	14.041	199.291	190.12
153.429	146.53	101.230	104.07	219.651	205.10	19.654	15.946	sublimed and melted sample	
155.620	148.53	103.079	105.45	Series 14		20.789	17.740		
157.745	150.60	Series 9		51.458	61.431	21.939	19.591	Series 29	
Series 4		104.949	106.85	53.397	63.571	23.105	21.503	187.284	185.49
159.931	152.59	106.850	108.42	54.967	65.232	24.292	23.462	188.348	187.52
162.093	154.73	108.727	109.90	56.523	66.812	Series 21		189.461	190.24
164.230	156.87	110.581	111.27	58.044	68.382	14.022	7.737	190.605	193.43
166.387	159.03	112.459	112.70	59.573	69.909	15.155	9.246	191.471	196.46
168.563	161.29	114.364	114.18	61.113	71.344	16.338	10.899	192.043	199.33
170.717	163.60	116.248	115.66	62.648	72.843	17.524	12.633	192.598	202.73
172.854	165.87	118.112	117.18	64.185	74.331	18.724	14.478	193.136	207.25
174.974	168.29	119.971	118.65	65.742	75.647	19.920	16.375	193.669	208.85
177.114	170.75	Series 10		67.319	77.107	21.113	18.250	194.206	201.47
179.273	173.41	116.646	115.94	68.905	78.503	22.311	20.199	194.752	196.11
181.410	176.38	119.536	118.27	70.475	79.884	23.517	22.186	195.306	193.07
183.520	179.37	121.996	120.12	72.029	81.161	24.732	24.183	195.859	191.58
185.649	182.59	Series 11		73.594	82.532	Series 22		196.693	190.35
187.795	186.42	167.071	159.49	75.145	83.762	21.983	19.641	Series 30	
189.955	191.09	168.073	160.68	76.688	85.031	23.168	21.574	189.949	191.44
192.121	198.23	169.090	161.76	78.224	86.303	24.373	23.544	191.053	195.01
194.313	200.52	170.141	162.87	79.754	87.473	25.599	25.537	192.087	199.51
196.515	192.22	171.228	163.91	81.303	88.765	Series 23		192.621	201.61
198.679	190.77	172.355	165.23	82.847	89.977	26.845	27.628	192.721	202.54
200.840	191.22	173.522	166.52	84.388	91.148	28.106	29.627	192.829	203.63
202.991	192.04	174.730	167.98	Series 15		29.383	31.666	192.940	204.74
205.132	193.46	175.957	169.33	3.732	0.184	30.671	33.715	193.052	205.69
207.263	194.91	177.177	170.79	3.873	0.239	31.965	35.765	193.164	206.94
209.394	196.46	178.394	172.23	3.991	0.268	33.266	37.775	193.275	208.30
Series 5		179.607	173.66	Series 16		34.590	39.748	193.387	209.50
210.577	197.08	180.807	175.25	4.627	0.321	35.929	41.715	193.501	209.35
213.355	199.13	182.015	176.98	5.073	0.425	37.298	43.709	193.614	209.55
		183.231	178.75	5.491	0.536	38.699	45.627	193.726	208.13

Table 1. (Continued)

T	$C_{p,m}$	T	$C_{p,m}$	T	$C_{p,m}$	T	$C_{p,m}$	T	$C_{p,m}$
K	J K^{-1} mol^{-1}	K	J K^{-1} mol^{-1}	K	J K^{-1} mol^{-1}	K	J K^{-1} mol^{-1}	K	J K^{-1} mol^{-1}
216.112	201.75	184.437	180.65	5.882	0.635	40.101	47.563	193.839	206.00
218.845	204.04	185.646	182.52	6.285	0.759	41.509	49.465	193.950	204.54
221.560	206.31	186.861	184.59	Series 17		42.928	51.319	194.063	202.34
224.244	208.60	188.067	186.85	3843	0.207	44.344	53.107	194.174	201.13
226.936	211.01	189.277	189.40	4.079	0.222	45.747	54.813	194.285	199.73
229.619	213.39	Series 12		4.436	0.287	47.109	56.480	194.396	198.26
232.307	216.14	190.003	190.22	4.838	0.369	48.460	58.096	194.506	197.15
235.026	218.32	190.250	191.46	5.235	0.467	49.838	59.713	195.088	194.20
237.725	220.77	190.520	191.88	5.610	0.576	51.207	61.229		
240.404	223.51	190.806	192.90	Series 18		Series 24			
Series 6		191.106	193.95	4.077	0.221	52.567	62.714		
243.063	225.35	191.415	194.89	4.422	0.278	53.948	64.261		
245.714	227.74	191.726	196.09	4.790	0.363	55.328	65.649		

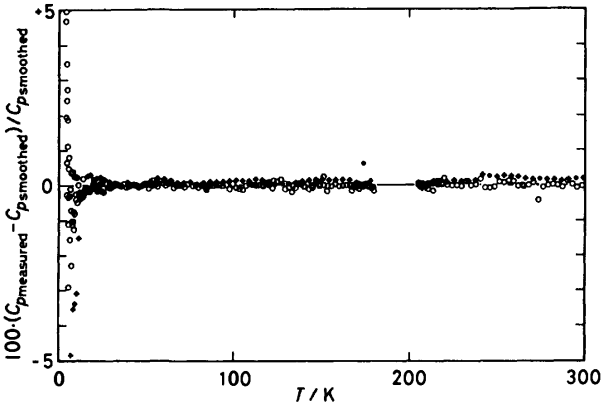

Fig. 3. Deviations of the measured values from the smooth curve determined from the present data for p-terphenyl; O, present work; ◆, Chang.[40]

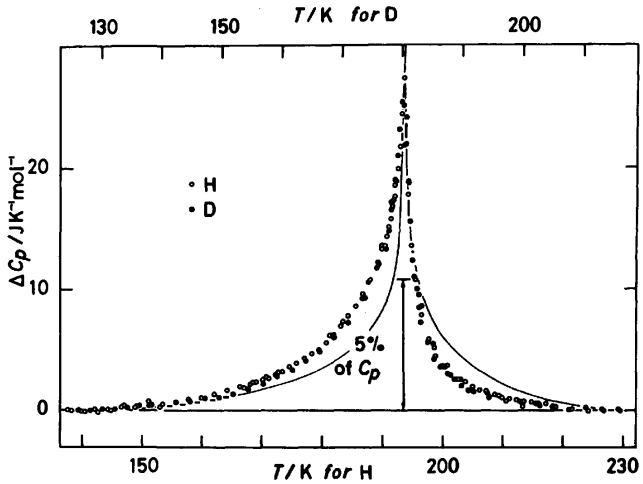

Fig. 4. Excess heat capacities due to the twist transition of p-terphenyl (O) and p-terphnyl-d_{14} (●).

Some thermodynamic quantities calculated from the present results are given at rounded temperatures in Tables 3 and 4, where small contributions below 4 K were estimated by extrapolating the heat capacity curve from the high temperature side smoothly.

Anomaly Due to Phase Transition. As clearly seen in Fig. 1, the twist transition is observed as a λ-shaped anomaly with a maximum at (193.5±0.1) K for p-terphenyl and (180.3±0.1) K for p-terphenyl-d_{14}. The transition temperature of the H compound reported by Chang[40] (193.55 K) agrees well with our result. The general shape of the anomaly is also in good agreement. The C_p maximum determined by Cailleau and Dworkin[39] occurred at 193.33 K, whereas they gave 191.0 K from DSC experiment. Cailleau and Dworkin also reported the transition temperature of the D compound as 178.8 K from DSC. In spite of sharp rise in heat capacity, no latent heat was detected in agreement with the results reported by Cailleau and Dworkin,[39] and Chang.[40] By assuming the normal portions of heat capacity as shown by the solid lines in Fig. 1, the excess parts were separated. This can be seen in Fig. 4 and the anomaly ranges from 145 K to 225 K (p-terphenyl) and 130 K to 210 K (p-terphenyl-d_{14}). The values of the enthalpies and the entropies of transition obtained by graphical integration are given in Table 5 and compared with the literature values.[39,40] Small differences between ours and those reported by Chang[40] are mainly due to the difference in estimation of the normal portion of heat capacity. As the estimation of the excess parts is more or less artificial in cases of structural phase transitions, it is considered that these values are in reasonable agreement. Thus, the entropy of transition of p-terphenyl is much larger than that of biphenyl (0.129 J·K^{-1}·mol^{-1})[18-20] which undergoes a displacive type of transition. This fact is consistent with an order-disorder nature of the transition of p-terphenyl. The detailed comparison of the properties of the twist transitions of biphenyl, p-terphenyl, and p-quaterphenyl was given in a previous paper.[23]

The critical exponent α for heat capacity was determined by plotting the excess heat capacities

$$\Delta C_p^{\infty} |T - T_c|^{-\alpha}$$

Table 2. Measured Molar Heat Capacities of *p*-Terphenyl-d_{14}

T	$C_{p,m}$	T	$C_{p,m}$	T	$C_{p,m}$	T	$C_{p,m}$	T	$C_{p,m}$
K	$J K^{-1} mol^{-1}$	K	$J K^{-1} mol^{-1}$	K	$J K^{-1} mol^{-1}$	K	$J K^{-1} mol^{-1}$	K	$J K^{-1} mol^{-1}$
Series 1		Series 4		83.618	95.826	4.519	0.296	24.063	25.303
142.267	150.48	279.816	299.94	85.388	97.317	4.839	0.359	25.287	27.439
144.794	153.56	282.655	302.99	87.152	98.842	5.192	0.463	26.497	29.520
147.334	156.47	285.502	306.32	88.910	100.47	5.558	0.565	27.712	31.555
149.665	158.99	288.352	309.64	90.677	101.93	5.936	0.714	28.927	33.609
152.056	161.76	291.174	313.32	Series 8		6.342	0.869	30.140	35.636
154.573	164.81	294.009	315.59	182.115	203.82	6.753	1.068	31.362	37.661
157.063	167.87	296.862	318.24	183.211	201.27	7.168	1.268	32.617	39.710
159.418	170.97	299.698	321.16	184.327	200.84	7.549	1.502	33.940	41.746
161.791	174.03	Series 5		185.440	200.68	Series 13		35.319	43.847
164.181	177.40	91.195	102.03	186.551	201.29	6.149	0.830	36.883	46.212
166.546	180.78	93.075	103.75	187.659	201.91	6.573	0.990	38.322	48.250
168.889	184.39	94.948	105.45	188.782	202.69	7.004	1.244	39.533	49.948
171.228	188.13	96.816	107.06	189.925	203.43	7.442	1.421	40.866	51.805
173.583	192.67	98.711	108.73	191.065	204.32	7.893	1.736	42.205	53.627
175.931	197.74	100.633	110.38	Series 9		Series 14		43.587	55.481
178.266	205.75	102.585	111.84	173.981	193.16	7.378	1.377	45.003	57.230
180.605	213.00	104.553	114.02	176.192	198.38	7.799	1.663	46.463	59.014
182.942	203.25	106.523	115.67	177.476	201.00	8.248	1.999	47.950	60.875
185.250	201.87	108.483	117.52	177.849	202.93	8.757	2.402	49.351	62.591
187.531	202.89	110.431	119.24	178.215	205.09	9.360	2.931	50.676	64.101
Series 2		112.369	121.05	178.579	206.24	10.069	3.632	52.022	65.602
187.146	201.92	114.299	122.72	178.942	208.32	10.924	4.532	53.393	67.179
189.571	203.70	116.236	124.58	179.304	210.69	11.869	5.644	54.795	68.648
192.027	205.25	Series 6		179.663	213.16	12.858	6.878	Series 20	
194.514	207.51	116.432	125.01	180.022	215.83	13.939	8.403	177.334	200.67
197.057	210.10	118.359	126.66	180.379	215.97	Series 15		178.121	201.93
199.680	212.87	120.292	128.72	180.737	215.33	8.032	1.844	178.246	202.69
202.363	215.69	122.251	130.46	181.096	210.46	8.463	2.179	178.368	201.06
205.077	218.47	124.224	132.27	181.457	207.66	8.964	2.588	178.496	202.09
207.832	221.30	126.209	134.21	181.819	204.79	Series 16		178.627	202.17
210.595	224.50	128.206	136.13	182.183	203.68	10.569	4.126	178.760	204.15
213.330	227.39	130.215	138.23	182.548	203.27	11.381	5.073	178.896	204.23
216.071	231.42	132.287	140.32	182.914	202.14	12.342	6.238	179.032	204.44
218.647	233.40	134.353	142.47	184.172	201.70	13.372	7.594	179.166	205.76
221.162	236.11	136.368	144.67	Series 10		Series 17		179.301	207.58
223.936	238.89	138.399	146.73	3.955	0.205	14.286	9.005	179.434	209.39
226.839	242.18	140.446	148.97	4.233	0.267	15.205	10.365	179.567	210.85
229.707	245.29	142.509	151.18	4.599	0.316	16.317	12.033	179.700	210.80
232.554	249.10	144.589	153.51	4.962	0.401	17.483	13.932	179.833	211.06
235.392	251.79	Series 7		5.325	0.518	18.657	15.896	179.967	211.99
238.209	255.00	55.803	69.701	5.702	0.639	19.863	17.955	180.099	211.82
241.003	257.48	57.703	71.753	6.096	0.783	21.130	21.131	180.231	212.56
243.829	260.69	59.411	73.517	6.501	0.954	Series 18		180.364	213.68
Series 3		61.058	75.264	6.899	1.152	14.082	8.687	180.497	211.43
245.835	262.31	62.739	76.782	Series 11		15.169	10.325	180.630	211.20
248.683	265.60	64.447	78.554	3.921	0.186	16.215	11.889	180.763	209.40
251.509	268.74	66.162	80.104	4.245	0.250	17.287	13.602	180.896	208.35
254.342	271.74	67.914	81.788	4.604	0.319	18.402	15.467	181.030	206.38
257.182	274.92	69.660	83.441	4.965	0.431	19.544	17.417	181.164	205.34
260.001	278.28	71.408	85.110	5.283	0.490	20.739	19.469	181.299	203.20
262.830	281.33	73.158	86.590	5.624	0.601	22.015	21.650	181.433	202.35
265.691	284.55	74.912	88.235	5.988	0.729	23.289	23.931		
268.533	287.87	76.648	89.721	Series 12		24.493	26.040		
271.358	291.07	78.371	91.207	3.789	0.145	Series 19			
274.188	294.01	80.105	92.711	3.981	0.191	21.611	20.968		
276.997	297.81	81.853	94.290	4.219	0.240	22.837	23.127		

Table 3. Molar Thermodynamic Functions of *p*-Terphenyl

T	$C_{p,m}$	$[H^\circ_m(T)-H^\circ_m(0)]/T$	$S^\circ_m(T)-S^\circ_m(0)$	$-[G^\circ_m(T)-H^\circ_m(0)]/T$
K	J K^{-1} mol^{-1}	J K^{-1} mol^{-1}	J K^{-1} mol^{-1}	J K^{-1} mol^{-1}
5	0.392	0.101	0.131	0.030
10	3.27	0.82	1.08	0.27
20	16.49	5.07	7.01	1.95
30	32.67	11.57	16.75	5.19
40	47.44	18.75	28.23	9.49
50	59.86	25.76	40.19	14.44
60	70.28	32.33	52.05	19.73
70	79.46	38.43	63.59	25.17
80	87.72	44.08	74.74	30.67
90	95.57	49.37	85.53	36.17
100	103.19	54.37	96.00	41.64
110	110.81	59.15	106.19	47.05
120	118.63	63.78	116.16	52.39
130	126.68	68.31	125.98	57.68
140	134.84	72.77	135.66	62.90
150	143.45	77.19	145.26	68.08
160	152.70	81.62	154.81	73.20
170	162.77	86.09	164.36	78.28
180	174.45	90.66	173.98	83.33
190	191.06	95.47	183.81	88.35
200	190.33	100.43	193.81	93.39
210	196.86	104.86	203.24	98.40
220	204.98	109.22	212.58	103.37
230	213.81	113.57	221.88	108.32
240	222.75	117.93	231.17	113.25
250	231.85	122.31	240.45	118.16
260	241.23	126.70	249.72	123.03
270	250.91	131.12	259.01	127.90
280	260.71	135.58	268.31	132.74
290	270.30	140.06	277.63	137.58
300	279.90	144.56	286.95	142.40
298.15	278.12	143.72	285.23	141.52

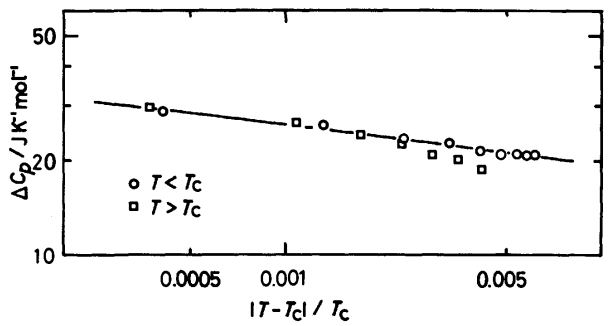

Fig. 5. Determination of the critical exponent α.

measured in series 26 in Table 1 as shown in Fig. 5. The temperature interval between adjacent points is about 0.1 K. The same value, $\alpha=0.13$, was obtained below and above the transition. This value is more like that of three-dimensional Ising model, and the positive sign of the exponent should result in an infinite heat capacity at the transition point. However, the measured heat capacity is finite at the transition point. Chang[40] reported an apparent rounding of the anomaly using a smaller temperature increment (0.025 K). He gave a larger α of 0.55 below the phase transition from a very detailed study close to the C_p maximum. It was not possible to obtain α for *p*-terphenyl-d_{14} because scatter of the measured points was larger.

Now, we will compare thermodynamic properties of the twist transitions in crystalline *p*-terphenyl and *p*-terphenyl-d_{14}. The shapes of the anomalies and the values of the entropies of transition indicate that the two compounds undergo the transition of the same mechanism and therefore the same model should apply. On the other hand, the transition temperature lowers on deuteration by about 13 K. The lowering of the transition temperature on deuteration also occurs in biphenyl.[18-20,58] Since the inter- and the intramolecular interactions are expected almost the same in the crystals of hydrogenated and deuterated compounds, these isotope effects reflect the roles of the molecular mass and/or moment of inertia in the twist transition though Raich and Bernstein[53] ruled out such a dynamical origin of the isotope effect. It is noteworthy that *p*-terphenyl-2,2″,3,3″,4,4″,5,5″,6,6″-d_{10} (C_6D_5-C_6H_4-C_6D_5) shows the twist transition at an intermediate temperature, 185.3 K.[47] Relative importance of the moment of inertia and the molecular mass in the mechanism of the transition will be experimentally demonstrated if one performs a study on

Table 4. Molar Thermodynamic Functions of *p*-Terphenyl-d_{14}

T	$C_{p,m}$	$[H^\circ_m(T)-H^\circ_m(0)]/T$	$S^\circ_m(T)-S^\circ_m(0)$	$-[G^\circ_m(T)-H^\circ_m(0)]/T$
K	J K^{-1} mol^{-1}	J K^{-1} mol^{-1}	J K^{-1} mol^{-1}	J K^{-1} mol^{-1}
5	0.421	0.109	0.142	0.033
10	3.56	0.89	1.17	0.28
20	18.19	5.59	7.71	2.12
30	35.41	12.68	18.37	5.68
40	50.64	20.32	30.69	10.38
50	63.30	27.68	43.39	15.71
60	74.10	34.53	55.91	21.37
70	83.77	40.89	68.09	27.18
80	92.67	46.81	79.84	33.03
90	101.22	52.39	91.25	38.87
100	109.83	57.69	102.36	44.66
110	118.88	62.85	113.25	50.40
120	128.26	67.90	123.99	56.09
130	137.97	72.92	134.64	61.72
140	148.43	77.94	145.24	67.31
150	159.32	82.99	155.85	72.86
160	171.76	88.14	166.52	78.38
170	185.90	93.46	177.34	83.88
180	215.90	99.21	188.59	89.38
190	203.50	104.70	199.60	94.90
200	213.19	109.87	210.27	100.40
210	223.79	115.04	220.93	105.98
220	234.82	120.24	231.59	111.36
230	245.72	125.46	242.27	116.82
240	256.22	130.69	252.95	122.27
250	266.93	135.92	263.63	127.71
260	278.16	141.17	274.31	133.14
270	289.48	146.46	285.03	138.57
280	300.54	151.76	295.75	143.99
290	311.27	157.08	306.49	149.41
300	321.55	162.39	317.22	154.82
298.15	319.66	161.41	315.23	153.82

Table 5. Properties of the Twist Transitions of *p*-Terphenyl and *p*-Terphenyl-d_{14}

		This work	Chang[40]	Dworkin and Cailleau[39]
p-Terphenyl	T_{trs}/K	193.5±0.1	193.55	193.33
	region/K	145—225	140—240	(175—200)[a]
	$\Delta_{trs}H$/J·mol^{-1}	304±20	334	
	$\Delta_{trs}S$/J·K^{-1}·mol^{-1}	1.63±0.10	1.80	0.49
p-Terphenyl-d_{14}	T_{trs}/K	180.3±0.1		178.8[b]
	region/K	130—210		
	$\Delta_{trs}H$/J·mol^{-1}	288±20		
	$\Delta_{trs}S$/J·K^{-1}·mol^{-1}	1.63±0.10		1.08[b]

a) Read from Fig. 1 of Ref. 39. b) Determined by DSC.

p-terphenyl-4,4″-d_2.

Although Chen et al.[38] suggested that there is another phase transition at about 8 K based from their EPR experiments, any anomalous behavior was not observed in the present experiments.

Anisotropy of Interaction The examination of crystal structures of poly(*p*-phenylene)s makes us suspect that the interaction within the ab plane (a, b, and c refer, hereafter, to the crystal axes of the room temperature phase) is much stronger than in the direction of the c axis because the nearest neighbor distance is much shorter in the ab plane than that along the c axis. Furthermore, in view of the order-disorder mechanism, it is also expected that inter-"spin" interaction, i.e. a part of the intermolecular interaction which depends on molecular twisting is much stronger within the ab plane than along the c axis since the interatomic distance between two neighboring molecules in the c direction changes little upon twisting of one of them. Indeed, two-dimensionality of interaction has been reported experimentally.[43–45]

In order to see the anisotropic interaction, we now examine the low temperature ordered structure.[9] The

structure viewed along the c axis is schematically shown in Fig. 6, where Roman numerals distinguish translationally inequivalent molecules. The solid line represents the triclinic unit cell of the low-temperature phase and the broken line the monoclinic unit cell of the room-temperature phase. All of the molecules shown there lie at the same height. Since the "spin" in this case corresponds to twisting of the central phenyl ring with respect to the outer rings, the atomic position of "wrong" molecules were determined from those of "right" molecules which are known by experiment.[9] The intermolecular interactions were then calculated assuming that it may be expressed by the sum of interatomic potentials of Buckingham type.[60] Summation was made over all the atom pairs between the two adjacent molecules under consideration.

The calculated intermolecular and inter-"spin" interactions are summarized in Table 6, where the inter-"spin" interaction energy J is defined by

$$J=\frac{1}{2}(E_{r-r}+E_{w-w})-\frac{1}{2}(E_{r-w}+E_{w-r}).$$

It is evident that interactions within the ab plane are much stronger than those along the c axis. Thus, a two-dimensional Ising model will apply to the twist transition of *p*-terphenyl at least in the first approximation. Indeed, the experimental excess heat capacity is well reproduced with a two-dimensional Ising mdel as shown in Fig. 4.

It is well-known that the heat capacity of any two dimensional Ising model diverges as $\ln|T-T_c|$ at T_c and shows the critical exponent $\alpha=0$. However, the experimental value determined in this study is not 0 but 0.13. However, the discrepancy is not crucial because the exact formula of the heat capacity gives a slope of about 0.1 at $|T-T_c|/T_c\simeq 0.001$, where the experiments were done.

Figure 7 shows the calculated heat capacity of, for

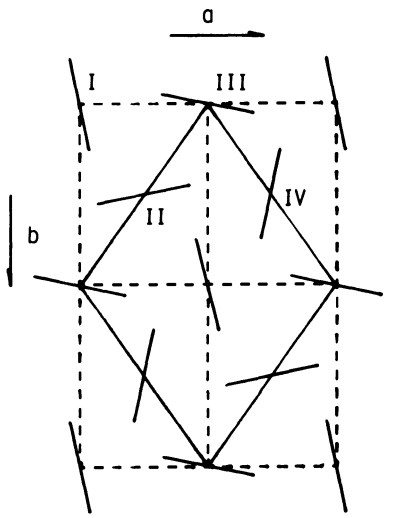

Fig. 6. Crystal structure of the low temperature phase viewed along the c axis (schematic). Broken line represents the unit cell of the room temperature phase.

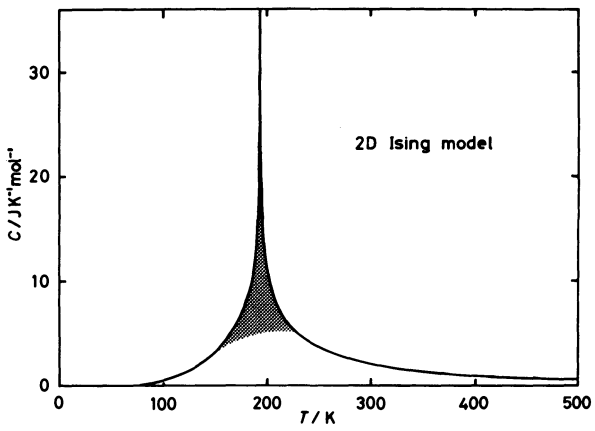

Fig. 7. Calculated heat capacity of the two-dimensional square lattice of Ising model with a critical temperature of 193.5 K.

Table 6. Calculated Inter-"spin" Interaction Energies within the ab Plane (upper) and along the c Axis (Lower)
r, "right" molecule; w, "wrong" molecule
$J=\frac{1}{2}(E_{r-r}+E_{w-w})-\frac{1}{2}(E_{r-w}+E_{w-r})$

	E_{r-r}	E_{r-w}	E_{w-r}	E_{w-w}	J
	kJ·mol^{-1}	kJ·mol^{-1}	kJ·mol^{-1}	kJ·mol^{-1}	kJ·mol^{-1}
I-II	−39.54	−39.46	−39.72	−39.75	−0.06
II-III	−39.98	−39.91	−37.64	−39.21	−1.17
III-IV	−38.75	−36.86	−36.59	−37.97	−1.64
IV-I	−39.80	−38.60	−39.00	−38.89	−0.55
I-III	−28.59	−22.72	−13.90	−28.55	−10.26
II-IV	−28.28	−20.65	−25.43	−28.32	−5.26
I-I	−7.25	−7.34	−7.34	−7.34	0.00
II-II	−7.28	−7.14	−7.14	−6.97	0.02
III-III	−7.40	−7.10	−7.10	−6.76	0.02
IV-IV	−7.16	−7.13	−7.13	−7.06	0.02

simplicity, the two-dimensional square lattice of Ising model[61] with the critical temperature of 193.5 K (J=709 J·mol^{-1}). There exist large tails on both the lower and the higher temperature sides of the transition. Remember that the experimental excess heat capacity was separated by drawing the smooth interpolating curve. For the sake of consistent comparison, therefore, the theoretical "excess" heat capacity should be separated also in the same manner as the experimental. This was done in the transition region determined experimentally (145 K to 225 K). The "excess part" is shaded in Fig. 7 and compared with the experimental one in Fig. 4. While the general agreement between the calculated and experimental curves in Fig. 4 shows that the transition may be approximated by a two-dimensional order-disorder model, discrepancies at the tail parts indicates that there is room for improvement in the model; extending the range of interaction beyond the nearest neighbors and/or introducing a small contribution of the third dimension.

It is noted that the ideal value of entropy of transition, Rln2, is obtained only when one integrates C/T between zero and high-temperature limits. This will be one of the reasons why the entropy of transition is smaller than Rln2.

Finally, a comment is in order about the change in the nature of the twist transitions of poly(*p*-phenylene)s from a displacive phase transition in crystalline biphenyl to order-disorder transitions in *p*-terphenyl and in *p*-quaterphenyl. In the case of biphenyl, the substitution of *p* and *p'* hydrogens with fluorine atoms[56,59] or hydroxyl groups[57] mainly modifies the intramolecular potential for the twisting motion and the twist transition disappears owing to the stabilization of the planar conformation that favors greater π-conjugation. This suggests that the twist transition of *p*-terphenyl may change its nature from an order-disorder type to a displacive type upon such substitutions. Thus, it is interesting to investigate the properties of suitably substituted *p*-terphenyls in order to elucidate the nature of displacive and order-disorder types of phase transitions.

References

1) J. Dale, *Acta Chem. Scand.*, **11**, 640 (1957).
2) H. Suzuki, *Bull. Chem. Soc. Jpn.*, **33**, 109 (1960).
3) S. Hino, K. Seki, and H. Inokuchi, *Chem. Phys. Lett.*, **36**, 335 (1976).
4) A. J. Grumadas, D. P. Poshkus, and A. V. Kiselev, *J. Chem. Soc., Faraday Trans. 2*, **78**, 2013 (1982).
5) H. M. Rietveld, E. N. Maslen, and C. J. B. Clews, *Acta Crystallogr., Sect. B*, **26**, 693 (1970).
6) J. L. Baudour, *Acta Crystallogr., Sect. B*, **28**, 1649 (1972).
7) J. L. Baudour, H. Cailleau, and W. B. Yelon, *Acta Crystallogr., Sect. B*, **33**, 1773 (1977).
8) J. L. Baudour, L. Toupet, Y. Delugeard, and S. Ghemid, *Acta Crystallogr., Sect. C*, **42**, 1211 (1987).
9) J. L. Baudour, Y. Delugeard, and H. Cailleau, *Acta Crystallogr., Sect. B*, **32**, 150 (1976).
10) J. Trotter, *Acta Crystallogr.*, **14**, 1135 (1961).
11) G. B. Robertson, *Nature (London)*, **191**, 593 (1961).
12) A. Hargreaves and S. H. Rizvi, *Acta Crystallogr.*, **15**, 365 (1962).
13) V. M. Kozhin and K. V. Mirskaya, *Sov. Phys. Crystallogr.*, **14**, 938 (1970).
14) G. P. Charboneau and Y. Delugeard, *Acta Crystallogr., Sect. B*, **32**, 1420 (1976).
15) G. P. Charboneau and Y. Delugeard, *Acta Crystallogr., Sect. B*, **33**, 1586 (1977).
16) H. Cailleau, J. L. Baudour, and C. M. E. Zeyen, *Acta Crystallogr., Sect. B*, **35**, 426 (1979).
17) J. L. Baudour and M. Sanquer, *Acta Crystallogr., Sect. B*, **39**, 75 (1983).
18) T. Atake and H. Chihara, *Solid State Commun.*, **35**, 131 (1980).
19) T. Atake, K. Saito, and H. Chihara, *Chem. Lett.*, **1983**, 493.
20) K. Saito, T. Atake, and H. Chihara, *Bull. Chem. Soc. Jpn.*, in press.
21) Y. Delugeard, J. Desuche, and J. L. Baudour, *Acta Crystallogr., Sect. B*, **32**, 702 (1976).
22) J. L. Baudour, Y. Delugeard, and P. Rivet, *Acta Crystallogr., Sect. B*, **34**, 625 (1978).
23) K. Saito, T. Atake, and H. Chihara, *J. Chem. Thermodyn.*, **17**, 539 (1985).
24) B. Wyncke, F. Brehat, and A. Hadni, *J. Phys. (Paris)*, **38**, 1171 (1977).
25) A. Girard, H. Cailleau, Y. Marqueton, and C. Ecolivet, *Chem. Phys. Lett.*, **54**, 479 (1978).
26) B. A. Bolton and P. N. Prasad, *Chem. Phys.*, **35**, 331 (1978).
27) D. Kirin, S. L. Chaplot, G .A. Mackenzie, and G. S. Pawley, *Chem. Phys. Lett.*, **102**, 105 (1983).
28) C. Ecolivet, B. Toudic, and M. Sanquer, *J. Chem. Phys.*, **81**, 599 (1984).
29) H. Cailleau, A. Girard, J. C. Messager, Y. Delugeard, and C. Vettier, *Ferroelectrics*, **54**, 257 (1984).
30) A. Girard, M. Sanquer, and Y. Delugeard, *Chem. Phys.*, **96**, 427 (1986).
31) A. Girard, Y. Delugeard, and H. Cailleau, *J. Phys. (Paris)*, **48**, 1751 (1987).
32) J. Fünfschilling, L. Altwegg, I. Z. Granacher, M. Chabr, and D. F. Williams, *J. Chem. Phys.*, **70**, 4622 (1979).
33) J. O. Williams, *Chem. Phys. Lett.*, **42**, 171 (1976).
34) Z. Burshtein and D. F. Williams, *J. Chem. Phys.*, **68**, 983 (1978).
35) N. I. Wakayama, *Chem. Phys. Lett.*, **70**, 397 (1980).
36) N. I. Wakayama, S. Matsuzaki, and M. Mizuno, *Chem. Phys. Lett.*, **74**, 37 (1980).
37) N. I. Wakayama, S. Matsuzaki, and M. Mizuno, *Chem. Phys. Lett.*, **75**, 587 (1980).
38) M. C. Chen, A. S. Cullick, R. E. Gerkin, and A. P. Lundstedt, *Chem. Phys.*, **46**, 423 (1980).
39) H. Cailleau and A. Dworkin, *Mol. Cryst. Liq. Cryst.*, **50**, 217 (1979)
40) S. S. Chang, *J. Chem. Phys.*, **79**, 6229 (1983).
41) H. Cailleau, J. L. Baudour, A. Girard, and W. B. Yelon, *Solid State Commun.*, **20**, 577 (1976)

42) H Cailleau, J. L. Baudour, W. B. Yelon, A. Girard, Y. Delugeard, and J. Desuche, *J. Phys. (Paris), Colloq.*, **37**, C1-233 (1976).
43) R. E. Lechner, B. Toudic, and H. Cailleau, *J. Phys. C*, **17**, 405 (1984).
44) B. Toudic and R. E. Lechner, *J. Phys. C*, **17**, 5503 (1984).
45) T. Gullion M. S. Conradi, and A. Rigamonti, *Phys. Rev. B*, **31** 4388 (1985).
46) H. Cailleau, A. Heidemann, and C. M. E. Zeyen, *J. Phys. C*, **12**, L411 (1979).
47) B. Toudic, H. Cailleau, R. E. Lechner, and W. Petry, *Phys. Rev. Lett.*, **56**, 347 (1986).
48) Z. Pajak, N. Pislewski, and J. Wasicki, Proc. XI-th Sem. NMR, 190 (1980).
49) K. Kohda, N. Nakamura, and H. Chihara, *J. Phys. Soc. Jpn.*, **51**, 3936 (1982).
50) B. Toudic, J. Gallier, P. Rivet, and H. Cailleau, *Solid State Commun.*, **47**, 291 (1983).
51) T. Gullion and M. S. Conradi, *Phys. Rev. B*, **30**, 1133 (1984).
52) S. Ramdas and J. M. Thomas, *J. Chem. Soc., Faraday Trans. 2*, **72**, 1251 (1976).
53) J. C. Raich and E. R. Bernstein, *Mol. Phys.*, **53**, 597 (1984)
54) K. Saito, T. Atake, and H. Chihara, *Chem. Lett.*, **1984**, 521.
55) K. Saito, H. Chihara. T. Atake, and Y. Saito, *Jpn. J. Appl. Phys.*, **24**, Suppl. **24-2**, 838 (1985).
56) K. Saito, T. Atake, and H. Chihara, *J. Chem. Thermodyn.*, **18**, 407 (1986).
57) K. Saito, T. Atake, and H. Chihara, *Thermochim. Acta*, **109**, 45 (1986).
58) K. Saito, T. Atake, and H. Chihara, *J. Chem. Thermodyn.*, **19**, 633 (1987).
59) K. Saito. T. Atake, and H. Chihara, *Acta Crystallogr., Sect. B*, **43**, 383 (1987).
60) D. E. Williams, *J. Chem. Phys.*, **47**, 4680 (1967).
61) L. Onsager, *Phys. Rev.*, **65**, 117 (1944).

 © 1988 The Chemical Society of Japan Bull. Chem. Soc. Jpn., 61, 2337—2341 (1988)

Molecular and Crystal Structure of the Bilayer-Forming Lipid-Model Amphiphile, Ditetradecyldimethylammonium Bromide Monohydrate

Kenji Okuyama,* Naomi Iijima, Kiyoshi Hirabayashi, Toyoki Kunitake,† and Masami Kusunoki††
Faculty of Technology, Tokyo University of Agriculture and Technology, Koganei, Tokyo 184
†Faculty of Engineering, Kyushu University, Fukuoka 812
††Crystallographic Research Center, Institute for Protein Research, Osaka University, Suita 565
(Received February 2, 1988)

The conformation and molecular packing of ditetradecyldimethylammonium bromide monohydrate ($2C_{14}N^+2C_1Br^-\cdot H_2O$), $C_{30}H_{62}NBr\cdot H_2O$, has been determined by the X-ray diffraction method. The crystals are triclinic with the space group $P\bar{1}$, $Z=2$, $a=2.9827(9)$, $b=0.7847(3)$, $c=0.7480(3)$ nm, $\alpha=104.69(4)$, $\beta=90.64(7)$, and $\gamma=90.84(6)°$. The structure was determined by direct methods and refined by the least-squares procedure: $R=0.07$ ($R_w=0.07$) for 3335 observed reflections. Two amphiphile molecules of the unit cell are related by centrosymmetry and pack tail to tail in a bilayer structure. The hydrocarbon chains tilt about 45° with respect to the bilayer normal. There are statistically four water molecules with half occupancies in a unit cell. Water molecules and bromide anions make hydrogen-bonding networks along the c-axis in the hydrophilic layer. The above molecular and crystal structure of $2C_{14}N^+2C_1Br^-\cdot H_2O$ was quite similar to those of $2C_{18}N^+2C_1Br^-\cdot H_2O$.

The fundamental organization of biomembrane is based on the bilayer structure of lipid molecules. Although lipid molecules in biomembranes are in the form of liquid crystal, the bilayer structures of this form are closely related to those of the gel (crystal) form. For better understanding of the bilayer structure and its properties, it is essential to accumulate detailed knowledge about preferred molecular and crystal structures of various types of bilayer-forming amphiphiles. It has, however, been difficult to get single crystals of amphipathic molecules suitable for X-ray structure analyses which could provide the most detailed and accurate information about molecular and crystal structures.

Since one of the authors (T. Kunitake) succeeded in formation of the biomembrane-like bilayer structure from totally synthetic amphiphiles,[1,2] a large number of other long-chain mono-, di-, and trialkyl amphiphiles were shown to form bilayer structures. These synthetic bilayer membranes, especially dialkylammonium membranes, has been intensively investigated their structures and physicochemical properties by means of electronmicroscopy, X-ray diffraction, differential scanning calorimetry, and so on.[3,4] Recently, we succeeded in growing single crystals of dialkyldimethylammonium bromides[5] and the detailed crystal structure of dioctadecyldimehylammonium bromide has been determined.[6] According to the structure of this compound, two amphiphile molecules pack tail to tail in a bilayer structure with tilting hydrocarbon chains by about 45° to the bilayer surface. In the hydrophilic layer bromide anions make hydrogen-bonding networks along the c-axis with water molecules contained statistically in a unit cell.

In this paper we discuss detailed structure of ditetradecyldimethylammonium bromide, $2C_{14}N^+2C_1Br^-$, which has the shortest alkyl chains among the homologs crystallized so far. Because of the short alkyl chains, the crystal liquid-crystal transition temperature, T_c, is rather low, 16 °C in dilute aqueous solution.

Experimental and Structure Determination

Ditetradecyldimethylammonium bromide, $2C_{14}N^+2C_1Br^-$, was prepared by step-wise alkylation of dimethylamine. Detailed procedures have been reported elsewhere.[1] $2C_{14}N^+2C_1Br^-$ (50 mg) was dissolved in 1 ml of dichloromethane. After complete dissolution, 4 ml of hexane was added. Transparent, plate-like crystals formed by keeping the solution for several days at about 8 °C. The size of the crystal used for the intensity measurement was about 0.8 mm×0.5 mm×0.01 mm.

Lattice parameters and diffraction intensities were measured on a Rigaku four-circle diffractometer with Ni-filtered Cu $K\alpha$ radiation ($\lambda=0.1542$ nm). The lattice parameters were refined by the least-squares fit using 24 reflections in the 2θ range of 11°—35°. By using the ω-scan mode at a scan rate of 6° min^{-1}, intensities of 5037 reflections were measured up to 120° in 2θ. The scan width was $\Delta\omega=(1.8+0.15\tan\theta)°$. Three reference reflections monitored every 53 reflections showed no significant intensity deterioration during the data collection. Corrections were made for the Lorentz and polarization factors, but not for absorption and extinction effects. A total of 3344 reflections greater than $3\sigma(F_o)$ were used in the following analysis.

Density was measured by flotation method using aqueous solution of sodium chloride. Since the specimen dissolved a little during the measurement, the value of the obtained density was not accurate and reliable. However, we could not find out more stable solution than aqueous sodium chloride for this compound. On the basis of the measured density and a unit cell volume, the unit cell contains two $2C_{14}N^+2C_1Br^-$ molecules. In the process of X-ray structure analysis, the monohydrated structure was revealed as shown

in the following section.

Crystal Data: $C_{30}H_{64}NBr \cdot H_2O$, F.W.=534, triclinic, space group $P\bar{1}$, Z=2, a=2.9827(9), b=0.7847(3), c=0.7480(3) nm, α=104.69(4), β=90.64(7), γ=90.84(6)°, V=1.693(1) nm^3, D_x=0.91, D_m=1.01 g cm^{-3}, μ(Cu $K\alpha$)=18.5 cm^{-1}.

Determination and Refinement of the Structure

The direct method with the MULTAN 78 program[7] was applied for $P1$ and $P\bar{1}$, space groups. For the both space groups, two planar zigzag alkyl chains could be readily discerned. In the former space group, the revealed structure consisted of two amphiphile molecules related by a centrosymmetry, which supported $P\bar{1}$ space group for the $2C_{14}N^+2C_1Br^- \cdot H_2O$ crystal. After several cycles of block-diagonal least-squares refinement starting from the coordinates of all the non-hydrogen atoms of the amphiphile obtained by the direct method, difference Fourier syntheses revealed two peaks, which were assumed to be oxygen atoms of water molecules. After another several cycles including these newly found water positions, a full-matrix least-squares calculation was performed to investigate occupancies of two water oxygen atoms, since the short distances between these oxygens (OW1···OW2, 0.18 nm and OW2···OW2, 0.22 nm) made it impossible to accomodate both of them simultaneously in the same unit cell. It was found from this calculation that two water molecules with half occupancies were most preferable and they were accomodated statistically in an asymmetric unit.

At this stage, all the magnitudes of the observed structure factors for the (h00) reflections with $h \leqq 9$ were consistently smaller than those of the calculated ones. This systematic disagreement was attributable to the absorption effect originated from the plate-like crystal shape and its long lattice constant a directed normal to the plate surface, and fairly large absorption coefficient of this compound. Therefore, these 9 reflections were excluded from the reflection data set during the following calculations. After an anisotropic refinement of non-hydrogen atoms, hydrogen atoms located on their calculated positions with isotropic temperature factors were included in the refinement. The quantity minimized was $\sum w$

Table 1. Fractional Coordinates and Equivalent Isotropic Temperature Factors[13] for Non-Hydrogen Atoms of $2C_{14}N^+2C_1Br^- \cdot H_2O$ with Estimated Standard Deviations in Parentheses

Atom	x	y	z	$B_{eq} \times 10^4$/nm^2
Br	0.0656(0)	0.2466(1)	0.6782(1)	700
N	0.0745(2)	−0.4446(8)	0.2456(8)	566
C(1)	0.0344(2)	−0.5667(12)	0.2294(11)	714
C(2)	0.0643(3)	−0.3061(11)	0.1407(11)	720
C(31)	0.0822(2)	−0.3566(9)	0.4511(9)	557
C(32)	0.1214(3)	−0.2258(9)	0.4917(10)	589
C(33)	0.1351(3)	−0.1783(10)	0.6972(10)	686
C(34)	0.1542(2)	−0.3305(10)	0.7655(10)	594
C(35)	0.1975(2)	−0.4049(10)	0.6799(9)	605
C(36)	0.2120(2)	−0.5642(10)	0.7467(10)	593
C(37)	0.2560(3)	−0.6404(10)	0.6704(10)	648
C(38)	0.2689(3)	−0.8047(10)	0.7332(10)	646
C(39)	0.3132(3)	−0.8806(10)	0.6657(10)	656
C(310)	0.3257(3)	−1.0444(10)	0.7282(11)	701
C(311)	0.3704(3)	−1.1192(11)	0.6622(11)	697
C(312)	0.3830(3)	−1.2822(11)	0.7271(11)	739
C(313)	0.4279(3)	−1.3537(12)	0.6600(13)	860
C(314)	0.4414(4)	−1.5133(14)	0.7264(16)	1159
C(41)	0.1147(2)	−0.5470(10)	0.1594(9)	571
C(42)	0.1281(2)	−0.7002(9)	0.2386(10)	582
C(43)	0.1715(2)	−0.7768(9)	0.1629(9)	551
C(44)	0.1846(2)	−0.9362(9)	0.2317(10)	576
C(45)	0.2293(2)	−1.0132(9)	0.1643(10)	571
C(46)	0.2407(2)	−1.1765(9)	0.2305(10)	577
C(47)	0.2854(2)	−1.2539(9)	0.1662(10)	596
C(48)	0.2965(2)	−1.4182(10)	0.2287(10)	596
C(49)	0.3410(2)	−1.4961(10)	0.1651(11)	632
C(410)	0.3521(3)	−1.6598(10)	0.2279(11)	651
C(411)	0.3975(3)	−1.7323(10)	0.1683(11)	703
C(412)	0.4094(3)	−1.8972(11)	0.2327(12)	744
C(413)	0.4543(3)	−1.9655(13)	0.1776(15)	955
C(414)	0.4668(4)	−2.1260(15)	0.2435(17)	1129
OW1	−0.0001(5)	0.0763(14)	0.2959(18)	1020
OW2	−0.0292(6)	0.0501(18)	0.0826(22)	1337

$B_{eq}=4\times(B_1\times a^2+B_2\times b^2+B_3\times c^2)/3$, where B_1, B_2, and B_3 are diagonal components of the anisotropic thermal parameters.

$(|F_o|-|F_c|)^2$ with $w=1.0$ for all reflections. After several cycles some hydrogen atoms with unacceptable geometry were excluded from further calculations. The final R value was 0.070 (R_w=0.067) for all non-hydrogen atoms and 61 hydrogen atoms. The final fractional coordinates and equivalent thermal parameters of the non-hydrogen atoms are given in Table 1.[8]

The atomic scattering factors were taken from International Tables for X-Ray Crystallography, Vol.IV.[9] Computations were done on an ACOS 700 S computer at the Crystallographic Research Center, Institute for Protein Research, Osaka University and on a HITAC M-280 H computer at the Computer Center, University of Tokyo with the help of the programs in UNICS III.[10]

Results and Discussion

Molecular Conformation of $2C_{14}N^+2C_1Br^-$. Figure 1 shows the molecular structure of $2C_{14}N^+2C_1$ viewed parallel (a and b) and perpendicular (c) to the zigzag plane. It also shows bond lengths, bond angles and dihedral angles together with the atom numbering following that of $2C_{18}N^+2C_1Br^-$.[6] The average C-C bond distance and C-C-C bond angle in the molecule

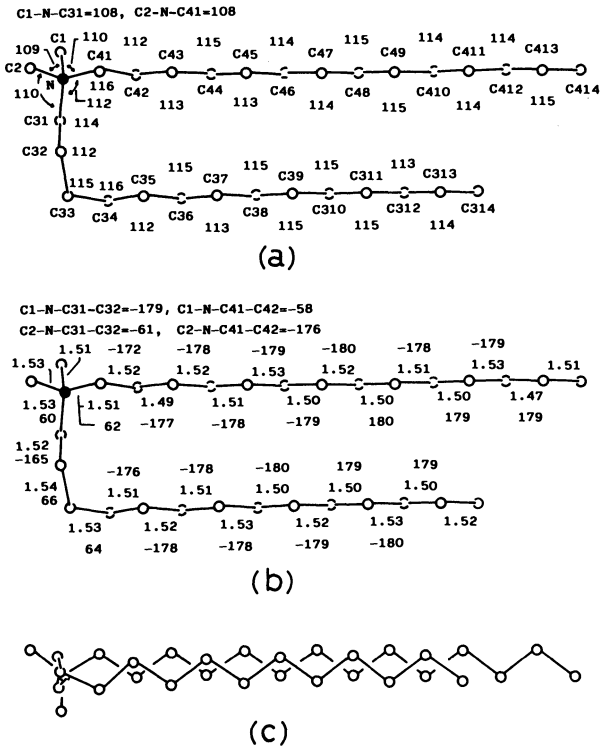

Fig. 1. (a) Atomic labelling and bond angles (/°), and (b) bond lengths (1×10/nm) and dihedral angles (/°) in $2C_{14}N^+2C_1Br^-$. Maximum estimated standard deviations for bond lengths, bond angles and dihedral angles are 0.002 nm, 1° and 1°, respectively. (c) Molecular conformation viewed from the direction normal to the zigzag plane.

are 0.151(1) nm and 114(1)°, respectively. The average bond distance is shorter by 0.002 nm and the average bond angle is wider by 2° than the corresponding values of $2C_{18}N^+2C_1Br^-$. These are still in good agreement with those previously reported for the long hydrocarbon chains of the amphiphilic compounds.[11,12] All the dihedral angles are within the range of 180°±2°, with exception in the connection parts between the head portion (N, C(31), C(32), C(33)) and the zigzag plane, C(33)-C(34)-C(35)-C(36) (−176°) and N-C(41)-C(42)-C(43) (−172°). One of the hydrocarbon chains (C(31), C(32), C(33), ···, C(314)) is bent at the C(33) atom at almost right angles. Since the quaternary nitrogen atom can be regarded as a carbon atom in the geometrical point of view, the molecular structure may be taken as one hydrocarbon chain from C(414) to C(314) folding at the bilayer surface just like polyethylene folding at the surface of the single crystal. Short atomic interactions between two chains in the same molecule are 0.405 (C(35)···C(42)), 0.407 (C(37)···C(44)), 0.407 (C(39)··· C(46)), 0.409 (C(311)··· C(48)), and 0.413 nm (C(313)···C(410)). The values of equivalent isotropic temperature factors (B_{eq}) of the chain carbon atoms gradually increase along the hydrocarbon chains. This kind of disorder was commonly observed in the bimolecular structures built up with amphiphilic molecules.[6,11,12] The detailed molecular structure of $2C_{14}N^+2C_1$ is quite similar to that of $2C_{18}N^+2C_1$, including the folding pattern (G, G, T, G, G) in the head portion.

Crystal Structure of $2C_{14}N^+2C_1Br^-$. The packing arrangement of $2C_{14}N^+2C_1Br^-$ viewed along the c-axis is shown in Fig. 2 together with short interatomic distances between neighbouring hydrocarbon chains and those between a bromide anion and the head portion of the amphiphile. There are two amphiphile molecules in a unit cell, arranged tail to tail fashion in a bilayer structure with tilting long hydrocarbon chains by about 45° to the layer surface. The molecules of the two opposite bilayer halves are related by centrosymmetry. The short intermolecular contacts between carbon atoms at the tail portions are 0.378 (C(413)···C(413)), 0.401 (C(314)···C(414)), and 0.427 nm (C(413···C(313)). While in the hydrophilic region, the bromide anion is in contact with many atoms with fairly short distances, 0.382 (C(41)), 0.391 (C(42)), 0.394 (C(31)), 0.409 and 0.388 (C(1)), 0.411 (C(2)), 0.401 (C(32)), 0.399 (C(33)), 0.345 (OW2), and 0.342 and 0.322nm (OW1). Though the direction of a-axis is slightly different from each other, the above detailed packing structure of $2C_{14}N^+2C_1Br^-$ is quite similar to that of $2C_{18}N^+2C_1Br^-$,[6] including hydrogen bonding networks between the bromide anions and water oxygens, mentioned below.

There are statistically four water oxygen atoms with half occupancies in a unit cell. Because of the short atomic contacts of OW1···OW2 (0.177 nm) or OW2···

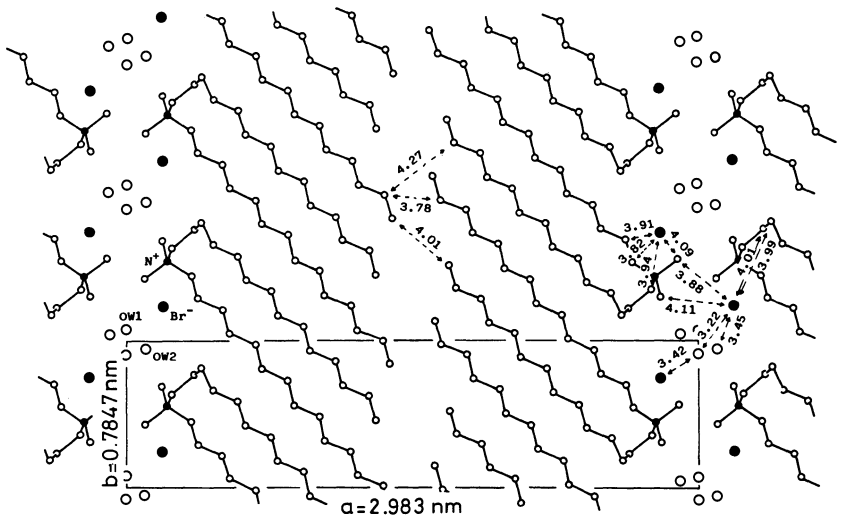

Fig. 2. Packing of $2C_{14}N^{+}2C_1Br^{-}\cdot H_2O$ projected onto the *ab*-plane (ORTEP[14] drawing). Four water oxygen atoms, OW1 and OW2 and their centrosymmetrical mates, are located on their positions in the unit cell. Distances (1×10/nm) between arrowed atoms are indicated short contacts in the structure.

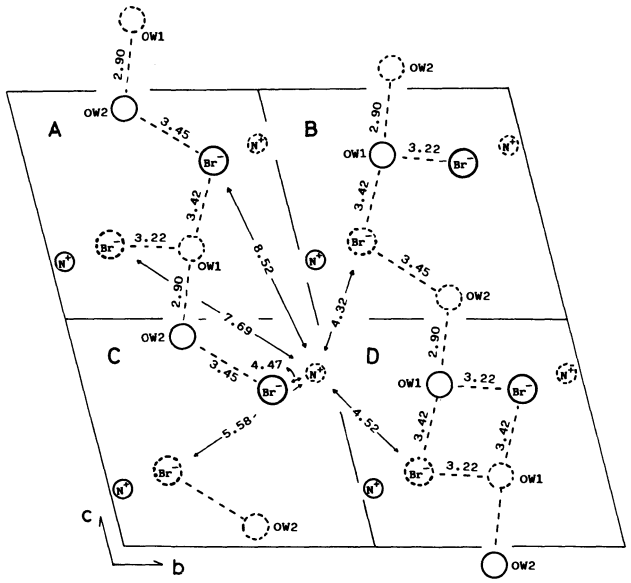

Fig. 3. Schematic illustration of hydrophillic layer of $2C_{14}N^{+}2C_1Br^{-}\cdot H_2O$ projected onto the *bc*-plane. Two water oxygen atoms are accomodated in a unit cell. Each unit cell, A, B, C, and D, has a different pair of water oxygens and hydrogen bonding scheme. Hydrogen bonds between bromide anions and water oxygen atoms are indicated by broken lines together with their bond lengths (1×10/nm). Solid and broken circles represent atoms on the upper and lower side of the hydrophillic layer, respectively. The unit cell is shifted by 0.5 along the *b*-axis for the comparison with that of $2C_{18}N^{+}2C_1Br^{-}$.

OW2 (the centrosymmetric mates at the origin) (0.219 nm), only four types of arrangement for water molecules are possible (Fig. 3). To make a comparison between $2C_{14}N^{+}2C_1Br^{-}$ and $2C_{18}N^{+}2C_1Br^{-}$, the unit cell in Fig. 3 was translated by 0.5 along the *b*-axis. Type A and B contain two water oxygen atoms, OW1 and OW2, with full occupancies. While type C or D contains a pair of centrosymmetrically related OW2 or OW1, respectively. In these arrangement, the water oxygen OW1 links to two Br^{-} and OW2 by hydrogen bonds with bond length of 0.342 and 0.322, and 0.290 nm, respectively. While the other water OW2 links to a bromide anion and OW1 by hydrogen bonds with 0.345 and 0.290 nm, respectively. Depending on the combination of the unit cell type, hydrogen-bonding networks are continuous (AA, BB, BD, DA) along the *c*-direction.

Both ammonium cations and bromide anions make a plane parallel to the bilayer surface (Fig. 2 and Table 1). There are two such planes in a hydrophilic layer. An ammonium cation is surrounded by three bromide anions, two in the same plane (0.432 and 0.452 nm) and one in the other plane (0.447 nm) (Fig. 3). Since distances to the other bromide anions are larger than 0.55 nm, the plus charge on an ammonium cation seems to be exclusively cancelled by these bromide anions.

From the analyses of $2C_nN^{+}2C_1Br^{-}$ (n=18,14) single crystal, it was found that the bilayer structure of $2C_nN^{+}2C_1Br^{-}$ is stabilized by the hydrogen bonding networks between water molecules and bromide anions, the electrostatic fources between bromide anions and ammonium cations, and the hydrophobi c interactions between long alkyl chains. It is suggested that single crystals of $2C_nN^{+}2C_1Br^{-}$ could be obtained by the above stabilizing fources.

References

1) T. Kunitake, Y. Okahata, K. Tamaki, F. Kumamaru

and M. Takayanagi, *Chem. Lett.*, **1977**, 387.

2) T. Kunitake and Y. Okahata, *J. Am. Chem. Soc.*, **99**, 3860 (1977).

3) T. Kajiyama, A. Kumano, M. Takayanagi, Y. Okahata and T. Kunitake, "Contemporary Topics in Polymer Science," ed by W. J. Bailey and T. Tsuruta, Plenum (1984), Vol. 4, pp. 829—854.

4) Y. Okahata, R. Ando and T. Kunitake, *Ber. Bunsenges. Phys. Chem.*, **85**, 789 (1981).

5) K. Okuyama, Y. Soboi, K. Hirabayashi, A. Harada, A. Kumano, T. Kajiyama, M. Takayanagi, and T. Kunitake, *Chem. Lett.*, **1984**, 2117.

6) K. Okuyama, Y. Soboi, N. Iijima, K. Hirabayashi, T. Kunitake and T. Kajiyama, *Bull. Chem. Soc. Jpn.*, **61**, 1485 (1988).

7) P. Main, S. E. Hull, L. Lessinger, G. Germain, J. P. Declercq, and M. M. Woolfson, MULTAN 78. "A System of Computer Programs for the Automatic Solution of Crystal Structures from X-ray Diffraction Data," Univs. of York, England, and Louvain, Belgium (1978).

8) Tables of anisotropic thermal parameters, coordinates of hydrogen atoms, and observed and calculated structure factors are kept at the Chemical Society of Japan, Document No. 8807

9) International Tables for X-ray Crystallography, Vol. IV, Kynoch Press, Birmingham (1974), p. 71.

10) T. Sakurai and K. Kobayashi, *Rep. Inst. Phys. and Chem. Res.*, **55**, 69 (1978).

11) S. Abrahamsson, B. Dahlen, and I. Pascher, *Acta Crystallogr., Sect. B*, **33**, 2008 (1977).

12) I. Pascher and S. Sundell, *Biochim. Biophys. Acta*, **855**, 68 (1986).

13) W. C. Hamilton, *Acta Crystallogr.*, **12**, 609 (1959).

14) C. K. Johnson, ORTEP II, Report ORNL-5138, Oak Ridge National Laboratory, Tennessee (1976).

 © 1988 The Chemical Society of Japan Bull. Chem. Soc. Jpn., 61, 2343—2346 (1988)

Structural Study of Lithium, Magnesium, and Barium Vanadate Glasses by Means of Mössbauer Spectroscopy

Tetsuaki NISHIDA,* Setsuko SARUWATARI, and Yoshimasa TAKASHIMA
Department of Chemistry, Faculty of Science, Kyushu University 33,
Hakozaki, Higashiku, Fukuoka 812
(Received August 1, 1987)

All the isomer shifts for Li_2O–, MgO–, and BaO–V_2O_5 glasses containing 10 mol% Fe_2O_3 are in a range of 0.39—0.37 mm s^{-1}, indicating that iron is present as tetrahedral Fe^{3+} ions. This suggests that all the Fe^{3+} ions are present at the substitutional sites of tetrahedral V^{5+} or V^{4+} ions constituting the skeleton of each glass matrix. Distinct decreases in the quadrupole splitting and the glass transition temperatures are observed when Li_2O is incorporated into V_2O_5 matrix, suggesting a gradual change of the glass matrix from the layer structure originally composed of VO_5 tetragonal pyramids to a chain structure composed of VO_4 tetrahedra. This structural change is essentially the same as that of Na_2O– and K_2O–V_2O_5 glasses. On the other hand, simultaneous increases in the quadrupole splitting and the glass transition temperatures are observed with increasing MgO or BaO content in the case of MgO– and BaO–V_2O_5 glasses. This suggests a gradual change of the glass matrix from the original layer structure to a highly complicated three-dimensional network structure composed of VO_4 tetrahedra, similarly to the case of P_2O_5–V_2O_5 glasses.

It is well known that V_2O_5 has a layer structure composed of distorted VO_5 tetragonal pyramids, which can also be viewed as distorted trigonal bipyramids.[1,2] Each V^{5+} (or V^{4+}) ion is known to be present at the center of the tetragonal pyramids, surrounded by five oxygen atoms. An IR study of several vanadate (V_2O_5-based) glasses performed by Dimitriev et al.[3] revealed that introduction of alkali or alkaline earth oxides into the V_2O_5 matrix results in a destruction of the layer structure followed by a formation of tetrahedral VO_4 units. Furthermore, Dimitriev et al.[3] elucidated that only VO_4 units are present in the skeleton of metavanadate glasses having alkali or alkaline earth oxide to V_2O_5 ratio equal to unity. The same conclusion was obtained by Segel and Creel[4] in an NMR study of KVO_3 glass. Considering that alkali metavanadate crystals (e.g. KVO_3 crystal) have a one-dimensional chain structure composed of VO_4 tetrahedra,[5] it is not surprising that alkali metavanadate glasses have a chain structure composed of VO_4 tetrahedra. These results are consistent with the recent Mössbauer results of alkali vanadate (K_2O–V_2O_5[6] and Na_2O–V_2O_5[7]) glasses containing 10 mol% Fe_2O_3, obtained by the present authors. In the K_2O– and Na_2O–V_2O_5 glasses,[6,7] all the Fe^{3+} ions proved to be present at the substitutional sites of the V^{5+} or V^{4+} ions constituting VO_4 tetrahedra. In the recent Mössbauer study of phosphorus vanadate (P_2O_5–V_2O_5) glasses,[8] it was concluded that introduction of P_2O_5 into the V_2O_5 matrix results in a structural change of the glass matrix from the layer structure originally composed of VO_5 tetragonal pyramids to a three-dimensional network structure composed of VO_4 tetrahedra. In contrast to these results, a neutron diffraction study performed by Wright et al.[9] showed that V^{5+} or V^{4+} ion is surrounded by five oxygen atoms in P_2O_5–V_2O_5, BaO–V_2O_5, and PbO–V_2O_5 glasses and that the vanadate glasses are composed of interconnected and distorted VO_5 tetragonal pyramids. A similar conclusion was obtained in EXAFS and XANES[10] and NMR and ESR[11] studies of P_2O_5–V_2O_5 glasses.

The present Mössbauer study was performed in order to elucidate the structural change of lithium, magnesium, and barium vanadate glasses, brought about by incorporating Li_2O, MgO, and BaO into V_2O_5 matrix. DTA measurements were performed in order to examine the structural change, such as a change in the coordination number of V^{5+} or V^{4+} ions and a formation of nonbridging oxygen atoms, through the composition dependency of the glass transition temperatures (T_g).

Experimental

Lithium, magnesium, and barium vanadate glasses containing 10 mol% Fe_2O_3 were prepared by melting the individual mixtures (1 g) of commercially available Li_2CO_3, $MgCO_3$, $BaCO_3$, V_2O_5, and Fe_2O_3, of guaranteed reagent grade. Each of the mixture was melted at 950—1000 °C for 1 h in an electric muffle furnace under the ambient atmosphere. Ten mol% Fe_2O_3 was incorporated into the individual mixture as a Mössbauer probe. After the fusion, each melt in a platinum crucible was quenched with ice-cold water. All the vanadate glasses prepared in the present study are almost black in color, having a metallic luster. Mössbauer and DTA measurements were performed on the pulverized glasses, according to the procedures reported in the previous papers.[6,8] A piece of metallic iron foil enriched with ^{57}Fe was used as a reference for the isomer shift. Powder of Al_2O_3 was used as a standard material in the DTA measurements.

Results and Discussion

A Mössbauer spectrum of Li_2O–V_2O_5 glass measured at room temperature is shown in Fig. 1, which indicates only the presence of paramagnetic Fe^{3+} ions of high spin state.[12,13] No absorption peak due to Fe^{2+} ions nor magnetic species is observed in any of

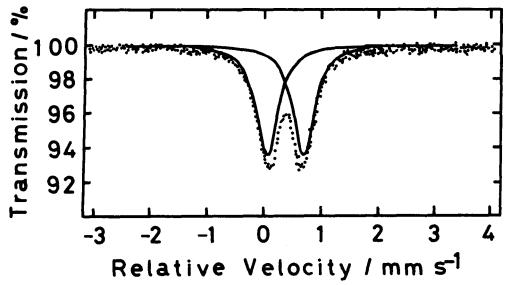

Fig. 1. Mössbauer spectrum of $30Li_2O \cdot 60V_2O_5 \cdot 10Fe_2O_3$ glass measured at room temperature.

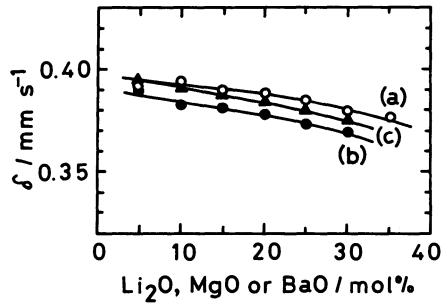

Fig. 2. Composition dependencies of the isomer shift (δ) of Fe^{3+} ions in (a) Li_2O–, (b) MgO–, and (c) $BaO-V_2O_5$ glasses containing 10 mol% Fe_2O_3.

the Mössbauer spectra. The linewidth (FWHM) is characteristic of the absorption peak due to iron in glasses, being in a range of 0.59—0.46 mm s^{-1}. All the isomer shifts of Fe^{3+} ions are located in a small range of 0.39—0.37 mm s^{-1} with respect to metallic iron, as is shown in Fig. 2. Earlier Mössbauer studies of several glasses[14–16] have shown that Fe^{3+} ions are present at tetrahedral environments in borate and silicate glasses. This is the case for the recent Mössbauer results on borate[17–20] and borosilicate[20–22] glasses obtained by the present authors' group. In these glasses,[17–22] all the isomer shift values are located in a range of 0.38—0.22 mm s^{-1} with respect to metallic iron. The experimental error for the isomer shift is usually estimated to be ± 0.01 mm s^{-1}. Judging from the experimental results shown in these reviews and papers,[14–22] it is concluded that all the Fe^{3+} ions are present at tetrahedral environments in the Li_2O–, MgO–, and $BaO-V_2O_5$ glasses, forming FeO_4 tetrahedra. This conclusion indicates the presence of tetrahedral VO_4 units, because Fe^{3+} ions should be present either at the substitutional sites of the V^{5+} (or V^{4+}) ions constituting the skeleton of the glass matrix or at the interstitial sites in the glass matrix. (The presence of V^{4+} ions has already been confirmed by ESR measurements of several vanadate glasses, e.g., $P_2O_5-V_2O_5$ glasses.[8]) It is considered that coordination number of metal ions present at interstitial sites is usually larger than that of the metal ions at substitutional sites. The same conclusion on the presence of VO_4 tetrahedra has been obtained in the

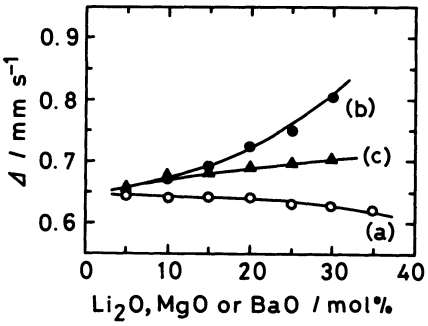

Fig. 3. Composition dependencies of the quadrupole splitting (Δ) of Fe^{3+} ions in (a) Li_2O–, (b) MgO–, and (c) $BaO-V_2O_5$ glasses containing 10 mol% Fe_2O_3.

recent Mössbauer studies of K_2O–, Na_2O–, and $P_2O_5-V_2O_5$ glasses containing 10 or 5 mol % Fe_2O_3.[6–8] The isomer shift values show a distinct decrease with increasing Li_2O, MgO, or BaO content (Fig. 2). Similar composition dependency of isomer shift observed in $K_2O-V_2O_5$[6] and $Na_2O-V_2O_5$[7] glasses was ascribed to a formation of nonbridging oxygen atoms in VO_4 tetrahedra, because a simultaneous decrease in the isomer shift and the quadrupole splitting of Fe^{3+} ions was observed with increasing K_2O or Na_2O content. This is true in the case of $Li_2O-V_2O_5$ glasses studied in the present paper, where a simultaneous decrease in the isomer shift (Fig. 2) and the quadrupole splitting (Fig. 3) is observed with increasing Li_2O content. The experimental error for the quadrupole splitting is estimated to be ± 0.02 mm s^{-1}. The decrease in the quadrupole splitting of Fe^{3+} ions is well ascribed to an increased symmetry of the iron-oxygen tetrahedra, because high-spin Fe^{3+} ions have a symmetric electron configuration of $3d^5$ in the outermost orbital and the electric field gradient brought about by the neighboring atoms or ions should primarily cause the nuclear quadrupole interaction. The simultaneous decrease in the isomer shift (Fig. 2) and the quadrupole splitting (Fig. 3) observed in $Li_2O-V_2O_5$ glasses is therefore ascribed to a formation of nonbridging oxygen atoms in VO_4 tetrahedra. Also, it is considered that a structural change of the glass matrix occurs from the two-dimensional layer structure originally composed of VO_5 tetragonal pyramids to a chain structure composed of VO_4 tetrahedra, similarly to the case of $K_2O-V_2O_5$[6] and $Na_2O-V_2O_5$[7] glasses.

On the other hand, increases in the quadrupole splitting are observed in the case of MgO– and $BaO-V_2O_5$ glasses (Fig. 3). A similar phenomenon was observed in $P_2O_5-V_2O_5$ glasses containing 5 mol% Fe_2O_3,[8] where an increase in the quadrupole splitting of Fe^{3+} ions, indicating a decreased symmetry of the FeO_4 (and VO_4) tetrahedra, was ascribed to a gradual change of the glass matrix from the layer structure originally composed of VO_5 tetragonal pyramids to

the three-dimensional network structure composed of VO_4 tetrahedra. The same conclusion was drawn from the similar composition dependency of the glass transition temperatures of the P_2O_5-V_2O_5 glasses.[8] The increase in the quadrupole splitting of Fe^{3+} ions, observed in the case of MgO- and BaO-V_2O_5 glasses (Fig. 3), is therefore ascribed to a gradual change of the glass matrix from the two-dimensional network structure composed of VO_5 tetragonal pyramids to a highly complicated three-dimensional network structure composed of VO_4 tetrahedra. In contrast to Li_2O-V_2O_5 glasses, it is considered that nonbridging oxygen atoms are rarely formed in the VO_4 tetrahedra constituting the skeleton of MgO- and BaO-V_2O_5 glasses, because the quadrupole splitting values show a continuous increase with increasing MgO or BaO content. It is therefore concluded that fraction of nonbridging oxygen atoms decreases with increasing MgO or BaO content in the MgO- and BaO-V_2O_5 glasses. It can be seen from Fig. 3 that the quadrupole splitting of Fe^{3+} ions in the MgO-V_2O_5 glasses shows a more distinct composition dependency than that of the Fe^{3+} ions in the BaO-V_2O_5 glasses. This will be due to a large ionic potential of Mg^{2+} ion. (The ionic potential is generally denoted by Z/r, where Z is the charge of cation and r is the ionic radius.) It is speculated that cations having large ionic potential will bring about an increased chemical bond strength between the cations and neighboring oxygen atoms. As a result, the resultant structure will become more complicated.

Regarding the short-range (local) structure of vanadate glasses, all the recent[6-8] and present Mössbauer results are consistent with the IR results obtained by Dimitriev et al.[3] and also with the NMR results obtained by Segel and Creel.[4] (In these studies,[3,4] it was reported that all the vanadate glasses are composed of VO_4 tetrahedra.) Regarding the middle- or long-range structure, it is concluded that structure of the glass matrix (skeleton) strongly depends on the type of so-called "network modifier," and that the glass matrix of alkaline earth vanadate glasses has highly complicated three-dimensional network structure. This structural change is similar to that of P_2O_5-V_2O_5 glasses.[8] It is interesting to compare the present results on MgO- and BaO-V_2O_5 glasses with the previous results obtained by different methods, such as a neutron diffraction[9] result on P_2O_5- and BaO-V_2O_5 glasses, an EXAFS and XANES[10] result on P_2O_5-V_2O_5 glasses, and an NMR and ESR[11] result on P_2O_5-V_2O_5 glasses. In these studies,[9-11] coordination number of V^{5+} or V^{4+} ions was reported to be always 5 irrespective of the composition. It seems that apparently higher coordination number (5) was obtained in those studies[9-11] owing to a highly complicated three-dimensional network structure of the glass matrix.

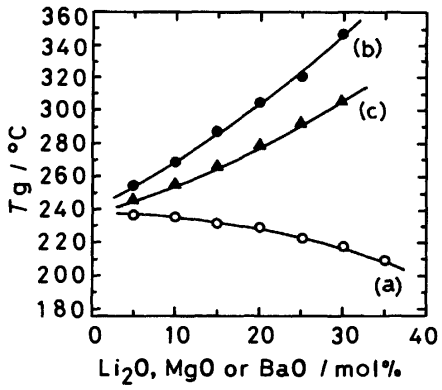

Fig. 4. Composition dependencies of the glass transition temperature (T_g) of (a) Li_2O-, (b) MgO-, and (c) BaO-V_2O_5 glasses containing 10 mol% Fe_2O_3.

Each DTA curve of the Li_2O-, MgO-, and BaO-V_2O_5 glasses containing 10 mol% Fe_2O_3 consists of an endothermic peak due to glass transition and one or a few exothermic peak(s) due to crytallization, similarly to the case of several vanadate glasses studied recently.[6-8] All the glass transition temperatures (T_g) are plotted in Fig. 4 against Li_2O, MgO, or BaO content. Previous Mössbauer and DTA studies of K_2O-V_2O_5[6] and Na_2O-V_2O_5[7] glasses revealed that T_g shows a distinct decrease when coordination number of V^{5+} or V^{4+} ions decreases from 5 to 4 and when nonbridging oxygen atoms are formed in the VO_4 tetrahedra. This is the case for the Li_2O-V_2O_5 glasses studied in the present paper, where the T_g shows a continuous decrease from 236 to 209 °C with increasing Li_2O content (Fig. 4). Considering the NMR result on KVO_3 glass[4] described above, i.e. the glass has a chain structure composed of VO_4 tetrahedra, the present Mössbauer and DTA results on the Li_2O-V_2O_5 glasses lead to the conclusion that a gradual structural change occurs from the two-dimensional layer structure originally composed of VO_5 tetragonal pyramids to the one-dimensional chain structure composed of VO_4 tetrahedra. (This corresponds to the decrease in the coordination number of V^{5+} and V^{4+} ions from 5 to 4.) It can be seen from Fig. 4 that a formation of nonbridging oxygen atoms in the VO_4 and FeO_4 tetrahedra is also reflected as a continuous decrease in T_g of the Li_2O-V_2O_5 glasses. On the other hand, an increase in T_g is observed with increasing MgO or BaO content in the MgO- and BaO-V_2O_5 glasses (Fig. 4). This is in good agreement with the Mössbauer results described above, i.e., a gradual change of the glass matrix occurs from the original layer structure composed of VO_5 tetragonal pyramids to the three-dimensional network structure composed of VO_4 tetrahedra. It should be noted that the T_g shows a distinct increase in spite of the decreased coordination number of V^{5+}or V^{4+} ions

from 5 to 4, as described above. Similar results were obtained in the DTA measurements of P_2O_5–V_2O_5 glasses[8] having a three-dimensional network structure. The difference in the structural change between alkali and alkaline earth vanadate glasses will be caused by the different positive charges of alkali (+1) and alkaline earth (+2) metal ions present at the interstitial sites. It is also considered that higher ionic potential of alkaline earth metal ions (e.g. Mg^{2+} ions) causes the formation of highly complicated three-dimensional network structure.

It is concluded that all the Fe^{3+} ions are tetrahedrally coordinated with oxygen atoms and are present at the substitutional sites of V^{5+} or V^{4+} ions, which constitute the skeleton of vanadate glasses in the form of VO_4 tetrahedra. It is also concluded that introduction of Li_2O into V_2O_5 matrix results in a gradual change of the glass matrix from the original layer structure composed of VO_5 tetragonal pyramids (or trigonal bipyramids) to the chain structure composed of VO_4 tetrahedra. It is considered that VO_4 tetrahedra have some nonbridging oxygen atoms and that the structural change of Li_2O–V_2O_5 glasses is essentially the same as that of Na_2O- and K_2O–V_2O_5 glasses. On the other hand, it is concluded that introduction of MgO or BaO into the V_2O_5 matrix results in a gradual change of the glass matrix from the original layer structure composed of VO_5 tetragonal pyramids to the highly complicated three-dimensional network structure composed of VO_4 tetrahedra, similarly to the structural change of P_2O_5–V_2O_5 glasses.

The authors are grateful to Dr. Koji Yamada of Hiroshima University and Dr. Hiroshi Hirashima of Keio University for their useful comments and discussion. One of the authors (TN) is grateful to Corning Research Grant, Nakamura Research Grant, Yoshida Research Grant, and a Grant-in-Aid for Scientific Research No. 61740350 from the Ministry of Education, Science and Culture.

References

1) A. Byström, K. A. Wilhelmi, and O. Brotzen, *Acta Chem. Scand.*, **4**, 1119 (1950).
2) K. Jansen and G. Sperlich, *Phys. Status Solidi B*, **55**, 495 (1973).
3) Y. Dimitriev, V. Dimitrov, M. Arnaudov, and D. Topalov, *J. Non-Cryst. Solids*, **57**, 147 (1983).
4) S. L. Segel and R. B. Creel, *Can. J. Phys.*, **48**, 2673 (1970).
5) H. T. Evans, *Z. Kristallogr.*, **114**, 257 (1960).
6) T. Nishida and Y. Takashima, *Bull. Chem. Soc. Jpn.*, **60**, 941 (1987).
7) T. Nishida, M. Ogata, and Y. Takashima, *Bull. Chem. Soc. Jpn.*, **60**, 2887 (1987).
8) T. Nishida, M. Ogata, and Y. Takashima, *J. Non-Cryst. Solids*, **94**, 229 (1987).
9) A. C. Wright, C. A. Yarker, P. A. V. Johnson, and R. N. Sinclair, *J. Non-Cryst. Solids*, **76**, 333 (1985).
10) S. Stizza, I. Davoli, O. Gzowski, L. Murawski, M. Tomellini, A. Marcelli, and A. Bianconi, *J. Non-Cryst. Solids*, **80**, 175 (1986).
11) F. R. Landsberger and P. J. Bray, *J. Chem. Phys.*, **53**, 2757 (1870).
12) N. N. Greenwood and T. C. Gibb, "Mössbauer Spectroscopy," Chapman and Hall Ltd., London (1971) Chap. 3.
13) R. Ingalls, F. Van der Woude, and G. A. Sawatzky, "Iron and Nickel," in "Mössbauer Isomer Shifts," ed by G. K. Shenoy and F. E. Wagner, North-Holland Pub Co., Amsterdam (1978), Chap. 7.
14) C. R. Kurkjian, *J. Non-Cryst. Solids*, **3**, 157 (1970).
15) J. M. D. Coey, *J. Phys.*, **35**, C6-89 (1974).
16) W. Müller-Warmuth and H. Eckert, *Phys. Rep.*, **88**, 91 (1982).
17) T. Nishida and Y. Takashima, *J. Non-Cryst. Solids*, **37**, 37 (1980).
18) T. Nishida, T. Shiotsuki, and Y. Takashima, *J. Non-Cryst. Solids*, **41**, 161 (1980).
19) T. Nishida, T. Hirai, and Y. Takashima, *J. Non-Cryst. Solids*, **43**, 221 (1981).
20) T. Nishida and Y. Takashima, "Application of Mössbauer Effect on the Crystallization of Several Glasses," in "Industrial Applications of the Mössbauer Effect," ed by G. J. Long and J. G. Stevens, Plenum Press, New York and London (1986), pp. 409—422.
21) T. Nishida, T. Hirai, and Y. Takashima, *Phys. Chem. Glasses*, **22**, 94 (1981).
22) T. Nishida, T. Hirai, and Y. Takashima, *Bull. Chem. Soc. Jpn.*, **54**, 3735 (1981).

Structural Study of Potassium Gallate Glasses by Mössbauer Spectroscopy and Differential Thermal Analysis

Tetsuaki NISHIDA,* Setsuko SARUWATARI, and Yoshimasa TAKASHIMA
Department of Chemistry, Faculty of Science, Kyushu University 33,
Hakozaki, Higashiku, Fukuoka 812
(Received December 4, 1987)

Mössbauer spectra of a series of potassium gallate (Ga_2O_3-based) glasses, containing 10 mol% Fe_2O_3 as a Mössbauer probe, consist of two types of quadrupole doublet peaks due to tetrahedral Fe^{3+} ions bonded with nonbridging and bridging oxygen atoms and those bonded only with bridging oxygen atoms. This indicates that all the Fe^{3+} ions are present at the substitutional sites of the tetrahedral Ga^{3+} ions constituting the skeleton of network structure. An increase in the K_2O content results in an increased fraction of the FeO_4 (and GaO_4) tetrahedra bonded with nonbridging oxygen atom(s). A Mössbauer spectrum of $70K_2O \cdot 20Ga_2O_3 \cdot 10Fe_2O_3$ glass consists of only one quadrupole doublet peak due to the FeO_4 tetrahedra having nonbridging oxygen atom(s). This suggests that each of the Fe^{3+} (and also Ga^{3+}) ions is tetrahedrally bonded with at least one nonbridging oxygen atom. Structural information obtained from the Mössbauer measurements is confirmed by DTA measurements of the gallate glasses, T_g of which shows a drastic decrease from 647 to 555 °C when the K_2O content is changed from 35 to 70 mol%.

Recently, Dumbaugh and Tyndell[1,2] and Kokubo et al.[3–5] revealed that ternary gallate glasses are easily prepared by the conventional crucible-melting technique when alkali or alkaline earth oxides are incorporated into the Ga_2O_3 matrix with so-called middle oxides such as Nb_2O_5, Ta_2O_5, and TiO_2. It was also revealed that gallate glasses have an excellent optical transparency ranging from UV to IR (about 7 or 8 μm).[1–5] Structural study of gallate glasses was performed using IR[3–5] and Raman scattering,[6,7] where most of the Ga^{3+} ions were reported to be tetrahedrally coordinated with oxygen atoms. In addition to the tetrahedral GaO_4 units, it was considered that a small amount of GaO_6 octahedra might be present in gallate glasses when the alkali or alkaline earth oxides content is low.[3–7] In the IR[3–5] and Raman[6,7] studies it was discussed that so-called three-fold coordinated oxygen atoms will be present in gallate glasses. Besides the IR and Raman spectroscopies, often used for the structural study of glasses, ^{57}Fe-Mössbauer spectroscopy has been utilized for the structural study of several kinds of glasses, such as borate,[8,10] borosilicate,[11–12] and vanadate[13–15] glasses. As a result, some useful information on the short-range (local) structure has been obtained, concerned with the coordination number of network-forming atoms and a formation of nonbridging oxygen atoms in BO_4, SiO_4, and VO_4 tetrahedra.[8–15]

The present Mössbauer study was carried out in order to elucidate the short-range structure of potassium gallate glasses and a structural change caused by K_2O molecules incorporated into the Ga_2O_3 matrix. Potassium gallate glasses were chosen as one of the representative example of alkali gallate glasses. Differential Thermal Analysis (DTA) measurements were performed in order to examine the structural change in the gallate glasses, e.g., a change in the coordination number of Ga^{3+} ions and a formation of nonbridging oxygen atom(s).

Experimental

Potassium gallate glasses denoted by $xK_2O \cdot (90-x)Ga_2O_3 \cdot 10Fe_2O_3$ were prepared by fusing the individual mixtures (2g) of commercially available K_2CO_3, Ga_2O_3, and Fe_2O_3, of a guaranteed reagent grade, in an electric muffle furnace. Each mixture in a platinum crucible was fused in the ambient atmosphere at 1400 °C for 2.5 — 8.5 h, depending on the K_2O content. During the fusion, each of the platinum crucibles was covered with a piece of platinum foil to prevent the mixture from evaporating. The x value was changed from 30 to 75 at 5 intervals. Ten mol% Fe_2O_3 was incorporated into the individual mixture as a Mössbauer probe. After the fusion, each melt in a platinum crucible was quickly quenched by immersing the crucible into ice-cold water. As a result, homogeneous glass samples were prepared in the compositional region $35 \leqq x \leqq 70$. (Only glass-ceramics were obtained when x was 30 and 75.) All the gallate glasses obtained in this way are transparent and dark brown in color, being hygroscopic. Mössbauer measurements were performed on the pulverized glasses under a dry nitrogen atmosphere, according to the procedures shown in the previous papers.[8–15] In the Mössbauer measurement, a piece of metallic iron foil enriched with ^{57}Fe was used as a reference of the isomer shift and for calibrating the velocity of the spectrometer. DTA measurements were performed under a nitrogen atmosphere, using Al_2O_3 powder as a standard material. Glass transition temperatures (T_g) were obtained from the DTA measurements performed in the range of room temperature to 800 °C. Each of the glass samples was heated with a heating rate of 5 °C min^{-1}.

Results and Discussion

Most of the Mössbauer spectra observed in the present study consist of two types of quadrupole doublet peaks, as indicated with broken lines in Fig. 1. No magnetic absorption peak is observed in the potassium gallate glasses, similarly to the case of several iron-containing oxide glasses so far studied by the present authors.[8–15] In the case of potassium gallate glasses containing 10 mol% Fe_2O_3, it is

Table 1. Mössbauer Parameters of K_2O-Ga_2O_3-Fe_2O_3 Glasses

Composition	δ[a]	Δ[b]	Γ[c]	A[d]
	mm s^{-1}	mm s^{-1}	mm s^{-1}	%
$35K_2O \cdot 55Ga_2O_3 \cdot 10Fe_2O_3$	0.24	1.32	0.58	61.1
	0.32	0.78	0.58	38.9
$40K_2O \cdot 50Ga_2O_3 \cdot 10Fe_2O_3$	0.23	1.32	0.59	55.2
	0.31	0.68	0.45	44.8
$45K_2O \cdot 45Ga_2O_3 \cdot 10Fe_2O_3$	0.25	1.29	0.59	64.7
	0.34	0.72	0.40	35.3
$50K_2O \cdot 40Ga_2O_3 \cdot 10Fe_2O_3$	0.23	1.26	0.52	66.1
	0.30	0.77	0.46	33.9
$55K_2O \cdot 35Ga_2O_3 \cdot 10Fe_2O_3$	0.23	1.25	0.46	66.8
	0.32	0.71	0.43	33.2
$60K_2O \cdot 30Ga_2O_3 \cdot 10Fe_2O_3$	0.23	1.28	0.59	69.2
	0.33	0.73	0.42	30.8
$65K_2O \cdot 25Ga_2O_3 \cdot 10Fe_2O_3$	0.23	1.23	0.61	85.5
	0.29	0.65	0.42	14.5
$70K_2O \cdot 20Ga_2O_3 \cdot 10Fe_2O_3$	0.23	1.17	0.68	100.0

a) Isomer shift. b) Quadrupole splitting. c) Linewidth. d) Absorption intensity (area).

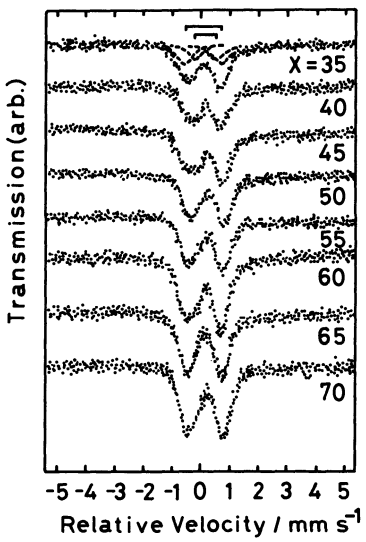

Fig. 1. Mössbauer spectra of $xK_2O \cdot (90-x)Ga_2O_3 \cdot 10Fe_2O_3$ glasses measured at room temperature.

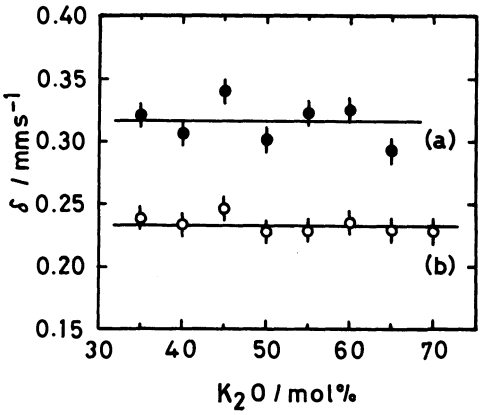

Fig. 2. Composition dependencies of the isomer shift (δ) of (a) inner and (b) outer doublet peaks shown in Fig. 1.

expected that all the iron (Fe^{3+} ions) should be present either at the substitutional sites of the Ga^{3+} ions constituting the skeleton of network structure or at the interstitial sites in the network structure. All the Mössbauer parameters obtained for the $xK_2O \cdot (90-x)Ga_2O_3 \cdot 10Fe_2O_3$ glasses are summarized in Table 1. It can be seen from Table 1 that the linewidth (FWHM), ranging from 0.40 to 0.68 mm s^{-1}, is characteristic of the absorption peak due to iron in glasses. This means that all the Fe^{3+} ions are homogeneously distributed in the glass matrix and are not forming a precipitate or aggregate which shows a magnetic hyperfine interaction. It is generally known that isomer shift indicates whether the Mössbauer nuclei (^{57}Fe in the present study) are present at the tetrahedral or octahedral environments.[8-18] All the isomer shift values obtained for one or two types of quadrupole doublets are shown in Fig. 2. Figure 2 and Table 1 indicate that all the isomer shifts obtained for the $xK_2O \cdot (90-x)Ga_2O_3 \cdot 10Fe_2O_3$ glasses are much smaller than 0.39 or 0.40 mm s^{-1} which is the boundary of isomer shift between octahedral and tetrahedral Fe^{3+} ions.[8-18] The experimental error of isomer shift is usually estimated to be ± 0.01 mm s^{-1}. Experimental results shown in Fig. 2 and Table 1 suggest that all the Fe^{3+} ions are present at the tetrahedral environments. This means that all the Fe^{3+} ions are present at the substitutional sites of the tetrahedral Ga^{3+} ions in the skeleton of network structure. When the isomer shift indicates the presence of octahedral Fe^{3+} ions, we can conclude that such Fe^{3+} ions are present at the interstitial sites of network structure composed of several GaO_4 tetrahedra. It is easily understood from Fig. 2 that the skeleton of network structure of gallate glasses, other than $70K_2O \cdot 20Ga_2O_3 \cdot 10Fe_2O_3$ glass, is composed of two types of FeO_4 (and GaO_4) tetrahedra having the isomer shifts of about 0.32 (inner doublet) and 0.23 mm s^{-1} (outer doublet). Figure 2 demonstrates that isomer shift values of inner (a) and outer

(b) doublets are constant irrespective of the K_2O content. Recently, Fukunaga et al.[6,7] revealed that several nonbridging oxygen atoms are present in the GaO_4 tetrahedra and each of the GaO_4 tetrahedra has at least one nonbridging oxygen atom when CaO content exceeds about 67 mol%, which corresponds to a composition $2CaO \cdot Ga_2O_3$. Taking into account the Raman results,[6,7] we can conclude that two types of the quadrupole doublets having different isomer shift values are concerned with the FeO_4 (and GaO_4) tetrahedra with and without nonbridging oxygen atoms.

This conclusion is consistent with the structural information obtained from composition dependencies of the quadrupole splitting (Fig. 3). The quadrupole splitting of outer doublets (b) shows a distinct decrease with increasing K_2O content. On the other hand, the quadrupole splitting of inner doublets (a) shows a less distinct decrease with increasing K_2O content. The experimental error of the quadrupole splitting is usually estimated to be ± 0.02 mm s^{-1}. Decrease in the quadrupole splitting of Fe^{3+} ions is ascribed to an increase in the symmetry of FeO_4 tetrahedra, because high-spin Fe^{3+} ion has a symmetric electron configuration of $3d^5$ in the outermost orbital. In such a case, the electric field gradient brought about by the neighboring oxygen atoms will primarily cause the quadrupole interaction (splitting).[8–15] It is generally considered that symmetry of the FeO_4 tetrahedra having nonbridging oxygen atom(s) is much higher than that of the FeO_4 tetrahedra bonded only with bridging oxygen atoms, because nonbridging oxygen atoms have higher degree of freedom. In the recent Mössbauer studies, the formation of nonbridging oxygen was observed as a decrease in the quadrupole splitting of Fe^{3+} ions.[8–15] The experimental results indicate that nonbridging oxygen atom(s) are present at less distorted sites than bridging oxygen. On the contrary, the quadrupole splitting of outer doublets (Fig. 3b) concerned with the nonbridging oxygen atom(s) is much greater than that of inner doublets (Fig. 3a) concerned only with bridging oxygen atoms. The large quadrupole splitting values observed for the outer doublets (Fig. 3b) may be concerned with so-called three-fold coordinated oxygen atoms proposed in IR[3–5] and Raman[6,7] studies. Three-fold coordinated oxygen atoms, if present, will greatly decrease the symmetry of the FeO_4 and GaO_4 tetrahedra because of higher distortion and lower degree of freedom. The FeO_4 and GaO_4 tetrahedra bonded with three-fold coordinated oxygen atom(s) will be present in more distorted (and highly energetic) states than those bonded with ordinary two-fold coordinated oxygen atoms. Therefore, it is concluded that large quadrupole splitting values of Fe^{3+} ions (Fig. 3b) are observed because the Fe^{3+} (and Ga^{3+}) ions are simultaneously bonded with so-called three-fold coordinated oxygen and nonbridging oxygen atoms. Further investigation will clarify the presence and role of the unfamiliar three-fold coordinated oxygen atoms. The continuous decrease in the quadrupole splitting of outer doublets (Fig. 3b) is concluded to be due to an increased fraction of nonbridging oxygen atoms in the FeO_4 (and GaO_4) tetrahedra. Small isomer shift values of the Fe^{3+} ions bonded with nonbridging oxygen atom(s) are ascribed to a decreased interatomic distance and therefore increased covalency between the Fe^{3+} ion and nonbridging oxygen atom. The peak assignment of the FeO_4 (and GaO_4) tetrahedra described above is confirmative when we see the distinct composition dependency of the relative absorption intensity of the Fe^{3+} ions bonded with nonbridging oxygen atom(s). This is shown in Fig. 4, where the relative absorption intensity (area) of the FeO_4 (and GaO_4) tetrahedra having nonbridging oxygen atom(s) (outer doublet) is increased with increasing K_2O content, and becomes 100% when the K_2O content is close to 70 mol%. A Mössbauer spectrum of $70K_2O \cdot 20Ga_2O_3 \cdot 10Fe_2O_3$

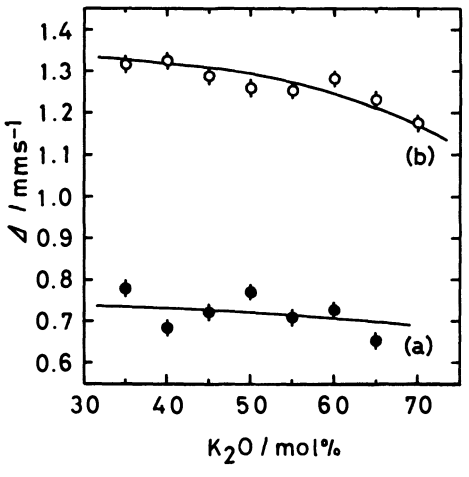

Fig. 3. Composition dependencies of the quadrupole splitting (Δ) of (a) inner and (b) outer doublet peaks shown in Fig. 1.

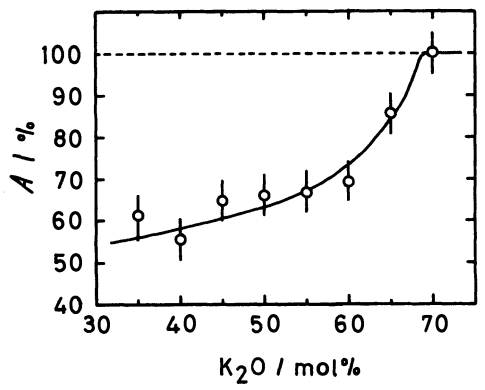

Fig. 4. Composition dependency of the relative absorption intensity of the outer doublets shown in Fig. 1.

glass is composed of only one quadrupole doublet corresponding to the outer doublet (Fig. 1). The experimental results on the formation and fraction of nonbridging oxygen atoms in the FeO_4 and GaO_4 tetrahedra are consistent with the Raman results recently obtained by Fukunaga et al.[6,7] In the Raman[6,7] and IR[3-5] studies, it was suggested that small amounts of octahedral GaO_6 units are present in the alkali or alkaline earth gallate glasses. In the present Mössbauer study, however, no absorption peak due to FeO_6 (and GaO_6) octahedra has been observed even in the low K_2O-content glasses. This is also in contrast to the ^{71}Ga-NMR results obtained by Zhong and Bray[19] recently, who elucidated that a large number of GaO_6 octahedra are present in caesium gallate glasses when the Cs/Ga ratio is smaller than unity. From the unambiguous NMR-spectral change of the caesium gallate glasses, Zhong and Bray[19] suggested that a gradual change of local structure from GaO_6 octahedra to GaO_4 tetrahedra was caused by caesium oxide molecules introduced into the Ga_2O_3 matrix. The NMR-spectral change is somewhat similar to the gradual change of Mössbauer spectra (Fig. 1), ascribed to the formation of nonbridging oxygen atoms in the FeO_4 and GaO_4 tetrahedra. If the NMR result of caesium gallate glasses[19] is taken into account, the absence of Mössbauer absorption peak due to FeO_6 (and GaO_6) octahedra in the present study may be responsible for the chemical property of iron in alkali gallate glasses. Fe^{3+} ions may be preferentially substituted for tetrahedral Ga^{3+} ions than octahedral Ga^{3+} ions. In such a case, a Mössbauer spectrum will be obtained only due to the tetrahedral FeO_4 (and also GaO_4) units. On the other hand, if Fe^{3+} ions are equivalently substituted for octahedral and tetrahedral Ga^{3+} ions, we can conclude that the fraction of GaO_6 octahedra in alkali (potassium) gallate glasses is too small to be detected by Mössbauer spectroscopy. Considering the precision of Mössbauer spectroscopy, we can estimate that the fraction of GaO_6 octahedra is less than several percent and that the skeleton of the $xK_2O\cdot(90-x)Ga_2O_3\cdot 10Fe_2O_3$ glasses is composed of only GaO_4 (and FeO_4) tetrahedra.

Each DTA curve of the potassium gallate glasses containing 10 mol% Fe_2O_3 consists of a weak endothermic peak due to glass transition and an exothermic peak due to crystallization. All the glass transition temperatures (T_g) of the $xK_2O\cdot(90-x)Ga_2O_3\cdot 10Fe_2O_3$ glasses are shown in Fig. 5, where the T_g shows a drastic decrease with increasing K_2O content. Similar composition dependency of T_g has recently been observed in K_2O-V_2O_5,[13] Na_2O-V_2O_5,[14] and Li_2O-V_2O_5[15] glasses containing 10 mol% Fe_2O_3. It should be noted that the decrease in T_g of potassium gallate glasses (Fig. 5) is much greater than that of alkali vanadate glasses.[13-15] In alkali vanadate

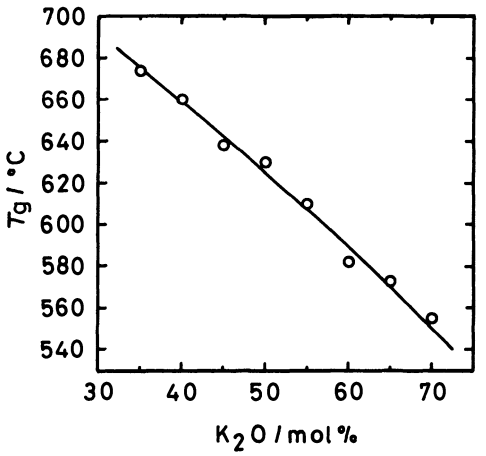

Fig. 5. Composition dependency of the glass transition temperature (T_g) of $xK_2O\cdot(90-x)Ga_2O_3\cdot 10Fe_2O_3$ glasses.

glasses,[13-15] the decrease in T_g was ascribed to a formation of nonbridging oxygen atoms in VO_4 and FeO_4 tetrahedra, followed by a gradual change of the glass matrix from the two-dimensional layer structure, originally composed of VO_5 tetragonal pyramids, to the one-dimensional chain structure composed of VO_4 tetrahedra. Mössbauer and DTA results obtained for alkali vanadate glasses[13-15] suggest that the pronounced decrease in T_g of potassium gallate glasses (Fig. 5) is closely correlated with a formation of nonbridging oxygen atoms in GaO_4 (and FeO_4) tetrahedra. In alkali vanadate glasses,[13-15] a continuous decrease in T_g amounting to about 30—60 °C was observed when the alkali oxide content was changed from 0 to 35 mol%. On the other hand, a drastic decrease in T_g amounting to more than 120 °C is observed in the potassium gallate glasses when K_2O content is changed from 35 to 70 mol% (Fig. 5). This suggests that fraction of nonbridging oxygen atoms in the GaO_4 tetrahedra constituting alkali gallate glasses is much greater than that in the VO_4 tetrahedra constituting alkali vanadate glasses. In Fig. 5, the increasing fraction of nonbridging oxygen atoms in the GaO_4 and FeO_4 tetrahedra is observed as a drastic and apparently linear decrease of T_g. The formation of nonbridging oxygen atoms is considered to be equivalent to a depolymerization of the glass matrix. Regarding the relationship between the structure and physical properties of gallate glasses, it is speculated that high optical transparency of gallate glasses ranging from UV to IR[1-5] may be concerned with the extraordinarily high fraction of nonbridging oxygen atoms in the GaO_4 tetrahedra constituting the skeleton of network structure.

The authors are grateful to Profs. Sumio Sakka and Tadashi Kokubo of Kyoto University and Prof. Jiro Fukunaga of Kyoto Institute of Technology for their

useful comments and discussion. One of the authors (TN) is indebted to Yoshida Science Foundation for the financial support.

References

1) W. H. Dumbaugh and B. P. Tyndell, U. S. US4, 456, 692, June 26, 1984.
2) W. H. Dumbaugh and B. P. Tyndell, U. S. US4, 483, 931, Nov. 20, 1984.
3) T. Kokubo, Y. Inaka, and S. Sakka, *J. Non-Cryst. Solids*, **80**, 518 (1986).
4) T. Kokubo, Y. Inaka, and S. Sakka, *J. Non-Cryst. Solids*, **81**, 337 (1986).
5) T. Kokubo, Y. Inaka, and S. Sakka, Proc. VI Int. Conf. Phys. Non-Cryst. Solids (Kyoto, 1987); *J. Non-Cryst. Solids*, **95/96**, 547 (1987).
6) Xiu-J. Zhao, J. Fukunaga, N. Yoshida, and M. Ihara, *Yogyo Kyokai Shi*, **93**, 708 (1985).
7) J. Fukunaga and R. Ota, Proc. VI Int. Conf. Phys. Non-Cryst. Solids (Kyoto, 1987); *J. Non-Cryst. Solids*, **95/96**, 271 (1987).
8) T. Nishida and Y. Takashima, *J. Non-Cryst. Solids*, **37**, 37 (1980).
9) T. Nishida, T. Shiotsuki, and Y. Takashima, *J. Non-Cryst. Solids*, **41**, 161 (1980).
10) T. Nishida, T. Hirai, and Y. Takashima, *J. Non-Cryst. Solids*, **43**, 221 (1981).
11) T. Nishida, T. Hirai, and Y. Takashima, *Phys. Chem. Glasses*, **22**, 94 (1981).
12) T. Nishida, T. Hirai, and Y. Takashima, *Bull. Chem. Soc. Jpn.*, **54**, 3735 (1981).
13) T. Nishida and Y. Takashima, *Bull. Chem. Soc. Jpn.*, **60**, 941 (1987).
14) T. Nishida, M. Ogata, and Y. Takashima, *Bull. Chem. Soc. Jpn.*, **60**, 2887 (1987).
15) T. Nishida, M. Ogata, and Y. Takashima, Proc. VI Int. Conf. Phys. Non-Cryst. Solids (Kyoto, 1987); *J. Non-Cryst. Solids*, **95/96**, 241 (1987).
16) C. R. Kurkjian, *J. Non-Cryst. Solids*, **3**, 157 (1970).
17) J. M. D. Coey, *J. Phys.*, **35**, C6-89 (1974).
18) W. Müller-Warmuth and H. Eckert, *Phys. Rep.*, **88**, 91 (1982).
19) J. Zhong and P. J. Bray, *J. Non-Cryst. Solids*, **94**, 122 (1987).

The Spectrofluorometric Determination of Anthraquinone with Hydroxylamine in the Dimethyl Sulfoxide Medium Containing Sodium Methoxide and Methanol

Masaki TACHIBANA* and Motohisa FURUSAWA
Faculty of Engineering, Yamanashi University, Takeda, Kofu 400
(Received December 15, 1987)

Anthraquinone reacts with hydroxylamine in the dimethyl sulfoxide (DMSO) medium containing sodium methoxide and methanol. Since the reaction product is fluorescent in the medium, this reaction can be used for the fluorometric determination of anthraquinone. A DMSO solution of a sample was mixed with a DMSO solution of hydroxylamine hydrochloride and a methanolic solution of sodium methoxide. The mixture was then allowed to stand for 20 min at 60 °C in a volumetric flask with a tightly fitting stopper. After cooling and dilution to the mark with DMSO, the fluorescence intensity of the solution was measured at 597 nm, with excitation at 494 nm. The intensity was stable for at least 2 h in the tightly stoppered flask. The determination limit of anthraquinone was 100 ng. By the application of this spectrofluorimetry, anthraquinone in 9,10-phenanthrenequinone could be successfully determined over the content range from 0.2 to 4%.

Anthraquinone, which is known as an oxidation product of anthracene, is of great value as a starting material for the manufacture of vat dyes. It is also utilized in the pulp industry as a catalyst for delignification. On the other hand, trace amounts of anthraquinone may be contained as an impurity in chemicals made from coal tar because anthracene is one of the main components of tar. As a result, there is great interest in monitoring the level of the anthraquinone content in such industrial products, intermediates, and wastes. A sensitive method for the determination of anthraquinone is, therefore, of importance. Several methods for determination have been developed, including gas chromatography,[1,2] liquid chromatography,[3-5] polarography,[6,7] and spectrophotometry.[8-10] The method using spectrofluorimetry has, however, been little discussed in the literature.

In the present paper, the reaction conditions of anthraquinone with hydroxylamine are investigated for the spectrofluorometric determination. This reaction proceeded advantageously in the dimethyl sulfoxide (DMSO) medium containing sodium methoxide and methanol. Anthraquinone could be determined by measuring the fluorescence intensity of the reaction product at 597 nm, with excitation at 494 nm. The product, however, could not be identified in the present research because of difficulties in isolating it from the reaction system. As a result of the application of this fluorimetry, anthraquinone in 9,10-phenanthrenequinone could be successfully determined.

Experimental

Reagents. DMSO was cooled to a temperature below the freezing point (18.5 °C). When about 90% of the DMSO had been frozen, the liquid remaining without solidification was removed. After the solid thus obtained had been completely melted, the same process was repeated 3 times. The DMSO finally obtained was stored in a tightly stoppered vessel because of its hygroscopicity. Anthraquinone and 9,10-phenanthrenequinone were purified by zone melting. Hydroxylamine hydrochloride was of a guaranteed reagent grade purchased from Tokyo Kasei Kogyo Co., Ltd. A methanolic solution of sodium methoxide was prepared by the dilution of a commercial chemical (sodium methoxide, about 28% in methanol, purchased from Wako Pure Chemical Industries, Ltd.) with proper amounts of methanol. The exact concentration of the commercial sodium methoxide solution was determined by titration.

Apparatus. All the fluorometric measurements were carried out using a Hitachi 650-40 fluorescence spectrophotometer. A 150-W Xenon lamp was used as the exciting source.

Procedure. Five milliliters of a sample solution containing less than about 2 μg of anthraquinone in 5 ml of DMSO was transferred into a 10-ml volumetric flask. Then, 2 ml of a 0.1 M (1 M=1 mol dm^{-3}) solution of hydroxylamine hydrochloride dissolved in DMSO was added to the flask. After stirring, 0.7 ml of a 3.5 M methanolic solution of sodium methoxide was added. The mixture was allowed to stand for 20 min at 60 °C in the tightly stoppered flask, with occasional stirring, and then it was diluted to the mark with DMSO after cooling in tap water. The anthraquinone was determined by measuring the fluorescence intensity of the resultant solution at 597 nm, with excitation at 494 nm. A DMSO solution containing 2.00 μg of anthraquinone per 5 ml was treated under the same conditions and at the same time; the fluorescence was used as the standard.

Results and Discussion

Fluorescence Spectra. The fluorescence spectra of the reaction product of anthraquinone with hydroxylamine are shown in Fig. 1. The excitation spectrum has maxima at 396, 471, and 494 nm. The emission spectrum exhibits a maximum at 597 nm. In order to minimize the interferences of diverse substances, 494 nm was selected as the excitation wavelength for the determination. The fluorescence intensity of the reagent blank was negligibly small. At the present stage, little is known about the structure of the fluorescent product. By a comparison of the

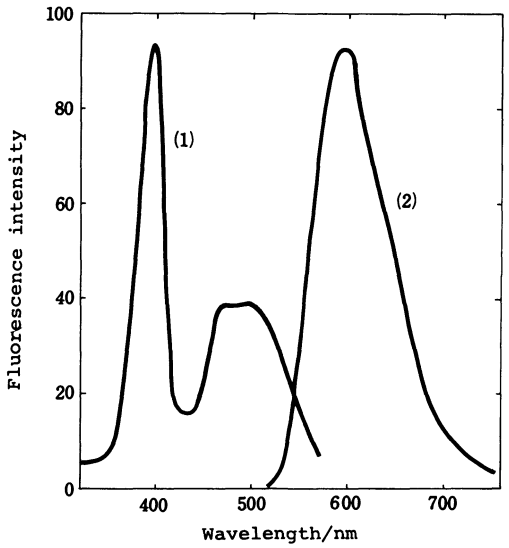

Fig. 1. Fluorescence spectra of the reaction product of anthraquinone.
(1): Excitation spectrum; (2): emission spectrum; uncorrected.

absorption and fluorescence spectra, however, the product was found not to be anthraquinone oxime, the formation of which is commonly predictable from a reaction with hydroxylamine.

Effects of Sodium Methoxide and Methanol. The reaction of anthraquinone with hydroxylamine proceeded well in DMSO containing sodium methoxide and methanol. Sodium methoxide was employed in order to make the DMSO medium strongly basic and methanol in order to increase the solubility of the sodium methoxide in the medium. The concentrations of these reagents had a relatively large influence on the fluorescence intensity of the reaction product. To study the effects of these reagents, various amounts of sodium methoxide (0.5—4.7 mmol) were added to 7 ml of a DMSO solution containing anthraquinone (2 μg) and hydroxylamine hydrochloride (0.2 mmol), together with 0.5, 0.7, and 1.0 ml of methanol. The fluorescence intensities were measured after the mixtures had stood for 20 min at 60 °C and had then been diluted to 10 ml with DMSO. The results of these experiments are shown in Fig. 2. Figure 2 indicates that an increase in the amount of methanol results in a decrease in the fluorescence intensity, and further that the increase requires more amounts of sodium methoxide for the maximum intensity to be reached. Therefore, it is necessary to take into account the simultaneous effects of these two reagents on the determination of anthraquinone. The maximum intensity observed in the presence of 0.7 ml of methanol is not so weak compared with that of 0.5 ml, and it is approximately constant over the broad range of 2—3 mmol of sodium methoxide. It is recommended, therefore, that a mixture of 0.7 ml of methanol and approximately 2.5 mmol of sodium

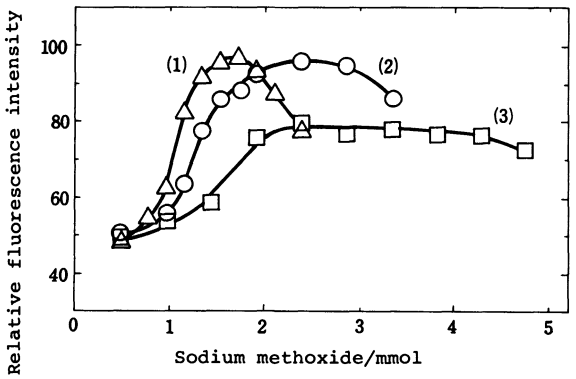

Fig. 2. Effects of the amounts of sodium methoxide and methanol.
Standard: fluorescence intensity of an ethanolic solution of Rhodamine B (20 ng ml^{-1}) was taken as 90.0 div.; anthraquinone: 2.00 mg/10 ml; (1): added along with 0.5 ml of methanol; (2): 0.7 ml; (3): 1.0 ml.

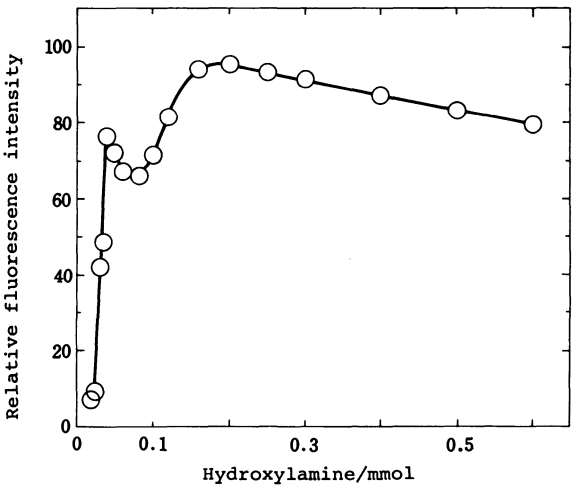

Fig. 3. Effect of the amount of hydroxylamine hydrochloride.
Standard: the intensity of the solution of Rhodamine B (20 ng ml^{-1}) was taken as 90.0 div.; anthraquinone: 2.00 μg/10 ml.

methoxide be used for the determination. In the determination procedure, 0.7 ml of a 3.5 M methanolic solution of sodium methoxide was added to a sample solution.

Effect of Hydroxylamine. Hydrochloride of hydroxylamine was used as the reaction reagent because of facility in handling. The effect of hydroxylamine was measured by varying the amount over the wide range from 20 μmol to 1 mmol in the presence of 2 μg of anthraquinone (approximately 10 nmol) and 2.5 mmol of sodium methoxide. These experiments showed that a large excess of hydroxylamine caused the fluorescence intensities to decrease. A milky turbidity appeared when more than 0.5 mmol of hydroxylamine hydrochloride had been added. In the region less than about 0.1 mmol, on the other hand, the fluorescence spectra were distinct from those

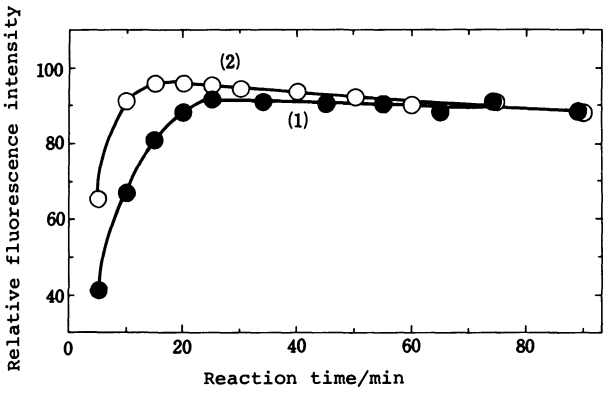

Fig. 4. Effects of reaction time and temperature. Standard: the intensity of the solution of Rhodamine B (20 ng ml^{-1}) was taken as 90.0 div.; anthraquinone: 2.00 mg/10 ml; (1): reacted at 50 °C; (2): 60 °C.

shown in Fig. 1. The fluorescence intensities of the reaction product, as measured over the range of hydroxylamine hydrochloride up to 0.6 mmol, are illustrated in Fig. 3. The maximum fluorescence intensity was obtained when approximately 0.2 mmol of the hydrochloride was added. Another unique peak is further observed at the approximate amount of 0.04 mmol in Fig. 3. Judging from the spectra, it seems likely that the peak was due to the formation of the mono-reacted species. The species, however, was unstable under these conditions, and the intensity decreased rapidly. Therefore, 2 ml of a 0.1 M DMSO solution of hydroxylamine hydrochloride was used in the determination procedure.

Effects of Reaction Temperature and Time. The reaction temperature and the time are important variables for the determination. The effects of these variables on the fluorescence intensity of the product were studied under various conditions. Figure 4 illustrates the results obtained by varying the standing time from 5 to 90 min at the reaction temperatures of 50 and 60 °C. All the measurements were carried out in a 10-ml volumetric flask with a tightly fitting stopper. As is shown in Fig. 4, the reaction of anthraquinone with hydroxylamine at temperatures of 50 and 60 °C is completed by letting it stand for approximately 25 and 15 min respectively. If the flask was left open, however, the fluorescence intensity was unstable and in some cases increased with the increase in the standing time without arriving at a constant value until at least 2 h. Therefore, this reaction was performed by letting the mixture stand for 20 min at 60 °C in the tightly stoppered flask.

Stability of the Fluorescence. In order to investigate the stability of fluorescence of the reaction product, 5 ml of a DMSO solution containing 2 μg of anthraquinone was allowed to react according to the determination procedure. The solution was cooled in tap water, diluted to the mark with DMSO, and then allowed to stand at room temperature. The fluorescence intensity of this solution was measured at adequate time intervals. The intensity was consequently constant for at least 2 h in the tightly stoppered flask. When the stopper was opened, however, the intensity became relatively unstable. This unstability may be attributable to atmospheric oxygen, carbon dioxide, and/or moisture, but no obvious conclusion could be drawn even from additional experiments.

Calibration Curve and Reproducibility. A calibration curve for the determination of anthraquinone was prepared from its DMSO solutions containing 0—2.00 μg per 5 ml according to the determination procedure. The solution with the highest concentration was used as the standard. The calibration curve thus prepared was linear between the fluorescence intensity and the concentration of anthraquinone. According to this curve, 0.1—2 μg of anthraquinone could be determined. The reproducibility of this method was measured by using 2.00 μg of anthraquinone. The relative standard deviation was 1.7% on 20 measurements over a several-day period. In these experiments, an ethanolic solution of Rhodamine B was used as the standard.

Behavior of Other Quinones and Polynuclear Aromatic Carbonyl Compounds. Since it seemed reasonable to assume that this reaction is applicable to other quinones, additional research was undertaken. Several aromatic compounds which have carbonyl groups were selected in order to investigate their reactivities with hydroxylamine. The spectral data of the resulting fluorescent products of these compounds are shown in Table 1. In this research, approximately 10—20 μg of each compound was treated under the same conditions as anthraquinone. *p*-Benzoquinone and 9-fluorenone were indistinct where the fluorescent substances were produced under the present conditions. Table 1 indicates that most of the quinones react with hydroxylamine much like anthraquinone, even though the conditions are not the optimum ones. Therefore, there is a good possibility that such nonfluorescent compounds can be determined by fluorimetry using hydroxylamine as the reaction reagent.

Effects of Diverse Substances. The effects of 16 different substances were studied for the determination of anthraquinone. Table 2 summarizes the effects on the fluorescence intensity of the reaction product of anthraquinone. The measurements of the intensity are not interfered with by the presence of even 100-fold amounts of biphenyl, naphthalene, acenaphthene, phenanthrene, dibenzofuran, dibenzothiophene, and carbazole. Pyrene and fluoranthene give negative errors, and fluorene, a positive one. Since anthracene changes in part to anthraquinone by oxidation during the determination process, the presence of large

Table 1. Fluorescence Excitation and Emission Maxima of the Reaction Products of a Variety of Quinones and Polynuclear Aromatic Carbonyl Compounds

Substances	Excitation maxima	Emission maxima
	nm	nm
2-Methylanthraquinone	396*, 472, 493	601
2-Ethylanthraquinone	397*, 471, 492	601
9,10-Phenanthrenequinone	291, 314, 367*, 420(s)	532
Acenaphthenequinone	322, 375, 460(s), 469*	545
1,2-Naphthoquinone	353	476
1,4-Naphthoquinone	292, 349*, 395	494
Vitamin K_1	297, 363*, 390(s)	509
Vitamin K_2	297, 364*, 395(s)	512
Vitamin K_3	295, 358*, 390(s)	501
Anthrone	393*, 471, 485(s)	567, 600(s)
9-Fluorenone	obscure	
p-Benzoquinone	obscure	

The most intense maximum in each spectrum is indicated by *, and the shoulder, by (s); uncorrected.

Table 2. Effects of Diverse Substances

Substances added		Relative fluorescence intensity[a]	Difference
	μg		
None		100.0	
Biphenyl	206	100.7	+0.7
Naphthalene	208	102.2	+2.2
Acenaphthene	207	100.7	+0.7
Phenanthrene	219	98.8	−1.2
Dibenzofuran	200	103.5	+3.5
Dibenzothiophene	212	100.3	+0.3
Carbazole	209	99.3	−0.7
Pyrene	22	95.5	−4.5
	45	94.2	−5.8
9-Fluorenone	11	97.5	−2.5
	22	95.2	−4.8
Anthracene	1.1	99.4	−0.6
	4.2	96.5	−3.5
	21	102.9	+2.9
	42	121.2	+21.2
1,4-Naphthoquinone	1.1	102.5	+2.5
	4.2	105.9	+5.9
Acenaphthenequinone	1.1	96.4	−3.6
	2.2	93.9	−6.1
Fluoranthene	0.42	96.3	−3.7
	1.1	94.3	−5.7
Fluorene	0.41	103.0	+3.0
	1.0	105.7	+5.7
Acridine	0.35	96.6	−3.4
	0.70	94.8	−5.2
Anthrone	0.045	102.2	+2.2
	0.11	105.5	+5.5

a) The fluorescence intensity of a solution of the reaction product (2.00 μg anthraquinone per 10 ml) was taken as 100 div.

amounts of anthracene gives a positive error. Quinones and the other carbonyl compounds have an observable effect on the determination of anthraquinone, for these substances also react with hydroxylamine. Acridine has a relatively large influence, much as do fluoranthene, fluorene, and the quinones. Anthrone is the most influential of all these substances.

Determination in 9,10-Phenanthrenequinone. The fluorometric method was applied to the determination of anthraquinone in 9,10-phenanthrenequinone (9,10-PQ). The influence of 9,10-PQ on the determination was first studied. A DMSO solution containing 2.00 μg of anthraquinone per 5 ml was treated, according to the determination procedure, in the presence of 0—110 μg of 9,10-PQ. Blank experiments were also carried out in the presence of 9,10-PQ at the same time. The results of these experiments are

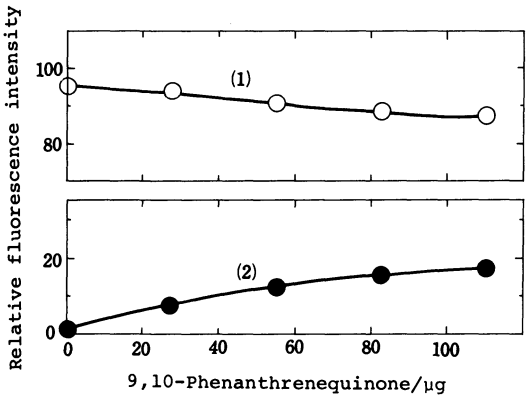

Fig. 5. Effect of the amount of 9,10-phenanthrenequinone.
Standard: the intensity of the solution of Rhodamine B (20 ng ml^{-1}) was taken as 90.0 div.; (1): 9,10-phenanthrenequinone solution containing anthraquinone (2.00 mg/10 ml); (2): 9,10-phenanthrenequinone alone.

Table 3. Analytical Results for Anthraquinone in Synthetic Mixtures of 9,10-Phenanthrenequinone

Content %	Relative fluorescence intensity[a)]	Found %	
0.20	15.0, 15.9	0.2_0, 0.2_5	
0.40	19.3, 19.2	0.4_2, 0.4_1	
0.80	27.8, 26.9	0.8_4, 0.8_0	
1.60	42.0, 42.0	1.5_5, 1.5_5	
2.40	57.8, 58.9	2.3_4, 2.4_0	
3.20	74.4, 74.7	3.1_7, 3.1_9	
4.00	91.0, 92.5	4.0_1, 4.0_8	
4.00	89.6, 90.9	3.9_4, 4.0_0	
4.00	88.1, 88.9	3.8_6, 3.9_0	$\bar{\chi}=3.9_8$
4.00	89.0, 90.3	3.9_1, 3.9_7	$\sigma=0.06_3$
4.00	91.2, 89.9	4.0_2, 3.9_5	R.S.D.=1.6%
4.00	91.0, 92.0	4.0_1, 4.0_6	

a) The fluorescence intensity of the product (2.00 μg anthraquinone per 10 ml) was taken as 95.0 div.

shown in Fig. 5. Figure 5 indicates that the fluorescence intensity of the reaction product of anthraquinone decreases with an increase in the amount of 9,10-PQ, but that the intensity of the blank solution increases. This apparently conflicting influence of 9,10-PQ is because the negative interference is greater than the positive one, which is based on the fluorescence of the reaction product of 9,10-PQ with hydroxylamine. For the determination of anthraquinone it is necessary to reduce such interference due to 9,10-PQ. In case it is present in small amounts, however, the effect can be corrected by the use of a calibration curve prepared in the presence of 9,10-PQ. Therefore, a calibration curve for anthraquinone (0—2 μg) was prepared in the presence of 50 μg of 9,10-PQ according to the procedure. The solution obtained by treating 2.00 μg of anthraquinone was used as the standard. The curve thus obtained was linear between the fluorescence intensity and the concentration of anthraquinone. However, the curve did not intersect at the point of origin, and its gradient was smaller than that for anthraquinone alone because of the influence of 9,10-PQ. The analytical results for anthraquinone in synthetic mixtures of 9,10-PQ are shown in Table 3. Each synthetic mixture contains 2% of phenanthrene, carbazole, and 9-fluorenone, as well as 0.2% of 1,4-naphthoquinone, acenaphthenequinone, dibenzofuran, dibenzothiophene, acridine, biphenyl, naphthalene, acenaphthene, anthracene, fluoranthene, and pyrene. Table 3 indicates that the anthraquinone in 9,10-PQ can be determined over the range from 0.2 to 4%. In addition, anthraquinone in 3 different chemicals of 9,10-PQ was determined; the resulting contents were 0.4, 4.0, and below 0.2%. The emission spectrum of the solution used for the determination agreed well with that of the solution prepared in the presence of 9,10-PQ. From the results of these experiments, the present fluorimetry can be applied to the determination of small amounts of anthraquinone in 9,10-PQ.

The authors are grateful to the Eisai Company, Ltd., for its gift of vitamin K_2.

References

1) V. I. Bogomolov and V. A. Fridman, *Metody Anal. Kontrolya Proizvod. Khim. Prom-sti.*, **7**, 6 (1977).
2) L. G. Harruff and M. A. Vazquez, *TAPPI*, **64**, 109 (1981).
3) D. N. Armentrout, *TAPPI*, **64**, 165 (1981).
4) K. H. Nelson and D. Schram, *J. Chromatogr. Sci.*, **21**, 218 (1983).
5) N. Kiba, M. Takamatsu, and M. Furusawa, *J. Chromatogr.*, **328**, 309 (1985).
6) S. D. Popescu, *Anal. Lett.*, **12**, 1565 (1979).
7) J. O. Broenstad, K. H. Schroeder, and H. O. Friestad, *Anal. Chim. Acta*, **119**, 243 (1980).
8) Gh. Ciuhandu, M. Diaconovici, and T. Fagasan, *Z. Anal. Chem.*, **196**, 270 (1963).
9) S. Iwasaki, M. Furusawa, and M. Sano, *Nippon Kagaku Kaishi*, **1973**, 2302.
10) J. E. Doyle and A. F. A. Wallis, *Appita*, **36**, 122 (1982).

 © 1988 The Chemical Society of Japan Bull. Chem. Soc. Jpn., 61, 2359—2364 (1988)

Structure and Racemization of Optically Active *mer*-(3-Azapentane-1,5-diamine or 3-methyl-3-azapentane-1,5-diamine)(ethylenediamine-*N*-acetato)cobalt(III) Complexes

Hiroshi KAWAGUCHI,* Hironobu FUKAKI, Tomoharu AMA, Takaji YASUI, Ken-ichi OKAMOTO,*,† and Jinsai HIDAKA†

Department of Chemistry, Faculty of Science, Kochi University, Akebono-cho, Kochi 780

†Department of Chemistry, University of Tsukuba, Tsukuba, Ibaraki 305

(Received February 3, 1988)

The crystal structure of $(-)^{CD}_{500}$-*mer*-[Co(edma)(dien)]$Br_2 \cdot 2/3CH_3OH \cdot 2/3H_2O$ was determined by the X-ray diffraction method. The crystal is triclinic, space group $P\bar{1}$, a=13.824(8), b=13.814(8), c=8.055(3) Å, α=101.18(6), β=101.17(6), γ=116.32(5)°, and Z=3. All of the crystallographically independent complex cations, in which the terdentate ligands coordinate meridionally, have a δ spiral configuration, and the asymmetric nitrogen donor atoms of the edma ligands take an *S* configuration. The racemization reactions due to the inversion at the secondary amine nitrogen atom of the edma ligand in $(-)^{CD}_{500}$-*mer*-[Co(edma)(dien)]$^{2+}$ and $(-)^{CD}_{514}$-*mer*-[Co(edma)(mdien)]$^{2+}$ were studied at 20—35 °C in the pH range of 6.10—7.24. The rate law for both complexes was described as $R=k$[OH^-][complex]. The activation parameters at 30.0 °C were ΔH^* of 94.9 kJ mol^{-1} and ΔS^* of 126 J K^{-1} mol^{-1} for the dien complex and ΔH^* of 73.8 kJ mol^{-1} and ΔS^* of 62.0 J K^{-1} mol^{-1} for the mdien complex.

Four possible geometrical isomers for each of [Co(edma)(dien)]$^{2+}$ and [Co(edma)(mdien)]$^{2+}$ (edma, dien, and mdien denote ethylendiamine-*N*-acetate, 3-azapentane-1,5-diamine, and 3-methyl-3-azapentane-1,5-diamine, respectively) have been separated and resolved into their optically active isomers.[1] Two pairs of enantiomers are possible for *mer*-[Co(edma)(dien)]$^{2+}$ and *mer*-[Co(edma)(mdien)]$^{2+}$ as shown in Fig. 1, where the enantiomers are designated by the combination of the *R* or *S* configuration due to the asymmetric nitrogen atom of the edma ligand and the δ or λ spiral configuration due to the arrangement of the two trans N-H groups in *mer*-[Co(edma)(dien)]$^{2+}$ or due to the arrangement of the trans N-H and N-CH_3 groups in *mer*-[Co(edma)(mdien)]$^{2+}$. However, it is difficult to determine spectrochemically their absolute configurations, and then we determined the crystal structure of $(-)^{CD}_{500}$-*mer*-[Co(edma)(dien)]$Br_2 \cdot 2/3CH_3OH \cdot 2/3H_2O$ by the X-ray diffraction method. A preliminary report has been presented.[2]

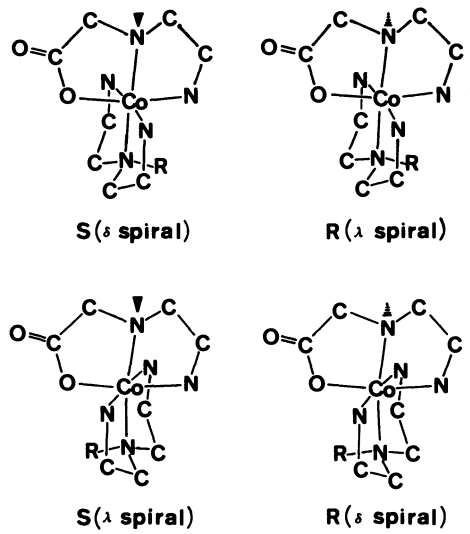

Fig. 1. Two pairs of enantiomeric isomers in *mer*-[Co(edma)(dien)]$^{2+}$ (R=H) and *mer*-[Co(edma)(mdien)]$^{2+}$ ($R=CH_3$).

Similar cases have been reported for *mer*-[Co(aepn)(dien)]$^{3+}$ (aepn; 3-azahexane-1,6-diamine) and *mer*-[$Co(dien)_2$]$^{3+}$. Two pairs of enantiomers are possible for *mer*-[Co(aepn)(dien)]$^{3+}$ and the absolute configuration of the $(-)^{CD}_{474}$ isomer has been determined by Ishii et al.[3] On the other hand, a pair of enantiomers are possible for mer-[$Co(dien)_2$]$^{3+}$ and designated as δ and λ spiral configurations. Their absolute configurations have been determined by Okiyama et al.[4] The kinetics of racemization due to δ spiral$\rightleftarrows\lambda$ spiral change for *mer*-[$Co(dien)_2$]$^{3+}$ has been studied by Searle and Keene.[5] The bis(dien) complex racemizes with inversion[6] at one of the two secondary amine nitrogen (sec-N) centers. The racemization process was described by a rate law of $R=k$[OH^-][complex], and a mechanism of Scheme 1 has been proposed.

In the case of *mer*-[Co(edma)(dien)]$^{2+}$, the inversion at the sec-N center in the coordinating edma results in $S(\delta$ spiral$)\rightleftarrows R(\lambda$ spiral) or $S(\lambda$ spiral$)\rightleftarrows R(\delta$ spiral) change (racemization) (Fig. 1). While, the inversion at the sec-N center in the coordinating dien results in $S(\delta$ spiral$)\rightleftarrows S(\lambda$ spiral) or $R(\delta$ spiral$)\rightleftarrows R(\lambda$ spiral) change (epimerization); the vicinal CD contribution due to the asymmetric sec-N of the coordinating edma

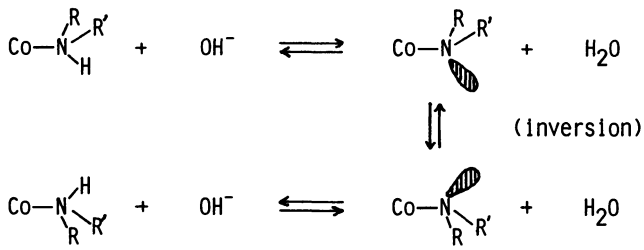

Scheme 1.

remains. These configurational changes must involve the dissociation of the N-H bonds.[5] Therefore, in the case of *mer*-[Co(edma)(mdien)]$^{2+}$ only inversion at the sec-N center in the coordinating edma is possible; racemization occurs. The present paper is concerned with the structure and racemization of the two mer edma complexes.

Experimental

Complexes. The complexes used in the present work were prepared and resolved according to the methods described in our previous paper:[1] $(-)^{CD}_{500}$-*mer*-[Co(edma)(dien)]Br·2/3CH_3OH·2/3H_2O ($\Delta\varepsilon_{500}$=−0.437, $\Delta\varepsilon_{450}$=+0.705), $(-)^{CD}_{514}$-*mer*-[Co(edma)(mdien)]Cl_2·H_2O ($\Delta\varepsilon_{514}$=−0.490, $\Delta\varepsilon_{460}$=+0.730).

Racemization. The racemization reactions were followed spectropolarimetrically with a JASCO J-22 spectropolarimeter. A reaction vessel with a jacket and a water-jacket cell mounted in the cell compartment of the spectropolarimeter were thermostated at a constant temperature (±0.1 °C) with circulating water from a constant-temperature bath. During the kinetic runs, the temperature and the pH of the reaction solution were checked with a thermistor-type thermometer (Takara D-221) and a pH meter (Toa TSC-10A), respectively. The reaction was started by dissolving the complex in 20 cm^3 of a buffered solution in the reaction vessel. About 3 cm^3 of this solution was quickly transferred into the cell in order to record the decrease of the CD intensity at a suitable wavelength (450 nm for *mer*-[Co(edma)(dien)]$^{2+}$ and 460 nm for *mer*-[Co(edma)(mdien)]$^{2+}$). The following conditions were set: pH 6.0—7.0 (Na_2HPO_4-KH_2PO_4 and collidine-HNO_3 buffers), complex concentration 1.8×10^{-3} M (M=mol dm^{-3}), ionic strength 1.0 M ($NaNO_3$), and temperature 19.9—40.0 °C. The ionic product of water at the appropriate temperature was obtained from the literature[7] and the appropriate activity coefficient corrections for ionic strength were made using the data from the same source. The hydroxide concentration could then be calculated.

For the racemization processes of both *mer*-[Co(edma)(dien)]$^{2+}$ and *mer*-[Co(edma)(mdien)]$^{2+}$, plots of $\ln[(L_0-L_{eq})/(L_t-L_{eq})]$ vs. time, where L represents the CD intensity at the subscripted time, gave straight lines over three half-lives, from which the pseudo-first-order rate constant k_{obsd}(s^{-1}) were obtained. Analyses of the kinetic data were carried out on an NEC PC-9801F computer using the least-squares method. In each of the kinetic data analysis, the value of the standard error was within ±1% of the rate constant.

X-Ray Data Collection. Unit cell parameters and intensity data for the single crystal (ca. 0.30×0.32×0.63 mm^3) were measured on a Rigaku-denki four-circle diffractometer (AFC-5) with graphite-monochromatized Mo Kα radiation. The unit cell parameters were determined by a least-squares refinement based on 49 reflections (24 reflections; 8.7°<2θ<11.7° and 25 ones; 20°<2θ<25°). Systematic absences led to the space group $P1$. Crystal data: $C_8H_{22}N_5O_2Br_2Co$·2/3CH_4O·2/3H_2O, M.W.=472.4, triclinic, space group $P1$, a=13.824(8), b=13.814(8), c=8.055(3) Å,

Table 1. Positional and Thermal Parameters (with e.s.d.'s)

Atom	x	y	z	B_{eq}/Å^2[a]	Atom	x	y	z	B_{eq}/Å^2[a]
CoA	0.4288	0.6477	0.2867	1.69	CB7	0.297(1)	1.028(1)	0.922(2)	3.11
OA1	0.2964(8)	0.5588(8)	0.347(1)	2.53	CB8	0.264(1)	1.107(1)	1.024(2)	3.42
OA2	0.2019(8)	0.5710(8)	0.538(1)	3.26	CoD	0.8508(2)	0.2956(2)	0.3100(3)	1.67
NA1	0.4784(9)	0.7490(9)	0.525(1)	2.12	OD1	0.8929(8)	0.4277(8)	0.501(1)	2.40
NA2	0.5736(9)	0.7566(10)	0.262(1)	2.23	OD2	1.0003(9)	0.5232(8)	0.787(1)	3.40
NA3	0.3479(9)	0.7165(10)	0.168(1)	2.28	ND1	0.9038(9)	0.2464(9)	0.498(1)	2.01
NA4	0.3759(10)	0.5349(10)	0.053(2)	2.59	ND2	0.8165(9)	0.1515(9)	0.144(1)	2.21
NA5	0.4962(10)	0.5558(9)	0.370(1)	2.40	ND3	0.9992(10)	0.3758(9)	0.269(1)	2.16
CA1	0.282(1)	0.611(1)	0.480(2)	2.25	ND4	0.7899(10)	0.3490(9)	0.130(1)	2.71
CA2	0.374(1)	0.740(1)	0.570(2)	2.43	ND5	0.6917(9)	0.2295(10)	0.324(2)	2.75
CA3	0.563(1)	0.871(1)	0.533(2)	2.97	CD1	0.960(1)	0.442(1)	0.650(2)	2.30
CA4	0.643(1)	0.849(1)	0.438(2)	2.96	CD2	0.997(1)	0.350(1)	0.647(2)	2.13
CA5	0.293(1)	0.649(1)	−0.033(2)	3.16	CD3	0.941(1)	0.163(1)	0.425(2)	2.68
CA6	0.266(1)	0.527(1)	−0.053(2)	2.92	CD4	0.840(1)	0.082(1)	0.250(2)	3.06
CA7	0.364(1)	0.428(1)	0.079(2)	3.22	CD5	0.987(1)	0.429(1)	0.123(2)	3.39
CA8	0.475(1)	0.462(1)	0.216(2)	3.31	CD6	0.893(1)	0.459(1)	0.134(2)	3.29
CoB	0.0767(2)	0.8735(2)	0.9113(3)	1.68	CD7	0.698(1)	0.363(1)	0.169(2)	2.91
OB1	0.1649(8)	0.8294(8)	1.059(1)	2.40	CD8	0.618(1)	0.250(1)	0.192(2)	3.68
OB2	0.1530(9)	0.7237(9)	1.238(1)	3.32	BR1	0.5328(2)	0.9458(2)	0.0710(3)	3.77
NB1	−0.0263(9)	0.8197(9)	1.047(1)	2.09	BR2	0.0446(2)	0.1914(2)	−0.0100(3)	3.72
NB2	−0.0333(9)	0.9073(9)	0.778(1)	2.06	BR3	0.5503(2)	0.6389(2)	0.8219(3)	3.55
NB3	0.0075(9)	0.7236(10)	0.722(1)	2.02	BR4	0.7204(2)	0.1741(2)	0.7238(3)	3.58
NB4	0.1894(10)	0.9335(10)	0.790(2)	2.66	BR5	0.7786(2)	0.6797(2)	0.3972(3)	3.74
NB5	0.1685(9)	1.0331(9)	1.087(1)	2.51	BR6	1.0855(2)	0.0039(2)	0.4553(3)	3.56
CB1	0.111(1)	0.763(1)	1.140(2)	2.28	CE1	0.279(5)	0.288(5)	0.639(8)	20.42[b]
CB2	−0.016(1)	0.727(1)	1.101(2)	2.34	CE2	0.419(4)	0.059(4)	0.576(7)	17.03[b]
CB3	−0.146(1)	0.784(1)	0.935(2)	2.77	OE1	0.298(3)	0.320(3)	0.490(5)	21.07[b]
CB4	−0.125(1)	0.885(1)	0.864(2)	3.11	OE2	0.407(4)	0.090(4)	0.432(6)	26.74[b]
CB5	0.072(1)	0.736(1)	0.588(2)	3.17	OW1	0.661(3)	0.436(3)	0.686(4)	18.45[b]
CB6	0.197(1)	0.831(1)	0.693(2)	2.74	OW2	0.452(4)	0.271(4)	0.808(5)	24.95[b]

a) $B_{eq}=8\pi^2(U_{11}+U_{22}+U_{33})/3$. b) Isotropic temperature factor.

α=101.18(6), β=101.17(6), γ=116.32(5)°, V=1282(2) Å^3, D_x= 1.835 g cm^{-3}, D_m=1.82 g cm^{-3}, Z=3, and μ(Mo $K\alpha$)=60.08 cm^{-1}.

The intensity data were collected by the ω-2θ scan technique up to 2θ=60° with scan rate of 3° min^{-1}. The intensity data were converted to the F_o data in the usual manner. Absorption corrections were not applied. A total of 5001 independent reflections with $|F_o|>3\sigma(|F_o|)$ of the measured 8064 reflections were considered as "observed" and used for the structure analysis.

Determination of the Crystal Structure. The X-ray analysis calculations were carried out on a FACOM M-382 computer at University of Tsukuba. The positions of three cobalt and six bromide atoms were determined by the direct method (program MULTAN[8]) was used). The difference-Fourier maps based on the three cobalt and six bromide positions revealed the other all non-hydrogen atoms. The structure was refined by a full-matrix least-squares refinement using the positional parameters, the anisotropic thermal parameters of the non-hydrogen atoms of the complex ions, and the isotropic thermal parameters of the non-hydrogen atoms of the water molecules (program RFINE by Finger[9]) was used). The atomic scattering factors for all the non-hydrogen atoms were taken from the literature.[10] The final residual values were R=0.049 and R_w=0.058, respectively. We attempted to determine the absolute configuration of the complex ions by an anomalous-scattering technique. When the refinements were carried out by use of a set of the atomic parameters containing the δ spiral configuration of the complex cations, the residual values converged to R=0.047 and R_w=0.056, respectively. On the contrary, the refinements in the enantiomeric atomic parameters (the λ spiral configuration) resulted in the residual values of R=0.054 and R_w=0.062, respectively. These facts suggest that the former is probably the correct choice, namely, the complex cation takes the δ spiral configuration. A similar relationship was observed for the determination of the absolute configration for the cobalt(III) complexes.[11,12]

The final positional parameters are listed in Table 1. A list of structure factors (Table A) and anisotropic thermal parameters of non-hydrogen atoms (Table B) are kept at the Chemical Society of Japan as Document No. 8810.

Results and Discussion

Description of the Structure. A perspective drawing of the [Co(edma)(dien)]$^{2+}$ cation (CoA species) is shown in Fig. 2, together with the numbering scheme. The bond distances and angles (with standard deviations) are summarized in Table 2. There are three crystallographically independent complex cations in an asymmetric unit, though their shapes and sizes remarkably resemble one another. The cobalt atom is octahedrally surrounded by an oxygen atom and five nitrogen atoms. The ethylenediamine-*N*-acetate and 3-azapentane-1,5-diamine coordinate meridionally to

Table 2. Interatomic Distances and Bond Angles (with e.s.d.'s) for $(-)^{CD}_{500}$-*mer*-[Co(edma)(dien)]$Br_2\cdot 2/3CH_3OH\cdot 2/3H_2O$

(a) Bond distance (l/Å)

	A	B	D
Co-O1	1.92(1)	1.91(1)	1.91(1)
Co-N1	1.92(1)	1.93(1)	1.93(1)
Co-N2	1.98(1)	1.97(1)	1.96(1)
Co-N3	1.99(1)	1.99(1)	1.98(1)
Co-N4	1.96(1)	1.96(1)	1.96(1)
Co-N5	2.02(2)	2.02(1)	2.01(1)
O1-C1	1.27(2)	1.28(2)	1.29(2)
O2-C1	1.23(2)	1.23(2)	1.24(2)
N1-C2	1.51(2)	1.49(2)	1.50(1)
N1-C3	1.54(2)	1.52(2)	1.52(2)
N2-C4	1.50(2)	1.50(2)	1.49(2)
N3-C5	1.54(2)	1.52(2)	1.52(2)
N4-C6	1.54(2)	1.54(2)	1.55(2)
N4-C7	1.47(2)	1.47(1)	1.46(2)
N5-C8	1.49(2)	1.52(2)	1.48(2)
C1-C2	1.57(2)	1.55(2)	1.55(3)
C3-C4	1.56(3)	1.54(3)	1.56(2)
C5-C6	1.53(3)	1.55(2)	1.54(3)
C7-C8	1.52(2)	1.53(3)	1.54(2)
CE1-OE1	1.39(8)		
CE2-OE2	1.32(8)		

(b) Bond angle (ϕ/°)

	A	B	D
O1-Co-N1	83.6(4)	83.8(5)	84.1(5)
O1-Co-N2	171.0(4)	170.4(5)	170.7(5)
O1-Co-N3	89.7(5)	89.6(5)	90.5(5)
O1-Co-N4	93.5(4)	93.5(6)	92.7(5)
O1-Co-N5	88.7(5)	88.9(5)	88.2(5)
N1-Co-N2	87.4(5)	86.7(6)	86.6(5)
N1-Co-N3	96.3(5)	95.6(5)	96.3(5)
N1-Co-N4	175.4(6)	176.1(4)	175.3(6)
N1-Co-N5	92.7(5)	93.4(5)	94.0(6)
N2-Co-N3	91.0(5)	90.3(5)	90.4(5)
N2-Co-N4	95.5(5)	96.1(6)	96.5(5)
N2-Co-N5	92.1(6)	92.7(5)	92.6(5)
N3-Co-N4	87.2(6)	87.1(5)	87.1(6)
N3-Co-N5	170.6(4)	170.7(5)	169.4(6)
N4-Co-N5	83.6(5)	83.8(5)	82.5(6)
Co-O1-C1	115.9(8)	115.1(10)	115.0(11)
Co-N1-C2	108.2(7)	108.3(11)	108.1(9)
Co-N1-C3	108.9(9)	108.8(9)	109.6(9)
C2-N1-C3	113.2(13)	114.0(10)	113.5(12)
Co-N2-C4	107.9(9)	108.2(10)	108.8(8)
Co-N3-C5	109.3(11)	109.5(8)	109.7(10)
Co-N4-C6	105.9(10)	105.5(9)	105.4(9)
Co-N4-C7	109.0(9)	109.1(10)	109.5(11)
C6-N4-C7	115.3(10)	115.1(14)	114.8(13)
Co-N5-C8	110.2(10)	109.9(9)	111.5(10)
O1-C1-O2	126.5(11)	124.4(15)	125.3(17)
O1-C1-C2	115.2(13)	115.7(15)	115.4(12)
O2-C1-C2	118.3(14)	119.8(14)	119.2(14)
N1-C2-C1	104.2(13)	104.8(11)	105.0(12)
N1-C3-C4	101.6(12)	102.4(10)	101.4(14)
N2-C4-C3	109.8(11)	108.8(16)	109.5(11)
N3-C5-C6	107.2(13)	106.4(11)	106.7(15)
N4-C6-C5	106.1(10)	105.8(15)	105.6(14)
N4-C7-C8	105.4(10)	105.5(13)	104.6(15)
N5-C8-C7	106.8(15)	105.9(12)	105.7(11)

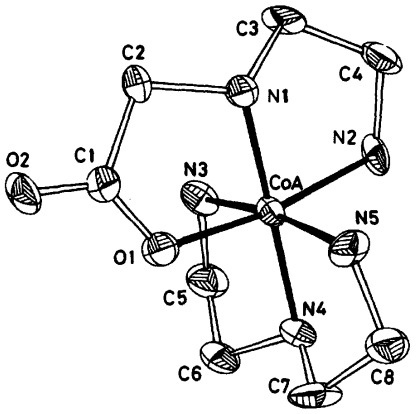

Fig. 2. Perspective view of $(-)^{CD}_{500}$-*mer*-[Co(edma)(dien)]$^{2+}$ ion.

the cobalt atom as terdentate ligands. For the *mer*-[Co(edma)(dien)]$^{2+}$ isomers, two pairs of enantiomers are possible, where the enantiomers are designated by the combination of the *R* or *S* configuration due to the asymmetric nitrogen donor atom of the edma ligand and the δ or λ spiral configuration due to the arrangement of the two trans N-H groups as in the case of *mer*-[Co(ida)(dien)]$^{+}$ (ida; iminodiacetate).[11] The absolute configuration of the asymmetric nitrogen donor atom in the present complex cation, which has the δ spiral configuration, was determined to be *S* (Fig. 2). This seems to indicate that one of two pairs of enantiomers, *S*(δ spiral) and *R*(λ spiral) isomers, were selectively formed in the crystalline state, because both of the *R*(δ spiral) and *S*(λ spiral) isomers have a significantly intramolecular steric interaction between the amino group in the edma ligand and the two methylene groups in the dien ligand.

The bond distances and angles for the coordinating dien in the three crystallographically independent complex cations are quite similar to those for *mer*-[Co(mida)(dien)]$^{+}$[11] and *mer*-[Co(dien)$_2$]$^{3+}$.[4] The bond distances and angles for the N1-O1 chelate moiety in the edma ligand also resemble to those for the cobalt(III) complexes with amino carboxylates,[11-13] although the Co-O1 distance (av. 1.91(1) Å) is somewhat longer and the Co-N1 one is somewhat shorter (av. 1.93(1) Å) than those of the corresponding distances. The conformations of the edma and dien ligands in the three complex cations resemble one another. The N1-O1 chelate ring in the edma ligand takes an envelope form with λ conformation as in the case of the cobalt(III) complexes with amino carboxylates,[11-13] and the diamine chelate ring N1-N2 takes an asymmetric skew form with δ conformation. Two coupled chelate rings in the dien ligand take asymmetric skew forms with δ and λ conformations, respectively, which somewhat differ from *mer*-[Co(mida)(dien)]$^{+}$[11] and *mer*-[Co(dien)$_2$]$^{3+}$.[4]

CD Spectra. Figure 3 shows the absorption and CD spectra of optically active *mer*-[Co(edma)(dien)]$^{2+}$ and *mer*-[Co(edma)(mdien)]$^{2+}$ measured in 0.1 M HCl at room temperature. These optically active isomers were stable in acidic solution and exhibited no measurable absorption and CD spectral changes. However, these isomers easily racemized in neutral or basic solution. Similar behavior was observed for the optically active isomers of complexes such as [Co(sar)(NH$_3$)$_4$]$^{2+}$ (sar; sarcosinate anion)[14] and *mer*-[Co(dien)$_2$]$^{3+}$.[5] The CD curves of $(+)^{CD}_{500}$ and $(-)^{CD}_{500}$ isomers of *mer*-[Co(edma)(dien)]$^{2+}$ are exactly symmetrical each other, indicating that these isomers are in an enantiomeric relation; the configuration of the $(+)^{CD}_{500}$ isomer is assigned to *R*(λ spiral).

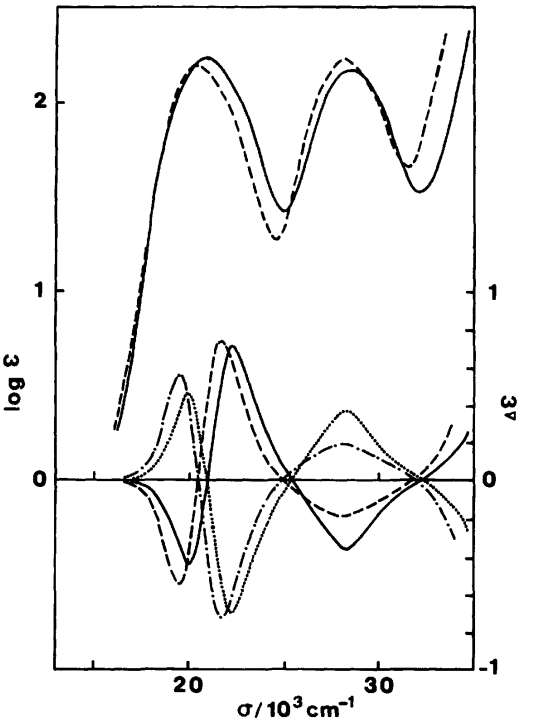

Fig. 3. Absorption (AB) and CD spectra: $(-)^{CD}_{500}$ (——) and $(+)^{CD}_{500}$ (·····) isomers of *mer*-[Co(edma)(dien)]$^{2+}$ and $(-)^{CD}_{514}$ (– – –) and $(+)^{CD}_{514}$ (– – – –) isomers of *mer*-[Co(edma)(mdien)]$^{2+}$. Solvent: water for AB measurements and 0.1 M HCl for CD measurements.

$(-)^{CD}_{514}$- and $(+)^{CD}_{514}$-[Co(edma)(mdien)]$^{2+}$ show very similar CD spectra to those for $(-)^{CD}_{500}$ and $(+)^{CD}_{500}$ dien analogues, respectively (Fig. 3). Accordingly, *S*(δ spiral) is assigned to the $(-)^{CD}_{514}$ isomer of *mer*-[Co(edma)(mdien)]$^{2+}$ and *R*(λ spiral) to the $(+)^{CD}_{514}$ one.

Both *mer*-[Co(edma)(dien)]$^{2+}$ and *mer*-[Co(edma)(mdien)]$^{2+}$ have two CD contributions, one from the spiral configuration and the other from the so-called vicinal effect due to the asymmetric sec-N in the edma ligand. The CD intensities in the first band region for these complexes are stronger than those for *mer*-[Co(dien)$_2$]$^{3+}$[5] and *mer*-[Co(ida)(dien)]$^{+}$[11] having only the CD contribution from the spiral configuration.

Racemization. Figure 4 shows CD spectral change

with time of $(-)^{CD}_{500}$-*mer*-[Co(edma)(dien)]$^{2+}$ in phosphate buffered solution at 39.9 °C. The initial CD curve almost coincided with the CD curve measured in 0.1 M HCl. The isocircular dichroism points lay on the base line and the values of CD intensities at various wavelengths decreased in the same ratio. The CD spectrum almost disappeared after 2 h. The absorption spectrum changed little during the CD measurement, indicating that no isomerization and/or decomposition occurred. In the $(-)^{CD}_{500}$-*S*(δ spiral) isomer of *mer*-[Co(edma)(dien)]$^{2+}$, the inversion at the sec-N in the dien ligand brings about the *S*(δ spiral)$\rightleftarrows$*S*(λ spiral) change (epimerization). In this case, however, the vicinal CD contribution due to the asymmetric sec-N of the edma ligand is expected to remain. On the other hand, the inversion at the sec-N center of the edma ligand leads to the *S*(δ spiral)$\rightleftarrows$*R*(λ spiral) change (racemization). The CD decrease in Fig. 4 conforms to the *S*(δ spiral)$\rightleftarrows$*R*(λ spiral) change, that is, the inversion at the sec-N of edma. This result, therefore, means that (1) the *S*(δ spiral)$\rightarrow$*S*(λ spiral) change is very slow compared with the *S*(δ spiral)$\rightarrow$*R*-(λ spiral) change or (2) the *S*(δ spiral)$\rightleftarrows$*S*(λ spiral) equilibrium extremely lies to the *S*(δ spiral) side if the rate of the *S*(δ spiral)$\rightarrow$*S*(λ spiral) change is comparable to that of the *S*(δ spiral)$\rightarrow$*R*(λ spiral) change. In $(-)^{CD}_{514}$-*mer*-[Co(edma)(mdien)]$^{2+}$, only the inversion at the sec-N center of the edma ligand is expected to occur. In fact, this complex showed the decrease of the CD intensity in the same pattern as $(-)^{CD}_{500}$-[Co(edma)(dien)]$^{2+}$ did.

The progress of the racemization was followed by monitoring the decrease of the CD intensity at 450 nm for *mer*-[Co(edma)(dien)]$^{2+}$ and at 460 nm for *mer*-[Co(edma)(mdien)]$^{2+}$. Kinetic data are summarized in Table 3. The values of the racemization rate constant $k(=k_{obsd}/[OH^-])$ for *mer*-[Co(edma)(dien)]$^{2+}$ at 39.9 °C are essentially constant, so the rate law is described as $R=k[OH^-][complex]$. Activation energies E_a were computed by least-squares analysis of the Arrhenius plots of *k*. The activation parameters calculated for the two complexes are given in Table 4. The close similarity in the activation parameters between the *mer*-[Co(edma)(dien)]$^{2+}$ and *mer*-[Co(dien)$_2$]$^{3+}$ complexes, as compared in Table 4, strongly suggests that a common mechanism takes place (Scheme 1). The racemization rate of *mer*-[Co(edma)(dien)]$^{2+}$ is about twice faster than that of *mer*-[Co(dien)$_2$]$^{3+}$. The difference in the rates of racemization might be explained by the electronic and conformational properties of the chelates. The electronegative carboxyl group decreases the electron density on the sec-N center. Consequently, the pre-equilibrium of Scheme 1 displaces to the deprotonated form and the rate of racemization increases. The glycinate chelate ring in *mer*-[Co(edma)(dien)]$^{2+}$ has a little conformational deformation out of the N-Co-O plane, whereas the ethylenediamine chelate rings in *mer*-[Co(dien)$_2$]$^{3+}$ is markedly puckered; therefore, the conformational interchange may be easier in the edma ring than in the dien ring for *mer*-[Co(edma)(dien)]$^{2+}$.

The racemization rate of *mer*-[Co(edma)(mdien)]$^{2+}$ is about one order faster than that of *mer*-[Co(edma)(dien)]$^{2+}$ (Table 3), and the activation enthalpy of the former is smaller than that of the latter (Table 4). It seems likely that the electron donative

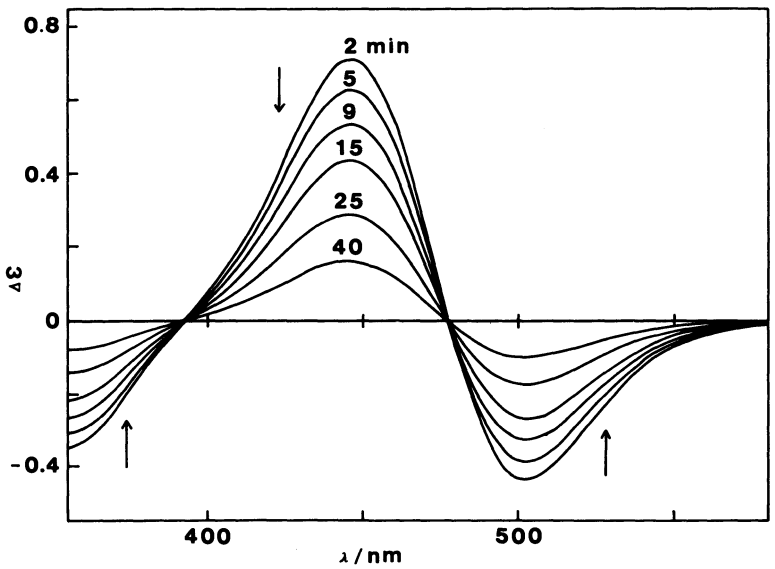

Fig. 4. The CD spectral change of $(-)^{CD}_{500}$-*mer*-[Co(edma)(dien)]$^{2+}$ measured under the conditions of pH 7.06 (phosphate buffer), ionic strength 1.0 M ($NaNO_3$), and 39.9 °C. The curves show the spectra measured at 2, 5, 9, 15, 25, and 40 min.

Table 3. The Rate Constants for Racemization of *mer*-$[Co(L_1)(L_2)]^{n+}$ Ions in Phosphate Buffered Solutions

Complex	T / °C	pH	k_{obsd} / 10^{-4} s^{-1}	k / 10^2 M^{-1} s^{-1}
$[Co(edma)(dien)]^{2+}$ [a]	30.0	7.05	0.464	2.16
	34.9	7.09	1.40	4.15
	39.9	7.05	3.18	7.36
	39.9	7.09	3.36	7.09
	39.9	6.45	0.803	7.40
	39.9	6.10	0.360	7.43
	39.9	7.24	2.69	4.48 [c]
$[Co(edma)(mdien)]^{2+}$ [a]	30.0	7.15	4.43	16.4
	25.0	7.12	1.66	9.61
	19.9	7.11	0.686	6.01
$[Co(dien)_2]^{3+}$ [b]	35	6.42	0.086	1.54
	40	6.44	0.297	3.6
	40	7.31	2.89	4.7 [c]

a) I=1.0 M($NaNO_3$). b) Reference 5. I=2.0 M($NaNO_3$). c) Collidine buffer.

Table 4. The Activation Parameters for Racemization of *mer*-$[Co(L_1)(L_2)]^{n+}$ Ions

Complex	T / °C	ΔH^* / kJ mol^{-1}	ΔS^* / J K^{-1} mol^{-1}
$[Co(edma)(dien)]^{2+}$ [a]	34.9	94.8±3.3	125±10
$[Co(edma)(mdien)]^{2+}$ [a]	30.0	73.8±4.0	62.0±13.5
$[Co(dien)_2]^{3+}$ [b]	35	98.3±1.7	121±8.4

a) Phosphate buffer. I=1.0 M($NaNO_3$). b) Reference 5. Collidine-HNO_3 buffer. I=2.0 M($NaNO_3$).

CH_3 group exerts a trans effect in *mer*-$[Co(edma)(mdien)]^{2+}$, enhancing the racemization rate.

The racemization of optically active $[Co(sar)(NH_3)]^{2+}$ has been studied in a number of buffers.[14] The rate was about twice slower in phosphate buffer rather than in collidine buffer, and this feature was rationalized on the basis of ion pairing; the complex reacts with the phosphate anion (HPO_4^{2-} or $H_2PO_4^-$) to give an ion pair which no longer reacts with OH^- at a rate comparable to that of the original complex, so that the racemization rate would be consequently diminished. In the case of $[Co(dien)_2]^{3+}$, the racemization rate in phosphate buffer was also slower than that in collidine buffer, but the difference between their rates was slight. However, in the present complex, the reverse tendency is observed (Table 3), so that the proposal given in the case of the racemization reaction of $[Co(sar)(NH_3)_4]^{2+}$ is inapplicable to the racemization reaction of the present complex. The reason is unknown at present. The studies for the factors such as the orientation of the complex ion in the ion pairing and the catalytic ability of phosphate anion may be required.

References

1) T. Yasui, T. Shikiji, N. Koine, T. Ama, and H. Kawaguchi, *Bull. Chem. Soc. Jpn.*, **60**, 595 (1987).
2) K. Okamoto, T. Yasui, and J. Hidaka, *Chem. Lett.*, **1987**, 1561.
3) M. Ishii, S. Sato, Y. Saito, and M. Nakahara, *Bull. Chem. Soc. Jpn.*, **57**, 3094 (1984).
4) K. Okiyama, S. Sato, and Y. Saito, *Acta Crystallogr., Sect. B*, **35**, 2389 (1979).
5) G. H. Searle and F. R. Keene, *Inorg. Chem.*, **11**, 1006 (1972).
6) We use the term "inversion" here to describe the configurational change about a sec-N center in meridionally coordinated dien.
7) H. S. Harned and W. J. Hamer, *J. Am. Chem. Soc.*, **55**, 2194 (1933).
8) G. Germain, P. Main, and M. M. Woolfson, *Acta Crystallogr., Sect. A*, **27**, 368 (1971).
9) L. W. Finger, RFINE-2, Geophysical Lab. Carnegie Institute, Washington, D. C. (1972).
10) a) "International Tables for X-Ray Crystallography," Kynoch Press, Birmingham (1974). Vol. IV; b) D. T. Cromer and J. B. Mann, *Acta Crystallogr., Sect. A*, **24**, 321 (1968).
11) K. Okamoto, T. Yasui, and J. Hidaka, *Chem. Lett.*, **1987**, 551.
12) K. Okamoto, M. Suzuki, H. Einaga, and J. Hidaka, *Bull. Chem. Soc. Jpn.*, **56**, 3513 (1983).
13) K. Okamoto, K. Matsutani, and Y. Fujii, *Bull. Chem. Soc. Jpn.*, **58**, 3486 (1985).
14) B. Halpern, A. M. Sargeson, and K. R. Turnbull, *J. Am. Chem. Soc.*, **88**, 4630 (1966).

Asymmetric Grignard Cross-Coupling Reaction Using Chiral Ligands Derived from Carbohydrates

Akihito IIDA and Mitsuji YAMASHITA*
Department of Applied Chemistry, Faculty of Engineering, Shizuoka University, Hamamatsu 432
(Received September 18, 1987)

Chiral diphenylphosphine and diphenylphosphinite derivatives of carbohydrates such as D-glucose, D-galactose, and L-rhamnose were used as the ligand of metal catalysts for asymmetric Grignard cross-coupling reaction. Coupling of *s*-butylmagnesium bromide with bromobenzene was carried out in the presence of nickel or palladium chloride with the chiral ligand. The highest optical yield was observed when D-galactose ligand was used.

Investigation of good chiral ligands is very important field in catalytic asymmetric reactions such as asymmetric hydrogenations and asymmetric coupling reactions.[1] A wide variety of ligands were used for asymmetric hydrogenations, where many monodentate and bidentate chiral phosphines such as CAMP, DIOP, and Norphos afforded chiral products in excellent optical yields.[2] For asymmetric Grignard cross-coupling reactions the ligands gave the product in poor to fair optical yields.[3] Chiral carbohydrate ligands, which can be easily prepared from readily available carbohydrates without optical resolution, are not so well investigated.[1),4] Some of the ligands showed potential ability for asymmetric induction in prochiral olefins.[4] To spread the application of carbohydrate ligands in the field for asymmetric synthesis we now tried to use them for cross-coupling reactions.

Coupling reactions of 1-phenylethylmagnesium halides with vinyl halides were successful using ferrocene[5] and amino acid derivatives[6] as the chiral ligand. But couplings of *s*-butylmagnesium halides with halobenzenes were unsuccessful so far. The coupling reactions, where phenyl groups in the Grignard reagents are absent, are competed with isomerization and elimination reactions.[7,8] This paper deals with asymmetric Grignard cross-coupling reaction using carbohydrate ligands of catalysts.

Carbohydrates exist widely in nature and they have some advantages for asymmetric synthesis in such properties as ready availability, rigidity of the structure, and chirality of the framework. Some ligands derived from carbohydrates were used for asymmetrical catalytic hydrogenations,[2,4,9,10] however, they were scarcely applied to asymmetric coupling reactions.[3] It is suggested that diphenylphosphinite derivatives afford higher optical yields than corresponding diphenylphosphine derivatives do, and that diphenylphosphinite derivatives can easily be synthesized through a shorter pathway than corresponding diphenylphosphine derivatives by at least two steps from starting carbohydrates having free hydroxyl groups.

Results and Discussion

Synthesis of Chiral Phosphino Ligands from Carbohydrates. Compounds **1**, **2**; **3**; and **4**, **7** were prepared from D-galactose; L-rhamnose; and D-glucose, respectively by known methods.[10] Reaction of glucose **6** with diphenylphosphinous chloride in the presence of sodium hydride in dry ether afforded not only diphosphino compound **7**, but also monophosphino compound **5** (Eq. 1). These ligands were immediately used for coupling reaction without isolation.

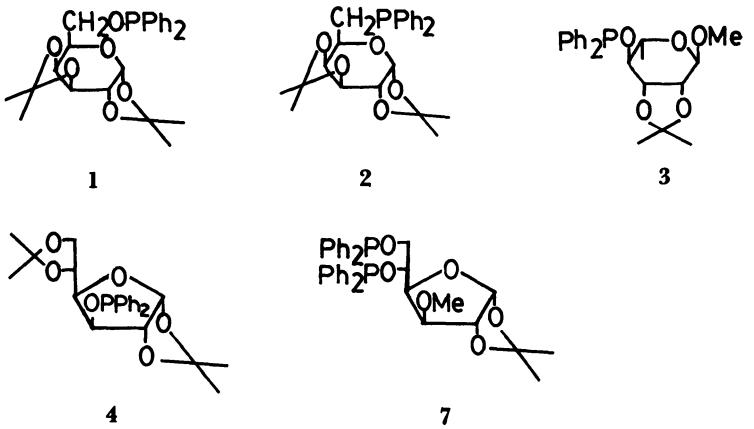

1 2 3

4 7

Scheme 1.

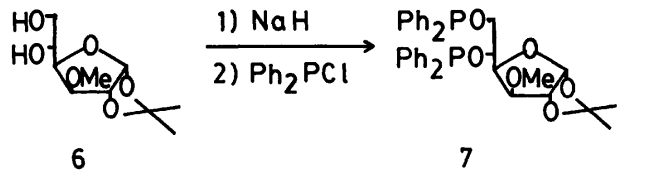

6 7

monophosphino deriv. 5 (1)

Asymmetric Grignard Cross-Coupling Reaction. Nickel- or palladium-catalyzed cross-coupling reaction of *s*-butylmagnesium bromide **8** with bromobenzene **9** using chiral ligands was carried out (Eq. 2). The reaction conditions and results are summarized in Table 1.

$$\underset{\mathbf{8}}{s\text{-BuMgBr}} + \underset{\mathbf{9}}{\text{PhBr}} \longrightarrow \underset{\mathbf{10}}{s\text{-BuPh}} + \underset{\mathbf{11}}{n\text{-BuPh}} \quad (2)$$

Table 1 shows that non-isomerized product **10** was obtained in higher yield than isomerized product **11**. The ratio of **10** to **11** obtained is higher than that reported using monodentate triphenylphosphine ligand.[11] This reason may be attributable to the property of the ligand having P-O-C bond, where electron density of phosphorus atom is lower than that of P-C bond.[7] Indeed the diphenylphosphinite ligand used in Entries 1 and 2 afforded less isomerized product than the corresponding diphenylphosphine ligand did in Entries 3 and 4. In asymmetric induction, the carbohydrate ligand having phosphorus atom out of the hemiacetal ring induced higher optical yield than the ligand having phosphorus atom in the hemiacetal ring did. Especially, D-galactose ligands **1** and **2** afforded the highest optical yields (Entries 2 and 3). These results confirmed that carbohydrate ligands are accessible for asymmetric cross-coupling reaction as chiral sources.

Experimental

Measurements. ^{1}H NMR spectra were measured on a Hitachi R-24B (60 MHz) spectrometer with tetramethylsilane as an internal standard, and IR spectra on a Japan Spectroscopic Co., Ltd., A-3 infrared spectrometer. Optical rotations were measured on a Japan Spectroscopic Co., Ltd., DIP-4 digital polarimeter. Isolation of coupling products was performed by a Yanaco Gas Chromatograph G 1800, equipped with a 1.5 m stainless steel column packed with silicone gum SE30 (30% on chromosorb W) at 100 °C (column) and 175 °C (injection).

Preparation of 6-*O*-(Diphenylphosphino)-1,2:3,4-di-*O*-isopropylidene-α-D-galactopyranose (1). To a solution of 1,2:3,4-di-*O*-isopropylidene-α-D-galactopyranose 0.39 g (1.50 mmol) in dry ether was added 72 mg (1.8 mmol) of sodium hydride, and the mixture was stirred for 12 h at room temperature under argon atmosphere. Diphenylphosphinous chloride (1.5 equiv) was added to the reaction mixture through a septum cap. After 24 h the mixture was filtered and the filtrate was successively washed with water and brine. The solution was dried over sodium sulfate and evaporated in vacuo. Crude product **1** (0.50 g) was obtained

Table 1. Asymmetric Cross-Coupling Reaction of **8** with **9**[a]

Entry	Ligand	Metal	Conversion/%[b]	Chemical yield/%[c]	
				10	**11**
1	**1**	Pd	91	17	4.3
2	**1**	Ni	58	15	Trace
3	**2**	Ni	98	5.5	9.4
4	**2**	Pd	77	6.6	9.6
5	**7**	Pd	96	3.4	3.6
6	**4**	Ni	54	5.1	2.1
7	**4**	Pd	90	10	10
8	**3**	Ni	69	7.0	3.0
9	**3**	Pd	76	20	4.3

Entry	$[\alpha]_D^t$/° (Concentration)[d]	Optical yield/%[e] (Configuration)
1	$[\alpha]^{16}$= −2.48 (*c* 1.05)	8.5 (*R*)
2	$[\alpha]^{20}$=−15.6 (*c* 0.397)	53 (*R*)
3	$[\alpha]^{20}$=+28.9 (*c* 0.993)	99 (*S*)
4	$[\alpha]^{21}$= −1.73 (*c* 0.980)	5.9 (*R*)
5	$[\alpha]^{21}$= −9.60 (*c* 0.177)	33 (*R*)
6	$[\alpha]^{30}$= −3.58 (*c* 0.520)	12 (*R*)
7	$[\alpha]^{16}$= −2.73 (*c* 0.880)	9.3 (*R*)
8	$[\alpha]^{16}$= −3.35 (*c* 0.925)	11 (*R*)
9	$[\alpha]^{29}$= −1.08 (*c* 1.15)	3.7 (*R*)

a) Reaction condition: ratio of **8** to **9** was 2:1 except for Entry 2 (**8** to **9** was 1.05:1 for Entry 2); and ratio of **9** to MCl_2 was 50:1. Reactions were carried out for about 40 h at 35 °C under argon atmosphere. b) Conversion was calculated on a basis of **9** recovered. c) Yield was calculated on a basis of **9** reacted. d) Benzene was used as the solvent. Less than 7% concentration dependence of $[\alpha]_D$ value was observed. e) Optical yield was calculated based on the specific rotation of (*S*)-2-phenylbutane: $[\alpha]_D^{25}$=+29.26° (neat).[8]

in 74% yield. The purity was checked by TLC on silica gel (eluent: ethyl acetate; R_f=0.74). IR ν_{max}^{neat} (cm^{-1}), 1442 (P-Ph), 1080 (P-O-C). ^1H NMR ($CDCl_3$) δ=1.32, 1.42, 1.46, (3s, 12H, $2CMe_2$), 3.7—4.8 (m, 6H, $C_{2-6,6'}$-H), 5.56 (d, 1H, $J_{H_1H_2}$=5.0 Hz, C_1-H), and 7.2—7.7 (m, 10H, PPh_2).[10b]

Preparation of Other Diphenylphosphinite Ligands. Methyl 4-*O*-(diphenylphosphino)-2,3-*O*-isopropylidene-α-L-rhamnopyranoside (**3**), 3-*O*-(diphenylphosphino)-1,2:5,6-di-*O*-isopropylidene-α-D-glucofuranose (**4**), and 5,6-di-*O*-(diphenylphosphino)-1,2-*O*-isopropylidene-3-*O*-methyl-α-D-glucofuranose (**7**) were prepared almost in pure form except **7** by the same procedure as above from the corresponding precursors. Crude product **7** showed two spots of TLC on silica gel (R_f; 0.88 and 0.71 (ethyl acetate)). They were monophosphino and diphosphino derivatives, respectively, and were used for the coupling reaction without isolation. Spectral data for **7**: ^1H NMR ($CDCl_3$) δ=1.20, 1.31 (2s, 6H, CMe_2), 3.30 (s, 3H, OMe), 3.5—4.4 (m, 5H, $C_{3-6,6'}$-H), 4.42 (d, 1H, $J_{H_1H_2}$= 3.5 Hz, C_2-H), 5.75 (d, 1H, $J_{H_1H_2}$=3.5 Hz, C_1-H), 7.0—8.0 (m, 20H, $2PPh_2$); IR ν_{max}^{neat} (cm^{-1}), 1442 (P-Ph), 1030 (P-O-C); MS *m/z*, 602 (M^+).

Preparation of 6-*C*-(Diphenylphosphino)-1,2:3,4-di-*O*-isopropylidene-α-D-galactopyranose (2). Through a septum cap a solution of 0.248 g (0.60 mmol) of the 6-*O*-*p*-toluenesulfonyl derivative in dry THF was added to refluxing THF solution of lithium diphenylphosphinide prepared by the treatment of 0.157 g (0.60 mmol) of triphenylphosphine with lithium under argon atmosphere.[11] The mixture was further refluxed for 4 h and cooled to room temperature. The product was extracted with ether and washed with water and brine. The solution was dried with sodium sulfate and evaporated in vacuo to give 0.257 g (quantitative yield) of crude **2**, which was contaminated with the tosylate, used without further purification. IR ν_{max}^{neat} (cm^{-1}), 1440 (P-Ph), 722 (C-P). ^1H NMR ($CDCl_3$) δ=1.30, 1.35, 1.46, 1.50 (4s, 12H, $2CMe_2$), 1.7—2.2 (m, 2H, $C_{6,6'}$-H), 3.6—4.7 (m, 4H, C_{2-5}-H), 5.45 (d, 1H, $J_{H_1H_2}$=5.0 Hz, C_1-H), 7.2—8.2 (m, 10H, PPh_2).

General Procedure for Coupling Reactions. In a 50 ml two-necked flask equipped with a stirring bar, a septum cap, and a stopcock was placed 13.0 mg of nickel chloride (0.1 mmol=2.0 mol%) or 17.7 mg of palladium chloride. The reaction vessel was filled with argon after evacuation and a solution of 0.2 mmol of ligand **1**, **2**, **3**, or **4**, or of 0.1 mmol of ligand **7** in freshly distilled 2—3 ml of THF was added via syringe through the ceptum cap. The reaction mass was refluxed for 1 h and cooled to 0 °C. To the solution were added 0.52 ml (5.0 mmol) of bromobenzene and solution of *s*-butylmagnesium bromide (prepared from 10 mmol of *s*-butyl bromide and magnesium in 10 ml of dry ether under nitrogen atmosphere) via a syringe through the septum cap. The reaction mixture was again refluxed for about 40 h and hydrolyzed with 8 ml of 10% hydrochloric acid. Extraction of the product with ether (6 ml×3) followed by successive washing the organic layer with aq. sodium hydrogencarbonate (4 ml×2) and water (5 ml), drying over anhydrous sodium sulfate, and removal of low boiling materials (bp<120 °C) afforded crude analytical sample. Unreacted bromobenzene and *s*- and *n*-butylbenzenes were isolated from the sample by gas chromatography. The structures of all the products were confirmed by ^1H NMR.

References

1) H. B. Kagan, "Asymmetric Synthesis," ed. by J. D. Morrison, Academic Press, Inc., Orlando (1985), Vol. 5, Chap. 1.

2) K. E. Koenig, "Asymmetric Synthesis," ed. by J. D. Morrison, Academic press, Inc., Orlando (1985), Vol. 5, Chap. 3.

3) T. Hayashi and M. Kumada, "Asymmetric Synthesis," ed. by J. D. Morrison, Academic Press, Inc., Orlando (1985), Vol. 5, Chap. 5.

4) M. Yamashita, M. Kobayashi, M. Sugiura, K. Tsunekawa, T. Oshikawa, S. Inokawa, and H. Yamamoto, *Bull. Chem. Soc. Jpn.*, **59**, 175 (1986).

5) T. Hayashi, M. Konishi, M. Fukushima, T. Mase, M. Kagotani, M. Tajika, and M. Kumada, *J. Am. Chem. Soc.*, **104**, 180 (1982).

6) T. Hayashi, M. Fukushima, M. Konishi, and M. Kumada, *Tetrahedron Lett.*, **21**, 79 (1980).

7) K. Tamao, Y. Kiso, K. Sumitani, and M. Kumada, *J. Am. Chem. Soc.*, **94**, 9268 (1972).

8) G. Consiglio, F. Morandini, and O. Piccolo, *Tetrahedron*, **39**, 2699 (1983).

9) a) T. Iwai, T. Yoshida, and M. Sato, *Nippon Kagaku Kaishi*, **1976**, 1652; b) W. R. Cullen and Y. Sugi, *Tetrahedron Lett.*, **1978**, 1635; c) Y. Sugi, and W. R. Cullen, *Chem. Lett.*, **1979**, 39; d) T. H. Johnson and G. Rangarajan, *J. Org. Chem.*, **45**, 62 (1980).

10) a) M. Yamada and M. Yamashita, *Carbohydr. Res.*, **95**, C9 (1981); b) M. Yamashita, K. Hiramatsu, M. Yamada, N. Suzuki, and S. Inokawa, *Bull. Chem. Soc. Jpn.*, **55**, 2917 (1982); c) M. Yamashita, M. Kobayashi, K. Tsunekawa, M. Sugiura, and T. Oshikawa, *Carbohydr. Res.*, **131**, C6 (1984).

11) T. Hayashi, M. Konishi, Y. Kobori, M. Kumada, T. Higuchi, and K. Hirotsu, *J. Am. Chem. Soc.*, **106**, 158 (1984).

12) a) A. M. Aguiar, J. Beisler, and A. Mills, *J. Org. Chem.*, **27**, 1001 (1962); b) A. M. Aguiar and J. Beisler, *J. Org. Chem.*, **29**, 1660 (1964).

Total Synthesis of Elaiophylin (Azalomycin B)

Kazunobu TOSHIMA, Kuniaki TATSUTA, and Mitsuhiro KINOSHITA*
Department of Applied Chemistry, Faculty of Science and Technology, Keio University, Hiyoshi, Kohoku-ku, Yokohama 223
(Received November 4, 1987)

Antibiotic elaiophylin (**1**) has been first synthesized by a convergent route involving aldol coupling of (5*R*,6*R*,7*R*)-5-*O*-[2-deoxy-3,4-bis-*O*-(isopropyldimethylsilyl)-α-L-fucopyranosyl]-6-ethyl-7-*O*-(diethylisopropylsilyl)-5,7-dihydroxy-3-octanone (**25f**) and (7*S*,8*S*,15*S*,16*S*:3*E*,5*E*,11*E*,13*E*)-8,16-bis[(1*R*)-1-formylethyl]-7,15-dimethyl-1,9-dioxa-3,5,11,13-cyclohexadecatetraene-2,10-dione (**3**), followed by desilylation. The appropriately O-protected segment **25f** and the macrocyclic dialdehyde **3** were synthesized from D-glucose and 2-deoxy-L-fucose.

The anti-Gram-positive bacterial antibiotic elaiophylin (**1**) was first isolated in 1959 by Arcamone et al.[1] and then isolated as azalomycin B in 1960 by Arai.[2] The chemical structure was elucidated partially by Takahashi et al.[3–5] and fully by Kaiser and Keller-Schierlein,[6] and the absolute configuration was established by X-ray crystallography.[7,8] Elaiophylin (**1**) belongs to a group of C_2-symmetrical 16-membered macrodiolides.[9] Of this class of natural products, the molecule of **1** has the most complex side chain with a glycosidated β-hydroxy hemiacetal structure. The similar side chain structure has also been found in other class of macrolide antibiotics such as concanamycins.[10] The isolation of the cyclic methyl acetal aglycon derivative **2′** from the methanolysis products of **1** and the total synthesis of **2′** from chiral carbon sources other than carbohydrate have been reported in 1985 by Seebach et al.[11,12] Other synthetic efforts toward **1** have been made by Wakamatsu et al.[13] As a synthetic challenge, we have been interested in **1** which is so sensitive to acid and base that its free aglycon **2** has never been isolated.[4–6,12] Herein we wish to describe, in full,[14] the total synthesis of elaiophylin (**1**) (azalomycin B), which makes use of carbohydrates as chiral source.

The retrosynthetic analysis of **1** is shown in Scheme 1 along with our synthesis plan. The synthesis of **1** through the glycosidation of free aglycon **2** would be impossible because of the extraordinary instability of **2**,[12] whereas it would be possible to synthesize an

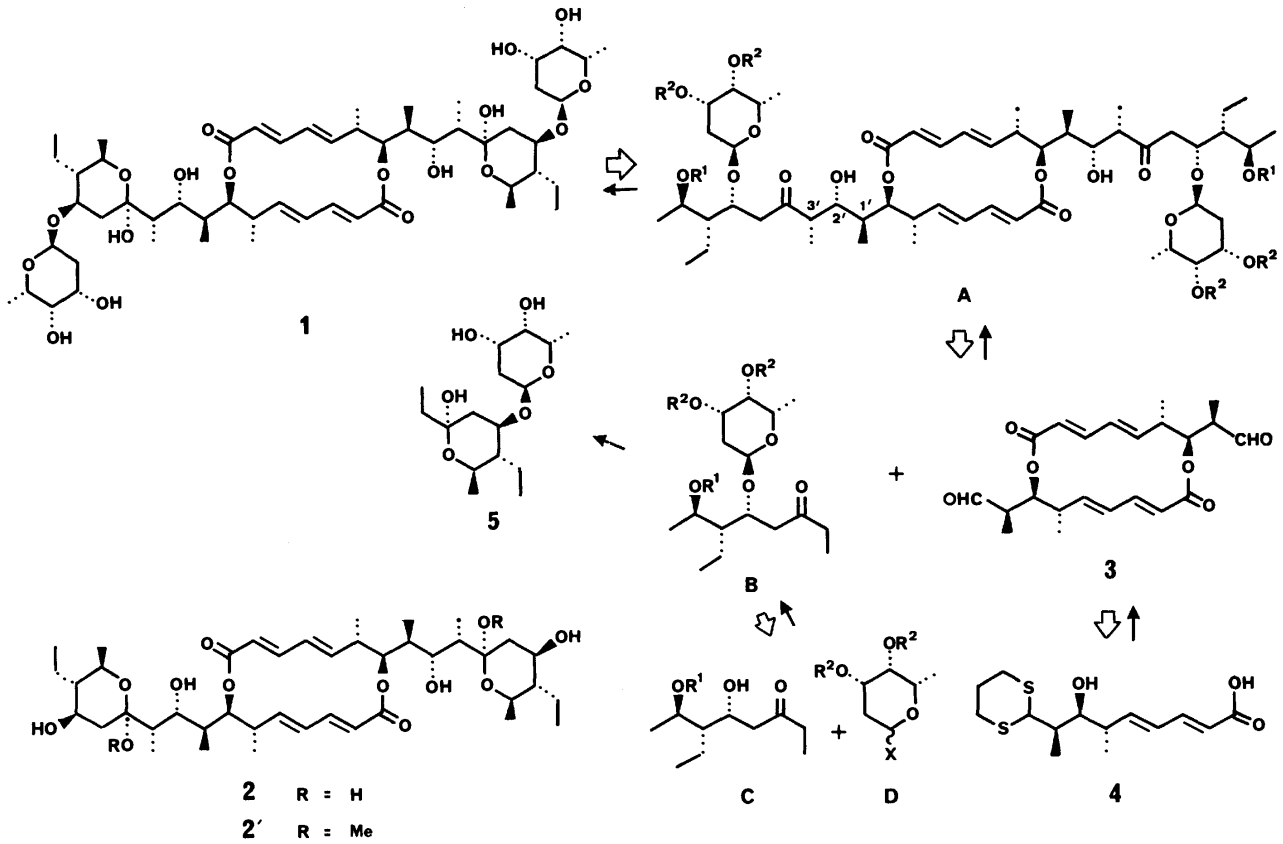

Scheme 1.

appropriately protected segment **B** from a more stable β-hydroxy ketone **C** and a sugar derivative **D**. The aldol coupling of **B** with the macrocyclic dialdehyde **3** which is obtainable through the dimerization of **4** would give a key intermediate **A**. The target compound **1** then will be obtainable, if the deprotection of **A** followed by the hemiacetalization produced smoothly without any decomposition of **1** formed. In this case, **B** (a synthetic segment of **A**) should have appositely chosen protecting groups (R^1 and R^2) to afford effectively the hemiacetal compound **5** by its deprotection under conditions in which **1** is stable. The conversion of **A** into **1** is presumably achieved under almost the same conditions as used in the deprotection of **B**. Thus it would be required to find the ideal protective groups for the segment **B** to make a success of the elaiophylin synthesis by our plan. Furthermore, it would be a formidable[15] but challenging task to realize the highly stereocontrolled aldol coupling of **B** and **3** in the penultimate step to the aforesaid deprotection.

Preparation of the Segment B. The starting material **6**[16] was obtainable in large scale by the reaction of methyl 2,3-anhydro-4,5-*O*-benzylidene-α-D-mannopyranoside[17] and ethylmagnesium chloride in ether. The reaction product was once recrystallized from ethyl acetate–hexane to afford a 7:1 mixture of **6** and the by-product **6′**.[16] The yields of **6** and **6′** from the starting 2,3-anhydro sugar derivative were assumed to be ca. 64 and 9%, respectively. The complete isolation of **6** from **6′** by further recrystallization or column chromatography was impracticable at this stage. The facile one-step conversion of the crude **6** into the furanose derivative **7** was well-achieved by the direct treatment of **6** with a catalytic amount of boron trifluoride etherate in acetone; an 80% yield of the pure **7** was obtained after chromatography. Selective 5,6-de-*O*-isopropylidenation of **7** with 75% aqueous acetic acid afforded **8** in 85% yield. The periodate oxidation of **8** followed by sodium borohydride reduction of the resulting aldehyde **9** gave **10** in 97% yield. The alcohol **10** was converted into the mesylate **11** by the usual way, which was immediatelly reduced with lithium aluminium hydride (LAH) in ether to afford **12** in 72.5% yield from **10**. Hydrolysis of **12** with 50% aqueous acetic acid gave the free sugar **13** in 82% yield, which was treated with LAH in THF to afford **14** in 95% yield. The triol **14** was directly subjected to the one-step epoxidation[18] of vicinal diol with triphenylphosphine, diethyl azodicarboxylate (DEAD), and 3A Molecular Sieves in refluxed benzene to yield **15**. The crude sample of **15** isolated through a short silica-gel column was contaminated with a considerable amount of *N,N*-bis(ethoxycarbonyl)hydrazine. Since further chromatographic purification of this sample was not practicable, the crude **15** was *t*-butyldimethylsilylated to obtain the pure sample of **16a** in 57% overall yield from **14**. The reaction of **16a** with 5 equivalents of 2-ethyl-2-lithio-1,3-dithiane in THF afforded a 90% yield of essentially pure **17a**. The dithioacetal group of **17a** was cleaved with a 1:1 mixture of $HgCl_2$ and HgO to generate the ethyl ketone **18a** in 93% yield.

We have now in our hand the segment **C** in which R^1 is *t*-butyldimethylsilyl (TBS), a most useful silyl protective group. In our preliminary deprotection experiments for the TBS group of **18a**, it was found that **18a** was smoothly deprotected by tetrabutylammonium fluoride[19] (TBAF) in THF to give the hemiacetal **19**, but the tetrahydropyranyl (THP) derivative **20**, which was prepared from **18a** by the usual way, afforded under the similar desilylation conditions the unsaturated ketone **21** in 48% yield instead of the expected **22**. It was also observed that the mild acidic hydrolysis (3:1:3 AcOH–H_2O–THF,[20] 0 °C, 3 h or 22 °C, 2.5 h) of **20** yielded **19** (20%), **22** (16%), and considerable amounts of **18a** and **21**. These results suggested that the 5-*O*-glycosidation of **18a** may lead to a β-eliminated desilylation product under the basic conditions (TBAF in THF), furthermore, under the acidic conditions (3:1:3 AcOH–H_2O–

6 R = Et
6′ R = H
7 R^1,R^2 = Me_2C
8 R^1 = R^2 = H
9 R = CHO
10 R = CH_2OH
11 R = CH_2OMs
12 R = Me
13

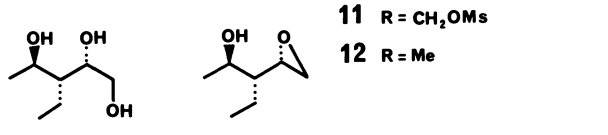

14 **15**

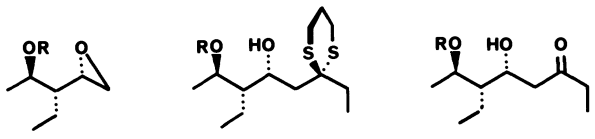

16a~f **17a~f** **18a~f**

R	a TBS	b TES	c IPDMS	d IPDPS	e DIPMS	f DEIPS

TBS = *t*-$BuMe_2Si$- , TES = Et_3Si- , IPDMS = *i*-$PrMe_2Si$-
IPDPS = *i*-Pr(*n*-Pr)$_2$Si-, DIPMS = (*i*-Pr)$_2$MeSi- , DEIPS = *i*-$PrEt_2Si$-

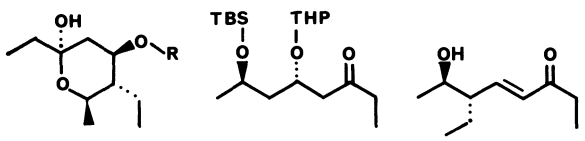

19 R = H
22 R = THP
20 **21**

THF), the rate of hydrolytic cleavage of the TBS ether linkage may be rather slower than that of the cleavage of the glycosidic linkage with the 2-deoxysugar moiety. In this respect, it was noteworthy that azalomycin B[21] (**1**) was immediately decomposed by TBAF in THF even at lower temperature, but it was hardly affected by 3:1:3 AcOH–H_2O–THF, recovering the unchanged **1** after evaporation of the resulting mixture and subsequent silica-gel column chromatography. Although the TBS group thus seemed to be not apposite as the protective group (R^1) of the segment **C**, we first pursued the 5-*O*-glycosidation of **18a** with a 3,4-di-*O*-protected 2-deoxy-L-fucose derivative. Treatment of 2-deoxy-D-fucose with di-2-pyridyl disulfide and tributylphosphine[22] followed by silylation[23] with TBS triflate and 2,6-lutidine in DMF afforded the α-thioglycoside **23** along with the minor β-anomer. 2-Propanol reacted with **23** in acetonitrile in the presence of *N*-bromosuccinimide (NBS) and 4A Molecular Sieves[24] to give only the α-glycoside **24a** in 55% yield. However, the reaction of **18a** and **23** provided no glycoside **25a** under the similar conditions or with $Pb(ClO_4)_2$ in acetonitrile, recovering **18a** in 71% yield. Desilylation of **24a** in an acidic conditions (6.9% aqueous 46% HF in acetonitrile,[25] 20 °C, 16 h) failed, resulting in only the cleavage of glycosidic bond of **24a**. We next pursued the glycosidation of **18a** with the glycal derivative **26a** which was obtained by the silylation[23] of L-fucal[26] in 52% yield. The glycosidation of **18a** with **26a** was first accomplished by the method[27] which was previously developed in our laboratories. The reaction of **18a** and **26a** in the presence of NBS afforded a ca. 3:1 mixture of α- and β-anomeric bromo derivative, which was chromatographed on silica gel to separate the desired α-anomer **27a** in 65% yield. Debromination of **27a** with tributylstannane and α,α'-azobisisobutyronitrile (AIBN) in benzene afforded **25a** in 73% yield (47.5% overall yield from **18a**). The synthetic route to segment **B** (R^1=R^2=TBS) was thus confirmed. However, as had been predicted by the desilylation experiment for **20** and **24a**, **25a** was decomposed with TBAF in THF at 20 °C to give no deprotected hemiacetal **5** (Scheme 1), while **25a** was hardly affected with 3:1:3 AcOH–H_2O–THF at 25 °C for 7 h.

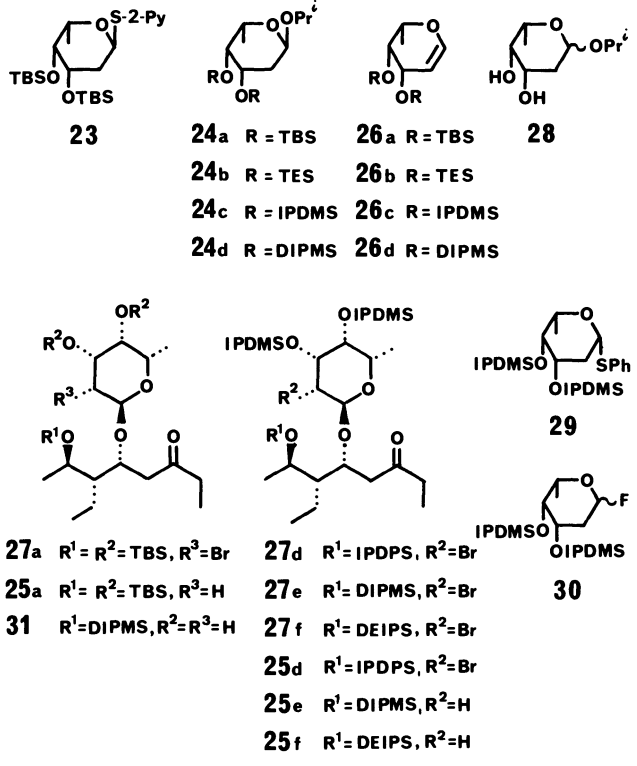

23

24a R = TBS **26a** R = TBS **28**
24b R = TES **26b** R = TES
24c R = IPDMS **26c** R = IPDMS
24d R = DIPMS **26d** R = DIPMS

29

30

27a R^1 = R^2 = TBS, R^3 = Br
25a R^1 = R^2 = TBS, R^3 = H
31 R^1 = DIPMS, R^2 = R^3 = H
27d R^1 = IPDPS, R^2 = Br
27e R^1 = DIPMS, R^2 = Br
27f R^1 = DEIPS, R^2 = Br
25d R^1 = IPDPS, R^2 = Br
25e R^1 = DIPMS, R^2 = H
25f R^1 = DEIPS, R^2 = H

Our selection of the ideal silyl protective group for the segment **B** was aided by the classical reasoning that the rate of acidic hydrolysis of alkylsilyl ether should be subtly influenced by steric effects of alkylsilyl ligands on silicon.[28] We examined the alkylsilyl groups less hindered than TBS, such as triethylsilyl (TES), isopropyldimethylsilyl (IPDMS), diisopropylmethylsilyl (DIPMS), isopropyldipropylsilyl (IPDPS), and diethylisopropylsilyl (DEIPS). The silylating agents, DIPMS-Cl[29] and unknown reagents, IPDPS-Cl and DEIPS-Cl, were prepared from the appropriate chlorosilanes according to the reactions (1,2,3) shown in Scheme 2, respectively. The silylation of the crude **15** using TES-Cl, IPDMS-Cl,[30] IPDPS-Cl, DIPMS-Cl, and DEIPS-Cl with imidazole in dichloromethane afforded **16b**, **16c**, **16d**, **16e**, and **16f**, respectively, which were converted into the corresponding dithiane derivatives, **17b**, **17c**, **17d**, **17e**, and **17f** in good yields. Among them **17d**, **17e**, and **17f** were smoothly dedithioacetalized with $HgCl_2$–H_2O to give **18d**, **18e**, and **18f** in 91, 80, and 79% yields, respectively, whereas **17b** and **17c** afforded **18b** (58%) and **18c** (44%) together with hemiacetal **19** (30 and 46%), respectively. From a preparative point of view, the silyl derivatives, **18d**, **18e**, and **18f**, were more suitable for the segment **C**.

The glycal derivatives, **26b**, **26c**, and **26d**, were prepared by treatment of L-fucal with the corresponding silylating agents and imidazole in DMF. The model glycosides (**24b**, **24c**, **24d**) were then prepared

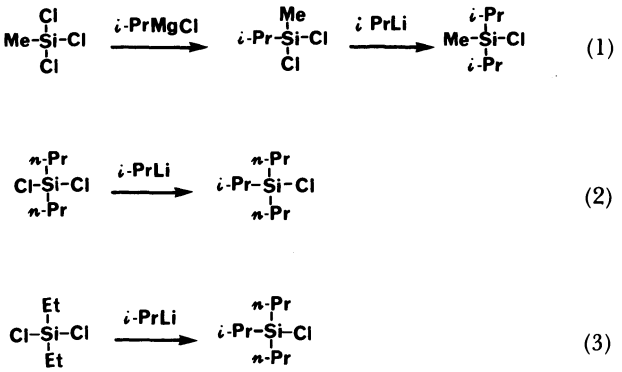

Scheme 2.

from the corresponding glycals and 2-propanol by the procedure described in the preparation of **25a**. Based on the facilities in the formation of the desilylation products **28** from **24b**, **24c**, and **24d** under the acidic conditions (8:1:8 AcOH-H_2O-THF, 30 °C, 24 h),[31] the most apposite protective group for the sugar moiety of **B** was assumed to be IPDMS, therefore **26c** became the most promising glycal derivative.

Each of the selected ketone derivatives, **18d**, **18e**, and **18f**, were subjected to glycosidation with **26c** followed by debromination to afford the glycosides, **25d** (24% via **27d**), **25e** (38% via **27e**), and **25f** (30% via **27f**), respectively. The glycosidation of **18f** with fluoride **30** did not proceed because the thioglycoside **29**, a precursor of **30**, was completely deprotected under the conditions of its fluoridation with (dimethylamino)-sulfur trifluoride (DAST) and NBS.[24,32] However, we found that the treatment of **18f** (1 equiv) with the glycal **26c** (3.5 equiv) and *dl*-10-camphorsulfonic acid (CSA) (0.36 equiv) in dichloromethane containing 4A Molecular Sieves[33] by modification of the Wakamatsu's methods[13a] afforded **25f** as a sole anomer in 80% yield.

Finally, thus obtained **25d**, **25e**, and **25f** were subjected to a deprotection test to determine the most favorable compound for the segment **B**. Exposure of **25d** to 2:1:2 AcOH-H_2O-THF (28 °C, 6 h) or 2:1:2 AcOH-aq 0.46% HF-THF (28 °C, 4 h) afforded mainly **5** accompanied by a small amount of partially deprotected product and 2-deoxy-L-fucose, which were detectable on TLC. Treatment of **25e** with 3:1:3 AcOH-H_2O-THF (25 °C, 20 h) or 2:1:2 AcOH-aq 0.46% HF-THF (26 °C, 6 h) gave mainly **5** and the same Kind of by-products. Exposure of **25e** to 8:1:8 AcOH-H_2O-THF (26 °C, 11 h) yielded mainly **31** in 45% yield. Treatment of **25f** with 2:1:2 AcOH-H_2O-THF (24—26 °C, 12—18 h) also afforded **5** as major product. In view of the minimal formation of by-products observed in the deprotection test, **25f** was considered to be the most promising segment **B**. In fact, **25f** provided a 64% yield of **5** on treatment with 3:1:4 AcOH-aq 1% HF·KF-THF (30 °C, 14 h). Under this conditions, natural azalomycin **B** was confirmed to be stable. The synthesis of the segment **B** was accomplished.

Preparation of the Segment 3. The synthesis of the second segment **3**[11,12] started from **32** which was previously prepared from D-glucose in our laboratories.[34] Deisopropylidenation of **32** with 50% aqueous acetic acid afforded the crystalline triol **33** in 90% yield. Treatment of **33** with lead tetraacetate[35] gave the aldehyde **34** (ca. 95% yield) which was allowed to react with [(2*E*)-3-methoxycarbonyl-2-propenyliden]triphenylphosphorane[36] in toluene at 80 °C to yield (2*E*,4*E*)-dienoic ester **35** and its (4*Z*)-isomer **36** in 51 and 21% overall yields from **33**, respectively, after chromatographic separation. The (4*Z*)→(4*E*) isomerization of **36** proceeded in benzene

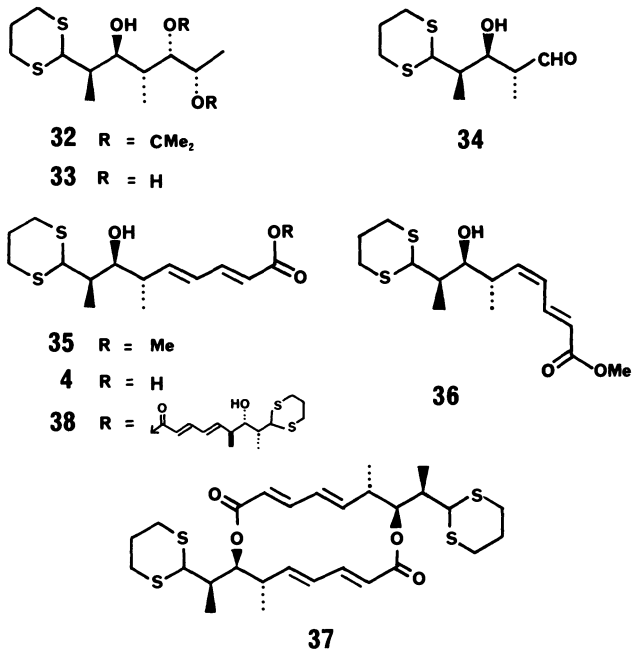

37

with a catalytic amount of iodine[37] at 25 °C for 1 m to afford **35** and **36** in 37.4 and 27% isolated yields, respectively. Saponification of **35** with lithium hydroxide gave the hydroxy dienoic acid **4** in quantitative yield. The dimerization of **4** was best effected by the Yamaguchi's method[38,39] to afford the crystalline diolide **37** in 31% yield. It was found that the reaction of **4** with 1-chloro-2-methylpyridinium iodide and triethylamine according to the Mukaiyama's method[40] gave the anhydride **38** in 85.5% yield, which was treated with 4-(dimethylamino)pyridine (DMAP) in acetonitrile to afford the diolide **37** in 9.4% overall yield from **4**. Dedithioacetalization of **37** with 1:1 $HgCl_2$-HgO (red) was carried out with irradiation in the water bath of an ultrasound laboratory cleaner to give the crystalline dialdehyde **3** in 70% yield.

Aldol Coupling of 25f and 3, and Synthesis of Elaiophylin. In the synthesis of 6-deoxyerythronolide B, Masamune et al.[41] have found that the aldol coupling of chiral aldehyde **39** and (*Z*)-lithium enolate prepared from ethyl ketone **40** with lithium bis-(trimethylsilyl)amide (LBTMSA) give the anti-Cram-syn aldol **41** in 88% yield and 94% diastereomeric purity. The aldol coupling of **25f** and **3** was first pursued according to this procedure. The lithium enolate was prepared by treatment of **25f** (2.4 equiv) with LBTMSA (2.4 equiv) in THF at −78 °C for 0.5 h. This was added slowly to a THF solution of **3** (1 equiv) at −78 °C and the resulting colorless mixture was stirred at −78 °C for 2 h. By careful chromatographic purification of the reaction products, three diastereomeric aldols, **43** (5.2%), **44** (8.9%), and **45** (6.3%), could be obtained in low yields. The minor aldol **43** proved to be the desired precursor **A** to elaiophylin **1** as will be described in the next paragraph. When inversely was added the aldehyde **3**

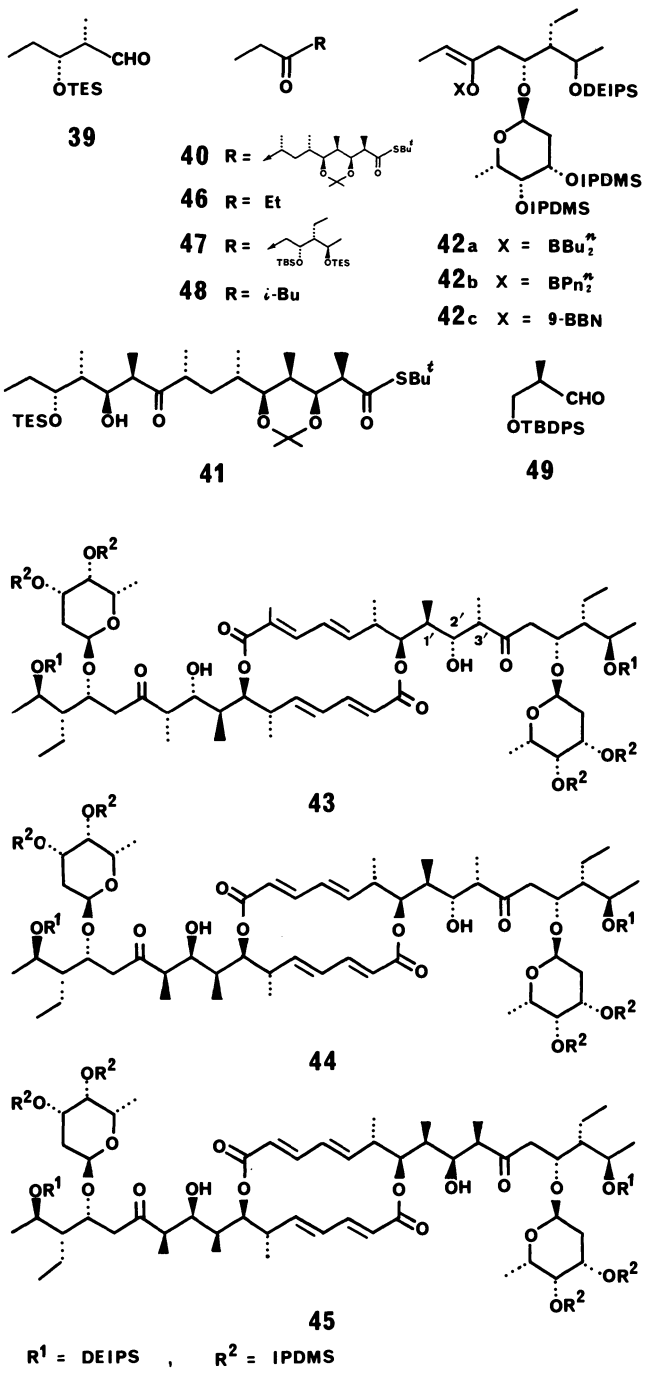

to the lithium enolate solution at −78 °C, the resulted red-colored reaction mixture afforded only poor yields of the aldol products. It was revealed that **3** was very sensitive to the strong base such as lithium enolate.

It has also been known that dibutylboryl triflate[42] reacts with ethyl ketones such as **46** and **47**[11,12] in the presence of weak base *i*-Pr2NEt to give with high stereoselectivity the (*Z*)-boron enolates[43] which add to aldehydes to provide syn aldols.[12,42-44] The coupling of **25f** and **3** was next carried out by this procedure using dialkylboryl triflates. The (*Z*)-boron enolate **42a** was prepared under the standard conditions[43] (*n*-Bu2BOTf, *i*-Pr2NEt, ether, −78 °C, 0.5 h). The reaction was performed by addition of an etherial solution of **42a** (4 equiv) to an etherial solution of **3** (1 equiv) at −78 °C under argon. It was allowed to warm to −10 °C and stirred for 2 h. Quenching with a phosphate buffer (pH 7) (25 °C, 3 min)[45] followed by chromatographic isolation afforded the three aldols, **43**, **44**, and **45** in 13, 24, and 26% yields, respectively. The ^{1}H NMR examination of these products revealed that **43** and **45** were C_2 symmetric, while **44** was unsymmetric (see Experimental). Upon treatments of these products with 3:1:3 AcOH–1% aqueous HF·KF–THF at 30 °C for 18 h, only **43** gave a 22% yields of **1**. The TLC behavior of **1** was coincidental with azalomycin B, and after two recrystallizations from ethyl acetate there was obtained colorless needles, mp 179—182 °C, $[\alpha]_D$ −53° which compared well with natural material. Comparison of ^{1}H NMR spectra at 400 MHz showed both materials to be identical. Unexpectedly, we could not obtain the diastereomers[46] of **1** from the aldol diastereomers **44** and **45** under the same deprotection conditions. Having thus assigned **43** as the bis(1′,2′-anti-2′,3′-syn)-product, **45** and **44** were assumed to be the bis(1′,2′-syn-2′3′-syn)- and (1′,2′-anti-2′,3′-syn:1″,2″-syn-2″,3″-syn)-products, respectively.

The reaction of **3** with other (*Z*)-boron enolates **42b** and **42c** which were prepared from **25f** and the corresponding boryl triflates were carried out by the procedure described above to afford **43** (12 and 5%), **44** (25.5 and 16.5%), and **45** (19 and 39%), respectively. The reaction of **3** with **42a** in the presence of $ZnCl_2$ in THF gave **43** (14%), **44** (31%), and **45** (21%). Moreover, the Mukaiyama's aldol reaction of **3** with **25f** via divalent tin enolate[47] gave **43** (6.5%), **44** (21%), and **45** (28%).

With the goal of obtaining the desired anti-Cram (1′,2′-anti) product **43** in high yield, we also examined the aldol reaction with the boron enolate of **25f** with chiral ligands attached to boron. A model coupling reaction of **48** and **49** using the chiral boryl triflate **50**[48,49] was carried out under the Paterson's conditions[49] (*i*-Pr2NEt, ether, 0 °C) to afford a 2:1 mixture of **51** (anti-Cram product[51]) and **52** (Cram product[51]) in 30% yield. While the coupling using achiral boryl triflates, *n*-Bu2BOTf and 9-BBNOTf, gave 2.3:1 and 1.2:1 mixture of **51** and **52** in 59 and 93% yields, respectively. The (−)-diisopinocampheylboron enolate of **48** showed to be of little help for enhancement of the expected *si*-face selectivity[50] in direction of the inherent 1,2-asymmetric induction on addition of achiral boron enolates to the α-chiral aldehyde **49**. Furthermore, on the reaction of **49** and **25f** using **50**, there could not be obtained any aldol products. The enolization of the large ethyl ketone **25f** with the bulky boryl triflate **50** seemed to be quite difficult. An extensive study by Masamune[52] revealed that Cram/anti-Cram selectivity in the coupling of boron enolate

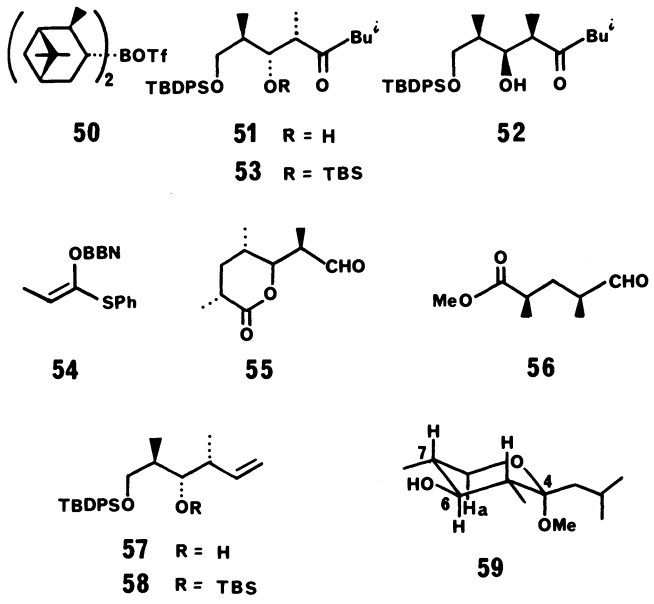

50 51 R = H 52

53 R = TBS

54 55 56

57 R = H

58 R = TBS

59

54 with chiral aldehydes depended on the aldehydes employed: the reaction of **54** with lactone aldehyde **55** afforded the Cram product in a 1.9—2.5:1 selectivity, whereas the reaction with linear aldehyde **39** or **56** gave the anti-Cram product in a 1.5:1 or 55:45 selectivity, respectively. The Cram selectivity observed in the coupling of **3** with **42c** and the anti-Cram selectivity in the reaction of **49** with 9-BBN enolate of **48** appeared to be in line with the Masamune's observation. The rationalization for these results is now not available.

Although the closing stages of this total synthesis of **1** were sullied by the minor preponderance of the unwanted Cram (1′2′-syn) product **45** over the anti-Cram (1′2′-anti) product **43** in the aldol reaction step, the synthesis of elaiophylin (**1**) which was sensitive to acid and base was first achieved via **43** by using the appropriate O-protecting groups such as DEIPS and DMIPS.

Experimental

Melting points were determined on a micro hot-stage Yanaco MP-S3 and were uncrrected. Optical rotations were measured with a Carl Zeiss photoelectric polarimeter or a JAS.CO DIP-360 photoelectric polarimeter in chloroform unless otherwise stated. IR spectra were recorded on a Hitachi Perkin-Elmer 225 spectrometer, UV spectra on a JAS.CO UVIDEC-1 spectrometer, and ^{1}H NMR spectra on a Varian EM-390, a Bruker WM 250, or a JEOL GX-400 spectrometer in $CDCl_3$ using TMS as internal standard unless otherwise stated. Mass spectra were measured with a Hitachi M-80 mass spectrometer or a Hitachi RMU-6M mass spectrometer. TLC was carried out on Merck TLC plates (60F-254, 0.25 mm). Column chromatography was performed on silica gel, Wakogel C-200 and Merck Kiesel gel 60 (230—400 mesh) for "Flash Chromatography". In general, organic solvents were purified and dried by the appropriate procedure, and evaporation and concentration were carried out under reduced pressure below 35 °C, unless otherwise noted.

3-Deoxy-3-*C*-ethyl-1,2:5,6-di-*O*-isopropylidene-β-D-altrofranose (7). To a solution of the crude sample of **6** (32.2 g) containing ca. 12.5% of **6′** in dry acetone (1.29 l) was added $BF_3 \cdot Et_2O$ (6.04 ml, 65.4 mmol) under ice-cooling. After being kept at room temperature for 15 h, the reaction mixture was neutralized with Et_3N under ice-cooling and then concentrated to afford a yellow syrup, which was chromatographed on silica gel (2 kg) with 6:1 toluene–ethyl acetate to give **7** (21.3 g, 80% based on **6**) as colorless needles. R_f=0.41 (9:1 toluene–ethyl acetate); mp 63—64 °C; $[\alpha]_D^{22}$ +16° (*c* 1.07); ^{1}H NMR (90 MHz) δ=1.00 (3H, t, 3-$CH_2C\underline{H}_3$, *J*=6.6 Hz), 1.30, 1.35, 1.40, and 1.53 (each 3H, each s, CMe_2×2), 1.2—1.8 (2H, m, 3-$C\underline{H}_2CH_3$), 2.37 (1H, dt, H-3, *J*=2.4, 7.5 Hz), 3.6—4.4 (4H, m, H-4, 5, 6, 6′), 4.43 (1H, d, H-2, *J*=4.5 Hz), and 5.77 (1H, d, H-1, *J*=4.5 Hz).

Found: C, 61.74; H, 8.88%. Calcd for $C_{14}H_{24}O_5$: C, 61.63; H, 8.71%.

3-Deoxy-3-*C*-ethyl-1,2-*O*-isopropylidene-β-D-altrofuranose (8). A solution of **7** (671 mg, 2.46 mmol) in aqueous 75% acetic acid (13.4 ml) was stirred at 30 °C for 4 h and then concentrated to give a crude syrup (684 mg) which was chromatographed on silica gel (21 g) with 1:1 toluene–ethyl acetate to afford **8** (487 mg, 85%) as a colorless surup: R_f=0.12 (3:2 toluene–ethyl acetate); $[\alpha]_D^{28}$ +13° (*c* 1.18); ^{1}H NMR (90 MHz) δ=1.00 (3H, t, 3-$CH_2C\underline{H}_3$, *J*=6.3 Hz), 1.30 and 1.53 (each 3H, each s, CM_2), 1.2—1.8 (2H, m, 3-$C\underline{H}_2CH_3$), 2.25—2.7 (2H, m, H-3 and OH), 2.87 (1H, d like, OH), 3.65—4.15 (4H, m, H-4.5, 6, 6′), 4.43 (1H, d, H-2, *J*=3.9 Hz), and 5.80 (1H, d, H-1, *J*=3.9 Hz).

Found: C, 56.71; H, 8.32%. Calcd for $C_{11}H_{20}O_5$: C, 56.88; H, 8.68%.

3-Deoxy-3-*C*-ethyl-1,2-*O*-isopropylidene-β-D-arabinofuranose (10). To an ice-cooled solution of **8** (4.55 g, 19.5 mmol) in acetone (45.5 ml) was slowly added a solution of $NaIO_4$ (8.35 g, 39.1 mmol) in water (83.5 ml). After being stirred at room temperature for 30 min, the mixture was concentrated to remove the acetone. The residue was diluted with water (100 ml), extracted with ethyl acetate (50 ml×3), and the extracts were washed with saturated aqueous NaCl (50 ml), dried and concentrated to afford a crude sample of **9** (4.35 g) as pale yellow needles, which was used without further purification. Powdered $NaBH_4$ (1.64 g, 43.5 mmol) was slowly added to a stirred ice-cooled solution of the crude sample of **9** (4.35 g) in methanol (43.5 ml), and then the mixture was stirred at room temperature for 10 min. The reaction mixture was neutralized with CO_2 (solid) and concentrated. The residue was triturated with chloroform, and the chloroform solutions were evaporated to give a pale yellow syrup, which was chromatographed on silica gel (110 g) with 1:1 toluene–ethyl acetate to afford **10** (3.83 g, 97% from **8**) as a colorless syrup. R_f=0.46 (1:1 toluene–ethyl acetate); $[\alpha]_D^{27}$ +11° (*c* 0.90); ^{1}H NMR (90 MHz) δ=1.00 (3H, t, 3-$CH_2C\underline{H}_3$, *J*=6.6 Hz), 1.30 and 1.53 (each 3H, each s, CMe_2), 1.25—1.55 (2H, m, 3-$C\underline{H}_2CH_3$), 1.9—2.2 (1H, m, H-3), 2.2—2.45 (1H, br, OH), 3.55—4.1 (3H, m, H-4,5,5′), 4.42 (1H, dd, H-2, *J*=1.5, 4.5 Hz), and 5.81 (1H, d, H-1, *J*=4.5 Hz).

Found: C, 59.71; H, 8.88%. Calcd for $C_{10}H_{18}O_4$: C, 59.39; H, 8.97%.

3-Deoxy-3-*C*-ethyl-1,2-*O*-isopropylidene-5-*O*-methylsulfonyl-β-D-arabinofuranose (11). To a solution of **10** (4.50 g, 22.2 mmol) in dry pyridine (45.0 ml) was added methanesulfonyl chloride (2.07 ml, 26.7 mmol) under ice-cooling. After being stirred at room temperature for 0.5 h, the reaction mixture was poured into cold water (50 ml), extracted with ethyl acetate (20 ml×3), washed with saturated aqueous NaCl (30 ml), dried, and concentrated to afford a crude sample of **11** (6.40 g) as yellow needles which was suitable for the next synthesis. Analytical sample was obtained after silica-gel column chromatography with 3:1 benzene-ethyl acetate. R_f=0.40 (3:1 toluene-ethyl acetate); mp 69.5—70 °C (ethyl acetate-hexane); $[\alpha]_D^{33}$ +25° (*c* 0.88); ^{1}H NMR (90 MHz) δ=1.00 (3H, t, 3-$CH_2C\underline{H}_3$, *J*=6.6 Hz), 1.30 and 1.58 (each 3H, each s, CMe_2), 1.25—1.7 (2H, m, 3-$C\underline{H}_2CH_3$), 2.10 (1H, dt, H-3, *J*=3.0, 1.5 Hz), 3.10 (3H, s, OMs), 4.0—4.75 (4H, m, H-2,4,5,5′), and 5.83 (1H, d, H-1, *J*=3.3 Hz).

Found: C, 46.92; H, 7.00%. Calcd for $C_{11}H_{20}O_6S$: C, 47.13; H, 7.19%.

3,5-Dideoxy-3-*C*-ethyl-1,2-*O*-isopropylidene-β-D-arabinofuranose (12). To an ice-cooled solution of the crude sample of **11** (6.40 g) in dry ether (96.0 ml) was slowly added powdered $LiAlH_4$ (2.60 g, 68.5 mmol) under stirring. The stirring was continued at room temperature for 5 h and to the reaction mixture were successively added dropwise water (2.60 ml), aqueous 15% NaOH (2.60 ml) and water (7.80 ml) under ice-cooling. The resulting mixture was then filtered, and the filter cake was washed with chloroform. The filtlate and washings were combined, and concentrated (10 °C, 40 mmHg; 1 mmHg≈133.322 Pa) to give a syrup (15.8 g) which was chromatographed on silica gel (790 g) with 10:1 hexane-acetone to afford **15** (3.00 g, 72.5% from **10**) as a colorless syrup. Analytical sample was obtained by distillation [bp_5 78—80 °C (bath temp)]. R_f=0.63 (5:1 toluene-ethyl acetate); $[\alpha]_D^{25}$ 0°, $[\alpha]_{365}$ +4.2° (*c* 1.19); ^{1}H NMR (90 MHz) δ=1.00 (3H, t, 3-$CH_2C\underline{H}_3$, *J*=6.6 Hz), 1.25—1.55 (2H, m, 3-$C\underline{H}_2CH_3$), 1.30 and 1.53 (each 3H, each s, CMe_2), 1.37 (3H, d, 4-Me, *J*=7.5 Hz), 1.75—2.1 (1H, m, H-3), 3.87 (1H, dq, H-4, *J*=7.5, 1.5 Hz), 4.37 (1H, dd, H-2, *J*=4.5, 1.5 Hz), and 5.72 (1H, d, H-1, *J*=4.5 Hz).

Found: C, 64.64; H, 9.52%. Calcd for $C_{10}H_{18}O_3$: C, 64.49; H, 9.74%.

3,5-Dideoxy-3-*C*-ethyl-β-D-arabinofuranose (13). A solution of **12** (9.90 g, 53.2 mmol) in aqueous 50% acetic acid (9.90 ml) was stirred at 100 °C for 0.5 h and then concentrated to give a syrup (8.20 g) which was subsequently chromatographed on silica gel (390 g) with 3:2 hexane-acetone to afford **13** (6.41 g, 82%) as a colorless syrup. Analytical sample was obtained by distillation [bp_2 100—110 °C (bath temp)]. R_f=0.33 (3:2 hexane-acetone); $[\alpha]_D^{29}$ −44° (*c* 1.41, after 2 d); ^{1}H NMR (90 MHz) δ=1.00 and 1.02 (3H, each t, 3-$CH_2C\underline{H}_3$ of α and β anomers, each *J*=6.6 Hz), 1.31 and 1.33 (3H, each d, 4-Me of α and β anomers, each *J*=6.3 Hz), 1.3—1.85 (3H, m, 3-$C\underline{H}_2CH_3$, H-3), 2.83 (2H, br s, OH×2), 3.45—4.15 (2H, m, H-2,4), 5.19 and 5.27 (1H, each d, H-1 of α and β anomers, *J*=4.5, 2.0 Hz).

Found: C, 57.30; H, 9.36%. Calcd for $C_7H_{14}O_3$: C, 57.51; H, 9.65%.

(2*S*,3*R*,4*R*)-3-Ethyl-1,2,4-pentanetriol (14). To an ice-cooled solution of **13** (6.41 g, 43.8 mmol) in dry THF (256 ml) was slowly added powdered $LiAlH_4$ (3.33 g, 87.6 mmol) under stirring. The stirring was continued at 70 °C for 2 h and to the reaction mixture were added dropwise water (3.3 ml), aqueous 10% NaOH (3.3 ml) and water (9.9 ml) successively under ice-cooling. The resulting mixture was then filtered, and filter cake was washed with chloroform. The filtrate and washings were combined, and concentrated to give a crude syrup (8.64 g) which was chromatographed on silica gel (400 g) with 11:1 chloroform-methanol to afford **14** (6.18 g, 95%) as a colorless syrup. R_f=0.32 (11:1 chloroform-methanol); $[\alpha]_D^{26}$ −4.4° (*c* 1.00, CH_3OH); ^{1}H NMR (90 MHz) δ=0.97 (3H, br t, 3-$CH_2C\underline{H}_3$), 1.28 (3H, d, H-5, *J*=6.6 Hz), 1.15—1.85 (3H, m, 3-$C\underline{H}_2CH_3$, H-3), and 3.4—4.45 (7H, m, H-1,1′,2,4, OH×3).

Found: C, 56.43; H, 10.60%. Calcd for $C_7H_{16}O_3$: C, 56.73; 10.88%.

(2*R*,3*R*,4*S*)-2-*O*-(*t*-Butyldimethylsilyl)-4,5-epoxy-3-ethyl-2-pentanol (16a). According to the procedure described by Achab and Das,[18] **14** (331 mg, 2.23 mmol) was directly epoxidated with triphenylphosphine (644 mg, 2.45 mmol) and DEAD (0.387 ml, 2.45 mmol) in refluxing benzene containing 3A Molecular Sieves (0.9 g) to afford the crude epoxide **15** (347 mg) which was contaminated by a considerable amount of *N*,*N*-bis(ethoxycarbonyl)hydrazine. To a solution of the crude sample of **15** (347 mg) and imidazole (219 mg, 3.21 mmol) in dry CH_2Cl_2 (2.46 ml) was added *t*-butyldimethylsilyl chloride (456 mg, 3.02 mmol) under ice-cooling. The reaction mixture was stirred at room temperature for 9 h, and then poured into cold water (10 ml) and extracted with CH_2Cl_2 (8 ml×3). The extracts were washed with saturated aqueous NaCl (8 ml), dried, and concentrated. The residue was chromatographed on silica gel (40 g) with benzene to afford a pure sample of **16a** (329 mg, 57% from **14**) as a colorless syrup. R_f=0.55 (benzene); $[\alpha]_D^{20}$ −14.3° (*c* 0.95); ^{1}H NMR (90 MHz) δ=0.87 (9H, s, *t*-Bu), 0.97 (3H, t, 3-$CH_2C\underline{H}_3$, *J*=7.2 Hz), 1.16 (3H, d, H-1, *J*=6.0 Hz), 1.1—1.3 (1H, m, H-3), 1.57 (2H, dq, 3-$C\underline{H}_2CH_3$, *J*=7.2, 1.0 Hz), 2.45—2.55 (1H, m, H-4), 2.7—3.0 (2H, m, H-5,5′), and 3.93 (1H, q, H-2, *J*=6.0, 2.3 Hz).

Found: C, 63.92; H, 11.28%. Calcd for $C_{13}H_{28}O_2Si$: C, 63.88; H, 11.54%.

(2*R*,3*R*,4*S*)-4,5-Epoxy-3-ethyl-2-*O*-(diethylisopropylsilyl)-2-pentanol (16f). By the procedure described in the preparation of **16a**, the crude sample of **15** (1.42 g) was silylated with DEIPS-Cl (1.63 ml, 8.82 mmol) and imidazole (651 mg, 9.56 mmol) to give a pure sample of **16f** (1.37 g, 72% from **14**) as a colorless syrup. R_f=0.53 (10:1 hexane-ethyl acetate); $[\alpha]_D^{20}$ −9° (*c* 1.10); ^{1}H NMR (90 MHz) δ=0.5—0.8 (4H, m, $Si(C\underline{H}_2CH_3)_2$), 0.8—1.15 (16H, m, $\underline{i\text{-}Pr}Si(CH_2C\underline{H}_3)_2$, 3-$CH_2C\underline{H}_3$).

Found: *m*/*z* 229.1622. Calcd for $C_{12}H_{25}O_2Si$: M−Et, 229.1622.

2-[(2*R*,3*R*,4*R*)-4-*O*-(*t*-Butyldimethylsilyl)-3-ethyl-2,4-dihydroxypentyl]-2-ethyl-1,3-dithiane (17a). A solution of 2-ethyl-1,3-dithiane (997 mg, 6.73 mmol) in dry THF (9.97 ml) was cooled to −40 °C under argon. A solution of 1.42 M butyllithium (1 M=1 mol dm^{-3}) in hexane (4.74 ml, 6.73 mmol) was added to the solution dropwise under stirring. After being stirred for an additional 2 h at −20 °C, the mixture was again cooled to −50 °C. A solution of **16a** (329 mg, 1.35 mmol) in dry THF (0.99 ml) was then added dropwise to this solution, and stirring was continued at −50 °C→−20 °C for 4 h. The reaction mixture was poured into cold water (20 ml) and extracted with chloroform

(10 ml×3). The extracts were washed with saturated aqueous NaCl (10 ml), dried, and concentrated. The residual syrup (1.40 g) was chromatographed on silica gel (210 g) with benzene to afford **17a** (474 mg, 90%) as a colorless syrup. R_f=0.43 (benzene); ^{1}H NMR (90 MHz) δ=0.87 (9H, s, *t*-Bu), 0.88 (3H, t, 2-$CH_2C\underline{H}_3$, J=7.2 Hz), 1.07 (3H, t, 3′-$CH_2C\underline{H}_3$, J=7.5 Hz), 1.30 (3H, d, H-5′, J=6.0 Hz), 1.15—1.35 (1H, m, H-3′), 1.4—1.8 (2H, m, 3′-$C\underline{H}_2CH_3$), 1.75—2.35 (6H, m, 2-$CH_2C\underline{H}_3$, H-1′, $SCH_2C\underline{H}_2$), 2.75—2.95 (4H, m, $SC\underline{H}_2CH_2C\underline{H}_2S$), 3.47 (1H, s, OH), 4.10 (1H, dq, H-4′, J=7.5, 3.0 Hz), and 4.3—4.7 (1H, m, H-3′).

(5*R*,6*R*,7*R*)-7-*O*-(*t*-Butyldimethylsilyl)-6-ethyl-5,7-dihydroxy-3-octanone (18a). To a mixture of **17a** (23.4 mg, 0.0596 mmol), mercury(II) oxide (56.8 mg, 0.262 mmol) and 80% aqueous acetone (1.64 ml) was added mercury(II) chloride (71.2 mg, 0.262 mmol) under ice-cooling with efficient stirring. The reaction mixture was stirred under ice-cooling for 0.5 h and filtered through a Celite. The filter cake was washed with acetone, and then the filtrate and the washings were combined. After removal of the acetone under reduced pressure (0 °C), to the aqueous residue was added aqueous 10% KI until orange color was disappeared. The mixture was then extracted with chloroform (7 ml×3) and the extracts were washed with saturated aqueous NaCl (10 ml), dried, and concentrated to give a crude syrup (22.6 mg) which was chromatographed on silica gel (2 g) with 8:1 hexane–ethyl acetate to afford a pure sample of **18a** (16.7 mg, 93%) as a colorless syrup. R_f=0.30 (benzene); $[\alpha]_D^{29}$ −2.9° (*c* 1.18); IR ($CHCl_3$) 1710 cm^{-1}; ^{1}H NMR (90 MHz) δ=0.89 (9H, s, *t*-Bu), 0.93 (3H, t, H-1, J=6.0 Hz), 1.03 (3H, t, 6-$CH_2C\underline{H}_3$, J=7.2 Hz), 1.30 (3H, d, H-8, J=6.0 Hz), 1.40 (2H, q, 6-$C\underline{H}_2CH_3$, J=7.2 Hz), 1.2—1.4 (1H, m, H-6), 2.2—2.95 (4H, m, H-2,2′,4,4′), 3.63 (1H, br s, OH), 4.17 (1H, dq, H-7, J=3.0, 6.0 Hz), and 4.5—4.85 (1H, m, H-5).

Found: C, 63.75; H, 11.10%. Calcd for $C_{16}H_{34}O_3Si$: C, 63.52; H, 11.33%.

2-Pyridinyl 3,4-Bis-*O*-(*t*-butyldimethylsilyl)-2-deoxy-1-thio-α-L-fucoside (23) and β-Anomer (23-β). To a solution of 2-deoxy-L-fucose[26] (35.2 mg, 0.238 mmol) in dry THF (0.70 ml) was added *n*-Bu_3P (88.8 µl, 0.357 mmol) dropwise and PySSPy (38.5 mg, 0.357 mmol) under ice-cooling. After being stirred under ice-cooling for 2 h, *n*-Bu_3P (29.6 µl, 0.119 mmol) and PySSPy (26.2 mg, 0.119 mmol) was added to the reaction mixture and stirred at room temperature (25 °C) for 1 h. The resulting mixture was concentrated to a crude syrup (0.3 g) which was chromatographed on silica gel (27 g) with 2:1 chloroform–acetone to afford a pale yellow syrup (39 mg). To an ice-cold solution of this sample (0.495 g, 2.15 mmol) in dry CH_2Cl_2 (4.95 ml) was added successively 2,6-lutidine (1.57 ml, 8.20 mmol) and TBDMSOTf (1.27 ml, 10.9 mmol) and the mixture was stirred under ice-cooling for 0.5 h. The reaction mixture was dilluted with ethyl acetate (20 ml) and water (10 ml) and extracted with saturated aqueous NaCl (20 ml), dried, and concentrated to give a crude syrup (1.6 g) which was chromatographed on silica gel (80 g) with 10:1 hexane–acetone to afford **23** (0.773 g, 80%) and **23-β** (0.173 g, 18%) as pale yellow syrup.

23: R_f=0.54 (10:1 hexane–acetone); ^{1}H NMR (90 MHz) δ=0.93 and 0.97 (each 9H, each s, *t*-Bu×2), 1.17 (3H, d, 5-Me, J=6.2 Hz), 1.82 (1H, ddd, H-2_{eq}, J=13.0, 4.5, 1.5 Hz), 2.58 (1H, ddd, H-2_{ax}, J=15.0, 13.0, 6.0 Hz), 3.63 (1H, br, H-4), 3.85—4.30 (2H, m, H-3,5), 6.27 (1H, dd, H-1, J=6.0, 1.5 Hz), 6.9—7.15 (1H, m), 7.2—7.7 (2H, m), and 8.4—8.7 (1H, m).

23-β: R_f=0.54 (10:1 hexane–acetone); ^{1}H NMR (90 MHz) δ=0.93 and 0.97 (each 9H, each s, *t*-Bu×2), 1.28 (3H, d, 5-Me, J=6.2 Hz), 1.7—1.95 (1H, m, H-2_{eq}), 2.05—2.25 (1H, m, H-2_{ax}), 3.55—4.15 (3H, m, H-3,4,5), 5.35 (1H, dd, H-1, J=12.6, 2.3 Hz), 6.6—6.9 (1H, m), 7.0—7.35 (1H, m), 7.35—7.75 (1H, m), and 7.95—8.15 (1H, m).

3,4-Bis-*O*-(*t*-butyldimethylsilyl)-L-fucal (26a). To a solution of L-fucal (48.4 mg, 0.372 mmol) and 2,6-lutidine (0.173 ml, 1.49 mmol) in dry CH_2Cl_2 (0.484 ml) was added TBDMSOTf (0.216 ml, 1.12 mmol) under ice-cooling. The resulting suspension was stirred at the same temperature for 20 min, and then the reaction mixture was poured into cold water (5 ml) and extracted with ethyl acetate (5 ml×3). The extracts were washed with saturated aqueous NaCl (10 ml), dried, and concentrated to a crude syrup (200 mg). The syrup was chromatographed on silica gel (10 g) with 70:1 hexane–ethyl acetate to afford **26a** (68.8 mg, 51.6%) as a colorless syrup. R_f=0.65 (50:1 hexane–ethyl acetate); $[\alpha]_D^{25}$ +31° (*c* 1.00); ^{1}H NMR (90 MHz) δ=0.90 (18H, s, *t*-Bu×2), 1.30 (3H, d, 5-CH_3, J=6.0 Hz), 3.75—3.9 (1H, m, H-4), 4.07 (1H, dq, H-5, J=6.0, 1.5 Hz), 4.25—4.35 (1H, m, H-3), 4.57 (1H, dd, H-2, $J_{1,2}$=6.3, $J_{2,3}$=2.0 Hz), and 6.20 (1H, dd, H-1, $J_{1,2}$=6.3, $J_{1,3}$=1.5 Hz).

Found: C, 60.49; H, 10.56%. Calcd for $C_{18}H_{38}O_3Si_2$: C, 60.28; H, 10.68%.

(5*R*,6*R*,7*R*)-5-*O*-[2-*C*-Bromo-3,4-bis-*O*-(*t*-butyldimethylsilyl)-2-deoxy-α-L-fucosyl]-7-*O*-(*t*-butyldimethylsilyl)-6-ethyl-5,7-dihydroxy-3-octanone (27a). To a mixture of **18a** (46.0 mg, 0.156 mmol) and **26a** (273 mg, 0.760 mmol) in dry CH_3CN (0.273 ml) was added NBS (135 mg, 0.760 mmol) under ice-cooling. The reaction mixture was stirred under ice-cooling for 0.5 h and then stirred at room temperature (25 °C) for 2 h. The solution was poured into cold saturated aqueous $NaHCO_3$ (5 ml) and extracted with ethyl acetate (5 ml×3). The extracts were washed with saturated aqueous NaCl (7 ml), dried, and concentrated to give a syrup (509 mg) which was chromatographed on silica gel (80 g) with 12:1 hexane–ethyl acetate to afford **27a** (72.9 mg, 65%) and **27a-β** (23.0 mg, 16%) as a colorless syrup, respectively.

27a: R_f=0.53 (10:1 hexane–ethyl acetate); ^{1}H NMR (90 MHz) δ=0.87 and 0.97 (30H, m, *t*-Bu×3, 6-$CH_2C\underline{H}_3$), 1.01, 1.15, and 1.24 (each, 3H, each d, H-1,8, 5′-Me, each J=6.0 Hz), 1.0—1.65 (3H, m, H-6, 6-$C\underline{H}_2CH_3$), 2.3—3.15 (4H, m, H-2,4), 3.35—3.4 (1H, m, H-4′), 3.8—4.15 (3H, m, H-2′,3′,5′), 4.15—4.55 (2H, m, H-5,7), and 5.02 (1H, d, H-1′, J=2.8 Hz).

27a-β: R_f=0.42 (10:1 hexane–ethyl acetate); ^{1}H NMR (90 MHz) δ=0.8—1.7 (42H, m, *t*-Bu×3, H-1,8,6, 5-CH_2CH_3), 2.3—3.2 (4H, m, H-2,2′,4,4′), and 3.3—4.7 (7H, m, H-5,7,1′,2′,3′,4′,5′).

(5*R*,6*R*,7*R*)-5-*O*-(*t*-Butyldimethylsilyl)-[3,4-bis-*O*-(*t*-butyldimethylsilyl)-2-deoxy-α-L-fucosyl]-6-ethyl-5,7-dihydroxy-3-octanone (25a). To a solution of **27a** (53.4 mg, 0.0722 mmol) in dry benzene (0.379 ml) was added *n*-Bu_3SnH (46.5 µl, 0.173 mmol) and AIBN (1.42 mg, 0.00866 mmol) and then stirred at 60 °C for 1 h under argon. The solution was cooled and concentrated to give a syrup which was chromatographed on silica gel (16 g) with 12:1:0.6 hexane–ethyl acetate–chloroform to afford **25a** (34.9 mg, 73% from **18a**) as a colorless syrup. R_f=0.30 (12:1:0.6 hexane–ethyl acetate–chloroform); $[\alpha]_D^{20}$ −46° (*c* 1.36); IR ($CHCl_3$) 1710 cm^{-1}; ^{1}H NMR (90 MHz) δ=0.75—1.7 (42H,

m, *t*-BuX3, H-1,6,8,6-CH_2CH_3, 5'-Me), 1.7—3.0 (6H, m, H-2,4,2'), 3.2—3.25 (1H, m, H-4'), 3.6—4.6 (4H, m, H-5,7,3',5'), and 4.97 (1H, m, H-1').

Found: C, 61.61; H, 10.77%. Calcd for $C_{34}H_{72}O_6Si_3$: C, 61.76; H, 10.98%.

(5*R*,6*R*,7*R*)-6-Ethyl-7-*O*-(diethylisopropylsilyl)-5,7-dihydroxy-3-octanone (18f). By the procedure described in the preparation of **18a** from **16a** via **17a**, a sample of **16f** (1.60 g, 6.19 mmol) was converted into crude **17f** (2.66 g) which was dedithioacetalized and worked up to afford a crude syrup of **18f** (1.84 g) which was chromatographed on silica gel (180 g) with 6:1 hexane–ethyl acetate to afford a pure sample of **18f** (1.54 g, 79% from **16f**) as a colorless syrup. R_f=0.16 (8:1 hexane–ethyl acetate); IR ($CHCl_3$) 1710 cm^{-1}; $[\alpha]_D^{26}$ 0°, $[\alpha]_{435}$ +3.8°, $[\alpha]_{365}$ +19.8° (*c* 1.01); ^1H NMR (90 MHz) δ=0.6—0.85 (4H, m, Si($C\underline{H}_2CH_3$)$_2$), 0.9—1.15 (16H, m, *i*-PrSi($CH_2C\underline{H}_3$)$_2$, 6-$CH_2C\underline{H}_3$), 1.30 (3H, d, H-8, *J*=6.0 Hz), 1.2—1.75 (3H, m, H-6, 6-$C\underline{H}_2CH_3$), 2.2—2.9 (4H, m, H-2,2',4,4'), 3.63 (1H, s, OH), 4.0—4.35 (1H, m, H-7), and 4.6—4.75 (1H, m, H-5).

Found: *m/z* 273.1856. Calcd for $C_{14}H_{29}O_3Si$: M−*i*-Pr, 273.1884. Found: *m/z* 287.2010. Calcd for $C_{15}H_{31}O_3Si$: M−Et, 287.2040.

3,4-Bis-*O*-(isopropyldimethylsilyl)-L-fucal (26c). To a solution of L-fucal (500 mg, 3.84 mmol) and imidazole (654 mg, 9.60 mmol) in dry DMF (7.5 ml) was added IPDMS-Cl (1.42 ml, 9.60 mmol) under ice-cooling. The resulting homogeneous solution was kept at room temperature for 2 h, and then the reaction mixture was poured into cold water (10 ml) and extracted with ethyl acetate (10 mlX3). The extracts were washed with saturated aqueous NaCl (15 ml), dried, and concentrated to a crude syrup (1.92 g). The syrup was chromatographed on silica gel (96 g) with 40:1 hexane–ethyl acetate to afford **26c** (820 mg, 65%) as a colorless syrup. R_f=0.57 (30:1 hexane–ethyl acetate); $[\alpha]_D^{26}$ +31° (*c* 1.07, acetone); ^1H NMR (90 MHz) δ=0.97 (14H, s, *i*-PrX2), 1.28 (3H, d, 5-Me, *J*=6.3 Hz), 3.70 (1H, ddd, H-4, $J_{4,2}$=2.0, $J_{4,3}$=3.6, $J_{4,5}$=2.0 Hz), 4.02 (1H, dq, H-5, *J*=6.3, 2.0 Hz), 4.3—4.5 (1H, m, H-3), 4.50 (1H, ddd, H-2, $J_{2,1}$=6.3, $J_{2,3}$=2.0, 2.0 Hz), and 6.23 (1H, dd, H-1, $J_{1,3}$=1.5 Hz).

Found: *m/z* 330.2018. Calcd for $C_{16}H_{34}O_3Si_2$: M, 330.2044.

(5*R*,6*R*,7*R*)-5-*O*-[2-Deoxy-3,4-bis-*O*-(isopropyldimethylsilyl)-α-L-fucosyl]-6-ethyl-7-*O*-(diethylisopropylsilyl)-5,7-dihydroxy-3-octanone (25f). Method A: By the procedure described in the preparation of **27a**, glycosidation of **18f** (1.04 g, 3.29 mmol) with **26c** (3.80 g, 11.5 mmol) and NBS (2.05 g, 11.5 mmol) afforded a crude sample of **27f** (983 mg) which was contaminated by a considerable amount of by-product, and a pure sample of the β-anomer of **27f** (501 mg, 21%) as colorless syrup. To a solution of the crude sample of **27f** (938 mg) in dry benzene (9.38 ml) was added *n*-Bu_3SnH (834 μl, 3.10 mmol) and AIBN (25.4 mg, 0.155 mmol) and then stirred at 60 °C for 0.5 h under argon. The solution was cooled and concentrated to give a syrup (2.04 g) which was chromatographed on silica gel (300 g) with 3:1:0.1 hexane–chloroform–ethyl acetate to afford **25f** (630 mg, 30% from **18f**) as a colorless syrup. R_f=0.39 (10:1 hexane–ethyl acetate); $[\alpha]_D^{20}$ −46° (*c* 1.36); IR ($CHCl_3$) 1710 cm^{-1}; ^1H NMR (250 MHz) δ=0.04, 0.05, 0.055, 0.07 (each 3H, each s, SiMeX4), 0.55—0.7 (4H, m, Si($C\underline{H}_2CH_3$)$_2$), 0.8—1.3 (7H, m, 6-$CH_2C\underline{H}_3$, H-6, Me), 1.13 (3H, d, Me, *J*=6.8 Hz), 1.23 (3H, d, Me, *J*=6.5 Hz), 1.35—1.55 (3H, m, 6-$C\underline{H}_2CH_3$, H-2'$_{eq}$), 1.99 (1H, ddd, H-2'$_{ax}$, *J*=12.8, 11.5, 3.8 Hz), 2.43 (2H, dq, H-2X2, *J*=7.5 and 2.3 Hz), 2.54 (1H, dd, H-4$_{AorB}$, *J*=16.0, 4.5 Hz), 2.82 (1H, dd, H-4$_{AorB}$, *J*=16.0, 8.8 Hz), 3.5—3.55 (1H, m, H-4'), 3.84 (1H, dq, H-5', *J*=6.5, 0.3 Hz), 3.93 (1H, ddd, H-3', *J*=12.5, 4.5, 2.5 Hz), 4.01 (1H, dq, H-7, *J*=7.3, 3.3 Hz), 4.18 (1H, ddd, H-5, *J*=4.5, 4.3, 8.8 Hz), and 4.94 (1H, dd, H-1', *J*=3.3, 1.2 Hz).

Found: C, 61.55; H, 10.61%. Calcd for $C_{33}H_{70}O_6Si_3$: C, 61.25; H, 10.90%.

Method B: To a mixture of **18f** (498 mg, 1.57 mmol), **26c** (1.82 g, 4.71 mmol), 4A Molecular Sieves (0.91 g), and dry CH_2Cl_2 (28.1 ml) was added *dl*-10-camphorsulfonic acid (128 mg, 0.471 mmol) under ice-cooling. After being stirred under ice-cooling for 1 h, *dl*-10-camphorsulfonic acid (25.6 mg, 0.0942 mmol) was added to the reaction mixture and stirred at the same temperature for 1 h. To the reaction mixture was then added dropwise triethylamine (76.8 μl) and water (30 ml) and then the mixture was extracted with ethyl acetate (30 mlX1 and 15 mlX2). The combined extracts were washed with saturated aqueous NaCl (30 ml), dried, and concentrated to give a crude syrup (2.45 g) which was chromatographed on silica gel (270 g) with 3:1:0.1 hexane–chloroform–ethyl acetate to afford **25f** (819 mg, 80%) as a colorless syrup.

(2*S*,4*R*,5*R*,6*R*)-4-*O*-(2-Deoxy-α-L-fucosyl)-2,5-diethyl-3,4,5,6-tetrahydro-2,4-hydroxy-6-methyl-2*H*-pyran (5). A solution of **25f** (63.4 mg, 0.0979 mmol) in 3:1:3 acetic acid–aqueous 1% HF·KF–THF (1.9 ml) was stirred at 30 °C for 14 h. The reaction mixture was concentrated to afford crude syrup which was chromatographed on silica gel (9 g) with 6:1 chloroform–methanol to afford **5** (19.9 mg, 64%) as colorless crystals. R_f=0.30 (6:1 chloroform–methanol); mp 55—62 °C (dichloromethane–hexane); $[\alpha]_D^{32}$ −96.1° (*c* 1.30); ^1H NMR (250 MHz) δ=0.88 (3H, t, 2-$CH_2C\underline{H}_3$, *J*=7.5 Hz), 0.95 (3H, t, 5-$CH_2C\underline{H}_3$, *J*=7.3 Hz), 1.15—1.3 (1H, m, H-5), 1.19 (3H, d, Me, *J*=6.3 Hz), 1.27 (3H, d, Me, *J*=6.5 Hz), 1.35—1.55 (2H, m, 5-$C\underline{H}_2CH_3$), 1.55—1.70 (1H, m, H-2'$_{eq}$), 1.63 (2H, q, 2-$C\underline{H}_2CH_3$, *J*=7.5 Hz), 1.75—1.9 (2H, m, H-3$_{AorB}$, H-2'$_{ax}$), 2.18 (1H, dd, H-3$_{AorB}$, *J*=12.5, 5.0 Hz), 3.6—3.7 (1H, br, H-4'), 3.8—4.1 (4H, m, H-4,6,3',5'), and 5.06 (1H, dd, H-1', *J*=2.8, 2.5 Hz).

Found: C, 60.07; H, 9.23%. Calcd for $C_{16}H_{30}O_6$: C, 60.36; H, 9.50%.

Preparation of DEIPS-Cl. To a solution of Li (1.90 g) in petroleum ether (130 ml) was added slowly a solution of *i*-PrCl (11.9 ml, 130 mmol) in dry petroleum ether (38 ml). The mixture was irradiated in the sonicator (65 W, 48 kHz) at 30—50 °C for 45 min to afford about 0.53 M *i*-PrLi–petroleum ether. To this 0.53 M *i*-PrLi–petroleum ether (120 ml) was added Et_2SiCl_2 (9.91 ml, 63.1 mmol) and stirred at 50 °C for 1 h. The reaction mixture was cooled to room temperature and LiCl was filtered off under argon. The filtrate was distilled at atmospheric pressure to remove solvent and then the residue distilled to give DEIPS-Cl (8.14 g, 92%) as a colorless liquid. Bp_{32} 73—74.5 °C.

Preparation of DPIPS-Cl. This experiment was carried out under the conditions described in the preparation DEIPS-Cl. DPIPS-Cl (3.12 g, 75%) was obtained as a colorless liquid from *n*-Pr_2SiCl_2 (4.14 ml). Bp_{26} 96.5—97.0 °C.

Preparation of DIPMS-Cl. To a suspension of Mg (3.97 g, 0.164 mmol) in dry THF (127 ml) was added dropwise $MeSiCl_3$ (30.0 ml, 0.256 mol) and *i*-PrCl (11.6 ml,

0.128 mol) and the reaction mixture was then refluxed for 14 h. The mixture was cooled to room temperature and the solvent was removed by distillation under atmospheric pressure. To the residue was added dry ether (150 ml), and $MgCl_2$ was filtered off under argon. The filtrate was distilled to give *i*-Pr(Me)$SiCl_2$ (5.17 g, bp 88—90 °C) as a colorless liquid. Next experiment to introduce the *i*-Pr group to this sample was carried out under the conditions described in the preparation DEIPS-Cl. DIPMS-Cl (2.99 g, 11%) was given as a colorless liquid. Bp 141—143 °C.

(2*R*,3*R*,4*S*,5*S*,6*R*)-4-Methyl-6-(1,3-dithian-2-yl)-2,3,5-heptanetriol (33). A solution of **32** (416 mg, 1.30 mmol) in aqueous 50% acetic acid (8.31 ml) was stirred at 50 °C for 1 h and then concentrated to give a syrup which was chromatographed on silica gel (20 g) with 10:1 chloroform–methanol to afford **33** (327 mg, 90%) as colorless needles. R_f=0.43 (10:1 chloroform–methanol); mp 134.9—135.2 °C (acetone–hexane); $[\alpha]_D^{21}$ 0°, $[\alpha]_{405}$ +1.9°, $[\alpha]_{315}$ +3.7°, (*c* 0.67); ^{1}H NMR (90 MHz, CD_3OD) δ=0.83 and 1.03 (each 3H, each d, Me×2, each *J*=7.2 Hz), 1.05—1.2 (3H, m, Me), 1.45—2.35 (4H, m, H-4,6, $SCH_2C\underline{H}_2$), 2.65—3.0 (4H, m, $SC\underline{H}_2CH_2C\underline{H}_2S$), 3.55—4.1 (3H, m, H-2,3,5), and 4.17 (1H, d, H-2′, *J*=8.4 Hz).

Found: C, 51.60; H, 8.41; S, 22.99%. Calcd for $C_{12}H_{24}O_3S_2$: C, 51.39; H, 8.63; S, 22.87%.

Methyl (6*S*,7*S*,8*R*)-(2*E*,4*E*)-7-Hydroxy-6-methyl-8-(1,3-dithian-2-yl)-2,4-nonadienoate (35) and (4*Z*)-Isomer (36). To a suspension of **33** (263 mg, 9.38 mmol) and potassium acetate (463 mg, 4.69 mmol) in dry CH_3CN (21.8 ml) was added lead tetraacetate (462 mg, 0.938 mmol) at −25 °C and then stirred for 3 min. The resulting mixture was chromatographed on Florisil (10 g) with ether to afford a crude sample of **34** (208 mg) which was suitable for the next synthesis. A mixture of the crude sample of **34** (319 mg) and [(2*E*)-3-methoxycarbonyl-2-propenylidene]triphenylphosphorane (980 mg, 2.72 mmol) in dry toluene (15.9 ml) was stirred at 80 °C for 0.5 h. The reaction mixture was concentrated and the residue (1.42 g) was chromatographed on silica gel (210 g) with 9:1 dichloromethane–ethyl acetate to afford **35** (232 mg, 51% from **33**) and **36** (93.4 mg, 21% from **33**) as colorless syrups.

35: R_f=0.51 (8:1 dichloromethane–ethyl acetate); $[\alpha]_D^{22}$ −22° (*c* 1.06); IR ($CHCl_3$) 1705 cm^{-1}; UV (EtOH) λ_{max} nm (log ε) 261 (4.39); ^{1}H NMR (90 MHz) δ=1.03 and 1.13 (each 3H, each d, Me×2, each *J*=7.2 Hz), 1.85—2.25 (4H, m, H-8, $SCH_2C\underline{H}_2$, OH), 2.30—2.65 (1H, m, H-6), 2.7—3.05 (4H, m, $SC\underline{H}_2CH_2C\underline{H}_2S$), 3.65—3.95 (1H, m, H-7), 3.77 (3H, s, COOMe), 4.17 (1H, d, H-2′, *J*=7.5 Hz), 5.83 (1H, d, H-2, *J*=15.3 Hz), 6.1—6.35 (2H, m, H-4,5), and 7.15—7.50 (1H, m, H-3).

Found: C, 56.71; H, 7.55; S, 20.08%. Calcd for $C_{15}H_{24}O_3S_2$: C, 56.93; H, 7.64; S, 20.26%.

36: R_f=0.56 (8:1 dichloromethane–ethyl acetate); ^{1}H NMR (90 MHz) δ=1.02 and 1.17 (each 3H, each d, Me×2, each *J*=7.2 Hz), 1.7—2.65 (5H, m, H-6,8, $SCH_2C\underline{H}_2$, OH), 2.7—3.05 (4H, m, $SC\underline{H}_2CH_2C\underline{H}_2S$), 3.75 (3H, s, COOMe), 4.05—4.3 (2H, m, H-8,2′), 5.7—6.45 (2H, m, H-4,5), 5.91 (1H, d, H-2, *J*=15.3 Hz), and 7.65 (1H, dd, H-3, $J_{2,3}$=15.3 and $J_{3,4}$=12.0 Hz).

Isomerisation of 36 to 35. A solution of **36** (2.11 g, 6.67 mmol) and iodine (8.4 mg) in dry benzene (51.3 ml) was stirred at room temperature (25 °C) in daylight for about a month. The reaction mixture was then washed with a saturated aqueous sodium thiosulfate solution (50 ml) and extracted with ethyl acetate (30 ml×3). The extracts were washed with saturated aqueous NaCl (40 ml), dried, and then concentrated to a crude syrup which was chromatographed on silica gel (300 g) with 9:1 dichloromethane–ethyl acetate to afford the (*E*,*E*)-diene **35** (790 mg, 37.4%) and the starting diene **36** (570 mg, 27%).

(6*S*,7*S*,8*R*)-7-Hydroxy-6-methyl-8-(1,3-dithian-2-yl)-2,4-nonadienoic Acid (4). To a solution of the methyl ester **35** (232 mg, 0.733 mmol) in 50% THF–H_2O (8.81 ml) was added 0.2 M LiOH/50% THF–H_2O (6.41 ml, 1.28 mmol) and the mixture was kept at 24 °C for 7 h. The solution was then neutralized with CG-50 resin (H^+ type) under ice-cooling, and filtered. The filterate and methanolic washings were combined and concentrated to give a crude syrup (0.5 g) which was chromatographed on silica gel (20 g) with 10:1:0.2 chloroform–acetone–acetic acid to afford **4** (220 mg, 100%) as a white form. R_f=0.26 (10:1:0.1 chloroform–acetone–acetic acid); $[\alpha]_D^{20}$ −31° (*c* 1.04); IR ($CHCl_3$) 1640 and 1685 cm^{-1}; UV (EtOH) λ_{max} nm (log ε) 254 (4.28); ^{1}H NMR (90 MHz) δ=1.03 and 1.12 (each 3H, each d, Me×2, each *J*=7.2 Hz), 1.75—2.2 (3H, m, H-8, $SCH_2C\underline{H}_2$), 2.3—2.65 (1H, m, H-6), 2.7—3.0 (4H, m, $SC\underline{H}_2CH_2C\underline{H}_2S$), 3.87 (1H, dd, H-7, *J*=8.4, 2.8 Hz), 4.18 (1H, d, H-2′, *J*=7.5 Hz), 5.85 (1H, d, H-2, *J*=15.3 Hz), 6.1—6.4 (2H, m, H-4,5), 6.4—6.95 (2H, br, OH, COOH), and 7.15—7.55 (1H, m, H-3).

Found: C, 55.86; H, 7.23; S, 20.96%. Calcd for $C_{14}H_{22}O_3S_2$: C, 55.60; H, 7.33; S, 21.20%.

(7*S*,8*S*,15*S*,16*S*:3*E*,5*E*,11*E*,13*E*)-7,15-Dimethyl-8,16-bis-[(1*R*)-1-(1,3-dithian-2-yl)ethyl]-1,9-dioxa-3,5,11,13-cyclohexadecatetraene-2,10-dione (37). Method A: A solution of **4** (208 mg, 0.688 mmol) in THF (2.98 ml) was treated with triethylamine (115 μl, 0.826 mmol) and 2,4,6-trichlorobenzoyl chloride (185 mg, 0.757 mmol) and the mixture was then stirred at room temperature for 2 h. The triethylamine hydrochloride was then filtered off and the filtrate diluted with dry toluene (344 ml). This solution was then added at 35 °C over a period of 2 h to a solution of 4-(dimethylamino)pyridine (505 mg, 4.13 mmol) in dry toluene (68.8 ml). After the addition had completed, the mixture was stirred at 35 °C for an additional 2.5 h, and then diluted with ether (300 ml). The mixture was washed with saturated aqueous citric acid (300 ml), saturated aqueous $NaHCO_3$ (300 ml), and finally saturated aqueous NaCl (300 ml). The organic layer was dried and concentrated to a syrup (290 mg) which was chromatographed on silica gel (43 g) with 5:1 dichloromethane–ethyl acetate to afford a pure sample of **37** (57.9 mg, 31%) as colorless crystals. R_f=0.44 (2:1 hexane–acetone); mp 262.0—263.5 °C (dichloromethane–hexane); $[\alpha]_D^{30}$ +75° (*c* 1.16); IR (KBr) 1640 and 1710 cm^{-1}; ^{1}H NMR (250 MHz) δ=1.07 and 1.19 (each 3H×2, each d, 7-Me, 15-Me, 1′-Me×2, each *J*=7.2 Hz), 1.86 (1H×2, ddq, H-1′×2, $J_{1',Me}=J_{1',2'}$=7.2 and $J_{1',8\text{or}16}$=10.6 Hz), 2.0—2.3 (2H×2, m, $SCH_2C\underline{H}_2$×2), 2.44 (1H×2, ddq, H-7,15, *J*=7.2, 1.1, 11.4 Hz), 2.75—2.95 (4H×2, m, $SC\underline{H}_2CH_2C\underline{H}_2SC\underline{H}_2S$×2), 4.02 (1H×2, d, H-2″×2, *J*=7.2 Hz), 5.18 (1H×2, dd, H-8,16, *J*=10.6, 1.1 Hz), 5.60 (1H×2, d, H-3,11, *J*=15.2 Hz), 5.62 (1H×2, dd, H-6,14, *J*=9.5, 15.0 Hz), 6.00 (1H×2, dd, H-5,13, *J*=15.0, 11.4 Hz), and 6.98 (1H×2, dd, H-4,12, *J*=11.4, 15.2 Hz); MS *m/z* 568 (M^+).

Found: C, 58.83; H, 6.82; S, 22.80%. Calcd for $C_{28}H_{40}O_4S_4$:

C, 59.12; H, 7.09; S, 22.55%.

Method B: To a solution of **4** (48.2 mg, 0.159 mmol) in dry CH_3CN (12.7 ml) was added triethylamine (0.176 ml, 1.28 mmol) and the mixture was added to a solution of 2-chloro-1-methylpyridinium iodide (163 mg, 0.638 mmol) in dry CH_3CN (16 ml) for 15 min. After being stirred at 25 °C, the reaction mixture was concentrated to give a syrup which was subsequently chromatographed on silica gel (20 g) with 2:1 hexane-acetone to afford **38** (40.0 mg, 85.5%) as a colorless syrup. R_f=0.30 (2:1 hexane-acetone); IR (CH_3Cl_3) 1710 and 1765 cm^{-1}; To a solution of **38** (9.60 mg, 0.0164 mmol) in dry CH_3CN (0.192 ml) was added 4-(dimethylamino)pyridine (5.20 mg, 0.00425 mmol) and the reaction mixture was stirred at room temperature (26 °C) for 30 min. Then the mixture was poured into cold water (1 ml) and extracted with ethyl acetate (0.5 ml×3) and the combined extracts were washed with saturated aqueous NaCl (1 ml), dried, and concentrated. The residue was chromatographed on silica gel (1 g) with 3:1 hexane-acetone to afford **37** (0.5 mg, 11% from **38**).

(7*S*,9*S*,15*S*,16*S*:3*E*,5*E*,11*E*,13*E*)-8,16-Bis[(1*R*)-1-formylethyl]-7,15-dimethyl-1,9-dioxa-3,5,11,13-cyclohexadecatetraene-2,10-dione (3). To a mixture of **37** (30.6 mg, 0.159 mmol) and mercury(II) oxide (51.7 mg, 2.39 mmol) in 4:7 CH_2Cl_2–80% aqueous acetone was added mercury(II) chloride (64.9 mg, 2.39 mmol) at room temperature. The mixture was ultrasonificated in the sonicator (65 W, 48 kHz) at 30—50 °C for 8 h, cooled, and filtered through a Celite. The filter cake was washed with acetone, and the filtrate and the washing were combined. After the subsequent removal of the acetone by concentration, to the aqueous residue was added aqueous 10% KI until orange color disappeared and extracted with chloroform (30 ml×3). The extracts were washed with saturated aqueous NaCl (20 ml), dried, and concentrated to give crude crystals which was chromatographed on silica gel (10 g) with 5:1 chloroform-ethyl acetate to afford the pure sample of **3** (43.1 mg, 70%) as colorless crystals. R_f=0.19 (10:1 chloroform-ethyl acetate); mp 152—156 °C (dichloromethane-hexane); $[\alpha]_D^{25}$ +46.8° (*c* 0.35, MeOH after 45 min); IR (KBr) 1710 cm^{-1}; UV (EtOH) λ_{max} nm (log ε) 253 (4.74); ^{1}H NMR (90 MHz) δ=1.10 and 1.19 (each 3H×2, each d, 7-Me, 15-Me, 2′-Me×2, each *J*=7.2 Hz), 2.3—2.9 (2H×2, m, H-7,15,2′×2), 5.39 (1H×2, dd, H-8, 16, *J*=10.8, 2.8 Hz), 5.56 (1H×2, d, H-3,11, *J*=15.6 Hz), 6.07 (1H×2, dd, H-5,13, *J*=15.0, 10.8 Hz), 6.98 (1H×2, dd, H-4,12, *J*=15.6, 10.8 Hz), and 9.69 (1H×2, s, CHO×2).

Found: C, 67.06; H, 7.30%. Calcd for $C_{22}H_{28}O_6 \cdot 1/4H_2O$: C, 67.24; H, 7.31%.

After drying the crystalline **3** over CaH_2 at 65 °C for 14 h gave an anhydrous sample of **3** as an orange-red colored solid whose ^{1}H NMR spectra was superimposesable to that of the crystalline sample of **3** except for the signals ascribed to water.

Found: C, 67.98; H, 7.35%. Calcd for $C_{22}H_{28}O_6$: C, 68.02; H, 7.26%.

(7*S*,8*S*,15*S*,16*S*:3*E*,5*E*,11*E*,13*E*)-8,16-Bis[(1*S*,2*R*,3*S*,6*R*,7*R*,8*R*)-6-*O*-[2-deoxy-3,4-bis-*O*-(isopropyldimethylsilyl)-α-L-fucosyl]-7-ethyl-8-*O*-(diethylisopropylsilyl)-2,6,8-trihydroxy-1,3-dimethyl-4-oxononyl]-7,15-dimethyl-1,9-dioxa-3,5,11,13-cyclohexadecatetraene-2,10-dione (43), Isomers 44 and 45. (A) With *n*-Bu_2BOTf: To a solution of *n*-Bu_2OTf (24.1 μl, 0.0958 mmol) and *N*,*N*-diisopropylethylamine (16.7 μl, 0.0958 mmol) in dry ether (0.192 mmol) was added dropwise a solution of **25f** (61.4 mg, 0.0958 mmol) in dry ether (0.012 ml) at −78 °C under argon with stirring. After being stirred for 30 min, the mixture was added dropwise to a solution of **3** (9.30 mg, 0.0239 mmol) in dry THF (0.186 ml) at −30 °C with stirring and then stirred at −10 °C for 2 h. To the reaction mixture was added pH 7 phosphate buffer[47] (0.5 ml) at −10 °C, and the mixture was stirred at 25 °C for 3 min, and then extracted with ether (0.5 ml×3). The extracts were washed with saturated aqueous NaCl (1.5 ml), dried, and concentrated to give a syrup (80.0 mg) which was purified by flash chlomatography on silica gel (20 g) with 6:1 benzene-ethyl acetate and then 3.5:1 benzene-ethyl acetate to afford **43** (5.1 mg, 12.7%), **44** (9.8 mg, 24.3%), and **45** (10.6 mg, 26.3%) as a colorless glassy solid respectively and recovered **25f** (22.1 mg, 36.0%). **43**: R_f=0.10 (6:1 benzene-ethyl acetate); $[\alpha]_D^{20}$ −9.3° (*c* 0.41); ^{1}H NMR (400 MHz) δ=0.03 (6H, s, SiMe×2), 0.035 (6H, s, SiMe×2), 0.04 (6H, s, SiMe×2), 0.06 (6H, s, SiMe×2), 0.55—0.70 (8H, m, $Si(CH_2CH_3)_2$×2), 0.80—1.30 (62H, m, $Si(CH_2CH_3)_2$×2, *i*-PrSi×6,7′-CH_2CH_3×2, H-7′×2), 0.87 (6H, d, Me×2, *J*=7.2 Hz), 1.04 (6H, d, Me×2, *J*=7.2 Hz), 1.11 (6H, d, Me×2, *J*=6.8 Hz), 1.12 (6H, d, Me×2, *J*=6.8 Hz), 1.26 (6H, d, Me×2, *J*=6.4 Hz), 1.35—1.45 (4H, m, 7′-CH_2CH_3), 1.45—1.55 (2H, m, H-2″$_{eq}$×2), 1.85—1.95 (2H, m, H-1′×2), 1.97 (2H, ddd, H-2′$_{ax}$×2, *J*=12.8, 12.0, 3.8 Hz), 2.45—2.65 (6H, m, H-5′$_{AorB}$×2, H-3′×2, H-7,15), 2.99 (2H, dd, H-5′$_{AorB}$×2, *J*=16.4, 8.8 Hz), 3.36 (2H, d, OH×2, *J*=3.2 Hz), 3.50—3.55 (2H, br, H-4″×2), 3.72 (2H, ddd, H-2′×2, *J*=9.2, 3.2, 3.2 Hz), 3.38 (2H, q, H-5″×2, *J*=6.2 Hz), 3.90 (2H, ddd, H-3″×2, *J*=12.0, 4.0, 2.0 Hz), 4.00 (2H, dq, H-8′, *J*=6.8, 3.6 Hz), 4.15—4.25 (2H, m, H-6′×2), 4.91 (2H, dd, H-1″×2, *J*=3.6, 0.8 Hz), 5.04 (2H, dd, H-8,16, *J*=10.4, 1.2 Hz), 5.62 (2H, d, H-3,11, *J*=15.6 Hz), 5.65 (2H, dd, H-6,14, *J*=9.5, 15.0 Hz), 6.07 (2H, dd, H-5,13, *J*=15.0, 11.4 Hz), 6.97 (2H, dd, H-4,12, *J*=11.4, 15.6 Hz). **44:** R_f=0.31 (6:1 benzene-ethyl acetate); $[\alpha]_D^{20}$ −13.3° (*c* 1.05); ^{1}H NMR (400 MHz) δ=0.021 (3H, s, SiMe), 0.027 (3H, s, SiMe), 0.028 (3H, s, SiMe), 0.035 (6H, s, SiMe×2), 0.04 (6H, s, SiMe×2), 0.06 (3H, s, SiMe), 0.55—0.70 (8H, m, $Si(CH_2CH_3)_2$×2), 0.80—1.30 (71H, m, $Si(CH_2CH_3)_2$, *i*-PrSi×6, Me×3, 7′-CH_2CH_3×2, H-7′×2), 0.86 (3H, d, Me, *J*=7.2 Hz), 1.03 (3H, d, Me, *J*=7.2 Hz), 1.05—1.15 (9H, m, Me×3), 1.19 (3H, d, Me, *J*=6.4 Hz), 1.26 (3H, d, Me, *J*=6.4 Hz), 1.35—1.55 (6H, m, 7′-CH_2CH_3×2, H-2″$_{eq}$×2), 1.85—2.05 (4H, m, H-1′×2, H-2″$_{ax}$×2), 2.45—2.65 (4H, m, H-5′$_{(16)AorB}$, H-7, 15, H-3′$_{(16)}$), 2.66 (1H, dd, H-5′$_{(8)AorB}$, *J*=16.4, 3.6 Hz), 2.82 (1H, dd, H-5′$_{(8)AorB}$, *J*=16.4, 8.8 Hz), 2.96 (1H, d, OH$_{(8)}$, *J*=3.2 Hz), 3.00 (1H, dd, H-5′$_{(16)AorB}$, *J*=16.4, 8.8 Hz), 3.05 (1H, dq, H-3′$_{(8)}$, *J*=7.2, 1.6 Hz), 3.32 (1H, d, OH$_{(16)}$, *J*=3.2 Hz), 3.45—3.50 (1H, br, H-4″$_{(8)}$), 3.50—3.55 (1H, br, H-4″$_{(16)}$), 3.65—3.75 (2H, m, H-2′$_{(8)\text{ and }(16)}$), 3.75—3.85 (2H, m, H-5″$_{(8)\text{ and }(16)}$), 3.85—3.95 (2H, m, H-3″$_{(8)\text{ and }(16)}$), 3.95—4.05 (2H, m, H-8′$_{(8)\text{ and }(16)}$), 4.15—4.25 (2H, m, H-6′$_{(8)\text{ and }(16)}$), 4.69 (1H, dd, H-8, *J*=10.4, 1.2 Hz), 4.82 (1H, dd, H-1″$_{(8)}$, *J*=3.0, 0.8 Hz), 4.92 (1H, dd, H-1″$_{(16)}$, *J*=3.0, 0.8 Hz), 5.09 (1H, dd, H-16, *J*=10.4, 1.2 Hz), 5.59 (1H, d, H-3, *J*=16.0 Hz), 5.60 (1H, dd, H-6, *J*=15.2, 9.5 Hz), 5.62 (1H, d, H-11, *J*=15.6 Hz), 5.64 (1H, dd, H-14, *J*=15.0, 9.5 Hz), 6.044 (1H, dd, H-5, *J*=15.2, 12.0 Hz), 6.047 (1H, dd, H-13, *J*=15.0, 11.6 Hz), 6.91 (1H, dd, H-4, 16.0, 12.0 Hz), 6.95 (1H, dd, H-12, *J*=15.0, 11.6 Hz).

Found: C, 62.91; H, 9.70%. Calcd for $C_{88}H_{168}O_{18}Si_6$: C,

62.81; H, 10.06%.

45: R_f=0.46 (6:1 benzene-ethyl acetate); $[\alpha]_D^{20}$ −22.4° (*c* 0.98); ^{1}H NMR (400 MHz) δ=0.01 (6H, s, SiMe×2), 0.02 (6H, s, SiMe×2), 0.035 (6H, s, SiMe×2), 0.04 (6H, s, SiMe×2), 0.55—0.70 (8H, m, Si($C\underline{H}_2CH_3$)$_2$×2), 0.80—1.30 (74H, m, Si($CH_2C\underline{H}_3$)$_2$×2, *i*-PrSi×6, Me×4, 7′-$CH_2C\underline{H}_3$×2, H-7′×2), 1.11 (12H, d, Me×4, *J*=6.8 Hz), 1.19 (6H, d, Me×2, *J*=6.4 Hz), 1.35—1.55 (6H, m, 7′-$C\underline{H}_2CH_3$×2, H-2″$_{eq}$×2), 1.90—2.00 (2H, m, H-1′), 1.92 (2H, ddd, H-2″$_{ax}$×2, *J*=12.8, 12.0, 3.8 Hz), 2.45—2.60 (2H, m, H-7,15), 2.66 (2H, dd, H-5′$_{AorB}$×2), 2.82 (2H, dd, H-5′$_{AorB}$×2), 2.94 (2H, d, OH×2, *J*=3.2 Hz), 3.05 (2H, dq, H-3′×2, *J*=7.2, 1.6 Hz), 3.45—3.50 (2H, br, H-4″×2), 3.73 (2H, ddd, H-2′×2, *J*=9.2, 3.2, 3.2 Hz), 3.79 (2H, q, H-5″×2, *J*=6.8 Hz), 3.88 (2H, ddd, H-3″×2, *J*=12.0, 4.0, 2.0 Hz), 3.99 (2H, dq, H-8′×2, *J*=6.8, 3.6 Hz), 4.20—4.25 (2H, m, H-6′×2), 4.72 (2H, dd, H-8,16, *J*=10.4, 1.2 Hz), 4.83 (2H, dd, H-1″×2, *J*=3.0, 0.8 Hz), 5.59 (2H, d, H-3,11, *J*=16.0 Hz), 5.60 (2H, dd, H-6,14, *J*=15.2, 10.0 Hz), 6.04 (2H, dd, H-5,13, *J*=15.2, 12.0 Hz), 6.91 (2H, dd, H-4,12, *J*=16.0, 12.0 Hz).

Found: C, 63.10; H, 9.99%. Calcd for $C_{88}H_{168}O_{18}Si_6$: C, 62.81; H, 10.06%.

In the case of the aldol coupling of **25f** and **3** in the presence of $ZnCl_2$, 4 molar equivalents of $ZnCl_2$ was first added to the THF solution of **3** and then to this mixture was added the ethereal boron enolate mixture prepared from **25f** with *n*-Bu_2BOTf by the aforesaid procedure.

(B) With Sn(OTf)$_2$: To a suspension of $Sn(OTf)_2$ (25.8 mg, 0.0618 mmol) and 1-ethylpiperidine (0.0093 ml, 0.060 mmol) in dry CH_2Cl_2 (0.124 ml) was added dropwise **25f** (39.6 mg, 0.0618 mmol) in CH_2Cl_2 (0.124 ml) at −78 °C under argon with stirring. After the mixture was stirred for 30 min, the solution was added dropwise to a solution of **3** (6.0 mg, 0.0155 mmol) in dry CH_2Cl_2 (0.060 ml) at −78 °C and then stirred at −78 °C for 30 min and at −78 °C→−10 °C for 2.5 h. To the reaction mixture was added pH 7 posphate buffer (0.5 ml) at −10 °C and then stirred at room temperature for 3 min, and extracted with CH_2Cl_2 (0.5 ml×3). The extracts were washed with saturated aqueous NaCl (1 ml), dried, and concentrated to give a crude syrup which was purified by flash chromatography on silica gel (10 g) with 6:1 benzene-ethyl acetate and 3.5:1 benzene-ethyl acetate to afford **43** (1.7 mg, 6.5%), **44** (5.4 mg, 20.8%), and **45** (7.2 mg, 27.7%) and recoverd **25f** (17.6 mg, 44.4%).

(C) With LiN(TMS)$_2$: To a solution of **25f** (24.6 mg, 0.0383 mmol) in dry THF (0.0766 ml) was added dropwise 1 M LiN(TMS)$_2$-THF (0.0383 ml, 0.0383 mmol) at −78 °C under argon with stirring. After the mixture was stirred for 30 min, the solution was added dropwise to a solution of **3** (6.2 mg, 0.0160 mmol) in dry THF (0.124 ml) at −78 °C and then stirred for 2 h at the same temperature. To the reaction mixture was added saturated aqueous NH_4Cl (0.4 ml), warmed to room temperature and extracted with ether (0.5 ml×3). The extracts were washed with saturated aqueous NaCl (1 ml), dried, and concentrated to give a crude syrup (30 mg) which was chromatographed on silica gel (10 g) with 4:1 benzene-ethyl acetate to afford fraction A (**25f**, **44**, **45**, 12.4 mg), fraction B (**43**, **3**, 2.0 mg), and **3** (1.7 mg, 6.3%). Further, fraction A was purified by flash chromatography on silica gel (2.5 g) with benzene-ethyl acetate to afford **25f** (8.3 mg, 33.7%), **45** (2.4 mg, 8.9%), and **44** (1.7 mg, 6.3%). Fraction B was purified by flash chromatography on silica gel (1 g) with 3:1 benzene-ethyl acetate to afford **43** (1.4 mg, 5.2%).

Elaiophylin (1). A solution of **43** (9.5 mg, 0.00565 mmol) in 3:1:3 acetic acid-aqueous 1% HF·KF-THF (0.380 ml) was stirred at 30 °C for 18 h. To the reaction mixture was added water (0.5 ml) and chloroform (0.5 ml) and then extracted with chloroform (0.5 ml×3). The extracts were washed with saturated aqueous NaCl (1 ml), dried, and concentrated to crude crystals (10.0 mg) which were purified by flash chlomatography on silica gel (2.5 g) with 6:1 chloroform-methanol to afford **1** (1.3 mg, 22.4%) as colorless crystals. R_f=0.31 (6:1 chloroform-methanol); $[\alpha]_D^{20}$ −53° (*c* 0.26, MeOH); mp 179—182 °C (AcOEt); mixture mp 179—182 °C; The ^{1}H NMR spectra (400 MHz, 5:1 $CDCl_3$-CD_3OD) was identical with that of the authentic sample of azalomycin B.

We are grateful to Prof. Sumio Umezawa, Institute of Bioorganic Chemistry, and the late Prof. Hamao Umesawa, Institute of Microbial Chemistry for their generous support of our program. The present work was partially supported by a Grant-in-Aid for Scientific Research No. 60470091 from the Ministry of Education, Science and Culture, the Japan Antibiotics Research Association Research Grant, and Sankyo Foundation of Life Science. We are indebted to Dr. Hiroshi Naganawa, Institute of Microbial Chimistry for 400 MHz ^{1}H NMR spectral analyses. We also thank Mr. Saburo Nakada and Mr. Hisao Arita of Keio University for elemental analyses and Messrs. Ken Ishiyama and Mutsumi Horikoshi for their technical assistance.

References

1) F. M. Arcamone, C. Bertazzoli, M. Ghione, and T. Scotti, *Giorn. Microbiol.*, **7**, 207 (1959).

2) M. Arai, *J. Antibiot. Ser. A*, **13**, 46, 51 (1960).

3) S. Takahashi, M. Arai, and E. Ohki, *Chem. Pharm. Bull.*, **15**, 1651 (1967).

4) S. Takahashi, M. Kurabayashi, and E. Oki, *Chem. Pharm. Bull.*, **15**, 1657 (1967).

5) S. Takahashi and E. Ohki, *Chem. Pharm. Bull.*, **15**, 1657 (1967).

6) H. Kaiser and W. Keller-Schierlein, *Helv. Chim. Acta*, **64**, 407 (1981).

7) K. Neupert-Laves and M. Dobler, *Helv. Chim. Acta*, **65**, 262 (1982).

8) S. V. Leg, D. Neuhaus, and D. J. Williams, *Tetrahedron Lett.*, **23**, 1207 (1982).

9) M. A. Sutter and D. Seebach, *Liebigs Ann. Chem.*, **1983**, 939.

10) H. Kinashi, K. Someno, and K. Sakaguchi, *J. Antibiot.*, **37**, 1333 (1984).

11) D. Seebach, H.-F. Chow, R. F. W. Jackson, M. A. Sutter, S. Thaisrivongs, and J. Zimmenmann, *J. Am. Chem. Soc.*, **107**, 5292 (1985).

12) D. Seebach, H.-F. Chow, R. F. W. Jackson, M. A. Sutter, S. Thaisrivongs, and J. Zimmermann, *Liebigs Ann. Chem.*, **1986**, 1281.

13) a) T. Wakamatsu, H. Nakamura, E. Nara, and Y. Ban,

Tetrahedron Lett., **27**, 3895 (1986); b) T. Wakamatsu, S. Yamada, H. Nakamura, and Y. Ban, *Heterocycles*, **25**, 42 (1987).

14) K. Toshima, K. Tatsuta, and M. Kinoshita, *Tetrahedron Lett.*, **27**, 4741 (1986).

15) a) S. Masamune, W. Choy, J. S. Petersen, and L. R. Sita, *Angew. Chem., Int. Ed. Engl.*, **24**, 1 (1985); b) R. W. Hoffmann and U. Weidmann, *Chem. Ber.*, **118**, 3966 (1985).

16) T. D. Inch and G. L. Lewis, *Carbohydr. Res.*, **15**, 1 (1970).

17) a) G. J. Robertson and C. F. Griffith, *J. Chem. Soc.*, **1935**, 1193; b) L. F. Wiggins, *Methods Carbohyd. Chem.*, **2**, 188 (1963).

18) S. Achab and B. C. Das, *Synth. Commun.*, **12**, 931 (1982) and references cited therein.

19) E. J. Corey and A. Venkateswarlu, *J. Am. Chem. Soc.*, **94**, 6190 (1972).

20) E. J. Corey and H. E. Ensley, *J. Org. Chem.*, **38**, 3187 (1973).

21) We thank Dr. M. Arai (Sankyo Co., Ltd.) for a generous gift of natural azalomycin B and its spectral data.

22) R. B. Woodward et al., *J. Am. Chem. Soc.*, **103**, 3215 (1981).

23) E. J. Corey, H. Cho, C. Rucker, and D. H. Hua, *Tetrahedron Lett.*, **22**, 3455 (1981).

24) K. C. Nicolaou, S. P. Seitz, and D. P. Papahatjis, *J. Am. Chem. Soc.*, **105**, 2430 (1983).

25) R. F. Newton and D. P. Reynold, *Tetrahedron Lett.*, **41**, 3981 (1979).

26) B. Iselin and T. Reichstein, *Helv. Chem. Acta*, **27**, 1200 (1944).

27) K. Tatsuta, K. Fujimoto, M. Kinoshita, and S. Umezawa, *Carbohydr. Res.*, **54**, 85 (1977).

28) a) L. H. Sommer, "Stereochemistry, Mechanism and Silicon," McGraw Hill, New York (1965), p. 130; b) R. H. Cunico and L. Bedell, *J. Org. Chem.*, **45**, 4797 (1980).

29) K. K. Ogilvie, S. L. Beaucage, D. W. Entwistle, E. A. Thompson, M. A. Quilliam, and J. B. Westmor, *J. Carbohydrates Nucleosides Nucleotides*, **3** (4), 197 (1976).

30) E. J. Corey and R. K. Varma, *J. Am. Chem. Soc.*, **93**, 7319 (1971).

31) T. W. Hart, D. A. Metcalfe, and F. Scheinmann, *J. Chem. Soc., Chem. Commun.*, **1979**, 156.

32) K. C. Nicolaou, R. E. Dolle, D. P. Papahatjis, and J. L. Randall, *J. Am. Chem. Soc.*, **106**, 4189 (1984).

33) The absense of the molecular sieves[13a] resulted in 30% yield of **25f**.

34) M. Nakata, H. Takao, Y. Ikeyama, T. Sakai, and M. Kinoshita, *Bull. Chem. Soc. Jpn.*, **54**, 1749 (1981).

35) E. J. Corey, L. O. Weigel, A. R. Chamberlin, and B. Lipshutz, *J. Am. Chem. Soc.*, **102**, 1439 (1980).

36) E. Buchta and F. Andree, *Chem. Ber.*, **92**, 3111 (1959).

37) I. Ernest, A. J. Main, and R. Menassi, *Tetrahedron Lett.*, **23**, 167 (1982).

38) J. Inagawa, K. Hirata, H. Katsuki, and M. Yamaguchi, *Bull. Chem. Soc. Jpn.*, **52**, 1989 (1979).

39) R. F. W. Jackson, M. A. Sutter, and D. Seebach, *Liebigs Ann. Chem.*, **1985**, 2313.

40) T. Mukaiyama, M. Usui, and K. Saigo, *Chem. Lett.*, **1976**, 49.

41) S. Masamune, M. Hirama, S. Mori, S. A. Ali, and D. S. Garvery, *J. Am. Chem. Soc.*, **103**, 1568 (1981).

42) T. Inoue and T. Mukaiyama, *Bull. Chem. Soc. Jpn.*, **53**, 174 (1980).

43) D. A. Evans, J. V. Nelson, E. Vogel, and T. R. Taber, *J. Am. Chem. Soc.*, **103**, 3099 (1981).

44) S. Masamune, S. A. Ali, D. L. Snitman, and D. S. Garvey, *Angew. Chem., Int. Ed. Engl.*, **19**, 557 (1980).

45) C.-H. Hsiao, S. P. Ashuburn, and M. J. Miller, *Tetrahedron Lett.*, **26**, 4855 (1985).

46) Our result was contrasted with the Seebach's observation[12] in the deprotections of the precursor products of **2** and of its diastereomers.

47) T. Mukaiyama, R. W. Stevens, and N. Iwasawa, *Chem. Lett.*, **1982**, 353.

48) H. C. Brown and B. Singaram, *J. Org. Chem.*, **49**, 945 (1984).

49) A. I. Meyers and Y. Yamamoto, *J. Am. Chem. Soc.*, **103**, 4278 (1986).

50) a) I. Paterson, M. A. Lister, and C. K. McClure, *Tetrahedron Lett.*, **27**, 4787 (1986); b) I. Paterson and C. K. McClure, *ibid.*, **28**, 1229 (1987).

51) The aldol **51** was converted into silyl ether **53**. According to the procedure reported by Roush et al.,[53] **49** was allowed to react with diisopropyl (*R*)-tartrate modified (*Z*)-crotylboronate to give **57** (69% yield, 77% ds), whose silyl ether **58** was transformed into **53** by the reaction sequence involving ozonolysis, Grignard coupling with *i*-BuMgBr, and PCC oxidation. The sample of **53** from **51** proved to be identical with that of **53** derived from **49** by ^{1}H NMR (400 MHz). The structure of **51** was thus established as depicted. The structure of **52** was confirmed by its transformation into **59** whose structure was unambiguously determined by its 400 MHz ^{1}H NMR spectra ($J_{5,6}$=9.9 or 12.0, $J_{6,7}$=12.0 or 9.9, $J_{7,8a}$=12.8 Hz).

52) S. Masamune, Y. Mori, M. Hirama, and D. Garvey, 23th Symposium on the Chemistry of Natural Products., Nagoya, October 1980, Symposium paper, pp. 250—257.

53) W. R. Roush, A. D. Palkowitz, and M. A. Palmer, *J. Org. Chem.*, **52**, 316 (1987).

 © 1988 The Chemical Society of Japan Bull. Chem. Soc. Jpn., 61, 2383—2386 (1988)

Selective Preferential Esterification of the Dicarboxylic Acids with Longer Carbon Chain by Diazomethane in the Presence of Dicarboxylic Acids with Shorter Carbon Chain by Adsorbing and Aligning the Acids on Alumina

Haruo OGAWA,* Nobuo HIRAGA, Teiji CHIHARA,† Shousuke TERATANI, and Kazuo TAYA

Department of Chemistry, Tokyo Gakugei University, Koganei-shi, Tokyo 184
†The Institute of Physical and Chemical Research, Wako-shi, Saitama 351-01

(Received November 6, 1987)

Selective monoesterification of a dicarboxylic acid with longer carbon chains by diazomethane in a mixture of dicarboxylic acids, [dodecanedioic acid (C_{12}) plus glutaric acid (C_5), adipic acid (C_6), pimelic acid (C_7), suberic acid (C_8), or sebacic acid (C_{10})] was achieved by adsorbing and aligning the acids on alumina. The larger the difference in the number of carbon atoms, the higher the selectivity. In the case of the combination of C_{12} and C_5 the highest selectivity was observed and the preferential 89% formation of the monomethyl ester of C_{12} was obtained in contrast to the 9% formation for the monomethyl ester of C_5. Selective reactions were also observed in the case of the combination of C_{10} and C_4, and that of C_{12} and *trans*-1,4-cyclohexanedicarboxylic acid.

The use of solid adsorbents such as alumina and silica gel as a reaction medium is becoming increasingly widespread in organic synthesis.[1-6] Usually it is the reagents that are supported. Reagent-doped adsorbents can be used to achieve some very mild and consequently selective organic transformations. Recent examples are given for the use of solid adsorbents as substrate support. Solid adsorbents are used deliberately as the reaction field for substrates to achieve highly selective reaction, in which the substrate molecules orient and/or are captured with suppression of translational movement on the surface of the solid adsorbents. This gives rise to the chance for highly selective reactions, for example ozonolysis of aliphatic ester,[7] terminal (ω) chlorination of octanoic acid,[8] enone photocycloaddition,[9] selective synthesis of crown ether,[10] *O*-methylation of alcohol[11] and monomethyl esterification of dicarboxylic acid.[12]

Fatty acids in general, when adsorbed on air–water interfaces, occupy an area of 0.205 nm^2 per molecule independent of chain length or molecular weight.[13] The molecules are aligned with their axis perpendicular to the interface in a close-packed, rigid array. We could develop a method for selective synthesis of the monomethyl esters of dicarboxylic acids with the aid of this phenomenon.[12] Aliphatic dicarboxylic acids were considered to be adsorbed as a monomolecular layer on alumina and to form a stable membranelike structure with the aid of van der Waals interactions between the methylene groups as in Fig. 1a.

If two kinds of dicarboxylic acids are adsorbed as in Fig. 1b, a facile reaction of the non-adsorbed carboxyl group of the longer chain dicarboxylic acid is easily recognized, while the shorter one would be expected to be hardly reactive. We reported briefly this new type of selective reaction proceeding on an aluminum surface on which the monomethyl esterification of dodecanedioic acid (C_{12}) proceeded preferentially in the presence of other shorter chain acids.[14] This paper presents details of this reaction and application of this adsorption-reaction procedure to other dicarboxylic acids.

Results and Discussion

Effect of Surface Coverage (θ) on Monomethyl Esterification of Suberic Acid (C_8). Figure 2 shows the formation of monomethyl ester of C_8 under the various θ values of C_8 on alumina. The value of θ is estimated as follows; θ=adsorption amount of C_8/

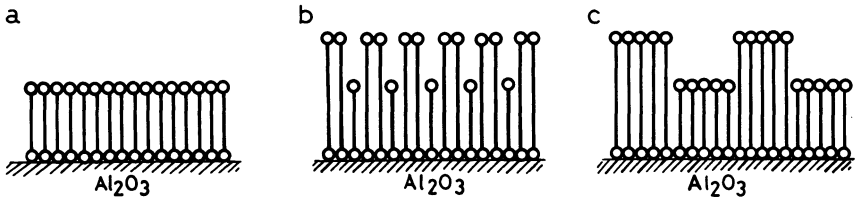

Fig. 1. Models for the aggregation of aliphatic dicarboxylic acids adsorbed on alumina, open circle represents carboxyl group and thick line represents aliphatic carbon chain: a) monomolecular layer of the acid; b) well-mixed aggregation of the mixture of two kinds of the acids; c) mosaic aggregation of the mixture of two kinds of the acids.

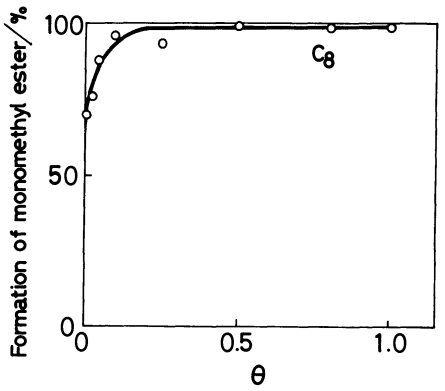

Fig. 2. Dependence of surface coverage (θ) on monomethyl ester formation for suberic acid (C_8): θ= adsorption amount of C_8/saturation amount (4.0×10^{-4}mol g-$Al_2O_3^{-1}$). The adsorption sample was suspended in cyclohexane. About 6 molar equivalents of diazomethane was added at room temperature.

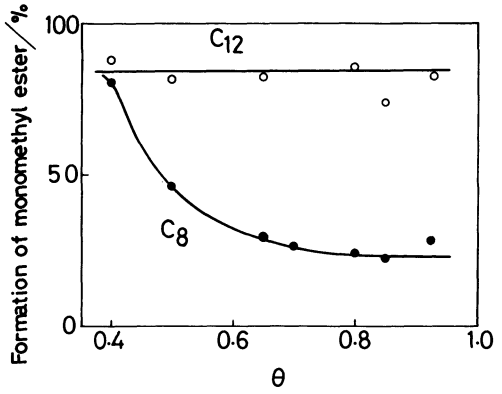

Fig. 3. Dependence of surface coverage (θ) on preferential monomethyl esterification of dodecanedioic acid (C_{12}) (○) in a mixture of C_{12} and suberic acid (C_8) (●): θ=adsorption amount (C_{12}+C_8)/saturation amount (4.0×10^{-4} mol g-$Al_2O_3^{-1}$). The adsorbed sample contained C_{12} and C_8 in a molar ratio of 2 to 1. Cyclohexane was used as a suspending agent. About 6 molar equivalents of diazomethane was added at room temperature.

saturation amount (4.0×10^{-4} mol g-$Al_2O_3^{-1}$).[12] The monomethyl ester was formed quantitatively in the range where the θ value exceeds 0.4 while the monomethyl ester was not formed quantitatively in the range where the value is less than 0.4. Quantitative formation of the monomethyl ester in the higher range of the θ value suggests that the adsorbed molecules would form the monomolecular layer in which one of the two carboxyl groups is chemisorbed on alumina with the rest of the carboxyl group in a position remote from the surface as shown in Fig. 1a.

Effect of θ on Selective Reaction. Selective monomethyl esterification of one of the dicarboxylic acids in a mixed system was attempted, and the effect of the surface coverage was examined by use of C_{12} and C_8 in a 2:1 molar ratio. As shown in Fig. 3, the difference

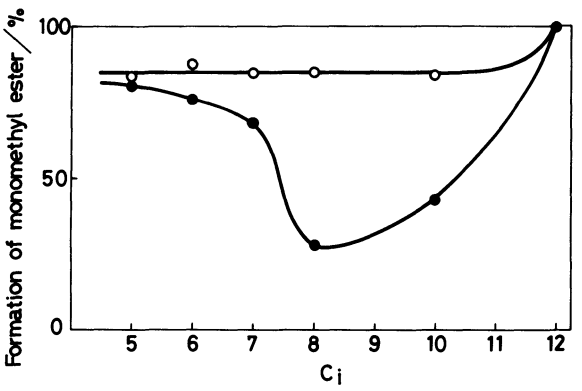

Fig. 4. Monomethyl ester formation for dodecanedioic acid (C_{12}) (○) and shorter chain acid (C_i) (●) adsorbed in the molar ratio of 2 to 1 where C_i means the aliphatic dicarboxylic acid having i carbons. The adsorbed sample consisted of a total of 0.32 mmol of the acids per gram of alumina (θ=0.8). About 6 molar equivalents of diazomethane was added at room temperature.

in reactivities of C_{12} and C_8 developed with increase in θ value. The formation of the monomethyl ester of C_8 decreased with increase in the θ value, and the formation for the monomethyl ester of C_{12} and that of C_8 became constant where the θ value exceeded about 0.8. The value of 0.8 was an adequate value for a sufficiently selective reaction, in which preferential 89% formation for the monomethyl ester of C_{12} was obtained in contrast to the 28% formation for the monomethyl ester of C_8 besides 1% formation for the dimethyl ester of C_{12}, 10% intact C_{12} and 72% intact C_8.

The same reactivity of the carboxyl groups of C_{12} and C_8 was confirmed in the following way. In a homogeneous reaction in a 1% DMF solution, the reactivities of C_{12} and C_8 were the same yielding the monomethyl esters in about 50% maximum yield at the same conversion.

Effect of Carbon Chain Length for the Selectivity at Low Ratio of C_{12}/Shorter Chain Dicarboxylic Acid (C_i). Various kinds of dicarboxylic acids were tested by combining with C_{12} for the selective monomethyl esterification of C_{12}. Figure 4 shows that the combination of C_{12} and C_8 was most effective for selective monomethyl esterification, 89% formation for the monomethyl ester of C_{12} and 28% formation for that of C_8, when the adsorption sample containing C_{12} and C_i in 2/1 molar ratio was used. From the alternative model as shown in Fig. 1b, the shorter chain dicarboxylic acids would be expected to be hardly reactive. But actually in the case of glutaric acid (C_5), adipic acid (C_6), and pimelic acid (C_7), the shorter the carbon chain of the dicarboxylic acids, the lower the selectivity became. Nonselective reaction occurred in the case of the combination of C_{12} and C_5.

Nonselective reaction was also observed even in a case of the combination of C_{12} and C_8 when the same

quantity of C_{12} and C_8 was used, and equal amounts of their monomethly esters were obtained quantitatively. The determining factor for the selective reaction appears to be the state of aggregation of the components acids. Selective reaction occurs when the two kinds of acids are adsorbed as in Fig. 1b. Based on the measurement of the surface pressures of mixed monolayers of pentadecanoic acid with acetates of its near neighbors in chain length, Matuo et al. found the interaction between the two components in a mixed monolayer decreased with an increase in the difference in chain length between the two components.[15] The formation of the aggregate as shown in Fig. 1b seems to be acceptable in the case of the combination of C_{12} and C_{10}, but in the case of the combination of the C_{12} and the much shorter carbon chain acids the formation of the aggregate seems to be difficult. Probably each acid might aggregate independently. The low selectivities in the combination of C_{12} and the much shorter carbon chain acids are considered to be due to the formation of "island"[16] aggregates of each kind of acids as shown in Fig. 1c.

Selective Monomethyl Esters Formation of C_{12} and C_i in Various Molar Ratios of Acids. As mentioned above, the selectivity decreased when the same quantity of C_{12} and C_8 was used. The effect of the molar ratio of C_{12} to C_i was examined. Figure 5 shows the selective monomethyl esterification of C_{12} with the increase in the molar ratio. The amount of the monomethyl ester of C_{12} formed was held preferentially high and constant regardless of the ratios, while that of the shorter carbon chain acids drastically changed. In the case of the combination of C_{12} and C_5 the higher ratio ($\geqslant 6$, more than six) of C_{12}/C_5 led to a decrease of monomethyl ester of C_5 formed, though the formation of the monomethyl ester could not be suppressed at a lower ratio (less than 4). In the case of the combination of C_{12}/C_8 the formation of the monomethyl ester of C_8 was sufficiently suppressed even at the lower ratio. In a region higher than 6/1 the formation for the monomethyl esters of both of the shorter carbon chain acids sufficiently decreased, and their values became constant; 28% for C_8, 9% for C_5. Two kinds of acids in both of the combinations at the higher molar ratio might be adsorbed on alumina as in Fig. 1b, in which shorter carboxylic acid molecules are surrounded with the longer on alumina surface. It is considered that in the combination of C_{12} and C_5 the state of aggregation of the acid mixture changed from the aggregate as shown in Fig. 1c to that of Fig. 1b with increase in the ratio, and the selective reaction then occurred.

Effect of Chain Length of Acid on the Selective Formation of Monomethyl Eater of C_{12} at High Ratio of C_{12}/C_i. A molar ratio of 6/1 for C_{12} to shorter chains was a large enough ratio to ensure an adequate protection of the shorter chain acids. Accordingly we tried the selective monomethyl esterification using this ratio. The results shown in Fig. 6 illustrate the selective preferential monomethyl esterification of C_{12}. Figure 6 presents a great contrast from Fig. 4 in that differences in the chain length of the shorter chain acids affected their reactivities. On the other hand, most of C_{12} reacted in every case. The larger the difference in the number of carbon atoms, the higher the selectivity obtained. The combination of C_{12} and C_5 was most effective for selective monomethyl esterification. An 89% yield of the monomethyl ester of C_{12} was obtained in contrast to a 9% yield for the monomethyl ester of C_5.

This method was applied to the other combination of acids. The formation of each monomethyl ester under the same reaction conditions described in this paragraph was as follows; C_{10}/C_6=81%/21% and C_{12}/*trans*-cyclohexanedicarboxylic acid=88%/45%.

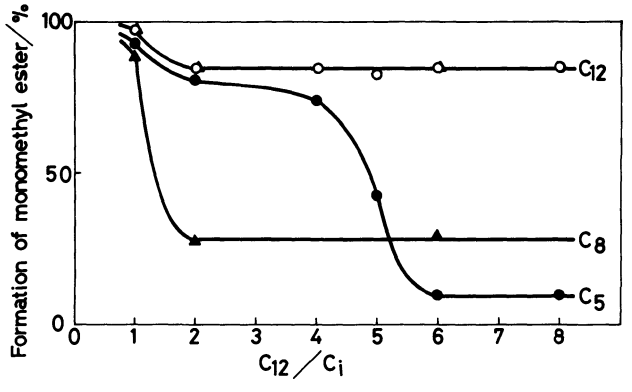

Fig. 5. Effect of the molar ratio of C_{12} to C_i on the formations of monomethyl esters: samples containing C_{12} (○) and C_5 (●); samples containing C_{12} (△) and C_8 (▲), respectively. The adsorbed sample consisted of a total of 0.32 mmol of the acids per gram of alumina (θ=0.8). About 6 molar equivalents of diazomethane was added at room temperature.

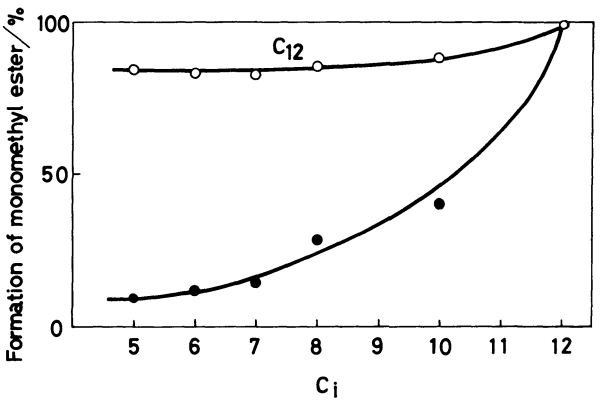

Fig. 6. Selective monomethyl ester formation for dodecanedioic acid (C_{12}) (○) and C_i (i=5—8,10) (●) adsorbed in the molar ratio 6:1 and a total of 0.32 mmol of the acids per gram of alumina (θ=0.8) where C_i is the aliphatic acid having i carbon atoms. About 6 molar equivalents of diazomethane was added at room temperature.

Interestingly, in the former case (the combination of C_{10} and C_6) 60% for the difference between the formation of each monomethyl ester was observed as in the case of C_{12}/C_8. These two values for the two systems are similar, and the difference in carbon number (the number 4) between two components acids is the same in both systems. This agreement demonstrates the adequate protection of shorter chain acids in which the differences in chain length of the shorter chain acids affects the reactivity of the shorter chain. No selective monomethyl esterification was observed in the case of the combination of C_{12}/terephthalic acid and C_{12}/isophthalic acid.

Experimental

Materials. Diazomethane was prepared from *N*-methyl-*N*-nitroso-*p*-toluenesulfonamide[17] without ether and was carried in a stream of nitrogen through a dry tube containing potassium hydroxide pellets and then into the reaction vessel. Alumina {the reference catalyst of the Catalysis Society of Japan (JRC-ALO-5);γ-type, 60—200 mesh, modal pore diameter 5.5 nm, Na_2O content 0.02%, adsorption capacity of 4.0×10^{-4} mol g^{-1} [12] of aliphatic dicarboxylic acid} was dried at 110 °C for a day and stored in a desiccator. Other materials were commercially available and used without further purification.

Preparation of Adsorption Samples. One gram of alumina powder was added to a 10 mL of *N,N*-dimethylformamide (**DMF**) solution containing 0.32 mmol of total amounts of two different carboxylic acids, dodecanedioic acid (C_{12}) plus glutaric acid (C_5), adipic acid (C_6), pimelic acid (C_7), suberic acid (C_8), sebacic acid (C_{10}), *trans*-1,4-cyclohexanedicarboxylic acid, terephthalic acid, or isophthalic acid to produce 80% surface saturation. The mixture was allowed to stand for 8 h at 30 °C with occasional shaking. The DMF was then slowly removed under reduced pressure.

Reaction Procedure. About 6 molar equivalents of diazomethane was introduced in a stream of dry nitrogen into a vigorously agitated reaction vessel containing 500 mg of the adsorbed sample and about 5 g of cyclohexane at room temperature. After all the diazomethane had been consumed or passed through the reaction vessel (about 45 min), the alumina was transferred to a glass column and eluted with **DMF**. After the eluate had been concentrated under reduced pressure, the products were analyzed by GSC with a Chromosorb 101 column, and/or HPLC with a ODS column. No reaction other than esterification was observed. Any other information about experimental section was described in the previous work.[12]

References

1) A. McKillop and D. W. Young, *Synthesis,* **1979**, 401; **1979**, 481.
2) G. H. Posner, *Angew. Chem., Int. Ed. Engl.,* **17**, 487 (1978).
3) A. Cornelis and P. Laszlo, *Synthesis,* **1985**, 909.
4) M. Hojo, *Yuki Gousei Kagaku Kyoukai Shi,* **42**, 635 (1984).
5) T. Ando, J. Ichihara, and T. Hanafusa, *Kagaku Sousetsu,* **47**, 166 (1985).
6) T. Chihara and H. Ogawa, *Shokubai,* **28**, 519 (1986).
7) A. L. J. Beckwith, C. L. Bodkin, and T. Duong, *Aust. J. Chem.,* **30**, 2177 (1977); A. L. J. Beckwith and T. Duong, *J. Chem. Soc., Chem. Commun.,* **1978**, 413; **1979**, 690.
690.
8) N. C. Deno, R. Fishbein, and C. Pierson, *J. Am. Chem. Soc.,* **92**, 1451 (1970).
9) R. Farwaha, P. de Mayo, and Y. C. Toong, *J. Chem. Soc., Chem. Commun.,* **1983**, 739.
10) J. Yamawaki and T. Ando, *Chem. Lett.,* **1980**, 533.
11) H. Ogawa, T. Hagiwara, T. Chihara, S. Teratani, and K. Taya, *Bull. Chem. Soc. Jpn.,* **60**, 627 (1987).
12) H. Ogawa, T. Chihara, and K. Taya, *J. Am. Chem. Soc.,* **107**, 1365 (1985).
13) N. K. Adam, *Proc. R. Soc. London, Ser. A,* **101**, 452 (1922).
14) H. Ogawa, T. Chihara, S. Teratani, and K. Taya, *J. Chem. Soc., Chem. Commun.,* **1986**, 1337.
15) H. Matuo, K. Motomura, and R. Matuura, *Bull. Chem. Soc. Jpn.,* **54**, 2205 (1981).
16) J. T. Davies and E. K. Rideal, "Interfacial Phenomena," Academic Press, New York and London (1961), Chap. 5, p. 234.
17) Th. J. de Boer and H. J. Backer, *Org. Synth.* Coll. Vol. IV, 250 (1963).

 © 1988 The Chemical Society of Japan Bull. Chem. Soc. Jpn., 61, 2387—2391 (1988)

Reaction of 1,1,2,2-Tetrachloro-2,2aα,4α,8bα-tetrahydrocyclobuta[c]quinolin-3(1*H*)-one with Nucleophiles; Reaction, Product Structure, and Mechanism[1)]

Shinji NONOYAMA, Noriyuki YONEZAWA,† Kazuhiko SAIGO, Masaki HASEGAWA,* and Tsuneo HIRANO*

Department of Synthetic Chemistry, Faculty of Engineering, University of Tokyo, Hongo, Bunkyo-ku, Tokyo 113

(Received November 11, 1987)

2a-Substituted dichlorodihydrocyclobuta[c]quinolin-3(4*H*)-one (**3**) and trichlorovinyl-2-quinolone (**4**) were obtained from the cross photocycloadduct of 2-quinolone and tetrachloroethylene. The position of the substituent on **3** was determined from the NOE volumes in the NOESY spectrum in comparison with the AM1 geometries. The reaction of the photoadduct (**1**) with a base or nucleophile, yielding **3** and/or **4**, was interpreted to proceed via a cyclobutene intermediate formation followed by an S_N2' displacement or [2+2] cycloreversion.

The reactivity of a heterocyclic ring, such as a coumarin ring, shows enhanced reactivity when a cyclobutane ring is fused to that ring by photochemical cyclobutanation. We have reported high reactivities of coumarin dimers and their lactone-opened derivatives.[2,3)] In previous papers,[4)] we showed unique reaction behaviors of the photocycloadduct of coumarin with tetrachloroethylene, such as (a) ring contraction from a [4,6,6]- to a [4,5,6]-fused ring system through a lactone-opening, (b) cyclobutene formation, followed by an intramolecular S_N2' displacement, and (c) a [2+2] cycloreversion at the cyclobutene intermediate, yielding trichlorovinylcoumarin. These behaviors were ascribed to the strain in lactone ring induced by the adjacent cyclobutane ring.

As a part of a continuing study of compounds having a [4,6,6]-fused ring system, we investigated the reaction of 1,1,2,2-tetrachloro-2,2aα,4α,8bα-tetrahydrocyclobuta[c]quinolin-3(1*H*)-one (**1**), a cyclobutane-fused quinolone derivative. Contrary to our expectation, based on the reaction behavior of the cycloadduct from coumarin with tetrachloroethylene,[4)] **1** gave a new cyclobutene compound and trichlorovinyl-2-quinolone, but gave no ring-contracted product.

We report here the reaction of **1** with nucleophiles or bases, the structure of the product, and molecular orbital (MO) geometry calculations.

Experimental

Measurements. All melting points were measured on a MELTEMP micro melting point apparatus and are uncorrected. IR spectra were recorded on a JASCO IR-810 spectrophotometer. NMR spectra were observed on a JEOL GX-400 spectrometer at 400 MHz. The chemical shifts for ^1H and ^{13}C NMR spectra are given in ppm in reference to the internal tetramethylsilane (TMS) signal.

2D (COSY and NOESY) spectra were recorded with a 3.1 s recycle time, 8 transitions correlated for each t_1 value, and accumulations of 512 spectra each consisting of 2048 data points.

Theoretical Calculations. Semiempirical AM1[5)] and MNDO[6)] calculations were performed on a HITAC M-680 or M-682 with the MOPAC package, version 3.1, of J. J. P. Stewart[7)] with complete geometry optimization.

Reactions. All the reagents and solvents were purified by methods described in the literature.[8)]

Photoirradiation was performed with an Eiko-sha EHB-WI(F)-500 high-pressure mercury lamp (500 W).

Unless specified otherwise, the reactions were carried out under an argon atmosphere. The extracts were washed with saturated aqueous sodium chloride and dried overnight over an appropriate deciccant. The deciccant was removed by filtration and the solvents were stripped off on a flash evaporator at a temperature below 10 °C. The conversions were determined from the ^1H NMR spectra of the reaction products dissolved in $CDCl_3$. Separations of the products were carried out by column chromatography using silica gel (Wako-gel C-200, 100—200 mesh).

1,1,2,2-Tetrachloro-2,2aα,4α,8bα-tetrahydrocyclobuta[c]-quinolin-3(1*H*)-one (1): 2-Quinolone (5.81 g, 40.0 mmol) and benzophenone (1.24 g, 6.8 mmol) were dissolved in a mixture of 1327.9 g (8.0 mol) of tetrachloroethylene and 1000 ml of dichloromethane. The solution was irradiated by a 500-W high-pressure mercury lamp through a Pyrex filter for 87 h. The reaction mixture was concentrated under reduced pressure and then passed through a silica-gel column (Wako C-200) with benzene as an eluent. Recrystallization from dichloromethane gave 5.64 g (43.9%) of pure **1**: Mp 285.0 °C (decomp).

1,2-Dichloro-2aα-methoxy-2aα,8bα-dihydrocyclobuta[c]-quinolin-3(4*H*)-one (3a): To a stirred methanol solution (20 ml) of **1** (31.0 mg, 0.10 mmol), 1 M NaCl (1.0 ml) (1 M =1 mol dm^{-3}) was added at room temperature. After stirring for 16 h at room temperature, the reaction mixture was poured into 1 M HCl (20 ml). The resultant solution was concentrated until the methanol was removed; then, the products were extracted three times with $CHCl_3$ (20 ml each). All extracts were combined, dried ($MgSO_4$), and concentrated under reduced pressure to leave a white solid. The residue was dissolved in $CDCl_3$. Based on the integrated intensities of the ^1H NMR lines of the residues, the content of **3a** was calculated to be 89% and that of **4** to be 11%.

† Present address: Advanced Technology Research Center, Nippon Kokan K.K.

Evaporation of $CDCl_3$ followed by recrystallization from CH_2Cl_2–hexane gave **3a** as white needles (15.1 mg, 56%): Mp 183 °C (decomp); IR (KBr) 1680, 1640, 1100, and 780 cm^{-1}; ^1H NMR ($CDCl_3$) δ=3.51 (3H, s, methoxyl protons), 4.21 (1H, s, cyclobutene ring proton), 7.00—7.14 (2H, m, aromatic protons), 7.23—7.32 (2H, m, aromatic protons), and 9.51 (1H, s, NH proton); ^{13}C NMR ($CDCl_3$) δ=53.2 (d), 54.3 (q), 80.7 (s), 116.6 (d), 118.3 (s), 123.9 (d), 126.2 (s), 128.5 (d), 129.3 (d), 131.9 (s), 135.3 (s), and 166.0 (s). Found: C, 53.24; H, 3.39; N, 5.18%. Calcd for $C_{12}H_9Cl_2NO_2$: C, 53.36; H, 3.36; N, 5.19%.

1,2-Dichloro-2aα-ethoxy-2aα,8bα-dihydrocyclobuta[*c*]-quinolin-3(4*H*)-one (3b): To a stirred ethanol solution (60 ml) of **1** (31.0 mg, 0.10 mmol), 1 M NaOH (1.0 ml) was added at room temperature. After stirring for 16 h at room temperature, the reaction mixture was poured into 1 M HCl (20 ml). The solution was concentrated until the ethanol was removed; then, the products were extracted three times with CH_2Cl_2 (20 ml each). The extracts were combined, dried ($MgSO_4$), and concentrated under reduced pressure. The residue was recrystallized from $CHCl_3$ to give white needles of **3b** (49.6 mg, 35%):Mp 190 °C (decomp); ^1H NMR ($CDCl_3$) δ=1.30 (3H, t, ethoxyl methyl protons), 3.70 (2H, m, ethoxyl methylene protons), 4.01 (1H, s, cyclobutene ring proton), 6.80—7.30 (4H, m, aromatic protons), and 9.72 (1H, s, NH proton); ^{13}C NMR ($CDCl_3$) δ=15.3 (q), 54.2 (d), 63.0 (t), 80.0 (s), 116.8 (d), 118.4 (s), 123.8 (d), 126.5 (s), 128.4 (d), 129.2 (d), 131.6 (s), 135.4 (s), and 166.7 (s). Found: *m/z* 283.0161. Calcd for $C_{13}H_{11}Cl_2NO_2$:M, 283.0167, (rel intensity, M:M+2:M+4=8.8:5.7:1.0).

1,2-Dichloro-2aα-butylamino-2aα,8bα-dihydrocyclobuta[*c*]-quinolin-3(4*H*)-one (3c): To a stirred acetone solution (50 ml) of **1** (155.0 mg, 0.50 mmol), butylamine (365.7 mg, 5 mmol) was added at room temperature. After stirring for 7 h at room temperature, the solution was concentrated to give a black solid. The residue was washed by hexane (50 ml), dissolved in 1 M NaOH (30 ml). The products were extracted three times with CH_2Cl_2 (50 ml each). The extracts were combined, dried ($MgSO_4$), and concentrated to leave colorless glass, which was washed with hexane to give **3c** (140.2 mg, 90%): Glass; ^1H NMR ($CDCl_3$) δ=0.90 (3H, t, *J*=7.5 Hz, $CH_2CH_2CH_2\underline{CH_3}$), 1.32—1.43 (2H, m, $CH_2CH_2\underline{CH_2}$-CH_3), 1.49—1.57 (2H, m, $CH_2\underline{CH_2}CH_2CH_3$), 2.58—2.66 (2H, m, $\underline{CH_2}CH_2CH_2CH_3$), 4.20 (1H, s, cyclobutene ring proton), 6.68 (1H, br s, amine proton), 6.89—7.18 (2H, m, aromatic protons), 7.20—7.29 (2H, m, aromatic protons), and 9.12 (1H, s, amide proton). Found: *m/z* 310.0638. Calcd for $C_{15}H_{16}Cl_2NO_2$:M, 310.0640, (rel intensity, M:M+2:M+4=9.0:6.2:1.0).

3-(Trichlorovinyl)-2-quinolone (4): Triethylamine (4.5 g, 45.0 mmol) was added to a stirred benzene solution (300 ml) of **1** (311.0 mg, 1.0 mmol) at room temperature. After stirring at room temperature for 15 min, the reaction mixture was poured into water (50 ml). The products were extracted three times with $CHCl_3$ (50 ml each). The extracts were combined, dried ($MgSO_4$), and concentrated under reduced pressure to leave a white solid. Recrystallization from acetone gave **4** as parallelepiped: Mp 276—278 °C; IR (KBr) 1660, 1570, and 1430 cm^{-1}; ^1H NMR (DMSO-d_6) δ=7.21—7.37 (2H, m, aromatic protons), 7.55—7.76 (2H, m, aromatic protons), and 8.27 (1H, s, olefinic proton). Found: C, 47.92; H, 2.20; N, 5.09%. Calcd for $C_{11}H_6Cl_3NO$: C, 48.13; H, 2.20; N, 5.10%.

Results and Discussion

Reaction of 1 with a Nucleophile and/or a Base. Cross adduct **1** was obtained from 2-quinolone and tetrachloroethylene under irradiation with a 500-W high-pressure mercury lamp. The yield of **1** based on 2-quinolone was 43.9%. Our procedure gives a higher yield than the method described by Evanega and Fabiny.[9]

Upon treatment of **1** with a nucleophile and/or a base, we obtained two products, a cyclobutene compound **3** and trichlorovinyl-2-quinolone (**4**), in place of the expected compound having a [4,5,6]-fused ring system.[4] The ratio of **3** to **4** in the products was influenced by the nucleophile used. The results of the reaction are summarized in Table 1. For the reaction of **1** with NaOH in methanol, the yields of **3** and **4** based on **1** were 70 and 7%, respectively. When NaOMe was used as a nucleophile, the conversion and yield were almost the same as those for the reaction of **1** with NaOH in methanol. Using NaH or Et_3N as a base in aprotic solvent benzene we obtained **4** exclusively, which is similar to the results of the reaction of the coumarin-tetrachloroethylene photoadduct with a non-nucleophilic base.[4] From the reaction of **1** with NaOH in aqueous acetone, **4** was also formed quantitatively. When butylamine was used in aprotic solvent acetone, **3** was obtained

Table 1. Reactions of **1** with Various Bases (See Experimental Section for Detailed Reaction Conditions)

Base	Equiv. to **1**	Solvent	Time/h	Conv. (Yield)/%[a]	
				3	**4**
NaOH	10	MeOH	16	89(70)	11(7)
NaOMe	900	MeOH	14	86(70)	14(5)
$NaHCO_3$	23	MeOH	23	40(32)	60(50)
NaOH	10	EtOH	7	40(35)	60(51)
NaOH	1900	Acetone (aq.)	16	0	100(85)
NaH	15	Benzene	5	0	100(90)
NEt_3	45	Benzene	7	0	100(92)
$BuNH_2$	10	Acetone	7	100(97)	0

a) Based on **1**.

exclusively. Thus the fraction of the cyclobutene compound **3** in the products was different, depending on the nucleophile employed. The highest ratio and yield of **3** in the products was observed for butylamine nucleophile. When methoxide and ethoxide anions were used, the ratio of **3** was lower than that observed for butylamine. Methoxide anion gave a higher ratio of **3** than the ethoxide anion. No product attacked by an OH^- anion at the carbon α to the carbonyl carbon, nor at β, was obtained when **1** was treated with an alkaline solution in alcohols.

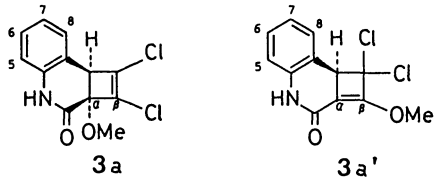

Fig 1. The candidate structures, **3a** and **3a'**, for the cyclobutene product **3** (Nu = OMe).

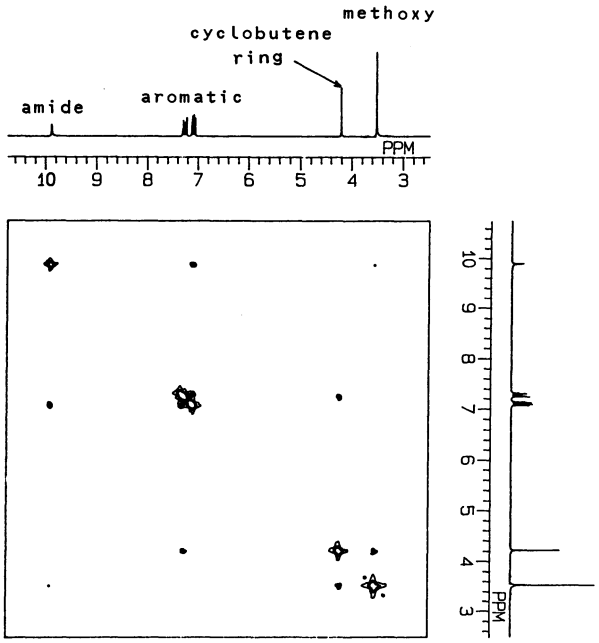

Fig 2. 400 MHz proton NOESY NMR spectrum of **3** in $CDCl_3$ at 27 °C. Data matrix by 1024 points with a frequency range of 5000 Hz in both dimensions was zero-filled to 2048.

Structure of the Cyclobutene Compound. For the cyclobutene compound **3** (Nu=OMe) two possible structures can be considered (Fig. 1). One is compound **3a** having a methoxyl group on the α carbon with respect to the carbonyl carbon formed as a result of the S_N2' replacement reaction. The other is **3a'**, where the chlorine atom at the β position to the carbonyl carbon is substituted by the methoxyl group via a 1,4-addition reaction. To determine which is the structure of the cyclobutene product, **3a** or **3a'**, we studied the Nuclear Overhauser Effect (NOE) by 2D NMR spectroscopy[10] and compared the results with the fully optimized geometries predicted by the AM1[5] and MNDO[6] MO calculations. Under the condition that the NMR T_1 values of the compared nuclei are almost the same, the NOE value becomes approximately proportional to $1/R^6$ for the correlated nuclei couple separated by a distance R.[11] The relative values of NOE can be determined from the volume of the cross-peak in the NOESY spectrum and, hence, candidate geometries predicted by MO calculations can be checked by the observed cross-peak volumes.

The NOESY contour plot observed for compound **3** ($Nu=OCH_3$) is shown in Fig. 2. In the COSY spectrum, no off-diagonal peak due to proton-proton J coupling was observed, except for those among aromatic protons. Thus, the correlation between the peaks at 3.5 ppm (methoxyl protons) and 4.2 ppm (cyclobutene ring proton) in the NOESY spectrum indicates that the geometrical distance between these protons is very short (less than 4 Å). The cross peak between 4.2 ppm (cyclobutene ring proton) and 7.2 ppm (one of the aromatic protons) indicates that these protons are also closely located. Furthermore, a correlation was observed between one of the aromatic protons and the amide proton (9.93 ppm). NOE values for these three correlations were determined from the cross-peak volumes in the NOESY spectrum and are given in Table 2, where the volumes of the cross peaks are given in relative to those between the cyclobutene proton and one of the aromatic protons (a proton at C8 in Fig. 1). Since the aromatic protons

Table 2. Observed Relative NOE Volumes of the Product **3** (Nu = OCH_3), and Expected Distance R and Relative $1/R^6$ for **3a** and **3a'**

Proton pair	Relative NOE volume	Relative $1/R^6$ (Distance/Å)[a] **3a**	**3a'**
H(cyclobutene)-H(Aro)[b]	1.0	1.0 (2.589)[c]	1.0 (2.979)[c]
H(cyclobutene)-H(OMe)	2.0	1.9 (2.418 / 3.936 / 3.461)	0.3 (4.967 / 6.626 / 5.532)
H(NH)-H(Aro)[b]	1.3	1.6 (2.392)[d]	3.6 (2.411)[d]

a) Calculated for the AM1 optimized geometries. b) Aro stands for one of the aromatic protons. c) Aromatic proton is assumed on the C8 in the phenyl ring (Fig. 1). d) Aromatic proton is assumed on the C5 in the phenyl ring (Fig. 1).

give a complex multiplet structure, as shown in the one-dimensional spectrum, the cross-peak volumes involving aromatic protons were determined after the line assignments as an ABCD 4-spin system had been performed with the aid of the LAOCN3 program.[12] Table 2 also shows the relative values of $1/R^6$, together with the proton-proton distance R, calculated for the geometries predicted from AM1 MO calculations. A good correlation between each NOE volume and the corresponding relative $1/R^6$ value is found for the candidate structure **3a**. It follows that the methoxyl group is situated at the α position with respect to the carbonyl carbon. Product **3** is, therefore, confirmed to be 1,2-dichloro-2aα-methoxy-2aα,8bα-dihydrocyclobuta-[*c*]quinolin-3(4*H*)-one (**3a**) (Fig. 3).

Reaction Mechanism. In the case of the [4,6,6] lactone-fused ring system studied before,[4] the first step of the reaction with a nucleophile is the lactone-ring-opening reaction. The second and third steps are a dehydrochlorination and an intramolecular S_N2' displacement to form the [4,5,6] fused ring system.[4] On the contrary, a lactam-ring-opening at **1** dose not occur under the mild conditions employed in this study, since the amide linkage in the lactam ring is known to be far stronger than the ester linkage in the corresponding lactone ring. Thus, the first step should be dehydrochlorination to yield the unstable intermediate **2**, although we did not try to isolate **2**.

For a reaction from **2** to the cyclobutene product **3** (i.e. **3a** or **3a'**), we calculated the heats of formation of these two candidates by the MNDO and AM1 MO methods. The heat of formation of **3a** (−0.6 kcal mol^{-1} from AM1, and −23.3 kcal mol^{-1} from MNDO) was slightly higher than that of 1,4-adduct **3a'**

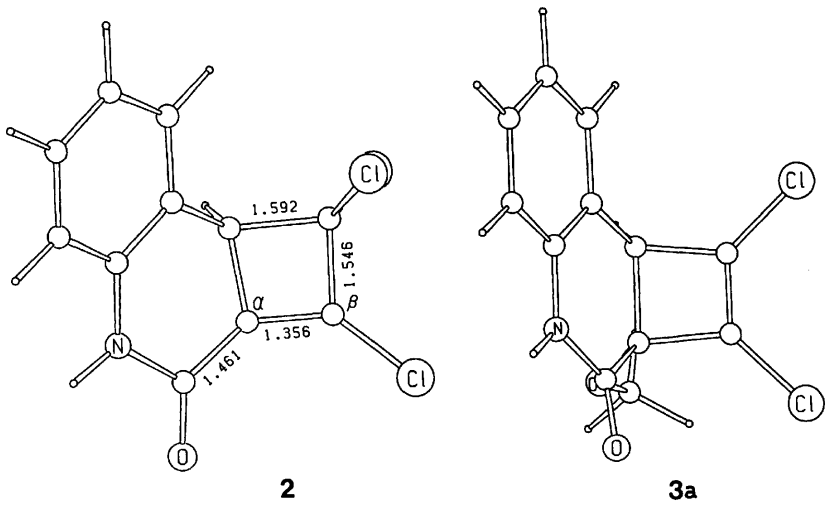

Fig 3. ORTEP[13] perspective view of **2** and **3a**, determined by the AM1 MO calculations.

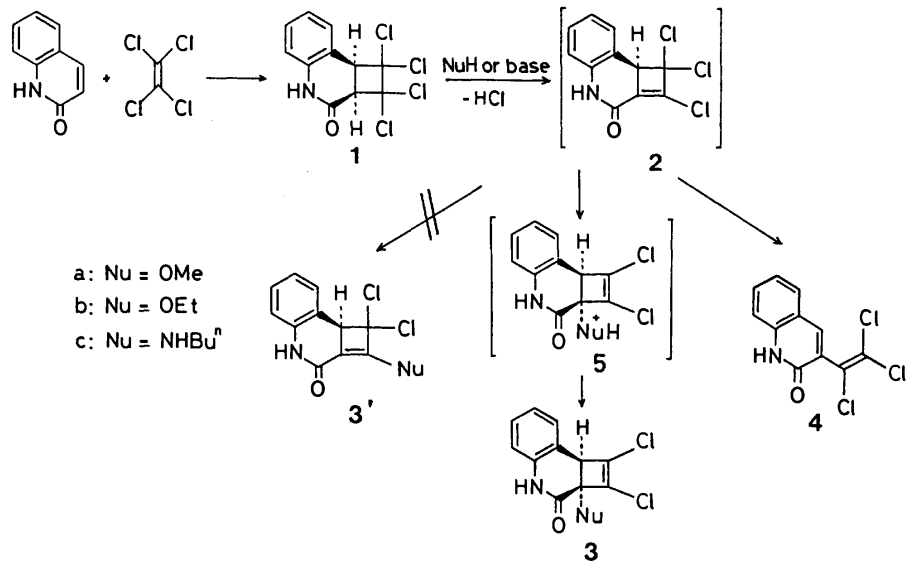

Scheme 1.

(-3.4 kcal mol^{-1} from AM1, and -26.9 kcal mol^{-1} from MNDO), suggesting that **3a** was thermodynamically less stable than **3a'**. Since **3a'** was not detected experimentally, as discussed in the previous section, the reaction of **2** with a nucleophile is not a thermodynamically equilibrium reaction. The lactam ring of **2** at the AM1 geometry (Fig. 3) is folded in against the cyclobutene ring by 51 ° while the benzene ring is on the same plane with the lactam ring. All these geometrical features indicate that the carbonyl group and the cyclobutene double bond are not well conjugated, which is also suggested from the calculated π-π overlap population. In these situations, a 1,4-addition of the attacking methoxide anion to the β position with respect to the carbonyl carbon should be improbable. Thus, molecular orbital calculations again support the conclusion from the NOE measurements described in the previous section that the cyclobutene product is **3a**.

Based on the information given above, the following reaction mechanism can be drawn (Scheme 1). In the first step of the reaction from **1**, dehydrochlorination leading to **2**, i.e. cyclobutene formation, takes place. In the second step, two possible routes can be considered. One is an S_N2' displacement by an attack of a nucleophile at the α carbon with respect to the carbonyl carbon in the cyclobutene intermediate **2**, resulting in another cyclobutene compound **3** by way of the assumed intermediate **5**. The other is the [2+2] cycloreversion of **2**, yielding trichlorovinyl-2-quinolone **4**. Since **2** should be very unstable due to the high steric strain expected for the AM1 geometry, the succeeding competitive reactions, i.e. a nucleophilic substitution reaction or the cycloreversion of the cyclobutene ring, may take place immediately when **2** is produced.

We wish to thank Mr. Hiroshi Tsuchiya, Mr. Mikio Kaihara, and Dr. Hiroaki Mametsuka (Advanced Technology Research Center, Nippon Kokan K. K) for the measurement of high mass spectra.

References

1) Preliminary communication, S. Nonoyama, N. Yonezawa, K. Saigo, T. Hirano, and M. Hasegawa, *Chem. Lett.*, **1987**, 487.

2) N. Yonezawa and M. Hasegawa, *Bull. Chem. Soc. Jpn.*, **56**, 367 (1983); N. Yonezawa, T. Yoshida, and M. Hasegawa, *J. Chem. Soc., Perkin Trans. 1*, **1983**, 1083; N. Yonezawa, Y. Ikebe, T. Yoshida, T. Hirai, K. Saigo, and M. Hasegawa, *Bull. Chem. Soc. Jpn.*, **57**, 1608 (1984); N. Yonezawa, T. Yamashita, T. Kanoe, K. Saigo, and M. Hasegawa, *Ind. Eng. Chem., Prod. Res. Dev.*, **24**, 593 (1985).

3) M. Hasegawa, K. Saigo, H. Katsuki, N. Yonezawa, and T. Kanoe, *J. Polym. Sci., Polym. Chem. Ed.*, **21**, 2345 (1983); N. Yonezawa, T. Kanoe, K.Saigo, Y. Chen, K. Tachibana, and M. Hasegawa, *J. Polym. Sci., Polym. Lett. Ed.*, **23**, 617 (1985); K. Saigo, Y. Chen, N. Yonezawa, T. Kanoe, K. Tachibana, and M. Hasegawa, *Macromolecules*, **19**, 1552 (1986); Y. Chen, K. Saigo, N. Yonezawa, and M. Hasegawa, *Bull. Chem. Soc. Jpn.*, **60**, 1895 (1987).

4) N. Yonezawa, S. Nonoyama, K. Saigo, and M. Hasegawa, *J. Org. Chem.*, **50**, 3026 (1985); S. Nonoyama, N. Yonezawa, K. Saigo, Y. Iitaka, and M. Hasegawa, *Bull. Chem. Soc. Jpn.*, **60**, 349 (1987).

5) M. J. S. Dewar and D. M. Storch, *J. Am. Chem. Soc.*, **107**, 3898 (1985); M. J. S. Dewar, E. G. Zoebisch, E. F. Healy, and J. J. P. Stewart, *J. Am. Chem. Soc.*, **107**, 3902 (1985).

6) M. J. S. Dewar and W. Thiel, *J. Am. Chem. Soc.*, **99**, 4899 (1977).

7) A HITAC version converted from the Vax version MOPAC supplied from J. J. P. Stewart, Frank J. Seiler Research Laboratory, U.S. Air Force Academy, Colorado Springs, Colorado, U.S.A.

8) D. D. Perrin, W. L. F. Armarego, and D. R. Perrin, "Purification of Laboratory Chemicals," 2nd ed., Pergamon Press, Oxford (1980).

9) G. R. Evanega and D. L. Fabiny, *J. Org. Chem.*, **35**, 1757 (1970).

10) a) W. Braun, C. Bösch, L. R. Brown, N. Go, and K. Wüthrich, *Biochim. Biophys. Acta*, **667**, 377 (1981); S. Macura and R. R. Ernst, *Mol. Phys.*, **41**, 95 (1980); J. H. Noggle and R. E. Schirmer, "The Nuclear Overhauser Effect," Academic Press, New York (1971). b) A. A. Bothner-By, "Biological Applications of Magnetic Resonance," ed by R. G. Shulman, Academic Press, New York (1979).

11) The volume of a cross peak a_{AB} in the NOESY spectrum can be related to the distance R_{AB} between two correlated atoms A and B as,[10b]

$$a_{AB} = f(\tau_m) \cdot \sigma$$

$$\sigma = \frac{1}{10} \cdot \frac{\gamma^4 \hbar^2}{R_{AB}^6} \cdot \left[\frac{6\tau_c}{1 + 16\pi^2 \nu^2 \tau_c^2} - \tau_c \right]$$

where τ_m is the mixing time, $f(\tau_m)$ a function of the τ_m, σ the cross-relaxation rate, γ the gyro-magnetic ratio, ν the observed frequency, and τ_c the correlation time which is inversely proportional to the relaxation time T_1.

12) A. A. Bothner-By and S. M. Castellano, "Computer Programs for Chemistry," Vol. 1, ed by D. F. DeTar, Benjamin, New York (1968), pp. 10—53.

13) C. K. Johnson, ORTEP, Report ORNL-3794, Oak Ridge National Laboratory, Oak Ridge, Tennessee, U.S.A., 1965.

Novel Preparation of 1- and 3-Substituted Bicyclo[3.2.2]nona-3,6,8-trien-2-ones from Tropones and 2,3-Bis(methoxycarbonyl)-7-oxabicyclo-[2.2.1]heptadiene by High-Pressure Cycloaddition-Thermal Cycloreversion Procedure

Guan Rong TIAN,† Shigeru SUGIYAMA, Akira MORI, and Hitoshi TAKESHITA*
Institute of Advanced Material Study, 86, Kyushu University,
Kasuga-koen, Kasuga, Fukuoka 816
(Received November 12, 1987)

The Diels-Alder adduct of tropone with 2,3-bis(methoxycarbonyl)-7-oxabicyclo[2.2.1]hepta-2,5-diene formed homobarrelenone on heating at 130 °C. Similarly prepared were 1-hydroxy-, 3-methoxy-, 1-chloro-, and 3-chlorohomobarrelenones. High-pressure cycloaddition improved the yields of the Diels-Alder adducts. In reactions of 2-methoxy- and 2-chlorotropones with the 7-oxanorbornadiene derivative, the endo-isomers were predominantly produced together with the exo-isomers.

There have been a number of Diels-Alder[1] and retro-Diels-Alder[2] reactions applied to organic syntheses. However, particularly important is the development of a synthon equivalent to acetylene for the cycloaddition reactions, since there seems to still be no versatile procedure; oxidative decarboxylations of Diels-Alder adducts from maleic acid were successful only in limited instances,[3] or reductive eliminations of halogens from dihaloethene adducts sometimes have limitations, depending on the other functional groups in the molecule.[4] A recently developed two-step sequence, Diels-Alder reaction of dienes to 1,2-bis(phenylsulfonyl)ethene[5] and β-nitrosulfonylethene[6] and subsequent reductive elimination with sodium amalgam or tributyltin hydride, usually gave good results; however, the use of mercury would be undesirable from environmental points of view.

Since it is well-known that cycloadducts of furans have a tendency to cyclorevert,[7] 7-oxabicyclo[2.2.1]-heptadiene, which corresponds to the Diels-Alder adduct of furan and acetylene,[8] should serve as a substitute for acetylene.

In fact, the 1,3-dipole additions of 7-oxabicyclo-[2.2.1]heptadiene derivatives and 1,3-dipoles have given five-membered heteroaromatic compounds via

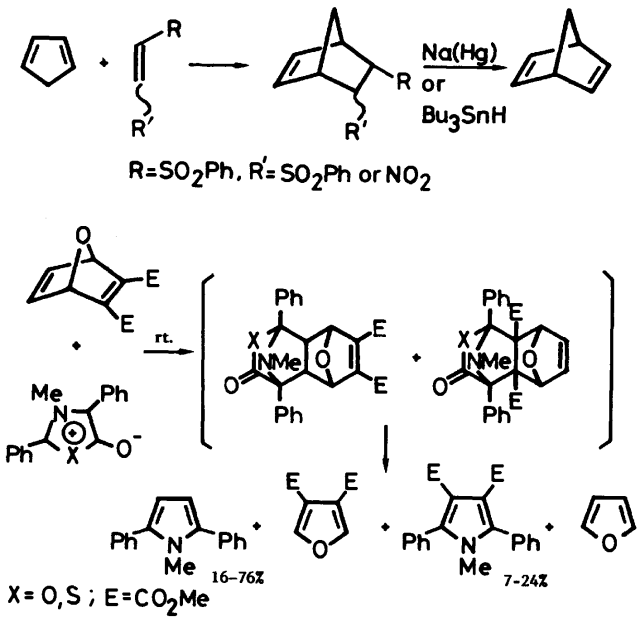

Scheme 1.

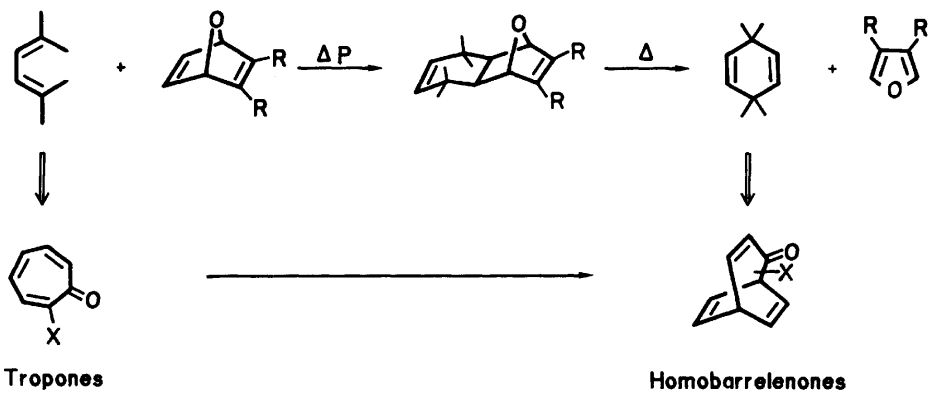

Scheme 2.

† On leave from Yanbian University, Yanji, Jilin, People's Republic of China.

the cycloaddition-fragmentation reactions.[9] We herein describe the synthesis of homobarrelenones **3a**,[10] **3b**, **3d**, **4c**, and **4d** by the thermolyzing the Diels-Alder adducts obtained from 2,3-bis(methoxycarbonyl)-7-oxabicyclo[2.2.1]heptadiene (**1**)[11] and tropones **2a—d** under high-pressure conditions. To date, only a few derivatives of **3** have been prepared,[12-14] including the 6,7-bis(methoxycarbonyl) derivative by the Diels-Alder addition of **2a** with dimethyl butynedioate.[14,15] Since the derivatives of **3** were recently utilized in natural product syntheses,[12] a versatile synthesis of **3** must be worthwhile.

Results and Discussion

Thermal Reaction of 1 and Tropone. In 1972, Sasaki et al.[16] described the Diels-Alder reaction of tropone **2a** with **1** to form a 1:1-adduct **5a**. However, we have found, through a repeated experiment, a formation of three other products **3a**, **6**, and **7a** together with the expected adduct **5a** even under the Diels-Alder conditions. The ^{1}H NMR data of **3a** were in accord with those reported,[10] and the structures of **6** and **7a** were deduced to be 3,4-bis(methoxycarbonyl)-furan and 1-indanone, respectively, from their NMR data. The reaction also gave better results under high-pressure conditions; at a pressure of 3000 bar, the yield of the Diels-Alder adduct was improved to 88%. Therefore, a retro-Diels-Alder fragmentation of **5a** to **3a** and **6** might be quite facile and the process can be used for the synthesis of derivatives of **3**.

Thermal Reaction of 1 and Tropolone. The reaction of tropolone **2b** with **1** at 130 °C under 1 bar similarly gave, together with the adduct **5b**[16] in 50% yield, fragmentation products 1-hydroxyhomobarrelenone (**3b**), 7-hydroxy-1-indanone (**7b**), and **6**. Again, a reaction under 3000 bar afforded **5b** in 67% yield. The structure of **3b** was confirmed by the NMR data and that of **7b** was identified by a comparison with the authentic sample.[17]

Thermal Reactions of 1 and 2-Methoxy- and 2-Chlorotropones. This high-pressure reaction could be further extended to 2-methoxytropone (**2c**) and 2-chlorotropone (**2d**) with **1**; in both cases, three adducts **5c**, **8c**, and **9c** from **2c** and **5d**, **8d**, and **9d** from **2d** formed under 3000 bar. On the other hand, the reactions at 1 bar with **2c** and **2d** were rather complicated; new types of Diels-Alder adducts **10c** and **10d** were isolated together with the cycloreversed homobarrelenones **3d**, **4c**, and **4d** and indanones **7c** and **7d**. Table 1 summarized the results of Diels-Alder reactions.

The structures of Diels-Alder adducts from **2c** and **2d** were established by the ^{1}H and ^{13}C NMR spectroscopies. The chemical shifts and the coupling constants are summarized in Tables 2 and 3. Since the NMR spectra of the main product **5c** resembled those of **5a** and **5b**, the structure of **5c** was determined to be an endo-exo [4+2]π-adduct[18] with a substituent on the bridge-head carbon.

From the splitting patterns of H_2 and H_7 ($J_{1,2}$=0 Hz and $J_{7,8}$=1.5 Hz) and those of H_3 and H_6 ($J_{2,3}$=$J_{6,7}$=0 Hz), the structure of **8c** was deduced to be another endo-exo [4+2]π-adduct with a chlorine substituent at C-10.

While **9c** also had a substituent on C-10 and the signals of H_3 and H_6 appeared as two singlets, the coupling constants of $J_{1,2}$ (5.5 Hz) and $J_{7,8}$ (5.5 Hz) suggested that H_2 and H_7 had an endo configuration in bicyclo[3.2.2] framework. Therefore, **9c** was the exo-exo [4+2]π-adduct.

The structure of **10c** was the exo-exo [4+2] π-adduct

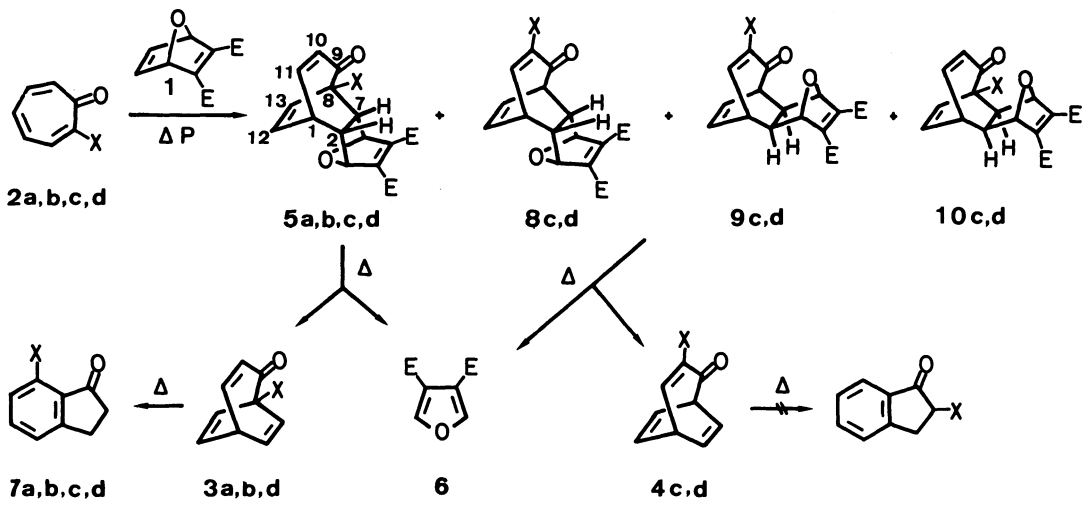

Scheme 3.

Table 1. Diels–Alder Reactions of **1** and **2**

2	Conditions (°C, h)	Product (Yield/%)[c] 5	8	9	10	3	4	6	7	Endo/Exo	Site selectivity
2a	100, 11[a]	88									
	130, 12[b]	64				11		21	5		
2b	120, 12[a]	67									
	130, 12[b]	50				11		14	2		
2c	120, 12[a]	34	12	4						11.5	2.1[d]
	130, 12[b]	24	11	3.4	2.6		3	16	4	5.8(8.5)[e]	1.6[d]
	130, 20[b]	25					17	26	10		
2d	120, 12[a]	44	20	7				14		9.1	1.6
	130, 20[b]	28	13	5	6	11	6	35	8	3.7(6.9)[e]	2.2[d]

a) Under 3000 bar. b) Under 1 bar. c) Yield was based on consumed **2**. d) These values were ratios including homobarrelenones and indanones. e) These values were ratios adding the yields of **6** to those of endo-adducts.

Table 2. NMR Data of 1:1-Adducts

	5a	**5b**	**5c**	**5d**	**8c**	**8d**	**9c**	**9d**	**10c**	**10d**
R_1	H	OH	OMe	Cl	H	H	H	H	OMe	Cl
R_2	H	H	H	H	OMe	Cl	OMe	Cl	H	H
H-1	3.44	3.61	3.43	3.48	3.5	3.54	3.7	3.7	3.61	3.63
H-2	2.50	2.24	2.64	2.62	2.48	2.52	2.6	2.7	2.60	2.69
H-3	4.92	4.70	4.91	4.96	4.90	4.90	4.86	4.90	4.86	4.90
H-6	5.01	5.52	5.41	5.69	4.98	5.02	4.92	4.95	5.07	5.09
H-7	2.70	2.58	2.64	2.76	2.68	2.74	2.6	2.7	2.72	3.03
H-8	3.68	OH	OMe	Cl	3.8	3.94	3.7	3.98	OMe	Cl
H-10	5.70	5.88	5.74	5.90	OMe	Cl	OMe	Cl	6.05	6.16
H-11	7.18	7.30	7.14	7.26	6.16	7.48	5.81	7.16	6.88	6.92
H-12	6.24	6.32	6.37	6.44	6.51	6.48	6.64	6.64	6.61	6.59
H-13	6.10	5.92	6.06	6.04	6.08	6.16	6.14	6.22	6.27	6.19
C-1	48.2	49.1	47.1	49.8	48.8	47.8	46.9	46.8	44.2	45.6
C-2	39.7	39.7	39.7	38.8	36.7	39.5	35.1	38.0	38.0	37.3
C-3[a]	85.9	83.4	83.5	85.9	85.7	85.6	81.5	81.8	80.1	80.4
C-4[a]	145.7	145.4	145.7	145.6	145.4	145.5	145.4	145.2	144.8	145.3
C-5[a]	146.1	145.8	146.1	146.4	146.3	146.1	145.8	145.8	146.3	145.6
C-6[a]	86.7	85.3	85.9	86.3	86.6	86.7	83.9	83.8	83.2	83.6
C-7	41.8	46.3	45.8	48.9	41.7	41.5	45.4	46.0	52.5	57.4
C-8	57.0	82.1	88.4	81.1	54.9	55.9	55.1	54.9	90.2	80.8
C-9	196.3	195.3	195.1	187.7	191.8	189.0	192.3	189.7	193.2	187.0
C-10	126.8	125.7	128.6	127.7	151.1	132.7	154.9	136.4	132.3	132.8
C-11	153.7	155.8	152.8	153.8	120.8	150.0	114.0	144.1	146.4	146.8
C-12	136.1	133.8	133.5	135.0	137.6	136.1	141.0	139.6	138.2	138.3
C-13	129.5	132.6	130.3	132.5	126.2	127.0	129.0	129.9	133.5	136.3

a) Assignments of C-3, C-6, C-4, and C-5 could be reversed.

Table 3. Coupling Parameters (Hz) of 1:1-Adducts

	5a	**5b**	**5c**	**5d**	**8c**	**8d**	**9c**	**9d**	**10c**	**10d**
$J_{1,2}$	0	0	0	1	—	—	5.5	5.5	5.9	5.9
$J_{1,10}$	2	0	1	0.7	—	—	×	×	0.7	0.7
$J_{1,11}$	8	8	8.5	8	9.5	9	9.5	9	8.8	8.8
$J_{1,12}$	8	7	7	7.5	7.5	7.5	7	7	7.0	7.3
$J_{2,3}$	1	0	1.5	1.5	0	0	0	1	1.1	1.1
$J_{2,7}$	8	8	—	7.5	8	8	8.5	8	8.8	8.8
$J_{6,7}$	1	0	1.5	1.5	0	0	0	1	1.1	1.1
$J_{7,8}$	0	×	×	×	1.5	1.5	5.5	3.5	×	×
$J_{8,13}$	8	×	×	×	7.5	7.5	7.5	7	×	×
$J_{10,11}$	11	11	11	11	×	×	×	×	11.0	11.0
$J_{12,13}$	8	8	9	9	7.5	7.5	8	8.5	8.8	8.8

—: Not observed. ×: Not existed.

from the presence of four olefinic protons and the value of the coupling constant ($J_{1,2}$=5.9 Hz, $J_{2,3}$=$J_{6,7}$= 1.1 Hz). Similarly, the structures of four 1:1-adducts **5d**, **8d**, **9d**, and **10d** from **1** and **2d** were confirmed from the NMR data, as shown in Scheme 3.

In addition, the structures of homobarrelenones **3d**, **4c**, and **4d** were also clarified by their NMR analysis. All ^{13}C NMR displayed seven lines. Since the ^{1}H NMR spectrum of **3d** showed six olefinic protons, **3d** was deduced to be 1-chlorohomobarrelenone. In **4c** and **4d**, the appearance of five olefinic and two methine protons determined the structures to be 3-methoxy- and 3-chlorohomobarrelenones, respectively.

The indanone **7c** was identified to be 7-methoxy-1-indanone by a direct comparison with the authentic sample.[17]

Pressure Effect on the Cycloaddition Reaction. Table 1 shows the pressure effect on the endo/exo ratio and the site selectivity [(**5**+**10**):(**8**+**9**)] in the reactions between **1** and **2c** or **2d**. In both cases, the pressure did not affect to the site selectivity under 3000 bar, but the endo/exo ratio was larger as roughly twice than that under 1 bar. When the time-course of the cycloreversion of the endo-adduct **5d** and exo-adduct **10d** in toluene-d_8 was monitored by ^{1}H NMR spectroscopy, the formation of **6** was observed in ca. 40% conversion from **5d** and in less than 1% conversion from **10d** after heating at 130 °C for 24 h. Therefore, an endo/exo ratio under 1 bar could be estimated to be larger than the observed value (5.8 for **2c** and 3.7 for **2d**). If all of **6** was formed by the cycloreversion of endo-adducts and the yields of **6** were added to the yields of endo-adducts, the endo/exo ratios became 8.5 and 6.9 in the reactions between **1** and **2c** or **2d**, respectively. This means that the change of the endo/exo ratio was insignificant within the present pressure range.

Thermal Cycloreversion of Adducts. To obtain homobarreleones, the adducts were thermolyzed at 130 °C for a prolonged period; e.g., **5a** gave **3a**, **7a**, and **6** in 26, 22, and 48% yields, respectively. The results are summarized in Table 4. The isolated yields for **3** and **4** were relatively low. This was due to their volatility and a facile isomerization to indanone derivatives. Therefore, in order to avoid any further transformation of **3** to **7**, we thermolyzed **5** in a flow system and could improve the yield of **3a** to 64% without indanone formation. This was applicable to preparing other homobarrelenones **3b** and **3d**.

Table 4. Pyrolysis of Adducts

Adducts	Condition		Product (Yield/%)[a]		
5a	130 °C,	15 h	**3a** (26)	**7a** (22)	**6** (48)
5b	120 °C,	6 d	**3b** (39)	**7b** (36)	**6** (81)
5c	120 °C,	7 d		**7c** (95)	**6** (100)
8c+**9c**	130 °C,	7 d	**4c** (50)		**6** (50)
5d	130 °C,	12 h	**3d** (17)	**7d** (17)	**6** (62)
8d+**9d**	130 °C,	6 d	**4d** (86)		**6** (88)

a) Yield was based on comsumed adduct.

An attempted fragmentation of **5c**, the major product from **2c**, resulted only the formation of **7c**; however **5d**, the major adduct from **2d**, produced **3d** and 7-chloro-1-indanone (**7d**).[19] Thus, the electron-releasing group on the bridge-head carbon facilitates the indanone formation.

Mechanism of Thermal Rearrangement. The mechanism of thermal isomerization, homobarrelenones to dihydroindenones, has already been proposed;[15] a [3,3] sigmatropic shift of a homobarrelenone to the 7-*syn*-norcaradienylketene intermediate (**A**) followed by a [3,5] sigmatropic shift (antarafacial or Möbius) to a dihydroindenone. If an intermediate (**B**) like **A** was involved, there should be two routes (a and b) to indanones. However, an exclusive formation of 7-substituted indanones is consistent only with path a from **B**, as illustrated in Scheme 4. The methoxyl group of 1-methoxyhomobarrelenone would assist the formation of the tricyclic intermediate (**C**) and the bond a cleavage to 7-methoxyindanone. Such an intermediate **C** has been noticed in the photochemical isomerization of 5-hydroxytricyclo[3.3.2.0^{2,4}]deca-7,9-dien-6-one[20] and 5-alkyl-1-hydroxy-8-oxabicyclo[3.2.1]-octa-3,6-dien-2-ones.[21]

The by-products **8c** and **9c** from **2c** and **8d** and **9d** from **2d** were, respectively, converted to **4c** and **4d** by cycloreversion. However, **4c** and **4d** gave no indanones, unlike 1-substituted homobarrelenones. A simi-

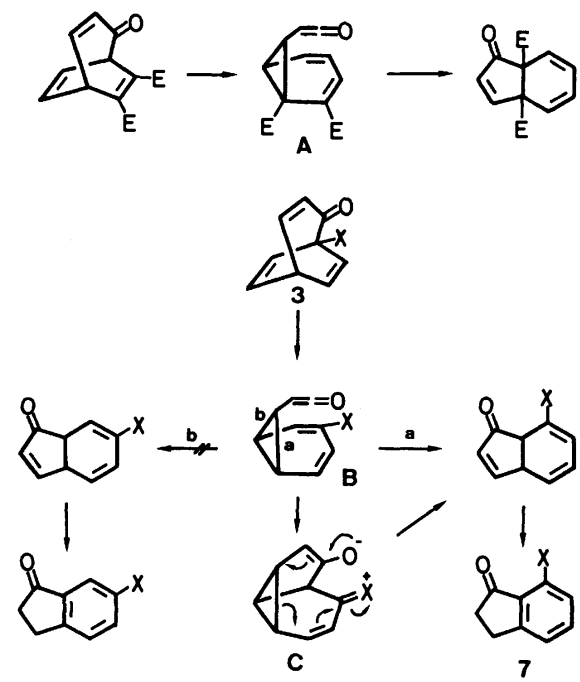

Scheme 4.

lar result has been observed in the pyrolysis of 9-isopropyl-1-methoxy-6,7-bis(methoxycarbonyl)bicyclo-[3.2.2]hepta-3,6,8-trien-2-one (**D**) and 9-isopropyl-3-methoxy-6,7-bis(methoxycarbonyl)bicyclo[3.2.2]hepta-3,6,8-trien-2-one (**E**); **D** gave a dihydroindenone derivative in 74% yield, while **E** did not give any products.[13] Probably, the electron-releasing methoxyl group at the α-position rather increased the electron density of the α,β-unsaturated ketone moiety. No occurrence of an indanone from **4d** could also be explained by the mesomeric effect of the chlorine atom on the α-position of the enone.

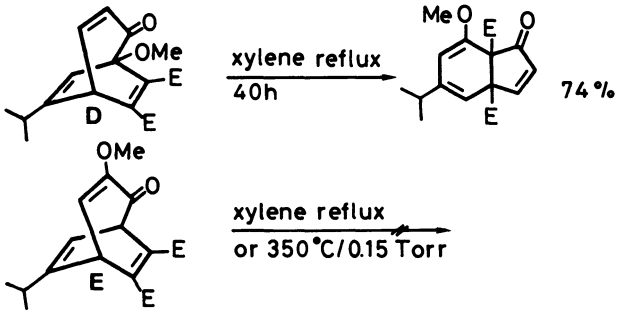

Scheme 5.

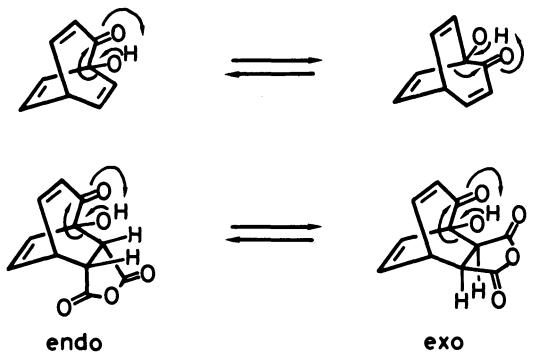

Scheme 6.

It is interesting that 1-hydroxyhomobarrelenone (**3b**) could be isolated after the thermal reactions, as shown in Table 1; probably, this would be attributable to a suppression of the rearrangement to indanone due to an alternative rearrangement, thermal acyloin rearrangement, which has been detected in the Diels–Alder adducts of maleic anhydride with tropolones.[22]

The NMR Spectral Analysis of Homobarrelenones. The ^1H and ^{13}C NMR chemical shifts of homobarrelenones prepared were systematically analyzed. As compiled in Table 5, the ^{13}C NMR chemical shifts of C-7(8) in **3b** and **3d** were at lower fields by ca. 6 ppm than the corresponding carbon in **3a**. Similar low-field shifts were observed for C-13 in 1:1-adducts summarized in Table 2. The chemical shift of the carbonyl carbon in **3a** was 189.7 ppm and the hydroxyl group at C-1 and the methoxyl group at C-3 did not affect the chemical shift of the carbonyl carbons, while the chlorine atom at C-1 and C-3 made the chemical shift of the carbonyl carbon higher by 6—8 ppm. These high field shifts can be explained in terms of the supressed polarization of the carbonyl group due to the polar substituent, the chlorine atom, at the α-position. Similar high field shifts were also observed in other 1:1-adducts (Table 2).

In the ^1H NMR spectra, protons H_3 in **3b** and **3d** and H_1 in **4c** and **4d** appeared at lower fields by ca. 0.3—0.4 ppm than those in **3a**. Protons H_8 and H_{10} in **8** and **5** behaved similarly. Thus, the substituent, being across the carbonyl group, caused a considerable change in the proton chemical shift.

Conclusion

As mentioned above, the Diels–Alder and the retro-Diels–Alder reactions provided a versatile two-step synthesis of structurally interesting bicyclic ketones, homobarrelenones. Substituted homobarrelenones at

Table 5. NMR Data of Homobarrelenones

	3a	**3b**	**3d**	**4c**	**4d**
R_1	H	OH	Cl	H	H
R_2	H	H	H	OMe	Cl
H-1	4.15	OH	Cl	4.38(0.23)	4.52(0.37)[a]
H-3	5.04	5.42(0.38)	5.34(0.30)	OMe	Cl
H-4	7.02	7.22(0.20)	7.14(0.12)	6.16(−0.96)	7.36(0.34)
H-5	3.85	4.04(0.19)	3.90(0.05)	3.96(0.11)	4.02(0.17)
H-6,9	6.67	6.66(−0.01)	6.76(0.09)	6.82(0.15)	6.82(0.15)
H-7,8	6.33	6.28(−0.05)	6.34(0.01)	6.42(0.09)	6.48(0.15)
C-1	59.4	86.0(26.6)	77.3(17.9)	54.5(−4.9)	58.4(−1.0)
C-2	189.7	189.9(0.2)	181.5(−8.2)	187.1(−2.6)	183.9(−5.8)
C-3	124.9	121.9(−3.0)	123.5(−1.4)	146.1(21.2)	127.3(2.4)
C-4	153.2	155.2(2.0)	153.4(0.2)	120.1(−33.1)	149.6(−3.6)
C-5	41.5	41.9(0.4)	40.2(−1.3)	38.3(−3.2)	41.2(−0.3)
C-6,9	138.5	137.7(−0.8)	136.0(−2.5)	140.2(1.7)	138.7(0.2)
C-7,8	128.9	134.4(5.5)	135.2(6.3)	128.7(−0.2)	129.1(0.2)

a) Figures shown in the parentheses were chemical shift differences with unsubstituted **3a**.

the bridge-head carbon tended to rearrange to the indanones, while 3-isomers did not.

This procedure, high-pressure cycloaddition and thermal fragmentation, may be widely applicable, and **1** will conveniently serve as a substitute for acetylene.

Experimental

The elemental analyses were performed by Miss S. Hirashima of Institute of Advanced Material Study, Kyushu University. NMR spectra were measured using a JEOL 100 and 270H spectrometer in $CDCl_3$ solution (unless otherwise specified); chemical shifts are expressed in the unit δ. Mass spectra were measured with a JEOL OlSG-2 spectrometer. IR spectra were taken as a $CHCl_3$ solution using a Jasco IR-A 102 spectrometer. UV spectra were measured by a Hitachi U-3200 spectrophotometer.

Preparation of 1 under 3000 bar. An ether solution (12 cm^3) of furan (13.1 g) and dimethyl butynedioate (5.80 g) was kept at room temperature under 3000 bar for 20 h. The solvent was evaporated in vacuo and the residue was chromatographed on a silica-gel column to give **1** [colorless oil, 5.53 g, 66%] together with two 1:1-adducts [4.31 g, 34%] between **1** and furan.

Thermal Reaction of 2a and 1. a) A chlorobenzene (CB) solution (1.5 cm^3) of **2a** (109 mg) and **1** (267 mg) was heated at 100 °C under 3000 bar for 11 h. The solvent was evaporated in vacuo and the residue was chromatographed on a silica-gel column to give **5a** [colorless crystals, mp 100—102 °C, (lit,[16] 100—102 °C), 271 mg, 88%. ^{1}H NMR δ=2.50 (1H, d, J=8 Hz), 2.70 (1H, d, J=8 Hz), 3.44 (1H, tm,J=8 Hz), 3.68 (1H, d, J=8 Hz), 3.78 (3H, s), 3.80 (3H, s), 4.92 (1H, d, J=1 Hz), 5.01 (1H, d, J=1 Hz), 5.70 (1H, dd, J=11, 2 Hz), 6.10 (1H, t, J=8 Hz), 6.24 (1H, t, J=8 Hz), and 7.18 (1H, dd, J=11, 8 Hz)] and recovered **1** [61.4 mg].

b) A CB solution (3 cm^3) of **2a** (303 mg) and **1**(611 mg) was heated at 130°C for 12 h. The solvent was evaporated in vacuo and the residue was chromatographed on a silica-gel column to give **3a** [colorless needles, mp 45 °C (lit,[10] 44 °C), 44.6 mg, 11%. ^{1}H NMR δ=3.85 (1H, m), 4.15 (1H, tq, J=6.5, 1.5 Hz), 5.04 (1H, ddd, J=11, 2, 1 Hz), 6.33 (2H, ddd, J=8, 6.5, 1.5 Hz), 6.67 (2H, ddd, J=8, 6.5, 1.5 Hz), and 7.02 (1H, dd, J=11, 8 Hz)], **5a** [582 mg, 64%], **6** [110 mg, 21%], and **7a** [a colorless oil, 21 mg, 5%. ^{1}H NMR δ=2.6—2.8 (2H, m), 3.0—3.2 (2H, m), and 7.3—7.8 (4H, m)].

Thermal Reaction of 2b and 1. a) A CB solution (2 cm^3) of **2b** (244 mg) and **1** (426 mg) was heated at 120 °C under 3000 bar for 12 h. The mixture gave **5b** [mp 114—115 °C, (lit,[16] 114—115 °C), 394 mg, 67%], recovered **2b** [28 mg], and **1** [22.4 mg].

b) A CB solution (1 cm^3) of **2b** (122 mg) and **1** (210 mg) was heated at 130 °C for 12 h. The mixture gave **3b** [a colorless oil, 14.3 mg, 11%. Found: m/z, 148.0523 (M^+). Calcd for $C_9H_8O_2$: 148.0523. IR ν: 3450 and 1670 cm^{-1}. UV λ_{max}^{MeOH}: 202 nm (ε=11700), 229 (3500), and 282 (540)], **5b** [165 mg, 50%], **6** [25.4 mg, 14%], and **7b** [colorless crystals, mp 111—112 °C (lit,[17] 111 °C), 3 mg, 2%. ^{1}H NMR δ=2.7—2.8 (2H, m), 3.0—3.2 (2H, m), 6.71 (1H, d, J=7.5 Hz), 6.89 (1H, d, J=7.5 Hz), 7.43 (1H, t, J=7.5 Hz), and 9.02 (1H, s). UV λ_{max}^{MeOH}: 221 nm (ε=21750), 255 (10600), and 314 (3400)].

Thermal Reaction of 2c and 1. a) A CB solution (2 cm^3) of **2c** (358 mg) and **1** (680 mg) was heated at 120 °C under 3000 bar for 12 h. The mixture gave **5c** [colorless crystals, mp 102—103 °C, 306 mg, 34%. Found: C, 62.20; H, 5.23%. Calcd for $C_{18}H_{18}O_7$: C, 62.42; H, 5.24%. IR ν: 1720 cm^{-1}. UV λ_{max}^{MeOH}: 221 nm (ε=12100)], **8c** [colorless crystals, mp 129—131 °C, 99 mg, 12%. Found: C, 62.29; H, 5.21%. Calcd for $C_{18}H_{18}O_7$: C, 62.42; H, 5.24%. IR ν: 1730, 1710, and 1675 cm^{-1}. UV λ_{max}^{MeOH}: 234 nm (ε=9000) and 287 (2700)], and **9c** [colorless crystals, mp 176.5—178 °C, 33 mg, 4%. Found: C, 62.39; H, 5.22%. Calcd for $C_{18}H_{18}O_7$: C; 62.42; H, 5.24%. IR ν: 1775 cm^{-1}. UV λ_{max}^{MeOH}: 232 nm (ε=6600) and 292 (2050)].

b) A CB solution (1 cm^3) of **2c** (126 mg) and **1** (214 mg) was heated at 130 °C for 12 h to give **4c** [a colorless oil, 4.1 mg, 3%. Found: m/z, 162.0682 (M^+). Calcd for $C_{10}H_{10}O_2$: 162.0681. IR ν: 1720, 1680, 1640, 1605, and 1120 cm^{-1}. UV λ_{max}^{MeOH}: 201 nm (ε=9150), 239 (2600), and 305 (990)], **5c** [76.6 mg, 24%], **6** [27.3 mg, 16%], **7c** [colorless plates, mp 98.5—100°C (lit,[17] 102—103 °C), 6 mg, 4%. ^{1}H NMR δ=2.6—2.75 (2H, m), 3.0—3.15 (2H, m), 4.90 (3H, s), 6.76 (1H, d, J=7.5 Hz), 6.96 (1H, d, J=7.5 Hz), and 7.50 (1H, t, J=7.5 Hz)], **8c** [36 mg, 11%], **9c** [11 mg, 3.4%], and **10c** [colorless crystals, mp 142—143 °C, 9.1 mg, 2.4%. Found: C, 62.37; H, 5.21%. Calcd for $C_{18}H_{18}O_7$: C, 62.42: H, 5.24%. IR ν: 1725, 1675, and 1230 cm^{-1}. UV λ_{max}^{MeOH}: 220 nm (ε=9500) and 289 (1250)].

c) A CB solution (2 cm^3) of **2c** (273 mg) and **1** (448 mg) was heated at 130 °C for 20 h to give **4c** [54.8 mg, 17%], **6** [96 mg, 26%], **5c** [170 mg, 25%], and **7c** [34 mg, 10%].

Thermal Reaction of 2d and 1. a) A CB solution (2 cm^3) of **2d** (281 mg) and **1** (420 mg) was heated at 120 °C under 3000 bar for 12 h. The mixture gave **5d** [colorless needles, mp 146—147 °C, 231 mg, 44%. Found: C, 58.10; H, 4.32%. Calcd for $C_{17}H_{15}O_6Cl$: C, 58.21; H, 4.31%. IR ν: 1740, 1720, 1685, 1640, and 1225 cm^{-1}. UV λ_{max}^{MeOH}: 227 nm (ε=11000)], **8d** [colorless needles, mp 122—123 °C, 106.5 mg, 20%. Found: C, 58.23; H, 4.31%. Calcd for $C_{17}H_{15}O_6Cl$: C, 58.21; H, 4.31%. IR ν: 1730, 1715, and 1680 cm^{-1}. UV λ_{max}^{MeOH}: 234 nm (ε=9700)], **9d** [colorless needles, mp 157—159 °C, 37.3 mg, 7%. Found: C, 58.10; H, 4.33%. Calcd for $C_{17}H_{15}O_6Cl$: C, 58.21; H, 4.31%. IR ν: 1720 and 1670 cm^{-1}. UV λ_{max}^{MeOH}: 224 nm (ε=7800) and 268 (3400)], **6** [38.8 mg, 14%], and unreacted **2d** [70.3 mg].

b) A CB solution (5 cm^3) of **2d** (234 mg) and **1** (350 mg) was heated for 130 °C for 12 h to give **3d** [colorless needles, mp 67—69 °C, 14 mg, 6%. Found: m/z, 166.0160 and 168.0154 (M^+). Calcd for C_9H_7OCl: 166.0183 and 168.0154. IR ν: 1680 cm^{-1}. UV λ_{max}^{MeOH}: 203 nm (ε=12800), 227 (3250), and 283 (700)], **4d** [colorless needles, mp 85.5—87 °C, 23.5 mg, 11%. Found: m/z, 166.0179 and 168.0146 (M^+). Calcd for C_9H_7OCl: 166.0183 and 168.0154. IR ν: 1680 and 1630 cm^{-1}. UV λ_{max}^{MeOH}: 203 nm (ε=9800), 241 (3600), and 295 (900)], **5d** [128.5 mg, 28%], **8d** [61 mg, 13%], **9d** [24 mg, 5%], **10d** [colorless needles, mp 152—153 °C, 27.5 mg, 6%. Found: C, 58.32; H, 4.27%. Calcd for $C_{17}H_{15}O_6Cl$: C, 58.21; H, 4.31%. IR ν: 1730 cm^{-1}. UV λ_{max}^{MeOH}: 224 nm (ε=7600)], **6** [84 mg, 35%], **7d** [colorless needles, mp 92—93.5 °C (lit,[19] 95 °C), 17.3 mg, 8%. ^{1}H NMR δ=2.6—2.9 (2H, m), 3.0—3.3 (2H, m), and 7.2—7.5 (3H, m)], and unreacted **2d** [52 mg].

Thermal Reaction of 5a. a) A CB solution (1.5 cm^3) of **5a** (254 mg) was heated at 130 °C for 15 h. The solvent was evaporated in vacuo and the residue was chromatographed on a silica-gel column to give **3a** [5 mg, 25%], **6** [13 mg, 48%], **7a** [4.3 mg, 22%], and **5a** [208 mg].

b) Crystalline **5a** (130 mg) was placed in a tube equipped with a dry-ice cold finger and thermolyzed at 160—170 °C for 2 h under 50 mmHg (1 mmHg=133.322 Pa). The thermolysate deposited on a wall was washed with ether and chromatographed on a PTLC to give **3a** [28.9 mg, 64%] and **6** [45.2 mg, 70%]. 21 mg of **5a** was remained in a tube.

Thermal Reaction of 5b. a) A CB solution (1 cm^3) of **5b** (175.5 mg) was heated at 120 °C for 6 d to give **3b** [17.4 mg, 39%], **6** [45 mg, 81%], **7b** [16 mg, 36%], and **5b** [75.5 mg].

b) Crystalline **5b** (160 mg) was thermolyzed at 180—185 °C for 2 h under 50 mmHg to give **3b** [42 mg, 59%], **6** [60 mg, 68%], and **7b** [18 mg, 25%].

Thermal Reaction of 5c. A CB solution (1 cm^3) of **5c** (132 mg) was heated at 120 °C for 7 d to give **7c** [40 mg, 95%], **6** [48 mg, 100%], and **5c** [42 mg].

Thermal Reaction of a Mixture of 8c and 9c. A xylene (XL) solution (1 cm^3) of a 3:1-mixture of **8c** and **9c** (105 mg) was heated at 130 °C for 7 d to give **4c** [14.7 mg, 50%], **6** [18.4 mg, 50%], and a mixture of **8c** and **9c** [35 mg].

Thermal Reaction of 5d. a) A XL solution (1 cm^3) of **5d** (141 mg) was heated at 130 °C for 12 h. The solvent was evaporated in vacuo and the residue was chromatographed on a silica-gel column to give **3d** [6 mg, 17%], **6** [24.8 mg, 62%], **7d** [6 mg, 17%], and **5d** [65.5 mg].

b) Crystalline **5d** (108 mg) was heated at 180—190 °C for 1.5 h under 50 mmHg to gvie **3d** [21.3 mg, 44%], **6** [37 mg, 62%], and **7d** [17.5 mg, 36%].

Thermal Reaction of a Mixture of 8d and 9d. A XL solution (1 cm^3) of a 2.6:1-mixture of **8d** and **9d** (98 mg) was heated at 130 °C for 6 d to give **4d** [31 mg, 86%], **6** [35 mg, 88%], and unreacted **8d** and **9d** [22 mg].

References

1) G. Desimoni, G. Tacconi, A. Barco, and G. P. Pollini, "Natural Products Synthesis Through Pericyclic Reactions," (ACS Monograph 180), Am. Chem. Soc., Washington D. C. (1983), pp. 119—254.

2) M. Karpf, *Angew. Chem., Int. Ed. Engl.*, **25**, 414 (1986).

3) S. Masamune, H. Cuts, and M. G. Hogben, *Tetrahedron Lett.*, **1966**, 1017; E. Grovenstein, Jr., D. V. Rao, and J. W. Taylor, *J. Am. Chem. Soc.*, **83**, 1705 (1961).

4) C. G. Scouten, F. E. Barton, Jr., J. R. Burgess, P. R. Story, and J. F. Garst, *J. Chem. Soc., Chem. Commun.*, **1969**, 78; J. F. King and R. G. Pews, *Can. J. Chem.*, **42**, 1294 (1964).

5) O. De Lucchi, V. Lucchini, L. Pasquato, and G. Modena, *J. Org. Chem.*, **49**, 596 (1984).

6) N. Ono, A. Kamimura, and A. Kaji, *Tetrahedron Lett.*, **27**, 1595 (1986).

7) R. B. Woodward and H. Baer, *J. Am. Chem. Soc.*, **70**, 1161 (1948).

8) H. Prinzbach and H. Babsch, *Angew. Chem., Int. Ed. Engl.*, **14**, 753 (1975).

9) H. Matsukubo and H. Kato, *J. Chem. Soc., Perkin Trans. 1*, **1976**, 2565 and D. Cristina, M. De Amici, C. De Micheli, and R. Gandolfi, *Tetrahedron*, **37**, 1349 (1981).

10) M. J. Goldstein and B. G. Odell, *J. Am. Chem. Soc.*, **89**, 6356 (1967).

11) G. Stork, E. E. van Tamelen, L. J. Friedman, and A. W. Burgstahler, *J. Am. Chem. Soc.*, **75**, 384 (1953).

12) T. Uyehara, Y. Kawai, J. Yamada, and T. Kato, *Chem. Lett.*, **1987**, 137.

13) T. Uyehara, S. Miyakoshi, and Y. Kitahara, *Bull. Chem. Soc. Jpn.*, **52**, 2023 (1979).

14) e.g., J. Ciabattoni, J. E. Crowley, and A. S. Kende, *J. Am. Chem. Soc.*, **89**, 2778 (1967).

15) T. H. Kinstle and P. D. Carpenter, *Tetrahedron Lett.*, **1969**, 3943.

16) T.Sasaki, K. Kanematsu, and K. Hayakawa, *J. Chem. Soc., Perkin Trans. 1*, **1972**, 1951.

17) J. D. Loudon and R. K. Razdan, *J. Chem. Soc.*, **1954**, 4299.

18) The former notation expresses the stereochemistry of bicyclo[3.2.2] part and the latter one that of bicyclo[2.2.1] part.

19) R. Miller, *Ber.*, **23**, 1893 (1890).

20) T. Uyehara, Y. Kayama, M. Taniguchi, C. Kabuto, and Y. Kitahara, *Chem. Lett.*, **1977**, 569.

21) H. Takeshita, A. Mori, and S. Kasai, *Bull. Chem. Soc. Jpn.*, **61**, 2259 (1988).

22) S. Itô, H. Takeshita, Y. Shoji, Y. Toyooka, and T. Nozoe, *Tetrahedron Lett.*, **1968**, 3215; S. Itô, A. Mori, Y. Shoji, and H. Takeshita, *ibid.*, **1972**, 2685.

A New Method of Synthesizing 7-(2-Hydroxy-5-oxo-1-cyclopentenyl)heptanoic Acid and Related Compounds

Hirokazu NAORA,* Takashi OHNUKI, and Asao NAKAMURA
Applied Research Dept., Central Laboratories, Ajinomoto Co., Inc.,
1-1, Suzuki-cho, Kawasaki, Kanagawa 210
(Received December 1, 1987)

A useful prostanoid synthon, 7-(2-hydroxy-5-oxo-1-cyclopentenyl)heptanoic acid (**3**), was prepared from commercially available cyclooctanone in two steps. Nine other related cyclopentanoids which are also valuable synthons for prostaglandins were obtained from **3** in reasonable yields via several steps. The procedure is capable of generating these useful synthons on a laboratory scale.

New methods of constructing of cyclopentane derivatives **3**—**7** are highly desirable, since these compounds have served as useful precursors in the synthesis of the naturally occurring prostaglandins and their congeners. In a preliminary report,[1] we described a synthesis of the 15-dehydroPGB$_1$ methyl ester from 7-(2-bromo-5-oxo-1-cyclopentenyl)heptanoate (**4a**) and 1-octen-3-one. Furthermore, some prostaglandin derivatives have been prepared from methyl 7-(2-bromo-3-hydroxy-5-oxo-1-cyclopentenyl)-heptanoate (**5b**) in our laboratory.[2] PGB$_1$ was obtained[3] from 7-(2-hydroxy-5-oxo-1-cyclopentenyl)-heptanoic acid (**3**) and ω-chain moieties via a Grignard reaction as a key step. PGE$_1$, PGF$_1$ and their analogues were prepared from methyl 7-(3-hydroxy-5-oxo-1-cyclopentenyl)heptanoate (**6b**)[4] by means of a Michael-type reaction with several ω-chain moieties, and 11-deoxyPGE$_1$, 11-deoxyPGF$_1$, and their derivatives were derived from methyl 7-(5-oxo-1-cyclopentenyl)heptanoate (**7**).[5]

Recently, we reported[6] the use of the Cleisen condensation of dimethyl 4-oxo-1,12-undecanedioate in preparing methyl 7-(2-hydroxy-5-oxo-1-cyclopentenyl)heptanoate (**3'**). Novák et al.[7] converted **3'** to **4c** by phosphorus trichloride in a 70% yield, and dechlorinated **4c** with a silver–zinc couple to give **7** in a 62% yield. Compound **6b** was prepared via several steps from methyl 7-(2-oxocyclopentyl)heptanoate by Alvarez et al.[8] In this report, we will describe in detail an entirely novel method for the preparation of **3** and the derivation of other prostanoid synthons **4**—**7**.

The precursors **2** were prepared[9] from commercially available starting substances. The yields and conditions are shown in Scheme 1. 1-Cyclooctenyl acetate (**2a**) was allowed to react with succinic anhydride to afford 7-(2-hydroxy-5-oxo-1-cyclopentenyl)heptanoic acid (**3**). The reaction was achieved in 1,2-dichloroethane mediated by aluminium trichloride. The yield, via two steps from cyclooctanone (**1**), was 23%. Compound **3** was obtained from **2b**—**2d** under almost the same conditions (Table 1). The reaction may include Friedel–Crafts-type C–C bond-formations and acid-catalyzed hydrolysis with a C–C bond-cleavage.[10]

Succinyl dichloride instead of succinic anhydride could be available, but the yield of the product was lower. Aluminium tribromide could also mediate the reaction. As for the reaction solvents, the reaction occurred in 1,1,2-trichloroethane, 1,1,2,2-tetrachloroethane, nitromethane, and nitrobenzene. When chlorotrimethylsilane was added to the reaction system, an improvement in its yield was observed.

Compound **3** was converted to **4a** in one pot by bromination with dibromotriphenylphosphorane and subsequent esterification with absolute methanol. 7-(2-Bromo-5-oxo-1-cyclopentenyl)heptanoic acid (**4b**) was obtained by a similar method without methanol. After the removal of the triphenylphosphine oxide by silica-gel chromatography, pure **4a** or **4b** was obtained in a 68 or 67% yield respectively. Methyl 7-(2-chloro-5-oxo-1-cyclopentenyl)heptanoate (**4c**) was obtained from **3** in a 55% yield by chlorination with phosphorus trichloride and by subsequent esterification. Methyl 7-(2-iodo-5-oxo-1-cyclopentenyl)-

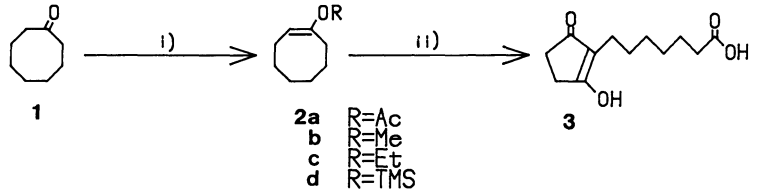

i) a) Isopropenyl acetate, p-TsOH, 115 °C, 95%; b) $HC(OMe)_3$, p-TsOH, r.t., 75%;
c) $HC(OEt)_3$, p-TsOH, r.t., 45%; d) TMSCl, Et_3N, DMF, reflux, 80%.
ii) Succinic anhydride, $AlCl_3$, 1,2-dichloroethane, 80 °C.

Scheme 1.

Table 1. Synthesis of **3** from **2**

	Starting material	Condition[a]				Yield/%	
		Catalyst	Solvent	Time/h	Temp/°C	Crude	Recrystal.
1	**2a** (R=Ac)	$AlCl_3$	A	28	80	20	18
2	**2a** (R=Ac)	$AlCl_3$	A	92	80	42	22
3[b]	**2a** (R=Ac)	$AlCl_3$	A	28	80	47	24
4	**2a** (R=Ac)	$AlCl_3$	B	24	110	31	16
5	**2a** (R=Ac)	$AlCl_3$	C	24	110	27	12
6	**2a** (R=Ac)	$AlCl_3$	D	3	100	16	10
7	**2a** (R=Ac)	$AlCl_3$	E	3	100	19	13
8	**2a** (R=Ac)	$AlBr_3$	A	28	80	20	18
9	**2b** (R=Me)	$AlCl_3$	A	63	80	27	17
10	**2c** (R=Et)	$AlCl_3$	A	92	80	16	10
11	**2d** (R=TMS)	$AlCl_3$	A	28	80	29	13

a) Catalyst: 1.95 equiv to **2**. Solvent: A: 1,2-dichloroethane; B: 1,1,2-trichloroethane; C: 1,1,2,2-tetrachloroethane; D: nitromethane; E: nitrobenzene. b) TMSCl was added (2.3 equiv to **2a**).

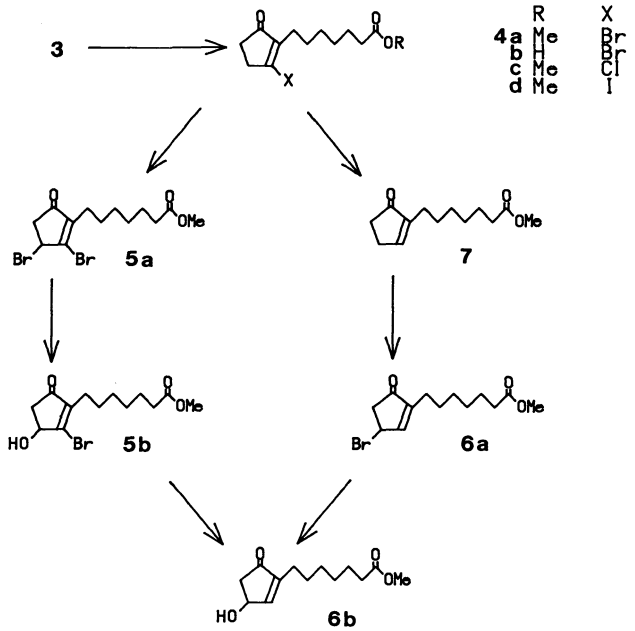

Scheme 2.

heptanoate (**4d**) was derived from methyl 7-(2-bromo-5-oxo-1-cyclopentenyl)heptanoate (**4a**) with sodium iodide quantitatively.

Methyl 7-(2,3-dibromo-5-oxo-1-cyclopentenyl)-heptanoate (**5a**) was obtained in a 51% yield from **4a** by allyl bromination with *N*-bromosuccinimide in tetrachloromethane. The substitution of the 3-bromo group of **5a** to the 3-hydroxyl group was achieved by the treatment of silver perchlorate, giving methyl 7-(2-bromo-3-hydroxy-5-oxo-1-cyclopentenyl)heptanoate (**5b**) in an 86% yield. Compound **5b** could be converted to methyl 7-(3-hydroxy-5-oxo-1-cyclopentenyl)heptanoate (**6b**) in a 90% yield by debromination with a silver-zinc couple.

Methyl 7-(2-bromo-5-oxo-1-cyclopentenyl)heptanoate (**4a**) was debrominated by a method similar to that described above to give a known prostaglandin intermediate **7** in a 96% yield. Methyl 7-(3-bromo-5-oxo-1-cyclopentenyl)heptanoate (**6a**) was obtained from **7** with *N*-bromosuccinimide in a 43% yield and converted to **6b** in a 92% yield with silver perchlorate.

The outlined synthesis represents a short and facile route to prostaglandin synthons **3**—**7**, because the starting materials are easily accessible and the operations of the reactions and purifications are suitable for the preparation of a sample.

Experimental

The ^1H NMR spectra were measured with a Varian EM-390 (90 MHz) spectrometer. The chemical shifts are expressed in parts per million (ppm) (δ) downfield from tetramethylsilane. The infrared spectra were obtained using a JASCO IR-810 Spectrometer. The low-resolution mass spectra (MS) and high-resolution mass spectra (HRMS) were determined on a JEOL G-300 Mass Spectrometer. The melting points and boiling points are uncorrected.

7-(2-Hydroxy-5-oxo-1-cyclopentenyl)heptanoic Acid (3).[3] Succinic anhydride (1.00 g: 10.0 mmol) was added to a suspension of 2.60 g (19.5 mmol) of aluminium trichloride in 1,2-dichloroethane, and the mixture was stirred for 1.5 h at room temperature. At 0 °C, to the resultant mixture were added dropwise 1.70 g (10.0 mmol) of 1-cyclooctenyl acetate (**2a**) and 2.50 g of chlorotrimethylsilane successively. The reaction mixture was then stirred at room temperature for 24 h, heated at 80 °C for 28 h, and then poured into 1.5 M (1 M=1 mol dm^{-3}) HCl with ice, and extracted with 40 ml of ethyl acetate five times. The combined organic layer was washed with 20 ml of water and extracted with 80 ml of aq. sat. $NaHCO_3$ and 20 ml of water. The resultant inorganic layer was adjusted to pH 1.5 and extracted with 40 ml of ethyl acetate four times. After washing with 30 ml of brine, the solvents were removed to give 1.06 g of a solid (47%). Recrystallization from water gave 0.54 g (24%) of **3**; mp 154.5—156 °C (lit,[3] mp 156—157 °C). ^1H NMR (acetone-d_6) δ=4.2—2.5 (br, 2H), 2.37 (s, 4H), 2.36—2.00 (m, 4H), and 1.8—1.2 (m, 8H); (methanol-d_4) δ=2.43 (s, 4H), 2.4—1.9 (m, 4H), and 1.8—1.2 (m, 8H); IR (KBr) 3400, 2900, 2830, 1690, 1550, and 1360 cm^{-1}.

Methyl 7-(2-Bromo-5-oxo-1-cyclopentenyl)heptanoate (4a). At 0 °C, to a stirred solution of 28.8 g (0.11 mol) of triphenylphosphine in 700 ml of benzene was added 110 ml of a 1 M bromine-benzene solution drop by drop, over a

15-min period. To the resultant mixture were then added 10 ml of triethylamine and 11.3 g of **3**. The reaction mixture was stirred at room temperature for 17 h, and then 10 ml of absolute methanol was added. After stirring for 15 min, the reaction mixture was poured into 300 ml of water. After ethereal extraction, the removal of the solvents gave crude **4a**. Silica-gel column chromatography (Merck Kieselgel 60 No. 7734: 300 g; hexane:ethyl acetate=2:1) gave 10.3 g (68%) of pure **4a**; bp 122 °C/0.15 mmHg (1 mmHg=133.322 Pa). ^{1}H NMR (chloroform-d_1) δ=3.56 (s, 3H), 2.95—2.7 (m, 2H), 2.65—2.4 (m, 2H), 2.4—2.15 (m, 4H), and 1.8—1.2 (m, 8H); IR (film) 2930, 2850, 1735, 1705, and 1630 cm^{-1}; Found: C, 51.41; H, 6.35; Br, 26.48%. Calcd for $C_{13}H_{19}O_3Br$ (Mw=303.2): C, 51.50; H, 6,32; Br, 26.35%. MS *m/z* 304, 302 (M^+), 273, 271 (M−MeO), and 223 (M−Br).

7-(2-Bromo-5-oxo-1-cyclopentenyl)heptanoic Acid (4b). To a solution of 288 mg of triphenylphosphine in 10 ml of benzene was added 1.1 ml of a 1 M bromine-benzene solution, drop by drop, at 0 °C. After the mixture had then been stirred for 15 min at room temperature, 0.15 ml of triethylamine and 113 mg of **3** were added at 0 °C. The reaction mixture was then stirred for 24 h at room temperature and poured into 20 ml of ice water. The mixture was extracted with 20 ml of ether three times. The organic layer was washed with equal volumes of water and brine, and then dried. After the evaporation of the solvent, the residue was purified on silica-gel chromatography (benzene:acetone=1:1) to give 97 mg (67%) of **4b**; ^{1}H NMR (chloroform-d_1) δ=3.0—2.8 (m, 2H), 2.60—2.43 (m, 2H), 2.30 (t, J=7 Hz, 2H), 2.20 (t, J=6 Hz, 2H), and 1.9—1.25 (m, 8H); IR (film) 3100 (br), 2920, 2840, 1730, 1700, and 1620 cm^{-1}.

To a solution of 50 mg of **4b** in 5 ml of methanol was added an excess of an ethereal diazomethane solution. An ordinary work-up and purification by means of silica-gel column chromatography (LiChroprep Si 60) gave 39 mg (78%) of methyl 7-(2-bromo-5-oxo-1-cyclopentenyl)heptanoate (**4a**); The ^{1}H NMR and IR spectra of this agreed with those of an authentic sample.

Methyl 7-(2-Chloro-5-oxo-1-cyclopentenyl)heptanoate (4c).[7] At 0 °C, to a stirred suspension of 2.24 g of 7-(2-hydroxy-5-oxo-1-cyclopentenyl)heptanoic acid (**3**) in 10 ml of benzene (dried with zeolite A-4) were added 2 ml of phosphorus trichloride and 2.02 g of triethylamine successively. The reaction mixture was then stirred for 30 min at room temperature and heated under reflux for 2 h. Methanol (1 ml) and then 10 ml of water were stirred in, drop by drop, at 0 °C. The reaction mixture was extracted with 10 ml of ether three times. A combined organic layer was washed with equal volumes of water, 0.1 M $NaHCO_3$ (twice), water, and brine successively, and then dried. Silica-gel column chromatography (LiChroprep Si 60, hexane:ethyl acetate=2:1) gave 1.42 g (55%) of **4c**; ^{1}H NMR (chloroform-d_1) δ=3.60 (s, 3H), 2.85—2.67 (m, 2H), 2.60—2.40 (m, 2H), 2,35 (t, J=6.6 Hz, 2H), 2.22 (t, J=6.6 Hz, 2H), and 1.8—1.1 (m, 8H); IR (film) 2920, 2850, 1735, 1705, and 1630 cm^{-1}; MS *m/z* 260, 258 (M^+), 229, 227 (M−MeO), 223 (M−Cl), and 191 (M−Cl−MeOH).

Methyl 7-(2-Iodo-5-oxo-1-cyclopentenyl)heptanoate (4d). Sodium iodide (0.5 g) which had been dried at 100 °C under 1 mmHg for 3 h and 0.05 g of *p*-toluenesulfonic acid were added to a solution of 100 mg of methyl 7-(2-bromo-5-oxo-1-cyclopentenyl)heptanoate (**4a**) in acetone dried by zeolite A-4. The reaction mixture was then stirred at room temperature for 21 h. The resultant mixture was filtered, and the precipitate was washed with 20 ml of ether. The combined solution was concentrated under reduced pressure. Ether and water (10 ml and 5 ml respectively) were added to the residue. After vigorous shaking, the separated inorganic layer was extracted with 5 ml of ether twice. The combined ethereal layer was washed with equal volumes of water four times and with brine twice, and then dried. The removal of the solvents gave 116 mg (100%) of **4d**; bp 143 °C/0.3 mmHg; ^{1}H NMR (chloroform-d_1) δ=3.60 (s, 3H), 2.95 (m, 2H), 2.43 (m, 2H), 2.27 (t, J=6 Hz, 2H), 2.23 (t, J=6 Hz, 2H), and 1.8—1.2 (m, 8H); IR (film) 2920, 2840, 1730, 1700, and 1605 cm^{-1}; Found: C, 44.61; H, 5.48; I, 35.24%. Calcd for $C_{13}H_{19}O_3I$ (Mw=350.2): C, 44.59; H, 5.47; I, 35.60%.

Methyl 7-(2,3-Dibromo-5-oxo-1-cyclopentenyl)heptanoate (5a). *N*-Bromosuccinimide (0.8 g) and 0.03 g of benzoyl peroxide were added to a solution of 1.21 g of methyl 7-(2-bromo-5-oxo-1-cyclopentenyl)heptanoate (**4a**) in 20 ml of tetrachloromethane (distilled from P_2O_5), and the resultant mixture was heated under reflux for 3 h. Furthermore, 0.4 g of *N*-bromosuccinimide and 0.01 g of benzoyl peroxide were added at room temperature, and the mixture was heated under reflux for 1.5 h. The reaction mixture was then filtered, and the precipitates were washed with 10 ml of tetrachloromethane. After the subsequent removal of the solvents, silica-gel column chromatography (LiChroporep Si 60; hexane:ethyl acetate=2:1) gave 0.78 g (51%) of the oily title compound **5a**; bp 85 °C/0.18 mmHg. ^{1}H NMR (chloroform-d_1) δ=4.98 (dd, J=6, 3 Hz, 1H), 3.60 (s, 3H), 3.13 (dd, J=6, 18 Hz, 1H), 2.93 (dd, J=18, 3 Hz, 1H), 2.27 (t-like, J=7.5 Hz, 4H), and 1.8—1.2 (m, 8H); IR (film) 2940, 2860, 1740, 1720, and 1620 cm^{-1}; MS *m/z* 353, 351, 349 (M−MeO), 303, 301 (M−Br), and 271, 269 (M−Br−MeOH); (HRMS) Found: *m/z* 352.9392, 350.9452, 348.9471. Calcd for $C_{12}H_{15}O_2Br_2$: (M−MeO): 352.9398, 350.9441, 348.9940; Found: C, 40.73; H, 4.87; Br, 42.22%. Calcd for $C_{13}H_{18}O_3Br_2$ (Mw=382.1):C, 40.87; H, 4.75; Br, 41.82%.

Methyl 7-(2-Bromo-3-hydroxy-5-oxo-1-cyclopentenyl)-heptanoate (5b). To a solution of 0.76 g of methyl 7-(2,3-dibromo-5-oxo-1-cyclopentenyl)heptanoate (**5a**) in 21 ml of aq. acetone (acetone:water=20:1) was added 1 g of silver perchlorate at room temperature under argon. The reaction mixture was stirred at room temperature for the first 50 min and at 50 °C for the next hour. To the mixture was then added 0.5 g of $NaHCO_3$ at room temperature, after which the mixture was stirred for 3 min. The reaction mixture was filtered, and the filtrate, with 70 ml of ether added, was washed with an equal volume of aq.sat.$NaHCO_3$, water and brine, and dried. The subsequent removal of the solvents gave 0.55 g (86%) of the oily title compound **5d**; ^{1}H NMR (chloroform-d_1) δ=4.77 (m, 1H), 3.58 (s, 3H), 2.87 (dd, J=18, 6 Hz, 1H), 2.6—2.1 (m, 5H), and 1.9—1.2 (m, 8H); IR (film) 3450 (br), 2940, 2860, 1740, 1720, and 1630 cm^{-1}; MS *m/z* 240 (M+H−Br), 222 (M+H−Br−H_2O), 208 (M+H−Br−MeOH), and 190 (M+H−Br−MeOH−H_2O); (HRMS) Found: *m/z* 240.1373. Calcd for $C_{13}H_{20}O_4$: (M+H−Br), 240.1362.

Methyl 7-(3-Hydroxy-5-oxo-1-cyclopentenyl)heptanoate (6b).[5] To a solution of 48 mg of silver acetate in 1 ml of glacial acetic acid at 100 °C was added 107 mg of zinc powder which had been activated by 10% HCl. The reaction

mixture was then stirred at 100 °C for 30 min. The supernatant liquid was removed by decantation at room temperature, after which the precipitate was washed with 1 ml of acetic acid twice and with 2 ml of ether five times. To the resultant precipitate was added a solution of 100 mg of methyl 7-(2-bromo-3-hydroxy-5-oxo-1-cyclopentenyl)-heptanoate (**5b**) in 2 ml of methanol, and the mixture was heated under reflux while being vigorously stirred for 2 h. The reaction mixture was filtered through a sintered-glass filter (G-4). The precipitate was then washed with methanol, and the washing was combined with the mother liquid. The resultant solution was concentrated under reduced pressure to dryness, and 5 ml of ether was added. The precipitate was separated, dissolved in 5 ml of 1 M HCl, and extracted three times by the use of 5 ml of ether. The ethereal layers thus obtained were washed with water and brine, and dried. The removal of the solvents from the combined ethereal layer gave 61 mg (90%) of **6b**. The ^{1}H NMR and IR spectra of this substance agreed with those in the literature.[5]

Methyl 7-(5-Oxo-1-cyclopentenyl)heptanoate (7).[7] To a solution of 49 mg of silver acetate in 5 ml of glacial acetic acid at 100 °C was added 1 g of zinc powder which had been activated by 10% HCl. The reaction mixture was then stirred at 100 °C for 7 min. The supernatant liquid was removed by decantation at room temperature. The precipitate was washed with 5 ml of acetic acid once and with 5 ml of ether five times. To the resultant precipitate was added a solution of 700 mg of methyl 7-(2-bromo-5-oxo-1-cyclopentenyl)-heptanoate (**4a**) in 5 ml of methanol. The reaction mixture was then stirred at 60 °C for 24 h and filtered through a sintered-glass filter (G-4). The precipitate was washed with methanol, and the washing was combined with the mother liquid. The resultant solution was concentrated under reduced pressure to dryness, and 10 ml of ether was added. The precipitate was dissolved in 10 ml of 1 M HCl and extracted with 10 ml of ether three times. The extracts thus obtained were washed with water and brine, and then dried. The subsequent removal of the solvents gave 496 mg (96%) of **7**. The ^{1}H NMR and IR spectra of this substance agreed with those in the literature.[7]

Methyl 7-(3-Bromo-5-oxo-1-cyclopentenyl)heptanoate (6a).[11] A solution of 780 mg of methyl 7-(5-oxo-1-cyclopentenyl)heptanoate (**7**), 682 mg of *N*-bromosuccinimide, and 24 mg of benzoyl peroxide in 35 ml of anhydrous tetrachloromethane was heated under reflux for 2.5 h under argon. The reaction mixture was then filtered, and the precipitate was washed with 50 ml of tetrachloromethane. After the removal of the solvents from the combined mother liquid and washing, purification by silica-gel column chromatography (LiChroprep Si 60; hexane:ethyl acetate=2:1) gave 450 mg (43%) of the oily title compound. The ^{1}H NMR and IR spectra of this substance agreed with those in the literature.[11]

Conversion to 6b from 6a. To a solution of 450 mg of methyl 7-(3-bromo-5-oxo-1-cyclopentenyl)heptanoate (**6a**) in 18 ml of aq. acetone (acetone:water=15:3) at 0 °C was added 306 mg of silver perchlorate under argon, after which the reaction mixture was stirred for 1 h. To the reaction mixture was then added 175 mg of $NaHCO_3$, and the mixture was stirred for 5 min. After the filtration of the AgBr, the filtrate was extracted with 20 ml of ether. The ethereal extracts were washed with equal volumes of aq. sat.$NaHCO_3$, water, and brine successively, and then dried. After the subsequent removal of the solvents, 326 mg (92%) of the title compound was obtained. The ^{1}H NMR and IR spectra of this substance agreed with those in the literature.[5]

References

1) H. Naora, T. Ohnuki, and A. Nakamura, *Chem. Lett.*, **1988**, 143.

2) The method will be reported in detail in the near future.

3) P. W. Collins, C. J. Jung, and R. Pappo, *Isr. J. Chem.*, **6**, 839 (1968); J. Katsube and M. Matsui, *Agric. Biol. Chem.*, **33**, 1078 (1969); Y. Yura and J. Ide, *Chem. Pharm. Bull.*, **17**, 408 (1969); B. D. Polis, S. Kwong, E. Polis, G. Nelson, and H. W. Shmukler, *Physiol. Chem. Phys.*, **11**, 109 (1979).

4) C. J. Sih, J. B. Heather, and G. P. Peruzzotti, *J. Am. Chem. Soc.*, **95**, 1676 (1973); C. Luthy, P. Konstantin, and K. G. Untch, *ibid.*, **100**, 6211 (1978).

5) M. B. Floyd and M. J. Weiss, *Prostaglandins*, **3**, 921 (1973); C. J. Sih, R. G. Solomon, P. Price, R. Sood, G. Peruzzotti, *J. Am. Chem. Soc.*, **97**, 857 (1975).

6) H. Naora, T. Ohnuki, and A. Nakamura, *Bull. Chem. Soc. Jpn.*, **61**, 993 (1988).

7) L. Novák, G. Baán, J. Marosfalvi, and C. Szántay, *Chem. Ber.*, **113**, 2939 (1980).

8) F. S. Alvarez, D. Wren, and A. Prince, *J. Am. Chem. Soc.*, **94**, 7823 (1972).

9) N. J. Leonard and F. H. Owens, *J. Am. Chem. Soc.*, **80**, 6039 (1958); R. A. Wohl, *Synthesis*, **1974**, 39; H. O. House, L. J. Czuba, M. Gall, and H. D. Olmstead, *J. Org. Chem.*, **34**, 2324 (1969); G. M. Rubottom and R. C. Mott, *ibid.*, **44**, 1731 (1979).

10) F. Merényi and M. Nilsson, *Acta Chem. Scand.*, **18**, 1368 (1964); V. J. Grenda, G. W. Lindberg, N. L. Wendler, and S. H. Pines, *J. Org. Chem.*, **32**, 1236 (1967).

11) L. Heslinga, M. V. Gorkom, and D. A. VanDorp, *Recl. Trav. Chim. Pays-Bas*, **87**, 1421 (1968).

The Synthesis of Methyl (15*S*)-16-Hydroxydehydroabietate and Its (15*R*)-Epimer

Takashi MATSUMOTO,* Sachihiko IMAI, and Noriaki HAYASHI
Department of Chemistry, Faculty of Science, Hiroshima University,
Higashisenda-machi, Naka-ku, Hiroshima 730
(Received December 5, 1987)

In order to elucidate the absolute configuration of C-15 in natural 16-hydroxydehydroabietic acid, a metabolite of (+)-dehydroabietic acid in rabbits, methyl (+)-dehydroabietate was transformed into methyl (15*S*)-16-hydroxy-8,11,13-abietatrien-18-oate (**3a**) and its (15*R*)-epimer (**3b**). The synthetic **3a** was identical with a methyl ester derived from the natural acid. Thus, the absolute configuration of C-15 in natural 16-hydroxydehydroabietic acid was conclusively assigned as an *S*-configuration.

16-Hydroxydehydroabietic acid (**1**), a biotransformation product of (+)-dehydroabietic acid (**2**), has been isolated independently as its methyl ester (**3**) by three groups, Ekman and Sjöholm,[1] Asakawa et al.,[2] and Nakashima et al.[3] However the absolute configuraion of C-15 in the biotransformation product has remained unsettled. In order to elucidate the unknown stereochemistry at C-15, we have now attempted the syntheses of methyl (15*S*)-16-hydroxy-8,11,13-abietatrien-18-oate (**3a**) and its (15*R*)-epimer (**3b**) starting from methyl (+)-dehydroabietate (**4**).

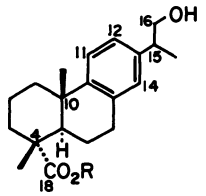

1 R=H
3 R=Me

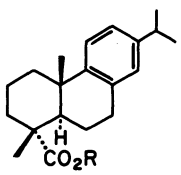

2 R=H
4 R=Me

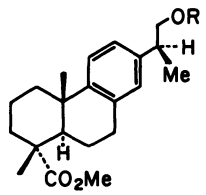

3a
20a

R=H
R=COC$_6$H$_4$NO$_2$(p)

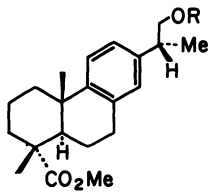

3b
20b

Dehydrogenation of **4** with 2,3-dichloro-5,6-dicyano-1,4-benzoquinone in refluxing 1,4-dioxane afforded the corresponding isopropenyl compound (**5**) which was immediately submitted to hydroboration-oxidation to give a mixture of the desired C-15 epimeric methyl 16-hydroxy-8,11,13-abietatrien-18-oates (**3**) in 39% yield from **4**. Compound **3** was then transformed into a mixture of the corresponding benzoates (**6**) by heating with benzoyl chloride in pyridine in a quantitative yield. Since a separation of the C-15 epimers in the mixture of **3** or **6** was unsuccessful, the benzoate **6** was converted into a C-15 epimeric mixture (ca. 1:1 ratio) of 12-acetyl compounds **7a,b** by Friedel–Crafts acylation using acetyl chloride and anhydrous aluminum chloride in dichloromethane in 86% yield. This mixture of **7a,b** was carefully separated by repeated column chromatography on silica gel and recrystallization to afford a pure crystalline methyl 12-acetyl-16-benzoyloxy-8,11,13-abietatrien-18-oate (**7a**), mp 113—114 °C, and its C-15 epimer (**7b**), mp 140—141.5 °C. The absolute configuration of C-15 in these diastereomers **7a** and **7b** were determined by the following chemical correlation. The Baeyer–Villiger oxidation of **7a** and **7b** with *m*-chloroperbenzoic acid and *p*-toluenesulfonic acid in refluxing 1,2-dichloroethane, followed by hydrolysis of the resulting acetates, **8a** (91%) and **8b** (85%), with aqueous sodium hydroxide in refluxing methanol, afforded the C-15 epimeric methyl 12,16-dihydroxy-8,11,13-abietatrien-18-oates **9a** (98%) and **9b** (92%), respectively. For the protection of the hydroxyl groups, the 12,16-diol **9a** was treated with a mixture of chloromethyl methyl ether, potassium iodide, and anhydrous potassium carbonate in refluxing ethyl methyl ketone to give a 12,16-methylenedioxy compound **10a** (55%) together with a 12,16-bis(methoxymethyl) ether **11a** (4%) and a 16-methoxymethyl ether **12a** (18%). The hydrolysis of **12a** with dilute hydrochloric acid in refluxing tetrahydrofuran produced **9a** and **10a** in 62 and 27% yields, respectively. A reduction of **10a** with lithium aluminum hydride in ether followed by tosylation of the resulting alcohol with *p*-toluenesulfonyl chloride in pyridine afforded the tosylate **13a** (95%). This was further treated with sodium iodide and zinc powder in *N,N*-dimethylformamide at 120—125 °C to give a 4,4-dimethyl compound **14a** (64%). The hydrolysis of **14a** with dilute hydrochloric acid in refluxing ethanol produced the known (15*S*)-16-hydroxyferruginol(**15a**)[4,5] in 78% yield. Thus, the absolute configurations of C-15 in **7a** and its derivatives **8a—14a** were assigned as the same *S*-configuration.

Similarly, the 12,16-diol **9b** was also converted into the known (15*R*)-16-hydroxyferruginol (**15b**).[4,5] Thus, the absolute configurations of C-15 in **7b** and its

derivatives **8b**—**14b** were also assigned as the same *R*-configuration.

Subsequently, syntheses of methyl (15*S*)-16-hydroxy-8,11,13-abietatrien-18-oate (**3a**) and its (15*R*)-epimer (**3b**) were carried out as follows. Partial hydrolysis of methyl (15*S*)-12-acetoxy-16-benzoyloxy-8,11,13-abietatrien-18-oate (**8a**) with dilute hydrochloric acid in refluxing methanol afforded methyl (15*S*)-16-benzoyloxy-12-hydroxy-8,11,13-abietatrien-18-oate (**16a**) in 87% yield. In order to remove the C-12 hydroxyl group, the phenolic compound **16a** was converted into the corresponding 1-phenyl-5-tetrazolyl ether **17a** (91%) by refluxing with 5-chloro-1-phenyl-1*H*-tetrazole and anhydrous potassium carbonate in ethyl methyl ketone. However, an attempt to hydrogenolyze this ether **17a** over 10% Pd–C in ethanol at room temperature gave no deoxygenation product and only the starting **17a** was recovered. Therefore, the 12,16-diol **9a** was treated with 5-chloro-1-phenyl-1*H*-tetrazole under the same conditions to produce methyl (15*S*)-16-hydroxy-12-(1-phenyl-1*H*-tetrazol-5-yloxy)-8,11,13-abietatrien-18-oate (**18a**: 48%) together with a dihydrobenzofuran derivative **19a** (37%) which was identical with authentic methyl (15*S*)-12,16-epoxy-8,11,13-abietatrien-18-oate.[6] Catalytic hydrogenolysis of **18a** over 10% Pd–C in ethanol at room temperature under an atmosphere of hydrogen afforded the desired methyl (15*S*)-16-hydroxy-8,11,13-abietatrien-18-oate (**3a**: 39%[7]), which gave a 4-nitrobenzoate (**20a**), mp 116—117 °C.

Similarly, methyl (15*R*)-12-acetoxy-16-benzoyloxy-8,11,13-abietatrien-18-oate (**8b**) was also transformed into methyl (15*R*)-16-hydroxy-8,11,13-abietatrien-18-oate (**3b**), which gave a 4-nitrobenzoate (**20b**), mp 133—134 °C. The methyl ester of the metabolite of (+)-dehydroabietic acid (**2**) in rabbits[2] and its 4-nitrobenzoate (mp 116—117 °C) were identical with the synthetic **3a** and **20a**, respectively.

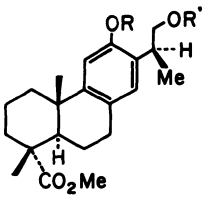

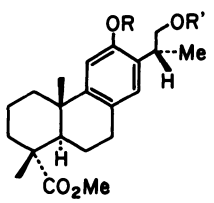

8a	R=Ac, R'=Bz	8b
9a	R=R'=H	9b
10a	R·R'=$-CH_2-$	10b
11a	R=R'=CH_2OMe	11b
12a	R=H, R'=CH_2OMe	12b
16a	R=H, R'=Bz	16b
17a	R=Pt, R'=Bz	17b
18a	R=Pt, R'=H	18b

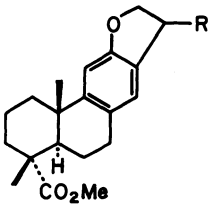

Bz = COC_6H_5

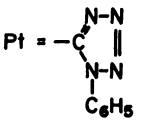

19a R=β-Me
19b R=α-Me

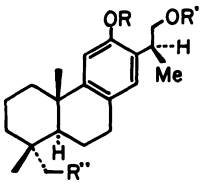

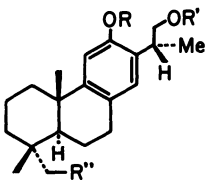

13a	R·R'=$-CH_2-$, R''=OTs	13b
14a	R·R'=$-CH_2-$, R''=H	14b
15a	R=R'=R''=H	15b

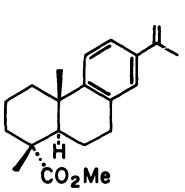

5

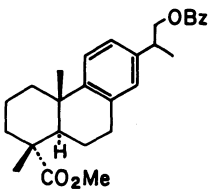

6

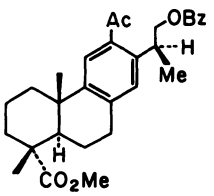

7a

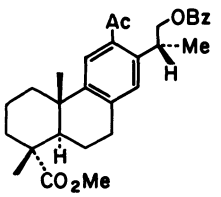

7b

Experimental

All melting points are uncorrected. The IR spectra and optical rotations were measured in chloroform, and the ^1H NMR spectra in carbon tetrachloride at 60 MHz, with tetramethylsilane as an internal standard, unless otherwise stated; s: singlet, bs: broad singlet, d: doublet, bd: broad doublet, dd: double doublet, m: multiplet. The column chromatography was performed using Merck silica gel (0.063 mm).

Methyl 8,11,13,15-Abietatetraen-18-oate (5). A mixture of methyl (+)-dehydroabietate (**4**) (21.07 g) and 2,3-dichloro-5,6-dicyano-1,4-benzoquinone (96%: 19.01 g) in 1,4-dioxane (210 ml) was refluxed for 4 h. The mixture was passed through an alumina (Merck Act. II—III, 200 g) column and the column was washed with benzene (600 ml). The eluate was evaporated in vacuo to give a crude **5** (16.88 g) as an oil, which was used, without purification, in the next reaction. IR 1715 and 1625 cm^{-1}, ^1H NMR δ=1.19 (3H, s, $C_{10}-CH_3$), 1.22 (3H, s, C_4-CH_3), 2.08 (3H, bs, $C_{15}-CH_3$), 3.61 (3H, s,

$-CO_2CH_3$), 4.88 (1H, bs) and 5.17 (1H, bs) ($-C(CH_3)=C\underline{H}_2$), 6.93 (1H, s) and 7.05 (2H, s) (aromatic protons).

Methyl 16-Hydroxy-8,11,13-abietatrien-18-oate (3). A solution of borane-tetrahydrofuran complex (1 mol dm^{-3}: 27.0 ml) was added to a stirred solution of the crude **5** (16.88 g) in dry tetrahydrofuran (170 ml) at −15—−10 °C for 20 min under a stream of nitrogen. After the mixture had been stirred at −10—0 °C for 10 min and at 0—5 °C for 3 h, there were added successively aqueous tetrahydrofuran (50%: 11.8 ml), aqueous sodium hydroxide (12%: 11.8 ml), and hydrogen peroxide (30%: 11.8 ml) at −15—−5 °C. The mixture was stirred at −5—0 °C for 30 min and then at room temperature for 1 h, diluted with brine, and extracted with ether. The ether extract was washed with brine, dried over sodium sulfate, and evaporated in vacuo. The residue was chromatographed on silica gel (0.063—0.200 mm, 200 g), using ether-benzene (3:97) as an eluent, to give mainly methyl dehydroabietate (**4**) (6.97 g). Further elution with ether-benzene (3:97 and then 6:94) afforded a mixture of C-15 epimers **3** (8.64 g: 39.0% from **4**) as an oil which, after standing at room temperature, was solidified. IR 3580, 3450, and 1720 cm^{-1}; ^1H NMR (90 MHz, $CDCl_3$) δ=1.19 (3H, s, C_{10}-CH_3), 1.23 (3H, d, J=7 Hz, C_{15}-CH_3), 1.27 (3H, s, C_4-CH_3), 3.67 (2H, d, J=7 Hz, $-C\underline{H}_2OH$), 3.67 (3H, s, $-CO_2CH_3$), 6.86 (1H, bs, C_{14}-H), 6.96 (1H, dd, J=9 and 2 Hz, C_{12}-H), 7.18 (1H, d, J=9 Hz, C_{11}-H). Found: C, 76.14; H, 9.38%. Calcd for $C_{21}H_{30}O_3$: C, 76.32; H, 9.15%.

Methyl 16-Benzoyloxy-8,11,13-abietatrien-18-oate (6). A mixture of **3** (7.992 g) and benzoyl chloride (4.18 ml) in pyridine (15.0 ml) was heated at 75—80 °C for 1.5 h. The mixture was cooled, poured into ice-dilute hydrochloric acid, and extracted with ether. The ether extract was washed successively with dilute hydrochloric acid, aqueous sodium hydrogencarbonate, and brine. The dried solution was evaporated in vacuo. The residue was chromatographed on silica gel (0.063—0.200 mm, 200 g), using hexane-benzene (2:8) as an eluent, to give an oily mixture of C-15 epimeric benzoates **6** (10.337 g: 98.4%). IR 1720 cm^{-1},^1H NMR (90 MHz, $CDCl_3$) δ=1.19 (3H, s, C_{10}-CH_3), 1.26 (3H, s, C_4-CH_3), 1.36 (3H, d, J=7 Hz, C_{15}-CH_3), 3.14 (1H, m, C_{15}-H), 3.65 (3H, s, $-CO_2CH_3$), 4.27 (1H, dd, J=11 and 7 Hz) and 4.41 (1H, dd, J=11 and 7 Hz) (C_{15}-CH_2O-), 6.92 (1H, bs, C_{14}-H), 7.00 (1H, dd, J=9 and 2 Hz, C_{12}-H), 7.18 (1H, d, J=9 Hz, C_{11}-H), 7.25—7.6 (3H, m) and 7.98 (2H, dd, J=8 and 2 Hz) ($-OCOC_6H_5$). Found: C, 77.54; H, 8.19%. Calcd for $C_{28}H_{34}O_4$: C, 77.39; H, 7.89%.

Methyl (15S)-12-Acetyl-16-benzoyloxy-8,11,13-abietatrien-18-oate (7a) and Its (15R)-Epimer (7b). Anhydrous aluminum chloride (1.70 g) was added at −10 °C to a stirred solution of **6** (1.387 g) and acetyl chloride (0.91 ml) in dichloromethane (15 ml). The mixture was stirred at this temperature for 15 min and then at room temperature for 64 h, poured into ice-dilute hydrochloric acid, and extracted with ether. The ether extract was washed successively with aqueous sodium hydrogencarbonate and brine, dried, and evaporated in vacuo. The residue was chromatographed on silica gel (50 g), using hexane-chloroform (2:8) as an eluent, to give a C-15 epimeric mixture (ca. 1:1 ratio) of methyl 12-acetyl-16-benzoyloxy-8,11,13-abietatrien-18-oate (**7a,b**) (1.314 g: 86.4%). The mixture (**7a,b**) was separated into the pure **7a**, mp 113—114 °C (from methanol), $[\alpha]_D$ +49.2° (*c* 2.32), IR 1718 and 1680 cm^{-1}, and **7b**, mp 140—141.5 °C (from methanol), $[\alpha]_D$ +49.1° (*c* 3.95), IR 1718 and 1680 cm^{-1}, by repeated column chromatography on silica gel and recrystallization. ^1H NMR of **7a** (90 MHz) δ=1.19 (3H, s, C_{10}-CH_3), 1.22 (3H, s, C_4-CH_3), 1.31 (3H, d, J=7 Hz, C_{15}-CH_3), 2.47 (3H, s, C_{12}-$COCH_3$), 3.62 (3H, s, $-CO_2CH_3$), 3.87 (1H, m, C_{15}-H), 4.33 (2H,d, J=7 Hz, C_{15}-CH_2O-), 7.03 (1H, s, C_{14}-H), 7.39 (1H, s, C_{11}-H), 7.2—7.45 (3H, m) and 7.92 (2H, dd, J=8 and 2 Hz) ($-OCOC_6H_5$). Anal. of **7a**; Found: C, 75.72; H, 7.89%. Calcd for $C_{30}H_{36}O_5$: C, 75.60; H, 7.61%. ^1H NMR of **7b** (90 MHz) δ=1.19 (3H, s, C_{10}-CH_3), 1.22 (3H, s, C_4-CH_3), 1.32 (3H, d, J=7 Hz, C_{15}-CH_3), 2.47 (3H, s, C_{12}-$COCH_3$), 3.62 (3H, s, $-CO_2CH_3$), 3.88 (1H, m, C_{15}-H), 4.30 (2H, d, J=7 Hz, C_{15}-CH_2O-), 7.02 (1H, s, C_{14}-H), 7.39 (1H, s, C_{11}-H), 7.2—7.45 (3H, m) and 7.92 (2H, dd, J=8 and 2 Hz) ($-OCOC_6H_5$). Anal. of **7b**; Found: C, 75.42; H, 7.91%. Calcd for $C_{30}H_{36}O_5$: C, 75.60; H, 7.61%.

Methyl (15S)-12-Acetoxy-16-benzoyloxy-8,11,13-abietatrien-18-oate (8a) and Its (15R)-Epimer (8b). a): A mixture of **7a** (1.655 g), *m*-chloroperbenzoic acid (80%: 1.498 g), and *p*-toluenesulfonic acid (30 mg) in 1,2-dichloroethane (15 ml) was refluxed for 3 h. The mixture was cooled, diluted with ether, and the ether solution was washed successively with aqueous potassium iodide, aqueous sodium thiosulfate, aqueous sodium hydrogencarbonate, and brine. The dried solution was evaporated in vacuo. The residue was chromatographed on silica gel (18 g), using ether-benzene (3:97) as an eluent, to give **8a** (1.552 g: 90.8%) which was recrystallized from methanol, mp 126—128 °C, $[\alpha]_D$ +33.5° (*c* 3.17), IR 1755 and 1718 cm^{-1}, ^1H NMR δ=1.23 (6H, s, C_4-CH_3 and C_{10}-CH_3), 1.28 (3H, d, J=7 Hz, C_{15}-CH_3), 2.25 (3H, s, C_{12}-$OCOCH_3$), 3.25 (1H, m, C_{15}-H), 3.62 (3H, s, $-CO_2CH_3$), 3.75—4.5 (2H, m, C_{15}-CH_2O-), 6.77 (1H, s) and 6.90 (1H, s) (C_{11}-H and C_{14}-H), 7.27—7.54 (3H, m) and 7.95 (2H, dd, J=8 and 2 Hz) ($-OCOC_6H_5$). Found: C, 72.83; H, 7.50%. Calcd for $C_{30}H_{36}O_6$: C, 73.14; H, 7.37%.

b): A mixture of **7b** (1.804 g), *m*-chloroperbenzoic acid (80%: 1.470 g), and *p*-toluenesulfonic acid (30 mg) in 1,2-dichloroethane (20 ml) was refluxed for 3.5 h. After the work-up (as described in **a**)) the crude product was purified by column chromatography on silica gel (40 g), using ether-benzene (3:97) as an eluent, to give the recovered **7b** (152 mg) and an oily **8b** (1.585 g: 85.1%) $[\alpha]_D$ +66.8° (*c* 5.79), IR 1753 and 1718cm^{-1} , ^1H NMR δ=1.20 (3H, s) and 1.24 (3H, s) (C_4-CH_3 and C_{10}-CH_3), 1.29 (3H, d, J=7 Hz, C_{15}-CH_3), 2.25 (3H, s, C_{12}-$OCOCH_3$), 3.27 (1H, m, C_{15}-H), 3.60 (3H, s, $-CO_2CH_3$), 3.9—4.5 (2H, m, C_{15}-CH_2O-), 6.78 (1H, s) and 6.90 (1H, s) (C_{11}-H and C_{14}-H), 7.25—7.6 (3H, m) and 7.97 (2H, dd, J=8 and 2 Hz) ($-OCOC_6H_5$). Found: C, 73.35; H, 7.45%. Calcd for $C_{30}H_{36}O_6$: C, 73.14; H, 7.37%.

Methyl (15S)-12,16-Dihydroxy-8,11,13-abietatrien-18-oate (9a) and Its (15R)-Epimer (9b). a): A mixture of **8a** (544 mg) and aqueous sodium hydroxide (20%: 1.5 ml) in methanol (6.0 ml) was refluxed for 1 h. The mixture was cooled, acidified with dilute hydrochloric acid, and extracted with ether. The ether extract was washed successively with aqueous sodium hydrogencarbonate and brine, dried, and evaporated in vacuo. The residue was chromatographed on silica gel (10 g), using ether-benzene (1:9) as an eluent, to give **9a** (375 mg: 98.0%) which was recrystallized from ether-hexane, mp 105—107 °C, $[\alpha]_D$ +50.0° (*c* 3.20), IR 3600, 3325, and 1720 cm^{-1}; ^1H NMR (90 MHz) δ=1.13 (3H, s, C_{10}-CH_3), 1.19 (3H, d, J=7 Hz,

C_{15}-CH_3), 1.20 (3H, s, C_4-CH_3), 3.02 (1H, m, C_{15}-H), ca. 3.6 (2H, m, overlap, C_{15}-CH_2OH), 3.61 (3H, s, -CO_2CH_3), 6.57 (2H, s, C_{11}-H and C_{14}-H). Found: C, 72.63; H, 8.86%. Calcd for $C_{21}H_{30}O_4$: C, 72.80; H, 8.73%.

b): A mixture of **8b** (1.207 g) and aqueous sodium hydroxide (20%: 3.0 ml) in methanol (10 ml) was refluxed for 1 h. After the work-up (as described in **a**)) the crude product was purified by column chromatography on silica gel (16 g), using ether–benzene (1:9) as an eluent, to give an oily **9b** (662 mg: 91.9%), $[\alpha]_D$ +65.5° (*c* 8.11), IR 3600, 3325, and 1720 cm^{-1}; ^1H NMR (90 MHz) δ=1.11 (3H, s, C_{10}-CH_3), 1.17 (3H, d, *J*=7 Hz, C_{15}-CH_3), 1.19 (3H, s, C_4-CH_3), 3.02 (1H, m, C_{15}-H), ca. 3.6 (2H, m, overlap, C_{15}-CH_2OH), 3.60 (3H, s, -CO_2CH_3), 6.57 (2H, s, C_{11}-H and C_{14}-H). Found: C, 72.78; H, 8.85%. Calcd for $C_{21}H_{30}O_4$: C, 72.80; H, 8.73%.

Reactions of 9a and 9b with Chloromethyl Methyl Ether. a): A stirred mixture of **9a** (584.0 mg), chloromethyl methyl ether (0.89 ml), potassium iodide (2.34 g), and anhydrous potassium carbonate (2.34 g) in ethyl methyl ketone (10 ml) was refluxed for 5 h. The mixture was cooled, diluted with water, and extracted with ether. The ether extract was washed successively with aqueous sodium thiosulfate and brine, dried, and evaporated in vacuo. The residue was chromatographed on silica gel (20 g), using ether–benzene (1:99) as an eluent, to give methyl (15*S*)-12,16-methylenedioxy-8,11,13-abietatrien-18-oate (**10a**) (332.0 mg: 54.8%) which was recrystallized from methanol, mp 154—155 °C, $[\alpha]_D$ +27.2° (*c* 1.62), IR 1715 cm^{-1}, ^1H NMR (90 MHz) δ=1.19 (3H, s) and 1.21 (3H, s) (C_4-CH_3 and C_{10}-CH_3), 1.28 (3H, d, *J*=7 Hz, C_{15}-CH_3), 2.6—3.0 (3H, m, C_7-H_2 and C_{15}-H), 3.53 (1H, dd, *J*=12 and 2 Hz) and 3.82 (1H, dd, *J*=12 and 4 Hz) (C_{15}-CH_2O-), 3.61 (3H, s, -CO_2CH_3), 4.52 (1H, d, *J*=7 Hz) and 5.16 (1H, d, *J*=7 Hz) (-OCH_2O-), 6.65 (1H, s, C_{14}-H), 6.72 (1H, s, C_{11}-H). Found: C, 73.59; H, 8.63%. Calcd for $C_{22}H_{30}O_4$: C, 73.71; H, 8.44%.

Subsequent elution with ether–benzene (2:98) gave methyl (15*S*)-12,16-bis(methoxymethoxy)-8,11,13-abietatrien-18-oate (**11a**) as an oil (29.0 mg: 4.0%), $[\alpha]_D$ +52.7° (*c* 0.74), IR 1720 cm^{-1}, ^1H NMR δ=1.19, (3H, s, C_{10}-CH_3), 1.20 (3H, d, *J*=7 Hz, C_{15}-CH_3), 1.23 (3H, s, C_4-CH_3), 3.20 (3H, s, C_{16}-OCH_2OCH_3), 3.42 (3H, s, C_{12}-OCH_2OCH_3), 3.60 (3H, s, -CO_2CH_3), 4.46 (2H, s, C_{16}-OCH_2OCH_3), 5.03 (2H, s, C_{12}-OCH_2OCH_3), 6.67 (1H, s) and 6.78 (1H, s) (C_{11}-H and C_{14}-H). Found: C, 69.28; H, 9.06%. Calcd for $C_{25}H_{38}O_6$: C, 69.09; H, 8.81%.

Further elution with ether–benzene (5:95) afforded methyl (15*S*)-12-hydroxy-16-methoxymethoxy-8,11,13-abietatrien-18-oate (**12a**) (119.5 mg: 18.2%) which was recrystallized from acetone–hexane, mp 81.5—82.5 °C, $[\alpha]_D$ +50.3° (*c* 1.53), IR 3325 and 1720 cm^{-1}, ^1H NMR δ=1.17 (3H, s, C_{10}-CH_3), 1.22 (3H, s, C_4-CH_3), 1.26 (3H, d, *J*=7 Hz, C_{15}-CH_3), 3.23 (3H, s, C_{16}-OCH_2OCH_3), 3.60 (3H, s, -CO_2CH_3), 4.54 (2H, s, C_{16}-OCH_2OCH_3), 6.57 (2H, bs, C_{11}-H and C_{14}-H), 6.69 (1H, s, C_{12}-OH). Found: C, 70.98; H, 8.97%. Calcd for $C_{23}H_{34}O_5$: C, 70.74; H, 8.78%.

b): A stirred mixture of **9b** (572.0 mg), chloromethyl methyl ether (0.87 ml), potassium iodide (2.28 g), and anhydrous potassium carbonate (2.28 g) in ethyl methyl ketone (10 ml) was refluxed for 5 h. After the work-up (as described in **a**)) the crude product was purified by column chromatography on silica gel (16 g), using ether–benzene (2:98) as an eluent, to give methyl (15*R*)-12,16-methylenedioxy-8,11,13-abietatrien-18-oate (**10b**) (213.0 mg: 36.0%) which was recrystallized from methanol, mp 134—135 °C, $[\alpha]_D$ +93.3° (*c* 2.53), IR 1718 cm^{-1}, ^1H NMR (90 MHz) δ=1.16 (3H, s, C_{10}-CH_3), 1.20 (3H, s, C_4-CH_3), 1.24 (3H, d, *J*=7 Hz, C_{15}-CH_3), 2.65—3.0 (3H, m, C_7-H_2 and C_{15}-H), 3.56 (1H, dd, *J*=12 and 2 Hz) and 3.78 (1H, dd, *J*=12 and 4 Hz) (C_{15}-CH_2O-), 3.61 (3H, s, -CO_2CH_3), 4.57 (1H, d, *J*=7 Hz) and 5.12 (1H, d, *J*=7 Hz) (-OCH_2O-), 6.63 (1H, s, C_{14}-H), 6.71 (1H, s, C_{11}-H). Found: C, 73.62; H, 8.74%. Calcd for $C_{22}H_{30}O_4$: C, 73.71; H, 8.44%.

Subsequent elution gave methyl (15*R*)-12,16-bis(methoxymethoxy)-8,11,13-abietatrien-18-oate (**11b**) as an oil (72.2 mg: 10.1%), $[\alpha]_D$ +54.2° (*c* 2.59), IR 1720 cm^{-1}, ^1H NMR δ=1.18 (3H, s, C_{10}-CH_3), 1.18 (3H, d, *J*=7 Hz, C_{15}-CH_3), 1.21 (3H, s, C_4-CH_3), 3.21 (3H,s, C_{16}-OCH_2OCH_3), 3.42 (3H, s, C_{12}-OCH_2OCH_3), 3.59 (3H, s, -CO_2CH_3), 4.43 (2H, s, C_{16}-OCH_2OCH_3), 5.03 (2H, s, C_{12}-OCH_2OCH_3), 6.67 (1H, s) and 6.79 (1H, s) (C_{11}-H and C_{14}-H). Found: C, 68.89; H, 8.95%. Calcd for $C_{25}H_{38}O_6$: C, 69.09; H, 8.81%.

Further elution with ether–benzene (5:95) afforded methyl (15*R*)-12-hydroxy-16-methoxymethoxy-8,11,13-abietatrien-18-oate (**12b**) (162.9 mg: 25.3%) which was recrystallized from acetone–hexane, mp 118—119 °C, $[\alpha]_D$ +61.2° (*c* 2.06), IR 3330 and 1720 cm^{-1}, ^1H NMR δ=1.15 (3H, s, C_{10}-CH_3), 1.22 (3H, s, C_4-CH_3), 1.26 (3H, d, *J*=7 Hz, C_{15}-CH_3), 3.26 (3H, s, C_{16}-OCH_2OCH_3), 3.60 (3H, s, -CO_2CH_3), 4.54 (2H, s, C_{16}-OCH_2OCH_3), 6.57 (2H, bs, C_{11}-H and C_{14}-H), 6.77 (1H, s, C_{12}-OH). Found: C, 70.79; H, 9.04%. Calcd for $C_{23}H_{34}O_5$: C, 70.74; H, 8.78%.

Hydrolyses of 11b, 12a, and 12b. a): A mixture of **11b** (20.0 mg) and dilute hydrochloric acid (15%: 0.15 ml) in tetrahydrofuran (1.5 ml) was refluxed for 2.5 h. The mixture was cooled, diluted with ether, and the ether solution was washed with brine. The dried solution was evaporated in vacuo. The residue was chromatographed on silica gel (6 g), using ether–benzene (1:9) as an eluent, to give a 12,16-diol (12.8 mg: 80.3%), the IR and ^1H NMR spectra of which were identical with those of the authentic **9b**.

b): A mixture of **12a** (68.0 mg) and dilute hydrochloric acid (15%: 0.3 ml) in tetrahydrofuran (3.0 ml) was refluxed for 2.5 h. After the work-up (as described in **a**)) the crude product was chromatographed on silica gel (10 g), using ether–benzene (3:97) as an eluent, to give a 12,16-methylenedioxy compound (16.6 mg: 26.6%), the IR and ^1H NMR spectra of which were identical with those of the authentic **10a**. Further elution with ether–benzene (1:9) afforded a 12,16-diol (37.4 mg: 62.0%), the IR and ^1H NMR spectra of which were identical with those of the authentic **9a**.

c): A mixture of **12b** (111.0 mg) and dilute hydrochloric acid (15%: 0.4 ml) in tetrahydrofuran (4.0 ml) was refluxed for 2.5 h. After the work-up (as described in **a**)) the crude product was chromatographed on silica gel (8 g), using ether–benzene (3:97) as an eluent, to give a 12,16-methylenedioxy compound (22.9 mg: 22.5%), the IR and ^1H NMR spectra of which were identical with those of the authentic **10b**. Further elution with ether–benzene (1:9) afforded a 12,16-diol (67.4 mg: 68.4%), the IR and ^1H NMR spectra of which were identical with those of the authentic **9b**.

(15*S*)-12,16-Methylenedioxy-18-tosyloxy-8,11,13-abietatriene (13a) and Its (15*R*)-Epimer (13b). a): A mixture of

10a (146 mg) and lithium aluminum hydride (20 mg) in dry ether (4.0 ml) was stirred at room temperature for 1 h. The mixture was poured into ice-dilute hydrochloric acid and extracted with ether. The ether extract was washed with brine, dried, and evaporated in vacuo to give a crude alcohol (134 mg) as an oil, IR 3630 and 3475 cm^{-1}.

A mixture of the above crude alcohol (134 mg) and *p*-toluenesulfonyl chloride (93 mg) in pyridine (1.5 ml) was heated at 80—85 °C for 4 h. The mixture was cooled, poured into ice-dilute hydrochloric acid, and extracted with ether. The ether extract was washed successively with aqueous sodium hydrogencarbonate and brine, dried, and evaporated in vacuo. The residue was chromatographed on silica gel (8 g), using ether-benzene (2:98) as an eluent, to give **13a** (188 mg: 95.3%) which was recrystallized from methanol, mp 113—114 °C, $[\alpha]_D$ +16.1 ° (*c* 2.36), IR 1360 and 1178 cm^{-1}, ^1H NMR δ=0.88 (3H, s, C_4-CH_3), 1.17 (3H, s, C_{10}-CH_3), 1.28 (3H, d, *J*=7 Hz, C_{15}-CH_3), 2.44 (3H, s, -$C_6H_4CH_3$), 3.3—4.0 (4H, m, C_4-CH_2OTs and C_{15}-CH_2O-), 4.51 (1H, d, *J*=7 Hz) and 5.15 (1H, d, *J*=7 Hz) (-OCH_2O-), 6.66 (1H, s, C_{14}-H), 6.72 (1H, s, C_{11}-H), 7.28 (2H, d, *J*=9 Hz) and 7.74 (2H, d, *J*=9 Hz) (-$C_6H_4CH_3$). Found: C, 69.60; H, 7.75%. Calcd for $C_{28}H_{36}O_5S$: C, 69.40; H, 7.48%.

b): A mixture of **10b** (182 mg) and lithium aluminum hydride (25 mg) in dry ether (5.0 ml) was stirred at room temperature for 1 h to give a crude alcohol (170 mg) as an oil, IR 3625 and 3460 cm^{-1}

The above crude alcohol (170 mg) was tosylated with *p*-toluenesulfonyl chloride (116 mg) in pyridine (2.0 ml) at 80—85 °C for 4 h. After the work-up (as described in **a**)) the crude product was purified by column chromatography on silica gel (8 g), using ether-benzene (1:99) as an eluent, to give **13b** (220 mg: 89.4%) which was recrystallized from methanol, mp 155—156 °C, $[\alpha]_D$ +70.7 ° (*c* 2.05), IR 1358 and 1174 cm^{-1}, ^1H NMR δ=0.87 (3H, s, C_4-CH_3), 1.13 (3H, s, C_{10}-CH_3), 1.24 (3H, d, *J*=7 Hz, C_{15}-CH_3), 2.43 (3H, s, -$C_6H_4CH_3$), 3.3—4.0 (4H, m, C_4-CH_2OTs and C_{15}-CH_2O-), 4.51 (1H, d, *J*=7 Hz) and 5.08 (1H, d, *J*=7 Hz) (-OCH_2O-), 6.61 (1H, s, C_{14}-H), 6.69 (1H, s, C_{11}-H), 7.24 (2H, d, *J*=9 Hz) and 7.68 (2H, d, *J*=9 Hz) (-$C_6H_4CH_3$). Found: C, 69.55; H, 7.68%. Calcd for $C_{28}H_{36}O_5S$: C, 69.40; H, 7.48%.

(15*S*)-12,16-Methylenedioxy-8,11,13-abietatriene (14a) and Its (15*R*)-Epimer (14b). a): A stirred mixture of **13a** (163.0 mg), sodium iodide (252 mg), and zinc powder (220 mg) in *N*,*N*-dimethylformamide (3.0 ml) was heated at 120—125 °C for 6 h. The mixture was cooled, diluted with ether, and then filtered. The filtrate was poured into dilute hydrochloric acid and extracted with ether. The ether extract was washed successively with aqueous sodium thiosulfate and brine, dried, and evaporated in vacuo. The residue was chromatographed on silica gel (7 g), using benzene as an eluent, to give an oily **14a** (68.0 mg: 64.4%), $[\alpha]_D$ +33.9 ° (*c* 3.30), ^1H NMR δ=0.94 (6H, s, -$C(CH_3)_2$), 1.16 (3H, s, C_{10}-CH_3), 1.28 (3H, d, *J*=7 Hz, C_{15}-CH_3), 3.35—3.95 (2H, m, C_{15}-CH_2O-), 4.50 (1H, d, *J*=7 Hz) and 5.13 (1H, d, *J*=7 Hz) (-OCH_2O-), 6.62 (1H, s, C_{14}-H), 6.71 (1H, s, C_{11}-H). Found: C, 80.48; H, 9.53%. Calcd for $C_{21}H_{30}O_2$: C, 80.21; H, 9.62%. Further elution with ether-benzene (6:94) afforded the recovered **13a** (24.9 mg: 15.3%).

b): A stirred mixture of **13b** (150.0 mg), sodium iodide (232 mg), and zinc powder (202 mg) in *N*,*N*-dimethylformamide (4.0 ml) was heated at 120—125 °C for 6 h. After the work-up (as described in **a**)) the crude product was purified by column chromatography on silica gel (8 g), using benzene as an eluent, to give an oily **14b** (59.2 mg: 60.8%), $[\alpha]_D$ +101 ° (*c* 1.91), ^1H NMR δ=0.94 (6H, s, -$C(CH_3)_2$), 1.14 (3H, s, C_{10}-CH_3), 1.26 (3H, d, *J*=7 Hz, C_{15}-CH_3), 3.35—3.95 (2H, m, C_{15}-CH_2O-), 4.54 (1H, d, *J*=7 Hz) and 5.13 (1H,d, *J*=7 Hz) (-OCH_2O-), 6.63 (1H, s, C_{14}-H), 6.72 (1H, s, C_{11}-H). Found: C, 80.15; H, 9.55%. Calcd for $C_{21}H_{30}O_2$: C, 80.21; H, 9.62%.

Further elution with ether-benzene (6:94) afforded the recovered **13b** (32.1 mg: 21.4%) and (15*R*)-12,16-methylenedioxy-8,11,13-abietatrien-18-ol (9.9 mg: 9.7%).

(15*S*)-16-Hydroxyferruginol (15a) and Its (15*R*)-Epimer (15b). a): A mixture of **14a** (63.0 mg) and dilute hydrochloric acid (15%: 0.2 ml) in ethanol (2.0 ml) was refluxed for 6 h. The mixture was cooled and diluted with ether. The ether solution was washed with brine, dried, and evaporated in vacuo. The residue was chromatographed on silica gel (7 g), using ether-benzene (1:9) as an eluent, to give **15a** (47.4 mg: 78.4%) which was recrystallized from acetone-hexane, mp 177—178 °C, $[\alpha]_D$ +45.5 ° (*c* 0.51), IR (KBr) 3555 and 3275 cm^{-1}, ^1H NMR (90 MHz, $CDCl_3$) δ=0.91 (6H, s, -$C(CH_3)_2$), 1.16 (3H, s, C_{10}-CH_3), 1.26 (3H, d, *J*=7 Hz, C_{15}-CH_3), 3.15 (1H, m, C_{15}-H), 3.64 (1H, dd, *J*=10 and 7 Hz) and 3.88 (1H, dd, *J*=10 and 4 Hz) (C_{15}-CH_2OH), 6.74 (2H, s, C_{11}-H and C_{14}-H). Found: C, 79.31; H, 10.18%. Calcd for $C_{20}H_{30}O_2$: C, 79.42; H, 10.00%. The physical and spectral data of **15a** were identical with those of the authentic (15*S*)-16-hydroxyferruginol.[4,5]

b): A mixture of **14b** (50.2 mg) and dilute hydrochloric acid (15%: 0.2 ml) in ethanol (2.0 ml) was refluxed for 5.5 h. After the work-up (as described in **a**)) the crude product was purified by column chromatography on silica gel (6 g), using ether-benzene (1:9) as an eluent, to give **15b** (38.1 mg: 78.9%) which was recrystallized from ether-hexane, mp 139—140 °C, $[\alpha]_D$ +65.7° (*c* 0.34), IR (KBr) 3520 and 3300 cm^{-1}, ^1H NMR (90 MHz, $CDCl_3$) δ=0.89 (3H, s) and 0.91 (3H, s) (-$C(CH_3)_2$), 1.13 (3H, s, C_{10}-CH_3), 1.24 (3H, d, *J*=7 Hz, C_{15}-CH_3), 3.15 (1H, m, C_{15}-H), 3.64 (1H, dd, *J*=10 and 7 Hz) and 3.88 (1H, dd, *J*=10 and 4 Hz) (C_{15}-CH_2OH), 6.72 (2H, s, C_{11}-H and C_{14}-H). Found: C, 79.24; H, 10.28%. Calcd for $C_{20}H_{30}O_2$: C, 79.42; H, 10.00%. The physical and spectral data of **15b** were identical with those of the authentic (15*R*)-16-hydroxyferruginol.[4,5]

Methyl (15*S*)-16-Benzoyloxy-12-hydroxy-8,11,13-abietatrien-18-oate (16a) and Its (15*R*)-Epimer (16b). a): A mixture of **8a** (1.412 g) and dilute hydrochloric acid (15%: 2.0 ml) in methanol (20 ml) was refluxed for 1 h. After removal of the methanol in vacuo, the residue was dissolved in ether and washed successively with brine, aqueous sodium hydrogencarbonate, and brine. The dried solution was evaporated in vacuo. The residue was chromatographed on silica gel (23 g), using ether-benzene (2:98) as an eluent, to give **16a** (1.123 g: 87.0%) as an oil, $[\alpha]_D$ +25.8° (*c* 3.96), IR 3600, 3400, and 1718 cm^{-1}; ^1H NMR δ=1.12 (3H, s, C_{10}-CH_3), 1.22 (3H, s, C_4-CH_3), 1.34 (3H, d, *J*=7 Hz, C_{15}-CH_3), 3.63 (3H, s, -CO_2CH_3), 3.9—4.7 (2H, m, C_{15}-CH_2O-), 6.62 (1H, s, overlap, C_{12}-OH), 6.62 (1H, s) and 6.71 (1H, s) (C_{11}-H and C_{14}-H), 7.2—7.6 (3H, m) and 7.99 (2H, dd, *J*=7 and 2 Hz) (-$OCOC_6H_5$). Found: C, 74.53; H, 7.67%. Calcd for $C_{28}H_{34}O_5$: C, 74.64; H, 7.61%.

b): A mixture of **8b** (308 mg) and dilute hydrochloric

acid (15%: 0.4 ml) in methanol (4.0 ml) was refluxed for 1 h. After the work-up (as described in **a**)) the crude product was chromatographed on silica gel (8 g), using ether-benzene (1:99) as an eluent, to give **16b** (279 mg: 98.9%) which was recrystallized from acetone-hexane, mp 75—78 °C, $[\alpha]_D$ +78.6° (*c* 2.10), IR 3600, 3400, and 1715 cm^{-1}, ^1H NMR δ=1.14 (3H, s, C_{10}-CH_3), 1.21 (3H, s, C_4-CH_3), 1.35 (3H, d, *J*=7 Hz, C_{15}-CH_3), 3.62 (3H, s, -CO_2CH_3), 3.8—4.7 (2H, m, C_{15}-CH_2O-), 6.20 (1H, s, C_{12}-OH), 6.59 (1H, s) and 6.69 (1H, s) (C_{11}-H and C_{14}-H), 7.2—7.6 (3H, m) and 8.03 (2H, dd, *J*=7 and 2 Hz) (-$OCOC_6H_5$). Found: C, 74.58; H, 7.83%. Calcd for $C_{28}H_{34}O_5$: C, 74.64; H, 7.61%.

Methyl (15*S*)-16-Benzoyloxy-12-(1-phenyl-1*H*-tetrazol-5-yloxy)-8,11,13-abietatrien-18-oate (17a) and Its (15*R*)-Epimer (17b). a): A stirred mixture of **16a** (980 mg), 5-chloro-1-phenyl-1*H*-tetrazole (97%: 810 mg), and anhydrous potassium carbonate (3.013 g) in ethyl methyl ketone (15 ml) was refluxed for 10 h. The mixture was cooled, diluted with water, and extracted with ether. The ether extract was washed with brine, dried, and evaporated in vacuo. The residue was chromatographed on silica gel (20 g), using hexane-benzene (1:3) and ether-benzene (5:95) as eluents, to give an oily **17a** (1.179 g: 91.1%), $[\alpha]_D$ +61.1° (*c* 2.96), IR 1720 cm^{-1}, ^1H NMR ($CDCl_3$) δ=1.21 (3H, s) and 1.28 (3H, s) (C_4-CH_3 and C_{10} -CH_3), 1.33 (3H, d, *J*=7 Hz, C_{15}-CH_3), 3.39 (1H, m, C_{15}-H), 3.67 (3H, s, -CO_2CH_3), 4.31 (2H, d, *J*=7 Hz, C_{15}-CH_2O-), 7.02 (1H, s, C_{14}-H), 7.22 (1H, s, C_{11}-H), 7.3—8.1 (10H, m, 2 -C_6H_5). Found: C, 70.98; H, 6.59; N, 9.42%. Calcd for $C_{35}H_{38}O_5N_4$: C, 70.68; H, 6.44; N, 9.42%.

b): A stirred mixture of **16b** (582 mg), 5-chloro-1-phenyl-1*H*-tetrazole (97%: 480 mg), and anhydrous potassium carbonate (1.785 g) in ethyl methyl ketone (10 ml) was refluxed for 10 h. After the work-up (as described in **a**)) the crude product was purified by column chromatography on silica gel (10 g), using benzene and ether-benzene (1:9) as eluents, to give an oily **17b** (726 mg: 94.6%), $[\alpha]_D$ +45.4° (*c* 3.46), IR 1720 cm^{-1}, ^1H NMR ($CDCl_3$) δ=1.23 (3H, s) and 1.29 (3H, s) (C_4-CH_3 and C_{10}-CH_3), 1.33 (3H, d, *J*=7 Hz, C_{15}-CH_3), 3.39 (1H, m, C_{15}-H), 3.67 (3H, s, -CO_2CH_3), 4.31 (2H, d, *J*=7 Hz, C_{15}-CH_2O-), 7.04 (1H, s, C_{14}-H), 7.24 (1H, s, C_{11}-H), 7.3—8.1 (10H, m, 2 -C_6H_5). Found: C, 70.87; H, 6.38; N, 9.40%. Calcd for $C_{35}H_{38}O_5N_4$: C, 70.68; H, 6.44; N, 9.42%.

Hydrolyses of 17a and 17b. a): A mixture of **17a** (1.090 g), sodium carbonate (291 mg), water (4.0 ml), and methanol (40 ml) was stirred at room temperature for 2.5 h. The mixture was acidified with dilute hydrochloric acid and then evaporated in vacuo to remove most of the methanol. The residue was extracted with ether. The ether extract was washed successively with aqueous sodium hydrogencarbonate and brine, dried, and evaporated in vacuo. The residue was chromatographed on silica gel (30 g), using ether-benzene (8:92) as an eluent, to give the recovered **17a** (507 mg: 46.5%). Subsequent elution with ether-benzene (1:9) gave a 12,16-diol (74 mg: 11.7%, 21.8%[7]), the IR and ^1H NMR spectra of which were identical with those of the authentic **9a**. Further elution with ether-benzene (1:9 and then 3:7) afforded methyl (15*S*)-16-hydroxy-12-(1-phenyl-1*H*-tetrazol-5-yloxy)-8,11,13-abietatrien-18-oate (**18a**) as an oil (366 mg: 40.7%, 76.1%[7]), $[\alpha]_D$ +34.0° (*c* 2.62), IR 3425 and 1720 cm^{-1}, ^1H NMR (90 MHz, $CDCl_3$) δ=1.18 (3H, d, *J*=7 Hz, C_{15}-CH_3), 1.19 (3H, s, C_{10}-CH_3), 1.25 (3H, s, C_4-CH_3), 3.11 (1H, m, C_{15}-H), 3.64 (2H, d, *J*=7 Hz, C_{15}-CH_2OH), 3.66 (3H, s, -CO_2CH_3), 7.00 (1H, s, C_{14}-H), 7.16 (1H, s, C_{11}-H), 7.45—7.9 (5H, m, -C_6H_5). Found: C, 68.75; H, 7.26; N, 11.17%. Calcd for $C_{28}H_{34}O_4N_4$: C, 68.55; H, 6.99; N, 11.42%.

b): A mixture of **17b** (620 mg), sodium carbonate (166 mg), water (3.0 ml), and methanol (30 ml) was stirred at room temperature for 2 h. After the work-up (as described in **a**)) the crude product was chromatographed on silica gel (20 g), using ether-benzene (1:9) as an eluent, to give the recovered **17b** (306 mg: 49.4%) and a 12,16-diol (35 mg: 9.7%, 19.1%[7]), the IR and ^1H NMR spectra of which were identical with those of the authentic **9b**. Further elution with ether-benzene (1:9 and then 3:7) afforded methyl (15*R*)-16-hydroxy-12-(1-phenyl-1*H*-tetrazol-5-yloxy)-8,11,13-abietatrien-18-oate (**18b**) (200 mg: 39.1%, 77.2%[7]) which was recrystallized from acetone-hexane, mp 169—170 °C, $[\alpha]_D$ +74.7° (*c* 1.78), IR 3425 and 1720 cm^{-1}, ^1H NMR (90 MHz, $CDCl_3$) δ=1.19 (3H, s, C_{10}-CH_3), 1.20 (3H, d, *J*=7 Hz, C_{15}-CH_3), 1.25 (3H, s, C_4-CH_3), 3.12 (1H, m, C_{15}-H), 3.64 (2H, d, *J*=7 Hz, C_{15}-CH_2OH), 3.66 (3H, s. -CO_2CH_3), 7.00 (1H, s, C_{14}-H), 7.16 (1H, s, C_{11}-H), 7.45—7.9 (5H, m, -C_6H_5). Found: C, 68.36; H, 7.18; N, 11.44%. Calcd for $C_{28}H_{34}O_4N_4$: C, 68.55; H, 6.99; N, 11.42%.

Reactions of 9a and 9b with 5-Chloro-1-phenyl-1*H*-tetrazole. a): A stirred mixture of **9a** (145 mg), 5-chloro-1-phenyl-1*H*-tetrazole (97%: 156 mg), and anhydrous potassium carbonate (579 mg) in ethyl methyl ketone (5.0 ml) was refluxed for 10 h. After the work-up (as described above) the crude product was chromatographed on silica gel (8 g), using hexane-benzene (2:3) as an eluent, to give a dihydrobenzofuran derivative (51.3 mg: 37.3%) which was identical with authentic methyl (15*S*)-12,16-epoxy-8,11,13-abietatrien-18-oate (**19a**).[6] ^1H NMR (90 MHz, $CDCl_3$) δ=1.18 (3H, s, C_{10}-CH_3), 1.25 (3H, s, C_4-CH_3), 1.28 (3H, d, *J*=7 Hz, C_{15}-CH_3), 3.47 (1H, m, C_{15}-H), 3.66 (3H, s, -CO_2CH_3), 3.99 (1H, dd, *J*=8 and 7 Hz) and 4.62 (1H, t, *J*=8 Hz) (C_{15}-CH_2O-), 6.67 (1H, s, C_{11}-H), 6.78 (1H, s, C_{14}-H). Further elution with ether-benzene (15:85) afforded **18a** (98.5 mg: 48.0%), the IR and ^1H NMR spectra of which were identical with those of the authentic sample.

b): A stirred mixture of **9b** (67.8 mg), 5-chloro-1-phenyl-1*H*-tetrazole (97%: 70.8 mg), and anhydrous potassium carbonate (271 mg) in ethyl methyl ketone (3.0 ml) was refluxed for 10 h. After the work-up (as described above) the crude product was chromatographed on silica gel (12 g), using hexane-benzene (1:3) as an eluent, to give a dihydrobenzofuran derivative (24.2 mg: 37.6%) which was identical with authentic methyl (15*R*)-12,16-epoxy-8,11,13-abietatrien-18-oate (**19b**).[6] ^1H NMR (90 MHz, $CDCl_3$) δ=1.18 (3H, s, C_{10}-CH_3), 1.25 (3H, s, C_4-CH_3), 1.27 (3H, d, *J*=7 Hz, C_{15}-CH_3), 3.47 (1H, m, C_{15}-H), 3.66 (3H, s, -CO_2CH_3), 4.00 (1H, dd, *J*=8 and 7 Hz) and 4.62 (1H, t, *J*=8 Hz) (C_{15}-CH_2O-), 6.68 (1H, s, C_{11}-H), 6.80 (1H, s, C_{14}-H). Further elution with ether-benzene (1:4) afforded **18b** (28.5 mg: 29.6%), mp 169—170 °C (from acetone-hexane), the IR and ^1H NMR spectra of which were identical with those of the authentic sample.

Methyl (15*S*)-16-Hydroxy-8,11,13-abietatrien-18-oate (3a) and Its (15*R*)-Epimer (3b). a): A mixture of **18a** (219.0 mg) and 10% Pd-C (300 mg) in ethanol (15 ml) was hydrogenated at room temperature under an atmosphere of

hydrogen for 85 h. After the usual work-up, the crude product was chromatographed on silica gel (10 g), using ether–benzene (5:95) as an eluent, to give an oily **3a** (37.6 mg: 25.5%, 39.3%[7]) which was allowed to stand at room temperature to give a solid, mp 51—53.5 °C, $[\alpha]_D$ +44.7° (*c* 1.37). IR 3590, 3475, and 1718 cm^{-1}; ^1H NMR (90 MHz) δ=1.16 (3H, s, C_{10}-CH_3), 1.17 (3H, d, *J*=7 Hz, C_{15}-CH_3), 1.22 (3H, s, C_4-CH_3), 1.39 (1H, s, C_{16}-OH), 3.50 (2H, d, *J*=7 Hz, C_{15}-CH_2OH), 3.60 (3H, s, -CO_2CH_3), 6.77 (1H, bs, C_{14}-H), 6.84 (1H, dd, *J*=8 and 2 Hz, C_{12}-H), 7.07 (1H, d, *J*=8 Hz, C_{11}-H). Found: C, 76.18; H, 9.03%. Calcd for $C_{21}H_{30}O_3$: C, 76.32; H, 9.15%. Further elution with ether–benzene (1:9) afforded a 12,16-diol **9a** (21.6 mg: 14.0%, 21.6%[7]), and the recovered **18a** (77.1 mg: 35.2%).

b): A mixture of **18b** (105.0 mg) and 10% Pd-C (110 mg) in ethanol (7.0 ml) was hydrogenated at room temperature under an atmosphere of hydrogen for 64 h. After the usual work-up, the crude product was chromatographed on silica gel (8 g), using ether–benzene (1:9) as an eluent, to give **3b** (64.6 mg: 91.4%) which was recrystallized from hexane, mp 71.5—73 °C, $[\alpha]_D$ +65.8° (*c* 1.57), IR 3590, 3475, and 1718 cm^{-1}; ^1H NMR (90 MHz) δ=1.16 (3H, s, C_{10}-CH_3), 1.17 (3H, d, *J*=7 Hz, C_{15}-CH_3), 1.22 (3H, s, C_4-CH_3), 1.32 (1H, s, C_{16}-OH), 3.50 (2H, d, *J*=7 Hz, C_{15}-CH_2OH), 3.60 (3H, s, -CO_2CH_3), 6.77 (1H, bs, C_{14}-H), 6.84 (1H, dd, *J*=8 and 2 Hz, C_{12}-H), 7.07 (1H, d, *J*=8 Hz, C_{11}-H). Found: C, 76.21; H, 9.33%. Calcd for $C_{21}H_{30}O_3$: C, 76.32; H, 9.15%.

Methyl (15*S*)-16-(4-Nitrobenzoyloxy)-8,11,13-abietatrien-18-oate (20a) and Its (15*R*)-Epimer (20b). a): A mixture of **3a** (25.0 mg) and 4-nitrobenzoyl chloride (28.1 mg) in pyridine (1.0 ml) was heated at 70—80 °C for 2.5 h. After the usual work-up, the crude product was chromatographed on silica gel (8 g), using benzene as an eluent, to give **20a** (35.0 mg: 96.5%) which was recrystallized from hexane, mp 116—117 °C, $[\alpha]_D$ +9.2° (*c* 2.95), IR 1720, 1530, and 1350 cm^{-1}; ^1H NMR (90 MHz, $CDCl_3$) δ=1.18 (3H, s, C_{10}-CH_3), 1.26 (3H, s, C_4-CH_3), 1.35 (3H, d, *J*=7 Hz, C_{15}-CH_3), 3.18 (1H, m, C_{15}-H), 3.67 (3H, s, -CO_2CH_3), 4.41 (2H, d, *J*=7 Hz, C_{15}-CH_2O-), 6.90 (1H, bs, C_{14}-H), 7.01 (1H, dd, *J*=8 and 2 Hz, C_{12}-H), 7.20 (1H, d, *J*=8 Hz, C_{11}-H), 8.10 (2H, d, *J*=8 Hz) and 8.28 (2H, d, *J*=8 Hz) (-$C_6H_4NO_2$). Found: C, 70.34; H, 7.17; N, 2.62%. Calcd for $C_{28}H_{33}O_6N$: C, 70.12; H, 6.94; N, 2.92%.

b): A mixture of **3b** (38.0 mg) and 4-nitrobenzoyl chloride (42.7 mg) in pyridine (1.5 ml) was heated at 70—80°C for 2.5 h. After the usual work-up, the crude product was chromatographed on silica gel (6 g), using benzene as an eluent, to give **20b** (53.3 mg: 96.7%) which was recrystallized from hexane, mp 133—134 °C, $[\alpha]_D$ +66.4° (*c* 2.23), IR 1720, 1530, and 1350 cm^{-1}; ^1H NMR (90 MHz, $CDCl_3$) δ=1.18 (3H, s, C_{10}-CH_3), 1.26 (3H, s, C_4-CH_3), 1.36 (3H, d, *J*=7 Hz, C_{15}-CH_3), 3.18 (1H, m, C_{15}-H), 3.67 (3H, s, -CO_2CH_3), 4.41 (2H. d, *J*=7 Hz, C_{15}-CH_2O-), 6.90 (1H, bs, C_{14}-H), 7.01 (1H, dd, *J*=8 and 2 Hz, C_{12}-H), 7.20 (1H, d, *J*=8 Hz, C_{11}-H), 8.10 (2H, d, *J*=8 Hz) and 8.28 (2H, d, *J*=8 Hz) (-$C_6H_4NO_2$). Found: C, 70.38; H, 7.14; N, 2.93%. Calcd for $C_{28}H_{33}O_6N$: C, 70.12; H, 6.94; N, 2.92%.

c): Methyl (+)-16-hydroxydehydroabietate[2] (20.0 mg) ($[\alpha]_D$ +48.6° (*c* 1.11)[8]), a methyl ester of a metabolite of (+)-dehydroabietic acid (**2**) in rabbits, was treated with 4-nitrobenzoyl chloride (23.0 mg) in pyridine (1.5 ml) at 70—80°C for 2.5 h. After the usual work-up, the crude product was chromatographed on silica gel (7 g), using benzene as an eluent, to give a 4-nitrobenzoate (28.7 mg: 99.0%) which was recrystallized from hexane, mp 116—117°C, $[\alpha]_D$ +9.5° (*c* 1.16), IR 1720, 1530, and 1350 cm^{-1}; ^1H NMR (90 MHz, $CDCl_3$) δ=1.18 (3H, s, C_{10}-CH_3), 1.26 (3H, s, C_4-CH_3), 1.35 (3H, d, *J*=7 Hz, C_{15}-CH_3), 3.18 (1H, m, C_{15}-H), 3.67 (3H, s, -CO_2CH_3), 4.41 (2H, d, *J*=7 Hz, C_{15}-CH_2O-), 6.90 (1H, bs, C_{14}-H), 7.01 (1H, dd, *J*=8 and 2 Hz, C_{12}-H), 7.20 (1H, d, *J*=8 Hz, C_{11}-H), 8.10 (2H, d, *J*=8 Hz) and 8.28 (2H, d, *J*=8 Hz) (-$C_6H_4NO_2$). Found: C, 70.37; H, 7.15; N, 2.76%. Calcd for $C_{28}H_{33}O_6N$: C, 70.12; H, 6.94; N, 2.92%.

The physical and spectral data of the natural 4-nitrobenzoate were identical with those of the synthetic (15*S*)-isomer **20a.**

The authors are grateful to Dr. Takashi Ishida, The Hiroshima Institute of Technology, for a generous gift of natural methyl (+)-16-hydroxydehydroabietate.

References

1) R. Ekman and R. Sjöholm, *Acta Chem. Scand., Ser. B,* **33**, 76 (1979).
2) Y. Asakawa, T. Ishida, M. Toyota, and T. Takemoto, *Xenobiotica,* **16**, 753 (1986).
3) Y. Shigemasa, H. Hakata, H. Saimoto, and R. Nakashima, The Meeting of the Chugoku-Shikoku and Kyushu Branches, Chemical Society of Japan, Tokushima, November 1986.
4) T. Matsumoto, S. Imai, S. Miuchi, and H. Sugibayashi, *Bull. Chem. Soc. Jpn.,* **58**, 340 (1985).
5) T. Matsumoto, S. Imai, and T. Yoshinari, *Bull. Chem. Soc. Jpn.,* **58**, 1165 (1985).
6) T. Matsumoto, S. Imai, T. Yoshinari, and K. Tsuruta, *Bull. Chem. Soc. Jpn.,* **60**, 2401 (1987).
7) Yields are based on the starting material consumed.
8) The optical rotation was measured in our laboratory.

Synthesis of 1,10-Disubstituted 1,4,7,10,13,16-Hexaazacyclooctadecanes and Their Extractability for Metal Cations

Masayuki TAKADA,† Kazuhiko SAIGO,* Teruhisa HIRAI, Ikuro OHCHI,
Masayuki TAJIMA, Manabu SENO,† and Masaki HASEGAWA
Department of Synthetic Chemistry, Faculty of Engineering, The University of Tokyo,
Hongo, Bunkyo-ku, Tokyo 113
†Institute of Industrial Science, The University of Tokyo, 7-22-1, Roppongi, Minato-ku, Tokyo 106
(Received December 9, 1987)

1,10-Disubstituted 1,4,7,10,13,16-hexaazacyclooctadecanes (hexaaza-18-crowns) having lipophilic groups were synthesized from 1,2-ethanediamine as a starting material. Cyclization of 3,6-ditosyl-3,6-diazaoctanedioyl dichloride and 3,6-ditosyl-3,6-diazaoctane-1,8-diamine under the high dilution conditions, followed by diborane reduction of the amide carbonyl, gave the macrocyclic precursor. A series of reactions, i.e., acylation, diborane reduction, and detosylation, afforded 1,10-disubstituted hexaaza-18-crowns. Their extractability for metal cations was examined by spectrophotometric analysis. They showed relatively high extractability for Ag^{+}, Zn^{2+}, and Cd^{2+}.

An understanding of the underlying factors for metal ion recognition by organic substrates is important in wide-ranging ramifications, especially in the areas of chemistry and biochemistry. Cyclic ligands can be further "tuned" by adjusting the macrocyclic hole-size until an optimum fit is achieved for a metal ion of interest. Such macrocyclic hole-size variation is considerably interest, and many studies of this type are directed to cyclic polyether ligands and typical metal ions.[1] Recently, similar studies directed to transition metal ions have received attention.[2] Further, by introducing additional ligating groups into a macrocycle its properties can be modified, so that its specificity in metal ion binding increases and/or its solubility changes.[3]

Macrocyclic polyamines have been synthesized and their binding properties toward metal cations are described; most of the works concern tetraaza-12(or 14)-membered ring systems.[4] For example, 12-membered **1** gives stable alkali and alkaline earth metal ion complexes[5] whereas the unsubstituted ligand binds only transition metal ions. Macrocycle **2**, of which a long lipophilic side chain makes the ligand and its metal ion complex soluble in organic solvents, can be used in extraction of metal ions from an aqueous solution to an organic phase.[6]

Tetraazamacrocyclic ligands containing a single pendant-arm have been synthesized based on template methods.[7] Macrobicyclic polyamines are also synthesized by a sequential two-step pathway[8] or by direct macrobicyclization via tripode-tripode coupling reaction.[9] But, there is no report on the selective introduction of two lipophilic groups in 1,4,7,10,13,16-hexaazacyclooctadecane (hexaaza-18-crown) at the symmetrical, e.g., 1,10-positions. Here we report the synthesis and extractability of macrocyclic polyamines, which are characterized by the parent azacrown ring and "arms".

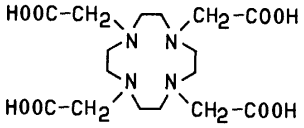

1

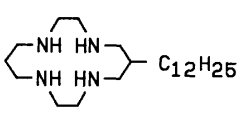

2

Results and Discussion

Synthesis of 1,10-Disubstituted Hexaaza-18-crowns. According to the literature,[10] 3,6-ditosyl-3,6-diazaoctanedioyl dichloride (**6**) was prepared from 1,2-ethanediamine via 1,2-bis(tosylamino)ethane (**3**), dimethyl 3,6-ditosyl-3,6-diazaoctanedioate (**4**) and then 3,6-ditosyl-3,6-diazaoctanedioic acid (**5**). The melting point of **6** was lower than that in the literature[10b] by 100 °C, but the structure of **6** was confirmed by IR and ^{1}H NMR spectra, and elemental analysis.

Diacid dichloride **6** was treated with excess liquid ammonia in dichloromethane to give the corresponding diamide **7** in 77% yield, which was converted into 3,6-ditosyl-3,6-diazaoctane-1,8-diamine (**8**) by the reduction with diborane (64% yield). Cyclization of **6** and **8** in dichloromethane under the high dilution conditions in the presence of triethylamine as a condensing agent gave cyclic diamide, 4,7,13,16-tetratosyl-1,4,7,10,13,16-hexaazacyclooctadecane-2,9-dione (**9**) in 50% yield. The macrocyclic precursor, 1,4,10,13-tetratosyl-1,4,7,10,13,16-hexaazacyclooctadecane (**10**) was obtained by reduction of **9** with diborane in 56% yield. 1,10-Dialkyl-4,7,13,16-tetratosyl-1,4,7,10,13,16-hexaazacyclooctadecanes (**12a, b**) were synthesized by acylation with benzoyl chloride and octanoyl chloride, respectively, in the presence of triethylamine in dichloromethane, followed by the reduction with diborane.

Hydrolysis with hydrogen bromide in acetic acid in the presence of phenol and reductive elimination with lithium aluminium hydride are known to be effective for detosylation of *N*-tosylated amine derivatives. But, detosylation of **12** by these reagents gave

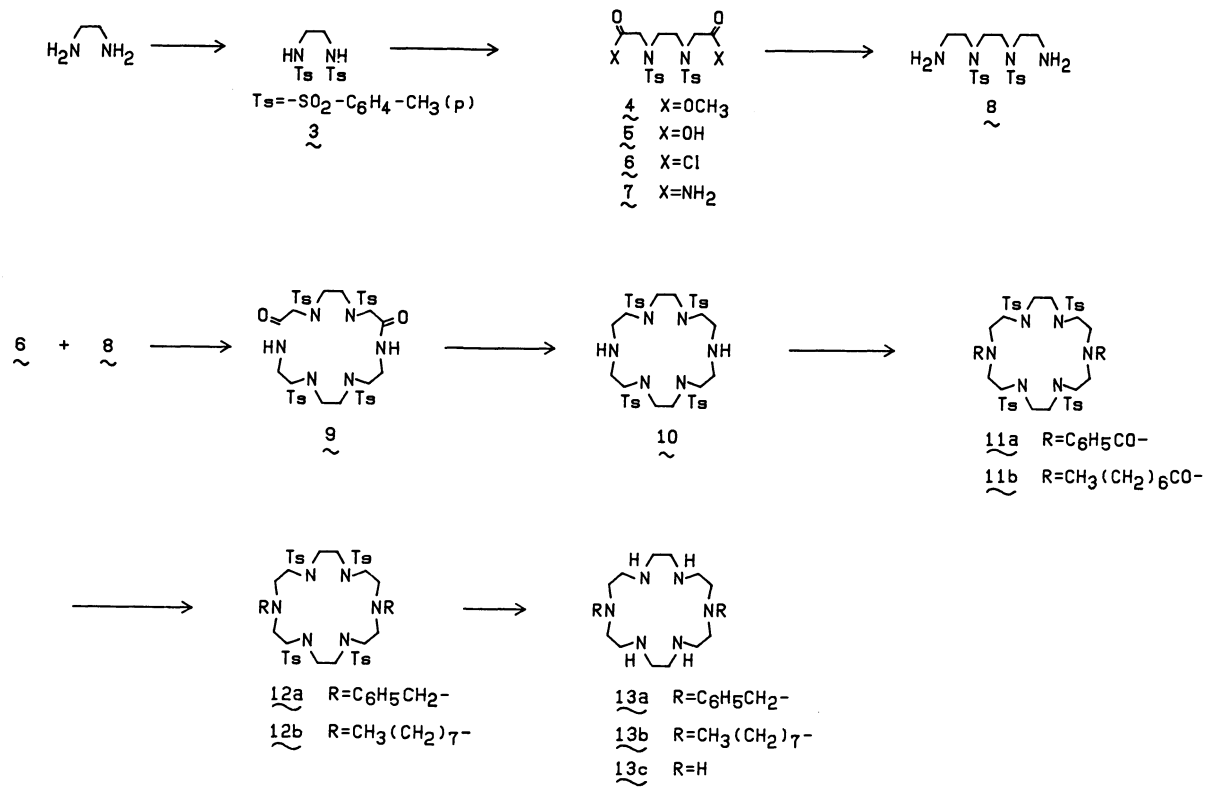

Table 1. Extractability of Hexaaza-18-crowns for Metal Cations

R%[a]	Li^+	Na^+	K^+	Ca^{2+}	Ba^{2+}
$PhCH_2$	14.8	13.0	14.4	15.7	16.1
C_8H_{17}	16.1	14.8	17.5	21.3	26.2
H	8.8	8.1	8.9	9.3	5.4

R%[b]	Li^+	Na^+	K^+	Rb^+	Cs^+	Mg^{2+}	Ca^{2+}	Ba^{2+}
$PhCH_2$	15.2	15.9	18.3	20.1	16.6	15.7	17.7	19.6
C_8H_{17}	18.9	19.3	21.7	23.1	21.0	18.9	21.4	23.4
H	5.0	4.2	3.9	2.4	2.9	3.7	8.5	4.6

R%[b]	Cu^+	Ag^+	Cu^{2+}	Zn^{2+}	Cd^{2+}	Fe^{3+}	Co^{2+}	NH_4^+
$PhCH_2$	22.5	43.4	22.4	39.8	36.4	19.7	27.1	23.3
C_8H_{17}	27.9	39.4	25.8	37.6	41.7	21.3	28.2	23.0
H	4.5	13.7	4.9	12.2	13.4	5.7	6.2	1.6

Conditions: a) [crown]=5×10^{-5} M (1 M=1 mol dm^{-3}), [MOH]=5×10^{-5} M, [$M(OH)_2$]=2.5×10^{-5} M, [picric acid]=5×10^{-5} M. b) [crown]=5×10^{-5} M, [MCl]=5×10^{-5} M, [MCl_2]=2.5×10^{-5} M, [MCl_3]=1.7×10^{-5} M, except for Ag^+~[$AgNO_3$]=5×10^{-5} M and Mg^{2+}~[$MgSO_4$]=2.5×10^{-5} M, [NaOH]=5×10^{-5} M, [picric acid]=5×10^{-5} M.

only complex mixtures. Finally, hydrolysis with concd. sulfuric acid at about 100 °C was found to be effective, giving 1,10-dialkyl-1,4,7,10,13,16-hexaazacyclooctadecane (1,10-disubstituted hexaaza-18-crown) (**13a, b**) in moderate yields.

Extractability. Metal cation-binding property of 1,10-disubstituted hexaaza-18-crowns **13a, b** and unsubstituted **13c** was investigated by equilibrating a dichloromethane solution of **13** with an aqueous solution of metal picrate, which was chosen as a metal cation source, at 25 °C. The results on the extraction of metal picrates with **13** are summarized in Table 1.

Metal picrates could not be extracted into a dichloromethane phase in the absence of **13**. Then, metal picrates may be extracted by the interaction with **13**, and the degree of extraction into a dichloromethane phase would reflect the cation-binding ability of **13**.

As shown in Table 1, **13a** and **13b** exhibited enhanced extraction efficiency compared with **13c**.

For alkali metal and alkaline earth metal cations the orders of the extractability of **13a** and **13b** were $Rb^+>K^+>Cs^+\geqq Na^+\simeq Li^+$ and $Ba^{2+}>Ca^{2+}>Mg^{2+}$, while unsubstituted **13c** exhibited metal cation selectivity in the orders of $Li^+\simeq Na^+\simeq K^+>Cs^+\simeq Rb^+$ and $Ca^{2+}>Ba^{2+}>Mg^{2+}$. On the other hand, the size of hexaaza-18-crown ring was found to be almost equal to that of 1,4,7,10,13,16-hexaoxacyclooctadecane (18-crown-6) on the basis of the structural analysis using CPK molecular models. The cation selectivities of 18-crown-6 are $Ba^{2+}>Ca^{2+}>Mg^{2+}$ and $K^+>Na^+$ and are well explained on the basis of the cation size vs. the cavity size correlation.[11] Then, the difference in extractability between **13a**, **b** and **13c**, which have the same binding site structure, and between **13** and 18-crown-6, which have similar ring size to each other, indicates that both of the side arms and the heteroatoms in the macrocycle play an important role in the incorporation of cations into the cavity of **13** and in the extraction to the organic phase.

The extractability of **13a** and **13b** for transition metal cations was higher than that for typical metal cations. The similar tendency was obtained for **13c**. This phenomenon can be explained by hard soft acid base principle; rather soft nitrogen atom has stronger affinity toward soft transition metal cations than hard typical metal cations. It is noticeable that **13** shows relatively high extractability for Ag^+, Zn^{2+}, and Cd^{2+}.

In most cases, the extractability of dioctylated hexaaza-18-crown **13b** for metal cations was a little higher than that of dibenzylated hexaaza-18-crown **13a**. Octyl group is probably more flexible and lipophilic than benzyl group. Then, **13b** would be liable to incorporate metal cations and its metal cation complexes would be more soluble in the organic phase in comparison with **13a**. The distinct reverse tendency in Ag^+ would result from π-interaction of Ag^+ with phenyl group in **13a**.

These 1,10-disubstituted hexaaza-18-crowns would wrap around the guest cations in such a way that the arms provide axial capping of the guest cations coordinated with the parent hexaaza-18-crown ring. The mobility of the arms attached to hexaaza-18-crown ring may permit dynamic complexation and decomplexation.

Experimental

Measurement. All melting points were measured on a Laboratory Devices MEL-TEMP apparatus and are uncorrected. IR spectra were recorded on a JASCO IR-810 spectrometer. ^1H NMR spectra were recorded on a Hitachi R-40 spectrometer in $CDCl_3$ or DMSO-d_6 using TMS as an internal standard. UV spectra were measured on a Shimadzu UV-260 spectrometer.

Materials. 3,6-Ditosyl-3,6-diazaoctanedioic acid (**5**) was prepared from 1,2-ethanediamine by the method in the literature.[10]

1,4,7,10,13,16-Hexaazacyclooctadecene (hexacyclen) (**13c**) was prepared from commercially available hexacyclen trisulfate (Aldrich Chem. Co.) by the method in the literature.[12]

Solvents were purified and dried by the standard procedures.

3,6-Ditosyl-3,6-diazaoctanedioyl Dichloride (6). 3,6-Ditosyl-3,6-diazaoctanedioic acid (**5**) (8.00 g, 16.5 mmol) was heated with thionyl chloride (100 ml) under reflux until the solution became clear. The excess thionyl chloride was evaporated at 60 °C. The remaining brownish crystals were repeatedly recrystallized from benzene to give **6** (7.30 g, 85% yield) as white crystals: mp 143—144 °C; IR (KBr) 2920, 2850, 1720, 1600, 1450, 1400, 1360, 1160, 1090, 1060, 960, 910, 805, 790, 750, 720 cm^{-1}; ^1H NMR ($CDCl_3$) δ=2.40 (6H, s), 3.26 (4H, s), 3.97 (4H, s), 7.50 (4H, d, J=7.5 Hz), and 7.59 (4H, d, J=7.5 Hz). Found: C, 46.26; H, 4.06; N, 5.31%. Calcd for $C_{20}H_{22}N_2O_6S_2Cl_2$: C, 46.07; H, 4.25; N, 5.37%.

3,6-Ditosyl-3,6-diazaoctanediamide (7). To a solution of **6** (72.2 g, 0.13 mol) in 700 ml of dichloromethane was introduced gaseous ammonia for 2 h at −78 °C to give white precipitates. After the excess ammonia was removed, the precipitates were collected by filtration, washed with water until the washing was no longer alkaline, and dried in vacuo. The precipitates were recrystallized from 2-methoxyethanol to give **7** as white crystals (48.6 g, 77%): mp 243.5—244.5 °C; IR (KBr) 3400, 3180, 2950, 2920, 1670, 1600,1500, 1460, 1420, 1360, 1310, 1290, 1250, 1190, 1160, 1120, 1090, 1050, 1020, 940, 900, 820, 790, 730 cm^{-1}; ^1H NMR (DMSO-d_6) δ=2.36 (6H, s), 3.26 (4H, s), 3.72 (4H, s), 6.97 (4H, brs), 7.42 (4H, d, J=7.5 Hz), and 7.51 (4H, d, J=7.5 Hz). Found: C, 49.99; H, 5.64; N, 11.33%. Calcd for $C_{20}H_{26}N_4O_6S_2$: C, 49.78; H, 5.43; N, 11.61%.

3,6-Ditosyl-3,6-diazaoctane-1,8-diamine (8). To a well-stirred suspension of 8.20 g (0.22 mol) of pulverized sodium borohydride in 300 ml of tetrahydrofuran (THF) containing 38.6 g (0.08 mmol) of **7** was added 55 ml (0.44 mol) of boron trifluoride etherate in 55 ml of dry THF in a period of 2 h at 0 °C under nitrogen atmosphere, then the mixture was refluxed for 12 h. After cooling at room temperature, the excess hydride was decomposed with water (60 ml), and 80 ml of 6 mol·dm^{-3} HCl solution was added. The solution was concentrated under reduced pressure. The residue was basified about pH 10 with 5 mol·dm^{-3} NaOH solution and extracted with dichloromethane (100 ml×3). Removal of the solvent gave solid mass. The crude product was recrystallized from methanol to afford white needles (23.2 g, 64%): mp 139—140 °C; IR (KBr) 3400, 2920, 2850, 1620, 1590, 1490, 1450, 1340, 1310, 1290, 1160, 1090, 1010, 960, 860, 810, 760, 720, 700 cm^{-1}; ^1H NMR (DMSO-d_6) δ=1.70 (4H, brs), 2.40 (6H, s), 2.65 (4H, t, J=7 Hz), 3.07 (4H, t, J=7 Hz), 3.22 (4H, s), 7.50 (4H, d, J=7.5 Hz), and 7.59 (4H, d, J=7.5 Hz). Found: C, 53.07; H, 6.68; N, 12.12%. Calcd for $C_{20}H_{30}N_4O_4S_2$: C, 52.84; H, 6.65; N, 12.32%.

4,7,13,16-Tetratosyl-1,4,7,10,13,16-hexaazacyclooctadecane-2,9-dione (9). A solution of **6** (7.30 g, 14 mmol) in dichlomethane (280 ml) and a solution of **8** (6.36 g, 14 mmol) and triethylamine (7.8 ml, 56 mmol) in dichloromethane (280 ml) were simultaneously added to a vigorously stirred dichloromethane (1700 ml) in a period of 12 h at the same dropping rate at 0 °C. Stirring was continued at 0 °C for additional 2 h. The solution was then washed with

water, dried with magnesium sulfate, and concentrated under reduced pressure to give the crude product. Purification by alumina column chromatography (the eluent: CH_2Cl_2) gave **9** as a white solid mass (6.33 g, 50%): IR (KBr) 3420, 2950, 2920, 1670, 1600, 1530, 1490, 1450, 1340, 1310, 1290, 1160, 1100, 1040, 1020, 1000, 930, 870, 820, 760, 720, 700 cm^{-1}; ^1H NMR ($CDCl_3$) δ=2.40 (12H, s), 3.31 (16H, brs), 3.72 (4H, s), 7.36 (8H, d, J=7.5 Hz), 7.45 (8H, d, J=7.5 Hz), and 8.11 (2H, brs). For the preparation of **10** the chromatographed **9** was used without further purification.

1,4,10,13-Tetratosyl-1,4,7,10,13,16-hexaazacyclooctadecane (10). To a well-stirred suspension of 1.14 g (30 mmol) of sodium borohydride in 120 ml of THF containing 4.15 g (5 mmol) of **9** was added 10 ml of boron trifluoride etherate (11.2 g, 80 mmol) in 40 ml of THF in a period of 1 h under nitrogen atmosphere at 0 °C, and the reaction mixture was refluxed for 24 h. After cooling at room temperature, the mixture was treated with water (25 ml) to decompose the excess hydride. The solution was concentrated under reduced pressure and extracted with dichloromethane (50 ml×5). The dichloromethane was evaporated, and 30 ml of 6 mol·dm^{-3} HCl solution was added to the residue. The acidic solution was heated at 80 °C for 1 h. After removal of excess HCl, saturated Na_2CO_3 solution was added until the evolution of gas ceased, and the product was extracted with dichloromethane (50 ml×3). The extracts were combined, dried, concentrated, and purified by alumina column chromatography (the eluent: CH_2Cl_2) to give **10** in 81%. The product was recrystallized from acetonitrile to give **10** (2.43 g, 56%): mp 208—212 °C; IR (KBr) 3420, 2940, 2860, 1590, 1500, 1450, 1340, 1310, 1290, 1190, 1160, 1120, 1090, 1040, 1010, 980, 920, 810, 760, 720 cm^{-1}; ^1H NMR ($CDCl_3$) δ=1.57 (2H, brs), 2.40 (12H, s), 2.73 (8H, t, J=5.0 Hz), 3.13 (8H, t, J=5 Hz), 3.31 (8H, s), 7.36 (8H, d, J=7.5 Hz), and 7.45 (8H, d, J=7.5 Hz). Found: C, 55.14; H, 6.31; N, 9.58%. Calcd for $C_{40}H_{54}N_6O_8S_4$: C, 54.90; H, 6.22; N, 9.60%.

1,10-Dibenzoyl-4,7,13,16-tetratosyl-1,4,7,10,13,16-hexaazacyclooctadecane (11a). To a stirred solution of **10** (0.60 g, 0.68 mmol) and triethylamine (0.40 ml, 2.8 mmol) in dichloromethane (30 ml) was added a solution of benzoyl chloride (0.38 ml, 2.8 mmol) in dichloromethane (5 ml) at 0 °C. After stirring for 8 h at room temperature, the reaction mixture was washed with water, dried, and concentrated under reduced pressure. The product was purified by silica-gel column chromatography (the eluent: CH_2Cl_2) to give **11a** (0.61 g, 83%): IR (KBr) 3070, 3040, 2940, 2870, 1720, 1640, 1600, 1500, 1450, 1420, 1350, 1310, 1160, 1120, 1100, 1040, 1020, 980, 910, 820, 740, 720, 700, 660 cm^{-1}; ^1H NMR ($CDCl_3$) δ=2.30 (12H, s), 3.0—3.9 (16H, m), 3.54 (8H, t, J=5 Hz), 7.37 (2H, dd, J=2 Hz, J'=9.5 Hz), 7.42 (4H, dd, J=7 Hz, J'=9.5 Hz), 7.43 (8H, d, J=7.5 Hz), 7.51 (8H, d, J=7.5 Hz), and 8.08 (4H, dd, J=2 Hz, J'=7 Hz).

1,10-Dioctanoyl-4,7,13,16-tetratosyl-1,4,7,10,13,16-hexaazacyclooctadecane (11b). The synthesis of **11b** was carried out in a similar manner to that of **11a**. Silica-gel chromatographic purification (the eluent: CH_2Cl_2) afforded **11b** in 94% yield: IR (KBr) 2930, 2850, 1720, 1640, 1600, 1460, 1420, 1350, 1310, 1160, 1090, 1040, 1020, 980, 910, 820, 740, 720, 700, 600 cm^{-1}; ^1H NMR ($CDCl_3$) δ=0.87 (6H, t, J=5 Hz), 1.27 (16H, brs), 1.63 (4H, t, J=5 Hz), 2.40 (12H, s), 3.08—3.81 (16H, m), 3.54 (8H, t, J=5 Hz), 7.43 (8H, d, J=7.5 Hz) and 7.51 (8H, d, J=7.5 Hz).

1,10-Dibenzyl-4,7,13,16-tetratosyl-1,4,7,10,13,16-hexaazacyclooctadecane (12a). To a solution of 0.70 g (0.64 mmol) of **11a** in 6 ml of THF was slowly added a solution of 11 ml of 1 mol·dm^{-3} diborane in THF (Aldrich Chem. Co.) at 0 °C under nitrogen atmosphere. The solution was then refluxed for 24 h. After cooling to room temperature, 10 ml of water was added to the solution, and the THF was evaporated. To the remaining residue was added 2 ml of 6 mol·dm^{-3} HCl solution, and the mixture was heated at 80 °C for 30 min. After concentration of the solution, the residue was basified with 10% LiOH solution (5 ml) and extracted with dichloromethane (30 ml×5). The extracts were concentrated under reduced pressure to give the crude product. Crystallization from benzene gave pure **12a** (0.49 g, 72%): mp 185—189 °C (decomp.); IR (KBr) 3060, 3030, 2930, 2860, 1630, 1600, 1500, 1460, 1400, 1340, 1310, 1160, 1100, 980, 920, 820, 740, 720, 700, 660 cm^{-1}; ^1H NMR ($CDCl_3$) δ=2.40 (12H, s), 2.65 (8H, t, J=7 Hz), 3.14 (8H, t, J=7 Hz), 3.24 (8H, s), 3.62 (4H, s), 7.35 (10H, s), 7.43 (8H, d, J=7.5 Hz), and 7.51 (8H, d, J=7.5 Hz). Found: C, 64.86; H, 6.41; N, 6.88%. Calcd for $C_{54}H_{66}N_6O_8S_4 \cdot 3/2C_6H_6$: C, 64.53; H, 6.45; N, 7.17%.

1,10-Dioctyl-4,7,13,16-tetratosyl-1,4,7,10,13,16-hexaazacyclooctadecane (12b). In a similar manner mentioned above, **12b** was synthesized. Recrystallization from acetonitrile gave pure **12b** in 81% yield: mp 160—163 °C (decomp); IR (KBr) 2930, 2850, 1630, 1600, 1500, 1460, 1350, 1310, 1160, 1100, 980, 820, 750, 710, 660 cm^{-1}; ^1H NMR ($CDCl_3$) δ=0.87 (6H, t, J=5 Hz), 1.25 (24 H, brs), 2.41 (12 H, s), 2.65 (12H, t, J=7 Hz), 3.14 (8H, t, J=7 Hz), 3.24 (8H, s), 7.43 (8H, d, J=7.5 Hz), and 7.51 (8H, d, J=7.5 Hz). Found: C, 61.32; H, 8.02; N, 7.94%. Calcd for $C_{56}H_{86}N_6O_8S_4$: C, 61.17; H, 7.88; N, 7.64%.

1,10-Dibenzyl-1,4,7,10,13,16-hexaazacyclooctadecane (13a). A solution of **12a** (106 mg, 0.1 mmol) in 0.7 ml of concd. H_2SO_4 was heated at 100 °C for 10 h. The solution was poured into an ice-cold water and basified with 10 mol·dm^{-3} NaOH solution, followed by extraction with dichloromethane (20 ml×5). The extracts were combined, dried, and concentrated under reduced pressure. The residue was chromatographed on an alumina column (the eluent: CH_2Cl_2) to give **13a** (30 mg, 69%): IR (neat) 3320, 3050, 2950, 2830, 1660, 1600, 1500, 1460, 1280, 1120, 1030, 910, 740, 700 cm^{-1}; ^1H NMR ($CDCl_3$) δ=2.50—2.95 (16H, m), 2.75 (8H, s), 3.62 (4H, s), 4.33 (4H, brs), and 7.25 (10H, s).

1,10-Dioctyl-1,4,7,10,13,16-hexaazacyclooctadecane (13b). In a similar manner, **13b** was prepared from **12b** in 60% yield: IR (neat) 3320, 2930, 2850, 1660, 1460, 1280, 1110, 910, 800, 740 cm^{-1}; ^1H NMR ($CDCl_3$) δ=0.88 (6H, t, J=5 Hz), 1.25 (24H, brs), 2.39—2.92 (16H, m), 2.82 (8H, s), and 3.98 (4H, brs).

Extraction Procedure. Extractability of unsubstituted and 1,10-disubstituted hexaaza-18-crowns for metal cations was examined in a similar manner to the method described in the literature.[13] A dichloromethane solution (5 ml) of hexaaza-18-crown (5×10^{-5} mol·dm^{-3}) and an aqueous solution (5 ml) containing equivalents of metal hydroxide (or metal chloride+sodium hydroxide) and picric acid were agitated at 25 °C for 1 h. An aliquot of the upper aqueous solution was withdraw, and UV spectrum was recorded. A similar extraction was performed without hexaaza-18-crown. The extractability was determined on the basis of the absorbance of picrate ion in the aqueous solutions by means

of the following equation:

$$\text{extractability } (\%) = [(A_0 - A)/A_0] \times 100$$

where A_0 is the absorbance in the absence of hexaaza-18-crown and A is the absorbance in the presence of hexaaza-18-crown.

The present work was partially supported by a Grant-in-Aid for Scientific Research No. 61226004 from the Ministry of Education, Science and Culture.

References

1) J.-M. Lehn, *Struct. Bonding (Berlin)*, **16**, 1 (1973); J. J. Christensen, D. J. Eatough, and R. M. Izatt, *Chem. Rev.*, **74**, 351 (1974); L. F. Lindoy, *Chem. Soc. Rev.*, **5**, 421 (1975); G. R. Newkome, J. D. Sauer, J. M. Roger, and D. C. Hager, *Chem. Rev.*, **77**, 513 (1977).

2) K. R. Adam, A. J. Leong, L. F. Lindoy, H. C. Lip, B. W. Skelton, and A. H. White, *J. Am. Chem. Soc.*, **105**, 4645 (1983).

3) D. M. Dishong, C. J. Diamond, and G. W. Gokel, *J. Chem. Soc., Chem. Commun.*, **1980**, 1053; D. M. Dishong, C. J. Diamond, M. I. Cinoman, and G. W. Gokel, *J. Am. Chem. Soc.*, **105**, 586 (1983).

4) J. E. Richman and T. J. Atkins, *J. Am. Chem. Soc.*, **96**, 2268 (1974); H. E. Simmons and C. M. Park, *J. Am. Chem. Soc.*, **90**, 2428 (1968); N. F. Curtis, *Coord. Chem. Rev.*, **3**, 3 (1968); E. Kimura, M. Kodama, and T. Yatsunami, *J. Am. Chem. Soc.*, **104**, 3182 (1982); E. Kimura, A. Watanabe, and M. Kodama, *J. Am. Chem. Soc.*, **105**, 2613 (1983); T. H. Kaden, *Top. Curr. Chem.*, **121**, 157 (1984).

5) H. Stetter and W. Frank, *Angew. Chem.*, **88**, 760 (1976); H. Stetter, W. Frank, and R. Mertens, *Tetrahedron*, **37**, 767 (1981); R. Delgado and J. J. F. Dasilva, *Talanta*, **29**, 815 (1982).

6) F. R. Muller and H. Handel, *Tetrahedron Lett.*, **23**, 2769 (1982).

7) N. W. Alcock, K. P. Balakrishnan, and P. Moore, *J. Chem. Soc., Chem. Commun.*, **1985**,1731.

8) B. Dietrich, J.-M. Lehn, and J.-P. Sauvage, *Tetrahedron Lett.*, **1969**, 2885; B. Dietrich, J.-M. Lehn, J.-P. Sauvage, and J. Blanzat, *Tetrahedron*, **29**, 1629 (1973).

9) B. Dietrich, M. W. Hosseini, J.-M. Lehn, and R. B. Sessions, *Helv. Chim. Acta*, **68**, 289 (1985).

10) a) H. Stetter and E. Roos, *Chem. Ber.*, **87**, 566 (1954); b) H. Stetter and K. Mayer, *ibid.*, **94**, 1410 (1961).

11) R. M. Izatt, R. E. Terry, B. L. Haymore, L. D. Hansen, N. K. Dalley, A. G. Avondet, and J. J. Christensen, *J. Am. Chem. Soc.*, **98**, 7620 (1976).

12) J. E. Richman, T. J. Atkins, and F. W. Oettle, *Org. Synth.*, **58**, 86 (1978).

13) C. J. Pedersen, *Federation Proceeding*, **27**, 1305 (1968); S. Akabori, Y. Habata, Y. Sakamoto, M. Sato, and S. Ebine, *Bull. Chem. Soc. Jpn.*, **56**, 537 (1983).

Synthesis and Structure of 6,7-Dihydro-2,3-disubstituted 5*H*-2a-Thia(2*a*-S^{IV})-2,3,4a,7a-tetraazacyclopent[*cd*]indene-1,4(2*H*,3*H*)-dithione

Noboru MATSUMURA,* Masaaki TOMURA, Osamu MORI, Yuko TSUCHIYA, Shigeo YONEDA,* and Koshiro TORIUMI†

Department of Applied Chemistry, College of Engineering, University of Osaka Prefecture, Sakai, Osaka 591

†Institute for Molecular Science, Myodaiji, Okazaki 444

(Received December 23, 1987)

Symmetrical tetraazapentalene derivatives **5** and **6** were synthesized by a convenient one-pot reaction using lithium thioureide/phenacyl chloride/alkyl (or allyl) isothiocyanate system. Unsymmetrical tetraazapentalene derivatives **8** were prepared by the reaction of various isothiocyanates with thiadiazolopyrimidine derivatives **7** which were derived from symmetrical tetraazapentalene derivatives. The structure of **5c** was determined by a single crystal X-ray diffraction.

Chemistry of π-hypervalent heterocyclic systems related to 6a-thia(S^{IV})pentalene has been of considerable current interest, and several systems containing S–S^{IV}–S, S–S^{IV}–O, or N–S^{IV}–N bond and 10π-electrons in the framework were synthesized.[1] We have recently reported that the dianion **3** of 3,4,5,6,-tetrahydro-2(1*H*)-pyrimidinethione (**1**) reacted with methyl isothiocyanate to give 6,7-dihydro-2,3-dimethyl-5*H*-2a-thia(*2a*-S^{IV})-2,3,4a,7a-tetraazacyclopent[*cd*]indene-1,4-(2*H*,3*H*)-dithione (**5a**)[2] in low yield. Compounds of this type[3] containing π-hypervalent sulfur and 12π-electrons in the framework are of interest, because the structure, stability, and reactivity should be different from those of the other 6a-thia(S^{IV})pentalene analogs mentioned above. Recently, we have established general preparation of the symmetrical and unsymmetrical tetraazapentalene derivatives reported as preliminary communications.[4] In this paper, we describe the detail of preparation of symmetrical tetraazapentalene derivatives **5** and **6**, the first example of the X-ray crystallographic structure of a new heteropentalene, 6,7-dihydro-2,3-diethyl-5*H*-2a-thia-(*2a*-S^{IV})-2,3,4a,7a-tetraazacyclopent[*cd*]indene-1,4(2*H*, 3*H*)-dithione (**5c**), and the smooth conversion of the symmetrical tetraazapentalene derivatives to the unsymmetrical ones **8** via selective elimination of alkyl (or allyl) isothiocyanate followed by 1,3-dipolar cycloaddition.

Results and Discussion

Synthesis of Symmetrical Tetraazapentalene Derivatives. Cyclic thioureas **1** and **2** were treated with two molar equivalents of butyllithium in tetrahydrofuran (THF) at 0 °C under argon. When the resulting dianions **3** and **4** were reacted with a molar equivalent of phenacyl chloride to give intermediate **A**, followed by addition of isothiocyanate (three molar equivalents), the tetraazapentalene derivatives **5** and **6** were obtained as colorless solids in good yields. These compounds are stable under the atmosphere.

The yields of products are shown in Table 1. The structures of **5** and **6** were determined by IR, ^{1}H NMR, ^{13}C NMR, mass spectra, and elemental analyses.

Scheme 1 shows a possible reaction mechanism for the formation of tetraazapentalenes, **5** and **6**. In this reaction, the formation of acetophenone was recognized. The yields of products depended on the ring size of cyclic thiourea and on the bulkiness of the alkyl group of alkyl isothiocyanate. When phenyl or *t*-butyl isothiocyanate was used in this reaction, no tetraazapentalene derivative was produced. The dianion **3**

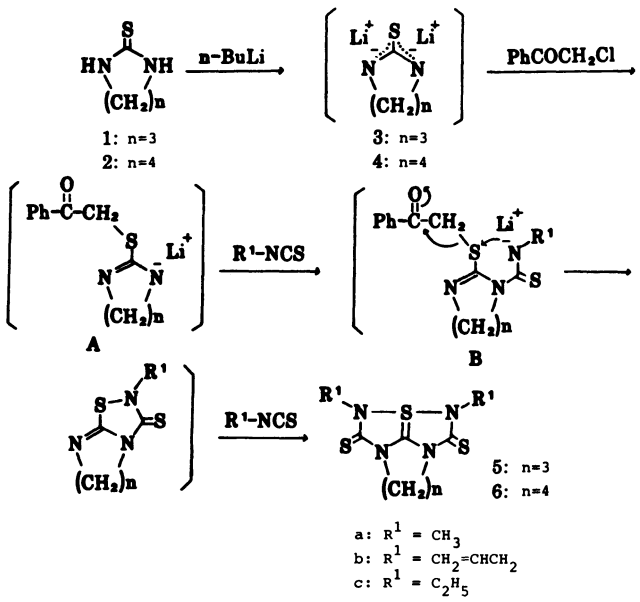

Scheme 1.

Table 1. Preparation of Tetraazapentalene Derivatives[a]

Entry	Dianion	R in R-NCS	Product	Yield/%[b]
1	**3**	CH_3	**5a**	74
2	**3**	CH_2=$CHCH_2$	**5b**	65
3	**3**	C_2H_5	**5c**	64
4	**4**	CH_3	**6a**	27
5	**4**	CH_2=$CHCH_2$	**6b**	9
6	**4**	C_2H_5	**6c**	14

a) The reactions were carried out in tetrahydrofuran at room temperature for 24 h under argon. b) Isolated yield.

derived from the 6-membered ring thiourea **1** gave tetraazapentalene derivatives more effectively than the dianion **4** derived from the 7-membered ring thiourea **2**. On the other hand, when a dianion derived from the 5-membered ring thiourea, 2-imidazolidinethione, was used in this reaction, tetraazapentalene derivative was not obtained. The intermediate derived from the 2-imidazolidinethione could not have favorable conformation for the attack of the nitrogen atom to the sulfur atom.

Synthesis of Unsymmetrical Tetraazapentalene Derivatives. The thermolysis or oxidation reaction of 6,7-dihydro-2,3-dimethyl-5*H*-2a-thia(2*a*-S^{IV})-2,3,4a,7a-tetraazacyclopent[*cd*]indene-1,4(2*H*,3*H*)-dithione (**5a**) gave easily 6,7-dihydro-2-methyl-5*H*-1,2,4-thiadiazolo[4,5-*a*]pyrimidine-3(2*H*)-thione (**7a**). Furthermore, **7a** was found to undergo a 1,3-dipolar cycloaddition with various isothiocyanates to give unsymmetrical tetraazapentalene derivatives having different groups at 3,4-positions (Scheme 2).

When the compounds **5** were heated at 170 °C under reduced pressure (2 mmHg, 1 mmHg≈133.322 Pa) or treated at room temperature with sodium periodate in methanol, the products **7** were obtained in moderate yields. The yields are shown in Table 2.

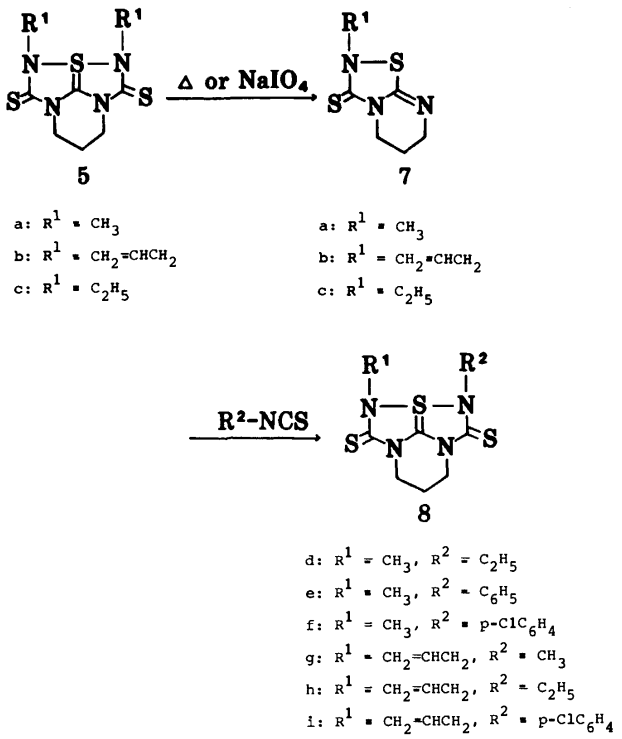

Scheme 2.

The thermolysis under reduced pressure (method A) is preferable to the oxidation reaction using $NaIO_4$ (method B) for the preparation of **7**. The structure of **7** was determined by IR, ^{1}H NMR, mass spectra, and elemental analyses. The compound **7** reacted smoothly with the isothiocyanates to give the unsymmetrical tetraazapentalene derivatives **8**. When the reaction of various isothiocyanates (1.5 times molar quantity of **7**) with **7** were carried out in refluxing chloroform for 3 h, the unsymmetrical tetraazapentalene derivatives **8** were obtained in good yields. The yields are shown in Table 3. All compounds were characterized by IR, ^{1}H NMR, ^{13}C NMR, UV, mass spectra, and elemental analyses.

Structure of Tetraazapentalene Derivatives. In order to establish the structure of the tetraazapentalene derivatives, a single crystal X-ray diffraction of **5c** was performed. The crystal of **5c** was most suitable for an X-ray diffraction among those of **5**, **6**, and **8**. Figure 1 shows the molecular structure of **5c**. Selected bond lengths and angles are listed in Table 4.

Figure 2 shows the molecular structure of **5c** viewed along the S(2)-C(1) bond and Table 5 shows the distance to the plane from the atoms in the molecule. The X-ray crystallographic analysis provides the following structural characteristics: (i) The S(1)-C(2) bond length [1.705 Å] is fairly shorter than the usual S(6a)-C(3) bond length [1.75 Å][5] of 6a-thia(S^{IV})pentalene analogs; (ii) the S(1)-N(1) [1.927 Å] and S(1)-N(2) [1.891 Å] bond lengths differ from each

Table 2. Preparation of Thiadiazolopyrimidine Derivatives **7**

	R^1	Method	Product	Yield/%
5a	CH_3	A[a]	**7a**	69
5a	CH_3	B[b]	**7a**	33
5b	CH_2=$CHCH_2$	A	**7b**	75
5b	CH_2=$CHCH_2$	B	**7b**	27
5c	CH_3CH_2	A	**7c**	62
5c	CH_3CH_2	B	**7c**	13

a) The compound was heated at 170 °C under reduced pressure (2 mmHg). b) Sodium periodate was used as an oxidizing agent.

Table 3. Preparation of Unsymmetrical Tetraazapentalene Derivatives **8**[a]

Entry	Thiadiazolopyrimidine	R^2 in R^2-NCS	Product	Yield/%[b]
1	**7a**	CH_3CH_2	**8d**	84
2	**7a**	C_6H_5	**8e**	85
3	**7a**	*p*-ClC_6H_4	**8f**	63
4	**7b**	CH_3	**8g**	63
5	**7b**	CH_3CH_2	**8h**	86
6	**7b**	*p*-ClC_6H_4	**8i**	66

a) The reactions were carried out in refluxing chloroform for 3 h. b) Isolated yield.

other, and it means that **5** has an unsymmetrical structure; (iii) the S–N bond length [1.91 Å, average] is 9% longer than the usual S–N single bond length [1.74 Å];[6] the external C=S double bond length [1.68 Å, average] is 4% longer than the usual C=S double bond length [1.61 Å];[6] and (v) the tetraazapentalene framework can be regarded as planar, because the maximum distance between the framework atoms and the plane is only 0.013 Å as seen in Table 5. Figure 3 shows the drawing of the molecular packing.

In spite that the tetraazapentalene **5c** formally has four tertiary nitrogen atoms, the framework was elucidated to be planar by X-ray crystallographic analysis. This fact indicates much contribution from polar resonance contributors to the electronic structure of **5** as illustrated in Scheme 3. The extension of the external C=S double bond length is due to such polar resonance contributors. In accord with the planarity of the framework, the four nitrogen atoms may have nature of the sp^2 configuration. In the conjugated π-system, twelve π-electrons are well delocalized on the tetraazapentalene framework.

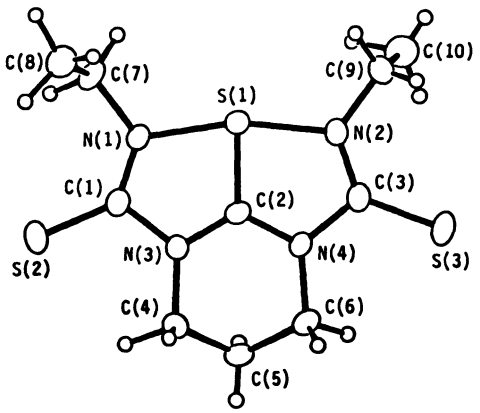

Fig. 1. Molecular structure of **5c** with numbering scheme.

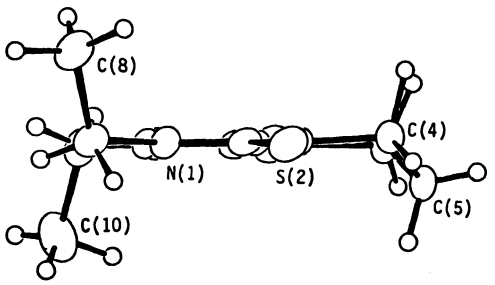

Fig. 2. Molecular structure of **5c** viewed along the S(2)–C(1) bond.

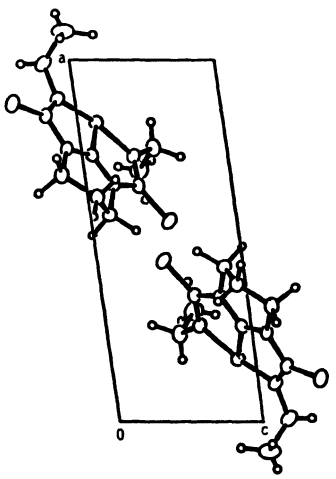

Fig. 3. Crystal packing diagram.

Table 4. Selected Bond Lengths and Angles of **5c** with Their Estimated Standard Deviations

	Distance/Å		Angle/°
S(1)–N(1)	1.927(4)	N(1)–S(1)–N(2)	165.5(2)
S(1)–N(2)	1.891(4)	N(1)–S(1)–C(2)	82.0(2)
S(1)–C(2)	1.705(4)	N(1)–C(1)–N(3)	108.7(4)
S(2)–C(1)	1.683(5)	N(1)–C(1)–S(2)	130.4(4)
S(3)–C(3)	1.674(5)	N(1)–C(7)–C(8)	112.5(4)
N(1)–C(1)	1.289(6)	N(2)–S(1)–C(2)	83.5(2)
N(1)–C(7)	1.461(6)	N(2)–C(3)–N(4)	108.5(4)
N(2)–C(3)	1.311(6)	N(2)–C(3)–S(3)	129.5(4)
N(2)–C(9)	1.438(7)	N(2)–C(9)–C(10)	112.1(5)
N(3)–C(1)	1.428(6)	N(3)–C(2)–N(4)	123.8(4)
N(3)–C(2)	1.327(6)	N(3)–C(4)–C(5)	108.9(4)
N(3)–C(4)	1.469(6)	N(4)–C(6)–C(5)	109.2(4)
N(4)–C(2)	1.339(6)	S(1)–N(1)–C(1)	116.0(3)
N(4)–C(3)	1.417(6)	S(1)–N(1)–C(7)	119.0(3)
N(4)–C(6)	1.469(6)	S(1)–N(2)–C(3)	115.7(3)
C(4)–C(5)	1.505(7)	S(1)–N(2)–C(9)	119.6(3)
C(5)–C(6)	1.519(7)	S(1)–C(2)–N(3)	119.0(3)
C(7)–C(8)	1.524(8)	S(1)–C(2)–N(4)	117.3(3)
C(9)–C(10)	1.494(8)	S(2)–C(1)–N(3)	120.9(3)
		S(3)–C(3)–N(4)	122.1(3)
		C(1)–N(1)–C(7)	125.1(4)
		C(1)–N(3)–C(2)	114.3(4)
		C(1)–N(3)–C(4)	125.5(4)
		C(2)–N(4)–C(3)	115.0(4)
		C(2)–N(3)–C(4)	120.2(4)
		C(2)–N(4)–C(6)	121.2(4)
		C(3)–N(2)–C(9)	124.5(4)
		C(3)–N(4)–C(6)	123.7(4)
		C(4)–C(5)–C(6)	110.7(4)

Table 5. Distances to the Plane from the Atoms in the Molecule

Atom	Distance/Å	Atom	Distance/Å
S(1)	0.002	S(3)	−0.015
N(1)	0.000	C(4)	−0.076
N(2)	−0.013	C(5)	0.629
N(3)	−0.006	C(6)	0.034
N(4)	0.010	C(7)	−0.027
C(1)	−0.002	C(8)	−1.413
C(2)	−0.003	C(9)	0.027
C(3)	−0.001	C(10)	1.422
S(2)	0.045		

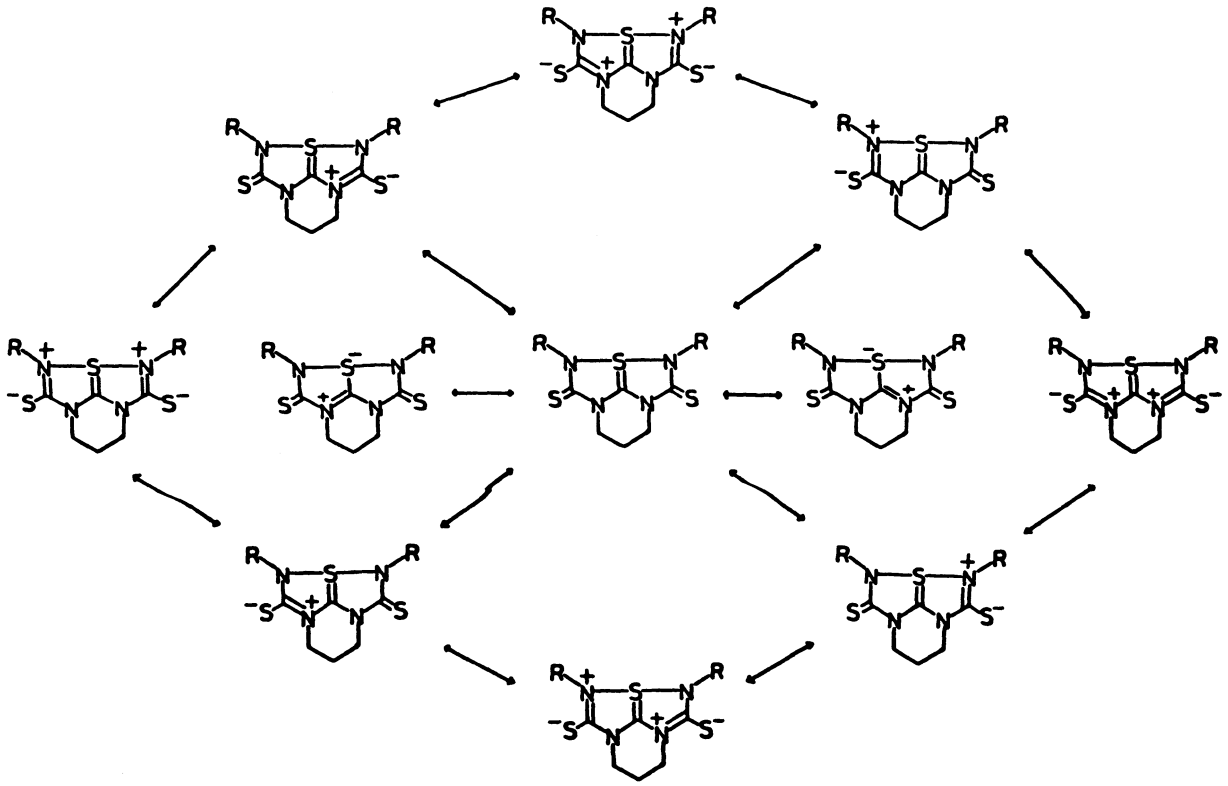

Scheme 3.

Experimental

General. Melting points were determined on a Yanagimoto melting point apparatus and were uncorrected. Proton magnetic resonance (^{1}H NMR) spectra were obtained using a Hitachi Perkin-Elmer R-24 spectrometer (60 MHz), JEOL FX-90Q (90 MHz), and JEOL JNM-GX270 (270 MHz). ^{13}C NMR spectra were obtained using a JEOL FX-90Q and JEOL JNM-GX270. Chemical shifts are reported in ppm from TMS as an internal standard and are given in δ units. The IR and UV spectra were determined on a Hitachi 215 Grating infrared spectrometer and Hitachi 124 spectrometer, respectively. Mass spectra were obtained with a SHIMADZU-LKB 9000 instrument equipped with a solid injector; the ionizing voltage was 70 eV. Purifications of products were conducted by column chromatography on silica gel (Wakogel C-300) or by preparative TLC on silica gel (Merck Kieselgel 60 GF_{254}).

General Procedure for the Preparation of Symmetrical Tetraazapentalene Derivatives 5 and 6. To a cooled THF solution (0 °C, 25 ml) of cyclic thiourea **1** or **2** (2.0 mmol) was added a hexane solution of butyllithium (4.4 mmol) with stirring at 0 °C under argon, and the mixture was stirred for 1 h under the same conditions. To the resulting dianion **3** or **4** was added dropwise a THF solution (5 ml) of phenacyl chloride (2.0 mmol). The solution immediately became wine red, and the reaction mixture was refluxed for 1 h under argon. After cooling to room temperature, the 5 ml of solution of alkyl isothiocyanate (6.0 mmol) in THF was added, and the reaction mixture was stirred at room temperature for 20 h under argon. After THF was evaporated, the residue was poured into an aqueous ammonium chloride. The solution was extracted with chloroform, and the extract was washed with water, dried over anhydrous Na_2SO_4, and condensed under reduced pressure. The residue was chromatographed on a silica-gel column or preparative TLC using dichloromethane as an eluent to give tetraazapentalene derivatives **5** or **6**. All tetraazapentalene derivatives were recrystallized from hexane–chloroform.

Spectroscopic data of 6,7-dihydro-2,3-dimethyl-5*H*-2a-thia(*2a*-S^{IV})-2,3,4a,7a-tetraazacyclopent[*cd*]indene-1,4(2*H*,3*H*)-dithione (**5a**) and 6,7-dihydro-2,3-diethyl-5*H*-2a-thia-(2a-S^{IV})-2,3,4a,7a-tetraazacyclopent[*cd*]indene-1,4(2*H*,3*H*)-dithione (**5c**) coincided with previously reported data.[2]

6,7-Dihydro-2,3-diallyl-5*H*-2a-thia(*2a*-S^{IV})-2,3,4a,7a-tetraazacyclopent[*cd*]indene-1,4(2*H*,3*H*)-dithione (5b). Mp 177—180 °C (decomp); IR (KBr) 2960, 1580, 1530, 1470, 1180, and 1160 cm^{-1}; ^{1}H NMR ($CDCl_3$) δ=2.37 (m, 2H, $NCH_2\underline{CH_2}CH_2N$), 4.36 (t of d, 4H, J=1.5 and 6.0 Hz, $2\times CH_2$=$CH\underline{CH_2}N$), 4.37 (t, 4H, J=6.0 Hz, $N\underline{CH_2}CH_2\underline{CH_2}N$), 5.20—5.28 (m, 4H, $2\times\underline{CH_2}$=$CHCH_2N$), and 5.88—6.02 (m, 2H, $2\times CH_2$=$\underline{CH}$-CH_2N); ^{13}C NMR ($CDCl_3$) δ=19.99, 44.84, 47.79, 118.10, 132.20, 156.66, and 169.57; UV (CH_3CN) 260 (log ε 4.52) nm; MS *m/z* (rel intensity) 213 (M^+-CH_2=$CHCH_2NCS$; 30), 99 (83), 72 (39), and 41 (100). Found: C, 46.02; H, 5.11; N, 17.91%. Calcd for $C_{12}H_{16}N_4S_3$: C, 46.12; H, 5.16; N, 17.93%.

5,6,7,8-Tetrahydro-2,3-dimethyl-2a-thia(*2a*-S^{IV})-2,3,4a,8a-tetraazacyclopent[*cd*]azulene-1,4(2*H*,3*H*)-dithione (6a). Mp 187—190 °C (decomp); IR (KBr) 2910, 1550, 1530, 1500, 1190, 1120, 1090 and 970 cm^{-1}; ^{1}H NMR ($CDCl_3$) δ=2.20 (m, 4H, $NCH_2\underline{CH_2}\underline{CH_2}CH_2N$), 3.15 (s, 6H, $2\times CH_3$), and 4.95 (m, 4H, $N\underline{CH_2}CH_2CH_2\underline{CH_2}N$); ^{13}C NMR ($CDCl_3$) δ=24.01, 31.49, 48.33, 161.49, and 170.78; UV (CH_3CN) 264 (log ε 4.56) nm; MS *m/z* (rel intensity) 201 (M^+-CH_3NCS; 91), 168 (32), 73 (100), 72 (81), and 69 (58). Found: C, 39.73; H, 5.19; N,

20.02%. Calcd for $C_9H_{14}N_4S_3$: C, 39.42; H, 5.15; N, 20.43%.

5,6,7,8-Tetrahydro-2,3-diallyl-2a-thia(2*a*-S^{IV})-2,3,4a,8a-tetraazacyclopent[*cd*]azulene-1,4(2*H*,3*H*)-dithione (6b). Mp 145—148 °C (decomp); IR (KBr) 2930, 2880, 1530, 1480, 1405, 1175, 1130, 1090, and 970 cm^{-1}; ^1H NMR ($CDCl_3$) δ=2.25 (m, 4H, $NCH_2C\underline{H}_2C\underline{H}_2CH_2N$), 4.33 (t of d, 4H, J=6.0 and 1.5 Hz, $2\times CH_2$=$CHC\underline{H}_2N$), 5.00 (m, 4H, $NC\underline{H}_2CH_2CH_2C\underline{H}_2N$), 5.20—5.27 (m, 4H, $2\times C\underline{H}_2$=$CHCH_2N$), and 5.87—6.02 (m, 2H, $2\times CH_2$=$C\underline{H}CH_2N$); ^{13}C NMR ($CDCl_3$) δ=23.96, 48.22, 48.38, 118.19, 132.01, 162.25, and 170.80; MS *m/z* (rel intensity) 227 (M^+-CH_2=$CHCH_2NCS$; 48), 194 (28), 114 (39), 99 (100), 72 (90), and 55 (50). Found: C, 47.30; H, 5.58; N, 17.01%. Calcd for $C_{13}H_{18}N_4S_3$: C, 47.82; H, 5.56; N, 17.16%.

5,6,7,8-Tetrahydro-2,3-diethyl-2a-thia(2*a*-S^{IV})-2,3,4a,8a-tetraazacyclopent[*cd*]azulene-1,4(2*H*,3*H*)-dithione (6c). Mp 159—162 °C (decomp); IR (KBr) 2960, 2920, 1550, 1530, 1430, 1190, 1080, and 980 cm^{-1}; ^1H NMR($CDCl_3$) δ=1.32 (t, 6H, J=7.3 Hz, $2\times CH_2C\underline{H}_3$), 2.24 (m, 4H, $NCH_2C\underline{H}_2C\underline{H}_2CH_2N$), 3.75 (q, 4H, J=7.3 Hz, $2\times C\underline{H}_2CH_3$), and 5.00 (m, 4H, J=5.6 Hz, $NC\underline{H}_2CH_2CH_2C\underline{H}_2N$); ^{13}C NMR ($CDCl_3$) δ=13.68, 24.01, 40.30, 48.08, 161.72, and 169.81; UV (CH_3CN) 264 (log ε 4.54) nm; MS *m/z* (rel intensity) 215 ($M^+-CH_3CH_2$-NCS; 65), 182 (17), 114 (25), 87 (100), 72 (62), 59 (61), and 55 (54). Found: C, 43.73; H, 6.30; N, 18.20%. Calcd for $C_{11}H_{18}N_4S_3$: C, 43.68; H, 6.00; N, 18.52%.

General Procedure for the Preparation of Thiadiazolopyrimidine Derivatives 7. Method A (Thermolysis of **5**): Thermolysis of **5** (200 mg) using sublimation apparatus was carried out at 170 °C for 5 h under reduced pressure (2 mmHg). Then the sublimation products were collected with chloroform and chromatographed on a preparative TLC (dichloromethane:ethyl acetate=4:1 as an eluent) to give **7** as a colorless solid. Method B (Oxidation of **5** with $NaIO_4$): To a methanol solution (50 ml) of **5** (0.23 mmol) was added a sodium periodate (0.33 mmol) with stirring at room temperature under argon. After the stirring was continued for 5 h, methanol was removed in vacuo. To the residual mixture was added chloroform (50 ml), stirred for 1 min, and the resulting suspension was filtered. After the filtrate was condensed under reduced pressure, the residue was chromatographed on a preparative TLC (dichloromethane:ethyl acetate=4:1 as an eluent) to give **7** as a colorless solid.

6,7-Dihydro-2-methyl-5*H*-1,2,4-thiadiazolo[4,5-*a*]pyrimidine-3(2*H*)-thione (7a). Mp 119—122 °C (decomp); IR(KBr) 2925, 2850, 1640, 1480, 1350, 1290, 1110, 945, and 750 cm^{-1}; ^1H NMR($CDCl_3$) δ=1.90 (m, 2H, $NCH_2C\underline{H}_2CH_2N$), 2.35 (s, 3H, CH_3), 3.55 (t, 2H, J=6.0 Hz, C=NCH_2), and 3.90 (t, 2H, J=6.0 Hz, NCH_2); MS *m/z* (rel intensity) 187 (M^+; 100), 154 (23), 72 (33), 69 (38), and 41 (26).

Picrate of 7a. Mp 196—200°C (decomp); Found: C, 34.60; H, 2.85; N, 20.12%. Calcd for $C_{12}H_{12}N_6O_7S_2$: C, 34.61; H, 2.90; N, 20.18%.

6,7-Dihydro-2-allyl-5*H*-1,2,4-thiadiazolo[4,5-*a*]pyrimidine-3(2*H*)-thione (7b). Mp 92—95 °C (decomp); IR (KBr) 2920, 2840, 1645, 1415, 1360, 1215, 1120, 855, and 835 cm^{-1}; ^1H NMR ($CDCl_3$) δ=2.10 (m, 2H, $NCH_2C\underline{H}_2CH_2N$), 3.65 (m, 2H, C=$NCH_2$), 4.00 (m, 2H, NCH_2), 4.55 (m, 2H, $NC\underline{H}_2CH$=CH_2), 5.20—5.65 (m, 2H, NCH_2CH=$C\underline{H}_2$), and 5.75—6.35 (m, 1H, $NCH_2C\underline{H}$=CH_2); MS *m/z* (rel intensity) 213 (M^+; 65), 180 (27), 128 (28), 100 (28), 99 (29), 72 (44), and 41 (100).

Picrate of 7b. Mp 171—174 °C (decomp); Found: C, 37.94; H, 3.02; N, 19.02%. Calcd for $C_{14}H_{14}N_6O_7S_2$: C, 38.01; H, 3.20; N, 18.99%.

6,7-Dihydro-2-ethyl-5*H*-1,2,4-thiadiazolo[4,5-*a*]pyrimidine-3(2*H*)-thione (7c). Mp 86—88 °C (decomp); IR (KBr) 2920, 2850, 1640, 1480, 1295, 1215, 1120, and 855 cm^{-1}; ^1H NMR ($CDCl_3$) δ=1.30 (t, 3H, J=7.0 Hz, $CH_2C\underline{H}_3$), 2.05 (m, 2H, $NCH_2C\underline{H}_2CH_2N$), 3.55 (t, 2H, J=6.0 Hz, C=NCH_2), 3.95 (q, 2H, J=7.0 Hz, $C\underline{H}_2CH_3$), and 4.35 (t, 2H, J=6.0 Hz, NCH_2); MS *m/z* (rel intensity) 201 (M^+; 100), 83 (43), 72 (50), 55 (39), and 41 (42).

Picrate of 7c. Mp 207—209 °C (decomp); Found: C, 36.24; H, 3.17; N, 19.16%. Calcd for $C_{13}H_{14}N_6O_7S_2$: C, 36.28; H, 3.28; N, 19.52%.

General Procedure for the Preparation of Unsymmetrical Tetraazapentalene Derivatives 8. A mixture of **7** (0.3 mmol) and isothiocyanate (0.45 mmol, 1.5 times molar quantity of **7**) in chloroform (30 ml) was refluxed for 3 h. After the solvent was removed, the residue was chromatographed on a preparative TLC (dichloromethane as an eluent) to give **8**. Recrystallization from hexane-chloroform gave a pure sample as a colorless solid.

6,7-Dihydro-2-methyl-3-ethyl-5*H*-2a-thia(2*a*-S^{IV})-2,3,4a,7a-tetraazacyclopent[*cd*]indene-1,4(2*H*,3*H*)-dithione (8d). Mp 200—202 °C (decomp); IR (KBr) 2960, 2920, 1575, 1540, 1495, 1310, 1240, 1185, and 1120 cm^{-1}; ^1H NMR($CDCl_3$) δ=1.32 (t, 3H, J=7.2 Hz, $CH_2C\underline{H}_3$), 2.36 (m, 2H, $NCH_2C\underline{H}_2CH_2N$), 3.22 (s, 3H, CH_3), 3.78 (q, 2H, J=7.2 Hz, $C\underline{H}_2CH_3$), and 4.41 (t, 4H, J=6.0 Hz, $NC\underline{H}_2CH_2C\underline{H}_2N$); ^{13}C NMR($CDCl_3$) δ=13.86, 20.04, 31.15, 39.89, 44.67, 44.85, 156.00, 168.72, and 169.52; UV (CH_3CN) 259 (log ε 4.53) nm; MS *m/z* (rel intensity) 201 (M^+-CH_3NCS; 17), 187 ($M^+-CH_3CH_2NCS$; 25), 116 (22), 87 (100), 73 (89), 72 (45), 69 (22), and 59 (43). Found: C, 39.59; H, 5.31; N, 19.93%. Calcd for $C_9H_{14}N_4S_3$: C, 39.42; H, 5.15; N, 20.43%.

6,7-Dihydro-2-methyl-3-phenyl-5*H*-2a-thia(2*a*-S^{IV})-2,3,4a,7a-tetraazacyclopent[*cd*]indene-1,4(2*H*,3*H*)-dithione (8e). Mp 179—182 °C (decomp); IR (KBr) 2920, 1570, 1530, 1450, 1320, 1245, 1165, 1130, 955, and 785 cm^{-1}; ^1H NMR($CDCl_3$) δ=2.35 (m, 2H, $NCH_2C\underline{H}_2CH_2N$), 3.20 (s, 3H, CH_3), 4.40 (m, 4H, $NC\underline{H}_2CH_2C\underline{H}_2N$), and 7.30 (s, 5H, aromatic); UV (CH_3CN) 257 (log ε 4.49) nm; MS *m/z* (rel intensity) 249 (M^+-CH_3NCS; 2), 187 ($M^+-C_6H_5NCS$; 58), 154 (16), 135 (100), 77 (62), 72 (26), and 69 (29). Found: C, 48.36; H, 4.45; N, 17.37%. Calcd for $C_{13}H_{14}N_4S_3$: C, 48.42; H, 4.38; N, 17.37%.

6,7-Dihydro-2-methyl-3-(*p*-chlorophenyl)-5*H*-2a-thia(2*a*-S^{IV})-2,3,4a,7a-tetraazacyclopent[*cd*]indene-1,4(2*H*,3*H*)-dithione (8f). Mp 188—191 °C(decomp); IR(KBr) 3040, 1560, 1515, 1495, 1305, 1240, 1120, 835, and 680 cm^{-1}; ^1H NMR ($CDCl_3$) δ=2.40 (m, 2H, $NCH_2C\underline{H}_2CH_2N$), 3.25 (s, 3H, CH_3), 4.40 (m, 4H, $NC\underline{H}_2CH_2C\underline{H}_2N$), and 7.30 (s, 4H, aromatic); ^{13}C NMR($CDCl_3$) δ=20.06, 31.44, 45.06, 45.23, 126.55, 129.44, 132.48, 137.40, 156.88, 169.27, and 170.23; UV(CH_3CN) 268 (log ε 4.49) nm; MS *m/z* (rel intensity) 283 (M^+-CH_3NCS; 1), 187 (M^+-p-ClC_6H_4NCS; 41), 171 (36), 169 (100), 154 (10), 113 (13), 111 (36), 75 (24), 72 (19), and 69 (19). Found: C, 43.45; H, 3.69; N, 15.50%. Calcd for $C_{13}H_{13}N_4S_3Cl$: C, 43.75; H, 3.67; N, 15.70%.

6,7-Dihydro-2-methyl-3-allyl-5*H*-2a-thia(2*a*-S^{IV})-2,3,4a,7a-tetraazacyclopent[*cd*]indene-1,4(2*H*,3*H*)-dithione (8g). Mp

185—188 °C(decomp); IR(KBr) 2930, 1570, 1530, 1485, 1305, 1235, 1180, 1115, 935, and 840 cm^{-1}; ^1H NMR($CDCl_3$) δ=2.37 (m, 2H, $NCH_2C\underline{H}_2CH_2N$), 3.22 (s, 3H, CH_3), 4.34—4.40 (m, 2H, $NC\underline{H}_2CH{=}CH_2$), 4.42 (t, 4H, J=6.0 Hz, $NC\underline{H}_2CH_2C\underline{H}_2N$), 5.20—5.28 (m, 2H, $NCH_2CH{=}C\underline{H}_2$), and 5.88—6.03 (m, 1H, $NCH_2C\underline{H}{=}CH_2$); MS m/z (rel intensity) 213 (M^+-CH_3NCS; 23), 187 ($M^+-CH_2{=}CHCH_2NCS$; 54), 99 (72), 73 (51), 72 (72), and 41 (100). Found: C, 42.08; H, 4.87; N, 19.12%. Calcd for $C_{10}H_{14}N_4S_3$: C, 41.89; H, 4.92; N, 19.54%.

6,7-Dihydro-2-ethyl-3-allyl-5*H*-2a-thia(2*a*-S^{IV})-2,3,4a,7a-tetraazacyclopent[*cd*]indene-1,4(2*H*,3*H*)-dithione (8h). Mp 186—189 °C (decomp); IR (KBr) 2960, 2900, 1575, 1535, 1485, 1305, 1235, 1180, and 1120 cm^{-1}; ^1H NMR($CDCl_3$) δ=1.30 (t, 3H, J=7.0 Hz, $CH_2C\underline{H}_3$), 2.35 (m, 2H, $NCH_2C\underline{H}_2CH_2N$), 3.75 (q, 2H, J=7.0 Hz, $C\underline{H}_2CH_3$), 4.20—4.50 (m, 6H, $NC\underline{H}_2CH{=}CH_2$ and $NC\underline{H}_2CH_2C\underline{H}_2N$), 5.00—5.35 (m, 2H, $NCH_2CH{=}C\underline{H}_2$), and 5.70—6.20 (m, 1H, $NCH_2C\underline{H}{=}CH_2$); MS m/z (rel intensity) 213 ($M^+-CH_3CH_2NCS$; 23), 201 ($M^+-CH_2{=}CHCH_2NCS$; 81), 99 (55), 87 (90), 72 (85), 59 (61), and 41 (100). Found: C, 43.40; H, 5.49; N, 18.65%. Calcd for $C_{11}H_{16}N_4S_3$: C, 43.97; H, 5.37; N, 18.64%.

6,7-Dihydro-2-allyl-3-(*p*-chlorophenyl)-5*H*-2a-thia(2*a*-S^{IV})-2,3,4a,7a-tetraazacyclopent[*cd*]indene-1,4(2*H*,3*H*)-dithione (8i). Mp 140—142 °C (decomp); IR (KBr) 1575, 1520, 1500, 1455, 1315, 1240, 1220, 1150, 1080, 955, 915, and 835 cm^{-1}; ^1H NMR ($CDCl_3$) δ=2.35 (m, 2H, $NCH_2C\underline{H}_2CH_2N$), 4.20—4.55 (m, 6H, $NC\underline{H}_2CH_2C\underline{H}_2N$ and $NC\underline{H}_2CH{=}CH_2$), 5.00—5.35 (m, 2H, $NCH_2CH{=}C\underline{H}_2$), 5.50—6.00 (m, 1H, $NCH_2C\underline{H}{=}CH_2$), and 7.20 (s, 4H, aromatic); MS m/z (rel intensity) 283 ($M^+-CH_2{=}CHCH_2NCS$; 2), 213 (M^+-p-ClC_6H_4NCS; 29), 171 (43), 169 (100), 111 (41), 99 (21), 75 (29), 72 (23), and 41 (48). Found: C, 46.94; H, 3.85; N, 14.42%. Calcd for $C_{15}H_{15}N_4S_3Cl$: C, 47.05; H, 3.95; N, 14.63%.

X-Ray Crystallographic Analysis of 5c.[7] A colorless crystal of **5c** was grown from hexane–chloroform solution. The crystal shape was a hexagonal prism. A single crystal of dimensions 0.52×0.24×0.17 mm was selected for X-ray investigations. Data were collected on a Rigaku AFC-5 diffractometer using Mo $K\alpha$ radiation. Reflections in the range $2\theta \leq 55°$ were measured by the ω/θ–2θ scan technique with a scan width of $1.4°+0.5°\tan\theta$. The structure was solved by the direct method with MULTAN 78[8] and refined by block-diagonal least-squares to final R value of 0.043 for 1315 absorption corrected[9] independent reflection [$|F_o|>3\sigma(F_o)$]. The weighting scheme $w=[\sigma^2_{count}+(0.03|F_o|)^2]^{-1}$ was employed. Crystal data for **5c** are as follows: $C_{10}H_{16}N_4S_3$, M=288.433, monoclinic, space group $P2_1$, a=13.060(5) Å, b=9.988(3) Å, c=5.211(2) Å, β=98.31(3)°, U=672.6(4) Å^3, Z=2, D_c=1.42 g cm^{-3}, $F(000)$=304, μ(Mo $K\alpha$)=5.19 cm^{-1}.

References

1) Y. Yamamoto and K. Akiba, *Heterocycles*, **13**, 297 (1979); M. Yokoyama, T. Shiraishi, H. Hatanaka, and K. Ogata, *J. Chem. Soc., Chem. Commun.*, **1985**, 1704; J. Goerdeler, H. Hohage, and I. Zeid, *Chem. Ber.*, **109**, 3108 (1976); D. H. Reid, *J. Chem. Soc. C*, **1971**, 3187; D. H. Reid and J. D. Symon, *J. Chem. Soc., Chem. Commun.*, **1969**, 1314; D. H. Reid and R. G. Webster, *ibid.*, **1972**, 1283; A. S. Ingram, D. H. Reid, and J. D. Symon, *J. Chem. Soc., Perkin Trans. 1*, **1974**, 242; E. Klingsberg, *J. Org. Chem.*, **33**, 2915 (1968); J. -L. Derocque, M. Perrier, and J. Vialle, *Bull. Soc. Chim. Fr.*, **1968**, 2062.

2) N. Matsumura, M. Tomura, R. Mando, Y. Tsuchiya, and S.Yoneda, *Bull. Chem. Soc. Jpn.*, **59**, 3693 (1986).

3) R. J. S. Beer, N. H. Holmes, and A. Naylor, *J. Chem. Soc., Perkin Trans. 1*, **1979**, 2909; R. J. S. Beer and A. Naylor, *Tetrahedron Lett.*, **1973**, 2989; R. J. S. Beer, H. Singh, D. Wright, and L. K. Hansen, *Tetrahedron*, **37**, 2485 (1981).

4) N. Matsumura, M. Tomura, S. Yoneda, and K. Toriumi, *Chem. Lett.*, **1986**, 1047; N. Matsumura, M. Tomura, Y. Tsuchiya, S. Yoneda, and M. Nakamura, *Chem. Express*, **1**, 487 (1986); N. Matsumura, M. Tomura, O. Mori, and S. Yoneda, *Chem. Lett.*, **1987**, 1065.

5) K. Akiba and N. Inamoto, *Kagaku No Ryoiki, Zokan*, **124**, 93 (1980).

6) L. Pauling, "The Nature of Chemical Bond," 3rd ed, Cornell University Press, Ithaca (1960).

7) Tables of atomic parameters, mean square displacement tensor of atoms, and bond distances are deposited as Document No. 8805 at the Office of the Editor of Bull. Chem. Soc. Jpn.

8) P. Main, S. E. Hull, L. Lessinger, G. Germain, J. P. Declercq, and M. M. Woolfson, MULTAN 78, A System of Computer Programs for the Automatic Solution of Crystal Structures from X-Ray Diffraction Data, University of York (1978).

9) W. R. Busing and H. A. Levy, *Acta Crystallogr.*, **10**, 180 (1957).

Reaction of Rifamycins with Sodium Sulfinates[1)]

Masahiro TAGUCHI,* Norio AIKAWA, Kenzaburo YOSHIDA, Mikiya KITAMURA, and Goro TSUKAMOTO
Pharmaceuticals Research Center, Kanebo, Ltd., Tomobuchi-cho, Miyakojima-ku, Osaka 534
(Received January 5, 1988)

The reaction of rifamycin S and the quinonic 3-(hydrazonomethyl)rifamycin derivatives with sodium sulfinates under neutral conditions were found to afford the hydroquinone-type 4-*O*-sulfonyl derivatives of rifamycin. 3-Amino-4-deoxo-4-iminorifamycin S also gave rise to the hydroquinone-type 4-deoxy-4-sulfonylamino derivatives of rifamycin when treated with sodium sulfinates. Under acidic conditions, rifamycin S and 3-bromorifamycin S produced the hydroquinone- and quinone-type 3-sulfonyl derivatives of rifamycin, respectively, by reactions with sodium sulfinates. Some of sodium salts of 4-*O*-sulfonylrifamycin SV derivatives afforded rifamycin S and sodium sulfinates and/or sodium sulfonates when heated in AcOEt.

We have recently reported on the reaction of rifamycin S (**1A**) with sodium sulfite.[2)] In connection with this work, we investigated the reaction of **1A** with sodium *p*-toluenesulfinate (**2a**), which is anticipated to formally resemble sodium sulfite, and found the unusual formation of sulfonic ester sodium salt **4Aa** under neutral conditions. This paper describes the reaction of **1A** with **2a** under various conditions (alkaline, neutral, or acidic), the formation of sulfonic ester sodium salts **4**, sulfonic esters **5** and sulfonamides **9**, and the decomposition of some of **4A** in AcOEt.

Results and Discussion

Reaction of 1A with 2a. We have reported that the reaction of **1A** with sodium sulfite under mild alkaline conditions gives the 3-substituted product, sodium rifamycin SV-3-sulfonate.[2)] In connection with this

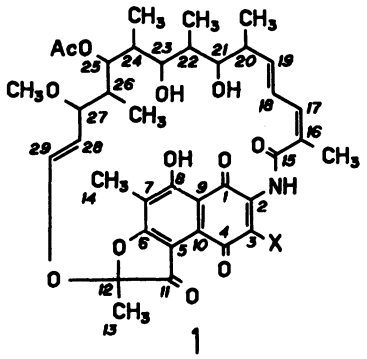

1

RSO_2Na

2

RSO_3Na

3

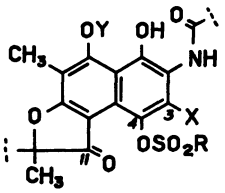

4: Y = Na

5: Y = H

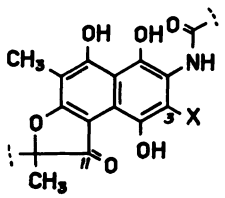

6

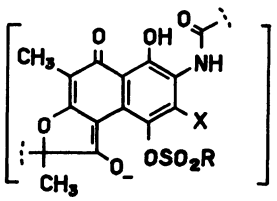

7

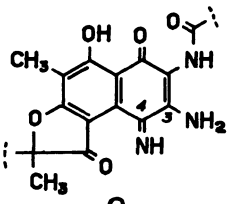

8

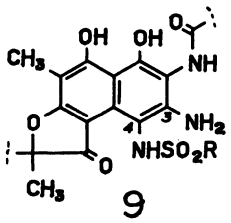

9

A : X = H

B : X = Br

C : X = -CH=NN(CH_3)$_2$

D : X = -CH=NN⬠

E : X = -CH=NN⬡

F : X = -SO_2-⬡-CH_3

G : X = -SO_2-⬡

H : X = -SO_2CH_3

a : R = -⬡-CH_3

b : R = -⬡

c : R = -⬡-Ac

d : R = -⬡-Cl

e : R = -⬡-OH

f : R = -⬡-OCH_3

g : R = -⬡-NO_2

h : R = -⬡-$N(CH_3)_2$

i : R = CH_3

j : R = n-C_4H_9

k : R = iso-C_4H_9

l : R = cyclo-C_5H_9

m : R = n-C_8H_{17}

n : R = n-$C_{12}H_{25}$

observation, **1A** was allowed to react with **2a** in an aq $NaHCO_3$–DMSO mixture (mild alkaline conditions). As a result, no products formed. However, in the absence of $NaHCO_3$ (neutral conditions) the reaction proceeded smoothly and almost quantitatively to produce a compound which fluoresced an orange color on a silica-gel TLC plate under an UV lamp (365 nm).[3] The reaction solution was poured into aq NaCl, and the extraction with AcOEt gave the sulfonic ester sodium salt **4Aa** in 85% yield. Sodium salt **4Aa** was converted to the corresponding acid form **5Aa** by acidification. The 4-*O*-sulfonyl structure of **5Aa** was deduced as follows. The UV spectrum (Table 2, footnote d) of **5Aa** resembling that[4] of rifamycin SV (**6A**), confirmed the 1,4-naphthalenediol derivative structure for **5Aa**; the NMR spectrum ($CDCl_3$) showed the signal at δ 7.42, which unfortunately overlapped with the signals of the *p*-tolyl group, but was attributed to the proton at the 3-position; the IR spectrum (KBr) showed the characteristic band of sulfonic ester at 1176 cm^{-1} ($\nu_s SO_2$). These spectral data suggested the 4-*O*-sulfonyl structure for **5Aa**, but the 1-*O*-sulfonyl structure is also possible. In order to distinguish these two possible structures, the 25-*O*-deacetyl derivative of **5Aa** was prepared from 25-*O*-deacetylrifamycin S[5] and **2a**. The IR spectrum ($CDCl_3$) of the 25-*O*-deacetyl derivative of **5Aa** clearly showed the furanone νC(11)=O band at 1709 cm^{-1} without disturbance of the 25-*O*-acetyl νC=O band.[6] This observation confirms the 4-*O*-sulfonyl structure for **5Aa**, because if **5Aa** takes the 1-*O*-sulfonyl structure the furanone νC(11)=O band should appear at ca. 1650 cm^{-1} due to the intramolecular hydrogen-bonding between the furanone C(11)=O group and the 4-OH group.[7] The furanone νC(11)=O band of the 25-*O*-deacetyl derivative of sodium salt **4Aa** in $CDCl_3$ appeared at 1675 cm^{-1}. A decrease of νC(11)=O in the salt form should be accounted for by the contribution of structure **7Aa**.

The formation mechanism of sulfonic ester is not clear, but the oxidation potential of **1A** seems to play an important role, because rifamycinol[5] (the 11-deoxo-11-hydroxy derivative of **1A**) did not react with **2a** under the same conditions as that described above.[8]

The reaction of **1A** with **2a** in aq AcOH (acidic conditions) produced 3-(*p*-tolylsulfonyl)rifamycin SV (**6F**) as a main product (9% yield) along with many complex products in which a trace amount of **5Aa** could be detected (analytical TLC). The IR spectrum ($CDCl_3$) of **6F** showed the characteristic bands of sulfone at 1292 ($\nu_{as}SO_2$) and 1137 cm^{-1} ($\nu_s SO_2$), and the singlet at δ 7.82 due to the proton at the 3-position of **1A** was absent in the NMR spectrum ($CDCl_3$).

Formation of Sulfonic Ester Sodium Salts 4A and Their Acid Form 5A, and Decomposition of Some of 4A in AcOEt. Similarly to **2a**, various sodium sulfinates were also found to react with **1A** under neutral conditions to afford sulfonic ester sodium salts **4A**, which upon acidification produced **5A**. The results are summarized in Tables 1 and 2. All sulfonic esters, except for **5Ac** and **5Ag**, fluoresced similarly to

Table 1. Sulfonic Ester Sodium Salts **4A**

Compound[a]	Yield/%	$\nu_s SO_2$/cm^{-1} (KBr)	Formula	Analysis[b]
4Aa	85	1176	$C_{44}H_{52}NNaO_{14}S \cdot 2H_2O$	C, H, N
4Ab	76	1188	$C_{43}H_{50}NNaO_{14}S \cdot H_2O$	C, H, N
4Ac	87	1190	$C_{45}H_{52}NNaO_{15}S \cdot 2H_2O$	C, H, N
4Ad	77	1186	$C_{43}H_{49}ClNNaO_{14}S$	C, H, N
4Ae	62	1166	$C_{43}H_{50}NNaO_{15}S \cdot 3H_2O$	C, H, N
4Af	80	1169	$C_{44}H_{52}NNaO_{15}S \cdot H_2O$	C, H, N
4Ag	76	1185	$C_{43}H_{49}N_2NaO_{16}S \cdot 3/2H_2O$	C, H, N
4Aj	85	1168	$C_{41}H_{54}NNaO_{14}S \cdot 3/2H_2O$	C, H, N

a) The melting points could not be specified due to gradual decomposition during heating. b) The values were within ±0.3% of the calculated theoretical values.

Table 2. Sulfonic Esters **5A**

Compound[a]	Procedure[b]	Yield/%	$\nu_s SO_2$/cm^{-1} (KBr)	Formula	Analysis[c]
5Aa[d]	A	84	1176	$C_{44}H_{53}NO_{14}S \cdot 1/2H_2O$	C, H, N
5Ab	B	32	1192	$C_{43}H_{51}NO_{14}S \cdot 3/2H_2O$	C, H, N, S
5Ac	A	91	1193	$C_{45}H_{53}NO_{15}S \cdot 3/2H_2O$	C, H, N
5Ad	C	31	1192	$C_{43}H_{50}ClNO_{14}S \cdot H_2O$	C, H, N, S
5Ae	C	16	1166	$C_{43}H_{51}NO_{15}S \cdot H_2O$	C, H, N, S
5Af	A	75	1169	$C_{44}H_{53}NO_{15}S \cdot 3/2H_2O$	C, H, N
5Ag	A	84	1192	$C_{43}H_{50}N_2O_{16}S \cdot 3/2H_2O$	C, H, N
5Aj	A	92	1166	$C_{41}H_{55}NO_{14}S \cdot 3/2H_2O$	C, H, N

a) The melting points could not be specified due to gradual decomposition during heating. b) See Experimental. c) The values were within ±0.3% of the calculated theoretical values. d) UV λ_{max} (pH 7.0 phosphate buffer) 226 (log ε 4.65), 296 (4.28), and 414 nm (4.24).

5Aa. The formations of **4A** proceeded very cleanly, but **4A** and **5A** were proved to decompose during work up. Accordingly, the decomposition of some of **4A** in AcOEt, which was used as an extraction solvent, was next investigated. The sodium salts **4Aa**, **4Ac**, **4Ad**, and **4Af** were heated at 70 °C in a solution of AcOEt for several hours. As a result, each salt decomposed to afford **1A** as a main product and many complex compounds along with the formation of precipitates. The precipitate from **4Ac** was found to be sodium *p*-acetylbenzenesulfinate (**2c**) by a comparison of the NMR spectra (D_2O) with that of the authentic sample. The identification was also confirmed by the reaction of **1A** with the precipitate to afford the compound identical with **4Ac** (analytical TLC). The IR spectra (KBr) of the precipitates from **4Aa** and **4Af** showed the sulfonate $\nu_s SO_2$ bands at 1200 and 1190 cm^{-1}, respectively; these precipitates were confirmed to be sodium *p*-toluenesulfonate (**3a**) and sodium *p*-methoxybenzenesulfonate (**3f**), respectively, by comparing the NMR spectra (D_2O) with those of the authentic samples. The IR spectrum (KBr) of the precipitate from **4Ad** showed the sulfonate $\nu_s SO_2$ band at 1200 cm^{-1}, while its NMR spectrum (D_2O) showed that it consisted of two sorts of the compounds, sodium *p*-chlorobenzenesulfinate (**2d**) and sodium *p*-chlorobenzenesulfonate (**3d**) (molar ratio, 1:ca. 2). The results are summarized in Table 3. It is of interest that the decomposition reactions of sodium salts **4Aa**, **4Ac**, **4Ad**, and **4Af** in AcOEt commonly afforded **1A**, while the oxidation states of the precipitates were different depending upon the nature of the substituent involved in the phenylsulfonyl group. The mechanism of decomposition is not clear. Heating of **5Aa** in AcOEt at 70 °C for 4 h resulted in the decomposition of **5Aa** into many complex compounds in which **1A** could not be detected (analytical TLC).

Formation of Sulfones 6G and 6H. Sodium benzenesulfinate (**2b**) was allowed to react with **1A** in aq AcOH to afford 3-(phenylsulfonyl)rifamycin SV (**6G**) in 5% yield. On the other hand, it was observed by TLC analysis that the 1,4-naphthoquinone derivative **1G** could be produced in good yield by the reaction of 3-bromorifamycin S[9] (**1B**) with **2b** in aq AcOH. Indeed, 3-(methylsulfonyl)rifamycin SV (**6H**) was obtained in 63% yield by the reaction of **1B** with sodium methanesulfinate (**2i**) in aq AcOH followed by reduction with L-ascorbic acid.

Formation of Sulfonic Esters 5C—E. The reactions of the 3-(hydrazonomethyl)rifamycin derivatives **1C—E** with some of **2** under neutral conditions followed by acidification, afforded the corresponding sulfonic esters **5C—E**. The sulfonic ester structures of **5C—E** were supported by the characteristic $\nu_s SO_2$ bands of the sulfonic esters. The results are summarized in Table 4.

Formation of Sulfonamides 9. When 3-amino-4-deoxo-4-iminorifamycin S[10] (**8**) were treated with some of **2** under neutral conditions, the reaction proceeded almost quantitatively to afford sulfona-

Table 3. Decomposition of Sulfonic Ester Sodium Salts **4Aa**, **4Ac**, **4Ad**, and **4Af** in AcOEt at 70°C

Compound	Time/h	Isolation yield/% of **1A**	Identification of the precipitate (Yield/%)
4Aa	5.75	46	**3a** (ca. 71)
4Ac	4.75	70	**2c** (ca. 80)
4Ad	4	49	**2d** and **3d** (ca. 98)[a]
4Af	6.25	37	**3f** (ca. 67)

a) The molar ratio of **2d** to **3d** was 1:ca. 2 (determined by the NMR spectrum in D_2O on the basis of integration of the signals of aromatic protons).

Table 4. Sulfonic Esters **5C—E**

Compound[a]	Yield/%	$\nu_s SO_2$/cm^{-1} (KBr)	Formula	Analysis[b]
5Ce	52	1166	$C_{46}H_{57}N_3O_{15}S \cdot H_2O$	C, H, N, S
5Cf	51	1169	$C_{47}H_{59}N_3O_{15}S$	C, H, N, S
5Ch	41	1167	$C_{48}H_{62}N_4O_{14}S$	C, H, N, S
5Cj	33	1167	$C_{44}H_{61}N_3O_{14}S \cdot 1/2H_2O$	C, H, N, S
5Cl	45	1164	$C_{45}H_{61}N_3O_{14}S$	C, H, N, S
5Cn	24	1163	$C_{52}H_{77}N_3O_{14}S$	C, H, N, S
5Dj	41	1164	$C_{46}H_{63}N_3O_{14}S$	C, H, N, S
5Dk	41	1161	$C_{46}H_{63}N_3O_{14}S$	C, H, N, S
5Dm	31	1165	$C_{50}H_{71}N_3O_{14}S$	C, H, N, S
5Dn	29	1163	$C_{54}H_{79}N_3O_{14}S$	C, H, N, S
5Ej	51	1164	$C_{47}H_{65}N_3O_{14}S \cdot 1/2H_2O$	C, H, N

a) The melting points could not be specified due to gradual decomposition during heating. b) The values were within ±0.3% of the calculated theoretical values.

Table 5. Sulfonamides **9**

Compound[a]	Yield/%	$\nu_s SO_2/cm^{-1}$ ($CHCl_3$)	Formula	Analysis[b]
9d	67	1162	$C_{43}H_{52}ClN_3O_{13}S \cdot H_2O$	C, H, N, S
9g	66	1168	$C_{43}H_{52}N_4O_{15}S$	C, H, N, S
9h	70	1152	$C_{45}H_{58}N_4O_{13}S \cdot H_2O$	C, H, N, S
9j	69	1148	$C_{41}H_{57}N_3O_{13}S \cdot 1/2H_2O$	C, H, N, S
9k	62	1148	$C_{41}H_{57}N_3O_{13}S \cdot H_2O$	C, H, N, S
9l	74	1145	$C_{42}H_{57}N_3O_{13}S \cdot H_2O$	C, H, N, S

a) The melting points could not be specified due to gradual decomposition during heating. b) The values were within ±0.3% of the calculated theoretical values.

mides **9** after acidification. The sulfonamide structures of **9** were supported by the characteristic $\nu_s SO_2$ bands of the sulfonamides. The results are summarized in Table 5. All sulfonamides in Table 5, except for **9g**, fluoresced similarly to **5Aa**.

Conclusion

Quinone- and quinone imine-type derivatives of rifamycin were found to react with sodium sulfinates under neutral conditions, giving the sulfonic esters and the sulfonamides, respectively. To our knowledge, only limited numbers of reports are concerned with the formation of sulfonic esters and sulfonamides in the reactions of quinonic or quinoniminic compounds with sulfinic acids or their salts.[11] Novel examples of such reactions are provided as described above.

Experimental

Analytical TLC was performed on Silica gel 60 F_{254} pre-coated plates (0.25 mm, Merck), using $CHCl_3$–CH_3OH (10:1 or 4:1) as a developing solvent. Preparative TLC was performed on Silica gel 60 F_{254} pre-coated plates (2 mm, Merck). IR spectra were measured on a JASCO IRA-1, a Shimadzu IR-440 spectrometer, or a Hitachi 270-50 infrared spectrometer. UV spectra were taken with a Shimadzu UV-210 spectrometer. Measurements of NMR spectra were carried out using a JEOL PS-100, a Hitachi R-24A spectrometer, or a Hitachi R-24B spectrometer. Tetramethylsilane was used as an internal reference for a solution of $CDCl_3$. NMR spectra of sodium sulfinates or sodium sulfonates were recorded in a solution of D_2O without an internal reference. Elemental analyses were performed with a Yanagimoto CHN-CORDER MT-3 or at the Elemental Analysis Center of Kyoto University.

Rifamycin Derivatives 1C—E. These compounds were prepared by oxidation of compounds[12] **6C—E** in $CHCl_3$ with MnO_2 (70%, Wako Pure Chemical Ind., Ltd.) followed by washing with dil H_2SO_4.

Sodium Sulfinates 2a—n and Sodium Sulfonates 3a, 3d, and 3f. Compounds **2a**, **2b**, **3a**, and **3d** were purchased. Compounds **2d**,[13a] **2g**,[13b] **2i**,[14b] **2j**,[14b] and **2k—n**[15] were prepared by the methods reported. Compounds **2c** and **2f** were prepared as **2d** from the corresponding sulfonyl chloride.[14a,16] Compound **2e** was prepared as **2g** from *p*-hydroxybenzenesulfonyl chloride.[17] Compound **2h** was prepared[18] from the corresponding sulfonyl chloride.[13c,d] Compound **3f** was prepared by hydrolysis of *p*-methoxybenzenesulfonyl chloride with $NaHCO_3$

Preparation of Sulfonic Ester Sodium Salts in Table 1 and the 25-*O*-Deacetyl Derivative of 4Aa. General Procedure: A solution of an excess amount of **2** in H_2O was added to a solution of **1A** in DMSO. After being stirred for several hours, the reaction mixture was poured into aq NaCl, and extracted with AcOEt. The combined extracts were washed with aq NaCl, dried over Na_2SO_4, then evaporated in vacuo. The resulting residue was precipitated from AcOEt–hexane, AcOEt–benzene, or AcOEt–benzene–hexane to afford **4A**, tabulated in Table 1. As a typical run, the preparation of **4Aa** is described below.

A solution of **2a** (2.16 g, 12 mmol) in H_2O (10 ml) was added to a solution of **1A** (2.00 g, 2.9 mmol) in DMSO (50 ml). After being stirred at r.t. for 3 h, the reaction mixture was treated according to the general procedure to afford 2.24 g (85% yield) of **4Aa** as a dark yellow powder after precipitation from AcOEt–benzene–hexane.

The 25-*O*-deacetyl derivative of **4Aa** was obtained from 25-*O*-deacetylrifamycin S[5] and **2a** in 82% yield. The 25-*O*-deacetyl derivative of **4Aa**: IR (KBr) 1175 cm^{-1} ($\nu_s SO_2$). IR ($CDCl_3$) 1675 cm^{-1} (νC(11)=O). Anal. ($C_{42}H_{50}NNaO_{13}S \cdot 1/2H_2O$) C, H, N.

Preparation of Sulfonic Esters 5Aa, 5Ac, 5Af, 5Ag, 5Aj and the 25-*O*-Deacetyl Derivative of 5Aa (Procedure A). General Procedure: A sodium salt **4A** was dissolved in AcOEt, then aq NaCl acidified with H_2SO_4 (acidic aq NaCl) was added to the solution. The mixture was shaken, and the organic layer was separated, washed with aq NaCl, dried over Na_2SO_4 or $MgSO_4$, and evaporated in vacuo. The resulting residue was precipitated from AcOEt–hexane or AcOEt–benzene–hexane to afford the title compounds. As a typical run, the preparation of **5Aa** is described below.

A solution of 1.13 g of **4Aa** in 80 ml of AcOEt was treated according to the general procedure, and the resulting residue was precipitated from AcOEt–hexane to afford 0.91 g (85% yield) of **5Aa** as a yellow powder. **5Aa:** ^1H NMR ($CDCl_3$) δ=2.33 (3H, s, the methyl protons of the *p*-tolylsulfonyl group), 7.04 (2H, d, the aromatic protons of the *p*-tolylsulfonyl group), 7.34—7.52 (3H, signals due to the aromatic protons of the *p*-tolylsulfonyl group and the proton at the 3-position).

The 25-*O*-deacetyl derivative of **5Aa** was obtained from the 25-*O*-deacetyl derivative of **4Aa** in 83% yield. The 25-*O*-deacetyl derivative of **5Aa**: IR (KBr) 1176 cm^{-1} ($\nu_s SO_2$). IR ($CDCl_3$) 1709 cm^{-1} (νC(11)=O). Anal. ($C_{42}H_{51}NO_{13}S \cdot H_2O$) C, H, N.

Preparation of Sulfonic Ester 5Ab (Procedure B). A solution of **2b** (0.19 g, 1.2 mmol) in H_2O (1 ml) was added to

a solution of **1A** (0.20 g, 0.29 mmol) in DMSO (8 ml). After being stirred overnight at r.t., the reaction mixture was poured into acidic aq NaCl. The resulting precipitate was collected, washed with acidic aq NaCl, and dissolved in AcOEt. The ethyl acetate solution was washed with aq NaCl, dried over $MgSO_4$, then evaporated in vacuo. The resulting residue was precipitated from AcOEt–benzene–hexane to afford 0.08 g (32% yield) of **5Ab** as a dark yellow powder.

Preparation of Sulfonic Esters 5Ad and 5Ae (Procedure C). As a typical run, the preparation of **5Ad** is described below.

A solution of **2d** (0.27 g, 1.4 mmol) in H_2O (1.5 ml) was added to a solution of **1A** (0.20 g, 0.29 mmol) in DMSO (7 ml). After being stirred overnight at r.t., the reaction mixture was treated by the same procedure as that described for **5Ab.** The resulting residue was separated on preparative TLC plates (4:1 $CHCl_3$–CH_3OH). The yellow band was collected and extracted with CH_3OH. AcOEt was added to the methanolic extract. The ethyl acetate solution was washed successively with acidic aq NaCl and aq NaCl, dried over $MgSO_4$, and evaporated in vacuo. The resulting residue was precipitated from AcOEt–hexane to afford 0.08 g (31% yield) of **5Ad** as a pale-yellow powder.

Compound **5Ae** was obtained from **1A** and **2e** in 16% yield.

Preparation of 3-Sulfonylrifamycin Derivatives 6F and 6G. As a typical run, the preparation of **6F** is described below.

A solution of **2a** (2.5 g, 14 mmol) in H_2O (20 ml) was added to a solution of **1A** (0.70 g, 1.0 mmol) in AcOH (30 ml). After being stirred at r.t. for 12 h, the reaction mixture was poured into H_2O. The resulting precipitate was collected, washed with H_2O, and dissolved in AcOEt. The ethyl acetate solution was washed with aq NaCl, dried over Na_2SO_4, and evaporated in vacuo. The resulting residue was separated on preparative TLC plates (two developments with 200:20:1 $CHCl_3$–EtOH–AcOH). The orange band was collected and extracted with CH_3OH. The methanolic solution was diluted with AcOEt, and the organic mixture was washed successively with acidic aq NaCl and aq NaCl, dried over Na_2SO_4, and evaporated in vacuo. The resulting residue was recrystallized from acetone to afford 0.08 g (9% yield) of **6F** as orange crystals. Mp ca. 180 °C (decomp). IR ($CDCl_3$) 1292 ($\nu_{as}SO_2$) and 1137 cm^{-1} (ν_sSO_2). ^1H NMR ($CDCl_3$) δ=2.41 (3H, s, the methyl protons of the *p*-tolylsulfonyl group), 7.28 (2H, d, the aromatic protons of the *p*-tolylsulfonyl group), 7.88 (2H, d, the aromatic protons of the *p*-tolylsulfonyl group). Anal. ($C_{44}H_{53}NO_{14}S \cdot 1/2H_2O$) C, H, N.

Physical data of **6G** are as follows. Mp ca. 174 °C (decomp). IR ($CDCl_3$) 1295 ($\nu_{as}SO_2$) and 1140 cm^{-1} (ν_sSO_2). ^1H NMR ($CDCl_3$) δ=7.3—7.7 (3H, m, the aromatic protons of the phenylsulfonyl group), 7.9—8.1 (2H, d, the aromatic protons of the phenylsulfonyl group). Anal. ($C_{43}H_{51}NO_{14}S \cdot H_2O$) C, H, N.

Preparation of 3-(Methylsulfonyl)rifamycin SV (6H). A solution of **2i** (0.47 g, 4.6 mmol) in H_2O (1 ml) was added to a solution of 3-bromorifamycin S[9] (**1B**) (0.50 g, 0.65 mmol) in AcOH (6 ml). After being stirred at r.t. for 40 min, the reaction mixture was poured into H_2O. The resulting precipitate was collected, washed with H_2O, and dissolved in AcOEt. The ethyl acetate solution was added to a solution of 2.5 g of L-ascorbic acid in aq CH_3OH. The mixture was shaken for several min, washed with aq NaCl, dried over $MgSO_4$, and evaporated in vacuo. The resulting residue was purified by preparative TLC in a similar manner to that described for **6F**, affording 0.32 g (63% yield) of **6H** as an orange powder after precipitation from AcOEt–ligroine. Mp ca. 204 °C (decomp). IR ($CDCl_3$) 1290 ($\nu_{as}SO_2$) and 1125 cm^{-1} (ν_sSO_2). ^1H NMR ($CDCl_3$) δ=3.50 (3H, s, the methyl protons of the methylsulfonyl group). Anal. ($C_{38}H_{49}NO_{14}S$) C, H, N.

Decomposition of Sulfonic Ester Sodium Salts 4Aa, 4Ac, 4Ad, and 4Af in AcOEt. As a typical run, the decomposition of **4Aa** is described below.

A 300 mg of **4Aa** was dissolved in 20 ml of AcOEt. After being stirred at 70 °C for 5.75 h, the resulting precipitate was collected by filtration and washed with AcOEt, affording 46 mg of a brownish powder. IR (KBr) 1200 cm^{-1}. The NMR spectrum in D_2O was identical with that of the authentic sample of **3a**. The filtrate and the washings were combined and evaporated in vacuo. The resulting residue was separated by a preparative TLC plate (10:1 $CHCl_3$–CH_3OH). The yellow band was collected and extracted with CH_3OH. The methanolic solution was diluted with AcOEt, and the organic mixture was washed successively with a mixture of a pH 4 buffer and aq NaCl and aq NaCl, dried over $MgSO_4$, and evaporated in vacuo. The resulting residue was crystallized from *i*-C_3H_7OH to afford 116 mg of yellow crystals. The IR spectrum in $CHCl_3$ was identical with that of **1A**.

Preparation of Sulfonic Esters in Table 4. These compounds were prepared from 3-(hydrazonomethyl)rifamycin derivatives **1C—E** and **2** by a similar procedure to that described for **5Ad**. As developing solvents for preparative TLC, AcOEt–CH_3OH (60:1—20:1) or $CHCl_3$–CH_3OH (10:1) was used. AcOEt–hexane or AcOEt–ligroine was used as a crystallizing solvent.

Preparation of Sulfonamides in Table 5. General Procedure: A solution of an excess amount of **2** in H_2O was added to a solution of 3-amino-4-deoxo-4-iminorifamycin S[10] (**8**) in DMSO. After being stirred at r.t. for several min, the reaction mixture was poured into aq NaCl and extracted with $CHCl_3$. The chloroform extracts were combined and reextracted with H_2O. The aqueous layers were extracted again with $CHCl_3$ under acidic conditions which were made by addition of dil H_2SO_4. The combined extracts were washed with aq NaCl, dried over Na_2SO_4, and evaporated in vacuo. The resulting residue was precipitated from $CHCl_3$–hexane to afford a sulfonamide **9** in Table 5. As a typical run, the preparation of **9h** is described below.

A solution of **2h** (0.13 g, 0.59 mmol) in H_2O (0.4 ml) was added to a solution of **8** (0.14 g, 0.20 mmol) in DMSO (2.4 ml). After being stirred at r.t. for 5 min, the reaction mixture was treated according to the general procedure, affording 0.13 g (70% yield) of sulfonamide **9h** as a yellow powder.

References

1) This work was reported at the 106th Annual Meeting of Pharmaceutical Society of Japan, Chiba, April 1986.

2) M. Taguchi, T. Kawashima, N. Aikawa, and G. Tsukamoto, *Chem. Pharm. Bull.*, **33**, 1982 (1985).

3) Rifamycin derivatives **1A-H**, **6A-H**, and **8** show no fluoresce under the described conditions.

4) The maximum absorption of **6A** in a pH 7.3 buffer has been reported as follows: 223 ($E^{1\%}_{1cm}$=555), 304 (275) and 425 nm (220). P. Sensi, R. Ballotta, A. M. Greco, and G. G. Gallo, *Farmaco Ed. Sci.*, **16**, 165 (1961).

5) W. Kump and H. Bickel, *Helv. Chim. Acta*, **56**, 2323 (1973).

6) In the IR spectrum ($CDCl_3$) of **5Aa**, the 25-*O*-acetyl νC=O band appeared at 1712 cm^{-1}, and this band obscured the presence of the furanone νC(11)=O band in the same region.

7) P. Ferrari and G. G. Gallo, *Farmaco Ed. Sci.*, **30**, 676 (1975).

8) The oxidation potential of rifamycinol is much lower than those of **1A** and other rifamycins **1B-H**, because rifamycins **1A-H** are readily reduced with L-ascorbic acid, being different from rifamycinol.

9) M. F. Dampier, C-W. Chen, and H. W. Whitlock, Jr., *J. Am. Chem. Soc.*, **98**, 7064 (1976); L. Marsili, V. Rossetti, and C. Pasqualucci, Ger. Offen. 2548128 (1976); *Chem. Abstr.*, **85**, 46783r (1976); Alfa Farmaceutici S. p. A., Belg. Patent 872294 (1979); *Chem. Abstr.*, **91**, 74658w (1979).

10) L. Marsili, V. Rossetti, and C. P. Ucci, Ger. Offen. 2620782 (1976); *Chem. Abstr.*, **86**, 106682q (1977).

11) M. V. Gorelik, *Zh. Ves. Khim. Obshchest.*, **11**, 586 (1966); *Chem. Abstr.*, **67**, 2933p (1967); M. V. Gorelik and I-H. Han, *Zh. Org. Khim.*, **14**, 414 (1978); *Chem. Abstr.*, **89**, 75362r (1978); K. T. Finley, P. S. Kaiser, R. L. Reeves, and G. Werimont, *J. Org. Chem.*, **34**, 2083 (1969).

12) Lepetit S. p. A., Neth. Appl.6509961 (1966); *Chem Abstr.*, **65**, 5462 (1966).

13) a) F. Muth, "Methoden der Organischen Chemie (Houben-Weyl)," Band IX, ed. by E. Muller, Georg Thieme Verlag, Stuttgart (1955), p. 306; b) *ibid.*, p. 309; c) *ibid.*, p. 570; d) *ibid.*, pp. 441, 442, p. 465.

14) a) M. Kobayashi, "Shin Jikken Kagaku Kohza," Vol. 14, ed. by the Chemical Society of Japan, Maruzen, Tokyo (1978), p. 1788; b) *ibid.*, p. 1812.

15) P. Allen, Jr., *J. Org. Chem.*, **7**, 23 (1942).

16) Ferrania S. p. A., Brit. Patent 1071180 (1967); *Chem. Abstr.*, **67**, 91689d (1967).

17) R. W. Campbell and H. W. Hill, Jr., *J. Org. Chem.*, **38**, 1047 (1973).

18) L. Field and F. A. Grunwald, *J. Org. Chem.*, **16**, 946 (1951).

Reaction of Rifamycin S with Hexahydro-1,3,5-triazines Prepared from Formaldehyde and Primary Aliphatic Amines

Masahiro TAGUCHI,* Norio AIKAWA, and Goro TSUKAMOTO
Pharmaceuticals Research Center, Kanebo, Ltd., Tomobuchi-cho, Miyakojima-ku, Osaka 534
(Received January 5, 1988)

Rifamycin S (**1**) and 25-*O*-deacetylrifamycin S reacted with 1,3,5-tri-*t*-butylhexahydro-1,3,5-triazine to give deep-blue compounds. The structures of the deep-blue compounds are discussed based on ^{13}C NMR data, and it is concluded that the earlier structures[1] should be partly re-revised. The mechanism of formation of the deep-blue compounds and the reaction of **1** with several hexahydro-1,3,5-triazines, which were prepared from formaldehyde and primary aliphatic amines, are also described.

We previously reported[1] that rifamycin S (**1**) was allowed to react with 1,3,5-tri-*t*-butylhexahydro-1,3,5-triazine (**2c**) to afford a characteristic deep-blue colored compound, which was identical with the compound prepared according to the method of Marsili and Pasqualucci,[2] who proposed that the structure of the deep-blue compound was **3c**. We suggested[1] that the deep-blue compound did not consist of an oxazinium ring but, rather, a dihydropyrimidinium ring. We partly revised the earlier structure, **4c**, suggested by Maggi et al.,[3-5] in which the 4-hydroxyl group was dissociated, to the enolized structure, **5c**, based on the IR spectral data and the interpretation[3] of Maggi et al. on a polarographic oxidation wave.[1] Here, we report that the structure of the deep-blue compound should be re-revised based on the ^{13}C NMR data to **6c** in which the 8-hydroxyl group is dissociated. Moreover, the mechanism of formation of the deep-blue compound and the reaction of **1** with several hexahydro-1,3,5-triazines **2** prepared from formaldehyde and aliphatic primary amines are reported.

Results and Discussion

The Structure of the Deep-Blue Compound Obtained in the Reaction of 1 with 2c. We previously suggested that the deep-blue compound, **A**, which was obtained in the reaction of **1** with **2c**, had the enolized structure **5c**.[1] The suggestion was based on the IR spectral data of **A** and its 25-*O*-deacetyl derivative **B** (no furanone νC(11)=O band was observed at ca. 1740 cm^{-1}; the amide νC(15)=O band was observed at ca. 1660 cm^{-1}) and the interpretation of Maggi et al.[3] on a polarographic oxidation wave. Later, we prepared *N*-methylrifamycin S (**8**),[6] 25-*O*-deacetyl-4-*O*-(*p*-tolylsulfonyl)rifamycin SV (**9**) and its sodium salt (**10**),[7] and from their IR spectral data ($CDCl_3$) we knew that the amide νC(15)=O band might appear at rather low frequency, owing to a structural factor of the amide group (**8**, tertiary amide, 1659 cm^{-1}) and that the furanone νC(11)=O band also might appear at rather low frequency, owing to a dissociation of the 8-hydroxyl group (**9**, 1709cm^{-1}; **10**, 1675 cm^{-1}). Moreover, it has been known that the occurrence of a polarographic two-step oxidation wave can be interpreted as being due to the presence of a stable intermediate radical,[8] but not due to the nonequivalence of the hydroquinone hydroxyls, the interpretation of Maggi et al.[3] This information brought us another possible structure, **6c**, in which the 8-hydroxyl group was dissociated, to the chromophores of **A** and **B**. The structure **6c** can be used to interpret the IR

Table 1. ^1H NMR Data of Compound **A** (**6c**) in $CDCl_3$ (Concn ca. 10^{-2} mol dm^{-3}) at 300 MHz

Proton	Multipl.	*J*/Hz	δ	Proton	Multipl.	*J*/Hz	δ
OH-1	s		16.57	H-25	dd	25,26=5[b]	4.95
OH-4	s		14.87	H-26	c)	26,27=3	2.10
CH=N^+	s		8.98	H-27	ddd	27,28=5	3.66
H-13	s		1.77	H-28	dd	28,29=12	5.27
H-14	s		2.08	H-29	dd	27,29=1.5	6.11
H-17	b.d	17,18=11	5.88	H-30	b.s	30,17=n.d.	2.14
H-18	a)	18,19=15.5	5.31	H-31	d	31,20=7	0.74
H-19	dd	19,20=4	6.01	H-32	d	32,22=7	0.95
H-20	ddq	20,21=9.5	2.25	H-33	d	33,24=7	0.71
H-21	b.d	21,22=n.d.	3.28	H-34	a)	34,26=n.d.	0.70
OH-21	b.	21,OH=n.d.	4.27	H-36	s		2.12
H-22	a)	22,23=n.d.	1.63	H-37	s		3.17
H-23	b.d	23,24=8.5	3.23	H-2′(α)[d]	d	2′(α),2′(β)=12	4.55
OH-23	b.	23,OH=n.d.	3.57	H-2′(β)[d]	d	2′(α),2′(β)=12	6.56
H-24	a)	24,25=6[b]	2.03	*t*-butyl	s		1.66

s: singlet, d: doublet, q: quartet, b.: broad, n.d.: not determined. a) This signal partly overlapped on another signal. b) These coupling constants may be interchanged. c) This signal entirely overlapped on another signal. d) The determination of the configuration was made by reference to the literature.[13]

spectral data of **A** and **B**, as well as their characteristic ^{1}H NMR spectral data, which showed two singlets due to the phenolic hydroxyl protons in the very low field (**A**, δ 16.57 and 14.87; **B**, δ 16.44 and 14.74). Namely, the amide νC(15)=O band appears at a rather low frequency (ca. 1660 cm^{-1}), owing to the structural factor of the amide group (tertiary amide), not owing to an intramolecular hydrogen bonding between the amide C(15)=O and the 1-hydroxyl group. The furanone νC(11)=O band appears at low frequency, perhaps at ca. 1590 cm^{-1} owing to dissociation of the 8-hydroxyl group and an intramolecular hydrogen bonding between the furanone C(11)=O and 4-hydroxyl group. The large chemical shift values of the two phenolic hydroxyl protons are due to strong intramolecular hydrogen bonding between the ionized 8-hydroxyl group and the 1-hydroxyl group and between the furanone C(11)=O and the 4-hydroxyl group (the oxygen atom of the furanone C(11)=O is considered to be charged much negatively due to contribution of a limiting structure **7c**). The possible structure of **6c** was substantiated by ^{13}C NMR data. Chemical shifts and assignments in ^{1}H and ^{13}C NMR spectra of **A** (**6c**) and **B** (25-OH-**6c**) in $CDCl_3$ are summarized in Tables 1—3. Assignments for protons and carbon atoms, except for two phenolic hydroxyl protons and all quaternary carbon atoms, were made based on H–H and C–H correlation spectroscopy. For assignments of quaternary carbon atoms, proton nondecoupling spectra were recorded, and assignments were performed with reference to the chemical shifts and the multiplicities of the quaternary carbon atoms of rifampicin (**11**) and 3-[(dimethylhydrazono)methyl]rifamycin SV.[9] The assignments for the

Table 2. ^{1}H NMR Data of Compound **B** (25-OH-**6c**) in $CDCl_3$ (Concn ca. 10^{-2} mol dm^{-3}) at 300 MHz

Proton	Multipl.	J/Hz	δ	Proton	Multipl.	J/Hz	δ
OH-1	s		16.44	H-25	dd	25,26=8.5	3.78
OH-4	s		14.74	OH-25	b.		4.13
CH=N$^+$	s		9.15	H-26	ddq	26,27=4.5	1.95
H-13	s		1.79	H-27	ddd	27,28=6	3.89
H-14	s		2.08	H-28	dd	28,29=12.5	5.13
H-17	dq	17,18=11	5.77	H-29	dd	27,29=1	6.19
H-18	dd	18,19=15.5	5.26	H-30	d	30,17=1	2.13
H-19	dd	19,20=6.5	5.87	H-31	d	31,20=7	0.94
H-20	ddq	20,21=3	2.66	H-32	d	32,22=7	0.93
H-21	dd[a]	21,22=6	3.23	H-33	d	33,24=7	0.86
OH-21	b.	21,OH=n.d.	3.09	H-34	d	34,26=7	0.69
H-22	ddq	22,23=7.5	1.30	H-37	s		3.29
H-23	dd[a]	23,24=5	3.16	H-2′(α)[b]	d	2′(α),2′(β)=12.5	4.51
OH-23	b.	23,OH=n.d.	4.11	H-2′(β)[b]	d	2′(α),2′(β)=12.5	6.69
H-24	ddq	24,25=2	1.59	t-butyl	s		1.72

s: singlet, d: doublet, q: quartet, b.: broad, n.d.: not determined. a) After treatment with D_2O. b) The determination of the configuration was made by reference to the literature.[13]

Table 3. ^{13}C NMR Chemical Shifts of Compound **A** (**6c**) and Compound **B** (25-OH-**6c**) in $CDCl_3$ at 75.47 MHz

Compound	C-1	C-2	C-3	C-4	C-5	C-6	C-7	C-8	C-9
A[a]	146.75	122.26	107.42	154.83	99.58	172.09	107.87	183.29	112.50
B[b]	147.11	121.67	107.58	153.24	98.79	172.04	107.36	183.39	113.50
Compound	C-10	C-11	C-12	C-13	C-14	C-15	C-16	C-17	C-18
A[a]	119.16	188.94	107.97	22.09	7.53	170.46	129.42	130.97	122.04
B[b]	118.92	188.56	106.69	21.99	7.35	172.09	128.96	130.84	124.75
Compound	C-19	C-20	C-21	C-22	C-23	C-24	C-25	C-26	C-27
A[a]	140.20	37.31	74.02	35.89	79.41	37.76	76.43	39.97	79.41
B[b]	139.49	37.00	78.87	41.86	79.28	36.21	72.46	39.06	83.43
Compound	C-28	C-29	C-30	C-31	C-32	C-33	C-34	C-35	C-36
A[a]	112.86	140.13	21.02	14.57	11.27	11.93	12.69	171.78	20.85
B[b]	106.90	140.78	20.45	17.85	14.40	11.50	12.99	—	—
Compound	C-37	CH=N$^+$	C-2′	$\underline{C}(CH_3)_3$	$C(\underline{C}H_3)_3$				
A[a]	57.30	154.27	56.32	64.79	27.50				
B[b]	57.13	155.86	55.36	65.02	27.27				

a) Concn ca. 10^{-2} mol dm^{-3}. b) Concn ca. 10^{-1} mol dm^{-3}.

Table 4. ^{13}C NMR Chemical Shifts and Multiplicities of Quaternary Carbon Atoms in a Proton Non-Decoupling Spectrum of Compound **B** (25-OH-**6c**) in $CDCl_3$ (Concn ca. 10^{-1} mol dm^{-3}) and Change of Multiplicities by Long-Range Selective Proton Decoupling (LSPD)

Chemical shift	Multiplicity (J/Hz)	Assignment	Change of Multiplicity (J/Hz) by LSPD		
			$CH{=}N^+$ (δ=9.09)	OH-4 (δ=14.59)[a]	OH-1 (δ=16.44)
188.56	q(2)	C-11	—	—	—
183.39	q(3.5)	C-8	—	—	—
172.09	n.d.	C-15	—	—	—
172.04	q(4)	C-6	—	—	—
153.24	n.d.	C-4	—	—	—
147.11	d(4)	C-1	—	—	s
128.96	dq(2, 7)	C-16	—	—	—
121.67	d(6)	C-2	—	—	s
118.92	d(1)	C-10	—	s	—
113.50	n.d.	C-9	—	—	—
107.58	dd(2.5, 6.5)	C-3	d(6.5)	d(2.5)	—
107.36	q(6)	C-7	—	—	—
106.69	quintet(4.5)	C-12	—	—	—
98.79	s	C-5	—	—	—

s: singlet, d: doublet, q: quartet, n.d.: not determined. a) This chemical shift was slightly different from the value on Table 2, maybe, due to different concentration.

two phenolic hydroxyl protons were carried out by long-range selective proton decoupling (LSPD) experiments. The results of LSPD experiments for **B** (25-OH-**6c**) are summarized in Table 4.[10] The LSPD of the δ 14.59 proton affected the signals at 118.92 and 107.58, which were attributed to C-10 and C-3, respectively; hence, the δ 14.59 proton are assigned to the 4-hydroxyl proton. This implies that the 4-hydroxyl proton is not dissociated. The LSPD of the δ 16.44 proton affected the signals at 147.11 and 121.67, which were attributed to C-1 and C-2, respectively; hence, the 1-hydroxyl proton is also not dissociated. Therefore, the remaining 8-hydroxyl proton must be dissociated. The signals due to C-8 of **A** (**6c**) and **B** (25-OH-**6c**) are shifted downfield compared with that of **11** for 14 ppm (**A**, 183.29; **B**, 183.39; **11**, 169.19). This phenomenon is interpreted in terms of the contribution of a limiting structure **7c**,[11] and supports the structure of **6c**, in which the 8-hydroxyl group is completely dissociated. Thus, the structures of the deep-blue compounds, which have been reported by Marsili and Pasqualucci,[2] Maggi et al.,[3-5] and the authors,[1,12,13] should be revised to structures comprising a dihydropyrimidinium ring in which the 8-hydroxyl group is dissociated.

Mechanism of the Formation of Compound 6c. The process of the reaction of **1** with **2c** in pyridine at 63 °C was investigated by analytical silica-gel TLC. In the early stages of the reaction (after ca. 30 min from beginning) an intermediate product **C**, **6c** and the remaining starting material **1** were detected. At the end of the reaction (after ca. 1.5 h from beginning) **C** and **1** disappeared, while 3-[(*t*-butylamino)methylene]rifamycin (**12c**)[14] and rifamycin SV (**14**) as well as **6c** were detected. From this reaction mixture, **6c** was isolated in 38% yield. The intermediate product **C** was detected more clearly when the reaction was carried out at r.t., and it was considered that **C** was an intermediate for **6c**, because two-dimensional TLC showed that **C** gradually transformed on TLC plates into several compounds in which **6c** was included. Attempts to isolate **C** were not successful, due to its instability. However, it was observed by TLC that L-ascorbic acid reduced **C**, while the resulting reduction product **D** reverted to **C** upon treatment with MnO_2. The reduction product **D** was also observed by TLC to be the same compound which was formed by reduction of **6c** with $NaBH_4$ in EtOH. Additionally, it was observed by TLC that 3-[(*t*-butylamino)methyl]rifamycin S (**13c**), which was prepared by oxidation of 3-[(*t*-butylamino)methyl]rifamycin SV (**15c**) with MnO_2, transformed immediately and completely into **C** by treatment with **2c** in pyridine at r.t., and after warming at 62 °C for 1 h **6c** was obtained in 41% yield.[15] These facts imply that the structure of the intermediate product **C** can be assigned to **17c**, and it is concluded that in the reaction of **1** with **2c** the Mannich derivative **13c** is formed at first, then **17c**, and finally **6c** is formed by isomerization of **17c**. The formation of **17c** from **13c** is very fast, and this is the reason for the failure of the detection of **13c** by TLC. It is described above that **12c** and **14** were also detected at the end of the reaction of **1** with **2c**. This is interpreted as meaning that **6c** partly underwent aminolysis into **16c** by the action of *t*-butylamine, which was released during the course of the reaction; then, the redox reaction between the resulting **16c** and the remaining **1** proceeded to afford **12c** and **14**. In fact, it was observed by TLC that **12c** and **14** were formed by treating **6c** with *t*-butylamine

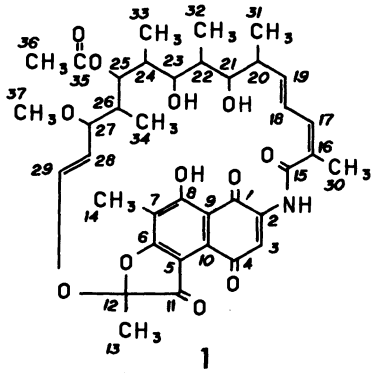

1

a: R = CH_3
b: R = C_2H_5
c: R = t-C_4H_9
d: R = t-C_5H_{11}
e: R = cyclo-C_6H_{11}

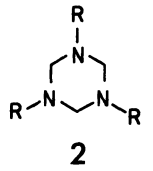

2

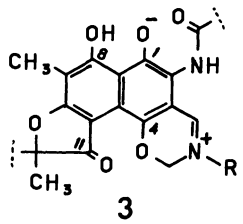

3

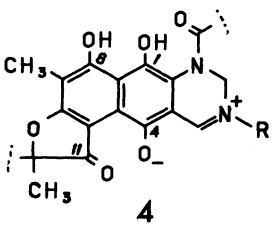

4

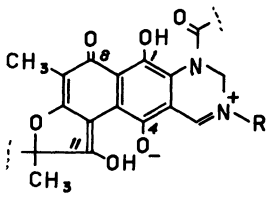

5

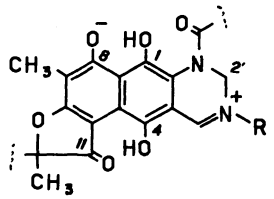

6

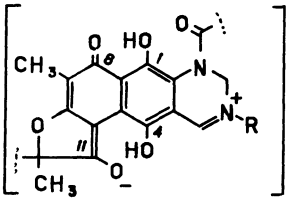

7

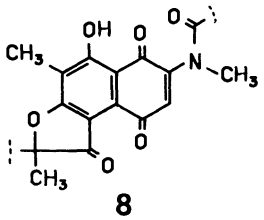

8

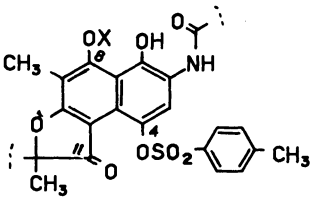

9: X = H (25-O-deacetyl)
10: X = Na (25-O-deacetyl)

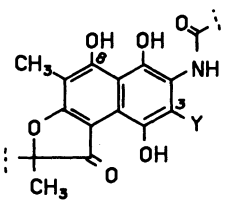

11: Y = -CH=NN⟨⟩NCH$_3$
14: Y = H
15: Y = -CH_2NHR
16: Y = -CH=NR

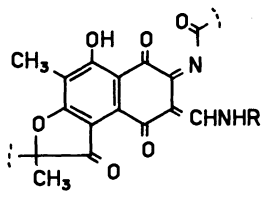

12

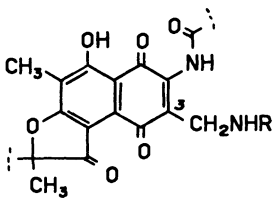

13

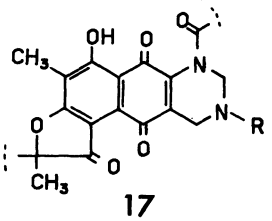

17

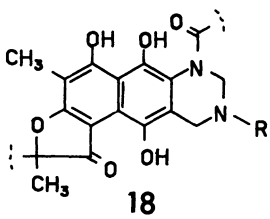

18

in the presence of **1** in pyridine at 65 °C.

Reaction of 1 with Other Hexahydro-1,3,5-triazines 2. Hexahydro-1,3,5-triazine **2d** reacted with **1** exactly like **2c**, and at the end of the reaction **6d**, **12d** and **14** were detected by TLC. The isolation yield of **6d** was 48%. Hexahydro-1,3,5-triazines **2a**, **2b**, or **2e** also reacted with **1**, but the results of the reaction were very different from the results described for **2c** and **2d**. The yields of compounds **6a**, **6b**, or **6e** were very low and the major products were observed by TLC to be the hydroquinone-type derivatives **18a**, **18b**, or **18e** and **14**. The formations of **12a**, **12b**, or **12e** were not observed. These different results from that of a reaction of **1** with **2c** or **2d** are attributed to the reducing power of hexahydro-1,3,5-triazines **2a**, **2b**, and **2e**.[12] As a representative example the result of the reaction of **1** with **2a** is interpreted as follows. At first, compound **17a** is formed via **13a**, then isomerizes into **6a**; however, the iminium bond of **6a** is reduced with the remaining **2a**, and **18a** is formed. The redox reaction between **18a** and the remaining **1** results in the formation of **17a** and **14**. Thus, the transformation of **1** into **18a** and **14** continues until **1** disappears; at the end of the reaction, **18a** and **14** are formed as major

Table 5. Reaction of Rifamycin S (**1**) with Hexahydro-1,3,5-triazines **2**

2 (Molar ratio to **1**)	Reaction condition[a]		Product	Yield/%
	Temp/°C	Time/h		
2a (1.9)	r.t.	48	**6a**	2
2b (2.0)	r.t.	48	**6b**	2
2c (0.69)	63	1.5	**6c**	38
2c (2.0)[b]	60	1.5	25-OH-**6c**	31
2d (2.4)	40	3.5	**6d**	48
2e (4.0)	r.t.	3.5	**6e**	4

a) Pyridine was used as a solvent. b) The 25-O-deacetyl derivative of **1** was used.

products, while **6a** is obtained in very low yield. The results are summarized in Table 5.

Experimental

Analytical TLC was performed on silica gel 60 F_{254} pre-coated plates (layer thickness 0.25 mm, Merck), using $CHCl_3$–CH_3OH (10:1) as a developing solvent. Preparative TLC was performed on silica gel 60 F_{254} pre-coated plates (layer thickness 0.5 mm, Merck). ^1H NMR spectra were recorded on a JEOL PS-100 spectrometer or a Bruker AM-300 spectrometer and TMS was used as an internal reference. ^{13}C NMR spectra were recorded on a Bruker AM-300 spectrometer and TMS was used as an internal reference. IR spectra were obtained with a Hitachi Perkin-Elmer model 225 spectrometer. UV spectra were obtained with a Shimadzu UV-210A spectrometer. Melting points were measured with a Yanagimoto micro melting-point apparatus and are uncorrected. Elemental analyses were performed with a Yanagimoto CHN-CORDER MT-3 or at the Elemental Analysis Center of Kyoto University.

Preparation of Hexahydro-1,3,5-triazines 2a—e. A similar method to that described by Smolin and Rapoport[16] was employed. Under cooling with ice-cold water, formalin was gradually added to an equimolar amount of amine. Isolation procedures were as follows.

2a, 2b, and 2d: A powder of K_2CO_3 was added to the reaction solution, and the products were extracted with $CHCl_3$. The extract was dried over K_2CO_3, evaporated in vacuo, and the residue was distilled. **2a**: Bp 40—42 °C/15 mmHg.** **2b**: Bp 63 °C/7 mmHg. In the case of **2d**, *N*-methylene-*t*-pentylamine (bp 92—93 °C) was obtained by distillation; however, this *N*-methyleneamine trimerized spontaneously into **2d** on standing.

2c: Pellets of NaOH were added to the reaction solution, and the resulting organic layer was separated, dried over KOH, and distilled in the presence of *d*-10-camphorsulfonic acid to afford *N*-methylene-*t*-butylamine (bp 67—68 °C); however, this *N*-methyleneamine trimerized spontaneously into **2c** on standing.

2e: The reaction products were extracted with ether, then the extract was dried over NaOH, evaporated in vacuo, and the residue was recrystallized from hexane. Mp 72—73 °C.

Reaction of 1 with Hexahydro-1,3,5-triazines 2a—e. As a typical run, the reaction of **1** with **2c** is described below.

To a solution of 300 mg of **1** in 3 ml of pyridine was added 76 mg of **2c**. After being stirred at 63 °C for 1.5 h, the reaction solution was poured into 10% AcOH, and the products were extracted with AcOEt. The extract was washed with 10% AcOH, brine, dried over Na_2SO_4, and evaporated in vacuo, then preparative TLC was carried out using $CHCl_3$–CH_3OH (20:1) as a developing solvent. The deep blue band was collected, and extracted with $CHCl_3$–CH_3OH (10:1). The extract was evaporated in vacuo, and the residue was further purified by column chromatography (Wakogel C-200, 10 g, Wako Pure Chemical Ind., Ltd.) using $CHCl_3$–CH_3OH (100:1, then 50:1) as an eluent. The deep-blue eluate was collected, and evaporated in vacuo to afford 133 mg (yield, 38%) of **6c** as a deep-blue powder. The reaction conditions and yields of **6a—e** are summarized in Table 5. The 25-*O*-deacetyl derivative of **6c** was prepared from 25-*O*-deacetylrifamycin S[17] and **2c**. Compounds **6a,b**, and **6e** were identical with authentic samples.[12] ^1H and ^{13}C NMR data of **6c** and its 25-*O*-deacetyl derivative are summarized in Tables 1—4. Other physical data of **6c** and its 25-*O*-deacetyl derivative have already been reported.[1] **6d**: UV λ_{max} (CH_3OH) 225 (log ε 4.58), 276 (4.35), 314 (sh, 4.17), 360 (4.28), and 600 nm (4.03); IR ($CHCl_3$) 3440, 1720, 1655 and 1580 cm^{-1}; ^1H NMR ($CDCl_3$) δ=9.00 (1H, s, iminium proton), 15.02 (1H, s, 4-OH), and 16.52 (1H, s, 1-OH). Found: C, 61.66; H, 6.95; N, 3.12%. Calcd for $C_{44}H_{58}N_2O_{12}\cdot 3H_2O$: C, 61.38; H, 7.14; N, 3.25%.

Preparation of 15c. To a solution of 8.0 g of 3-formylrifamycin SV[18–20] in 50 ml of pyridine was added 4.0 g of *t*-butylamine. The mixture was stirred at r.t. for 10 min; then 0.5 g of $NaBH_4$ was added to the mixture at 0 °C. After being stirred at 0 °C for 10 min, the reaction mixture was added to 1 l of cold 10% H_2SO_4. The products were extracted with AcOEt, and the extract was washed with H_2O, dried over Na_2SO_4, and evaporated in vacuo. The residue was dissolved in $CHCl_3$–AcOEt (1:1), and the solution was concentrated in vacuo to afford 2.0 g (yield, 22%) of **15c** as orange crystals. ^1H NMR ($CDCl_3$, after treatment with D_2O) δ=1.51 (9H, s, *t*-butyl), 3.76 (1H, d, *J*=11 Hz, $C\underline{H}_2NH$), and 4.15 (1H, d, *J*=11 Hz, $C\underline{H}_2NH$). Found: C, 62.08; H, 7.35; N, 3.62%. Calcd for $C_{42}H_{58}N_2O_{12}\cdot 3/2H_2O$: C, 62.28; H, 7.59; N, 3.45%.

Reaction of 13c with 2c. To a solution of 200 mg of **15c** in 20 ml of $CHCl_3$ was added 2.0 g of MnO_2 (70%, Wako Pure Chemical Ind., Ltd.). After being stirred at r.t. for 15 min, the mixture was filtered, and the filtrate was evaporated in vacuo. The residue, in which **13c** and **12c** were included,[15] was dissolved in 4 ml of pyridine, and to the solution 23 mg of **2c** was added. After being stirred at 62 °C for 1 h, the reaction mixture was extracted with AcOEt under acidic conditions (10% AcOH). The extract was washed with brine, dried over Na_2SO_4, and evaporated in

** (1 mmHg≈133.33 Pa.)

vacuo; then, preparative TLC was carried out using $CHCl_3$–CH_3OH (10:1) as a developing solvent. From the orange band 40 mg (yield, 20%) of **12c** was obtained (AcOEt was used as an eluent). From the deep-blue band 85 mg (yield, 41%) of **6c** was obtained (10:1 $CHCl_3$–CH_3OH was used as an eluent).

The authors wish to express their thanks to Mr. Yukinobu Yamane, Development Research Laboratories, Kanebo, Ltd., for obtaining the NMR spectra and his helpful discussions.

References

1) G. Tsukamoto, N. Aikawa, and M. Taguchi, *Chem. Lett.*, **1979**, 1313.

2) L. Marsili and C. Pasqualucci, Ger. Offen. 2428387 (1975) and 2433105 (1975); *Chem. Abstr.*, **83**, 10188v (1975) and **82**, 156407s (1975). They obtained deep-blue colored compounds in satisfactory yields by treating **1** with *N,N*-bis(alkoxymethyl)alkylamines, and used the deep-blue compounds as synthetic intermediates for rifampicin (**11**), which has been a most valuable drug for the treatment of tuberculosis.

3) N. Maggi, G. G. Gallo, and A. Vigevani, *Tetrahedron Lett.*, **1968**, 1763.

4) Gruppo Lepetit S. p. A., Brit. Patent 1226050 (1971); *Chem. Abstr.*, **75**, 20428x (1971).

5) N. Maggi, Brit. Patent 1276482 (1972); *Chem. Abstr.*, **77**, 114449y (1972).

6) M. Taguchi and G. Tsukamoto, *Chem. Pharm. Bull.*, **33**, 3133 (1985).

7) M. Taguchi, N. Aikawa, M. Kitamura, K. Yoshida, and G. Tsukamoto, *Bull. Chem. Soc. Jpn.*, **61**, 2425 (1988).

8) M. Koide, "Polarography," ed. by I. Tachi, Iwanami, Ltd., Tokyo (1954), pp. 298—300.

9) M. Taguchi, Y. Yamane, N. Aikawa, and G. Tsukamoto, *Chem. Pharm. Bull.*, to be submitted.

10) Compound **B** is more soluble in $CDCl_3$ than compound **A**, and therefore LSPD experiments were performed only for compound **B**.

11) G. E. Maciel and R. V. James, *J. Am. Chem. Soc.*, **86**, 3893 (1964).

12) G. Tsukamoto, M. Taguchi, and N. Aikawa, *Chem. Pharm. Bull.*, **28**, 2309 (1980).

13) M. Taguchi, N. Aikawa, and G. Tsukamoto, *Chem. Pharm. Bull.*, **32**, 4388 (1984).

14) Compounds **12** are the quinonoid form of **16**. The formation and structure of **12** has been reported by Maggi et al.[3] Authentic samples of **12** could also be obtained by MnO_2 oxidation of **16** in $CHCl_3$; compounds **16** were obtained by the reaction of an excess amount of primary amines with 3-formylrifamycin SV[18–20] in $CHCl_3$ followed by washing with dilute aq. H_2SO_4 solution.

15) Compound **13c** employed in this reaction was contaminated with **12c**. Contamination of **12c** into **13c** is not avoid, because **13c** is rather unstable and easily undergoes disproportionation into **12c** and **15c**. The latter compound **15c** reverts into **13c** during the preparation of **13c**. The disproportionation of **13c** into **12c** and **15c** is considered as that **13c** isomerizes into **16c** in a similar way described for **17c** into **6c**, then the redox reaction between the resulting **16c** and the remaining **13c** affords **12c** and **15c**.

16) E. M. Smolin and L. Rapoport, "s-Triazines and Derivatives" in "The Chemistry of Heterocyclic Compounds," ed. by A. Weissberger, Interscience Publishers Inc., New York (1967), p. 477.

17) W. Kump and H. Bickel, *Helv. Chim. Acta*, **56**, 2323 (1973).

18) N. Maggi and P. Sensi, Fr. Patent 1457435 (1966); *Chem. Abstr.*, **68**, 104836x (1968).

19) N. Maggi and P. Sensi, *Farmaco. Ed. Sci.*, **22**, 316 (1967).

20) A. Gianantonio, A. Fabrucci, S. Sacerdoti, and A. Soutzo, S. African Patent 6803308 (1968); *Chem. Abstr.*, **71**, 50008v (1969).

The Synthesis of *C*-Methyl Branched-Chain Deoxy Sugar Nucleosides by the Deoxygenative Methylation of *O*-Tosylated Adenosines with Grignard Reagents[1)]

Masajiro KAWANA,* Kikuko TAKEUCHI, Takayo OHBA, and Hiroyoshi KUZUHARA
RIKEN (The Institure of Physical and Chemical Research),
Wako, Saitama 351-01
(Received January 7, 1988)

The reaction of appropriately protected 2′-*O*-tosyladenosines with methylmagnesium bromide (or iodide) gave 9-(2-deoxy-3-*C*-methyl-β-D-*threo*-pentofuranosyl)adenine after deprotection. The same reaction on 3′-*O*-tosyladenosine derivatives afforded an epimeric pair of 2′-*C*-methyl-3′-deoxy sugar nucleosides. The modified structures of the sugar moieties were determined unambiguously.

There has been considerable interest during the past decade in the synthesis and chemistry of branched-chain sugar nucleosides,[2)] because modification of the sugar moieties has produced compounds with biologically interesting properties. Walton et al.[3)] reported that 2′-*C*- and 3′-*C*-methyladenosines were resistant to adenosine deaminase (adenosine aminohydrolase; EC 3.5.4.4) and that they exhibited inhibitory activity against KB cells in a culture. These findings prompted us to develop a convenient method for synthesizing a new type of adenosine analogue, branched-chain deoxy sugar nucleosides.

Previously we have described that methyl 5-*O*-benzyl-2-*O*- or -3-*O*-tosyl-β-D-ribofuranosides reacted with methylmagnesium iodide (MeMgI) to produce the corresponding 2-deoxy-3-*C*- or 3-deoxy-2-*C*-methyl branched-chain sugar furanosides in an efficient one-pot procedure.[4)] These reactions involved a [1,2]-hydride shift and a concerted elimination of a sulfonyloxy group, as is depicted in **A** (Scheme 1).[5)] The resulting α-deoxygenated keto sugar **B** was converted into products in the presence of an excess of MeMgI.[6)] We have now extended the scope of this reaction to the preparation of adenosine analogues. (A preliminary report on this work has been published.)[7)] During the course of this work, a report on the preparation of 1-(2-deoxy-3-*C*-methyl-5-*O*-trityl-β-D-*erythro*-pentofuranosyl)uracil by using 2′-*O*-tosyl-5′-*O*-trityluridine and MeMgI appeared.[8)]

Results and Discussion

Appropriately protected 2′-*O*- and 3′-*O*-tosyladenosines were prepared from adenosine by the operations outlined in Scheme 2. Thus, the silylation of adenosine with *t*-butyldimethylsilyl chloride according to the method of Ogilvie et al.[9)] gave a mixture of 3′,5′-di-*O*- and 2′,5′-di-*O*-sililated adenosines (**1** and **2**), along with a 2′,3′,5′-tri-*O*-protected derivative; the compounds were isolated in a ratio of 51:41:8 by silica-gel column chromatography. The protection of an NH_2 group in **1** with 4,4′-dimethoxytrityl chloride (DMTrCl) afforded the corresponding N^6-(4,4′-dimethoxytrityl) derivative **3** in a good yield. A similar reaction conducted with **2** and DMTrCl gave the N^6-protected compound **6**. The conventional tosylation of **3**, followed by deprotection with tetrabutylammonium fluoride,[9b)] gave N^6-(4,4′-dimethoxytrityl)-2′-*O*-tosyladenosine (**4**). Alternatively, **4** was prepared from N^6,$O^{5'}$-bis(4,4′-dimethoxytrityl)-2′-*O*-tosyladenosine[6i)] (**5**) by the selective detritylation of **5** with pyridinium *p*-toluenesulfonate (PPTS).[10)] Similarly, N^6-(4,4′-dimethoxytrityl)-3′-*O*-tosyladenosine (**7**) was obtained from **6** or N^6,$O^{5'}$-bis(4,4′-dimethoxytrityl)-3′-*O*-tosyladenosine (**8**).[6i)] The conventional tritylation of 2′-*O*-tosyladenosine provided the corresponding 5′-*O*-trityl derivative **9**.[6c,11)]

The deoxygenative methylations of **4**, **5**, and **7**—**9** were carried out in dry benzene with methylmagnesium bromide (MeMgBr; in tetrahydrofuran) or MeMgI (in diethyl ether) at room or an elevated temperature (Scheme 3). The products were not purified but were directly deblocked with 80% acetic acid or zinc bromide ($ZnBr_2$);[12)] in the former case, a depurination from 2′-deoxy nucleosides took place to some extent during the reaction and work-up. The

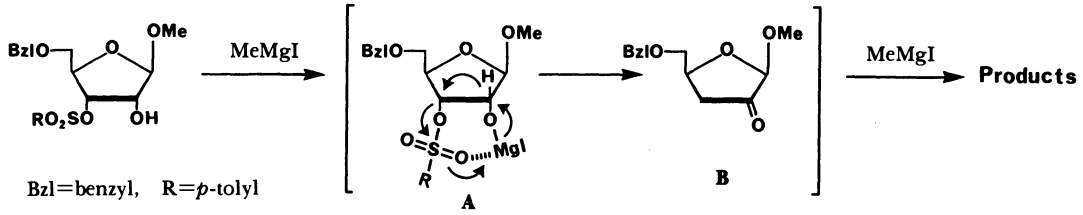

Scheme 1.

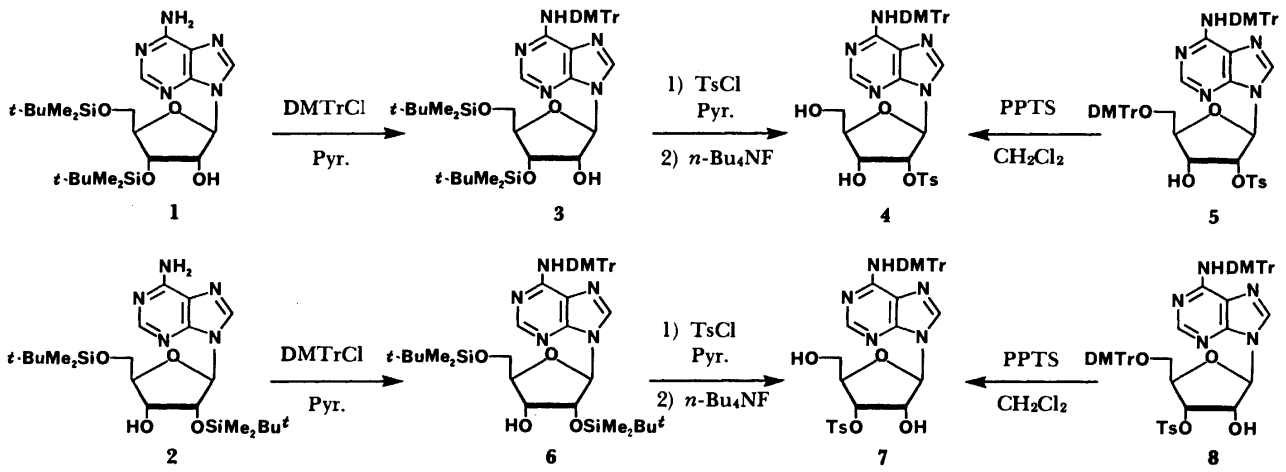

DMTr=4,4-dimethoxytrityl; PPTS=pyridinium *p*-toluenesulfonate; Ts=tosyl.

Scheme 2.

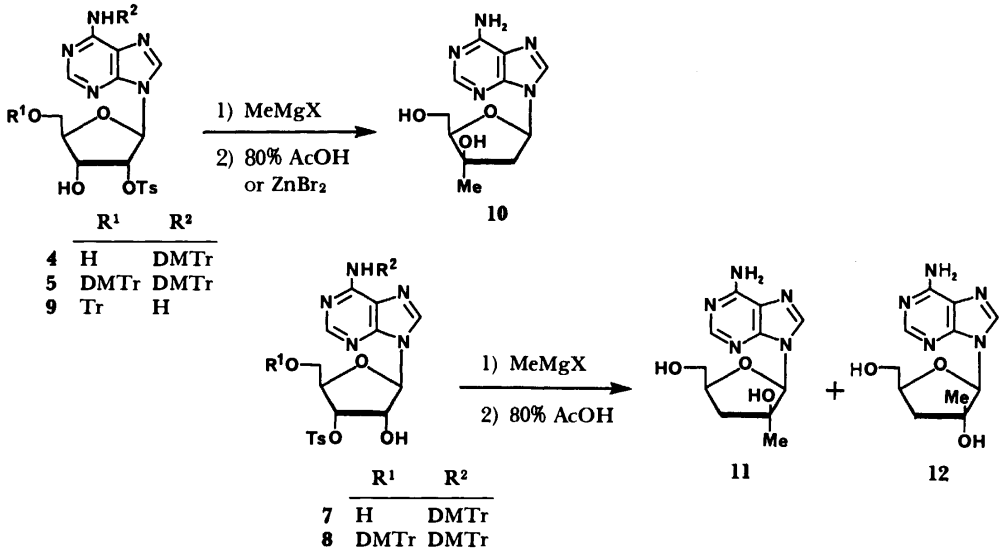

Tr=trityl; X=Br or I.

Scheme 3.

deprotection of the 5′-trityl group in the product derived from **9** was achieved with $ZnBr_2$ at 65 °C without the depurination. The resulting free nucleosides were isolated by means of ion-exchange [Dowex-1 (OH^- form)] column chromatography. In these operations, **4**, **5**, and **9** were successfully converted into 9-(2-deoxy-3-*C*-methyl-β-D-*threo*-pentofuranosyl)adenine (**10**). The results are summarized in Table 1.

The structure of the modified sugar moiety in **10** was established on the basis of its elemental analyses, the UV and ^1H NMR spectral data, and the fact that the methanolysis of **10** gave isomeric mixtures of methyl pentosides, whose ^1H NMR spectrum was identical with those of specimens prepared from the known methyl 2-deoxy-3-*C*-methyl-β-D-*threo*-pentofuranoside[4] except for the intensity of the signals. No erythro isomer with the 3′-"up"-methyl group could be detected in the deoxygenative methylation of **4**, **5**, and **9**. In the case of the uridine derivative,[8] however, the erythro (3′-"up"-methyl group) derivative was the main product. The steric course of the methyl group in these reactions was strongly influenced by the nature of the base moiety attached to the anomeric position,[13] but the reason for this is not clear at this time. On the other hand, the reactions of **7** and **8** with MeMgBr or MeMgI proceeded at elevated temperatures to produce a pair of isomers, 9-(3-deoxy-2-*C*-methyl-β-D-*threo*- and -*erythro*-pentofuranosyl)adenine (**11** and **12**), after the deprotection (Table 1). Satisfactorily elemental analyses and spectral data were obtained for these products. The structure of the sugar moiety in **11** was correlated with that for the known methyl 3-deoxy-2-*C*-methyl-β-D-*threo*-pento-

Table 1. The Synthesis of Branched-Chain Deoxy Sugar Nucleosides with Grignard Reagents[a]

Starting material (mmol)	Grignard reaction			Deprotection			Product (Yield/%)
	Reagent (mmol)	Temp[b]	Time	Reagent	Temp[b]	Time	
4 (0.5)	MeMgBr (3)	rt	17 h	$ZnBr_2$	rt	2.5 h	**10** (17)
(0.5)	MeMgI (8)	1) rt 2) 65 °C	8 h 50 min	$ZnBr_2$	rt	2.5 h	**10** (53)
5 (2.0)	MeMgBr (12)	rt	5 h	AcOH	rt	0.5 h	**10** (55)
(0.5)	MeMgBr (11)	rt	5 h	$ZnBr_2$	rt	2.5 h	**10** (58)
(2.0)	MeMgI (12)	rt	8.5 h	$ZnBr_2$	rt	2.5 h	**10** (41)
9 (0.6)	MeMgBr (12)	80 °C	20 min	$ZnBr_2$	65 °C	1 h	**10** (51)
7 (0.7)	MeMgBr (4)	65 °C	30 min	AcOH	rt	2.5 h	**11** (40), **12** (19)
(0.8)	MeMgI (11)	rt	4 h	AcOH	rt	45 min	**11** (65), **12** (19)
8 (0.9)	MeMgBr (5)	65 °C	40 min	AcOH	rt	35 min	**11** (62), **12** (8)
(1.0)	MeMgI (17)	65 °C	15 min	AcOH	rt	60 min	**11** (67), **12** (15)

a) Some of the reaction conditions are described in the Experimental Section. b) rt=room temperature.

furanoside[4] by the methanolysis. In addition, the ^{1}H NMR spectrum (in DMSO-d_6) of **12** showed that the signal due to the methyl protons shifted upfield by 0.45 ppm relative to that for the corresponding protons in **11**, while the H-8 signal shifted downfield by 0.25 ppm. Similar shifts were observed in the ^{1}H NMR spectrum measured in MeOH-d_4. These facts indicated that, in **12**, the methyl group and the imidazole ring in a base moiety were located close to each other; the erythro structure of **12** was thus established.

Very recently Koole et al.[14] have reported the synthesis of **11** by the stereoselective addition of MeMgI to a protected 3′-deoxy-2′-keto nucleoside, followed by deprotection: the keto nucleoside was prepared from 5′-*O*-(4-methoxytrityl)-9-(3-deoxy-β-D-*erythro*-pentofuranosyl)adenine. The ^{1}H NMR (in MeOH-d_4) spectral data of **11** prepared by our method were almost identical with those previously reported.[14]

The reactions of 2′- or 3′-*O*-tosyladenosine derivatives with Grignard reagents other than MeMgI or MeMgBr gave various products, depending on the structure of the organic residues in the reagents; the preliminary results have been previously published.[7]

Experimental

General. The melting points were determined in capillary tubes with a Yamato micro melting-point apparatus and are uncorrected. The optical rotations were measured with a Perkin-Elmer Model 241MC polarimeter in a 1-dm cell. The UV spectra were measured with a Varian Cary 2200 apparatus using a 1-cm cell. The ^{1}H NMR spectra were recorded with a JEOL JNM-GX 400 spectrometer, using tetramethylsilane as the internal standard. The coupling constants were measured directly from the spectra or were calculated from the peak listing. The TLC was performed on precoated plates (0.25 mm) of Silica Gel 60 F_{254} (Merck). Detection was done by means of UV (254 nm) or by spraying the plates with a solution of methanol–sulfuric acid–*p*-anisaldehyde (85:15:5, v/v), followed in the latter case by heating at above 200 °C. The column chromatography was effected on Silica Gel 60 (Merck 70—230 mesh, ASTM). The elemental analyses were performed by the Microanalytical Laboratory of this Institute. The solvent extracts were dried with anhydrous magnesium sulfate, and the solutions were evaporated under diminished pressure at 40—45 °C. The analytical samples were dried at 60 °C for 4 h in vacuo over diphosphorus pentaoxide. The Grignard reagents were purchased from the Tokyo Chemical Industry Co., Ltd.

3′,5′-Bis-*O*-(*t*-butyldimethylsilyl)adenosine (1) and Its 2′,5′-Isomer (2). The method of Ogilvie et al.[9] was slightly modified.

To a stirred solution of adenosine (2.67 g, 10 mmol) in a mixture of dry pyridine (4 ml) and DMF (10 ml), we added silver nitrate (3.40 g, 20 mmol), after which the mixture was stirred at room temperature for 2 h. After cooling with iced water, THF (20 ml), and *t*-butyldimethylsilyl chloride (3.02 g, 20 mmol) were added and the mixture was stirred at room temperature for 1 h. The undissolved materials were removed by filtration through a Celite pad and washed with THF. The combined filtrate and washings were diluted with ether containing a small amount of chloroform. The mixture was then washed successively with aq. sodium hydrogencarbonate and water (three times), dried, and concentrated. The pyridine was removed by repeated co-evaporation with toluene. The residue was chromatographed on a silica-gel column with benzene–ethyl acetate (7:3). The compound emerging first was 2′,3′,5′-tris-*O*-(*t*-butyldimethylsilyl)adenosine (427 mg, 7%). The second product eluted with the same solvent system (1:1) was **2** (1.74 g, 35%). The elution of **1** (2.18 g, 44%) was effected with benzene–ethyl acetate–methanol (25:25:1).

1: ^{1}H NMR ($CDCl_3$) δ=0.07 and 0.09 (3H, each s, 3′-SiMe), 0.17 (6H, s, 2×5′-SiMe), 0.90 (9H, s, 3′-SiBu^t), and 0.95 (9H, s, 5′-SiBu^t), 3.43 (1H, br d, OH), 3.77 (1H, dd,

J=2.9 and 11.4 Hz, H-5′), 3.93 (1H, dd, J=3.5 and 11.4 Hz, H-5″), 4.13 (2H, br s, H-2′ and H-3′), 5.94 (2H, br s, NH_2), 6.04 (1H, d, J=4.3 Hz, H-1′), 8.10 (1H, s, H-2), and 8.34 (1H, s, H-8).

2: ^{1}H NMR ($CDCl_3$) δ=−0.12 and −0.05 (3H, each s, 2′-SiMe), 0.14 and 0.15 (3H, each s, 5′-SiMe), 0.84 (9H, s, 2′-*t*-Bu), 0.96 (9H, s, 5′-SiBu^t), 2.85 (1H, d, J=4.3 Hz, OH), 3.86 (1H, dd, J=2.4 and 11.5 Hz, H-5′), 4.02 (1H, dd, J=2.4 and 11.5 Hz, H-5″), 4.22 (1H, m, H-4′), 4.29 (1H, m, H-3′), 4.64 (1H, t, J=5.0 Hz, H-2′), 5.92 (2H, br s, NH_2), 6.12 (1H, d, J=5.2 Hz, H-1′), 8.23 (1H, s, H-2), and 8.35 (1H, s, H-8).

3′,5′-Bis-*O*-(*t*-butyldimethylsilyl)-N^6-(4,4′-dimethoxytrityl)adenosine (3). Compound **1** (3.14 g, 6.33 mmol) was dried by co-evaporation with dry pyridine-toluene. This product was then dissolved in dry pyridine (30 ml), and 4,4′-dimethoxytrityl chloride (2.79 g, 8.2 mmol) was added. The mixture was then stirred at room temperature for 17 h. After cooling, 50% aq. pyridine was added; the products were extracted with ether. The extracts were washed with water, dried, and concentrated. The residual pyridine was removed by co-evaporation with chloroform–toluene, and the residue was chromatographed on a silica-gel column with toluene–ethyl acetate–triethylamine (9:1:0.1) to give **3** (4.34 g, 86%) as a foam. A portion of the product was dissolved in a small amount of dichloromethane and precipitated by the addition of the dichloromethane solution to an excess of pentane under vigorous stirring. The resulting precipitates were collected and dried to afford an analytical sample: amorphous powders: $[\alpha]_D^{22}$ −23.1° (*c* 0.49, $CHCl_3$); UV λ_{max}^{MeOH} 275 nm (ε 20200); ^{1}H NMR ($CDCl_3$) δ=0.03 and 0.07 (3H, each s, 3′-SiMe), 0.16 (6H, s, 2×5′-SiMe), 0.88 (9H, s, 3′-SiBu^t), 0.94 (9H, s, 5′-SiBu^t), 3.29 (1H, d, J=6.4 Hz, OH), 3.78 (6H, s, 2×OMe), 3.75 (1H, dd, J=2.9 and 11.2 Hz, H-5′), 3.89 (1H, dd, J=3.8 and 11.2 Hz, H-5″), 4.10 (1H, m, H-4′), 4.58 (2H, m, H-2′ and H-3′), 5.97 (1H, d, J=4.6 Hz, H-1′), 6.76—7.43 (14H, m, Arom. and NH), and 8.00 and 8.05 (1H, each s, H-2 and H-8). Found: C, 64.77; H, 7.43; N, 8.70; Si, 7.04%. Calcd for $C_{43}H_{59}N_5O_6Si_2$: C, 64.71, H, 7.45; N, 8.77; Si, 7.04%.

N^6-(4,4′-Dimethoxytrityl)-2′-*O*-tosyladenosine (4). From **3.** Compound **3** (2.85 g, 3.6 mmol) was dried by co-evaporation with dry pyridine–toluene. This was then dissolved in dry pyridine (32 ml), and tosyl chloride (2.75 g, 14.3 mmol) was added. The mixture was stirred at room temperature for 5 d and then quenched with 50% aq. pyridine. The products were extracted with diethyl ether containing a small amount of chloroform. The extracts were washed successively with water, aq. sodium hydrogencarbonate, and water, and then dried. The solvents were evaporated, and the residual pyridine was removed by repeated co-evaporation with toluene. The residue was dissolved in THF (30 ml), and tetrabutylammonium fluoride (1 mol dm^{-3} solution in THF; 7.2 ml) was added. The mixture was then stirred at room temperature for 30 min. After cooling, it was diluted with diethyl ether and a small amount of chloroform. The solution was washed three times with water, dried, and concentrated. The residue was chromatographed on a silica-gel column with chloroform–ethyl acetate (9:1), followed with chloroform–ethyl acetate–methanol (9:1:0.1), to give amorphous **4** (2.12 g, 82%). Precipitation from dichloromethane–pentane gave an analytical sample: amorphous powders: $[\alpha]_D^{23}$ −13.9° (*c* 0.49, $CHCl_3$); UV λ_{max}^{MeOH} 275 nm (ε 22700); ^{1}H NMR ($CDCl_3$) δ=2.24 (3H, s, CMe), 3.28—3.37 (1H, br s, 5′-OH), 3.78 (6H, s, OMe), 3.63 (1H, br t, J=12 Hz, H-5′), 3.81 (1H, br d, J=11 Hz, H-5″), 4.21 (1H, br s, H-4′), 4.63 (1H, dd, J=1.7 and 4.4 Hz, H-3′), 5.47 (1H, dd, J=4.4 and 7.8 Hz, H-2′), 5.93 (1H, d, J=7.8 Hz, H-1′), 6.37 (1H, dd, J=2.0 and 12.0 Hz, 3′-OH), 6.78—7.44 (18H, Arom. and NH), 7.68 (1H, s, H-2), and 7.84 (1H, s, H-8). Found: C, 63.06; H, 5.25; N, 9.40; S, 4.38%. Calcd for $C_{38}H_{37}N_5O_8S$: C, 63.06; H, 5.15; N, 9.68; S, 4.43%.

From **5.** A solution of PPTS (450 mg, 1.8 mmol) in dichloromethane (8 ml) was added to a solution of **5** (4.56 g, 4.4 mmol) in dichloromethane (40 ml). The mixture was stirred at room temperature for 3 h and then diluted with dichloromethane. The solution was washed successively with aq. sodium carbonate and water, dried, and concentrated. The residue was chromatographed on a silica-gel column with chloroform–ethyl acetate (9:1), followed with chloroform–ethyl acetate–methanol (9:1:0.1), to give **4** (2.56 g, 80%).

2′,5′-Bis-*O*-(*t*-butyldimethylsilyl)-N^6-(4,4′-dimethoxytrityl)-adenosine (6). Compound **2** (2.94 g, 5.9 mmol) was treated under conditions similar to those used in the preparation of **3.** The usual work-up and purification by silica-gel column chromatography [toluene–ethyl acetate–triethylamine (9:1:0.1)] gave **6** as crystals: mp 186 °C (sintered), 193.5—194.5 °C (benzene–hexane); $[\alpha]_D^{22}$ −29.7° (*c* 0.52, $CHCl_3$); UV λ_{max}^{MeOH} 275 nm (ε 24700); ^{1}H NMR ($CHCl_3$) δ=−0.17 and −0.07 (3H, each s, 2′-SiMe), 0.12 and 0.14 (3H, each s, 5′-SiMe), 0.80 (9H, s, 2′-SiBu^t), 0.95 (9H, s, 5′-SiBu^t), 2.71 (1H, d, J=3.9 Hz, OH), 3.78 (6H, s, 2×OMe), 3.84 (1H, dd, J=2.5 and 11.3 Hz, H-5′), 4.00 (1H, dd, J=2.8 and 11.3 Hz, H-5″), 4.19 (1H, m, H-4′), 4.26 (1H, m, H-3′), 4.65 (1H, t, J=5.1 Hz, H-2′), 6.05 (1H, J=5.1 Hz, H-1′), 6.76—7.34 (14H, m, Arom. and NH), 8.04 (1H, s, H-2), and 8.11 (1H, s, H-8). Found: C, 64.62; H, 7.41; N, 8.66; Si, 6.84%. Calcd for $C_{43}H_{59}N_5O_6Si_2$: C, 64.71; H, 7.45; N, 8.77; Si, 7.04%.

N^6-(4,4′-Dimethoxytrityl)-3′-*O*-tosyladenosine (7). From **6.** Compound **6** (1.78 g, 2.2 mmol) was treated under condition similar to those described for the synthesis of **4** from **3**, giving **7** (1.37 g, 85%): amorphous powders; $[\alpha]_D^{21}$ −29.6° (*c* 0.64, $CHCl_3$); UV λ_{max}^{MeOH} 275 nm (ε 21100); ^{1}H NMR ($CDCl_3$) δ=2.46 (3H, s, CMe), 3.05—3.2 (1H, br s, OH), 3.76 and 3.77 (6H, s, 2×OMe), 3.55 (1H, br t, J=13 Hz, H-5′), 3.82 (1H, d, J=13.7 Hz, H-5″), 4.37 (1H, m, H-4′), 5.11 (2H, m, H-2′ and H-3′), 5.76 (1H, d, J=7.1 Hz, H-1′), 6.72—7.34 (15H, m, Arom., NH, and OH), 7.39 (2H, d, J=8.6 Hz, Arom.), 7.85 (2H, d, J=8.5 Hz, Arom.), 7.76 (1H, s, H-2), 7.95 (1H, s, H-8). Found: C, 62.92; H, 5.14; N, 9.57; S, 4.33%. Calcd for $C_{38}H_{37}N_5O_8S$: C, 63.06; H, 5.15; N, 9.68; S, 4.43%.

From **8.** A solution of PPTS (270 mg, 1.08 mmol) in dichloromethane (5 ml) was added to a solution of **8** (2.77 g, 2.7 mmol), and the mixture was stirred at room temperature for 8 h. The resulting fine crystals of 3′-*O*-tosyladenosine tosylate salt[6i] were filtered off, and the filtrate was diluted with dichloromethane. The solution was washed successively with aq. sodium carbonate and water, dried, and concentrated. The residue was chromatographed on a silica-gel column with chloroform–ethyl acetate (9:1), followed by chromatography with chloroform–ethyl acetate–methanol (9:1:0.4), to afford **7** (1.33 g, 68%).

9-(2-Deoxy-3-*C*-methyl-β-D-*threo*-pentofuranosyl)adenine

(10). Some of the reaction conditions and the results are summarized in Table 1.

To a stirred mixture of MeMgI (2 mol dm^{-3} solution in diethyl ether) or MeMgBr (1 mol dm^{-3} solution in THF) and dry benzene (3 ml), we added a solution of **4**, **5**, or **9** (ca.0.5 mmol) in dry benzene (3 ml) at room temperature, after which the mixture was stirred at the given temperature for the given reaction time. After cooling, aq. ammonium chloride was added, and the products were extracted with diethyl ether containing a small amount of chloroform. The extracts were then washed with water, dried, and concentrated. The residue was dissolved in chloroform (2.5 ml), and the solution was added to a solution of $ZnBr_2$ (450 mg, 2 mmol) in a mixture of methanol (0.54 ml) and chloroform (2.2 ml).[12] After the mixture had been stirred at the given temperature for the given reaction time, it was diluted with methanol and then concentrated to a few ml at room temperature in vacuo. The residue was chromatographed on a silica-gel column with chloroform–methanol (9:1 → 8:2). The combined eluates containing the product were concentrated to about 10 ml, and then the concentrate was diluted with methanol. This solution was then concentrated to a few ml and placed in an ion-exchange column (Dowex 1X-2, OH^-, 100—200 mesh) made up with water. Elution with the same solvent gave **10**: mp 166—167 °C (from MeOH–diisopropyl ether); $[\alpha]_D^{25}$ +4.7° (*c* 0.44, H_2O); UV λ_{max}^{MeOH} 259 nm (ε 15100); ^1H NMR (DMSO-d_6) δ=1.34 (3H, s, Me), 2.36 (1H, dd, *J*=2.7 and 14.4 Hz, H-2′), 2.65 (1H, dd, *J*=8.8 and 14.4 Hz, H-2″), 3.55—3.73 (3H, m, H-4′ and H-5′, 5″), 4.67 (1H, t, *J*=5.5 Hz, 5′-OH), 6.06 (1H, s, 3′-OH), 6.20 (1H, dd, *J*=2.8 and 8.7 Hz, H-1′), 7.36 (2H, br s, NH_2), 8.14 (1H, s, H-2), and 8.35 (1H, s, H-8). Found: C, 49.00; H, 5.70; N, 26.32%. Calcd for $C_{11}H_{15}N_5O_3 \cdot 0.2H_2O$: C, 49.14; H, 5.77; N, 26.05%.

9-(3-Deoxy-2-*C*-methyl-β-D-*threo*-pentofuranosyl)adenine (11) and Its Erythro Isomer (12). Some of the reaction conditions and the results are listed in Table 1.

Compound **7** or **8** (ca. 0.5 mmol), was subjected to a Grignard reaction under conditions similar to those used in the synthesis of **10**. After the reaction mixture had been worked up, the residue was dissolved in 80% acetic acid (10 ml) and the solution was stirred at room temperature for the given reaction time. The acetic acid was removed by repeated co-evaporation with ethanol–toluene, the residue was partitioned between chloroform and water. The water solution was washed with chloroform and then concentrated. The residue was chromatographed on a column of ion-exchange resin (Dowex 1X-2, OH^- form, 100—200 mesh) packed with water. Elution with the same solvent gave **12**, and then **11**.

11: Mp 218—219 °C (from MeOH–diisopropyl ether); $[\alpha]_D^{27}$ +34.9° (*c* 0.45, H_2O); UV λ_{max}^{MeOH} 259 nm (ε 16200); ^1H NMR (DMSO-d_6) δ=1.30 (3H, s, Me), 2.17 (2H, m, H-3′,3″), 3.55—3.70 (2H, m, H-5′,5″), 4.16 (1H, m, H-4′), 5.34 (1H,s, 2′-OH), 5.36 (1H, t, *J*=4.9 Hz, 5′-OH), 5.88 (1H, s, H-1′), 7.24 (2H, br s, NH_2), 8.13 (1H, s, H-2), and 8.28 (1H, s, H-8); (MeOH-d_4) δ=1.38 (3H, s, Me), 2.26 (1H, dd, *J*=5.5 and 13.4 Hz, H-3′), 2.37 (1H, dd, *J*=8.5 and 13.4 Hz, H-3″), 3.72 (1H, dd, *J*=3.7 and 11.9 Hz, H-5′), 3.87 (1H, dd, *J*=2.8 and 11.9 Hz, H-5″), 4.33 (1H, m, H-4′), 6.01 (1H, s, H-1′), 8.19 (1H, s, H-2), and 8.43 (1H, s, H-8). Found: C, 48.72; H, 5.65; N, 26.12%. Calcd for $C_{11}H_{15}N_5O_3 \cdot 0.3H_2O$: C, 48.81; H, 5.81; N, 26.12%.

12: Mp 233—234 °C (from EtOH); $[\alpha]_D^{22}$ −32.3° (*c* 0.54, H_2O); UV λ_{max}^{MeOH} 259 nm (ε 14900); ^1H NMR (DMSO-d_6) δ=0.85 (3H, s, Me), 1.84 (1H, dd, *J*=4.9 and 13 Hz, H-3′), 1.87 (1H, br t, *J*=12 Hz, H-3″), 3.63 (1H, m, H-5′), 3.84 (1H, m, H-5″), 4.40 (1H, m, H-4′), 5.22 (1H, t, *J*=5.1 Hz, 5′-OH), 5.55 (1H, s, 2′-OH), 5.92 (1H, s, H-1′), 7.29 (2H, br s, NH_2), 8.14 (1H, s, H-2), and 8.53 (1H, s, H-8); (MeOH-d_4) δ=0.97 (3H, s, Me), 1.95 (1H, dd, *J*=5.0 and 13.3 Hz, H-3′), 2.32 (1H, dd, *J*=11.3 and 13.1 Hz, H-3″), 3.77 (1H, dd, *J*=2.9 and 12.4 Hz, H-5′), 4.04 (1H, dd, *J*=2.6 and 12.4 Hz, H-5″), 4.55 (1H, m, H-4′), 6.06 (1H, s, H-1′), 8.20 (1H, s, H-2), and 8.64 (1H, s, H-8). Found: C, 49.19; H, 5.70; N, 26.51%. Calcd for $C_{11}H_{15}N_5O_3 \cdot 0.1H_2O$: C, 49.47; H, 5.74; N, 26.22%.

Methanolysis of Methyl 2-Deoxy-3-*C*-methyl-β-D-*threo*-pentofuranoside and 10. A mixture of methyl 2-deoxy-3-*C*-methyl-β-D-*threo*-pentofuranoside[4] (15 mg, 0.09 mmol) and Dowex 50W-X8 (125 mg, H^+ form, 100—200 mesh) in methanol (1.5 ml) was stirred at room temperature for 6 h. The resin was then removed by filtration through a Celite pad and washed with methanol. The combined filtrate and washings were concentrated to give methyl 2-deoxy-3-*C*-methyl-α- and -β-D-*threo*-pentosides (14 mg, 93%): ^1H NMR ($CDCl_3$) δ=1.23 (0.6H, s, CMe), 1.36 (1.1H, s, CMe), 1.39 (0.3H, s, CMe), 1.43 (1.0H, s, CMe), 3.39, 3.40, 3.446, and 3.448 (each s, OMe), 4.62 (0.4H, dd, *J*=3.4 and 6.6 Hz, H-1), 4.81 (0.2H, br d, *J*=3.2 Hz, H-1), 5.02 (0.1H, dd, *J*=2.1 and 3.5 Hz, H-1), and 5.16 (0.3H, dd, *J*=3.2 and 5.9 Hz, H-1).

The methanolysis of **10** (32 mg, 0.012 mmol) with Dowex 50W-X8 (127 mg, H^+ form, 100—200 mesh) in methanol (1.5 ml) was carried out at room temperature for 2.3 h. A work-up similar to that described above gave methyl pentosides (17 mg, 89%), whose thin-layer chromatographic behavior and ^1H NMR spectrum were identical with those for the pentosides prepared by the methanolysis of methyl 2-deoxy-3-*C*-methyl-β-D-*threo*-pentofuranoside.

Methanolysis of Methyl 3-Deoxy-2-*C*-methyl-β-D-*threo*-pentofuranoside and 11. A mixture of methyl 3-deoxy-2-*C*-methyl-β-D-*threo*-pentofuranoside[4] (15 mg, 0.09 mmol) and Dowex 50W-X8 (126 mg, H^+ form, 100—200 mesh) in methanol (1 ml) was stirred first at room temperature for 1.5 h and then at 50 °C for 5.5 h. The resin was removed by filtration and washed with methanol. The combined filtrate and washings were concentrated to give methyl 3-deoxy-2-*C*-methyl-α- and -β-D-*threo*-pentosides (13 mg, 89%): ^1H NMR ($CDCl_3$) δ=1.34 (s, CMe), 1.35 (s, CMe), 1.86 (0.74H, dd, *J*=2.7 and 13.4 Hz, H-3a,b), 1.94 (0.52H, d, *J*=7.6 Hz, H-3a,b), 2.25 (0.74H, dd, *J*=10.0 and 13.4 Hz, H-3a,b), 3.36 (s, OMe), 3.50 (s, OMe), 3.57 (0.74H, dd, *J*=1.7 and 11.7 Hz, H-5a,b), 3.71 (0.26H, dd, *J*=2.7 and 11.7 Hz, H-5a,b), 3.91 (0.74H, dd, *J*=2.1 and 11.6 Hz), 4.40 (0.25H, s, H-1), and 4.59 (0.75H, s, H-1).

A similar methanolysis of **11** (41 mg, 0.15 mmol) with Dowex 50W-X8 (H^+ form, 130 mg) in methanol (2 ml) afforded the pentosides (22 mg, 92%), whose thin-layer chromatographic behavior and ^1H NMR spectrum were identical with those for the pentosides prepared from methyl 3-deoxy-2-*C*-methyl-β-D-*threo*-pentofuranoside.

We wish to thank Dr. Jun Uzawa and Mrs. Tamiko Chijimatsu for the measurement of the ^1H NMR spectra, and Dr. Hiroshi Yamazaki and his staff for the

elemental analyses. This work was supported, in part, by a Research Grant for Life Science granted by this Institute.

References

1) Presented at the 8th Japanese Carbohydrate Symposium, Kyoto, July 1985, Abstr., p. 97.

2) S. N. Mikhailov, L. N. Beigelman, G. V. Gurskaya, N. S. Padyukova, G. I. Yakovlev, and M. Y. Karpeisky, *Carbohydr. Res.*, **124**, 75 (1983), and the references cited therein; V. Nelson and H. S. El Khadem, *J. Med. Chem.*, **26**, 1527 (1983); M. Iwakawa, O. R. Martin, and W. A. Szarek, *Carbohydr. Res.*, **121**, 99 (1983); H. P. Albrecht, G. H. Jones, and J. G. Moffatt, *Tetrahedron*, **40**, 79 (1984); T. Kurihara, A. Ota, H. Hayashi, M. Inoue, and T. Ishida, *J. Heterocycl. Chem.*, **21**, 259 (1984); T. Suami, H. Sasai, K. Matsuno, and N. Suzuki, *Carbohydr. Res.*, **143**, 85 (1985); T. Sano, S. Shuto, H. Inoue, and T. Ueda, *Chem. Pharm. Bull.*, **33**, 3617 (1985); H. Usui and T. Ueda, *ibid.*, **34**, 15 (1986); *ibid.*, **34**, 1518 (1986); H. Usui, A. Matsuda, and T. Ueda, *ibid.*, **34**, 1961 (1986); J. Kimura, H. Kobayashi, O. Miyahara, and O. Mitsunobu, *Bull. Chem. Soc. Jpn.*, **59**, 869 (1986); O. Sakanaka, T. Ohmori, S. Kozaki, and T. Suami, *ibid.*, **60**, 1057 (1987), and the references cited therein; H. Hayakawa, H. Tanaka, N. Itoh, M. Nakajima, T. Miyasaka, K. Yamaguchi, and Y. Iitaka, *Chem. Pharm. Bull.*, **35**, 2605 (1987); L. N. Beigelman, B. S. Ermolinsky, G. V. Gurskaya, E. N. Tsapkina, M. Ya. Karpeisky, and S. N. Mikhailov, *Carbohydr. Res.*, **166**, 219 (1987).

3) E. Walton, S. R. Jenkins, R. F. Nutt, M. Zimmerman, and F. W. Holly, *J. Am. Chem. Soc.*, **88**, 4524 (1966); R. F. Nutt, M. J. Dickinson, F. W. Holly, and E. Walton, *J. Org. Chem.*, **33**, 1789 (1968).

4) M. Kawana, T. Koresawa, and H. Kuzuhara, *Bull. Chem. Soc. Jpn.*, **56**, 1095 (1983).

5) M. Kawana and S. Emoto, *Tetrahedron Lett.*, **1975**, 3395; *Bull. Chem. Soc. Jpn.*, **53**, 222 (1980).

6) For synthetic applications of the deoxygenative [1,2]-rearrangement in carbohydrate chemistry, see a) M. Kawana and S. Emoto, *Chem. Lett.*, **1977**, 597; b) H. Ohrui and H. Kuzuhara, *Agric. Biol. Chem.*, **44**, 907 (1980); c) F. Hansske and M. J. Robins, *J. Am. Chem. Soc.*, **105**, 6736 (1983); d) T. Haradahira, M. Maeda, Y. Kai, H. Omae, and M. Kojima, *Chem. Pharm. Bull.*, **33**, 165 (1985); e) R. W. Binkley, *J. Carbohydr. Chem.*, **4**, 227 (1985); f) H. H. Baer, D. J. Astles, H.-C. Chin, and L. Siemsen, *Can. J. Chem.*, **63**, 432 (1985); g) H. H. Baer and M. Mekarska-Falicki, *ibid.*, **63**, 3043 (1985); h) P. Herdewijn, J. Balzarini, E. De Clercq, R. Pauwels, M. Baba, S. Broder, and H. Vanderhaeghe, *J. Med. Chem.*, **30**, 1270 (1987); i) M. Kawana and H. Kuzuhara, *Tetrahedron Lett.*, **28**, 4075 (1987); j) P. Herdewijn, M. Baba, J. Balzarini, and E. De Clercq, *J. Med. Chem.*, **30**, 2123 (1987); k) M. Kawana, N. Yamasaki, M. Nishikawa, and H. Kuzuhara, *Chem. Lett.*, **1987**, 2419.

7) M. Kawana, K. Takeuchi, T. Ohba, and H. Kuzuhara, *Nucleic Acids Res. Symp. Ser.*, No. 17, **1986**, 37.

8) A. Grouiller, H. Essadig, H. Pacheco, S. Juntunene, and J. Chattopadhyaya, *Angew. Chem., Int. Ed. Engl.*, **24**, 52 (1985).

9) a) K. K. Ogilvie, S. L. Beaucage, A. L. Schifman, N. Y. Theriault, and K. L. Sadana, *Can. J. Chem.*, **56**, 2768 (1978); b) G. H. Hakimelahi, Z. A. Proba, and K. K. Ogilvie, *ibid.*, **60**, 1106 (1982).

10) M. Miyashita, A. Yoshikoshi, and P. A. Grieco, *J. Org. Chem.*, **42**, 3772 (1977).

11) M. Kawana and H. Kuzuhara, to be submitted.

12) V. Kohli, H. Blöcker, and H. Köster, *Tetrahedron Lett.*, **21**, 2683 (1980); M. D. Matteucci and M. H. Caruthers, *ibid.*, **21**, 3243 (1980); R. Kierzek, H. Ito, R. Bhatt, and K. Itakura, *ibid.*, **22**, 3761 (1981).

13) For example, see A. Mete, J. B. Hobbs, D. I. C. Scopes, and R. F. Newton, *Tetrahedron Lett.*, **26**, 97 (1985); H. Hayakawa, H. Tanaka, Y. Maruyama, and T. Miyashita, *Chem. Lett.*, **1985**, 1401.

14) L. H. Koole, H. M. Buck, H. Bazin, and J. Chattopadhyaya, *Tetrahedron*, **43**, 2989 (1987).

Intramolecular End-to-End Reactions of Photoactive Terminal Groups Linked by Poly(oxyethylene) Chains

Kazuo ASHIKAGA, Shinzaburo ITO, Masahide YAMAMOTO,* and Yasunori NISHIJIMA
Department of Polymer Chemistry, Faculty of Engineering, Kyoto University,
Yoshida, Sakyo-ku, Kyoto 606
(Received January 8, 1988)

The triplet-sensitized photochemical reaction using a series of poly(oxyethylene) chains with a pair of photoactive terminal groups, dibenz[*b,f*]azepine (DBA) chromophores (DBA-$COCH_2CH_2(OCH_2CH_2)_nOCH_2$-$CH_2CO$-DBA, n=0—10) was examined. The photoirradiation of bichromophoric compounds caused either intra- or intermolecular reactions. These reactions were kinetically analyzed by two different methods: the measurement of deactivation processes of the reaction intermediates (excited triplet state of DBA) by nanosecond laser photolysis and the quantitative analysis of the reaction products by GPC. The intramolecular deactivation rate constant, k^{intra}, showed a remarkable chain-length dependence; the maximum k^{intra} value appeared at n=5 and it was found to be 5.9×10^4 s^{-1}. On the other hand, the intramolecular cyclization rate also depends on the chain length; the maximum quantum yield, ϕ_d^{intra}, was given at n=7 (ϕ_d^{intra}=0.51). The chain length for the maximum cyclization yield shifted slightly to the longer region than that for the maximum k^{intra} value due to the restriction of the terminal structure (anti-configuration). The results obtained for this reaction system are compared with those obtained for the previously reported polymethylene system and the effect of chain flexibility on the intramolecular ring-closure reaction is discussed.

Previously, we reported on the intra- and intermolecular end-to-end photochemical reactions of a pair of terminal dibenz[*b,f*]azepine (DBA) chromophores linked by polymethylene chains.[1,2] The probing DBA chromophore undergoes photodimerization via an excited triplet intermediate under the sensitized conditions and gives an anti-cyclobutane dimer as a unique reaction product.[3,4] In contrast with other intramolecular ring-closure reactions reported in the past,[5–15] these characteristics of DBA chromophore give the following features to this reaction system: (1) The reaction intermediate, the triplet state of DBA chromophore, has a long lifetime, 17 μs, so a wide range of chain lengths can be pursued for the cyclization reaction. (2) Ring-closure probability of specific chain conformation can be obtained, since two terminal DBA groups must approach each other from an opposite side for the cycloaddition reaction to make the anti-cyclobutane ring.

Our previous results, obtained for the polymethylene system, demonstrated that the intramolecular cyclization rate is pronouncedly controlled by the chain length connecting a pair of terminal DBA groups and that the terminal direction of a molecular chain exerts a great influence upon the chain-length dependence of the intramolecular ring-closure reaction.[1] That is, we concluded in the previous work that the intramolecular reaction yield is determined by the equilibrium ring-closure probability of a molecular chain. Generally, the cyclization reaction is considered to be affected not only by the chain length, but also by the chain nature. Sisido et al. carried out intrachain reactions of a pair of reactive groups attached to both ends of the polysarcosine chain,[16] and poly(oxyethylene) chain[17] and the intrachain reactivities were compared among the polymer chains. They showed that the intrachain reaction of the polysarcosine chain proceeds more effectively than that of the poly(oxyethylene) chain and that the intrachain reaction of the polysarcosine chain is more efficient than that of the polymethylene chain by two or three times. The flexibility of a molecular chain is expected to be one of the most important nature in determining the reaction yield of the cyclization; that is, a flexible molecular chain will show a higher cyclization yield than a rigid one.

In the present work, we investigated the intra- and intermolecular end-to-end reaction of bichromophoric poly(oxyethylene) compounds, as shown in Fig. 1. These compounds are denoted as DE-n (n=0—10, l=3n+5). Hereafter, "n" represents the number of

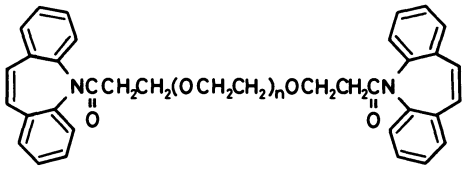

DE-n (n=0~10, l=3n+5)

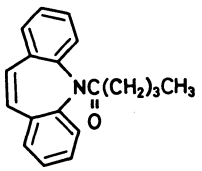

5-Valeryl-DBA

Fig. 1. A series of poly(oxyethylene) compounds having a pair of DBA groups as the terminal reactants, DE-n (n=0—10). Monomeric compound, 5-valeryl-DBA, is also shown.

oxyethylene units, and "l" the number of atoms in the poly(oxyethylene) chain. The experimental results obtained for this system were compared with those obtained for the polymethylene system and the effect of chain nature on the intramolecular cyclization was examined.

Experimental

Materials. Bichromophoric Compounds: A series of poly(oxyethylene) compounds having a pair of dibenz[*b,f*]-azepine (DBA) as the terminal groups were synthesized according to the procedure reported by Kricka et al.,[18] i.e., by an acylation reaction of the corresponding poly(oxyethylene)dicarboxylic acid dichloride with 5*H*-DBA. For example, 5,5′-(4,7,10,13,16,19-hexaoxadocosanedioyl)bisdibenz[*b,f*]azepine (DE-5) was prepared as follows. Hexaoxadocosanedicarboxylic acid dichloride (1.1 g) in dry benzene was added dropwise to a stirred benzene solution of 5*H*-DBA (1.0 g, Aldrich) at room temperature. The reaction mixture was refluxed for 5 h, then cooled and washed with water. A solution of the reaction mixture was dried with calcium chloride, and evaporation of the solvent afforded a yellow oily product. The product was purified by column chromatography on neutral alumina eluted with the mixture of dichloromethane and methanol (500:3). A series of other bichromophoric compounds, except for DE-0, were prepared by the same procedure as DE-5. DE-0 was obtained by an acylation reaction of 5*H*-DBA with 3,3′-oxybis-(propanoyl chloride). All obtained compounds were identified by IR, UV, and NMR spectra. The spectra for the obtained bichromophoric compounds showed the same characteristic spectra. The data were as follows: IR (KBr); 3100, 2850, 1660, 1600, 1490, 1370, 1100, 800, and 760 cm^{-1}, UV (CH_2Cl_2); λ_{max}=287 nm, ^1H NMR (CD_2Cl_2); δ=1.8—2.8 (m, $-COCH_2CH_2-$), 3.2—3.8 (m, $-OCH_2CH_2O-$), 6.9 (s, $-CH=CH-$), 7.2—7.5 (m, aromatic). The reaction yields of all obtained compounds were about 60%. The purity of the compounds was confirmed by TLC (one spot, on neutral alumina).

Poly(oxyethylene)dicarboxylic Acid Dichlorides: Each poly(oxyethylene)dicarboxylic acid dichloride was prepared from the corresponding poly(oxyethylene)dicarboxylic acid by a reaction with thionyl chloride; e.g., 3,6,9,12,15,18-hexaoxaeicosanedicarboxylic acid dichloride was obtained as follows. 3,6,9,12,15,18-Hexaoxaeicosanedicarboxylic acid dissolved in thionyl chloride was heated at 50°C for 1 h under stirring. When the evolution of hydrogen chloride stopped, the excess thionyl chloride was removed by distillation and an acid chloride was obtained. A series of other acid chlorides were obtained by the same procedure as 3,6,9,12,15,18-hexaoxaeicosanedicarboxylic acid dichloride.

Poly(oxyethylene)dicarboxylic Acids: Each poly(oxyethylene)dicarboxylic acid was prepared by the hydrolysis of the corresponding poly(oxyethylene)dicarbonitrile with hydrochloric acid; e.g., 3,6,9,12,15,18-hexaoxaeicosanedicarboxylic acid was obtained as follows. 3,6,9,12,15,18-Hexaoxaeicosanedinitrile was dissolved in hydrochloric acid (12 M (1 M=1 mol dm^{-3})) and was refluxed for 5 min; then the water was removed by distillation. The residue was extracted by dichloromethane and the evaporation of dichloromethane afforded 3,6,9,12,15,18-hexaoxaeicosanedicarboxylic acid. A series of acids were obtained by the same procedure as 3,6,9,12,15,18-hexaoxaeicosanedicarboxylic acid.

Poly(oxyethylene)dicarbonitriles: Each poly(oxyethylene)-dicarbonitrile was prepared by an addition reaction of acrylonitrile to poly(ethylene glycol); e.g., 3,6,9,12,15,18-hexaoxaeicosanedinitrile was prepared as follows. Acrylonitrile in benzene was added dropwise to the benzene solution of pentaethylene glycol under stirring in the presence of potassium hydroxide as a catalyst. The reaction mixture was stirred for 1 h at room temperature. After the insoluble substance was filtered off, benzene was evaporated to yield 3,6,9,12,15,18-hexaoxaeicosanedinitrile. A series of other nitriles were obtained by the same procedure as 3,6,9,12,15,18-hexaoxaeicosanedinitrile.

Polyethylene Glycols: Commercial polyethylene glycols (Tokyo Kasei) were used for the shorter chains than tetraethylene glycol. A series of polyethylene glycols longer than tetraethylene glycol were prepared according to the procedure of Pedersen,[19] i.e., by the Williamson method. For example, pentaethylene glycol was prepared as follows. Potassium hydroxide was dissolved in excess ethylene glycol (Wako) under stirring. 1,2-Bis(2-chloroethoxy)ethane (Tokyo Kasei) was added to the solution and heated at 80 °C for 48 h. The reaction mixture was cooled to room temperature and potassium chloride was filtered off. After unreacted ethylene glycol was removed by distillation under reduced pressure, pentaethylene glycol was obtained by fractional distillation under highly reduced pressure. Other polyethylene glycols were obtained by a similar procedure.

Benzophenone (BP, Wako) used as the triplet sensitizer was purified by recrystallization from ligroin several times and dried in vacuo.

Dichloromethane used as the solvent was purified as follows. Dichloromethane was washed with sulfuric acid and water, and then washed with 10% sodium hydroxide aqueous solution and with water till it became neutral. Dried 1,2-dichloroethane with calcium chloride was distilled twice over calcium hydride.

Laser Photolysis. An NEC SLG 2009 ruby laser was used for laser photolysis.[20] The concentration of the deaerated sample solutions was in the range 5.0×10^{-4} to 2.0×10^{-3} mol l^{-1} in chromophore units. The concentration of BP used as the triplet sensitizer was 2.5×10^{-3} mol l^{-1} for all sample solutions. Samples were excited by the second-harmonic pulse (347 nm, 16 ns, 3.02×10^{-8} einstein/pulse). The laser power was attenuated by a suitable combination of filters, so that the absorbance of the $T_n\leftarrow T_1$ absorption was less than 0.2. Under such conditions, the T–T annihilation process became negligibly small.

Photoirradiation. Photoirradiation was carried out for 0.5 h in a thermostat kept at 25 °C. A Toshiba 300-W high-pressure mercury lamp was used as the excitation source. A 365-nm mercury line was selected through a combination of filters: a Toshiba UVD-2 and a Corning C.S. 0-52. The concentration of bichromophoric compounds in the deaerated solution was adjusted to be 2.0×10^{-3} mol l^{-1} with respect to the chromophore concentration. The concentration of BP was 2.5×10^{-3} mol l^{-1}. All sample solutions were filled in a 1-cm quartz cell and deaerated by several freeze-pump-thaw cycles at ca. 10^{-6} Torr (1 Torr=133.322 Pa).

The number of photons at 365 nm was measured to be 1.89×10^{-9} Einstein cm^{-2} s^{-1} by the potassium trioxalatofer-

rate(III) actinometry.[21]

Product Analysis. Intra- and intermolecular photoreaction products were analyzed by a Toyo Soda HLC 802 UR gel permeation chromatograph with double G2000H columns eluted by THF. UV, IR, NMR spectra of the products were measured by a Shimadzu UV-200 S double-beam spectrophotometer, by a JASCO IR-G infrared spectrophotometer, and by a JEOL FX-90 Q NMR spectrometer using TMS as an internal standard, respectively. The spectroscopic data for the obtained products were as follows. The IR spectra for the intra- and intermolecular products showed the same characteristic spectra: IR (KBr); 1660 (s, C=O), 1450 cm^{-1} (m, CH). All intermolecular reaction products showed the same characteristic ^1H NMR spectra: ^1H NMR (CD_2Cl_2); δ=1.9—2.7 (m, methylene), 3.4—3.7 (m, oxyethylene), 6.9 (s, ethylenic), 7.1—7.5 (m, aromatic). For all intramolecular cyclomers the chemical shifts of the ^1H NMR spectra were as follows: ^1H NMR (CD_2Cl_2); δ=2.5—4.1 (m, oxyethylene), 4.0 (s, methine), 6.9—7.7 (m, aromatic).

Results and Discussion

Intra- and Intermolecular End-to-End Interactions Measured by Nanosecond Laser Photolysis. The absorption spectra of a series of bichromophoric compounds, DE-n (n=0—10), in dichloromethane were found to be independent of the chain length (l) and were identical with the monomeric compound, 5-valeryl-DBA (λ_{max}=287 nm).[4] This fact shows that a pair of terminal DBA groups of these bichromophoric compounds do not have any specific interaction with each other in the ground state.

Intra- and intermolecular end-to-end interactions in the excited triplet state were examined by nanosecond laser photolysis through the kinetic analysis of the deactivation processes of the terminal DBA triplet. Benzophenone (BP) sensitized $T_n \leftarrow T_1$ absorption spectra of the bichromophoric compounds in dichloromethane at room temperature were independent of the chain length (l) and identical with those of the bichromophoric polymethylene compounds reported previously.[1] The $T_n \leftarrow T_1$ absorption band of the DBA triplet for DE compounds (λ_{max}=420 nm) hardly overlaps with that of the BP triplet (λ_{max}=520 nm). Therefore, the decay curves at 400 nm and 520 nm were unambiguously analyzed. Figure 2 shows the scheme of BP sensitization and the deactivation processes of the sensitized DBA triplet in the bichromophoric compounds. In this figure, BP and $^3BP^*$ represent benzophenone in the ground state and in the excited triplet state, respectively. DBA-DBA represents a bichromophoric molecule in the ground state and $^3DBA^*$-DBA in the excited triplet state of the bichromophoric molecule. The rate constant, k_n^s, is the sum of the rate constants for all unimolecular decay processes of the triplet BP, and k_t the rate constant for the triplet-triplet (T-T) energy transfer from BP to a terminal DBA group. The rate constant, k_n, is the sum of the rate constants for all unimolecular decay processes of the excited triplet state of DBA, k_n^{intra} the rate constant of the triplet deactivation by intramolecular quenching, and k_d^{intra} the rate constant of the intramolecular ring-closure reaction, and k_n^{inter} the rate constant of the deactivation by intermolecular quenching, k_d^{inter} the rate constant of intermolecular cycloaddition reaction. The decay processes are roughly divided into two routes: one is a decay path in which the excited triplet DBA group is self-quenched and gives no reaction product, a kind of genuine concentration quenching process; the other is a decay path in which the terminal DBA group in the excited state reacts with that in the ground state and gives the photoproducts. Each decay path consists of intramolecular and intermolecular processes.

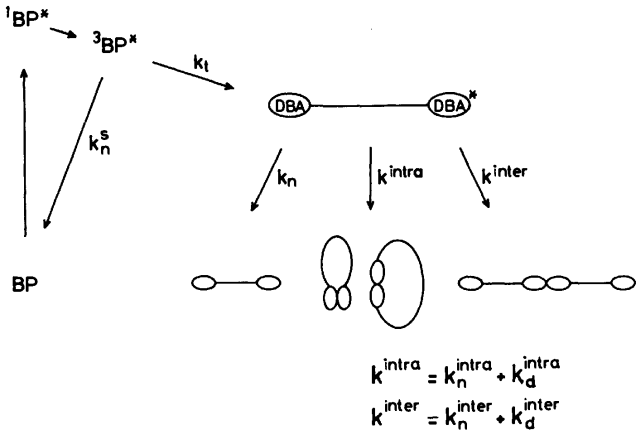

Fig. 2. T-T energy transfer from benzophenone to the bichromophoric compounds and deactivation processes of the excited triplet state of the bichromophoric compounds.

The lifetime of the BP triplet (τ^D) was measured at several concentrations of DE molecules which were the triplet energy acceptor. The Stern-Volmer equation for the lifetime of the BP triplet is expressed as follows:

$$\tau_0^D/\tau^D = 1 + \tau_0^D k_t[DBA], \quad (1)$$

where τ_0^D is the lifetime of the BP triplet in the absence of the DE molecule (τ_0^D=3.6×10^{-6} s),[4] and [DBA] the concentration of DBA chromophore. The plot of τ_0^D/τ^D against the concentrations of DBA chromophore for all DE compounds showed a straight line, and from the slope of the line the rate constant for a T-T energy transfer, k_t, was estimated for each DE compound. Figure 3 shows the chain-length dependence of the k_t value. The k_t value is almost independent of the chain length of DE compounds and is close to the diffusion-controlled rate constant ($k_t \simeq 2\times10^9$ M^{-1} s^{-1}). This tendency and the k_t value itself are almost the same as those for the polymethylene system.[1] In this low-molecular-weight region, the diffusion rate constant is presumed to be independent of the molecular size.[22]

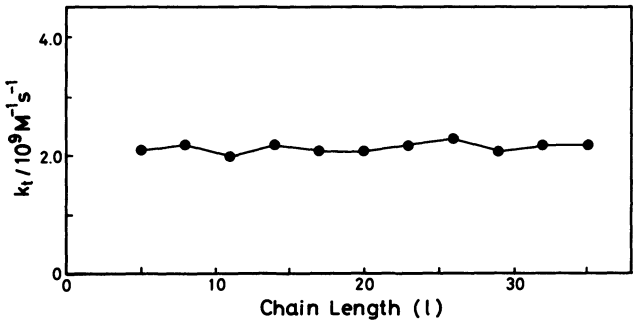

Fig. 3. Chain length dependence of the rate constant of T-T energy transfer, k_t, from benzophenone to a terminal DBA group of poly(oxyethylene) compound in dichloromethane at room temperature.

The lifetime of the terminal DBA triplet, τ^A, in this reaction system is represented by the following equation:

$$1/\tau^A = k_n + k^{intra} + k^{inter}[DBA], \quad (2)$$

where k^{intra} is the sum of the rate constants of k_n^{intra} and k_d^{intra} ($k^{intra}=k_n^{intra}+k_d^{intra}$), k^{inter} the sum of k_n^{inter} and k_d^{inter} ($k^{inter}=k_n^{inter}+k_d^{inter}$). The lifetime of the terminal DBA triplet was measured for several concentrations of the DE compound, and the plot of $1/\tau^A$ against the concentration of the terminal DBA group gave a straight line for each compound. From the intercept in this plot, the k_n+k^{intra} value was obtained. The k^{intra} value for each bichromophoric compound was determined by subtracting the k_n value from the k_n+k^{intra} value, since the k_n value is considered to be inherent to the DBA chromophore. In this case, the k_n value is assumed to be equal to the k_n^A value obtained for the monomeric compound, 5-valeryl DBA, which was reported previously ($k_n=k_n^A=5.9\times10^4$ s^{-1}).[4] Figure 4 shows a plot of the k^{intra} value obtained in this reaction system against the chain length of the bichromophoric compounds, together with the results obtained in the previous polymethylene system. In this figure, it is apparent that the k^{intra} value is strongly dependent on the chain length. The peak of the k^{intra} value corresponding to the first peak in the polymethylene system was not observed in the poly(oxyethylene) system. In the present system, the shortest chain length (l) was 5 (n=0). Therefore, the first peak for intramolecular interaction exists presumably at a chain length shorter than l=5.

In the range of the chain length l=5 to 11, the k^{intra} values are very small compared with those of other chain lengths. This tendency in this system is almost the same as that in the polymethylene system reported previously. This means that poly(oxyethylene) chains in this region can hardly take a favorable or stable ring conformation intramolecularly.

On the other hand, the k^{intra} value increases with increasing chain length beyond l=11 and the maximum value appears at l=20. This indicates that

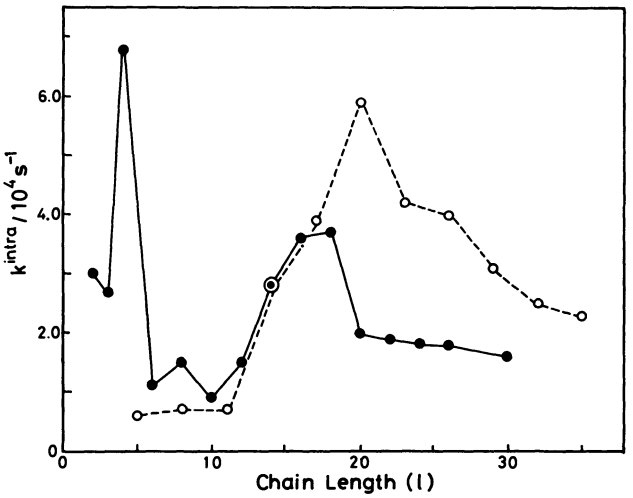

Fig. 4. Chain length dependence of the rate constant of intramolecular interaction, k^{intra}, for poly(oxyethylene) system (○), and polymethylene system (●) at room temperature.

a strong interaction occurs intramolecularly between a pair of terminal DBA groups with this extent of separation. At this chain length, the poly(oxyethylene) chain takes a favorable conformation for the terminal DBA groups to interact with each other. This experimental finding indicates that ring-closure probability of a poly(oxyethylene) chain reaches the maximum at the chain length l=20. For the poly(oxyethylene) system, the chain length which gives the maximum value of k^{intra} is slightly longer than that for the polymethylene system. This effect is due to an increasing contribution of k_d^{intra} to the k^{intra} value, which will be discussed in the following section. That is, the k_d^{intra} value increases sharply at l=20 in the poly(oxyethylene) system and the chain length for the maximum value of k^{intra} shifts to a longer region than that for the polymethylene system.

A theoretical treatment for the intramolecular ring-closure probability of a poly(oxyethylene) chain (C-O-(-C-C-O-)$_m$-C, m=3—20) was carried out by Sisido et al.[23] They calculated the ring-closure probability of a poly(oxyethylene) chain by the Monte Carlo Method. In their calculation, the maximum ring-closure probability appears at m=4 or 5 (the number of atoms in the chain is 15 or 18) under the critical distance between the chain ends, r_0=6 or 4 Å, respectively. The calculated result is different from their experimental findings. They concluded that this discrepancy is attributed to the effect of the bulky terminal groups attached to the poly(oxyethylene) chain. In our experimental examination, the maximum k^{intra} value appears at n=5 (l=20). This chain length is also longer than the chain length of the maximum ring-closure probability calculated by the Monte Carlo Method. The difference between our experimental findings in the present system and their

calculated results may be attributed to the effect of the terminal DBA groups.

In the region of the chain length $l \geqq 17$, the k^{intra} values in this system are larger than those in the polymethylene system. This indicates that the collisional frequency of the terminal reactants in the poly(oxyethylene) system is higher than that in the polymethylene system. The difference of collisional frequencies in the two systems is due to the difference of the flexibility between two molecular chains connecting terminal DBA groups. Yamakawa et al. have investigated the chain stiffness of flexible chain polymers on the basis of helical wormlike chains.[24,25] They defined the parameters λ^{-1} and τ/τ^0 as the static chain stiffness and the dynamic chain stiffness, respectively, where τ and τ^0 are the correlation time of a flexible chain and that of the monomer unit, respectively. The larger the parameter λ^{-1}, the statically stiffer the chain, and the larger the parameter τ/τ^0, the dynamically stiffer the chain. They showed that there is a good correlation between the dynamic stiffness τ/τ^0 and the static stiffness λ^{-1}; τ/τ^0 is a monotonically increasing function of λ^{-1}. According to their theoretical estimate, the value λ^{-1} is 14.5 and 12.0 Å for the polymethylene chain and for the poly(oxyethylene) chain, respectively. Hence, the poly(oxyethylene) chain is considered to be more flexible than the polymethylene chain from a dynamic standpoint as well as from a static one. Our experimental results agree well with their theoretical prediction.

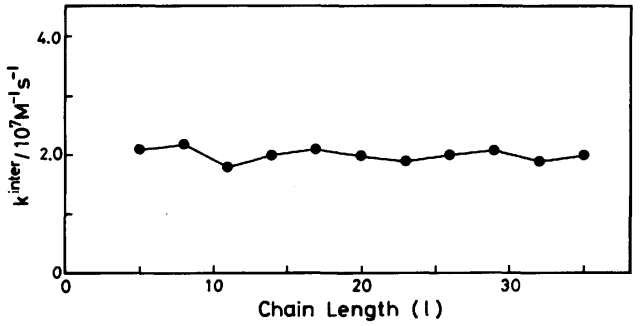

Fig. 5. Chain length dependence of the rate constant of intermolecular interaction, k^{inter}, for bichromophoric poly(oxyethylene) compounds in dichloromethane at room temperature.

The rate constant, k^{inter}, was determined from the slope of the straight line obtained by the plot of $1/\tau^A$ against the DBA concentration. Figure 5 shows a plot of the k^{inter} value against the chain length of the DE compounds. It is apparent that the rate constant for the deactivation by intermolecular interaction k^{inter}, is independent of the chain length of the poly(oxyethylene) chain. The k^{inter} values in this system are nearly equal to those in polymethylene system reported previously ($(1—2)\times10^7$ M^{-1} s^{-1}).[1] The absence of the influence of chain length on the rate constant k^{inter} is partly due to an activation-controlled process[26] and partly due to the rather small molecular weights of the bichromophoric compounds.

In this section, the ring-closure probability of a poly(oxyethylene) chain was examined through an analysis of the intramolecular deactivation rate constant, k^{intra}; the experimental results indicate that the flexibility of a moleculr chain exerts a great influence upon the ring-closure probability.

Intra- and Intermolecular End-to-End Cycloaddition Reactions. A series of bichromophoric compounds, DE-n (n=0—10), which are excited by a T-T energy transfer from BP, have two kinds of reaction paths (Fig. 2): intramolecular ring-closure reaction and intermolecular dimer formation reaction.

Figure 6 shows typical GPC diagrams of the reaction products obtained after 0.5 h irradiation. For DE-1, only one intermolecular reaction product **2** was

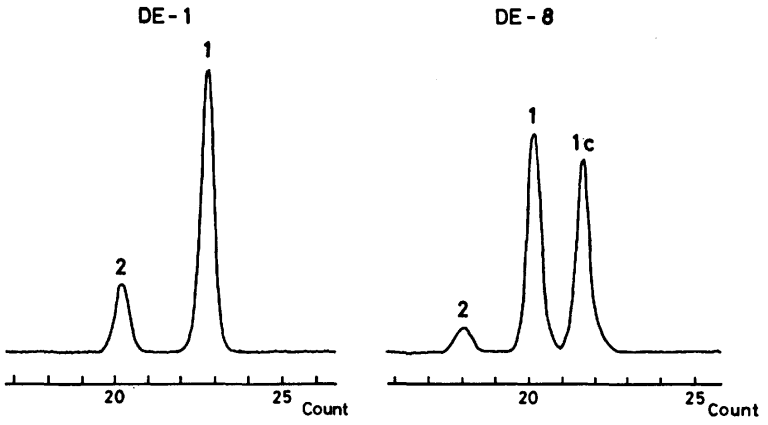

Fig. 6. Typical GPC diagrams of photoreaction products obtained by 0.5 h irradiation of bichromophoric compounds, DE-1 and DE-8. Unreacted monomer **1**, intramolecular ring-closure product **1c**, and intermolecular dimer **2**.

detected at 20.2 counts, together with the residual unreacted monomer **1** at 22.7 counts. This situation is the same as that for the shorter-chain compounds. The intramolecular reaction does not occur, since the oxyethylene chain is too short for a pair of terminal DBA group to form intramolecularly. On the other hand, with longer-chain compounds, such as DE-8, not only the intermolecular reaction product **2** at 18.0 counts but also the intramolecular ring-closure product **1c** at 21.6 counts was detected together with the unreacted monomer **1** at 20.0 counts. A GPC analysis showed that an intramolecular ring-closure product is produced for samples of $l \geqq 14$, but not for samples of $l \leqq 11$. These experimental facts can be explained in terms of the configuration of the terminal groups; DBA group forms only anti-cyclobutane ring[4] and for the compounds having an oxyethylene chain shorter than $l=14$, a pair of terminal DBA groups cannot take a favorable orientation to form an anti-cyclobutane ring intramolecularly. Such a chain-length dependence of the intramolecular ring-closure reaction for this system is almost the same as that for the polymethylene system; in the polymethylene system, the intramolecular ring-closure product cannot be detected for the compounds having a chain shorter than $l=14$.[1]

The quantum yields of both the intra-and intermolecular cycloaddition reactions in each bichromophoric compound were determined by the quantitative analyses of the reaction products with GPC. In these BP-sensitized systems, the quantum yields for the intramolecular ring-closure product (ϕ_d^{intra}) and for the intermolecular dimer (ϕ_d^{inter}) are defined as follows:

ϕ_d^{intra} = the number of intramolecular ring-closure products/the number of photons absorbed by BP,

ϕ_d^{inter} = the number of intramolecular dimers/the number of photons absorbed by BP.

As described in the previous section, the rate constant of a T–T energy transfer, k_t, is almost independent of the chain length, and the efficiency of a triplet energy transfer from BP to the terminal DBA group is close to unity. Therefore, the values, ϕ_d^{intra} and ϕ_d^{inter}, are nearly equal to the quantum yields defined by the ratio of the number of the product molecules to the number of initial molecules in the excited triplet state.

The effect of the chain-length dependence of the intramolecular ring-closure reaction was examined. Figure 7 shows a plot of the quantum yield for intramolecular ring-closure reaction against the chain length, l ($l=3n+5$) for the poly(oxyethylene) system, together with the values obtained for the polymethylene system. The quantum yield increases sharply for a chain length $l=20$ and the maximum quantum yield of the intramolecular ring-closure reaction appears at $l=26$ (DE-7). The chain length that gives the

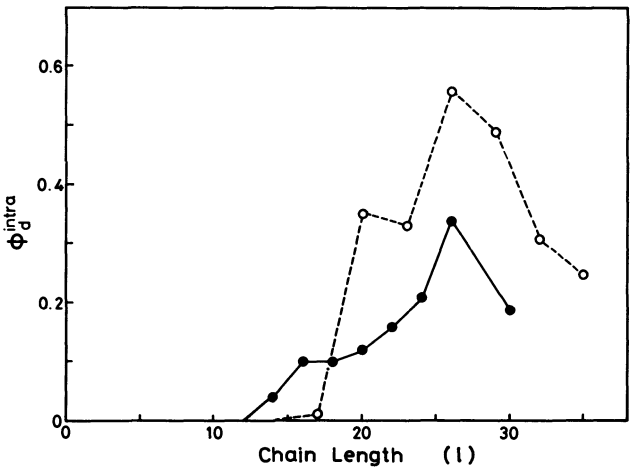

Fig. 7. Chain length dependence of the quantum yield of intramolecular ring-closure reaction, ϕ_d^{intra}, for bichromophoric compounds, poly(oxyethylene) system (○), and polymethylene system (●), in dichloromethane at 25°C.

maximum quantum yield of the intramolecular ring-closure reaction is different from that of the intramolecular end-to-end interaction: in other words, the chain length for the maximum quantum yield of intramolecular ring-closure reaction shifts to chains longer than that for the maximum intramolecular deactivation rate constant. The NMR examination shows that a pair of terminal DBA groups of intramolecular ring-closure products forms an anti-cyclobutane ring. This suggests that a pair of terminal DBA groups take the most favorable orientation for the anti-cyclobutane formation at the chain length $l=26$, i.e., the ring-closure probability for a pair of terminal bonds to be put in an opposite direction becomes maximum at $l=26$. The chain length which gives the maximum quantum yield ϕ_d^{intra} for the poly(oxyethylene) system is in fair agreement with that for the polymethylene system.

Figure 8 shows a plot of the quantum yield of the intermolecular dimerization against the chain length. In this figure, the ϕ_d^{inter} values show a marked dependence on the chain length. This is in contrast to the independence of the k^{inter} value on the chain length in the previous section (Fig. 5). This chain-length dependence of the ϕ_d^{inter} value is probably due to the influence of the triplet lifetime of the terminal DBA group. The lifetime is mainly determined by the k^{intra} value. Compounds $l \geqq 14$ have large k^{intra} values compared with compounds $l \leqq 11$. This therefore reduces the intermolecular reaction rate for the longer-chain compounds. That is, because of the short lifetime for $l \geqq 14$, these compounds have little chance to react with other DBA groups intermolecularly. Hence, ϕ_d^{inter} values are low in this region of chain length. In addition, the ϕ_d^{inter} values in the poly(oxyethylene) system are nearly the same as those of the previous polymethylene system in the range of

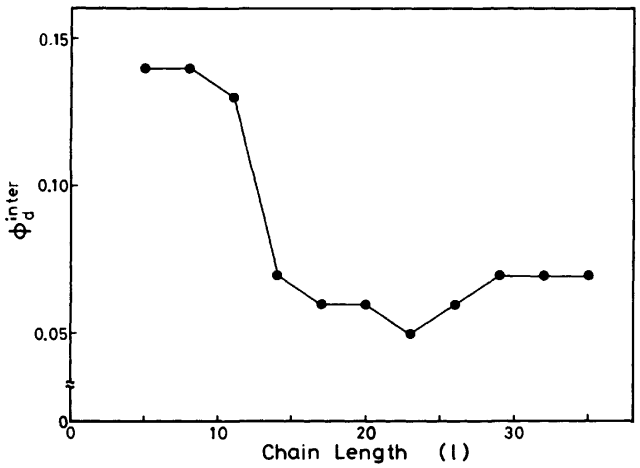

Fig. 8. Chain length dependence of the quantum yield of intermolecular dimerization, ϕ_d^{inter}, for bichromophoric poly(oxyethylene) compounds in dichloromethane at 25°C.

the short chain length ($\phi_d^{inter} \simeq 0.14$). This trend implies that intermolecular dimerization is not affected by the nature of a molecular chain: it is controlled by the lifetime of the terminal reactants.

In the present work, the chain length which gives the highest ring-closure probability of a poly(oxyethylene) chain was found to be l=20 (n=5) by laser photolysis. On the other hand, the maximum quantum yield for the ring-closure reaction appears at a longer chain length, l=26 (n=7): that is, a longer chain length is needed for the intramolecular ring-closure reaction. In this case, the terminal bonds must point to opposite directions to take anti-configuration, that is, the chain length which yields the maximum quantum yield for the ring-closure reaction shifts to a longer chain length. In the present system, the steric factor of a pair of terminal groups must be considered in an examination of the intramolecular reaction probability. It is concluded that the reaction yield of the intramolecular ring-closure reaction is determined by the equilibrium ring-closure probability of a molecular chain with a certain direction of terminal bonds. Furthermore, the ϕ_d^{intra} values for the poly(oxyethylene) system are larger than those for the polymethylene system. This means that the effective concentration of a terminal group of poly(oxyethylene) in the vicinity of the other terminal group is higher than that in a polymethylene system, i.e., the ring-closure probability of a poly(oxyethylene) chain in equilibrium is higher than that of a polymethylene chain. The flexibility of a molecular chain is said to be one of the most important factors in determining intrachain reactivity.

This work was supported by a Grant-in-Aid for Special Project Research, No. 61123006, from the Ministry of Education, Science and Culture.

References

1) K. Ashikaga, S. Ito, M. Yamamoto, and Y. Nishijima, *J. Am. Chem. Soc.*, **110**, 198 (1988).
2) K. Ashikaga, S. Ito, M. Yamamoto, and Y. Nishijima, *Polym. J.*, **19**, 727 (1987).
3) T. Taga, N. Yamamoto, K. Ashikaga, and Y. Nishijima, *Acta Crystallogr., Sect. C*, **42**, 840 (1986).
4) K. Ashikaga, S. Ito, M. Yamamoto, and Y. Nishijima, *J. Photochem.*, **38**, 321 (1987).
5) J. Put and F. C. De Schryver, *J. Am. Chem. Soc.*, **95**, 137 (1973); F. C. De Schryver, J. Put, L. Leenders, and H. Loos, *ibid.*, **96**, 6994 (1974); N. Boens, M. De Brackeleire, J. Huybrehts, and F. C. De Schryver, *Z. Phys. Chem., N. F.*, **101**, S417 (1976); F. C. De Schryver, K. Demeyer, and S. Toppet, *Macromolecules*, **16**, 89 (1983).
6) A. Castellan, J. M. Lacoste, and H. Bouas-Laurent, *J. Chem. Soc., Perkin Trans. 2*, **1974**, 411; H. Bouas-Laurent, A. Castellan, and J. P. Desvergene, *Pure Appl. Chem.*, **52**, 2663 (1980).
7) N. J. Leonard, K. Golankiewicz, R. S. McCredie, S. M. Johnson, and I. C. Paul, *J. Am. Chem. Soc.*, **91**, 5855 (1969).
8) C. Galli, G. Illuminati, and L. Mandolini, *J. Am. Chem. Soc.*, **95**, 8374 (1973); G. Illuminati, L. Mandolini, and B. Maci, *ibid*, **99**, 6308 (1977).
9) M. A. Winnik, S. N. Basu, C. K. Lee, and D. S. Sanders, *J. Am. Chem. Soc.*, **98**, 2928 (1974); P. Srirskaya, J. Danhelka, A. E. C. Redpath, and M. A. Winnik, *Polymer*, **24**, 319 (1983).
10) Y. Imanishi, *Macromol. Rev.*, **14**, 1 (1979).
11) K. Horie, W. Schnabel, I. Mita, and H. Ushiki, *Macromolecules* **14**, 1422 (1981).
12) M. Yamamoto, K. Goshiki, T. Kanaya, and Y. Nishijima, *Chem. Phys. Lett.*, **56**, 333 (1978); T. Kanaya, K. Goshiki, M. Yamamoto, and Y. Nishijima, *J. Am. Chem. Soc.*, **104**, 3580 (1982).
13) Y. Hatano, M. Yamamoto, and Y. Nishijima, *J. Phys. Chem.*, **82**, 367 (1978).
14) K. Shimada and M. Szwarc, *J. Am. Chem. Soc.*, **97**, 3313 (1975).
15) K. Zachariasse and W. Kühnle, *Z. Phys. Chem., N. F.*, **101**, 267 (1976).
16) M. Sisido, T. Mitamura, Y. Imanishi, and T. Higashimura, *Macromolecules*, **9**, 316 (1976).
17) M. Sisido, E. Yoshikawa, Y. Imanishi, and T. Higashimura, *Bull. Chem. Soc. Jpn.*, **51**, 1464 (1978).
18) L. J. Kricka, C. Lambert, and A. Ledwith, *J. Chem. Soc., Perkin Trans. 2*, **1974**, 52.
19) C. P. Pedersen, *J. Am. Chem. Soc.*, **89**, 7017 (1967); C. P. Pedersen, *ibid.*, **92**, 386 (1970).
20) A. Tsuchida, M. Yamamoto, and Y. Nishijima, *J. Phys. Chem.*, **88**, 5062 (1984).
21) C. G. Hatchard and C. A. Parker, *Proc. R. Soc, London, Ser. A*, **235**, 518 (1956).
22) K. Horie and I. Mita, *Polym. J.*, **9**, 201 (1977).
23) M. Sisido, Y. Imanishi, and T. Higashimura, *Bull. Chem. Soc. Jpn.*, **51**, 1469 (1978).
24) M. Fujii, K. Nagasaka, J. Shimada, and H. Yamakawa, *Macromolecules*, **16**, 1613 (1983).
25) H. Yamakawa, T. Yoshizaki, and M. Fujii, *J. Chem. Phys.*, **84**, 4693 (1986).
26) A. Okamoto, K. Toyoshima, and I. Mita, *Eur. Polym. J.*, **19**, 341 (1983).

Syntheses and Properties of Dipyridylnorbornadienes

Yoshiro YAMASHITA,* Takaaki HANAOKA, Yasuyuki TAKEDA, Toshio MUKAI, and Tsutomu MIYASHI
Department of Chemistry, Faculty of Science, Tohoku University, Aramaki, Sendai 980
(Received January 9, 1988)

2,3-Dipyridylnorbornadienes were prepared using the Diels–Alder reaction of the HBF_4 salts of dipyridylacetylenes with cyclopentadiene. Their absorptions extend to 380 nm and are red-shifted in an acidic media. They underwent photocyclization to give quadricyclanes which reverted to norbornadienes upon heating or encountering a Co(II)–TPP catalyst. 2,3-Bis(1-methylpyridinio)norbornadienes were also prepared by a Diels–Alder reaction of bis(1-methylpyridinio)acetylenes with cyclopentadiene. Irradiation of 1-methyl-2-pyridinio and 1-methyl-3-pyridinio derivatives led to the photostationary state between them and the corresponding quadricyclanes, while a 1-methyl-4-pyridinio derivative gave a water or methanol adduct in the presence of water or methanol. Electron-transfer reactions of bis(1-methylpyridinio)norbornadienes were investigated by cyclic voltammetry. The radical cations formed by their reduction were unstable compared with those of the corresponding *trans*-bis(1-methylpyridinio)ethylenes. Steric factors were shown to strongly affect the reactivities.

Valence isomerization between norbornadienes and quadricyclanes has attracted considerable attention from the viewpoint of the reaction mechanism[1] as well as solar energy storage.[2] Since norbornadiene, itself, does not have absorptions above 300 nm, many derivatives have been prepared to extend the absorptions to longer wavelengths.[2] 2,3-Dicyano-1,5,6-trimethyl derivative **1** is a typical compound which shows absorption extending to 400 nm, due to an intramolecular charge-transfer interaction between the dicyanoethylene and dimethylethylene parts.[2c] The mechanism for the photochemical cyclization to give the corresponding quadricyclane was investigated in detail and the high quantum yield could be attributed to the excited state having a charge-transfer property.[3] In this connection, 2,3-dipyridyl derivatives **2** are of interest since they can be easily led to the quaternary salts **3** in which the intramolecular interaction resulting in the shifts of absorptions to longer wavelengths is possible. The photochemistry of **2** and **3**, which contain a cis-fixed dipyridylethylene moiety, is intriguing for comparisons with that of dipyridylethylenes in which a cis–trans isomerization occurs.[4] The redox reactions of bis(1-methylpyridinio) derivatives **3** are also interesting since they have a Weitz-type redox system,[5] which is regarded as a viologen analogue. The particularly interesting point is that the bis(1-methylpyridinio)ethylene part is cis-fixed and cannot undergo cis–trans isomerization. The C_5–C_6 double bond may affect the redox reactions. From these viewpoints, we have prepared dipyridylnorbornadienes and investigated their properties.[6]

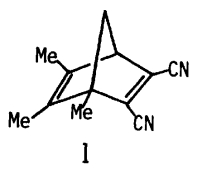

1

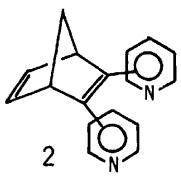

2

a; 4-pyridyl
b; 3-pyridyl
c; 2-pyridyl

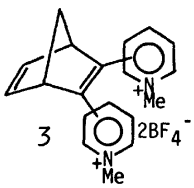

3

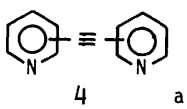

4

a; 4-pyridyl
b; 3-pyridyl
c; 2-pyridyl

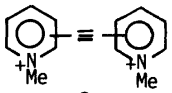

6

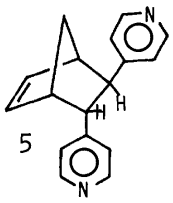

5

Results and Discussion

Preparation of Dipyridylnorbornadienes. 2,3-Dipyridylnorbornadienes (**2**) were considered to be prepared by a Diels–Alder reaction of dipyridylacetylenes with cyclopentadiene. However, dipyridylacetylenes are weak dienophiles and the reported examples only involve reactions of the 2-pyridyl derivative with tetraphenylcyclopentadienone[7] and coumarin,[8] which require severe conditions. In fact, dipyridylacetylenes

4a—**c**[9] did not undergo a Diels–Alder reaction with cyclopentadiene at all. Therefore, we tried the reaction of the HBF_4 salts of **4a**—**c**, which are considered to be stronger dienophiles due to the more electron-withdrawing property of the pyridinium substituents lowering the LUMO level of the acetylene moiety. The reaction of the HBF_4 salts of **4a**—**c** with cyclopentadiene followed by a treatment with an aqueous sodium hydrogencarbonate solution gave 2,3-dipyridylnorbornadienes **2a**—**c**. The reactivity of the conjugated acid of **4** as a dienophile for the Diels–Alder reaction was dependent on the position of the nitrogen atom in the pyridyl substituents, as can be seen in the reaction conditions listed in Table 1. 2-Pyridyl derivative is the most reactive, while a reaction of the 3-pyridyl derivative requires severe conditions and the yield is poor. The poor reactivity of 3-pyridyl derivative can be explained by considering that the positive charge on the nitrogen atom cannot be delocalized to the acetylenic bond at the meta position. Similarly, the reactivity of *trans*-dipyridylethylene as a dienophile in the Diels–Alder reaction could be enhanced by protonation. Thus, *trans*-di-4-pyridylethylene was recovered upon heating with cyclopentadiene under toluene reflux for 24 h; however, the HBF_4 salt gave *trans*-5,6-di-4-pyridylnorbornene (**5**) in 90% yield upon heating with cyclopentadiene under acetonitrile reflux for 24 h followed by neutralization.

Bis(1-methylpyridinio)acetylenes (**6**) were prepared by the reaction of **4** with trimethyloxonium tetrafluoroborate in good yields. The reaction of **6** with cyclopentadiene under the conditions shown in Table 1 gave 2,3-bis(1-methylpyridinio)norbornadienes (**3**).

Properties of Dipyridylnorbornadienes. The electronic spectra of dipyridylnorbornadienes **2a**—**c** are shown in Fig. 1. All of the norbornadienes **2a**—**c** have end-absorptions around 380 nm, indicating that the introduction of the pyridyl groups shifts the absorption maxima to longer wavelengths. The absorptions are red-shifted in the acidic medium relative to those in a neutral solvent. The 4-pyridyl derivative **2a** has an absorption maximum at 360 nm in an acidic medium. The spectrum of the 2-pyridyl derivative is pH dependent (as shown in Fig. 1), but those of **2a** and **2b** are not. The pH dependence may be attributed to the fact that the conjugated acid has two separate pK_a values, which were determined to be 1.1 and 7.2 by an absorptiometric method. This behavior can be explained by considering that the two pyridyl groups interpose a proton, as shown in the structure **7**,[10] since the absorption of the monoprotonated species is red-shifted compared with that of the di-protonated species; such separate pK_a values are observed in chelate reagents such as 2,2′-bipyridyl and 1,10-phenanthroline. The spectra of 1-methylpyridinium derivatives **3a**,**b**, shown in Fig. 2, are similar to those of the corresponding protonated species. The red shifts caused by quaternarization indicate the presence of a charge-transfer interaction between two olefinic parts. This is also supported by the fact that the absorption of **3a** is red-shifted compared with the corresponding norbornene **8**. On

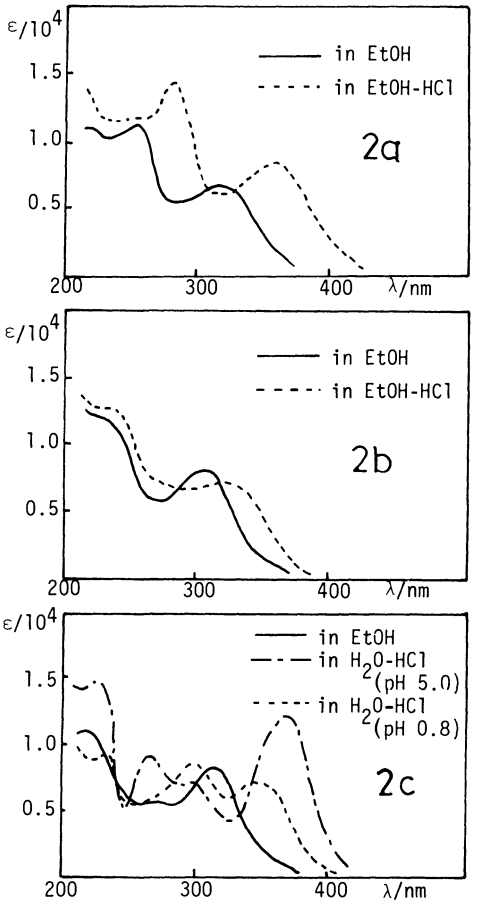

Fig. 1. Electronic spectra of 2,3-dipyridylnorbornadienes (**2**).

Table 1. Diels–Alder Reactions of Dipyridylacetylenes with Cyclopentadiene

Compound	Condition	Product	Yield[a]/%
4a-$(HBF_4)_2$	MeCN reflux 8 h	**2a**	85[b]
4b-$(HBF_4)_2$	MeCN 150 °C 2 d	**2b**	15[b]
4c-$(HBF_4)_2$	MeCN 50 °C 30 min	**2c**	60[b]
6a	MeCN reflux 12 h	**3a**	80
6b	MeCN reflux 2 d	**3b**	30
6c	MeCN 50 °C 10 h	**3c**	80

a) Isolated yield. b) Obtained after treatment with aq $NaHCO_3$.

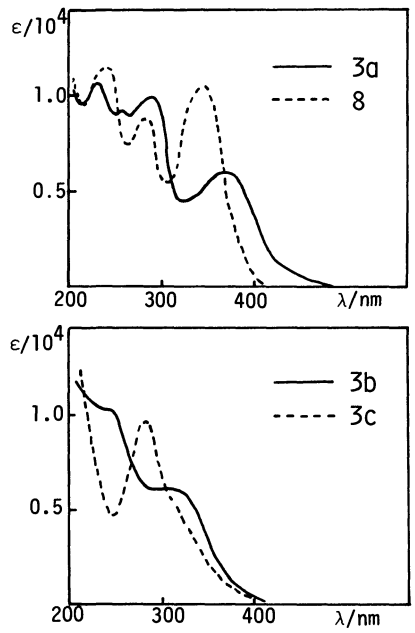

Fig. 2. Electronic spectra of 2,3-bis(1-methylpyridinio)norbornadienes (**3**) and norbornene (**8**).

the other hand, the absorption maximum of **3c** is rather blue-shifted compared with that of the neutral species **2c**. This fact may be attributed to the twisting structure of the 1-methylpyridinium derivative, resulting in a loss of the conjugation of the pyridinium groups with the double bond.

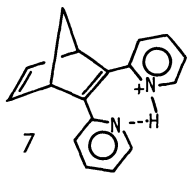

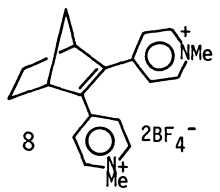

Pyridine derivatives, such as 2,2′-bipyridyl, are well-known to be good ligands for metal ions and to form complexes. In the presence of CuCl or $FeSO_4$, red shifts of the absorptions of 4- and 2-pyridyl derivatives **2a** and **2c** were observed, indicating that coordination occurs. On the other hand, the spectrum of 3-pyridyl derivative **2b** was not changed by the addition of CuCl or $FeSO_4$. The reason for no coordination in **2b** is still ambiguous.

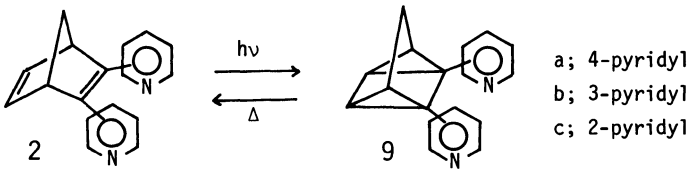

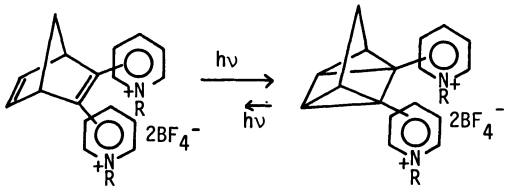

3b; 3-pyridinio, R=Me
3c; 2-pyridinio, R=Me
11b; 3-pyridinio, R=H
10b; 3-pyridinio, R=Me
10c; 2-pyridinio, R=Me
12b; 3-pyridinio, R=H

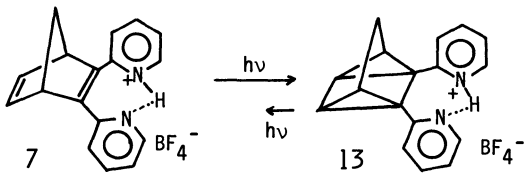

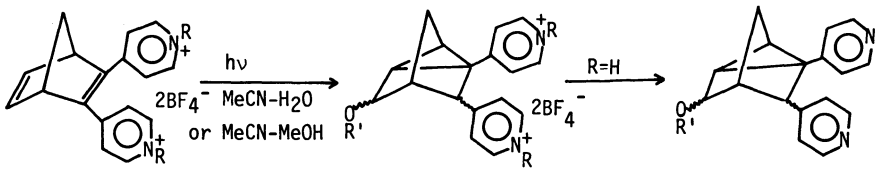

3a; R=Me
11a; R=H

14a; R=Me, R'=H
14b; R=R'=Me
14c; R=R'=H
14d; R=H, R'=Me

15a; R'=H
15b; R'=Me

Valence Isomerization Reaction. Irradiation of an acetonitrile solution of **2a—c** with Rayonet RUL-3000 Å lamps gave quadricyclanes **9a—c** quantitatively. The quantum yields in acetonitrile were very high and insensitive to the substituents (**2a**; ϕ 0.72, **2b**; ϕ 0.78, **2c**; ϕ 0.79). The yields in cyclohexane were nearly equal (**2a**; ϕ 0.72, **2b**; ϕ 0.71). The photoreaction was affected neither by triplet quenchers, such as 2,5-dimethyl-2,4-hexadiene, 1,3-cyclohexadiene, and oxygen, nor by biacetyl which sensitizes the cis-trans isomerization of dipyridylethylenes. This fact suggests that the reaction proceeds via a singlet state. This is consistent with the fact that the intersystem crossing in dipyridylethylenes is inefficient.[11] The photoisomerization of **2a** also proceeded in a solid state quantitatively when a KBr pellet of **2a** was irradiated with a 300-W xenon lamp.

Irradiation of the dimethyl derivatives **3b, c** with Rayonet RUL- 3500 Å lamps led to a photostationary state between **3b, c** and quadricyclanes **10b, c** (**3b**:**10b**=1:4, **3c**:**10c**=2:5). This can be explained by the fact that the resulting quadricyclanes **10b, c** have end-absorptions around 350 nm and undergo cycloreversion under the irradiation conditions. A similar photostationary state was observed upon irradiating a diprotonated derivative **11b** with RUL-3500 Å lamps (**11b**: quadricyclane **12b**=3:7). The irradiation of a monoprotonated derivative **7** with RUL-3000 Å lamps led to a photostationary state between **7** and quadricyclane **13** (**7**:**13**=1:4). However, irradiation with RUL-3500 Å lamps gave **13** quantitatively. This wavelength dependence is explicable by the fact that quadricyclane **13** has no absorption around 350 nm and is stable under the irradiation conditions with 3500 Å lamps. In contrast, irradiation of 4-pyridyl derivative **3a** with RUL-3500 Å lamps in acetonitrile gave a complex mixture of products. Irradiation in the presence of a small amount of water or methanol led to the formation of a water adduct **14a** or a methanol adduct **14b**, respectively.[12] In the case of diprotonated derivative **11a**, **15a** or **15b** was isolated after neutralization.[12] A treatment of quadricyclane **9a** with HBF_4 in acetonitrile containing methanol followed by neutralization gave **15b**. This result suggests that adducts **14** are formed by a nucleophilic attack of water or methanol on the initially formed quadricyclanes.

Quadricyclanes **9a—c** underwent a cycloreversion reaction to give norbornadienes **2a—c** upon heating. The activation parameters were calculated (Table 2) from the first-order rate constants determined by a UV spectroscopic method in ethanol. Those values indicate that the introduction of the two pyridyl groups significantly lowers the activation energy compared with that of dicyano[13] and bis(methoxycarbonyl) substituents.[14] The position of nitrogen of pyridyl substituents has little effect on the reactivities. The salts **10b, c, 12b**, and **13** also underwent a cycloreversion reaction upon heating at 60 °C in acetonitrile.

Transition metals are well-known to catalyze the cycloreversion reaction of quadricyclanes to norbornadienes.[15] However, $Mo(CO)_6$, $Fe_2(CO)_9$, Rh/C, $RhCl(PPh_3)_3$, $Pd(PPh_3)_2Cl_2$, and Fe-TPP (tetraphenylporphyrin) were ineffective for the cycloreversion of quadricyclanes **9a—c** to norbornadienes **2a—c**. Only Co(II)-TPP catalyzed the reaction. The activity of Co(II)-TPP may be attributed to a radicophilic attack of the metal to the electronegative substituted quadricyclanes, as reported by Yoshida et al.[16] On the other hand, Co(II)-TPP did not catalyze the cycloreversion of dications **10b, c** and **12b** although it catalyzed that of monocation **13**. This fact may be caused by a Coulomb repulsion which makes it difficult for the catalyst to approach the dications.

Electron-Transfer Reactions of 2,3-Bis(1-methylpyridinio)norbornadienes (3). Norbornadienes **3** possess a Weitz-type redox system,[5] as shown in Scheme 1. The electron-transfer reactions of **3**, which have a cis-fixed bis(1-methylpyridinio)ethylene skeleton, are of particular interest since bis(1-methylpyridinio)ethylenes usually undergo cis-trans isomerization upon reduction.[17] The reduction potentials of **3a—c** and norbornene **8** measured by cyclic voltammetry (c.v.) are summarized in Table 3. The waves for **3a, 3c**, and **8** are reversible or quasi-reversible for the following reasons. The current ratios, i_{pa}/i_{pc}, were near unity. They and the half-wave reduction potentials, $E^{red}_{1/2}$, were independent on the scan rates, v. The cathodic peak current, i_{pc}, was proportional to $v^{1/2}$. In contrast, the wave for **3b** was irreversible. Since the i_{pc} was proportional to $v^{1/2}$, the irreversible property can be attributed to the lability of a product formed by the reduction on the c.v. time scale. This seems to be

Table 2. Activation Parameters for Cycloreversion of Quadricyclanes

R	E_a/kJ mol^{-1}	log A	ΔS/J K^{-1}[a]
4-pyridyl (**9a**)	115.1	13.0	−5.3
3-pyridyl (**9b**)	113.0	12.7	−11.0
2-pyridyl (**9c**)	116.3	13.2	−1.4
H[b]	160.2	15.0	—
CO_2Me[b]	146.0	14.3	—
CN[c]	141.4	7.5	—

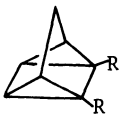

a) At 60 °C. b) In toluene.[14] c) In acetonitrile.[13]

Table 3. Data for the Cyclic Voltammetry[a]

Compound	Solvent	$E^{red}_{1/2}$/V vs. SCE	$E_{p/2}$/V	(E_1-E_2/V[b])	log K_{sem}[c]
3a	DMF	−0.59	0.061	0.04	0.68
	MeCN	−0.67	0.079	0.08	1.4
	CH_2Cl_2	−0.43, −0.52	—	0.095[d]	1.6
3b	DMF	−1.05[e]	—	—	—
	MeCN	−1.12[e]	—	—	—
	CH_2Cl_2	−0.90[e]	—	—	—
3c	DMF	−0.70	0.050	0.02	0.34
	MeCN	−0.78	0.040	0	0
	CH_2Cl_2	−0.57	0.040	0	0
8	MeCN	−0.74	0.085	0.085	1.4
	CH_2Cl_2	−0.50, −0.60	—	0.10[d]	1.7

a) 0.1 mol dm^{-3} Et_4NClO_4 in MeCN or DMF, or 0.1 mol dm^{-3} Bu_4NBF_4 in CH_2Cl_2, Pt electrode, scan rate 100 mV s^{-1}. b) Analyzed by Myers and Shain's method.[19] c) log $K_{sem}=(E_1-E_2)/0.059$. d) Observed value. e) Irreversible.

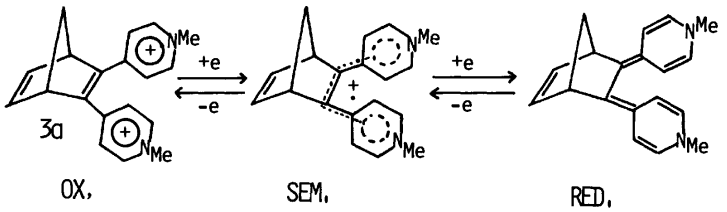

Scheme 1.

related to the nature of the meta-derivative in which the cation or radical cannot conjugate with the double bond.

Since norbornadiene **3a** has the same electron-accepting part as norbornene **8**, the differences in the behavior of the electron-transfer reactions are considered to reflect the difference in the structures. Both of their c.v. revealed only one wave in *N,N*-dimethylformamide (DMF) and acetonitrile. However, the peak widths, $\Delta E_{p/2}$, are different from that for the usual one-electron transfer (56.5 mV), suggesting that a one-electron transfer occurs closely in two stages. In fact, the separated potentials were observed in dichloromethane. The cation radical species are more stabilized in dichloromethane than in acetonitrile.[18] The differences between the first and second reduction potentials (E_1-E_2) were calculated according to the Myers and Shain's method,[19] as shown in Table 3. The semiquinone formation constants, K_{sem}, calculated as log $K_{sem}=(E_1-E_2)/0.058$ are also shown in Table 3. Those values are much smaller than that of *trans*-bis(1-methylpyridinio)ethylenes whose pyridinio groups are coplanar.[20] The first reduction potential of **3a** is a little higher than that of **8**. This may be caused by the interaction between the two olefinic parts, which lowers the LUMO level of the bis(1-methylpyridinio)ethylene moiety.

On the other hand, the c.v. of 2-pyridinio derivative **3c** revealed one peak with small values of $\Delta E_{p/2}$ even in dichloromethane. The (E_1-E_2) values determined by Myers and Shain's method are zero or nearly zero as shown in Table 3. This fact shows that a one-electron transfer occurs very closely in two stages or a two-electron transfer occurs in one stage. The reason for this may be attributed to a steric effect for the 1-methyl groups, decreasing the conjugation between the 2-pyridinio groups and the double bond.

The radical cations of **3a** and **8**, generated electrochemically in degassed acetonitrile containing 0.1 mol dm^{-3} of tetraethylammonium perchlorate, were observed in the ESR spectrum. The *g*-values were both 2.0025, which were determined using 2,2-diphenyl-1-picrylhydrazyl as a standard. Interestingly, the lifetime for the radical cation of **3a** ($t_{1/2}$=104 s at 20 °C) was longer than that for the radical cation of **8** ($t_{1/2}$=36 s at 18 °C). The decay of the former obeyed second-order kinetics, indicating disproportionation, while that of the latter was first-order, indicating a reaction with a substance such as the solvent or the electrolyte. This result shows that the nonconjugated double bond decreased the reactivity of the radical cation species.

Experimental

Electronic spectra were obtained on a Hitachi 340 spectrophotometer. IR spectra were taken on a Shimadzu IR-27G spectrometer. Mass data were collected on a Hitachi M-52 mass spectrometer. ^1H and ^{13}C NMR spectra were obtained at 90 MHz on a Varian EM-390 and at 50 MHz on a Varian XL-200 spectrometer, respectively. Redox potentials were measured on a Yanako p-1000 voltammetric analyzer. Dichloromethane and acetonitrile were distilled from calcium hydride. Melting points are uncorrected.

HBF_4 Salts of Dipyridylacetylenes (4). To a solution of

200 mg (1.1 mmol) of di-4-pyridylacetylene (**4a**) in 200 ml of ether, 1 ml of 42% HBF_4 was added with vigorous stirring. The precipitated colorless solid was collected by filtration and dried to give 370 mg (88%) of the HBF_4 salt of **4a**: mp 260—270 °C (decomp). Found: C, 40.64; H, 2.82; N, 8.10%. Calcd for $C_{14}H_{18}N_2BF_4$: C, 40.51; H, 2.83; N, 7.87%. Similarly, the HBF_4 salts of **4b** and **4c** were obtained as colorless solids. **4b**-2HBF_4: mp 240—270 °C (decomp). Found: C, 40.90; H, 2.88; N, 8.42%. Calcd for $C_{14}H_{18}N_2BF_4$: C, 40.51; H, 2.83; N, 7.87%. **4c**-2HBF_4: mp 235—245 °C (decomp). Found: C, 40.00; H, 2.91; N, 8.25%. Calcd for $C_{14}H_{18}N_2BF_4$: C, 40.51; H, 2.83; N, 7.87%.

2,3-Di-4-pyridylbicyclo[2.2.1]hepta-2,5-diene (2a). A solution of 302 mg (0.85 mmol) of the HBF_4 salt of **4a** and 1.1 ml of cyclopentadiene in 30 ml of dry acetonitrile was refluxed for 8 h. After the solvent was removed, 50 ml of water containing a small amount of HBF_4 was added and the mixture was extracted with dichloromethane (3×30 ml). The aqueous layer was neutralized with $NaHCO_3$ and extracted with dichloromethane (4×30 ml). The organic extract was dried over Na_2SO_4 and the solvent was removed to give 178 mg (85%) of **2a**, which was recrystallized from hexane to give **2a** as colorless needles: mp 110—111 °C; IR (KBr) 1620, 1591, 1551, 1529, 1492, 1443, 1408, 1391, 1210, 1068, 1050, 978, 943, 872, 850, 800, 718 cm^{-1}; UV (EtOH) 243 nm (log ε 4.06), 315 (3.83); MS (25 eV) *m/z* (relative intensity) 246 (M^+, 100%), 181 (78%); ^1H NMR ($CDCl_3$, 90 MHz) δ=2.15 (dt, 1H, *J*=6.3, 3.0 Hz), 2.39 (dt, 1H, *J*=6.3, 3.0 Hz), 3.92 (m, 2H), 6.99 (m, 6H), 8.43 (m, 4H); ^{13}C NMR ($CDCl_3$) δ=57.23, 71.45, 121.95, 143.15, 144.75, 150.60, 151.26. Anal. ($C_{17}H_{14}N_2$) C, H, N.

2,3-Di-3-pyridylbicyclo[2.2.1]hepta-2,5-diene (2b). A mixture of 318 mg (0.83 mmol) of the HBF_4 salt of **4b** and 3 ml of cyclopentadiene in 15 ml of argon-purged dry acetonitrile was sealed in a Pyrex tube. Heating at 160 °C for 3 d and similar workup as for **2a** gave a yellow oil, which was separated by thin-layer chromatography on alumina (4:1 dichloromethane–ether) to give 32 mg (16%) of **2b**. Recrystallization from hexane gave **2b** as colorless leaflets: mp 100—101 °C; IR (KBr) 3040, 2980, 2950, 1565, 1483, 1405, 1284, 1012, 722, 680 cm^{-1}; UV (MeCN) 231 nm (log ε 4.08), 252 (3.96), 306 (3.92); MS (25 eV) *m/z* (relative intensity) 246 (M^+, 58), 181 (100), 180 (81); ^1H NMR ($CDCl_3$) δ=2.13 (dm, 1H, *J*=6.0 Hz), 2.42 (dm, 1H, *J*=6.0 Hz), 3.90 (m, 2H), 6.95 (m, 2H), 7.30 (dd, 2H, *J*=7,5, 4.5 Hz), 7.85 (dm, 2H, *J*=7.5 Hz), 8.2—8.6 (m, 4H). Anal. ($C_{17}H_{14}N_2$) C, H, N.

2,3-Di-2-pyridylbicyclo[2.2.1]hepta-2,5-diene (2c). A solution of 596 mg (1.56 mmol) of the HBF_4 salt of **4c** and 1 ml of cyclopentadiene in 80 ml of dry acetonitrile was heated under nitrogen at 50 °C for 30 min. A similar workup as that for **2a** gave 224 mg (54%) of **2c**, which was recrystallized from hexane to give colorless needles: mp 72—73 °C; IR (KBr) 1582, 1576, 1452, 1428, 1419, 1282, 1269, 771, 761, 730, 713, 676, 668 cm^{-1}; UV (EtOH) 223 nm (log ε 4.06), 316 (3.93); MS (25 eV) *m/z* (relative intensity) 245 (M^+, 100), 181 (34), 168 (73); ^1H NMR ($CDCl_3$) δ=2.10 (dt, 1H, *J*=6.2, 3.0 Hz), 2.42 (dt, 1H, *J*=6.2, 3.0 Hz), 4.20 (m, 2H), 7.18 (m, 8H), 8.55 (m, 2H). Anal. ($C_{17}H_{14}N_2$) C, H, N.

***trans*-5,6-Di-4-pyridylbicyclo[2.2.1]hept-2-ene (5).** A solution of 150 mg (0.42 mmol) of the HBF_4 salt of *trans*-1,2-di-4-pyridylethylene and 2 ml of cyclopentadiene in 100 ml of dry acetonitrile was heated under reflux for 24 h. A similar workup as that for **2a** gave 94 mg (90%) of **5** as colorless needles: mp 92—94 °C (from hexane); IR (KBr) 3000, 1600, 1553, 1412, 1335, 985, 845, 830, 795, 770, 725, 640, 590 cm^{-1}; MS (25 eV) *m/z* (relative intensity) 248 (M^+, 14), 183 (100), 180 (50).

Bis(1-methylpyridinio)acetylenes (6a—c). A mixture of 2.1 g (14 mmol) of trimethyloxonium tetrafluoroborate and 500 mg of di-4-pyridylacetylene (**4a**) in 18 ml of nitromethane was stirred under nitrogen at r.t. for 2 d. After 2 ml of methanol was added, the mixture was stirred for an additional 2 h and poured into 300 ml of ether with vigorous stirring to give 1.06 g (100%) of **6a**. Recrystallization from acetonitrile–dichloromethane–ether gave **6a** as colorless needles: mp 270—280 °C (decomp). Anal. ($C_{14}H_{14}N_2B_2F_8$) C, H, N. In a similar manner, 3-pyridyl derivative **6b** and 2-pyridyl derivative **6c** were prepared. **6b**: mp 255—265 °C (decomp). Anal. ($C_{14}H_{14}N_2B_2F_8$) C, H, N. **6c**: mp 260—268 °C (decomp). Anal. ($C_{14}H_{14}N_2B_2F_8$) C, H, N.

2,3-Bis(1-methyl-4-pyridinio)bicyclo[2.2.1]hepta-2,5-diene Bis(tetrafluoroborate) (3a). A solution of 165 mg (0.42 mmol) of acetylene **6a** and 1.5 ml of cyclopentadiene in 20 ml of dry acetonitrile was heated during reflux under nitrogen for 12 h. The cooled mixture was poured into 200 ml of ether to give 152 mg (90%) of **3a**: mp 220—225 °C (decomp) (from acetonitrile–ether); IR (KBr) 3050, 1640, 1560, 1520, 1470, 1285, 1050, 840, 730, 530, 515 cm^{-1}; UV (MeCN) 223 nm (log ε 4.03), 255 (3.98), 286 (4.00), 364 (3.80); ^1H NMR (CD_3CN) δ=2.23 (dm, 1H, *J*=7.5 Hz), 2.57 (dm, 1H, *J*=7.5 Hz), 4.20 (m, 2H), 4.35 (s, 6H), 7.08 (t, 2H, *J*=1.5 Hz), 7.68 (d, 4H, *J*=6.0 Hz), 8.45 (d, 4H, *J*=6.0 Hz). ^{13}C NMR (CD_3CN) δ=46.68, 58.58, 72.66, 126.48, 143.68, 146.41, 152.27, 156.32. Anal. ($C_{19}H_{20}N_2B_2F_8$) C, H, N.

2,3-Bis(1-methyl-3-pyridinio)bicyclo[2.2.1]hepta-2,5-diene Bis(tetrafluoroborate) (3b). A solution of 184 mg (0.48 mmol) of acetylene **6b** and 2 ml of cyclopentadiene in 20 ml of dry acetonitrile was heated during reflux under nitrogen for 2 d. A similar work-up as that for **3a** gave 32 mg of **3b**: mp 180—185 °C (decomp) (from acetonitrile–ether); IR (KBr) 3300, 1630, 1552, 1468, 1280, 1250, 1050, 795, 670, 515 cm^{-1}; UV (MeCN) 245 nm (log ε 4.03), 280 sh (3.84), 314 (3.79); ^1H NMR (CD_3CN) δ=2.20 (dm, 1H, *J*=6.0 Hz), 2.55 (dm, 1H, *J*=6.0 Hz), 4.05 (tm, 2H, *J*=1.5 Hz), 4.25 (s, 6H), 7.10 (tm, 2H, *J*=1.5 Hz), 7.85 (dm, 2H, *J*=7.5 Hz), 8.20 (dm, 2H, *J*=7.5 Hz), 8.45—8.60 (m, 4H). Anal. ($C_{19}H_{20}N_2B_2F_8$) C, H, N.

2,3-Bis(1-methyl-2-pyridinio)bicyclo[2.2.1]hepta-2,5-diene Bis(tetrafluoroborate) (3c). A solution of 130 mg (0.36 mmol) of acetylene **6c** and 2 ml of cyclopentadiene in 15 ml of dry acetonitrile was heated under nitrogen at 50 °C for 10 h. A similar workup as that for **3a** gave 119 mg (74%) of **3c**: mp 235—255 °C (decomp) (acetonitrile–ether); IR (KBr) 3100, 1625, 1580, 1510, 1455, 1265, 1050, 778, 762, 735, 720, 512 cm^{-1}; UV (MeCN) 284 nm (log ε 3.99), 328 (3.64); ^1H NMR (CD_3CN) δ=2.35 (dm, 1H, *J*=7.0 Hz), 2.80 (dm, 1H, *J*=7.0 Hz), 4.10 (s, 6H), 4.30 (tm, 2H, *J*=1.5 Hz), 7.10 (t, 2H, *J*=1.5 Hz), 7.52 (dm, 2H, *J*=8.0 Hz), 7.85 (ddm, 2H, *J*=8.0, 6.0 Hz), 8.25 (tm, 2H, *J*=8.0 Hz), 8.65 (dm, 2H, *J*=6.0 Hz). Anal. ($C_{19}H_{20}N_2B_2F_8$) C, H, N.

2,3-Di-4-pyridylbicyclo[2.2.1]hept-2-ene. In a hydrogenation apparatus, 202 mg (0.82 mmol) of norbornadiene **2a** was hydrogenated in 22 ml of ethyl acetate with 5 ml of 5% Pd-C. Removal of the catalyst and solvent followed by recrystallization from hexane gave 115 mg (57%) of a norbornene derivative as colorless needles: mp 121—123 °C;

IR (KBr) 3075, 2980, 2870, 1592, 1538, 1414, 1271, 1115, 810, 760, 588, 518 cm^{-1}; UV (MeCN) 227 (log ε 4.06), 239 (3.97), 288 (3.98); MS (25 eV) *m/z* (relative intensity) 248 (M^+, 46%), 220 (100%); ^1H NMR ($CDCl_3$) δ=1.2—1.4 (m, 3H), 1.6—2.1 (m, 5H), 3.30 (brs, 2H), 7.05 (dm, 4H, *J*=6.0 Hz), 8.46 (dm, 4H, *J*=6.0 Hz); ^{13}C NMR ($CDCl_3$) δ=26.40, 47.90, 49.55, 123.14, 144.17, 144.64, 150.89. Anal. ($C_{17}H_{16}N_2$) C, H, N.

2,3-Bis(1-methyl-4-pyridinio)bicyclo[2.2.1]hept-2-ene Bis(tetrafluoroborate) (8). A solution of 76 mg (0.31 mmol) of 2,3-di-4-pyridylnorbornene and 250 mg (1.68 mmol) of trimethyloxonium tetrafluoroborate in 8 ml of nitromethane was stirred at room temperature for 2 d. After 1 ml of methanol was added, the mixture was stirred for 1 h, concentrated to 4 ml, and then poured into 80 ml of ether with vigorous stirring. The resulting crystals were filtered and washed with cold acetone to give 74 mg (53%) of **8** as colorless needles: mp 220—225 °C, IR (KBr) 2950, 1640, 1520, 1470, 1270, 1050, 832, 513 cm^{-1}; UV (MeCN) 238 nm (log ε 4.08), 280 (3.96), 341 (4.04); ^1H NMR (CD_3CN) δ=1.35—1.6 (m, 4H), 1.8—2.2 (m, 2H), 3.50 (m, 2H), 4.26 (s, 6H), 7.70 (d, 4H, *J*=7.5 Hz), 8.47 (d, 4H, *J*=7.5 Hz). ^{13}C NMR (CD_3CN) δ=25.91, 48.58, 48.68, 50.43, 127.28, 146.31, 147.94, 151.99. Anal. ($C_{19}H_{22}N_2B_2F_8$) C, H, N.

1,5-Di-4-pyridyltetracyclo[3.2.0.0^{2,7}.0^{4,6}]heptane (9a). A solution of 102 mg (0.61 mmol) of norbornadiene **2a** in 70 ml of acetonitrile was irradiated through a Pyrex filter with Rayonet RUL-3000 Å lamps under nitrogen bubbling for 1 h. Removal of the solvent followed by recrystallization from pentane gave 86 mg (84%) of **9a** as colorless needles: mp 92.5—93 °C; IR (KBr) 1588, 1531, 1491, 1405, 1200, 1141, 972, 797, 780, 761, 502 cm^{-1}; UV (EtOH) 261 nm (log ε 3.99); MS (25 eV) *m/z* (relative intensity) 246 (M^+, 100), 181 (97), 66 (93); ^1H NMR (CCl_4) δ=2.00 (m, 2H), 2.38 (m, 4H), 6.72 (m, 4H), 8.24 (m, 4H). Anal. ($C_{17}H_{14}N_2$) C, H, N.

In a similar manner, 3-pyridyl derivative **9b** and 2-pyridyl derivative **9c** were obtained in 80—90% yields. **9b**: mp 95—98 °C; IR (KBr) 3050, 1570, 1482, 1420, 1150, 1010, 822, 798, 708, 617 cm^{-1}; UV (MeCN) 246 nm (log ε 3.89), 270 (3.79); MS (25 eV) *m/z* (relative intensity) 246 (M^+, 58), 181 (100), 180 (81); ^1H NMR ($CDCl_3$) 1.95 (dm, 2H, *J*=4.5 Hz), 2.28 (dm, 1H, *J*=12.0 Hz), 2.33 (d, 2H, *J*=4.5 Hz), 2.48 (dm, 1H, *J*=12.0 Hz), 7.07 (ddm, 2H, *J*=7.5, 4.5 Hz), 7.27 (dt, 2H, *J*=7.5 Hz), 8.2—8.5 (m, 4H). Anal. ($C_{17}H_{14}N_2$) C, H, N. **9c**: mp 61—62 °C; IR (KBr) 1582, 1558, 1468, 1428, 819, 769, 751, 738 cm^{-1}; UV (EtOH) 239 nm (log ε 3.92), 273 (3.85); MS (25 eV) *m/z* (relative intensity) 246 (M^+, 93), 181 (44), 168 (100); ^1H NMR ($CDCl_3$) δ=2.20 (m, 3H), 2.50 (m, 3H), 6.93 (m, 4H), 7.35 (m, 2H), 8.37 (m, 2H). Anal. ($C_{17}H_{14}N_2$) C, H, N.

Irradiation of the HBF_4 Salt 7. A solution of 30 mg (0.090 mmol) of **7** in nitrogen-purged acetonitrile was irradiated with Rayonet RUL-3500 Å lamps for 30 min. Removal of the solvent gave quadricyclane **13** as yellow needles quantitatively: mp 245—250 °C (decomp); IR (KBr) 1610, 1590, 1480, 1432, 890, 778, 765, 585, 515 cm^{-1}; ^1H NMR (CD_3CN) δ=2.37 (dm, 1H, *J*=6.0 Hz), 2.58 (d, 2H, *J*=4.0 Hz), 2.60 (dm, 1H, *J*=6.0 Hz), 2.94 (d, 2H, *J*=4.0 Hz), 7.05 (dm, 2H, *J*=9.0 Hz), 7.43 (tm, 2H, *J*=7.5 Hz), 7.97 (ddm, 2H, *J*=9.0, 7.5 Hz), 8.63 (dm, 2H, *J*=6.0 Hz). Anal. ($C_{17}H_{15}N_2BF_4$) C, H, N.

Irradiation of Dimethyl Derivatives 3b, c. A solution of 30 mg (0.067 mmol) of **3b** in 5 ml of argon-purged acetonitrile was irradiated with Rayonet RUL-3500 Å lamps for 1 h. Removal of the solvent gave a mixture of **3b** and quadricyclane **10b** whose ^1H NMR spectrum showed the ratio of **3b** and **10b** to be 1:4. The ratio was not changed by prolonged irradiation. Similarly, irradiation of **3c** with Rayonet RUL-3500 Å lamps gave a mixture of **3c** and **10c** whose ratio was 2:5 from the ^1H NMR spectrum.

Irradiation of Dimethyl Derivative 3a. A solution of 30 mg (0.067 mmol) of **3a** in argon-purged acetonitrile–methanol (3:1) was irradiated through a Pyrex filter with Rayonet 3500 Å lamps for 1 h. Removal of the solvent gave a yellow solid of **14b** whose structure was deduced from the ^1H NMR spectrum: (CD_3CN) δ=1.8—2.3 (m, 5H), 2.7—2.9 (m, 1H), 3.19 (s, 2.2H), 3.34 (s, 0.8H), 3.8—4.0 (m, 1H), 4.14 (s, 3H), 4.27 (s, 3H), 7.46 (d, 2H, *J*=6.0 Hz), 7.71 (d, 2H, *J*=6.0 Hz), 8.33 (d, 2H, *J*=6.0 Hz), 8.49 (d, 2H, *J*=6.0 Hz).

Irradiation of the HBF_4 Salt 11a. A solution of 80 mg (0.19 mmol) of **11a** in 10 ml of nitrogen-purged acetonitrile through a Pyrex filter with Rayonet RUL-3500 Å lamps for 30 min. A mixture obtained after removal of the solvent was dissolved in water, neutralized with $NaHCO_3$, and then extracted with dichloromethane. After the organic extract was dried over Na_2SO_4, removal of the solvent gave **15a** as a pale yellow oil, whose structure was deduced from the ^1H NMR spectrum: ($CDCl_3$) δ=1.5—2.3 (m, 7H), 3.9—4.2 (m, 1H), 6.84 (m, 2H), 7.02 (m, 2H), 8.3—8.5 (m, 4H).

Similarly, irradiation of **11a** in acetonitrile–methanol (3:1) gave **15b** as a yellow oil: ^1H NMR ($CDCl_3$) δ=1.6—1.9 (m, 2H), 2.0—2.5 (m, 3H), 3.19 (s, 2.2H), 3.34 (s, 0.8H), 3.4—4.9 (m, 2H), 6.79 (dm, 2H, *J*=6.0 Hz), 6.99 (dm, 2H, *J*=6.0 Hz), 8.38 (m, 4H).

Quantum Yield Determinations. Samples were irradiated with an Ushio 150-W xenon lamp on a Hitachi MPF-4 spectrometer (λ_{ex}=334±10 nm). The number of photons incident on the samples were determined by using a potassium trioxalatoferrate(III) actinometer. The reactions were followed by the electronic spectra.

Rate Constant Determinations. Solutions of 0.9—1.3×10^{-4} mol dm^{-3} of quadricyclanes **9a**—c in absolute ethanol were heated in a thermostat (RAUDA-WB20D). The rate constants were determined by an absorptiometric method.

The authors thank Dr. Kimio Akiyama and Professor Yusaku Ikegami at Tohoku University for providing the measurements of the ESR spectra.

References

1) N. J. Turro, W. R. Cherry, M. F. Mirbach, and M. J. Mirbach, *J. Am. Chem. Soc.*, **99**, 7388 (1977); H. D. Roth, M. L. M. Schilling, and G. Jones, II, *ibid*, **103**, 1246 (1981).

2) a) T. Toda, E. Hasegawa, T. Mukai, H. Tsuruta, T. Hasegawa, and T. Yoshida, *Chem. Lett.*, **1982**, 1551; b) H. Hirao, A. Ando, T. Hamada, and O. Yonemitsu, *J. Chem. Soc., Chem. Commun.*, **1984**, 300; c) Z. Yoshida, *J. Photochem.*, **29**, 27 (1985); d) K. Maruyama, H. Tamiaki, and T. Yanai, *Bull. Chem. Soc. Jpn.*, **58**, 781 (1985); P. G. Gassman and J. W. Hershberger, *J. Org. Chem.*, **52**, 1337 (1987) and references cited therein.

3) H. Ikezawa, C. Kutal, K. Yasufuku, and H. Yamazaki, *J. Am. Chem. Soc.*, **108**, 1589 (1986).

4) D. G. Whitten and Y. J. Lee, *J. Am. Chem. Soc.*, **94**, 9142 (1972); T. W. Ebbesen, C. M. Previtali, T. Karatsu, T.

Arai, and K. Tokumaru, *Chem. Phys. Lett.*, **119**, 489 (1985).

5) K. Deuchert and S. Hünig, *Angew. Chem., Int. Ed. Engl.*, **17**, 875 (1978).

6) The preparation and photoreactions of the dipyridylnorbornadienes were reported as a communication. Y. Yamashita, T. Hanaoka, Y. Takeda, and T. Mukai, *Chem. Lett.*, **1986**, 1279.

7) G. R. Newkome, N. B. Islam, and J. M. Robinson, *J. Org. Chem.*, **40**, 3514 (1975).

8) G. R. Newkome, N. B. Roper, and J. M. Robinson, *ibid.*, **45**, 4380 (1980).

9) **4a**; M. Tanner and A. Ludi, *Chimia*, **34**, 23 (1980), **4b**; T. Teitel, D. Wells, and W. H. F. Sasse, *Aust. J. Chem.*, **26**, 2129 (1973), **4c**; D. Jerchel and W. Melloh, *Liebigs Ann. Chem.*, **622**, 53 (1959); K. Sonegashira, Y. Tohda, and N. Hagihara, *Tetrahedron Lett.*, **1975**, 4467.

10) The pK_a values of **2a** were between 5.5 and 6.5, but the exact values could not be obtained since the pK_{a1} and pK_{a2} values are too close. The pK_a values of **2b** could not be measured because of the small difference in absorption between the neutral and acidic species.

11) D. G. Whitten and M. T. McCall, *J. Am. Chem. Soc.*, **91**, 5097 (1969).

12) The stereochemistry of **14** and **15** could not be determined.

13) J. R. Edman, *J. Org. Chem.*, **32**, 2920 (1967).

14) D. S. Kabakoff, J-C. G. Bunzli, J. F. M. Oth, W. B. Hammond, and J. A. Berson, *J. Am. Chem. Soc.*, **97**, 1510 (1975).

15) K. C. Bishop, III, *Chem. Rev.*, **76**, 461 (1976); K. Maruyama and H. Tamiaki, *J. Org. Chem.*, **51**, 602 (1986).

16) S. Miki, T. Ohno, H. Iwasaki, and Z. Yoshida, *Tetrahedron Lett.*, **26**, 3487 (1985).

17) J. W. Happ, J. A. Ferguson, and D. G. Whitten, *J. Org. Chem.*, **37**, 1485 (1972).

18) The similar stabilization in dichloromethane has been reported by Bard et al. A. J. Bard and J. Phelps, *J. Electroanal. Chem.*, **25**, App. 2 (1970).

19) R. L. Myers and I. Shain, *Anal. Chem.*, **41**, 980 (1969).

20) S. Hünig and J. Gross, *Tetrahedron Lett.*, **1968**, 2599.

The Preparation of Photoresponsive Cyclobutanocrown Ethers by Means of Intramolecular [2+2]Photocycloaddition

Sadatoshi AKABORI,* Takeshi KUMAGAI, Yoichi HABATA, and Sadao SATO†
Department of Chemistry, Faculty of Science, Toho University, Funabashi, Chiba 274
†Analytical and Metabolic Research Laboratories, Sankyo Co., Ltd., Hiromachi, Shinagawa-ku, Tokyo 140
(Received January 9, 1988)

The reaction of *o*-bis(3-hydroxy-1-oxapropyl)benzene (**7b**) with 3,3′-(trimethylenedi-4,1-phenylene)bis[2-propenoyl chloride] gave 8,9-benzo-4,7,10,13-tetraoxa[16.3]paracyclopha-1,8,15-triene-3,14-dione (**8b**) in a 6.5% yield, together with its dimer in a 12.3% yield. Also, 5,6-benzo-4,7-dioxa[10.3]paracyclopha-1,5,9-triene-3,8-dione (**8a**) and 11,12-benzo-4,7,10,13,16,19-hexaoxa[22.3]paracyclopha-1,11,21-triene-3,20-dione (**8c**) were obtained by the same method in 7.0 and 8.0% yields, together with their respective dimers (**9a**: 6.0%, **9c**: 10.8%). X-Ray analysis of **8b** revealed the two double bonds to be trans and the distances between the two olefinic carbon atoms (C_{17}–C_{35}) and (C_{18}–C_{34}) to be 5.341(11) and 5.906(9) Å respectively. These distances are too long for intramolecular [2+2]photocycloaddition to occur in the crystalline state. However, the irradiation of the solutions of the crown ethers **8a** and **8b** in acetonitrile by Pyrex-filtered UV light (>300 nm) gave two intramolecular [2+2]photocycloadducts, cyclobutanocrown ethers **10a** and **10b**, in 95.7 and 91.8% yields respectively. Subsequently, **10a** and **10b** were transformed to **8a** and **8b** in 37 and 29% yields respectively upon irradiation with 220 nm UV light. The structures of **10a** and **10b** were confirmed to be the β-form.

Both intermolecular and intramolecular [2+2]photocycloadditions of a large number of olefinic compounds have recently been investigated extensively by many research groups from the points of view of molecular design and the synthetic method for novel organic compounds.[1] Several kinds of photoresponsive crown ethers have been investigated by several research groups with the aim of controlling the extraction ability of crown ethers by light or thermal means.[2-4] It is well-known that macrocyclic polyethers can be complexed with various metal ions, although the corresponding open chain polyethers show poor complexing abilities.[5] Recently, several kinds of cyclobutanocrown ethers formed by the intramolecular [2+2]photocycloaddition of open-chain polyethers which contain two vinyl or vinyloxy groups at both terminals have received much attention in connection with the synthetic method for crown ethers.[6-9] However, these reports did not discuss the possibility of a photoreversible cleavage of the cyclobutanocrown ethers in order to control the complexing abilities. Egerton et al.[10] reported that the irradiation of cinnamic acid with >300 nm UV light gave a dimer by means of intermolecular [2+2]photocycloaddition, while the irradiation of the dimer with 200 nm UV light gave, on the contrary, the corresponding starting monomer. In connection with this finding, we ourselves reported on the syntheses of cyclobutanocrown ethers by means of the intramolecular [2+2]photocycloaddition of α,ω-dicinnamoyl polyethylene glycol derivatives **1** with >300 nm UV light and their photoreversible reactions with 220 nm light.[11] However, the rates of the intramolecular [2+2]photocycloaddition of the dicinnamates were extremely slow (e.g., the half-life periods of **1a**, **1b**, and **1c** were 590.7, 98.7, and 105.9 min respectively), and the structures of the main cycloadducts **2** were of the δ-form which is disadvantageous for complexation with metal cations. We will, therefore, present in this paper the syntheses of new types of photoresponsive cyclobutanocrown ethers **10** by means of the intramolecular [2+2]photocycloaddition of **8** and their photoreversible cleavage reaction in order to deal with the above problems.

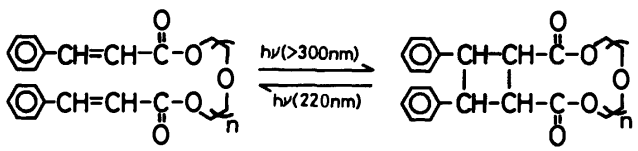

1a: n=0 **2a**: n=0
1b: n=1 **2b**: n=1
1c: n=2 **2c**: n=2

Results and Discussion

Syntheses of 8. Compound **6** was prepared by the following methods. Dialdehyde **4** was obtained in a 95% yield as a pale yellow oil by the Sommelet reaction of the corresponding dibromide **3** according to the method in the literature.[12] The reaction of **4** with malonic acid in the presence of piperidine in pyridine gave **5** in a 91% yield as a colorless powder. The carboxyl groups of **5** were chlorinated with thionyl chloride to give **6** in a 71% yield.[13] The condensation of **6** with **7a** gave **8a** in a 7.0% yield, together with its dimer **9a** in a 6.0% yield. Also, **8b**, **8c**, **9b**, and **9c** were obtained by the same method. The structures of these products were established by their ^{1}H NMR and elemental analysis and mass spectral data and/or gel-permeation chromatography. As is shown in Fig. 1, the ^{1}H NMR spectrum of **8b** showed the signals of the trimethylene protons at δ 2.72(t, J=5.8 Hz, 4H) and 2.24—2.17(m, 2H) respectively, and the signals of the *p*-phenylene protons as a pair in the A_2B_2 pattern at δ 6.95(d, J=8.2 Hz, 4H) and 6.71(d, J=8.2 Hz, 4H) together with the signals of the olefinic protons as a pair in the A_2B_2 pattern at δ 7.52(d,

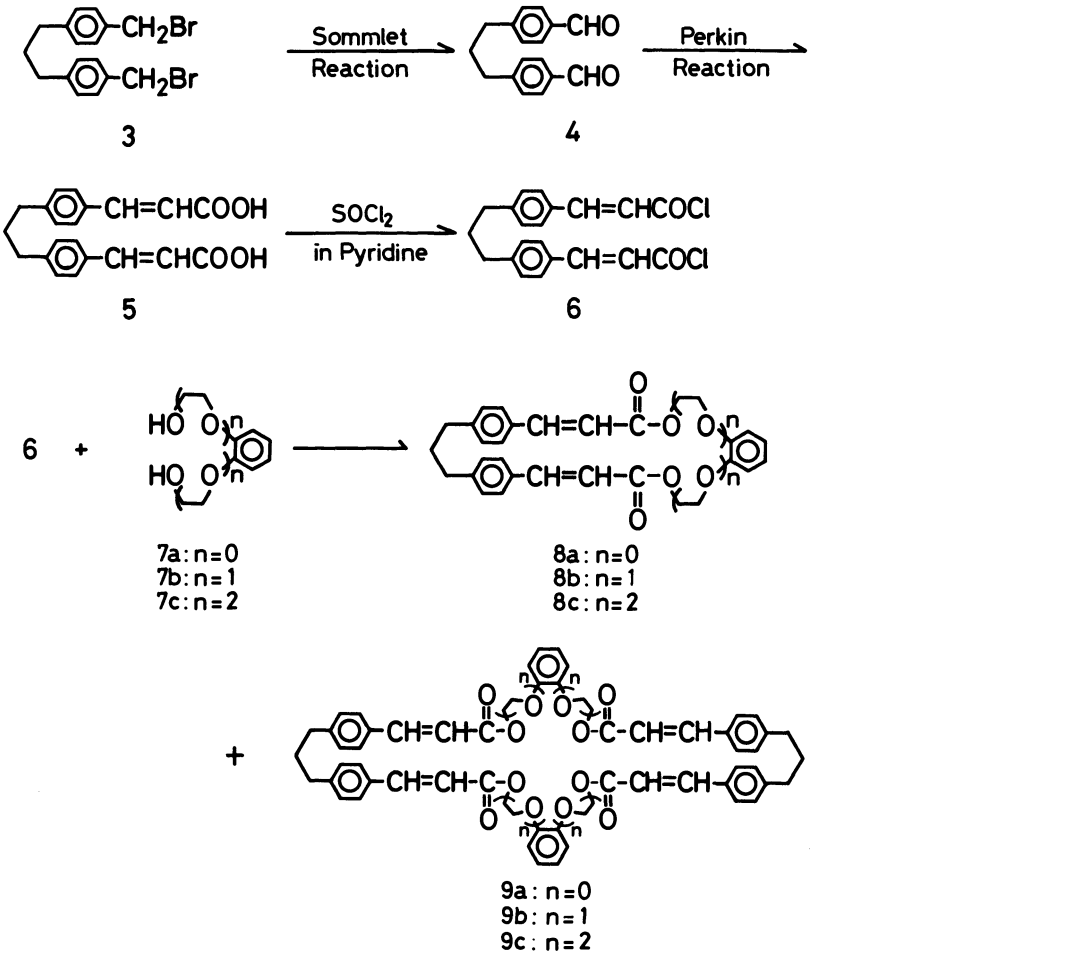

J=16.0 Hz, 2H) and 6.24(d, J=16.0 Hz, 2H). However, the signals of the *p*-phenylene protons of the dimers **9a**—**c** shifted upfield (ca. 0.50 ppm) compared with those of its monomers as a result of decreases in the anisotropic effect of the opposite aromatic rings upon each other. Furthermore, the parent peaks of the dimers of the mass spectra could not be obtained, although the M^+ values of the corresponding monomers agreed well with the calculated values. We then examined the gel-permeation chromatography of **9a**—**c**. Compounds **9a**—**c** had a longer retention time than the corresponding compounds **8a**—**c**. The molecular weights of **9a**—**c**, which were calculated from the retention times using the calibration curves, were nearly all consistent with the expected values of the dimers.

Conversion of 8 to 10. The intramolecular [2+2]-photocycloaddition of **8a**—**c** was carried out as follows, while the yields were calculated from the intensity of the absorption band at 275 nm in the steady state. The irradiation of **8b** in acetonitrile for 1 h with a 450W high-pressure mercury lamp through a Pyrex filter in the absence of any sensitizer gave **10b** in a 91.8% yield (isolated yield: 71.3%). The irradiation of **8a** (0.25 h) also yielded **10a** in a 95.7% yield (isolated yield: 18%). It is well known that the trans–cis

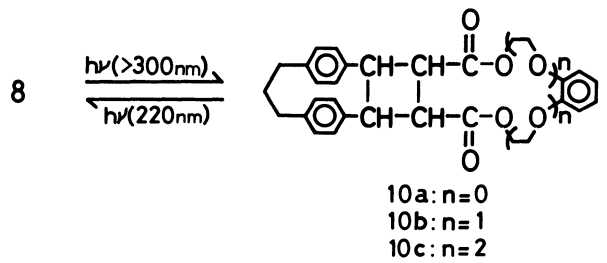

isomerization of the carbon–carbon double bonds in ethyl cinnamate generally competes with the photodimerization.[1] In the above photoreaction, however, the isolated intramolecular [2+2]photocycloadducts were β-isomers, as will be described below, although very tiny side reaction products were observed by means of TLC. Therefore, the intramolecular [2+2]photocycloaddition of **8a** and **8b** can be said to proceed because of the proximity of the two carbon–carbon double bonds prior to the trans–cis isomerization of the carbon–carbon double bonds. However, **10c** could not be obtained because the irradiation of **8c** gave many tiny products. The solutions of **8a** and **8b** were measured by means of their UV spectra at appropriate intervals during irradiation. The change in the UV spectra of **8b** is

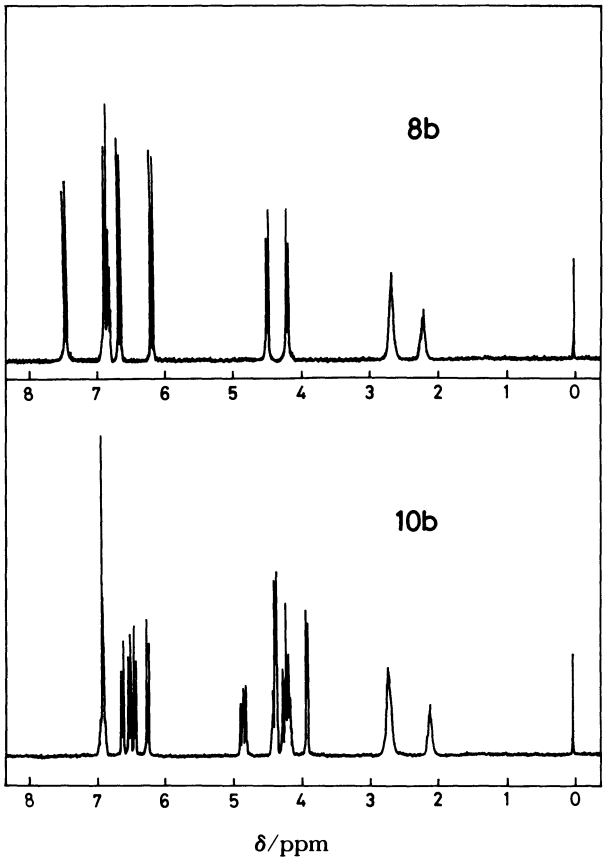

Fig. 1. 400 MHz ^{1}H NMR spectra of **8b** and **10b**.

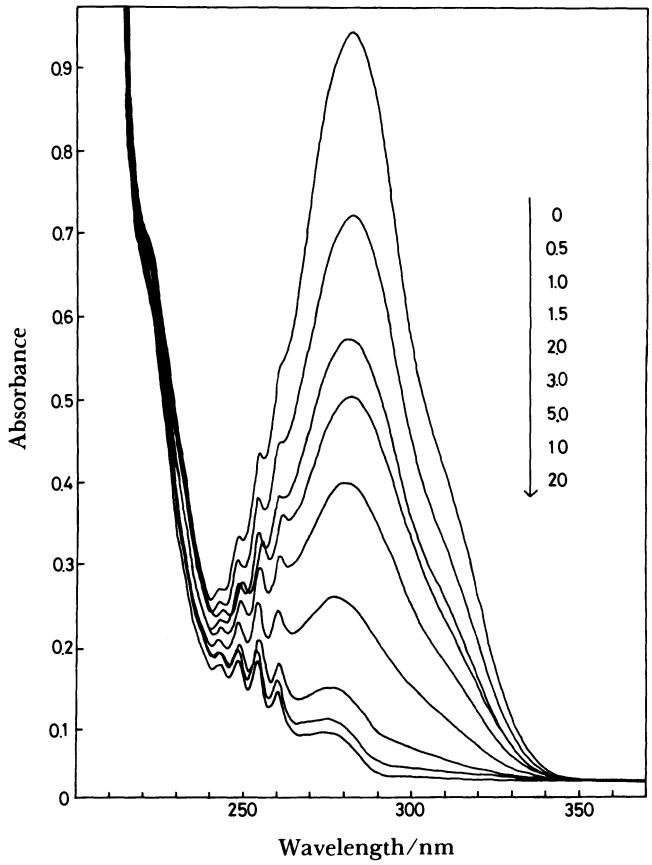

Fig. 2. Spectral changes of **8b** to **10b** in acetonitrile (4×10^{-5} mol dm^{-3}). The numbers beside the arrow are the elapse of irradiation time (min).

shown in Fig. 2. The half-life periods of the intramolecular [2+2]photocycloaddition of **8a** and **8b** were only 29 min and 40 s respectively; these values are very fast compared with those of the corresponding open-chain dicinnamates **1a** and **1b**. The difficulty in the ring closure of **8c** to **10c** is due to the longer intramolecular distance between the two double bonds compared with those of **8a** and **8b**. Therefore, the photoreaction of **8c** caused the intramolecular [2+2]-photocycloaddition, together with other side reactions (for example, trans–cis isomerization, intramolecular [2+2]photocycloaddition of the cis isomerized products, the intermolecular addition of **8c**, and the cleavage of ester groups). The template-type intramolecular [2+2]photocycloaddition of **8** in the presence of the alkali metal ion was also determined; however, the yields were not improved. This fact agrees with the finding that **8** lacks any extraction ability, as will be described below, because if **8** were complexed with an alkali metal cation, the rate of photocyclization would be improved due to the approach of the two double bonds.

Structures of 8 and 10. In order to investigate this problem in more detail, the structure of **8b** was confirmed by means of single crystal X-ray analysis. The conformation of **8b** is illustrated in Fig. 3 together with its atomic numbering, while the selected bond distances and bond angles are summarized in

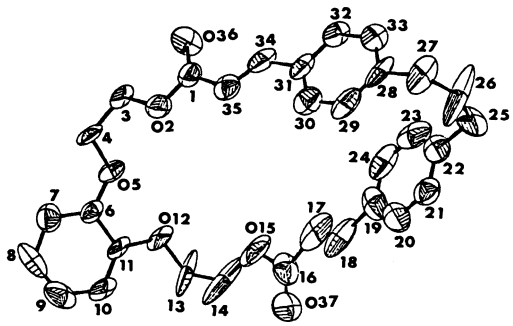

Fig. 3. **ORTEP** drawing of the molecule **8b** with atomic numbering scheme.

Tables 1 and 2 respectively. As is shown in Fig. 3, the two double bonds are trans and are situated in such positions relative to each other as to make the ring closure possible. The torsion angles of C_{16}–C_{17}–C_{18}–C_{19} and C_{33}–C_{34}–C_{35}–C_{36} are −179.8(5) and 179.7(5)° respectively. Also, the torsion angles of O_2–C_3–C_4–O_5 and C_{12}–C_{13}–C_{14}–C_{15} are −73.7(4) and −24.8(11)° respectively. The two benzene rings are face-to-face, albeit slightly distorted, and the dihedral angle is 20.6(2)°. The distances between the two olefinic carbon atoms (C_{17}–C_{35} and C_{18}–C_{34}) are 5.341(11) and 5.906(9) Å respectively. These values are significantly

Table 1. Fractional Atomic Coordinates ($\times 10^4$) and Thermal Parameters, with Estimated Standard Deviations in Parentheses

Atom	x	y	z	B_{eq}/Å^2	Atom	x	y	z	B_{eq}/Å^2
C(1)	2148(4)	7594(5)	7683(5)	5.7	C(20)	−2890(4)	4316(5)	5991(5)	6.4
O(2)	2850(3)	6489(3)	7785(3)	5.9	C(21)	−3501(4)	5187(5)	5396(5)	6.2
C(3)	3606(4)	6642(5)	8629(5)	5.9	C(22)	−3749(4)	6535(5)	5807(5)	6.4
C(4)	4353(4)	5342(5)	8569(5)	5.7	C(23)	−3367(5)	6932(5)	6837(5)	7.3
O(5)	3638(3)	4447(3)	9162(3)	5.5	C(24)	−2761(4)	6022(6)	7411(5)	7.4
C(6)	4112(4)	3124(5)	8996(4)	4.6	C(25)	−4427(5)	7467(6)	5141(6)	9.4
C(7)	5276(4)	2648(5)	8555(5)	5.7	C(26)	−3869(6)	8064(10)	4220(7)	17.7
C(8)	5646(5)	1285(6)	8387(5)	7.5	C(27)	−2846(5)	8456(7)	3772(5)	9.4
C(9)	4868(5)	425(5)	8656(5)	7.8	C(28)	−1934(4)	8367(6)	4528(5)	6.8
C(10)	3716(5)	876(5)	9114(5)	6.9	C(29)	−1126(4)	7243(6)	4442(5)	6.8
C(11)	3331(4)	2221(5)	9300(4)	5.0	C(30)	−310(4)	7181(5)	5151(5)	6.3
O(12)	2216(3)	2782(3)	9755(3)	6.7	C(31)	−272(4)	8269(5)	5946(4)	5.3
C(13)	1427(6)	1957(8)	10229(9)	15.6	C(32)	−1093(5)	9407(5)	6025(5)	6.9
C(14)	551(7)	1894(8)	9990(7)	14.6	C(33)	−1905(5)	9449(6)	5321(5)	7.5
O(15)	−121(3)	2933(4)	9524(4)	9.0	C(34)	585(4)	8312(5)	6709(5)	5.9
C(16)	−729(4)	2459(6)	8750(5)	7.2	C(35)	1353(4)	7336(5)	6874(5)	5.5
C(17)	−1374(5)	3691(7)	8334(6)	9.8	O(36)	2167(3)	8637(4)	8240(4)	9.1
C(18)	−1815(5)	3576(7)	7545(5)	8.4	O(37)	−773(3)	1307(4)	8523(4)	9.0
C(19)	−2508(4)	4696(6)	6986(5)	6.7					

Table 2. Bond Lengths (Å) and Angles(°), with Estimated Standard Deviations in Parentheses

Bond length	(l/Å)	Bond length	(l/Å)	Bond angle	(ϕ/°)	Bond angle	(ϕ/°)
C(1)-O(2)	1.325(7)	C(17)-C(18)	1.140(9)	O(2)-C(1)-C(35)	111.8(4)	C(18)-C(19)-C(20)	116.9(5)
C(1)-C(35)	1.484(8)	C(18)-C(19)	1.555(9)	O(2)-C(1)-O(36)	121.1(6)	C(18)-C(19)-C(24)	125.4(5)
C(1)-O(36)	1.201(7)	C(19)-C(20)	1.362(8)	C(35)-C(1)-O(36)	127.0(6)	C(20)-C(19)-C(24)	117.7(5)
O(2)-C(3)	1.460(7)	C(19)-C(24)	1.366(8)	C(1)-O(2)-C(3)	115.1(3)	C(19)-C(20)-C(21)	123.6(6)
C(3)-C(4)	1.471(8)	C(20)-C(21)	1.365(8)	O(2)-C(3)-C(4)	107.0(4)	C(20)-C(21)-C(22)	119.3(5)
C(4)-O(5)	1.434(6)	C(21)-C(22)	1.383(7)	C(3)-C(4)-O(5)	106.8(4)	C(21)-C(22)-C(23)	117.5(5)
O(5)-C(6)	1.363(6)	C(22)-C(23)	1.402(8)	C(4)-O(5)-C(6)	115.3(3)	C(21)-C(22)-C(25)	118.1(4)
C(6)-C(7)	1.383(8)	C(22)-C(25)	1.499(9)	O(5)-C(6)-C(7)	124.7(5)	C(23)-C(22)-C(25)	124.4(6)
C(6)-C(11)	1.397(7)	C(23)-C(24)	1.372(8)	O(5)-C(6)-C(11)	115.4(5)	C(22)-C(23)-C(24)	121.3(6)
C(7)-C(8)	1.375(9)	C(25)-C(26)	1.353(11)	C(7)-C(6)-C(11)	119.9(5)	C(19)-C(24)-C(23)	120.6(5)
C(8)-C(9)	1.356(9)	C(26)-C(27)	1.345(11)	C(6)-C(7)-C(8)	119.4(5)	C(22)-C(25)-C(26)	120.1(7)
C(9)-C(10)	1.368(10)	C(27)-C(28)	1.513(9)	C(7)-C(8)-C(9)	119.7(7)	C(25)-C(26)-C(27)	142.7(13)
C(10)-C(11)	1.361(8)	C(28)-C(29)	1.367(9)	C(8)-C(9)-C(10)	121.7(6)	C(26)-C(27)-C(28)	117.9(5)
C(11)-O(12)	1.354(7)	C(28)-C(33)	1.385(8)	C(9)-C(10)-C(11)	119.7(6)	C(27)-C(28)-C(33)	119.5(6)
O(12)-C(13)	1.390(9)	C(29)-C(30)	1.382(9)	C(6)-C(11)-C(10)	119.5(6)	C(27)-C(28)-C(29)	121.6(5)
C(13)-C(14)	1.136(13)	C(30)-C(31)	1.393(8)	C(6)-C(11)-O(12)	115.6(5)	C(29)-C(28)-C(33)	118.9(5)
C(14)-O(15)	1.428(10)	C(31)-C(32)	1.388(8)	C(10)-C(11)-O(12)	124.8(6)	C(28)-C(29)-C(30)	120.5(6)
O(15)-C(16)	1.354(7)	C(31)-C(34)	1.474(8)	C(11)-O(12)-C(13)	118.6(4)	C(29)-C(30)-C(31)	120.9(6)
C(16)-C(17)	1.524(9)	C(32)-C(33)	1.374(9)	O(12)-C(13)-C(14)	126.1(11)	C(30)-C(31)-C(32)	118.2(4)
C(16)-O(37)	1.185(7)	C(34)-C(35)	1.299(8)	C(13)-C(14)-O(15)	125.5(11)	C(30)-C(31)-C(34)	124.8(6)
				C(14)-O(15)-C(16)	113.2(4)	C(32)-C(31)-C(34)	117.0(5)
				O(15)-C(16)-C(17)	106.1(4)	C(31)-C(32)-C(33)	120.2(6)
				O(15)-C(16)-O(37)	124.7(7)	C(28)-C(33)-C(32)	121.3(7)
				C(17)-C(16)-O(37)	129.1(6)	C(31)-C(34)-C(35)	127.8(6)
				C(16)-C(17)-C(18)	120.0(8)	C(1)-C(35)-C(34)	119.4(5)
				C(17)-C(18)-C(19)	127.9(9)		

longer than the value of 4.0 Å for the compounds in which intermolecular [2+2]photocycloaddition in the crystalline state occurred.[1] Indeed, the attempted intramolecular [2+2]photocycloaddition of **8** in the solid state failed. These facts suggest that the intramolecular [2+2]photocycloaddition of **8b** in the solution occurred after the distance between the two double bonds was closed within 4.0 Å due to the molecular flexibility of **8** in the solution. The respective configurations of the photoadducts were elucidated by a comparative ^{1}H NMR study of **10a,b** and the corresponding starting materials **8a** and **8b**. As is shown in Fig. 1, the ^{1}H NMR spectrum of **10b** showed the signals of the trimethylene protons at δ 2.11 (bs, 2H) and 2.71 (bs, 4H), the signals of the oxyethylene protons at δ 4.23—4.27 (m, 4H) and 4.84—4.88 (m, 4H), and the signals of the methine protons of the cyclobutane ring at δ 3.92 (m, 2H) and 4.38 (m,

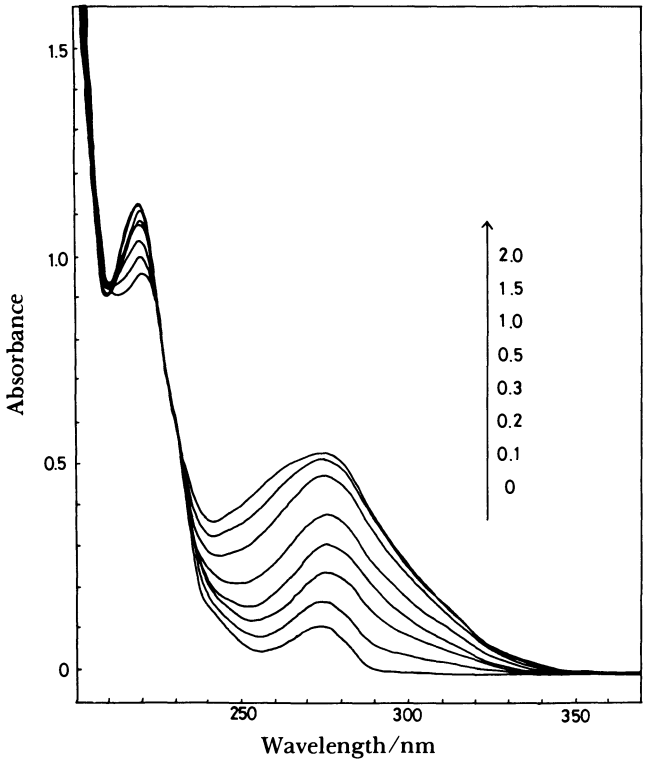

Fig. 4. Spectral changes of **10b** to **8b** in acetonitrile (4×10^{-5} mol dm^{-3}). The numbers beside the arrow are the elapse of irradiation time (h).

2H) as the AA'BB' pattern, together with the aromatic ring protons, due to the *p*-phenylene groups and the catechol moiety, at δ 6.26—6.66 (two pairs of A_2B_2, 8H) and 6.95 (A_2B_2, 4H) respectively. The aromatic protons of the *p*-phenylene groups shifted upfield (ca. 0.3—0.5 ppm) compared with those of the starting material **8b**. This upfield shift and the two pairs of *p*-phenylene protons in the A_2B_2 pattern suggest that the two benzene rings are opposite each other in the solution. Furthermore, the chemical shifts and the split pattern of the cyclobutane ring protons are consistent with those of the dimethyl β-toluxinate reported by Ben-Efrain et al.[14] Also, the trimethylene group of **8a—c** is too short to allow the formation of a δ-isomer. Therefore, these intramolecular [2+2]-photocycloadducts must be β-isomers.

Photoreversible Reaction between 10 and 8. An acetonitrile solution of the pure **10b** was irradiated with a 220 nm UV light. As is shown in Fig. 4, the UV spectra of the solution were then measured at appropriate intervals. The absorption band at 275 nm increased with the UV irradiation of the solution, and a steady state was attained within 2 h. The structures of the irradiated products were confirmed by a direct comparison of the values of TLC and the spectral data with those of authentic samples. The irradiation of the pure **10a** was also carried out by the same method. The photoreversible cleavages of **10a** and **10b** gave **8a** and **8b** in 37 and 29% yields respectively, calculated

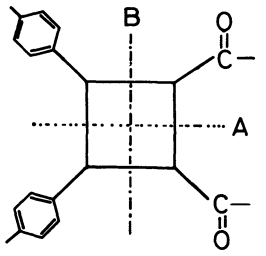

Fig. 5.

from the intensities of the absorption bands at 275 nm in the steady state. Also, the yields of the reversible reactions (**8**⟷**10**) were measured by means of irradiation by >300 nm and 220 nm UV lights one after the other. As has been described above, the irradiation of acetonitrile solutions of **8a** and **8b** with >300 nm UV light gave **10a** and **10b** in 95.7 and 91.8% yields respectively. The subsequent irradiation of the above irradiated mixtures of **8a** and **8b** with 220 nm UV light gave **8a** and **8b** in 39.0 and 22.0% yields respectively. Furthermore, one more irradiation of the above solutions with >300 nm UV light gave **10a** and **10c** in 43.8 and 54.0% yields respectively. The absolute concentrations of **8** and **10** under the photoirradiation were derived from these values of the UV spectra. The yields of **10**→**8** are relatively low compared with those of **8**→**10**. The results suggest that, in the photoreaction of **10**→**8**, the cleavage (Fashion A) of the C–C single bonds in the cyclobutane ring[10] occurred together with the cleavage (Fashion B) of the C–C bonds, as is shown in Fig. 5, although another cleavage cannot be ruled out. The above results imply that the photoreversible reaction of **10**⟷**8** can be controlled by UV light, although the yields of the reversible reactions are relatively low because of the side reactions.

Extraction Abilities of 8 and 10. The extraction abilities of **8** and **10** toward alkali and alkaline earth metal cations were examined according to Pedersen's method.[15] These results are summarized in Table 3. An irradiated mixture of **8c** was used instead of pure **10c**, because **10c** could not be isolated, as has been described above. Compound **8c** and the irradiated mixture of **8c** showed a significant extraction ability toward alkali and alkaline earth metal ions, although the extraction ability of **8b** and **10b** toward these metal ions was negligible. The insignificant extraction ability of **8b** and **10b** may be attributed to the smaller number of oxygen atoms which can effect the complexing ability. Only two oxygen atoms of the four in the crown ether moiety of **8b** can contribute to the complexing ability, for the electron density of the two oxygen atoms of the ester groups is lower than that of the ether-linkage oxygen atom. Also, the negligible extraction ability of **10b** can be ascribed to the same reason, although a CPK model suggests that the hole size of **10b** would fit better than that of **8b** to

Table 3. Extraction of Metal Picrates from the Aqueous to the Organic Phase(%)

Compd	Li^+	Na^+	K^+	Rb^+	Cs^+	Mg^{2+}	Ca^{2+}	Sr^{2+}	Ba^{2+}
8b	0	0	0	0	0	0	0	0	0
10b	0	0	0	0	0	0	1	0	0
8c	1	1	3	4	3	3	4	3	5
Irradiated mixtures of **8c**	8	7	7	7	7	7	7	7	5

incorporate the guest metal ions. In **8c** there are four ether-linkage oxgen atoms. Therefore, the extraction ability of **8c** is higher than that of **8b**, although the values are relatively poor because of the presence of the ester moieties in the macrocycle, as has been described in a previous paper.[11] The extraction ability of the irradiated mixture of **8c** is slightly higher than that of **8c**. However, the reason for this higher extraction ability has not been defined, for the irradiated mixture contain several products as has been described above. The above results suggest that the photoreversible crown ethers **8** and **10** showed low or negligible extraction abilities and could not, therefore, control the extraction ability toward alkali and alkaline earth metal ions.

Experimental

The melting points are uncorrected. The UV spectra were obtained on a Hitachi 330 spectrometer. The IR spectra were measured on a JASCO IRA-2 Diffraction Grating Infrared Spectrometer. The ^1H NMR spectra were obtained on a JEOL GX400 Spectrometer, with TMS as the internal standard. For the irradiation of **8** on a preparative scale, the solution was charged with dry nitrogen for 10 min and then internally irradiated with an USHIO high-pressure mercury lamp (HPL)(UM-452). Also, the photocleavage of **10** to **8** was carried out by means of a 220 nm UV light using a grating monochromator (Model JASCO CT-10), with a 500W xenon lamp (JASCO PS-X500) and a band width of 0.5 nm. The gel-permeation chromatography was carried out on a Hitachi 635 high-pressure liquid chromatograph using a Hitachi Gelpack W-520 apparatus as the GLC column (10.7×30 mm L). Chloroform was used as the eluting solvent. UV was detected at 254 nm.

Materials. *o*-Bis(2-hydroxyethoxy)benzene (**7b**),[16] and *o*-bis[2-(2-hydroxyethoxy)ethoxy]benzene (**7c**),[17] and 1,3-bis-(*p*-formylphenyl)propane (**4**)[12] were prepared according to the methods in the literature. The other reagents employed were either commercial or prepared by the usual methods. The solvents were purified by distillation.

3,3′-(Trimethylenedi-4,1-phenylene)bis[2-propenoic acid] (5): A solution of 1,3-bis(*p*-formylphenyl)propane (**4**) (6.25 g, 24.8 mmol) and malonic acid (18.0 g, 182.7 mmol) in dry pyridine (60 cm^3) was refluxed for 8 h in the presence of piperidine (2.2 cm^3). The reaction mixture was cooled to room temperature and then was added to a mixture of ice (100 g) and concentrated hydrochloric acid (80 cm^3). The resulting precipitate was filtered, washed with water, and dried. Recrystallization from acetic acid gave **5** in a 91% yield as a white powder. Mp 262.0—266.0 °C. Found: C, 73.42, H, 6.22%. Calcd for $C_{21}H_{20}O_4 \cdot 1/4CH_3COOH$: C, 73.42, H, 5.98%. MS (70 eV) *m/z* 336 (M^+). ^1H NMR (DMSO-d_6) δ=7.57 (d, *J*=16.0 Hz, 2H), 7.69—7.06 (A_2B_2 pattern, m, 8H), 6.44 (d, *J*=16.0 Hz, 2H), 1.75 (bs, 2H), and 2.14—1.60 (m, 4H).

3,3′-(Trimethylenedi-4,1-phenylene)bis[2-propenoyl chloride] (6): A mixture of thionyl chloride (20 cm^3) and **5** (1.50 g, 4.5 cm^3) was stirred for 2 h at 30—35 °C. The excess of thionyl chloride was removed in vacuo, and the residual solid was used for the next reaction without further purification.

Reaction of 6 with 7. Compound **6** (1.90 g, 5.1 mmol) in benzene (100 cm^3) and **7a** (1.01 g, 5.1 mmol) in benzene (100 cm^3) were added to a benzene solution (400 cm^3) containing pyridine (9 cm^3) at the same rate over a period of 27 h and then refluxed further for 15 h. The reaction mixture was cooled and evaporated, and the residue was extracted with chloroform. The extract was washed with aqueous 10% hydrochloric acid and water, dried, and evaporated in vacuo. The residue was chromatographed on silica gel, using chloroform as the eluent. The first fraction was collected and concentrated. The recrystallization of the residual oil from benzene–hexane gave **8a** in a 7.0% yield as colorless needles. Mp 240.0—242.0 °C. Found: C, 80.00, H, 5.74%. Calcd for $C_{27}H_{22}O_4 \cdot 1/2C_6H_6$:C, 80.15, H, 5.62%. ^1H NMR ($CDCl_3$) δ=7.63 (d, *J*=16.0 Hz, 2H), 6.37 (d, *J*=16.0 Hz, 2H), 7.28 (s, 4H), 6.97 (d, *J*=8.2 Hz, 4H), 6.75 (d, *J*=8.2 Hz, 4H), 2.76 (t, *J*=5.8 Hz, 4H), and 2.25—2.16 (m, 2H). Crude **9a** was obtained from the second fraction. Recrystallization from toluene gave **9a** in a 6.0% yield as a colorless powder. Mp 245.0—247.0 °C. Found: C, 78.12, H, 5.52%. Calcd for $C_{54}H_{44}O_8 \cdot 1/2H_2O$: C, 78.15, H, 5.46%. ^1H NMR ($CDCl_3$) δ=7.80 (d, *J*=16.0 Hz, 2H), 7.31—7.26 (A_2B_2 pattern, 4H), 7.41 (d, *J*=8.2 Hz, 4H), 7.14 (d, *J*=8.2 Hz, 4H), 2.62 (t, *J*=7.8 Hz, 4H), and 1.90 (q, *J*=7.8 Hz, 2H).

Compounds **8b**, **8c**, **9b**, and **9c** were obtained by a method similar to that described above.

8b. Yield, 6.5%. Mp 213.0—214.0 °C. Found: C, 74.50, H, 6.25%. Calcd for $C_{31}H_{30}O_6$: C, 74.68, H, 6.07%. MS (70 eV) *m/z* 471 (M^+). ^1H NMR ($CDCl_3$) δ=7.52 (d, *J*=16.0 Hz, 2H), 6.24 (d, *J*=16.0 Hz, 2H), 6.95—6.86 (A_2B_2 pattern, 4H), 6.95 (d, *J*=8.2 Hz, 4H), 6.71 (d, *J*=8.2 Hz, 4H), 2.72 (t, *J*=5.7 Hz, 4H), 2.24—2.17 (m, 2H), 4.56 (t, *J*=4.3 Hz, 4H), and 4.27 (t, *J*=4.3 Hz, 4H).

9b. Yield, 12.3%, Mp 193.5—194.5 °C. Found: C, 74.81, H, 6.01%. Calcd for $C_{62}H_{60}O_{12}$: C, 74.63, H, 6.07%. ^1H NMR ($CDCl_3$) δ=7.53 (d, *J*=16.0 Hz, 2H), 6.38 (d, 16.0 Hz, 2H), 7.06—6.91 (A_2B_2 pattern, 4H), 7.42 (d, *J*=8.2 Hz, 4H), 7.10 (d, *J*=8.2 Hz, 4H), 2.52 (t, *J*=7.6 Hz, 4H), 1.84—1.74 (q, *J*=7.6 Hz, 2H), 4.46 (t, *J*=4.9 Hz, 4H), and 4.26 (t, *J*=4.9 Hz, 4H).

8c. Yield, 8.0%. Mp 111.0—112.5 °C. Found: C, 70.43, H, 6.51%. Calcd for $C_{35}H_{38}O_8 \cdot 1/2H_2O$: C, 70.57, H, 6.43%. MS

(70 eV) m/z 586 (M^+). ^1H NMR ($CDCl_3$) δ=7.55 (d, J=16.0 Hz, 2H), 6.27 (d, J=16.0 Hz, 2H), 6.97—6.86 (A_2B_2 pattern, 4H), 7.07 (d, J=8.2 Hz, 4H), 6.77 (d, J=8.2 Hz, 4H), 2.71 (t, J=6.0 Hz, 4H), 2.19 (m, 2H), 4.36 (t, J=4.9 Hz, 4H), 4.21 (t, J=4.9 Hz, 4H), 3.93 (t, J=4.8 Hz, 4H), and 3.87 (t, J=4.8 Hz, 4H).

9c. Yield, 10.8%. Mp 145.5—146.5 °C. Found: C, 71.43,H, 6.75%. Calcd for $C_{70}H_{76}O_{16}$: C, 71.65, H, 6.53%. ^1H NMR ($CDCl_3$) δ=7.64 (d, J=16.0 Hz, 2H), 6.39 (d, J=16.0 Hz, 2H), 6.93—6.88 (A_2B_2 pattern, 4H), 7.37 (d, J=8.0 Hz, 4H), 7.11 (d, J=8.0 Hz, 4H), 2.58 (t, J=7.6 Hz, 4H), 1.87 (q, J=7.6 Hz, 2H), 4.37 (t, J=4.8 Hz, 4H), 4.18 (t, J=4.8 Hz, 4H), 3.90 (t, J=4.8 Hz, 4H), and 3.87 (t, J=4.9 Hz, 4H).

Gel-Permeation Chromatography. Compounds **8a**, **8b**, **8c**, **9a**, **9b**, and **9c** were submitted to gel-permeation chromatography. The retention times were 12.83, 11.89, 11.48, 10.84, 10.40, and 10.13 min respectively. The molecular weights of **8** and **9** were obtained from the calibration curves of the polyethylene glycols and epoxy resins of known molecular weights.

Preparation of 10 by the Photoreaction of 8. A solution of **8b** in acetonitrile (4×10^{-5} M; 1 M=1 mol dm^{-3}) was irradiated internally with a high-pressure mercury lamp (450 W) through a Pyrex filter at the temperature of running water for 1.0 h. The solvent was then evaporated, and the residue was chromatographed on silica gel, using chloroform as the eluent. The first fraction was concentrated and recrystallized from acetonitrile to give **10b** as white leaves. Yield, 71.3%. Mp 218.0—219.0 °C. Found: C, 74.39, H, 6.46%. Calcd for $C_{31}H_{30}O_6$: C, 74.68, H, 6.06%. MS (70 eV) m/z 498 (M^+). ^1H NMR ($CDCl_3$) δ=6.98—6.92 (m, A_2B_2 pattern, 4H, aromatic H), 6.66—6.26 (m, two pair of A_2B_2 pattern, 8H, aromatic H), 4.90—4.16 (m, 8H, -OCH_2-), 4.40—4.36 (m, 2H, C_α-H), 3.95—3.90 (m, 2H, C_β-H), 2.71 (bs, 4H, -CH_2-), and 2.11 (bs, 2H, -CH_2-).

10a was also obtained by the method described above. Yield, 18%. Mp 148.0—150.0 °C. Found: C, 78.40, H, 5.39%. Calcd for $C_{27}H_{22}O_4$: C, 79.01, H, 5.40%. MS (70 eV) m/z 410 (M^+). ^1H NMR ($CDCl_3$) δ=7.49—7.37 (m, A_2B_2 pattern 4H, aromatic H), 6.55 (d, J=8.1 Hz, 4H, aromatic H), 6.33—5.99 (m, A_2B_2 pattern, 4H, aromatic H), 4.66—4.63 (m, 2H, C_α-H), 3.53—3.49 (m, 2H, C_β-H), 2.77—2.59(m 4H, -CH_2-), and 2.12—2.04 (m, 2H, -CH_2-).

Photoreversible Cleavage of 10. An acetonitrile solution of **10** (4.0×10^{-5} M) was placed in a quartz cell (1×1×4 cm) and irradiated at room temperature with a 220 nm UV light using a grating monochromater with a xenon lamp (500 W). The UV spectral changes were recorded during irradiation and a steady state was attained within 2 h. The solution was then checked on thin-layer chromatography, using chloroform as the eluent, and the results were compared with the R_f values of authentic samples **8a** and **8b**. The photoreversible yields of **10** were calculated from the intensity of the absorption band at 275 nm in the steady state. The yields of **8a** and **8b** were 37 and 29% respectively.

Photoreversible Reaction between 8 and 10. An acetonitrile solution of **8** (4.0×10^{-5} M) was irradiated by means of high-pressure mercury lamp through a Pyrex filter at the temperature of running water for 1 h. The yields of the irradiated products, **10a** and **10b**, were 95.7 and 91.8% respectively. A part of this solution was placed in a quartz cell (1×1×4 cm) and irradiated at 220 nm UV light, using a grating monochromator with a 500 W xenon lamp, for 2 h. The photoreversible yields of **8a** and **8b** were 39.0 and 20.0% respectively. Furthermore, the solutions were irradiated again with 300 nm UV light to give **10a** and **10b** in 43.8 and 54.0% yields respectively. These values were calculated from the intensity of the absorption band at 275 nm in the steady state. The structures of the irradiated product **10a** and **10b**, and of the photoreversible products, **8a** and **8b**, were confirmed by a comparison of the R_f values of the silica-gel TLC, the melting points, and the spectral data of the authentic samples.

Solvent Extraction. Equal volumes (5 cm^3) of dichloromethane containing 7×10^{-4} M of crown ethers **8b** and **8c** and a photoirradiated mixture of **8b** and **8c**, and an aqueous solution containing 1×10^{-1} M metal nitrate and 7×10^{-5} M picric acid were agitated. The solution was then separated by the use of a centrifugal separator. The upper solution was then withdrawn, and its electronic spectrum was recorded. A similar extraction was performed with pure dichloromethane. Similar extraction abilities were calculated by means of the following equation:

$$\text{Extraction ability}=(A_0-A)/A_0\times100.$$

A_0 was the absorbance in the absence of metal nitrate, while A was the absorbance in its presence.

X-Ray Crystallography. A crystal with dimensions of 0.4×0.2×0.15 mm was used for the X-ray crystallography. The crystal data are as follows: $C_{31}H_{30}O_6$, Mw=498.6, triclinic, $P\bar{1}$, a=11.880(1), b=10.085(1), c=11.480(1) Å, α=93.65(1), β=78.60(1), γ=82.62(1)°, U=1331.5 Å^3, Z=2, D_x=1.24 g cm^{-1}, μ(Cu $K\alpha$)=6.6 cm^{-1}. The intensity data for $2\theta<128°$ were recorded on a Rigaku AFC-5R apparatus with graphite monochromatized Cu $K\alpha$ irradiation. A total of 4440 independent reflections was corrected for Lorentz and polarization factors, but not for absorption. The structure was solved by direct methods using MULTAN84,[19] and refined by block diagonal least-square methods. The positions of the hydrogen atoms were estimated using standard geometry. The final refinements, with anisotropic temperature factors for the non-hydrogen atoms and isotropic temperatures for the hydrogen atoms, were lowered R values 0.113 (R_w=0.096, $w=1/\sigma2(F_o)$, 3125 observed reflections within $F_o\geq2\sigma(F_o)$). The parameters for the bond lengths, angles, and structure factors (observed and calculated) are kept at the Chemical Society of Japan (Document No. 8804).

We are grateful to Mr. Hisashi Kumagai of Toho University for his kind help in the synthesis of **8**. We also wish to thank Mr. Yoshiyuki Mukoyama of the Ibaragi Research Center, Hitachi Kasei Kogyo Co., Ltd., for his kind help in the measurement of the gel-permeation chromatography. The present work was supported by a Grant-in-Aid for Scientific Research (No. 61540384) from the Ministry of Education, Science and Culture.

References

1) M. Hasegawa, *Chem. Rev.*, **83**, 507 (1983).
2) S. Shinkai, T. Minami, Y. Kusano, and O. Manabe, *J. Am. Chem. Soc.*, **104**, 1967 (1982); S. Shinkai, T. Nakaji, T.

Ogawa, K. Shigematsu, and O. Manabe, *J. Am. Chem. Soc.*, **103**, 111 (1981).

3) H. Sasaki, A. Ueno, J. Anzai, and T. Osa, *Bull. Chem. Soc. Jpn.*, **59**, 1953 (1986).

4) M. Irie and M. Kato, *J. Am. Chem. Soc.*, **107**, 1024 (1985).

5) F. de Jhon and D. N. Reinhouldt, "Stability and Reactivity of Crown-ether Complexes," Academic Press, New York (1981).

6) K. Mizuno, T. Hashizume, and Y. Otsuji, *J. Chem. Soc., Chem. Commun.*, **1983**, 977.

7) M. Kimura, M. Kishimoto, and S. Morosawa, 48 th National Meeting of the Chemical Society of Japan, April **1983**, Kyoto, Abstr., No. 1E32.

8) M. Shirai, A. Ueda, and M. Tanaka, *Makromol. Chem.*, **186**, 493 (1985); M. Shirai, J. Orikata, and M. Tanaka, *Makromol. Chem., Rapid Commun.*, **4**, 65 (1983); *J. Polym. Sci., Polym. Chem. Ed.*, **23**, 463 (1985).

9) K. Hiratani and S. Aiba, *Bull. Chem. Soc. Jpn.*, **57**, 2657 (1984).

10) P. L. Egerton, E. Pitts, and A. Reiser, *Macromolecules*, **14**, 95 (1981); P. L. Egerton, E. M. Hyde, J. Trigg, A. Payne, P. Begnon, M. V. Mijovic, and A. Reiser, *J. Am. Chem. Soc.*, **103**, 3895 (1981).

11) S. Akabori, Y. Habata, M. Nakasawa, Y. Yamada, Y. Shindo, T. Sugimura, and S. Sato, *Bull. Chem. Soc. Jpn.*, **60**, 3453 (1987).

12) J. N. Ashley, H. J. Barber, A. J. Evins, G. Newberg, and A. D. H. Self, *J. Chem. Soc.*, **1942**, 103 (A42).

13) R. C. Fuson and J. T. Walker, *Org. Synth.*, Coll. Vol. 2, 169 (1984).

14) D. A. Ben-Efraim and B. S. Green, *Tetrahedron*, **30**, 2357 (1974).

15) C. J. Pedersen, *Federation Proceedings*, **27**, 1305 (1968).

16) R. E. Rinndfusz, P. M. Ginnings, and V. L. Harnack, *J. Am. Chem. Soc.*, **42**, 163 (1920).

17) S. Kopolow, T. E. Hegen Esch, and J. Smid, *Macromolecules*, **6**, 133 (1973).

18) P. Main, G. Germain, and M. M. Woolfson, "MULTAN84: A System of Computer Programs for the Automatic Solution of Crystal Structures from X-Ray Diffraction Data," Universities of York, England, and Louvain, Belgium (1984).

Synthesis of α-Helices Having a Positively Charged Random Coil-Block on Either N- or C-Terminal

Sho TAKAHASHI,* Takeshi HIBINO, and Seiji SAWADA†
Institute for Chemical Research, Kyoto University, Uji, Kyoto 611
†Department of Science, Kyoto University of Education, Fujinomori, Fushimi-ku, Kyoto 612
(Received January 13, 1988)

To study a charge-induced stabilization of α-helix, α-helical peptides having a positively charged random-coil block on either N- or C-terminal of the helix, and having a strictly defined length, $(Ala)_{20}(X)_{20}Phe$ and $(X)_{20}(Ala)_{20}Phe$ (X=Lys or Orn), were synthesized. Component dipeptides were coupled on *p*-(oxymethyl)-phenylacetamidomethyl polystyrene.

A peptide bond is not symmetric and a polypeptide chain has a direction. As a consequence, properties inherent to α-helix and extrinsic effects of surrounding groups exerting upon α-helix might be different at the N- and C- terminal parts of a helix. We intended to discriminate the difference, and tried to approach the problem by studying the stabilities of polyalanine helix having a negatively charged random coil block either on an N- or C-terminal side of the helix.[1,2] The result showed that the difference in stabilities of two polymers was not solely depended on an enthalpic term (electrostatic interaction between external charges and a helix dipole) but also contributed from an entropic term, suggesting a contribution of helix-intrinsic properties on helical stability was different at the parts near N- and C-terminals. Since the stabilities of secondary structures are fundamental problem to study protein folding, asymmetry in the stability of α-helix has been called much attention recently[3] and a study of a system similar to that stated above but with positive charges has been requested.[4] If we could estimate a stability of polyalanine helix having a positively charged block on either N- or C-terminal, a combined analysis with the previous result for the helix with negative charges would make a comparison of the effects of opposite electric charges on the stability of α-helix possible. Furthermore, an estimation of intrinsic stabilities of α-helix at N- and C-terminal parts will be possible, under an assumption that the effect of positive and negative charges on an electric dipole was symmetric.

From a standpoint of peptide synthesis, preparations of homooligopeptides meet troubles not encountered in synthesis of peptides which incorporate various amino acid residues as naturally occurring ones. An application of a solution method for the preparation of oligopeptides having identical amino acid residues is sometimes extremely difficult, as such a peptide became less and less soluble in most of the solvents used in peptide chemistry when the number of residues increased. The other choice, a solid-phase method, is free from such a problem, however, purification of the product is difficult since immature peptides (namely, peptides having lesser numbers of residues than that was intended) will have similar properties with the desired one. Since the number of residues included in a peptide is most critical to stabilities of peptide secondary structures, it is crucial to have peptides with strictly defined length for a study of peptide conformation. In the present paper, we tried a coupling of dipeptide unit with a solid-phase methodology: in this case, immature peptides lacked two or multiples of two residues were expected to be discriminated more readily from the desired peptide.

Results and Discussion

Synthesis of $(Ala)_{20}(Lys)_{20}Phe$, (1), $(Lys)_{20}(Ala)_{20}Phe$, (2), $(Ala)_{20}(Orn)_{20}Phe$, (3), and $(Orn)_{20}(Ala)_{20}Phe$, (4). Merrifield's solid-phase procedure with *p*-(oxymethyl)-phenylacetamidomethyl (PAM)-resin[6] was used to synthesize **1—4**. The peptides have a general formula, $(L\text{-}Ala)_n(L\text{-}X)_nPhe$ or $(L\text{-}X)_n(L\text{-}Ala)_nPhe$ (X=Lys or Orn), in which poly-L-alanine block assumes α-helix (at least partly), and a block of positively charged lysine or ornithine forms a random-coil. The number of residues, *n*, was 20, which was consistent with the previous work.[1] The side chain of lysine is long and a hydrophobic nature of alkyl chain sometimes induces ordered structures, for example, β-structure. As we hoped to minimize such a possibility in the following study, peptides containing ornithine, which had one less methylene group were also synthesized. C-Terminal phenylalanine was incorporated as an internal marker during the synthesis. As the length of α-helix is most critical to its stability, dipeptide coupling was employed to ensure the desired product free from immature peptides. With dipeptide coupling, the inmature peptides differed by two amino acid residues and separation from the desired peptide was expected easier.[5] PAM-resin[6] was prepared with a slight modification: *p*-(bromomethyl)phenylacetic acid phenacyl ester was obtained from phenacyl alcohol (readily prepared from styrene oxide and dimethyl sulfoxide[7]) and trifluoroacetic anhydride, the procedure simpler and with higher yield. Dipeptide coupling was carried out with dicyclohexyl-

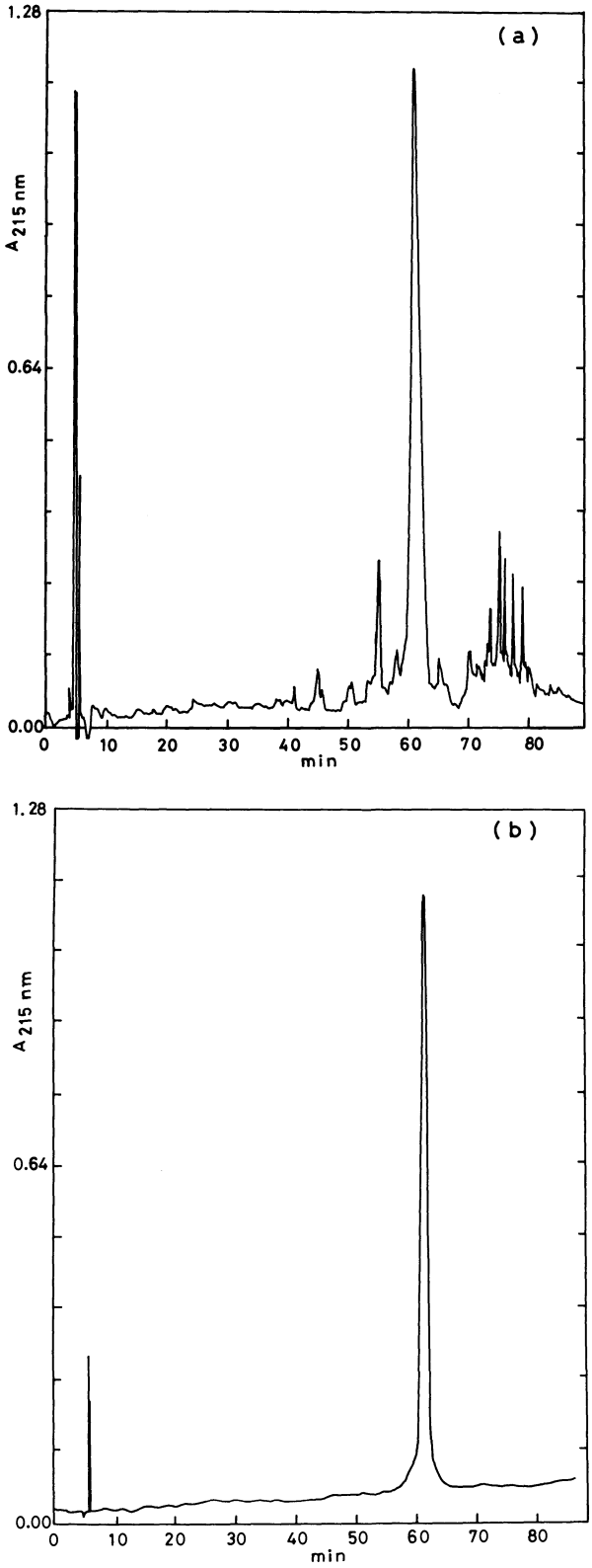

Fig. 1. HPLC analysis (Cosmosil 5C_{18}-P, 4.6×150 mm) of **1**.
(a) Crude product obtained by HF-cleavage. (b) After purification with preparative HPLC.
Peptide was eluted with an H_2O–acetonitrile gradient containing 0.05% TFA (10 to 20% acetonitrile over a period of 0 to 60 min and 20 to 40% acetonitrile from 60 to 90 min). Flow rate, 1 ml min^{-1}.

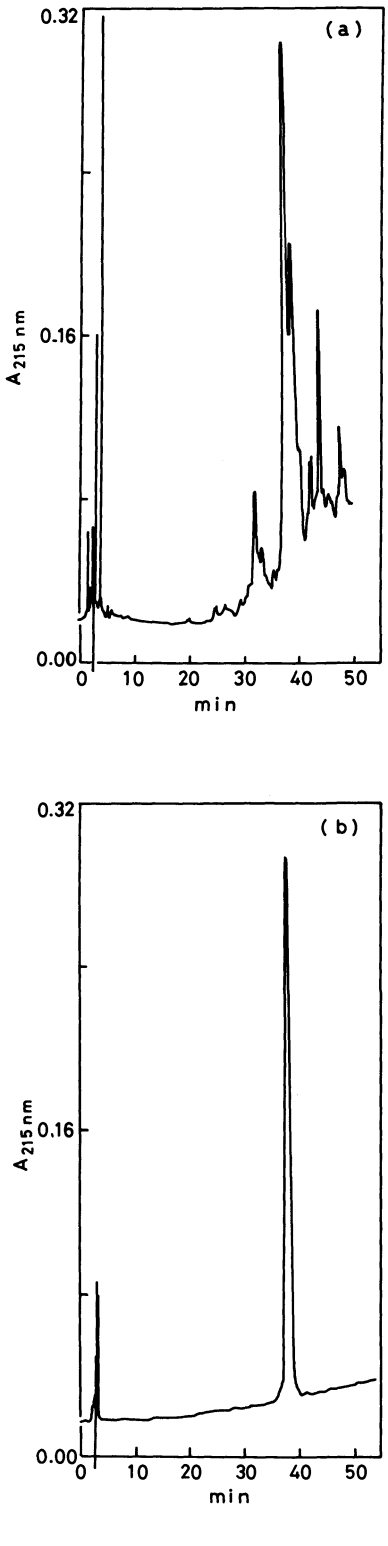

Fig. 2. HPLC analysis (Cosmosil 5C_{18}-P, 4.6×150 mm) of **2**.
Peptide was eluted with an H_2O–acetonitrile gradient containing 0.05% TFA (20 to 30% acetonitrile over a period of 0 to 30 min and 30 to 40% acetonitrile from 30 to 45 min). Flow rate, 1 ml min^{-1}.
(a) Crude product obtained by HF-cleavage. (b) After purification with preparative HPLC.

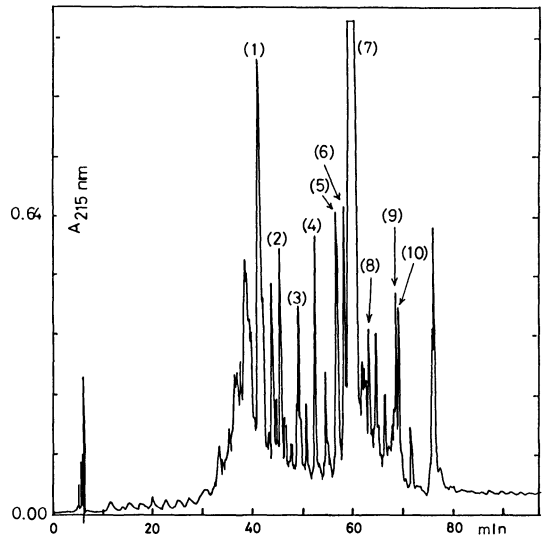

Fig. 3. Demonstration of resolution in HPLC of crude **1**.
Column: Cosmosil 5C_{18}-P, 10×250 mm, flow rate, 3 ml min^{-1}. Linear gradient elution: 0.05% aq.TFA: CH_3CN (100:0)→(67:23) for 0→80 min. About 2 mg of peptide was loaded. Peak assignment follows amino acid analysis: (1) $Ala_{2\,or\,4}Lys_{14\,or\,16}Phe$, (2) $Ala_6Lys_{18}Phe$, (3) $Ala_{8\,or\,10}Lys_{18}Phe$, (4) $Ala_{12}Lys_{18}Phe$, (5) $Ala_{16}Lys_{18}Phe$, (6) $Ala_{18}Lys_{20}Phe$, (7) peptide, **1**, (8) $Ala_{18}Lys_{16}Phe$, (9) $Ala_{20}Lys_{18}Phe$, (10) $Ala_{20}Lys_{16}Phe$.

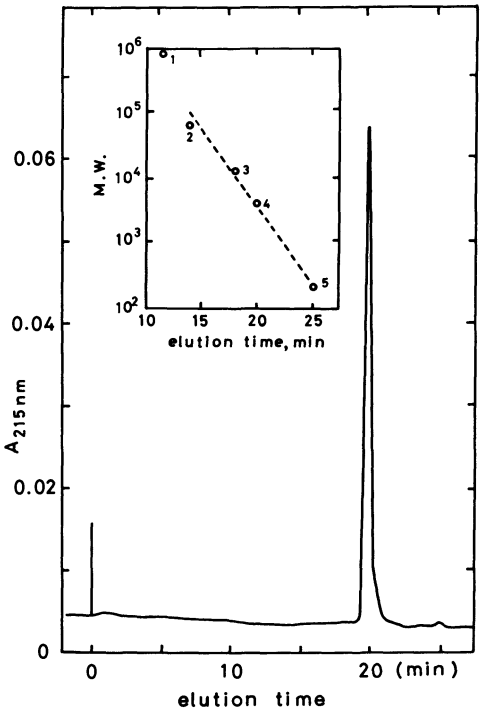

Fig. 4. Size exclusion chromatography of peptide **2**. Column: TSK Gel G2000SWXL (7.5×300 mm), elution with 0.1% TFA–0.2M KCl at a flow rate of 0.5 ml min^{-1}, at room temperature. Sample: 2 μg in 1 μl of 0.1% of TFA. Inset, Calibration of the column. 1, Blue Dextran (Pharmacia); 2, bovine serum albumin; 3, bovine pancreatic ribonuclease A; 4, peptide **2**, 5, GlyHis. M.W.: molecular weight, in logarithmic scale.

carbodiimide in the presence of 1-hydroxybenzotriazole. After the desired number of coupling, the products were cleaved from resin support with HF and were purified with high-performance liquid chromatography (HPLC). The results for peptides **1** and **2** are shown in Figs. 1 and 2, respectively. We characterized some of the satellite products and confirmed separation of the desired 41-residue peptides from immature peptides. As an example, the case of peptide **1** is shown in Fig. 3. Ion-exchange chromatography with carboxymethylcellulose was also employed to check the purity of HPLC-purified materials. We found only a single symmetric peak in every case. The overall yield of peptide **1**—**4** was from 9 to 19%.

Gel filtraion profiles of peptides **1**—**4** with TSK Gel G2000 (or 3000) SW may need some remarks. Each of the peptides gave a single peak at the position of expected elution position (as a typical example, Fig. 4 shows a chromatogram for peptide **2**, nearly identical results were obtained for the other peptides), but it was much retarded at higher pH. In the case of polylysines having molecular weights higher than 50000, such retardation of peak position as observed even at pH 3.0. The observed molecular weights of peptides **1** and **2** in solution derived from sedimentation equilibrium analysis at pH 4.65 (0.01 M KH_2PO_4–0.1 M KCl 1 M=1 mol dm^{-3}) were 4100 (c=0.668 mg ml^{-1}) and 4130 (c=0.789 mg ml^{-1}), respectively.

Check of Racemization. Athough 1-hydroxybenzotriazole[8] was included in dicyclohexylcarbodiimide-mediated coupling of dipeptide, racemization at the C-terminal amino acid of dipeptide might be a problem. We checked the content of D-amino acids with a modified[5] Manning-Moore procedure,[9] coupled with an HPLC separation of diastereomeric peptides.[10] The amounts (± 0.5%) of D-amino acids detected were: Ala in **1** or **3**, 0.7%; Ala in **2**, 1.0%; Ala in **4**, 0.6%; Orn in **3**, 1.5%; Orn in **4**, 1.9%; Lys in **1**, 1.0%; Lys in **2**, 0.8%.

Experimental†

All amino acids are of L-configuration. Melting points were measured on a micro hotplate and described without correction. Dipeptides, N^{α}-Boc-Lys(N^{ε}-*o*-Cl-Z)-Lys(N^{ε}-*o*-Cl-Z)-OH, N^{α}-Boc-Orn(N^{ε}-*o*-Cl-Z)-Orn(N^{ε}-*o*-Cl-Z)-OH, and Boc-AlaAla-OH, were prepared from Boc-amino acid succinimido esters. Elemental analysis and melting points are summarized in Table 1.

$BrCH_2C_6H_4CH_2COOH$. A solution of *p*-tolylacetic acid (25 g, 0.17 mol) and Br_2 (29.5 g, 1.1 equiv) in 200 ml CCl_4

† Abbreviations used: Boc, *t*-butyloxycarbonyl; *o*-Cl-Z, *o*-chlorobenzyloxycarbonyl; DCC, dicyclohexylcarbodiimide; DCHA, dicyclohexylamine; DIEA, *N*,*N*-diisopropylethylamine; DMF, *N*,*N*-dimethylformamide; HOBT, 1-hydroxybenzotriazole; TLC, thin-layer chromatography.

Table 1.

Compound	Melting point/°C[a]	Formula
N^{α}-Boc-Lys(N^{ε}-*o*-Cl-Z)-OSu	102—103 (AcOEt-Et_2O)	$C_{23}H_{30}O_8N_3Cl$
N^{α}-Boc-[Lys(N^{ε}-*o*-Cl-Z)]$_2$-OH·DCHA	142—143 (EtOH-AcOEt)	$C_{45}H_{67}O_9N_5Cl_2$
H-Orn(N^{δ}-*o*-Cl-Z)-OH	245—250 decomp (H_2O)	$C_{13}H_{17}O_4N_2Cl$
N^{α}-Boc-Orn(N^{δ}-*o*-Cl-Z)-OH	122—123 (AcOEt)	$C_{18}H_{25}O_6N_2Cl$
N^{α}-Boc-Orn(N^{δ}-*o*-Cl-Z)-OSu	152—156 (EtOH)	$C_{22}H_{28}O_8N_3Cl$
N^{α}-Boc-[Orn(N^{δ}-*o*-Cl-Z)]$_2$-OH	130 (MeOH-H_2O)	$C_{31}H_{40}O_9N_4Cl$
N^{α}-Boc-[Orn(N^{δ}-*o*-Cl-Z)]$_2$-OH·DCHA	166—169 (AcOEt)	$C_{43}H_{63}O_9N_5Cl_2$
Boc-Phe-$OCH_2C_6H_4CH_2CO_2CH_2COC_6H_5$	80—82 (AcOEt)	$C_{31}H_{33}O_7N$
Boc-Phe-$OCH_2C_6H_4CH_2CO_2H$	100—102 (Et_2O-pet.ether)	$C_{23}H_{27}O_6N$

Compound	Calcd			Found		
	C%	H%	N%	C%	H%	N%
N^{α}-Boc-Lys(N^{ε}-*o*-Cl-Z)-OSu	53.96	5.91	8.21	54.01	5.95	8.25
N^{α}-Boc-[Lys(N^{ε}-*o*-Cl-Z)]$_2$-OH·DCHA	60.46	7.67	7.83	60.33	7.55	7.52
H-Orn(N^{δ}-*o*-Cl-Z)-OH	51.92	5.70	9.32	51.94	5.59	9.37
N^{α}-Boc-Orn(N^{δ}-*o*-Cl-Z)-OH	53.93	6.29	6.99	53.91	6.18	7.02
N^{α}-Boc-Orn(N^{δ}-*o*-Cl-Z)-OSu	53.06	5.67	8.44	53.00	5.70	8.42
N^{α}-Boc-[Orn(N^{δ}-*o*-Cl-Z)]$_2$-OH	54.47	5.90	8.20	54.54	5.88	8.12
N^{α}-Boc-[Orn(N^{δ}-*o*-Cl-Z)]$_2$-OH·DCHA	59.71	7.34	8.10	59.44	7.42	8.06
Boc-Phe-$OCH_2C_6H_4CH_2CO_2CH_2COC_6H_5$	70.04	6.26	2.64	70.31	6.27	2.64
Boc-Phe-$OCH_2C_6H_4CH_2CO_2H$	66.81	6.58	3.39	66.93	6.43	3.30

a) Solvent for recrystallization in parentheses.

was stirred at room temperature and illuminated with a 60-W reflector lamp. The distance between the lamp and the reaction vessel was determined to give a moderate reaction. As the separated crystals of the product inhibited the reaction by reflecting back the incident light, the reaction mixture was filtered three times to collect crystals during 24 h of the photoreaction. If the solution became colorless, up to 3 ml of Br_2 was added to the reaction mixture. After the reaction had been completed (checked with TLC), the solvent was evaporated to give an additional amount of *p*-(bromomethyl)phenylacetic acid, which was recrystallized from acetone-hexane. Yield, 72%; mp 179—180 °C.

Br$CH_2C_6H_4CH_2COOCH_2COC_6H_5$. *p*-(Bromomethyl)-phenylacetic acid, 2.29 g, and 2.5 ml of trifluoroacetic anhydride were dissolved in 5 ml of benzene with warming. The mixture was kept at room temperature for 1 h and evaporated. The residue was dissolved in a mixture of 5 ml benzene and 1.55 g of phenacyl alcohol[7] with warming. Unreacted bromo acid was recovered with filtration after 3 h at room temperature and the filtrate was washed with aq. $NaHCO_3$ and concentrated to afford the phenacyl ester, which was recrystallized from ethyl acetate-cyclohexane, mp 88—90 °C. Yield, 79% (after correction of recovered acid).

Boc-Phe-$OCH_2C_6H_4CH_2COOCH_2COC_6H_5$. A solution of 2.8 g (8 mmol) of *p*-(bromomethyl)phenylacetic acid phenacyl ester, 4.25 g (16 mmol) of Boc-Phe-OH, and 2.8 ml (16 mmol) of DIEA in 60 ml DMF was stirred at room temperature for 24 h. After 8 h from the start of the reaction, TLC showed the bromo ester was consumed. Evaporation of DMF afforded an oil, which was dissolved in AcOEt (filtration was sometimes necessary to remove a mass of DIEA·HBr) and washed successively with 5% aq. citric acid and 0.5 M carbonate buffer, pH 10. Concentration of AcOEt layer gave needles, which were recrystallized from AcOEt. Yield, 93%.

Boc-Phe-$OCH_2C_6H_4CH_2COOH$. The compound was synthesized by a Zn-reduction of *p*-[(Boc-phenylalanyl)oxymethyl]phenylacetic acid phenacyl ester in a similar way as described in Ref. 6. Yield, 69%.

Boc-Phe-$OCH_2C_6H_4CH_2CONHCH_2$-Resin. Polystyrene beads (BioRad SX-1, 200—400 mesh) were aminomethylated according to the method described.[6] The content of amino group was 0.3 mmol g^{-1} resin from picric acid titration of the product. The resin was coupled[6] to Boc-Phe-OCH_2-$C_6H_4CH_2COOH$ and treated with 1-acetylimidazole (3 g/20 g resin) to block the residual free amino groups, if any. The product, which showed 0.285 mmol phenylalanine per g of resin on amino acid analysis, was used for the solid-phase peptide synthesis.

Solid-Phase Synthesis of H-$(Lys)_{20}(Ala)_{20}$Phe-OH, (1); H-$(Ala)_{20}(Lys)_{20}$Phe-OH, (2); H-$(Orn)_{20}(Ala)_{20}$Phe-OH, (3); and H-$(Ala)_{20}(Orn)_{20}$Phe-OH, (4). Solid-phase peptide synthesis was carried out according to the schedule outlined in Table 2. Double coupling was applied in every cycle except first 3 cycles of **1** and **3**. After each cycle was finished, an aliquot of the peptide resin was removed and checked by the Kaiser test.[11] Another aliquot was hydrolyzed and analyzed on an amino acid analyzer. After completion of required cycles, peptide resin was first treated with 50% TFA in dichloromethane, then with HF-20% anisole at 0 °C for 1 h. The residue was extracted with water (peptides **2** and **4**) or with 30% AcOH (peptides **1** and **3**). In the latter case, extracts were dialyzed against water and centrifuged to remove insolubles. The lyophilized peptides were dissolved in 0.05% TFA and purified with HPLC on a C_{18} column, with a linear gradient of acetonitrile containing 0.05% of TFA. The final yield of the purified peptide: **1**, 10%; **2**, 19%; **3**, 8.6%; **4**, 13.4%. Amino acid composition: **1**, Ala:Lys: Phe=21.4:21.0:1.0; **2**, Ala:Lys:Phe=20.6:19.3:1.0; **3**, Ala: Orn:Phe=20.8:20.2:1.0; **4**, Ala:Orn:Phe=19.3:19.4:1.0.

Check of Racemization. Peptide-resin and free peptides (about 1 μ mol peptide) were hydrolyzed with concd HCl-propionic acid (1:1, v/v, 110 °C, 24—48 h) or 6M HCl-0.15% phenol (110 °C, 24—48 h), respectively. To the hydrolyzate

Table 2.

1. Wash. CH_2Cl_2, 2 min×3.
2. Deprotection. 50% TFA in CH_2Cl_2, 30 min×1.
3. Wash. CH_2Cl_2, 2 min×5.
4. Neutralization. 5% DIEA in CH_2Cl_2, 2 min×2 (or 3[a]) for first coupling, 2 min×1 for second coupling.
5. Wash. CH_2Cl_2, 2 min×5.
6. Dipeptide,[b] 2 min.
7. HOBT[c] in DMF, 2 min.
8. DCC[d] in CH_2Cl_2. 6—18 h[e] for first coupling, 7—9 h for second coupling.
9. Wash. CH_2Cl_2–DMF(1:1) 2 min×2; CH_2Cl_2, 2 min×3.
10. Kaiser test.

The synthesis was started with 5 g (equivalent to 1.5 mmol of Boc-Phe groups) of Boc-Phe-PAM-resin. The volume of solvent was gradually increased from 50 to 80 ml according to swelling of the resin. First and second coupling mean the respective cycles when double coupling was employed. When a second coupling was employed, the step 4 and so on followed the step 10.

a) At the cycle later than the 5th. b) 4.5 mmol in the first coupling, 2.3 mmol in the second coupling. Boc-AlaAla-OH was dissolved in 30 ml of 30% DMF in CH_2Cl_2, lysine- and ornithine-dipeptides were dissolved in CH_2Cl_2. c) One and a half equivalent to dipeptide was used as a solution in 5 ml. d) An equivalent amount to dipeptide was used as a solution in 5 ml. e) 6—9 h for the first 5 cycles for **1** and **3** (coupling of BocAlaAlaOH) and first 10 cycles for **2** (coupling of BocLys(*o*-Cl-Z)Lys(*o*-Cl-Z)OH); 12—18 h for the other cycles.

were added 1.2 ml of 1 M $NaHCO_3$ and 50 μl of Boc-L-leucine succinimido ester (0.4 g/5 ml CH_3CN or 0.25 mmol ml^{-1}. 0.25 equiv to amino groups) and the mixture was evaporated after standing at room temperature for 2 h. The residue was treated with TFA or HCl and analyzed by HPLC in a similar way as described by Takaya et al.[10] Separation of diastereomeric peptides was achieved with Cosmosil $5C_{18}$-P (4.6×150 mm) at a flow rate of 1 ml min^{-1}. Elution times (min) of L-Leu-(X) were: (with 0.01 M potassium phosphate, pH 3.5) X=L-Lys, 16.5; D-Lys, 18.1; L-Orn, 8.5; D-Orn, 9.5; (with 0.01 M potassium phosphate, pH 3.5–CH_3CN=97:3) L-Ala, 5.5; D-Ala, 16.0. After a necessary correction for racemization during acid hydrolysis (estimated from free amino acids exposed to the same hydrolytic conditions), the degrees of racemization were estimated.

Chromatography. A Jasco Trirotar liquid chromatograph system was used for HPLC. For purification of peptides, Cosmosil $5C_{18}$-P (10×250 mm, Nakarai Chem. Co.) or YMC-ODS 5 μm (20×250 mm, Yamamura Kagaku), for analytical purpose, Cosmosil $5C_{18}$-P (4.6×150 mm), and for gel filtration, TSK G2000SWXL (7.5×300 mm, TOSO Co.) or G3000SW (7.5×600 mm) columns were used. Peptides were detected by UV absorption at 215 nm. For carboxymethylcellulose chromatography, the procedure described by Erickson and Merrifield[12] was followed.

Amino Acid Analysis. Peptide-resin and peptides were hydrolyzed at 130 °C for 12—24 h in concd HCl–propionic acid (1:1, v/v) or in TFA–concd HCl (9:1, v/v). In the latter case, a correction of amino acid recovery under the conditions was made: Ala, 98.4%; Phe, 96.4%; Orn, 75%; Lys, 97%, after 24 h. Amino acid analysis was carried out with a Jasco amino acid analyzer (single column operation, pH 5.25 ($[Na^+]$=0.2 M) and pH 5.0 ($[Na^+]$=1.6 M) buffers used).

Ultracentrifuge Analysis. Sedimentation equilibrium analysis was carried out with a Beckman Spinco E analytical ultracentrifuge, at 29500 rpm.

Encouragement by Prof. Tatsuo Ooi, Kyoto University, and ultracentrifuge analysis by Mr. E.-H. Kim are greatly acknowledged. This work was supported in part by a grant from the Ministry of Education, Science and Culture.

References

1) S. Takahashi, S.Ihara, and T.Ooi, *Nature (London)*, **276**, 735 (1978).
2) S.Ihara, T.Ooi, and S.Takahashi, *Biopolymers*, **21**, 131 (1982).
3) H. A. Scheraga, *Proc. Natl. Acad. Sci. U. S. A.*, **82**, 5585 (1985).
4) K. R. Shoemaker, P. S. Kim, D. N. Brems, S. Marqusee, E. J. York, I. M, Chaiken, J. M. Stewart, and R. L. Baldwin, *Proc. Natl. Acad. Sci. U. S. A.*, **82**, 2349 (1985).
5) S. Takahashi, *Bull. Chem. Soc. Jpn.*, **50**, 3344 (1977).
6) A. R. Mitchell, S. B. H. Kent, M. Engelhard, and R. B. Merrifield, *J. Org. Chem.*, **43**, 2845 (1978).
7) T. Tsuji, *Tetrahedron Lett.*, **1966**, 2413.
8) W. Konig and R. Geiger, *Chem. Ber.*, **103**, 788 (1970).
9) J. M. Manning, *Meth. Enzymol.*, **25**, 9 (1972).
10) T. Takaya, Y. Kishida, S. Sakakibara, *J. Chromatogr.*, **215**, 279 (1981).
11) E. Kaiser, R. L. Colescott, C. D. Bossinger, P. I. Cook, *Anal. Biochem.*, **34** 595 (1970).
12) B. W. Erickson and R. B. Merrifield, *J. Am. Chem. Soc.*, **95**, 3757 (1973).

 © 1988 The Chemical Society of Japan Bull. Chem. Soc. Jpn., 61, 2473—2479 (1988)

The Knoevenagel Reactions of Aldehydes with Carboxy Compounds. I. Reactions of *p*-Nitrobenzaldehyde with Active Methine Compounds

Mayumi TANAKA,* Osamu OOTA,† Hideo HIRAMATSU, and Kazuyoshi FUJIWARA
College of Industrial Technology, Nihon University,
Izumi-cho, Narashino-shi, Chiba 275
(Received January 21, 1988)

The Knoevenagel reactions of *p*-nitrobenzaldehyde (**1**) with β-keto acids, methylmalonic (**2a**) and α-methylacetoacetic acids (**2b**) were carried out in the presence of a tertiary amine such as pyridine. We have isolated the corresponding β-hydroxy intermediate (**3a**) by the reaction of **2a** which positively suggested the reaction proceeded by the Hann and Lapworth mechanism. A kinetic study using ^{1}H NMR revealed the existence of the reversibility between the starting materials and the β-hydroxy intermediate and that the rate determining step was decarboxylattion. But, when using the secondary amine, both the β-hydroxy acid and the corresponding condensation product were obtained via this reaction. These findings led to the conclusion that the reaction proceeded according to the two competing mechanisms, i.e., the Hann and Lapworth and Knoevenagel mechanisms. It was further clarified that either the decarboxylation step or the formation of the bis(dialkylamino) derivative was the rate determining step. The stereoselectivity of the β-hydroxy saturated compound has been closely related to the fact that the conformation of the intermediate possesses an intramolecular hydrogen bond to a hydroxyl group.

Some mechanisms,[1] depending on the kind of amine catalysts, have been proposed for the Knoevenagel reaction between an aldehyde and an active methylene compound. The Hann and Lapworth mechanisms[2] containing a β-hydroxy intermediate was expected when using tertiary amines. The Knoevenagel mechanism[3] has been predicted for the reaction which gives a condensation product via a bis(dialkylamino) derivative formed from a secondary amine and an aldehyde. However, these expectations were not realized because the condensation product was mainly obtained in both mechanisms.

For active methylene compounds such as malonic, cyanoacetic, and acetoacetic acids which accompanies decarboxylation, it is not yet clear that either dehydration or decarboxylation preferentially proceeds from the β-hydroxy intermediate in the presence of a tertiary amine.

An active methine compound such as β-keto acid was reacted with an aromatic aldehyde instead of an active methylene one. Gensler et al.[4] have reported that reaction of *p*-nitrobenzaldehyde with methylmalonic acid at 90 °C in the presence of piperidine–pyridine gave the corresponding cinnamic acid, but Fujiwara et al.[5] obtained 3-hydroxy-2-methyl-3-(*p*-nitrophenyl)propionic acid via the same reaction in pyridine. Yuan et al.[6] have considered the reaction mechanism operated by both catalysts at room temperature. However, the intermediate could not be confirmed in all cases. Tanikaga et al.[7] have reported that various aromatic aldehydes reacted with active methylene compounds in the presence of piperidine to isolate bispiperidides and that this reaction proceeded via the Knoevenagel mechanism. Lopez et al.[8] have shown that 2,3-*O*-isopropylidene-D-glyceraldehyde and α-methylacetoacetic acid reacted in toluene in the presence of diethylamine to give the β-ketol and α,β-enone. Inoue et al.[9] have stated that the reaction of *m*-nitrobenzaldehyde with *p*-nitrophenylacetic acid in the presence of secondary amines also proceeded via the Hann and Lapworth mechanism, i.e., the reaction proceeded via the β-hydroxy intermediate as in the case of tertiary amine catalysts. Thus, the mechanism for the Knoevenagel reaction accompanying decarboxylation is not yet clear.

To elucidate these problems, we carried out the Knoevenagel reactions of *p*-nitrobenzaldehyde (**1**) with methylmalonic (**2a**) and α-methylacetoacetic acids (**2b**) using secondary and tertiary amines. We report the isolation of the β-hydroxy intermediate and the mechanistic determination of the role of amines.

Results and Discussion

Synthesis of the β-Hydroxy Intermediate 3a and the β-Hydroxy Acid 4a. To a mixture of **1** (0.03 mol) and **2a** (0.06 mol), pyridine (0.18 mol) was added at room temperature and the mixture was kept for 6 h. The reaction time was determined in advance by ^{1}H NMR. From the residue remaining after the removal of the unreacted substances the β-hydroxy intermediate, **3a**, was isolated in a 54% yield after extraction with ether under acidic conditions (pH 2).

The β-hydroxy acid, **4a**, was obtained in a 46% yield by decarboxylation of the corresponding β-hydroxy intermediate. The structure of **4a** was identified with ^{1}H NMR, IR, and elemental analyses. The threo- and erythro-compound, **4a**, have been distinguished and their configurations were established by ^{1}H NMR at 4.89 (J=8.4 Hz) and 5.71 (J=4.2 Hz), respectively.

It may be affirmed by the isolation of **3a** that this

† Present address: Sanwa Kagaku Kenkyusho Co., Ltd., Higashisotobori-cho, Higashi-ku, Nagoya.

reaction proceeded via the Hann and Lapworth mechanism.

Kinetic Studies on Addition and Decarboxylation Stages. A mixture of **1**, **2a** (1.04 mmol, each) and pyridine-d_5 (3.11 mmol) was put into a sealed NMR tube and the reaction was run for 30 days at room temperature, then the ^{1}H NMR spectra of the mixture were measured. The signals were assigned as follows (Scheme 1): A, A′, and A″ are methyl proton signals of **2a**, **3a**, and **4a**, respectively, B for α-CH signal of **2a**, and B′ and B″ for β-CH signals of **3a** and **4a**, respectively and G refers to the proton signal of an aldehyde, where the intergral of B″ was calculated by the total amount of β-CH signals of the threo- and erythro- β-hydroxy acids. The integrated intensities of their signals are the mean values of more than three observed values. Relative concentrations of the compounds were calculated by the total amount of the groups (A+A′+A″).

Time dependences of the relative concentration of **3a** and **4a** measured by ^{1}H NMR during 30 days are shown in Fig. 1. The concentration of the β-hydroxy intermediate, **3a**, showed a maximum in about 3.5 h, while the β-hydroxy acid, **4a**, began to appear after 24 h.

The different formation times between **3a** and **4a** have suggested that the rate of the decarboxylation reaction was slower than that of the addition reaction at room temperature under these reaction conditions.

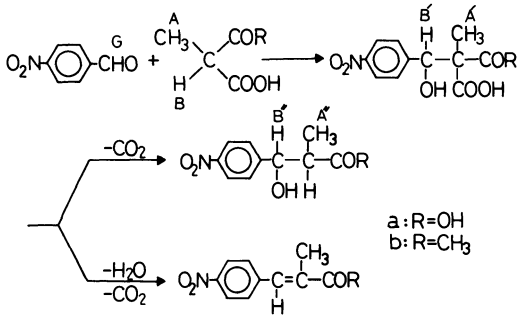

Scheme 1.

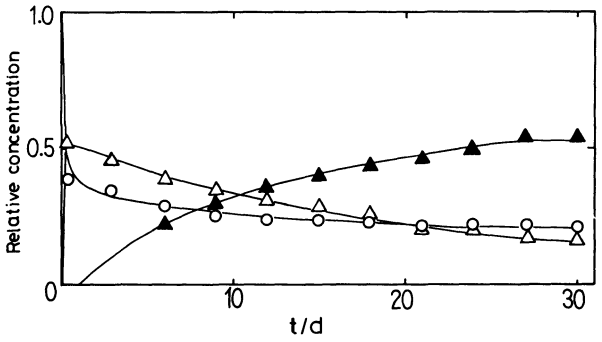

Fig. 1. Reaction of **1** with **2a** in the presence of pyridine and DMSO at room temperature. O: Starting material, △: β-hydroxy intermediate, ▲: β-hydroxy acid.

Figure 2 shows the initial part of Fig. 1. From this figure it can be assumed that the concentrations of **3a** become almost unchangeable after 200 min. Further, when the **3a** isolated in pure form was dissolved in pyridine at room temperature, a part of **3a** was cleaved into **1** and **2a**. This result has suggested the reversible reaction between starting materials and the intermediate, in accordance with the reports by Kinastowski et al.[10] They have demonstrated that there is a linear relation between the rate constant and the concentration of the catalyst at an addition stage and that the catalytic rate was fairly faster than the rate of the spontaneous chemical reaction. In practice, we have experienced great difficultly in calculating the rate sequence, **1**+**2**⇄**3**→**4**. To overcome this difficulty, an analysis based on a preequilibrium was considered. We tried to conveniently determine the apparent reaction rates at a constant catalytic concentration by dividing it into two stages: (a) the addition stage, and (b) the decarboxylation stage.

(a) The Addition Stage. From Fig. 2, we assumed that there exists a reversibility between second-order (forward reaction k_1) and first-order (reverse reaction k_2) rates and that the concentration of an aldehyde (C_1) is equal to that of an active methine compound (C_2), that is, $C_1=C_2$. The rate constants are expressed by:

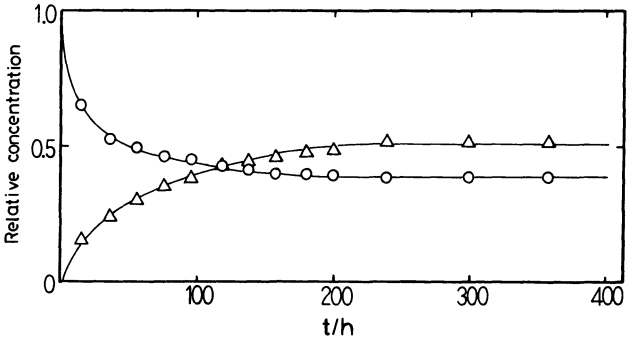

Fig. 2. Reaction of **1** with **2a** in the presence of pyridine and DMSO at room temperature. O: Starting material, △: β-hydroxy intermediate

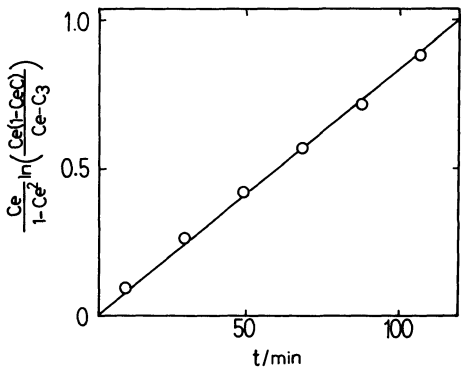

Fig. 3. Second-order plots vs. time in the reaction of **1** with **2a**.

$$k_1 t = \frac{C_e}{1 - C_e} \ln \frac{C_e(1 - C_e C_3)}{C_e - C_3}, \quad (1)$$

$$k_2 = \frac{k_1(C_0 - C_e)^2}{C_e}, \quad (2)$$

where C_0 is the initial concentration of aldehyde, and C_3 and C_e are the concentration and the preequilibrium concentrations of the β-hydroxy intermediate, respectively. In Fig. 3, the right side of Eq. 1 is plotted against reaction time. The plot gives a satisfactory straight line passing through the origin, from which the rate constants, k_1=4.56×10^{-1} and k_2=1.98×10^{-1} h^{-1}, and the preequilibrium constant, $K(=k_1/k_2)$= 2.30, could be estimated.

(b) The Decarboxylation Stage. By using the C_e value determined from Fig. 2, the rate of decarboxylation originating from the β-hydroxy intermediate was calculated by assuming a first-order reaction (k_3):

$$k_3 t = \ln \frac{C_e}{C_e - C_4}, \quad (3)$$

where C_4 is the concentration of the β-hydroxy acid. Figure 4 shows the relation between the right side in Eq. 3 and reaction time. As shown in this figure, a satisfactory straight line was also suggested by the results of a regression analysis. The rate constant, k_3, was 4.17×10^{-3} h^{-1}. The decarboxylation rate in this system was 10^{-2}-fold slower than the addition one. The reactions of *p*-substituted (cf. CN, Br) benzaldehydes with **2a** showed the same results.

We may firmly suggest that there is a reversibility between the starting materials and the β-hydroxy intermediate, and that the decarboxylation process is the rate determining step. The careful and exact observations by NMR have indicated that the β-hydroxy acid consisted of threo and erythro isomers and that the reaction rate of threo isomer was faster than that of the erythro. These details will be demonstrated later.

The Knoevenagel Reaction in the Presence of Piperidine. For the Knoevenagel reaction in the presence of a tertiary amine, the Hann and Lapworth mechanism was firmly demonstrated by our experiments. On the other hand, for the reaction promoted by the presence of secondary amines, another mechanism has been proposed by Knoevenagel himself; the catalyst reacts with an aldehyde to form a bis(dialkylamino) derivative, which then reacts with an active methylene compound to produce an unsaturated compound. However, the Knoevenagel reaction catalyzed by a secondary amine as reported by Lopez or Inoue et al. cannot be explained only by the Knoevenagel mechanism. To elucidate the complete mechanism of the reaction conducted in the presence of secondary amines, we studied similar reaction at room temperature by the use of ^{1}H NMR. To a solution of **1** and **2a** (1.04 mmol, each) in CD_3CN, piperidine was added dropwise (1/10, 1/3 and 1 mole per mole of aldehyde). Time dependences of the relative concentrations of **3a**, **4a** and α,β-unsaturated compound **6a** measured with ^{1}H NMR during 100 h are shown in Fig. 5. In all cases of the added piperidine, the β-CH-proton signal of **3a** appeared at δ 5.5 immediately after the initiation of the reaction. The concentration of this intermediate increased with increasing piperidine. After the appearance of the β-CH signal, **6a** was recognized. The product, **4a**, increased as the piperidine was decreased (1/10 and 1/3 mole per mole of an aldehyde). But, since the

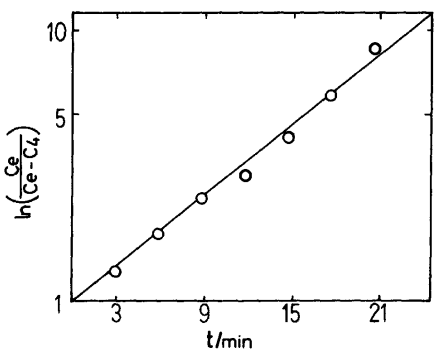

Fig. 4. First-order plots vs. time in the reaction of **1** with **2a**.

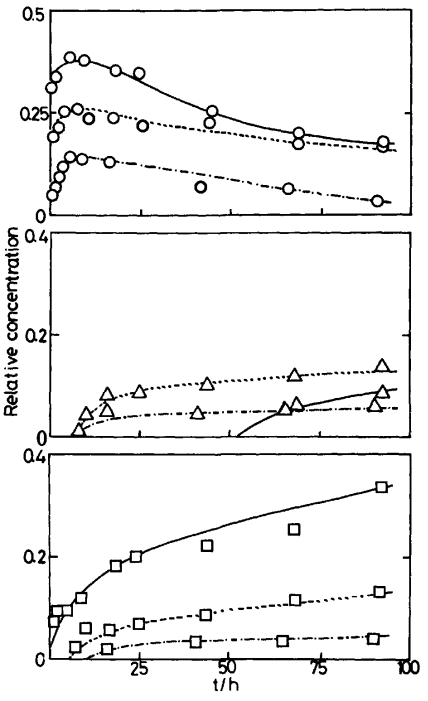

Fig. 5. Reaction of **1** with **2a** in the presence of piperidine. Piperidine concn. (mole per mole of aldehyde): —— (1 equiv), ------ (1/3 equiv), -·-·- (1/10 equiv). ○: β-Hydroxy intermediate, △: β-hydroxy acid, □: α,β-unsaturated compound.

dehydration from both the β-hydroxy intermediate and the β-hydroxy acid is usually difficult to occur under such reaction conditions, we have no convictions about the formation of **6a**. Therefore, the reactions of the β-hydroxy intermediate with amine catalysts were subsequently carried out.

Reaction from the β-Hydroxy Intermediate 3a. The reactions using **3a** (1.04 mmol) as a starting material were carried out in an NMR tube at room temperature with the $CDCl_3$–DMSO-d_6 solutions of piperidine (0.35 mmol) or pyridine (1.04 mmol). Time dependences of the relative concentrations of reactants in the presence of piperidine measured with ^1H NMR for 200 h are shown in Fig. 6. In both systems, **1** and **2a** were immediately produced and **4a** was obtained in a small amount. In the presence of piperidine, **6a**, which was not obtained in the presence of pyridine, was produced after the formation of **1** and **2a**. Further, when piperidine (2 mmol) was added to a solution of **1** (1 mmol) in $CDCl_3$, this solution showed the CH-proton signal of bispiperidide (**5a**) at δ 3.5. **6a** was produced immediately after addition of **2a** to the CD_3CN solution of **5a**. It gave additional credence that **3a** was easily decomposed into **1** and **2a** in the presence of piperidine, whereas only **4a** was obtained in the presence of pyridine. The product ratio, **4a**/**6a**, was dependent on the quantity of added piperidine. Judging from this fact, we may safely say that a slight amount of piperidine promotes the decarboxylation of **3a**, as supported by the study of Patai et al.[11] In other words, **6a** was not directly supplied by either the dehydration of **3a** or **4a**, but produced by the reaction via the Knoevenagel mechanism. From the above results there may exist a different mechanism between the presence of pyridine or piperidine. Therefore, we can advance the suggestion that the reaction accompanying the decarboxylation in the presence of piperidine proceeds by two competing mechanisms; the Hann and Lapworth(path A) and the Knoevenagel (path B) mechanisms as shown in Scheme 2, and that both decarboxylation from **3a** and the formation of **5a** are the rate determining steps of these competing reactions.

Reaction in the Presence of Various Secondary Amine Catalysts. Several reactions of **1** with **2a** were carried out in toluene–DMSO at room temperature using several kinds of secondary amines such as piperidine, morpholine, diethylamine, and dicyclohexylamine, in order to make a comparison with the reaction using the tertiary amine such as pyridine. The results are shown in Table 1. In all cases using the secondary amines as a catalyst, the mixture of **4a** and **6a** was obtained, but in pyridine, **6a** was not formed. The product ratio, **4a**/**6a**, depended on the type of the secondary amine catalyst, i.e., the yield of **6a** was somewhat higher than that of **4a**, when piperidine and morpholine were used, while that of **4a** was preferentially produced when diethylamine and dicyclohexylamine were used.

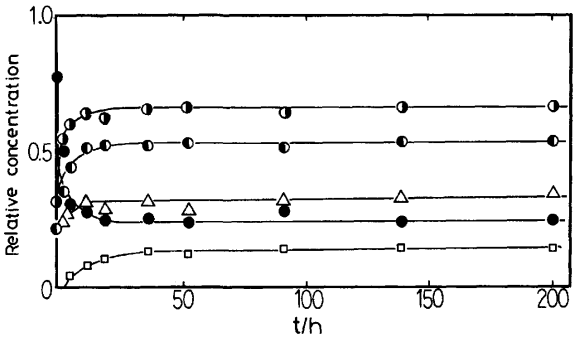

Fig. 6. Reaction from β-hydroxy intermediate in the presence of piperidine (1/3 equiv). ●: β-Hydroxy intermediate, ◐: **1**, ◑: **2a**, △: β-hydroxy acid, □: α,β-unsaturated compound.

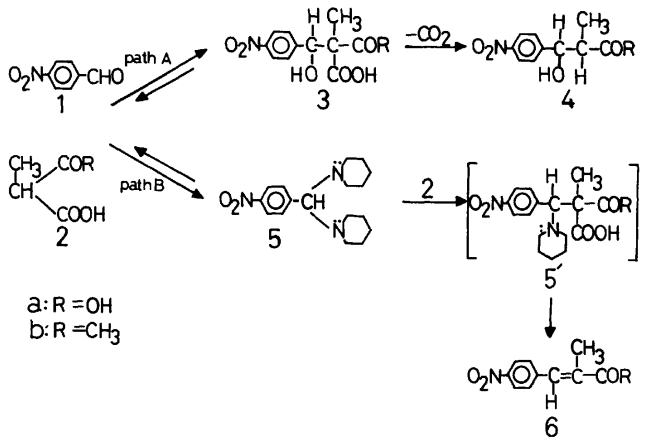

Scheme 2.

Table 1. Reaction of **1** with **2a**

Catalyst	pK_a	Yield/%		Selectivity	
		4a	**6a**	Erythro	: Threo
Pyridine	5.2	92.1	—	16	84
Piperidine	11.2	42.2	54.4	12	88
Morpholine	8.5	35.9	58.7	16	84
Diethylamine	10.8	81.3	15.5	10	90
Dicyclohexylamine	11.2	85.4	8.3	7	93
—[a]		—	—	59	41

a) This is not estimated from isolated product.

These results have given active support to the existence of the two competing mechanisms. In the reactions of **1** with diethylamine or dicyclohexylamine in $CDCl_3$ solutions in an NMR tube at room temperature, the bis(dialkylamino) derivatives can be hardly recognized. The order of the difficulty for detection of bis(dialkylamino) derivatives is as follows: dicyclohexylamine>diethylamine≫morpholine, piperidine.

We may thus conclude that the yield of the bis(dialkylamino) derivative increased by decreasing the steric hindrance of the secondary amines in accordance with the previously mentioned results.

Reaction of α-Methylacetoacetic Acid (2b). To verify the existence of another rate determining step, namely the difficulty of the decarboxylation, the reaction of **1** with **2b**, which was easier than **2a** during decarboxylation, was carried out using various secondary and tertiary amines in toluene. The reaction finished at −18 °C for a short period, about 2 days, compared well with the reaction of **2a** done for one month at room temperature. The β-hydroxy intermediate could not be determined due to the rapid decarboxylation. The yields of **4b** and **6b** are shown in Table 2. **4b** was preferentially obtained in all cases, but of these, **6b** was slightly produced using only secondary amines. The ratio of **4b** to **6b** varied with the kind of secondary amines and this tendency was somewhat similar to that of the reaction with **2a**.

We concluded that **1** reacted with α-substituted active methine compounds accompanying decarboxylation in the presence of secondary amines to afford the preferential formation of the β-hydroxy acid, when the active methine compound possible for decarboxylation and/or bulky amines were used. The existence of competing pathways in the reaction mentioned above was thus reconfirmed.

Stereochemistry of the Knoevenagel Reaction. In the Knoevenagel reaction of **1** with **2a**, the stereochemical data were also tabulated in Tables 1 and 2. The threo/erythro ratios were determined by ^1H NMR and compared with the results of Yuan et al. It was inconclusive that the stereoselective formation of the product was explainable by kind, bulkiness, and pK_a of the catalyst. But, we could draw a clear distinction between the presence or the absence of catalysts in both cases. Also, there was a subtle difference between the two active methine compounds. The ratio of the erythro isomer in the case of the reaction with **2b** is somewhat high.

Moreover, the reactions with **2b** were run with varying amounts of pyridine, giving the results shown in Table 3. The formation of the threo isomer was inclined to increase with an increase in pyridine while using 9-fold moles of pyridine, the *threo*-**4b** was obtained exclusively, although **2b** itself is apt to evolve carbon dioxide, resulting in a lower yield of **4b**. The basicity of the reaction system may contribute to this trend.

In general, the β-hydroxy intermediate obtained by the Knoevenagel reaction in the presence of a tertiary amine would be a mixture of diastereomers. For the Knoevenagel reaction with a planar prochiral compound, e.g., **1**, **3b** may include the threo isomer equivalent to the erythro, although **3b** could not be isolated. The fact will be experimentally verified in a subsequent paper on the reaction of **1** with *p*-nitrophenylacetic acid.[12] So, when the difference in the stereoselectivity of the saturated product can be detected, the fact is undoubtedly due to the decarboxylation stage initiated from the intermediate. In this reaction, it is theorized that the conformations cannot be exchanged in the course of the decarboxylation since we believe that the reaction conditions are hard to produce epimerization between threo and erythro isomers.[13] In addition, the coupling constants of **4b** (J=8.0 and 4.0 Hz) also correspond to those of **4a**. On an analogous discussion of Yuan et al., **3b** seems to possess an intramolecular hydrogen bonding.

Table 3. Reaction of **1** with **2b** in Pyridine

Pyridine/mol[a]	Yield/% **4b**	Selectivity Erythro	: Threo
0.1	60.1	33	67
0.5	57.8	50	50
1.5	31.4	25	75
4.0	32.7	16	84
9.0	28.7	0	100

a) Per mole of aldehyde.

Table 2. Reaction of **1** with **2a** in Toluene

Catalyst	pK_a	Yield/% **4a**	**6b**	Selectivity Erythro	: Threo
Pyridine	5.2	88.9	—	37	63
2,6-Lutidine[a]	6.7	93.7	—	8	92
DABCO[a]	8.6	98.1	—	15	85
Piperidine	11.2	83.7	14.3	12	88
Morpholine	8.5	82.9	17.0	27	73
Diethylamine	10.8	89.0	9.5	22	78
Dicyclohexylamine	11.2	94.0	4.9	27	73
—		64.1	—	67	33

a) These reactions were carried out without toluene.

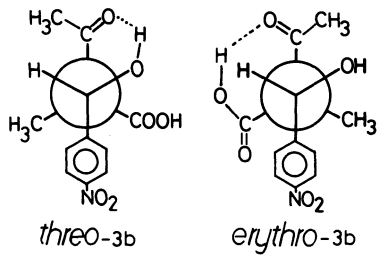

Scheme 3.

The intramolecular hydrogen bonding suggests to us the reactivity or stability of the intermediate, which will be demonstrated in a forthcoming report.

Taking into account the above statements, the conformations of **3b** are illustrated in Scheme 3. Each is invariable during decarboxylation. Further, the conformations of the corresponding saturated compounds were deduced by Karplus' equation.

When β-keto acids are used as the active methine compounds, we must consider the decarboxylation from a few types; the keto acid[14] or the hydroxy acid type,[15] and in the presence or in the absence of amine catalysts. The acetyl group of **3b** is able to be linked to both hydroxyl and carboxyl groups by intramolecular hydrogen bonding. In the absence of amine catalysts, we may propose the mechanism which would induce the spontaneous decarboxylation of the keto acid type instead of the hydroxy acid one. This argument is suggested by the fact that the erythro isomer was preferentially obtained. The representation of the erythro isomer is then carried out by a figure of conformation of the intramolecular bonding between acetyl and carboxyl groups.

On the contrary, the acetyl group of the threo conformation prefers the hydroxyl group to the carboxyl. This conformation is more stable than the other in the presence of amine catalysts, since the reverse reaction forming starting materials is relatively difficult to produce owing to the hydrogen bond.

Accordingly, the amine catalyst at first draws a free proton from the carboxyl group, and subsequently accelerates the decarboxylation of *threo*-**3b**, while it acts on the reversible reaction of *erythro*-**3b**. This might be supported by the fact that the appearance of *threo*-**4b** was easier and that in excess pyridine the threo isomer was exclusively produced.

Experimental

The melting points were measured with a Yanagimoto Melting-point Apparatus and are presented without correction. Solvents and other commercially obtained materials were purified by distillation. The IR spectra were recorded with a Shimadzu IRA-435 spectrometer and the ^{1}H NMR spectra using a JEOL JNM-MH100 (100 MHz) or a JEOL GX-400 (400 MHz) spectrometer with TMS as an internal standard. GLC analysis was performed on a Shimadzu GC-6AM gas chromatography using FID detector. All analyses were carried out on 2 m×3 mm in 10% Silicone SE-30.

β-Hydroxy Intermediate 3a. A mixture of **1** (0.03 mmol), **2a** (0.06 mmol), and pyridine (0.18 mmol) was kept at room temperature for 6 h. To the mixture was added 4 M HCl (1 M=1 mol dm^{-3}) until pH 2. Then the mixture, except pyridine, was extracted with ether. After the ether was evaporated, dil. Na_2CO_3 was added to the residue to pH 11, then an unreacted aldehyde was extracted with benzene. The remaining aqueous solution was acidified (pH 2) with concd. HCl, extracted with ether, and the ether solution was washed with water, and dried with anhydrous Na_2SO_4. After removing the remaining ether, pale yellowish crystals obtained were recrystallized from methanol–water solution (4.36 g, 54% yield). Mp 130—131 °C; Found: C, 49.29; H, 4.12; N, 5.04%. Calcd for $C_{11}H_{11}O_7N$: C, 49.08; H, 4.12; N, 5.20%. ^{1}H NMR (400 MHz) δ=1.289 (s, 3H), 5.534 (s, 1H), 7.619, 8.137 (2d, 4H), 10.285 (s, 3H). IR(KBr) 3500, 1710, 1350 cm^{-1}.

3-Hydroxy-2-methyl-3-(*p*-nitrophenyl)propionic Acid (4a). A mixture of **1** (0.03 mol), **2a** (0.06 mol) and pyridine (0.18 mol) was kept at room temperature for a month, and was added 4 M HCl until pH 2. The mixture was extracted with ether. After the ether was evaporated, dil. Na_2CO_3 was added to the residue to pH 11, then an unreacted aldehyde was extracted with benzene. The aqueous solution was acidified (pH 2) with concd. HCl and again was extracted with ether. The extract was washed with water, and dried with anhydrous Na_2SO_4. Ether was evaporated and the residue was recrystallized from methanol–water solution. (3.10 g, 46% yield); mp 139—141 °C. Found: C, 53.41; H, 5.01; N, 6.01%. Calcd for $C_{10}H_{11}O_5N$; C, 53.33; H, 4.93; N, 6.22%; ^{1}H NMR($CDCl_3$) δ=5.66 (br, 1H), 8.97 (br, 1H), 8.16, 7.58 (dd, 4H), 5.71 (d, β-CH, J=4.2 Hz, erythro), 4.89 (d, β-CH, J=8.4 Hz, threo), 2.80 (m, α-CH,erythro), 2.67 (m, α-CH, threo), 1.15 (d, CH_3, erythro), 0.95 (d, CH_3, threo); IR (KBr) 3500, 1710, 1350 cm^{-1}.

Bispiperidide (5a). A mixture of **1** (1 mol) and piperidine (3 mol) was kept at room temperature for about 5 h, and subsequently the reaction mixture was freeze-dried to yield quantitatively red brown crystals. Mp 79—82 °C; ^{1}H NMR ($CDCl_3$) δ=8.15—7.35 (dd, 4H), 3.65 (s, 1H), 2.30, 1.45 (dd, 10H).

Preparation of 6a from 5a and 2a. A mixture of (0.041 mol) **2a** and **5a** (0.041 mol) was kept at room temperature for about 4 days, and into the mixture 4M HCl was poured until pH 2 to yield crude yellowish crystals. They were recrystallized from methanol–water solution (7.38 g, 87% yield). Mp 205—206 °C; ^{1}H NMR ($CDCl_3$) δ=8.15, 7.35 (dd, 4H), 7.72 (s, 1H), 2.00 (s, 3H); IR (KBr) 1710, 1680, 1510, 1350, 860 cm^{-1}.

α-Methylacetoacetic Acid (2b). To α-methylacetoacetic acid ethyl ester (0.1 mol) 1 M NaOH aqueous solution (110 ml) was dropped at room temperature for about 12 h, the solution was extracted with ether (50 ml×2), concentrated until one-third volume, to which dil. H_2SO_4 (H_2SO_4=15 ml:3.5 ml) was added in the ice bath, saturated with NaCl, and extracted with ether. The extraction was continued until no α-methylacetoacetic acid in water layer was detected with $FeCl_3$ test. The extract was dried with anhydrous Na_2SO_4. Ether was evaporated in the ice-water bath to obtain the product (8.8 g, 76% yield). ^{1}H NMR

($CDCl_3$) δ=7.6—8.0 (br, 1H), 3.4 (q, 1H), 2.2 (s, 3H), 1.3 (d, 3H).

4-Hydroxy-3-methyl-4-(*p*-nitrophenyl)-2-butanone (4b) and 3-Methyl-4-(*p*-nitrophenyl)-3-buten-2-one (6b). A mixture of **1** (0.05 mol), **2b** (0.1 mol), and pyridine (0.025 mol) was kept at −50 °C in the Dry Ice bath, to −18 °C for 48 h under closed pressure, and opened in the nitrogen atmosphere. The reaction was continued until a disappearance of an aldehyde signal of **1** in an NMR spectrum. The unreacted catalyst was excluded from the solution in vacuo and the residue was washed with benzene to precipitate yellowish crystals, 4-hydroxy-3-methyl-4-(*p*-nitrophenyl)-2-butanone (4.21 g, 37.8% yield). Mp 93—95 °C; ^{1}H NMR ($CDCl_3$) δ=8.24, 7.60 (dd, 4H), 5.32 (d, β-CH, J=4.0 Hz, erythro), 4.92 (d, β-CH, J=8.0 Hz, threo), 4.60 (br, 1H), 2.96 (q, 1H), 2.26 (s, CH_3, erythro), 2.24 (s, CH_3, threo), 1.04 (d, α-CH_3, erythro), 0.98 (d, α-CH_3, threo); IR (KBr) 3400, 1710, 1510, 1350 cm^{-1}.

On the other hand, using piperidine–pyridine (0.1 mol, each) the same method was performed to obtain the mixture **4b** and **6b**. The residue was washed with benzene, and with additional methanol to yield crystals, 3-methyl-4-(*p*-nitrophenyl)-3-buten-2-one (0.27 g, 2.6% yield). Mp 205—206 °C; ^{1}H NMR ($CDCl_3$) δ=8.28—7.76 (dd+s, 5H), 2.40 (s, 3H, E), 2.00 (s, 3H); IR (KBr) 1650, 1510, 1350 cm^{-1}

References

1) G. Jones, "Organic Reactions," John Wiley and Sons, Inc., NY. (1967), Vol. 15, p. 204.
2) A. C. O. Hann and A. Lapworth, *J. Chem. Soc.*, **85**, 46 (1904).
3) E. Knoevenagel, *Ber.*, **32**, 2585 (1898).
4) W. J. Gensler and E. Berman, *J. Am. Chem. Soc.*, **80**, 4949 (1958).
5) K. Fujiwara and K. Naruse, *Nippon Kagaku Zasshi*, **83**, 1051 (1961).
6) K. Yuan and J. Zhu, *Acta Chim. Sinica*, **42**, 536 (1984); K. Yuan, G. Chen, and L. Kong, *ibid.*, **42**, 664 (1984).
7) R. Tanikaga, T. Tamura, Y. Nozaki, and A. Kaji, *J. Chem. Soc., Chem. Commun.*, **1984**, 87.
8) F. J. Lopez Aparicio, R. Garcia Mendosa, and F. Zorrilla Benitez, *Anal. Quim.*, **80**, 83 (1984).
9) K. Inoue, T. Imai, and M. Kakimoto, *Nippon Kagaku Kaishi*, **1985**, 1495.
10) S. Kinastowski and W. Mroczyk, *Bull. Acad. Pol. Sci., Ser. Sci. Chim.*, **27**, 95 (1979).
11) S. Patai, *J. Am. Chem. Soc.*, **76**, 3441 (1954).
12) M. Tanaka, H. Osawa, H. Hiramatsu, and K. Fujiwara, in preparation.
13) D. S. Noyce and K. S. Brauman, *J. Am. Chem. Soc.*, **90**, 5218 (1968).
14) J. Kenyon and W. A. Ross, *J. Chem. Soc.*, **1951**, 3407; C. G. Swain, R. F. W. Bader, R. M. Esteve, Jr., and R. N. Griffin, *J. Am. Chem. Soc.*, **83**, 1951 (1961).
15) S. Patai, "The Chemistry of Carboxylic Acids and Esters," John Wiley and Sons, Inc., (1969), p. 589.

Synthesis of Isoindoles. Acid or Base Induced Cyclization of 2-Cyanobenzaldehyde with Alcohols

Ryu SATO,* Michiko OHMORI, Fumiko KAITANI, Akiko KUROSAWA, Toshihide SENZAKI, Takehiko GOTO, and Minoru SAITO
Department of Resource Chemistry, Faculty of Engineering, Iwate University, Morioka 020
(Received January 25, 1988)

Various 3,3-dialkoxy-2,3-dihydro-1-hydroxy-1*H*-isoindoles (**2**) were obtained by treating 2-cyanobenzaldehyde (**1**) with alcohols in the presence of an acid catalyst such as silica gel. In the reaction using a base catalyst such as triethylamine and 1,8-diazabicyclo[5.4.0]undec-7-ene (DBU), 3-alkoxy-2,3-dihydro-1*H*-isoindol-1-ones (**4**) were formed via 3-alkoxy-1,3-dihydro-1-isobenzofuranimine (**3**). The use of 1,4-diazabicyclo[2.2.2]octane (DABCO) and *N,N,N',N'*-tetramethylethylenediamine (TMEDA) gave **2** besides **3** and **4**. A convenient and selective synthesis of isoindoles and its derivatives are described.

In the recent extensive studies on the chemistry of isoindoles, many chemists have directed their attention to the synthesis of 2,3-dihydro-1*H*-isoindol-1-ones and its derivatives, some of which are recognized to exhibit pharmacological and pesticidal activities.[1] In the previous paper we described the one-step formation of 3-amino-2,3-dihydro-1*H*-isoindol-1-ones from 2-cyanobenzaldehyde (**1**) with various amines and the 2-alkylation of the isoindole by the phase-transfer catalyst system.[2] To our knowledge, there have been only a few papers for the syntheses of 3-alkoxy-2,3-dihydro-1*H*-isoindol-1-ones by alkoxylation of 2,3-dihydro-3-hydroxy-1*H*-isoindol-1-one, which was prepared by electrolytic reduction from phthalimide, and its related reactions.[3] Hence our attention centered on the direct synthesis of the isoindoles and its derivatives having an alkoxy group on the isoindole ring by cyclization of **1** with alcohols. It is well-known that the nucleophilicities of alcohols are very poor, compared with those of amines. Therefore, based on the our previous results,[2] activation of substrates or reagents is necessary to bring about the reaction at ambient temperature. Recent interesting investigations on silica gel induced reactions[4] encouraged us to explore a facile formation of some isoindoles and its derivatives by acid, e.g. silica gel, or base, e.g. DABCO, induced cyclization of **1** with various alcohols. Here we describe the novel selective synthesis of isoindoles and its related compounds.

Results and Discussion

Reaction of 1 with Alcohols in the Presence of Acid Catalysts. Without catalyst, **1** did not react at all with any alcohols even under reflux conditions (Table 1, Run 1, Scheme 1), whereas in the presence of acid

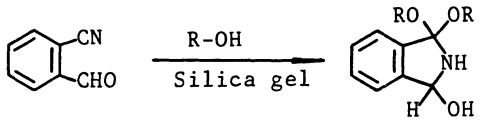

1 2

Scheme 1.

Table 1. Reactions of 2-Cyanobenzaldehyde (**1**) with Alcohol in the Presence of Various Catalysts

Run[a]	Alcohol R	Condition		Catalyst	mmol	Yield of **2**/%[b]
		Temp/°C	Time/h			
1	CH_3-	Reflux	24	—		0
2	CH_3-	Reflux	24	Phenol	0.5	95 **2a**
3	CH_3-	Reflux	24	Silica gel(C)[c]	0.1	97 **2a**
4	CH_3-	Reflux	16	Silica gel(G)[d]	0.1	99 **2a**
5	CH_3-	Reflux	24	$AlCl_3$	0.5	—
6	CH_3-	20	5(min)	12N-HCl	0.5(ml)	—
7	CH_3-	Reflux	5	Al_2O_3	0.5	82 **2a**
8	CH_3-	Reflux	7	Bu_4NI	0.1	79 **2a**
9	CH_3CH_2-	Reflux	12	Silica gel(G)	1.0	100 **2b**
10	$CH_3CH_2CH_2$-	Reflux	22	Silica gel(G)	1.0	86 **2c**
11	$(CH_3)_2CH$-	Reflux	48	Silica gel(G)	1.0	—
12	$CH_3CH_2CH_2CH_2$-	Reflux	52	Silica gel(G)	1.0	85 **2d**
13	$(CH_3)_3C$-	Reflux	75	Silica gel(G)	1.0	—
14	$(CH_3)_2CHCH_2$-	Reflux	75	Silica gel(G)	1.0	91 **2e**

a) Substrate: 0.5 mmol, alcohol: 4 ml. b) Isolated yields based on the substrate. c) Wako gel G-300 (200—300 mesh). d) Wako gel G (30—50 mesh).

catalysts (phenol and silica gel) **1** readily reacted with methyl alcohol to give 2,3-dihydro-1-hydroxy-3,3-dimethoxy-1*H*-isoindole (**2**) in high yields (Runs 2—4). In this reaction the use of silica gel of large grain size (Wako gel G), even if the silica gel was employed without drying, gave a better yield of **2** than that when a small grain size silica gel (Wako gel C-300) which was dried at 150 °C for 5 h under vacuum was used (Runs 3 and 4). Other solid acid catalyst, for example, alumina (neutral) also catalyzed this reaction (Run 7). Interestingly, tetrabutylammonium iodide behaved similarly to other acid catalysts to give **2** in good yield (Run 8). The use of aluminium chloride and hydrogen chloride gave, however, an acetal compound, 2-cyanobenzaldehyde dimethyl acetal (Runs 5 and 6). Thus, the catalytic effect of silica gel for cyclization of **1** with methyl alcohol was confirmed and a generality of this procedure was also shown in Table 1 (Runs 9—14). Characteristically, butyl and isobutyl alcohols also gave **2** in good yields, but isopropyl and *t*-butyl alcohols did not react with **1** under the same conditions. These results suggest that a steric bulkiness of alcohols used is an important factor in this reaction. Although, unfortunately, α,ω-alkanediols such as ethylene glycol did not react with **1** even at high temperature such as 100 °C, the present silica gel induced cyclization of **1** with various alcohols should provide a novel and convenient synthetic method for new isoindoles such as **2a—e**.

Reactions of 1 with Alcohols in the Presence of Base Catalysts. Compound **1** was treated with various alcohols in the presence of base catalysts such as triethylamine, DBU, DABCO, and TMEDA. In the presence of triethylamine, interesting product, isobenzofurans **3a,b** and **d** were obtained in yields as shown in Table 2. To our surprise, however, **2b** and **2d**, which were the same type of products in the silica gel induced reactions, were also obtained (Runs 2 and 3). Next we employed DBU as a strong base in the reaction of **1** with methanol. Thus, in the reaction at

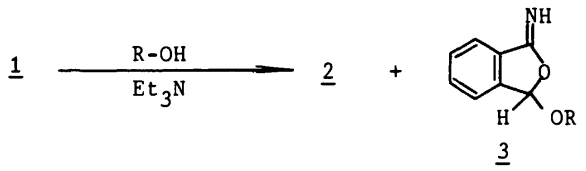

Scheme 2.

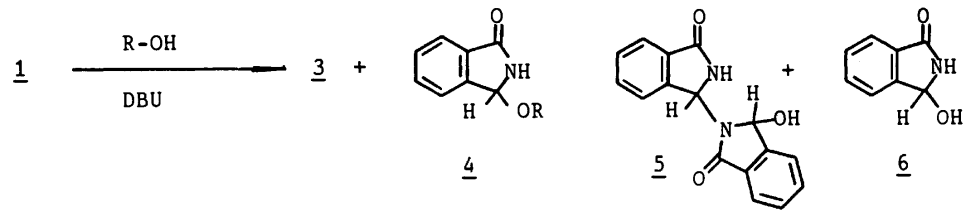

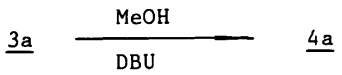

Scheme 3.

Table 2. Reactions of **1** with Alcohols in the Presence of Base Catalysts

Run[a]	Alcohol R	Condition		Catalyst	mmol	Yield of Product/%[b]		
		Temp/°C	Time/h			2	3	4
1	CH_3-	20	12	Et_3N	0.5	—	98 **3a**	—
2	CH_3CH_2-	30	48	Et_3N	0.5	13 **2b**	63 **3b**	—
3	$CH_3CH_2CH_2CH_2$-	30	49	Et_3N	0.5	24 **2d**	71 **3d**	
4	CH_3-	15	12	DBU	0.1	—	27 **3a**	58 **4a**
5	CH_3-	30	5	DBU	0.1	—	—	87 **4a**
6	CH_3CH_2-	50	7	DBU	0.2	—	—	20 **4b**
7	CH_3CH_2-	50	78	DBU	0.2	—	—	30 **4b**
8	$CH_3CH_2CH_2CH_2$-	40	45	DBU	0.2	—	—	29 **4d**
9	CH_3-	15	16	DABCO	0.1	52 **2a**	35 **3a**	—
10	CH_3-	Reflux	0.5	DABCO	0.1	97 **2a**	—	—
11	CH_3CH_2-	60	20	DABCO	0.2	83 **2b**	17 **3b**	—
12	$CH_3CH_2CH_2CH_2$-	60	20	DABCO	0.2	69 **2d**	31 **3d**	—
13	CH_3-	40	5	TMEDA	0.1	—	100 **3a**	—
14	CH_3CH_2-	40	30	TMEDA	0.1	67 **2b**	33 **3b**	—
15	$CH_3CH_2CH_2CH_2$-	40	30	TMEDA	0.1	52 **2d**	42 **3d**	—

a) Substrate: 0.5 mmol, alcohol: 4 ml. b) Isolated yields based on the substrate.

15 °C, **3a** was obtained in yield of 27% together with 2,3-dihydro-3-methoxy-1*H*-isoindol-1-one (**4a**, 58%) (Run 4), while only **4a** was given at 30 °C in yield of 87% (Run 5). In order to confirm an intermediacy, **3a** was actually treated with methanol in the presence of DBU under the same conditions, to afford the expected **4a** quantitatively. In the reaction of **1** with ethanol in the presence of DBU, a little different results were obtained. Thus, desired isoindole, 3-ethoxy-2,3-dihydro-1*H*-isoindol-1-one (**4b**), was given in a 30% yield. Furthermore, we found that 3′-hydroxy-1,2′-bi-2*H*-isoindole-1′,3(1*H*)-dione (**5**) was formed in 66% yield at 50 °C for 78 h together with 2,3-dihydro-3-hydroxy-1*H*-isoindol-1-one (**6**) (trace) when a small amount of water was present in the system (Scheme 3). To clarify the pathway of the formation of **5** and **6**, we carried out some related reactions. Compound **6** was obtained quantitatively when **1** was treated with water in the presence of DBU at room temperature. It is very interesting that **6** reacted easily with **1** at 50 °C for 3 h under the same conditions, to give **5** quantitatively (see Experimental). This result suggests that the NH group of **6** was activated with DBU and then reacted with **1** as a nucleophile to give **5**. Further evidence for the formation of **5** was obtained by the reaction of **1** with 2,3-dihydro-3-hydroxy-2-methyl-1*H*-isoindol-1-one (**7**) under the similar conditions. Thus, **7** did not react at all with **1**, and **7** was recovered completely. Based on these results, the formations of **5** and **6** are illustrated as shown in Scheme 4.

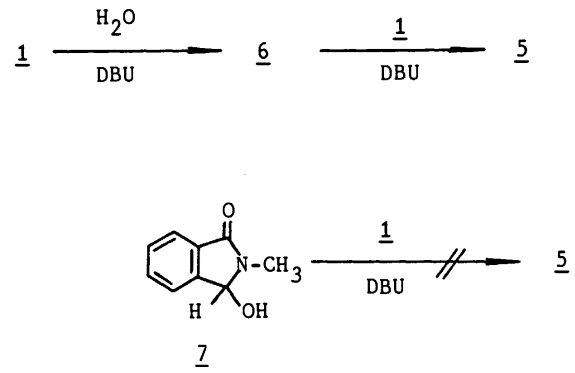

Scheme 4.

It should be noted that unexpected products **2**, which were given by the silica gel induced reaction, were obtained as major product when **1** was treated with methanol in the presence of DABCO (Table 2, Run 9). Moreover, 2,3-dihydro-3,3-dimethoxy-1-hydroxy-1*H*-isoindole (**2a**) was formed exclusively under reflux (Table 2, Run 10). In contrast to these results, upon treating **1** with methanol in the presence of TMEDA, **3a** was exclusively obtained (Run 13), though the reactions with other alcohols, e.g. ethanol (Run 14) and 1-butanol (Run 15), gave a mixture of **2** and **3**. Based on these results, it seems that methanol behaves as a special nucleophile in connection with the points of reactivity and stereochemistry. In the reaction of **1** with alcohols, there are apparently two pathways, i. e., (1) double nucleophilic additions of alcohol toward cyano group involving cyclization (Scheme 5, path A) and (2) nucleophilic attack of alcohol toward formyl group and sequent intramolecular rearrangement after cyclization (Scheme 5, path B). Therefore, it is possible that in the presence of an acid catalyst the reaction path A is predominant, while both reactions, path A and B, could take place simultaneously in the presence of a base catalyst. These results also suggest that triethylamine, DABCO, and TMEDA can serve as conjugated acids.[5]

In conclusion, the selective synthesis of isoindoles, such as **2** and **4**, was performed by the reaction of **1** with alcohols in the presence of various acid or base catalysts.

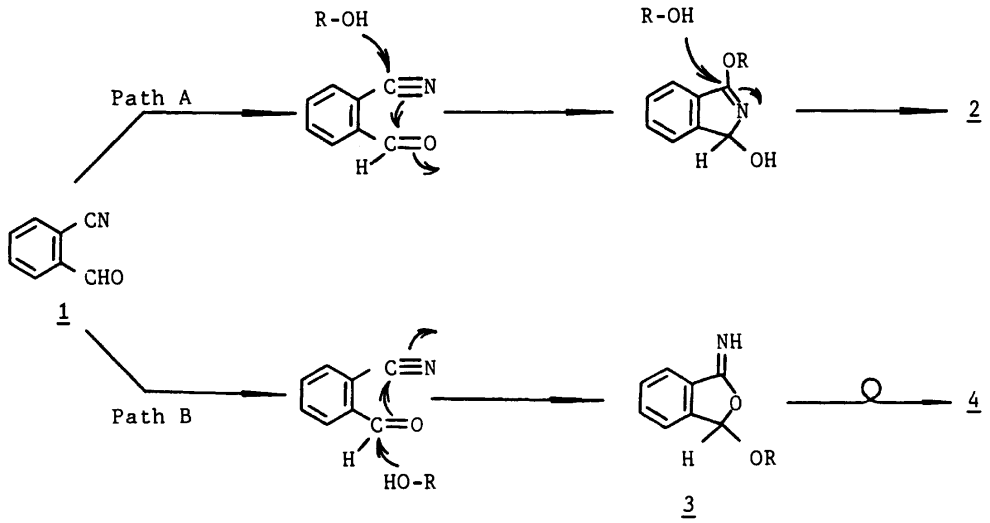

Scheme 5.

Experimental

All melting points were uncorrected. IR spectra were obtained on a Hitachi 295 spectrophotometer and ^{1}H NMR spectra were obtained on a Hitachi R-22 spectrometer using tetramethylsilane as an internal standard. Mass spectra were taken with a Hitachi RMU-6M mass spectrometer. Elemental analyses were carried out with a Yanagimoto MT-3. All reactions were monitored by TLC (Merck Kiesel gel 60-GF 254).

Materials. All reagents were obtained from Wako Pure Chemical Industries Ltd., Tokyo Kasei Co., Ltd., or Aldrich Chemical Co. The reagents used were further purified by usual methods such as recrystallization or distillation. The silica gel used as an acidic catalyst (Wako gel G) was employed without drying, but Wako gel C-300 was dried under vacuum at 150 °C for 5 h.

General Procedure for Synthesis of 2 by Reactions of 1 with Alcohols in the Presence of Silica Gel. To a solution of **1** (66 mg, 0.5 mmol) in 4 ml of an alcohol was added silica gel (60 mg, Wako gel G) and the mixture was refluxed for 16—75 h. After filtration and evaporation of the alcohol, the residue obtained was chromatographed on silica gel using the mixture of chloroform and methyl alcohol (8/1, v/v) as an eluent to give **2a—e.**

2,3-Dihydro-1-hydroxy-3,3-dimethoxy-1*H*-isoindole (2a): Colorless crystals ($CHCl_3$); mp 97 °C; IR (KBr) 3175 and 3400 cm^{-1}; ^{1}H NMR ($CDCl_3$) δ=3.37 (6H, s, CH_3×2), 5.66 (1H, s, CH), 6.15 (1H, br, OH), 6.90 (1H, br, NH), and 7.30—7.70 (m, 4H, arom); MS *m/z* 164 (M^+—OMe). Found: C, 61,48; H, 6.73; N, 7.15%. Calcd for $C_{10}H_{13}NO_3$: C, 61.53; H, 6.71; N, 7.18%.

3,3-Diethoxy-2,3-dihydro-1-hydroxy-1*H*-isoindole (2b): Colorless crystals (CH_2Cl_2); mp 99 °C; IR (KBr) 3180 and 3375 cm^{-1}; ^{1}H NMR ($CDCl_3$) δ=1.23 (6H, t, *J*=7.0 Hz, CH_3×2), 3.62 (4H, q, *J*=7.0 Hz, CH_2×2), 5.83 (1H, s, CH), 6.00 (1H, br, OH), 7.10 (1H, br, NH), and 7.23—7.80 (4H, m, arom); MS *m/z* 178 (M^+—OCH_2CH_3). Found: C, 64.55; H, 7.65; N, 6.34%. Calcd for $C_{12}H_{17}NO_3$: C, 64.55; H, 7.67; N, 6.27%.

2,3-Dihydro-1-hydroxy-3,3-dipropoxy-1*H*-isoindole (2c): Colorless crystals ($CHCl_3$); mp 70 °C; IR (KBr) 3175 and 3370 cm^{-1}; ^{1}H NMR ($CDCl_3$) δ=0.94 (6H, t, *J*=7.0 Hz, CH_3×2), 1.65 (4H, quint, *J*=7.0 Hz, CH_2×2), 3.55 (4H, dt, *J*=7.0 and 3.1 Hz, CH_2×2), 5.78 (1H, s, CH), 6.10 (1H, br, OH), 7.22 (1H, br, NH), and 7.33—7.83 (4H, m, arom); MS *m/z* 192(M^+—OPr). Found: C, 67.26; H, 8.23; N, 5.83%. Calcd for $C_{14}H_{21}NO_3$: C, 66.91; H, 8.42; N, 5.57%.

3,3-Dibutoxy-2,3-dihydro-1-hydroxy-1*H*-isoindole (2d): Colorless crystals ($CHCl_3$); mp 72 °C; IR (KBr) 3180 and 3325 cm^{-1}; ^{1}H NMR ($CDCl_3$) δ=0.90 (6H, t, *J*=7.5 Hz, CH_3×2), 1.20—1.76 (8H, m, CH_2×4), 3.45—3.73 (4H, m, CH_2×2), 5.78 (1H, s, CH), 6.03 (1H, br, OH), and 7.28—7.82 (5H, m, NH and arom); MS *m/z* 206 (M^+—OBu). Found: C, 68.87; H, 8.85; N, 5.27%. Calcd for $C_{16}H_{15}NO_3$: C, 68.79; H, 9.02; N, 5.27%.

2,3-Dihydro-1-hydroxy-3,3-diisobutoxy-1*H*-isoindole (2e): Colorless crystals ($CHCl_3$); mp 93 °C; IR(KBr) 3180 and 3395 cm^{-1}; ^{1}H NMR ($CDCl_3$) δ=0.96 (12H, d, *J*=7.0 Hz, CH_3×4), 1.75—2.15 (2H, m, *J*=7.0 Hz, CH×2), 3.36 (4H, dd, *J*=7.0 and 1.5 Hz, CH_2×2), 5.81 (1H, s CH), 6.10 (1H, br, OH), and 7.31—7.90 (4H, m, arom and NH); MS *m/z* 206 (M^+—OBu-i). Found: C, 68.89; H, 9.26; N, 5.02%. Calcd for $C_{16}H_{25}NO_3$: C, 68.79; H, 9.02; N, 5.01%.

General Procedure for Synthesis of 3 and 4 by Reactions of 1 with Alcohols in the Presence of Base Catalyst. To a solution of **1** (66 mg, 0.5 mmol) in 4 ml of an alcohol was added triethylamine, DBU, DABCO, or TMEDA (0.1—0.5 mmol, respectively) and the mixture was stirred at 15—60 °C for 0.5—16 h. After evaporation of the alcohol, the residue obtained was chromatographed on silica gel using the mixture of chloroform and methyl alcohol (8/1, v/v) as eluent, to give **3** and **4**.

1,3-Dihydro-1-imino-3-methoxyisobenzofuran (3a): Colorless crystals ($CHCl_3$); mp 129 °C; IR (KBr) 1640 and 3200 cm^{-1}; ^{1}H NMR ($CHCl_3$) δ=4.10 (3H, s, CH_3), 6.10 (1H, s, CH), and 7.30—7.90 (5H, m, arom and NH); MS *m/z* 132(M^+—OMe). Found: C, 65.82; H, 5.53; N, 8.49%. Calcd for $C_9H_9NO_2$: H, 66.25; H, 5.56; N, 8.58%.

3-Ethoxy-2,3-dihydro-1-iminoisobenzofuran (3b): Colorless crystals ($CHCl_3$); mp 112 °C; IR (KBr) 1620 and 3140 cm^{-1}; ^{1}H NMR ($CDCl_3$) δ=1.48 (3H, t, *J*=7.0 Hz, CH_3), 4.51 (2H, q, *J*=7.0 Hz,-CH_2-), 6.15 (1H, s, CH), and 7.30—7.73 (5H, m, NH and arom); MS *m/z* 177 (M^+). Found: C, 67.69; H, 6.15; N, 7.96%. Calcd for $C_{10}H_{11}NO_2$: C, 67.76; H, 6.26; N, 7.90%.

3-Butoxy-2,3-dihydro-1-iminoisobenzofuran (3d): Colorless crystals ($CHCl_3$); mp 63 °C; IR (KBr) 1620 and 3100 cm^{-1}; ^{1}H NMR ($CDCl_3$) δ=1.02 (3H, t, *J*=7.0 Hz, CH_3), 1.02—2.03 (4H, m, -CH_2CH_2-), 4.46 (2H, t, CH_2), 6.16 (1H, s, CH), and 7.30—7.72 (5H, m, NH and arom); MS *m/z* 205 (M^+). Found: C, 70.04; H, 7.49; N, 6.64%. Calcd for $C_{12}H_{15}NO_2$: C, 70.22; H, 7.37; N, 6.82%.

4a: Colorless crystals ($CHCl_3$); mp 100 °C (lit, 99 °C[3]).

4b: Colorless crystals ($CHCl_3$); mp 105 °C (lit, 108 °C[3]).

4d: Colorless crystals ($CHCl_3$); mp 92 °C; IR (KBr) 1720 and 3170 cm^{-1}; ^{1}H NMR ($CDCl_3$) δ=1.88 (3H, t, *J*=7.0 Hz, CH_3), 1.13—1.76 (4H, m, -CH_2CH_2-), 3.18—3.66 (2H, m, CH_2), 5.96 (1H, s, CH), and 7.36—8.04 (5H, m, NH and arom); MS *m/z* 205 (M^+). Found: C, 70.25; H, 7.45; N, 6.80%. Calcd for $C_{12}H_{15}NO_2$: C, 70.22; H, 7.37; N, 6.82%.

Reaction of 3a with Methanol in the Presence of DBU. To a solution of **3a** (82 mg, 0.5 mmol) in methanol (4 ml) was added DBU (15 mg, 0.1 mmol) and the solution was stirred at 20 °C for 3 h. After evaporation of methanol, the residue was chromatographed on silica gel using mixture of chloroform and ether (8/1, v/v), to give **4a** (81 mg, ca. 100%).

Reaction of 1 with Water in the Presence of DBU. To a solution of **1** (66 mg, 0.5 mmol) in water (4 ml) was added DBU (45 mg, 0.3 mmol) and the solution was heated at 50 °C for 3 h with stirring. After evaporation of water under vacuum, the residue was chromatographed on silica gel using the mixture of chloroform and methanol (10/1, v/v), to give **6** (70 mg, 93%) and **5** (5 mg, 7%).

Reaction of 1 with 6 in the Presence of DBU. To a solution of **1** (33 mg, 0.25 mmol) and DBU (30 mg, 0.2 mmol) in ethanol (4 ml) was added **6** (37 mg, 0.25 mmol) and the mixture was heated at 50 °C for 3 h with stirring. After evaporation of ethanol the residue was chromatographed on silica gel using the mixture of chloroform and methanol (10/1, v/v), to give **5** quantitatively (70 mg, 100%).

5: Colorless crystals (MeOH); mp 225 °C; IR (KBr) 1700 and 3220 cm^{-1}; ^{1}H NMR (DMSO-d_6) δ=5.74 (1H, d, *J*=9.1 Hz, CH), 6.45 (1H, s, CH), 6.63 (1H, d, *J*=9.1 Hz,

OH), 7.40—7.80 (8H, m, arom), and 8.77 (1H, s, NH); MS *m/z* 148 and 132. Found: C, 68.30; H, 4.29; N, 9.76%. Calcd for $C_{16}H_{12}N_2O_3$: C, 68.57; H, 4.32; N, 9.99%.

6: Colorless crystals (MeOH); mp 165 °C (lit, 178,[3] 184[6] °C); IR (KBr) 1700 and 3450 cm^{-1}; ^1H NMR (DMSO-d_6) δ=5.86 (1H, d, J=9.1 Hz, CH), 6.29 (1H, d, J=9.1 Hz, OH), 7.40—7.80 (4H, m, arom), and 8.70—9.00 (1H br, NH); MS *m/z* 149 (M^+). Found: C, 64.22; H, 9.36; N, 4.67%. Calcd for $C_8H_7NO_2$: C, 64.42; H, 9.39; N, 4.73%.

7: This compound was synthesized by alkylation of phthalimide followed by reduction with sodium borohydride according to the method as shown in the literature.[6] Colorless crystals ($CHCl_3$); mp 130 °C (lit, 129 °C[7]).

References

1) Fujimoto, Japan Kokai Tokkyo Koho, 188567 (1982) [*Chem. Abstr.*, **98**, 179215x (1983)]; P. N. Giraldi and G. Nannini, Ger. Offen, 2154525 (1971) [*Chem. Abstr.*, **77**, 88292v (1972)]; P. N. Giraldi and V. Mariotti, S. Afr. Patent., 3624206 (1971) [*Chem. Abstr.*, **70**, 68156f (1969)]; G. Sacchetti, Farmaco ED Prat., **27**, 708 (1972) [*Chem. Abstr.*, **78**, 119448c (1973)]; M. Takeda, *Oyo Yakuri.*, **7**, 903, 1073 (1973); T. Mukai, *Jpn. T. Phatmacol.*, **31**, 1073 (1973); P. Aeberli and J. Houlihan, *J. Org. Chem.*, **34**, 165 (1969); C. A. Demerson and I. L. Jikovsky, U. S. Patent., 4355031 (1982) [*Chem. Abstr.*, **98**, 160738y (1983)]; M. Los, Eur. Pat. Appl. EP., 135711 (1985) [*Chem. Abstr.*, **103**, 87875f (1985)]; M. Los, Eur. Pat. Appl. EP., 519603 (1985) [*Chem. Abstr.*, **103**, 87872c (1985)]; M. Waniak, H. C. van der Plas, and S. Haskema, *J. Org. Chem.*, **50**, 3435 (1985).

2) R. Sato, T. Senzaki, T. Goto, and M. Saito, *Chem. Lett.*, **1984**, 1599; R. Sato,T. Senzaki, T. Goto, and M. Saito, *Bull. Chem. Soc. Jpn.*, **59**, 2950 (1986).

3) B. Sakurai, *Bull. Chem. Soc. Jpn.*, **5**, 184 (1930); M. M. Dunet and A. Willemart, *Bull. Soc. Chim. Fr.*, **1948**, 887 and 889.

4) Y. Kamitori, M. Hojo, R. Masuda, and T. Yoshida, *Tetrahedron Lett.*, **27**, 4767 (1986); Y. Kamitori, M. Hojo, R. Masuda, T. Kimura, and T. Yoshida, *J. Org. Chem.*, **51**, 1427 (1986). As review: D. W. Young, *Synthesis*, **1979**, 481; M. Hojo and R. Masuda, *Yuki Gosei Kagaku Kyokai Shi*, **37**, 689 (1979)

5) F. Toda and K. Tanaka, *Chem. Lett.*, **1986**, 1905.

6) D. A. Burnett, J. K. Choi, D. J. Hart, and Y. M. Tsai, *J. Am. Chem. Soc.*, **106**, 8201 (1984); A. O. Stewart and R. M. Williams, *ibid.*, **107**, 4289 (1985).

7) F. Englaender, H. Funten, P. Rieger, K-D. Steffen, G. Weigerber, and G. Zoche, *Chem.-Ztg.*, **103**, 9 (1979).

 © 1988 The Chemical Society of Japan Bull. Chem. Soc. Jpn., 61, 2487—2491 (1988)

The Crystal and Molecular Structures of 2,2,4,6-Tetraphenyldihydro-1,3,5-triazine Acetone Solvate and 2-Propanol Solvate

Yukie MORI, Yuji OHASHI, and Koko MAEDA*
Department of Chemistry, Faculty of Science, Ochanomizu University,
Otsuka, Bunkyo-ku, Tokyo 112
(Received January 29, 1988)

The crystal and molecular structures of 2,2,4,6-tetraphenyldihydro-1,3,5-triazine acetone solvate (**1**) which turns red on exposure to UV light, and 2-propanol solvate (**2**) which shows no photocoloration, have been determined by the X-ray method. The crystals of both inclusion compounds are monoclinic. For **1** the space group is $P2_1/n$; Z=4, with a=16.385(2), b=11.987(2), c=12.939(2) Å, and β=92.24(2)°. For **2** the space group is $C2/c$; Z=8, with a=21.967(3), b=13.418(1), c=19.576(4) Å, and β=118.73(1)°. The final R values were 0.082 and 0.083 for **1** and **2** respectively. In both crystals, the dihydrotriazine ring exists in 2,3-dihydro form, which is one of the two possible tautomeric forms. In **1** each acetone molecule interacts with only one molecule of tetraphenyldihydrotriazine by N(3)–H(3)···O hydrogen bond, while in **2** tetraphenyldihydrotriazine and 2-propanol molecules are alternately connected by N(3)–H(3)···O and N(5)···H–O hydrogen bonds to construct a ribbon-like structure. It was suggested that the N(3)–H(3)···O–H···N(5) hydrogen bonds which exist in **2** but not in **1** inhibit photocoloration of **2**.

2,2,4,6-Tetraphenyldihydro-1,3,5-triazine (hereafter abbreviated as triazine) was synthesized by Lottermoser in 1896 and reported to exhibit photochromism in the solid state,[1] but the structure of the colored species has been undetermined. It has been reported that triazine exists in an equilibrium mixture of 2,3-dihydro (a) and 2,5-dihydro (b) forms, which are

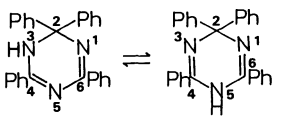

(a) (b)

prototropic tautomers, in solutions and in the solid state.[2] During the course of the investigation on the photocoloration of triazine we found that triazine forms crystalline inclusion compounds with various solvent molecules having one hetero atom with molar ratio of 1:1 on the recrystallization. These inclusion compounds could be classified into two types in terms of their photochemical behavior. The inclusion compounds composed of acetone, chloroform, tetrahydrofuran or 2-methyltetrahydrofuran turned red or reddish violet on exposure to UV light and the color faded gradually in the dark, while the ones composed of ethanol, 2-propanol or propylamine showed no photocoloration. The crystal and molecular structure of 2,2,4,6-tetraphenyldihydro-1,3,5-triazine ethanol solvate (**3**) has been determined and it was assumed that two types of hydrogen bonds might inhibit the photocoloration of the crystals.[3] In order to confirm the assumption and to reveal the structural differences between photo-active and photo-inactive inclusion compounds, the molecular and crystal structures of the title compounds were determined.

Experimental

Triazine was synthesized by the method of Lottermoser.[1] Colorless plate-like crystals of **1** and **2** were obtained by recrystallization of triazine from acetone or 2-propanol, respectively. In both cases a crystal was sealed in a glass capillary and set up on a RIGAKU AFC-4 diffractometer. Cell parameters were refined by least squares on the basis of 16 and 18 independent 2θ values for **1** and **2** respectively. Crystal data and some experimental conditions are listed in Table 1. Intensities were measured with graphitemonochromated Mo $K\alpha$ or Cu $K\alpha$ radiation, using the ω–2θ scan technique. Background counts were accumulated for 5 s before and after each scan. Three standard reflections were monitored for every 50 reflections and no significant variations in intensities were observed. Reflections of $|F_o|>3\sigma(|F_o|)$ were considered as observed and used for structure determination. Corrections for the Lorentz and polarization factors were made, but no correction for absorption was applied.

The structure of **1** was solved by the direct method with the program MULTAN 78[4] and refined by the full-matrix least squares with the program SHELX 76.[5] All the hydrogen atoms were found on the difference map. The atoms of acetone molecule were disordered between three sets of positions and were treated as rigid molecules with the usual geometry. The occupancy factor for each set was fixed to 0.33333, considering from the temperature factors. The final refinement was made with the anisotropic temperature factors for non-hydrogen atoms of triazine molecule and the isotropic ones for hydrogen atoms and the atoms of acetone molecule. The quantity minimized was $\sum w(|F_o|-|F_c|)^2$ and $w=[\sigma^2(|F_o|)+0.0021|F_o|^2]^{-1}$. The final R and R_w values became 0.082 and 0.092 for 3488 observed reflections. No peaks higher than 0.35 e Å^{-3} were found on the final difference map.

The procedure of the structure determination for **2** was similar to that for **1**. Some of hydrogen atoms were found on the difference map. The others were calculated geometrically and refined with C–H distances constrained to 1.00 Å. The atoms of 2-propanol molecule were disordered between three sets of positions but were refined with no constraint. The occupancy factors were fixed to 0.5 for one set and 0.25 for the other two sets. The final refinement was made with the anisotropic temperature factors for non-hydrogen atoms of triazine molecule and the isotropic ones for hydrogen

Table 1. Crystal Data and Experimental Conditions of **1** and **2**

	1	**2**
Formula	$C_{27}H_{21}N_3 \cdot C_3H_6O$	$C_{27}H_{21}N_3 \cdot C_3H_8O$
F.W.	445.55	447.56
Crystal size/mm	0.7×0.5×0.3	0.5×0.3×0.2
Crystal system	Monoclinic	Monoclinic
Space group	$P2_1/n$	$C2/c$
a/Å	16.385(2)	21.967(3)
b/Å	11.987(2)	13.418(1)
c/Å	12.939(2)	19.576(4)
β/°	92.24(2)	118.73(1)
V/Å^3	2539.5(6)	5059.5(14)
Z	4	8
D_x/g cm^{-3}	1.17	1.17
λ/Å	0.71069 (Mo$K\alpha$)	1.54184 (Cu$K\alpha$)
μ/cm^{-1}	0.39 (Mo$K\alpha$)	4.87 (Cu$K\alpha$)
F (000)	944.0	1904.0
T/K	293	293
$2\theta_{max}$/°	50.0	125.0
Scanning rate/° min^{-1}	4 (2θ)	8 (2θ)
Scan width/°	1.0+0.35tanθ	0.8+0.15tanθ

Table 2. Final Atomic Coordinates Multiplied by 10^4 and Equivalent Thermal Parameters, B_{eq}(Å^2), for Non-Hydrogen Atoms of Acetone Solvate (**1**). All the Occupancy Factors for the Three Acetone Molecules, O(31)-C(34), O(31′)-C(34′), and O(31″)-C(34″), Are Fixed to be 0.33333

$$B_{eq} = \frac{4}{3} \sum_i \sum_j B_{ij} a_i a_j$$

Atom	x	y	z	B_{eq}	Atom	x	y	z	B_{eq}
N(1)	2068(1)	840(2)	10286(2)	3.5	C(22)	1315(3)	4649(3)	9324(3)	5.6
C(2)	2581(2)	1782(2)	10611(2)	3.3	C(23)	2032(3)	4321(3)	8923(3)	5.7
N(3)	3414(2)	1643(2)	10239(2)	3.8	C(24)	2463(2)	3418(3)	9338(3)	4.7
C(4)	3564(2)	992(2)	9437(2)	3.2	C(25)	2652(2)	1835(3)	11803(2)	3.6
N(5)	3014(1)	351(2)	8996(2)	3.7	C(26)	2388(2)	977(3)	12397(3)	4.8
C(6)	2291(2)	261(2)	9520(2)	3.1	C(27)	2509(3)	1013(4)	13471(3)	6.1
C(7)	1741(2)	−654(2)	9135(2)	3.3	C(28)	2885(3)	1912(4)	13932(3)	6.6
C(8)	2008(2)	−1484(3)	8500(2)	3.9	C(29)	3144(3)	2785(4)	13339(3)	6.3
C(9)	1485(2)	−2333(3)	8148(3)	4.8	C(30)	3022(2)	2741(3)	12280(3)	5.1
C(10)	695(3)	−2344(3)	8426(3)	5.4	O(31)	4654(5)	3622(7)	1107(6)	7.9
C(11)	414(3)	−1524(3)	9075(3)	6.1	C(32)	5230(8)	3890(11)	1671(9)	13.7
C(12)	938(2)	−685(3)	9430(3)	4.8	C(33)	5808(8)	4818(12)	1378(12)	11.2
C(13)	4404(2)	988(3)	9038(2)	3.7	C(34)	5504(10)	3182(14)	2596(11)	13.6
C(14)	4949(2)	1836(4)	9241(3)	5.5	O(31′)	4727(7)	3072(10)	1573(12)	18.2
C(15)	5732(3)	1783(5)	8859(4)	7.0	C(32′)	5311(6)	3661(8)	1792(9)	7.0
C(16)	5956(3)	896(4)	8270(3)	6.4	C(33′)	5286(10)	4916(8)	1631(14)	12.2
C(17)	5417(2)	68(4)	8058(3)	5.8	C(34′)	6058(8)	3210(13)	2387(14)	13.0
C(18)	4649(2)	111(3)	8440(3)	4.7	O(31″)	4836(4)	3010(6)	1382(5)	5.5
C(19)	2167(2)	2836(2)	10165(2)	3.4	C(32″)	5413(7)	3329(13)	1920(7)	11.6
C(20)	1447(2)	3193(3)	10576(3)	4.3	C(33″)	6081(8)	4056(16)	1496(11)	14.6
C(21)	1019(2)	4084(3)	10163(3)	5.5	C(34″)	5521(8)	2998(12)	3049(6)	9.4

atoms and the atoms of 2-propanol. The weighting scheme was $w=[\sigma^2(|F_o|)+0.0313|F_o|^2]^{-1}$. The final R and R_w values became 0.083 and 0.110 for 2997 observed reflections. No peaks higher than 0.31 e Å^{-3} were found on the final difference map. The atomic scattering factors were taken from the International Tables for X-Ray Crystallography.[6] The final atomic coordinates and equivalent isotropic temperature factors for non-hydrogen atoms are given in Tables 2 and 3. The lists of the anisotropic temperature factors for non-hydrogen atoms, atomic coordinates and temperature factors for hydrogen atoms, and the observed and calculated structure factors are kept in the office of the Chemical Society of Japan (Document No. 8814). The computation was carried out on HITAC M-280 computer at the Computer Center of the University of Tokyo.

Results and Discussion

The structure of triazine with the atom-numbering in **1** is shown in Fig. 1. For **2** the same numbering

Table 3. Final Atomic Coordinates Multiplied by 10^4 and Equivalent Thermal Parameters, B_{eq}(Å^2), for Non-Hydrogen Atoms of 2-Propanol Solvate (**2**). All the Occupancy Factors for the Three 2-Propanol Molecules, O(31)-C(34), O(31′)-C(34′), and O(31″)-C(34″), Are Fixed To Be 0.5, 0.25, and 0.25 Respectively

$$B_{eq} = \frac{4}{3}\sum_i\sum_j B_{ij}a_ia_j$$

Atom	x	y	z	B_{eq}	Atom	x	y	z	B_{eq}
N(1)	8552(1)	1388(2)	1762(1)	4.5	C(22)	9723(3)	2639(4)	4477(2)	8.0
C(2)	8360(1)	2299(2)	2011(2)	4.1	C(23)	9026(3)	2777(4)	4176(2)	7.7
N(3)	7617(1)	2258(2)	1819(1)	4.1	C(24)	8576(2)	2681(3)	3387(2)	5.9
C(4)	7331(1)	1383(2)	1806(1)	3.5	C(25)	8432(1)	3183(3)	1553(2)	4.3
N(5)	7624(1)	528(2)	1811(1)	5.4	C(26)	8274(2)	3029(3)	778(2)	5.9
C(6)	8205(1)	596(2)	1707(2)	3.8	C(27)	8308(2)	3829(4)	347(2)	6.6
C(7)	8412(2)	−347(3)	1473(2)	4.4	C(28)	8484(2)	4753(4)	649(2)	7.5
C(8)	7970(2)	1160(3)	1227(2)	5.4	C(29)	8622(3)	4926(4)	1406(3)	8.6
C(9)	8132(3)	−2038(3)	976(2)	6.6	C(30)	8595(3)	4131(3)	1847(2)	7.1
C(10)	8757(3)	−2096(4)	974(3)	7.9	O(31)	7051(2)	4186(3)	1874(2)	5.7
C(11)	9202(3)	−1302(4)	1218(3)	8.0	C(32)	6657(5)	4813(8)	1202(6)	9.5
C(12)	9038(2)	−424(3)	1464(3)	6.4	C(33)	5940(4)	4931(7)	1138(5)	8.6
C(13)	6630(1)	1350(2)	1744(1)	4.0	C(34)	6641(5)	4432(7)	520(6)	9.4
C(14)	6411(2)	2088(3)	2073(2)	5.0	O(31′)	7014(4)	4159(6)	1907(5)	5.9
C(15)	5754(2)	2014(3)	2019(3)	6.4	C(32′)	6533(5)	4736(8)	1245(6)	4.8
C(16)	5332(2)	1226(4)	1640(2)	6.5	C(33′)	5850(6)	4671(11)	1245(7)	6.1
C(17)	5541(2)	506(4)	1299(3)	6.1	C(34′)	6498(5)	4049(9)	496(6)	5.0
C(18)	6192(2)	555(3)	1357(2)	5.0	O(31″)	7172(3)	4255(5)	1884(3)	3.7
C(19)	8827(1)	2429(3)	2889(2)	4.4	C(32″)	6627(5)	4762(9)	1224(6)	4.7
C(20)	9539(2)	2302(4)	3200(2)	8.0	C(33″)	7009(8)	5531(12)	1048(10)	7.8
C(21)	9977(3)	2384(6)	3985(3)	9.6	C(34″)	6191(10)	4047(16)	599(11)	9.9

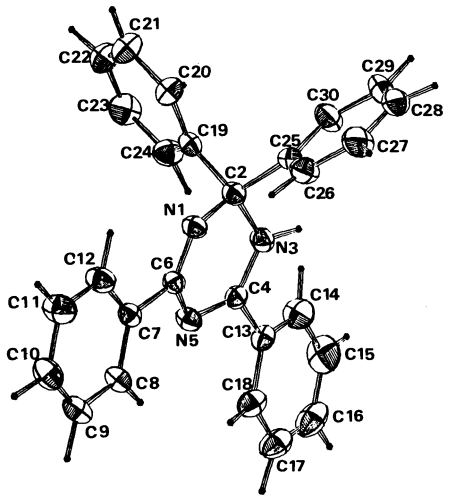

Fig. 1. ORTEP[7] plot of tetraphenyldihydrotriazine molecule in **1** with the atom-numbering. The anisotropic ellipsoids for non-H atoms enclose 30% probability.

Table 4. Selected Bond Distances (Å) and Angles (deg)

	1	**2**	**3**[3]
N(1)-C(2)	1.460(4)	1.453(4)	1.465(3)
C(2)-N(3)	1.474(4)	1.488(4)	1.481(3)
N(3)-C(4)	1.329(4)	1.327(4)	1.336(3)
C(4)-N(5)	1.299(4)	1.314(4)	1.312(3)
N(5)-C(6)	1.393(4)	1.387(4)	1.396(3)
N(1)-C(6)	1.274(4)	1.282(4)	1.278(3)
C(2)-C(19)	1.535(4)	1.530(5)	1.537(4)
C(2)-C(25)	1.544(4)	1.540(5)	1.527(4)
C(4)-C(13)	1.489(4)	1.486(4)	1.490(4)
C(6)-C(7)	1.493(4)	1.489(5)	1.490(4)
N(1)-C(2)-N(3)	110.4(2)	110.1(2)	109.2(2)
C(2)-N(3)-C(4)	121.6(3)	119.4(3)	119.5(2)
N(3)-C(4)-N(5)	123.0(3)	123.1(3)	122.0(2)
C(4)-N(5)-C(6)	114.9(2)	115.0(3)	114.6(2)
N(5)-C(6)-N(1)	127.7(3)	126.4(3)	127.2(2)
C(6)-N(1)-C(2)	117.8(2)	117.9(3)	116.2(2)

scheme is used. The crystal structures of **1** and **2** are shown in Fig. 2. Selected bond distances and angles of **1** and **2** are listed in Table 4, and the torsion angles, the dihedral angles and the hydrogen bond distances of **1** and **2** are listed in Table 5, together with the corresponding ones of **3**.[3] The molecular structures of **1** and **2** are closely similar to that of **3**. During the refinements the difference maps showed that N(3), not N(5), is bound to a hydrogen atom, that is, the dihydrotriazine exists in 2,3-dihydro form, in both **1** and **2**, as was reported in **3**. The triazine structure is also confirmed by the bond distances: N(3)-C(4) is longer than N(5)-C(4). The dihydrotriazine ring in **1** and **2** was found to exist in the boat conformation with the apexes of C(2) and N(5), as was observed in **3**, but the dihedral angles between the least-squares plane of N(1), C(6), C(4), and N(3) and the plane through N(1), C(2), and N(3) or that through C(4), N(5), and C(6) varied with the kind of included solvent. In **1** these dihedral angles are smaller than

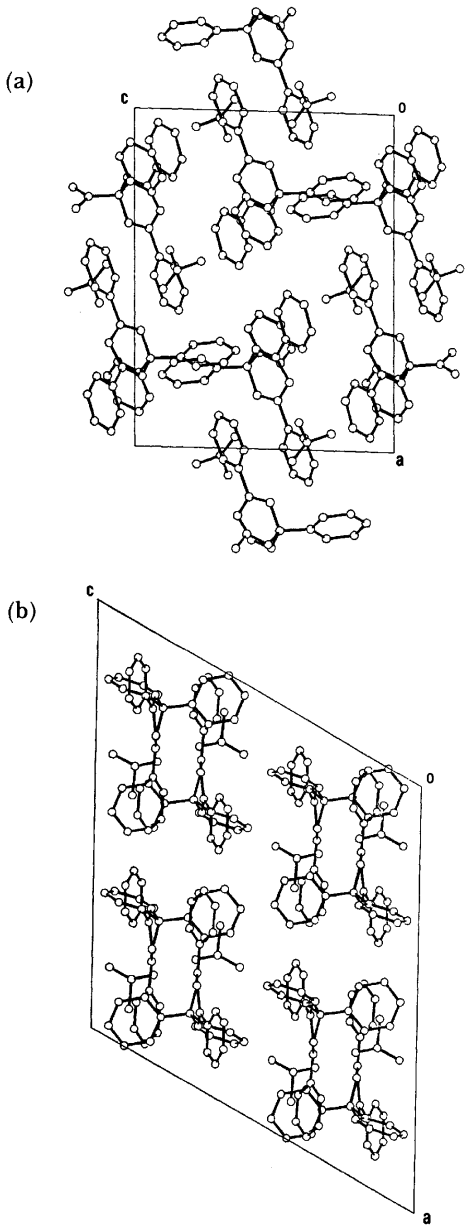

Fig. 2. Crystal structure viewed along the b axis. (a) **1** and (b) **2**. For the solvent molecules the atoms with prime or double prime are omitted.

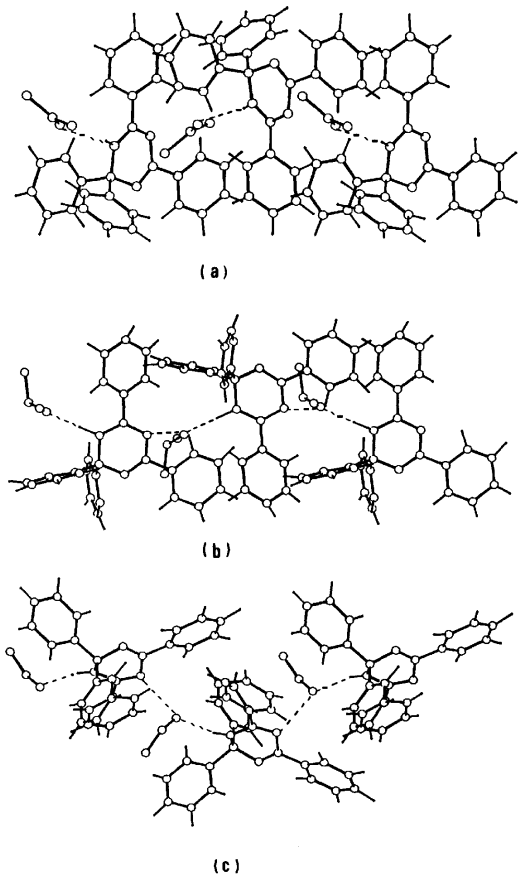

Fig. 3. Hydrogen bonding scheme drawn schematically for (a) **1**, (b) **2**, and (c) **3**. The hydrogen bonds are indicated by broken lines. For the solvent molecules the atoms with prime or double prime are omitted.

those in **2** or **3**, which means that the dihydrotriazine ring in **1** is more planar. The corresponding bond distances and angles of the three inclusion compounds are almost consistent within experimental error, except that the angle C(2)-N(3)-C(4) of **1** (121.6°) is slightly larger than that of **2** (119.4°) or of **3** (119.5°). In the three inclusion compounds the torsion angles N(5)-C(6)-C(7)-C(8) and N(3)-C(4)-C(13)-C(14) are relatively small, indicating that the two phenyl rings at 4- and 6-positions are nearly coplanar with the dihydrotriazine ring. On the other hand, the two phenyl rings at 2-position are perpendicular to the dihydrotriazine ring. The two perpendicular phenyl rings serve to prevent the close packing of triazine molecules and in both crystals of **1** and **2** each acetone or 2-propanol molecule is placed in a cavity which is formed by phenyl rings of neighboring triazines, respectively. In both crystals solvent molecules are disordered, probably since there is enough space around them. Oxygen atoms in both solvent molecules are located near N(3) of triazine and involved in hydrogen bonds. However, the hydrogen bonding scheme is significantly different between **1** and **2**. As is shown in Fig. 3(b), the triazine and solvent molecules in **2** are alternately connected to form an infinite helix around the two-fold screw axis by the two types of hydrogen bond: N(3)-H(3)···O and N(5)···H-O. This hydrogen bonding scheme was also seen in **3** (Fig. 3(c)) and the pitch of the helix, that is, the value of b of **2** (13.418 Å) is similar to that of **3** (13.527 Å). On the other hand, in the case of **1**, although the crystal packing is similar to that of **2** or **3**, each acetone molecule interacts with one triazine molecule by the hydrogen bond of N(3)-H(3)···O and each hydrogen bonding pair is isolated (Fig. 3(a)). The distances N(5)···O and N(3)···O of **2** are similar to those of **3**, but the distance N(3)···O of **1** is longer as is shown in

Table 5. Comparison of the Torsion Angles, the Dihedral Angles[a] (deg) and the Hydrogen Bond Distances (Å)

	1	2	3[3]
N(5)-C(6)-C(7)-C(8)	14.6(4)	12.6(5)	20.3(4)
N(3)-C(4)-C(13)-C(14)	−19.8(5)	−32.5(5)	−20.1(4)
[1]	83.4(1)	79.0(2)	96.4(1)
[2]	56.0(1)	69.5(2)	73.9(1)
[3]	18.6(3)	24.2(3)	28.9(2)
[4]	8.2(3)	10.0(4)	11.5(3)
N(3)-O(31)	3.29(1)[b]	2.90(1)	2.86(1)
N(3)-O(31′)	3.20(2)	2.92(1)	3.01(3)
N(3)-O(31″)	3.17(1)	2.88(1)	
O(31)-N(5)		2.94(1)	2.90(1)
O(31′)-N(5)		2.92(1)	2.78(2)
O(31″)-N(5)		2.90(1)	

a) [1]: the angle between the least-squares plane of N(1), C(6), N(3), and C(4) (plane A) and that of C(19), C(20), C(21), C(22), C(23), and C(24), [2]: the angle between the plane A and the least-squares plane of C(25), C(26), C(27), C(28), C(29), and C(30), [3]: the angle between the plane A and the plane of N(1), C(2), and N(3), [4]: the angle between the plane A and the plane of C(4), N(5), and C(6). b) The distances of O(31)···H(3), O(31′)···H(3), and O(31″)···H(3) are 2.51(3), 2.35(4), and 2.31(3)Å, respectively.

Table 5. In **2** and **3** the solvent molecules seem to interact more strongly with triazine through the two types of hydrogen bonds than in **1**. Except for the hydrogen bonds, there are no unusually short contacts in **1** and **2** as well as **3**.

On the basis of the crystal structures of the three inclusion compounds **1**, **2**, and **3** and the molecular structures of triazine in them, the difference in the photochemical behavior between the two types of inclusion compounds is probably ascribable to the difference in the hydrogen bonding scheme. Although the structure of the colored species is still open to the question, it is strongly suggested that the N(3)-H(3)···O-H···N(5) hydrogen bonds, by which triazine and solvent molecules are alternately connected in **2** and **3**, inhibit the photocoloration. If the colored species is formed on irradiation, because of the instability of the electronic state, it would easily change back to the stable initial state due to the chain like hydrogen bonds. On the other hand, the crystal of **1** exhibits the photocoloration because each N(3)-H(3)···O hydrogen bond is isolated.

References

1) A. Lottermoser, *J. Prakt. Chem.*, **54**, 113 (1896).

2) K. Maeda, N. Kihara, and N. Ishimura, *J. Chem. Soc., Perkin Trans. 2*, **1985**, 887.

3) Y. Mori, Y. Ohashi, and K. Maeda, *Acta Crystallogr., Sect. C*, in press.

4) P. Main, S. E. Hull, L. Lessinger, G. Germain, J.-P. Declercq, and M. M. Woolfson, MULTAN78. A System of Computer Programs for the Automatic Solution of Crystal Structures from X-ray Diffraction Data. Univs. of York, England, and Louvain, Belgium (1978).

5) G. M. Sheldrick, SHELX76. Program for Crystal Structure Determination. Univ. of Cambridge, England (1976).

6) "International Tables for X-ray Crystallography," Kynoch Press, Birmingham (1974), Vol. IV.

7) C. K. Johnson, ORTEP, Report ORNL-3794, Oak Ridge National Laboratory, Tennessee (1965).

 © 1988 The Chemical Society of Japan Bull. Chem. Soc. Jpn., 61, 2493—2497 (1988)

Studies on Lignan Lactone Antitumor Agents. V. 1-*O*-(Aminoethyl) Ether of 4′-*O*-Demethyl-1-epipodophyllotoxin

Hitoshi SAITO, Yoshio NISHIMURA,* Shinichi KONDO, Keiko KOMURO, and Tomio TAKEUCHI
Institute of Microbial Chemistry, 3-14-23 Kamiosaki, Shinagawa-ku, Tokyo 141
(Received February 2, 1988)

1-*O*-(2-Aminoethyl)-4′-*O*-demethyl-1-epipodophyllotoxin derivatives were synthesized by a stereoselective BF_3-catalyzed coupling of 4′-*O*-benzyloxycarbonyl-1-epipodophyllotoxin with the corresponding 2-aminoethanol derivatives, and with ethylene glycol followed by reductive amination of its aldehyde. Some 1-*O*-(2-aminoethyl) ethers of 4′-*O*-demethyl-1-epipodophyllotoxin prolonged markedly survival periods in mice with leukemia L-1210.

Due to the clinical efficacy and intriguing mechanism of action, the synthetic podophyllotoxin glycosides, VP-16-213 (**1**) and VM-26 (**2**)[1,2] have attracted considerable interest in the synthesis of new active analogues of podophyllotoxin. In the previous paper of this series,[3-5] the systematic chemical modification of podophyllotoxin and α-peltatin based on glycosidation with amino sugar derivatives were reported. 2-Amino-, 3-amino-, and 2-dimethylamino-β-D-glucosidic variants (**3**, **4**, and **5**) were found to have the superior antitumor activity to **1**.

Changes in the 1-*O*-glycosyl group are also interest for simplified structure which might retain the activity of **3**, **4**, and **5**, and be accessible to practical industrialization. The basic amino substituent of the sugar moiety is proved to be important for increasing the activity, but considerable simplification in the sugar structure might be permitted so long as the amino group is retained in the same distance from the linkage at C-1. In the chemical modification of podophyllotoxin glycosides, it also appears that β-configuration at C-1 of aglycone, podophyllotoxin, is indispensable for increasing an antitumor activity and decreasing a toxic side effect.[1]

Here we wish to present the synthesis of 1-*O*-(aminoethyl)-4′-*O*-demethyl-1-epipodophyllotoxin derivatives (**8a—8j** and **12k—12m**) having a β-configuration at C-1, and their biological activities. Acid-catalyzed coupling using boron trifluoride diethyl etherate, as a key step, was successfully used in these syntheses. The synthesis was achieved by the following three methods. Condensation of 4′-*O*-benzyloxycarbonyl-4′-*O*-demethyl-1-epipodophyllotoxin (**6**) with 2-(benzyloxycarbonylamino)ethanol analogues (**7a**, **7b**, and **7c**) in dichloromethane in the presence of $BF_3 \cdot OEt_2$,[6,7] followed by removal of the masking groups gave the corresponding 1-*O*-(2-aminoethyl)-4′-*O*-demethyl-1-epipodophyllotoxins (**8a**, **8b** and **8c**), respectively, in good yields. Compound **8a** was further transformed into dimethylamino and diethylamino derivatives **8e** and **8f** upon a reductive amination with the corresponding aldehydes using sodium cyanotrihydroborate.[8] Alternative BF_3-catalyzed coupling was successfully accomplished when **6** was added into a solution of 2-(phenylamino)-ethanol (**7d**) and 2-(dialkylamino)ethanol analogues (**7e—7j**) with $BF_3 \cdot OEt_2$ in dichloromethane. Thus, 1-*O*-[2-(phenylamino)ethyl]-4′-*O*-demethyl-1-epipodophyllotoxin (**8d**) and 1-*O*-[2-(dialkylamino)ethyl]-4′-*O*-demethyl-1-epipodophyllotoxins (**8e—8j**) were synthesized by one step in excellent yields. BF_3-catalyzed coupling in dichloromethane was also successful in a formation of an ether bond with ethylene glycol, and 1-*O*-(2-hydroxyethyl)-4′-*O*-benzyloxycarbonyl-4′-*O*-demethyl-1-epipodophyllotoxin (**9**) was obtained in an excellent yield. Compound **9** was converted to an aldehyde **10** by Swern oxidation, and the successive reduction with the corresponding alkylamines **11c**, **11f**, and **11k—12m** by sodium cyanotrihydroborate gave 1-*O*-[2-(alkylamino)ethyl]-4′-*O*-demethyl-1-epipodophyl-

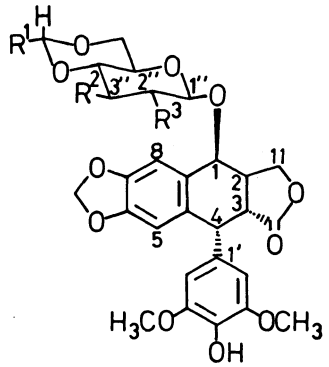

1 : R^1=CH_3, R^2=R^3=OH (Etoposide)
2 : R^1= , R^2=R^3=OH (Teniposide)
3 : R^1=CH_3, R^2=OH, R^3=NH_2
4 : R^1=CH_3, R^2=NH_2, R^3=OH
5 : R^1=CH_3, R^2=OH, R^3=$N(CH_3)_2$

Fig. 1.

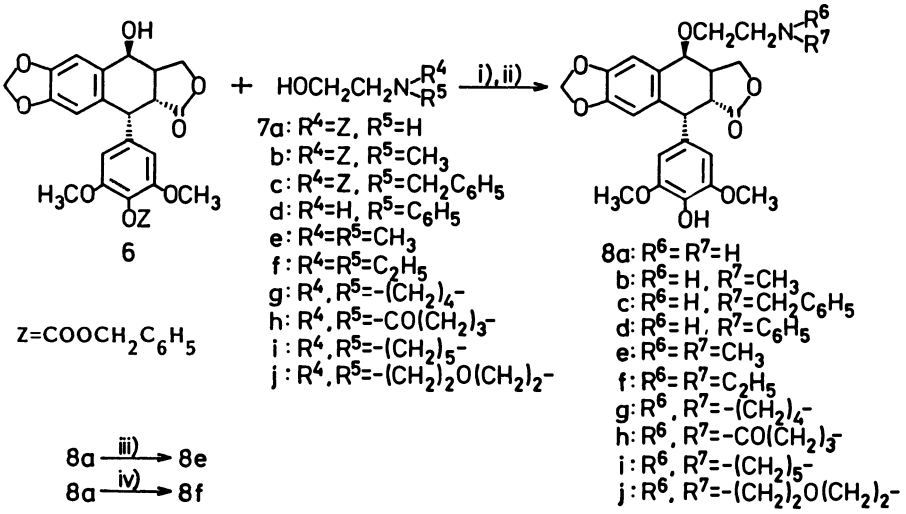

Scheme 1.

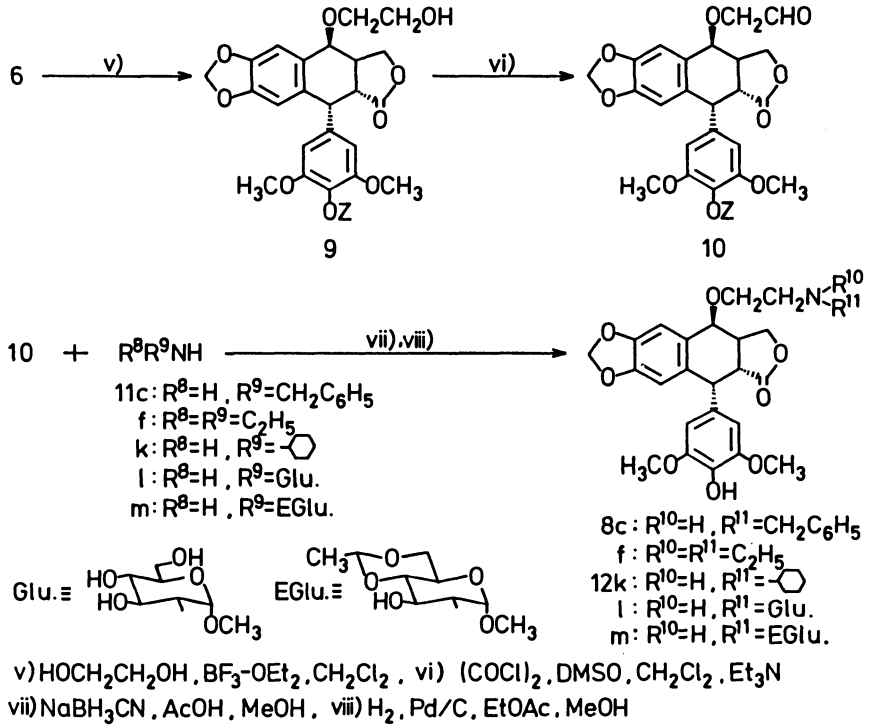

Scheme 2.

Table 1. The Antitumor Activities of **1**, **5**, and 1-*O*-(2-Aminoethyl) Ethers of 4′-*O*-Demethyl-1-epipodophyllotoxin (T/C%)

Dose (μg/mouse)	Compound No.														
	1	**5**	**8a**	**8b**	**8c**	**8d**	**8e**	**8f**	**8g**	**8h**	**8i**	**8j**	**12k**	**12l**	**12m**
25	184	438	130	188	139	109	270	139	72	113	145	172	108	95	102
6.25	139	164	162	271	108	103	141	108	72	104	133	135	108	95	102

The T/C values are the percentage ratios of the mean survival period of five treated mice to the mean survival period of the control group. L-1210 cells (10^6 cells) were inoculated intraperitoneally and the intraperitoneal treatment was started on day 1 and continued for 10 days.

lotoxins (**8c**, **8f**, and **12k—12m**) in good overall yields. Condensations in all cases were carried out stereoselectively by the same fashion through a benzyl cation at C-1 generated by $BF_3 \cdot OEt_2$ as has been reported in a previous synthesis.[4,6,9]

Synthesized compounds **8a—8j** and **12k—12m**, compared with **1** and **5**, were screened for antitumor activities using lymphocytic leukemia L-1210 in mice. Test results are shown in Table 1. Compounds **8a**, **8b**, **8e**, **8i**, and **8j** produced a good survival time increase in mice with leukemia L-1210. Interestingly, prototypal structures such as **8b** and **8e** showed a significant antitumor activity alongside **1** and **5**. These results suggest further elaboration of the amino side chain to optimize their structures. Further study for antitumor activity of synthesized compounds is in progress.

Experimental

General Methods. Melting points were determined with a Yamato apparatus and were uncorrected. IR spectra were determined on a Hitachi Model 260-10 and Jasco IR-810 spectrophotometers. Optical rotations were measured with a Perkin-Elmer Model 241 polarimeter. ^1H NMR spectra were recorded with Varian EM-390, Jeol GX-270 and Jeol GX-400 spectrometers. Chemical shifts are expressed in δ values (ppm) with tetramethylsilane as an internal standard. The mass spectra was taken by a Jeol D-300 for fast atom bombardment (FAB).

1-*O*-(2-Aminoethyl)-4′-*O*-demethyl-1-epipodophyllotoxin (8a). To a solution of a mixture of **6** (320 mg) and 2-(benzyloxycarbonylamino)ethanol (142 mg) in dichloromethane (8 ml) was added $BF_3 \cdot OEt_2$ (200 μl) at −10 °C, and the mixture was stirred at −10 °C for 1 h. After being quenched with pyridine (200 μl), the solution was washed with water and dried over $MgSO_4$. Evaporation of the solvent gave a solid. The solid was dissolved in ethyl acetate–methanol (1:1, 30 ml), and the solution was stirred under atmosphere of hydrogen in the presence of 10% Pd/C (40 mg) at room temperature for 1 h. After removal of catalyst, the solvent was evaporated to afford a solid. The solid was chromatographed on a column of silica gel with chloroform–methanol (4:1) to give a solid of **8a** (191 mg, 72%). The solid was recrystallized from methanol to give a crystal of **8a**: mp 182—184 °C; $[\alpha]_D^{23}$ −46° (*c* 0.4, MeOH); IR (KBr) 1775, 1760, 1483 1230, and 1110 cm^{-1}; ^1H NMR (C_5D_5N, 270 MHz) δ=3.18 (3H m, H-2 and $-OCH_2C\underline{H}_2N-$), 3.58 (1H dd, *J*=5 and 14 Hz, H-3), 3.71 (6H s, $2\times OCH_3$), 3.84 and 3.98 (1H each m, $-OC\underline{H}_2CH_2N-$), 4.39 (1H t, *J*=8 Hz, H-11), 4.51 (1H dd, *J*=8 and 11 Hz, H-11), 4.62 (1H d, *J*=3.0 Hz, H-1), 4.76 (1H d, *J*=5 Hz, H-4), 5.98 (2H d, methylene), 6.66 (2H s, H-2′ and 6′), 6.74 (1H s, H-5), and 7.15 (1H s, H-8); MS (FAB) *m/z* 444 (M^++H) and 383.

1-*O*-[2-(Dimethylamino)ethyl]-4′-*O*-demethyl-1-epipodophyllotoxin (8e). To a solution of 2-(dimethylamino)-ethanol (30 mg) in dichloromethane (1 ml) was added $BF_3 \cdot OEt_2$ (110 μl) at −15 °C and the mixture was stirred at −15 °C for 10 min. Then to the mixture was added dropwise a solution of **6** (108 mg) in dichloromethane (1 ml) at −15 °C, and the mixture was stirred at −15 °C for 30 min. The similar work-up and purification to those used for preparation of **8a** were used (43% overall yield).

From **8a**: To a solution of **8a** (88 mg) in methanol (3 ml) was added 37% aqueous solution of formaldehyde (50 μl) and sodium cyanoborohydride (30 mg), and the mixture was stirred at room temperature for 30 min. After being diluted with dichloromethane (10 ml), the solution was washed with water, dried over $MgSO_4$, and filtered. The filtrate was evaporated to give a solid, which was subjected to preparative thin-layer chromatography on silica gel developed with chloroform–methanol (4:1). A solid of **8e** was obtained in a yield of 90%. The solid was recrystallized from methanol to give a crystal of **8e**: 195—197 °C; $[\alpha]_D^{22}$ −57° (*c* 0.5, MeOH); IR (KBr) 1760, 1483, 1227, 1108, and 1080 cm^{-1}; ^1H NMR ($CDCl_3$, 270 MHz) δ=2.27 (6H s, $2\times NCH_3$), 2.53 (2H t, *J*=6 Hz, $-OCH_2C\underline{H}_2N-$), 2.87 (1H m, H-2), 3.39 (1H dd, *J*=5.1 and 14 Hz, H-3), 3.61 and 3.80 (1H each m, $-OC\underline{H}_2CH_2N-$), 3.77 (6H s, $2\times OCH_3$), 4.35 (2H m, H-11), 4.45 (1H d, *J*=3.4 Hz, H-1), 4.59 (1H d, *J*=5.1 Hz, H-4), 5.95 and 5.99 (2H ABq, *J*=1.5 Hz, methylene), 6.26 (2H s, H-2′ and 6′), 6.54 (1H s, H-5), and 6.84 (1H s, H-8); MS (FAB) *m/z* 472 (M^++H) and 383.

1-*O*-(2-Hydroxyethyl)-4′-*O*-benzyloxycarbonyl-4′-*O*-demethyl-1-epipodophyllotoxin (9). To a solution of **6** (1 g) and ethylene glycol (0.2 ml) in dichloromethane (15 ml) was added dropwise a solution of $BF_3 \cdot OEt_2$ (0.6 ml) in dichloromethane (1 ml) at −15 °C, and the mixture was stirred at −15 °C for 2 h. After being quenched with pyridine (0.6 ml), the solution was washed with water and dried over $MgSO_4$. Evaporation of the solvent gave a solid, which was subjected to column chromatography on silica gel. Elution with toluene–acetone (5:1) gave **9** (980 mg, 90%), which was recrystallized from methanol: mp 182—183 °C; $[\alpha]_D^{22}$ −51° (*c* 0.66, $CHCl_3$); IR (KBr) 1770, 1602, 1482, 1234, and 1125 cm^{-1}; ^1H NMR ($CDCl_3$, 270 MHz) δ=2.88 (1H m, H-2), 3.40 (1H dd, *J*=14 and 5.1 Hz, H-3), 3.68 (6H s, $2\times OCH_3$), 4.51 (1H, d, *J*=3 Hz, H-1), 4.64 (1H d, *J*=5.1 Hz H-4), 5.26 (2H s, $OC\underline{H}_2Ph$), 6.28 (2H s, H-2′ and 6′), 6.55 (1H s, H-5), 6.85 (1H s, H-8), and 7.15—7.45 (5H, Ph); MS (FAB) *m/z* 579 (M^++H), 517, and 443.

1-*O*-(2-Oxoethyl)-4′-*O*-demethyl-1-epipodophyllotoxin (10). A solution of dichloromethane (0.5 ml) and dimethyl sulfoxide (120 μl) was added to a stirred solution of dichloromethane (2 ml) and oxallyl dichloride (70 μl) at −60 °C. To the solution was added a solution of **9** (360 mg) in dichloromethane (2 ml) within 5 min, and the mixture was stirred at −60 °C for 15 min. Triethylamine (0.4 ml) was added and the reaction mixture was stirred for 5 min and then allowed to warm to room temperature. After being quenched with water, the mixture was extracted with dichloromethane (10 ml). The organic layer was washed with a saturated NaCl solution and dried over $MgSO_4$. The filtered solution was evaporated to give a solid, which was subjected to a column chromatography on silica gel. Elution with toluene–acetone (2:1) gave a solid of **10** (250 mg, 69%). The solid was crystallized from methanol: mp 96—98 °C; $[\alpha]_D^{22}$ −57 ° (*c* 0.48, $CHCl_3$); IR (KBr) 1770, 1602, 1482, 1235, and 1127 cm^{-1}; ^1H NMR ($CDCl_3$, 90 MHz) δ=3.67 (6H s, $2\times OCH_3$), 5.26 (2H s, $OC\underline{H}_2Ph$), 5.98 (2H s, methylene), 6.28 (2H s, H-2′ and 6′), 6.59 (1H s, H-8), 7.25—7.50 (5H broad s, Ph), and 9.66 (1H s, CHO); MS (FAB) *m/z* 599 (M^++Na) and 517.

Methyl 2-Amino-2-deoxy-4,6-*O*-ethylidene-α-D-glucopyranoside (11m). To a suspension of methyl 2-benzyloxy-

carbonylamino-2-deoxy-α-D-glucopyranoside (100 mg) and acetaldehyde diethyl acetal (0.3 ml) in dichloromethane (5 ml) was added *p*-toluenesulfonic acid (5 mg) at room temperature, and the mixture was stirred for 2 h. The solution was washed with a saturated $NaHCO_3$ solution and water, and dried over $MgSO_4$. Evaporation of the filtered solution gave a solid, which was crystallized from methanol to give a crystal of methyl 2-benzyloxycarbonylamino-2-deoxy-4,6-*O*-ethylidene-α-D-glucopyranoside (**13**) (88 mg, 81%): mp 176—177 °C; $[\alpha]_D^{22}$ +65° (*c* 0.5, $CHCl_3$). Compound **13** (70 mg) was dissolved in ethanol (5 ml), and the solution was stirred under atmosphere of hydrogen in the presence of 10% Pd/C (10 mg) at room temperature for 1 h. After removal of catalyst, the solvent was evaporated to afford solid. The solid was subjected to a next step without purification.

13: IR (KBr) 1693, 1542, 1280, and 1130 cm^{-1}; ^1H NMR ($CDCl_3$, 90 MHz) δ=1.36 (3H d, CH_3 of ethylidene), 3.34 (3H s, OCH_3), 5.13 (2H s, OCH_2Ph), and 7.3—7.5 (5H m, Ph); MS (FAB) *m/z* 354 (M^++H) and 322.

1-*O*-[2-(Cyclohexylamino)ethyl]-4′-*O*-demethyl-1-epipodophyllotoxin (12k). A solution of cyclohexylamine (20 mg) and sodium cyanoborohydride (10 mg) in methanol (2 ml) was adjusted pH value to 4—5 with acetic acid, and to the solution was added **10** (58 mg), and then the mixture was stirred at room temperature for 1 h. After dilution with chloroform (10 ml), the mixture was washed with a saturated $NaHCO_3$ solution and water, and dried over $MgSO_4$. Evaporation of the solvent gave a solid, which was dissolved in ethyl acetate–methanol (1:1). The mixture was stirred under atmosphere of hydrogen in the presence of 10% Pd/C (10 mg) at room temperature for 1 h. After removal of catalyst, evaporation of the solvent gave a solid. The solid was subjected to preparative thin-layer chromatography on silica gel with chloroform–methanol (4:1) to give a solid of **12k** (34 mg, 64%). The solid was recrystallized from methanol to give a crystal of **12k**: mp 169—171 °C; $[\alpha]_D^{22}$ −57° (*c* 0.5, $CHCl_3$); IR (KBr) 2935, 1765, 1482, 1228, and 1110 cm^{-1}; ^1H NMR ($CDCl_3$, 90 MHz) δ=1.0—2.0 (10H m, methylene protons of cyclohexyl), 2.45 (1H m, methine proton of cyclohexyl), 2.83 (2H t, *J*=5 Hz, $-OCH_2C\underline{H}_2N-$), 3.40 (1H dd, *J*=5 and 14 Hz, H-3), 3.77 (6H s, 2×OCH_3), 4.34 (2H d, *J*=9 Hz, H-11), 4.46 (1H d, *J*=3 Hz, H-1), 4.60 (1H d, *J*=5 Hz, H-4), 5.97 (2H m, methylene), 6.28 (2H s, H-2′ and 6′), and 6.55 (1H s, H-5); MS (FAB) *m/z* 526 (M^++H) and 383.

8b: **8b** was obtained from **6** (0.6 mmol) and 2-benzyloxycarbonyl-2-(methylamino)ethanol (0.7 mmol) by the similar procedure for the preparation of **8a** (yield 73%): mp 182 °C (crystallized from ethanol); $[\alpha]_D^{23}$ −60° (*c* 0.5, MeOH); IR (KBr) 1775, 1480, 1328, 1227 and 1115 cm^{-1}; ^1H NMR ($CDCl_3$, 270 MHz) δ=2.45 (3H s, NCH_3), 2.77 (2H m, $OCH_2C\underline{H}_2N$), 2.87 (1H m, H-2), 3.37 (1H dd, *J*=5.4 and 14 Hz, H-3), 3.64 and 3.82 (1H each m, $-OC\underline{H}_2CH_2N-$), 3.76 (6H s, 2×OCH_3), 4.34 (2H d, *J*=9 Hz, H-11), 4.45 (1H d, *J*=3.4 Hz, H-1), 4.76 (1H d, *J*=5.4 Hz, H-4), 5.97 (2H d, methylene), 6.26 (2H s, H-2′ and 6′), 6.54 (1H s, H-5), and 6.81 (1H s, H-8); MS (FAB) *m/z* 458 (M^++H) and 383.

8c: **8c** was obtained from **6** (0.6 mmol) and 2-benzyloxycarbonyl-2-(benzylamino)ethanol (0.7 mmol) by the similar procedure for the preparation of **8a** (yield 70%). **8c** was also prepared from **10** (0.1 mmol) and benzylamine (0.2 mmol) by the similar procedure for the preparation of **12k** (yield 75%): mp 146—148 °C (recrystallized from methanol); $[\alpha]_D^{22}$ −51° (*c* 0.5, $CHCl_3$); IR (KBr) 1763, 1482, 1228, and 1108 cm^{-1}; ^1H NMR ($CDCl_3$, 90 MHz) δ=2.82 (2H t, *J*=5 Hz, $-OCH_2C\underline{H}_2N-$), 3.10 (1H m, H-2), 3.36 (1H dd, *J*=5 and 14 Hz, H-3), 3.75 (6H s, 2×OCH_3), 3.81 (2H s, $OC\underline{H}_2Ph$), 4.32 (2H d, *J*=9 Hz, H-11), 4.43 (1H d, *J*=3 Hz, H-1), 4.59 (1H d, *J*=5 Hz, H-4), 5.95 (2H m, methylene), 6.26 (2H s, H-2′ and 6′), 6.53 (1H s, H-5), and 6.81 (1H s, H-8); MS (FAB) *m/z* 534 (M^++H) and 383.

8d: **8d** was obtained from **6** (0.2 mmol) and 2-(phenylamino)ethanol (0.3 mmol) by the similar procedure for the preparation of **8e** from **6** (yield 67%): mp 157—158 °C (recrystallized from methanol); $[\alpha]_D^{20}$ −60° (*c* 0.4, $CHCl_3$); IR (KBr) 1779, 1619, 1520, 1498, 1240, and 1121 cm^{-1}; ^1H NMR ($CDCl_3$, 270 MHz) δ=2.87 (1H m, H-2), 3.35 (3H m, H-3 and $-OCH_2C\underline{H}_2N-$), 3.73 and 3.87 (1H each m, $-OC\underline{H}_2CH_2N-$), 3.76 (6H s, 2×OCH_3), 4.30 (2H m, H-11), 4.45 (1H d, *J*=3.4 Hz, H-1), 4.61 (1H d, *J*=5 Hz, H-4), 5.40 (1H broad s, 4′-OH), 5.97 and 5.99 (2H ABq, *J*=1.3 Hz, methylene), 6.25 (2H s, H-2′ and 6′), 6.56 (1H s, H-5), 6.61, 6.74 and 7.19 (2H, 1H and 2H each m, Ph), and 6.77 (1H s, H-8); MS (FAB) *m/z* 520 (M^++H) and 383.

8f: **8f** was obtained from **6** (0.2 mmol) and 2-(diethylamino)ethanol (0.3 mmol) by the similar procedure for the preparation of **8e** from **6**, and from **8c** (0.2 mmol) by the similar procedure for the preparation of **8e** from **8a** in yields of 80 and 88%, respectively. **8f** was also prepared from **10** (0.1 mmol) and diethylamine (0.2 mmol) by the similar procedure for the preparation of **12k** (yield 69%): mp 196—198 °C (recrystallized from methanol); $[\alpha]_D^{22}$ −73° (*c* 0.5, $CHCl_3$); IR (KBr) 1760, 1482, 1228, and 1110 cm^{-1}; ^1H NMR ($CDCl_3$ 90 MHz) δ=1.05 (6H t, *J*=7 Hz, 2×$-NCH_2C\underline{H}_3$), 2.62 (4H q, *J*=7 Hz, 2×$NC\underline{H}_2CH_3$), 2.70 (2H t, *J*=6 Hz, $-OCH_2C\underline{H}_2N-$), 2.90 (1H m, H-2), 3.37 (1H dd, *J*=5 and 14 Hz, H-3), 3.77 (6H s, 2×OCH_3), 4.36 (2H d, *J*=9 Hz, H-11), 4.47 (1H d, *J*=3 Hz, H-1), 4.60 (1H d, *J*=5 Hz, H-4), 5.98 (2H m, methylene), 6.27 (2H s, H-2′ and 6′), 6.54 (1H s, H-5), and 6.86 (1H s, H-8); MS (FAB) *m/z* 500 (M^++H) and 383.

8g: **8g** was obtained from **6** (0.2 mmol) and 2-(cyclopentylamino)ethanol (0.3 mmol) by the similar procedure for the preparation of **8e** from **6** (yield 81%): mp 227—228 °C (recrystallized from methanol); $[\alpha]_D^{22}$ −48° (*c* 0.5, MeOH); IR (KBr) 1758, 1610, 1482, 1225, 1108, and 1080 cm^{-1}; ^1H NMR ($CDCl_3/C_5D_5N$=2/1, 270 MHz) δ=1.8—2.0 and 2.9—3.4 (4H and 8H each m, H-2, H-3 and pyrrolidine), 3.68 (6H s, 2×OCH_3), 3.96 and 4.06 (1H each m, $-OC\underline{H}_2CH_2N-$), 4.31 (2H m, H-11), 4.59 (1H d, *J*=3.8 Hz, H-1), 5.92 (2H s, methylene), 6.36 (2H s, H-2′ and 6′), 6.59 (1H s, H-5), and 6.97 (1H s, H-8); MS (FAB) *m/z* 498 (M^++H) and 383.

8h: **8h** was obtained from **6** (0.2 mmol) and 2-(2-hydroxyethyl)pyrrolidone (0.3 mmol) by the similar procedure for the preparation of **8e** from **6** (yield 91%): mp 212—214 °C (recrystallized from ethanol); $[\alpha]_D^{22}$ −82° (*c* 0.8, $CHCl_3$); IR (KBr) 1762, 1682, 1610, 1480, 1220, and 1110 cm^{-1}; ^1H NMR ($CDCl_3$, 270 MHz) δ=1.99 (2H m, $-NCOCH_2C\underline{H}_2-$), 2.38 (2H t, *J*=8 Hz, $-NCOC\underline{H}_2CH_2-$), 2.89 (1H m, H-2), 3.77 (6H s, 2×OCH_3), 4.29 (2H m, H-11), 4.47 (1H d, *J*=3 Hz, H-1), 4.60 (1H d, *J*=5.1 Hz, H-4), 5.40 (1H s, 4′-OH), 5.98 and 6.00 (2H ABq, *J*=1.3 Hz, methylene), 6.24 (2H s, H-2′ and 6′), 6.56 (1H s, H-5), and 6.77 (1H s, H-8); MS (FAB) *m/z*

512 (M^++H) and 383.

8i: **8i** was obtained from **6** (0.2 mmol) and 1-piperidineethanol (0.3 mmol) by the similar procedure for the preparation of **8e** from **6** (yield 73%): mp 199—200 °C (recrystallized from methanol); $[\alpha]_D^{23}$ −73° (*c* 0.4, $CHCl_3$); IR (KBr) 1772, 1481, 1237, 1223, and 1120 cm^{-1}; ^1H NMR ($CDCl_3$, 270 MHz) δ=1.4—1.65 (6H m, piperidine), 2.45 (4H t, *J*=4 Hz, 2X-NCH_2- of piperidine), 2.56 (2H t, *J*=6 Hz, -OCH_2CH_2N-), 2.85 (1H m, H-2), 3.37 (1H dd, *J*=5.1 and 14 Hz, H-3), 3.76 (6H s, 2XOCH_3), 4.35 (2H m, H-11), 4.45 (1H d, *J*=3.0 Hz, H-1), 4.60 (1H d, *J*=5.1 Hz, H-4), 5.40 (1H s, 4'-OH), 5.95 and 5.98 (2H ABq, *J*=1.3 Hz, methylene), 6.26 (2H s, H-2' and 6'), 6.53 (1H s, H-5), and 6.88 (1H s, H-8); MS (FAB) *m/z* 512 (M^++H).

8j: **8j** was obtained from **6** (0.2 mmol) and 4-(2-hydroxyethyl)morpholine (0.3 mmol) by the similar procedure for the preparation of **8e** from **6** (yield 80%): mp 220—224°C (recrystallized from methanol); $[\alpha]_D^{23}$ −73° (*c* 0.5, $CHCl_3$); IR (KBr) 1774, 1480, 1230, and 1120 cm^{-1}; ^1H NMR ($CDCl_3$, 90 MHz) δ=2.4—2.7 (6H m, -OCH_2CH_2N- and 2X-NCH_2- of morpholine), 2.92 (1H m, H-2), 3.40 (1H dd, *J*=5 and 14 Hz, H-3), 3.77 (6H s, 2XOCH_3), 4.46 (1H d, *J*=3 Hz, H-1), 4.63 (1H d, *J*=5 Hz, H-4), 6.00 (2H broad s, methylene), 6.30 (2H s, H-2' and 6'), 6.56 (1H s, H-5), and 6.89 (1H s, H-8); MS (FAB) *m/z* 514 (M^++H) and 383.

12l: **12l** was obtained from **10** (0.1 mmol) and methyl 2-amino-2-deoxy-α-D-glucopyranoside (0.2 mmol) by the similar procedure for the preparation of **12k** (yield 73% based on **10**): mp 178—180 °C (recrystallized from methanol); $[\alpha]_D^{23}$ +14° (*c* 0.5, MeOH); IR (KBr) 1763, 1482, 1230, and 1112 cm^{-1}; ^1H NMR ($CDCl_3$, 90 MHz) δ=3.36 and 3.76 (3H and 6H each s, 3XOCH_3), 4.33 (2H d, *J*=9 Hz, H-11), 4.46 (1H d, *J*=3 Hz, H-1), 4.60 (1H d, *J*=5 Hz, H-4), 5.86 (1H d, *J*=3 Hz, H-1 of glucopyranoside), 5.97 (2H broad s, methylene), 6.26 (2H s, H-2' and 6'), 6.56 (1H s, H-5), and 6.81 (1H s, H-8); MS (FAB) *m/z* 620 (M^++H) and 383.

12m: **12m** was obtained from **10** (0.1 mmol) and methyl 2-amino-2-deoxy-4,6-*O*-ethylidene-α-D-glucopyranoside (0.2 mmol) by the similar procedure for the preparation of **12k** (yield 59% based on **10**): mp 179—181 °C (recrystallized from methanol); $[\alpha]_D^{22}$ +7° (*c* 0.5, $CHCl_3$); IR (KBr) 1762, 1482, 1228, and 1110 cm^{-1}; ^1H NMR ($CDCl_3$, 90 MHz) δ=1.36 (3H d, *J*=5 Hz, CH_3 of ethylidene), 3.36 and 3.76 (3H and 6H each s, 3XOCH_3), 4.35 (2H d, *J*=9 Hz, H-11), 4.46 (1H d, *J*=3 Hz, H-1), 4.61 (1H d, *J*=5 Hz, H-4), 5.98 (2H m, methylene), 6.27 (2H s, H-2' and 6'), 6.56 (1H s, H-5), and 6.81 (1H s, H-8); MS (FAB) *m/z* 646 (M^++H) and 607 and 515.

This work was supported in part by a Grant-in-Aid for Cancer Research No. 62010013 from the Ministry of Education, Science and Culture, Japan, and No. 61-21 from the Ministry of Health and Welfare, Japan.

References

1) For review: See I. Jardine "Podophyllotoxins in Anticancer Agents Based on Natural Products Models," Academic Press, Inc., New York (1980), pp. 319—351.

2) For review: See B. F. Issell, *Cancer Chemother. Pharmacol.*, **7**, 87 (1982).

3) H. Saito, H. Yoshikawa, Y. Nishimura, S. Kondo, T. Takeuchi, and H. Umezawa, *Chem. Pharm. Bull.*, **34**, 3733, 3741 (1986).

4) H. Saito, Y. Nishimura, S. Kondo, and H. Umezawa, *Chem. Lett.*, **1987**, 799.

5) H. Saito, Y. Nishimura, S. Kondo, T. Takeuchi, and H. Umezawa, *Bull. Chem. Soc. Jpn.*, in press.

6) M. Kuhn and A. von Wartburg, *Helv. Chim. Acta*, **51**, 163 (1968); **52**, 948 (1969).

7) C. Keller-Juslén, M. Kuhn and A. von Wartburg, *J. Med. Chem.*, **14**, 936 (1971).

8) For review: R. U. Hutchins and N. R. Natale, *Org. Prep. Proc. Int.*, **11**, 201 (1979).

9) Y. Nishimura, *Yuki Gosei Kagaku Kyokai Shi*, **45**, 873 (1987).

Synthesis and Structural Analysis of 5-Deoxy-3-*O*-methyl-5-*C*-[(*R*)- and (*S*)-phenylphosphinothioyl]-α- and β-D-xylopyranoses

Tadashi HANAYA, Nobuyuki SHIGETOH, and Hiroshi YAMAMOTO*
Department of Chemistry, Faculty of Science, Okayama University,
Tsushima, Okayama 700
(Received February 3, 1988)

Treatment of 5-deoxy-5-iodo-1,2-*O*-isopropylidene-3-*O*-methyl-α-D-xylofuranose with ethyl phenylphosphinothioate in the presence of NaH in DMF gave a 1:1 mixture of the 5-deoxy-5-*C*-[(*R*)- and (*S*)-(ethoxy)phenylphosphinothioyl] derivatives. Reduction of these D-xylofuranoses with sodium dihydrobis(2-methoxyethoxy)aluminate, followed by the acid hydrolysis, provided the title compounds, which are the first sugar analogues having a phosphinothioyl group in the hemiacetal ring. These compounds were converted into four, separable 1,2,4-tri-*O*-acetates, the structures and conformations of which were established by spectroscopy. The corresponding per-*O*-acetyl-5-deoxy-5-*C*-[(*R*)- and (*S*)-phenylphosphinyl] analogues were also prepared and their previously presented structures were revised. Complete ^{1}H NMR (500-MHz) parameters of these two types of compounds are given for a comparative, structural study.

A large number of sugar analogues having a phosphorus atom in place of oxygen in the hemiacetal ring have been prepared in recent years:[1] e.g., D-glucopyranose type **1**[2] and D-ribofuranose type **2**.[3] Such compounds are of interest from the viewpoint of their physicochemical properties and potential biological activity.[1] All of these analogues possess an alkyl-, aryl-, or hydroxyphosphinyl group in the hemiacetal ring, but no derivatives containing a phosphinothioyl group in the ring have been prepared so far. On the other hand, it is well-known that many organophosphorus insecticides of P=S type, such as fenithion[4] (**3**) and EPN[5] (**4**), are in wide use and the P=S functional group of these compounds is effective in the relatively facile permeability through the skin of insects and then the slow oxidative desulfurization to generate the active P=O form by the action of a microsomal oxidase in vivo.[6] In this paper we wish to describe a detailed study on the two synthetic routes to the first sugar analogue having a phosphinothioyl group in the hemiacetal ring, as well as a comparative study with the corresponding 5-*C*-(phenylphosphinyl) derivatives, taking a 3-*O*-methyl-D-xylopyranose analogue as a model compound.[7]

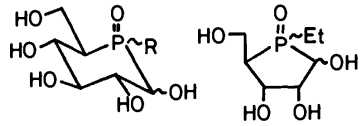

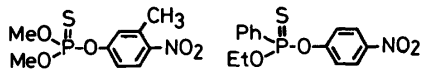

Results and Discussion

After examination of various reaction conditions, introduction of a phosphinothioyl group to the model compound was found to be best achieved by the reaction of 5-deoxy-5-iodo-1,2-*O*-isopropylidene-3-*O*-methyl-α-D-xylofuranose[8] (**5**) with ethyl phenylphos-

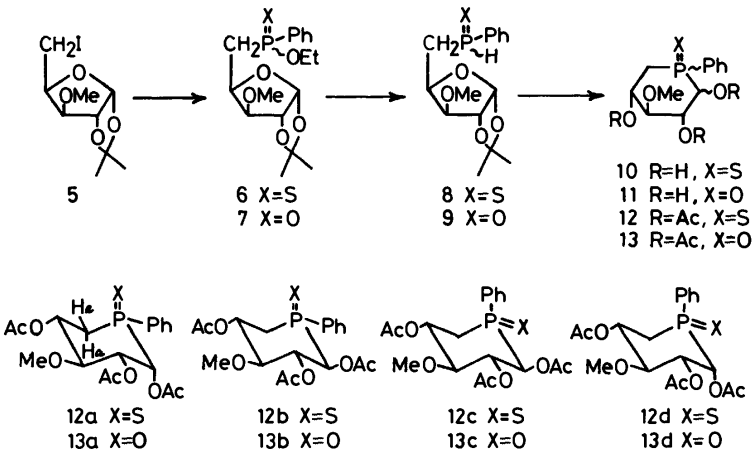

Scheme 1. Synthesis of 5-deoxy-3-*O*-methyl-5-*C*-(phenylphosphinothioyl)-D-xylopyranoses.

phinothioate[9] in dry *N,N*-dimethylformamide (DMF) containing an equivalent of sodium hydride at 0 °C for 3 h under argon (see Scheme 1). Thus the 5-*C*-[(*R*)- and (*S*)-(ethoxy)phenylphosphinothioyl] derivatives **6a,b** were obtained in 84% yield as a 1:1 mixture which were chromatographically inseparable. Compound **6** was obtained in less satisfactory yields when the reaction was carried out at room temp in DMF (3 h, 40% yield) or at elevated temps in benzene or xylene (19 h, ca. 9% yield). Complete ^{1}H NMR spectral parameters of both **6a** and **6b** were obtained at 500-MHz and are summarized in Table 1, by taking into consideration the similar spectral data of the 5-*C*-[(ethoxy)phenylphosphinyl] analogues **7a** and **7b** which were separable by chromatography (see later). On inspecting the molecular models of these *P*-epimers (see formulas **6a** and **6b**), the characteristic upfield shift of the δ value for MeO-3 of **6a** (δ 2.99) from the normal value of **6b** (δ 3.41) strongly suggests the most likely configurations of the P atom of **6a** and **6b** to be (*R*) and (*S*), respectively, because a stronger shielding effect on the MeO-3 group apparently exists in **6a** by the *P*-phenyl group in the vicinity.

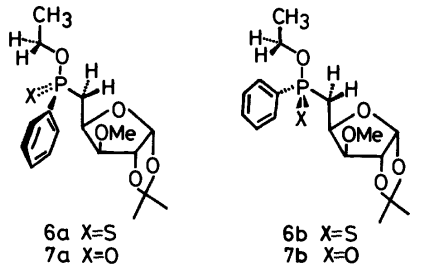

Reduction of **6** with sodium dihydrobis(2-methoxyethoxy)aluminate (SDMA) in dry benzene or tetrahydrofuran (THF) was found to proceed much slower than that of the alkoxyphosphinyl analogues which normally completes within 30 min at 0 °C.[1-3] Thus, the reduction was carried out at 20 °C for 17 h to give the unstable 5-*C*-(phenylphosphinothioyl) compound **8**. Other conditions such as with SDMA in benzene (at 50 °C for 30 h or 20 °C for 35—44 h), SDMA in THF (0 °C, 26 h) or $LiAlH_4$ in ether (20 °C, 60 h) have been found so far to result in less satisfactory yields of **8** from **6**; in most cases the starting material **6** remains unchanged. The acid-catalyzed deprotection of 1,2-*O*-isopropylidene group of **8** and the subsequent ring-transposition in oxygen-free 0.5 M HCl-EtOH (1:1 v/v) (1 M=1 mol·dm^{-3}) at 80 °C for 2 h provided 5-deoxy-3-*O*-methyl-5-*C*-(phenylphosphinothioyl)-D-xylopyranoses (**10**).

The structural assignment of **10** was made by converting them into the 1,2,4-tri-*O*-acetates **12** by treatment with acetic anhydride-pyridine at 20 °C for 20 h as in the case of the previous phosphorus-containing sugar analogues.[1-3] Purification of the crude mixture by column chromatography on silica gel using ethyl acetate-hexane as eluant and then recrystallization gave four, crystalline diastereomers: 5-deoxy-3-*O*-methyl-5-*C*-[(*S*)-phenylphosphinothioyl]-α-D-xylopyranose (**12a**, 1.8% overall yield from **6**), the 5-*C*-[(*S*)-P]-β- (**12b**, 1.8% yield), the 5-*C*-[(*R*)-P]-β- (**12c**, 3.4% yield), and the 5-*C*-[(*R*)-P]-α-isomer (**12d**, 2.3% yield). The identical molecular composition ($C_{18}H_{23}O_7PS$) of **12a—d** was confirmed by the high-resolution MS. The precise configurations and the $^4C_1$(D) conformation of **12a—d** were established on the basis of the 500-MHz ^{1}H NMR spectra by taking into account the known parameters of structurally similar compounds obtained before; e.g., the four diastereomers (with respect to the C-1 and ring-P atom) of per-*O*-acetyl-5-deoxy-5-*C*-(methoxyphosphinyl)-3-*O*-methyl-D-xylopyranoses[8,10] (**14**) and other related compounds such as 5-*C*-[(*S*)-(phenylphosphinyl)]-α-L-idopyranoses[11] (**15**) and L-iditol[11] (**16**). The complete NMR assignments of **12a—d** are listed in Table 1 and will be discussed later.

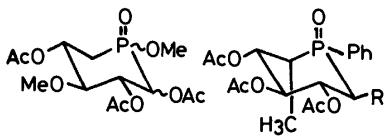

14 15 R=OAc 16 R=H

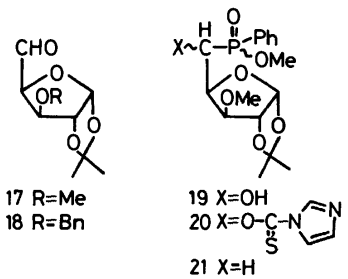

Meanwhile, the corresponding four 5-*C*-phenylphosphinyl derivatives **13a—d** of the above thioyl compounds have been prepared by Seo,[12] employing 1,2-*O*-isopropylidene-3-*O*-methyl-α-D-*xylo*-pentodialdo-1,4-furanose[13] (**17**) as the starting material by sequence **17**→**19**→**20**→**21**→**9**→**11**→**13**; structural assignments of the final products were made on the evidence of the insufficiently resolved 60-MHz ^{1}H NMR data and the values of optical rotations.[12] Having found some ambiguity in a part of the reported NMR assignments for **13a—d** and felt necessity of a comparative study of the exact parameters of **12a—d** with those of **13a—d** for further structural proof for the former compounds, we decided to prepare **13a—d**, by using **7** as the starting material. Thus, **7** was readily obtained from **5**[14] by the Michaelis-Arbusov reaction with diethyl phenylphosphonite in 91% yield as a 1:1 mixture of the two

Table 1. ^{1}H NMR (500-MHz) Parameters for **6**, **7**, **12**, and **13** in $CDCl_3$[a]

Compd	H-1	H-2	H-3	H-4	H-5 (H_a-5	H-5′ H_e-5)	Me_2C–O-1,2 (AcO-1,2,4)[b]		
6a	5.80	4.49	3.49	4.62	2.69	2.58	1.50,	1.30	
6b	5.75	4.53	3.73	4.39	2.78	2.49	1.40,	1.28	
7a	5.80	4.50	3.52	4.53	2.47	2.38	1.47,	1.29	
7b	5.78	4.53	3.66	4.32	2.52	2.31	1.39,	1.28	
12a	5.68	5.90	3.67	5.68	(2.91	2.60)	(1.94,	2.14,	2.03)
12b	5.79	5.78	3.57	5.65	(2.44	2.61)	(1.91,	2.09,	2.07)
12c	5.77	5.08	3.53	4.92	(2.37	3.23)	(2.16,	2.14,	2.07)
12d	6.11	4.77	3.65	4.83	(2.56	3.16)	(2.31,	2.14,	2.04)
13a	5.76	5.62	3.69	5.54	(2.49	2.68)	(1.98,	2.12,	2.04)
13b	5.60	5.75	3.58	5.53	(2.05	2.70)	(1.93,	2.09,	2.07)
13c	5.80	5.09	3.57	4.99	(2.33	3.01)	(2.15,	2.08,	2.05)
13d	6.10	4.78	3.70	4.86	(2.55	3.00)	(2.25,	2.15,	2.06)

Compd	MeO-3	HC–O–P	H′C–O–P	Me–C–O–P	Ph(*o*, *m*, *p*)		
6a	2.99	4.12	3.78	1.28	7.92,	7.43,	7.53
6b	3.41	4.12	3.79	1.27	7.93,	7.48,	7.53
7a	3.06	4.09	3.86	1.29	7.81,	7.48,	7.55
7b	3.39	4.11	3.89	1.31	7.81,	7.48,	7.55
12a	3.51				7.83,	7.49,	7.57
12b	3.51				7.89,	7.51,	7.58
12c	3.47				7.95,	7.56,	7.58
12d	3.47				7.86,	7.59,	7.59
13a	3.52				7.72,	7.50,	7.60
13b	3.53				7.75,	7.52,	7.60
13c	3.49				7.95,	7.57,	7.64
13d	3.48				7.89,	7.60,	7.65

Coupling constant

Compd	$J_{1,2}$	$J_{1,P}$	$J_{1,5e}$	$J_{2,3}$	$J_{2,P}$	$J_{3,4}$	$J_{4,5a}$ ($J_{4,5}$	$J_{4,5e}$ $J_{4,5'}$	$J_{4,P}$	$J_{5a,5e}$ $J_{5,5'}$	$J_{5a,P}$ $J_{5,P}$	$J_{5e,P}$ $J_{5'P}$)
6a	3.0			0		3.0	(9.1	4.4	8.7	14.5	10.6	17.8)
6b	3.9			0		3.0	(8.7	4.6	9.5	14.2	15.5	14.2)
7a	3.9			0		3.1	(9.5	4.7	6.4	14.8	12.8	17.7)
7b	3.9			0		3.1	(9.0	5.0	7.2	14.9	16.6	14.8)
12a	2.8	7.5	2.3	10.2	0	9.7	11.8	3.9	3.0	13.1	10.4	15.9
12b	11.0	0.3	0	9.4	3.4	9.7	11.8	4.2	3.3	13.8	8.5	16.7
12c	10.9	6.6	0	8.8	5.2	9.4	11.9	4.1	3.9	15.3	13.8	15.3
12d	2.6	7.2	2.2	10.1	0	9.4	12.1	4.2	2.8	15.2	15.1	14.5
13a	2.8	10.8	2.3	10.1	0	9.7	12.0	4.3	2.2	14.0	6.4	18.3
13b	11.0	2.7	0	9.5	2.8	9.6	12.3	4.3	2.9	14.5	4.2	19.5
13c	10.3	11.3	0	8.3	5.8	8.9	11.4	4.3	5.5	15.1	17.5	15.4
13d	2.6	8.9	2.0	9.3	3.6	8.7	11.2	4.3	5.5	15.0	18.5	15.0

Compd	*P*-OEt					*P*-Ph					
	$J_{H,H'}$	$J_{P,H}$	$J_{H,Me}$	$J_{P,H'}$	$J_{H',Me}$	$J_{P,2}$	$J_{P,3}$	$J_{P,4}$	$J_{2,3}$	$J_{3,4}$	J_m[c]
6a	10.2	9.8	7.1	8.5	7.0	13.1	3.3	1.8	7.0	7.5	1.5
6b	10.2	9.8	7.1	8.7	7.0	13.1	3.3	1.8	7.0	7.5	1.5
7a	10.1	7.1	7.1	7.1	7.1	12.1	3.3	1.4	8.3	7.5	1.5
7b	10.1	7.1	7.1	7.1	7.1	11.8	3.3	1.5	7.5	7.5	1.5
12a						13.4	3.5	1.8	7.5	7.7	1.5
12b						13.9	3.3	2.0	7.3	7.5	1.5
12c						12.8	3.3	1.8	8.1	7.8	1.5
12d						12.8	3.2	2.0	8.0	7.5	1.5
13a						11.8	3.3	1.5	7.5	7.5	1.5
13b						12.5	3.3	1.7	7.5	7.5	1.5
13c						11.8	3.3	1.7	7.7	7.7	1.5
13d						12.1	3.2	1.6	7.5	7.7	1.5

a) The assignments of all signals were made by employing a first-order analysis with the aid of decoupling technique and the parameters were confirmed by a computer-assisted simulation analysis. Very slight corrections were made on a few of the parameters for **12c, d** that were reported in Ref. 7, because the spectra of pure **12c** and **12d** have now become available. b) The assignments of acetoxyl groups may have to be interchanged. c) Approximate J values for meta-coupling of the *P*-phenyl ring protons: $J_{2,4'}$, $J_{2,6'}$, and $J_{3,5}$.

diastereomers, which were separable by chromatography into pure components **7a** and **7b**. From the analysis of the complete ^{1}H NMR data (see Table 1) the most likely configuration of the phosphorus atom of **7a** and **7b** were assigned to (*R*) and (*S*), respectively, on the same grounds taken into consideration in the case of **6a,b** shown above.

For the preparative purpose, however, the crude mixture **7** (without separation) can be subjected to the reduction with SDMA, because both **7a** and **7b** afford the identical 5-deoxy-5-*C*-phenylphosphinyl compound **9**[12] (see Scheme 1). Thus, after following the usual procedures,[1-3] **9** was led to **11** and then to **13**, from which the four diastereomers, **13a** (colorless needles, mp 202—203 °C, 11% overall yield from **7**), **13b** (colorless needles, mp 296—298 °C, 11% yield), **13c** (colorless syrup, 5% yield), and **13d** (colorless needles, mp 148—149 °C, 6% yield) were separated by silica-gel chromatography. As in the case of **12a—d** shown above, these compounds were characterized by MS and 500-MHz ^{1}H NMR (see Table 1 for the summarized parameters) as 5-deoxy-3-*O*-methyl-5-*C*-[(*S*)-phenylphosphinyl]-α-D-xylopyranose (**13a**), 5-*C*-[(*S*)-P]-β- (**13b**), 5-*C*-[(*R*)-P]-β- (**13c**), and 5-*C*-[(*R*)-P]-α- isomer (**13d**), in contrast to the previously reported assignments[12] of the structures 5-*C*-[(*R*)-P]-β-, 5-*C*-[(*R*)-P]-α-, 5-*C*-[(*S*)-P]-β-, and 5-*C*-[(*S*)-P]-α- isomer, respectively.

The ^{1}H NMR data of **12** and **13** generally follow the characteristic features in the δ and *J* values for 5-deoxy-5-*C*-(alkyl-, aryl-, and methoxyphosphinyl)-D-aldopyranoses approximately in the $^4C_1$(D) conformation.[1-3] Namely, the axial orientations (*S*) of the ring P=S and P=O groups in **12a,b** and **13a,b** are established by the downfield shift (0.7—1.1 ppm) of the H-2 and H-4 signals from those of **12c,d** and **13c,d** having equatorial P=S and P=O groups (see the δ values in Table 1). The α-orientation of C-1 is derived by considering the small magnitudes of $J_{1,2}$ (2.6—2.8 Hz) and $J_{1,5e}$ (2.0—2.3 Hz) values of **12a,d** and **13a,d**, whereas the β-anomers **12b,c** and **13b,c** show large $J_{1,2}$ (10.3—11.0 Hz) and negligible $J_{1,5e}$. It is noteworthy to mention some characteristic features in the spectral data of **12** and **13** more in detail for the purpose of comparison:

1) The proton signals of H-2 and H-4 of **12a** and **12b** appear at a slightly lower field (0.1—0.3 ppm) compared with those of **13a** and **13b**. The axial P=S group in the $^4C_1$(D) conformation therefore seems to excert a larger down-field shift on the signals of protons at the 1,3-diaxial positions in comparison with the same effect by the axial P=O group.

2) Appreciable differences in the magnitudes of the $J_{1,P}$, $J_{5a,P}$, and $J_{5e,P}$ are observed between the corresponding diastereomers of **12a—d** and **13a—d** (e.g., compare the $J_{1,P}$ values of **12a** and **13a**).

3) All of the AcO-1 signals of **12a,b** and **13a,b** appear at a rather high field (δ 1.91—1.99), indicating that these acetoxyl groups are most likely to be situated at the positions above the plane of the vicinal, equatorial *P*-phenyl ring. Significant down-field shifts (ca. 0.4 ppm) are observed for the δ values of H_a-5 of **12a,b** from those of the corresponding **13a,b** which seem to have normal values. Taking into consideration of the known values of the torsion angles (determined by X-ray crystallography[1,11]) between the P=O bond and the plane of the *P*-phenyl ring of compounds **15** and **16** (see Fig. 1), the most probable torsion angle between P=S and the plane of the *P*-phenyl ring of **12a** and **12b** in $CDCl_3$ solution is illustrated in Fig. 1, which would account for the above unusual δ values of H_a-5 and AcO-1 of these compounds.

However, exact reasons for these interesting features of the NMR parameters of the P=S compounds compared with those of the P=O analogues have remained to be further clarified employing a larger number of similar sugar analogues; particularly, the relation to their $^4C_1$(D) conformational deviations as well as intrinsic characters of P=S bonding affecting

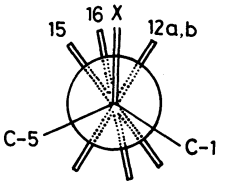

Fig. 1. "Newman" projection down the P–C(phenyl) bond illustrating the phenyl ring. [The digits mark the phenyl rings for compounds **15** (15, X=O),[11] **16** (16, X=O),[11] **12a**, and **12b** (12a, b, X=S)].

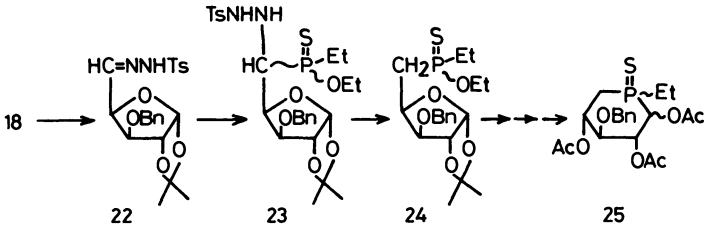

Scheme 2. Synthesis of 5-deoxy-3-*O*-benzyl-5-*C*-(ethylphosphinothioyl)-D-xylopyranoses.

the δ and J values of the neighboring groups would be of interest. Nevertheless, these exact parameters for **12a—d** are certainly of value in determining other 5-deoxy-5-*C*-phosphinothioyl-D-aldopyranoses that are still unknown.

Another approach for the synthesis of the sugar analogues having a P=S group in the ring was also made (see Scheme 2) utilizing a similar scheme employed for the synthesis of D-ribofuranose analogues[3] **2**. Namely, condensation of 3-*O*-benzyl-1,2-*O*-isopropylidene-α-D-*xylo*-pentodialdo-1,4-furanose[15] (**18**) with tosylhydrazine in methanol at 20 °C for 2 h gave the hydrazone **22** (85% yield), which was treated with ethyl ethylphosphinothioate[9] in the presence of trifluoromethanesulfonic acid at 0—20 °C for 7 h, thus affording the 5-*C*-[(ethoxy)ethylphosphinothioyl] derivative **23** (73%). Although reduction of **23** with sodium borohydride in THF was repeatedly examined at 25—50 °C for 7—48 h, the desired compound **24** was obtained in fluctuating yields (10—55%) besides a large amount of unidentified by-products. The same treatment of **24** (as in the case of **6** and **7**) with SDMA, followed by the 0.5 M HCl-EtOH and then acetic anhydride-pyridine afforded a diastereomeric mixture of 1,2,4-tri-*O*-acetyl-3-*O*-benzyl-5-deoxy-5-*C*-[(*R*)- and (*S*)-ethylphosphinyl]-α,β-D-xylopyranoses (**25**, colorless syrup) in only 1.6% overall yield from **24**. Compounds **25** were not separable into each diastereomers by chromatography. Therefore the synthetic approach shown in Scheme 2 seems to be less satisfactory than that described in Scheme 1.

Although improvement of the yields of some steps particularly of the reduction and the subsequent ring-enlargement reactions of the D-xylofuranoses **6** and **24** remains to be done, present work demonstrates an effective way for the preparation of 5-deoxy-5-*C*-(phenylphosphinothioyl)-D-xylopyranoses from an appropriate precursor. This scheme is therefore expected to be applicable to the preparation of various other 5-deoxy-5-*C*-phosphinothioyl-D- and L-aldofuranoses and pyranoses, which is currently under investigation.

Experimental

Melting points were determined with a Yanagimoto MP-S3 instrument and were uncorrected. All reactions were monitored by TLC (Merck silica gel 60F, 0.25 mm) with an appropriate solvent. Column chromatography was performed with Wako C-200 silica gel [or Merck Lobar prepacked silica gel (Size A) for rechromatography of **12** and **13**]. The ^{1}H NMR spectra were measured in $CDCl_3$ with a Hitachi R-600 (60-MHz, FT) or Varian VXR-500 instrument (500-MHz, the CS-NMR Lab., Okayama Univ.) at 27 °C. Chemical shifts (at 60-MHz unless otherwise specified) were recorded as δ values relative to tetramethylsilane as internal standard. The mass spectra were taken on a Shimadzu LKB-9000 low-resolution or a JEOL JMX-HX100 high-resolution instrument and were given in terms of m/z (rel intensity) compared with the base peak.

5-Deoxy-5-*C*-[(*R*)- and (*S*)-(ethoxy)phenylphosphinothioyl]-1,2-*O*-isopropylidene-3-*O*-methyl-α-D-xylofuranoses (6a, b). In a 100 cm^3 two-necked flask was placed sodium hydride (60% in oil, 688 mg, 1.2 equiv), which was then washed twice with dry hexane under argon and diluted with dry DMF (10 cm^3). To this suspension was dropwise added a solution of ethyl phenylphosphinothioate[9] (4.00 g, 1.5 equiv) in dry DMF (10 cm^3) at room temp under argon. After the consumption of sodium hydride to form the sodium salt of the thioate, a solution of **5**[8] (4.50 g) in dry DMF (10 cm^3) was dropwise added at 0 °C, followed by stirring at this temp for 3 h. The solvent was evaporated in vacuo (pump). The residue was dissolved in chloroform and washed with water. The organic layer was dried (Na_2SO_4) and evaporated in vacuo. The residue was purified by column chromatography with 1:3 AcOEt-hexane, giving an inseparable, 1:1 (by ^{1}H NMR) mixture of **6a** and **6b** (presumably 5-*C*-[(*R*)-P] and (*S*)-P diastereomer, respectively): A colorless syrup (4.50 g, 84%); R_f=0.65 (1:2 AcOEt-hexane); ^{1}H NMR (500-MHz), see Table 1; MS m/z 373 (M+1; 27.5), 372 (≃0), 340 (42), 312 (12), 311 (15), 287 (17), 282 (25), 186 (100), 185 (18), 157 (39), 153 (41), and 142 (21).

Found: m/z 373.1190. Calcd for $C_{17}H_{26}O_5PS$: M+1, 373.1239.

1,2,4-Tri-*O*-acetyl-5-deoxy-3-*O*-methyl-5-*C*-[(*R*)- and (*S*)-phenylphosphinothioyl]-α,β-D-xylopyranoses (12a—d). A solution of SDMA (490 mg, 70% in toluene, 3.0 equiv) in dry benzene (3 cm^3) was dropwise added into a solution of **6** (300 mg) in dry benzene (5 cm^3) at 5 °C under argon, followed by stirring at 20 °C for 18 h. Cold water (ca. 0.5 cm^3) was slowly added at 0 °C under stirring to decompose excess SDMA. The resulting white ppt was centrifuged and washed with benzene. Combined benzene solutions were concentrated in vacuo to give crude 5-deoxy-1,2-*O*-isopropylidene-3-*O*-methyl-5-*C*-[(*R*)- and (*S*)-phenylphosphinothioyl]-α-D-xylofuranoses (**8**) as a colorless syrup.

This was immediately dissolved in oxygen-free ethanol (5 cm^3) and 0.5 M hydrochloric acid (5 cm^3). The mixture (pH ca. 1) was degassed with argon and then refluxed for 2 h. The cooled mixture was neutralized by adding enough Amberlite IRA-45. The resin was filtered off and washed with aq ethanol. The filtrate was evaporated in vacuo to give crude 5-deoxy-3-*O*-methyl-5-*C*-[(*R*)- and (*S*)-phenylphosphinothioyl]-α,β-D-xylopyranoses (**10**) as a colorless syrup.

This was dissolved in pyridine (2 cm^3) and acetic anhydride (1 cm^3) at 5 °C. The mixture was stirred at 20 °C overnight, diluted with a small amount of cold water, and concentrated in vacuo. The residue was dissolved in chloroform and washed with water. The organic layer was dried (Na_2SO_4) and evaporated in vacuo. The residue was chromatographed with 1:2 AcOEt-hexane to give **12a—d**; **12d** was separated from **12c** by recrystallization (three times).

12a (5-*C*-[(*S*)-Phosphinothioyl]-α-isomer): Colorless needles (6.0 mg, 1.8% overall yield from **6**); mp 177—178 °C (from 1:1 AcOEt-hexane); R_f=0.24 (1:1 AcOEt-hexane); ^{1}H NMR (500-MHz), see Table 1; MS m/z 414 (M$^+$; 12.5), 382 (12), 356 (16), 355 (38), 324 (29), 323 (56), 322 (57), 313 (20), 294 (19), 281 (52), 280 (100), 265 (27), 264 (28), 239 (43), 238 (28), 222 (31), 171 (22), 87 (23), 71 (31), and 43 (68).

Found: m/z 414.0930. Calcd for $C_{18}H_{23}O_7PS$: M, 414.0902.

12b (5-*C*-[(*S*)-Phosphinothioyl]-β-isomer): Colorless needles (6.0 mg, 1.8% yield from **6**); mp 166.5—167 °C (from 1:1 AcOEt–hexane); R_f=0.31 (1:1 AcOEt–hexane); ^{1}H NMR (500-MHz), see Table 1; MS *m/z* 414 (M^+; 8.3), 355 (14), 323 (14), 322 (56), 281 (35), 280 (100), 239 (29), 238 (29), and 43 (51).

Found: *m/z* 414.0825. Calcd for $C_{18}H_{23}O_7PS$: M, 414.0902.

12c (5-*C*-[(*R*)-Phosphinothioyl]-β-isomer): Colorless needles (7.7 mg, 2.3% yield from **6**); mp 231—232 °C (from 1:1 AcOEt–hexane); R_f=0.44 (1:1 AcOEt–hexane); ^{1}H NMR (500-MHz), see Table 1; MS *m/z* 414 (M^+; 2.5), 355 (13), 354 (38), 295 (72), 294 (45), 254 (19), 253 (100), 252 (66), 157 (20), 155 (66), 113 (68), and 43 (72).

Found: *m/z* 414.0914. Calcd for $C_{18}H_{23}O_7PS$: M, 414.0902.

12d (5-*C*-[(*R*)-Phosphinothioyl]-α-isomer): Colorless needles (11.3 mg, 3.4% yield from **6**); mp 181—182 °C (from 1:1 AcOEt–hexane); R_f=0.44 (1:1 AcOEt–hexane); ^{1}H NMR (500-MHz), see Table 1; MS *m/z* 414 (M^+; 30.7), 354 (16), 296 (24), 295 (54), 294 (49), 281 (23), 253 (94), 252 (79), 237 (53), 128 (40), 127 (45), 113 (96), 71 (84), and 43 (100).

Found: *m/z* 414.0902. Calcd for $C_{18}H_{23}O_7PS$: M, 414.0902.

5-Deoxy-5-*C*-[(*R*)- and (*S*)-(ethoxy)phenylphosphinyl]-1,2-*O*-isopropylidene-3-*O*-methyl-α-D-xylofuranoses (7a,b). A mixture of **5** (500 mg) and diethyl phenylphosphonite (1.58 g, 5.0 equiv) was heated at 160 °C for 4 h under nitrogen and then concentrated below ca. 80 °C in vacuo. The residue was dissolved in ether and washed with water. The organic layer was dried (Na_2SO_4) and evaporated in vacuo. The residue was chromatographed with 1:1 AcOEt–hexane to give a 1:1 (by ^{1}H NMR) mixture of **7a** and **7b** as a colorless syrup (516 mg, 91% yield). The mixture was separated by careful rechromatography into the pure diastereomers.

7a (5-*C*-[(*R*)-P] isomer): Colorless syrup (170 mg, 30%); R_f=0.28 (2:1 AcOEt–hexane); ^{1}H NMR (500-MHz), see Table 1; MS *m/z* 356 (M^+).

7b (5-*C*-[(*S*)-P] isomer): Colorless syrup (190 mg, 34%); R_f=0.23 (2:1 AcOEt–hexane); ^{1}H NMR (500-MHz), see Table 1; MS *m/z* 356 (M^+).

1,2,4-Tri-*O*-acetyl-5-deoxy-3-*O*-methyl-5-*C*-[(*R*)- and (*S*)-phenylphosphinyl]-α,β-D-xylopyranoses[12] (13a—d). Similar procedures to those for **12** from **6** were employed. Thus, **7** (320 mg) was treated with SDMA (218 mg, 1.2 equiv) at 5 °C for 30 min, giving **9** as a colorless syrup. This was refluxed with 1:1 ethanol–0.5 M HCl (10 cm^3, oxygen-free) to afford **11** as colorless syrup. This was acetylated with Ac_2O–pyridine to give a mixture of **13**, which was separated by column chromatography with a gradient solution of 2:1 AcOEt–hexane→AcOEt→19:1 AcOEt–EtOH.

13a (5-*C*-[(*S*)-Phenylphosphinyl]-α-isomer): Colorless needles (39 mg, 11% yield from **7**); mp 202—203 °C (from 1:1 AcOEt–hexane, Ref. 12, mp 295—296 °C); R_f=0.44 (AcOEt); ^{1}H NMR (500-MHz), see Table 1; MS *m/z* 398 (M^+).

13b (5-*C*-[(*S*)-P]-β-isomer): Colorless needles (40 mg, 11% yield from **7**); mp 296—298 °C (from 1:1 AcOEt–hexane, Ref. 12, mp 200—200.5 °C); R_f=0.44 (AcOEt); ^{1}H NMR (500-MHz), see Table 1; MS *m/z* 398 (M^+).

13c (5-*C*-[(*R*)-P]-β-isomer): Colorless syrup (17 mg, 5% yield from **7**); R_f=0.33 (AcOEt); ^{1}H NMR (500-MHz), see Table 1; MS *m/z* 398 (M^+).

13d (5-*C*-[(*R*)-P]-α-isomer): Colorless needles (20 mg, 6% yield from **7**); mp 148—149 °C (from AcOEt–hexane, Ref. 12, syrup); R_f=0.22 (AcOEt); ^{1}H NMR (500-MHz), see Table 1; MS *m/z* 398 (M^+).

3-*O*-Benzyl-1,2-*O*-isopropylidene-α-D-*xylo*-pentodialdo-1,4-furanose 5-Tosylhydrazone (22). To a solution of **18**[15] (300 mg) in dry methanol (15 cm^3) was added tosylhydrazine (200 mg, 1.07 equiv) at 0 °C. The mixture was stirred at room temp for 2 h and then evaporated in vacuo. The residue was dissolved in chloroform, dried (Na_2SO_4), concentrated in vacuo, and then purified by column chromatography, giving **22** as colorless needles (406 mg, 85% yield): mp 129—132 °C (from AcOEt–hexane); R_f=0.68 (1:1 AcOEt–hexane); ^{1}H NMR δ=1.31, 1.48 (6H, 2s, Me_2C), 2.42 (3H, s, Me-C_6-S), 4.02—4.80 (5H, m, H-2,3,4, CH_2-O-3), 5.94 (1H, d, $J_{1,2}$=3.4 Hz, H-1), 7.15, 7.82 (2H, each, 2brd, *J*=8 Hz, C_6H_4-S), 7.25 (6H, brs, C_6H_5-C-O-3, NH), and 8.13 (1H, s, H-5); MS *m/z* 446 (M^+).

(*R*)- and (*S*)-3-*O*-Benzyl-5-deoxy-1,2-*O*-isopropylidene-5-*C*-[(*R*)- and (*S*)-(ethoxy)ethylphosphinothioyl]-5-*C*-[(2-tosyl)-hydrazino]-α-D-*xylo*-pentofuranose (23). A mixture of **22** (200 mg) and ethyl ethylphosphinothioate[9] (320 mg, 5 equiv) was degassed with argon. Trifluoromethanesulfonic acid (25 mg, 0.4 equiv) was dropwise added to the above mixture at 0 °C with stirring under argon, followed by stirring at 20 °C for 7 h. The mixture was diluted with chloroform (ca. 30 cm^3) and neutralized by washing with cold, saturated aq $NaHCO_3$. The organic layer was dried (Na_2SO_4) and concentrated in vacuo. The residue was purified by column chromatography with 1:2 AcOEt–hexane, giving **23** as a yellow syrup (192 mg, 73%): R_f=0.68 (1:1 AcOEt–hexane); ^{1}H NMR δ=0.65—1.65 (6H, m, MeC-P, MeC-O-P), 1.28, 1.48 (6H, 2s, Me_2C), 1.7—2.4 (2H, m, C-CH_2-P), 2.39 (3H, s, MeC_6-S), 3.4—5.0 (7H, m, H-2,3,4, CH_2-O-P, NH), 4.64 (2H, s, CH_2-O-3), 5.93 (1H, d, $J_{1,2}$=3.5 Hz, H-5), and 6.8—7.9 (10H, m, H-5, C_6H_5-C-O-3, C_6H_4-S); MS *m/z* 584 (M^+).

3-*O*-Benzyl-5-deoxy-1,2-*O*-isopropylidene-5-*C*-[(*R*)- and (*S*)-(ethoxy)ethylphosphiothioyl]-α-D-xylofuranose (24). To a solution of **23** (100 mg) in dry THF (10 cm^3) was slowly added sodium borohydride (32 mg) at 5 °C. The mixture was degassed with argon, stirred at 50 °C for 13 h, and then refluxed for 9 h (under argon). It was diluted with ether and an aq saturated solution of Na_2SO_4 was added. After separation, the aq layer was extracted with ether. The combined ethereal layer was dried (Na_2SO_4) and evaporated in vacuo. The residue was purified by column chromatography to give **24** as a yellow syrup (38 mg, 55% yield): R_f=0.6 (1:2 AcOEt–hexane); ^{1}H NMR δ=0.8—1.6 (6H, m, MeC-P, MeC-O-P), 1.34, 1.49 (6H, 2s, Me_2C), 1.6—2.4 (4H, m, 2H-5, CH_2-P), 3.5—4.9 (5H, m, H-2,3,4, CH_2-O-P), 4.58, 4.66 (2H, 2s, CH_2-O-3), 5.91 (1H, d, $J_{1,2}$=3.8 Hz, H-1), and 7.34 (5H, s, C_6H_5-C-O-3); MS *m/z* 400 (M^+).

1,2,4-Tri-*O*-acetyl-3-*O*-benzyl-5-deoxy-5-*C*-[(*R*)- and (*S*)-ethylphosphinothioyl]-α,β-D-xylopyranoses (25). The same procedures as those for **12** and **13** were employed. Thus, **24** (66 mg) was treated with SDMA (0.05 cm^3) at 5 °C for 5.5 h, followed by the usual procedures, giving an inseparable mixture of **25** as a pale yellow syrup (1.2 mg, 1.6% yield from **24**): R_f=0.5—0.7 (1:1 AcOEt–hexane); ^{1}H NMR δ=0.8—1.6 (3H, m, MeC-P), 1.6—2.1 (2H, m, $MeCH_2$-P), 1.88, 2.02, 2.09 (9H, 3brs, 3AcO), 2.2—3.5 (2H, m, 2H-5), 3.5—4.0 (1H, m, H-3), 4.60 (2H, brs, CH_2O-3), and 4.8—6.0 (3H, m, H-1,2,4); MS *m/z* 442 (M^+; 28.1), 383 (9), 336 (14), 332 (19), 305

(13), 292 (14), 262 (30), 245 (59), 203 (29), 185 (100), 157 (20), 138 (23), 137 (21), 109 (38), 91 (81), and 43 (33).

Found: *m/z* 442.1243. Calcd for $C_{20}H_{27}O_7PS$: M, 442.1208.

We are grateful to Mr. Shin-ichi Takekuma (Kinki University) for the measurement of mass spectra.

References

1) For a review, see H. Yamamoto and S. Inokawa, *Adv. Carbohydr. Chem. Biochem.*, **42**, 131 (1984).

2) H. Yamamoto, K. Yamamoto, S. Inokawa, M. Yamashita, M.-A. Armour, and T. T. Nakashima, *J. Org. Chem.*, **48**, 435 (1983); H. Yamamoto, T. Hanaya, S. Inokawa, M. Yamashita, M.-A. Armour, and T. T. Nakashima, *Carbohydr. Res.*, **128**, C5 (1984); H. Yamamoto, T. Hanaya, H. Kawamoto, S. Inokawa, M. Yamashita, M.-A. Armour, and T. T. Nakashima, *J. Org. Chem.*, **50**, 3516 (1985).

3) H. Yamamoto, Y. Nakamura, S. Inokawa, M. Yamashita, M.-A. Armour, and T. T. Nakashima, *J. Org. Chem.*, **49**, 1364 (1984).

4) Y. Nishizawa, K. Fujii, T. Kadota, J. Miyamoto, and H. Sakamoto, *Agric. Biol. Chem.*, **25**, 605 (1961).

5) A. G. Jelinek, U. S. Patent 2503390 (1950); *Chem. Abstr.*, **44**, 6435f (1950). N. Shindo, S. Wada, K. Ota, F. Suzuki, and Y. Ohata, U. S. Patent 3327026 (1967); *Chem. Abstr.*, **67**, 64531q (1968).

6) M. Eto, *Yuki Gosei Kagaku Kyokai Shi*, **45**, 549 (1987), and references cited therein.

7) A part of the results have been preliminarily reported as a communication: H. Yamamoto, T. Hanaya, N. Shigetoh, H. Kawamoto, and S. Inokawa, *Chem. Lett.*, **1987**, 2081.

8) H. Yamamoto, T. Hanaya, S. Inokawa, K. Seo, M.-A. Armour, and T. T. Nakashima, *Carbohydr. Res.*, **114**, 83 (1983).

9) J. Michalshi and Z. Tulimowski, *Rocz. Chem.*, **36**, 1781 (1962); K. A. Petrov, A. A. Basyuk, V. P. Evdakov, and L. I. Mizrakh, *Zh. Obshch. Khim.*, **34**, 2226 (1964).

10) H. Yamamoto, T. Hanaya, S. Inokawa, and M.-A. Armour, *Carbohydr. Res.*, **124**, 195 (1983).

11) H. Yamamoto, K. Yamamoto, H. Kawamoto, S. Inokawa, M.-A. Armour, and T. T. Nakashima, *J. Org. Chem.*, **47**, 191 (1982); S. Inokawa, K. Yamamoto, H. Kawamoto, H. Yamamoto, M. Yamashita, and P. Luger, *Carbohydr. Res.*, **106**, 31 (1982); H. Yamamoto, S. Inokawa, and P. Luger, *ibid.*, **113**, 31 (1983).

12) K. Seo, *Carbohydr. Res.*, **119**, 101 (1983); the author appears to have made the structural assignments of **13a—d** somewhat erroneously (see the main text).

13) R. Schaffer and H. S. Isbell, *J. Res. Natl. Bur. Stand.*, **56**, 191 (1956).

14) Compound **7** had been obtained, apparently as a mixture of two isomers at the phosphorus atom, in 90% yield from 5-bromo derivative of **5**: S. Inokawa, Y. Tsuchiya, H. Yoshida, and T. Ogata, *Bull. Chem. Soc. Jpn.*, **43**, 3224 (1970).

15) T. Iida, M. Funabashi, and J. Yoshimura, *Bull. Chem. Soc. Jpn.*, **46**, 3203 (1973).

Addition of Diphenyldiazomethane to Unsubstituted and Chloro-Substituted 1,4-Benzoquinones. Effects of Chloro Substituents on the Addition Modes

Takumi OSHIMA* and Toshikazu NAGAI
Institute of Chemistry, College of General Education, Osaka University, Toyonaka, Osaka 560
(Received February 3, 1988)

Unsubstituted 1,4-benzoquinone (**1a**) reacted with diphenyldiazomethane (DDM) at the C=C double bonds to give dihydroxy-3*H*-indazole (**2a**) and its benzhydryl ether (**3a**) together with benzodipyrazole derivative (**4a**). Similarly, reactions of 2-chloro- and 2,3-dichloro-1,4-benzoquinones (**1b** and **1c**) with DDM yielded the corresponding dihydroxy-3*H*-indazoles (**2b**, **2b'**, and **2c**) and their benzhydryl ethers (**3b**, **3b'**, and **3c**) along with 5—13% benzophenone (**6**). On the other hand, reaction of 2,6-dichloro-1,4-benzoquinone (**1e**) with DDM gave bicyclic **5e** and tricyclic diones (**7e**), together with benzophenone dimethyl acetal (**9**) in the presence of added methanol. In the same conditions, 2,3,5-trichloro-1,4-benzoquinone (**1f**) provided bicyclic dione (**5f**) and **9**. Formation of **6** and **9** was interpreted as arising from the hydrolysis and methanolysis of the 1:1 betaine intermediates given by the addition of DDM to the quinonoid C=O double bonds. The C=O addition increased with increasing chlorine substituents.

Additions of diazoalkanes to quinones are of synthetic and mechanistic interest because quinones, with the conjugated C=C and C=O double bonds, show two possible modes of addition which are markedly affected by the substituents and structural natures of these reactants, affording various types of products.[1] Diphenyldiazomethane (DDM), one of the most familiar diazoalkanes, is reported to add only to the C=C double bond of 1,4-benzoquinone (**1a**) giving 3*H*-indazole derivative **2a**.[2] Recently, it has been found that DDM reacts with 2,5-dichloro-1,4-benzoquinone (**1d**) at the C=C and C=O double bonds to yield bicyclic dione **5d** and poly(2,5-dichlorohydroquinone benzhydryl ether), respectively.[3] Further, tetrachloro-1,4-benzoquinone (**1g**) is known to undergo the addition of DDM only at the C=O double bond to afford poly(tetrachlorohydroquinone benzhydryl ether).[4] These striking changes in the reaction fashions with increasing chlorine substituents of 1,4-benzoquinones prompted us to extend the reaction of DDM to all of other chloro-substituted 1,4-benzoquinones. In this paper, we wish to report a systematic investigation of the products of reaction of DDM with 2-chloro-, 2,3- and 2,6-dichloro-, and 2,3,5-trichloro-1,4-benzoquinones, together with a reinvestigation of the product in the prior study of DDM and unsubstituted 1,4-benzoquinone. The effects of the substitution patterns of the chlorines on the addition modes of these quinones are also discussed.

Results and Discussion

Reaction of DDM with 1,4-Benzoquinone (1a), 2-Chloro- (1b) and 2,3-Dichloro-1,4-benzoquinone (1c). In 1931 Fieser and his co-worker have reported that DDM adds to 1,4-benzoquinone (**1a**) to give in nearly quantitative yield dihydroxy-3*H*-indazole (**2a**).[2] However, besides **2a** (40%), two additional products, benzhydryl ether **3a** (39%) of **2a** and bis(3*H*-pyrazole) adduct **4a** (9%), were obtained in the present equimolar reaction in same benzene solution at 25 °C (Scheme 1).

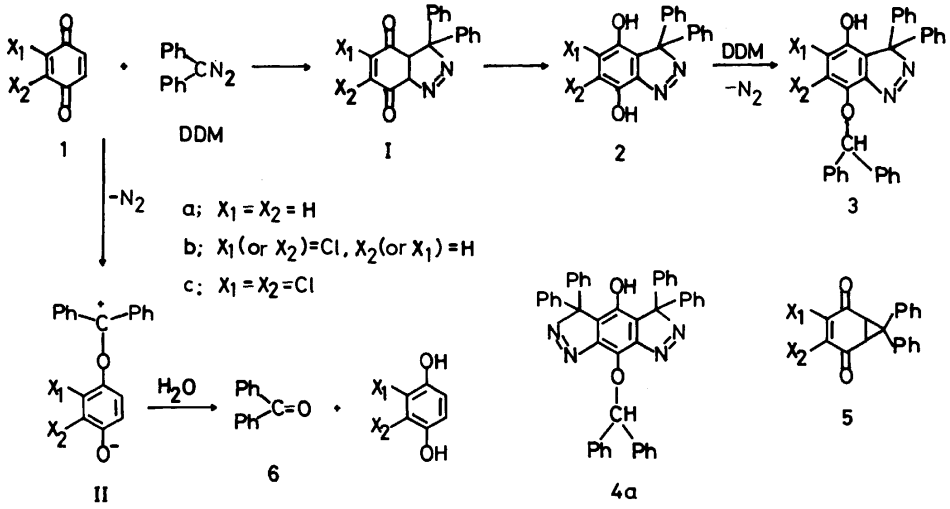

Scheme 1.

This reaction consists in dipolar addition of DDM to **1a** and dienolization of the first product, pyrazoline (**Ia**). The compound **3a** appears to be the secondary product formed from the resulting **2a** and DDM. Indeed, equimolar reaction of **2a** and DDM yielded **3a** in 77% yield. Here, it seems likely that DDM prefers the unhindered phenolic OH of **2a** to avoid the steric repulsion due to the bulky diphenylmethylene moiety. With respect to the formation of **4a**, two possible routes can be put forward. One is the dehydrogenative conversion of **Ia** and/or **2a** into a 3*H*-indazole-4,7-dione (**III**) which would undergo addition of DDM to lead a precursor **IV** of **4a** after dienolization. Another

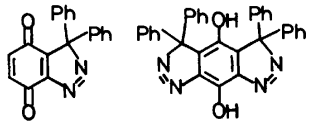

III IV

one is direct addition of DDM to **Ia** followed by dehydrogenation and dienolization yielding **IV**. The symmetric orientation of **4a** was established by the ^{13}C NMR spectrum which contains six signals for the twelve unprotonated C-atoms of the aromatic rings and one signal for the two diphenyl-substituted C-atoms of the 3*H*-pyrazole rings, respectively; asymmetric one would require nine and two signals for the corresponding C-atoms.

Similarly, equimolar reaction of DDM with **1b** and **1c** gave two principal products, 3*H*-indazole derivatives (**2b**, its regioisomer **2b'**, and **2c**) and their benzhydryl ethers (**3b**, **3b'**, and **3c**), together with 5—13% amounts of benzophenone (**6**) (Scheme 1). The **1b**, as expected, allowed the two addition direction at the unchlorinated C=C bond and thus provided the two sets of isomers, **2b** and **2b'**, **3b** and **3b'**. Each of the isomers could be isolated by column chromatography on silica gel, but it is not yet possible to make the structural assignments. In contrast with the above unchlorinated **1a**, these chlorinated **1b** and **1c** afforded **6**; the yield of **6** for dichlorinated **1c** was nearly twice that for the monochlorinated **1b**. The origin of **6** appears to be water-sensitive 1 : 1 betaine intermediates **II** given by addition of DDM to the C=O double bond. Such hydrolyzable betaines were the key intermediates in the previous reactions of DDM with tetrachloro-1,4-benzoquinone (**1g**)[4] and 2,3-dichloro-5,6-dicyanobenzoquinone (DDQ),[5] where the additions take place only at the C=O bonds. It is also noted that the chlorinated C=C bonds of **1b** and **1c** remain intact for the dipolar addition of DDM. According to FMO (Frontier Molecular Orbital) theory, cycloadditions of simple diazoalkanes to electron-deficient olefins are classified as being controlled by the interaction of the highest occupied molecular orbitals (HOMOs) of diazoalkanes and the lowest unoccupied molecular

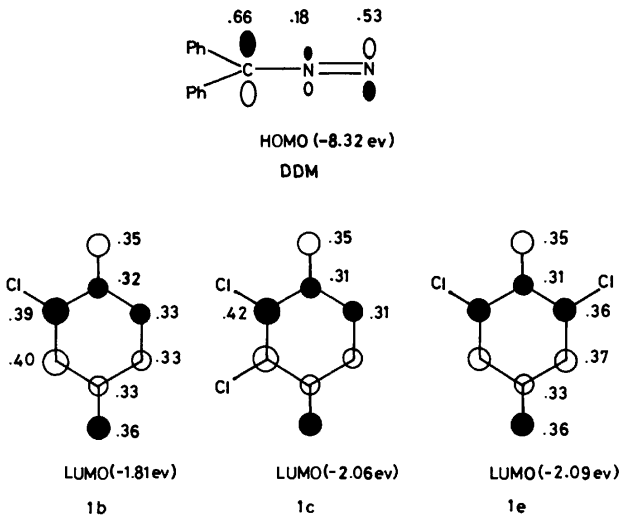

Fig. 1. MNDO π-orbital shapes and energies (in parentheses) of DDM and of 2-chloro-(**1b**), 2,3-dichloro-(**1c**), and 2,6-dichloro-1,4-benzoquinones (**1e**). Only coefficients of diazo function are shown for DDM.

orbitals (LUMOs) of olefins.[6] Figure 1 denotes the HOMO of DDM and LUMO of some quinones by MNDO calculation.[7] The concept of FMO predicts addition of DDM to the chloro-substituted C=C bonds rather than to the unsubstituted ones of **1b** and **1c**, because of the larger LUMO coefficients. This discrepancy is apparently attributable to the steric repulsion due to the chlorine substituents.

It has been found that, in refluxing benzene, these reaction systems of DDM and quinones **1a—c** showed no substantial changes in the product distributions except the formation of small amounts of nitrogen free bicyclic diones, **5a** (12%), **5b** (15%), and **5c** (5%). The **5a—c** supposedly arise by nitrogen release from **I** or by addition of diphenylcarbene to **1a—c**.[8]

Reaction of DDM with 2,6-Dichloro- (1e) and 2,3,5-Trichloro-1,4-benzoquinones (1f). We have previously reported that DDM and 2,5-dichloro-1,4-benzoquinone (**1d**) yield bicyclic dione **5d** and hydroquinone acetal (**8d**) in the presence of added methanol,[3] as shown in Scheme 2. The **5d** is the product given by loss of nitrogen from the initial dipolar adduct, pyrazoline (**Id**), whose chloro substituent prohibits the rearrangement into 3*H*-indazole derivative. While, the **8d** can be accounted for on the basis of a 1:1 betaine intermediate **IId**. Here, methanol was added as a capture of **IId**, otherwise, **IId** tends to polymerize into poly(2,5-dichlorohydroquinone benzhydryl ether).[3]

A study has now been made of reactions of DDM with 2,6-dichloro- (**1e**) and 2,3,5-trichloro-1,4-benzoquinones (**1f**), both of which are designed to avoid dienolization upon the dipolar addition to the C=C bonds as well as above **1d**. In the presence of 5 equiv of methanol, quinone **1e** reacted with DDM to give

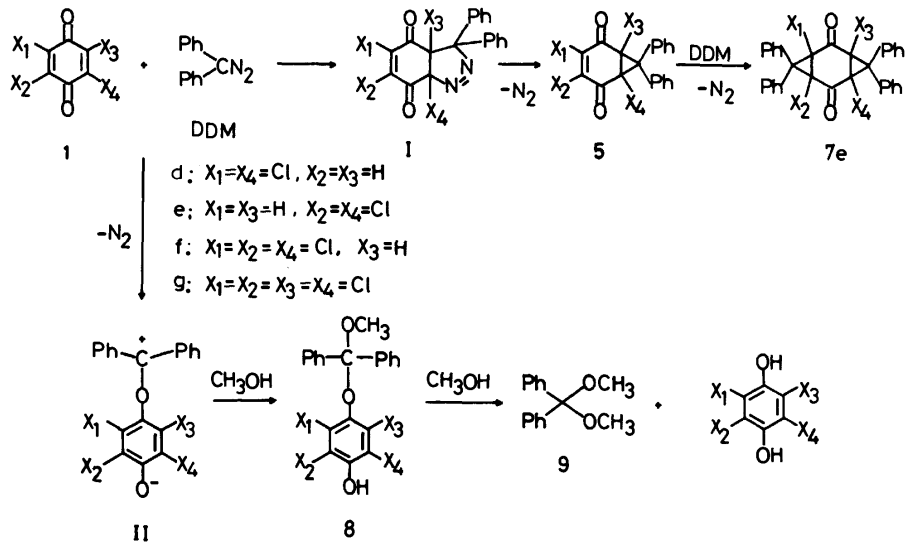

Scheme 2.

Table 1. Effects of the Chloro Substituents on the Addition Modes of 1,4-Benzoquinones (**1a—g**) to DDM in Benzene

Quinone	Temp/°C	Substituted position	Addition mode/%	
			C=C addition	C=O addition
1a	25	—	100	0
1a	80	—	100	0
1b	25	2-	91[a]	9
1b	80	2-	90[a]	10
1c	25	2,3-	78[a]	22
1c	80	2,3-	83[a]	17
1d[b]	30	2,5-	49	51
1e	25	2,6-	50[c]	50
1f	25	2,3,5-	40[d]	60
1g[e]	30	2,3,5,6-	0	100

a) For unchlorinated C=C bond. b) Ref. 3. c) Estimated as the sum of **5e** and **7e**. d) For monochlorinated C=C bond. e) Solvent: tetrahydrofuran, see Ref. 4.

bicyclic dione **5e** (43%) and tricyclic dione **7e** (5%) in addition to benzophenone dimethyl acetal **9** (45%). Apparently, the behavior of **1e** is different from that of above **1d** in that the former involved the dipolar addition to both the C=C bonds to give **7e** and caused the redoxical acetalization into **9** and 2,6-dichlorohydroquinone. Indeed, bicyclic dione **5e** reacted slowly with DDM to provide **7e**; $k=1.57\times10^{-4}/s^{-1}\,mol^{-1}$ (30 °C, benzene). This value of k is only one twentieth of the overall rate ($k=3.36\times10^{-3}$) for the reaction of DDM and **1e**,[9] reflecting the above product distribution. However, **5d** derived from **1d** remained unchanged even on 2 day's standing with DDM under the same conditions. The stereochemistry of tricyclic dione **7e** is unknown. The ^1H NMR spectrum of **7e** (δ=2.66, s, two bridgehead H) can not allow the stereochemical assignment in view of the fact that the corresponding protons of similar tricyclic diones, *syn*- and *anti*-tricyclo[5.1.0.$0^{3,5}$]octane-2,6-diones, do not resonate with each other.[10]

As for the process giving the 1:1 betaine **IIe**, it is more likely that DDM preferably attacks the C=O bond meta to the chloro-substituents in the light of the steric effects and of the results of the MNDO calculation[7] of **1e** which indicates slightly larger LUMO coefficients for this meta C=O bond (Fig. 1). Such an addition appears to be responsible for the higher reactivity of **8e**, because the combination of two meta chlorine substituents do make the diphenylmethylene moiety more positive than do the combination of ortho and meta chlorine-substituents in the comparable **8d**.

Introduction of one more chlorine atom to the quinone nucleus of **1e** brought about slight increase of the relative reactivity of the C=O to the C=C bonds, as exhibited by the product ratio (55:37) of acetal **9** to bicyclic dione **5f** for the reaction of 2,3,5-trichloro-1,4-benzoquinone (**1f**).

The product distributions are shown in Table 1. This table clearly shows the increase of C=O additions

with increasing Cl substituents as well as the lack of temperature effects (i.e., **1a—c**).

Experimental

All the melting points were uncorrected. The IR, ^{1}H NMR, ^{13}C NMR, and mass spectra were recorded on a Perkin Elmer 983 G, a Varian EM 390, a Hitachi 90 H, and a Hitachi RMU 6E spectrometers respectively.

Materials. The diphenyldiazomethane (DDM) was prepared by the oxidation of benzophenone hydrazone with yellow mercury oxide and recrystallized from petroleum ether; mp 29—30 °C. All quinones were purified before use by column chromatography on silica gel (hexane–benzene (3:1) as an eluent) and recrystallization from a mixture of hexane and benzene. The 1,4-benzoquinone (**1a**) and 2-chloro-1,4-benzoquinone (**1b**) were of commercial origin; mp 113—115 °C and 57—58 °C respectively. The 2,3-dichloro- (**1c**) and 2,6-dichloro-1,4-benzoquinone (**1e**), and 2,3,5-trichloro-1,4-benzoquinone (**1f**) were prepared according to the literature methods; mp 100—101 °C (lit,[11] 100—101 °C), 121—122 °C (lit,[12] 120.5—121 °C), and 167—168 °C (lit,[13] 169—170 °C) respectively.

4,7-Dihydroxy-3,3-diphenyl-3*H*-indazole (2a), 7-Benzhydryloxy-4-hydroxy-3,3-diphenyl-3*H*-indazole (3a), and 8-Benzhydryloxy-3,6-dihydro-4-hydroxy-3,3,5,5-tetraphenylbenzo[1,2-*c*:5,4-*c*']dipyrazole (4a). To begin with, it should be kept in mind that all the yields are based on DDM used. A benzene solution (10 ml) of DDM (540 mg, 2.78 mmol) and 1,4-benzoquinone **1a** (300 mg, 2.78 mmol) was allowed to stand for 10 h at 25 °C. The solvent was removed and the residue was column-chromatographed on silica gel. Elution with hexane–benzene (20 to 100%) gave successively recovered **1a** (20 mg), **4a** (55 mg, 9%), and **3a** (255 mg, 39%). Further elution with benzene–ether (10%) yielded **2a** (339 mg, 40%). Recrystallization of **2a** from a mixture of hexane and ether gave yellow crystals: mp 208—209 °C (lit,[2] 210 °C); IR (KBr) 3405, 1501, 1454, 1272, 696 cm^{-1}; ^{1}H NMR (acetone-d_6) δ=6.60 (s, 1H, aromatic H), 6.87 (s, 2H, aromatic H), 7.2—7.5 (m, 9H, aromatic H), 8.23 (s, 1H, OH, exchangeable with CD_3OD), 9.07 (s, 1H, OH, exchangeable with CD_3OD); MS, *m/z* 302 (M^+). Anal. ($C_{19}H_{14}O_2N_2$) C, H, N. The compound **3a** was recrystallized from a mixture of hexane and benzene: mp 188—190 °C, yellow plates; IR (KBr) 3423, 1500, 1274, 697 cm^{-1}; ^{1}H NMR ($CDCl_3$) δ=4.80 (s, 1H, OH, exchangeable with CD_3OD), 6.6—7.6 (m, 23H, aromatic H+$Ph_2C\underline{H}$); MS, *m/z* 468 (M^+). Anal. ($C_{32}H_{24}O_2N_2$) C, H, N. Recrystallization of **4a** from a mixture of hexane and benzene provided pale yellow prisms: mp 201—203 °C; IR (KBr) 3534, 1490, 1185, 1022, 754, 697 cm^{-1}; ^{1}H NMR ($CDCl_3$) δ=4.50 (s, 1H, OH, exchangeable with CD_3OD), 6.9—7.8 (m, 30H, aromatic H), 7.93 (s, 1H, $Ph_2C\underline{H}$); ^{13}C NMR ($CDCl_3$) δ=87.1 ($Ph_2\underline{C}H$), 101.8 ($Ph_2\underline{C}$=), 127.0, 127.5, 127.9, 128.1, 128.5, 128.9 (protonated aromatic C), 134.7, 135.9, 138.8, 140.7, 141.3, 150.5 (unprotonated aromatic C); MS, *m/z* 660 (M^+). Anal. ($C_{45}H_{32}O_2N_2$) C, H, N.

7,7-Diphenylbicyclo[4.1.0]hept-3-ene-2,5-dione (5a). To a refluxing benzene (5 ml) containing **1a** (300 mg, 2.78 mmol) was added dropwise over 10 min a benzene solution (5 ml) of DDM (540 mg, 2.78 mmol). After 1 h refluxing, the solvent was removed and the residue was column-chromatographed on silica gel. Elution with hexane–benzene (30%) provided benzophenone azine (35 mg, 7%) and recovered **1a** (30 mg). The bicyclic dione **5a** (91 mg, 12%) was eluted with hexane–benzene (50%). The **4a** (25 mg, 4%), **3a** (282 mg, 43%), and **2a** (252 mg, 30%) were yielded on further chromatographic treatment as above. Recrystallization of **5a** from a mixture of hexane and benzene yielded pale yellow needles: mp 173—174 °C; IR (KBr) 1666, 1493, 1302, 707 cm^{-1}; ^{1}H NMR ($CDCl_3$) δ=3.33 (s, 2H, cyclopropyl H), 6.18 (s, 2H, vinyl H), 7.2—7.6 (m, 10H, aromatic H); MS, *m/z* 274 (M^+). Anal. ($C_{19}H_{14}O_2$) C, H.

5- or 6-Chloro-4,7-dihydroxy-3,3-diphenyl-3*H*-indazole (2b or 2b') and 7-Benzhydryloxy-5- or 6-chloro-4-hydroxy-3,3-diphenyl-3*H*-indazole (3b or 3b'). A benzene solution (20 ml) of DDM (700 mg, 3.61 mmol) and 2-chloro-1,4-benzoquinone **1b** (515 mg, 3.61 mmol) was allowed to stand for 10 h at 25 °C. The solvent was removed and the residue was column-chromatographed on silica gel. Elution with hexane–benzene (20 to 100%) gave successively benzophenone **6** (35 mg, 5%), recovered **1b** (100 mg), **3b** (248 mg, 27%), and **3b'** (265 mg, 29%). Further elution with benzene–ether (5%) yielded **2b'** (210 mg, 17%) and **2b** (85 mg, 7%). The **2b** and **2b'** were converted into **3b** and **3b'** respectively, when treated with DDM. Recrystallization of **2b** from benzene provided yellow crystals: mp 180 °C (decomp); IR (KBr) 3473, 1460, 1401, 1242, 696 cm^{-1}; ^{1}H NMR ($CDCl_3$) δ=2.05 (broad s, 1H, OH, exchangeable with CD_3OD), 5.50 (broad s, 1H, OH, exchangeable with CD_3OD), 7.1—7.4 (m, 11H, aromatic H); MS *m/z* 336 (M^+). Anal. ($C_{19}H_{13}O_2N_2Cl$) C, H, N. Recrystallization of **2b'** from benzene gave yellow crystals: mp 172—174 °C; IR (KBr) 3398, 1493, 1452, 1228, 696 cm^{-1}; ^{1}H NMR ($CDCl_3$) δ=1.83 (broad s, 1H, OH, exchangeable with CD_3OD), 5.40 (broad s, 1H, OH, exchangeable with CD_3OD), 7.2—7.4 (m, 11H, aromatic H); MS, *m/z* 336 (M^+). Anal. ($C_{19}H_{13}O_2N_2Cl$) C, H, N. Recrystallization of **3b** from a mixture of hexane and benzene provided yellow crystals of mp 86—88 °C; IR (KBr) 3429, 1480, 1460, 1230, 1040, 697 cm^{-1}; ^{1}H NMR ($CDCl_3$) δ=5.33 (s, 1H, OH, exchangeable with CD_3OD), 7.00 (s, 1H, $Ph_2C\underline{H}$), 7.1—7.7 (m, 21H, aromatic H); MS, *m/z* 502 (M^+). Anal. ($C_{32}H_{23}O_2N_2Cl$) C, H, N. Recrystallization of **3b'** from benzene yielded yellow crystals which decomposed at 178 °C (decomp); IR (KBr) 3429, 1491, 1460, 1240, 697 cm^{-1}; ^{1}H NMR ($CDCl_3$) δ=4.77 (s, 1H, OH, exchangeable with CD_3OD), 6.87 (s, 1H, $Ph_2C\underline{H}$), 6.9—7.8 (m, 21H, aromatic H); MS, *m/z* 502 (M^+). Anal. ($C_{32}H_{23}O_2N_2Cl$) C, H, N.

3-Chloro-7,7-diphenylbicyclo[4.1.0]hept-3-ene-2,5-dione (5b). To a refluxing benzene (10 ml) containing **1b** (515 mg, 3.61 mmol) was added dropwise over 10 min a benzene solution (10 ml) of DDM (700 mg, 3.61 mmol). After 1 h refluxing, the solvent was removed and the residue was column-chromatographed on silica gel. Elution with hexane–benzene (20—50%) gave successively **6** (40 mg, 6%), recovered **1b** (90 mg), and benzophenone azine (25 mg, 4%). The bicyclic dione **5b** (171 mg, 15%) was eluted with hexane–benzene (50%) and recrystallized from a mixture of hexane and benzene to yield pale yellow prisms: mp 104—105 °C; IR (KBr) 1684, 1661, 1595, 707 cm^{-1}; ^{1}H NMR ($CDCl_3$) δ=3.2—3.3 (m, 2H, cyclopropyl H), 6.33 (d, *J*=1.5 Hz, 1H, vinyl H), 7.0—7.3 (m, 10H, aromatic H); MS, *m/z* 308 (M^+). Anal. ($C_{19}H_{13}O_2Cl$) C, H. The **3b** (205 mg, 23%), **3b'** (230 mg, 25%), **2b'** (125 mg, 10%), and **2b** (63 mg, 5%) were obtained on further column-chromatographic treatment as above.

5,6-Dichloro-4,7-dihydroxy-3,3-diphenyl-3*H*-indazole (2c) and 7-Benzhydryloxy-5,6-dichloro-4-hydroxy-3,3-diphenyl-3*H*-indazole (3c). A benzene solution (10 ml) of DDM (290 mg, 1.49 mmol) and 2,3-dichloro-1,4-benzoquinone **1c** (260 mg, 1.47 mmol) was allowed to stand for 10 h at 25 °C. The solvent was removed and the residue was column-chromatographed on silica gel. Elution with hexane–benzene (30 to 100%) gave successively **6** (35 mg, 13%), recovered **1c** (120 mg), and **3c** (240 mg, 60%). Further elution with benzene–ether (5%) yielded 2,3-dichlorohydroquinone (13 mg, 5%) and **2c** (93 mg, 17%). Recrystallization of **2c** from a mixture of hexane and ether provided yellow glanulates: mp 173—174 °C; IR (KBr) 3427, 1451, 1099, 696 cm^{-1}; ^1H NMR (acetone-d_6) δ=2.9 (broad s, 1H, OH, exchangeable with CD_3OD), 7.30 (s, 10H, aromatic H), 8.30 (broad s, 1H, OH, exchangeable with CD_3OD); MS, *m/z* 370 (M^+). Anal. ($C_{19}H_{12}O_2N_2Cl_2$) C, H, N. Recrystallization of **3c** from a mixture of hexane and benzene provided pale yellow crystals: mp 166—168 °C; IR (KBr) 3431, 1438, 696 cm^{-1}; ^1H NMR ($CDCl_3$) δ=5.48 (s, 1H, OH, exchangeable with CD_3OD), 7.0—7.7 (m, 20H, aromatic H), 7.80 (s, 1H, $Ph_2C\underline{H}$); MS, *m/z* 536 (M^+). Anal. ($C_{32}H_{22}O_2N_2Cl$) C, H, N.

3,4-Dichloro-7,7-diphenylbicyclo[4.1.0]hept-3-ene-2,5-dione (5c). To a refluxing benzene (5 ml) containing **1c** (260 mg, 1.47 mmol) was added dropwisely over 10 min a benzene solution (5 ml) of DDM (290 mg, 1.49 mmol). After 1 h refluxing, the solvent was removed and the residue was column-chromatographed on silica gel. Elution with hexane–benzene (30%) gave successively **6** (30 mg, 11%), recovered **1c** (75 mg), and bicyclic dione **5c** (25 mg, 5%). Recrystallization from benzene yielded pale yellow prisms: mp 237—238 °C; IR (KBr) 1691, 1561, 1277, 708 cm^{-1}; ^1H NMR ($CDCl_3$) δ=3.38 (s, 2H, cyclopropyl H), 7.2—7.5 (m, 10H, aromatic H); MS, *m/z* 343 (M^+). Anal. ($C_{19}H_{12}O_2Cl_2$) C, H. The **3c** (212 mg, 53%), 2,3-dichlorohydroquinone (15 mg, 6%), and **2c** (125 mg, 23%) were obtained on further column-chromatographic treatment as above.

1,3-Dichloro-7,7-diphenylbicyclo[4.1.0]hept-3-ene-2,5-dione (5e), 1,3-Dichloro-4,4,8,8-tetraphenyltricyclo[5.1.0.$0^{3,5}$]-octane-2,6-dione (7e), and Benzophenone Dimethyl Acetal (9). A benzene solution (10 ml) of DDM (350 mg, 1.80 mmol), 2,6-dichloro-1,4-benzoquinone **1e** (320 mg, 1.81 mmol), and 5 equiv of methanol (300 mg) was allowed to stand for 15 h at 25 °C. The solvent was removed and the pasty residue was immediately submitted for ^1H NMR measurement. The absolute yields of bicyclic dione **5e** (43%), tricyclic dione **7e** (5%), and benzophenone dimethyl acetal **9** (45%) were determined by the integral ratios with 1,1,1,2-tetrachloroethane (δ=4.20) as an internal standard. Extraction with pentane (5 ml×3) left solid residue. Combined pentane extracts were column-chromatographed on alumina to yield acetal **9** (83 mg, 20%) and hydrolyzed **6** (60 mg, 18%) with hexane–benzene (20%). The structure of **9** was confirmed by comparison of the IR and NMR spectra with those of authentic sample. The solid residue was column-chromatographed on silica gel to give successively **7e** (49 mg, 5%) and **5e** (235 mg, 38%) with hexane–benzene (50%), and 2,6-dichlorohydroquinone (135 mg, 42%) with benzene–ether (10%). Recrystallization of **5e** from a mixture of hexane and benzene gave pale yellow prisms: mp 149—151 °C; IR (KBr) 1706, 1671, 709 cm^{-1}; ^1H NMR ($CDCl_3$) δ=3.54 (d, *J*=1.8 Hz, 1H, cyclopropyl H), 6.45 (d, *J*=1.8 Hz, 1H, vinyl H), 7.1—7.6 (m, 10H, aromatic H); MS, *m/z* 342 (M^+). Anal. ($C_{19}H_{12}O_2Cl_2$) C, H. Recrystallization of **7e** from a mixture of hexane and benzene yielded pale yellow prisms: mp 285 °C (decomp); IR (KBr) 1710, 1693, 706 cm^{-1}; ^1H NMR ($CDCl_3$) δ=2.66 (s, 2H, cyclopropyl H), 7.2—7.4 (m, 20H, aromatic H); MS, *m/z* 508 (M^+). Anal. ($C_{32}H_{22}O_2Cl_2$) C, H.

1,3,4-Trichloro-7,7-diphenylbicyclo[4.1.0]hept-3-ene-2,5-dione (5f). A benzene solution (10 ml) of DDM (440 mg, 2.27 mmol), 2,3,5-trichloro-1,4-benzoquinone **1f** (480 mg, 2.27 mmol), and 5 equiv of methanol (360 mg) was allowed to stand for 15 h at 25 °C. The solvent was removed and the pasty residue was submitted for ^1H NMR measurement to determine the absolute yields of bicyclic dione **5f** (37%) and **9** (55%). After complete hydrolysis of **9** by adding few drops of dilute hydrochloric acid, the reaction products were column-chromatographed on silica gel. Elution gave successively **6** (195 mg, 47%) and **5f** (290 mg, 34%) with hexane–benzene (30%), and 2,3,5-trichlorohydroquinone (265 mg, 55%) with benzene–ether (20%). Recrystallization of **5f** from a mixture of hexane–benzene yielded pale yellow prisms: mp 189—190 °C; IR (KBr) 1698, 1257, 1103, 712 cm^{-1}; ^1H NMR ($CDCl_3$) δ=3.73 (s, 1H, cyclopropyl H), 7.0—7.5 (m, 10H, aromatic H); MS, *m/z* 376 (M^+). Anal. ($C_{19}H_{11}O_2Cl_3$) C, H.

References

1) a) C. D. Gutsche, *Org. React.*, **8**, 364 (1954); b) K. T. Finley, "The Chemistry of the Quinonoid Compounds," ed by S. Patai, John Wiley & Sons (1974), Chap. 17; c) D. S. Wulfman, G. Linstrumell, and C. F. Cooper, "The Chemistry of Diazonium and Diazo groups," ed by S. Patai, John Wiley & Sons (1978), Chap. 18; d) M. Regitz and H. Heydt, "1,3-Dipolar Cycloaddition Chemistry," ed by A. Padwa, John Wiley & Sons (1984), Chap. 4; e) B. Eistert, J. Riedinger, G. Kuffner, and W. Lazik, *Chem. Ber.*, **106**, 727 (1973), and other papers in this series; f) F. M. Dean, L. E. Houghton, R. Nayyir-Mashir, and C. Thebtaranonth, *J. Chem. Soc., Perkin Trans. 2*, **1980**, 1994, and other papers in this series; g) T. Oshima and T. Nagai, *Bull. Chem. Soc. Jpn.*, **59**, 3865 (1986), and a series of preceding papers.

2) L. F. Fieser and M. A. Peters, *J. Am. Chem. Soc.*, **53**, 4080 (1931).

3) T. Oshima and T. Nagai, *Bull. Chem. Soc. Jpn.*, **55**, 551 (1982).

4) T. Oshima and T. Nagai, *Bull. Chem. Soc. Jpn.*, **53**, 3284 (1980).

5) a) T. Oshima and T. Nagai, *Bull. Chem. Soc. Jpn.*, **54**, 2039 (1981); b) T. Oshima, R. Nishioka, and T. Nagai, *Tetrahedron Lett.*, **1980**, 3919; c) T. Oshima, R. Nishioka, S. Ueno, and T. Nagai, *J. Org. Chem.*, **47**, 2114 (1982).

6) a) K. N. Houk, J. Sims, C. R. Watts, and L. J. Luskus, *J. Am. Chem. Soc.*, **95**, 7301 (1973); b) R. Sustmann, *Tetrahedron Lett.*, **1971**, 2717.

7) a) W. Thiel, *QCPE*, **11**, 353 (1978); b) Y. Beppu and I. Ninomiya, *QCPE*, **14**, 409 (1981); c) Y. Sasaki, T. Takagi, A. Tanaka, and R. Tokura, *Bulletin of Computation Center Osaka University*, **14**, 103 (1985). Geometries of **1b**, **1c**, and **1e** were taken from the X-ray crystal data; P. B. Ress, *Acta Crystallogr. Sect. B*, **26**, 1292 (1969); *Sect. B*, **26**, 1298, 1304 (1970).

8) F. M. Dean et al. obtained tricyclic dione by heating a mixture of DDM and 2-methyl-1,4-naphthoquinone at

100 °C and argued that the product could have resulted from diphenylcarbene formed by preliminary loss of nitrogen from the diazoalkane; *J. Chem. Soc.*, **1963**, 5336.

9) T. Oshima and T. Nagai, *Tetrahedron Lett.*, **1985**, 4785.

10) J. Heller, A. Yoger, and A. S. Dreiding, *Helv. Chim. Acta*, **55**, 1003 (1972).

11) J. B. Conant and L. F. Fieser, *J. Am. Chem. Soc.*, **45**, 2194 (1923).

12) H. van Erp, *Ber.*, **58**, 663 (1925).

13) H. Biltz and W. Giese, *Ber.*, **37**, 4010 (1904).

 © 1988 The Chemical Society of Japan Bull. Chem. Soc. Jpn., 61, 2513—2524 (1988)

Cycloaddition Reactions of Highly Stabilized Isoquinolinium Methylides to Nonactivated Olefins and Electron-Rich Olefins

Otohiko TSUGE,* Shuji KANEMASA, Kazushige SAKAMOTO, and Shigeori TAKENAKA
Institute of Advanced Material Study, and Department of Molecular Science and Technology,
Interdisciplinary Graduate School of Engineering Sciences,
Kyushu University, Kasugakoen, Kasuga 816
(Received February 3, 1988)

Highly stabilized isoquinolinium methylides bearing two electron-withdrawing substituents at the ylide carbon undergo cycloadditions with aryl-substituted olefins (acenaphthylene, (*E*)- and (*Z*)-stilbenes, indene, and styrene), alkyl-substituted olefins (norbornene, (*Z*)-3-hexene-1,6-dinitrile, 1-hexene, 2-propen-1-ol, and 3-(trimethylsilyloxy)propene), and electron-rich olefins (vinylene carbonate, butyl vinyl ether, and phenyl vinyl sulfide). These cycloadditions proceed in an exclusively regioselective and mostly stereoselective manner.

Heteroaromatic *N*-ylides belong to highly reactive and easily accessible azomethine ylide 1,3-dipoles.[1] Their cycloadditions to electron-deficient activated olefins take place frequently in regio- and stereoselective manners to produce stereochemically pure fused pyrrolidine rings.[2] However the cycloadducts are not often highly stable since cycloaddition stage of heteroaromatic *N*-ylides involves loss of aromaticity of the heterocyclic ring. A major route of decomposition of the cycloadducts involves cleavage of the carbon–carbon bond newly formed in the cycloaddition step generating betaine intermediates. Anion-stabilizing substituents (R=EWG) introduced from the olefin dipolarophiles must accelerate this cleavage.[3]

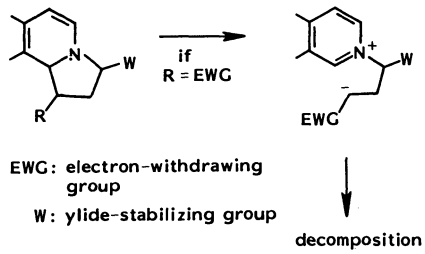

Several attempts to increase the stability of cycloadducts were previously applied to avoid the undesired decomposition.[4] Replacement of the electron-withdrawing substituent R=EWG with such an ordinary substituent as aryl, alkyl, or electron-donating moiety can be an effective method of stabilization. Formally such stabilized cycloadducts would be accessible from the cycloadditions of heteroaromatic *N*-ylides to the olefins bearing no electron-withdrawing substituent.

Introduction of two anion-stabilizing substituents at the ylide carbon of heteroaromatic *N*-ylides lowers both levels of the highest occupied molecular orbital (HOMO) and the lowest unoccupied molecular orbital (LUMO) so that the reactivity with electron-deficient activated olefins may be decreased but the reactivity with electron-rich olefins may be increased instead. So highly stabilized and isolable heteroaromatic *N*-ylides are expected to undergo cycloadditions with electron-rich olefins under a control of $LUMO_{dipole}$–$HOMO_{dipolarophile}$ interaction.[5]

Although several examples have been reported for the cycloadditions of azomethine ylides with nonactivated olefins,[6–8] the reactivity of heteroaromatic *N*-ylides with nonactivated olefins is unknown. The only example is the reaction of isoquinolinium bis(ethoxycarbonyl)methylide with enamines.[9]

The present paper describes the first example of cycloadditions of highly stable and isolable isoquinolinium ylides with aryl-substituted, alkyl-substituted, and electron-rich olefins. These reactions are found to be exclusively regioselective regardless of the ylide-stabilizing substituent, and mostly stereoselective when the ester-stabilized ylides are employed.

Results and Discussion

Three types of isoquinolinium methylides **1a—c** were employed in the present work. They are all stable enough to be isolated: Bis(methoxycarbonyl)-**1a** and cyano(methoxycarbonyl)methylide **1c** can be prepared via *N*-alkylisoquinolinium bromides and such a weak base as isoquinoline, triethylamine, or aqueous potassium carbonate, and dicyanomethylide **1b** is directly accessible from isoquinoline and tetracyanooxirane. A mixture of ylide and olefin is heated in dry toluene or xylene under nitrogen and the reaction is monitored on TLC. After removal of the solvent, the crude reaction mixture is inspected by means of ^{1}H NMR spectrum to see the content of isomeric cycloadducts.

Two geometric isomers, (*E,Z*)-**1c** and (*E,E*)-**1c**, are possible for the cyano(methoxycarbonyl)methylide **1c** as shown below. As it is already known that the anti forms (or *E,Z*-forms) of carbonyl-stabilized heteroaromatic *N*-ylides show relatively high stability by 1,5-dipole stabilization and are exclusively involved in their cycloadditions to electron-deficient olefins,[2,10] the selective participation of isomer (*E,Z*)-**1c** is anticipated.

Both ^{1}H and ^{13}C NMR spectra of ylide **1c** measured in deuteriochloroform show no contamination by any

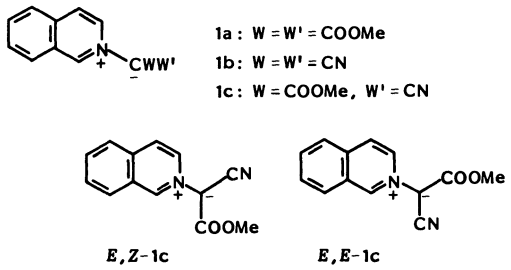

isomeric form, indicating either its existence in a single isomeric form, probably in an *E,Z*-form, or a free rotation around the ylide carbon–nitrogen bond. Since both the ester groups of bis(methoxycarbonyl)-methylide **1a** are magnetically equivalent as shown in its ^{1}H and ^{13}C NMR spectra measured at room temperature, the energy barrier for the ylide isomerization of such highly stabilized heteroaromatic *N*-ylides as **1a—c** may not be high so as to restrict the rotation.

Though NMR spectra of dicyanomethylide **1b** was not available due to its low solubility in organic solvent, the other two **1a** and **1c** as well as 2-[bis(methoxycarbonyl)methyl]isoquinolinium bromide as a precursor of **1a** gave informative ^{1}H and ^{13}C NMR spectra. Both 1- and 3-Cs of cyano(methoxycarbonyl)methylide **1c** (1-C: δ=137.56 and 3-C: 132.88) appear in much upper field than those of bis(methoxycarbonyl)-methylide **1a** (1-C: 153.41 and 3-C: 141.32), indicating that the ylide anion of **1a** hardly flows into the isoquinoline ring but is stabilized by delocalization through the two ester moieties. Thus ylide **1a** and the precursor salt of **1a** show 1-C (**1a**: δ=153.41 and the precursor: 152.85) very close to each other. Stabilization of the anion of ylide **1c** is mainly made by its conjugation with the isoquinoline π-orbitals rather than the delocalization through the ylide-stabilizing cyano and ester moieties so that electron density at the 1-position is relatively increased.

On the other hand, ^{1}H chemical shifts of **1a** and **1c** are inconsistent with the corresponding ^{13}C chemical shifts. Ylide **1c** shows its 1- and 3-Hs (1-H: δ=10.11 and 3-H: 8.83) in much lower field than those of **1a** (1-H: 9.32 and 3-H: 8.33). The low-field shifts of 1- and 3-Hs are presumably caused by anisotropy from the ylide-stabilizing ester moiety. The ester moiety of **1c** can stay in the same plane to the isoquinoline ring so that the 1- and 3-Hs are strongly deshielded. However, the plane including the ylide carbon and two ester moieties of ylide **1a** is forced to cross to the isoquinoline plane due to a considerable steric congestion, deshielding of the 1- and 3-Hs from the ester groups being relatively decreased.

Cycloadditions to Aryl-Substituted Olefins. Heating isoquinolinium bis(methoxycarbonyl)methylide (**1a**) or dicyanomethylide (**1b**), under reflux in toluene, with acenaphthylene as a symmetrically aryl-substituted cyclic olefin produced the cycloadduct **2** or **3**. Though the cycloadduct **2** was obtained as a single isomer, **3** consists of two stereoisomers (3:1 by ^{1}H NMR) whose separation from each other through column chromatography was unsuccessful (Scheme 1 and Table 1). Compared to the major isomer **3A** (5-H: δ=6.02, 6-H: 6.49, and 14c-H: 4.99), the minor isomer **3B** shows strong magnetic shieldings at 5-H (5.03) and 6-H (5.87) as well as deshielding at 14c-H (5.22) from the fused acenaphthylene ring, confirming the exo and endo structures of **3A** and **3B**, respectively.

Similar reactions of the ylides **1a**, **1b**, and isoquinolinium cyano(methoxycarbonyl)methylide (**1c**) with (*E*)- and (*Z*)-stilbenes produced *E*-specific **4—6** and *Z*-specific cycloadducts **7**, **8**, respectively, while **1a** could not be trapped by (*Z*)-stilbene and recovered in 52% yield under reflux in toluene for 72 h (Scheme 1 and Table 1). Heating **1b** with (*Z*)-stilbene under reflux in toluene or xylene for 71 or 76 h gave 34 or 45% yield of cycloadduct **7**, respectively, but no cycloadduct was formed at 110 °C in *N,N*-dimethylformamide (DMF).[11] Thus polar solvents are disfavored in these cycloadditions.

Both relatively small trans couplings for J_{1-2} (2.0 Hz) and J_{1-10b} (6.2 Hz) of **4** and big trans couplings for J_{1-2} (11.3 Hz) and J_{1-10b} (8.0 Hz) of **5**

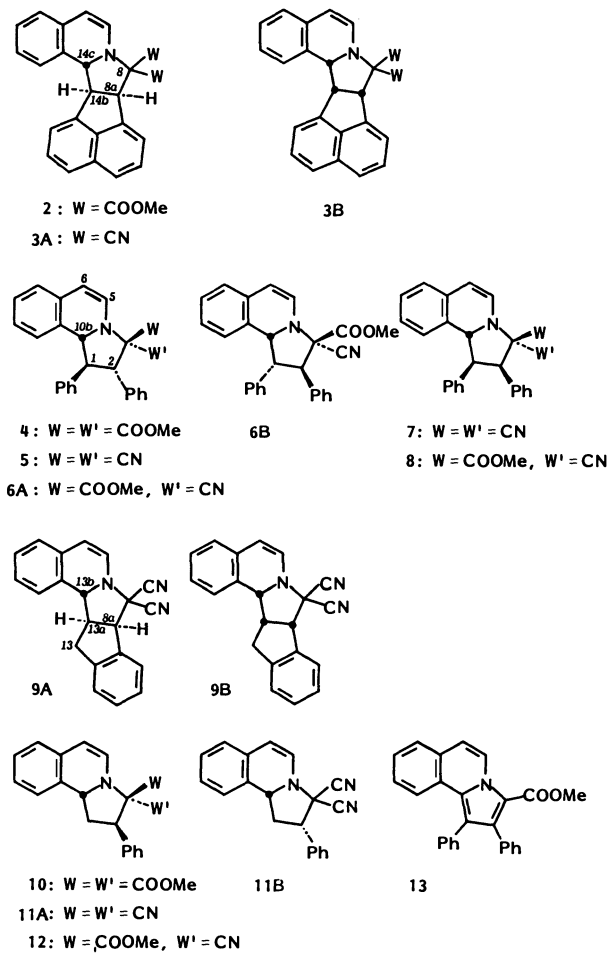

Scheme 1.

result from the same 1-exo-2-endo substitution as shown in the following discussion using molecular models: When the 3-endo substituent W′ is small, the most stable conformation of the fused pyrrolidine ring of the 1-exo-2-endo-cycloadduct of ylide **1** to an (*E*)-olefin ($R^1CH=CHR^2$) has trans diaxial geometry between the adjacent two of 10b-, 1-, and 2-Hs (conformer **A** in Fig. 1). The cycloadduct **5** occupies this conformation **A** (W=W′=CN, $R^1=R^2$=Ph) showing two big vicinal couplings J_{1-2} and J_{1-10b}. If the 3-endo substituent W′ becomes bulkier in the conformer **A**, the substituent W′ can not stay at the congested axial position and goes outside by rotations around the C(1)-C(2) and C(2)-C(3) bond leading to conformer **B**. The cycloadduct **4** occupies this conformation **B** (W=W′=COOMe, $R^1=R^2$=Ph) in which very small J_{1-2} (2.0 Hz) is observed.

The cycloadduct of **1c** to (*E*)-stilbene includes two isomers **6A** and **6B** in a 42:33 ratio of isolated products, although two more isomers are possible in this case depending upon the geometry at the 3-position. Both the isomers **6A** and **6B** exhibit big vicinal couplings for J_{1-2} (**6A**: 12.1 and **6B**: 10.9 Hz) which are assigned to a typical trans diaxial geometry. Together with magnetic shielding of the 3-COOMe of **6B** (δ=3.25) by the adjacent 2-phenyl, **6A** and **6B** are assigned to be 1-exo-2-endo and 1-endo-2-exo cycloadducts to the *E,Z*-form of ylide **1c**, respectively. The other big vicinal couplings J_{1-10b} (**6A**: 9.1 and **6B**: 8.2 Hz) are consistent with the assigned stereochemistry. Thus **6A** and **6B** exist as conformations **A** and **C**, respectively (Scheme 1 and Fig. 1, $R^1=R^2$=Ph, W=COOMe, W′=CN).

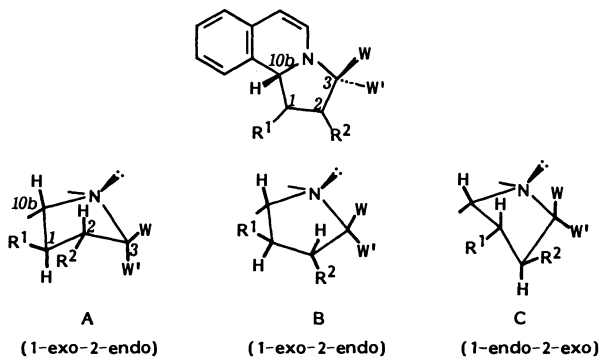

Fig. 1. Stable conformation of the cycloadducts of **1** to (*E*)-olefins.

The cycloadducts **7** and **8** to (*Z*)-stilbene bear trans diaxial stereochemistry between 1-H and 10b-H (J_{1-10b}=10.0 Hz) and are assigned to be the exo-cycloadducts.

The side product **13** obtained together with **4** in the reaction of **1a** with (*E*)-stilbene was assigned as methyl 1,2-diphenylpyrrolo[2,1-*a*]isoquinoline-3-carboxylate. Its formation presumably arose from **4** by homolytic thermal decarboxylation since **4** was quantitatively converted into **13** on treatment with chloranil under reflux in toluene for 0.5 h.[12]

Ylides **1** similarly react with such unsymmetrically aryl-substituted olefins as indene and styrene. In the cycloaddition of **1b** to indene an inseparable mixture of two cycloadducts was obtained in a 3:2 ratio (^{1}H NMR). As both the isomers show 8a-H and 13b-H as doublets, they are stereoisomeric mixtures of regioselective cycloadducts **9A** and **9B** (Scheme 1 and Table 1). The major isomer **9A** showing relatively big $J_{13a-13b}$ (9.5 Hz) and the major one **9B** showing smaller $J_{13a-13b}$ (5.2 Hz) are assigned to be the exo- and endo-cycloadducts, respectively.

The cycloadditions with styrene are also regioselective. Though ester-stabilized ylides **1a** and **1c** produced 2-exo-phenyl-substituted cycloadducts **10** and **12** as single products (Scheme 1 and Table 1), dicyanomethylide **1b** afforded a 3:2 mixture of two stereoisomers (by ^{1}H NMR of the crude reaction mixture). When this mixture is chromatographed over silica gel (hexane:ethyl acetate=10:1 v/v), the major isomer **11A** is isolated in 88% yield, indicating that the minor isomer **11B** has isomerized into **11A** during the chromatographic procedure.

This epimerization is most likely to be acid-

Table 1. Cycloadditions of Isoquinolinium Ylides **1** to Aryl-Substituted Olefins

Olefin	Equiv	Ylide	Solvent	Time/h	Product (Yield/%)[a]	Isomer ratio[b]
Acenaphthylene	3	**1a**	Toluene	3	**2** (42)	
Acenaphthylene	1	**1b**	Toluene	42	**3** (58)	**3A**: **3B**=3:1[c]
(*E*)-Stilbene	1.5	**1a**	Toluene	37	**4** (23)+**13** (6)	
(*E*)-Stilbene	1.2	**1b**	Toluene	48	**5** (61)	
(*E*)-Stilbene	2	**1c**	Toluene	24	**6** (75)	**6A**: **6B**=42:33
(*Z*)-Stilbene	1.2	**1b**	Xylene	76	**7** (45)[d]	
(*Z*)-Stilbene	1.5	**1c**	Toluene	48	**8** (62)	
Indene	1.2	**1b**	Toluene	6.5	**9** (59)	**9A**: **9B**=3:2[e]
Styrene	1	**1a**	Toluene	6	**10** (90)	
Styrene	1	**1b**	Toluene	1.5	**11** (88)	**11A**:**11B**=3:2[e,f]
Styrene	1	**1c**	Toluene	3	**12** (100)	

a) Yield of isolated products. b) Isomer ratio of isolated products. c) Inseparable mixture whose ratio was determined by ^{1}H NMR spectrum. d) Recovered **1b**: 19%. e) Isomer ratio of the crude reaction mixture (^{1}H NMR). f) Compound **11B** isomerizes into **11A** on silica-gel chromatography.

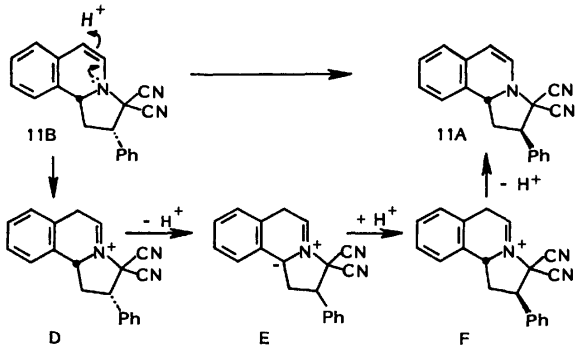

Fig. 2. Possible mechanism for the isomerization of **11B** into **11A**.

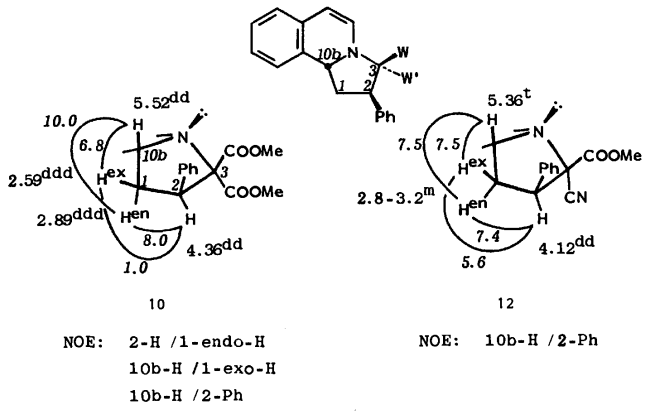

Fig. 3. Stereostructures of two styrene adducts **10** and **12**.

catalyzed via azomethine ylide 1,3-dipole intermediate **D** (Fig. 2). Although neither acetic acid nor phenol in aprotic solvents such as chloroform and dimethyl sulfoxide effects this epimerization, the epimerization is completed on treatment of the mixture of **11A** and **11B** (2:1) with Molecular Sieves 4A in dichloromethane for 3 days or with a catalytic amount of trifluoroacetic acid in ethanol for 1 day, both at room temperature. The epimerization on chromatography is found to be most effective.

Stereostructures of **10** and **12** were determined as the 2-exo-phenyl cycloadducts of **1a** and (*E*,*Z*)-**1c**, respectively, on the basis of the spectral data in which NOE difference spectrum was most informative. Thus notable NOE's were observed between 10b-H/2-phenyl of **10** and **12**, 2-H/1-endo-H of **10**, and 10b-H/1-exo-H of **10** indicating the 2-exo-phenyl substitution. Both cycloadducts **10** and **12** exhibit quite different coupling patterns among the methylene and methine hydrogens on the newly constructed fused pyrrolidine ring as shown in Fig. 3. This difference arises from the bulkiness of the 3-endo substituent W' (**10**: COOMe and **12**: CN).

Since **11A** and **11B** derived from dicyanomethylide **1b** and styrene are thermodynamic and kinetical

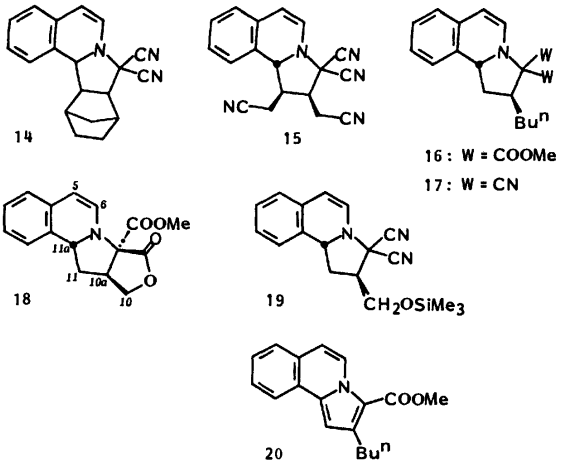

Scheme 2.

products as described above, respectively, the 2-exo-phenyl structure for **11A** and 2-endo-phenyl structure for **11B** are reasonable. Coupling patterns of **11A** (J_{1-2}=8.0, 7.0 and J_{1-10b}=8.0, 7.8 Hz) are close to those of **12** which is carrying a small cyano group as the 3-endo substituent, confirming the 2-exo-phenyl stereochemistry of **12**. The 2-endo-phenyl isomer **11B** has the anti diaxial relationship between 10b-H and 1-endo-H and between 1-endo-H and 2-H as confirmed on the basis of the coupling patterns (J_{1-2}=12.0, 6.6 and J_{1-10b}=9.0, 5.9 Hz).

Cycloadditions to Alkyl-Substituted Olefins. Norbornene as a symmetrically substituted olefin of nonactivated type is so reactive to ylide **1b** that 89% yield of the cycloadduct **14** was produced under reflux in toluene for 0.7 h (Scheme 2 and Table 2). The product **14** consists of two stereoisomers in a 3:1 ratio which can not be separated from each other by silica-gel column chromatography. Among four possible stereostructures (exo, exo-, exo, endo-, endo, exo-, and endo, endo-isomers) in respect of the ylide (exo or endo)-norbornene (exo or endo) approach, **14** would be assigned to be the exo-exo and exo-endo stereoisomers on the basis of the exo-selective cycloadditions of ylides **1** with alkyl-substituted olefins discussed below.

Contrary to the high reactivity of strained norbornene, (*Z*)-3-hexene-1,6-dinitrile as a 1,2-disubstituted acyclic (*Z*)-olefin is less reactive. Heating ylide **1b** with this olefin at reflux in toluene for 8 days under nitrogen gave 24% yield of cycloadduct **15** as a single stereoisomer and 55% of the starting ylide **1b** was recovered. 1-Hexene as an unsymmetrically substituted 1-olefin regioselectively traps the ylide **1a** and **1b** to furnish 2-exo-butyl-substituted cycloadducts **16** and **17**. In the former case, part of the cycloadduct **16** was again aromatized by the elimination of an ester moiety at the 3-position to give **20**.

The reaction of ylide **1a** with O-unprotected 2-propen-1-ol takes place under similar conditions to

Table 2. Cycloadditions of Isoquinolinium Ylides **1** to Alkyl-Substituted Olefins

Olefin	Equiv	Ylide	Solvent	Time/h	Product (Yield/%)[a]	Isomer ratio
Norbornene	1.2	**1b**	Toluene	0.7	**14** (89)	3:1[b]
(*Z*)-3-Hexene-1,6-dinitrile	1	**1b**	Toluene	8d	**15** (24)[c]	
1-Hexene	4	**1a**	Xylene	5	**16** (21)+**20** (11)	
1-Hexene	1.3	**1b**	Toluene	24	**17** (85)	
2-Propen-1-ol	3.6	**1a**	Toluene	12	**18** (32)	
3-(Trimethylsilyl-oxy)propene	2	**1b**	Toluene	2.5	**19** (60)	

a) Yield of isolated products. b) Inseparable mixture whose ratio was determined by ^{1}H NMR spectrum. c) Recovered **1b**: 55%.

Table 3. Cycloadditions of Isoquinolinium Ylides **1** to Electron-Rich Olefins

Olefin	Equiv	Ylide	Solvent	Time/h	Product (Yield/%)[a]	Isomer ratio[b]
Vinylene carbonate	3	**1a**	Toluene	42	**21** (32)	
Vinylene carbonate	1.3	**1b**	Toluene	75	**22** (53)	**22A**:**22B**=40:13
Vinylene carbonate	1.2	**1c**	Toluene	21	**23** (23)	
Butyl vinyl ether	2.7	**1a**	Toluene	3	**24** (68)	
Butyl vinyl ether	1.2	**1b**	Toluene	4	**25** (97)	
Butyl vinyl ether	3.3	**1c**	Toluene	3	**26** (61)	34:27[c]
Phenyl vinyl sulfide	1	**1a**[d]	Toluene	44	**27** (30)+**29** (15)[c]	
Phenyl vinyl sulfide	1	**1c**	Toluene	6	**28** (97)	

a) Yield of isolated products. b) Ratio of isolated isomers. c) Mixture of two 3-epimers **26A**+**26B**. d) Ylide **1a** was in situ generated from the corresponding isoquinolinium bromide and triethylamine. e) Inseparable mixture.

provide a lactone **18** in 32% yield (Scheme 2 and Table 2), indicating the regio- and stereoselective formation of 2-exo-hydroxymethyl-substituted cycloadduct followed by an internal lactonization with the 3-exo-ester group. The stereostructure of **18** is confirmed by the shielding of 11a-H (δ=4.12) from the carbonyl group of the fused lactone ring. Similarly 3-(trimethylsilyl-oxy)propene as O-protected 2-propen-1-ol reacts with ylide **1b** to give the 2-exo-substituted cycloadduct **19**.

Cycloadditions to Electron-Rich Olefins. The strained and electron-rich double bond of vinylene carbonate undergoes cycloadditions with electron-deficient ylides **1a—c** under reflux in toluene to give the corresponding cycloadducts **21—23** (Scheme 3 and Table 3). Though **21** and **23** are single isomers, **22** consists of exo- **22A** and endo-cycloadduct **22B** in a 40:13 ratio of isolated products. The major isomer **22A** which shows 11b-H as a singlet signal ($J_{11a-11b}$=0 Hz) is determined to be the exo structure; the single product **23** produced from ylide **1c** is also assigned as the exo-cycloadduct based upon the zero coupling between 11a-H and 11b-H.

The cycloadduct **21** bearing two relatively bulky ester groups at the 8-position must occupy a conformation different from that for the other two exo-cycloadducts **22A** and **23** which bear a small cyano moiety as the 8-endo substituent. The 8-endo-ester group would move to outer side in order to avoid steric congestion so that the coupling between 11a-H and 11b-H becomes bigger. Thus **21** was assigned as the exo-cycloadduct whose $J_{11a-11b}$ is 5.5 Hz. Similar

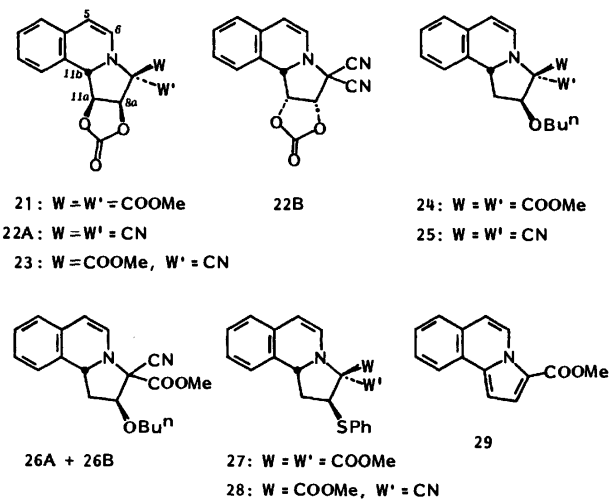

Scheme 3.

difference has been observed above between the two exo-cycloadducts to acenaphtylene **2** and **3A** ($J_{14b-14c}$: **2**: 7.8 and **3A**: 0 Hz).

Butyl vinyl ether or phenyl vinyl sulfide as an electron-rich olefin readily reacts with ylides **1a—c** to give the regio- and stereoselective 2-exo-butoxy- **24—26** or 2-exo-phenylthio-substituted cycloadducts **27,28** (Scheme 3 and Table 3). The cycloadduct **27** is thermally labile so as to undergo eliminative and decarboxylative aromatization leading to methyl [2,1-*a*]isoquinoline-3-carboxylate (**29**). An authentic sample of **29** is available in the reaction of **1a** with

phenyl vinyl sulfoxide in good yield.

The 2-exo-butoxy stereochemistry of **24** was confirmed on the basis of NOE difference spectrum which showed clear NOE's between 1-endo-H and 2-H and between 1-exo-H and 10b-H. Coupling constants $J_{1\text{-}10b}$(trans)=10.6 and $J_{1\text{-}2}$(trans)=0 Hz are also consistent with the assigned structure.

The other cycloadducts **25**, **27**, and **28** show similar coupling patterns to those of the cycloadducts to 1-hexene **16—17** and are assigned to be the 2-exo-substituted cycloadducts as shown in Scheme 3. Resemblance of the coupling patterns of the isomeric cycloadducts **26A** and **26B** indicates the same configuration, and even almost the same conformation, around the 1-, 2-, and 10b-positions. They are assigned as the 3-epimers each other, while it was unsuccessful to determine which is which.

Regioselectivity. As described above, the cycloadditions of highly stabilized isoquinolinium ylides **1a—c** with aryl- and alkyl-substituted and electron-rich olefins proceeded all in regioselective manners to give the single regioisomers of cycloadducts **10—12**, **16—19**, and **24—28** bearing the substituent from olefins at the 2-position.

This exclusive regioselection can be explained in terms of frontier molecular orbital (FMO) theory.[13] Interaction between LUMO of ylides **1** and HOMO of olefins would predominantly control reactivity and regioselectivity of their cycloadditions since the ylides **1** are electron-deficient and the olefins are relatively electron-rich. The LUMOs of ylides **1** must carry larger atomic orbital coefficients at the γ-carbon rather than the ylide carbon; β-coefficients must be larger than those at the α-carbons in HOMOs of the olefins employed in the present work (Fig. 4).

Stereoselectivity. Cycloadditions of bis(methoxycarbonyl)methylide **1a** were exclusively stereoselective: The exo-cycloadducts **2** and **21**, 1-exo-2-endo-cycloadduct **4**, and 2-exo-cycloadducts **10**, **16**, **18**, **24**, and **27** were produced. Though there are a few exceptions the *E,Z*-ylide isomer of cyano(methoxycarbonyl)methylide **1c** was mostly involved in its stereoselective cycloadditions with olefins leading to **8**, **12**, **23**, and **28**: Only in the reactions with (*E*)-stilbene and butyl vinyl ethers two isomeric cycloadducts **6** and **26** were formed. Compared with these stereoselective reactions of ester-stabilized ylides **1a** and **1c**, cycloadditions using dicyanomethylide **1b** are frequently poor in stereoselectivity: Mixtures of two isomeric cycloadducts **3**, **9**, **11**, **14**, and **22** were formed in the reactions with acenaphthylene, indene, styrene, norbornene, and vinylene carbonate.

In several cases, stereoselectivity can be explained on the basis of secondary orbital interaction and steric repulsion as shown below.

There are two approaches possible for the cycloaddition of ylides **1a—c** to (*E*)-stilbene, 1-exo-2-endo **G** and 1-endo-2-exo approach **H** (Fig. 5). Attractive secondary orbital interaction would work between the phenyl and the ester moiety W′ (=COOMe in the approach **G**) or W (=COOMe in **H**), while repulsion would be present in the approach **H** between the phenyl and the isoquinolinium ring. Thus ylide **1a** (W=W′=COOMe) and **1b** (W=W′=CN) react with (*E*)-stilbene through 1-exo-2-endo-selective approach **G** furnishing **4** and **5**. On the other hand, the approach **G** competes with **H** since steric repulsion caused by one of the phenyls is cancelled by attractive interaction working between the ester W (=COOMe) and the other phenyl plane.

The exo-selective cycloadditions of ylides **1b** and **1c** to (*Z*)-stilbene via approach **I** are reasonable from the standpoints of steric repulsion and attractive interaction (Fig. 5).

The ylides **1a** and **1c** which carry at least one ester moiety underwent exo-selective cycloadditions to styrene affording **10** and **12**. Attractive interaction between the phenyl of styrene and the ester W (=COOMe) probably determined the stereoselectivity. If such attraction is absent, both exo and endo approaches occur. Thus two stereoisomers **11A** and

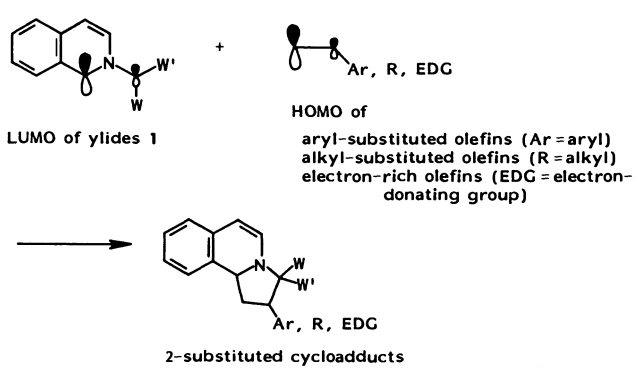

Fig. 4. $LUMO_{ylide}$–$HOMO_{dipolarophile}$ interaction leading to regioselective cycloadducts.

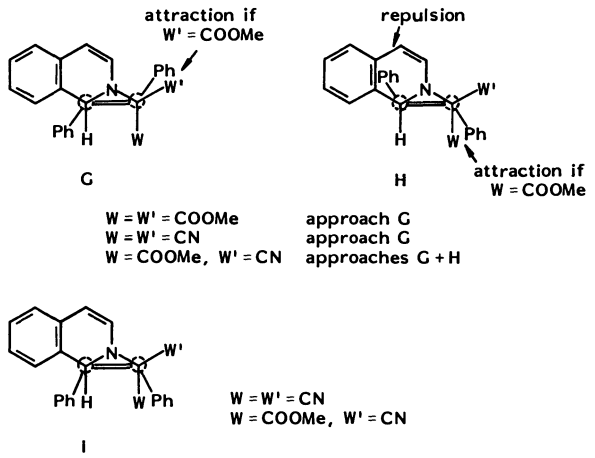

Fig. 5. Stereoselectivity between ylides **1** and (*E*)- and (*Z*)-stilbenes.

11B were formed in the reaction of dicyanomethylide **1b** with styrene.

The competitive formation of sterically unfavorable endo-cycloadducts **3B 9B**, one of **14**, and **22B** in the cycloadditions of dicyanomethylide **1b** can not be interpreted so far. The decrease of ylide-specificity observed in the reaction of ylide **1c** with butyl vinyl ether leading to **26A** and **26B** is not be solved yet.

Use of Other Heteroaromatic N-Ylides. At an early stage of the present work, several derivatives of pyridinium methylides were employed. Compared to satisfactory reactivity of the three isoquinolinium methylides **1a—c**, their pyridinium analogs are absolutely inert to nonactivated olefins: Thus pyridinium dicyanomethylide was recovered intact in the reactions with styrene (reflux in toluene for 33 h), butyl vinyl ether (reflux in toluene for 84 h or at 140 °C for 20 h), and vinylene carbonate (reflux in toluene for 66 h). Attempted cycloadditions of 3,5-dimethylpyridinium bis(methoxycarbonyl)methylide with styrene, vinylene carbonate, or butyl vinyl ether as well as that of 4-methoxypyridinium bis(methoxycarbonyl)methylide with styrene produced no corresponding cycloadducts, but decomposition of the ylides was observed.

Both energy levels of LUMO (+2.046 eV) and HOMO (−8.792 eV) of pyridinium methoxycarbonylmethylide are calculated to be higher than those of isoquinolinium methoxycarbonylmethylide (LUMO: +0.588 and HOMO: −9.082 eV).[14] Accordingly pyridinium methylides must show relatively less enhanced reactivity than the corresponding isoquinolinium methylides, especially in the cycloadditions under control of $LUMO_{dipole}$–$HOMO_{dipolarophile}$. The observed low reactivity of these pyridinium methylides is the case.

Experimental

General. Melting points were determined on a Yanagimoto melting point apparatus and are uncorrected. IR spectra were taken with a JASCO IRA-1 or a JASCO A-702 spectrometer. ^{1}H NMR spectra were recorded on a Hitachi R-40 (90 Hz), a JEOL FX-100 (100 MHz), or a JEOL GSX-270 instrument (270 MHz) and ^{13}C NMR on a JEOL FX-100 (25.05 MHz) or a GSX-270 spectrometer (67.94 MHz). Chemical shifts are expressed in parts per million downfield from tetramethylsilane as an internal standard. Mass spectra were measured with a JEOL-01SG-2 spectrometer at 70 eV of ionization energy. High resolution mass spectra were also obtained on the same instrument. Elemental analyses were performed on a Hitachi 026 CHN analyzer. For preparative column chromatography, Wakogel C-200, C-300 (Wako), and Silicagel 60 (Merck) were employed. Flash chromatography was carried out on an EYELA EF-10 apparatus using a Lobar column (20×180 mm) packed with Silicagel 60 (Merck, size: 0.04—0.063 mm). Solvents were evaporated with a Tokyo Rikakikai rotary evaporator type-V at about 50 °C unless otherwise stated.

Materials. Isoquinolinium dicyanomethylide (**1b**)[15] or cyano(methoxycarbonyl)methylide (**1c**)[16] is directly available from the reaction of isoquinoline with tetracyanooxirane or methyl 2-bromocyanoacetate, respectively, according to the reported method. 2-[Bis(methoxycarbonyl)methyl]isoquinolinium bromide[16] can be prepared from isoquinoline and dimethyl bromomalonate. Ylide **1a**[16] is either isolated on treatment of the salt with aqueous potassium carbonate or generated in situ by the action with triethylamine in an appropriate reaction solvent. 2-[Bis(methoxycarbonyl)methyl]isoquinolinium bromide: ^{1}H NMR (DMSO-d_6) δ=3.92 (6H, s, COOMe), 7.55 (1H, br s, CH), 8.0—9.1 (6H, m, Ar), and 10.50 (1H, br s, 1-H); ^{13}C NMR (DMSO-d_6) δ=54.45 (COOMe), 71.68 (ylide C), 124.78, 126.36, 127.30, 131.08, 131.44, 136.31, 137.75, 138.35, 152.85 (1-C), and 163.05 (COOMe). **1a:** ^{1}H NMR ($CDCl_3$) δ=3.75 (6H, s, COOMe), 7.7—8.3 (5H, m, 3-, 4-, 5-, 6-, and 7-H), 8.33 (1H, dd, J=8.0 and 1.0 Hz 3-H), and 9.32 (1H, s, 1-H); ^{13}C NMR ($CDCl_3$) δ=50.65 (COOMe), 97.26 (ylide C), 123.44, 126.75, 127.66, 129.67, 130.10, 135.53, 136.28, 141.32 (3-C), 153.41 (1-C), and 165.70 (COOMe); **1c:** ^{1}H NMR ($CDCl_3$) δ=3.80 (3H, s, COOMe), 7.7—8.1 (5H, m, 4-, 5-, 6-, 7-, and 8-H), 8.83 (1H, dd, J=8.0 and 1.0 Hz, 3-H), and 10.11 (1H, s, 1-H); ^{13}C NMR ($CDCl_3$) δ=50.81 (COOMe), 121.02 (CN), 124.29, 126.69, 128.02, 128.49, 130.67, 130.88, 132.11, 132.88 (3-C), 137.56 (1-C), and 165.00 (COOMe).

General Procedure for the Cycloadditions of Isoquinolinium Methylides 1 to Olefins. A mixture of isoquinolinium methylide **1** (1 mmol) and olefin in dry toluene or xylene was heated at reflux under nitrogen. After the reaction was over, the reaction mixture was cooled to room temperature. When some precipitate appeared, it was collected on a filter. The filtrate was evaporated in vacuo and the residue as chromatographed over silica gel by using hexane–ethyl acetate.

2: The residue obtained from the crude reaction mixture by evaporation of the solvent was chromatographed over silica gel with hexane–ethyl acetate (10:1 v/v) to give **2**: Pale yellow prisms (benzene–hexane); mp 209—210 °C; IR (KBr) 1750, 1723, 1610, 1250, 1230, and 770 cm^{-1}; ^{1}H NMR ($CDCl_3$) δ=3.07, 3.86 (each 3H, s, COOMe), 4.68 (1H, dd, J=8.0 and 7.8 Hz, 14b-H), 4.81 (1H, d, J=8.0 Hz, 8a-H), 5.17 (1H, d, J=7.8 Hz, 14c-H), 5.71 (1H, d, J=7.6 Hz, 5-H), 6.65 (1H, d, J=7.6 Hz, 6-H), and 6.9—7.7 (10H, m, Ar); ^{13}C NMR ($CDCl_3$) δ=50.53 (d, 8a-C), 51.82, 53.36 (each q, COOMe), 55.95 (d, 14b-C), 67.18 (d, 14c-C), 76.65 (s, 8-C), 106.06 (d, 5-C), 120.07, 121.48, 123.48, 123.66, 123.95, 124.54, 126.30, 127.74, 128.25, 131.60, 131.89, 133.83, 134.89, 139.12, 141.30, 144.60, and 169.59 (s, 2C of COOMe); MS m/z (rel intensity, %) 411 (M^+, 19), 260 (16), 259 (base peak), 201 (38), and 143 (25). Found: C, 76.05; H, 5.16; N, 3.46%. Calcd for $C_{26}H_{21}NO_4$: C, 75.90; H, 5.14; N, 3.40%.

3A+3B: The crude reaction mixture was chromatographed, after evaporation of the solvent in vacuo, over silica gel with hexane–ethyl acetate (10:1 v/v) to give an inseparable mixture of **3A** and **3B** (3:1 by ^{1}H NMR): Colorless solid; IR (KBr) 2360, 1620, 1250, 1169, 783, and 773 cm^{-1}; ^{1}H NMR ($CDCl_3$) **3A**: δ=4.48 (1H, d, J=6.9 Hz, 8a-H), 4.82 (1H, dd, J=8.8 and 6.9 Hz, 14b-H), 4.99 (1H, d, J=8.8 Hz, 14c-H), 6.02 (1H, d, J=7.6 Hz, 5-H), 6.49 (1H, d, J=7.6 Hz, 6-H), and 7.0—8.0 (10H, m, Ar). **3B**: δ=4.6—4.8 (2H, m, 8a- and 14b-H), 5.03 (1H, d, J=7.6 Hz, 5-H), 5.22 (1H, d, J=6.0 Hz, 14c-H), 5.87 (1H, d, J=7.6 Hz, 6-H), and 7.0—8.0 (9H, m, Ar); MS m/z (rel intensity, %) 345 (M^+, 3),

194 (16), 193 (base peak), 166 (17), 152 (48), 139 (16), 129 (21), 128 (19), and 102 (13). Found: C, 83.38; H, 4.38; N, 12.15%. Calcd for $C_{24}H_{15}N_3$: C, 83.46; H, 4.38; N, 12.16%.

4 and 13: When the crude reaction mixture was subjected to column chromatography over silica gel with hexane-ethyl acetate (10:1 v/v), a mixture of **4** and **13** was obtained. This mixture was again chromatographed with hexane-ethyl acetate (20:1 v/v) to give **13** (6%) and then **4** (23%). As compound **4** is so susceptible as to suffer from ready decarboxylative aromatization leading to **13**, only ^{1}H NMR spectrum is available. **4**: ^{1}H NMR ($CDCl_3$) δ=3.08, 3.72 (each 3H, s, COOMe), 3.97 (1H, dd, J=6.2 and 2.0 Hz, 1-H), 4.58 (1H, d, J=2.0 Hz, 2-H), 5.53 (1H, d, J=7.5 Hz, 6-H), 5.99 (1H, d, J=6.2 Hz, 10b-H), 6.34 (1H, br d, J=7.5, 10-H), 6.63 (1H, d, J=7.5 Hz, 5-H), and 6.5—7.4 (13H, m, Ar). **13**: Colorless prisms (diethyl ether); mp 223—224 °C; IR (KBr) 1690, 1430, 1365, 1245, 1190, 1065, and 700 cm^{-1}; ^{1}H NMR ($CDCl_3$) δ=3.59 (3H, s, COOMe), 7.00 (1H, d, J=7.5 Hz, 6-H), 7.1—7.7 (15H, m, Ar), and 9.33 (1H, d, J=7.5 Hz, 5-H); MS m/z (rel intensity, %) 377 (M^+, 99), 346 (15), 320 (13), 319 (41), 318 (20), 317 (33), 316 (18), 315 (19), 227 (16), 226 (base peak), and 168 (13). Found: C, 82.85; H, 5.16; N, 3.90%. Calcd for $C_{26}H_{19}NO_2$: C, 82.74; H, 5.07; N, 3.71%.

5: Part of **5** precipitated out when the crude solution was cooled to room temperature. Silica-gel chromatography of the filtrate, after evaporation of the solvent in vacuo, with hexane-ethyl acetate (10:1 v/v) afforded major part of **5**. Colorless prisms (diethyl ether); mp 182—182.5 °C; IR (KBr) 2220, 1630, 1454, 1294, 1256, 1167, 779, 761, and 706 cm^{-1}; ^{1}H NMR ($CDCl_3$) δ=4.09 (1H, dd, J=11.3 and 1.0 Hz, 1-H), 4.27 (1H, dd, J=11.3 and 8.0 Hz, 2-H), 5.32 (1H, br d, J=8.0 Hz, 10b-H), 5.95 (1H, d, J=7.8 Hz, 6-H), 6.40 (1H, d, J=7.8 Hz, 5-H), and 6.6—7.5 (14H, m, Ar); MS m/z (rel intensity, %) 373 (M^+, 2), 194 (14), 193 (base peak), 180 (32), 179 (50), 178 (34,) 166 (22), 165 (35), 139 (16), 129 (24), 128 (24), 115 (12), 103 (13), and 102 (20). Found: C, 83.66; H, 5.12; N, 11.20%. Calcd for $C_{26}H_{19}N_3$: 83.62; H, 5.13; N, 11.25%.

6A and 6B: Column chromatography of the crude reaction mixture over silica gel with hexane-ethyl acetate (15:1 v/v) provided **6A** and then **6B**. **6A**: Pale yellow needles (benzene-diethyl ether); mp 215—215 °C; IR (KBr) 3020, 1750, 1620, 1240, and 770 cm^{-1}; ^{1}H NMR ($CDCl_3$) δ=3.84 (3H, s, COOMe), 3.99 (1H, d, J=12.1 Hz, 2-H), 4.26 (1H, dd, J=12.1 and 9.1 Hz, 1-H), 5.47 (1H, d, J=9.1 Hz, 10b-H), 5.72 (1H, d, J=7.5 Hz, 6-H), 6.12 (1H, d, J=7.5 Hz, 5-H), and 6.6—7.4 (14H, m, Ar); ^{13}C NMR ($CDCl_3$) δ=54.18 (q, COOMe), 55.29 (d, 2-C), 61.83 (d, 1-C), 64.00 (d, 10b-C), 71.77 (s, 3-C), 106.71 (d, 6-C), 115.66 (s, CN), 124.07, 124.48, 126.83, 127.95, 128.18, 128.89, 129.00, 129.13, 129.36, 132.25, 138.18, and 167.71 (s, COOMe); MS m/z (rel intensity, %) 406 (M^+, 4), 227 (13), 226 (base peak), 168 (29), 143 (18), 140 (13), and 115 (10). Found: C, 79.82; H, 5.55; N, 6.83%. Calcd for $C_{27}H_{22}N_2O_2$: C, 79.78; H, 5.46; N, 6.89%. **6B**: Pale yellow prisms (benzene-hexane); mp 160—162 °C; IR (KBr) 3010, 1750, 1610, 1440, 1290, 1220, 770, and 700 cm^{-1}; ^{1}H NMR ($CDCl_3$) δ=3.25 (3H, s, COOMe), 4.11 (1H, d, J=10.9 Hz, 2-H), 4.30 (1H, dd, J=10.9 and 8.2 Hz, 1-H), 5.32 (1H, d, J=8.2 Hz, 10b-H), 5.74 (1H, d, J=7.8 Hz, 6-H), 6.28 (1H, d, J=7.8 Hz, 5-H), and 6.6—7.4 (14H, m, Ar); ^{13}C NMR ($CDCl_3$) δ=53.30 (q, COOMe), 53.42 (d, 2-C), 63.83 (d, 1-C), 64.24 (d, 10b-C), 70.06 (s, 3-C), 107.07 (d, 6-C), 117.83 (s, CN), 123.83, 124.36, 126.77, 127.95, 128.24, 128.83, 129.01, 129.42, 129.89, 131.01, 132.60, 133.95, 138.72, and 165.83 (s, COOMe); MS m/z (rel intensity, %) 406 (M^+, 5), 227 (15), 226 (base peak), 217 (10), 168 (27), 143 (19), and 140 (13). Found: C, 79.85; H, 5.46; N, 6.87%. Calcd for $C_{27}H_{22}N_2O_2$: C, 79.78; H, 5.46; N, 6.89%.

7: Unreacted **1b** (19%) was recovered when the mixture was cooled to room temperature. The filtrate was chromatographed over silica gel by using hexane-ethyl acetate (10:1 v/v) to give **7**. Colorless prisms (diethyl ether-hexane); mp 155—156 °C; IR (KBr) 2220, 1628, 1489, 1454, 1294, 1261, 1137, 785, and 698 cm^{-1}; ^{1}H NMR ($CDCl_3$) δ=4.03 (1H, d, J=7.0 Hz, 2-H), 4.53 (1H, dd, J=10.0 and 7.0 Hz, 1-H), 5.54 (1H, d, J=7.0 Hz, 10b-H), 6.06 (1H, d, J=7.0 Hz, 6-H), 6.48 (1H, d, J=7.0 Hz, 5-H), and 6.7—7.3 (14H, m, Ar); ^{13}C NMR ($CDCl_3$) δ=55.03 (d, 2-C), 59.33 (d, 1-C), 59.86 (d, 10b-C), 60.25 (s, 3-C), 111.33 (d, 6-C), 112.21, 115.00 (each s, CN), 124.12, 125.10, 126.22, 127.93, 128.22, 128.37, 128.80, 128.91, 129.00, 129.20 129.98, 131.05, 133.05, and 135.49; MS m/z (rel intensity, %) 373 (M^+, 20), 194 (17), 193 (base peak), 180 (34), 179 (57), 178 (39), 166 (15), 165 (32), 154 (24), 153 (13), 139 (11), 129 (18), 128 (29), 127 (21), 115 (13), 103 (29), and 102 (20). Found: C, 83.50; H, 5.15; N, 11.19%. Calcd for $C_{26}H_{19}N_3$: C, 83.62; H, 5.13; N, 11.25%.

8: Column chromatography of the reaction mixture over silica gel with hexane-ethyl acetate (10:1 v/v) gave **8**. Colorless prisms (ethyl acetate-hexane); mp 225—227 °C; IR (KBr) 1760, 1650, 1245, 770, and 705 cm^{-1}; ^{1}H NMR ($CDCl_3$) δ=3.40 (3H, s, COOMe), 4.05 (1H, d, J=7.0 Hz, 2-H), 4.57 (1H, dd, J=10.0 and 7.0 Hz, 1-H), 5.71 (1H, d, J=10.0 Hz, 10b-H), 5.89 (1H, d, J=7.5 Hz, 6-H), 6.49 (1H, d, J=7.5 Hz, 5-H), 6.58 (1H, br d, J=7.0 Hz, 10-H), and 6.7—7.2 (13H, m, Ar); ^{13}C NMR ($CDCl_3$) δ=53.47 (q, COOMe), 55.12 (d, 2-C), 60.24 (d, 1-C),69.95 (d, 10b-C), 108.95 (d, 6-C), 118.36 (s, CN), 60.24 (d, 1-C), 69.95 (d, 10b-C), 108.95 (d, 6-C), 118.36 (s, CN), 124.24, 124.41, 127.07, 127.42, 127.89, 128.25, 128.42, 128.60, COOMe); MS m/z (rel intensity, %) 406 (M^+, 6), 227 (16), 226 (base peak), 168 (82), and 143 (12). Found: C, 79.65; H, 5.46; N, 7.00%. Calcd for $C_{27}H_{22}N_2O_2$: C, 79.78; H, 5.46; N, 6.89%.

9A and 9B: The crude reaction mixture was chromatographed over silica gel with chloroform to give a mixture of **9A** and **9B** (59%, 3:2 by ^{1}H NMR). This mixture was separated through flash chromatography in a Lobar column with hexane-ethyl acetate (20:1 v/v) to give **9A** and then **9B**. **9A:** Colorless prisms (diethyl ether-hexane); mp 148—149 °C; IR (KBr) 1620, 1480, 1450, 1410, 1290, 1240, and 1160 cm^{-1}; ^{1}H NMR ($CDCl_3$) δ=3.11 (1H, dd, J=16.0 and 3.3 Hz, 13-exo-H), 3.50 (1H, dd, J=16.0 and 9.4 Hz, 13-endo-H), 3.6—3.7 (1H, m, 13a-H), 4.36 (1H, d, J=8.4 Hz, 8a-H), 4.64 (1H, d, J=10.3 Hz 13b-H), 5.97 (1H, d, J=7.7 Hz, 5-H), 6.48 (1H, d, J=7.7 Hz, 6-H), and 7.1—7.6 (8H, m, Ar); MS m/z (rel intensity, %) 309 (M^+, 10), 194 (16), 193 (base peak), 166 (18), 139 (21), 129 (16), 128 (17), 116 (69), and 115 (77). Found: C, 81.75; H, 4.66; N, 13.39%. Calcd for $C_{21}H_{15}N_3$: C, 81.53; H, 4.89; N, 13.58%. **9B**: Pale yellow prisms (diethyl ether-hexane); mp 115—156 °C; IR (KBr) 1620, 1450, 1400, 1290, 1240, and 1180 cm^{-1}; ^{1}H NMR ($CDCl_3$) δ=3.26 (1H, dd, J=16.0 and 9.2 Hz, 13-endo-H), 3.34 (1H, dd, J=16.0 and 7.0 Hz, 13-exo-H), 3.8—3.9 (1H, m, 13a-H), 4.43 (1H, d, J=7.7 Hz, 8a-H), 5.07 (1H, d, J=5.1 Hz, 13b-H), 5.79 (1H, d, J=7.7 Hz, 5-H), 6.36 (1H, d, J=7.7 Hz, 6-H), and 7.0—7.5 (8H m, Ar); MS m/z (rel intensity, %) 309 (M^+, 8), 193 (95), 166 (22), 139 (21), 129 (24), 128 (29), 116 (77), 115 (base peak), 89 (23), 77 (22), and 63 (26). Found: C, 81.34; H, 4.72; N,

13.43%. Calcd for $C_{21}H_{15}N_3$: C, 81.53; H, 4.89; N, 13.58%.

10: The crude reaction mixture was chromatographed, after evaporation of the solvent in vacuo, over silica gel with hexane-ethyl acetate (5:1 v/v) to afford **10**: Colorless prisms (ethyl acetate-hexane); mp 164 °C; IR (KBr) 1757, 1734, 1608, 1454, 1288, 1271, 1227, 1207, 1038, 769, and 706 cm^{-1}; ^1H NMR ($CDCl_3$) δ=2.59 (1H, ddd, J=12.5, 6.8, and 1.0 Hz, 1-endo-H), 2.89 (1H, ddd, J=12.5, 10.0, and 8.0 Hz, 1-exo-H), 3.20, 3.67 (each 3H, s, COOMe), 4.36 (1H, dd, J=8.0 and 1.0 Hz, 2-H), 5.52 (1H, dd, J=10.0 and 6.8 Hz, 10b-H), 5.62 (1H, d, J=7.5 Hz, 6-H), 6.61 (1H, d, J=7.5 Hz, 5-H), 6.7—7.4 (4H, m, Ar), and 7.22 (5H, s, Ph); ^{13}C NMR ($CDCl_3$) δ=37.00 (t, 1-C), 50.47 (d, 2-C), 51.95, 52.83 (each q, COOMe), 60.36 (d, 10b-C), 103.77 (d, 6-C), 123.07, 123.36, 125.83, 127.36, 128.48, 128.72, 131.19, 132.89, 133.30, 140.72, 168.78 (q, COOMe), and 169.07 (q, COOMe); MS m/z (rel intensity, %) 363 (M^+, 17), 304 (35), 245 (20), 244 (78), 243 (33), 201 (29), 167 (64), 166 (24), 143 (88), 130 (25), 129 (46), 128 (38), 116 (26), 115 (73), 104 (72), and 103 (32). Found: C, 72.65; H, 5.94; N, 4.09%. Calcd for $C_{22}H_{21}NO_4$: C, 72.71; H, 5.82; N, 3.85%.

11A: The crude product obtained by evaporation of the solvent in vacuo was subjected to ^1H NMR measurement which showed a 3:2 mixture of **11A** and **11B**, and then chromatographed over silica gel with hexane-ethyl acetate (10:1 v/v) to provide 88% of **11A** as a single product: Colorless prisms (diethyl ether); IR (KBr) 2773, 2229, 1618, 1456, 1406, 1290, 1253, 1217, 773, and 702 cm^{-1}; ^1H NMR ($CDCl_3$) δ=2.90 (1H, dd, J=8.0 and 7.0 Hz, one of 1-H), 2.92 (1H, dd, J=8.0 and 7.8 Hz, the other of 1-H), 4.08 (1H, dd, J=8.0 and 7.0 Hz, 3-H), 4.94 (1H, dd, J=8.0 and 7.8 Hz, 10b-H), 6.01 (1H, d, J=7.5 Hz, 6-H), 6.47 (1H, d, J=7.5 Hz, 5-H), 6.9—7.3 (4H m, Ar), and 7.42 (5H, s, Ph); ^{13}C NMR ($CDCl_3$) δ=33.36 (t, 1-C), 54.83 (d, 2-C), 59.00 (d, 10b-C), 61.00 (s, 3-C) 110.77 (d, 6-C), 123.60, 124.95, 127.71, 128.25, 128.54, 129.36, 129.48, 129.66, 131.36, and 134.54; MS m/z (rel intensity, %) 297 (M^+, 13), 194 (16), 193 (base peak), 166 (13), 129 (15), 128 (17), 115 (16), 104 (916), 103 (14), 102 (12), and 77 (15). Found: C, 80.80; H, 5.10; N, 14.06%. Calcd for $C_{20}H_{15}N_3$: C, 80.78; H, 5.08; N, 14.13%.

^1H NMR spectrum ($CDCl_3$) of **11B** which was abstracted from the spectrum of the mixture with **11A**: δ=2.7—3.0 (2H, m, 1-H), 4.14 (1H, dd, J=12.0 and 6.6 Hz, 2-H), 5.10 (1H, dd, J=9.0 and 5.9 Hz, 10b-H), 5.87 (1H, d, J=7.3 Hz, 6-H), and 6.33 (1H, d, J=7.3 Hz, 5-H).

12: The reaction mixture was evaporated in vacuo to dryness to give residue which solidified on standing: Colorless prisms (diethyl ether); mp 130—132 °C; IR (KBr) 2240, 1750, 1605, 1450, 1220, 1210, 765, and 700 cm^{-1}; ^1H NMR ($CDCl_3$) δ=2.8—3.2 (2H, m, 1-H), 3.38 (3H, s, COOMe), 4.12 (1H dd, J=7.4 and 5.6 Hz, 2-H), 5.36 (1H, t, J=7.5 H, 10b-H), 5.86 (1H, d, J=7.5 Hz, 6-H), 6.34 (1H, d, J=7.5 Hz, 5-H), 6.8—7.5 (4H, m, Ar), and 7.29 (5H, s, Ph); ^{13}C NMR ($CDCl_3$) δ=35.65 (t, 1-C), 53.06 (q, COOMe), 54.47 (d, 2-C), 59.65 (d, 10b-C), 70.42 (s, 3-C), 107.89 (d, 6-C), 117.71 (s, CN), 123.42, 124.13, 126.95, 127.60, 128.36, 128.77, 129.77, 130.95, 131.83, 136.72, and 165.72 (s, COOMe); MS m/z (rel intensity, %) 330 (M^+, 56), 329 (29), 271 (45), 227 (17), 226 (base peak), 168 (29), 143 (98), 129 (22), and 115 (26). Found: C, 76.27; H, 5.58; N, 8.41%. Calcd for $C_{21}H_{18}N_2O_2$: C, 76.34; H, 5.49; N, 8.48%.

14 (an inseparable mixture of two stereoisomers (3:1 by ^1H NMR)): The crude reaction mixture was evaporated in vacuo and the residue was chromatographed over silica gel with hexane-ethyl acetate (5:1 v/v) to give **14** as a 3:1 mixture of two isomers): Colorless crystals (diethyl ether); IR (KBr) 2964, 1622, 1483, 1456, 1409, 1284, 1250, 1178, 777, and 710 cm^{-1}; ^1H NMR ($CDCl_3$) δ=1.0—2.0 (6H, m, CH_2), 2.4—3.0 (4H, m, CH), 4.15 (3/4H, d, J=5.9 Hz, 10b-H), 4.83 (1/4H, d, J=6.1 Hz, 10b-H), 5.72 (1/4H, d, J=8.0 Hz, =CH), 5.91 (3/4H, d, J=7.8 Hz, =CH), 6.33 (1/4H, d, J=8.0 Hz, =CHN), 6.42 (3/4H, d, J=7.8 Hz, =CHN), and 6.9—7.3 (4H, m, Ar); ^{13}C NMR ($CDCl_3$) major isomer: δ=27.59, 28.47, 34.37 (each t, CH_2), 38.72, 39.21, 52.88 (each d, CH), 57.67 (d and s, CH and q-C), 63.87 (d, CHN), 110.55 (d, =CH), 112.74, 114.65 (each s, CN), 123.48, 124.75, 127.54, 128.07, 128.76, 131.15, and 131.74; minor isomer: δ=27.59, 29.25, 34.96 (each t, CH_2), 36.67, 40.67, 47.02, 56.59 (each d, CH), 57.32 (s, q-C), 62.65 (d, CHN), 108.40 (d, =CH), 112.04, 113.50 (each s, CN), 125.20, 125.82, 126.86, 129.69, and 132.56; MS m/z (rel intensity, %) 287 (M^+, 7), 194 (19), 193 (73), 166 (32), 165 (21), 139 (24), 129 (base peak), 128 (36), 103 (21), 102 (45), 91 (20), 79 (63), and 77 (52). Found: C, 79.20; H, 5.94; N, 14.56%. Calcd for $C_{19}H_{17}N_3$: C, 79.41; H, 5.96; N,14.62%.

15: Unreacted ylide **1b** precipitated out when the reaction mixture was cooled to room temperature. The filtrate was evaporated in vacuo and chromatographed over silica gel with hexane-ethyl acetate (3:1 v/v) to afford **15.** The fraction eluted with hexane-ethyl acetate (1:1 v/v) gave additional **1b** (The combined yield of recovered **1b** was 55%): Colorless plates (diethyl ether-hexane); mp 151—152 °C; 2220, 1620, 1405, 1280, 1245, 1170, and 770 cm^{-1}: ^1H NMR ($CDCl_3$) δ=2.6—3.6 (6H, m, 1-, 2-H, and CH_2), 5.14 (1H, d, J=4.9 Hz, 10b-H), 5.72 (1H, d, J=7.5 Hz, 6-H), 6.63 (1H, d, J=7.5 Hz, 5-H), and 6.9—7.3 (4H, m, Ar); MS m/z (rel intensity, %) 299 (M^+, 6), 194 (15), 193 (base peak), 192 (10), and 129 (14). Found: C, 72.08; H, 4.37; N, 23.16%. Calcd for $C_{18}H_{13}N_3$: C, 72.23; H, 4.38; N, 23.40%.

16: The reaction mixture was chromatographed, after evaporation of the solvent in vacuo, over silica gel with hexane-ethyl acetate (8:1 v/v) to give **16** and then **20: 16**: Colorless liquid; IR (neat) 2980, 1750, 1740, 1610, 1455, and 770 cm^{-1}; ^1H NMR ($CDCl_3$) δ=0.7—1.6 (9H, m, n-Bu), 2.40 (2H, dd, J=8.1 and 4.5 Hz, 1-H), 2.8—3.2 (1H, m, 2-H), 3.65, 3.77 (each 3H, s, COOMe), 4.91 (1H, t, J=8.1 Hz, 10b-H), 5.49 (1H, d, J=7.5 Hz, 6-H), 6.50 (1H, d, J=7.5 Hz, 5-H), and 6.7—8.2 (4H, m, Ar); ^{13}C NMR ($CDCl_3$) δ=13.94 (q, n-Bu), 22.59, 29.30, 30.06 (each t, n-Bu), 33.24 (t, 1-C), 44.36 (d, 2-C), 52.47, 52.83 (each q, COOMe), 58.77 (d, 10b-C), 77.71 (s, 3-C), 102.30 (d, 6-C), 123.07, 123.30, 125.54, 127.36, 131.07, 133.13, 133.89, 169.25 (s, COOMe), and 169.72 (s COOMe); MS m/z (rel intensity, %) 343 (M^+, 10), 284 (17), 132 (90), 100 (18), 85 (71), and 83 (base peak). HRMS Found: m/z 343.1778. Calcd for $C_{20}H_{25}NO_4$: M, 343.1782. **20**: Colorless prisms (hexane); mp 80—81 °C; IR (KBr) 2980, 1680, 1440, and 1350 cm^{-1}; ^1H NMR ($CDCl_3$) δ=0.8—1.1 (3H, m, n-Bu), 1.2—2.0 (4H, m, n-Bu), 3.00 (2H, t, J=7.5 Hz, n-Bu), 3.96 (3H, s, COOMe), 6.88 (1H, s, 1-H), 6.92 (1H d, J=7.5 Hz, 6-H), 7.3—7.7 (3H, m, Ar), 7.9—8.2 (1H, m, Ar), and 9.20 (1H, d, J=7.5 Hz, 5-H); MS m/z (rel intensity, %) 281 (M^+, 48), 239 (base peak), 181 (20), 180 (42), and 41 (25). Found: C, 76.62; H, 6.84; N, 4.72%. Calcd for $C_{18}H_{19}NO_2$: C, 76.84; H, 6.81; N, 4.98%.

17: The crude mixture was chromatographed over silica gel by using hexane-ethyl acetate (10:1 v/v) to provide **17**: Colorless viscous liquid; IR (neat) 2958, 2926, 2210, 1618,

1456, 1406, 1256, 1178, and 775 cm^{-1}; ^1H NMR ($CDCl_3$) δ=0.8—3.0 (12H, m, 1-, 2-H, and *n*-Bu), 4.59 (1H, dd, *J*=8.2 and 7.5 Hz, 10b-H), 5.90 (1H, d, *J*=7.5 Hz, 6-H), 6.42 (1H, d, *J*=7.5 Hz, 5-H), and 6.8—7.3 (4H, m, Ar); ^{13}C NMR ($CDCl_3$) δ=13.82 (q, *n*-Bu), 22.53, 29.77, 31.06 (each t, *n*-Bu), 33.00 (t, 1-C), 49.47 (d, 2-C), 58.36 (d, 10b-C), 59.00 (s, 3-C), 110.13 (d, 6-C), 111.77, 114.00 (each s, CN), 123.60, 124.83, 127.54, 128.18, 128.48, 131.19, and 131.66; MS *m/z* (rel intensity, %) 277 (M^+, 18), 276 (11), 194 (16), and 193 (base peak). HRMS Found: *m/z* 277.1583. Calcd for $C_{18}H_{19}N_3$: M, 277.1578.

18: The crude reaction mixture was chromatographed over silica gel with hexane-ethyl acetate to afford **18**: Pale yellow prisms (diethyl ether-hexane); mp 158—159 °C; IR (KBr) 1760, 1740, 1610, 1240, 1175, 1020, and 760 cm^{-1}: ^1H NMR ($CDCl_3$) δ=2.3—2.7 (2H, m, 11-H), 3.3—3.6 (1H, m, 10a-H), 3.79 (3H, s, COOMe), 4.12 (1H, dd, *J*=9.5 and 4.5 Hz, 11a-H), 4.61 (1H, dd, *J*=9.5 and 3.0 Hz, one of 10-H), 4.67 (1H, dd, *J*=9.5 and 5.0 Hz, the other of 10-H), 5.60 (1H, d, *J*=7.8 Hz, 5-H), 6.68 (1H, *J*=7.8Hz, 6-H), and 6.8—7.2 (4H, m, Ar); ^{13}C NMR ($CDCl_3$) δ=34.41 (t, 11-C), 44.18 (d, 10a-C), 53.42 (q, COOMe), 59.18 (d, 11a-C), 71.83 (s 7a-C), 72.24 (t, 10-C), 104.13 (d, 5-C), 123.48, 123.77, 126.07, 127.89, 130.30, 131.95, 133.30, 168.54 (s, 8-C), and 172.03 (s, COOMe); MS *m/z* (rel intensity, %) 285 (M^+, 50), 284 (base peak), 226 (40), 182 (13), 181 (20), 180 (27), 168 (19), 167 (47), 143 (28), 129 (41), 128 (21), and 115 (29). Found: C, 67.39; H, 5.34; N, 4.86%. Calcd for $C_{16}H_{15}NO_4$: C, 67.36; H, 5.30; N, 4.91%.

19: The crude mixture was chromatographed over silica gel with hexane-ethyl acetate (7:1 v/v) to give **19**: Colorless prisms (hexane); mp 92—93 °C; IR (KBr) 2950, 1610, 1470, 1450, 1400, 1245, 1080, 855, and 830 cm^{-1}; ^1H NMR ($CDCl_3$) δ=0.19 (9H, s, $SiMe_3$), 2.13 (1H, ddd, *J*=12.1, 7.5, and 5.9 Hz, 1-endo-H), 2.53 (1H, ddd, *J*=12.1, 10.0, and 8.5 Hz, 1-exo-H), 3.0—3.2 (1H, m, 2-H), 3.89 (1H, d, *J*=8.4 Hz, one of 2-CH_2), 3.90 (1H, d, *J*=7.0 Hz, the other of 2-CH_2), 4.58 (1H, dd, *J*=8.5 and 7.5 Hz, 10b-H), 5.91 (1H, d, *J*=7.5 Hz, 6-H), 6.49 (1H, d, *J*=7.5 Hz, 5-H), and 6.8—7.3 (4H, m, Ar); ^{13}C NMR ($CDCl_3$) δ=0.64 (q, $SiMe_3$), 29.12 (t, 1-C), 51.53 (d, 2-C), 57.53 (s, 3-C), 58.95 (d, 10b-C), 62.24 (t, CH_2O), 110.18 (d, 6-C), 111.24, 114.01 (each s, CN), 123.77, 125.01, 127.66, 128.42, 128.83, 131.48, and 131.83; MS *m/z* (rel intensity, %) 323 (M^+, 11), 308 (19), 281 (15), 220 (29), 194 (12), 193 (60), 145 (12), 144 (base peak), and 73 (14). Found: C, 66.62; H, 6.60; N, 12.80%. Calcd for $C_{18}H_{21}N_3OSi$: C, 66.84; H, 6.54; N, 12.99%.

21: This compound was obtained by column chromatography of the crude reaction mixture over silica gel with hexane-ethyl acetate (5:1 v/v): Colorless viscous liquid; IR (neat) 2960, 1820, 1750, 1620, 1560, 1440, and 780 cm^{-1}; ^1H NMR ($CDCl_3$) δ=3.67, 3.84 (each 3H, s, COOMe), 5,03 (d, *J*=5.5 Hz, 11b-H), 5.43 (1H, dd, *J*=7.5 and 5.5 Hz, 11a-H), 5.72 (1H, d, *J*=7.5 Hz, 8a-H), 5.75 (1H, d, *J*=7.8 Hz, 5-H), 6.52 (1H d, *J*=7.8 Hz, 6-H), and 6.8—7.3 (4H, m, Ar); ^{13}C NMR ($CDCl_3$) δ=53.59 (q, 2C, COOMe), 66.54 (d, 11b-C) 75.59 (s, 8-C), 80.01, 81.77 (each d, 8a- and 11a-C), 107.66 (d, 5-C), 120.77, 123.12, 124.42, 127.19, 128.65, 131.19, 132.18, 153.13 (s, 10-C), 165.77, and 166.37 (each s, COOMe); MS *m/z* (rel intensity, %) 345 (M^+, 5), 259 (9), 226 (16), 225 (base peak), 194 (32), 167 (34), 166 (26), 139 (18), 129 (82), 128 (20), 102 (20), and 91 (17). HRMS Found: *m/z* 345.0846. Calcd for $C_{17}H_{15}NO_7$: M, 345.0847.

22A and 22B: When the reaction mixture was cooled to room temperature, less soluble **22A** precipitated out. The filtrate was evaporated in vacuo and the residue was chromatographed over silica gel by using hexane-ethyl acetate (10:1 v/v) to provide **22B**. **22A:** Pale yellow prisms (benzene-ethanol); mp 177—178 °C; IR (KBr) 1813, 1632, 1377, 1255, 1167, 1093, 962, 777, and 761 cm^{-1}; ^1H NMR (DMSO-d_6:$CDCl_3$=1:4 v/v) δ=4.78 (1H, br s, 11b-H), 5.85, 5.87 (each 1H, s, 8a- and 11a-H), 5.98 (1H, d, *J*=7.8 Hz, 5-H), 6.46 (1H, d, *J*=7.8 Hz, 6-H), and 7.0—7.4 (4H, m, Ar); MS *m/z* (rel intensity, %) 279 (M^+, 8), 194 (15), 193 (base peak), 129 (24), and 128 (13). Found: C, 64.53; H, 3.50; N, 14.99%. Calcd for $C_{15}H_9N_3O_3$: C, 64.52; H, 3.25; N, 15.05%. **22B**: Pale yellow needles (benzene-ethanol); mp 193—194 °C; IR (KBr) 1808, 1628, 1182, 1159, 1149, and 775 cm^{-1}; ^1H NMR ($CDCl_3$) δ=4.82 (1H, d, *J*=3.6 Hz, 11b-H), 5.46 (1H, d, *J*=6.5 Hz, 8a-H), 5.64 (1H, dd, *J*=6.5 and 3.6 Hz, 11a-H), 6.02 (1H, d, *J*=8.0 Hz, 5-H), 6.42 (1H, d, *J*=8.0 Hz, 6-H), and 7.0—7.2 (4H, m, Ar); MS *m/z* (rel intensity, %) 279 (M^+, 5), 193 (54), 166 (11), 130 (12), 129 (81), 128 (52), 115 (15), 103 (19), 102 (40), and 86 (base peak). Found: C, 64.55; H, 3.41; N, 14.89%. Calcd for $C_{15}H_9N_3O_3$: C, 64.52; H, 3.25; N, 15.05%.

23: The reaction mixture was chromatographed, after evaporation of the solvent in vacuo, over silica gel with hexane-ethyl acetate (3:1 v/v) to give **23**: Colorless prisms (diethyl ether); mp 154—156 °C; IR (KBr) 2220, 1830, 1795, 1770, 1620, 1210, 1140, and 755 cm^{-1}; ^1H NMR ($CDCl_3$) δ=3.95 (3H, s, COOMe), 5.22 (1H, br s, 11b-H), 5.53 (2H, m, 8a- and 11a-H), 5.94 (1H, d, *J*=7.5 Hz, 5-H), 6.33 (1H, d, *J*=7.5 Hz, 6-H), and 6.9—7.2 (4H, m, Ar); MS *m/z* (rel intensity, %) 312 (M^+, 8), 227 (15), 226 (base peak), 209 (15), 168 (36), 144 (40), 143 (26), 129 (30), 128 (18), and 115 (14). HRMS Found: *m/z* 312.0749. Calcd for $C_{16}H_{12}N_2O_5$: M, 312.0745.

24: The mixture was evaporated in vacuo and the residue was chromatographed over silica gel with hexane-ethyl acetate (10:1 v/v) to give **24**: Pale yellow prisms (diethyl ether-hexane); mp 101—102 °C; IR (KBr) 2970, 1770, 1740, 1600, 1460, 1420, 1210, 1120, 1070, and 765 cm^{-1}; ^1H NMR ($CDCl_3$) δ=0.8—1.7 (7H, m, *n*-Bu), 2.26 (1H, ddd, *J*=12.5, 10.6 and 4.1 Hz, 1-endo-H), 2.64 (1H, dd, *J*=12.5 and 5.0 Hz, 1-exo-H), 3.3—4.0 (2H, m OCH_2), 3.64, 3.76 (each 3H, s, COOMe), 4.63 (1H, d, *J*=4.1 Hz, 2-H), 5.06 (1H, dd, *J*=10.6 and 5.0 Hz, 10b-H), 5.45 (1H, d, *J*=7.5 Hz, 6-H), 6.51 (1H, d, *J*=7.5 Hz, 5-H), and 6.8—7.1 (4H, m, Ar); ^{13}C NMR ($CDCl_3$) δ=13.82 (q, *n*-Bu), 19.30, 31.88 (each t, *n*-Bu), 35.59 (t, 1-C), 52.59, 52.95 (each q, COOMe), 59.42 (d, 10b-C), 70.42 (t, OCH_2), 78.30 (s, 3-C), 82.95 (d, 2-C), 101.78 (d, 6-C), 123.12, 123.48, 125.54, 127.48, 130.95, 133.01, 133.95, 167.95 (s, COOMe), and 168.30 (s, COOMe); MS *m/z* (rel intensity, %) 359 (M^+, 38), 358 (20), 300 (30), 259 (22), 226 (27), 225 (22), 201 (22), 167 (34), 143 (base peak), and 130 (11). Found: C, 67.39; H, 5.34; N, 4.86%. Calcd for $C_{20}H_{25}NO_5$: C, 67.36; H, 5.30; N, 4.91%.

25: The crude reaction mixture was chromatographed over silica gel with hexane-ethyl acetate (10:1 v/v) to provide **25**: Pale yellow prisms (diethyl ether-hexane); mp 79—80 °C; IR (KBr) 2933, 1622, 1456, 1402, 1254, 1182, 1108, and 777 cm^{-1}; ^1H NMR ($CDCl_3$) δ=0.93 (3H, t, *J*=6.9 Hz, *n*-Bu), 1.2—1.8 (4H, m, *n*-Bu), 2.59 (2H, dd, *J*=8.0 and 5.0 Hz, 1-H), 3.5—4.0 (2H, m, OCH_2), 4.51 (1H, t, *J*=5.0 Hz, 10b-H), 4.85 (1H, t, *J*=8.0 Hz, 2-H), 5.85 (1H, d, *J*=7.5Hz, 6-H), 6.35 (1H, d, *J*=7.5 Hz, 5-H), and 6.8—7.3 (4H, m, Ar); ^{13}C NMR ($CDCl_3$) δ=13.82 (q, *n*-Bu), 19.14, 31.59 (each t,

n-Bu), 35.84 (t, 1-C), 58.25 (d, 10b-C), 59.62 (s, 3-C), 72.27 (t, OCH_2), 85.74 (d, 2-C), 109.62 (d, 6-C), 111.13, 113.67 (each s, CN), 123.78, 124.90, 127.59, 127.93, 128.27, 130.86, and 131.45; MS *m/z* (rel intensity, %) 293 (M^+, 3), 193 (33), 58 (40), and 42 (base peak). Found: C, 73.55; H, 6.54; N, 14.31%. Calcd for $C_{18}H_{19}N_3O$: C, 73.70; H, 6.53; N, 14.32%.

26A and 26B: The crude mixture was chromatographed over silica gel with hexane–ethyl acetate (10:1 v/v) to give **26A** and **26B** which are still contaminated by each other. They were further purified by preparative thin-layer chromatography using the same eluent to give pure **26A** and **26B**. **26A**: Colorless liquid; IR (neat) 2970, 2200, 1760, 1740, 1620, 1560, and 770 cm^{-1}; ^1H NMR ($CDCl_3$) δ=0.8—1.7 (7H, m, *n*-Bu), 2.50 (1H, ddd, *J*=13.0, 9.5, and 5.0 Hz, 1-endo-H), 2.77 (1H, ddd, *J*=13.0, 6.0, and 2.0 Hz, 1-exo-H), 3.4—3.8 (2H, m, OCH_2), 3.88 (3H, s, COOMe), 4.54 (1H, dd, *J*=5.0 and 2.0 Hz, 2-H), 5.22 (1H, dd, *J*=9.5 and 6.0 Hz, 10b-H), 5.66 (1H, d *J*=7.5 Hz, 6-H), 6.26 (1H, d, *J*=7.5 Hz, 5-H), and 6.8—7.3 (4H, m, Ar); ^{13}C NMR ($CDCl_3$) δ=13.77 (q, *n*-Bu), 19.12, 31.65 (each t, *n*-Bu), 37.00 (t, 1-C), 53.65 (q, COOMe), 58.83 (d, 10b-C), 69.89 (s, 3-C), 71.30 (t, OCH_2), 85.24 (d, 2-C), 105.59 (d, 6-C), 116.95 (s, CN), 123.71, 124.18, 126.60, 127.77, 129.83, 130.72, 132.18, and 165.07 (s, COOMe); MS *m/z* (rel intensity, %) 326 (M^+, 24), 227 (21), 226 (96), 195 (18), 194 (22), 193 (72), 192 (56), 168 (97), 167 (20), 143 (base peak), 140 (23), 139 (19), 129 (37), 128 (33), and 115 (38). HRMS Found: *m/z* 326.1627. Calcd for $C_{19}H_{22}N_2O_3$: M, 326.1629. **26B**: Colorless liquid; IR (neat) 2970, 2200, 1750, 1620, 1560, 1455, 1240, and 760 cm^{-1}; ^1H NMR ($CDCl_3$) δ=0.8—1.8 (7H, m, *n*-Bu), 2.50 (1H, dd, *J*=9.5 and 5.5 Hz, 1-endo-H), 2.54 (1H, dd, *J*=6.8 and 2.8 Hz, 1-exo-H), 3.4—4.0 (2H, m, OCH_2), 3.81 (3H, s, COOMe), 4.40 (1H, dd, *J*=5.5 and 2.8 Hz, 2-H), 4.92 (1H, dd, *J*=9.5 and 6.8 Hz, 10b-H), 5.34 (1H, d, *J*=7.5 Hz, 6-H), 6.34 (1H, d, *J*=7.5 Hz, 5-H), and 6.8—7.3 (4H, m, Ar); MS *m/z* (rel intensity, %) 326 (M^+, 10), 269 (14), 227 (19), 226 (88), 194 (24), 193 (base peak), 192 (56), 168 (61), 167 (23), 143 (54), 140 (25), 129 (40), 128 (33), and 115 (33). HRMS Found: *m/z* 326.1630. Calcd for $C_{19}H_{22}N_2O_3$: M, 326.1629.

27 and 29: The crude mixture was chromatographed over silica gel with hexane–ethyl acetate (5:1 v/v) to give a mixture of **27** and **29**. As compound **27** was so susceptible as to suffer from the decarboxylative aromatization leading to **29**, only ^1H NMR spectrum was measured. **27**: ^1H NMR ($CDCl_3$) δ=2.6—2.8 (2H, m, 1-H), 3.60, 3.64 (each 3H, s, COOMe), 4.54 (1H, m, 10b-H), 5.10 (1H, dt, *J*=8.0, 8.0, and 1.0 Hz, 2-H), 5.47 (1H, d, *J*=7.0 Hz, 6-H), 6.48 (1H, d, *J*=7.0 Hz, 5-H), and 6.6—7.7 (9H, m, Ar). Authentic sample of **29** was synthesized according to the following procedure: A mixture of 1-[bis(methoxycarbonyl)methyl]isoquinolinium bromide (0.34 g, 1 mmol), phenyl vinyl sulfoxide (0.152 g, 1 mmol), and triethylamine (0.14 ml, 1 mmol) in dry toluene (5 ml) was heated under reflux for 64 h. The mixture was poured into water (100 ml), extracted with dichloromethane (30 ml×2), the combined extracts were dried over magnesium sulfate, and evaporated in vacuo. The residue was chromatographed over silica gel by using hexane to give diphenyl disulfide (0.051 g, 47%) and the fraction eluted with hexane–ethyl acetate (10:1 v/v) afforded **29** (0.102 g, 45%). **29**: Colorless prisms (diethyl ether); mp 111—112 °C; IR (KBr) 1685, 1530, 1355, 1260, 1190, 1110, 785, and 745 cm^{-1}; ^1H NMR ($CDCl_3$) δ=3.89 (3H, s, COOMe), 6.9—7.2 (2H, m), 7.3—7.8 (4H, m), 8.0—8.2 (1H, m), and 9.20 (1H, d, *J*=7.7 Hz); MS *m/z* (rel intensity, %) 225 (M^+, 90), 194 (57), 167 (base peak), 166 (69), 140 (33), and 139 (51). Found: C, 74.55; H, 4.96; N, 6.20%. Calcd for $C_{14}H_{11}NO_2$: C, 74.65; H, 4.92; N, 6.22%.

28: The crude reaction mixture was chromatographed over silica gel by using hexane–ethyl acetate (4:1 v/v) to give **28**: Colorless prisms (diethyl ether); mp 109—111 °C; IR (KBr) 2220, 1775, 1620, 1250, and 780 cm^{-1}; ^1H NMR ($CDCl_3$) δ=2.84 (1H, ddd, *J*=13.0, 7.2, and 4.0 Hz, 1-endo-H), 3.02 (1H, ddd, *J*=13.0, 8.0, and 6.5 Hz, 1-exo-H), 3.74 (3H, s, COOMe), 4.24 (1H, dd, *J*=6.5 and 4.0 Hz, 10b-H), 5.17 (1H, dd, *J*=8.0 and 7.2 Hz, 2-H), 5.76 (1H, d, *J*=7.3 Hz, 6-H), 6.25 (1H, d, *J*=7.3 Hz, 5-H), and 6.7—7.8 (9H, m, Ar); MS *m/z* (rel intensity, %) 362 (M^+, 8), 253 (39), 226 (20), 194 (27), 193 (base peak), 192 (43), 168 (28), 167 (27), 143 (23), 129 (22), 110 (22), and 109 (56). Found: C, 69.80; H, 5.03; N, 7.68%. Calcd for $C_{21}H_{18}N_2O_2S$: C, 69.61; H, 4.97; N, 7.73%.

The present research was financially supported in part by a Grant-in-Aid for Scientific Research No. 62101008 from the Ministry of Education, Science and Culture.

References

1) I. Zugravescu and M. Petrovanu, "N-Ylide Chemistry," McGraw-Hill Internatl. New York (1976); J. W. Lown, "Azomethine Ylides", as chapter 6 of "1,3-Dipolar Cycloaddition Chemistry," ed by A. Padwa, A Wiley-Interscience Publication, New York, Chichester, Brisbane, Toronto, Shingapore (1984), Vol. 2, pp. 653—732; R. M. Kellogg, *Tetrahedron*, **32**, 2165 (1976); C. G. Stuckwisch, *Synthesis*, **1973**, 469.

2) O. Tsuge, S. Kanemasa, and S. Takenaka, *Bull. Chem. Soc. Jpn.*, **58**, 3137, 3320 (1985) and references cited therein; M. Hori, T. Kataoka, H. Shimizu, E. Imai, Y. Matsumoto, M. Kawachi, and K. Kuratani, *J. Chem. Soc., Perkin Trans. 1*, **1987**, 1211.

3) O. Tsuge, S. Kanemasa, S. Kuraoka, and S. Takenaka, *Chem. Lett.*, **1984**, 281; O. Tsuge, S. Kanemasa, S. Takenaka, and S. Kuraoka, *ibid.*, **1984**, 465; O. Tsuge, S. Kanemasa, and S. Takenaka, *Bull. Chem. Soc. Jpn.*, **60**, 1489 (1987).

4) O. Tsuge, S. Kanemasa, and S. Takenaka, *J. Org. Chem.*, **51**, 1853 (1986); O. Tsuge, S. Kanemasa, and S. Takenaka, *Bull. Chem. Soc. Jpn.*, **59**, 3631 (1986).

5) R. Sustmann, *Tetrahedron Lett.*, **1971**, 2717.

6) Cycloadditions of azomethine ylides to the following olefins of nonactivated types are known: with norbornene: R. Huisgen, W. Scheer, G. Szeimies, and H. Huber, *Tetrahedron Lett.*, **1966**, 397; J. A. Deyrup and G. S. Kuta, *J. Org. Chem.*, **43**, 501 (1978). With acenaphthylene: R. Huisgen, H. Gotthardt, and H. O. Bayer, *Chem. Ber.*, **103**, 2368 (1970); R. Grigg and S. Thianpatanagul, *J. Chem. Soc., Chem. Commun.*, **1984**, 180. With styrene: O. Tsuge, S. Kanemasa, M. Ohe, and S. Takenaka, *Chem. Lett.*, **1986**, 973; O. Tsuge, S. Kanemasa, M. Ohe, and S. Takenaka, *Bull. Chem. Soc. Jpn.*, **60**, 4079 (1987). With vinylene carbonate and vinyl ethers: P. Deshong, D. A. Kell, and D. R. Sidler, *J. Org. Chem.*, **50**, 2309 (1985); P. Deshong, D. R. Sidler, D. A. Kell, and N. N. Aronson, Jr., *Tetrahedron Lett.*, **26**, 3734 (1985).

7) Nonstabilized azomethine ylides generated from *N*-oxides and an alkyllithium are highly reactive to nonactivated olefins: R. Beugelmans, G. Negron, and G.

Roussi, *J. Chem. Soc., Chem. Commun.*, **1983**, 31; J. Chastanet and G. Roussi, *Heterocycles*, **23**, 653 (1985); R. Beugelmans, L. B.-Iguertsira, J. Chastanet, G. Negron, and G. Roussi, *Can. J. Chem.*, **63**, 725 (1985); J. Chastanet and G. Roussi, *J. Org. Chem.*, **50**, 2910 (1985).

8) R. Huisgen and K. Niklas, *Heterocycles*, **22**, 21 (1984).

9) N. S. Basketter and A. O. Plunkett, *J. Chem. Soc., Chem. Commun.*, **1973**, 188.

10) O. Tsuge, S. Kanemasa, and S. Takenaka, *Heterocycles*, **20**, 1907 (1983).

11) The ylide **1b** decomposes quite readily when heated in DMF at 110 °C. Only (*Z*)-stilbene was recovered in a good yield after the reaction in DMF.

12) Homolytic dehydrogenation by DDQ has been already discussed: A. J. Fatiadi, "Preparation and Synthetic Applications of Cyano Compounds," as chapter 26 of "The Chemistry of Triple-Bonded Functional Groups," ed by S. Patai and Z. Rappoport, John Wiley and Sons, Chichester, New York, Brisbane, Toronto, Singapore (1983), p. 1210.

13) K. N. Houk, J. Sims, R. E. Duke, Jr., R. W. Strozier, and J. K. George, *J. Am. Chem. Soc.*, **95**, 7287 (1973); K. N. Houk, J. Sims, C. R. Watts, and L. J. Luskus, *ibid.*, **95**, 7301 (1973); K. N. Houk, *Acc. Chem. Res.*, **8**, 361 (1975).

14) G. Surpateanu and A. L.-Combier, *Heterocycles*, **22**, 2079 (1984).

15) W. J. Linn, O. W. Webster, and R. E. Benson, *J. Am. Chem. Soc.*, **87**, 3651 (1965).

16) Y. Kobayashi, T. Kutsumura, K. Morinaga, M. Fugita, and Y. Hanzawa, *Chem. Pharm. Bull.*, **18**, 2489 (1970).

Stereoselective Syntheses of 1,3,5-Trihydroxy-2,4-dimethylpentane Equivalents from Methyl α-Mannopyranosides

Kuniaki TATSUTA,* Yoshihito KOGUCHI, and Motohiro KASE
Department of Applied Chemistry, Faculty of Science and Technology, Keio University, Hiyoshi, Kohoku, Yokohama 223
(Received February 12, 1988)

The optically active 1,3,5-trihydroxy-2,4-dimethylpentane equivalents: methyl 2,4-dideoxy-2,4-di-*C*-methyl-α-D-ido- and talopyranosides and their enantiomers, which should be suitable for the syntheses of propionate-derived natural products, were stereo- and regioselectively prepared from methyl α-D- and L-mannopyranosides through the reactions of the 3,4-anhydro-2-*O*-mesyl- and 3,4-anhydro-2-*C*-methyl-altropyranoside derivatives with methylmagnesium bromide and methylmagnesium chloride.

In recent years an impressive number of natural products have been synthesized from carbohydrate derivatives.[1] The syntheses have required fragments with the correct relative and absolute configurations, together with functionality which allows them to be incorporated into the synthetic schemes. Especially, such chiral fragments as 1,3,5-trihydroxy-2,4-dimethylpentane units **1** and **2** can be found in the structures of biologically active natural products including erythromycin A,[2] monensin,[3] rifamycin S,[4] ionomycin,[5] and tirandamycin.[6] Several methods have been developed to affect these stereoselective syntheses by mainly using 1,6-anhydro-β-D-glucopyranose[7] as a chiral source, although alternative strategies including aldol type reactions[8] have been recently reported.

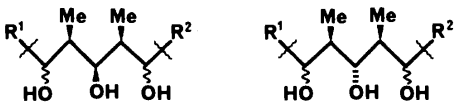

In this paper, we report the novel stereoselective syntheses of such fragment equivalents (**12ab**, **14ab**, **15**, and **16**) and their enantiomers from readily and enantiomerically available methyl α-mannopyranoside derivatives. Repeated alkylation of the intermediary epoxides with methylmagnesium bromide–*t*-butyl bromide and methylmagnesium chloride–CuCl[7c] reagents results in the stereo- and regiospecific introduction of *C*-methyl groups through the trans diaxial opening of their epoxide rings.

The study commenced with the synthesis of the 6-deoxy derivatives **12a** (in the a-series, R=H) and **14a** from methyl α-D-mannopyranoside (**3**). Methyl α-D-mannopyranoside (**3**) was converted by the published procedure[9] into the corresponding 6-iodo compound **4**, which was mesylated to give exclusively the 2,3-di-*O*-mesyl derivative **5** in a quantitative yield. The compound **5** was dehalogenated by tributylstannane to methyl 6-deoxy-2,3-di-*O*-mesyl-α-D-mannopyranoside (**6a**).

The corresponding L-enantiomer (**6'a**) of **6a** could be directly obtained by mesylation of methyl α-L-rhamnopyranoside[10] in a 90% yield for the L-series.

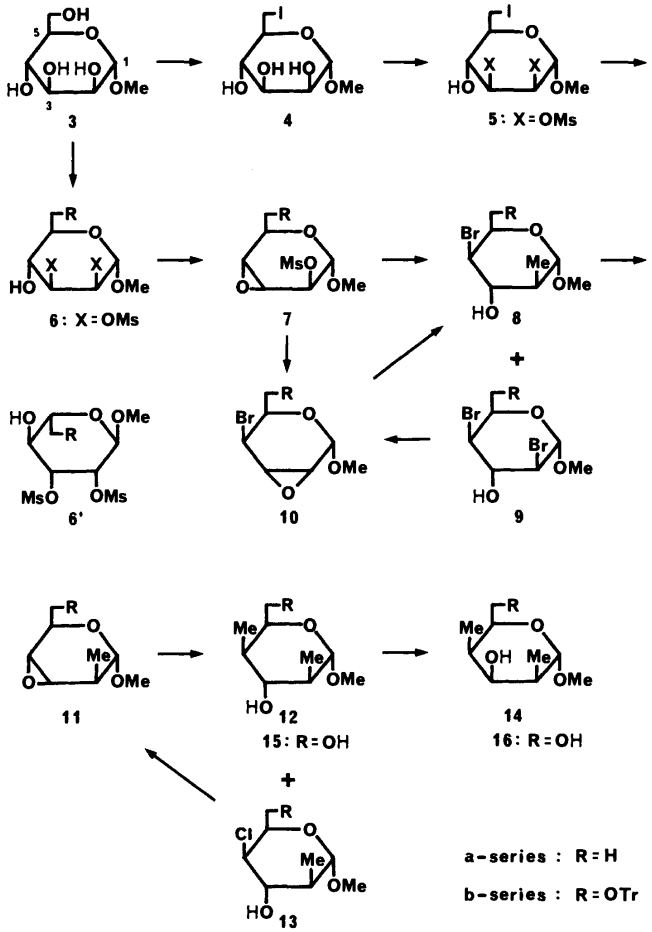

The compound **6a** was treated with sodium methoxide to give methyl 3,4-anhydro-6-deoxy-2-*O*-mesyl-α-D-altropyranoside (**7a**) in an 86% yield. Treatment of the 3,4-epoxide **7a** in dichloromethane with an ethereal methylmagnesium bromide solution and *t*-butyl bromide gave methyl 4-bromo-2,4,6-trideoxy-2-*C*-methyl-α-D-idopyranoside (**8a**) and methyl 2,4-dibromo-2,4,6-trideoxy-α-D-idopyranoside (**9a**) in 56 and 29% yields, respectively, both of which could be reasonably formed by the following sequence: (i) an attack of the Br anion on the C-4 position with the first diaxial opening of the epoxide; (ii) an adjacent attack of the intermediary hydroxide anion on the C-2 position with the *O*-mesyl group leaving to give the

2,3-epoxide **10a**; (iii) an attack of the methyl anion or Br anion on the C-2 position with the second diaxial opening of the epoxide to give **8a** and **9a**. This epoxide-swinging reaction could be traced by the stepwise reactions as follows. The compound **7a** reacted with LiBr to give the same methyl 2,3-anhydro-4-bromo-4,6-dideoxy-α-D-gulopyranoside (**10a**) in an 80% yield, which was converted into the compounds **8a** and **9a** in 62 and 24% yields by the aforesaid conditions using methylmagnesium bromide and *t*-butyl bromide. Then, the by-product **9a** was selectively led to the 2,3-epoxide **10a** by treatment with sodium methoxide in an 83% yield and recycled to the desired compound **8a**.

In the transformation of **7a** into **8a**, other couples[7] of organometallic reagents (methylmagnesium iodide, methylmagnesium bromide, methylmagnesium chloride, lithium dimethylcuprate(I) and methyllithium) and additives (tetrabutylammonium bromide, LiBr, CuI, CuBr, CuCl, $MgBr_2$, Li_2CuCl_4, phenylmagnesium iodide, phenylmagnesium chloride, *t*-butyl bromide, and trimethylsilyl bromide) were investigated in several solvents (ether, dichloromethane, dibromomethane, THF, and dioxane), but they gave **8a** only in lower yields.

The compound **8a** was converted by NaH into the 3,4-epoxide, methyl 3,4-anhydro-2,6-dideoxy-2-*C*-methyl-α-D-altropyranoside (**11a**) in an 85% yield, which was treated with methylmagnesium chloride and CuCl in THF to give methyl 2,4,6-trideoxy-2,4-di-*C*-methyl-α-D-idopyranoside **12a** and methyl 4-chloro-2,4,6-trideoxy-2-*C*-methyl-α-D-idopyranoside **13a** in 60 and 28% yields, respectively, as results of the diaxial opening of the epoxide. Also, in the latter reaction, a large number of variables[7] including reagents, additives and solvents were assayed as mentioned above, but in vain. The by-product **13a** was recycled to **12a** through **11a**, which was obtained by treatment with NaH.

The stereochemistry of **12a** was confirmed by the ^1H NMR analysis. In the $CDCl_3$ solution, the spectrum showed $J_{1,2}$=4.0 Hz, $J_{2,3}=J_{3,4}$=5.5 Hz, and $J_{4,5}$=4.5 Hz, supporting that the idopyranoside **12a** could exist in the C_1^4 chair form[11] (Fig. 1) due to an intramolecular hydrogen-bond between the C-1 and C-3 position, as suggested by Lemieux and Levine,[12] rather than other possible conformations including the C_4^1 chair form.[11] However, in the deuterated acetone solution, the spectrum showed $J_{1,2}$=7.4 Hz, $J_{2,3}=J_{3,4}$=9.1 Hz, and $J_{4,5}$=5.6 Hz, indicating that **12a** existed in the C_4^1 form as shown in Fig. 1.[12]

Inversion of the stereochemistry at the C-3 position of **12a** was cleanly achieved by oxidation to the corresponding ketone with pyridinium chlorochromate followed by borohydride reduction to give methyl 2,4,6-trideoxy-2,4-di-*C*-methyl-α-D-talopyranoside (**14a**) in an 82% yield with a little of **12a**. The coupling constants ($J_{1,2}$=3.5 Hz, $J_{2,3}=J_{3,4}$=4.8 Hz, and $J_{4,5}$=4.2 Hz) in the $CDCl_3$ solution supported that **14a** was favoured in the C_1^4 chair form spread by a strong repulsion between the C-2 and C-4 methyl groups. Consequently, **12a** and **14a** are equivalent to the pentane units **1** and **2**, respectively.

The corresponding L-isomers of **12a** and **14a**, which are equivalent to the antipodes of **1** and **2**, were derived from methyl α-L-rhamnoside through **6'a** by the same conditions as described above.

On the other hand, the 6-hydroxy derivatives **15** and **16** were also synthesized from methyl α-D-mannopyranoside (**3**) by the similar manner with the aforesaid sequences.

Tritylation of **3** followed by mesylation afforded methyl 2,3-di-*O*-mesyl-6-*O*-trityl-α-D-mannopyranoside (**6b**: in the b-series, R=OTr), which was converted into the 3,4-epoxide (**7b**) in a 73% overall yield. The epoxide **7b** was treated with methylmagnesium bromide and *t*-butyl bromide to give methyl 4-bromo-2,4-dideoxy-2-*C*-methyl-6-*O*-trityl-α-D-idopyranoside (**8b**) and methyl 2,4-dibromo-2,4-dideoxy-6-*O*-trityl-α-D-idopyranoside (**9b**) in 55 and 27% yields, respectively. The latter product **9b** was recycled into **8b** through **10b** in a 54% overall yield as described in the recovery of **8a** through **10a**. Reaction of **8b** with NaH afforded the 3,4-epoxide **11b** in an 89% yield, which was treated with methylmagnesium chloride and CuCl to give methyl 2,4-dideoxy-2,4-di-*C*-methyl-6-*O*-trityl-α-D-idopyranoside (**12b**) and methyl 4-chloro-2,4-dideoxy-2-*C*-methyl-6-*O*-trityl-α-D-idopyranoside (**13b**) in 60 and 29% yields. The by-product **13b** was also recycled to **12b** through **11b**. The compound **12b** was transferred into the C-3 epimer **14b** by pyridinium chlorochromate oxidation and borohydride reduction. Removal of *O*-trityl group in **12b** and **14b** by acidic conditions did not give the desired products **15** and **16**, but the

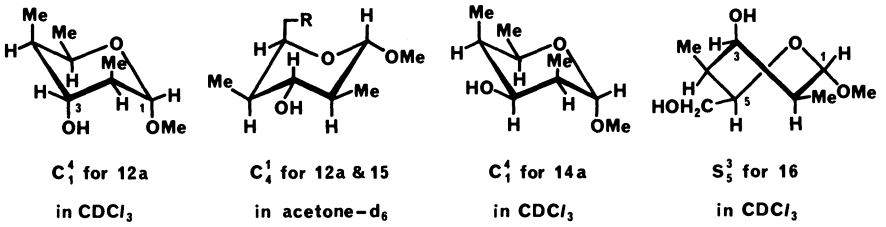

Fig. 1. Preferred conformations of **12a**, **14a**, **15**, and **16** in $CDCl_3$ or acetone-d_6.

corresponding 1,6-anhydro derivatives. Then, by hydrogenolysis with palladium hydroxide, methyl 2,4-dideoxy-2,4-di-*C*-methyl-α-D-ido- and talopyranosides (**15** and **16**) were obtained in 75 and 87% yields, respectively.

The stereochemistry of **15** and **16** was confirmed by their ^{1}H NMR spectra, the coupling constants (see the Experimental section) of which revealed that **15** existed in the C_4^1 chair form in the deuterated acetone solution and **16** in the S_5^3-like skew conformation[11] in the $CDCl_3$ solution as shown in Fig. 1. Hence, **15** and **16** are equivalent to the chiral units **1** and **2**, respectively.

The enantiomers of **15** and **16** could be reasonably derived from methyl α-L-mannopyranoside by the same reaction sequences to generate the antipode units of **1** and **2**.

In conclusion, an efficient, stereo- and regiospecific preparation of synthetic equivalents of the structural fragments **1** and **2** and their enantiomeric fragments have been developed, starting from methyl α-D- and L-mannopyranosides.

Experimental

Melting points were determined on a micro hot-stage Yanaco MP-S3 and were uncorrected. Optical rotations were measured with a JASCO DIP-360 photoelectric polarimeter in chloroform unless otherwise stated. IR spectra were recorded on a Hitachi Perkin-Elmer 225 spectrometer, and ^{1}H NMR spectra on a Varian EM-390, a Bruker WM 250 or a JEOL GX-400 spectrometer in $CDCl_3$ using TMS as internal standard unless otherwise noted. Mass spectra were measured with a Hitachi M-80 mass spectrometer or a Hitachi RMU-6M mass spectrometer. TLC was carried out on Merck TLC plates (60F-254, 0.25 mm). Column chromatography was performed on silica gel, Wakogel C-200. In general, organic solvents were purified and dried by the appropriate procedures, and evaporation and concentration were carried out under reduced pressure below 35 °C, unless otherwise noted.

Methyl 6-Deoxy-6-iodo-2,3-di-*O*-mesyl-α-D-mannopyranoside (5). The starting methyl 6-deoxy-6-iodo-α-D-mannopyranoside (**4**) was prepared from methyl α-D-mannopyranoside (**3**) according to the reported procedure.[9]

To a stirred and ice-cooled solution of **4** (88.8 g) in pyridine (620 ml) were added 4-dimethylaminopyridine (17.8 g) and mesyl chloride (68 ml), and stirring was continued at room temperature for 24 h. After addition of ethanol (52 ml), the mixture was evaporated and co-evaporated with toluene to a residue, which was partitioned between ethyl acetate and a saturated aqueous $NaHCO_3$ solution. The combined layers were evaporated to a residue, which was chromatographed on silica gel (670 g) with 2:1 benzene–ethyl acetate to give an amorphous solid of **5** (130.8 g, 97%): R_f 0.36 (2:1 benzene–ethyl acetate); $[\alpha]_D^{31}$ +29° (*c* 0.60); IR (KBr): 1350 cm^{-1} (OMs); ^{1}H NMR (400 MHz): δ=2.79 (1H, d, OH-4, $J_{4,OH}$=4.5 Hz), 3.15 and 3.17 (each 3H, s, Ms), 3.37 (1H, dd, H-6, $J_{5,6}$=7.7 Hz, $J_{6,6'}$=10.9 Hz), 3.48 (3H, s, OMe), 3.56 (1H, ddd, H-5, $J_{4,5}$=9.5 Hz, $J_{5,6'}$=2.9 Hz), 3.63 (1H, dd, H-6′), 3.82 (1H, dt, H-4, $J_{3,4}$=9.5 Hz), 4.92 (1H, d, H-1, $J_{1,2}$=1.6 Hz), 4.92 (1H, dd, H-3, $J_{2,3}$=3.5 Hz), and 4.96 (1H, dd, H-2); MS *m/z* 460 (M$^+$).

Methyl 6-Deoxy-2,3-di-*O*-mesyl-α-D-mannopyranoside (6a). A solution of **5** (58.2 g) in toluene (466 ml) was stirred with tributylstannane (51.2 ml) and α,α′-azobis(isobutyronitrile) (2.08 g) at 90 °C for 3 h under argon. The resulting solution was evaporated and co-evaporated with ethyl acetate to a solid, which was recrystallized from ethyl acetate–hexane to give a solid of **6a** (36.7 g, 87%), which was used for the next step.

An analytically pure sample was obtained by chromatography on silica gel with 3:2 benzene–ethyl acetate followed by recrystallization from ether to afford cubes of **6a**: R_f 0.31 (2:1 benzene–ethyl acetate); mp 143—145 °C; $[\alpha]_D^{34}$ +6.9° (*c* 0.94); IR (KBr): 1347 cm^{-1} (OMs); ^{1}H NMR (400 MHz): δ=1.38 (3H, d, Me-5, $J_{5,Me}$=6.0 Hz), 2.64 (1H, d, OH-4, $J_{4,OH}$), 3.15 and 3.17 (each 3H, s, Ms), 3.41 (3H, s, OMe), 3.66 (1H, dt, H-4, $J_{3,4}$=9.4 Hz, $J_{4,5}$=9.4 Hz), 3.74 (1H, dq, H-5), 4.83 (1H, d, H-1, $J_{1,2}$=1.6 Hz), 4.85 (1H, dd, H-3, $J_{2,3}$=3.0 Hz), and 4.92 (1H, dd, H-2).

Found: C, 32.50; H, 5.32%. Calcd for $C_9H_{18}O_9S_2$: C, 32.33; H, 5.43%.

Methyl 6-Deoxy-2,3-di-*O*-mesyl-α-L-mannopyranoside (6′a). A solution of methyl α-L-rhamnopyranoside[10] (0.94 g) in pyridine (9.4 ml) was stirred with mesyl chloride (0.86 ml) at room temperature for 4 h. After addition of ethanol (1 ml), the resulting mixture was evaporated and co-evaporated with toluene to a residue, which was chromatographed on silica gel with 15:1 chloroform–methanol followed by recrystallization from ether to give cubes of **6′a** (1.61 g, 90%): mp 142—145 °C; $[\alpha]_D^{30}$ −6.9° (*c* 1.0). The physicochemical properties were identical with those of **6a** except for the sign of the optical rotation.

Methyl 3,4-Anhydro-6-deoxy-2-*O*-mesyl-α-D-altropyranoside (7a). A solution of **6a** (7.93 g) in chloroform (79 ml) was stirred with a 28% methanolic sodium methoxide solution (6.0 ml) at room temperature for 48 h. The reaction mixture was partitioned between chloroform and water, and the combined organic layers were dried and evaporated to a residue. This was chromatographed on silica gel (85 g) with 4:1 benzene–ethyl acetate followed by recrystallization from ethyl acetate–hexane to give plates of **7a** (4.85 g, 86%): R_f 0.55 (2:1 benzene–ethyl acetate); mp 88—90 °C; $[\alpha]_D^{33}$ +64° (*c* 0.98); IR (KBr): 1345 cm^{-1} (OMs); ^{1}H NMR (400 MHz): δ=1.45 (3H, d, Me-5, $J_{5,Me}$=7.2 Hz), 3.09 (1H, d, H-4, $J_{3,4}$=3.5 Hz, $J_{4,5}$=0 Hz), 3.12 (3H, s, OMs), 3.42 (3H, s, OMe), 3.44 (1H, d, H-3, $J_{2,3}$=0 Hz), 4.31 (1H, q, H-5), 4.56 and 4.63 (each 1H, d, H-1 and H-2, vice versa, $J_{1,2}$=4.2 Hz).

Found: C, 40.34; H, 5.86%. Calcd for $C_8H_{14}O_6S$: C, 40.33; H, 5.92%.

Methyl 4-Bromo-2,4,6-trideoxy-2-*C*-methyl-α-D-idopyranoside (8a) and Methyl 2,4-Dibromo-2,4,6-trideoxy-α-D-idopyranoside (9a). A) From 7a: To a stirred and ice-cooled solution of **7a** (105 mg) in dichloromethane (0.53 ml) were added *t*-butyl bromide (0.149 ml) and dropwise a 3 M† ethereal methylmagnesium bromide solution (1.48 ml) under argon, and stirring was continued at the same temperature for 15 min and then at room temperature for 2.5 h. After the reaction was quenched with a saturated aqueous NH_4Cl solution (1.5 ml), the reaction mixture was extracted with ethyl acetate (1.5 ml×3). The combined

† 1 M=1 mol dm^{-3}.

extracts were dried and evaporated to a residue, which was chromatographed on silica gel (10 g) with 6:1 benzene–ethyl acetate to give **8a** (59 mg, 56%) and **9a** (39 mg, 29%) having the R_f-values of 0.35 and 0.48 (6:1 benzene–ethyl acetate) respectively.

8a: Needles from ether–hexane; mp 116—118 °C; $[\alpha]_D^{34}$ +114° (*c* 0.93); ^{1}H NMR (400 MHz): δ=1.28 (3H, d, Me-2, $J_{2,Me}$=7.4 Hz), 1.37 (3H, d, Me-5, $J_{5,Me}$=6.7 Hz), 1.95 (1H, m, H-2), 3.33 (1H, d, OH, $J_{3,OH}$=8.0 Hz), 3.41 (3H, s, OMe), 3.92 (1H, dt, H-3, $J_{2,3}$=$J_{3,4}$=4.8 Hz), 4.04 (1H, dd, H-4, $J_{4,5}$=3.5 Hz), 4.28 (1H, dq, H-5), 4.51 (1H, d, H-1, $J_{1,2}$=3.5 Hz).

Found: C, 40.02; H, 6.16%. Calcd for $C_8H_{15}O_3Br$: C, 40.19; H, 6.32%.

9a: Needles from ether–hexane; mp 95—97 °C; $[\alpha]_D^{27}$ +72° (*c* 0.67); ^{1}H NMR (400 MHz): δ=1.48 (3H, d, Me-5, $J_{5,Me}$=7.0 Hz), 2.88 (1H, broad d, OH, $J_{3,OH}$=3.8 Hz), 3.49 (3H, s, OMe), 3.76 (1H, dd, H-2, $J_{1,2}$=7.4 Hz, $J_{2,3}$=8.6 Hz), 4.07 (1H, dd, H-4, $J_{3,4}$=8.6 Hz, $J_{4,5}$=5.4 Hz), 4.12 (1H, dt, H-3), 4.37 (1H, dq, H-5), 4.80 (1H, d, H-1).

Found: C, 27.93; H, 3.97%. Calcd for $C_7H_{12}O_3Br_2$: C, 27.66; H, 3.98%.

B) From 10a: To a stirred and ice-cooled solution of **10a** (3.80 g) in dichloromethane (19 ml) was added dropwise a 3 M ethereal methylmagnesium bromide solution (42 ml) under argon, and stirring was continued at room temperature for 2 h. After the reaction was quenched with a saturated aqueous NH_4Cl solution (38 ml), the mixture was partitioned between ethyl acetate and water. The combined organic layers were dried and evaporated to a residue, which was chromatographed on silica gel (133 g) with 7:1 benzene–ethyl acetate to give **8a** (2.52 g, 62%) and **9a** (1.23 g, 24%).

Methyl 2,3-Anhydro-4-bromo-4,6-dideoxy-α-D-gulopyranoside (10a). A) From 7a: A solution of **7a** (4.29 g) in 1,4-dioxane (43 ml) was stirred with LiBr (3.13 g) under argon at 100 °C for 68 h. The salt was filtered and washed with dichloromethane. The filtrates and washings were combined and partitioned between dichloromethane and water. The combined organic layers were dried and evaporated to a residue, which was chromatographed on silica gel (80 g) with 4:1 hexane–ethyl acetate to give a solid of **10a** (3.20 g, 80%), which was used for the next step.

An analytically pure sample was obtained by distillation under reduced pressure (bath temp 85 °C/4 mmHg††) as a syrup which was changed into cubes of **10a**: R_f 0.60 (5:1 benzene–ethyl acetate); mp 56 °C; $[\alpha]_D^{32}$ −14° (*c* 1.0); ^{1}H NMR (90 MHz): δ=1.30 (3H, d, Me-5, $J_{5,Me}$=7 Hz), 3.60 (1H, m, H-3), 3.65 (3H, s, OMe), 3.82 (1H, dd, H-2, $J_{1,2}$=3.3 Hz, $J_{2,3}$=2.7 Hz), 4.16 (1H, dq, H-5, $J_{4,5}$=2 Hz), 4.41 (1H, t, H-4, $J_{3,4}$=2 Hz), and 5.17 (1H, d, H-1).

Found: C, 37.42; H, 4.86%. Calcd for $C_7H_{11}O_3Br$: C, 37.69; H, 4.97%.

B) From 9a: A solution of **9a** (6.47 g) in 1,4-dioxane (97 ml) was stirred with a 28% methanolic sodium methoxide solution (5.2 ml) at room temperature for 1 h. The reaction mixture was partitioned between chloroform and water, and the combined organic layers were dried and evaporated to a residue. This was chromatographed on silica gel (145 g) with 5:1 hexane–ethyl acetate to give a solid of **10a** (3.94 g, 83%).

Methyl 3,4-Anhydro-2,6-dideoxy-2-*C*-methyl-α-D-altropyranoside (11a). A) From 8a: A solution of **8a** (3.06 g) in 1,2-dimethoxyethane (46 ml) was stirred with a 55% oily NaH powder (670 mg) at room temperature for 30 min. After addition of ethanol (1 ml), the resulting mixture was partitioned between ethyl acetate and a saturated aqueous NaCl solution, and the combined organic layers were dried and evaporated under atmospheric pressure to give a residue. This was purified by distillation under reduced pressure (bath temp 86 °C/2—3 mmHg) to give a syrup of **11a** (1.71 g, 85%): R_f 0.32 (6:1 benzene–ethyl acetate); bp ca. 66 °C (2 mmHg); $[\alpha]_D^{32}$ +122° (*c* 0.54); ^{1}H NMR (90 MHz): δ=1.17 (3H, d, Me-2, $J_{2,Me}$=7.5 Hz), 1.44 (3H, d, Me-5, $J_{5,Me}$=7.2 Hz), 2.27 (1H, dq, H-2, $J_{1,2}$=3.0 Hz, $J_{2,3}$=0 Hz), 3.11 (2H, apparently s, H-3 and H-4, $J_{3,4}$=4 Hz), 3.50 (3H, s, OMe), 4.38 (1H, q, H-5, $J_{4,5}$=0 Hz), and 4.43 (1H, d, H-1). MS *m/z* 127 (M^+−31).

B) From 13a: A sample of **13a** (611 mg) was treated by the procedure described in the preparation from **8a** and then worked up to give a syrup of **11a** (432 mg, 87%).

Methyl 2,4,6-Trideoxy-2,4-di-*C*-methyl-α-D-idopyranoside (12a) and Methyl 4-Chloro-2,4,6-trideoxy-2-*C*-methyl-α-D-idopyranoside (13a). A 3 M methylmagnesium chloride solution (37 ml), which was prepared in situ from magnesium (2.7 g) and a large excess of methyl chloride in THF, was added dropwise to a suspension of **11a** (1.60 g) with CuCl (400 mg) in THF (8 ml) with stirring at 5 °C under argon, and then stirring was continued at room temperature for 18 h. After the reaction was quenched with a saturated aqueous NH_4Cl solution (50 ml), the resulting mixture was partitioned between ethyl acetate and water. The combined organic layers were dried and evaporated to a residue, which was chromatographed on silica gel (88 g) with 5:2 benzene–ethyl acetate to give **12a** (1.05 g, 60%) and **13a** (0.55 g, 28%) having the R_f-values of 0.19 and 0.36 (3:1 hexane–ethyl acetate) respectively.

12a: Needles from ethyl acetate–hexane; mp 102—104 °C; $[\alpha]_D^{35}$ +111° (*c* 1.04); ^{1}H NMR (400 MHz): δ=1.00 and 1.08 (each 3H, d, Me-2 and Me-4, vice versa, *J*=7.0 and 7.4 Hz), 1.17 (3H, d, Me-5, $J_{5,Me}$=6.8 Hz), 1.77 (2H, m, H-2 and H-4), 2.62 (1H, d, OH, $J_{3,OH}$=8.2 Hz), 3.40 (1H, dt-like, H-3, $J_{2,3}$=$J_{3,4}$=5.5 Hz), 3.40 (3H, s, OMe), 4.23 (1H, dq, H-5, $J_{4,5}$=4.5 Hz), and 4.40 (1H, d, H-1, $J_{1,2}$=4.0 Hz); ^{1}H NMR (400 MHz, acetone-d_6): δ=0.93, 1.01, and 1.12 (each 3H, d, Me-2, Me-4, and Me-5, vice versa, *J*=7.2 Hz, *J*=6.7 Hz, and *J*=6.7 Hz), 1.44 (1H, m, H-2), 1.68 (1H, m, H-4), 2.80 (1H, broad s, OH), 3.10 (1H, t, $J_{2,3}$=$J_{3,4}$=9.1 Hz), 3.32 (3H, s, OMe), 4.08 (1H, dq, H-5, $J_{4,5}$=5.6 Hz, $J_{5,Me}$=6.7 Hz), and 4.22 (1H, d, H-1, $J_{1,2}$=7.4 Hz).

Found: C, 61.84; H, 10.23%. Calcd for $C_9H_{18}O_3$: C, 62.04; H, 10.41%.

13a: Needles from ether–hexane: mp 93—94 °C; $[\alpha]_D^{32}$ +117° (*c* 0.91); ^{1}H NMR (400 MHz): δ=1.25 (3H, d, Me-2, $J_{2,Me}$=7.5 Hz), 1.34 (3H, d, Me-5, $J_{5,Me}$=6.5 Hz), 1.97 (1H, m, H-2), 3.40 (3H, s, OMe), 3.43 (1H, d, OH, $J_{3,OH}$=8.0 Hz), 3.85 (1H, m, H-3), 3.91 (1H, dd, H-4, $J_{3,4}$=3.5 Hz, $J_{4,5}$=3.0 Hz), 4.40 (1H, dq, H-5), and 4.56 (1H, d, H-1, $J_{1,2}$=2.3 Hz).

Found: C, 49.09; H, 7.58%. Calcd for $C_8H_{15}O_3Cl$: C, 49.36; H, 7.77%.

Methyl 2,4,6-Trideoxy-2,4-di-*C*-methyl-α-D-talopyranoside (14a). To a stirred and ice-cooled solution of **12a** (22.4 mg)

†† 1 mmHg≅133.322 Pa.

in dichloromethane (0.45 ml) were added Molecular Sieves 3A powder (193 mg) and pyridinium chlorochromate (111 mg), and stirring was continued at room temperature for 1 h. The mixture was diluted with ether and passed through a silica-gel column (1.0 g) with ether to give a crude syrup (23 mg) of the keto compound.

The syrup was stirred with $NaBH_4$ (9.7 mg) in methanol (0.49 ml) at room temperature for 1 h. The reaction mixture was neutralized with Amberlite CG-50 (H type), filtered and then evaporated to a residue, which was chromatographed on silica gel (2.2 g) with 3:1 hexane–ethyl acetate to afford **14a** (18 mg, 82%) and the starting **12a** (2.2 mg, 10%) having R_f-values of 0.24 and 0.19 (3:1 hexane–ethyl acetate) respectively.

14a: syrup; $[\alpha]_D^{31}$ +107° (*c* 0.69); ^{1}H NMR (400 MHz): δ=0.97 and 1.05 (each 3H, d, Me-4 and Me-2, $J_{4,Me}=J_{2,Me}$=7.2 Hz), 1.22 (3H, d, Me-5, $J_{5,Me}$=6.7 Hz), 1.51 (1H, broad s, OH), 1.90 (2H, m, H-2 and H-4), 3.36 (3H, s, OMe), 3.99 (1H, t, H-3, $J_{2,3}=J_{3,4}$=4.8 Hz), 4.04 (1H, dq, H-5, $J_{4,5}$=4.2 Hz), and 4.51 (1H, d, H-1, $J_{1,2}$=3.5 Hz). HRMS Found: *m/z* 174.1229. Calcd for $C_9H_{18}O_3$: M, 174.1255.

Methyl 3,4-Anhydro-2-*O*-mesyl-6-*O*-trityl-α-D-altropyranoside (7b). To a stirred and ice-cooled solution of **3** (40.4 g) in pyridine (400 ml) were added 4-dimethylaminopyridine (1.26 g) and trityl chloride (63.2 g), and stirring was continued at room temperature for 24 h. After cooling again, mesyl chloride (33.7 ml) was added, and the resulting mixture was allowed to stand with stirring at room temperature for 8 h. After addition of ethanol (23 ml), the mixture was evaporated and co-evaporated with toluene to a residue, which was partitioned between ethyl acetate and a saturated aqueous $NaHCO_3$ solution. The combined organic layers were washed with a saturated aqueous NaCl solution, dried, and evaporated to give a crude syrup of **6b** (approximately 150 g): R_f 0.28 (6:1 benzene–ethyl acetate).

To an ice-cooled solution of the crude syrup in chloroform (750 ml) was added dropwise a 28% methanolic sodium methoxide solution (65.7 ml) with stirring, and the mixture was stirred at room temperature for 14 h and then partitioned between chloroform and water. The combined organic layers were washed with water, dried and evaporated to a residue, which was chromatographed on silica gel (1 kg) with 10:1 benzene–ethyl acetate followed by recrystallization from benzene–ethyl acetate to give cubes of **7b** (75.4 g. 73% overall yield from **3**): R_f 0.30 (20:1 benzene–ethyl acetate); mp 150—151 °C; $[\alpha]_D^{31}$ +17° (*c* 1.0); IR (KBr): 1367 and 1176 cm^{-1} (OMs); ^{1}H NMR (400 MHz): δ=3.09 (3H, s, Ms), 3.27 (1H, d, H-4, $J_{3,4}$=3.5 Hz, $J_{4,5}$=0 Hz), 3.37 (3H, s, OMe), 3.47 (1H, dd, H-6, $J_{5,6}$=4.3 Hz, $J_{6,6'}$=10.3 Hz), 3.51 (1H, dd, H-6′, $J_{5,6'}$=4.3 Hz), 3.53 (1H, d, H-3, $J_{2,3}$=0 Hz), 4.22 (1H, t, H-5), 4.65 (1H, d, H-1, $J_{1,2}$=4.5 Hz), 4.82 (1H, d, H-2), and 7.24—7.47 (15H, m, Tr).

Found: C, 65.10; H, 5.60%. Calcd for $C_{27}H_{28}O_7S$: C, 65.31; H, 5.68%.

Methyl 4-Bromo-2,4-dideoxy-2-*C*-methyl-6-*O*-trityl-α-D-idopyranoside (8b) and Methyl 2,4-Dibromo-2,4-dideoxy-6-*O*-trityl-α-D-idopyranoside (9b). A) From 7b: A sample of **7b** (1.26 g) was treated by the procedure described in the preparation of **8a** and **9a** from **7a**, and then worked up to give amorphous solids of **8b** (694 mg, 55%) and **9b** (386 mg, 27%) having the R_f-values of 0.41 and 0.47 (20:1 benzene–ethyl acetate) respectively.

8b: $[\alpha]_D^{27}$ +25° (*c* 1.0); ^{1}H NMR (400 MHz): δ=1.27 (3H, d, Me-2, $J_{2,Me}$=7.2 Hz), 1.99 (1H, m, H-2), 3.24 (1H, dd, H-6, $J_{5,6}$=4.8 Hz, $J_{6,6'}$=9.8 Hz), 3.43 (3H, s, OMe), 3.44 (1H, d, OH, $J_{3,OH}$=8.0 Hz), 3.52 (1H, dd, H-6′, $J_{5,6'}$=6.7 Hz), 3.91 (1H, dt, H-3, $J_{2,3}=J_{3,4}$=3.2 Hz), 4.02 (1H, t, H-4, $J_{4,5}$=3.2 Hz), 4.14 (1H, m, H-5), 4.57 (1H, broad s, H-1, $J_{1,2}$=0 Hz), and 7.22—7.49 (15H, m, Tr); MS *m/z* 498 and 496 (M$^+$).

9b: $[\alpha]_D^{31}$ +37° (*c* 1.0); ^{1}H NMR (400 MHz): δ=2.96 (1H, d, OH, $J_{3,OH}$=5.2 Hz), 3.49 (3H, s, OMe), 3.52 (1H, dd, H-6, $J_{5,6}$=3.8 Hz, $J_{6,6'}$=10.7 Hz), 3.63 (1H, dd, H-6′, $J_{5,6'}$=5.4 Hz), 3.78 (1H, dd, H-2, $J_{1,2}$=6.4 Hz, $J_{2,3}$=7.5 Hz), 4.04 (1H, dd, H-4, $J_{3,4}$=7.5 Hz, $J_{4,5}$=4.6 Hz), 4.15 (1H, m, H-5), 4.37 (1H, dt, H-3), 5.10 (1H, d, H-1), and 7.23—7.49 (15H, m, Tr); MS *m/z* 564, 562, and 560 (M$^+$), and 482 (M$^+$−Br).

B) From 10b: A sample of **10b** (172 mg) was treated by the procedure described in the preparation of **8a** and **9a** from **10a**, and then worked up to give **8b** (114 mg, 64%) and **9b** (54 mg, 27%).

Methyl 2,3-Anhydro-4-bromo-4-deoxy-6-*O*-trityl-α-D-gulopyranoside (10b). A sample of **9b** (294 mg) was treated by the procedure described in the preparation of **10a** from **9a**, and then worked up to give a syrup of **10b** (213 mg, 85%): R_f 0.58 (20:1 benzene–ethyl acetate); $[\alpha]_D^{31}$ −31° (*c* 0.99); ^{1}H NMR (400 MHz): δ=3.04 (1H, dd, H-6, $J_{5,6}$=5.8 Hz, $J_{6,6'}$=9.3 Hz), 3.39 (1H, dd, H-6′, $J_{5,6'}$=6.4 Hz), 3.45 (1H, dd, H-2, $J_{1,2}$=2.9 Hz, $J_{2,3}$=3.9 Hz), 3.50 (3H, s, OMe), 3.62 (1H, dd, H-3, $J_{3,4}$=2.0 Hz), 4.09 (1H, m, H-5), 4.41 (1H, t, H-4, $J_{4,5}$=2.0 Hz), 4.98 (1H, d, H-1), and 7.21—7.45 (15H, m, Tr); MS *m/z* 482 and 480 (M$^+$).

Methyl 3,4-Anhydro-2-deoxy-2-*C*-methyl-6-*O*-trityl-α-D-altropyranoside (11b). A) From 8b: A sample of **8b** (1.32 g) was treated by the procedure described in the preparation of **11a** from **8a**, and then worked up to give an amorphous solid of **11b** (987 mg, 89%): R_f 0.33 (20:1 benzene–ethyl acetate); $[\alpha]_D^{30}$ +44° (*c* 1.1); ^{1}H NMR (400 MHz): δ=1.15 (3H, d, Me-2, $J_{2,Me}$=8.0 Hz), 2.20 (1H, dq, H-2, $J_{1,2}$=2.4 Hz, $J_{2,3}$=0 Hz), 3.05 and 3.20 (each 1H, d, H-3 and H-4, vice versa, $J_{3,4}$=4.5 Hz, $J_{4,5}$=0 Hz), 3.33 (3H, s, OMe), 3.36 (1H, dd, H-6, $J_{5,6}$=4.8 Hz, $J_{6,6'}$=9.5 Hz), 3.43 (1H, dd, H-6′, $J_{5,6'}$=4.8 Hz), 4.13 (1H, t, H-5), 4.37 (1H, d, H-1), and 7.22—7.49 (15H, m, Tr); MS *m/z* 417 (M$^+$+1).

B) From 13b: A sample of **13b** (1.01 g) was treated by the procedure described in the preparation of **11a** from **8a** or **13a**, and then worked up to give **11b** (931 mg, 99%).

Methyl 2,4-Dideoxy-2,4-di-*C*-methyl-6-*O*-trityl-α-D-idopyranoside (12b) and Methyl 4-Chloro-2,4-dideoxy-2-*C*-methyl-6-*O*-trityl-α-D-idopyranoside (13b). A sample of **11b** (1.88 g) was treated by the procedure described in the preparation of **12a** and **13a** from **11a**, and then worked up to give amorphous solids of **12b** (1.17 g, 60%) and **13b** (587 mg, 29%) having the R_f-values of 0.25 and 0.44 (3:1 hexane–ethyl acetate) respectively.

12b: $[\alpha]_D^{33}$ +25° (*c* 1.1); ^{1}H NMR (400 MHz): δ=0.80 and 1.06 (each 3H, d, Me-2 and Me-4, vice versa, *J*=7.2 Hz), 1.75—1.92 (2H, m, H-2 and H-4), 2.91 (1H, dull d, OH, $J_{3,OH}$=7.8 Hz), 3.02 (1H, dd, H-6, $J_{5,6}$=4.5 Hz, $J_{6,6'}$=9.8 Hz), 3.33 (1H, dd, H-6′, $J_{5,6'}$=6.9 Hz), 3.42 (1H, m, H-3), 3.49 (3H, s, OMe), 4.26 (1H, dt, H-5, $J_{4,5}$=4.5 Hz), 4.52 (1H, d, H-1, $J_{1,2}$=2.7 Hz), and 7.20—7.50 (15H, m, Tr); MS *m/z* 433 (M$^+$+1).

13b: $[\alpha]_D^{33}$ +23° (*c* 0.69); ^{1}H NMR (400 MHz): δ=1.22 (3H, d, Me-2, $J_{2,Me}$=7.8 Hz), 1.99 (1H, ddq, H-2, $J_{1,2}$=1 Hz,

$J_{2,3}$=2.5 Hz), 3.28 (1H, dd, H-6, $J_{5,6}$=4.9 Hz, $J_{6,6'}$=10.0 Hz), 3.43 (3H, s, OMe), 3.46 (1H, d, OH, $J_{3,OH}$=8.3 Hz), 3.52 (1H, dd, H-6′, $J_{5,6'}$=6.4 Hz), 3.82 (1H, ddd, H-3, $J_{3,4}$=2.9 Hz), 3.95 (1H, t, H-4, $J_{4,5}$=2.9 Hz), 4.26 (1H, m, H-5), 4.58 (1H, broad s, H-1), and 7.21—7.49 (15H, m, Tr); MS *m/z* 453 and 452 (M^+).

Methyl 2,4-Dideoxy-2,4-di-*C*-methyl-6-*O*-trityl-α-D-talopyranoside (14b). A sample of **12b** (99 mg) was treated by the successive procedure in the preparation of **14a** through the keto compound, and then worked up to give **14b** (83 mg, 84%) and the starting **12b** (7.7 mg, 7.6%) having the R_f-values of 0.30 and 0.25 (3:1 hexane–ethyl acetate) respectively.

14b: syrup; $[\alpha]_D^{33}$ +59° (*c* 0.30); ^{1}H NMR (400 MHz): δ=0.73 (3H, d, Me-4, $J_{4,Me}$=7.4 Hz), 1.04 (3H, d, Me-2, $J_{2,Me}$=7.0 Hz, 1.88 (1H, m, H-2), 1.96 (1H, d, OH, $J_{3,OH}$=6.2 Hz), 2.04 (1H, m, H-4), 3.16 (1H, dd, H-6, $J_{5,6}$=4.2 Hz, $J_{6,6'}$=10.2 Hz), 3.29 (1H, dd, H-6′, $J_{5,6}$=6.4 Hz), 3.49 (3H, s, OMe), 3.89 (1H, dt, H-3, $J_{2,3}$=$J_{3,4}$=4.4 Hz), 4.03 (1H, dt, H-5, $J_{4,5}$=4.2 Hz), 4.65 (1H, d, H-1, $J_{1,2}$=4.1 Hz), and 7.21—7.51 (15H, m, Tr); MS *m/z* 433 (M^++1).

Methyl 2,4-Dideoxy-2,4-di-*C*-methyl-α-D-idopyranoside (15). A solution of **12b** (152 mg) in ethanol (3.6 ml) was shaken with palladium hydroxide on carbon and 3-atm hydrogen at room temperature for 38 h, filtered and evaporated to give a residue. This was chromatographed on silica gel (8 g) with ethyl acetate followed by recrystallization from ethyl acetate to give needles of **15** (49.8 mg, 75%): R_f 0.33 (ethyl acetate); mp 149—150 °C; $[\alpha]_D^{31}$ +99° (*c* 1.0); ^{1}H NMR (400 MHz): δ=1.00 and 1.11 (each 3H, d, Me-2 and Me-4, vice versa, *J*=7.2 Hz), 1.81—1.96 (3H, m, H-2, H-4, and OH-3), 2.99 (1H, broad signal, OH-6), 3.42 (1H, m, H-3), 3.42 (3H, s, OMe), 3.58 (1H, dd, H-6, $J_{5,6}$=3.6 Hz, $J_{6,6'}$=11.2 Hz), 3.76 (1H, dd, H-6′, $J_{5,6'}$=9.0 Hz), 4.19 (1H, dt, H-5, $J_{4,5}$=3.6 Hz), and 4.51 (1H, d, H-1, $J_{1,2}$=2.9 Hz); ^{1}H NMR (400 MHz, acetone-d_6): δ=0.99 (3H, d, Me-4, $J_{4,Me}$=6.8 Hz), 1.02 (3H, d, Me-2, $J_{2,Me}$=6.8 Hz), 1.55 (1H, m, H-2), 1.77 (1H, m, H-4), 3.17 (1H, dt, H-3, $J_{2,3}$=8.8 Hz, $J_{3,4}$=$J_{3,OH}$=6.8 Hz), 3.35 (3H, s, OMe), 3.47 (1H, dd, OH-6, $J_{6,OH}$=6.4 Hz, $J_{6',OH}$=4.4 Hz), 3.57 (1H, ddd, H-6, $J_{5,6}$=4.9 Hz, $J_{6,6'}$=11.2 Hz), 3.67 (1H, d, OH-3), 3.70 (1H, ddd, H-6′, $J_{5,6'}$=7.3 Hz), 3.99 (1H, dt, H-5, $J_{4,5}$=4.9 Hz), and 4.35 (1H, d, H-1, $J_{1,2}$=6.8 Hz).

Found: C, 56.63; H, 9.25%. Calcd for $C_9H_{18}O_4$: C, 56.82; H, 9.54%.

Methyl 2,4-Dideoxy-2,4-di-*C*-methyl-α-D-talopyranoside (16). A sample of **14b** (97.5 mg) was treated by the procedure described in the preparation of **15**, and then worked up to give a syrup of **16** (37.3 mg, 87%): R_f 0.40 (ethyl acetate); $[\alpha]_D^{32}$ +106° (*c* 1.0); ^{1}H NMR (400 MHz): δ=0.99 (3H, d, Me-2, $J_{2,Me}$=7.1 Hz), 1.05 (3H, d, Me-4, $J_{4,Me}$=7.2 Hz), 1.82 (1H, ddq, H-2, $J_{1,2}$=5.8 Hz, $J_{2,3}$=3.6 Hz), 2.13 (1H, m, H-4), 2.25—2.50 (2H, broad signal, OH-3 and OH-6), 3.43 (3H, s, OMe), 3.67 (1H, dd, H-6, $J_{5,6}$=3.3 Hz, $J_{6,6'}$=11.2 Hz), 3.85 (1H, dd, H-6′, $J_{5,6'}$=6.6 Hz), 3.87 (1H, dd, H-3, $J_{2,3}$=3.6 Hz, $J_{3,4}$=7.4 Hz), 3.99 (1H, ddd, H-5, $J_{4,5}$=5.3 Hz), and 4.63 (1H, d, H-1); MS *m/z* 190 (M^+).

We are grateful to Prof. Sumio Umezawa, Institute of Bioorganic Chemistry, and the late Prof. Hamao Umezawa, Institute of Microbial Chemistry for their generous support of our program. Financial support by the Ministry of Education, Science and Culture (Grant-in-Aid for Scientific Research) is gratefull acknowledged.

References

1) K. Tatsuta, Y. Amemiya, S. Maniwa, and M. Kinoshita, *Tetrahedron Lett.*, **21**, 2837 (1980); K. Tatsuta, Y. Amemiya, Y. Kanemura, and M. Kinoshita, *Tetrahedron Lett.*, **22**, 3997 (1981); S. Hanessian, *Acc. Chem. Res.*, **12**, 159 (1979); I. Paterson and M. M. Mansuri, *Tetrahedron*, **41**, 3569 (1985).

2) D. R. Harris, S. G. McGeachin, and H. H. Mills, *Tetrahedron Lett.*, **1965**, 679; M. Kinoshita, M. Arai, K. Tomooka, and M. Nakata, *Tetrahedron Lett.*, **27**, 1811, 1815 (1986) and references cited therein; H. Tone, T. Nishi, Y. Oikawa, M. Hikota, and O. Yonemitsu, *Tetrahedron Lett.*, **28**, 4569 (1987).

3) A. G. Agtarap, J. W. Charnberlain, M. Pinkerton, and L. Steinrauf, *J. Am. Chem. Soc.*, **89**, 5737 (1967); T. Fukuyama, K. Akasaka, D. S. Karanewsky, C.-L. J. Wang, G. Schmid, and Y. Kishi, *ibid.*, **101**, 259 (1979).

4) W. Oppolzer and V. Prelog, *Helv. Chim. Acta.*, **56**, 2287 (1973); H. Nagaoka, W. Rutsch, G. Schmid, H. Iio, M. R. Johnson, and Y. Kishi, *J. Am. Chem. Soc.*, **102**, 7962 (1980); M. Nakata, S. Wada, K. Tatsuta, and M. Kinoshita, *Bull. Chem. Soc. Jpn.*, **58**, 1801 (1985).

5) B. K. Toeplitz, A. I. Cohen, P. T. Funke, W. L. Parker, and J. Z. Gougoutas, *J. Am. Chem. Soc.*, **101**, 3344 (1979).

6) D. J. Duchamp, A. R. Branfman, A. C. Button, K. L. Rinehart, Jr., *J. Am. Chem. Soc.*, **95**, 4077 (1973).

7) a) S. Challenger and G. Procter, *Tetrahedron Lett.*, **27**, 391 (1986); b) T. Ogawa, N. Takasaka, and M. Matsui, *Carbohydr. Res.*, **60**, C4 (1978); c) A. G. Kelly and J. S. Roberts, *J. Chem. Soc., Chem. Commun.*, **1980**, 228; d) N. K. Kochetkov, A. F. Sviridov, and M. S. Ermolenko, *Tetrahedron Lett.*, **22**, 4315 (1981); e) A. F. Sviridov, G. E. Berdimbetova, and N. K. Kochetkov, *Izv. Akad. Nauk SSSR, Ser. Khim.*, **1982**, 2572; *Chem. Abstr.*, **98**, 179765b (1983); f) L. Magdzinski, B. Cweiber, and B. Fraser-Reid, *Tetrahedron Lett.*, **24**, 5823 (1983); g) M. P. Edwards, S. V. Ley, S. G. Lister, and B. D. Palmer, *J. Chem. Soc., Chem. Commun.*, **1983**, 630; h) P. J. Hodges and G. Procter, *Tetrahedron Lett.*, **26**, 4111 (1985); i) T. Wakamatsu, H. Nakamura, Y. Nishikimi, K. Yoshida, T. Noda, M. Taniguchi, and Y. Ban, *Tetrahedron Lett.*, **27**, 6071 (1986).

8) S. Masamune, T. Sato, B. M. Kim, and T. A. Wollman, *J. Am. Chem. Soc.*, **108**, 8279 (1986); W. R. Roush and A. D. Palkowitz, *ibid.*, **109**, 953 (1987).

9) P. J. Garegg and B. Samuelsson, *J. Chem. Soc., Chem. Commun.*, **1979**, 978.

10) K. Tatsuta, K. Akimoto, M. Annaka, Y. Ohno, and M. Kinoshita, *Bull. Chem. Soc. Jpn.*, **58**, 1699 (1985).

11) L. Hough and A. C. Richardson, "Conformational Analysis of The Monosaccharides," in "Rodd's Chemistry of Carbon Compounds," ed by S. Coffey, Elsevier Publishing Co., Amsterdam (1967), pp. 87—124.

12) R. U. Lemieux and S. Levine, *Can. J. Chem.*, **42**, 1473 (1964).

Synthesis and Reactions of 2-Arylhydrazinotropones. I. Preparation of 2-(2-Arylhydrazino)tropones and the 4-Substituted Derivatives[1)]

Tetsuo NOZOE,* Kimiaki IMAFUKU,*,† Bing-Zhu YIN,†,a) Masaaki HONDA,†,b) Yasutomo GOTO,†,c) Yasushi HARA,††,d) Takayoshi ANDOH,†† and Hiroshi YAMAMOTO*,††

Tokyo Research Laboratories, Kao Corporation, Bunka, Sumida-ku, Tokyo 131
†Department of Chemistry, Faculty of Science, Kumamoto University, Kurokami, Kumamoto 860
††Department of Chemistry, Faculty of Science, Okayama University, Tsushima, Okayama 700

(Received March 9, 1988)

A wide variety of 2-(2-arylhydrazino)tropones were prepared by the reactions of 2-tosyloxytropone with arylhydrazines. The dimeric compounds 6,6′-bis(arylhydrazono)-1,1′-bi(2,4-cycloheptadiene)-7,7′-diones, 2-anilinotropones, and 3-(2-arylhydrazino)tropones were isolated as minor products in some cases. Similarly, starting with 2-tosyloxytropones bearing an isopropyl, isopropenyl, (1-acetamidoethyl), and protected acetyl group at the 5-position, 4-substituted 2-(2-arylhydrazino)tropones were obtained as the major products by the abnormal substitution reaction. These 2-(2-arylhydrazino)tropones are expected to effectively serve as precursors for a convenient synthesis of 5-aryl-substituted tropolones via benzidine-type rearrangement. ^{1}H NMR (200 or 500-MHz) parameters for these 4-substituted 2-(2-arylhydrazino)tropones are given for their unambiguous structural assignments.

Many hydrazoarenes and 1,2-diarylhydrazines (ArNHNHAr′) are prepared by reduction of nitro-, azo-, and azoxyarenes.[2)] As for troponoids,[3)] several arylhydrazinotropones have been reported to be made by the substitution reaction of 2-methoxy-,[4)] 2-chloro-,[1a)] and 2-tosyloxytropones[1b,5)] with arylhydrazines. Meanwhile, it became known that some 2-(2-arylhydrazino)-tropones exhibited interesting physiological activity but were somewhat unstable towards acid.[6)] We wish to describe in this paper a detailed study on preparation of a wide variety of 2-(2-arylhydrazino)tropones with or without a *C*-substituent at the 4-position. These compounds are expected to be valuable as the precursors for our attempt to exploit a convenient, general method of preparing B-ring-open colchicine analogues of type **2**, by utilizing a novel benzidine type rearrangement of these 2-(2-arylhydrazino)tropones.[1)] This is because colchicine itself (**1**), though possessing highly important biological activity,[7)] is often too toxic clinically and thus various analogues of **1** are drawing an increasing interest from the viewpoint of pharmacological activity.[8)]

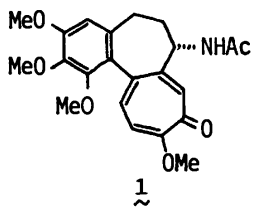

1

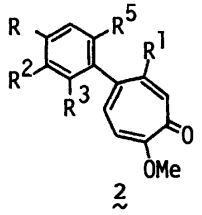

2

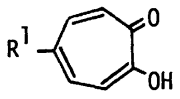

3

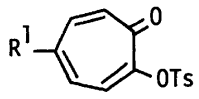

4

3,4	R^1
a	H
b	i-Pr
c	isopropenyl
d	Ac
e	-CHMeNHAc
f	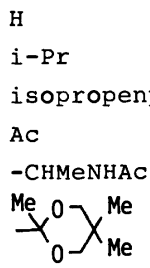

Results and Discussion

As model compounds for the synthetic study on the B-ring-open analogues of type **2**, six kinds of tropolones **3a—f** were chosen as the starting materials: namely, those bearing no substituent, an isopropyl, isopropenyl, acetyl, (1-acetamidoethyl), and a protected acetyl group at the 5-position. Among these, 5-(1-acetamidoethyl)- (**3e**) and 5-(2,5,5-trimethyl-1,3-dioxan-2-yl)tropolone (**3f**) were newly synthesized from 5-acetyltropolone[9)] (**3d**) by an application of the three-step procedure[10,11)] (i.e., by the reaction with hydroxylamine, followed by hydrogenation over Pd-C and then acetylation with acetic anhydride) and by treatment with 2,2-dimethyl-1,3-propanediol in the presence of acid, respectively; the overall yields of these products are given in Table 1. These tropolones were then led to the tosylates **4a—f** by the reaction with tosyl chloride in pyridine (see Table 1 for the

Present address: a) Yanbian University, Yanji, Jilin, China. b) Koei Chemical Co., Ltd., Osaka 536. c) Fuji Photo Film Co., Ltd., Fujinomiya 418. d) Tosoh Co., Ltd., Shin-Nanyo-shi 746.

Table 1. Preparation of Tropolones and Tropolone Tosylates

Starting material	Product	Yield/%
3a	**4a**[a]	100
3b	**4b**[b]	100
3c	**4c**[c]	97
3d	**4d**[d]	21
3d	**3e** 47[e]	**4e**[f] 70
3d	**3f** 70	**4f**[g] 89

a) Ref. 17. b) Ref. 13. c) Ref. 14. d) Moisture-sensitive at 20 °C. e) Overall yield from **3d**. f) From **3e**. g) From **3f**.

yields of **4**).

The tosylates **4** were treated with an excess (2—3 equiv) of various arylhydrazines **6a—o** (hydrochloride) either in refluxing methanol (or ethanol) for 6—24 h or in *N,N*-dimethylformamide (DMF) at 0—25 °C for 3—48 h in the presence of an excess (3—4 equiv) of triethylamine under nitrogen (see Scheme 1). After the usual work-up procedures including chromatographic separation, 27 kinds of 2-(2-arylhydrazino)tropones **7a—z'** were isolated mostly as the main product in good to moderate yields. Besides **7**, certain amounts of by-products **8a—g, j—o, 9a,l**, and **10—13** were

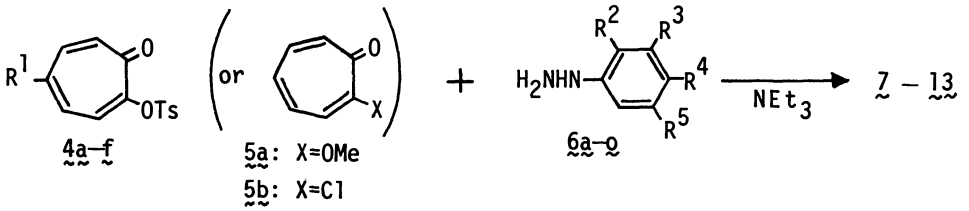

6-9	R^1	R^2	R^3	R^4	R^5
a	H	H	H	H	H
b	H	Me	H	H	H
c	H	H	Me	H	H
d	H	H	H	Me	H
e	H	OMe	H	H	H
f	H	H	OMe	H	H
g	H	H	H	OMe	H
h	H	OMe	OMe	H	H
i	H	OMe	OMe	H	Me
j	H	Cl	H	H	H
k	H	H	Cl	H	H
l	H	H	H	Cl	H
m	H	NO_2	H	H	H
n	H	H	NO_2	H	H
o	H	H	H	NO_2	H
p	i-Pr	H	H	H	H
q		H	H	H	H
r	"	Me	H	H	H
s	"	H	Me	H	H
t	"	MeO	H	H	H
u	"	H	MeO	H	H
v	"	MeO	MeO	H	H
w	"	MeO	MeO	H	Me
x	NHAc	MeO	H	H	H
y	"	H	MeO	H	H
z	"	MeO	MeO	H	H
z'		MeO	H	H	H

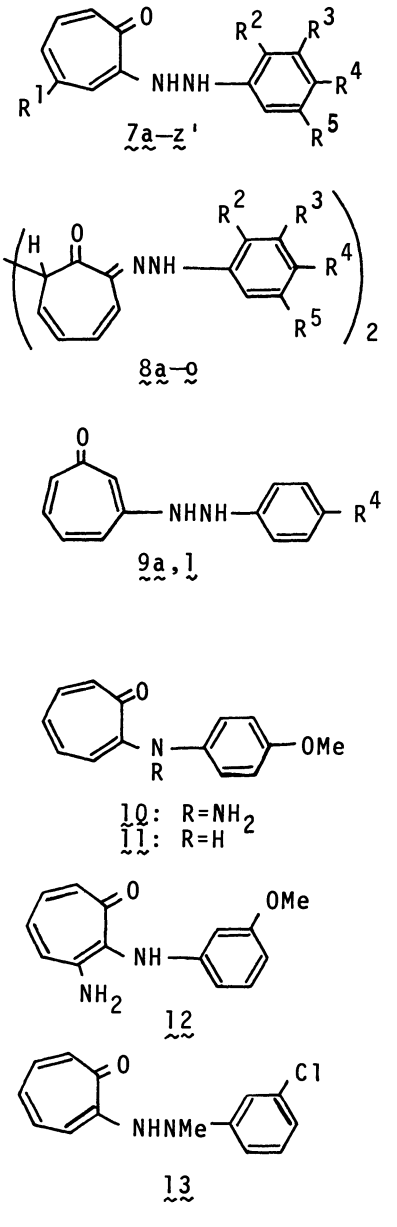

Scheme 1.

isolated by the additional or unusual reactions of **4a** with some kinds of **6**; for further discussion on these minor products **8—13**, see below. The yields of these products are summarized in Table 2. 5-Acetyltropolone tosylate (**2d**), which was rather unstable at room temp, did not afford any of the expected 4-acetyl-2-(2-arylhydrazino)tropones. Also, the reaction of 2-methoxytropone (**5a**) with some of the arylhydrazines **6** was conducted in refluxing methanol. However, the yields of the products by this combination tend to become lower than those obtained by the reaction starting with tosylate **4a** and the corresponding arylhydrazines, as had also been observed in the case[1a] with 2-chlorotropone (**5b**) (see Table 2).

Structures of these products were established by spectroscopy [UV, IR, ^{1}H NMR, MS, and ^{13}C NMR (for some compds)] and elemental analysis; their exact data and the rational assignments for the spectral parameters are described in the Experimental section. The unequivocal assignments of the *C*-substituents of **7p—z′** to the 4-position, not 5-position, were based on the careful analysis of the 200 or 500-MHz ^{1}H NMR data by taking into account the parameters established earlier for similar compounds, such as 4-substituted 2-methoxytropones.[11] Characteristic features in the δ and J values for these 4-substituted 2-(2-arylhydrazino)-tropones are summarized in Table 3. These data are obviously of considerable value in precisely determining the positions of substituents even of hitherto unreported polysubstituted troponoids, such as those of type **2**.[12] It should be noticed that the 4-substituted products **7p—z′** were smoothly derived by the abnormal (ciné) substitution reactions of 5-substituted tropolone tosylates **4b—f** with arylhydrazines at room temperature in a polar aprotic solvent (DMF) as in the case of the reaction of **4b,c** with liquid ammonia.[13,14]

By taking the parent tosylate **4a** as a representative, model compound, an effort to isolate the minor products **8—13** was made for the purpose of machanistic study on this rather subtle, substitution reactions with primary arylhydrazines.[15] The dimeric structures, 6,6′-bis(arylhydrazino)-1,1′-bi(2,4-cycloheptadiene)-7,7′-diones, were assigned for **8** primarily on the ground of their elemental analysis, IR, and doubly overlapping NMR signals, although MS gave no molecular ions but two intense fragment peaks presumably assignable to moieties **7** (m/z $M^+/2+1$) and the corresponding 2-arylazotropones (m/z $M^+/2-1$) derived from **8** as the result of facile fission by a disproportionation reaction. The dimers **8** are considered to be produced by oxidation of the monomeric arylhydrazinotropones **7**, since **8a** was obtained in 93% yield by refluxing **7a** in benzene in the presence of benzoyl peroxide.[15]

Another type of the minor products obtained in the case of the reaction of **4a** with **6a** and **6l** were 3-(2-arylhydrazino)tropones **9a** (6% yield) and **9l** (10%), respectively. These products are apparently derived as the result of the abnormal attack of the hydrazino

Table 2. Synthesis of 2-(2-Arylhydrazino)tropones

Starting material	Product					
	Yield/%[a,b]		Yield/%		Yield/%	
4a (**5a**, **5b**)	**7a**	66 (28[c], 48[d])	**8a**	3	**9a**	6
4a (**5a**, **5b**)	**7b**	82 (31, 34[d])	**8b**	Trace		
4a (**5a**, **5b**)	**7c**	72 (12, 57[d])	**8c**	Trace		
4a (**5a**)	**7d**	63 (24)	**8d**	Trace		
4a	**7e**	56	**8e**	2		
4a	**7f**	80	**8f**	Trace	**12**	29[e]
4a	**7g**	47	**8g**	8	**10**	7
4a			**10**	10[f]	**11**	33[f]
4a	**7h**	22				
4a	**7i**	31				
4a	**7j**	64	**8j**	Trace		
4a	**7k**	80	**8k**	2	**13**	3
4a	**7l**	80	**8l**	1	**9l**	10
4a	**7m**	21	**8m**	Trace		
4a (**5b**)	**7n**	62 (53[d])	**8n**	Trace		
4a	**7o**	51	**8o**	Trace		
4b	**7p**	40				
4c	**7q**	63				
4c	**7r**	57				
4c	**7s**	77				
4c	**7t**	59				
4c	**7u**	60				
4c	**7v**	71				
4c	**7w**	61				
4e	**7x**	58				
4e	**7y**	57				
4e	**7z**	74				
4f	**7z′**	50				

a, b) Values in parentheses are for starting materials **5a** and **5b**, respectively. c) Ref. 4. d) Ref. 1a. e, f) Values obtained when the free bases **6f** and **6g** were used, respectively.

Table 3. Characteristic Features in the δ and J Values (Hz) for 4-Substituted 2-(2-Arylhydrazino)tropones **7p—z′**

Proton	δ	J
NH-2	8.3—8.1	
H-3	7.0—7.3	$J_{3,5}\simeq 1.5$
R-4	a, b, c, d)	
H-5	6.7—6.95	$J_{5,6}=9.5$, $J_{5,7}\simeq 1.0$
H-6	7.2—7.3	$J_{6,7}=11.5$—12.0
H-7	7.05—7.15	
NH-1′	5.6—6.3	
H-2′	6.3—6.8	$J_{2',3'}=8.0$—8.5, $J_{2',4'}\simeq J_{2',6'}\simeq 2$
H-3′	6.9—7.35	$J_{3',4'}=7.5$—8.0
H-4′	6.2—6.9	$J_{4',5'}=7.5$—8.0, $J_{4',6'}=1.5$—2.0
H-5′	6.9—7.25	$J_{5',6'}=7.5$—8.0
H-6′	6.3—6.8	

a) For *i*-Pr: δ=1.66 (6H, d, J=7.0 Hz) and 2.81 (1H, sept). b) For Isopropenyl: δ=2.02—2.05 (3H, dd or t, J=1.0—1.5 Hz), 5.09—5.13 (1H, dq or quint, J=1.0—1.5 Hz), and 5.13—5.20 (1H, brs). c) For (1-acetamido)ethyl: δ=1.3—1.4 (3H, d, J=7.0 Hz) 1.85—1.9 (3H, s), 4.8—4.9 (1H, brq), and 5.7—6.3 (1H, brd, J=6.5 Hz). d) For 2,5,5-trimethyl-1,3-dioxan-2-yl: δ=0.55 (3H, s), 1.20 (3H, s), 1.47 (3H, s), and 3.19 (4H, brs).

group at C-3 of **4a** as was observed[16] in the case of the initial step of the degradative alkaline hydrolysis of **5b** to salicylaldehyde.

The reaction of **4a** with the hydrochloride of **6g** gave, besides **7g** and **8g** (see Table 2), 2-(*N*-amino-4-methoxyanilino)tropone (**10**) in 7% yield. However, 2-(4-methoxyanilino)tropone (**11**) was mainly obtained (33% yield) besides **10** (10%) when **6g** hydrochloride had been converted to the free base with triethylamine before being treated with **4a**; it was later confirmed that compound **10** was converted into **11** in refluxing methanol in the presence of hydrochloric acid. Similarly, the reaction of free **6f** with **4a** gave 3-amino-2-(3-methoxyanilino)tropone (**12**) in 29% yield. These results indicate that *m*- and *p*-methoxyphenylhydrazines (**6f,g**) tend to afford much more complex products depending upon the reaction conditions, whereas *o*-methoxyphenylhydrazine (**6e**) appears to give no product of the anilino-substituted type.

From the reaction of **4a** with **6k**, 2-[2-(3-chlorophenyl)-2-methylhydrazino]tropone (**13**) was also isolated in 3% yield, the reason for which, however, remains to be clarified.[15]

The 2-(2-arylhydrazino)tropones thus conveniently obtained in the present study are considered to be not only of interest from the view point of their potential biological activity but also useful precursors to various 5-aryl-substituted troponoids via benzidine-type rearrangement reaction, which is currently under intensive investigation.[12]

Experimental

Melting points were determined with a Yanagimoto MP-S3 instrument and are uncorrected. All reactions were monitored by TLC (Merck silica gel 60F, 0.25 mm) with appropriate solvent systems (mostly with MeOH–$CHCl_3$, $CHCl_3$–AcOEt, ether–benzene, and/or AcOEt–hexane). Preparative TLC and column chromatography were performed with Merck Kiesel Gel 60G and Wako C-200 silica gel, respectively. Yields of **3**, **4**, and **7**—**13** are given in Tables 1 and 2. The IR spectra were taken with a JASCO A-102 or Hitachi 215 spectrometer in chloroform (unless otherwise stated). The UV spectra were recorded in MeOH with a Hitachi EPS-3T spectrophotometer. The ^1H NMR spectra were measured in $CDCl_3$ (unless otherwise stated) with a Hitachi R-24 or R-600 (60-MHz), JEOL-FX200 (200-MHz, Kinki University), and/or Varian VXR-500 instrument (500-MHz, the SC-NMR Lab., Okayama University) at 27 °C. Chemical shifts are reported as δ values rel to tetramethylsilane as the internal standard measured at 60-MHz (unless otherwise stated). The assignment of all signals were made by employing a first-order analysis with the aid of decoupling technique and the parameters were confirmed by a computer-assisted simulation analysis. ^{13}C NMR spectra were recorded with a JEOL FX-100 (25-MHz, Kyushu Univ.). Mass spectra were taken on a JEOL DX-300 low resolution, or JEOL JMX-HX100 (with a JEOL JMA-DA5000 mass data system) high-resolution instrument and are given in terms of *m/z* (rel intensity) compared with the base peak.

5-(1-Acetamidoethyl)tropolone (3e). A slightly modified procedure of Nozoe et al.[10,11] for 4-cinnamoyltropolones was applied. Thus, a solution of **3d**[9] (211 mg, 1.29 mmol) and hydroxylammonium chloride (168 mg, 2.42 mmol) in dry ethanol (7 cm^3) was refluxed under argon for 1 h. After cooling, the precipitate was filtered off and washed with cold water to give the oxime of **3d** as a brown powder. This was dissolved in acetic acid (7 cm^3) containing concd HCl (0.5 cm^3) and then hydrogenated in the presence of 5% Pd on carbon (127 mg). The catalyst was filtered off and washed thoroughly with hot ethanol. The filtrate was evaporated in vacuo. The residue was dissolved in acetic anhydride (3 cm^3) and heated at 60 °C for 5 min. The excess acetic anhydride was evaporated in vacuo. The residue was chromatographed in a column of silica gel with $CHCl_3$, giving 5-(1-acetamidoethyl)-2-acetoxytropone as an amber oil (160 mg, 50% overall yield from **3d**): ^1H NMR δ=1.40 (3H, d, J=7.0 Hz, MeC-5), 1.98 (3H, s, AcN), 2.35 (3H, s, AcO), 4.92 (1H, brquint, J=7 Hz, HC-5), and 6.9—7.45 (5H, m, aromatic H, NH).

A mixture of this acetate (160 mg), ethanol (3 cm^3), and 1 M KOH (1.5 cm^3) (1 M=1 mol·dm^{-3}) was stirred under argon overnight at 20 °C. The solvent was evaporated in vacuo. The residue was diluted with cold water, taken to pH 4 with dil HCl at 5 °C, and extracted with CH_2Cl_2. The combined organic layers were dried (Na_2SO_4) and evaporated in vacuo, giving **3e** as a pale yellow syrup: ^1H NMR δ=1.41 (3H, d, J=7.0 Hz, MeC-5), 1.98 (3H, s, AcN), 4.93 (1H, brquint, $J\simeq$7 Hz, HC-5), 7.0 (1H, brm, NH), 7.35 (2H, d, J=11 Hz, H-3,7), 7.40 (2H, d, J=11 Hz, H-4,6), and 7.98 (1H, brm, OH); MS *m/z* 207 (M^+; 100) and 148 (72).

Found: *m/z* 207.0861. Calcd for $C_{11}H_{13}NO_3$: M, 207.0895.

5-(2,5,5-Trimethyl-1,3-dioxan-2-yl)tropolone (3f). A solution of **3d** (50 mg, 0.31 mmol) and 2,2-dimethyl-1,3-propanediol (40 mg, 0.39 mmol) in dry benzene (3 cm^3) containing *p*-toluenesulfonic acid (6 mg) was refluxed for 13 h (using a Dean-Stark apparatus). After cooling, the mixture was diluted with cold water and then extracted with $CHCl_3$. The combined organic layers were extracted with 2 M NaOH. The aq layer was taken to pH 4 with 3 M HCl and then extracted with CH_2Cl_2. The combined organic layers were dried (Na_2SO_4) and evaporated in vacuo. The residue was chromatographed in a column of silica gel with 1:19 MeOH–$CHCl_3$ to give **3f** as colorless needles: mp 109—110 °C (from cyclohexane); IR (KBr) 3205 (OH) and 1615 cm^{-1} (C=O); ^1H NMR δ=0.63 [3H, s, (*Z*)-Me-5′], 1.24 [3H, s, (*E*)-Me-5′], 1.52 (3H, s, Me-2′), 3.39 (4H, brs, 2H-4′,6′), 7.37 (2H, d, J=11 Hz, H-3,7), 7.66 (2H, d, J=11 Hz, H-4,6), and 8.75 (1H, brm, OH); MS *m/z* 250 (M^+; $\simeq$0), 235 (100), 167 (21), and 149 (50).

Found: *m/z* 235.0959. Calcd for $C_{13}H_{15}O_4$: M−CH_3, 235.0970.

General Procedure for the Preparation of 5-Substituted Tropolone Tosylates (4a—f). To a cold solution of a 5-substituted tropolone **3** (1.00 g) in dry pyridine (2.5 cm^3) was added tosyl chloride (1.1—1.2 equiv mol) at 5 °C. The mixture was stirred at 20 °C for 10—16 h (but 20 min for **4d**), and then diluted with cold water. The precipitate was filtered off and washed with cold water to give **4**. The filtrate was concentrated in vacuo and extracted with CH_2Cl_2, giving an additional **4** after chromatographic

purification in a column of silica gel.

2-Tosyloxytropone[17] (4a): Colorless needles; mp 155.5—157 °C lit,[17] 159—159.5 °C).

5-Isopropyl-2-tosyloxytropone[13] (4b): Colorless needles; mp 120.5—121.5 °C (from benzene–hexane, lit,[13] 122—123 °C); ^{1}H NMR δ=1.22 (6H, d, J=7.0 Hz, Me_2C-5), 2.46 (3H, s, Me-4′), 2.85 (1H, sept, J=7 Hz, HC-5), 6.89 (1H, dd, $J_{3,4}$=9.5, $J_{4,6}$=1.5 Hz, H-4), 7.17 (1H, d, $J_{6,7}$=11.0 Hz, H-7), 7.23 (1H, dd, H-6), 7.39 (2H, brd, J=8.5 Hz, H-3′,5′), 7.47 (1H, d, H-3), and 7.98 (2H, brd, J=8.5 Hz, H-2′,6′).

5-Isopropenyl-2-tosyloxytropone[14] (4c): Colorless crystals; mp 125.5—126.5 °C (from benzene–hexane, lit,[14] mp 126—127 °C); ^{1}H NMR δ=2.10 (3H, brd, $J\simeq$1.0 Hz, MeC-5), 2.44 (3H, s, Me-4′), 5.29 [1H, brs, (*E*)-HC=C-5], 5.38 [1H, brs, (*Z*)-HC=C-5], 7.00 (1H, dd, $J_{3,4}$=11.0, $J_{4,6}$=1.5 Hz, H-4), 7.12 (1H, d, $J_{6,7}$=12.5 Hz, H-7), 7.35 (2H, brd, J=8.5 Hz, H-3′,5′), 7.41 (1H, dd, H-6), 7.44 (1H, d, H-3), and 7.92 (2H, brd, J=8.5 Hz, H-2′,6′).

5-Acetyl-2-tosyloxytropone (4d): Pale yellow prisms; mp 115—115.5 °C (from AcOEt–cyclohexane); ^{1}H NMR δ=2.47 (3H, brs, Me-4′), 2.61 (3H, s, Ac), 7.19 (1H, d, $J_{6,7}$=12.5 Hz, H-7), 7.37 (2H, brd, J=8.5 Hz, H-3′,5′), 7.55 (1H, brd, $J_{3,4}\simeq$11.5 Hz, H-3), 7.68 (1H, brdd, $J_{4,6}$=1.5 Hz, H-4), 7.84 (1H, brdd, H-6), and 7.91 (2H, brd, J=8.5 Hz, H-2′,6′); MS m/z 318 (M^+; ≃0), 254 (37), 164 (27), 155 (57), 149 (15), 139 (16), 121 (17), 91 (100), 65 (20), and 43 (18). **4d** decomposes on setting aside at room temp (or rapidly on silica gel).

Found: m/z 254.0939. Calcd for $C_{16}H_{14}O_3$: M−SO_2, 254.0943.

5-(1-Acetamidoethyl)-2-tosyloxytropone (4e): A pale yellow syrup; ^{1}H NMR δ=1.39 (3H, d, J=7.0 Hz, MeC-5), 1.97 (3H, s, AcN), 2.46 (3H, s, Me-4′), 4.82 (1H, brquint, J=7 Hz, HC-5), 6.97 (1H, brm, NH), 6.98 (2H, brd, $J_{3,4}\simeq J_{6,7}\simeq$10.5 Hz, H-3,7), 7.27 (1H, brd, H-4), 7.31 (1H, brd, H-6), 7.35 (2H, brd, J=8.5 Hz, H-3′,5′), and 7.98 (2H, brd, J=8.5 Hz, H-2′,6′); MS m/z 361 (M^+; 5.5), 302 (17), 295 (100), 239 (18), 238 (42), and 139 (25).

Found: m/z 361.0957. Calcd for $C_{18}H_{19}NO_5S$: M, 361.0984.

5-(2,5,5-Trimethyl-1,3-dioxan-2-yl)-2-tosyloxytropone (4f): Colorless crystals (89% yield from **3f**); mp 114—116 °C (from EtOH); IR 1632 cm^{-1} (C=O); ^{1}H NMR δ=0.67 [3H, s, (*Z*)-Me-5″], 1.22 (3H, s, (*E*)-Me-5″], 1.49 (3H, s, Me-2″), 2.48 (3H, s, Me-4′), 3.39 (4H, brs, 2H-4″,6″), 7.28—7.62 (4H, m, aromatic H), 7.37 (2H, brd, J=8 Hz, H-3′,5′), and 7.98 (2H, brd, J=8 Hz, H-2′,6′); MS m/z 404 (M^+; ≃0), 389 (27), 361 (22), 341 (27), 340 (100), 326 (15), 325 (60), 275 (15), 249 (11), 155 (23), 129 (25), 107 (9), 91 (17), and 69 (19).

Found: m/z 389.1049. Calcd for $C_{20}H_{21}O_6S$: M−CH_3, 389.1059.

General Procedure for the Preparation of 2-(2-Arylhydrazino)tropones (7a—z′) (with the Formation of By-products 8—13). A. Procedure for 7a—o: A mixture of **4a** (1.38 g, 5 mmol) and an arylhydrazine **6** (or its hydrochloride, 10 mmol) in methanol (or ethanol for **6m—o**, 150 cm^3) was refluxed for 6—24 h under nitrogen in the presence of triethylamine (5 mmol, or 15 mmol when the arylhydrazine hydrochloride was used).

B. Procedure for 7p—z′: To a solution of a 5-substituted 2-tosyloxytropone **4** (250 mg) in dry DMF (6 cm^3) were successively added, under argon at −20 °C, arylhydrazine hydrochloride **6** (3.0 equiv mol) and triethylamine (4.0 equiv mol, dropwise), followed by stirring at −20 °C for 1 h and then at 20 °C for 7—20 h.

C. Procedure Using Free 6f,g: Triethylamine (1.01 g, 10 mmol) was added to a suspension of hydrochloride (1.75 g, 10 mmol) of **6** in methanol (150 cm^3). To the resulting solution was added **4a** (1.38 g, 5 mmol), and the mixture was refluxed for 8 h under nitrogen.

D. Procedure for 7b—d Using 5a as the Starting Material: The same method as **A** described above was employed except for using **5a** (in place of **4a**).

When the starting material **4** or **5** almost disappeared (by TLC), the solvent was evaporated in vacuo. The residue was diluted with cold water and extracted with CH_2Cl_2 or $CHCl_3$. The organic layer was dried (Na_2SO_4) and evaporated in vacuo. The residue (when it was a solid) was recrystallized from an appropriate solvent (see below) to give the corresponding product **7**; the filtrate was concentrated in vacuo and the residue was chromatographed on preparative thin-layer plates (with $CHCl_3$–AcOEt) or in a column of silica gel (with MeOH–$CHCl_3$ or AcOEt–hexane), giving an additional amount of **7** and other by-products.

2-(2-Phenylhydrazino)tropone[1a,4] (7a): Yellow prisms (by Procedure **A**); mp 163—165 °C (from benzene, lit,[1a,4] 168 °C).

2-[2-(*o*-Tolyl)hydrazino]tropone[1a] (7b): Brown prisms (by Procedures **A** and **D**); mp 90—91 °C (from benzene, lit,[1a]

2-[2-(*m*-Tolyl)hydrazino]tropone[1a] (7c): Yellow prisms (by Procedures **A** and **D**); mp 148 °C (from benzene, lit,[1a] 147 °C).

2-[2-(*p*-Tolyl)hydrazino]tropone[1a] (7d): Yellow prisms (by Procedures **A** and **D**); mp 162—164 °C (from benzene, lit,[1a] 158 °C).

2-[2-(2-Methoxyphenyl)hydrazino]tropone (7e): Yellow prisms (by Procedure **A**); mp 118—119 °C (from benzene); IR 3300 (NH) and 1605 cm^{-1} (C=O); UV λ_{max} 250 (log ε 4.58), 339 (4.12), and 402 nm (4.10); ^{1}H NMR δ=3.48 (3H, s, MeO-2′), 6.25 (1H, brm, NH-1′), 6.5—7.3 (9H, m, aromatic H), and 8.2 (1H, brm, NH-2); MS m/z 242 (M^+; 93), 123 (100), 122 (49), and 108 (48).

Found: m/z 242.1045. Calcd for $C_{14}H_{14}N_2O_2$: M, 242.1055.

2-[2-(3-Methoxyphenyl)hydrazino]tropone (7f): Yellow prisms (by Procedures **A** and **C**); mp 148—150 °C (from benzene); IR 3305 (NH) and 1605 cm^{-1} (C=O); UV λ_{max} 248 (log ε 4.50), 339 (4.47), and 406 nm (4.07); ^{1}H NMR δ=3.71 (3H, s, MeO-3′), 6.15 (1H, brm, NH-1′), 6.3—7.4 (9 H, m, aromatic H), and 8.3 (1H, brm, NH-2).

Anal. ($C_{14}H_{14}N_2O_2$) C, H, N.

2-[2-(4-Methoxyphenyl)hydrazino]tropone (7g): Yellow prisms (by Procedures **A** and **C**); mp 137—139 °C (from benzene); IR 3300 (NH) and 1605 cm^{-1} (C=O); UV λ_{max} 250 (log ε 4.51), 339 (4.07), and 405 nm (4.08); ^{1}H NMR δ=3.71 (3H, s, MeO-4′), 5.7 (1H, brm, NH-1′), 6.5—6.9 (1H, m, H-5), 6.71 (4H, s, H-2′,3′,5′,6′), 6.9—7.4 (4H, m, H-3,4,6,7), and 8.25 (1H, brm, NH-2).

Anal. ($C_{14}H_{14}N_2O_2$) C, H, N.

2-[2-(2,3-Dimethoxyphenyl)hydrazino]tropone (7h): Yellow prisms (by Procedure **A** using **6h**[18]); mp 103—105 °C (from benzene–hexane); IR 3305 (NH) and 1605 cm^{-1} (C=O); UV λ_{max} 250 (log ε 4.49), 339 (4.04), and 405 nm (4.07); ^{1}H NMR δ=3.83 (3H, s, MeO-3′), 3.90 (3H, s, MeO-2′), 6.25—6.65 (3H, m, H-4′,5′,6′), 6.35 (1H, brm, NH-1′), 6.7—7.4 (5H, m, aromatic H), and 8.23 (1H, brm, NH-2); MS m/z 272 (M^+; 100), 153 (92), 153 (31), 138 (57), and 137 (29).

Found: m/z 272.1156. Calcd for $C_{15}H_{16}N_2O_3$: M, 272.1161.

2-[2-(2,3-Dimethoxy-5-methylphenyl)hydrazino]tropone (7i): Yellow prisms (by Procedure **A** using **6i**[18]); mp 73—75 °C (from benzene–hexane); IR 3305 (NH) and 1605 cm^{-1} (C=O); UV λ_{max} 250 (log ε 4.54), 339 (4.08), and 405 nm (4.11); ^1H NMR δ=2.15 (3H, s, Me-5′), 3.84 (3H, s, MeO-3′), 3.88 (3H, s, MeO-2′), 6.16 (1H, d, J=1.8 Hz, H-4′), 6.28 (1H, d, J=1.8 Hz, H-6′), 6.35 (1H, brm, NH-1′), 6.5—7.5 (5H, m, aromatic H), and 8.2 (1H, brm, NH-2); MS m/z 286 (M^+; 100), 167 (76), 166 (28), 152 (66), 151 (24), 139 (25), 138 (21), and 123 (21).

Found: m/z 286.1304. Calcd for $C_{16}H_{18}N_2O_3$: M, 286.1317.

2-[2-(2-Chlorophenyl)hydrazino]tropone (7j): Yellow prisms (by Procedure **A**); mp 91—93 °C (from benzene); IR 3320 (NH) and 1595 cm^{-1} (C=O); UV λ_{max} 249 (log ε 4.58), 338 (4.12), and 402 nm (4.14); ^1H NMR δ=6.35 (1H, brm, NH-1′), 6.5—7.4 (9H, m, aromatic H), and 8.25 (1H, brm, NH-2); MS m/z 248 (M^+; 19), 246 (M^+; 58), 129 (33), and 127 (100).

Found: m/z 246.0561. Calcd for $C_{13}H_{11}ClN_2O$: M, 246.0566.

2-[2-(3-Chlorophenyl)hydrazino]tropone (7k): Yellow prisms (by Procedure **A**); mp 159—161 °C (from benzene); IR 3320 (NH) and 1595 cm^{-1} (C=O); UV λ_{max} 248 (log ε 4.38), 338 (3.91), and 403 nm (3.93); ^1H NMR δ=6.25 (1H, brm, NH-1′), 6.5—7.4 (9H, m, aromatic H), and 8.35 (1H, brm, NH-2).

Anal. ($C_{13}H_{11}ClN_2O$) C, H, N.

2-[2-(4-Chlorophenyl)hydrazino]tropone (7l): Yellow prisms (by Procedure **A**); mp 118—120 °C (from ethanol–benzene); IR 3300 (NH) and 1595 cm^{-1} (C=O); UV λ_{max} 251 (log ε 4.48), 338 (4.00), and 403 nm (4.02); ^1H NMR δ=5.9 (1H, brm, NH-1′), 6.7—7.4 (5H, m, H-3—7), 6.71 (2H, brd, J=8.5 Hz, H-2′,6′), 7.18 (2H, brd, J=8.5 Hz, H-3′, 5′), and 8.3 (1H, brm, NH-2).

Anal. ($C_{13}H_{11}ClN_2O$) C, H, N.

2-[2-(2-Nitrophenyl)hydrazino]tropone (7m): Yellow prisms (by Procedure **A**); mp 178—179 °C (from benzene); IR 3320 (NH) and 1610 cm^{-1} (C=O); UV λ_{max} 245 (log ε 4.57), 327 (4.11), and 405 nm (4.25); ^1H NMR δ=6.5—7.8 (8H, m, aromatic H), 8.23 (1H, m, H-3′), and 9.55 (2H, brm, NH-1-,2).

Anal. ($C_{13}H_{11}N_3O_3$) C, H, N.

2-[2-(3-Nitrophenyl)hydrazino]tropone[1a] **(7n):** Yellow prisms (by Procedure **A**); mp 178—180 °C (from ethanol, lit,[1a] 180 °C).

2-[2-(4-Nitrophenyl)hydrazino]tropone[1a] **(7o):** Yellow prisms (by Procedure **A**); mp 185 °C decomp (from ethanol, lit,[1a] 191 °C).

4-Isopropyl-2-(2-phenylhydrazino)tropone (7p): Pale yellow needles (by Procedure **B** with phenylhydrazine free base); mp 152.5—153.5 °C (from EtOH); ^1H NMR (200-MHz) δ=1.16 (6H, d, J=7.0 Hz, Me_2C-4), 2.81 (1H, sept, J=7.0 Hz, HC-4), 5.71 (1H, brs, NH-1′), 6.73 (1H, brd, $J_{5,6}$=9.5 Hz, H-5), 6.82 (2H, brd, $J_{2',3'}=J_{5',6'}$=8.0 Hz, H-2′,6′), 6.93 (1H, brt, $J_{3',4'}=J_{4',5'}$=7.0 Hz, H-4′), 7.11 (1H, d, $J_{6,7}$=12.0 Hz, H-7), 7.13 (1H, d, $J_{3,5}$=1.5 Hz, H-3), 7.25 (2H, brdd, H-3′,5′), 7.29 (1H, dd, H-6), and 8.31 (1H, brs, NH-2); MS m/z 254 (M^+; 74), 211 (4), 163 (7), 163 (7), 105 (9), 93 (100), and 77 (30).

Found: m/z 254.1422. Calcd for $C_{16}H_{18}N_2O$: M, 254.1419.

4-Isopropenyl-2-(2-phenylhydrazino)tropone (7q): Yellow needles (by Procedure **B**); mp 176—178 °C (from EtOH); ^1H NMR (200-MHz) δ=2.04 (3H, brt, $J\simeq$1.2 Hz, MeC-4), 5.12 [1H, brquint, $J\simeq$1.5 Hz, (*E*)-HC=C-4], 5.17 [1H, brs, (*Z*)-HC=C-4], 5.17 (1H, brs, NH-1′), 6.81 (2H, brd, $J_{2',3'}=J_{5',6'}$=8.5 Hz, H-2′,6′), 6.81 (1H, brd, $J_{5,6}$=9.5 Hz, H-5), 6.92 (1H, brt, $J_{3',4'}=J_{4',5'}$=7.5 Hz, H-4′), 7.14 (1H, dd, $J_{6,7}$=11.5, $J_{5,7}$=1.0 Hz, H-7), 7.25 (2H, brdd, H-3′,5′), 7.28 (1H, d, $J_{3,5}$=1.5 Hz, H-3), 7.30 (1H, dd, H-6), and 8.30 (1H, brs, NH-2); MS m/z 252 (M^+; 72.8), 161 (11), 93 (100), and 77 (33).

Found: m/z 252.1271. Calcd for $C_{16}H_{16}N_2O$: M, 252.1263.

4-Isopropenyl-2-[2-(*o*-tolyl)hydrazino]tropone (7r): Yellow needles (by Procedure **B**); mp 141—142 °C (from ether); ^1H NMR (200-MHz) δ=2.05 (3H, brt, J=1.2 Hz, MeC-4), 2.29 (3H, s, Me-2′), 5.12 [1H, brquint, J=1.2 Hz, (*E*)-HC=C-4], 5.17 [1H, brs, (*Z*)-HC=C-4], 5.64 (1H, brs, NH-1′), 6.75 (1H, brd, $J_{5',6'}$=8.0 Hz, H-6′), 6.86 (1H, brd, $J_{5,6}$=9.5 Hz, H-5), 6.87 (1H, td, $J_{3',4'}=J_{4',5'}$=7.5, $J_{4',6'}$=1.0 Hz, H-4′), 7.11 (1H, brt, H-5′), 7.14 (1H, brd, H-3′), 7.14 (1H, d, $J_{6,7}$=11.5 Hz, H-7), 7.28 (1H, d, $J_{3,4}$=1.5 Hz, H-3), 7.32 (1H, dd, H-6), and 8.28 (1H, brs, NH-2); MS m/z 266 (M^+; 52.5), 161 (8), 145 (4), 133 (13), 107 (100), 106 (55), and 91 (16).

Found: m/z 266.1397. Calcd for $C_{17}H_{18}N_2O$: M, 266.1419.

4-Isopropenyl-2-[2-(*m*-tolyl)hydrazino]tropone (7s): Yellow needles (by Procedure **B**); mp 165—167 °C (from ether); ^1H NMR (200-MHz) δ=2.05 (3H, brt, $J\simeq$1.2 Hz, MeC-4), 2.27 (3H, s, Me-3′), 5.13 [1H, qd, J=1.5, 1.0 Hz, (*E*)-HC=C-4], 5.19 [1H, brs, (*Z*)-HC=C-4], 5.65 (1H, brs, NH-1′), 6.62 (1H, brd, $J_{4',5'}$=8.5 Hz, H-4′), 6.64 (1H, brs, H-2′), 6.74 (1H, brd, $J_{5',6'}$=7.5 Hz, H-6′), 6.86 (1H, brd, $J_{5,6}$=9.5 Hz, H-5), 7.15 (1H, brdd, H-5′), 7.16 (1H, brdd, $J_{6,7}$=11.5, $J_{5,7}\simeq$1.0 Hz, H-7), 7.26 (1H, brd, $J_{3,5}$=1.5 Hz, H-3), 7.31 (1H, dd, H-6), and 8.28 (1H, brs, NH-2); MS m/z 266 (M^+; 43.1), 223 (5), 161 (4), 145 (6), 133 (15), 132 (12), 107 (100), and 91 (20).

Found: m/z 266.1432. Calcd for $C_{17}H_{18}N_2O$: M, 266.1419.

4-Isopropenyl-2-[2-(2-methoxyphenyl)hydrazino]tropone (7t): Yellow needles (by Procedure **B**); mp 122—123.5 °C (from ether–light petroleum); ^1H NMR (500-MHz) δ=2.05 (3H, brd, J=1.5 Hz, MeC-4), 3.92 (3H, s, MeO-2′), 5.11 [1H, brquint, J=1.5 Hz, (*E*)-HC=C-4], 5.17 [1H, brs, (*Z*)-HC=C-4], 6.24 (1H, brm, NH-1′), 6.74 (1H, brd, $J_{3',4'}$=7.4 Hz, H-3′), 6.84 (1H, brd, $J_{5,6}$=9.5 Hz, H-5), 6.83—6.88 (3H, m, H-5′,4′,6′), 7.12 (1H, brd, $J_{6,7}$=11.7 Hz, H-7), 7.26 (1H, brd, $J_{3,5}$=1.5 Hz, H-3), 7.29 (1H, dd, H-6), and 8.22 (1H, brm, NH-2); MS m/z 282 (M^+; 69.2), 161 (10), 132 (21), 123 (100), 122 (42), 108 (42), 94 (97), and 80 (43).

Found: m/z 282.1364. Calcd for $C_{17}H_{18}N_2O_2$: M, 282.1368.

4-Isopropenyl-2-[2-(3-methoxyphenyl)hydrazino]tropone (7u): Yellow needles (by Procedure **B**); mp 165—166 °C (from ether); ^1H NMR (200-MHz) δ=2.03 (3H, brd, J=1.5 Hz, MeC-4), 3.71 (3H, s, MeO-3′), 5.08 [1H, brq, J=1.5 Hz, (*E*)-HC=C-4], 5.13 [1H, brs, (*Z*)-HC=C-4], 5.65 (1H, brs, NH-1′), 6.30 (1H, t, $J_{2',4'}\simeq J_{2',6'}\simeq$2.0 Hz, H-2′), 6.35 (1H, ddd, $J_{4',5'}$=8.0, $J_{4',6'}$=1 Hz, H-4′), 6.40 (1H, dd, $J_{5',6'}$=8.0 Hz, H-6′), 6.79 (1H, ddd, $J_{5,6}$=9.5, $J_{3,5}$=1.5, $J_{5,7}$=1.0 Hz, H-5), 7.05 (1H, dd, $J_{6,7}$=12.0 Hz, H-7), 7.07 (1H, t, H-5′), 7.19 (1H, d, H-3), 7.23 (1H, dd, H-6), and 8.19 (1H, brs, NH-2); MS m/z 282 (M^+; 53.3), 161 (8), 132 (18), 123 (100), 122 (43), 108 (38), 94 (82), and 80 (50).

Found: m/z 282.1365. Calcd for $C_{17}H_{18}N_2O_2$: M, 282.1368.

4-Isopropenyl-2-[2-(2,3-dimethoxyphenyl)hydrazino]tropone (7v): A yellow oil (by Procedure **B**); ^1H NMR (200-MHz) δ=2.02 (3H, dd, J=1.5, 1.0 Hz, MeC-4), 3.85 (3H, s, MeO-3′), 3.90 (3H, s, MeO-2′), 5.09 [1H, qd, J=1.5, 1.0 Hz, (*E*)-HC=C-4], 5.16 [1H, quint, J=1.0 Hz, (*Z*)-HC=C-4], 6.27 (1H, brs, NH-1′), 6.36 (1H, dd, $J_{4',5'}$=8.0, $J_{4',6'}$=1.5 Hz, H-4′), 6.40 (1H, dd, $J_{5',6'}$=8.0 Hz, H-6′), 6.82 (1H, ddd, $J_{5,6}$=9.5,

$J_{3,5}$=1.5, $J_{5,7}$=1 Hz, H-5), 6.87 (1H, t, H-5′), 7.09 (1H, dd, $J_{6,7}$=12.0 Hz, H-7), 7.22 (1H, d, H-3), 7.27 (1H, dd, H-6), and 8.17 (1H, brs, NH-2); MS *m/z* 312 (M^+; 3), 153 (72), and 138 (100).

Found: *m/z* 312.1470. Calcd for $C_{18}H_{20}N_2O_3$: M, 312.1474.

4-Isopropenyl-2-[2-(2,3-dimethoxy-5-methylphenyl)hydrazino]tropone (7w): A yellow oil (by Procedure **B**); ^{1}H NMR (200-MHz) δ=2.07 (3H, brs, MeC-4), 2.19 (3H, s, Me-5′), 3.85 (3H, s, MeO-3′), 3.88 (3H, s, MeO-2′), 5.12, 5.20 (1H each, both brs, H_2C=C-4), 6.21 (1H, brd, $J_{4',6'}$=1.5 Hz, H-4′), 6.24 (1H, brs, NH-1′), 6.30 (1H, brd, H-6′), 6.84 (1H, ddd, $J_{5,6}$=9.5, $J_{3,5}$=1.5, $J_{5,7}$≃0.5 Hz, H-5), 7.13 (1H, d, $J_{6,7}$=12.0 Hz, H-7), 7.28 (1H, d, H-3), 7.29 (1H, dd, H-6), and 8.18 (1H, brs, NH-2); MS *m/z* 326 (M^+; 90), 331 (8), 295 (5), 175 (14), 167 (100), 161 (48), 152 (97), 136 (84), and 91 (57).

Found: *m/z* 326.1611. Calcd for $C_{19}H_{22}N_2O_3$: M, 326.1630.

4-(1-Acetamidoethyl)-2-[2-(2-methoxyphenyl)hydrazino]tropone (7x): A pale amber syrup (by Procedure **B**); ^{1}H NMR δ=1.41 (3H, d, *J*=7.5 Hz, MeC-4), 1.88 (3H, s, AcN), 3.97 (3H, s, MeO-2′), 4.87 (1H, brquint, *J*=7.5 Hz, HC-4), 5.6 (1H, brd, *J*≃6.5 Hz, HNC-4), 6.3 (1H, brs, NH-1′), 6.65—7.40 (8H, m, aromatic H), and 8.10 (1H, brs, NH-2); MS *m/z* 327 (M^+; 81), 268 (42), 124 (100), and 107 (91).

Found: *m/z* 327.1556. Calcd for $C_{18}H_{21}N_3O_3$: M, 327.1583.

4-(1-Acetamidoethyl)-2-[2-(3-methoxyphenyl)hydrazino]tropone (7y): A yellow oil (by Procedure **B**); ^{1}H NMR (200-MHz) δ=1.34 (3H, d, *J*=7.0 Hz, MeC-4), 1.86 (3H, s, AcN), 3.72 (3H, s, MeO-3′), 4.80 (1H, brquint, *J*≃7 Hz, HC-4), 5.77 (1H, brd, *J*≃6.5 Hz, HNC-4), 5.83 (1H, brs, NH-1′), 6.28 (1H, brt, $J_{2',4'}$≃$J_{4',6'}$≃2.0 Hz, H-2′), 6.33 (1H, brdt, $J_{4',5'}$=8.0, $J_{4',6'}$=2 Hz, H-4′), 6.40 (1H, brdd, $J_{5',6'}$=8.0 Hz, H-6′), 6.71 (1H, brd, $J_{5,6}$=9.5 Hz, H-5), 6.99 (1H, brd, $J_{3,5}$≃1 Hz, H-3), 7.05 (1H, brd, $J_{6,7}$=12.0 Hz, H-7), 7.08 (1H, t, H-5′), 7.22 (1H, dd, H-6), and 8.21 (1H, brs, NH-2); MS *m/z* 327 (M^+; 92), 268 (63), 124 (100), and 107 (88).

Found: *m/z* 327.1565. Calcd for $C_{18}H_{21}N_3O_3$: M, 327.1583.

4-(1-Acetamidoethyl)-2-[2-(2,3-dimethoxyphenyl)hydrazino]tropone (7z): A yellow oil (by Procedure **B**); ^{1}H NMR (200-MHz) δ=1.33 (3H, d, *J*=7.0 Hz, MeC-4), 1.87 (3H, s, AcN), 3.88 (3H, s, MeO-3′), 3.95 (3H, s, MeO-2′), 4.83 (1H, brquint, *J*=7 Hz, HC-4), 5.72 (1H, brd, *J*=6.5 Hz, HNC-4), 6.30 (1H, brs, NH-1′), 6.37 (1H, brdd, $J_{4',5'}$=8.0, $J_{4',6'}$=1.5 Hz, H-4′), 6.49 (1H, brdd, H-6′), 6.76 (1H, brd, $J_{5,6}$=9.5 Hz, H-5), 6.89 (1H, t, $J_{5',6'}$=8.0 Hz, H-5′), 6.96 (1H, brd, $J_{3,5}$≃1.5 Hz, H-3), 7.10 (1H, brdd, $J_{6,7}$=11.5, $J_{5,7}$=1.0 Hz, H-7), 7.26 (1H, dd, H-6), and 8.22 (1H, brs, NH-2); MS *m/z* 357 (M^+; 69), 298 (39), 206 (28), 163 (32), 153 (100), and 138 (49).

Found: *m/z* 357.1736. Calcd for $C_{19}H_{23}N_3O_4$: M, 357.1689.

4-(2,5,5-Trimethyl-1,3-dioxan-2-yl)-2-[2-(2-methoxyphenyl)hydrazino]tropone (7z′): Yellow needles (by Procedure **B**); mp 145—146.5 °C (from ether–light petroleum); IR (KBr) 3320 (NH) and 1598 cm^{-1} (C=O); ^{1}H NMR δ=0.54 [3H, s, (*Z*)-Me-5″], 1.20 [3H, s, (*E*)-Me-5″], 1.47 (3H, s, Me-2″), 3.19 (4H, brs, 2H-4″,6″), 3.92 (3H, s, MeO-2′), 6.27 (1H, m, NH-1′), 6.80 (1H, d, $J_{5,6}$≃9.5 Hz, H-5), 6.55—7.0 (4H, m, H-3′,4′,5′,6′), 7.16 (1H, brd, $J_{6,7}$≃11 Hz, H-7), 7.23 (1H, brs, H-3), 7.30 (1H, brdd, H-6), and 8.29 (1H, m, HN-2); MS *m/z* 370 (M^+; 100), 355 (14), 129 (30), 123 (50), 108 (17), 69 (13), and 43 (18).

Found: *m/z* 370.1892. Calcd for $C_{21}H_{26}N_2O_4$: M, 370.1893.

6,6′-Bis(phenylhydrazono)-1,1′-bi(2,4-cycloheptadiene)-7,7′-dione (8a): Bright yellow needles (by Procedure **A**); mp 183—184 °C decomp (from benzene); IR 3350 (NH) and 1635 cm^{-1} (C=O); ^{1}H NMR (100-MHz) δ=3.82 (2H, brt, $J_{1,2}$=3.0, $J_{1,3}$=2.5 Hz, H-1,1′), 5.48 (2H, brddd, $J_{2,3}$=9.0, $J_{2,4}$=2.5 Hz, H-2,2′), 6.33 (2H, m, $J_{4,5}$=11.0, $J_{3,5}$=2.0 Hz, H-5,5′), 6.34 (2H, m, $J_{3,4}$=2.5 Hz, H-3,3′), 6.66 (2H, brdt, H-4,4′), 6.9—7.4 (10H, m, 2Ph), and 13.6 (2H, brm, NH-6,6′); ^{13}C NMR δ=50.3 (C-1), 115.5, 123.4, 124.2, 124.8, 129.2, 129.4, 129.9, 135.0 (C-1′), 142.4 (C-6), and 187.6 (C-7); MS *m/z* 212 (41), 210 (97), 193 (24), 182 (19), 181 (22), 154 (26), 119 (38), and 91 (100).

Anal. ($C_{26}H_{22}N_4O_2$) C, H, N.

6,6′-Bis[(*o*-tolyl)hydrazono]-1,1′-bi(2,4-cycloheptadiene)-7,7′-dione (8b): Bright yellow needles (by Procedure **A**); mp 161—162 °C decomp (from benzene); IR 3450 (NH) and 1635 cm^{-1} (C=O); ^{1}H NMR δ=1.95 (6H, s, 2 Me-2″), 3.8—3.95 (2H, m, H-1,1′), 5.3—5.7 (2H, m, H-2,2′), 6.15—7.8 (14H, m, aromatic H), and 13.9 (2H, brm, NH-6,6′).

Anal. ($C_{28}H_{26}N_4O_2$) C, H, N.

6,6′-Bis[(*m*-tolyl)hydrazono]-1,1′-bi(2,4-cycloheptadiene)-7,7′-dione (8c): Bright yellow needles (by Procedure **A**); mp 179—181 °C decomp (from benzene); IR 3410 (NH) and 1630 cm^{-1} (C=O); ^{1}H NMR δ=2.22 (6H, s, 2Me-3″), 3.65—3.85 (2H, m, H-1,1′), 5.2—5.6 (2H, m, H-2,2′), 6.1—7.2 (14H, m, aromatic H), and 14.4 (2H, brm, NH-6,6′).

Anal. ($C_{28}H_{26}N_4O_2$) C, H, N.

6,6′-Bis[(*p*-tolyl)hydrazono]-1,1′-bi(2,4-cycloheptadiene)-7,7′-dione (8d): Bright yellow needles (by Procedure **A**); mp 174—175 °C decomp (from benzene); IR 3450 (NH) and 1630 cm^{-1} (C=O); ^{1}H NMR δ=2.30 (6H, s, 2Me-4″), 3.65—3.9 (2H, m, H-1,1′), 5.3—5.7 (2H, m, H-2,2′), 6.15—7.3 (6H, m, H-3,3′,4,4′,5,5′), 7.20 (8H, m, 2H-2″,3″,5″,6″), and 13.8 (2H, brm, NH-6,6′).

Anal. ($C_{28}H_{26}N_4O_2$) C, H, N.

6,6′-Bis[(2-methoxyphenyl)hydrazono]-1,1′-bi(2,4-cycloheptadiene)-7,7′-dione (8e): Bright yellow needles (by Procedure **A**); mp 174—176 °C decomp (from benzene); IR 3400 (NH) and 1640 cm^{-1} (C=O); ^{1}H NMR δ=3.40 (6H, s, 2MeO-2″), 3.90 (2H, m, H-1,1′), 5.3—5.6 (2H, m, H-2,2′), 6.2—7.8 (14H, m, aromatic H), and 13.4 (2H, brm, NH-6,6′).

Anal. ($C_{28}H_{26}N_4O_4$) C, H, N.

6,6′-Bis[(3-methoxyphenyl)hydrazono]-1,1′-bi(2,4-cycloheptadiene)-7,7′-dione (8f): Bright yellow needles (by Procedure **A**); mp 162—163 °C decomp (from benzene); IR 3390 (NH) and 1635 cm^{-1} (C=O); ^{1}H NMR δ=3.65—3.85 (2H, m, H-1,1′), 3.70 (6H, s, 2MeO-3″), 5.3—5.6 (2H, m, H-2,2′), 6.1—7.3 (14H, m, aromatic H), and 13.75 (2H, brm, NH-6,6′).

Anal. ($C_{28}H_{26}N_4O_4$) C, H, N.

6,6′-Bis[(4-methoxyphenyl)hydrazono]-1,1′-bi(2,4-cycloheptadiene)-7,7′-dione (8g): Bright yellow needles (by Procedure **A**); mp 158—160 °C decomp (from benzene); IR 3200 (NH) and 1630 cm^{-1} (C=O); ^{1}H NMR δ=3.7—3.8 (2H, m, H-1,1′), 3.71 (6H, s, 2MeO-4″), 5.25—5.6 (2H, m, H-2,2′), 6.15—7.35 (6H, m, H-3,3′,4,4′,5,5′), 6.73 (4H, brd, *J*=8.5 Hz, 2H-3″,5″), 7.11 (4H, brd, *J*=8.5 Hz, 2H-2″,6″), and 14.0 (2H, brm, NH-6,6′).

Anal. ($C_{28}H_{26}N_4O_4$) C, H, N.

6,6′-Bis[(2-chlorophenyl)hydrazono]-1,1′-bi(2,4-cycloheptadiene)-7,7′-dione (8j): Bright yellow needles (by Procedure **A**); mp 173—175 °C decomp (from benzene); IR 3450 (NH) and 1635 cm^{-1} (C=O); ^{1}H NMR δ=3.9—4.05 (2H, m, H-1,1′), 5.15—5.55 (2H, m, H-2,2′) 6.1—7.7 (14H, m, aromatic H), and 13.6 (2H, brm, NH-6,6′).

Anal. ($C_{26}H_{20}Cl_2N_4O_2$) C, H, N.

6,6′-Bis[(3-chlorophenyl)hydrazono]-1,1′-bi(2,4-cycloheptadiene)-7,7′-dione (8k): Bright yellow needles (by Procedure **A**); mp 180—181 °C decomp (from benzene); IR 3415 (NH) and 1630 cm^{-1} (C=O); ^1H NMR δ=3.85—3.95 (2H, m, H-1,1′), 5.45—5.8 (2H, m, H-2,2′), 6.3—7.75 (14H, m, aromatic H), and 13.6 (2H, brm, NH-6,6′).

Anal. ($C_{26}H_{20}Cl_2N_4O_2$) C, H, N.

6,6′-Bis[(4-chlorophenyl)hydrazono]-1,1′-bi(2,4-cycloheptadiene)-7,7′-dione (8l): Bright yellow needles (by Procedure **A**); mp 175—176 °C decomp (from benzene); IR 3410 (NH) and 1630 cm^{-1} (C=O); ^1H NMR δ=3.7—3.95 (2H, m, H-1,1′), 5.4—5.75 (2H, m, H-2,2′), 6.3—7.0 (6H, m, H-3,3′,4,4′,5,5′), 7.35 (8H, s, 2H-2″,3″,5″,6″), and 14.1 (2H, brm, NH-6,6′).

Anal. ($C_{26}H_{20}Cl_2N_4O_2$) C, H, N.

6,6′-Bis[(2-nitrophenyl)hydrazono]-1,1′-bi(2,4-cycloheptadiene)-7,7′-dione (8m): Bright yellow needles (by Procedure **A**); mp 182—184 °C decomp (from ethyl acetate); IR 3390 (NH) and 1655 cm^{-1} (C=O); ^1H NMR almost insoluble for the measurement.

Anal. ($C_{26}H_{20}N_6O_6$) C, H, N.

6,6′-Bis[(3-nitrophenyl)hydrazono]-1,1′-bi(2,4-cycloheptadiene)-7,7′-dione (8n): Bright yellow needles (by Procedure **A**); mp 180—182 °C decomp (from ethyl acetate); IR 3420 (NH) and 1640 cm^{-1} (C=O); ^1H NMR δ=3.65—3.75 (2H, m, H-1,1′), 5.25—5.45 (2H, m, H-2,2′), 6.2—8.4 (14H, m, aromatic H), and 13.85 (2H, brm, NH-6,6′).

Anal. ($C_{26}H_{20}N_6O_6$) C, H, N.

6,6′-Bis[(4-nitrophenyl)hydrazono]-1,1′-bi(2,4-cycloheptadiene)-7,7′-dione (8o): Bright yellow needles (by Procedure **A**); mp 189—191 °C decomp (from ethyl acetate); IR 3450 (NH) and 1640 cm^{-1} (C=O); ^1H NMR δ=3.65—3.8 (2H, m, H-1,1′), 5.2—5.6 (2H, m, H-2,2′), 6.2—8.4 (14H, m, aromatic H), and 13.85 (2H, brm, NH-6,6′).

Anal. ($C_{26}H_{20}N_6O_6$) C, H, N.

3-(2-Phenylhydrazino)tropone (9a): Pale yellow crystals; mp 140—142 °C (from benzene); IR 3250 (NH) and 1600 cm^{-1} (C=O); UV λ_{max} 248 (log ε 4.19), 305 (4.06), and 354 nm (4.39); ^1H NMR δ=6.6—7.6 (9H, m, aromatic H), 7.35 (1H, brm, NH-1′), 7.63 (1H, s, H-2), and 10.82 (1H, brm, NH-3).

Anal. ($C_{13}H_{12}N_2O$) C, H, N.

3-[2-(4-Chlorophenyl)hydrazino]tropone (9l): Brownish yellow crystals; mp 168—170 °C (from benzene); IR 3320 (NH) and 1600 cm^{-1} (C=O); UV λ_{max} 242 (log ε 4.15), 316 (4.21), and 355 nm (4.40); ^1H NMR δ=6.7—7.8 (8H, m, aromatic H), 8.24 (1H, s, H-2), and 10.25 (2H, brm, NH-3, NH-1′); MS *m/z* 248 (M^+; 29), 246 (M^+; 100), 127 (94), and 126 (53).

Found: *m/z* 246.0546. Calcd for $C_{13}H_{11}ClN_2O$: M, 246.0560.

2-(*N*-Amino-4-methoxyanilino)tropone (10): Reddish orange prisms; mp 105—107 °C (from hexane); IR 3350 (NH) and 1615 cm^{-1} (C=O); UV λ_{max} 250 (log ε 4.22), 285 sh (3.94), 368 (3.83), and 428 nm (3.93); ^1H NMR δ=3.80 (3H, s, MeO-4′), 4.8 (2H, brm, NH_2), 6.5—7.5 (5H, m, aromatic H), 6.82 (2H, brd, *J*=9.0 Hz, H-3′,5′), and 7.16 (2H, brd, *J*=9.0 Hz, H-2′,6′).

Anal. ($C_{14}H_{14}N_2O_2$) C, H, N.

2-(4-Methoxyanilino)tropone (11): Yellow prisms; mp 74—75 °C (from light petroleum); IR 3300 (NH) and 1605 cm^{-1} (C=O); UV λ_{max} 246 (log ε 4.39), 284 sh (3.85), 350 (4.02), and 411 nm (4.19); ^1H NMR δ=3.81 (3H, s, MeO-4′), 6.4—7.3 (5H, m, H-3—7), 6.97 (2H, brd, *J*=9.5 Hz, H-3′,5′), 7.19 (2H, brd, *J*=9.5 Hz, H-2′,6′), and 8.6 (1H, brm, NH).

Anal. ($C_{14}H_{13}NO_2$) C, H, N.

3-Amino-2-(3-methoxyanilino)tropone (12): Orange needles; mp 145—147 °C (from benzene); IR 3450, 3375, 3275 (NH), and 1600 cm^{-1} (C=O); UV λ_{max} 242 (log ε 4.41), 250 sh (4.38), 346 (3.91), and 413 nm (4.16); ^1H NMR δ=3.82 (3H, s, MeO), 3.9 (2H, brm, NH_2), 6.5—6.9 (4H, m, H-4—7), and 8.6 (1H, brm, NH-2).

Anal. ($C_{14}H_{14}N_2O_2$) C, H, N.

3-[2-(3-Chlorophenyl)-2-methylhydrazino]tropone (13): Red needles; mp 118—120 °C (from benzene); IR 3350 (NH) and 1600 cm^{-1} (C=O); UV λ_{max} 269 (log ε 3.76) and 363 (4.10); ^1H NMR δ=3.86 (3H, s, MeN), 5.6—7.5 (9H, m, aromatic H), and 7.59 (1H, brm, NH); MS *m/z* 262 (M^+; 34), 260 (M^+; 100), 247 (15), 245 (46), 134 (40), 111 (64), and 91 (35).

Found: *m/z* 260.0729. Calcd for $C_{14}H_{13}ClN_2O$: M, 260.0716.

Conversion of 10 to 11. A solution of **10** (33 mg) in methanol (5 cm^3) containing concd HCl (0.2 cm^3, 2 equiv) was refluxed for 8 h, diluted with water, neutralized with a saturated aq $NaHCO_3$, and extracted with chloroform. The combined organic layers were washed with water, dried (Na_2SO_4), and evaporated in vacuo. The residue was purified by preparative TLC with chloroform to give **11** (4 mg, 13%) and the recovered **10** (36%).

We are very grateful to Dr. Yukio Sugimura (Sankyo Co., Ltd., Tokyo) and Professor Kahai Takese (Tohoku University) for their valuable advice and help. Thanks are also due to Professor Hitoshi Takeshita (Kyushu Univ.) for the measurement of the ^{13}C NMR spectrum, Mr. Shin-ich Takekuma (Kinki Univ.) for 200-MHz ^1H NMR and MS, and Dr. Hiromichi Matsuura (Wakunaga Pharmaceutical Co., Ltd.) for the high-resolution mass spectra. The present work was partially supported by Grant-in-Aids for Scientific Research Nos. 60540331 (to H. Y.), 60540336, and 61540381 (to K. I.) from the Ministry of Education, Science and Culture.

References

1) A part of the results has been preliminarily presented: a) H. Saito, M. Yasunami, M. Ando, K. Takase, and T. Nozoe, 37th National Meeting of the Chemical Society of Japan, Tokyo, April 1978, Abstr. No. 2D32; H, Saito, M. Sc. Thesis, Tohoku Univ. (1978); b) T. Nozoe, K. Takase, H. Saito, H. Yamamoto, and K. Imafuku, *Chem. Lett.*, **1986**, 1577 and references cited therein.

2) B. T. Newbold, "The Chemistry of the Hydrazo, Azo, and Azoxy Groups," ed by S. Patai, Wiley, London (1975), Part 2, pp. 599—641; I. G. Laing, "Rodd's Chemistry of Carbon Compounds," 2nd ed., ed by S. Coffey, Elsevier, Amsterdam (1978), Vol. 3C, pp. 217—247.

3) T. Nozoe, K. Takase, H. Matsumura, T. Asao, K. Kikuchi, and S. Ito, "Dai Yuki Kagaku (Comprehensive Organic Chemistry)," ed by M. Kotake, Asakura, Tokyo (1960), Vol. 13, pp. 1—692; F. Pietra, *Chem. Rev.*, **73**, 293 (1973); D. Lloyd, "Non-benzenoid Conjugated Carbocyclic Compounds," Elsevier, Amsterdam (1984), pp. 107—125.

4) N. Soma, J. Nakazawa, T. Watanabe, Y. Sato, and G. Sunagawa, *Chem. Pharm. Bull.*, **13**, 457 (1965).

5) K. Imafuku, K. Kamachi, Y. Matsuda, and H. Matsumura, *Bull. Chem. Soc. Jpn.*, **52**, 2447 (1979).

6) N. Kitano, S. Sugawara, Y. Kishida, F. Kondo, Y. Sugimura, and N. Soma, Nippon Kokai Tokkyo Koho JP. 49-94816 (1974); *Chem. Abstr.*, **81**, 176148r (1974).

7) See B. Bhattacharyya and J. Wolff, *J. Biol. Chem.*, **259**, 11836 (1984) and references cited therein.

8) See e.g., T. J. Fritzgerald, *Biochem. Pharmacol.*, **25**, 1383 (1976); M. Rossi, J. Link, and C. Lee, *Arch. Biochem. Biophys.*, **231**, 470 (1984); C.-P. Mak and G. Büchi, *J. Org. Chem.*, **46**, 1 (1981).

9) T. Nozoe, K. Takase, and M. Ogata, *Chem. Ind. (London)*, **1957**, 1070; H, Yamamoto, A. Hara, A. Noguchi, H. Kawamoto, S. Inokawa, and T. Nozoe, *Bull. Chem. Soc. Jpn.*, **55**, 1594 (1982).

10) T. Nozoe, *Experientia, Suppl. VII*, **1957**, 306; T. Nozoe, K. Takase, N. Kawabe, T. Asao, and H. Yamamoto, *Bull. Chem. Soc. Jpn.*, **56**, 3099 (1983) and references cited therein.

11) H. Yamamoto, A. Hara, S. Inokawa, and T. Nozoe, *Bull. Chem. Soc. Jpn.*, **56**, 3106 (1983).

12) T. Nozoe, K. Takase, M. Yasunami, M. Ando, H. Saito, K. Imafuku, B.-Z. Yin, M. Honda, Y. Goto, T. Hanaya, Y. Hara, and H. Yamamoto: To be published (in preparation).

13) T. Sato, *Nippon Kagaku Zasshi*, **80**, 1058 (1959).

14) T. Nozoe, T. Mukai, and T. Asao, *Bull. Chem. Soc. Jpn.*, **33**, 1452 (1960).

15) The detailed mechanistic study on this substitution reaction as well as the oxidation of **7** to **8** will be reported later: K. Imafuku, S. Hirose, Y. Imai, and T. Nozoe.

16) E. J. Forbes, D. C. Warrell, and W. J. Fry, *J. Chem. Soc. C*, **1967**, 1693.

17) W. von E. Doering and C. F. Hiskey, *J. Am. Chem. Soc.*, **74**, 5688 (1952).

18) M. Tsutsumi, M. Hojo, I. Takasu, and T. Nozoe, to be published.

Promoter Effect of Platinum on Liquid-Phase Dehydrogenation of 2-Propanol by a Nickel Fine-Particle Catalyst

Michio NODA,* Sumio SHINODA,† and Yasukazu SAITO
Institute of Industrial Science, University of Tokyo,
7-22-1 Roppongi, Minato-ku, Tokyo 106
(Received November 2, 1987)

A platinum-deposited nickel fine-particle catalyst was shown to be more active than a nickel-alone catalyst. A study of the temperature dependence of a rate constant revealed that platinum increased the frequency factor of the rate constant. An experiment regarding poisoning showed that the number of active sites was the same for the two catalysts. Thus the promoter effect was ascribed to an increase in the frequency factor per active site.

Liquid-phase dehydrogenation of 2-propanol proceeded by means of a metallic catalyst[1-4] or a complex catalyst in solution[5-9] or on a support.[10,11]

$$(CH_3)_2CHOH \longrightarrow (CH_3)_2CO + H_2$$

Nickel fine particles that were prepared by a gas-evaporation method[12,13] were also a suitable catalyst for the reaction.[14,15]

The surface modification of a metallic catalyst with a platinum-group metal has long been applied in order to increase the reaction rate. For example, platinum salts promoted hydrogenation activity of the Raney nickel catalyst.[16,17] In the present work, the promoter effect was studied through catalysis using nickel fine particles, since their shape and components are sufficiently simple to provide a clear explanation.

Experimental

1. Materials. Nickel fine particles were prepared by means of a gas-evaporation method of Vacuum Metallurgical Co., Ltd. (Chiba Pref., Japan). They comprised black, light powder. Their average diameter and BET surface area were 19.7 nm and 43.8 $m^2 g^{-1}$. Their surfaces were covered with oxide layers in order to prevent the particles from burning in air. Partial reduction of the surface oxide by heating nickel fine particles under hydrogen was necessary in order to reveal catalytic activity.[18]

Bis(acetylacetonato)platinum(II) ($Pt(acac)_2$) was purchased from Nippon Engelhard Ltd..

2. Pretreatment. Nickel fine particles were pretreated and a reaction rate was measured using the technique described in a previous paper.[15] A prescribed amount (200 mg) of nickel fine particles was put into a round-bottom three-neck flask. After evacuation, the nickel fine particles were heated under hydrogen up to 160 °C in 15 min, held at 160 °C for 1 min and rapidly cooled. The amount of consumed hydrogen was measured with a gas buret. After evacuation, a prescribed amount (200 ml) of 2-propanol was added under nitrogen or argon. The nickel fine-particle catalyst was suspended in 2-propanol by means of vibration with a supersonic cleaner.

Platinum was deposited on the catalyst as follows: A prescribed amount (9 mg) of $Pt(acac)_2$ was dissolved in 2-propanol beforehand. After a nickel fine-particle catalyst was suspended in the solvent, hydrogen was blown into the stirred suspension through a glass straw for 30 min at room temperature. Hydrogen reduced any divalent platinum in the complex. If part of a catalyst suspension was placed on a magnet, the nickel fine particles contained in it precipitated during a day. The visible and ultraviolet spectra of a supernatant were recorded with a Shimadzu UV-365 spectrometer. An XRD pattern of the catalyst was recorded with a Rigaku-Denki Geigerflex D-9C X-ray diffractometer.

3. Measurement. A catalyst suspension was heated under boiling conditions with stirring. The height of the level of the suspension equaled that of an oil bath in which the reactor was soaked. A gas buret was connected to the reactor through a water-cooled condenser. The reaction rate was determined by the volume of gas that accumulated in the gas buret. Products in a gas phase and in the liquid phase were analyzed by gas chromatography using an active carbon column and a PEG-1000 column, respectively.

The temperature dependence of the reaction rate was investigated by addition of hexane to a catalyst suspension, since hexane reduces the boiling point of a solvent. The frequency factor and the coefficient of exponential T^{-1} were determined for the rate constant k and the equilibrium constant of acetone adsorption K.[4]

The number of active sites of a nickel fine-particle catalyst was estimated by means of poisoning. The reaction rate was plotted against an amount of a poison such as water, triethylamine, pyridine, thiophene, or triphenylphosphine. Each poison was easily dissolved in 2-propanol and was added to a catalyst suspension.

Results and Discussion

1. Promoter Effect of $Pt(acac)_2$. Platinum chloride promoted catalytic activity of the Raney nickel in various hydrogenation reactions.[16,17] Nevertheless, a slight amount of $PtCl_2$ extremely retarded any liquid-phase dehydrogenation of 2-propanol that was catalyzed by nickel fine particles. Instead of $PtCl_2$, $Pt(acac)_2$ was selected as a supply source of platinum. Platinum was deposited on a nickel fine-particle catalyst by means of reducing the complex with hydrogen. The disappearance of a characterestic peak of $Pt(acac)_2$ at 344 nm in visible and ultraviolet spectra

† Present address: Department of Industrial Chemistry, Faculty of Engineering, Seikei University, 3-3-1 Kichijyoji-Kitamachi, Musashino-Shi, Tokyo 180.

of a supernatant indicated that the platinum in the complex was reduced. No platinum peak was observed in the XRD pattern of the catalyst after a reaction. This showed that the reduced platinum did not form a particle.

A platinum-deposited nickel fine-particle catalyst was more active than a nickel-alone catalyst, as shown in Fig. 1. Both catalysts exclusively produced hydrogen and acetone.

2. Retardation Effect of Acetone. A gradual decrease in the reaction rate was observed for various nickel catalysts in liquid-phase dehydrogenation of 2-propanol. The decrease in activity was ascribed to an adsorptive retardation of the produced acetone. Reaction rates are well expressed by

$$v = k/(1 + K[\text{acetone}]), \qquad (1)$$

where k is a rate constant and K is an equilibrium constant of acetone adsorption.[1-4,15] Symbol [acetone] refers to the amount of acetone, expressed in units of mmol.

Equation 1 also expressed the reaction rate provided by a platinum-deposited nickel fine-particle catalyst. Though the boiling point of the solvent decreased from 82.4 to 80.7 °C after a 5-h reaction, this change hardly affected the constants k and K. Figure 2 illustrates a linear relation between v^{-1} and the amount of acetone, into which data of Fig. 1 were converted. Values of k and K were determined from the section and the slope of Fig. 2; k was 330 mmol h^{-1} g^{-1} and K was 0.0403 $mmol^{-1}$. As for a nickel-alone catalyst, k was 116 mmol h^{-1} g^{-1} and K was 0.0301 $mmol^{-1}$.[15]

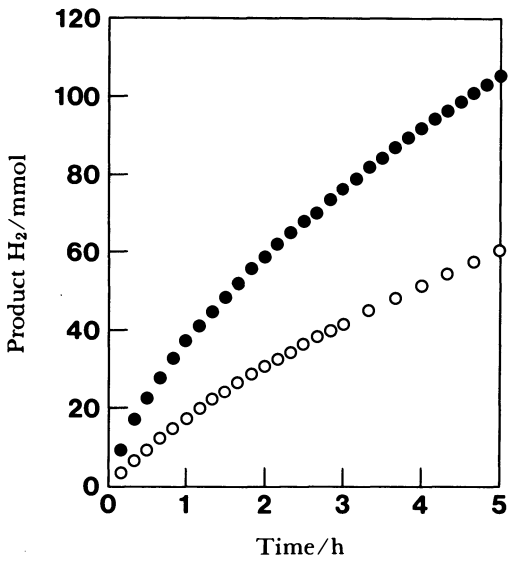

Fig. 1. The time course of H_2 evolution in the liquid-phase dehydrogenation of 2-propanol by a nickel fine-particle catalyst. Nickel alone (○) or platinum-deposited nickel (●) in 2-propanol (200 mg/200 ml).

3. Temperature Dependence of the Reaction Rate. It is already known that a normal alkane does not adsorb on nickel near the boiling point of 2-propanol and does not affect the reaction rate.[3] Mears and Boudart have reported that the addition of hexane (48 vol%) to 2-propanol reduces the boiling point to 62 °C and that Eq. 1 holds for the reaction of a suspended nickel boride catalyst in the solvent.[4] The method of adding hexane was followed in the present study.

The boiling point of a mixture of 2-propanol (200 ml) and hexane (7, 15, 25, and 40 ml) decreased to

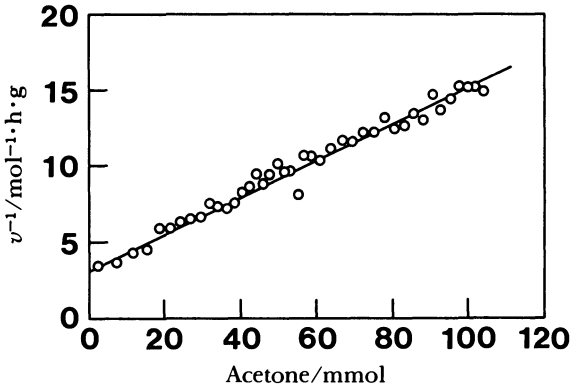

Fig. 2. The analysis of the retardation effect of produced acetone on a platinum-deposited nickel fine-particle catalyst. Data of Fig. 1 were converted into the form of Eq. 1.

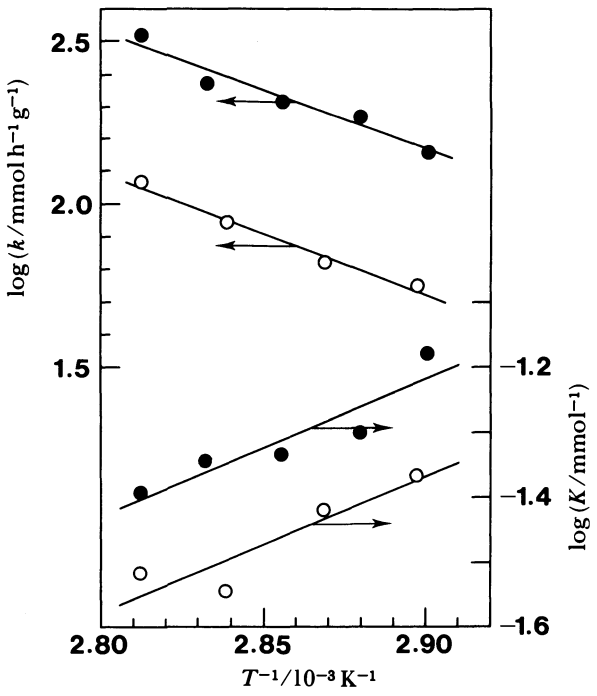

Fig. 3. The temperature dependence of the rate constant k and the equilibrium constant of acetone adsorption K of a nickel fine-particle catalyst. Nickel alone (○) and platinum-deposited nickel (●).

79.9, 77.0, 74.1, and 71.4 °C from the boiling point of 2-propanol (82.4 °C). The reaction rate was measured for 5 h at each temperature. Values of k and K were determined in terms of Eq. 1 and are plotted against T^{-1} in Fig. 3. Data regarding the nickel-alone catalyst are those found in the previous paper.[15]

Figure 3 shows that a pair of lines were parallel; the correlation coefficients in the least-square method were 0.913—0.981 for plots of v^{-1} against [acetone] and 0.973—0.991 for the Arrhenius plots in Fig. 3. The value of the activation energy or adsorption heat of acetone was much the same between the platinum-deposited nickel and the nickel-alone catalysts. On the other hand, the frequency factor of k of the former catalyst was larger than that of the latter catalyst. Hence, the increase in the activity of the platinum-deposited nickel catalyst could be ascribed to an increase in the frequency factor of the rate constant k.

The accumulated acetone lowered the boiling point of a solvent mixture slightly (0.3—1.7 degrees) in a 5-h run. Values of the frequency factors of k and K, the activation energy and the adsorption heat of acetone were determined in terms of the least-square method while taking account of all the experimental values of the rates and boiling points in the five runs. Consequently, the activation energy was 79.3 kJ mol^{-1} and the adsorption heat of acetone was −24.7 kJ mol^{-1} for a platinum- deposited nickel fine-particle catalyst. These values were similar to those of other metallic catalysts.[1,4,15] The activation energy slightly surpassed the enthalpy change of this endothermic reaction (69.9 kJ mol^{-1}).

4. Effect of Poisons. The effects of five kinds of poisons were studied. Water of 1.0 mmol or triethylamine of 1.4 mmol did not change the reaction rate, but the other three poisons affected the activity of a nickel fine-particle catalyst. A prescribed amount of a poison such as pyridine, thiophene, or triphenylphosphine was continually added to a catalyst suspension, and the reaction rate was plotted against the amount of accumulated poison. Table 1 shows the amount of a poison that made a rate half per 200 mg of a nickel fine-particle catalyst.

A plot of v^{-1} against the amount of a poison resembled Fig. 2 for a small amount of poison. Thus the reaction rate could be expressed by

$$v = k/(1 + K'[\text{poison}]). \quad (2)$$

The initial rate was substituted for the rate constant k, because the two values were approximately the same under conditions of no poison and little acetone in the initial state. Table 1 shows the inhibition constant of a poison K'. This table also contains the equilibrium constant of acetone adsorption K and the amount of acetone producing half the rate, for the purpose of comparison.

The retardation effect of triphenylphosphine and thiophene was strong and the effect of pyridine was intermediate. Equation 2 fitted experimental data up to 0.05 mmol of pyridine, but it did not fit the data for more than 0.01 mmol of triphenylphosphine and thiophene. According to the principle of hard and soft acids and bases, soft bases adsorb on metal surfaces which are a soft acid.[19] The order of the effect of the poisons, that is,

triphenylphosphine, thiophene>pyridine>acetone, triethylamine, water

corresponded to the order of softness as a base and was explained in terms of the principle. This fact showed that the properties of active sites of this catalyst could be explained by concepts of usual metallic catalysts.[20]

The value of the inhibition constant of every poison in Table 1 or its amount which produced half the rate was almost the same between the platinum-deposited nickel and the nickel-alone catalysts. This fact showed that the number of active sites was almost the same for the two catalysts. Therefore, the increase in the frequency factor of the rate constant k of a platinum-deposited nickel fine-particle catalyst was ascribed to a change of the frequency factor per active site. Probably the change also caused a slight difference in the frequency factor of an equilibrium constant of acetone adsorption K between the two catalysts.

5. Properties of Active Sites. As shown in studies of bonding orbitals of a metal-hydrogen cluster, the 5d orbitals chiefly work in a platinum cluster, though the 4s orbital of nickel works more than its 3d orbitals.[21-23] The difference in the frequency factor or reaction probability per active site can be ascribed to a

Table 1. Effect of Poisons on the Reaction Rate

Poison	Half-rate amount[a]/mmol		K'[b]/mmol^{-1}	
	Ni	Pt/Ni	Ni	Pt/Ni
Acetone[c]	33	25	0.0301	0.0403
Pyridine	0.014	0.011	57	76
Thiophene	0.006	0.009	169	113
Triphenylphosphine	0.006	0.006	178	191

a) The amount of a poison producing half the rate per 200 mg of a platinum-deposited nickel or a nickel-alone fine-particle catalyst. b) The inhibition constant of Eq. 2. c) The value of a half-rate amount was calculated from the constant K of Eq. 1.

difference in a valence orbital working in the rate-determining step.

The platinum-deposited nickel and nickel-alone fine-particle catalysts were similar to other metallic catalysts, because the values of activation energy and adsorption heat of acetone resembled the reported ones, in addition to the fact that the time course of the reaction rate fitted Eq. 1. The cleavage of a methine C-H bond was regarded as the rate-determining step of liquid-phase dehydrogenation of 2-propanol by means of a nickel boride catalyst.[4] We also think that the cleavage of a methine C-H bond is the most important among the elementary steps.

Appendix

1. Effect of Experimental Conditions. The rate constant k and the equilibrium constant of acetone adsorption K depended on the reducing conditions and on the amount of a catalyst or a solvent, as summarized in Table 2.

The usual pretreatment under hydrogen removed about 10% of the oxygen from surface-oxide layers of nickel fine particles. When a pretreatment under hydrogen was continued for 30 min at 160 °C, about 50% of the oxygen was removed. This severe reducing condition made values of k and K large.

A catalyst of 100 mg showed large values of k and K, in spite of the usual pretreatment. Nickel fine particles piled on the bottom of a reactor (a flask) through a hydrogen pretreatment. When the amount of particles was 100 mg, the particles were sufficiently exposed to hydrogen. Probably the surface oxide of 100-mg particles was considerably reduced after much exposure to hydrogen.

The amount of 2-propanol was varied from 200 ml to 6.4 ml. A reactor of different size was selected in response to it. The rate constant k decreased with the volume of the solvent, or rather, the reactor. The reaction and boiling essentially required heat, which was transmitted through the wall of the reactor soaked in an oil bath. Probably any decrease in a thermal-conduction area reduced heat supply and, consequently, the rate constant k. The heat supply was so small that the boiling of 2-propanol was suppressed when the thermal-conduction area was 22 or 28 cm^2.

The decrease in the amount of 2-propanol increased the value of K by about two orders of magnitude. However, any comparison should be based on a common measure, namely, molarity. If the amount of acetone is expressed in units of molarity, the units of K become $mmol^{-1} \cdot l$ and the value of K has to be multiplied by the volume of the solvent. In fact, the value of K multiplied by the volume of 2-propanol was almost constant as shown in Table 2, suggesting that the conversion of the value of K was reasonable.

2. Other Attempts for Promoting Catalysis with $Pt(acac)_2$. The divalent platinum in 9 mg of $Pt(acac)_2$ was also reduced, when a catalyst suspension containing the complex was held at about 40 °C for 2 h with stirring. The reductant was 2-propanol at that time. Constants k and K were 325 $mmol\ h^{-1}\ g^{-1}$ and 0.0430 $mmol^{-1}$. This method resulted in much the same promoter effect as that of reducing platinum by means of blowing hydrogen into a catalyst suspension. The two methods seemed to sufficiently draw out a promoter effect from 9 mg of $Pt(acac)_2$.

A mixture of 60 ml of acetone and 140 ml of 2-propanol dissolved 100 mg of $Pt(acac)_2$. After the reduction of platinum, acetone was removed under vacuum and then 2-propanol was added to make up for the lost volume. An observed promoter effect, however, did not surpass that of 9 mg of $Pt(acac)_2$; k was 226 $mmol\ h^{-1}\ g^{-1}$ and K was 0.0463 $mmol^{-1}$. Furthermore, a peak of platinum appeared in the XRD pattern of the catalyst after a reaction. Probably, excessive platinum coagulated and scarcely showed a promoter effect. The promoter effect of platinum reached a limit when the amount of $Pt(acac)_2$ was 9 mg.

Table 3 shows the reaction rate in a high mole fraction of acetone. The value was compared with that calculated from Eq. 1, by taking account the temperature dependence of k and K for a catalyst promoted by 9 mg of $Pt(acac)_2$ or a nickel-alone catalyst. The two values were approximately the same. This is consistent with the fact that coagulated platinum scarcely showed a promoter effect.

Table 2. Effect of Experimental Conditions on the Reaction Rate

Ni/mg	2-Propanol/ml	Thermal-conduction area/cm^2	k[a]/$mmol\ h^{-1}\ g^{-1}$	K[b]/$mmol^{-1}$
100	200	120	180	0.062
200[c]	200	120	164	0.089
200	200	120	116	0.030
200	100	94	94	0.046
200	30	28	79	0.268
200	6.4	22	51	1.321

a) The rate constant of Eq. 1. b) The equilibrium constant of acetone adsorption of Eq. 1. c) Surface oxide was severely reduced at 160 °C for 30 min.

Table 3. Reaction Rates in a High Mole Fraction of Acetone

$Pt(acac)_2$/mg	Mole fraction of acetone	Acetone/mmol	Bp/°C	Rate[a]/$mmol\ h^{-1}\ g^{-1}$ Obsd	Calcd[b]
0	0.3	296	70	2.9	3.8
100	0.3	296	70	3.7	8.1
100	0.5	1361	64	0.8	1.0

a) The nickel fine-particle catalyst (200 mg) in an acetone/2-propanol solvent (200 ml). b) Calculation using Eq. 1 and the kinetic data of k and K of a catalyst promoted by 9 mg of $Pt(acac)_2$ or a nickel-alone catalyst.

References

1) F. Claes and J. C. Jungers, *Bull. Soc. Chim. Fr., Ser. 5*, **25**, 1167 (1958).
2) F. Velasco, *Chim. Ind. (Milan)*, **81**, 521 (1959).
3) S. L. Kiperman, N. V. Nikolaeva, and I. R. Davydova, *Kinetika i Kataliz*, **4**, 723 (1963).
4) D. E. Mears and M. Boudart, *AIChE J.*, **12**, 313 (1966).
5) H. B. Charman, *J. Chem. Soc. B*, **1970**, 584.
6) A. Dobson and S. D. Robinson, *J. Organomet. Chem.*, **87**, C52 (1975); *Inorg. Chem.*, **16**, 137 (1977).
7) C. W. Jung and P. E. Garrou, *Organometallics*, **1**, 658 (1982).
8) H. Moriyama, T. Aoki, S. Shinoda, and Y. Saito, *J. Chem. Soc., Perkin Trans. 2*, **1982**, 369.
9) S. Shinoda, T. Kojima, and Y. Saito, *J. Mol. Catal.*, **18**, 99 (1983).
10) W. K. Rybak and J. J. Ziólkowski, *J. Mol. Catal.*, **11**, 367 (1981).
11) S. Shinoda, Y. Tokushige, T. Kojima, and Y. Saito, *J. Mol. Catal.*, **17**, 81 (1982).
12) S. Kashu, M. Nagase, C. Hayashi, R. Uyeda, N. Wada, and A. Tasaki, *Jpn. J. Appl. Phys.*, Suppl. 2, Part. 1, 491 (1974).
13) M. Hida, N. Wada, H. Maeda, H. Terauchi, Y. Tsu, and N. Kamijo, *Jpn. J. Appl. Phys.*, **24**, L3 (1985).
14) M. Noda, S. Shinoda, and Y. Saito, *Nippon Kagaku Kaishi*, **1984**, 1017.
15) M. Noda, S. Shinoda, and Y. Saito, *Bull. Chem. Soc. Jpn.*, **61**, 961 (1988).
16) S. Taira, "Gensobetsu Shokubai Binran," ed by Catalysis Society, Chijin Shokan, Tokyo (1967), pp. 489—490.
17) M. Preifelder, "Practical Catalytic Hydrogenation," John Wiley & Sons Inc., New York (1971), pp. 61—63.
18) T. Hayashi and T. Nagayama, *Nippon Kagaku Kaishi*, **1984**, 1050.
19) S. Arland, J. Chatt, and N. Davis, *Quart. Rev.*, **12**, 265 (1958); R. G. Pearson, *J. Am. Chem. Soc.*, **85**, 3533 (1963).
20) J. R. Anderson, "Structure of Metallic Catalysts," Academic Press Inc., New York (1975).
21) C. F. Melius, J. W. Moskovitz, A. P. Mortola, M. B. Baillie, and M. A. Ratner, *Surf. Sci.*, **59**, 279 (1976).
22) R. P. Messmer, D. R. Salahub, K. H. Johnson, and C. Y. Yang, *Chem. Phys. Lett.*, **51**, 84 (1977).
23) G. Henrici-Olivé and S. Olivé, "The Chemistry of the Catalyzed Hydrogenation of Carbon Monoxide," Springer-Verlag, Berlin (1984), pp. 9—17.

Synthesis of C_3 and C_4 Paraffins from Synthesis Gas with Hybrid Catalyst

Kaoru FUJIMOTO,* Hitoshi SAIMA, and Hiro-o TOMINAGA
Department of Synthetic Chemistry, Faculty of Engineering, University of Tokyo,
7-3-1, Hongo, Bunkyo-ku, Tokyo 113
(Received December 24, 1987)

Hybrid catalysts composed of the physical mixture of methanol synthesis catalysts and Y-type zeolites gave C_3 and C_4 paraffins from synthesis gas at 2.1 MPa, with a selectivity higher than 70%. The product contained small methane and little aromatic hydrocarbons. The hydrid catalyst kept its activity and selectivity at almost constant level for 50 h. The yield of hydrocarbon was much higher than the level estimated from the thermodynamic equilibrium of methanol formation from synthesis gas. The yield of hydrocarbon increased monotonically with the increase in temperature while the carbon number distribution of the product shifted to lower side between 523 and 623 K. The production of hydrocarbon was accompanied by the nearly equal amount of CO_2.

Several attempts to make LPG (C_3 and C_4 paraffins) selectively from synthesis gas have been made by using catalysts such as a supported Fe-Mn-Cu,[1] a fused iron,[2] and a supported molybdenum.[3] However, since these catalysts are so-called Fischer-Tropsch catalysts their product distributions closely follow the Anderson-Schulz-Flory distribution law,[4] the selectivity of LPG is only about 33% at most and 18% of methane selectivity is inevitable.[4]

It has been reported that the synthesis gas reaction on a hybrid catalyst comprising physical mixtures of methanol synthesis catalysts and zeolites gives hydrocarbon mixtures whose composition are much different from those of a Fischer-Tropsch synthesis.[5-10] In the hybrid catalyst system, methanol formed on the methanol synthesis catalyst is successively converted in situ to hydrocarbons on the zeolite catalyst. We have already reported that on the hybrid catalyst composed of a Cu-Zn mixed oxide catalyst and H-ZSM-5 or DAY (dealuminated Y-type zeolite), aliphatic paraffins with 3—6 carbon atoms were predominantly produced from synthesis gas with a low methane selectivity,[10] while the hybrid catalyst composed of a Pd/SiO_2 and H-ZSM-5 or mordenite gave aromatic hydrocarbons with high selectivity.[8]

This study focused on developing hybrid catalysts which make C_3 and C_4 hydrocarbons selectively and clarifying the effects of several operating factors which control the product selectivity.

Experimental

The methanol synthesis catalyst, Cu-Zn (H) was prepared according to the method described by Shimomura et al.[11] The catalysts composition was Cu:40, Zn:23, Al:27 (atm%). Cu-Zn (C) was commercially available one (BASF S8-45). Dealuminated Y-type zeolite (DAY) was supplied by Shokubai Kasei Co. REY was obtained by calcining Linde type SK-500 in air at 723 K for 3 h. Pt-Y was prepared from SK-40 by ion exchanging with aqueous ammonium hexachloroplatiniate and the loading was 0.1 wt%. Some of the physical properties of the zeolites are shown in Table 1.

The hybrid catalysts were prepared as follows: Equal weights of methanol synthesis catalyst and zeolite were physically mixed and were powdered under 100 mesh. Then, they were pressed to a disk and were finally crushed to granules with 20/40 mesh. About 2.0 g of the hybrid catalyst was placed in a tubular reactor with a 6 mm inner diameter and was activated in a hydrogen flow at 723 K.

A pressurized, flow-type reaction apparatus was used for the synthesis gas reaction.[6]

Results and Discussion

Synthesis of Hydrocarbons with a Variety of Hybrid Catalysts. Table 2 shows the catalytic properties of a variety of hybrid catalyst prepared by combining Pd/SiO_2, Cu-Zn(H), and Cu-Zn(C) with Y-type zeolite and ZSM-5. It is clear from the data that any Y-type zeolite exhibited an excellent LPG selectivity of C_3 and C_4 hydrocarbons, while the activity itself was strongly influenced by the methanol synthesis catalyst. ZSM gave a small amount of aromatic hydrocarbons which was mainly composed of tri- and tetramethylbenzenes.

The high selectivity of LPG fraction on the Y-type zeolite system should be attributed to the quick

Table 1. Physical Properties of Zeolites Used for Preparing Hybrid Catalyst

Zeolite	SiO_2/Al_2O_3 mole ratio	Pore size	Content of Al_2O_3	Acidity
		Å	mmol g^{-1}	meq. g^{-1}
H-ZSM-5	50.2	6	1.2	1.74
DAY	7.6	13	3.6	4.22
REY	4.9	13	4.5	4.31
PtY	4.8	13	5.0	4.55

Table 2. Synthesis Gas Conversion on Hybrid Catalysts

Methanol cat.	Cu-Zn(H)				Cu-Zn(C)
Zeolite	DAY	RE-Y	Pt-Y	ZSM-5	DAY
Product yield (carbon %)					
Hydrocarbons	15.9	17.6	19.6	17.0	35.7
Oxygenates	1.5	1.2	0.2	0.6	5.3
CO_2	14.7	16.6	16.4	16.2	30.7
Coke	0.4	—	—	—	—
Hydrocarbon distribution (carbon %)					
Aliphatics					
C_1	3.2	1.4	0.9	7.7	3.2
C_2	8.5	11.8	14.8	13.5	10.7
C_3	17.8	18.0	22.0	26.9	24.7
C_4	49.4	48.3	42.8	12.7	49.6
C_5	12.6	12.4	12.7	9.1	8.2
C_6^+	8.5	9.0	6.8	26.4	3.7
Aromatics	0	tr.	0	3.8	tr.

Methanol catalyst/zeolite: 1/1 (weight ratio), temperature: 573 K, pressure: 2.06 MPa, H_2/CO: 2/1 (mole ratio), W/F: 3.4 g-cat h mol^{-1}.

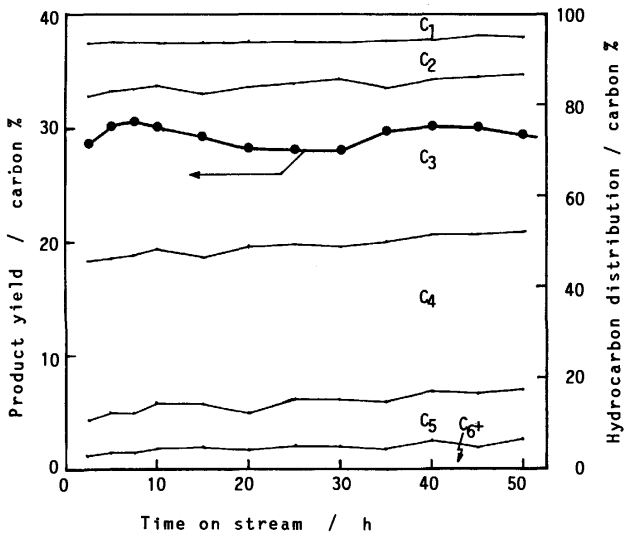

Fig. 1. Durability of hybrid catalyst: Cu-Zn(H)+DAY (1/1 by weight); Temperature 623+5 K; pressure 2.1 MPa; W/F=3.1 g-cat h mol^{-1}; H_2/CO=2/1 (mole ratio).

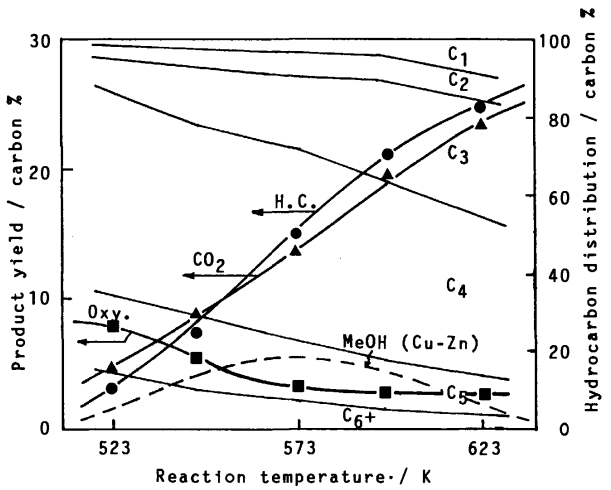

Fig. 2. Product yield and hydrocarbon distribution as a function of reaction temperature: Cu-Zn(H)+DAY (1/1 by weight); pressure 2.1 MPa; W/F=3.1 g-cat h mol^{-1}; H_2/CO=2/1 (mole ratio).

diffusion of olefins, which are the primary products of methanol conversion and their hydrogenation on the methanol synthesis catalyst.[10]

Durability of Hybrid Catalyst. Figure 1 shows the results of the synthesis gas reaction over a hybrid catalyst composed of Cu-Zn (H) and DAY. The catalytic activity was kept at almost a constant level over 50 hours, while a slight change in the hydrocarbon distribution occurred.

The level of synthesis gas conversion might be controlled by the activity of either catalyst of the hybrid catalyst, because the synthesis gas is first converted to methanol on the methanol synthesis catalyst and then the methanol is converted to hydrocarbons. Since the rate of synthesis gas conversion was substantially controlled by the rate of methanol formation in the present case, the constant activity of the present case should be attributed to the constant activity of the methanol synthesis catalyst. If the activity of DAY dropped quickly, which usually occur during the methanol conversion on the Y-type zeolite,[12] the product distribution should change quickly. The data in Fig. 1 indicate that the decrease in the zeolite activity was also quite slow. The slow deactivation of the zeolite should be attributed to the quick hydrogenation of olefins on the methanol synthesis catalyst,[8] which inhibits the polymerization of olefins to aromatics or coke.

Operational Factors Controlling Catalyst Activity and Product Selectivity. The catalytic activity and the product selectivity of the hybrid catalyst are influenced by several operational factors as demonstrated in figures through 2 to 5.

a. Temperature. As shown in Fig. 2, the hydro-

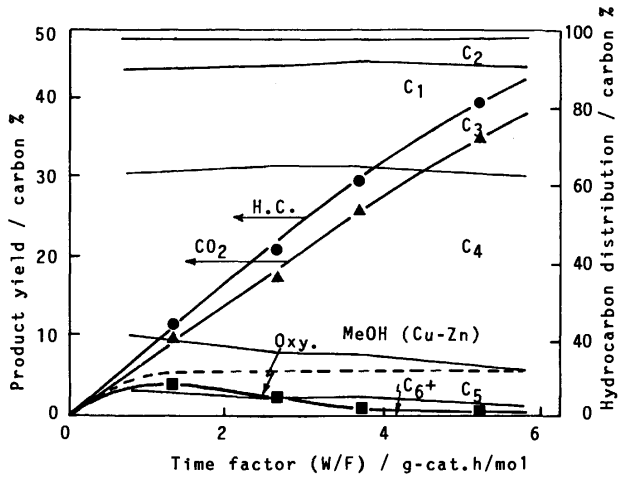

Fig. 3. Product yield and hydrocarbon distribution as a function of time factor: Cu-Zn(H)+DAY (1/1 by weight); temperature 623 K; pressure 2.1 MPa; $H_2/CO=2/1$ (mole ratio).

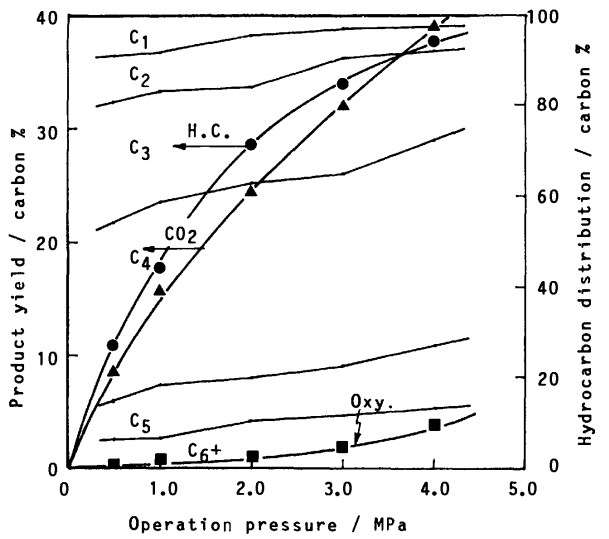

Fig. 4. Product yield and hydrocarbon distribution as a function of time factor: Cu-Zn(H)+DAY (1/1 by weight); temperature 623 K; W/F=3.1 g-cat h mol^{-1}; $H_2/CO=2/1$ (mole ratio).

carbon yield increased monotonically and the yield of oxygenated compounds decreased with increasing reaction temperature while the product yield from the synthesis gas conversion on Cu-Zn(H) alone (broken line) reached a maximum level (ca. 5%) at approximately 573 K and then decreased due to the thermodynamic limitation of the methanol formation from synthesis gas. The high level of synthesis gas conversion on the hybrid catalyst could be attributed to the successive conversion of methanol to hydrocarbons on the zeolite as shown below.

$$2nCH_3OH \rightleftarrows nCH_3OCH_3 \longrightarrow C_nH_m + nH_2O$$

Product distribution is also strongly influenced by reaction temperature. At 573 K or lower, a significant amount of oxygenates (mostly dimethyl ether) was observed in the product suggesting the incomplete conversion of methanol to hydrocarbons on DAY at such low temperatures. The degree of carbon chain growth decreased monotonically with an increase in temperature. It is characteristic that the selectivity of C_4 paraffins was extraordinarily high and reached a maximum as high as 50% at 573 K. Among C_4 paraffins, the fraction of isobutane was about 3 times higher than that of normal butane. This value is much higher than that of the butane mixture in thermodynamic equilibrium. The reason is not clear yet.

b. Contact Time. The hydrocarbon yield was almost proportional to the contact time (W/F) as shown in Fig. 3, while methanol yield on the Cu-Zn(H) catalyst was independent of the time factor (dotted line). It suggests that products such as light paraffins or carbon dioxide have little suppressive effect on either methanol formation or methanol conversion to hydrocarbons. Also, the hydrocarbon distribution was never affected by the contact time, which suggests that apparently no significant secondary reactions of product hydrocarbon took place.

c. Reaction Pressure. Figure 4 shows how the reaction pressure affects the synthesis gas conversion on the hybrid catalyst. The hydrocarbon yield increased monotonically with an increase in the pressure, however, the promotional effect of pressure on this catalyst is not as remarkable as that on the Pd/SiO_2 based catalyst.[8] A slight increase in the hydrocarbon formation and a marked increase in the oxygenated formation above 3 MPa could be attributed to the relative rate of methanol formation and its conversion. The increase in the reaction pressure contributes only to the increase in the methanol formation. However, since the rate-determining step on this hybrid catalyst (Cu-Zn(H)/DAY=1/1 by weight) is the conversion of methanol to hydrocarbon,[12] the increase in methanol formation should have little effect on hydrocarbon formation but it should contribute to the increase in the oxygenates formation.

d. Composition of Synthesis Gas. The composition of synthesis gas (H_2/CO ratio) exhibited a complicated effect on the product yield and selectivity (Fig. 5). The hydrocarbon yield was in the similar level between $H_2/CO=3/1$, and 2/1 and then decreased markelly with decreased H_2/CO ratio, while that of oxygenates decreased drastically when the H_2/CO ratio in the feed was decreased from 3/1 to 1/1.

These phenomena are explained as follows: in principle, the rate of methanol formation is proportional to the partial pressure of hydrogen,[13] and thus the product yield should be higher at high H_2/CO ratios. The hydrocarbon yield at $H_2/CO=3/1$, however, was in the same level to that at $H_2/CO=2/1$.

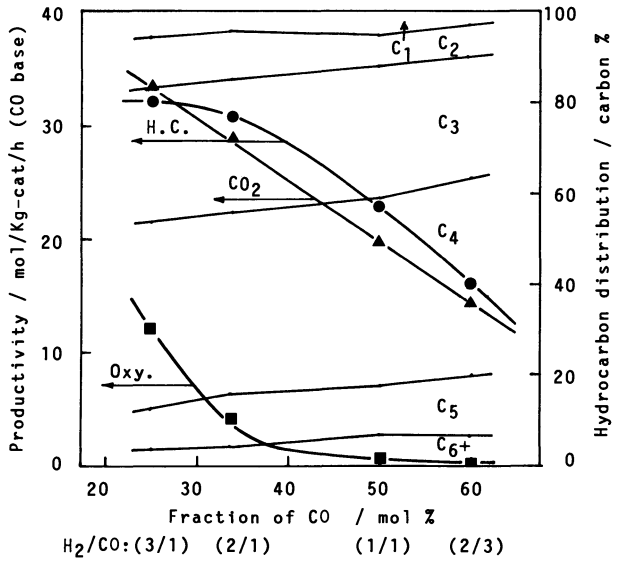

Fig. 5. Space time yield of each product and hydrocarbon distribution as a function of feed gas composition: Cu-Zn(H)+DAY (1/1 by weight); temperature 623 K; pressure 2.1 MPa; W/F=3.1.

The phenomena can be attributed to the fact that the rate-determining step of the present hybrid catalyst, where the hybrid catalyst is composed of equal weights of Cu-Zn(H) and DAY, is the methanol conversion step. Thus, the high H_2/CO ratio contributes only to the increase in the methanol (and DME) concentration in the catalyst bed. In fact, the yield of DME was much higher with the feed gas at $H_2/CO=3/1$. On the other hand, when the H_2/CO ratio is 1/1 or lower the methanol formation should be the rate limiting and thus, the rate of hydrocarbon formation decreases with the decrease in the H_2/CO ratio. The idea is also supported by the fact that little oxygenates is formed when the H_2/CO ratio is 1/1 or lower.

Conclusion

It has been confirmed that the hybrid catalysts composed of Cu-Zn mixed oxide methanol synthesis catalyst and Y-type zeolite exhibits a highly active, selective and stable catalysis for making LPG from synthesis gas. The catalytic activity is substantially controlled by the activity of the methanol synthesis catalyst. Other catalytic properties such as the product selectivity, the temperature characteristic, the pressure characteristic are explained in terms of the relative rate of methanol synthesis and its conversion to hydrocarbons.

References

1) S. Kodama, K. Tarama, A. Mishima, A. Fujita, and M. Yasuda, *Kogyo Kagaku Zasshi*, **46**, 69 (1943).
2) J. C. Foogendorn, Preprint of "IGT Symposium" (1973).
3) C. B. Murchison and D. A. Murdick, *Hydrocarbon Processing, Jan.*, **1981**, 160.
4) G. H. Olive and S. Olive, *Angew. Chem., Int. Ed. Engl.*, **15**, 136 (1976).
5) C. D. Chang, W. H. Lang, and A. J. Silvertri, *J. Catal.*, **56**, 268 (1979).
6) K. Fujimoto, Y. Kudo, and H. Tominaga, *Nippon Kagaku Kaishi*, **1982**, 206.
7) C. D. Chang, J. N. Miale, and R. F. Socha, *J. Catal.*, **90**, 84 (1984).
8) K. Fujimoto, Y. Kudo, and H. Tominaga, *J. Catal.*, **87**, 136 (1984).
9) T. Inui, T. Hagiwara, and Y-Takegami, *J. Jpn. Petrol. Inst.*, **27**, 228 (1984).
10) K. Fujimoto, H. Saima, and H. Tominaga, *Bull. Chem. Soc. Jpn.*, **58**, 1485 (1985).
11) K. Shimomura, K. Ogawa, M. Oba, and Y. Kotera, *J. Catal.*, **52**, 191 (1978).
12) K. Fujimoto, T. Shikada, and Tominaga, *Nippon Kagaku Kaishi*, **1982**, 229.
13) K. Fujimoto, H. Saima, and H. Tominaga, *Ind. Eng. Chem. Research*, in press.

 © 1988 The Chemical Society of Japan Bull. Chem. Soc. Jpn., 61, 2551—2557 (1988)

The Polymerization of Benzene Catalyzed by a Copper(I) Chloride-Aluminium Chloride-Oxygen System

Naoki TOSHIMA,* Keiichi KANAKA, Atsunori KOSHIRAI, and Hidefumi HIRAI
Department of Industrial Chemistry, Faculty of Engineering, The University of Tokyo, Hongo, Bunkyo-ku, Tokyo 113
(Received January 6, 1988)

The polymerization of benzene to poly(1,4-phenylene) (PPP) has been done successfully using copper(I) chloride and aluminium chloride as catalysts under oxygen. Since copper(I) chloride and aluminium chloride form a double salt (aluminium copper(I) chloride, $AlCuCl_4$) and are soluble in benzene, a high homogeneity of the reaction system has been achieved and the polymerization reaction proceeds without any evolution of hydrogen chloride. The polymerization products contained an insoluble dark brown solid and a benzene-soluble tarry mass. The solid product has been determined to be PPP by comparison with an authentic sample. The product PPP was obtained in a yield of more than 100%, based on the molar quantity of copper(I) chloride, by controlling the quantity of aluminium chloride. For example, the treatment of benzene with aluminium chloride and copper(I) chloride (20:3:1 in molar ratio) under 1 atm of oxygen at 70 °C for 24 h gave PPP in a 187% yield, based on copper(I) chloride. This reaction could be carried out by the use of oxidants other than oxygen and by the use of low-valent metal salts other than copper(I) chloride, although a copper(I) chloride–aluminium chloride–oxygen system is most suitable for the polymerization of benzene in terms of the yield of PPP and the convenience of the reaction.

The aromatic hydrocarbon polymer is an interesting organic material in that it is thermally stable[1] and can be electrically conductive upon doping with various dopants.[2] Poly(1,4-phenylene) (PPP) has a structure characteristic of this type of polymer. The methods of synthesizing it and its character have been investigated for a long time.[1,2]

Several methods for the direct synthesis of PPP from benzene have been investigated. One well-known procedure is the oxidative cationic polymerization of benzene by a Lewis acid-oxidant system reported by Kovacic et al.;[3]

$$n\,C_6H_6 + 2n\,CuCl_2 \xrightarrow{AlCl_3} (C_6H_4)_n + 2n\,CuCl + 2n\,HCl \quad (1)$$

Usually, aluminium chloride is used as a Lewis acid, and copper(II) chloride, as an oxidant.[4] Molybdenium(V) chloride[5] and iron(III) chloride,[6] which have functions of both a Lewis acid and an oxidant, are also used. In this method, the polymerization reaction proceeds under mild conditions, and the yield of PPP is fairly high. The polymerization of alkylbenzenes, such as toluene,[7] halogenated benzenes,[8] and thiophenes,[9] has also been attempted by the use of this method. However, the vigorous evolution of a large amount of hydrogen chloride is unavoidable in this method, since the polymerization of 1 mol of benzene produces 2 mol of hydrogen chloride, according to Eq. 1. Furthermore, it is difficult to stir the reaction mixtures, even at the beginning of the reaction, because the metal salts do not dissolve in benzene, resulting in slurried conditions. Since the oxidizing metal salts are consumed during the reaction, the yield of PPP based on the oxidant is always less than 100%. Recently, the polymerization of benzene by the use of a superacid composed of aluminium chloride and copper(II) chloride was reported,[10] although the evolution of hydrogen chloride is unavoidable in this method also. The electrolytic polymerization of benzene in the presence of a supporting electrolyte was found to produce a film of PPP.[11] The structure-definite PPP was synthesized by the dehalogenation of dihalogenated benzene in the presence of nickel-complex catalysts.[12]

The direct polymerization of benzene by Kovacic's method does not give the PPP in so high a molecular weight. The heterogeneity of the reaction system and the insolubility of PPP in organic solvents might be the reasons for this lower molecular weight. Against this background, the methods via a soluble precusor polymer have been investigated. It has previously been reported that PPP could be synthesized by the dehydrogenation of the polymer of 1,3-cyclohexadiene.[13] However, the yield of PPP synthesized by this method was also low, and the purification of the polymer was difficult. Recently, it was also reported that the polymer of acylated 3,5-cyclohexadiene-1,2-diol, which can be synthesized by a biotechnical procedure, is thermally converted into PPP with a high molecular weight.[14] By this method, it is possible to make films at the stage of the precusor polymer.

The present authors have now tried to polymerize benzene to PPP by taking advantage of aluminium copper(I) chloride ($AlCuCl_4$), which is known to be soluble in various aromatic compounds[15] and which should be formed at the termination step in Kovacic's method. Thus, the polymerization of benzene was attempted by producing the active species (Cu(II) ion) for polymerization by using $AlCuCl_4$ and an oxidant under highly homogeneous conditions, where copper(I) chloride would be expected to work as a catalyst. The present paper reports on the synthesis of PPP in a

system of aluminium chloride, copper(I) chloride, and an oxidant, where not only $AlCuCl_4$ but also excess $AlCl_3$ and an oxidant are required by the reaction. The syntheses by the use of double salts other than $AlCuCl_4$ have also been successful.

Experimental

Materials. The aluminium chloride (Kishida Chemical Co.) was purified by vacuum sublimation. The copper(I) chloride (Koso Chemical Co.) was reprecipitated from an aqueous hydrochloric acid solution by the addition of distilled water, followed by successive washing with ethanol and diethyl ether; it was then dried in vacuo at 100 °C for 24 h. The aluminium bromide, copper(I) bromide, cobalt(II) chloride, nickel(II) chloride, and copper(II) chloride were commercially (guaranteed grades) obtained and were used without further purification.

The benzene was distilled over metallic sodium. The 1-bromopropane was distilled after drying by anhydrous magnesium sulfate.

The chloranil and potassium permanganate were commercially obtained (guaranteed and extra pure grade respectively) and were used without further purification. The 18-crown-6 (1,4,7,10,13,16-hexaoxacyclooctadecane) was purified by recrystallization from acetonitrile. The oxygen was passed through columns of Molecular Sieves 3A and diphosphorus pentaoxide before use.

Analysis. The ^1H NMR spectrum was obtained with a JEOL model FX 90Q spectrometer at 89.55 MHz. The infrared absorption spectra (KBr disks and liquid film with KBr plates) were obtained with a JASCO model A-3 spectrometer. The GPC was recorded on a TOYO SODA model HLC-802UR chromatograph equipped with two TSK-GEL 2000H columns.

Polymerization of Benzene by a $CuCl$-$AlCl_3$-O_2 System. One gram (10.1 mmol) of copper(I) chloride, 4.04 g (30.3 mmol) of aluminium chloride, and 18.2 cm^3 (202 mmol) of benzene were placed in a 100 cm^3 Kjeldahl flask, and the mixture was stirred at room temperature for 2 h under dry nitrogen. In this stage, the copper(I) chloride was dissolved completely and a highly homogeneous solution was obtained, leaving some excess aluminium chloride. The reaction was carried out by replacing the solution atmosphere with oxygen at 60 °C for 24 h. As the reaction proceeded, the color of the reaction mixture changed from yellow to dark brown at the beginning of the reaction. At the end of the reaction, brownish black precipitates appeared at the bottom of the reaction vessel. During the reaction, no evolution of hydrogen chloride was observed. Polymerization was terminated by adding an 18% hydrochloric acid solution to the reaction mixtures. After the filtration of the reaction mixtures with a sintered glass disk, the remaining solid was repeatedly washed with a boiling solution of 18% hydrochloric acid and then with boiling water. The subsequent drying of the dark brown solid product at 100 °C for 24 h, yielded 0.458 g (119% yield based on the charged copper(I) chloride) of PPP. The filtrate was extracted by benzene, and the benzene solution was also washed several times with an 18% hydrochloric acid solution and water. After the evaporation of the benzene under reduced pressure and then drying for 24 h, 0.177 g (46.0% yield based on charged CuCl) of a reddish brown, tarry product was obtained.

The solid product was quite insoluble in various organic solvents. The elemental analysis data are shown in Table 3. The IR spectra of the solid product showed bands at 800 (C–H out-of-plane vibration of a para-disubstituted benzene ring), 1000 (C–H in-plane vibration of the same species), and 1480 cm^{-1} (C=C skeletal in-plane vibration).

The results of the elemental analysis of the benzene-soluble product were: C, 85.4; H, 6.3; Cl, 3.2%. Thus, the C/H ratio is 1.14, between the calculated values of $(C_6H_4)_n$ (1.50) and $(C_6H_6)_n$ (1.00). The IR spectrum has bands at 700, 760, 800, 1450, 1500, 1600, 2870, 2950, 3040, and 3070 cm^{-1}. The ^1H NMR spectrum in $CDCl_3$ shows its peaks at δ 1.25, 5.4—5.5, and 7.2—7.3 (refer to TMS).

Polymerization of Benzene by the Use of Other Metal Salts and Oxidants. In the case of using other metal salts, polymerization was carried out by the procedure described above. Polymerization by the use of copper(II) chloride was carried out according to Kovacic's method.[4]

When potassium permanganate was used as an oxidant, the reaction was carried out in the presence of 18-crown-6, thus enabling this oxidant to dissolve in benzene. When chloranil was used as an oxidant, unreactive chloranil was removed from the solid product by extraction with benzene using a Soxhlet extractor. The experimental conditions are shown in Tables 4 and 5, as well as the yield of polymers.

Alkylation of PPP. The alkylation of PPP was achieved by 1-bromopropane according to the method in the literature.[16]

Elemental analysis:

Alkylated PPP prepared by the $CuCl$-$AlCl_3$-O_2 method:
Found: C, 87.9; H, 9.9; Cl, 0.7% (C/H ratio, 0.75).
Calcd for $[C_6H_2(C_3H_7)_2]_n$: C, 89.9; H, 10.1% (C/H ratio, 0.75).

Alkylated PPP prepared by Kovacic's method:
Found: C, 84.8; H, 9.0; Cl, 0.6% (C/H ratio, 0.79).
Calcd for $[C_6H_{2.5}(C_3H_7)_{1.5}]_n$: C, 90.6; H, 9.5% (C/H ratio, 0.81).

Results and Discussion

Synthesis of PPP by the Use of the $CuCl$-$AlCl_3$-Oxygen System. The direct polymerization of benzene to PPP by a copper(II)-aluminium chloride ($CuCl_2$-$AlCl_3$) system, as reported by Kovacic et al., is one of the best known methods. However, this method has some problems: (1) the vigorous evolution of hydrogen chloride, (2) difficulty in stirring the slurried reaction mixtures caused by the insolubility of the metal salts in benzene, and (3) the limited yield of PPP based on $CuCl_2$ because of the consumption of the $CuCl_2$ used as a reagent. As copper(I) chloride ($CuCl$) is a by-product of the preparation of PPP from benzene in this method, it is considered that polymerization can be continued if this $CuCl$ is oxidized to Cu(II) species again. Thus, copper chloride is thought to be able to participate repeatedly in the polymerization as a catalyst. On the other hand, it is known that $AlCl_3$ and $CuCl$ can form a double salt of aluminium copper(I) chloride ($AlCuCl_4$),

which is soluble in benzene by the coordination of benzene to the salt.[15] From this point of view, the polymerization of benzene might proceed efficiently because of the homogeneity of the reaction system.[17]

Table 1 shows the results of polymerization using CuCl-$AlCl_3$ (1:1 in charged molar ratio) and adding various oxidants. Though oxygen, iodine, and potassium permanganate ($KMnO_4$) were added as oxidants, polymerization did not occur. Even when $CuCl_2$ was added, PPP was not obtained at all. These results indicate that $AlCl_3$ loses its activity as a Lewis-acid catalyst by forming the double salt $AlCuCl_4$.

The polymerization was successfully attempted by the addition of an excess of $AlCl_3$ with respect to the CuCl under oxygen. The results are shown in Table 2. The addition of the excess $AlCl_3$ caused benzene to polymerize smoothly, resulting in a dark brown solid. The structure of this solid product has been proved by IR spectral measurements to be almost identical with that of the PPP synthesized by Kovacic's method. However, under nitrogen, no reaction at all occurred in spite of the use of an excess of $AlCl_3$ relative to CuCl. These results indicate that oxygen is required for polymerization. When more than twice as much $AlCl_3$ as CuCl was used, PPP was obtained in a yield of more than 100%, based on the CuCl. This result clearly indicates that CuCl works as a catalyst.

On the other hand, when $AlCl_3$ and benzene (3:20 in charged molar ratio) were treated at 60 °C under oxygen without CuCl, the yield of PPP was only about 1% of that in the presence of CuCl. This result demonstrates that the polymerization is not achieved by only $AlCl_3$ and oxygen, but that it is greatly promoted by copper(I) species in cooperation with oxygen in this reaction system. The necessity of oxygen for polymerization is well supported by the consumption of oxygen during polymerization. For example, when 258 mmol of benzene was polymerized by the use of 12.8 mmol of CuCl and 38.6 mmol of $AlCl_3$ at 70 °C for 24 h, at the beginning of the reaction no appreciable amount of oxygen was consumed, but as the reaction proceeded further, the uptake of oxygen gradually increased, in all, about 12 mmol of oxygen was consumed, resulting in PPP. The yield of PPP (16.5 mmol) nearly corresponds to twice amount of oxygen consumed. The time course of the oxygen uptake is comparable to the change in

Table 1. Polymerization of Benzene by Aluminium Copper(I) Chloride with Various Oxidants[a]

Run	Charged molar ratio[b]		Yield/%
	$AlCuCl_4$	Oxidant	
1	1.0	— (O_2)[c]	0
2	0.5	0.25 (I_2)	0
3	0.5	0.1 ($KMnO_4$)	0
4	1.0	0.5 ($CuCl_2$)	0

a) Reaction time=2 h; reaction temperature=40 °C. b) Benzene=10.0. c) Under 1 atm of oxygen.

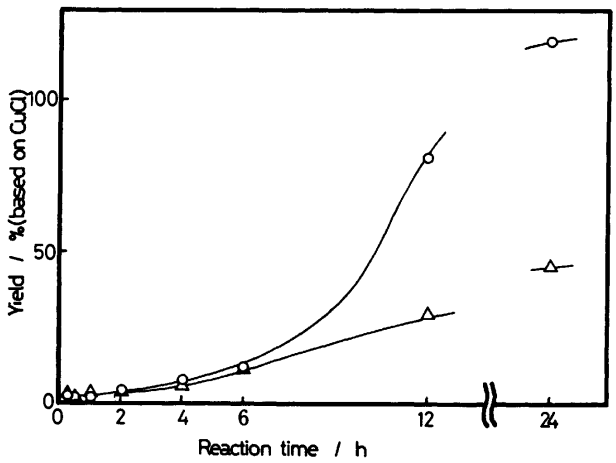

Fig. 1. Changes in the yields of PPP, insoluble (○) and soluble (△) portions in benzene, with reaction time by a CuCl-$AlCl_3$-O_2 method. Charged molar ratio of CuCl-$AlCl_3$-benzene was 1:3:20 and reaction temperature was 60 °C.

Table 2. Polymerization of Benzene Catalyzed by Copper(I) Chloride-Aluminium Chloride under Oxygen[a]

Run	Charged molar ratio[b]		Temp	Yield/%[c]		
	$AlCuCl_4$	Excess $AlCl_3$	°C	Insoluble[d]	Soluble[d]	Total
5[e]	1.0	2.0	50	0	0	0
6	1.0	2.0	40	5	4	9
7	1.0	2.0	50	43	22	65
8	1.0	2.0	60	119(3.0)[g]	46(1.1)	165(4.1)
9	1.0	2.0	70	187	41	228
10	1.0	1.0	60	56	11	67
11	0.5	1.0	60	111	47	158
12	2.0	4.0	60	139	51	190
13	1.0	2.0+3.8[f]	60	649	154	803
14	0.0	3.0	60	−(0.04)[g]	−(0.05)	−(0.09)

a) Reaction time=24 h except Run 13. b) Benzene=20.0. c) Based on CuCl. d) The products are insoluble or soluble in benzene. e) Reaction under nitrogen. f) After the reaction with a 2.0 excess (molar ratio) of aluminium chloride for 24 h, a 3.8 excess (molar ratio) of aluminium chloride was added, after which the reaction was continued for a further 24 h. g) The % values shown in parentheses are calculated based on the charged amount of benzene.

the yield of PPP with the reaction time (Fig. 1).

The yield of PPP was strongly influenced by the quantity of the excess $AlCl_3$; that is, the more the quantity of excess $AlCl_3$ used, the higher the yield of PPP. Furthermore, the yield increased up to 803% by the extra addition of a 3.8-fold quantity of $AlCl_3$ after a 24-h reaction and continuous stirring for another 24 h. These results indicate that excess $AlCl_3$ is consumed during the reaction. $AlCl_3$ is considered to be deactivated by water generated from oxygen and protons which will be eliminated from benzene in the course of the reaction.

The yield of PPP rose drastically with a rise in the reaction temperature. In contrast, the molar ratio of benzene to CuCl had little influence on the yield of PPP. The reaction under dry air also gave PPP, but the yield was remarkably low in comparison with that obtained by the reaction under pure oxygen. The yield of PPP also increased with a lengthening of the reaction time. In the initial stage of the reaction, however, a few hours' induction period was observed (Fig. 1).

Structure of PPP. Table 3 shows the results of the elemental analyses of the various polymerization products prepared by a $CuCl-AlCl_3-O_2$ system as well as a $CuCl_2-AlCl_3$ system. The C/H ratio of the PPP prepared at 50 °C was 1.50, identical with that of an ideal PPP structure, $(C_6H_4)_n$. The C/H ratios of the other products were also near to that of PPP. The contamination of chlorine may be due to the partial chlorination of the aromatic rings of the polymers. The C/H ratio and the content of chlorine atoms increased as the reaction temperature rose.

In the present polymerization reaction, a product which was soluble in benzene was obtained as well as an insoluble solid product. In the IR spectrum, remarkable peaks located at 700 and 760 cm^{-1} were observed; they were attributed to the C-H in-plane vibration of a mono-substituted benzene ring. From the IR spectrum, the molecular weight of this benzene-soluble product was proved to be very low. On the other hand, the peaks located at 2870 and 2950 cm^{-1} indicated that the benzene-soluble product was not completely aromatized, for these peaks were attributable to the C-H stretching vibration of alkanes. This consideration was also supported by the ^1H NMR spectroscopy, that is, the peaks assigned to nonaromatic and vinyl protons were observed around δ 1.25 and 5.4—5.5 respectively. The proposed structure for the soluble product is shown in Fig. 2 as well as that for the insoluble product. This structure of the soluble product is also supported by the experimental result that the soluble product could be rearomatized by oxidation with the $CuCl-AlCl_3-O_2$ system in carbon tetrachloride, producing insoluble PPP.

Molecular Weight of PPP. PPP exhibits characteristic infrared absorptions around 650—900 cm^{-1} corresponding to the C-H out-of-plane vibration of a benzene ring. These absorptions involve the peaks at 760 and 800 cm^{-1}, as for a monosubstituted and a para-disubstituted benzene ring respectively. The former peak arises from the end phenyl units of PPP, and the latter, from the internal phenylene units. By a comparison of the ratios of the two peak intensities, it

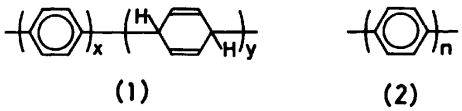

(1) (2)

Fig. 2. The proposed structure for the soluble (1) and insoluble (2) product of PPP.

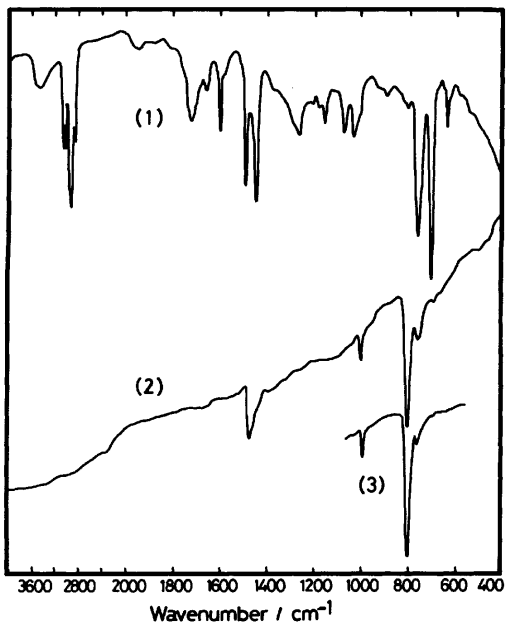

Fig. 3. Infrared spectra of PPP prepared by a $CuCl-AlCl_3-O_2$ method (soluble portion (1) and insoluble portion (2) in benzene) and by a Kovacic's method (3).

Table 3. The Elemental Analysis Data of Solid PPP Prepared by Various Methods

Method	Temp	Weight/%			C/H
	°C	C	H	Cl	Atomic ratio
$CuCl_2-AlCl_3$	40	92.90	5.25	1.24	1.48
$CuCl-AlCl_3-O_2$	50	90.70	5.08	0.86	1.50
$CuCl-AlCl_3-O_2$	60	92.70	5.02	1.08	1.55
$CuBr-AlBr_3-O_2$	50	86.65	4.44	5.17(Br)	1.64
Calcd for $(C_6H_4)_n$		94.70	5.30	0.00	1.50

is possible to estimate the molecular weight of PPP.[16] As is depicted in Fig. 3, the PPP prepared by using CuCl-$AlCl_3$-O_2 shows a little stronger absorption at 760 cm^{-1} than that prepared by using $CuCl_2$-$AlCl_3$, suggesting that the molecular weight of the former PPP is a little lower than that of the latter PPP.

The Friedel-Crafts alkylation of these PPPs by 1-bromopropane resulted in the dissolution in organic solvents. In either case, the alkylated PPP showed a light brown color and could be dissolved in various organic solvents. It was estimated, on the basis of the results of the elemental analyses, that the number of alkyl groups introduced to benzene rings of PPP prepared by the CuCl-$AlCl_3$-O_2 method was 2 per benzene ring, in contrast with 1.5 per ring in the case of Kovacic's PPP, where the degree of polymerization was 15.[16] Figure 4 shows some typical GPC spectra of the alkylated PPPs. From these GPC spectra, it has become apparent that the PPP prepared by the CuCl-$AlCl_3$-O_2 method has a somewhat lower molecular weight than does Kovacic's PPP.

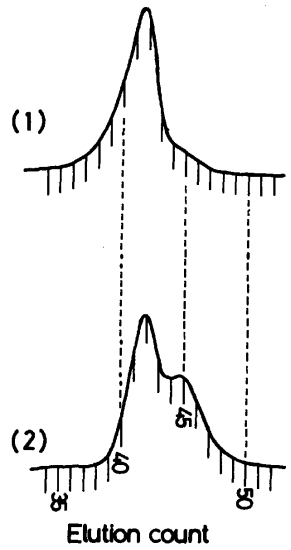

Fig. 4. Gel permeation chromatograms (chloroform as a carrier) of PPP alkylated by 1-bromopropane in the presence of $AlCl_3$. The original PPP were prepared by a Kovacic's method (1) and a CuCl-$AlCl_3$-O_2 method (2).

Syntheses of PPP by CuCl and $AlCl_3$ Using Other Oxidants. The successful preparation of PPP by the use of excess $AlCl_3$ with respect to CuCl under oxygen as an oxidant suggested that PPP could also be prepared using other oxidants under the same conditions. Table 4 shows the results of the polymerization of benzene using $KMnO_4$, chloranil, iodine, and so on as oxidants. When $KMnO_4$ was used instead of oxygen, polymerization occurred without CuCl. However, the yield of PPP got higher in the presence of CuCl. That is to say, the combination of CuCl and $KMnO_4$ influenced the acceleration of the polymerization reaction. When chloranil was used instead of oxygen, the acceleration of the reaction by a combination of CuCl and chloranil was not observed, since the 44% yield based on chloranil was achieved only with $AlCl_3$ in Kovacic's method.[18] This result indicates that the polymerization of benzene occurs independently in the absence of $AlCuCl_4$ when chloranil is used. In the case of iodine as an oxidant, the yield of the insoluble solid product was high. However, the content of iodine in the product was also very high (86.1%).

The polymerization using chloranil or iodine as an oxidant is supposed not to be suitable for the synthesis of PPP because of the difficulty of removing the oxidant from the polymer. When sodium periodate was used instead of oxygen, only a little PPP was obtained.

Syntheses of PPP by Other Metal Salts under Oxygen. It has become possible to polymerize benzene to PPP catalytically by the use of low-valent copper(I) chloride, $AlCl_3$, and oxygen. Low-valent metal salts other than CuCl were examined for the polymerization of benzene. Table 5 shows the results of these examinations. When cobalt(II) chloride ($CoCl_2$) and nickel(II) chloride ($NiCl_2$) were stirred with an excess of $AlCl_3$ in benzene, the color of the solution turned green[19] and deep yellow respectively, resulting in the formation of double salts with $AlCl_3$ and a consequent dissolution in benzene. By the use of these metal salts instead of CuCl, benzene could be polymerized to produce PPP. However, the yield of a benzene-soluble product was relatively high in

Table 4. Polymerization of Benzene Catalyzed by a Copper(I) Chloride-Aluminium Chloride-Oxidant System[a]

Run	Charged molar ratio[b]			Temp	Yield/%[c]	
	CuCl	$AlCl_3$	Oxidant	°C	Insoluble	Soluble
15	1.0	3.0	— (O_2)[d]	27	4	5
16	1.0	3.0	0.4 ($KMnO_4$)	27	112 (56)	2 (1)
17	0.0	3.0	0.4 ($KMnO_4$)	27	— (21)	— (1)
18	0.5	1.5	2.0 (Chloranil)	27	132 (33)	— (—)
19	0.8	2.4	1.0 (I_2)	50	168 (84)	— (—)
20	0.9	2.7	0.5 ($NaIO_4$)	50	2 (2)	— (—)

a) Reaction time=24 h. b) Benzene=20.0. c) Based on CuCl. The values shown in parentheses are calculated based on the charged oxidants. d) Under 1 atm of oxygen.

Table 5. Polymerization of Benzene by Various Metal Salts under Oxygen[a]

Run	Charged molar ratio[b]			Yield/%[c]	
	Salt A	Salt B	B/A	Insoluble	Soluble
20	$CoCl_2$	$AlCl_3$	4.0	25	45
21	$NiCl_2$	$AlCl_3$	4.0	19	20
6	CuCl	$AlCl_3$	2.0	43	22
22	CuCl	$AlBr_3$	2.0	21	21
23	CuBr	$AlBr_3$	2.0	19	20

a) Reactions were carried out at 50 °C under 1 atm of oxygen for 24 h. b) Salt A: benzene=1:20. c) Based on salt A.

comparison with the case of $AlCuCl_4$, even though the yield of a benzene-insoluble product was not changed. In these reactions, the solubility of these salts in benzene is less than that of $AlCuCl_4$, resulting in less effective polymerization. The use of aluminium bromide ($AlBr_3$) instead of $AlCl_3$ made the double salts much more soluble in benzene than in the case of $AlCl_3$. The yield of benzene-insoluble PPP, however, was lower than that when $AlCl_3$ was used. The rearomatization of the polymeric precursor is thought to take place inefficiently in the case of $AlBr_3$ because the oxidation power of the copper ion is lowered by an increase in the charge density on copper caused by the lower electronegativity of bromine than chlorine. As is shown in Table 3, the PPPs prepared by metal bromides are highly contaminated with bromine atoms and give a high C/H ratio because of the bromination of the benzene rings.

Mechanism for Polymerization. In the polymerization of benzene by using $CuCl_2$ and $AlCl_3$, Kovacic et al. proposed that the polymerization was initiated by the generation of the benzene-cation radical,[20] propagated by the coordination of an appreciable number of benzene nuclei as stair-steps, and terminated by rearomatization by means of the oxidative elimination of protons by $CuCl_2$ from the delocalized stair-step cation radical (stair-step mechanism).[21]

In the method reported here, the polymerization has occurred under oxygen by the use of excess $AlCl_3$ with respect to CuCl, in contrast to no polymerization under nitrogen in spite of the presence of excess $AlCl_3$. Thus, the present reaction is described by Eq. 2, not by Eq. 1 as in the case of the Kovacic reaction:

$$2n\,C_6H_6 + n\,O_2 \xrightarrow{AlCl_3/CuCl} 2(C_6H_4)_n + 2n\,H_2O \quad (2)$$

Furthermore, when the molar ratio of $AlCl_3$ to CuCl was unity in the present system, benzene did not polymerize at all, not even under oxygen. These results suggest that the cooperation of excess $AlCl_3$ and the oxygenated copper(I) ion produces the cation radical species and initiates the polymerization. The induction period of only a few hours in this reaction is thought to be due to the lowering of the initiation activity of the benzene-cation radicals because of the interaction of the radicals with $AlCl_3$.

By the ESR experiments in the present system, the cation radical has been proved to be produced before the reaction atmosphere is replaced by oxygen. Thus, the signal observed under nitrogen with excess $AlCl_3$ (g=2.0025) has been identified as an organic radical. After the reaction under oxygen for 24 h, no additional signal was observed except that for the organic radical (g=2.0026). This result indicates that the copper(II) species do not take part in the polymerization reaction. Presumably, the oxygen activated by $AlCuCl_4$ participates in the reaction to withdraw hydrogen in the rearomatization step. The fact that a considerable amount of the benzene-soluble product was obtained in the present reaction is attributable to the weaker oxidative power of the activated oxygen than $CuCl_2$ in Kovacic's method.

As has been described before, the yield of PPP can be raised by increasing the quantity of excess $AlCl_3$ or by the addition of extra $AlCl_3$ in the course of the reaction. These results suggest the generation of water, by which $AlCl_3$ is consumed during the reaction. That is to say, the water is considered to be produced by oxygen and protons eliminated from the dihydropolymer in the termination stage.

References

1) Reviews: G. K. Noren and J. K. Stille, *J. Polym. Sci., Macromol. Rev.*, **5**, 385 (1971); Y. Imai, *Yuki Gosei Kagaku Kyokai Shi*, **42**, 1061 (1984).

2) D. M. Ivory, G. G. Miller, J. M. Sowa, L. W. Shacklette, R. R. Chance, and R. H. Baughman, *J. Chem. Phys.*, **71**, 1506 (1979); R. H. Baughman, J. L. Bredas, R. R. Chance, R. L. Elsenbaumer, and L. W. Shacklette, *Chem. Rev.*, **82**, 209 (1982).

3) P. Kovacic and M. B. Jones, *Chem. Rev.*, **87**, 357 (1987).

4) P. Kovacic and A. Kyriakis, *J. Am. Chem. Soc.*, **85**, 454 (1963).

5) P. Kovacic and R. M. Lange, *J. Org. Chem.*, **28**, 968 (1963).

6) P. Kovacic and F. W. Koch, *J. Org. Chem.*, **28**, 1864 (1963).

7) P. Kovacic and J. S. Ramsey, *J. Polym. Sci., Pt. A-1*, **7**, 111 (1969).

8) P. Kovacic, J. T. Uchic, and L.-C. Hsu, *J. Polym. Sci., Pt. A-1*, **5**, 945 (1967).

9) J. S. Ramsey and P. Kovacic, *J. Polym. Sci., Pt. A-1*, **7**, 127 (1969).

10) N. Kitajima, Y. Hakone, and Y. Ono, *Chem. Lett.*, **1982**, 871.

11) I. Rubinstein, *J. Electrochem. Soc.*, **130**, 1506 (1983); M. Tabata, M. Satoh, K. Kaneto, and K. Yoshino, *J. Phys. Soc. Jpn.*, **55**, 1305 (1986).

12) T. Yamamoto, Y. Hayashi, and A. Yamamoto, *Bull. Chem. Soc. Jpn.*, **51**, 2091 (1978).

13) C. S. Marvel and G. E. Hartzell, *J. Am. Chem. Soc.*, **81**, 448 (1959); D. A Frey, M. Hasegawa, and C. S. Marvel, *J.*

Polym. Sci., Pt. A, **1**, 2057 (1963).
14) D. G. H. Ballard, A. Courtis, I. M. Shirley, and S. C. Taylor, *J. Chem. Soc., Chem. Commun.*, **1983**, 954.
15) R. W. Turner and E. L. Amma, *J. Am. Chem. Soc.*, **88**, 1877 (1966).
16) M. B. Jones, P. Kovacic, and D. Lanska, *J. Polym. Sci., Polym. Chem. Ed.*, **19**, 89 (1981).
17) H. Hirai, N. Toshima, K. Kanaka, and A. Koshirai, *Chem. Lett.*, **1987**, 1461.
18) P. Kovacic and J. Oziomek, *J. Org. Chem.*, **29**, 100 (1964).
19) D. E. O'Reilly, C. P. Poole, Jr., R. F. Belt, and H. Scott, *J. Polym. Sci., Pt-A*, **2**, 3257 (1964).
20) G. G. Engstrom and P. Kovacic, *J. Polym. Sci., Polym. Chem. Ed.*, **15**, 2453 (1977).
21) P. Kovacic and W. B. England, *J. Polym. Sci., Polym. Lett. Ed.*, **19**, 359 (1981).

Crystal and Molecular Structure of Tetrabutylammonium Bis(1,4-dithiin-2,3-dithiolato)nickelate(III), (Bu^n_4N)[Ni(ddt)$_2$]

Hyernjoo KIM,* Akiko KOBAYASHI, Yukiyoshi SASAKI, Reizo KATO,†
Hayao KOBAYASHI,† Tadashi NAKAMURA,†† Takashi NOGAMI,††
and Yasuhiko SHIROTA††
Department of Chemistry, Faculty of Science, The University of Tokyo, Hongo, Bunkyo-ku, Tokyo 113
†Department of Chemistry, Faculty of Science, Toho University, Funabashi, Chiba 274
††Department of Applied Chemistry, Faculty of Engineering, Osaka University, Yamadaoka, Suita, Osaka 565
(Received November 9, 1987)

The crystal structure of tetrabutylammonium salt of a new multi-sulfur 1,3-dithiolene complex, (Bu^n_4N)[Ni(ddt)$_2$] (ddt=1,4-dithiin-2,3-dithiolato) has been determined by the single-crystal X-ray diffraction technique. Crystals are monoclinic, space group $C2/c$, a=66.107(40), b=9.182(5), c=19.119(12) Å, β=147.29(3)°, V=6271(1) Å^3, and Z=8. The structure was solved by the heavy atom method, and refined by a block-diagonal least-squares method to R=0.070. There are two crystallographically independent molecules of Ni(ddt)$_2$, molecule-A and molecule-B. Molecule-B forms segregated uniform stacks along the b-axis. The (Bu^n_4N)$^+$ cations are located between two molecular planes of molecule-A. The Ni(ddt)$_2$ molecules are almost planar except two terminal vinylene moieties, which are folded to opposite side each other and the folding angles of molecule-A and molecule-B are 28° and 39°, respectively.

The intermolecular transverse interaction between multi-chalcogen π-donor and/or π-acceptor molecules is essential to enhance the dimensionality of the molecular metals, which is useful for the suppression of the Peierls instability which is the characteristic of the quasi-one-dimensional molecular metals. The structure of BEDT-TTF (BEDT-TTF=bis(ethylenedithio)tetrathiafulvalene) complexes clearly showed the way to introduce the transverse interactions and therefore to obtain 2-dimensional (2D) molecular conductors.[1] The superconductors, θ- and κ-(BEDT-TTF)$_2$I$_3$ are the most successful examples.[2,3] Recently, the 1D molecular metals without metal instabilities became to be noticed. In these systems, "multi-Fermi surface" nature of the molecular metals has been found to be important for supressing the Peierls instability and stabilizing the metallic state down to low temperature.[4,5] Two superconductors of metal 1,3-dithiolene complex (TTF)[Ni(dmit)$_2$]$_2$,[4] and [$(CH_3)_4N$][Ni(dmit)$_2$]$_2$[6] (dmit=2-thioxo-1,3-dithiolene-4,5-dithiolato) have been reported to be the examples of multi-Fermi surface systems. The stable metallic state of (DMe-DCNQI)$_2$Cu has been proposed to be originated from the same reason.[5]

Although a considerable number of studies have been made on the physical properties of the M(mnt)$_2$ (mnt=1,2-dicyano-1,2-ethylnendithiolato) and M(dmit)$_2$ compounds (M=Ni, Pd, Pt), reports on the syntheses of a new type of metal dithiolene complex are very few. A new multi-sulfur dithiolene complexes (Ni and Pd complexes of ddt; ddt=1,4-dithiin-2,3-dithiolato), which are expected to be a possible candidate to give highly conducting organic complexes, have been synthesized recently.[7] In this paper, the crystal structure of tetrabutylammonium salt of Ni(ddt)$_2$, (Bu^n_4N)[Ni(ddt)$_2$] will be reported.

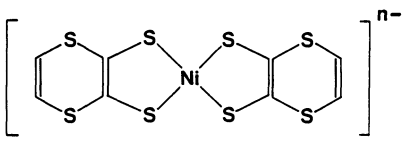

[Ni(ddt)$_2$]$^{n-}$

Experimental

Brown needle-type crystals of (Bu^n_4N)[Ni(ddt)$_2$] were prepared by the method reported previously.[7] The unit cell parameters were determined by a least-squares fit of 2θ angles for 20 reflections (17°<2θ<30°) measured with Mo $K\alpha$ radiation on an automated Rigaku AFC-6 four-circle diffractometer.

Details of the crystal data and experimental parameters along with data collection are summarized in Table 1. Three standard reflections were monitored every 100 reflections and their intensities showed random variation of ±0.6% throughout the data collection. The intensity data were corrected for Lorentz and polarization factors but not for absorption because of the small size of the crystal (<0.25 mm).

The structure was solved by Patterson method, and refined by a block-diagonal least-squares method. From the sharpened Patterson map, the positions of the nickel atoms were determined. A total of 33 non-hydrogen atoms were identified in the Fourier map calculated from the structure factors phased with heavy atoms. All the coordinates of the hydrogen atoms were calculated and were included in the final refinement cycles. Anisotropic thermal parameters were adopted for non-hydrogen atoms and the hydrogen atoms were refined isotropically. The weighting scheme $w=(1.0+0.004|F_o|^2)^{-1}$ for $|F_o|<12.0$ and $(\sigma(|F_o|)^2+0.004|F_o|^2)^{-1}$ for $|F_o|\geq 12.0$ was employed. The atomic scattering factors were taken from International Tables for X-ray Crystallography.[8] All the calculations were performed on HITAC M-680H computer at the Computer Centre of the University of Tokyo, using the program UNICS III.[9]

Table 1. Crystal Data and Experimental Parameters for the X-Ray Diffraction Study of $(Bu^n_4N)[Ni(ddt)_2]$

Formula	$C_{24}H_{44}NS_8Ni$
Formula weight	657.1
Crystal system	Monoclinic
Space group	$C2/c$
Cell constant	
a/Å	66.107(40)
b/Å	9.182(5)
c/Å	19.119(12)
β/°	147.29(3)
V/Å^3	6271(1)
Z	8
X-Ray	Mo$K\alpha$ vadiation (λ=0.71069Å)
Monochromator	Graphite
$d_{cal.}$/g cm^{-1}	1.39
μ(Mo$K\alpha$)/cm^{-1}	11.5
Crystal size/mm^3	0.13×0.025×0.025
Scan technique	2θ-ω scan
Scan rate/° min^{-1}	2
Scan width (ω)	$1.23+0.5\tan\theta$
Scan range	$2\theta \leqq 50°$
Number of reflections measured	5258
Number of reflections used in the calculation ($\|F_o\| > 3\sigma(\|F_o\|)$)	1494
R value[a]	0.070
R_2 value[b]	0.087
Goodness of fit (g.o.f.)[c]	1.09

a) $R=\sum\||F_o|-|F_c\|/\sum|F_o|$. b) $R_2=[\sum w(|F_o|-|F_c|)^2/\sum|F_o|^2]^{1/2}$. c) g.o.f.$=[\sum w(|F_o|-|F_c|)^2/(N-M)]^{1/2}$, where N=number of reflections, M=number of parameters.

Results and Discussion

The atomic coordinates are listed in Table 2.** The bond distances and angles are shown in Fig. 1. The crystal structure is shown in Fig. 2.

There are two types of $Ni(ddt)_2$ molecules (A and B) which are crystallographically independent. Both of them are located on the centers of the symmetry. The monoclinic unit cell contains eight $Ni(ddt)_2$ molecules (four molecule-As and four molecule-Bs), and eight $(Bu^n_4N)^+$ cations. The averaged Ni–S distances are 2.148 Å in molecule-A and 2.137 Å in molecule-B, which are close to those of other monoanionic dithiolato-nickelate.[10] The $Ni(ddt)_2$ molecules are almost planar except the terminal vinylene moieties while the VT molecules in usual cases are not planar (bis(vinylenedithio)tetrathiafulvalene, BVDT-TTF, is abbreviated as VT; in $Ni(ddt)_2$, the central C=C double bond of VT is replaced by the Ni atom). The planarity of $Ni(ddt)_2$ molecules is better than that of the $VT^{+1/2}$ molecules in VT_2PF_6 which is better than that of VT^0 molecules in neutral VT.[11] The two terminal vinylene groups of the each side of a $Ni(ddt)_2$ molecule are folded to opposite side each other, and the folding angles of molecule-A and molecule-B are 28° and 39°, respectively. The shapes of $Ni(ddt)_2$) molecules (A and B) and the folding angles are shown in Fig. 1.

The molecule-B forms the independent uniform stacks along the b-axis on the position of x/a=0, 1/2. The interplanar distances within the stacks of molecule-B are 4.03 Å. $(Bu^n_4N)^+$ cations are located between two molecular planes of molecule-A. There is

Table 2. Fractional Atomic Coordinates (×10^4) with Estimated Standard Deviations in Parentheses

Atom	x/a	y/b	z/c	B_{eq}/Å^2[a]	Atom	x/a	y/b	z/c	B_{eq}/Å^2[a]
Ni1	2500	2500	5000	5.9	N	1510(3)	−980(11)	3250(10)	4.0
Ni2	5000	5000	5000	7.1	C(N)1	1575(5)	−2315(16)	3908(16)	5.4
S1	2125(2)	2129(5)	3050(5)	6.7	C(N)2	1779(4)	−937(15)	3422(13)	4.3
S2	2068(2)	3584(5)	4328(5)	6.8	C(N)3	1590(4)	412(16)	3909(13)	4.9
S3	1326(2)	2561(7)	425(5)	8.5	C(N)4	1103(4)	−1027(15)	1835(13)	4.6
S4	1269(2)	4146(5)	1849(6)	8.1	C(N)5	1968(4)	−2596(17)	5318(14)	5.5
S5	5203(2)	3640(6)	6408(5)	8.6	C(N)6	1772(4)	−2310(16)	2941(15)	5.4
S6	4575(1)	3454(6)	3490(5)	8.1	C(N)7	1342(5)	605(20)	3845(17)	6.9
S7	4964(2)	933(7)	6397(7)	11.3	C(N)8	976(5)	259(18)	1025(18)	7.9
S8	4308(2)	642(6)	3298(7)	10.3	C(N)9	2012(5)	−3979(16)	5837(17)	6.2
C1	1697(5)	2794(14)	2091(17)	6.1	C(N)10	2047(5)	−2104(14)	3116(16)	5.6
C2	1682(5)	3445(16)	2698(17)	5.9	C(N)11	1433(6)	2128(25)	4437(19)	9.5
C3	1030(5)	3882(24)	−196(21)	9.9	C(N)12	589(5)	−98(28)	−392(20)	13.4
C4	993(6)	4538(19)	309(22)	9.9	C(N)13	2410(5)	−4291(22)	7172(16)	8.3
C5	4893(5)	2171(20)	5489(19)	8.4	C(N)14	2084(5)	−3524(16)	2811(16)	6.0
C6	4619(4)	2130(24)	4237(19)	9.8	C(N)15	1204(6)	2458(32)	4407(22)	13.0
C7	4845(7)	−631(21)	5653(23)	10.6	C(N)16	443(9)	968(48)	−1174(36)	23.1
C8	4575(5)	−802(21)	4377(21)	9.7					

a) $B_{eq}=(4/3)(B_{11}a^2+B_{22}b^2+B_{33}c^2+B_{12}ab\cos\gamma+B_{13}ac\cos\beta+B_{23}bc\cos\alpha)$.

** The coordinates of the hydrogen atoms, the anisotropic thermal parameters of the non-hydrogen atoms and the F_o–F_c tables have been deposited as a Document No. 8806 at the Office of the Editor of Bull. Chem. Soc. Jpn.

no short intermolecular S···S (<3.70 Å) contacts within the $Ni(ddt)_2$ molecules.

The amplitudes of LUMO (lowest unoccupied molecular orbital) of $[Ni(ddt)_2]^-$ anion were calculated on the basis of extended Hückel approximation (Fig. 3). The LUMO of $[Ni(ddt)_2]^-$ has the same symmetry as those of $[Ni(dmit)_2]^-$, the well-known metal 1,3-dithiolene complex, and $[Ni(dddt)_2]^-$.[12] In the case of $[Ni(dmit)_2]^-$, shown in Table 3, the amplitudes of LUMO of the "outer sulfur atoms" (a_o) are one-fifth as small as those of the "inner sulfur atoms" (a_i) therefore the side-by-side interactions of the $Ni(dmit)_2$ molecules are not so strong.[4] In the case of $[Ni(dddt)_2]^-$, which have ethylene moieties instead of thioxo group of $Ni(dmit)_2$ in the outer side of the molecule, the ratio of a_o, to a_i are one-half. Consequently, compared with $[Ni(dmit)_2]^-$, $[Ni(dddt)_2]^-$ is considered to be liable to form the 2D molecular conductor. In the case of $[Ni(ddt)_2]^-$, the

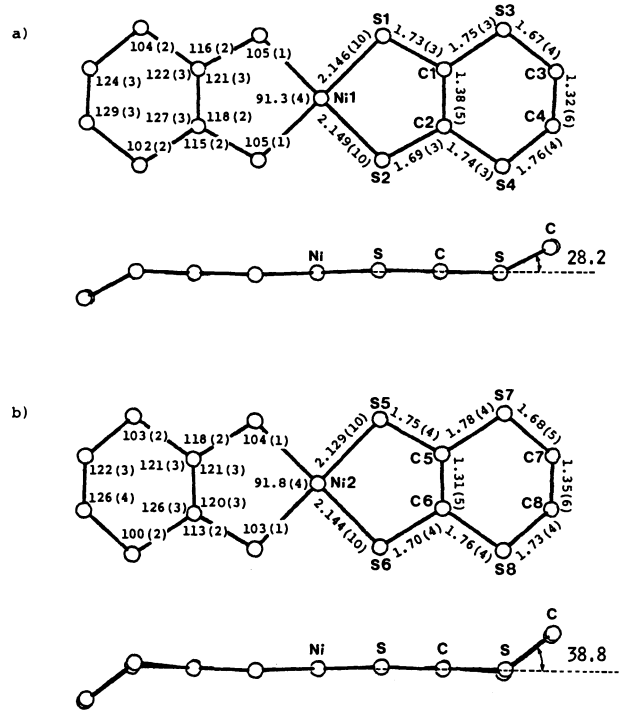

Fig. 1. Molecular structure, bond distances (l/Å), bond angles (ϕ/°), and folding angles (ϕ/°) of a) molecule-A and b) molecule-B of $Ni(ddt)_2$.

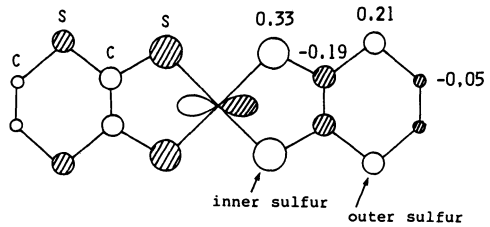

Fig. 3. Schematic drawing of LUMO of $[Ni(ddt)_2]^-$.

Table 3. Comparison of the a_i and a_o Values of the Monoanionic Dithiolatonickelates

	a_i	a_o	a_o/a_i
$[Ni(ddt)_2]^-$	0.33	0.21	64%
$[Ni(dddt)_2]^-$	0.37	0.18	49%
$[Ni(dmit)_2]^-$	0.42	0.08	19%

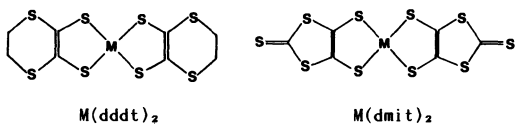

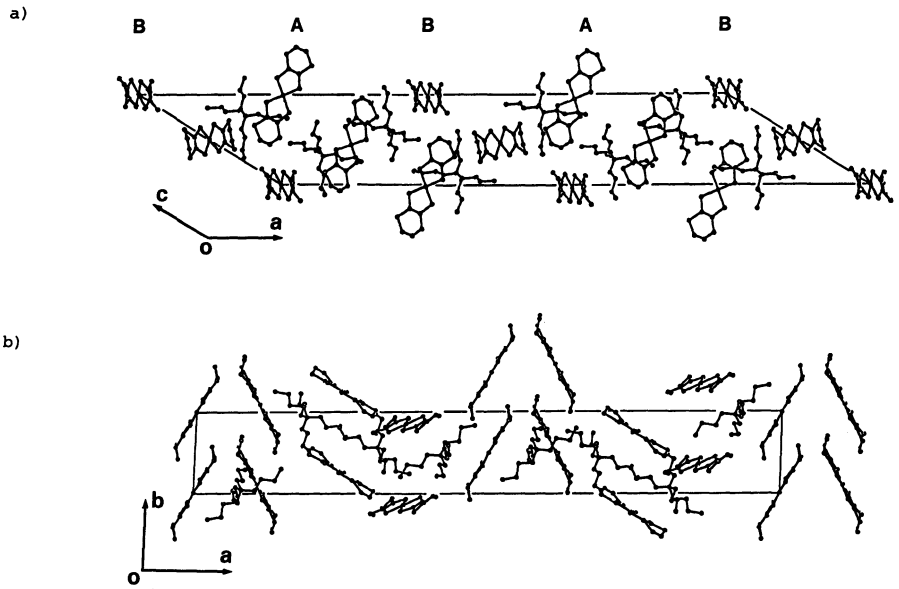

Fig. 2. Crystal structure of $(Bu^n_4N)[Ni(ddt)_2]$ projected along a) the b-axis and b) the c*-axis.

ratio of a_o to a_i is three-fifth which is larger than that of $[Ni(dddt)_2]^-$. But in case of synthesizing the real molecular conductor, the electrochemical property of $Ni(ddt)_2$ molecule become an important factor. As reported by Nakamura et al.,[7] the $\Delta E(=E_1-E_2)$[13] value of $[Ni(ddt)_2]^-$, which is a measure of the on-site Coulomb repulsion, lies between that of $[Ni(dmit)_2]^-$ and that of $[Ni(dddt)_2]^-$.

References

1) H. Kobayashi, A. Kobayashi, Y. Sasaki, G. Saito, T. Enoki, and H. Inokuchi, *J. Am. Chem. Soc.*, **105**, 297 (1983); H. Kobayashi, R. Kato, and A. Kobayashi, *Synthetic Metals*, **19**, 623 (1987).

2) H. Kobayashi, R. Kato, A. Kobayashi, Y. Nishio, K. Kajita, and W. Sasaki, *Chem. Lett.*, **1986**, 789; H. Kobayashi, R. Kato, A. Kobayashi, Y. Nishio, K. Kajita, and W. Sasaki, *ibid.*, **1986**, 833; R. Kato, H. Kobayashi, A. Kobayashi, Y. Nishio, K. Kajita, and W. Sasaki, *ibid.*, **1986**, 957; A. Kobayashi, R. Kato, H. Kobayashi, S. Moriyama, Y. Nishio, K. Kajita, and W. Sasaki, *ibid.*, **1986**, 2017.

3) A. Kobayashi, R. Kato, H. Kobayashi, S. Moriyama, Y. Nishio, K. Kajita, and W. Sasaki, *Chem. Lett.*, **1987**, 459; R. Kato, H. Kobayashi, A. Kobayashi, S. Moriyama, Y. Nishio, K. Kajita, and W. Sasaki, *ibid.*, **1987**, 507.

4) A. Kobayashi, H. Kim, Y. Sasaki, R. Kato, and H. Kobayashi, *Solid State Commun.*, **62**, 57 (1987).

5) A. Kobayashi, R. Kato, H. Kobayashi, T. Mori, and H. Inokuchi, *Solid State Commun.*, **64**, 45 (1987).

6) A. Kobayashi, H. Kim, Y. Sasaki, R. Kato, H. Kobayashi, S. Moriyama, Y. Nishio, K. Kajita, and W. Sasaki, *Chem. Lett.*, **1987**, 1819.

7) T. Nakamura, T. Nogami, and Y. Shirota, *Bull. Chem. Soc. Jpn.*, **60**, 3447 (1987).

8) International Tables for X-Ray Crystallography, Vol. IV, Kynoch Press, Birmingham (1974).

9) T. Sakurai and K. Kobayashi, *Rep. Inst. Phy. Chem. Res.*, **55**, 69 (1979).

10) A. Kobayashi and Y. Sasaki, *Bull. Chem. Soc. Jpn.*, **50**, 2650 (1977); O. Lindqvist, L. Anderson, J. Sieler, G. Steimecke, and E. Hoyer, *Acta Chem. Scand., Ser. A*, **36**, 855 (1982); C. T. Vance, R. D. Bereman, J. Bordner, W. H. Hatfield, and J. H. Helms, *Inorg. Chem.*, **24**, 2905 (1985).

11) H. Kobayashi, A. Kobayashi, T. Nakamura, T. Nogami, and Y. Shirota, *Chem. Lett.*, **1987**, 559.

12) H. Kim, A. Kobayashi, Y. Sasaki, R. Kato, and H. Kobayashi, *Bull. Chem. Soc. Jpn.*, **61**, 579 (1988).

13) E_1 and E_2 are the redox potentials of $[ML_2]^{2-} \overset{E_1}{\rightleftharpoons} [ML_2]^- \overset{E_2}{\rightleftharpoons} [ML_2]^0$, where ML_2 is a metal 1,3-dithiolene complex.

 © 1988 The Chemical Society of Japan Bull. Chem. Soc. Jpn., 61, 2563—2567 (1988)

The Crystal Structure of 1,5-Dithioniabicyclo[3.3.0]octane Bis(trifluoromethanesulfonate). The First Structural Characterization of Dithionia Dication and Strong S···O Interactions between Cations and Anions

Fujiko Iwasaki,* Nobuhiko Toyoda, Ryouichi Akaishi,† Hisashi Fujihara,† and Naomichi Furukawa†

Department of Applied Physics and Chemistry, University of Electro-Communications, Chofu-shi, Tokyo 182

†Department of Chemistry, The University of Tsukuba, Tsukuba-shi, Ibaraki 305

(Received December 26, 1987)

The crystal structure of 1,5-dithioniabicyclo[3.3.0]octane bis(trifluoromethanesulfonate) has been determined by the X-ray method to elucidate the structure of a dithionia dication. Crystal data; $C_6S_2H_{12}^{2+}\cdot 2CF_3SO_3^-$, F_w=446.43, orthorhombic, Pccb, a=16.775(2), b=9.893(3), c=19.592(3) Å, V=3251(1) Å^3, Z=8, D_x=1.825 Mg m^{-3}. There are two independent dications, **A** and **B**, in the crystals, each of which has a crystallographic twofold axis. The mean S$^+$–S$^+$ distance is 2.124 Å. The conformation of the eight-membered ring is a distorted chair-chair form. Very strong interactions were observed between S$^+$ of dications and O atoms of counter anions. The average distance of S$^+$···O is 2.724 Å and colinear arrangements of O···S–S···O are formed with the central twofold axis. Other weak S···O interactions (2.903—3.153 Å) were also observed between dications and anions. The coordination around S is a roughly distorted octahedron with two C and two O atoms in a plane and apical S and O atoms.

The presence of cyclic dithionia dications was reported by means of spectroscopic studies.[1] No crystallographic studies of these salts have been reported because of the difficulties to obtain stable crystals. Recently the title salt could be isolated from a reaction of 1,5-dithiacyclooctane *S*-oxide and $(CF_3SO_2)O$ in CH_2Cl_2.[2] The X-ray analysis was undertaken to confirm the existence of a dication and to reveal a structural feature of a transanuular effect between sulfurs. Some sulfur-bonded 1-thionia-5-thiacyclooctane salts and 1,5-dithiacyclooctanes have been found to have a relatively short transannular S···S contact in the range 3.121—3.271 Å[3] because of the hypervalency of the sulfur atom.[4] It is also interesting to compare the structure of 1,5-dithioniacyclooctane with those of 1,5-dithiacyclooctanes. This is the first report about the structure of a cyclic dithionia dication.

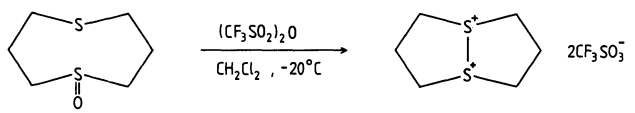

Experimental

Colorless plate with dimension of 0.45×0.30×0.15 mm was sealed in a thin glass capillary because crystals were unstable in air. Crystal data and some experimental conditions are listed in Table 1. Intensities were collected on a Rigaku automatic diffractometer with graphite-monochromated Mo$K\alpha$ (λ=0.71073 Å) radiation, using ω–2θ scan technique. At both ends of the scan range 10 s background counts were taken for each reflection. Three reflections were monitored for each 50 reflections. Variation of intensities of the monitored reflections were within 2%. Reflections with $|F_o|\geq 3\sigma(F)$ were considered to be observed. No absorption nor extinction corrections were applied. Three S atoms were picked up from the E-map obtained by MULTAN78.[5] The other atoms were obtained from the succesive F- and D-maps. Block-diagonal least-squares were carried out with anisotropic temperature factors for non-H and isotropic ones for H atoms. Four strong reflections considered to be affected by an extinction effect

Table 1. Crystal Data and Some Experimental Conditions

	$C_6H_{12}S_2^{2+}\cdot 2CF_3SO_3^-$
F_w	446.43
Crystal system	Orthorhombic
Space group	Pccb
a/Å	16.775(2)
b/Å	9.893(3)
c/Å	19.592(3)
V/Å^3	3251.2(11)
Z	8
D_x/Mg m^{-3}	1.825
F(000)	1808
Temperature/K	292
Crystal size/mm	0.45×0.30×0.15
Radiation	Mo$K\alpha$
μ/mm^{-1} (Mo$K\alpha$)	0.646
$2\theta_{max}$/°	55
Scan width $\Delta\omega$/°	1.3+0.5 tan θ
Scan speed 2θ/° min^{-1}	4
Max. h,k,l	21, 12, 25
No. of reflections	
measured	3966
unique	3735
observed	2200
refined	2196
R (Observed)	0.069
R (Refined)	0.065
wR (Refined)	0.071

were omitted from the final refinement. $\Sigma w(|F_c|-k^{-1}|F_o|)^2$ was minimized with $w=1/(9.1852-0.1234|F_o|+0.0013|F_o|^2)$. The final R was 0.065 for 2196 refined reflections and an R value for 2200 reflections with $|F_o|\geq 3\sigma(F)$ was 0.069. Atomic scattering factors were taken from International Tables for X-Ray Crystallography.[6] All computations were performed on a HITAC M260 Computer of the Data Processing Center of the University of Electro-Communications with the programs UNICS III,[7] ORTEP II.[8]

Results and Discussion

Crystal Structure. The final atomic parameters are listed in Table 2.[9] There are two independent dications, **A** and **B**, in the crystals, each of which has a crystallographic twofold symmetry as shown in Fig. 1(a). Thus there are two halves of the dications and two independent anions in an asymmetric unit. These two independent dications are related with each other by a local pseudo mirror at $x=0.125$. The molecules are stacked along the a axis in a manner of **AABBAA**···. The environment of the anion **A** is different from that of **B**: the anions **A** are located between methylene groups of the two dications while the anions **B** are located between sulfur atoms. Figure 1(b) shows the molecular arrangement viewed along the a axis.

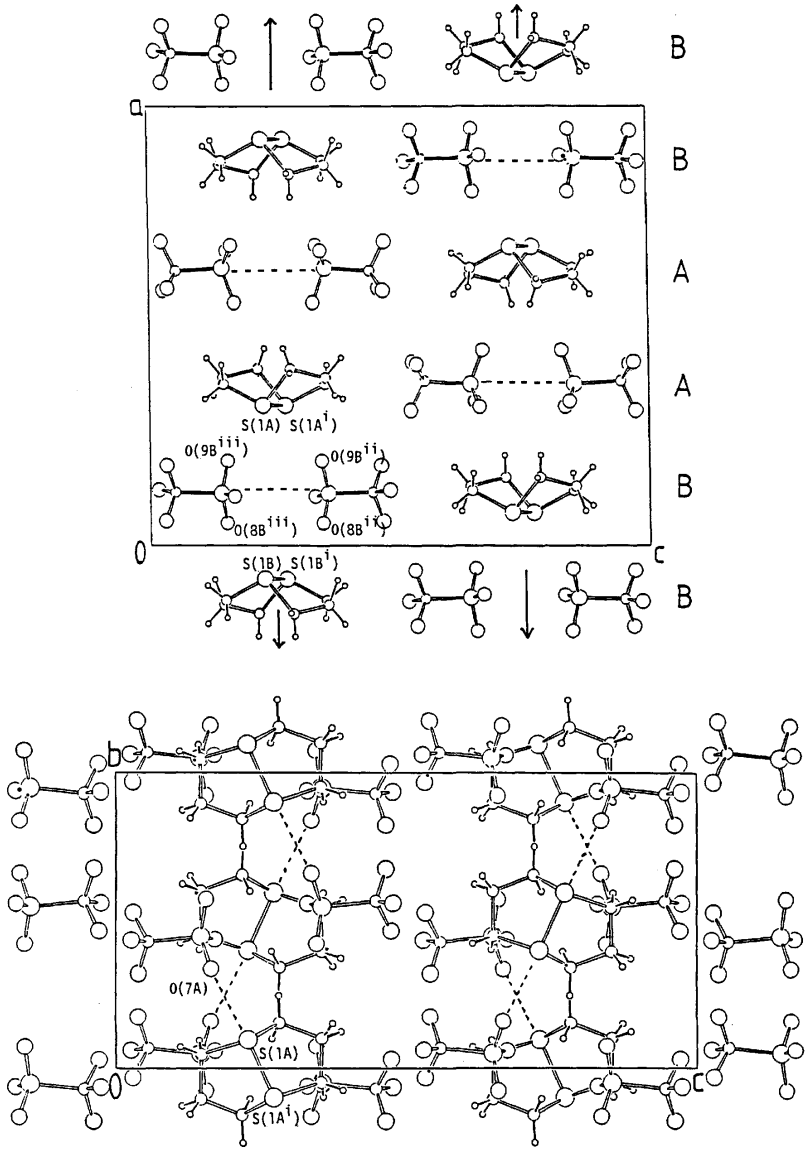

Fig. 1. The projection of the crystal structure, (a) viewed along the b axis within the range from $x=0.0$ to 0.5. Dotted lines show the pseudo local mirror between the dications **A** and **B**. (b) Viewed along the a axis within the range from $x=0.25$ to 0.75. Only dications **A** and anions **A** are shown in this range. Dotted lines show the S···O interaction between dications **A** and anions **A**.

Structure of Dication. The structure of the dication with the atom-numbering is shown in Fig. 2 and the bond distances and angles are listed in Table 3. The S(1)-S(1^{i}) (i=x,$-y$,1/2$-z$) lengths are 2.126(3) and 2.122(3) Å,[10] for **A** and **B**, respectively, which are only slightly longer than the normal S-S single bond (2.08 Å). Therefore a bond formation of S^{+}-S^{+} is confirmed unequivocally and the structure of the dication is not an open cyclooctane ring but a bicyclooctane. On the other hand relatively short transannular S···S contacts in some sulfur-bonded 1-thionia-5-thiacyclooctane salts and 1,5-dithiacyclooctanes are in the range of 3.121—3.271 Å.[2] The S-C lengths are 1.842(7) and 1.828(6) Å for the dication **A** and 1.829(7) and 1.830(6) Å for **B**. These values are also slightly longer than the normal S-C single bond length, while C-C lengths are slightly shorter than the normal Csp^3-Csp^3 bond. The bond angles of C-S-C are 104.1(3)° and 104.6(3)° for **A** and **B**, respectively and those of S-S-C are 92.7(2)—95.9(2)°. The torsion angles of the dications are listed in Table 4. The conformation of the eight-membered ring is a

Table 2. Atomic Coordinates (×10^4) and Equivalent Isotropic Temperature Factors[a] for Non-H Atoms

The esd's in parenthses refer to last digits.

Atom	x	y	z	B_{eq}/Å^2
S(1A)	3205(1)	982(1)	2280(1)	2.52(3)
C(2A)	4036(4)	1553(6)	2824(3)	3.1(1)
C(3A)	3836(4)	1026(7)	3526(3)	3.6(2)
C(4A)	3687(3)	−478(6)	3517(3)	2.9(1)
S(1B)	−752(1)	984(1)	2285(1)	2.41(3)
C(2B)	−1555(4)	1570(6)	2844(3)	3.2(2)
C(3B)	−1351(4)	1023(7)	3546(3)	3.4(1)
C(4B)	−1254(4)	−511(6)	3509(3)	2.9(1)
S(5A)	3681(1)	4500(2)	1468(1)	3.4(1)
C(6A)	3749(6)	4308(10)	553(4)	5.9(3)
O(7A)	3166(3)	3390(5)	1652(3)	5.0(2)
O(8A)	3288(4)	5758(6)	1561(4)	7.2(2)
O(9A)	4460(3)	4393(11)	1715(4)	10.2(3)
F(10A)	4139(5)	3232(8)	385(4)	12.4(3)
F(11A)	3081(4)	4371(12)	261(3)	13.3(4)
F(12A)	4189(5)	5309(9)	293(4)	12.5(3)
S(5B)	−1194(1)	4775(1)	1431(1)	2.6(1)
C(6B)	−1216(5)	4507(9)	518(4)	5.1(2)
O(7B)	−1125(3)	3446(5)	1697(3)	5.3(2)
O(8B)	−515(2)	5631(5)	1540(3)	4.2(1)
O(9B)	−1947(2)	5437(5)	1558(2)	3.8(1)
F(10B)	−1838(3)	3726(7)	346(3)	8.0(2)
F(11B)	−558(4)	3863(8)	315(3)	9.7(2)
F(12B)	−1272(4)	5620(7)	178(3)	9.3(2)

a) $B_{eq}=4/3\sum_i\sum_j\beta_{ij}\boldsymbol{a}_i\boldsymbol{a}_j$.

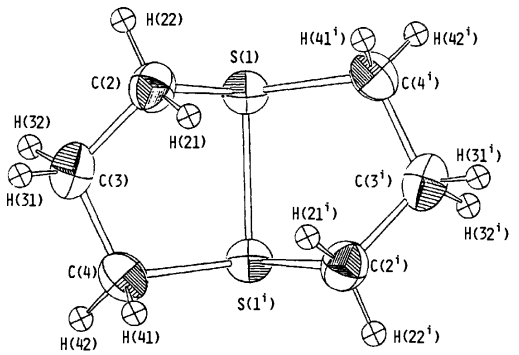

Fig. 2. The structure of dication **A** with the atom-numbering. The thermal ellipsoids for non-H atoms are drawn at 50% probability.

Table 3. Bond Lengths (l) and Angles (θ)

Cation Distance	**A** l/Å	**B** l/Å	Cation Angle	**A** θ/°	**B** θ/°
S(1)-S(1^{i})	2.126(3)	2.122(3)	S(1^{i})-S(1)-C(2)	92.6(2)	93.1(2)
S(1)-C(2)	1.842(7)	1.829(7)	S(1^{i})-S(1)-C(4^{i})	95.6(2)	95.9(2)
S(1)-C(4^{i})	1.828(6)	1.830(6)	C(2)-S(1)-C(4^{i})	104.1(3)	104.6(3)
C(2)-C(3)	1.509(9)	1.516(9)	S(1)-C(2)-C(3)	104.7(4)	105.3(4)
C(3)-C(4)	1.509(9)	1.527(9)	C(2)-C(3)-C(4)	111.5(5)	109.6(5)
			C(3)-C(4)-S(1^{i})	110.6(4)	110.1(4)
Anion Distance	**A** l/Å	**B** l/Å	**Anion Angle**	**A** θ/°	**B** θ/°
S(5)-C(6)	1.807(10)	1.809(9)	C(6)-S(5)-O(7)	101.9(4)	103.2(4)
S(5)-O(7)	1.443(6)	1.419(6)	C(6)-S(5)-O(8)	104.4(4)	104.5(4)
S(5)-O(8)	1.419(7)	1.435(5)	C(6)-S(5)-O(9)	106.0(6)	102.7(4)
S(5)-O(9)	1.397(11)	1.444(5)	O(7)-S(5)-O(8)	111.0(4)	115.3(3)
C(6)-F(10)	1.292(13)	1.340(11)	O(7)-S(5)-O(9)	114.6(5)	115.4(3)
C(6)-F(11)	1.259(15)	1.335(12)	O(8)-S(5)-O(9)	117.2(6)	113.6(3)
C(6)-F(12)	1.336(13)	1.291(11)	S(5)-C(6)-F(10)	111.8(7)	110.4(6)
			S(5)-C(6)-F(11)	112.9(8)	110.3(7)
			S(5)-C(6)-F(12)	109.6(7)	112.7(7)
			F(10)-C(6)-F(11)	112.1(10)	107.1(8)
			F(10)-C(6)-F(12)	103.5(9)	107.9(8)
			F(11)-C(6)-F(12)	106.3(10)	108.2(8)

Superscript (i) x, $-y$, 1/2$-z$.

distorted chair-chair form, while in the case of 1-thionia-5-thiacyclooctanes and 1,5-dithiacyclooctanes a chair-boat conformation is dominant.

S···O Interaction between Cations and Anions. Very strong interactions were observed between S^+ of the dications and O(7) atoms of the counter anions. The distance of $S^+ \cdots O$ are 2.682(6) and 2.766(6) Å for **A** and **B**, respectively, which are remarkablely shorter than the van der Waals contact of 3.35 Å. The angles of S-S···O are 176.3(2) and 166.8(1)°, for **A** and **B**, respectively. Nearly colinear interactions of O···S-S···O, especially in **A**, are formed with the central two fold symmetry as shown in Fig. 3. A linear O···S-S arrangement with a short S···O distance is a typical feature of the hypervalent sulfur compounds.[4] Intramolecular interactions with such a linear O···S-S···O interaction have been reported in 3,5-diacetamido-1,2-dithiolium bromide,[11] bis(*o*-nitrophenyl) disulfide,[12] dimethyl 2,2′-dithiodibenzoate,[13] and N,N′-dimethyl-2,2′-dithiodibenzamide.[14] The S···O distances of these compounds are 2.52—2.89 Å.

Other short nonbonded interactions between dications and anions are also shown in Fig. 3. S(1**A**) has nonbonded contacts to O(9**B**^{ii}) and O(9**B**^{iii}) (ii=$-x$, $y-1/2$, $1/2-z$; iii=$-x$, $1/2-y$, z) at the distances of 3.151(5) and 2.903(5) Å, respectively. These oxygen atoms, in turn, have bifurcate contacts with S(1**A**) and S(1**A**^{i}). The similar situation is observed between S(1**B**) and O(8**B**). The distances of S(1**B**)···O(8**B**^{ii}) and S(1**B**)···O(8**B**^{iii}) are 3.153(5) and 3.034(5) Å, respectively. Thus the coordination around S(1) is a roughly distorted octahedron with two C and two O atoms in a plane and an apical S-S bond and S···O contact. Some interatomic distances and angles related with the S···O interactions are summalized in Table 5. S(1**A**) deviates by 0.277 Å from the plane defined by four atoms C(2**A**), C(4**A**^{i}), O(9**B**^{ii}), and O(9**B**^{iii}). The angle between this plane and S(1**A**)···O(7**A**) is 67.9°. The corresponding deviation and the angle for the dication **B** are 0.260 Å and 56.1°, respectively.

All the O atoms of the anion **B**, which is located between S atoms of both dications **A** and **B**, coordinate

Table 4. Torsion Angles (τ) of Dications

Torsion angle	**A** τ/°	**B** τ/°
C(2)-S(1)-S(1^i)-C(2^i)	−81.6(3)	85.1(3)
C(4)-S(1)-S(1^i)-C(4^i)	127.2(3)	−124.9(3)
C(2)-S(1)-S(1^i)-C(4^i)	22.8(3)	−19.9(3)
C(4^i)-S(1)-C(2)-C(3)	−140.3(4)	140.1(4)
S(1^i)-S(1)-C(2)-C(3)	−43.8(4)	43.3(4)
S(1)-C(2)-C(3)-C(4)	54.2(5)	−55.9(5)
C(2)-C(3)-C(4)-S(1^i)	−34.8(6)	38.7(5)
C(3)-C(4)-S(1^i)-S(1)	2.1(4)	−6.6(4)
C(3)-C(4)-S(1^i)-C(2^i)	96.3(4)	−101.3(4)

Superscript (i) x, $-y$, $1/2-z$.

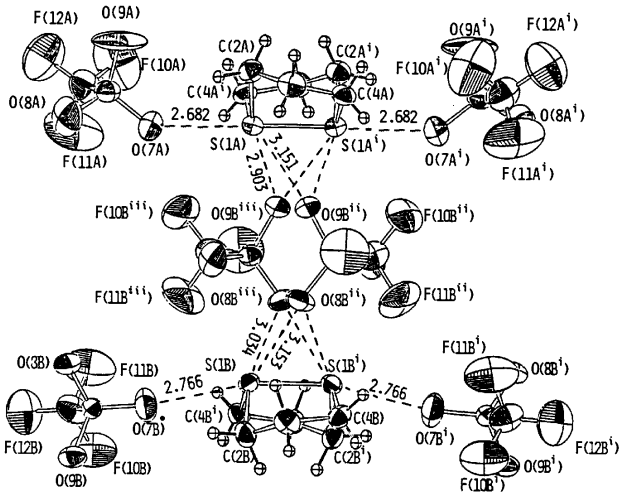

Fig. 3. S···O interactions between dications and anions.

Table 5. S···O Interactions between Cations and Anions Distances (l) and Angles (θ)

	Cation **A**	Cation **B**
Distance	l/Å	l/Å
S(1)···O(7)	2.682(6)	2.766(6)
Angle	θ/°	θ/°
S(1^i)-S(1)···O(7)	176.3(2)	166.8(1)
C(2)-S(1)···O(7)	90.7(2)	78.7(2)
C(4^i)-S(1)···O(7)	82.0(2)	76.5(2)

	Cation **A**		Cation **B**	
X	O(9B^{ii})	O(9B^{iii})	O(8B^{ii})	O(8B^{iii})
Distance	l/Å	l/Å	l/Å	l/Å
S(1)···**X**	3.151(5)	2.903(5)	3.153(5)	3.034(5)
Angle	θ/°	θ/°	θ/°	θ/°
S(1^i)-**S**(1)···**X**	63.3(1)	75.8(1)	67.0(1)	73.0(1)
C(2)-S(1)···**X**	98.1(2)	168.5(2)	95.4(2)	166.1(2)
C(4^i)-S(1)···**X**	150.1(2)	76.9(2)	154.5(2)	77.2(2)
O(7)···S(1)···**X**	117.8(2)	100.9(2)	123.7(2)	114.9(2)
X···**S**(1)···**X**′	77.4(1)		79.7(1)	

Superscript (i) x, $-y$, $1/2-z$, (ii) $-x$, $-1/2+y$, $1/2-z$, (iii) $-x$, $1/2-y$, z.

to the sulfur atoms. On the other hand for the anion **A** only O(7) is used for the coordination. These facts relate with a larger deviation from the linearity of O···S–S···O and a longer S···O distance in the case of **B** rather than those of **A**. The temperature factors of O atoms of the anion **B** and O(7**A**) are smaller than those of the other O and F atoms. This is another evidence of the strong interactions between S^+ and O. It may be attributed to these strong interactions between the dications and the anions to obtain the crystals of this salt successfully, since an attempt to obtain stable crystals with different anions such as $H_2SO_4^{2-}$ and BF_4^- was failed.

This work was supported in part by a Grand-in-Aid for Scientic Research from the Ministry of Education, Science and Culture. F. I. would like to thank Japan Securities Scholarship Foundation for financial support.

References

1) J. T. Doi and W. K. Musker, *J. Am. Chem. Soc.*, **103**, 1159 (1981). N. Furukawa, A. Kawada, and T. Kawai, *J. Chem. Soc., Chem. Commun.*, **1984**, 1151.

2) H. Fujihara, R. Akaishi, and N. Furukawa, *J. Chem. Soc., Chem. Commun.*, **1987**, 930.

3) S. M. Johnson, C. A. Maier, and I. C. Paul, *J. Chem. Soc. B*, **1970**, 1603. W. K. Musker, M. M. Olmstead, and M. H. Goodrow, *Acta Crystystallogr., Sect. C*, **39**, 887 (1983). M. M. Olmstead, K. A. Williams, and W. K. Musker, *J. Am. Chem. Soc.*, **104**, 5567 (1982). F. Iwasaki and N. Furukawa, *Acta Crystallogr., Sect. C*, **43**, 80 (1987).

4) J. I. Musher, *Angew. Chem.*, **81**, 68 (1969); *Angew. Chem., Int. Ed. Engl.*, **8**, 54 (1969).

5) P. Main, S. E. Hull, L. Lessinger, G. Germain, J. P. Declercq, and M. M. Woolfson, MULTAN78. A System of Computer Programs for the Automatic Solution of Crystal Structures from X-ray Diffraction Data. Univs. of York, England and Louvain-la-Neuve, Belgium (1978).

6) "International Tables for X-ray Crystallography," Vol. IV. Birmingham: Kynoch Press (1974).

7) T. Sakurai and K. Kobayashi, *Rikagaku Kenkyusho Houkoku*, **55**, 69 (1979).

8) C. K. Johnson, ORTEP II, Report ORNL-5138, Oak Ridge National Laboratory, Tennessee (1976).

9) Tables of atomic parameters for H-aroms, thermal parameters for non-H atoms and the F_o-F_c list are deposited as Document No. 8813 at the Office of the Editor of the Bulletin of the Chemical Society of Japan.

10) Here and after the last decimal figure in parenthesis shows e.s.d.

11) A. Hordvik and H. M. Kjoge, *Acta Chem. Scand.*, **20**, 1923 (1966).

12) J. S. Ricci and I. Bernal, *J. Chem. Soc. B*, **1970**, 806.

13) A. Kúcsmán, I. Kapovits, L. Parkanyi, G. Argay, and A. Kálmán, *J. Mol. Struct.*, **125**, 331 (1984).

14) F. Iwasaki, N. Toyoda, and N. Yamazaki, to be published.

Solid-State ^2H NMR Study of Discotic Benzenehexayl Hexaheptanoate. Conformational Transition of Alkyl Side Chains

Hirokazu TORIUMI,* Toru SHIMMURA, Hiroshi WATANABE, and Hazime SAITÔ†
Department of Chemistry, College of Arts and Sciences, University of Tokyo,
Komaba, Meguro-ku, Tokyo 153
†Biophysics Division, National Cancer Center Research Institute,
Tsukiji 5-chome, Chuo-ku, Tokyo 104
(Received January 21, 1988)

A ^2H NMR study of discotic benzenehexayl hexaheptanoate carrying perdeuterated alkyl side chains (BH7-d_{78}) is reported. Solid-state ^2H NMR measurements reveal that the conformational transition of the heptanoate chains takes place at 230 K from nearly static to mobile state. The chains above 230 K undergo flip-flop type reorientational motion, with the degree increasing upon heating. This temperature coincides with the solid-to-solid phase transition temperature, indicating that the phase transition takes place accompanied by the conformational melting of the flexible alkyl side chains. A spectrum measured in the discotic mesophase is also reported.

Extensive efforts have been devoted to characterize the conformational properties of alkyl chains appended to liquid crystalline molecules. In particular, their effects on the structure and stability of liquid crystals have been of both theoretical and practical interest. It is now generally recognized that the chain flexibility has a major contribution to the entropy of melting, hence it exerts significant influence on the phase transition behavior of liquid crystals. The deuterium NMR (^2H NMR) has emerged during the course of these studies as a powerful technique for investigating the conformational and dynamic properties of molecules in the mesomorphic state.[1,2] Yet, so far, only little is known about the alkyl chain conformation in the solid state and therefore its effect on the solid to liquid crystal phase transition is still open to debate.

For a homologous series of disc-like liquid crystals, benzenehexayl hexaalkanoates (BHn), $C_6(OCOC_{n-1}H_{2n-1})_6$, Sorai et al.[3-5] have carried out heat capacity measurements and shown that these compounds undergo a series of solid-state phase transitions before forming the discotic mesophase. These transitions are ascribed to the conformational melting of pendent alkyl chains, and the formation of the discotic mesophase of BHn is suggested to be a phenomenon appearing as one stage of successive phase transition driven by the side-chain conformational changes. In this communication, we report a solid-state ^2H NMR study of benzenehexayl hexaheptanoate (BH7) and show how the conformational melting of flexible alkyl chains proceeds in the solid phases.

Experimental

The sample of BH7-d_{78}, carrying perdeuterated heptanoate chains, was synthesized from tetrahydroxy-*p*-benzoquinone and heptanoic-d_{13} acid (MSD isotopes) according to the published method.[6,7] The reaction product was purified by repeated recrystallization from absolute ethanol and dried under vacuum to give white needle crystals of BH7-d_{78}. Solid-state ^2H NMR spectra were recorded on a Bruker CXP-300 spectrometer at 46.07 MHz using the quadrupole echo pulse sequence ($90^\circ_{\pm x}$-τ-90°_{y}-τ-echo) with a 90° pulse duration of 4.0 μs and a delay time τ=50 μs. Typically 100—200 spectra were accumulated with a repetition time of 0.2—0.5 s. The ^2H NMR spectrum of BH7-d_{78} in the mesomorphic state was measured by a JEOL GSX-270 spectrometer at 41.27 MHz using the single pulse sequence with a 90° pulse length of 5.0 μs. In both experiments, the temperature of the sample was controlled within ±1 °C with nitrogen gas flow.

Results and Discussion

Figure 1 shows the temperature dependence of the ^2H NMR spectrum of BH7-d_{78} in the solid state. The spectra at low temperatures consist of superposition of two axially symmetric quadrupolar powder patterns. The outer component is assigned to the methylene deuterons of pendent heptanoate chains and the inner component is assigned to the methyl deuterons. Although the parallel shoulders of the outer powder component (arising from methylene deuterons with C-D bond vectors oriented parallel to the field direction; θ=0° orientation) are lost outside of the spectrum, the perpendicular peaks (corresponding to θ=90° orientation) are clearly resolved with a peak separation of 123 kHz. Since a rigid-limit axially-symmetric powder spectrum of polycrystalline sample appears as superposition of properly weighted quadrupolar doublets, each of which has a spacing[8]

$$\Delta\nu = \frac{3}{2}\frac{e^2qQ}{h}P_2(\cos\theta) \qquad (1)$$

(e^2qQ/h is the quadrupolar coupling constant), the separation between perpendicular peaks (θ=90°) measures a value (3/4)(e^2qQ/h). The observed peak separation $\Delta\nu$=123 kHz yields e^2qQ/h=164 kHz, which is in good agreement with the literature value of the quadrupolar coupling constant of methylene deuterons.[8] The separation between parallel edges of the

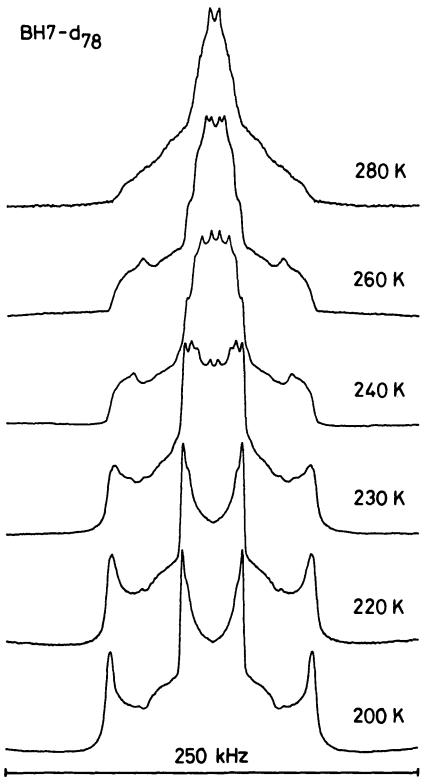

Fig. 1. Temperature dependence of solid-state ^{2}H NMR spectrum of BH7-d_{78} carrying perdeuterated heptanoate side chains.

methyl powder pattern ($\Delta\nu$=71.8 kHz) is just twice as large as its perpendicular peak separation ($\Delta\nu$= 35.8 kHz) in accord with the prediction of Eq 1. If the terminal methyl group, having the tetrahedral geometry (with the C-C-D bond angle β=109.47°), undergoes rapid rotation about its C_3 symmetry axis, separation of peaks is scaled down by a factor $|(1/2)(3\cos^2\beta-1)|=1/3$. The observed peak separation (35.8 kHz) is however slightly smaller than the expected value (41.0 kHz). This additional reduction in $\Delta\nu$ is indicative of either a departure of the methyl group structure from the ideal tetrahedral geometry or the presence of librational motions of the methyl symmetry axis.[9,10] Nevertheless, for the heptanoate chain as a whole, the degree of reorientational motion should be quite low (or the rate is slow on the ^{2}H NMR frequency scale), since the quadrupolar coupling constant observed for the inner methylene deuterons is large and reproduces its rigid-limit value.

Above 230 K the spectral shape changes substantially. A sizable build-up of intensity occurs in the central part of the spectrum, while the intensity of the outermost peaks is decreased and the linewidth is broadened. The 230 K spectrum shows several pairs of powder-pattern peaks in the central pattern indicating that the inner methylene segments aquire the reorientational freedom at this temperature. The narrowing of the central spectral component proceeds

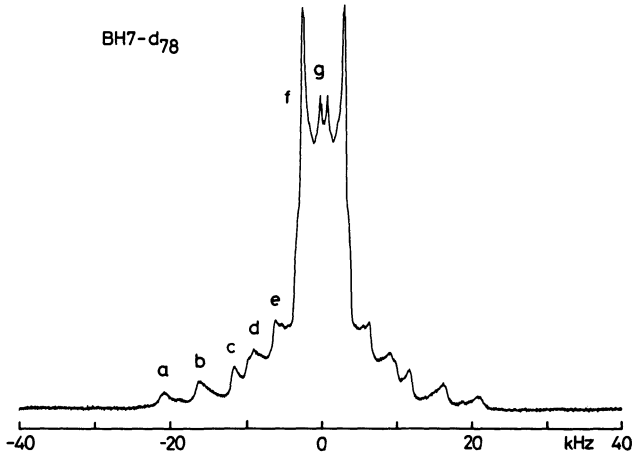

Fig. 2. ^{2}H NMR spectrum of BH7-d_{78} in the discotic mesophase at 354 K.

continuously with increasing temperature, and eventually results in the line shape such as that observed at 280 K. This pattern, i.e., the biaxial powder pattern which would arise when the C-D bond axis jumps rapidly between discrete sites, suggests the flip-flop type motion of the heptanoate chain. In this connection, it is noteworthy that the 280 K spectrum still preserves a broad component with a separation between extreme edges of ca. 110 kHz. The coexistence of spectral components with widely varying quadrupolar coupling constants is consistent with the flip-flop motion of the chain suggested above; namely, the methylene segment undergoes an increasing degree of motion as it approaches to the chain terminal.

The onset of the aforementioned changes in the ^{2}H NMR line shape was observed at 230 K. This temperature coincides with the first-order solid-to-solid phase transition temperature (230.81 K) determined calorimetrically by Sorai and Suga.[4] They have also reported the results of infrared measurements and pointed out that the molecular and crystal structures are different between these two solid phases. Our present ^{2}H NMR studies clearly demonstrate that the melting of the alkyl chain conformation takes place at this temperature from nearly static state (the chain being in the lowest energy all-trans conformation) to mobile state (undergoing the flip-flop motion). The spectral shape remains essentially unchanged above room temperature (except for the occurrence of continuous narrowing) until the transition to the discotic mesophase at 353.79 K.

Shown in Fig. 2 is the ^{2}H NMR spectrum of BH7-d_{78} recorded in the discotic mesophase. For the measurement the sample was first heated to the isotropic liquid phase (T_{iso}=359.28 K), then cooled down slowly to turn into the mesophase. The spectrum shows five discrete quadrupolar doublets (a—e) with $\Delta\nu$ values ranging from 42 to 12 kHz,

which are attributable to the five methylene groups. The innermost doublet (g) with $\Delta\nu$=0.96 kHz is then assigned to the terminal methyl group by taking account of the signal intensity. These discrete quadrupolar doublets arise from BH7-d_{78} molecules oriented uniaxially in the field. Elucidation of the average alkyl chain conformation from the $\Delta\nu$ pattern is possible in terms of the theories described previously.[11,12] However, these doublet patterns are dominated by an intense powder-like component (f). Its peak separation $\Delta\nu$=5.6 kHz is comparable to a value $\Delta\nu$=6.6 kHz observed for peaks in the solid-state spectrum at 280 K in Fig. 1. Obviously, there should coexist unoriented molecules. Corresponding ^2H NMR spectra reported for triphenylene-type discotic liquid crystals exhibit only discrete quadrupolar doublets.[13,14] The coexistence of "oriented" and "unoriented" components in our spectrum suggests that the diamagnetic anisotropy of the central benzene core of BH7-d_{78} is not larger than that of the triphenylene core and thereby cannot suffice to cause homogeneous orientation.

In summary, we have demonstrated that the solid-state deuterium NMR is successful in analyzing the conformational properties of flexible alkyl chains appended to liquid crystalline molecules. The observed ^2H NMR line shape shows marked differences between phases, reflecting the changes in the mode and degree of reorientational motions of alkyl side chains. Lifshitz, et al.[15] have recently carried out ^2H NMR measurements of BH6 (a hexanoate homologue of BH7) and shown that the hexanoate side chains undergo very similar solid-state conformational transitions. Thus, the sequential melting of side-chain conformation at the phase transition appears to be a general characteristic of this class of disc-like liquid-crystalline molecules.

We thank Professor M. Sorai of Osaka University for directing our attention to this problem and for valuable informations concerning the sample synthesis. We are also grateful to JEOL for measuring the spectrum in Fig. 2.

References

1) "Nuclear Magnetic Resonance of Liquid Crystals," ed by J. W. Emsley, D. Reidel, Dordrecht (1985).
2) J. W. Doane, "Magnetic Resonance of Phase Transition," ed by F. J. Owens, C. P. Poole, and H. A. Farach, Academic Press, New York (1979).
3) M. Sorai, K. Tsuji, H. Suga, and S. Seki, *Mol. Cryst. Liq. Cryst.*, **59**, 33 (1980).
4) M. Sorai and H. Suga, *Mol. Cryst. Liq. Cryst.*, **73**, 47 (1981).
5) M. Sorai, H. Yoshioka, and H. Suga, *Mol. Cryst. Liq. Cryst.*, **84**, 39 (1982).
6) I. E. Neifert and E. Bartow, *J. Am. Chem. Soc.*, **65**, 1770 (1943).
7) A. J. Fatiadi and W. F. Sager, *Org. Synth.*, Coll. Vol. 5, 595 (1973).
8) H. H. Mantsch, H. Saitô, and I. C. P. Smith, *Prog. Nucl. Magn. Reson. Spectrosc.*, **11**, 211 (1977).
9) L. S. Batchelder, C. H. Niu, and D. A. Torchia, *J. Am. Chem. Soc.*, **105**, 2228 (1983).
10) H. Saitô, R. Tabeta, A. Kuzuhara, and T. Asakura, *Bull. Chem. Soc. Jpn.*, **59**, 3383 (1986).
11) E. T. Samulski and H. Toriumi, *J. Chem. Phys.*, **79**, 5194 (1983).
12) B. Janik, E. T. Samulski, and H. Toriumi, *J. Phys. Chem.*, **91**, 1842 (1987).
13) D. Goldfarb, Z. Luz, and H. Zimmermann, *J. Chem. Phys.*, **78**, 7065 (1983).
14) D. Goldfarb, E. Lifshitz, H. Zimmermann, and Z. Luz, *J. Chem. Phys.*, **82**, 5155 (1985).
15) E. Lifshitz, D. Goldfarb, S. Vega, Z. Luz, and H. Zimmermann, *J. Am. Chem. Soc.*, **109**, 7280 (1987).

 © 1988 The Chemical Society of Japan Bull. Chem. Soc. Jpn., 61, 2573—2578 (1988)

Thermal and Ferroelectric Properties of Novel Ferroelectric Liquid Crystals Containing α-Methylcinnamoyl Moiety in the Core Structure

Jun NAKAUCHI* and Yoshitaka KAGEYAMA
Tokyo Research Laboratory, Mitsubishi Rayon Co. Ltd., Noborito, Tama-ku, Kawasaki, Kanagawa 214
(Received February 10, 1988)

Six homologous series of novel ferroelectric liquid crystals containing α-methylcinnamoyl moiety in the core structure:

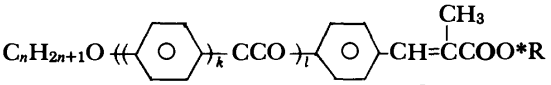

(IA: k=1, l=1, *R=-$CH_2^*CHC_2H_5$, n=8—16; IB: k=1, l=1, *R=$^*CHC_6H_{13}$, n=8—16; IIA: k=1, l=2, *R=-$CH_2^*CHC_2H_5$, n=9—16; IIB: k=1, l=2, *R=$^*CHC_6H_{13}$, n=8—14; IIIA: k=2, l=1, *R=-$CH_2^*CHC_2H_5$, n=9—16; IIIB: k=2, l=1, *R=$^*CHC_6H_{13}$, n=9—16) have been synthesized and their thermal and ferroelectric properties have been investigated. The mesomorphic transition temperatures and the spontaneous polarization for the homologous series (IA, IB, IIA, IIB, IIIA, and IIIB) depend on the core structure, the chiral group, and the terminal alkoxyl chain length. These homologous series show the chiral smectic C phase over wide temperature ranges including room temperature and the values of their maximum spontaneous polarization are in the range of 30 to 800 μC m^{-2}. The thermal stability of the mesophase and the magnitude of the spontaneous polarization have been discussed from the view point of the molecular structure and the local molecular interactions.

It was recently shown that the thin cell containing ferroelectric liquid crystals was applied to high-speed switching devices.[1] Since then, much attention has been given to the synthesis of ferroelectric liquid crystals which show the chiral smectic C (Sm*C) phase over a wide temperature range including room temperature and have large spontaneous polarization.[2-6] However, there are few liquid crystals which exhibit the Sm*C phase in the region of lower temperature than room temperature and have large spontaneous polarization. Therefore, eutectic mixtures which show the enantiotropic Sm*C phase over a wide temperature range covering room temperature have been prepared by mixing several compounds.[7-10] In addition to such practical approach, the synthesis of novel compounds and the investigation of the correlation between the physical properties and the molecular structure are necessary in order to design the materials with higher quality than those reported so far. In the previous paper,[11] we reported that the homologues with longer alkoxyl chain of (*S*)-2-methylbutyl esters or 4-(4-*n*-alkoxybenzoyloxy)-α-methylcinnamic acid (IA homologues shown below) show enantiotropic Sm*C phase around room temperature. In addition to these homologues (IA), we have synthesized other five homologous series (IB, IIA, IIB, IIIA, and IIIB) as shown in the following general formula:

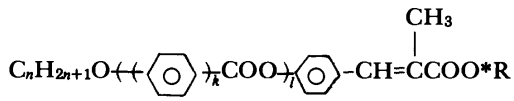

IA: k = 1, l = 1, *R = -$CH_2^*CHC_2H_5$, n = 8—16,

IB: k = 1, l = 1, *R = $^*CHC_6H_{13}$, n = 9—16,

IIA: k = 1, l = 2, *R = -$CH_2^*CHC_2H_5$, n = 9—16,

IIB: k = 1, l = 2, *R = $^*CHC_6H_{13}$, n = 8—14,

IIIA: k = 2, l = 1, *R = -$CH_2^*CHC_2H_5$, n = 9—16,

IIIB: k = 2, l = 1, *R = $^*CHC_6H_{13}$, n = 9—16,

In the present paper, we discuss the effect of the core, the chiral part, and the terminal alkoxyl chain in the molecular structure on the mesomorphic transition temperatures and the magnitude of the spontaneous polarization in the Sm*C phase.

Experimental

Preparation of Materials. All the reagents purchased from Tokyo Kasei Co., Ltd. were used without further purification. *p*-Hydroxy-α-methylcinnamic acid was prepared by a Perkin reaction according to the literature.[12] (*S*)-2-Methylbutyl or (*R*)-1-methylheptyl ester of *p*-hydroxy-α-methylcinnamic acid were synthesized by an esterification reaction of *p*-acetoxy-α-methyl-cinnamoyl chloride with (*S*)-2-methyl-1-butanol or (*R*)-1-methyl-1-heptanol using triethylamine as a base, followed by the hydrolysis of the acetoxyl group selectively in the mixed solvent of tetrahydrofuran and methanol (volume ratio : 9/1) containing equimolar 1 mol dm^{-3} LiOH. The specific rotations $[\alpha]_D$ measured in chloroform at 23 °C were 3.56° and −26.73° for the (*S*)-2-methylbutyl ester and the (*R*)-1-methylheptyl ester, respectively. 4′-Alkoxy-1-biphenylcarboxylic acids were synthesized by the hydrolysis of the 4′-alkoxy-4-cyanobiphenyls, which were synthesized by a reaction or 4′-cyanobiphenyl-4-ol with the corresponding alkyl bromides in cyclohexanone containing K_2CO_3, in NaOH–H_2O–ethylene glycol solution. (*S*)-2-Methylbutyl or (*R*)-1-methylheptyl esters of *p*-hydroxybenzoyloxy-α-methylcinnamic acid were synthesized by an esterification reaction of *p*-acetoxybenzoyl chloride with (*S*)-2-methylbutyl or (*R*)-1-methylheptyl esters of *p*-hydroxy-α-methylcinnamic acid using triethylamine as a base, followed by the hydrolysis of the acetoxyl group selectively in the mixed solvent of tetrahydrofuran and methanol (volume ratio: 9/1) containing equimolar 1 mol dm^{-3} LiOH at room temperature.

Table 1. Elemental Analyses for Homologous Series IB, IIA, IIB, IIIA, and IIIB

(IB Homologues)

Carbon No. *n*	Calcd (%)		Found (%)	
	C	H	C	H
9	76.08	9.01	75.84	9.21
10	76.33	9.15	76.33	9.32
11	76.56	9.28	76.49	9.55
12	76.78	9.40	76.91	9.40
14	77.19	9.63	77.17	9.64
16	77.38	9.78	77.32	10.02

(IIA Homologues)

Carbon No. *n*	Calcd (%)		Found (%)	
	C	H	C	H
9	74.23	7.55	74.22	7.69
10	74.50	7.69	74.38	7.66
11	74.72	7.85	74.71	8.04
12	74.96	7.98	75.16	8.27
14	75.39	8.25	75.20	8.33
16	75.80	8.49	75.63	8.79

(IIB Homologues)

Carbon No. *n*	Calcd (%)		Found (%)	
	C	H	C	H
8	74.74	7.84	74.95	7.97
9	74.97	7.98	75.25	8.15
10	75.19	8.11	75.02	8.38
11	75.41	8.24	75.59	8.44
12	75.61	8.36	75.70	8.54
14	76.00	8.60	76.00	8.77

(IIIA Homologues)

Carbon No. *n*	Calcd (%)		Found (%)	
	C	H	C	H
9	77.85	8.13	77.84	8.29
10	78.05	8.27	78.32	8.49
11	78.23	8.42	78.43	8.44
12	78.40	8.55	78.68	8.78
14	78.71	8.81	78.86	8.98
16	79.00	9.04	78.93	9.23

(IIIB Homologues)

Carbon No. *n*	Calcd (%)		Found (%)	
	C	H	C	H
9	78.40	8.55	78.67	8.59
10	78.54	8.64	78.68	8.94
11	78.71	8.81	78.84	8.82
12	78.86	8.93	78.89	9.10
14	79.14	9.16	79.04	9.31
16	79.38	9.36	79.25	9.60

The homologous series (IB, IIA, IIB, IIIA, and IIIB) were prepared by an esterification reaction of the *p*-hydroxy-α-methylcinnamates or the 4-(4-hydroxybenzoyloxy)-α-methylcinnamates with the corresponding *p*-alkoxybenzoyl chlorides or 4′-alkoxy-1-biphenylcarboxylic acid chlorides using triethylamine as a base. The products were purified by column chromatography (silica gel, benzene–hexane), followed by the recrystallization from ethanol.

Their elementary analysis data are listed in Table 1.

Measurement of Physical Properties. An identification of the mesophase was carried out using a Nikon polarizing microscope equipped with a Mettler FP-52 heating stage. Transition temperatures were measured using a Daini Seikosha SSC-560 differential scanning calorimeter (DSC) at a scanning rate of 2.5 °C min^{-1} under N_2 atmosphere. The spontaneous polarization (Ps) was determined by a triangular wave method reported by Miyasato et al.[13] The frequency, the maximum amplitude, and the cell thickness were 10 Hz, 150 V, and 50 μm, respectively.

Results and Discussion

The melting points and the mesomorphic transition temperatures for the homologous series (IA, IB, IIA, IIB, IIIA, and IIIB) are summarized in Table 2. All the homologous series except a IA homologue with terminal octyloxyl chain and IB homologues with shorter alkoxyl chains (n=8—10) exhibit the enantiotropic Sm*C phase. Their phase sequences above Sm*C are isotropic (Iso)-smectic A(SmA)-Sm*C for the homologues (IA, IB, IIB, IIIA, and IIIB) and IIA homologues with longer alkoxyl chains (n=14,16) and are Iso-cholesteric(Ch)-SmA-Sm*C for IIA homologues with shorter alkoxyl chains (n=9—12). The IB homologues with longer alkoxyl chains (n=11—16) and the IIIA and IIIB homologues with shorter alkoxyl chains (n=9—12) exhibit other smectic phases (Sm 3) below the Sm*C. However, these phases have not been determined at this stage, yet. As is

Table 2. Phase Transition Temperatures for Homologous Series (IA—IIIB)

Series	Carbon No. (n)	Mp θ_m/°C	Phase transition temperature (°C)[a] Sm3–Sm*C	Sm*C–SmA	SmA–Iso(Ch)	Ch–Iso
IA	8	34.2	—	—	72.1	—
	9	30.4	—	31.0	72.3	—
	10	32.9	—	36.0	74.2	—
	11	33.9	—	41.0	74.2	—
	12	29.4	—	44.6	75.6	—
	14	41.9	—	44.7	74.4	—
	16	44.9	—	50.2	74.4	—
IB	8	29.8	—	—	37.8	—
	9	7.3	—	(5.5)[b]	35.3	—
	10	20.6	—	(14.7)	38.2	—
	11	22.2	(6.0)	26.4	35.8	—
	12	22.0	(6.2)	27.0	37.8	—
	14	16.7	(7.7)	29.2	35.5	—
	16	30.5	24.2	34.0	37.0	—
IIA	9	78.5	—	93.1	178.9	189.4
	10	77.5	—	117.0	178.2	185.0
	11	76.7	—	128.0	177.1	181.7
	12	78.1	—	139.0	176.7	179.4
	14	76.7	—	142.0	173.1	—
	16	72.6	—	141.0	170.3	—
IIB	8	54.8	—	53.5	155.3	—
	9	63.5	—	94.1	151.6	—
	10	62.6	—	105.9	149.3	—
	11	73.5	—	116.5	144.7	—
	12	62.6	—	117.1	142.9	—
	14	60.3	—	119.6	136.0	—
IIIA	9	51.6	62.1	159.8	196.3	—
	10	52.6	64.6	151.5	196.5	—
	11	64.4	(59.8)	152.9	192.7	—
	12	64.8	(60.2)	150.0	189.0	—
	14	74.4	—	150.0	197.7	—
	16	80.4	—	152.0	193.6	—
IIIB	9	27.4	62.1	128.1	160.2	—
	10	57.4	58.8	131.8	157.6	—
	11	48.4	(47.5)	128.3	156.6	—
	12	56.2	(41.6)	131.9	148.4	—
	14	62.1	—	122.3	140.2	—
	16	70.3	—	126.0	138.8	—

a) Sm3; unidentified smectic phase, Sm*C; chiral smectic C, SmA; smectic A, Ch; cholesteric, Iso; isotropic liquid.
b) ( ); monotropic transition.

evident from the table, the transition temperatures from the SmA phase to the Sm*C one for IB homologues are very low and the temperature range of the enantiotropic Sm*C phase for the homologous series IIA and IIIA is significantly wide. Such mesomorphic properties are comparable with those for the well-known MORE series with broad-band Sm*C phase, although their values of the spontaneous polarization are very small.[14,15] The IB homologue with terminal nonyloxyl chain exhibits the lowest transition temperature from SmA phase to Sm*C at 5°C monotropically, and the IIIA homologue with the terminal nonyloxyl chain exhibits the widest temperature range of the enantiotropic Sm*C phase from 62.1 to 159.8 °C. These results indicate that the α-methylcynnamoyl moiety is a suitable structure for the appearance of the Sm*C phase.

The transition temperatures from SmA phase to Iso or from SmA phase to Ch against the carbon number in terminal alkoxyl chain are plotted in Fig. 1. Compared with the transition temperatures for the homologous series IIA, IIB, IIIA, and IIIB, those for the homologous series IA and IB are little dependent on the terminal alkoxyl chain length. This result can be interpreted as follows: the thermal stability of SmA phase of the IA and IB homologues is a little affected by the thermal motion of the flexible alkoxyl chain because of their transition temperatures much lower than those for the other homologous series. Another characteristic feature is the effect of the chiral groups

on the transition temperatures. On changing a 2-methylbutyl group to a 1-methylheptyl group, the Ch phase observed in the homologous series IIA disappears in the homologous series IIB, and the transition temperatures for the homologous series IB, IIB, and IIIB become about 30—50 °C lower than those for the corresponding homologous series IA, IIA, and IIIA. The effects of the chain branching on the thermal stability of the mesophase have been investigated on the Schiff base compounds with branched alkylcinnamate moieties by Gray and Harrison and have been discussed in terms of a steric effect between the branched methyl group and the ester group.[16] Our results are similar to those reported previously[16] and can be interpreted in terms of the difference of the steric hindrance between the 1-methyl branch and the 2-methyl branch. The former interacts with the carbonyl oxygen much stronger than the latter and lies out of the plane of the mesogen, thus leading to decrease greatly both Ch and SmA thermal stabilities.

The transition temperatures from Sm*C phase to SmA against the carbon number in the terminal alkoxyl chain are plotted in Fig. 2. As is pointed out by McMillan,[17] de Jue,[18] and Patel and Goodby,[19] the transition temperatures from Sm*C to SmA depend strongly on the core structure with local dipole moments and the terminal chain length. As seen in Fig. 2, the transition temperatures for IA and IB homologues gradually increase with the terminal alkoxyl chain length and those for IIA and IIB homologues increase steeply with the terminal alkoxyl chain length in the range of lower carbon number and are approaching to the constant value in the region of higher carbon number. On the other hand, the transition temperatures for IIIA and IIIB homologues slightly decrease with the terminal alkoxyl chain length. These facts indicate that the effect of the terminal alkoxyl chain on the thermal stability of the Sm*C phase is quite different if the compounds have different core structures. The effect of the chiral group on the thermal stability of the Sm*C is a little different from that of the SmA phase, that is, the degree of depression of the transition temperature from Sm*C to SmA by replacing the 2-methylbutyl group into the 1-methylheptyl group is not so large as that from Iso or Ch phase to SmA and depends on the core structures. These facts also indicate that the position of the bulky methyl branch

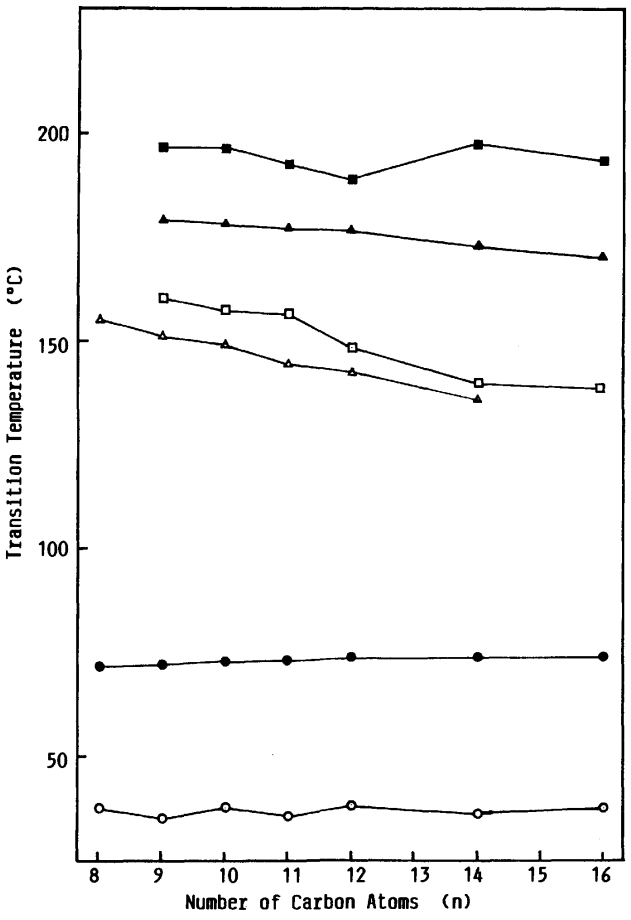

Fig. 1. Plots of the transition temperatures from SmA phase to Iso or Ch phse against the number of carbon atoms in the *n*-alkoxyl chain of the homologous series IA(-●-), IB(-○-), IIA(-▲-), IIB(-△-), IIIA(-■-), and IIIB(-□-).

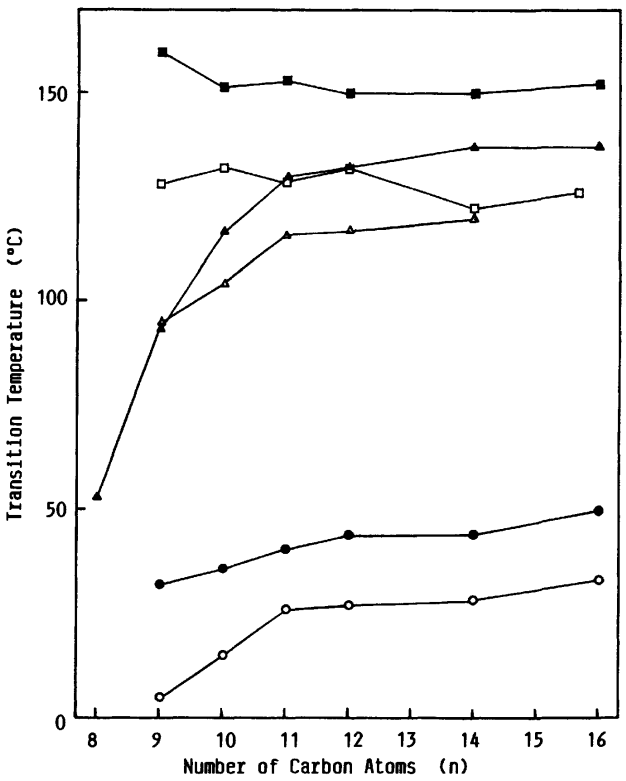

Fig. 2. Plots of the transition temperatures from Sm*C phase to SmA against the number of carbon atoms in the *n*-alkoxyl chain of the homologous series IA(-●-), IB(-○-), IIA(-▲-), IIB(-△-), IIIA(-■-), and IIIB(-□-).

and the chain length of the chiral group play some role for the appearance of Sm*C phase as well as the core structure and the terminal alkoxyl chain length.

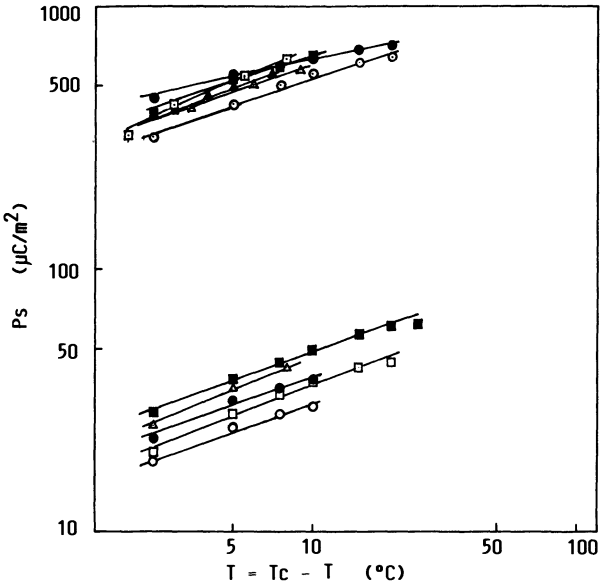

Fig. 3. Logarithmic plots of the temperature dependence of the spontaneous polarization for the homologous series IA and IB: n=9(-○-); n=10(-●-); n=11(-□-); n=12(-■-); n=14(-△-); n=16(-▲-). The cell thickness, the frequency, and the maximum amplitude of applied voltage are 50 μm, 10 Hz, and 150 V, respectively.

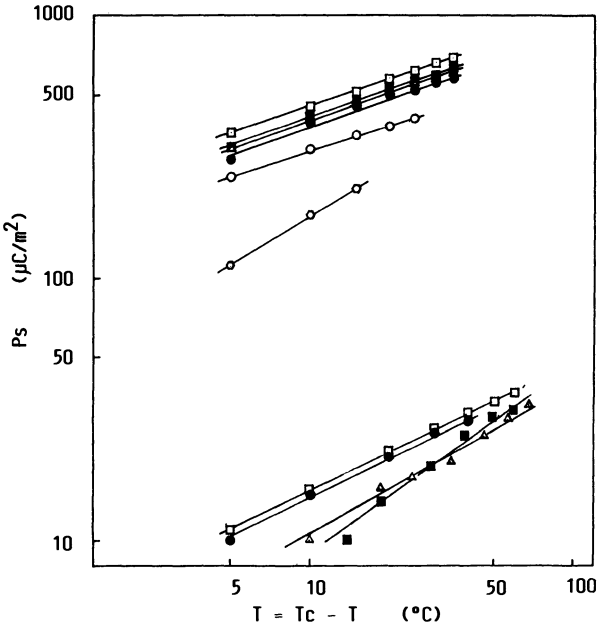

Fig. 4. Logarithmic plots of the temperature dependence of the spontaneous polarization for the homologous series IIA and IIB: n=8(-○-); n=9(-○-); n=10(-●-); n=12(-■-); n=14(-△-). The cell thickness, the frequency, and the maximum amplitude of applied voltage are 50 mm, 10 Hz, and 150 V, respectively.

The temperature dependence of the spontaneous polarization in the Sm*C phase for a number of the homologues in the homologous series (IA and IB), (IIA and IIB), and (IIIA and IIIB) are shown in Figs. 3, 4, and 5, respectively. It is clearly shown that the temperature dependence of the measured values for all the IA, IB, IIA, IIB, and IIIB homologues except that for IIIA homologues is represented by the expression $P_s=A(\Delta T)^a$. The log-log plots of P_s vs. ΔT for the IIIA homologues form nonlinear curve, which could be divided into two linear lines with different gradient. This fact may indicate that two processes concerned with the temperature dependence of the spontaneous polarization exist in the Sm*C phase of the IIIA homologues.

As is expected from the effect of the position or the asymmetric carbon in the chiral part on the spontaneous polarization reported so far,[20,21] the magnitude of the spontaneous polarization for the homologous series IB, IIB, and IIIB with 1-methylheptyl group is one order higher than that for the corresponding homologous series IA, IIA, and IIIA with 2-methylbutyl group. Some relation between the spontaneous polarization and the core structure is also seen among the homologous series (I, II, and III), that is, the values of the spontaneous polarization for the homologous series I, II, and III are approximately in the order of III>I>II. Additionally, in each homologous series, the magnitude of the spontaneous polarization shows the maximum value at a certain length of the terminal alkoxyl chain.

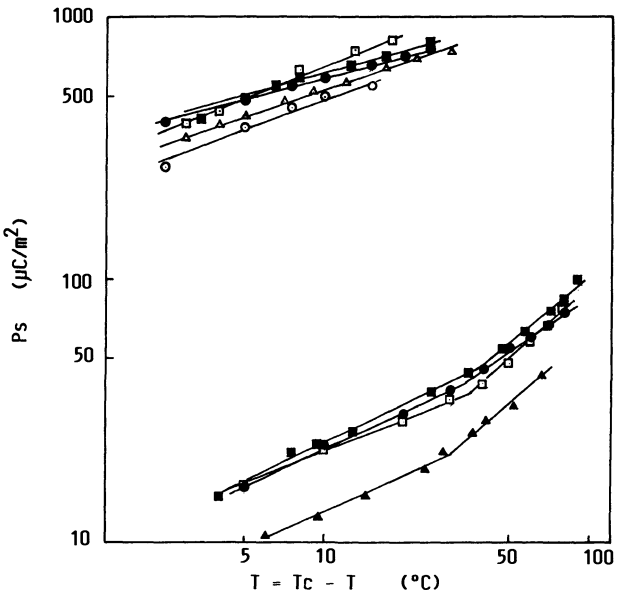

Fig. 5. Logarithmic plots of the temperature dependence of the spontaneous polarization for the homologous series IIIA and IIIB: n=9(-○-); n=10(-●-); n=11(-□-); n=12(-■-); n=14(-△-); n=16(-▲-). The cell thickness, the frequency, and the maximum amplitude of applied voltage are 50 μm, 10 Hz, and 150 V, respectively.

The magnitude of the spontaneous polarization is considered to depend on the size of the lateral component of dipole moment of the ester group adjacent to the chiral part and on the degrees of the restriction of a rotation about the molecular long axis and of an internal rotation around the bond between the chiral part and the core. The effect of the restriction of the internal rotation around the bond between the chiral part and the core on the spontaneous polarization is clearly seen in the homologous series A with the 1-methyl branch and in the series B with the 2-methyl branch. In comparison with the 2-methyl branch in the chiral group, the 1-methyl branch restricts the internal rotation around the bond between the chiral part and the core more strongly due to the steric hindrance. The difference of the values of the spontaneous polarization among the homologous series (I, II, and III) with the same chiral group is not so large. This result may be attributed to the reason that the core structure near the chiral part for the homologous series I, II, and III is identical, and then, the size of the net dipole moment related to the spontaneous polarization is considered to be almost same. However, the effect of the core and the terminal alkoxyl chain length on the magnitude of the spontaneous polarization cannot be well explained at this stage, because the temperature range of Sm*C phase among these homologous series is quite different one another, therefore the degree of the restriction of the rotation about the molecular long axis cannot be estimated.

More detailed study on the molecular motion and the structure in the Sm*C phase must be necessary in order to elucidate the correlation between the spontaneous polarization and the molecular structure.

The authors thank Dr. Toshio Yoshihara for his helpful discussion and also thank Mrs. Mioko Uematsu and Mr. Yoshihiro Sako for their assistance of experiments.

References

1) N. A. Clark and S. T. Lagewall, *Apll. Phys. Lett.*, **36**, 899 (1980).
2) T. Sakurai, N. Mikami, R. Higuchi, M. Honma, M. Ozaki, and K. Yoshino, *J. Chem. Soc., Chem. Commum.*, **1986**, 979.
3) T. Sakurai, N. Mikami, M. Ozaki, and K. Yoshino, *J. Chem. Phys.*, **85**, 585 (1986).
4) T. Inukai, S. Saitoh, H. Inoue, K. Miyazawa, K. Terashima, and K. Furukawa, *Mol. Cryst. Liq.Cryst.*, **141**, 251 (1986).
5) K. Terashima, M. Ichihashi, M. Kikuchi, K. Furukawa, and T. Inukai, *Mol. Cryst. Liq. Cryst.*, **141**, 237 (1986).
6) K. Yoshino, M. Ozaki, H. Taniguchi, M. Ito, K. Satoh, N. Yamasaki, and T. Kitazume, *Jpn. J. Appl. Phys.*, **26**, L-77 (1987).
7) K. Kondo, S. Era, M. Isogai, and A. Mukoh, *Jpn. J. Appl. Phys.*, **24**, 1389 (1985).
8) J. P. Le Pesant, J. N. Perbert, B. Mourey, M. Hareng, G. Decobert, and J. C. Dubois, *Mol. Cryst. Liq. Cryst.*, **129**, 61 (1985).
9) W. Kuczynski, S. T. Lagerwall, M. Matuszezyk, K. Skarp, B. Stebler, and J. Wahl, *Mol. Cryst. Liq. Cryst.*, **146**, 173 (1987).
10) K. Mohr, S. Köhler, K. Worm, G. Pelzl, S. Diele, H. Zaschke, D. Demus, G. Andersson, I. Dahl, S. T. Lagerwall, K. Skarp, and B. Stebler, *Mol. Cryst. Liq. Cryst.*, **146**, 151 (1987).
11) J. Nakauchi, Y. Kageyama, M. Uematsu, and S. Minami, *Bull. Chem. Soc. Jpn.*, **60**, 4239 (1987).
12) J. R. Johnson, "Organic Reaction" ed by R. Adams, W. E. Bachman, J. R. Johnson, L. F. Fieser, H. R. Snyder, Robert E. Krieger Pub., Huntington, New York (1978), Vol. 1, p. 210.
13) K. Miyasato, S. Abe, H. Takezoe, A. Fukuda, and E. Kuze, *Jap. J. Appl. Phys.*, **2**, L-661 (1983).
14) A. Hallsby, M. Nilsson, and B. Otterholn, *Mol. Cryst. Liq. Cryst.*, **82**, 61 (1982).
15) K. Skarp, K. Flatischler, K. Kondo, Y. Sato, K. Miyasato, H. Takezoe, A. Fukuda, and E. Kuze, *Jpn. J. Appl. Phys.*, **22**, 566 (1982).
16) G. W. Gray and K. J. Harrison, *Sym. Faraday Soc.*, **5**, 54 (1971).
17) W. L. McMillan, *Phys. Rev. A*, **8**, 1921 (1973).
18) W. H. de Jeu, *J. Phys.(Paris)*, **38**, 1265 (1977).
19) J. S. Patel and J. W. Goodby, *Mol. Cryst. Liq. Cryst.*, **144**, 117 (1987).
20) R. B. Meyer, L. Liebert, L. Strzelecki, and P. Keller, *J. Phys.(Paris)*, **36**, L-69 (1975).
21) T. Sakurai, K. Sakamoto, M. Honma, K. Yoshino, and M. Osaki, *Ferroelectrics*, **58**, 21 (1984).

Rotational Lattice Vibrations of Tetramethyl- and Tetramethyl-d_{12}-pyrazine Crystals

Masayoshi MAEHARA, Toshikazu HIEIDA, Yoshinori NIBU, Hiroko SHIMADA,* and Ryoichi SHIMADA†

Department of Chemistry, Faculty of Science, Fukuoka University, Nanakuma, Jonan-ku, Fukuoka 814-01

†Department of Chemistry, Faculty of Science, Kyushu University 33, Hakozaki, Higashi-ku, Fukuoka 812

(Received February 29, 1988)

The low-frequency Raman bands of the tetramethyl- and tetramethyl-d_{12}-pyrazine crystals and their hydrated crystals were studied at various temperatures between 4.2 and 298 K. The isotopic factors and the temperature effects on the frequencies of the Raman bands indicate that the low-frequency Raman bands observed in the crystal are to be ascribed to the rotational lattice vibrations. A smooth curve of the plot of the Raman frequency versus temperature suggests that no apparent temperature-induced phase transition takes place in the tetramethylpyrazine crystal. Classification of the rotational lattice vibrations into symmetry species was made based on the polarization behavior of the Raman bands. It was also observed that tetramethylpyrazine hydrates quite easily with a trace of moisture in the air.

The low-frequency Raman bands due to the lattice vibrations of the aromatic compounds in crystals have been studied by many workers.[1-6] Ito et al. observed the low-frequency Raman bands of the benzene and pyrazine crystals and calculated the mean square amplitudes of the rotational motions of the molecules in the crystals.[3,4] Suzuki et al.[5] and Bonadeo et al.[6] observed the polarized Raman spectra of the naphthalene and benzene crystals, respectively, and classified the Raman bands arising from the rotational lattice vibrations into symmetry species. Recently, Calvé et al. studied the temperature effects on the frequencies of the lattice vibrations of the 4-methylpyridine crystal and discussed about the phase transition.[7] They also observed the temperature dependence of the torsional vibration of the methyl group and showed that the rotation of the methyl group is free in the crystal phases above 100 K, while the rotation is hindered in the phase below 100 K.

Braam et al. determined the crystal structure of tetramethylpyrazine and showed that four molecules are involved in the unit cell.[8] Thus, based on the knowledge of the crystal structure, the lattice vibrations of the tetramethylpyrazine crystal can easily be distinguished from the torsional vibrations of the methyl group, which will be observed in the same low-frequency region, by measuring the temperature effects and isotopic factors of the frequencies of the Raman bands.

The intramolecular vibrations of tetramethylpyrazine were studied through the analyses of the polarized Raman and infrared spectra and the assignments of the normal vibrations were made based on the oriented gas model approximation.[9] It was known that when the tetramethylpyrazine crystal is grown in aqueous solution, one obtains the trihydrated crystal.[10] It is interesting to investigate whether the oriented gas model approximation can be applied to the assignments of the intermolecular vibrations or not, and to study how the lattice vibrations are affected by hydration.

In this paper the lattice vibrations of the tetramethyl- and tetramethyl-d_{12}-pyrazine crystals are discussed based on the isotopic factors and temperature effects on the Raman frequencies and the polarization behavior of the Raman bands, and then the effects of hydration on the lattice vibrations are studied.

Experimental

Material. Tetramethyl-d_{12}-pyrazine (TMP-d_{12}) was synthesized by the exchange reaction of tetramethylpyrazine (TMP-d_0) obtained from Aldrich Chemical Co. with D_2O. The isotopic purity of the product was confirmed by the nuclear magnetic resonance measurement. The samples were purified by zone refining of about 100 passages. The hydrated crystals were prepared by adjusting the amount of moisture adding to the TMP-d_0 and TMP-d_{12} crystals.

Optical Measurements. The sample was sealed in a glass tube of about 3 mm in diameter and was excited with the 514.5 nm line from an Ar^+ ion laser. The Raman spectra were observed with a JEOL 400 T Laser Raman Spectrophotometer at various temperatures between 298 and 155 K. The temperature was regulated with an automatic temperature controller of JEOL Model RS-VTC 41. The Raman scattering and excitation light beams were at right angles. The Raman spectra were also observed at 77 and 4.2 K. The preparation of the single crystal and the method of the measurement of the polarized Raman spectrum were exactly the same as those described previously.[9]

Results and Discussion

Tetramethylpyrazine crystallizes in the orthorhombic space group D_{2h}^{15} with four molecules in the unit cell, each molecules being located at the site of symmetry C_i.[8] There are twenty one optical branches of the lattice vibrations, of which nine are the vibrations of the translational modes and twelve are of the rotational modes. According to the group theory the six lattice vibrations of the nine translational modes are infrared active and the three of them are

inactive both in the infrared and Raman spectra, while the twelve lattice vibrations of the rotational modes are all Raman active. The twelve rotational lattice vibrations are classified into four symmetry species A_g, B_{1g}, B_{2g}, and B_{3g}, and three vibrations belong to each symmetry species. Each mode of the rotational lattice vibrations can be represented by a linear combination of the in-phase and out-of-phase rotational oscillations of the four molecules in the unit cell about the u, v, and w axes of the molecule. The u axis is taken perpendicular to the molecular plane and the v and w axes are in the plane with the w axis passing through the nitrogen atoms.

The Raman spectra of the TMP-d_0 and TMP-d_{12} crystals in the low-frequency region observed at 4.2 K are shown in Fig. 1. The twelve Raman bands were clearly observed and their frequencies are given in Fig. 1 and Table 1. If the low-frequency Raman bands are ascribable to the rotational lattice vibrations, the isotopic factor of the corresponding bands of the TMP-d_0 and TMP-d_{12} crystals is given by $\tilde{\nu}(d_0)/\tilde{\nu}(d_{12})=\{I_r(d_{12})/I_r(d_0)\}^{1/2}$, where $\tilde{\nu}$ is the Raman frequency and I_r the moment of inertia of the molecule about the axis r (=u, v, or w). The values of the moments of inertia of the TMP-d_0 and TMP-d_{12} molecules were calculated

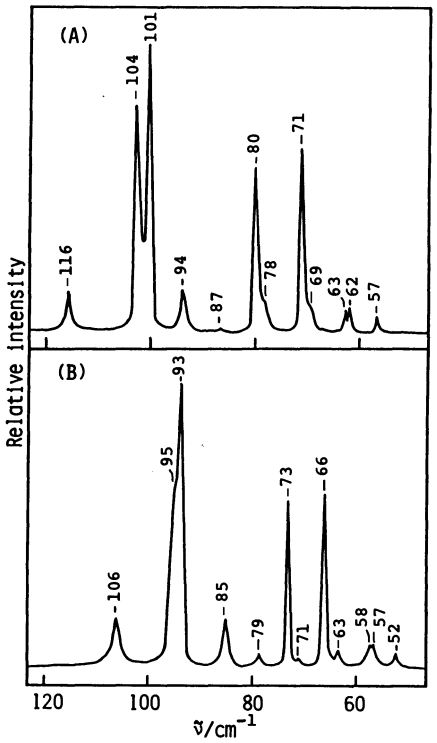

Fig. 1. The Raman spectra of the tetramethyl-(A) and tetramethyl-d_{12}-pyrazine(B) crystals in the low-frequency region observed at 4.2 K.

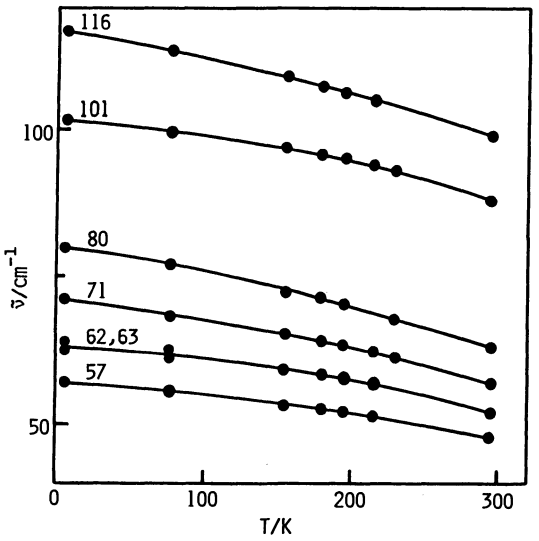

Fig. 2. Temperature effects on the frequencies of the Raman bands of the tetramethylpyrazine crystal.

Table 1. Raman Frequencies of Rotational Lattice Vibrations of Tetramethyl-d_0- and Tetramethyl-d_{12}-pyrazine Crystals

4.2 K				77 K				298 K				
TMP-d_0		TMP-d_{12}		TMP-d_0		TMP-d_{12}		TMP-d_0		TMP-d_{12}		Assign
$\tilde{\nu}$/cm^{-1}	I	$\tilde{\nu}$/cm^{-1}	I	$\tilde{\nu}$/cm^{-1}	I	$\tilde{\nu}$/cm^{-1}	I	$\tilde{\nu}$/cm^{-1}	Pol	$\tilde{\nu}$/cm^{-1}	Pol	
57	w	52	w	55	w	50	w	48	cc, aa	43	cc, aa	Ag
62	w	57	w	61	w							
						56	w	52	bc	47	bc	B_{3g}
63	w	58	w	62	w							
69	sh	63	sh	66	sh	60	sh	55	ac	50	ac	B_{2g}
71	s	66	s	68	s	63	s	57	aa, bb, cc	52	aa, bb, cc	Ag
78	sh	71	sh									
80	s	73	s	77	s	71	m	63	bc	58	bc	B_{3g}
87	vw	79	w					66	ab	60	ab	B_{1g}
94	w	85	w	92	w	83	w	82	ab	74	ab	B_{1g}
101	vs	93	vs	99	vs	91	vs	88	cc, aa, bb	80	cc, aa, bb	Ag
104	vs	95	vs	101	vs	92	vs	91	ac	83	ac	B_{2g}
116	w	106	w	113	w	104	w	99	bc	91	bc	B_{3g}

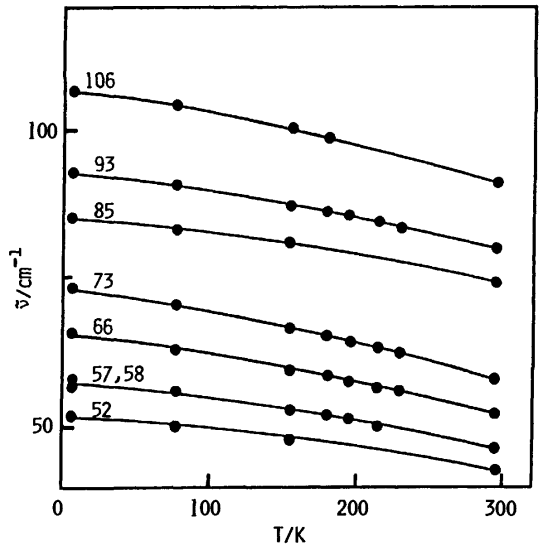

Fig. 3. Temperature effects on the frequencies of the Raman bands of the tetramethyl-d_{12}-pyrazine crystal.

using the molecular structure give by Braam.[8] The values are ranged in a order $I_u > I_w > I_v$. The isotopic factors were calculated to be 1.09, 1.09, and 1.10 at 100 and 300 K for the rotational lattice vibrations about the u, v, and w axes, respectively. The observed Raman frequencies for the TMP-d_0 and TMP-d_{12} crystals at 4.2, 77, and 298 K are given in Table 1 and the temperature effects on the frequencies of the Raman bands are shown in Figs. 2 and 3 for TMP-d_0 and TMP-d_{12}, respectively. The spectral structures observed at various temperatures are exactly the same as that observed at 4.2 K except for the width of the bands, which increases with increasing temperature. It is readily seen from Table 1 and Figs. 2 and 3 that (1) the observed isotopic factors are about 1.1 for all the corresponding Raman bands, (2) the frequencies increase with decreasing temperature, and (3) the observed Raman frequencies lie on a smooth curve against temperature within the experimental errors. These facts suggest that (1) the observed low-frequency Raman bands can be ascribed to the rotational lattice vibrations in the crystals and (2) no apparent phase transition takes place between 298 and 4.2 K in the TMP crystal. This is consistent with the fact that the crystal structure of TMP belongs to the space group D_{2h}^{15} at 300 and 100 K.[8] Calvé et al. observed the Raman bands arising from the torsional vibration of the methyl group in the 4-methylpyridine crystal at various temperatures between 4.2 and 100 K and pointed out that the isotopic factor of the torsional vibration of the methyl group is about 1.4 and the frequency increases with increasing temperature, unlike the behavior of the rotational lattice vibrations.[7] The Raman bands giving such high value of the isotopic factor could not be observed in our experiment.

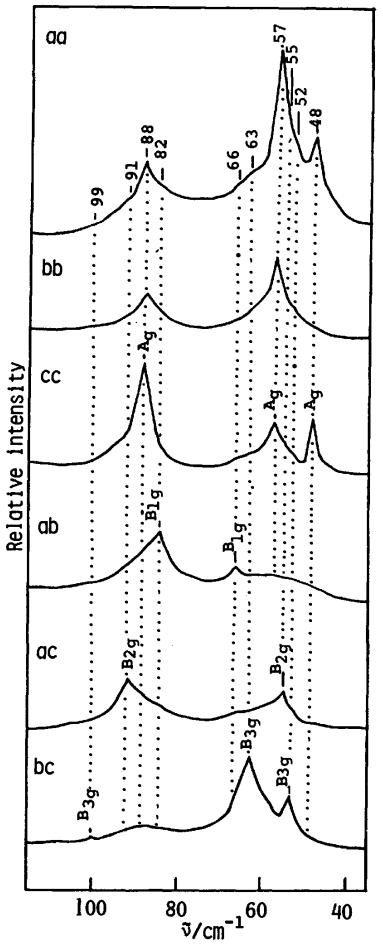

Fig. 4. The polarized Raman spectra of the tetramethylpyrazine crystal in the low-frequency region observed at 298 K.

The polarized Raman spectra of the TMP-d_0 and TMP-d_{12} crystals observed at 298 K are given in Figs. 4 and 5, respectively. Notations of the spectra such as aa and bb are exactly the same as those given in the previous paper reported on the intramolecular vibrations of TMP-d_0.[9] The observed polarization behavior of the Raman bands arising from the rotational lattice vibrations of the TMP-d_0 crystal is the same as that of the TMP-d_{12} crystal. The calculated squared values of the elements of the Raman (derived polarizability) tensor based on the oriented gas model for the TMP crystal are given in Table 2.[9] According to Table 2, the lattice vibrations belonging to the symmetry species A_g will be observed in the aa, bb, and cc spectra and those belonging to the B_{1g}, B_{2g}, and B_{3g} species in the ab, ac, and bc spectra, respectively. Figures 4 and 5 show that the Raman bands having frequencies of 52(47), 63(58), and 99(91) cm^{-1} are clearly observed in the bc spectrum, those of 55(50) and 91(83) cm^{-1} are in the ac spectrum, those of 66(60) and 82(74) cm^{-1} are in the ab spectrum, and those of 48(43), 57(52), and 88(80) cm^{-1} are in the aa, bb, and cc spectra, where the first numbers refer to

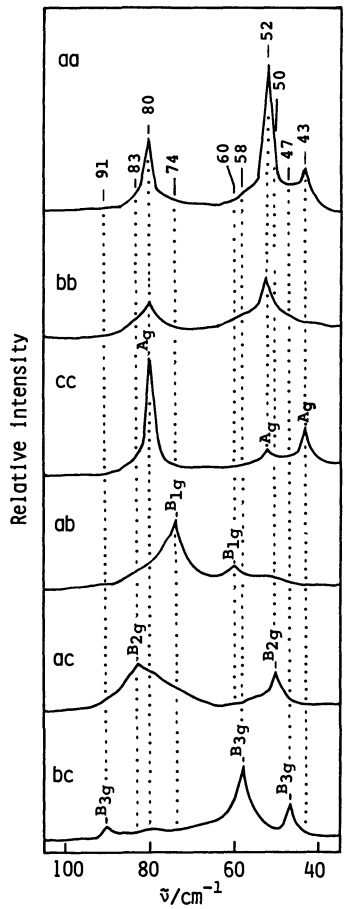

Fig. 5. The polarized Raman spectra of the tetramethyl-d_{12}-pyrazine crystal in the low-frequency region observed at 298 K.

Table 2. Squared Values of Elements of Raman Tensor for Tetramethylpyrazine

Crystal		Molecule		
		$b_{1g}(R_w)$	$b_{2g}(R_v)$	$b_{3g}(R_u)$
A_g	$(A_{aa})^2$	0.19	0.76	0.10
	$(A_{bb})^2$	0.08	0.06	0.91
	$(A_{cc})^2$	0.53	0.39	0.41
B_{1g}	$(A_{ab})^2$	0.40	0.15	0.05
B_{2g}	$(A_{ac})^2$	0.10	0.01	0.24
B_{3g}	$(A_{bc})^2$	0.10	0.23	0.00

the frequencies for the TMP-d_0 crystal and the numbers in parentheses to the TMP-d_{12} crystal. These observed facts indicate that the 52(47), 63(58), and 99(91) cm^{-1} bands are to be assigned to the B_{3g} lattice vibrations, the 55(50), 91(83) cm^{-1} bands to the B_{2g} vibrations, the 66(60) and 82(74) cm^{-1} bands to the B_{1g} vibrations, and the 48(43), 57(52), and 88(80) cm^{-1} bands to the A_g vibrations. These assignments are given in Table 1 and Figs. 4 and 5. Table 2 also indicates that for the A_g rotational lattice vibrations the relative intensities of the Raman bands arising from the rotational oscillations of the molecule about

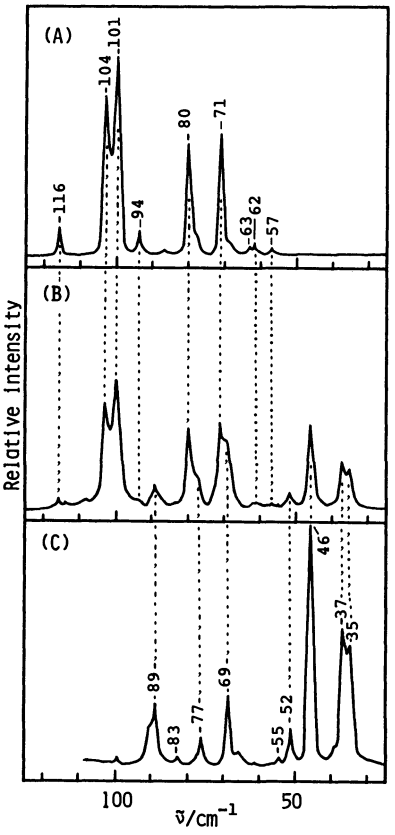

Fig. 6. The Raman spectra of the unhydrated(A), partially hydrated(B), and completely hydrated(C) tetramethylpyrazine crystals.

Table 3. Root Mean Square Amplitudes (degree) of Rotational Lattice Vibrations of Tetramethyl-d_0- and Tetramethyl-d_{12}-pyrazine Crystals about v Axis

	4.2 K	77 K	298 K
TMP-d_0	1.5	1.8	3.6
TMP-d_{12}	1.5	1.8	3.6

the u, v, and w axes are strongest in the bb, aa, and cc spectra, respectively. However, the observed relative intensities are not consistent with the expectation, although the observed intensities of the bands for the intramolecular vibrations are quantitatively consistent with the expected values.[9] This phenomenon may be caused by mode mixing among the rotational lattice vibrations about the u, v, and w axes and also by coupling of the rotational lattice vibrations with the torsional vibrations of the methyl groups. This means that the oriented gas model is rather a poor approximation for the determination of modes of the rotational lattice vibrations.

The moment of inertia of TMP about the v axis is smaller than those about the u and w axes, and linear combinations of the in-phase and out-of-phase rotational oscillations of four molecules about the v axis in the crystal give four rotational lattice

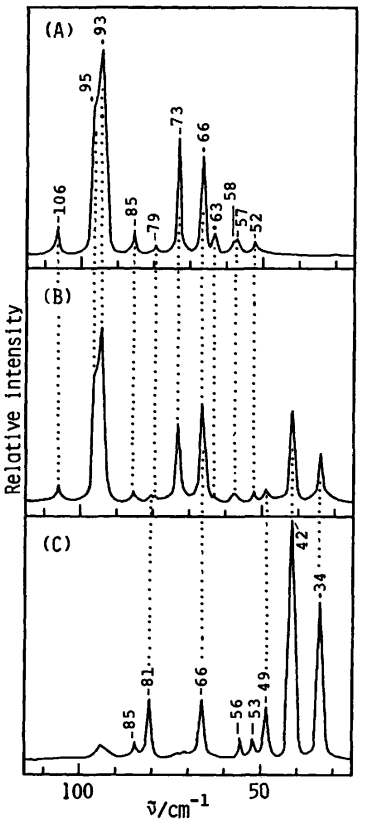

Fig. 7. The Raman spectra of the unhydrated(A), partially hydrated(B), and completely hydrated(C) tetramethyl-d_{12}-pyrazine crystals.

vibrations belonging to symmetry species A_g, B_{1g}, B_{2g}, and B_{3g}. Thus, the Raman bands observed at 82, 88, 91, and 99 cm^{-1} in the TMP crystal could be assigned to the lattice vibrations arising mainly from the oscillation about the v axis, because these bands are located in the higher wavenumber region than the other bands and showed the B_{1g}, A_g, B_{2g}, and B_{3g} polarization behavior, respectively, although these vibrations might couple with the rotational motions about the u and w axes as described above. The mean square amplitudes of the rotational motions about the v axis of the molecule in the crystal can be calculated. Calculation was made using the equation given by Cruickshank[11] and the results are given in Table 3. The values of the rotational mean square amplitude decrease with decreasing temperature.

It has been known that TMP crystallizes with three molecules of water of crystallization when the crystal is grown in aqueous solution.[10] The Raman spectra of the hydrated TMP-d_0 and TMP-d_{12} crystals in the low-frequency region are shown in Figs. 6 and 7, respectively. The spectra shown in (A), (B), and (C) of the figures are for the unhydrated, partially hydrated, and completely hydrated TMP crystals, respectively. The crystal structure of the trihydrated TMP crystal belongs to the monoclinic space group C_{2h}^5 with four molecules in the unit cell and thus, the rotational lattice vibrations are all Raman active. The Raman bands arising from the rotational lattice vibrations of the hydrated crystal were located in the lower wavenumber region of the bands of the unhydrated crystal. This may be due to differences of the mass and potential field of the hydrated TMP from those of the unhydrated TMP in crystals. The Raman bands arising from the lattice vibrations of the hydrated TMP crystal are observed when the unhydrated TMP crystal is exposed in the humid air. Thus, the preparation of the TMP crystal was made in the air free from moisture.

References

1) D. W. J. Cruickshank. *Rev. Mod. Phys.*, **30**, 163 (1958).
2) P. A. Bazhulin, A. V. Rakov, and A. A. Rakhimov, *Opt. and Spektrosk.*, **16**, 554 (1964).
3) M. Ito and T. Shigeoka, *Spectrochim. Acta*, **22**, 1029 (1966).
4) M. Ito and T. Shigeoka, *J. Chem. Phys.*, **44**, 1001 (1966).
5) M. Suzuki, T. Yokoyama, and M. Ito, *Spectrochim. Acta*, **24A**, 1091 (1968).
6) H. Bonadeo, M. P. Marzocchi, E. Castellucci, and S. Califano, *J. Chem. Phys.*, **57**, 4299 (1972).
7) N. Le. Calvé, B. Pasquier, G. Braathen, L. Soulard, and F. Fillaux, *J. Phys. C*: Solid State Phys., **19**, 6695 (1986).
8) A. W. M. Braam, A. Eshuis, and Aafje Vos, *Acta Crystallogr., Sect. B*, **37**, 730 (1981).
9) Y. Ishibashi, F. Arakawa, H. Shimada, and R. Shimada, *Bull. Chem. Soc. Jpn.*, **56**, 1327 (1983).
10) A. W. M. Braam, J. C. Eikelenboom, G. van Dijk, and Aafje Vos, *Acta Crystallogr., Sect. B*, **37**, 259 (1981).
11) D. W. J. Cruickshank, *Acta Crystallogr.*, **9**, 1005 (1956).

Crystal Face Anisotropy of Propylene Oxidation on Molybdenum Trioxide

Shigeo Ted OYAMA†
Catalytica, 430 Ferguson Drive, Building 3, Mt. View, CA 94305, U.S.A.
(Received February 23, 1987)

Samples of MoO_3 consisting of unsupported oriented crystallites exposing primarily the (010) plane and of randomly oriented powders were used to study the partial oxidation of propylene and allyl iodide. The materials were characterized by scanning electron microscopy, X-ray diffraction, infrared spectroscopy, laser Raman spectroscopy, temperature programmed desorption of ammonia and surface area measurements. The unoriented powders were twice as active as the oriented crystallites in the oxidation of propylene, but both were similar in activity in the oxidation of allyl iodide. Thus, the reactions depended only slightly on the structure of the MoO_3.

The concept of structure-sensitivity has been useful in the study of the catalytic activity of metals, but has been little exploited in the case of nonmetallic catalysts such as sulfides or oxides. The bonding in nonmetals is more highly localized and directional than on metals. Thus, on nonmetals geometrical constraints for surface intermediates are likely to be greater than on metals, and surface structure might be expected to play a greater role in nonmetal reactivity. Investigations of the catalytic activity of different faces of nonmetal single crystals were pioneered by Tanaka and Okuhara[1-3] who found that isomerization and hydrogen exchange of olefins proceed on the edge planes of MoS_2 whereas the isomerization of 2-methyl-1-butene occurs on the basal planes. Berlowitz and Kung[4] report that dehydrogenation of 2-propanol to acetone on zinc oxide proceeds three to five times faster on polar crystal faces where zinc atoms are exposed than on similar polar faces where oxygen is exposed.

Structure-sensitive reactions may be defined to be those whose rates change appreciably with the atomic structure of the surface.[5-8] There is no clear dividing line between structure-sensitive and insensitive reactions, although the former on metals often show activity differences of tens, hundreds, it not thousands, between samples of different structure. Structure-sensitive reactions studied over different crystalline faces of a solid should also show pronounced reactivity differences, and this will be referred to as crystal face anisotropy.

In recent years there have been a number of attempts to study this topic, with MoO_3 receiving considerable attention. Volta et al., have investigated the oxidation of propylene on oriented crystallites of MoO_3 supported on graphite[9-13] and have concluded that the various faces catalyze different reactions. They correlated small changes in selectivity to the amounts of different exposed crystal faces determined from microphotographs and inferred that for propylene oxidation the (010) basal face produces exclusively carbon oxides, while the (100) and (101) edge faces produce acrolein.[13] The present paper seeks to examine these conclusions and reopen the question of the crystal face anisotropy of the reaction. The investigation is carried out on oriented crystallites of MoO_3, materials similar to the ones used by Volta et al., except that they leave out the support and, therefore, its possible influence.

Tatibouët and Germain have used the same system, unsupported crystallites of MoO_3 preferentially exposing different faces, in the oxidation of methanol[14] and ethanol.[15,16] These investigators concluded that the (010) face carries active centers for the oxidative dehydrogenation of methanol to formaldehyde. Ohuchi et al., have compared the temperature-programmed reaction and desorption of methanol from MoO_3 single crystals and powder.[17,18] These investigators found formaldehyde desorbing from the powder and only methanol desorbing from the (010) face of the single crystal. From this they reached an opposite conclusion from that of Tatibouët and Germain, namely, that the (010) face is inactive for the partial oxidation of methanol. These studies on MoO_3 have inspired theoretical work by Ziólkowski[19] and by Allison and Goddard.[20] The latter propose that the molybdenum dioxo groups found on the (010) plane are particularly effective for the oxidation of methanol, thus supporting the findings of Tatibouët and Germain.

The unit cell of MoO_3 is orthorhombic with lattice parameters a_o=396.28±0.07 pm, b_o=1385.5±0.3 pm, and c_o=369.64±0.06 pm.[21] Figure 1 illustrates the crystal structure. The structure consists of double layers of MoO_6 octahedra held together by covalent forces in the (100) and (001) directions, but by van der Waals forces in the (010) direction. As a consequence, large MoO_3 crystallites have elongated slab-like habits preferentially exposing the (010) direction.

Experimental

Reagent grade MoO_3 powder (Mallinckrodt, 99.95%) was used as received. Propylene (Linde, 99.0%) was purified by passage through a reduced Ni/SiO_2 trap and through a Molecular Sieve 3A trap. Allyl iodide (Aldrich, 98%), high purity ammonia (Linde, 99.995%), oxygen (Linde, 99.99%), nitrogen (Linde, 99.998%), and helium (Linde, 99.995%) were used without further purification.

† Present address: Dept. of Chemical Engineering, Clarkson Univ., Potsdam, New York 13676, U.S.A.

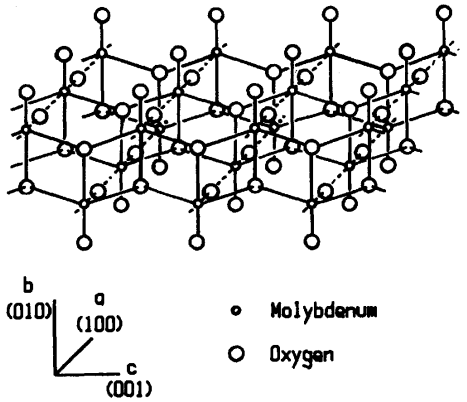

Fig. 1. Structure of orthorhombic MoO_3.
Terminal oxygen atoms extend in the (010) direction, two-fold coordinate oxygen atoms in the (100) direction and three-fold coordinate oxygen atoms in the (001) direction.

X-Ray diffraction patterns were taken with a Norelco 12206/7 spectrometer using Cu Kα radiation. Samples were lightly pressed onto a shallow indentation in an aluminium sample holder to provide a flat 1 cm×1 cm surface. Infrared spectra of the powder were taken with a Perkin Elmer 1330 spectrometer with about 0.1 wt% of the sample pressed in KBr pellets. Laser Raman spectra were obtained with a Cary 81 spectrometer equipped with 90° optics and using the 632.8 nm output of a 50 mW He-Ne laser. Scanning electron micrographs were measured with a JEOL JSM 35 microscope with samples sprayed with a palladium gold coating to prevent charging effects. Surface area and temperature-programmed desorption measurements were carried out in a flow system equipped with a single-filament TC detector (Hewlett-Packard 19302-60530), with samples treated in flowing He at 473 K prior to measurement. Absolute absorbate amounts were obtained by comparing the areas under the desorption peaks to those under standard calibration pulses from a sampling valve. Single-point BET areas were obtained by equilibrating the sample with a 30 mol% N_2 in He stream at liquid nitrogen temperatures followed by flash desorption of the adsorbed nitrogen. Ammonia TPD spectra were obtained by saturating samples held at 273 K with NH_3, purging the samples in the He carrier and then monitoring the desorption peaks as the temperature was raised linearly at 0.17 K s^{-1}. Because of the use of a thermal conductivity detector the possibility of NH_3 oxidation as well as desorption cannot be ruled out. However, the technique was used primarily to show differences between samples.

Reactivity measurements were carried out in two separate reactor systems of almost identical design which could be used in both flow and pulse modes. The only difference between the systems was that for analysis of products one used an on-line gas chromatograph (Hewlett-Packard 5880 GC) whereas the other used an on-line mass spectrometer (Hewlett-Packard 5995 GC-MS). The reactor with the gas chromatograph was used in a flow mode for the propylene oxidation work, whereas the reactor with the mass spectrometer was used primarily in a pulse mode for the allyl iodide oxidation investigations. However, propylene oxidation data taken in one system could readily be reproduced in the other. The gas chromatograph used an octane on Porasil C column and an OV-101 column which were respectively connected to a TC and a FI detector. The mass spectrometer simultaneously monitored the ion masses of all product species. Injections of pulses of N_2 as a standard allowed the calibration of the sensitivity of the mass spectrometer prior to each run and, thus, the quantification of the products of the reaction. For the pulse reaction an average reaction rate was obtained by integrating the concentration of each species through the duration of each pulse (60 s).

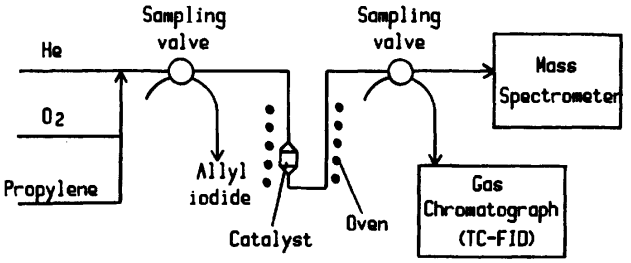

Fig. 2. Schematic diagram of the flow reactor apparatus.

A schematic diagram common to both flow systems is presented in Fig. 2. Electronic mass flow controllers (Brooks 5850) delivered gases in precise proportions. For the allyl iodide experiments a sampling valve injected pulses of He carrier gas containing the vaporized liquid reactant. The catalysts were in packed beds held in Pyrex or 316 stainless steel tubes by either sintered glass frits or packed glass wool. Furnaces surrounded the tubes and heated them. Thermocouples clamped to the outside of the tubes monitored the temperature of the beds. Heated transfer lines led the effluent to the analyzers.

Table 1 summarizes the conditions at which the steady-state propylene oxidation data were obtained. Flow rates are expressed in units of μmol s^{-1} which can be converted to units of cm^3 (NTP) min^{-1} by multiplication by 1.5. The contact time is defined as the bed volume divided by the volumetric flow rate. To compare accurately the reactivity of the needles and powder, quantities of catalyst corresponding to the same total surface area of 0.18 m^2 were employed. Furthermore, since the MoO_3 powder was denser than the needles, the former was diluted with inert, acid-washed ground quartz to achieve equal bed volumes of 2.2 cm^3. Rates are reported as areal rates, i.e., per unit surface area.

The allyl iodide oxidation data were obtained with amounts of catalyst and conditions similar to those employed for the propylene oxidation measurements. The flow rate of the helium and oxygen were 60 and 6 μmol s^{-1}, and the delivery rate of allyl iodide was 0.13 μmol s^{-1}. This delivery rate corresponds to the injection of pulses containing 7.6 μmol of allyl iodide every 60 s.

Neither reactor material nor shape had an influence on the results except at the highest temperatures (>800 K). Above this temperature blank runs with acid washed quartz showed there was some contribution to the reactivity from the reactor or from homogeneous gas phase reactions. All conclusions from this study will be drawn from the lower

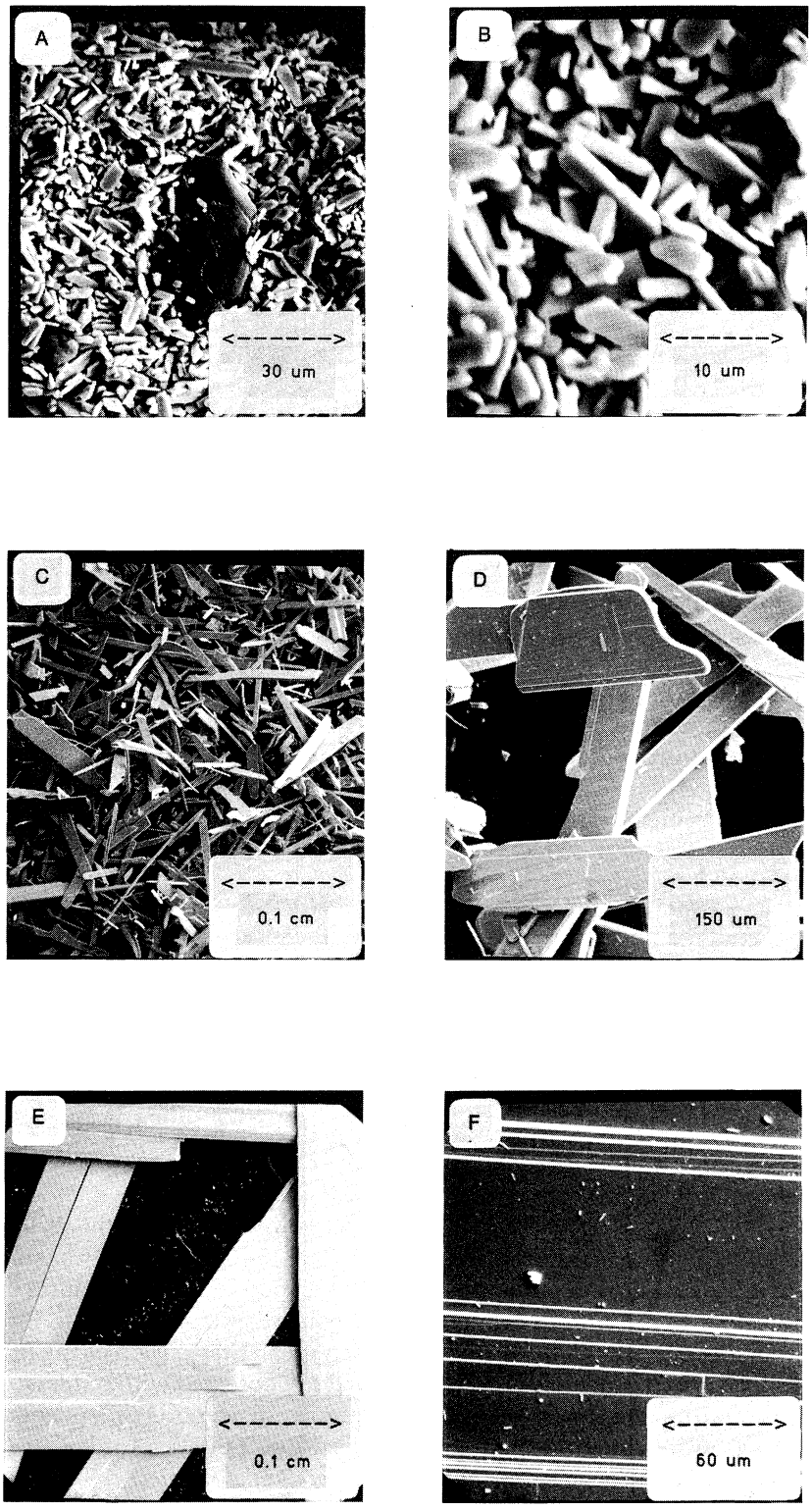

Fig. 3. Scanning electron micrographs of MoO_3 samples.
High and low magnification pictures of the powder (a and b), needles (c and d), and slabs (e and f).

Table 1. Reaction Conditions for Propylene Oxidation

Temperature = 300—900 K	Amount of catalyst = 0.18 m^2
Pressure = 101 kPa	Bed volume = 2.2 cm^3
Flow rate He = 60 μmol s^{-1}	Contact time = 1.3 s
Flow rate O_2 = 3—12 μmol s^{-1}	Conversion = 0—90%
Flow rate C_3 = 3 μmol s^{-1}	

Table 2. Physical Properties of the MoO_3 Samples

Sample	Dimension	Basal plane	Edge plane	Surface area/$m^2 g^{-1}$ Calculated	Measured
Powder	1×3×3 μm	60	40	0.72	0.81
Needle	10×100×700 μm	90	10	0.047	0.080
Slab	0.03×0.2×3 cm	90	10	0.0025	—

temperature, lower conversion region of the data. At all conversions carbon mass balances of 100±5% were obtained.

Results

Synthesis of MoO_3 Single Crystals. Single crystals of MoO_3 were prepared following the method reported by Wanklyn,[22] consisting of vaporizing a MoO_3 powder and condensing the product crystals a short distance away. Approximately 50 g of MoO_3 were loaded in a shallow, covered alumina crucible which was placed in a temperature-controlled oven. Unlike in the work of Wanklyn who used a constant temperature of 993 K, the temperature here was allowed to oscillate between 987 and 997 K. This resulted in the formation of larger crystallites, probably by an Ostwald ripening process.

Different products were obtained depending on the duration of the synthesis. From an initial micrometer-sized powder, hundred-fold larger needle-shaped crystallites could be collected after 40 hours. After 150 hours even larger, centimeter-sized single crystal slabs were formed. In the following sections these materials will be simply referred to as powders, needles, and slabs. Because of the low surface area of the slabs, the catalytic work will concentrate on the powder and needles.

Characterization. Figure 3 shows scanning electron micrographs of the three samples at various magnifications that indicate the variation in external morphology of the powder, needles, and slabs. Table 2 summarizes the physical characteristics of the samples. The size of the crystallites in the samples is estimated without carrying out a statistical analysis. The dimensions are used to roughly calculate the relative proportions of basal and edge planes, as well as the surface areas. The measured surface areas are also reported.

Figure 4 compares the X-ray diffraction patterns of the MoO_3 powders and needles. The MoO_3 powder displays a pattern characteristic of randomly oriented crystallites. The needles, however, exhibit a pattern

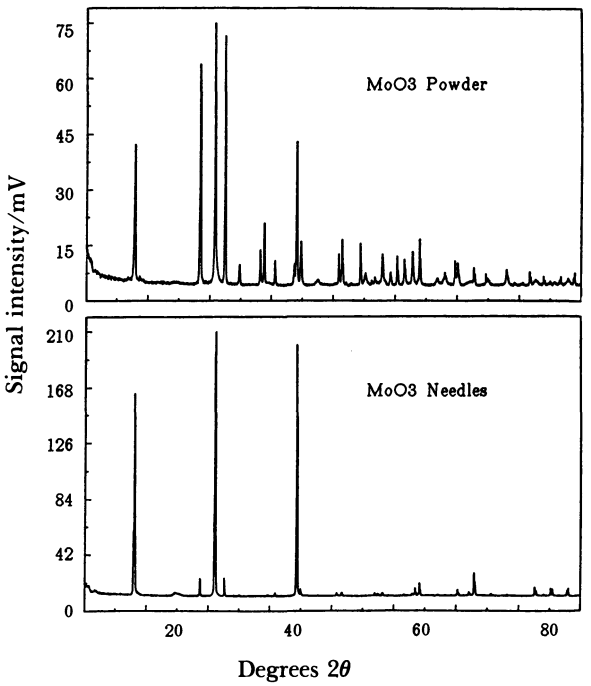

Fig. 4. X-Ray diffraction patterns of MoO_3 samples. Top, MoO_3 powder. Bottom, MoO_3 needles.

with strong intensity in the (020) family of reflections.

Figure 5 shows the transmission infrared and Raman spectra of molybdenum trioxide powder taken at room temperature. It is interesting to note the much greater resolution of the Raman spectra. This is generally observed with oxides.

Figure 6 reports the temperature-programmed desorption (TPD) profiles of ammonia from the needles and powder. The needles had a single desorption peak at 330 K whereas the powder had two desorption peaks at 320 and 430 K. Integration of the areas under the desorption peaks allowed the calculation of the surface number density of ammonia molecules absorbed. These values were 4.0×10^{19} m^{-2} for the needles and 6.7×10^{19} m^{-2} for the powder.

Reactivity Results. Figures 7 and 8 present the

propylene oxidation data for the needles and powder at various oxygen partial pressures. The only products that were detected were acrolein and carbon dioxide. For both catalysts the rate of carbon dioxide production per unit surface area was similar. As the temperature was raised, this rate increased to a plateau and then slowly decreased. The rate in the region of the plateau varied with the first order of the oxygen

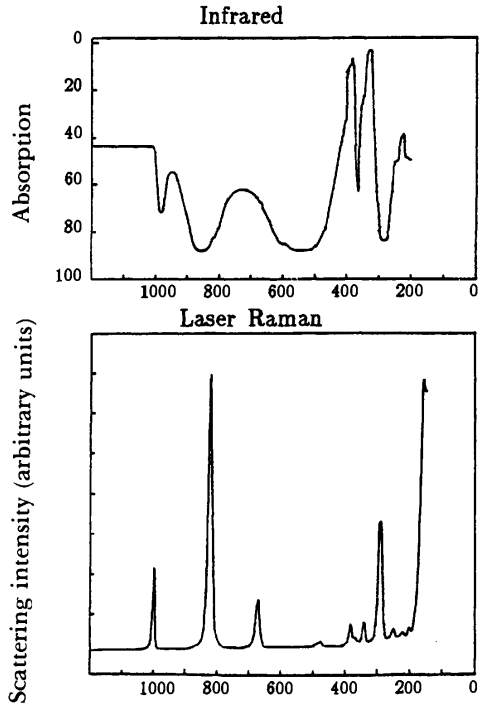

Fig. 5. Vibrational spectra of MoO_3 powder.
Top, infrared spectrum. Bottom, laser Raman spectrum.

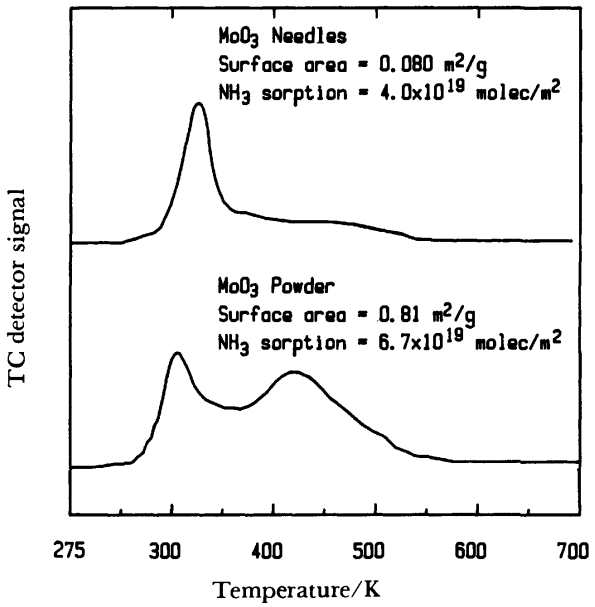

Fig. 6. Ammonia temperature programmed desorption spectra of the MoO_3 needles and powder.
Top, MoO_3 needles. Bottom, MoO_3 powder.

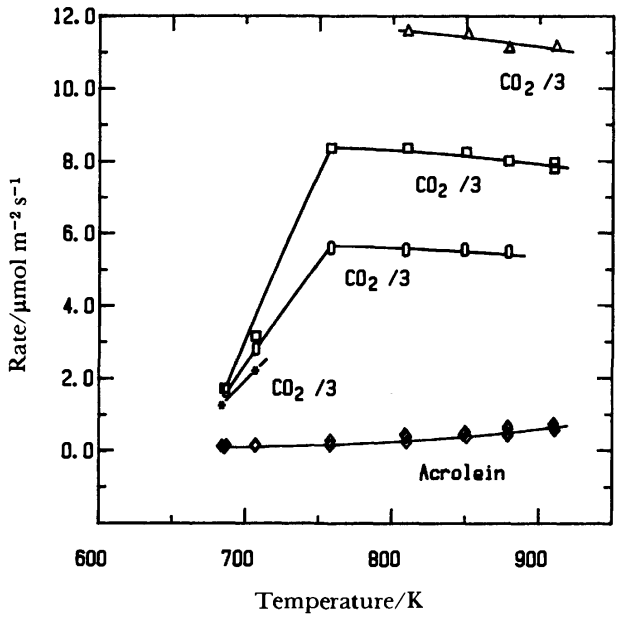

Fig. 7. Steady-state propylele oxidation on MoO_3 needles.
Total pressure=101 kPa. Partial pressure propylene= 4 kPa, partial pressure oxygen=4 kPa (✳), 8 kPa (○), 12 kPa (□), and 16 kPa (△), partial pressure helium= balance. Acrolein production (◇) was independent of oxygen pressure.

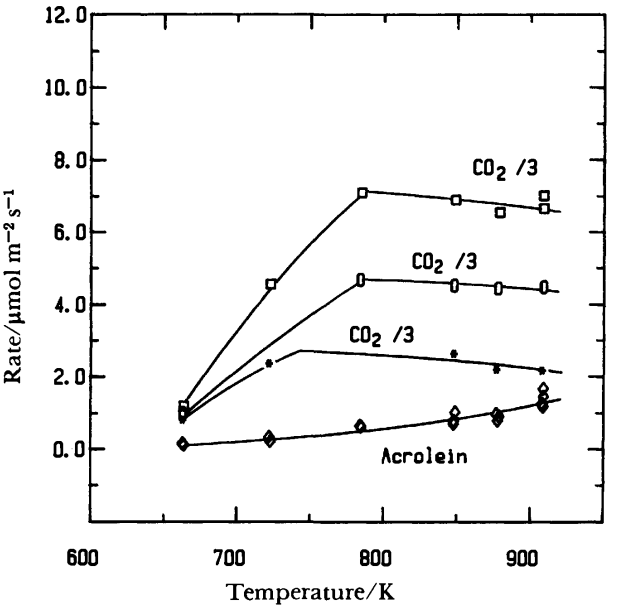

Fig. 8. Steady-state propylene oxidation on MoO_3 powder.
Total pressure=101 kPa. Partial pressue propylene= 4 kPa, partial pressue oxygen=4 kPa (✳), 8 kPa (○), and 12 kPa (□), partial pressure helium=balance. Acrolein production (◇) was independent of oxygen partial pressure.

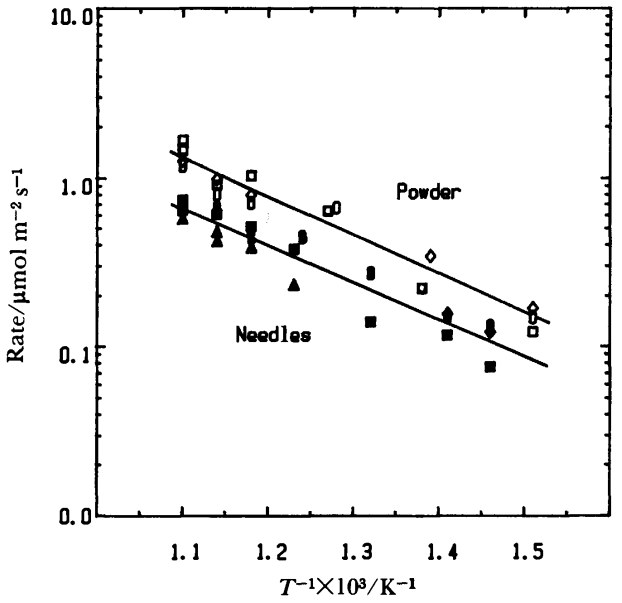

Fig. 9. Steady-state propylene oxidation to acrolein on MoO_3 powder and needles.
Total pressure=101 kPa. Partial pressure propylene= 4 kPa, partial pressure oxygen=4 kPa (◇), 8 kPa (○), 12 kPa (□), and 16 kPa (△), partial pressure helium=balance. Powder=open symbols, needles= filled symbols.

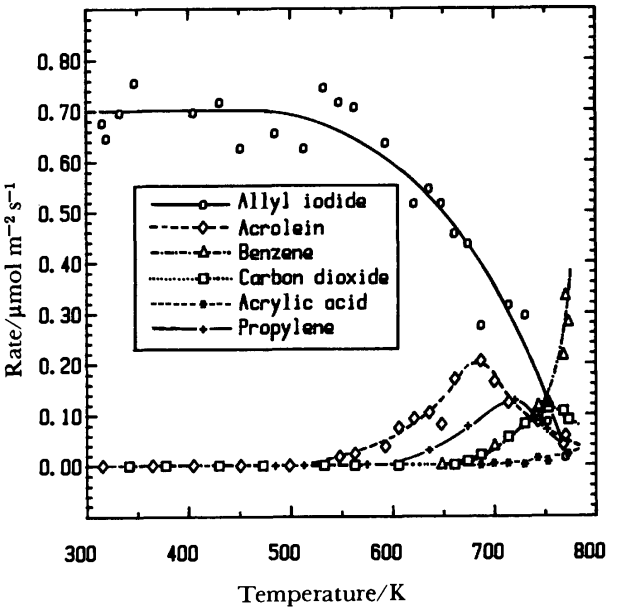

Fig. 10. Allyl iodide pulse oxidation on MoO_3 needles.
Total pressure=101 kPa. Partial pressure oxygen= 9 kPa, partial pressure helium=balance. Allyl iodide pulse size=7.6 μmol.

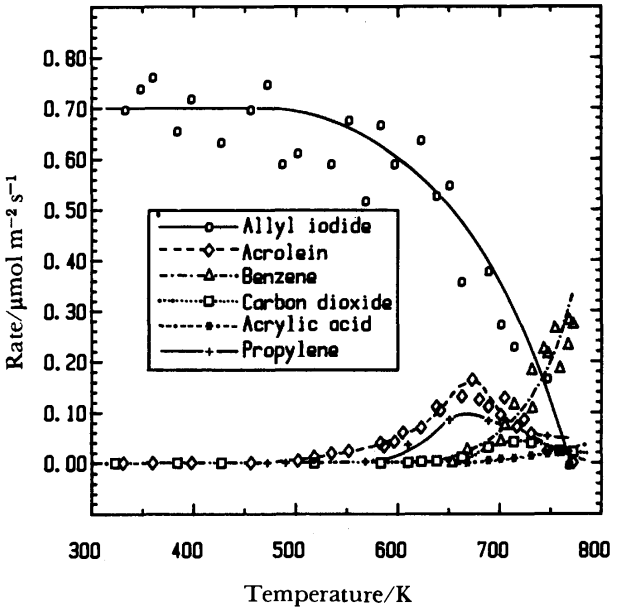

Fig. 11. Allyl iodide pulse oxidation on MoO_3 powder.
Total pressure=101 kPa. Partial pressure oxygen= 9 kPa, partial pressure helium=balance. Allyl iodide pulse size=7.6 μmol.

partial pressure, $v_{CO_2}=kP_{O_2}^{1.0}$.

The data for the rate of acrolein production in Figs. 7 and 8 are presented in Arrhenius form in Fig. 9. The rate was independent of oxygen partial pressure, $v_{ACR}=kP_{O_2}^{0}$, and was uniformly higher by a factor of about 2 on the powder than on the needles. The apparent activation energy, E_{APP}, was the same for both samples within experimental error (±2 kJ mol^{-1}), 43 kJ mol^{-1} for the powder and 42 kJ mol^{-1} for the needles.

The allyl iodide oxidation data taken in a pulse mode are presented in Figs. 10 and 11. The oxidation produced a number of products, acrolein, benzene, carbon dioxide, acrylic acid and propylene. The behavior of the needles and the powder was very similar, although at higher conversions the needles produced more acrolein than the powder (0.21 vs. 0.16 μmol m^{-2} s^{-1}).

Discussion

Structure of the Catalysts. Transmission infrared spectroscopy and laser Raman spectroscopy characterize the bulk of the MoO_3 crystallites; scanning electron microscopy and X-ray diffraction reveal the external macroscopic morphology and orientation; and TPD of ammonia gives information about their surface.

The scanning electron micrographs of the MoO_3 powder and needles show that the samples have different morphologies. The powder consists of small crystallites with little tendency to expose a preferred orientation. The needles consist of larger crystallites with a substantial proportion of flat faces. The X-ray

diffraction pattern of the needles shows that the flat faces are those perpendicular to the (010) direction. The high intensity of the diffraction peaks in that direction are due to preferential orientation of the flat crystallites in the plane of the sample holder.

The surface areas of the materials was calculated from the average size of the crystallites obtained from the scanning electron micrographs. This was done by first calculating the number of such crystallites in one gram using the bulk density of MoO_3 (4.692 g cm^{-3}), and then calculating the corresponding geometric area of the crystallites using their known dimensions. This gave calculated surface areas for the powder and needles of 0.72 and 0.047 $m^2 g^{-1}$. These are in reasonable agreement with the measured values of 0.81 and 0.080 $m^2 g^{-1}$. The lower calculated value for the needles is probably due to underestimating the number of smaller crystallites.

The TPD spectra of ammonia provide direct evidence that the surfaces of the samples are significantly different and that, hence, the samples are appropriate for investigating crystal face anisotropy. The needles show a single desorption feature at 330 K, whereas the powder shows a similar feature at 320 K and a broad desorption peak centered at 430 K. The peak at 320—330 K in both samples is probably due to desorption of ammonia from the basal (010) planes. For the powder the broad peak at 430 K is probably due to the presence of a substantial proportion of other planes, as was shown by the scanning electron micrographs. The surface number density of adsorbed ammonia was 4.0×10^{19} m^{-2} for the needles and 6.7×10^{19} m^{-2} for the powder. The number density of exposed surface molybdenum atoms on the low index planes of MoO_3 are 7.81×10^{18} m^{-2} for the (100) plane, 6.83×10^{18} m^{-2} for the (010) plane and 7.28×10^{18} m^{-2} for the (001) plane. Because of the MoO_3 stoichiometry the total surface atom density, including oxygen atoms, will be roughly four times the above values. Thus, the quantity of adsorbed ammonia corresponds approximately to a monolayer.

General Aspects of the Allylic Oxidation of Propylene. There are two features of the selective oxidation of propylene on molybdate catalysts that are generally accepted. The first feature is that the rate-determining step in the reaction is the abstraction of an allylic hydrogen atom to form an adsorbed allyl radical.[23-27] This will be discussed in more detail below. The second feature is that the oxygen species responsible for selective oxygenation is lattice oxygen.[26-29] Absorbed oxygen species, especially those that are electrophilic in nature (O_2^-, O_2^{2-}, O^{2-}), are thought to be responsible for complete oxidation.[30,31]

Our results for the propylene oxidation reaction agree with the above view. The lack of dependence of acrolein formation on oxygen partial pressure is consistent with the participation of lattice oxygen in the reaction. Similarly, the dependence of carbon dioxide formation on oxygen partial pressure is consistent with the reaction of propylene or some propylene-derived species with absorbed oxygen. Indeed, it is precisely in the region where CO_2 is observed, 700—900 K, that $^{16}O_2$–$^{18}O_2$ exchange, and thus probably chemisorption, on MoO_3 is found to begin.[32,33] The observation in this study of a decrease in the rate of formation of CO_2 in the region of the plateau can be explained by the expected decrease in the amount of chemisorbed oxygen as the temperature increases.

Molybdenum trioxide is generally described as a selective but inactive catalyst for propylene oxidation. In this study the low selectivity obtained is probably due to the high temperatures employed. The activation energy obtained for the production of acrolein, close to 43 kJ mol^{-1}, is low. This is understandable as the value is an apparent activation energy that includes contributions from a number of reactions, including the further oxidation of acrolein.

Allyl Iodide Oxidation. The results obtained in this study for the oxidation of allyl iodide are similar to those found in previous examinations of the reaction by the group of Haber[34] and by Burrington and Grasselli.[35] In the present work, however, provision was taken to cofeed oxygen so as to maintain the surface of the catalyst oxidized. In molybdenum trioxide alteration of the structure on reduction occurs by a crystallographic shear mechanism[36,37] in which corner-sharing octahedra become

Table 3. Summary of Results on Propylene Oxidation

Steady-state selectivity (%) (This work)			
T=673 K Conversion=9%			
	Acrolein	CO_2	Others
(020) MoO_3 crystallites	3	97	—
Non-oriented MoO_3 crystallites	6	94	—
Initial selectivity (%) (Refs. 10, 11)			
T=648 K Conversion<1%			
	Acrolein	CO_2	Others
(020) MoO_3 crystallites	4	94	1
Non-oriented MO_3 crystallites	10	86	4

Table 4. Summary of Results on Allyl Oxidation

MoO_3 crystallites (This work)			
T=593 K Conversion=7%	Contact time=1.3 s		
	Acrolein	CO_2	Others
(020) MoO_3 crystallites	99	—	1
Non-oriented MoO_3 crystallites	99	—	1
MoO_3 Powder (Ref. 34)			
T=593 K Conversion=100%			
	Acrolein	CO_2	Others
MoO_3 powder	98	2	0.1
MoO_3 powder (Ref. 35)			
T=593 K Conversion=100%	Contact time=4 s		
	Acrolein	CO_2	Others
MoO_3 powder	93	0.4	7

edge sharing by the loss of an oxygen atom. This is characterized by the formation of striations in the crystals. In this study, X-ray diffraction patterns of the used catalysts revealed no evidence for this phenomenon. The catalysts did exhibit a purple colored discoloration, probably from deposition of iodine. There was no change in activity as the catalysts were taken to high temperature and then brought down.

The selectivity results obtained here agree well with those in the work cited above (Table 4). In those investigations, conducted mainly at 593 K in the absence of oxygen, the main product was acrolein, with side products consisting of propylene, and traces of acrylic acid, acetaldehyde, 1,5-hexadiene and phenol. In this study the last three products were not observed, probably due to their further oxidation in the presence of oxygen. At higher temperatures substantial amounts of benzene were obtained. The observed product distribution at these temperatures are unlikely to be due to gas-phase free-radical reactions because of the absence of the characteristic products, propylene oxide and acetaldehyde.[38] In this study a lower conversion of propylene was obtained than in the previous work. At 593 K the conversion was 7% as opposed to 100% for the other measurements. This is probably due to the use of a significantly lesser quantity of catalyst than previously. This work used a total of 0.18 m^2, whereas the other studies used 5.3 m^2 and 8 m^2.

Burrington and Grasselli have indicated that allyl iodide does not produce free allyl radicals as suggested by the group of Haber. Rather they propose that allyl iodide adsorbs on MoO_3 prior to reaction. Whatever the mechanism, the crucial observation is that allyl iodide reacts much more readily than propylene by bypassing the difficult hydrogen atom abstraction step. An intermediate resembling adsorbed allyl radical is likely.

Crystal Face Specificity of Propylene Oxidation on MoO_3. Figure 9 reports the rate of acrolein formation on unsupported MoO_3 needles and powder. Table 3 takes part of this data at low temperature and compares it to findings obtained on a similar system, oriented MoO_3 crystallites supported on graphite.[10,11] The results in both studies are very similar, the selectivity to acrolein is higher on the non-oriented samples by a factor of about two. On the basis of this selectivity difference and a statistical analysis of exposed planes, Volta et al., concluded that the various planes of MoO_3 catalyze different reactions.[13]

A similar analysis can be made here using the estimated average dimensions of the powder and needle crystallites. From these dimensions it can be calculated that there is approximately four times more edge plane surface area on the powder than on the needles (Table 2). If these are the planes solely responsible for acrolein formation, as Volta et al., suggest, the results here are in qualitative agreement with this suggestion. This study finds that the powder is twice as selective as the needles in the oxidation of propylene, and the approximate factor of four can account for this. However, noting that it is difficult to accurately measure the quantity of exposed planes by electron microscopy and, furthermore, recognizing that the differences between samples is exceedingly small, we defer here the question of determining crystal face specificity by this type of analysis until a more definitive study is undertaken.

The low selectivity to the product of interest in propylene oxidation (<ca. 10%) raises the question of whether a possible greater crystal face specificity is erased by the combination of the high temperatures employed and the presence of the unselective total oxidation reaction. For this reason it is desirable to examine the behavior of more reactive probe molecules. Table 5 reports the results obtained in the allylic oxidation of a number of propylene analogues on oriented and unoriented samples of MoO_3. There is a notable trend of increasing overall selectivity toward allylic oxidation products as the allylic bond strength decreases. In addition, in comparing the basal and edge oriented samples, there is less

Table 5. Allylic Oxidation of Propylene Analogues

Molecule	Bond energy / kJ mol^{-1}	Selectivity/% Basal sample	Selectivity/% Edge sample	Selectivity ratio	Ref.
CH_2=CH-CH_2-H Propylene	361[39]	3	6	2	This work
CH_2=CH-CH(CH_3)-H 1-Butene	345[39]	9	12	1.3	Ref. 13[a,b]
CH_2=C(CH_3)-CH_2-H Isobutene	322[40]	27	36	1.3	Ref. 13[a,c]
CH_2=CH-CH_2-I Allyl iodide	184[41]	99	99	1	This work

a) Basal sample=85% (010) plane, 15% edge planes. b) Edge sample=55% (010) plane, 45% edge planes. c) Edge sample=61% (010) plane, 39% edge planes.

variability in the selectivities as the bond strength decreases. For propylene, 1-butene, isobutene, and allyl iodide oxidation the selectivities change by factors of only 2, 1.3, 1.3, and 1, respectively. This is understandable as those molecules whose allylic positions are easier to activate are expected to show lesser sensibility to the structure of the surface. Factors like the above are small in catalysis, and they suggest that allylic oxidation on MoO_3 is only slightly sensitive to the structure of the surface. However, the differences are reproducible[10,11] and do demonstrate trends, indicating a variability of the rate with the structure of the surface. Thus, we must recognize here a contribution of the structure to the reactivity, even though it is outside the confines of a range of variation of rate characteristic of structure-sensitive reactions.

Conclusion

Oriented crystallites of MoO_3 in the shape of needles and a random powder were used to investigate the partial oxidation of propylene and allyl iodide. Only a small difference in reactivity of both materials in propylene oxidation is observed, indicating that the reaction depends only slightly on the structure of the MoO_3.

The author thanks Dr. Leo Volpe for taking the scanning electron micrographs, Prof. Richard W. Gaver for the usage of the Cary 81 Raman spectrometer, Prof. Michel Boudart for extensive discussions, and Catalytica for permission to publish this work.

References

1) K. Tanaka and T. Okuhara, "Proc. 3rd Int. Conf. Molybdenum, The Chemistry and Uses of Molybdenum," ed by H. F. Barry and P. C. H. Mitchell, Climax Molybdenum Co., 1979, p. 170.
2) K. Tanaka and T. Okuhara, *J. Catal.*, **65**, 1 (1980).
3) K. Tanaka and T. Okuhara, *J. Catal.*, **78**, 155 (1982).
4) P. Berlowitz and H. H. Kung, *J. Am. Chem. Soc.*, **108**, 3533 (1986).
5) H. S. Taylor, *Proc. R. Soc. London, Ser. A*, **108**, 105 (1925).
6) M. Boudart, A. Aldag, J. E. Benson, N. A. Dougharty, and C. Girvin Harkins, *J. Catal.*, **6**, 92 (1966).
7) M. Boudart, *Adv. Catal.*, **20**, 153 (1969).
8) M. Boudart, "Proc. 6th Int. Cong. Catal.," London, 1976, Vol. 1, p. 1 ed by G. C. Bond, P. B. Wells, and F. C. Tomkins, Chemical Society, London, 1977.
9) J. C. Volta, W. Desquesnes, B. Moraweck, and G. Coudurier, *React. Kinet. Catal. Lett.*, **12**, 241 (1979).
10) J. C. Volta and B. Moraweck, *J. Chem. Soc., Chem. Commun.*, **1980**, 338.
11) J. C. Volta, W. Desquesnes, B. Moraweck, and J. M. Tatibouët, "Proc. 7th Int. Cong. Catal.," Tokyo, 1980, Part B. p. 1398, ed by T. Seiyama and K. Tanabe, Elsevier, Amsterdam, 1981.
12) J. C. Volta, M. Forissier, F. Theobald, and T. P. Pham, *Farad. Disc. Chem. Soc.*, **72**, 225 (1981).
13) J. C. Volta, J. M. Tatibouët, C. Phichitkul, and J. E. Germain, "Proc. 8th Int. Cong. Catal.," Berlin 1984, Vol. 4, p. 451, Verlag Chemie, 1984.
14) J. M. Tatibouët and J. E. Germain, *J. Catal.*, **72**, 375 (1981).
15) J. M. Tatibouët and J. E. Germain, *J. Chem. Res. (S)*, **1981**, 268.
16) J. M. Tatibouët and J. E. Germain, *J. Chem. Res. (M)*, **1981**, 3070.
17) F. Ohuchi and U. Chowdhry, "Proceedings of the 12th North American Thermal Analysis Society Conference," Paper #103, Williamsburg, Virginia, September 1983.
18) F. Ohuchi, L. E. Firment, U. Chowdhry, and A. Ferretti, *J. Vac. Sci. Technol.*, **A2**, 1022 (1984).
19) J. Ziólkowski, *J. Catal.*, **80**, 263 (1983).
20) J. N. Allison and W. A. Goddard, III, *J. Catal.*, **92**, 127 (1985).
21) L. Kihlborg, *Arkiv Kemi*, **21**, 357 (1963).
22) B. Wanklyn, *J. Crystal Growth*, **2**, 251 (1968).
23) C. R. Adams and T. J. Jennings, *J. Catal.*, **2**, 63 (1963).
24) C. R. Adams and T. J. Jennings, *J. Catal.*, **3**, 549 (1964).
25) W. M. H. Sachtler and N. H. de Boer, "Proc. 3rd Int. Cong. Catal," Amsterdam, 1964, Vol. I, p. 252, ed by W. M. H. Sachtler, G. C. A. Schuit and P. Zwietering, North Holland Publ. Co., Amsterdam, 1965.
26) J. Haber, B. Grzybowska, *J. Catal.*, **28**, 489 (1973).
27) J. Haber, M. Sochacka, B. Grzybowska, and A.

Goleobiowsky, *J. Mol. Catal.*, **1**, 35 (1975).
28) G. N. Keulks, *J. Catal.*, **19**, 232 (1970).
29) Y. Morooka, "Proc. Fifth Int. Cong. Catal.," Miami Beach, 1972, Vol. 2, p. 981, ed by J. W. Hightower, North Holland Publ. Co., Amsterdam-London, American Elsevier Co. Inc., New York, 1973.
30) L. Ya. Margolis, *Catal. Rev. Sci. Eng.*, **8**, 241 (1973).
31) A. Bielanski and J. Haber, *Catal. Rev. Sci. Eng.*, **19**, 1 (1979).
32) L. A. Kassatkina and G. K. Boreskov, *Zhur. Fiz. Khim.*, **29**, 455 (1959).
33) J. Haber, *Z. Chem.*, **13**, 241 (1973).
34) B. Grzybowska, J. Haber, and J. Janas, *J. Catal.*, **49**, 150 (1977).
35) J. D. Burrington and R. K. Grasselli, *J. Catal.*, **59**, 79 (1979).
36) P. L. Gai, "Proc. 3rd Int. Conf. Molybdenum, The Chemistry and Uses of Molybdenum," p. 143, ed by H. F. Barry and P. C. H. Mitchell, Climax Molybdenum Co., 1979.
37) P. L. Gai, *Philos. Mag. A*, **43**, 841 (1981).
38) J. H. Jones, T. E. Daubert, and M. R. Fenske, *Ind. Engl. Chem. Prod. Res. Develop.*, **8**, 196 (1969).
39) D. F. McMillen and D. M. Golden, *Annual Rev. Phys. Chem.*, **33**, 493 (1982).
40) V. I. Vedeneyev, L. V. Gurvich, V. N. Kondratyev, V. A. Medvedev, and Ye. L. Frakevich, "Bond Energies, Ionization Potentials and Electron Affinities," English translation by Scripta Technica Ltd., St. Martin's Press, New York (1966).
41) K. W. Egger and A. T. Cocks, *Helv. Chim. Acta*, **56**, Fasc. 5, 1516 (1973).

Conductance Study of Alkali Metal Chlorides and Ammonium Chloride in 1,2-Dimethoxyethane-Water Mixtures at 25 °C

P. V. S. S. PRABHU*,† and M. V. RAMANAMURTI
Department of Chemistry, Faculty of Science, Banaras Hindu University, Varanasi-221005, India
(Received September 21, 1987)

Conductance data for alkali metal chlorides and ammonium chloride in 1,2-dimethoxyethane (DME)-water mixtures (14.00<dielectric constant<56.76) at 25 °C are reported in the concentration range 0.0001—0.06 mol·dm^{-3}. The data have been analyzed by Fuoss (1978) conductance-concentration relation. Preferential solvation of cations by water does not show systematic trend depending on the cationic size. Walden product variations indicated the complex dependence of conductance of alkali metal cations on solvent sorting and structural effects. The energy (E_s) values suggest that alkali metal cations and chloride ions in majority exist as contact pairs in these solutions.

A series of investigations[1-6] on the influence of solvent structure on limiting ionic mobilities of alkali metal cations and halide ions in water-organic solvent mixtures have been carried out in the recent past. Of these the most important contributions are by Kay et al.[1-3] and also Petrella et al.[4-6] In their studies the ionic Walden products have been analyzed in terms of the short range ion-solvent interactions. For cations (alkali metal) and anions (halide) they found that the curves for W_p (designated by us), the ratio of the limiting Walden product for the mixture to that of water, show maxima in water-rich regions where the long range order of water is increased by the addition of organic solvent. However, for anions the W_p values are less than unity in solvent mixtures where structure breaking occurs. Also a systematic decrease of W_p value with the increase in cationic or anionic sizes was observed irrespective of the type of change induced by the cosolvent on water structure. With the objective to examine how far these observations could be reproducible for alkali metal chlorides and ammonium chloride in 1,2-dimethoxyethane (DME)-water mixtures analogous conductance studies have been undertaken. DME is a dipolar aprotic solvent and weakly interacts with anions.[7] The electrolytes in the present study have chloride (Cl^-) as the common anion so that the variations observed in Walden products are considered to be mainly due to the alkali metal cations only. This paper, therefore, deals with the conductance study of LiCl, NaCl, KCl, RbCl, CsCl, and NH_4Cl in 1,2-dimethoxyethane-water mixtures at 25 °C.

Experimental

Conductivity water (κ=0.2—0.5×10^{-6} mho cm^{-1}) was prepared by distillation of double distilled water in the presence of $KMnO_4$ in an all Pyrex glass set.

1,2-Dimethoxyethane (Riedel-De-Haenag) was kept two days over KOH and then refluxed for 24 h. This was distilled over sodium and refluxed again for 24 h. Then the sample was distilled and middle fraction was directly used for measurements.[8]

Lithium chloride (AR), sodium chloride (AR, BDH), rubidium chloride (E. Merck), cesium chloride (E. Merck), and ammonium chloride (AR, BDH) were recrystallized twice from conductivity water and dried in a vacuum desiccator. Potassium chloride (AR, BDH) was recrystallized as suggested by Hawes and Kay.[9]

Results and Discussion

The physical properties, density (ρ), viscosity (η) and dielectric constant (D) of DME-water mixtures are given in Table 1. The molar conductance values Λ (S·cm^2·mol^{-1}) as a function of concentration C (mol·dm^{-3}) in six compositions of DME-water mixtures at 25 °C are shown in Table 2. Conductance data in the present investigation are analyzed by the Fuoss conductance-concentration relation.[10] The use of any other equation or incorporation of slight modification[11] may introduce small changes in the individual fitting parameters but will not alter the overall conclusions which can be deduced from trends in these parameters. For a set of conductance data (C_j, Λ_j; J=1, N) the three adjustable parameters (Λ_o, K_Λ, and R) are derived from the following three equations:

$$\Lambda = p[\Lambda_o(1 + \Delta X/X) + \Delta\Lambda_e] \quad (1)$$

$$\gamma = 1 - K_\Lambda C \gamma^2 f^2 \quad (2)$$

Table 1. Physical Properties of the Solvent Mixtures (DME-Water) at 25 °C

Mole fraction of DME	D	ρ/g cm^{-3}	$\eta/10^{-2}$P
0.00	78.54	0.9908	0.8903
0.09	56.75	0.9837	1.9861
0.20	40.01	0.9754	1.9905
0.30	31.05	0.9456	1.5632
0.40	24.00	0.9292	1.2161
0.50	17.53	0.9147	0.9503
0.60	14.00	0.9031	0.7725

† Present address: Lithium Battery Section, Central Electrochemical Research Institute, Karaikudi-623006, Tamil Nadu, India.

Table 2. Conductance Data in DME–Water Mixtures at 25°C

$C/10^{-4}$ mol·dm^{-3} (1)	Λ/S cm^2 mol^{-1} (2)	$C/10^{-4}$ mol·dm^{-3} (3)	Λ/S cm^2 mol^{-1} (4)	$C/10^{-4}$ mol·dm^{-3} (5)	Λ/S cm^2 mol^{-1} (6)
1. Lithium chloride					
0.09 mole fraction DME		0.20 mole fraction DME		0.30 mole fraction DME	
601.0	28.01	262.2	29.01	116.5	36.12
500.7	29.78	218.5	30.58	97.0	37.59
429.2	31.35	187.3	31.91	83.2	38.83
375.5	32.73	163.9	33.12	72.8	39.92
300.4	35.17	145.7	34.25	58.2	41.69
250.3	37.22	131.1	35.23	41.6	44.30
187.7	40.58	109.2	36.85	32.3	46.15
150.2	43.26	93.6	38.40	24.2	48.20
125.1	45.47	81.9	39.67	28.8	49.23
107.3	43.35	72.8	40.78	18.2	60.07
83.4	50.40	65.5	41.73	14.5	51.42
62.5	53.84	54.6	43.39	12.1	52.44
0.40 mole fraction DME		0.50 mole fraction DME		0.60 mole fraction DME	
55.0	39.25	14.8	34.10	6.3	46.10
45.8	40.75	12.3	35.85	5.2	48.44
39.3	41.89	10.6	37.37	4.5	50.43
34.4	42.92	9.2	38.79	3.9	51.15
27.5	44.61	7.4	41.81	3.1	55.40
22.9	45.91	6.1	42.82	2.6	57.56
19.6	47.08	5.1	44.72	2.2	59.61
17.2	48.00	4.6	45.79	1.9	61.35
15.2	48.76	3.7	47.98	1.7	62.88
11.4	50.58	3.0	49.73	1.5	64.18
8.6	52.27	2.3	52.38	1.3	66.49
6.8	53.47	2.0	53.40	1.1	68.68
2. Sodium chloride					
0.09 mole fraction DME		0.20 mole fraction DME		0.30 mole fraction DME	
606.8	35.28	206.0	35.16	98.8	34.29
505.7	36.85	171.7	36.79	82.3	35.71
433.4	38.35	147.1	38.20	70.5	36.99
337.1	40.71	128.7	39.45	61.7	38.06
252.8	43.66	114.4	40.41	49.4	39.735
189.6	46.81	85.8	42.91	41.1	41.24
151.7	49.38	75.5	44.02	35.2	42.43
126.4	51.54	64.3	45.30	30.8	43.49
108.3	53.38	51.5	47.21	24.7	45.13
84.2	56.48	42.9	48.58	17.6	47.45
63.2	60.06	32.1	50.80	13.7	49.07
47.4	63.58	25.7	52.38	10.2	50.68
0.40 mole fraction DME		0.50 mole fraction DME		0.60 mole fraction DME	
74.6	27.82	20.2	44.20	10.7	39.73
62.2	29.16	16.8	45.48	9.5	40.85
53.3	30.29	14.4	46.45	8.6	41.86
41.4	32.25	12.6	47.28	7.1	43.72
31.1	34.56	11.2	48.11	6.1	45.26
23.3	36.75	18.1	48.76	5.3	46.67
18.6	38.51	8.4	49.95	4.7	41.91
15.5	39.92	7.2	50.86	4.3	49.04
11.6	42.08	6.3	51.67	3.9	50.06
9.3	43.73	5.0	52.93	3.5	57.02
6.5	46.07	4.2	53.96	2.9	53.18
5.1	47.54			2.6	54.19
3. Potassium chloride					
0.09 mole fraction DME		0.20 mole fraction DME		0.30 mole fraction DME	
604.8	36.77	238.4	40.00	115.1	51.28
549.8	37.91	216.7	40.93	102.2	52.25
465.2	39.78	198.5	41.82	95.9	52.89
432.0	40.62	170.3	43.39	79.9	54.43

Table 2. (Continued)

$C/10^{-4}$ mol·dm^{-3} (1)	Λ/S cm^2 mol^{-1} (2)	$C/10^{-4}$ mol·dm^{-3} (3)	Λ/S cm^2 mol^{-1} (4)	$C/10^{-4}$ mol·dm^{-3} (5)	Λ/S cm^2 mol^{-1} (6)
378.0	42.34	149.0	44.76	68.5	55.62
336.0	43.94	132.4	46.03	59.9	56.70
302.4	45.41	119.2	47.19	53.3	57.65
252.0	47.93	99.3	49.19	47.9	58.43
216.0	50.18	85.2	50.82	39.9	59.89
189.0	52.12	74.5	52.31	36.9	60.57
168.0	53.95	66.2	53.61	34.2	61.20
151.2	55.70	54.1	55.84	31.9	61.65
0.40 mole fraction DME		0.50 mole fraction DME		0.60 mole fraction DME	
48.6	53.81	24.1	49.70	9.3	46.30
44.2	54.60	19.9	51.72	7.7	48.39
37.4	56.28	18.6	52.51	6.6	50.09
32.4	57.70	15.5	54.55	5.4	52.37
28.6	58.93	13.3	56.39	4.9	53.74
25.6	60.03	11.6	51.81	4.2	55.62
22.1	61.38	10.3	59.19	3.5	57.70
18.7	62.89	9.3	68.42	3.1	59.64
16.2	64.03	7.7	62.49	2.7	61.32
12.8	66.11	6.6	64.20	2.4	62.83
11.0	67.20	5.8	65.65	2.1	64.72
8.6	69.01	4.2	69.18	1.9	65.95
4. Rubidium chloride					
0.09 mole fraction DME		0.20 mole fraction DME		0.30 mole fraction DME	
600.6	36.65	208.6	38.54	97.9	41.08
500.5	38.76	173.8	40.55	81.4	42.69
429.0	40.58	149.0	42.26	69.9	44.08
375.4	42.29	130.3	43.77	61.2	45.23
300.4	45.28	115.9	45.12	54.4	46.25
250.2	47.81	86.9	48.42	48.9	47.16
214.5	50.03	74.5	50.20	40.8	48.70
116.8	53.72	65.2	51.74	34.9	49.97
115.1	58.27	57.9	53.05	27.2	51.97
107.2	60.68	52.1	54.24	24.4	52.70
83.4	64.70	43.4	56.27	20.4	54.15
62.5	69.32	37.2	58.01	15.3	56.05
0.40 mole fraction DME		0.50 mole fraction DME		0.60 mole fraction DME	
48.3	34.37	17.3	46.02	10.5	45.51
40.2	36.05	14.4	48.01	8.7	47.58
34.5	37.50	12.3	49.62	7.5	49.39
30.1	38.69	10.8	51.08	6.5	57.05
26.8	39.79	9.6	52.32	5.8	52.53
24.1	40.77	8.6	53.44	5.2	53.90
20.1	42.47	7.2	55.36	4.3	56.22
17.2	43.89	6.1	56.95	3.7	58.09
13.4	46.13	4.8	59.47	3.2	59.95
10.0	48.71	3.6	62.18	2.6	62.73
8.6	50.02	2.4	65.65	2.1	65.14
6.7	52.04	1.8	67.84	1.8	67.18
5. Cesium chloride					
0.09 mole fraction DME		0.20 mole fraction DME		0.30 mole fraction DME	
515.2	63.03	327.3	43.31	305.7	37.14
436.8	63.74	273.2	43.99	252.8	37.92
362.5	64.49	225.1	44.71	201.2	38.78
270.7	65.61	186.3	45.42	150.3	39.85
200.3	66.22	119.7	47.02	104.8	41.31
140.1	67.74	100.9	47.61	80.7	42.37
105.1	68.53	75.7	48.55	64.3	43.26
67.1	69.60	50.4	49.65	52.0	44.07
50.1	70.21	37.2	50.56	35.6	45.41
32.0	71.00	25.3	51.42	21.6	46.99
16.8	71.89	15.8	52.35	11.5	48.58

Table 2. (Continued)

$C/10^{-4}$ mol·dm^{-3} (1)	Λ/S cm^2 mol^{-1} (2)	$C/10^{-4}$ mol·dm^{-3} (3)	Λ/S cm^2 mol^{-1} (4)	$C/10^{-4}$ mol·dm^{-3} (5)	Λ/S cm^2 mol^{-1} (6)
0.40 mole fraction DmE		0.50 mole fraction DME		0.60 mole fraction DME	
98.1	34.59	32.0	25.75	31.9	17.57
82.1	35.71	27.1	26.89	26.4	18.74
68.1	36.88	23.1	28.09	21.2	20.18
57.5	37.91	20.1	29.02	17.8	21.41
49.2	38.85	15.7	30.98	15.2	22.54
42.3	39.74	13.0	32.45	11.5	24.69
34.8	40.87	10.7	34.03	9.4	26.31
27.7	42.12	8.5	35.84	7.7	28.03
22.2	43.29	7.0	37.42	5.8	30.50
18.3	44.26	5.5	39.46	4.5	32.89
13.1	45.82	3.8	42.21	3.4	35.54
9.6	47.11	2.3	45.70	2.2	39.60
6. Ammonium chloride					
0.09 mole fraction DME		0.20 mole fraction DME		0.30 mole fraction DME	
583.7	41.11	208.4	40.65	98.8	34.43
486.4	43.08	173.7	42.43	82.3	35.15
416.9	44.82	148.9	43.88	70.5	35.80
364.8	46.40	130.2	45.20	54.9	36.75
291.8	49.16	115.8	46.49	49.4	37.11
243.2	51.51	104.2	47.49	41.1	37.75
208.4	53.48	86.8	49.32	35.2	38.32
162.1	57.07	74.4	50.79	30.8	38.74
121.6	61.23	65.1	52.06	27.4	39.05
104.2	63.51	57.9	53.11	17.6	40.16
91.2	65.52	52.1	54.06	10.2	41.43
72.9	68.87	43.4	55.72	8.8	41.69
0.40 mole fraction DME		0.50 mole fraction DME		0.60 mole fraction DME	
74.6	28.47	16.8	38.87	12.1	40.49
62.2	29.51	13.3	40.11	10.3	42.22
53.3	30.40	11.4	41.06	8.6	44.05
46.6	31.11	10.2	41.71	7.2	45.98
37.3	32.35	9.2	42.29	6.2	47.61
31.1	33.34	8.5	42.73	4.8	50.28
23.3	34.86	7.2	43.56	3.6	53.28
18.6	35.98	6.3	44.29	3.0	54.88
13.3	37.51	5.6	44.86	2.7	56.20
10.3	38.65	4.5	45.89	2.3	57.53
7.7	39.80	4.2	46.26	1.8	60.06
5.1	41.20	3.5	47.03	1.3	62.56

$$\ln f = -\beta\kappa/2(1 + \kappa R) \quad (3)$$

Here $\Delta X/X$ and $\Delta\Lambda_e$ are the relaxation and electrophoretic terms respectively and expressions used for these terms are the same as these used by Fuoss.[10] The detailed method of analysis of the data has been described earlier.[12] Various parameters thus derived from the conductance data are assembled in Table 3. Limiting molar conductance values obtained in our present investigation for all the electrolytes, viz., chlorides of Li, Na, K, Rb, Cs, and NH_4 in water at 25 °C are in agreement with the reported values.[13–17] Also the Λ_o values for CsCl in DME–water mixtures obtained in present work are in good agreement with the already reported values.[18] These facts substantiate the accuracy of our experimental results and the computational procedures.

The limiting molar conductance variations as well as the viscosity variation with the mole fraction of DME are depicted in the Fig. 1. DME has been characterized as a structure promoter in water rich mixtures through viscosity studies.[19] On structural characteristics of DME–water mixtures no further information is available in the literature. A decrease in limiting molar conductance for each electrolyte with a corresponding increase in viscosity of the solvent mixtures has been observed both in the water rich and DME rich mixtures. The maximum viscosity and the minimum in the limiting molar conductance ($\Lambda_{o_{min}}$) of any electrolyte does not occur at the same mole fraction of DME and also $\Lambda_{o_{min}}$ is shifted towards the DME rich region. This is because of the pre-

Table 3. Derived Conductance Parameters

Mole fraction of DME	$\Lambda_o \pm \Delta\Lambda_o$	K_A	K_R	K_S	R	σ%	$\Lambda_o \cdot \eta$	E_s/kT
	$S \cdot cm^2\ mol^{-1}$				Å		$\Omega^{-1}\ cm \cdot mol^{-1}P$	J^{-1}
(1)	(2)	(3)	(4)	(5)	(6)	(7)	(8)	(9)
1. Lithium chloride								
0.00	115.12±0.01	0.79	0.71	0.11	5.12	0.023	1.024	+2.20
0.09	79.31±0.02	120.60	3.16	37.10	6.50	0.009	1.575	−3.61
0.20	65.06±0.10	158.39	6.43	23.61	7.04	0.056	1.294	−3.16
0.30	61.69±0.01	152.93	11.81	11.94	7.51	0.01	0.964	−2.47
0.40	62.53±0.03	282.30	38.60	6.31	14.53	0.044	0.760	−1.84
0.50	69.78±0.07	1988.21	73.28	26.13	7.69	0.052	0.663	−3.26
0.60	91.00±0.04	4172.51	146.37	27.50	9.49	0.021	0.703	−3.31
2. Sodium chloride								
0.00	126.53±0.01	0.81	0.79	0.02	5.56	0.018	1.126	+3.91
0.09	90.36±0.06	185.83	31.24	4.94	19.55	0.036	1.794	−1.59
0.20	64.04±0.08	107.04	7.45	13.36	8.01	0.080	1.274	−2.59
0.30	60.07±0.04	218.38	25.12	7.69	14.00	0.051	0.938	−2.03
0.40	57.86±0.03	467.28	28.90	15.16	5.56	0.045	0.703	−2.71
0.50	64.56±0.06	703.35	272.17	1.58	4.53	0.045	0.613	−0.45
0.60	83.88±0.05	5008.83	890.83	4.62	5.06	0.015	0.648	−1.53
3. Potassium chloride								
0.00	149.90±0.01	0.56	0.45	0.24	4.65	0.012	1.334	+1.42
0.09	117.87±0.47	283.57	20.67	10.53	16.52	0.044	2.341	−2.35
0.20	83.10±0.06	211.68	34.51	5.13	18.61	0.024	1.653	−1.63
0.30	77.69±0.12	148.17	51.19	1.89	2.53	0.072	1.214	−0.63
0.40	81.82±0.08	240.92	24.41	8.86	8.80	0.063	0.994	−2.18
0.50	90.75±0.10	1203.74	195.13	5.16	4.95	0.047	0.862	−1.64
0.60	104.64±0.16	8296.77	1592.20	4.21	4.54	0.036	0.808	−1.43
4. Rubidium chloride								
0.00	153.64±0.01	0.26	0.19	0.36	3.35	0.011	1.367	+1.02
0.09	108.14±0.11	177.75	14.08	11.62	14.03	0.028	2.147	−2.45
0.20	80.20±0.05	168.87	11.05	14.28	10.48	0.025	1.596	−2.65
0.30	67.62±0.04	155.55	11.81	12.16	7.51	0.040	1.057	−2.49
0.40	66.55±0.04	532.58	24.28	20.92	7.02	0.035	0.809	−3.04
0.50	79.67±0.01	1052.82	61.31	16.17	10.54	0.015	0.757	−2.78
0.60	79.67±0.15	4440.91	593.66	6.48	5.53	0.050	0.743	−1.86
5. Cesium chloride								
0.00	153.04±0.02	0.62	0.58	0.06	3.62	0.015	1.362	+2.81
0.09	74.36±0.01	11.18	6.80	0.64	10.02	0.008	1.477	+0.44
0.20	55.65±0.02	13.71	5.85	1.34	3.54	0.056	1.107	−0.29
0.30	52.84±0.02	39.41	18.54	1.12	3.52	0.061	0.826	−0.11
0.40	54.74±0.01	201.79	46.88	3.30	16.55	0.010	0.665	−1.93
0.50	57.98±0.07	1417.99	75.40	17.80	7.51	0.069	0.551	−2.87
0.60	64.64±0.13	5357.60	142.52	36.58	19.04	0.051	0.498	−3.59
6. Ammonium chloride								
0.00	149.75±0.01	0.35	0.29	0.20	4.12	0.018	1.333	+1.60
0.09	108.20±0.01	187.18	27.31	5.85	18.52	0.026	2.148	−1.76
0.20	72.73±0.09	96.76	5.19	17.61	5.03	0.058	1.447	−2.86
0.30	45.22±0.03	76.24	26.76	1.84	14.52	0.092	0.707	−0.60
0.40	46.77±0.02	224.91	29.27	6.68	11.52	0.041	0.568	−1.89
0.50	55.35±0.03	563.46	471.01	2.29	5.15	0.041	0.526	−0.82
0.60	77.61±0.03	2302.65	145.84	14.78	19.52	0.023	0.599	−2.69

ferential solvation of cations (Cl^- common anion) by water as DME is less polar than water. The shift in $\Lambda_{o_{min}}$ towards the DME rich region may be due to gradual replacement of water molecules by DME molecules in the cationic shells as a result of breakdown of the water polymeric structure at higher concentrations of DME.

The Walden product ($\Lambda_o \cdot \eta$) maximum is observed around 0.1 mole fraction of DME (Fig. 2) for all the alkali metal cations and ammonium ion (Cl^- being the common anion). This behavior of alkali metal cations is similar to that observed by Kay et al., for the

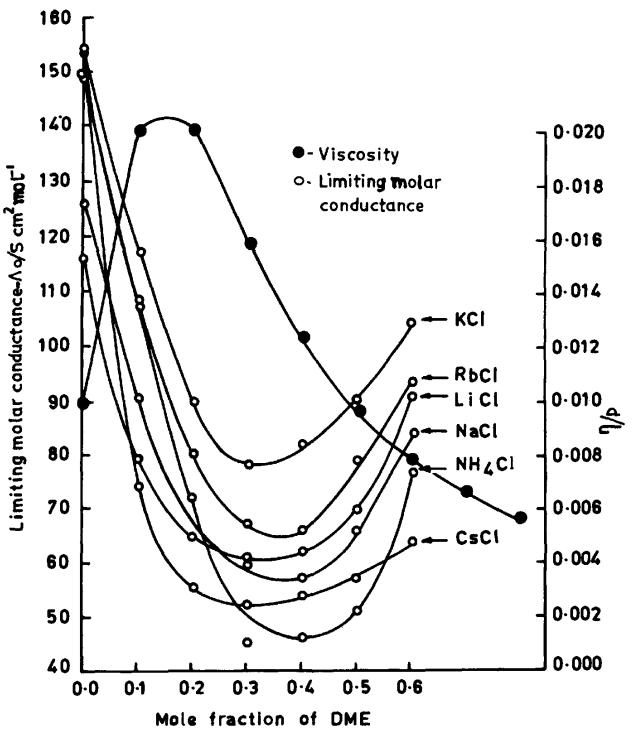

Fig. 1. Variation of viscosity (η) and limiting molar conductances (Λ_o) of alkali metal chlorides and ammonium chloride with mole fraction of DME in water.

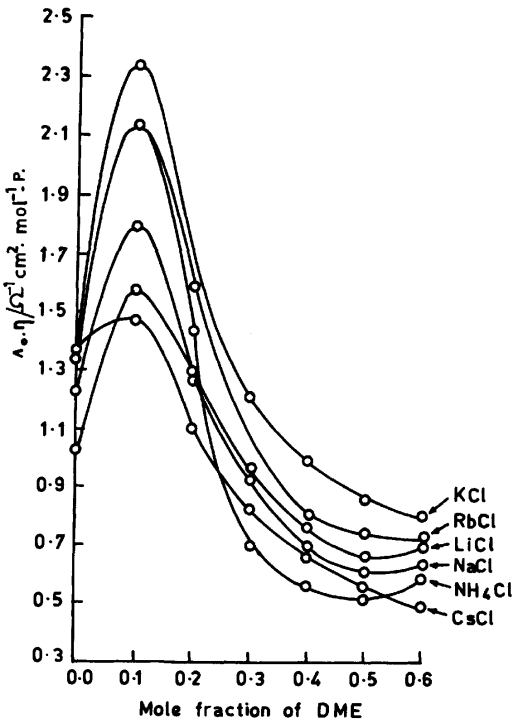

Fig. 2. Variation of Walden products ($\Lambda_o \cdot \eta$) of alkali metal chlorides and ammonium chloride with respect to mole fraction of DME in water.

same ions in other aqueous binary mixtures of the solvents dioxane,[1] ethanol,[2] and *t*-butyl alcohol.[3] Petrella et al. have also observed similar Walden product maxima for alkali metal cations and halide ions in sulfolane-water,[4] acetonitrile-water,[5] and dimethyl sulfoxide-water[6] mixtures. They have explained the existence of maximum on the basis of Kay's "solvent sorting model".[2] Several other significant reasons[20-22] were also suggested for this variation, and their mathematical treatments[23-30] also have been given by different workers from time to time. The most recent model proposed by Nakahara et al.[30] demonstrates the superiority of residual friction coefficient ($\Delta\zeta$) over the Walden product to explain long range interactions in the case of smaller ions. However, due to the lack of experimental data on intermediate frequency dielectric constants (ε_c) and infinite frequency dielectric constants (ε_∞) for these electrolyte solutions of DME-water mixtures it would not be possible to follow the method of Nakahara. Alternatively, the Walden product maximum observed in the present study has been explained by Kay's model.

In water-DME mixtures the ion water interactions are stronger than ion DME interactions, and therefore in the ionic cosphere there is a higher percentage of water than in the bulk mixture. Due to preferential solvation of these ions by water in this region of the solvent mixtures, viscosity of the solvent in the vicinity of these ions is lower than that of the bulk solvent. Since the bulk viscosity value is used in the calculation of Walden product, the calculated values of $\Lambda_o \cdot \eta$ are too high up to the point corresponding to the viscosity maximum after which they are low, and therefore a maximum in Walden product occurs. The bulk viscosity of DME - water mixtures also goes through a maximum and since the alkali metal cations as well as ammonium ion have water-rich solvation shells in dilute DME - water mixtures, the observed behavior of these ions is consistent with Kay's model.

However, the height of the Walden product maximum relative to that in pure water (designated as W_p), does not show systematic dependence on the cationic size in the present results (Fig. 2). This is in contrast to the earlier observations.[1-6] The observed order of variation of W_p value, i.e.

$$W_p(Cs^+) < W_p(Li^+) < W_p(Na^+) < W_p(Rb^+) \approx W_p(NH_4^+) < W_p(K^+),$$

cannot be explained on the basis of sorting mechanism alone. Petrella et al.[3-6] have shown that alkali metal cations are sensitive to sorting effect and halide ions are influenced by structural effects. Parker et al.[31] have however concluded through their analogous conductance studies that the behavior of ions (cations and anions) is quite complex and may be influenced by a combination of such factors as solvent

sorting and structural changes due to the solvent mixing. Therefore, a plausible explanation may be given as follows for the observed order of variation of W_p value. Let us first consider the Li^+ and Cs^+ ions. As the sorting effect will be more accentuated in the case of smaller ions the order $W_p(Li^+)>W_p(Cs^+)$ is consistent with the sorting model. However, in the case of Na^+ and K^+ ions the order $W_p(K^+)>W_p(Na^+)$ is not in agreement with this model. Na^+ and K^+ ions behave as structure breakers in water. As DME-water mixtures are more structured than water, Na^+ and K^+ may behave as better structure breakers in the mixtures than in water. The largest ion will show the greatest increase and hence the order observed for Na^+ and K^+ ions. In the case of NH_4^+ and Rb^+ the magnitudes of heights of Walden product maxima are equal, which suggests that the contribution of structure breaking effect of these two ions of equal size is the same in these solutions. These results indicate that alkali metal cations are not only sensitive to sorting effect but also influenced by structural effects.

Association constant values (K_A) for all the electrolytes given in Table 3 are greater than 10 indicating significant association in DME-water mixtures. This pairing constant (K_A) is the product of two terms,[10] one (K_R) of which depends explicitly on dielectric constant of the solvent. While the other (K_S) is system-specific depending on short-range ion-ion and ion-solvent interactions. The relationship is represented as,

$$K_A = K_R(1 + K_S). \tag{4}$$

Where

$$K_R = \frac{4\pi N \cdot R^3}{3000} \exp(e^2/RDkT), \tag{5}$$

and

$$K_S = \frac{\alpha}{1-\alpha} = \exp(-E_s/k \cdot T) = \exp(-\varepsilon). \tag{6}$$

N is Avogadro's number, e is electronic charge, k is Boltzmann's constant, D is dielectric constant, R is cosphere (Gurney) diameter, and T is absolute temperature. The plot of $\log K_R$ vs. $1/D$ is therefore expected to show linear variation (Fig. 3) in the present study. But the variation of E_s/kT vs. $1/D$ will not be linear (Fig. 4) as K_S depends on specific ion-solvent interactions.[32] If α is the time average fraction of diffusion pairs (for which $a \leqslant r \leqslant R$) which are in contact, the equilibrium between solvent separated pairs and contact pairs is described[32] by Eq. 6, where E_s is the difference in free energy between states defined as $r=R$ and $r=a$. The magnitude of E_s may give an insight into the mechanism of process of ionic association in these solutions. The values of K_R, K_S, and E_s are shown in Table 3 for all the electrolytes in DME-water mixtures. A remarkable decrease in E_s values from pure water to those of mixtures for all the electrolytes is observed (Fig. 4). Also there is no systematic decrease in these values with the increase in content of DME in the mixtures. This pattern of behavior of E_s becoming less positive as polarizability of the solvent decreases was observed in other systems[32] also. This suggests the predominance of

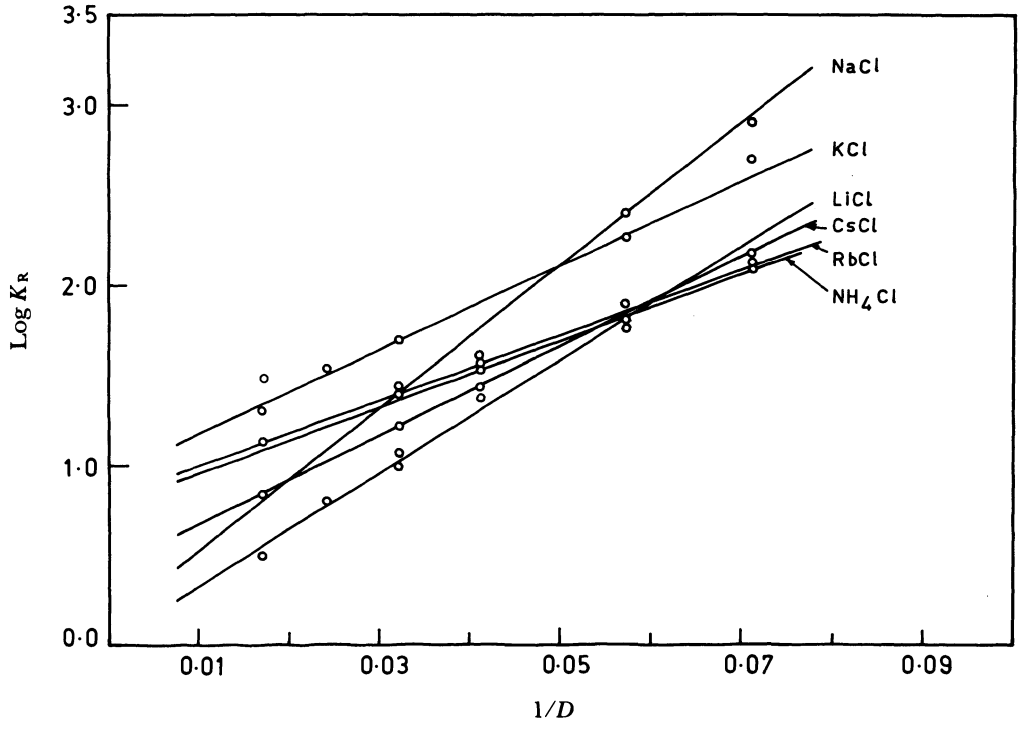

Fig. 3. Plot of $\log K_R$ vs. $1/D$.

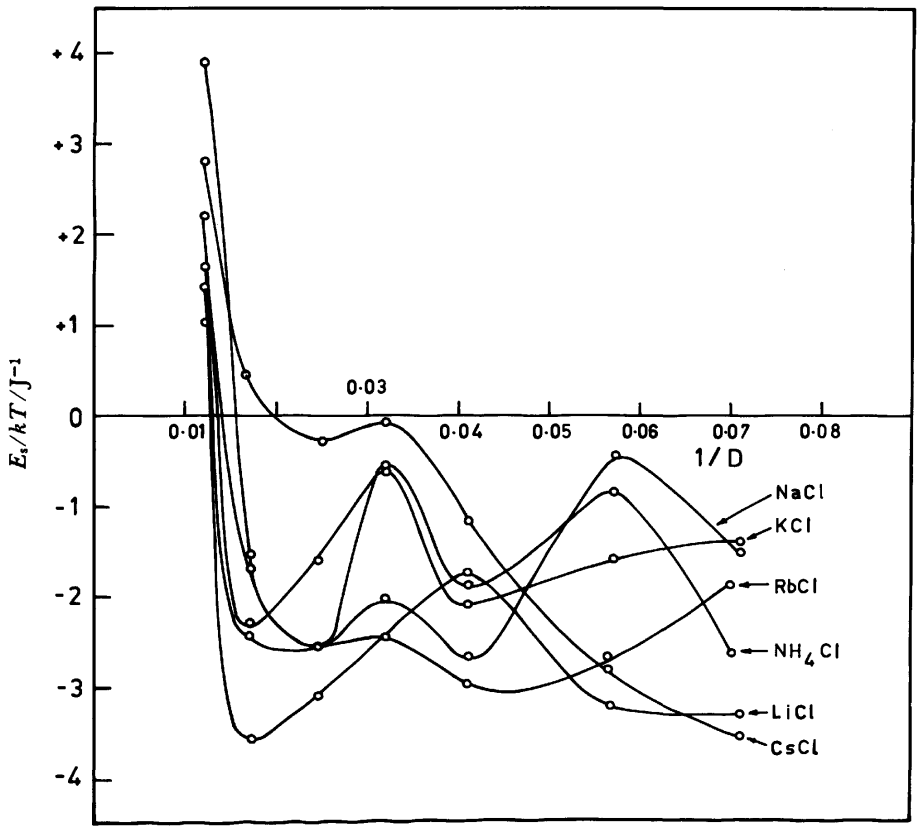

Fig. 4. Variation of E_s/kT with the reciprocal of dielectric constant ($1/D$).

electrostatic effect in the E_s and indicate formation of more contact ion pairs. Even though there is every possibility for the formation of solvent separated ion pairs through the donor-acceptor type of interaction[33-37] in these electrolyte solutions, as there are two bonding oxygen sites available in DME, the trend of the variation in E_s values suggests that alkali metal cations and chloride ions in majority exist as contact pairs. This may be due to the less polarizability of DME which allows the interionic attraction to become greater in these solutions. However, the variations of E_s/kT vs. $1/D$ are not systematic (Fig. 4) because of the competition between the donor-acceptor interactions and electrostatic interactions.

One of the authors (PVSSP) thank CSIR, New Delhi for the award of Senior Research Fellowship and the Head, Department of Chemistry, Banaras Hindu University, for providing necessary facilities. Thanks are also due to the authorities, Computer Centre, B.H.U. for help in computational work using ICL 1904 S Computer.

References

1) R. L. Kay and T. L. Broadwater, *Electrochimica Acta*, **16**, 667 (1971).
2) R. L. Kay and T. L. Broadwater, *J. Solar Chem.*, **5**, 57 (1976).
3) T. L. Broadwater and R. L. Kay, *J. Phys. Chem.*, **74**, 3802 (1970).
4) G. Petrella, A. Sacco, M. Castagnolo, M. Della Monica, and A. DeGiglio, *J. Soln. Chem.*, **6**, 13 (1977).
5) G. Petrella, M. Castagnolo, A. Sacco, and M. Petrella, *J. Soln. Chem.*, **9**, 331 (1980).
6) F. Petrella, M. Petrella, M. Castagnolo, Angelo Dell'Atti, and Angelo DeGiglio, *J. Soln. Chem.*, **10**, 129 (1981).
7) A. J. Parker, *Chem. Rev.*, **69**, 1 (1969).
8) W. J. Wallace and A. L. Mathews, *J. Chem. Engg. Data*, **8**, 496 (1963).
9) J. L. Hawes and R. L. Kay, *J. Phys. Chem.*, **69**, 2420 (1965).
10) R. M. Fuoss, *J. Phys. Chem.*, **82**, 2427 (1978).
11) L. Bahadur and M. V. Ramanamurti, *J. Electrochem. Soc.*, **128**, 339 (1981).
12) M. V. Ramanamurti and L. Bahadur, *Electrochimica Acta*, **25**, 601 (1980).
13) C. F. Mattina and R. M. Fuoss, *J. Phys. Chem.*, **79**, 1604 (1975).
14) Y. C. Chin and R. M. Fuoss, *J. Phys. Chem.*, **72**, 4123 (1968).
15) R. W. Kunze and R. M. Fuoss, *J. Phys. Chem.*, **67**, 914 (1963).
16) J. C. Justice and R. M. Fuoss, *J. Phys. Chem.*, **67**, 1707 (1963).
17) R. C. Paul, J. P. Singla, D. S. Gill, and S. P. Narula, *Indian J. Chem.*, **9**, 981 (1971).
18) E. Renard and J. C. Justice, *J. Soln. Chem.*, **3**, 633 (1974).

19) M. V. Ramanamurti, P. V. S. S. Prabhu, and Lal Bahadur, *Bull. Chem. Soc. Jpn.*, **59**, 2341 (1986); P. V. S. S. Prabhu and M. V. Ramanamurti, *Ind. J. Chem.*, **26A**, 609 (1987).
20) L. Bahadur and M. V. Ramanamurti, *J. Chem. Soc., Faraday Trans. 1*, **76**, 1409 (1980).
21) L. Bahadur and M. V. Ramanamurti, *Canad. J. Chem.*, **62**, 1051 (1984).
22) D. Singh, L. Bahadur, and M. V. Ramanamurti, *J. Soln. Chem.*, **6**, 703 (1977).
23) A. D'Aprano and R. M. Fuoss, *J. Phys. Chem.*, **67**, 1704 (1963); **67**, 1722 (1963).
24) R. Zwanzing, *J. Chem. Phys.*, **52**, 3675 (1970).
25) P. Hemmes, *J. Phys. Chem.*, **78**, 907 (1974).
26) A. D'Aprano and R. M. Fuoss, *J. Soln. Chem.*, **4**, 175 (1975).
27) D. F. Evans, T. Tominaga, J. B. Hubbard, and P. G. Wolynes, *J. Phys. Chem.*, **83**, 2669 (1979).
28) J. H. Chen and S. A. Adelman, *J. Chem., Phys.*, **72**, 2819 (1980).
29) J. B. Hubbard and R. F. Kayser, *J. Chem. Phys.*, **74**, 3535 (1981).
30) M. Nakahara and K. Ibuki, *J. Phys. Chem.*, **90**, 3026 (1986).
31) P. Singh, I. D. MacLeod, and A. J. Parker, *J. Soln. Chem.*, **13**, 103 (1984).
32) Silvia Schiavo, R. M. Fuoss, G. Narrosu, and G. Guida, *J. Soln. Chem.*, **8**, 557 (1979).
33) R. H. Cox and H. W. Terry, Jr., *J. Magn. Reson.*, **14**, 317 (1974).
34) J. F. Coetzee and W. R. Sharpe, *J. Soln. Chem.*, **1**, 77 (1972).
35) B. S. Krumgalz, *J. Soln. Chem.*, **11**, 283 (1982).
36) G. W. Stockton and J. S. Martin, *J. Am. Chem. Soc.*, **94**, 6921 (1972).
37) C. C. Addison, D. M. Amos, and D. Sutton, *J. Chem. Soc. A*, **9**, 2285 (1968).

 © 1988 The Chemical Society of Japan Bull. Chem. Soc. Jpn., 61, 2605—2608 (1988)

Electrical Conductance of a Mixture of Sodium and Potassium Thiocyanates in Aqueous Medium at 25 °C

Ratan Lal GUPTA and Kochi ISMAIL*
Department of Chemistry, North-Eastern Hill University,
Bijni Campus, Laitumkhrah, Shillong 793003, India
(Received September 28, 1987)

Electrical conductance measurements of $[x\mathrm{NaSCN}+(1-x)\mathrm{KSCN}]+R\mathrm{H_2O}$ system were made as functions of x and R at 25 °C. The mixed alkali effect was found to be negligible when $R>10$ and it increased sharply with increase in concentration in the range $R\leqslant 10$. The concentration dependence of molar conductance (Λ) has been described satisfactorily by the expression, $\Lambda=\Lambda_{FH}\exp(Bm+Cm^2)$ where Λ_{FH} is the Falkenhagen-Leist-Kelbg equation for Λ, m is the molality and the parameters B and C are the empirical constants.

In a glassy or molten medium containing mixed alkali ions deviations from additivity are observed in isotherms of various physical properties as a function of composition which is varied by progressively replacing one alkali ion by another.[1,2] This phenomenon is termed as the mixed alkali effect (MAE) and it is most pronounced for properties related to ionic transport. For instance, in glasses of constant alkali content the electrical conductivity of mixed glasses can be reduced by a factor of about 10^4 or 10^5 in comparison with the conductivity of single alkali glasses measured at the same temperature.[3] According to Ingram et al.[4] such large departures from additivity indicate a major breakdown of the principle of independent migration of ions which works well for dilute aqueous electrolytes.

Recently attempts have been made to look for MAE in media other than glassy or molten media. Aqueous medium is one of such suitable medium. There are some very old reports on the conductivities of mixed aqueous electrolytes containing alkali halides and nitrates.[5] In recent years only one report is made on the study of MAE in aqueous medium.[4] One of the characteristics of MAE is that it shows a complicated dependence on the total alkali ion concentration.[6] With a view to understanding better the dependence of MAE on the total alkali ion concentration we have made in the present study measurement of electrical conductance of a mixture of NaSCN and KSCN in aqueous medium with varying amounts of water.

Experimental

Molal solutions were prepared using recrystallized NaSCN (SD, R grade) and KSCN (SD, R grade). Before using these salts they were dried for several days over $CaCl_2$ in vacuum desiccator. Conductivity measurements were made using the CDM83 conductivity meter (Radiometer, Copenhagen) and a dip-type CDC304 conductivity cell. The instrument was calibrated by adjusting the cell constant knob of the instrument till the specific conductance value of the reference solution (0.1 M KCl (1 M=1 mol dm^{-3})) was displayed. For measuring density a calibrated glass pycnometer was used. All measurements were made in a thermostated (±0.02 °C) water bath.

Results and Discussion

The experimental values of molar conductance (Λ) at 25 °C of $[x\ \mathrm{NaSCN}+(1-x)\ \mathrm{KSCN}]+R\mathrm{H_2O}$ system as functions of x and R are presented in Table 1. The molar concentrations (c) of these solutions are also evaluated using the measured density values and are included in Table 1. The present values of Λ of NaSCN and KSCN solutions are found to be in good agreement with the reported data[7,8] as apparent from Fig. 1. In the case of KSCN solution since the literature values of Λ at 25 °C were not readily available, the comparison of the experimental and reported data[8] was made at 20 °C. The measured values of conductance were found to be reproducible within ±0.75% accuracy.

Variation of Λ with x. The variation of Λ with x at different R values is shown in Fig. 2. Λ tends to deviate more and more from additivity as R decreases. The non-additivity in Λ are represented here in terms of r-factor defined as $r=[x\Lambda_1+(1-x)\Lambda_2]/\Lambda$, where Λ_1 is

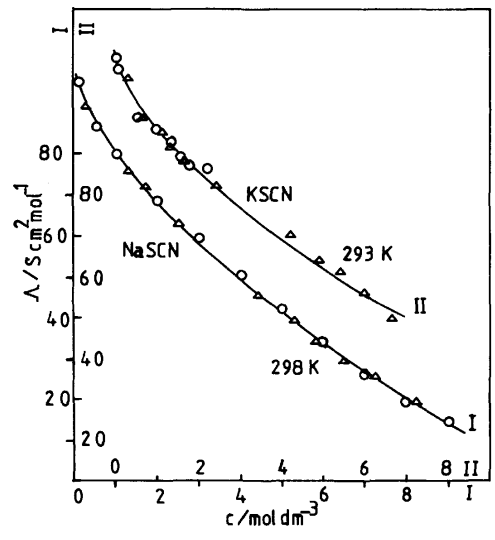

Fig. 1. Plots of Λ vs. molar concentration for NaSCN and KSCN solutions (Δ-experimental, O-reported).

Table 1. Molar Conductance of $[x\ NaSCN+(1-x)KSCN]+RH_2O$ System at 25 °C as Functions of x and R

x	$\Lambda \pm 0.75\%$/S cm² mol⁻¹				
	R=4	R=5	R=6	R=7	R=8
0.0	44.1	53.1	60.2	65.0	68.8
	(7.8275)	(6.8685)	(6.1212)	(5.4788)	(4.9751)
0.1	41.1	50.0	56.6	61.7	65.8
	(7.8902)	(6.898)	(6.1481)	(5.5052)	(5.0184)
0.2	37.8	46.5	53.1	58.3	62.4
	(7.9436)	(6.9511)	(6.1832)	(5.5310)	(5.0329)
0.3	34.5	43.2	49.6	54.8	58.1
	(8.0101)	(6.987)	(6.2264)	(5.5665)	(5.0591)
0.4	31.5	40.2	46.6	51.6	54.9
	(8.0733)	(7.0397)	(6.2246)	(5.5909)	(5.0913)
0.5	29.0	37.2	43.4	48.5	52.1
	(8.1166)	(7.0815)	(6.2838)	(5.6295)	(5.1169)
0.6	26.2	34.5	40.5	45.0	49.0
	(8.1845)	(7.1194)	(6.3132)	(5.678)	(5.1478)
0.7	24.5	32.0	37.1	41.9	46.4
	(8.2228)	(7.1529)	(6.3786)	(5.7185)	(5.1554)
0.8	22.4	29.6	34.4	38.8	43.5
	(8.2805)	(7.1959)	(6.4192)	(5.7601)	(5.226)
0.9	21.1	27.1	31.8	36.1	40.6
	(8.3073)	(7.2473)	(6.4659)	(5.7903)	(5.2509)
1.0	19.0	25.3	29.0	33.5	38.0
	(8.3774)	(7.2761)	(6.5308)	(5.8305)	(5.2775)

x	$\Lambda \pm 0.75\%$/S cm² mol⁻¹				
	R=10	R=20	R=30	R=100	R=200
0.0	75.4	89.3	95.8	108.2	—
	(4.2205)	(2.3948)	(1.6684)	(0.5324)	
0.1	72.2	86.3	—	—	110.3
	(4.2479)	(2.3968)			(0.2705)
0.2	68.7	83.2	90.0	103.4	108.8
	(4.2647)	(2.409)	(1.6738)	(0.5328)	(0.2705)
0.3	65.3	81.3	—	—	106.1
	(4.2835)	(2.4145)			(0.2708)
0.4	62.5	78.3	—	97.6	103.3
	(4.3022)	(2.4175)		(0.5334)	(0.2710)
0.5	59.1	76.3	83.8	95.5	101.5
	(4.3268)	(2.4325)	(1.6781)	(0.5338)	(0.2713)
0.6	56.0	73.1	81.2	93.0	100.1
	(4.341)	(2.4365)	(1.6812)	(0.534)	(0.2709)
0.7	53.2	—	79.3	—	97.2
	(4.3434)		(1.6849)		(0.2708)
0.8	50.1	67.4	77.2	86.6	95.6
	(4.3949)	(2.4546)	(1.6874)	(0.5342)	(0.2710)
0.9	47.6	64.7	75.0	85.3	—
	(4.3983)	(2.4603)	(1.6917)	(0.5351)	
1.0	45.1	62.7	71.1	82.4	90.8
	(4.4232)	(2.4801)	(1.6994)	(0.5359)	(0.2713)

Molar concentration data are within the parentheses.

the molar conductance of NaSCN solution and Λ_2 that of KSCN solution. The dependence of r on concentration is illustrated in Fig. 3 for x=0.5. r varies negligibly upto a particular concentration and thereafter increases sharply with increasing concentration. Similar trend in the variation of r-factor with R is found at other x values also. Such a dependence of r on R therefore clearly indicates that the MAE is dependent on the total alkali ion concentration. For the system under study the value of r appears to increase sharply above ca. 10R (ca. 5.6 m) concentration. It is interesting to note that this concentration falls in the range where the specific conductance of NaSCN solution becomes maximum. Moreover, in this concentration range the viscosity of NaSCN solution starts increasing exponentially with concentration.[7,9] Every electrolytic solution exhibits a particular concentration range of this type and it is identified as the region where a transition from primitive structure to quasi-crystalline structure takes

place.[10,11] For KSCN solution such a concentration range of structural transition falls around ca. 6R (ca. 9.2 m). In a mixed electrolyte containing NaSCN and KSCN a quasi-crystalline type structure may therefore be considered to start appearing from ca. 10R and the extent of quasi-crystallinity keeps on increasing beyond this concentration. Therefore in aqueous medium the MAE seems to become significant when the solution attains a quasi-crystalline type structure. This inference is in accordance with the empirical fact that the MAE is much prominant in the glassy media having very rigid-like structure. In the present system of interest the MAE observed for the highest concentration (=4R) studied is about 8.6%, i.e., the percentage of deviation of Λ from additivity.

The dependence of r-factor or MAE on concentration may be explained in terms of the anion polarization model.[12,13] According to this model, the MAE is due to the asymmetry created in the electrical field around the thiocyanate ion owing to its competitive polarization by the unlike cations. Such a competitive polarization can cause significant MAE only when the ionic concentration is large enough. Moreover, the effect of competitive polarization is expected to be maximum when the two cations are in equal concentration. This is, in fact, observed as evident from the plot (Fig. 3) of r vs. x which passes through a maximum in the range x=ca. 0.5.

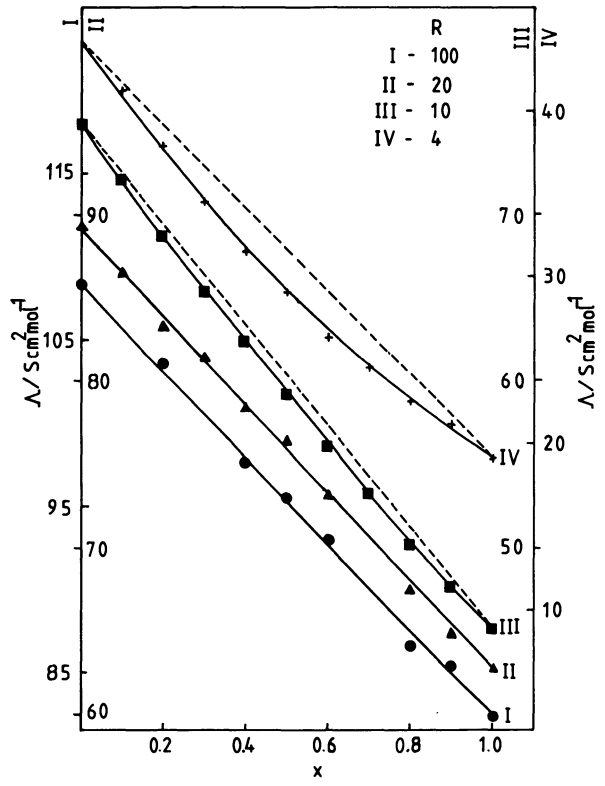

Fig. 2. Variation of Λ of [x NaSCN+(1−x)KSCN]+ RH$_2$O system with x at different R values.

Variation of Λ with R. A successful theoretical expression is not available to describe the concentration dependence of Λ in the higher concentration range. Recently we have reported[11] an expression of the form

$$\Lambda = A\exp(Bm + Cm^2) \quad (1)$$

for describing the conductance of aqueous electrolytes upto very high concentrations. In Eq. 1 A, B, and C are adjustable parameters. This equation was shown to be obtainable from the Adam-Gibbs configurational entropy model.[14] However, Eq. 1 was found to be only partly successful in describing the conductance data of concentrated aqueous solutions. The incomplete success of Eq. 1 was attributed to the fact that this expression accounts only for the short-range interactions in the solution. An attempt has been made here to improve Eq. 1 by accounting for the long-range interactions. This is achieved by substituting Λ_{FH} term for Λ where Λ_{FH} refers to the Falkenhagen-Leist-Kelbg[15] equation for Λ and is of the form

$$\Lambda_{FH} = (\Lambda_o - \frac{B_1c^{1/2}}{1 + B_oa_oc^{1/2}})(1 - \frac{B_2c^{1/2}F}{1 + B_oa_oc^{1/2}}) \quad (2)$$

B_1=82.501/$\eta_o(DT)^{1/2}$, B_2=82.04×10^4/$(DT)^{3/2}$, B_o=50.29/$(DT)^{1/2}$, and F=(exp(0.2929B_oa_o)−1)/0.2929B_oa_o. Λ_o is the equivalent conductance of the solution at infinite dilution, η_o is the vicosity of water, D is the dielectric constant of water, and T is the absolute temperature. a_o is a term which accounts for the finite size of the ions and is known as the ion-size parameter. The conductance data of the system under study were therefore least squares fitted to the equation

$$\Lambda = \Lambda_{FH}\exp(Bm + Cm^2). \quad (3)$$

For least-squares fitting the conductance data to Eq. 3,

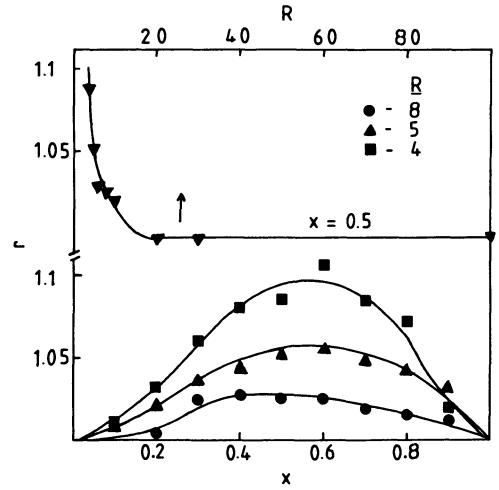

Fig. 3. Variation of r of [xNaSCN+(1−x)KSCN]+ RH$_2$O system with R and x.

Table 2. Best-Fit Values of the Parameters of Eq. 3 for the Molar Conductance of $[x\mathrm{NaSCN}+(1-x)\mathrm{KSCN}]+R\mathrm{H_2O}$ System at 25 °C

x	Λ_o/S cm^2 mol^{-1}	$a_o\times10^8$	B	$C\times10^2$	Std. dev. in Λ
0.0	139.6[a]	5.78	−0.0325	−0.1022	0.212
0.1	137.3[b]	5.05	−0.0293	−0.1394	0.270
0.2	135.0[b]	5.57	−0.0403	−0.0984	0.150
0.3	132.7[b]	5.28	−0.0418	−0.1193	0.511
0.4	130.4[b]	4.99	−0.0425	−0.1423	0.520
0.5	128.1[b]	5.25	−0.0490	−0.1338	0.877
0.6	125.7[b]	5.58	−0.0588	−0.1059	0.737
0.7	123.4[b]	5.57	−0.0661	−0.0791	0.999
0.8	121.1[b]	5.31	−0.0677	−0.1026	1.4111
0.9	118.8[b]	5.43	−0.0780	−0.0499	1.478
1.0	116.5[a]	5.27	−0.0798	−0.0799	1.257

a) Literature value. b) Estimated values using additivity principle.

we have chosen in the case of solutions with $x=0$ and $x=1$ the reported values of Λ_o and for compositions with x values other than 0 or 1 the Λ_o values are estimated using the additivity principle. Therefore Eq. 3 becomes an expression with three adjustable parameters. The best-fit values of a_o, B, and C corresponding to the lowest standard deviations were computed and are given in Table 2.

The value of a_o=5.27 Å for NaSCN solution is comparable with the value 5.5 Å reported for this solution by Janz et al.[7] The higher value for a_o= 5.78 Å of KSCN is expected due to the larger ionic size of the K^+ ion. For the mixed electrolyte, however, no regular trend in the variation of a_o with x has been observed. It may be pointed out as suggested by others[17] also that a_o behaves more like an adjustable parameter than a physically significant parameter.

The value of B appears to decrease with increasing x. A comparison of Eq. 3 with the Wishaw-Stokes[18] equation reveals that the exponential part of Eq. 3 is related to the viscosity of the solution. Accordingly, a decrease in the value of B with increasing x appears to be due to the increasing viscosity of the solution as the content of NaSCN increases. We also made an attempt to estimate the viscosity of NaSCN solution at different concentrations by equating $\exp(Bm+Cm^2)$ to the reciprocal of the relative viscosity. The viscosity of NaSCN solution estimated in this fashion was found to be in agreement with the experimental values[7] only at lower concentrations. This envisages that the Wishaw-Stokes equation[18] can describe the conductance data only at concentrations where the relative viscosity is low.[19] Furthermore, it may be seen that Eq. 3 reduces to the form of Postler equation[20] at low concentrations.

We acknowledge the financial support received from the Council of Scientific & Industrial Research (New Delhi) to carry out this work.

References

1) J. O. Isard, *J. Non-Cryst. Solids*, **1**, 235 (1969).
2) D. E. Day, *J. Non-Cryst. Solids*, **21**, 343 (1976).
3) L. P. Boesch, Ph. D. Thesis, Catholic University of America (1975).
4) M. D. Ingram, K. King, D. Kranbuehl, and M. Adel-Hadadi, *J. Phys. Chem.*, **85**, 289 (1981).
5) P. V. Rysselberghe and L. Nutting, *J. Am. Chem. Soc.*, **59**, 333 (1937).
6) C. T. Moynihan, *J. Electrochem. Soc.*, **126**, 2144 (1979).
7) G. J. Janz, B. G. Oliver, G. R. Lakshminarayanan, and G. E. Mayer, *J. Phys. Chem.*, **74**, 1285 (1970).
8) R. C. Weast, "Handbook of Chemistry and Physics," 58th ed, CRC Press, Cleveland, OH (1977).
9) M. L. Miller and M. Doran, *J. Phys. Chem.*, **60**, 186 (1956).
10) S. Mahiuddin and K. Ismail, *J. Phys. Chem.*, **87**, 5241 (1983).
11) S. Mahiuddin and K. Ismail, *J. Phys. Chem.*, **88**, 1027 (1984).
12) C. T. Moynihan and R. W. Laity, *J. Phys. Chem.*, **68**, 3312 (1964).
13) C. T. Moynihan, "Ionic Interactions," ed by S. Petrucci, Academic Press, New York (1971), Vol. I, p. 261.
14) G. Adam and J. H. Gibbs, *J. Chem. Phys.*, **43**, 139 (1965).
15) H. Falkenhagen, M. Leist, and G. Kelbg, *Ann. Phys.*, **6**, 51 (1952).
16) A. L. Horvath, "Handbook of Aqueous Electrolyte Solutions," Ellis Horwood Ltd., West Sussex (1985).
17) N. P. Yao and D. N. Bennion, *J. Phys. Chem.*, **75**, 3586 (1971).
18) B. F. Wishaw and R. H. Stokes, *J. Am. Chem. Soc.*, **76**, 2065 (1954).
19) M. D. Monica, A. Ceglie, and A. Agostiano, *Electrochim. Acta*, **29**, 933 (1984).
20) M. Postler, *Collec. Czech. Chem. Commun.*, **35**, 535 (1970).

 © 1988 The Chemical Society of Japan Bull. Chem. Soc. Jpn., 61, 2609—2613 (1988)

Molecular Orbital Treatment of Some Amino Acids

R. Abu-Eittah,*,† A. Obaid, S. Basahl, and E. Diefallah
Department of Chemistry, Faculty of Science, King Abdulaziz University, Jeddah, Saudi Arabia
(Received October 14, 1987)

INDO-molecular orbital calculations have been performed on a number of amino acids, namely, alanine, phenylalanine, some tyrosines and histidine. Computations on *N*-acetylhistidine are included for comparison. The results obtained for the charge densities and dipole moments were used to get a "structure-function" correlation.

Proteins perform virtually all types of work in an organism. The standard amino acids, constituting proteins, differ only with respect to their side chain. Each side chain is so specific that it cannot be replaced by another one.

Several CNDO/2 calculations predict that the neutral form of glycine is more stable than the ionic form.[1-3] Conformational analysis performed with CNDO/2[4-7] and INDO[8] as well as the corresponding ab initio calculations,[9-11] reveals a number of interesting results. CNDO/2 calculations on systems of two, three, and four members (-$CONHCH_2$-) were carried out and the most stable conformation of glycine trimer was predicted.[5] Cooperative conformational studies have been carried out on glycine.[12]

Luke et al.[13] have studied the STO-3G and STO-3G* optimized structures of glycine and found that it has three or four low-lying stable conformations. The molecule can easily rearrange to any of them. Intermediate water structures in the solution of alanine dipeptide were investigated.[14] With the ST2 water model, the solute, alanine dipeptide, is hydrated.

Ladik et al.[15] have presented some new results on the quantum mechanical investigation using localized orbitals of DNA. The results show an excellent localization of the occupied orbitals and a rather good one for the virtuals (both for the σ- and π-orbitals) of the four nucleotide bases. Interaction energy calculations between a polyglycine chain in different conformations and polynucleotide chain were performed.

In the last years, substantial progress has been achieved in the quantum mechanical investigation of DNA including the water and ion structure around it,[16] and band structure calculations using a whole nucleotide as a unit cell.[17] Pilot calculations have been performed to assess the effect of water structure on a nucleotide base stack[18] for the investigation of polynucleotide-polypeptide (polyglycine) interaction[19] and for the treatment of a periodicity in DNA macromolecules.[20]

The negative factor counting technique in its ab initio form[21] was used to calculate the total density of states of nonperiodic polynucleotides and polypeptides.[22] Computations were performed on a periodic and nonperiodic poly(-gly-cys-asp-ser-) chain.

A number of theoretical investigations have been devoted to the determination of the energy band stuctures and of the possible pathway for electron delocalization in proteins.[23] All calculations were represented by the very simple periodic models, mostly poly(gly) with the exception of MINDO/3 all-valence electron crystal orbital calculations of aperiodic β-polypeptide.[24] The effect of some factors on the energy band structure on some protein models was calculated with the aid of the CNDO/2 crystal orbital method.[25]

In this work INDO-molecular orbital calculations have been carried out on a number of amino acids in an attempt to understand the "structure-function" relationship for them. Such a study has not been reported before.

Method of Calculations. INDO-CI procedures have been followed, details and parameterization of the procedures are found elsewhere.[26] Interaction was considered between nine configurations which correspond to electronic transitions between the three highest occupied molecular orbitals and the three lowest unoccupied molecular orbitals.

Results and Discussion

A. Alanine and Phenylalanine. Alanine is considered as the α-amino acid with the smallest nonpolar side chain whereas phenylalanine is the amino acid with the largest nonpolar side chain. Figure 1 shows the configuration used in MO calculations with the INDO values of total charge in units of 10^{-3} e. Table 1 gives the values of some of the calculated parameters. It can be seen that phenylalanine has a weaker dipole than alanine indicating that the polarization of the benzene ring is in the opposite direction to that of the -COOH group. The total charge densities on the groups: $-NH_2$, -OH, and -COOH are only slightly higher than they are in alanine. This result explains the fact that phenylalanine is a stronger acid (K_a=6.7×10^{-3}) than alanine (K_a=4.89×10^{-3}).[27] The built up of a slight negative charge on the benzene ring (0.052) suggests that phenylalanine can act as electron donor as well as an electron acceptor.

† Present adress: Department of Chemistry, Faculty of Science, University of Cairo, Giza-Egypt.

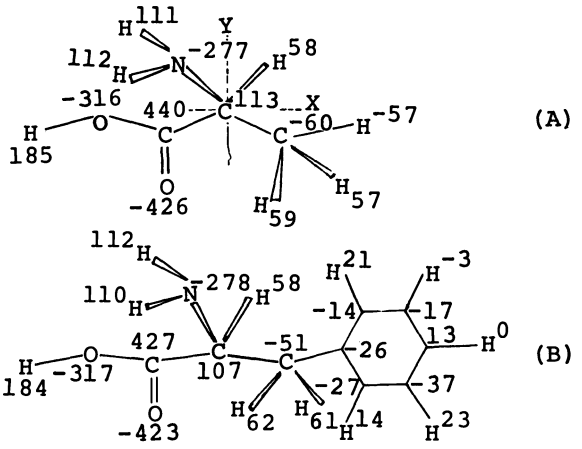

Fig. 1. Configuration and total charge density($\times 10^3$) on: (A) alanine, (B) phenylalanine.

Figures 2 and 3 show the electronic absorption spectra of alanine and phenylalanine using methanol as a solvent. A weak band appears in the spectrum of alanine (240—290 nm) which agrees satisfactory with the calculated transition energy (3.88 eV). The spectrum of phenylalanine shows two absorption bands, the lower energy one (ca. 260 nm) shows the characteristic vibrational components of the $^1L_b \leftarrow {}^1A$ transition of the benzene nucleus. The correspondance between the calculated (4.91, 5.70 eV) and the experimental (4.81, 5.90 eV) transition energies is satisfactory.

B. Tyrosine and Hydroxytyrosines. Figures 4A,B and 5 show the configurations of the molecules and the calculated total charge density in units 10^{-3} e. Table 2 gives the values of the calculated parameters. It can be seen that tyrosines have strong dipoles and hence their position and sequence in proteins is totally different from those of alanine and phenyl-

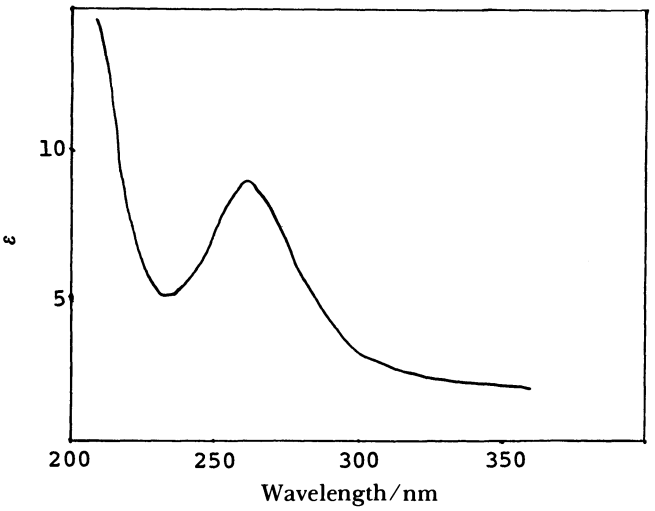

Fig. 2. Electronic absorption spectrum of alanine in methanol.

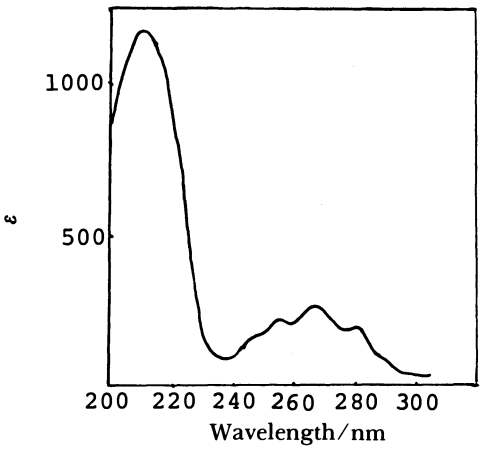

Fig. 3. Electronic absorption spectrum of phenylalanine in methanol.

Table 1. Values of Calculated Parameters of Alanine and Phenylalanine

Calcd parameter	Alanine	Phenylalanine
Dipole moment, *D*		
atomic[a]	1.6555	1.5009
polarization[b]	2.0866	1.9098
total	2.5622	2.2909
Total charge density ($\times 10^3$ e)		
$-NH_2$	−56	−57
-OH	−130	−133
-COOH	−126	−130
Ph ring	—	−52
Energy/eV		
HOMO	−10.2289	−9.3201
LUMO	−0.3975	−0.8001
Transition energy and Osc. str.	3.88(0.01)	4.90(0.12)
	7.80(0.08)	5.70(0.54)

a) $\vec{\mu}_{ch}$. b) $\vec{\mu}_{hyb}$ (Ref. 26).

Table 2. Values of Calculated Parameters of the Studied Tyrosines

Parameter	Tyrosine	3-Hydroxytyr	3,5-Dihydroxytyr
Dipolemoment, *D*			
atomic	1.9437	2.1552	2.2027
polarization	2.7567	3.5154	4.6785
total	4.1873	5.1414	6.6757
Total charge density ($\times 10^3$ e)			
$-NH_2$	−57	−57	−57
-OH	−134	−134	−133
-COOH	−131	−132	−131
-OH(a)[a]	−136	−131	−125
-OH(b)	—	−96	−95
-OH(c)	—	—	−136
-Ph ring	89	184	256
-Side Chain[b]	−47	−43	−100
Energy/eV			
HOMO	−9.4268	−9.3141	−9.2292
LUMO	−0.8692	−0.9555	−1.0378
Trans. energy and Osc. str.	5.04(0.01)	4.70(0.03)	4.79(0.01)
	5.48(0.56)	5.51(0.50)	5.36(0.60)
	6.17(0.45)	6.15(0.50)	6.18(0.50)

a) See Figs. 4A, B and 5. b) Net total charge on the side chain.

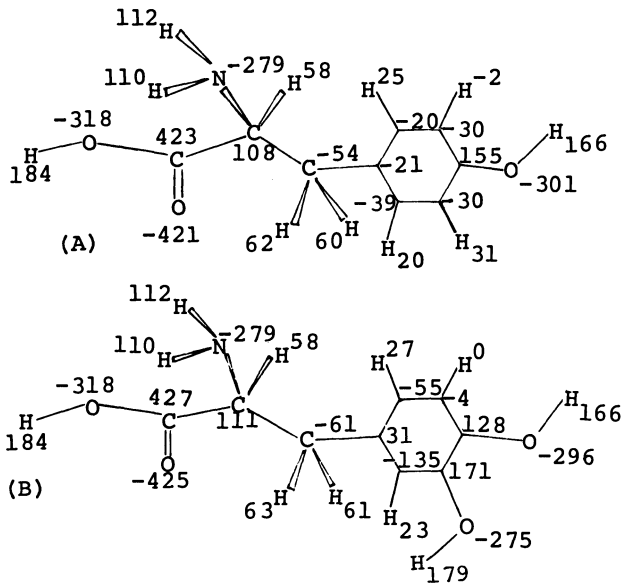

Fig. 4. Configuration and total INDO charge density($\times 10^3$ e): (A) tyrosine, (B) 3-hydroxytyrosine.

alanine. The charge densities on different functional groups ($-NH_2$, -OH, and -COOH) did not differ significantly from tyrosine to hydroxytyrosines. However, a net negative charge is built up on the side chain and increases in the order: 3,5-dihydroxytyrosine>tyrosine>3-hydroxytyrosine. On the other hand a net positive charge is built on the benzene ring and increases in the order: 3,5-dihydroxytyrosine>3-hydroxytrosine>tyrosine. Tyrosine is a much stronger acid ($K_{a_1}=6.7\times10^{-3}$) than 3-hydroxytyrosine ($K_{a_1}=1.32\times10^{-5}$).

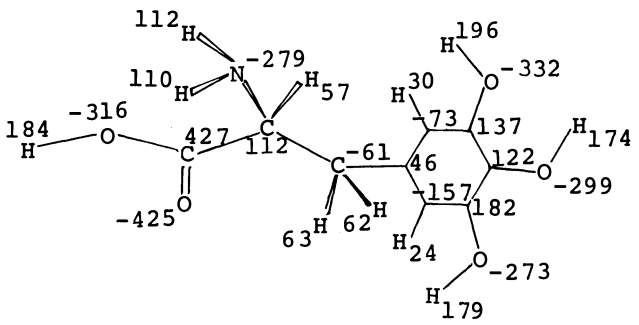

Fig. 5. Configuration and total INDO charge density($\times 10^3$ e) for 3,5-dihydroxytyrosine.

Figure 6 shows the absorption spectrum of tyrosine in methanol. Two electronic transitions are observed and correspond to the $^1L_b \leftarrow {}^1A$ and $^1L_a \leftarrow {}^1A$ of the perturbed benzene nucleus. The correspondance between the observed transition energies (4.51, 5.51 eV) and the calculated (5.04, 5.48) seems to be satisfactory.

C. Histidine and *N*-Acetylhistidine. The presence of imidazole ring in the side chain of histidine is a determining factor in the properties of histidine. Table 3 gives the calculated parameters and Fig. 7 shows the total charge density on the different atoms of the molecule. Computations on *N*-acetylhistidine are included for comparison. Acetylation led to a pronounuced increase in the dipole moment and a decrease of charge density on the imidazole ring compared to histidine.

The results of calculations (Table 3) show that histidine has a much stronger dipole than tyrosine or

Table 3. Numerical Values of the Calculated Parameters of Histidine and *N*-Acetylhistidine

Parameter	Histidine	*N*-Acetylhistidine
Dipole moment, *D*		
atomic	4.2880	6.8581
polarization	2.5580	3.1215
total	6.3829	9.8934
Total charge density ($\times 10^3$ e)		
$-NH_2$	−157	−158(-NH)
-OH	−167	−175
-COOH	−226	−242
Imidazole ring	−147	−35
Energy/eV		
HOMO	−9.1263	−9.0382
LUMO	−2.3710	−2.4539
Trans. Energy and Osc. Str.	3.97(0.003)	4.01(0.02)
	4.87(0.001)	5.19(0.37)
	5.21(0.37)	5.86(0.02)
	6.09(0.01)	5.99(0.02)
	6.22(0.39)	6.70(0.05)

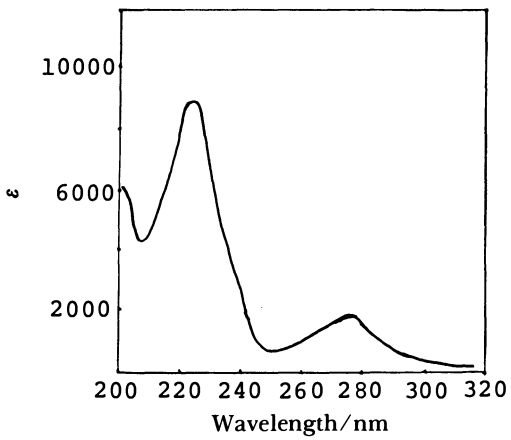

Fig. 6. Electronic absorption spectrum of tyrosine in methanol.

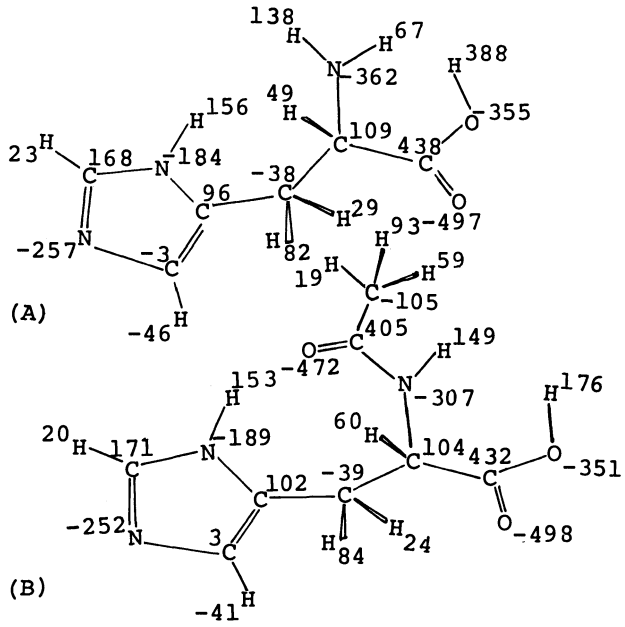

Fig. 7. Configuration and INDO total charge density($\times 10^3$ e): (A) histidine, (B) *N*-acetylhistidine.

hydroxytyrosine. This explains the activity of the acid and its existence in the most active center of the enzyme. The net negative charge built on the functional groups is higher than on the same groups in tyrosine and hydroxytyrosines. A net negative charge is built on the imidazole ring of histidine contorary to the net positive charge built on the benzene ring of phenylalanine and tyrosines. Histidine can act as an electron donor.

The electronic absorption spectrum of histidine (Fig. 8) shows two electronic transitions at 3.97 and 5.21 eV which corresponds nicely with the calculated (3.97 and 5.21 eV).

Conclusion

The position and function of the amino acid in the protein series is dependent on its electronic structure in addition to other properties as size, geometry and nature of its side chain. The results of this work explains many experimental observations. Calculations showed that phenylalanine has a weaker dipole than alanine. There is a weak built up of negative charge density on the benzene nucleus (−0.052) and this renders phenylalanine to act as an electron donor as well as an electron acceptor. Phenylalanine is a stronger acid than alanine which could be due to the higher charge densities of the functional groups in phenylalanine.

Tyrosines have strong dipoles and this determines their position in the protein series. A net positive charge is built on the benzene nucleus and tyrosines

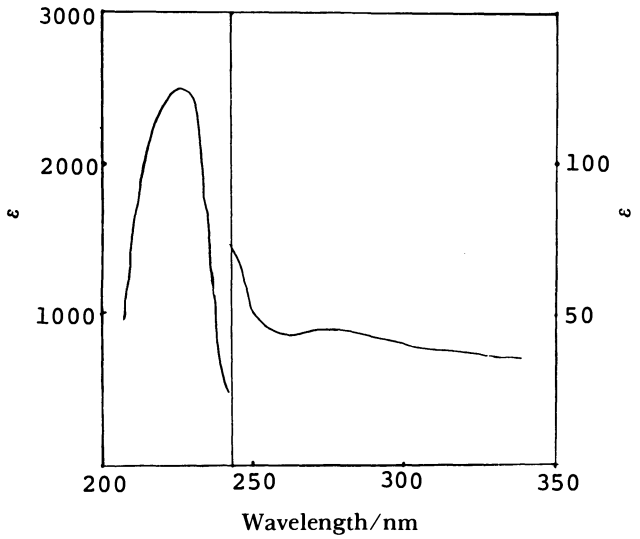

Fig. 8. Electronic absorption spectrum of histidine in methanol.

act as electron acceptors. The theoretical results account for the activity of histidine and its existence at the active center of the enzyme. Histidine can act as an electron donor, a net negative charge is built on its imidazole ring. Acetylation decreases this charge.

References

1) A. Imamura, H. Fujita, and C. Nagata, *Bull. Chem. Soc. Jpn.*, **42**, 3118 (1969).
2) B. Pullman, J. L. Conbeils, D. Conveira, and D. Perahia, *Theore. Chim. Acta*, **22**, 11 (1971).
3) W. R. Oegerle and J. R. Sabin, *J. Mol. Struct.*, **15**, 131 (1973).
4) H. Fujita and I. Imamura, *J. Chem. Phys.*, **53**, 4555 (1970).
5) K. Morkuma, *Chem. Phys. Lett.*, **9**, 129 (1971).
6) M. Bossa, A. Damiani, R. Fidenzi, S. Gili, R. Leli, and G. Ramcenni, *Theoret. Chim. Acta*, **20**, 299 (1971).
7) J. Ladik, *Int. J. Quantum Chem., Quantum Biol. Symp.*, **1**, 5 (1974).
8) D. L. Beveridge, I. Jan, and J. Ladik, *J. Chem. Phys.*, **56**, 4744 (1972).
9) H. Berthod and A. Pullman, *Chem. Phys. Lett.*, **14**, 217 (1972).
10) D. A. Kleier and W. N. Lipscomb, *Int. J. Quantum Chem., Quantum Biol. Symp.*, **4**, 73 (1977).
11) L. L. Shipman and R. E. Christoffersen, *J. Am. Chem. Soc.*, **95**, 1408 (1973).
12) C. Petrongolo, *Gazz. Chim. Ital.*, **108**, 445 (1978).
13) B. T. Luke, A. G. Gupta, G. H. Loew, J. G. Lawless and D. H. White, *Int. J. Quantum Chem., Quantum Biol. Symp.*, **11**, 117 (1984).
14) C. No Yoon and Mu S. Jhon, *Int. J. Quantum Chem., Quantum Biol. Symp.*, **12**, 33 (1986).
15) J. Ladik, P. Otto, and W. Forner, *Int. J. Quantum Chem., Quantum Biol. Symp.*, **10**, 73 (1983).
16) E. Clementi, "Structure and Dynamics of Nucleic Acids and Proteins," ed by E. Clementi and H. Sharma, Adenine Press, Philadelphia (1983); E. Clementi, "Computational techniques for large Chemical Systems," in "Lecture Notes in Chemistry," Vol. 19, Springer-Verlag, Berlin (1980); G. Corongiu and E. Clementi, *Biopolymers*, **20**, 551 (1981).
17) J. Ladik and S. Suhai, *Inter. J. Quantum Chem., Quantum Biol. Symp.*, 181 (1980).
18) P. Otto, J. Ladik, G. Corongiu, S. Suhai, and W. Ferner, *J. Chem. Phys.*, **77**, 5026 (1982).
19) P. Otto, E. Clementi, J. Ladik, and F. Martino, *J. Chem. Phys.*, **80**, 5294 (1984).
20) R. S. Day and J. Ladik, *Inter, J. Quantum Chem.*, **21**, 917 (1982).
21) R. S. Day and F. Martino, *Chem. Phys. Lett.*, **84**, 86 (1981); J. Ladik, *Int. J. Quantum Chem.*, **23**, 1073 (1983).
22) J. Ladik, P. Otto, A. K. Bakhshi, and M. Seel, *Int. J. Quantum Chem.*, **29**, 597 (1986).
23) J. Ladik, "Electronic Structure of Polymers and Molecular Crystals," ed by J.-M. Ander and J. Ladik, Plenum, New York (1975), p. 663.
24) S. Suhai, J. Kasper, and J. Ladik, *Int. J. Quantum Chem.*, **17**, 995 (1980).
25) Xiao Yi and ChenRun-Sheng, *Int. J. Quantum Chem.*, **28**, 573 (1985).
26) J. A. Pople and D. L. Beveridge "Approximate Molecular Orbital Theory," McGrawhill, New York (1970).
27) A. E. Martel and R. M. Smith, "Critical Stability Constants," Vol. 5, First Sublement, Plenum Press, New York (1982).

Complete Computer Analysis of NQR Data

Bolesław NOGAJ†
Institute of Physics, A. Mickiewicz University, Grunwaldzka 6, 60-780 Poznań, Poland
(Received June 6, 1987)

Theories explaining temperature dependences of frequency, line width and spin-lattice relaxation times in Nuclear Quadrupole Resonance (NQR) spectroscopy have been presented in the form of mathematical expressions. Hence a complete analysis of experimental data can easily be implemented on any microcomputer. This was demonstrated by the results obtained from ^{35}Cl NQR studies of *p,p'*-DDT. The computer analysis allowed to separate different mechanisms of quadrupole relaxation and determine characteristic parameters: moments of inertia of the molecule, librational frequencies and activation energies of rotating molecular groups. Besides numerical values, the printer working with the computer can produce plots of experimental points in different coordinate systems as well as the fit curves.

The parameters most frequently studied in NQR spectroscopy are the resonance frequency (ν_Q), line width ($\delta\nu_Q$), and spin-lattice relaxation time (T_1). Temperature studies of these parameters allow for determination of molecular dynamics in solids, mainly librations and hindered rotations of atomic groups. There are many theories relating individual spectroscopic parameters to molecules and their dynamics. All these theories can be expressed as more or less complex mathematical formulas. The accurate fit of experimental results to these expressions allows for a direct determination of physical parameters of interest. The aim of this paper is to show that the complete numerical and graphical analysis of NQR data can successfully be achieved on any accessible microcomputer.

Temperature Dependences of Basic Parameters in NQR Spectroscopy

Let us consider the influence of molecular motions on individual parameters of NQR spectrum studied as a function of temperature. As is known from infrared studies, the librational frequencies in molecular crystals range from 10^{11} Hz to 10^{13} Hz, so they exceed considerably the NQR frequencies of 10^6—10^8 Hz. Therefore the librational motions cause only an averaging of electric field gradient seen by the resonant nuclei. Bayer[1] assumed that NQR frequency decreases with increasing temperature only due to an increase in the amplitude of librational motions. He treated a molecule as a quantum harmonic oscillator and obtained the following expression for a temperature dependence of NQR frequency:

$$\nu_Q(T) = a - \frac{b}{\exp(c/T) - 1}, \tag{1}$$

$$a = \nu_Q(0), \tag{2}$$

$$b = \frac{6\hbar\nu_Q(0)}{4I\omega_l - 3\hbar}, \tag{3}$$

$$c = \frac{\hbar\omega_l}{k}. \tag{4}$$

$\nu_Q(0)$ is the NQR frequency at 0 K, I is the relevant moment of inertia, ω_l is the librational frequency of the molecule. However, experiments have yielded only qualitative agreement with Bayer's theory. Better agreement with the theory could have been obtained if other types of molecular vibrations as well as thermal expansion had been taken into account. This has been done by Kushida, Benedek and Bloembergen (KBB),[2] who have come to the following relation:

$$\nu_Q(T) = a_0 + a_1T + a_2T^{-1}, \tag{5}$$

$$a_0 = \nu_Q^S, \tag{6}$$

$$a_1 = -\frac{3}{2}k\nu_Q^S\sum_{i=1}^{M}\frac{A_i}{\omega_i^2}, \tag{7}$$

$$a_2 = -\frac{\hbar^2}{8k}\nu_Q^S\sum_{i=1}^{M}A_i, \tag{8}$$

where ν_Q^S is the resonance frequency in a fictitious "static" lattice, ω_i is the frequency of the i-th lattice vibrational mode, and A_i is a coefficient which for librations is equal to the reciprocal of the relevant moment of inertia.

A few years later Brown[3] took into account anharmonicity of librations, assuming a linear temperature dependence of librational frequency:

$$\omega_i = \omega_i^0(1 - g_iT). \tag{9}$$

Moreover Brown limited his considerations to the appropriately high temperatures for which the term a_2T^{-1} of Eq. 5 can be neglected. Under this assumption he obtained:

$$\nu_Q(T) = a_0 + a_1T + a_2T^2, \tag{10}$$

$$a_0 = \nu_Q(0), \tag{11}$$

$$a_1 = -\frac{3}{2}k\nu_Q(0)\sum_{i=1}^{M}\frac{A_i}{(\omega_i^0)^2}, \tag{12}$$

$$a_2 = -3k\nu_Q(0)\sum_{i=1}^{M}\frac{g_iA_i}{(\omega_i^0)^2}. \tag{13}$$

† For correspondence: Solid State Spectroscopy Laboratory, Institute of Physics, A. Mickiewicz University, Grunwaldzka 6, 60-780 Poznań, Poland.

As this dependence describes quite well most of experimentally obtained data $\nu_Q(T)$ for the temperatures above 77 K, we attempted to extend this approach to study the influence of molecular motions on NQR frequency in the temperatures lower than 77 K. After the calculations similar to those of Brown[3] and taking into account the term a_2T^{-1} in Eq. 5 we have come to:

$$\nu_Q(T) = a_0 + a_1T + a_2T^2 + a_3T^{-1}, \quad (14)$$

$$a_0 = \nu_Q^S, \quad (15)$$

$$a_1 = -\frac{3}{2}k\nu_Q^S\sum_{i=1}^{M}\frac{A_i}{(\omega_i^0)^2}, \quad (16)$$

$$a_2 = -3k\nu_Q^S\sum_{i=1}^{M}\frac{g_iA_i}{(\omega_i^0)^2}, \quad (17)$$

$$a_3 = -\frac{\hbar^2}{8k}\nu_Q^S\sum_{i=1}^{M}A_i. \quad (18)$$

In IR and Raman spectroscopy the square dependence of librational frequency on temperature has been observed for a significant number of compounds:

$$\omega_i = \omega_i^0(1 - g_iT - f_iT^2). \quad (19)$$

Taking into account Eq. 19 in our calculations we obtain:

$$\nu_Q(T) = a_0 + a_1T + a_2T^2 + a_3T^3, \quad (20)$$

$$a_0 = \nu_Q(0), \quad (21)$$

$$a_1 = -\frac{3}{2}k\nu_Q(0)\sum_{i=1}^{M}\frac{A_i}{(\omega_i^0)^2}, \quad (22)$$

$$a_2 = -3k\nu_Q(0)\sum_{i=1}^{M}\frac{g_iA_i}{(\omega_i^0)^2}, \quad (23)$$

$$a_3 = -3k\nu_Q(0)\sum_{i=1}^{M}\frac{f_iA_i}{(\omega_i^0)^2}. \quad (24)$$

Equation 20 can be applied to appropriately high temperatures similarly as the Brown's relation—Eq. 10. Extending the above treatment of the influence of librations on NQR spectrum to very low temperatures we obtain:

$$\nu_Q(T) = a_0 + a_1T + a_2T^2 + a_3T^3 + a_4T^{-1}, \quad (25)$$

$$a_0 = \nu_Q^S, \quad (26)$$

$$a_1 = -\frac{3}{2}k\nu_Q^S\sum_{i=1}^{M}\frac{A_i}{(\omega_i^0)^2}, \quad (27)$$

$$a_2 = -3k\nu_Q^S\sum_{i=1}^{M}\frac{g_iA_i}{(\omega_i^0)^2}, \quad (28)$$

$$a_3 = -3k\nu_Q^S\sum_{i=1}^{M}\frac{f_iA_i}{(\omega_i^0)^2}, \quad (29)$$

$$a_4 = -\frac{\hbar^2}{8k}\nu_Q^S\sum_{i=1}^{M}A_i. \quad (30)$$

As follows from the above theories, the accurate fit of experimentally obtained NQR frequencies vs. temperature to the relations found allows one to determine the librational frequencies and the corresponding moments of inertia of the molecules studied.

The other NQR spectroscopy parameters—the line width ($\delta\nu_Q$) and spin-lattice relaxation time (T_1)—are sensitive to greater changes in electric field gradient caused by hindered rotations of (i) atomic groups or molecules including the resonant nuclei or (ii) atomic groups or molecules situated in the neighborhood of the resonant nuclei. In general, we can state that the line width is a resultant effect of static broadening (both electric and magnetic) associated with a crystal lattice, and dynamic broadening associated with some kind of motion (e.g., with a hindered rotation). If the resonant nuclei rotate, the line becomes broadened, and if neighboring groups containing protons rotate the NQR line narrows. In general, the line width observed can be expressed as:[4,5]

$$(\delta\nu_Q)^{observ.} = (\delta\nu_Q)^{static} + (\delta\nu_Q)^{narrow.} + (\delta\nu_Q)^{broad.}, \quad (31)$$

$$(\delta\nu_Q)^{narrow.} = -A\exp(-E_a'/RT), \quad (32)$$

$$(\delta\nu_Q)^{broad.} = B\exp(-E_a/RT), \quad (33)$$

where A and B are constants and E_a and E_a' are the activation energies for hindered rotations analyzed, R is the gas constant.

Let us now consider the nuclear quadrupole spin-lattice relaxation. According to Bayer[1] as well as Woessner and Gutowsky[6] the fluctuations of electric field gradient caused by librational motions lead to the following relation between the relaxation time T_1 and temperature (T):

$$T_1^{-1} = aT^n \quad (34)$$

where a is a constant and $n\approx2$.

Abrupt changes in electric field gradient due to hindered rotation of molecular groups containing quadrupole nuclei (e.g., CCl_3 group) lead to the exponential temperature dependence of the relaxation time:[7]

$$T_1^{-1} = b\exp(-E_a/RT) \quad (35)$$

where b is a constant, E_a is the activation energy for hindered rotation.

If atomic groups in the neighborhood of the resonating nuclei undergo a rotation with a frequency close to the observed NQR freguency, then in the temperature dependence of T_1 a so-called modulation minimum is observed that can be described by the formula:[6,8]

$$T_1^{-1} = [d\exp(E_a'/RT) + g\exp(-E_a'/RT)]^{-1} \quad (36)$$

where

$$d = 3\tau_0\left(\frac{q'_{zz}}{q_{zz}}\right)^{-2}, \quad (37)$$

$$g = \frac{3}{\omega_Q^2\tau_0}\left(\frac{q'_{zz}}{q_{zz}}\right)^{-2}. \quad (38)$$

E'_a is the activation energy for hindered rotation of the corresponding molecular groups, τ_0 is the correlation time at infinitely high temperature, and q'_{zz} is the contribution of motions of adjacent groups or molecules to the whole electric field gradient q_{zz}.

The Application of Microcomputer in Analysis of NQR Data

After discussion of the present theories we may state that in most cases the fit of experimental data to the above relations is sufficient for determination of searched parameters. All these relations have been reduced to a few general equations:

$$y = a - b[\exp(c/x) - 1]^{-1} \quad (39)$$

$$y = a_0 + a_1x + a_2x^2 + \cdots + a_px^p \quad (40)$$

$$y = a_0 + a_1x + a_2x^2 + \cdots + a_{p-1}x^{p-1} + a_px^{-1} \quad (41)$$

$$y^{-1} = ax^n \quad (42)$$

$$y^{-1} = b\exp(-c/x) \quad (43)$$

$$y^{-1} = ax^n + b\exp(-c/x) + A[d\exp(f/x) + g\exp(-f/x)]^{-1} + B[k\exp(m/x) + l\exp(-m/x)]^{-1} \quad (44)$$

$$y = h + d\exp(f/x) + g\exp(-m/x) \quad (45)$$

Eqs. 39—41 refer to the NQR frequency, Eqs. 42—44 to the T_1 relaxation time and Eq. 45 to the NQR line width.

A SINCLAIR ZX81 microcomputer with a memory extended to 64 kB and with High Resolution Graphics add-on was used to do all the calculations. The programs prepared in ZX81 BASIC are based on the standard least squares approximation and the gradient method. The programs applied allow to determine the parameters of interest as well as the quality of the fit by error analysis. The quality of the fit may also be observed on the monitor, as the fit curve is displayed together with the experimental points. The diagrams may be plotted in the following systems of coordinates: x, $\ln x$, $1/x$, x^n (the same refers to the y axis). Each diagram seen on the monitor may be copied by a printer. Experimental data may be entered manually or loaded from a cassette-recorder.

An Example of NQR Data Analysis

The computer analysis will be demonstrated by results obtained from ^{35}Cl NQR studies of *p,p'*-DDT/1,1,1-trichloro-2,2-bis(*p*-chlorophenyl)ethane; $CCl_3CH(C_6H_4Cl)_2$/. The ^{35}Cl NQR data for *p,p'*-DDT include all the effects discussed previously. We deal here with hindered rotation of the resonant nuclei (CCl_3 groups) and with the influence of rotating neighboring groups (phenyl rings). The motion of phenyl rings leads to a narrowing of ^{35}Cl NQR line, while the hindered rotation of CCl_3 groups is observed as a rapid broadening of the resonance lines. In the temperature dependences of the relaxation times we observe two modulation minima due to the rotating phenyl rings. Molecular dynamics of *p,p'*-DDT and the results of ^{35}Cl NQR studies are reported in more

Table 1. Parameters of the Fit of Experimental $\nu_Q^3(T)$ Values for *p,p'*-DDT to the Proper Theories-Formulas: Eqs. 1, 5, 10, 14, 20, and 25. For the Sake of Clarity All Parameters Standing at T^{-1} in Formulas Are Denoted by a Common Symbol d

Formula	Notation of $\nu_Q(T)$ curves in Figs. 1—6	a_0 or a	a_1	a_2
		MHz	10^{-3} MHz K^{-1}	10^{-6} MHz K^{-2}
$\nu_Q(T)=a_0+a_1T+a_2T^2+a_3T^3+dT^{-1}$	F	38.629	−1.606	−1.293
$\nu_Q(T)=a_0+a_1T+a_2T^2+dT^{-1}$	D	38.599	−1.164	−3.373
$\nu_Q(T)=a_0+a_1T+a_2T^2$	A	38.583	−1.051	−3.578
$\nu_Q(T)=a_0+a_1T+a_2T^2+a_3T^3$	E	38.582	−1.001	−3.708
$\nu_Q(T)=a-\frac{b}{\exp(c/T)-1}$	B	38.538	—	—
$\nu_Q(T)=a_0+a_1T+dT^{-1}$	C	38.797	−2.854	—

Formula	a_3	d	b	c	Standard deviation
	10^{-9} MHz K^{-3}	MHz K	MHz	K	kHz
$\nu_Q(T)=a_0+a_1T+a_2T^2+a_3T^3+dT^{-1}$	−2.990	−0.799	—	—	2.91
$\nu_Q(T)=a_0+a_1T+a_2T^2+dT^{-1}$	—	−0.340	—	—	3.51
$\nu_Q(T)=a_0+a_1T+a_2T^2$	—	—	—	—	3.96
$\nu_Q(T)=a_0+a_1T+a_2T^2+a_3T^3$	+0.210	—	—	—	3.98
$\nu_Q(T)=a-\frac{b}{\exp(c/T)-1}$	—	—	0.827	257.8	15.08
$\nu_Q(T)=a_0+a_1T+dT^{-1}$	—	−3.914	—	—	24.39

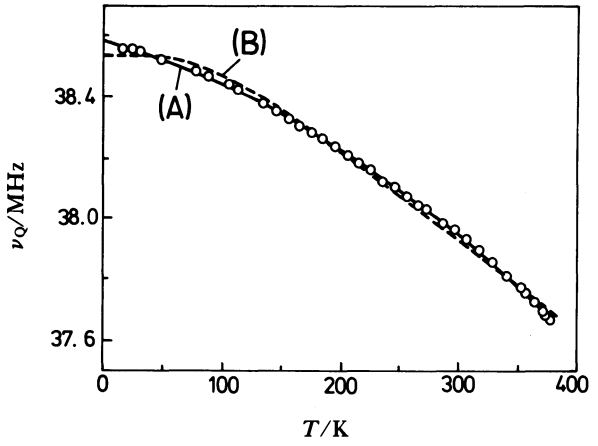

Fig. 1. Comparison of the fits of temperature dependence of ^{35}Cl NQR frequency for ν_Q^3 line in p,p'-DDT to: (A)—Brown's relation (Eq. 10 or 40 for p=2), (B)—Bayer's relation (Eq. 1 or 39); O—experimental points.

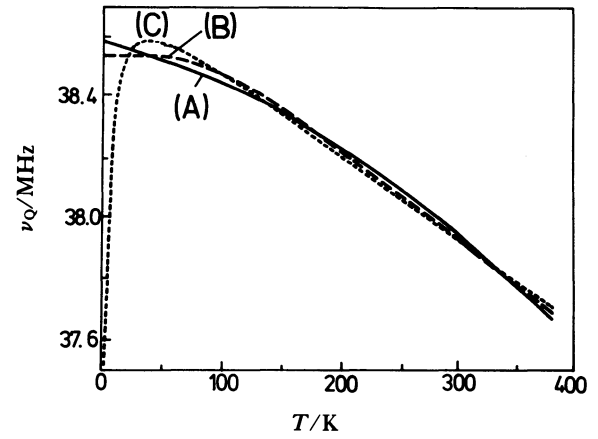

Fig. 2. Comparison of the fits of temperature dependence of ^{35}Cl NQR frequency for ν_Q^3 line in p,p'-DDT to: (A)—Brown's relation (Eq. 10 or 40 for p=2), (B)—Bayer's relation (Eq. 1 or 39), (C)—KBB relation (Eq. 5 or 41 for p=2).

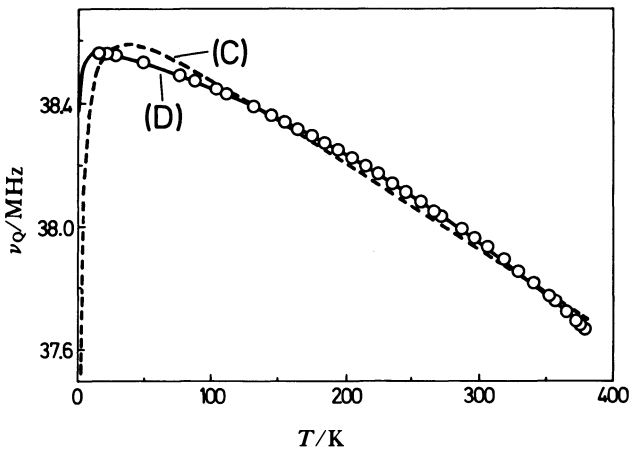

Fig. 3. Comparison of the fits of temperature dependence of ^{35}Cl NQR frequency for ν_Q^3 line in p,p'-DDT to: (C)—KBB relation (Eq. 5 or 41 for p=2), (D)—Eq. 14 or 41 for p=3; O—experimental points.

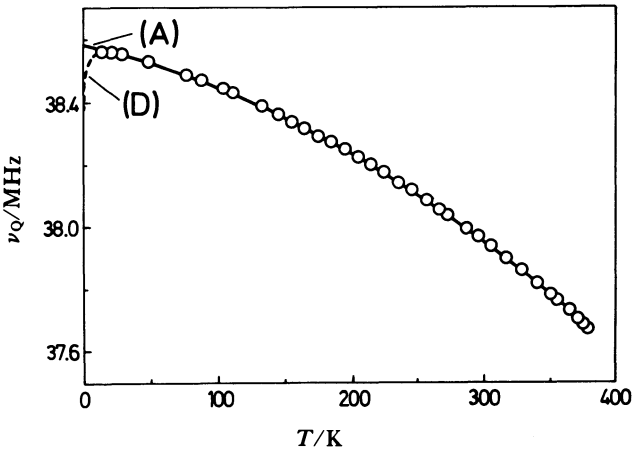

Fig. 4. Comparison of the fits of temperature dependence of ^{35}Cl NQR frequency for ν_Q^3 line in p,p'-DDT to: (A)—Brown's relation (Eq. 10 or 40 for p=2), (D)—Eq. 14 or 41 for p=3; O—experimental points.

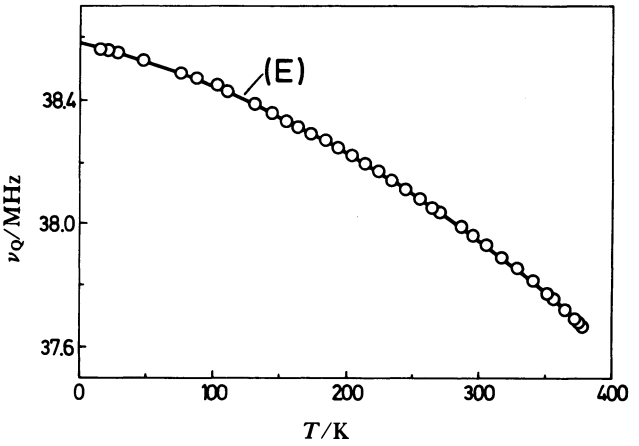

Fig. 5. Temperature dependence of ^{35}Cl NQR frequency for ν_Q^3 line in p,p'-DDT. O—experimental points; solid line (E)—fit to Eq. 20 or 40 for p=3.

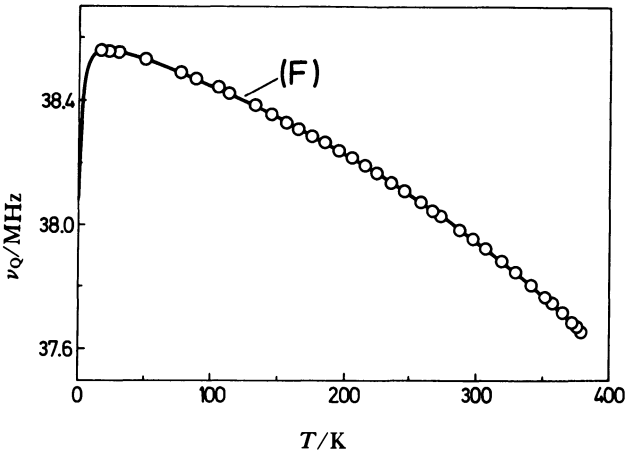

Fig. 6. Temperature dependence of ^{35}Cl NQR frequency for ν_Q^3 line in p,p'-DDT. O--experimental points; solid line (F)—fit to Eq. 25 or 41 for p=4 (best fit).

Table 2. The Values of Parameters Determining Temperature Dependence of Mean Librational Frequency (ν_l) of the Chlorine Atom (of CCl_3 Group in p,p'-DDT) Obtained from the Fit of Experimental Data $\nu_Q^3(T)$ to Individual Theories-Formulas: Eqs. 10, 14, 20, and 25

Formula	Determined parameter			Notation of $\nu_l(T)$ in Fig. 7
	ν_1^0	g	f	
	cm^{-1}	$10^{-4}\,K^{-1}$	$10^{-7}\,K^{-2}$	
		$\nu_l=\nu_1^0(1-gT)$		
$\nu_Q(T)=a_0+a_1T+a_2T^2$	112.85	17.028	—	(1)
$\nu_Q(T)=a_0+a_1T+a_2T^2+a_3T^{-1}$	107.26	14.495	—	(2)
		$\nu_l=\nu_1^0(1-gT-fT^2)$		
$\nu_Q(T)=a_0+a_1T+a_2T^2+a_3T^3$	114.01	18.009	−1.020	(3)
$\nu_Q(T)=a_0+a_1T+a_2T^2+a_3T^3+a_4T^{-1}$	91.32	4.024	9.308	(4)

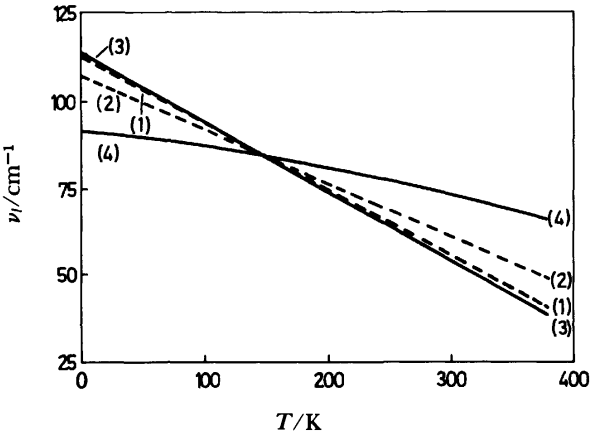

Fig. 7. Temperature dependence of mean librational frequency (ν_l) for chlorine atom (of the CCl_3 group in p,p'-DDT) obtained from fitting the $\nu_Q^3(T)$ data to the proper theories-formulas: Eqs. 10, 14, 20, and 25. The line (1) and (2) represent the dependence $\nu_l=\nu_1^0(1-gT)$ while the lines (3) and (4) stand for $\nu_l=\nu_1^0(1-gT-fT^2)$. The values of ν_1^0, g and f are given in Table 2.

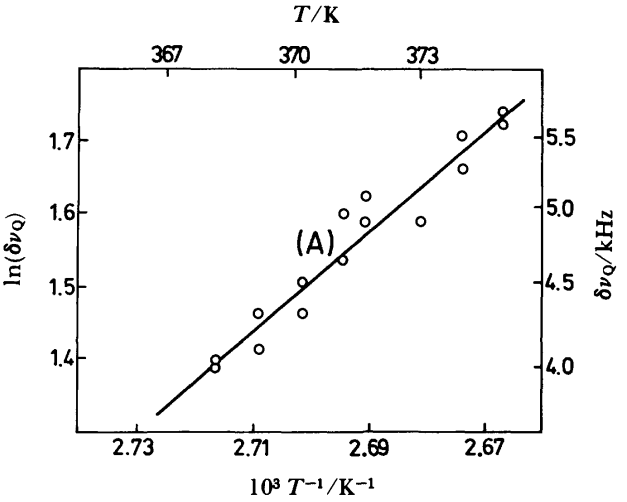

Fig. 8. Temperature dependence of ^{35}Cl NQR line width for rotating chlorines of the CCl_3 group (lines ν_Q^3, ν_Q^4, ν_Q^5 in p,p'-DDT). O—experimental points; solid line (A)—fit to Eq. 33 or 45 for $h=0$ and $d=0$.

detail in Refs. 9—13. In this paper we shall concentrate on the analysis of some experimental results.

We shall illustrate the temperature dependence of ^{35}Cl NQR frequency for the ν_Q^3 line which is one of the five resonance lines observed for p,p'-DDT.[9-13] The parameters of the fit of the experimental dependence $\nu_Q=\nu_Q^3=f(T)$ to individual theories — formulas are given in Table 1 while Figs. 1—6 illustrate the quality of the fits. The formulas in Table 1 are arranged according to increasing standard deviation. As follows from Table 1 the best agreement between the experimental data and the three basic theories (Bayer, KBB, and Brown) was obtained for Brown's formula, Figs. 1 and 2. Thus, it validated the introduction of anharmonicity of vibrations through the linear temperature dependence of their frequencies. The fit improves when we modify the Brown's dependence to extend its validity also at relatively low temperatures, Eq. 14, see curves (D) in Figs. 3 and 4. However, the best fit has been obtained by assuming the square temperature dependence of librational frequency, Eq. 25, see curve (F) in Fig. 6 and Table 1. Despite some really good fits of $\nu_Q(T)$ obtained, none of the equations applied does describe the experimental dependence sufficiently well in very low temperatures, below 20 K. Nevertheless, using these fits we can find the appropriate moments of inertia, librational frequencies and the parameters describing the temperature dependence of librational frequency. Table 2 presents the appropriate parameters for linear and square temperature dependences of mean librational frequency of the Cl atom considered, while Fig. 7 illustrates $\nu_l(T)$ dependences. Curve (4) in Fig. 7 shows the dependence $\nu_l(T)$ obtained from the best fit of $\nu_Q(T)$. The square temperature dependence of librational frequency presented as curve (4) in Fig. 7 is the closest approximation of the real situation for the p,p'-DDT. A detailed analysis of other parameters obtained from individual fits of $\nu_Q(T)$ is given in Refs. 9, 10, and 13.

The width of the resonance line ($\delta\nu_Q$) may be analyzed with the help of the computer program finding the fit of $\delta\nu_Q(T)$ to Eq. 45. As an example we shall analyze the width of the resonance lines due to

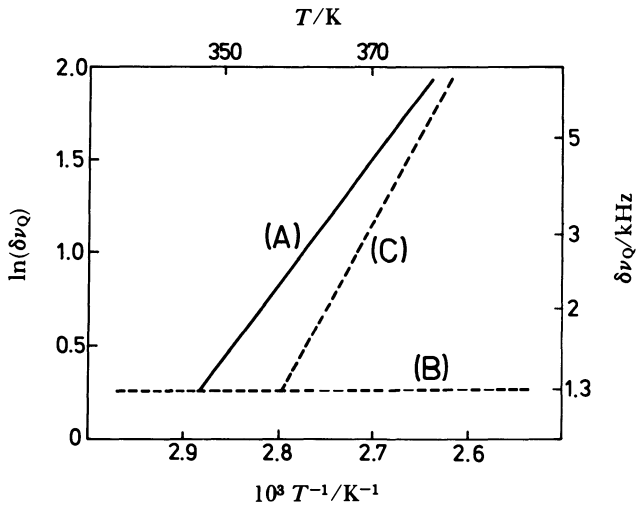

Fig. 9. Separation of ^{35}Cl NQR line width observed (line (A) in Figs. 8 and 9) into line width related to hindered rotation of CCl_3 groups (line (C)) and line width being the resultant effect of static line width and dynamical narrowing due to hindered rotation of phenyl rings in *p,p'*-DDT (line (B)).
$(\delta\nu_Q)^{observed} = (\delta\nu_Q)' + B\exp(-E_a/RT)$
(A) (B) (C)

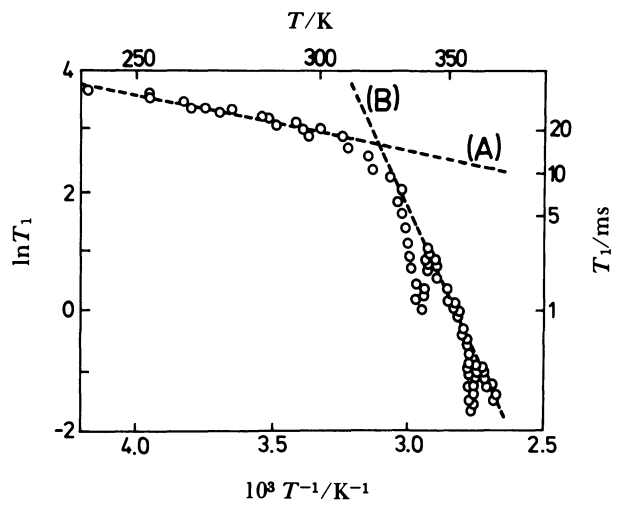

Fig. 10. Temperature dependence of nuclear quadrupole spin-lattice relaxation time (T_1) (lines ν_Q^3, ν_Q^4, ν_Q^5 in *p,p'*-DDT). O—experimental points; (A)—fit function taking into account only librations (Eq. 34 or 42); (B)—fit function taking into account only hindered rotations of CCl_3 groups (Eq. 35 or 43).

chlorine atoms of CCl_3 group in *p,p'*-DDT. As a result of growing rate of hindered rotation of CCl_3 group with increasing temperature the lines undergo significant broadening, which is shown in Fig. 8. The separation of line width being the resultant effect of static line width and dynamical narrowing from the observed line width leads to obtaining the pure effect of line broadening due to hindered rotation of CCl_3 group (see Fig. 9). This procedure also allows us to determine the activation energy for hindered rotation of CCl_3 group which in the case considered is 77.9 kJ mol^{-1}. The computer analysis of resonance line widths in *p,p'*-DDT is given in more detail in Refs. 9, 10, and 13.

As an example of the computer analysis of quadrupole relaxation time T_1 let us consider the relaxation times studied on chlorine nuclei of CCl_3 group in *p,p'*-DDT. We shall consider the temperature range from 200 to 378 K, within which there are several relaxation mechanisms: the mechanism associated with librations of Cl atoms of CCl_3 group, another associated with hindered rotation of CCl_3 groups and the modulation mechanism associated with hindered rotation of the two dynamically nonequivalent groups of phenyl rings. All these mechanisms influence the measured relaxation times T_1:

$$(T_1^{-1})^{observed} = (T_1^{-1})^{librations} + (T_1^{-1})^{CCl_3\ rot.} + (T_1^{-1})_I^{modul.} + (T_1^{-1})_{II}^{modul.} \quad (46)$$

Using Eqs. 34—36 we come to:[12]

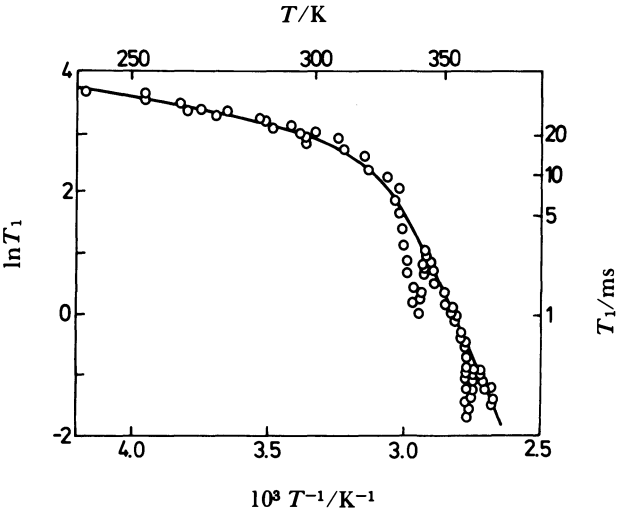

Fig. 11. Temperature dependence of nuclear quadrupole spin-lattice relaxation time (T_1) (lines ν_Q^3, ν_Q^4, ν_Q^5 in *p,p'*-DDT). O—experimental points; solid line-fit function taking into account both librations and hindered rotations of CCl_3 groups (Eq. 44 for $A=0$ and $B=0$).

$$(T_1^{-1})^{observed} = aT^n + b\exp(-E_a/RT) + [d\exp(E_a'/RT) + g\exp(-E_a'/RT)]^{-1} + [k\exp(E_a''/RT) + l\exp(-E_a''/RT)]^{-1} \quad (47)$$

The most important parameters in the above equation are activation energies for hindered rotation of individual atomic groups: E_a for CCl_3 group, E_a' and E_a'' for the two groups of phenyl rings. Figures 10—14 show the computer fit of the experimentally obtained $T_1(T)$ to Eqs. 47 and 44 where various mechanisms are

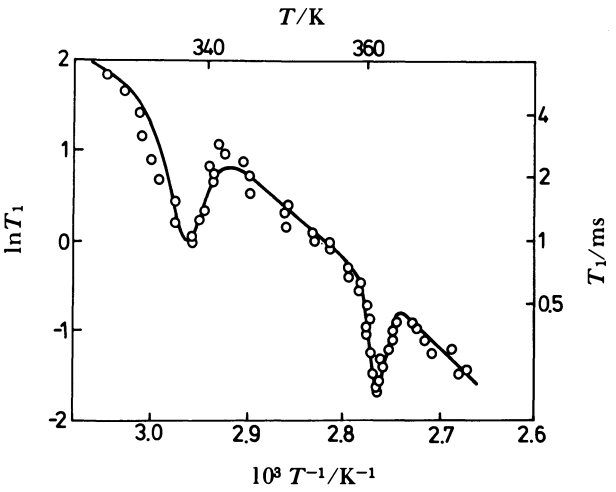

Fig. 12. Temperature dependence of nuclear quadrupole spin-lattice relaxation time (T_1) (lines ν_Q^3, ν_Q^4, ν_Q^5 in *p,p'*-DDT). O—experimental points; solid line-fit function taking into account librations, hindered rotations of CCl_3 groups and the influence of rotating two nonequivalent phenyl groups (two modulation minima) (Eq. 44 for $A=1$ and $B=1$ or Eq. 47).

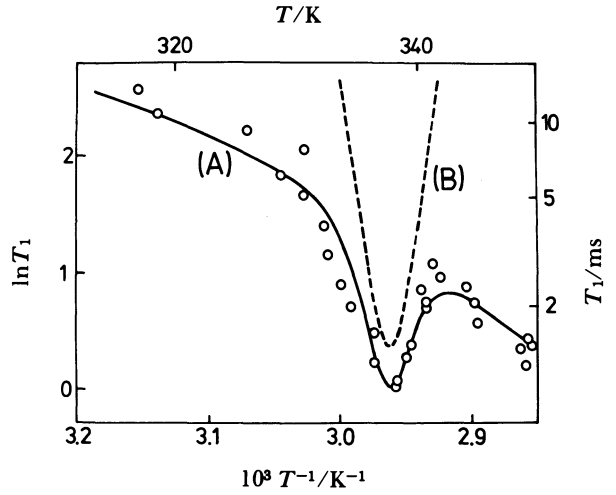

Fig. 13. Temperature dependence of nuclear quadrupole spin-lattice relaxation time (T_1) (lines ν_Q^3, ν_Q^4, ν_Q^5 in *p,p'*-DDT)—the first modulation minimum. O—experimental points; (A)—fit function taking into account librations, hindered rotations of CCl_3 groups and the influence of rotating phenyl rings (Eq. 44 for $A=1$ and $B=1$ or Eq. 47); (B)—function describing only the modulation effect due to rotation of one group of phenyl rings (Eq. 36 or 44 for $a=0$, $b=0$, $A=1$, and $B=0$).

taken into account. From these fits we determined the following activation energies: E_a=86.6 kJ mol^{-1}, E'_a= 84.5 kJ mol^{-1}, and E''_a=91.0 kJ mol^{-1}.[12] Moreover, derived mathematical expression for the curve $T_1^{-1}=f(T)$ allows us to determine accurately the temperature at which the relaxation time reaches its minimum value. This, in turn, enables finding activation energy of the atomic group as well as contribution of the modulated (due to phenyl rings

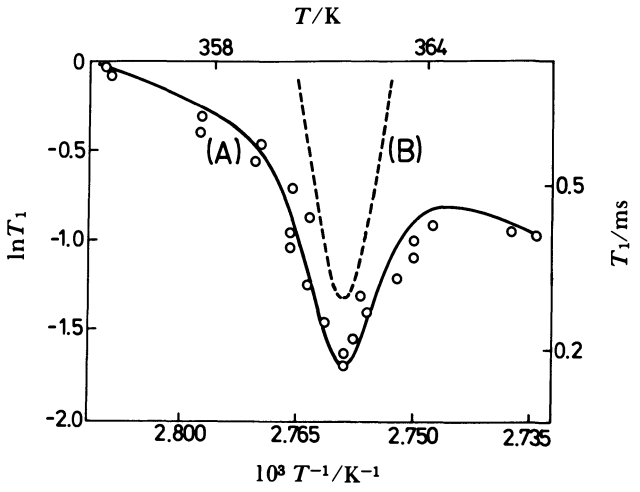

Fig. 14. Temperature dependence of nuclear quadrupole spin-lattice relaxation time (T_1) (lines ν_Q^3, ν_Q^4, ν_Q^5 in *p,p'*-DDT)—the second modulation minimum. O—experimental points; (A)—fit function taking into account librations hindered rotations of CCl_3 groups and the influence of rotatings (Eq. 44 for $A=1$ and $B=1$ or Eq. 47); (B)—function describing only the modulation effect due to rotation of one (the other than in Fig. 13) group of phenyl rings (Eq. 36 or 44 for $a=0$, $b=0$, $A=0$, and $B=1$).

rotation) q'_{zz} gradient to the total electric field gradient q_{zz} on the chlorine nucleus.[12] Complete analysis of the results obtained from the computer fits of $T_1(T)$ data is given in Refs. 10 and 12.

In conclusion we can say that all kinds of temperature dependences of fundamental parameters in NQR spectroscopy may be described by more or less complex mathematical formulas. Further, it is sufficient to perform an accurate computer fit which may be done even with the help of a personal computer. The parameters determined from the fits are the functions of the physical parameters describing the electronic structure and dynamics of the molecules studied.

References

1) H. Bayer, *Z. Physik*, **130**, 227 (1951).
2) T. Kushida, G. B. Benedek, and N. Bloembergen, *Phys. Rev.*, **104**, 1364 (1956).
3) R. J. C. Brown, *J. Chem. Phys.*, **13**, 116 (1960).
4) Y. Ayant, *Ann. Phys.*, **10**, 487 (1955).
5) M. Buyle-Bodin, *Ann. Phys.*, **10**, 533 (1955).
6) D. E. Woessner and H. S. Gutowsky, *J. Chem. Phys.*, **39**, 440 (1963).
7) S. Alexander and A. Tzalmona, *Phys. Rev.*, **138**, 845 (1965).
8) A. Zussman and S. Alexander, *J. Chem. Phys.*, **48**, 3534 (1968).
9) B. Nogaj and J. R. Brookeman, In Proceedings of the XVI Seminar on NMR and Its Applications, Cracow 1983; Institute of Nuclear Physics: Cracow, 1984; Report No. 1237/PL, pp. 138, 145.
10) B. Nogaj, In Proceedings of the XVII Seminar on

NMR and Its Applications, Cracow 1984; Institute of Nuclear Physics: Cracow, 1985; Report No. 1287/PL, p. 191.
11) B. Nogaj, In Proceedings of the RAMIS-85 Conference, Poznań 1985; Adam Mickiewicz University: Poznań 1985; pp. 587, 593.
12) B. Nogaj, *J. Phys. Chem.*, **91**, 1236 (1987).
13) B. Nogaj, *J. Phys. Chem.*, **91**, 1241 (1987).

 © 1988 The Chemical Society of Japan Bull. Chem. Soc. Jpn., 61, 2623—2628 (1988)

Kinetics of Substitution of Aqua-Ligands from *cis*-Diaquobis(ethylenediamine)-cobalt(III) Complex by β-Alanine and DL-Valine in Various EtOH-Water Mixtures

Debabrata CHATTERJEE and G. S. DE*
Department of Chemistry, University of Burdwan, Burdwan 713104, India
(Received July 30, 1987)

The kinetics of above titled reaction has been studied spectrophotometrically in various water-ethanol mixtures at different temperatures (45—60 °C). The following rate law has been established in the pH range 3.2 to 4.5.

$$\frac{d[Co(en)_2(H_2O)(LH)^{3+}]}{dt} = \frac{k_a K_E [Co(en)_2(H_2O)_2^{3+}]_T [LH]}{1 + K_E[LH]}$$

where LH represents the zwitterionic form of the amino acids viz. β-alanine and DL-valine. K_E is the ion-pair equilibrium constant between substrate complex ion and zwitterionic ligand the values of which increase with the increase of organic component of medium, where reverse is true for k_a, the interchange rate constant from outersphere complex to innersphere product. It was observed that at higher ligand concentration a limiting rate is attained, which has been explained due to completion of ion-pair formation. Increasing effect of pH and special catalytic effect of NO_3^- have been observed. Activation parameters (ΔH^* and ΔS^*) have been calculated and compared with isotopic water exchange reaction and other deaquation reactions. A dissociative interchange mechanism (I_d) involving ion-pair formation has been suggested.

Elucidation of the mechanism of deaquation reactions on Co(III) center in still a lively issue. No single mechanism can be adequate to explain the variety of observations in the water replacement reactions on Co(III) complexes. However, thorough survey[1-7] reveals a general pattern of the mechanism in which replacement of water molecule occurred through either purely dissociative or dissociative interchange pathway. In case of dissociative interchange process, substrate Co(III) complex ion first forms an ion pair with incoming ligand in a very rapid step, then in a slower rate determining step interchange between coordinated water molecule and incoming ligand occurs to give final product. Deviations from the above mechanism are also noticed in which associative (A) and associative interchange (I_a) mechanism have been suggested.[8-10] Therefore the controversy regarding mechanism in water replacement reactions of well studied cobalt(III) aqua-amine (or ammine) system still persists. The variation of substitution rate with solvent composition has also been proved useful for diagnosis of mechanism in octahedral substitution reactions.[11-14] In response to the above fact we have studied the kinetic behavior of *cis*-$[Co(en)_2(H_2O)_2]^{3+}$ with amino acid ligands viz. glycine,[15] DL-alanine,[16] and L-serine[17] which behaved as good bidentate ligands (NO). The present work is a continuation of our earlier studies having the purpose of assessing the role of solvent composition on water replacement reactions in octahedral Co(III) complex.

Experimental

Substrate complex *cis*-$[Co(en)_2(H_2O)_2](NO_3)_3$ was prepared by following the literature method[18] and characterized by elemental analysis and spectral data obtained were compared with the data reported in literature.[19] Crystal forms of reaction products were not separated due to their hygroscopic nature. To determine the composition of the reaction product in each case equal volume of solution of substrate complex (0.01 M†) and ligand (β-alanine, DL-valine) was mixed separately in three different molar ratios 1:1, 1:2, and 1:3 at fixed pH 4.2. The mixtures were kept at 50 °C for 24 hours. Absorption spectra of all the mixtures were taken and spectral data obtained were compared with the data shown for the product complexes. There is very little difference in absorbances between our product complexes and those cited in literature.[20] Further 1:1 metal-ligand composition of reaction products in solution was verified by Job's method in both cases. There are three possible products expected in solution: (a) $[Co(en)_2L]^{2+}$, (b) $[Co(en)_2(H_2O)(LH)]^{3+}$, and (c) $[Co(en)_2(LH)_2]^{3+}$. Experiment on Job's method of continuous variation, ruled out the possibility of formation of $[Co(en)_2(LH)_2]^{3+}$. To establish the composition of the product between (a) and (b) we have performed pH metric titration with the reaction product in solution. The result indicates the formation of (b), i.e. $[Co(en)_2(H_2O)(LH)]^{3+}$. Thus the zwitterionic ligand ^-OOC-R-NH_3^+ coordinated to metal center through its O- end.

Kinetic Run. The course of the reaction was followed by a HILGER UVISPEK spectrophotometer at 495 nm bacause substantial differences exist in the absorption of substrate complex and it's reaction product (Fig. 1). Equal volume of Complex 1 (substrate complex) and amino acid ligand [LH]≫[Co] was mixed as such that the pseudo-first-order condition is applicable and the pseudo-first-order rate constant values (k_{obs}) were obtained by plotting $\log[(A_\alpha - A_0)/(A_\alpha - A_t)]$ against time, where A_0, A_t, and A_∞ are the absorbance values initially, after time t, and after the

† 1 M=1 mol dm^{-3}.

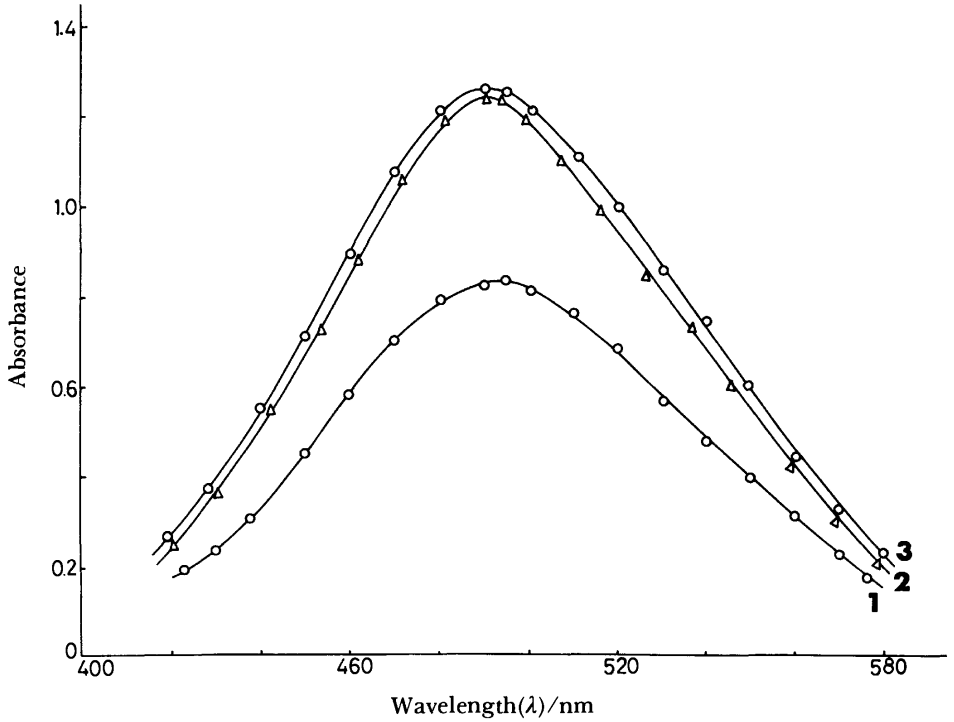

Fig. 1. Spectra of substrate complex *cis*-$[Co(en)_2(H_2O)_2]^{3+}$ (**1**) and it's products $[Co(en)_2(H_2O)$-(valH)$]^{3+}$ (**2**) and $[Co(en)_2(H_2O)(\beta$-alaH$)]^{3+}$ (**3**).

completion of the reaction respectively. The plot of $\log[(A_\alpha-A_0)/(A_\alpha-A_t)]$ vs. time t gave a good straight line passing through the origin. This linearity is observed from start to finish of the reaction which ruled out the possibility of any consecutive reactions.

Results and Discussion

i) Effect of [Complex 1] on Rate. At fixed ligand concentration [Complex 1] was varied in the range 0.0025 to 0.0075 M keeping pH and ionic strength of the medium fixed at 4.2 and 0.05 M respectively. It is seen that the values of $k_{obs}\times(10^4\ s^{-1})$ are 2.60, 2.61, and 2.64 at [Complex 1]=0.0025, 0.005, and 0.0075 M, where anating ligand is β-alanine. In case of ligand valine pseudo-first order rate constant $k_{obs}\times10^4\ s^{-1}$ values are 1.92, 1.90, and 1.94 at 0.0025, 0.005, and 0.0075 M complex concentrations respectively. These k_{obs} values at different Complex 1 concentrations are in good agreement with the first order rate law with respect to the Complex 1 concentration.

ii) Effect of Varying pH on Rate. When the anating ligand is β-alanine the values of k_{obs} $(\times10^4\ s^{-1})$ are 0.73, 0.95, 1.63, 2.61, and 3.5 at pH 3.2, 3.5, 3.8, 4.2, and 4.5 respectively and for DL-valine k_{obs} $(\times10^4\ s^{-1})$ are 0.87, 1.1, 1.42, 1.90, and 2.30 at the above mentioned pH respectively. Now in the studied pH range 3.2 to 4.5 both the ligand β-alanine and DL-valine exist in zwitterionic forms as β-alaH and DL-valH respectively in solution.[21] Therefore ligands nature is not altered appreciably in the solution. Acid dissociation equilibrium of substrate complex can be represented as follows.

$$cis\text{-}[Co(en)_2(H_2O)_2]^{3+} \overset{K_1}{\rightleftharpoons} cis\text{-}[Co(en)_2(OH)(H_2O)]^{2+} + H^+$$

where the value of pK_1 is 5.8 at 25 °C.[22]

Now considering the above equilibrium effect of pH on observed rate constant can be expressed as follows.

$$k_{obs} = k_1 + k_2K_1[H^+]^{-1} \quad (1)$$

where k_1 is the observed rate constant when reacting species is diaquo complex and k_2 is the observed rate constant for hydroxoaquo complex. It is seen from Eq. 1 that the increase in pH i.e. decrease in hydrogen ion concentration increases the reaction rate. Plot of k_{obs} vs. $1/[H^+]$ gave a good straight line and deperture from linearity started at higher pH. Actually in the studied pH range 3.2 to 4.5 percentage of diaquo complex in the solution is maximum, however increase in small amount of hydroxaquo complex increases the reaction rate because hydroxoaquo complex is much more reactive (reacts 60 times more faster than diaquo complex)[22] than diaquo species. Again hydroxide ion facilitates the formation of very reactive hydroxo complex which also increases the reaction rate.

iii) Effect of Variation of Ligand Concentration on Rate. The ligand concentration was varied in the range 0.05 to 0.15 M at four different temperatures

Table 1. Values of k_{obs} in Various Ethanol-Water Mixtures at Different Temperatures $[Co(en)_2(H_2O)_2^{3+}]$=0.005 M, pH=4.2, Ionic Strength=0.03 M

Ligand concentration	Temp	$k_{obs}\times10^4/s^{-1}$					
		β-Alanine			DL-Valine		
M	°C	% of ethanol (v/v)			% of ethanol (v/v)		
		10	20	30	10	20	30
0.050	45	0.32	0.37	0.43	0.24	0.27	0.35
	50	0.75	0.84	0.96	0.35	0.41	0.57
	55	1.32	1.61	1.85	1.11	1.32	1.50
	60	2.51	3.05	3.47	2.05	2.32	2.64
0.075	45	0.52	0.59	0.67	0.37	0.41	0.47
	50	1.21	1.30	1.40	0.49	0.62	0.76
	55	2.01	2.34	2.61	1.52	1.72	1.90
	60	3.60	4.20	4.79	3.13	3.40	3.90
0.100	45	0.65	0.70	0.76	0.45	0.52	0.57
	50	1.65	1.78	1.91	0.66	0.85	0.98
	55	2.61	2.98	3.19	1.98	2.25	2.52
	60	4.61	5.60	6.14	3.98	4.25	4.60
0.125	45	0.76	0.85	0.92	0.55	0.59	0.65
	50	1.85	2.00	2.15	0.87	1.00	1.15
	55	3.02	3.40	3.62	2.36	2.71	3.10
	60	6.55	6.80	7.16	4.67	4.97	5.40
0.150	45	0.88	0.95	1.05	0.59	0.65	0.72
	50	2.10	2.32	2.50	0.95	1.10	1.25
	55	3.47	3.83	4.27	2.69	2.98	3.32
	60	6.71	7.32	7.67	5.31	5.62	6.01

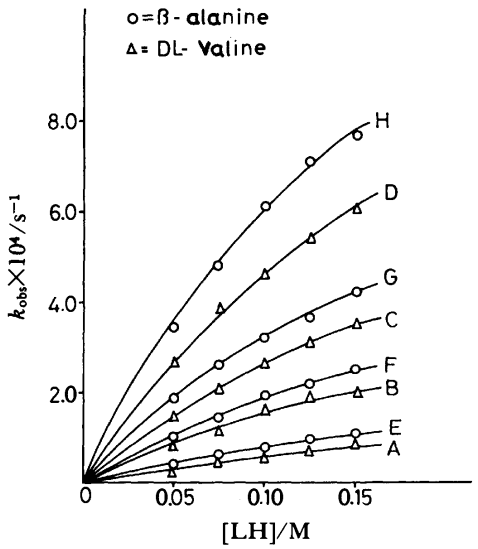

Fig. 2. Effect of ligand concentration (LH) on rate constant (k_{obs}) at different temperatures A) 45 °C, B) 50 °C, C) 55 °C, D) 60 °C; E) 45 °C, F) 50 °C, G) 55 °C, and H) 60 °C.

keeping Complex 1 (0.005 M), pH (4.2) and ionic strength (0.03 M) fixed. The result shown in Table 1 exhibits that for both β-alanine and DL-valine the rate increases with the increase of ligand concentration and reaches a limiting value at higher ligand concentration (Fig. 2). This is due to completion of ion pair formation with the substrate complex ion and amino acid ligands through its negative end. Actually when the zwitterionic amino acid ligand is brought to react with the triply charged substrate complex ion it occupies the near vicinity of complex ion replacing the solvent molecule. Thus an ion pair species is formed in a very rapid process. Then ligand molecule occupies the site vacated by the leaving water molecule in a slower rate determining step. Now increase in ligand concentration increases the concentration of ion pair in the solution and lastly at certain ligand concentration ion pair formation is completed. Further addition of ligand increases it's amount in bulk solution.

The following scheme commensurating the above fact can be set up to explain the variation of rate with ligand concentration.

$$cis\text{-}[Co(en)_2(H_2O)_2]^{3+} + LH \overset{K_E}{\rightleftharpoons} \underset{IP}{cis\text{-}[Co(en)_2(H_2O)_2]^{3+}\cdot LH}$$

$$cis\text{-}[Co(en)_2(H_2O)_2]^{3+}\cdot LH \xrightarrow{k_a} cis\text{-}[Co(en)_2(H_2O)(LH)]^{3+} + H_2O$$

Considering ion pair equilibrium (K_E) and rate determining step (k_a) a familiar rate expression has been established

$$\frac{d[Co(en)_2LH^{3+}]}{dt} = \frac{k_a K_E [Co(en)_2(H_2O)_2^{3+}]_T [LH]}{1 + K_E[LH]}$$

$$= k_{obs}[Co(en)_2(H_2O)_2^{3+}] \qquad (2)$$

Now

$$k_{obs} = \frac{k_a K_E[LH]}{1 + K_E[LH]} \quad (3)$$

or

$$1/k_{obs} = 1/k_a + 1/k_a K_E[LH] \quad (4)$$

Here $[Co(en)_2(H_2O)_2^{3+}]_T$=concentration of total unreacted complex, and [LH] represents the concentration of β-alanine or DL-valine in their respective zwitterionic forms.

From Eq. 3 plot of $1/k_{obs}$ vs. 1/[LH] at a constant pH gives a straight line (Fig. 3) with an intercept $1/k_a$ and slope $1/k_aK_E$. The values of k_a are given in Table 2. K_E values were found to be more or less temperature independent, but at a given temperature K_E values increase with the increase in organic component i.e. lowering of dielectric constant of the medium, range from 1.8 to 6.2 M^{-1}. In proposing the above scheme it was resonably assumed that under experimental conditions only cis-diaquo complex is involved in the reaction.

iv) Effect of Ionic Strength on Rate Constant. At fixed [Complex 1] (0.005 M), [ligand] (0.075 M) and pH 4.2 the ionic strength of the medium was varied by adding (a) $NaNO_3$ and (b) $NaClO_4$. It is observed that at 55 °C k_{obs} values increase with the increase in NO_3^- concentration. The values of $k_{obs}(\times 10^4\ s^{-1})$ at 55 °C are 2.61, 2.93, 3.11, 3.43, and 3.93 (for β-alanine) and 1.90, 2.10, 2.98, 3.64, and 4.60 (for DL-valine) at different ionic strengths 0.03, 0.1, 0.25, 0.5, and 1.0 M respectively. Whereas ClO_4^- ion cannot make any change in the k_{obs} values. Considering the net charge of the zwitterionic amino acid ligands being zero the reaction rate should have been independent of ionic strength of the medium,[23] hence the variation of ionic strength made by adding ClO_4^- did not produce any change in rate constant values. But it was shown by Brown and Harris[2] that NO_3^- has greater tendency to attack coordinated water molecule rather than water molecules attached to the ligands and this facilitates Co-OH_2 bond fission and thus increase of rate occurs.

v) Effect of Variation of Dielectric Constant on Rate Constant. Effect of solvent composition on the water replacement reactions of *cis*-$[Co(en)_2(H_2O)_2]^{3+}$ with amino acids was studied in three different ethanol-water mixtures (10, 20, and 30% v/v). Table 2 shows that at a particular temperature the values of interchange rate constant k_a decrease with the increase

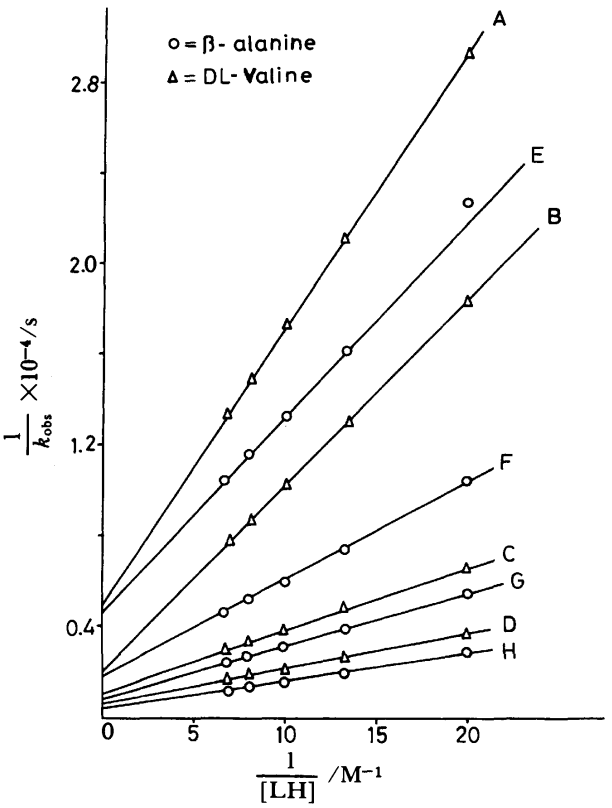

Fig. 3. Plot of $1/k_{obs}$ vs. 1/[LH] at different temperatures A) 45 °C, B) 50 °C, C) 55 °C, and D) 60 °C; E) 45 °C, F) 50 °C, G) 55 °C, and H) 60 °C.

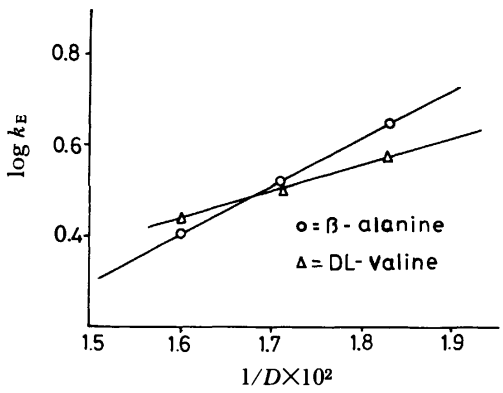

Fig. 4. Plot of log K_E vs. $1/D$ at 55 °C.

Table 2. Values of k_a at Different Temperatures in Various Ethanol-Water Mixtures

Temp	$k_a \times 10^4/s^{-1}$					
	β-Alanine			DL-Valine		
°C	% of ethanol (v/v)			% of ethanol (v/v)		
	10	20	30	10	20	30
45	3.13	2.77	2.12	2.97	2.51	2.01
50	7.24	6.35	5.18	6.85	5.63	5.00
55	12.30	11.31	10.10	11.90	10.10	9.52
60	25.30	22.81	21.30	25.10	22.30	20.00

of organic component of the medium. But reverse is true for K_E values ranging from 1.8 to 6.2 M^{-1}. Actually this is in good agreement with the ion pair formation that lowering of dielectric constant i.e., increases in organic component of the medium increases the forces of attraction between two ions, which favors the ion pair formation (Fig. 4).

According to the electrostatic theory, the dependence of the rate constant of the ion dipole typed reaction on the dielectric constant of the medium is best represented by the Laidler-Eyring equation.[23] In our case considering the total charge on the amino acid ligand is zero the Laidler-Eyring equation can be represented in a simplified way.

$$\frac{d \ln k_a}{d(1/D)} = \frac{e^2Z^2}{2kT}(1/r_1 - 1/r_2) \quad (5)$$

Here, Z is the charge on the complex ion, r_1 and r_2 represent the effective radii of the ion pair in the ground state and in activated state (activated ion pair) respectively, k=Boltzmann constant, T=temperature in absolute degree and D represents the changing dielectric constant. It is seen from Eq. 5, that if $r_2 < r_1$, plot of ln k_a vs. $1/D$ will give a straight line having a negative slope. Now for dissociative interchange process one water molecule is lost in the activated state consequently size of the activated species is lowered i.e. r_2 becomes smaller than r_1. Had it been followed an associative path, the elongation of metal-water bond in the activated states increases the size of the activated species i.e. r_2 becomes larger than r_1. In practice we got a good straight line by ploting ln k_a against $1/D$ with a small negative slope (Fig. 5). This is because r_1 and r_2 do not differ markedly since size of lost water molecule is small in comparison to the large complex ion. Another equation[13] which shows the relation between the rate constant of the ion-dipole reaction and dielectric constant of the medium is as follows:

$$\frac{d \ln k_a}{d(1/D)} = -\frac{Z^2 e^2}{kTr_0^2}\mu_{LH}\cos\theta \quad (6)$$

Here μ_{LH} is the dipole moment of the amino acid ligand, θ is the angle which the negative end of the dipole makes with the line joining the center of the dipole to the complex ion. r_0 is the critical ion-dipole distance which is more or less the same in ground state or activated state as stated earlier. In case of dissociative interchange mechanism one water molecule is dissociated from the metal ion and as a result metal ion attracts the negatively charged oxygen atom in carboxylate group of the amino acid ligand towards on itself. Consequently in this case the value of angle θ cannot exceed the value 90° and thus plot of ln k_a against $1/D$ always gives a straight line with a negative slope. In case of associative interchange process θ may be greater than 90° because complete detachment of water molecule dose not occur in activated state, which increases the steric effect that pushes the negative end of the dipole far from its equilibrium position. However, the small difference obtained in the values of k_a (Table 2) may be due to other non-electrostatic solvent-solute interaction. An interesting point to be noted here is that the values of k_{obs} (Table 1) increase with the increase in organic component of the medium. This is due to increasing effect of K_E on k_{obs} is larger than that of opposite effect of k_a on k_{obs} (Eq. 4).

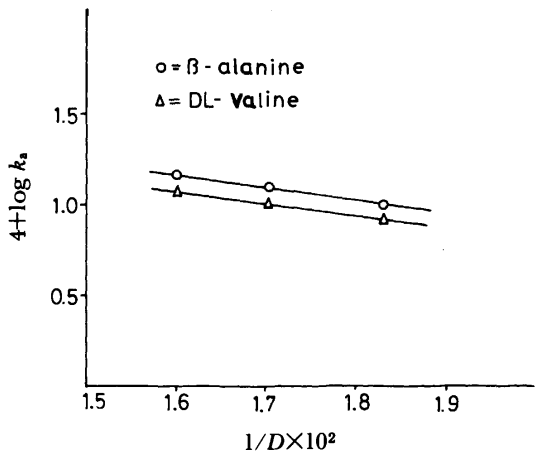

Fig. 5. Plot of log k_a vs. $1/D$ at 55°C.

vi) Effect of Temperature on Rate Constant. The reactions were studied at four different temperatures for media of three different dielectric constants. Activation parameters were calculated by using the Eyring equation and the data obtained were checked by a least squares method and compared with data shown for isotopic water exchange process[25] and other substitution reactions (Table 3). It is seen from Table 3 that the $\Delta H^{\neq}$ and $\Delta S^{\neq}$ values increase with as the dielectric constant of the medium decreases.

Table 3. Values of $\Delta H^{\neq}$ and $\Delta S^{\neq}$ in Different Ethanol-Water Mixtures

% of ethanol (v/v)	β-Alanine		DL-Valine	
	$\Delta H^{\neq}$	$\Delta S^{\neq}$	$\Delta H^{\neq}$	$\Delta S^{\neq}$
	kcal mol^{-1}	cal deg^{-1}	kcal mol^{-1}	cal deg^{-1}
10	26.2	13.3	25.8	12.2
20	27.7	14.1	27.4	13.9
30	30.0	18.1	29.1	15.7

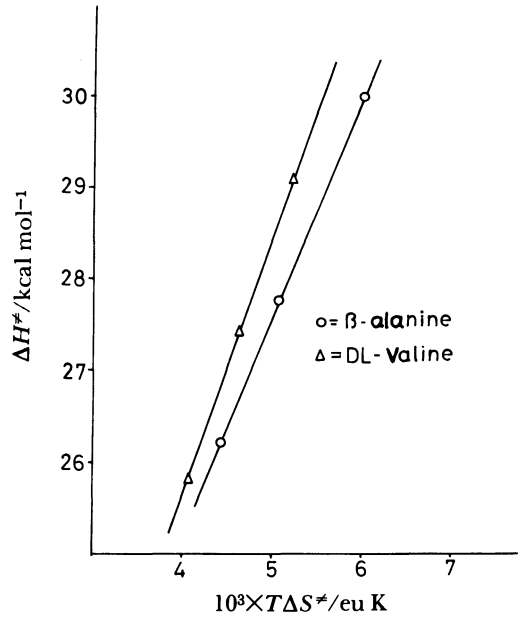

Fig. 6. Isokinetic plot of $\Delta H^{\neq}$ vs. $T\Delta S^{\neq}$.

Though the reactions are performed in water rich media, but crowding of non-polar solvent molecule in the outersphere zone diminishes the rate of Co–OH_2 bond dissociation and thus higher activation energy is required, which is reflected from Table 3. Again increase in organic component effects the solvation of reacting species as well as activated species. Increase in $\Delta S^{\neq}$ values observed is mainly due to change in solvation of the system concerned. Interestingly plots of $\Delta H^{\neq}$ vs. $T\Delta S^{\neq}$ are linear for both the water replacement reactions (Fig. 6). It may be inferred that the similar transition states are formed in the studied range of the composition of the solvent pair.

Conclusion

Basing the above facts a dissociative interchange mechanism (I_d) has been suggested in which complex *cis*-$[Co(en)_2(H_2O)_2]^{3+}$ first forms an ion pair with the incoming amino acid ligands viz. β-alanine and DL-valine in a very rapid step, then slow replacement of water molecule occurs through a dissociative pathway in which amino acid ligand takes the position vacated by leaving water molecule.

We are thankful to CSIR for senior research fellowship to DC.

References

1) P. Basolo and R. G. Pearson, "Mechanism of Inorganic Reactions," 2nd ed, Wiley Estern Ltd., New York (1977).
2) P. M. Brown and G. M. Harris, *Inorg. Chem.*, **7**, 1872 (1968).
3) R. V. Eldic and G. M. Harris, *Inorg. Chem.*, **18**, 1887 (1979).
4) A. C. Dash and M. S. Dash, *J. Coord. Chem.*, **10**, 79 (1980).
5) V. Holba and M. Talapka, *Chem. Zvesti.*, **70(1)**, 83 (1981).
6) M. C. Ghosh and P. Banerjee, *J. Chem. Research (Synop)*, **1980**, 284.
7) A. C. Dash and R. K. Nanda, *J. Coord. Chem.*, **12(2)**, 91 (1983).
8) A. Ghoshal and S. K. Siddhanta, *Indian J. Chem.*, **20A**, 611 (1981).
9) C. Choudhuri and S. K. Siddhanta, *Indian J. Chem.*, **21A**, 1079 (1982).
10) A. Ganguli and G. S. De, *Indian J. Chem.*, (in press).
11) J. Burgess and M. G. Price, *J. Chem. Soc. A*, 3108 (1971).
12) V. V. Udovenko, L. G. Reiter, and E. P. Shkurman, *Russ. J. Inorg. Chem.*, **18**, 1296 (1973).
13) V. Holba and O. Granicova, *J. Inorg. Nucl. Chem.*, **43**, 2071 (1981).
14) M. N. Bishnu, B. Chakravarti, R. N. Banerjee, and D. Banerjea, *J. Coord. Chem.*, **13**, 63 (1983).
15) D. Chatterjee and G. S. De, *J. Indian Chem. Soc.*, **62**, 526 (1985).
16) D. Chatterjee and G. S. De, *Indian J. Chem.*, **25A**, 350 (1986).
17) D. Chatterjee and G. S. De, *Trans. Met. Chem.*, **12(3)**, 193 (1987).
18) F. P. Dwyer, A. M. Sergeson, and L. K. Reid, *J. Am. Chem. Soc.*, **85**, 1219 (1963).
19) R. D. Gillard and G. Wilkinson, *J. Chem. Soc.*, **1963**, 3193.
20) J. Meisenheimer, *Justus Liebigs Ann. Chem.*, **438**, 217 (1924); M. Kojima, H. Takayanagi, and J. F. Fujita, *Bull. Chem. Soc. Jpn.*, **50**, 1891 (1977).
21) A. E. Martel and R. M. Smith, "Critical Stability Constant, Vol. 1, (Amino Acids)," Plenum Press, London (1974), pp. 9, 20.
22) J. Bjerrum and S. E. Rasmussen, *Acta Chem. Scand.*, **16**, 1265 (1952).
23) S. Glasstone, "A Text Book of Physical Chemistry," Macmillan, London (1977), p. 116.
24) E. S. Amis and J. F. Hinton, "Solvent Effect on Chemical Phenomena," Academic Press, New York and London (1973), Vol. 1, p. 245.
25) W. Kruse and H. Taube, *J. Am. Chem. Soc.*, **83**, 1281 (1961).

Molecular Rearrangements. XXVIII. Thermolysis and Photolysis of Some Hydroxamic Acid Derivatives

M. Z. A. Badr, A. M. Fahmy,* S. A. Mahgoub, and M. M. Aly
Chemistry Department, Faculty of Science, Assiut University, Assiut, Egypt, A.R.E.
(Received July 7, 1987)

Thermolysis and photolysis of benzohydroxamic acid and some of its derivatives have been investigated. Thermolysis of benzohydroxamic acid (BHA) either by heating in air or in a sealed tube gives NH_3, H_2O, CO, benzil, aniline, *o*- and *p*-aminophenols, phenoxazine, benzanilide, and benzoic acid. Whereas, thermolysis of *N*-(benzyloxy)benzamide (BBA) affords toluene, benzaldehyde, bibenzyl, stilbene, phenanthrene, acridine, and *o*- and *p*-aminodiphenylmethane in addition to the previous products. Analogous products were also obtained on pyrolysis of phenylacetohydroxamic acid. Photolysis of BHA and BBA in acetonitrile gives similar results to those of pyrolysis. A free-radical mechanism involving homolysis at different sites was postulated to account for the formation of such products.

Hydroxamic acids which have long been used for treatment of recurrent kidney stone formation were incriminated as potential carcinogens.[1] The current concept is that the carcinogenic activity is further enhanced by *O*-esterification. The base-catalyzed rearrangement of hydroxamic acids to primary amines was first described by Lossen.[2] Later, Tiemann[3] reported the noncatalyzed Lossen rearrangement where he obtained aniline and CO_2 by the destructive distillation of benzohydroxamic acid. Moreover, refluxing of some hydroxamic acid derivatives in dimethyl sulfoxide as polar solvent was reported[4,5] to proceed through an ionic mechanism, where *o*-(aroyloxy)arenecarboxanilides were obtained from *N,O*-diacyl-*N*-phenylhydroxylamine through heterolysis of the N-O bond. This prompted us to study the thermal and photostability characteristics of such class of compounds.

Thermolysis of benzohydroxamic acid (BHA) by heating in air at 240 °C for 30 min. leads to the formation of ammonia, water, carbon monoxide, benzil, aniline, *o*- and *p*-aminophenols, phenoxazine, benzanilide, benzoic acid, and ammonium benzoate (Table 1).

Similary, thermolysis of *N*-(benzyloxy)benzamide (BBA) under the same conditions gives the above mentioned products in addition to toluene, benzaldehyde, benzyl alcohol, bibenzyl, stilbene, phenanthrene, *o*- and *p*-aminodiphenylmethane, and acridine (Table 1).

Phenylacetohydroxamic acid (PAH) on similar treatment gives ammonia, toluene, benzaldehyde, bibenzyl, stilbene, phenanthrene, and *N*-benzylphenylacetamide (Table 2). When pyrolysis of PAH was affected by heating at 270 °C for 10 h in a sealed tube under nitrogen, the same products except benzaldehyde were also obtained, in addition to another unknown by-product with mp 147—148 °C; ν_{NH_2} at 3320 and 3120 cm^{-1} and $\nu_{C=O}$ at 1625 cm^{-1}, whereas its microanalysis result points to the formula $C_{12}H_{13}NO_2$.

The formation of the identified products strongly points to a free radical mechanism starting by the preferential homolysis of the N-O bond of BHA (Scheme 1, route a) rather than C-N bond (route b) forming benzoylaminyl and hydroxyl free radicals on basis of bond energy values being of the order 48 and 70 kcal mol^{-1} respectively as observed by other workers.[5] The benzoylaminyl radicals undergo rearrangement into *N*-phenylaminocarbonyl free radicals through a process of 1,2-phenyl shift involving a bridged radical intermediate. Subsequent decarbonylation of such radical leads to the formation of phenylaminyl radical which passes into aniline, *o*- and *p*- aminophenols, and phenoxazine as shown in Scheme 1.

Further evidence for the intermediate formation of *N*-phenylaminocarbonyl free radicals is the results obtained from pyrolysis of *N,N'*-diphenyloxamide in presence of naphthalene as solvent where substitution of the *N*-phenylaminocarbonyl radicals on the naphthalene nucleus occurs at position-1 forming 1-naphthanilide in addition to other fragmentation products of such radicals namely aniline, *N*-phenyl-1-naphthylamine, and carbon monoxide.

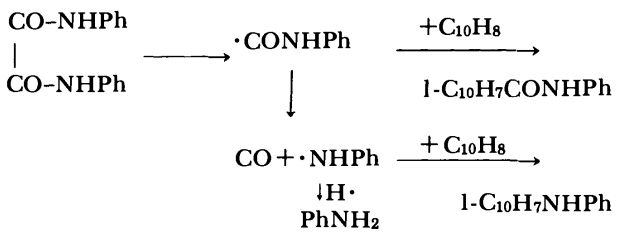

The observed low yield of *o*-aminophenol can be attributed to its incorporation in the formation of phenoxazine, ammonia and water. The formation of phenyl isocyanate was ruled out due to the absence of its condensation product with aniline, namely, *N,N'*-diphenylurea among the pyrolysis products. The probability of homolysis of the C-N bond (route b) into benzoyl and hydroxyaminyl radicals is worth considering to account for the formation of benzil, benzoic acid, and benzanilide as shown in Scheme 1. The benzoyl free radicals are involved in the formation of benzil, benzoic acid, and benzanilide

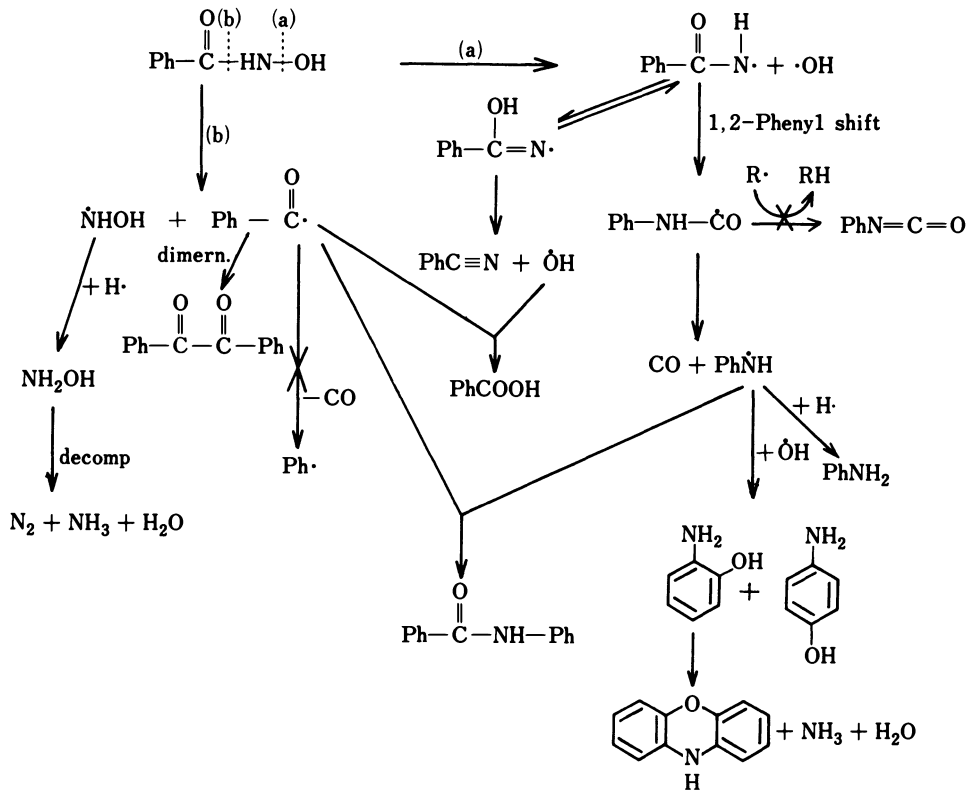

Scheme 1. Pyrolysis of BHA.

through processes of dimerization or coupling with hydroxyl or phenylaminyl radicals respectively. On the other hand, the hydroxyaminyl radicals undergo H-abstraction forming hydroxylamine, which ultimately decomposes into ammonia and water.[6]

Thermolysis of BBA is suggested to proceed through homolysis of the N–O bond (route a; Scheme 2) forming benzyloxyl and benzoylaminyl radical pairs. The benzyloxyl radical are the precursor of benzaldehyde and benzyl alcohol through a disproportionation process, whereas the benzoylaminyl radical is transformed into benzonitrile. Other fates of benzoylaminyl radicals such as fragmentation into phenyl radicals and isocyanic acid, which ultimately undergoes hydrolysis by water to give ammonia and carbon dioxide, were ruled out due to the absence of CO_2 and biphenyl among the products.

However, formation of products derived from benzyl radicals necessitates another pathway, involving homolysis of the benzyl–O bond (route b, Scheme 2) forming benzyl and benzohydroxamoyl radical pairs. The benzyl radicals are involved in the formation of toluene, bibenzyl, stilbene, and phenanthrene through processes of H-abstraction and/or dimerization, followed by dehydrogenation and cyclization respectively.

The formation of *o*- and *p*-aminodiphenylmethanes can be assumed to take place through attack of benzyl radicals on aniline formed in the reaction medium. Radical oxidative cyclization of some *o*-aminodiphenylmethane will ultimately lead to the formation of acridine.[7] A result which explains the low yield of *o*-aminodiphenylmethane as compared with its *p*-isomer. On the other hand, benzohydroxamoyl free radicals abstract hydrogen to form benzohydroxamic acid which passes into the products identified in Scheme 1, namely; benzil, benzoic acid, benzanilide, aniline, *o*- and *p*-aminophenols, phenoxazine, carbon monoxide, ammonia, and water.

The products formed from pyrolysis of PAH by refluxing imply the homolysis of the $-\overset{O}{\overset{\|}{C}}-\overset{H}{\overset{|}{N}}-$ bond (route a), forming phenylacetyl and hydroxyaminyl radical paris (Scheme 3).

The phenylacetyl radicals decarbonylate[8] mainly into benzyl free radicals which are considered as the precursor of toluene, benzaldehyde, bibenzyl, stilbene, and phenanthrene as shown previously, whereas some of the phenylacetyl radicals form phenylacetic acid on coupling with hydroxyl free radicals which are considered as intermediates in the decomposition of hydroxylamine.[6]

The formation of benzaldehyde can be reasonably assumed to be through atmospheric oxidation of benzyl radicals since absence of air on heating PAH in a sealed tube in nitrogen atmosphere does not give benzaldehyde among the products. The formation of *N*-benzylphenylacetamide necessitates homolysis of

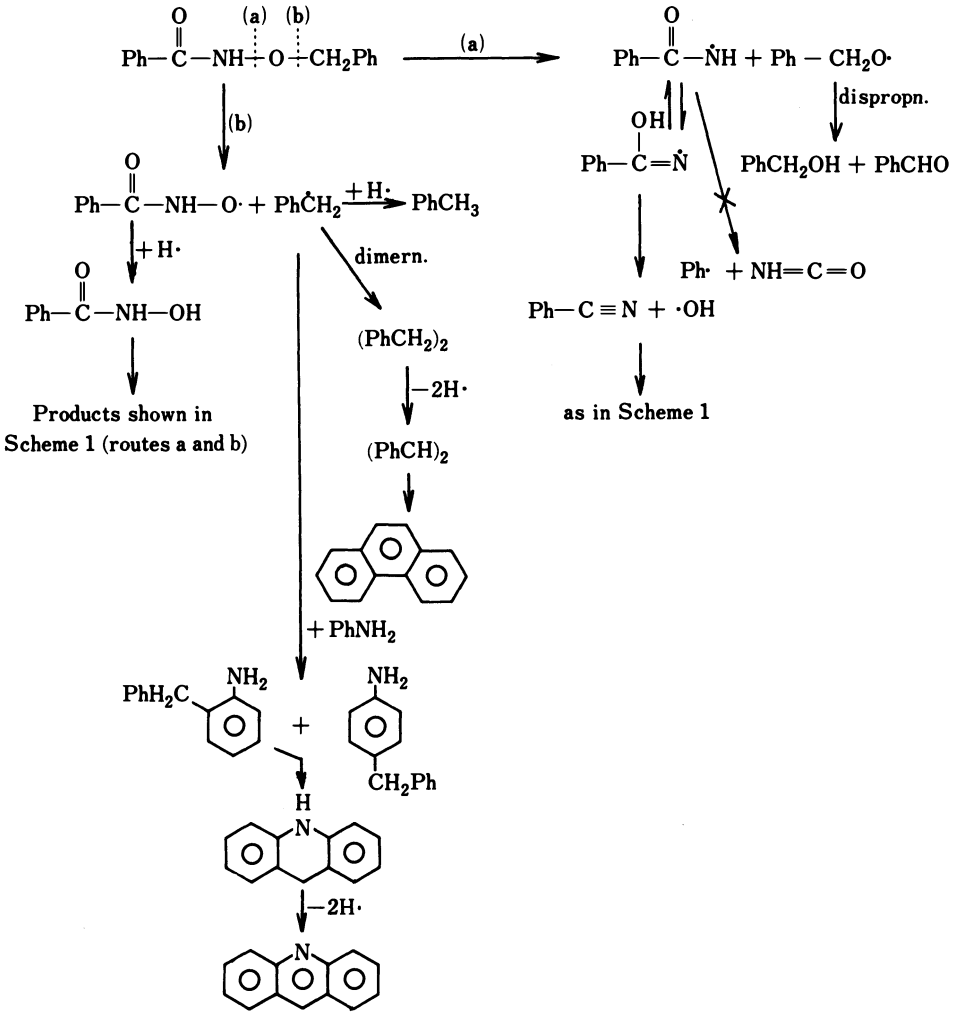

Scheme 2. Pyrolysis of BBA.

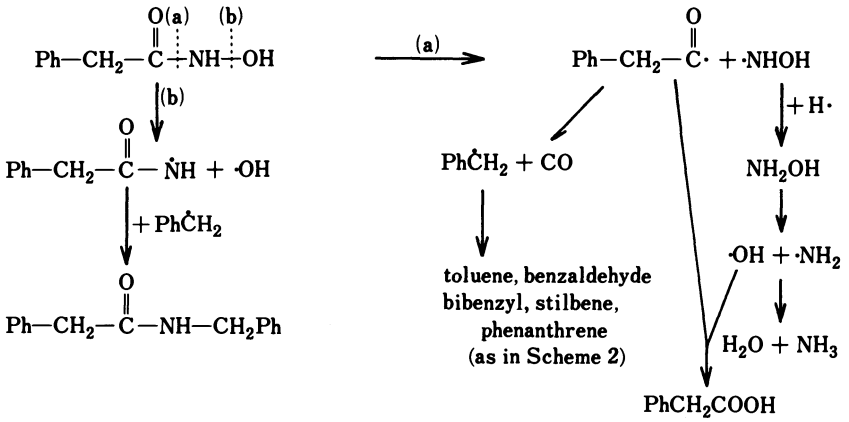

Scheme 3. Pyrolysis of PHA.

the N–OH bond (route b) forming hydroxyl and phenylacetylaminyl radicals. The latter subsequently couples with the benzyl radical. The normal fate of hydroxyaminyl free radicals is the formation of hydroxylamine as shown in case of BHA.

N-(Benzyloxy)phenylacetamide (BPAA) on pyrolysis by reflux in air gives the same products in addition to benzyl alcohol and benzaldehyde which are suggested to be formed through homolysis of the $-\overset{O}{\overset{\|}{C}}-\overset{|}{N}-$ bond forming phenylacetyl and benzyloxyaminyl free radicals.

The normal fate of phenylacetyl free radicals was discussed previously (Scheme 3), whereas the benzyl-

oxyaminyl radical abstracts hydrogen to form *O*-benzylhydroxylamine which subsequently undergoes homolysis of the N-O bond as shown in (Scheme 4). This was further confirmed by the results obtained from pyrolysis of *O*-benzylhydroxylamine where NH_3, H_2O, benzyl alcohol, and benzaldehyde were identified among the products.

Photolysis of BHA and BBA in acetonitrile solution at 280 nm at 25 °C affords analogous products to those obtained on pyrolysis. Hence it is reasonable to assume that the photolysis of these hydroxamic acid derivatives involves the homolytic cleavage of the N-O bond in the excited state forming aroylamino and alkyloxyl free radicals, which either react within the solvent cage affording the rearrangement products or escape out of the cage to give the fragmentation products so identified.

Experimental

All melting points are uncorrected. The IR spectroscopic

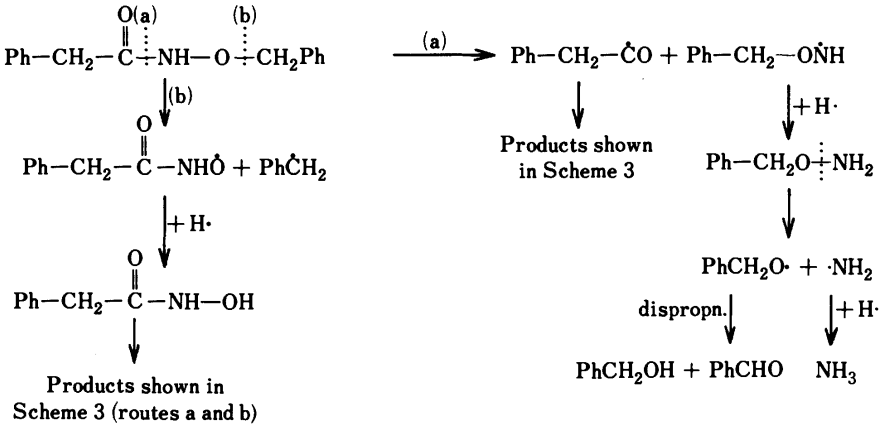

Scheme 4. Pyrolysis of BPAA.

Table 1. Thermolysis Products of Benzohydroxamic Acid and Its *O*-Benzyl Derivatives in Gram (%)

Expt. No.[a]			1	2
Expt. conditions			Reflux in air (30 min)	Reflux in air (5 h)
Products in gram (%)	Bp θ_b/°C/5 mmHg[p]	Mp θ_m/°C		
Ammonia			Evolved	Evolved
Carbon monoxide			Evolved	Evolved
Water			Drops	Drops
Toluene[b]			—	0.3(3.0)
Benzaldehyde[c]	45—55		—	0.7(7.0)
Benzyl alcohol[d]	60—70			0.8(8.0)
Bibenzyl[e]	108—122	52—53	—	0.4(4.0)
trans-Stilbene[f]	140—148	124	—	0.3(3.0)
Benzil[g]		95	0.2(2.0)	Trace*
Aniline[h]	62—75		3.2(32)	1.5(15)
o- and *p*-Aminodiphenyl methanes[i]	162—170		—	0.9(9.0)
Acridine[j]	192—200	107—110	—	0.2(2.0)
Phenoxazine[k]		153—155	0.4(4.0)	Trace
Benzanilide[l]		160—163	1.1(11)	1.5(15)
o- and *p*-Aminophenols[m]			1.5(15)	0.8(8.0)**
Benzoic acid[n]		120—122	1.4(14)	0.2(2.0)
Phenanthrene[o]		100	—	0.7(7.0)
Residue			1.1(11)	0.8(8.0)

a) Experiment 1 using benzohydroxamic acid and 2 using *N*-(benzyloxy)benzamide. b) 2,4-Dinitro derivative mixture mp 72 °C. c) Benzaldehyde estimated in the mixture by DNP formation mp 230—232 °C. d) n_D^{20} 1.5395; 3,5-dinitrobenzoate mp 113 °C. e) Mixture mp 52 °C, 4,4′-dinitro derivative mixture mp 179—180 °C. f) Mixture mp 124 °C. g) Mixture mp 96 °C.* Identified by preparative TLC using pet. ether (60—80°C)-acetone (5:1) v/v as eluent, *trans*-stilbene R_f=0.66, benzil R_f=0.9. h) n_D^{20} 1.5836; acetyl derivative mixture mp=113—114 °C. i) Separated by column chromatography on silica gel (100—150 mesh) using benzene as eluent, *o*-isomer 0.2 g, acetyl derivative mmp 135 °C and *p*-isomer 0.6 g, picrate mmp 179 °C. j) Mixture mp 111 °C. k) Mixture mp 152—153 °C. l) Mixture mp 161—163 °C. m) Separated by column chromatography silica gel (100—150 mesh) using benzene-ether (4:1) v/v as eluent, *o*-isomer 0.2 g, mmp 174 °C and *p*-isomer 1.2 g mmp 186 °C in case of benzohydroxamic acid; 0.15 g of *o*-isomer, 0.5 g of *o*-isomer in case of *O*-benzyl derivative**, *N*-benzyl derivative mmp 167 °C, 153—154 °C respectively. n) Mixture mp 120 °C. o) Mixture mp 109 °C; picrate derivative mp and mmp 143 °C. p) 1 mmHg=133.322 Pa.

analysis were carried out on a Pye-Unicam IR spectrophotometer, Model Sp. 200 G. GLC was carried out using a Pye-Unicam gas chromatograph series 104, with dual flame ionization detector, Model 24 and the column used was 20% SE 30 on Chromosorb W (35—80 mesh) at temperature 185 °C using nitrogen as carrier gas. Molecular weight determination of some reaction products was carried out by mass spectrophotometer, Model A.E.I.M.S. 902. Ultraviolet irradiation was carried out using Mallinkrodt 150 W mercury discharge lamp and the solutions were contained in open topped Pyrex beakers. ^{1}H NMR spectrum for some reaction products were obtained using EM-390 90 MHz NMR spectrometer.

Thermolysis of Arene-, Arylalkanehydroxamic Acids and *O*-Benzyl Derivatives: The arene- and arylalkanehydroxamic acid (10 g) was heated on an oil bath (bath temp 240 °C) for 30 min where frothing takes place or in a sealed tube under nitrogen atmosphere. The carbon monoxide evolved was detected by platinum chloride test paper. The ammonia gas evolved was detected by HCl. The products were separated into neutral, basic, phenolic and acidic components as in a previous work.[7] The separated products were subjected to further separation into their constituents by column chromatography and identified by TLC and GLC or by comparison of their infrared spectra with those of authentic samples.

The *O*-benzyl derivatives of these hydroxamic acids were pyrolyzed by refluxing for 5 h in air whereby ammonia and carbon monoxide were evolved and detected by chemical means. The pyrolysate was separated and detected as described before. The results are given in Tables 1 and 2.

Photolysis of Benzohydroxamic Acid and *O*-Benzyl Derivatives: A solution of BHA or BBA (1 g) in dry acetone (50 ml) was irradiated at room temperature (25 °C) for 20 h. The photolysate was separated as indicated in a previous work[9] into amine, acid and neutral products and analyzed by GLC as compared with authentic samples using nitrobenzene as internal standard. The results are summarized in Table 3.

Pyrolysis of *O*-Benzylhydroxylamine: *O*-Benzylhydroxylamine (10 g) was refluxed for 10 h. The ammonia evolved was detected by chemical means. The dark brown viscous product was subjected to fractional distillation under reduced pressure whereby the following products were obtained:

Product	Bp θ_b/°C /100 mmHg	gram(%)
NH_3	Evolved	—
Benzaldehyde	68	3.0(30)
Benzyl alcohol	85	3.15(31.5)
Unchanged hydroxylamine		2.80(28)

Pyrolysis of *N,N'*-Diphenyloxamide: A mixture of *N,N'*-diphenyloxamide (10 g) and naphthalene (20 g) was refluxed for 3 h whereby CO was evolved and detected by turning platinum chloride test paper grey. The dark brown viscous product obtained was subjected to distillation under reduced pressure where excess naphthalene (16 g) come over

Table 3. Photolysis Products of Benzohydroxamic Acid and Its *O*-Benzyl Derivatives

	BHA	BBA
Products, in gram (%)		
NH_3, CO gas	Exist	Exist
Benzaldehyde	—	0.15(15)
Bibenzyl	—	0.10(10)
Benzanilide	0.32(32)	0.25(25)
Benzoic acid	0.2(20)	0.15(15)
BHA	0.23(23)	0.10(10)
Unknown solid[a]	0.10(10)	0.08(8.0)
Ammonium benzoate	Trace	Trace

a) Unknown mp 119—120 °C. Analysis C, 69.78; H, 6.15; N, 11.53. ν band at 3350, 3150, >C=, at 1695, 1615 cm^{-1}.

Table 2. Thermolysis Products of Phenylacetohydroxamic Acid and Its *O*-Benzyl Derivatives in Gram (%)

Expt. No.[a]			1	2	3
Expt. conditions			Reflux in air (4 h)	Sealed tube at 270 °C (10 h)	Reflux in air (5 h)
Products in gram (%)	Bb θ_b/°C/5 mmHg	Mp θ_m/°C			
Ammonia			Evolved	Evolved	Evolved
Carbon monoxide			Evolved	Evolved	Evolved
Water			Drops	Drops	Drops
Toluene[b]	40—55		0.3(3.0)	0.8(8.0)	Trace
Benzaldehyde[c]			0.6(6.0)	—	2.1(21)
Benzyl alcohol[d]	60—70		—	—	0.9(9.0)
Bibenzyl[e]	110—125		1.2(12)	0.5(5.0)	0.8(8.0)
trans-Stilbene[f]	130—152		0.7(7.0)	0.3(3.0)	0.6(6.0)
Phenantherene[g]			0.5(5.0)	0.2(2.0)	Traces
N-Benzylphenylacetamide[h]		116—118	3.5(35)	3.1(31)	2.3(23)
Unknown solid[i]		147—148	—	2.6(26)	—
Phenylacetic acid[j]		77—78	0.2(2.0)	0.3(3.0)	Trace
Residue			1.4(14)	0.5(5.0)	1.5(15)

a) Experiments 1, 2 using phenylacetohydroxamic acid and 3 using *N*-(benzyloxy)phenylacetamide. b—g) As in footnote Table 1. h) Identified by mol. wt. determination (*m/z* 225), elemental analysis Calcd for $C_{15}H_{15}NO$: C, 80.00; H, 6.6, N, 6.2; Found: C, 79.88; H, 6.6; N, 6.3%, mixture mp and IR absorption spectrum are coincident with that of an authentic sample. i) Solid separated from (g) by column chromatography on silica gel (100—150 mesh) using pet. ether (60—80°) acetone (4:1 v/v) as eluent, analysis, C, 71.1; H, 6.4; N, 7.4%. j) Mixture mp 78 °C.

at first followed by aniline (2.5 g) bp 80 °C/10 mmHg and *N*-phenyl-1-naphthylamine (1.2 g), bp 200 °C/10 mmHg, which was triturated with pet. ether (40—60 °C) and crystallized from ligroine mp 62 °C. The residue was crystallized from ethanol to give 1-naphthanilide (3.2 g) mp and mixed mp 160—162 °C.

Reference Compounds: Benzohydroxamic acid,[10] crystals from ethanol, mp 129—130 °C.

N-(Benzyloxy)benzamide:[11] crystals from pet. ether (60—80 °C) mp 103—104 °C.

Phenylacetohydroxamic acid:[12] crystals from ethanol, mp 140—142 °C.

N-(Benzyloxy)phenylacetamide:[11] crystals from ethanol mp 71—72 °C.

trans-Stilbene:[13] crystals from ethanol, mp 123—4 °C.

Bibenzyl:[14] crystals from ethanol, mp 52 °C, 4,4′-dinitroderivatives, mp 180 °C.

Phenoxazine:[15] crystals from ethanol mp 152—154 °C.

o-Aminodiphenylmethane:[16] crystals from pet. ether (40—60 °C) mp 52 °C, *N*-acetyl derivative mp 135 °C.

p-Aminodiphenylmethane:[17] bp 165—167 °C/3 mmHg, crystals from pet. ether (40—60 °C) mp 34—36 °C, picrate, mp 179 °C.

N-Benzylphenylacetamide:[18] crystals from ethanol, mp 116—118 °C.

o-Benzylhydroxylamine:[19] bp 118—119 °C/30 mmHg; hydrochloride mp 238 °C.

N,N′-Diphenyloxamide:[20] crystals from benzene, mp 254 °C.

N,-Phenyl-1-naphthylamine:[21] crystals from ligroine mp 62 °C.

1-Naphthanilide:[22] crystals from ethanol, mp 160—161 °C.

References

1) J. A. Miller, "Chemical Carcinogenesis," Part A, ed by Paul O. P. Ts'O and J. A. Di Paolo, Marcel Dekker. Inc., N. Y. (1974), p. 61; T. Ohta, K. Shudo, and T. Okamoto, *Tetrahedron Lett.*, **33**, 1983 (1978).

2) H. Lossen, *Justus Liebigs Ann. Chem.*, **150**, 314 (1869); W. Lossen, *Ber.*, **16**, 873 (1883).

3) F. Tiemann, *Ber.*, **24**, 4162 (1891).

4) D. B. Denny and D. Z. Denny, *J. Am. Chem. Soc.*, **82**, 1389 (1960).

5) T. Sarkurai, S. Yamada, and H. Inoue, *Chem. Lett.*, **1983**, 975.

6) J. Betts and R. A. Back, *Can. J. Chem.*, **43**, 2678 (1965).

7) M. Z. A. Badr and M. M. Aly, *Can. J. Chem.*, **52**, 293 (1974); M. Z. A. Badr, M. M. Aly, G. M. El-Naggar, and A. M. Fahmy, *Z. Naturforsch.*, **34b**, 1128 (1979).

8) M. Z. A. Badr, M. M. Aly, and S. S. Salem, *Tetrahedron*, **33**, 3155 (1977); M. Z. A. Badr, M. M. Aly, and A. M. Fahmy, *Can. J. Chem.*, **58**, 1229 (1980).

9) M. Z. A. Badr, M. M. Aly, A. M. Fahmy, and F. F. Abdel-Latif, *Acta Chim. Sci. Hung.*, **109**, 223 (1982).

10) L. W. Jones and C. D. Hurd, *J. Am. Chem. Soc.*, **43**, 244 (1921).

11) J. H. Cooley, W. D. Bills, and J. R. Throckmorton, *J. Org. Chem.*, **25**, 1734 (1960).

12) W. M. Wise and W. W. Brandt, *J. Am. Chem. Soc.*, **77**, 1058 (1955).

13) D. A. Ballard and W. M. Dehn, *J. Am. Chem. Soc.*, **54**, 3969 (1932).

14) L. Cannizzaro and G. Rossi, *Justus Liebigs Ann. Chem.*, **121**, 251 (1862).

15) K. Hawas and G. Mougin, *Ber.*, **47**, 1884 (1893).

16) C. L. Hewett, L. J.; Lermit, H. T. Openshaw, A. R. Todd, A. H. Williams, and F. N. Woodward, *J. Chem. Soc.*, **1948**, 292.

17) W. J. Hickinbotton, *J. Chem. Soc.*, **1937**, 119.

18) A. H. Cook and I. M. Heilbron, "Chemistry of Penicillin," ed by H. T. Clarke, (1949), p. 921.

19) E. L. Schumann, R. V. Heinzelman, M. E. Greig, and W. Veldkamp, *J. Med. Chem.*, **7**, 329 (1964).

20) J. T. Bornwater, *Rec. Trav. Chim.*, **31**, 108 (1912).

21) E. Knoevenagel, *J. Prakt. Chem.*, **89**, 17 (1914).

22) R. T. Howard and A. Simons, *J. Chem. Soc.*, **1952**, 2849.

The Effect of "Chemiluminescence Quenching" on the Chemiluminescence Quantum Yields from 9-Benzylacridine and 9-Benzyl-10-methylacridinium Iodide

Isao KAMIYA,* Takashi SUGIMOTO, and Kuniaki YAMABE†
Department of Chemistry, College of General Education, Nagoya University, Chikusa-ku, Nagoya 464-01
†Department of Industrial Chemistry, Sasebo Technical College, Sasebo 857-11
(Received October 29, 1987)

Synopsis. A visible chemiluminescence (CL) has been found from the air oxidation of 9-benzyl-10-methylacridinium iodide, in contrast to the case of 9-benzylacridine, from which only a feeble CL could be detected. The difference in the CL quantum yields from the acridinium salt and acridine is interpreted in terms of a "CL quenching" of the chemiexcited species by benzaldehyde generated simultaneously in a solvent cage.

We have found a visible chemiluminescence (CL) of 9-benzyl-10-methylacridinium iodide[1] (**1**) upon base-catalyzed air oxidation: a solution of potassium *t*-butoxide (*t*-BuOK) in *t*-butyl alcohol (*t*-BuOH) (2×10^{-2} mol dm^{-3}, 0.2 cm^3) was added to an aerated solution of **1** in *N*,*N*-dimethylformamide (DMF) (1.0×10^{-4} mol dm^{-3}, 2.0 cm^3) at 313 K. The CL emission with a peak at 415 nm showed the same spectral distribution as that of the fluorescence of 10-methylacridone (**3**) and the spent reaction mixture. Benzaldehyde was detected as one of the reaction products by gas chromatography. The overall CL quantum yield was determined to be 2.5×10^{-3}. The reaction pathway involving the cleavage of 10-methyl-4′-phenylspiro[acridine-9(10*H*),3′-[1,2]-dioxetane] **2** shown in Scheme 1 seems most probable for the CL of **1**, since **2** is known to give singlet, excited 10-methylacridone (**3***), together with benzaldehyde, on decomposition.[2] In a previous paper,[3] a similar reaction pathway via the cleavage of a dioxetane intermediate **5** to give excited singlet acridone anion (**6***), shown as Scheme 2, was presented as the mechanism[4] for the CL of 9-alkylacridines. Among these, 9-methylacridine (**4c**) produced the excited product **6*** in a relatively high CL quantum yield (6.3×10^{-3}), while 9-benzylacridine (**4a**) and 9-(diphenylmethyl)acridine (**4b**) produced **6*** in extremely low yields (1.5×10^{-6} and 1.1×10^{-5} respectively), in spite of the high yield of unexcited acridone anion (**6**). Thence, there remained the problem of why the CL quantum yields from **4a** and **4b** are far lower than those from **4c** and **1**.

Recently, Perkizas and Nikokavouras[5] have proposed a "CL quenching" process of an excited moiety by the simultaneously produced leaving moiety in a solvent cage: an efficient quenching would arise through molecular collision inside the solvent cage if the quenching probability per collision were great. This paper will present some experimental results giving support to the idea that the low CL quantum yields from **4a** and **4b** are due to a CL quenching.

When the CL quenching arises through the collision of two moieties produced inside a solvent cage, the apparent CL quantum yield (Φ) is given approximately by the following equation:

$$\Phi = \Phi^\circ k_{-d}/(k_{-d} + k_e)$$

where Φ° is the proper CL quantum yield, obtained as the product of the yield of the excited product from the substrate and the fluorescence quantum yield of the

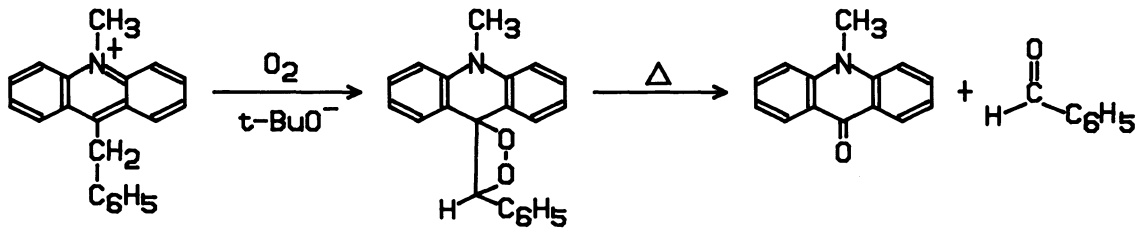

Scheme 1.

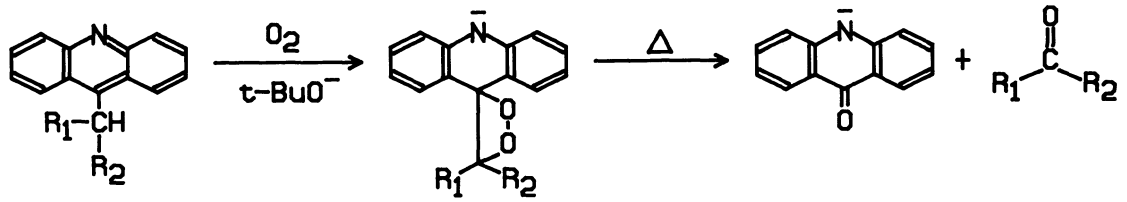

Scheme 2.

excited product, k_{-d} is the rate constant of the moieties to get out of the cage, and k_e is the rate constant for energy transfer by collision.

The Stern-Volmer constant (K_{sv}) for the quenching is given by the following convenient equation:

$$K_{sv} = (I_0/I - 1)/[Q] = k_q\tau$$

where I_0 and I are the fluorescence intensities of an excited species in the absence and in the presence of a quencher Q at a given concentration [Q], k_q is the quenching rate constant, and τ is the lifetime of the excited species in the absence of Q. When the quenching arises via a diffusion controlled encounter in a solvent cage, k_q is given approximately by the following equation:

$$k_q = k_d k_e/(k_e + k_{-d}) = k_d p$$

where k_d is the rate constant for the molecular diffusion in the fluid solution and p is the quenching probability per encounter. Thus, Φ is given by:

$$\Phi = \Phi^\circ(1 - k_q/k_d) = \Phi^\circ(1 - p)$$

If the two CL systems, I and II, are assumed to posses similar k_d and Φ°, the following relation is established:

$$\Phi(\mathrm{I})/\{1 - p(\mathrm{I})\} = \Phi(\mathrm{II})/\{1 - p(\mathrm{II})\} = \Phi^\circ$$

Thus, the effect of the CL quenching on the CL quantum yield can be interpreted by taking account of the value of p ($=k_q/k_d$) obtained from the Stern-Volmer analysis.

The plot of $I_0/I-1$ versus [Q] for the quenching of **3*** and **6*** by benzaldehyde and of **6*** by benzophenone in DMF solutions containing *t*-BuOK and *t*-BuOH at 313 K were determined; the slopes of the lines gave the values of K_{sv}(**1**)=10.3, K_{sv}(**4a**)=145, and K_{sv}(**4b**)=144 $dm^3\,mol^{-1}$.[6] From the values of K_{sv} and τ (7.6×10^{-9} s)[7,8], k_q(**1**), k_q(**4a**), and k_q(**4b**) were calculated to be 1.4×10^9, 1.9×10^{10} and 1.9×10^{10} $dm^3\,mol^{-1}\,s^{-1}$ respectively.

These experimental values give the following relation:

$$1.5\times10^{-6}/\{1 - p(\mathbf{4a})\} = 1.1\times10^{-5}/\{1 - p(\mathbf{4b})\} = 2.5\times10^{-3}/\{1 - p(\mathbf{1})\} = \Phi^\circ$$

Since $\Phi^\circ \geqq 2.5\times10^{-3}$, the values of $1-p$(**4a**) and $1-p$(**4b**) might be very small, indicating that $k_d \sim k_q$(**4a**)$\sim k_q$(**4b**)$\sim 1.9\times10^{10}$ $dm^3\,mol^{-1}\,s^{-1}$, though the value is somewhat larger than that calculated by the use of $k_d = 8RT/3\eta$.[9] Taking $k_d = 1.90\times10^{10}$ $dm^3\,mol^{-1}\,s^{-1}$, a large value of $1-p$(**1**) is obtained by the following calculation:

$$1 - p(\mathbf{1}) = 1 - 1.4\times10^9/1.9\times10^{10} = 0.93$$

It is, therefore, reasonable to conclude that an efficient CL quenching arises in the CL system of **4a** and **4b** because of the extremely low value of $1-k_q/k_d$ whereas no remarkable CL quenching occurs in the CL of **1** because of the large value of $1-k_q/k_d$.

No appreciable quenching of **6*** by formaldehyde[10] was observed. Thence, the much higher CL quantum yield from **4c** than from the analogues seems to be attributable to the absence of "CL quenching".

Experimental

Materials. The 10-methyl-9(10*H*)-acridone (Aldrich) and 9(10*H*)-acridone (Tokyo Kasei) were chromatographically pure. The luminol was recrystallized from dilute hydrochloric acid prior to use. The benzaldehyde and benzophenone were purified by distillation prior to use.

Measurement of CL and Fluorescence. The intensity and spectrum of CL were measured on a Opelecs CLS-1 chemiluminescence spectrophotometer equipped with a R446 photomultiplier and 1200/mm grating. The overall CL quantum yield, defined as (total light per unit volume)/(the initial concentration of the substrate), was determined from the ratio of the total light emitted from the CL of the substrate to that from a standard luminol solution in the same way as has been described previously.[3] The fluorescence spectrum was measured on a Hitachi MPF-2A fluorescence spectrophotometer.

We wish to express our gratitude to Prof. Jiro Tanaka and Dr. Nobuaki Kanamaru (Department of Chemistry, Faculty of Science, Nagoya University) for the measurement of the lifetime of the excited species and to Prof. Motoo Yasuda and Mr. Kiyoshi Mizutani (Department of Chemistry, College of General Education, Nagoya University) for the measurement of the viscosity.

References

1) H. Decker and T. Hock, *Chem. Ber.*, **37**, 1565 (1904).

2) F. McCapra, I. Beheshti, A. Burford, R. A. Hann, and K. A. Zaklika, *J. Chem. Soc., Chem. Commun.*, **1977**, 944; C. Lee and L. A. Singer, *J. Am. Chem. Soc.*, **102**, 3823 (1980).

3) I. Kamiya, T. Sugimoto, and K. Yamabe, *Bull. Chem. Soc. Jpn.*, **57**, 1735 (1984).

4) An analogous mechanism was proposed by E. H. White and M. J. Harding in *Photochem. Photobiol.*, **4**, 1129 (1965).

5) G. Perkizas and J. Nikokavouras, *Monatsh. Chem.*, **117**, 89 (1986).

6) For the quenching of **3*** by benzaldehyde, we use the symbol K_{sv}(**1**), since **3*** and benzaldehyde are produced from **1**. Similarly, K_{sv}(**4a**) and K_{sv}(**4b**) are used to symbolize the quenching of **6*** by benzaldehyde and benzophenone respectively.

7) Since the values of τ of **3*** and **6***, as determined on a nano-second fluorimeter equipped with a Lomonics TE-type XeCl Laser (excited at 308 nm), were both ca. 1×10^{-8} s, the value (7.6×10^{-9} s) in the literature[8] was employed for the calculation of k_q.

8) K. D. Legg and D. M. Hercules, *J. Am. Chem. Soc.*, **91**, 1902 (1969).

9) The viscosity of DMF containing *t*-BuOK and *t*-BuOH was determined to be 6.6×10^{-4} $kg\,m^{-1}\,s^{-1}$ at 313 K. Using the value, k_d was calculated to be 1.1×10^{10} $dm^3\,mol^{-1}\,s^{-1}$.

10) A solution of formaldehyde in DMF (ca. 0.5 mol dm^{-3}, 0.2 cm^3), prepared by dissolving gaseous formaldehyde (*Org. Synth.*, Coll. Vol. 1, p. 80), was added to 2.0 cm^3 of a solution of acridone anion or 10-methylacridone in DMF containing *t*-BuOK.

The ^1H and ^{13}C NMR of the Tetraphenylcyclopentadienone Dianion

Masatoshi HIRAYAMA,* Kazuhiko KOIWAI, Kazumi TAKEMURA, Masaaki KOBAYASHI, Akihiko SEKI, and Kensuke TAKAHASHI†
Department of Chemistry, Faculty of Science, Ibaraki University, 2-1-1 Bunkyo, Mito 310
†Department of Applied Chemistry, Nagoya Institute of Technology, Gokiso-cho, Showa-ku, Nagoya 446
(Received December 1, 1987)

Synopsis. The stable monomer dianion of the title compound was formed by the contact of its tetrahydrofuran-d_8 or 1,2-dimethoxyethane-d_{10} solution with sodium metal at 5 °C and was characterized by means of its ^1H and ^{13}C NMR spectra.

It has been known that the alkali metal salts of aromatic ketyls ($A^{\cdot-}M^+$) generated by alkali-metal reduction in an ethereal solvent tend to change competitively to a diamagnetic dimer dianion ($A_2^{2-}2M^+$) and a diamagnetic monomer dianion ($A^{2-}2M^+$) via a paramagnetic ketyl dimer $(A^{\cdot-}M^+)_2$[1] and that the latter change is dominant in 2-methyltetrahydrofuran, generally causing a pronounced ion pairing with alkali metal.[1a] Recently, the monomer dianion of fluorenone has been precisely investigated by means of NMR in our laboratory.[2] We wish to report here on the monomer dianion of sterically hindered tetraphenylcyclopentadienone (**1**).

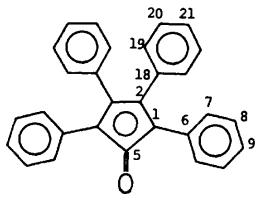

1

Experimental

Compound **1** (Aldrich Co., Ltd.) was used without further purification. Tetrahydrofuran(THF)-d_8 and 1,2-dimethoxyethane(DME)-d_{10} (Canada MSD Co., Ltd.) used as the solvents were dried, degassed, and stored over sodium/potassium in vacuo. 0.2 mol dm^{-3} THF-d_8 and DME-d_{10} solutions of **1** were in contact with a clean sodium mirror in high vacuum at 5 °C in a Pyrex cell fused with an NMR tube. The ^1H NMR spectra were measured on JEOL GX-400 (400 MHz) and Varian XL-200 (200 MHz), and the ^{13}C NMR spectra on JEOL FX-90Q (22.5 MHz) and Varian VXR-300 (75 MHz) at room temperature. The ESR and ENDOR spectra were observed on JEOL JES-FE1XG and Varian E-1700, respectively in order to confirm the disappearance of the ketyl radical of **1**. The MO calculation of the charge density was performed on HITAC M-240H at Ibaraki University, the program used for the CNDO calculation being Y4CB04[3] in the library programs of the University of Tokyo.

Results and Discussion

The contact of **1** with sodium in THF-d_8 or DME-d_{10} gave first a reddish-purple species revealing an ESR and an ENDOR spectra, which can be identified with the radical anion of **1**.[4] Upon continued contact, it gradually turned orange, the ESR signal of $\mathbf{1}^{\cdot-}$ disappeared, and a new NMR spectrum developed simultaneously. The ^1H and ^{13}C NMR spectra of this new diamagnetic species **1a**, as observed in THF-d_8 after complete reduction, are shown in Figs. 1 and 2 respectively, along with those of **1**. The addition of a reducible aromatic compound, 2-nitroacetophenone, to **1a** led to the ESR spectrum of the radical anion of this compound, while the quenching of **1a** with oxygen gas regenerated **1**. The ^1H spectrum of **1a** consists of two sets of AA'BB'C patterns separated from each other; they can be clearly distinguished in terms of the H-H shift correlation 2D NMR, and its spectral center of gravity shifts toward a field higher by 0.29 ppm than that of **1** (Table 1). The observed number of lines in the ^{13}C spectrum of **1a** is equal to that in **1**; furthermore, a line with a particularly weak intensity is included, as in **1**. Its center of gravity was found to shift toward a field higher by 5.73 ppm than that of **1**. The fact that both the ^1H and ^{13}C NMR patterns of the orange species produced in THF are completely identical with those in THF-d_8 implies that **1a** does not arise from a possible diamagnetic anion formed by the subtraction of a proton from the solvent. The ^{13}C line with a particularly weak intensity appears at a field much lower than an aliphatic region, although it shifts toward a considerably higher field than that of **1**. These experimental

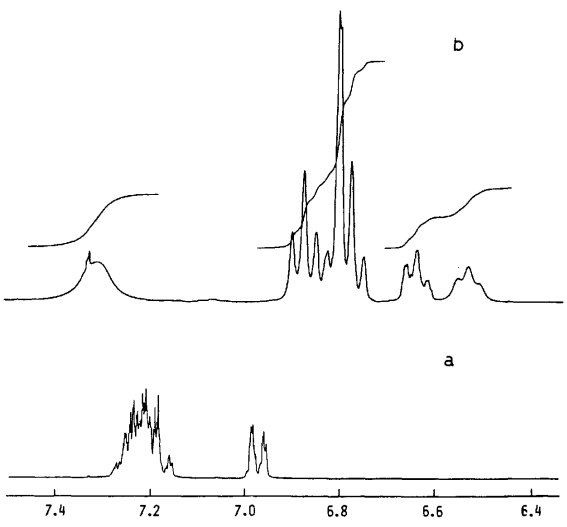

Fig. 1. ^1H NMR spectra of **1** (a) (400 MHz) and $\mathbf{1}^{2-}$ (b) (200 MHz) in THF-d_8.

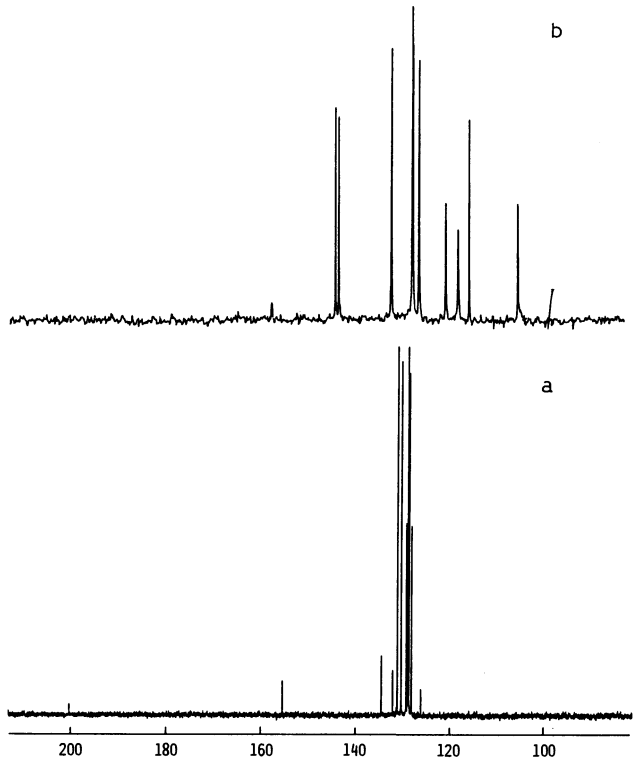

Fig. 2. ^{13}C NMR spectra of **1** (a) (75 MHz) and $\mathbf{1}^{2-}$ (b) (22.5 MHz) in THF-d_8.

Table 1. Chemical Shifts in ppm[a)]

	δ_N	δ_D	$\Delta\delta$[a)]
H7	7.21±0.05	7.31	−0.01±0.05
8	7.21±0.05	6.88	0.33±0.05
9	7.21±0.05	6.58	0.63±0.05
19	6.98	6.80	0.18
20	7.21±0.05	6.78	0.43±0.05
21	7.21±0.05	6.64	0.57±0.05
C1	126.07	116.16	9.91
2	155.37	105.97	49.40
5	200.20	157.82	42.38
6	134.41	143.68[c)]	−9.27[c)]
7	131.03	128.13	2.90
8	128.59	128.02	0.57
9	129.19	118.54	10.65
18	132.01	144.38[c)]	−12.37[c)]
19	130.21	132.52	−2.31
20	128.83	126.67	2.16
21	128.06	121.09	6.97

a) Relative to TMS. Positive signs denote low-field shifts. δ_N: **1**, δ_D: $\mathbf{1}^{2-}$. b) $\Delta\delta=-(\delta_D-\delta_N)$. c) Assigned tentatively.

results thus show that **1a** can be attributed to a monomer dianion of **1**, $\mathbf{1}^{2-}$, or its disodium salt, $\mathbf{1}^{2-}2Na^+$, and that the formation of a possible pinacolate-type dimer dianion can, therefore, be ruled out.

The higher-field doublet in the ^1H NMR of **1** was assigned to H_{19} using lanthanoid-induced shifts due to Eu(fod)$_3$. In the ^1H spectrum of $\mathbf{1}^{2-}$ it may be considered that an AA'BB'C group with a much lower-field doublet corresponds to the C_6—C_{11} ring, considering the anisotropic effect of the carbonyl group. The assignment of the ^{13}C spectrum of **1** was that in the literature.[5)] For $\mathbf{1}^{2-}$, all the tertiary carbons were assigned using the C–H shift correlation 2D NMR combined with proton assignments. C_5 can be distinguished from the other quaternary carbons in terms of its long T_1, as in **1**. The MO calculations by the INDO method[6)] reveal that most of the excess π-charge densities of $\mathbf{1}^{2-}$ from **1**, Δq_c^{π}'s, occupy the cyclopentadienone moiety; the calculated ^{13}C shifts of $\mathbf{1}^{2-}$ from **1** ($\Delta\delta_c$), estimated using the standard value of k_c, 160 ppm/electron, in $\Delta\delta_c=k_c\cdot\Delta q_c^{\pi}$, are 19.5, 62.5, and 46.6 ppm for C_1, C_2, and C_5 respectively.[7)] With the aid of these results, the lines appearing at δ 116.16 and 105.97 were assigned to C_1 and C_2 respectively, while those at δ 144.59 and 143.59 were assigned to C_6 and C_{18}, but C_6 and C_{18} were indistinguishable from each other. Thus, the observed ^{13}C shift pattern of $\mathbf{1}^{2-}$ is, on the whole, consistent with that expected from theoretical considerations.

References

1) a) N. Hirota and S. I. Weissman, *J. Am. Chem. Soc.*, **86**, 2538 (1964); b) N. Hirota, *ibid.*, **89**, 32 (1967); c) K. S. Chen, S. W. Mao, K. Nakamura, and N. Hirota, *ibid.*, **93**, 6004 (1971); d) T. Takeshita and N. Hirota, *ibid.*, **93**, 6421 (1971).

2) M. Hirayama, H. Suzuki, and H. Ohhata, *Chem. Lett.*, **1987**, 413; M. Hirayama and H. Ohhata, *Bull. Chem. Soc. Jpn.*, **60**, 2751 (1987).

3) This program was prepared on the basis of J. A. Pople, D. C. Beveridge, and P. A. Dobosh, *J. Am. Chem. Soc.*, **90**, 4201 (1968).

4) To be published.

5) L. Knothe and H. Prinzbach, *Liebigs Ann. Chem.*, **1977**, 687.

6) The averaged atomic coordinates from the crystallographic data (J. A. Potenza, R. J. Johnson, R. Chirico, and A. Efraty, *Inorg. Chem.*, **16**, 2354 (1977)) were used.

7) For the phenyl carbons, the pattern of the values of $\Delta\delta$(calcd) does not correlate well with that of $\Delta\delta$(obsd). Also, for the ring protons, the values of $\Delta\delta_H$ calculated using k_H=10.7 ppm/electron in $\Delta\delta_H=k_H\cdot\Delta q_c^{\pi}$ does not correspond well with those of $\Delta\delta_H$(obsd). These results may be accounted for by the fact that the polarization effect of the excess π-charge density at a carbon atom on the ^1H or ^{13}C shift does not become predominant over some other contributions to the ^1H or ^{13}C shift of the dianion from its neutral precursor, for the excess π-charges in the phenyl rings decrease considerably because of the very weak π-conjugation between the cyclopentadienyl and phenyl rings.

Studies of the Stabilities of Scandium, Yttrium, and Lanthanoid-Ion Complexes of 2-Nitroso-5-(*N*-propyl-3-sulfopropylamino)phenol

Isao YOSHIDA,* Fumio SAGARA, and Keihei UENO
Department of Industrial Chemistry, Kumamoto Insutitute of Technology,
Ikeda 4-22-1, Kumamoto 860
(Received December 4, 1987)

Synopsis. The stability constants of the 1:1 complexes formed by 2-nitroso-5-(*N*-propyl-3-sulfopropylamino)phenol (NPSAP: H_2L) with tervalent scandium, yttrium, and lanthanoids, but not promethium, have been determined potentiometrically in aqueous solutions at an ionic strength of 0.1 with potassium nitrate and at 25 °C. The stability constants of the 1:1 complexs increased with the increase in the atomic number of the lanthanoid, with the slight decrease at gadolinium. The stability constant of the 1:1 complex of scandium was the highest among the metal complexes investigated, while that of the yttrium complex was found to be between those of the cerium and praseodymium complexes.

Many studies have been reported on the complexing behavior of *o*-nitrosonaphthols,[1-6] such as 2-nitroso-1-naphthol-4,8-disulfonic acid with tervalent lanthanoid ions, and the stability constants for these complexes, including those for scandium(III) and yttrium(III) complexes,[5] have been discussed with respect to the structures of the ligands, the basicity of the donor atoms, and the relative sizes of central metal ions.[4]

Recently, 2-nitroso-5-(*N*-propyl-3-sulfopropylamino) phenol (NPSAP: H_2L) has been synthesized as a water-soluble nitrosophenol derivative and found to be a useful chromogenic reagent for iron[7] and cobalt.[8] The chelating behavior of the reagent with some bi- and ter-valent metal ions has also been described.[9] This paper will report on the chelating behavior of this particular ligand for tervalent lanthanoid ions, including scandium(III) and yttrium(III) ions, in order to provide more detailed information on the nature of *o*-nitrosophenols as ligands.

Experimental

The apparatus and methods were the same as those described in a recent paper.[9] All the measurements were carried out at 25±0.5 °C and at an ionic strength of 0.1 with potassium nitrate. All of the 0.01 M (1 M=1 mol dm^{-3}) stock solutions of the metal ions, except for those of thulium and lutetium, were prepared by dissolving their chlorides or nitrates in water. As to the two metal ions mentioned, their oxides were dissolved in hydrochloric acid; the solution was then boiled to dryness to expel the excess hydrochloric acid and subsequently diluted with water. The metal-ion concentrations, of the stock solutions were determined by EDTA titration.[10] The mathematical analysis of the chelating behavior of the ligand and the calculations of their stability constants were carried out by the use of the SUPERQUAD program[11] on potentiometric data, using $\log K_1^H=8.23$ and $\log K_2^H=2.61$ as the protonation constants of the ligand.[9]

Results and Discussion

The interpretation of the potentiometric data obtained from the titration of a 3:1 (ligand-to-metal) mixture of NPSAP with each of the lanthanoids, scandium, and yttrium ions indicated that, in most cases, only 1:1 complexes were formed when $-\log[H^+]$ was raised to about 4.8 by adding potaasium hydroxide. The results obtained on the stability constants for the 1:1 complexes are given in Table 1, as $\log \beta_1$, where $\beta_1=[ML^+]/[M^{3+}][L^{2-}]$, together with their computed standard deviations. The formation of the 2:1 complexes was observed on some metal ions; these results are also given in Table 1, as $\log \beta_2$, where $\beta_2=[ML_2^-]/[M^{3+}][L^{2-}]^2$.

No protonated or polynuclear complex species could be found in this system. It was impossible to increase the value for $-\log[H^+]$ to such an extent that any reliable data for the possible higher complexes could be found. The increase in the ligand-to-metal ratio would result in the formation of higher complexes; however, the titrations on such a mixture were not carried out in this experiment. A series of stability constants for the 1:1 complexes with fourteen lanthanoid metal ions is illustrated in Fig. 1, together

Table 1. Stability Constants of 1:1 Metal Complexes of Scandium, Yttrium, and Lanthanoid Ions with 2-Nitroso-5-(*N*-propyl-3-sulfopropylamino)-phenol at 25 °C and at I=0.1 (KNO_3)

Metal ion M^{3+}	$\log \beta_1$ (st. dev.)
Sc	7.48 (0.007)
Y[a]	5.52 (0.006)
La	5.09 (0.003)
Ce	5.43 (0.003)
Pr	5.61 (0.003)
Nd	5.70 (0.003)
Sm	5.86 (0.002)
Eu	5.85 (0.001)
Gd[b]	5.70 (0.006)
Tb	5.81 (0.003)
Dy	5.85 (0.003)
Ho	5.86 (0.003)
Er	5.94 (0.003)
Tm	6.03 (0.005)
Yb	6.13 (0.001)
Lu[c]	6.03 (0.007)

a) $\log \beta_2$=10.06(0.03). b) $\log \beta_2$=10.06(0.15). c) $\log \beta_2$=11.01(0.07).

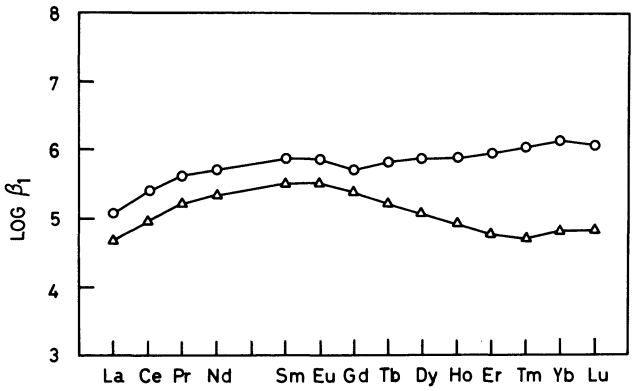

Fig. 1. Stability constants of the 1:1 complexes of lanthanoid ions with NPSAP (-○-) and 2-nitroso-1-naphthol-4,8-disulfonic acid (-△-) at 25°C and at I=0.1 (KNO_3).

with the corresponding values for 2-nitroso-1-naphthol-4,8-disulfonic acid.[4]

It seems from this figure that the stability trends of the complexes with the earlier half of the series of metal ions resemble each other among the two ligands. However, as to the later half of the series, the stability trends of the complexes with both ligands show a rather noticeable difference. The stability constants of the NPSAP complexes increase very slightly with an increase in the atomic number from gadolinium to ytterbium, whereas those of 2-nitroso-1-naphthol-4,8-disulfonic acid decrease from gadolinium to thulium.

According to Moeller et al., the trends in the stability-constant data for the lanthanoid elements heavier than gadolinium can be divided qualitatively into three groups; a group of ligands for which there is a regular increase in the stability constants, a group of ligands for which the stability constants have nearly the same values, and a group of ligands for which the stability constants decrease slightly.[12] The stability trend of NPSAP may be classified as that of the second group of ligands.

It has also been pointed out by the same authors that the value of the stability constant of the yttrium complex of this group of ligands was among those for light lanthanoid elements. The fact that the position of the stability constant of the yttrium complex with NPSAP was found between cerium and praseodymium complexes also suggests that NPSAP belongs to the second group.

The stability constants of the NPSAP comlexes with all of the lanthanoid ions are higher than that of 2-nitroso-1-naphthol-4,8-disulfonic acid, as is shown in Fig. 1. The relatively higher values of the stability constants of NPSAP compared with those for nitrosonaphthols were also observed on other metal ions, such as zinc(II) and copper(II).[9] Such a high stability of the NPSAP complexes may be ascribed to its higher basicity of phenolic oxygen compared to that of nitrosonaphthols.[9]

The stability constant of the scandium(III) complex is markedly higher than those of the lanthanoid complexes; this may be due to the smaller ionic radius of the scandium ion compared to those of the lanthanoid ions.[13]

The stability constants of the yttrium and lanthanum complexes of NPSAP are found to be in the order of $Cu^{2+}>Ni^{2+}>Y^{3+}>La^{3+}>Zn^{2+}$,[9] just as one can see in the case of the nitroso R acid complexes.[14]

References

1) O. Makitie, *Suom. Kemistil. B*, **40**, 267 (1967).
2) O. Makitie, *Suom. Kemistil. B*, **41**, 31 (1968).
3) R. Petrola and O. Makitie, *Suom. Kemistil. B*, **46**, 10 (1973).
4) H. Saarinen, *Suom. Kemistil. B*, **46**, 250 (1973).
5) H. Saarinen, *Suom. Kemistil. B*, **46**, 333 (1973).
6) H. Saarinen, *Acta Chem. Scand.*, **A28**, 589 (1974).
7) S. Saito, D. Horiguchi, and K. Kina, *Bunseki Kagaku*, **30**, 635 (1981).
8) I. Yoshida and K. Ueno, *Bunseki Kagaku*, **34**, 77 (1985).
9) I. Yoshida, F. Sagara, and K. Ueno, *Anal. Sci.*, **4**, 41 (1988).
10) K. Ueno,. "Kire-to Tekitei-ho," Nankodo, Tokyo (1956).
11) P. Gans, A. Sabatini, and A. Vacca, *J. Chem. Soc., Dalton Trans.*, **1985**, 1195.
12) T. Moeller, O. F. Martin, L. C. Thompson, R. Ferrus, G. R. Feistel, and W. J. Randall, *Chem. Rev.*, **65**, 1 (1965).
13) Y. Sasada, "Kagaku Binran, Kiso II," ed. by Nippon Kagaku Kai, Maruzen, Tokyo(1984), p. 717, and the references cited therein.
14) O. Makitie, *Suom. Kemistil. B*, **40**, 27 (1967).

The Thermal Decomposition of 1-Methyl-1-phenylethyl 2,2-Dimethylperoxypropionate in Cumene

Takeshi KOMAI, Kenji KATO, and Kazuo MATSUYAMA*
Chemical & Explosives Research Laboratory, Nippon Oil & Fats Co., Ltd.,
Taketoyo-cho, Chita-gun, Aichi-ken 470-23
(Received October 29, 1987)

Synopsis. The thermal decomposition of 1-methyl-1-phenylethyl 2,2-dimethylperoxypropionate was studied in cumene. Based on the kinetic parameters and the decomposition products, it was concluded that the peroxyester was decomposed mainly by means of the radical process in cumene.

Most studies[1] concerning the thermal decomposition mechanism of 1-methyl-1-phenylethyl peroxyesters have indicated that these peroxyesters are rather decomposed ionically as is shown in Eq. 1, compared with 1,1-dimethylethyl analogues which

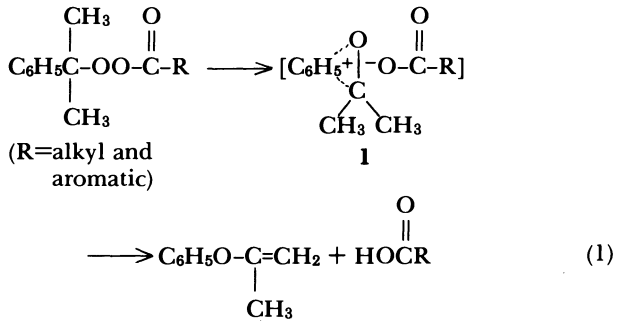

are decomposed by a radical process.[2] Leffler and Scrivener[3] have reported that 1-methyl-1-phenylethyl peroxyacetate is decomposed in toluene by means of competing radical (75%) and ionic (25%) pathways, based on the decomposition product. However, several reports[4] and patents[5] published more recently, have indicated that 1-methyl-1-phenylethyl 2,2-dimethylperoxypropionate (**2**) and 2,2-dimethylperoxyoctanoate can initiate the radical polymerization of vinyl monomers, such as methyl methacrylate, vinyl chloride, and ethylene. For the purpose of understanding this contradiction, we studied the thermal decomposition of **2** in cumene.

Results and Discussion

The rates of the thermal decomposition of **2** in cumene were determined by following the decrease in the peroxycarbonyl in the infrared spectra. The first-order rate constants were obtained with no appreciable change for a 10-fold increase in the peroxyester concentration. The results are given in Table 1 in order to compare them with those of the 1,1-dimethylethyl analogue.[2b] The liquid part of the decomposition products was analyzed using GLC; the results are shown in Table 2. In a separate analysis with HPLC, phenol was detected, but the amount was only 0.004 mol per mol of the decomposed peroxyester. These results indicate that the **2** was decomposed almost quantitatively by means of the radical process in cumene. The first reason is that the activation parameters are similar to those of the 1,1-dimethylethyl analogue (Table 1). This means that **2** in cumene decomposes homolytically in the same

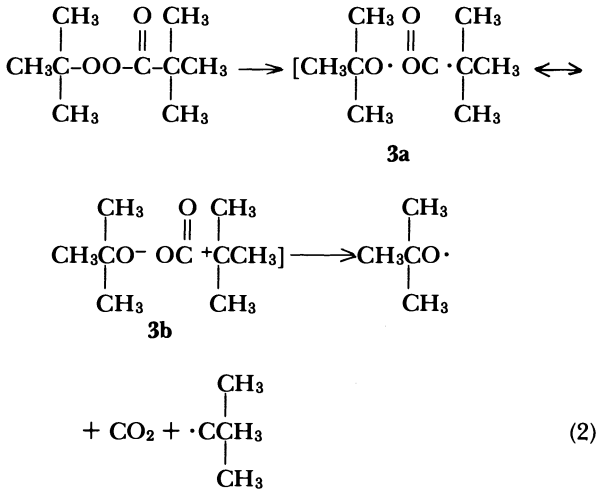

Table 1. Decomposition Rates and Activation Parameters in Cumene

R in $RC(CH_3)_2OOCC(CH_3)_3$	Concn M[a]	Initial temp °C	Rate const. $10^5 k_d/s^{-1}$	Activation parameter ΔH^*/kJ mol^{-1}	Activation parameter ΔS^*/J K^{-1} mol^{-1}
C_6H_5	0.051	40	0.691±0.020	115±1	22±1
	0.019	50	2.80±0.03		
	0.051	50	2.74±0.03		
	0.217	50	3.11±0.04		
	0.051	60	10.32±0.24		
	0.051	70	35.7±1.64		
CH_3[b]	—	60	2.95	118±1	23±3

a) 1 M=1 mol dm^{-3}. b) See Ref. 2b.

Table 2. Decomposition Products of **2** in Cumene[a)]

Product	Amount mol/mol of **2**
2-Phenyl-2-propanol	0.94
Acetophenone	0.04
1-Methyl-1-phenylethyl 1,1-dimethylethyl ether	0.02
2,3-Dimethyl-2,3-diphenylbutane	0.63
2-Phenyl-1-propene	0.005

a) Decomposition conditions: initial concentration of **2**, 0.050 mol dm^{-3}; decomposition, 96 h at 50 °C under a nitrogen atmosphere.

fashion to the 1,1-dimethylethyl analogue (Eq. 2), because the ionic decomposition of peroxyesters has a considerably smaller activation entropy than does the radical one.[1d)] The second reason involves the decomposition products. That is, the products in Table 2 can be explained as having been obtained from the 1-methyl-1-phenylethoxyl radical. Criegee rearrangement products, such as 2-phenoxypropene, phenol and 2,2-dimethylpropionic acid, could be detected in only small amounts; not at all. The higher yield of 2-phenyl-2-propanol compared with Leffler's results may be explained by the decomposition temperature and the disproportionation of the radicals in the solvent cage. Our experiment was done at a lower temperature (50 °C). The ratio of the β-scission of the alkoxyl radical to the hydrogen abstraction increased with the reaction temperature.[6)] The alkoxyl radical is much more likely to disproportionate with the 1,1-dimethylethyl radical than with the methyl radical in the solvent cage.[7)]

The peroxyester **2** decomposes more homolytically than does 1-methyl-1-phenylethyl peroxyacetate.[3)] This may be correlated with the acidity of the parent acids. Because the dissociation constant[8)] of 2,2-dimethylpropionic acid (8.91×10^{-6}) was smaller than that of acetic acid (1.23×10^{-5}), the peroxyester **2** is less acceptable as an ionic intermediate **1**, as is shown in Eq. 1. The rate constants in the decomposition of 1,1-dimethylethyl and 1-methyl-1-phenylethyl peroxyacetates in diphenylmethane and toluene at 100 °C were 1.23×10^{-5} [9)] and 3.43×10^{-5} s^{-1}, [1d)] respectively, and the later decomposed about 2.8 times faster than the former. However, the peroxyester **2** decomposed about 3.5 times faster than the 1,1-dimethylethyl analogue (Table 1). These differences indicate that the polar structure of **2**, similar to **3b**, may be stabilized by the electron-withdrawing phenyl substituent and that the contribution of the exothermic decarboxylation to the transition state may accelerate the homolitic decomposition of **2**.[10)]

Experimental

The peroxyester **2** was prepared by the reaction of 2,2-dimethylpropionyl chloride with 1-methyl-1-phenylethyl hydroperoxide in the presence of a 20% KOH aqueous solution in a method similar to that in the reference.[10)] The cumene was purified by the method described in Ref. 11. The decomposition rates were determined by following the carbonyl band of **2** at 1767 cm^{-1}. The decomposition products were determined by means of standard analytical techniques[10)] using gas-liquid chromatography (GLC) and high-performance liquid chromatography (HPLC).

References

1) a) N. V. Yakova, N. A. Yablokov, and V. K. Mamushkin, *Zh. Obshch. Khim.*, **9**, 82 (1973); *Chem. Abstr.*, **78**, 110288t (1973); b) N. V. Yablokova, V. A. Yablokov, and V. A. Shushunov, *Kinetika i Kataliz*, **7**, 165 (1966); *Chem. Abstr.*, **64**, 17378e (1966); c) J. T. Barbas and J. E. Leffler, *J. Org. Chem.*, **50**, 705 (1985); d) E. Hedaya and S. Winstein, *J. Am. Chem. Soc.*, **89**, 1661 (1967).

2) a) T. Koenig, "Free Radicals," Vol. I, ed. by J. K. Kochi, Wiley-Interscience, Chap. 3 (1973); b) T. Komai, M. Ishigaki, and K. Matsuyama, *Bull. Chem. Soc. Jpn.*, **58**, 2431 (1985).

3) J. E. Leffler and F. E. Scrivener, Jr., *J. Org. Chem.*, **37**, 1794 (1972).

4) a) G. P. Sterling, *Mod. Plast.*, **59**, 66, 71 (1982); b) D. Peterson, *Mod. Plast.*, **62**, 92, 95 (1985); c) Anon, Res. *Riscl.*, **249**, 42 (1981).

5) a) V. R. Kamath and C. S. Sheppard (Pennwalt Corp.), Ger. Offen., 2942383 (1980); *Chem. Abstr.*, **93**, 95908j (1980); b) Sumitomo Chemical Co., Ltd., Jpn. Kokai Tokkyo Koho 58-134104 (1983); *Chem. Abstr.*, **100**, 68925u (1984); c) Mistui Toatsu Chemicals Inc., Jpn. Kokai Tokkyo Koho, 58-120611 (1983); *Chem. Abstr.*, **100**, 7396a (1984).

6) C. Walling and P. J. Wagner, *J. Am. Chem. Soc.*, **86**, 3368 (1964).

7) R. A. Sheldon and J. K. Kochi, *J. Am. Chem. Soc.*, **92**, 5175 (1970).

8) Y. Iwakura and K. Nagaoka, "Constants of Organic Compounds," ed. by M. Kotake, Asakura Publishing Co., (1963), p. 614.

9) T. Koami and S. Suyama, *Bull. Chem. Soc. Jpn.*, **58**, 3045 (1985).

10) T. Komai, K. Matsuyama, and M. Matsushima, *Bull. Chem. Soc. Jpn.*, in press; we showed in this report that the relation of the Taft equation (log $(k_d/k_{d0})=\rho^*\sigma^*+(\Delta n)h$) was recognized in the homolytic decomposition of *t*-alkyl 2,2-dimethylperoxypropionates, in which $\rho^*=0.67$ and $h=0.058$. The relation indicates that an electron-withdrawing substituent in the *t*-alkyl group accelerates the decomposition.

11) T. Komai and K. Matsuyama, *Bull. Chem. Soc. Jpn.*, **58**, 2207 (1985).

Pinacol-Pinacolone Rearrangement Promoted by Polyphosphoric Acid Trimethylsilyl Ester (PPSE)

Masa-aki KAKIMOTO,* Takuya SERI, and Yoshio IMAI
Department of Organic and Polymeric Materials, Tokyo Institute of Technology, Meguro-ku, Tokyo 152
(Received November 16, 1987)

Synopsis. Pinacols afforded the corresponding pinacolones in high yields in the presence of the polyphosphoric acid trimethylsilyl ester (PPSE) at a temperature above 80 °C. Tetraphenylethylene oxide, in addition to benzopinacolone, was obtained in the reaction of benzopinacol under milder conditions. The solvent effect suggested that the rearrangement proceeded via the carbonium-ion intermediate.

Pinacol-pinacolone rearrangement has been known as an acid-catalyzed rearrangement which involves the carbonium-ion intermediate.[1] Strong acids, such as sulfuric acid,[2] iodine-acetic acid,[3] and trifluoroborane,[4] have been used as catalysts. We have previously investigated the reactivity of the polyphosphoric acid trimethylsilyl ester (PPSE), which is readily soluble in aprotic solvents. Because PPSE has the characteristics of both a Lewis acid and a dehydrating agent, it has been successfully applied to the Pummerer rearrangement of sulfoxides,[5] to the synthesis of dithioacetals from carbonyl compounds and thiols,[6] and to the synthesis of amidines from carboxylic acids and amines.[7] In this article, we describe the pinacol-pinacolone rearrangement promoted by PPSE.

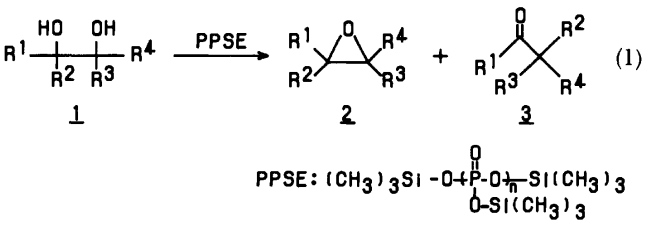

Results and Discussion

The results of the pinacol-pinacolone rearrangement are summarized in Table 1. Benzopinacol (**1a**) afforded both tetraphenylethylene oxide (**2a**) and benzopinacolone (**3a**) in a ratio depending markedly on the reaction conditions as shown in Entries 1—3. The use of an excess amount of PPSE or a higher reaction temperature (150 °C) afforded **3a** in a high yield. These results suggested that epoxide **2a** was an intermediate of the final rearrangement product **3a**. In fact, **2a** was completely converted into **3a** by treatment with an equimolar amount of PPSE in dichloroethane at 150 °C for 2 h. The acceleration effect of a polar solvent, tetrahydrothiophene 1,1-dioxide, sug-

Table 1. Pinacol-Pinacolone Rearrangement Using PPSE

Entry	Pinacol	Equivalent of PPSE	Solvent	Reaction temp/°C	Reaction time/h	Yield/%[a]	
						2	3
1	**1a**	1.0	$(CH_2Cl)_2$	80	2	61	26
2	**1a**	4.0	$(CH_2Cl)_2$	80	2	27	60
3	**1a**	1.0	$(CH_2Cl)_2$	150	2	0	97
4	**1a**	1.0	$(CH_2)_4SO_2$	80	2	0	95
5	**1b**	4.0	—	150	2	0	73
6	**1c**	1.0	$(CH_2Cl)_2$	150	2	0	88
7	**1c**	1.0	$(CH_2)_4SO_2$	80	2	0	95

a) Isolated yield.

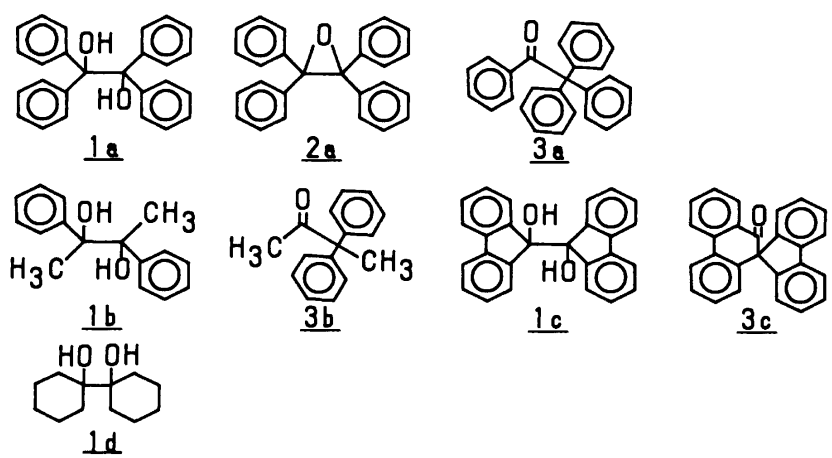

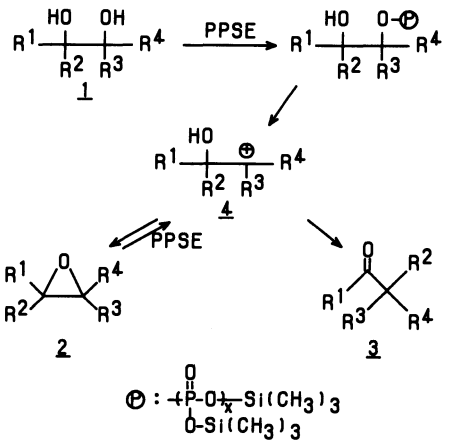

Scheme 1.

gested that the rearrangement proceeded via an ionic intermediate (Entries 4 and 7). In the reaction of pinacols **1b** and **1c**, the corresponding epoxides **2** were not obtained, and the reactions afforded only pinacolones **3b** and **3c**, respectively, in high yields. The reaction of aliphatic pinacol **1d** and PPSE afforded an unknown mixture whose IR spectrum indicated that it did not include either alcohols or carbonyl functions. The formation of olefins with the elimination of water was a possible reaction from the NMR spectrum, but it did not succeed in isolating the olefinic products.

As shown in Scheme 1, the present reaction should involve the paths of the phosphorylation of a pinacol and the formation of the carbonium ion **4** by the elimination of the silylated phosphoric acid. There are two possible paths starting from **4**. One is the direct formation of pinacolone **3**, and the other is the formation of epoxide **2**. Epoxide **2** is also rearranged in the presence of PPSE via the carbonium ion **4**.

The details of the reaction mechanism will be reported in the near future. The pinacol-pinacolone rearrangement promoted by PPSE should have a wide range of application in organic synthesis, because the reaction proceeds under more neutral and milder conditions than usual acid-catalyzed rearrangements.

Experimental

A typical procedure was as follows: PPSE (20.00 mmol) was prepared in 10 ml of 1,2-dichloroethane as has been described in a previous paper.[7] To this solution, 1.830 g (5.00 mmol) of benzopinacol (**1a**) was added, and the mixture was stirred at 80 °C for 5 h. The resulting solution was poured into 100 ml of a 1 M aqueous sodium hydroxide solution (1 M=1 mol dm^{-3}) and then extracted with dichloromethane. Benzopinacolone (**3a**) (1.046 g, 60%), and tetraphenylethylene oxide (**2a**) (0.471 g, 27%), were obtained by the column chromatography (Silica gel, dichloromethane/hexane=1/2) of the crude product.

3a: mp 179—180 °C (lit, 180—181 °C);[8] IR (KBr plate) ν/cm^{-1}=1680, 1590, 1490.

2a: mp 206—207 °C (lit, 205—206 °C);[8] IR (KBr plate) ν/cm^{-1}=1590, 1480, 895.

References

1) J. March, "Advanced Organic Chemistrt: Reactions, Mechanism and Structure," McGraw-Hill (1977), p. 969.
2) C. J. Collins, *J. Am. Chem. Soc.*, **77**, 5517 (1955).
3) W. E. Bachmann, *Org. Synth.*, Coll. Vol. 2, 71 (1943).
4) E. J. Corey, R. L. Danheiser, and S. Chandrasekaran *J. Org. Chem.*, **41**, 260 (1976).
5) M. Kakimoto and Y. Imai, *Chem. Lett.*, **1984**, 1831.
6) M. Kakimoto, T. Seri, and Y. Imai, *Synthesis*, **1987**, 164.
7) S. Ogata, A. Mochizuki, M. Kakimoto, and Y. Imai, *Bull. Chem. Soc. Jpn.*, **59**, 2171 (1986).
8) H. J. Gebhart, Jr. and K. H. Adams, *J. Am. Chem. Soc.*, **76**, 3925 (1954).

Reinvestigation of the Diastereoselectivity of Kinetic Aldol Condensation of Cyclohexanone Lithium Enolate with Benzaldehyde

Masahiro HIRAMA,* Takeshi NODA, Shoichi TAKEISHI, and Shô ITÔ
Department of Chemistry, Tohoku University, Sendai 980
(Received January 21, 1988)

Synopsis. Aldol condensation of cyclohexanone lithium enolate with benzaldehyde has been shown to give a considerably higher stereoselectivity at low temperature than that reported previously.

It has been well-established that the aldol condensations from lithium (*E*)-enolates exhibit rather low anti diastereoselectivity.[1] In particular, lithium enolate of cyclohexanone with benzaldehyde has been recorded to give 1:1[2] anti/syn ratio at −20 °C and 1.1:1[3] even at −72 °C. Accordingly several devices using other metal ions have been developed to improve the selectivity.[2b,4] In connection with our synthetic study on a stereocontrolled construction of hexahydrobenzofuran subunit of the avermectins and the milbemycins, we examined the diastereoselectivity of kinetic aldol condensation of cyclohexanone lithium enolate with α,β-unsaturated aldehyde **1**, and have found that it gives a complete anti selectivity (Eq. 1).[5] These extreme results prompted us to reinvestigate the kinetic aldol reaction of the cyclohexanone lithium enolate with benzaldehyde (Eq. 2).

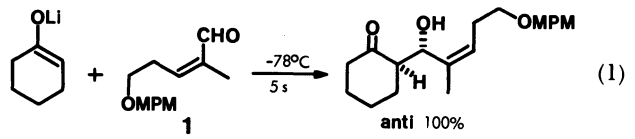

(1)

As the stereoselectivity might depend strongly on reaction temperature, the temperature of reaction mixture in a flask was controlled carefully and directly monitored by digital thermometer. The anti/syn ratios obtained under various conditions are summarized in Table 1. Contrary to the previous result,[3] considerably high ratios were obtained at low temperature in a short reaction period (entries 1, 3). The apparent ratio (ca. 5:1) at −78 °C is likely to be kinetic at this temperature because equilibration appears to be slow at −78 °C (entry 2), only reasonably rapid at −50 °C (entries 3, 4) and very rapid at −20 °C (entry 5). The temperature of reaction mixture was found to rise by up to 5 °C at the moment benzaldehyde was added to the enolate solution, even though the aldehyde solution was precooled.

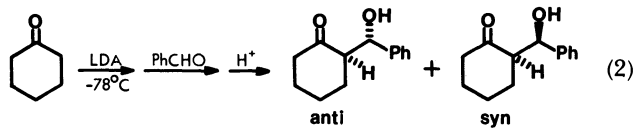

(2)

Thus, the rapid equilibration of the lithium ketone enolates requires careful temperature control and short reaction period to get kinetic stereoselectivity in the condensation of cyclohexanone lithium enolate with benzaldehyde, as recognized in the condensations of other ketones such as propiophenone.[3]

Kinetic stereoselectivities with crotonaldehyde, isobutyraldehyde and trans isomer of **1**[5] at −78 °C were also obtained to be 7.0:1,[6] 28:1, and 20:1, respectively, which suggest that steric bulk owing to methyl group at α-position of α,β-unsaturated aldehydes such as **1** would play an important role for high kinetic diastereoselectivity.

Experimental

^{1}H NMR spectra were run for $CDCl_3$ solutions with Me_4Si as the internal standard on Varian XL200 and JEOL FX-90Q spectrometers. Infrared spectra were recorded on a JASCO IRA-2 diffraction grating spectrophotometer. Melting points were measured on a Yanaco MP-S3 hot stage melting point apparatus and were uncorrected. Elemental analyses were performed at Instrumental Analysis Center for Chemistry, Tohoku University. Reaction temperature was measured on a DELTA MC-20R digital thermometer with MC-20R-01 sensor (Pt 100 Ω).

THF was distilled from sodium benzophenone ketyl. Merck silica gel 60 (230—400 mesh) was used for column chromatography. Analytical thin-layer chromatography (TLC) was performed by using plates precoated with Wako silica gel 70 F_{254} (0.25 mm thick). HPLC analysis (column: Develosil 30-3, 15 cm×4 mm; solvent: Et_2O:hexane=3:2, 2 ml min^{-1}) was performed on a GILSON HPLC system (Model 302—802) with GILSON 111B UV detector (254 nm)

Table 1. Diastereoselectivity of Aldol Condensation of Cyclohexanone Lithium Enolate with Benzaldehyde

Entry	Reaction condition[a]	anti : syn	Yield[b]/%
1	−78 °C, 3 s	4.7—5.4 : 1[c,d]	68—78
2	−78 °C, 30 min	4.3 : 1[d]	87
3	−50 °C, 3 s	4.6 : 1[e]	63
4	−50 °C, 5 min	1.5 : 1[d]	92
5	−20 °C, 3 s	0.7 : 1[e]	65

a) Precooled (−78 °C) benzaldehyde solution was added to enolate solution quickly by syringe or via cannula. b) Cambined isolated yield for anti and syn products. c) The highest and the lowest ratio among four runs. d) Ratio determined by HPLC analysis. e) Ratio determined by ^{1}H NMR spectroscopy.

and Shimadzu Chromatopac C-R3A. All reactions were carried out in a three or two necked 10 ml flask equipped with the sensor of digital thermometer under an argon atmosphere.

General Procedure: A 1.61 M† hexane solution of butyllithium (0.650 ml, 1.05 mmol) was added to a solution of diisopropylamine (0.154 ml, 1.1 mmol) in dry THF (2 ml) at −78 °C and stirred at 0 °C for 10 min. To this LDA solution was added dropwise a solution of cyclohexanone (98 mg, 1.0 mmol) in dry THF (0.5 ml) at −78 °C. After 20 min at this temperature, a cooling bath was replaced to set the solution at a specific temperature. After the temperature became specific, to this solution was added quickly a cold (−78 °C) solution of an aldehyde (0.112 ml, 1.0 mmol) in dry THF (0.5 ml) by a syringe or via a cannula at the temperature. After 3 s, a saturated aqueous NH_4Cl (5 ml) was added and the mixture was warmed up to room temperature, extracted with ether (3×10 ml). The combined organic layer was dried over $MgSO_4$ and concentrated. A diastereomer ratio of the aldol was determined by ^1H NMR spectroscopy (relative intensity of carbinol methine proton) or HPLC analysis of crude product. The crude mixture was chromatographed on SiO_2 column with AcOEt/hexane (1:3) as an eluent to give pure aldols from benzaldehyde in the yield shown in Table 1 or a mixture of diastereomers (70% yield) from the other aldehydes.

2-(α-Hydroxybenzyl)cyclohexan-1-one; syn isomer: R_f= 0.42 (AcOEt/hexane=1:2); colorless needles; mp 105—106.5 °C (hexane-ether) (lit, mp 102—103 °C[2b]); ^1H NMR δ=1.31—2.79 (9H, m), 3.00 (1H, d, J=3.3 Hz, OH), 5.38 (1H, m, benzylic CH, collapsed to doublet, J=2.2 Hz, when D_2O added), 7.30 (5H, m); IR (KBr) 3570, 1695, 1500, 1450, 1130, 1060, 985, 700 cm^{-1}; Calcd for $C_{13}H_{16}O_2$: C, 76.44; H, 7.86%, Found: C, 76.26; H, 7.89%. Anti isomer: R_f=0.36 (AcOEt/hexane=1:2); colorless plates; mp 76—77 °C (hexane-ether) (lit, mp 74—75 °C); ^1H NMR δ=1.08—2.79 (9H, m), 3.93 (1H, d, J=2.9 Hz, OH), 4.78 (1H, dd, J=2.9 and 8.7 Hz, benzylic CH), 7.31 (5H, m); IR (KBr) 3520, 1685, 1500, 1450, 1130, 1040, 1010, 700 cm^{-1}; Calcd for $C_{13}H_{16}O_2$: C, 76.44; H, 7.86%, Found: C, 76.37; H, 8.16%.

2-(*trans*-1-Hydroxy-2-butenyl)cyclohexan-1-one (7.0:1 anti/syn mixture): colorless oil; ^1H NMR δ=1.2—2.2 (6H, m), 1.72 (3H, dd, J=6.3, 1.5 Hz), 2.2—2.6 (3H, m), 3.60 (1H, br, OH), 4.21 (1H, br t, J=8.0 Hz, CHOH), 4.49 (syn CHOH, br m), 5.46 (1H, ddq, J=15.3, 8.0, 1.5 Hz), 5.72 (1H, dqd, J=15.3, 6.3, 0.7 Hz); IR (film) 3430, 2930, 2860, 1700, 1450, 1310, 1215, 1115, 965 cm^{-1}; MS m/z 169 (M^++1, 20), 151 (34), 135 (50), 98 (100), 83 (63), 70 (100).

2-(1-Hydroxy-2-methylpropyl)cyclohexan-1-one (28:1 anti/syn mixture): colorless oil; ^1H NMR δ=0.91 (3H, d, J=6.9 Hz), 1.01 (3H, d, J=6.9 Hz), 1.1—2.2 (7H, m), 2.2—2.6 (3H, m), 3.32 (1H, br d, J=4.5 Hz, OH), 3.56 (1H, br dt, J=7.5, 4.5, 4.0 Hz, CHOH), 3.74 (syn CHOH, br dd, J=9.5, 2 Hz); IR (film) 3550, 2940, 2860, 1695, 1445, 1395, 1240, 1130, 990, 840 cm^{-1}; MS m/z 170 (M^+, 2), 151 (55), 136 (43), 126 (100), 98 (23).

2-[*trans*-1-Hydroxy-2-methyl-5-(4-methoxybenzyloxy)-2-pentenyl]cyclohexan-1-one (20:1 anti/syn mixture): colorless oil; ^1H NMR δ=1.53—2.18 (6H, m), 1.63 (3H, br s), 2.29—2.55 (3H, m), 2.37 (2H, br q, J=6.9 Hz), 3.47 (2H, td, J=6.9, 1.4 Hz), 3.60 (1H, br s, OH), 3.82 (3H, s), 4.20 (1H, d, J=9.2 Hz, CHOH), 4.60 (syn CHOH, d, J=3 Hz), 4.45 (2H, s), 5.43 (1H, br t, J=6.9 Hz), 6.90 (2H, br d, J=8.8 Hz), 7.27 (2H, br d, J=8.8 Hz); IR (film) 3500, 2940, 2860, 1700, 1610, 1515, 1240, 1090, 1030, 815 cm^{-1}; MS m/z 314 (M^+-H_2O), 234, 178, 137, 136, 122, 121, 108, 99, 98, 83, 70.

† 1 M=1 mol dm^{-3}.

References

1) C. H. Heathcock, "Asymmetric Synthesis," ed by J. D. Morrison, Vol. 3, Academic Press, Orlando, Florida (1984), p. 111.

2) a) H. O. House, D. S. Crumrine, A. Y. Teranishi, and H. D. Olmstead, *J. Am. Chem. Soc.*, **95**, 3310 (1973); b) D. A. Evans, E. Vogel, and J. V. Nelson, *J. Am. Chem. Soc.*, **101**, 6120 (1979).

3) C. H. Heathcock, C. T. Buse, W. A. Kleschick, M. C. Pirrung, J. E. Sohn, and J. Lampe, *J. Org. Chem.*, **45**, 1066 (1980).

4) Y. Yamamoto, H. Yatagai, and K. Maruyama, *Tetrahedron Lett.*, **23**, 2387 (1982).

5) M. Hirama, T. Noda, and S. Itô, *J. Org. Chem.*, **53**, 706 (1988).

6) Similar extent of anti-selectivity has been observed in aldol condensation with 2-cyclohexenone derivatives. See: W. C. Still, *J. Am. Chem. Soc.*, **101**, 2493 (1979); S. Torii, T. Inokuchi, and H. Ogawa, *Bull. Chem. Soc. Jpn.*, **52**, 1233 (1979).

Convenient Synthesis of *N*-Protected Amino Acid Amides[1)]

Sukekatsu NOZAKI* and Ichiro MURAMATSU†
Faculty of Pharmaceutical Sciences, Josai University, Sakado, Saitama 350-02
†Department of Chemistry, College of Science, Rikkyo University, Nishi-Ikebukuro, Tokyo 171
(Received February 19, 1988)

Synopsis. Boc- or Z-amino acids were conveniently amidated at room temperature by a one-pot procedure employing ammonium hydrogencarbonate and *N*-ethoxycarbonyl-2-ethoxy-1,2-dihydroquinoline in yields of 81—96%. The benzyl ester-type protector for the side chains of aspartic acid and glutamic acid was not affected by the procedure.

Amino acid amides, an important starting material in peptide synthesis, are usually prepared by ammonolysis of amino acid esters, or by coupling of *N*-protected amino acids with ammonia.[2)] The former procedure is somehow inconvenient, since ammonia, a reagent often troublesome for handling, is required and the reaction is rather slow. In the latter, care must be paid to prevent possible racemization during activation of the amino acids, especially when mixed anhydride method[3)] was employed for the purpose.

We report here that by addition of ammonium hydrogencarbonate and *N*-ethoxycarbonyl-2-ethoxy-1,2-dihydroquinoline (EEDQ),[4,5)] a mild mixed anhydride-type coupling reagent stable to amines,[5)] Boc- or Z-amino acids in chloroform are conveniently converted to the corresponding amides at room temperature.

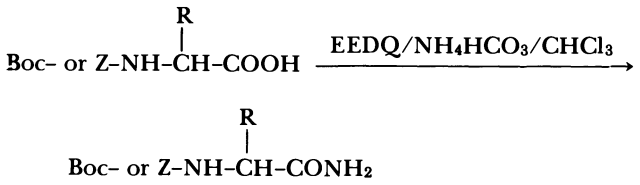

The reaction proceeded smoothy with gentle evolution of carbon dioxide, although ammonium hydrogencarbonate is scarcely soluble in the solvent. The amides were readily isolated in satisfactory yields after removal of the excess ammonium hydrogencarbonate by washing the reaction mixture with water. By this procedure, the benzyl ester-type protecting group for the β- or γ-carboxylic acid part of aspartic acid or glutamic acid, respectively, was not affected. No racemization occurred during the amidation when an *N*-protected amino acid with a urethane-type protector was employed as the starting compound. However, this method cannot be applied to the preparation of a peptide amide consisting of an optically active amino acid at the C-terminal, since in a test preparation, Boc-L-leucyl-L-leucine gave a considerable amount of the diastereomeric product (14%), Boc-L-leucyl-D-leucinamide. The data are summarized in Table 1.

Experimental

Melting points were uncorrected. Merck precoated silica-gel plates were used for TLC analysis with a solvent system of chloroform–MeOH (19:3). For HPLC analysis, a LiChrosorb RP-18 column (4×250 mm) was employed with a solvent system of MeOH–water (1:1) at a flow rate of 1.83 ml min^{-1}. The column effluent was monitored at 220 nm, and the peak area was recorded by a Shimadzu C-R3A integrator.

Preparation of Boc-Glu(OBzl)-NH_2 (General Procedure).

Table 1. Preparation of *N*-Protected Amino Acid Amides

Product[a)]	Yield/%	Mp θ_m/°C	Solvent for recrystallization	$[\alpha]_D^{26}$/° (*c* 1, EtOH)
Boc-Ala-NH_2	89	124—125	AcOEt–hexane	−2.7
Boc-Val-NH_2[b)]	88	155—157	AcOEt–hexane	<±0.05
Boc-Leu-NH_2	82	144—146	AcOEt–hexane	−11.4
Boc-Ile-NH_2	88	166—167	AcOEt–hexane	−3.0
Boc-Ser(Bzl)-NH_2	81	101—102	AcOEt–hexane	+27.8
Boc-Thr(Bzl)-NH_2	91	135—136	AcOEt–hexane	+38.6
Boc-Lys(Z)-NH_2[c)]	89	137—142	AcOEt–hexane	+1.7
Boc-Asp(OBzl)-NH_2	89	157—160	AcOEt	−2.6
Boc-Glu(OBzl)-NH_2	90	120—122	AcOEt–hexane	+4.0
Boc-Phe-NH_2	91	142—149	AcOEt–hexane	+16.7
Z-Phe-NH_2[d)]	94	161—162	AcOEt–hexane	−2.6
Boc-Tyr(Bzl)-NH_2	96	170—171	AcOEt	+16.0
Boc-Trp-NH_2	85	133—136	AcOEt–hexane	+7.7
Z-Trp-NH_2[e)]	96	188—189	AcOEt	−4.0
Boc-Pro-NH_2	81	104—106	Ether–hexane	−43.4

a) Each compound gave a single spot on TLC. Satisfactory data of microanalysis was obtained for each compound within an error range of ±0.3%. b) Mp 156—157 °C in lit;[6)] mp 157—158 °C in lit.[7)] c) Mp 142 °C, $[\alpha]_D^{25}$ +1.6° (*c* 1, MeOH) in lit.[8)] d) Mp 161—162 °C in lit;[9)] mp 164—165 °C, $[\alpha]_D^{20}$ −4.9° (*c* 1.5, 80% AcOH) in lit;[10)] mp 163—164 °C, $[\alpha]_D^{25}$ −6.3° (*c* 2, DMF) in lit.[11)] e) Mp 187—188 °C in lit.[12)]

Boc-Glu(OBzl)-OH (0.675 g, 2 mmol), EEDQ (0.544 g, 2.2 mmol), and ammonium hydrogencarbonate (0.474 g, 6 mmol) were suspended in chloroform (5 ml), and the mixture was stirred overnight at room temperature. The mixture was then washed with water (2 ml×1, 1 ml×1) and evaporated to give a solid, which was recrystallized from ethyl acetate-hexane; 0.603 g (90%); mp 120—122 °C. Found: C, 61.00; H, 7.39; N, 8.22%. Calcd for $C_{17}H_{24}O_5N_2$: C, 60.70; H, 7.19; N, 8.33%.

Preparation of Boc-Ala-NH_2 and Boc-Pro-NH_2. Prepared according to the general procedure with modification: the aqueous washing phase was extracted with chloroform (2 ml×6) to recover the water soluble products. The desired amides were obtained from the combined organic layer.

Preparation of Z-Trp-NH_2. Prepared according to the general procedure with modification: a larger volume of chloroform (25 ml) was used as the solvent because of the poor solubility of the product.

Racemization Test. a) In Amidation of Amino Acid: Boc-Leu-NH_2 (0.326 g, 1.42 mmol) prepared by the general procedure described above was dissolved in 4 M† HCl/dioxane (5 ml) at room temperature. After 15 min, the mixture was evaporated and the residue was triturated in ether to give a solid (0.232 g), which was then dissolved in chloroform (10 ml) and triethylamine (0.20 ml, 1.44 mmol). To this solution was added Boc-Leu-ONSu (0.473 g, 1.44 mmol) and the mixture was stirred overnight at room temperature. The mixture was then washed successively with 0.1 M HCl (2 ml×1, 1 ml×1), water (2 ml), 0.5 M $NaHCO_3$ (2 ml×1, 1 ml×1), and water (2 ml×2). An aliquot (0.002 ml) of the chloroform solution was analyzed by the HPLC to determine the ratio of Boc-Leu-Leu-NH_2 (the retention time of the authentic sample, 24 min) and Boc-Leu-D-Leu-NH_2 (30 min). Similarly Boc-Phe-NH_2 obtained was converted to Boc-Leu-Phe-NH_2 and the purity of the product was also examined by the HPLC (the retention time of an authentic Boc-Leu-Phe-NH_2, 34 min; Boc-Leu-D-Phe-NH_2, 44 min). In either case, no peak corresponding to the D-amino acid containing peptide was observed (less than 0.2%).

b) In Amidation of Peptide: Boc-Leu-Leu-OH (0.344 g, 1 mmol), EEDQ (0.272 g, 1.1 mmol), and ammonium hydrogencarbonate (0.237 g, 3 mmol) were allowed to react in chloroform (5 ml) overnight at room temperature. The reaction mixture was washed with water (2 ml×1, 1 ml×1) and evaporated to give an oil, which was then dissolved in AcOEt. By addition of hexane, a viscous oil was separated. The oil collected by decantation was dissolved in MeOH and analyzed by the HPLC.

† 1 M=1 mol dm^{-3}.

References

1) Amino acids with no prefix are of L-configuration. Following abbreviations were used; Boc=*t*-butoxycarbonyl, Z=benzyloxycarbonyl, Bzl=benzyl ether, OBzl=benzyl ester, ONSu=*N*-hydroxysuccinimide ester.

2) E. Schröder and K. Lübke, "The Peptides," Academic Press (1965), Vol. 1, p. 67.

3) G. W. Anderson, J. E. Zimmerman, and F. M. Callahan, *J. Am. Chem. Soc.*, **89**, 5012 (1967).

4) B. Belleau, R. Martel, G. Lacasse, M. Ménard, N. L. Weinberg, and Y. G. Perron, *J. Am. Chem. Soc.*, **90**, 823 (1968).

5) B. Belleau and G. Malek, *J. Am. Chem. Soc.*, **90**, 1651 (1968).

6) R. Schwyzer, A. Costopanagiotis, and P. Sieber, *Helv. Chim. Acta*, **46**, 870 (1963).

7) M. Bodanszky, K. W. Funk, and M. L. Fink, *J. Org. Chem.*, **38**, 3565 (1973).

8) A. Eberle, J-L. Fauchère, G. I. Tesser, and R. Schwyzer, *Helv. Chim. Acta*, **58**, 2106 (1975).

9) J. M. Davey, A. H. Laird, and J. S. Morley, *J. Chem. Soc.*, **1966**, 555.

10) E. Wünsch and K-H. Deimer, *Hoppe-Seyer's Z. Physiol. Chem.*, **353**, 1246 (1972).

11) M. Bodanszky and S. Natarajan, *J. Org. Chem.*, **40**, 2495 (1975).

12) E. L. Smith and W. J. Polglase, *J. Biol. Chem.*, **180**, 1209 (1949).

Selective Synthesis of Ethylene by Dehydrogenative Coupling of Methane by Use of Thermal Diffusion Column

Tatsuaki YAMAGUCHI* and Chiaki SAITO
Laboratory of Organic Chemistry, Chiba Institute of Technology,
Tsudanuma, Narashino-shi, Chiba 275
(Received February 8, 1988)

Synopsis. Ethylene was found to be obtained dehydrogenatively from methane in extremely high selectivities (91.5% at 9.4% conversion of methane) with the downward introduction to the modified thermal diffusion column with electrically heated tungusten wire at 1200 °C.

From the challenging viewpoint of the utilization of natural gas, the partial oxidative conversion of methane into more useful chemicals such as ethylene[1] and methanol[2] has been investigated more and more extensively. Nevertheless, less attention has been now taken on the direct dehydrogenative coupling of methane to ethylene because it requires temperatures higher than 1000 °C. But the by-production of hydrogen is the advantage of this process over the oxidative one.

$$2CH_4 \longrightarrow CH_2{=}CH_2 + 2H_2$$

Half a century ago, Clusius and Dickel invented a powerful separation column based on thermal diffusion and thermal convection.[3] A few years later Hirota applied this separation column to the thermal polymerization of methane and succeeded in getting condensed hydrocarbon oil in a good yield.[4]

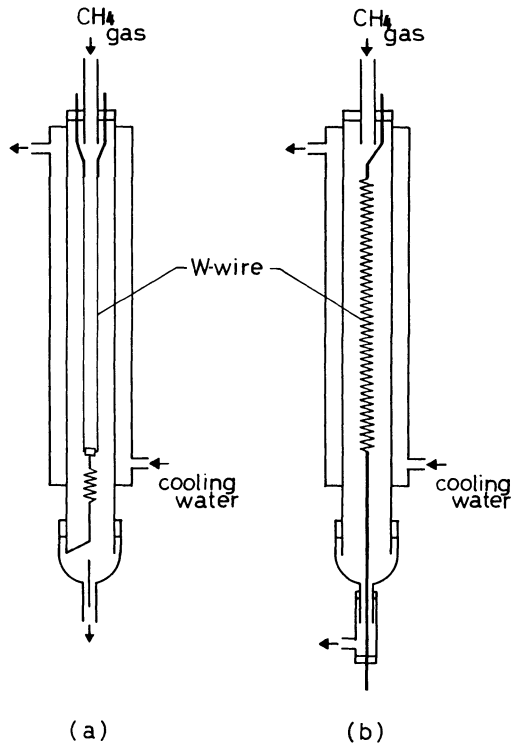

Fig. 1. Clusius-Dickel type thermal diffusion column reactor. The tungsten wire is modified in a) U-type, b) spiralled type.

By the upward flow (linear velocity 3.8 m h^{-1}) of methane in a water-cooled Pyrex-glass column of 1 m in length and 2 cm in diameter centering a straight tungsten wire of 70 cm in length and 0.5 mm in diameter, which was heated electrically at 1200 °C on surface, we could fully reproduce Hirota's results obtaining hydrocarbon oil in the yield of 62% of methane feeded. However, the operation in downward flow of methane with the similar apparatus in the same conditions was found to give a quite different result. Thus, ethylene was obtained in the yield of 5.4% with 90% selectivity at 1200 °C accompanying with far less amount of oily matter.[5]

With intent of enhancing the methane conversion, the shape of the tungsten wire is now modified from a straight line to a U-type (Fig. 1a) or a spiral (Fig. 1b) in this paper.

Experimental

Deoxygenated methane gas was introduced from the top of the thermal diffusion column (Fig. 1, length 40 cm, inner diameter 2.0 cm) without preheating under ordinary pressure, and the out-let gas from the bottom was analyzed by a gaschromatograph (Shimadzu GC-9A). The surface temperature of the tungsten wire was measured pyroptically by a radiation pyrometer (Minolta IR-120). And the amount of the alternating current was measured by a clamp tester (SOAR Model 2220).

Results and Discussion

The results are summarized in Table 1 with experimental details. In the case of Run 1, substantially 100% selectivity to total C_2 compounds was obtained. But in other cases oily matter condensed on the cold wall of column as by-products. Especially carbonaceous product was observed in Run 7. This means too much heating of the gas phase causes unfavorable results on ethylene selectivity. As expected, increasing the contact chance of methane molecule on the high-temperature tungsten surface gave the favorable effect increasing the methane conversion and the hydrogen yield with high selectivities of ethylene (Runs 1—3). The ethane yields were as low as 0.3% in every run.

Figure 2 shows variations of the product yields with the linear velocity of gas flow in the column with U-type tungsten wire. The higher linear velocity resulted in decrease of the methane conversion and increase of the ethylene selectivity. The maximum of the ethylene yield was given around 6 m h^{-1} with this type of reactor. The ethane productions were limited in a very low yield in this case again.

Table 1. Results with the Modified Column

Run No.	W wire length	Heating zone	Electric power	Methane conv.	Ethylene		Ethane		Hydrogen yield
					yield	selec.	yield	selec.	
	cm	cm	W	%	%	%	%	%	%
1	30	30	150	2.6	2.3	89.5	0.3	10.5	5
2	60[a)]	30	450	9.4	8.6	91.5	0.3	3.4	27
3	120[b)]	30	675	14.2	12.6	88.8	0.3	2.0	43
4	30[c)]	24	150	3.5	2.9	82.1	0.3	8.6	8
5	30[c)]	18	150	4.2	3.8	90.6	0.3	6.6	11
6	30[c)]	12	150	9.1	7.1	78.1	0.3	2.9	23
7	30[c)]	6	150	26.1	15.0	58.1	0.2	0.7	56

Methane feed rate 1.8 dl h^{-1}, linear velocity 5.76 m h^{-1}, average surface temperature of W wire 1200 °C. Values for selectivities were based on the methane conversion. Yields of ethylene and ethane were defined as the product of the conversion and the selectivity. Hydrogen yields were calculated from the molar ratio of produced hydrogen to methane feeded. a) Folded in U-type. b) Folded in W-type. c) Spiralled 4 mm in diameter.

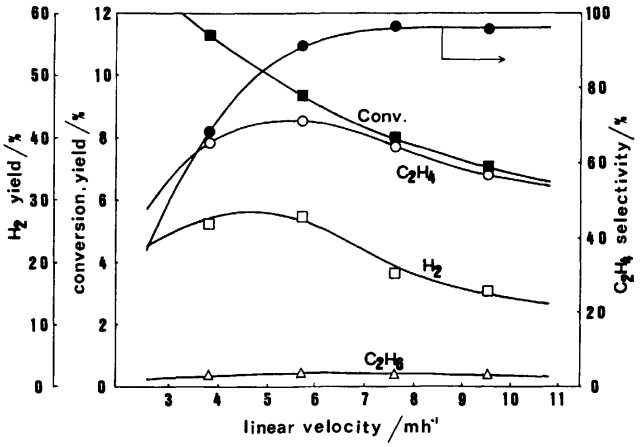

Fig. 2. The influence of the linear velocity of methane in the column.
Tungsten wire 0.5 mm×60 cm, U-type (heating zone 30 cm), surface temperature 1200 °C. Methane conversion: ■. Ethylene selectivity: ●. Yields: ○, ethylene; △, ethane; □, hydrogen.

The phenomenon giving high selectivity of ethylene production may be understood in terms of two theoretical considerations. First, the thermodynamic data give the favorable free energy change for the gas-phase conversion of methane to ethylene at 1200 °C over that to ethane. This is suggested from the fact of the very low yield of ethane throughout the experiments at this temperature. Secondly, the thermal diffusion due to the temperature gradient between the surfaces of the heated tungsten wire and the cold wall of the column permits the produced ethylene molecule, which is of the highest molecular weight in the system, to leave the heated surface for the cold wall. Following by the thermal convection the ethylene molecule is driven downward along with the cold wall and the hydrogen molecule driven upward as pointed out by Clusius. The observation of less brightness in the upper part of the tungsten wire suggests a higher concentration of hydrogen around this part of the column. By this effect the produced ethylene may be prevented from the recombination with hydrogen. Further polymerization of ethylene which occured by its recycling to the high-temperature surface may be limited because its downward direction along the cold wall is with the current when the overall feed flow in the column is downward.

From the practical viewpoint, it should be noted that the electric power required in this procedure would be rather low since it is not necessary to heat the whole gas phase up to 1200 °C.

References

1) a) G. E. Keller and M. M. Bhasin, *J. Catal.*, **73**, 9 (1982); b) T. Ito and J. H. Lunsford, *Nature (London)*, **314**, 721 (1985); c) E. Iwamatsu, T. Moriyama, N. Takasaki, and K. Aika, *J. Chem. Soc., Chem. Commun.*, **1987**, 19; d) K. Otsuka and T. Komatsu, *J. Chem. Soc., Chem. Commun.*, 1987, 388.

2) a) H. D. Gesser and N. R. Hunter, *Chem. Rev.*, **85**, 235 (1985); b) R. Pitchai and K. Klier, *Catal. Rev. Sci. Eng.*, **28**, 13 (1986).

3) K. Clusius and G. Dickel, *Naturwiss.*, **26**, 546 (1938).

4) K. Hirota, *Bull. Chem. Soc. Jpn.*, **16**, 274 (1941).

5) T. Yamaguchi, A. Kadota, and C. Saito, *Chem. Lett.*, **1988**, 681.

Diverse Kinetic Behaviors of the β-Structure Formation. A Study on Poly(*S*-carboxymethyl-L-cysteine)

Kazuhiro FUKADA,* Hideyuki HATTORI, Hiroshi MAEDA,* and Shoichi IKEDA*
Department of Chemistry, Faculty of Science, Nagoya University, Nagoya 464-01
(Received December 4, 1987)

Synopsis. The pH jump kinetics of random coil-to-β-structure convertsion of poly(*S*-carboxymethyl-L-cysteine) were examined on two samples of degree of polymerization (DP) of 330 and 560. Various kinetic behaviors were observed depending on polymer chain length and concentration: single exponential with or without a lag and two exponential behavior. In unbuffered solutions, the rate enhancement of β-formation was confirmed.

Kinetics of the β-structure formation of polypeptides have been studied mainly on two polypeptides; poly(L-lysine)(PLL)[1-5] and poly(L-tyrosine) (PLT).[6,7] Conversion from the α-helix to the β-structure of PLL with degree of polymerization (DP) 240 or 1000 by a temperature change followed first-order kinetics and the rate was independent of concentration below about 10—20 mg L^{-1}.[2] In the kinetics of coil-to-β conversion of PLL (DP=700) induced by an isothermal pH jump at high temperature, however, there was a slow initiation step and the progress of reaction was sigmoidal.

In the case of β-formation by pH jump of PLT, the kinetics were described in terms of superposition of two exponential terms without any sigmoidal behavior.

These results show that two polypeptides behave differently with respect to kinetics of chain folding. This aspect was already pointed out[6] and hence diverse kinetic behaviors are ascribed to different kinds of side chains of the polypeptides. However, it will be shown in the present study that various kinetic behaviors previously found on PLL and PLT were all observed on the kinetics of pH induced coil-to-β conversion of poly(*S*-carboxymethyl-L-cysteine) (poly[Cys(CH_2COOH)]), another well characterized model β-polypeptide.[8-10]

Experimental

Average degrees of polymerization (DP) of the two samples of poly[Cys(CH_2COOH)] used in the present study were 330 and 560. Residue ellipticity at 210 nm, $[\theta]_{210}$, varied from $-(4—5)\times10^3$ to $(1.0—1.1)\times10^4$ and that at 205 nm, $[\theta]_{205}$, varied from $-(8—10)\times10^3$ to $(2.6—2.9)\times10^4$ accompanying to coil-to-β conversion. The conversion occurred at about pH 4.9 in 50 mM sodium salt aqueous solutions (1M=1 mol dm^{-3}). We used $[\theta]_{210}$ or $[\theta]_{205}$ as a measure of the β-formation. Circular dichroism (CD) was recorded on a Jasco J-40A circular dichrograph at 25(±0.1) °C, using cells of 2, 10 and 20 mm light paths.

Kinetics of the β-formation were carried out as follows. The solution in a test tube containing poly[Cys(CH_2COOH)] and 50 mM $NaClO_4$, with or without sodium acetate buffer (pH≈7), was brought to acid pH (between 4.7—4.9) by the addition of a small amount of 0.1 M HCl followed by immediate mixing. It took only a few seconds to attain complete mixing. A part of the mixed solution was introduced into the cell and $[\theta]_{210}$ or $[\theta]_{205}$ was continuously recorded for about 1.5×10^3 s. The earliest reliable readings were obtained at about 15 s after the pH jump. Afterward, CD spectra (200—260 nm) were measured at selected time intervals until the reaction was completed. The rest of the solution was used for pH measurement. An Iwaki M 225 pH meter was used to determine the pH when the reaction were completed.

Results and Discussion

Diverse Kinetic Behaviors of the β-Formation of Poly[Cys(CH_2COOH)]. Kinetic study of the β-formation in acetate buffer solutions was performed at two polymer concentrations (C_p) on the sample of DP=330 (see Fig. 1). The dependence of the rate of β-formation on pH is shown in Fig. 1(a). At a C_p of 5×10^{-4} M (80 mg L^{-1}), the β-formation proceeded faster as the pH became lower, where β-structure carried a smaller number of charges. The effect of concentration can be seen in Fig. 1(b), where β-formation is slower at the polymer concentration of 1×10^{-4} M (16 mg L^{-1}) than at 5×10^{-4} M. Figure 1(b) further indicates that the β-formation at $C_p=1\times10^{-4}$ M hardly proceeds within 5×10^3 s (a time lag) and the whole kinetic curve is sigmoidal.

These kinetic data were analyzed as follows. The extent of unreacted fraction after pH jump is given with Eq. 1 as a function of time.

$$f(t) = ([\theta]_{210}(\infty) - [\theta]_{210}(t))/([\theta]_{210}(\infty) - [\theta]_{210}(0)) \quad (1)$$

Here, $[\theta]_{210}(t)$ denotes the residue ellipticity at time t, and $[\theta]_{210}(\infty)$ is the value at equilibrium. Semilogarithmic plots of f versus time are indicated in the insets of Fig. 1(a) and (b). As shown in the inset of Fig.1 (a), at $C_p=5\times10^{-4}$ M the time course $f(t)$ could not be fitted with a single exponential term but by the superposition of two exponential terms shown below

$$f(t) = A\exp(-t/\tau_1) + (1 - A)\exp(-t/\tau_2) \quad (2)$$

Here, τ_1 and τ_2 are the phenomenological time constants for the fast and slow processes, and A is the amplitude of the fast process. It was confirmed that the two-term exponential decay curves gave better fit to all the experimental data shown in Fig. 1(a) than single exponential curves. This kinetic pattern is in accord with the kinetics of PLT.[6,7]

At $C_p=1\times10^{-4}$ M, on the other hand, the reaction approximately follows a single exponential decay after a time lag (see inset of Fig. 1(b)). Single exponential decay with a lag was also found in the isothermal pH jump kinetics of PLL. It is to be noted that the lag in the case of PLL was obtained with light scattering and fluorescence but not with optical activity as was done in the present study.[5] It was expected that at very dilute solutions such as

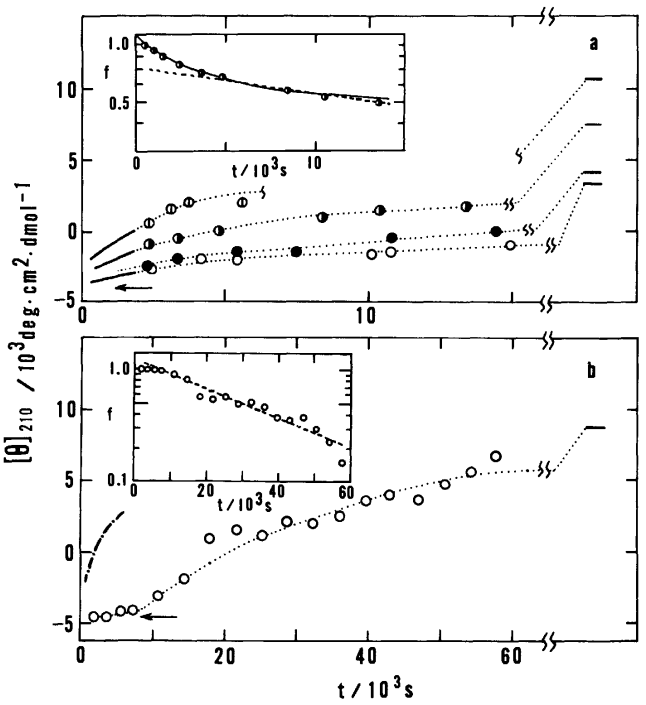

Fig. 1. Kinetics of the β-formation of the sample of DP=330 in 20 mM sodium acetate buffer +50 mM $NaClO_4$. Values of $[\theta]_{210}$ are represented with various circles and with solid thick lines for the initial stage where measurements were carried out continuously. Arrows indicate the initial value of $[\theta]_{210}$.
(a) $C_p=5\times10^{-4}$ M; pH=4.90 (○), 4.87 (●), 4.84 (◑), and 4.74 (Φ). Inset: A semilogarithmic plot of the unreacted fraction f (defined by Eq. 1) versus time of the data at pH 4.84. A solid line indicates the two-term exponential curve, i.e., $f=0.42\exp(-t/2700)+0.58\exp(-t/140000)$. A broken line indicates the single exponential decay curve fitted to the data of long time region.
(b) $C_p=1\times10^{-4}$ M; pH=4.76. A chain line indicates the data at $C_p=5\times10^{-4}$ M (pH=4.74). Inset: A semilogarithmic plot of f versus time. A broken line indicates the single exponential decay curve with a lag time of 5×10^3 s.

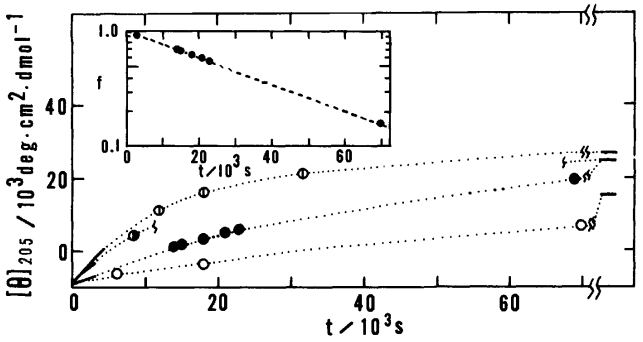

Fig. 2. Kinetics of the β-formation of the sample of DP=560 at different values of pH and concentrations. $C_p=2\times10^{-4}$ M; 10 mM sodium acetate buffer +50 mM $NaClO_4$: pH=4.86 (○) and 4.79 (◑). $C_p=5\times10^{-5}$ M; 2 mM sodium acetate buffer +50 mM $NaClO_4$: pH=4.74 (●) and 4.71 (Φ). Inset: A semilogarithmic plot of f versus time for the data at pH 4.74 ($C_p=5\times10^{-5}$ M).

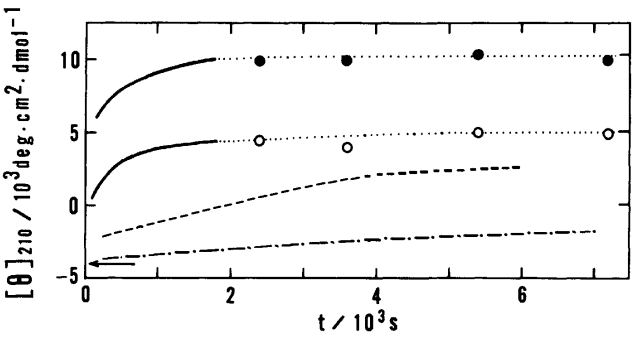

Fig. 3. Kinetics of the β-formation in unbuffered solutions at $C_p=5\times10^{-4}$ M in 50 mM $NaClO_4$ for the sample of DP=330. (○) pH 4.90 and (●) pH 4.80. Solid thick lines represent the values of $[\theta]_{210}$ for initial stage where measurements were carried out continuously. The broken (chain) curve represents the kinetic data at similar concentration in acetate buffer of similar ionic strength at pH 4.74 (4.90). Those data are taken from Fig. 1(a) and given for the sake of comparison.

1×10^{-4} M, β-formation of poly[Cys(CH_2COOH)] proceeded by two-step mechanism of slow nucleation followed by fast growth.

In Fig. 2, kinetic data of the sample of DP=560 are summarized for different pH and concentrations. No lag was observed even at lower concentration of 5×10^{-5} M (8 mg L^{-1}) for this long chain sample. All kinetics shown in Fig. 2 followed the first-order rate law, as indicated in the inset for an example. The first-order kinetic behavior is consistent with the case of thermally induced α→β conversion of PLL.[2-4] Thermal coil-to-β conversion of poly[Cys(CH_2COOH)] showed kinetic behavior too complex to be described with two exponential terms.[12]

From these results, it was confirmed that various kinetic behaviors previously found on PLL and PLT were all observed in the β-formation of poly[Cys(CH_2COOH)] depending on polymer chain length and concentration: single exponential behavior with or without a lag and two exponential behavior. Therefore, we expect that diverse kinetic behaviors accompanying the β-formation originate rather from diverse aspects of the kinetics of polypeptide chains in general than from different kinds of side chains as has been supposed to be. It is to be noted that the β-formation of homopolypeptide chains consists of many elementary steps and hence various kinetic behaviors manifest themselves depending on which step is rate-limiting. In addition, the polydispersity of samples may possibly contribute to the diverse behaviors. A simple kinetic theory explicable of diverse kinetic patterns of intramolecular β-formation has been recently presented.[13]

Rate Enhancement of the β-Formation in Unbuffered Solutions. In Fig. 3, the rates of β-formation in unbuffered solutions are compared with those in buffer at similar conditions. At the same pH of 4.90, the rate of the β-formation is faster in the absence of

acetate buffer. Within 4×10^3 s the β-formation is completed at both pH 4.80 and pH 4.90 in the case of unbuffered solution.

It was confirmed that acetate buffer had little effect on the stability of the β-structure of poly[Cys-(CH_2COOH)],[11] hence its specific effect on the kinetics can be ignored.

The observed rate enhancement could be explained in terms of either or both of the two mechanisms: the seeding effect and the different pathways. The formation of seed may occur as follows. When 0.1 M HCl is added to and mixed with the polymer solution, the added 0.1 M HCl will be dispersed in a number of small drops, hence microscopic inhomogeniety with respect to pH will result. In the presence of buffer, this inhomogeniety disappears rapidly due to the fast diffusion of both H^+ and acetate ions. In the absence of buffer, however, this equilibration process takes a long time. At the early stage of the process, the conversion of polymer molecules from random coils to the β-structure nuclei takes place in the interface region between the low pH small drops and the polymer solution. There remain these nuclei, more or less, after pH becomes uniform. They play the role of the seed in the folding of unfolded molecules.

On the other hand, it is likely that the reaction proceeds via different pathways for buffered and unbuffered solutions. While the coil-to-β conversion proceeds at constant pH in buffered solutions, it proceeds at nearly constant charges in the case of unbuffered solutions (random coil polymers are protonated at first by the added acid, and then converted to β-structure under the constant charges).

We carried out pH jump kinetic experiments with unbuffered solutions using a mixing unit for stopped-flow apparatus (MODEL MX-7, Union Giken Company, Osaka) which mixed solutions at most within 0.1 s. The rate enhancement was again observed by means of this device nearly to the same extent as with manual mixing. This result supports the latter mechanism rather than the former, unless the β-structure nuclei were formed within 0.1 s.

References

1) B. Davidson and G. D. Fasman, *Biochemistry*, **6**, 1616 (1967).
2) S.-Y. C. Wooly and G. Holzwarth, *Biochemistry*, **9**, 3604 (1970).
3) C. R. Snell and G. D. Fasman, *Biochemistry*, **12**, 1017 (1973).
4) H.-A. Arfmann, R. Labitzke, and K. G. Wagner, *Biopolymers*, **16**, 1815 (1977).
5) R. Hartman, R. C. Schwaner, and J. Hermans, Jr., *J. Mol. Biol.*, **90**, 415 (1974).
6) H. E. Auer and E. Patton, *Biophys. Chem.*, **4**, 15 (1976).
7) H. E. Auer and H. Miller-Auer, *Biopolymers*, **25**, 1607 (1986).
8) H. Maeda, K. Kadono, and S. Ikeda, *Macromolecules*, **15**, 822 (1982).
9) K. Saito, H. Maeda, and S. Ikeda, *Biophys. Chem.*, **16**, 67 (1982).
10) H. Maeda, Y. Gatto, and S. Ikeda, *Macromolecules*, **17**, 2031 (1984).
11) K. Fukada, H. Maeda, and S. Ikeda, Int. *J. Biol. Macromol.*, **9**, 87 (1987).
12) K. Fukada, H. Maeda, and S. Ikeda, *Polymer*, **28**, 1887 (1987).
13) H. Maeda, *Bull. Chem. Soc. Jpn.*, **60**, 3895 (1987).

The Lowest Triplet States of 2-Amino- and 2-Amino-d_2-pyrimidines

Yoshinori NIBU, Masayoshi MAEHARA,† Hiroko SHIMADA,† and Ryoichi SHIMADA*
Department of Chemistry, Faculty of Science, Kyushu University 33,
Hakozaki, Higashi-ku, Fukuoka 812
†Department of Chemistry, Faculty of Science, Fukuoka University,
Nanakuma, Jonan-ku, Fukuoka 814-01
(Received December 12, 1987)

Synopsis. The vibrational analyses of the sublevel phosphorescence spectra of 2-amino- and 2-amino-d_2-pyrimidines were made. The result shows that the lowest triplet $^3A_1(\pi,\pi^*)$ state is strongly perturbed by closely lying $^3B_1(n,\pi^*)$ and $^3A_2(n,\pi^*)$ states and the polarization of the very weak 0–0 bands in the dark sublevel spectra suggests that the symmetry of the molecular structure in the lowest triplet state is slightly lowered from the point group C_{2v} to the C_2.

Kleinwacher et al.[1] studied the absorption and emission spectra of 2-aminopyrimidine and assigned the lowest triplet state to a $^3A_1(\pi,\pi^*)$ state based on the polarization behavior of the phosphorescence. Since $^3B_1(n,\pi^*)$ and $^3A_2(n,\pi^*)$ states were considered to lie closely above the phosphorescent state,[2,3] it was expected that the lowest triplet state would be strongly perturbed by these two $^3(n,\pi^*)$ states. Nishi and Kinoshita[4] studied the individual sublevels of the lowest triplet state of 2-aminopyrimidine by the microwave induced delayed phosphorescence method and showed that the short-, medium-, and long-lifetime phosphorescences originate from the y, z, and x sublevels, respectively. They analyzed the phosphorescence spectrum based on the normal vibrations determined by Lafaix and Lebas[5] and concluded that the most effective phosphorescence mechanism for the y sublevel of the phosphorescent state is the first-order spin-orbit coupling between the $^1B_1(n,\pi^*)$ and $^3A_1(\pi,\pi^*)$ states, and that of the z sublevel is the second-order spin-orbit-vibronic coupling between the $^1A_1(\pi,\pi^*)$ and $^3A_1(\pi,\pi^*)$ states via the $^3A_2(n,\pi^*)$ state.

Very recently we reexamined the assignments of the normal vibrations of 2-amino- and 2-amino-d_2-pyrimidines and gave new assignments.[6] In this paper the vibrational analyses of the sublevel phosphorescence spectra of 2-amino- and 2-amino-d_2-pyrimidines are discussed based on the polarization behavior of the phosphorescence bands and normal vibrations newly determined and the phosphorescence processes of these molecules are restudied.

Experimental

Materials. 2-Amino-d_2-pyrimidine was obtained by the exchange reaction of 2-aminopyrimidine (Tokyo Kasei) with D_2O. The samples were purified by repeated distillation under reduced pressure. The solvent, benzene (Dotite Spectrosol Grade), was completely desiccated with an alloy of sodium and potassium because 2-amino-d_2-pyrimidine turned into 2-amino-d_1- and/or 2-aminopyrimidines quite easily by the exchange reaction with water containing in the solvent.

Optical Measurements. The phosphorescence lifetimes and the time-resolved phosphorescence spectra of 2-amino- and 2-amino-d_2-pyrimidines were measured in benzene matrices at 1.4 K. Using the relative values of the populations and radiative rate constants and the lifetimes for the lowest triplet sublevels of 2-aminopyrimidine determined by Nishi and Kinoshita,[4] the intensity ratio of the 0–0 bands of the phosphorescence spectra originating from the y, z, and x sublevels was calculated changing the sampling time after interrupting the excitation. The calculated intensity ratios indicate that the three sublevel phosphorescence could be mechanically separated if the adequate sampling time was chosen.

The short-lifetime phosphorescence was observed by sampling the emission from 3 ms to 40 ms after the cessation of the excitation. For the observation of the medium- and long-lifetime phosphorescences, the sampling times were set at 300—400 ms and 4000—5000 ms, respectively, after cutting off the exciting light.

The polarized phosphorescence spectrum was observed in a benzene host crystal at 1.4 K in the same way as described previously.[7] Since we have no knowledge about the orientation of the 2-aminopyrimidine molecule in the benzene single crystal, the polarized phosphorescence spectrum was observed with a rotatable polarizer whose orientation was set in such a way that the intensity of the 0–0 band in the short-lifetime spectrum became strongest and the rotation of the polarizer by 90° made the intensity weakest. The spectra observed at the former and latter orientations of the polarizer are drawn with solid and dotted lines and are referred to as solid and dotted spectra hereafter, respectively. The optical and electric apparatus used for the measurements of the time-resolved phosphorescence spectra, the polarized phosphorescence spectra and the phosphorescence lifetimes are exactly the same as those described previously.[7–9]

Results and Discussion

The phosphorescence lifetimes of 2-amino- and 2-amino-d_2-pyrimidines in benzene at 1.4 K were determined through the analysis of the phosphorescence decays. The short-, medium-, and long-lifetimes obtained for 2-amino-d_2-pyrimidine were 35, 395, and 1500 ms, respectively, and the lifetimes obtained for 2-aminopyrimidine were approximately equal to the sublevel lifetimes determined by Nishi and Kinoshita in p-xylene.[4] The mechanically resolved sublevel phosphorescence spectra of 2-amino- and 2-amino-d_2-pyrimidines in benzene at 1.4 K are shown in Figs. 1 and 2, respectively, where the intensity of the strongest band in each spectrum is normalized to unity.

The vibrational analysis of the short-lifetime phosphorescence spectrum of 2-aminopyrimidine will be discussed first. The shortest wavelength band at 27646 cm^{-1}, whose intensity is the strongest in the spectrum, was taken as the 0–0 band. The strong bands

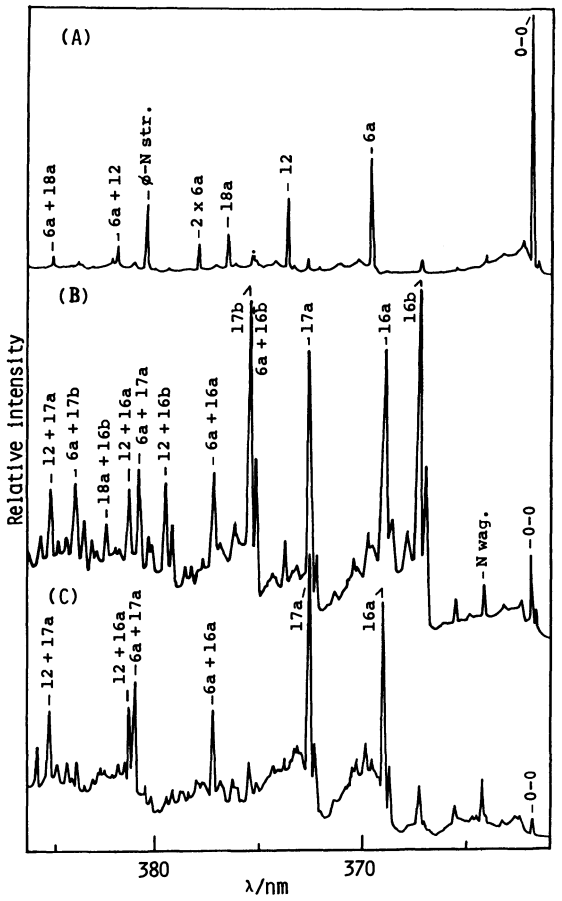

Fig. 1. The (A) short-, (B) medium-, and (C) long-lifetime phosphorescence spectra of 2-aminopyrimidine in benzene at 1.4 K.

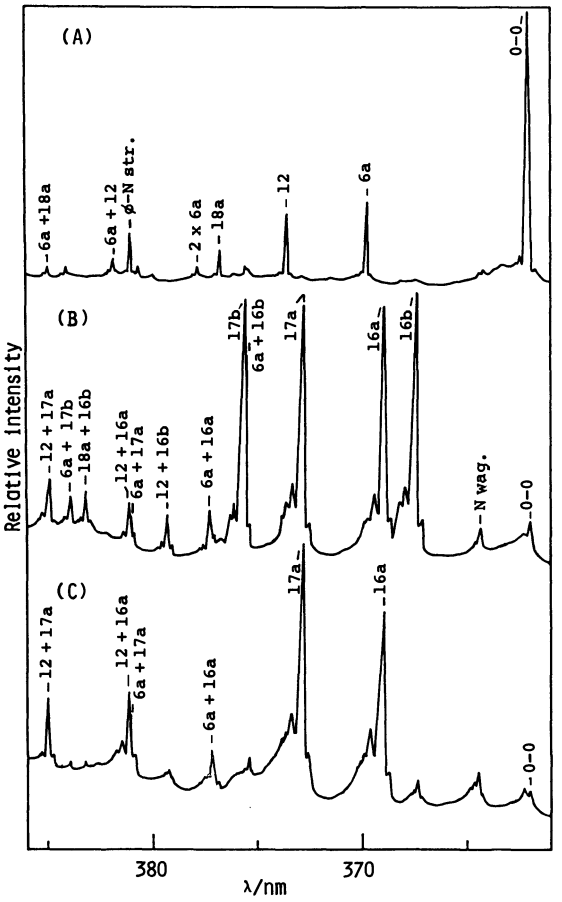

Fig. 2. The (A) short-, (B) medium-, and (C) long-lifetime phosphorescence spectra of 2-amino-d_2-pyrimidine in benzene at 1.4 K.

separated by 586, 876, 1090, and 1357 cm^{-1} from the 0–0 band were assigned to the totally symmetric ν_{6a}, ν_{12}, ν_{18a}, and ϕ–N stretching vibrations, respectively. The overtone and combination bands of these vibrations were also observed with medium or weak intensity.

The polarized time-resolved phosphorescence spectra of a benzene single crystal doped with 2-aminopyrimidine are shown in Fig. 3. For the 0–0 and totally symmetric ν_{6a} and ν_{12} bands observed in the polarized short-lifetime spectrum, the intensity of the solid spectrum is stronger than that of the dotted one. Since the symmetry representation of the y sublevel is B_1, the 0–0, ν_{6a}, and ν_{12} bands are to be polarized along the x direction. The x-polarized bands were also observed at 532 and 807 cm^{-1} from the 0–0 bands in the polarized long-lifetime spectrum. Since the symmetry representation of the x sublevel is B_2, these bands should be assigned to the a_2 vibration. We assigned these bands to the ν_{16a} and ν_{17a} vibrations. The ν_{16a} and ν_{17a} vibronic bands were also observed in the medium-lifetime spectrum where the band intensity of the dotted spectrum is stronger than that of the solid one. The z sublevel belongs to the symmetry representation A_2 and thus these bands are to be polarized along the z direction. The z-polarized bands were also observed at 190, 409, and 1000 cm^{-1} from the 0–0 band in the short-lifetime spectrum. These bands should be ascribed to the b_1 vibration and thus the bands were assigned to the N wagging, ν_{16b}, and ν_{17b} vibrations, respectively. The ν_{16b} and ν_{17b} vibronic bands were strongly observed in the medium-lifetime spectra with nearly equal intensity of the solid and dotted spectra. These bands are to be polarized along the y direction. The observed characteristic polarization behavior of these vibronic bands in the time-resolved phosphorescence spectra clearly shows that the main bands observed in the short-, medium-, and long-lifetime spectra are the bands originating from the y, z, and x sublevels, respectively.

The spectral structure of the sublevel phosphorescence spectra of 2-amino-d_2-pyrimidine is essentially the same as that of 2-aminopyrimidine. The strong bands separated by 570, 848, 1076, and 1366 cm^{-1} from the 0–0 band located at 27619 cm^{-1} in the short-lifetime spectrum were assigned to the ν_{6a}, ν_{12}, ν_{18a}, and ϕ–N stretching vibrations, respectively. The prominent bands separated by 522 and 785 cm^{-1} from the 0–0 band in the long-lifetime spectrum were assigned to the ν_{16a} and ν_{17a}, vibrations, respectively. In addition to the ν_{16a} and ν_{17a} bands, relative strong bands were observed at 407 and 990 cm^{-1} from the 0–0 band in the medium-lifetime spectrum and these bands were assigned to the ν_{16b} and ν_{17b} vibrations, respectively.

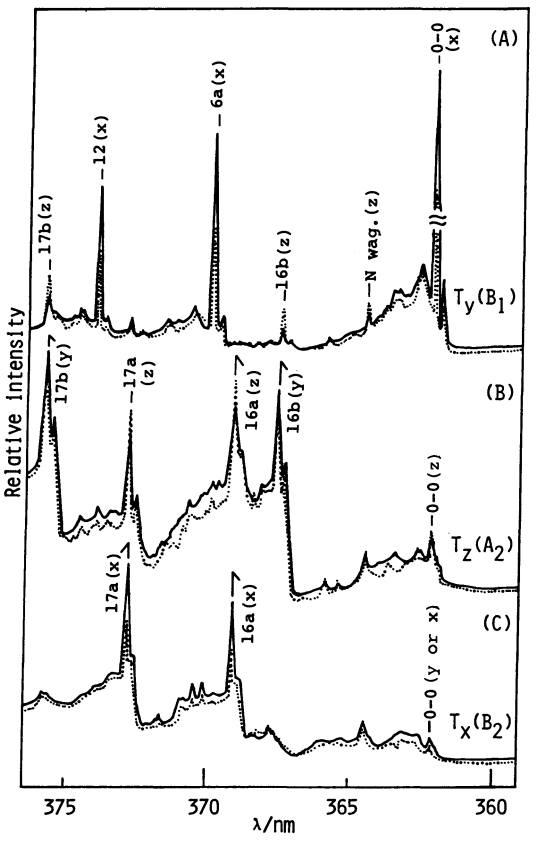

Fig. 3. The polarized (A) short-, (B) medium-, and (C) long-lifetime phosphorescence spectra of 2-aminopyrimidine in a benzene single crystal at 1.4 K. (x), (y), and (z) indicate the polarization directions of the bands.

The detailed vibrational analyses are given in Figs. 1 and 2.

The vibrational analyses made on two molecules distinctly indicate that (1) the emission from the y sublevel borrows the intensity from the $^1B_1(n,\pi^*)$-$^1A_1$ transition through the first-order spin-orbit coupling, (2) the emission from the z sublevel borrows the intensity almost equally from the $^1A_1(\pi,\pi^*)$-$^1A_1$ and $^1B_2(\pi,\pi^*)$-$^1A_1$ transitions via the $^3A_2(n,\pi^*)$ and $^3B_1(n,\pi^*)$ states, respectively, through the second-order spin-orbit-vibronic coupling, although Nishi and Kinoshita considered only the second-order process via the $^3A_2(n,\pi^*)$ state as the main perturbing process, and (3) the emission from the x sublevel borrows the intensity from the $^1B_1(\sigma,\pi^*)$-$^1A_1$transition via the $^3A_2(n,\pi^*)$ state. The dominant vibronic coupling is expected to take place among the triplet states because of the small energy separation between the $^3A_1(\pi,\pi^*)$ and $^3A_2(n,\pi^*)$ or $^3B_1(n,\pi^*)$ states.

A question that may be asked is: why do the dark $z(A_2)$ and $x(B_2)$ sublevels give the 0–0 bands polarized along the z and y(or x) directions, respectively? If the symmetry of the molecular structure reduces to the point group C_s due to the amino-substitution, the symmetry representations of the y, z, and x sublevels turn into the symmetry species A′, A″, and A″, respectively. This molecular geometry gives the 0–0 bands polarized along the y direction in both the z and x sublevel spectra contrary to the observaton. If the molecular structure reduces to the point group C_2, the symmetry representations of the y, z, and x sublevels turn into the species B, A, and B, and the z and x sublevel spectra could show the 0–0 bands polarized along the z direction and in the xy plane, respectively, in accord with the observation. However, the distortion of the molecular geometry, which may be caused by the vibronic coupling or the crystal force, should be small because the intensity of the 0–0 bands is much weaker than that of the a_2 and b_1 vibronic bands in the dark sublevel spectra, and the overtone bands of the ν_{16a} and ν_{17a} vibrations belonging to the a_2 symmetry species could not be observed. In the parent molecule, pyrimidine, whose lowest triplet state is the $^1B_1(n,\pi^*)$ state, the molecular distortion and the second-order spin-orbit-vibronic coupling give almost equal contributions to the phosphorescence processes for the dark sublevel.[7]

References

1) V. Kleinwachter, J. Drobnik, and L. Augenstein, *Photochem. Photobiol.*, **5**, 579 (1966).
2) L. Goodman, *J. Mol. Spectry.*, **6**, 109 (1961).
3) R. M. Hochstrasser and C. J. Marzzacco, *J. Mol. Spectry.*, **42**, 75 (1972).
4) N. Nishi and M. Kinoshita, *Chem. Phys. Lett.*, **27**, 342 (1974).
5) A. J. Lafaix and J. M. Lebas, *Spectrochim. Acta*, **26A**, 1243 (1970).
6) M. Maehara, S. Nakama, Y. Nibu, H. Shimada, and R. Shimada, *Bull. Chem. Soc. Jpn.*, **60**, 2769 (1987).
7) M. Umemoto, T. Ogata, H. Shimada, and R. Shimada, *Bull. Chem. Soc. Jpn.*, **57**, 3300 (1984).
8) Y. Urabe, T. Watanabe, Y. Ishibashi, H. Shimada, and R. Shimada, *Mem, Fac. Sci. Kyushu Univ., Ser. C*, **13**, 1 (1981).
9) T. Watanabe, H. Shimada, and R. Shimada, *Bull. Chem. Soc. Jpn.*, **55**, 2564 (1982).

Spherical Aromaticity of Buckminsterfullerene

Jun-ichi AIHARA* and Haruo HOSOYA†
Department of Chemistry, Faculty of Science, Shizuoka University, Oya, Shizuoka 422
†Department of Chemistry, Ochanomizu University, Bunkyo-ku, Tokyo 112
(Received December 14, 1987)

Synopsis. Aromatic stabilization of buckminsterfullerene is not large enough to guarantee isolation in macroscopic amounts. This does not rule out the possibility that such carbon clusters are formed in sooting flames and/or in dark interstellar space.

Carbon clusters are produced in a pulsed supersonic beam apparatus using laser vaporization of a graphite disk.[1] Kroto et al. presented evidence for the existence of a remarkably stable C_{60} cluster in the vaporization products.[2-4] The stability has been presumed to arise from the ability of a graphitic sheet to close into a spheroidal shell, thereby eliminating its reactive edges.[2-4] The structure proposed was a truncated icosahedron with 12 pentagons and 20 hexagons arranged on the surface of a sphere. The ultraviolet spectrum of C_{60}[5] and the photoelectron spectrum of its anion[6] are apparently consistent with this structure. Kroto et al. named the molecule having this structure (**1**) buckminsterfullerene.[2,7] If the C_{60} cluster is really buckminsterfullerene, it will be of great interest in connection with the problem of spherical aromaticity.

Various molecular orbital (MO) methods have been used to obtain the energy structure of buckminsterfullerene.[8-24] Dewar resonance energy was estimated by use of Herndon-Simpson and conjugated circuit resonance theories[10,12] and by the Hess-Schaad method based on Hückel MO theory.[10,13] The topological resonance energy (TRE) is known to be an excellent measure of aromatic stabilization.[25-29] It can be calculated exactly within the Hückel framework. However, no one has ever calculated the TRE of buckminsterfullerene because it is not easy to evaluate the non-adjacent numbers[30,31] of a very large conjugated system.

The situation has changed recently. Hosoya overcame this difficulty,[32] and succeeded in construct ing the matching polynomial (i.e., the reference polynomial[25]) of buckminsterfullerene, which is shown below:[32]

$$\begin{aligned}R(X)=&X^{60}-90X^{58}+3825X^{56}-102120X^{54}+1922040X^{52}\\&-27130596X^{50}+298317860X^{48}-2619980460X^{46}\\&+18697786680X^{44}-109742831260X^{42}+534162544380X^{40}\\&-2168137517940X^{38}+7362904561730X^{36}\\&-20949286202160X^{34}+49924889888850X^{32}\\&-99463457244844X^{30}+165074851632300X^{28}\\&-227043126274260X^{26}+256967614454320X^{24}\\&-237135867688980X^{22}+176345540119296X^{20}\\&-104113567937140X^{18}+47883826976580X^{16}\\&-16742486291340X^{14}+4310718227685X^{12}\\&-783047312406X^{10}+94541532165X^{8}-6946574300X^{6}\\&+269272620X^{4}-4202760X^{2}+12500\end{aligned} \quad (1)$$

According to our standard interpretation,[25-29] this is a characteristic polynomial for an olefinic reference structure of buckminsterfullerene. Here, an olefinic reference structure stands for a hypothetical molecule obtained by replacing all bonds in a given molecule by those found in acyclic polyenes.

Hückel MO calculations of buckminsterfullerene have been published repeatedly.[8-13,16,18,19,33] Total π-electron energy of this molecule is $60\alpha+93.1616\beta$. That of its olefinic reference structure is $60\alpha+91.5189\beta$, which was obtained from the roots of the equation $R(X)=0$. The TRE is then given as the difference between these two energies. It is 1.6427β for buckminsterfullerene. Since this molecule is more stable than its olefinic reference structure, it can be classified as an aromatic molecule or a molecule of spherical aromaticity.

However, an aromatic molecule is not always stable enough to exist in the condensed phase. In order to see relative stabilities of buckminsterfullerene and related molecules, we evaluated the percent resonance energies (%RE's). The %RE of a given molecule is defined as 100 times the TRE, divided by the total π-electron energy of its olefinic reference structure.[28,34-36] Owing to the wide variation in the size of molecules compared, we feel that %RE is a better way of comparing stabilities than using the total TRE's. The %RE's calculated for buckminsterfullerene and related species are listed in Table 1.

The %RE of buckminsterfullerene is 1.79, which is smaller than those of typical benzenoid hydrocarbons

Table 1. Topological Resonance Energies of Buckminsterfullerene and Related Hydrocarbons

Species	TRE/β	%RE
Buckminsterfullerene (**1**)	1.643	1.79
Buckminsterfullerene*	1.010	1.10
Buckminsterfullerene^{2+}	0.530	0.58
Buckminsterfullerene^{2-}	1.489	1.63
Corannulene (**2**)	0.735	2.63
Naphthacene	0.553	2.27
Pentacene	0.630	2.11
Hexacene	0.706	1.99
Heptacene	0.783	1.91
Acenaphthylene (**3**)	0.354	2.18
Cyclopenta[*cd*]pyrene (**4**)	0.565	2.27
Pyracylene (cyclopent[*fg*]-acenaphthylene) (**5**)	0.106	0.55

(2.2—3.3).[35,36] In the benzenoid hydrocarbons, a %RE of this size does not guarantee stability or isolability in macroscopic amounts.[28] In the polyacene series, even hexacene and heptacene have a larger %RE. Note that hexacene (%RE=1.99) must be handled under nitrogen and that heptacene (%RE=1.91) is so unstable that it has never been obtained in a pure state. Hess and Schaad also noted insufficient stability of buckminsterfullerene.[13] Thus, this molecule is predicted not to be isolable although it has as many as 12500 Kekulé structures.[10,12,32]

Each carbon in buckminsterfullerene is equivalent to every other carbon, being the vertex joining one pentagon and two hexagons. As in graphite, each atom is involved in two single bonds and one double bond to its neighbors. Graphite has a total π-electron energy per carbon of $\alpha+1.5746\beta$.[37] If we assume that the olefinic reference structures of buckminsterfullerene and graphite have the same total π-electron energy per carbon, the %RE of graphite is calculated to be 3.23, which is slightly less than twice the %RE of buckminsterfullerene. This again suggests insufficient stability of the icosahedral C_{60} cluster.

To make matters worse, each C-C resonance integral in buckminsterfullerene cannot take the standard value (β) since all C-C bonds are bent on the surface of the sphere. Taking this structural factor into account, Haddon et al. showed that the resonance integrals in buckminsterfullerene must be reduced to 0.877β.[11] This further decreases the TRE of buckminsterfullerene. The TRE of buckminsterfullerene in Table 1 must likewise be multiplied by 0.877.

The structural unit of the truncated icosahedron is a pentagon surrounded by five hexagons. Corannulene (**2**) is a hydrocarbon in such a structure. This molecule is shaped like a bowl,[38] and isolable in accord with its large %RE (2.63). As stated by Hess and Schaad,[13] the isolation of corannulene which has a considerably larger %RE than buckminsterfullerene does not imply the potential isolation of buckminsterfullerene.

Heath et al. obtained evidence for the formation of stable complexes of the formula $C_{60}M$ by laser evaporation of a graphite disk impregnated with M, where M=La, Ba, Sr, Ca, etc.[39] Stability of the dianion in a supersonic beam might be rationalized well by the %RE, which is comparable to that of the neutral species. As can be seen from the structure, buckminsterfullerene has a nonalternant hydrocarbon skeleton but without hydrogens. The dication has a much smaller %RE than the dianion.

Kroto et al. speculated about the possibility that the C_{60} cluster might be the carrier of the diffuse interstellar ultraviolet band.[2,40] As in a supersonic beam, buckminsterfullerene may be formed somewhere in the hydrogen-deficient interstellar or circumstellar medium. At present, there is no reason to doubt the existence of this molecule in dark interstellar space. In fact, the C_{60} cluster in a supersonic beam is very resistant to chemical attack by such small molecules as NO, H_2, CO, SO_2, O_2, and NH_3.[3]

Léger and Puget[41] and Allamandola et al.[42] proposed recently that there must be abundant polycyclic aromatic hydrocarbons (PAH's) in the interstellar medium. In previous papers,[35,36] Aihara suggested that such interstellar PAH's must have a large %RE both in the ground and excited states since they are placed in the intense radiation field. As shown in Table 1, the %RE of buckminsterfullerene is very small in the first excited state. Therefore, it does not seem stable enough to exist in the intense radiation field. Buckminsterfullerene* in Table 1 indicates the excited-state species.

Soot is formed by incomplete combustion of organic matter. One of the striking features known about soot is that it is almost always found in the form of spheres, arranged in strands of beads or more complicated structures.[2,43] The polycyclic hydrocarbons are detectable in high concentrations in sooting flames. They may adopt pentagonal rings as they grow, so as to generate spheroidal structures which maximize the number of C-C linkages.[2]

Acenaphthylene (**3**) and cyclopenta[*cd*]pyrene (**4**) are formed in sooting flames.[43] Even pyracylene (cyclopent[*fg*]acenaphthylene) (**5**) is suspected to exist in flames.[43] These molecules are not highly aromatic PAH's. Synthetic pyracylene is far from isolable from solution.[44,45] Fluorene and indene are also detectable in flames.[43] Since in flames there are many such hydrocarbons with pentagonal rings, it seems likely that soot or large spheroidal carbon clusters are formed starting from these molecules. However, this does not imply that buckminsterfullerene is isolable even if it is formed in flames.[46] As pointed out above, the %RE of buckminsterfullerene is too small.

Localization energy is a typical reactivity index for aromatic molecules.[47] The cation and anion localization energies of buckminsterfullerene are 2.767 and 2.490, respectively, at all constituent carbons. These values are very large as compared with those at the peripheral carbons of polycyclic benzenoid hydrocarbons (1.90—2.55).[47] It should be noted that most reactions of benzenoid hydrocarbons occur at these peripheral carbons. If in future buckminsterfullerene is found to be isolable, the stability will be ascribed to the absence of peripheral reactive carbons,

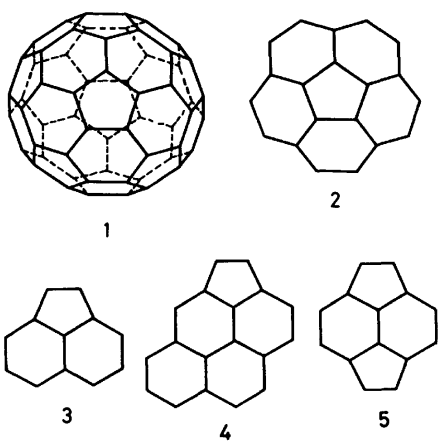

thereby being kinetic rather than thermodynamic in nature.

In this connection, Iijima prepared a spherical particle of graphitic carbon by arc discharge between two carbon rods, and found that there seems to be a C_{60} cluster at the core of the particle.[48] The innermost carbon cluster is obviously protected from danger by many outer spheres made of carbon atoms.

References

1) E. A. Rohlfing, D. M. Cox, and A. Kaldor, *J. Chem. Phys.*, **81**, 3322 (1984).
2) H. W. Kroto, J. R. Heath, S. C. O'Brien, R. F. Curl, and R. E. Smalley, *Nature (London)*, **318**, 162 (1985).
3) Q. Zhang, S. C. O'Brien, J. R. Heath, Y. Liu, R. F. Curl, H. W. Kroto, and R. E. Smalley, *J. Phys. Chem.*, **90**, 525 (1986).
4) R. M. Baum, *Chem. Eng. News*, **63**, 20 (Dec. 23, 1985).
5) J. R. Heath, R. F. Curl, and R. E. Smalley, *J. Chem. Phys.*, **87**, 4236 (1987).
6) S. H. Yang, C. L. Pettiette, J. Conceicao, O. Cheshnovsky, and R. E. Smalley, *Chem. Phys. Lett.*, **139**, 233 (1987).
7) A very lengthy IUPAC systematic name can be assigned to buckminsterfullerene: J. Castells and F. Serratosa, *J. Chem. Educ.*, **63**, 630 (1986).
8) A. D. J. Haymet, *Chem. Phys. Lett.*, **122**, 421 (1985).
9) A. D. J. Haymet, *J. Am. Chem. Soc.*, **108**, 319 (1986).
10) D. J. Klein, W. A. Seitz, and T. G. Schmaltz, *Nature (London)*, **323**, 703 (1986).
11) R. C. Haddon, L. E. Brus, and K. Raghavachari, *Chem. Phys. Lett.*, **125**, 459 (1986).
12) T. G. Schmalz, W. A. Seitz, D. J. Klein, and G. E. Hite, *Chem. Phys. Lett.*, **130**, 203 (1986).
13) B. A. Hess, Jr., and L. J. Schaad, *J. Org. Chem.*, **51**, 3902 (1986).
14) R. L. Disch and J. M. Schulman, *Chem. Phys. Lett.*, **125**, 465 (1986).
15) S. Nagase and K. Ito, *Chem. Phys. Lett.*, **126**, 43 (1986).
16) M. Ozaki and A. Takahashi, *Chem. Phys. Lett.*, **127**, 242 (1986).
17) S. Satpathy, *Chem. Phys. Lett.*, **130**, 545 (1986).
18) R. C. Haddon, L. E. Brus, and K. Raghavachari, *Chem. Phys. Lett.*, **131**, 165 (1986).
19) P. W. Fowler, *Chem. Phys. Lett.*, **131**, 444 (1986).
20) H. P. Lüthi and J. Almlöf, *Chem. Phys. Lett.*, **135**, 357 (1987).
21) I. László and L. Udvardi, *Chem. Phys. Lett.*, **136**, 418 (1987).
22) S. Larsson, A. Volosov, and A. Rosén, *Chem. Phys. Lett.*, **137**, 501 (1987).
23) J. M. Schulman, R. L. Disch, M. A. Miller, and R. C. Peck, *Chem. Phys. Lett.*, **141**, 45 (1987).
24) M. L. McKee and W. C. Herndon, *J. Mol. Struct. (Theochem)*, **153**, 75 (1987).
25) J. Aihara, *J. Am. Chem. Soc.*, **98**, 2750 (1976).
26) I. Gutman, M. Milun, and N. Trinajstić, *J. Am. Chem. Soc.*, **99**, 1692 (1977).
27) J. Aihara, *J. Am. Chem. Soc.*, **99**, 2048 (1977).
28) J. Aihara, *Pure Appl. Chem.*, **54**, 1115 (1982).
29) J. Aihara, *Netsu Sokutei*, **12**, 61 (1985).
30) H. Hosoya, K. Kawasaki, and K. Mizutani, *Bull. Chem. Soc. Jpn.*, **45**, 3415 (1972).
31) H. Hosoya, *Theor. Chim. Acta*, **25**, 215 (1972).
32) H. Hosoya, *Comput. Math. Appls.*, **12B**, 271 (1986).
33) I. V. Stankevich, M. V. Nikerov, and D. A. Bochvar, *Russ. Chem. Rev.*, **53**, 640 (1984).
34) J. Aihara, *Bull. Chem. Soc. Jpn.*, **53**, 2689 (1980).
35) J. Aihara, *Bull. Chem. Soc. Jpn.*, **60**, 3143 (1987).
36) J. Aihara, *Bull. Chem. Soc. Jpn.*, **60**, 3581 (1987).
37) S. E. Stein and R. L. Brown, *J. Am. Chem. Soc.*, **109**, 3721 (1987).
38) W. E. Barth and R. G. Lowton, *J. Am. Chem. Soc.*, **93**, 1730 (1971).
39) J. R. Heath, S. C. O'Brien, Q. Zhang, Y. Liu, R. F. Curl, H. W. Kroto, F. K. Tittel, and R. E. Smalley, *J. Am. Chem. Soc.*, **107**, 7779 (1985).
40) H. W. Kroto, "Polycyclic Aromatic Hydrocarbons and Astrophysics," ed by A. Léger, L. d'Hendecourt, and N. Boccara, Reidel, Dordrecht (1987), pp. 197—206.
41) A. Léger and J. Puget, *Astron. Astrophys.*, **137**, L5 (1984).
42) L. J. Allamandola, A. G. G. M. Tielens, and J. R. Barker, *Astrophys. J.*, **290**, L25 (1985).
43) J. B. Howard and J. P. Longwell, "Polynuclear Aromatic Hydrocarbons: Formation, Metabolism and Measurement," ed by M. Cooke and A. J. Dennis, Battelle Press, Columbus (1983), pp. 27—62.
44) B. M. Trost and G. M. Bright, *J. Am. Chem. Soc.*, **89**, 4244 (1967).
45) B. M. Trost, G. M. Bright, C. Frihart, and D. Brittelli, *J. Am. Chem. Soc.*, **93**, 737 (1971).
46) P. Gerhardt, S. Löffler, and K. H. Homann, *Chem. Phys. Lett.*, **137**, 306 (1987).
47) A. Streitwieser, Jr., "Molecular orbital Theory for Organic Chemists," Wiley, New York (1961), Chap. 11.
48) S. Iijima, *J. Phys. Chem.*, **91**, 3466 (1987).

Absorption and CD Spectral Properties of Bis(ethylenediamine)cobalt(III) Complexes with *O*-Bonded Sulfoxide and Seleninate

Takumi KONNO,* Ken-ichi OKAMOTO, and Jinsai HIDAKA
Department of Chemistry, University of Tsukuba, Tsukuba, Ibaraki 305
(Received December 17, 1987)

Synopsis. The absorption and CD spectral behavior of $[Co\{OS(CH_3)CH_2CH_2NH_2\}(en)_2]^{3+}$ and $[Co\{OSe(O)CH_2CH_2NH_2\}(en)_2]^{2+}$ was discussed. The *O*-bonded seleninato isomer, Λ-$(+)_{500}^{CD}$-$[Co\{OSe(O)CH_2CH_2NH_2\}(en)_2]^{2+}$, showed racemization at the chiral selenium atom in an aqueous solution and a shift of the equilibrium between the (*R*) and (*S*) configurations of the chiral selenium atom through the protonation on the pendant oxygen atom.

Several bis(diamine)cobalt(III) complexes containing a coordinated chiral sulfur or selenium atom have been investigated,[1-11] and some stereochemical differences between cobalt(III) complexes with a selenium-containing ligand and those with a sulfur-containing ligand have been reported.[8-10] Recently, the two diastereomers due to the non-coordinated chiral sulfur atom, $\Lambda(R)$ and $\Lambda(S)$,[12] have been isolated for the *O*-bonded sulfinato complex, $[Co\{OS(O)CH_2CH_2NH_2\}(en)_2]^{2+}$.[13] On the other hand, the single crystal X-ray analysis indicated that the chiral selenium atom in the corresponding *O*-bonded seleninato complex, $(-)_{500}^{CD}$-$[Co\{OSe(O)CH_2CH_2NH_2\}(en)_2]^{2+}$, selectively takes the (*S*) configuration in the crystal state.[14]

Here we report on the stereochemical behavior of Λ-$(+)_{500}^{CD}$-$[Co\{OSe(O)CH_2CH_2NH_2\}(en)_2]^{2+}$ in solution, together with that of the newly prepared two diastereomers of the *O*-bonded sulfoxide complex, $\Lambda(R)$- and $\Lambda(S)$-$[Co\{OS(CH_3)CH_2CH_2NH_2\}(en)_2]^{3+}$. The absorption and CD spectra of the *O*-bonded seleninato complex are discussed in comparison with those of the corresponding *O*-bonded sulfinato and sulfoxide complexes.

Experimental

Complexes. (1) Λ-$(+)_{500}^{CD}$-$[Co\{OSe(O)CH_2CH_2NH_2\}(en)_2](ClO_4)_2$. Fairly large crystals of this complex were prepared by the method described in a previous paper.[14]

(2) $\Lambda(S)$-$(-)_{500}^{CD}$-$[Co\{OS(CH_3)CH_2CH_2NH_2\}(en)_2](ClO_4)_3\cdot H_2O$ and $\Lambda(R)$-$(+)_{500}^{CD}$-$[Co\{OS(CH_3)CH_2CH_2NH_2\}(en)_2](ClO_4)_3$. These isomers were prepared by a procedure similar to that used for $[Co\{OS(CH_3)CH_2CH_2NH_2\}(en)_2]^{3+}$,[6,15] using $\Lambda(R)$- and $\Lambda(S)$-$[Co\{S(O)CH_2CH_2NH_2\}(en)_2](ClO_4)_2$[9] instead of $[Co\{S(O)CH_2CH_2NH_2\}(en)_2](ClO_4)_2$. To a dimethyl sulfoxide solution (3 cm^3) of $\Lambda(R)$- or $\Lambda(S)$-$[Co\{S(O)CH_2CH_2NH_2\}(en)_2](ClO_4)_2$ (0.15 g) was added an excess amount of CH_3I (1.0 g); the mixture was then allowed to stand at room temperature for three days. After the excess CH_3I and dimethyl sulfoxide had been extracted with diethyl ether, to the remaining oily product was added a small amount of water, after which the solution was passed through a column (2.5 cm×25 cm) of QAE-Sephadex A-25 (ClO_4^- form) while being eluted with water. The reddish eluate was concentrated to a small volume with a rotary evaporator. The addition of a small amount of ethanol to the concentrate, followed by cooling in a refrigerator overnight, yielded crystals of the desired *O*-bonded sulfoxide isomer. The $(-)_{500}^{CD}$ and $(+)_{500}^{CD}$ isomers thus obtained showed the same absorption spectrum as the racemic $[Co\{OS(CH_3)CH_2CH_2NH_2\}(en)_2]^{3+}$.[6,15] No CD spectral change was observed for the two isomers, at least for one day. Found for the $\Lambda(S)$ isomer: C, 13.97; H, 4.49; N, 11.67%. Calcd for $[Co\{OS(CH_3)CH_2CH_2NH_2\}(en)_2](ClO_4)_3\cdot H_2O=C_7H_{27}N_5O_{14}SCl_3Co$: C, 13.95; H, 4.52; N, 11.62%. Found for the $\Lambda(R)$ isomer: C, 14.45; H, 4.31; N, 11.98%. Calcd for $[Co\{OS(CH_3)CH_2CH_2NH_2\}(en)_2](ClO_4)_3=C_7H_{25}N_5O_{13}SCl_3Co$: C, 14.38; H, 4.31; N, 11.97%. Attempts to prepare the corresponding selenoxide complex, $[Co\{OSe(CH_3)CH_2CH_2NH_2\}(en)_2]^{3+}$, by the reaction of $\Lambda(R)$-$[Co\{Se(O)CH_2CH_2NH_2\}(en)_2](ClO_4)_2$[9] (0.1 g) with CH_3I (0.7 g) were unsuccessful; instead, the selenide complex, $\Lambda(R)$-$[Co\{Se(CH_3)CH_2CH_2NH_2\}(en)_2]^{3+}$,[9] was formed. An SP-Sephadex chromatographic investigation of the reaction solution (after ca. 10 min) revealed the formation of the selenolato complex, Λ-$[Co(SeCH_2CH_2NH_2)(en)_2]^{2+}$,[9] besides the selenide complex.

Measurements. The electronic absorption spectra were recorded with a JASCO UVIDEC-1 spectrophotometer, and the CD spectra with a JASCO J-20 spectropolarimeter in an aqueous solution at room temperature. The ^1H and ^{13}C NMR spectra were recorded with a JEOL JNM-FX-100 or -FX-90Q NMR spectrometer in a D_2O or $HClO_4$–D_2O solution at room temperature. Sodium 2,2-dimethyl-2-silapentane-5-sulfonate (DSS) was used as the internal reference.

Results and Discussion

The two isomers of the *O*-bonded sulfoxide complex, $(-)_{500}^{CD}$- and $(+)_{500}^{CD}$-$[Co\{OS(CH_3)CH_2CH_2NH_2\}(en)_2]^{3+}$, were prepared by the reaction of $\Lambda(R)$- and $\Lambda(S)$-$[Co\{S(O)CH_2CH_2NH_2\}(en)_2]^{2+}$ respectively with CH_3I. As shown in Fig. 1 their absorption spectra show an intense shoulder at ca. 37.0×10^3 cm^{-1} besides the first absorption band (ca. 19.5×10^3 cm^{-1}) and the second absorption band (ca. 27.5×10^3 cm^{-1}). In the first absorption band region, the CD patterns of the *O*-bonded sulfoxide isomers coincide well with those of the parental $\Lambda(R)$ and $\Lambda(S)$ sulfenato isomers[9] (Fig. 1), suggesting that the isomers retain the Λ configuration of the parental sulfenato isomers. The $(-)_{500}^{CD}$ isomer derived from the $\Lambda(R)$ sulfenato isomer exhibits a sharp ^1H NMR peak arising from the methyl group of the ligand at 2.93 ppm, while the $(+)_{500}^{CD}$ isomer derived from the $\Lambda(S)$ isomer exhibits a peak at 2.83 ppm. Furthermore, the methylation of $[Co\{S(O)CH_2CH_2NH_2\}(en)_2]^{2+}$ to $[Co\{OS(CH_3)CH_2CH_2NH_2\}(en)_2]^{3+}$ is known to proceed with a retention of the absolute configuration at the chiral sulfur atom.[15,16] Taking these facts into consideration, it is probable that the methylation reaction of the $\Lambda(S)$ and $\Lambda(R)$ sulfenato isomers produce the $\Lambda(R)$ and $\Lambda(S)$ *O*-bonded sulfoxide isomers respectively. The $\Lambda(R)$ and $\Lambda(S)$ isomers of $[Co\{OS(CH_3)CH_2CH_2NH_2\}(en)_2]^{3+}$

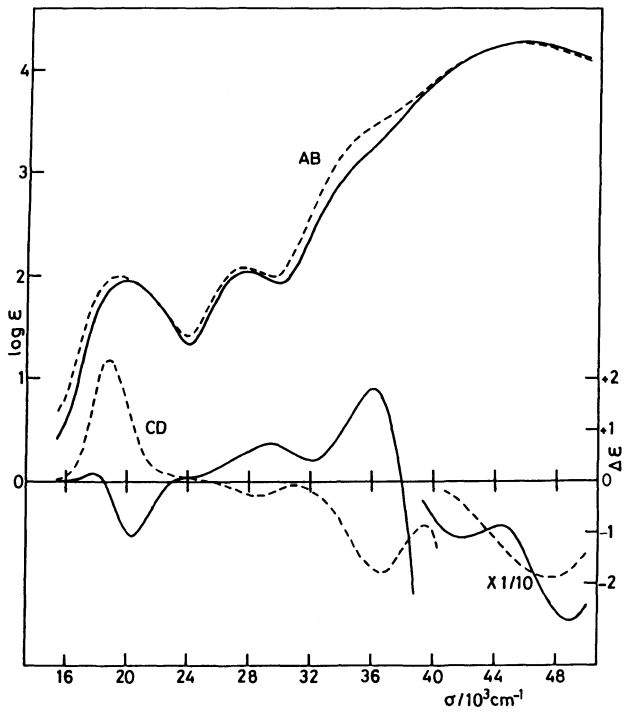

Fig. 1. Absorption and CD spectra of $\Lambda(S)$-[Co{OS(CH$_3$)CH$_2$CH$_2$NH$_2$}(en)$_2$]$^{3+}$ (——) and $\Lambda(R)$-[Co{OS(CH$_3$)CH$_2$CH$_2$NH$_2$}(en)$_2$]$^{3+}$ (----).

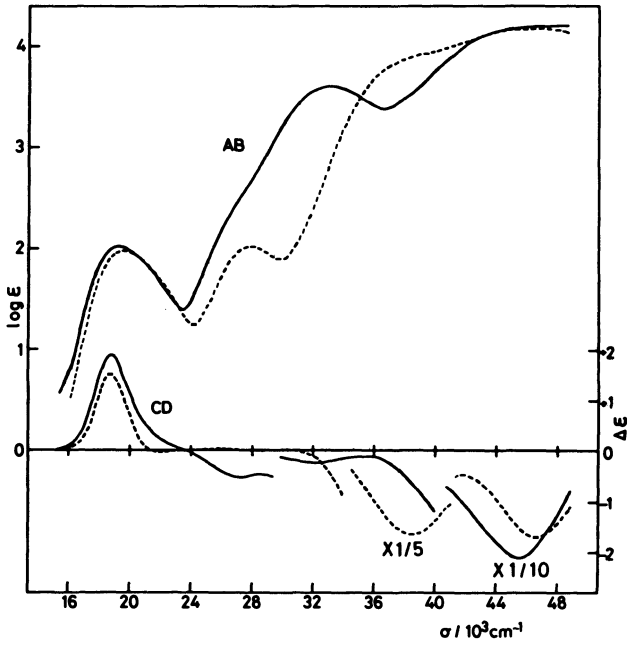

Fig. 2. Absorption and CD spectra of Λ-(+)$^{CD}_{500}$-[Co{OSe(O)CH$_2$CH$_2$NH$_2$}(en)$_2$]$^{3+}$ in water (——) and Λ-(+)$^{CD}_{500}$-[Co{OSe(OH)CH$_2$CH$_2$NH$_2$}(en)$_2$]$^{3+}$ in 6% HClO$_4$ (----).

show almost enantiomeric CD spectra in the region of 18—38×10^3 cm^{-1} (Fig. 1), indicating that the non-coordinated chiral sulfur atom in the sulfoxide complex contributes significantly to the CD spectrum, just as in the case of the coordinated chiral sulfur atoms in [Co{S(O)CH$_2$CH$_2$NH$_2$}(en)$_2$]$^{2+}$,[9] and [Co{S(OH)CH$_2$CH$_2$NH$_2$}(en)$_2$]$^{3+}$.[8] The methylation of the selenenato complex, $\Lambda(R)$-[Co{Se(O)CH$_2$CH$_2$NH$_2$}(en)$_2$]$^{2+}$, produced the selenide complex, $\Lambda(R)$-[Co{Se(CH$_3$)CH$_2$CH$_2$NH$_2$}(en)$_2$]$^{3+}$; no selenoxide complex was detected. The presence of the selenolato complex, Λ-[Co(SeCH$_2$CH$_2$NH$_2$)(en)$_2$]$^{2+}$, in the reaction solution (after ca. 10 min) besides the selenide complex suggests that the selenide complex was formed via the intermediate, Λ-[Co(SeCH$_2$CH$_2$NH$_2$)(en)$_2$]$^{2+}$, which retained the Λ configuration of $\Lambda(R)$-[Co{Se(O)CH$_2$CH$_2$NH$_2$}(en)$_2$]$^{2+}$.

The *O*-bonded seleninato complex, [Co{OSe(O)CH$_2$CH$_2$NH$_2$}(en)$_2$]$^{2+}$, shows an instantaneous and reversible absorption spectral change with the pH change in an aqueous solution. The pK_a value for this complex at 25 °C and μ=1.0 mol dm^{-3} (NaClO$_4$) has been determined to be 1.91±0.05 in a previous paper.[14] For the *O*-bonded seleninato complex, there are three possible protonation sites: the coordinated oxygen atom, the pendant oxygen atom, and the selenium atom. As shown in Fig. 2 the first absorption band of the protonated complex is quite similar to that of the parental *O*-bonded seleninato complex, suggesting that the coordinated oxygen atom is not protonated. The charge-transfer band at ca. 33×10^3 cm^{-1} characteristic of the *O*-bonded seleninato complex[14] disappears in the protonated complex. Furthermore, the protonated complex exhibits a new intense shoulder at ca. 39×10^3 cm^{-1} and the second absorption band at 27.86×10^3 cm^{-1}. This absorption spectral behavior of the protonated complex is in good agreement with that of the corresponding *O*-bonded sulfoxide complex, [Co{OS(CH$_3$)CH$_2$CH$_2$NH$_2$}(en)$_2$]$^{3+}$ (Figs. 1 and 2). Taking account of the fact that the absorption spectra of [Co{Se(OH)CH$_2$CH$_2$NH$_2$}(en)$_2$]$^{3+}$ and [Co{S(CH$_3$)CH$_2$CH$_2$NH$_2$}(en)$_2$]$^{3+}$ behave quite similarly to each other,[8] it is probable to consider that the protonation of the *O*-bonded seleninato complex occurs on the pendant oxygen atom to form [Co{OSe(OH)CH$_2$CH$_2$NH$_2$}(en)$_2$]$^{3+}$.

In the crystal state, the chiral selenium atom in the *O*-bonded seleninato isomer, Δ-(−)$^{CD}_{500}$-[Co{OSe(O)CH$_2$CH$_2$NH$_2$}(en)$_2$]$^{2+}$, takes selectively the (*S*) configuration with the axial pendant oxygen atom.[14] Thus, the Λ-(+)$^{CD}_{500}$ isomer should have the (*R*) configurational selenium atom in the crystal state. When the Λ-(+)$^{CD}_{500}$ isomer was dissolved in water, a slight intensity change in the CD spectrum (ca. 12% decrease at 500 nm) was observed and the solution attained equilibrium after ca. 10 min. No change in the absorption spectrum was observed during the CD measurement. The ^{13}C NMR spectrum of Λ-(+)$^{CD}_{500}$-[Co{OSe(O)CH$_2$CH$_2$NH$_2$}(en)$_2$]$^{2+}$ in a D$_2$O solution exhibits ten peaks for the six carbon atoms of the complex (Fig. 3(a)). This ^{13}C NMR spectral behavior is similar to that of a mixture of the $\Lambda(R)$ and $\Lambda(S)$ isomers of the corresponding *O*-bonded sulfinato complex, [Co{OS(O)CH$_2$CH$_2$NH$_2$}(en)$_2$]$^{2+}$; the peaks at 32.94, 45.45, 46.86, 47.08, and 51.09 ppm correspond to those for the $\Lambda(R)$ *O*-bonded sulfinato isomer, and

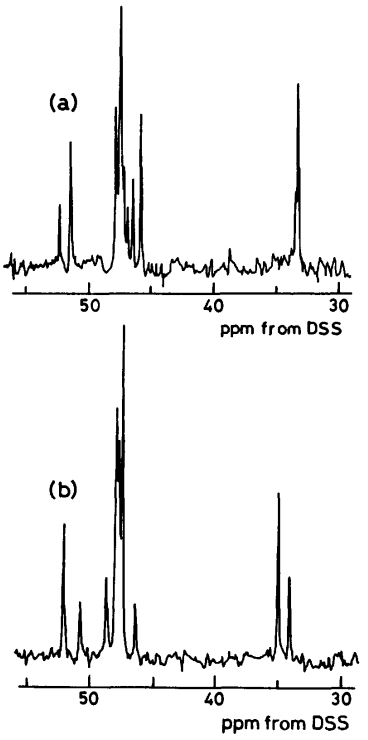

Fig. 3. ^{13}C NMR spectra of Λ-(+)$^{CD}_{500}$-[Co{OSe(O)-$CH_2CH_2NH_2$}$(en)_2]^{2+}$ in D_2O (a) and Λ-(+)$^{CD}_{500}$-[Co·{OSe(OH)CH_2CH_2NH}$(en)_2]^{3+}$ in 6% $HClO_4$–D_2O (b).

the peaks at 33.10, 46.10, 46.53, 47.51, and 51.95 ppm to those for the $\Lambda(S)$ isomer.[13] These facts mean that Λ-(+)$^{CD}_{500}$-[Co{OSe(O)$CH_2CH_2NH_2$}$(en)_2]^{2+}$ exists in a mixture of the $\Lambda(R)$ and $\Lambda(S)$ isomers in an aqueous solution because of the inversion at the chiral selenium atom. The $\Lambda(R)$ isomer seems to be dominant in the mixture, considering the intensity of the ^{13}C NMR peaks for the two isomers. In order to confirm the presence of the two isomers, the SP-Sephadex column chromatographic separation was attempted for Λ-(+)$^{CD}_{500}$-[Co{OSe(O)$CH_2CH_2NH_2$}$(en)_2]^{2+}$. However, only one absorbed band appeared, and all of its fractions showed the same CD spectra, though the corresponding *O*-bonded sulfinato isomers, $\Lambda(R)$- and $\Lambda(S)$-[Co{OS(O)$CH_2CH_2NH_2$}$(en)_2]^{2+}$, have been separated by the use of an SP-Sephadex column.[13] These facts indicate that the inversion at the chiral selenium atom in [Co{OSe(O)$CH_2CH_2NH_2$}$(en)_2]^{2+}$ is faster than that at the chiral sulfur atom in [Co{OS(O)CH_2-CH_2NH_2}$(en)_2]^{2+}$.

The Λ-(+)$^{CD}_{500}$ *O*-bonded seleninato isomer shows an instantaneous and reversible CD spectral change with the pH change corresponding to the absorption spectral change. The positive CD band at 18.76×10^3 cm^{-1} in the first absorption band region of the protonated (+)$^{CD}_{500}$-[Co{OSe(OH)$CH_2CH_2NH_2$}$(en)_2]^{3+}$ suggests that the protonation reaction proceeds with a retention of the Λ configuration (Fig. 2). The ^{13}C NMR spectrum of Λ-(+)$^{CD}_{500}$-[Co{OSe(OH)CH_2CH_2-NH_2}$(en)_2]^{3+}$ exhibits nine peaks for the six carbon atoms of the complex (Fig. 3(b)). This ^{13}C NMR spectral behavior indicates the coexistence of the $\Lambda(R)$ and $\Lambda(S)$ isomers as the parental Λ-(+)$^{CD}_{500}$-[Co{OSe-(O)$CH_2CH_2NH_2$}$(en)_2]^{2+}$. For each pair of peaks at ca. 34 and 51 ppm, however, the peak at the higher magnetic field appears weaker than that at the lower one, in contrast with the case of the parental Λ-(+)$^{CD}_{500}$-[Co{OSe(O)$CH_2CH_2NH_2$}$(en)_2]^{2+}$ (Fig. 3). Furthermore, the CD spectrum of Λ(+)$^{CD}_{500}$-[Co{OSe(OH)CH_2-CH_2NH_2}$(en)_2]^{3+}$is quite similar to that of $\Lambda(R)$-[Co-{OS$(CH_3)CH_2CH_2NH_2$}$(en)_2]^{3+}$ (Figs. 1 and 2), where the (*R*) configuration of the latter complex corresponds to the (*S*) configuration of the former one.[16] The ^{13}C NMR and CD spectral behavior suggests that a shift of the equilibrium between the (*R*) and (*S*) configurations taskes place through the protonation reaction and that the protonated Λ-(+)$^{CD}_{500}$ isomer takes the (*S*) configuration dominantly.

References

1) W. G. Jackson, A. M. Sargeson, and P. O. Whimp, *J. Chem. Soc., Chem. Commun.*, **1976**, 934.
2) K. Yamanari, J. Hidaka, and Y. Shimura, *Bull. Chem. Soc. Jpn.*, **50**, 2299 (1977).
3) R. C. Elder, G. J. Kennard, M. D. Payne, and E. Deutsch, *Inorg. Chem.*, **17**, 1296 (1978).
4) D. L. Herting, C. P. Sloan, A. W. Cabral, and J. H. Krueger, *Inorg. Chem.*, **17**, 1649 (1978).
5) I. K. Adzamli, K. Libson, J. D. Lydon, R. C. Elder, and E. Deutsch, *Inorg. Chem.*, **18**, 303 (1979).
6) J. D. Lydon and E. Deutsch, *Inorg. Chem.*, **21**, 3180 (1982).
7) M. Kita, K. Yamanari, and Y. Shimura, *Bull. Chem. Soc. Jpn.*, **55**, 2873 (1982).
8) T. Konno, K. Okamoto, H. Einaga, and J. Hidaka, *Chem. Lett.*, **1983**, 969.
9) T. Konno, K. Okamoto, and J. Hidaka, *Bull. Chem. Soc. Jpn.*, **57**, 3104 (1984).
10) T. Konno, K. Okamoto, H. Einaga, and J. Hidaka, *Bull. Chem. Soc. Jpn.*, **58**, 1119 (1985).
11) K. Okamoto, T. Konno, H. Einaga, and J. Hidaka, *Bull. Chem. Soc. Jpn.*, **60**, 393 (1987).
12) The symbols (*R*) and (*S*) denote the absolute configuration of the chiral sulfur or selenium atom.
13) K. Yamanari and Y. Shimura, *Chem. Lett.*, **1984**, 761.
14) K. Okamoto, T. Konno, M. Nomoto, H. Einaga, and J. Hidaka, *Bull. Chem. Soc. Jpn.*, **57**, 1494 (1984).
15) G. J. Gainsford, W. G. Jackson, and A. M. Sargeson, *J. Am. Chem. Soc.*, **104**, 137 (1982).
16) According to the sequence rule for labeling chiral centers, the designations, (*R*) and (*S*), for the chirality at sulfur atom in [Co{OS$(CH_3)CH_2CH_2NH_2$}$(en)_2]^{3+}$ correspond to those, (*S*) and (*R*), in [Co{S(O)$CH_2CH_2NH_2$}-$(en)_2]^{2+}$.

A New Method for Determining Cyclodextrin Complex Formation Constants with Electrolytes in Aqueous Medium

Isao SANEMASA,* Motohisa FUJIKI, and Toshio DEGUCHI
Department of Chemistry, Faculty of Science, Kumamoto University,
Kurokami 2-39-1, Kumamoto 860
(Received December 24, 1987)

Synopsis. By making use of the volatilization rate of iodine from aqueous into gaseous phase, association constants of α-cyclodextrin with electrolytes (chlorides, nitrates, and perchlorates) have been determined at 25 °C; the counter cations are found to be largely responsible for the association.

Among several methods so far available for determining cyclodextrin (CyD) complex formation constants, four techniques, i.e., conductometry,[1-3] calorimetry,[4] kinetic inhibition,[5] and spectral competitive inhibition[6-9] have been used for the systems where electrolytes having neither absorption nor fluorescence are involved.

We have studied CyD associations with volatile guests such as iodine, benzene, alkylbenzenes, naphthalenes.[10-12] The present work is concerned with a further development of the study; iodine is used as a volatile guest which serves as an indicator and α-CyD is used as a host.

By introducing an inert gas at a constant flow rate into aqueous solutions, iodine molecules are driven out into the gaseous phase. The volatilization rate is reduced in the presence of CyD owing to the host-guest association. The decrease in rate gives the complex formation constant. Now consider the presence of an electrolyte which does not interact with iodine, but does associate with CyD. Under such a circumstance, the iodine volatilization rate is expected to be accelerated as a result of competition with the electrolyte.

Associations of some inorganic electrolytes with CyD have been well demonstrated and anions are thought to be responsible for the association. Is there any contribution of the counter cation? It is another object of this work to elucidate the effect of counter cation.

Experimental

Distilled deionized water was used throughout this work. Electrolytes, NaCl, KCl, HNO_3, $NaNO_3$, $HClO_4$, $LiClO_4$, $NaClO_4$, $KClO_4$, and $(CH_3)_4NClO_4$, of analytical reagent grade were used as purchased and each stock solution was, when necessary, standardized by alkalimetry after passing a suitable portion of the stock solution through H^+-form cation-exchange resin. Preparations of α-CyD (Nakarai Chemical Co.) and iodine aqueous solutions, the iodine standardization method, experimental procedures, and apparatus were described in the previous paper.[10]

A brief statement of the experimental procedure will be made here. A 50 cm^3 portion of the sample solution in which both iodine and electrolyte to be studied are present with or without CyD, was transferred into a 2.5φ×25 cm cylindrical glass tube immersed in a bath thermostated at 25.0±0.1 °C. N_2 gas was blown in the sample solution through a capillary glass tube at a constant flow rate of 600 $cm^3\ min^{-1}$. The I_2 concentration in this work was lower than that used in our previous study, and N_2 gas was blown at a much higher flow rate to expel I_2 effectively. The N_2 gas flow rate was kept the same irrespective of the presence of CyD. The iodine carried out of the solution by N_2 gas stream was trapped in a 5×10^{-4} M $Na_2S_2O_3$ solution of 20 cm^3 and the amount of I_2 expelled during a fixed time, ΔQ_{I_2}, was determined.

The concentration in M unit (M≡ mol dm^{-3}) used in most of the runs was as follows; iodine (1.57×10^{-5}), α-CyD (1.57×10^{-4}), NaCl (2.12×10^{-2}), KCl (1.00×10^{-2}), HNO_3 (5.00×10^{-2}), $NaNO_3$ (5.00×10^{-2}), $HClO_4$ (5.04×10^{-2}), $LiClO_4$ (4.24×10^{-2}), $NaClO_4$ (5.00×10^{-2}), $KClO_4$ (5.45×10^{-2}), and $(CH_3)_4NClO_4$ (3.51×10^{-2}). The association constants were determined on average of three or four measurements.

Results and Discussion

It is well established that both the molecular iodine and the electrolyte used in this study form 1:1 complex with α-CyD. Then, the reactions that should be taken into account are:

$$CyD + I_2 \rightleftharpoons CyD\cdot I_2, \quad K_{I_2}, \tag{1}$$

$$CyD + X \rightleftharpoons CyD\cdot X, \quad K_X, \tag{2}$$

and

$$I_2(aq) \longrightarrow I_2(gas), \quad k, \tag{3}$$

where K_{I_2} and K_X are association constants with iodine and electrolyte (X), respectively, and k is the rate constant for the transfer of iodine molecules from aqueous to gaseous phase. The iodine molecules expelled into the gaseous phase are collected successively by the absorbent, and the total amount, Q_{I_2}, which is the sum of ΔQ_{I_2}, is measured as a function of aeration time, t. The iodine volatilization rate at a constant N_2 gas flow rate is of the first-order with respect to the concentration of free iodine species in the solution as follows:

$$dQ_{I_2}V^{-1}/dt = k[I_2], \tag{4}$$

where V is the volume of the aqueous solution.

The mass-balance equations are:

$$C_{CyD} = [CyD] + [CyD\cdot I_2] + [CyD\cdot X] = [CyD](1 + K_{I_2}[I_2] + K_X[X]), \tag{5}$$

and

$$C_{I_2} = [I_2] + [CyD\cdot I_2] + Q_{I_2}V^{-1} = [I_2](1 + K_{I_2}[CyD]) + Q_{I_2}V^{-1} \tag{6}$$

where C_{CyD} and C_{I_2} denote the total concentration of CyD and that of iodine, respectively. Substituting Eq.

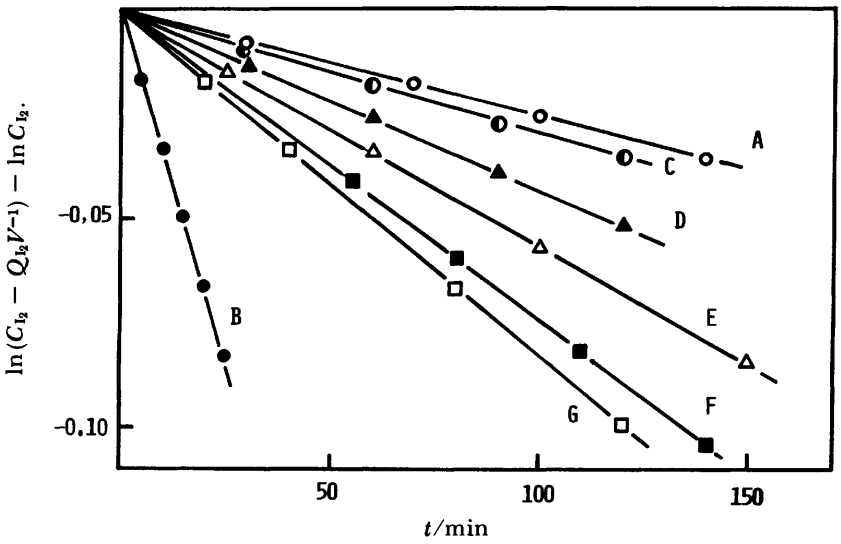

Fig. 1. The plots of $\ln(C_{I_2}-Q_{I_2}V^{-1})-\ln C_{I_2}$ vs. t in the presence (A) and absence (B) of CyD. N_2 flow rate: 600 $cm^3 min^{-1}$; C_{I_2}: 1.57×10^{-5} M, C_{CyD}: 7.99×10^{-4} M; Electrolyte ($C_X/10^{-2}$ M): (C) $(CH_3)_4NClO_4$ (3.51), (D) $LiClO_4$ (4.24), (E) $NaClO_4$ (5.00), (F) $KClO_4$ (5.45), (G) $HClO_4$ (5.04).

6 into Eq. 4 and integration ($Q_{I_2}=0$ at $t=0$) yield

$$\ln(C_{I_2} - Q_{I_2}V^{-1}) = -kt/(1 + K_{I_2}[CyD]) + \ln C_{I_2}. \quad (7)$$

Here we set experimental conditions as follows: the equilibrium concentration of iodine is sufficiently low so that the product $K_{I_2}[I_2]$ can be neglected and that of electrolyte is so large that [X] can be taken as its total concentration, C_X. Then, Eq. 7 becomes

$$\ln(C_{I_2} - Q_{I_2}V^{-1}) = -kt/\{1 + K_{I_2}C_{CyD}(1 + K_XC_X)^{-1}\} + \ln C_{I_2}. \quad (8)$$

Plots of $\ln(C_{I_2}-Q_{I_2}V^{-1})$ vs. t (Fig. 1) gave straight lines over the aeration time investigated; the slope corresponds to $-k$ in the absence of CyD, to $-k/(1+K_{I_2}C_{CyD})$ in the absence of the associating electrolyte, and to $-k/\{1+K_{I_2}C_{CyD}(1+K_XC_X)^{-1}\}$ in the presence of both CyD and electrolyte. The K_{I_2} value thus determined was 1.5×10^4 M^{-1}, which agrees with our previous result.[10] The association constants of CyD with the electrolytes studied here are given in Table 1 together with literature values available.

The association constants determined in this work seem to be significantly larger than the literature data. It is not clear at present whether or not the present results are reasonable, because the data so far available are limited and, moreover, considerable disagreement exists among them.

It is generally accepted that the CyD association constant decreases in the order, ClO_4^->SCN^->I^->Br^->NO_3^-.[7] As for the cation, on the other hand, little attention has been paid. For instance, K_X was reported for α-CyD-ClO_4^- system without specifying the counter cation.[6] In spite of different cation being used, the relative magnitude of K_X value of a given anion was compared for α- and β-CyDs.[7] Based on the data obtained by the spectral competitive inhibition method, Buvári and Barcza pointed out the importance of the counter cation: potassium salts associate more strongly with β-CyD than the sodium salts.[8]

Table 1. Association Constants for the Complex Formation between Electrolytes and α-Cyclodextrin at 25°C

Electrolyte	Association constant/M^{-1}	
	This work[a]	Literature
NaCl	3	negligible[4]
KCl	5	
HNO_3	11	
$NaNO_3$	4	1.4 (KNO_3)[1]
$HClO_4$	60	39.8[4]
$LiClO_4$	22	
$NaClO_4$	35	20.4,[4] 30.6[2]
$KClO_4$	48	28.9,[1] 37[9]
$(CH_3)_4NClO_4$	8	

a) The relative standard deviation is roughly estimated to be 30% for the association constant lower than 5 and 15% for that higher than 10.

The present study indicates that the counter cation plays an important role in the α-CyD association with electrolytes; the association constant decreases in the order, H^+>K^+>Na^+>Li^+>$(CH_3)_4N^+$. In light of the order of anions, this order of alkali ions is understandable: counter cation with less affinity with water is favorable to association with CyD. The behavior of H^+ is particular and should be ascribed to hydrogen bonding to CyD; H^+ bound to primary or secondary alcohol group of the CyD rim attracts its counter anion and holds it inside the CyD cavity, when the anion has low affinity with water. The

small K_X observed for $(CH_3)_4N^+$ ion may be attributable to that this ion cannot enter into the α-CyD cavity.[3] The counter cation effect is thus explainable on the assumption that electrolyte exists as ion-pair inside or in the entrance of CyD cavity with anion preferentially included in the cavity, although there has been no direct experimental evidence supporting this idea.

There are two essential requirements for the present method to be successufully applied. One is that the difference between the tow slopes, $-k$ at $C_{CyD}=0$ and $-k/(1+K_{I_2}C_{CyD})$ at $C_X=0$, be as large as possible. Any volatile guest substance with sufficiently large association constant can be used as an indicator; iodine is suitable for α-CyD, but not for β-CyD; in the latter case different guest should be used. Another requirement is that the product, K_XC_X, should not be too small compared with unity. When K_X is small, as is the present case, C_X should be made large. In such a case, care must be taken for the so-called salt effect.

The spectral competitive inhibition method makes use of the fact that the presence of electrolyte shifts the CyD association equilibrium with a certain guest substance as an indicator, usually, azo dye. Our method resembles this spectral method with respect to competing the electrolyte with the indicator guest for the CyD bonding site. It should be noted that, as was pointed out by Mochida et al.,[13] the presence of electrolyte does not always inhibit the indicator guest association with CyD, but, on the contrary, promotes the association by reducing the activity of water surrounding the indicator guest molecule. It depends on the nature of both cation and anion constituting the electrolyte which governs promotion or inhibition. The spectral method usually needs electrolyte of high concentration to cause measurable absorbance changes of the indicator guest. If a counter ion has more or less a promoting effect, the K_X value for this electrolyte is to be underestimated. These situations hold for the present method. It is, however, easy to study the salt effect by our method. The volatilization rate of the indicator guest is measured in the presence of salt of desired concentration and is compared with that in the absence of salt. If there is no change between them, the salt effect can be ignored. The salt concentration used in this work did not affect the iodine volatilization rate constant, k.

When iodine is used as an indicator guest, association constants of such electrolytes as SCN^-, I^-, and Br^- cannot be determined by the present method.

References

1) J. F. Wojcik and R. P. Rohrbach, *J. Phys. Chem.*, **79**, 2251 (1975).

2) H. Høiland, L. H. Hald, and O. J. Kvammen, *J. Solution Chem.*, **10**, 775 (1981).

3) K. Miyajima, M. Sawada, T. Ueda, and M. Nakagaki, *Nippon Kagaku Kaishi*, **1984**, 527.

4) E. A. Lewis and L. D. Hansen, *J. Chem. Soc., Perkin Trans. 2*, **1973**, 2081.

5) W. Hirsch and S. Petrucci, *J. Molecular Liquids*, **28**, 14 (1984).

6) F. Cramer, W. Saenger, and H.-Ch. Spatz, *J. Am. Chem. Soc.*, **89**, 14 (1967).

7) R. P. Rohrbach, L. J. Rodriguez, E. M. Eyring, and J. F. Wojcik, *J. Phys. Chem.*, **81**, 944 (1977).

8) Á. Buvári and L. Barcza, *Inorg. Chim. Acta*, **33**, L179 (1979).

9) R. I. Gelb, L. M. Schwartz, B. Cardelino, and D. A. Laufer, *Anal. Biochem.*, **103**, 362 (1980).

10) I. Sanemasa, Y. Nishimoto, A. Tanaka, and T. Deguchi, *Bull. Chem. Soc. Jpn.*, **59**, 2269 (1986).

11) I. Sanemasa and Y. Akamine, *Bull. Chem. Soc. Jpn.*, **60**, 2059 (1987).

12) M. Fujiki, T. Deguchi, and I. Sanemasa, *Bull. Chem. Soc. Jpn.*, **61**, 1163 (1988).

13) K. Mochida, A. Kagita, Y. Matsui, and Y. Date, *Bull. Chem. Soc. Jpn.*, **46**, 3703 (1973).

X-Ray Crystal Structure and Electrochemical Property of a Novel Monohydroxo-Bridged Binuclear Cobalt(II) Complex with *N,N',N'',N'''*-Tetrakis(2-aminoethyl)-1,4,8,11-tetraazacyclotetradecane

Masahiro MIKURIYA,* Sigeo KIDA,*,†,†† Takamitsu KOHZUMA,†† and Ichiro MURASE†††
Department of Chemistry, School of Science, Kwansei Gakuin University, Uegahara, Nishinomiya 662
†Department of Chemistry, Faculty of Science, Kyushu University 33, Hakozaki, Higashi-ku, Fukuoka 812
††Coordination Chemistry Laboratories, Institute for Molecular Science, Myodaiji, Okazaki 444
†††Laboratory of Chemistry, College of General Education, Kyushu University 01, Ropponmatsu, Chuo-ku, Fukuoka 810
(Received February 17, 1988)

Synopsis. The crystal structure of a binuclear cobalt(II) complex of *N,N',N'',N'''*-tetrakis(2-aminoethyl)-1,4,8,11-tetraazacyclotetradecane (taec), $[Co_2(taec)(OH)](ClO_4)_3$, was determined by the single-crystal X-ray diffraction method. The two cobalt ions are bridged by a single hydroxide ion in the cavity of taec. The cyclic voltammogram showed an irreversible profile with two anodic peaks at ca. 1.4 and 1.8 V vs. SCE.

In the previous paper, we reported the preparation of the μ-hydroxo-bridged cobalt(II) complexes with an octadentate ligand, *N,N',N'',N'''*-tetrakis(2-aminoethyl)-1,4,8,11-tetraazacyclotetradecane (abbreviated as taec), $[Co_2(taec)(OH)]X_3$ (X=ClO_4 and PF_6).[1] The taec ligand exclusively forms binuclear complexes where each metal ion is coordinated by two cyclam-ring nitrogens and two pendant amino nitrogens.[1-6] On the basis of infrared and electronic spectra and magnetic susceptibility data, we assumed that the two cobalt ions are bridged by only one hydroxide ion in the "cavity" of taec. Monohydroxo-bridged complexes are rare, although recently some examples have been reported for copper(II) complexes.[7] Interestingly these cobalt(II) complexes are inert toward aerobic or chemical oxidation. Attempts to obtain cobalt(III) species of taec were all unsuccessful. We assumed that the resistance to oxidation is due to the sterical difficulty in achieving six-coordination.[1] In this study, we have examined the electrochemical property and the X-ray crystal structure of $[Co_2(taec)(OH)](ClO_4)_3$ in order to confirm our assumption.

Experimental

The crystals were prepared as described in Ref. 1.

X-Ray Structure Determination. A Rigaku AFC-5

Table 1. Crystal Data and Data Collection Details

Complex	$[Co_2(taec)(OH)](ClO_4)_3$
Formula	$C_{18}H_{45}Cl_3Co_2N_8O_{13}$
Fw	805.82
Crystal system	Monoclinic
Space group	$P2_1/a$
a/Å	20.481(3)
b/Å	16.394(2)
c/Å	9.275(1)
β/°	91.23(1)
V/Å^3	3113.6(7)
Z	4
D_c/g cm^3	1.719
D_m/g cm^3	1.68
$F(000)$	1672
Radiation	Graphite-mnochromated Mo$K\alpha$ (λ=0.71073 Å)
Crystal size/mm	0.15×0.27×0.48
μ(Mo$K\alpha$)/cm^{-1}	13.9
Scan type	θ-2θ
Scan speed/° min^{-1}	3
Scan width/°	1.1+0.5 tan θ
2θ range/°	1.5—55.0
Total number of observed reflections	7472
Number of unique reflections with $\lvert F_o\rvert > 3\sigma(\lvert F_o\rvert)$	3123
Final number of variables	398
Final residuals	
R	0.046
R_w	0.052
Weighting scheme	$w=[\sigma_{count}^2+(0.015\lvert F_o\rvert)^2]^{-1}$
Largest peak on final difference map	0.77 e Å^{-3} (near Cl(1))

Table 2. Atomic Coordinates ($\times 10^4$) and Thermal Parameters

Atom	x	y	z	B_{eq}/Å^2	Atom	x	y	z	B_{eq}/Å^2
Co(1)	2765(1)	868(1)	7559(1)	2.2	N(5)	2891(3)	140(3)	5685(6)	3.6
Co(2)	1009(1)	1464(1)	7492(1)	2.3	N(6)	3060(3)	−60(3)	9017(6)	3.7
Cl(1)	1471(1)	−1239(1)	7525(2)	3.7	N(7)	448(3)	838(3)	9098(5)	3.5
Cl(2)	−1458(1)	152(1)	7415(2)	3.6	N(8)	446(3)	943(3)	5819(6)	3.8
Cl(3)	4718(1)	−559(1)	7489(2)	3.8	C(1)	3806(3)	2081(4)	7393(7)	3.1
O(1)	1819(2)	871(2)	7821(5)	3.5	C(2)	3488(3)	2336(4)	8783(7)	3.2
O(2)	1173(3)	−2022(3)	7537(5)	5.0	C(3)	2569(3)	1963(4)	10311(6)	2.9
O(3)	1510(5)	−904(5)	8896(7)	12.7	C(4)	2089(3)	2517(4)	9511(7)	2.7
O(4)	2103(3)	−1271(4)	7061(9)	11.1	C(5)	1411(3)	2492(4)	10097(7)	3.2
O(5)	1122(5)	−722(4)	6703(12)	17.1	C(6)	869(3)	3240(4)	8101(7)	3.4
O(6)	−1997(3)	704(3)	7413(7)	7.1	C(7)	665(3)	3099(4)	6588(7)	3.3
O(7)	−1532(3)	−329(4)	6157(6)	8.5	C(8)	1723(3)	2834(4)	5502(7)	3.6
O(8)	−1504(3)	−357(4)	8645(6)	7.7	C(9)	2232(3)	2179(4)	5165(7)	3.0
O(9)	−870(3)	571(5)	7427(7)	9.9	C(10)	2916(3)	2420(4)	5753(8)	4.0
O(10)	4841(6)	225(5)	7494(11)	18.3	C(11)	3641(3)	1256(5)	5196(7)	3.7
O(11)	5197(4)	−1095(7)	7189(10)	16.1	C(12)	3196(3)	628(4)	4533(7)	3.7
O(12)	4176(3)	−717(4)	6615(9)	10.8	C(13)	3533(3)	1103(4)	10263(7)	3.6
O(13)	4550(5)	−736(6)	8890(8)	13.4	C(14)	3229(3)	278(4)	10458(7)	3.8
N(1)	3312(2)	1737(3)	6358(5)	2.8	C(15)	245(3)	2291(4)	9579(7)	3.8
N(2)	3100(2)	1654(3)	9386(5)	2.5	C(16)	203(3)	1428(5)	10175(7)	4.0
N(3)	892(2)	2460(3)	8937(5)	2.5	C(17)	764(3)	2162(4)	4501(7)	4.1
N(4)	1081(2)	2477(3)	5862(5)	2.7	C(18)	214(3)	1569(5)	4773(8)	4.3

automated four-circle diffractometer was used for all measurements at 25±1 °C. Crystal data and details of the data collections are given in Table 1. Lattice constants were determined by least-squares refinement based on 50 reflections with $20°<2\theta<30°$. The intensity data were corrected for Lorentz-polarization effects and for absorption. The structure was solved by the direct method. Refinements were carried out by the block-diagonal least-squares method. Hydrogen atoms were inserted in their calculated positions and fixed at their positions. The final discrepancy factors, $R=\sum||F_o|-|F_c||/\sum|F_o|$ and $R_w=[\sum w(|F_o|-|F_c|)^2/\sum w|F_o|^2]^{1/2}$ are listed in Table 1. The thermal parameters of the ClO_4^- ions are high probably due to the partial disorder. The hydrogen atom of the bridging hydroxide ion could not be located on a final difference Fourier map.

The atomic scattering factors for all the atoms and the anomalous dispersion corrections for all the nonhydrogen atoms were taken from Ref. 8. All the calculations were carried out on the HITAC M-680H computer at the Computer Center of the Institute for Molecular Science using a local version of the MULTAN 78,[9] UNICS-III,[10] and ORTEP[11] programs. Atomic coordinates and thermal parameters of nonhydrogen atoms are listed in Table 2. The anisotropic thermal parameters of nonhydrogen atoms, the atomic coordinates and thermal parameters of hydrogen atoms, and the F_o-F_c tables have been deposited at the Office of the Chemical Society of Japan as a Document No. 8812.

Physical Measurement. Cyclic voltammetric measurement was carried out by using a Hokuto Denko HA-501 potentiostat with a Hokuto Denko HF-201 function generator and a Yokogawa 3086-11 X-Y recorder. A three-electrode cell consisting of a glassy carbon electrode, a platinum-flug counter electrode, and a saturated caromel references electrode (SCE) was used.

Results and Discussion

The crystal consists of binuclear cations $[Co_2(taec)(OH)]^{3+}$ and perchlorate ions. A perspective view of $[Co_2(taec)(OH)]^{3+}$ is shown in Fig. 2. The coordination mode of taec is the same as that of $[Cu_2(taec)Y](ClO_4)_3$ (Y=F, Br, I, N_3, NCO, NO_2).[1,5,6] The two

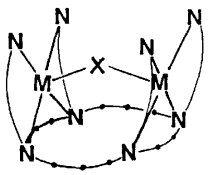

Fig. 1. Coordination mode of taec.

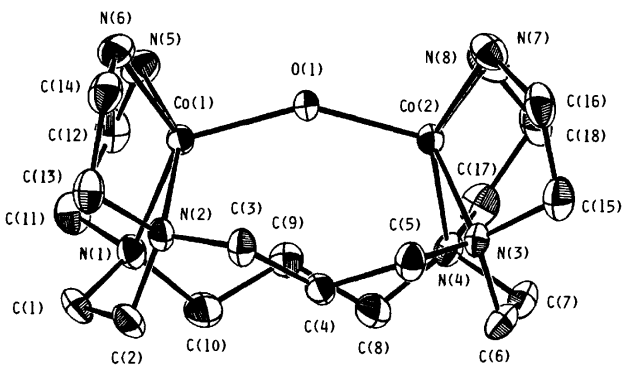

Fig. 2. ORTEP diagram of $[Co_2(taec)(OH)]^{3+}$.

cobalt ions are bridged by a single hydroxide ion. The geometry around each cobalt ion can be described as a distorted square pyramid. The basal plane is formed by two nitrogens of the cyclam ring and two pendant amino nitrogens. The deviations of the basal atoms from the mean plane are within ±0.22 Å, and Co(1) and Co(2) are displaced by 0.66 and 0.69Å, respectively, from the mean planes toward the hydroxide ion. The Co(1)-Co(2) distance of 3.727(1) Å is significantly shorter than the Cu-Cu distances of $[Cu_2(taec)Y](ClO_4)_3$ (4.299(2)—4.841(3) Å).[1,5,6] This may be attributed to the fact that the cobalt ions are further apart from the basal planes than are the copper ions of

Table 3. Selected Interatomic Distances (l/Å) and Bond Angles (ϕ/°)

Co(1)-Co(2)	3.727(1)	Co(2)-O(1)	1.942(4)
Co(1)-O(1)	1.958(4)	Co(2)-N(3)	2.128(5)
Co(1)-N(1)	2.139(5)	Co(2)-N(4)	2.252(5)
Co(1)-N(2)	2.226(5)	Co(2)-N(7)	2.161(5)
Co(1)-N(5)	2.128(5)	Co(2)-N(8)	2.096(5)
Co(1)-N(6)	2.115(5)		
Co(1)-O(1)-Co(2)	145.7(2)	N(3)-Co(2)-N(4)	82.4(2)
N(1)-Co(1)-N(2)	81.6(2)	N(3)-Co(2)-N(7)	82.1(2)
N(1)-Co(1)-N(5)	82.8(2)	N(4)-Co(2)-N(8)	81.2(2)
N(2)-Co(1)-N(6)	81.4(2)	N(7)-Co(2)-N(8)	91.4(2)
N(5)-Co(1)-N(6)	94.7(2)	O(1)-Co(2)-N(3)	113.1(2)
O(1)-Co(1)-N(1)	126.4(2)	O(1)-Co(2)-N(4)	114.0(2)
O(1)-Co(1)-N(2)	101.2(2)	O(1)-Co(2)-N(7)	96.8(2)
O(1)-Co(1)-N(5)	103.9(2)	O(1)-Co(2)-N(8)	111.5(2)
O(1)-Co(1)-N(6)	101.1(2)		

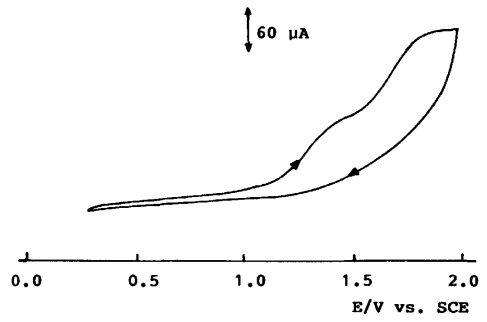

Fig. 3. Cyclic voltammogram of $[Co_2(taec)(OH)](ClO_4)_3$ (1/2 mM) (1 M=1 mol dm^{-3}) in acetonitrile containing 0.1 M $(C_2H_5)_4NBF_4$. The scan rate is 100 mV s^{-1}.

$[Cu_2(taec)Y](ClO_4)_3$ (0.37—0.48 Å).[1,5,6] In this structure, the sixth coordination site of the cobalt ion is blocked by the methylene groups of taec. Thus, the result also consists with our previous assumption that the strong resistivity to the oxidation from Co(II) to Co(III) in these complexes arises mainly from prohibition against six-coodination which stabilizes Co(III) oxidation state characteristically.[1]

Cyclic voltammetric measurements were carried out with a glassy carbon electrode in acetonitrile solution. The cyclic voltammogram showed an irreversible profile with two anodic peaks at ca. 1.4 and 1.8 V vs. SCE (Fig. 3). The remarkable high oxidation potentials agree with the fact that the chemical oxidation of the cobalt(II) of this complex is very difficult. The complex was oxidized electrolytically at ca. 1.4 V vs. SCE in acetonitrile solution. The solution turned from purple to reddish orange yielding an amorphous precipitate at the anode. Attempts to obtain a cobalt(III) complex were unsuccessful. The degradation of ligand seemed to take place with the oxidation.

The present work was partially supported by a Grant-in-Aid for Scientific Research No. 62540478 from the Ministry of Education, Science and Culture.

References

1) I. Murase, M. Mikuriya, H. Sonoda, Y. Fukuda, and S. Kida, *J. Chem. Soc., Dalton Trans.*, **1986**, 953.
2) I. Murase, M. Mikuriya, H. Sonoda, and S. Kida, *J. Chem. Soc., Chem. Commun.*, **1984**, 692.
3) S. Kida, I. Murase, C. Harada, L. Daizeng, and M. Mikuriya, *Bull. Chem. Soc. Jpn.*, **59**, 2595 (1986).
4) M. Mikuriya, S. Kida, and I. Murase, *J. Chem. Soc., Dalton Trans.*, **1987**, 1261.
5) M. Mikuriya, S. Kida, and I. Murase, *Bull. Chem. Soc. Jpn.*, **60**, 1355 (1987).
6) M. Mikuriya, S. Kida, and I. Murase, *Bull. Chem. Soc. Jpn.*, **60**, 1681 (1987).
7) M. S. Haddad, S. R. Wilson, D. J. Hodgson, and D. N. Hendrickson, *J. Am. Chem. Soc.*, **103**, 384 (1981); P. L. Burk, J. A. Osborn, and M. -T. Youinou, *J. Am. Chem. Soc.*, **103**, 1273 (1981); P. K. Coughlin and S. J. Lippard, *J. Am. Chem. Soc.*, **103**, 3228 (1981); M. G. B. Grew, M. McCann, S. M. Nelson, *J. Chem. Soc., Dalton Trans.*, **1981**, 1868.
8) "International Tables for X-Ray Crystallography," Kynoch Press, Birmingham (1974), Vol. 4.
9) P. Main, S. E. Hull, L. Lessinger, G. Germain, J. P. Declercq, and M. M. Woolfson, MULTAN 78, A System of Computer Programs for the Automatic Solution of Crystal Structures from X-Ray Diffraction Data, University of York (1978).
10) T. Sakurai and K. Kobayashi, *Rikagaku Kenkyusho Hokoku*, **55**, 69 (1979).
11) C. K. Johnson, Report No. ORNL 3794, Oak Ridge National Laboratory, Oak Ridge, Tennessee (1965).

A Convenient Synthesis of Spironorcamphors

Kimihiko HORI, Naotake TAKAISHI,* and Yoshiaki INAMOTO
Tochigi Research Laboratories, Kao Corporation,
2606 Akabane, Ichikaimachi, Tochigi 321-34
(Received November 30, 1987)

Synopsis. The effects of the base, molar ratio of the reagent, solvent and reaction temperature on the cycloalkylation of norcamphor with 1,4-dibromobutane were explored, and optimum conditions for the preparation of spiro[bicyclo[2.2.1]heptane-2,1′-cyclopentan]-3-one have been established. 3-*exo*-(4-Bromobutyl)norcamphor was isolated and characterized as a reaction intermediate. A series of spironorcamphors with various ring sizes were obtained in good yields using a 1:1.5:2.5 ratio of norcamphor/α,ω-dibromoalkanes /$NaNH_2$ in Et_2O.

The syntheses and reactions of spiro compounds have attracted considerable attention in recent years.[1] As one part of our continuing interest in the chemistry of tricycloundecane derivatives,[2] we have required a convenient method for the preparation of spiro[bicyclo[2.2.1]heptane-2,1′-cyclopentan]-3-one (**3c**).[2d] It seemed that the most direct route to **3c** would be cycloalkylation[1b,3] of norcamphor (bicyclo[2.2.1]heptan-2-one **1**) with 1,4-dibromobutane (**2c**) in the presence of the base.

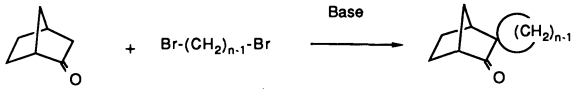

1 **2** **3**

a : n=3
b : n=4
c : n=5
d : n=6
e : n=7

Although a lot of examples for the synthesis of spiroketones via cycloalkylation have been described,[1b] a survey of the literature has indicated that only one example has been reported by Sauers et al.,[4] on the reaction of **1**, giving spiro[bicyclo[2.2.1]heptane-2,1′-cyclobutan]-3-one (**3b**) in low yield by treatment with 1,3-dibromopropane (**2b**) in the presence of $NaNH_2$. We now report on a general method for the synthesis of spironorcamphors (**3**) involving the cycloalkylation of **1** with α,ω-dibromoalkanes (**2**) in the presence of a base.

Initial attempts to alkylate **1** with **2c** to the spiroketone **3c** were carried out under similar conditions employed for the preparation of **3b**.[4] Treatment of **1** with $NaNH_2$ (3 equiv) in Et_2O gave an enolate which upon treatment with **2c** (10 equiv) at ambient temperature for 48 h afforded **3c** (48%) along with monoalkylated product, 3-*exo*-(4-bromobutyl)-norcamphor (*exo*-**4c**, 31%) (Table 1, entry 1). The structure of **3c** was confirmed by a comparison of the physical properties with previously reported data.[2d] The configuration of the substituent of *exo*-**4c** was evidenced by comparing the ^{13}C NMR chemical shifts with those of the related 3-alkylnorcamphors.[5] A marked upfield shift at C-7 was observed due to the presence of an exo substituent at C-3 in *exo*-**4c**, which can be classified as a γ-syn effect.[5]

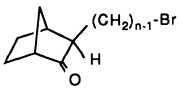

exo- **4**

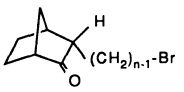

endo- **4**

Table 1. Reaction of Norcamphor (**1**) with 1,4-Dibromobutane (**2c**)

Entry	Equiv of **2c**	Base (equiv)	Solvent	Reaction temp	Reaction time/h	Yield/%[a]	
						3c	*exo*-**4c**
1	10	$NaNH_2$ (3.0)	Et_2O	r.t.	48	48	31
2	10	$NaNH_2$ (2.5)	Et_2O	Reflux	24	48	31
3	6	$NaNH_2$ (2.5)	Et_2O	Reflux	24	55	26
4	3	$NaNH_2$ (2.5)	Et_2O	Reflux	24	67	
5	1.5	$NaNH_2$ (2.5)	Et_2O	Reflux	24	67	
6	1.5	$NaNH_2$ (3.0)	Et_2O	Reflux	24	67	
7	1.5	$NaNH_2$ (2.5)	Hexane	Reflux	12	48	
8	1.5	$NaNH_2$ (2.5)	Toluene	Reflux	1	24	
9	1.5	$NaNH_2$ (2.5)	Toluene	40°C	12	41	
10	1.5	*t*-BuOK (2.5)	Benzene	Reflux	3	53	
11	10	*t*-BuOK (2.5)	Benzene	Reflux	3	45	9
12	1.5	LDA (2.5)	THF	−78°C→r.t.	60	8	33
13	1.2	LDA (1.2)	THF	−78°C→r.t.	60	12	41

a) Determined by GLC analysis using dodecane as an internal standard.

The exclusive formation of the *exo*-**4c** is rationalized based on a selective exo attack of the alkylating reagent **2c**.[6] The isolated ketone *exo*-**4c** was cyclized in the presence of $NaNH_2$ to afford **3c** in 89% yield.[7] This means that *exo*-**4c** is the intermediate in the above-mentioned cycloalkylation reaction. The lack of its epimer, *endo*-**4c**, implies a rapid cyclization of the enolate anion derived from *exo*-**4c**, compared to a proton-exchange reaction.[8]

Various efforts were devoted to optimize the yield of **3c**. Similar results were obtained through a treatment of a mixture of **1** and **2c** with $NaNH_2$ in boiling Et_2O[9] (entry 2). However, the yield and selectivity of **3c** were highly increased upon decreasing the amounts of **2c** (entries 3—6). The highest yield of **3c** could be attained when the reaction was performed using a 1:1.5:2.5 ratio of **1**/**2c**/$NaNH_2$ in Et_2O (entry 5). A large excess of **2c** caused side reactions with $NaNH_2$.

The use of hexane (entry 7) or toluene (entries 8 and 9) instead of Et_2O gave a decreased yield of **3c**. It has been reported[10] that cyclohexanone affords spiro[4.5]-decan-6-one in 70% yield when treated with **2c** in the presence of potassium *t*-butoxide (*t*-BuOK). By using these conditions, we obtained a slightly decreased yield of **3c** (entries 10 and 11). On the other hand, upon treatment with lithium diisopropylamide (LDA),[11] *exo*-**4c** was obtained as a major product (entries 12 and 13).

These improved reaction conditions (entry 5) were successfully applied to a reaction of **1** with other α,ω-dibromoalkanes **2**, giving the corresponding spironorcamphors **3** in moderate to good yields. Interestingly, **3b** was isolated in 52% yield as compared to 3% reported in the literature.[4] Although none of the monoalkylated product, 3-*exo*-(3-bromopropyl)norcamphor (*exo*-**4b**), was detected in the products, allylation[12] became a significant side reaction, a fact possibly attributable to the formation of allyl bromide by the ready dehydrobromination of **2b** compared to the other α,ω-dibromoalkanes. A mixture of allylated compounds, 3-*exo*-allylnorcamphor (*exo*-**5**, 7%),[11b,c] 3-*endo*-allylnorcamohor (*endo*-**5**, 4%), and 3,3-diallylnorcamphor (**6**, 1%) was isolated as by-products. Enol ether, which would be derived from *exo*-**4b** by intramolecular O-alkylation, was not observed.[13]

It is noteworthy that spiro[bicyclo[2.2.1]heptane-2,1′-cycloheptan]-3-one (**3e**) containing a seven-membered ring was produced in moderate yield, since the corresponding spirocyclohexanone has been obtained in only 8% yield from cycloalkylation of cyclohexanone with **2e**.[14] Although the preparation of a three-membered ring by alkylation is a kinetically favored process,[3a] we were not able to isolate the spiro[bicyclo[2.2.1]heptane-2,1′-cyclopropan]-3-one (**3a**).[15]

In conclusion, spironorcamphors (**3**) can now be easily obtained in good yields from the reaction of norcamphor (**1**) with α,ω-dibromoalkane (**2**) in the presence of $NaNH_2$. This ready availability should enhance the attractiveness of these compounds as starting materials for several reactions, including dehydration-rearrangement reactions.[1a,2b]

Experimental

Preparation of Spironorcamphors (3). General Procedure. To a magnetically stirred solution of norcamphor (**1**) (5.51 g, 50 mmol) and α,ω-dibromoalkane (**2**) (75 mmol) in dry Et_2O (150 ml) was added $NaNH_2$ (4.88 g, 125 mmol) in one portion. After being refluxed under a nitrogen atmosphere for 24 h, the reaction mixture was cooled to room temperature and poured into cold water (150 ml). The organic layer was separated, and the aqueous portion was extracted two times with Et_2O. The ethereal extracts were washed with a saturated NaCl solution, dried over Na_2SO_4, filtered and concentrated in vacuo. Purification of the residue by column chromatography on silica gel using hexane–Et_2O (10:1) as an eluent afforded **3** as a colorless liquid.

Spiro[bicyclo[2.2.1]heptane-2,1′-cyclobutan]-3-one (3b): Yield 52%; IR (neat) 2975, 1750, 1465 cm^{-1}; ^1H NMR δ= 1.30—2.25 (m, 12H), 2.45—2.60 (m,2H); ^{13}C NMR δ=15.1 (t), 21.9 (t), 24.4 (t), 25.4 (t), 30.4 (t), 34.1 (t), 45.4 (d), 49.6 (d), 54.4 (s), 221.3 (s); MS *m/z* 150 (M^+), 122, 84, 81,67.

Capillary GLC analysis of the crude reaction mixture at 90 °C showed that 7% of 3-*exo*-allylnorcamphor (*exo*-**5**), 4% of 3-*endo*-allylnorcamphor (*endo*-5) and 1% of 3,3-diallylnorcamphor (**6**) were present as by-products. The mass spectrum and GLC retention time of *exo*-**5** were identical with those of an authentic sample, which was prepared by alkylation of **1** with allyl bromide in the presence of LDA. The other products, *endo*-**5** and **6**, isolated by preparative GLC, had the following properties:

***exo*-5**:[11b,c] IR (neat) 2975, 1755, 920 cm^{-1}; ^1H NMR δ=1.26—2.13 (m, 8H), 2.25—2.61 (m, 3H), 4.97—5.11 (m, 2H), 5.70—5.89 (m, 1H); ^{13}C NMR δ=23.9 (t), 28.0 (t), 33.3 (t), 34.6 (t), 38.5 (d), 49.6 (d), 53.2 (d), 116.1 (t), 136.4 (d), 219.0 (s); MS *m/z* 150 (M^+), 109, 81, 67, 41.

***endo*-5**: IR (neat) 2975, 1755, 920 cm^{-1}; ^1H NMR δ=1.32—2.18 (m, 8H), 2.43—2.67 (m, 3H), 4.97—5.11 (m, 2H), 5.70—5.89 (m, 1H); ^{13}C NMR δ=21.0 (t), 25.3 (t), 30.6 (t), 37.0 (t), 38.2 (d), 50.5 (d), 53.3 (d), 115.8 (t), 136.4 (d), 218.9 (s); MS *m/z* 150 (M^+), 109, 81, 67, 41; Found: *m/z*, 150.1039. Calcd for $C_{10}H_{14}O$: M, 150.1045

6: IR (neat) 3000, 1740, 920 cm^{-1}; ^1H NMR δ=1.40—2.71 (m, 12H), 4.95—5.23 (m, 4H), 5.72—5.96 (m, 2H); ^{13}C NMR δ=23.2 (t), 25.4 (t), 34.6 (t), 36.0 (t), 36.7 (t), 43.4 (d), 50.3 (d), 52.5 (s), 117.5 (t), 117.9 (t), 133.9 (d), 134.1 (d), 220.1 (s); MS *m/z* 190 (M^+), 93, 79, 67, 41; Found: *m/z*, 190.1350. Calcd for $C_{13}H_{18}O$: M, 190.1358.

Spiro[bicyclo[2.2.1]heptane-2,1′-cyclopentan]-3-one (3c): Yield 63%; IR (neat) 2980, 1750, 1470 cm^{-1}; ^1H NMR δ=1.30—2.00 (m, 14H), 2.24 (bs, 1H), 2.50—2.60 (m, 1H); ^{13}C NMR δ=23.9 (t), 25.5 (t), 26.4 (t), 26.8 (t), 32.7 (t), 36.0 (t), 36.4 (t), 46.5 (d), 49.8 (d), 59.0 (s), 223.9 (s); MS *m/z* 164 (M^+), 95, 68, 67, 41. Anal. ($C_{11}H_{16}O$) C, H.

Spiro[bicyclo[2.2.1]heptane-2,1′-cyclohexan]-3-one (3d): Yield 54%; IR (neat) 2950, 1750, 1455 cm^{-1}; ^1H NMR δ=1.10—2.00 (m, 16H), 2.40—2.70 (m, 2H); ^{13}C NMR δ=22.4 (t), 22.5 (t), 22.7 (t), 24.7 (t), 25.8 (t), 30.3 (t), 30.5 (t), 34.9 (t), 40.9 (d), 50.4 (d), 51.5 (s), 221.9 (s); MS *m/z* 178 (M^+), 109, 82, 67, 41. Anal. ($C_{12}H_{18}O$) C, H.

Spiro[bicyclo[2.2.1]heptane-2,1′-cycloheptan]-3-one (3e): Yield 48%; IR (neat) 2950, 1755, 1475 cm^{-1}; ^1H NMR δ=1.10—2.00 (m, 18H), 2.40—2.70 (m, 2H); ^{13}C NMR δ=23.0 (t), 24.1 (t), 24.5 (t), 25.4 (t), 29.2 (t), 29.3 (t), 32.7 (t), 33.5 (t), 34.7 (t), 43.6 (d), 50.1 (d), 53.5 (s), 223.1 (s); MS *m/z* 192 (M^+), 123, 81, 67, 55; Found: *m/z*, 192.1511. Calcd for $C_{13}H_{20}O$: M,192.1514.

Reaction of 1,4-Dibromobutane (2c) with Enolate Generated from 1 and $NaNH_2$ (Table 1, Entry 1). A variation of the procedure of Sauers et al.[4] was utilized. To a magnetically stirred solution of **1** (1.10 g, 10 mmol) and dodecane(0.85 g, 5 mmol; internal standard) in dry Et_2O (40 ml) was added $NaNH_2$ (1.17 g, 30 mmol) in one portion. After reflux under a nitrogen atmosphere for 4.5 h, the resulting mixture was poured onto **2c** (21.59 g, 100 mmol) and stirred at room temperature for 2 days. The reaction mixture was poured into cold water (50 ml), and the organic layer was separated. The aqueous portion was extracted two times with Et_2O. The combined organic extracts were washed with a saturated NaCl solution and dried over Na_2SO_4. A GLC analysis showed the presence of two major products [48% of **3c** and 31% of 3-*exo*-(4-bromobutyl)norcamphor (*exo*-**4c**)], which were purified by preparative GLC. *exo*-**4c**: IR (neat) 2975, 1750, 1470 cm^{-1}; ^1H NMR δ=1.10—2.08 (m, 13H), 2.35—2.70 (m, 2H, CH-CO-CH), 3.42 (t, J=6.6 Hz, 2H, CH_2Br); ^{13}C NMR δ=24.0 (t), 26.9 (t), 28.0 (t), 28.3 (t), 32.6 (t), 33.5 (t), 34.8 (t), 39.2 (d), 49.5 (d), 53.7 (d), 219.9 (s); MS *m/z* 246 (M^++2), 244 (M^+), 95, 82, 67, 41; Found: *m/z*, 244.0442. Calcd for $C_{11}H_{17}OBr$: M, 244.0462.

Reaction of 1 with 2c in the Presence of Potassium *t*-Butoxide (*t*-BuOK)[10] (Table 1, Entry 10). To a magnetically stirred solution of **1** (1.10 g, 10 mmol), **2c** (3.24 g, 15 mmol) and dodecane (0.85 g, 5 mmol; internal standard) in dry benzene (40 ml) was added *t*-BuOK (2.81 g, 25 mmol) in one portion. The resulting mixture was heated 3 h at reflux under a nitrogen atmosphere. Upon cooling to room temperature, the reaction mixture was poured into water (50 ml). The organic layer was separated and the aqueous portion was extracted two times with Et_2O. The combined organic extracts were washed with a saturated NaCl solution and dried over Na_2SO_4. A GLC analysis showed the presence of **3c** as the main product (53% yield).

Reaction of 1 with 2c in the Presence of Lithium Diisopropylamide (LDA)[11] (Table 1, Entry 12). A 1.6 M (1 M=1 mol dm^{-3}) hexane solution of butyllithium (7.8 ml, 12.5 mmol) was added to a stirred solution of diisopropylamine in dry THF (10 ml) at −78 °C. The solution was stirred at −78 °C for 1 h and at 0 °C for an additional 1 h, and again cooled to −78°C. To the resulting LDA solution was added dropwise a solution of **1** (0.55 g, 5 mmol) in dry THF (10 ml). After stirring for 1 h at −78 °C, a solution of **2c** (1.62 g, 7.5 mmol) in dry THF (5 ml) was added into the mixture. The reaction mixture was allowed to warm to 0 °C, stirred at that temperature for 1 h and at room temperature for 60 h, and then poured into water (50 ml). The mixture was extracted three times with Et_2O. The combined extracts were washed with saturated NaCl solution and dried over Na_2SO_4. GLC analysis of the solution indicated the formation of **3c** (8%) and *exo*-**4c** (33%).

Cyclization of *exo*-4c to 3c in the Presence of $NaNH_2$. To a magnetically stirred solution of *exo*-**4c** (0.50 g, 2.04 mmol) and dodecane (0.185 g, 1.08 mmol; internal standard) in dry ether (15 ml) was added $NaNH_2$ (0.12 g, 3.06 mmol) in one portion. The resulting mixture was refluxed under nitrogen for 24 h, allowed to cool, and then poured into water (50 ml). The organic layer was separated and the aqueous portion was extracted two times with Et_2O. The combined extracts were washed with saturated NaCl solution and dried over Na_2SO_4. A GLC analysis showed that **3c** was formed in 87% yield.

References

1) a) W. R. Dolbier, Jr., "Mechanisms of Molecular Migrations," ed by B. S. Thyagarajan, Wiley-Interscience, New York (1971), Vol. 3, p. 1; b) A. P. Krapcho, *Synthesis*, **1974**, 383; c) A. P. Krapcho, *Synthesis*, **1976**, 425; d) B. M. Trost and B. R. Adams, *J. Am. Chem. Soc.*, **105**, 4849 (1983); e) R. D. Bach and R. C. Klix, *J. Org. Chem.*, **50**, 5438 (1985).

2) a) N. Takaishi, Y. Inamoto, and K. Aigami, *Chem. Lett.*, **1979**, 803 and references cited therein; b) N. Takaishi, Y. Inamoto, and K. Aigami, *J. Org. Chem.*, **45**, 2254 (1980); c) Y. Fujikura, N. Takaishi, and Y. Inamoto, *Tetrahedron*, **37**, 4465 (1981); d) N. Takaishi, H. Takahashi, and Y. Inamoto, *Tetrahedron Lett.*, **26**, 2361 (1985).

3) a) H. O. House, "Modern Synthetic Reactions," 2nd ed, Benjamin, Inc., Menlo Park, CA, (1972), Chapter 9; b) R. M. Moriarity, C. C. Chien, and T. B. Adams, *J. Org. Chem.*, **44**, 2206 (1979).

4) R. R. Sauers and A. Shurpik, *J. Org. Chem.*, **32**, 3120 (1967).

5) a) J. B. Grutzner, M. Jautelat, J. B. Dence, R. A. Smith, and J. D. Roberts, *J. Am. Chem. Soc.*, **92**, 7107 (1970); b) J. B. Stothers, "Carbon-13 NMR Spectroscopy," Academic Press, New York (1972), p. 181.

6) a) E. J. Corey, R. Hartmann, and P. A. Vatakencherry, *J. Am. Chem. Soc.*, **84**, 2611 (1962); b) J.Wolinski, D. R. Dimmel, and T. W. Gibson, *J. Org. Chem.*, **32**, 2087 (1967).

7) No reaction intermediate has been isolated in the cycloalkylation of the other cyclic ketones with **2**.

8) The enolate from 3-*exo*-methylnorcamphor with LDA, when quenched with acetic acid, has afforded 3.5:1 mixture of endo and exo with endo predominating: X. Creary, F. Hudock, M. Keller, J. F. Kerwin, Jr., and J. P. Dinnocenzo, *J. Org. Chem.*, **42**, 409 (1977).

9) For similar procedures, see: a) J. M. Conia, *Rec. Chem. Prog.*, **24**, 43 (1963); b) H. O. House and V. Kramar, *J. Org. Chem.*, **28**, 3362 (1963); c) J. S. McConaghy, Jr. and J. J. Bloomfield, *J. Org. Chem.*, **33**, 3425 (1968).

10) M. Mousseron, R. Jacquier, and H. Christol, *Bull. Soc. Chim. Fr.*, **1957**, 346.

11) a) W. Kreiser and L. Janitschke, *Chem. Ber.*, **112**, 408 (1979); b) R. Bloch, *Tetrahedron Lett.*, **1979**, 3945; c) P. Barraclough, *Tetrahedron Lett.*, **21**, 1897 (1980); d) J. E. Baldwin and T. C. Barden, *J. Am. Chem. Soc.*, **105**, 6656 (1983).

12) Similar allylated ketone formations have been reported for the reaction of cyclohexanone with **2b** in the presence of *t*-BuOK, where no spiroketone was observed; see: Ref. 10.

13) Formation of enol ethers has been observed in the intramolecular alkylation of 2-(3-bromopropyl)cyclohexanone or 2-(3-bromopropyl)cyclopentanone with *t*-BuOK: S. J. Etheredge, *J. Org. Chem.*, **31**, 1990 (1966).

14) H. Christol, M. Mousseron, and F. Plenat, *Bull. Soc. Chim. Fr.*, **1959**, 543.

15) The spironorcamphor **3a** has been prepared by acid-catalyzed oxirane rearrangement: D. H. Aue and R. N. Reynolds, *J. Am. Chem. Soc.*, **95**, 2027 (1973).

Stereospecific Synthesis of 3-Oxo-α-bourbonene and the Cisoid Isomer for Structural Determination of the Toxic Component of *Lansium domesticum*

Tadao UYEHARA,* Ichiro SUZUKI, and Yoshinori YAMAMOTO
Department of Chemistry, Faculty of Science, Tohoku University, Aramaki-Aoba, Sendai 980
(Received December 2, 1987)

Synopsis. The cis-cisoid-cis isomer of 3-oxo-α-bourbonene, (**1**), the original structure proposed for the toxic principle of *Lansium domesticum*, has been prepared from (−)-mintsulfide. Neither spectral data of **1** nor of 3-oxo-α-bourbonene itself, derived from β-bourbonene, are not identical with those of the toxic componet.

Recently, it has been reported that one of the toxic principles (fish poisons) of *Lansium domesticum* Jack v.duku, a Meliaceous plant, is the cis-cisoid-cis isomer of 3-oxo-α-bourbonene, (**1**).[1] Because of this unique cisoid-[5-4-5] fused-ring skeleton, we have designed a stereospecific synthesis of **1** starting from the sulfur-bridged sesquiterpene, (−)-mintsulfide (**2**) whose absolute stereostructure had been established.[2] We report herein the synthesis of **1** from **2**, a similar transformation of β-bourbonene (**4**) into 3-oxo-α-bourbonene (**5**), and the findings that the toxic component has not any [5-4-5] fused ring skeleton.

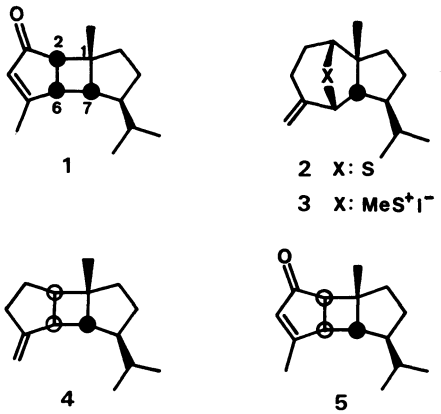

Results and Discussion

The methylsulfonium iodide of (−)-mintsulfide, (**3**),[3] is the actual starting material of the synthesis of **1**. By treating with alkyllithium, **3** reacts in competitively. One is the [2,3]sigmatropic rearrangement of the resulting sulfonium methylide to give the homologous sulfur-bridged compound. The other is the sulfide extrusion to yield the cis-cisoid-cis isomer of β-bourbonene, **6**, and the [5-7] fused-ring diene **7** via the hypothetical diradical intermediate.[3,4] The ratio of these products was reported to depend upon the reaction conditions, while **6** was the minor product.[3] After several attempts, the yield of **6** was increased up to 41% by treating with methyllithium at 0 °C.

Ozonization of **6** in ethanol followed by treatment with zinc dust gave the cyclopentanone (**8**) in 85% yield. In order to transform **8** into the α,β-unsaturated ketone **9** by palladium-catalyzed oxidation,[5] the allyl enol carbonate was derived from **8** using potassium *t*-butoxide and allyl chloroformate. Treatment of the carbonate with palladium acetate (10%) in boiling acetonitrile gave **9** in 84% overall yield from **8**. Conversion of **9** into **1** was achieved by consecutive treatment with methyllithium and pyridinium chlorochromate (PCC)[6] in 85% yield.

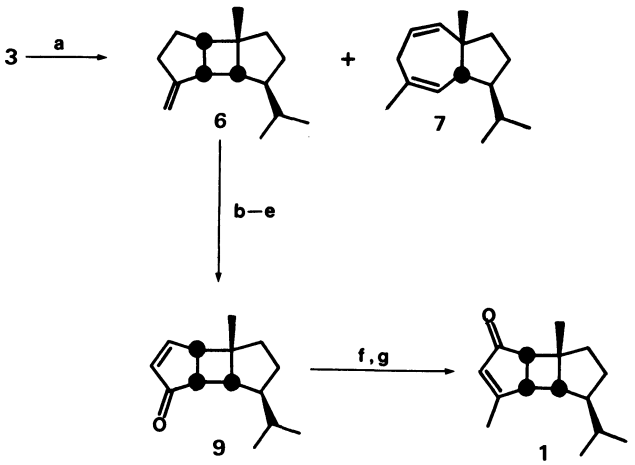

Scheme 1. Preparation of *cis-cisoid-cis*-3-oxo-α-bourbonene (**1**).
(a): MeLi, THF, (b): O_3, EtOH, (c): Zn, AcOH, EtOH–H_2O, (d) *t*-BuOK, THF, $ClCOOCH_2CH=CH_2$, (e): $Pd(OAc)_2$, CH_3CN, (f): MeLi, ether, (g): PCC, CH_2Cl_2.

Compound **1** shows reasonable spectral characteristics. The cis-cisoid-cis arrangement of **1** is clearly supported by the ^1H NMR spectrum ($J_{2,6}$=5.8 Hz and $J_{6,7}$=9.6 Hz) and the NOEDIF spectra which show certain interactions between the C-1 methyl protons (δ=1.33) and the C-2 proton (δ=2.60), the C-2 proton and the C-6 proton (δ=3.24), and the C-6 proton and the C-7 proton (δ=2.33). Upon irradiation of the C-1 methyl protons, NOE enhancement was also observed at C-7 proton. However, the spectral data of **1** are completely different from those of the toxic principle of *Lansium domesticum*.

Cis-transoid-cis isomer of **1**, namely **5**,[7] has been prepared in a similar manner as above starting from β-bourbonene (**4**) which was derived photochemically from (−)-germacrene-D.[8] The spectral characteristics of **5**, including ^{13}C NMR spectrum, are also different from those of that fish poison. Now it is clear that the

toxic principle has no [5-4-5] fused ring skeletons. Remaining candidates for the toxic principle seem to be ylangene or copaene type compounds containing an *r*-1, *t*-2, *c*-3, *t*-4-tetrasubstituted cyclobutane ring.

Experimental

General. Melting points were determined with a Yamato MP-21 capillary melting point apparatus and are uncorrected. UV and IR spectra were recorded on Hitachi Model 323 and 215 spectrometers, respectively. NMR spectra were obtained on JEOL JNM-PMX60, Varian EM-390, Varian XL-200, and JEOL GX-400 NMR spectrometers, using tetramethylsilane as an internal standard. The mass spectral studies were conducted using a Hitachi M-52 spectrometer and a JEOL DX-303 mass spectrometer. Optical rotations were measured on a Perkin-Elmer 241 Polarimeter. Elemental analyses were performed by the Microanalytical Laboratory of Tohoku University. All reactions were monitored by analytical TLC using E. Merck precoated silica gel $60F_{254}$ plates. Column chromatography was carried out with E. Merck silica gel 60 (70—230 mesh ASTM). Ozone was generated using a Nippon Ozone type O-1-2 laborastory ozonator.

(1*S*)-*cis*-1-*cisoid*-1,2-*cis*-2-Bourbonene ((1*S*)-*cis*-8-Isopropyl-1-methyl-5-methylenetricyclo[5.3.0.$0^{2,6}$]decane 6). The procedure used for preparation of **6** was essentially that of Ohnuma[9] with following modification. To a mixture of methylsulfonium iodide of mintsulfide (**3**, 4.42 g, 11.7 mmol) and THF (40 ml) was added 1 M methyllithium solution (1 M=1 mol dm^{-3}) in ether (14 ml, 1.2 equiv) at 0 °C under argon and stirred for 30 min. To the reaction mixture was added saturated aqueous ammonium chloride solution and extracted with three portions of ether. The combined extracts were washed with water and saturated brine, and dried over $MgSO_4$. After removal of the solvent, the remaining oil (2.61 g) was chromatographed on silica gel (50 g; hexane) to yield a mixture of hydrocarbons (1.85 g). Silver nitrate impregnated silica-gel chromatography (50 g; hexane) of the mixture gave **6** (0.946 g, 4.74 mmol, 41% yield) **7** (0.579 g, 2.83 mmol, 24% yield), and a mixture of them (0.109 g). **6**: Colorless oil; $[\alpha]_D^{25}$+188.41° (*c* 0.0820, $CHCl_3$); IR (CCl_4) 3070 (w), 1640 (w), and 890 (m) cm^{-1}; ^1H NMR ($CDCl_3$) δ=0.83 (3H, d, *J*=6.8 Hz), 0.86 (3H, d, *J*=6.8 Hz), 1.12 (3H, s), 1.1—1.8 (9H, m), 1.86 (1H, m), 2.3—2.5 (2H, m), 3.12 (1H, dd, *J*=9.5 and 8.1 Hz), 4.68 (1H, broad s, $W_{1/2}$=4.0 Hz), and 5.00 (1H, $W_{1/2}$=4.0 Hz); ^{13}C NMR ($CDCl_3$) δ=21.86 (q), 21.98 (q), 27.73 (t), 30.23 (q), 31.79 (t), 33.02 (t), 34.48 (d), 36.32 (t), 41.49 (d), 44.72 (s), 46.20 (d), 49.50 (d), 52.10 (d), 107.73 (t), and 155.15 (s). Found: C, 88.42; H, 11.73%. Calcd for $C_{15}H_{24}$: C, 88.16; H, 11.84%.

(1*R*)-*cis*-8-Isopropyl-1,5-dimethyl-*cis*-bicyclo[5.3.0]deca-2.5-diene 7: Colorless oil; $[\alpha]_D^{25}$ −97.80° (*c* 1.452, $CHCl_3$); IR (CCl_4) 1460 (w), 820 (w), 730 (w), 705 (m), and 680 (w) cm^{-1}; ^1H NMR (CCl_4) δ=0.85 (3H, d, *J*=6.8 Hz), 0.88 (3H, d, *J*=6.8 Hz), 1.09 (3H, s), 1.72 (3H, broad s), 1.1—2.2 (7H, m), 2.63 (1H, dd, *J*=21.3 and 3.3 Hz), 2.83 (1H, broad d. *J*=21.3 Hz. $W_{1/2}$=7.8Hz), 5.25 (1H, d, *J*=12.0 Hz), and 5.00 (1H, $W_{1/2}$=4.0 Hz). Found: C, 88.15: H, 11.90%. Calcd for $C_{15}H_{24}$: C, 88.16; H, 11.84%.

(1*R*)-*cis*-10-Isopropyl-7-methyl-*cis*-1-*cisoid*-1,2-*cis*-2-tricyclo[5.3.0.$0^{2,6}$]decan-3-one (8). To a solution of **6** (844.1 mg, 4.13 mmol) in ethanol (20 ml) at −78 °C was treated with ozone until it was faintly blue. The reaction mixture was diluted with water (30 ml) and then treated with zinc (1.37 g) and acetic acid (2.4 ml). The resulting suspension was stirred at room temperature for 2 h and then filtered. The filtrate was diluted with saturated aqueous ammonium chloride solution and extracted with three portions of ether. The combined extracts were washed with saturated sodium hydrogencarbonate solution and saturated brine, and dried over $MgSO_4$. Removal of the solvent followed by chromatography of the remaining oil (847.3 ml) on silica gel (25 g; 10:1 hexane–ethyl acetate) gave **8** (720.3 mg, 3.49 mmol, 85% yield); colorless oil; $[\alpha]_D^{20}$ +251.2° (*c* 0.400, $CHCl_3$) 1720cm^{-1}; ^1H NMR (CCl_4) δ=0.87 (6H, d, *J*=6.0 Hz), 1.18 (3H, s), and 1.2—2.8 (13H, m). Found *m/z* 206.1668. Calcd for $C_{14}H_{22}O$: M, 206.1670.

(1*R*)-*cis*-10-Isopropyl-7-methyl-*cis*-1-*cisoid*-1,2-*cis*-2-tricyclo[5.3.0.$0^{2,6}$]dec-4-en-3-one (9). To a solution of potassium *t*-butoxide (580 mg, 6.10 mmol) in THF (20 ml) was added a solution of **8** (614.4 mg, 3.0 mmol) in THF (20 ml) at −70°C under argon and the resulting mixture was stirred for 1 h. Allyl chloroformate (0.80 ml, 909 mg, 8.0 mmol) was added to the deep yellow solution and the mixture was stirred for 1 h at −78°C and then allowed to warm to room temperature. After stirring overnight, the mixture was treated with saturated aqueous NH_4Cl solution (40 ml) and then extracted with three portions of ether. The combined extracts were washed with saturated brine, dried over $MgSO_4$, and concentrated. Chromatography of the remaining oil (1.105 g) on silica gel (30 g; 20:1 hexane–ethyl acetate) gave the allyl enol carbonate (743.4 mg, 3.00 mmol) as a colorless oil.

Palladium acetate (67 mg, 0.30 mmol) was added to a solution of the carbonate in acetonitrile (10 ml) and the mixture was heated at 80 °C for 1 h under nitrogen. After filtration through a Celite layer, the solvent was romoved in vacuo. Chromatography of the residue on silica gel (50 g; 20:1 hexane–ethyl acetate) gave **9** (510.3 mg, 2.50 mmol, 84%); colorless oil; $[\alpha]_D^{20}$ +487.8° (*c* 1.07, $CHCl_3$); IR ($CHCl_3$) 1685 (s) cm^{-1}; ^1H NMR δ=0.85 (3H, d, *J*=6 Hz), 0.92 (3H, d, *J*=6 Hz), 1.33 (3H, s), 2.13 (1H, broad dd, *J*=11.7 and 3.8 Hz), 2.77 (1H, dd, *J*=11.7 and 5.9 Hz), 2.77 (1H, dddd, *J*=5.9, 3.3, 1.2, and 0.9 Hz), 6.25 (1H, dd, *J*=5.6 and 1.8 Hz), and 7.48 (1H, ddd, *J*=5.6, 3.3, and 0.7 Hz); MS *m/z* (rel intensity) 204 (M^+, 12.5), 189 (8.1), 161 (48.8), 123 (100), and 81 (95). Found *m/z* 204.1514. Calcd for $C_{14}H_{20}O$: M, 204.1513.

(1*S*)-*cis*-8-Isopropyl-1,5-dimethyl-*cis*-1-*cisoid*-1,2-*cis*-2-tricyclo[5.3.0.$0^{2,6}$]dec-4-en-3-one (1). To a solution of **9** (314.6 mg, 1.54 mmol) in THF (10 ml) was added 1 M methyllithium solution in ether (3 ml) at −78 °C under argon and stirred for 30 min. To the reaction mixture was added saturated aqueous ammonium chloride solution and extracted with three portions of ether. The combined extracts were washed with saturated brine, and dried over $MgSO_4$. Removal of the solvent gave a colorless oil (351 mg). To a solution of PCC (665 mg, 3.08 mmol) in dichloromethane (16 ml) was added a solution of the product in dichloromethane (12 ml) and the mixture was stirred for 3.2 h. The resulting mixture was diluted with ether (40 ml) and the supernatant was decanted from the black solid. The residue was washed with several portions of ether. The combined ethereal solutions were washed successively with 5% NaOH solution, 5% HCl, saturated $NaHCO_3$ solution, and saturated brine, dried over $MgSO_4$, and concentrated. Chromatography of the residue (389 mg) on silica gel (23 g; 10:1 hexane–ethyl acetate)gave **1** (289.5 mg, 1.31 mmol, 85% yield); colorless prisms; mp 50.5—51.5 °C (ether); $[\alpha]_D^{20}$ −331.5° (*c* 0.97); UV (EtOH) λ_{max} 238 (ε 9370) and 318 nm (94); IR ($CHCl_3$) 1680 (broad s) and 1610 (m) cm^{-1}; ^1H NMR ($CDCl_3$) δ=0.86 (3H, d, *J*=6.2 Hz), 0.90 (3H, d, *J*=6.4 Hz), 1.25—1.52 (4H, m), 1.33 (3H, s), 1.54—1.68 (2H, m), 2.11 (3H, broad s, $W_{1/2}$=2.5 Hz), 2.23 (1H, dd, *J*=9.6 and 3.8 Hz), 2.60 (broad, d, *J*=5.8 Hz, $W_{1/2}$=2 Hz), 3.24 (1H, dddd, *J*=9.6, 5.8, 0.8, and 0.8 Hz), and

6.11 (1H, brosd s, $W_{1/2}$=3.5 Hz); ^{13}C NMR ($CDCl_3$) δ=19.29 (5-Me), 20.85 (-CHMe-Me), 21.94 (-CHMe-Me), 28.70 (1-Me), 32.12 (9 or 10), 33.33 (-CHMe$_2$), 35.58 (9 or 10), 41.96 (6), 46.65 (1), 50.03 (8), 50.90 (7), 52.90 (2), 135.68 (4), 179.35 (5), and 211.08 (3). MS *m/z* (rel intensity) 218 (M^+, 12.3), 203 (6.5), 189 (4.0), 175 (20.5), 149 (18.0), 123 (100), and 81 (69.5). Found *m/z* 218.1671. Calcd for $C_{15}H_{22}O$: M, 218.1670.

Transformation of β-Bourbonene (4) into 3-Oxobourbonene ((1*S*)-*cis*-8-Isopropyl-1,5-dimethyl-*cis*-1-*transoid*-1,2-*cis*-2-tricyclo[5.3.0.0^{2,6}]dec-4-en-3-one (5)). β-Bourbonene was derived photochemically by using the literature procedure[7] from (−)-germacrene-D which was isolated from peppermint oil (*Mentha peperita*). In a procedure similar to that employed for the synthesis of **9**, **4** was transformed into (1*R*)-*cis*-10-isopropyl-7-methyl-*cis*-1-*transoid*-1,2-*cis*-tricyclo-[5.3.0.0^{2,6}]dec-4-en-3-one (^{1}H NMR ($CDCl_3$) δ=0.88 (3H, d, *J*=6.5 Hz), 0.90 (3H, d, *J*=6.5 Hz), 1.03 (3H, s), 1.30 (1H, d-sept, *J*=9.5 and 6.5 Hz), 1.58 (1H, ddd, *J*=13.0, 10.5, and 6.8 Hz), 1.65 (1H, m, 10-H), 1.72 (1H, ddd, *J*=13.0, 6.8, and 3.5 Hz), 1.80 (1H, dddd, *J*=16.5, 7.0, 3.5, and 1.0 Hz), 1.93 (1-H, broad s), 1.96 (1H, ddd, *J*=13.4, 10.8, and 6.5), 2.33 (2-H, ddd, *J*=4.9, 3.8, and 0.2 Hz), 2,97 (6-H, ddd, *J*=4.9, 3.2, and 1.2 Hz), 6.40 (4-H, ddd, *J*=5.6, 1.2, and 0.2 Hz), and 7.73 (5-H, ddd, *J*=5.6, 3.2, and 0.3 Hz); Found *m/z* 204.1519). This α,β-unsaturated ketone was converted into **5** in a manner similar to that adopted to prepare **1** from **9**. **5**: Colorless oil; $[\alpha]_D^{20}$ +336.3° (*c* 0.30, $CHCl_3$); UV (EtOH)λ_{max} 234 (ε 11700) and 315 nm (95); IR ($CHCl_3$) 1675 (s) and 1615 cm^{-1}; ^{1}H NMR ($CDCl_3$) δ=0.90 (3H, d, *J*=6.3 Hz), 0.91 (3H, d, *J*=6.3 Hz), 1.07 (3H, s), 1.34 (1H, d-sept, *J*=9.2 and 6.3 Hz), 1.50 (ddd, *J*=13.0, 11.0 and 6.5 Hz), 1.52—1.62 (1H, m), 1.78 (1H, dddd, *J*=13.0, 6.8, 3.0, and 0.8 Hz), 1.82 (1H, $W_{1/2}$=5 Hz), 1.93 (1H, dddd, *J*=13.0, 11.0, 6.5, and 6.5 Hz), 2.12 (3H, d, *J*=1.2 Hz), 2.57 (2,6-H, broad s, $W_{1/2}$=1.5 Hz), and 5.98 (4-H, q, *J*=1.2 Hz); ^{13}C NMR ($CDCl_3$) δ=17.08 (5-Me), 21.26 (-CHMe-Me), 21.65 (-CHMe-Me), 24.12 (1-Me), 29.35 (9 or 10), 30.54 (-CHMe$_2$), 40.72 (9 or 10), 45.79 (1), 47.06 (2 or 6), 50.82 (8), 53.32 (2 or 6), 54.60 (7), 132.10 (4), 180.87 (5), and 211.20 (3); MS (25 eV) *m/z* (rel intensity) 218 (M^+, 0.8), 175 (15.9), 124 (5.1), 123 (100), 122 (25.0), and 81 (47.3). Found *m/z* 218.1663. Calcd for $C_{12}H_{22}O$: M, 218.1670.

We wish to thank Professor Yuji Hayashi of Osaka City University for fruitful discussion and Takasago Perfumery Co., Ltd., for generous gift of peppermint oil (*Mentha piperita*). We also thank Professor Kuninobu Kabuto of Tohoku University for measurement of optical rotations.

References

1) H. Ikeda, M. Nishizawa, T. Tokuyama, and Y. Hayashi, 31 st Symposium on the Chemistry of Terpenes, Essential Oils, and Aromatics, Kyoto, September 1987, Symposium paper, pp. 209—211.

2) Y. Yoshida, S. Muraki, K. Takahashi, T. Kato, C. Kabuto, T. Suzuki, T. Uyehara, and T. Ohnuma, *J. Chem. Soc., Chem. Commun.*, **1979**, 512.

3) T. Uyehara, T. Ohnuma, T. Saito, T. Kato, T. Yoshida, and K. Takahashi, *J. Chem. Soc., Chem. Commun.*, **1981**, 127.

4) T. Uyehara, M. Takahashi, and T. Kato, *Tetrahedron Lett.*, **25**, 3003 (1984); **26**, 1241 (1985).

5) J. Tsuji, I. Minami, I. Shimizu, and H. Kataoka, *Chem. Lett.*, **1984**, 1133.

6) W. G. Dauben and D. M. Michno, *J. Org. Chem.*, **42**, 682 (1977).

7) M. Brown, *J. Org. Chem.*, **33**, 162 (1968).

8) K. Yoshihara, Y. Ohta, T. Sakai, and Y. Hirose, *Tetrahedron Lett.*, **1969**, 2263.

9) T. Ohnuma, Master Thesis, Tohoku University, 1980; Ref. 3.

Radical Cyclization to Seleno-Substituted Thiahomoprotoadamantanone and Its Unexpected Conversion to the Vinyl Selenide

Takeshi TORU,* Toshiya KANEFUSA, Eturô MAEKAWA, Yoshio UENO, Kazumoto KONDO,† and Shoji EGUCHI*,†

Department of Applied Chemistry, Faculty of Engineering, Nagoya Institute of Technology, Gokiso, Showa-ku, Nagoya 466

†Institute of Applied Organic Chemistry, Faculty of Engineering, Nagoya University, Furo-cho, Chikusa-ku, Nagoya 464

(Received December 8, 1987)

Synopsis. Heating *Se*-phenyl bicyclo[3.3.1]non-6-ene-3-(selenothioperoxy)carboxylate with AIBN gives 5-phenylseleno-3-thia-2-homoprotoadamantan-2-one which is unexpectedly converted to the vinyl selenide via the selenoxide by oxidation with hydrogen peroxide or *m*CPBA.

Se-Phenyl (selenothioperoxy)carboxylates are useful reagents for introducing both a thioester and a phenylseleno group into a molecule. Intermolecular addition of *Se*-phenyl(selenothioperoxy)benzoate to olefins gave addition products, i.e. *S*-phenylselenoalkyl thiobenzoate,[1] whereas *Se*-phenyl (selenothioperoxy)carboxylates bearing an unsaturated bond resulted in intramolecular selenothiolactonization to give phenylseleno-substituted thiolactones.[2] These reactions proceed via a free-radical pathway[1] involving the inter- or intramolecular attack of initially formed thiyl radical on the olefinic carbon and subsequent chain transfer of the carbon radical with the (selenothioperoxy)carboxylate. The construction of polycyclic molecules such as adamantane analogs could be of great interest because of their unique structures and reactivities.[3] We here disclose a new free-radical cyclization of *Se*-phenyl bicyclo[3.3.1]non-6-ene-3-(selenothioperoxy)carboxylate (**1**) into 5-phenylseleno-3-thia-2-homoprotoadamantan-2-one (5-phenylseleno-3-thiatricyclo[5.3.1.$0^{4,9}$]undecan-2-one) (**2**) and also an oxidative conversion of **2** to unexpected 5-phenylseleno-3-thia-2-homoprotoadmant-5-en-2-one (**5**).

(Selenothioperoxy)carboxylate **1** was prepared[4] in 87% overall yield according to the following sequence: Bicyclo[3.3.1]non-6-ene-3-carboxylic acid[5] was converted to acid chloride, which was then transformed to thiocarboxylic acid. The thiocarboxylic acid was treated with *N*-(phenylseleno)phthalimide to give compound **1**. A 0.04 M (1 M=1 mol dm^{-3}) solution of (selenothioperoxy)carboxylate **1** in benzene was heated under reflux for 4 h in the presence of azobis(isobutyronitrile) (AIBN) (10 mol%). After removing the solvent the mixture was purified by chromatography to give 5-phenylseleno-3-thia-2-homoprotoadamantan-2-one (**2**) in 97% yield. There was no indication of the formation of any significant amount of 4-thiahomoadamantan-5-one derivative **3**. Compound **2** was shown to be homogeneous by an inspection of its ^{13}C NMR spectrum, although the configuration of the phenylseleno group in **2** is uncertain at present.[6] We have observed the formation of both trans and cis isomers in the selenothiolactonization[2] as well as in the addition reactions of *Se*-phenyl (selenothioperoxy)benzoate to cycloalkenes.[1] But in the present case there must exist a stronger steric requirement for a chain transfer of the intermediate carbon radical, leading to the exclusive formation of one isomer.

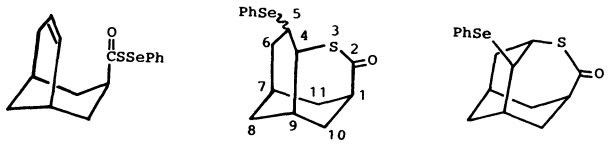

1 **2** **3**

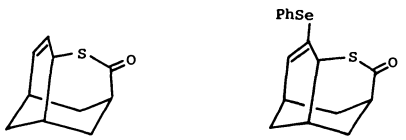

4 **5**

The present cyclization shows a notable reaction feature via a radical intermediate; i.e. the cyclization led to thiahomoprotoadamantanone **2**, but not to thiahomoadamantanone **3**. These results seem to be in accord with the predominant cyclization of 1-hexenyl radicals to five-membered rings.[7] Thus, the cyclization to thiahomoprotoadamantanone **2** can probably be ascribed to the stereoelectronically more favorable approach of the thiyl radical to the C-6 olefinic carbon than to the C-7 carbon, although a theoretical calculation is not presently available. In contrast, the ionic ring-closure of bicyclo[3.3.1]non-6-enes carrying internal nucleophiles at the 3-position generally results in an exclusive formation of homoadamantane ring systems, e.g., 4-thiahomoadamantane[8] from 3-mercaptomethylbicyclo[3.3.1]non-6-ene epoxide, 4-oxahomoadamantane[9] from 3-hydroxymethylbicyclo[3.3.1]non-6-ene, 2-bromo-4-oxatricyclo-[4.3.1.$1^{3,8}$]undecan-5-one[10] from the corresponding 3-carboxylic acid derivative.

Anticipating the formation of thiahomoprotoadamantenone **4**, we attempted on oxidation of the seleno group in **2** by hydrogen peroxide in the presence of pyridine in dichloromethane at ambient temperature, followed by heating the crude selenoxide under reflux in benzene for 1.5 h. This reaction, however, did not lead to the elimination of benzeneselenenic acid (PhSeOH), which would give thiahomoprotoadamantenone **4**. Instead, it gave unexpected selenothiahomoprotoadamantenone **5** bearing a vinyl selenide moiety in 82% yield. Oxidation of selenide **2** by *m*-

chloroperbenzoic acid (*m*CPBA) in dichloromethane at −40°C and subsequent heating under reflux with pyridine in benzene also gave vinyl selenide **5** in 70% yield. The spectral data showed an assigned structure that was concretely confirmed by the X-ray analysis (see Tables 1 and 2).

It is noteworthy that the oxidation of selenide **2** under conditions which usually induce the PhSeOH elimination to an olefin,[11] did not result in the formation of olefin **4** but, instead, gave vinyl selenide **5**. Sterically compressed steroidal sulfoxides have been reported[12] to give vinyl sulfoxides under the Pummerer reaction conditions involving the inevitable step of acylation of the corresponding sulfoxides. Another example is the oxidation of α-silyl selenides via the silyl rearrangement to the oxygen of the selenoxides, the reaction course of which is similar to that of the Pummerer reaction.[13] The present conversion of selenide **2** to vinyl selenide **5** via the selenoxide was carried out under conditions different from those for the typical Pummerer reaction. The selenoxide could not undergo a smooth syn-elimination of PhSeOH, probably because of its highly strained arrangement. Instead, it afforded vinyl selenide **5** through a possible proton-abstraction from the α-carbon attached to the selenoxide. Unfortunately, there is presently insufficient evidence to permit an equivocal conclusion regarding the mechanism. Further experiments are now in progress that are designed to assess the steric factor in the above reaction as well as in the radical cyclization of bridged bicyclic compounds.

Experimental

***Se*-Phenyl Bicyclo[3.3.1]non-6-ene-3-(selenothioperoxy)-carboxylate (1).** To a suspension of sodium hydride (60% oil dispersion, 29 mg, 0.73 mmol), washed three times with pentane, in tetrahydrofuran (0.8 ml) was added at 0 °C a solution of bicyclo[3.3.1]non-6-ene-3-carboxylic acid (110 mg, 0.66 mmol) in tetrahydrofuran (0.5 ml). The reaction mixture was stirred for further 15 min after the evolution of hydrogen had ceased. The solvent was evaporated under reduced pressure and to the residual solid was added dry benzene (1.2 ml) and pyridine (0.1 ml). Then, oxalyl dichloride (0.17 ml, 1.97 mmol) was added to the ice-cooled mixture over a period of 6 min and the mixture was stirred for 20 min at that temperature, while white precipitate appeared. The mixture was filtered and solvent was removed by evaporation under reduced pressure to leave crude acid chloride. The acid chloride was taken up to tetrahydrofuran (2 ml) and the solution was added dropwise at 5 °C under vigorous stirring to a solution of sodium hydrogensulfide (70% purity, 265 mg, 3.31 mmol) in 80% aqueous ethanol (0.34 ml). The mixture was stirred for 5 min after the addition and, then, concentrated under reduced pressure. To the residue were added diethyl ether (15 ml) and water (5 ml). The aqueous layer was acidified with 1 M HCl (1 M=1 mol dm^{-3}). The organic layer was separated and the aqueous layer was extracted with diethyl ether (10 ml). The combined ethereal extracts were washed with brine several times, dried over anhydrous $MgSO_4$, and concentrated under reduced pressure to give crude thiocarboxylic acid as a colorless solid. It was dissolved in dichloromethane (2 ml) and the solution was added to a solution of *N*-(phenylseleno)phthalimide (240 mg, 0.79 mmol) in dichloromethane (0.5 ml) at −70 °C. The reaction was completed within a minute. Hexane (15 ml) was then added and the resultant precipitate was filtered off. Evaporation under reduced pressure gave a crude product, which was purified by flash column chromatography (silica gel 18 g, hexane/ethyl acetate 200:1 and then 99:1) to give (selenothioperoxy)carboxylate **1** (194 mg, 87%). ^{1}H NMR (CCl_4) δ=1.48—2.93 (m, 11H), 4.89—5.70 (m, 2H), 7.00—7.75 (m, 5H); IR (film) 1715 cm^{-1}; MS (70 eV) *m/z* (rel intensity) 338, 336 (M^+, ^{80}Se, 17, ^{78}Se, 9), 314, 312 ($(PhSe)_2$, ^{80}Se, 9, ^{78}Se, 5), 189, 187 ($PhSeS^+$, ^{80}Se, 10, ^{78}Se, 7), 181 (24), 157, 155 ($PhSe^+$, ^{80}Se, 69, ^{78}Se, 34), 149 (100), 121 (99). Found: C, 56.83; H, 5.52%. Calcd for $C_{16}H_{18}OSSe$: C, 56.97; H, 5.38%.

5-Phenylseleno-3-thiatricyclo[5.3.1.0^{4,9}]undecan-2-one (2). A mixture of (selenothioperoxy)carboxylate **1** (185 mg, 0.55 mmol) and azobis(isobutyronitrile) (9 mg, 0.055 mmol) in degassed benzene (13 ml) was heated for 7 h. After removing the solvent by evaporation under reduced pressure, the residue was purified by flash column chromatography (silica gel 5 g, hexane/ethyl acetate 95:5) to give thiahomoprotoadamantanone **2** (180 mg, 97%), mp 57—58 °C (from diethyl ether). ^{1}H NMR (500 MHz, $CDCl_3$) δ=1.57 (dddd, *J*=13.0, 5.6, 3.6, 1.6 Hz, C-8H), 1.96 (ddd, *J*=13.7, 6.3, 4.9 Hz, C-11H), 1.99 (m, C-11H′), 2.00 (ddd, *J*=13.6, 6.3, 4.9 Hz, C-10H), 2.07 (m, C-10H′), 2.12 (dddd, *J*=14.3, 3.9, 2.5, 1.9 Hz, C-6H), 2.14—2.22 (m, C-7H, C-8H), 2.43 (m, C-9H), 2.88 (ddd, *J*=14.3, 6.3, 3.8 Hz, C-6H′), 3.08 (tt, *J*=6.3, 2.5 Hz, C-1H), 3.17 (ddd, *J*=6.3, 2.5, 1.0 Hz, C-5H), 4.10 (dddd, *J*=1.9, 1.6, 1.0, 0.1 Hz, C-4H), 7.25—7.60 (m, phenyl H); ^{13}C NMR ($CDCl_3$) δ=26.4 (CH), 29.5 (CH_2), 29.8 (CH_2), 31.4 (CH_2), 32.4 (CH), 34.4 (CH_2), 40.9 (CH), 50.7 (CH), 52.7 (CH), 127.9 (CH), 129.5 (CH), 129.7 (C), 133.9 (CH), 209.7 (C=O); IR (KBr) 1653 cm^{-1}; MS (70 eV) *m/z* (rel intensity) 338, 336 (M^+, ^{80}Se, 3, ^{78}Se, 2), 306 (13), 278 (12), 261 (5), 181 (100), 157 (15), 155 (8), 149 (40). Found: C, 50.07; H, 5.58%. Calcd for $C_{16}H_{18}OSSe$: C, 56.97; H, 5.38%.

5-Phenylseleno-3-thiatricyclo[5.3.1.0^{4,9}]undec-5-en-2-one (5). Method A: To a solution of (selenothioperoxy)carboxylate **1** (54 mg, 0.16 mmol) and pyridine (54 μl, 0.66 mmol) in dichloromethane (7 ml) was added 35% hydrogen peroxide (150 μl, 0.87 mmol) under vigorous stirring at room temperature and the mixture was stirred until all the starting selenide was converted to the selenoxide, which could easily be confirmed by TLC (selenide; R_f=0.28, hexane/ethyl acetate 9:1, selenoxide; R_f=0.38, chloroform/methanol 95:5). After 1 h diethyl ether (30 ml) was added to the mixture and the resulting solution was washed succesively with water and brine. The organic solution was dried over anhydrous $MgSO_4$. The solvent was removed by evaporation under reduced pressure. Benzene (3 ml) was then added to the residue and the solution was refluxed for 1.5 h. The residue obtained after removing the solvent by evaporation under reduced pressure was purified by flash column chromatography to give vinyl selenide **5** (45 mg, 82%).

Method B: To a solution of (selenothioperoxy)carboxylate **1** (23 mg, 0.068 mmol) in dichloromethane (0.5 ml) was added *m*CPBA (80% purity, 16 mg, 0.74 mmol) at −40 °C. The mixture was stirred for 10 min at this temperature. After the cooling bath had been removed, pyridine (22 μl, 0.27 mmol) and benzene (1 ml) were added to the mixture. The reaction mixture was then heated under reflux for 6 h. The mixture was allowed to cool to room temperature and solvent was removed by evaporation under reduced pressure to give a residue which was purified as mentioned above to afford vinyl selenide **5** (16 mg, 70%). ^{1}H NMR (200 MHz,

Table 1. Bond Angles for 5[a)]

Bond angle (ϕ/deg)			
C(2)-C(1)-C(10)	110.2(6)	C(6)-C(5)-Se(13)	120.3(4)
C(2)-C(1)-C(11)	115.1(6)	C(5)-C(6)-C(7)	120.3(6)
C(10)-C(1)-C(11)	112.1(6)	C(6)-C(7)-C(8)	106.3(6)
C(1)-C(2)-S(3)	117.6(5)	C(6)-C(7)-C(11)	114.1(6)
C(1)-C(2)-O(12)	124.0(6)	C(8)-C(7)-C(11)	111.3(6)
S(3)-C(2)-O(12)	118.3(5)	C(7)-C(8)-C(9)	109.1(6)
C(2)-S(3)-C(4)	100.2(3)	C(4)-C(9)-C(8)	110.7(5)
S(3)-C(4)-C(5)	105.2(4)	C(4)-C(9)-C(10)	112.1(5)
S(3)-C(4)-C(9)	114.8(4)	C(8)-C(9)-C(10)	107.2(6)
C(5)-C(4)-C(9)	113.9(5)	C(1)-C(10)-C(9)	109.0(6)
C(4)-C(5)-C(6)	121.6(5)	C(1)-C(11)-C(7)	116.3(6)
C(4)-C(5)-Se(13)	117.8(4)	C(5)-Se(13)-C(14)	98.6(3)

a) Labeling corresponds to that indicated in Figure. Estimated standard deviations in parentheses.

Table 2. Bond Lengths for 5[a)]

Bond length (l/Å)			
C(1)-C(2)	1.494(10)	C(7)-C(8)	1.492(11)
C(1)-C(10)	1.523(10)	C(7)-C(11)	1.529(11)
C(1)-C(11)	1.543(10)	C(8)-C(9)	1.526(10)
C(2)-S(3)	1.788(7)	C(9)-C(10)	1.530(9)
C(2)-O(12)	1.213(8)	Se(13)-C(14)	1.914(6)
S(3)-C(4)	1.846(6)	C(14)-C(15)	1.394(9)
C(4)-C(5)	1.497(8)	C(14)-C(19)	1.382(10)
C(4)-C(9)	1.570(9)	C(15)-C(16)	1.391(13)
C(5)-C(6)	1.322(9)	C(16)-C(17)	1.368(15)
C(5)-Se(13)	1.922(6)	C(17)-C(18)	1.397(13)
C(6)-C(7)	1.496(9)	C(18)-C(19)	1.377(11)

a) Labeling corresponds to that indicated in figure. Estimated standard deviations in parentheses.

$CDCl_3$) δ=1.72—2.32 (m, 5H), 2.49 (m, 2H), 2.79 (m, 1H), 2.95 (m, 1H), 4.08 (d, J=9.9 Hz, 1H), 6.33 (d, J=8.0 Hz, 1H), 7.12—7.65 (m, 5H); ^{13}C NMR ($CDCl_3$) δ=26.9 (CH), 28.9 (CH_2), 31.1 (CH), 35.8 (CH_2), 36.0 (CH_2), 47.3 (CH), 50.2 (CH), 127.3 (CH), 129.3 (CH), 129.4 (C), 132.8 (CH), 138.1 (C), 141.3 (CH), 208.2 (C=O); IR ($CHCl_3$ solution) 1665 cm^{-1}; MS (70 eV) m/z (rel intensity) 336, 334 (M^+, ^{80}Se, 100, ^{78}Se, 49), 157 (61), 155 (33). Found: C, 57.25; H, 4.92%. Calcd for $C_{16}H_{16}OSSe$: C, 57.31; H, 4.81%.

Crystallographic Study of Vinyl Selenide 5. Crystal was obtained by slow crystallization from diethyl ether-hexane. D_m was measured by flotation. A Rigaku automated four-circles diffractometer AFC-5 was used with graphite monochromated Cu radiation (Cu K=1.5418 Å).

$C_{16}H_{16}OSSe$, M_r=335.32; monoclinic, *Pbca*, a=12.835(1) Å, b=18.190(2) Å, c=12.137(2) Å, α=90.03(1)°, β=89.99(1)°, γ=90.01(1)°, V=2837 Å^3, D_x=1.570 g cm^{-3}, D_m=1.574 g cm^{-3}; Z=8; Crystal size, 0.10×0.20×0.40 mm; 2687. Intensities were collected, $2\theta_{max}$=126°.

Structures were solved by the Monte-Carlo direct method with the aids of MULTAN78 program system using 2089 non-zero unique reflections, and refined by the full-matrix least-squares program with the analytical absorption correction. Non-hydrogen atoms were assigned anisotropic temperature factors. All the atoms were located by using a difference Fourier map and refined with the equivalent isotropic temperature factor to that for the bonded carbon atoms. R=0.0681, $S=[\sum w(|F_o|^2-|F_c|^2)^2/(m-n)]^{1/2}$=1.4, $w=1/\sigma^2(F^2)$, $\Delta\rho_{max}$=5.6 e Å^{-3}. Atomic scattering factors from International Tables for X-Ray Crystallography, Kynoch press, Birmingham, England (1974), Vol. 4. All calculations were made on a FACOM M-382 at the computer center of Nagoya University. Selected bond lengths and bond angles for **5** are shown in Tables 1 and 2.

The present work was partially supported by a Grant-in-Aid for Scientific Research No. 61470086 from the Ministry of Education, Science and Culture.

References

1) T. Toru, T. Seko, and E. Maekawa, *Tetrahedron Lett.*, **26**, 3263 (1985).
2) T. Toru, T. Kanefusa, and E, Maekawa, *Tetrahedron Lett.*, **27**, 1583 (1986).
3) R. C. Fort, Jr., "Adamantane: The Chemistry of Diamond Molecules," Marcel Dekker, New York (1976).
4) T. Toru, M. Nishigaki, T. Seko, T. Kanefusa, and E. Maekawa, *Synthesis*, **1985**, 879.
5) A. C. Udding, H. Wynberg, and J. Strating, *Tetrahedron Lett.*, **1968**, 5719; T. Sasaki, S. Eguchi, and T. Toru, *J. Am. Chem. Soc.*, **91**, 3390 (1969).
6) The ^{1}H NMR study in which each proton was assigned by the double resonance technique showed that the cyclohexane ring bearing a phenylseleno group might adopt a pseudo boat form since C-4 proton attached to the thio ester showed two long range couplings with C-6 and C-8 protons. Furthermore, from the model study the vicinal coupling constants between C-5 proton, attached to the phenylseleno group, and protons at C-4, C-6, and C-6′ position are more likely in accord with those anticipated from their dihedral angles in the structure having the anti configuration.
7) A. L. J. Beckwith, *Tetrahedron*, **37**, 3073 (1981); **41**, 3925 (1985); B. Giese, "Radicals in Organic Synthesis: Formation of Carbon-Carbon Bonds," Pergamon Press, Oxford (1986).
8) T. Sasaki, S. Eguchi, and H. Ban, *J. Org. Chem.*, **48**, 4073 (1983).
9) M. A. Mckervey, D. Faulkner, and H. Hamill, *Tetrahedron Lett.*, **1970**, 1971.
10) Takeshi Toru, Ph. D. Thesis, Nagoya University, Nagoya, Japan, 1971; W. H. Staas and L. A. Spurlock, *J. Org. Chem.*, **39**, 3822 (1974).
11) D. N. Jones, D. Mundy, and R. D. Whitehouse, *J. Chem. Soc., Chem. Commun.*, **1970**, 86; K. B. Sharpless, M. W. Young, and R. F. Lauer, *Tetrahedron Lett.*, **1973**, 1979; H. J. Reich, J. M. Renga, and I. L. Reich, *J. Am. Chem. Soc.*, **97**, 5434 (1975).
12) D. N. Jones, E. Helmy, and R. D. Whitehouse, *J. Chem. Soc., Perkin Trans. 1*, **1972**, 1329.
13) H. J. Reich and S. K. Shah, *J. Org. Chem.*, **42**, 1773 (1977).

^{13}C NMR Spectra and Anomerization of *cis*- and *trans*-5-Arylamino-3-isopropyl-1,2,4-trioxanes

Hiroshi YAMAMOTO,* Masatoshi HIRAYAMA,† Masamoto AKUTAGAWA,†† Takehiko NISHIO,†††
Choji KASHIMA,††† and Yoshimori OMOTE†††
Faculty of Education, Ibaraki University, Bunkyo, Mito 310
†Department of Chemistry, Ibaraki University, Bunkyo, Mito 310
††Faculty of Education, Kumamoto University, Kurokami, Kumamoto 860
†††Department of Chemistry, The University of Tsukuba, Tsukuba, Ibaraki 305
(Received December 4, 1987)

Synopsis. The cis and trans isomers of 3-isopropyl-6,6-dimethyl-5-arylamino-1,2,4-trioxanes have been clearly identified and the anomerization of arylaminotrioxanes has been detected by the ^{13}C NMR spectra in chloroform-*d*.

The 1,2,4-trioxanes have interested researchers since they play the active role in Arteannuin (Qinghosu),[1] an antimalarial remedy. Several methods for synthesizing 1,2,4-trioxanes have been reported;[2] recentry we obtained 5-arylamino-3-isopropyl-1,2,4-trioxanes (**3**) from one-pot reactions of arylamines (**1a—p**) and 2-methylpropanal (**2**) (molar ratio 1:3) in the presence of oxygen.[3] (Scheme 1) After purification by column chromatography, the liquid trioxanes were found by NMR spectra to be a mixture of two isomers. From a hexane, or occasionally a hexane-ethyl acetate, solution of the liquid, one of the isomers of **3** slowly crystallized into colorless prisms. Based on X-ray crystal-structure analyses of the prisms, the structures of the trioxane ring in **3a**[4] and **3k**[5] were found to be different from each other. The structure of **3a** was the chair conformation of the trioxane ring with the naphthylamino group bonding at an equatorial position (cis isomer), while that of **3k** bonded to the 2-chloroanilino group occupying an axial position (trans isomer). We now report on the distinction between these cis and trans isomers of **3** on the basis of ^{13}C NMR spectra.

Results and Discussion

The sixteen synthesized trioxanes (**3**) were divided into three groups according to ^{13}C NMR chemical shifts (Table 1). The *gem*-dimethyl groups at C-6 of **3** were assigned by comparing their NMR signals with those of other trioxanes having one methyl at C-6 (5-arylamino-6-methyl-6-phenyl-3-(1-phenylethyl)-1,2,4-trioxanes[6]). The trioxanes of group 1, including **3a**, exhibited the C-3 signals at a lower field (δ 107.3—107.1) than those of the group 2, including **3k** (δ 99.7—99.4), whereas axial methyl signals at C-6 of group 1 appeared at higher fields (δ 17.7—17.4) than those of group 2 (δ 23.8—23.6). Since the C-3 and axial methyl carbons are in the γ-position relative to the nitrogen, the difference between these chemical shifts may be interpreted according to the suggestion that the γ-gauche-effect is stronger than the γ-trans-effect for nitrogen.[7] When the $CDCl_3$ solutions of group 1 were allowed to stand at room temperature for a long time, new ^{13}C signals appeared in the higher fields where the trioxanes of group 2 had shown signals. Similarly, when the $CDCl_3$ solutions of group 2 were allowed to stand, new ^{13}C signals were observed in the lower fields where those of group 1 had appeared. (These new signals are shown in parentheses in Table 1.) These changes in the spectra can be explained in terms of the establishment of an equilibrium between cis and trans isomers: the change is caused by an anomerization at C-5 of the 1,2,4-trioxane ring. Since the intensity ratio of the two isomers reached a constant value within about two days, it may be reasonable to assume that these two isomers reached equilibrium during this period. Molar fractions of cis isomer (x_{cis} were derived from average intensities of distinguishable ^{13}C signals at

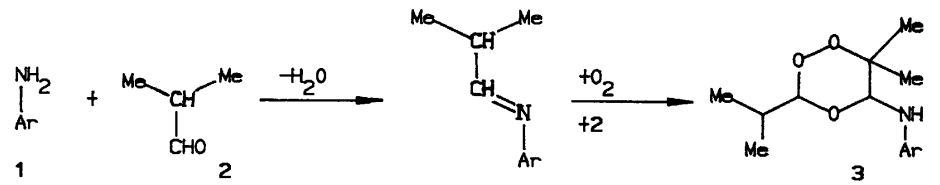

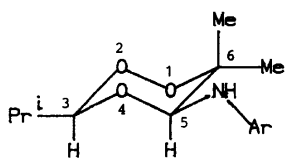

3 (cis)

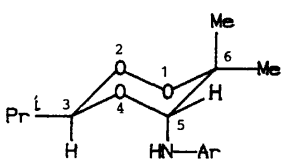

3 (trans)

Ar=a; 1-naphthyl b; 2-methyl-4-chlorophenyl c; 2,4-xylyl d; 2,5-xylyl e; 4-chlorophenyl f; 4-bromophenyl g; 4-ethoxycarbonylphenyl h; 4-acetylphenyl i; 3-acetylphenyl j; 2-methyl-3-chlorophenyl k; 2-chlorophenyl l; *o*-tolyl m; phenyl n; 9-anthryl o; mesityl p; 2,6-xylyl

Scheme 1.

Table 1. ^{13}C NMR Chemical Shifts of 5-Arylamino-1,2,4-trioxanes (**3**) in $CDCl_3$ at 25 °C (δ/ppm from Me_4Si)[a]

	C-3	CH	Me, Me	C-5	eq. Me	C-6	ax. Me
Group 1							
3a-cis	107.1	31.0	16.9, 16.7	86.7	22.0	80.0	17.6
trans	(99.5)	(30.6)		(81.6)	(22.7)		(23.6)
3b-cis	107.1	31.0	16.9, 16.8	86.5	22.0	79.8	17.5
trans	(99.4)	(30.6)		(81.3)	(22.7)		(23.6)
3c-cis	107.3	31.1	17.0	87.1	22.2	80.2	17.5
trans	(99.5)	(30.8)		(81.8)	(22.9)		(23.8)
3d-cis	107.3	31.1	17.0	86.6	22.1	80.1	17.7
trans	(99.5)	(30.8)		(81.5)	(22.9)		(23.8)
3e-cis	107.2	31.0	16.8	86.4	21.8	79.8	17.4
trans	(99.5)	(30.6)		(81.2)	(22.4)	(79.7)	(23.6)
3f-cis	107.2	31.0	16.8	86.2	21.8	79.8	17.5
trans	(99.5)	(30.6)		(81.1)	(22.4)		(23.6)
3g-cis	107.3	31.0	16.9, 16.8	85.5	21.9	79.7	17.5
trans	(99.7)	(30.6)		(80.4)	(22.3)		(23.2)
3h-cis	107.1	31.0	16.8, 16.7	85.5	21.8	79.7	17.5
trans	(99.7)	(30.6)		(80.5)	(22.3)		(23.6)
3i-cis	107.2	31.0	16.8	86,2	21.8	79.9	17.5
trans	(99.6)	(30.5)		(81.0)	(22.4)	(79.8)	(23.7)
Group 2							
3j-trans	99.5	30.6	16.8	81.4	22.8	79.9	23.6
cis	(107.2)	(31.0)		(86.5)	(22.0)		(17.6)
3k-trans	99.5	30.6	16.8, 16.6	81.1	22.5	79.6	23.6
cis	(107.1)	(31.0)		(85.8)	(21.9)	(79.7)	(17.5)
3l-trans	99.4	30.6	16.8	81.4	22.7	79.9	23.6
cis	(107.1)	(31.0)		(86.5)	(22.0)		(17.5)
3m-trans	99.7	30.7	17.0	81.4	22.6	80.0	23.8
cis	(107.4)	(31.1)		(86.5)	(22.0)		(17.6)
Group 3							
3n-cis	107.0	31.0	16.9, 16.5	92.1	22.6	81.2	17.6
3o-cis	106.9	31.2	16.7	90.7	22.2	81.0	17.2
3p-cis	106.9	31.2	16.8	90.4	22.2	81.0	17.2

a) Newly appeared signals in solution are given in parentheses.

equilibrium. Thus, the free-energy difference of this change ($G°_{cis}-G°_{trans}$) was evaluated from x_{cis} by the equation $G°_{cis}-G°_{trans}=RT\ln(1-x_{cis})/x_{cis}$ at 25 °C (Table 2). These $G°_{cis}-G°_{trans}$ values were very close to those of 2-(arylamino)tetrahydropyrans.[8] Thus, there would be no appreciable dipole interaction between arylamino substituent and the three oxygen atoms of the trioxane ring.

When the $CDCl_3$ solutions of the trioxanes of group 3 were allowed to stand at room temperature, no ^{13}C signal of another isomer (corresponding to trans) was observed in solution, and only signals of the prducts of trioxane decomposition (acetone and 2-methylpropanal) were observed. The observed spectra of group 3 were very similar to those of group 1 except for the C-5 signal which shifted to a lower field. All trioxanes of group 3 are bonded with a 2,6-disubstituted arylamino group at C-5. These low-field shifts in ^{13}C NMR spectra, having the above similarity, have been recognized in the methyl signal of *N*-methylaniline derivatives having two substituents at ortho positions (Table 3). Therefore, it is considered that in group 3 there exists only a cis isomer with an arylamino group rotated along the N-C bond.

Table 2. Equilibration of 5-Arylamino-3-isopropyl-1,2,4-trioxanes (**3**) in $CDCl_3$ at 25 °C

Trioxane	cis isomer, %	$G°_{cis}-G°_{trans}$/kJ mol^{-1}
3a	78±2	3.1±0.1
3b	80±1	3.4±0.1
3c	82±1	3.8±0.1
3d	82±1	3.8±0.1
3e	80±5	3.4±0.2
3f	87±3	5.1±0.1
3g	93±2	6.4±0.1
3h	91±1	5.7±0.1
3i	80±2	3.4±0.1
3j	80±3	3.4±0.1
3k	75±3	2.7±0.1
3l	79±2	3.3±0.1
3m	79±3	3.3±0.1

Experimental

Melting points are all uncorrected. Spectral characterization was carried out with the following instruments. ^{13}C NMR: JEOL JNM-FX100 and Varian CFT-20 spectrometers using tetramethylsilane as an internal standard;

Table 3. Chemical Shifts of Methyl-Carbon of *N*-Methylanilines in $CDCl_3$ (δ/ppm from Me_4Si)

Compd	$R^1=R^2=H$[9]	$R^1=H, R^2=Me$[9]	$R^1=R^2=Me$[10]
$\underline{C}H_3$-N	30.4	30.4	35.3

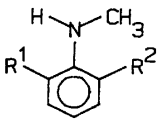

^1H NMR: Hitachi R-20A spectrometer; MS: JEOL JMS-DX300 mass spectrometer using a direct insertion probe at 20 eV and 100 μA of ionization energy; IR: Hitachi 215 spectrometer.

Materials. The general preparation of 5-arylamino-1,2,4-trioxanes has recently been reported and trioxanes **3a**,**3c—d** and **3k—p** have been described.[3]

5-(4-Chloro-2-methylanilino)-3-isopropyl-6,6-dimethyl-1,2,4-trioxane (3b): prisms from hexane–ethyl acetate (yield 38%), mp 103—104 °C (decomp); IR (Nujol) 3440, 1300, 1255, 1150, and 1050 cm^{-1}; ^1H NMR of cis isomer ($CDCl_3$) δ=0.95 (6H, d, J=6.5 Hz), 1.19 (3H, s), 1.52 (3H, s), ca. 1.9 (1H, m), 2.12 (3H, s), 3.71 (1H, d, J=10 Hz), 4.77 (1H, d, J=10 Hz), 5.06 (1H, d, J=5.5 Hz), and 6.5—7.2 (3H, m) DI-MS (20 eV) m/z (%) 301, 299 (M^+, 7:23), 172, 170 (24:100); Found: C,60.34; H,7.39; N, 4.63%. Calcd for $C_{15}H_{22}NO_3Cl$: C, 60.09; H, 7.39; N, 4.67%.

5-(4-Chloroanilino)-3-isopropyl-6,6-dimethyl-1,2,4-trioxane (3e): prisms from hexane (yield 17%), mp 54—55 °C (decomp); IR(Nujol) 3410, 1310, 1250, 1155, and 1070 cm^{-1}; ^1H NMR of cis isomer ($CDCl_3$) δ=0.92 (6H, d, J=7 Hz), 1.15 (3H, s), 1.46 (3H, s), ca. 1.8 (1H, m), 3.92 (1H, d, J=10 Hz), 4.75 (1H, d, J=10 Hz), 5.02 (1H, d, J=5.5 Hz), and 6.5—7.3 (4H, m); DI-MS (20 eV) m/z (%) 287, 285 (M, 6:17), 158, 156 (33:100); Found: C, 58.94; H, 7.09; N, 4.85%. Calcd for $C_{14}H_{20}NO_3Cl$: C, 58.84 H, 7.05; N, 4.90%.

5-(4-Bromoanilino)-3-isopropyl-6,6-dimethyl-1,2,4-trioxane (3f): prisms from hexane (yield 31%), mp 49—51 °C (decomp); IR (Nujol) 3420, 1290, 1250, 1155, 1140, and 1070 cm^{-1}; ^1H NMR of cis isomer ($CDCl_3$) δ=0.95 (6H, d, J=7 Hz), 1.17 (3H, s), 1.49 (3H, s), ca. 1.9 (1H, m), 3.95 (1H, d, J=10 Hz), 4.79 (1H, d, J=10 Hz), 5.04 (1H, d, J=5.5 Hz), and 6.4—7.4 (4H, m); DI-MS (20 eV) m/z (%) 331, 329 (M^+, 23:23), 202, 200 (94:100); Found: C, 50.95; H, 6.18; N, 4.21%. Calcd for $C_{14}H_{20}NO_3Br$: C, 50.92; H, 6.10 N, 4.24%.

5-(4-Ethoxycarbonylanilino)-3-isopropyl-6,6-dimethyl-1,2,4-trioxane(3g): prisms from hexane (yield 17%), mp 99—101 °C (decomp); IR (Nujol) 3420, 1680, 1290, 1270, 1180, 1150, and 1060 cm^{-1}; ^1H NMR of cis isomer ($CDCl_3$) δ=0.93 (6H, d, J=6.5 Hz), 1.15 (3H, s), 1.32 (3H, t, J=7 Hz) 1.49 (3H, s), ca. 1.8 (1H, m), 4.24 (2H, q, J=7 Hz), 4.37 (1H, d, J=10 Hz), 4.78 (1H, d, J=10 Hz), 5.04 (1H, d, J=5.5 Hz), and 6.5—7.9 (4H, m); DI-MS (20 eV) m/z (%) 323 (M^+ ,8), 194 (100); Found: C, 63.22; H, 7.85; N, 4.40%. Calcd for $C_{17}H_{25}NO_5$: C, 63.13; H, 7.79; N, 4.33%.

5-(4-Acetylanilino)-3-isopropyl-6,6-dimethyl-1,2,4-trioxane (3h): prisms from hexane–ethyl acetate (yield 35%), mp 105—106 °C (decomp); IR (Nujol) 3430, 1670, 1280, 1265, 1150, and 1060 cm^{-1}; ^1H NMR of cis isomer ($CDCl_3$) δ=0.96 (6H, d, J=6.5 Hz), 1.20 (3H, s), 1.53 (3H, s), ca. 1.9 (1H, m), 2.51 (3H, s), 4.50 (1H, d, J=10 Hz), 4.96 (1H, d, J=10 Hz), 5.13 (1H, d, J=5.5 Hz), and 6.7—8.0 (4H, m); DI-MS (20 eV) m/z (%) 293 (M^+ ,10), 164 (100); Found: C, 65.41; H, 7.91; N, 4.65%. Calcd for $C_{16}H_{23}NO_4$: C, 65.50; H, 7.90; N, 4.77%.

5-(3-Acetylanilino)-3-isopropyl-6,6-dimethyl-1,2,4-trioxane (3i): prisms from hexane–ethyl acetate (yield 42%), mp 82—84 °C (decomp); IR (Nujol) 3440, 1680, 1295 (w), 1270, 1150, and 1050 cm^{-1}; ^1H NMR of cis isomer ($CDCl_3$) δ=0.96 (6H, d, J=6.5 Hz), 1.21 (3H, s), 1.53 (3H, s), ca. 1.8 (1H, m), 2.58 (3H, s), 4.21 (1H, d, J=10 Hz), 4.96 (1H, d, J=10 Hz), 5.16 (1H, d, J=5.5 Hz), and 6.6—7.5 (4H, m); DI-MS (20 eV) m/z (%) 293(M^+ ,8), 164 (100); Found: C, 65.31; H, 8.05; N, 4.65%. Calcd for $C_{16}N_{23}NO_4$: C, 65.50; H, 7.90; N, 4.77%.

5-(3-Chloro-2-methylanilino)-3-isopropyl-6,6-dimethyl-1,2,4-trioxane (3j): prisms from hexane (yield 4.2%, yield of crude liquid 41%), mp 37—38 °C (decomp); IR (Nujol) 3450, 1300, 1250, 1155, 1130, and 1050 cm^{-1}; ^1H NMR of trans isomer ($CDCl_3$) δ=0.95 (6H, d, J=7 Hz), 1.19 (3H, s), 1.52 (3H, s), ca. 1.9 (1H, m), 2.20 (3H, s), 4.84 (1H, d, J=10 Hz), 4.80 (1H, d, J=10 Hz), 5.11 (1H, d, J=5.5 Hz), and 6.5—7.3 (3H, m); DI-MS (20 eV) m/z (%) 301, 299 (M^+, 5:14), 172, 170 (31:100); Found: C, 60.08; H, 7.47; N, 4.72%. Calcd for $C_{15}H_{22}NO_3Cl$: C, 60.09; H, 7.39; N ,4.67%.

We are indebted to Mr. Mamoru Sekine of the Department of Chemistry, Ibaraki University, and Mr. Hideto Suzuki of the Analytical Center, the University of Tsukuba, for obtaining the ^1H and ^{13}C NMR spectra. This research was partially supported by a Grant-in-Aid for Special Project Research from the Ministry of Education, Science and Culture (Ibaraki University, 1986).

References

1) Xu Xing-xiang, Zhu Jie, Huang Da-zhong, and Zhou Wei-shan, *Acta Chimica Sinica*, **41**, 574 (1983); G. Schmid and W. Hofheinz, *J. Am. Chem. Soc.*, **105**, 624 (1983).

2) G. B. Payne and C. W. Smith, *J. Org. Chem.*, **22**, 1682 (1957); W. Adam and A. Rios, *J. Chem. Soc., Chem. Commun.*, **1971**, 822; R. M. Wilson, E. J. Gardner, R. C. Elder, R. H. Squire, and L. R. Florian, *J. Am. Chem. Soc.*, **96**, 2955 (1974); M. Miura, M. Nojima, and S. Kusabayashi, *J. Chem. Soc., Chem. Commun.*, **1981**, 581; C. W. Jefford, D. Jaggi, J. Boukouvalas, and S. Kohmoto, *J. Am. Chem. Soc.*, **105**, 6497 (1983); C. W. Jefford, J. Boukouvalas, and S. Kohmoto, *Helv. Chim. Acta*, **66**, 2615 (1983); C. W. Jefford, J. Boukouvalas, and S. Kohmoto, *J. Chem. Soc., Chem. Commun.*, **1984**, 523.

3) H. Yamamoto, M. Akutagawa, H. Aoyama, and Y. Omote, *J. Chem. Soc., Perkin Trans. 1*, **1980**, 2300.

4) H. Yamamoto, H. Aoyama, Y. Omote, M. Akutagawa, A. Takenaka, and Y. Sasada, *J. Chem. Soc., Chem. Commun.*, **1977**, 63; A. Takenaka, Y. Sasada, and H. Yamamoto, *Acta Crystallogr., Sect. B*, **33**, 3564 (1977).

5) H. Yamamoto, I. Nakai, C. Kashima, Y. Omote, and M. Akutagawa, *Chem. Lett.*, **1983**, 1841.

6) Preparation of these trioxanes were reported in ref 3), but their ^{13}C NMR spectra have been unpublished. In 5-arylamino-6-methyl-6-phenyl-3-(1-phenylethyl)-1,2,4-trioxanes, the axial methyl signals at C-6 appeared at δ 15.5—15.8 in the cis isomer and at δ 25.7—26.7 in the trans isomer.

7) F. W. Wehrli and T. Wirthlin, "Interpretation of Carbon-13 NMR Spectra," Heyden, London (1976), p. 37.

8) D. Barbry, D. Couturier, and G. Ricart, *J. Chem. Soc., Perkin Trans. 2*,, **1982**, 249.

9) Sadtler Standard Carbon-13 NMR Spectra, Philadelphia (1976).

10) *N*-methyl-2,6-xylidine was prepared from 2,6-xylidine and dimethyl sulfate: bp 100—103 °C (3330—3600 Pa); ^1H NMR ($CDCl_3$) δ=2.28 (s, 6H), 2.76(s, 3H), 2.9 (s, 1H), and 6.6—7.1 (m, 3H); MS m/z (%) 135 (M^+, 42), 120 (100).

Halogenation Using Quaternary Ammonium Polyhalides. XI.[1] Bromination of Acetanilides by Use of Tetraalkylammonium Polyhalides

Shoji KAJIGAESHI,* Takaaki KAKINAMI,† Hiromichi YAMASAKI, Shizuo FUJISAKI, and Tsuyoshi OKAMOTO†

Department of Industrial Chemistry, Faculty of Engineering, Yamaguchi University, Tokiwadai, Ube 755

†Department of Industrial Chemistry, Ube Technical College, Tokiwadai, Ube 755

(Received January 11, 1988)

Synopsis. The reaction of acetanilides with tetraalkylammonium polyhalides, such as tetrabutylammonium tribromide, benzyltrimethylammonium tribromide, and benzyltrimethylammonium chlorobromate(1−), in dichloromethane-methanol at room temperature gave bromo-substituted acetanilides in good yields, respectively.

In general, bromo-substituted acetanilides (**2**) have been prepared from the acetylation of bromoanilines with acetyl chloride,[2] or acetic anhydride in acetic acid,[3] further, from the reaction of acetanilides (**1**) with bromine in acetic acid.[4] As a special brominating agent for **1**, *N*,*N*-dibromobenzenesulfonamide has also been used instead of bromine.[5]

Recently, we have shown that benzyltrimethylammonium tribromide (BTMA Br_3) (**3b**) is a useful brominating agent to anilines.[6] In the present paper, we wish to report on the bromination of **1**, *N*-acetyl-protected anilines, by the use of tetraalkylammonium polyhalides, such as tetrabutylammonium tribromide (TBA Br_3) (**3a**), **3b** and benzyltrimethylammonium chlorobromate(1−) (BTMA Br_2Cl) (**3c**).

Results and Discussion

The reaction of **1** with **3a**,[7] **3b**,[8] and **3c** in dichloromethane-methanol at room temperature gave **2** in good yields, respectively.

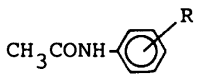

1

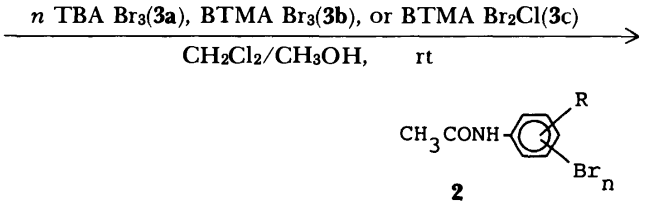

2

The results are summarized in Table 1. This table shows that **3c** is the strongest brominating agent to **1**, and that these brominations of **1**, except hydroxy- and amino-substituted acetanilides (e.g., **1h**, **1i**, and **1j**), have usually given predominantly the corresponding para-bromo derivatives.[15] The reaction of hydroxy- or amino-substituted acetanilides with these brominating agents gave mono-, di-, or tribromo-substituted derivatives which were products controlled mainly by the effect of the hydroxy or amino group on the orientation.

Recently, Berthelot et al.[16] reported that the bromination of **1a** with **3a** in chloroform at room temperature did not proceeded at all. However, as shown in the table, in the presence of methanol, the reaction of **1** with **3** in dichloromethane at room temperature easily gave **2** in good yields. In these cases, it can be presumed that the active species is probably the methyl hypobromite produced from the reaction of **3** with methanol.[17]

Since aminophenols and phenylenediamines are so sensitive for **3**, isolations of mono-, di-, or tribromo derivatives of these compounds are considerably difficult. However, the selective brominations of *N*-acetyl-protected anilines, such as 2-hydroxyacetoanilide (**1h**), 3-hydroxyacetanilide (**1i**), and 3-aminoacetanilide (**1j**), by use of **3** under mild conditions occured most readily, as shown in the table. Accordingly, bromo-substituted aminophenols and phenylenediamines should be obtained by the hydrolyses of these corresponding acetanilides.

We believe that these tetraalkylammonium polyhalides such as TBA Br_3, BTMA Br_3, and BTMA Br_2Cl are more useful brominating agents for **1** than bromine or *N*,*N*-dibromobenzenesulfonamide, because of their solid character, stability and nontoxicity.

Experimental

Benzyltrimethylammonium Chlorobromate(1−) (BTMA Br_2Cl) (3c). To a solution of bromine (15.98 g, 0.1 mol) in dichloromethane (100 ml) was added dropwise a solution of benzyltrimethylammonium chloride (18.57 g, 0.1 mol) in water (100 ml) under stirring at room temperature. After the mixture was stirred for 30 min, the dichloromethane layer was separated and dried with magnesium sulfate, and then evaporated in vacuo to give a residue which was recrystallized from dichloromethane-ether (10:1) affording BTMA Br_2Cl as stable orange crystals; yield 24.50 g (71%); mp 101—102 °C. Found: C, 34.88; H, 4.63; N, 4.01; Br_2Cl, 56.31%. Calcd for $C_{10}H_{16}NBr_2Cl$: C, 34.76; H, 4.67; N, 4.05; Br_2Cl, 56.51%.

4-Bromoacetanilide (2a); Typical Procedure: To a solution of acetanilide (**1a**) (0.50 g, 3.70 mmol) in dichloromethane (50 ml)-methanol (20 ml) was added **3c** (1.41 g, 4.08 mmol) at room temperature. The mixture was stirred for 20 min until a decoloration of the orange color took place. The solvent was distilled and to the obtained residue was added water (20 ml). The mixture was extracted with ether (40 ml×4). The ether layer was then dried with

Table 1. Bromination of Acetanilides by Use of Tetraalkylammonium Polyhalides

	Substrate 1	Product 2	Molar ratio 3/1	3 used	Reaction time	Yield[a]/%	Mp θ_m/°C Found	Mp θ_m/°C Reported
a	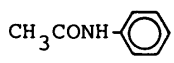	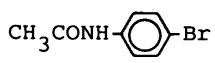	1.1	**3a**	12 h	95		
				3b	2 h	97	163—164	168.8[9]
				3c	20 min	97		
b	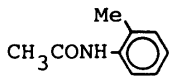	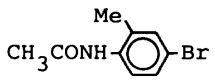	1.1	**3a**	36 h	91		
				3b	27 h	87	160	158—159[10]
				3c	10 h	99		
c	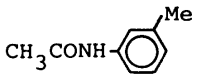	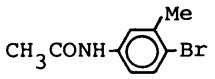	1.1	**3a**	1 h	98		
				3b	3 h	96	103—104	103—104[11]
				3c	15 min	99		
d	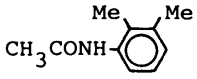	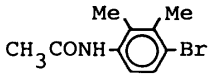	1.1	**3a**	12 h	95		
				3b	2 h	96	159—160	161—162[3]
				3c	2 h	89		
e	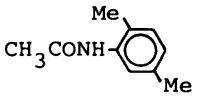	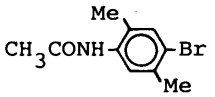	1.1	**3a**	12 h	96		
				3b	2 h	95	188	187[4]
				3c	20 min	93		
f	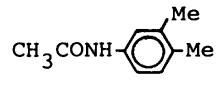	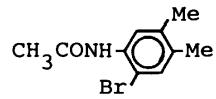	1.1	**3a**	12 h	91		
				3b	16 h	92	163—164	164[12]
				3c	15 min	91		
g	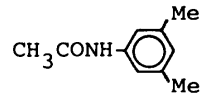	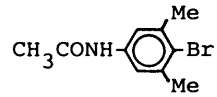	1.1	**3a**	10 min	97		
				3b	2 min	96	180—181	—
				3c	1 min	96		
h-1	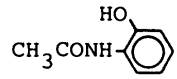	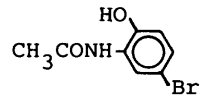	1.0	**3a**	15 min	97		
				3b	2 min	99	175—176	175—175.5[13]
				3c	1 min	96		
h-2		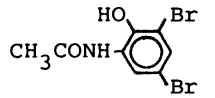	2.1	**3a**		—[b]		
				3b		—[b]	174	174—175[14]
				3c	2 h	89		
i-1	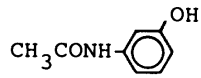	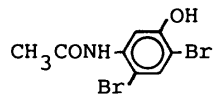	2.0	**3a**	1 h	93		
				3b	1 h	92	237—238	—
				3c	2 min	88		
i-2		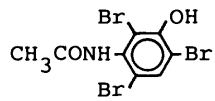	3.1	**3a**		—[c]		
				3b	24 h	69	205	—
				3c	14 h	93		
j-1	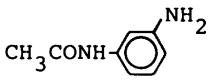	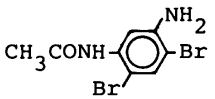	2.0	**3a**	10 min	96		
				3b	3 min	91	162—163	—
				3c	—[d]	96		
j-2		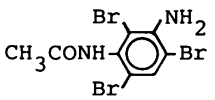	3.1	**3a**		—[c]		
				3b	21 h	57	218—218.5	—
				3c	3 h	98		

a) Yield of isolated product. b) A mixture of mono- and dibromo compounds was obtained. c) A mixture of di- and tribromo compounds was obtained. d) Product **2j-1** precipitated almost immediately as soon as the solution of **3c** was added into the solution of **1j**.

magnesium sulfate and evaporated in vacuo to give a residue which was recrystallized from ethanol-water (1:3) affording **2a** as colorless crystals; yield 0.77 g (97%); mp 163—164 °C (lit,[9] mp 168.8 °C).

4-Bromo-3,5-dimethylacetanilide (2g). Compound **2g** was prepared from the reaction of 3,5-dimethylacetanilide (**1g**) with equimolecular amount of **3** by a similar procedure to that discribed above: colorless crystals; mp 180—181 °C (ethanol-water (1:3)): IR (KBr) 1670 cm^{-1} (CO); ^1H NMR ($CDCl_3$) δ=2.05 (3H, s, $COCH_3$), 2.34 (6H, s, 3 and 5-CH_3), 7.34 (2H, s, 2 and 6-H), 9.63 (1H, br. s, NH). Found: C, 49.58; H, 4.92; N, 5.74%. Calcd for $C_{10}H_{12}NOBr$: C, 49.61; H, 4.99; N, 5.79%.

2,4-Dibromo-5-hydroxyacetanilide (2i-1). Compound **2i-1** was prepared from 3-hydroxyacetanilide (**1i**) and 2 equiv of **3** by a similar procedure to that discribed above: colorless

crystals; mp 237—238 °C (ethanol–water (1:3)); IR (KBr) 1680 cm^{-1} (CO); ^1H NMR ($CDCl_3$) δ=2.17 (3H, s, CH_3), 7.55 (1H, s, 6-H), 7.75 (1H, s, 3-H), 8.38 (1H, br. s, OH), 10.08 (1H, br. s, NH). Found: C, 30.98; H, 2.19; N, 4.49%. Calcd for $C_8H_7NO_2Br_2$: C, 31.10; H, 2.29; N, 4.53%.

3-Hydroxy-2,4,6-tribromoacetanilide (2i-2). Compound **2i-2** was prepared similary from **1i** and 3 equiv of **3b** or **3c**: colorless crystals, mp 205 °C (ethanol–water (1:3)); IR (KBr) 1675 cm^{-1} (CO); ^1H NMR ($CDCl_3$) δ=2.08 (3H, s, CH_3), 3.50 (1H, br. s, OH), 7.73 (1H, s, 5-H), 9.69 (1H, br. s, NH). Found: C, 24.81; H, 1.60; N, 3.60%. Calcd for $C_8H_6NO_2Br_3$: C, 24.77; H, 1.56; N, 3.61%.

5-Amino-2,4-dibromoacetanilide (2j-1). Compound **2j-1** was prepared similary from **1j** and 2 equiv of **3**: colorless crystals, mp 162—163 °C (ethanol–water (1:3)); IR (KBr) 1655 cm^{-1} (CO); ^1H NMR ($CDCl_3$) δ=2.12 (3H, s, CH_3), 4.25 (2H, br. s, NH_2), 7.38 (1H, s, 6-H), 7.45 (1H, s, 3-H), 8.67 (1H, br. s, NH). Found: C, 30.97; H, 2.52; N, 8.90%. Calcd for $C_8H_8N_2OBr_2$: C, 31.20; H, 2.62; N, 9.10%.

3-Amino-2,4,6-tribromoacetanilide (2j-2). Compound **2j-2** was prepared similary from **1j** and 3 equiv of **3b** or **3c**: colorless crystals, mp 218—218.5 °C (ethanol–water (1:3)); IR (KBr) 1675 cm^{-1} (CO); ^1H NMR ($CDCl_3$) δ=2.10 (3H, s, CH_3), 4.28 (2H, br. s, NH_2), 7.62 (1H, s, 5-H),9.48 (1H, br. s, NH). Found: C, 24.97; H, 1.79; N, 6.98%. Calcd for $C_8H_7N_2OBr_3$: C, 24.84; H, 1.82; N, 7.24%.

We wish to thank Dr. Mamoru Nakai and Mr. Katsumasa Harada, Ube Laboratory, Ube Industries, Ltd., for elemental analysis.

References

1) Part X, S. Kajigaeshi, T. Kakinami, M. Moriwaki, S. Fujisaki, K. Maeno, and T. Okamoto, *Synthesis*, in press.
2) P. W. Robertson, *J. Chem. Soc.*, **115**, 1210 (1919).
3) M. Cachia and H. Wahl, *Bull. Soc. Chim. Fr.*, **1958**, 1418.
4) A. S. Wheeler and E. W. Constable, *J. Am. Chem. Soc.*, **45**, 1999 (1923).
5) S. Ito and T. Oya, *Bull. Chem. Soc. Jpn.*, **40**, 418 (1967).
6) S. Kajigaeshi, T. Kakinami, K. Inoue, M. Kondo, H. Nakamura, M. Fujikawa, and T. Okamoto, *Bull. Chem. Soc. Jpn.*, **61**, 597 (1988).
7) S. Kajigaeshi, T. Kakinami, T. Okamoto, and S. Fujisaki, *Bull. Chem. Soc. Jpn.*, **60**, 1159 (1987).
8) S. Kajigaeshi, T. Kakinami, H. Tokiyama, T. Hirakawa, and T. Okamoto, *Bull. Chem. Soc. Jpn.*, **60**, 2667 (1987).
9) R. J. Hartman, E. W. Kanning, and J. E. Weber, *J. Am. Chem. Soc.*, **62**, 1304 (1940).
10) F. B. Dains, O. O. Malleis, and J. T. Meyers, *J. Am. Chem. Soc.*, **35**, 975 (1913).
11) E. Bemberger, *Ber.*, **57**, 2089 (1924).
12) W. H. Mills and I. G. Nixon, *J. Chem. Soc.*, **1930**, 2524.
13) L. C. Raiford and J. Linsk, *J. Am. Chem. Soc.*, **67**, 879 (1945).
14) L. C. Raiford, *J. Am. Chem. Soc.*, **41**, 2076 (1919).
15) Exceptionally, the brominations of 3,4-dimethylacetanilide (**1f**), in which the para-position was occupied by methyl group, with **3** gave orthobromo derivative, 2-bromo-4,5-dimethylacetanilide (**2f**), respectively.
16) J. Berthelot, C. Guette, M. Essayegh, P. L. Desbene, and J. J. Basselier, *Synth. Commun.*, **16**, 1641 (1986).
17) S. Kajigaeshi, T. Kakinami, H. Tokiyama, T. Hirakawa, and T. Okamoto, *Chem. Lett.*, **1987**, 627.

Efficient Reduction of Acyl Chlorides with $Zn(BH_4)_2$/*N,N,N',N'*-Tetramethylethylenediamine

Hiyoshizo KOTSUKI,* Yasuyuki USHIO, Naka YOSHIMURA, and Masamitsu OCHI
Department of Chemistry, Faculty of Science, Kochi University,
Akebono-cho, Kochi 780
(Received January 21, 1988)

Synopsis. Aliphatic and aromatic acyl chlorides were efficiently reduced to give the corresponding alcohols when treated with $Zn(BH_4)_2$ in the presence of *N,N,N',N'*-tetramethylethylenediamine. The reactions with other bases were also examined.

The reductive synthesis of primary alcohols from carboxylic acid derivatives is a very common procedure in organic chemistry and numerous reagents have been developed.[1] In our separate work, we have required methods for the selective and mild reduction of acyl chloride function in the presence of esters.[2] The use of a well-known reagent such as $LiAlH_4$ was not satisfactory for our purpose because of its strong reducing ability. As previously reported, however, the use of $Zn(BH_4)_2$ with *N,N,N',N'*-tetramethylethylenediamine (TMEDA) was found to be a remarkably mild method for the reduction of acyl chlorides to the corresponding alcohols.[3] In this paper we would like to report a more detailed study of this reaction.

Contrary to the description given in the literature,[4] the reduction of benzoyl chloride with $Zn(BH_4)_2$ was very slow and showed less synthetic utility. Fortunately, we found that the reaction was highly accelerated by using one equivalent of TMEDA and gave a clean product. As listed in Table 1 for a comparison, this new reagent system is superior to the usual reagents. Under these conditions a wide variety of aliphatic and aromatic acyl chlorides could be efficiently reduced into the corresponding alcohols in high yields (Table 2). Only one exception was phthaloyl dichloride, which gave a considerable amount of phthalide along with the desired diol. Since under the same conditions phthalide was not reduced, this product must be formed by intramolecular acylation. In these reductions the functional selectivity is particularly noteworthy. Thus, chloro, nitro, ester, and conjugated double bonds were not affected by this reagent system. The limitation is a compound containing an isolated double bond, such as 3-cyclohexenecarbonyl chloride, because of the concomitant hydroboration on this function.

Coupled with this observation, we found that a TMEDA·$(BH_3)_2$ complex,[15] mp 179—180 °C (lit,[16] 179—179.5 °C), was also formed under these reactions, although the yield depended upon the runs (usually in around 40 %). As is well-known, this complex is not only exceedingly stable toward the conventional workup conditions but is insoluble in most organic solvents.[16] Therefore, the product alcohols can be simply separated from the mixture by filtration. From this evidence we concluded that during the reaction borane was generated and trapped by TMEDA. Namely, TMEDA can be regarded as an effective borane scavenger leading to clean reactions, as illustrated in Scheme 1.

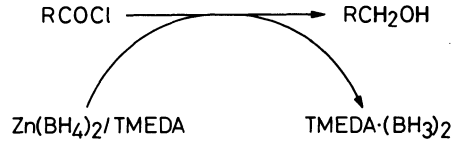

Scheme 1.

With these results in hand we have examined the effect of amine on the reduction of *m*-chlorobenzoyl chloride. The result is summarized in Table 3. It will be apparent that among the several amines TMEDA is the best one. DABCO also showed a comparable yield, probably due to a similar stability of its borane complex.[16] Interestingly, the use of *N,N*-dimethylaniline or 2,6-lutidine gave *m*-chlorobenzyl *m*-chlorobenzoate as a major product. The formation of this ester probably accounts for the fast esterification of the starting acyl chloride with the formed alcohol catalyzed with these amines. However, attempts to develop this finding as a general procedure have been unsuccessful.

Though cyclohexene and 2,5-norbornadiene were also employable as a borane scavenger,[17] in these cases the isolation of alcohols from the mixture was not so easy.

Although there are several methods available for the reduction of acyl chlorides, we believe that the present method offers considerable advantages in terms of simpleness, functional selectivity, readily available reagents, and very mild conditions.

Experimental

An ethereal solution of $Zn(BH_4)_2$ was prepared from

Table 1. Reduction of Benzoyl Chloride to Benzyl Alcohol with Several Reducing Agents

Reducing agent	Solvent	Reactn conditions: temp (°C)/time (h)	Yield (%)	Ref.
$LiAlH_4$	Ether	Reflux	72	5
$NaBH_4$	Dioxane	100/1—2	76	6
$NaBH(OMe)_3$	Ether	Reflux/4	66	7
Bu_4NBH_4	CH_2Cl_2	−78/0.25	98	8
$NaBH_4$/Alumina	Ether	25/2—4	90	9
$Zn(BH_4)_2$/TMEDA	Ether	40/4.5	95	

Table 2. Reduction of Acyl Chlorides with $Zn(BH_4)_2$/TMEDA

Acyl chloride	Reactn conditions:[a] temp (°C)/time (h)	Product[b]	Yield (%)[c]	Mp (°C) or bp (°C) (mmHg)[d] Found	Reported[Ref]
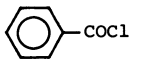	40/4.5	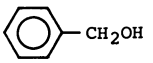	95	101—102(14)	93(10)[10]
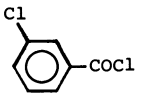	0/0.5[e]	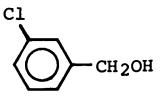	98	59—60(0.9)	119(10)[11]
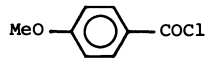	0/0.5	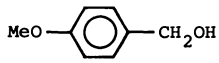	89	99—100(0.6)	134—135(12)[10]
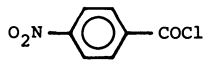	0/0.25[e]	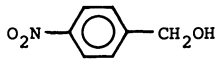	93	91—92	92—93[12]
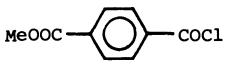	0/0.25[e]	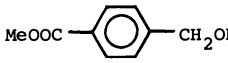	95	49—49.5	49.5—50[13]
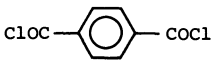	40/24	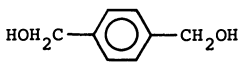	75	115—116	115—116[10]
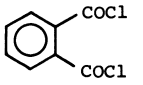	40/4.5	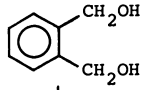	36	62—63	65—66[10]
		+ 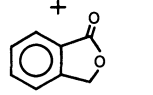	39	72—74	75[10]
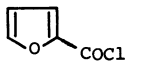	40/72	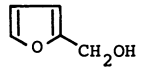	80[f]	66—67(17)	68—69(20)[10]
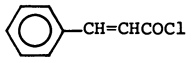	0/0.5[e]	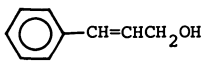	86	94(1.5)	127—128(10)[10]
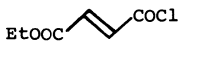	0/0.5	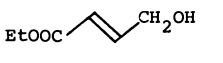	88	96—98(5)	115—120(15)[14]
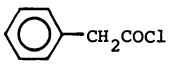	0/0.5	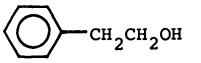	98	113—114(14)	97.4(10)[10]
$CH_3(CH_2)_8COCl$	25/5	$CH_3(CH_2)_8CH_2OH$	96	92—93(1.7)	107—108(7)[10]
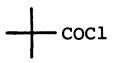	25/2	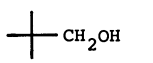	(88)	113—114	114—116[10]
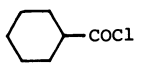	0/6	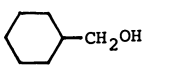	93	85(15)	83(14)[10]

a) Ether as solvent, unless otherwise stated. b) Identified by GLC, IR, ^1H NMR, and high resolution mass spectrometry. c) Yields represent pure isolated products, value in parentheses was determined by GLC. d) Kugelrohr distillation bath temperature. All melting points and boiling points are uncorrected. e) THF/ether as solvent. f) After 92% conversion.

$NaBH_4$ and $ZnCl_2$ according to the literature method;[18] the concentration was determined by injecting aliquots of the solution into water and then measuring the evolved hydrogen.

General Procedure for the Reduction of Acyl Chlorides with $Zn(BH_4)_2$/TMEDA. To a THF or ether solution (1.8 ml) of acyl chloride (1 mmol) at 0 °C were added successively $Zn(BH_4)_2$ (0.21 M†; 6.7 ml, 1.4 mmol) and TMEDA (1 mmol). The mixture was then stirred at 0 °C or at the indicated temperature (see Table 2) until completion of the reaction, as monitored by TLC or GLC analysis. During the reaction, a white insoluble substance was gradually formed. After quenching by the addition of dilute HCl, the mixture was extracted with AcOEt. The extracts were washed with dilute HCl, satd $NaHCO_3$, and satd NaCl, dried ($MgSO_4$), and evaporated. The obtained crude product was filtered in order to remove any insoluble TMEDA·$(BH_3)_2$ complex. Then, the filtrate was purified by distillation or flash column chromatography, providing the corresponding alcohol. All of the products were known compounds and were identified by comparisons with authentic samples.

Reduction of *m*-Chlorobenzoyl Chloride with $Zn(BH_4)_2$/*N,N*-Dimethylaniline. To a THF solution (1.8 ml) of *m*-chlorobenzoyl chloride (175 mg, 1 mmol) at 0 °C were added $Zn(BH_4)_2$ (6.7 ml, 1.4 mmol) and *N,N*-dimethylaniline

† 1 M=1 mol dm^{-3}.

Table 3. Effect of Amine on the Reduction of *m*-Chlorobenzoyl Chloride with $Zn(BH_4)_2$[a]

Amine	Product yield (%)[b]	
	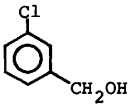	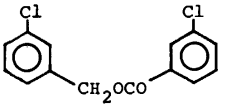
TMEDA[c]	98	—
DABCO[c,d]	93	—
Triethylamine	91	—
Pyridine	83	—
N-Methylmorpholine	86	11
N,*N*-Dimethylaniline[e]	14	81
2,6-Lutidine	18	64

a) All reactions were carried out in ether–THF using 1 equiv of $Zn(BH_4)_2$ and 2 equiv of amine at 0 °C for 30 min unless otherwise stated. b) Isolated yields based on the consumed starting material. c) One equiv of amine was used. d) DABCO = 1,4-diazabicyclo[2.2.2]-octane. e) Reaction time = 40 min.

(0.3 ml, 2 mmol). After stirring for 40 min at this temperature, the excess reagent was quenched by the addition of dilute HCl and extracted with AcOEt. The extracts were washed with dilute HCl, satd $NaHCO_3$, and satd NaCl, dried ($MgSO_4$), and evaporated. The crude product was purified by preparative TLC (hexane:AcOEt= 2:1) to give 114 mg (81 %) of *m*-chlorobenzyl *m*-chlorobenzoate (R_f=0.67) and 20 mg (14 %) of *m*-chlorobenzyl alcohol (R_f=0.40).

***m*-Chlorobenzyl *m*-Chlorobenzoate:** bp 120—121 °C (0.32 mmHg††); IR (neat) 1725, 1600, 1580, 1290, 1280, 1255, 1130, and 750 cm^{-1}; ^1H NMR ($CDCl_3$) δ=5.31 (2H, s), 7.2—7.6 (6H, m), 7.8—8.0 (2H, m); HRMS Found: *m/z* 283.9977 and 280.0032. Calcd for $C_{14}H_{10}O_2Cl_2$: M, 283.9999 and 280.0058.

This work was supported in part by the Ministry of Education, Science and Culture, Grant-in-Aid for Scientific Research (C) (Grant No. 62540410). We also thank Dr. Ayumi Ohsaki of Kinki University for performing the high-resolution mass spectra measurements.

†† 1 mmHg=133.322 Pa.

References

1) a) J. March, "Advanced Organic Chemistry," 3rd ed, Wiley-Interscience, New York, N. Y. (1985), pp. 1093—1120. b) M. Hudlicky, "Reductions in Organic Chemistry," John Wiley & Sons, New York, N. Y. (1984). c) W. Carruthers, "Some Modern Methods of Organic Synthesis," 2nd ed, Cambridge Univ. Press, London (1978), Chap. 7. For reviews see, d) H. C. Brown and S. Krishnamurthy, *Tetrahedron*, **35**, 567 (1979). e) E. R. H. Walker, *Chem. Soc. Rev.*, **5**, 23 (1976).

2) H. Kotsuki, Y. Mori, T. Ohtsuka, H. Nishizawa, M. Ochi, and K. Matsuoka, *Heterocycles*, **26**, 2347 (1987).

3) H. Kotsuki, Y. Ushio, N. Yoshimura, and M. Ochi, *Tetrahedron Lett.*, **27**, 4213 (1986).

4) N. M. Yoon, H. J. Lee, H. K. Kim, and J. Kang, *Taehan Hwahak Hoechi*, **20**, 59 (1976); *Chem. Abstr.*, **85**, 4641n (1976). See also Ref. 1e.

5) R. F. Nystrom and W. G. Brown, *J. Am. Chem. Soc.*, **69**, 1197 (1947).

6) S. W. Chaikin and W. G. Brown, *J. Am. Chem. Soc.*, **71**, 122 (1949).

7) H. C. Brown and E. J. Mead, *J. Am. Chem. Soc.*, **75**, 6263 (1953).

8) D. J. Raber and W. C. Guida, *J. Org. Chem.*, **41**, 690 (1976).

9) E. Santaniello, C. Farachi, and A. Manzocchi, *Synthesis*, **1979**, 912.

10) "CRC Handbook of Chemistry and Physics," 65 th ed, ed by R. C. Weast, CRC Press, Boca Raton, FL (1984—1985).

11) "Beilsteins Handbuch der Organischen Chemie," 4 th ed, Springer-Verlag, Berlin (1966), Vol. 6, III 1555.

12) W. W. Hartman and E. J. Rahrs, *Org. Synth.*, Coll. Vol. III, 652 (1955).

13) J. M. Goldwasser and C. C. Lezmoff, *Can. J. Chem.*, **56**, 1562 (1978).

14) T. Kato and H. Kimura, *Chem. Pharm. Bull.*, **25**, 2692 (1977).

15) Satisfactory microanalyses obtained.

16) H. C. Brown and L. T. Murray, *Inorg. Chem.*, **23**, 2746 (1980).

17) Cf. E. J. Corey and A. G. Myers, *J. Am. Chem. Soc.*, **107**, 5574 (1985).

18) W. J. Gensler, F. A. Johnson, and A. D. B. Sloan, *J. Am. Chem. Soc.*, **82**, 6074 (1960). T. Nakata, Y. Tani, M. Hatozaki, and T. Oishi, *Chem. Pharm. Bull.*, **32**, 1411 (1984).

Dehydrooligopeptides. IX. Syntheses and Conversions of α-Dehydroglutamine Derivatives to *N*-Carboxy-α-dehydroglutamine Anhydride and Δ^1-Dehydroglutaminyldipeptides[1)]

Yasuchika YONEZAWA, Nobuo TAKEFUJI, Nobuyuki TAKAHASHI, and Chung-gi SHIN*
Laboratory of Organic Chemistry, Faculty of Technology, Kanagawa University, Rokkakubashi, Kanagawa-ku, Yokohama 221
(Received January 29, 1988)

Synopsis. Various kinds of Cbz-α-dehydroglutamine derivatives were synthesized by the reaction of Cbz-α-dehydroglutamic acids with a few primary amines, including L-α-amino acid ester, and subsequently transformed to *N*-carboxy-α-dehydroglutamine anhydride and several Δ^1-dehydroglutaminyldipeptides.

In connection with the syntheses and reactions of α-dehydroamino acids (DHA) and dehydrooligopeptides (DHP), *N*-carboxy-α-dehydroamino acid anhydride (ΔNCA), derived by the cyclization of *N*-benzyloxycarbonyl (Cbz)-DHA with $SOCl_2$, were found to be a very important substrate for the transformation to various kinds of other DHA and DHP.[2-4)] So far, we reported on the syntheses of various kinds of ΔNCAs, derived from neutral (alkyl and aryl), acidic, and basic DHAs, which corresponded to the proteinic L-α-amino acid (AA).[5-8)] However, at present, the DHA and its ΔNCA corresponding to α,β-unsaturated derivatives of asparagine and glutamine, for example, α-dehydroglutamine (ΔGln) and its *N*-carboxy-α-dehydroglutamine anhydride (ΔGln·NCA) have never been synthesized.

In this paper, we wish to report on the syntheses of various kinds of Cbz-α-dehydroglutamine derivatives [Cbz-ΔGln(R)-OY: **2** (Y=Bu^t) and **3** (Y=H); **a**; R=H, **b**; R=Bu^t, **c**; R=NHBu^t, **d**; R=CH_2COOMe] and X-ΔGln(Bu^t)·NCA derivatives (**4**; X=H and **5**; X=Boc), by utilizing (*Z*)-isomer of Cbz-α-dehydroglutamic acid *t*-butyl ester (Cbz-ΔGlu-OBu^t) (**1**).[6)] Moreover, the coupling of DHA (**3b**) with an appropriate L-α-AA-OMe was also tried successfully to give the Δ^1-dehydrodipeptides.

The starting compound **1** was derived from α-oxoglutaric acid in six steps, according to a method reported previously.[6)] For the subsequent amidation of γ-carboxyl group of the side chain in ΔGlu, first a treatment of **1** with *N*-hydroxysuccinimide (HOSu) in tetrahydrofuran (THF) was carried out in the presence of *N,N'*-dicyclohexylcarbodiimide (DCC) to form the expected γ-active ester as an intermediate. It was found that the γ-ester, thus yielded, reacted smoothly with aqueous ammonium to give Cbz-α-dehydroglutamine *t*-butyl ester (Cbz-ΔGln-OBu^t) (**2a**) in 86% yield. In a similar manner, the reaction of the active ester with *t*-butylamine was worked up to give Cbz-ΔGln(Bu^t)-OBu^t (**2b**) in 74% yield. Furthermore, the coupling of the above ester with H-AA-OMe, e.g., glycine methyl ester in the presence of both DCC and HOSu also proceeded to give Cbz-ΔGln(CH_2COOMe)-OBu^t (**2d**) in 84% yield. In the case of *t*-butyloxycarbonylhydrazine, however, compound **1** was directly treated in the presence of DCC to give Cbz-ΔGln(NHBoc)-OBu^t (**2c**) in 85% yield.

On the other hand, in order to obtain α-acid free Cbz-ΔGln derivatives, which are anticipated to convert to the corresponding ΔNCA, the α-ester cleavage of ΔGln-OBu^t (**2**) was carried out. When compounds **2a, b, d** were treated, respectively, with gaseous hydrogen chloride in THF or ethyl acetate, the corresponding Cbz-ΔGln-OH derivatives **3a, b, d** were readily obtained in ca. 87% yield.

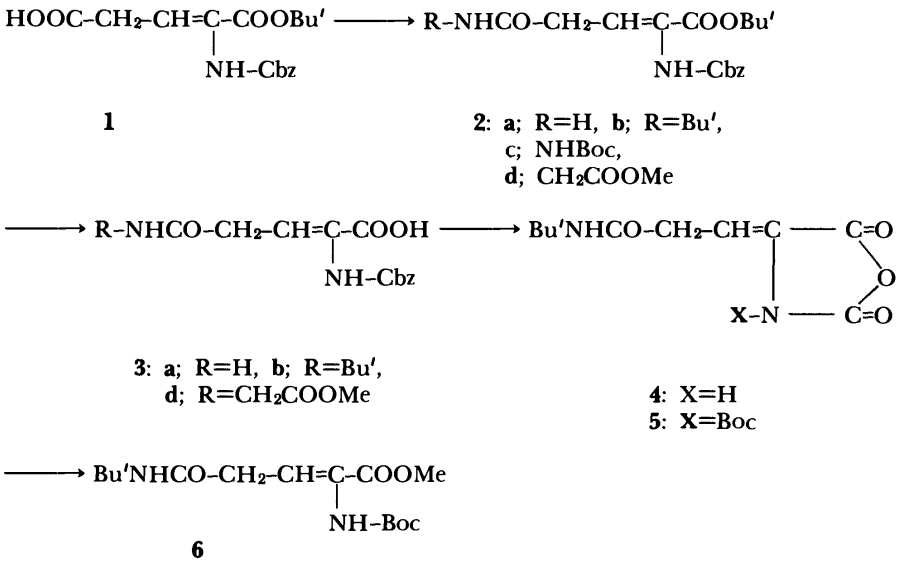

Scheme 1.

Table 1. *N*-Blocked α-Dehydroglutamine Derivatives (**2** and **3**)

Compound[a] No.	Yield %	Mp θ_m/°C	IR, ν/cm^{-1} in KBr -NHCO-	IR, ν/cm^{-1} in KBr -C=C-	^{1}H NMR, δ in $CDCl_3$ -CH= (J/Hz)	^{1}H NMR, δ in $CDCl_3$ -NH- (bs) (J/Hz)
2a	86	145—146[b]	1665	1625	6.64t	6.60
			1540		(7.0)	5.96
2b	74	syrup[c]	1660	1650	6.68t	6.98
			1520		(7.0)	6.43
2c	85	syrup[d]	1685	1650	6.52t	8.70
			1550		(7.0)	7.06, 6.92
2d	84	syrup[c]	1665	1660[f]	6.68t	7.16t
			1520		(7.0)	(7.0)
3a	85	144—145[e]	1660	1620	6.66t	7.47
			1520		(7.0)	7.00
3b	89	160—161[e]	1665	1620	6.56t	8.72
			1540		(7.0)	7.61
3d	85	135—136[c]	1640	1640[g]	6.60t	8.52t
			1515		(7.0)	(7.0)

a) All the compounds were analyzed for C, H, and N, and were within ±0.3% of theoretical values. b) Colorless needles from diisopropyl ether–ethyl acetate. c) Pale yellow. d) Yellow. e) Colorless prisms from diisopropyl ether–ethyl acetate. f) Shoulder. g) Overlapped.

Table 2. (*Z*)-Cbz-ΔGln(Bu^t)-AA-OMe (**7**)

Compound[a] No.	AA	Yield %	Mp θ_m/°C	IR, ν/cm^{-1} in KBr -CONH-	^{1}H NMR, δ in $CDCl_3$ -CH= (J/Hz)	^{1}H NMR, δ in $CDCl_3$ -NH-CH-CO- (J/Hz)	$[\alpha]_D^{20}$ in MeOH (c 1)
7a	Gly	70	syrup[b]	1670	4.49t	4.06d	—
				1540	(7.0)	(7.5)	
7b	Ala	75	syrup[b]	1670	6.34t	4.52dq	−2.5°
				1550	(7.0)	(7.5, 4.5)	
7c	Leu	78	96—97[c]	1670	6.42t	4.64m	−12.6°
				1530	(7.0)		
7d	Phe	73	154—155[c]	1690	6.24t	4.84dt	−6.1°
				1530	(7.0)	(8.0, 5.0)	

a) All the compounds were analyzed for C, H, and N, and were within ±0.3% of theoretical values. b) Colorless. c) Colorless needles from hexane–ethyl acetate.

Subsequently, in order to synthesize the ΔGln·NCA derivative by a method reported previously,[5] compound **3b** was chosen and then treated with $SOCl_2$ to give the desired ΔGln(Bu^t)·NCA (**4**) in 70% yield. Subsequent *N*-acylation of **4** with di-*t*-butyl dicarbonate [$(Boc)_2O$] was carried out to form Boc-ΔGln·NCA (**5**) as an intermediate, which was treated in situ with methanol to give Boc-ΔGln(Bu^t)-OMe (**6**) almost quantitatively, as illustrated in Scheme 1. Consequently, it was found that compound **4** also had a high reactivity with alcohol, such as the hitherto obtained ΔNCA derivatives.[5]

As summarized in Table 1, it can be seen that the yields of **2** and **3** were very high with an average value of 84%. In addition, the spectral data of **2** and **3** show the configurational structure of DHA to be a (*Z*)-isomer remain unchanged during the amidation and consecutive ester cleavage.

Futhermore, according to Scheme 2, the synthesis of Cbz-Δ^1-dehydroglutaminyldipeptides were successfully tried by the usual peptide synthetic method. The coupling of **3b** with an appropriate H-AA-OMe (AA=Gly, Ala, Leu, Phe) was carried out to give

3b + H-AA-OMe ⟶ Cbz-ΔGln(Bu^t)-AA-OMe

7: AA; **a**; Gly, **b**; Ala, **c**; Leu, **d**; Phe

Scheme 2.

Cbz-ΔGln(Bu^t)-AA-OMe (**7**) in a good yield, as summarized in Table 2.

In conclusion, it is firmly believed that the synthesis of the ΔGln·NCA derivative is surely available for the synthesis of various kinds of DHP containing the ΔGln residue.

Experimental

Melting points were determined with a Yamato (Model Mp-21) micro melting-point apparatus, and were not corrected. IR spectra were recorded with a Hitachi EPI-G2 grating spectrometer. ^{1}H NMR spectra were measured with a JEOL JMN PS-100 spectrometer in a $CDCl_3$ solution with tetramethylsilane as the internal standard. The specific rotations were measured in a 0.5-dm tube using a JASCO DIP-4 polarimeter (Japan Spectroscopic Co., Ltd.).

General. To a solution of **1** (45.0 mmol) and HOSu (50.0 mmol) in diethylene glycol dimethyl ether (65 ml) was added portionwise DCC (51.0 mmol) under cooling. After stirring the resulting solution at room temperature for 12 h, the solution was again cooled at 5—10 °C. After removal of the *N,N'*-dicyclohexylurea separated out, the filtrate was concentrated under reduced pressure to give the corresponding active ester as an intermediate, which was utilized for the following amidation.

Preparation of 2a. To a solution of the active ester, thus obtained, in THF (50.0 ml) was added, with stirring, 28% aqueous ammonium (11.0 ml) at −10 °C. After continuing the stirring for 15 min and then at room temperature 15 min, the reaction solution was concentrated under reduced pressure. The residual product was dissolved with chilled ethyl acetate (30.0 ml) and then HOSu deposited was filtered off. The filtrate was further diluted with ethyl acetate (40 ml) and the resultant solution was washed twice with 15% NaCl aqueous solution and then dried over anhydrous Na_2SO_4. After removal of the solvent under reduced pressure, the residual crystals were collected and then recrystallized from diisopropyl ether–ethyl acetate to give **2a** as colorless needles.

Preparation of 2b and 2d. To a solution of the active ester in CH_2Cl_2 (40 ml) was added drop by drop, with stirring, a solution of *t*-butylamine or glycine methyl ester (50.0 mmol) in CH_2Cl_2 (15 ml) under cooling. After stirring for 30 min and then at room temperature for 1 h, the reaction mixture was concentrated under reduced pressure. The residue, thus obtained, was dissolved with chilled ethyl acetate (30 ml) and then HOSu deposited was filtered off. The filtrate was again diluted with ethyl acetate (40 ml) and the resulting solution was washed successively with 10% citric acid, saturated $NaHCO_3$ aqueous solution, and then water and finally dried over anhydrous Na_2SO_4. After removal of the solvent under reduced pressure, the residual syrup was purified on silica-gel column using a mixture of $CHCl_3$ and acetone (20:1 v/v) as the eluent. The fraction was concentrated to give **2b** or **2d** as a pale-yellow syrup.

Preparation of 2c. A solution of **1** (2.7 mmol) in CH_2Cl_2 (10 ml) was cooled at −5 °C and then DCC (3.0 mmol) was added, with stirring, for 30 min. To the resultant solution was added Boc-$NHNH_2$ (3.0 mmol) with stirring; then the reaction solution was stirred continuously at room temperature for 12 h. After removing the solvent and then adding chilled ethyl acetate (5 ml) to the residue, the *N,N'*-dicyclohexylurea deposited was filtered off. The filtrate was diluted with ethyl acetate (15 ml); then the resultant solution was washed successively with 10% citric acid, saturated $NaHCO_3$ aqueous solution, 15% NaCl aqueous solution, and then water and finally dried over anhydrous Na_2SO_4. After concentrating the solution under reduced pressure, the residual syrup was purified on a silica-gel column using a mixture of chloroform and acetone (20:1 v/v) as the eluent. The concentration of the fraction gave **2c** as a yellow syrup.

Preparation of 3a, b, d. A solution of **2** (10.0 mmol) in THF (50 ml) was saturated with HCl gas under cooling and then allowed to stand at room temperature for 1 h. After removing the solvent under reduced pressure, the residual substance was dissolved in $CHCl_3$ (30 ml) and the resultant solution was again concentrated. The crude crystals, thus obtained, were collected by using diisopropyl ether. Recrystallization from diisopropyl ether–ethyl acetate gave **3a, b, d** as colorless prisms.

Preparation of 4. To thionyl chloride (15 ml) was added a suspension of **3b** (5.0 mmol) in diethyl ether (15 ml), drop by drop, with stirring at −10 °C. After stirring vigorously for 30 min at −5—−8 °C. After removing the excess $SOCl_2$ under reduced pressure below 30 °C, the residue, thus obtained, was dissolved in carbon tetrachloride and the resultant solution was again condensed. This procedure was repeated three times and then the final residue, thus obtained, was purified on a silica-gel column using $CHCl_3$ to give crystalline product. Recrystallization from a mixture of benzene and ethyl acetate gave **4** as colorless prisms, yield 75%, mp 150—151 °C. ν_{max}^{KBr} 1840, 1780 (-CO-O-CO-), 1640 (C=C) cm^{-1}. ^1H NMR δ=5.86 (t, 1H, -CH=), 7.62 [s, 1H, -NH- (ring)]. Found: C, 53.28; H, 6.19; N, 12.45%. Calcd for $C_{10}H_{14}N_2O_4$: C, 53.09; H, 6.24; N, 12.38%.

Preparation of 6. To a solution of **4** (2.2 mmol) in THF (8 ml) was added $(Boc)_2O$ (2.6 mmol) and pyridine (30 µl) under cooling. After stirring for 4 h, the solution prepared was treated with methanol (8 ml) and then made to pH 8—9. The reaction mixture was further stirred at room temperature for 12 h and then concentrated under reduced pressure. The residual syrup, thus obtained, was dissolved in ethyl acetate (30 ml) and the resultant solution was washed successively with 10% citric acid, saturated $NaHCO_3$ aqueous solution, and then water, and finally dried over anhydrous Na_2SO_4. After removing the solvent under reduced pressure, the residue, thus obtained, was purified on a silica-gel column using a mixture of $CHCl_3$ and acetone (15:1 v/v) to give **6** as colorless syrup. Yield 95%. ν_{max}^{KBr} 1650, 1545 (-NHCO-), 1640 (C=C) cm^{-1}. ^1H NMR δ=6.56 (bs, 1H, 2 -NH-), 6.74 (t, 1H, -CH=). Found: C, 57.22; H, 8.53; N, 9.07%. Calcd for $C_{15}H_{26}N_2O_5$: C, 57.31; H, 8.34; N, 8.91%.

Preparation of 7. A suspension of an appropriate H-AA-OMe·HCl (1.80 mmol) in THF (6 ml) in the presence of TEA (1.80 mmol) was stirred under cooling for 30 min. To the prepared suspension was successively added **3b** (1.50 mmol), HOSu (1.70 mmol), and DCC (1.70 mmol); the resulting solution was returned to room temperature and then stirred for 2 h. After removing the solvent under reduced pressure, ethyl acetate (15 ml) was added to the residue obtained and the resultant solution was chilled and then filtered. The filtrate was washed successively with 10% citric acid, saturated $NaHCO_3$ aqueous solution, and water and then dried over anhydrous Na_2SO_4. After concentrating the solution under reduced pressure, the residual crystalline product was collected by using diisopropyl ether. Recrystallization from a mixture of hexane and ethyl acetate gave colorless needles. When the residue was syrup, purification on a silica-gel column using a mixture of $CHCl_3$ and ethyl acetate gave **7** as a colorless syrup. See Table 2.

References

1) Part VIII. C. Shin, Y. Yonezawa, T. Obara, and H. Nishio, *Bull. Chem. Soc. Jpn.*, **61**, 885 (1988).
2) C. Shin, Y. Yonezawa, and J. Yoshimura, *Chem. Lett.*, **1981**, 1635.
3) C. Shin, T. Yamada, and Y. Yonezawa, *Tetrahedron Lett.*, **24**, 2175 (1983).
4) C. Shin, Y. Yonezawa, and M. Ikeda, *Bull. Chem. Soc. Jpn.*, **59**, 3573 (1986).
5) C. Shin, Y. Yonezawa, and T. Yamada, *Chem. Pharm. Bull.*, **32**, 3934 (1984).
6) C. Shin, Y. Yonezawa, and E. Watanabe, *Tetrahedron Lett.*, **26**, 85 (1985).
7) C. Shin. Y. Yonezawa, and T. Obara, *Heterocycles*, **24**, 1561 (1986).
8) C. Shin, T. Obara, S. Segami, and Y. Yonezawa, *Tetrahedron Lett.*, **28**, 3827 (1987).

Electrophilic and Nucleophilic Substitutions of 2-Amino- and 2-Hydroxy-1,3-diazaazulenes

Seiji EBINE,* Kazuko TAKAHASHI,† and Tetsuo NOZOE††
Department of Chemistry, Faculty of Science, Saitama University, Urawa 338
†Department of Chemistry, Faculty of Science, Tohoku University, Sendai 980
††Tokyo Research Laboratories, Kao Corporation, Bunka, Sumida-ku, Tokyo 131
(Received February 2, 1988)

Synopsis. 2-Amino- (**2**) and 2-hydroxy-1, 3-diazaazulenes (**3**) underwent smoothly electrophilic bromination under basic conditions to give 2-amino-4,6,8-tribromo- (**4**) and 6-bromo-2-hydroxy-1,3-diazaazulenes (**7**), respectively. Bromo derivatives **4** and **7** underwent some nucleophilic substitutions, e.g., **4** reacted with ease with sodium methoxide to give 2-amino-4,6,8-trimethoxy-1,3-diazaazulene (**10**).

1,3-Diazaazulene (cycloheptimidazole) (**1**) and its derivatives are of theoretical interest in relation to the structural chemistry of nonbenzenoid aromatics and of biological interest in relation to naturally occurring cycloheptimidazole derivatives such as zoanthoxanthin[1a] epizoanthoxanthin,[1b] and paragracine.[1c]

1,3-Diazaazulene (**1**) would be difficult of undergoing an electrophilic substitution, because **1** has a large contribution of dipolar structure (**1a**) to the ground state[2] causing an enhanced diatropicity of the seven-membered ring and moreover the electron-rich 1- and 3-positions are blocked by nitrogen atoms. In fact it has been reported that, on treatment with bromine in chloroform or acetic acid, **1**,[3] 2-amino- (**2**),[4] and 6-amino-1,3-diazaazulene[5] give the corresponding diazaazulene-bromine molecular compounds which easily decompose regenerating respective starting diazaazulenes without giving any bromo-substituted product. There has appeared only one paper dealing with the electrophilic substitution in which 2-dimethylamino-1,3-diazaazulene affords brominated products in chloroform but in very poor yields.[6a] Most derivatives of **1**, therefore, have to be synthesized by condensation of the corresponding substituted 2-chloro- or 2-methoxytropones with guanidine or thiourea.[3,4,6-8] However, we have presumed that **2** and 2-hydroxy-1,3-diazaazulene (**3**),[3] carrying an electron-donating substituent at the 2-position and being in equilibrium with imino (**2a**) and keto (**3a**) forms,[9] respectively, may undergo effectively electrophilic substitutions at the seven-membered ring if any suitable reaction conditions are explored.[10] In order to clarify the fundamental reactivities of **2** and **3**, and to develop a new synthetic method for the preparation of 1,3-diazaazulene derivatives, we have now carried out a brief study on the electrophilic and nucleophilic substitution reactions of **2** and **3**, which is dealt with herein.

When 2-amino-1,3-diazaazulene (**2**) was allowed to react with an excess amount of bromine (4 molar equivalents) in pyridine solution at room temperature, 2-amino-4,6,8-tribromo-1,3-diazaazulene (**4**) was formed in good yield.[11] Even when a lesser amount of bromine was employed in this reaction, the same tribromo compound **4** was obtained in low yield, neither monobromo- nor dibromo-substituted product being obtained. The position of the bromo substituents of **4** is elucidated by the ^{1}H NMR spectrum which showed only one singlet in the region of the ring protons, and further by the formation of **4** on bromination of known compounds **5**[6b,12] and **6**[7] in pyridine.

The bromination of **3** in aq sodium hydroxide solution gave 6-bromo-2-hydroxy-1,3-diazaazulene (**7**) in moderate yield. Contrary to the case of **2**, neither dibromo- nor tribromo-substituted product of **3** was produced even when an excess amount of bromine was applied. The position of the bromo substituent of **7** was evidenced by the A_2B_2 type of signals in the ^{1}H NMR spectrum and by the fact that **7** was converted to known **11**[7] (vide post).

It has also been known that the substituent at the seven-membered ring of **5**[6b,12] and **6**[7] undergoes nucleophilic substitution, which is quite reasonable on considering the significant contribution of **1a** to the ground state of **1**. In order to obtain a further insight into the influence of an electron-donating amino or hydroxyl group on nucleophilic substitution, the solvolysis of **4** and **7** was then examined. When an aq acetic acid solution of **4** was heated to reflux, 2-amino-4,6-dibromo-8-hydroxy-1,3-diazaazuene (**8**) was formed in moderate yield. The ^{1}H NMR of **8** showed two unequivalent signals in the region of ring protons and the catalytic hydrogenation of **8** over Pd-C gave a known debrominated compound **9**,[6b,12] elucidating the structure of **8**. This fact indicates that **4** is attacked by a nucleophile first at the 4- (or 8-) position, presumably via the intermediate formation of a hydrogen-bonded chelate bridge among the nucleophile, protonated N-1 and electropositive C-8.[13] More interestingly when a methanolic solution of **4** was refluxed with sodium methoxide, 2-amino-4,6,8-trimethoxy-1,3-diazaazulene (**10**) was formed in good yield. The ^{1}H NMR spectrum of **10** showed only one singlet for the seven-membered ring protons (H-5,7). It is worthy of special notice that all the bromo substituents of **4** are easily replaced by the nucleophile even under the influence of the electron-donating 2-amino group. Similarly, reflux of an aq acetic acid solution of **7** afforded **11**.[7]

As a consequence, it has been proved that, although 1,3-diazaazulene (**1**) is electron-deficient at the seven-membered ring, the derivatives of **1** carrying an electron-donating amino or hydroxyl group at the 2-position, e.g., **2** and **3**, are reactive enough to undergo smooth electrophilic bromination under basic conditions, and that bromo-substituted 2-amino- and 2-

hydroxy-1,3-diazaazulenes, e.g., **4** and **7**, are capable of undergoing nucleophilc substitution with considerable ease under both acidic and basic conditions (despite the electron-donating influence of the 2-substituent).

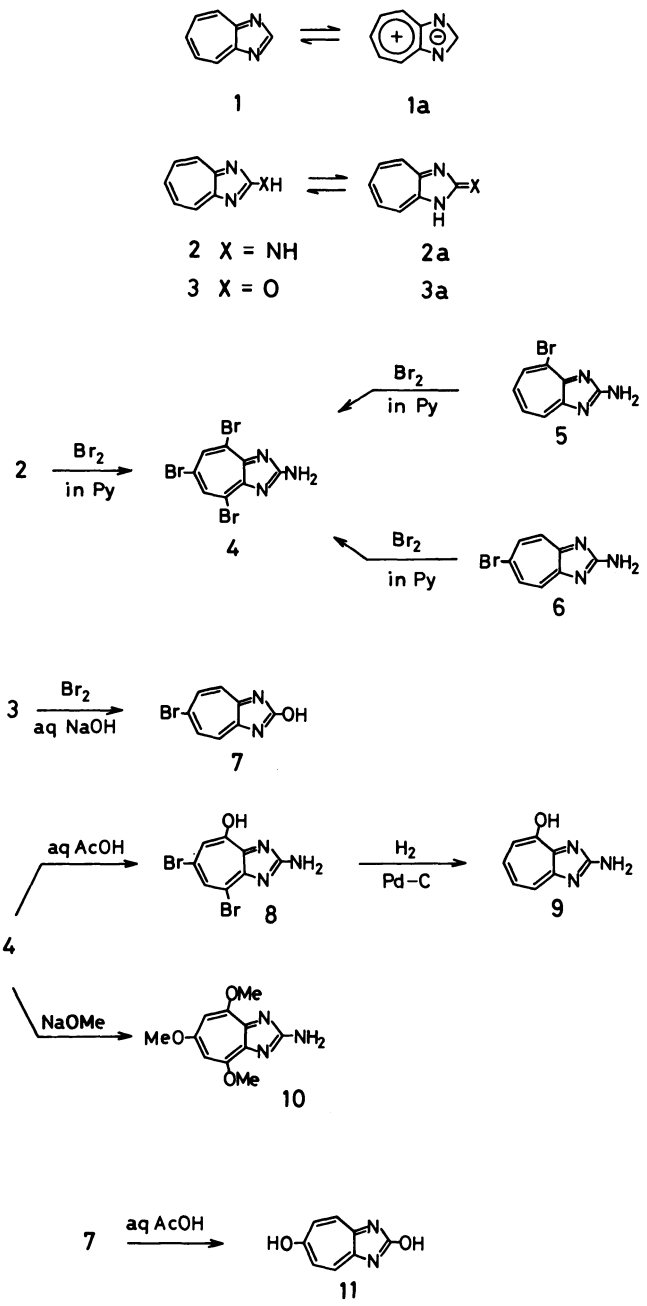

Experimental

2-Amino-4,6,8-tribromo-1,3-diazaazulene (4). a) Bromination of 2-Amino-1,3-diazaazulene (2): Into a suspension of 2[4] (1 g, 6.89 mmol) in pyridine (40 ml) was dropped a solution of bromine (6.9 g, 42 mmol) in pyridine (10 ml) at room temperature in a 10 min period, during which time the suspension went into solution and then a yellow powder precipitated again. After being diluted with water (20 ml), the precipitate was collected and washed with methanol to give crude **4**, yellow powder (2.1—2.3 g, 80—87% yield). An analytical sample of **4** was obtained by recrystallization from pyridine as yellow needles, mp>350°C. IR (KBr) 3340, 3130, 1685, 1522, 1508, 1362, 1010, 879 (m), 843, 830 cm^{-1}. ^1H NMR (CF_3COOH) δ=9.10 (2H, s, H-5,7), 7.6 (br. $\overset{+}{N}H_3$). Found: C, 25.05; H, 1.35; N, 10.75%. Calcd for $C_8H_4N_3Br_3$: C, 25.16; H, 1.06; N, 11.01%.

b) Bromination of 2-Amino-4-bromo-(5) and 2-Amino-6-bromo-1,3-diazaazulene (6): A suspension of 5[6b,12] or 6[7] (200 mg, 0.893 mmol) in pyridine (10 ml) was treated with a solution of bromine (430 mg, 2.7 mmol) in pyridine (1 ml). The same work-up as described in a) afforded **4** (240—260 mg, 70—75% yield).

6-Bromo-2-hydroxy-1,3-diazaazulene (7). Into a solution of 3[3] (200 mg, 1.37 mmol) in 0.2 M sodium hydroxide (8 ml) (1 M=1 mol dm^{-3}) was dropped a solution of bromine (440 mg, 2.75 mmol) in 2 M sodium hydroxide (3 ml) at room temperature. Neutralization with dilute hydrochloric acid gave a precipitate, which was collected and recrystallized from saturated sodium hydrogencarbonate solution to give **7** (160 mg, 51.9% yield) as a yellow crystalline powder, mp>330 °C. Soluble in both dilute hydrochloric acid and dilute alkali. IR (KBr) 3450, 3020 2600, 1695, 1618, 1590, 1542 (m), 1467, 1430, 1387, 1355, 1322, 1295, 1055 (m), 955 848, 780 cm^{-1}. ^1H NMR (CF_3COOH) δ=8.98 (2H, d, J=10.5 Hz, H-5,7 or H-4,8), 8.51 (2H, d, J=10.5 Hz, H-4,8 or H-5,7). Found: C, 42.96; H, 2.29; N, 12.27%. Calcd for $C_8H_5ON_2Br$: C, 42.70; H, 2.24; N, 12.45%.

2-Amino-4,6-dibromo-8-hydroxy-1,3-diazaazulene (8). A suspension of **4** (500 mg, 1.31 mmol) in 95% acetic acid (50 ml) was refluxed for 3 h. The resulting solution was concentrated, diluted with water and a precipitate which separated was collected and recrystallized from glacial acetic acid (50 ml) to give **8**, yellow fibrous needles (260 mg, 62.2% yield), mp>320 °C. IR (KBr) 3430, 3095, 1978, 1580 (m), 1550, 1520 (m), 1490, 1393 (m), 1286, 913 (m) cm^{-1}. ^1H NMR (CF_3COOH) δ=8.31 (1H, d, J=1.3 Hz, H-5), 8.15 (1H, d, J=1.3 Hz, H-7), 7.6 (br. $\overset{+}{N}H_3$). Found: C, 30.21; H, 1.57; N, 13.30%. Calcd for $C_8H_5ON_3Br_2$: C, 30.12; H, 1.58; N, 13.18%.

Debromination of 8 to 2-Amino-4-hydroxy-1,3-diazaazulene (9). A solution of **8** (100 mg, 0.314 mmol) in 5% potassium hydroxide (20 ml) was shaken with hydrogen over 5% Pd-charcoal (50 mg) and 2 equivalents (14 ml) of hydrogen were uptaken. Usual work-up gave pale yellow needles of **9** (40 mg, 79% yield), identical in all respects with an authentic sample.[6b,12]

2-Amino-4,6,8-trimethoxy-1,3-diazaazulene (10). Compound **4** (500 mg, 1.31 mmol) was suspended in a sodium methoxide solution prepared from sodium (92 mg, 0.004 atom) and anhydrous methanol (40 ml) and then refluxed for 2.5 h. The methanol was evaporated and the residue was recrystallized from water (10 ml) to give **10** (250 mg, 66.0% yield), deep yellow needles, dp 240—245 °C. IR (KBr) 3370, 3300, 3120, 1643, 1610, 1563, 1515, 1458 (m), 1422 (m), 1378, 1250, 1208 (m), 1073 (m), 990, 839 (m), 778 (w) cm^{-1}. ^1H NMR (CF_3COOH) δ=4.34 (3H, s, OMe-6), 4.42 (6H, s, OMe-4,8), 7.40 (2H, s, H-5,7), 7.90 (br. $\overset{+}{N}H_3$). Found: C, 45.63; H, 6.39; N, 14.89%. Calcd for $C_{11}H_{13}O_3N_3 \cdot 3H_2O$: C, 45.63; H, 6.62; N, 14.53%.

2,6-Dihydroxy-1,3-diazaazulene (11). A suspension of **7** (200 mg, 0.889 mmol) in 95% acetic acid (20 ml) was refluxed for 3 h. Concentration of the resulting solution and recrystallization of a separated precipitate from water afforded **11** (110 mg, 68.7% yield) as yellow fibrous needles, entirely identical with an authentic sample.[7]

The authors are grateful to Assistant Professor Juzo Nakayama for his technical assistance.

References

1) a) L. Cariello, S. Crescenzi, G. Prota, S. Capasso, F. Giordana, and L. Mazzarella, *Tetrahedron*, **30**, 3281 (1974). b) L. Cariello, S. Crescenzi, G. Prota, and L. Zanetti, *ibid.*, **30**, 4191 (1974). c) Y. Komoda, S. Kaneko, M. Yamamoto, M. Ishikawa, A. Itai, and Y. Iitaka, *Chem. Pharm. Bull.*, **23**, 2464 (1975).

2) Dipole moment of 1,3-diazaazulene, 4.03 D. Y. Kurita and M. Kubo, *J. Am. Chem. Soc.*, **79**, 5460 (1957).

3) T. Nozoe, T. Mukai, I. Murata, *J. Am. Chem. Soc.*, **76**, 3352 (1954).

4) T. Nozoe, T. Mukai, K. Takase, I. Murata, K. Matsumoto, *Proc. Jpn. Acad.*, **29**, 452 (1953).

5) T. Nozoe, M. Sato, S. Ito, and K. Matsui, *Proc. Jpn. Acad.*, **29**, 565 (1953).

6) a) H. Nakao and G. Sugawara, *Chem. Pharm. Bull.*, **13**, 465 (1965). b) H. Nakao, N. Soma, Y. Sato, and G. Sugawara, *ibid.*, **13**, 473 (1965).

7) T. Nozoe, T. Mukai, T. Asao, *Bull. Chem. Soc. Jpn.*, **35**, 1188 (1962).

8) K. Kikuchi and T. Muroi, *Nippon Kagaku Zassi*, **77**, 1081 (1956) [*Chem. Abstr.*, **53**, 5250 (1959)]. T. Muroi, *ibid.*, **77**, 1084 (1956) [*Chem. Abstr.*, **53**, 5249 (1959)]. H. Akino, K. Sato, and Y. Suzuki, *Sci. Repts. Tohoku Univ., First Ser.*, **40**, 92 (1956) [*Chem. Abstr.*, **51**, 17948 (1957)].

9) T. Nozoe, T. Mukai, and I. Murata, *Proc. Jpn. Acad.*, **30**, 482 (1954). I. Murata, *Sci. Repts. Research Insts. Tohoku Univ.*, Ser. A, **12**, 271 (1960) [*Chem. Abstr.*, **55**, 519 (1961)].

10) Treatment of diethyl 2-amino- and 2-hydroxyazulene-1,3-dicarboxylates with bromine in chloroform or acetic acid gave the corresponding 6-bromo-substituted products. T. Nozoe, S. Seto, and S. Matsumura, *Bull. Chem. Soc. Jpn.*, **35**, 1990 (1962). T. Nozoe, T. Asao, and M. Oda, *ibid.*, **47**, 681 (1974).

11) Attempted condensation of 3,5,7-tribromo-2-methoxytropone with guanidine in the presence of potassium hydroxide failed to give desired **4** due to steric hindrance, but produced a rearranged product, methyl 2,4,6-tribromobenzoate.

12) K. Matsumoto, Master's Thesis, Tohoku Univ., 1955.

13) Supposed intermediate.

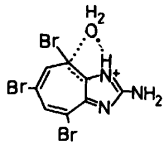

Hydrostannation and Hydrogermylation of Allenes

Yoshifumi ICHINOSE, Koichiro OSHIMA,* and Kiitiro UTIMOTO
Department of Industrial Chemistry, Faculty of Engineering, Kyoto University, Yoshida, Kyoto 606
(Received February 26, 1988)

Synopsis. Treatment of allenes with Ph_3SnH or Ph_3GeH in the presence of $Pd(PPh_3)_4$ catalyst provides the corresponding allylic stannanes or allylic germanes in good yields. Et_3B induced radical addition of Ph_3SnH or Ph_3GeH to allenes are also described.

Previously reported reaction of Ph_3SnH or Ph_3GeH with acetylenic compounds in the presence of a catalytic amount of palladium[1] or Et_3B[2] affords a simple and general access to the corresponding vinylic triphenylstannanes or vinylic triphenylgermanes. In furhter extension of these techniques, we have examined the reaction of allenic compounds with Ph_3SnH or Ph_3GeH.

Treatment of allenic compounds with triphenylstannane or triphenylgermane[3] in the presence of a catalytic amount of $Pd(PPh_3)_4$ resulted in exclusive formation of allylic triphenylstannanes or allylic triphenylgermanes. The typical results are summarized in Table 1. We are tempted to assume the following reaction mechanism: (1) Oxidative addition of Ph_3SnH (Ph_3GeH) to Pd(0), (2) stannylpalladation (germylpalladation) to give vinylpalladium, and (3) reductive elimination to produce allylic stannanes (allylic germanes) and regenerate the palladium(0) (Scheme 1). Palladium always attacked the central carbon of allenic linkage and Ph_3Sn (Ph_3Ge) group added to end carbon in the stannylpalladation (germylpalladation) step. The distribution of two regioisomeric products, allylic stannanes or allylic germanes,

Table 1. Hydrostannation and Hydrogermylation of Allenes

Entry	Allene	Ph_3SnH (Ph_3GeH)	Catalyst	Product (Yield/%)
1	$CH_2=C=CH_2$[a]	Ph_3SnH	$Pd(PPh_3)_4$	$CH_2=CHCH_2SnPh_3$ (40) **5**
2		Ph_3GeH	$Pd(PPh_3)_4$	$CH_2=CHCH_2GePh_3$ (88) **6**
3		Ph_3SnH	Et_3B	**5** (36) $CH_2=C(Me)SnPh_3$ (24)
4		Ph_3GeH	Et_3B	**6** (57)
5	n-$C_{10}H_{21}CH=C=CH_2$	Ph_3GeH	$Pd(PPh_3)_4$	n-$C_{10}H_{21}CH(GePh_3)CH=CH_2$ (53)
6		Ph_3SnH	Et_3B	n-$C_{10}H_{21}CH=C(Me)SnPh_3$ **7** (E/Z=3/2, 51) n-$C_{10}H_{21}CH_2C(SnPh_3)=CH_2$ **8** (10) n-$C_{10}H_{21}CH=CHCH_2SnPh_3$ **9** (5)
7		Ph_3GeH	Et_3B	n-$C_{10}H_{21}CH=CHCH_2GePh_3$ (82)
8	$PhCH=C=CH_2$	Ph_3SnH	$Pd(PPh_3)_4$	$PhCH_2CH=CHSnPh_3$ (100)
9	$PhMe_2SiCH=C=CH_2$	Ph_3SnH	$Pd(PPh_3)_4$	$PhMe_2SiCH=CHCH_2SnPh_3$ (40)
10		Ph_3GeH	$Pd(PPh_3)_4$	$PhMe_2SiCH=CHCH_2GePh_3$ **10** (57) $PhMe_2SiCH(GePh_3)CH=CH_2$ **11** (38)
11		Ph_3SnH	Et_3B	$PhMe_2SiCH_2C(SnPh_3)=CH_2$ **12** (62) $PhMe_2SiCH=C(Me)SnPh_3$ **13** (33)
12		Ph_3GeH	Et_3B	**10** (69) $PhMe_2SiCH=C(Me)GePh_3$ **14** (28)
13	6,7-Tridecadiene	Ph_3GeH	$Pd(PPh_3)_4$	n-$C_5H_{11}CH=CHCH(GePh_3)$-C_5H_{11} (79)
14		Ph_3SnH	Et_3B	n-$C_5H_{11}CH=C(SnPh_3)CH_2$-$C_5H_{11}$ (E/Z=32/68, 81)
15	1,2-Cyclononadiene	Ph_3SnH	Et_3B	1-(Triphenylstannyl)cyclononene (74)

a) Excess (3.0 mmol) of 1,2-propadiene was employed. Yields were based on an amount of Ph_3SnH (or Ph_3GeH) employed.

depended on the nature of the substitution pattern of the starting allenic compounds. For instance, hydrogermylation of 1,2-tridecadiene afforded 3-triphenylgermyl-1-tridecene selectively, while 1-dimethylphenylsilyl-1,2-propadiene gave a mixture of 1-dimethylphenylsilyl-3-triphenylgermyl-1-propene and 3-dimethylphenylsilyl-3-triphenylgermyl-1-propene upon treatment with Ph_3GeH–Pd(0).

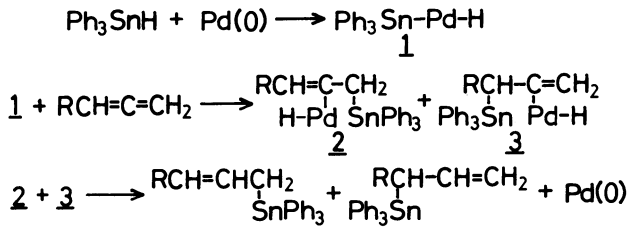

Scheme 1.

The formation of (*Z*)-3-phenyl-1-triphenylstannyl-1-propene from 1-phenyl-1,2-propadiene presumably is explained by the following reaction path: Elimination of palladium hydride from vinylpalladium species **4** and subsequent readdition in the opposite end of 1,2-diene, followed by reductive elimination (Scheme 2). The exclusive generation of (*Z*)-olefin as a single stereoisomer may be ascribed to the selective readdition of Pd–H to $PhCH{=}C{=}CHSnPh_3$ from less hindered face.

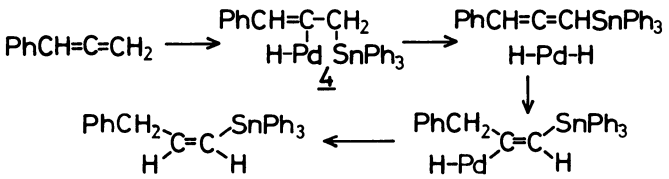

Scheme 2.

On the other hand, triphenylstannyl radical attacked allenes at the center carbon of monosubstituted allenes, $RCH{=}C{=}CH_2$, or disubstituted ones, $RCH{=}C{=}CHR$ to give vinylic stannanes selectively,[4] in the case of Et_3B induced radical reaction. With unsubstituted 1,2-propadiene, triphenylstannyl radical added to both end and middle carbons to give a mixture of allyltriphenylstannane and 2-triphenylstannyl-1-propene. Triphenylgermyl radical was less reactive than triphenylstannyl radical and disubstituted allenes were reluctant to react with Et_3B–Ph_3GeH system. Reaction of unsubstituted or monosubstituted allenes afforded allylic germanes selectively.

Experimental

The IR spectra were determined on a JASCO IR-810 spectrometer, the ^1H NMR and ^{13}C NMR spectra were recorded on a Varian XL-200 spectrometer. The chemical shifts of the proton NMR are given in δ with TMS as an internal standard. The analyses were performed at the Elemental Analyses Center of Kyoto University. Tetrahydrofuran was dried in benzophenone ketyl and distilled.

General Procedure for the Reaction of Allenic Compounds with Triphenylstannane (or Triphenylgermane) in the Presence of $Pd(PPh_3)_4$. The reaction of 1,2-tridecadiene with Ph_3GeH is representative. $Pd(PPh_3)_4$ (58 mg, 0.05 mmol) was added to a solution of 1,2-tridecadiene (0.18 g, 1.0 mmol) and Ph_3GeH (0.37 g, 1.2 mmol) in tetrahydrofuran (10 ml) under an argon atmosphere. The reaction mixture was stirred at 25 °C for 5 h, then poured into water, and extracted with ethyl acetate (3×20 ml). The combined organic extracts were dried (Na_2SO_4) and concentrated in vacuo. Purification by preparative TLC on silica gel provided 3-triphenylgermyl-1-tridecene (0.26 g) in 53% yield: IR (neat) 3066, 3048, 2994, 2922, 2850, 2034, 1484, 1431, 1091, 998, 732, 697 cm^{-1}; ^1H NMR ($CDCl_3$) δ=0.88 (t, *J*=6.5 Hz, 3H), 1.06—1.44 (m, 16H), 1.55—1.83 (m, 2H), 2.60—2.78 (m, 1H), 4.90—5.03 (m, 2H), 5.80 (m, 1H), 7.28—7.43 (m, 9H), 7.43—7.61 (m, 9H); ^{13}C NMR ($CDCl_3$) δ=14.1, 22.7, 29.0, 29.1, 29.3, 29.5, 29.6, 29.9, 31.9, 34.5, 113.6, 128.0, 128.8, 135.5, 136.3, 139.6.

General Procedure for the Et_3B-Induced Radical Reaction of Ph_3SnH (or Ph_3GeH) with Allenes. The reaction of 1,2-tridecadiene with Ph_3GeH is representative. A hexane solution of Et_3B (1.0 M, 1 M=1 mol dm^{-3}, 1.2 ml, 1.2 mmol) was added to a solution of Ph_3GeH (0.37 g, 1.2 mmol) and 1,2-tridecadiene (0.18 g, 1.0 mmol) in benzene (10 ml) at 25 °C. After stirring for 2 h at 25 °C, the reaction mixture was poured into water and extracted with ethyl acetate. Purification by preparative tlc gave (*E*)-1-triphenylgermyl-2-tridecene (0.40 g, 82% yield) as a colorless oil: IR (neat) 3064, 3048, 2920, 2850, 1654, 1484, 1465, 1431, 1091, 1026, 998, 963, 732, 696 cm^{-1}; ^1H NMR ($CDCl_3$) δ=0.88 (t, *J*=6.1 Hz, 3H), 1.04—1.45 (m, 16H), 1.79—1.99 (m, 2H), 2.40 (d, *J*=7.4 Hz, 2H), 5.35 (dt, *J*=15.2, 6.4 Hz, 1H), 5.51 (dt, *J*=15.2, 7.4 Hz, 1H), 7.30—7.44 (m, 9H); ^{13}C NMR ($CDCl_3$) δ=13.7, 19.5, 22.7, 29.1, 29.4, 29.6, 29.9, 30.0, 31.9, 32.7, 125.1, 128.1, 128.9, 131.0, 135.0, 136.9. Found: C, 77.12; H, 8.66%. Calcd for $C_{31}H_{40}Ge$: C, 76.73; H, 8.31%.

Allyltriphenylstannane, 2-Triphenylstannyl-1-propene, Allyltriphenylgermane. The reaction of 1,2-propadiene[5] with Ph_3SnH (Ph_3GeH) gave the title compounds whose spectral data were identical with the authentic samples.[6,7]

(*Z*)-2-Triphenylstannyl-2-tridecene (7Z), (*E*)-2-Triphenylstannyl-2-tridecene (7E), and 2-Triphenylstannyl-1-tridecene (8) (a 35:50:15 Mixture): IR (neat) 3062, 3046, 2922, 2850, 1637, 1480, 1458, 1429, 1074, 1022, 997, 726, 697 cm^{-1}; ^1H NMR ($CDCl_3$) δ=0.89 (t, *J*=6.0 Hz, 3H), 1.06—1.50 (m, 16.3H), 1.86—2.08 (m, 2.5H, $=CCH_3$ (**7E**) and $=CCH_2$ (**7E**)), 2.13—2.31 (m, 1.75H, $=CCH_3$ (**7Z**) and $=CCH_2$ (**7Z**)), 2.36—2.48 (m, 0.3H, $=CCH_2$ (**8**)), 5.08—5.12 (m, 0.15H, $=CH_2$ (**8**)), 5.78—5.89 (m, 0.5H, =CH (**7E**)), 5.94—5.99 (m, 0.15H, $=CH_2$ (**8**)), 6.33—6.43 (m, 0.35H, =CH (**7Z**)), 7.31—7.52 (m, 9H), 7.52—7.77 (m, 6H); ^{13}C NMR ($CDCl_3$) δ=14.2, 22.7, 28.6, 29.4, 29.6, 29.7, 32.0, 33.3, 116.9, 128.5, 128.6, 128.8, 128.89, 128.93, 136.8, 137.1, 137.2, 138.8, 143.1. Found: C, 70.09; H, 7.68%. Calcd for $C_{31}H_{40}Sn$: C, 70.07; H, 7.59%.

(*E*)-1-Triphenylstannyl-2-tridecene (9). The compound was separated from other three isomers (**7E**, **7Z**, **8**) by preparative thin layer chromatography in pure form. ^1H NMR ($CDCl_3$) δ=0.89 (t, *J*=6.0 Hz, 3H), 1.06—1.50 (m, 16H), 1.85—2.04 (m, 2H), 2.41 (d, *J*=8.0 Hz, 2H), 5.31—5.58 (m, 1H), 5.58—5.80 (m, 1H), 7.31—7.52 (m, 9H), 7.52—7.77 (m, 6H).

(*Z*)-1-Triphenylstannyl-3-phenyl-1-propene: Mp 69 °C; IR (KBr) 3060, 3014, 2986, 1636, 1494, 1481, 1429, 1075, 1045, 1022, 997, 959, 749, 727, 696 cm^{-1}; ^1H NMR ($CDCl_3$) δ=2.62 (d, *J*=7.9 Hz, 2H), 6.33 (d, *J*=15.7 Hz, 1H), 6.49 (dt, *J*=15.7, 7.9 Hz, 1H), 7.09—7.34 (m, 5H), 7.34—7.51 (m, 9H), 7.51—7.78 (m, 6H); ^{13}C NMR ($CDCl_3$) δ=17.6, 125.5, 126.2, 127.7,

128.1, 128.4, 128.6, 129.1, 137.1, 138.2, 138.3. Found: C, 69.14; H, 5.01%. Calcd for $C_{27}H_{24}Sn$: C, 69.41; H, 5.18%.

1-Dimethylphenylsilyl-3-triphenylstannyl-1-propene: IR (neat) 3062, 2950, 1597, 1429, 1247, 1111, 1075, 997, 843, 822, 726, 697 cm^{-1}; ^1H NMR ($CDCl_3$) δ=0.20 (s, 6H), 2.59 (dd, J=8.2, 1.1 Hz, 2H), 5.66 (dt, J=18.2, 1.1 Hz, 1H), 6.34 (dt, J=18.2, 8.2 Hz, 1H), 7.20—7.46 (m, 12H), 7.46—7.95 (m, 8H); ^{13}C NMR ($CDCl_3$) δ=—2.4, 21.7, 124.8, 127.6, 128.5, 128.6, 129.0, 129.1, 133.8, 137.1, 137.2, 138.2. Found: C, 66.09; H, 5.60%. Calcd for $C_{29}H_{30}SiSn$: C, 66.30; H, 5.76%.

A Mixture of 1-Dimethylphenylsilyl-3-triphenylgermyl-1-propene (10) and 3-Dimethylphenylsilyl-3-triphenylgermyl-1-propene (11) (a 61:39 Mixture): IR (neat) 3064, 3044, 2952, 1604, 1485, 1430, 1248, 1113, 1091, 827, 732, 697 cm^{-1}; ^1H NMR ($CDCl_3$) δ=—0.01 (s, 3.66H, Me_2Si (**10**)), 0.18 (s, 2.34H, Me_2Si (**11**)), 0.98 (d, J=12 Hz, 0.39H, CH (**11**)), 2.58 (dd, J=1.2, 8.0 Hz, 1.22H, CH_2 (**10**)), 4.82 (dd, J=2.0, 16.5 Hz, 0.39H, =CH_2 (**11**)), 4.86 (dd, J=2.0, 10.0 Hz, 0.39H, =CH_2 (**11**)), 5.65 (dt, J=18.4, 1.3 Hz, 0.61H, =CHSi (**10**)), 5.88 (ddd, J=10.0, 12.0, 16.5 Hz, 0.39H, =CH (**11**)), 6.20 (dt, J=18.4, 8.0 Hz, 0.61H, =CH (**10**)), 5.68—6.08 (m, 20H); ^{13}C NMR ($CDCl_3$) δ=—2.0, 24.6, 25.0, 114.3, 127.5, 127.6, 127.9, 128.2, 128.3, 128.65, 128.72, 128.9, 129.0, 133.8, 134.1, 135.0, 135.4, 136.4, 136.5, 137.2, 138.7, 143.1, 144.9. Found: C, 72.63; H, 6.25%. Calcd for $C_{29}H_{30}GeSi$: C, 72.68; H, 6.31%.

A Mixture of 3-Dimethylphenylsilyl-2-triphenylstannyl-1-propene (12) and 1-Dimethylphenylsilyl-2-triphenylstannyl-1-propene (13) (a 68:32 Mixture): IR (neat) 3060, 2950, 1480, 1428, 1247, 1112, 1074, 997, 833, 808, 726, 697 cm^{-1}; ^1H NMR ($CDCl_3$) δ=0.14 (s, 4.08H, Me_2Si (**12**)), 0.41 (s. 1.92H, Me_2Si (**13**)), 2.13—2.25 (m, 2.32H, CH_2 (**12**) and =CCH_3 (**13**)), 5.30—5.41 (m, 0.68H, =CH_2 (**12**)), 5.78—5.84 (m, 0.68H, =CH_2 (**12**)), 6.31—6.38 (m, 0.32H, =CH (**13**)), 7.20—7.48 (m, 14H), 7.48—7.73 (m, 6H); ^{13}C NMR ($CDCl_3$) δ=—2.8, 29.2, 127.7, 127.8, 128.0, 128.1, 128.5, 128.6, 128.8, 128.9, 133.6, 133.7, 136.8, 137.2, 138.7, 143.1. Found: C, 66.11; H, 6.06%. Calcd for $C_{29}H_{30}SiSn$: C, 66.30; H, 5.76%.

8-Triphenylgermyl-6-tridecene: IR (neat) 2952, 2922, 2852, 1654, 1485, 1458, 1431, 1090, 969, 732, 697 cm^{-1}; ^1H NMR ($CDCl_3$) δ=0.85 (t, J=5.5 Hz, 6H), 0.99—1.34 (m, 14H), 1.81—1.99 (m, 2H), 2.50—2.68 (m, 1H), 5.125—5.39 (m, 2H), 7.26—7.41 (m, 9H), 7.41—7.58 (m, 6H); ^{13}C NMR ($CDCl_3$) δ=13.3, 22.5, 22.6, 25.6, 28.7, 29.4, 30.5, 31.2, 31.4, 32.6, 33.1, 127.9, 128.7, 130.2, 130.7, 135.5, 136.7. Found: C, 76.73; H, 8.34%. Calcd for $C_{31}H_{40}Ge$: C, 76.73; H, 8.31%.

A Mixture of (*Z*)-7-Triphenylstannyl-6-tridecene and (*E*)-Isomer (a 65:35 Mixture): IR (neat) 3062, 2952, 2922, 2850, 1618, 1578, 1480, 1458, 1428, 1377, 1074, 1022, 997, 725, 697 cm^{-1}; ^1H NMR ($CDCl_3$) δ=0.65—0.82 (m, 6H), 0.82—1.51 (m, 14H), 1.89—2.08 (m, 1.3H, =$C(SnPh_3)CH_2$ (*Z*)), 2.12—2.33 (m, 2H, =CCH_2 (*E* and *Z*)), 2.39 (t, J=7.3 Hz, 0.7H, =$C(SnPh_3)CH_2$ (*E*)), 5.80 (t, J=7.1 Hz, 0.35H, =CH (*E*)), 6.29 (t, J=7.3 Hz, 0.65H, =CH (*Z*)), 7.47—7.51 (m, 9H), 7.51—7.76 (m, 6H); ^{13}C NMR ($CDCl_3$) δ=13.9, 14.0, 22.4, 22.5, 22.6, 28.6, 28.7, 29.0, 29.6, 30.3, 30.7, 31.3, 31.5, 31.6, 32.9, 35.7, 40.3, 127.9, 128.4, 128.6, 128.7, 128.8, 136.4, 137.0, 137.2, 137.4, 139.7, 140.2, 143.5. Found: C, 70.17; H, 7.64%. Calcd for $C_{31}H_{40}Sn$: C, 70.07; H, 7.59%.

1-(Triphenylstannyl)cyclononene: Mp 88—89 °C; IR (KBr) 3060, 3012, 2984, 2922, 2850, 1480, 1074, 726, 698 cm^{-1}; ^1H NMR ($CDCl_3$) δ=1.20—1.65 (m, 10H), 2.06—2.40 (m, 2H), 2.45—2.65 (m, 2H), 6.03 (t, J=8.0 Hz, 1H), 7.20—7.75 (m, 15H); ^{13}C NMR ($CDCl_3$) δ=24.6, 25.46, 25.52, 25.8, 26.0, 27.7, 31.3, 128.4, 128.7, 128.9, 137.2, 137.5, 139.1, 145.0. Found: C, 68.43; H, 6.39%. Calcd for $C_{27}H_{30}Sn$: C, 68.53; H, 6.39%.

Financial support by the Ministry of Education, Science, and Culture, Japanese Government (Grant-in-Aid for Scientific Research No. 61850153) is acknowledged.

References

1) Y. Ichinose, H. Oda, K. Oshima, and K. Utimoto, *Bull. Chem. Soc. Jpn.*, **60**, 3468 (1987).

2) K. Nozaki, K. Oshima, and K. Utimoto, *J. Am. Chem. Soc.*, **109**, 2547 (1987); *Bull. Chem. Soc. Jpn.*, **60**, 3465 (1987); Y. Ichinose, K. Nozaki, K. Wakamatsu, K. Oshima, and K. Utimoto, *Tetrahedron Lett.*, **28**, 3709 (1987).

3) The reaction of phenoxyallene with Et_3GeH has been reported. G. S. Lyashenko, A. Kh. Filippova, I. D. Kalikhman, V. V. Keiko, O. A. Kruglaya, and N. S. Vyyazankin, *Izv. Akad. Nauk, SSSR, Ser. Khim.*, **1981**, 874.

4) Free radicals have been reported to attack allenes most often at the end, though attack at the middle has also been reported. PhS radical: K. Griesbaum, A. A. Oswald, E. R. Quiram, and W. Naegele, *J. Org. Chem.*, **28**, 1952 (1963); H. J. Van der Ploeg, J. Knotnerus, and A. F. Bickel, *Recl. Trav. Chim. Pays-Bas*, **81**, 775 (1962). $CH(CN)_2$ radical: H. M. Bartels and P. Boldt, *Justus Liebigs Ann. Chem.*, **1981**, 40. PhSe radical: T. Masawaki, A. Ogawa, N. Kambe, I. Ryu, and N. Sonoda, *Chem. Lett.*, **1987**, 2407.

5) H. N. Cripps and E. F. Kiefer, *Org. Synth.*, Coll., Vol. 5, 22 (1973).

6) T. Nonaka, Y. Okuda, S. Matsubara, K. Oshima, K. Utimoto, and H. Nozaki, *J. Org. Chem.*, **51**, 4716 (1986).

7) R. J. P. Corriu and C. Guerin, *J. Organomet. Chem.*, **197**, C19 (1980).

Structure of Physalin M Isolated from *Physalis alkekengi* var. *francheti*

Masao KAWAI,* Toichi OGURA, Masaki NAKANISHI, Taketoshi MATSUURA,
Yasuo BUTSUGAN,* Yuji MORI,† Ken'ichi HARADA,†
and Makoto SUZUKI†
Department of Applied Chemistry, Nagoya Institute of Technology,
Showa-ku, Nagoya 466
†Faculty of Pharmacy, Meijo University, Tenpaku-ku, Nagoya 468
(Received March 15, 1988)

Synopsis. The structure of physalin M, isolated from *Physalis alkekengi* var. *francheti* was determined as 7-deoxyphysalin L by spectroscopic studies and chemical correlation with a known compound. Physalin M exhibited weak cytotoxicity against tumor cells.

Since the isolation of the first physalin, a novel 13,14-seco-16,24-cyclosteroid, from *Physalis alkekengi* var. *francheti* (Japanese name; Hôzuki),[1] more than ten physalins were isolated from *Physalis* plants grown in Japan[2-4] and in India.[5-11] Physalins were also isolated from *Witheringia coccoloboides* as cytotoxic constituents against tumor cells.[12] Very recently we reported the isolation and structure determination of a new physalin named physalin L (**1**) as a constituent of *P. alkekengi* var. *francheti*.[13] Unlike other physalins **1** possesses a conjugated diene structure in the A-B ring moiety instead of the conjugated cyclohexenone structure. In this note we will also report the isolation and structure determination of another new physalin which is structurally closely related to **1**.

From the extract of *P. alkekengi* var. *francheti*[13] a new compound, whose R_f value in SiO_2-TLC was the same as that of physalin B in benzene-ethyl acetate system but was lower than that of physalin B in chloroform-methanol system, was isolated and named physalin M (**2**). The new physalin **2** crystallized from 2-propanol as colorless prisims, mp 224—227 °C, and its molecular formula was established as $C_{28}H_{32}O_9$ by high-resolution mass spectroscopy and elemental analysis. Spectral data of **2** indicated that **2** possesses the similar structural characteristics to those of **1** as follows: i) Chemical shifts of olefinic protons (δ=5.67, 5.70, and 6.08) in the ^{1}H NMR spectrum (CD_3SOCD_3) and carbonyl stretching frequencies (1775, 1760, 1730, and 1695 cm^{-1}) in the IR spectrum indicated absence of the conjugated cyclohexenone moiety which is present in all known physalins except **1**. ii) Presence of a trisubstituted conjugated diene moiety was demonstrated by the UV absorption band at 228 nm (ε 11000) and by the three olefinic proton signals in the ^{1}H NMR spectrum. iii) Presence of a secondary methyl group (δ=1.14, d, J=7 Hz) in addition to three tertiary methyl groups (δ=1.18, 1.27, and 1.76) was also shown by the ^{1}H NMR spectrum. Assuming that **2** possesses the skeletal structure of physalins, the secondary methyl group was located at C(27) position as are the cases for **1** and also for the cytotoxic physalin from *Witheringia* species, namely 25-epi-25,27-dihydrophysalin C (**3**). Regarding the configuration of the secondary methyl group, a correlation between the stereochemistry at C(25) and the proton chemical shifts of C(27) and C(28) methyl groups was proposed;[12,13] i.e., in CD_3SOCD_3 solution C(27) methyl protons resonate at δ=1.07—1.10 and C(28) methyl protons at δ=1.42—1.48 for the compounds with the secondary methyl group in α-configuration, while C(27) and C(28) methyl protons resonate at δ=1.13—1.26 and at δ=1.14—1.30, respectively, for those with a β-methyl group. From the chemical shifts of C(27) and C(28) methyl groups of **2** (δ=1.14 and 1.27, respectively), β-configuration was assigned to the C(27) methyl group of **2**. The conjugated diene carrying three olefinic hydrogens could be placed only in the A-B ring moiety of the physalin skeleton. Thus two possible structures of **2** were obtained, i.e., one with the double bonds at C(3)-C(4) and C(5)-(6) positions and the other at C(4)-C(5) and C(6)-C(7). The former structure corresponds to the analog of **1** in which the secondary hydroxyl group is replaced by a hydrogen, namely 7-deoxyphysalin L, while the latter (**4**) is the known compound which was obtained by acid dehydration of tetrahydrophysalin A.[3] Spectral

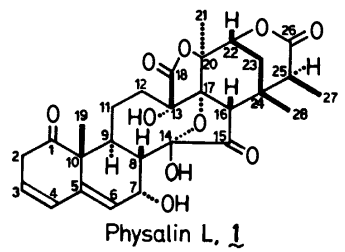
Physalin L, 1

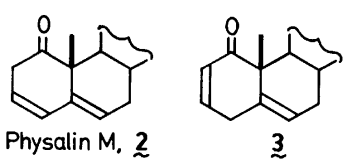
Physalin M, 2 3

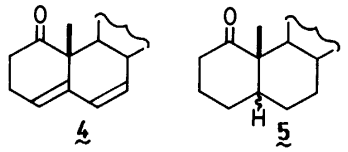
4 5

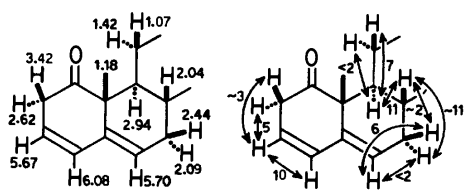

Fig. 1. Chemical shifts (δ) and vicinal coupling constants (Hz) of protons in the A-B ring moiety of physalin M (**2**) measured in CD_3SOCD_3 solution.

comparison clearly indicated that **2** is different from **4**, while the IR, UV, and ^1H and ^{13}C NMR spectral data of **2** resembled closely to those of **1**. The structure of physalin M (**2**) was thus reasonably assumed to be 7-deoxyphysalin L.

Detailed analysis of 400 MHz ^1H NMR spectrum of **2** was performed to ascertain the assumed structure. Homonuclear spin-spin decoupling experiment in combination with COSY analysis enabled the assignment of all of the 32 protons, and their chemical shifts and coupling constants were consistent with the 7-deoxyphysalin A structure. The results of ^1H NMR analysis in CD_3SOCD_3 solution concerning the A-B ring moiety of **2** is given in Fig. 1. Out of 28 carbons of the structure of **2**, 27 carbon resonances were observed in the ^1H noise-decoupled ^{13}C NMR spectrum recorded in CD_3SOCD_3 solution and remaining one carbon, which overlapped solvent signals, could be detected by DEPT (distortionless enhancement by polarization transfer) method. Chemical shifts of all the 4 methyl, 5 methylene, 8 methine, and 11 quaternary carbons were in consistent with the proposed structure as given in the experimental part.

In order to confirm the structure further, chemical tansformation of **2** to the known compound was attempted. Catalytic hydrogenation of **2** in methanol in the presence of palladium-charcoal was found to afford the expected tetrahydro derivative **5**, which was identical in all respects with the known 25-epi-7-deoxy-2,3,5,6,25,27-hexahydrophysalin A.[3,14] Thus, the structure of physalin M (**2**) has been established unequivocally as 7-deoxyphysalin A, namely 25-epi-3,4-dehydro-7-deoxy-2,3,25,27-tetrahydrophysalin A.

Physalins are of interest because of their antitumor activities.[12,13] The new physalin **2**, however, was found to show only very weak cytotoxicity against HeLa cells (IC_{50} 27.6 μg ml^{-1}). The low activity was not unexpected considering the lack of cytotoxicity of the 7-hydroxy analog **1**.[13] Taking into account the potential in vivo and in vitro activity of the double bond isomer (**3**) of **2**, having a double bond at C(2)-C(3) instead of C(3)-C(4),[12] it has been concluded that the conjugated cyclohexenone moiety at the A ring is quite important for the antitumor activity of physalins.

Experimental

Column chromatography and TLC were performed using SiO_2 (Merck, Silicagel 60, 7734) and precoated SiO_2 plates (Merck, Silica Gel 60 F_{254}), respectively. Melting points were determined with a Yanagimoto micro melting point apparatus and uncorrected. Optical rotation and UV spectrum were measured using a JASCO DIP-4 digital polarimeter and HITACHI 124 spectrophotometer, respectively. IR spectrum of **2** was recorded on a JASCO IRA-1 spectrometer with a KBr disk and FT-IR spectra of **5** were recorded on a JEOL JIR-100 spectrometer using a diffuse reflectance accessory. High-resolution MS was measured with a Hitachi M-80 mass spectrometer. ^1H NMR (400 MHz) and ^{13}C NMR (100 MHz) were recorded on a JEOL JNM-GX 400 spectrometer, respectively. Elemental analysis was performed at Elemental Analysis Center of Kyoto University and cytotoxicity test was performed at Pharmaceuticals Laboratory, Life Science Research Sector, Research Center of Mitsubishi Chemical Industries Ltd.

Isolation of Physalin M (2). Water-$CHCl_3$ extract (10 g) of *P. alkekengi* var. *francheti*[13] was subjected to repeated column chromatography with the solvent systems $CHCl_3$-CH_3OH and C_6H_6-$CH_3CO_2C_2H_5$ to give a fraction (350 mg) which showed a single spot (R_f 0.75) on TLC with C_6H_6-$CH_3CO_2C_2H_5$ (3:7), but it showed two spots (R_f 0.70 and 0.58) when developed with $CHCl_3$-CH_3OH (9:1). Column chromatography of the fraction using $CHCl_3$-CH_3OH as eluent afforded physalin B (130 mg) and physalin M (**2**, 140 mg), and the latter was crystallized from 2-propanol to give colorless prisms of **2**: mp 224—227 °C; R_f 0.58 ($CHCl_3$:CH_3OH=9:1); $[\alpha]_D^{24}$ −106° (*c* 0.34, CH_3COCH_3); IR (KBr) 3480, 1775, 1760, 1730, and 1695 cm^{-1}; UV (CH_3OH) 228 nm (ε 11000); ^1H NMR (CD_3SOCD_3) δ=1.04 (6H, d, *J*=6 Hz, 2-propanol), 1.07 (1H, m, H-11β), 1.14 (3H, d, $J_{27,25}$=7 Hz, CH_3-27), 1.18 (3H, s, CH_3-19), 1.27 (3H, s, CH_3-28), 1.42 (1H, dd, $J_{11\alpha,11\beta}$=17 and $J_{11\alpha,12\alpha}$=9 Hz, H-11α), 1.64 (1H, d, $J_{23,23'}$=15 Hz, H-23), 1.76 (3H, s, CH_3-21), 1.86 (1H, dd, $J_{12\beta,12\alpha}$=16 and $J_{12\beta,11\beta}$=6 Hz, H-12β), 2.04 (1H, m, H-8), 2.08 (1H, m, H-23′), 2.09 (1H, m, H-7α), 2.18 (1H, ddd, $J_{12\alpha,12\beta}$=16, $J_{12\alpha,11\beta}$=12, and $J_{12\alpha,11\alpha}$=9 Hz, H-12α), 2.44 (1H, br dd, $J_{7\beta,7\alpha}$=15 and $J_{7\beta,6}$=6 Hz, H-7β), 2.62 (1H, dd, $J_{2\alpha,2\beta}$=20 and $J_{2\alpha,3}$=5 Hz, H-2α), 2.70 (1H, q, $J_{25,27}$=7 Hz, H-25), 2.78 (1H, s, H-16), 2.94 (1H, dd, $J_{9,8}$=11 and $J_{9,11\beta}$=7 Hz, H-9), 3.42 (1H, H-2β, partially overlapping H_2O signal), 3.77 (1H, m, 2-propanol), 4.35 (1H, d, *J*=4 Hz, 2-propanol), 4.48 (1H, d, $J_{22,23'}$=3 Hz, H-22), 5.67 (1H, m, H-3), 5.70 (1H, br d, $J_{6,7\beta}$=6 Hz, H-6), 6.08 (1H, br d, $J_{4,3}$=10 Hz, H-4), 6.20 (1H, s, OH), and 6.47 (1H, s, OH); ^{13}C NMR (CD_3SOCD_3) δ=16.6 and 18.0 (C-27 and C-28), 20.8 (C-19), 24.2 (C-11), 25.4 (2-propanol), 25.5 (C-21), 25.7, 26.1, and 29.0 (C-7, C-12, and C-23), 32.4 (C-9), 34.3 (C-24), 39.5 (C-2), 40.8 and 40.9 (C-8 and C-25), 54.0 (C-16), 55.1 (C-10), 62.0 (2-propanol), 76.4 (C-22), 78.8, 82.0, and 82.3 (C-13, C-17, and C-20), 101.2 (C-14), 122.5, 126.4, and 128.0 (C-3, C-4, and C-6), 140.4 (C-5), 171.7 and 172.2 (C-18 and C-26), 209.6 (C-1), and 215.8 (C-15). Found: C, 63.31; H, 6.84%; *m/z* 512.2031. Calcd for $C_{28}H_{32}O_9 \cdot C_3H_8O \cdot H_2O$: C, 63.04; H, 7.17%. Calcd for $C_{28}H_{32}O_9$: M, 512.2043.

Hydrogenation of Physalin M. Physalin M (9 mg) in CH_3OH (5 ml) was hydrogenated at room temperature and atmospheric pressure over platinum black (2 mg) for 18 h. TLC of the product showed two spots (R_f 0.65 and 0.55, $CHCl_3$:CH_3OH=9:1) and the compound having lower R_f value (3 mg) was isolated by column chromatography using $CHCl_3$ as eluent. Crystallization from CH_3COCH_3 gave colorless prisms: mp>300 °C. The FT-IR spectra of this product and authentic 25-epi-7-deoxy-2,3,5,6,25,27-hexahydrophysalin A (**5**)[3] prepared from physalin A were indistinguishable.

The authors are grateful to Mr. Jun'ichi Ohya of Pharmaceuticals Laboratory, Mitsubishi Chemical Industries Ltd. for the assay of cytotoxic activity and to FT-IR division of Instrument Center, Nagoya Institute of Technology for FT-IR measurement. Thanks are also to Professor Teruo Matsuura of Kyoto University and Professor Ruka Nakashima of Tottori University for helpful discussions.

References

1) T. Matsuura, M. Kawai, R. Nakashima, and Y. Butsugan, *Tetrahedron Lett.*, **1969**, 1083.

2) T. Matsuura and M. Kawai, *Tetrahedron Lett.*, **1969**, 1765.

3) T. Matsuura, M. Kawai, R. Nakashima, and Y. Butsugan, *J. Chem. Soc. C*, **1970**, 664.
4) M. Kawai and T. Matsuura, *Tetrahedron*, **26**, 1743 (1970).
5) S. S. Subramanian and P. D. Sethi, *Curr. Sci.*, **40**, 85 (1971).
6) E. Glotter, I. Kirson, A. Abraham, P. D. Sethi, and S. S. Subramanian, *J. Chem. Soc., Perkin Trans. 1*, **1975**, 1370.
7) R. R. Alluri, R. J. Miller, W. H. Shelver, and S. K. W. Khalil, *Lloydia*, **39**, 405 (1970).
8) L. R. Row, N. S. Sarma, T. Matsuura, and R. Nakashima, *Phytochemistry*, **17**, 1641 (1978).
9) L. R. Row, N. S. Sarma, K. S. Reddy, T. Matsuura, and R. Nakashima, *Phytochemistry*, **17**, 1647 (1978).
10) L. R. Row, K. S. Reddy, N. S. Sarma, T. Matsuura, and R. Nakashima, *Phytochemistry*, **19**, 1175 (1980).
11) K. K. Purushothaman and S. Vasanth, *Ind. J. Chem., Sect. B*, **20B**, 89 (1981).
12) M. D. Antoun, D. Abramson, R. L. Tyson, C. Chang, J. L. McLaughlin, G. Peck, and J. M. Cassady, *J. Nat. Prod.*, **44**, 579 (1981).
13) M. Kawai, T. Matsuura, S. Kyuno, H. Matsuki, M. Takenaka T. Katsuoka, Y. Butsugan, and K. Saito, *Phytochemistry*, **26**, 3313 (1987).
14) The stereochemistry at C(25) of **4** was not given in Ref. 3, but β-methyl configuration was assigned in Ref. 13 considering the chemical shifts of C(27) and C(28) methyl groups.

 © 1988 The Chemical Society of Japan Bull. Chem. Soc. Jpn., 61, 2701—2706 (1988)

The Study of Partition Coefficients. The Prediction of Log *P* Value Based on Molecular Structure

Kenji KASAI,* Hideaki UMEYAMA,† and Atsushi TOMONAGA††
Biomedical Research Laboratory, Kureha Chemical Industry Co., Ltd.,
3-26-2, Hyakunin-cho, Shinjuku-ku, Tokyo 160
†School of Pharmaceutical Sciences, Kitasato University, Shirokane,Minato-ku, Tokyo 108
††Intelligence & Development for Research Depart., Kureha Chemical Industry Co., Ltd.,
3-25-1, Hyakunin-cho, Shinjuku-ku, Tokyo 160
(Received October 30, 1987)

An effort has been made to determine the partition coefficients from the physical quantities based on the molecular structure. The quantities are representatives of energies which constitute the solvation energy of the solute molecule. The log *P* value is expressed with them as

$$\log P = -1.26 + 3.78\,\phi_{ct} - 0.72\,\mu_1 - 1.28\,\mu_2$$
(N=244, R=0.959, S.D.=0.54, F=934).

For the practical use, the following equation is recommended:

$$\log P = -1.36 + 3.89\,\phi_{ct} - 1.09\,\mu_2 - 0.085U_H + 0.021U_C - 0.134U_N - 0.198U_O$$
(N=244, R=0.976, S.D.=0.42, F=787).

Here, ϕ_{ct} is the representative related to the charge-transfer energy and μ_1, μ_2, U_H, U_C, U_N, and U_O are those related to the electrostatic energy. The molecular structure of the solute molecule has been shown to be very important in the determination of the log *P* value. A log *P* value with a higher precision can be obtained by modifying the approximations used.

For almost one hundred years, many investigators have been carrying out studies of partition coefficients in both basic and applied fields.[1] However, the results of their studies were not sufficiently good to satisfy all of the investigators. For example, despite the fact that a partition coefficient is a physicochemical quantity, it still cannot be elucidated theoretically and universally. The difficulties in calculating it are due to the complexity of the phenomena in a liquid; the system is a cluster of many characteristic particles. These particles have a diversity of structures and electronic states. The collective state of molecules in a liquid or a solution shows properties over a wide range, from order to disorder. It is difficult to provide systematic explanations for such complexity. These days, however, progress in computer systems is enabling researchers to directly approach the subject.

The partition coefficients have been explained by a linear free-energy relationship. Under this relationship, the logarithm of the partition coefficient of a molecule, log *P* value, has been determined by the sum of the values given to the molecular fragment, the so-called fragment constants.[2] In recent years, this method has been refined[3] and the fragment constants have been specified as various values.[4] Although this method is convenient to use, the physicochemical and microscopical significance of the fragment constants are not clear. The calculation techniques were inadequate during the initial stage of the physicochemical study.[5] The trials[6,7] which determine the fragment constant using the physicochemical method did not make the essence of the subject clear. Those trials should reveal the inherent limit of the method. There is a method which expresses the log *P* value by using the observed physical quantities;[8] however, it is not useful for the designed molecules.

Thus, it is necessary to formulate a partition coefficient faithfully along the general concept of the free energy. The log *P* value of a solute molecule is derived from the transfer energy which is the difference in the standard free energy between two phases. The standard free energy of a solute in a solvent corresponds to the solvation energy in an infinite dilution.

By modifying the previous studies[9,10] in our present study, the solvation energy could be expressed by the summation of various types of energy in a molecular system which consists of a solute molecule and solvent molecules. The representatives of each of the energies could be obtained by examining each energy type. The solvation energy is represented by a linear combination of these representatives. Some approximations were introduced in order to determine the representatives. As a result, in some cases there may be a disagreement between the observed and the calculated values, since the approximation is not appropriate for these particular molecules. Such results suggest the elimination of the approximation, or at least an improvement in it. Thus, these modifications provided a better understanding of the phenomena. It is therefore important to discuss the applied approximation and its result.

To use alternatively both the molecular dynamics method and the super molecular approach method is desired as a technical method for calculations, but it is difficult on account of the costly computer facilities. The method stated in the report has been worked out, taking into account the first solvation layer and the continuum model.[11]

Method

The partition coefficient P of a non-associated solute molecule is given by the transfer energy $\Delta\mu_{12}^{\circ}$ per solute molecule between two phases, the solvent 1 and 2,[12]

$$\log P_{12} = -\Delta\mu_{12}^{\circ}/2.303\ kT, \tag{1}$$

where k is Boltzmann's constant, and T is the absolute temperature. If solvent 1 and 2 are water and 1-octanol, respectively, $\log P_{12}$ is the so-called $\log P$.

Solvation Energy and Transfer Energy. The solvation energy $\Psi(\mathrm{M})$ of a solute molecule is given by

$$\Psi(\mathrm{M}) = \psi_{\mathrm{M}}(\mathrm{M}) + \psi_{\mathrm{S}}(\mathrm{M}) + \psi_{\mathrm{MS}}(\mathrm{M}), \tag{2}$$

where M represents the state of the solute in the solvent S. $\psi_{\mathrm{M}}(\mathrm{M})$ is the intramolecular free energy of the solute in state M. $\psi_{\mathrm{S}}(\mathrm{M})$ is the free energy of cavity formation of the solute in the solution.[13] $\psi_{\mathrm{MS}}(\mathrm{M})$ is the sum of the interaction energies between the solute and the solvent molecules. The transfer energy is given by

$$\Delta\mu_{12}^{\circ} = \Psi_2(\mathrm{M2}) - \Psi_1(\mathrm{M1}), \tag{3-1}$$

$$= \phi_{\text{solute}} + \phi_{\text{solution}} + \phi_{\text{inter}}. \tag{3-2}$$

The energies expressed in Eq. 3-2 are given by following equations:

$$\phi_{\text{solute}} = \psi_{\mathrm{M}}(\mathrm{M2}) - \psi_{\mathrm{M}}(\mathrm{M1}), \tag{4-1}$$

$$\phi_{\text{solution}} = \psi_{\mathrm{S}_2}(\mathrm{M2}) - \psi_{\mathrm{S}_1}(\mathrm{M1}), \tag{4-2}$$

and

$$\phi_{\text{inter}} = \psi_{\mathrm{MS}_2}(\mathrm{M2}) - \psi_{\mathrm{MS}_1}(\mathrm{M1}), \tag{4-3}$$

where subscripts 1 snd 2 denote solvents 1 and 2, respectively.

Linear Free Energy Relationship. The linear free energy relationship from Eqs. 1 and 3-2 are obtained as follows:

$$\log P = \sum_i f(i)/2.303\ kT, \tag{5}$$

where $f(i)$ is the energy of the i-th element. The additivity of the $\log P$ value is attributed to the property of the energy. If the energy, $f(i)$, is a linear combination of a physicochemical quantity, Q_{ij}, which itself corresponds to each of the energies, then the value of $\log P$ is given as

$$\log P = \sum_i \sum_j \alpha_{ij} \cdot Q_{ij}, \tag{6}$$

where α_{ij} is the coefficient of Q_{ij}. α_{ij} is determined deductively by the physical meaning or inductively by the least squares method when the $\log P$ values are observed.

Analysis

Approximations. Calculations of the $\log P$ values are almost impossible without using approximations. A water-methane system can be considered in place of a water-1-octanol system (approx. 1), since the dielectric properties of methane resemble that of 1-octanol, compared to water. The size and shape of methane gives merit to the calculation, and leaves no problem in the theory. Water and methane are hereinafter considered to be the two solvents, 1 and 2, respectively.

The transfer energy $\Delta\mu_{12}^{\circ}$ can be explained by three terms: ϕ_{solute}, ϕ_{solution}, and ϕ_{inter}. If the structure of a solute molecule in methane is assumed to be the same as that in water, then $\phi_{\text{solute}}=0$ (approx. 2). The contribution of ϕ_{solution} is neglected, since there is insufficient information regarding the configuration and the orientation of solvent molecules on the solute surface (approx. 3). As for ϕ_{inter}, the attractive forces are generally the main interactions in the liquid state. They are the induction energy, dispersion energy, charge-transfer energy, and electrostatic energy. The induction energy can be neglected, since it is usually small.[14] The dispersion energy can also be neglected because of the difficulty in its estimation. The charge-transfer energy, which is a short-range interaction, and the electrostatic energy, which is a long-range interaction, are denoted by Ect and Ecoul, respectively. Thus, the interaction energy is given by

$$E = E_{\mathrm{ct}} + E_{\mathrm{coul}} \quad \text{(approx. 4)}. \tag{7}$$

This is known as the Klopman-Hudson equation.[15]

$\psi_{\mathrm{MS}}(\mathrm{M})$ in Eq. 2 is given by the summation of all interactions among the solute molecule and all of the solvent molecules surrounding it:

$$\psi_{\mathrm{MS}}(\mathrm{M}) = \sum_j \sum_k E_{jk} \cdot \Delta\tau_j \cdot \Delta\tau_k, \tag{8}$$

where $\Delta\tau_j$ and $\Delta\tau_k$ are the volume elements, and E_{jk} is the interaction energy between the volume elements. Generally speaking, the contribution of the solvent outside the solvation layer is negligible. In order to simplify the calculation, solvent molecules are estimated only in the first layer (approx. 5). If the thickness of the layer is fixed, the summation in Eq. 8 is replaced by that on the surface of the solute. The solvent accessible surface (SAS)[16] is adopted as the molecular surface.

Representatives of Charge-Transfer Energy. In order to simplify the calculation, the orientation of a solvent molecule is assumed to be such that an atom in the solvent molecule faces the solute molecule in proportion to its ratio, R_k, covering the surface of the solvent one. The total charge-transfer energy, ψ_{ct}, then, is given as follows according to Eq. 8:

$$\psi_{\mathrm{ct}} = \sum_j \sum_k \sum_p \sum_q [E_{\mathrm{ct}}]_{pq} \cdot \delta_{pj} \cdot \delta_{qk} \cdot \Delta s_j \cdot R_k, \tag{9-1}$$

where

$$R_k = \Delta s_k / S_{\mathrm{slv}}, \tag{9-2}$$

and δ_{pj} and δ_{qk} are Kronecker's δ; thus, $\delta_{pj}=1$ if the

p-th STO of the solute molecule belongs to the j-th atom of the same molecule, and $\delta_{pj}=0$ otherwise. The existing probability of a solvent molecule in the volume element $\Delta\tau_j$ is proportional to the surface area element Δs_j if the thickness of the layer is fixed. $\sum_j$ corresponds to the sum of all the solvent molecules in the first solvation layer. $\delta_{qk}=1$ if the q-th STO of the solvent molecule belongs to the atom in the volume element $\Delta\tau_k$, and $\delta_{qk}=0$ otherwise. $\sum_k$ indicates the sum for taking the average of the orientation of the solvent. S_{slv} is the total surface area of the solvent molecule, and Δs_k is the surface area element. $[E_{ct}]_{pq}$ is given as follows:[15]

$$[E_{ct}]_{pq} = -2\left(\sum_m^{Oc.}\sum_n^{Un.} - \sum_m^{Un.}\sum_n^{Oc.}\right)\frac{C_{mp}^2 \cdot C_{nq}^2}{\varepsilon_n - \varepsilon_m}\beta_{pq}^2 \quad (10)$$

The resonance integral β_{pq} is strongly dependent on the interatomic distance. Therefore, it is sufficient to take only the atoms exposed to the molecular surface, as the object of the calculation of β_{pq}. The sum of two van der Waals radii[17] of atoms, which face each other across the solute surface, is used as the interatomic distance in the calculation.

Thus, the contribution of the charge-transfer energy in the water-methane system is given by

$$\phi_{ct}=\psi_{2,ct}-\psi_{1,ct}, \quad (11)$$

where $\psi_{1,ct}$ and $\psi_{2,ct}$ are the charge-transfer energy in the water and methane solvent, respectively.

Representatives of Electrostatic Energy. Since a methane molecule is minimally polarized in such a mild field as the solution, the electrostatic energy between the solute and the solvent molecules in the methane solvent is negligible for any solutes:

$$\psi_{2,coul}=0.$$

The contribution of the electrostatic energy is given by

$$\phi_{coul} = \psi_{2,coul} - \psi_{1,coul} = -\psi_{1,coul}, \quad (12)$$

where $\psi_{1,coul}$ is the electrostatic energy in water. The simplest form of $\psi_{1,coul}$ is given as

$$\psi_{1,coul}=-\boldsymbol{\mu}\cdot\boldsymbol{E}, \quad (13)$$

where $\boldsymbol{\mu}$ is the molecular dipole moment of the solute and $\boldsymbol{E}$ is the electric field applied to the solute. If $\boldsymbol{E}$ is fixed over any solute molecules, $\psi_{1,coul}$ depends on $\boldsymbol{\mu}$. The molecular dipole moment is calculated as the sum of two terms,[18]

$$\boldsymbol{\mu}=\boldsymbol{\mu}_1+\boldsymbol{\mu}_2, \quad (14)$$

where the first contribution term $\boldsymbol{\mu}_1$ is obtained from the net charges located at the nuclear position and the second contribution term $\boldsymbol{\mu}_2$ is essentially a hybridization term. Thus, the absolute values of $\boldsymbol{\mu}_1$ and $\boldsymbol{\mu}_2$ are adopted as the representatives of $\phi_{1,coul}$.

$$\mu_1=|\boldsymbol{\mu}_1|, \quad \mu_2=|\boldsymbol{\mu}_2|. \quad (15)$$

Multiple Linear Regression. Thus, ϕ_{ct}, μ_1, and μ_2 are representatives of the energies based on the molecular structure. These are not on the same level as the approximations. According to Eq. 6, the $\log P$ value is given by a linear combination of these representatives. The relationship is obtained by applying a multiple linear regression analysis.

Observed Log P Values and Molecular Structures. The observed $\log P$ values used in the analysis are those of 265 molecules. These were selected according to the order of the molecular size with the following atomic types of H, C, N, and O atoms on the Hansch-Leo data base.[19]

All of the structures of the 265 molecules were geometrically optimized by using the MNDO method.[20] The analyses on the conformation were carried out for 26 molecules, and there was a wide gap between the observed value and the calculated one in the preliminary work. One of the criteria used in the conformational analysis was the total energy for the optimized structure; another one was the stabilization owing to the solvation. The former was obtained directly by a MNDO calculation, but the latter was not so easily obtained. Some conformers, ranging from the lowest energy to one about 3 kcal mol^{-1} higher, are the objects of investigations. As for tautomers, the structures generally considered were fully optimized by the MNDO calculation.

A solvent molecule with a radius of 1.50 Å was used in order to calculate the area of the SAS. The molecular volume was defined as that of the space surrounded by SAS. The other molecular properties were obtained by NNDO calculations.

Results

The following equation was obtained by using the representatives of ϕ_{ct}, μ_1, and μ_2:

$$\log P = -1.26(\pm0.17)+3.78(\pm0.15)\phi_{ct} - 0.72(\pm0.03)\mu_1 - 1.28(\pm0.07)\mu_2 \quad (16)$$
$$(N=244,\ R=0.959,\ \text{S.D.}=0.54).$$

In addition, an equation for more practical use than Eq. 16 is

$$\log P = -1.36(\pm0.17)+3.89(\pm0.19)\phi_{ct} - 0.085(\pm0.014)U_H + 0.021(\pm0.008)U_C - 0.134(\pm0.017)U_N - 0.198(\pm0.018)U_O - 1.09(\pm0.06)\mu_2 \quad (17)$$
$$(N=244,\ R=0.976,\ \text{S.D.}=0.42),$$

where U_H, U_C, U_N, and U_O are the representatives instead of μ_1. Figure 1 shows the relationship between the observed $\log P$ value and the calculated one through Eq. 17.

Derivations of U_H, U_C, U_N, and U_O, and the values of each parameter in Eqs. 16 and 17 are deposited as Document No. 8808 at the Office of the Editor of Bull. Chem. Soc. Jpn.

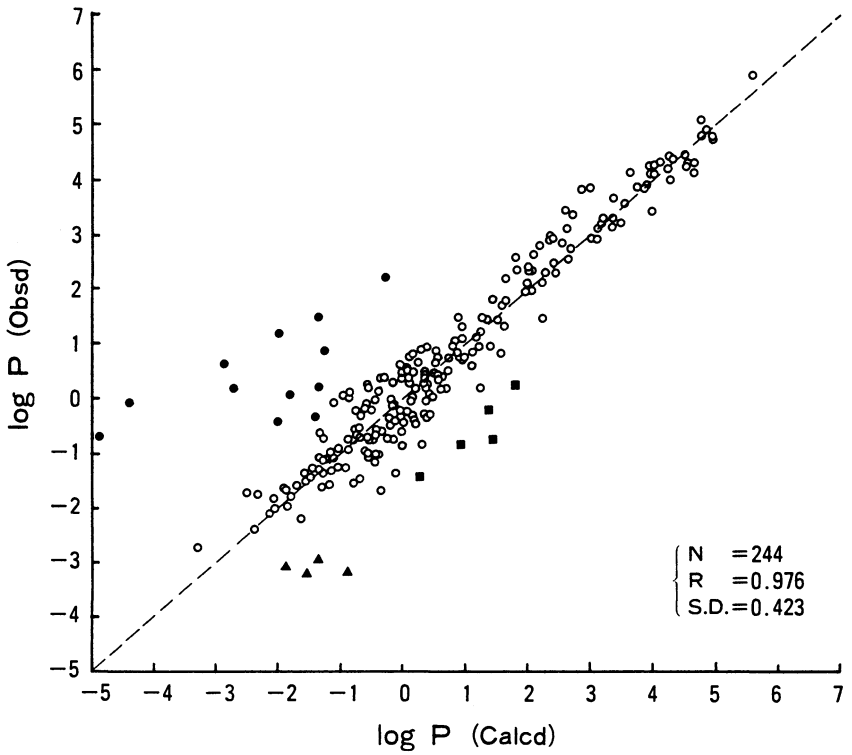

Fig. 1. Observed log$P$ values plotted against values calculated through Eq. 17. ○: Molecules in the group A, B, C, D, and E, ●: Nitro compounds (Group F), ▲: Amino acids (Group G), ■: Symmetrical molecules (Group H). For details of the groups, Document should be referred to.

Discussion

The results showed excellent agreement between the observed and calculated log$P$ values for 244 molecules among 265. The remaining 21 molecules could not be the objects of the analysis.

Characteristics of the 21 Molecules. There were 12 nitro compounds, 4 amino acids, and 5 molecules with a high structure symmetry. In the nitro compounds, the molecular structures optimized by the MNDO method were geometrically unnatural; the C-NO_2 bond is too long (e.g. MNDO; 1.546 Å, 6-31G; 1.479 Å). Therefore, the representatives calculated from the molecular structure may be inappropriate for applications to the analysis. Amino acids are not appropriate for approx.2; the conformations in two solvents are considered to be different. In molecules with high symmetry, the contribution due to the dipole moment is of no value.

Limitation of Fragment Constant Method. If $f(i)$ in Eq. 5 is the energy of the i-th fragment in a molecule, and all fragments are independent of one another, the fragment constant method is valid. This method is, however, invalid if the procedure for dividing the molecule into fragments is inappropriate, and/or if the intra- and the intermolecular interactions involve long-range interactions. For example, though the hydrocarbons are satisfied with the additivity in the log$P$ values, it is difficult to validate the additivity in molecules, having hetero atoms like nitrogen and oxygen atoms.

Correlations of S, V, and ϕ_{ct}. There is a close correlation between the molecular surface area S and the volume V (e.g. R=0.998, N=244). There is also a close correlation between ϕ_{ct} and V (e.g. R=0.984, N=244). The former fact is the reason that the radius of each atom in the molecule is almost the same. As for the latter, if E_{ct} in Eq. 9-1 is fixed, ϕ_{ct} is directly proportional to S, so that ϕ_{ct} has a close correlation with V. Thus, S. V, and ϕ_{ct} have close correlations to one another in a molecule without any long-range interaction, such as the electrostatic interaction.

The interactions of the saturated hydrocarbons, except for the dispersion energy, must be negligible. The log$P$ values in these molecules also seem to depend on ϕ_{ct} in Eqs. 16 and 17. The dependency is considered to be derived from the energies represented by S and/or V. The energies may be the dispersion energy and/or the energy of the cavity formation. Although these energies are not taken up here, the dependency suggests that they are significant for the saturated hydrocarbons.

Log P Value and Molecular Structure. The strength of the intra- and the intermolecular interaction depends upon the molecular structure, so thst a molecular property like the log$P$ value is also

changed.

i) Conformer: Table 1 shows the value of the intramolecular energy, the magnitude of the dipole moment, and the observed and the calculated log *P* values of various conformers of three molecules: urea, dioxane, and cyclohexane.

The typical conformers of urea are shown in Fig. 2. Although conformer A1 has the lowest energy in the planar forms, the calculated log *P* value does not agree with the observed value. The calculated log *P* value of conformer A2 is the nearest to the observed one. Dioxane has two typical conformers: a chair form and a boat form. The energy of the chair form is lower than that of the boat form, but the observed value of log *P* shows better agreement with the calculated value of the boat form than that of the chair form. In cyclohexane, the calculated log *P* values are similar to both the chair and the boat forms, but the energy of the chair form is clearly lower than that of the boat form.

ii) Tautomer: Table 2 and Fig. 3 show an example of the tautomer in tetrazole. The observed log *P* value is closer to the calculated one of the 2*H*-type than that of the 1*H*-type. On the other hand, the results of the 6-31G**, calculated by Mazurek and Osman[21] reverse the evaluation of the energy in comparison with the MNDO calculations.

Table 1. Conformers

No.	Molecule	Structure		Heat of form. kcal mol^{-1}	Total energy hartree	Dipole moment debye	log P Obsd	log P Calcd
39	Urea	Planar form	A_1	−44.4	−223.4561[a)]	3.04	−2.11	−0.857
			A_2	−42.6		3.98		−2.132
			A_3	−39.6		3.92		−2.360
		Non-planar form	B	−36.1	−223.4010[a)]	2.57		−1.610
			C	−33.7	−223.3984[a)]	0.42		−1.686
			D	−31.2	−223.3944[a)]	4.44		−2.924
291	Dioxane	Chair form		−88.5		0.42	−0.27	0.944
		Boat form		−87.5		1.23		0.381
815	Cyclohexane	Chair form		−34.7		0.00	3.44	2.608
		Boat form		−32.2		0.00		2.609

a) 4-21G: C. A. Alsenoy, J. O. Williams, and L. Schafer, *J. Mol. St.*, **78**, 179 (1981).

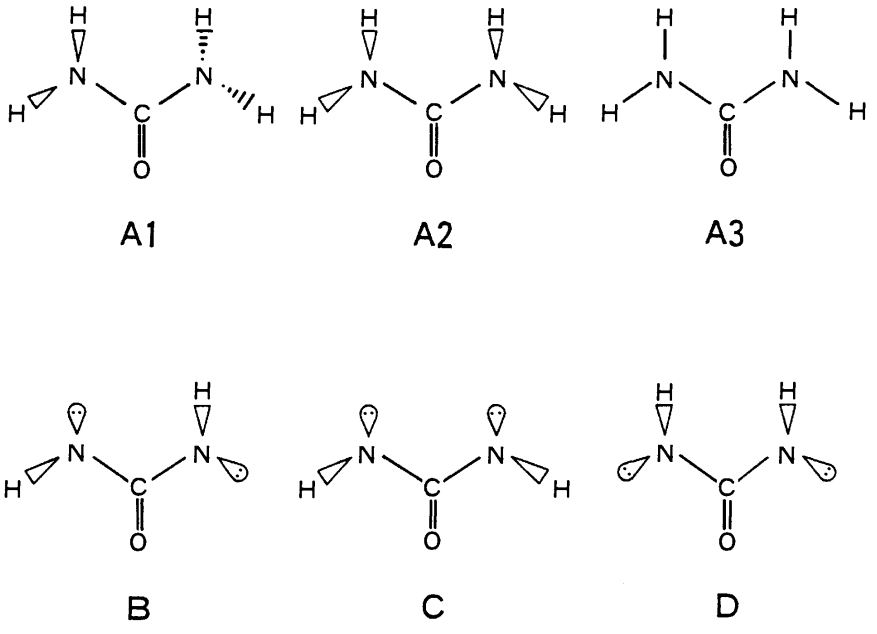

Fig. 2. Conformers of urea. A1, A2, A3: Planar form, B, C, D: Nonplanar form.

Table 2. Tautomers

No.	Molecule	Structure	Heat of form. kcal mol^{-1}	Total energy hartree	Dipole moment debye	log P Obsd	log P Calcd
28	tetrazole	1H-type	54.0	−256.7573[a)]	5.10 5.63[a)]	−0.60	−2.614
		2H-type	58.3	−256.7601[a)]	1.89 2.24[a)]		−0.023

a) 6-31G**: A. P. Mazurek and R. Osman, *J. Phys. Chem.*, **89**, 460 (1985).

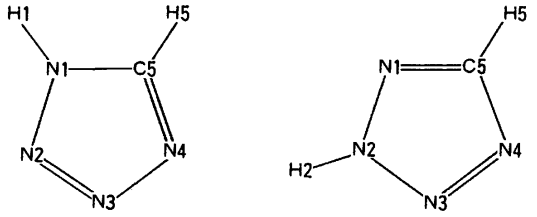

1H-Tetrazole 2H-Tetrazole

Fig. 3. Tautomers of tetrazole.

Conclusion

The partition coefficient of the solute molecule is determined by the transfer energy which is the difference of the standard free energy between two phases. The standard free energy consists of the intramolecular free energy of the solute molecule, the free energy of the cavity formation, and the interaction energy between the solute molecule and the solvent ones. These energies depend on the molecular structure of the solute. The log P values are represented by linear combination of the representatives of each energy.

This method has a characteristic of being applicable to the molecules, regardless of their types. In the analysis for instance, the log P value was investigated over the wide range of about −3 to 6, where 38% of the molecules were found to have a negative log P value.

References

1) A. Leo, C. Hansch, and D. Elkins, *Chem. Rev.*, **71**, 525 (1971).
2) A. Leo, P. Y. C. Jow, C. Silipo, and C. Hansch, *J. Med. Chem.*, **18**, 865 (1975).
3) J. T. Chou and P. C. Jurs, *J. Chem. Inf. Comput. Sci.*, **19**, 172 (1979).
4) G. Klopman, K. Namboodiri, and M. Schochet, *J. Comput. Chem.*, **6**, 28 (1985).
5) A. Cammarata and K. S. Rogers, *J. Med. Chem.*, **14**, 269 (1971).
6) A. J. Hopfinger and R. D. Battershell, *J. Med. Chem.*, **19**, 569 (1976).
7) A. K. Ghose and G. M. Crippen, *J. Comput. Chem.*, **7**, 565, (1986).
8) R. W. Taft, M. H. Abraham, R. M. Doherty, and M. J. Kamlet, *Nature (London)*, **313**, 384 (1985); *J. Am. Chem. Soc.*, **106**, 466 (1984).
9) K. Kasai and A. Tomonaga, "QSAR and Strategies in the Design of Bioactive Compounds" ed by J. K. Seydel, VCH (1985), p. 277; 12th Symp. Struc. -Act. Relat. Osaka, p. 267 (1984).
10) K. Kasai, A. Tomonaga, and H. Umeyama, 13th Symp. Struc. -Act. Relat. Kanazawa, p. 262 (1985).
11) M. Born, *Z. Phys.*, **1**, 45 (1920).
12) J. N. Murrell and E. A. Boucher, "Properties of Liquids and Solutions," John Wiley & Sons (1982), p. 146.
13) H. Reiss, H. L. Frisch, E. Felfand, and J. L. Lebowittz, *J. Chem. Phys.*, **32**, 119 (1960).
14) a) J. O. Hirschfelder, C. F. Curtiss, and R. B. Bird, "Molecular Theory of Gases and Liquids," John Wiley & Sons (1964), p. 988. b) T. Yonezawa, T. Nagata, H. Kato, A. Imamura, and K. Morokuma, "Ryoshi Kagaku Nyumon," Kagaku Dojin (1983), p. 599.
15) R. F. Hudson and G. Klopman, *Tetrahedron Lett.*, **1967**, 1103.
16) B. Lee and F. M. Richards, *J. Mol. Biol.*, **55**, 379 (1971).
17) A. Bondi, *J. Phys. Chem.*, **68**, 441 (1964).
18) J. A. Pople and D. L. Beveridge, "Approximate Molecular Orbital Theory," McGraw-Hill (1970), p. 87.
19) "Log P and Parameters Data Base," Comtex Scientific Corporation, N. Y. (1983).
20) W. Thiel; QCPE 353.
21) A. P. Mazurek and R. Osman, *J. Phys. Chem.*, **89**, 460 (1985).

 © 1988 The Chemical Society of Japan Bull. Chem. Soc. Jpn., 61, 2707—2710 (1988)

A Conductance Study of 1 : 1 Complexes of 1,2-Bis[2-(2-methoxyethoxy)-ethoxy]benzene (Noncyclic Polyether) with Alkali Metal Ions in Nonaqueous Solvents

Yasuyuki TAKEDA,* Shinichi SAKAMOTO, Naohiko OHASHI, and Naoaki FUKADA
Department of Chemistry, Faculty of Science, Chiba University, Yayoi-cho, Chiba 260
(Received November 18, 1987)

Conductivities of alkali metal salts in the presence of 1,2-bis[2-(2-methoxyethoxy)ethoxy]benzene (AC·B18C6), which is a linear counterpart of benzo-18-crown-6 (B18C6), were measured at 25 °C in acetonitrile, propylene carbonate, and methanol. Formation constants and limiting ionic molar conductivities of the 1 : 1 AC·B18C6–alkali metal ion complexes were determined. Selectivity of AC·B18C6 for alkali metal ions is lower than that of B18C6. The selectivity order of AC·B18C6 for K^+, Rb^+, and Cs^+ is consistent entirely with that of B18C6 ($K^+ > Rb^+ > Cs^+$), but the selectivity order of AC·B18C6 for Na^+ differs from that of B18C6. The AC·B18C6–alkali metal ion complex is less stable than the corresponding B18C6 complex. The AC·B18C6 complex may be entropy-destabilized due to the two flexible arms. The AC·B18C6–alkali metal ion complex is more mobile than the corresponding B18C6 complex; the mobility of the AC·B18C6 complex is less sensitive to a variety of the alkali metal ions in the complexes than that of the B18C6 complex. This indicates that the alkali metal ion in the AC·B18C6 complex is coordinated with the two arms and the surface charge of the alkali metal ion in the AC·B18C6 complex is more effectively shielded than that in the B18C6 complex.

In order to clarify the macrocyclic effect (i.e., enhanced stabilities of crown compound-cationic species complexes), complexation reactions of crown compounds and their corresponding open-chain analogs with metal ions have been studied from thermodynamic and kinetic points of view.[1] However, few data on solvation behavior and structures in solutions of the resulting complexes have been reported. In this study, conductivities of alkali metal salts in the presence of 1,2-bis[2-(2-methoxyethoxy)ethoxy]benzene (AC·B18C6), which is a linear counterpart of benzo-18-crown-6 (B18C6), were measured at 25 °C in acetonitrile, propylene carbonate, and methanol. Formation constants and limiting ionic molar conductivities of the 1 : 1 AC·B18C6-alkali metal ion complexes were determined. Stabilities and mobilities of the AC·B18C6 complexes in the solvents were compared with those of the B18C6 complexes to obtain information on the macrocyclic effect of B18C6, and solvation properties and structures in solutions of the AC·B18C6 complexes.

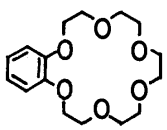

B18C6

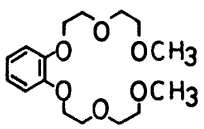

AC·B18C6

Experimental

Materials. AC·B18C6 was prepared by the reaction of catechol with 2-(2-methoxyethoxy)ethyl chloride in aqueous sodium hydroxide–1-butanol mixture according to the literature method.[2,3] The crude light yellow oil was distilled three times to give colorless viscous oil: 65%; bp 225—230 °C/19 Torr (1 Torr≃133.322 Pa); MS m/z, 314 (M^+). Found: C, 60.97; H, 8.20%. Calcd for $C_{16}H_{26}O_6$: C, 61.13; H, 8.34%. Extremely pure $LiCl \cdot H_2O$, NaCl, KCl, RbCl, and CsCl were obtained from Merck Japan Ltd., and were used without further purification. Rubidium and caesium perchlorates were prepared by adding a little excess of perchloric acid to aqueous solutions of the RbCl and CsCl, respectively. Lithium, sodium, and potassium perchlorates were purchased from Merck Japan Ltd. All the perchlorates were recrystallized four times from distilled water. The alkali metal chlorides and perchlorates were, prior to use, dried at 150 °C in a vacuum oven.

The method of purification of acetonitrile,[4] propylene carbonate,[5] and methanol[6] was previously described. Middle 70% of distillate of the solvents was used. Conductivities of the purified acetonitrile, propylene carbonate, and methanol were less than 3×10^{-7}, 6×10^{-8}, and 3×10^{-7} $\Omega^{-1}cm^{-1}$, respectively.

Alkali metal chlorides were employed for the methanol system and alkali metal perchlorates for the other solvent systems.

Apparatus and Procedure. The conductance measurements were made on a Fuso conductivity apparatus, model 362A, in a water bath thermostated at 25±0.005 °C. Three cells were used with cell constants of 0.13545, 0.090741, and 0.031112 cm^{-1}.

The experimental procedure to obtain formation constants and limiting ionic molar conductivities of AC·B18C6–alkali metal ion complexes was almost the same as that described in a previous paper.[5]

Results and Discussion

The procedure for obtaining formation constants (K_{ML^+}) and limiting ionic molar conductivities (λ^0) of AC·B18C6–alkali metal ion complexes was just the same as that reported in a previous paper,[5] where $K_{ML^+}=[ML^+]/[M^+][L]$. M^+ and L denote an alkali metal ion and AC·B18C6, respectively. In this study, it is assumed that the association between a cation and an anion is negligible and that AC·B18C6 forms the 1 : 1 complex with an alkali metal ion. Corrections for viscosity changes were neglected. The log K_{ML^+} and λ^0

Table 1. Log (K_{ML^+}/mol^{-1} dm^3) Values of AC·B18C6- and B18C6-Alkali Metal Ion Complexes at 25 °C

	AN[a]		PC[b]		CH_3OH	
	AC·B18C6	B18C6	AC·B18C6	B18C6	AC·B18C6	B18C6
Li^+	—	—	1.93±0.08	—	—	—
Na^+	2.85±0.02	4.9[7]	3.07±0.03	5.3[7]	1.44[3]	4.5[7]
K^+	2.619±0.005	5.3[7]	2.544±0.009	5.4[7]	2.25±0.03 2.15[3]	5.7[7]
Rb^+	2.403±0.006	4.4[7]	2.12±0.02	4.5[7]	2.116±0.008	5.1[7]
Cs^+	1.75±0.11	3.8[7]	1.82±0.06	3.6[7]	1.83±0.03 1.66[3]	4.1[7]

a) Acetonitrile. b) Propylene carbonate.

Table 2. λ^0/Ω^{-1} cm^2 mol^{-1} Values of AC·B18C6- and B18C6-Alkali Metal Ion Complexes at 25 °C

	AN[a]		PC[b]	
	AC·B18C6	B18C6	AC·B18C6	B18C6
Na^+	$58._6$	$53._1$[8]	8.1_7	7.2_9[8]
K^+	$58._1$	$56._5$[8]	8.5_3	7.9_0[8]
ClO_4^-	103.7[9]		18.2$_8$[10]	

a) Acetonitrile. b) Propylene carbonate.

values of the AC·B18C6-alkali metal ion complexes are summarized in Tables 1 and 2, respectively, together with the literature values.

The molar conductivity (Λ) vs. $[L]_t/[M]_t$ plots in acetonitrile, propylene carbonate, and methanol are given in Figs. 1, 2, and 3, $[L]_t$ and $[M]_t$ being total concentrations of AC·B18C6 and an alkali metal ion, respectively. The Λ vs. $[L]_t/[M]_t$ plots show a decrease in Λ with an increase in the AC·B18C6 concentration, except for all the Li^+ systems and the Na^+-CH_3OH system. This indicates that the moving entity of the AC·B18C6-alkali metal ion complex is larger than that of the corresponding alkali metal ion. In the case of the Li^+ system, a small increase in Λ is found with an increase in the AC·B18C6 concentration, indicating that, if a complex is formed between AC·B18C6 and Li^+, the moving entity of the AC·B18C6-Li^+ complex is smaller than that of Li^+. For the Na^+-CH_3OH system, scarcely any change in Λ is observed in spite of an increase in the AC·B18C6 concentration. Consequently, the conductometric determination of the complex-formation constant is impossible for the Li^+-acetonitrile and -methanol systems and the Na^+-methanol system. From the fact that the AC·B18C6-Na^+ complex is formed in CH_3OH,[3] the changeless Λ may be caused by low stability of the AC·B18C6 complex and/or nearly equal mobilities of the AC·B18C6 complex and Na^+ in CH_3OH.

It can be seen from Figs. 1, 2, and 3 that no clear breaking point is observed at $[L]_t/[M]_t=1$; whereas, the reverse holds for B18C6 systems.[7] This is attributed largely to much lower stabilities of AC·B18C6-alkali metal ion complexes compared with B18C6-alkali metal ion complexes (Table 1).

Stabilities of AC·B18C6 Complexes. The difference in logK_{ML^+} values of AC·B18C6 between neighboring alkali metal ions in the periodic table in the same solvent is smaller than that of B18C6 except for the cases of Rb^+, Cs^+ in acetonitrile and Na^+, K^+ in propylene carbonate. The difference between the

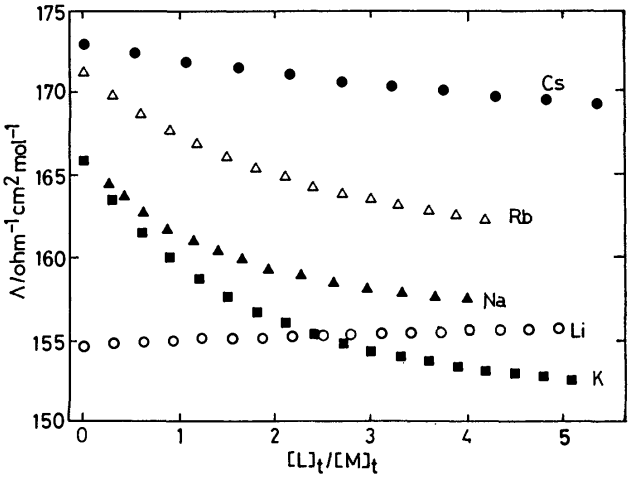

Fig. 1. Λ vs. $[L]_t/[M]_t$ curves for AC·B18C6-alkali metal perchlorate systems in acetonitrile at 25 °C. $[M]_t=1.5\times10^{-3}$ mol dm^{-3}.

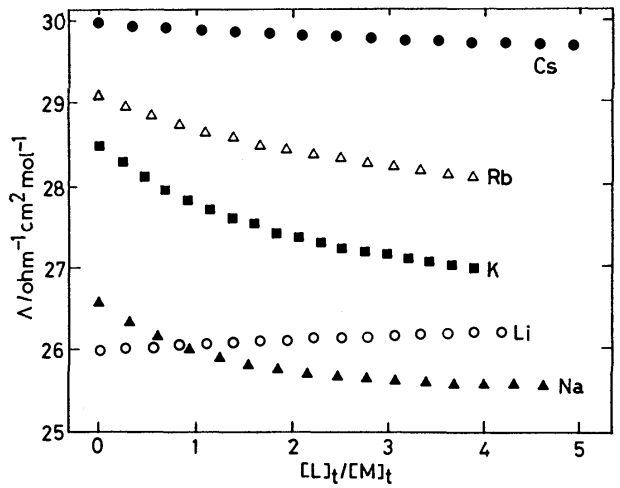

Fig. 2. Λ vs. $[L]_t/[M]_t$ curves for AC·B18C6-alkali metal perchlorate systems in propylene carbonate at 25 °C. $[M]_t=1.5\times10^{-3}$ mol dm^{-3}.

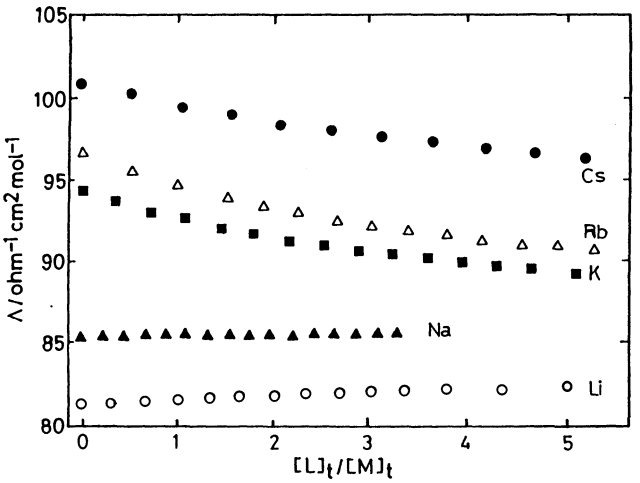

Fig. 3. Λ vs. $[L]_t/[M]_t$ curves for AC·B18C6–alkali metal chloride systems in methanol at 25 °C. $[M]_t=1.5\times10^{-3}$ mol dm^{-3}.

largest and the smallest $\log K_{ML^+}$ values of AC·B18C6 complexes among alkali metal ions in a given solvent is smaller than that of B18C6. Thus, the selectivity of AC·B18C6 for alkali metal ions is lower than that of B18C6. Since AC·B18C6 has two relatively flexible arms, each of which contains three donor ether oxygen atoms, AC·B18C6 may trap the alkali metal ion with the two arms and adopt the most favorable conformation according to the size of the alkali metal ion at the complexation reaction. Thus, since smaller alkali metal ions may attract the donor oxygen atoms of the two arms of AC·B18C6 more strongly than larger alkali metal ions, values of both enthalpy ($\Delta H°$) and entropy ($\Delta S°$) of complexation are expected to be negative and small for smaller alkali metal ions and are expected to be negative and large for larger alkali metal ions. By way of example, values of thermodynamic quantities of pentaethylene glycol dimethyl ether–Na^+ and K^+ complexes in 99 wt.% methanol at 25 °C are as follows.

	$\log K_{ML^+}$	$\Delta H°$/kJ mol^{-1}	$T\Delta S°$/kJ mol^{-1}
Na^+ [11]	1.0	−38.2	−32
K^+ [12]	2.27	−34.1	−21.2

However, it seems that differences in $\Delta H°$ and $\Delta S°$ among AC·B18C6–alkali metal ion complexes are not so large on account of its flexible structure compared with the case of rigid B18C6. The same tendency for $\Delta H°$ and $\Delta S°$ values is found for relatively rigid 18C6- and flexible dibenzo-24-crown-8–alkali metal ion complexes.[1] Consequently, enthalpy and entropy changes compensate each other, resulting in lower selectivity of AC·B18C6 for alkali metal ions.

The selectivity order of AC·B18C6 for K^+, Rb^+, and Cs^+ is consistent entirely with that of B18C6 ($K^+ > Rb^+ > Cs^+$), but the selectivity order of AC·B18C6 for Na^+ among alkali metal ions differs from that of B18C6. This shows that, in the cases of K^+, Rb^+, and Cs^+, the size and shape of a pseudocavity formed by the two arms at the ortho position may be similar to those of the B18C6 cavity, and that a smaller Na^+ ion may cause a larger conformational change on complexation with AC·B18C6 than K^+, Rb^+, and Cs^+ compared with the case of B18C6.

As can be seen from Table 1, an AC·B18C6–alkali metal ion complex is less stable than the corresponding B18C6 complex in the same solvent. Since the two arms of AC·B18C6 are flexible, the entropy contribution seems to play a more dominant role in destabilizing the AC·B18C6–alkali metal ion complex compared with the case of the corresponding B18C6 complex.

For each of the AC·B18C6–Na^+, K^+, and Rb^+ complexes, the $\log K_{ML^+}$ value in CH_3OH is the smallest of all the solvents, and $\log K_{ML^+}$ values in the three solvents of the AC·B18C6–Cs^+ complex are almost the same; however, for each of the B18C6–K^+, Rb^+, and Cs^+ complexes, the $\log K_{ML^+}$ value in CH_3OH is the largest. This may be attributed to stronger hydrogen bonding between uncomplexed AC·B18C6 and CH_3OH compared with the case of B18C6. On the basis of a thermodynamic study on Ni^{2+} complexes in water of tetramine ligands, Hinz and Margerum proposed that a cyclic ligand, being much more compact, is less solvated than a noncyclic, and consequently less energy is expended at its desolvation step.[13] It was reported that, from the data of transfer activity coefficients of Na^+, Na^+ is solvated most strongly in CH_3OH among all the solvents used here.[7] This may be responsible for the fact that $\log K_{ML^+}$ value of the B18C6–Na^+ complex in CH_3OH is the smallest of all the solvents.

Transport Phenomena of AC·B18C6 Complexes. Limiting molar conductivities (Λ_0) of AC·B18C6 complexes determined in this study are as follows:

	Λ_0/Ω^{-1} cm^2 mol^{-1} values at 25 °C	
	Propylene carbonate	Acetonitrile
(Na·AC·B18C6)ClO_4	26.45±0.09	162.3±0.9
(K·AC·B18C6)ClO_4	26.81±0.08	161.8±0.7

Although, when the two arms of AC·B18C6 form a pseudocavity, the size and shape of AC·B18C6 are similar to those of B18C6, an AC·B18C6–alkali metal ion complex is more mobile than the corresponding B18C6 complex (Table 2). This indicates that the alkali metal ion in the AC·B18C6 complex is coordinated with the two arms, and the surface charge of the alkali metal ion in the AC·B18C6 complex is more effectively shielded than that in the B18C6 complex. The effective shielding seems to be ascribed to high flexibility of the two arms. For Na^+, λ^0 values of the complex increase from B18C6 to AC·B18C6 by $10._3$ and $12._0$% in acetonitrile and propylene carbonate, respectively; for K^+, λ^0 values of the complex increase from B18C6 to AC·B18C6 by 2.8_3 and 7.9_7% in acetonitrile and propylene carbonate, respectively. For the

rate of increase in λ^0 values of the complex from B18C6 to AC·B18C6, Na^+ is much larger than K^+. Since Na^+ is smaller than K^+, Na^+ may attract the two flexible arms of AC·B18C6 more strongly than K^+, resulting in more efficient shielding of Na^+ in the complex by the two arms from surrounding solvent molecules on going from B18C6 to AC·B18C6 compared with the case of K^+.

Mobilities of AC·B18C6-Na^+ and K^+ complexes in acetonitrile are almost the same; λ^0 values of AC·B18C6 and B18C6 complexes in propylene carbonate increase from Na^+ to K^+ by 4.4 and 8.4%, respectively; the λ^0 value of the B18C6 complex in acetonitrile increases by 6.4%. Mobilities of the B18C6 complexes vary with a variety of metal ions in the complexes much more than those of the AC·B18C6 complexes. These data support the above discussion, i.e., much more effective shielding of surface charge of the metal ion in the AC·B18C6 complex owing to the two flexible arms compared with the case of B18C6.

Walden products of the AC·B18C6 complexes with Na^+ and K^+ at 25 °C are as follows:

	Acetonitrile	Propylene carbonate
η_0/mP	3.39[14]	25.3[14]
Na^+	0.19_8	0.20_6
K^+	0.19_6	0.21_5

where η_0 denotes viscosity and 1 P = 0.1 Pa s. Walden products of the AC·B18C6-alkali metal ion complexes in propylene carbonate, dielectric constant of which (64.4 at 25 °C[14]) is larger than that of acetonitrile (35.95 at 25 °C[14]), are slightly greater than those in acetonitrile.

References

1) G. A. Melson, "Coordination Chemistry of Macrocyclic Compounds," Plenum Press, New York (1979).
2) C. J. Pedersen, *J. Am. Chem. Soc.*, **89**, 7017 (1967).
3) G. Chaput, G. Jeminet, and J. Juillard, *Can. J. Chem.*, **53**, 2240 (1975).
4) Y. Takeda, *Bull. Chem. Soc. Jpn.*, **56**, 866 (1983).
5) Y. Takeda, H. Yano, M. Ishibashi, and H. Isozumi, *Bull. Chem. Soc. Jpn.*, **53**, 72 (1980).
6) Y. Takeda and H. Yano, *Bull. Chem. Soc. Jpn.*, **53**, 1720 (1980).
7) Y. Takeda, Y. Ohyagi, and S. Akabori, *Bull. Chem. Soc. Jpn.*, **57**, 3381 (1984).
8) Y. Takeda, *Bull. Chem. Soc. Jpn.*, **58**, 1259 (1985).
9) C. H. Springer, J. F. Coetzee, and R. L. Kay, *J. Phys. Chem.*, **73**, 471 (1969).
10) N. Matsuura, K. Umemoto, and Y. Takeda, *Bull. Chem. Soc. Jpn.*, **48**, 2253 (1975).
11) P. U. Früh and W. Simon, "Protides of the Biological Fluids-20th Colloquium," ed by H. Peeters, Pergamon Press, New York (1973).
12) J. D. Lamb, Ph. D. Dissertation, Brigham Young University, Provo, Utah (1978).
13) F. P. Hinz and D. W. Margerum, *Inorg. Chem.*, **13**, 2941 (1974).
14) G. J. Janz and R. P. T. Tomkins, "Nonaqueous Electrolytes Handbook," Academic Press, New York and London (1972), Vol. 1.

 © 1988 The Chemical Society of Japan Bull. Chem. Soc. Jpn., 61, 2711—2714 (1988)

Electrochemical Oxidation of Ruthenium and Iron Complexes at Rotating Disk Electrode in Acetonitrile Solution

Masayuki MORITA,* Yoshinori TANAKA, Keisuke TANAKA,
Yoshiharu MATSUDA, and Takeko MATSUMURA-INOUE†
Department of Industrial Chemistry, Faculty of Engineering, Yamaguchi University, Tokiwadai, Ube 755
†Department of Chemistry, Nara University of Education, Takabatake-cho, Nara 630
(Received December 9, 1987)

The diffusion coefficient and the apparent rate of charge-transfer have been determined for various ruthenium and iron complexes in an acetonitrile solution by using a rotating disk electrode (RDE) method. The diffusion coefficients of $[Ru(bpy)_3]^{2+}$, $[Ru(acac)_3]$, and $[Fe(bpy)_3]^{2+}$ (bpy: 2,2′-bipyridine, acac: acetylacetone), being similar to each other, were about 2×10^{-10} m^2 s^{-1} in acetonitrile containing 0.1 mol dm^{-3} $(C_2H_5)_4NBF_4$. The apparent rate of electrochemical oxidation increased in the order $[Ru(bpy)_3]^{2+}<[Ru(acac)_3]<[Fe(bpy)_3]^{2+}$. The order of the rates was reciprocal to the order of their oxidation potentials in the same electrolyte.

The electrochemistry of transition-metal complexes with organic ligands has been widely investigated by many workers.[1] Some complexes such as Fe, Co, Ru, and Os with 2,2′-bipyridine (bpy), ethylenediamine (en), and 1,10-phenanthroline (phen) as ligands are oxidized and reduced reversibly. The multi-step valence changes of these complexes can be utilized in a rechargeable battery system.[2] The authors have proposed new-type redox batteries consisting of Ru complexes as active materials and organic electrolyte solutions.[3,4] It has been found that the performances of such redox batteries are greatly influenced by the electrochemical reversibility, i.e. the rates of charge-transfer and the diffusion of the electroactive species. The heterogeneous rate constants of Ru complexes have been determined at Pt or a dropping mercury electrode (DME) in aqueous and nonaqueous solutions by some workers.[5,6] However, to our knowledge, the diffusion coefficients and rate constants at the carbon electrode in organic media have not been reported. This paper presents the diffusion coefficients and the heterogeneous charge-transfer rates of some Ru and Fe complexes in an acetonitrile solution. These parameters have been determined by using a rotating disk electrode (RDE) method which would be useful to estimate the parameters simultaneously.

Experimental

The metal complexes used here were tris(2,2′-bipyridine)-ruthenium(II) tetrafluoroborate, $[Ru(bpy)_3](BF_4)_2$, tris(acetylacetonato)ruthenium(III), $[Ru(acac)_3]$, and tris(2,2′-bipyridine)iron(II) tetrafluoroborate, $[Fe(bpy)_3](BF_4)_2$. These were prepared and purified by methods described in the literature.[7-9] The solvent acetonitrile (CH_3CN) was dehydrated and purified by the usual distillation method.[10] The supporting electrolyte was tetraethylammonium tetrafluoroborate (Et_4NBF_4). The concentration of the supporting electrolyte was 0.1 mol dm^{-3} throughout the experiments. The solution contained 0.5×10^{-3}—2.0×10^{-3} mol dm^{-3} of the metal complex.

A one-compartment glass cell (ca. 200 cm^3 volume) was used for the electrochemical measurements. The working electrode was a Pt ring-glassy carbon (GC) disk electrode, whose surface areas were 0.24 and 0.22 cm^2, respectively. Before use, the working electrode was mechanically polished with fine powder of alumina, throughly washed with distilled water and with acetone in a ultrasonic cleaner, and finally rinsed with a test solution. A Pt wire was used as the counterelectrode. The reference electrode was an SCE, which was connected to the working electrode through a salt bridge and a Luggin capillary filled with the test solution. Thus, the electrode potential in this paper is indicated with respect to the SCE. Dry N_2 was introduced into the electrolytic solution for about 30 min before a measurement in order to purge any O_2 dissolved in the electrolyte: then the top of the cell was filled with dry N_2 throughout the measurements.

The current-potential relations were measured by using cyclic voltammetry and an RDE method. The rate of the potential sweep during voltammetry measurements was usually 0.1 or 0.3 V s^{-1}. The potential of the ring-disk electrode and the rotation rate of the electrode were controlled by a dual-potentio/galvanostat (Nikko Keisoku DPGS-1) and a rotation controller unit (Nikko Keisoku RRDE-1, SC-1), respectively. The rotation rate, N, of the electrode was varied from 0 to 4500 rpm (rotation per minute). In some experiments the error in the electrode potential due to uncompensated solution resistance was estimated by a current-interrupting technique: it was negligibly small in most cases. These electrochemical experiments were carried out at room temperature (17—21 °C). The viscosity of the electrolytic solution was measured by a modified Ostwald viscometer in a water bath thermostatted at 20 °C.

Results and Discussion

The cyclic voltammograms for $[Ru(bpy)_3](BF_4)_2$, $[Fe(bpy)_3](BF_4)_2$ and $[Ru(acac)_3]$ at the stationary GC-disk electrode (N=0 rpm) are shown in Fig. 1. The shapes of the voltammograms are quite consistent with those shown in previous work.[11-14] The peak couples are attributable to simple one-electron transfer reactions of the complexes. The potential difference (ΔE_p) of each redox couple apparently showed that the reaction proceeds almost reversibly (ΔE_p=59—62 mV).

Figure 2 shows the voltammograms for $[Ru(bpy)_3](BF_4)_2$ at a rotating ring-disk electrode (RRDE). The increase in the disk current at 1.2 V or above is based on the oxidation of Ru(II) to Ru(III), and the ring current corresponds to the reverse reaction. The col-

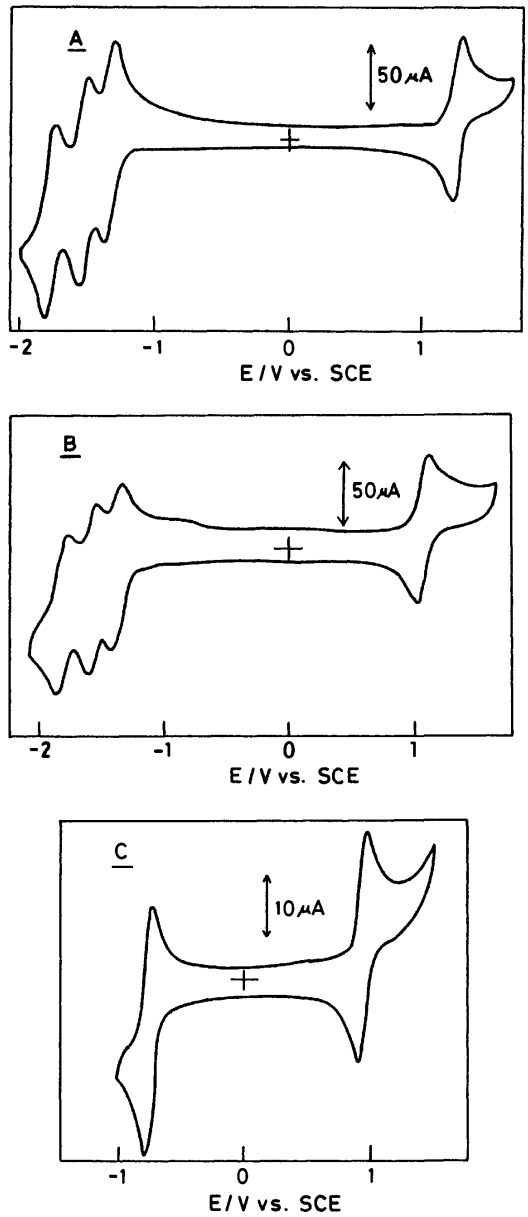

Fig. 1. Cyclic voltammograms for $[Ru(bpy)_3](BF_4)_2$, $[Fe(bpy)_3](BF_4)_2$, and $[Ru(acac)_3]$ at a stationary GC disk electrode in 0.1 mol dm^{-3} Et_4NBF_4/CH_3CN. Surface area of the disk electrode; 0.096 cm^2. Sweep rate; 0.3 V s^{-1}. (A): $[Ru(bpy)_3](BF_4)_2$ (2.0×10^{-3} mol dm^{-3}), (B): $[Fe(bpy)_3](BF_4)_2$ (2.0×10^{-3} mol dm^{-3}), (C): $[Ru(acac)_3]$ (8.0×10^{-4} mol dm^{-3}).

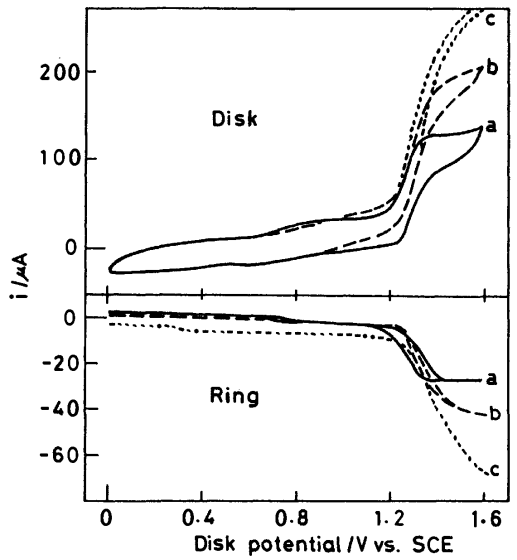

Fig. 2. Voltammograms for $[Ru(bpy)_3](BF_4)_2$ at RRDE in 0.1 mol dm^{-3} Et_4NBF_4/CH_3CN. Surface area of the electrode; 0.22 cm^2 (GC disk) and 0.24 cm^2 (Pt ring). Sweep rate of the disk potential; 0.1 V s^{-1}. Ring potential; 0.3 V vs. SCE. Rate of the electrode rotation (rpm); a: 300, b: 1000, c: 3000.

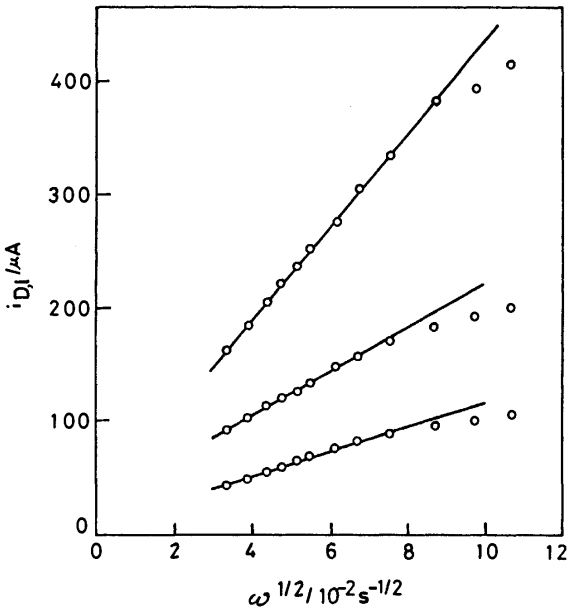

Fig. 3. Typical $i_{D,l}$ vs $\omega^{1/2}$ plots for the anodic oxidation of $[Ru(bpy)_3]^{2+}$. Concentration of the complex (10^{-3} mol dm^{-3}); a: 0.5, b: 1.0, c: 2.0.

lection efficiency obtained experimentally was in good agreement with that calculated from the electrode geometry: this also suggested the reaction is reversible. The steady-state limiting current at the disk electrode, $i_{D,l}$, depended on the rotation rate of the electrode: that is, it yielded the Levich equation:

$$i_{D,l} = 0.62\pi r^2 nFD^{3/2}\nu^{-1/6}\omega^{1/2}c, \quad (1)$$

where r, n, F, D, ν, ω, and c are the radius of the disk electrode, number of transferred electron (here, n=1), Faraday constant, diffusion coefficient of the complex ion, kinematic viscosity of the solution, rate of the electrode rotation (ω=120 πN, where N is rotation per minute), and concentration of the complex, respectively. Figure 3 shows a typical $i_{D,l}$ vs. $\omega^{1/2}$ plot. The diffusion coefficient, D, was determined from the slope of the plot. Table 1 summarizes the D's of $[Ru(bpy)_3]^{2+}$, $[Fe(bpy)_3]^{2+}$, and $[Ru(acac)_3]$ in Et_4NBF_4/CH_3CN. In the present electrolyte system, D was dependent neither on the central metal cation nor on the ligand of the complex. That is, there is little difference in the size of the diffusing species among the three complexes, in spite of some differences in the

Table 1. Diffusion Coefficient (D) of the Complex Ion Determined at an RDE in 0.1 mol dm^{-3} Et_4NBF_4/CH_3CN at 20 °C

Concn of complex/ 10^{-3} mol dm^{-3}	$D/10^{-10}$ m^2 s^{-1}		
	$[Ru(bpy)_3]^{2+}$	$[Re(bpy)_3]^{2+}$	$[Ru(acac)_3]$
0.5	2.4	2.4	2.3
1.0	1.8	2.3	2.3
2.0	2.1	2.1	2.1

ionic radius of the metal and in the size of the ligand. This is probably due to some compensation effects of the solvent, though details have not yet been made clear.[13]

As shown in Fig. 3, plots of $i_{D,l}$ vs. $\omega^{1/2}$ slightly deviate from a straight line that intersects the origin. This suggests that some kinetic step is involved in the electron transfer reaction.[15] The inconsistency of the results obtained at the RDE with those from cyclic voltammetry may be attributed to a difference in the experimental conditions. That is, the reaction rates observed under the steady-state condition of the RDE method might be somewhat different from those of cyclic voltammetry. If the disk current is considered to be formally expressed by Eq. 2, which is applicable to a totally irreversible reaction,

$$1/i_D = 1/i_{D,k} + 1/i_{D,l}, \quad (2)$$

where $i_{D,k}$ represents the current in the absence of mass transfer effects, the intercepts of the $1/i_D$ vs. $\omega^{-1/2}$ plots will give the disk current at $\omega \to \infty$, i_D^{∞} ($=i_{D,k}$). Figure 4 is an example of the $1/i_D$ vs. $\omega^{-1/2}$ plots, where the intercept of each line indicates $1/i_D^{\infty}$ at a given potential. The plots of log (i_D^{∞}) against the disk potential gave Tafel relations, which are shown in Figs. 5, 6, and 7. The Tafel slope, b, was about 0.2 V/decade for each anodic line. Thus, the apparent exchange current, $i_{0,app}$, is obtained by extrapolation of anodic log (i_D^{∞})—E_D curve to the reversible potential, E_r, which had previously determined by the cyclic voltammogram at the stationary electrode. The resulting $i_{0,app}$'s are

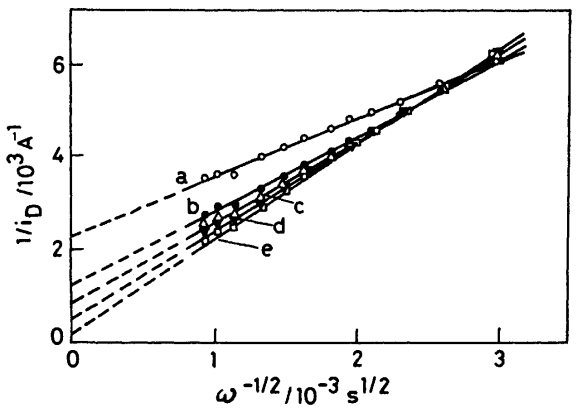

Fig. 4. Typical $1/i_D$ vs. $\omega^{-1/2}$ plots for the anodic oxidation of 2×10^{-3} mol dm^{-3} $[Ru(bpy)_3]^{2+}$. Disk potential (V vs. SCE); a: 1.35, b: 1.40, c: 1.45, d: 1.50, e: 1.60.

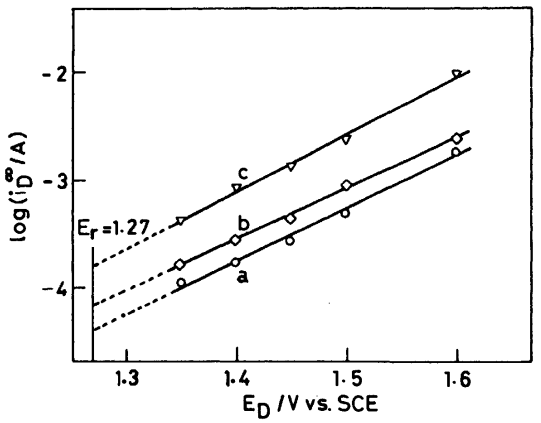

Fig. 5. Plots of log(i_D^{∞}) against disk potential (Tafel plots) for the anodic oxidation of $[Ru(bpy)_3]^{2+}$. Concentration of the complex (10^{-3} mol dm^{-3}); a: 0.5, b: 1.0, c: 2.0.

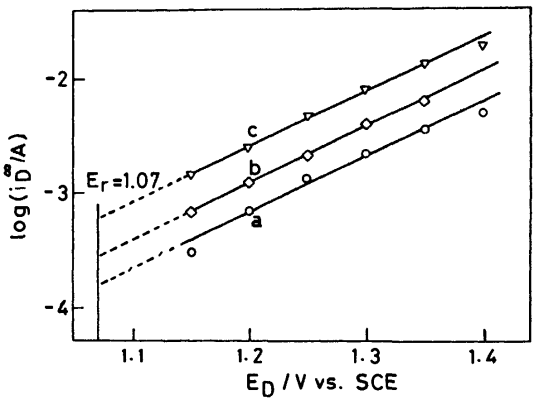

Fig. 6. Plots of log(i_D^{∞}) against disk potential (Tafel plots) for the anodic oxidation of $[Fe(bpy)_3]^{2+}$. Concentration of the complex (10^{-3} mol dm^{-3}); a: 0.5, b: 1.0, c: 2.0.

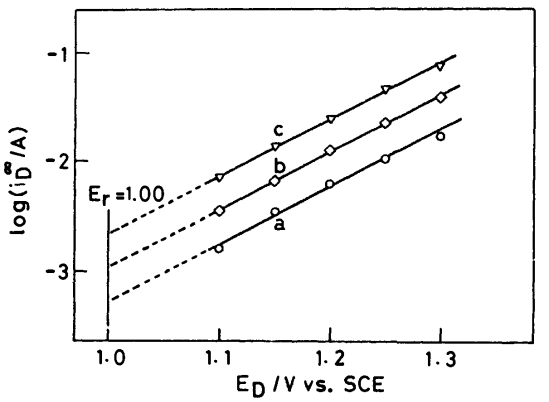

Fig. 7. Plots of log(i_D^{∞}) against disk potential (Tafel plots) for the anodic oxidation of $[Ru(acac)_3]$. Concentration of the complex (10^{-3} mol dm^{-3}); a: 0.5, b: 1.0, c: 2.0.

summarized in Table 2. If one tentatively estimates the heterogeneous rate constant, k, from Eq. 3,

$$i_0 = nFkc \quad (3)$$

k will be 3.4×10^{-5} m s^{-1} for the $[Ru(bpy)_3]^{2+}$ system. This value is rather small compared with those deter-

Table 2. Apparent Exchange Current ($i_{0,app}$) for the Anodic Oxidation of the Complex in 0.1 mol dm^{-3} Et_4NBF_4/CH_3CN at 20 °C

Concn of complex/ 10^{-3} mol dm^{-3}	$i_{0,app}/10^{-3}$ A cm^{-2}		
	$[Ru(bpy)_3]^{2+}$	$[Fe(bpy)_3]^{2+}$	$[Ru(acac)_3]$
0.5	0.16	0.68	2.2
1.0	0.33	1.3	4.5
2.0	0.64	2.7	9.1

mined previously in similar nonaqueous systems, but by different methods.[7,16] A possible reason for this is that the apparent i_0 obtained in this work is essentially based on the deviation of the rate equation from that for a totally reversible reaction.[15] Thus, the apparent rate, $i_{0,app}$, might involve a somewhat different meaning from the heterogeneous rate constant that were previously determined by cyclic voltammetry. However, a discussion of $i_{0,app}$ obtained under a steady-state condition will also be meaningful from the standpoint of any application of the redox system to a practical battery.[3,4]

The rate varies significantly with both the central metal cation and the ligand, in contrast to little variation of the diffusion constant among the complexes. The order of the rates,

$$[Ru(bpy)_3]^{2+} < [Fe(bpy)_3]^{2+} < [Ru(acac)_3],$$

was in agreement with the reciprocal order of the redox (reversible) potentials,

$$[Ru(bpy)_3]^{2+/3+}\ (1.27\ V) > [Fe(bpy)_3]^{2+/3+}\ (1.07\ V) > [Ru(acac)_3]^{0/+}\ (1.00\ V),$$

The reason for this result has not yet been made clear. The relation between the redox potential and the electronic structure of the complex among the series of analogs has been widely investigated by means of cyclic voltammetry and polarography.[13,14,17–20] However, only a few studies have been carried out concerning the correlation between the charge-transfer rate and the structure of the complex.[5] This is probably due to the insufficiency of reliable data concerning the rate constant. Our present interest is how the rates of charge transfer and diffusion of the complexes influence the charge-discharge performance of the redox batteries with this type of complex. Some experiments are now in progress and the results will be reported in the near future.

Summary

The diffusion coefficients and the electron-transfer rates of some Ru and Fe complexes have been measured at a rotating disk electrode. The results are summarized as follows:

1. The cyclic voltammetry shows that the heterogeneous redox reactions of $[Ru(bpy)_3]^{2+}$, $[Fe(bpy)_3]^{2+}$, and $[Ru(acac)_3]$ proceed reversibly in an acetonitrile-based electrolyte.

2. The diffusion rate was almost constant among the complexes examined, while the current based on the electron transfer varied according to the structure of the complex.

3. The rate of electron transfer tended to increase with the decrease in the redox potential.

This work was financially supported by Grants-in-Aid for Scientific Research Nos. 59040053, 60040055, and 61040019 from the Japanese Ministry of Education, Science and Culture. We also wish to thank Dr. Yoshio Takasu and Mr. Masaki Okada for their participation in discussion on this work.

References

1) e.g. C. J. Pickett, "Electrochemistry," ed by D. Pletcher, The Royal Society of Chemistry, London (1983), Vol. 8, Chap. 3; C. J. Pickett, "Electrochemistry," ed by D. Pletcher, The Royal Society of Chemistry, London (1984), Vol. 9, Chap. 4.

2) P. Singh, *J. Power Sources*, **11**, 135 (1984).

3) Y. Matsuda, Y. Takasu, M. Morita, K. Tanaka, M. Okada, and T. Matsumura-Inoue, *Denki Kagaku*, **53**, 632 (1985).

4) Y. Matsuda, K. Tanaka, and M. Morita, *J. Appl. Electrochem.*, in press.

5) T. Saji and S. Aoyagui, *J. Electroanal. Chem.*, **63**, 31 (1975).

6) C. R. Martin, I. Rubinstein, and A. J. Bard, *J. Electroanal. Chem.*, **151**, 267 (1983).

7) C. F. Liu, N. C. Liu, and J. C. Bailar, Jr., *Inorg. Chem.*, **3**, 1085 (1964).

8) P. Pfeiffer and Fr. Tappermann, *Z. Anorg. Chem.*, **215**, 273 (1933).

9) E. A. Seddon and K. R. Seddon, "The Chemistry of Ruthenium (Topics in Inorganic and General Chemistry, Vol. 19)," Elsevier, Amsterdam (1984), p. 201.

10) C. K. Mann, "Electroanalytical Chemistry," ed by A. J. Bard, Marcel Dekker, New York (1969), Vol. 3, p. 57.

11) N. E. Tokel-Takvoryan, R. E. Hemingway, and A. J. Bard, *J. Am. Chem. Soc.*, **95**, 6582 (1973).

12) T. Matsumura-Inoue, C. Ishida, M. Kasai, and N. Kuroda, *Nippon Kagaku Kaishi*, **1982**, 72.

13) M. Iwamura-Kasai, *Nippon Kagaku Kaishi*, **1983**, 1456.

14) Y. Ohsawa, K. W. Hanck, and M. K. DeArmond, *J. Electroanal. Chem.*, **175**, 229 (1984).

15) A. J. Bard and L. R. Faulkner, "Electrochemical Methods," John Wiley & Sons, New York (1980), p. 290.

16) T. Saji, T. Yamada, and S. Aoyagui, *Bull. Chem. Soc. Jpn.*, **48**, 1641 (1975).

17) T. Kubota, H. Miyazaki, K. Ezumi, and M. Yamakawa, *Bull. Chem. Soc. Jpn.*, **47**, 491 (1974).

18) T. Saji and S. Aoyagui, *J. Electroanal. Chem.*, **58**, 401 (1975).

19) T. Saji and S. Aoyagui, *J. Electroanal. Chem.*, **60**, 1 (1975).

20) T. Matsumura-Inoue, H. Tomono, M. Kasai, and T. Tominaga-Morimoto, *J. Electroanal. Chem.*, **95**, 109 (1979).

21) R. J. Klingler and J. K. Kochi, *J. Phys. Chem.*, **85**, 1731 (1981).

 © 1988 The Chemical Society of Japan Bull. Chem. Soc. Jpn., 61, 2715—2719 (1988)

Dielectric Properties of the Hydrogen-Bonded Liquids. Steric Effects on Dielectric Properties in Isomeric Methylcyclohexanols

Kimiya TAKESHITA, Eiji IKADA,* and Michio ASHIDA
Department of Industrial Chemistry, Faculty of Engineering, Kobe University, Nada, Kobe 657
(Received December 28, 1987)

The dielectric properties of 2- and 4-methylcyclohexanols were studied in order to elucidate the molecular geometric dependences of the dielectric properties of alcohols. The Kirkwood correlaton factors g of the trans isomers are larger than those of the cis isomers. Especially the g of *cis*-2-methylcyclohexanol at 298 K is 0.75. The dielectric relaxation of all the methylcyclohexanols studied shows the characteristics of the Debye-like behavior frequently reported for primary alcohols. The activation energy of dielectric relaxation of 2-methylcyclohexanol is much larger than that of the other methylcyclohexanols. These facts are discussed in terms of the difference of the steric hindrance for the association through the hydrogen bond.

It is well-known that alcohol molecules in a liquid state are generally self-associated by intermoleculer hydrogen bonding; therefore, the alcohols show abnormal physical properties.[1] The abnormal behaviors in dielectric properties have been revealed in earlier investigations.[2]

The dielectric susceptibility of many organic liquids can be predicted from the magnitude of their dipole moments while that of the alcohols can not. This can be explained by the fact that the dipoles of alcohol molecules do not follow an electric field independently, owing to the self-association through the hydrogen bond. Further, their dielectric relaxation times are longer than those of many organic molecules in a liquid state due to the large interaction of the hydrogen bond. In the dielectric relaxation process, the dipoles of many organic molecules reorient independently under an alternative electric field, while the dipoles of alcohol molecules reorient cooperatively for the hydrogen bond. After all, the abnormal dielectric behavior of the alcohols also results from the hydrogen bond.

The association through the hydrogen bond and the hydrogen bond network system governing the dielectric relaxation have been investigated by changing the molecular geometry of alcohols: Secondary alcohols and tertiary alcohols, with the more sterically hindered association in a liquid state, are known to have different tendencies of dielectric properties from primary alcohols. Many investigators have mainly studied linear alcohols and have discussed the steric effect for the association and the dielectric relaxation.[3,4] Most of these linear molecules, however, have a freedom of intramolecular dipolar rotation for the dipole, which is considered to denature the association and the hydrogen bond system, itself. Therefore, these investigators have neglected the significance of the change of the molecular geometry and did not separate the segmental dipolar reorientation process from the whole dielectric relaxation.

In order to discuss the different tendencies of secondary alcohols and tertiary alcohols in further detail, we studied the dielectric properties of cyclohexanol derivatives which have less freedom of the segmental dipolar reorientation motion and of changing the molecular geometry than the linear molecules.

Experimental

2-Methylcyclohexanol. The trans isomer (Guaranteed reagent, Tokyo Kasei Co.) and the cis isomer synthesized according to the literature[5] were used to prepare the isomeric mixture. The commercial isomeric mixture (Extra pure reagent, 23% cis content by GC, Tokyo Kasei Co.) was also used.

3-Methylcyclohexanol. The commercial isomeric mixture (Extra pure reagent, 67% cis content by GC, Tokyo Kasei Co.) was used.

4-Methylcyclohexanol. The trans isomer (Analytical reagent, Aldrich Chemical Co.) and the cis isomer (Analytical reagent, Aldrich Chemical Co.) were used to prepare the isomeric mixture. The commercial isomeric mixture (Extra pure reagent, 37% cis content by GC, Tokyo Kasei Co.) was also used.

Purification. Dielectric measurments are sensitive to water as an inpurity, so that all these alcohols were dried by refluxing over calcium hydride before distillation. These purities were checked using a Hitachi GC-063 gas chromatograph with a thermal conductivity detecter and a stainless-steel column (1m long, 3mm diameter) packed with PEG 20M.

Dielectric Measurements. The measurements were carried out using a ratio-arm transformer bridge (TR-1C, Ando Electric Co.) and a glass cell with a platinum concentric electrode over a frequency range from 100 Hz to 3 MHz. Dipole measurements were carried out by the Halverstadt-Kumler method[6] in CCl_4 using another more precise ratio-arm transformer bridge (TR-10C, Ando Electric Co.). The accuracy of the temperature control was maintained within 0.1 K. All data regarding dielectric relaxation were analyzed with a least-square method.

Viscosity Measurement. Measurements were carried out with an Ostwald-type viscometer calibrated with the "standard liquid" (Cosmo Oil Co.). The accuracy of the temperature control was maintained within 0.1 K.

Results and Discussion

Static Dielectric Constants and the Association. The

temperature dependences of static dielectric constants of 2-methylcyclohexanol and 4-methylcyclohexanol studied are shown in Fig. 1. There are linear correlations between the static dielectric constants and the reciprocal absolute temperature for the trans isomer of these two isomers, while small deviations from the linear correlation can be seen for the cis isomers. Such deviations have been frequently found in the neighborhood of the melting temperature. The melting temperature of a cis isomer is generally higher than that of the trans isomer.[7] The maximum point is found for *cis*-2-methylcyclohexanol, whose melting temperature is ca. 280 K.[8]

As is shown in Fig. 1, a very weak dependence of the dielectric constant on temperature was found for *cis*-2-methylcyclohexanol. This phenomenon is peculiar for the alcohols, i.e. associated molecules, though it is generally found for nonpolar molecules. Upon mixing one substance with an associated one, a correlation between the dielectric constant and its mole fraction maintains an experimentally linear relationship since the density is almost the same.[9] Figure 2 shows the change in the dielectric constants with the mixing

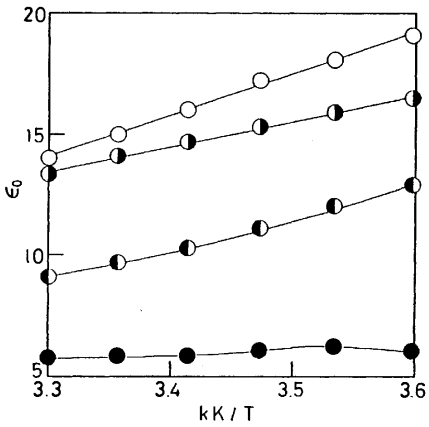

Fig. 1. Dielectric constants for some methylcyclohexanols as a function of T^{-1}. ○: *trans*-2-methyl, ◐: *trans*-4-methyl, ◑: *cis*-4-methyl, ●: *cis*-2-methyl.

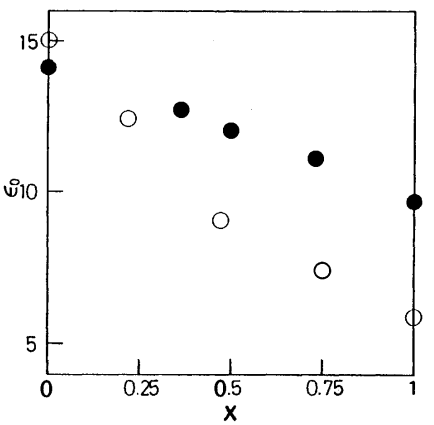

Fig. 2. Dielectric constants for some methylcyclohexanols as a function of x at 298 K. ○: 2-methyl, ●: 4-methyl.

ratio of the cis isomer and the trans isomer. x is the mole fraction of the cis isomer. A linear correlation was also found in a mixture of these two isomers. This fact shows that the cis isomer associates with the trans isomer and that such a self-association of these alcohols could also be confirmed by an IR spectroscopic study.

The dielectric constant generally depends on the temperature, density and dipole moment. For associated molecules, however, an estimation of the orientational angle between the two neighboring dipoles is important for a determination of the dielectric constant. The Kirkwood theory for liquid dielectrics includes this correlation factor, g, which is used to evaluate the dipole-dipole correlation:[10]

$$g = 1 + z\langle\cos\theta\rangle = \frac{9kTV}{4\pi N\mu^2}\,\frac{(\varepsilon_0-\varepsilon_\infty)(2\varepsilon_0+\varepsilon_\infty)}{\varepsilon_0(\varepsilon_\infty+2)^2}, \quad (1)$$

where z is the number of nearest-neighbor dipoles, θ the orientational angle between a dipole and its nearst neighbors, k the Boltzmann constant, T the absolute temperature, V the molar volume, N Avogadro's number, and μ the gas-phase dipole moment ε_0 and ε_∞ are, respectively, the static dielectric constant and the high-frequency limiting value of ε, and the bracket indicates the average over the ensemble. We used $\varepsilon_\infty=1.1\,n_D^2$ according to Dannhauser and Bahe,[11] and μ in CCl_4 solution instead of that in gas phase. Since z is not known for almost all organic molecules, g was used to estimate and discuss the dipole-dipole correlation. It is difficult to estimate the degree of aggregation of dipoles from g, but it gives a criterion for cluster formation. The calculated experimental g is shown in Table 1.

The g of both trans isomers in this table is larger than unity, indicating a parallel alignment of these dipoles. This phenomenon is similar to that of primary alcohols, which generally form a linear chain multimer of various lengths. On the other hand, the g of these cis isomers does not have the same characteristic as that of their trans isomers. The g of *cis*-4-methylcyclohexanol is larger than unity, that is the same case of the trans isomer. The g of *cis*-2-methylcyclohexanol, however, is smaller than unity, which indicates the possibility that *cis*-2-methylcyclohexanol forms a cyclic multimer.

In order to discuss the steric hindrance for the association through the hydrogen bonding, we took the

Table 1. Dielectric Properties for Some Methylcyclohexanols at 298 K

Isomer	d[a]/g cm^{-3}	ε_0	n_D	μ/D[b]	g
cis-2-Methyl	0.93181	5.85	1.4608	1.88	0.75
trans-2-Methyl	0.92085	15.0	1.4589	1.74	2.91
cis-4-Methyl	0.9147	9.68	1.4578	1.76	1.73
trans-4-Methyl	0.9080	14.1	1.4535	1.85	2.46
Cyclohexanol[a]	0.9684	15.0	1.4684	1.86	2.10

a) From Ref. 25. b) 1 D=3.3356×10^{-30} C m.

role of the conformation of these methylcyclohexanols into account.

Cyclohexane skeletons have been well-studied in stereo chemistry. The structure of such a molecule can be roughly divided into the two types of conformations: a boat and a chair form. The latter conformation is more stable than the former one. Here, we consider only the chair conformation while discussing the dielectric properties of this alcohol since this form is predominant at room temperature. A substituent has two positions: axial and equatorial. The former position has an "1,3-diaxial" interaction, a large steric repulsion of a methyl substituent with the two axial hydrogen atoms on the same side of a cyclohexane skeleton. For this reason a large substituent prefers the equatorial position to the axial one.

There have been many conformational studies of these methylcyclohexanols.[12-14] The predominant position of the two substituents is determined as follows: The hydroxyl group has an axial position and the methyl group, which is larger than hydroxyl group, has an equatorial position for the cis isomer, while both these substituents have an equatorial position for the trans isomer. Therefore, the cis isomer, having an 1,3-diaxial interaction, can be said to have a larger steric hindrance for the association than the trans isomer. 2-Methyl isomer evidently has a larger steric hindrance for the hydroxyl group than the 4-methyl isomer, which is considered to have the absence of a direct steric hindrance.[7]

Alcohols with a strong steric hindrance have the tendency to form a cyclic dimer or trimer.[15,16] The position of the methyl group attached to the same or the neighboring carbon with the hydroxyl group has been reported to make the g smaller than unity for the case of secondary alcohols.[3,4] Therefore, the g of *cis*-2-methylcyclohexanol is smaller than unity. However, that of *cis*-4-methylcyclohexanol, having the 1,3-diaxial interaction as well as *cis*-2-methylcyclohexanol, is larger than unity. It can be, therefore, considered that the steric hindrance of the 1,3-diaxial interaction enlarges the average dipolar orientation angle, though this hindrance is not sufficient to form a cyclic multimer.

It is strange to say that the larger the number of carbon atoms for the homolog of the primary alcohol, the larger is g.[17] This suggests that the steric hindrance is favorable for making the g larger upon forming a linear multimer. This may be the reason why *trans*-2-methylcyclohexanol has a larger g than *trans*-4-methylcyclohexanol. It is interesting to see how strong the association is sterically hindered to form the cyclic multimer.

Dielectric Relaxation. The typical dielectric relaxation for the methylcyclohexanol investigated is shown in Fig. 3. In general, the dielectric relaxation for monohydric alcohol is reported as a Debye type, formulated in Eq. 2, while a dielectric relaxation for diol and triol is reported as a Davidson-Cole type, formulated in Eq. 3:

$$\varepsilon^* = \varepsilon_0 + \frac{\varepsilon_0 - \varepsilon_\infty}{1 + i\omega\tau_m} \tag{2}$$

and

$$\varepsilon^* = \varepsilon_0 + \frac{\varepsilon_0 - \varepsilon_\infty}{(1 + i\omega\tau_m)^\beta} \tag{3}$$

where ε^* is the complex dielectric constant, ω the angular frequency, $\tau_m=(2\pi f_m)^{-1}$ the relaxation time, and β the Davidson-Cole parameter. The Davidson-Cole type is used in the following discussion because the standard deviation of the residual of the Davidson-Cole type is smaller than that of the Debye type with an analysis by the least-square method.

Fitted parameters are shown in Table 2. The β are nearly equal to unity, indicating a "Debye-like" behavior of the relaxation frequently reported for the

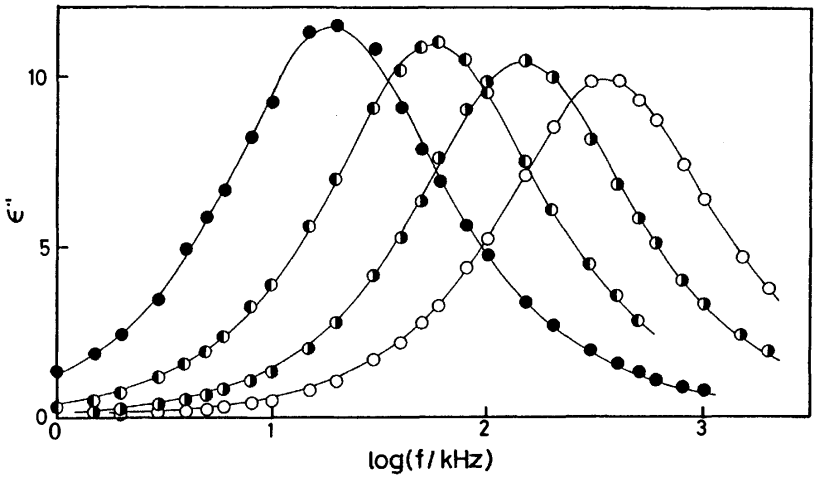

Fig. 3. Dielectric losses for 2-methylcyclohexanol (x=0.23) as a function of frequency. Circles show observed values and real lines are estimated by using observed values. ○: at 253 K, ○: at 248 K, ○: at 243 K, ●: at 238 K.

Table 2. The Davidson-Cole Parameters for Some Methylcyclohexanols

T/K	x	f_m/kHz	β	ε_0	ε_∞
		2-Methylcyclohexanol			
228	0.62	8.43	0.78	24.9	3.73
233	0.23	5.85	0.91	28.4	4.07
	0.62	28.9	0.80	22.8	3.10
238	0.23	17.4	0.89	27.3	3.30
	0.62	87.7	0.81	21.0	3.00
243	0.23	52.8	0.91	26.2	3.51
248	0.23	135	0.92	24.7	3.03
253	0.23	340	0.94	23.3	3.14
		4-Methylcyclohexanol			
228	0.36	25.9	0.85	24.8	2.83
	0.50	15.9	0.89	25.4	3.00
	0.73	19.9	0.80	24.7	3.37
233	0.36	46.3	0.90	24.0	3.04
	0.50	39.1	0.90	24.3	3.19
	0.73	50.6	0.83	23.5	3.16
238	0.36	104	0.91	23.0	3.08
	0.50	94.5	0.91	23.2	3.08
	0.73	121	0.86	22.2	3.31
243	0.36	213	0.90	22.1	2.86
	0.50	203	0.93	22.2	3.19
	0.73	262	0.86	21.1	3.22
248	0.36	428	0.91	21.2	2.80
	0.50	402	0.90	21.3	2.83
	0.73	502	0.82	20.1	2.86

monohydric alcohols. The relaxation time of 2-methylcyclohexanol is larger than that of the 4-methyl isomer, but the dependence of that on the fraction of the cis isomer cannot be estimated because of a lack of data points. Activation parameters of the dielectric relaxation process are shown in Table 3. The activation energy and the preexponential factor of 2-methylcyclohexanol are larger than those of 4-methyl isomers, although they depend on the fraction of the cis isomer. The spectral shape parameters,[19] m and n, are shown in Table 4. m is the index of "correlation of the intercluster exchange of relaxation motions," and n is that of "the intracluster correlation of relaxation motions." These parameters of all the methylcyclohexanol investigated are approximately the same regardless of the fraction of the cis isomer; this fact shows that the motion of an intercluster exchange of the dipole is almost free and that the motion of the dipole in its local environment couples weakly.

The Debye-like behavior for monohydric alcohols is explained on "the dipole relaxation of clusters of alcohol molecules hydrogen-bonded with each

Table 3. Dielectric and Viscous Activation Parameters for Some Methylcyclohexanols

Isomer	x	$\Delta E_\varepsilon^{\neq}$	A_ε	$\Delta E_\eta^{\neq}$	A_ε
		kJ mol^{-1}	Hz	kJ mol^{-1}	Hz
2-Methyl	0.23	99.8	8×10^{26}	54.7	1×10^{14}
	0.62	106	9×10^{28}		
3-Methyl	0.67	67.2	5×10^{20}	40.9	6×10^{11}
4-Methyl	0.36	67.0	4×10^{20}	47.9	7×10^{12}
	0.50	76.3	3×10^{22}		
	0.73	76.3	4×10^{22}		
Cyclohexanol		55.0[a]	10^{18}[a]		
		49.2[b]	6×10^{16}[b]		

a) From Ref. 26. b) From Ref. 27.

Table 4. Spectral Shape Parameters with Standard Deviations of Residual for Some Methylcyclohexanols

Isomer	x	m	n
2-Methyl	0.23	1.04(0.07)	0.21(0.03)
	0.62	0.92(0.03)	0.31(0.04)
3-Methyl	0.67	0.99(0.02)	0.19(0.02)
4-Methyl	0.36	0.91(0.01)	0.25(0.02)
	0.50	0.97(0.02)	0.26(0.04)
	0.73	0.97(0.02)	0.29(0.03)
Cyclopentanol[a]		0.85	0.28
Cyclohexanol[a]		0.61	0.41

a) From Ref. 26.

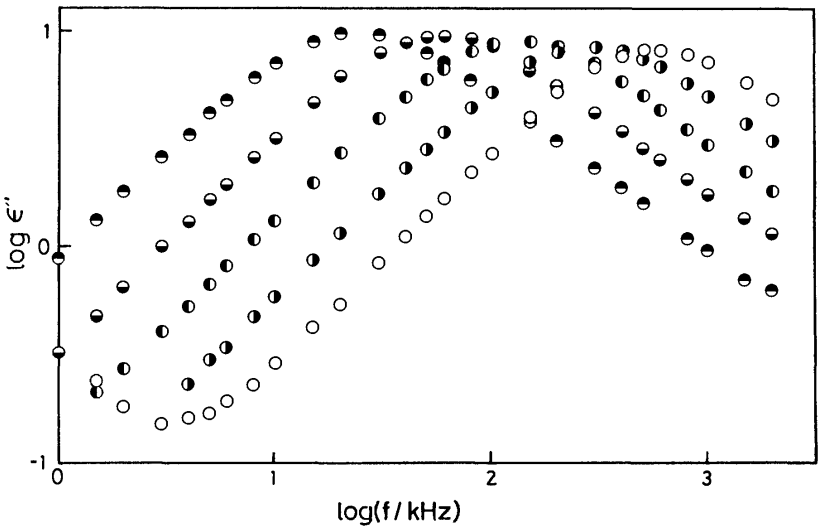

Fig. 4. Dielectric losses for 4-methylcyclohexanol (x=0.73) as a function of frequency. ○: at 248 K, ◑: at 243 K, ◐: at 238 K, ◒: at 233 K, ◓: at 228 K.

Table 5. Dielectric and Viscous Activation Energies for Some Alcohols

Alcohol	$\Delta E_\varepsilon^{\neq}$ / kJ mol^{-1}	Ref.	$\Delta E_\eta^{\neq}$ / kJ mol^{-1}	Ref.
1-Propanol	23.0	21	18.5	22
1-Pentanol	34.2	4	20.9	23
2-Methyl-2-butanol	52.1	4	30.5	23
1-Octanol	36.8	21		
2-Octanol	56.6	24		
3-Octanol	71.2	24		
5-Methyl-3-heptanol	82.1	24		
6-Methyl-3-heptanol	79.7	24		

other."[20] The relaxation time of primary alcohols can be evaluated by Bertolini et al. using the hydrogen bond lifetime and the probability that the bond is randomly intact.[4] The relaxation time of secondary alcohols and tertiary alcohols, however, could not be evaluated; this suggests an additional intramolecular relaxation of dipoles with the intermolecular one.

Secondary and tertiary alcohols have the same tendencies for the dielectric relaxation in that the activation energy and the preexponential factor are larger than primary alcohols having the same number of carbon atoms, as shown in Table 5. At first glance, the activation energy and the preexponential factor become larger with the increasing size of the alkyl group and the increasing degree of branching. Our results in Table 3 are similar to this tendency with respect to the point of the degree of the branching. The large activation energy cannot be attributed to the additional intramolecular relaxation because the activation entropy of the relaxation of these methylcyclohexanols, ca. 400—500 J mol^{-1} K^{-1}, is too large for such an additional intramolecular relaxation motion of the dipole. There seems to be another reason for the large activation energy.

Crossely et al. found a large Eyring activation enthalpy, ca. 60—100 kJ mol^{-1} for the dielectric relaxation of some simple hydrocarbons at temperatures just above their glass temperatures, T_g.[28] They concluded that this phenomenon resulted from a dipolar cooperative reorientation in the amorphous clusters and that the activation enthalpy reflected the ability of the molecules to interact. However, the activation enthalpy of methylcyclohexane in their work is almost equal to that of 3- and 4-methylcyclohexanol which clearly have a larger interaction than methylcyclohexane.

The dielectric relaxation process, which can be regarded as a molecular rotation process, is often discussed in contrast with viscosity or a shear process. The activation energies of the shear process are also listed in Table 3. The dependence on the fraction of the cis isomer cannot be evaluated due to the small quantity to be measured. The difference between the dielectric activation energy and the viscous activation energy of 2-methylcyclohexanol is larger than that of 3- or 4-methyl isomer. The difference between the two activation energies may be explained by the difference of hydrogen-bond breaking and reforming mechanisms between rotation and translation. From this point of view, the larger activation energy and the longer relaxaton time of 2-methylcyclohexanol are attributed to the steric effect of the neighboring methyl group for the hydrogen bond as well as the association.

References

1) See, e.g., G. C. Pimentel and A. L. McClellan, "The Hydrogen Bond," W. H. Freeman & Company, San Francisco (1960).
2) S. Mizushima, *Sci. Pap. I. P. C. R.*, **9**, 209 (1928).
3) W. Dannhauser, *J. Chem. Phys.*, **48**, 1911 (1968).
4) A. D'Aprano, D. I. Donato, G. D'Arrigo, D. Bertolini, M. Cassettari, and G. Salvetti, *Mol. Phys.*, **55**, 475 (1985).
5) H. C. Brown and S. Krishnamurthy, *J. Am. Chem. Soc.*, **94**, 7159 (1972).
6) "Jikken Kagaku Kouza," Maruzen Co., Ltd., Tokyo (1957), Vol. 3, p. 26.
7) M. Hanack, "Conformational Theory," Academic Press Inc., New York (1965), p. 142.
8) "Kagaku Binran," Maruzen Co., Ltd., Tokyo (1984), Vol. 1, p. 376.
9) K. Baba and K. Kamiyoshi, *Bull. Res. Inst. Sci. Measurement, Tohoku Univ.*, **29**, 121 (1981).
10) J. G. Kirkwood, *J. Chem. Phys.*, **7**, 911 (1939).
11) W. Dannhauser and L. W. Bahe, *J. Chem. Phys.*, **40**, 3058 (1964).
12) A. R. H. Cole, P. R. Jefferies, and G. T. A. Mueller, *J. Chem. Soc.*, **1959**, 1222.
13) E. L. Eliel and C. A. Luckach, *J. Am. Chem. Soc.*, **79**, 5986 (1957).
14) S. Winstein and N. J. Holness, *J. Am. Chem. Soc.*, **77**, 5574 (1955).
15) A. D'Aprano, D. I. Donato, P. Migliardo, F. Alliotta, and C. Vasi, *Mol. Phys.*, **58**, 213 (1986).
16) C. Boudéron, J. J. Péron, and C. Sandorfy, *J. Chem. Phys.*, **76**, 869 (1972).
17) A. D'Aprano, D. I. Donato and E. Caponetti, *J. Solution Chem.*, **8**, 135 (1979).
18) D. W. Davidson and R. H. Cole, *J. Chem. Phys.*, **19**, 1484 (1951).
19) R. M. Hill, *Phys. Status Solidi B*, **103**, 319 (1981).
20) R. Minami, K. Ito, H. Takahashi, and K. Higasi, *J. Chem. Phys.*, **73**, 3396 (1980).
21) W. Dannhauser, L. W. Bahe, R. Y. Lin, and A. F. Flueckinger, *J. Chem. Phys.*, **43**, 257 (1965).
22) J. Miyazaki, Master Thesis, Kobe University, Kobe, Japan, 1984.
23) A. D'Aprano, D. I. Donato, and V. Agrigento, *J. Solution Chem.*, **10**, 673 (1981).
24) W. Dannhauser, *J. Chem. Phys.*, **48**, 1918 (1968).
25) J. A. Riddick and W. A. Bunger, "Organic Solvents," Wiley-Interscience, New York (1970).
26) M. Shablakh, L. H. Dissado, and R. M. Hill, *J. Chem. Soc., Faraday Trans. 2*, **79**, 369 (1983).
27) K. Baba and K. Kamiyoshi, *Bull. Res. Inst. Sci. Measurement, Tohoku Univ.*, **10**, 51 (1961).
28) M. S. Ahmed, J. Chao, J. Crossley, M. S. Hossain, and S. Walker, *J. Chem. Soc., Faraday Trans. 2*, **80**, 1047 (1984).

 © 1988 The Chemical Society of Japan Bull. Chem. Soc. Jpn., 61, 2721—2726 (1988)

Surface Properties of Microcrystalline Hydrous Titanium Oxide as Obtained by Thermal Hydrolysis from a $TiCl_4$ Solution

Kenta Ooi,* Yoshitaka Miyai, Shunsaku Katoh, and Kazuhiko Sugasaka
Government Industrial Research Institute, Shikoku, 2-3-3 Hananomiya-cho, Takamatsu-shi 761
(Received January 20, 1988)

The surface properties of hydrous titanium oxides (HTiO's), as obtained by refluxing $TiCl_4$ or urea-containing $TiCl_4$ solutions at 373 K, were examined by means of nitrogen adsorption/desorption at 77 K and of fluoride ion adsorption. Their crystal phases and particle shapes were investigated by X-ray diffraction analyses and electronmicroscopic observations, respectively. The HTiO obtained from a 0.03 or 0.1 mol·dm^{-3} $TiCl_4$ solution was of an anatase type, consisting of small (about 10 nm) particles. They had pores that were 2 nm in radius, with an narrow size distribution. The HTiO obtained from a 1.0 mol·dm^{-3} $TiCl_4$ solution was of a rutile type, consisting of acicular particles. It had pores that were greater than 2 nm in radius, with a broad size distribution. All of the HTiO's obtained from ($TiCl_4$+urea) solutions were anatase types. The most probable pore radius increased from 1.9 to 3.6 nm with the increase in the initial $TiCl_4$ concentration from 0.03 to 1.0 mol·dm^{-3}. The surface properties of the anatase-type HTiO's were discussed based on the sizes and shapes of the primary crystallites and on their spatial distribution.

The adsorptive or catalytic activity of HTiO depends strongly on its surface properties. These surface properties themselves vary depending on the preparation method and conditions. There have been many studies of the surface properties of the HTiO's obtained through different methods of preparation.[1-20]

The thermal hydrolysis of titanium(IV) salt in solution is one of the most common methods for the preparation of HTiO. However, the physical properties of the HTiO precipitated vary widely, depending on the starting titanium(IV) salt compound and on the precipitation conditions.[14] Moreover, the addition of a water-soluble material during precipitation results in HTiO's with different physicochemical properties.[5] The addition of HCl helps to make a stabilized rutile structure, while the addition of sulfate ions accelerates anatase formation. The anatase formation can be explained by the fact that the formation of sulfate complexes ($Ti(OH)_3HSO_4$, $Ti(OH)_2HSO_4^+$) prefers the growth of a monofunctional complex of anatase.[16] Aqueous dispersions of monodispersed titanium dioxide spheres with modal diameters of 1 to 4 μm have been obtained by the thermal hydrolysis of highly acidic solutions of $TiCl_4$ in the presence of sulfate ions.[17] A method involving the addition of urea has also been tried[18] by analogy with the homogeneous precipitation method. The added urea stabilizes the anatase structure and depresses any change in the pore structure during heat aging.[19]

The HTiO's with high surface areas can be classified into two types in terms of their crystal phases: the amorphous and micro-crystalline types. The former is X-ray amorphous and can be thought to have a structure of a three-dimensional network of $-\overset{|}{\underset{|}{Ti}}-O-\overset{|}{\underset{|}{Ti}}-$ chains.[3] Therefore, its pore structure may depend on the degree of closslinking of the $-\overset{|}{\underset{|}{Ti}}-O-\overset{|}{\underset{|}{Ti}}-$ chains. The latter type has an X-ray diffraction pattern of anatase, rutile, or brookite, with a character of broad diffraction peaks. Since they are aggregates consisting of extremely small crystallites, their pore structures are controlled both by the size and shape of the primary crystallites and by their spatial distribution.[21]

In the present study, we investigated the surface properties of the HTiO's obtained through the thermal hydrolysis method. The effects of the initial concentration of $TiCl_4$ and of the addition of urea during thermal hydrolysis on the surface properties of HTiO were studied. The surface properties were examined by means of nitrogen adsorption/desorption at 77 K and of fluoride ion adsorption. Since the HTiO's obtained by this method are usually microcrystalline anatase or rutile, the difference in the pore structures was discussed based on a packing model for small spheres.

Experimental

Preparation of HTiO. A $TiCl_4$ solution of 0.03, 0.1, 0.3, or 1.0 mol·dm^{-3}, prepared by diluting a stock solution of 3.0 mol·dm^{-3} $TiCl_4$, was refluxed with vigorous stirring at 373 K. After 7 hours of reflux, a white precipitate which had thus been precipitated was left standing for 10 hours at room temperature, washed with water, air-dried, crushed, and sieved to a 200—300 mesh size. The products were named H-0.03, H-0.1, etc. so that the numbers corresponded to the starting $TiCl_4$ concentrations.

The concentration of the titanium(IV) ions in the reacting solution was determined by atomic absorption spectrometry in order to determine a given fraction of precipitated HTiO.

In the case of urea addition, HTiO's were prepared by the same procedure using solutions of urea-containing $TiCl_4$. The molar concentrations of urea were adjusted to twice those of $TiCl_4$. The products were named N-0.03, N-0.1, etc. as above.

The water, urea, and chloride-ion contents of the products were measured as has previously been reported.[19,20]

X-Ray Diffraction Analysis and Electronmicroscopic Observation. X-Ray diffraction analyses were made on a Rigaku-Denki D3F X-ray diffractometer using Cu $K\alpha$ radia-

tion. Transmission electronmicroscopic observations were carried out by use of a Hitachi H-800 electron microscope at 200 kV.

Nitrogen Adsorption/Desorption Isotherm. Nitrogen adsorption/desorption isotherms were obtained on a Carlo Erba 1800 Sorptomatic apparatus with samples outgassed for 4 hours below 10^{-3} mmHg (1 mmHg≈133.322 Pa) at 333 K. V_l-t plots were made from adsorption isotherms using de Boer's t-values (Al_2O_3 standard).[22] The pore-size distribution curves were calculated from the desorption branches using the method of Mikhail et al., assuming cylindrical pores.[23]

Fluoride Ion Adsorption. The amounts of the surface hydroxyl group were determined by means of fluoride ion adsorption from a acetic acid-sodium acetate buffer solution (pH 4.6)[24] using a fluoride ion-selective electrode.

Results and Discussion

Bulk Properties. The rate of HTiO precipitation was fast and was independent of the starting $TiCl_4$ concentration and of the urea concentration. More than 90% of the titanium(IV) ions were precipitated by heating for 1 hour.

The urea and chloride ion contents were less than 0.1% for all of the HTiO's. The water contents are given in Tables 1 and 2. The crystal phases varied from anatase (H-0.03, H-0.1), mixture of anatase and rutile (H-0.3), to rutile (H-1) with the increase in the initial $TiCl_4$ concentration in the case of $TiCl_4$ solutions (Fig. 1). The H-0.03 and H-1 samples correspond to the microcrystalline anatase and rutile, respectively, reported in a previous paper.[21] A previous paper showed a conversion of anatase phase into rutile during heat-aging at 353 K in the case of a 1.0 mol·dm^{-3} $TiCl_4$ solution.[19] The conversion proceeds by means of a dissolution/recrystallization mechanism. The concentrations of free titanium(IV) ions in

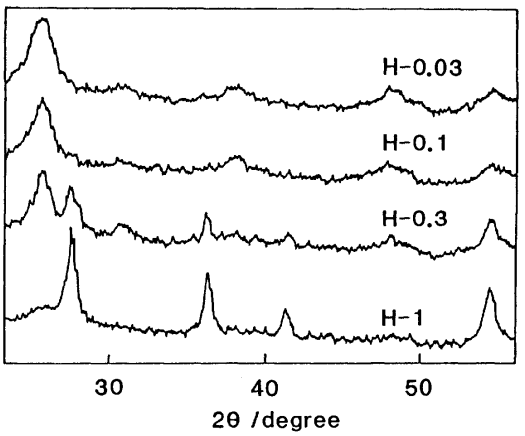

Fig. 1. X-Ray diffraction patterns of the HTiO's obtained from $TiCl_4$ solutions. Initial $TiCl_4$ concentration; H-1: 1.0 mol dm^{-3}, H-0.3: 0.3 mol dm^{-3}, H-0.1: 0.1 mol dm^{-3}, H-0.03: 0.03 mol dm^{-3}.

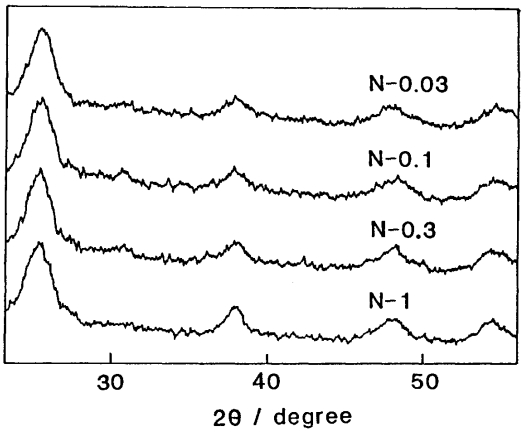

Fig. 2. X-Ray diffraction patterns of the HTiO's obtained from urea-containing $TiCl_4$ solutions. Initial $TiCl_4$ concentration; N-1: 1.0 mol dm^{-3}, N-0.3: 0.3 mol dm^{-3}, N-0.1: 0.1 mol dm^{-3}, N-0.03: 0.03 mol dm^{-3}.

Table 1. Properties of HTiO's Obtained from $TiCl_4$ Solutions

Sample	Water content	D_c	S_{BET}	S_t	V_p	N_{OH}	D_{OH}
	%	nm	$m^2 \cdot g^{-1}$	$m^2 \cdot g^{-1}$	$cm^3 \cdot g^{-1}$	$mmol \cdot g^{-1}$	nm^{-2}
H-0.03	17.4	5.5[a]	212	204	0.170	1.43	4.0
H-0.1	15.9	5.3[a]	211	200	0.195	1.38	3.9
H-0.3	13.1	9.4[b]	146	143	0.155	1.02	4.2
H-1	10.6	11.0[b]	116	108	0.244	0.87	4.5

D_c: Crystallite size estimated from X-ray diffraction pattern, a); anatase (101), b); rutile (101), S_{BET}: BET surface area, S_t: surface area obtained from V_l-t plot, V_p: pore volume, N_{OH}: amount of surface hydroxyl group, D_{OH}: surface density of hydroxyl group=N_{OH}/S_{BET}.

Table 2. Properties of HTiO's Obtained from ($TiCl_4$+Urea) Solutions

Sample	Water content	D_c	S_{BET}	S_t	V_p	N_{OH}	D_{OH}
	%	nm	$m^2 \cdot g^{-1}$	$m^2 \cdot g^{-1}$	$cm^3 \cdot g^{-1}$	$mmol \cdot g^{-1}$	nm^{-2}
N-0.03	16.8	5.3[a]	209	214	0.182	1.36	3.9
N-0.1	17.3	5.3[a]	210	208	0.201	1.38	3.9
N-0.3	15.5	5.2[a]	229	223	0.263	1.41	3.7
N-1	13.2	5.0[a]	256	240	0.382	1.41	3.4

Symbols are the same as those in Table 1.

the mother solutions were measured in the present case, after a 3-hour reflux, as 1.9, 2.0, 10, and 13 mmol·dm^{-3} at the $TiCl_4$ concentrations of 0.03, 0.1, 0.3, and 1 mol·dm^{-3}, respectively. A comparison of the solubility data with the crystal phases of the HTiO's suggests that the conversion takes place at a $TiCl_4$ concentration above 0.3 mol·dm^{-3}, while only a reinforcement of the primary particles is dominant below 0.1 mol·dm^{-3}. The crystallite sizes calculated using the Scherrer equation[25] were about 5 nm for the anatase-type HTiO's (Table 1). In the case of the ($TiCl_4$+urea) solutions, all of the HTiO's showed the X-ray diffraction patterns corresponding to that of anatase (Fig. 2).

Electronmicrographs showed that the rutile type was an aggregate of acicular particles, while the anatase types were aggregates of extremely small, nearly spherical particles (Figs. 3a and 3b). The shapes of the particles differed slightly between N-1 and N-0.03; the particles were less spherical, and their boundaries were less clear for N-1. H-0.3 was a mixture of irregular-shaped particles about 100 nm in size and spherical particles about 10 nm in size.

Surface Properties of HTiO's Obtained from $TiCl_4$ Solutions. The nitrogen adsorption/desorption isotherms were classified as being the BDDT IV type for all of the samples (Fig. 4); this is a characteristic of mesoporous materials.[26] Hysteresis loops existed at a relative pressure of around either 0.5 or 0.9; this cor-

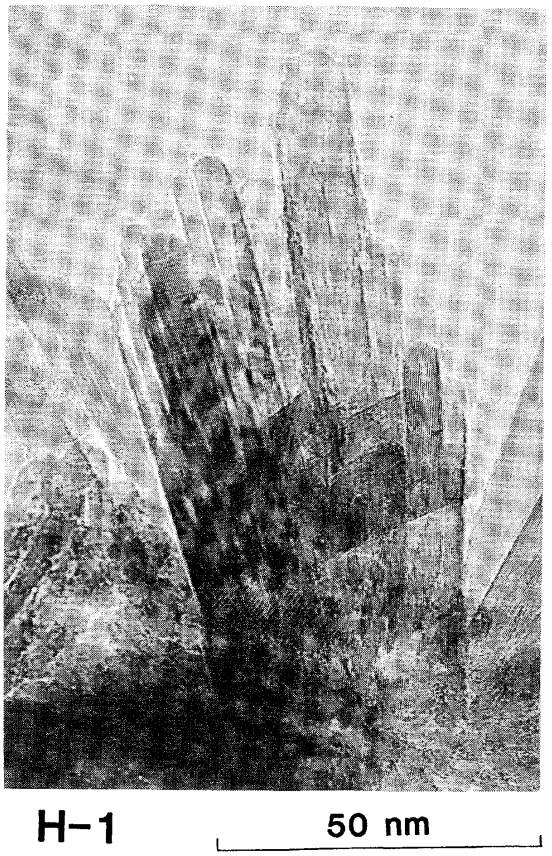

Fig. 3a. Electronmicrograph of H-1.

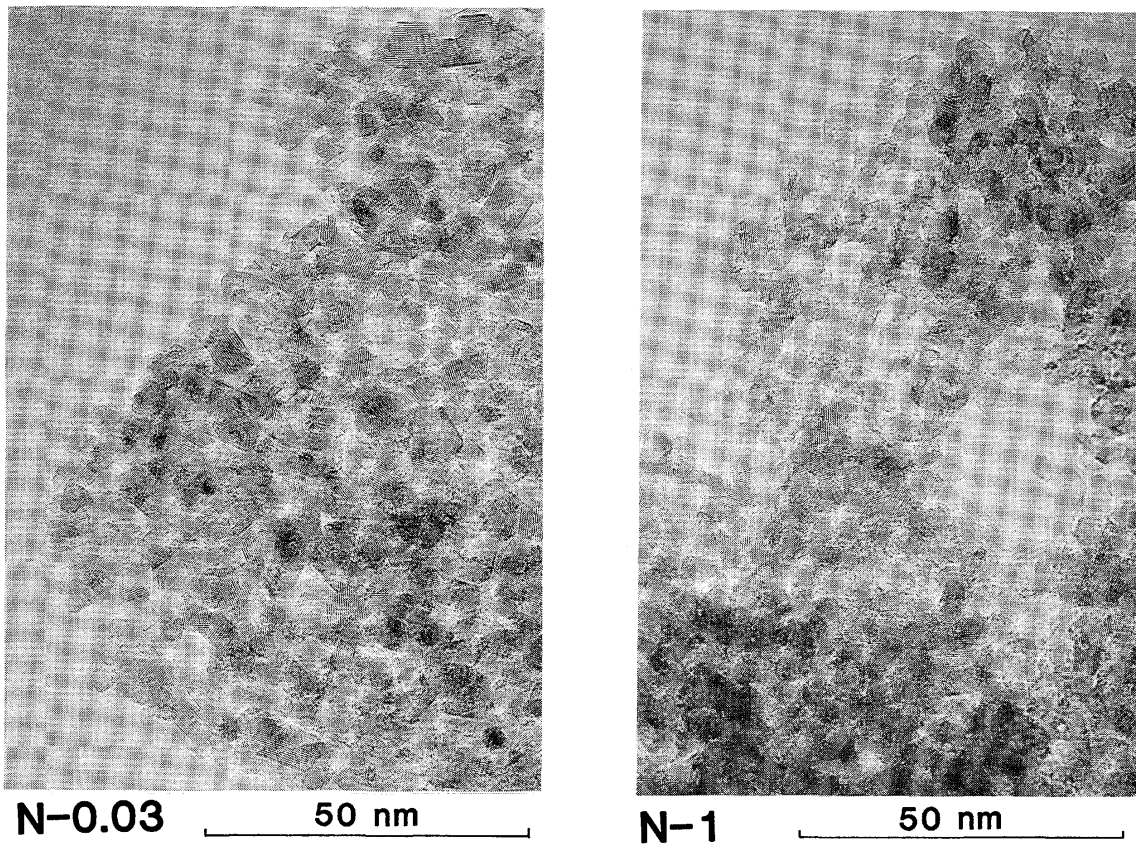

Fig. 3b. Electronmicrographs of N-1 and N-0.03.

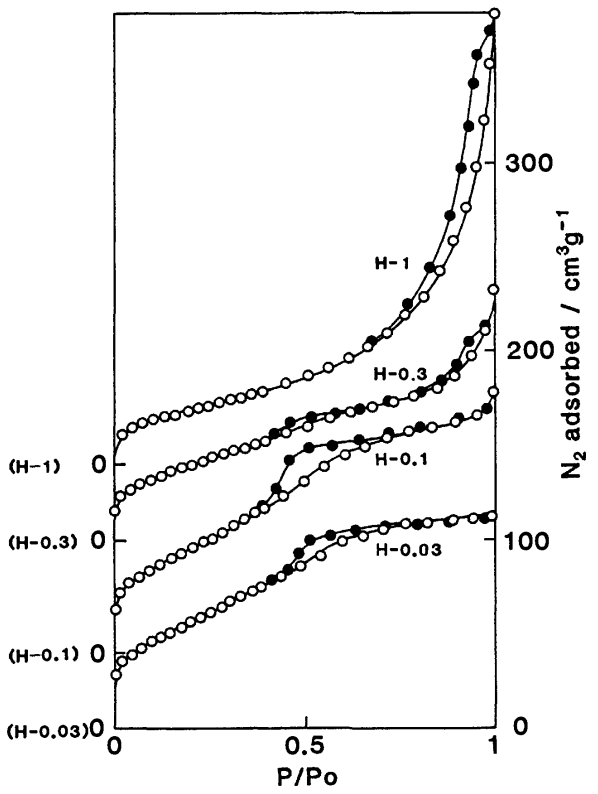

Fig. 4. Nitrogen adsorption/desorption isotherms. ○: adsorption, ●: desorption.

responds to the presence of two types of pores in these HTiO's. The BET surface area showed a tendency to decrease with an increase in the initial $TiCl_4$ concentration, probably because of the increase in the crystallite size. The V_l-t plots for H-1 and H-0.1 showed upward deviations from straight lines at $t>0.65$ and $t>0.54$ nm, respectively, due to the capillary condensation of nitrogen in the mesopores (Fig. 5). At a still higher value of t, the slope of the plot for H-0.1 tended to decrease because of the filling of the pores with liquid nitrogen. The V_l-t plots for H-0.03 and H-0.3 showed downward deviations at $t>0.57$ nm due to pore filling of nitrogen. The surface areas calculated from the slopes of the straight lines (St) agreed well with the corresponding BET surface areas (Table 1). The pore-volume distribution curves showed the presence of two types of pores: pores of a 2-nm radius with a narrow size distribution and pores with radii greater than 2 nm with a broad size distribution (Fig. 6). The former were found for the anatase-type HTiO's, and the latter, for the rutile-type HTiO. The difference in the crystal phase of the product may be responsible for the variation in pore structure in the case of $TiCl_4$ solution. The broad size distribution of the pores in the rutile-type HTiO may be caused by an irregular orientation of the rod-like particles in an aggregate.

The amounts of the surface hydroxyl group (N_{OH}) are given in Table 1. The surface densities of the hydroxyl group per unit area (D_{OH}) were calculated by using the S_{BET} values. The D_{OH} values were about 4

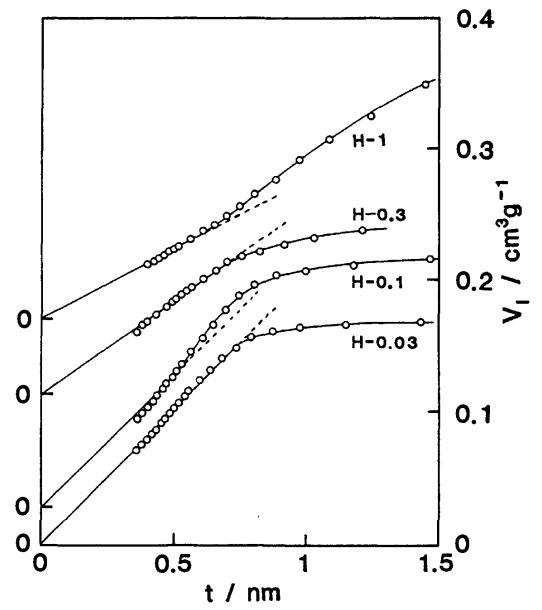

Fig. 5. V_l-t plots from nitrogen adsorption data.

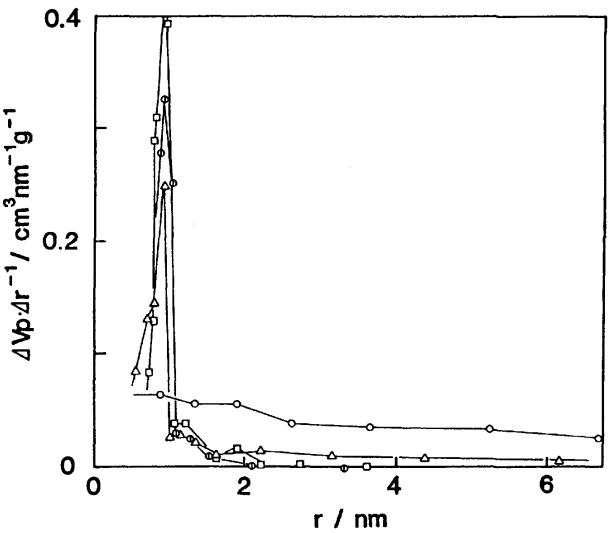

Fig. 6. Pore volume distribution curves. ○: H-1, △: H-0.3, □: H-0.01, ⊕: H-0.03.

OH/nm^2 for the anatase types, while it was slightly larger (4.5 OH/nm^2) for the rutile type (Table 1).

Surface Properties of HTiO's Obtained from ($TiCl_4$+ Urea) Solutions. The nitrogen adsorption/desorption isotherms also belonged to the BDDT IV classification for all of the HTiO's (Fig. 7). The hysteresis loop shifted to a higher relative pressure with an increase in the initial $TiCl_4$ concentration, indicating an increase in the pore size. The BET surface area increased slightly with an increase in the $TiCl_4$ concentration, while the pore volume increased markedly. The V_l-t plots showed upward deviations from straight lines at $t>0.57$ nm for N-0.1, N-0.3, and N-1 (Fig. 8). At a still higher value of t, however, the slopes of the plots for N-0.1 and N-0.3 tended to decrease. The V_l-t plot showed a downward deviation for N-

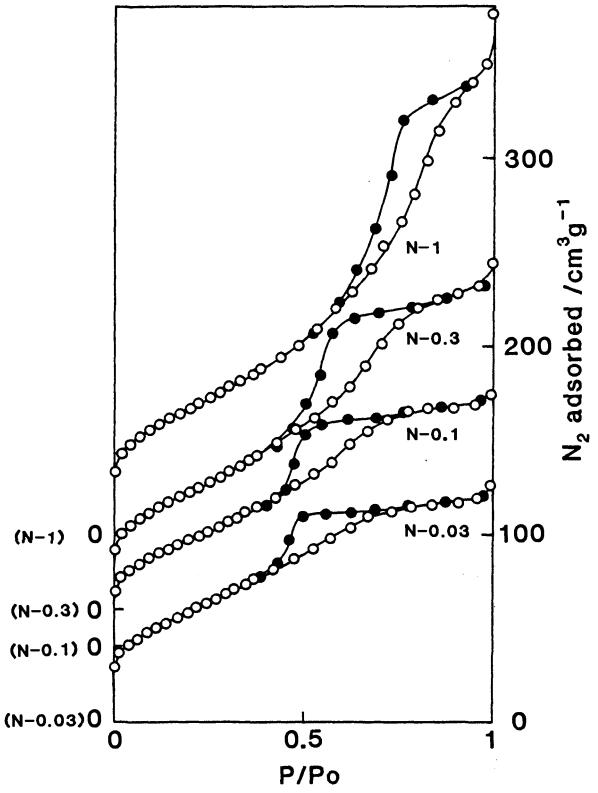

Fig. 7. Nitrogen adsorption/desorption isotherms. ○: adsorption, ●: desorption.

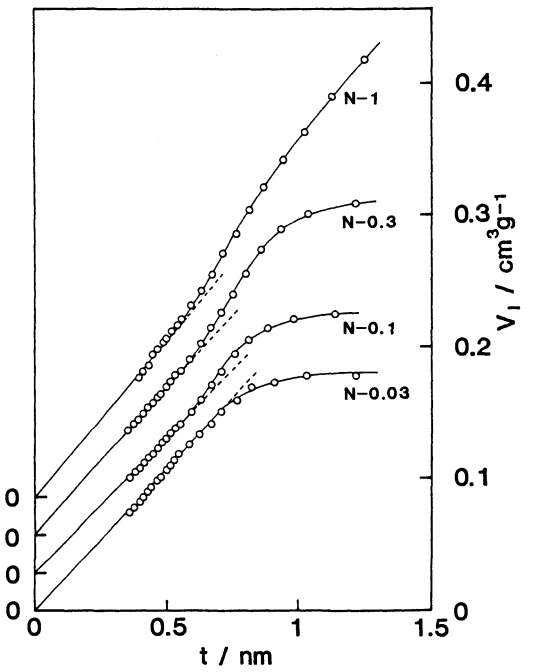

Fig. 8. V_1–t plots from nitrogen adsorption data.

0.03. The pore-volume distribution curves showed that the most probable pore radius (R_p) increased from 1.9 to 3.6 nm with an increase in the initial $TiCl_4$ concentration, accompanied by a broadening of the distribution curve (Fig. 9).

A previous study has shown that the crystal phase

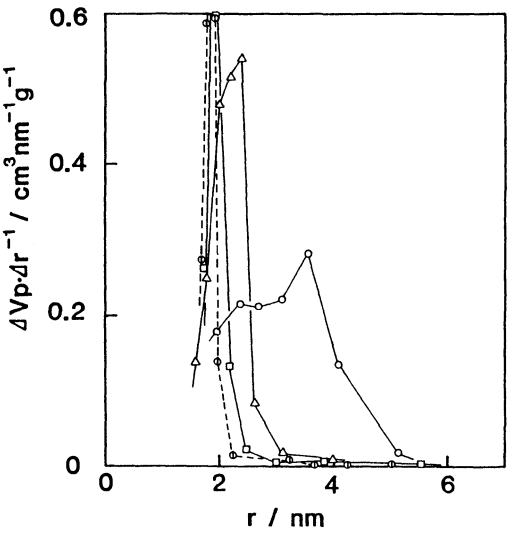

Fig. 9. Pore volume distribution curves. ○: N-1, △: N-0.3, □: N-0.1, ◇: N-0.03.

and pore structure of the precipitates are scarcely influenced by the step of heat-aging at 353 K in the case of a ($TiCl_4$+urea) solution.[19] Therefore, the pore structure is controlled mainly by the conditions during the step when the primary crystallites are precipitated and become an aggregate of a gel network. The increase in the porosity with the initial $TiCl_4$ concentration in the ($TiCl_4$+urea) system can be thought of as being due to the presence of urea at higher concentration. The addition of a water-soluble organic material before gel formation serves to provide a gel with a greater porosity.[12] Urea may play the same role.

Analysis Based on Packed-Sphere Model. The previous calculations of the surface areas of microcrystalline anatase and rutile showed that the BET surface areas correspond mainly to the external surface of the primary crystallites.[21] Therefore, their pore structures can be represented by the spatial distribution of the primary crystallites. The pore distributions of the anatase-type HTiO's could be analyzed by the use of a packed-sphere model, in which a system consisting of spherical particles of a uniform size was assumed.[27,28] According to this model, the radius of the circle (R') inscribed in the throat of the cavity among spheres can be calculated as a function of the cordination number (n) between the particles.[28] A crude estimation of the n-value can be derived from the porosity (P) of a material; this can be evaluated from the pore volume (V_p) and the particle density (ρ) as:

$$P(\%) = 100 \cdot V_p/((1/\rho) + V_p). \quad (1)$$

The porosity of the HTiO increased from 41 to 59% with an increase in the initial $TiCl_4$ concentration from 0.03 to 1 mol·dm^{-3} in the case of a urea-containing $TiCl_4$ system (the particle densities were assumed to be equal to that of anatase, ρ=3.8 g·ml^{-1})[29] (Table 3). This indicated a looser packing of the anatase crystallites with an increase in the initial

Table 3. Porosity (P), Coordination Number (n), and Pore Radius Evaluated by the Packed-Sphere Model

Sample	P	n	R'	R_p
	%		nm	nm
N-0.03	41	8	1.3	1.9
N-0.1	43	8		2.0
N-0.3	50	6		2.3
N-1	59	4—6	1.2—2.1	3.6

The packing model used was that of Avery and Ramsay.[28]
R': Radius of circle inscribed in the throat of a cavity, R_p: most probable pore radius in Fig. 9.

$TiCl_4$ concentration. The increase in the porosity corresponded to a decrease in the cordination number (n) from 8 to about 5.

The R' values could be calculated using the averaged particle radii, which could themselves be evaluated by studying the electronmicrographs of 100 particles (3.2 nm for N-0.03 and 2.9 nm for N-1). In the case of N-0.03, the calculated R' value agreed comparatively well with the most probable pore radius (R_p), as determined by the nitrogen isotherm (Table 3). This suggested the validity of the application of the packed-sphere model to anatase-type HTiO. However, the agreement between the R_p- and R'-values was not so good in the case of N-1; the R_p value was about twice as large as the R' value. The larger R_p value in N-1 may be due to an irregular packing of the crystallites compared to the theoretical packing of primitive cubic (n=6) or tetrahedral (n=4). The irregular packing could be presumed from the broadening of the pore distribution of N-1 in Fig. 9.

The above calculations suggest the suitability of the packed-sphere model for describing the pore structure of anatase-type HTiO when the packing of the microcrystallites is relatively compact ($n>8$). In the case of a looser packing ($n<6$), however, it may be necessary to consider the diversity of the coordination number in describing an appropriate packing image of the pore structure.

The authors are grateful to Hitachi, Ltd., for its helpful support of the electronmicroscopic observation.

References

1) S. J. Gregg and M. I. Pope, *Kolloid-Z*, **174**, 27 (1961).
2) M. R. Harris and G. Whitaker, *J. Appl. Chem.*, **12**, 490 (1962).
3) M. R. Harris and G. Whitaker, *J. Appl. Chem.*, **13**, 348 (1963).
4) C. Heitner-Wirguin and A. Albu-Yaron, *J. Appl. Chem.*, **15**, 445 (1965).
5) J. P. Bonsack, *J. Colloid Interface Sci.*, **44**, 430 (1973).
6) G. D. Parfitt, K. S. W. Sing, and D. Urwin, *J. Colloid Interface Sci.*, **53**, 187 (1975).
7) A. Kurosaki and S. Okazaki, *Nippon Kagaku Kaishi*, **1976**, 1816.
8) J. Ragai, K. S. W. Sing, and R. Michail, *J. Chem. Tech. Biotech.*, **30**, 1 (1980).
9) J. Ragai and K. S. W. Sing, *J. Chem. Tech. Biotech.*, **32**, 988 (1982).
10) J. Ragai and K. S. W. Sing, *J. Colloid Interface Sci.*, **101**, 369 (1984).
11) T. M. El-Akkad, *J. Colloid Interface Sci.*, **76**, 67 (1980).
12) T. M. El-Akkad, *J. Colloid Interface Sci.*, **78**, 100 (1980).
13) M. Tsuji, M. Abe, and M. Orimo, *Bull. Chem. Soc. Jpn.*, **58**, 97 (1985).
14) K. Funaki and Y. Saeki, *Kogyo Kagaku Zasshi*, **59**, 1291 (1956).
15) K. Funaki and Y. Saeki, *Kogyo Kagaku Zasshi*, **59**, 1295 (1956).
16) E. Santacesaria, M. Tonello, G. Storti, P C. Pace, and S. Carra, *J. Colloid Interface Sci.*, **111**, 44 (1986).
17) E. Matijevic, M. Budnik, and L. Meites, *J Colloid Interface Sci.*, **61**, 302 (1977).
18) H. Suzuki, T. Iwai, T. Hasegawa, K. Okujima, C. Horie, and I. Koyama, *Nippon Kagaku Kaishi*, **1977**, 1063.
19) K. Ooi, T. Kitamura, S. Katoh, and K. Sugasaka, *Nippon Kagaku Kaishi*, **1983**, 1.
20) K. Ooi, T. Kitamura, S. Katoh, and K. Sugasaka, *Nippon Kagaku Kaishi*, **1984**, 534.
21) K. Ooi, S. Katoh, and K. Sugasaka, *J. Colloid Interface Sci.*, **119**, 595 (1987).
22) B. C. Lippens and J. H. de Boer, *J. Catal.*, **4**, 319 (1965).
23) R. Sh. Mikhail, S. Brunauer, and E. E. Bodor, *J. Colloid Interface Sci.*, **26**, 54 (1968).
24) H. P. Boehm, *Angew. Chem.*, **78**, 617 (1966).
25) H. P. Klug and L. E. Alexander, "X-ray Diffraction Procedure for Polycrystalline and Amorphous Materials," John Wiley and Sons, New York (1956), p. 491.
26) S. J. Gregg and K. S. W. Sing, "Adsorption, Surface Area, and Porosity," Academic Press, New York, (1982), p. 5.
27) D. C. Havard and R. Wilson, *J. Colloid Interface Sci.*, **57**, 276 (1976).
28) R. G. Avery and J. D. F. Ramsay, *J. Colloid Interface Sci.*, **42**, 597 (1973).
29) R. J. H. Clark, "Titanium," in "Comprehensive Inorganic Chemistry, Vol. 3," ed by J. C. Bailar, Pergamon Press, New York (1983), p. 376.

Binding Aspects of 2-(4-Hydroxyphenylazo)benzoic Acid to Bovine Serum Albumin in the Limited Mixing Ratio

Kunio TAKEDA,* Katsushi SASA, Kazuaki HACHIYA, Mamoru MURATA,† and Koichiro AOKI
Department of Applied Chemistry, Okayama University of Science, 1-1 Ridai-cho, Okayama 700
†Department of Applied Chemistry, Aichi Institute of Technology, Toyota 470-03
(Received January 20, 1988)

The binding of 2-(4-hydroxyphenylazo)benzoic acid (HABA) to bovine serum albumin (BSA) was studied in a dilute phosphate buffer of pH 7.0 and ionic strength 0.014 at 25 °C. Binding measurements were made for both undefatted BSA and defatted BSA (the protein naturally contains 2.4—2.5 mol/mol fatty acid). A metachromasy band appeared at 480 nm at the expense of the original absorption band at 350 nm in the presence of BSA. An isosbestic point in the absorption spectra was observed in the vicinity of 380 nm only in the limited range of the molar mixing ratios of HABA to BSA (D_0/P_0), where the ratio was 1—10 in the above buffer, regardless of the absence and presence of fatty acids. However, the isosbestic point was not observed by any feasible change of the D_0/P_0 ratio in a buffer containing 0.1 M NaCl. This fact seemed to indicate that the binding nature depended on the ionic strength as well as the D_0/P_0 ratio. Then, binding measurements were carried out in the limited range of D_0/P_0 ratios in a dilute phosphate buffer. The amount of HABA bound to BSA was determined by curve-fitting for changes of the apparent molar extinction coefficient, ε, between 300 and 550 nm, assuming one class of binding site: that is, only two species (free and bound dyes) contributing to the absorption changes. The simulated curves of ε were in good agreement with those obtained experimentally. By the use of the Scatchard plot, the binding parameters were determined. The binding constant was larger for defatted BSA than for undefatted BSA, the values being of the order of 10^5 M^{-1}. The number of binding sites of HABA was 1.4—1.5, not being affected very much by the absence and presence of fatty acids.

The azo dye, 2-(4-hydroxyphenylazo)benzoic acid (HABA) is well-known to exhibit a new absorption band characteristically, when it binds to serum albumin, which generally serves as a carrier protein for a wide variety of substances.[1] Consequently, the mode of interaction between HABA and serum albumin has been attracting renewed interest. During the last two decades, the system of HABA and bovine serum albumin (BSA) has often been studied.[2-7] The exhibition of a new band has been attributed to the azo-hydrazone tautomeric transition of the dye induced upon its binding to the protein.[2-9] However, most of these studies have been carried out by changing the HABA concentration over wide ranges, from 10^{-6} or 10^{-5} to 10^{-3} M (1 M=1 mol dm^{-3}), at a constant BSA concentration in rather concentrated buffers. In the present work, the interaction depended on both the ionic strength of the buffer and the molar mixing ratio of HABA to BSA, D_0/P_0. An isosbestic point in the absorption spectra of HABA was observed only over a limited range of the D_0/P_0 ratios and only in the buffer of low ionic strength. Some important facts seem to have been overlooked, probably because most of the preceding studies regarding the interaction were made under the above-stated experimental conditions. The present results suggest that a certain chemical equilibrium in the binding system exists only within a particular range of D_0/P_0 ratios.

Experimental

The crystalline BSA was purchased from Miles Laboratories Inc.[10] The preceding studies concerning this system emphasized the importance of the purity of the protein.[6] Therefore, the BSA sample was purified by passing it through Pharmacia MONOQ HR5/5 (ionic-exchange media) and Superose 12 (gel filtration media) using a Pharmacia high-performance liquid chromatography FPLC. HABA was purchased from Tokyo Kasei Co. and was purified by recrystallization from methanol before use. The protein concentration was determined spectrophotometrically using $E^{1\%}_{1\,cm}$=6.8 at 280 nm.[11] The molar extinction coefficient of HABA was assumed to be 18800 at 350 nm. A sodium phosphate buffer of pH 7.0 was extensively used. The final concentrations of NaH_2PO_4 and Na_2HPO_4 in the buffer were 3.33 and 3.56 mM, respectively; the ionic strength of the buffer was 0.014.[10]

The content of fatty acids in the present BSA was determined to be 2.4—2.5 mol/mol by the Dole method.[12] The removal of fatty acids was carried out by an acid-charcoal treatment.[13] The BSA fractionated as described above was mixed with charcoal, the amount of which was approximately half of that of the protein in weight. The pH of the BSA–charcoal solution was lowered to 3 by the addition of 0.2 M HCl. After the solution was stirred at 0—2 °C for 4 days, the charcoal was then removed by centrifugation. The period of 4 days was determined on the basis of a relation obtained between the stirring time and the quantity of fatty acids remaining in the BSA treated by charcoal. The clarified solution was brought to pH 7.0 by the addition of 0.2 M NaOH, and then dialyzed against the phosphate buffer of pH 7.0.

Absorbance measurements were made at 25 °C with a Hitachi double-beam spectrophotometer U-3200.

Results and Discussion

The binding properties of HABA to serum albumin have been studied so far by equilibrium dialysis,[2,5,9] rotating-disk polarography,[14] ultrafiltration,[14] spectrophotometric analysis,[3,5,6] and gel chromatography[7]

at rather high ionic strengths using mostly 0.05—0.1 M phosphate buffers.[2-9] The HABA concentration was in the range 10^{-6} or 10^{-5} to 10^{-3} M and the BSA concentration in the range 10^{-5} to 10^{-4} M in these preceding studies. When HABA binds to serum albumin, it exhibits a metachromasy band at 480 nm at the expense of the original absorption band at 350 nm, as has been observed by Baxter[2] and Moriguchi et al.[3,4] They concluded that the absorption band at 480 nm is due to the formation of a hydrazone form of HABA;[2-4] Terada et al. have supported this conclusion.[6] There are two kinds of binding sites for HABA in the protein. Sakurai et al. have shown that the absorption bands at 350 and 480 nm originate in HABA bound to a non-metachromasy site and a metachromasy site of BSA, respectively.[5] They have concluded that there are, at least, 5 binding sites consisting of 1.5—2 metachromasy sites and 3.5—3 non-metachromasy sites (Fig. 1 in Ref. 5).

Figure 1 shows the absorbances of 1×10^{-5} M HABA at various BSA concentrations in the present dilute buffer. The absorbance at the metachromatic band clearly increased with an increase in the BSA concentration up to a protein concentration of 1×10^{-5} M,

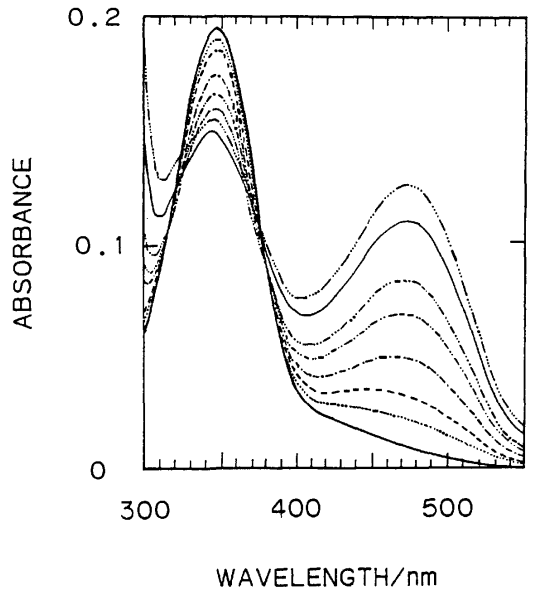

Fig. 1. Absorbance of 1.0×10^{-5} M HABA in the presence of defatted BSA of 0 (——), 1.0×10^{-6} (·····), 2.0×10^{-6} (– – –), 4.0×10^{-6} (–·–·–), 7.0×10^{-6} (–·····–), 1.0×10^{-5} (–·–·–·–), 2.0×10^{-5} (——), and 3.0×10^{-5} M (–·–·–·–) at 25°C.

showing an isosbestic point in the vicinity of 380 nm. However, when the BSA concentration was beyond 1.0×10^{-5} M against 1.0×10^{-5} M HABA, the spectrum did not pass through the isosbestic point. The absorption spectrum of HABA in 2×10^{-5} M BSA crossed the spectrum of HABA, itself, at a different wavelength from that of the isosbestic point obtained below 1×10^{-5} M BSA. The spectrum of HABA in 3×10^{-5} M BSA crossed the spectrum of HABA, itself, at another different wavelength. These results suggest that the HABA-BSA interaction, itself, differs with each other above and below this particular BSA concentration (1×10^{-5} M) at the constant HABA concentration: that is, the binding mechanism depends on the D_0/P_0 ratio.

Although absorbance measurements were also performed in a phosphate buffer of ionic strength 0.1 and in the present dilute buffer containing 0.1 M NaCl, the isosbestic point was not observed at any feasible concentration range of BSA at a constant concentration of HABA. In the present dilute buffer containing 0.1 M NaCl, the decreasing magnitude of the absorbance around 350 nm upon the addition of BSA was rather small (not shown) compared with that in a buffer without NaCl (Fig. 1). Figure 2 shows the effect of the added NaCl on the apparent molar extinction coefficients at 350 and 480 nm, ε_{350} and ε_{480}, in the presence of 1×10^{-5} M BSA. The value of ε_{350} increased and that of ε_{480} decreased with increasing NaCl concentration, indicating qualitatively that the increment of ionic strength inhibits the HABA binding to the protein.

The amount of HABA bound to BSA was determined spectrophotometrically by applying a curve-fitting method to the apparent molar extinction coefficient changes in the wavelength region 300—550 nm. This is the same method that has often been used to estimate the fractions of secondary structures, such as a helix in a polypeptide, using a reference circular dichroism spectra of the corresponding structures.[15-17] Assuming that only two species, the free HABA and the HABA bound to the protein, contribute to the absorption, the following relation is obtained:

$$\varepsilon_{obs}=f_{free}\,\varepsilon_{free}+f_{bound}\,\varepsilon_{bound},$$

where ε_{obs} is the experimentally observed apparent molar extinction coefficient of HABA in the presence of BSA; ε_{free} and ε_{bound} are the molar extinction coeffi-

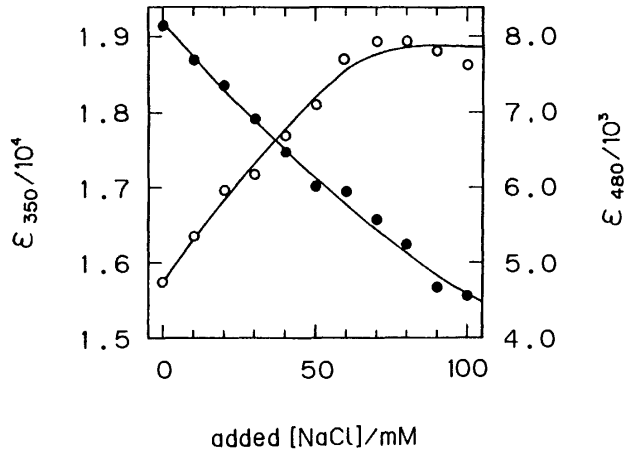

Fig. 2. Changes of extinction coefficients of HABA, ε_{350} (○) and ε_{480} (●) as a function of NaCl concentration added to the buffer of ionic strength 0.014 at 25°C. BSA concentration was kept at 1.0×10^{-5} M.

cients of the free and bound species, respectively. The notations of f_{free} and f_{bound} are fractions of the free and bound species, respectively, and $\sum f_i=1$. Since the solution of HABA obeyed Beer's law in the concentration range used here (in the order of 10^{-5} M), the value of ε_{free} was easily determined at each wavelength. However, it was actually impossible to obtain the value of ε_{bound} only by the spectrophotometrical method, since the absorbance of 1×10^{-5} M HABA continued to increase with increasing BSA concentration up to 1×10^{-3} M. Then, the values of ε_{bound} were determined by the combined use of the equilibrium dialysis at the particular ratios of D_0/P_0 which enable the absorption spectra of HABA to pass through the isosbestic point in Fig. 1. The binding quantity estimated by the equilibrium dialysis method corresponds to the total amount of HABA bound to both the metachromasy and non-metachromasy sites. However, the dye is considered to bind predominantly to the metachromasy site under the present experimental conditions, because the binding numbers obtained in the present work are similar to those already obtained spectrophotometrically so far (as stated below). When the total HABA concentration (free HABA+bound HABA) was 1×10^{-5} M in the presence of 1×10^{-5} M BSA, the concentration of bound HABA was determined to be 8.8×10^{-6} M by an interpolation of the binding data obtained by equilibrium dialysis. Thus, the value of ε_{bound} was obtained at an arbitrary wavelength. The simulated wavelength region covers the two characteristic absorption bands. This method seems to be more reliable than an estimation at a particular wavelength. Figure 3 shows an example of the fitting of the simulated molar extinction coefficient to the experimentally obtained value in the above-mentioned wavelength region. The calculated curve agrees excellently with the experimentally obtained curve. This good agreement and the existence of the isosbestic point might suggest that the dye binds to one class of binding site in BSA. The binding profile was also examined in a dilute buffer containing 0.1 M NaCl. In this case, the binding number of the dye to the defatted BSA was determined by changes of ε_{obs} between 400 and 550 nm, since the absorbance below 400 nm did not change systematically with a change in the BSA concentration in the presence of 0.1 M NaCl.

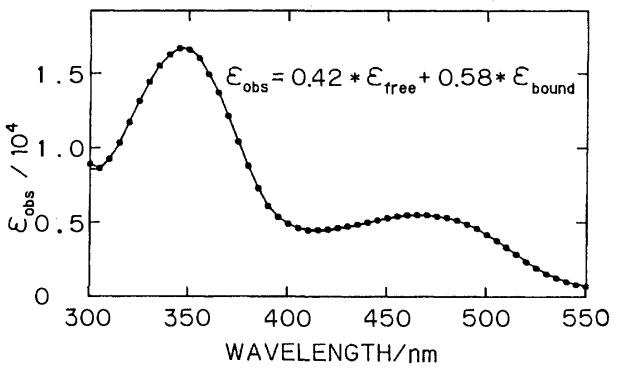

Fig. 3. Computed (——) and experimentally determined (-⊖-) molar extinction coefficient, ε_{obs}, of HABA in 5.3×10^{-6} M BSA. The scheme in the figure indicates that the computed spectrum consists of 42% of extinction coefficient of free HABA and 58% of extinction coefficient of bound HABA (see text). The binding quantity of HABA was calculated by the multiplication of the constant HABA concentration (1.0×10^{-5} M) by 0.58 and the subsequent division of it by the BSA concentration.

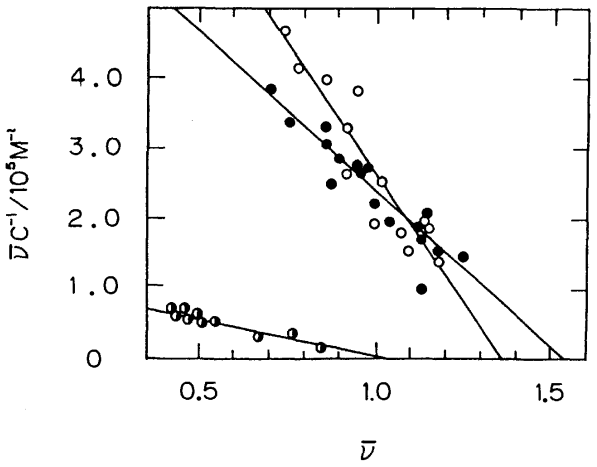

Fig. 4. Scatchard plot of binding of HABA to BSA. (O); defatted BSA, (●); undefatted BSA, (O); defatted BSA in 0.1 M NaCl. The binding data were taken in the range of D_0/P_0 between 1 and 10 at 25°C.

Scatchard plots for these three kinds of binding profiles are shown in Fig. 4. The intercept to the ordinate equals the product of nK (n: number of binding site, K: binding constant) according to the Scatchard equation. Each product was of the order of 10^5 M^{-1}. Accordingly, the values of K are of the order of 10^5 M^{-1}, being larger by one order than those so far reported.[2,3,5–7] The values of K and n are listed in Table 1.

The magnitude of K was influenced by the presence of 0.1 M NaCl. At a low ionic strength, the BSA molecule more or less expands. Thus, the protein is in a more expanded state at an ionic strength of 0.014 than at a higher ionic strength. The metachromasy of HABA has been considered to be caused by its binding to the hydrophobic interior of a BSA molecule.[2,4,6]

Table 1. Binding Parameters of HABA to BSA

	Native BSA	Defatted BSA	Defatted BSA in 0.1 M NaCl
K_{int}[a]/10^5 M^{-1}	4.55	7.44	1.05
n[b]	1.5	1.4	1.0

a) Intrinsic binding constant obtained from the Scatchard plot. b) Number of binding site obtained in the same plot.

The environmental change of the binding site due to the expansion might be the reason for the increase in K with a lowering of the ionic strength. As can be seen in Table 1, the value of K is appreciably larger for defatted BSA than for undefatted BSA. Spector and Imig have studied an effect of the palmitate concentration on HABA binding to human serum albumin by means of equilibrium dialysis.[9] In their Scatchard plot (Fig. 1 in Ref. 9), the intercept on the ordinate (corresponding to the value of nK) is clearly larger in the absence of palmitate than in its presence, indicating a similar effect of the fatty acid on K to that observed in the present work.

The values of n are substantially compatible with those obtained spectrophotometrically at higher ionic strengths by Sakurai et al. (Fig. 1 in Ref. 5) and by Terada et al.[6] As can be seen in Table 1, however, the addition of 0.1 M NaCl decreases the number of binding sites in defatted BSA. This might also be related to an expansion of the BSA molecule at a low ionic strength. On the other hand, the removal of the fatty acids causes no appreciable difference in the number of binding sites (Table 1). Thus, it is believed that HABA binds to the same metachromasy sites independently of the fatty acids, although the removal of the fatty acids increases the magnitude of K.

Using a medium of such low ionic strength, we encountered the fact that the isosbestic point was observed in the restricted range of D_0/P_0 ratios in a dilute buffer. Assuming only two species, a good agreement was observed between the curve of experimentally observed apparent extinction coefficients and that of simulated ones. These suggest that only one kind of binding site exists under the present restricted conditions. Therefore, the reason why such an isosbestic point is not observed at higher ionic strengths might be due to a simultaneous appearance of plural kinds of binding sites. The difference in the numbers of binding site classes seems to be caused by the expansion nature of BSA due to a decrease in the ionic strength. The binding nature of BSA appeared to be easily affected by the coexistence of fatty acids or electrolytes. We can state that this is one of the aspects of serum albumin which serves as a carrier protein for various substances.

This work was partly supported by a Grant-in-Aid for Scientific Research No. 61540342 to K. T. from the Ministry of Education, Science and Culture.

References

1) T. Peters, Jr., "The Plasma Proteins," ed by F. W. Putnam, 2nd ed., Academic Press, New York (1975), Vol. 1, pp. 133—181.
2) J. H. Baxter, *Arch. Biophys. Biochem.*, **108**, 375 (1964).
3) I. Moriguchi, S. Wada, and H. Sano, *Chem. Pharm. Bull. (Tokyo)*, **16**, 592 (1968).
4) I. Moriguchi, S. Fushimi, C. Ohshima, and N. Kaneniwa, *Chem. Pharm. Bull.*, **18**, 2447 (1970).
5) T. Sakurai, S. Tsuchiya, and H. Matsumaru, *J. Pharm. Dyn.*, **4**, 65 (1981).
6) H. Terada, K. Aoki, and M. Kamada, *Biochim. Biophys. Acta*, **342**, 41 (1974).
7) K. Murakami, T. Sano, S. Tsuchie, and T. Yasunaga, *Biophys. Chem.*, **21**, 127 (1985).
8) H. Terada, *Spectrochim. Acta*, **31A**, 945 (1975).
9) A. A. Spectar and B. Imig, *Mol. Pharmacol.*, **7**, 511 (1971).
10) K. Takeda, M. Miura, and T. Takagi, *J. Colloid Interface Sci.*, **82**, 38 (1981).
11) "Handbook of Biochemistry (Selected Data for Molecular Biology)," 2nd ed., ed by H. A. Sober and R. A. Harte, CRC Press, Cleveland, Ohio (1973), p. C-71.
12) V. P. Dole, *J. Clin. Invest.*, **35**, 150 (1956).
13) R. F. Chen, *J. Biol. Chem.*, **242**, 173 (1967).
14) Y. W. Chien, T. D. Sokoloski, C. L. Olson, D. T. Witiak, and R. Nazareth, *J. Pharm. Sci.*, **62**, 440 (1973).
15) N. Greenfield and G. D. Fasman, *Biochemistry*, **8**, 4108 (1969).
16) Y. H. Chen, J. T. Yang, and K. H. Chau, *Biochemistry*, **13**, 3350 (1974).
17) K. Takeda, *Biopolymers*, **24**, 683 (1985).

 © 1988 The Chemical Society of Japan Bull. Chem. Soc. Jpn., 61, 2731—2737 (1988)

Proton Transfer and Aggregation Reactions in Aqueous Solutions of Isobutylamine and Isopentylamine Studied by Ultrasonic Methods

Sadakatsu NISHIKAWA,* Yukio YOSHIDA, and Ayumi NAKANO
Department of Chemistry, Faculty of Science and Engineering, Saga University, Saga 840
(Received January 29, 1988)

Ultrasonic absorption and velocity measurements have been performed in aqueous solutions of isobutylamine and isopentylamine at 25 °C. Two different relaxation phenomena are observed in these sample solutions. One of them, observed at a high frequency range, has been attributed to a proton transfer reaction of amines from the concentration dependence of the relaxation frequency and the maximum excess absorption per wavelength. The rate and thermodynamic constants have been determined for ion-pair formation and dissociation. The other, observed at a low frequency range becomes more striking as the hydrophobicity of the solute increases; it has been considered that the cause of the relaxation may be associated with a hydrophobic interaction. The formation of small aggregates has been speculated in both solutions. The rate and thermodynamic constants for the association and dissociation reactions of nonionized amine molecules have been estimated from the concentration dependences of the relaxation frequency and the maximum excess absorption per wavelength. Furthermore, the coupling effect of the two relaxation processes has been discussed briefly.

In a previous study[1] concerning the ultrasonic absorption mechanisms in aqueous solutions of isomeric butylamines, we have shown the existence of two different relaxational processes in the frequency range from 6.5 to 220 MHz from the measurements of the absorption coefficients as a function of the frequency. One of these processes has been attributed to a perturbation of the $R\text{-}NH_3^+ + OH^- \leftrightarrow R\text{-}NH_3^+ \cdots OH^-$ equilibrium. We have predicted from some experimental facts that the other may be due to the aggregation reaction of a nonionized solute.[2] The ultrasonic property due to this reaction is very dependent on the size of the hydrophobic groups. Atkinson et al.,[3] on the other hand, have analyzed the ultrasonic absorption results in an aqueous solution of *t*-butylamine on the basis of the hydrolysis and fluctuation model proposed by Romanov et at.[4] In order to clarify the justification of the interpretation of the ultrasonic absorption results in aqueous solutions of various amines over a wide concentration range and in order to substantiate the effect of the size of the hydrophobic groups on the ultrasonic absorption properties, the accumulation of many ultrasonic absorption results has been earnestly desired. The purpose of the present investigation is to report the ultrasonic absorption and velocity results for aqueous solutions of isobutylamine and isopentylamine as a function of their concentrations and to provide information about the dynamics of their solutions. Further, the analytical procedure of the relaxation times for the studies of fast reactions in solutions is examined for a system where two relaxation processes are observed in an equivalent time region.

Experimental

The isobutylamine and isopentylamine were purchased from Wako Pure Chemicals and then distilled. The desired concentrations of the aqueous solutions were prepared with doubly distilled water by weight.

The ultrasonic measurements were performed over the frequency range from 3.5 to 220 MHz by the use of semiautomatic pulse equipment connected with an 8 bit microcomputer. The computer programs had been developed so as to obtain the absorption spectrum elegantly. It is necessary to see the linearity of the attenuation vs. the moving distance of the transducer in order to obtain the absorption coefficient accurately. Such plots are seen on a display just after the measurements; when the error of the plots is less than 2%, the absorption coefficient is stored. Once the measurements at the available frequencies are performed, the computer program goes to the determination of the ultrasonic parameters. The details of the calculation procedure have been described elsewhere.[5]

The sound velocity was measured by a sing around method at 1.92 MHz and by use of an interferometer at 2.5 MHz. The accuracies are within 1 $m\,s^{-1}$. The densities of the solutions were determined by the use of a pycnometer, volume of which was about 4 cm^3. The pH's of the solutions were measured by means of a Hitachi-Horiba pH meter with a glass electrode. All the ultrasonic and pH measurements were carried out under a dry nitrogen gas in order to prevent the contamination of the solutions with carbon dioxide.

Results and Discussion

In order to interpret the ultrasonic absorption mechanisms, there are several procedures. The most effective one is to see how the absorption coefficient, α, depends on the measurement frequency, f.[6] When the absorption is related to the fluctuation in solutions attributable to the critical mixtures, as is occasionally seen in various amine aqueous solutions, the absorption would show unusual tendencies, e.g., an abnormal increase in the absorption coefficient when the system is close to the critical point. However, in the amine solutions studied here, the absorption did not show such trends in our frequency range and the values of α/f^2 tend to show a plateau at a low frequency range. Therefore, the absorption coefficients, as a function of the frequency in the aqueous solutions of the two amines, have been tested by the equation

associated with the usual relaxation process.[6]

$$\alpha/f^2=\sum_i A_i/[1+(f/f_{ri})^2]+B, \quad (1)$$

or

$$\mu=\sum_i A_i fc/[1+(f/f_{ri})^2], \quad (2)$$

where f_{ri} is the relaxation frequency for the i-th process. μ the excess absorption per wavelength, c the sound velocity, and A_i and B the constants. Some typical ultrasonic spectra for isopentylamine and isobutylamine are shown in Figs. 1 and 2 respectively.

For the isopentylamine aqueous solution, a double relaxational equation (i=2 for Eq. 1 or 2) has been found to fit the experimental data well in the concentration range from 0.4 to 1.77 mol dm^{-3}. In the range less than 0.4 mol dm^{-3}, the ultrasonic spectra are well-expressed by a single relaxational equation, i.e. i=1 in Eq. 1 or 2. The ultrasonic parameters, f_{ri}, A_i, and B have been determined by means of a nonlinear least-mean-square method; the solid curves indicate the calculated values. The parameters obtained are listed in Table 1.

For the isobutylamine solution, the spectra in the concentrations below 0.719 mol dm^{-3} are well fitted to the single relaxational equation. Further, with increase in the concentration the spectra still look like those associated with a single relaxation process. Figures 3 and 4 show the amplitude of the excess absorption, A, and the relaxation frequency, f_r which have been determined by a single relaxational equa-

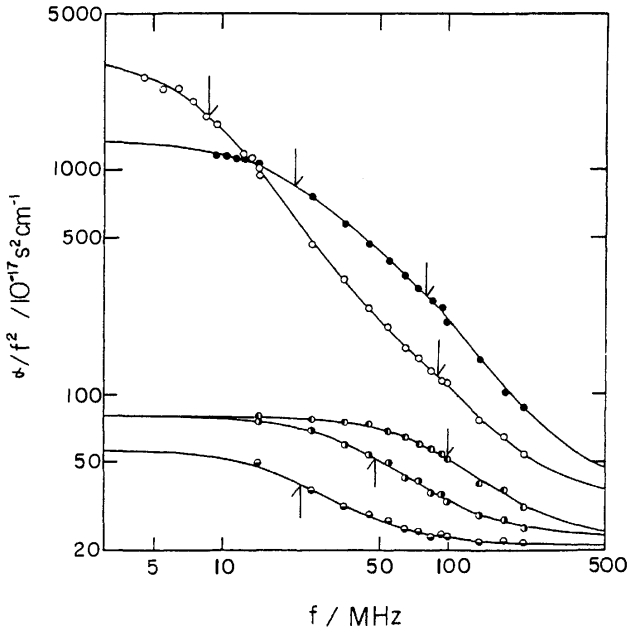

Fig. 1. The representative ultrasonic absorption spectra in aqueous solution of isopentylamine at 25 °C. ●: 1.50 mol dm^{-3}, ○: 0.700 mol dm^{-3}, ◐: 0.221 mol dm^{-3}, ◑: 0.050 mol dm^{-3}, ◒: 0.0070 mol dm^{-3}. The arrows show the positions of the relaxation frequency.

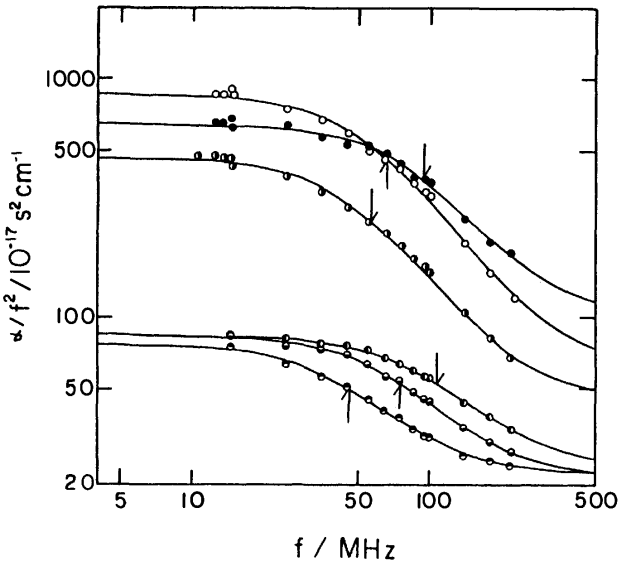

Fig. 2. The representative ultrasonic absorption spectra in aqueous solution of isobutylamine at 25 °C. ●: 2.75 mol dm^{-3}, ○: 1.75 mol dm^{-3}, ◑: 1.29 mol dm^{-3}, ◐: 0.566 mol dm^{-3}, ◒: 0.243 mol dm^{-3}, ◓: 0.0784 mol dm^{-3}.

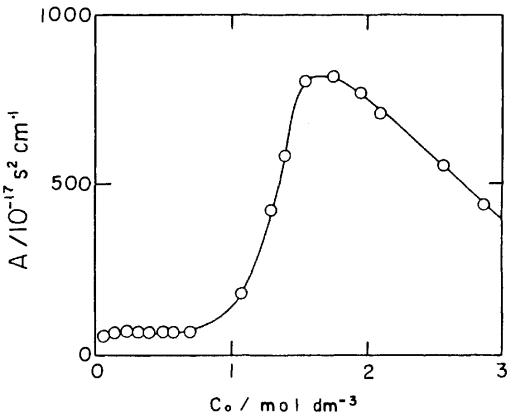

Fig. 3. Concentration dependence of the amplitude excess absorption, A, for aqueous solution of isobutylamine. They are those determined by a single relaxational equation.

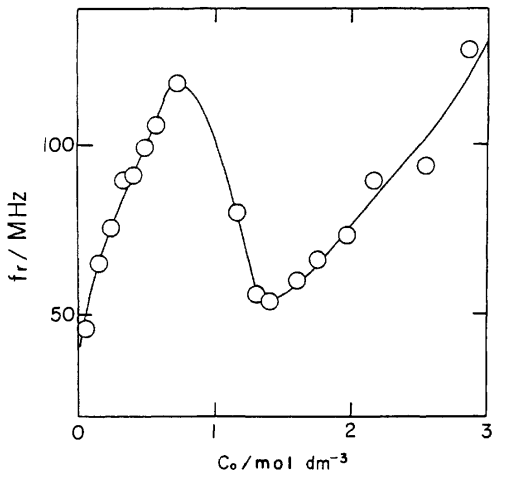

Fig. 4. Concentration dependence of the relaxation frequency f_r, for aqueous solution of isobutylamine.

Table 1. Ultrasonic and Thermodynamc Parameters for Aqueous Solutions of Isopentylamine and Isobutylamine at 25 °C

Concn	pH	ρ	c	f_{r1}	f_{r2}	A_1	A_2	B
mol dm^{-3}		g cm^{-3}	m s^{-1}	MHz		10^{-17} s^2 cm^{-1}		
			(Isopentylamine)					
0.0070	11.17	0.9970	1497	22		36		21
0.0097	11.25	0.9970	1496	25		40		22
0.0170	11.39	0.9969	1497	36		46		21
0.0283	11.51	0.9965	1498	38		52		22
0.0500	11.64	0.9964	1499	48		56		23
0.0997	11.80	0.9960	1503	64		60		21
0.119	11.84	0.9952	1503	78		60		21
0.150	11.89	0.9950	1508	83		64		19
0.221	11.98	0.9939	1509	100		58		22
0.350	12.09	0.9915	1524	124		68		18
0.601	12.31	0.9878	1498	109	6.4	84	3815	26
0.652	12.32	0.9858	1495	96	7.9	113	3957	26
0.700	12.33	0.9857	1492	90	8.8	114	3154	33
0.751	12.35	0.9849	1490	62	9.2	225	3502	41
0.800	12.36	0.9836	1489	73	12	184	2738	35
1.282	12.38	0.9700	1488	43	13	687	865	55
1.500	12.38	0.9660	1487	80	21	347	965	37
1.770	12.39	0.9600	1486	79	26	325	548	57
			(Isobutylamine)					
0.0784	11.60	0.9965	1501	46		56		22
0.158	11.78	0.9954	1505	65		63		21
0.243	11.90	0.9942	1513	75		64		21
0.322	11.97	0.9932	1515	90		61		22
0.403	12.04	0.9921	1522	91		61		23
0.482	12.08	0.9912	1529	99		64		22
0.566	12.16	0.9900	1534	106		61		23
0.719	12.22	0.9878	1543	118		68		21
1.13	12.32	0.9812	1560	142*	54	84*	118	21
				(80)		(181)		(32)
1.29	12.36	0.9811	1566	152*	44	87*	384	27
				(56)		(425)		(45)
1.40	12.38	0.9775	1569	157*	44	89*	546	30
				(54)		(580)		(51)
1.59	12.41	0.9744	1568	165*	54	91*	754	26
				(60)		(807)		(50)
1.75	12.42	0.9710	1564	168*	60	91*	764	38
				(66)		(815)		(62)
1.97	12.44	0.9672	1558	174*	66	91*	718	47
				(73)		(769)		(69)
2.16	12.45	0.9629	1549	177*	72	92*	640	64
				(79)		(705)		(81)
2.57	12.47	0.9562	1536	183*	83	92*	487	83
				(93)		(554)		(99)
2.87	12.48	0.9465	1522	186*	117	94*	355	63
				(127)		(439)		(71)

The ultrasonic parameters indicated in parentheses for the solution of isobutylamine are those calculated by a single relaxational equation. Those indicated by the super asterisk are calculated using Eqs. 4 and 7.

tion as a function of the analytical concentration, C_o, for the isobutylamine solution. As may be seen in these figures, the excess absorption amplitude, A, increases suddenly around 1 mol dm^{-3} and goes through a maximum. Further, the relaxation frequency also indicates an unusual trend at around 1 mol dm^{-3}. Therefore, it is considered that the cause of the absorption in the high concentration range differs from that in the low concentration range. Therefore, it may be necessary to distinguish the multiple relaxation processes, which we will describe later.

Firstly, in order to analyze the excess absorption mechanisms in the two solutions, the absorptions in a relatively low concentration range (less than 0.4 mol dm^{-3} for isopentylamine and less than 1 mol dm^{-3} for isobutylamine) are considered. The characteristic properties of the ultrasonic absorption are that the relaxation frequencies increase monotonously with the analytical concentration and that the amplitudes of the excess absorption indicate a plateau, as may be

seen in Table 1. Such dependences have been observed in various amine solutions, and the absorptions have been well analyzed by the reaction kinetics of the hydrolysis.[1,2,7-9] As has been pointed out in a previous report,[1] the amine hydrolysis in aqueous media proceeds through an intermediate, which is expressed by the next equilibria:

$$\mathrm{R\text{-}NH_3^+ + OH^-} \underset{k_{21}}{\overset{k_{12}}{\longleftrightarrow}} \mathrm{R\text{-}NH_3^+ \cdots OH^-} \underset{k_{32}}{\overset{k_{23}}{\longleftrightarrow}} \mathrm{R\text{-}NH_2 + H_2O} \quad (3)$$

This reaction mechanism was originally proposed by Eigen.[8] When the relaxation frequencies associated with the above two steps are close to each other, the coupling effects on the relaxation frequencies and the amplitudes of the relaxations should be taken into account. However, the observed ultrasonic absorption spectra is clearly expressed by a single relaxational equation. When the coupling effect is considered, an unreasonable dissociation constant, K_b, is obtained, which has been described in detail in Ref. 1. Therefore, we have assumed that the observed relaxation phenomena are due only to a perturbation of the equilibrium of the first step in Eq. 3. The relation between the relaxation frequency and the reactant concentration is simply expressed as:

$$2\pi f_{r1} = \gamma^2([\mathrm{R\text{-}NH_3^+}]+[\mathrm{OH^-}])k_{12} + k_{21}, \quad (4)$$

where f_{r1} is the relaxation frequency observed in the higher frequency range and γ the ion activity coefficient which is calculated by the use of the Davies equation.[10] Figure 5 shows the plots of f_{r1} vs. $\gamma^2[\mathrm{OH^-}]$, the intercept and slope of which provide the rate constants. These good linearities confirm that the cause of the excess absorption is the hydrolysis of the amines. The rate constants obtained are tabulated in Table 2. The dissociation constant, K_b, is related to each equilibrium constant as

$$K_b = K_{12}/(1+K_{32}^{-1}) \quad (5)$$

where $K_{12}=k_{21}/k_{12}$ and $K_{32}=k_{32}/k_{23}$. Therefore, K_{32} may be calculated; it is also shown in Table 2. The relation between the relaxation frequency and the analytical concentration is derived, under the same assumption, as:[1]

$$2\pi f_{r1} = k_{12}[-K_b + (-K_b^2 + 4\gamma^2 C_o K_b)^{1/2}] + k_{21}. \quad (6)$$

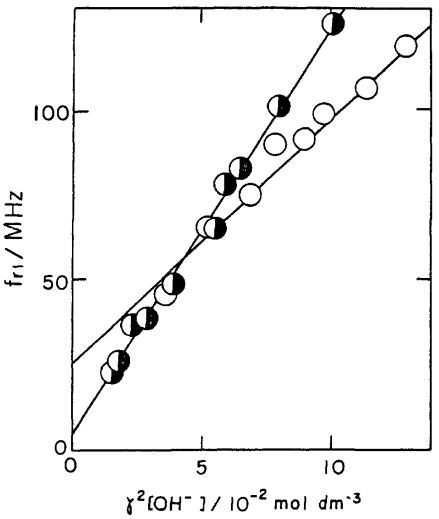

Fig. 5. The plots of f_{r1} vs. $\gamma^2[\mathrm{OH^-}]$ for the analysis of the proton transfer reaction. ◑: isopentylamine, ○: isobutylamine.

Using this equation, it is possible to estimate whether or not the above interpretation is reasonable. The dissociation constants, K_b, have been calculated; they are close to those in the literature.[11]

Another important parameter obtained by the ultrasonic absorption and velocity measurements is the maximum excess absorption per wavelength, μ_{m1};[6]

$$\mu_{m1} = 0.5A_1 f_{r1} c = \pi\rho c^2 \Gamma(\Delta V_1 - \alpha_p \Delta H/\rho C_p)^2/2RT, \quad (7)$$

where ρ is the solution density, ΔV_1 the standard volume change of the reaction, ΔH the standard enthalpy change of the reaction, α_p the thermal expansion coefficient at the high frequency limit, C_p the specific heat, and Γ the concentration term, which is expressed for the reaction under consideration as:

$$\Gamma = \{1/[\mathrm{R\text{-}NH_3^+}] + 1/[\mathrm{OH^-}] + 1/[\mathrm{R\text{-}NH_3^+ \cdots OH^-}]\}^{-1}. \quad (8)$$

Since the enthalpy term can be quite small compared with the volume term for proton transfer reactions in general, the enthalpy term is neglected. As a result, the plots of μ_{m1} vs. $\rho c^2\Gamma$, which are shown in Fig. 6, provide the standard volume change of the reaction. The results are also given in Table 2. The volume changes thus obtained are very close to those for other amine hydrolysis obtained by use of the ultrasonic method.[8]

Table 2. The Rate and Thermodynamic Constants for Proton Transfer Reaction in Aqueous Solutions of Isopentylamine and Isobutylamine at 25 °C

Solute	$10^{-10}\,k_{12}$ / mol^{-1} dm^3 s^{-1}	$10^{-8}\,k_{21}$ / s^{-1}	K_{32}	$10^4\,K_b$[a] / mol dm^{-3}	ΔV_1 / cm^3 mol^{-1}
Isobutylamine	2.3	1.7	0.035	2.5 (3.3)	27
Isopentylamine	3.7	0.39	0.51	3.7 (4.4)	26

a) The dissociation constants have been determined from the ultrasonic absorption measurements using Eq. 6. The values in parentheses are those in the literature.[11]

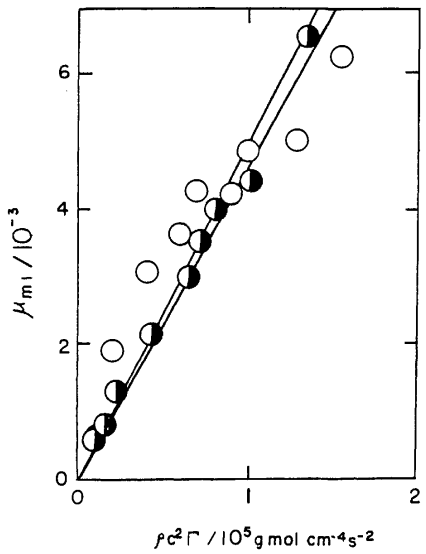

Fig. 6. The plots of μ_{m1} vs. $\rho c^2\Gamma$ for the determination of the standard volume change of the reaction. ◑: isopentylamine, O: isobutylamine.

However, they seem to be slightly larger than those obtained by the static method.[12] This might be because the latter are the over all results for the hydrolysis reaction, while the former are those for only the first step of the ion-pair formation process. The forward rate constants are reasonable for diffusion controlled reactions in the aqueous media. The equilibrium constant, K_{32}, which is smaller than unity, indicates that the intermediate concentration is small.

Secondly, the excess absorption mechanism in the concentrated solutions will now be considered. This phenomenon is observed in the lower frequency range. In the analysis of the absorption spectra, it is now necessary to distinguish the multiple relaxations. When two relaxation frequencies are far apart in a measured frequency range, it might be suitable to analyze the experimental results using eigher Eq. 1 or 2, as i=2. This may be appropriate in the case of the isopentylamine aqueous solution. The calculated ultrasonic parameters are listed in Table 1 in the concentration range above 0.6 mol dm^{-3}. However, for aqueous solutions of isobutylamine, the spectra look like a single relaxation one, so the above procedure for the determination of the ultrasonic parameters is not adequate. The parameters calculated using the single relaxational equation are indicated in the parentheses in Table 1 for the concentration range above 1 mol dm^{-3}. Fortunately, the excess absorption associated with the hydrolysis, which is observed in the higher frequency range and in the dilute solutions, may be expected to take place also in the concentrated solutions. Therefore, once the concentrations of the reactants for the hydrolysis are determined, the amplitude of the excess absorption and the relaxation frequency can be predicted by the use of Eqs. 4, 7, and 8. We have, then, assumed that the ultrasonic absorption due to the hydrolysis should be subtracted from the experimental data. As a result, it is possible to see if the residual absorptions fit Eq. 1 or 2. It is found that they have been well-analyzed by the single relaxational equation. The ultrasonic parameters obtained in this way are listed in Table 1 for the isobutylamine solutions in the concentration range above 1.13 mol dm^{-3}. Figure 7 shows an example of an absorption in which the two relaxation processes in the solution are distinguished. The experimental values all fit the calculated curves perfectly. There is some experimental evidence[2] concerning the excess absorption under consideration. (1) Such excess absorption is not observed in the aqueous solutions of propylamine and ethylamine. (2) The amplitude of the excess absorption increases and then decreases with the concentration; this is the so called "PSAC" (peak sound absorption concentration). This phenomenon becomes more striking with an increase in the hydrophobicity of the solute and is also observed in aqueous solutions of alcohols and ethers. (3) In an orgaic solvent, however, it is not found. (4) When the solute is ionized, the excess absorption disappears. These facts lead us to predict that the excess absorption may be associated with the hydrophobic effect of the nonionized solute molecules. The most plausible mechanism seems to be a molecular aggregation reaction by means of the hydrophobic interaction, which might be close to the micelle formation of surface active agents. However, such big micelles may not be formed because the hydrophobic groups of isobutylamine and isopentylamine are not very large. Actually, there have been several theories[13,14] to interpret the micelle formation

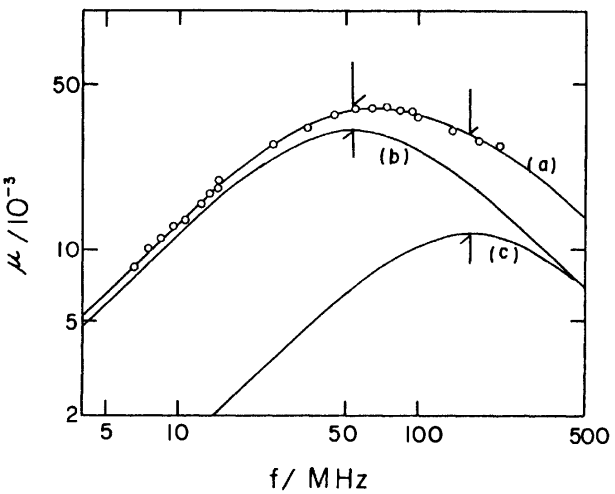

Fig. 7. The frequency dependence of the excess absorption per wavelength for 1.59 mol dm^{-3} isobutylamine aqueous solution. O's are the experimental values. The curve (c) is the calculated excess absorptions per wavelength associated with the proton transfer reaction and the curve (b) is those associated with the aggregation reaction. The solid curve (a) is the sum of the two relaxational curves, (b) and (c).

and breakage kinetics. However, they all assume the distribution of the aggregates, which is only applicable when the aggregation number is quite large. Therefore, we will simply consider the perturbation of the following equilibrium by the sound wave:

$$nA \underset{k_{43}}{\overset{k_{34}}{\longleftrightarrow}} A_n, \tag{9}$$

when n is the aggregation number. The relation between the relaxation frequency and the reactant concentration is given by the next equation:[15,16]

$$2\pi f_{r2} = 1/\tau = k_{34}n^2[A]^{(n-1)} + k_{43}, \tag{10}$$

where τ is the relaxation time and [A] the equilibrium concentration of the free nonionized solute. If the equilibrium constant (dissociation constant), K_b, in the concentration range is still satisfactorily expressed by $K_b=\gamma^2[R\text{-}NH_3^+][OH^-]/[R\text{-}NH_2]$, it is possible to determine the monomer concentration, [A], from the pH measurement, because the two equilibrium constants in Eq. 3 have been determined. Then, it may be possible to estimate the rate constants using an appropriate aggregation number, n. The plots of f_{r2} vs. $[A]^{(n-1)}$ are shown in Fig. 8. The best straight lines have been obtained for the aqueous solution of isobutylamine when n=4 and for that of isopentylamine when n=5. For the isobutylamine solution, the forward and backward rate constants have been determined from the slope and the intercept. They are listed in Table 3. However, the intercept of the plots for the isopentylamine solution is very close to zero. Therefore, it is not suitable for determining the backward rate constant. Equation 10 is also expressed in a different form with the analytical concentration as follows:[16]

$$2\pi f_{r2} = k_{43}n^2C_o/[A] + (1-n)k_{43}. \tag{11}$$

If the above procedure is correct, the same rate constant may be determined by the use of Eq. 11. For the isobutylamine solution, the values of k_{43} have been determined to be 2.7×10^8 s^{-1} from the slope and 3.0×10^8 s^{-1} from the intercept; these values are very close to that in Table 3. For the isopentylamine solution, the values have been determined to be 1.5×10^7 s^{-1} and 1.4×10^7 s^{-1} from the slope and the intercept respectively; the mean values are listed in Table 3.

Now, the concentration dependence of the maximum excess absorption per wavelength, μ_{m2}, will be explained. It is derived as follows:[16]

$$\mu_{m2} = \pi\rho c^2(\Delta V_2)^2 k_{34}[A]^n\tau/2RT, \tag{12}$$

where ΔV_2 is the standard volume change of the aggregation reaction. For simplicity, only the volume relaxation has been assumed. The plots of $\ln(\mu_{m2}/\rho c^2\tau)$ vs. $\ln[A]$ provide the aggregation numbers, which have been found to be 3.7±0.2 for the isobutylamine solution and 4.9±1.2 for the isopentylamine solution. These results also confirm that the cause of the excess absorption is the aggregation reaction by the nonionized solute molecules. The standard volume changes of the reaction, ΔV_2 have been calculated with the help of Eq. 12; they are listed in Table 3, along with the results for butylamine[16] and pentylamine[2] solutions. As may be seen in the table, the association rate constant tends to increase with an increase in the hydrophobicity of the solute. On the other hand, the dissociation rate constant seems to decrease with an increase in the carbon number. These results may reflect the stability of the aggregate. Cabani et al.[17] have studied in detail the volumetric properties in aqueous solutions of various nonelectrolytes including amines. They have speculated a presence of the solute-solute interaction of butylamines in aqueous solutions. We consider that such interacting molecules may corre-

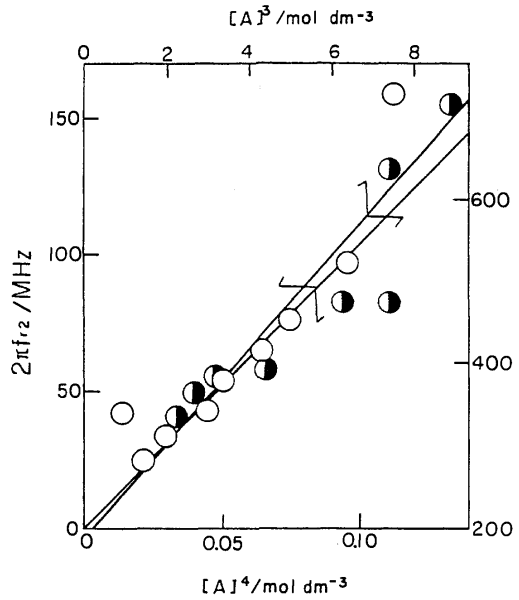

Fig. 8. The plots of $2\pi f_{r2}$ vs. $[A]^{(n-1)}$ for the two aqueous solutions. ◑: isopentylamine, ○: isobutylamine.

Table 3. The Rate Constants for the Aggregation Reaction for Aqueous Solutions of Butylamines and Pentylamines at 25 °C

Solute	n	$10^{-6}\,k_{34}$ / $(\text{mol}^{-1}\,\text{dm}^3)^{n-1}\,\text{s}^{-1}$	$10^{-7}\,k_{43}$ / s^{-1}	ΔV_2 / $\text{cm}^3\,\text{mol}^{-1}$	Reference
Isobutylamine	4	3.7	28	19	This work
Isopentylamine	5	4.1	1.4	22	This work
Butylamine	4	2.2	9.0	14	16
Pentylamine	5	4.7	3.0	17	2

spond to the aggregate under consideration.

As has been described previously, the coupling effect of the two reactions should be taken into account, as the processes of the hydrolysis and the aggregation reaction have been observed experimentally in the equivalent time range. The reaction mechanisms under consideration may be generally expressed as follows when the two reactions shown by Eqs. 3 and 9 are taken into account.

$$\mathrm{R\text{-}NH_3^+ + OH^- \underset{k_{21}}{\overset{k_{12}}{\longleftrightarrow}} R\text{-}NH_3^+ \cdots OH^- \underset{k_{32}}{\overset{k_{23}}{\overset{H_2O}{\longleftrightarrow}}}}$$

$$\mathrm{R\text{-}NH_2 \underset{k_{43}}{\overset{k_{34}}{\longleftrightarrow}} \frac{1}{n}(R\text{-}NH_2)_n}. \qquad (13)$$

As has been explained, the ultrasonic relaxation process due to the hydrolysis has been well-interpreted on the basis of the fact that the second step in the above reaction scheme may not affect the first step very much. We consider that the second step may be too fast to couple with the first step, as the second step is the intramolecular proton exchange. In our time region, the second step may be estimated to be in the steady state. The third step, associated with the aggregation reaction, is observed in a lower frequency range than the first step. Therefore, the third process may not be so affected by the second step. That is, the independent procedures of absorption analysis may be appropriate for the aqueous solutions of amines investigated in this study.

This work was partly supported by The Naito Foundation.

References

1) Y. Yoshida and S. Nishikawa, *Bull. Chem. Soc. Jpn.*, **59**, 1941 (1986).

2) S. Nishikawa, T. Yasunaga, and K. Takahashi, *Bull. Chem. Soc. Jpn.*, **46**, 2992 (1973).

3) G. Atkinson, M. M. Emara, H. Endo, and B. L. Atkinson, *J. Phys. Chem.*, **84**, 259 (1980).

4) V. P. Romanov and V. A. Solovev, *Sov. Phys. Acoust. (Engl. Transl.)*, **11**, 68 (1965).

5) S. Nishikawa and K. Kotegawa, *J. Phys. Chem.*, **89**, 2896 (1985). The computer programs, written in Basic Language are available on request to one of the authors (S.N.).

6) For example, "Physical Acoustics," Vol. II, Part A, ed by W. P. Mason, Academic Press, New York and London (1965); M. J. Blandamer, "Introduction to Chemical Ultrasonics," Academic Press, London and New York (1973).

7) R. D. White, L. J. Slutsky, and S. Pattison, *J. Phys. Chem.*, **75**, 161 (1971).

8) M. Eigen, G. Maass, and G. Schwarzt, Z. Phys, *Chem. (Frankfurt am Main)*, **74**, 319 (1971).

9) K. Applegate, L. J. Slutsky, and R. C. Parker, *J. Am. Chem. Soc.*, **90**, 6909 (1968).

10) C. W. Davies, "Ion Association," Butterworths, London (1962).

11) J. J. Christensen, R. M. Igatt, D. P. Wrathall, and L. D. Hansen, *J. Chem. Soc. A*, **1969**, 1212.

12) R. Zana, *J. Phys. Chem.*, **81**, 1817 (1977).

13) E. A. G. Aniansson and S. N. Wall, *J. Phys. Chem.*, **78**, 1024 (1974).

14) M. Teubner, *J. Phys. Chem.*, **83**., 2917 (1979).

15) G. K. Krescheck, E. Hammori, G. Davenport, and H. A. Scheraga, *J. Am. Chem. Soc.*, **88**, 246 (1966).

16) S. Nishikawa and T. Yasunaga, *Bull. Chem. Soc. Jpn.*, **46**, 1098 (1973).

17) S. Cabani, G. Conti, and L. Lepori, *J. Phys. Chem.*, **78**, 1030 (1974).

 © 1988 The Chemical Society of Japan Bull. Chem. Soc. Jpn., 61, 2739—2741 (1988)

New Mesomorphic Compounds: *N,N',N''*-Trialkanoyl-2,4,6-trimethyl-1,3,5-benzenetriamines

Yukimasa HARADA and Yoshio MATSUNAGA*
Department of Chemistry, Faculty of Science, Hokkaido University, Sapporo 060
(Received February 8, 1988)

The homologous series of *N,N',N''*-trialkanoyl-2,4,6-trimethyl-1,3,5-benzenetriamines has been prepared. The viscous birefringent melts are given by the butyryl to hexadecanoyl derivatives. The X-ray diffraction pattern recorded for the octanoyl derivative and the higher homologous members consists of two sharp inner peaks and a broad outer one assignable to the 100, 110, and 001 reflections respectively, indicating that the phase is hexagonal disordered columnar (D_{hd}). A more-structured high-temperature phase is displayed at lower temperatures by the nonanoyl to hexadecanoyl derivatives.

A number of single compounds composed of disk-like molecules are known to form stable or metastable mesophases. The first series, reported by Chandrasekhar et al. in 1977, consists of three homologous members of hexakis(alkanoyloxy)benzenes.[1] The hexaalkoxytriphenylenes, discovered by Billard et al., constitute the second series.[2] These disk-like molecules are made of a planar rigid core fully surrounded by a planar ring of paraffinic chains. Nevertheless, our earlier study revealed that *N,N',N''*-trialkyl-1,3,5-benzenetricarboxamides (**1**), the molecule of which has only three long alkyl groups and is far from the shapes of discogens discovered to date, can exhibit hexagonal disordered columnar (D_{hd}) mesophases.[3]

In this paper, we wish to describe a new series of mesomorphic compounds designed on the basis of their isomers: *N,N',N''*-trialkanoyl-1,3,5-benzenetriamines. Since the enthalpy change upon melting of *N,N'*-dioctadecanoyl-1,3-benzenediamine, 81 kJ mol^{-1}, is larger by about 70% than that of *N,N'*-dioctadecyl-1,3-benzenedicarboxamide,[4] the appearance of a mesophase in the above-mentioned isomeric compounds does not seem highly probable. However, the enthalpy change upon a transformation into an isotropic liquid can be considerably reduced by methyl substitution, as disclosed also by the same work. For example, *N,N'*-dioctadecanoyl-2-methyl-1,3-benzenediamine is transformed into an isotropic liquid with an enthalpy change of 26 kJ mol^{-1} and the corresponding 2,4,6-trimethyl compound with 0.7 kJ mol^{-1}. Consequently, *N,N',N''*-trialkanoyl-2,4,6-trimethyl-1,3,5-benzenetriamines (**2**) seemed to be good candidates for new mesomorphic compounds.

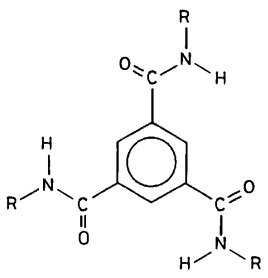

1 R = C_nH_{2n+1}

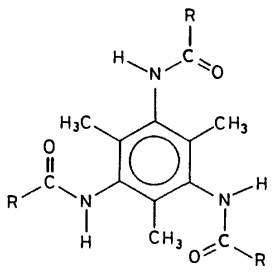

2

Experimental

Materials. Trinitromesitylene was prepared by the nitration of mesitylene with a mixture of concentrated sulfuric acid and fuming nitric acid.[5] The product was reduced with metallic tin and concentrated hydrochloric acid. The reaction between 2,4,6-trimethyl-1,3,5-benzenetriamine and acyl chloride was carried out in benzene by the addition of pyridine. The compounds were purified by repeated recrystallization from appropriate solvents: methanol for the propanoyl to octanoyl derivatives, ethanol for the nonanoyl to dodecanoyl derivatives, and mixtures of benzene and ethanol for the remaining two. The results of elemental analysis are in good agreement with the composition of the desired compounds. For example, Found: C, 71.79; H, 10.19; N, 8.33%. Calcd for $C_6(CH_3)_3(NHCOC_6H_{13})_3$: C, 71.81; H, 10.24; N, 8.37%.

Measurements. Calorimetric, X-ray, and NMR measurements were made as reported in our previous work.[4]

Results and Discussion

The compounds prepared for this investigation are listed in Table 1 along with their transition temperatures and the associated enthalpy changes. By an examination using a polarizing microscope the appearance of viscous birefringent melts was noted with the butyryl to hexadecanoyl derivatives. In addition,

Table 1. Transition Temperatures (°C) and Enthalpy Changes (kJ mol^{-1}) of Compounds **2**[a]

n[b]	K	M_2	M_1	I
2	·	421(45)		·
3	·	380(4)	· 410(35)	·
4	·	315(16)	· 380(34)	·
5	·	300(22)	· 357(30)	·
6	·	257(28)	· 357(16)	·
7	·	239(30)	· 346(15)	·
8	· 200(8)	· 222(19)	· 340(15)	·
9	· 189(5)	· 206(16)	· 342(15)	·
10	· 185(15)	· 191(15)	· 338(9)	·
11	· 183(14)	· 189(7)	· 342(11)	·
13	· 118(16)	· 182(19)	· 338(9)	·
15	· 120(28)	· 175(12)	· 328(9)	·

a) The latter quantities are in parentheses. b) The number of carbon atoms in the alkyl group.

another high-temperature phase, tentatively called a mesophase because of low rigidity, was observed at lower temperatures for the nonanoyl to hexadecanoyl derivatives. In this table, K, M_1, M_2, and I stand for crystalline, mesophases appearing at higher and lower temperatures, and isotropic phase respectively.

The mesophases (M_1) of the present series are thermally much more stable than those of the previously studied isomeric series **1**, the difference in the transition temperature between the corresponding members being greater than 100 °C. This stability enhancement may be ascribed to an increase in the intermolecular interaction by the substituents $NHCOC_nH_{2n+1}$ outweighing the decrease by three methyl groups. The steady and rather drastic falling of melting point (K-M_1 or K-M_2 transition temperature) is noted as the series is ascended. Nonetheless, its lowest temperature is comparable with the highest melting point observed for series **1**. The clearing point (M_1-I transition temperature) is also lowered by the increase of alkyl chain length, up to the octanoyl derivative, but no consistent variation has been found for the higher homologous members. Because of the high clearing point, compounds **2** are not stable above this temperature and the reversible transition cannot be recorded by calorimetry. The focal conic texture may be observed when the M_1 phase, heated to relatively high temperatures, is cooled. Finally, it may be added that the enthalpy change at the clearing point is much larger than that given by the corresponding *N,N'*-dialkanoyl-2,4,6-trimethyl-1,3-benzenediamine, reflecting the intermolecular interaction strengthened by the introduction of an extra $NHCOC_nH_{2n+1}$ group to the molecule.

Since the high-temperature phases of the lower homologous members are located at temperature ranges too high to carry out X-ray measurements, the diffraction patterns were recorded for the octanoyl to hexadecanoyl derivatives. The patterns observed with the unoriented M_1 phases are similar to those reported for compounds **1**.[3] The sharp innermost peak is strong and is accompanied by a weak peak, the spacing of which is about $1/\sqrt{3}$ times that given by the innermost peak. This ratio is characteristic of a hexagonal lattice. Such a symmetry may be achieved by the rotation of the molecular core around the columnar axis, even if the molecule has only three alkyl groups. The innermost peak may be assigned to the 100 reflection and the other one to the 110 reflection. The two spacings defined by these peaks are independent of the temperature. They increase linearly with the alkyl chain length. The spacing d_{100} given by the octanoyl derivative is 1.48 nm and that given by the hexadecanoyl derivative is 1.93 nm. A broad peak located at a large Bragg angle gives a spacing of about 0.46 nm throughout the series. This spacing is characteristic of the melted state of the paraffinic moieties in mesophases and gives the average stacking distance between

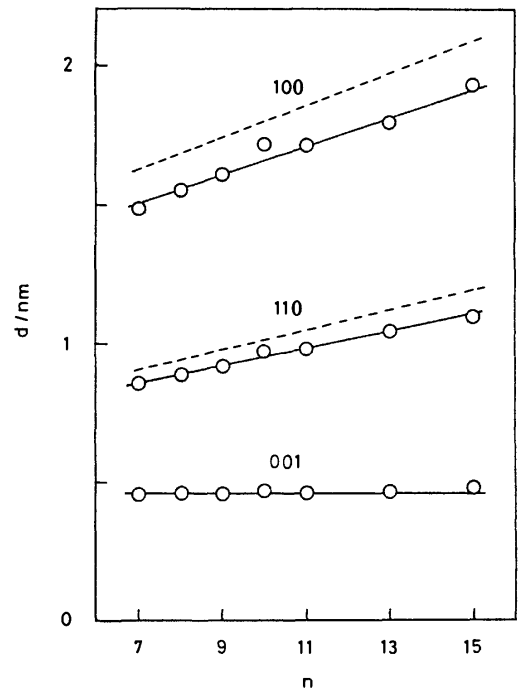

Fig. 1. Plots of spacings measured in M_1 phases against the number of carbon atoms in the alkyl group for compounds **2**. Broken lines indicate the corresponding spacings of compounds **1**.

the molecular planes irregularly spaced in a column. Thus, the observed feature is of the hexagonal disordered columnar (D_{hd}) structure. The M_1 phase, given by the heptanoyl derivative, is probably of the same nature; however, those exhibited by the butyryl to hexanoyl derivatives may be more-structured because of about twice larger enthalpy changes upon the transformation into an isotropic liquid.

In Fig. 1, the broken lines represent the spacings d_{100} and d_{110} plotted against the number of carbon atoms in the alkyl group measured for the mesophases of compounds **1**.[3] The spacings in the present series are consistently shorter than those of series **1**. For example, the spacing d_{100} of the octanoyl derivative (n=7) is 1.48 nm and that of the heptyl derivative in series **1** is 1.63 nm. The former value is essentially the same as that found for hexakis(octanoyloxy)benzene, 1.50 nm, reported by Chandrasekhar et al.[1] On the basis of these differences in the spacing, one might suggest that the alkyl chains in the present series of compounds are conformationally more disordered than those in series **1**. The enthalpy changes at the clearing point are 15 kJ mol^{-1} for the present compound, 12 kJ mol^{-1} for the corresponding compound **1**,[3] and 19 kJ mol^{-1} for the hexasubstituted compound.[1] It must be noted that the clearing point of the present compound, 328 °C, is appreciably higher than that of the previously studied one, 214 °C, and also that of the compound reported by Chandrasekhar et al., 83.4 °C. Therefore, the entropy changes at the clearing point in the former two are

actually close to each other but are smaller by a factor of two than that for hexakis(octanoyloxy)benzene. Three long alkyl groups carried by the molecules in our two series appear to be disordered nearly to the same extent in the mesophases; therefore, the shorter spacing may imply that the alkyl groups in series **2** are more interdigitated than those in series **1**.

The diffraction pattern recorded for the M_2 phase of the hexadecanoyl derivative shows four sharp peaks and two relatively broad ones. The sharp peak at the lowest Bragg angle is accompanied by its second and third order reflections. The spacing is markedly longer than that shown by the corresponding M_1 phase, namely 4.25 versus 1.93 nm. There are three peaks at relatively high Bragg angles giving spacings of 0.42, 0.46, and 0.55 nm respectively. The second one is sharp and the other two are rather broad. The shortest and the second shortest spacings are common to all the diffraction patterns of the M_2 phases. The spacing given by the innermost peak decreases almost linearly by the decrease in the alkyl chain length and 2.73 nm is obtained for the nonanoyl derivative. The diffraction pattern becomes more complicated as the series is descended. A few extra weak peaks appear in the intermediate Bragg angles. The phase is viscous but may have a three-dimensional lattice.[7] The innermost peak in the diffraction pattern recorded for the crystalline phases gives a spacing a little longer than that of the M_2 phase of the same compound; for example, 2.78 versus 2.73 nm for the nonanoyl derivative and 4.02 versus 3.81 nm for the tetradecanoyl derivative.

The conformational melting of the alkyl chains in the M_1 and M_2 phases is firmly supported by the small second moments of the broad-line proton NMR spectra (the mean-square widths of the resonance line), $<\Delta H^2>$, recorded above the melting point. The tetradecanoyl derivative gives a moment of about 12 G^2 (1 $G=10^{-4}$ T) at room temperature. The value decreases continuously to about 3 G^2 by the melting point and then rather abruptly to 0.5 G^2 of the M_2 phase. The moment remains at this value up to the M_2–M_1 transition temperature. The value as small as 0.03 G^2 observed for the M_1 phase is close to those observed for the mesophases of *N,N′,N″*-trioctyl- and *N,N′,N″*-trihexadecyl-1,3,5-benzenetricarboxamides and also *N,N′*-dihexadecanoyl-2,3,5,6-tetrakis(hexadecanoyloxy)-1,4-benzenediamine.[3,6] Their X-ray diffraction patterns are essentially the same and are attributable to the hexagonal disordered columnar structure.

This work was supported by a Grant-in-Aid for Scientific Research No. 60470001 from the Ministry of Education, Science and Culture.

References

1) S. Chandrasekhar, B. K. Sadashiva, and K. A. Suresh, *Pramana*, **9**, 471 (1977).
2) J. Billard, J. C. Dubois, Nguyen Huu Tinh, and A. Zann, *Nouv. J. Chim.*, **2**, 535 (1978).
3) Y. Matsunaga, N. Miyajima, Y. Nakayasu, S. Sakai, and M. Yonenaga, *Bull. Chem. Soc. Jpn.*, **61**, 207 (1988).
4) Y. Matsunaga and M. Terada, *Mol. Cryst. Liq. Cryst.*, **141**, 321 (1986).
5) R. Fittig, *Justus Liebigs Ann. Chem.*, **141**, 133 (1867).
6) Y. Kobayashi and Y. Matsunaga, *Bull. Chem. Soc. Jpn.*, **60**, 3515 (1987).
7) A. de Vries, *Mol. Cryst. Liq. Cryst.*, **63**, 215 (1981).

 © 1988 The Chemical Society of Japan Bull. Chem. Soc. Jpn., 61, 2743—2746 (1988)

Some Aspects through Sedimentation Study on the Extremely Elongated Micelle Formed in Cationic Surfactant-Aromatic Additive Systems

Yuko SAKAIGUCHI and Hirotaka HIRATA*
Niigata College of Pharmacy, Department of Physical Chemistry, 2-13-5 Kamishin'eicho Niigata 950-21
(Received February 12, 1988)

Sedimentation studies were carried out upon systems composed of HTAB or HPB, a cationic surfactant, and several aromatic additives which were accompanied by remarkable viscoelasticity in a solution in which the existence of extremely elongated gigantic rod-like micelles was previously established by the authors as images under an electron microscope. Those elongated rod-like micelle systems appeared to be separated into two components: one showed floatation and the other sedimentation under a 6×10^4 rpm force field, providing rather pertinent values of $S_{20\omega}$ in the order of 10^{-13}s, compared with several proteins or other polymeric substances. After attaining an equilibrium state during sedimentation, the micellar particle weight was deduced to be about 1.2×10^7 amu. The obtained values seemed to be considerably smaller than those expected from the electron microscope images where the length of the rod-like micelles were assumed to be infinitely elongated. The discrepancy is likely to have been brought about by a degradation of the micelle chain under a strong centrifugal force field.

Several cationic surfactants with appropriate chain lengths, such as hexadecyltrimethylammonium bromide (HTAB) and *N*-hexadecylpyridinium bromide (HPB), when added to various aromatic substances such phenolic derivatives like iodophenol and salicylic acid or its sodium salt, form infinitely elongated rod-like micelles. The occurrence of these extremely elongated rod-like micelles has been established through electron microscope studies[1,2] by the authors for a wide variety of pairs of surfactant-additive systems.[3] A solution composed of these substances possesses a remarkable viscoelasticity in solution, which reflects an entanglement of those extremely elongated rof-like micelles with each other.

These solution behaviors aroused the interest of several investigators who investigated the solution structure etc. in more detail through many field measurements of NMR,[4] light scattering,[5] neutron scattering,[6] flow[7] and electric birefringence[8] and dynamics.[9]

The values of the micelle length, obtained through these experiments are not very great, only several thousand Å at most. These values are far smaller than those which are suggested from observations of electron micrographs.

The reasons for this discrepancy are unknown. Whether it is caused by specimens being in a dry condition for electron microscopy, or in a wet condition for other measurements in solutions, is one of the most relevant problems that needs to be urgently solved. Hence, we intended to determine the micellar particle weights and selected a sedimentation measurement technique as an alternative direct method to approach this problem. A knowledge of the micellar particle weight is also a requisite in order to disclose the solution behavior as the remarkable viscoelasticity in these systems.

Experimental

Cationic surfactants, HTAB and HPB, were commercially available and used after one recrystallization from an acetone–methanol mixture. Aromatic additive substances were all of a special pure grade and used as purchased. Measurements of the sedimentation velocity and micellar particle weight in equilibrium were achieved by using a Hitachi Seisakusho Co. centrifugal separator attached to it with a UV scanner (ABS-7, Hitachi Co) under a controlled temperature of 20 °C. All analyses of the obtained data were automatically processed by a Hitachi data analyzer DA-7 online with the above apparatus. The progress of the sedimentation was detected by the UV absorption fitted to the appropriate absorption wavelength of the additive substances. The values of specific volume, $\bar{v}$, required to estimate the micellar particle weight which referred to $M=2RT/(1-\bar{v}\rho)\omega^2\cdot d\ln C/dr^2$ were measured as to the sediment deposited on the bottom of a centrifugal separation cell. The sediment was filled into a Lipkin–Devison type pycnometer held at 20 °C thermostat in which the densitometry deduced the values of $\bar{v}$.

The conductance measurement relied on a conductivity meter, CM-30ET (TOA Electronics Ltd.). Values were directly obtained by using a cell equipped with a meter for reading the specific conductivity in units of $S\,m^{-1}$ ($\Omega^{-1}\,m^{-1}$). Measurements were always carried out for solutions thermostated at 20 °C. For a frozen-dried sample of sediments prepared beforehand, an analysis of the surfactant content was carried out by a volumetric method in which any color change of congo red, an indicator, was detected as the end point by a wolframophosphoric acid solution of a known titer.

Results and Discussion

Measurements were mainly carried out upon systems containing HTAB–iodophenols, which showed rather clearer sedimentation profiles on diagrams for any analysis (Fig. 1), whereas HTAB-salicylic acid, the most typical viscoelastic system, showed no clear profiles of sedimentation under a 6×10^4 rpm centrifugal force field for an hour or so. In Fig. 1 it is obviously shown that these systems are composed of two entities, one of which moves to the upper part and the other to

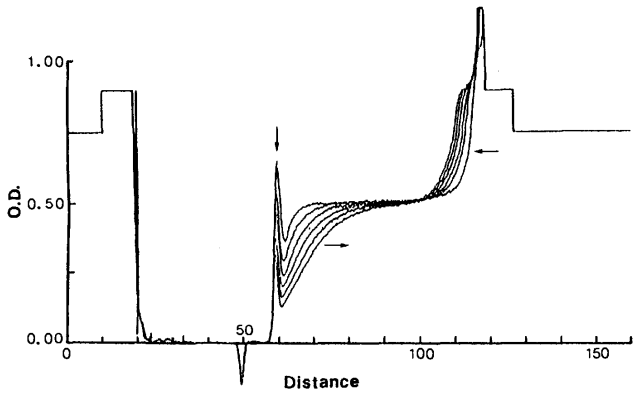

Fig. 1. Concentration traces observed for each ten minutes lapse in a system of HTAB-*o*-iodophenol under a 6×10^4 rpm centrifugal force field. HTAB concentration was 5×10^{-3} mol l^{-1} and the mixing molar ratio was unity. O. D. values were from 305 nm absorption of *o*-iodophenol. Arrows show the direction of the shift of the concentration traces with the lapse of time.

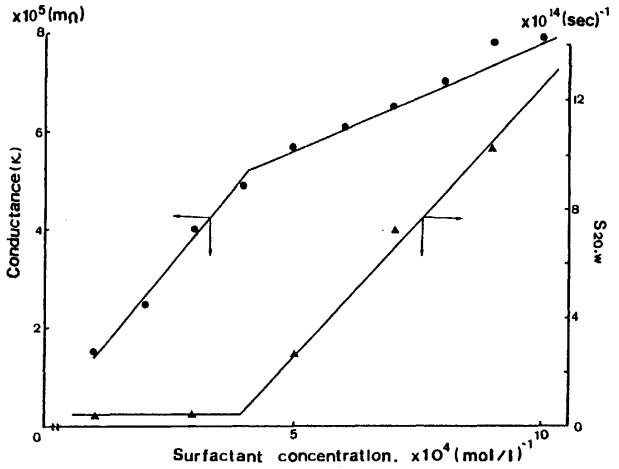

Fig. 2. The relation of conductance and $S_{20,\omega}$ vs. surfactant (CPB) concentration.

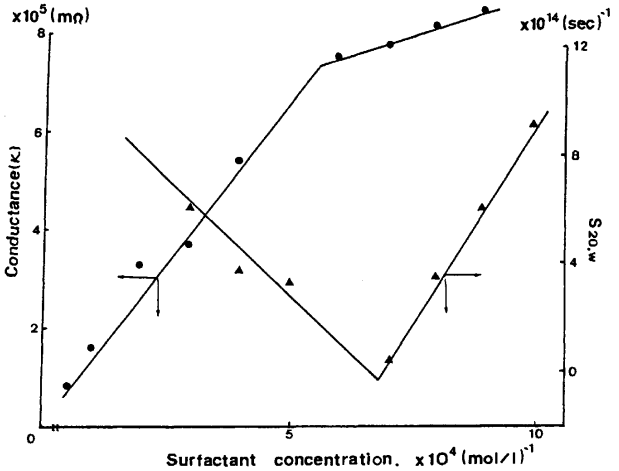

Fig. 3. The relation of conductance and $S_{20,\omega}$ vs. surfactant (CTAB) concentration.

the bottom side of a cell as time passes. The sedimentation coefficients, $S_{20\omega}$, obtained from each separated part in several systems, are summarized in Table 1; values having either a plus or minus sign show the sedimentation or the floatation, respectively. In ionic surfactants such values as $S_{20\omega}$, which indirectly suggest a state of surfactant aggregation, are sensitively affected by any surface charge. In order to avoid those effects arising from an electric charge which cause interactions between micellar particles, a supporting electrolyte is generally added to the systems to be studied. However, in our systems a special electrolyte was not added at all so as not to cause any inevitable changes in the aggregation states (shapes, degrees, or numbers etc.) due to the electrolyte added. Because viscoelastic extremely elongated gigantic micelles are also very sensitive to the coexistence of any other substance, such as electrolytes. The values of $S_{20\omega}$ appear, however, to fit the generally accepted magnitude, nearly of 10^{-13} s,[11] in their order.

In each system of HPB- and HTAB-*o*-iodophenol the dependence of $S_{20\omega}$ on the surfactant concentrations are shown in Figs. 2 and 3, respectively, in which the conductance behaviors are also exhibited in order to show the distinct relation of $S_{20\omega}$ or κ to the surfactant concentration. As is common knowledge, a conductivity measurement is one of the most reliable methods for estimating the cmc of any surfactant, which is represented as a sharp break point in a κ vs. concentration diagram. In both systems the curves of

Table 1. $S_{20,w}$ Values of Several Surfactant/Additive Systems

System surfactant/additive[a]	Concentration mol l^{-1}	$S_{20,w}$/s	
HTAB/*o*-iodophenol	1×10^{-3}	1.01×10^{-13}	-2.76×10^{-14}
	5×10^{-3}	1.13×10^{-13}	-5.47×10^{-14}
	1×10^{-2}	1.99×10^{-13}	
HTAB/*p*-iodophenol	5×10^{-3}	1.01×10^{-13}	-2.84×10^{-14}
	1×10^{-2}	1.89×10^{-13}	
HTAB/salicylic acid	1×10^{-3}		-2.16×10^{-13}
HTAB/sodium salicylate	1×10^{-2}	0.13×10^{-13}	
HTAB/sodium biphthalate	1×10^{-2}		-0.03×10^{-13}
HPB/*o*-iodophenol	5×10^{-3}	1.04×10^{-13}	-1.34×10^{-13}

a) Mixing molar ratios of each surfactant/additive systems are equal to unity.

conductance vs. surfactant concentration had clear break points which were assumed to be the cmc's of each surfactant-additive system, above which concentration the micelles were formed in those composed solutions. The values of the composed systems were a little smaller, but in good coincidence, compared with those for each single surfactant system of HPB[12] and HTAB[13] reported hitherto. Some lack of uniformity concerning $S_{20\omega}$ values was found over the low concentration range in an HTAB-*o*-iodophenol system, whereas no lack in HPB-*o*-iodophenol; this seems to be due to a difficulty in the appraisal of the sedimentation distance on a diagram of the former system necessary to determine the $S_{20\omega}$ value. Thus, we were provided with a good correspondence of aggregation states with $S_{20\omega}$ under a support of gradual increase of the micellar weight with an increase in the surfactant concentration above cmc, though it is imposed with several assumptions that micelle structure, say its form and density etc., is left unchanged during micelle growth. The same behavior of succeeding aggregation with an increase in the surfactant concentration in those viscoelastic systems has been reported by some investigators in various studies.[9,14]

The results of an analysis on the sediments deposited at the cell bottom under a 6×10^4 rpm centrifugal force for 1 h are presented in Table 2. It should be noted that the above-mentioned sediments do not refer to some crystalline or other materials. The sediments gathered at cell bottom were, of course, clear and appeared something like jelly in a test tube, being kept without flowing down in its up-side-down state. The sediments were a little enriched in iodophenol compared with those of the initial component ratio, increasing with an increase in the molar ratio of the surfactant/iodophenol until a level off at a ratio of 1.0. The values, however, suggest that in those systems the elongated micelles comprise two components of surfactant and iodophenol in a nearly unity composition at optimum states. This idea has been supported from many facts: e.g. the viscoelasticity[3,15] is most remarkably induced at a mixing molar ratio of unity with both components.

Table 2. Analyses of Sediments of HTAB/*o*-Iodophenol Systems

Original mixing molar ratio (HTAB/*o*-iodophenol)	HTAB weight %[a]	*o*-Iodophenol weight %[a]	Assayed value in molar ratio of HTAB/*o*-iodophenol
1/0.5	73.2	26.8	1/0.6
1/1	57.7	42.3	1/1.2
1/2	56.8	43.2	1/1.3

a) Water contents of the sediments were nearly the same to be given as averaged 97.1% in weight, values shown were referred to the frozen-dried samples as total materials.

In addition to the analyses of sediments, the densities of the sediments were measured by using a Lipkin-Devison type pycnometer, being determined at 20 °C to be 1.0035 $cm^{-3}g^{-1}$ for HTAB-iodophenol system referred to water at 20 °C. In our systems composed of HTAB or HPB and aromatics such as iodophenol, the values appeared to be much smaller compared with those of single surfactants reported concerning their micellar form, though the available data were very few, especially regarding cationics.

Studies of sedimentation equilibrium based on the Archibald method provided the particle weight of the elongated rod-like micelle by introducing the above obtained specific volume of the sedimentating micellar particle. An equilibrium state for those micellar systems was presumed to be attained after 30 h operation of the apparatus under 6000 rpm force. An averaged value of the micellar particle weight in several times trials resulted in 1.2×10^7 amu; this seemed to be very much smaller than that expected from the electron microscopic images.

It seems that there's no decisive conclusion about the variation of micellization under a centrifugal force field, especially in an electrically perturbed state of ionic surfactants: various effects concerning the concentration gradient on the micellar size, structure and/or a shift of aggregation equilibrium. While in our systems of HTAB- or HPB-aromatic additives, which provide an extremely elongated gigantic micelle, the circumstances are presumably very much similar to those explained by the concept of the Phase Separation Model. In other words, in the Mass Action Law Model or the Mutiple Equilibrium Model, the gigantic micelles are very stable and almost undissociable in solution: that is, equilibrium deviates extremely to the side of gigantic micelle formation having a large equilibrium constant. It cannot easily be moved to produce shorter, smaller aggregates or to be dissociated to single surfactant molecules with only a little change in the micellar and monomer concentrations. A smooth shift of the concentration traces (Fig. 1) with the centrifugation time lapses seems to prove this view point to be reasonable.

The apparent discrepancies between the obtained values and the expected one from the electron microscopic images might be due to some degradation effect of a long micellar chain into smaller fragments under a strong force field. Those micellar chains of infinite length are evidently in firmly entangled states, also as shown in the electron micrographs.[3] They can form a gigantic tight network structure all over the whole system. We were not able to obtain a sedimentation profile in HTAB-salicylic acid systems which showed the most typical viscoelastic behavior with some gel-like appearance. These micellar chains of HTAB-salicylic acid system seem to form too firm a frame-work in structure to suffer from fragmentation. The elongated micellar chain in a HTAB-iodophenol system is per-

haps easier than the micellar chain of HTAB-salicylic acid to be broken into fragments to become shorter chains of which micellar particle weight might be so reasonably decreased, as has been obtained as the above value. In electron micrographs the thickness of the micellar chain was evidently different from each other between these two systems, it being thinner in HTAB-iodophenol than in HTAB-salicylic acid.[3] The experimental fact support the result of sedimentation.

At any rate, the value was, however, not so much different from those which had been reported by several authors concerning several analogous viscoelastic systems by many different method.[4,13] Moreover, it was approximately one order larger compared with values[16] measured in these cationic surfactant systems added with a simple salt, such as NaBr etc. The particle weight obtained here implies that the micellar chain has a length of about 1710 nm from the following consideration and results based on a treatment[17] of a contour length estimation etc.: A rod-like micellar chain is cylindrically constructed by surfactant molecules accompanied by phenolic derivatives as ionic counterparts in about a one-to-one ratio, which are arranged with a hydrocarbon core surrounded by hydrophilic groups. The cylindrical micelle is assumed to be a stack of thin elementary discs composed of fewer surfactant molecules than twenty in a disc.[16] The molecular weight of the thin elementary disc is nearly 7×10^3 nm^{-1}, it being postulated that the additives are localized only at a micelle surface. Through this consideration, therefore, the stacking number of discs can be deduced to about 1940 by dividing the averaged micellar chain molecular weight by the elementary disc molecular weight; the micellar chain length can subsequently be derived, as described above, to be about 17100 Å through an appraisal of the disc thickness to be ca. 9 Å.[16]

Whether such a length of micellar chain is suitable for explaining the viscoelastic solution behavior is now yet ambiguous because of insufficiency of directly comparable data of both in qualities and in quantities. We are undertaking a more reasonable elucidation of the viscoelastic solution behavior, which might be reflected by the micellar structure etc. through more extensive and detailed data.

References

1) T. Shikata, Y. Sakaiguchi, H. Urakami, A. Tamura, and H. Hirata, *J. Colloid Interface Sci.*, **119**, 291 (1987).
2) Y. Sakaiguchi, T. Shikata, H. Urakami, A. Tamura, and H. Hirata, *Colloid Polym. Sci.*, **265**, 750 (1987).
3) Y. Sakaiguchi, T. Shikata, H. Urakami, A. Tamura, and H. Hirata, *J. Electron Microsc. (Tokyo)*, **36**, 168 (1987).
4) J. Ulmius, H. Wennerström, L. B. Johansson, G. Lindblom, and S. Gravsholt, *J. Phys. Chem.*, **83**, 2232 (1979).
5) H. Hoffmann, G. Platz, H. Rehage, and W. Schorr, *Ber. Bunsenges. Phys. Chem.*, **85**, 877 (1981).
6) J. Kalus, H. Hoffmann, K. Reizlein, W. Ulbricht, and K. Ibel, *Ber. Bunsenges. Phys. Chem.*, **86**, 37 (1982).
7) L. B. Johansson, G. Lindblom, and B. Norden, *J. Colloid Interface Sci.*, **69**, 358 (1979).
8) L. B. Johansson, A. Davidsson, G. Lindblom, and B. Norden, *J. Phys. Chem.*, **82**, 2604 (1978).
9) H. Hoffmann, G. Platz, W. Schorr, and W. Ulbricht, *Ber. Bunsenges. Phys. Chem.*, **85**, 225 (1981).
10) H. Hoffmann, M. Lobl, H. Rehage, and I. Wunderlich, *Tenside Detergents*, **22**, 290 (1985).
11) C. Tanford, "Physical Chemistry of Macromolecules," John Wiley & Sons Inc., (1961), p. 381.
12) M. Czerniawski, *Roczn. Chem.*, **39**, 1275 (1965).
13) M. Czerniawski, *Roczn. Chem.*, **40**, 1935 (1966).
14) K. L. Mittal and B. Lindman ed. "Surfactants in Solution," Plenum Press, (1984), Vol. 1, p.425.
15) T. Shikata, T. Kotaka, and H. Hirata, *Langmuir*, in press.
16) T. Imae and S. Ikeda, *J. Phys. Chem.*, **90**, 5216 (1986).
17) O. Kratky and G. Porod, *Recl. Trav. Chim. Pays-Bas.*, **68**, 1106 (1949).

 © 1988 The Chemical Society of Japan Bull. Chem. Soc. Jpn., 61, 2747—2752 (1988)

Catalytic Activity of Nonstoichiometric Niobium Oxide with Controlled Composition, $NbO_{2.488-2.500}$, for Butene Isomerization

Yasushi MURAKAMI, Yuji WADA, and Akira MORIKAWA*
Department of Chemical Engineering, Tokyo Institute of Technology, Meguro-ku, Tokyo 152
(Received February 26, 1988)

The composition of niobium oxide was controlled between $NbO_{2.488}$ and $NbO_{2.500}$ by treating with mixture of water vapor and hydrogen gas at 873K. X-ray diffraction (XRD) study of the treated niobium oxide showed that only a phase of nonstoichiometric T-Nb_2O_5 was found in the range of $NbO_{2.488-2.500}$ and a phase of NbO_2 coexisted with the T-Nb_2O_5 phase by further reduction. The catalytic activity of the oxide for *cis*-2-butene isomerization had a maximum value at the O/Nb ratio of 2.494. The electron spin concentration of Nb^{4+} ion, and the amount of nitrogen monoxide adsorbed on the niobium oxide also showed a maximum value at the O/Nb ratio of 2.496 and 2.494, respectively. Coincidence in the dependences, on the composition of the reduced niobium oxide, of the catalytic activity, the spin concentration of Nb^{4+} ion, and of the amount of adsorbed nitrogen monoxide shows that isolated Nb^{4+} ion with unsaturated coordination is a catalytically active site.

Niobium oxide has been often used as a promoter of catalysts, but has been recently examined as a main component of catalysts by several investigators.[1-10]

Morikawa et al. have reported that niobium oxide supported on silica became catalytically active for dimerization of ethylene both by UV light irradiation in the presence of olefin and by reduction with hydrogen at high temperature.[1] The catalytic activity of the niobium oxide catalyst activated by both the processes has been attributed to a reduced niobium species like Nb^{4+} ion. Many phases are present for reduced niobium oxide.[11] It has been reported that a specific phase of the various oxide catalysts, tungsten,[12-14] vanadium,[15] and rhenium oxides,[16] plays an important role on their obtaining catalytic activities. It is therefore supposed that the catalytic activity of niobium oxide should be closely related to the composition of niobium and oxygen atom, or the type of phase of the oxide.

We have found in this study that the composition of niobium oxide is controlled between $NbO_{2.488}$ and $NbO_{2.500}$ without change of its phase by the treatment with mixtures of water vapor and hydrogen gas in various ratios. The reaction experiment with the isomerization of butene carried out on the niobium oxide with the various controlled compositions have revealed the relationship between the structure of the oxide and its catalytic activity.

Experimental

Materials. A standard material of niobium oxide, $NbO_{2.500}$ was prepared from niobic acid manufactured by CBMM INT. LTDA. (#AD378). This niobic acid contained the impurities of Fe (40 ppm), Na (23 ppm), K (27 ppm), and Si (490 ppm). Niobic acid was dried in air at 673 K for 3 hours and calcined at 873 K for 30 hours. The X-ray diffraction (XRD) pattern of the oxide was attributed to the T-Nb_2O_5 structure.[17] Oxygen and hydrogen were purified by passing through 4A Molecular Sieve cooled to the Dry Ice temperature. Water and *cis*-2-butene were used after bulb-to-bulb distillation in vacuo.

Control of the Composition of Niobium Oxide. The treatment of niobium oxide for its control of the composition was carried out with a closed gas-circulation system. The standard oxide of 1 g was heated up to 873 K in the stream of oxygen gas. After the oxygen gas was evacuated for 30 min, the H_2O-H_2 mixture was brought into contact with the oxide. The H_2O-H_2 mixture was circulated by a magnetically driven piston pump installed in the gas-circulation loop. Excess amount of water was stored at U shape trap of the circulation system cooled at a temperature between 233 and 283 K to keep a constant partial pressure of water vapor in the H_2O-H_2 mixture. Initial pressure of hydrogen was 13.3 kPa. After the pressure drop of the gas was ceased, the sample was quenched by rapid cooling to 298 K. The composition of niobium oxide prepared by the treatment is calculated from the pressure decrease of the mixture. The composition is expressed by the atomic ratio, O/Nb, with precision of ±0.0005. The surface area (15 $m^2 g^{-1}$) of the oxide was unchanged by the treatment.

Reaction Experiments and Spectroscopy. The reaction of *cis*-2-butene was carried out at 298 K with a closed circulation system. The reaction mixture was analyzed by gas chromatography. XRD was measured with Rikadenki Rotaflex RU-200. Electron spin resonance (ESR) spectra were recorded at 77 K by JEOL-PE-IX spectrometer. The sample was transferred to an ESR tube and sealed in vacuo.

Results

Control of O-Nb Composition. In Fig. 1, the changes in the composition of niobium oxide indicated by the ratio, O/Nb, during the treatments at 873 K with the H_2O-H_2 mixtures of various H_2O/H_2 ratios are displayed. When the standard sample was treated in the H_2O-H_2 mixture of the partial pressure ratio of $P_{H_2O}/P_{H_2}=9.0\times10^{-3}$, the ratio of oxygen and niobium atom in the oxide was decreased up to the value of O/Nb=2.498 and no further reduction was observed. This composition did not change even after 6 hours of the treatment. When the sample which was preliminarily reduced to the ratio of O/Nb=2.482 was kept into contact with the H_2O-H_2 mixture of ratio, $P_{H_2O}/P_{H_2}=9.0\times10^{-3}$, the O/Nb value was increased to 2.498, which was coincident with the value observed when the standard sample with O/Nb=2.500 was

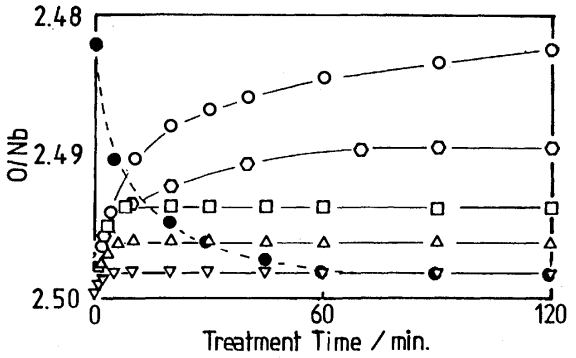

Fig. 1. Change in the O-Nb composition during the treatment with H_2O-H_2 mixture at 873 K. The ratios of the mixture, P_{H_2O}/P_{H_2}, are 2.0×10^{-3} (○), 4.0×10^{-3} (○), 8.0×10^{-3} (□), 3.0×10^{-2} (△), and 9.0×10^{-2} (▽). The broken line shows change in the composition of $NbO_{2.483}$, when it was treated with the H_2O-H_2 mixture of the P_{H_2O}/P_{H_2} ratio, 9.0×10^{-2} (●).

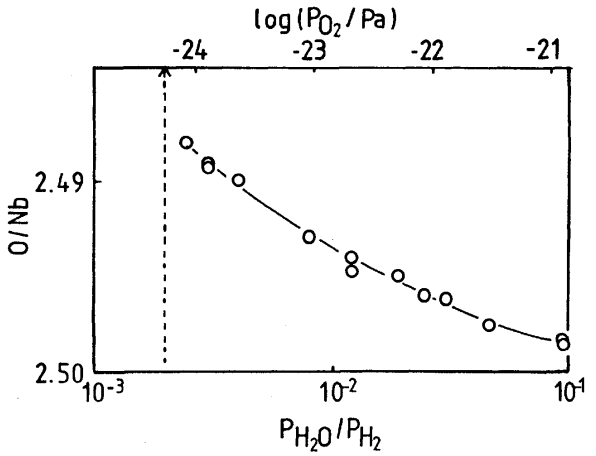

Fig. 2. Dependence of the equilibrium composition of niobium oxide on P_{H_2O}/P_{H_2} at 873 K. The partial pressure of oxygen is denoted by P_{O_2}.

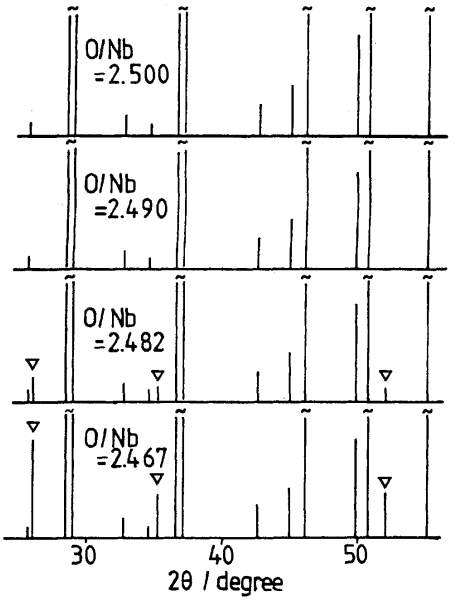

Fig. 3. XRD patterns of niobium oxide of the various composition obtained by the treatment. ($K\alpha$= 0.15418 nm).

treated by the H_2O-H_2 mixture of the same ratio. It is, therefore, stressed that oxidation and reduction of the oxide are reversible and the oxide is in equilibrium with the H_2O-H_2 mixture.

The treatment with the H_2O/H_2 mixture of the ratio 3.0×10^{-2}, 8.0×10^{-3}, or 4.0×10^{-3}, gave the reduced oxides with the corresponding O/Nb ratio, 2.496, 2.493, or 2.490, respectively. When the mixture of $P_{H_2O}/P_{H_2}=2.0\times10^{-3}$ was used, the O/Nb value continuously decreased and did not show a stable equilibrium composition. It was reduced to the O/Nb ratio further less than 2.475 by the treatment of 6 hours.

The careful examination of the O/Nb values corresponding to the various P_{H_2O}/P_{H_2} values of the reducing gas mixture in the range of 1.0×10^{-1}—2.5×10^{-3} yielded the result shown in Fig. 2. The partial pressure of oxygen calculated from the equilibrium of water decomposition is expressed in the figure. The value of the O/Nb ratio decreased with decrease in the ratio of P_{H_2O}/P_{H_2} between 1.0×10^{-1} and 2.5×10^{-3}. A discontinuity in the O-Nb phase at the O/Nb ratio of 2.488 was present in Fig. 2.

XRD Measurements of Niobium Oxide. Figure 3 shows X-ray diffraction patterns of niobium oxide which was rapidly quenched by cooling after the treatment described in the above section. The standard Nb_2O_5 (non-reduced) is identified as T-Nb_2O_5 type crystal structure by XRD pattern.[17] The observed XRD patterns show that niobium oxide reduced up to the composition of O/Nb=2.490 maintains the crystal structure of T-Nb_2O_5, although the careful analysis of the patterns revealed a slight lattice expansion by the reduction in respect to all the three crystal axes. It is, therefore, suggested that only a nonstoichiometric T-Nb_2O_5 phase is present in the range of the O/Nb ratio, 2.500—2.488.

When the oxide was further reduced to $NbO_{2.482}$, new peaks marked by ▽ signs in the figure appeared at d values of 0.343, 0.255, and 0.176 nm, which were attributed to NbO_2.[18] The intensity of the peaks due to NbO_2 increased with decrease in the O/Nb ratio of the oxide. Therefore, it is concluded that two phases coexist below the O/Nb ratio of 2.488 and the nonstoichiometric Nb_2O_5 phase is transformed into NbO_2 phase with decrease of the O/Nb ratio.

ESR Spectrum of Nb^{4+} Ion. No ESR signal was observed for the standard oxide. The ESR absorption by the oxide was induced by its reduction. An ESR spectrum of the niobium oxide reduced to the O/Nb ratio of 2.496 by the treatment was observed as shown in Fig. 4. Its g value was 1.85 ± 0.03. The spectrum was attributed to Nb^{4+} ion as discussed in the following section.

The intensity of the ESR signal changed as shown in Fig. 5 when the O/Nb composition of niobium

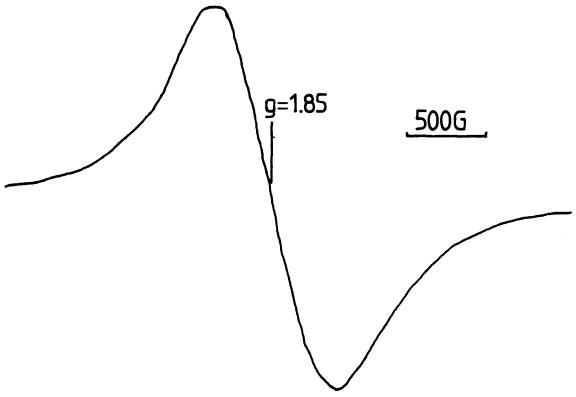

Fig. 4. ESR spectrum of niobium oxide (O/Nb=2.496) measured at 77 K after the treatment with the H_2O-H_2 mixture.

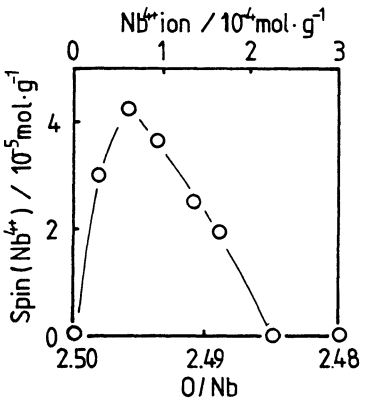

Fig. 5. Dependence of the spin concentration of Nb^{4+} ion upon the composition of niobium oxide. The spectrum was measured at 77 K. The concentration of Nb^{4+} ion estimated from the O/Nb ratio is shown.

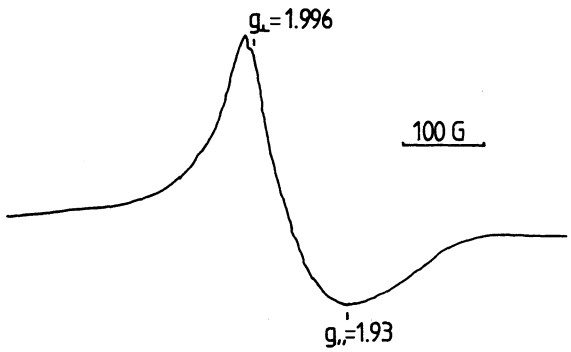

Fig. 6. ESR spectrum of nitrogen monoxide adsorbed on the treated niobium oxide (O/Nb=2.494) measured at 77 K.

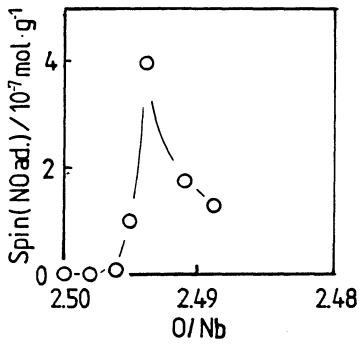

Fig. 7. Dependence of the spin concentration of nitrogen monoxide adsorbed on niobium oxide upon the composition of niobium oxide. The spectrum was measured at 77 K.

oxide was varied. The g value was independent of the composition. The spin concentration of Nb^{4+} ion increased with decrease of the O/Nb ratio and reached a maximum value at O/Nb=2.496. The spin concentration of Nb^{4+} determined by ESR was coincided well with the amount of Nb^{4+} ions estimated from the composition of the oxide only at the low extent of reduction. Further decrease of the O/Nb ratio depressed the spin concentration and, finally, no ESR signal was observed at the O/Nb ratio below 2.485.

Adsorption of NO. The asymmetric broad signal was observed by ESR spectroscopy after the adsorption of nitrogen monoxide on the niobium oxide of the O/Nb ratio between 2.489 and 2.498 as shown in Fig. 6. The perpendicular and parallel g values of the signal are 1.996 ±0.001 and 1.93±0.01, respectively.

Figure 7 shows the change of the spin concentration of nitrogen monoxide adsorbed on the niobium oxides of the various O/Nb compositions. The spin concentration showed a maximum at the O/Nb value of 2.494, while it is lowered for the O/Nb values both lower and higher than this value.

Isomerization of *cis*-2-Butene. The standard sample of niobium oxide was catalytically inactive for isomerization of *cis*-2-butene. Reduction of the oxide by the treatment with the H_2O-H_2 mixture induced its catalytic activity. Change in the amounts of isomers, *trans*-2-butene and 1-butene observed at 298K on the niobium oxide with the O/Nb ratio of 2.494, is displayed in Fig. 8. No other product was found. A short induction period was observed at the initial stage of the reaction, and the isomerization proceeded linearly to the reaction time. The slope of the linear part was taken as the rate of the isomerization of *cis*-2-butene to each isomer. The ratio of the amount of *trans*-2-butene to that of 1-butene produced was constant at the value of 10 during the reaction. The catalytic activity is represented by the rate of *trans*-2-butene formation observed at a constant pressure of the reactant, *cis*-2-butene, in this paper.

As shown in Fig. 9, the catalytic activity depended upon the O/Nb composition of niobium oxide. The catalytic activity increased with increase in the extent of the reduction, and reached a maximum value at O/Nb=2.494 and decreased with further decrease in the O/Nb value. The oxide with the O/Nb value less than 2.488 showed a very little, constant catalytic activity.

The catalytic activity observed on the oxide of the O/Nb ratio, 2.494, was poisoned completely by nitro-

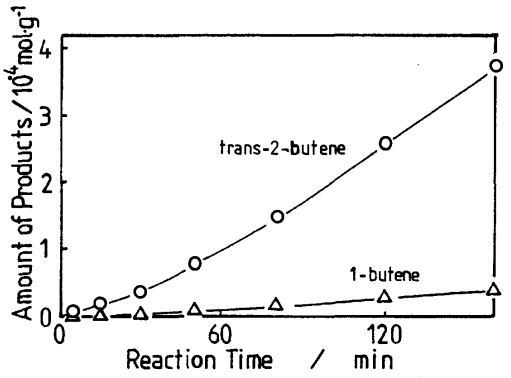

Fig. 8. Isomerization of *cis*-2-butene on the treated niobium oxide (O/Nb=2.494) along the reaction time at 298 K. Initial pressure of *cis*-2-butene was 13.3 kPa.

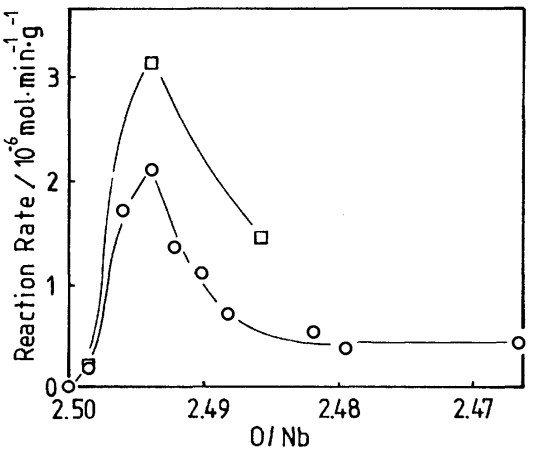

Fig. 9. Dependence of the reaction rate upon the composition of niobium oxide. The H_2O-H_2 mixture was evacuated at 298 K (○) or at 373 K (□) after the treatment.

gen monoxide of the amount, 5×10^{-6} mol, admitted both before and during the reaction.

Discussion

Crystal Structure of Niobium Oxide. It has been demonstrated that the composition of niobium oxide is controlled by the treatment with the H_2O-H_2 mixture at 873 K between the O/Nb ratio, 2.500 and 2.488. The oxide reaches in equilibrium with the H_2O-H_2 mixture in this range as described in the above section. XRD studies (Fig. 3) have clarified that the oxide maintains the T-Nb_2O_5 phase in the region between 2.500 and 2.488 of the O/Nb ratio. The continuous change of the O/Nb value against the ratio, P_{H_2O}/P_{H_2} (Fig. 2), with the slight expansion of the crystal lattice shows that T-Nb_2O_5 phase is nonstoichiometric. Continuous increase in the lattice parameters with increase in the extent of reduction observed by XRD ensures that the whole bulk of niobium oxide particles is homogeneously reduced by the treatment.

Phase relations, defect structures, and thermodynamic properties of the oxygen-niobium system above 1273 K have been reported by many investigators and have been intensively reviewed by Naito and Matsui.[11] Several oxide phases, $Nb_{12}O_{29}$, $Nb_{22}O_{54}$, $Nb_{47}O_{116}$, $Nb_{25}O_{62}$, and $Nb_{53}O_{132}$ have been recognized between NbO_2 and Nb_2O_5 at 1573—1673 K by Schäfer et al.[19] and Kimura.[20] At lower temperatures 1273—1373 K, Marucco has found only two phases $Nb_{12}O_{29}$ and $Nb_{25}O_{62}$ within the same composition range.[21] In the present work, however, niobium oxide with T-Nb_2O_5 phase structure directly transforms into NbO_2 at the O/Nb ratios less than 2.488 and no suboxide phase between NbO_2 and $NbO_{2.5}$ has been found. This absence of suboxide phases is explained by the discussion of Naito et al., who have reported that the several suboxide phases with the composition between NbO_2 and $NbO_{2.5}$ were less stable at temperature lower than 1273 K.[22]

The ESR absorption observed for niobium oxide of the O/Nb ratio, 2.496, obtained by the treatment with H_2O-H_2 mixture (Fig. 4) is attributed to reduced niobium ions. The ESR absorption due to Nb^{4+} ion in pure niobium oxide was observed for the first time owing to the controlled slight reduction by the treatment with the H_2O-H_2 mixture instead of that with hydrogen gas. An ESR study of Nb^{4+} ions in silicate glasses ($n$$Na_2O$·(98−$n$)$SiO_2$·2$Nb_2O_5$ n=11 and 22) has been reported by Yafaev and Garif'yanov.[23] The g value in our spectrum, 1.85±0.03, was close to their g values, 1.89 and 1.92. Their ESR spectrum of Nb^{4+} ions has hyperfine structure due to the interaction of a single 4d electron with the nucleus (I=9/2) of the natural niobium isotope ^{93}Nb. The parallel and perpendicular hyperfine constants were 310 and 145 Oe in Yafaev's results. In our experiment the hyperfine structure was not observed because the spectrum was extremely broad, in which the width of magnetic field of the absorption band was about 3000 Oe as shown in Fig. 4. The spectrum of Nb^{4+} ions in our system must have been broadened by various crystallographic environment of Nb^{4+} ions in the oxide so that the hyperfine structure has been indistinguishable.

As shown in Fig. 5, when the niobium oxide is reduced further from the value of the O/Nb ratio of 2.496, the spin concentration of Nb^{4+} ion measured by ESR is decreased in spite of increase in the extent of reduction. This inconsistency is attributed to a magnetic coupling between Nb^{4+} ions. Though Nb^{4+} ion is paramagnetic and hence its signal should be observed by ESR, no ESR signal of Nb^{4+} ion was observed for NbO_2. The crystal structure of NbO_2 is described as the distorted rutile structure, resulting Nb-Nb bonding.[24,25] Thus the pairs of Nb^{4+} ions bring about spin coupling resulting in a diamagnetic character of NbO_2. In the case of molybdenum oxide the concentration of Mo^{5+} ions determined by ESR spectroscopy is lower than that evaluated from the measurement of the composition,[26] and that deter-

mined by X-ray photoelectron spectroscopy.[27,28] Abdo et al. have suggested that the Mo^{5+} ions undetectable by ESR must be strongly, magnetically coupled.[29] Our result shows that Nb^{4+} ions are detectable by ESR in nonstoichiometric Nb_2O_5 phase, because they are isolated each other in the Nb_2O_5 matrix.

A simple interpretation is given for the result shown in Fig. 5. As far as the amount of Nb^{4+} ions is very small, isolated Nb^{4+} ion is increased in T-Nb_2O_5 structure when the oxide is progressively reduced. However, when the concentration of Nb^{4+} ions exceeds a certain value, Nb^{4+} ions couple each other, causing their magnetic character to be ESR-inactive. Thus, the spin concentration determined by ESR is less than that estimated from the O/Nb ratio at a large extent of reduction. No ESR signal is observed when most of Nb^{4+} ions couple at the ratio of O/Nb greater than 2.485.

Adsorption Site of NO. ESR spectrum of nitrogen monoxide adsorbed on the niobium oxide reduced by the H_2O-H_2 mixture was observed as shown in Fig. 6. Its shape is similar to that of nitrogen monoxide adsorbed on alumina reported by Lunsford.[30] Nitrogen monoxide adsorbed on niobium oxide should provide 30 hyperfine lines due to the interaction with the nucleus of ^{14}N (I=1) and ^{93}Nb (I=9/2), but this type of hyperfine structure was ambiguous in the present experiment.

According to Lunsford's work nitrogen monoxide is adsorbed on aluminum ion which is exposed to the surface with an oxygen ion vacancy. It is plausible that the adsorption of nitrogen monoxide occurs on the oxygen ion vacancy of reduced niobium oxide. Therefore, the change of the spin concentration of nitrogen monoxide adsorbed on the reduced niobium oxide depending on the O/Nb ratio reflects the change in the amount of Nb^{4+} ion which is exposed to the surface with an oxygen ion vacancy. The similar changes of the spin concentration of Nb^{4+} and of adsorbed nitrogen monoxide along with decrease in the O/Nb ratio lead us to a new assumption that isolated Nb^{4+} ion must provide an oxygen ion vacancy, in other words, isolated Nb^{4+} ions are coordinatively unsaturated. When the isolated Nb^{4+} ions are paired, they lose coordinatively unsaturation.

Active Sites for Isomerization. Isomerization of 1-butene on niobium oxide catalyst prepared by degassing of $Nb_2O_5 \cdot nH_2O$ has been studied by Iizuka et al.[2] $Nb_2O_5 \cdot nH_2O$ degassed at 373K exhibits a substantial catalytic activity for the isomerization, attributed to a very strong Brønsted acid. Degassing of $Nb_2O_5 \cdot nH_2O$ at temperatures higher than 773 K results in a remarkable decrease in the acidity and, therefore, niobium oxide prepared by calcination at 873 K exhibits little activity for the isomerization. Therefore, it is stressed that the catalytic activity for butene isomerization on the reduced niobium oxide observed in the present work originates hardly from its acid catalysis. Actually, the addition of ammonia of which amount was in excess of that of all the reduced species on the surface did not result in the complete loss of the activity, but reduced the activity to only one-half of its original value.

No catalytic activity was observed for the non-reduced niobium oxide, while the activity for the catalytic isomerization of butene was resulted from reduction of niobium oxides, indicating that the catalytically active site of the reduced niobium oxide catalyst is attributed to the reduced species of niobium ion. Thermodynamic data tell us that Nb^{5+} ion is reduced only to Nb^{4+} but not to a lower valence niobium ions in our experimental conditions. Formation of Nb^{4+} by the treatment with the H_2O-H_2 mixture was assured by ESR spectroscopy.

As discussed above, the observed spin concentration of Nb^{4+} reflects the amount of isolated and coordinatively unsaturated Nb^{4+}. Since nitrogen monoxide strongly poisons the catalytic activity, it was adsorbed on the catalytically active site of butene isomerization. It is concluded that the catalytically active site is identical with the nitrogen monoxide adsorption site, that is, isolated Nb^{4+} ion with coordinative unsaturation. This conclusion is supported by the general agreement between the catalytic activity and the amount of the adsorbed nitrogen monoxide (Figs. 7 and 9). The reason for the difference between these two measurements on the slightly reduced catalyst is ambiguous at present.

Among the tungsten oxide catalysts, WO_{3-x}, nonstoichiometric phase shows the high activity and selectivity for the reactions, for example, oxidation of propylene,[12] and allyl iodide,[13] and decomposition of N_2O.[14] On the other hand, stoichiometric oxides, WO_3, WO_2 or a tunnel structure oxide of $WO_{2.72}$, are less active or inactive for those reactions. Metathesis of propylene on ReO_3 catalyst is enhanced by a slight reduction of the catalyst with CO, but its catalytic activity is lowered when the extent of reduction exceeds a critical value.[16] Importance of nonstoichiometric phase for the catalysis demonstrated in these systems may be explained by the same idea that isolation of catalytically active species to keep the state of coordinative unsaturation is essential to maintain high catalytic activities as demonstrated in the present system.

We would like to thank CBMM INTERNACIONAL LTDA. for their kind supply of niobium samples and financial support.

References

1) A. Morikawa, T. Nakajima, I. Nishiyama, and K. Otsuka, *Nippon Kagaku Kaishi*, **1984**, 239; Proc. 8th Int. Congr. Catal., **IV**, 815 (1984).

2) T. Iizuka, K. Ogasawara, and K. Tanabe, *Bull. Chem. Soc. Jpn.*, **56**, 2927 (1983).

3) K. Ogasawara, T. Iizuka, and K. Tanabe, *Chem. Lett.*, **1984**, 645.
4) Z. Chen, T. Iizuka, and K. Tanabe, *Chem. Lett.*, **1984**, 1085.
5) T. Iizuka, S. Fujie, T. Ushikubo, Z. Chen, and K. Tanabe, *Appl. Catal.*, **28**, 1 (1986).
6) K. Asakura and Y. Iwasawa, *Chem. Lett.*, **1986**, 859.
7) M. Nishimura, K. Asakura, and Y. Iwasawa, *J. Chem. Soc., Chem. Commun.*, **1986**, 1660.
8) S. Okazaki and T. Okuyama, *Bull. Chem. Soc. Jpn.*, **56**, 2159 (1983).
9) G. Albanesi and P. Moggi, *Appl. Catal.*, **6**, 293 (1983).
10) P. Moggi and G. Albanesi, *React. Kinet. Catal. Lett.*, **22**, 247 (1983).
11) K. Naito and T. Matsui, *Solid State Ionics*, **12**, 125 (1984).
12) S. De Rossi, E. Iguchi, M. Schiavello, and R. J. D. Tilley, *Z. Phys. Chem., N. F.*, **103**, 193 (1976).
13) M. Schiavello, R. J. D. Tilley, S. De Rossi, and E. Iguchi, *Z. Phys. Chem., N. F.*, **104**, 165 (1977).
14) J. Haber, J. Janas, M. Schiavello, and R. J. D. Tilley, *J. Catal.*, **82**, 395 (1983).
15) A. Andersson and S. T. Lundin, *J. Catal.*, **58**, 383 (1979).
16) N. Tsuda and A. Fujimori, *J. Catal.*, **69**, 410 (1981).
17) S. Tamura, K. Kato, and M. Goto, *Z. Anorg. Allg. Chem.*, **410**, 313 (1974).
18) A. Magneli, G. Andersson, and G. Sundkvist, *Acta Chem. Scand.*, **9**, 1402 (1955).
19) H. Schäfer, D. Bergner, and R. Gruehn, *Z. Anorg. Allg. Chem.*, **365**, 31 (1969).
20) S. Kimura, *J. Solid State Chem.*, **6**, 438 (1973).
21) J. F. Marucco, *J. Chem. Phys.*, **70**, 649 (1979).
22) A. Naito, N. Kamegashira, and N. Sasaki, *J. Solid State Chem.*, **35**, 305 (1980).
23) N. R. Yafaev and N. S. Garif'yanov, *Fizika Tverdogo Tela*, **5**, 3025 (1963).
24) B. Marinder, *Ark. Kem.*, **19**, 435 (1962).
25) A. K. Cheetham and C. N. R. Rao, *Acta Crystallogr., Sect. B*, **32**, 1579 (1976).
26) W. K. Hall and M. LoJacono, Proc. 6th Int. Congr. Catal., **1976**, 246.
27) L. Petrakis, P. L. Meyer, and T. P. Debiies, *J. Phys. Chem.*, **84**, 1020 (1980).
28) T. A. Patterson, J. C. Carver, D. E. Leyden, and D. M. Hercules, *J. Phys. Chem.*, **80**, 1700 (1976).
29) S. Abdo, R. B. Clarkson, and W. K. Hall, *J. Phys. Chem.*, **80**, 2431 (1976).
30) J. H. Lunsford, *J. Catal.*, **14**, 379 (1969).

 © 1988 The Chemical Society of Japan Bull. Chem. Soc. Jpn., 61, 2753—2762 (1988)

A Systematic Investigation of the Effects of Axial Ligands and Peripheral Substituents on the Electronic Structures of Zinc(II) Tetraphenylporphyrin π-Cation Radicals: Electrochemical EPR and Spectroscopic Observation

Kohji Ichimori, Hiroaki Ohya-Nishiguchi,* and Noboru Hirota
Department of Chemistry, Faculty of Science, Kyoto University, Sakyo-ku, Kyoto 606
(Received February 29, 1988)

A detailed study of the effect of axial ligand and peripheral substituent on the π-system of zinc(II) tetraphenylporphyrin π-cation radical has been made using an electrochemical EPR technique. It is confirmed from the EPR spectra that most of the anions and bases examined coordinate the radicals axially. The spin density on the nitrogen nuclei in the radicals increases with the polarizability of the axial ligand estimated from the optical spectra of the parent neutral complexes. For the fourteen complexes with different substituents on the phenyl groups examined here, there is a linear correlation between the Hammett substituent constant and the spin density. It is also shown that the para position of the phenyl group carries the spin density comparable to that of the ortho position, which indicates considerable conjugation between the porphyrin ring and the phenyl groups. In most cases, there exist two kinds of radical species which give rise to broad and sharp EPR spectra at low temperature. It is suggested that the difference in the motional states of the phenyl groups in the radicals is responsible for the different EPR spectra.

The redox behavior of metalloporphyrins has been investigated widely from biological interest.[1,2] Metalloporphyrins are known to undergo two different kinds of redox reactions; the reaction of a central metal ion and of a porphyrin ring.[3] The redox properties of metalloporphyrins have been studied by making systematic variations in central metal ions,[4] peripheral substituents,[5-8] axial ligands and solvents.[9-12] Not only the metal-centered redox, but also the oxidation of a porphyrin ring are of great importance and π-cation radicals generated by the oxidation act as active species in biological systems.[13,14]

The electronic structures and characters of frontier orbitals of the π-cation radicals have been studied by means of EPR,[15,16] optical,[17,18] and MCD[19] spectroscopies combined with electrochemical techniques in addition to cyclic voltammetry.[3,17,18,20] There are two factors which influence the electronic state of the π-system: One is the axial ligand and the other is the peripheral substituent. The axial ligand are known to play important roles in the biological functions of metalloporphyrins, but their effects on the π-system have not been investigated sufficiently. The effects of peripheral substitution have been investigated in relation to basicity of free base,[21] redox potentials,[5,8,22] base addition reactions,[5,23-27] rates of metal incorporation,[28] chemical shifts,[29,30] and other physicochemical properties.[25,31-35] But their effects on the electron distribution of the π-system have not been studied directly.

Recently a systematic investigation was made on the effects of axial ligands and solvents on the π-cation radicals of 5,10,15,20-tetraphenylporphyrinatocobalt(III), $[Co(III)(tpp)]^{2+\cdot}$, in our laboratory using an electrochemical EPR technique.[36,37] It was demonstrated that axial ligands affect largely the hyperfine coupling constants (hfcc) of the nitrogen and cobalt nuclei. The changes in spin distributions caused by the axial ligands were determined directly from the analysis of the EPR spectra.

Since the zinc(II) porphyrin π-cation radicals are very stable, the techniques applied to the studies on the $[Co(III)(tpp)]^{2+\cdot}$ π-cation radical can be applied to this system as well. Moreover, zinc(II) porphyrins are free from metal-centered redox and d-π mixing in the frontier orbitals.[38] It is known that zinc(II) porphyrins can coordinate only one axial ligand.[38-42] The naturally abundant zinc nucleus carries no nuclear spin. Therefore, one can expect much simpler EPR spectra for zinc complexes than for cobalt ones. By making systematic variations of the axial ligand and peripheral substituent, their effects on the spin-density distribution of the π-cation radicals can be investigated in detail.

The EPR spectra of Zn(tpp) π-cation radical were first observed by Fajer et al., with electrochemical oxidation[43] and several works have been done subsequently.[44-47] It was shown that the π-cation radical can axially coordinate one halogen anion or one pyridine molecule,[45] but the effects of the axial ligand on the π-system have not been studied in detail. Here, we have investigated the effects of the axial ligand and peripheral substitution on the EPR spectra of the π-cation radical to see how these two factors affect the π-system.

In this paper we first describe the general feature of the EPR analysis of the zinc(II) tetraarylporphyrin π-cation radicals briefly. Second, we examine the EPR spectra of the Zn(II)(tpp) π-cation radicals obtained in the presence of various anions and bases and deduce their structures in solution. Electronic effects of the axial ligands on the π-system are also discussed. Third, the effects of the peripheral substituents on the electronic states of the Zn(tpp) π-cation radical exam-

ined are discussed by correlating the EPR parameters with the Hammett constants of the substituents. Finally the origin of the two paramagnetic species observed in most cases is discussed.

Experimental

Materials. 5,10,15,20-Tetraarylporphyrin free bases with various peripheral substituents, hereafter abbreviated as H_2 (substituents on phenyl groups)(tpp), were prepared by the literature procedures[23,51,56] followed by modified purification process. In Table 1, the absorption spectra of their zinc(II) complexes are summarized together with the preparative references of free bases.

The zinc(II) complexes of these porphyrins were prepared by the method of Adler et al.[57,58] and purified by chromatography on neutral alumina with CH_2Cl_2 or $CHCl_3$ as the eluent. All synthesized zinc complexes were recrystallized from mixed solvents such as CH_2Cl_2–CH_3OH and identified by elemental analysis, TLC, and optical spectra.

CH_2Cl_2 and butyronitrile of spectroscopic grade were distilled from CaH_2 and dried over activated neutral alumina for the use of EPR measurements. Tetrabutylammonium salts (TBAX, where X=BF_4, ClO_4, NO_3, and F) were obtained by the method reported previously.[37] The preparations of dibenzo-18-crown-6 complexes with potassium salts (DB18C6-KX, where X=CN, SCN, and OAc) were carried out according to the method given by Pedersen.[59] The other reagents were commercially obtained and used without further purification.

Apparatus and Procedure. The EPR spectra were taken with JEOL PE-3X and FE-3X spectrometers equipped with a temperature controller. The π-cation radicals were generated by electrochemical one-electron oxidation of the corresponding zinc complexes using various TBA salts as electrolytes with/without bases. The applied voltages was +1.7 to +3.0 V, depending on the peripheral substituent and solvent: The voltage in n-C_3H_7CN was ca. 0.4 V higher than that in CH_2Cl_2. The procedures for the electrochemical EPR measurement and the field calibration were previously described in detail.[37,60] A Takeda Riken TR5211 frequency counter was used for measuring precise microwave frequencies. The simulation of the EPR spectra was carried out by using the literature program.[61] Absorption spectra were measured with a Shimadzu UV-2005 spectrophotometer.

Table 1. Electronic Absorption Spectra of Zinc(II) Tetraarylporphyrins[a]

Substituents	Soret	λ_{max}/nm		$\varepsilon_\alpha/\varepsilon_\beta$[b]	Preparative Ref.
		β	α		
1. 4-OCH_3	427	554	589	0.311	48,56
2. 4-$C(CH_3)_3$	426	553	592	0.268	48,49
3. 4-CH_3	426	552	592	0.270	48
4. 4-H	424	551	590	0.186	48
5. 4-F	424	551	590	0.174	48,50
6. 4-Cl	426	552	591	0.175	48,50
7. 4-$COOCH_3$	427	552	592	0.193	25,48,51
8. 4-CF_3	424	551	590	0.141	48,52
9. 4-CN	427	552	592	0.156	48
10. 2-F	423	550	584(sh)	0.086	48,50
11. 2,4,6-OCH_3	428	554	589	0.100	48,50,53
12. 3,4,5-OCH_3	429	552	593	0.192	48,54
13. 2,4,6-CH_3	424	552	589	0.097	55
14. 2,3,4,5,6-F	422	548	582	0.218	25,48

a) In C_6H_6 at 20 °C. b) Intensity ratio between the vibronic components in Q band. See Ref. 42.

Results and Discussion

EPR Analysis. The EPR spectra of zinc(II) tetraarylporphyrin π-cation radicals depended on axial ligands, peripheral substituents, and temperature. In most cases the room-temperature spectra of the Zn(tpp) π-cation radical exhibited broad nine-line structures due to four equivalent pyrrole nitrogens, indicating that the unpaired electron resides in the a_{2u} π-orbital. At sufficiently low temperatures, the spectra were often resolved further.

Using $TBAClO_4$ as a supporting electrolyte in n-C_3H_7CN, a partially resolved spectrum has been observed at −55 °C, as was reported by Fajer et al.[44] This sectrum could not be simulated without assuming superposition of two spectra; a broad nine-line spectrum identical with that observed at room temperature and a sharp spectrum resolved further by phenyl protons but with the same nitrogen coupling constant as that for the former.

In the previous works by Fajer et al. the well resolved spectra of the π-cation radical were simulated by considering the splittings due to only eight ortho-phenyl protons, because it was considered that the phenyl groups are nearly perpendicular to the mean plane of the porphyrin ring and only the ortho protons give rise to hyperfine splittings (hfs) due to the direct overlap with the unpaired electron. In our systems of the acetate-ligated and para substituted π-cation radicals, it was confirmed that the para positions carry spin densities comparable to those of the ortho positions. In the present work, therefore, 4N and 12H are assumed in the simulations of the spectra of all Zn(II)(tpp) π-cation radicals.

Dual structures of the spectra were observed in most of our systems and we succeeded in the simulation by means of the superposition of sharp and broad components. In general, the intensity of the broad component was much higher than that of the sharp one and the sharp component often disappeared at room temperature, The cause for the existence of the two paramagnetic species responsible for these two species will be discussed in the last section.

The Effects of Axial Ligands on Zn(tpp) π-Cation Radical. The axial-ligand effects on the EPR spectra were examined using the unsubstituted tpp ring. The EPR spectra were delicately influenced by the coordination of the coexisting anion or base. The results obtained from the EPR spectra are summarized in Table 2. The structures and electronic states of the radicals in solution are described in the following five parts which are classified according to the coordinating power[37] and charges of the axial ligands. The effects of the axial ligands on the electronic states of

Table 2. The EPR Parameters of Zn(tpp) π-Cation Radical with Axial Ligands

Anion or base	Solvent	T/°C	Hfcc (mT)			g (±0.0002)	Ref.
			a_N	a_H[a)]	a_X[b)]		
ClO_4^-	$CHCl_3$		0.146			2.0025	16
	CH_2Cl_2		0.143	0.024		2.0025	16
	CH_2Cl_2		0.162	0.028			16
	DMF		0.157	0.028		2.0029	16
	C_6H_5CN		0.163	0.026		2.0026	16
	n-C_3H_7CN	25/−55	0.158	0.032		2.0025	16
Br^-	$CHCl_3$		0.160		0.818	2.0059	16
Cl^-	$CHCl_3$		0.162		0.166	2.0032	16
F^-	$CHCl_3$		0.161		0.878	2.0027	16
ClO_4^-	CH_2Cl_2	RT/−92	0.156	0.030		2.0031	This work
	n-C_3H_7CN	−44	0.158	0.029		2.0029	This work
BF_4^-	CH_2Cl_2	RT	0.155	0.030		2.0031	This work
	n-C_3H_7CN	−52	0.158	0.029		2.0029	This work
PF_6^-	CH_2Cl_2	RT/−56	0.155	0.030		2.0031	This work
NO_3^-	CH_2Cl_2	−55	0.158	0.033		2.0032	This work
F^-	CH_2Cl_2	−50	0.167	0.033	0.860	2.0031	This work
AcO^-/PF_6^-	CH_2Cl_2	−10	0.171	0.029		2.0033	This work
CN^-/PF_6^-	CH_2Cl_2	−70	0.192	0.034		2.0033	This work
SCN^-/PF_6^-	CH_2Cl_2	RT/−62	0.170	0.030	0.183	2.0033	This work
4-CNpy/PF_6^-	CH_2Cl_2	−70				2.0028	This work
4-CH_3py/PF_6^-	CH_2Cl_2	−75				2.0029	This work
$P(C_6H_5)_3/PF_6^-$	CH_2Cl_2	−60	0.176	0.032	3.284	2.0034	This work

a) In this work, a_H is determined by assuming the contribution from 12 equivalent protons otherwise noted, but 8 protons in other works. b) Hfcc due to the axial ligand.

the π-system are presented in the last part.

(1) Weak-Ligand Anions (ClO_4^-, BF_4^-, PF_6^-, and NO_3^-): When TBAX (X=ClO_4, BF_4, or PF_6) was used as a supporting electrolyte at room temperature, a nine-line spectrum was observed in both CH_2Cl_2 (Fig. 1a) and n-C_3H_7CN. The spectrum in $TBAClO_4/CH_2Cl_2$ could be simulated by assuming hyperfine coupling constants (hfcc) of 4N (0.156 mT) and unresolved 12H (0.030 mT). The hfcc of nitrogens (a_N) in the system is the smallest of all, which reflects the smallest axial perturbation. Furthermore, the change of the anions has no effect on the spectrum, indicating that the radical is free from an axial ligand. It was shown by X-ray and IR results[62] that a perchlorate ion is bound to the radical in CH_2Cl_2 as well as in the solid state. Therefore, it is considered that the perturbation caused by the perchlorate ion is negligibly small. When cooled in CH_2Cl_2, the spectrum remained broad down to ca. −85 °C, but a partially resolved spectrum was obtained at around −94 °C (Fig. 1c).

In n-C_3H_7CN the same spectra as reported by Fajer et al., were observed with these three anions. The fact that a_N in n-C_3H_7CN (0.158 mT) is slightly larger than that in CH_2Cl_2 (see Table 2) indicates solvent ligation. The coordination of nitrile to neutral Zn(tpp) has been established from the optical spectra by Nappa and Valentine.[42] Therefore, it is reasonable to conclude that the π-cation radical is ligated by the solvent and is not influenced by these weak anions.

When $TBANO_3$ was used as the supporting electrolyte in CH_2Cl_2, the spectrum was almost identical with that in $TBAClO_4/n$-C_3H_7CN system, indicating that the effects of a nitrate ion is similar to that of n-

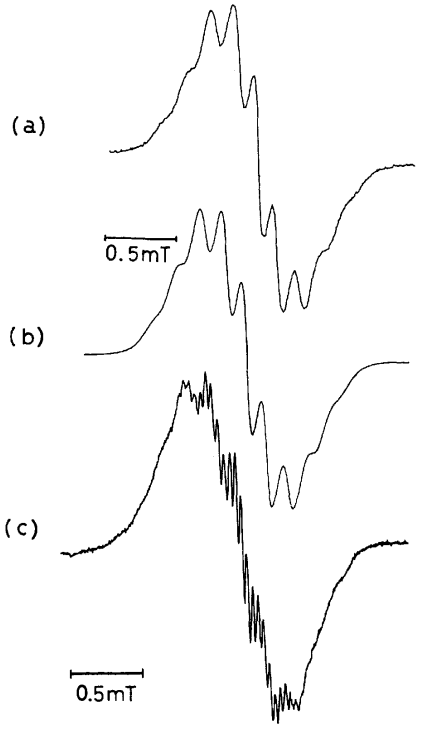

Fig. 1. The EPR spectra of the Zn(II)(tpp) π-cation radical in $TBAPF_6/CH_2Cl_2$ system, (a) observed at room temperature, (b) simulated, and (c) observed at −94 °C.

C_3H_7CN.

(2) Intermediate Anions (F^-, Cl^-, and Br^-): In the presence of the halogen anions, the spectra at room temperature in CH_2Cl_2 were broad. With lowering the temperature down to −50 °C, however, the spectrum for TBAF as the supporting electrolyte showed a partially resolved structure (Fig. 2a). The spectrum could

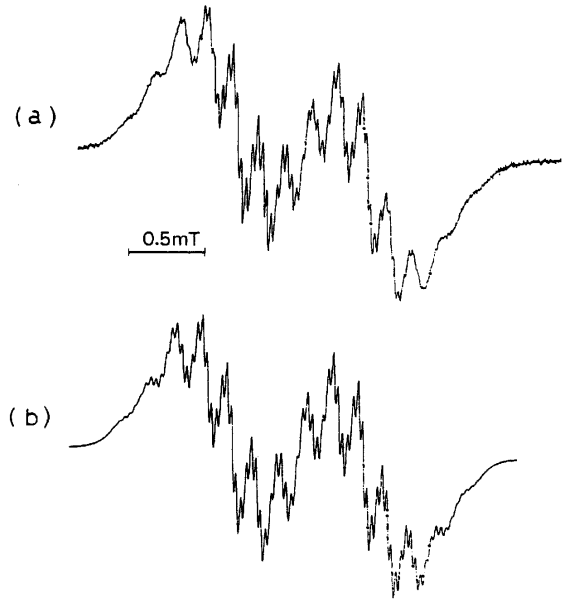

Fig. 2. The EPR spectra of the Zn(II)(tpp) π-cation radical in TBAF/CH_2Cl_2 system, (a) observed at −50 °C, and (b) simulated.

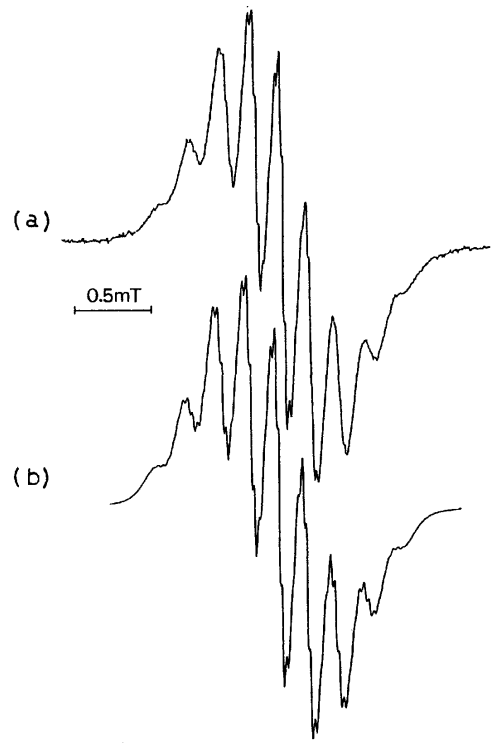

Fig. 3. The EPR spectra of the Zn(II)(tpp) π-cation radical in DB18C6-KCN(TBAPF$_6$)/CH_2Cl_2 system, (a) observed at −70 °C, and (b) simulated.

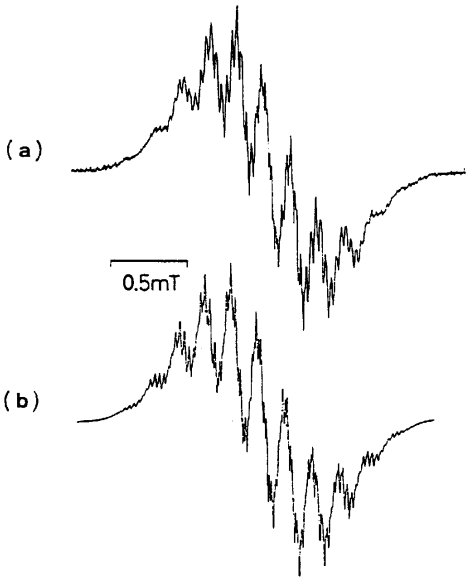

Fig. 4. The EPR spectra of the Zn(II)(tpp) π-cation radical in DB18C6-KSCN(TBAPF$_6$)/CH_2Cl_2 system, (a) observed at −62 °C, and (b) simulated.

be simulated with 4N, 12H, and 1F, which means that one fluoride ion ligates to the species responsible for both the sharp and broad spectra. In simulating the spectrum, coexistence of the two paramagnetic species with the same hfcc's but different linewidth was taken into account (Fig. 2b) with the ratio of the sharp and broad components being 1 : 206. The same phenomenon was observed at lower temperatures, when TBACl was used. In the case of TBABr, however, the spectrum consisting of broad four lines due to Br^- with I=3/2 was not resolved further on cooling.

(3) Strong Anions (CN^-, SCN^-, and AcO^-) in CH_2Cl_2: These anions were introduced in the form of DB18C6-KX complexes with TBAPF$_6$ as a supporting electrolyte as reported previously.[37] It was confirmed by the large spectral changes from the above cases (1) and (2) that these strong anions ligate the π-cation radical. The spectra in the presence of these anions also showed the dual structures at low temperatures. In the presence of cyanide, no spectrum could be observed at room temperature because of instability of the radical. But at around −70 °C, a spectrum with the largest a_N was observed, accompanied with the fine splittings due to phenyl protons (Fig. 3a). This indicates ligation by cyanide. The spectrum could be simulated by a set of 4N and 12H and assuming Sharp and Broad=1 : 289 (Fig. 3b).

In the presence of thiocyanide, a spectrum with eleven-line structure could be observed even at room temperature. This could be simulated by a set of 4N and 12H, and an additional nitrogen hfcc larger than that of the porphyrin ring. This indicates that thiocyanate ligates the π-cation radical by nitrogen, not by sulfur. At around −60 °C the spectrum was also resolved further and could also be simulated by using

the same set of hfcc, as shown in Fig. 4b (Sharp: Broad=1 : 45).

The spectrum in the presence of the acetate shows much different temperature dependence. Even at room temperature, the spectrum had a dual structure which could be simulated by a set of 4N and 12H with the sharp-to-broad ratio of 1 : 130 at −10 °C. With lowering the temperature, the spectrum was once broadened but the sharp component appeared again with a more complicated structure below −55 °C. Due to the broadening on both sides of the spectrum, the simulation could not reproduce the observed spectrum well. This results from the nitrogen m_I dependence of the linewidth of the sharp component.[63]

(4) Base Ligation: Besides the anionic ligands, the electrically neutral ligands such as 4-CNpy, 4-CH_3py, and $P(C_6H_5)_3$ were also examined using $TBAPF_6$ as the electrolyte. The radical generated by the electrooxidation in the presence of these bases was unstable and the EPR spectra was not observed at room temperature. When the pyridine derivatives were used as the base, the nine-line structure described above collapsed into broad single line with slight undulation. Such broadening is probably due to the hyperfine contribution from pyridine nitrogen.

A remarkable change was seen in the spectrum, when $P(C_6H_5)_3$ was added (Fig. 5a). The central broad line was due to the unligated radical species. On both sides of the central line, a pair of nine-line spectrum was observed, which indicates clearly the ligation of one phosphine with $I=1/2$ in $P(C_6H_5)_3$. In n-C_3H_7CN the lines on both sides were very weak compared with the central line. Such solvent dependence of the relative intensity supports the identification mentioned above.

Extensive works about the axial ligand effects on the redox potential have been done using nitrogenous bases[17,20] and the reactions of the radical in the presence of these nucleophile have been investigated in detail.[64] The EPR spectra of $Zn(tpp)^+$ with axial pyridine reported by Fujita et al.[45b] show that the complex formation of the radical with pyridine results in an 10% increase in a_N. This is in accord with the trend in the anion ligation described above.

(5) The Effect of Axial ligands on the Electronic States of the π-Cation Radical: In the previous work on the Co(III)(tpp) π-cation radical, it was noted that ligation by chloride or cyanide ion increases a_N from 0.18 mT to 0.28 mT.[37] This increase was rationalized on the bases of the result of a CNDO/2 calculation which predicts an increase of a_N with the increase of the axial ligand field. As shown in Table 2, a_N becomes larger when a strong anion coordinates to the π-cation radical. This trend qualitatively agrees with that found for the cobalt complex. However, the increase of a_N in the zinc complex is much smaller than in the cobalt one, which may be primarily due to the fewer charge of the metal cation and fewer numbers of the axial ligand.

The effects of the axial ligands on the electronic states of regular metalloporphyrins have been parametrized by means of the visible absorption spectra, which include so-called α and β bands (see Table 1).[65] In neutral Zn(tpp), considerable red shifts of these bands and the increase of the intensity ratio of α band over β band ($\varepsilon_\alpha/\varepsilon_\beta$) have been observed by introducing a wide variety of axial ligands.[42] It has been considered that $\varepsilon_\alpha/\varepsilon_\beta$ represents the electronic polarizability of the axial ligand: As more charge of the axial ligand transfers to the porphyrin ring through the metal ion, $\varepsilon_\alpha/\varepsilon_\beta$ becomes larger. We have examined the correlation between a_N and $\varepsilon_\alpha/\varepsilon_\beta$. The plot given in Fig. 6 clearly shows a correlation between these parameters except for the case of $P(C_6H_5)_3$ with neutral charge: a_N becomes larger with the increase of $\varepsilon_\alpha/\varepsilon_\beta$. It is therefore concluded that the spin density on the nitrogen nuclei increases as the polarizability of the axial ligand increases.

The Effects of Peripheral Substituents on the Zn(tpp) π-Cation Radicals. The EPR spectra of zinc-

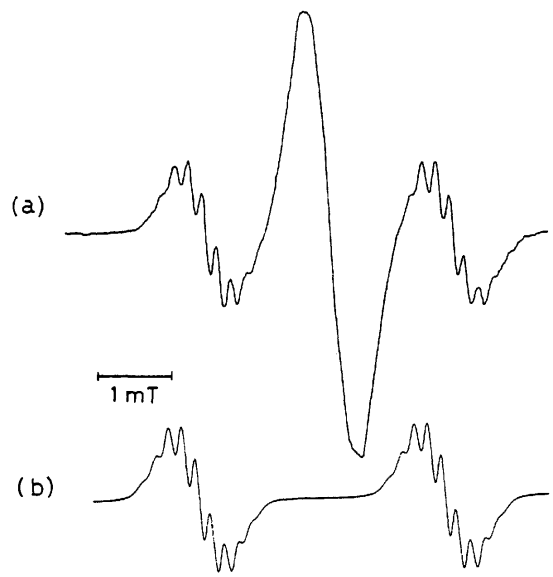

Fig. 5. The EPR spectra of the Zn(II)(tpp) π-cation radical in $P(C_6H_5)_3$($TBAPF_6$)/CH_2Cl_2 system, (a) observed at −80°C, and (b) simulated.

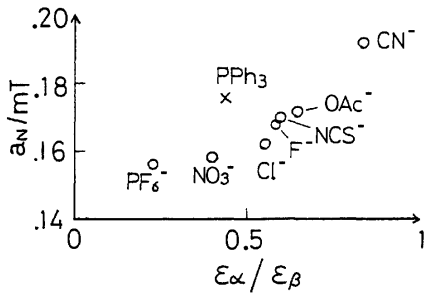

Fig. 6. Correlation between nitrogen hfcc (a_N) and the intensity ratio ($\varepsilon_\alpha/\varepsilon_\beta$). $\varepsilon_\alpha/\varepsilon_\beta$ was obtained from Ref. 42 or measured in C_6H_6.

(II) tetraarylporphyrin π-cation radicals also depended on the nature of peripheral substituents. Effects of peripheral substituents were examined with fourteen complexes by fixing the counter ion to nitrate and the solvent to CH_2Cl_2. Some typical spectra are shown in Fig. 7 to 9 and the results of the analysis are listed in Table 3.

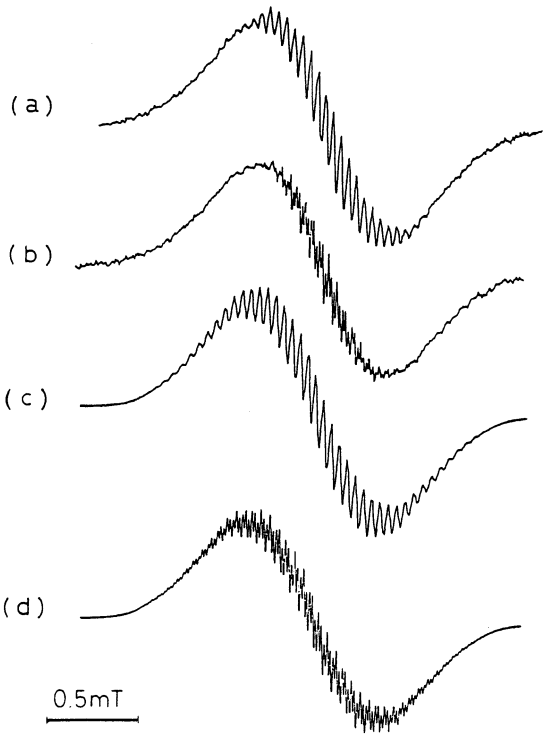

Fig. 7. The EPR spectra of the Zn(4-CH_3)(tpp) π-cation radical in $TBANO_3/CH_2Cl_2$ system, (a) observed at −60 °C and (b) observed at −80 °C. (c) and (d) are the simulated spectra corresponding to (a) and (b), respectively.

As shown in Fig. 7 and Table 3, hfs due to substituents are clearly observed in the 4-CH_3, 4-F, 4-CF_3, and 2-F complexes. This indicates that the spin density in the porphyrin ring permeates the phenyl rings and that the spin distribution can be influenced by the para substitution. This also supports our analysis which includes four para protons in simulating the spectra of the Zn(tpp) π-cation radicals.

These hfcc of the para substituents can be compared with those of the phenoxyl radical which has a_H=1.02 mT for the para proton.[66] By para substitution, a_H= 1.25 mT for 4-CH_3, a_F=2.70 mT for 4-F, and a_F=0.95 mT for 4-CF_3 have been obtained. The hfcc are amplified by factors of 1.23, 2.65, and 0.93, respectively. In the zinc complexes, the factors obtained from Table 3 are 1.33, 1.94, and 0.79, respectively. Thus the mechanism to produce the splittings due to the para substituents in both systems are quite similar. This result indicates that there is considerable conjugation between the phenyl groups and the porphyrin ring, possibly due to the wagging motion of the phenyl group. We can also conclude that the hfs of the phenyl protons are due to the spin polarization caused by the delocalized unpaired π-electron.

The dual structure mentioned in the previous section was also seen in several cases. The π-cation radicals with ortho substituents did not have sharp component. On the other hand, Zn(3,4,5-OCH_3)(tpp) π-cation radical showed a very sharp spectrum even at room temperature, as shown in Fig. 9 (Sharp : Broad= 2 : 1). The temperature at which the sharp component had the maximum intensity varied depending on the nature of substituent. These results are discussed in the last section.

Table 3. The EPR Parameters of Zn(tpp) π-Cation Radicals with Peripheral Substituents[a]

Substituent	4σ	T/°C	Hfcc (mT)			g (±0.0002)
1. 4-OCH_3	−1.08	10	4N : 0.163	8H : 0.040		2.0032
2. 4-$C(CH_3)_3$	−0.80	−50	4N : 0.161	8H : 0.040		2.0031
3. 4-CH_3[b]	−0.68	−80	4N : 0.158	8H : 0.033	12H : 0.044	2.0032
4. 4-H	0	−55	4N : 0.158	12H : 0.033		2.0032
5. 4-F	0.24	−16	4N : 0.156	8H : 0.029	4F : 0.064	2.0033
6. 4-Cl	0.92	0	4N : 0.158	8H : 0.028		2.0037
7. 4-$COOCH_3$	1.80	0	4N : 0.152	8H : 0.028		2.0031
8. 4-CF_3	2.16	−30	4N : 0.154	8H : 0.028	12F : 0.026	2.0030
9. 4-CN	2.64	−30	4N : 0.147	8H : 0.026		2.0032
10. 2-F		−40	4N : 0.136	8H : 0.026	4F : 0.106	2.0031
2-F[c]		25	4N : 0.12			
11. 2,4,6-OCH_3		0	4N : 0.147			2.0028
12. 3,4,5-OCH_3	−0.12[d]	10	4N : 0.159	8H : 0.030		2.0031
13. 2,4,6-CH_3		−20	4N : 0.160			2.0028
14. 2,3,4,5,6-F[e]		−20				2.0027

a) In $TBANO_3/CH_2Cl_2$ system. b) 8H : 0.032 at −60 °C. c) From Ref. 16. Counterion and solvent are not described. d) σ_p=0.262 and σ_m=0.12 are assigned for OCH_3 group. Therefore, $4\sigma=4(\sigma_p+2\sigma_m)=-0.12$ can be assumed for Zn(3,4,5-OCH_3)(tpp). e) This shows a broad spectrum without splittings. The a_N may be the smallest of all because this has the smallest total linewidth.

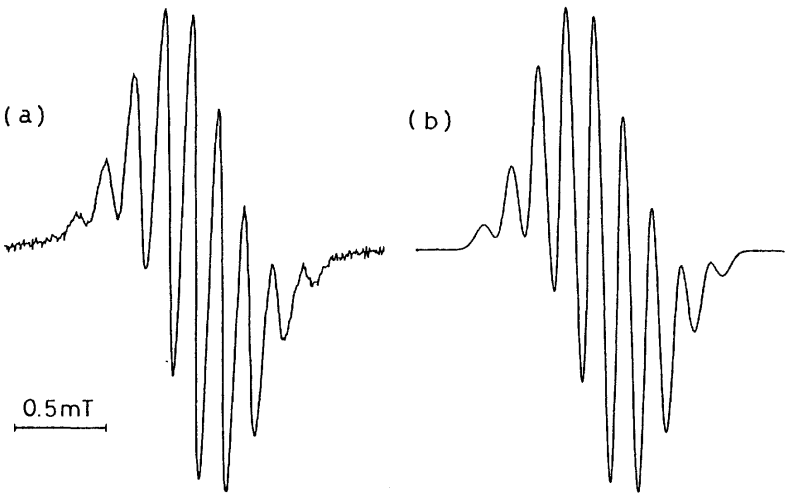

Fig. 8. The EPR spectra of Zn(2,4,6-OCH_3)(tpp) π-cation radical in $TBANO_3/CH_2Cl_2$ system, (a) observed at 0°C, and (b) simulated.

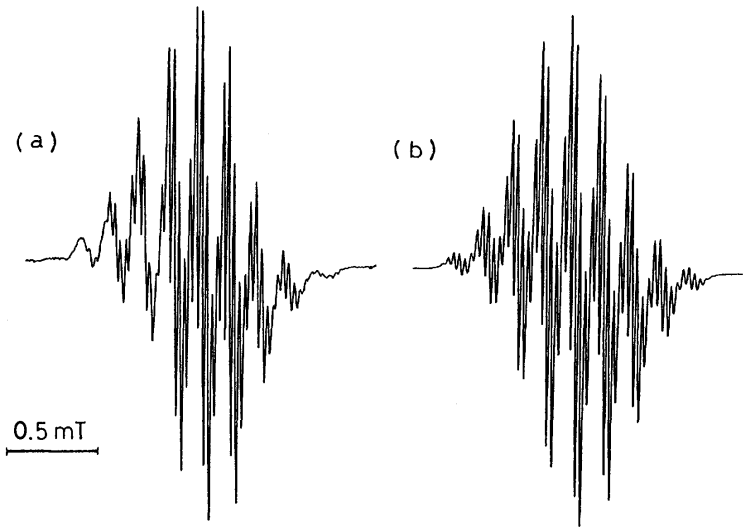

Fig. 9. The EPR spectra of Zn(3,4,5-OCH_3)(tpp) π-cation radical in $TBANO_3/CH_2Cl_2$ system (a) observed at 10°C, and (b) simulated.

The physical properties such as redox potentials and stability constants for complex formation measured in connection with the peripheral substitution have been shown to correlate with the sigma constant of the Hammett equation,[23]

$$P = 4\sigma\rho \quad (1)$$

where P is an observed physical property, σ the Hammett substituent constant, and ρ is a proportionality constant. From the analysis of base addition reactions[23,26] and minute NMR measurements,[29] it has been shown that there is a significant contribution from π-induction in the transmission of the phenyl substituent effect to the whole porphyrin π-system, despite the lack of coplanarity between the porphyrin ring and phenyl groups.[67] Thus a substantial effect may be detectable on a_N which is determined by the spin densities on the nitrogens of the π-cation radicals. The values of 4σ are listed in Table 3 together with the EPR parameters. The hfcc of a_N and a_H vs. 4σ are plotted in Fig. 10. We find considerable substituent effects on the EPR parameters and a clear Hammett linear relation between a_N and 4σ. It is seen that both a_N and a_H increase with the electron donating power of the para substituent. In the previous CNDO/2 calculations for the Co(III)(tpp)X_2 π-cation radical,[37] it was shown that the spin densities on the meso carbons increase together with those on nitrogen as the bond length between cobalt and axial ligands are shortened. This is consistent with the observed increase of a_N and a_H, because the spin density in the phenyl groups is brought by the conjugation through the meso carbons.

From the above discussion, 2,4,6-OCH_3 and 2,4,6-CH_3 are expected to have larger a_N than 4-CH_3, But

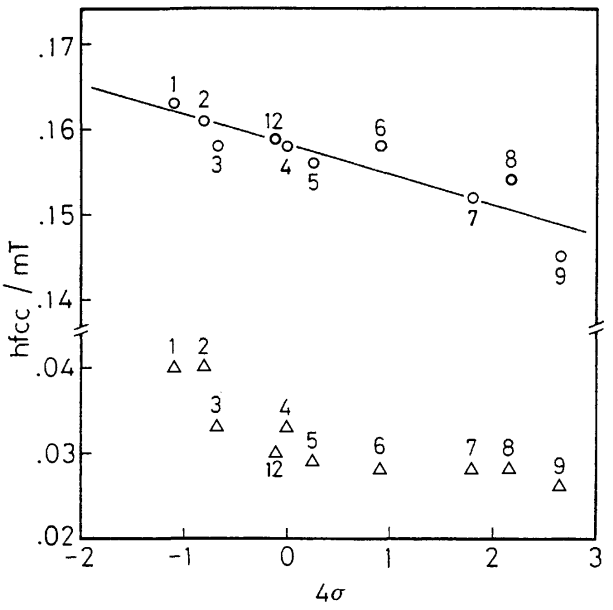

Fig. 10. Plots of a_N (O) and a_H (Δ) vs. Hammett constant (σ). Numbers in the figure refer to the π-cation radicals in Table 3.

2,4,6-OCH_3 and 2-F have smaller a_N values and 2,4,6-CH_3 has a comparable value compared with that of unsubstituted tpp. In these complexes the phenyl groups stand almost vertically to the porphyrin ring in so as disrupting π-conjugation. Therefore, deviations from the linear correlation between a_N and 4σ are expected in these complexes. This steric effect can also be seen in the decrease of the g-values from ca. 2.0031 to 2.0028.

Dual Structure of the Spectra. The EPR spectra of the π-cation radicals exhibit the dual structures in most cases as described above. The coexistence of the two paramagnetic species observed as the dual structure is interpreted by the equilibria between (1) the ligated and unligated radicals, (2) the radicals with different interactions with solvent, and (3) the radicals with different motional states of the phenyl groups. The most probable reason for the coexistence of two paramagnetic species is due to the change in the motional states of the phenyl groups. The ratio of the sharp and broad components is much dependent on the substituents on the phenyl groups. The π-cation radicals with ortho substituents do not have any sharp component. On the other hand, most of the other radicals exhibit substantially sharp component. Especially Zn(3,4,5-OCH_3)(tpp) π-cation radical shows the sharp component with high intensity ratio of 2 : 1 even at room temperature. Thus, it is likely that the broad component is related to the species with hindered rotations of the phenyl groups. When the rotation of the phenyl group is slow in the EPR time scale, broadening of each hyperfine line is expected because of the incomplete averaging of the unequivalent isotropic hfs as well as the anisotropic parts of hfs. The hindered rotations of the phenyl groups of the metalloporphyrins have been investigated by NMR[52,68] and the rates of the rotations and the activation energies have been determined for rutheniumcarbonyl, titanyl, indium, and gallium complexes.[34,35] These rates were indeed found to be slow in the EPR time scale. Thus it is reasonable to consider that the broad component is due to the species with hindered rotational state of the phenyl groups.

On the other hand, the sharp component in the dual structure is highly related to the free rotation of the phenyl groups. Fajer et al. have investigated the π-cation radical of Zn(II) *meso*-tetramethylporphyrin which has no sterically hindered phenyl groups,[69] and observed only the sharp component in the spectrum. It may be unlikely that the phenyl groups rotate freely. If four phenyl groups rotate cooperatively, however, apparent free rotation visualized as the sharp component becomes quite possible.

Concluding Remarks

We have investigated the effects of axial ligand and peripheral substituent on the EPR spectrum of the π-cation radical of Zn(tpp). It is shown that both the axial ligand and the peripheral substituent have large effects on the spin densities on the nitrogen atoms. The axial ligand is known to have a large effects on the behavior of the central metal ion,[33] but the present work shows that the π-system of the zinc complex is also affected by the axial ligand considerably as in the case of the cobalt complex.[37] The nitrogen hfs, a_N, is found to be sensitive to the peripheral substituent, different from the EPR[23,25] and Mössbauer[31,32] parameters of the central metal ions. A good correlation between a_N and the Hammett σ constant as well as the presence of the spin densities on the para positions indicates effective conjugation of the π-system between the porphyrin ring and the phenyl group. It is known that the energy level of the π-system is shifted by the peripheral substituents, but the present result directly shows the effect of the peripheral substitution on the π-system. It is suggested that the presence of the sharp and broad components of the EPR spectra are ascribed to the difference in the motional states of the phenyl groups.

The authors gratefully acknowledge Dr. Kiyoko Yamamoto of JEOL Co. for her kind advice to the sample preparations and kind gift of Zn(tpp) in early stage of this investigation. This work was partially supported by the Grant-in-Aid for Scientific Research on Priority Area of "Macromolecular Complexes (No. 62612005)" from the Ministry of Education, Science and Culture.

References

1) R. H. Felton, "Primary Redox Reactions of Metalloporphyrins," in "The Porphyrins," ed by D. Dolphin, Aca-

demic Press, New York (1979), Vol. 5, Chap. 3.
2) D. G. Davis, "Electrochemistry of Porphyrins," in "The Porphyrins," ed by D. Dorphin, Academic Press, New York (1979), Vol. 5, p. 127.
3) A. Worberg and J. Mannassen, *J. Am. Chem. Soc.*, **92**, 2982 (1970).
4) J. Fuhrhop, K. M. Kadish, and F. G. Davis, *J. Am. Chem. Soc.*, **95**, 5140 (1973).
5) F. A. Walker, D. Beroiz, and K. M. Kadish, *J. Am. Chem. Soc.*, **98**, 3484 (1976).
6) K. M. Kadish and M. M. Morrison, *Inorg. Chem.*, **15**, 980 (1976).
7) K. M. Kadish, M. M. Morrison, L. A. Constant, L. Dickens, and D. G. Davis, *J. Am. Chem. Soc.*, **98**, 8387 (1976).
8) S. Ni, L. Dickens, J. Tappan, L. Constant, and D. G. Davis, *Inorg. Chem.*, **17**, 228 (1978).
9) a) K. M. Kadish and L. A. Bottomley, *Inorg. Chem.*, **19**, 832 (1980); b) L. A. Bottomley and K. M. Kadish, *Inorg. Chem.*, **20**, 1348 (1981).
10) K. M. Kadish and D. Chang, *Inorg. Chem.*, **21**, 3614 (1982).
11) S. L. Kelly and K. M. Kadish, *Inorg. Chem.*, **21**, 3621 (1982).
12) K. M. Kadish, X. Q. Lin, and B. C. Han, *Inorg. Chem.*, **26**, 4161 (1987).
13) J. Fajer, D. C. Brune, M. S. Davis, A. Forman, and L. D. Spaulding, *Proc. Natl. Acad. Sci. U.S.A.*, **72**, 4956 (1975).
14) H. B. Dunford and J. S. Stillman, *Coord. Chem. Rev.*, **19**, 187 (1976).
15) J. Subramanian, "Electron Paramagnetic Resonance Spectroscopy of Porphyrins and Metalloporphyrins," in "Porphyrins and Metalloporphyrins," ed by K. M. Smith, Elsevier, Amsterdam (1975), p. 576.
16) J. Fajer and M. S. Davis, "Electron Spin Resonance of Porphyrin π Cations and Anions," in "The Porphyrins," ed by D. Dorphin, Academic Press, New York (1979), Vol. 4, p. 197 and references cited therein.
17) K. M. Kadish and R. H. Rhodes, *Inorg. Chem.*, **20**, 2961 (1981).
18) E. C. Johnson, T. Niem, and D. Dolphin, *Can. J. Chem.*, **56**, 1381 (1978).
19) W. R. Browett and M. J. Stillman, *Inorg. Chim. Acta*, **49**, 69 (1981).
20) K. M. Kadish, L. R. Shiue, R. K. Rhodes, and L. A. Bottomley, *Inorg. Chem.*, **20**, 1274 (1981).
21) W. S. Caughey, W. Y. Fujimoto, and B. P. Johnson, *Biochemistry*, **5**, 3830 (1966).
22) P. Worthington, P. Hambright, R. F. X. Williams, J. Reid, C. Burnham, A. Shamin, J. Turey, D. M. Bell, R. Kirkland, R. G. Little, N. Datta-Gupta, and U. Eisner, *J. Inorg. Biochem.*, **12**, 281 (1980).
23) F. A. Walker, E. Hui, and J. M. Walker, *J. Am. Chem. Soc.*, **97**, 2390 (1975).
24) F. A. Walker, M.-W. Lo, and M. T. Ree, *J. Am. Chem. Soc.*, **98**, 5552 (1976).
25) E. W. Baker, C. B. Storm, G. T. McGraw, and A. H. Corwin, *Bioinorg. Chem.*, **3**, 49 (1973).
26) G. A. McDermott and F. A. Walker, *Inorg. Chim. Acta*, **91**, 95 (1984).
27) V. L. Balke, F. A. Walker, and J. T. West, *J. Am. Chem. Soc.*, **107**, 1226 (1985).
28) J. B. Reid and P. Hambright, *Inorg. Chem.*, **16**, 968 (1977).
29) F. A. Walker, V. L. Balke, and G. A. McDermott, *Inorg. Chem.*, **21**, 3342 (1982).
30) F. A. Walker, V. L. Balke, and G. A. McDermott, *J. Am. Chem. Soc.*, **104**, 1569 (1982).
31) M. A. Torrens, D. K. Straub, and L. M. Epstein, *J. Am. Chem. Soc.*, **94**, 4160 (1972).
32) M. A. Torrens, D. K. Straub, and L. M. Epstein, *J. Am. Chem. Soc.*, **94**, 4162 (1972).
33) F. A. Walker, D. Reis, and V. L. Balke, *J. Am. Chem. Soc.*, **106**, 6888 (1984).
34) S. S. Eaton and G. R. Eaton, *J. Am. Chem. Soc.*, **99**, 6594 (1977).
35) S. S. Eaton, D. M. Fishwild, and G. R. Eaton, *Inorg. Chem.*, **17**, 1542 (1978).
36) H. Ohya-Nishiguchi, M. Kohno, and K. Yamamoto, *Bull. Chem. Soc. Jpn.*, **54**, 1923 (1981).
37) K. Ichimori, H. Ohya-Nishiguchi, N. Hirota, and K. Yamamoto, *Bull. Chem. Soc. Jpn.*, **58**, 623 (1985).
38) Zinc(II) porphyrins are classified into regular porphyrins: M. Gouterman, "Optical Spectra and Electronic Structure of Porphyrins and Related Rings," in "The Porphyrins," ed by D. Dolphin, Academic Press, New York (1979), Vol. 3, p. 1.
39) J. R. Miller and G. D. Dorough, *J. Am. Chem. Soc.*, **74**, 3977 (1952).
40) C. H. Kirsley, P. Hambright, and C. B. Storm, *Inorg. Chem.*, **8**, 2141 (1969).
41) G. C. Vogel and B. A. Beckmann, *Inorg. Chem.*, **15**, 483 (1976).
42) M. Nappa and J. S. Valentine, *J. Am. Chem. Soc.*, **100**, 5075 (1978).
43) R. H. Felton, D. Dolphin, D. C. Borg, and J. Fajer, *J. Am. Chem. Soc.*, **91**, 196 (1969).
44) J. Fajer. D. C. Borg. A. Forman, D. Dolphin, and R. H. Felton, *J. Am. Chem. Soc.*, **92**, 3451 (1970).
45) a) A. Forman, D. C. Borg, R. H. Felton, and J. Fajer, *J. Am. Chem. Soc.*, **93**, 2790 (1971); b) I. Fujita, L. K. Hanson, F. A. Walker, and J. Fajer, *J. Am. Chem. Soc.*, **105**, 3296 (1983).
46) Yu. V. Glazkov, A. G. Zhurzalev, P. V. Kuzovkov, and A. M. Shul'ga, *Zh. Prikl. Spectrosk.*, **18**, 117 (1974).
47) D. Lexa and M. Reix, *J. Chim. Phys.*, **71**, 24 (1974).
48) A. D. Adler, F. R. Longo, J. D. Finarelli, J. Goldmacher, J. Assour, and L. Korsakoff, *J. Org. Chem.*, **32**, 476 (1967).
49) *p-t*-Butylbenzaldehyde was synthesized according to the literature method: W. E. Smith, *J. Org. Chem.*, **37**, 3972 (1972).
50) J. B. Kim, J. J. Leonard, and F. R. Longo, *J. Am. Chem. Soc.*, **94**, 3986 (1972).
51) F. R. Longo, M. G. Finarelli, and J. B. Kim, *J. Heterocyclic Chem.*, **6**, 927 (1969).
52) S. S. Eaton and G. R. Eaton, *J. Am. Chem. Soc.*, **97**, 3660 (1975).
53) L. Vaska, A. R. Amundsen, R. Brady, B. R. Flynn, and H. Nakai, *Finn. Chem. Lett.*, **1974**, 66.
54) R-J. Cheng, L. Latos-Grazinski, and A. L. Balch, *Inorg. Chem.*, **21**, 2412 (1982).
55) J. T. Groves and T. E. Nemo, *J. Am. Chem. Soc.*, **105**, 6243 (1983).
56) G. H. Barnett, M. F. Hudson, and K. M. Smith, *J. Chem. Soc., Perkin Trans. 1*, **1975**, 1401.
57) A. D. Adler, F. R. Longo, F. Kampas, and J. Kim, *J.*

Inorg. Nucl. Chem. Lett., **32**, 2443 (1970).
58) A. D. Adler, F. R. Longo, and V. Varadi, *Inorg. Synth.*, **16**, 213 (1976).
59) C. J. Pedersen, *J. Am. Chem. Soc.*, **89**, 7017 (1967).
60) A. Terahara, H. Ohya-Nishiguchi, N. Hirota, and A. Oku, *J. Phys. Chem.*, **90**, 1564 (1986).
61) U. M. Oehler and E. G. Janzen, *Can. J. Chem.*, **60**, 1542 (1982).
62) L. D. Spaulding, P. G. Eller, J. A. Bertrand, and R. H. Felton, *J. Am. Chem. Soc.*, **96**, 982 (1974).
63) A. Carrington and A. D. McLachlan, "Introduction to Magnetic Resonance," Harper & Low, New York (1969), p. 197.
64) H. J. Shine, A. G. Padilla, and S. M. Wu, *J. Org. Chem.*, **44**, 4069 (1979).
65) M. Goutermann, F. P. Schwarz, P. D. Smith, and D. Dorphin, *J. Chem. Phys.*, **59**, 676 (1973).
66) "Landort-Boernstein," ed by H. Fischer and K.-H. Hellwege, Springer-Verlag, Berlin-Heidelberg (1979), Vol. 9, Part c2, p. 29.
67) J. L. Hoard, "Stereochemistry of Porphyrins and Metalloporphyrins," in "Porphyrins and Metalloporphyrins," ed by K. M. Smith, Elsevier, Amsterdam (1975), p. 317.
68) F. A. Walker and G. N. La Mar, *Ann. N. Y. Acad. Sci.*, **206**, 328 (1973).
69) J. Fajer, D. C. Borg, A. Forman, A. D. Adler, and V. Varedi, *J. Am. Chem. Soc.*, **96**, 1238 (1974).

 © 1988 The Chemical Society of Japan Bull. Chem. Soc. Jpn., 61, 2763—2766 (1988)

Synthesis, Properties, and Crystal and Molecular Structure of Chloro[*N*,*N*-bis(2-hydroxyethyl)glycinato]copper(II)

Hiromitsu YAMAGUCHI,* Makoto NAGASE, Yasuhiko YUKAWA,† Yoshie INOMATA, and Toshio TAKEUCHI
Department of Natural Sciences, Faculty of Science and Technology, Sophia University, 7-1 Kioi-cho, Chiyoda-ku, Tokyo 102
(Received March 8, 1988)

The crystal and molecular structure of the title copper(II) complex was determined by the X-ray diffraction method. The crystal is orthorhombic with the space group Pbca, Z=8, a=14.18(1), b=15.835(7), c=8.188(3) Å. Full matrix least-squares refinements have led to a final R value of 0.047 for 2128 reflections. The copper atom is in a trigonal-bipyramidal geometry, ligated by a nitrogen atom, an oxygen atom of carboxylato group, two hydroxyl oxygen atoms and a chlorine atom. The complex has three five-membered chelate rings which are formed by one copper, one nitrogen, one oxygen, and two carbon atoms. There are two hydrogen bonds formed between the non-coordinated carboxylato oxygen atom and the hydroxyl hydrogen atom. The powder diffuse reflection spectrum of this complex exhibits a band characteristic of trigonal bipyramidal structure at 1000 nm. In the far-infrared absorption spectra of this complex, the bands at 340, 317, and 275 cm^{-1} are assigned to the stretching vibrations of Cu-N, Cu-Cl, and Cu-O (carboxylato), respectively.

Some of the present authors have previously reported on the syntheses and properties of bivalent metal complexes of *N*,*N*-bis(2-hydroxyethyl)glycine (Hbheg).[1] In that work two copper(II) complexes with Hbheg have been prepared; one is [Cu(bheg)$_2$] and the other is [CuCl(bheg)].

Anan'eva et al. have determined by an X-ray diffraction study that in the former complex the copper atom occupied the center of inversion and that the coordination number was six in an elongated tetragonal bipyramid formed by two nitrogen atoms and four oxygen atoms from two ligands.[2]

As for the latter complex, it has been presumed that the copper atom is coordinated through an oxygen atom of the carboxylato group, a nitrogen atom and two oxygen atoms of two hydroxyl groups.[1]

However, there are many types of coordination for a hydroxyl group. For example, in the case of bis(triethanolamine)nickel(II) nitrate, the nickel atom is ligated by two oxygen atoms out of the three hydroxyl groups in one triethanolamine molecule, and the other oxygen atom is not associated with the coordination;[3] for bis(triethanolamine)strontium(II) nitrate, three hydroxyl oxygen atoms coordinate the identical strontium atom.[4]

It is therefore difficult to determine from the infrared spectra how these hydroxyl oxygen atoms coordinate the copper atom in [CuCl(bheg)].

In this work, the structure of [CuCl(bheg)] was determined by an X-ray diffraction study; the behavior of the two hydroxyl groups is discussed in detail. In addition, this structure is compared with the structure of copper(II) chloride complex with *N*,*N*-diethylglycine (Hdeg), [CuCl(deg)],[5] previously investigated in our laboratory, and an interpretation of the properties has been carried out based on the proposed structure.

† Present address: Division of Chemistry, General Education Department, Niigata University, 8050, Ikarashi, Ninocho, Niigata 950-21.

Experimental

Preparation of the Sample. The samples for the X-ray diffraction study were prepared as follows: equimolar amounts of $CuCl_2 \cdot 2H_2O$ and Hbheg were mixed in aqueous solution. Green crystals were obtained from this solution by keeping it in a desiccator containing ethanol for several days.

X-Ray Measurements and Structure Determination. The crystal data are given in Table 1. The reflection intensities were collected by the ω-2θ scan technique ($2\theta < 70°$) on a Rigaku AFC-6A automated four-circle diffractometer, with graphite monochromated Mo$K\alpha$ radiation (λ=0.71073 Å). The 2128 intensities ($|F_o| > 3\sigma(|F_o|)$) were corrected for Lorentz and polarization factors, but not for absorption, because of the low magnitude of μr($<$1.0).

All calculations were carried out on a Hitachi M-680H computer at the Computer Center of The University of Tokyo, using UNICS III[6] and ORTEP.[7] The scattering factors were taken from tables.[8] The structure was solved by the heavy-atom method. The position of the copper atom was obtained from the three-dimensional Patterson function, while the positions of all other non-hydrogen atoms were successively located by Fourier syntheses and were refined by a block-diagonal least-squares method and only in the last cycle by a full matrix least-squares method. The positions of hydrogen atoms were obtained by difference-Fourier syntheses. In the last cycle of the full matrix least-squares refinement with anisotropic temperature factors for all non-hydrogen atoms, all the parameter shifts were less than one-third of the corresponding standard deviations. The weighting scheme was $W = 1/\{a \times (|F_o|)^2 + b \times |F_o| + c\}$. These coefficients were automatically computed in the program system. The final R value was 0.047.

Powder Diffuse Reflection and Electronic Spectra. These

Table 1. Crystal Data

$CuCl(C_6H_{12}NO_4)$	F.W.=261.17
Orthorhombic	Pbca
a=14.18(1) Å	b=15.835(7) Å
c=8.188(3) Å	U=1838(2) Å^3
Z=8	
D_m=1.871(3) g cm^{-3}	D_x=1.887 g cm^{-3}
μ(Mo$K\alpha$)=26.6 cm^{-1}	

spectra were obtained from 800 to 1500 nm with a JASCO UVIDEC-590 spectrophotometer. The spectra from 400 to 800 nm were obtained with a Hitachi 624 digital spectrophotometer. Both spectrophotometers were equipped with a standard reflection attachment and a magnesium oxide standard for measurements of powder diffuse reflection spectra.

Infrared and Far-Infrared Absorption Spectra. Infrared absorption spectra from 4000 to 400 cm^{-1} were measured using a Hitachi spectrophotometer, type EPI-G_2. Far-infrared absorption spectra from 700 to 200 cm^{-1} were measured using a Hitachi spectrophotometer, type EPI-L. Samples were prepared as KBr disks and Nujol mulls. The spectra were calibrated with polystyrene and atmospheric water vapor.

Results and Discussion

Structure of [CuCl(bheg)]. The final atomic parameters are listed in Table 2,[9] the interatomic distances in Table 3,[9] and the bond angles in Table 4.

Table 2. Final Positional Parameters ($\times 10^4$) and Equivalent Isotropic Temperature Factors (B_{eq}/Å^2),[a] with the Estimated Standard Deviations in Parentheses[b]

Atom	X	Y	Z	B_{eq}/Å^2
Cu	1237.4(3)	916.0(3)	689.9(4)	2.1
Cl	1066.2(9)	767.5(7)	3349.0(1)	3.4
O(1)	2534(2)	1608(2)	703(4)	2.8
O(2)	213(2)	1844(2)	416(3)	2.1
O(3)	1200(3)	−294(2)	170(3)	3.3
O(4)	1337(2)	−1212(2)	−1831(3)	2.8
N	1384(2)	1065(2)	−1731(3)	1.9
C(1)	2126(3)	1707(3)	−2065(5)	2.8
C(2)	430(3)	1336(3)	−2321(4)	2.3
C(3)	1637(4)	231(2)	−2423(5)	2.6
C(4)	2932(3)	1603(3)	−902(5)	3.1
C(5)	54(4)	2027(3)	−1280(5)	2.7
C(6)	1369(3)	−478(2)	−1288(4)	2.2

a) The equivalent isotropic temperature factors for non-hydrogen atoms were computed using the following expression: $B_{eq}=4/3(B_{11}a^2+B_{22}b^2+B_{33}c^2)$. B_{ij}'s are in the form: $\exp\{-(h^2B_{11}+k^2B_{22}+l^2B_{33}+2klB_{23}+2hlB_{13}+2hkB_{12})\}$. b) Final atomic parameters of hydrogen atoms are deposited.[9]

Table 3. Interatomic Distances (*l*/Å), with the Estimated Standard Deviations in Parentheses[a]

Cu-Cl	2.203(1)	N-C(1)	1.487(5)
Cu-O(1)	2.140(4)	N-C(2)	1.499(5)
Cu-O(2)	2.078(3)	N-C(3)	1.481(5)
Cu-O(3)	1.963(3)	C(1)-C(4)	1.497(6)
Cu-N	2.007(3)	C(2)-C(5)	1.487(6)
O(1)-C(4)	1.430(5)	C(3)-C(6)	1.505(5)
O(2)-C(5)	1.437(5)	O(1)-H(O1)	0.63(6)
O(3)-C(6)	1.252(4)	O(2)-H(O2)	0.68(4)
O(4)-C(6)	1.246(4)		
O(1)-O(4)^{I}	2.652(4)	O(2)-O(4)^{II}	2.678(4)
O(1)-H(O1)^{I}	2.03(6)	O(2)-H(O2)^{II}	2.00(4)

Key to symmetry operations: I. 0.5−*x*, −*y*, 0.5+*z*; II. −*x*, −*y*, −*z*. a) Interatomic distances of C-H are deposited.[9]

Table 4. Bond Angles (ϕ/°), with the Estimated Standard Deviations in Parentheses

Cl-Cu-O(1)	98.3(1)	Cu-O(3)-C(6)	115.4(2)
Cl-Cu-O(2)	96.03(9)	O(3)-C(6)-O(4)	123.4(3)
Cl-Cu-O(3)	96.15(9)	O(3)-C(6)-C(3)	117.6(3)
Cl-Cu-N	179.29(9)	O(4)-C(6)-C(3)	119.0(3)
O(1)-Cu-O(2)	103.8(1)	Cu-N-C(1)	109.6(2)
O(1)-Cu-O(3)	121.6(2)	Cu-N-C(2)	105.0(2)
O(2)-Cu-O(3)	130.4(1)	Cu-N-C(3)	107.3(2)
O(1)-Cu-N	81.7(1)	C(1)-N-C(2)	112.5(3)
O(2)-Cu-N	83.3(1)	C(1)-N-C(3)	111.6(3)
O(3)-Cu-N	84.4(1)	C(2)-N-C(3)	110.6(3)
Cu-O(1)-C(4)	109.4(3)	O(1)-C(4)-C(1)	106.4(4)
Cu-O(2)-C(5)	110.9(2)	O(2)-C(5)-C(2)	110.5(3)
O(1)-H(O1)··O(4)^{I}	170(7)	O(2)-H(O2)··O(4)^{II}	175(4)

Key to symmetry operations: I. 0.5−*x*, −*y*, 0.5+*z*; II. −*x*, −*y*, −*z*.

Table 5. The Deviations of Atoms from the Least-Squares Planes (*l*/Å)

Plane (1)	[O(1), O(2), O(3)] Cu, 0.2405; Cl, 2.4427; N, −1.7657
Plane (2)	[Cu, O(1), N, C(1), C(4)] Cu, 0.1187; O(1), −0.1683; N, 0.2113; C(1), −0.2771; C(4), 0.2087
Plane (3)	[Cu, O(2), N, C(2), C(5)] Cu, 0.1615; O(2), −0.0106; N, −0.2371; C(2), 0.3006; C(5), −0.1415
Plane (4)	[Cu, O(3), N, C(3), C(6)] Cu, −0.0694; O(3), 0.0492; N, 0.1228; C(3), −0.1291; C(6), 0.0479; O(4), 0.1700
Plane (5)	[O(3), O(4), C(3), C(6)] Cu, 0.0997; O(3), −0.0014; O(4), −0.0014; N, 0.3872; C(3), −0.0011; C(6), 0.0040

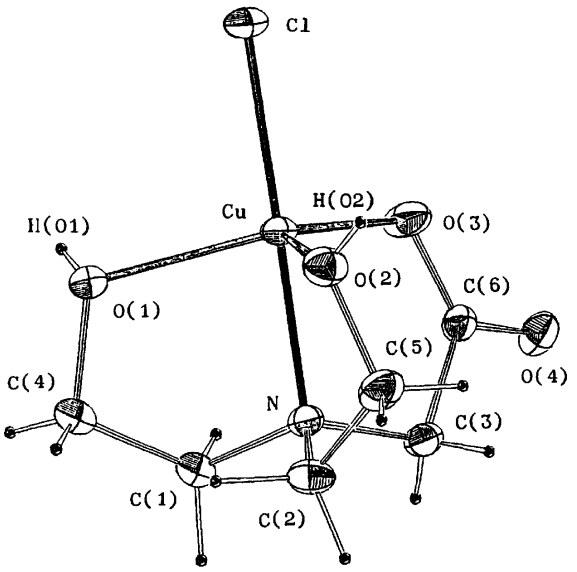

Fig. 1. The molecular structure of [CuCl(bheg)] and the numbering scheme of the atoms.

The deviations of atoms from least-squares planes are shown in Table 5. The molecular structure of the complex and the numbering scheme of the atoms, except alkyl hydrogen atoms, are shown in Fig. 1.

The stucture of the complex is trigonal-bipyramid.

The copper atom is surrounded by five atoms: one carboxylato oxygen atom, two hydroxyl oxygen atoms, one nitrogen atom and one chlorine atom. The nitrogen atom and the chlorine atom are at the apical position. The angle Cl-Cu-N is 179.29(9)° and three coordinated oxygen atoms form a triangle around the copper atom. The copper atom is 0.24 Å above the plane formed by the three ligating oxygen atoms. The bond length of Cu-O (carboxylato) (1.963 Å) is shorter than those of Cu-O (hydroxyl) (2.140 and 2.078 Å).

The complex has three five-membered *N*,*O*-chelate rings. They are all distorted because of the small N-Cu-O angles. As shown in Table 5, plane (4) shows the least deviation among the chelate rings because it includes one sp^2 carbon atom. All C-C bond lengths are slightly shorter than the usual general C-C bond lengths: this is the same trend as those of the free ligand already reported.[10] The three C-N bonds become shorter than those of the free ligand (1.508, 1.505, and 1.504 Å) because the nitrogen atom of the free ligand is protonated. The distances between carboxylato carbon atom and carboxylato oxygen atom: C(6)-O(3) (coordinated); 1.252(4) Å and C(6)-O(4) (non-coordinated), 1.246(4) Å, are not so different, since O(4) forms two hydrogen bonds with the neighboring unit. The bond lengths of the O-H are shorter than the usual general O-H bond lengths. The free ligand also has the same trend.[10]

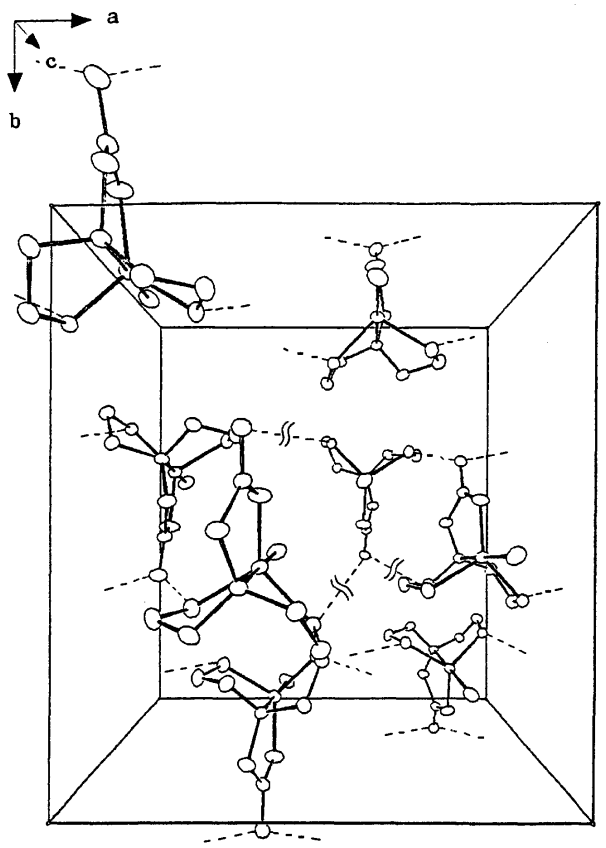

Fig. 2. The crystal structure of [CuCl(bheg)]. (----: Hydrogen bonding).

Let us now compare the structure of this complex with that of [CuCl(deg)]. The coordination number of [CuCl(deg)] is five,[5] like that of [CuCl(bheg)]. In [CuCl(deg)], the copper atom is surrounded by three carboxylato oxygen atoms, one nitrogen atom, and one chlorine atom, and the structure consists of a one-dimensional polymer chain bridged by only one carboxylato group of *N*,*N*-diethylglycine. This [CuCl(bheg)] has no bridging carboxylato groups and so is a monomer with the coordination of hydroxyl groups.

The molecular packing of the complex is shown in Fig. 2. There are no intermolecular interactions except at the two hydrogen bonds, which are formed between the non-coordinated carboxylato oxygen atom and the hydroxyl hydrogen atom. They are parallel to the ac plane. No intermolecular interactions parallel to b axis are found. This agrees with the easy cleavage of this crystal along this axis.

Powder Diffuse Reflection and Electronic Spectra. The reflection spectrum shows a broad band at about 1000 nm. This wavelength is different from those of copper(II) chloride complexes with *N*-substituted amino acids previously investigated in our laboratory, as shown in Table 6, but it is near to the value of the reflection band (900 nm) for 1-(2-ammonioethyl)piperazinediium pentachlorocuprate(II) dihydrate, which has a typical trigonal bipyramidal structure.[14] The electronic spectrum in aqueous solution shows a band at 760 nm. As this spectrum is similar to that of octahedral configurations, the structure of this complex seems to change in aqueous solution.

Infrared Absorption Spectra. There is a strong broad band at 3025 cm^{-1} for [CuCl(bheg)]. It is assigned to the OH stretching vibration, because of its disappearance on deuteration and the absence of bands in this region for [CuCl(deg)]. As this band is observed at a lower frequency region than for the free ligand (3186 and 3089 cm^{-1}), the strengths of the O-H bonds seem to become weaker on coordination.

For the free ligand, the COO^- antisymmetric and symmetric stretching vibrations appear at 1639 and 1401 cm^{-1}, respectively. In [CuCl(bheg)] the former

Table 6. Powder Diffuse Reflection Spectra of Copper(II) Chloride Complexes with *N*-Substituted Amino Acids

Complex	λ/nm	Coordination number[a]	Reference
CuCl(pro)·MeOH	754	5+1	11
CuCl(hpro)·H_2O	755	5+1	12
CuCl(pro)·H_2O	730	5	13
CuCl(deg)	626	4+1	5
CuCl(bheg)	1000	5	This work

Hpro=L-proline, Hhpro=4-hydroxy-L-proline.
a) Coordination Number: For example "5+1" stands for that the complex has 5 usual coordination bonds and 1 weak bond.

shifts to a somewhat lower frequency region (1578 cm^{-1}) and the latter shifts to a higher one (1406 cm^{-1}). The frequency separation between these two frequencies for [CuCl(bheg)] (172 cm^{-1}) is smaller than that of the free ligand. It has been reported that the frequency separation betweeen the two COO^- stretching vibrations in an unidentate complex is generally larger than that of a free ligand.[15] Though [CuCl(bheg)] shows an opposite tendency, this vibrational spectrum pattern is consistent with the result of X-ray analyses that the bond lengths of the C-O (coordinated) and the C-O (non-coordinated) are almost the same.

Far-Infrared Absorption Spectra. Two new bands (340 and 275 cm^{-1}) which were not observed in the ligand appear in [CuCl(bheg)]. They are assigned to Cu-N and Cu-O (carboxylato) stretching vibrations, by comparing this spectrum with those of [$Cu(bheg)_2$] and metal complexes with other amino acids.[16-18] From the molecular structure determined by X-ray analysis, it is clear that this molecule has a Cs symmetry. Therefore in view of the five atoms which form a trigonal-bipyramid around the copper atom, there are twelve normal vibrations. They are divided into two symmetries (8A'+4A") which are all infrared active. Since the bond lengths of the Cu-OH are longer than that of Cu-O (carboxylato), two Cu-OH stretching vibrations appear at a lower frequency region than where Cu-O (carboxylato) stretching vibration is observed. Therefore, it is reasonable to assign the band at 275 cm^{-1} to the Cu-O (carboxylato) stretching vibration.

The band at 317 cm^{-1} is assigned as a terminal Cu-Cl stretching vibration, by comparison with the spectra of [$Cu(bheg)_2$], [CuCl(deg)][5] (344 cm^{-1}) and other copper(II) complexes containing chlorine atoms.[19,20]

Such behavior in infrared and far-infrared spectra is in good agreement with the results of X-ray diffraction study of [CuCl(bheg)].

The authors wish to express their thanks to Professor Akira Ouchi of The University of Tokyo for X-ray diffractometer measurements. They would also like to thank Dr. F.S. Howell of Sophia University for correcting this manuscript.

References

1) Y. Inomata, T. Takeuchi, and T. Moriwaki, *Bull. Chem. Soc. Jpn.*, **49**, 1568 (1976).

2) N. N. Anan'eva, N. I. Samus, T. N. Polynova, M. A. Poraoi-Koshits, and N. D. Mitrofanova, *Zh. Strukt. Khim.*, **16**, 480 (1975).

3) K. Nielsen, R. G. Hazell, and S. E. Rasmussen, *Acta Chem. Scand.*, **26**, 889 (1972).

4) J. C. Voegele, J. Fischer, and R. Weiss, *Acta Crystallogr., Sect. B*, **30**, 66 (1974).

5) S. Nakagome, K. Aoyagi, Y. Yukawa, Y. Inomata, and T. Takeuchi, 52nd National Meeting of the Chemical Society of Japan, Kyoto, April 1986, Abstr., No. 4K27.

6) T. Sakurai and K. Kobayashi, *Rep. Inst. Phys. Chem. Res.*, **55**, 69 (1979).

7) C. K. Johnson, "ORTEP," Oak Ridge National Laboratory, ORNL- 3794 (1965).

8) International Tables for X-Ray Crystallography, Vol. IV. Kynoch Press, Birmingham (1974).

9) The final positional parameters and equivalent isotropic temperature factors of hydrogen atoms, the final thermal parameters and the final F_o-F_c table are deposited as Document No. 8819 at the Office of the Editor of the Bulletin of the Chemical Society of Japan.

10) V. Cody, J. Hazel, and D. Langs, *Acta Crystallogr., Sect. B*, **33**, 905 (1977).

11) Y. Yukawa, Y. Inomata, and T. Takeuchi, 34th Symposium on Coordination Chemistry, Nagaoka, Japan, October 1984, Abstr., No. 3A13.

12) S. Itoh, Y. Yukawa, Y. Inomata, and T. Takeuchi, *Bull. Chem. Soc. Jpn.*, **60**, 899 (1987).

13) Y. Yukawa, Y. Inomata, and T. Takeuchi, 50th National Meeting of the Chemical Society of Japan, Tokyo, April 1985, Abstr. 1K01.

14) L. Antolini, G. Marcotrigiano, L. Menabue, and G. C. Pellacani, *J. Am. Chem. Soc.*, **102**, 1303 (1980).

15) K. Nakamoto, "Infrared and Raman Spectra of Inorganic and Coordination Compounds," 4th ed, John Wiley and Sons, New York (1986), pp. 232—233.

16) K. Nakamoto, "Infrared and Raman Spectra of Inorganic and Coordination Compounds," 4th ed, John Wiley and Sons, New York (1986), pp. 236.

17) J. R. Ferraro, "Low-Frequency Vibrations of Inorganic and Coordination Compounds," Plenum Press, New York (1971), pp. 227—230.

18) J. R. Ferraro, "Low-Frequency Vibrations of Inorganic and Coordination Compounds," Plenum Press, New York (1971), pp. 97—99.

19) J. R. Ferraro, "Low-Frequency Vibrations of Inorganic and Coordination Compounds," Plenum Press, New York (1971), pp. 111—182.

20) A. Finch, P. N. Gates, K. Radcliffe, F. N. Dickson, and E. F. Bentley, "Chemical Applications of Far Infrared Spectroscopy," Academic Press, London and New York (1970), pp. 145—150.

 © 1988 The Chemical Society of Japan Bull. Chem. Soc. Jpn., 61, 2767—2772 (1988)

Structures and Properties of Divalent Metal Complexes of an N_2O_2 Type Ligand, 6,6′-Bis(benzoylamino)-2,2′-bipyridine

Masaki YAMADA, Koji ARAKI,* and Shinsaku SHIRAISHI*
Institute of Industrial Science, The University of Tokyo, 7-22-1 Roppongi, Minato-ku, Tokyo 106
(Received March 9, 1988)

Complex formations of an N_2O_2 tetradentate ligand, 6,6′-bis(benzoylamino)-2,2′-bipyridine ($babpH_2$) with various divalent metal ions were investigated. $BabpH_2$ complexes of Ni(II), Co(II), and Zn(II) were obtained as dinitrate and/or diacetate, and their deprotonated complexes, [Ni(babp)], [Co(babp)], and [Zn(babp)], where babp represents the deprotonated form of amide protons of $babpH_2$, were also isolated. The deprotonated complexes were shown to have high thermal stability up to 300 °C. The structures, stabilities, and spectral properties of these complexes were discussed in relation to the copper(II) complexes of $babpH_2$ and babp.

Recently we reported the syntheses, structures, and some properties of a new type of tetradentate N_2O_2 ligand, 6,6′-bis(acylamino)-2,2′-bipyridines and their copper(II) complexes.[1] Deprotonation of the amide protons of copper(II) complex **1a** takes place in weakly acidic to neutral pH range, giving the deprotonated complex **2a** which have a similar structure to those of salen complexes in their N_2O_2 tetradentate coordination sites, square-planar structure, and the anionic sites on oxygens. In addition, our preliminary results showed that the deprotonated type of the cobalt(II) complex of 6,6′-bis(benzoylamino)-2,2′-bipyridine ($babpH_2$), [Co(babp)], serves as a better catalyst for oxygenation of phenols by molecular oxygen compared to cobalt(II)-salen complexes.[2,3] In this report, complex formations of $babpH_2$ with various divalent metal ions including cobalt(II) and the structural elucidation of the complexes are described.

Results

Syntheses of Complexes. Syntheses of 1 : 1 complexes of $babpH_2$ with various divalent metal ions are shown in Scheme 1, and their characterization data are summarized in Table 1. $BabpH_2$ complexes of nickel(II) as a nitrate (**1b**), cobalt(II) and zinc(II) as acetates (**1′c** and **1′d**, respectively), were obtained by mixing $babpH_2$ with corresponding metal salts. The cobalt(II) (**1c**) and zinc(II) (**1d**) complexes were also obtained in nitrate form from **1′c** and **1′d**, respectively (see experimental section). All of the non-deprotonated complexes were soluble in water. The nitrate of the non-deprotonated nickel(II) complex **1b** was very stable in water even under highly acidic conditions, while the non-deprotonated complexes of cobalt(II) and zinc(II) acetates (**1′c** and **1′d**, respectively) or nitrates (**1c** and **1d**, respectively) released the metal ions in weakly acidic or even in neutral water to give metal-free $babpH_2$ quantitatively.

In the case of nickel(II), use of nickel(II) acetate directly yielded the deprotonated-type complex [Ni(babp)] (**2b**), being similar to the case of copper (II).[1] The deprotonated-type of cobalt(II) complex [Co(babp)] (**2c**) was obtained as a precipitate by addition of twice molar amount of KOH to **1′c** in methanol under anaerobic atmosphere.[4] Similar attempt to obtain the deprotonated-type complexe of zinc(II) from **1′d** resulted in recovery of metal-free $babpH_2$ (see experimental section). But the thermolysis of **1′d** (see thermal properties section) successfully afforded the zinc(II) complex [Zn(babp)] (**2d**). These deprotonated complexes, **2b—2d**, are insoluble in water and not release metal ions in acid-free water.

IR Spectra. The nitrates of the non-deprotonated complexes, **1b**, **1c**, and **1d**, showed quite similar IR spectra to that of the corresponding copper(II) complex **1a**,[1] and the deprotonated complexes, **2b**, **2c**, and **2d** to that of the corresponding copper(II) complex **2a** (Table 2),[1] showing that either $babpH_2$ or babp serves as a tetradentate N_2O_2 ligand in those complexes similarly to **1a** and **2a**.[1,5,6]

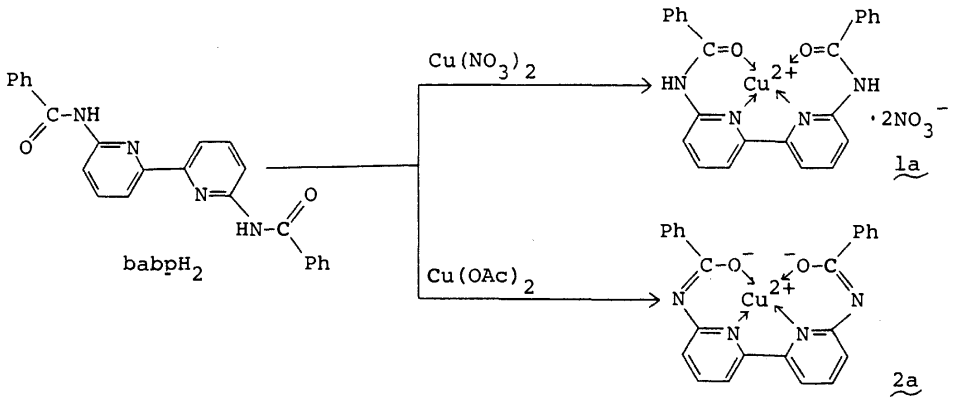

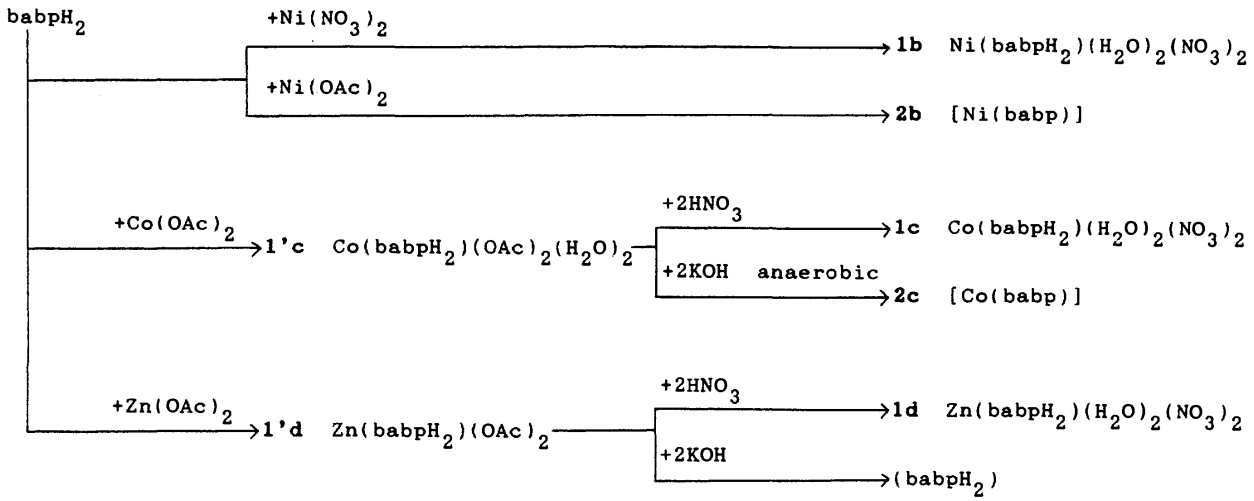

Scheme 1.

Table 1. Analytical Data of Isolated Complexes

Code	Appearance	Composition[a)]	E.A./%(Found(Calcd))		
			C	H	N
1b	Pale green plates	$Ni(babpH_2)(NO_3)_2(H_2O)_2$	46.84 (47.01)	3.88 (3.62)	13.63 (13.71)
2b	Orange needles	[Ni(babp)]	64.12 (63.90)	3.44 (3.57)	12.26 (12.42)
1'c	Pink powder	$Co(babpH_2)(OAc)_2(H_2O)_2$	55.73 (55.36)	4.15 (4.64)	8.64 (9.22)
1c	Pale brown powder	$Co(babpH_2)(NO_3)_2(H_2O)_2$	46.91 (46.99)	3.60 (3.61)	13.33 (13.70)
2c	Red needles	[Co(babp)]	63.54 (63.87)	3.42 (3.57)	12.43 (12.41)
1'd	White plates	$Zn(babpH_2)(OAc)_2$	58.01 (58.19)	4.07 (4.19)	9.58 (9.69)
1d	White needles	$Zn(babpH_2)(NO_3)_2(H_2O)_2$	46.85 (46.51)	3.40 (3.58)	13.13 (13.56)
2d	Yellow powder	[Zn(babp)]	63.52 (62.97)	3.53 (3.52)	12.30 (12.24)

a) Abbrebiation babp representates deprotonated (both of two amide protons) form of $babpH_2$.

Table 2. Characteristic IR Bands of Complexes in KBr Disks

Material	IR band/cm^{-1}				
	ν(N-H)	Amide band			Others
		I	II	III	
$babpH_2$[a)]	3310	1651	1521	1245	—
1a[a)]	3430	1615	1535	1323	1381 (ν(N-O) of nitrate)
1b	3406	1620 1647sh[b)]	1541	1317	1385 (ν(N-O) of nitrate)
1c	3284	1616 1645sh	1541	1315	1385 (ν(N-O) of nitrate)
1d	3398	1619 1640sh	1542	1317	1384 (ν(N-O) of nitrate)
2a[a)])	—	(1555)	(1366)	—	—
2b	—	(1562)	(1382)	—	—
2c	—	(1557)	(1381)	—	—
2d	—	(1562)	(1378)	—	—
1'c	3290	1653 1675	1537	1238	1579 (ν(C-O) of acetate)
1'd	3334	1658 1694	1538	1266	1578 (ν(C-O) of acetate)

a) Ref. 1. b) Shoulder peak.

On the other hand, IR spectra of the acetates of the non-deprotonated complexes, **1′c** and **1′d**, are quite different in amide carbonyl region (amide I) from those of nitrates (Table 2). The amide I bands of the acetates appear at higher wavenumber compared with that of metal-free babpH_2. Similar blue shift of the amide I band was reported for the non-deprotonated palladium(II) complex of 2-(acetylamino)pyridine in which the ligand coordinates only with its ring nitrogen but not with its amide oxygen.[6] Therefore, it may be implyed that babpH_2 in **1′c** and **1′d** coordinates to metal ions only with its ring nitrogens but not with its amide oxygens. The structures of the acetates are remained uncertain.

Electronic Spectra. The electronic spectra of the complexes in dimethyl sulfoxide (DMSO) are shown in Fig. 1. The acetates of the non-deprotonated complexes, **1′c** and **1′d**, showed the similar spectra to those of the corresponding deprotonated-type complexes (**2c** and **2d**, respectively). Therefore, it is quite likely that the amide protons of these complexes were dissociated under the measured conditions.

Dropwise addition of nitric acid to the solution of the deprotonated nickel(II) complex **2b** in DMSO up to twice molar amount caused gradual spectral change to that of **1b** in two-steps (Fig. 2). This result shows

$$[Ni(babpH_2)]^{2+} \underset{+H^+}{\overset{-H^+}{\rightleftharpoons}} [Ni(babpH)]^{+} \underset{+H^+}{\overset{-H^+}{\rightleftharpoons}} [Ni(babp)]$$

Scheme 2.

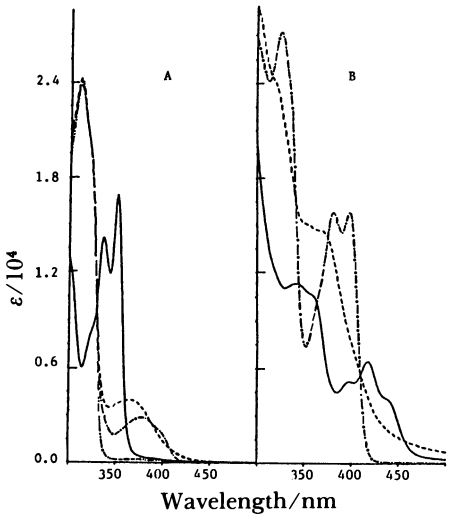

Fig. 1. The electronic spectra of (A) nitrate salts of the non-deprotonated complexes and (B) deprotonated complexes in DMSO (6.67×10^{-5} M) at 20°C. (——): nickel(II) complexes **1b** (A) and **2b** (B), (----): cobalt(II) complexes **1c** (A) and **2c** (B), (-·-·-): zinc(II) complexes **1d** (A) and **2d** (B), and (-···-···-): metal free babpH_2 (A).

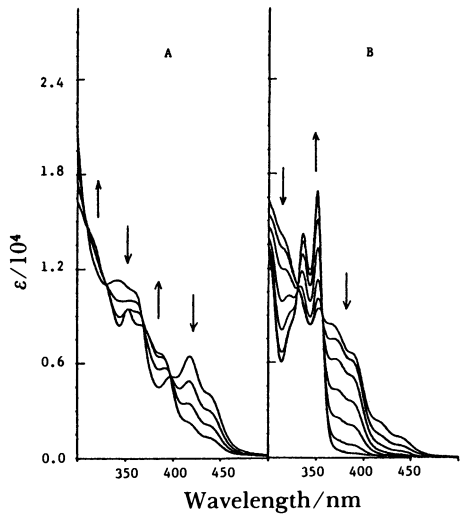

Fig. 2. The spectral change of **2b** in DMSO (6.67×10^{-5} M) by addition of nitric acid at 20°C. Molar ratio of added nitric acid were as follows; A: 0.0, 0.2, 0.4, and 0.6, B: 0.6, 0.8, 1.0, 1.2, 1.6, 1.8, and 2.0.

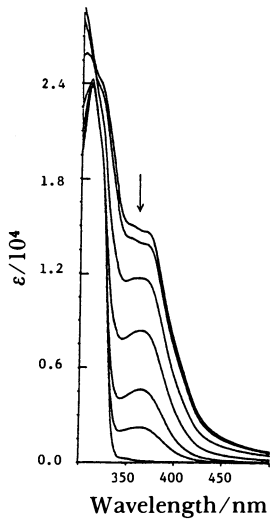

Fig. 3. The change of electronic spectra of **2c** by addition of nitric acid in DMSO (6.67×10^{-5} M) at 20°C. Molar ratio of added nitric acid were 0.0, 0.5, 1.0, 1.5, 2.0, 2.2, and 2.5.

that protonation to the deprotonated species **2b** in DMSO takes place stepwisely via intermediacy of monoprotonated species (Scheme 2). Similar result has been observed for the copper(II) complex **2a**.[1] The spectra of the cobalt(II) and zinc(II) complexes, **2c** and **2d**, in DMSO changed to that of metal-free babpH_2 by addition of nitric acid (Fig. 3).[7]

Thermal Properties of Complexes in Solid State. Thermal properties of the complexes were analyzed by TG and DTA, and the results are summarized in Table 3. Figure 4 represents the typical TG curves of the complexes, **1b**, **1′d**, and **2b**. Those of the copper(II) complexes are also included which were not reported in the preceding paper.[1]

Table 3. Thermal Properties of Complexes[a)]

Complex	Temperature/°C
1a	63—76($-H_2O$) 136—161($-H_2O$) 224—238($-2HNO_3\rightarrow$**2a**)
1b	72—85($-H_2O$) 166—186($-H_2O$) 254—303($-2HNO_3\rightarrow$**2b**)
1c	75—166($-2H_2O$) 228—248($-2HNO_3\rightarrow$decomp)
1d	77—110($-2H_2O$) 238—263($-2HNO_3\rightarrow$decomp)
1'c	96—203($-2H_2O$, $-2AcOH\rightarrow$**2c**)
1'd	200—258($-2AcOH\rightarrow$**2d**)
2a	337(mp)
2b	337(mp)
2c	333(mp)
2d	b)

a) Heating rate; 5 °C min^{-1}, under aerobic atmosphere. b) See text.

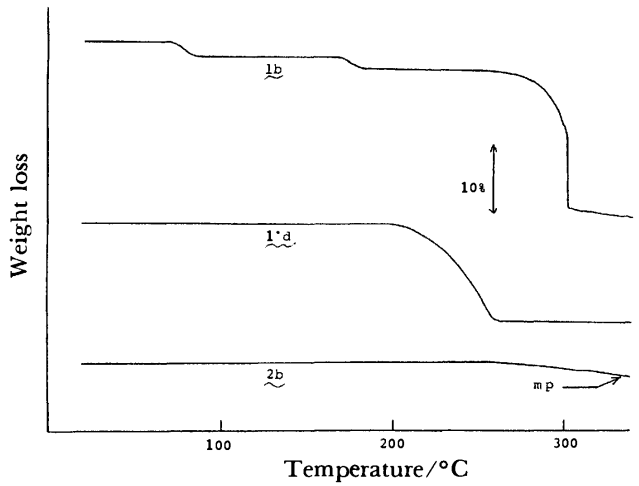

Fig. 4. Typical TG curves of the complexes, **1b**, **1'd**, and **2b**.

In the case of the nitrate salts of the non-deprotonated complexes, **1a—1d**, small weight loss during 50—190 °C accounted for loss of two water molecules took place endothermically. Further heating caused gradual weight decrease endothermically at above 220 °C, followed by abrupt weight loss with sharp exothermic peak in DTA. In the case of **1a** and **1b**, these weight losses were accounted for the loss of nitric acid, and IR spectra of the residual solids were identical to those of **2a** and **2b**, respectively. While, weight of **1c** and **1d** decreased much more than those accounted for loss of two nitric acid molecules indicating the thermal decomposition of the ligand, and, indeed, IR spectra of the residues were different from those of the deprotonated complexes. Instead, heating the acetate salts, **1'c** and **1'd**, up to 260 °C successfully afforded the deprotonated complexes of cobalt(II) and zinc(II), respectively, by elimination of acetic acid, though elimination took place more slowly in these cases. IR spectra of the residual solids were characteristic to those of the deprotonated complexes. Thus, it was shown that thermolysis of the non-deprotonated complexes yielded the corresponding deprotonated complexes. It is worth to note that the deprotonated complex **2d**, [Zn(babp)] was isolated only by thermolysis of **1'd** but not by deprotonation in solution under basic conditions.

The deprotonated complexes **2a—2c** showed clear melting points near 330 °C, and were stable up to these temperatures. Decomposition of these complexes were only observed when they were heated above their melting points. The deprotonated complex of zinc(II) **2d** did not show any weight loss up to 370 °C, and decomposed without showing any apparent melting above this temperature.

Discussion

Structure and Stability of the Complexes. The ligand $babpH_2$ is shown to coordinate as N_2O_2 tetradentate ligand to form two types of the complexes, one is the non-deprotonated type (nitrate salts), **1a—1d**, and the other the deprotonated ones, **2a—2d**. The structure of the complexes were elucidated by their IR spectra[1,5,6] and elemental analyses. In the case of acetates of the non-deprotonated complexes, **1'c** and **1'd**, however, $babpH_2$ was suggested to serve as an N_2 bidentate ligand from their IR spectra.

The non-deprotonated complexes of copper(II)[1] and nickel(II) were stable even in acidic aqueous solution, while those of cobalt(II) and zinc(II) were not stable in water. This difference in the stability of the non-deprotonated complexes were in agreement with Irving-Williams'[8] and Mellor-Malley's[9] laws. The deprotonated complexes, **2a—2d**, were stable enough not to suffer any change in neutral acid-free water.

Dissociation of Amide Protons. Amide proton is very weak acid and the pK_a is higher than 13 in most cases.[10] Complexation of metal ions at amide oxygen is known to increase their acidity.[10] Spectrometric titration of the nitrate salt of the non-deprotonated nickel(II) complex, **1b**, in water with pottasium hydroxide solution indicated that the two amide protons dissociated almost simultanously at pH 5.8 and the deprotonated complex **2a** precipitated. Titration of copper(II) complex **1a** by similar method showed that dissociation of both of its amide protons took place at pH 5.2.[1] Titration of the cobalt(II) complex could not be carried out because of its instability in water. Complexation of $babpH_2$ and cobalt(II) acetate gave the non-deprotonated complex, though com-

plexation with nickel(II) or copper(II) acetate gave the deprotonated complex, suggesting that the acidity of the amide protons of the cobalt(II) complex is lower than that of copper(II) or nickel(II) complex. Thus acidities of the amide protons of the $babpH_2$ complexes follow the order, Co(II)<Ni(II)<Cu(II). Acidities of metal-chelated amide protons in peptides were also known to follow this order.[10]

In most cases amide groups are known to coordinate to metal ions by their oxygens, while, amide groups in deprotonated form by their nitrogens. In the cases of $babpH_2$, however, both $babpH_2$ and babp served as an N_2O_2 tetradentate ligand, and high acidity of amide protons in nitrate salts of the non-deprotonated complexes were observed. One of the reason why the amide protons in the complexes of $babpH_2$ have high acidity might be due to the high stability of the deprotonated complexes. They are thought to be stabilized by intramolecular charge transfer because they contain strong O-donor (deprotonated amide oxygens) and heteroaromatic N-donor having relatively strong π-electron accepting abilities (2,2′-bipyridine moiety).[11] This effect has been proposed as "intramolecular mixed ligand" effect[10,12] to explain the stability of the complexes of 8-quinolinol[13] and the deprotonated palladium(II) complex of 2-(acetylamino)pyridine.[6,10]

Thermal Properties. The results of thermal analyses of the non-deprotonated complexes indicated that dissociation of amide protons took place by heating in solid state. In some cases, thermolysis is an effective process to obtain deprotonated complexes, because dissolution of the complexes in aqueous solution sometimes causes the release of the metal ions from the complexes.

It is noteworthy that the deprotonated complexes **2a—2d** are thermally stable up to 300°C under aerobic atmosphere. This also enable thermal dissociations of acid moieties of the non-deprotonated complexes to give deprotonated ones.[14]

Experimental

Materials. 6,6′-Bis(benzoylamino)-2,2′-bipyridine ($babpH_2$) was prepared from 6,6′-diamino-2,2′-bipyridine[15] and benzoyl chloride according to the method previously reported.[1] Other chemicals were obtained commercially, and some of them were purified by conventional methods prior to use.

Spectral Measurements. IR spectra were measured by JASCO IR-700 spectrophotometer. Electronic spectra were recorded on a JASCO UVIDEC-505 spectrophotometer at 20 °C. Measurement of cobalt(II) complexes in this report were carried out under anaerobic conditions because they interact with molecular oxygen in solution.[2,3]

Thermal Analyses. TG and DTA curves were recorded simultanously on Shimadzu DTG-30 Thermal Analyzer with heating rate of 5 °C min^{-1} under aerobic conditions.

Nickel(II) Complex 1b: This was obtained from 78 mg (0.2 mmol) of $babpH_2$ and 58 mg (0.2 mmol) of $Ni(NO_3)_2 \cdot 6H_2O$ by complexation in methanol in a similar manner to the preparation of copper(II) complex **1a**.[1] Recrystallization from water gave 83 mg (68%) of pale green plates of $Ni(babpH_2)(H_2O)_2(NO_3)_2$.

Nickel(II) Complex 2b: This was obtained from 78 mg (0.2 mmol) of $babpH_2$ and 50 mg (0.2 mmol) of $Ni(OAc)_2 \cdot 4H_2O$ by complexation in chloroform in a similar manner to the preparation of copper(II) complex **2a**.[1] Recrystallization from benzene gave orange needles of [Ni(babp)], yield 57 mg (63%).

Cobalt(II) Complex 1′c: A mixture of 78 mg (0.2 mmol) of $babpH_2$ and 50 mg (0.2 mmol) of $Co(OAc)_2 \cdot 4H_2O$ in 100 cm^3 of chloroform was stirred at room temperature until the suspension became a homogeneous brown solution. Then the solvent was removed by evaporation to leave pink powder, which was washed by benzene, yielding 80 mg (66%) of $Co(babpH_2)(OAc)_2(H_2O)_2$.

Zinc(II) Complex 1′d: A mixture of 78 mg (0.2 mmol) of $babpH_2$ and 44 mg (0.2 mmol) of $Zn(OAc)_2 \cdot 2H_2O$ in 100 cm^3 of tetrahydrofuran was stirred at room temperature until the suspension became a homogeneous pale brown solution. Then solvent was removed by evaporation. Residual white powder was recrystallized from benzene to give 72 mg (62%) of $Zn(babpH_2)(OAc)_2$.

Cobalt(II) Complex 1c and Zinc(II) Complex 1d: A mixture of 78 mg (0.2 mmol) of $babpH_2$ and 50 mg (0.2 mmol) of $Co(OAc)_2 \cdot 4H_2O$ in 100 cm^3 of tetrahydrofuran was stirred at room temperature until the suspension became a homogeneous brown solution. Then 0.4 cm^3 of 1M HNO_3 (1 M=1 mol dm^{-3}) was added and was allowed to stand for 24 h at room temperature. The precipitated pale brown powder was collected by filtration, yielding 110 mg (90%) of **1b**, $Co(babpH_2)(H_2O)_2(NO_3)_2$. Compound **1d** was obtained from 78 mg (0.2 mmol) of $babpH_2$ and 44 mg (0.2 mmol) of $Zn(OAc)_2 \cdot 2H_2O$ in a similar manner to the preparation of **1c**, yielding 98 mg (79%) of $Zn(babpH_2)(H_2O)_2(NO_3)_2$ as white needles. Non-deprotonated complxes **1c** and **1d** were not obtained pure form by direct complexation of $babpH_2$ and nitrate.

Cobalt(II) Complex 2c: Under nitrogen gas bubbling, a mixture of 78 mg (0.2 mmol) of $babpH_2$ and 50 mg (0.2 mmol) of $Co(OAc)_2 \cdot 4H_2O$ in 20 cm^3 of methanol was stirred at room temperature until the mixture became a homogeneous brown solution. To this solution, 0.8 cm^3 of 0.5 M-methanolic KOH was added. The color of the solution changed to dark red followed by precipitation of red solid. After stirring another 1 h under nitrogen atmosphere at room temperature, the red solid was collected by filtration. Recrystallization from benzene gave red needles of **2c**, [Co(babp)], yield 60 mg (67%). When similar process was performed under aerobic atmosphere or oxygen bubbling, reaction mixture retained homogeneous after addition of alkali, and removal of most of methanol gave 55 mg of yellow powder, which showed almost the same IR spectrum as that of **2c** except that the former has strong absorption band at 1403 cm^{-1}.

Zinc(II) Complex 2d: Compound **1′d** (116 mg, 0.2 mmol) was heated at 280 °C under reduced pressure for 20 h. Yellow powder of [Zn(babp)], **2d**, was obtained as a residue, yield 84 mg (92%). Compound **2d** was not obtained as a precipitate by addition of potassium hydroxide to a solution of **1d** or **1′d** in methanol. Extraction by benzene from residual solid after removal of methanol gave only metal free $babpH_2$ as extract and $Zn(OH)_2$ as insoluble solid.

References

1) M. Yamada, K. Araki, and S. Shiraishi, *Bull. Chem. Soc. Jpn.*, **60**, 3149 (1987).
2) M. Yamada, K. Araki, and S. Shiraishi, *J. Coord. Chem., Sect. B*, in press.
3) M. Yamada, K. Araki, and S. Shiraishi, *J. Chem. Soc., Chem. Commun.*, **1988**, 530.
4) Result under aerobic atmosphere, see experimental section.
5) M. B. Robin, F. A. Bovey, and H. Basch, "The Chemistry of Amide," ed by J. Zabicky, Interscience, London (1970), p. 1.
6) M. Nonoyama, S. Tomita, and K. Yamasaki, *Inorg. Chim. Acta*, **12**, 33 (1975).
7) The spectra after addition of twice amount of nitric acid were the same as those of corresponding nitrate salt of the non-deprotonated ones.
8) H. M. N. H. Irving and R. J. P. Williams, *J. Chem. Soc.*, **1953**, 3192.
9) D. P. Mellor and L. E. Maley, *Nature (London)*, **159**, 370 (1947); **161**, 436 (1948).
10) H. Sigel and R. B. Martin, *Chem. Rev.*, **82**, 385 (1982).
11) M. Yamada, K. Araki, and S. Shiraishi, *Bull. Chem. Soc. Jpn.*, **61**, 2208 (1988).
12) H. Sigel, B. E. Fischer, and B. Prijs, *J. Am. Chem. Soc.*, **99**, 4489 (1977).
13) L. G. Sillén and A. E. Martell, "Stability Constants," Chem. Soc. Spec. Publ., No. 17 (1964); No. 25 (1971).
14) In the case of cobalt(II) complex, **2c**, thermal stability enabled the complex to restore its catalytic activity for oxygenation by heating.[2,3]
15) N. Kishii, K. Araki, and S. Shiraishi, *Bull. Chem. Soc. Jpn.*, **57**, 2121 (1984).

 © 1988 The Chemical Society of Japan Bull. Chem. Soc. Jpn., 61, 2773—2778 (1988)

Effect of the *N*-Methylation of Dodecylammonium Chloride on the Adsorption from Its Micellar Solution

Makoto ARATONO,* Toru OKAMOTO, Norihiro IKEDA, and Kinsi MOTOMURA
Department of Chemistry, Faculty of Science, Kyushu University 33, Fukuoka 812
(Received April 6, 1988)

The surface tension of the aqueous solution of dodecylmethylammonium chloride (DMAC) and dodecyldimethylammonium chloride (DDAC) was measured as a function of temperature under atmospheric pressure at concentrations below and above the critical micelle concentration (cmc). The entropy and energy of adsorption from the monomeric state in the aqueous solution and the micellar state were evaluated by applying the thermodynamic equations of adsorption to the surface tension values. The thermodynamic quantities were compared with those of the aqueous solutions of dodecylammonium chloride (DAC) and dodecyltrimethylammonium chloride (DTAC). It was found that the successive *N*-methylation of DAC has a considerable effect on the adsorbed film with changes in its surface density, entropy, and energy brought about by changes in the geometry and the hydrophilicity of the polar head group.

The adsorption of dodecylammonium chloride (DAC) and dodecyltrimethylammonium chloride (DTAC) from their micellar solution at water/air interface has been investigated in our previous papers.[1,2] It has been shown that the thermodynamic quantity changes associated with the adsorption and micelle formation are greatly influenced by the chemical structure of the head group; for example, both entropy changes associated with adsorption from the monomeric state in the solution and the micellar state were negative for DAC and positive for DTAC, while the corresponding energy changes were positive for the two surfactants.

Now the systematic study is required on the effect of the chemical structure of the head group on the adsorption and micelle formation. In this paper we are concerned with the effect of the successive *N*-methylation of dodecylammonium chloride on the adsorption and micelle formation; the adsorption of dodecylmethylammonium chloride (DMAC) and dodecyldimethylammonium chloride (DDAC) at the aqueous solution/air interface at concentrations around the critical micelle concentrations is investigated in detail. The surface tension is measured as a function of temperature at fixed concentrations under atmospheric pressure. The thermodynamic quantities are evaluated by applying the thermodynamic equations developed previously[1] to the measured values of surface tension. By comparing the results with those of DAC and DTAC, the influence of the chemical structure of the head group is considered systematically.

Experimental

To synthesize dodecylmethylammonium chloride, dodecylmethylamine was prepared first according to the following way.[3] Acrylonitrile and dodecylamine were mixed slowly, stirred for 30 minutes, and refluxed for six hours. After removal of the excess acrylonitrile in vacuo, resulting *N*-(2-cyanoethyl)dodecylamine was obtained by the fractional distillation of the mixture under reduced pressure. The reaction of *N*-(2-cyanoethyl)dodecylamine with formic acid and formaldehyde yielded *N*-(2-cyanoethyl)-*N*-methyldocecylamine.[4] Its pyrolysis at 250—270 °C and 450 mmHg (1 mmHg≈133.322 Pa) followed by distillation under reduced pressure gave *N*-methyldodecylamine. As the second step the amine was neutralized by hydrochloric acid and the salt was purified by repeated recrystallization from ethanol–ethyl acetate mixture.

To obtain dodecyldimethylammonium chloride, *N,N*-dimethyldodecylamine was prepared as the first step as follows;[4] formic acid, ethanol solution of dodecylamine, and formaldehyde were mixed and, after reflux for 15 hours, neutralized by 25% aqueous sodium hydroxide solution, *N,N*-dimethyldodecylamine being separated as the upper phase. The amine was dried over sodium hydroxide and then distilled under reduced pressure. Dodecyldimethylammonium chloride was obtained by the reaction of the amine with hydrochloric acid and recrystallized from benzene–ethyl acetate mixture and then from ethanol–ethyl acetate mixture for five times. The purity of surfactants was confirmed by observing no minimum on the surface tension vs. concentration curves.

Water was distilled three times from alkaline permanganate solution. The surface tension was measured by the drop volume apparatus and procedure described previously,[5] and the experimental error was within 0.05 mN m^{-1}.

Results and Discussion

The surface tension γ was measured as a function of temperature T at constant molalities m_1 of the surfactant under atmospheric pressure. The surface tension value of the aqueous solution of DMAC is plotted against temperature in Fig. 1. Figure 2 shows the γ vs. m_1 curves depicted by taking up the γ values in Fig. 1 at a given temperature. It is seen that the curve has a sharp break point, of which the concentration is referred to as a critical micelle concentration (cmc). Looking at Fig. 1, it is observed that the γ vs. T curve has a minimum at a concentration between about 5 mmol kg^{-1} and the cmc, while it is a straight line with a slightly positive slope at a concentration above the cmc. Since the shape of γ vs. m_1 curve changes abruptly at the cmc, the γ vs. T curve has a break point as indicated by an arrow. For the aqueous DDAC

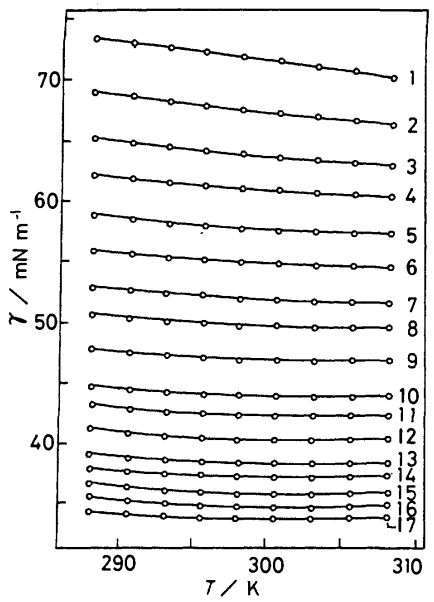

Fig. 1a. Surface tension vs. temperature curves of DMAC at constant concentration under atmospheric pressure: (1) m_1=0 mmol kg^{-1}; (2) 1.47; (3) 2.27; (4) 3.03; (5) 3.83; (6) 4.86; (7) 5.66; (8) 6.37; (9) 7.40; (10) 8.74; (11) 9.43; (12) 10.56; (13) 11.67; (14) 12.39; (15) 13.19; (16) 13.87; (17) 14.76.

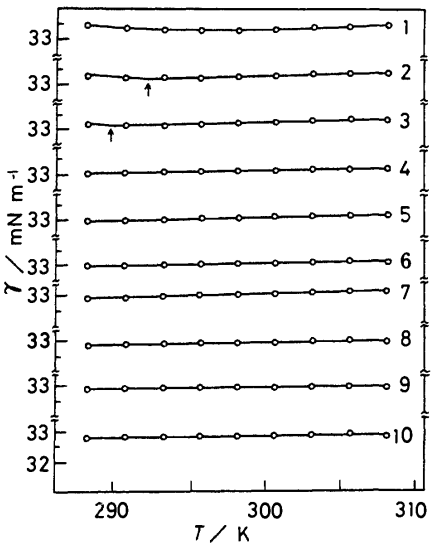

Fig. 1b. Surface tension vs. temperature curves of DMAC at constant concentration under atmospheric pressure: (1) m_1=14.94 mmol kg^{-1}; (2) 15.18; (3) 15.56; (4) 16.52; (5) 17.58; (6) 18.69; (7) 21.19; (8) 23.36; (9) 26.29; (10) 36.84.

solution/air interface, similar measurements were made; the γ vs. T curves at constant molalities and the γ vs. m_1 curves at constant temperatures are drawn in Figs. 3 and 2, respectively. Comparing the curves in Fig. 3 with those in Fig. 1, we notice that the γ vs. T curve of DDAC has no minimum at a concentration below the cmc and its slope remains negative at a concentration above the cmc.

In Figs. 4 and 5, respectively, the critical micelle concentration vs. temperature curves and the surface

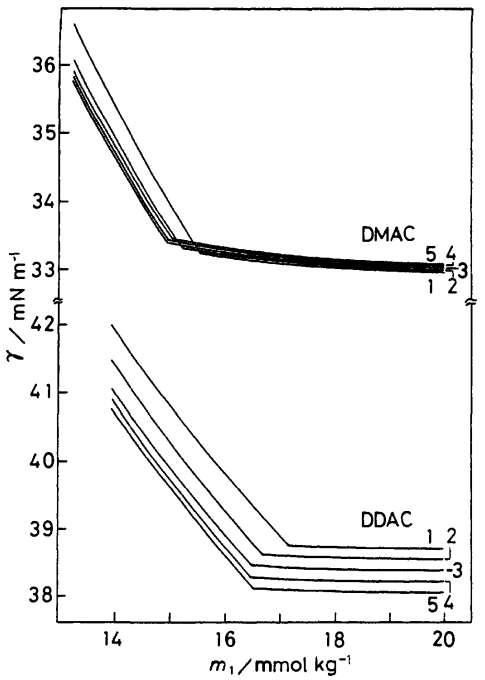

Fig. 2. Surface tension vs. concentration curves at constant temperature under atmospheric pressure: (1) T=288.15 K; (2) 293.15; (3) 298.15; (4) 303.15; (5) 308.15.

tension vs. concentration curves at 298.15 K of the aqueous solutions of DMAC and DDAC are shown with the corresponding curves of DAC and DTAC. It is seen that the temperature dependence of the cmc value is remarkably large and has a minimum. It is also seen that the cmc and its surface tension γ^{cmc} are correlated to the chemical structure of the polar headgroup of surfactant; the *N*-methylation of dodecylammonium chloride successively raises the cmc and

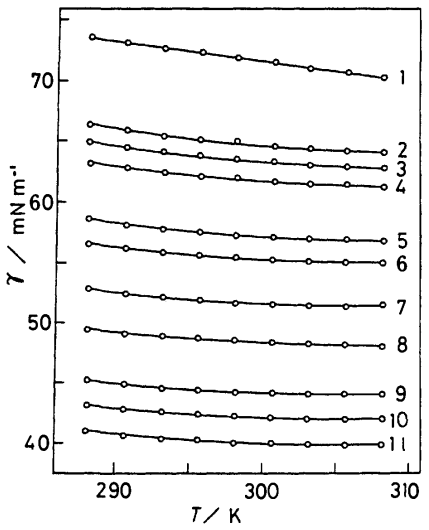

Fig. 3a. Surface tension vs. temperature curves of DDAC at constant concentration under atmospheric pressure: (1) m_1=0 mmol kg^{-1}; (2) 2.21; (3) 2.59; (4) 2.93; (5) 4.44; (6) 5.34; (7) 6.90; (8) 8.61; (9) 11.25; (10) 12.98; (11) 15.59.

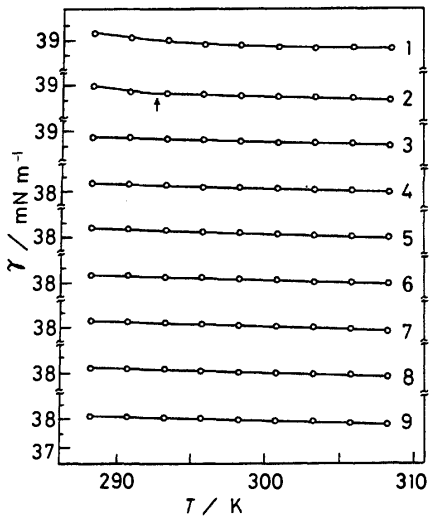

Fig. 3b. Surface tension vs. temperature curves of DDAC at constant concentration under atmospheric pressure: (1) m_1=16.17 mmol kg^{-1}; (2) 16.76; (3) 17.36; (4) 17.66; (5) 18.43; (6) 22.65; (7) 25.22; (8) 27.95; (9) 38.98.

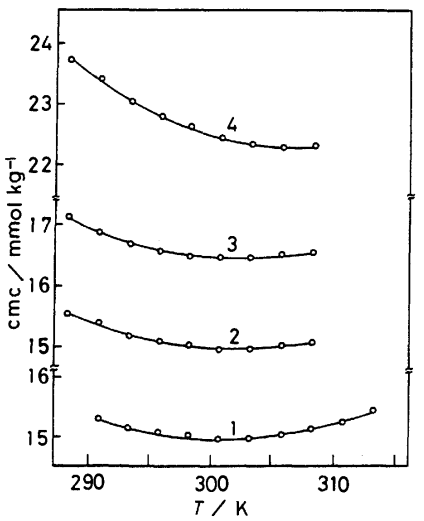

Fig. 4. Critical micelle concentration vs. temperature curves under atmospheric pressure: (1) DAC; (2) DMAC; (3) DDAC; (4) DTAC.

γ^{cmc} values and the differences in the cmc and the γ^{cmc} values seem to be remarkable between dodecyldimethylammonium chloride and dodecyltrimethylammonium chloride. Such a behavior was also observed in the case of the electric conductivity measurements of the surfactants.[6]

It has been shown that the derivative of surface tension with respect to temperature is the one of the useful quantities to elucidate the adsorption from the micellar solution.[1,2,5,7-9] The $-\partial\gamma/\partial T$ values obtained from Figs. 1 and 3 are shown as functions of molality at constant temperature in Fig. 6. At concentrations below the cmc, they decrease with increasing concentration and raising temperature. At concentrations above the cmc, however, they seem to be almost constant. It should be noted that the $-\partial\gamma/\partial T$ vs. m_1 curves change discontinuously at the cmc.

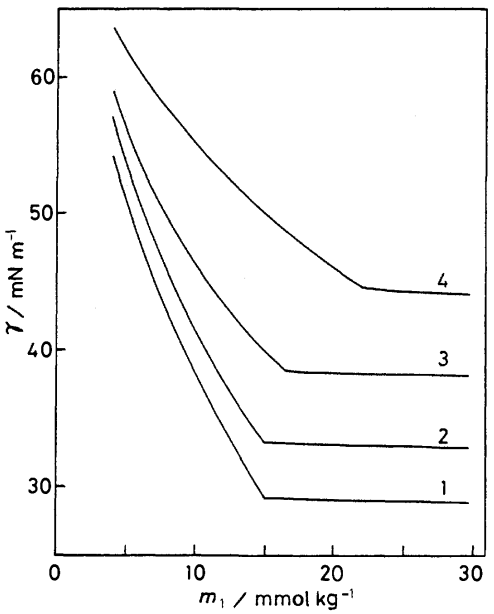

Fig. 5. Surface tension vs. concentration curves at 298.15 K under atmospheric pressure: (1) DAC; (2) DMAC; (3) DDAC; (4) DTAC.

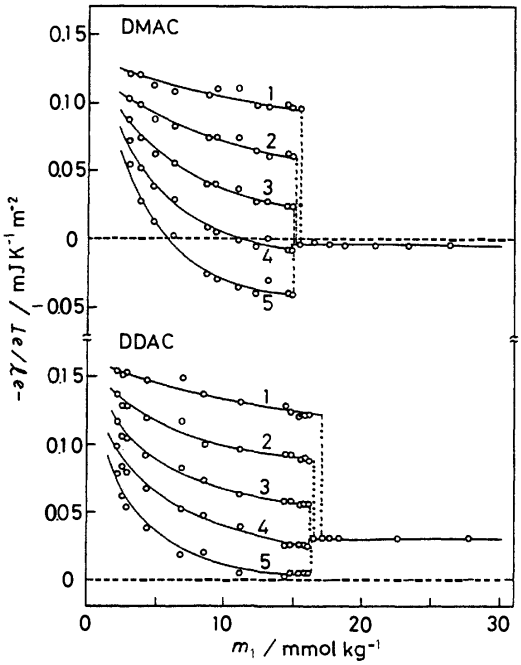

Fig. 6. Derivative of surface tension with respect to temperature vs. concentration curves at constant temperature under atmospheric pressure: (1) T=288.15 K; (2) 293.15; (3) 298.15; (4) 303.15; (5) 308.15.

Now we proceed to analyze the above results with the aid of the thermodynamics of the adsorption of surfactant from its micellar solution.[1] The adsorbed film is described by the excess thermodynamic quantities with reference to the two dividing plane surfaces

which make the excess numbers of moles of water and air zero. Defining as the thermodynamic quantities of the micelle particle the excess ones with reference to the dividing spherical surface which makes the excess number of moles of water zero, the micelle formation has been shown to be satisfactorily treated as if a new macroscopic phase appears in the solution. At a concentration below the cmc, the entropy change associated with the adsorption of surfactant from the monomeric state in the aqueous solution $\Delta s(1)$ defined by

$$\Delta s(1)=\Gamma_1^{\mathrm{H}}(s^{\mathrm{H}}/\Gamma_1^{\mathrm{H}}-s_1) \tag{1}$$

is evaluated by the derivative of surface tension with respect to temperature;

$$\Delta s(1)=-(\partial\gamma/\partial T)_{p,m_1},\ m_1<\mathrm{cmc}. \tag{2}$$

Here Γ_1^{H} and s^{H} are respectively the surface excess number of moles of surfactant and surface excess entropy per unit area and s_1 is the partial molar entropy of monomeric surfactant in the aqueous solution. At a concentration above the cmc, the entropy change associated with the adsorption of surfactant from the micellar state $\Delta s(\mathrm{M})$ defined by

$$\Delta s(\mathrm{M})=\Gamma_1^{\mathrm{H}}(s^{\mathrm{H}}/\Gamma_1^{\mathrm{H}}-s^{\mathrm{M}}/N_1^{\mathrm{M}}) \tag{3}$$

is evaluated by

$$\Delta s(\mathrm{M})=-(\partial\gamma/\partial T)_{p,m_1},\ m_1\geqq\mathrm{cmc}, \tag{4}$$

where N_1^{M} and s^{M} are the excess number of surfactant ions in the micelle and the excess molar entropy of micelle, respectively.

Bearing Eqs. 2 and 4 in mind and looking at the $-\partial\gamma/\partial T$ vs. m_1 curve in Fig. 6, we may say that the entropy change associated with the adsorption of surfactant from the monomeric state in the aqueous solution is strongly dependent on temperature and concentration, while the corresponding quantity from the micellar state is practically independent of both of them. Similar results have been obtained for the adsorption of DAC and DTAC.[1,2] It turns out, therefore, that the dependence of the entropy of surfactant on temperature and concentration in the adsorbed film is analogous to that in the micelle though different from that in the aqueous solution.

It is worth noting that the $\Delta s(\mathrm{M})$ value of DMAC is approximately zero and that of DDAC is obviously positive. Let us consider this point in further detail. Since the surface density of surfactant Γ_1^{H} usually is a large value at a concentration near the cmc, Eqs. 1 and 3 can be approximated respectively as

$$\Delta s(1)/\Gamma_1^{\mathrm{H}}=\bar{s}_1^{\mathrm{H}}-s_1 \tag{5}$$

and

$$\Delta s(\mathrm{M})/\Gamma_1^{\mathrm{H}}=\bar{s}_1^{\mathrm{H}}-\bar{s}_1^{\mathrm{M}}, \tag{6}$$

where $\bar{s}_1^{\mathrm{H}}$ and $\bar{s}_1^{\mathrm{M}}$ are the mean partial molar entropy of surfactant in the adsorbed film and the micelle, respectively.[8] Using the Γ_1^{H} vs. m_1 curve obtained by applying

$$\Gamma_1^{\mathrm{H}}=-(m_1/2RT)(\partial\gamma/\partial m_1)_{T,p} \tag{7}$$

to the γ vs. m_1 curve (Fig. 7), we can calculate the left hand sides of Eqs. 5 and 6. The resulting values are given as a function of molality at 298.15 K with those of DAC and DTAC in Fig. 8. It can be seen that the $\Delta s(\mathrm{M})/\Gamma_1^{\mathrm{H}}$ value varies regularly from a negative one for DAC to a positive one for DTAC with the *N*-methylation of dodecylammonium chloride. Therefore we may say that the *N*-methylation has a different effect on the entropy of surfactant in the adsorbed film from that in the micelle. This view is supported by the fact that the aggregation number of the DAC micelle is

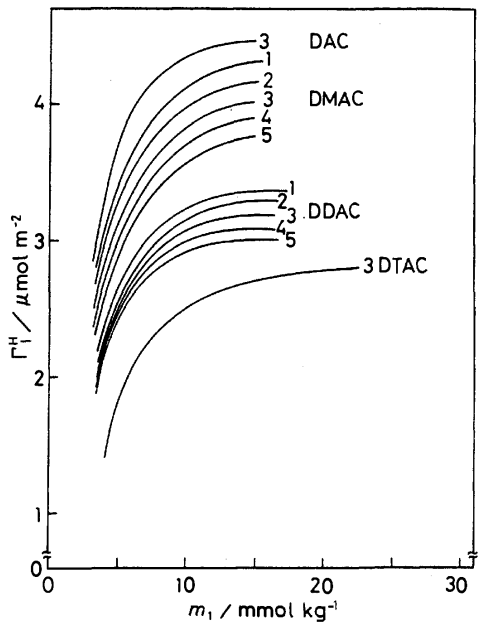

Fig. 7. Surface excess number of moles vs. concentration curves at constant temperature under atmospheric pressure: (1) T=288.15 K; (2) 293.15; (3) 298.15; (4) 303.15; (5) 308.15.

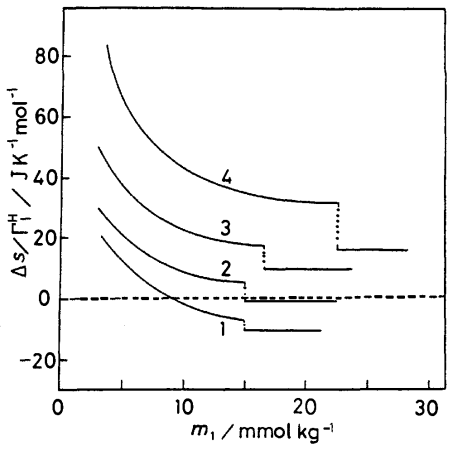

Fig. 8. Entropy change associated with the adsorption per mole of surfactant vs. concentration curves at 298.15 K under atmospheric pressure: (1) DAC; (2) DMAC; (3) DDAC; (4) DTAC.

more than 2 times that of the DTAC micelle at 298.15 K.[10] Figure 8 also shows that the $\Delta s(1)/\Gamma_1^H$ value of surfactants regularly varies with the *N*-methylation of the head group. Comparing with Fig. 7, it is understandable that the variation of $\Delta s(1)/\Gamma_1^H$ is primarily correlated to that of the saturated value of Γ_1^H and accordingly to the geometry of the head group.

Let us now consider the abrupt change of the temperature derivative of surface tension seen in Fig. 6. If the micelle formation can be treated like an appearance of a new phase in the aqueous solution, we have

$$[\Delta s(1)-\Delta s(M)]/\Gamma_1^H=-(2RT/\text{cmc})(\partial \text{cmc}/\partial T)_p. \quad (8)$$

In Fig. 9, the value of the left hand side, which was evaluated by using the $-\partial\gamma/\partial T$ vs. m_1 curve given in Fig. 6 and the Γ_1^H vs. m_1 curve given in Fig. 7, is plotted against temperature by the circle and, on the other hand, the value of the right hand side, which was evaluated from the slope of the cmc vs. T curve given in Fig. 4, is drawn by the full line. It is seen that the values of both sides are in fair agreement with each other within the experimental error. This finding justifies the validity of our thermodynamic treatment of the micelle formation.

Taking into account Eqs. 5 and 6, we have the relation

$$[\Delta s(1)-\Delta s(M)]/\Gamma_1^H=\bar{s}_1^M-s_1, \quad (9)$$

the right hand side being regarded as the entropy of micelle formation $\Delta_W^M s$. It is seen from Fig. 9 that the value $\Delta_W^M s$ decreases with increasing temperature and becomes negative. Noting that the value of $\Delta_W^H s$ defined by

$$\Delta_W^H s=\bar{s}_1^H-s_1 \quad (10)$$

also decreases with increasing temperature, we may say that the s_1 value increases remarkably with increasing temperature. Further it is seen that the difference in $\Delta_W^M s$ between DAC and DTAC is about 10 $J\,K^{-1}\,mol^{-1}$ while that in $\Delta_W^H s$ is about 40 $J\,K^{-1}\,mol^{-1}$ at 298.15 K. This observation supports the view that the adsorbed film at a plane interface is influenced more significantly by the *N*-methylation of DAC than the spherical micelle.

It is now useful to examine the adsorption of the surfactants from their micellar solutions from the viewpoint of energy. The energy changes associated with adsorption from the monomeric state in the aqueous solution $\Delta u(1)$ and from the micellar state $\Delta u(M)$ are evaluated by

$$\Delta u(1)=\gamma+T\Delta s(1)-p\Delta v(1) \quad (11)$$

and

$$\Delta u(M)=\gamma+T\Delta s(M)-p\Delta v(M), \quad (12)$$

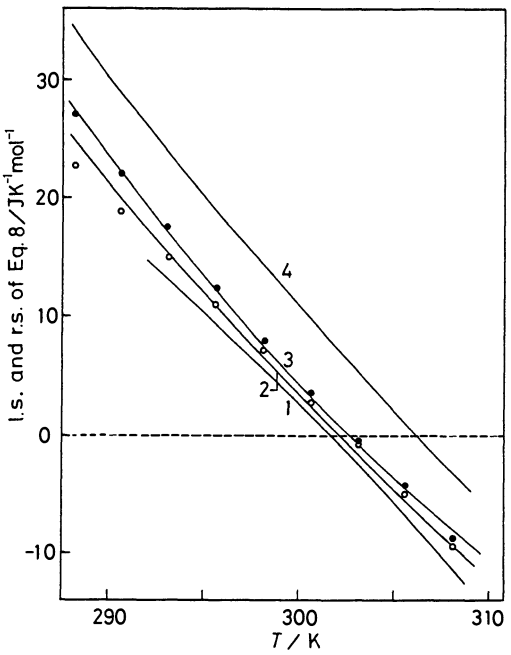

Fig. 9. Comparison between the left and the right side of Eq. 8: (○,●) left side; (——) right side; (1) DAC; (2) DMAC; (3) DDAC; (4) DTAC.

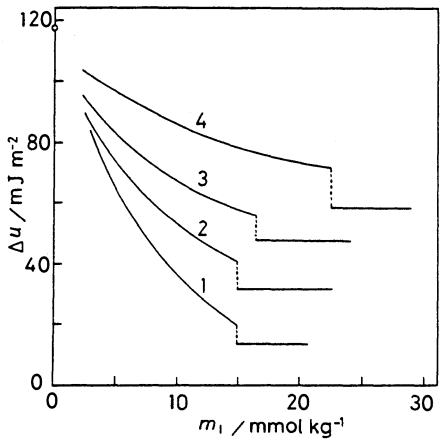

Fig. 10. Energy change associated with the adsorption vs. concentration curves at 298.15 K under atmospheric pressure: (1) DAC; (2) DMAC; (3) DDAC; (4) DTAC.

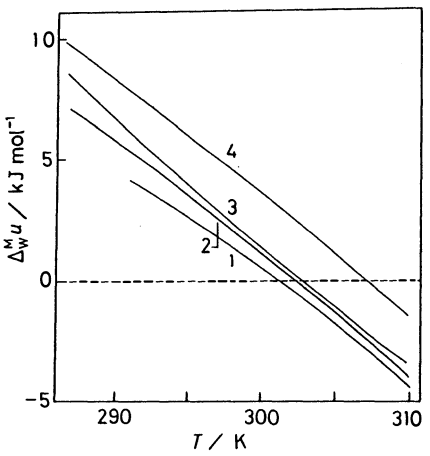

Fig. 11. Energy change of micelle formation vs. temperature curves under atmospheric pressure: (1) DAC; (2) DMAC; (3) DDAC; (4) DTAC.

respectively. Here $\Delta v(1)$ and $\Delta v(M)$ are the corresponding volume changes; the $p\Delta v$ terms are negligibly small compared with the others under atmospheric pressure.[11] The $\Delta u(1)$ and $\Delta u(M)$ values evaluated are shown as functions of concentration at 298.15 K under atmospheric pressure in Fig. 10. The curve appears to behave similarly to the Δs vs. m_1 curve; the *N*-methylation of dodecylammonium chloride regularly increases the values of $\Delta u(1)$ and $\Delta u(M)$. This behavior may be explicable by the increase in the hydrophilicity of the head group of surfactant by its successive *N*-methylation. On the other hand, energy of micelle formation $\Delta_W^M u$ defined by

$$\Delta_W^M u = \bar{u}_1^M - u_1, \tag{13}$$

where $\bar{u}_1^M$ and u_1 are respectively the mean partial molar energy in the micelle and the partial molar energy in the aqueous solution, is evaluated by use of the equation

$$\Delta_W^M u = [\Delta u(1) - \Delta u(M)]/\Gamma_1^H. \tag{14}$$

Its value is depicted in the form of $\Delta_W^M u$ vs. T plot in Fig. 11, which bears a striking resemblance to Fig. 9. Therefore we can say that the u_1 value increases remarkably with increasing temperature. In conclusion, it is possible to say that the successive *N*-methylation of DAC exercises considerable effect on the adsorbed film with changes in its surface density, entropy, and energy brought about by changes in the geometry and the hydrophilicity of the polar head group.

References

1) K. Motomura, S. Iwanaga, M. Yamanaka, M. Aratono, and R. Matuura, *J. Colloid Interface Sci.*, **86**, 151 (1982).
2) M. Aratono, T. Okamoto, and K. Motomura, *Bull. Chem. Soc. Jpn.*, **60**, 2361 (1987).
3) P. L. DuBrow and H. J. Harwood, *J. Org. Chem.*, **17**, 1043 (1952).
4) H. T. Clarke, H. B. Gillespie, and S. Z. Weisshause, *J. Am. Chem. Soc.*, **55**, 4571 (1933).
5) K. Motomura, S. Iwanaga, Y. Hayami, S. Uryu, and R. Matuura, *J. Colloid Interface Sci.*, **80**, 232 (1981).
6) A. W. Ralston, F. K. Broome, and H. J. Harwood, *J. Am. Chem. Soc.*, **69**, 671 (1949).
7) M. Yamanaka, M. Aratono, H. Iyota, K. Motomura, and R. Matuura, *Bull. Chem. Soc. Jpn.*, **55**, 2744 (1982).
8) M. Yamanaka, H. Iyota, M. Aratono, K. Motomura, and R. Matuura, *J. Colloid Interface Sci.*, **94**, 451 (1983).
9) K. Motomura, S. Iwanaga, S. Uryu, H. Matsukiyo, M. Yamanaka, and R. Matuura, *Colloids Surf.*, **9**, 19 (1984).
10) A. Malliaris, J. L. Moibne, J. Sturm, and R. Zana, *J. Phys. Chem.*, **89**, 2709 (1985).
11) M. Aratono, M. Yamanaka, N. Matubayasi, K. Motomura, and R. Matuura, *J. Colloid Interface Sci.*, **74**, 489 (1980).

 © 1988 The Chemical Society of Japan Bull. Chem. Soc. Jpn., 61, 2779—2783 (1988)

The Determination of a Small Amount of Biological Constituent by the Use of Chemiluminescence. XIII. High Sensitive Metal Chelate Affinity Chromatography

Tadashi HARA,* Kazuhiko TSUKAGOSHI, and Tatsunari YOSHIDA
Department of Chemical Engineering, Faculty of Engineering, Doshisha University, Karasuma Imadegawa, Kamigyo-ku, Kyoto 602
(Received September 10, 1987)

A chemiluminescence detector using a 1,10-phenanthroline-hydrogen peroxide-copper(II) system was successfully combined with a metal chelate affinity column. A mixture comprising bovine serum albumin, lysozyme, and bovine serum γ-globulin as model proteins was completely separated by the pH-gradient elution method on a TSK gel Chelate-5PW adsorbed with zinc ions, also, each protein could be quantitatively determined. According to the present method, using a 0.4 cm^3 column of bed volume, 1) the determinable concentration range for bovine serum γ-globulin was formed to be 1.0×10^{-4}—1.0×10^{-1} g dm^{-3} with a detection limit of 5 ng for a 50 mm^3 of injection volume, 2) the recovery of 1.0×10^{-3} g dm^{-3} bovine serum γ-globulin was 85% with 7.9% of the coefficient of variation (n=5), and 3) the time necessary for an analysis was about 50 min. The present method was about 200 times more sensitive than that using an ultraviolet detector and was also applicable to a human serumn sample.

In order to separate and determine each small amount of protein in the mixture by high-performance liquid chromatography (HPLC), highly sensitive HPLC was attempted using a chemiluminescence (CL) detector. In the present study, metal chelate affinity chromatography (MCAC) was used since the authors were interested in the affinity between metal ions and proteins;[1] MCAC using the affinity is a relatively new method for the separation of a mixture of various proteins.

The concept of metal chelate affinity chromatography was first described by Porath and co-worker.[2] Its sensitivity when using a conventional ultraviolet (UV) detector was still unsatisfactory for the determination of a small amount of biological constituent.

In order to improve the sensitivity of MCAC, an attempt to combine it with CL detection using a 1,10-phenanthroline (phen)-hydrogen peroxide (H_2O_2)-copper(II) (Cu(II)) catalyst system was carried out in the present study. The determination of a protein is based on a measurement of the decreasing catalytic activity of Cu(II) for a CL reaction in the presence of the protein.[3] In this case, the stable Cu(II)-protein complex formed as a result of heating caused a lowering of the free Cu(II) concentration.[1] Chemiluminescence detection, developed by the authors, is characterized by the following: 1) high sensitivity, 2) application to HPLC (including the determination of a small amount of protein without labeling), 3) a wide dynamic range, and 4) a relatively simple apparatus.[1,3,4]

By using a CL detector, which was developed by the authors for the determination of various proteins, they could be determined over a concentration range 5.0×10^{-6}—1.0×10^{-1} g dm^{-3}, with a detection limit of 250 pg (for a 50 mm^3 of injection volume).[3] Though the CL detector was shown by the authors to be applicable to immunoaffinity chromatography in which a specific single protein in a serum could be analyzed by an immune reaction,[4] no investigation has been made with regard to the applicability of the CL detector to the determination of a small amount of protein separated by HPLC.

The CL detector was shown to be highly sensitive and its response was influenced by the pH, salt content, solvent, flow-rate, and temperature.[3] Therefore, suitable conditions for elution using the CL detector were investigated, and the experimental conditions necessary for the acquisition of a well-defined chromatogram were optimized. A metal chelate affinity column was successfully connected to the CL detector (developed by the authors), and a mixed sample containing bovine serum albumin, lysozyme, and bovine serum γ-globulin as a model proteins was subjected to pH-gradient elution, followed by CL detection. The sensitivity of the present method was about 200 times as high as that of the conventional UV method.

Experimental

Reagents. All of the reagents used were of a commercially available special grade. Deionized water was distilled for use. A phen solution, a H_2O_2 solution, and a Cu(II) catalyst solution were prepared as described in a previous paper,[2] except for the use of a borate buffer of pH 12.19 for the preparation of a Cu(II) catalyst solution. The borate buffer solution (Buff-A; pH 8.04) contained 5.0×10^{-3} mol dm^{-3} boric acid (H_3BO_3), 5.0×10^{-4} mol dm^{-3} potassium hydroxide (KOH), and 2.0×10^{-1} mol dm^{-3} sodium chloride (NaCl). The borate buffer solution (Buff-B; pH 12.19) used for the preparation of a Cu(II) catalyst solution contained 2.0×10^{-1} mol dm^{-3} H_3BO_3 and 2.0×10^{-1} mol dm^{-3} KOH. An acetic acid solution for pH-gradient elution was prepared by dissolving 2.5×10^{-2} mol acetic acid in 1 dm^3 Buff-A. The sample solution of bovine serum albumin (BSA) (Sigma Chemical Co.), human serum albumin (HSA) (Sigma Chemical Co.), bovine serum α-globulin (BαG) (Sigma Chemical Co.), bovine serum γ-globulin (BγG) (Sigma Chemical Co.), lysozyme (from chicken egg white) (Sigma Chemical Co.), α_2-macroglobulin (from human) (Sigma Chemical Co.),

apoferritin (from human) (ICN Pharmaceuticals, Inc.), α-fetoprotein (AFP) (Midorijuji Co.), and control serum (Q-PAC-Chemistry Control Serum I) (HYLAND) were prepared by dissolving them in Buff-A and by diluting them with Buff-A.

Preparation of an MCAC Column. The following columns were used for MCAC: TSK gel Chelate-5PW (7.5 mm i.d.×75 mm) (Toyo Soda, Tokyo), and HR-5/5 (5 mm i.d.×50 mm) (Pharmacia) charged with Chelating Sepharose 6B (Pharmacia). Their bed volumes were 3.3 cm^3, 0.4 cm^3, in the above-mentioned order. All of the charged gel, which has an iminodiacetic acid group at the end of a spacer, showed a chelate-forming ability against such metal ions as Cu(II), zinc(II) (Zn(II)), and cobalt(II); each 1 cm^3 of the charged gel was capable of adsorbing at least a 20 μmol of the metal ion.

Zinc(II) was selected as an added metal ion in the present study because Zn(II) could not be detected in an eluate using a CL detector and several proteins were selectively adsorbed and eluted on the Zn(II) containing gel.

An MCAC column was prepared as follows: A definite volume of 0.03 mol dm^{-3} Zn(II) solution (pH 4), prepared by dissolving zinc chloride in a dilute acetic acid solution, was delivered into a column through a sampling loop. In practice, the column was loaded with Zn(II) calculated on the basis of its adsorbing capacity, only to 67% of its length in order to avoid any contamination of the eluate with Zn(II). Thereafter, the column was preconditioned by feeding Buff-A (equivalent to 15 times of a bed volume) at a flow rate of 1.0 cm^3 min^{-1}. All of the fundamental experiments for the elution of proteins from a column were carried out using a Zn(II) loaded TSK gel Chelate-5PW; HR-5/5 was in order to improve of the sensitivity, based upon a reduction of the bed volume.

Apparatus and Procedure. The MCAC method was carried out using the HPLC system (Fig. 1) equipped with a CL detector and an apparatus for the pH-gradient. The CL detector used was the same one as described in previous papers.[3,4] A 50 mm^3 portion of a protein sample solution was injected into the eluent solution line, that is, an MCAC column (j) through the sampling loop (i) and the six-way cock (g). Then, the protein was adsorbed on an MCAC column.

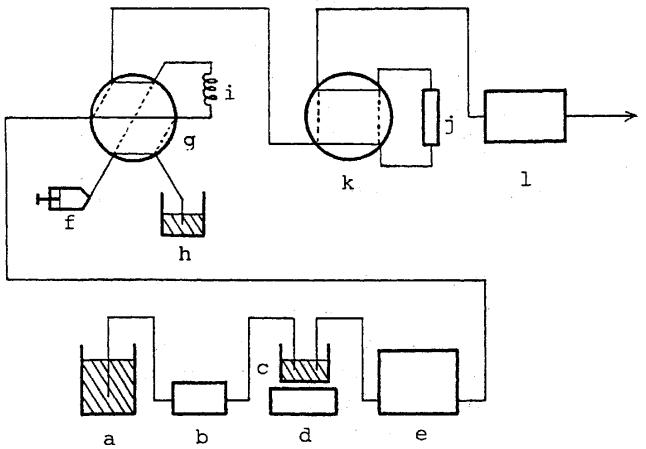

Fig. 1. Schematic diagram of the HPLC-CL system. a: Acetic acid solution, b: peristaltic pump, c: gradient-mixer, d: magnetic stirrer, e: constant flow pump, f: syringe, g: six-way cock, h : sample solution, i: sampling loop, j: MCAC column, k: four-way cock, and l: CL detector.

The pH-gradient elution was carried out as follows: The sample adsorbed on the MCAC column was eluted by a pH-gradient elution method. An acetic acid solution (a) for pH-gradient elution was fed into a gradient-mixer (c), which was charged with 50 cm^3 Buff-A at a flow rate of 0.5 cm^3 min^{-1} using a peristaltic pump (b). The solution in a gradient-mixer was well-stirred by a magnetic stirrer (d) and was fed into the MCAC column at a flow rate of 1.0 cm^3 min^{-1} using a constant flow pump (e). The protein eluted from the MCAC column was detected by a CL detector (l) as described in previous papers.[3,4]

The FIA method using direct-injection was carried out by injecting a sample solution (h) into the eluent line and by operating a four-way cock (k) and a six-way cock (g) equipped with a sampling loop (i).

Results and Discussion

Connection of the CL Detector with an MCAC Column. In a previous paper,[3] the optimum pH value of the solution during the CL reaction of a phen-H_2O_2-Cu(II) system was reported to be about 10.2 for the determination of a protein. Since the adsorption of a protein onto an MCAC column and the elution of a protein from it were usually carried out in the pH range of 8.0—4.0,[2,5-7] the pH value and buffer capacity of the solution during the CL reaction had to be adjusted to about pH 10.2 with a Cu(II) catalyst solution. Judging from the experimental result, this was accomplished by an adding a Cu(II) solution containing a borate buffer solution of pH 12.19 (Buff-B). A phen solution and a H_2O_2 solution were prepared as described in a previous paper.[2] Under these conditions, calibration curves for BSA, lysozyme, and BγG were obtained by an FIA method (Fig. 2). These proteins in a concentration range of 2.0×10^{-5}—1.0×10^{-1} g dm^{-3} could be determined by injecting each 50-mm^3 sample into an FIA system, with a detection limit of 1 ng (S/N=2) and a coefficient of variation (CV) of 5.9% (n=6) at 1.0×10^{-3} g dm^{-3} protein. Hereafter, the detection limit is based on S/N=2.

The different calibration curves of BSA, lysozyme, and BγG seemed to be due to differences between in their molecular structures. Relatively linear calibration curves were obtained in a previous study,[3] while the calibration curves shown in Fig. 2 are sigmoid. Since the concentration of NaCl was different in the experiment for the preparation of both calibration curves, the effect of NaCl on the form of the calibration curve was examined and a linear calibration curve was found to assume a sigmoid form with an increasing amount of NaCl. Though there might be some other causes for the sigmoid form, a calibration curve for protein by CL detection was mostly obtained as a sigmoid form.[8-10]

pH-Gradient. A protein adsorbed on an MCAC column can be eluted by such methods as 1) lowering

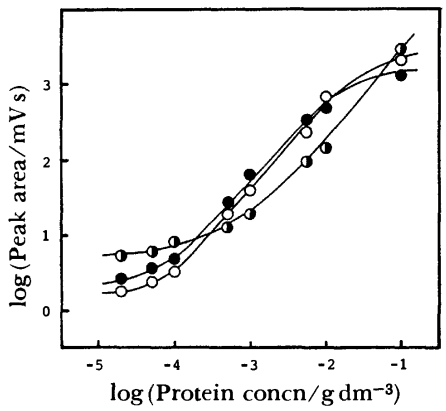

Fig. 2. Calibration curves for proteins by FIA. ○: BSA, ●: BγG, and ◑: lysozyme.

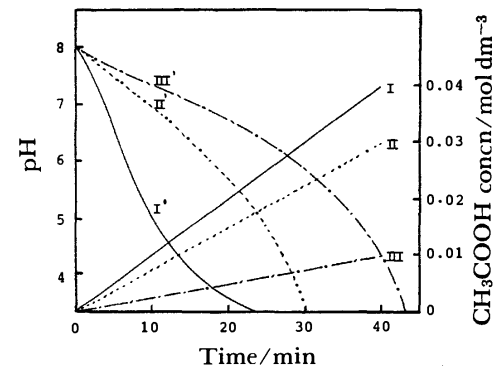

Fig. 3. Relationship among pH, time, and concentration of an acetic acid. Line-I, -II, and -III: relationship between C_A and t and curve-I′, -II′, and -III′: relationship between pH and t.

of the pH, 2) adding a competitor,[7] and 3) adding ethylenediaminetetraacetic acid. Among these methods, methods 2) and 3) were unsuitalbe for the present purpose because they did not give smooth base-lines on the CL detector, whereas method 1) was shown to be useful. Since any protein adsorbed on a Zn(II) column was eluted at an individual pH-band and all the proteins used in this study were completely eluted near pH 4, a pH-gradient method in which the pH of the eluent changed continuously from 8.0 to 4.0 was proposed. During the course of an investigation regarding the preparation of the pH-gradient, it was found that 1) the base-line of the CL detector was most stable as a result of adding a definite concentration of acetic acid to Buff-A and by lowering the pH of the eluent, and 2) that the stability of the CL detector was further improved by adding salt (NaCl) to Buff-A. The pH-gradient of the eluent was prepared by using the gradient apparatus based on principle of a single stage of a continuously stirred tank reactor; the optimum conditions could be obtained. The pH change of the eluate from the Zn(II) column against a linear increase in the concentration of acetic acid (C_A) in the eluent is shown in Fig. 3. Line-I,-II, and -III show the relationship between C_A and the feed time (t), while curve-I′, -II′, and -III′ show the relationship between pH and t. Line-III and curveIII′ were best for the separation of proteins since the base-line stability of the CL detector was excellent and an approximately linear pH-gradient could be applied.

Effect of NaCl. A definite amount of salt was usually added to the eluent in MCAC in order to avoid any undesirable ion exchange and any association between proteins. According to the preliminary experiment, the retention time of BSA, lysozyme, and BγG varied according to the concentration of NaCl. However, the sensitivity of the CL detector became lower upon increasing the amount of NaCl. Therefore, their relations were examined in detail. So far, it has been experimentally accepted that the base-line separation of a binary mixture is feasible if the peak resolution

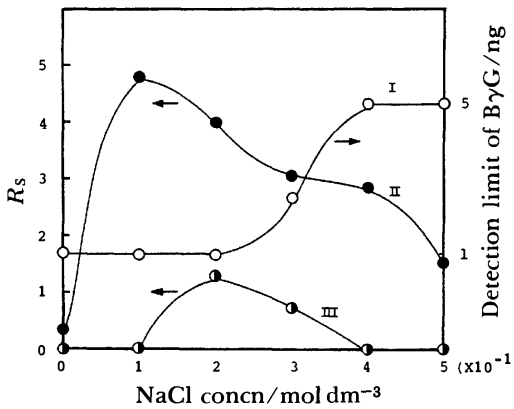

Fig. 4. Effect of NaCl on detection limit and R_S. ○: detection limit of BγG, ●: R_S between BSA and BγG, and ◑: R_S between BSA and lysozyme.

(R_S) exceeds 1.25 in a chromatogram.

The effect of the NaCl concentration on the detection limit of BγG and on the R_S between BSA and BγG as well as between BSA and lysozyme are shown in Fig. 4. As can be seen from curve-I in Fig. 4, the detection limit of BγG increases with increasing the concentration of NaCl. From curve-II in Fig. 4, BSA and BγG could also be completely separated when the eluent contained more NaCl than 0.1 mol dm^{-3} (R_S exceeded 1.25). From curve-III in Fig. 4, BSA and lysozyme could also be separated when the eluent contained 0.2 mol dm^{-3} NaCl (where R_S exceeded 1.25). On the basis of these results, an eluent containing 0.2 mol dm^{-3} NaCl was shown to be most suitable for a sensitive detection of BSA, lysozyme, and BγG as well as for the base-line separation of a BSA and BγG mixture or a BSA and lysozyme mixture. Therefore, an eluent containing 0.2 mol dm^{-3} NaCl was used for the separation of BSA, lysozyme, and BγG in the present experiment. Though the retention times of these proteins varied according to the concentration of NaCl in the eluent, the reason for such a phenomenon still remains unsolved.

Affinity against a Zn(II) Column. The affinity of various proteins against a Zn(II) column was examined under the above-mentioned conditions and the results are shown in Table 1. Judging from the retention time, 1) both BSA and HSA showed no affinity, 2) lysozyme showed moderate affinity, and 3) BαG, BγG, α_2-macroglobulin, and HγG showed strong affinity. α-Fetoprotein, a cancer marker, also showed no affinity.

Separation and Determination of Proteins by MCAC. As can be seen from the above results, BSA, lysozyme, and BγG, all the retention times that were mutually different, were selected as model proteins. The separation of a mixture consisting of the above-mentioned three proteins and the determination of individual proteins were carried out by MCAC. A protein mixture (50 mm^3) dissolved in Buff-A was injected onto a Zn(II) column, and pH-gradient elution was started 7 min after the injection of a sample solution. A chromatogram is shown in Fig. 5. As can be seen from Fig. 5, BSA, lysozyme, and BγG could be almost completely separated. Calibration curves of BSA, lysozyme, and BγG were obtained by MCAC using a Zn(II) column (Fig. 6). Both BSA and BγG in 50 mm^3 were determinable in the concentration range of 5.0×10^{-4}—1.0×10^{-1} g dm^{-3}, with a detection limit of each 25 ng. Lysozyme was also determinable in a concentration range of 8.0×10^{-4}—1.0×10^{-1} g dm^{-3}, with detection limit of 40 ng. Bovine serum γ-globulin of 1.0×10^{-3} g dm^{-3} was determined with an average recovery of 78% and a CV of 10.9% (n=6). The time necessary for an analysis was about 150 min. The detection limit of FIA method was 2.0×10^{-5} g dm^{-3} (1 ng) BγG but that of the MCAC method was 5.0×10^{-4} g dm^{-3} (25 ng) BγG. These differences seem to be due to the fact that the MCAC method is accompanied by an the extreme band broadening during separation, while the FIA method is not. The poor results in the above-mentioned average recovery and CV could be explained on the basis of the extreme band broadening. It was, therefore, concluded that the bed volume of a TSK gel Chelate-5PW was too large for the successful analysis of a low concentration of protein mixture using a CL detector.

Reduction of Bed Volume. In order to improve the detectability of a CL detector by reducing bed volume of a Zn(II) column, HR-5/5 having a bed volume 0.4 cm^3 was prepared and applied to a mixture of BSA, lysozyme, and BγG. Each calibration curve was obtained and is shown in Fig. 7. Both BSA and BγG

Table 1. Affinity Against a Zn(II) Column

Protein	Sample load/ng	Retention time/s
BSA	50	210
HSA	50	227
Apoferritin	50	227
AFP	38.8	287
Lysozyme	50	563
BαG	50	1487
BγG	50	1496
α_2-Macroglobulin	50	1559
HγG	50	1498

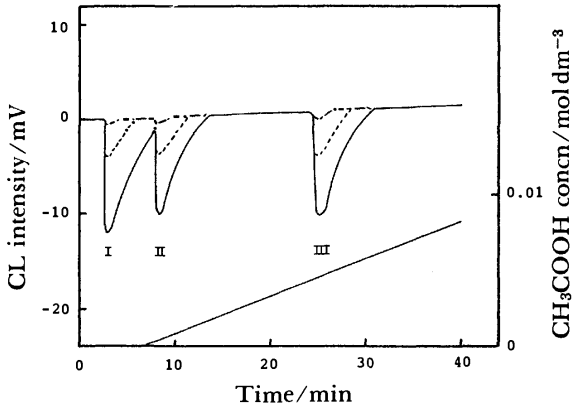

Fig. 5. A chromatogram of a BSA, lysozyme, and BγG mixture. I: BSA, II: lysozyme, and III: BγG, solid line: 1.0×10^{-1} g dm^{-3}, dotted line: 1.0×10^{-2} g dm^{-3}, broken line: 1.0×10^{-3} g dm^{-3}, and straight line: acetic acid concentration.

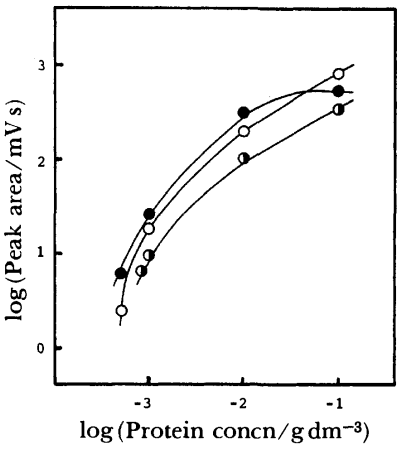

Fig. 6. Calibration curves for BSA, lysozyme, and BγG by MCAC. ○: BSA, ●: BγG, and ◑: lysozyme.

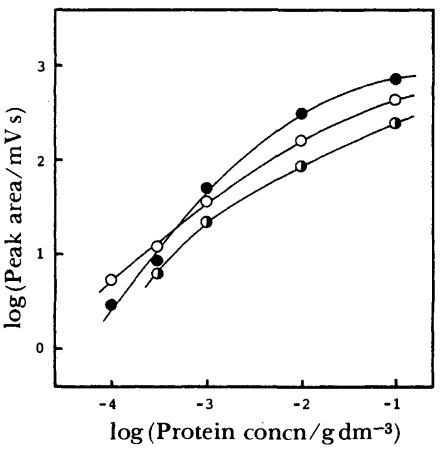

Fig. 7. Calibration curves for proteins by MCAC using a HR-5/5. ○: BSA, ●: BγG, and ◑: lysozyme.

in a 50 mm^3 sample solution were determinable in a concentration range of 1.0×10^{-4}—1.0×10^{-1} g dm^{-3}, with a detection limit of 5 ng each. Lysozyme was also determinable in the concentration range 3.0×10^{-4}—1.0×10^{-1} g dm^{-3}, with a detection limit of 15 ng. Bovine serum γ-globulin in a concentration of 1.0×10^{-3} g dm^{-3} could be determined with an average recovery of 85%, and a CV of 7.8% (n=5). The detection limit of BγG against HR-5/5 (0.4 cm^3 bed volume) was 5 ng whereas that of a TSK gel Chelate-5PW (3.3 cm^3 bed volume) was 25 ng under the same conditions. The time necessary for an analysis was about 60 min. Moreover, HR-5/5 could be confirmed from Fig. 7 to be satisfactorily usable for analyzing of a mixture consisting of a low concentration of proteins.

The lowest detectable concentration of BγG using a UV detector and a CL detector were compared under the same conditions using a TSK gel Chelate-5PW: 1.0×10^{-1} g dm^{-3} BγG for a UV detector, and 5.0×10^{-4} g dm^{-3} BγG for a CL detector. The sensitivity of a CL detector was about 200 times as high as that of a UV detector.

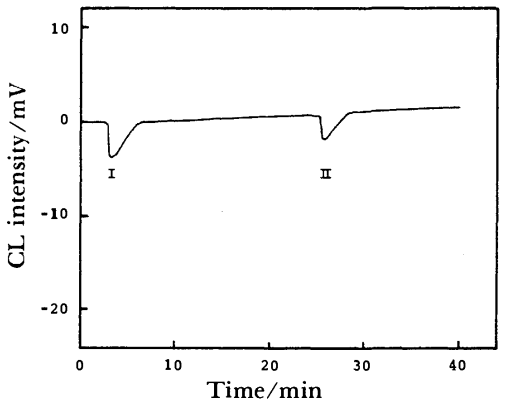

Fig. 8. A chromatogram of human serum. I: HSA and II: human serum globulins.

Finally, a control serum was diluted 5000 times with Buff-A and an aliquot (50 mm^3) was analyzed by the present method using a TSK gel Chelate-5PW (Fig. 8). As shown in the figure, there are two peaks: peak I corresponds to HSA and peak II to human serum globulins.

It has been concluded from the results that by the use of a CL detector and an MCAC column having a small bed volume, sensitive MCAC suitable for the separation and determination of low concentrations of proteins could be established. The present study suggests the possibility of combining a CL detector with a wide range of columns, including an MCAC column.

The authors wish to thank Tsutomu Hashimoto for providing TSK gel Chelate-5PW for the present study.

References

1) T. Hara, K. Tukagoshi, A. Arai, and T. Iharada, *Bull. Chem. Soc. Jpn.*, **59**, 3681 (1986).
2) J. Porath, J. Carlsson, I. Olsson, and G. Belfrage, *Nature (London)*, **258**, 598 (1975).
3) T. Hara, T. Ebuchi, A. Arai, and M. Imaki, *Bull. Chem. Soc. Jpn.*, **59**, 1833 (1986).
4) T. Hara, K. Tsukagoshi, A. Arai, and T. Iharada, *Bull. Chem. Soc. Jpn.*, **61**, 301 (1987).
5) E. S. Hemdm and J. Porath, *J. Chromatogr.*, **323**, 274 (1985).
6) E. S. Hemdm and J. Porath, *J. Chromatogr.*, **323**, 255 (1985).
7) Y. Koto, K. Nakamura, and T. Hashimoto, *J. Chromatogr.*, **324**, 511 (1986).
8) Y. Ikariyama and S. Suzuki, *Anal. Chem.*, **54**, 1126 (1982).
9) A. Patel, C. J. Devies, A. K. Campbell, and F. McCapra, *Anal. Biochem.*, **129**, 162 (1983).
10) T. Hara, M. Toriyama, and K. Tukagoshi, *Bull. Chem. Soc. Jpn.*, **56**, 1382 (1983).

 © 1988 The Chemical Society of Japan Bull. Chem. Soc. Jpn., 61, 2785—2790 (1988)

Relaxation of Short-Lived ^{57}Fe-Species in ^{57}Co-Labeled $Co(IO_3)_2$ Studied by Time-Resolved Emission Mössbauer Spectroscopy

Yasuo WATANABE,* Kazutoyo ENDO, and Hirotoshi SANO
Department of Chemistry, Faculty of Science, Tokyo Metropolitan University, Fukasawa, Setagaya, Tokyo 158
(Received January 5, 1988)

KX-Ray-gated and time resolved emission Mössbauer spectra of ^{57}Co-labeled $Co(IO_3)_2$ were measured at room temperature, using a coincidence technique. No remarkable difference was found on the relative intensity of Fe(II)/Fe(III) between the X-ray-gated and normal emission spectra. A lifetime for unstable ^{57}Fe(II)-species formed through EC-decay was estimated to be 43±5 ns and the initial distribution of Fe(II)/Fe(III) at 14.4 keV nuclear level to be 0.47±0.13 from the time-resolved emission Mössbauer spectrum. The results are discussed in terms of the chemical stability of the environments of the decayed ^{57}Fe-atoms.

Investigations on the lifetime and electronic state of short-lived chemical species provide very attractive fields for understanding chemical bond and reaction mechanism. Emission Mössbauer spectroscopy is useful for dynamic study of such short-lived chemical species in its nuclear lifetimes or the same order of magnitude; it has the advantage that it detects the chemical states of Mössbauer active atoms decayed from the parent nuclide in ultra-microquantities in the solid. The concentration of metastable or unstable species produced after EC-decay is usually too low to be detected by ordinary physicochemical techniques. By combining emission Mössbauer spectroscopy with a coincidence technique, more detailed and selected information can be provided. If a Mössbauer spectrum gated with a particular radiation among several ones associated with the de-excitation of nuclear or atomic states, we expect to extract information accompanied by the transition. In the present study, two simple coincidence systems were built to elucidate the relaxation processes of unstable chemical species formed through EC-decay. One of the systems involves an X,γ-coincidence and another a γ,γ-coincidence. In X,γ-ray coincidence, a Mössbauer spectrum gated with 6.4 keV KX-ray from decayed ^{57}Fe is observed, which reflects information relating the chemical effects of the KX-ray emission. Kobayashi and Friedt examined the effects of KX-ray emission on ^{57}Co-labeled $CoCl_2 \cdot nH_2O$ (n=2—6), finding a different chemical distribution of ^{57}Fe atoms between the normal and the X-ray-gated emission Mössbauer spectra.[1] In γ,γ-coincidence, the spectrum is taken at an appropriate time interval of the nuclear lifetime, which enables us to study dynamic chemical states of decayed ^{57}Fe atoms. Hoy et al. showed a filtering spectrum of a single resonance line,[2] and analyzed it based on Hamermesh's treatment.[3] Triftshäuser and Craig observed no time dependence of the intensity ratio of Fe(III)/Fe(II) on ^{57}Co-labeled CoO, $CoSO_4$, and $CoCl_2 \cdot 4H_2O$ on the time resolved Mössbauer spectra.[4] Gol'danskii's group estimated the intramolecular electron charge transfer rate from ^{57}Fe atoms to Fe(III) atoms in the system of $^{57}Co_3[Fe(III)(CN)_6]_2$.[5] Gütlich's group reported the lifetime of unstable high-spin Fe(II)-species formed in ^{57}Co-labeled $[Co(phen)_3](ClO_4)_2 \cdot 2H_2O$ at various temperatures.[6] In the present study, we examined the chemically unstable ^{57}Fe-species formed through EC-decay in ^{57}Co-labeled $Co(IO_3)_2$ using both coincidence systems. The labeled compound was selected because the iodate anion is highly oxidizable and its rather simple chemical structure is suitable for examining the stabilization mechamism of the decayed ^{57}Fe-species.

Experimental

Source Preparation. To prepare ^{57}Co-doped $Co(IO_3)_2 \cdot nH_2O$, the procedure described in the literature was modified for small scale synthesis.[7] $Co(NO_3)_2 \cdot 6H_2O$ was dissolved in dil. nitric acid containing ca. 3.0×10^6 Bq of ^{57}Co, and iodic acid was added dropwise to this solution. After heating the solution on a steam bath at 80 °C for ten minutes, the purple blue products were filtered, washed with distilled water and then dried under vacuum. The radioactivity of the sample was estimated to be ca. 2.2×10^6 Bq. Thermogravimetric analysis and X-ray diffraction of the product prepared without ^{57}Co by the same procedure proved it to be an anhydride.

Measurement of X,γ-Ray Coincidence Mössbauer Spectra. The X,γ-ray coincidence system used in the present experiment is shown in Fig. 1. For detecting the 6.4 keV KX-rays two NaI(Tl) crystals of 0.8 mm in thickness and 1″ in diameter were used, and a crystal of 1 mm×1″ NaI(Tl) crystal for 14.4 keV γ-rays. These scintillators were coupled to photomultipliers; Hamamatsu R580, of which cathodes were set to operate at the photocathode potential of −1200 V with respect to the ground. The magnetic shield of Hamamatsu-E989 was used for the photomultiplier, which was effective for fast timing operation to eliminate the magnetic field of the Mössbauer transducer. The bleeder strings assemblies were built by us using low noise resistors, and the current was 0.4 mA. The anode signals from two photomultipliers for detection of KX-rays were fed into fast discriminators (ORTEC-473A) and then each logic signal was summed. The pulses from the third photomultiplier for measuring the Mössbauer spectra were amplified in pulse-height by a linear amplifier (CANBERRA-2011) and then 14.4 keV γ-rays were selected with a timing-SCA (ORTEC-551). These signals were gated by the logic pulses (0.5 μs in pulse width) of the summed 6.4 keV KX-rays.

Measurement of γ,γ-Coincidence Mössbauer Spectra. The γ,γ-coincidence system used in the present experiment

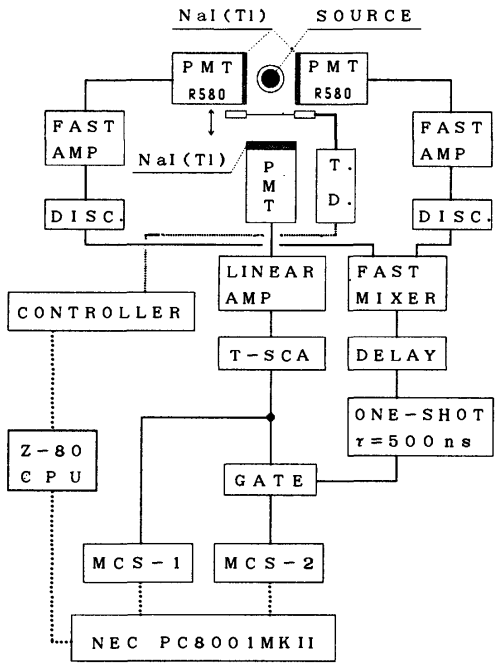

Fig. 1. Block diagram for the X,γ-ray coincidence Mössbauer system; memory units and a Mössbauer controller were governed by a Z-80 CPU. PMT=photomultiplier, AMP=amplifier, T.D.=transducer, T-SCA=timing single-channel analyzer, MIXER=sum circuit, DISC=fast discriminator, GATE=linear gate and stretcher, CONTROLLER=Austine S-600 Mössbauer controller, MCS-1,2=data acquisition system, CPU=central processing unit.

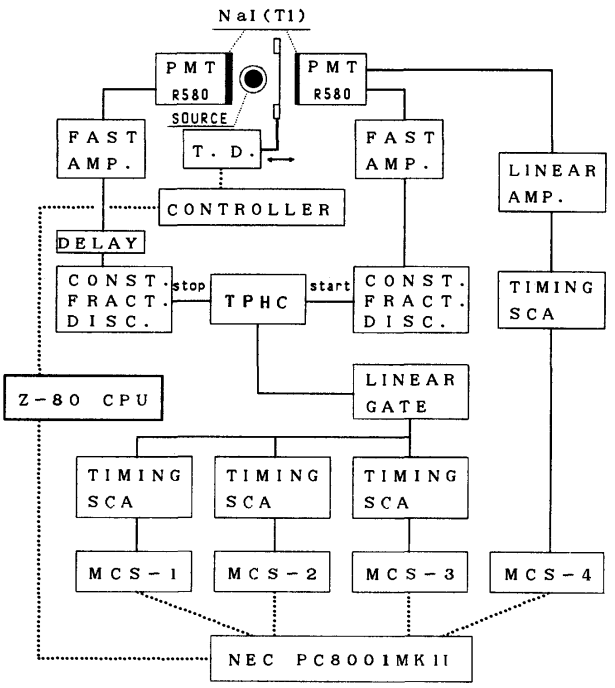

Fig. 2. Block diagram of the apparatus for the delayed coincidence Mössbauer experiments; a transducer controller and all memory units were supervised by a Z-80 CPU. PMT=photomultiplier, AMP=amplifier, T.D.=transducer, SCA=single-channel analyzer, TPHC=time-to-pulse height converter, CONST.FRACT.DISC=constant fraction discriminator, LINEAR GATE=linear gate and stretcher, CONTROLLER=Austine S-600 Mössbauer controller, MCS-1,2,3,4=data acquisition system, CPU=central processing unit.

is shown in Fig. 2. A NaI(Tl) crystal of 1″ in thickness and 1″ in diameter was used to detect 122 keV γ-ray and another crystal of 0.8 mm in thickness and 1″ in diameter for 14.4 keV γ-ray. Anode signals from each multiplier were fed into a fast amplifier (ORTEC-574), the constant fraction discriminator (ORTEC-473A) and then to TPHC (ORTEC-467) as start and stop signals, respectively. In order to reduce the dead time of the time conversion to amplitude at TPHC, the busy start signals of 122 keV were delayed with a coaxial cable for about 2.0×10^{-7} s. Voltage signals from the 11th dynode of the multiplier with a thinner scintillator were used for energy selection of 14.4 keV. With the gated signals of transmitted γ-ray, a Mössbauer spectrum were measured. An Austine Mössbauer spectrometer (S-600) was used together with a data taking system. The latter built by us was a four-channel parallel-mode (4×512 channel) system which is essentially a microprocesser(Z80)-aided multichannel scaler and a memory unit. A microcomputer NEC PC-8001MKII was used for an auxiliary controller of this data acquisition system. The time resolution of γ,γ-coincidence was estimated to be (10.0±0.3) ns using annihilation radiations of ^{22}Na. The windows of the timing SCA were set at the same condition as were used in ^{57}Fe Mössbauer measurement. The time-resolved Mössbauer spectra were measured at the time windows of A(0-45 ns), B(45-88 ns), D(88-148)ns, and E(0-infinity), or A(0-45 ns), C(45-148 ns), and E(0-infinity) in a separate run, respectively. The oscillation due to the time filtering effects on the time resolved Mössbauer spectrum was hardly observed, because the preset time window was rather wide. By subtracting the randomly-coincided fraction from the observed spectrum, the truly-coincided spectra were tentatively analyzed with two sets of quadrupole doublets using a least square fitting of a Gaussian function. Gauss-Newton iteration method was used in the "SALS" least square fitting program developed by Nakagawa and Oyanagi.[9]

Results and Discussion

X,γ-Ray Coincidence Spectrum. An emission Mössbauer spectrum gated with KX-ray is shown in Fig. 3, together with the normal emission spectrum. The former was obtained by subtracting the randomly coincided spectrum from the observed spectrum. The contribution of the random coincidence was estimated to be 30% in the present experimental conditions. The resulting X-ray-gated spectrum does not show remarkable difference from the normal one in their parameters. It has been reported that in various kinds of chemical compounds, an Auger process plays an important role in determining the final chemical state of hot atoms produced through the de-excitation associated with the nuclear transformation. The low energy electrons and/or vacancies produced in Auger cascades dissipate their energies to neighbouring atoms. The Auger process is expected to emit a large

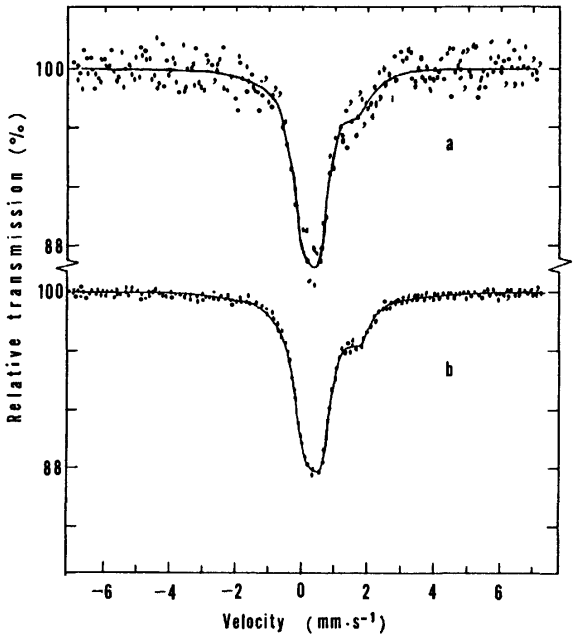

Fig. 3. (a) X,γ-Ray-gated and (b) normal emission Mössbauer spectra of ^{57}Co-labeled $Co(IO_3)_2$ at room temperature.

number of electrons than the competitive X-ray emission process; i.e., the former will give a large influence to the chemical species formed through the EC-decay. Multiple ionization will be larger in Auger electron emission than in X-ray emission. However, even if any unstable chemical species are formed by Auger processes and are different from those of the X-ray emission, such chemical species cannot be observed if their lifetimes are too short to be discriminated by the experimental set-up used. These considerations suggest that different chemical species to be discriminated by the present method are not formed in the labeled compound.

γ,γ-Coincidence. Line Width: Time-resolved Mössbauer spectra are shown in Fig. 4, together with a time integral spectrum for comparison. A gradual decrease was observed in the linewidth of both trivalent and divalent species with an increase in the delay time. This trend can be understood qualitatively from the uncertainty principle, as shown in Fig. 5. The line broadening has been observed in many source experiments. This effect arises from several factors. One is to use a thick absorber in order to increase the sensitivity of measurement. Secondly, it arises from superimposition of various kinds of hyperfine parameters corresponding to many electronically excited states formed through EC-decay in the insulator. Thirdly, it is caused by the slow relaxation time of spin-spin and spin-lattice interactions. The former effect is observed in some source experiments of a diamagnetic insulator host lattice where the decayed ^{57}Fe species are placed in a magnetically-diluted material. In the present work, a similar time-dependence of the line widths observed

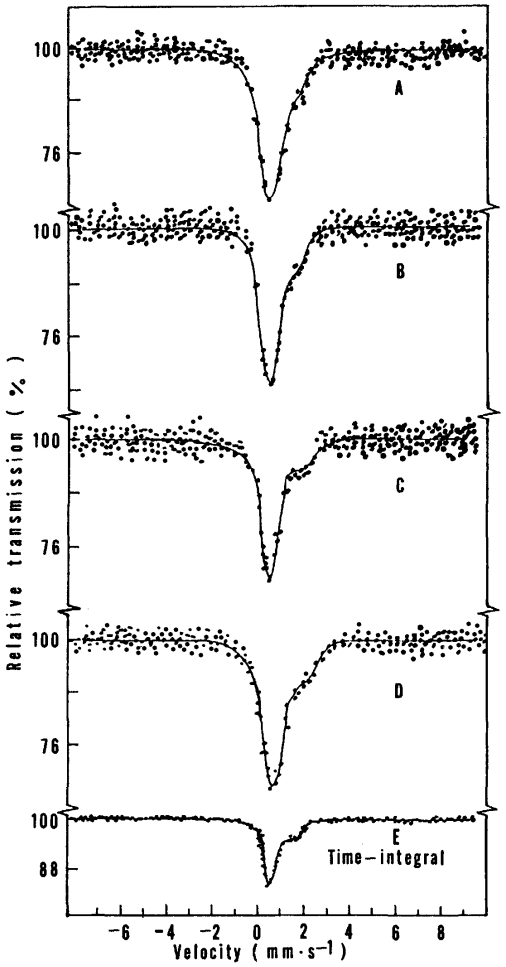

Fig. 4. Time-resolved Mössbauer spectra of ^{57}Co-labeled $Co(IO_3)_2$ at room temperature. The time windows were set to be A=0—45 ns, B=45—88 ns, C=45—148 ns, D=88—148 ns, E=0—infinity.

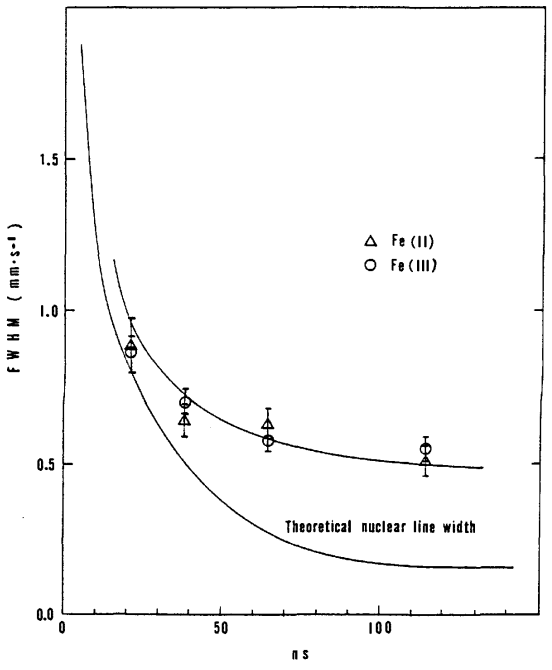

Fig. 5. Line width of the time resolved Mössbauer spectra plotted against the mean time of the windows. Theoretical line width (2Γ) is also plotted.

for the two species shows that the line broadening due to the uncertainty principal predominates over other factors such as the time-dependent population of given species in the present compound.

Evaluation of Relative Intensity on Time-Resolved Spectra: The ratio of the absorption peak area of ^{57}Fe(II) to ^{57}Fe(III) is plotted against the mean time, t, of the time windows in Fig. 6. The mean time for the time window was evaluated by the equation as

$$\frac{t}{\tau_N} = \int_{T_A}^{T_B} Te^{-T}\,dT \Big/ \int_{T_A}^{T_B} e^{-T}\,dT \qquad (1)$$

where t is the mean time in the interval $T_A \leqq t \leqq T_B$, and τ_N the mean nuclear lifetime of the first excited state of ^{57}Fe. The chemical decay constant of the unstable ^{57}Fe(II)-species is estimated in the following manner. Several factors are assumed to facilitate the discussion; Debye-Waller factors of ^{57}Fe(II)- and ^{57}Fe(III)-species are the same at every time window. Fe(II)-species decay with a pseudo-first order kinetics of a chemical decay constant, λ_c, and Fe(III) once formed are stable during the time in question, since the anion concentration in the vicinity of the decayed ^{57}Fe-atoms may be regarded as constant. The chemical reaction of ^{57}Fe(II)-species can be assumed to be the electron transfer from the species to the highly oxidizable iodate anion. Let the distributions of ^{57}Fe(II) and ^{57}Fe(III) be $P_2(t)$ and $P_3(t)$ at t after the emission of 122 keV γ-ray and their ratio at $t=0$ be R.
Then, $P_2(t)+P_3(t)=1$ and

$$R = P_2(0)/P_3(0). \qquad (2)$$

With the decay constant, λ_c, of the Fe(II)-species, the populations found at time t after the emission 122 keV gamma-ray can be written as

$$P_2(t) = P_2(0)e^{-\lambda_c t}, \qquad (3)$$

$$P_3(t) = P_2(0)(1-e^{-\lambda_c t}) + P_3(0). \qquad (4)$$

Since emission Mössbauer spectroscopy gives us information on the electronic states of "nucleogenic" probe atoms, the observable quantities with this probe at time t should be those of Eqs. 3 and 4 multiplied by $\exp(-\lambda_N t)$, where λ_N is the nuclear decay constant of ^{57}Fe at the 14.4 keV level.

Actually, time-resolved Mössbauer spectroscopy offers a spectrum integrated with respect to the preset time window between T_A and T_B. Then, Eqs. 3 and 4 should be written as

$$\int_{T_A}^{T_B} P_2(t)\,dt = \int_{T_A}^{T_B} P_2(0)e^{-\lambda_c t}dt, \qquad (5)$$

$$\int_{T_A}^{T_B} P_3(t)\,dt = \int_{T_A}^{T_B} [P_3(0) + P_2(0)(1-e^{-\lambda_c t})]dt. \qquad (6)$$

Due to the finite resolution of the equipment, the observed spectrum involves a time distribution of Gaussian type, $G(t-t', 2\tau_0)$, where $2\tau_0$ is a full width at half maximum of the time resolution and estimated to be 10.0±0.3 ns by the measurement of annihilation radiations of ^{22}Na in Al metal. Taking the resolution function into consideration, the observed intensity ratio of Fe(II) to Fe(III), at time interval between T_A and T_B, can be described as follows using Eqs. 2, 5, and 6.

$$\{I_2(t)/I_3(t)\}_{ob} \equiv \frac{R\int_{T_A}^{T_B}\left[\int_0^\infty e^{-\lambda_c t'}e^{-\lambda_N t'}G(t-t';2\tau_0)dt'\right]dt}{\int_{T_A}^{T_B}\left\{\int_0^\infty\left[1+R(1-e^{-\lambda_c t'})\right]e^{-\lambda_N t'}G(t-t',2\tau_0)dt'\right\}dt} \qquad (7)$$

where $G(t-t';2\tau_0) = \dfrac{1}{\sqrt{2\pi(2\tau_0)^2}} \exp\left\{\dfrac{-(t-t')^2}{(2\tau_0)^2}\right\}$

Numerical calculation of Eq. 7 was carried out with a computer. The initial distribution ratio of Fe(II)- to Fe(III)-species, R=0.46±0.13, and the chemical decay constant of Fe(II)-species, $\lambda_c = 2.33\times10^{-2}$ ns^{-1} (or τ_c= 43±5 ns), were obtained. In Fig. 6, the obtained and calculated relative intensities of spectral area are plotted vs. mean time t. The integral value, shown as oblique lines, is obtained by the normal emission Mössbauer spectrum without gate. The relative intensities of ^{57}Fe(II) and ^{57}Fe(III) against time calculated by using the values of R, λ_c, and Eqs. 3, 4 are shown in Fig. 7. The intensity of ^{57}Fe(III)-species just after the 122 keV γ-ray emission is taken as an unity. Although the present method for analyzing the relative intensity on the time resolved spectrum is similar to that used by Gütlich's group,[6] the initial distribution ratio of Fe(II)- to Fe(III)-species at 14.4 keV nuclear level was taken as an arbitrary parameter, R, in the present work.

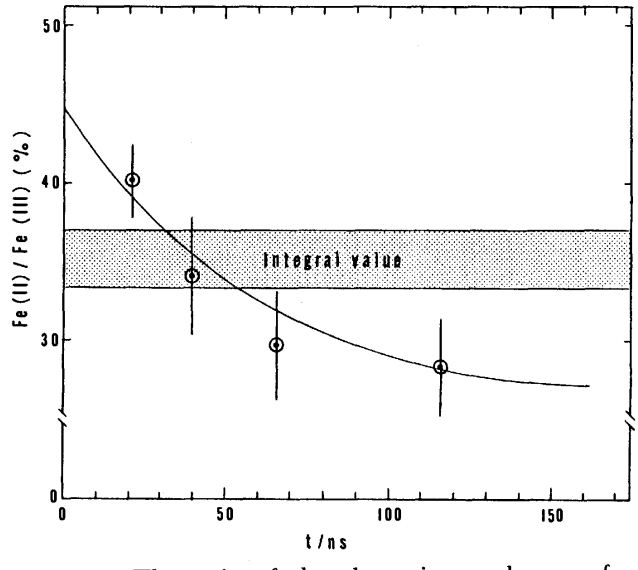

Fig. 6. The ratio of the absorption peak area of ^{57}Fe(II) to ^{57}Fe(III) plotted against the mean time, t, of the time windows. The line is the best-fitted values calculated using Eq. 7.

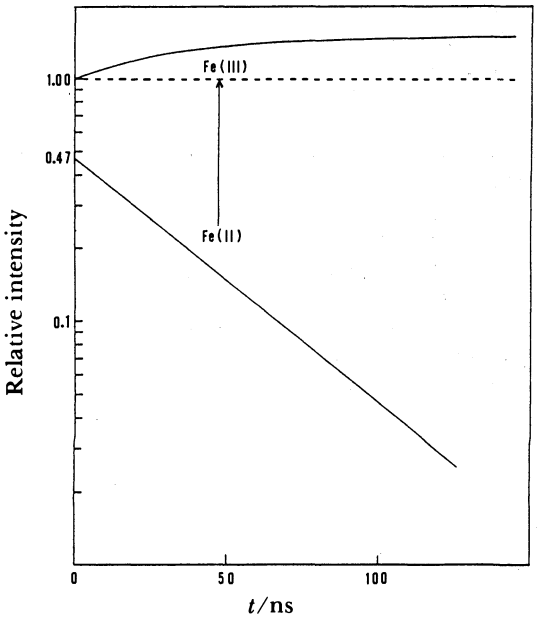

Fig. 7. Growth curve of ^{57}Fe(III)-species and decay curve of ^{57}Fe(II)-species are depicted based on Eqs. 3 and 4. The intensity of ^{57}Fe(III)-species just after the 122 keV γ-ray emission is taken as an unity.

Charge State of ^{57}Fe: The observed lifetime of the short-lived ^{57}Fe-species is 43±5 ns and the initial distribution of Fe(II)/Fe(III) at 14.4 keV level is obtained to be 0.46±0.13 by assuming the divalent ^{57}Fe-species are oxidized monotonically to trivalent species. Although the evaluation of the data for the time-resolved Mössbauer spectra is not the same as that used in the present work, Gol'danskii and his co-workers obtained the electron transfer rate of 1×10^8 or 5.5×10^7 s^{-1} in ^{57}Co-labeled $Co_3[Fe(CN)_6]_2$, and reporting the value of the mean lifetime of the order 10—20 ns.[5] They attributed such fast decay rate to the transition from an electronically excited level in a narrow well of Fe(II) to various kinds of levels in a deep well of $[Fe(II)(CN)_6]^{3-}$. Gütlich's group reported that the lifetime of anomalous high-spin species is of the order of 23.0±5.0 ns at 223 K in ^{57}Co-labeled $[Co(phen)_3](ClO_4)_2\cdot2H_2O$, assuming the initial distribution of high-spin Fe(II) equal to that of low-spin Fe(II). On the other hand, no time dependence has been observed on CoO, and $CoCl_2\cdot4H_2O$ as mentioned in the introduction. It seems likely from the results on many systems reported so far the normal emission spectroscopy that the stabilization of the ^{57}Fe charge state does not depend on the charge state of the parent cobalt atoms in their compounds but on the radiation stability of the neighboring atoms, ligands, and/or anions.[10-15] The present results may suggest that the chemical stability may affect the lifetime of the unstable Fe-species observed by time-resolved Mössbauer spectroscopy. In fact, Fe(II) iodate is very sensitive for oxidation even under nitrogen atmosphere.

In the decay of radioactive nuclide or nuclear transformations, the recoiled atoms are often found in aliovalent states. In the case of ^{57}Co EC-decay, the recoil energy associated with the 122 keV γ-ray emission and neutrino emission (600 keV maximum) are 0.14 and 3.5 eV, respectively, which is smaller than the displacement energy of ^{57}Co atoms in the solid. Then, the initial chemical effects in the EC-decay of ^{57}Co will be the electronic excitation of ^{57}Fe atoms. This excitation is caused by Anger cascade following the EC-decay. The Auger ionization processes have been calculated by Pollak, using Watson wave functions.[16] His result predicts a distribution of charge states ranging from Fe^{2+} to Fe^{7+} with most probability for a Fe^{5+} configuration for free $^{57}Co^{2+}$ and from Fe^{1+} to Fe^{6+} with a most probability for Fe^{4+} for free neutral ^{57}Co atoms. Highly-charged states other than Fe^{4+}, however, relax rapidly in the solid, even in insulators, and have not been observed with Mössbauer spectroscopy. It seems likely that the neutralization of such highly-charged states is much faster than the Mössbauer time scale. In addition, the initial distribution ratio of ^{57}Fe(II)/^{57}Fe(III)-species at 14.4 keV nuclear level indicated the short-lived ^{57}Fe(II)-species formed through EC-decay exhibits a relatively small distribution even immediately after the emission of 122 keV gamma-rays; i.e., since the second excited state of ^{57}Fe has a lifetime of 12.4 ns, the chemical species once formed and relaxed after the EC-decay can be observed by time-resolved Mössbauer spectrum.

Conclusion

No remarkable differences between X-ray gated and normal spectra were observed, although when a KX-ray is emitted, the total numbers of low energy electrons and vacancies generated by the Auger cascade are about a half compared with those generated when a K-Auger electron is emitted. In the present system, gate signals of 0.5 μs both for X-ray and 14.4 keV γ-ray were used in order to avoid the time filtering effect on the spectrum. It may be reasonable to conclude from the lifetime obtained that the unstable Fe(II)-species will fully relax or decay into the stable Fe(III)-species within the resolving time on X-ray-gated spectrum and that the chemical effects on X-ray emission will produce no remarkable difference in $Co(IO_3)_2$. It is also noted that the chemical lifetime and the distribution ratio of ^{57}Fe(II)/^{57}Fe(III) at 14.4 keV nuclear level are closely related to the chemical instability of the corresponding iron compound.

References

1) T. Kobayashi and J. M. Friedt, *Bull. Chem. Soc. Jpn.*, **59**, 631 (1986).

2) G. R. Hoy, D. W. Hamill, and P. P. Wintersteiner, "Mössbauer Effect Methodology," ed by I. J. Gruverman, Plenum, New York (1970), Vol. 6, p. 109.

3) F. J. Lynch, R. E. Holland, and M. Hamermesh, *Phys.*

Rev., **120**, 513 (1960).
4) W. Triftshäuser and P. P. Craig, *Phys. Rev.*, **162**, 274 (1967).
5) V. P. Alekseev, V. I. Gol'danskii, V. E. Prusakov, A. V. Nefed'ev, and R. S. Stukan, *JETP Lett.*, **16**, 43 (1972).
6) R. Grimm, P. Gütlich, E. Kankeleit, and R. Link, *J. Phys. Chem.*, **67**, 549 (1977).
7) J. K. Mulhem, D. Horvath, B. Molnar and D. L. Nagy, *Nucl. Instrum. and Method*, **199**, 277 (1982).
8) A. Meusser, *Ber.*, **34**, 2434 (1901).
9) T. Nakagawa and Y. Oyanagi, "Program System SALS for Nonlinear Least-Squares Fitting in Experimental Sciences," in Recent Developments in Statistical Inference and Data Analysis, ed by K. Matsushita, North Holland Publishing Company, (1980), pp. 221—225.
10) H. Sano, K. Sato, and H. Iwagami, *Bull. Chem. Soc. Jpn.*, **44**, 2570 (1971).
11) H. Sano and T. Ohnuma, *Chem. Phys. Lett.*, **26**, 348 (1974).
12) H. Sano and T. Ohnuma, *Bull. Chem. Soc. Jpn.*, **48**, 266 (1975).
13) H. Sano, M. Harada, and K. Endo, *Bull. Chem. Soc. Jpn.*, **51**, 2583 (1978).
14) K. Endo, M. Harada, Y. Sakai, and H. Sano, *J. Phys. C2*, 420 (**1979**).
15) Y. Sakai, K. Endo, and H. Sano, *Bull. Chem. Soc. Jpn.*, **53**, 1317 (1980); **54**, 3589 (1981).
16) H. Pollak, *Phys. Stat. Solid.*, **2**, 720 (1962).

Determination of Trace Metals in Seawater by Graphite Furnace Atomic Absorption Spectrometry after Preconcentration Using Synergistic Extraction

Kazumasa UEDA,* Katsutoshi KUBO, Osamu YOSHIMURA, and Yoshikazu YAMAMOTO
Department of Industrial Chemistry, Faculty of Technology, Kanazawa University, Kodatsuno, Kanazawa 920
(Received February 20, 1988)

Trace Cd, Mn, Pb, Co, Ni, and Cu have been quantitatively separated and concentrated from seawater matrices with a low concentration (mmol dm^{-3} level) of 1,1,1-trifluoro-4-mercapto-4-(2-thienyl)-3-buten-2-one and trioctylphosphine oxide cyclohexane solution. The synergistic extract was directly injected into the furnace and a reproducible signal with little memory effect was obtained. The extracted adduct enhanced the AAS sensitivity during thermal decomposition processes, and simultaneously resulted in depression of the interferences. The detection limits of the analytes ranged from several ng dm^{-3} to 100 ng dm^{-3}. The proposed technique provides both the preconcentration and determination for trace analysis by a single extraction using a small volume of sample. Coastal seawater samples were analyzed by the method.

The determination of trace metals in seawater, particulary toxic or neutrient elements, has received increasing attension in analytical and environmental chemistry. Graphite furnace atomic absorption spectrometry (GF-AAS) is one of the most widely used methods for this purpose. Since the concentrations of many elements are extremely low, adequate preconcentration techniques are usually required prior to GF-AAS measurement.[1-5] However, most of them are troublesome due to the use of a large volume of sample and often cause contamination or loss of the analytes. A simple and reliable preconcentration method is required.

The synergistic extraction is a useful technique for separation and concentration of trace metals. Although the analytical importance has been well recognized, the applications combined with AAS are relatively few.[6,7] Recently, Itoh et al.[8] reported a convenient method for determining cadmium in river water, in which synergistic extract with dithizone-tributylphosphine oxide was directly injected into the furnace. Direct analysis of the organic extract is highly desirable to simplify sample pretreatment steps. Though similar attempts in GF-AAS have been undertaken by utilizing the conventional extraction, e.g., ammonium 1-pyrrolidinecarbodithioate[9] and thiocyanate-zephiramine systems,[10] they were not sufficiently sensitive for accurate analysis of seawater.

In this study, synergistic extraction with 1,1,1-trifluoro-4-mercapto-4-(2-thienyl)-3-buten-2-one (STTA)-trioctylphosphine oxide (TOPO) is evaluated for the preconcentration followed by GF-AAS measurement. The extraction conditions and recovery of trace metals from saline waters are examined in detail.

Experimental

Apparatus. A Nippon Jarrel-Ash Model AA-8500 atomic absorption spectrophotometer with a FLA-10 graphite furnace atomizer was used. A deuterium lamp was used for background correction and tube temparature was measured with a Keisoku Electric Co. Model OPA optical pyrometer. Solvent extractions were carried out by a centrifuge tube (volume: 50 cm^3) with glass stopper. An Iwaki KM type shaker and a Kubota K80 centrifuge were also used.

Reagents. All reagents used were of analytical reagent or better grade. Deionized distilled water was used. The standard solutions (1000 mg dm^{-3}) for Cd, Mn, Pb, Co, Ni, and Cu were prepared by dissolving pure metals or their salts in 0.1 M (M=mol dm^{-3}) HNO_3. STTA was synthesized by the method of Berg et al.[11] and purified repeatedly by recrystallization from absolute ethanol. TOPO was purchased from Dojindo Co. Ltd. Stock reagent solutions (50 mM) for synergistic extraction were prepared by dissolving STTA and TOPO in cyclohexane. The working solution was prepared by mixing and diluting them with cyclohexane before use. HCl, HNO_3, and acetic acid were of extra pure grade purchased from Wako Chemical Co. Ltd., and NaOH was of suprapure grade from Merck. Buffer solutions were purified by washing with the extracting solution, and cyclohexane.

Seawater Samples. Surface seawater was collected at the coast of Noto Peninsula. The waters was filtered through a 0.45 μm Toyo Roshi membrane filter immediately after sampling, acidified to pH 1.5 with HNO_3 and stored in polyethylene bottles. Artificial seawater was prepared according to Japanese Industrial Standard K 2510. All glass wares and polyethylene bottles were rinsed well with pure water after soaking in (1+2) HNO_3 for over 3 days. Centrifuge tube was thoroughly washed with the extracting solution and cyclohexane just before use. Membrane filter was soaked in (1+1) HCl for over 5 days.

Analytical Procedure. An aliquot of seawater (up to 30 cm^3) was transferred into centrifuge tube and neutralized with 1 M NaOH. The pH was adjusted with 5 cm^3 of 0.1 M acetate or 0.05 M borax buffer solution; the total volume of the solution was controlled within the optimum volume for each metal. Then, 5.0 cm^3 of synergistic extracting solution was added and the mixture was shaked for 20 min. After centrifugal separation, 20 μL of the upper organic phase was directly injected into graphite furnace. The atomic absorption peak height for each metal was measured. The metal concentration was determined by the calibration method, except for Co by the standard addition method. Analytical conditions were determined for artificial or natural seawater by comparing the signal height with that for aqueous standard. Optimum analytical parameters obtained for furnace operation and synergistic extraction are shown in

Table 1. Optimum Analytical Parameters for Furnace Operation and SynergistiC Extraction

Condition	Cd	Mn	Pb	Co	Ni	Cu
Wavelength(nm)	228.8	279.5	283.3	240.7	232.0	324.8
Drying current and time/A-s	14-20	14-20	14-20	14-20	14-20	14-20
(final temp/°C)	(80)	(80)	(80)	(80)	(80)	(80)
Ashing current and time/A-s	30-40	60-60	90-60	60-60	40-40	60-40
(final temp/°C)	(300)	(640)	(1000)	(640)	(420)	640
Atomizing current and time/A-s	270-5	320-5	270-5	350-5	330-5	350-5
(final temp/°C)	(2200)	(2550)	(2200)	(2700)	(2600)	(2700)
Ar flow rate: 2.0 dm^3/min, Injection volume: 20 μL						
Exraction pH	8.0	9.3	5.5	5.5	8.0	5.5
STTA concentration/mM	5.0	2.0	1.0	1.0	5.0	1.0
TOPO concentration/mM	1.0	5.0	1.0	0.1	0.1	0.1
Volume ratio (V_{aq}/V_{org}): 4, Shaking time/min: 20						

Table 1.

Results and Discussion

Operating Conditions. Operating conditions for GF-AAS differ a little from those of the usual method, because synergistic extract is directly injected into the furnace. On graphite surface, the following chemical reactions will take place: evaporation of cyclohexane, fussion and decomposition of extracting reagents and adduct chelates, and vaporization of metals in drying, ashing, and atomization processes. The establishment of ashing temperature was especially important, because the extracting reagent acted as a flux. Figure 1 shows the effect of ashing current on the absorption signals of trace metals spiked into artificial seawater. The maximum absorbance was obtained at the current of 90 A (1000 °C) for Pb, up to 60 A (640 °C) for Mn and Co, and up to 100 A (1100 °C) for Cu. The signals for Cd and Ni markedly decreased even at low currents. Berg and Reed[11] have reported that the thermal stability of STTA chelate is relatively low. Although the thermal stability of TOPO adducts is not well-known, the abrupt decrease of Cd and Ni signals would be attributable to the sublimation of the adducts. On the other hand, the loss of Cu and Co by volatilization was little even at elevated temperatures, presumably due to forming a stable fussion product or metallic carbide during decomposition of chelating agents. The ashing temperature of each metal was set high enough to eliminate matrix interferences at the atomization step and ashing time was selected to make background signal became zero or minimum. The drying conditions were established by considering only the evaporation of cyclohexane.

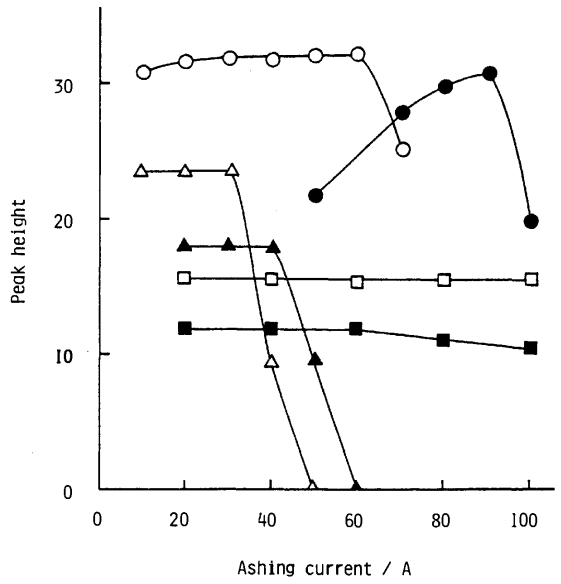

Fig. 1. Effect of ashing current on absorption signal of each metal. ○: Mn 40 ng, ●: Pb 125 ng, △: Cd 5 ng, ▲: Ni 300 ng, □: Cu 250 ng, ■: Co 100 ng.

Absorption Profiles. When the analyte spiked into alkali or alkaline earth metal chloride solution was directly supplied into the furnace, a background signal with multiple peaks appeared and a large depressive effect on the analyte peak was observed in the following sequence, Cs > Na > Mg > Ca. Whereas, when the synergistic extract was applied, a reproducible single peak with little memory effect was obtained, which was compatible with the aqueous analyte standard. Synergistic extraction was effective not only for preconcentration of trace metals from saline waters but also for reduction of the desired metal during thermal decomposition processes, because the synergist acted as a reductant. Furthermore, the extracted adduct showed favorable effects on the AAS measurement, e.g., extension of thermal contact area in the furnace, depression of analyte volatilization at the ashing step, prevention of metal oxide formation, and acceleration of thermal decomposition of the extracted matrix.

Selection of Synergistic Extractants. When a common fluorinated β-diketone, such as thenoyltrifluoroacetone (TTA) or benzoyltrifluoroacetone, was used as a chelating reagent, matrix elements in seawater were coextracted and the detection of the analyte, especially Cd, Mn and Pb, became difficult. However, the interferences could be almost neglected when a low concentration of STTA was used. Figure 2 shows the effect of Ca or Mg matrices on Mn and Pb signals. The constant signals were obtained by the STTA-TOPO extraction at the seawater level of Ca and Mg, whereas the TTA-TOPO extraction gave the decreased signals

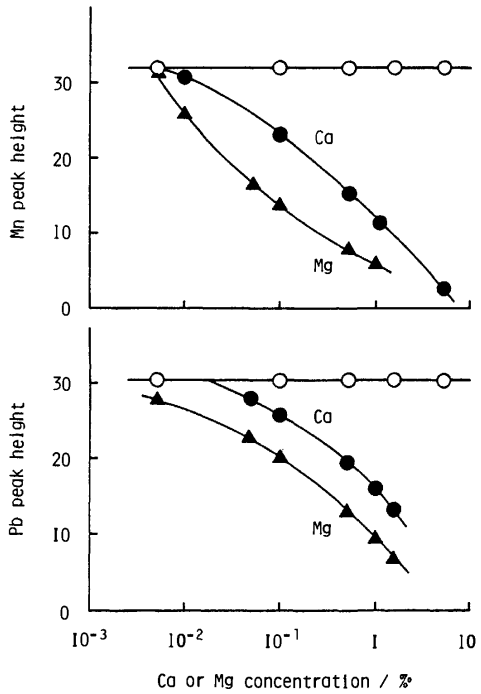

Fig. 2. Effect of Ca or Mg concentration on Mn and Pb absorption signals. Open symbols: 1 mM STTA–1 mM TOPO extraction. Closed symbols: 1 mM TTA–1 mM TOPO extraction.

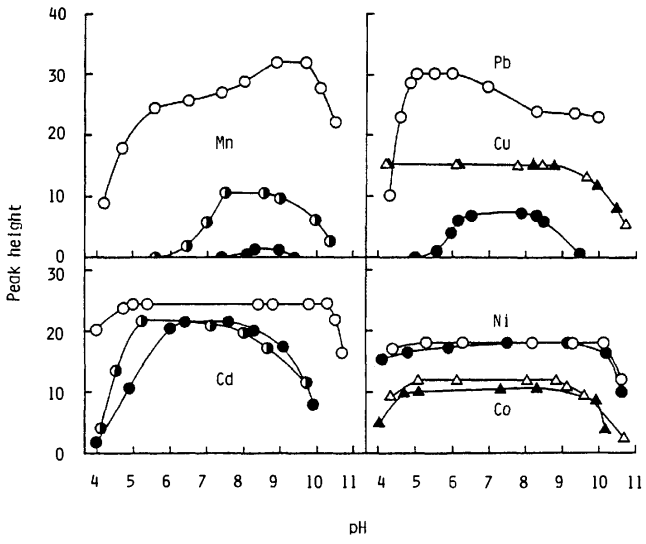

Fig. 3. Effect of extraction pH on absorption signals of each metal. Open and closed symbols denote the absorbances by STTA-TOPO and STTA extraction, respectively, except for STTA-TBP extraction (◑). The reagent and metal concentrations are identical to those shown in Table 1 and Fig. 1, respectively.

with the increase of matrix concentration, especially for Mg. Similar decreased signals were also recognized for Cd, Co and Ni, except for Cu. As a synergist, alkylphosphine oxides and pyridine bases were examined. The analyte peaks were generally enhanced in the following order: pyridine, piperidine < α-picoline, α-pipecoline, 2,6-lutidine < γ-picoline, γ-pipecoline, 2,4-lutidine ≪ tributyl phosphate (TBP) < TOPO. Although the order differed a little from the ordinary base effect for synergistic extraction,[12] TOPO showed a constant signal over wider pH region with the largest enhancement effect. As for the diluent, the signals were increased in the following sequence: chloroform < carbon tetrachloride < benzene < hexane < cyclohexane. Cyclohexane was easier to volatilize than chlorinated solvent, that showed the depressive effect in pH range over 9.

Effect of Extraction pH. Figure 3 shows the effect of pH on the signals of each metal by extraction with STTA-TOPO (or TBP) or STTA only. The maximum and constant absorbances were obtained over wider pH ranges of 8.9—9.7 for Mn, 5.0—10.3 for Cd, 5.0—6.0 for Pb, 4.2—8.5 for Cu, 5.3—10.1 for Ni, and 5.0—8.8 for Co, respectively. Comparing with the signal of STTA only, the peak height increased about 23-fold for Mn and 4.2-fold for Pb, and these enhancement effects were recognized in the following order: Mn ≫ Pb > Cd > Co > Ni ≈ Cu. The order agrees nearly with that of synergistic extractability, but Cu and Ni did not show any significant effect, presumably due to low stability of the adducts. In order to make the phenomena clearer, the extraction equilibria of the TOPO adducts were analyzed by the curve fitting method with 0.05 M STTA at μ=0.1 ($NaClO_4$). The extracted species of Cd, Pb and Zn were found to be $MR_2 \cdot L$ type adduct with one molecule of TOPO, and those of Mn and Co are of $MR_2 \cdot L_2$ type, while Ni formed an ambiguous adduct. Copper was completely extracted with STTA only even at pH 0.5 or below. The primary stability constants of the adducts increased in the order of Cd > Mn > Pb > Co > Zn. These facts suggest that the more STTA chelate is stabilized by adduct formation, the more the sensitivity for GF-AAS is increased.

STTA and TOPO Concentrations. The maximum and constant signals were obtained in the following STTA concentration ranges; 0.1—1 mM for Cu, 0.1—5 mM for Cd, 0.5—1 mM for Pb and Co, 1—5 mM for Mn, and 5—50 mM for Ni. Above the concentrations, the decreases of the signal height, except for Ni, were observed, especially for Mn and Pb. The effect of TOPO concentrations is shown in Fig. 4, where constant absorbances are obtained in the following ranges: 5—10 mM for Mn, 1—10 mM for Pb, 0.5—5 mM for Cd, up to 1 mM for Ni and 0.1 mM for Cu, and 0.1—10 mM for Co, respectively. Above 10 mM, the decreases of absorbance arising from the antagonism were observed for Cd, Ni, and Cu.

Shaking Time and Aqueous Phase Volume. The constant signals were obtained by shaking for over 5 min for Mn, Co, Ni and Cu, 10 min for Pb, and 15 min for Cd, respectively, up to 60 min in each case. The effect of aqueous phase volume was also examined by shaking for 20 min with 3.0 cm^3 of organic phase. The peak height of each metal was little affected by the

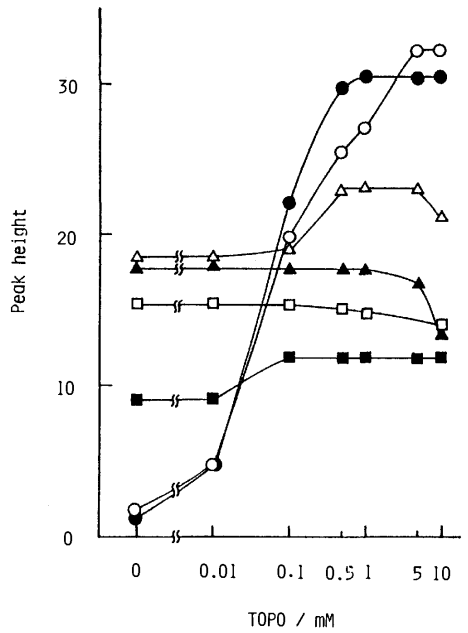

Fig. 4. Effect of TOPO concentration. Symbols and experimental conditions are identical to those shown in Fig. 1 and Table 1, respectively.

volume ratio (V_{aq}/V_{org}) up to 10, but at the ratio of 15, peak height of Cd, Mn, and Ni decreased by about 7, 8, and 15%, respectively.

Recovery of Spikes and Calibration Curves. Known amounts of metals were spiked into seawater aliquots (20 cm^3) to evaluate the net recovery of the extracted metals by comparing with the aqueous standards. The spikes were added before pH adjustment and the solutions were equilibrated for at least 6 h prior to extraction. The spikes were extracted into 5.0 cm^3 of organic phase with above 99% recovery at the concentration up to 5 ng for Cd, 40 ng for Mn, and 125 ng for Pb and Co, and below these concentrations, favorable linear relationships were obtained by a single extraction. The straight lines were also obtained for Cu up to 250 ng and Ni up to 400 ng, although the mean recovery fell to 94.5 and 87.3%, respectively. Since the spikes of Cu and Ni can be quantitatively extracted by synergistic extraction with 1 mM STTA-TOPO,[13] low recovery from seawater matrices would be attributed to the non-extractable metal species.[14] In practice, found values of Cu and Ni were corrected by the calibration graphs.

Table 2. Blanks and Detection Limits

	Blank/ng cm^{-3} a)	Detection limit/ng cm^{-3}
Cd	0.010±0.004	0.008
Mn	0.10±0.05	0.10
Pb	0.84±0.16	0.32
Co	<0.20	<0.20
Ni	0.3±0.1	0.2
Cu	0.5±0.1	0.2

a) Mean and standard deviation for five determinations.

Blanks and Detection Limits. The blank in the extraction procedure consists of metals in the reagents used as well as those introduced during sampling and extraction steps. A reagent blank was prepared by re-extracting the previously extracted seawater. A preextracted seawater sample (500 cm^3) was washed with two 10 cm^3 portions of cyclohexane, and the aliquots were submitted to the analysis. Replicate blanks for each metal studied are shown in Table 2. As for Co, the metal concentration corresponding to the peak unit of 0.1 is regarded as a blank, due to it's weak signal. The detection limits are based on twice the standard deviation of the blank, which are lower than those obtained by the dithiocarbamate extraction-GF-AAS.[9]

Analysis of Seawater. The analytical results of coastal seawater samples are summarized in Table 3. Each metal was determined within the relative standard deviation of 10%, but the concentration of Co was near or below the detection limit and the values found had poor analytical precision. The results of six elements were lower than those found in Seto Inland Sea and Tokyo Bay,[15] especially for Mn and Pb. The results of Monzen were compared with those obtained by the chelex-100 resin preconcentration-GF-AAS.[16] The concentrations obtained by two analytical methods were agreed closely with each other, indicating that the proposed method is accurate enough to apply to the determination of trace metals in seawater.

Conclusion

Synergistic extraction by using a low concentration synergist is useful for preconcentration of trace metals

Table 3. Analytical Results of Trace Metals in Seawater

	Concentration/ng cm^{-3} a)					
	Cd	Mn	Pb	Co	Ni	Cu
Wajima	0.038±0.001	0.92±0.08	1.84±0.08	0.35±0.05	1.2±0.1	1.1±0.1
Sosogi	0.033±0.003	0.80±0.03	0.71±0.03	0.17±0.03	1.1±0.1	1.4±0.1
Noroshi	0.031±0.002	0.96±0.02	0.66±0.03	0.29±0.04	1.2±0.1	1.4±0.1
Koiji	0.031±0.002	0.92±0.08	0.78±0.01	N.D.[b]	0.7±0.1	1.1±0.1
Anamizu	0.088±0.003	7.70±0.12	0.73±0.05	0.21±0.03	1.0±0.1	1.0±0.1
Monzen	0.029±0.005	0.66±0.03	0.71±0.04	N.D.	1.1±0.1	1.0±0.1
	0.025±0.005[c]	0.60±0.05	0.75±0.08	N.D.	1.2±0.1	0.8±0.1

a) Mean and standard deviation for three determinations. b) Not detected. c) Chelex-100 resin preconcentration method.[16]

in saline water. The method is convenient and rapid, as the extraction is carried out in a centrifuge tube and an aliquot of cyclohexane extract in the upper layer can be directly served for GF-AAS. This enables the use of smaller amounts of samples and reagents compared with those in the conventional methods. As an another merit of synergistic extraction, the group separation of trace metals is achievable, that is now under investigation for simultaneous multielement analyses.

References

1) Yu. A. Zolotov, N. M. Kuz'min, O. M. Petrukhin, and B. Ya. Spivakov, *Anal. Chim. Acta*, **180**, 137 (1986).
2) J. Komárek and L. Sommer, *Talanta*, **29**, 159 (1982).
3) E. A. Boyle and J. M. Edmond, *Anal. Chim. Acta*, **91**, 189 (1977).
4) R. E. Sturgeon, S. S. Berman, S. N. Willie, and J. A. H. Desaulniers, *Anal. Chem.*, **53**, 2337 (1981).
5) G. E. Batley and J. P. Matousek, *Anal. Chem.*, **52**, 1570 (1980).
6) I. Kojima, T. Uchida, M. Nanbu, and C. Iida, *Anal. Chim. Acta*, **93**, 69 (1977).
7) M. Sugiyama, O. Fujino, and M. Matsui, *Bunseki Kagaku*, **33**, E 123 (1984).
8) Y. Itoh, H. Kawamoto, and H. Akaiwa, *Bunseki Kagaku*, **36**, T 119 (1987).
9) S. C. Apte and A. M. Gunn, *Anal. Chim. Acta*, **193**, 147 (1987).
10) Y. Okamoto, T. Kumamaru, S. Hara, H. Matsuo, and M. Kiboku, *Bull. Chem. Soc. Jpn.*, **60**, 3053 (1987).
11) E. Berg and K. P. Reed, *Anal. Chim. Acta*, **36**, 372 (1966).
12) T. Honjo and T. Shigematsu, *Kagaku*, **23**, 708 (1968).
13) T. Honjo, S. Yashima, and T. Kiba, *Bull. Chem. Soc. Jpn.*, **46**, 3772 (1973).
14) R. E. Sturgeon, S. S. Berman, A. Desaulniers, and D. S. Russel, *Talanta*, **27**, 85 (1980).
15) C. J. Cheng, T. Akagi, and H. Haraguchi, *Bull. Chem. Soc. Jpn.*, **58**, 3229 (1985).
16) H. M. Kingston, I. L. Barnes, T. J. Brady, T. C. Rains, and A. M. Champ, *Anal. Chem.*, **50**, 2064 (1978).

 © 1988 The Chemical Society of Japan Bull. Chem. Soc. Jpn., 61, 2797—2804 (1988)

Mechanistic Study on the Photochemical Conversion of Disilanyliron(II) Complexes to Monosilyliron(II) Complexes

Hiromi Tobita, Keiji Ueno, and Hiroshi Ogino*
Department of Chemistry, Faculty of Science, Tohoku University, Sendai 980
(Received March 5, 1988)

Photolysis of a C_6D_6 solution of $CpFe(CO)_2SiMe_2SiMe_3$ ($Cp=\eta^5$-C_5H_5) or $(MeCp)Fe(CO)_2SiMe_2SiMe_3$ ($MeCp=\eta^5$-C_5H_4Me) resulted in the formation of monosilyl derivative, $CpFe(CO)_2SiMe_3$ or $(MeCp)Fe(CO)_2SiMe_3$ in 64 or 59% yield, respectively, together with small quantities of ferrocene and $Cp_2Fe_2(CO)_4$ or their methylated derivatives. The yield of $CpFe(CO)_2SiMe_3$ increased to 88% when the photolysis was carried out under a carbon monoxide atmosphere, while decreased to 22% when argon was vigorously bubbled through the reaction mixture. These results are consistent with a mechanism involving dissociation and recombination of a carbonyl ligand which are common processes in photoreactions of transition-metal carbonyl derivatives. Dimethylsilylene moiety released during the photolysis was tried to be trapped with a hydrosilane, diene, and cyclotrisiloxane, but none of the expected products from the trapping reactions was detected, even in a trace amount. Photolysis of $CpFe(CO)_2SiMe_2SiMeEt_2$ afforded, accompanying alkyl migration between silicon atoms, $CpFe(CO)_2SiMeEt_2$, $CpFe(CO)_2SiMe_2Et$, and $CpFe(CO)_2SiMe_3$ in 26, 33, and 4% yields, respectively. Photolysis of a 1 : 1 mixture of $CpFe(CO)_2SiMe_2SiMeEt_2$ and $(MeCp)Fe(CO)_2SiMe_2SiMe_3$ provided only products expected from intramolecular alkyl migration mechanism. A possible mechanism involving silyl(silylene)iron intermediates is proposed to explain these results.

Divalent silicon species, silylene, is important as a key intermediate for many reactions containing silicon compounds.[1,2] Its existence is well established by many trapping reactions as well as low-temperature matrix isolation techniques.[3-5] However, the only known divalent silicon species stable at room temperature are decamethylsilicocene, $(\eta^5$-$C_5Me_5)_2Si$,[6] and a metallocarborane, $[(Me_3Si)_2C_2B_4H_4]Si$,[7] and no usual σ-substituted silylene has been isolated so far under normal conditions because of its lability and instability. Carbene is also a very reactive species, but it is well known to be stabilized by coordination to a metal atom and becomes isolable.[8] Therefore, we can expect that silylene is also stabilized as a ligand on a transition metal.

There is no genuine silylene complex isolated at present,[9] although some neutral[10,11] and cationic[12] base-stabilized silylene complexes have been reported. There are also several reactions in which silylene complexes are proposed as reactive intermediates during the courses of reactions; e.g. decomposition reactions of silicon containing organometallic complexes,[13,14] metal-catalyzed reactions of organosilicon compounds,[15] and reactions of transition-metal ions with methylsilanes in gas phase.[16]

Recently, Pannell et al. suggested the formation of novel silyl(silylene)iron complexes as intermediates in the photochemical conversion of $CpFe(CO)_2SiMe_2SiPh_3$ to $CpFe(CO)_2SiPh_nMe_{3-n}$ (n=1—3).[17] Our independent study on the photoreaction of $CpFe(CO)_2SiMe_2SiMeR_2$ (R=Me, Et) (Eq. 1) led us to almost the same mechanism which we reported previously in a preliminary communication.[18] We now give the evidence for the intramolecular mechanism for this reaction as well as the full detail of the mechanistic study.

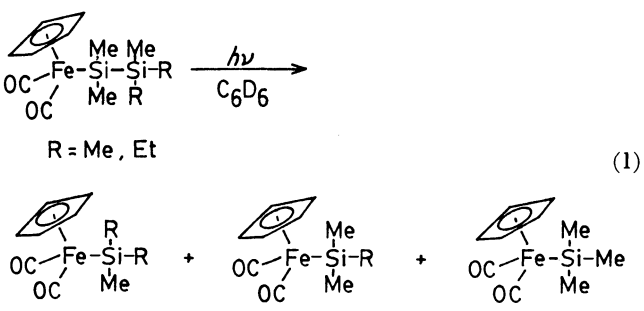

Experimental

General Details. All experiments were performed under a nitrogen atmosphere by using standard Schlenk techniques. Hexane, pentane, and tetrahydrofuran (THF) were reagent grade and were freshly distilled from sodium-benzophenone ketyl under nitrogen. Chlorotrimethylsilane, dichlorodimethylsilane, and ethyl bromide were obtained from Wako Pure Chemical Industries, Ltd. and distilled under nitrogen before use. 2,3-Dimethyl-1,3-butadiene was obtained from Tokyo Chemical Industry Co., Ltd. and used after distillation. Chloropentamethyldisilane,[19] 1-chloro-2,2-diethyl-1,1,2-trimethyldisilane,[20] chlorodiethylmethylsilane,[21] diethylmethylsilane,[22] $Cp_2Fe_2(CO)_4$,[23] $(MeCp)_2Fe_2(CO)_4$,[23] $CpFe(CO)_2SiMe_3$ (**2a**),[24] $CpFe(CO)_2SiMe_2SiMe_3$ (**1a**),[25] $(MeCp)Fe(CO)_2SiMe_3$ (**2b**),[26] and hexamethylcyclotrisiloxane[27] were prepared according to the published procedures.

Measurements. Electronic spectra were recorded on a Hitachi 330 or a Shimadzu UV-260 spectrophotometer using a quartz cell of 1 cm optical path length. Infrared spectra were recorded on a JASCO IRA-1 spectrophotometer, and gas chromatography-mass spectra (70 eV) on a JEOL JMS-D300 mass spectrometer. NMR spectra were measured on a JEOL FX-90Q Fourier-transform spectrometer in C_6D_6 at 25 °C. Gas chromatograms were obtained on a Hitachi 263-30 (FID) with a glass column (1 m) packed with 10% SE-30 using nitrogen as a carrier gas. The measurements of HPLC were carried out using a Hitachi 655 with a Gasukuro Kogyo UNISIL Q-30-5 silica-gel column (4.6 mm×250 mm), a

Hitachi 638-41 variable wavelength UV detector, and a Hitachi 655-61 data processor.

Preparation of Compounds. $CpFe(CO)_2SiMe_2SiMeEt_2$ (1c). A solution of $Na[FeCp(CO)_2]$ (5.2 mmol) in 15 cm^3 of THF was added dropwise over 30 min to a solution of 1-chloro-2,2-diethyl-1,1,2-trimethyldisilane (1.05 g, 2.6 mmol) in THF (15 cm^3) with vigorous stirring at room temperature. After the solution was stirred for additional 18 h, solvent was removed from the reaction mixture under reduced pressure and the dark brown residue was extracted with three 10 cm^3 portions of hexane. The extracts were filtered through a Celite pad, and the filtrates were combined and concentrated. Molecular distillation of the dark red residue at 0.15 Torr† and 80 °C yielded an orange oil of **1c** (1.29 g, 73%); ^1H NMR (C_6D_6) δ=4.14 (5H, s, Cp), 1.2—0.6 (10H, m, Et), 0.57 (6H, s, Me), 0.14 (3H, s, Me); ^{13}C NMR (C_6D_6) δ=215.9 (CO), 83.1 (Cp), 8.5 (CH_3 of Et), 6.4 (CH_2 of Et), 4.5 (Me), −5.2 (Me); MS *m/z* 336 (M^+, 16.3), 235 (34.0), 207 (15.6), 179 (12.5), 159 (100), 131 (95.2), 121 (24.0). Found: C, 50.15; H, 7.25%. Calcd for $C_{14}H_{24}FeO_2Si_2$: C, 50.00; H, 7.19%.

$CpFe(CO)_2SiMeEt_2$ (2c). In a similar manner, the reaction of $Et_2MeSiCl$ (0.73 g, 5.3 mmol) with $Na[FeCp(CO)_2]$ (5.2 mmol) in THF followed by molecular distillation at 0.02 Torr and 80°C gave an orange oil of **2c** (0.95 g, 68%); ^1H NHR (C_6D_6) δ=4.07 (5H, s, Cp), 1.3—0.7 (10H, m, Et), 0.44 (3H, s, Me); ^{13}C NMR (C_6D_6) δ=216.2 (CO), 83.2 (Cp), 14.4 (CH_2), 9.4 (Me), 2.2 (Me); MS *m/z* 278 (M^+, 10.8), 250 (4.8), 249 (3.6), 220 (9.3), 192 (24.9), 164 (11.6), 121 (11.8), 101 (48.0), 93 (23.3), 73 (100). Found: C, 52.05; H, 6.58%. Calcd for $C_{12}H_{18}FeO_2Si$: C, 51.81; H, 6.52%.

$CpFe(CO)_2SiMe_2Et$ (2d). To a solution of dichlorodimethylsilane (10.9 g, 84.5 mmol) in THF (50 cm^3) was added dropwise over 3 h a solution of ethylmagnesium bromide prepared from magnesium ribbon (2.48 g, 0.102 mol) and ethyl bromide (11.0 g, 0.101 mol) in THF (50 cm^3). After the reaction mixture was stirred at room temperature for 24 h, a solution of $Na[FeCp(CO)_2]$ (56 mmol) in THF (150 cm^3) was added dropwise over 2 h to the reaction mixture. The resulting mixture was stirred at room temperature for additional 12 h and then THF was removed in vacuo. To the reddish brown residue was added 200 cm^3 of hexane and the slurry was filtered through a Celite pad. After evaporation of hexane from the filtrate, the resultant dark red oil was purified by molecular distillation at 0.3 Torr and 90 °C yielding an orange oil of **2d** (10.1 g, 68%); ^1H NMR (C_6D_6) δ=4.04 (5H, s, Cp), 1.2—0.7 (5H, m, Et), 0.45 (6H, s, Me); ^{13}C NMR (C_6D_6) δ=216.1 (CO), 83.3 (Cp), 16.4 (CH_2), 9.2 (Me), 4.8 (Me); MS *m/z* 264 (M^+, 27.1), 236 (16.5), 208 (10.0), 206 (34.5), 180 (41.6), 178 (23.3), 121 (26.6), 93 (27.6), 87 (77.4), 59 (100). Found: C, 49.93; H, 6.06%. Calcd for $C_{11}H_{16}FeO_2Si$: C, 50.02; H, 6.11%.

$(MeCp)Fe(CO)_2SiMe_2SiMe_3$ (1b). This compound was prepared by a procedure similar to that of $CpFe(CO)_2SiMe_2SiMeEt_2$ (**1c**). $Me_3SiSiMe_2Cl$ (1.75 g, 10.5 mmol) and $Na[Fe(MeCp)(CO)_2]$ (5.24 mmol) were used as starting materials, and after the usual work-up, molecular distillation at 0.09 Torr and 65 °C gave an orange oil of **1b** (2.42 g, 72%): ^1H NMR (C_6D_6) δ=4.2—3.9 (4H, m, ring protons of MeCp), 1.52 (3H, s, Me of MeCp), 0.55 (6H, s, Me), 0.23 (9H, s, Me); ^{13}C NMR (C_6D_6) δ=216.3 (CO), 101.0 (ring carbon of MeCp), 13.2 (Me), 3.5 (Me), 0.5 (Me); MS *m/z* 322 (M^+, 11.0), 294 (5.0), 264 (11.4), 249 (45.4), 193 (11.3), 131 (100), 73 (50.0). Found: C, 48.20; H, 6.73%. Calcd for $C_{13}H_{22}FeO_2Si_2$: C, 48.45: H, 6.88%.

The IR and electronic spectral data of all disilanyl- and silyliron complexes which were used in this work were listed in Table 1.

Photolysis. Unless otherwise noted, photolysis was carried out as follows: Iron complex(es) and, in some cases, a trapping agent were placed in a Pyrex NMR sample tube (5 mm o.d.) and dissolved in deoxygenated C_6D_6. It was then immersed in the water at room temperature and irradiated with a 450 W medium pressure Hg arc lamp (Ushio UV-450) placed in a water-cooled, quartz jacket. The distance between the light source and the sample tube was about 3 cm. A ^1H NMR spectrum or gas chromatogram of the reaction mixture was taken periodically to monitor the reaction. Identification of products was accomplished by taking gas chromatograms, gas chromatography-mass spectra, ^1H NMR spectra and, in some cases, high performance liquid chromatograms of the reaction mixture and comparing them with the authentic samples prepared by the independent methods. Yields of products were determined by gas chromatography with dodecane as an internal standard and calculated for the consumed starting materials.

Results and Discussion

Photolyses of $CpFe(CO)_2SiMe_2SiMe_3$ (1a) and $(MeCp)Fe(CO)_2SiMe_2SiMe_3$ (1b). Irradiation of a solution of disilanyl complex $CpFe(CO)_2SiMe_2SiMe_3$ (**1a**) with a 450 W medium pressure Hg lamp in a Pyrex tube for 7 min at room temperature consumed 80% of **1a** and gave monosilyl complex $CpFe(CO)_2SiMe_3$ (**2a**) in 64% yield together with ferrocene (4%) and $Cp_2Fe_2(CO)_4$.[18] Similarly, the photolysis of methylcyclopentadienyl derivative $(MeCp)Fe(CO)_2SiMe_2SiMe_3$ (**1b**) for 3 min yielded $(MeCp)Fe(CO)_2$-

Table 1. IR and UV-Vis Spectral Data for Relevant Complexes

Complex	ν_{CO}/cm^{-1} (neat)		λ_{max} (hexane)/nm ($\varepsilon/(mol^{-1}\,dm^3\,cm^{-1})$)
$CpFe(CO)_2SiMe_2SiMe_3$ (**1a**)	1970	1920	284.0 (5000) 330sh (1900)
$CpFe(CO)_2SiMe_2SiMeEt_2$ (**1c**)	1990	1934	285.6 (5100) 330sh (1900)
$(MeCp)Fe(CO)_2SiMe_2SiMe_3$ (**1b**)	1985	1930	285.4 (4900) 330sh (1900)
$CpFe(CO)_2SiMe_3$ (**2a**)	1970	1910	270sh (3700) 322.0 (1600)
$CpFe(CO)_2SiMe_2Et$ (**2d**)	1986	1925	
$CpFe(CO)_2SiMeEt_2$ (**2c**)	1988	1929	
$(MeCp)Fe(CO)_2SiMe_3$ (**2b**)	1990	1932	

† 1 Torr≈133.322 Pa.

$SiMe_3$ (2b) (59%), 1,1′-dimethylferrocene (11%) and $[(MeCp)Fe(CO)_2]_2$ after 64% of **1b** was consumed (Eq 2).

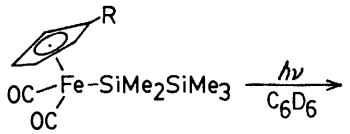

1a: R=H
1b: R=Me

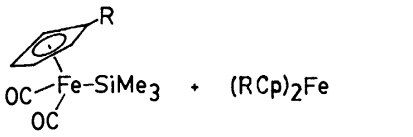

(2)

2a: R=H
2b: R=Me
+ $[(RCp)Fe(CO)_2]_2$

The reactions were monitored either by ^1H NMR spectroscopy or by gas chromatography. Figures 1 and 2 show the changes of ^1H NMR spectrum and gas chromatogram of the reaction mixture of **1a**, respectively. It can be seen that the ^1H NMR signals or the GC peak of **1a** is weakened and those of **2a** newly appear instead. The absence of well-resolved Si-Me signals except that of **2a** on the ^1H NMR spectrum of the final reaction mixture (conversion: 98%) implies that a dimethylsilylene unit, which is considered to be extruded from **1a**, forms a number of oligomeric and/or polymeric products. Results similar to this are also observed for the photolysis of **1b**.

Electronic spectra of disilanyliron complexes **1a—1c** show two characteristic absorption maxima at ca. 285 nm and ca. 330 nm (Table 1, Fig. 3). This fact suggests that the choice of the light source is critical. In fact, irradiation with a low pressure Hg lamp using a quartz NMR tube as a reaction vessel made the reaction more complicated.

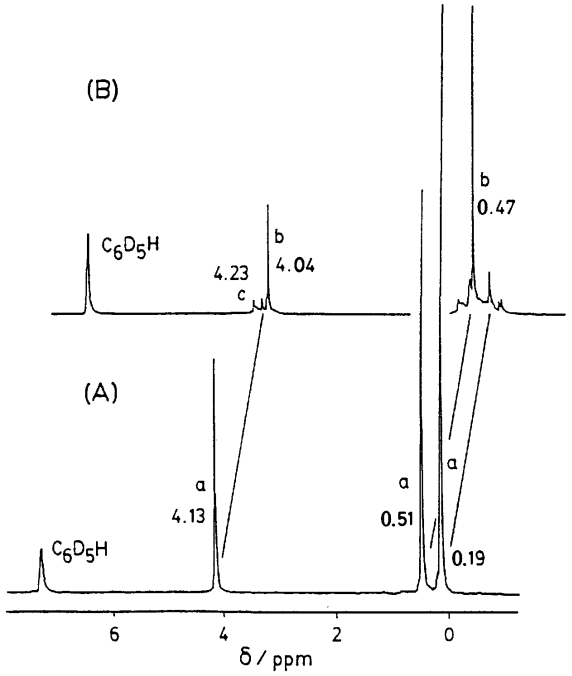

Fig. 1. ^1H NMR spectral change for the photolysis of $CpFe(CO)_2SiMe_2SiMe_3$ (**1a**) in C_6D_6. (A) Before irradiation; (B) after 8 min irradiation. a: $CpFe(CO)_2SiMe_2SiMe_3$, b: $CpFe(CO)_2SiMe_3$, c: $[CpFe(CO)_2]_2$.

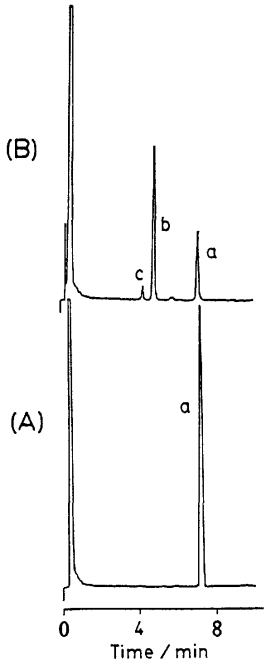

Fig. 2. Change of gas chromatogram for the photolysis of $CpFe(CO)_2SiMe_2SiMe_3$ (**1a**) in C_6D_6. (A) Before irradiation; (B) after 5 min irradiation. a: $CpFe(CO)_2SiMe_2SiMe_3$, b: $CpFe(CO)_2SiMe_3$, c: Cp_2Fe.

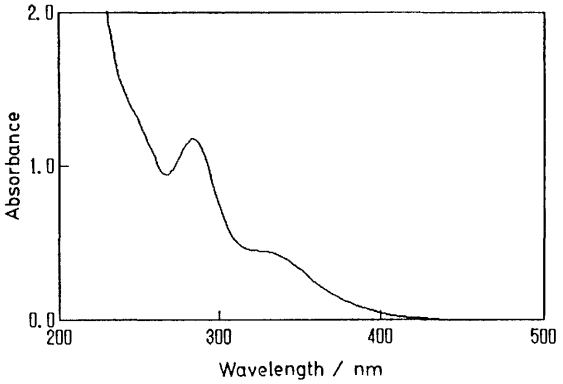

Fig. 3. Electronic spectrum of 2.3×10^{-4}M $CpFe(CO)_2SiMe_2SiMe_3$ (**1a**) in hexane.

Effect of CO Concentration on the Photoreaction of $CpFe(CO)_2SiMe_2SiMe_3$ (1a). $CpFe(CO)_2SiMe_3$ (**2a**) is known to lose one of the coordinated carbonyl ligands by near UV irradiation. Thus, the irradiation of **2a** in the presence of PPh_3 forms $CpFe(CO)(PPh_3)SiMe_3$ as a main product (Eq. 3).[24] By analogy with this reaction, the initial step of the photoreaction of **1a** is likely to be

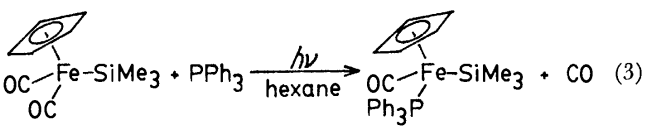

(3)

Table 2. Photolysis of $CpFe(CO)_2SiMe_2SiMe_3$ (**1a**) under a Nitrogen Atmosphere, a Carbon Monoxide Atmosphere, and with a Vigorous Argon Bubbling

Entry	Reaction condition	Conversion/%	Product and yields/%	
			(**2a**)	ferrocene
1	N_2 atmosphere, 7 min	80	64	4
2	CO atmosphere, 4 min	73	88	9
3	Ar bubbling,[a] 5 min	83	22	3

a) Dry argon saturated with benzene vapor was bubbled through the reaction mixture. Flow rate $>15\ cm^3\ s^{-1}$.

the loss of CO.

The effect of CO on the photoreaction of **1a** was investigated by the following two experimental procedures: In the first procedure a solution of **1a** was saturated with CO before irradiation. In the second procedure CO which was considered to be liberated from **1a** was efficiently removed from the system by vigorous argon bubbling through the reaction mixture.[28] The results of these experiments along with that of photolysis under nitrogen atmosphere are summarized in Table 2.

The large decrease of the yield of **2a** in entry 3 is in accord with the light-induced CO loss mechanism. In a preliminary experiment, irradiation of vigorously argon bubbled solution of **2a** in the same conditions as in entry 3 caused decomposition of only 14% of **2a**. Therefore the decrease of **2a** during the photolysis in entry 3 is considered to be almost negligible. The substantial increase of the yield of **2a** in entry 2 comes from the efficient bimolecular CO recombination process. An analogous photochemical behavior including dissociative loss and following recombination of CO is reported with respect to the photolyses of $Me_3SiCo(CO)_4$[29] and $(\eta^5\text{-}C_5Me_5)Fe(CO)_2SiMe_3$[30] in the presence of R_3SiH by Wrighton et al.

Photolysis of $CpFe(CO)_2SiMe_2SiMe_3$ (1a) in the Presence of Silylene-Trapping Agents. As mentioned above, the formation of monosilyl complex **2a** from disilanyl complex **1a** must be a result of expulsion of Me_2Si moiety. Thus, in hopes of trapping this Me_2Si moiety, we employed three different types of silylene-trapping agents, i.e., 2,3-dimethyl-1,3-butadiene (**3**),[31] diethylmethylsilane (**4**),[1] and hexamethylcyclotrisiloxane (**5**).[32] It is known that each of them undergoes a certain type of reaction with dimethylsilylene to give a specific product, **6**, **7**, or **8**, respectively (Eq. 4).

A benzene solution of $CpFe(CO)_2SiMe_2SiMe_3$ (**1a**) and two- to twenty-fold excess of a silylene-trapping agent was irradiated under conditions similar to those of the simple photolysis of **1a**. Contrary to our expectations, no silylene-trapped product was detected from each of those reaction mixtures by means of GC and GC-MS.

From the photolysis of **1a** in the presence of **3** or **5**, formation of a reasonable amount of **2a** was observed. On the other hand, the photolysis of **1a** in the presence of eighteen-fold excess of **4** provided significant amount of $CpFe(CO)_2SiMeEt_2$ (**2c**) (15%) besides **2a** (24%) (conversion: 90%). The formation of **2c** can be interpreted as a result of the silyl group exchange on iron complexes through successive oxidative addition and reductive elimination of hydrosilanes (Scheme 1).[29,30] In fact, when **2a** was irradiated in the presence

$$CpFe(CO)_2SiMe_2R \overset{h\nu}{\rightleftarrows} CpFe(CO)SiMe_2R + CO$$

1a: R=$SiMe_3$

2a: R=Me

$$CpFe(CO)SiMe_2R + Et_2MeSiH \rightleftarrows CpFe(CO)H(SiMe_2R)(SiMeEt_2)$$

$$CpFe(CO)H(SiMe_2R)(SiMeEt_2) \rightleftarrows CpFe(CO)SiMeEt_2 + RMe_2SiH$$

$$CpFe(CO)SiMeEt_2 + CO \overset{h\nu}{\rightleftarrows} CpFe(CO)_2SiMeEt_2 \quad (\mathbf{2c})$$

Scheme 1.

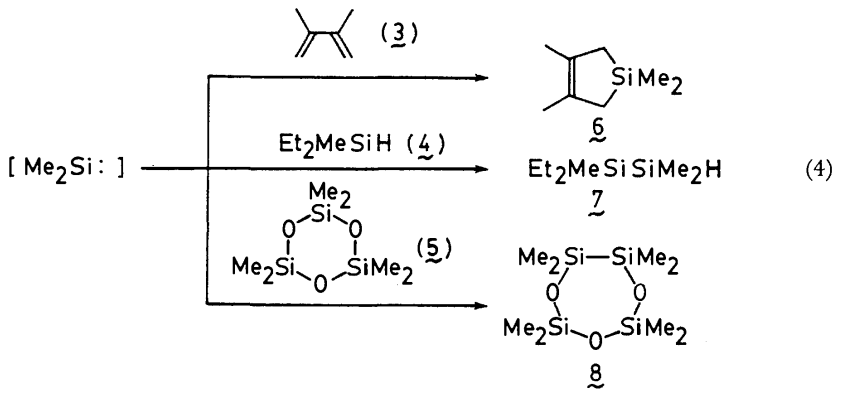

(4)

of 10 mol equiv of Et_2MeSiH, **2c** was formed in 53% yield based on 55% conversion of **2a**.

Carbon monoxide generated during the photolysis might be a silylene trapping agent. However, the following two respects seem to make this possibility unlikely: (a) The concentration of free carbon monoxide in the reaction mixture is thought to be extremely low compared with that of added trapping agent throughout the reaction; (b) since the yield of **2a** is 64% under a nitrogen atmosphere, the amount of extruded dimethylsilylene exceeds that of carbon monoxide liberated into the solution. This means that all dimethylsilylene can not be trapped by carbon monoxide if one carbon monoxide reacts with one dimethylsilylene. Therefore these results suggest the existence of some unknown route of excluding Me_2Si unit without generating free dimethylsilylene. Loss of Me_2Si unit from silylene-metal intermediate without being trapped with some trapping agents are also reported by Pannell et al. in the photolysis of $CpFe(CO)_2SiMe_2$-$SiPh_3$[17] and by Sakurai et al. in the pyrolysis of disilacyclohexadiene iron complexes (Eq. 5).[13]

Photolysis of $CpFe(CO)_2SiMe_2SiMeEt_2$ (1c). The fact that Me_2Si unit is extruded from **1a** without being trapped suggests the complexity of the mechanism of photochemical conversion from **1a** to **2a**. To probe the structure and reactivity of intermediates in this reaction, two methyl groups on **1a** was changed to ethyl groups and the diethyl derivative **1c** was photolyzed under the same reaction conditions. Surprisingly, after 69% conversion of **1c**, three monosilyliron complexes, $CpFe(CO)_2SiMeEt_2$ (**2c**), $CpFe(CO)_2SiMe_2Et$ (**2d**), and $CpFe(CO)_2SiMe_3$ (**2a**) were obtained in 26, 33, and 4% yields, respectively, together with 7% of ferrocene (Eq 6). Monosilyl complexes **2d** and **2a** can not be formed by only the cleavage of relatively weak Si-Si and Si-Fe bonds of **1c**. Therefore it is necessary to postulate the alkyl migration between silicon atoms, although that type of reaction is very rare. To our knowledge, there are two sorts of reactions accompanying alkyl migration between two silicon atoms: The one is the 1,3-migration of a methyl group between the two silicon atoms in a cationic intermediate generated in the reaction of $(Me_3Si)_3CSiR_2I$ with silver salts,[33] and the other is the [1,3]sigmatropic shifts of methyl and phenyl groups from a saturated Si atom to an unsaturated one in dimethyl[bis(trimethylsilyl)methylene]silane or its phenyl- or *t*-butyl-substituted derivatives.[34-37] Particularly, the degenerate [1,3]-sigmatropic shift of the methyl group in dimethyl[di-*t*-butylmethylsilyl(trimethylsilyl)methylene]silane (**9**) is fast enough even at 30°C to broaden the peaks in the ^1H NMR spectrum (Eq. 7).[37]

Concerted, symmetry-allowed reaction mechanism undoubtedly plays an important role for these systems to decrease the activation energy of alkyl migration. A

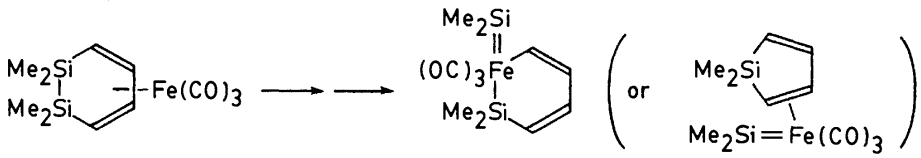

(5)

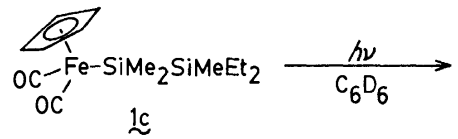

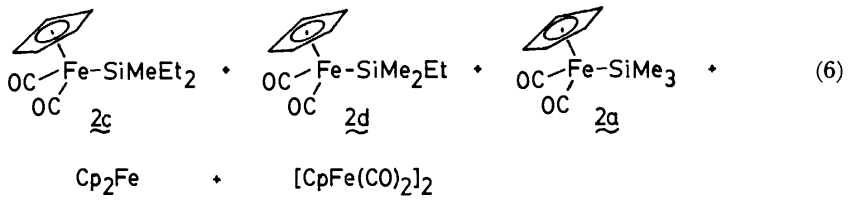

(6)

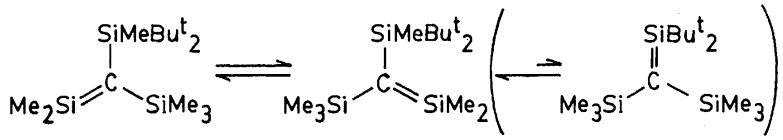

(7)

9

similar concerted mechanism and perhaps a similar structure of intermediates involving an unsaturated silicon atom seem to be necessary to explain the unusually fast shift of alkyl groups in the photoreaction of **1c**. A possible mechanism will be discussed later in datail.

Photolysis of a 1 : 1 Mixture of $(MeCp)Fe(CO)_2SiMe_2SiMe_3$ (1b) and $CpFe(CO)_2SiMe_2SiMeEt_2$ (1c). It is important to determine whether the photochemical conversion from disilanyl complex to monosilyl complex proceeds intramolecularly or intermolecularly. If only an intramolecular mechanism is operative in the reaction, we can discard some mechanisms including split intermediates such as radicals, solvent separated ion pairs, etc., and possible mechanisms can be greatly limited. The lack of triethylsilyl derivative $CpFe(CO)_2SiEt_3$ in the products of the photolysis of **1c** as shown in the previous section is suggestive of the intramolecular mechanism. Thus, to obtain more reliable answer to this question, we performed the cross reaction of two substrates, **1b** and **1c**, in which the former has an iron atom labeled with methylcyclopentadienyl ligand and a disilanyl group labeled with five methyls, while the latter has an iron atom labeled with unsubstituted cyclopentadienyl ligand and a disilanyl group labeled with two ethyls and three methyls. It is apparent from the result mentioned above that a methyl group on the cyclopentadienyl ligand has almost no effect on the photoreaction (Eq 2).

When a benzene solution of a 1:1 mixture of $(MeCp)Fe(CO)_2SiMe_2SiMe_3$ (**1b**) and $CpFe(CO)_2SiMe_2SiMeEt_2$ (**1c**) was irradiated under a nitrogen atmosphere, ferrocene, 1-methylferrocene, 1,1′-dimethylferrocene, $CpFe(CO)_2SiMe_3$ (**2a**), $(MeCp)Fe(CO)_2SiMe_3$ (**2b**) (39%), $CpFe(CO)_2SiMe_2Et$ (**2d**) (28%), and $CpFe(CO)_2SiMeEt_2$ (**2c**) (21%) were detected by GC-MS. Yields of ferrocenes and $CpFe(CO)_2SiMe_3$ (**2a**) were not determined because the GC peaks of them were not fully separated (Fig. 4).

Scheme 2 shows the products expected from intramolecular and intermolecular alkyl migrations. Here, the intermolecular alkyl migrations include not only the intermolecular migration of an alkyl group itself but also that of silyl groups, e.g., $SiMeEt_2$, $SiMe_2Et$, etc. None of the products which are expected only from intermolecular alkyl migrations was detected in the reaction mixture by GC-MS. Therefore the possibility of intermolecular alkyl migration mechanisms is effectively ruled out.

Mechanism of Photochemical Conversion from Disilanyliron Complexes to Monosilyliron Complexes. The following points were revealed in this study: (1) The reaction may be initiated by a light-induced CO loss and completed by a CO re-coordination; (2) unusually fast intramolecular alkyl migration from one silicon atom to the other occurs during the photoreaction, and the existence of concerted process such as the sigmatropic shift is suggested; (3) The R_2Si unit

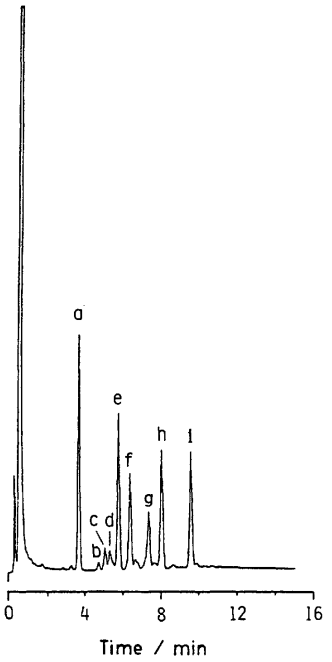

Fig. 4. Gas chromatogram after a 1:1 mixture of **1b** and **1c** was photolyzed for 8 min. a: dodecane, b: $FeCp_2$, c: FeCp(MeCp), d: $Fe(MeCp)_2$+$CpFe(CO)_2SiMe_3$, e: $(MeCp)Fe(CO)_2SiMe_3$, f: $CpFe(CO)_2SiMe_2Et$, g: $CpFe(CO)_2SiMeEt_2$, h: $(MeCp)Fe(CO)_2SiMe_2SiMe_3$, i: $CpFe(CO)_2SiMe_2SiMeEt_2$.

$$(MeCp)Fe(CO)_2SiMe_2SiMe_3 + CpFe(CO)_2SiMe_2SiMeEt_2$$
1b **1c**

$h\nu$ | C_6D_6

(a) $(MeCp)Fe(CO)_2SiMe_3$; $CpFe(CO)_2SiMe_3$, $CpFe(CO)_2SiMe_2Et$, $CpFe(CO)_2SiMeEt_2$

(b) $(MeCp)Fe(CO)_2SiMe_2Et$, $(MeCp)Fe(CO)_2SiMeEt_2$, $(MeCp)Fe(CO)_2SiEt_3$; $CpFe(CO)_2SiEt_3$

(a) Products expected from an intramolecular alkyl migration mechanism.
(b) Products expected from an intermolecular alkyl migration mechanism.

Scheme 2.

extruded in this photochemical conversion could not be trapped with usual silylene trapping agents. This fact implies the existence of some unknown route of excluding R_2Si unit without generating free silylene.

Although the third point is still obscure, we can construct the principal framework of the possible mechanism as shown in Scheme 3. The key intermediate is silyl(silylene)iron complex B which is very likely to be formed by 1,2-migration of the terminal silyl group to the 16e metal center of intermediate **A**. Moreover, it is worth noticing that this intermediate **B**

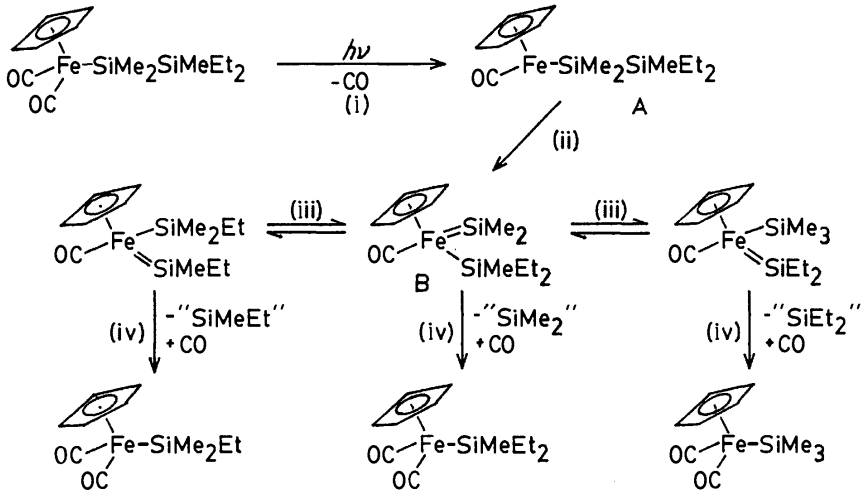

Scheme 3.

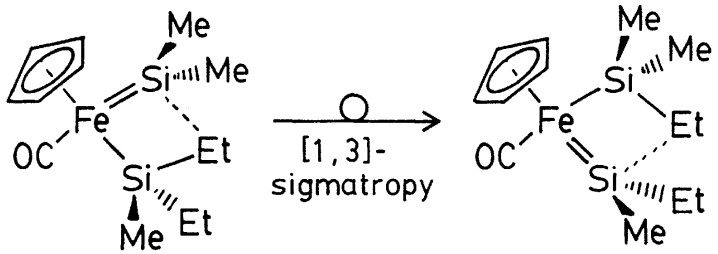

Scheme 4.

takes an ideal geometry for [1,3]sigmatropic shift of an alkyl group from a saturated Si atom to an unsaturated one as depicted in Scheme 4.

The mechanism contains four successive reactions which are essentially similar to those proposed by Pannell et al. for the photoreaction of $CpFe(CO)_2SiMe_2$-$SiPh_3$:[18] (i) Photochemically induced loss of CO to generate a coordinatively unsaturated complex A; (ii) 1,2-shift of the terminal silyl group to the Fe atom; the formation of a silyl(silylene)iron complex B; (iii) [1,3]sigmatropic alkyl shift from a saturated Si atom to an unsaturated one; and (iv) ligand substitution of dialkylsilylene by carbonyl.

The product ratio in the photolysis of $CpFe(CO)_2$-$SiMe_2SiMeEt_2$ turned out to be $CpFe(CO)_2SiMe_3$: $CpFe(CO)_2SiMe_2Et$: $CpFe(CO)_2SiMeEt_2$=0.7 : 6 : 4.7. Therefore interconversion between three silyl(silylene)-iron complexes (iii) seems to be quicker than the ligand substitution of dialkylsilylene by carbonyl, since the observed product ratio is relatively close to the statistically predicted product ratio after reaching an equilibrium of the interconversion: $CpFe(CO)_2Si$-Me_3 : $CpFe(CO)_2SiMe_2Et$: $CpFe(CO)_2SiMeEt_2$=1 : 6 : 3 on the assumption that methyl and ethyl groups behave identically.

Low-temperature photolysis of **1a** was carried out in hopes of observing the silyl(silylene)iron complexes. However, irradiation in a methylcyclohexane matrix at 77 K resulted in little net photoreaction. In comparison with the efficient photochemical conversion of $(\eta^5\text{-}C_5Me_5)Fe(CO)_2CH_2SiMe_2H$ to $(\eta^5\text{-}C_5Me_5)Fe(CO)$-$(CH_2SiMe_2)H$ at 77 K,[38] this low efficiency may be attributable to the difficulty of migration of bulky trimethylsilyl group in a relatively hard methylcyclohexane matrix.

The authors are greatly indebted to Prof. Hideki Sakurai, Tohoku University, for his warm encouragement and helpful discussion during the course of this work. This work has been supported by Grants-in-Aid for Special Project Research, No. 61125007, and for Scientific Research, Nos. 60430011 and 62740340, from the Ministry of Education, Science and Culture.

References

1) P. P. Gaspar, "Reactive Intermediates," ed by M. Jones, Jr., and R. A. Moss, Wiley-Interscience, New York (1978), Vol. 1, pp. 229—77 and (1981), Vol. 2, pp. 335—85.

2) P. P. Gaspar and B. J. Herold, "Carbene Chemistry," 2nd ed., ed by H. W. Kirmse, Academic Press, New York (1971), pp. 504—37.

3) T. J. Drahnak, J. Michl, and R. West, *J. Am. Chem. Soc.*, **101**, 5427 (1979).

4) T. J. Drahnak, J. Michl, and R. West, *J. Am. Chem. Soc.*, **103**, 1845 (1981); C. A. Arrington, K. A. Klingensmith, R. West, and J. Michl, *J. Am. Chem. Soc.*, **106**, 525 (1984).

5) A. S. Nazran, J. A. Hawari, D. Griller, I. S. Alnaimi, and W. P. Weber, *J. Am. Chem. Soc.*, **106**, 7267 (1984).

6) P. Jutzi, D. Kanne, and C. Krüger, *Angew. Chem., Int. Ed. Engl.*, **25**, 164 (1986).
7) N. S. Hosmane, P. de Meester, U. Siriwardane, M. S. Islam, and S. S. C. Chu, *J. Chem. Soc., Chem. Commun.*, **1986**, 1421.
8) H. Fischer, "The Chemistry of the Metal-Carbon Bond," ed by F. R. Hartley and S. Patai, Wiley, New York (1982), Vol. 1, pp. 181—231.
9) H. Sakurai, Y. Kamiyama, and Y. Nakadaira, *Angew. Chem., Int. Ed. Engl.*, **17**, 674 (1978). Professor Sakurai informed us that the silylene complex reported previously was in fact a disilanyliron complex. Details will be reported elsewhere.
10) G. Schmid and E. Welz, *Angew. Chem., Int. Ed. Engl.*, **16**, 785 (1977).
11) C. Zybill and G. Müller, *Angew. Chem., Int. Ed. Engl.*, **26**, 669 (1987).
12) D. A. Straus, T. D. Tilley, A. L. Rheingold, and S. J. Geib, *J. Am. Chem. Soc.*, **109**, 5872 (1987).
13) Y. Nakadaira, T. Kobayashi, and H. Sakurai, *J. Organomet. Chem.*, **165**, 399 (1979).
14) H. Sakurai, Y. Kamiyama, and Y. Nakadaira, *J. Organomet. Chem.*, **184**, 13 (1980); G. Thum and W. Malisch, *J. Organomet. Chem.*, **264**, C5 (1984).
15) K. Yamamoto, H. Okinoshima, and M. Kumada, *J. Organomet. Chem.*, **27**, C31 (1971); H. Okinoshima, K. Yamamoto, and M. Kumada, *J. Am. Chem. Soc.*, **94**, 9263 (1972); I. Ojima, S. Inaba, T. Kogure, and Y. Nagai, *J. Organomet. Chem.*, **55**, C7 (1973); H. Sakurai, Y. Kamiyama, and Y. Nakadaira, *J. Am. Chem. Soc.*, **99**, 3879 (1977).
16) H. Kang, D. B. Jacobson, S. K. Shin, J. L. Beauchamp, and M. T. Bowers, *J. Am. Chem. Soc.*, **108**, 5668 (1986).
17) K. H. Pannell, J. Cervantes, C. Hernandez, J. Cassias, and S. Vincenti, *Organometallics*, **5**, 1056 (1986).
18) H. Tobita, K. Ueno, and H. Ogino, *Chem. Lett.*, **1986**, 1777.
19) H. Sakurai, K. Tominaga, T. Watanabe, and M. Kumada, *Tetrahedron Lett.*, **1966**, 5493.
20) This compound was prepared owing to standard procedures shown in the following equation.

$$PhMe_2SiLi + Et_2MeSiCl \xrightarrow[THF]{} PhMe_2SiSiMeEt_2$$

$$\xrightarrow[benzene]{HCl,\ cat.\ AlCl_3} ClMe_2SiSiMeEt_2$$

21) F. P. Price, *J. Am. Chem. Soc.*, **69**, 2600 (1947).
22) J. W. Jenkins and H. W. Post, *J. Org. Chem.*, **15**, 556 (1950); A. G. Taylor and B. V. de G. Walden, *J. Am. Chem. Soc.*, **66**, 842 (1944).
23) R. B. King and F. G. A. Stone, *Inorg. Synth.*, **7**, 110 (1963).
24) R. B. King and K. H. Pannell, *Inorg. Chem.*, **7**, 1510 (1968).
25) R. B. King, K. H. Pannell, C. R. Bannett, and M. Ishaq, *J. Organomet. Chem.*, **19**, 327 (1969).
26) S. R. Berryhill, G. L. Clevenger, and F. Y. Burdurlu, *Organometallics*, **4**, 1509 (1985).
27) C. W. Young, P. C. Servais, C. C. Currie, and M. Hunter, *J. Am. Chem. Soc.*, **70**, 3758 (1948).
28) J. P. Blaha, B. E. Bursten, J. C. Dewan, R. B. Frankel, C. L. Randolph, B. A. Wilson, and M. S. Wrighton, *J. Am. Chem. Soc.*, **107**, 4561 (1985).
29) F. R. Anderson and M. S. Wrighton, *J. Am. Chem. Soc.*, **106**, 995 (1984).
30) C. L. Randolph and M. S. Wrighton, *J. Am. Chem. Soc.*, **108**, 3366 (1986).
31) W. H. Atwell and D. R. Weyenberg, *J. Am. Chem. Soc.*, **90**, 3438 (1968); P. P. Gaspar and R.-J. Hwang, *J. Am. Chem. Soc.*, **96**, 6198 (1974).
32) H. S. D. Soysa, H. Okinoshima, and W. P. Weber, *J. Organomet. Chem.*, **133**, C17 (1977).
33) C. Eaborn, D. A. R. Happer, S. P. Hopper, and K. D. Safa, *J. Organomet. Chem.*, **188**, 179 (1980); C. Eaborn, P. D. Lickiss, G. Marquina-Chidsey, and E. Y. Thorli, *J. Chem. Soc., Chem. Commun.*, **1982**, 1326.
34) G. Raabe and J. Michl, *Chem. Rev.*, **85**, 419 (1985).
35) C. Eaborn, D. A. R. Happer, R. B. Hitchcock, S. P. Hopper, K. D. Safa, S. S. Washburne, and D. R. M. Walton, *J. Organomet. Chem.*, **186**, 309 (1980).
36) M. Ishikawa, K. Nishimura, H. Ochiai, and M. Kumada, *J. Organomet. Chem.*, **236**, 7 (1982).
37) N. Wiberg, *J. Organomet. Chem.*, **273**, 141 (1984); N. Wiberg, G. Wagner, and G. Müller, *Angew. Chem., Int. Ed. Engl.*, **24**, 229 (1985).
38) C. L. Randolph, and M. S. Wrighton, *Organometallics*, **6**, 365 (1987).

 © 1988 The Chemical Society of Japan Bull. Chem. Soc. Jpn., 61, 2805—2810 (1988)

The Synthesis, and the Crystal and Molecular Structures of Tetraethylammonium [Aquaheptakis(thiocyanato)lanthanoidate(III)], $[(C_2H_5)_4N]_4[M(SCN)_7(H_2O)]$, (M=La, Ce, Pr; Nd, Dy, Er): The Complexes in a Cubic Octa-Coordination Geometry

Yoshikuni TATEYAMA,† Yasumitsu KUNIYASU,† Yasuo SUZUKI,† and Akira OUCHI*
Department of Chemistry, College of Arts and Sciences, The University of Tokyo, Komaba, Meguro-ku, Tokyo 153
†Department of Industrial Chemistry, Faculty of Engineering, Meiji University, Higashi-mita, Tama-ku, Kawasaki, Kanagawa 214
(Received March 5, 1988)

The title complexes have been synthesized, and their crystal and molecular structures were determined by the X-ray diffraction method using their single crystals. Among them, the crystals of the La, Ce, and Pr complexes are isomorphous; cubic, space group $Pm\bar{3}$, $Z=1$, and the cell constants of the Pr complex, for example, are $a=11.513(2)$ Å, $U=1526.1(5)$ Å^3, and the final R value was 0.093. The Nd, Dy, and Er complexes, another group of the isomorphous complexes obtained almost by the same synthetic method, are tetragonal, space group $I4/m$, $Z=2$, and the cell constants of the Er complex, for example, are $a=11.564(2)$, $c=22.627(4)$ Å, $U=3026(3)$ Å^3, and the final R value was 0.071. The coordination geometry around the metal atoms of both types of complexes are almost the same: seven thiocyanato nitrogen and one water oxygen atoms are coordinated in a cubic geometry, being disordered as if each ligating atomic position is equally occupied by 1/8 atom of the water oxygen and 7/8 atoms of the thiocyanato nitrogen. In the lattice of the former three complexes, the tetraethylammonium nitrogen atoms occupy all Cl^- ionic positions of the NaCl-type lattice, while the metal atoms only the apex Na^+ ionic positions; not the face-center ones. The unit cells of the latter three complexes are apparently consist of the two former cubic type cells being piled on the c-axis direction, where the arrangement of the atoms is different from the former only on the plane where two original cells are contact: metal and ammonium nitrogen positions slide 0.5 both to a- and b-axis directions. Thus each metal atom of the both type complexes is surrounded by six tetraethylammonium nitrogen atoms on both sides of the a, b, and c-axis directions.

Lanthanoids(III) are known to be very hard elements,[1] and oxygen-coordinating ligands are most easily bonded to them. However, it is known that some nitrogen-containing ligands are also capable of being ligated to the metal atoms, forming stable complexes, when they are synthesized in anhydrous medium:[2] the structures of lanthanoid complexes with some such ligands were already reported.[3-5]

A thiocyanate ion (SCN) shows a variety of very interesting behaviors in its metal complexes: depending on the hardness of the metal, it is coordinated with its nitrogen or sulfur atom. In other cases it forms anionic complexes of the type $(M^{m+}(SCN)_n]^{(n-m)-}$ or the polymeric complexes connected by the [M-SCN-M']-type bridgings.[6] In some anionic thiocyanato complexes, the structure changes sensitively depending on the kinds of counter cations. For example, in the case of the tris(thiocyanato)cadmates, its rubidium, cesium, and tetramethylammonium salts have the respective types of network strucrtures.[7,8]

Only a few structural data of the thiocyanato complexes of lanthanoids(III) have been reported so far. The structures of the tetrabutylammonium salts of hexakis(thiocyanato)lanthanoidates(III), where the metals are praseodymium through ytterbium or yttrium, were reported: their metal atoms are ligated with six SCN nitrogen atoms being in an octahedral geometry.[9] It is very interesting that the coordination number of the metal atom is of such low value, even though the SCN ion is not a massive ligand. On the other hand, Lazarev has reported the structures of some aqua-thiocyanato mixed complexes of neodymium and europium, where four water oxygen as well as four SCN nitrogen atoms are ligated in a square-antiprism geometry.[10] In cases of the SCN complexes of uranium(IV), $[(C_2H_5)_4N]_4[U(SCN)_8]$, the central metal atom is in a cubic geometry, while in its cesium salt, the metal atom is in a square-antiprism geometry.[11,12] Referring to these data, it was thought to be interesting to study in more detail the structures of the thiocyanato complexes of lanthanoids.

Since we could obtain the crystals of the title complexes, their crystal and molecular structures were determined by the X-ray diffraction method, using their single crystals.

Experimental

Synthesis of Tetraethylammonium [Aquaheptakis(thiocyanato)praseodymate(III)]. The metal and tetraethylammonium thiocyanates were obtained by metathesis reactions between their hydrated chlorides and potassium thiocyanate in methanolic medium, as in the cases of the other metal thiocyanates.[13] As the starting metal thiocyanate, the obtained methanolic solution was used directly without drying up.

To the methanolic solution of the praseodymium thiocyanate (15 cm^3, containing 2.0 mmol of Pr), tetraethylammonium thiocyanate (1.5 g, 8.0 mmol), and 0.5 cm^3 of water were added. The mixed solution was left standing in a silica gel desiccator until the volume of the solution reduced to about 8 cm^3, and the deposited crystals were separated, washed with a little portion of methanol, and dried in air. Yield: 1.3 g (1.2 mmol, 60%). Almost by the same way, the isomorphous lanthanum and cerium salts were obtained: starting from 2.0 mmol of the lanthanum(III) or cerium(III)

thiocyanate in methanolic solution, 0.5 cm^3 of water, and tetraethylammonium thiocyanate (1.5 g, 8.0 mmol), the yield of their complexes were 1.5 g (1.4 mmol, 69%), and 1.4 g (1.3 mmol, 65%), respectively.

Their elemental analyses are shown in Table 1.

Although these complex crystals were not deposited from the severely dried medium, several tenths of a gram of water per one mmol of metal salt is sufficient to synthesize the products: the included water was hardly removed, even when they were left standing in a silica gel desiccator for several days; however, they became dehydrated after a longer time. On the other hand, the use of the solvent containing more water (the authors have tried up to 2 : 1=v/v in concentration of the methanol-water mixture) gave the same product; however, as the complexes were readily soluble in such a solvent, we had to evaporate the solvent more, and the yield as well as the purity were inferior.

Attempts to synthesize such complexes of the heavier lanthanoids were not successful: in such cases, the complexes written in the following section were always obtained.

The Synthesis of Tetraethylammonium [Aquaheptakis(thiocyanato)erbate(III)]. The starting materials, metal and tetraethylammonium thiocyanates, were obtained in the same way. To a methanolic solution of erbium(III) thiocyanate (15 cm^3, including 2.0 mmol of Er), tetraethylammonium thiocyanate (1.5 g, 8.0 mmol), and 0.5 cm^3 of water were added and dissolved. The solution was kept in a silica-gel desiccator until about 80% of the solvent was evaporated off. The deposited crystals were separated, washed with a small portion of methanol, and dried in air. Yield: 1.2 g (1.1 mmol, 54%). The neodymium and the dysprosium salts were obtained almost in the same way: started from 2.0 mmol of neodymium or dysprosium thiocyanate in methanolic solution, the yields of the complexes were 1.6 g (1.5 mmol, 74%), and 1.4 g (1.3 mmol, 63%), respectively.

Their elemental analyses are shown in Table 1.

In these cases, too, when more water was added into the solution, the yields of the products were lowered. By this synthetic process, neither lanthanum through prasedymium complexes of this type were obtained.

X-Ray Structure Analysis. The crystallographic data, the sizes of the used crystals (approximately parallelepiped in shape, and the colors are; the Pr salt, pale green, the Nd salt, pale violet; the Er salt, pale pink; the others, colorless), and various experimental conditions are listed in Tables 2A and 2B. Reflections were collected on a Rigaku AFC-6A automated four-circle X-ray diffractometer with graphite monochromated Mo $K\alpha$ radiation (λ=0.71073 Å), ω-2θ scan technique being employed (scan speed was 4° min^{-1} (θ)). The intensities were corrected for Lorentz and polarization factors, but no correction was made for the absorption and extinction.

Table 1. Elemental Analyses of the Complexes $[(C_2H_5)_4N]_4[M(SCN)_7(H_2O)]$, $MC_{39}H_{82}N_{11}OS_7$ (M=La, Ce, Pr, Nd, Dy, and Er) (*n*/%)

M		M	C	H	N
La	Found	13.06	43.15	7.42	14.24
	Calcd	12.81	43.19	7.62	14.21
Ce	Found	12.66	42.69	7.36	13.89
	Calcd	12.91	43.14	7.61	14.19
Pr	Found	13.17	42.70	7.34	13.98
	Calcd	12.97	43.11	7.61	14.18
Nd	Found	13.11	42.87	7.37	14.19
	Calcd	13.23	42.98	7.58	14.14
Dy	Found	14.70	41.92	7.21	13.83
	Calcd	14.66	42.27	7.46	13.90
Er	Found	15.09	42.10	7.28	13.90
	Calcd	15.03	42.09	7.43	13.84

Table 2. Crystallographic Data and Various Experimental Conditions to Obtain the Reflection Intensities

A. Light Lanthanoid Complexes $[(C_2H_5)_4]_4[M(SCN)_7(H_2O)]$, $MC_{39}H_{82}N_{11}OS_7$, (M=La, Ce, Pr), Cubic, $Pm\bar{3}$, Z=1

M=	La	Ce	Pr
F. W.	1084.5	1085.7	1086.5
a(*l*/Å)	11.540(4)	11.530(4)	11.513(2)
U(*v*/Å^3)	1536.7(9)	1532.8(10)	1526.1(5)
D_m(*d*/g cm^{-3})	1.16(3)	1.19(3)	1.19(3)
D_x(*d*/g cm^{-3})	1.17	1.18	1.18
μ(Mo $K\alpha$)(*n*/cm^{-1})	9.74	10.15	10.65
N_m[a]	2266	3143	3137
N_c[b]	449	683	589
R[c]	0.124	0.099	0.093
V_c[d](*v*/mm^3)	0.30×0.30 ×0.15	0.20×0.35 ×0.12	0.30×0.20 ×0.25
S_W[e](θ/°)	1.30+0.5tanθ	1.10+0.5tanθ	1.30+0.5tanθ
S_R[f](2θ/°)	3—60	3—65	3—65

B. Heavy Lanthanoid Complexes $[(C_2H_5)_4]_4[M(SCN)_7(H_2O)]$, $MC_{39}H_{82}N_{11}OS_7$, (M=Nd, Dy, Er), Tetragonal, $I4/m$, Z=2

M=	Nd	Dy	Er
F. W.	1089.9	1108.1	1112.9
a(*l*/Å)	11.569(2)	11.556(2)	11.564(2)
c(*l*/Å)	22.755(4)	22.605(4)	22.627(4)
U(*v*/Å^3)	3046(2)	3018.7(11)	3026(3)
D_m(*d*/g cm^{-3})	1.19(3)	1.21(3)	1.21(3)
D_x(*d*/g cm^{-3})	1.19	1.22	1.23
μ(Mo $K\alpha$)(*n*/cm^{-1})	11.23	15.55	17.16
N_m[a]	3094	2207	3056
N_c[b]	839	783	793
R[c]	0.0771	0.0807	0.0707
V_c[d](*v*/mm^{-3})	0.30×0.30 ×0.25	0.40×0.20 ×0.20	0.35×0.22 ×0.22
S_W[e](θ/°)	1.12+0.5tanθ	1.30+0.5tanθ	1.21+0.5tanθ
S_R[f](2θ/°)	3—65	3—60	3—65

a) Number of reflections measured (all positive *hkl* region was surveyed). b) Reflections used for the calculation (reflections of $|F_o|>3\sigma(|F_o|)$ were used). c) $R=\sum||F_o|-|F_o||/\sum|F_o|$. d) Size of crystals used. e) Scan width. f) Scanned range.

Structure Determination. The crystal system of the La, Ce, and Pr complexes, which are isomorphous with each other, was ascertained by the facts that the respective Weisenberg photographs rotated around three unit-cell axes are the same, and that the measured intensities of the corresponding reflections are almost the same. The space group of the Nd, Dy, and Er complexes, which are isomorphous with each other, was ascertained by the regular extinction of the reflections, and the comparison of the measured intensities of the corresponding reflections of both the Weisenberg pho-

tographs rotated around the unit cell axes, as well as of the intensity data obtained by a diffractometer.

The structures of the praseodymium and the erbium salts were solved by the heavy-atom method, respectively. The positions of the metal and sulfur atoms were deduced from their three-dimensional Patterson map; other non-hydrogen atoms were located by successive Fourier syntheses. Their positional, isotropic and, then, anisotropic thermal parameters were refined by a block-diagonal least-squares method. All hydrogen atoms were excluded from the structure factor calculations. The structure analyses of the other isomorphous salts were started from their final positional and final isotropic thermal parameters of the praseodymium or the erbium complex; they were refined in the same way.

All calculations were carried out on a HITAC M-680H computer at the Computer Center of the University of Tokyo, using a local version of the UNICS progrm.[14] The atomic scattering factors were taken from Ref. 15.

In the case of the praseodymium complex, according to the request of the symmetry regulations of the space group, many positional as well as anisotropic thermal parameters were fixed or equated with each other. Other than the ruled ones, the x and z coordinates of C(11) and C(13) atoms are assumed to be equal to the x and y coordinates of the C(12) and C(14) atoms, respectively, because they take equivalent positions around the nitrogen atom from each other.

The metal atom is at the center of symmetry, 0 0 0, and the atoms of the SCN ions are restricted to be arranged on the [±1±1±1] axes. However, from the result of their elemental analyses, as well as from the charge balance aspect, each complex contains only seven SCN ions; one water atom is coordinated to the metal atom other than the SCN ions. Attempted structure analyses assuming other lower symmetry space groups did not result in much improvement, except in some cases where a slightly better R values were obtained. However, these may only have been due to increase in the number of parameters. Therefore, we have assumed the disorder of the water molecule and the thiocyanate ions: respective eight coordinating positions around the metal atom are occupied equally by 1/8 molecules of water and 7/8 ions of SCN. Excepting this comples, in $[Co(NCS)(NH_3)_5]Cl_2$[16] too, all six coordinating positions around the cobalt atom are occupied equally by a disordered SCN ion (1/6) and ammonia molecules (5/6). During the calculation, the input positional parameters of the ligating oxygen atom was fixed as if the atom was on the [111] axis, and the distance from the metal atom is the sum of the metal (coordination number is 8, valence is 3+), and an oxygen (coordination number is 2, valence is 2−) atomic radii proposed by Shannon.[17]

There are crystallographically two independent kinds of tetraethylammonium ions; their ethyl carbon atoms are also disordered. The positions of the carbon atoms around the N(11) and N(21) atoms are shown schematically in Figs. 1A and 1B, respectively. Although one possible selection of the four ethyl group position are shown in the respective figures by thick lines, there are many other possible selections keeping the tetrahedrally bonding geometry around the nitrogen atom as well as the sp^3 angles of the N-C-C bonds: we have assumed that all equivalent positions of the respective carbon atoms are equally occupied. The multiplicities of the respective atoms used in the calculation are shown in Table 3.

In the cases of the erbium and its isomorphous salts, their anionic complex ions are approximately in a cubic (though not exact cube) coordination geometry around their metal atoms, which are at the centers of symmetry, 0 0 0 and 0.5 0.5 0.5. To these complexes, too, the same type of disorder of the water molecule and of the SCN ions around each metal atom is assumed: each coordination position is occupied by 1/8 atom of the water oxygen and 7/8 atoms of the SCN nitrogen atoms. The position of the coordinated water oxygen atom was fixed as in the case of the light lanthanoid complexes. The ethyl carbon atoms around a central tetraethylammonium nitrogen atom are also disordered. Arrangements of the ethyl carbon atoms around both N(11) and N(21) atoms are in the type schematically shown in Fig. 1A, and the occupancies of the respective equivalent positions of the car-

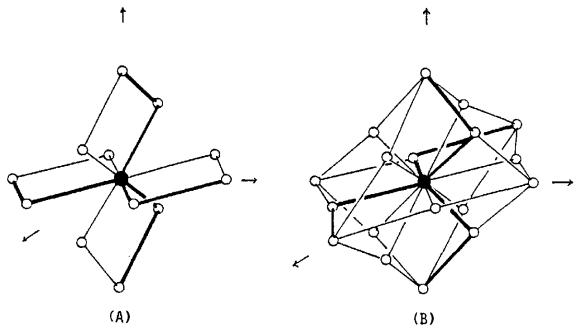

Fig. 1. Schematic presentation of the arrangements of the ethyl carbon atoms around, (A) N(11) atom of the praseodymium complex, and N(11) and N(21) atoms of the erbium complex; (B) N(21) atom of the praseodymium complex. ●, nitrogen atom; ○, carbon atom. Thick bonding lines mean one of the possible selection of the bondings.

Table 3. Final Atomic Coordinates (×10³), Multiplicities Used in the Calculation, and Equivalent Isotropic Temperature Factors (B_{eq}/Å²), with Estimated Standard Deviations in Parenthesess, of the Praseodymium Complex

Atom	G[g]	x	y	z	B_{eq}/Å²[h]
Pr	1/24	0	0	0	2.1_8
S(1)[i]	7/8	260.4(9)	260.4	260.4	10.6_9
C(1)[i]	7/8	186(3)	186	186	7.2_8
N(1)[i]	7/8	125(3)	125	125	12.2_3
N(11)	1/8	500	0	0	8.5_8
N(21)	1/24	500	500	500	5.7_8
C(11)[j]	1/4	421(3)	0	97(3)	10.6_3
C(12)[j]	1/4	421	97	0	10.6_3
C(13)[j]	1/4	500	0	214(3)	13.9_4
C(14)[j]	1/4	500	214	0	13.9_4
C(21)	1/6	410(5)	413(5)	500	8.1_5
C(22)	1/6	500	282(3)	500	9.2_5
O(1)[k]	1/8	12.4	12.4	12.4	8.0

g) Multiplicities. h) The equivalent isotropic temperature factors were computed using the following expression: $B_{eq}=4/3(B_{11}a^2+B_{22}b^2+B_{33}c^2)$. The B_{ij}'s are defined by: $T=\exp[-(h^2B_{11}+k^2B_{22}+l^2B_{33}+2hkB_{12}+2hlB_{13}+2klB_{23})]$. i) $x=y=z$. j) As C(11) and C(12), and C(13) and C(14) are equivalent respectively, x and z of the formers are defined to be the same as x and y of the latters, respectively. k) O(1) was fixed at the position.

bon atoms are assumed to be equal. The multiplicities used in the calculations are shown in Table 4. Attempts to perform structure factor calculations using other lower symmetry space groups did not yield improved results.

As shown in the results, the atomic positions as well as the temperature factors of these complexes did not converged well as the usual crystals: this was probably due to the existence of much disordering of the atoms.

Infrared Absorption Spectrum Measurements. They were obtained by means of JASCO A-202 grating infrared spectrophotometer, using liquid paraffin and hexachloro-1,3-butadiene mull.

Results and Discussion

The final positional parameters, their multiplicities used in the calculation, and their isotropic equivalent temperature factors of the praseodymium and erbium complexes are shown in Tables 3 and 4; selected interatomic distances as well as bond angles of the six complexes are shown in Tables 5 and 6. The perspective drawings of the praseodymium and the erbium complexes and their numbering scheme of the atoms are shown in Figs. 2 and 4, while their crystal packing diagrams in Figs. 3 and 5, respectively.[18]

In the praseodymium complex, the metal atom (at 0 0 0) is octa-coordinated being in a cubic geometry: seven SCN nitrogen atoms, and one water oxygen atoms are ligated to the metal atom, being disordered to occupy the eight positions equally, as shown in the previous paragraph. Since the SCN ions are arranged on the [±1±1±1] axes, the angles M-N(1)-C(1) as well as N(1)-C(1)-S(1) angles are 180°.

The Pr-N(1) bond length is 2.50(2) Å, which is shorter than the sum of their Shannon's ionic radii, 2.58 Å,[17] while the Pr-O(1) bond length is fixed as 2.477 Å.[17] The interatomic distance S(1)···S(1^{v}), the edge length of the complex anion cube, is 6.00(2) Å.

Table 4. Final Atomic Coordinates (×10^4), Multiplicities Used in the Calculation, and Equivalent Isotropic Temperature Factors (B/Å^2), with Estimated Standard Deviations in Parentheses, of the Erbium Complex

Atom	G[g]	x	y	z	B_{eq}/Å^2 [h]
Er	1/8	0	0	0	5.3_6
S(1)	7/8	2510(5)	2520(5)	1308(2)	12.0_5
C(1)	7/8	1755(13)	1794(13)	907(6)	8.9_4
N(1)	7/8	1171(16)	1211(18)	588(6)	17.4_7
N(11)	1/4	0	5000	0	11.6_8
N(21)	1/4	0	0	2576(8)	8.4_3
C(11)	1/4	939(43)	5686(42)	0	12.4_7
C(12)	1/4	1014(54)	4142(33)	0	14.3_1
C(13)	1/2	46(34)	4215(22)	511(12)	12.6_2
C(14)	1/2	2171(23)	4904(27)	0	14.5_4
C(15)	1/2	0	5000	1103(10)	15.1_8
C(21)	1/2	−22(44)	997(25)	2150(9)	10.7_0
C(22)	1/2	−59(41)	987(25)	2982(9)	10.6_7
C(23)	1/2	39(16)	2207(13)	2548(8)	13.3_1
O(1)[k]	1/8	118	118	60	4.0_3

g), h), and k): see the footnotes of Table 3.

Table 5. Selected Interatomic Distances and Bond Angles of the Light Lanthanoid Complexes with the Standard Deviations in Parentheses

A. Interatomic distances (l/Å) M=	La	Ce	Pr
M-N(1)	2.60(3)	2.568(16)	2.50(2)
M-N (Shannon)[l]	2.62	2.60	2.58
M-O(1)[m]	2.482	2.480	2.477
S(1)-C(1)	1.48(3)	1.538(14)	1.49(2)
C(1)-N(1)	1.14(4)	1.10(2)	1.21(3)
S(1)···S(1^{v})	6.03(3)	6.012(17)	6.00(2)
N(1)···N(1^{v})	3.007(1)	2.966(1)	2.888(1)
M··· N(11)	5.870(2)	5.765(2)	5.757(1)
B. Bond angles (ϕ/°) M=	**La**	**Ce**	**Pr**
M-N(1)-C(1)	180	180	180
N(1)-C(1)-S(1)	180	180	180
N(1)-M-N(1^{v})	70.5(8)	70.5(5)	70.5(7)
N(1)-M-N(1^{v})	109.5(8)	109.5(5)	109.5(7)

Key to the symmetry operations: i, −x, −y, z; v, x, y, −z. l) Sum of the Shannon's ionic radii.[17] m) O(1) atom is fixed assuming the M-O(1) bond length is the same as the sum of the metal and oxygen ionic radii.[17]

Table 6. Selected Interatomic Distances and Bond Angles of the Heavy Lanthanoid Complexes with the Standard Deviations in Parentheses

A. Interatomic distances (l/Å) M=	Nd	Dy	Er
M-N(1)	2.49(3)	2.40(3)	2.36(3)
M-N (Shannon)[l]	2.57	2.49	2.46
M-O(1)[m]	2.46	2.38	2.35
S(1)-C(1)	1.51(3)	1.49(3)	1.51(3)
C(1)-N(1)	1.15(4)	1.19(4)	1.20(4)
S(1)···S(1^{iv})	5.98(3)	5.93(3)	5.92(3)
S(1)···S(1^{ii})	5.912(13)	5.837(13)	5.817(12)
N(1)···N(1^{iv})	2.85(9)	2.74(8)	2.66(9)
N(1)···N(1^{ii})	2.88(4)	2.79(4)	2.76(4)
M···N(11)	5.785(1)	5.778(1)	5.782(1)
M···N(21)	5.81(2)	5.80(2)	5.828(17)
B. Bond angles (ϕ/°) M=	**Nd**	**Dy**	**Er**
M-N(1)-C(1)	179(3)	176(2)	177(2)
N(1)-C(1)-S(1)	176(3)	176(2)	179(2)
N(1)-M-N(1^{ii})	70.9(8)	71.0(8)	71.4(8)
N(1)-M-N(1^{i})	110.2(10)	110.4(10)	111.3(10)

Key to the symmetry operations: i, −x, −y, z; ii, −y, x, z; iv, x, y, −z. l) and m): see the footnote of Table 5.

As shown schematically in Fig. 6, the crystal lattice of this complex resembles that of rock salt. The tetraethylammonium nitrogen atoms occupy the Cl^- ionic position, the N(11) atoms are at the midpoints of the respective edges, and the N(21) atom is at the body center of the unit cell. The metal atoms occupy only the apex Na^+ ionic positions of the NaCl-type crystal lattice, and the face center positions are vacant. Therefore, each metal atom is surrounded by six N(11) atoms from both sides of the a, b, and c axis directions. No bridging was found between these anions and cations.

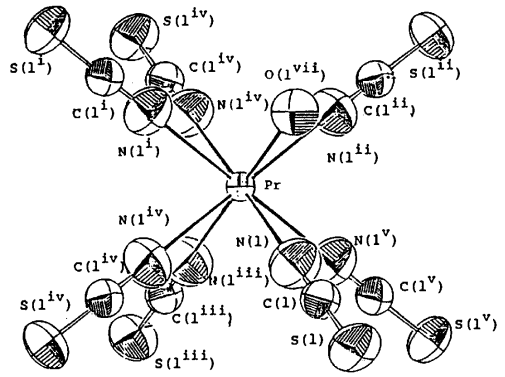

Fig. 2. A perspective drawing of the praseodymium complex around the metal atom (one of the possible arrangement). The key to the symmetry operations are: i, $-x$, $-y$, z; ii, $-x$, y, $-z$; iii, x, $-y$, $-z$; iv, $-x$, $-y$, $-z$; v, x, y, $-z$; vi, x, $-y$, z; vii, $-x$, y, z.

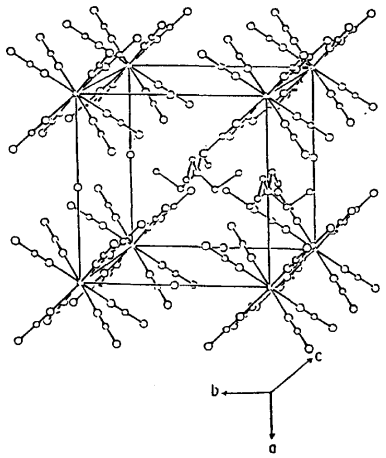

Fig. 3. Crystal packing diagram of the praseodymium complex.

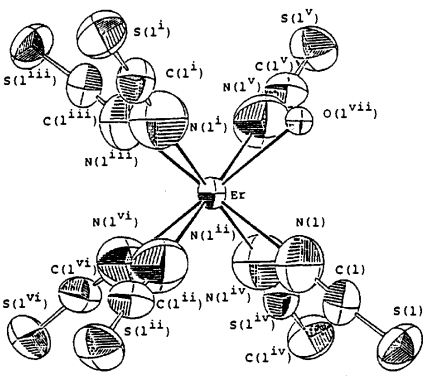

Fig. 4. A perspective drawing of the erbium complex around the metal atom (one possible arrangement). The key to the symmetry operations are: i, $-x$, $-y$, z; ii, $-y$, x, z; iii, $-x$, $-y$, $-z$; iv, x, y, $-z$; v, y, $-x$, $-z$; vi, $-y$, x, $-z$; vii, y, $-x$, z;

The structure of the isomorphous lanthanum and cerium complexes are fundamentally the same as that of the praseodymium complex. However, as the cell volume decreases, depending on the atomic number of the metal atom, the M···N(11) distance (the separation between the cation and anion) decreases in the order. The M-N(1) bond length (La-N(1), 2.60(3); Ce-N(1), 2.568(16); Pr-N(1), 2.50(2) Å) also decreases in the same order; it decreases more rapidly than the sum of their Shannon's ionic radii (La-N, 2.62; Ce-N, 2.60; Pr-N, 2.58 Å).[17]

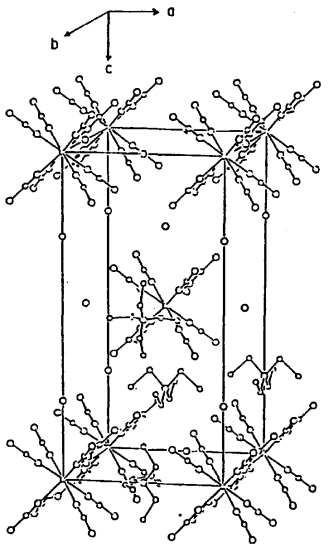

Fig. 5. Crystal packing diagram of the erbium complex.

The complex ion of the erbium salt has approximately the same structure as that of the light lanthanoid complexes. The metal atoms (at 0 0 0 and 0.5 0.5 0.5) are octa-coordinated, being approximately in a cubic geometry: seven SCN nitrogen and one water oxygen atoms are ligated to the metal atom, being disordered to occupy all eight coordinating positions equally.

The edge lengths of the complex anion cube are: S(1)···S(1^{ii}), 5.817(12); and S(1)···S(1^{iv}), 5.92(3) Å (key to the symmetry operations: ii, $-y$, x, z; iv, x, y, $-z$). The bond length of Er-N(1) is 2.36(3) Å, which is shorter than the sum of the Shannon's ionic radii, 2.46 Å.[17] The Er-O(1) distance was fixed as 2.35 Å.[17] The bond angles Er-N(1)-C(1), and N(1)-C(1)-S(1) are 177(2) and 179(2)°, respectively, which are almost 180°. The bond angles N(1)-Er-N(1^{i}) and N(1)-Er-N(1^{ii}) are 111.3(10) and 71.4(8)°, respectively (key to the symmetry operations: i, $-x$, $-y$, z; ii, $-y$, x, z).

As shown in Fig. 6, the crystal lattice of the erbium complex is a modified form of the praseodymium complex lattice. Its unit cell apparently consists of two latter cubic cells piled along the c-axis direction, and the positions of the metal and ammonium nitrogen atoms on the contact plane of the original two cells are shifted as shown in the following. The relative arrangement of the metal and the tetraethylammonium nitrogen atoms on the plane **1** and **2** (see Fig. 6) of the erbium complex, which are parallel to the ab-plane and intersect the c-axis at 0.0 and 0.5, is the same, but all of their positions on plane **2** are shifted

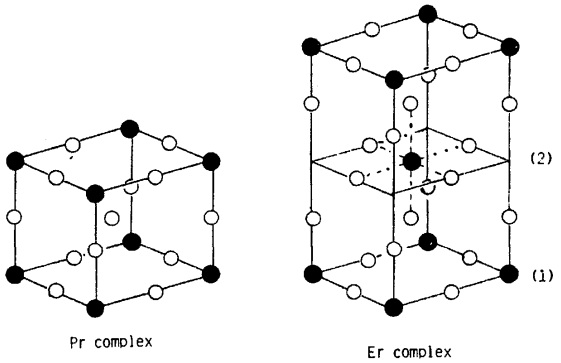

Fig. 6. Schematic presentation of the metal and tetraethylammonium nitrogen atomic positions in the crystal lattices of the praseodymium and erbium complexes. ●: metal atoms, ○: tetraethylammonium nitrogen atoms.

by 0.5 along both the a- and b-axis directins from the respective positions on plane 1. The **1** and **2** type planes appear alternately along the c-axis. On the other hand, in the erbium complex, the N(11) atoms at the midpoint of the c-edge as well as the body-centered N(21) atoms of the praseodymium complex are apparently kept at their positions: they are on the planes parallel to the ab-plane intersecting the c-axis at about 0.25 and 0.75, respectively.

As a result, as shown in Fig. 6, in the erbium complex, too, the metal atom is surrounded by six tetraethylammonium nitrogen atoms in about equidistances on both sides along a-, b-, and c-axis directions: Er···N(11), 5.782(1); Er···N(21), 5.828(17) Å.

The neodymium and dysprosium complexes have essentially the same type of structure. The M-N(1) bond lengths (Nd-N(1), 2.49(3); Dy-N(1), 2.40(3); and Er-N(1), 2.36(3) Å) are shorter than the respective sums of the Shannon's ionic radii (Nd-N, 2.57; Dy-N, 2.49; Er-N, 2.46 Å), and the differences are larger than the values found in the series of the light lanthanoid complexes. Therefore, it is likely that, through the both series of these complexes, the M-N(SCN) bonds have the more covalent-bonding character in the higher metal-atomic-number complexes.

The infrared absorption spectra of these complexes were examined. Not only the general feature, but also the maximum wavenumbers of the respective peaks of the title six complexes were not much different from each other. Therefore, the respective average wavenumbers of the peak maxima will be discussed.

Although some of them partially overlapped with the bands due to the tetraethylammomium ion, the typical bands due to the SCN ion were observed: ν(CN), 2050(s); ν(CS), 735(sh); and δ(NCS), 475(m) cm^{-1}, respectively (here, s, strong; sh, shoulder; m, medium). These values are all in a reasonable region for the bands of the N-bonded SCN ions.[19] The ν(OH) band of the coordinated water was found at about 3370 cm^{-1} in the spectra of all of these complexes, although it is broad and weak. The maximum wavenumbers of the tetraethylammonium ion peaks, 1490, 1440, 1393, 1170, 1050, 998, 780, and 720 cm^{-1}, were not much different from those of tetraethylammonium chloride.

The authors wish to thank the Shin-Etsu Chemical Ind. Co. Ltd., for presenting us with the highly pure lanthanoid oxides.

References

1) R. G. Pearson, *J. Chem. Educ.*, **45**, 581, 643 (1968).
2) J. H. Forsburg and T. Moeller, *Inorg. Chem.*, **8**, 883, 889 (1969).
3) J. G. Leipoldt, L. D. C. Bok, S. S. Basson, and A. E. Laubscher, *J. Inorg. Nucl. Chem.*, **38**, 1477 (1976).
4) G. H. Frost, F. A. Hart, C. Heath, and M. B. Hursthouse, *J. Chem. Soc. D*, **1969**, 1421.
5) A. Zazzetta and A. Greco, *Acta Crystallogr., Sect. B*, **35**, 457 (1979).
6) A. Wells, "Structural Inorganic Chemistry," 5th ed, Clarendon, Oxford, U. K. (1984), pp. 126, 935, 1159.
7) G. Thiele and D. Messer, *Z. Anorg. Allg. Chem.*, **464**, 255 (1980).
8) Y. Kuniyasu, Y. Suzuki, M. Taniguchi, and A. Ouchi, *Bull. Chem. Soc. Jpn.*, **60**, 179 (1987).
9) J. L. Martin, L. C. Thompson, L. J. Radonovich, and M. D. Glick, *J. Am. Chem. Soc.*, **90**, 4493 (1968).
10) P. I. Lazarev, L. A. Aslanov, V. M. Ionov, and M. A. Porai-Koshits, *Koord. Khim.*, **1**, 710 (1975); also in *Structure Report*, **41A**, 210 (1975).
11) R. Countryman and W. S. McDonald, *J. Inorg. Nucl. Chem.*, **33**, 2213 (1971).
12) G. Bombieri, P. T. Moseley, and D. Brown, *J. Chem. Soc., Dalton Trans.*, **1975**, 1520.
13) I. S. Ahuja and A. Garg, *J. Inorg. Nucl. Chem.*, **34**, 1929 (1972).
14) "Universal Crystallographic Computation Program System (UNICS)," ed by T. Sakurai, Crystallographic Society of Japan, Tokyo (1967).
15) "International Tables for X-Ray Crystallography," Kynoch Press, Birmingham (1974), Vol. IV, pp. 72, 150.
16) M. R. Snow and R. F. Boomsma, *Acta Crystallogr., Sect. B*, **28**, 1908 (1972).
17) R. D. Shannon, *Acta Crystallogr., Sect. A*, **32**, 751 (1976). According to this paper, the ionic radii are as follows: Metals (Coordination number is 8, valence is 3+); La, 1.160; Ce, 1.143; Pr, 1.126; Nd, 1.109; Dy, 1.027; and Er, 1.004 Å. Oxygen (coordination number is 2, valence is 2−), 1.35 Å Nitrogen (coordination number is 4, valence is 3−), 1.46 Å.
18) The atomic positional parameters of the lanthanum, cerium, neodymium, and dysprosium complexes, the thermal parameters, the final F_o-F_c tables and some additional data of bond lengths and bond angles of the all complexes are deposited as Document No. 8811 at the office of the Editor of Bull. Chem. Soc. Jpn.
19) K. Nakamoto, "Infrared and Raman Spectra of Inorganic and Coordination Compounds," 4th ed, John Wiley & Son, New York (1986), p. 283.

 © 1988 The Chemical Society of Japan Bull. Chem. Soc. Jpn., 61, 2811—2815 (1988)

The Effect of Water Vapor on the Thermal Decomposition of Various Tin(IV) *cyclo*-Phosphates

Hiroyuki NARIAI,* Itaru MOTOOKA, and Mitsutomo TSUHAKO†
Department of Chemistry, Faculty of General Education, Kobe University, Tsurukabuto, Nada-ku, Kobe 657
†Kobe Women's College of Pharmacy, Kitamachi, Motoyama, Higashinada-ku, Kobe 658
(Received March 2, 1988)

The process of the thermal decomposition of various tin(IV) *cyclo*-phosphates, $SnP_4O_{12}\cdot 4H_2O(P_{4m})$, $Sn_3(P_6O_{18})_2\cdot 12H_2O$ (P_{6m}), and $Sn_2P_8O_{24}\cdot 5H_2O(P_{8m})$, was investigated using X-ray analysis, DTA-TG, and HPLC-FIA. P_{4m} lost the water of crystallization at about 105 °C. In the region of 400—500 °C, P_{4m} changed to *cyclo*-triphosphate (P_{3m}) without any other species of phosphates. Therefore, the change of P_{4m} to P_{3m} probably proceeded as a radical reaction. At temperatures above 580 °C, P_{3m} changed to insoluble polyphosphates ($P_{high\ poly}$). P_{6m} lost the water of crystallization at about 110 °C. In the region of 500—570 °C, P_{6m} changed to $P_{high\ poly}$ through P_{3m}. P_{8m} lost the water of crystallization at about 140 °C. At about 255 °C, P_{8m} decomposed to oligo phosphates($n<8$)(P_{oligo}), soluble polyphosphates($15<n<20$)(P_{poly}), and amorphous insoluble polyphosphates ($P^*_{high\ poly}$). Under a higher water vapor pressure, these decomposition and subsequent condensation reactions proceeded rather faster than in a lower one. At about 300 °C, $P^*_{high\ poly}$ changed to P_{3m} again. At higher temperatures, P_{3m} changed to $P_{high\ poly}$.

It is well-known that, upon heating, phosphates hydrolyze or condense to form various kind of phosphates.[1-13] These reactions are affected by the kind of metal, the atmosphere, the temperature, the time and rate of heating, etc., thus resulting in the formation of different phosphates. In a previous paper,[14] we reported the effect of water vapor on the thermal decomposition of lead *cyclo*-tetraphosphate. As regards the thermal decomposition of tin(IV) *cyclo*-phosphates, though, little work has been reported. Therefore, in this paper, we wish to present the experimental results of the atmospheric dependence of the thermal decomposition of tin(IV) *cyclo*-phosphates and also discuss the mechanisms of their thermal decomposition. The process of the thermal decomposition of *cyclo*-phosphates was investigated by means of X-ray analysis, thermal analysis (DTA-TG), and high performance liquid chromatography-flow injection analysis (HPLC-FIA).

Experimental

Chemicals. The tin(IV) *cyclo*-phosphates—$SnP_4O_{12}\cdot 4H_2O$ (P_{4m}), $Sn_3(P_6O_{18})_2\cdot 12H_2O(P_{6m})$, and $Sn_2P_8O_{24}\cdot 5H_2O$ (P_{8m})— were prepared by methods similar to those described in the literature.[5,14-16] Tin(IV) *cyclo*-triphosphate(P_{3m}) could not be obtained by the above method. Unless otherwise stated, guaranteed reagents were used without further purification. The analytical procedures and apparatus were essentially the same as those used in the previous paper.[14]

Results and Discussion

Thermal Decomposition of $SnP_4O_{12}\cdot 4H_2O$ (P_{4m}). Figure 1 shows the DTA-TG curves of P_{4m} at atmospheric pressure. Three endothermic peaks at about 70 and 105 (with a weight loss), and at 580 °C, and an exothermic peak at about 630 °C were observed. To clarify these thermal changes at each temperature, X-ray measurements of the products on heating were performed. Figure 2 shows the X-ray diffraction patterns of products heated at various temperatures in an electric furnace for 30 min. In the 300—450 °C region, no change in the X-ray diffraction patterns was observed. In the 495—510 °C region, though, some new peaks began to appear. In the 610—660 °C region, other new peaks began to appear, gradually increasing with the heating temperature. From the X-ray diffraction pat-

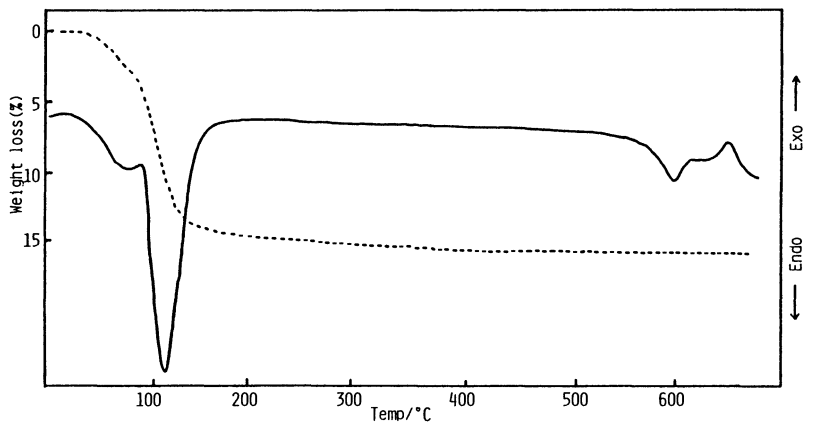

Fig. 1. DTA-TG curves of $SnP_{4m}\cdot 4H_2O$. Solid line: DTA, dotted line: TG.

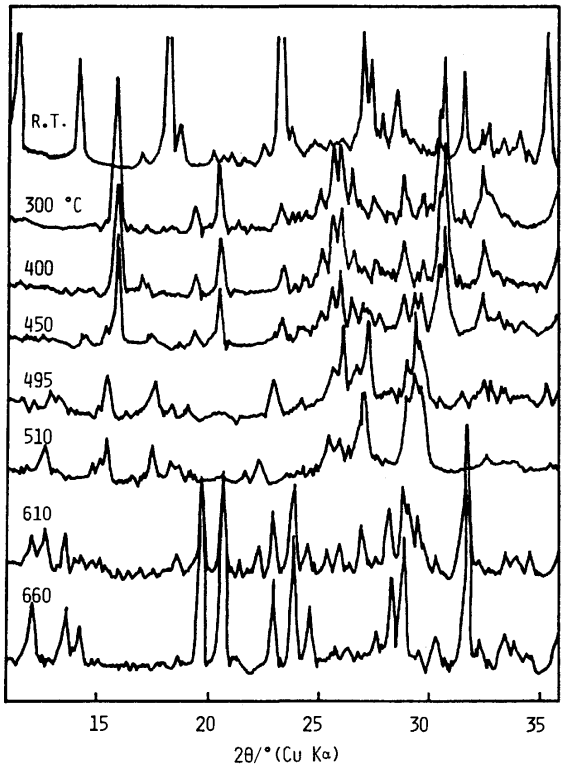

Fig. 2. X-Ray diffraction patterns of products on heating. Sample: $SnP_{4m}\cdot 4H_2O$.

terns and HPLC, it seems that P_{4m} dehydrated to form an anhydride at about 105 °C and that it thereafter remained unchanged up to 450 °C. At temperatures above 500 °C, P_{4m} began to decompose and changed to P_{3m} and/or $P_{high\ poly}$. Although the DTA-TG curves do not have a definite peak in Fig. 1, P_{4m} gradually decomposed above 500 °C. Therefore, the influence of water vapor upon thermal decomposition was investigated at 400 and 450 °C. Table 1 shows the changes in the amounts of phosphates in the samples heated at each temperature. At 400 °C in a dry air atmosphere (r.h.=0%), 35% of the starting material has already changed to P_{3m}, while in the 15—90% range of relative humidity (at 25 °C), about 12—15% of the starting material changed to P_{3m}. At 450 °C in a dry air atmosphere (r.h.=0%), most of the P_{4m} changed to P_{3m}, while in r.h.=15—90, 30—36% of that remained unchanged. From the X-ray diffraction pattern and the HPLC of the product heated at 610 °C, the endothermic peak at 580 °C shows the phase transition of P_{3m} to $P_{high\ poly}$, while the exothermic peak at 630 °C shows the crystallization of $P_{high\ poly}$. When P_{4m} changed to P_{3m}, no other species of phosphates except P_{4m} and P_{3m} were observed, indicating that its rearrangement probably proceeded radically.[17] For a reason similar to that noted above and from the fact that no weight change was observed in the TG curve (Fig. 1), the change of P_{3m} to $P_{high\ poly}$ probably proceeded radically.

Table 1. Changes in the Amounts of Phosphates (Starting Material: P_{4m})

Temp/°C	Compound R.H./%	P_{oligo} %	P_{4m} %	P_{3m} %	P_{poly} %	$P_{high\ poly}$ %
400	0	0	65.0	35.0	0	0
	15	0	84.3	15.7	0	0
	90	0	87.7	12.3	0	0
450	0	0	4.9	95.1	0	0
	15	0	30.9	69.1	0	0
	90	0	36.4	63.6	0	0

Thermal Decomposition of $Sn_3(P_6O_{18})_2\cdot 12H_2O$ (P_{6m}). Figure 3 shows the DTA-TG curves of P_{6m} at atmospheric pressure. Five endothermic peaks, at about 60 and 110 (with a weight loss), and at 550, 570, and 610 °C, were observed. From the results of HPLC, P_{6m} remained unchanged up to the 500 °C region, while in the region near 560 °C it completely decomposed to a mixture of P_{oligo}, P_{3m}, and $P_{high\ poly}$. Figure 4 shows the X-ray diffraction patterns of products heated at various temperatures in an electric furnace for 30 min. In the 210—500 °C region, only the peaks for anhydride were observed. In 570 °C, the diffraction pattern changed to another pattern, that of $P_{high\ poly}$. The higher the temperature, the more intense the peaks became. Table 2 shows the changes in the amounts of phosphates in the samples heated at 500 and 570 °C. At 500 °C, the temperature before the endothermic peak in Fig. 3, we expected a remarkable effect of the water vapor upon the decomposition of

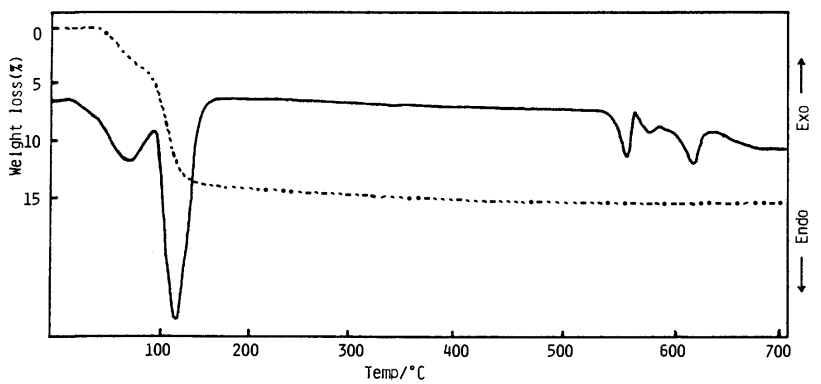

Fig. 3. DTA-TG curves of $Sn_3(P_{6m})_2\cdot 12H_2O$. Solid line: DTA, dotted line: TG.

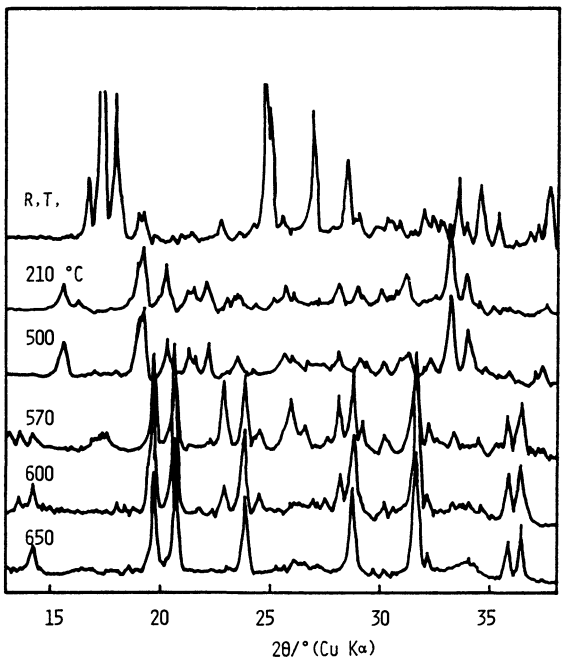

Fig. 4. X-Ray diffraction patterns of products on heating. Sample: $Sn_3(P_{6m})_2 \cdot 12H_2O$.

Table 2. Changes in the Amounts of Phosphates (Starting Material: P_{6m})

Temp/°C	Compound R.H./%	P_{oligo} %	P_{6m} %	P_{3m} %	P_{poly} %	$P_{high\ poly}$ %
500	0	0	84.6	15.4	0	0
	15	0	88.1	11.9	0	0
	90	0	91.0	9.0	0	0
570	0	1.7	0	44.5	1.4	52.4
	15	11.2	0	28.9	2.7	57.2
	90	5.6	0	30.3	1.9	62.2

P_{6m}. In a dry air atmosphere (r.h.=0%), the amounts of P_{6m} decreased and P_{3m} was formed in about a 15% yield. In a 15—90% relative humidity atmosphere (at 25 °C), P_{3m} was formed in about a 10% yield. The ratio of the amounts of P_{3m} to P_{6m} decreased with the increase in the humidity. At 570 °C, the P_{6m} completely disappeared throughout the humidity region and considerable amounts of P_{3m} and $P_{high\ poly}$ were produced along with some soluble linear phosphates (P_{oligo} and P_{poly}). The amount of $P_{high\ poly}$ in r.h.=15—90% was larger than that in r.h.=0%, while that of P_{3m} had an opposite tendency. It seems from the above results that P_{3m} begins to decompose and changes to $P_{high\ poly}$ at 550—570 °C, while P_{3m} completely decomposes at 610 °C near an endothermic peak and $P_{high\ poly}$ forms in a large quantity. When P_{6m} changed to $P_{high\ poly}$ through P_{3m}, scarcely no other species of phosphates were found in these reaction processes (maximum of P_{oligo}=10%). Consequently, these rearrangements probably proceed in the same manner as is the case with the P_{3m} system.

Thermal Decomposition of $Sn_2P_8O_{24} \cdot 5H_2O$ (P_{8m}). Figure 5 shows the DTA-TG curves of P_{8m} at atmospheric pressure. Four endothermic peaks — at about 65, 140, 270, and 635 °C — were observed. A large exothermic peak was shown at 320 °C. The endothermic peaks with a weight loss at 65 and 140 °C are attributable to the dehydration of the water of crystallization. From the results of the X-ray analysis and the HPLC of products heated at various temperatures, it seems that P_{8m} existed in anhydride at 180 °C and decomposed to P_{oligo} and $P^*_{high\ poly}$ in the 250—300 °C region, except for the changing of P_{8m}, in part, to P_{3m}. At higher temperatures, P_{3m} decomposed and then condensed $P_{high\ poly}$. Table 3 shows the changes in the amounts of phosphates in the samples heated at sev-

Table 3. Changes in the Amounts of Phosphates (Starting Material: P_{8m})

Temp/°C	Compound R.H./%	P_{oligo} %	P_{8m} %	P_{3m} %	P_{poly} %	$P^*_{high\ poly}$ %
255	0	23.8	18.9	3.9	26.8	26.6
	15	11.7	0	5.7	3.5	79.1
	90	15.5	0	5.7	3.5	75.3
300	0	5.0	0	84.8	1.6	14.8
	15	17.2	0	6.3	1.6	81.0
	90	26.9	0	7.6	2.1	69.5

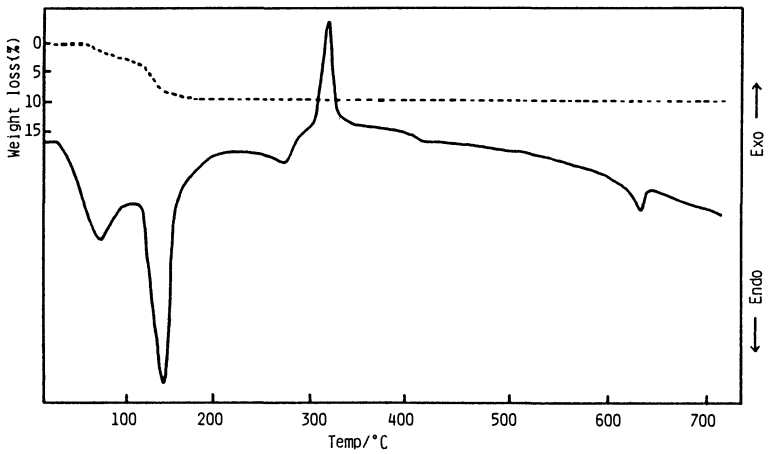

Fig. 5. DTA-TG curves of $Sn_2P_{8m} \cdot 5H_2O$. Solid line: DTA, dotted line: TG.

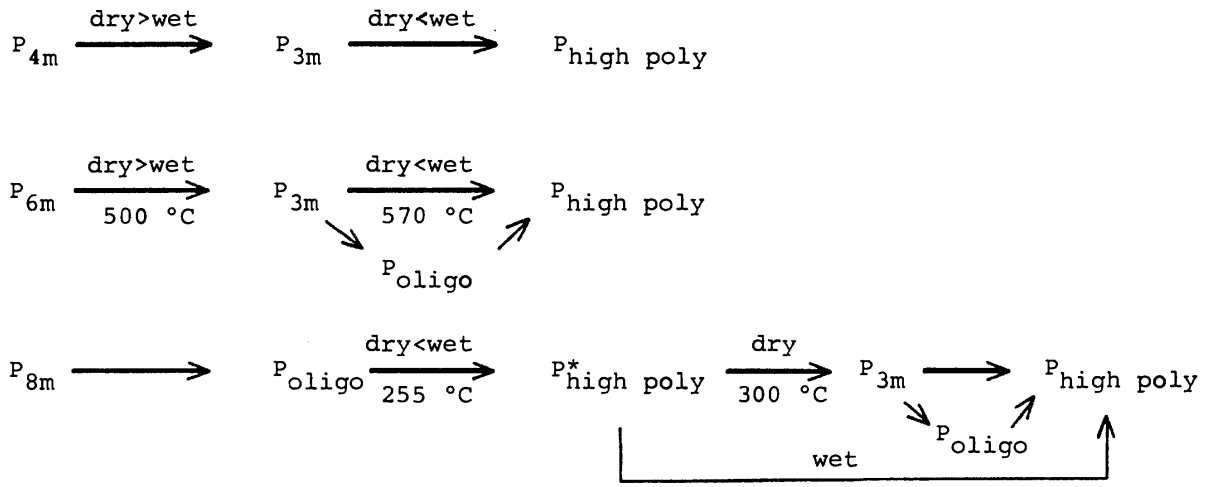

Scheme 1.

eral temperatures. At 255 °C in a dry air atmosphere (r.h.=0%), about 80% of the P_{8m} has already changed to P_{oligo}, P_{poly}, and $P^*_{high\ poly}$ in about equal quantities, while in a relative humidity of 15—90% (at 25 °C) the P_{8m} disappeared completely, while $P^*_{high\ poly}$ was formed in a large quantity. Further, at 300 °C in a dry air atmosphere (r.h.=0%), P_{3m} formed again in about a 85% yield with the decrease in P_{oligo}, P_{poly} and $P^*_{high\ poly}$, while in a relative humidity of 15—90% (at 25 °C), no remarkable change was observed in the amounts of phosphates as compared with the results at 255 °C. In the humid atmosphere, there might be a path of $P^*_{high\ poly}$ to $P_{high\ poly}$ without going through P_{3m}.

Based upon the results described above, the process of the thermal decomposition of tin(IV) *cyclo*-phosphates under several humid atmospheres may be summarized schematically as in Scheme 1. In a previous paper,[17] Takenaka et al. reported that, in a humid atmosphere, the radicals formed from P_{4m} may be considered to combine with water molecules in the atmosphere, so the water molecules could be expected to inhibit the radical polymerization. In this work, when P_{4m} decomposed in a humid atmosphere, the amount of the P_{3m} was small compared with that in a dried atmosphere. Consequently, P_{3m} is produced by the recyclization of the radicals which result from the cleavage of P_{4m}. Therefore, the mechanisms of P_{4m} to $P_{high\ poly}$ through P_{3m} may be considered to be as follows:

(1) $P_{4m} \xrightarrow[\text{lower temp}]{\text{decompn.}} \cdot\overset{\overset{\|}{O}}{\underset{|}{P}}\text{-O-}\overset{\overset{\|}{O}}{\underset{|}{P}}\text{-}\cdots\cdots\text{-O-}\overset{\overset{\|}{O}}{\underset{|}{P}}\text{-O}\cdot$

(Formation of radical)

(2) $3\ \cdot\overset{\overset{\|}{O}}{\underset{|}{P}}\text{-O-}\overset{\overset{\|}{O}}{\underset{|}{P}}\text{-}\cdots\cdots\text{-O-}\overset{\overset{\|}{O}}{\underset{|}{P}}\text{-O}\cdot \longrightarrow 4P_{3m}$

(Recyclization)

(3) $\cdot\overset{\overset{\|}{O}}{\underset{|}{P}}\text{-O-}\overset{\overset{\|}{O}}{\underset{|}{P}}\text{-}\cdots\cdots\text{-O-}\overset{\overset{\|}{O}}{\underset{|}{P}}\text{-O}\cdot + \text{H-O:H} \longrightarrow \text{H-O:}\overset{\overset{\|}{O}}{\underset{|}{P}}\text{-O-}\overset{\overset{\|}{O}}{\underset{|}{P}}\text{-}\cdots\cdots\text{-O-}\overset{\overset{\|}{O}}{\underset{|}{P}}\text{-O:H}$

(Stop of radical reaction)

(4) $P_{3m} \longrightarrow \cdot\overset{\overset{\|}{O}}{\underset{|}{P}}\text{-O-}\overset{\overset{\|}{O}}{\underset{|}{P}}\text{-}\cdots\text{O-}\overset{\overset{\|}{O}}{\underset{|}{P}}\text{-O}\cdot \xrightarrow{\text{radical polymn.}} P_{high\ poly}$

(5) $\text{H-O:}\overset{\overset{\|}{O}}{\underset{|}{P}}\text{-O-}\overset{\overset{\|}{O}}{\underset{|}{P}}\text{-}\cdots\text{O-}\overset{\overset{\|}{O}}{\underset{|}{P}}\text{-O:H} \xrightarrow[\text{higher temp.}]{\text{dehydration condensation, } -H_2O} \longrightarrow (\text{H-O-}\overset{\overset{\|}{O}}{\underset{|}{P}}\text{-O-}\overset{\overset{\|}{O}}{\underset{|}{P}}\text{-}\cdots\cdots\text{O-}\overset{\overset{\|}{O}}{\underset{|}{P}}\text{-O-H})_{high\ poly}$

Since no P_{oligo} was detected, and since the TG curve indicated no weight change, at a lower temperature, it seems that the thermal reaction of P_{4m} to P_{3m} proceeds mainly according to Processes (1) and (2), while at a higher temperature the thermal polymerization of P_{3m} to $P_{high\ poly}$ proceeds mainly by Process (4), not Process(5). In the case of P_{6m}, the thermal reactions probably proceed by similar mechanisms except for the formation of a small amount of P_{oligo}.

On the other hand, P_{8m} decomposes at a rather low temperature (at about 250 °C) compared with the other two *cyclo*-phosphates. Consequently, it can be said that the water vapor very much influenced the thermal reaction and that P_{oligo} is formed by Process (3), followed by the change to $P^*_{high\ poly}$ by means of the dehydration-condensation reaction (Process (5)). $P^*_{high\ poly}$ in a dry air atmosphere (r.h.=0%) changed radically to $P_{high\ poly}$ through P_{3m} by means of Process (4), while in a humid atmosphere it probably crystallizes or changes to $P_{high\ poly}$ by means of the dehydration-condensation reaction (Process (5)).

References

1) J. R. Van Wazer and E. Karl-Kroupa, *J. Am. Chem. Soc.*, **78**, 1772 (1956).
2) J. F. McCullough, J. R. Van Wazer, and E. J. Griffith, *J. Am. Chem. Soc.*, **78**, 4528 (1956).
3) R. P. Langguth, R. K. Osterheld, and E. Karl-Kroupa, *J. Phys. Chem.*, **60**, 1335 (1956).
4) E. Thilo and U. Schülke, *Z. Anorg. Allg. Chem.*, **341**, 293 (1965).
5) E. J. Griffith and R. L. Buxton, *Inorg. Chem.*, **4**, 549 (1965).

6) M. Watanabe, S. Sato, and H. Saito, *Bull. Chem. Soc. Jpn.*, **48**, 896 (1975).
7) H. Worzala, *Z. Anorg. Allg. Chem.*, **445**, 27 (1978).
8) M. Watanabe, M. Matsuura, and T. Yamada, *Bull. Chem. Soc. Jpn.*, **54**, 738 (1981).
9) H. Worzala and K. H. Jost, *Z. Anorg. Allg. Chem.*, **486**, 165 (1982).
10) U. Schülke, R. Kayser, and L. Arndt, *Z. Anorg. Allg. Chem.*, **504**, 77 (1983).
11) G. Kura, *Bull. Chem. Soc. Jpn.*, **56**, 3769 (1983).
12) I. Grunze and H. Grunze, *Z. Anorg. Allg. Chem.*, **512**, 39 (1984).
13) U. Schülke and R. Kayser, *Z. Anorg. Allg. Chem.*, **531**, 167 (1985).
14) H. Nariai, I. Motooka, Y. Kanaji, and M. Tsuhako, *Bull. Chem. Soc. Jpn.*, **60**, 1337 (1987).
15) R. N. Bell, L. F. Audrieth, and O. F. Hill, *Ind. Eng. Chem.*, **44**, 568 (1952).
16) U. Schülke, *Z. Anorg. Allg. Chem.*, **360**, 231 (1968).
17) A. Takenaka, I. Motooka, and H. Nariai, *Bull. Chem. Soc. Jpn.*, **60**, 4299 (1987).

 © 1988 The Chemical Society of Japan Bull. Chem. Soc. Jpn., 61, 2817—2823 (1988)

The Crystal Structures of Δ-, Λ-, and Pseudoracemic Forms of Bis(ethylenediamine)oxalatocobalt(III) Aspartates

Hideko KIRIYAMA*,† and Michihito IGAKI
Department of Chemistry, Faculty of Science, Kobe University, Nada, Kobe 657
(Received March 7, 1988)

The crystal structures of Δ-[Co(ox)(en)$_2$](L-Hasp)·3H$_2$O, Λ-[Co(ox)(en)$_2$](L-Hasp)·3H$_2$O and *rac*-[Co(ox)(en)$_2$](L-Hasp) have been determined by means of X-ray diffraction. The absolute configurations of (−)-and (+)-cations were assigned as Δ($\delta\lambda$) and Λ($\delta\lambda$), respectively, on the basis of that of L-Hasp$^-$ ion. The counter ion is extended with C-C-C-C near 180° in all cases, but the other torsion angles are somewhat affected by surroundings. Both α and β carboxyl groups of the anion are ionized, therefore its NH$_2$ group is protonated. In the three compounds, the cations and the anions are alternately arranged, forming a layer through N-H···O hydrogen bonds in a very similar way to each other. The lattice of the more soluble Δ-isomer consists of such single cation-anion layers, between which water molecules are inserted. In the less soluble Λ-diastereoisomer the cation-anion layers are doubled by N-H···O bonds between cations from neighboring layers. The less soluble racemic salt is anhydride where the similar cation-anion layers are connected by hydrogen bonds between cations and between anions alternately. In connection to optical resolution, the difference in solubility was discussed in terms of the density, unoccupied fraction and electrostatic energy.

An useful method to isolate one of the enantiomers for a racemic mixture is to add a suitable chiral reagent. When a cationic racemate is precipitated with an optically active anion, two different diastereoisomeric salts may result and sometimes their solubility difference allows both of them to be isolated. In view of this, Kuramoto et al. have developed structural studies of optical resolution on various pairs of diastereoisomeric salts.[1,2] Gajhede and Larsen have recently related the crystal structure to solubility for the diastereoisomeric salts which are obtained from bis(ethylenediamine)glycinatocobalt(III) and bis-μ-[(*R*,*R*)-tartrato(4−)]-diantimonate(III).[3] On the other hand, an application of L-amino acid anion as a resolving agent for some metal complexes was examined on the systems of (−)$_{589}$- and (+)$_{589}$-[Co(ox)(en)$_2$]X with X=L-hydrogenglutamate (L-Hglu$^-$) and L-hydrogenaspartate (L-Hasp$^-$) by Yamanari et al.[4] They determined these solubility phase diagrams and confirmed that the former anion L-Hglu$^-$ is an excellent resolving agent, while the latter anion L-Hasp$^-$ forms the pseudoracemate, *rac*-[Co(ox)(en)$_2$](L-Hasp). We have succeeded in preparing (−)$_{589}$-, (+)$_{589}$-, and *rac*-[Co(ox)(en)$_2$](L-Hasp) and also (−)$_{589}$- and (+)$_{589}$-[Co(ox)(en)$_2$](L-Hglu) salts as suitable single crystals for X-ray analysis. In the hydrogenaspartate system, [Co(ox)(en)$_2$](L-Hasp)·*n*H$_2$O, the (−)$_{589}$ diastereoisomer (*n*=3) **1** is more soluble than the (+)$_{589}$ isomer (*n*=3) **2** and the rac-complex (*n*=0) **3**; for example the values of solubility as expressed by grams of anhydrous salt in 100 g water are 71.0, 12.4, and 11.9 at 20 °C and 127, 44.8, and 18.8 at 60 °C for **1**, **2**, and **3**, respectively. On the other hand, in the hydrogenglutamate system [Co(ox)(en)$_2$](L-Hglu)·*n*H$_2$O the (−)$_{589}$ diastereoisomer (*n*=2) **4** is more soluble than the (+)$_{589}$ isomer (*n*=5) **5**. In order to understand such an appreciable difference in solubility the crystal structures of these five complexes have been determined by X-ray diffraction methods. The absolute configuration of the common cation [Co(ox)(en)$_2$]$^+$ was determined by reference to that of the L-amino acid anion. The present paper is concerned with the results of the hydrogenaspartates and the next with the hydrogenglutamate ones.

† Present address: Imajuku 1-12, Ogaki, Gifu 503.

Experimental

Preparation. The three aspartates were prepared by the methods described in the previous paper and recrystallized from water.[4] The density was measured by pycnometry with kerosine or floatation with kerosine-bromoform mixture. The number of water of crystallization was estimated by thermogravimetry and precisely determined from X-ray structure analysis. The prepared samples were identified by elemental analysis, thermal analysis, absorption and circular dichroism spectra.[4]

X-Ray Structure Determination. The lattice parameters and the space groups were determined preliminary with Weissenberg and precession cameras and confirmed by single crystal diffractometers. Intensity data were collected on Rigaku AFC-4 (Mo*Kα*, 30 kV, 200 mA) for **1** and **3** and on Rigaku AFC-5 (Mo*Kα*, 50 kV, 150 mA) for **2**. Graphite monochromated Mo*Kα* radiation (λ=0.71069 Å) and the ω-2θ scan technique (at 4° min^{-1} in ω) were used throughout the experiment. Intensities were corrected for Lorentz-polarization and absorption effects; empirical absorption correction factors on *F* were 0.993—1.013 about [c] axis for **1**, 1.009—1.034 about [b] for **2** and 1.020—1.131 about [c] for **3**.[5] Other experimental conditions and refinement details are listed in Table 1.

Every structure was solved by a direct method based on MULTAN78[6] and refined by block-diagonal least-squares on F. Most of O, N and C atoms were located by Fourier syntheses and their remaining atoms and most H atoms were found in difference Fourier maps. Anisotropic thermal parameters were applied to all non-hydrogen atoms in **1** and **2**, while they were only to Co atoms in **3** because of its poor intensity data. In the final refinements all H atoms were included at fixed positions (calculated from C-H=1.10,

Table 1. Experimental Conditions and Refinement Details

	1	2	3
Crystal size (mm)	0.06×0.12×0.18	0.10×0.12×0.20	0.06×0.13×0.18
Number of reflections and 2θ range(°) used for measuring lattice parameters	30 $17<2\theta<28$	25 $18<2\theta<24$	40 $15<2\theta<28$
$2\theta_{max}$ (°)	55	50	55
Ranges of h	−12 to 12	−16 to 16	−13 to 13
k	−14 to 14	−7 to 0	−16 to 16
l	−8 to 0	−12 to 12	0 to 7
Systematic absences	None	$0kl$: k odd	None
Standard reflections and their intensity variations	$00\bar{2}$,400,$03\bar{3}$ 0.970—1.023	$\bar{5}00$,220,003 0.943—1.009	003,$\bar{1}01$,$0\bar{4}1$ 0.981—1.053
$R_{int}=(\sum\|\|F\|-<\|F\|>\|)/\sum\|F\|$		0.052	
Number of reflections measured	4280	3643	3531
Number of unique reflections with $\|F_o\|>3\sigma(F_o)$	3732	1668	1780
$R=\sum(\|\|F_o\|-\|F_c\|\|)/\sum\|F_o\|$	0.050	0.034	0.078
$R_W=[\sum W(\|F_o\|-\|F_c\|)^2/\sum W\|F_o\|^2]^{1/2}$	0.051	0.043	0.050
Weight $W=[\sigma^2(F_o)+a\|F_o\|+b\|F_o\|^2]^{-1}$	$a=-0.0065$ $b=0.0009$	$a=0.0070$ $b=0.0008$	$a=0.0000$ $b=0.0000$
$S=[\sum W(\|F_o\|-\|F_o\|)^2/(m-n)]^{1/2}$	1.036	0.977	1.336
Number of observed reflections used for refinements, m	3732	1668	1169($2\theta<43°$)
Number of refined parameters, n	245	245	184
$(\Delta\rho)_{max}$, $(\Delta\rho)_{min}$ (e Å^{-3})	0.67, −0.59	0.34, −0.31	0.76, −0.68
$(\Delta/\sigma)_{av}$, $(\Delta/\sigma)_{max}$	0.08, 0.59	0.03, 0.21	0.08, 0.28

N–H=1.02 and O–H=0.96 Å) with isotropic temperature factors. Neutral atomic scattering factors and anomalous dispersion terms were taken from International Tables for X-ray Crystallography.[7] The programs MULTAN78, ORTEPII and UNICS-OSAKA were used for calculations at the Information Processing Center of Kobe University.[6,8,9] The final atomic parameters are listed in Tables 2—4.[10]

Crystal Data. Crystal data are as follows:

(**1**) $[Co(C_2O_4)(C_2H_8N_2)_2]^+$ $(C_4H_6NO_4)^-\cdot 3H_2O$, M_r=453.3, triclinic, $P\bar{1}$, a=8.968(3), b=9.953(4), c=6.084(2) Å, α=103.49 (3), β=79.17(3), γ=117.43(3)°, V=466.7(3) Å^3, Z=1, D_m=1.58 (2), D_x=1.61 g cm^{-3}, $F(000)$=238, T=298 K, μ(Mo $K\alpha$)=10.05 cm^{-1}.

(**2**) $[Co(C_2O_4)(C_2H_8N_2)_2]^+(C_4H_6NO_4)^-\cdot 3H_2O$, M_r=453.3, monoclinic, $P2_1$, a=14.319(4), b=6.1043(7), c=10.771(2) Å, β=96.96(3)°, V=934.5(3) Å^3, Z=2, D_m=1.61(2), D_x=1.61 g cm^{-3}, $F(000)$=476, T=298 K, μ(Mo $K\alpha$)=10.24 cm^{-1}.

(**3**) $[Co(C_2O_4)(C_2H_8N_2)_2]^+$ $(C_4H_6NO_4)^-$, M_r=399.2, triclinic, $P\bar{1}$, a=10.363(3), b=12.964(4), c=6.091(1) Å, α=102.78 (2), β=86.47(3), γ=104.59(3)°, V=772.4(3) Å^3, Z=2, D_m=1.73 (2), D_x=1.72 g cm^{-3}, $F(000)$=416, T=298 K, μ(Mo $K\alpha$)= 12.22 cm^{-1}.

Results and Discussion

Cation and Anion Geometries. The perspective drawings of the $(-)_{589}$- complex cation and the counter anion are given in Fig. 1 with the atomic numbering scheme. The absolute configurations of the $(-)_{589}$-$[Co(ox)(en)_2]^+$ and the $(+)_{589}$-$[Co(ox)(en)_2]^+$ cations were identified to be $\Delta(\delta\lambda)$ and $\Lambda(\delta\lambda)$, respectively, on the basis of L-aspartate ion as an internal reference. These configurations are consistent with the assignments made by analyses of the circular dichroism spec-

Table 2. Fractional Atomic Coordinates and Thermal Parameters (Å^2) of Non-Hydrogen Atoms (with e.s.d.'s) for Structure **1**

Atom	x	y	z	B_{eq}
Co	0.7082(1)	0.7212(1)	0.7189(2)	1.93(1)
O(1)	0.7321(4)	0.5324(3)	0.6169(5)	2.6(1)
O(2)	0.8097(4)	0.7394(3)	0.9805(5)	2.5(1)
O(3)	0.8315(5)	0.3951(4)	0.7307(6)	3.9(1)
O(4)	0.9143(4)	0.6170(4)	1.1216(5)	3.0(1)
O(5)	0.2809(4)	0.2015(4)	0.1491(7)	4.1(1)
O(6)	0.5209(5)	0.4117(4)	0.1121(6)	3.5(1)
O(7)	0.5017(4)	−0.0090(4)	0.6456(6)	3.6(1)
O(8)	0.6545(5)	0.0076(4)	0.3132(5)	3.7(1)
O(9)	0.1995(5)	0.9155(5)	0.8594(7)	4.5(1)
O(10)	0.0442(6)	0.3288(6)	0.2731(10)	7.2(1)
O(11)	0.2667(5)	0.7509(6)	0.1298(9)	6.1(1)
N(1)	0.9294(4)	0.8317(3)	0.5622(6)	2.4(1)
N(2)	0.7125(5)	0.9212(4)	0.8333(6)	2.5(1)
N(3)	0.4830(5)	0.6087(5)	0.8676(6)	2.8(1)
N(4)	0.5903(5)	0.6871(4)	0.4584(6)	2.6(1)
N(5)	0.7174(5)	0.3005(4)	0.1936(6)	2.6(1)
C(1)	0.8034(6)	0.5067(5)	0.7541(7)	2.5(1)
C(2)	0.8476(5)	0.6312(5)	0.9724(7)	2.3(1)
C(3)	0.9553(7)	0.9891(6)	0.5539(9)	3.4(1)
C(4)	0.8831(7)	1.0423(6)	0.7857(9)	3.8(1)
C(5)	0.3639(6)	0.5162(6)	0.6896(8)	3.3(1)
C(6)	0.4060(6)	0.6234(6)	0.5204(8)	3.2(1)
C(7)	0.4353(6)	0.2759(6)	0.1454(7)	2.8(1)
C(8)	0.5362(6)	0.1928(5)	0.1872(7)	2.4(1)
C(9)	0.4692(6)	0.1295(6)	0.4096(8)	2.9(1)
C(10)	0.5485(6)	0.0346(5)	0.4545(8)	2.6(1)

$B_{eq}=(4/3)\sum_i\sum_j\beta_{ij}\boldsymbol{a}_i\cdot\boldsymbol{a}_j$.
$T=\exp[-(\beta_{11}h^2+\beta_{22}k^2+\beta_{33}l^2+2\beta_{12}hk+2\beta_{13}hl+2\beta_{23}kl)]$.

Table 3. Fractional Atomic Coordinates and Thermal Parameters (Å^2) of Non-Hydrogen Atoms (with e.s.d.'s) for Structure **2**

Atom	x	y	z	B_{eq}
Co	0.68676(4)	0.23158(18)	0.71632(5)	1.94(1)
O(1)	0.6830(2)	0.2562(6)	0.5377(3)	2.4(1)
O(2)	0.6228(2)	−0.0438(6)	0.6808(3)	2.5(1)
O(3)	0.6355(2)	0.0642(7)	0.3654(3)	3.1(1)
O(4)	0.5654(2)	−0.2474(7)	0.5183(3)	2.8(1)
O(5)	0.0897(3)	0.3557(9)	0.5742(3)	4.8(1)
O(6)	0.2079(2)	0.2628(7)	0.4695(3)	3.1(1)
O(7)	0.2527(3)	0.2494(9)	1.0204(3)	4.1(1)
O(8)	0.3178(4)	0.0093(9)	0.9052(4)	6.0(1)
O(9)	0.9583(3)	0.2738(9)	0.3659(4)	5.9(1)
O(10)	0.9273(4)	0.3455(12)	0.1147(5)	7.3(1)
O(11)	0.0886(4)	0.4770(10)	0.0285(4)	6.3(1)
N(1)	0.5660(3)	0.3855(7)	0.7088(3)	2.4(1)
N(2)	0.6751(3)	0.1855(6)	0.8932(3)	2.6(1)
N(3)	0.8114(3)	0.0938(7)	0.7222(4)	2.8(1)
N(4)	0.7556(3)	0.5057(7)	0.7446(3)	2.4(1)
N(5)	0.3098(3)	0.0739(8)	0.6599(4)	3.1(1)
C(1)	0.6431(3)	0.0919(8)	0.4782(4)	2.3(1)
C(2)	0.6063(3)	−0.0846(8)	0.5641(4)	2.3(1)
C(3)	0.5377(4)	0.4033(10)	0.8373(5)	3.2(1)
C(4)	0.5735(3)	0.2034(12)	0.9075(4)	3.2(1)
C(5)	0.8808(3)	0.2662(10)	0.7010(5)	3.3(1)
C(6)	0.8577(4)	0.4608(10)	0.7769(5)	3.2(1)
C(7)	0.1669(3)	0.2654(9)	0.5646(4)	2.9(1)
C(8)	0.2139(3)	0.1458(9)	0.6810(4)	2.7(1)
C(9)	0.2189(4)	0.2857(9)	0.8000(4)	3.4(1)
C(10)	0.2652(4)	0.1703(9)	0.9178(4)	3.3(1)

$B_{eq}=(4/3)\sum_i\sum_j\beta_{ij}\boldsymbol{a}_i\cdot\boldsymbol{a}_j$.

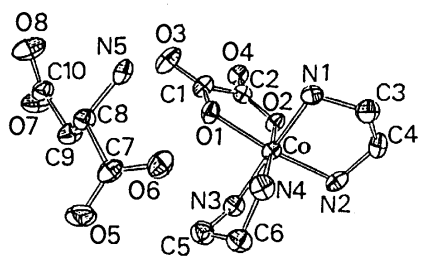

Fig. 1. Absolute configurations of (−)$_{589}$-[Co(ox)(en)$_2$]$^+$ cation and L-Hasp$^-$ anion.

tra of the complexes.[4] The assignments also agree with those in the compounds with various counter ions such as Br$^-$,[11] (+)$_{589}$-[Co(CN)$_2$(mal)(NH$_3$)$_2$]$^-$,[12] and H-*d*-tart$^-$.[1,2] It was therefore confirmed that the *lel-ob* conformation is the most stable form among the possible three, *lel-lel*, *lel-ob*, *ob-ob*, for the two ethylenediamine ligands. Selected bond lengths and angles within the ions are listed in Table 5. The corresponding values for the four complex cations are in fair agreement with each other, as well as with those found in the literature.[2,11]

The bond lengths and angles in the L-aspartate ion are consistent with the values reported for the free acid and its metal complexes.[13-15] In the present cases, the L-Hasp$^-$ ion is not coordinated to the Co(III) atom, but acts as a counter anion to the complex cation

Table 4. Fractional Atomic Coordinates and Thermal Parameters (Å^2) of Non-Hydrogen Atoms (with e.s.d.'s) for Structure **3**

Atom	x	y	z	B_{eq}[a]/B_{iso}
Co(A)	0.9633(3)	0.9456(3)	0.6160(6)	1.6(1)[a]
Co(B)	0.4409(3)	0.3530(3)	0.3215(6)	2.1(1)[a]
O(1A)	1.144(1)	0.936(1)	0.582(2)	1.9(3)
O(2A)	1.004(1)	1.008(1)	0.940(3)	2.8(3)
O(3A)	1.334(1)	0.993(1)	0.760(2)	2.6(3)
O(4A)	1.189(1)	1.054(1)	1.147(2)	2.3(3)
O(5A)	0.231(2)	0.710(1)	−0.267(3)	4.3(4)
O(6A)	0.114(1)	0.785(1)	0.016(2)	1.3(3)
O(7A)	0.695(1)	0.844(1)	0.028(3)	2.9(3)
O(8A)	0.577(1)	0.875(1)	0.349(3)	4.1(4)
O(1B)	0.256(1)	0.350(1)	0.381(2)	1.8(3)
O(2B)	0.390(1)	0.282(1)	0.032(2)	1.9(3)
O(3B)	0.060(1)	0.285(1)	0.188(2)	2.4(3)
O(4B)	0.218(1)	0.224(1)	−0.201(3)	2.9(3)
O(5B)	1.159(1)	0.567(1)	1.222(2)	1.5(3)
O(6B)	1.276(1)	0.489(1)	0.947(2)	2.2(3)
O(7B)	0.703(1)	0.404(1)	0.865(3)	3.3(4)
O(8B)	0.831(1)	0.449(1)	0.581(2)	1.2(3)
N(1A)	0.999(2)	1.077(1)	0.527(3)	2.5(4)
N(2A)	0.779(1)	0.961(1)	0.675(3)	1.3(3)
N(3A)	0.920(1)	0.791(1)	0.704(3)	3.0(4)
N(4A)	0.924(2)	0.859(1)	0.304(3)	1.5(3)
N(5A)[b]	0.296	0.798	0.312	3.0
N(1B)	0.396(2)	0.203(1)	0.410(3)	2.1(4)
N(2B)	0.617(2)	0.323(1)	0.254(3)	2.3(4)
N(3B)	0.479(1)	0.488(1)	0.248(3)	1.0(3)
N(4B)	0.488(2)	0.428(1)	0.626(3)	2.2(4)
N(5B)	1.089(1)	0.488(1)	0.630(3)	1.4(3)
C(1A)[b]	1.209	0.976	0.736	2.0
C(2A)[b]	1.128	1.011	0.955	2.0
C(3A)	0.866(2)	1.115(2)	0.506(4)	2.3(5)
C(4A)	0.774(2)	1.074(2)	0.714(4)	3.8(6)
C(5A)	0.922(2)	0.713(1)	0.493(3)	0.7(4)
C(6A)	0.849(2)	0.744(1)	0.321(3)	1.5(4)
C(7A)	0.224(2)	0.765(1)	−0.071(3)	1.5(4)
C(8A)	0.348(2)	0.839(2)	0.076(4)	2.4(5)
C(9A)	0.470(2)	0.793(1)	−0.005(3)	1.5(4)
C(10A)	0.590(2)	0.835(2)	0.134(4)	3.5(6)
C(1B)[b]	0.180	0.298	0.180	2.0
C(2B)[b]	0.271	0.263	−0.026	2.0
C(3B)	0.514(2)	0.172(2)	0.417(4)	3.5(6)
C(4B)	0.602(2)	0.209(2)	0.246(4)	1.7(4)
C(5B)	0.494(2)	0.575(2)	0.450(5)	4.6(6)
C(6B)	0.543(2)	0.544(2)	0.638(4)	3.8(6)
C(7B)	1.181(2)	0.519(2)	1.027(4)	3.9(6)
C(8B)	1.059(2)	0.520(2)	0.868(4)	1.5(4)
C(9B)	0.939(2)	0.440(2)	0.924(4)	2.0(5)
C(10B)	0.816(2)	0.431(2)	0.779(4)	2.4(5)

a) $B_{eq}=(4/3)\sum_i\sum_j\beta_{ij}\boldsymbol{a}_i\cdot\boldsymbol{a}_j$. b) Atom was not refined.

[Co(ox)(en)$_2$]$^+$. The anion is therefore extended with the carbon atom skeleton, C(7)-C(8)-C(9)-C(10), in almost planar, zigzag conformation. The molecule in the crystalline state of free L-aspartic acid (LASP) is in the zwitterionic form and the ionized α-carboxyl group and the un-ionized β-carboxyl group are clearly distinguished; the C-O distances in the ionized COO$^-$ group are 1.242 and 1.252 Å, whereas in the un-ionized COOH group they are 1.202 and 1.306 Å.[14] A comparison with these values indicates that both α and β car-

Table 5. Bond Lengths (l/Å) and Angles (ϕ/°)

	1	2	3	
			"A"	"B"
Co-O(1)	1.934(4)	1.924(3)	1.90(1)	1.92(1)
Co-O(2)	1.911(4)	1.930(3)	1.99(1)	1.84(1)
Co-N(1)	1.955(3)	1.961(4)	1.85(2)	2.06(2)
Co-N(2)	1.934(5)	1.953(4)	1.97(2)	1.96(2)
Co-N(3)	1.963(4)	1.967(4)	2.13(2)	1.85(2)
Co-N(4)	1.948(4)	1.947(4)	1.99(2)	1.92(2)
O(1)-C(1)	1.274(7)	1.286(6)	1.14	1.44
O(2)-C(2)	1.258(7)	1.274(5)	1.28	1.25
O(3)-C(1)	1.220(8)	1.218(5)	1.27	1.22
O(4)-C(2)	1.243(7)	1.226(6)	1.31	1.18
N(1)-C(3)	1.485(8)	1.492(6)	1.60(3)	1.39(3)
N(2)-C(4)	1.475(6)	1.485(6)	1.45(3)	1.43(3)
N(3)-C(5)	1.491(6)	1.484(7)	1.45(2)	1.46(3)
N(4)-C(6)	1.479(6)	1.487(6)	1.52(2)	1.45(3)
C(1)-C(2)	1.560(5)	1.554(7)	1.57	1.58
C(3)-C(4)	1.521(7)	1.493(9)	1.64(3)	1.43(3)
C(5)-C(6)	1.528(8)	1.502(8)	1.51(3)	1.45(4)
O(1)-Co-O(2)	85.0(2)	85.1(1)	86.6(6)	86.8(6)
N(1)-Co-N(2)	85.7(2)	86.0(2)	86.9(7)	83.3(7)
N(3)-Co-N(4)	85.5(2)	85.5(2)	84.5(7)	87.4(7)
Co-O(1)-C(1)	113.1(3)	113.2(3)	115.6	109.4
Co-O(2)-C(2)	113.4(3)	113.1(3)	103.7	120.0
Co-N(1)-C(3)	109.8(3)	109.5(3)	111.5(11)	108.2(13)
Co-N(2)-C(4)	109.9(4)	106.9(3)	111.4(12)	107.6(11)
Co-N(3)-C(5)	108.8(3)	108.3(3)	105.1(14)	110.8(15)
Co-N(4)-C(6)	110.5(3)	110.1(3)	107.4(13)	110.8(15)
O(1)-C(1)-O(3)	126.0(4)	125.9(5)	130.5	118.6
O(1)-C(1)-C(2)	113.3(5)	114.0(4)	113.3	112.2
O(3)-C(1)-C(2)	120.6(5)	120.1(4)	116.2	129.1
O(2)-C(2)-O(4)	125.5(4)	125.3(4)	119.7	132.0
O(2)-C(2)-C(1)	115.2(4)	114.6(4)	119.8	111.4
O(4)-C(2)-C(1)	119.3(5)	120.1(4)	120.1	116.6
N(1)-C(3)-C(4)	104.8(4)	107.2(4)	103.0(18)	109.0(22)
N(2)-C(4)-C(3)	108.0(4)	106.7(4)	101.6(17)	112.0(18)
N(3)-C(5)-C(6)	105.1(4)	106.3(4)	107.9(16)	111.8(21)
N(4)-C(6)-C(5)	107.2(5)	107.1(4)	106.1(14)	109.0(18)
O(5)-C(7)	1.233(6)	1.251(7)	1.26(2)	1.25(3)
O(6)-C(7)	1.253(6)	1.241(6)	1.29(2)	1.18(3)
O(7)-C(10)	1.265(6)	1.239(6)	1.23(3)	1.26(3)
O(8)-C(10)	1.240(6)	1.256(8)	1.31(3)	1.28(3)
N(5)-C(8)	1.480(5)	1.485(7)	1.65	1.45(3)
C(7)-C(8)	1.562(9)	1.534(7)	1.58(3)	1.65(3)
C(8)-C(9)	1.527(7)	1.534(7)	1.54(3)	1.48(3)
C(9)-C(10)	1.511(9)	1.531(7)	1.47(3)	1.56(3)
O(5)-C(7)-O(6)	127.0(6)	125.8(5)	122.8(17)	131.4(23)
O(5)-C(7)-C(8)	116.8(5)	116.5(4)	124.9(17)	106.8(19)
O(6)-C(7)-C(8)	116.2(4)	117.7(4)	111.1(15)	121.0(21)
N(5)-C(8)-C(7)	110.1(4)	109.7(4)	96.2(13)	111.7(16)
N(5)-C(8)-C(9)	109.5(4)	110.0(4)	106.5(17)	108.3(14)
C(7)-C(8)-C(9)	111.0(4)	112.9(4)	108.1(15)	107.1(18)
C(8)-C(9)-C(10)	114.8(4)	114.1(5)	117.5(17)	112.2(19)
O(7)-C(10)-O(8)	124.2(6)	123.7(5)	125.5(19)	122.0(20)
O(7)-C(10)-C(9)	115.0(5)	117.7(5)	114.9(21)	117.3(20)
O(8)-C(10)-C(9)	120.8(5)	118.4(5)	118.6(19)	120.8(17)

boxyl groups are ionized and consequently the amino groups are protonated in crystals of **1**, **2**, and **3**. The torsion angles of the L-Hasp$^-$ ions are compared in Table 6, where the corresponding values for LASP and DL-aspartic acid (DLASP) are also included.[14,15] The angles other than the carbon skeleton described above are more or less different from each other, possibly owing to the packing effect, especially to the hydrogen bonding scheme. The variation in torsion angle among the aspartates **1**, **2**, and **3** is considerably less than that between the two glutamates **4** and **5**, which are described in the next paper.

Crystal Structures. The crystal structures of the three aspartates are shown in Figs. 2—4. The distances and angles for intermolecular hydrogen bonds are given in Table 7.

***Δ*-(−)[Co(ox)(en)$_2$](L-Hasp)·3H$_2$O (1):** In the most soluble aspartate, (−)[Co(ox)(en)$_2$]$^+$ cations and L-Hasp$^-$ anions are arranged alternately to form a layer parallel to (100) and water molecules are sandwiched between these layers (Fig. 2). Each complex cation donates its eight NH hydrogen atoms to eight oxygen atoms of one cation, four anions and two water molecules, forming eight N-H···O hydrogen bonds with distances ranging from 2.79 to 3.27 Å (av 2.96 Å). The ammonio group -NH$_3^+$ of the anion is hydrogen bonded to three oxygen atoms from two cations and one water molecule with a mean N-H···O distance of 2.99 Å, while three kinds of water molecules form six O-H···O hydrogen bonds (av 2.86 Å) with six oxygen atoms of two cation, three anions and one water molecule. Thus, the two types of hydrogen bonds, N-H···O and O-H···O, contribute to stabilize the crystal lattice, in addition to electrostatic interaction.

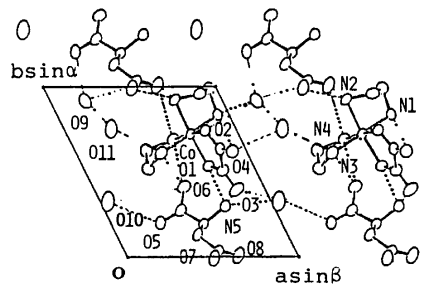

Fig. 2. Crystal structure of diastereoisomer **1** projected along [001]. Broken lines denote hydrogen bonds. Thermal ellipsoids are shown at 50% probability level.

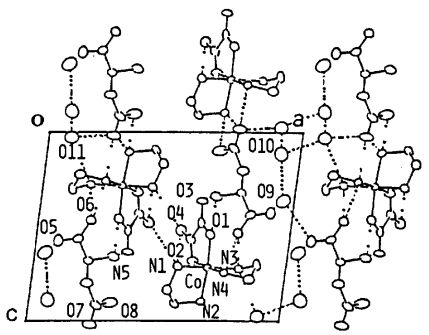

Fig. 3. Crystal structure of diastereoisomer **2** projected along [010]. Broken lines denote hydrogen bonds. Thermal ellipsoids are shown at 50% probability level.

Table 6. Torsion Angles (τ/°) of L-Aspartic Acid

Atom	1	2	3 "A"	3 "B"	LASP[14]	DLASP[15]
O(5)-C(7)-C(8)-N(5)	−176.0(4)	−172.5(4)	−135.5(17)	167.4(18)	144.8	172.3
O(6)-C(7)-C(8)-N(5)	3.9(6)	8.1(6)	57.6(17)	−3.9(30)	−37.8	−7.3
O(5)-C(7)-C(8)-C(9)	−54.6(6)	−49.4(6)	−26.0(26)	−73.8(23)	−94.2	−64.0
O(6)-C(7)-C(8)-C(9)	125.3(5)	131.2(5)	167.1(15)	114.9(24)	83.2	117.6
C(7)-C(8)-C(9)-C(10)	174.7(4)	179.8(4)	−168.5(16)	−178.6(18)	178.2	174.2
C(8)-C(9)-C(10)-O(7)	175.3(4)	−163.6(5)	−144.2(18)	−151.6(21)	131.4	3.1
C(8)-C(9)-C(10)-O(8)	−2.8(7)	20.5(7)	25.1(25)	29.4(31)	−51.3	−175.8
N(5)-C(8)-C(9)-C(10)	−63.5(6)	−57.2(5)	−66.4(20)	−57.7(24)	−61.9	−61.9

Table 7. Distances D···A(l/Å) and Angles D-H···A(ϕ/°) of Hydrogen Bonds

	D···A	D-H···A		D···A	D-H···A
(1) Δ-form			(2) Δ-form		
N(1)-H(1)···O(4^{iv})	2.995(6)	168	N(1)-H(1)···O(4^{iii})	3.038(6)	150
N(1)-H(2)···O(9^{ii})	2.986(6)	162	N(1)-H(2)···O(4^{xii})	3.011(6)	152
N(2)-H(3)···O(7^{iii})	2.785(6)	170	N(2)-H(3)···O(7^{xv})	2.965(7)	177
N(2)-H(4)···O(8^{viii})	2.865(6)	165	N(2)-H(4)···O(8^{xiii})	2.929(7)	132
N(3)-H(5)···O(6^{v})	2.888(6)	172	N(3)-H(5)···O(6^{xi})	2.878(6)	172
N(3)-H(6)···O(11^{v})	2.936(7)	154	N(3)-H(6)···O(11^{xi})	2.972(8)	156
N(4)-H(7)···O(6)	2.927(6)	145	N(4)-H(7)···O(6^{xii})	2.889(6)	153
N(4)-H(8)···O(8^{iii})	3.273(6)	166	N(4)-H(8)···O(7^{viii})	2.950(7)	152
N(5)-H(9)···O(1)	3.008(6)	180	N(5)-H(9)···O(1^{xi})	2.891(6)	179
N(5)-H(10)···O(3^{iv})	3.022(6)	180	N(5)-H(10)···O(3^{xii})	3.114(6)	179
N(5)-H(11)···O(10^{ii})	2.935(8)	145			
O(9)-H(12)···O(5^{viii})	2.823(6)	179	O(9)-H(12)···O(5^{ii})	2.794(8)	179
O(9)-H(13)···O(7^{iii})	2.618(6)	179	O(9)-H(13)···O(5^{xi})	2.740(8)	179
O(10)-H(14)···O(3^{i})	3.183(8)	180	O(10)-H(14)···O(9)	2.723(9)	178
O(10)-H(15)···O(5)	2.848(8)	180	O(10)-H(15)···O(11^{ii})	2.713(10)	177
O(11)-H(16)···O(4^{vi})	2.813(7)	179	O(11)-H(16)···O(7^{iv})	2.740(8)	177
O(11)-H(17)···O(9^{iv})	2.880(7)	179	O(11)-H(17)···O(10^{xiv})	2.722(10)	179
(3) Rac-form "A"			(3) Rac-form "B"		
N(1A)-H(1A)···O(4A^{iv})	2.96(2)	164	N(1B)-H(1B)···O(4B^{v})	2.92(2)	162
N(1A)-H(2A)···O(4B^{x})	2.90(2)	154	N(1B)-H(2B)···O(4A^{ix})	2.81(2)	164
N(2A)-H(3A)···O(7A^{v})	2.87(2)	163	N(2B)-H(3B)···O(7B^{iv})	2.81(2)	108
N(2A)-H(4A)···O(8A)	2.82(2)	158	N(2B)-H(4B)···O(8B)	2.98(2)	143
N(3A)-H(5A)···O(6A^{vii})	2.88(2)	174	N(3B)-H(5B)···O(6B^{vi})	2.88(2)	173
N(3A)-H(6A)···O(7A^{v})	3.07(3)	145	N(3B)-H(6B)···O(7B^{iv})	3.39(2)	144
N(4A)-H(7A)···O(6A^{ii})	2.76(2)	153	N(4B)-H(7B)···O(6B^{i})	2.99(2)	144
N(4A)-H(8A)···O(7A)	2.93(2)	136	N(4B)-H(8B)···O(7B)	2.85(2)	153
N(5A)-H(9A)···O(1A^{i})	2.86(2)	179	N(5B)-H(9B)···O(1B^{ii})	2.92(2)	178
N(5A)-H(10A)···O(5B^{vi})	2.91(2)	179	N(5B)-H(10B)···O(5A^{vii})	2.83(2)	177

(i) $-1+x$, y, z; (ii) $1+x$, y, z; (iii) x, $1+y$, z; (iv) x, y, $-1+z$; (v) x, y, $1+z$; (vi) $-1+x$, y, $-1+z$; (vii) $1+x$, y, $1+z$; (viii) x, $1+y$, $1+z$; (ix) $-1+x$, $-1+y$, $1+z$; (x) $1+x$, $1+y$, $1+z$; (xi) $1-x$, $-1/2+y$, $1-z$; (xii) $1-x$, $1/2+y$, $1-z$; (xiii) $1-x$, $1/2+y$, $2-z$; (xiv) $1-x$, $1/2+y$, $-z$; (xv) $1-x$, $-1/2+y$, $2-z$.

Recently, Miyoshi et al. have proposed an instructive mechanism of chiral recognition of octahedral metal complexes such as $[Co(en)_3]^{3+}$ and the related cations by bis-μ-(*d*-tartrato)-diantimonate(III) anion in solution.[16] It is pointed out in their association model that two amine protons of the octahedral cation are doubly hydrogen bonded to two oxygen atoms of the chiral $[Sb_2(d\text{-tart})_2]^{3-}$ ion along the C_3 or C_2 axis of the octahedron. In the present case three pairs of double hydrogen bonding are recognized between a given cation and the three surrounding anions; these are a pair of N(2)-H(3)···O(7^{iii}) and N(4)-H(8)···O(8^{iii}), a pair of N(3)-H(5)···O(6^{v}) and N(5^{v})-H(10^{v})···O(3) and a pair of N(4)-H(7)···O(6) and N(5)-H(9)···O(1), as can be seen in Table 7.

Δ-(+)[Co(ox)(en)$_2$](L-Hasp)·3H$_2$O (2): The less soluble aspartate has a crystal symmetry of $P2_1$ in contrast to $P1$ for compound 1. Owing to the presence of twofold screw axes 2_1, the complex cations and the counter anions are packed into double layers parallel to (100), between which layers water molecules are inserted as shown in Fig. 3. Four NH_2 groups of each cation form eight N-H···O hydrogen bonds (av 2.95 Å) with eight oxygen atoms from two cations, four anions and one water molecule. The NH_3 group of an anion participates in only two N-H···O hydrogen bonds with two oxygen atoms of two cations (av 3.00 Å), and the remaining NH hydrogen atom is free. Three kinds

of water molecules donate their six hydrdogen atoms to six oxygen atoms from three anions and three water molecules, forming O-H···O bonds with the average distance 2.74 Å.

In the complex **2**, three pairs of double N-H···O hydrogen bonds are also found between the cation and three surrounding anions in the same scheme as in **1**. Therefore, the formation of such double hydrogen bonds may not contribute to chiral discrimination. In both diastereoisomers, the chiral $[Co(ox)(en)_2]^+$ cations and L-Hasp$^-$ anions are alternately arranged into layers through N-H···O hydrogen bonds. Additionally, in the complex **2**, two cations which are related by the twofold screw axis are hydrogen bonded, giving rise to the double layered structure against the single layer in **1**.

***rac*-[Co(ox)(en)$_2$](L-Hasp) (3):** The least soluble pseudoracemate **3** is anhydride, different from the optically active diastereomers **1** and **2**. The unit cell contains the *Δ*-complex cation centered at Co(A) and the *Λ*-cation centered at Co(B) in the molar ratio 1 : 1, as shown in Fig. 4. Each complex cation is surrounded by six counter anions and vice versa, suggesting dominant electrostatic interaction. The cation labeled 'A' (or 'B') forms eight N-H···O hydrogen bonds with seven oxygen atoms of two cations, A and B, and of four anions A (or B); the average distance is 2.90 Å for cation A (or 2.95 Å for B). Anion A (or B) also acts as hydrogen donor to two oxygen atoms of one cation A (or B) and one anion B (or A) with an average N-H···O distance of 2.89 (or 2.88) Å.

In the pseudoracemate **3**, two pairs of double hydrogen bonds are also formed between either cation and the neighboring L-Hasp$^-$ ions; one pair is N(2A)-H(4A)···O(8A) and N(4A)-H(8A)···O(7A) and the other is N(4A)-H(7A)···O(6A^{ii}) and N(5A^{ii})-H(9A^{ii})···O(1A) for *Δ*-cation. As compared in Table 7, these schemes which are found in *Λ*-cation as well, are identical to two of three found in **1** and **2**. Two types of layers, one of which consists of *Δ*-cations and L-Hasp$^-$ ions and the other of *Λ*-cations and L-Hasp$^-$ ions, are stacked parallel to (010) plane. Thus formed layers are connected by hydrogen bonds between two different types of cations and between two anions alternately. Such anion-anion approach via N-H···O hydrogen bonds is recognized only in **3**. Besides these, no existence of water molecules provides the most dense packing for the least soluble **3**, as discussed later.

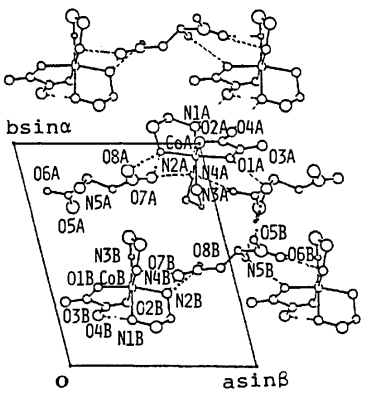

Fig. 4. Crystal structure of pseudoracemic salt **3** projected along [001]. Broken lines denote hydrogen bonds. Thermal ellipsoids are shown at 50% probability level.

Solubility and Crystal Structure. According to Yamanari et al. the *Δ*-salt is much more soluble in water than the other two aspartates.[4] Such difference in solubility must be caused by the difference in packing scheme, because the three complexes are composed of the same cations and the same anions. Moreover, the numbers of water molecule of crystallization are equally three for the two diastereoisomers. The present X-ray study revealed that the three salts possess a common structural principle such that $[Co(ox)(en)_2]^+$ cations and L-Hasp$^-$ anions form a layer by N-H···O hydrogen bonding in a very similar way to each other. The crystal lattice of *Δ*-isomer consists of such single cation-anion layers, while those of *Λ* and pseudoracemic salts contain doubled and multipled cation-anion layers, respectively. It was supposed that the difference in arrangement of ionic species and water molecules is responsible for the differences in density and solubility. However, the X-ray (or measured) densities are 1.61 (or 1.58), 1.61 (or 1.61), and 1.72 (or 1.73) for **1**, **2**, and **3**, respectively, indicating the increasing density is not necessarily correlated to the decreasing sulubility.

Another scale such as unoccupied (cavity) fraction CV/V where CV is the unoccupied space by atoms and V the unit cell volume was introduced to compare the extent of molecular packing. The calculation with van der Waals radii for peripheral atoms of ions or water molecules gave the values 31.3, 30.3, and 28.7% for **1**, **2**, and **3**, respectively.[17] Although the order of magnitude of CV/V is compatible with that of solubility, this measure is still not sufficient to account for the solubility difference relatively. If the solubility is governed by molecular packing, the solubility difference between the pseudoracemic and *Λ* compounds would be greater than the observation.[4]

In general, solubility is explicitly related to the change in the free energy upon solution. For the present diastereoisomers, fortunately, their entropy changes and hydration enthalpies would be equal and then the solubility difference would be attributed to the difference in enthalpy change. Such consideration lead us to estimate the electrostatic term of the lattice energy in accordance with the lattice sum method.[18] The lattice sum was carried out over 125 (5×5×5 along ***a***, ***b***, ***c*** axes) unit cells around a given unit cell. The calculation was based on the electroneutrality principle and distributions of the charges of the cation, anion and water molecule on their peripheral atoms.[19] The charge distributions for both ions were assigned from the elec-

tronegativity difference between bonding atoms as follows:[20] For the cation Co, −1.06; N, 0.23; H(N), 0.17; C(en), 0.05; H(C), 0.05; O(Co), 0.60; C(ox), 1.39; O(C), −1.20 and for the anion N, 0.35; H(N), 0.17; C(O), 1.39; O, −1.20; C(CH), 0.10; C(CH$_2$), −0.09; H(C), 0.05. On the other hand, the "ST 2" model proposed by Stillinger and Rahman was adopted for the formal charges on a water molecule.[21] Such a typical set of charge distribution yielded electrostatic energies of −1214, −1476, and −1246 kJ mol^{-1} for **1**, **2**, and **3**, respectively. This order of magnitude was unchanged even for the electronic structure with the extreme ionic bonds. It was therefore ascertained that the less soluble isomer is characterized by the electrostatic energy higher than that of the more soluble *Δ* isomer.

In conclusion, the solubility difference between the *Δ*- and *Λ*-diastereoisomers could be explained in terms of density, unoccupied fraction and electrostatic interaction. However, there remained some uncertainty with respect to the solubility of the pseudoracemate, because this salt is anhydride, different from the other two. Other factors such as hydration enthalpy, hydrogen bonding interaction and entropy changes must be taken into account, but these terms are too complicated to be considered.

References

1) M. Kuramoto, Y. Kushi, and H. Yoneda, *Bull. Chem. Soc. Jpn.*, **51**, 3251 (1978).

2) M. Kuramoto, Y. Kushi, and H. Yoneda, *Bull. Chem. Soc. Jpn.*, **53**, 125 (1980).

3) M. Gajhede and S. Larsen, *Acta Crystallogr., Sect. B*, **42**, 172 (1986).

4) K. Yamanari, M. Igaki, and Y. Shimura, *Bull. Chem. Soc. Jpn.*, **57**, 3007 (1984).

5) A. C. North, D. C. Phillips, and F. S. Mathews, *Acta Crystallogr., Sect. A*, **24**, 351 (1968).

6) P. Main, S. E. Hull, L. Lessinger, G. Germain, J.-P. Declercq, and M. M. Woolfson, Univs. of York, England, and Louvain, Belgium (1978).

7) "International Tables for X-ray Crystallography," Birmingham (1974), Vol. IV, Knoch Press (present distributor D. Reidel, Dordrecht).

8) C. K. Johnson, Report ORNL-5138. Oak Ridge National Laboratory, Tennessee (1976).

9) The Universal Crystallographic Computing System-Osaka (1979). The Computing Center, Osaka University.

10) The lists of structure factors, anisotropic thermal parameters of non-hydrdogen atoms and calculated positional parameters of hydrogen atoms are deposited as Document No. 8818 at the Office of the Editor of Bull. Chem. Soc. Jpn.

11) T. Aoki, K. Matsumoto, S. Ooi, and H. Kuroya, *Bull. Chem. Soc. Jpn.*, **46**, 159 (1973).

12) K. Toriumi, S. Sato, and Y. Saito, *Acta Crystallogr., Sect. B*, **33**, 1378 (1977).

13) I. Oonishi, S. Sato, and Y. Saito, *Acta Crystallogr., Sect. B*, **31**, 1318 (1975).

14) J. L. Derissen, H. J. Endeman, and A. F. Peerdeman, *Acta Crystallogr., Sect. B*, **24**, 1349 (1968).

15) S. T. Rao, *Acta Crystallogr., Sect. B*, **29**, 1718 (1973).

16) K. Miyoshi, S. Izumoto, and H. Yoneda, *Bull. Chem. Soc. Jpn.*, **59**, 3475 (1986).

17) The program to calculate unoccupied space was kindly supplied by Professor Yoshio Sasada at Tokyo Institute of Technology.

18) W. H. Baur, *Acta Crystallogr.*, **19**, 909 (1965).

19) L. Pauling, "The Nature of The Chemical Bond," 3rd ed, Cornell Univ. Press (1960), p. 172.

20) A. L. Allred and E. G. Rochow, *J. Inorg. Nucl. Chem.*, **5**, 264 (1958).

21) F. H. Stillinger and A. Rahman, *J. Chem. Phys.*, **60**, 1545 (1974).

Studies on the Reaction Products of Antitumor Platinum Complex with d(ApG), d(GpA), and d(pGpA). 2′-Deoxy Sugar Is Favourable for G-N7, A-N1 Chelation

Kenji INAGAKI,* Akihito TOMITA, and Yoshinori KIDANI
Faculty of Pharmaceutical Sciences, Nagoya City University, 3, Tanabe-dori, Mizuho-ku, Nagoya 467
(Received March 9, 1988)

The reaction products of dichloro[(1*R*,2*R*)-1,2-cyclohexanediamine]platinum(II), Pt(*R*,*R*-dach)Cl_2, with dinucleotides, d(ApG), d(GpA), and d(pGpA) have been separated by HPLC, and each product fractionated has been characterized by UV and CD spectral analyses. The reaction of Pt(*R*,*R*-dach)Cl_2 with d(ApG) yields Pt(*R*,*R*-dach)(d(ApG)-*N1(1),N7(2)*) (**1**, 16%), Pt(*R*,*R*-dach)(d(ApG)-*N7(1),N7(2)*) (**2**, 80%) and uncharacterized minor product (4%). The reaction with d(GpA) yielded two Pt(*R*,*R*-dach)(d(GpA)-*N7(1),N1(2)*), (**3**, 22% and **5**, 61%), and Pt(*R*,*R*-dach)(d(GpA)-*N7(1),N7(2)*), (**4**, 17%), but surprisingly **5** isomerizes very slowly to **3** and **4** under the subsequent incubation (half life of **5**; about 6 days at 37 °C). The reverse reaction (**3** and **4**→**5**) was not observed. The reaction with d(pGpA) also yielded two Pt(*R*,*R*-dach)(d(pGpA)-*N7(1),N1(2)*), (**3′**, 8% and **5′**, 80%) and Pt(*R*,*R*-dach)(d(pGpA)-*N7(1),N7(2)*), (**4′**, 12%). The adduct, **5′**, also isomerizes to **3′** and **4′**. The platinum adducts, **3′**, **4′**, and **5′**, are compatible with **3**, **4**, and **5**, respectively, after removal of the 5′-phosphate group upon treatment with alkaline phosphatase. A competition reaction between d(ApG) and d(GpA) for Pt(*R*,*R*-dach)Cl_2 indicates that d(ApG) was about 2 times more reactive than d(GpA). The reactivity decreases along the series; d(pGpA)>d(ApG)>d(GpA).

In the mechanism of action of antitumor platinum drugs, DNA has been considered to be the primary target.[1-3] Studies on the reactions with DNA and its constituents have indicated that the N7 of guanine base is a strongly preferred platinum binding site. The interaction between the bifunctional platinum compound and the guanine base, especially the intrastrand crosslink between two adjacent guanine bases,[4-8] appears to play an important role in cell killing.[9,10] The enzymatic digestion of platinum modified DNA has been indicated that such intrastrand crosslinked compound is the most prominent platinum adduct.[11-15] An intriguing observation is that only an intrastrand crosslinked compound between adjacent adenine and guanine base, d(ApG)-chelate, but no d(GpA)-chelate has been found after digestion in the reaction products with DNA.[12,13] The d(ApG)-chelate is a major platinum adduct next to the d(GpG)-chelate. An important question is why only the d(ApG)-chelate is found in the reaction with DNA, and this has led us to the present study.

In the previous paper,[16] we reported that the reaction of r(GpA) with *cis*-Pt$(NH_3)_2Cl_2$ gives two platinum adducts and that one of them is *cis*-Pt$(NH_3)_2$-(r(GpA)-*N7(1),N7(2)*).[17] Very recently, Chottard et al.[18] investigated *cis*-Pt$(NH_3)_2$-adducts with r(ApG) and r(GpA) by means of NMR, in which the reaction between *cis*-Pt$(NH_3)_2Cl_2$ and r(ApG) gave *cis*-Pt$(NH_3)_2$-(r(ApG)-*N7(1),N7(2)*) as a major platinum adduct (>95%). The reaction[18] of *cis*-Pt$(NH_3)_2Cl_2$ with r(GpA) yielded *cis*-Pt$(NH_3)_2$(r(GpA)-*N7(1),N7(2)*) (68%) and *cis*-Pt$(NH_3)_2$(r(GpA)-*N7(1),N1(2)*) (32%). The present paper describes about the reaction products of Pt(*R*,*R*-dach)Cl_2 with d(ApG), d(GpA), and d(pGpA) and the competition reaction between d(ApG) and d(GpA), with a common reactant Pt(*R*,*R*-dach)Cl_2. Our results are somewhat different from those obtained from the reaction[18] between *cis*-Pt$(NH_3)_2Cl_2$ and r(ApG) or r(GpA).

Experimental

The dinucleotides used were purchased from Pharmacia Co., Ltd. The platinum complexes, Pt(*R*,*R*-dach)Cl_2 and [Pt$(NH_3)_3$Cl]Cl, were prepared according to the literature.[19,20] For the purpose of characterization of the reaction products, the dinucleotide, d(ApG), d(GpA), or d(pGpA), was allowed to react with a stoichiometric amount of Pt(*R*,*R*-dach)Cl_2 in a deionized and distilled water at 37 °C for 1 day. The reaction products formed are separated and fractionated by a Hitachi 655 liquid chromatograph with Shimadzu Chromatopak C-R5A and with variable wavelength UV monitor. Fractions of 3—4 cm^3 were collected to characterize each product separated by HPLC. The parameters of the run of HPLC are as follows: Column, Cosmosil $5C_{18}$ (0.46 cm i.d.×15 cm); detector, UV at 260 nm; flow rate, 0.8 $cm^3\,min^{-1}$; mobil phase, 0.02 mol dm^{-3} phosphate buffer (pH=8.0) in 10% methanol solution. Retention time: **3**, 6.0

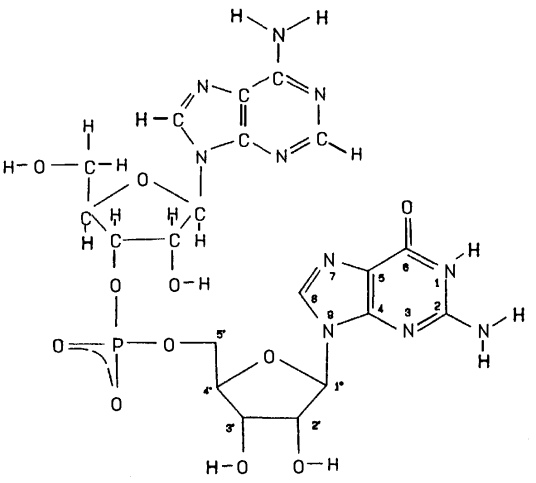

Fig. 1. Schematic structure of r(ApG) with the base and deoxyribose numbering scheme.

min; **4**, 12.2 min; **5**, 18.8 min; d(GpA), 23.2 min. For the competition reaction: Cosmosil $5C_{18}$ (0.46 cm i.d.×25 cm); Mobil phase, 0.25 mol dm^{-3} KH_2PO_4 in 9% methanol solution. Retention time: **1**, 12.2 min; **2**, 29.7 min; **3**, 12.2 min; **4**, 22.1 min; **5**, 19.8 min; **3′**, 12.0 min; **4′**, 31.1 min; **5′**, 13.5 min; d(ApG), 60.4 min; d(GpA), 62.2 min; d(pGpA), 17.4 min.

The platinum content of each product was determined by a Shimadzu AA-670G atomic absorption spectrometer. The UV and UV difference spectra were recorded on a Hitachi 557 dual-wavelength double beam spectrometer. In the measurement of UV difference spectrum, the reference cell contained a pH=5—6 solution of the each product. The CD spectrum was recorded on a JEOL J-40 spectrometer. The values are given per mole of platinum.

Results and Discussion

HPLC Analysis.[21] The reaction between Pt(*R*,*R*-dach)Cl_2 and d(ApG) yields two products, with a minor product (less than 4%). The two main platinum adducts are called **1** and **2**, according to their elution order. The reaction was followed at suitable time intervals by means of HPLC. The reactants are almost completely converted into **1** and **2** after 1 day reaction at 37 °C (see Figs. 8 and 9). The relative ratio of **1** (16 %) to **2** (80%) did not change throughout the reaction, suggesting parallel reaction. The Pt/base ratio (r=[Pt]/[Base], r=0.5 and 0.25) in the initial reaction solution also did not change the product ratio. The reaction of Pt(*R*,*R*-dach)Cl_2 with d(GpA) resulted in three platinum adducts, **3**, **4** and **5**. Figure 2 shows a time-dependence of the reaction. Relative ratios of each product to all the platinum adducts were almost constant for the first 10 hours, **3** (21—22%), **4** (16—18%) and **5** (62—59%). Afterward, the relative ratios, however, gradually change with the subsequent incubation because of an isomerization of **5** to **3** and **4**, as being mentioned later. The similar behaviour is also observed in the reaction between Pt(*R*,*R*-dach)Cl_2 and

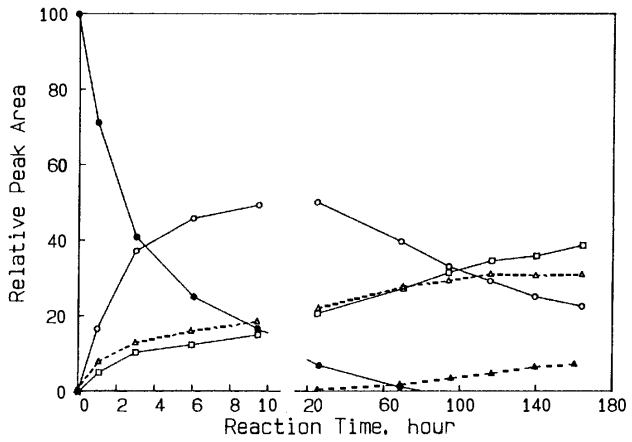

Fig. 2. Time-dependence of the reaction products of Pt(*R*,*R*-dach)Cl_2 with d(GpA) at 40 °C in water. (●), unreacted d(GpA); (○), Pt(*R*,*R*-dach)(d(GpA)-*N7(1),N1(2)*), **5**; (△), Pt(*R*,*R*-dach)(d(GpA)-*N7(1),N1(2)*), **3**; (▲), unknown; (□), Pt(*R*,*R*-dach)-(d(GpA)-*N7(1),N7(2)*), **4**.

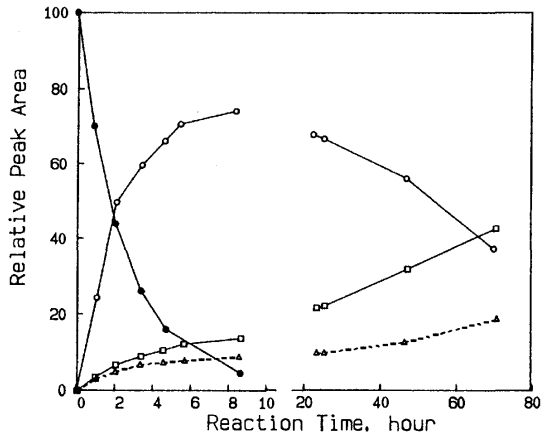

Fig. 3. Time-dependence of the reaction products of Pt(*R*,*R*-dach)Cl_2 with d(pGpA) at 40 °C in water. (●), unreacted d(pGpA); (○), Pt(*R*,*R*-dach)(d(pGpA)-*N7(1),N1(2)*), **5′**; (□), Pt(*R*,*R*-dach)(d(pGpA)-*N7(1),N7(2)*), **4′**: (△), Pt(*R*,*R*-dach)(d(pGpA)-*N7(1),N1(2)*), **3′**.

d(pGpA). The reaction also yielded three platinum adducts, **3′** (8—9%), **4′** (10—15%), and **5′** (81—77%), in which the figures in parenthesis indicate the product ratio obtained for the first 10 hours. The reaction products, **3′**, **4′**, and **5′** were identified by HPLC after treating with alkaline phosphatase. The resulting products were completely compatible with **3**, **4**, and **5**. It is noteworthy that the product ratio of **5′** is significantly greater, compared with that of **5**, i.e. formation of **5′** largely predominates due to the presence of the 5′-phosphate group. The reaction of Pt(*R*,*R*-dach)Cl_2 with r(GpA) yields four platinum adducts, **8**, **9**, **10**, and **11**. In the first 10 hours reaction, the relative ratios of each product to all the platinum adducts are as follows; **8** (6%), Pt(*R*,*R*-dach)(r(GpA)-*N7(1),N1(2)*); **9** (12%), Pt(*R*,*R*-dach)(r(GpA)-*N7(1),N1(2)*); **10** (44%), Pt(*R*,*R*-dach)(r(GpA)-*N7(1),N7(2)*); **11** (38%), Pt(*R*,*R*-dach)(r(GpA)-*N7(1),N1(2)*). Afterward, the product ratios gradually change because **11** isomerizes to **8**, **9**, and **10**.

Characterization of Platinum Adducts. In general, the possible binding sites for platination are expected to be guanine N7 and adenine N7 and N1. The 6-NH_2 group of adenine base is also a possible platinum binding site,[22] but it would be a very weak binding site for platination because the lone pair of electrons of the 6-NH_2 group delocalizes into the π-system of the purine ring. Table 1 shows the platinum binding sites of the products obtained in this work. The platinum adducts, **1**—**5**, were fractionated from HPLC, and their platinum binding sites were determined as follows.

(1) From UV and AAS spectrophotometry, a molar extinction coefficient of 23000—25000/mol Pt was calculated at 260 nm, suggesting a presence of the 1 : 1 species. (2) The UV spectrum of **1** was in agreement with that of **3**. The UV spectral pattern of **1** and **3** was also in agreement with the calculated UV spectrum of

Table 1. Platinum Adducts Obtained from the Reaction of Pt(*R*,*R*-dach)Cl_2 with d(ApG), d(GpA), and d(pGpA)

Reactants	Reaction product	Yield/%[a]
Pt(*R*,*R*-dach)Cl_2+d(ApG)	**1**, Pt(*R*,*R*-dach)(d(ApG)-*N1(1),N7(2)*)	16
	2, Pt(*R*,*R*-dach)(d(ApG)-*N7(1),N7(2)*)	80
Pt(*R*,*R*-dach)Cl_2+d(GpA)	**3**, Pt(*R*,*R*-dach)(d(GpA)-*N7(1),N1(2)*)	22[b]
	4, Pt(*R*,*R*-dach)(d(GpA)-*N7(1),N7(2)*)	17[b]
	5, Pt(*R*,*R*-dach)(d(GpA)-*N7(1),N1(2)*)	61[b]
Pt(*R*,*R*-dach)Cl_2+d(pGpA)	**3'**, Pt(*R*,*R*-dach)(d(pGpA)-*N7(1),N1(2)*)	8[b]
	4', Pt(*R*,*R*-dach)(d(pGpA)-*N7(1),N7(2)*)	12[b]
	5', Pt(*R*,*R*-dach)(d(pGpA)-*N7(1),N1(2)*)	80[b]
[Pt(NH_3)$_3$Cl]Cl+d(ApG)	**6**, Pt(NH_3)$_3$(d(ApG)-*N7(2)*)	>98
[Pt(NH_3)$_3$Cl]Cl+d(GpA)	**7**, Pt(NH_3)$_3$(d(GpA)-*N7(1)*)	>98
Pt(*R*,*R*-dach)Cl_2+r(GpA)	**8**, Pt(*R*,*R*-dach)(r(GpA)-*N7(1),N1(2)*)	6[b]
	9, Pt(*R*,*R*-dach)(r(GpA)-*N7(1),N1(2)*)	12[b]
	10, Pt(*R*,*R*-dach)(r(GpA)-*N7(1),N7(2)*)	44[b]
	11, Pt(*R*,*R*-dach)(r(GpA)-*N7(1),N1(2)*)	38[b]

a) Relative ratio of each product to all the platinum adducts.[21] b) The values obtained in the first 10 hours reaction.

Pt(NH_3)$_3$(G-*N7*) and Pt(NH_3)$_3$(A-*N1*),[16,23] suggesting platination at the *G-N7* and the *A-N1*. (3) The UV spectral pattern of **2** and **4** was in agreement with the calculated UV spectrum of Pt(NH_3)$_3$(G-*N7*) and Pt(NH_3)$_3$(A-*N7*),[16,23] suggesting platination at the *G-N7* and the *A-N7*. (4) From the pH-UV titration curve, the pK_a values at the N1 of the G base for **1**, **2**, **3**, **4**, and **5** were in the range of 8.0—8.5, a value significantly lower than the corresponding one of the unplatinated G base (pK_a ca. 9.6). Platination at the N7 of the G base results in the well-known lowering of the pKa of the N1. (5) No protonation reaction at the N7 of the G base was observed, suggesting that the N7 of the G base has already been occupied by the platinum atom. (6) The UV difference spectral change of **1**—**5** as a function of pH, — arising from the deprotonation reaction at the N1 of the G base —, agreed with that of the N7-platinated guanine derivatives.[16,23] These results ((4)—(6)) are good evidences for platination at the *G-N7*. (7) No protonation reaction at the N1 of the A base was observed for **1**, **3**, and **5**, suggesting platination at the N1 of the A base. (8) The pK_a values at the N1 of the A base of **2** and **4** were in the range of 1.7—1.9. Such decrease in the pK_a at the N1, compared with unplatinated A base (pK_a=3.6), is an evidence for platination at the N7 of the A base.[23-25] The binding sites of the platinum adducts containing r(GpA) were also determined by the same method described above.

Figures 4—6 show the CD spectra of the platinum dinucleotide adducts. The CD band in the 260 nm region is likely to arise from an interaction between the two purines. The CD spectrum of **2** is quite similar to that[18] of the structurally characterized compounds, *cis*-Pt(NH_3)$_2$(r(ApG)-*N7(1),N7(2)*) with A_{anti}, G_{anti}, which was characterized by NMR and CD spectroscopy.[18] Examination of the molecular models indicates that the interbase crosslink between the *A-N7* and *G-N7* seems to be favorable under the configuration of A_{anti} with the N-type conformer and G_{anti} with

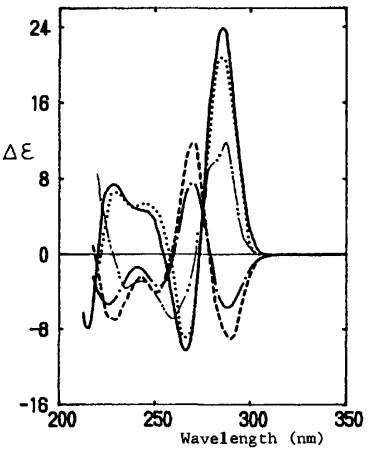

Fig. 4. Circular dichroism spectra of *G-N7*, *A-N7* platinum adducts (pH=4.6). (——), Pt(*R*,*R*-dach)(d(ApG)-*N7(1),N7(2)*), **2**; (-·-·-·-), Pt(*R*,*R*-dach)(d(GpA)-*N7(1),N7(2)*), **4**; (------), *cis*-Pt(NH_3)$_2$(r(ApG)-*N7(1),N7(2)*);[18] (----), Pt(*R*,*R*-dach)(r(GpA)-*N7(1),N7(2)*), **10**; (-·-·-), *cis*-Pt(NH_3)$_2$(r(GpA)-*N7(1),N7(2)*).[18]

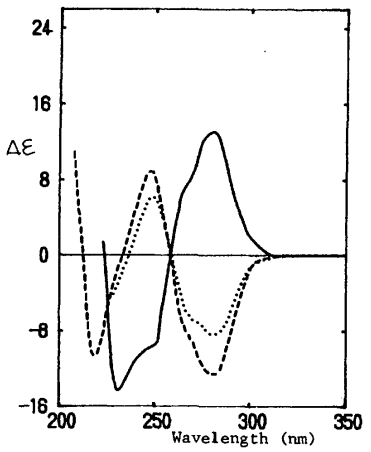

Fig. 5. Circular dichroism spectra of *G-N7*, *A-N1* platinum adducts (pH=4.6). (——), Pt(*R*,*R*-dach)(d(ApG)-*N1(1),N7(2)*), **1**; (------), Pt(*R*,*R*-dach)(d(GpA)-*N7(1),N1(2)*), **3**; (----), Pt(*R*,*R*-dach)(r(GpA)-*N7(1),N1(2)*), **9**.

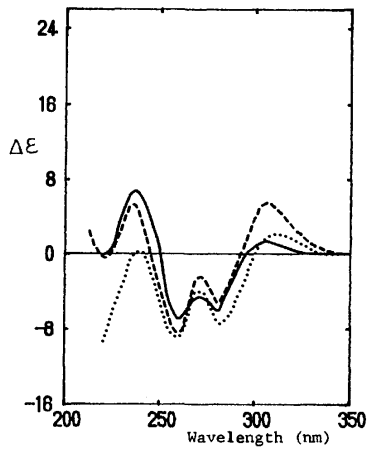

Fig. 6. Circular dichroism spectra of *G-N7*, *A-N1* platinum adducts (pH=4.6). (——), Pt(*R,R*-dach)(d(GpA)-*N7(1),N1(2)*), **5**; (----), Pt(*R,R*-dach)(r(GpA)-*N7(1),N1(2)*), **11**; (------), *cis*-$Pt(NH_3)_2$(r(GpA)-*N7(1),N1(2)*).[18]

the S-type conformer in the sugar moieties and that the product **2** is likely to have such sugar conformations because of the similarity of the CD spectra (see Fig. 4). Such conformation in the sugar moieties has been also found in *cis*-$Pt(NH_3)_2$(d(GpG)-*N7(1),N7(2)*).[4-7] Figure 4 also shows the CD spectra of Pt(*R,R*-dach)(r(GpA)-*N7(1),N7(2)*), (**10**), and *cis*-$Pt(NH_3)_2$(r(GpA)-*N7(1),N7(2)*).[17] The CD spectra of the both adducts are very similar to each other except for a difference in the intensity and are also similar to those of the sequence isomers, i.e. **2** and *cis*-$Pt(NH_3)_2$(r(ApG)-*N7(1),N7(2)*), except for an inversion of sign. That is, the CD spectral pattern of the adducts with platination at *G-N7* and *A-N7* have a common feature. However, the CD spectrum of **4** appears to be different from the other *G-N7* and *A-N7* adducts. This may be due to a presence of conformational isomers (probably, equilibrium mixture of syn and anti conformations).[18] In HPLC analysis, **4** shows an unusually broad peak (retention time of **4** (12.2 min) is shorter than that of **5** (18.8 min), and a half width of the peak of **4** is about 20 times larger than that of **5**.

The CD of **1** is almost mirror image of that of **3**, suggesting the reverse of the direction of the transition moments and the similarity in the overlap of the two purines (see Fig. 5). Inversion of CD bands in Fig. 5 has been also observed in the CD spectra of *cis*-$Pt(NH_3)_2$(r(GpC)-*N7(1),N3(2)*) and *cis*-$Pt(NH_3)_2$(r(CpG)-*N3(1),N7(2)*).[24] It should be stressed that the formation of the species **1** and **3** has not been found in the study of Chottard et al.[18] The species **1** and **3** are considered to be a platinum adduct with G_{anti} configuration. The CD spectral pattern of **3** is in agreement with that of *cis*-$Pt(NH_3)_2$(d(GpA)-*N7(1),N1(2)*)[27] with G_{anti} configuration which has been characterized by NMR. Figure 6 also shows CD spectra of the adducts with platination at *G-N7* and *A-N1*. They are characteristically observed in the platinum adducts with GA-sequence. The band above 300 nm, probably due to $n \rightarrow \pi^*$ electronic transition, may arises from a significant interaction between the 6-NH_2 group of the A base and O6 of the G base. The CD of **5** is also similar to that of Pt(*R,R*-dach)(r(GpA)-*N7(1),N1(2)*),(**11**) and *cis*-$Pt(NH_3)_2$(r(GpA)-*N7(1),N1(2)*).[18] Chottard et al. assigned *cis*-$Pt(NH_3)_2$(r(GpA)-*N7(1),N1(2)*) to the platinum adduct with G_{syn} configuration.[18] The CD spectral pattern of the Pt-adducts obtained in this work is hardly influenced by the presence and absence of the 2′-OH group of the sugar, though the CD of d(ApG) and d(GpA) are different from those of r(ApG) and r(GpA).[28]

Isomerization of 5. In the reaction of Pt(*R,R*-dach)Cl_2 with d(GpA), the relative ratios of each product for all the platinum adducts were almost constant at least for the first 10 hours. But the subsequent incubation results in a decrease of **5** and an increase of **3** and **4**. The platinum adduct, **5**, is not a monodentate intermediate but a chelate compound which platinum bound to *G-N7* and *A-N1* as described above. In order to make this point much clear, we performed further two experiments. (1) The reaction solution of Pt(*R,R*-dach)Cl_2 with d(GpA) was treated with snake venom phosphodiesterase.[14-16] The resulting solution gave dG and 5′-dAMP as an enzymatic digestion products, but **3**, **4**, and **5** were not digested at all by the enzyme. The dG and 5′-dAMP come from the enzymatic digestion of the unreacted d(GpA). This strongly suggests that **5** is a chelate compound.[29,30] The enzymatic digestion of $Pt(NH_3)_3$(d(GpA)-*N7(1)*) gave $Pt(NH_3)_3$(dG-*N7*) and 5′-dAMP under the same conditions. (2) The reaction of $[Pt(R,R\text{-dach})(OH_2)_2]^{2+}$ with d(GpA) gave the platinum adducts, **3**—**5**, via a monodentate intermediate, probably Pt(*R,R*-dach)(OH_2)(d(GpA)-*N7(1)*).

Isomerization of **5** was followed by means of HPLC. The solutions containing each **1**, **2**, **3**, **4**, and **5**, which were fractionated from HPLC, was incubated at 37°C. The product **5** was slowly converted into **3** and **4** (see Fig. 7), but the reverse reaction was not observed. This suggests that **3** and **4** are a thermodynamically more stable species and that **5** is likely to be a kinetically preferred species. The product **3** is further converted into unknown compound under further incubation. The half life of **5** was about 6 days at 37 °C. Addition of halogen ions (Cl^-, Br^-, and I^-) to the solution of **5** promotes the isomerization reaction. The more detail study is now under investigation.[31] Conversion between **1** and **2** was not observed.

Competition Reaction. In order to examine a relative reactivity of Pt(*R,R*-dach)Cl_2 with d(ApG) and d(GpA), a competition experiment was carried out. Stoichiometric amounts of d(ApG) and d(GpA) were incubated with half equivalent of Pt(*R,R*-dach)Cl_2 at 37 °C. Figure 8 shows a change of the unreacted dinucleotides and the products as a function of time. The reaction appeared to be complete within 1 day. Quan-

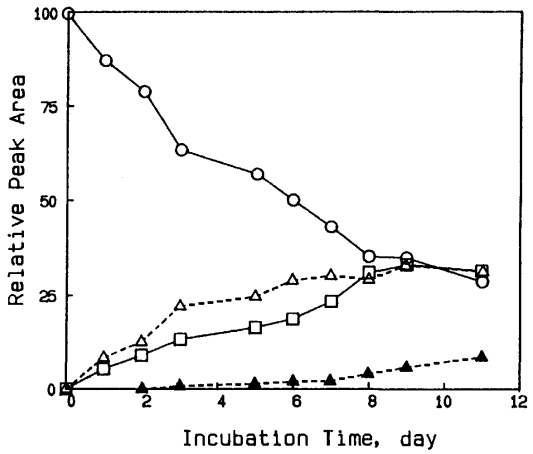

Fig. 7. Isomerization of Pt(*R,R*-dach)(d(GpA)-*N7(1),N1(2)*), **5**, to Pt(*R,R*-dach)(d(GpA)-*N7(1),N1(2)*), **3**, and Pt(*R,R*-dach)-(d(GpA)-*N7(1),-N7(2)*), **4**, at 37°C (pH=4.6). (○), Pt(*R,R*-dach)-(d(GpA)-*N7(1),N1(2)*), **5**; (△), Pt(*R,R*-dach)(d(GpA)-*N7(1),N1(2)*), **3**; (□), Pt(*R,R*-dach)(d(GpA)-*N7(1),-N7(2)*), **4**; (▲), unknown compound, which forms from **5** via **3**.

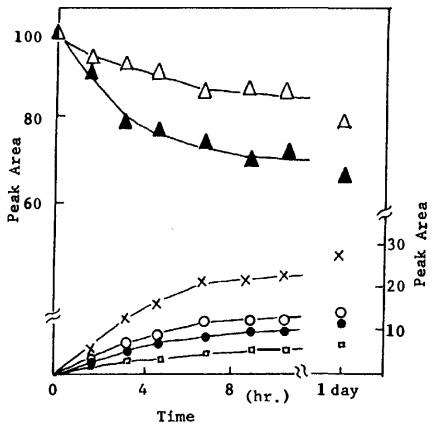

Fig. 8. Competition reaction of Pt(*R,R*-dach)Cl_2 with an equimolar mixture of d(ApG) and d(GpA) at 37°C (in water), r=0.25. (△), unreacted d(GpA); (▲), unreacted d(ApG); (×), **2**; (○), **5**; (●), **1**+**3**; (□), **4**.

titation result of the unreacted dinucleotides showed that d(ApG) is more reactive for platination than d(GpA) by a factor of about 1.7—1.9. The result is also supported by the quantitation result of the reaction products. The reaction between bifunctional platinum compound and d(ApG) or d(GpA) occurs via a two step mechanism.[32,33] The first step corresponds to formation of the 1 : 1 intermediate, and the second step to formation of the interbase crosslinked compound. In order to make the first step reaction clear, the reaction between monofunctional platinum complex, [Pt-(NH_3)$_3$Cl]Cl, and d(ApG) or d(GpA) was examined. The reaction product was exclusively Pt(NH_3)$_3$(d-(ApG)-*N7(2)*), (**6**), and Pt(NH_3)$_3$(d(GpA)-*N7(1)*), (**7**). The result agrees well with other studies.[34-36] Quantitation of the products in the competition reaction

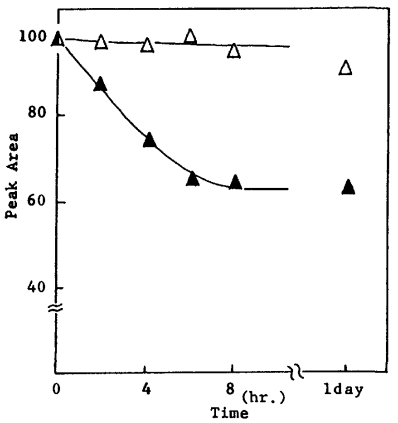

Fig. 9. Competition reaction of Pt(*R,R*-dach)Cl_2 with an equimolar mixture of d(ApG) and d(pGpA) at 37°C (in water), r=0.25. (△), unreacted d(ApG); (▲), unreacted d(pGpA).

indicated that formation of **6** is 2 times easier than that of **7**. This strongly suggests that the 1 : 1 intermediate formed in the reaction of Pt(*R,R*-dach)Cl_2 with d(ApG) or d(GpA) is the compound which platinum bound to the N7 of the G base, and that a preference in the reactivity is governed by a degree of formation of the 1 : 1 intermediate. The preference in the relative reactivity of d(ApG), compared with d(GpA), can be explained by an effect of the 5′-connected phosphodiester group, as being reported by Reedijk et al.[34] and Chottard et al.[18] i.e. interaction between the aquated platinum species and phosphodiester group on the 5′ side. To confirm the idea, the competition reaction between d(pGpA) and d(ApG) for Pt(*R,R*-dach)Cl_2 was also examined. As can be seen in Fig. 9, the reaction of Pt(*R,R*-dach)Cl_2 with d(pGpA) is much more reactive than that with d(ApG), i.e. the reactivity is greatly promoted by the presence of the 5′-phosphate group. This implies that a charge interaction, in addition to hydrogen bonding interaction, between the aquated platinum species and the 5′-phosphate group contributed to the reaction preference. It has been known that the reaction rate of *cis*-Pt(NH_3)$_2$(OH_2)$_2$ with 5′-dGMP is faster than that with 3′-dGMP.[37,38]

Concluding Remarks

The reaction between Pt(*R,R*-dach)Cl_2 and d(ApG) resulted in Pt(*R,R*-dach)(d(ApG)-*N7(1),N7(2)*) and Pt(*R,R*-dach)(d(ApG)-*N1(1),N7(2)*), i.e. **2** and **1**. The former product, **2**, contains 80% of the reaction products. Formation of the latter product has not been found in the reaction[18] between *cis*-Pt(NH_3)$_2$$Cl_2$ and r(ApG). The reaction of Pt(*R,R*-dach)Cl_2 with d(GpA) resulted in Pt(*R,R*-dach)(d(GpA)-*N7(1),N1(2)*),(**3** and **5**) and Pt(*R,R*-dach)(d(GpA)-*N7(1),N7(2)*), (**4**). The platinum adduct, **5**, isomerizes very slowly to **3** and **4**. The reaction between Pt(*R,R*-dach)Cl_2 and r(GpA) yields Pt(*R,R*-dach)(r(GpA)-*N7(1),N7(2)*), (**10**), and Pt(*R,R*-dach)(r(GpA)-*N7(1),N1(2)*), (**8**, **9**, and **11**), and

11 also isomerizes to **8**, **9**, and **10**. In the initial process of the reactions (up to 10 hours), the Pt(*R,R*-dach)(d(GpA)-*N7(1),N1(2)*) adducts contains more than 80% of all the reaction products, while the product ratio of the Pt(*R,R*-dach)(r(GpA)-*N7(1),N1(2)*) adducts is less than 60%. The interesting difference seems to arise from the difference at the C2′ position of the sugar (2′-deoxy and 2′-oxy). The absence of the 2′-OH group of the sugar seems to be favourable to the binding at the *A-N1*.

The two purine bases in **5** appears to have the same sugar orientations as *cis*-Pt(NH_3)$_2$(r(GpA)-*N7(1), N1(2)*)[18] because of the similarity of the both CD spectra. Examination of molecular model indicates that when the 1 : 1 intermediate has G_{syn} configuration with the N-type conformer, subsequent chelation is very likely to occur at the N1 of the A base. In general, the reaction between platinum complex and nucleic acid base appears to be controlled by kinetic rather than thermodynamic in character. The relative preference of **5** to **3** and **4** may originate from such a kinetic reason. Although the product **5** is a kinetically preferred species, it is thermodynamically unstable species. In the reaction of Pt(*R,R*-dach)Cl_2 with d(pGpA), formation of **5′** is much more preferred, compared with the case of the reaction with d(GpA). The presence of 5′-phosphate group may allows an increase of G_{syn} configuration, probably in the 1 : 1 intermediate.

In the reaction of antitumor platinum complex with DNA, formation of the platinum adduct,**5**, seems to be unfavorable because it requires large conformational changes of the sugar moiety. Moreover, the N1 of adenine base is involved in base pairing in double stranded DNA. This may be one of the reason why the d(GpA)-chelate was not found after the enzymatic digestion of the platinum modified DNA.

We thank Professor Jan Reedijk for helpful suggestions.

References

1) J. J. Robert and M. P. Pera, Jr., "Molecular Aspect of Anti-Cance Drug Action" ed by S. Neidle and M. J. Waring, The Macmillan Press Limited. London: (1983), pp. 183—231.
2) J. Reedijk, *Pure Appl. Chem.*, **59**, 181, (1987).
3) S. J. Lippard, *Pure Appl. Chem.*, **59**, 731, (1987).
4) S. E. Sherman, D. Gibson, A. H.-J. Wang, and S. J. Lippard, *Science*, **230**, 412 (1985).
5) G. Admiraal, J. L. van der Veer, R. A. G. de Graaff, J. H. J. den Hartog, and J. Reedijk, *J. Am. Chem. Soc.*, **109**, 592 (1987).
6) J. H. J. den Hartog, C. Altona, J. C. Chottard, J. P. Girault, J. Y. Lallemand, F. A. A. M. de Leeuw, A. T. M. Marcelis, and J. Reedijk, *Nucleic Acid Res.*, **10**, 4715 (1982).
7) J. P. Girault, G. Chottard, J. Y. Lallemand, and J. C. Chottard, *Biochemistry*, **21**, 1352 (1982).
8) K. Inagaki and Y. Kidani, *Inorg. Chem.*, **25**, 1 (1986).
9) A. L. Pinto and S. J. Lippard, *Proc. Natl. Acad. Sci. U. S. A.*, **82**, 4616 (1985); *Biochim. Biophys. Acta*, **780**, 167 (1985).
10) R. B. Ciccarelli, M. J. Solomon, A. Varshavsky, and S. J. Lippard, *Biochemistry*, **24**, 7533 (1985).
11) A. M. J. Fichinger-Schepman, P. H. M. Lohman, and J. Reedijk, *Nucleic Acids Res.*, **10**, 5345 (1982).
12) A. M. J. Fichinger-Schepman, J. L.vanderVeer, J. H. J.den Hartog, P. H. M. Lohman, and J. Reedijk, *Biochemistry*, **24**, 707 (1985).
13) A. Eastman, *Biochemistry*, **22**, 3927 (1983); **24**, 5027 (1985).
14) K. Inagaki, K. Kasuya, and Y. Kidani, *Chem. Lett.* **1984**, 171.
15) K. Inagaki and Y. Kidani, *Chem. Lett.*, **1986**, 233.
16) K. Inagaki and Y. Kidani, *Inorg. Chim. Acta*, **80**, 171 (1983).
17) In platinum adducts, the coordination atom(s) is indicated after the nucleotides, separated by a hyphen, e.g., Pt(*R,R*-dach)(d(GpA)-*N7(1),N1(2)*) indicates that Pt(*R,R*-dach)$^{2+}$ moiety binds to the N7 of the guanine base and the N1 of the adenine base. The number in the parenthesis is noted sequentially from the 5′- to the 3′-terminus.
18) B. van Hemelryck, J. P. Girault, G. Chottard, P. Valadon, A. Laoui, and J. C. Chottard, *Inorg. Chem.*, **26**, 787 (1987).
19) Y. Kidani, K. Inagaki, M. Iigo, A. Hoshi, and K. Kuretani, *J. Med. Chem.*, **21**, 1315 (1978).
20) A. L. Tshugaev, *J. Chem. Soc.*, **107**, 1247 (1915).
21) Yields of the reaction products were calculated from peak areas of the HPLC chromatograms. Although the extinction coefficients (at 260 nm) of the platinum adducts are not closely identical, they are expected to be similar to each other. Their extinction coefficients per mole of platinum are in the range of 23000—25000 $dm^3\ mol^{-1}\ cm^{-1}$.
22) S. Mansy, B. Rosenberg, and A. J. Thomson, *J. Am. Chem. Soc.*, **95**, 1633 (1973).
23) K. Inagaki, M. Kuwayama, and Y. Kidani, *J. Inorg. Biochem.*, **16**, 59 (1982).
24) M. D. Reily and L. G. Marzilli, *J. Am. Chem. Soc.*, **108**, 6785 (1986).
25) J. H. J. den Hartog, H. van den Elst, and J. Reedijk, *J. Inorg. Biochem.*, **21**, 83 (1984).
26) J. P. Girault, G. Chottard, J. Y. Lallemand, F. Huguenin, and J. C. Chottard, *J. Am. Chem. Soc.*, **106**, 7227 (1984).
27) J. Reedijk and F. J. Dijt, personal communication.
28) M. M. Warshaw and C. R. Cantor, *Biopolymers*, **70**, 1079 (1970).
29) K. Inagaki, K. Kasuya, and Y. Kidani, *Chem. Lett.*, **1983**, 1345.
30) A. Forsti, R. Laatikainen, and K. Hemminki, *Chem.-Biol. Interact.*, **63**, 1 (1987).
31) Kinetic parameters of the isomerization reaction imply that the isomerization proceeds via Pt-AN1 bond cleavage.
32) J. Reedijk, J. H. J.den Hartog, A. M. J. Fichtinger-Schepman, and A. T. M. Marcelis, "Platinum Coordination Complexe in Cancer Chemotherapy," ed by M. P. Hacker, D. P. Douple, and I. H. Krakoff, Martinuss Nijhoff Publishers, Boston (1984), pp. 39—50.
33) A. T. M. Marcellis, C. G. van Kralingen, and J. Reedijk, *J. Inorg. Biochem.*, **13**, 213 (1980).
34) J. L. van der Veer, H. van den Elst, J. H. J. den Hartog, A. M. J. Fichtinger-Schepman, and J. Reedijk,

Inorg. Chem., **25**, 4657 (1986).
35) J. L. van der Veer, H. P. J. M. Noteborn, H. van den Elst, and J. Reedijk, *Inorg. Chim. Acta*, **131**, 221 (1987).
36) E. L. M. Lempers, K. Inagaki, and J. Reedijk, Proc. 5th Int. Conf. Platinum Cancer Chemotherapy, **131**, 221 (1987).
37) A. T. M. Marcelis, C. Erkelens, and J. Reedijk, *Inorg. Chim. Acta*, **91**, 129 (1984).
38) S. Eapen, M. Green, and I. M. Ismail, *J. Inorg. Biochem.*, **24**, 233 (1985).

 © 1988 The Chemical Society of Japan Bull. Chem. Soc. Jpn., 61, 2833—2836 (1988)

Synthesis and Properties of Copper(II) Thiocyanato Complexes with Imino Oximes

Songping WAN,* Wasuke MORI,† Shoichiro YAMADA,† and Shun-Ichi MURAHASHI
Faculty of Engineering Science, Osaka University, Toyonaka 560
†College of General Education, Osaka University, Toyonaka 560
(Received March 14, 1988)

Reaction of copper(I) thiocyanate with imino oximes 3-[[2-(alkylamino)ethyl]imino]-2-butanone oximes or 3-[[2-(dialkylamino)ethyl]imino]-2-butanone oximes, (abbreviated as Hdox-enRR'), gave a series of copper(II) complexes which consist of binuclear complexes $[Cu_2(dox\text{-}enRR')_2(NCS)_2]$ with a thiocyanate anion coordinated to the copper(II) ion. The magnetic susceptibilities over the temperature range 77—320 K show a strong antiferromagnetic spin coupling through the N–O bridge for these complexes. The magnetic behavior can be explained by using the Bleaney–Bowers equation.

It has been shown previously that imino oximes (Hdox-enRR' **1**) form various transition metal complexes, in which they function in various manners, namely as bidentate, terdentate or bridging quadridentate ligands, depending upon the nature of the central metal ion on one hand and the substituents R and R' on the other.[1-4] We have reported that the reactions of nickel(II) thiocyanate with imino oximes **1** yield paramagnetic nickel(II) complexes, which are

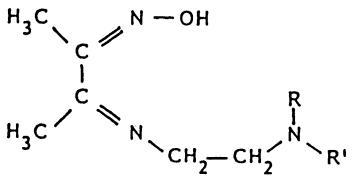

Hdox-enRR'
1

hexa-coordinated with two thiocyanate ions bonded to the metal ion in cis-positions.[1] This result is in contrast to the results on the corresponding nickel(II) halides and perchlorate complexes with the same ligands.[2-4] Examination has been extended to the corresponding copper(II) thiocyanate complexes in the present study. Since the stereochemistry of copper(II) complexes is known to be significantly different from, although similar in many ways to, that of nickel(II) complexes, it is interesting to compare the copper(II) imino oxime complexes with the corresponding nickel(II) complexes. For example, the behavior of the thiocyanate ion in the copper(II) complexes may be different from that in the nickel(II) complexes. Although copper(II) perchlorate complexes with these ligands were reported previously,[4] there remain important problems about related complexes. Moreover, it is worthwhile to investigate the effects of the anions on the structure and the bonding of copper(II) complexes formed. Another important feature often observed with the copper(II) complexes is the spin–spin interaction between copper(II) ions, whereas the interaction of a similar type rarely occurs in the corresponding nickel(II) complexes. The present paper describes synthesis and characterization of the copper(II) thiocyanato complexes, including examination of their magnetic properties.

Experimental

Materials. Biacetyl monoxime, *N*-alkylethylenediamine, *N,N*-dialkylethylenediamine, and copper(I) thiocyanate were commercially available and used as received.

Synthesis. Cu(dox-enMe)NCS (R'=H, R=Me; 2a). A mixture of biacetyl monoxime (1.11 g, 0.011 mol) and copper(I) thiocyanate (0.61 g, 0.005 mol) in 2-propanol (40 cm^3) was heated at 70 °C for 1 h. To the solution was added *N*-methylethylenediamine (0.74 g, 0.01 mol) at 60 °C and stirred for 2 h. Filtration and subsequent washing with ethanol gave dark-green crystalline complex (0.45 g) in 32% yield, which appeared green when ground. Mp 151 °C. Found: C, 34.55; H, 5.04; N, 20.05%. Calcd for $C_7H_{14}N_3OCuNCS$: C, 34.57; H, 5.07; N, 20.16%.

Cu(dox-enEt)NCS (R'=H, R=Et; 2b). A mixture of biacetyl monoxime (1.11 g, 0.011 mol) and copper(I) thiocyanate (0.61 g, 0.005 mol) in 2-propanol (40 cm^3) was heated at 70 °C for 1 h. To the solution was added *N*-ethylethylenediamine (0.88 g, 0.01 mol) at 60 °C and stirred for 2 h. The filtered solution was allowed to stand in a refrigerator. Dark-green crystalline complex (0.57 g) was obtained in 39% yield. Mp 143 °C. Found: C, 37.32; H, 5.68; N, 19.09%. Calcd for $C_8H_{16}N_3OCuNCS$: C, 37.04; H, 5.53; N, 19.29%.

Cu(dox-enPr)NCS (R'=H, R=Pr; 2c). A mixture of biacetyl monoxime (1.11 g, 0.011 mol) and copper(I) thiocyanate (0.61 g, 0.005 mol) in 2-propanol (40 cm^3) was heated at 70 °C for 1 h. To the solution was added *N*-propylethylenediamine (1.01 g, 0.01 mol) at 60 °C and stirred for 2 h. The reaction solution was evaporated spontaneously at room temperature and dark-green crystals were collected by filtration and washed with ethanol to give the complex (0.40 g) in 26% yield. Mp 145 °C. Found: C, 39.26; H, 5.88; N, 18.27%. Calcd for $C_9H_{18}N_3OCuNCS$: C, 39.26; H, 5.93; N, 18.32%.

Cu(dox-enMe$_2$)NCS (R'=R=Me; 2d). This complex was prepared by a similar method which was used for the preparation of Cu(dox-enMe)NCS, except that *N,N*-dimethylethylenediamine (0.88 g, 0.01 mol) was used in place of *N*-methylethylenediamine. Complex **2d** (1.36 g) was obtained in 93% yield. Mp 153 °C. Found: C, 37.32; H, 5.46; N,

Table 1. Main Spectral Data of Copper(II) Complexes

Complex	d-d band	IR(oxime)	IR(NCS)		
	10^3 cm^{-1}	cm^{-1}	cm^{-1}		
		ν(C=N)	ν(C-N)	ν(C-S)	δ(N-C-S)
2a	15.8	1642	2077	793	432
2b	15.4	1645	2080	797	425
2c	15.2	1648	2072	805	425
2d	15.9	1648	2077	776	457
2e	15.2	1643	2096	775	452
2f	16.3	1649	2087	786	453

19.44%. Calcd for $C_8H_{16}N_3OCuNCS$: C, 37.04; H, 5.53; N, 19.29%.

Cu(dox-enEt$_2$)NCS (R′=R=Et; 2e). To a solution of copper(I) thiocyanate (0.61 g, 0.005 mol) in ethanol (40 cm^3) was added a ligand (Hdox-enEt$_2$ 1.99 g, 0.01 mol) which was prepared beforehand.[1] The mixture was stirred at 60 °C for about 1 h. Filtration and washing with ethanol gave dark-green crystalline complex (1.52 g) in 95% yield. Mp 146 °C. Found: C, 41.51; H, 6.34; N, 17.63%. Calcd for $C_{10}H_{20}N_3$-OCuNCS: C, 41.29; H, 6.30; N, 17.51%.

Cu(dox-enBu$_2$)NCS (R′=R=Bu; 2f). A suspension of biacetyl monoxime (1.01 g, 0.01 mol) and *N,N*-dibutylethylenediamine (1.72 g, 0.01 mol) in 2-propanol (20 cm^3) was refluxed at 70 °C for 2 h. The resulting solution was added dropwise to a suspension of copper(I) thiocyanate (0.61 g, 0.005 mol) in ethanol (30 cm^3) and stirred at 60 °C for several hours. The solution was allowed to evaporate spontaneously at room temperature nearly to dryness. Dark needle-like crystals were filtered and washed with ethanol to yield 1.76 g (94%) of complex. Mp 115 °C. Found: C, 46.47; H, 7.21; N, 14.77%. Calcd for $C_{14}H_{28}N_3ONCS \cdot 1/2H_2O$: C, 46.79; H, 7.33; N, 14.55%.

Measurements. Electronic absorption spectra and infrared spectra were measured at room temperature on a Shimadzu MPS 5000 spectrophotometer and a Perkin-Elmer 938G infrared spectrophotometer, and all samples were mulled with Nujol. Magnetic susceptibilities were measured by the Gouy method at room temperature and by the Faraday method in a manner as described previously[5] at temperatures between 77K and 320K.

Results and Discussion

Synthesis and Characterization of the Thiocyanato (imino oximato)copper(II) Complexes. A possibility was explored in the present work to employ copper(I) thiocyanate as a starting compound for the preparation of copper(II) complexes with the imino oximes, partly because copper(II) thiocyanate was not available in the stable form. Reactions of copper(I) thiocyanate with the imino oximes yielded copper(II) complexes of the type Cu(dox-enRR′)NCS, copper(I) being oxidized to copper(II) by the atmospheric oxygen under the reaction conditions.

As discussed later in more detail, d-d bands and magnetic properties indicate that the products isolated are copper(II) complexes. It is important to note that this method using a copper(I) salt as a starting substance may be applied to the preparation of other copper(II) complexes, in case the copper(II) salts as a starting compounds are not available or do not give successful results.

Table 2. Magnetic Moments and Exchange Parameters of Copper(II) Complexes

Complex	μ	g	$-2J$	$N\alpha\times10^6$	p[a]
	BM		K	cm^{3}mol^{-1}	
2a	0.96	2.33	822	20	0.08
2b	1.05	2.23	719	65	
2c	0.99	2.34	792	37	
2d	0.92	2.24	830	65	
2e	0.76	2.32	938	18	
2f	0.66	2.32	1100	55	0.05

a) the percentage of the impurity species.

The composition determined from elemental analysis indicates that the imino oximes lose a proton on coordination to the copper(II) ion. This assumption is borne out by infrared spectra of these complexes, which exhibit no absorption bands due to the free oxime OH group in the region between 3000 and 3500 cm^{-1}. In other words, the imino oximes are coordinated to the copper(II) ion as monoanions. Moreover, the bands due to imino oxime C=N (Table 1) shift from the vibration 1623—1630 cm^{-1} of the free ligand indicating that imino oxime C=N is bound to the copper(II) ion. Infrared bands due to thiocyanate ions, as shown in Table 1 also indicate that the thiocyanate anion is coordinated to the copper(II) ion through the nitrogen atom.[6,7] Tentative assignments[8,9] are given in Table 1.

Their magnetic moments (0.66—1.05 BM) at room temperature are much lower than the spin-only moment (1.73 BM) for the d^9 system, as shown in Table 2. The subnormal magnetic moments imply that a sort of spin-spin interaction is present between copper(II) ions in these complexes.

All the findings discussed above indicate that one of the most probable structures for these copper(II) complexes is a binuclear one, as shown in **2**, in analogy to a copper(II) complex with a similar composition, Cu(dox-enMe$_2$)ClO$_4 \cdot$ H$_2$O having a subnormal magnetic moment (0.6 BM at room temperatuire).[10] Thus the copper(II) ion has a square-pyramidal coordination geometry, with one thiocyanate ion at the apex, as

also presumed from the infrared bands. This is also in agreement with the crystal structure analysis of one of the present complexes. According to preliminary results of the X-ray analysis,[11] Cu(dox-enPr)NCS in the crystalline state consists of binuclear complexes, represented by structure **2**. The coordination polyhed-

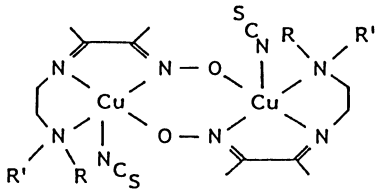

Cu(dox-enRR′)(NCS)
2

ron around the copper(II) ion is square-pyramidal with one thiocyanate ion at the apex, and the binuclear skeleton is somewhat distorted from the strictly planar structure. A similar binuclear structure may be assumed for the other complexes of the type Cu(dox-enRR′)NCS.

The maxima of the first d-d bands of the copper(II) complexes, as shown in Table 1, are consistent with the structure in which copper(II) ion is in the square-pyramidal environment with one thiocyanate ion at the apex.[12,13]

The discussion outlined above shows that copper(II) has a higher tendency to form binuclear complexes with the imino oximate N-O bridges in comparion with nickel(II). In this regard, it is interesting to note a marked difference in the structure between the copper(II) and nickel(II) complexes with these imino oximes. Hexa-coordinate copper(II) complexes have not been isolated in the present work, whereas nickel(II) forms hexa-coordinated complexes of the type *cis*-[Ni(NCS)$_2$(Hdox-enRR′)$_2$].[1] The present work indicates that the capacity of copper(II) ion with a $3d^9$ configuration to form hexa-coordinated complexes is obviously lower than that of nickel(II) ion having a $3d^8$ configuration. One of the main reasons for this may be the Jahn-Teller effect, which is operative in copper(II) complexes having a $3d^9$ configuration.

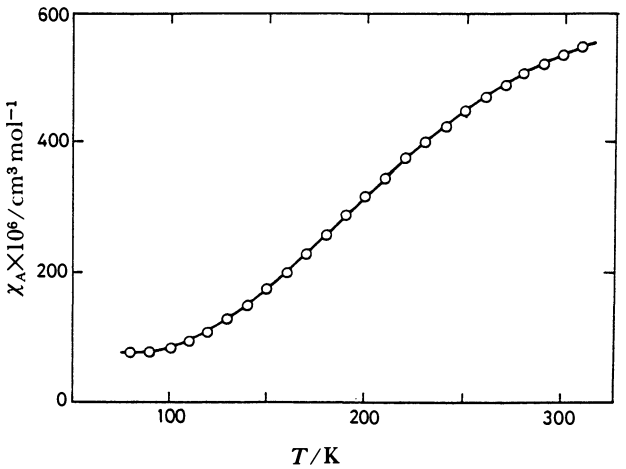

Fig. 1. Temperature dependence of the magnetic susceptibilities for Cu(dox-enEt)(NCS). The solid line was calculated from Eq. 1 with $2J=-719$ K, $N\alpha=65\times10^{-6}$ cm^3 mol^{-1}.

Magnetic Properties of Thiocyanato(imino oximato)-copper(II) Complexes. Variable-temperature magnetic susceptibilities of all the copper(II) complexes obey the Bleaney-Bowers equation for the pair of $S=1/2$ metal ions, Eq. 1,

$$\chi_A = \frac{Ng^2\beta^2}{kT}\,\frac{1}{3+\exp(-2J/kT)} + N\alpha \qquad (1)$$

or its modification, Eq. 2,

$$\chi_A = \frac{Ng^2\beta^2}{kT}\,\frac{1}{3+\exp(-2J/kT)}(1-p) + \frac{Ng^2\beta^2}{4kT}\cdot p + N\alpha \qquad (2)$$

where g, J, $N\alpha$, and p are, respectively, g factor, exchange integral, T. I. P. and percentage of the impurity species.

A typical example of the data is shown in Fig. 1. The figure shows that the experimental data fit to the theoretical expression given above. In Table 2 are also given the magnetic moments of the complexes and the values for the main parameters estimated from the variable-temperature data. All the copper(II) complexes in the present work exhibit large negative J values, showing antiferromagnetic interaction between copper(II) ions. The interaction is considered to arise from superexchange through the bridging N-O groups. The $|J|$ values of these copper(II) complexes are in the range reported for the related binuclear complex, for example, Cu(dox-enMe$_2$)ClO$_4\cdot$H$_2$O,[10] which also contain similar bridging N-O groups.

References

1) S. P. Wan, H. Kuma, and S. Yamada, *Synth. React. Met.-Org. Chem.*, **16**, 1049 (1986).
2) S. P. Wan, W. Mori, and S. Yamada, *Synth. React. Met.-Org. Chem.*, **16**, 1273 (1986).
3) H. Tanaka, H. Kuma, and S. Yamada, *Synth. React. Met.-Org. Chem.*, **15**, 699 (1985).
4) S. Baral and A. Chakravorty, *Proc. Indian Acad. Sci.*, **86A**, 45 (1977).
5) W. Mori, M. Kishita, and M. Inoue, *Inorg. Chim. Acta*, **42**, 11 (1980).
6) K. Nakamoto, "Infrared Spectra of Inorg. and Coord. Compounds," John Wiley, New York, 1978.
7) S. Yamada, "Structural Coordination Chemistry," Kagakudojin, Kyoto (1980), p. 183.
8) E. Uhlig, E. Dinjus, and M. Helbig, *Z. Anorg. Allg. Chem.*, **373**, 279 (1970).
9) S. Baral and A. Chakravorty, *Inorg. Chim. Acta*, **39**, 1 (1980).

10) M. Nasakkala, H. Saarinen, and J. Korvenranta, *Fin. Chem. Lett.*, **1980** (1), 6; *Chem. Abstr.*, **92**, 172842s (1980).
11) S. P. Wan, W. Mori, S. Yamada, and S.-I. Murahasi, Proceedings XXV. ICCC., Nanjing, C2-462, (1987).
12) M. Kato, Y. Muto, H. B. Jonassen, K. Imai, and T. Tokii, *Bull. Chem. Soc. Jpn.*, **43**, 1066 (1970).
13) B. J. Hathaway and A. A. G. Tomlinson, *Coord. Chem. Rev.*, **5**, 1 (1970).

 © 1988 The Chemical Society of Japan Bull. Chem. Soc. Jpn., 61, 2837—2846 (1988)

Photochemical Alkylation, Hydroxyalkylation, and Alkoxylation of Pyridinecarboxamides in Alcohol

Akira SUGIMORI,* Hiroshi ITOH, (the late) Mitsuharu KANAI, Nobuko ITOH, and Toru SUGIYAMA
Department of Chemistry, Faculty of Science and Technology, Sophia University, Kioi-cho 7-1, Chiyoda-ku, Tokyo 102
(Received August 7, 1987)

The UV-irradiation of 2- and 4-pyridinecarboxamides in alcohol brings about alkylation and/or hydroxyalkylation in the pyridine ring. In the irradiation of 3-pyridinecarboxamide in the presence of sulfuric acid, ionic reaction (alkoxylation at the 2- and 6-position) and radical reaction (alkylation at the 4- and 6-position) occur in parallel. The effects of quenchers indicate that two alkylation products originate from one excited triplet state which is quenched by energy-transfer mechanism and that two alkoxylation products originate from the excited singlet state.

In the preceding papers,[1-8] we have reported the remarkable photoreactivities of pyridinecarboxylic esters: parallel occurrence of ionic and radical reactions and simultaneous participation of several excited states of the same multiplicity. The most characteristic example is the photoreaction of methyl 3-pyridinecarboxylate in methanol in the presence of sulfuric acid.[2,3] It has been concluded that an excited singlet state, the n-π* triplet state, and the π-π* triplet state coexist and that the excited singlet state gives the products methoxylated at the 2- and 6-positions, while the π-π* and the n-π* triplet states give the methylation products at the 4- and 6-positions. The parallel occurrence of ionic and radical reactions has been observed in the photoreactions of 2-pyridinecarbonitrile in alcohol.[9]

In the present paper, we report the photoreactions of pyridinecarboxamides in alcohol, in order to compare their photochemical behavior with that of the esters.[10]

Results and Discussion

Types of Photoreactions of Pyridinecarboxamides. In the UV-irradiation of 2-pyridinecarboxamide (picolinamide, **1**) in methanol in the absence of added acid, methylation and hydroxymethylation occur in parallel. Irradiation in the presence of sulfuric acid gives a methylation product.

The position of the methylation depends on the presence and the absence of sulfuric acid. In the absence of the acid, the 5-position is methylated, whereas in the presence of sulfuric acid the 4-position is methylated.

The irradiation of 3-pyridinecarboxamide (nicotinamide, **2**) in alcohol brings about both the ionic reaction (alkoxylation) and the radical reaction (alkylation and hydroxyalkylation).

4-Pyridinecarboxamide (isonicotinamide, **3**) undergoes the hydroxymethylation in methanol either in the presence or in the absence of sulfuric acid.

With respect to the reaction types, the photoreactions of pyridinecarboxamides in alcohol are similar to those of pyridinecarboxylic esters in the following points: 1) Observed reactions are alkylation, hydroxy-

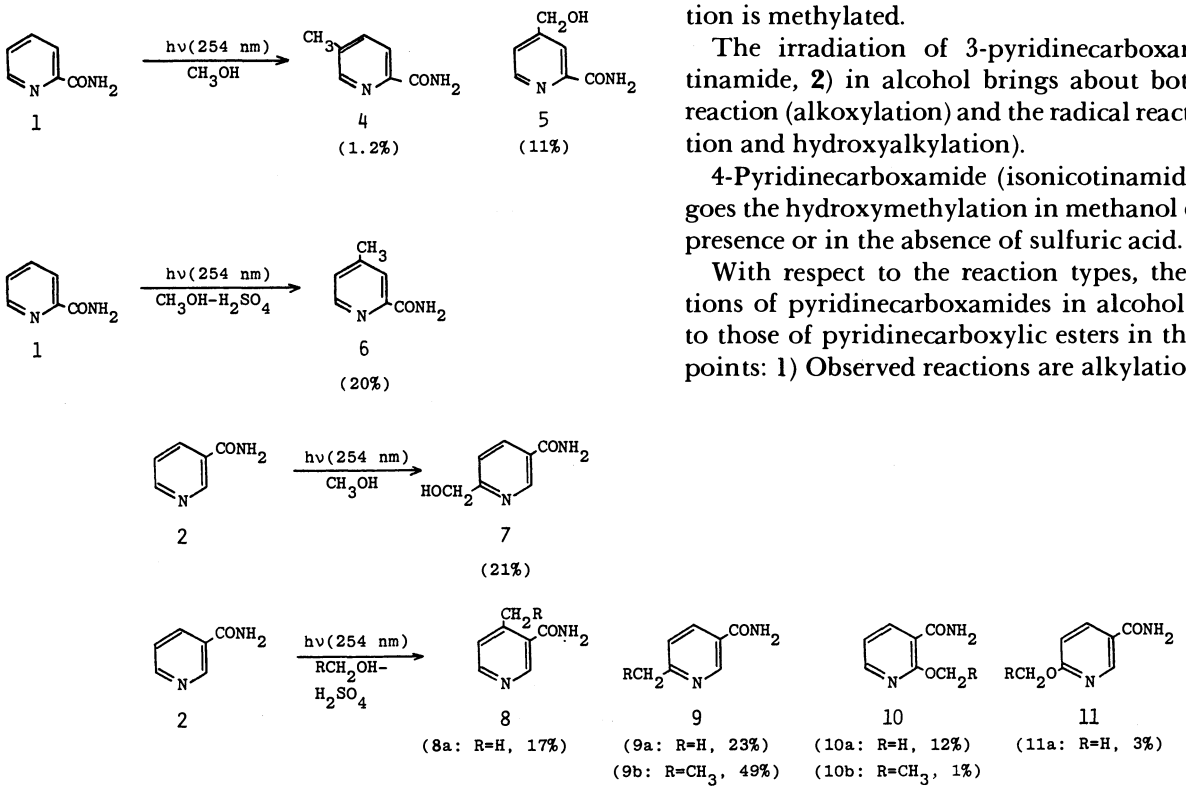

1 → 4 (1.2%), 5 (11%)
1 → 6 (20%)
2 → 7 (21%)
2 → 8 (8a: R=H, 17%), 9 (9a: R=H, 23%; 9b: R=CH3, 49%), 10 (10a: R=H, 12%; 10b: R=CH3, 1%), 11 (11a: R=H, 3%)

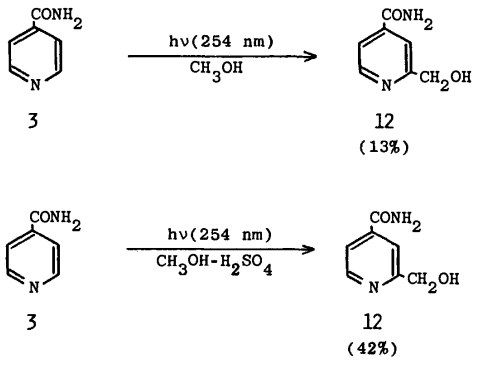

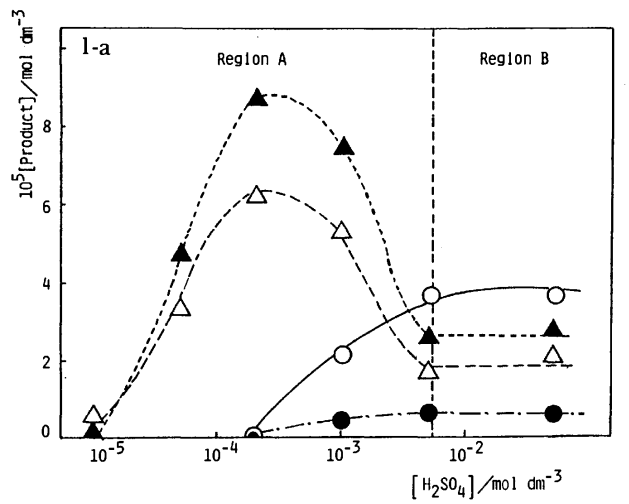

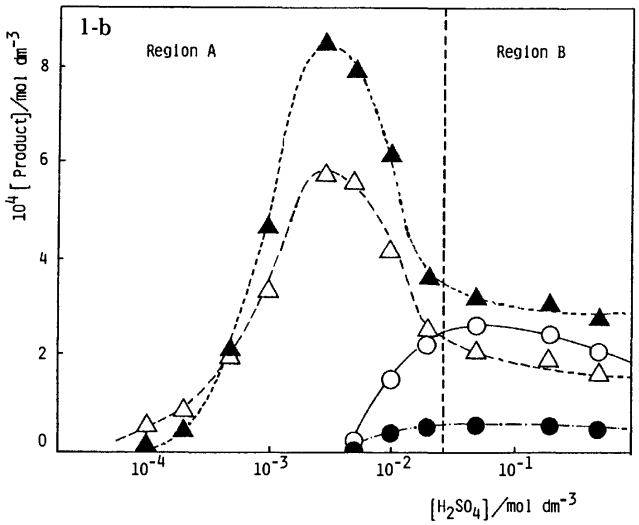

Fig. 1. Dependence of photoreactions of 3-pyridinecarboxamide (**2**) in methanol on the concentration of H_2SO_4. 1-a: [**2**]=1.0×10^{-2} mol dm^{-3}; 30 °C; irradiation time, 3 h. 1-b: [**2**]=1.0×10^{-3} mol dm^{-3}; 30 °C; irradiation time, 20 min. —△—, **8a**; ----▲----, **9a**; —○—, **10a**; ···●···, **11a**.

alkylation, and alkoxylation. In particular, the photoreactions of 3-pyridinecarboxamide (**2**) are very similar to those of the corresponding ester[2,3] (in the reaction type as well as in the positions of the reaction). 2) The change of alcohol from methanol to

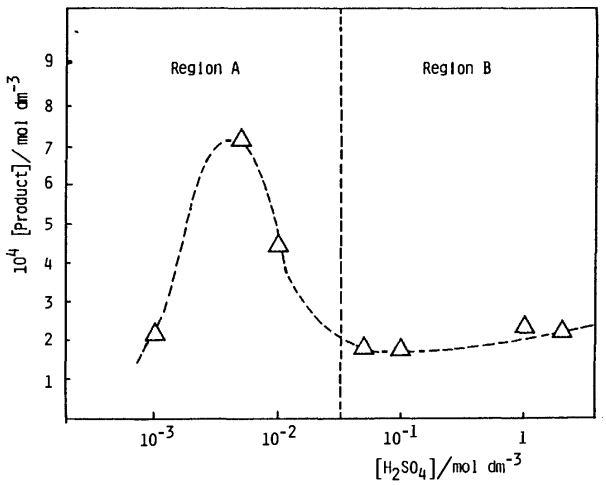

Fig. 2. Dependence of the photomethylation of 2-pyridinecarboxamide (**1**) at the 4-position on the concentration of H_2SO_4. [**1**]=1.0×10^{-2} mol dm^{-3}; irradiation time, 4 h.

ethanol causes the change in the product distribution in the photoreaction of 3-pyridinecarboxamide. In ethanol alkoxylation decreases, while alkylation increases. In ethanol alkoxylation occurs selectively at the 4-position. 3) Similar to methyl 2-pyridinecarboxylate,[4] 2-pyridinecarboxamide (**1**) undergoes the methylation at the 5-position in the absence of sulfuric acid but at the 4-position in its presence. Although the similarities should be stressed as a whole, the details of the photoreactivities of the amides are different from those of the esters: UV-irradiation of 2- and 4-pyridinecarboxamides gives only the products from radical reactions (alkylation or hydroxyalkylation), whereas the corresponding esters give alkoxylation products in addition to the alkylation and hydroxyalkylation products.[4,5]

Photoreactivity and Form of Substrate in Solution. The photoreactions of pyridinecarboxamides are controlled by an added acid. The photoreactions of 2- and 3-pyridinecarboxamide in the presence of sulfuric acid are different from those in its absence. The remarkable dependences of the photoreactions on the concentrations of added sulfuric acid are observed in cases of 2- and 3-pyridinecarboxamides (Figs. 1 and 2).

In UV-irradiation of 3-pyridinecarboxamide in methanol (Figs. 1-a and 1-b), the methylation occurs effectively at lower concentrations of sulfuric acid (Region A), while the methylation and methoxylation occur in parallel at higher concentrations of sulfuric acid (Region B). This type of acidity dependence is similar to that of methyl 3-pyridinecarboxylate.[3]

In Fig. 3 are shown the correlations between the molar absorption coefficient of **2** and the concentration of added sulfuric acid. The change in the molar absorption coefficient shows the change in the form of **2**. Figures 1 and 3 indicate that **2** exists in the pyridinium form in Region B and that the pyridinium form

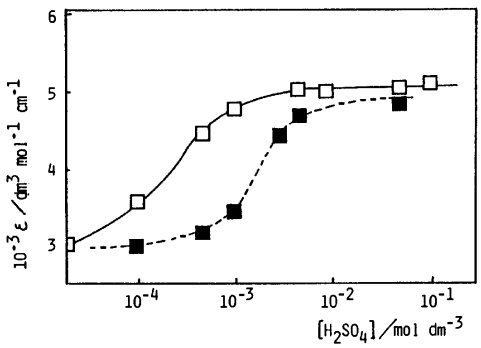

Fig. 3. Relation between molar absorption coefficient of 3-pyridinecarboxamide (**2**) at 262 nm and concentration of added sulfuric acid. —□—: [**2**]=1.0×10^{-3} mol dm^{-3}; ---■---: [**2**]=3.0×10^{-3} mol dm^{-3}.

and the free base form of **2** coexist in Region A. The correlation between the photoreactivity and the forms of **2** in solution is also similar to that for methyl 3-pyridinecarboxylate. However, there exists a remarkable difference between the amide and the ester: In methyl 3-pyridinecarboxylate the peak for the methylation in Region A becomes lower as the concentration of the substrate is lowered,[3] whereas in 3-pyridinecarboxamide such a dependence of the methylation on the concentration of the substrate was not observed.

Mechanism of Photoreactions of Pyridinecarboxamides. A significant feature of the photoreactions of pyridinecarboxylic esters is the simultaneous participation of various kinds of excited states. Do pyridinecarboxamides show the similar photochemical fea-

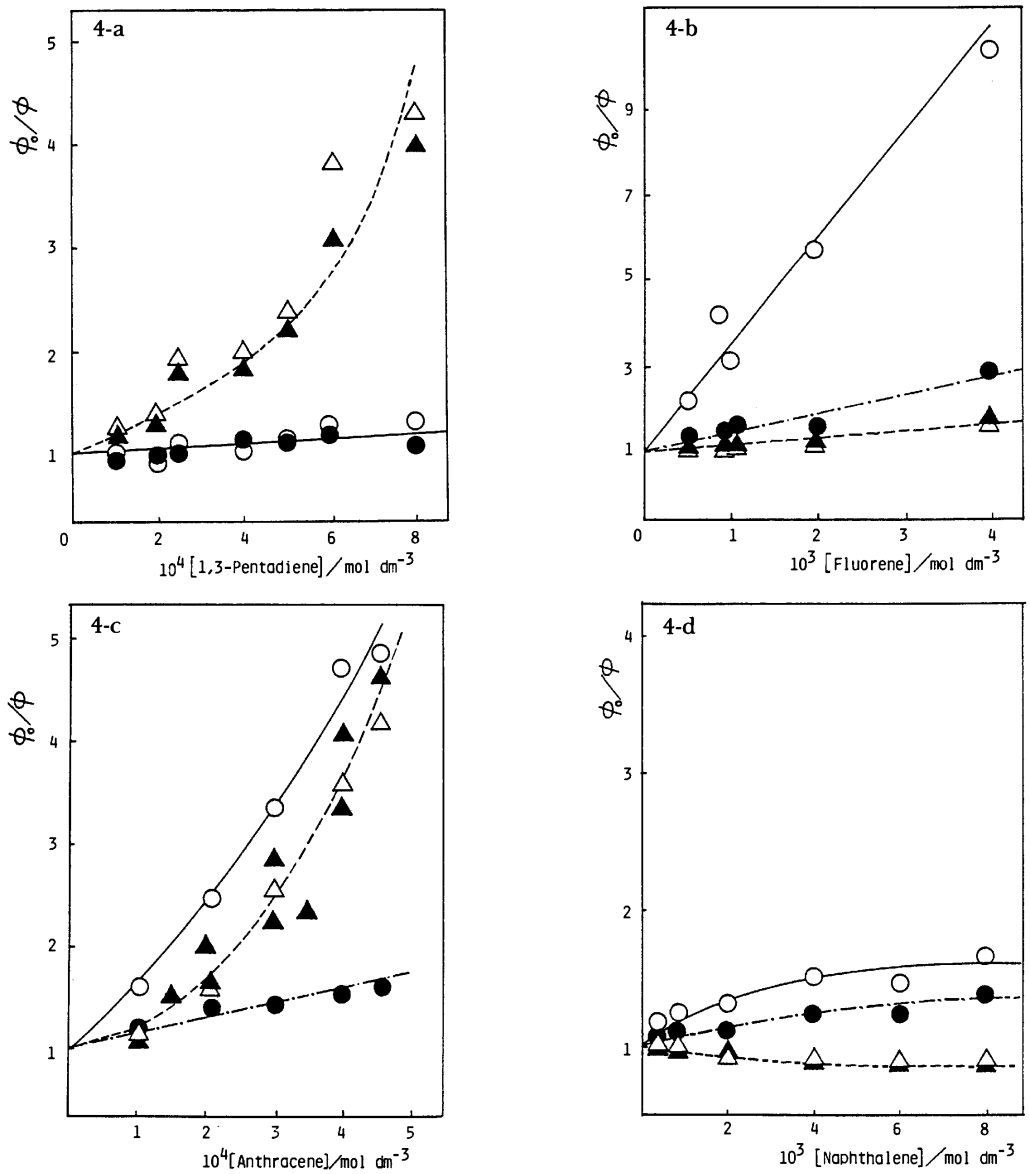

Fig. 4. Stern-Volmer plots for quenching of the photoreactions of 3-pyridinecarboxamide(**2**) in methanol by 1,3-pentadiene (4-a), fluorene (4-b), anthracene (4-c), and naphthalene (4-d). [**2**]=1.0×10^{-2} mol dm^{-3}; [H_2SO_2]=5×10^{-2} mol dm^{-3}; irradiation time, 3 h; 30 °C. ----△----, methylation at the 4-position; ----▲----, methylation at the 6-position; —○—, methoxylation at the 2-position; —●—, methoxylation at the 6-position.

ture? We analyze the photoreactions by means of the effects of quenchers in order to identify the excited states which may participate in the photoreactions.

For the Stern-Volmer analysis of the effects of additives, the quantum yields are calculated on the basis of the light quanta which are absorbed by the substrate.[11] The values Y and L are defined as,

$$Y = \frac{\text{Yield of product in the presence of quencher}}{\text{Yield of product in the absence of quencher}},$$

$$L = \frac{\text{Light absorbed by substrate}}{\text{Light absorbed by substrate and quencher}}.$$

Thus, $\phi_0/\phi = L/Y$.

Photoreaction of 3-Pyridinecarboxamide in Strongly Acidic Alcoholic Solution (Reaction in Region B in Fig. 1-a). The Stern-Volmer plots for the effects of 1,3-pentadiene, fluorene, naphthalene, and anthracene on the photoreactions of **2** in methanol in the presence of sulfuric acid ($[H_2SO_4]=5\times10^{-2}$ mol dm^{-3}; $[2]=1.0\times10^{-2}$ mol dm^{-3}) are shown in Figs. 4-a—4-d.

With respect to the effects of the additives, the photoreactions of 3-pyridinecarboxamide in strongly acidic methanolic solutions can be classified into 3 groups: the two methylation reactions (the formation of **8a** and **9a**), the methoxylation at the 2-position (the formation of **10a**), and the methoxylation at the 6-position (the formation of **11a**). The formation of **8a**

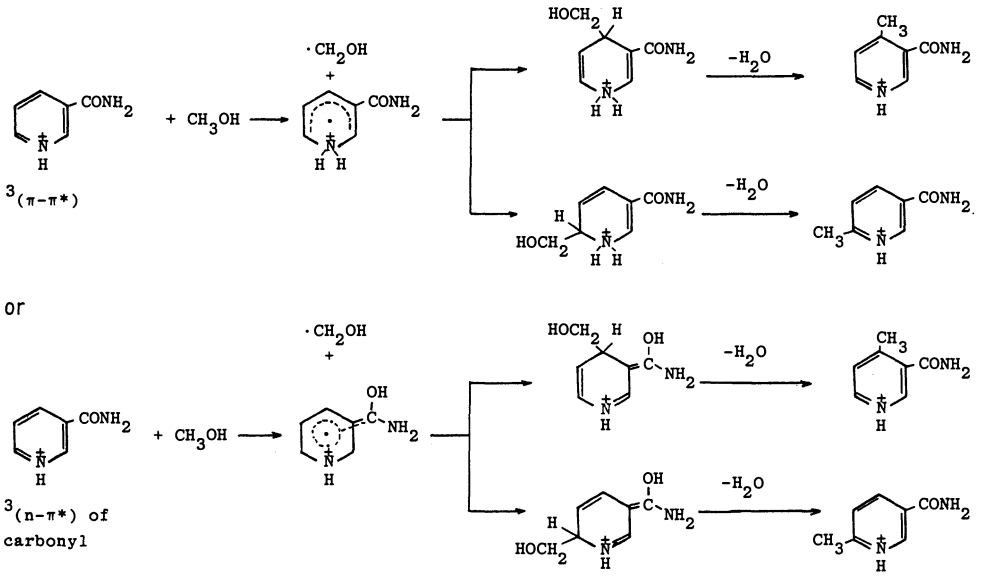

Scheme 1.

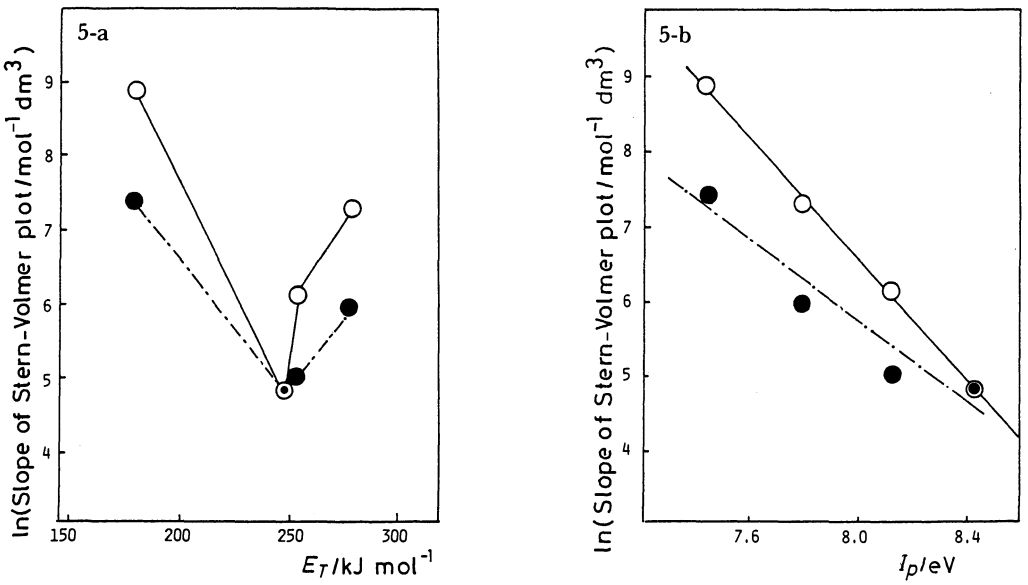

Fig. 5. Relations between the slope of Stern-Volmer plot and triplet energy (5-a) as well as between the slope of Stern-Volmer plot and ionization potential (5-b) of the additives in the quenching of the photomethoxylation of 3-pyridinecarboxamide in methanol. —○—, methoxylation at the 2-position; ···●···, methoxylation at the 6-position.

and **9a** is affected by the additives always to the same extent. The effects of quenchers on the methoxylation differ from those on the methylation and, furthermore, the effects of additives on the formation of **10a** and **11a** are different from each other.

The photomethylation reactions are quenched[12] by the additives with low triplet energies (anthracene: E_T=176 kJ mol^{-1}; 1,3-pentadiene: E_T=248 kJ mol^{-1})[13] but are slightly affected or even promoted by the additives with higher triplet energies (fluorene: E_T=285 kJ mol^{-1}; naphthalene: E_T=255 kJ mol^{-1}). These facts suggest that the methylation reactions originate from an excited triplet state. The photomethylation reactions at the 4- and 6-positions can be explained either by $^3(\pi\text{-}\pi^*)$ or by $^3(n\text{-}\pi^*)$ of carbonyl (Scheme 1).

The slopes of Stern-Volmer plots for photomethoxylation are plotted against the triplet energy values[13] (Fig. 5-a) and the ionization potential values[14] (Fig. 5-b) of the additives. The slopes correlate well with the I_p values of the quenchers, while those have no correlation with the E_T values of the quenchers.

The photomethoxylation reactions should originate from the excited singlet state(s), because the inhibition of the photomethoxylation is not correlated with the triplet energies of the quenchers.

The methoxylation is inhibited by the electron transfer from the electron-rich aromatic hydrocarbons to the excited states or precursors for the methoxylation products. The inhibition would not be due to the direct attack of the quencher to the excited singlet state of 3-pyridinecarboxamide, because the lifetime of the species to be quenched would be too long for an excited singlet state. The lifetime of the reactive species is in the order of 10^{-6} s, when we calculate it from the $k_q\tau$=2.6×10^3 mol^{-1} dm^3 (in the inhibition by fluorene) and the assumed k_q value of 10^9 mol^{-1} dm^3 s^{-1}. The inhibition of the photomethoxylation would occur in the attack of the quenchers to the certain intermediates which are formed from the excited singlet state of **2**.

The following fact also supports the above conclusion. In the presence of fluorene the methoxylation at the 2-position is inhibited but the both methylation reactions (via the excited triplet state) are not inhibited. If the singlet state itself is quenched, the yield of the excited triplet state, which is formed from the excited singlet state, should be decreased. Therefore, if we assume that the inhibition of the methoxylation is due to the quenching of the excited singlet state of the substate, the methylation reactions which originate from an excited triplet state should be inhibited by fluorene to the similar or greater extent than the methoxylation (the reaction from the excited singlet state). This type of phenomena was not observed in

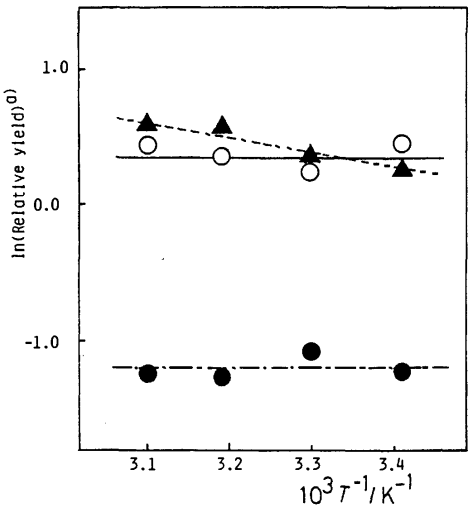

Fig. 6. Temperature dependence of the relative yields of the products from the photoreaction of 3-pyridinecarboxamide in methanol. ----▲----, yield of **9a**/yield of **8a**; —○—, yield of **10a**/yield of **8a**; —●—, yield of **11a**/yield of **8a**.

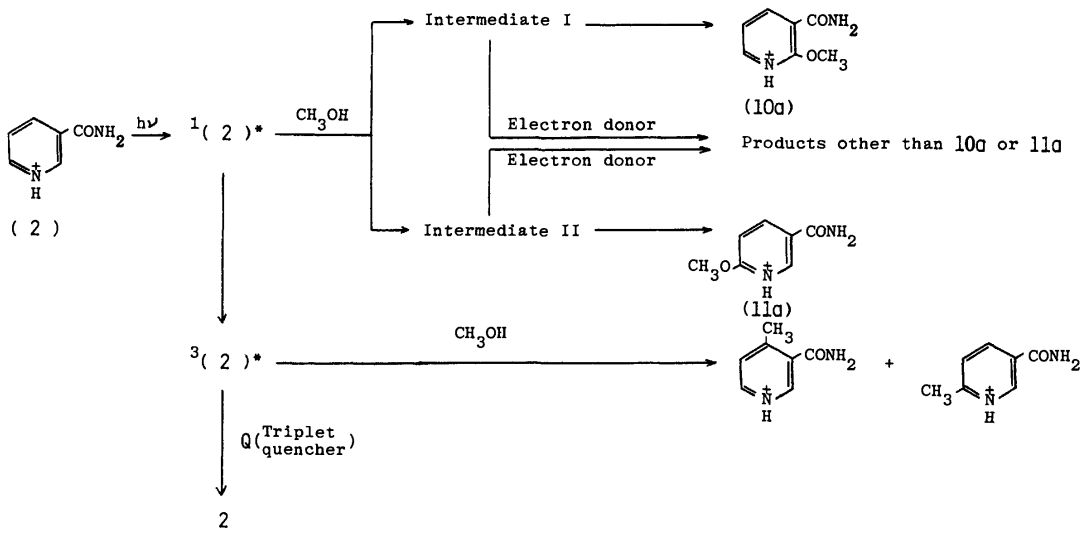

Scheme 2.

the quenching of the photoreaction of 3-pyridinecarboxamide by fluorene. The photoreaction of 3-pyridinecarboxamide shows no remarkable temperature dependence unlike that of the ester (Fig. 6).

The photoreactions of 3-pyridinecarboxamide in methanol acidified with sulfuric acid are summarized in Scheme 2.

Photoreaction of 3-Pyridinecarboxamide in the Presence of Chloride Ion. The UV-irradiation of 3-pyridinecarboxamide in alcohol in the presence of HCl resulted in the increase in the yields of the alkylation products and in the decrease in the yields of the alkoxylation products as shown in Table 1. This observation is similar to that in the photoreaction of methyl 3-pyridinecarboxylate.

More detailed studies by means of Stern-Volmer analysis by using LiCl as an additive in the photoreactions of 3-pyridinecarboxamide in the presence of sulfuric acid (Fig. 7) reveals that chloride ion inhibits the two types of photomethoxylation and, furthermore, to different extents. On the other hand, chloride ion promotes the methylation reactions at the 4- and 6-position to the same extent.

As the roles of chloride ions, we can consider two possibilities: 1) chloride ion accelerates the intersystem crossing of the excited 3-pyridinecarboxamide and 2) chloride ion donates an electron to the excited state(s) of 3-pyridinecarboxamide to give chlorine atom which would bring about the methylation in a radical process (Scheme 3).

We can not determine which process occurs actually. The fact that the isomeric ratio of the photomethylation products is not affected by chloride ion supports

Table 1. Difference in Effect of H_2SO_4 and HCl on Photoreaction of 3-Pyridinecarboxamide (**2**) in Alcohol[a)]

Alcohol	Acid	Irr. time	[Product]/10^{-4} mol dm^{-3}			
		h	**8**	**9**	**10**	**11**
MeOH[b)]	H_2SO_4	6	4.5	6.8	4.1	1.1
	HCl	1.5	4.9	6.9	0.4	0.0
EtOH[c)]	H_2SO_4	3		24	0.3	
	HCl	2		57		

a) [**2**]=1.0×10^{-2} mol dm^{-3}; [H_2SO_4]=5×10^{-2} mol dm^{-3} or [HCl]=5×10^{-1} mol dm^{-3}; temperature, 30 °C. b) Irradiated with a "merry-go-round" type irradiation apparatus. c) Irradiated separately at the center of a spiral type low pressure mercury lamp.

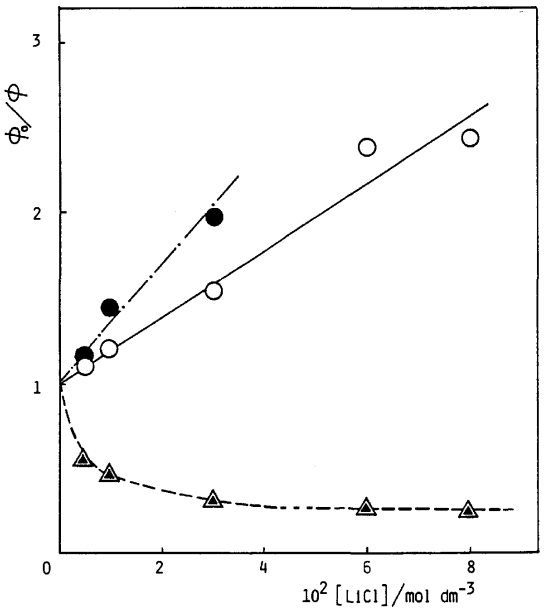

Fig. 7. Effect of LiCl on the photoreaction of 3-pyridinecarboxamide (**2**) in methanol.
[**2**]=1.0×10^{-2} mol dm^{-3}; [H_2SO_4]=5×10^{-2} mol dm^{-3}; irradiation time, 3 h. ----△----, methylation at the 4-position; ----▲----, methylation at the 6-position; —○—, methoxylation at the 2-position; —●—, methoxylation at the 6-position.

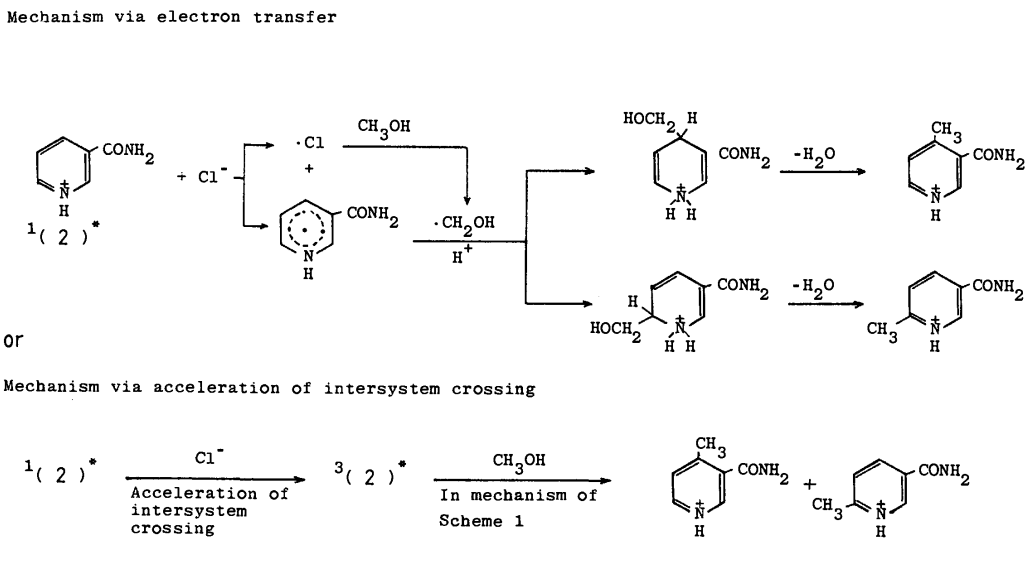

Scheme 3.

Table 2. Dependence of Yields of Products on Concentration of 3-Pyridinecarboxamide (**2**) in Photoreaction in Methanol in the Presence of Sulfuric Acid[a)]

[2]	[Product]/10^{-5} mol dm^{-3}			
mol dm^{-3}	**8a**	**9a**	**10a**	**11a**
2×10^{-4}	2.1	2.9	3.3	0.4
1×10^{-3}	1.6	2.4	3.4	0.5
1×10^{-2}	1.4	2.0	2.8	0.7

a) $[H_2SO_4]=5\times10^{-2}$ mol dm^{-3}; irradiation time, 18 min; temperature, 30 °C.

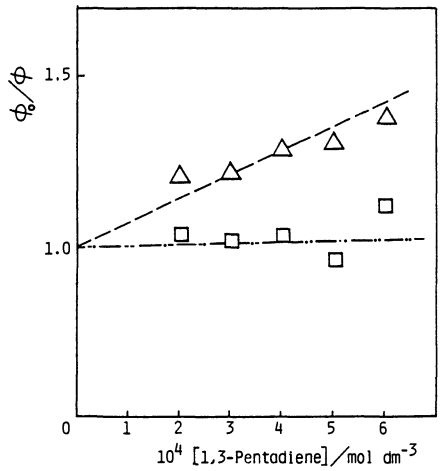

Fig. 8. Stern-Volmer plots for quenching of the photoreactions of 2-pyridinecarboxamide (**1**) by 1,3-pentadiene in the absence of sulfuric acid. [**1**]=9.9×10^{-3} mol dm^{-3}; irradiation time, 10 h. ----△----, methylation at the 5-position; -···□···-, hydroxymethylation at the 4-position.

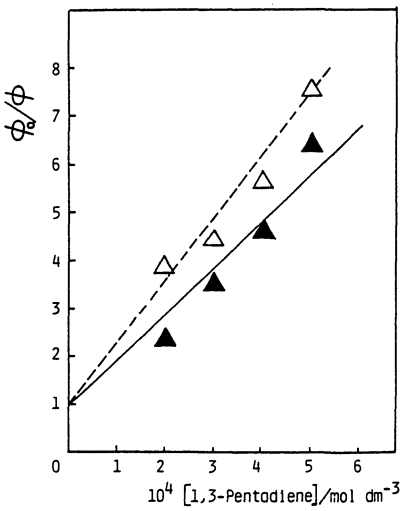

Fig. 9. Stern-Volmer plots for quenching of the photomethylation at the 4-position of 2-pyridinecarboxamide (**1**) by 1,3-pentadiene in the presence of sulfuric acid. [**1**]=1.0×10^{-2} mol dm^{-3}; irradiation time, 4 h. —▲—, $[H_2SO_4]=5\times10^{-3}$ mol dm^{-3}; --△--, $[H_2SO_2]=2\times10^{-1}$ mol dm^{-3}.

the mechanism of the acceleration of the intersystem crossing. However, the different quenchings of chloride ion on the two methoxylation reactions can not be explained by the acceleration of the intersystem crossing, but can be explained more easily by the electron transfer from the intermediates to chloride ion.

Dependence of Photoreaction on Concentration of 3-Pyridinecarboxamide. The photoalkoxylation reactions of 2-pyridinecarboxylic acid,[15] 2-pyridinecarboxylic ester,[4] and 2-pyridinecarbonitrile[9] are characterized by the dependences on the concentration. The reaction occurs effectively at the higher concentrations of the substrate. The alkoxylation reactions of these compounds have been explained by a mechanism via an excimer. The photoreactions of 3-pyridinecarboxamide, however, show only a small concentration dependence as shown in Table 2. It is suggested that an excimer plays no important role in the photoreactions of 3-pyridinecarboxamide in strongly acidic methanolic solutions.

Photoreaction of 2-Pyridinecarboxamide in Methanol. In contrast to methyl 2-pyridinecarboxylate, 2-pyridinecarboxamide (**1**) gives no methoxylation product (the products in ionic reaction). However, the radical type photoreactions of **1** are similar to those of the ester: the methylation at the 5-position in the absence of added acid and the methylation at the 4-position in the presence of H_2SO_4.

The effects of 1,3-pentadiene on the photoreactions of 2-pyridinecarboxamide in the absence of sulfuric acid (Fig. 8) suggest that the methylation at the 5-position and the hydroxymethylation at the 4-position occur from the different kinds of excited species: The formation of **4** is inhibited by a triplet quencher, 1,3-pentadiene, while that of **5** is not affected by 1,3-pentadiene. Therefore, the photoreaction of **1** in the absence of acid might occur via the triplet n-π^* state of amide carbonyl to give **4** but via the singlet n-π^* or π-π^* state of the pyridine ring to give **5**.

The photomethylation at the 4-position in the presence of sulfuric acid is quenched by 1,3-pentadiene (Fig. 9). Anthracene ([anthracene]=4×10^{-4} mol dm^{-3} for [**1**]=1.0×10^{-2} mol dm^{-3} and $[H_2SO_4]=0.2$ mol dm^{-3}) inhibits the formation of **6** completely. These facts suggest that the photomethylation at the 4-position originates from an excited triplet state.

The photomethylations at the 4- and 5-positions are explained by the hydrogen abstractions by the n-π^* of the amide carbonyl and π-π^* of the pyridinium, respectively (Scheme 4).

Photoreaction of 4-Pyridinecarboxamide. The photoreaction of 4-pyridinecarboxamide (**3**) is simpler than those of 2- and 3-pyridinecarboxamide. The UV-irradiation of **3** in methanol gives 2-hydroxymethyl-4-pyridinecarboxamide (**12**) either in the presence or in the absence of an added acid. The photohydroxymethylation was not inhibited by 1,3-pentadiene either

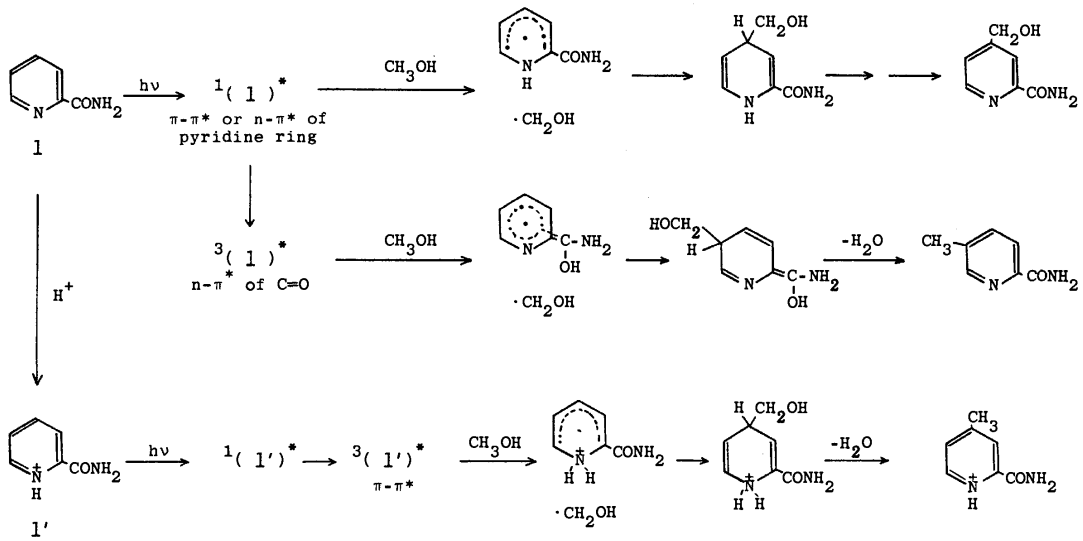

Scheme 4.

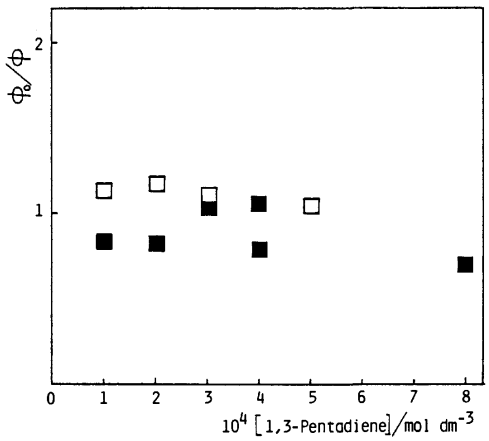

Fig. 10. Stern-Volmer plots for quenching of the photohydroxymethylation of 4-pyridinecarboxamide (**3**) in methanol by 1,3-pentadiene. [**3**]= 1.0×10^{-3} mol dm^{-3}. □, in the absence of sulfuric acid (irradiation time, 30 min); ■, in the presence of sulfuric acid ([H_2SO_2]=5×10^{-2} mol dm^{-3}; irradiation time, 90 min).

in the presence or in the absence of sulfuric acid (Fig. 10). The excited singlet states of protonated and non-protonated **3** might be responsible for the formation of **12**.

Experimental

Materials. Commercial 2- and 4-pyridinecarboxamide (GR-grade of Tokyo Kasei Co.) were purified by recrystallization from benzene and from benzene-ethanol, respectively. 3-Pyridinecarboxamide supplied by Yuki Gosei Yakuhin Co. was recrystallyzed from benzene-ethanol. 2-Pyridinecarboxamide, mp 106 °C; 3-pyridinecarboxamide, mp 126—127 °C; 4-pyridinecarboxamide, mp 152—153 °C.

1,3-Pentadiene (GR-grade of Wako Junyaku Co.), anthracene (analytical standard reagent of BDH Chemical Co.), naphthalene (Reagent for scintillator made by Dojindo Laboratories), and fluorene (zone-refined U.P. grade reagent of Tokyo Kasei Co.) were used without further purification.

UV-Irradiation. Methanolic or ethanolic solutions containing pyridinecarboxamide (in most cases, 1.0×10^{-2} mol dm^{-3}), sulfuric acid, and additives were deaerated by bubbling nitrogen or argon through for 40 min before irradiation.

In the quenching experiment with 1,3-pentadiene, the quencher was added after the deaeration of the substrate solutions in order to avoid the evaporation of the quencher during the bubbling of an inert gas.

For the quenching expeiment, a "merry-go-round" irradiation apparatus was employed, and the solutions (each 20 cm^3) were irradiated with a low-pressure mercury lamp at about 30 °C.

Isolation of Photoproducts. After the irradiation, the solvent was evaporated under reduced pressure. The solution was neutralized with sodium hydrogencarbonate (when the photoreaction has been carried out in the presence of sulfuric acid) and the products were extracted with ethyl acetate. The products were separated by means of TLC (plate, GF_{254} (Type 60) of E. Merck Co.; the developing solvent was ethyl acetate-methanol (9:1) for the products from 2- and 3-pyridinecarboxamides and ethyl acetate-methanol-NH_3 (9:1:small amount) for the products from 4-pyridinecarboxamide.). The separation of the photoproducts from 2- and 3-pyridinecarboxamides was carried out by HPLC (column, RP-18 of E. Merck Co.; eluent, methanol-water (2:8) for the products from 3-pyridinecarboxamide and methanol-water (35:65) for the products from 2-pyridinecarboxamide).

Identification of Photoproducts. The identification of 4-methyl-2-pyridinecarboxamide (**6**), 4-methyl-3-pyridinecarboxamide (**8a**), 6-methyl-3-pyridinecarboxamide (**9a**), and 2-hydroxymethyl-4-pyridinecarboxamide (**12**) was described in our earlier paper.[16]

2-Methoxy-3-pyridinecarboxamide (10a): Mp 131—133 °C; lit,[17] 130—131 °C); IR(KBr disk) 3460, 1670, and 1650 cm^{-1}; ^{1}H NMR (D_2O) δ=4.01 (3H, s), 7.12 (1H, t, J=6.2 Hz, H at the 5-position), and 8.20 (2H, d, J=6.2 Hz, H at the 4-and 6-positions).

2-Ethoxy-3-pyridinecarboxamide (10b) was identified by

the similarity of its spectra to those of **10a**. ^{1}H NMR (D_2O) δ=1.49 (3H, t, J=7.0 Hz), 4.51 (2H, q, J=7.0 Hz), 7.18 (1H, t, J=6.4 Hz, H at the 5-position), and 8.27 (2H, d, J=6.4 Hz, H at the 4- and 6-positions).

6-Methoxy-3-pyridinecarboxamide (11a): Mp 167—168 °C; IR(KBr disk) 3420, 3170, 1670, and 1625 cm^{-1}; ^{1}H NMR (D_2O) δ=4.03 (3H, s), 7.01 (1H, d, J=9.4 Hz, H at the 5-position), 8.16 (1H, dd, J=9.4 and 3.0 Hz, H at the 4-position), and 8.60 (1H, d, J=3.0 Hz, H at the 2-position). Found: C, 54.6; H, 5.3; N, 18.1%. Calcd for $C_7H_8N_2O_2$: C, 55.2; H, 5.3; N, 18.4%.

6-Ethyl-3-pyridinecarboxamide (9b): Mp 161—163 °C; IR(KBr disk) 3220 and 1655 cm^{-1}; ^{1}H NMR (D_2O) δ=1.30 (3H, t, J=7.2 Hz), 2.88 (2H, q, J=7.2 Hz), 7.40 (1H, d, J=8.0 Hz, H at the 5-position), 8.09 (1H, dd, J=8.0 and 2.0 Hz, H at the 4-position), and 8.84 (1H, d, J=2.0 Hz, H at the 2-position); Found: C, 63.7; H, 6.7; N, 18.9%. Calcd for $C_8H_{10}N_2O$: C, 64.0; H, 6.7; N, 18.7%.

5-Methyl-2-pyridinecarboxamide (4) was identified by the similarity of its spectra to those of methyl 5-methyl-2-pyridinecarboxylate. ^{1}H NMR ($CDCl_3$) δ=2.41 (3H, s), 7.62 (1H, dd, J=8.0 and 2.0 Hz, H at the 4-position), 8.08 (1H, d, J=8.0 Hz, H at the 3-position), and 8.37 (1H, d, J=2.0 Hz, H at the 6-position); MS (70 eV) m/z (rel intensity) 137 ($(M+1)^+$; 4), 136 (M^+; 51), 118 ($(M-NH_2)^+$; 8), 94 (7), 93 ($(M-CONH_2)^+$; 100), 92 (46), 66 (25), and 64 (30).

4-Hydroxymethyl-2-pyridinecarboxamide (5) was not obtained in pure form and was identified spectroscopically. ^{1}H NMR (CD_3COCD_3) δ=4.75 (2H, s), 7.50 (1H, dd, J=5.0 and 1.5 Hz, H at the 5-position), 8.08 (1H, d, J=1.5 Hz, H at the 3-position), and 8.49 (1H, d, J=5.0 Hz, H at the 6-position); MS (70 eV) m/z (rel intensity) 153 (5), 152 (M^+; 43), 109 (100), 108 ($(M-CONH_2)^+$; 23), 80 (21), and 78 (14).

Found: m/z 152.0562. Calcd for $C_7H_8N_2O_2$: M, 152.0584.

Quantitative Analysis of Photoproducts. The quantitative analyses of the photoproducts in the quenching experiments were carried out by means of gas chromatography for 4- and 5-methyl-2-pyridinecarboxamides (column, 1 m column of PEG 5%; column temperature, 160 °C). Analyses with HPLC were applied for 4-hydroxymethyl-2-pyridinecarboxamide and for the photoproducts from 3-pyridinecarboxamide (column, 25 cm column of Zorbax ODS of DuPont Co.; eluent, acetonitrile-water (1 : 9) buffered at pH=6.7—7.1 with phosphate buffer) and for the photoproducts from 4-pyridinecarboxamide (column, 25 cm column of Zorbax-ODS; eluent, methanol-water (2 : 8)).

The present work was partially supported by a Grant-in-Aid for Scientific Research No. 60470028 from the Ministry of Education, Science and Culture.

References

1) A review; A. Sugimori, *Yuki Gosei Kagaku Kyokai Shi*, **39**, 712 (1981).

2) T. Sugiyama, E. Tobita, K. Takagi, M. Sato, Y. Kumagai, G. P. Sato, and A. Sugimori, *Chem. Lett.*, **1980**, 131.

3) A. Sugimori, E. Tobita, Y. Kumagai, and G. P. Sato, *Bull. Chem. Soc. Jpn.*, **54**, 1761 (1981).

4) T. Sugiyama, T. Furihata, K. Takagi, M. Sato, S. Akiyama, G. P. Sato, and A. Sugimori, *Bull. Chem. Soc. Jpn.*, **54**, 3585 (1981).

5) T. Sugiyama, K. Yagi, Y. Ito, and A. Sugimori, *Chem. Lett.*, **1982**, 917; T. Sugiyama, Y. Kusano, K. Yagi, Y. Ito, and A. Sugimori, *Bull. Chem. Soc. Jpn.*, **57**, 1882 (1984).

6) A. Sugimori and M. Kanai, *Nippon Kagaku Kaishi*, **1984**, 37.

7) T. Sugiyama, M. Kanai, S. Takenaka, and A. Sugimori, *Bull. Chem. Soc. Jpn.*, **58**, 1331 (1985).

8) A. Sugimori, T. Ogishima, Y. Miyazawa, R. Hasegawa, and Y. Suzuki, *Bull. Chem. Soc. Jpn.*, **56**, 1817 (1983).

9) A. Sugimori, T. Furihata, S. Mikayama, M. Yoshida, and Y. Nakanishi, *Bull. Chem. Soc. Jpn.*, **55**, 2906 (1982).

10) Preliminary report on the photoreactions of 3-pyridinecarboxamide: A. Sugimori and H. Itoh, *Chem. Lett.*, **1986**, 209. The mechanism of the photoreaction of 3-pyridinecarboxamide was reinvestigated.

11) When the quencher absorbs the light, the effective concentration of the quencher might be smaller than the charged concentration, because a part of the quencher is in the excited state. However, the decrease in the effective concentrations of the quencher is negligible under our reaction conditions, where the stationary irradiation with a "merry-go-round" irradiation apparatus equipped with a 17 W low pressure mercury lamp was employed. The measured light quanta absorbed by 20 cm^3 of the solution was 4×10^{16} s^{-1} (3×10^{-6} mol dm^{-3} s^{-1}). If we consider the reported triplet lifetimes of the quenchers (for anthracene in ethanol: 3000+2000 μs (D. N. Dempstor, T. Morrow, and M. F. Quinn, *J. Photochem.*, **2**, 399 (1974) and 150±45 μs (G. Porter and M. W. Windsor, *Discuss. Faraday Soc.*, **17**, 178 (1954); for fluorene in hexane at 300 K: 150 μs (W. Heinzelmann and H. Laphart, *Chem. Phys. Lett.*, **4**, 20 (1969)) the stationary concentration of these quenchers in their excited states should be much lower than the charged concentration of the quenchers (ca. 10^{-4} mol dm^{-3}).

12) We observed the upward-curved Stern-Volmer plots for the quenching of the photomethylation reactions. It indicates that the inhibition of the photomethylation does not occur in a simple triplet energy transfer mechanism.

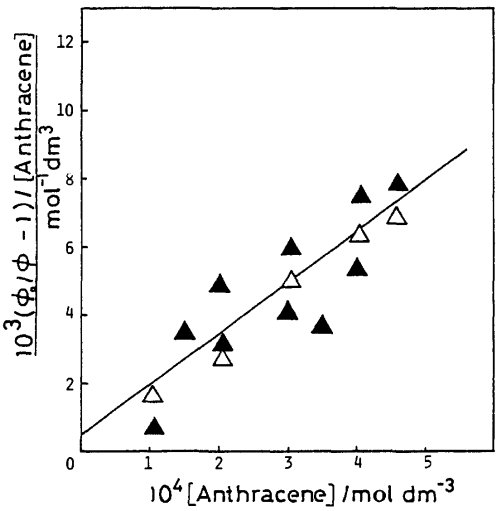

Fig. 11. Plot of $(\phi_0/\phi-1)$/[anthracene] vs. [anthracene] in the quenching of photomethylation reactions of **2** by anthracene. Reaction conditions are the same for Fig. 4-c. —△—, methylation at the 4-position; —▲—, methylation at the 6-position.

The Stern-Volmer plots curved upward are observed (1) in the case of the participation of the static quenching and (2) in the case of the participation of two excited states ((2.1) in the case where each of two states, whether in equilibrium or not, is quenched and the lower one is reactive and (2.2) in the case where two reactive states which are quenched react in parallel) (P. J. Wagner, "Energy Transfer Kinetics in Solution," in "Creation and Detection of the Excited State" ed by A. A. Lamola, Marcel Dekker, Inc. New York (1971), Vol. 1, part A, Chap. 4, pp. 173—212). The concentrations of 1,3-pentadiene in our reaction conditions for quenching (10^{-4}—10^{-3} mol dm^{-3}) are much lower than those which are required for the simple statistical chance that the reactant and the quencher will be nearest neighbors (it occurs under the conditions of [quencher]$>$0.1 mol dm^{-3}). The evidence for the formation of "a complex" between **2** and 1,3-pentadiene which will cause the static quenching at lower concentrations of the quencher has not been obtained in the careful examination of UV-vis. spectra of their mixtures. The Stern-Volmer plots curved upward can be explained by the mechanism (2.1) which involves two states (R_1^* and R_2^*) both of which are quenched and one of which is reactive.

$$R_1^* + Q \xrightarrow{k_{t1}} R_0 + Q_1^* \text{ (Q: Quencher)}$$

$$R_1^* \xrightarrow{k_i} R_0$$

$$R_1^* \xrightarrow{k_{t2}} R_2^*$$

$$R_2^* + Q \xrightarrow{k_{t2}} R_0 + Q_2^*$$

$$R_2^* \xrightarrow{k_d} R_0$$

$$R_2^* \xrightarrow{k_{r2}} I \longrightarrow P \text{ (I: Intermediate; P: product)}$$

When R_1^* and R_2^* are in equilibrium, we add,

$$R_2^* \xrightarrow{k_{21}} R_1^*$$

In this mechanism the Stern-Volmer plots should be parabolic and a linear relationship between $(\phi_0/\phi-1)/$[quencher] and [quencher] should be expected.

In the case where R_1^* and R_2^* are not in equilibrium,

$$\frac{(\phi_0/\phi-1)}{[Q]} = (k_{t1}\tau_1 + k_{t2}\tau_2) + k_{t1}\tau_1 k_{t2}\tau_2[Q].$$

In the case where R_1^* and R_2^* are in equilibrium,

$$\frac{(\phi_0/\phi-1)}{[Q]} = (X_2 k_{t2} + X_1 k_{t1})\tau_e + \frac{k_{t1}k_{t2}}{k_{12}+k_{21}}[Q].$$

In the equation, we define as $X_1=k_{21}/(k_{12}+k_{21})$ and $X_2=k_{12}/(k_{12}+k_{21})$, The apparent lifetime is expressed as τ_e.

The plot for the quenching of photomethylation by anthracene fits this kinetics (Fig. 11).

The participation of two excited triplet states in the photomethylation of 3-pyridinecarboxamide can be conceivable, because $^3(\pi-\pi^*)$ and $^3(n-\pi^*$ of carbonyl) states could contribute to the photomethylation. The photomethylation reactions at the 4- and 6-positions can be explained either by $^3(\pi-\pi^*)$ or by $^3(n-\pi^*$ of carbonyl) (Scheme 1). The fact that the ratio of the two photomethylation products is not affected by the quenchers supports that the reactive state to undergo methylation would be one of them (the lower excited triplet state). Therefore, the mechanism (2.2) which involve two reactive states is less probable.

We have not yet determine which of the excited triplet states, $^3(\pi-\pi^*)$ or $^3(n-\pi^*$ of carbonyl) undergoes the photomethylation reactions.

13) Triplet energy values of quenchers: S. L. Murov, "Handbook of Photochemistry," Marcel Dekker, NY (1973), pp. 3—7.

14) Inization potential values of quenchers: S. L. Murov, "Handbook of Photochemistry," Marcel Dekker, NY (1973), pp. 198—199.

15) H. Kurokawa, T. Furihata, F. Takeuchi, and A. Sugimori, *Tetrahedron Lett.*, **1973**, 2623.

16) A. Sugimori, M. Nishijima, and H. Itoh, *Bull. Chem. Soc. Jpn.*, **55**, 3055 (1982).

17) E. C. Taylor and A. J. Crovetti, *J. Am. Chem. Soc.*, **78**, 214 (1956).

 © 1988 The Chemical Society of Japan Bull. Chem. Soc. Jpn., 61, 2847—2852 (1988)

The Crystal and Molecular Structures of Dithia[4.3](6,9)(6′,9′)-purinophane, Dithia[4.4](6,9)(6′,9′)purinophane, and Dithia[3.3](6,9)(9′,6′)purinophane

Fumio SEYAMA, Yoshiteru SAKATA, Nobutami KASAI,*,† and Soichi MISUMI*
The Institute of Scientific and Industrial Research, Osaka University, Ibaraki, Osaka 567
†Department of Applied Chemistry, Faculty of Engineering, Osaka University, Suita, Osaka 565
(Received October 12, 1987)

Molecular structures of three purinophanes, dithia[4.3](6,9)(6′,9′)purinophane (**1**), dithia[4.4](6,9)(6′,9′)-purinophane (**2**), and dithia[3.3](6,9)(9′,6′)purinophane (**3**), have been determined by means of X-ray diffraction. **1**: monoclinic, space group $P2_1/n$, a=10.561(1), b=16.674(3), c=9.136(1) Å, β=90.29(1)°, V=1608.8(4) Å^3, D_c=1.529 g cm^{-3} for Z=4. **2**: monoclinic, space group $P2_1/n$, a=10.870(2), b=17.058(2), c=9,289(1) Å, β=94.15(1)°, V=1717.9(4) Å^3, D_c=1.487 g cm^{-3} for Z=4. **3**: monoclinic, space group $P2_1/n$, a=8.068(1), b=27.841(2), c=6.913(1) Å, β=111.0(1)°, V=1449.8(2) Å^3, D_c=1.631 g cm^{-3} for Z=4. All structures were solved by the direct method, and refined anisotropically by the least-squares procedure. Final R values are 0.045, 0.053, and 0.050 for **1**, **2**, and **3**, respectively. Molecular structures of **1** and **2** take very similar crossed form, whereas that of **3** reveals a different crossed form.

Previously, we reported syntheses and spectral properties of a few [*m.n*](6,9)purinophanes, in which two purine rings are intramolecularly stacked with each other, for studying relationship between such a base-to-base stacking structure and remarkable hypochromic effect (ca. 40%) in the electronic spectra of DNA.[1,2] In general, although two conformational isomers are theoretically expected for the stacking structures of all purinophanes, their structures can be presumed on the basis of chemical shifts of purine ring protons which would be shifted to higher field by magnetic anisotropy of faced another purine ring. The preferential formation of less overlapped conformer to decrease π-electron repulsive interaction was similarly proposed for all of the double-bridged purinophanes according to NMR assignment. For the confirmation of NMR determined structure and the structural relationship of hypochromism in electronic spectra, molecular structures of dithia[4.3](6,9)(6′,9′)-purinophane (**1**), dithia[4.4](6,9)(6′,9′)purinophane (**2**), and dithia[3.3](6,9)(9′,6′)purinophane (**3**) have been determined by means of X-ray diffraction.

Experimental

Crystal data: **1**, $C_{15}H_{14}N_8S_2$, M 370.45, monoclinic, space group $P2_1/n$, a=10.561(1), b=16.674(3), c=9.136(1) Å, β=90.29(1)°, V=1608.8(4) Å^3, D_c=1.529 g cm^{-3} for Z=4; **2**, $C_{16}H_{16}N_8S_2$, M 384.47, monoclinic, space group $P2_1/n$, a=10.870(2), b=17.058(2), c=9.289(1) Å, β=94.15(1)°, V=1717.9(4) Å^3, D_c=1.487 g cm^{-3} for Z=4; **3**, $C_{14}H_{12}N_8S_2$, M 356.43, monoclinic, space group $P2_1/n$, a=8.068(1), b=27.841(2), c=6.913(1) Å, β=111.0(1)°, V=1449.8(2) Å^3, D_c=1.631 g cm^{-3} for Z=4.

Colorless prismatic crystals with approximate dimensions of 0.25×0.20×0.20 (**1**), 0.25×0.20×0.10 (**2**), and 0.10×0.10×0.10 mm (**3**) were used. X-Ray experiments were carried out on a Rigaku automated, four-circle diffractometer combined with a rotating-anode X-ray generator at the Crystallographic Research Center, Institute for Protein Research, Osaka University. Nickel-filtered Cu $K\alpha$ radiation (λ=1.5418 Å) was used.

Intensity data of each crystal were collected by the θ-2θ scan technique at a 2θ scan rate of 8° min^{-1} and scan width $\Delta 2\theta$=(2.4+0.3 tan θ)°. Backgrounds were counted for 4 s at both ends of a scan. Three standard reflections were measured after every 60 reflections to monitor the stability and orientation of the crystal, which showed no significant decay throughout the data collection. Totals of 2130 reflections out of 2394 (**1**), 2478 out of 2561 (**2**), and 1842 out of 2150 (**3**) were observed ($|F_o|>3\sigma(F_o)$), where $\sigma(F_o)$ is the standard deviation obtained by the counting statistics of intensities. Usual Lorentz and polarization corrections were made but

Table 1. Final Atomic Parameters of Non-Hydrogen Atoms with Estimated Standard Deviations in Parentheses

1. Dithia[4.3](6,9)(6′,9′)purinophane

Atom	x	y	z	B_{eq}/Å^2
S(6)	0.60459(8)	0.06969(5)	0.09028(9)	3.3
S(6′)	0.8873(1)	0.03651(5)	0.2528(1)	4.3
N(1)	0.6908(3)	0.1116(2)	−0.1778(3)	3.5
C(2)	0.7272(4)	0.1680(2)	−0.2741(4)	3.9
N(3)	0.7245(3)	0.2475(2)	−0.2594(3)	3.7
C(4)	0.6761(3)	0.2691(2)	−0.1309(3)	2.9
C(5)	0.6268(3)	0.2176(2)	−0.0249(3)	2.7
C(6)	0.6427(3)	0.1364(2)	−0.0498(3)	2.8
N(7)	0.5850(3)	0.2603(2)	0.0962(3)	3.1
C(8)	0.6088(3)	0.3347(2)	0.0604(4)	3.4
N(9)	0.6653(3)	0.3450(2)	−0.0728(3)	3.2
N(1′)	0.8308(3)	0.1770(2)	0.3668(3)	3.5
C(2′)	0.8247(3)	0.2570(2)	0.3719(4)	3.6
N(3′)	0.8541(3)	0.3096(2)	0.2673(3)	3.2
C(4′)	0.8987(3)	0.2724(2)	0.1483(3)	2.5
C(5′)	0.9147(3)	0.1906(2)	0.1302(3)	2.6
C(6′)	0.8748(3)	0.1418(2)	0.2460(3)	3.1
N(7′)	0.9692(3)	0.1741(2)	−0.0048(3)	3.2
C(8′)	0.9817(3)	0.2455(2)	−0.0639(3)	3.2
N(9′)	0.9394(3)	0.3076(2)	0.0220(3)	3.0
C(61)	0.7057(4)	−0.0149(2)	0.0496(4)	3.5
C(62)	0.8459(4)	0.0027(2)	0.0692(4)	3.6
C(91)	0.7214(4)	0.4191(2)	−0.1296(4)	4.2
C(92)	0.8625(4)	0.4143(2)	−0.1471(4)	4.1
C(93)	0.9428(4)	0.3934(2)	−0.0129(4)	4.1

2. Dithia[4.4](6,9)(6′,9′)purinophane

Atom	x	y	z	B_{eq}/Å^2
S(6)	0.10416(6)	0.06026(4)	0.38499(6)	3.7
S(6′)	0.37646(7)	0.02478(4)	0.24613(7)	4.5
N(1)	0.1975(2)	0.09891(12)	0.6513(2)	4.0
C(2)	0.2307(3)	0.15251(16)	0.7551(3)	4.4
N(3)	0.2171(2)	0.23019(13)	0.7486(2)	4.2
C(4)	0.1638(3)	0.25336(14)	0.6230(3)	3.5
C(5)	0.1236(2)	0.20468(14)	0.5077(3)	3.4
C(6)	0.1443(2)	0.12509(13)	0.5272(3)	3.4
N(7)	0.0746(2)	0.24961(12)	0.3920(2)	3.8
C(8)	0.0854(3)	0.32123(15)	0.4383(3)	4.2
N(9)	0.1392(2)	0.32820(11)	0.5782(2)	3.9
N(1′)	0.3274(2)	0.16021(12)	0.1213(2)	4.2
C(2′)	0.3278(3)	0.23878(15)	0.1106(3)	4.3
N(3′)	0.3656(2)	0.29094(12)	0.2086(2)	3.9
C(4′)	0.4073(2)	0.25687(12)	0.3327(2)	3.0
C(5′)	0.4116(2)	0.17662(12)	0.3605(3)	3.1
C(6′)	0.3689(2)	0.12781(14)	0.2466(3)	3.5
N(7′)	0.4664(2)	0.16306(11)	0.4974(2)	3.7
C(8′)	0.4922(3)	0.23323(13)	0.5480(3)	3.6
N(9′)	0.4589(2)	0.29266(10)	0.4518(2)	3.2
C(61)	0.2021(3)	−0.02208(13)	0.4331(3)	4.2
C(62)	0.3384(3)	−0.00534(14)	0.4242(3)	4.3
C(91)	0.1812(3)	0.40024(15)	0.6514(3)	4.5
C(92)	0.3204(3)	0.40824(15)	0.6500(3)	4.3
C(93)	0.3641(3)	0.42078(13)	0.4992(3)	4.1
C(94)	0.4812(3)	0.37698(13)	0.4708(3)	3.8

3. Dithia[3.3](6,9)(9′,6′)purinophane

Atom	x	y	z	B_{eq}/Å^2
S(6)	0.97543(15)	0.29943(4)	0.41814(17)	3.1
S(6′)	1.48414(15)	0.41425(5)	0.00341(18)	3.4
N(1)	0.9746(5)	0.39583(12)	0.3992(6)	3.1
C(2)	1.0485(6)	0.43845(15)	0.3935(7)	3.2
N(3)	1.2136(5)	0.44830(12)	0.4105(6)	2.8
C(4)	1.3123(5)	0.40855(14)	0.4446(6)	2.5
C(5)	1.2569(6)	0.36172(14)	0.4657(6)	2.6
C(6)	1.0786(6)	0.35622(15)	0.4324(6)	2.7
N(7)	1.3946(5)	0.32964(13)	0.4970(6)	3.1
C(8)	1.5250(6)	0.35637(16)	0.4904(7)	3.0
N(9)	1.4854(4)	0.40430(12)	0.4585(5)	2.5
N(1′)	1.1491(5)	0.44506(12)	−0.0877(6)	3.2
C(2′)	0.9756(6)	0.43823(16)	−0.1157(7)	3.4
N(3′)	0.8941(5)	0.39737(13)	−0.1064(6)	3.3
C(4′)	1.0037(6)	0.35985(15)	−0.0691(7)	2.9
C(5′)	1.1812(6)	0.36096(15)	−0.0501(6)	2.9
C(6′)	1.2526(6)	0.40608(15)	−0.0514(6)	2.9
N(7′)	1.2559(6)	0.31542(13)	−0.0092(6)	3.8
C(8′)	1.1249(7)	0.28887(16)	−0.0046(7)	3.8
N(9′)	0.9678(5)	0.31310(13)	−0.0387(6)	3.3
C(61)	0.7819(6)	0.30835(15)	0.1813(8)	3.4
C(62)	0.8089(7)	0.29256(16)	−0.0140(8)	3.7
C(92)	1.5295(6)	0.46095(16)	0.2024(8)	3.5
C(91)	1.5981(6)	0.44120(15)	0.4217(7)	3.1

absorption correction was ignored [μ(Cu $K\alpha$)=30.9, 29.2, and 34.0 cm^{-1} for **1**, **2**, and **3**, respectively].

Structure Solution and Refinement

The structure of each crystal was established by the direct method (*MULTAN* 78),[3] and refined anisotropically by the block-diagonal least-squares procedure (*HBLS* V).[4] Hydrogen atoms could be located on the difference Fourier map, which were included in the refinement with isotropic temperature factors. Final R values were 0.045 (R_w=0.070) for **1** and 0.053 (R_w=0.079) for **2**, and 0.050 (R_w=0.064) for **3** for observed reflections. Weighting schemes used in the final cycles of the refinements were $\{\sigma^2(F_o)-0.0071|F_o|+0.0017|F_o|^2\}^{-1}$ for **1**, $\{\sigma^2(F_o)-0.2283|F_o|+0.0116|F_o|^2\}^{-1}$ for **2**, and $\{\sigma^2(F_o)-0.0281|F_o|+0.0001|F_o|^2\}^{-1}$ for **3** for observed reflections. Atomic parameters of non-hydrogen atoms are given in Table 1 with equivalent isotropic temperature factors.**[5] Atomic scattering factors were taken from those of International Tables for X-Ray Crystallography.[6] Calculations were done on ACOS 900 and ACOS 850 computers at the Crystallographic Research Center, Institute for Protein Research, Osaka University.

Results and Discussion

Molecular Structure. Throughout the three purinophanes the corresponding bond distances and bond angles in two purine rings are respectively equal within the range of error (Table 2). Each of these is not significantly different from the corresponding bond distances and bond angles in 6-(methylthio)-purine[8] and also from that in purine in the 2 : 1 complex of purine and urea.[9]

The characteristic feature of molecular structures of **1** and **2** is that these purinophanes take similar crossed form as to the overlapping of two purine rings (Fig. 1,a). However, because of the shorter -$(CH_2)_3$- bridge than -S-$(CH_2)_2$-S- the upper purine ring in **1** bent slightly convex upward (Fig. 1,b). Very close inter-purine ring nonbonded atomic distances are observed between atoms located near the -$(CH_2)_3$-bridge: the closest distance is 3.081(3) Å (between the N(9) and N(9′) atoms) and the others ranging from 3.172(4) Å (between the C(4) and N(9′) atoms) to 3.490(4) Å (between the N(1) and N(7′) atoms). Two purine rings in **2** are planar, and the tilting direction of the upper purine ring relative to the lower one differs from that in **1** because of the longer -$(CH_2)_4$- bridge. All the inter-purine nonbonded distances except N(1)···N(7′) [3.520(3) Å], N(3)···C(8)[3.489(3) Å], and C(5)···C(5′)-[3.538(3) Å] are longer than 3.6 Å.

Similar to the cyclophanes and heterophanes, the pyrimidine moiety of purine rings showed a tendency to be folded slightly at the N(1)···C(5) or N(1′)···C(5′) line while the imidazole moiety at the C(4)···C(8) or C(4′)···C(8′) line. The dihedral angle between the plane defined by the N(1), C(2), C(4), and C(5) atoms and that made by the N(1), C(5), and C(6) is only 4.8(3), which is the largest in **1**. In **2**, all the dihedral angles

** Tables of anisotropic temperature factors, atomic parameters of hydrogen atoms, and observed and calculated structure factors are kept at the Chemical Society of Japan, Document No. 8816.

Table 2. Selected Bond Distances and Bond Angles with Estimated Standard Deviations in Parentheses

	1	2	3		1	2	3
Bond distance (l/Å)							
N(1)-C(2)	1.345(4)	1.358(3)	1.335(6)	N(7')-C(8')	1.314(4)	1.309(3)	1.300(7)
N(1')-C(2')	1.336(4)	1.344(3)	1.356(6)	C(8)-N(9)	1.369(4)	1.392(3)	1.372(5)
N(1)-C(6)	1.342(4)	1.329(3)	1.354(6)	C(8')-N(9')	1.375(4)	1.382(3)	1.379(7)
N(1')-C(6')	1.336(4)	1.337(3)	1.337(6)	C(6)-S(6)	1.745(3)	1.753(2)	1.773(4)
C(2)-N(3)	1.333(4)	1.334(3)	1.323(6)	C(6')-S(6')	1.761(3)	1.760(2)	1.782(4)
C(2')-N(3')	1.335(4)	1.318(3)	1.327(6)	S(6)-C(61)	1.808(3)	1.799(3)	1.829(5)
N(3)-C(4)	1.332(4)	1.325(3)	1.334(5)	S(6')-C(62)	1.821(3)	1.809(3)	
N(3')-C(4')	1.339(4)	1.340(3)	1.332(6)	S(6')-C(92)			1.832(5)
C(4)-C(5)	1.398(4)	1.400(3)	1.403(6)	C(61)-C(62)	1.518(5)	1.517(4)	1.508(7)
C(4')-C(5')	1.385(4)	1.393(3)	1.391(6)	N(9)-C(91)	1.467(4)	1.462(3)	1.454(5)
C(4)-N(9)	1.376(4)	1.363(3)	1.370(5)	N(9')-C(93)	1.467(4)		
C(4')-N(9')	1.366(4)	1.349(3)	1.366(6)	N(9')-C(94)		1.467(3)	
C(5)-C(6)	1.382(4)	1.386(3)	1.382(6)	N(9')-C(62)			1.469(6)
C(5')-C(6')	1.401(4)	1.399(3)	1.383(6)	C(91)-C(92)	1.505(5)	1.520(4)	1.519(7)
C(5)-N(7)	1.390(4)	1.394(3)	1.381(6)	C(92)-C(93)	1.528(5)	1.526(4)	
C(5')-N(7')	1.391(4)	1.384(3)	1.389(6)	C(93)-C(94)		1.515(3)	
N(7)-C(8)	1.308(4)	1.298(3)	1.303(6)				
Bond angle (ϕ/°)							
C(2)-N(1)-C(6)	117.7(3)	117.8(3)	118.2(4)	C(5')-N(7')-C(8')	103.2(3)	104.1(2)	103.1(5)
C(2')-N(1')-C(6')	119.0(3)	118.3(3)	117.2(4)	N(7)-C(8)-N(9)	115.3(3)	114.3(3)	114.6(4)
N(1)-C(2)-N(3)	128.5(3)	127.8(3)	128.9(4)	N(7')-C(8')-N(9')	114.4(3)	113.5(2)	115.1(5)
N(1')-C(2')-N(3')	128.3(3)	128.7(3)	128.1(5)	C(4)-N(9)-C(8)	105.4(3)	105.4(2)	105.6(4)
C(2)-N(3)-C(4)	111.5(3)	112.1(3)	111.2(4)	C(4')-N(9')-C(8')	105.3(3)	105.8(2)	105.1(4)
C(2')-N(3')-C(4')	111.2(3)	111.8(3)	112.1(4)	C(4)-N(9)-C(91)	127.2(3)	126.7(2)	127.8(4)
N(3)-C(4)-C(5)	126.2(3)	126.1(3)	126.7(4)	C(4')-N(9')-C(93)	127.7(3)		
N(3')-C(4')-C(5')	126.7(3)	126.2(3)	126.1(5)	C(4')-N(9')-C(94)		126.7(2)	
C(5)-C(4)-N(9)	105.5(3)	106.2(2)	105.5(4)	C(4')-N(9')-C(62)			129.1(4)
C(5')-C(4')-N(9')	106.4(3)	106.6(2)	105.9(4)	C(8)-N(9)-C(91)	126.7(3)	127.1(2)	126.3(4)
N(3)-C(4)-N(9)	128.4(3)	127.7(3)	127.8(4)	C(8')-N(9')-C(93)	127.0(3)		
N(3')-C(4')-N(9')	126.9(3)	127.1(2)	127.9(4)	C(8')-N(9')-C(94)		127.4(2)	
C(4)-C(5)-C(6)	116.2(3)	116.3(2)	115.9(4)	C(8')-N(9')-C(62)			125.2(4)
C(4')-C(5')-C(6')	116.4(3)	116.1(2)	115.9(4)	C(6)-S(6)-C(61)	102.0(2)	101.2(2)	99.3(2)
C(4)-C(5)-N(7)	111.0(3)	110.1(2)	110.4(4)	C(6')-S(6')-C(62)	105.0(2)	105.5(2)	
C(4')-C(5')-N(7')	110.6(3)	110.0(2)	110.8(4)	C(6)-S(6')-C(92)			99.3(3)
C(6)-C(5)-N(7)	132.2(3)	133.5(3)	133.3(4)	S(6)-C(61)-C(62)	113.7(3)	113.7(3)	114.3(4)
C(6')-C(5')-N(7')	133.1(3)	133.8(2)	132.8(5)	S(6')-C(62)-C(61)	113.4(3)	113.1(2)	
N(1)-C(6)-C(5)	119.5(3)	119.9(2)	118.9(4)	N(9')-C(62)-C(61)			113.7(4)
N(1')-C(6')-C(5')	118.4(3)	119.0(3)	120.3(4)	S(6')-C(92)-C(91)			113.3(4)
N(1)-C(6)-S(6)	122.1(3)	120.7(2)	117.8(4)	N(9)-C(91)-C(92)	113.3(3)	110.4(2)	113.8(4)
N(1')-C(6')-S(6')	115.8(3)	115.1(2)	118.2(4)	N(9')-C(93)-C(92)	112.5(3)		
C(5)-C(6)-S(6)	118.4(2)	119.4(2)	123.2(4)	N(9')-C(94)-C(93)		112.5(3)	
C(5')-C(6')-S(6')	125.6(3)	125.7(2)	121.4(4)	C(91)-C(92)-C(93)	118.3(3)	113.4(3)	
C(5)-N(7)-C(8)	102.9(3)	104.0(2)	103.9(4)	C(92)-C(93)-C(94)		114.3(2)	

Table 3. Some Short Non-Bonded Distances between Two Purine Rings with Estimated Standard Deviations in Parentheses (l/Å)

	1	2		3
N(1)···N(7')	3.490(4)	3.520(3)	N(1)···N(3')	3.319(5)
N(3)···C(8')	3.243(4)	3.636(3)	C(2)···C(2')	3.354(7)
C(4)···C(4')	3.461(4)	3.913(3)	N(3)···N(1')	3.295(5)
C(4)···C(8')	3.306(4)	3.702(3)	C(4)···C(6')	3.288(6)
C(4)···N(9')	3.172(4)	3.743(3)	C(5)···C(5')	3.395(6)
C(5)···C(4')	3.398(4)	3.697(3)	C(6)···C(4')	3.300(6)
C(5)···C(5')	3.379(4)	3.538(3)	C(6)···N(9')	3.280(6)
C(6)···C(5')	3.424(4)	3.501(3)	N(7)···N(7')	3.293(6)
N(7)···N(3')	3.339(4)	3.766(3)	N(9)···C(6')	3.348(5)
N(7)···C(4')	3.351(4)	3.699(3)		
C(8)···N(3')	3.226(4)	3.878(3)		
C(8)···C(4')	3.327(4)	3.861(3)		
C(9)···C(4')	3.402(4)			
N(9)···N(9')	3.081(3)	3.796(3)		

Table 4. Torsional Angles in the Bridge Bonds (ϕ/°)

	1	2	3
C(6)-S(6)-C(61)-C(62)	292.9	292.7	268.2
S(6)-C(61)-C(62)-S(6')	302.5	303.9	
S(6)-C(61)-C(62)-N(9')			52.4
C(61)-C(62)-S(6')-C(6')	90.8	92.4	
N(9)-C(91)-C(92)-C(93)	33.7	66.7	
N(9)-C(91)-C(92)-S(6')			53.6
C(91)-C(92)-C(93)-N(9')	282.7		
C(91)-C(92)-C(93)-C(94)		219.8	
C(92)-C(93)-C(94)-N(9')			73.6
C(91)-C(92)-S(6')-C(6')			264.8

of this kind have small values which are not significant.

As the C(6) and C(6') atoms of purine rings are connected by the -S-$(CH_2)_2$-S- bridge in **1** and **2**, the C(6)-

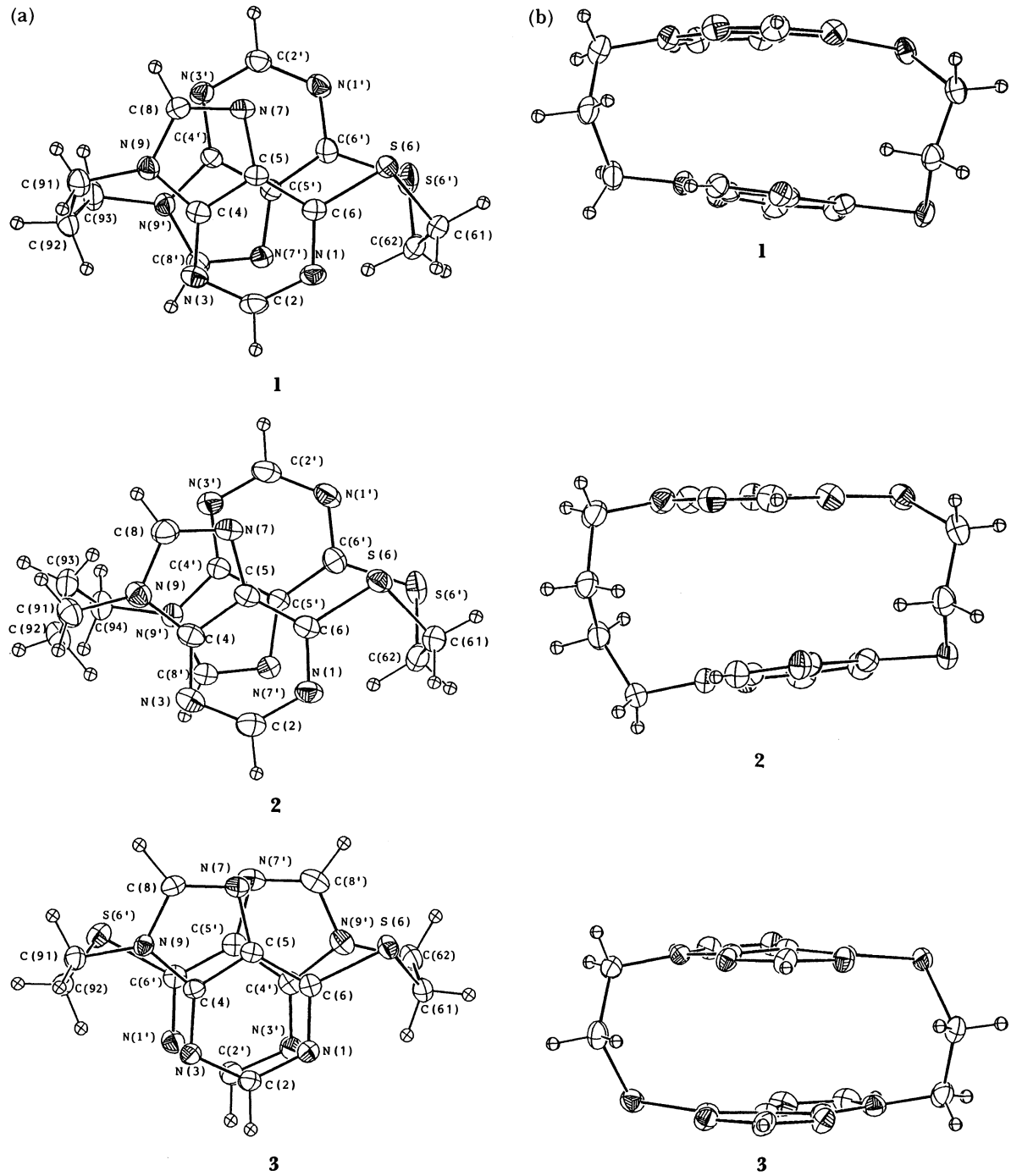

Fig. 1. Molecular structures[7] of three purinophanes, **1**, **2**, and **3**. Non-hydrogen atoms are expressed as thermal ellipsoids with 30% probability level, and hydrogen atoms as spheres with B=1.0 Å^2. a: projected onto the mean plane defined by the N(1), C(2), N(3), C(4), C(5), C(6), N(7), C(8), and N(9) atoms. b: projected along the line passing through the C(2) and C(5) atoms.

S(6) and C(6′)-S(6′) bonds are not parallel to the plane defined by the N(1), C(5), and C(6) atoms and that formed by the N(1′), C(5′), and C(6′) atoms, respectively, among which the largest angle is 4.8(3) in **2**. On the other hand, the N(9) and N(9′) atoms are connected by the -$(CH_2)_2$- (**1**) or -$(CH_2)_3$- (**2**) bridge. The angles between the N(9)-C(91) bond and the plane defined by the C(4), C(8), and N(9) atoms [7.4(3)(**1**) and 8.1(3)° (**2**)] are larger than the other two angles. The -S-$(CH_2)_2$-S- bridges in **1** and **2** have similar structures: corresponding bond distances, bond angles, and torsional angles are respectively equal within the range of error (Tables 2, 3, and 4).

The overlapping of two purine rings in **3** is another crossed form (Fig. 1, a). The molecule **3** has approximately two fold symmetry about the line passing

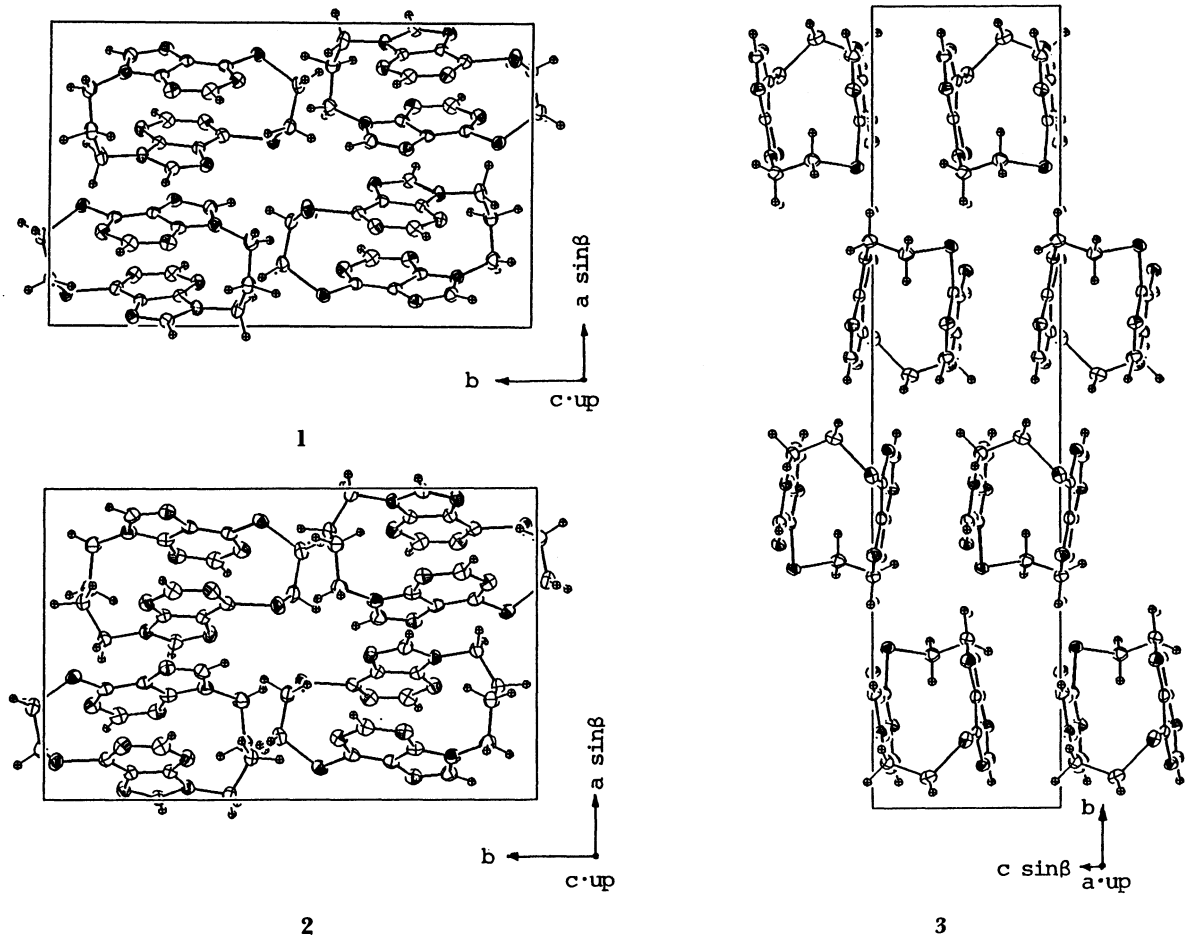

Fig. 2. Crystal structures[7] of three purinophanes, **1**, **2**, and **3**. Non-hydrogen atoms are drawn as thermal ellipsoids with 30% probability level, and hydrogen atoms as spheres with B=1.0 Å^2.

Table 5. Close Intermolecular Atomic Contacts (l/Å) less than 3.6 Å

In **1**			
C(2)···N(1′)[a]	3.467(4)	N(7)···C(2′)[d]	3.432(4)
N(3)···C(2′)[a]	3.540(4)	N(7)···N(1′)[d]	3.555(4)
N(3′)···C(61)[b]	3.431(4)	C(8)···N(1′)[d]	3.426(4)
S(6)···C(92)[c]	3.525(4)	N(9)···N(1′)[d]	3.592(4)
C(2)···N(9′)[d]	3.580(4)	N(9)···C(6′)[d]	3.486(4)
N(3)···C(4′)[d]	3.554(4)		
N(3)···C(5′)[d]	3.571(4)	Key	
C(4)···C(5′)[d]	3.573(4)	a) x, y, $-1+z$;	
C(5)···C(2′)[d]	3.348(4)	b) $1.5-x$, $0.5+y$, $0.5-z$;	
C(5)···N(3′)[d]	3.471(4)	c) $-0.5+x$, $0.5-y$, $0.5+z$;	
C(6)···N(3′)[d]	3.583(4)	d) $-0.5+x$, $0.5-y$, $-0.5+z$;	
In **2**			
N(1′)···C(2)[a]	3.490(3)	N(7)···C(2′)[d]	3.485(3)
C(2′)···N(3)[a]	3.492(3)	C(8)···N(1′)[d]	3.397(3)
C(8′)···N(7)[b]	3.269(3)	C(8)···C(2′)[d]	3.477(4)
C(61)···N(3′)[c]	3.508(3)	N(9)···N(1′)[d]	3.447(3)
C(2)···C(94)[d]	3.523(4)	N(3′)···C(61)[e]	3.508(3)
N(3)···C(4′)[d]	3.520(3)	Key	
N(3)···N(9′)[d]	3.516(3)	a) x, y, $-1+z$;	
C(4)···N(3′)[d]	3.476(3)	b) $0.5+x$, $0.5-y$, $0.5+z$;	
C(4)···C(4′)[d]	3.520(3)	c) $0.5-x$, $-0.5+y$, $0.5-z$;	
C(5)···C(2′)[d]	3.553(4)	d) $-0.5+x$, $0.5-y$, $0.5+z$;	
C(5)···N(3′)[d]	3.481(3)	e) $0.5-x$, $0.5+y$, $0.5-z$;	
In **3**			
N(1)···N(1′)[a]	3.586(5)		
N(1)···C(2′)[a]	3.553(6)		
C(2)···N(1′)[a]	3.386(6)	Key	
C(6)···C(5′)[a]	3.373(6)	a) x, y, $-1+z$;	
N(3)···C(91)[b]	3.443(6)	b) $-1+x$, y, z;	
N(1)···C(91)[c]	3.344(6)	c) $1+x$, y, z.	

through the midpoint of the C(2) and C(2′) atoms and that of the N(7) and N(7′), and two purine rings are approximately parallel to each other (Fig. 1, b). Close inter-purine nonbonded atomic distances observed are ranging from 3.289(6) Å (between the C(6) and N(9′) atoms) to 3.395(5) Å (between the C(5) and C(5′)).

Two purine rings in **3** are symmetrically connected by the -S(CH$_2$)$_2$- bridges. Only the dihedral angles concerned with the folding of the pyrimidine moiety have significant values. The angle made by the N(9)-C(91) (or N(9′)-C(93)) bond and the plane formed by the C(4), C(8), and N(9) (or C(4′), C(8′), and N(9′)) atoms [5.5(4)(or 6.7(5))°] is larger than the corresponding angle at the C(6)(or C(6′)) atom. In **3**, the

structures of two -S-$(CH_2)_2$- bridges are very similar to each other.

Based on the structures determined in this study, detailed discussions about the relationship between the stacked orientations of two purine rings and hypochromism values as well as the arguments of NMR determined structures are given in a separate paper.[10]

Crystal Structure. Crystal structures of **1**, **2**, and **3** are drawn in Fig. 2. Among the three, crystals of **1** and **2** show the similar mode of packings. Molecules are packed closely: the closest intermolecular atomic contacts are 3.348(4) Å [C(5)(x, y, z)···C(2′) ($-0.5+x$, $0.5-y$, $-0.5+z$)] and 3.397(3) Å [C(8′)(x, y, z)···N(7)($-0.5+x$, $0.5-y$, $0.5+z$)] in **1** and **2**, respectively (Table 5). In **3**, the shortest non-bonded distance between adjacent molecules is 3.344(6) Å [N(1)(x, y, z)···C(91)($1+x$, y, z)].

The authors wish to express their deep thanks to Miss Nobuko Kanehisa who helped them with computations at the final stage of the refinement and *ORTEP* drawings.

References

1) F. Hama, Y. Sakata, and S. Misumi, *Tetrahedron Lett.*, **22**, 1123 (1981); *Nucleic Acid Res., Spec. Publ.*, **8**, 131 (1980); **10**, 73 (1981).

2) F. Hama, Y. Sakata, S. Misumi, M. Aida, and C. Nagata, *Tetrahedron Lett.*, **23**, 3061 (1982).

3) P. Main, S. E. Hull, L. Lessinger, G. Germain, J. P. Declercq, and M. M. Woolfson, *MULTAN* 78, "A System of Computer Programs for the Automatic Solution of Crystal Structure from X-Ray Data," Univ. of York, England (1973).

4) T. Ashida, *HBLS* V, "The Universal Crystallographic Computing System-Osaka," The Computation Center, Osaka Univ., (1973), pp. 55—61.

5) W. C. Hamilton, *Acta Crystallogr.*, **12**, 609 (1959).

6) "International Tables for X-Ray Crystallography," Vol. IV, Kynoch Press, Birmingham (1974), p. 71.

7) C. K. Johnson, *ORTEP* II, Report ORNL-5138, Oak Ridge National Laboratory, Tennessee (1976).

8) W. J. Cook and C. E. Bugg, *J. Pharm. Sci.*, **64**, 221 (1975).

9) A. Itai, H. Yamada, T. Okamoto and Y. Iitaka, *Acta Crystallogr., Sect. B*, **33**, 1816 (1977).

10) F. Seyama, K. Akahori, Y. Sakata, S. Misumi, M. Aida, and C. Nagata, *J. Am. Chem. Soc.*, **110**, 2192 (1988).

 © 1988 The Chemical Society of Japan Bull. Chem. Soc. Jpn., 61, 2853—2858 (1988)

Iodine- or Iodine Monobromide-Catalyzed Alkoxy-Alkoxy Exchange Reactions of Alkylalkoxysilanes: Formation of the Catalyst-Alkoxysilane Complexes and the Reaction Mechanism

Katsuko Ito* and Takeshi Ibaraki
Department of Natural Science, Osaka Women's University, Daisen-cho 2-1, Sakai, Osaka 590
(Received December 7, 1987)

The formation of charge-transfer complexes of iodine and of iodine monobromide with alcohols and alkoxysilanes has been established spectroscopically, and the formation constants of iodine-ethoxytriethylsilane and iodine-diethoxydimethylsilane complexes has been determined as 0.55±0.01 and 0.61±0.02, respectively. On the basis of these observations and the kinetic information recently reported, the previously proposed mechanism for the iodine or iodine monobromide catalyzed alkoxy-alkoxy exchange reactions of alkoxysilanes is discussed afresh. It has been confirmed that a mechanism involving a four-centered transition state containing a CT-complex is most favorable.

In our previous work we disclosed that halogens and interhalogen compounds were extremely favorable catalysts for quantitative studies of the alcoholysis and redistribution reactions of alkoxysilanes.[1,2] These catalysts accelerate the alkoxy-alkoxy exchange reactions at ordinary temperature without any by-products, unlike conventional catalysts such as various acids and bases.

Among these catalysts, iodine and iodine monobromide that are easier to handle than others were preferred for the determination of alcoholysis and redistribution equilibrium constants, and the extensive data at 20 °C and 40 °C could be successfully observed.[1,2]

Since only a few redistribution equilibria have so far been examined at 150 °C[3,4] and 120 °C[5] in the absence of a catalyst and no alcoholysis equilibria have been examined, halogens and interhalogen compounds may be the first catalysts to make it possible to investigate these equilibria quantitatively at ordinary temperature.

A kinetic study on the following iodine-catalyzed alcoholysis was undertaken, in order to ascertain the catalytic activity of iodine quantitatively and to provide information about the mechanism of the reaction, $Et_3SiOBu^n+Bu^sOH \rightleftarrows Et_3SiOBu^s+Bu^nOH$ Both forward and reverse reactions were of first order with respect to butoxysilane, to butanol and also to iodine.[7]

Hologens and interhalogen compounds are expected to form charge-transfer complexes (CT-complexes) with alkoxysilanes as well as alcohols,[6] and the present reactions have been assumed to proceed via four-centered transition states containing such CT-complexes as intermediates.

To confirm the formation of these CT-complexes, we have now made spectrophotometric studies of iodine and iodine monobromide solutions in various alkoxysilanes, and determined the formation constants of iodine complexes with ethoxytriethylsilane and with diethoxydimethylsilane. Based on the results obtained here and of the kinetic studies mentioned above, the reaction mechanism previously proposed has been confirmed.

Results and Discussion

Studies on Alkoxy-Alkoxy Exchange Equilibria of Alkoxysianes. The following two iodine-catalyzed alcoholysis and three iodine monobromide-catalyzed redistribution equilibria of alkylalkoxysilanes were examined at 20 °C, and the equilibrium constants K were evaluated from the equilibrium compositions determined by gas chromatographic analysis.

No. 1

$$Et_3SiOBu^n+Bu^sOH \rightleftarrows Et_3SiOBu^s+Bu^nOH \quad (I_2)$$

$$K=\{[Et_3SiOBu^s][Bu^nOH]\}/\{[Et_3SiOBu^n][Bu^sOH]\}$$

No. 2

$$Me_2Si(OPr^n)_2+2Bu^nOH \rightleftarrows Me_2Si(OBu^n)_2+2Pr^nOH \quad (I_2)$$

$$K_1=\{[Me_2Si(OPr^n)(OBu^n)][Pr^nOH]\}/\{[Me_2Si(OPr^n)_2][Bu^nOH]\}$$

$$K_2=\{[Me_2Si(OBu^n)_2][Pr^nOH]\}/\{[Me_2Si(OPr^n)(OBu^n)][Bu^nOH]\}$$

No. 3

$$Me_2Si(OEt)_2+Me_2Si(OPr^n)_2 \rightleftarrows 2Me_2Si(OEt)(OPr^n) \quad (IBr, \text{ in hexane solution})$$

$$K=[Me_2Si(OEt)(OPr^n)]^2/\{[Me_2Si(OEt)_2][Me_2Si(OPr^n)_2]\}$$

Nos. 4 and 5

$$R_2Si(OEt)_2+Et_3SiOR' \rightleftarrows R_2Si(OEt)(OR')+Et_3SiOEt$$

$$R_2Si(OEt)(OR')+Et_3SiOR' \rightleftarrows R_2Si(OR')_2+Et_3SiOEt \quad (IBr)$$

$$R_2Si(OEt)_2+R_2Si(OR')_2 \rightleftarrows 2R_2Si(OEt)(OR')$$

$$K_1=\{[R_2Si(OEt)(OR')][Et_3SiOEt]\}/\{[R_2Si(OEt)_2][Et_3SiOR']\}$$

$$K_2=\{[R_2Si(OR')_2][Et_3SiOEt]\}/\{[R_2Si(OEt)(OR')][Et_3SiOR']\}$$

$$K_3=[R_2Si(OEt)(OR')]^2/\{[R_2Si(OEt)_2][R_2Si(OR')_2]\}$$

R=Et, R'=Pr^n (No. 4); R=Me, R'=Bu^n (No. 5)

In each of the Nos. 1, 2, and 3 reactions, equilibrium was approached from both directions. As for reaction No. 4 and 5, however, the following four processes were examined (A, B, C, and D-series).

A-series $R_2Si(OEt)_2+Et_3SiOR' \longrightarrow$
B-series $R_2Si(OEt)(OR')+Et_3SiOEt \longrightarrow$
C-series $R_2Si(OEt)(OR')+Et_3SiOR' \longrightarrow$
D-series $R_2Si(OR')_2+Et_3SiOEt \longrightarrow$

The results are summarized in Table 1.

Each reaction reached equilibrium within several hours at 20 °C without formation of any by-products, and equilibrium constants obtained from both directions agreed well with each other.

Catalytic Action of Iodine or Iodine Monobromide and of Conventional Catalysts. Various acids and bases have so far been used to promote alkoxy-alkoxy exchange reactions. As acid catalysts, *p*-toluenesulfonic acid[8,9] and others[10-14] are employed, while base catalysts such as sodium or sodium alkoxides[8,10,15-20] are most frequently utilized.

Catalyses of such acids and bases were examined by tracing the following reaction by means of gas-liquid partition chromatography (GLC). $Et_3SiOBu^n+Bu^sOH \rightleftarrows Et_3SiOBu^s+Bu^nOH$

Sodium exhibited little activity to this alcoholysis at ordinary temperature and reflux was required to cause the reaction to proceed.

A sample of one hour heating indicated little progress of the reaction, while a sample of thirty hours heating contained larger quantities of the products, along with fairly large amounts of impurities, especially the condensate $(Et_3Si)_2O$.

In general, acids promote alcoholysis more significantly than bases, but they also accelerate the condensation of alkoxysilanes markedly, if water coexists even slightly.[21,22] For example, *p*-toluenesulfonic acid (monohydrate) promoted the reaction appreciably at ordinary temperature, but a fair amount of condensed compound and other impurities were always formed. Trifluoroacetic acid[14] accelerated the reaction remarkably, but even in this case the concentration of the condensed compound increased with the lapse of time.

Halogen and interhalogen compounds such as iodine and iodine monobromide are favorable catalysts as mentioned above. Iodine monobromide is more active than iodine, and is well suited for promotion of the redistribution reactions and the alcoholyses associated with tertiary alcohols. Iodine is conveniently used in other alcoholyses.

Consequently, they are especially favorable catalysts for the quantitative work on the alkoxy-alkoxy exchange reactions of alkoxysilanes.

Absorption Spectra of Iodine or Iodine Monobromide Solutions in Alkoxysilanes or Disiloxanes. Since iodine and iodine monobromide exhibit excellent catalytic action in the present reactions, it is expected that specific interactions must occur between these catalysts and the alkoxysilanes.

Iodine and iodine monobromide appear to form CT-complexes with alkoxysilanes, and it can reasonably be assumed that these CT-complexes facilitate the reactions.

However little is known concerning the formation of such molecular complexes, except for the following spectroscopic study on the solvation of iodine. A solution of iodine in octamethylcyclotetrasiloxane $(Me_2SiO)_4$ is reddish violet, and the absorption maximum λ_{max} is observed at 518 nm. A solution in tetraethoxysilane is brown, having the λ_{max} at 475 nm.[23] This blue shift in the absorption spectrum may be attributed to the formation of a CT-complex in the latter solution.[28]

Iodine or iodine monobromide was dissolved in various alkoxysilanes and disiloxanes, and the λ_{max} values of these solutions were determined in order to see if CT-complexes were formed.

Table 1. Alcoholysis and Redistribution Equilibrium Constants of Alkylalkoxysilanes at 20 °C

Reaction system	Equilibrium constant				
	Forward reaction	Reverse reaction			Mean value
No. 1	K =0.45±0.02	0.44±0.02			0.45±0.02
No. 2	K_1=2.05±0.01	2.04±0.03			2.04±0.02
	K_2=0.48±0.01	0.47±0.01			0.48±0.01
No. 3	K = 4.1±0.1	4.0±0.1			4.0±0.1
	Equilibrium constant				
	A-series	B-series	C-series	D-series	Mean value
No. 4	K_1=1.90±0.02	1.92±0.01	1.90±0.01	1.90±0.01	1.91±0.02
	K_2=0.48±0.01	0.48±0.01	0.49±0.01	0.48±0.01	0.48±0.01
	K_3= 4.0±0.1	4.0±0.1	3.9±0.1	3.9±0.1	4.0±0.1
No. 5	K_1=1.90±0.02	1.91±0.02	1.90±0.06	1.89±0.01	1.90±0.02
	K_2=0.49±0.01	0.50±0.01	0.49±0.01	0.49±0.01	0.49±0.01
	K_3= 3.9±0.1	3.8±0.1	3.9±0.1	3.9±0.1	3.9±0.01

Absorption spectra of four disiloxane solutions of iodine were measured, and the absorption maxima were observed as follows.

$(Me_3Si)_2O$: 517—518 nm

$(Me_2EtSi)_2O$, $(MeEt_2Si)_2O$, $(Et_3Si)_2O$: 520 nm

The solutions are reddish violet and the λ_{max} values are around 520 nm similarly to the value in $(Me_2SiO)_4$ solution. A linear plot passing through the origin was always found between the absorbance at λ_{max} and iodine concentration in each solution, suggesting no interaction between iodine and disiloxane.

The λ_{max} in the visible region of the iodine or iodine monobromide spectrum in non-polar solvents is around 520 nm (I_2) or 490—500 nm (IBr). On the other hand, the λ_{max} values of alkoxysilane solutions were at 474—500 nm (I_2) or 425—455 nm (IBr), indicating blue shifts, and new peaks were also observed in the ultraviolet region. These results prove the formation of CT-complexes between iodine or iodine monobromide and alkoxysilanes.

The observed absorption maxima are given in Table 2.

In general, the peaks in the visible region are gently sloping, and some peaks are shifted a little with change of concentration.

Table 2. Wavelength of Absorption Peaks Observed on the Solutions of Iodine or Iodine Monobromide in Alkoxysilanes (λ_{max}/nm in ultraviolet and visible regions)

Alkoxysilane	λ_{max}/nm (I_2 solution)		λ_{max}/nm (IBr solution)	
	UV	Visible	UV	Visible
$Me_2Si(OEt)_2$	228	474	229	428
$Me_2Si(OEt)(Opr^n)$	243	474	244	428
$Me_2Si(OPr^n)_2$	233	478	238	428
$Me_2Si(OEt)(OBu^n)$	228	475	234	428
$Me_2Si(OBu^n)_2$	225	475	225	430
$Me_2Si(OEt)(OBu^s)$	230	482	223	430
$Me_2Si(OBu^s)_2$	237	492	218	436
$Me_2Si(OEt)(OBu^i)$	238	482	229	429
$Me_2Si(OBu^i)_2$	240	475	230	435
Et_3SiOEt	238	475	228	425
Et_3SiOPr^n	238	490	226	450
Et_3SiOBu^n	229	495	224	425
Et_3SiOBu^s	233	498	225	445
Et_3SiOBu^i	238	490	233	455

Formation Constants of Iodine-Ethoxytriethylsilane and Iodine-Diethoxydimethylsilane Complexes. As iodine-alkoxysilane complexes have absorption maxima at about 262 nm in carbon tetrachloride solutions, as shown in Fig. 1 and 2, the absorbances were measured at several wavelengths around the λ_{max} at about 22 °C.

Formation constants K_f were evaluated by employing the approximate equation developed by Ketelaar et al.[25]

$$C_I/(A-A_0) = 1/\{(\varepsilon_C-\varepsilon_I)K_f \cdot C_D\} + 1/(\varepsilon_C-\varepsilon_I)$$

where

A : Observed absorbance of the sample solution.
A_0 : Absorbance of I_2-CCl_4 solution.
C_I : Initial concentration of iodine.
C_D : Initial concentration of the alkoxysilane.
ε_C : Molar extinction coefficient of the complex.
ε_I : Molar extinction coefficient of iodine.

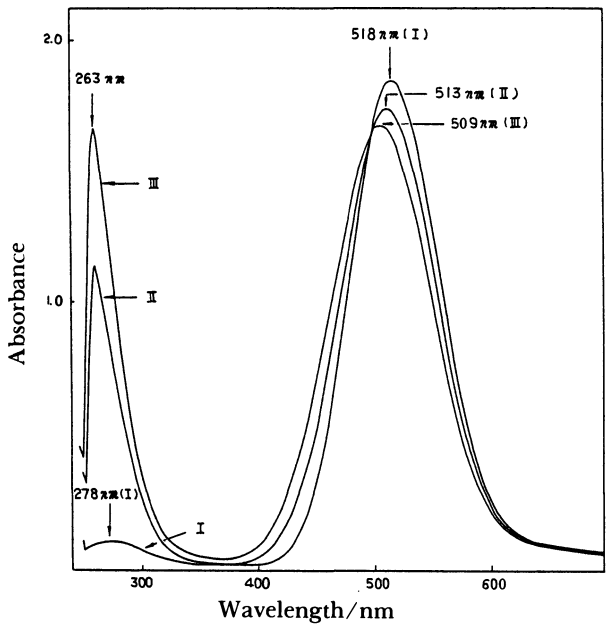

Fig. 1. The absorption spectra of the solutions I, II, III. I: iodine in carbon tetrachloride, II, III: ethoxytriethylsilane and iodine in carbon tetrachloride, $[I_2]=2\times10^{-3}$ mol dm^{-3}, $[Et_3SiOEt]=0.57$ (II), 1.01 (III) mol dm^{-3}.

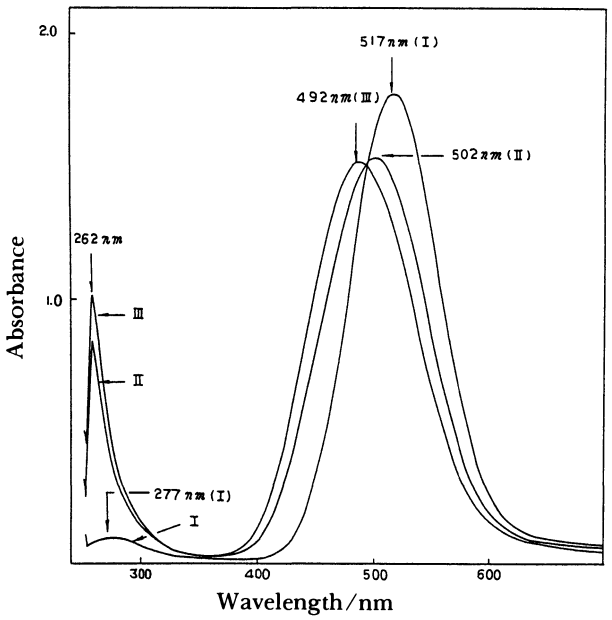

Fig. 2. The absorption spectra of the solutions I, II, III. I: iodine in carbon tetrachloride, II, III: diethoxydimethylsilane and iodine in carbon tetrachloride, $[I_2]=2\times10^{-3}$ mol dm^{-3}, $[Me_2Si(OEt)_2]=1.13$ (II), 2.10 (III) mol dm^{-3}.

This equation is derived with the approximation $C_D - C_C \fallingdotseq C_D$, as the complex concentration in which C_C is negligibly small compared to C_D under the operating conditions of $C_D \gg C_I$. The conditions of the present experiments satisfy the above approximation, because C_D/C_I is 50—200 (I_2-Et_3SiOEt-CCl_4 solutions) or 80—200 (I_2-$Me_2Si(OEt)_2$-CCl_4 solutions).

Typical examples of the results are illustrated in Fig. 3, and the formation constant of each complex was evaluated as follows.

K_f=0.55±0.01

(I_2-Et_3SiOEt complex in CCl_4 solutions).

K_f=0.61±0.02

(I_2-$Me_2Si(OEt)_2$ complex in CCl_4 solutions).

These are intermediate values between K_f=0.92 (20 °C) of iodine-ethanol complex in heptane solution[6] and K_f=0.176 (25 °C) of iodine-benzene complex in carbon tetrachloride solution.[26]

An alkoxysilane acts as a n-donor toward iodine, but the stability of this CT-complex seems to be lower than the iodine-ethanol complex, because of the smaller polarity of alkoxysilane than that of ethanol. This complex appears to be more stable than the iodine complex of benzene which is a π-donor. Consequently, the formation constants observed here may be regarded as reasonable.

Reconsideration of the Reaction Mechanism

The catalytic action of iodine or iodine monobromide was interpreted by a mechanism which involves a four-centered transition state containing a catalyst-alkoxysilane or alcohol CT-complex as an intermediate, as previously proposed.[1,2]

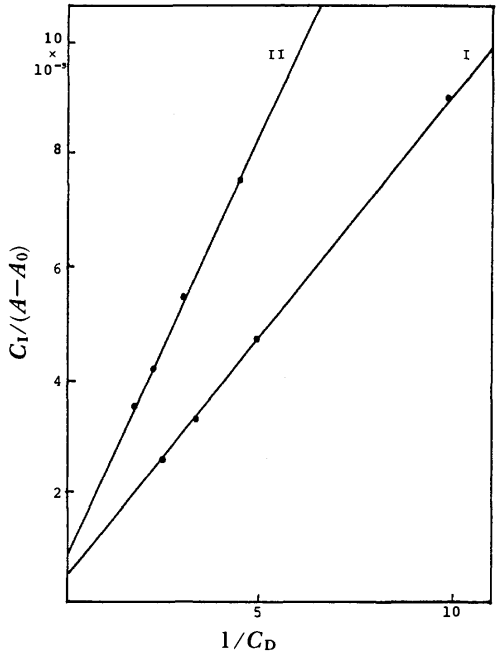

Fig. 3. Application to the Ketelaar's equation. Typical examples of plots of $C_I/(A-A_0)$ vs. $1/C_D$. I: I_2-Et_3SiOEt complex K_f=0.55, II: I_2-$Me_2Si(OEt)_2$ complex K_f=0.61.

Based on the results of the present spectroscopic work and the previously reported kinetic study on the alcoholysis,[7] together with the extensive work on the alkoxy-alkoxy exchange equilibria,[1,2] this mechanism is considered afresh.

Iodine and iodine monobromide promote both the alcoholysis and redistribution reaction of alkoxysilanes, with the latter catalyst being the more active. Therefore, it is proposed that in such a mechanism iodine and iodine monobromide promote both reactions in a similar manner, unlike the conventional mechanisms of base- or acid-catalyzed alcoholyses which can not apply to the redistribution reactions.

The mechanism should also satisfy the following requirements together with the above essential need.

(a) Iodine monobromide is more active than iodine.

(b) Alcoholyses proceed more rapidly than redistribution reactions in the presence of these catalysts.

(c) The reaction would be a bimolecular process, because the reaction is first order in both components at a constant catalyst concentration.

(d) The mechanism must proceed by a pathway via the transition state containing a catalyst molecule, as the reaction rate is first order with respect to the catalyst.

(e) The transition state should be of ionic character, because the rate constants of the alcoholysis increase with increasing alcohol contents, that is, with increasing polarity of the reaction mixture.

(f) The polarized transition state is also inferred from the large lowering of the activation entropy.

(g) Since alcohols as well as alkoxysilanes can form CT-complexes with iodine or iodine monobromide, such complexes should be used to form the transition state.

In regard to redistribution reactions among alkoxysilanes, no mechanism has been reported, but some mechanisms concerning the reactions with alkylsilanes or halosilanes or the like are reported in the literature. A mechanism involving a four-centered transition state has been proposed by Russell for the disproportionation of ethyltrimethylsilane catalyzed by aluminum bromide.[27] He concluded such a transition state with ionic character to be most favorable, based on arguments against other proposals. The present alcoholyses and redistribution reactions seem to be favorably interpreted by a mechanism analogous to this.

Iodine and iodine monobromide form charge-transfer complexes with alkoxysilanes as described above. A CT-complex is usually represented as a resonance hybrid of a no-bond form and a dative bond form. The dative bond forms of iodine or iodine monobromide-alkoxysilanes are regarded as $[(C_2H_5)_3SiOR\cdots I]^+I^-$ and $[(CH_3)_2Si(OR)_2\cdots I]^+ Br^-$, etc.

Since these CT-complexes are apparently of ionic character, and the silicon-alkoxy bond is considerably polar compared with the silicon-alkyl bond, the reaction systems involving alkoxysilanes can be shifted more smoothly.

The formation of such transition states will be followed by cleavage of a Si–O bond and not of a C–O bond, in a similar manner to the case of the acid-catalyzed redistribution between optically active di-*s*-butoxydimethylsilane and diethoxydimethylsilane.[9]

The following reaction mechanism may be satisfactorily assumed for the iodine monobromide-catalyzed redistribution reactions among dialkoxydimethylsilanes.

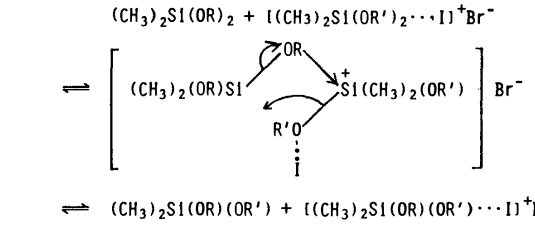

Iodine appears to form a complex with ethanol more readily than with alkoxysilanes, since the formation constants K_f of the iodine-ethanol complex in heptane solution is 0.92 (24 °C),[6] while the observed K_f values of iodine-ethoxytriethylsilane and -diethoxydimethylsilane complexes are 0.55 and 0.61, respectively. In addition, alkoxysilane-alcohol complexing has also been suggested.[28]

Consequently, the four-centered transition state can be more favorably realized in the alcoholysis of alkoxysilanes than in the redistribution reaction. Thus the reaction mechanism of the alcoholysis of alkoxytriethylsilane can be proposed as follows.

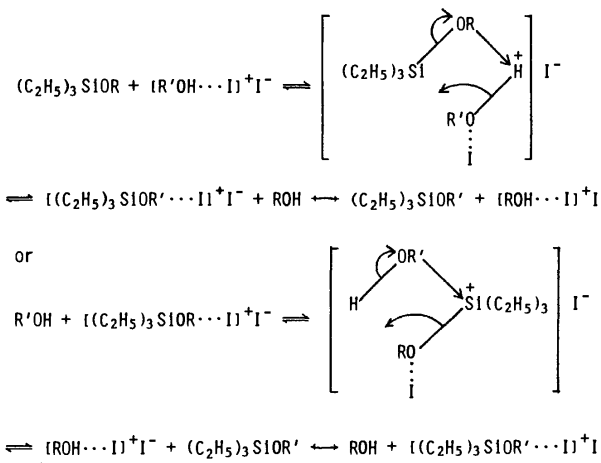

The redistribution reaction as well as the alcoholysis can be satisfactorily interpreted by an identical reaction mechanism involving a four-centered transition state, which meets the requirements as described above.

Experimental

Reagents. Ethoxytriethylsilane, diethoxydiethylsilane, triethoxyethylsilane, and ethoxytrimethylsilane were prepared by the reactions of tetraethoxysilane with ethyl- or methylmagnesium bromide.

Diethoxydimethylsilane was prepared by the reaction of octamethylcyclotetrasiloxane with tetraethoxysilane in the presence of potassium hydroxide.[29]

Other alkoxytriethylsilanes, dialkoxydiethylsilanes and dialkoxydimethylsilanes were prepared by iodine-catalyzed alcoholysis of the above ethoxysilanes.

Four disiloxanes used for the spectroscopic work were synthesized by condensation of the corresponding trialkylethoxysilanes.

The crude products were purified by repeated fractional distillation at atmospheric or reduced pressure.

Alcohols, iodine and iodine monobromide were purified by methods similar to those previously reported.[1,2]

Analysis. Analyses of the reaction mixtures were performed by GLC using a Shimadzu model GC-4B gas chromatograph with a thermal conductivity detector. The stationary phases of the packings used in these GLC analyses were PEG 1000 (Reaction No. 1, Table 1), PEG 4000 (Nos. 2 and 3), PEG 6000 (No. 4) and Shinchrom E-71 (No. 5). PEG 6000 was also employed in examining the catalytic actions of the conventional catalysts.

General Procedure. The equilibrium constants of the various exchange reactions were determined by methods similar to those previously reported.[1,2] The compositions of the reaction mixtures were as follows.

Nos. 1, 2 [Alkoxysilane]: [Alcohol]≒1 : 3—6; [I_2]<0.1 mol%
No. 3 [$Me_2Si(OEt)_2$]: [$Me_2Si(OPr^n)_2$]: [C_6H_{14}]≒1 : 1 : 16; [$Me_2Si(OEt)(OPr^n)$]: [C_6H_{14}]≒2 : 16; [IBr]=0.03—0.4 mol%
Nos. 4, 5 [dialkoxydialkylsilane]: [Alkoxytriethylsilane] ≒1 : 1 or 1 : 2; [IBr]=0.3—1 mol%

The compositions of the reaction mixtures used in examining the catalytic actions of the conventional catalysts were approximately as follows. Et_3SiOBu: 0.013 mol; BuOH: 0.05 mol; Na: 0.01 mol, or acids: 10^{-3}—10^{-4} mol.

Spectrophotometric Measurements. The absorption spectra were measured with a Shimadzu model UV-200 double-beam spectrophotometer, using stoppered silica cells with a path length of 10 mm at 20—22 °C.

The compositions of the sample solutions for determining the formation constants of CT-complexes were as follows.

I_2–Et_3SiOEt–CCl_4 solutions
C_I (Iodine concentration)≒2×10^{-3} mol dm^{-3}
C_D (Alkoxysilane concentration)≒0.1, 0.2, 0.3, 0.4 mol dm^{-3}

I_2–$Me_2Si(OEt)_2$–CCl_4 solutions
C_I≒2.8×10^{-3} mol dm^{-3}
C_D≒0.22, 0.34, 0.45, 0.56 mol dm^{-3}

References

1) T. Ibaraki and K. Ito, *Bull. Chem. Soc. Jpn.*, **54**, 3234 (1981).

2) K. Ito and T. Ibaraki, *Bull. Chem. Soc. Jpn.*, **55**, 2973 (1982); **56**, 295 (1983).

3) K. Moedritzer and J. R. Van Wazer, *Inorg. Chem.*, **3**, 268 (1964).

4) J. R. Van Wazer and K. Moedritzer, *J. Inorg. Nucl.*

Chem., **26**, 737 (1964).
5) D. N. Dolan and G. Nickless, *J. Chromatog.*, **37**, 1, (1964).
6) L. M. Julien, W. E. Bennett, and W. B. Person, *J. Am. Chem. Soc.*, **91**, 6915 (1969).
7) K. Ito and T. Ibaraki, *Int. J. Chem. Kinet.*, **19**, 841 (1987).
8) B. Helferich und W. Reimann, *Chem. Ber.*, **80**, 163 (1946).
9) R. H. Krieble and C. A. Burkhard, *J. Am. Chem. Soc.*, **69**, 2689 (1947).
10) D. F. Peppard, W. G. Brown, and W. C. Johnson, *J. Am. Chem. Soc.*, **68**, 73, 77 (1969).
11) H. Gilman and G. N. R. Smart, *J. Org. Chem.*, **19**, 441 (1954).
12) M. G. Voronkov and B. N. Dolgov, *Bull. Acad. Sci. USSR., Div. Chem. Sci.*, **1957**, 1153.
13) M. G. Voronkov and L. A. Zhagata, *J. Gen. Chem. USSR.*, **37**, 2630 (1967).
14) G. Tschernko und H. Hamann, *Z. Chem. (DDR)*, **18**, 64 (1978).
15) J. L. Speier, *J. Am. Chem. Soc.*, **74**, 1003 (1952).
16) E. Larsson, *Chem. Ber.*, **86**, 1382 (1953).
17) E. Larsson, *Acta Chem. Scand.*, **8**, 898 (1954).
18) B. N. Dolgov, N. P. Kharitonov, and M. G. Voronkov, *J. Gen. Chem. USSR.*, **24**, 1169 (1954).
19) L. H. Sommer and H. Fujimoto, *J. Am. Chem. Soc.*, **90**, 982 (1968).
20) H. G. Emblem and K. Hargreaves, *J. Inorg. Nucl. Chem.*, **30**, 721 (1968).
21) P. A. DiGiorgio, W. A. Strong, L. H. Sommer, and F. C. Whitmore, *J. Am. Chem. Soc.*, **68**, 1380 (1946).
22) W. H. Daudt and J. F. Hyde, *J. Am. Chem. Soc.*, **74**, 386 (1952).
23) K. Shinoda and J. H. Hildebrand, *J. Phys. Chem.*, **61**, 789 (1957).
24) L. J. Andrews and R. M. Keefer, *Adv. Inorg. Chem. Radiochem.*, **3**, 91 (1952).
25) J. A. A. Ketelaar, C. Van de Stolpe, A. Goudsmit, and W. Dzcubas, *Recl. Trav. Chim. Pays-Bas*, **71**, 1104 (1952).
26) I. D. Kunsts, Jr., F. P. Gasparro, M. D. Johnston, Jr., and R. P. Taylor, *J. Am. Chem. Soc.*, **90**, 4778 (1968).
27) G. A. Russell, *J. Am. Chem. Soc.*, **81**, 4815 (1959).
28) J. Nagy, S. Ferenczi-Gresz, F. Farkas, und T. Gábor, *Z. Anorg. All. Chem.*, **377**, 328 (1970).
29) M. G. Voronkov, *J. Gen. Chem. USSR.*, **29**, 890 (1959).

A Novel Synthesis of (±)-Prostaglandin B_1 Methyl Ester

Hirokazu NAORA,* Takashi OHNUKI, and Asao NAKAMURA
Applied Research Dept., Central Laboratories, Ajinomoto Co., Inc., 1-1, Suzuki-cho, Kawasaki, Kanagawa 210
(Received January 8, 1988)

Five simple preparative methods of (±)-prostaglandin B_1 (PGB_1) methyl ester are described. All routes were started from a common intermediate, 7-(2-hydroxy-5-oxo-1-cyclopentenyl)heptanoic acid derived from cyclooctanone via two steps. The key reaction of these routes is a palladium-catalyzed vinylation. The methods provided other PGB_1 congeners and are applicable to synthesize 11-functionalized PG systems.

PGB_x[1] is an oligomeric mixture of prostaglandin B series, and has unique biological activities which are quite different from the ordinary prostaglandin activities. For example, it conserves oxidative phosphorylation in rat liver mitochondria in vitro and reverses the damaging effect of experimentally induced ischemia in heart and brain of monkey and dog in vivo.[1] 15-DehydroPGB_1 methyl ester (**3a**) is usually used as a monomer for the synthesis of PGB_x. Instead of **3a**, PGB_1 methyl ester (**1a**), 13, 14-cisPGB_1 methyl ester (**2**), and 13,14-dehydroPGB_1 methyl ester (**4a**) can also be used (Scheme 1). To elucidate structures and biological activities of the oligomers, it is necessary to prepare various PGB_x from some closely related monomers. Although the total syntheses of PGB_1 or its equivalents have already been known,[2-4] multi-step reactions and severe conditions are required in most of the cases. For the study of new biologically active features of PGB_x, it is important to develop a novel synthetic method by which enough amount of PGB_1 and the starting materials for PGB_x can be obtained in a few steps and in simple procedures.

As the preliminary investigation of a new short synthetic sequence to prepare (±)-PGB_1 methyl ester and its related compounds, we have already reported synthesis of 15-dehydroPGB_1 methyl ester (**3a**) via four steps.[5] We have also reported the synthetic methods to obtain the key intermediate **7** from commercially available cyclooctanone via two steps and to derive other synthons for prostaglandins from **7** (Scheme 2).[6]

In this report, we describe the facile synthetic method to form a sort of PGB_1 methyl esters from the key intermediate **8** and its application to a 11-functionalized PG analogue in detail (Schemes 3 and 4).

The ω-chain moieties of PGB_1 methyl esters were successfully introduced to the synthetic intermediates **8** by applying the palladium-catalyzed vinylation reaction.[7] Coupling reaction of methyl 7-(2-bromo-5-oxo-1-cyclopentenyl)heptanoate (**8**) with (±)-3-(*t*-butyldimethylsiloxy)-1-octene (**12b**) gave (±)-methyl 15-(*t*-butyldimethylsiloxy)-9-oxoprost-8(12),13-dienoate {(±)-15-(*t*-butyldimethylsiloxy)PGB_1 methyl ester} (**1b**) in a 92% yield. The reaction was catalyzed by a few molar percent of the mixture of palladium diacetate and triphenylphosphine (1: 2 mole ratio). Triethylamine was also added for trapping hydrogen bromide. Desilylation of **1b** with tetrabutylammonium fluoride gave (±)-PGB_1 methyl ester (**1a**) in a 96% yield.

Coupling reaction of methyl 7-(2-bromo-5-oxo-1-cyclopentenyl)heptanoate (**8**) with 1-octen-3-one (**12c**) gave 15-dehydroPGB_1 methyl ester (**3a**) in an 80% yield

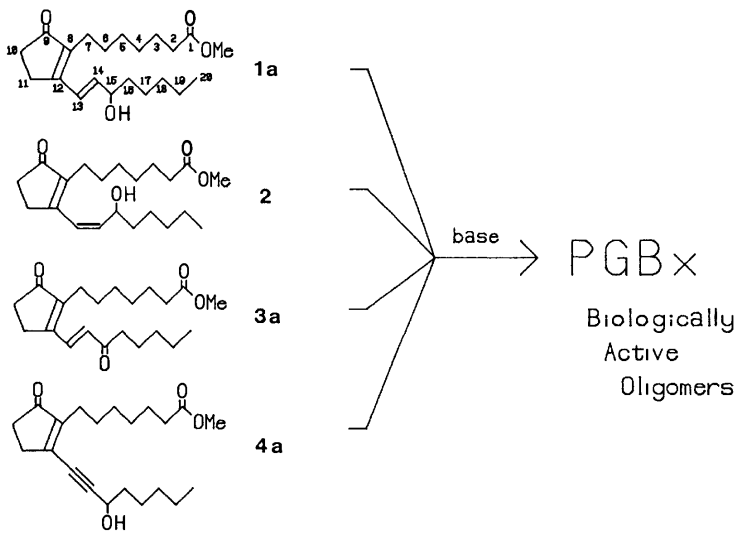

Scheme 1.

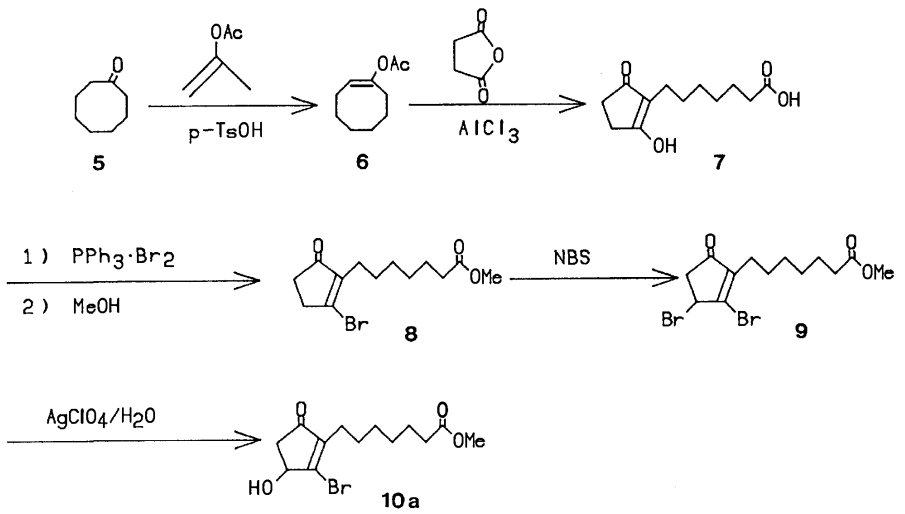

Scheme 2.

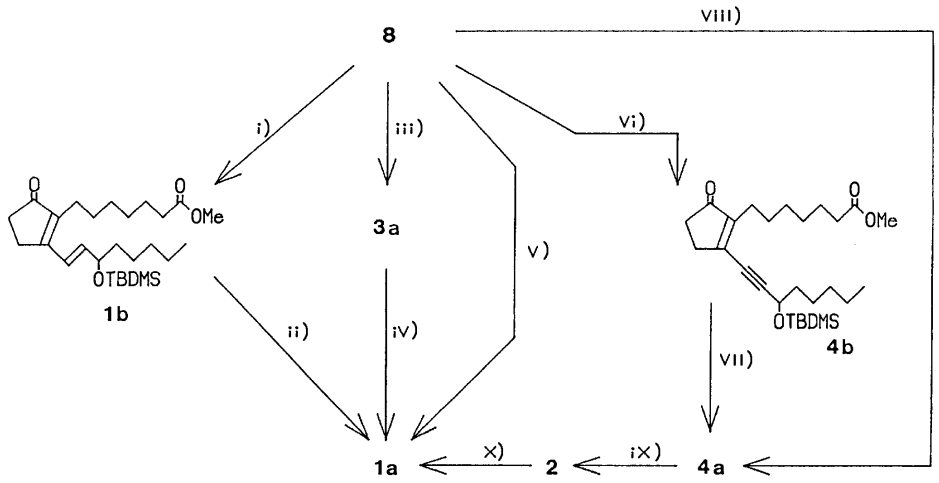

Scheme. 3. i)[a] (±)-3-(*t*-Butyldimethylsiloxy)-1-octene (**12b**). ii) Bu_4NF/THF. iii)[a] 1-Octen-3-one (**12c**). iv) $NaBH_4/CH_3OH$. v)[a] (±)-1-Octen-3-ol (**12a**). vi)[a] (±)-3-(*t*-Butyldimethylsiloxy)-1-octyne (**13b**). vii) Bu_4NF/THF. viii)[a] (±)-1-Octyn-3-ol (**13a**). ix) H_2, Lindlar catalyst/CH_3CH_2OH. x) I_2/C_6H_{12}, $CHCl_3$. a) $Pd(OAc)_2 \cdot 2PPh_3$ and Et_3N were used.

and 15-dehydro-13,14-dihydroPGB$_1$ methyl ester (**3b**) as a by-product in a 3% yield. Compound **3a** was easily converted to **1a** by the reduction with sodium borohydride in a 78% yield.

(±)-PGB$_1$ methyl ester (**1a**) could be obtained by the coupling reaction of **8** and (±)-1-octen-3-ol (**12a**) directly in a 42% yield. Under the reaction conditions, the double-bond isomer [15-dehydro-13,14-dihydro-PGB$_1$ methyl ester (**3b**)] and the oxidized compound [15-dehydroPGB$_1$ methyl ester (**3a**)] were obtained in 24 and 11% yields, respectively.

(±)-Methyl 15-(*t*-butyldimethylsiloxy)-9-oxoprost-8(12)-en-13-ynoate {(±)-15-(*t*-butyldimethylsiloxy)-13,14-dehydroPGB$_1$ methyl ester} (**4b**) was obtained from methyl 7-(2-bromo-5-oxo-1-cyclopentenyl)heptanoate (**8**) and (±)-3-(*t*-butyldimethylsiloxy)-1-octyne (**13b**) in a 50% yield (69% based on the consumed **8**). Desilylation of **4b** with tetrabutylammonium fluoride gave (±)-13,14-dehydroPGB$_1$ methyl ester (**4a**) in a 97% yield.

(±)-13,14-DehydroPGB$_1$ methyl ester (**4a**) was also obtained directly from **8** and (±)-1-octyn-3-ol (**13a**) in a 33% yield. In this case, 15-dehydroPGB$_1$ methyl ester (**3a**) was obtained in a 10% yield. The α,β-enone **3a** is an isomer of the β,γ-ynol **4a**.

Hydrogenolysis of (±)-13,14-dehydroPGB$_1$ methyl ester (**4a**) over Lindlar catalyst gave (±)-13,14-cisPGB$_1$ methyl ester (**2**) in an 89% yield. Any other isomeric compounds, such as (±)-8,12-dihydro-, (±)-13,14-dihydro-, and (±)-13,14-transPGB$_1$ methyl ester, were not detected in this reaction.

Double-bond isomerization of **2** was achieved with iodine in a 98% yield. That is, (±)-13,14-cisPGB$_1$ methyl ester (**2**) was converted to (±)-PGB$_1$ methyl

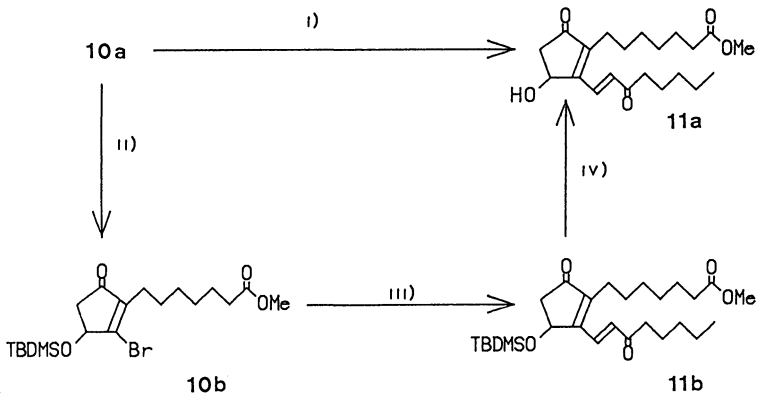

Scheme. 4. i)[a] 1-Octen-3-one (**12c**). ii) TBDMSCl, Et_3N, DMAP/CH_2Cl_2. iii)[a] 1-Octen-3-one (**12c**). iv) Bu_4NF/THF. a) $Pd(OAc)_2 \cdot 2PPh_3$ and Et_3N were used.

ester (**1a**) by treating with iodine in dark at 40 °C for 13 h. In this case, equilibrium was completely inclined to the trans isomer.

The synthetic strategy described above was also extended to the 11-functionalized PG systems (Scheme 4).

Reaction of (±)-methyl 7-(2-bromo-3-hydroxy-5-oxo-1-cyclopentenyl)heptanoate (**10a**) with 1-octen-3-one (**12c**) gave directly (±)-15-dehydro-11-hydroxyPGB_1 methyl ester (**11a**) in a 15% yield. Reaction of (±)-methyl 7-[2-bromo-3-(*t*-butyldimethylsiloxy)-5-oxo-1-cyclopentenyl]heptanoate (**10b**), which was derived from **10a**, and 1-octen-3-one (**12c**) gave (±)-11-(*t*-butyldimethylsiloxy)-15-dehydroPGB_1 methyl ester (**11b**) in a 76% yield. Desilylation of **11b** with tetrabutylammonium fluoride gave (±)-15-dehydro-11-hydroxy-PGB_1 methyl ester (**11a**) in a 49% yield.

Experimental

Instrumentation. The ^1H NMR spectra were measured with a Varian EM-390 (90 MHz) spectrometer. The chemical shifts are expressed in parts per million (ppm) (δ) downfield from tetramethylsilane. The infrared spectra were obtained using a JASCO IR-810 Spectrometer. The low-resolution mass spectra (MS) and the high-resolution mass spectra (HRMS) were determined on a JEOL D-300 Mass Spectrometer. The boiling points are uncorrected.

Materials and Substances. 1-Octen-3-one (**12c**)[8] was obtained from (±)-1-octen-3-ol (**12a**) by the Jones' oxidation. (±)-3-(*t*-Butyldimethylsiloxy)-1-octene (**12b**)[9] and (±)-3-(*t*-butyldimethylsiloxy)-1-octyne (**13b**)[10] were obtained from (±)-1-octen-3-ol (**12a**) and (±)-1-octyn-3-ol (**13a**), respectively with *t*-butylchlorodimethylsilane. Solvents were dried over Zeolite A-3 or A-4 when necessary.

(±)-15-(*t*-Butyldimethylsiloxy)PGB_1 Methyl Ester (1b). A mixture of methyl 7-(2-bromo-5-oxo-1-cyclopentenyl)heptanoate [**8**; 119.5 mg (0.39 mmol)], (±)-3-(*t*-butyldimethylsiloxy)-1-octene [**12b**; 158.3 mg (0.65 mmol)], and triethylamine [72.0 mg (0.71 mmol)] with 8.5 mg of the palladium catalyst (a mixture of palladium diacetate and triphenylphosphine; 1 : 2 mole ratio) was heated to 100 °C in a reaction tube under Ar for 24 h. The reaction mixture was dissolved in 3 ml of ether and insoluble components were filtered off. After evaporation, the reaction mixture was separated by a medium-pressure silica-gel column chromatography (LiChroprep Si 60), and 167. 2 mg (92.0%) of **1b** was obtained. Starting material **8** (3.9 mg: 1.3%) was also recovered.

1b: ^1H NMR ($CDCl_3$) δ=6.69 (d, J=15 Hz, 1H), 6.13 (dd, J=15, 5.4 Hz, 1H), 4.25 (m, 1H), 3.55 (s, 3H), 2.1—2.7 (m, 8H), 1.15—1.75 (m, 16H), 0.90 (s, 9H), 0.75—1.0 (m, 3H), 0.06 (s, 3H) and 0.03 (s, 3H); IR (film) 2930, 2860, 1740, 1695, and 1640 cm^{-1}; Found: m/z 464.3340. Calcd for $C_{27}H_{48}O_4Si$: M, 464.3323.

15-DehydroPGB$_1$ Methyl Ester (3a).[2] A mixture of methyl 7-(2-bromo-5-oxo-1-cyclopentenyl)heptanoate [**8**; 146.3 mg (0.48 mmol)], 1-octen-3-one [**12c**; 142.7 mg (1.15 mmol)], and triethylamine [156.4 mg (1.55 mmol)] with 5.6 mg of the palladium catalyst was heated to 100 °C in a reaction tube under Ar for 24 h. The reaction mixture was dissolved in 3 ml of ether and insoluble components were filtered off. After evaporation, separation with medium-pressure silica-gel column chromatography (LiChroprep Si 60) gave 133.0 mg (79.6%) of **3a** and 4.9 mg (2.6%) of 15-dehydro-13,14-dihydroPGB_1 methyl ester (**3b**).[3] Starting material **8** (9.8 mg: 6.7%) was also recovered.

3a: ^1H NMR ($CDCl_3$) δ=7.51 (d, J=16.5 Hz, 1H), 6.45 (d, J=16.5 Hz, 1H), 3.60 (s, 3H), 2.15—2.75 (m, 10H), 1.2—1.9 (m, 14H), and 0.90 (t, J=6 Hz, 3H); IR (film) 2930, 2850, 1735, 1705, and 1630 cm^{-1}.

3b: ^1H NMR ($CDCl_3$) δ=3.67 (s, 3H), 2.05—2.75 (m, 14H), 1.1—1.8 (m, 14H), and 0.89 (t, J=6.6 Hz, 3H); IR (film) 2930, 2860, 1740, 1720, 1700, and 1640 cm^{-1}.

(±)-15-(*t*-Butyldimethylsiloxy)-13,14-dehydroPGB_1 Methyl Ester (4b). A mixture of methyl 7-(2-bromo-5-oxo-1-cyclopentenyl)heptanoate [**8**; 304.7 mg (1.01 mmol)], (±)-3-(*t*-butyldimethylsiloxy)-1-octyne [**13b**; 264.2 mg (1.10 mmol)], and triethylamine [106.7 mg, (1.06 mmol)] with 37.5 mg of the palladium catalyst was heated to 100 °C in a reaction tube under Ar for 23 h. Ether (3 ml) was added and filtrated. By medium-pressure silica-gel column chromatography (LiChroprep Si 60), 230.1 mg (49.5%) of **4b** was afforded. Compound **8** (88.0 mg: 28.9%) was recovered.

4b: Bp 122 °C/0.15 mmHg (1 mmHg=133.322 Pa); ^1H NMR ($CDCl_3$) δ=4.5 (t, J=6 Hz, 1H), 3.6 (s, 3H), 2.2—2.6 (m, 8H), 1.2—1.9 (m, 16H), 0.93 (s, 9H), 0.8—0.95 (m, 3H), and

0.16 (s, 6H); IR (film) 2950, 2930, 2860, 1740, 1705, and 1615 cm^{-1}; Found: C, 69.97; H, 10.04%. Calcd for $C_{27}H_{46}O_4Si$: C, 70.08; H, 10.02%.

(±)-13,14-DehydroPGB$_1$ Methyl Ester (4a).[2,4] a) To a solution of 0.37 g (0.80 mmol) of **4b** in 20 ml of THF was added 2 ml of 1 M (1 M=1 mol dm^{-3}) tetrabutylammonium fluoride in THF. The reaction mixture was stirred at room temperature for 2 h. To the resultant mixture was added 20 ml of ether. The ethereal layer was washed with equal volumes of water twice and brine, dried over anhydrous magnesium sulfate. After medium-pressure silica-gel column chromatography (LiChroprep Si 60), 0.27 g (97%) of (±)-13,14-dehydroPGB$_1$ methyl ester (**4a**) was obtained.

b) A mixture of methyl 7-(2-bromo-5-oxo-1-cyclopentenyl)-heptanoate [**8**; 62.0 mg (0.20 mmol)], (±)-1-octyn-3-ol [**13a**; 39.9 mg (0.32 mmol)], and triethylamine [26.0 mg (0.26 mmol)] with 2.0 mg of palladium diacetate and 4.6 mg of triphenylphosphine was heated to 100 °C in a reaction tube under Ar for 5 h. Ether (3 ml) was added and filtrated. Separation with medium-pressure silica-gel column chromatography (LiChroprep Si 60) gave 23.5 mg (33.0%) of **4a** and 7.0 mg (10%) of 15-dehydroPGB$_1$ methyl ester (**3a**). Starting material **8** (1.9 mg: 3%) was also recovered.

4a: ^{1}H NMR ($CDCl_3$) δ=4.6 (t, J=6 Hz, 1H), 3.6 (s, 3H), 2.2—2.8 (m, 8H), 1.2—1.9 (m, 16H), and 0.9 (t, J=6 Hz, 3H); IR (film) 3400, 1735, 1700, 1600, 1435, and 1360 cm^{-1}.

(±)-13,14-cisPGB$_1$ Methyl Ester (2).[2,4] Hydrogenolysis of 0.50 g (1.4 mmol) of (±)-13,14-dehydroPGB$_1$ methyl ester (**4a**) was achieved over Lindlar catalyst[11] in ethanol under atmospheric pressure. The reaction mixture was filtered and after removal of ethanol, ether (30 ml) was added. The resultant solution was washed with 20 ml of 0.1 M HCl three times, 20 ml of water three times and brine, and dried. Removal of solvents gave 0.45 g (89%) of (±)-13,14-cisPGB$_1$ methyl ester (**2**).

2: ^{1}H NMR ($CDCl_3$) δ=6.38 (d, J=12 Hz, 1H), 5.75 (dd, J=12, 9 Hz, 1H), 4.6 (m, 1H), 3.6 (s, 3H), 2.6—2.85 (m, 2H), 2.1—2.5 (m, 6H), 1.2—1.8 (m, 16H), and 0.9 (t, J=6 Hz, 3H); IR (film) 3400, 1730, 1690, 1620, 1585, 1330, and 1260 cm^{-1}.

(±)-PGB$_1$ Methyl Ester (1a).[2-4] a) To a solution of 142.0 mg of **1b** in 20 ml of THF and 2 ml of water was added 1 ml of 1 M tetrabutylammonium fluoride/THF solution. The reaction mixture was stirred at room temperature for 7 days and poured into 30 ml of water. The reaction mixture was extracted with 100 ml and then 50 ml of ether. Combined organic layer was washed with 50 ml of water twice and dried. After evaporation, the mixture was separated with medium-pressure silica-gel column chromatography, and 102.7 mg (95.9%) of (±)-PGB$_1$ methyl ester (**1a**) was obtained.

b) A solution of 20 mg of sodium borohydride in dry methanol (2 ml) was added dropwise at 0 °C to a solution of 98.1 mg (0.28 mmol) of 15-dehydroPGB$_1$ methyl ester (**3a**) in methanol (3 ml). After stirring for 15 min at 0 °C, 0.5 ml of acetone was added. The reaction mixture was poured into 5 ml of water and extracted with 5 ml of ether three times. Combined ethereal layer was washed with equal volumes of water three times and brine, and dried. After evaporation, separation with medium-pressure silica-gel column chromatography (LiChroprep Si 60) gave 76.2 mg (78%) of (±)-PGB$_1$ methyl ester (**1a**).

c) A mixture of methyl 7-(2-bromo-5-oxo-1-cyclopentenyl)heptanoate [**8**; 83.3 mg (0.28 mmol)], (±)-1-octen-3-ol [**12a**; 47.3 mg (0.37 mmol)], and triethylamine [42.1 mg (0.42 mmol)] with 1.4 mg of palladium diacetate and 3.6 mg of triphenylphosphine was heated to 100°C in a reaction tube under Ar for 22 h. Ether (3 ml) was added and filtrated. The reaction mixture was separated with medium-pressure silica-gel column chromatography (LiChroprep Si 60), and 40.1 mg (41.7%) of **1a**, 10.3 mg (10.8%) of 15-dehydroPGB$_1$ methyl ester (**3a**), and 22.6 mg (23.5%) of 15-dehydro-13,14-dihydroPGB$_1$ methyl ester (**3b**) were obtained. Starting material **8** (12.0 mg: 14.4%) was also recovered.

d) To a solution of 0.42 g (1.2 mmol) of (±)-13,14-cisPGB$_1$ methyl ester (**2**) in 2 ml of a solvent (cyclohexane: chloroform=20: 1) was added 2 ml of iodine solution (0.5% w/v in the solvent described above) and allowed to stand in dark at 40 °C for 13 h. The reaction mixture was diluted with 20 ml of ether and washed with 10 ml of sodium thiosulfate three times and brine, and dried. Removal of solvents gave 0.41 g (98%) of (±)-PGB$_1$ methyl ester (**1a**).

1a: ^{1}H NMR ($CDCl_3$) δ=6.73 (d, J=16 Hz, 1H), 6.20 (dd, J=16.6 Hz, 1H), 4.3 (m, 1H), 3.6 (s, 3H), 2.5—2.7 (m, 2H), 2.2—2.5 (m, 6H), 1.2—1.7 (m, 16H), and 0.9 (t, J=6 Hz, 3H); IR (film) 3450, 1735, 1690, 1635, 1590, and 1370 cm^{-1}.

(±)-11-(*t*-Butyldimethylsiloxy)-15-dehydroPGB$_1$ Methyl Ester (11b). (±)-Methyl 7-(2-bromo-3-hydroxy-5-oxo-1-cyclopentenyl)heptanoate [**10a**: 0.50 g (1.6 mmol)] was silylated in dichloromethane by *t*-butylchlorodimethylsilane [0.69 g (4.6 mmol)] with triethylamine [0.51 g (5.1 mmol)] and 4-(dimethylamino)pyridine [40 mg (0.33 mmol)] to give (±)-methyl 7-[2-bromo-3-(*t*-butyldimethylsiloxy)-5-oxo-1-cyclopentenyl]heptanoate [**10b**; 0.62 g (91%)]; ^{1}H NMR ($CDCl_3$) δ=4.63 (dd, J=6, 3 Hz, 1H), 3.49 (s, 3H), 2.70 (dd, J=16.5, 6 Hz, 1H), 2.0—2.4 (m, 5H), 1.2—1.8 (m, 8H), 0.8 (s, 9H), 0.1 (s, 3H), and 0.06 (s, 3H); IR (film) 2950, 2940, 2860, 1740, 1720, and 1635 cm^{-1}; Found: m/z 377.0604, 375.0674. Calcd for $C_{15}H_{24}O_4BrSi$: M−C_4H_9, 377.0606, 375.0720. A mixture of (±)-methyl 7-[2-bromo-3-(*t*-butyldimethylsiloxy)-5-oxo-1-cyclopentenyl]heptanoate [**10b**; 439.6 mg (1.01 mmol)], 1-octen-3-one [**12c**; 143.6 mg (1.14 mmol)], and triethylamine [124.2 mg (1.23 mmol)] with 15.8 mg of the palladium catalyst was heated to 100 °C in a reaction tube under Ar for 80 h. Ether (3 ml) was added and filtrated. Separation by medium-pressure silica-gel column chromatography (LiChroprep Si 60) gave 370.0 mg (76.2%) of **11b**; ^{1}H NMR ($CDCl_3$) δ=7.45 (d, J=16.5 Hz, 1H), 6.78 (d, J=16.5 Hz, 1H), 5.11 (dd, J=3, 6 Hz, 1H), 3.71 (s, 3H), 2.0—2.9 (m, 8H), 1.2—1.9 (m, 14H), 1.0 (s, 9H), 0.9—1.1 (m), 0.33 (s, 3H), and 0.27 (s, 3H); IR (film) 2940, 2860, 1740, 1705, 1675, and 1590 cm^{-1}; MS m/z 478 (M^+), 447 (M−MeO), 421 (M−Bu+H), 389 (M−Bu−MeO); Found m/z 478.3132. Calcd for $C_{27}H_{46}O_5Si$: M, 478.3114.

(±)-15-Dehydro-11-hydroxyPGB$_1$ Methyl Ester (11a).[3] a) A mixture of (±)-methyl 7-(2-bromo-3-hydroxy-5-oxo-1-cyclopentenyl)heptanoate [**10a**; 75.8 mg (0.32 mmol)], (±)-1-octen-3-ol [**12a**; 42.4 mg (0.34 mmol)], and triethylamine [43.4 mg (0.43 mmol)] with 2.4 mg of the palladium catalyst was heated to 100 °C in a reaction tube under Ar for 48 h. Ether (3 ml) was added and filtrated. After purification with medium-pressure silica-gel column chromatography (LiChroprep Si 60), 13.2 mg (15.3%) of **11a** was obtained; ^{1}H NMR ($CDCl_3$) δ=7.39 (d, J=15 Hz, 1H), 6.89 (d, J=15 Hz, 1H), 5.05 (m, 1H), 3.60 (s, 3H), 2.15—3.0 (m, 8H), 1.1—1.9 (m, 14H), and 0.9 (t, J=6 Hz, 3H); IR (film) 3450, 2930, 2860, 1740, 1705, and 1590 cm^{-1}; MS m/z 364 (M^+), 346 (M−H_2O), 314 (M−H_2O−MeOH); Found: m/z 364.2239. Calcd for

$C_{21}H_{32}O_5$: M, 364.2247.

b) To a solution of 20.4 mg of (±)-11-(*t*-butyldimethylsiloxy)-15-dehydroPGB$_1$ methyl ester (**11b**) in 3 ml of THF was added 0.06 ml of 1 M tetrabutylammonium fluoride/THF solution, and the mixture was stirred at room temperature for 10 min. To the resultant mixture was added 10 ml of ether and water. The organic layer was washed with equal volumes of water and brine, and dried. After removal of solvents, silica-gel column chromatography gave 7.6 mg (50%) of (±)-15-dehydro-11-hydroxyPGB$_1$ methyl ester (**11a**).

References

1) B. D. Polis, E. Polis, and S. Kwong, *Proc. Natl. Acad. Sci. U. S. A.*, **76**, 1598 (1979); E. T. Angelakos, R. L. Riley, and B. D. Polis, *Physiol. Chem. Phys.*, **12**, 81 (1980); B. D. Polis and E. Polis, *ibid.*, **8**, 429 (1976); **11**, 3 (1979); B. D. Polis, S. Kwong, E. Polis, and G. L. Nelson, *ibid.*, **12**, 167 (1980); H. W. Shmuckler, S. F. Kwong, E. Polis, M. G. Zawryt, and E. Soffer, *ibid.*, **12**, 551 (1980).

2) B. D. Polis, S. Kwong, E. Polis, G. Nelson, and H. W. Shmuckler, *Physiol. Chem. Phys.*, **11**, 109 (1979).

3) M. Miyano, *J. Org. Chem.*, **35**, 2314 (1970).

4) J. Katsube and M. Matsui, *Agric. Biol. Chem.*, **33**, 1078 (1969); P. Collins, C. J. Jung, and R. Pappo, *Isr. J. Chem.*, **6**, 839 (1968); Y. Yura and J. Ide, *Chem. Pharm. Bull.*, **17**, 408 (1969).

5) H. Naora, T. Ohnuki, and A. Nakamura, *Chem. Lett.*, **1988**, 143.

6) H. Naora, T. Ohnuki, and A. Nakamura, *Bull. Chem. Soc. Jpn.*, **61**, 2401 (1988).

7) F. H. Heck, *Org. React.*, **27**, 345 (1982).

8) Beilstein IV, Band I, 3468.

9) Bp 76 °C/4 mmHg; ^{1}H NMR ($CDCl_3$) δ=5.73 (ddd, J=18, 12, 6 Hz, 1H), 4.8—5.2 (m, 2H), 4.0 (brq, J=4.5 Hz, 1H),1.2—1.7 (m, 8H), 0.9 (s, 9H), 0.85—1.15 (m, 3H), 0.07 (s, 3H), and 0.03 (s, 3H); IR (film) 2960, 2940, 2830, 1470, and 1460 cm^{-1}; Found: m/z 242.2091. Calcd for $C_{14}H_{30}OSi$: M, 242.2066.

10) Bp 77 °C/2.7 mmHg; ^{1}H NMR ($CDCl_3$) δ=4.40 (t of d, J=6, 3 Hz, 1H), 2.43 (d, J=3 Hz, 1H), 1.2—2.0 (m, 8H), 1.02 (s, 9H), 0.85—1.15 (m, 3H), 0.25 (s, 3H), and 0.20 (s, 3H): IR (film) 3320, 2960, 2940, 2860, 1750, 1475, and 1465 cm^{-1}; Found: m/z 240.1917. Calcd for $C_{14}H_{28}OSi$: M, 240.1910.

11) Lindlar catalyst was prepared from 35 mg of 5% palladium over barium sulfate and 18 mg of equinoline is 4 mol of methanol under hydrogen with stirring for 1.5 h.

 © 1988 The Chemical Society of Japan Bull. Chem. Soc. Jpn., 61, 2865—2873 (1988)

Direct Synthesis of Ethylene Glycol from Carbon Monoxide and Hydrogen by Use of Rhodium Catalyst. The Effect of Amine Promoters and Their Roles

Takashi MASUDA,* Kazuhisa MURATA, and Akio MATSUDA
National Chemical Laboratory for Industry, Higashi, Tsukuba, Ibaraki 305
(Received January 23, 1988)

The influence of addition of amines on the direct synthesis of ethylene glycol (EG) has been investigated using a rhodium catalyst under a high pressure (1800 kg cm^{-2}). The addition of amines improved the catalyst activity and selectivity for the EG formation and the stability of the catalyst. The addition of amines further resulted in glycerol (GL) formation. Optimum amine/rhodium ratios for the EG formation were 50—100 in tetrahydrofuran solvent with a low polarity and 1—3 in γ-butyrolactone solvent with a high polarity. Optimum N/Rh ratios and IR spectra of reaction solutions suggested that amine promoters serve to accelerate the formation of mononuclear Rh species from the catalyst precursor. It was also suggested that amines promote formation of a Rh-CH_2OH complex and insertion of CO. Bulky amines such as triisobutylamine, *N*-ethylcarbazole, triisopropanolamine, and tribenzylamine were especially effective promoters for the formation of EG and GL. The effectiveness of bulky amines as the promoter is discussed.

Attention is focused on the direct synthesis of ethylene glycol (EG) as one of researches on the synthesis of useful chemicals from synthesis gas.[1] Researchers of Union Carbide discovered that rhodium compounds are useful as catalyst precursors for the EG direct synthesis. Further, they have so far made many proposals on promoters for improving the activity and selectivity of Rh catalysts for the EG formation.[1] Amine is one of such promoters. Amines promote the formation of anionic rhodium complex as proton bases.[1b] Rhodium cluster anion has been postulated to be the catalyst or its immediate precursor for the EG formation.[1b] Kaplan[2] has proposed that ion pairing between rhodium complex anions and counterions, R_3NH^+, has an adverse effect on the catalytic activity for the EG formation. However, details on the role of amine promoters are still left unclear. Deluzarche et al.[3] have reported that rhodium-2-hydroxypyridine catalyst system shows an effect on the GL formation. Keim et al.[4] have reported that the catalytic activity of iridium for hydrogenation of carbon monoxide is largely enhanced by addition of amines. And amines act as inhibitors in cobalt-catalyzed hydrogenation of carbon monoxide.[4]

In this study, the influence of addition of amines on the direct synthesis of EG was investigated at a high pressure (1800 kg cm^{-2}) to elucidate the behavior of amine promoters. We describe some roles of the amine promoter and effects of bulky amines on the EG formation.

Experimental

All reagents were commercially available. All experiments were carried out in a 20 ml rocking batch reactor made of Inconel Alloy at a constant pressure. Oxygenated compounds, i.e., methyl alcohol (MeOH), ethylene glycol (EG), methyl formate (MF), ethyl alcohol (EtOH), and glycerol (GL), were formed as products. The products were analyzed by gas chromatography using a Chromosorb 102 column. Sulfolane was used as an internal standard. Infrared spectra of catalytic reaction solutions were measured in a KRS cell under ambient conditions after reaction. Rates of formation of products were given in turnover frequency, defined as the number of moles of the product formed per gram-atom of metal per hour. The turnover frequency of EG, *N*(EG), is obtained by

$$N(\mathrm{EG}) = \mathrm{mol(EG)}/(\text{g-atom Rh})\mathrm{h}.$$

Product selectivity is defined as the carbon efficiency on the basis of reduced carbon monoxide in a product obtained. The selectivity value of EG, Sel.(EG), is obtained by

$$\mathrm{Sel.(EG)} = \frac{2\mathrm{EG} \times 100}{\mathrm{MeOH} + \mathrm{MF} + 2(\mathrm{EtOH} + \mathrm{EG}) + 3\,\mathrm{GL}}.$$

Results and Discussion

Influence of Some Solvents on the EG Formation. Table 1 shows the influence of solvents on the EG formation in the presence of triethylamine (Et_3N). An addition of Et_3N to a nonpolar solvent such as tetrahydrofuran (THF) or toluene in a molar ratio of Et_3N to Rh of 100 improved the activity and selectivity for the EG formation to a great extent (Nos. 2 and 4). When γ-butyrolactone (γ-BL) having a high polarity, on the other hand, is employed, an addition of Et_3N (N/Rh=100) remarkably decreased the catalytic activity (No. 6). From these results, it is suggested that the effect of addition of amines varies with the polarity of solvents to a considerable extent.

Influence of Amines on the $Rh_4(CO)_{12}$-THF System. Table 2 shows the influence of addition of some amines (N/Rh=100) on the $Rh_4(CO)_{12}$-THF system. Triisobutylamine ($(i\text{-Bu})_3N$) gave a remarkable effect on the activity and selectivity for the EG formation (No. 5) compared to straight-chain trialkylamines. (i-$Bu)_3N$ showed a remarkable effect also on the GL formation.

Table 1. Influence of Some Solvents on the EG Formation[a)]

Expt. No.	Solvent (7ml)	Et_3N mmol	Product/mmol MeOH	MF	EtOH	EG	GL	N(EG)	Sel.(EG)
1	Toluene	—	7.55	3.15	0	0.14	0	1.4	2.6
2	Toluene	10	15.24	1.21	0.10	4.74	0	47.5	36.3
3	THF	—	9.32	3.55	0	1.28	0	12.8	16.6
4	THF	10	13.23	0.96	0.09	7.47	0.18	74.7	50.1
5	γ-BL	—	1.83	0.17	0.07	0.24	0	2.4	18.3
6	γ-BL	10	0.03	0	0	trace	0	0.04	21.1

a) Reaction conditions: 1800 kg cm^{-2}, P_{H_2}/P_{CO}=1, $Rh_4(CO)_{12}$ 0.1 mg-atom, 230 °C, 1 h.

Table 2. Effect of Amines on the $Rh_4(CO)_{12}$–THF System[a)]

Expt. No.	R_3N (10 mmol)	Product/mmol MeOH	MF	EtOH	EG	GL	N(EG)	Sel.(EG)	Sel.(GL)
1	—	9.32	3.55	0	1.28	0	12.8	16.6	0
2	Et_3N	13.23	0.96	0.09	7.47	0.18	74.7	50.1	1.8
3	$(n\text{-Bu})_3N$	10.97	0.80	0.03	6.52	0.21	65.2	51.2	2.5
4	$(n\text{-}C_8H_{17})_3N$	9.99	0.73	0.05	6.09	0.31	60.9	50.9	3.9
5	$(i\text{-Bu})_3N$	3.10	0.34	0	9.19	1.24	91.9	72.0	14.6

a) Reaction conditions: 1800 kg cm^{-2}, P_{H_2}/P_{CO}=1, solvent THF (7 ml), $Rh_4(CO)_{12}$ 0.1 mg-atom, 230 °C, 1 h.

Table 3. Effect of Branched-Chain Amines on the $Rh_4(CO)_{12}$–THF System[a)]

Expt. No.	R_3N (10 mmol)	Product/mmol MeOH	MF	EtOH	EG	GL	N(EG)	Sel.(EG)	Sel.(GL)
1	—	9.32	3.55	0	1.28	0	12.8	16.6	0
2	Et_3N	13.23	0.96	0.09	7.47	0.18	74.7	50.1	1.8
3	$(i\text{-Pr})_2EtN$	10.16	0.63	0.08	7.01	0.36	70.1	53.8	4.2
4	$(i\text{-Bu})_3N$	3.10	0.34	0	9.19	1.24	91.9	72.0	14.6
5	$(i\text{-}C_5H_{11})_3N$	10.42	0.83	0.04	6.69	0.65	66.9	50.2	7.3
6	Ph_3N	9.64	2.81	0	0.94	0	9.4	13.1	0
7	$(PhCH_2)_3N$	2.05	0.11	0	8.00	2.00	80.0	66.2	24.8
8	*N*-Ethylcarbazole	5.00	1.23	0	7.36	0.15	73.6	68.8	2.1

a) Reaction conditions: 1800 kg cm^{-2}, P_{H_2}/P_{CO}=1, solvent THF (7 ml), $Rh_4(CO)_{12}$ 0.1 mg-atom, 230 °C, 1 h.

Table 4. Effect of (Hydroxyalkyl)amines on the $Rh_4(CO)_{12}$–THF System[a)]

Expt. No.	R_3N (10 mmol)	Product/mmol MeOH	MF	EtOH	EG	GL	N(EG)	Sel.(EG)	Sel.(GL)
1	—	9.32	3.55	0	1.28	0	12.8	16.6	0
2	$(HOCH_2CH_2)_3N$	5.16	0.23	0.46	3.20	0.49	32.0	45.1	10.4
3	$[CH_3CH(OH)CH_2]_3N$	2.95	0.10	0.11	9.76	2.87	97.6	62.2	27.4
4	$CH_2CH(OH)CH_2OH$	3.58	0.40	0.07	4.62	0.78	46.2	58.9	14.0

a) Reaction conditions: 1800 kg cm^{-2}, P_{H_2}/P_{CO}=1, solvent THF (7 ml), $Rh_4(CO)_{12}$ 0.1 mg-atom, 230 °C, 1 h.

Then, we have investigated the effect of addition of amines having branched alkyl groups. As shown in Table 3, an addition of amines having α- or β-branched alkyl group such as *N*,*N*-diisopropylethylamine (No. 3), *N*-ethylcarbazole (No. 8), or tribenzylamine (No. 7) gave an improving effect on the selectivity for the EG formation. Tribenzylamine showed a remarkable effect also on the GL formation. The sum of the selectivities to EG and GL exceeded 90%.

No effect was observed by addition of triphenylamine (No. 6). Triisopentylamine having γ-branched alkyl groups produced a relatively small effect on the selectivity to EG (No. 5). The selectivity to EG was

almost the same as that attained by addition of the straight-chain alkylamines.

Table 4 shows the effect of (hydroxyalkyl)amines on the $Rh_4(CO)_{12}$-THF system. Triisopropanolamine (No. 3) and 3-(1-pyrrolidinyl)-1,2-propanediol (No. 4) which have a β-substituent gave an improving effect on the activity and selectivity for the EG formation, compared to triethanolamine (No. 2). Triisopropanolamine and 3-(1-pyrrolidinyl)-1,2-propanediol showed an effect also on the GL formation. The results of Tables 2 to 4 show that bulky amines are effective as the promoter for C-C bond formation.

We have further investigated the influence of amounts of Et_3N and $(i\text{-}Bu)_3N$ on the $Rh_4(CO)_{12}$-THF system. The addition of the amines increased the selectivity to EG and decreased the selectivities to MeOH and MF (Figs. 1 and 2). The rate of decrease in the selectivity to MF was larger than that of decrease in the selectivity to MeOH. The addition of Et_3N increased the yield of MeOH as well as EG up to the N/Rh ratio of about 100 (Fig. 1). Consequently, the EG selectivity was as much as 60% or lower. The addition of $(i\text{-}Bu)_3N$, on the other hand, suppressed the formation of MeOH and MF (Fig. 2). As a result, the EG selectivity exceeded 70%. $(i\text{-}Bu)_3N$ showed a remarkable effect also on the GL formation compared to Et_3N.

Influence of CO Partial Pressure on the $Rh_4(CO)_{12}$-THF System. Increase in CO partial pressure increased the selectivities to EG and MF as shown in Fig. 3. On the contrary, it decreased the selectivity to MeOH. Fahey[5] has reported that formaldehyde is trapped as its ethylene glycol acetal in a Rh-catalyzed direct synthesis of EG. Therefore, a reaction path con-

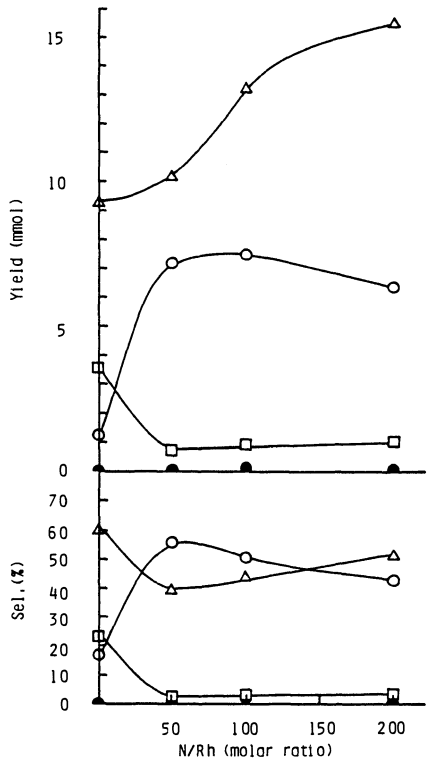

Fig. 1. Influence of Et_3N/Rh ratio. 1800 kg cm^{-2}, P_{H_2}/P_{CO}=1, THF (7 ml), 230°C, $Rh_4(CO)_{12}$ 0.1 mg-atom, 1 h. ○: EG, △: MeOH, □: MF, ●: GL.

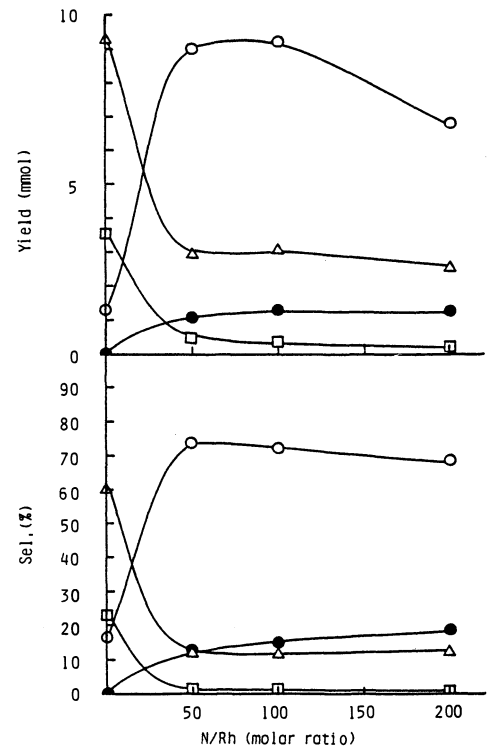

Fig. 2. Influence of $(i\text{-}Bu)_3N$/Rh ratio. 1800 kg cm^{-2}, P_{H_2}/P_{CO}=1, THF (7 ml), 230°C, $Rh_4(CO)_{12}$ 0.1 mg-atom, 1 h. ○: EG, △: MeOH, □: MF, ●: GL.

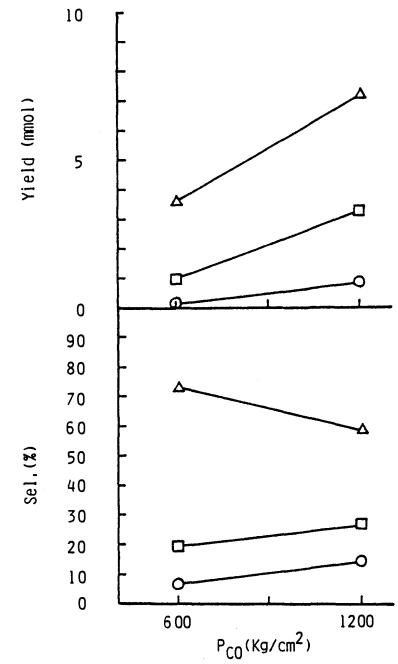

Fig. 3. Influence of CO partial pressure. THF (7 ml), $Rh_4(CO)_{12}$ 0.1 mg-atom, P_{H_2}=600 kg cm^{-2}, 230°C, 1 h. ○: EG, △: MeOH, □: MF.

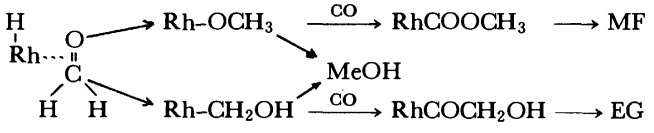

(1)

taining hydroxymethyl and methoxy intermediates, like that of the $Co_2(CO)_8$-toluene system already reported,[6] is suggested for the formation of EG, MF, and MeOH in the $Rh_4(CO)_{12}$-THF system. That is, the increase in CO partial pressure is considered to promote the insertion of CO and increase the selectivities to EG and MF.

In the $Co_2(CO)_8$-toluene system, the increase in CO partial pressure decreases the amount of MeOH and increases the amounts of EG and MF.[6] On the contrary, the increase in CO partial pressure increased the amount of MeOH as well as EG and MF in Fig. 3. This increase in the amount of MeOH can be explained by considering that the increase in CO partial pressure serves to improve the formation of the active species in the $Rh_4(CO)_{12}$-THF system.

As shown in Figs. 1 and 2, the addition of amines increases the selectivity to EG and decreases the selectivities to MeOH and MF. The rate of decrease in MF selectivity is larger than that in MeOH selectivity. This larger rate of decrease in MF selectivity and the improvement of EG selectivity by the addition of amines suggest that amines contribute advantageously to the formation of $Rh-CH_2OH$ intermediate compared to $Rh-OCH_3$ intermediate in the sequence

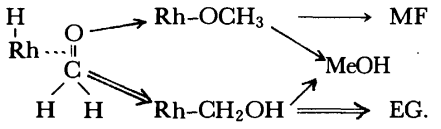

(2)

The decrease in MeOH selectivity and the increase in EG selectivity by the addition of amines in Figs. 1 and 2 suggest that the insertion of CO is promoted by the amines. The contribution of amines to the formation of $Rh-CH_2OH$ intermediate in Eq. 2 can be explained in terms of a nucleophilic attack on the carbonyl C atom of formaldehyde by Rh whose electron density is increased by amine coordination.

Amines show an effect also on the GL formation. The GL formation can be explained on the basis of the sequence

$$Rh-COCH_2OH \xrightarrow{H_2} Rh-CH(OH)CH_2OH \xrightarrow{CO} Rh-COCH(OH)CH_2OH,$$

$$Rh-COCH(OH)CH_2OH \xrightarrow{H_2} Rh-CH(OH)CH(OH)CH_2OH \xrightarrow{H_2} GL, \quad (3)$$

including $Rh-CH(OH)CH_2OH$ and $Rh-CH(OH)CH(OH)CH_2OH$ intermediates similar to $Rh-CH_2OH$ intermediate.

Influence of Catalyst Concentration. Figures 4 and 5 show the influence of catalyst concentrations on the $Rh_4(CO)_{12}$-Et_3N-THF and $Rh_4(CO)_{12}$-$(i\text{-}Bu)_3N$-THF systems, respectively. The $Rh_4(CO)_{12}$-Et_3N-THF system was affected by the catalyst concentration to a large extent. The selectivities to EG and GL were decreased and the MeOH selectivity was increased with increase in catalyst concentration. It is suggested that MeOH is formed advantageously at a high catalyst concentration by the diatomic reaction

$$Rh-CH_2OH + Rh-H \longrightarrow MeOH. \quad (4)$$

On the contrary, the influence of the catalyst concentration on the selectivities to EG, GL, and MeOH was small in the $Rh_4(CO)_{12}$-$(i\text{-}Bu)_3N$-THF system. It is suggested that the diatomic reaction mentioned above is relatively unlikely to proceed in the $Rh_4(CO)_{12}$-$(i\text{-}Bu)_3N$-THF system because of the bulkiness of $(i\text{-}Bu)_3N$ ligand. $(i\text{-}Bu)_3N$ which gives a

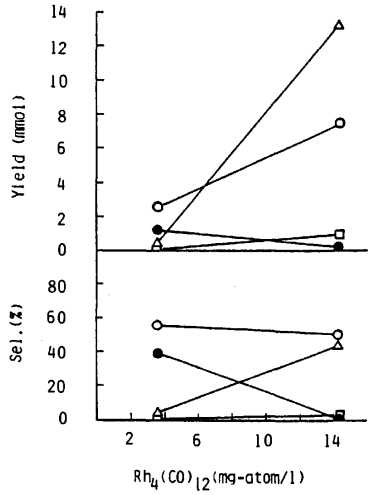

Fig. 4. Influence of catalyst concentration in $Rh_4(CO)_{12}$-Et_3N-THF system. 1800 kg cm^{-2}, P_{H_2}/P_{CO}=1, THF (7 ml), 230°C, N/Rh=100, 1 h. ○: EG, △: MeOH, □: MF, ●: GL.

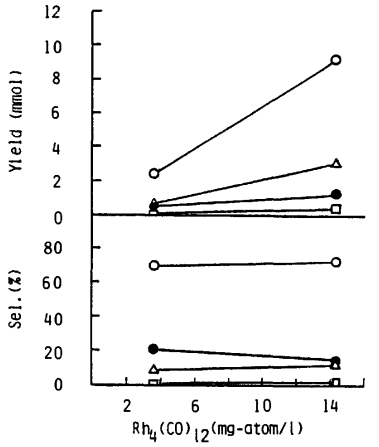

Fig. 5. Influence of catalyst concentration in $Rh_4(CO)_{12}$-$(i\text{-}Bu)_3N$-THF system. 1800 kg cm^{-2}, P_{H_2}/P_{CO}=1, THF (7 ml), 230°C, N/Rh=100, 1 h. ○: EG, △: MeOH, □: MF, ●: GL.

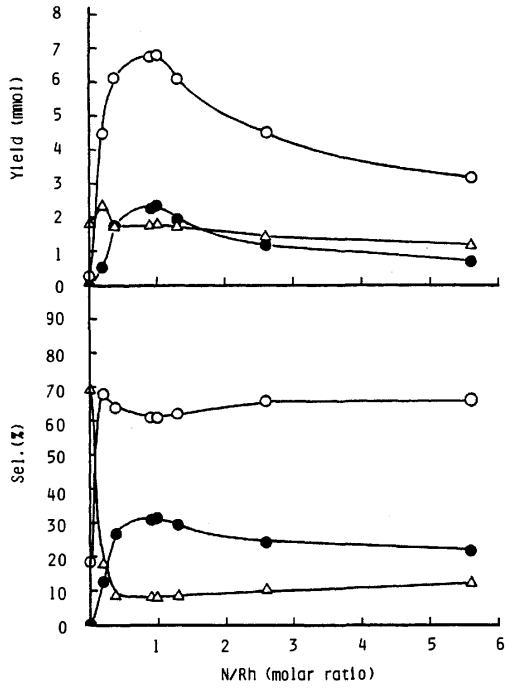

Fig. 6. Influence of $(n\text{-Bu})_3N/Rh$ ratio. 1800 kg cm^{-2}, P_{H_2}/P_{CO}=1, γ-BL (7 ml), 230 °C, $Rh_4(CO)_{12}$ 0.1 mg-atom, 1 h. ○: EG, △: MeOH, ●: GL.

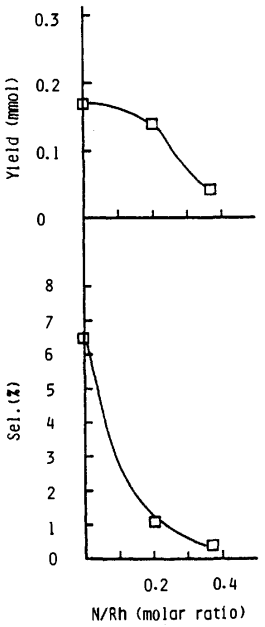

Fig. 7. Influence of $(n\text{-Bu})_3N/Rh$ ratio. 1800 kg cm^{-2}, P_{H_2}/P_{CO}=1, γ-BL (7 ml), 230 °C, $Rh_4(CO)_{12}$ 0.1 mg-atom, 1 h. □: MF.

higher EG selectivity at a high catalyst concentration can give a high space time yield (STY: g EG/l h) of EG. Amines that can provide a high STY are favorable as the promoter from the practical point of view. Tribenzylamine (No. 7, Table 3), *N*-ethylcarbazole (No. 8, Table 3), and triisopropanolamine (No. 3, Table 4) which give higher EG selectivities as compared with Et_3N, are also favorable promoters.

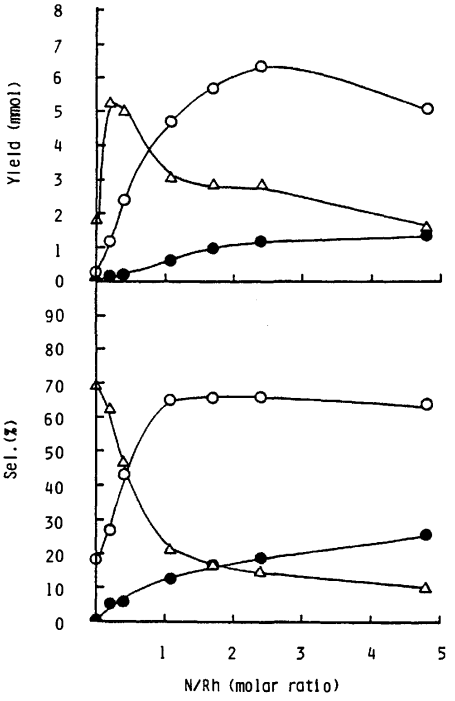

Fig. 8. Influence of $(i\text{-Bu})_3N/Rh$ ratio. 1800 kg cm^{-2}, P_{H_2}/P_{CO}=1, γ-BL (7 ml), 230 °C, $Rh_4(CO)_{12}$ 0.1 mg-atom, 1 h. ○: EG, △: MeOH, ●: GL.

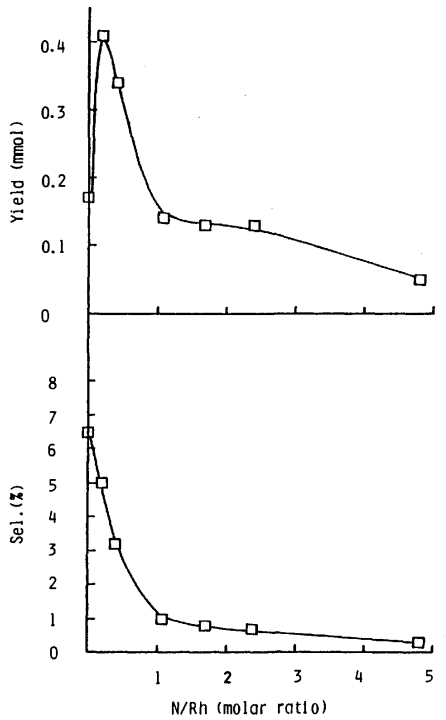

Fig. 9. Influence of $(i\text{-Bu})_3N/Rh$ ratio. 1800 kg cm^{-2}, P_{H_2}/P_{CO}=1, γ-BL (7 ml), 230 °C, $Rh_4(CO)_{12}$ 0.1 mg-atom, 1 h. □: MF.

Influence of Amines on the $Rh_4(CO)_{12}$-γ-BL System. The influence of amounts of amines was also investigated using γ-BL with a high polarity as a solvent. Figures 6 and 7 illustrate the relationship of

Table 5. Effect of Et_3N on the $Rh_4(CO)_{12}$-TGM System[a)]

Expt. No.	Et_3N (mmol)	Temp °C	Product/mmol					N(EG)	Sel.(EG)
			MeOH	MF	EtOH	EG	GL		
1	—	230	6.40	1.14	0.09	0.91	0	9.1	19.1
2	—	250	4.79	0.32	0.30	0.14	0	1.4	4.7
3	10	250	16.70	2.28	0.80	18.68	1.71	186.8	59.2

a) Reaction conditions: 1800 kg cm^{-2}, P_{H_2}/P_{CO}=1, solvent TGM (7 ml), $Rh_4(CO)_{12}$ 0.1 mg-atom, 1 h.

yields of MeOH, MF, EG, and GL and their selectivities with the amount of $(n\text{-Bu})_3N$ added. The yields of EG and GL increase with increase in N/Rh ratio (Fig. 6). The maximum value of the yields of EG and GL was obtained at the N/Rh ratio of 1. On the other hand, the yield of MeOH showed the maximum value at the N/Rh ratio of about 0.2. And the yield of MF decreased with increase in N/Rh ratio (Fig. 7). An increasing tendency of the MeOH selectivity was observed in Fig. 6 when the N/Rh ratio exceeded 1. A suppression of the coordination of an additional CO leading to the C_2 species may be caused by an excessive amount of $(n\text{-Bu})_3N$. This tendency of MeOH selectivity is similar to that of Fig. 1 at N/Rh ratios ranging from 100 to 200. The GL selectivity decreased with increasing amount of $(n\text{-Bu})_3N$ at N/Rh ratios above 1 (Fig. 6). This variation of GL selectivity will not contradict with the tendency of MeOH selectivity.

Figures 8 and 9 illustrate the relationship of yields of MeOH, MF, EG, and GL and their selectivities with the amount of $(i\text{-Bu})_3N$ added. The addition of $(i\text{-Bu})_3N$ also improved the selectivities to EG and GL and decreased the selectivities to MeOH and MF. The optimum N/Rh ratio for the EG formation was in the range from 2 to 3. This optimum N/Rh ratio for the EG formation in γ-BL solvent with a high polarity is remarkably smaller than that obtained in THF solvent with a low polarity (Fig. 2).

The addition of a small amount of $(n\text{-Bu})_3N$ increases the yield of MeOH (Fig. 6). This effect became more remarkable in the case of $(i\text{-Bu})_3N$ as shown in Fig. 8. The activity for the MeOH formation became maximum at N/Rh ratios ranging from 0.2 to 0.4. Simultaneously, the activity for the MF formation became maximum at the same N/Rh molar ratio (Fig. 9). The $Rh_4(CO)_{12}$-tribenzylamine-γ-BL system also showed the same effects. The maximum value for the yields of MeOH and MF was obtained at the N/Rh ratio of about 0.5.[7)]

The effectiveness order for the EG selectivity derived from the maximum activities for the EG formation in Figs. 6 and 8 is $(i\text{-Bu})_3N > (n\text{-Bu})_3N$. However, the difference in EG selectivity between $(i\text{-Bu})_3N$ and $(n\text{-Bu})_3N$ in γ-BL solvent is not so much as that obtained in THF solvent (Figs. 1 and 2 and Table 2). One possible explanation for this small difference in EG selectivity in γ-BL solvent is that the diatomic reaction (Eq. 4) is relatively unlikely to proceed in the $Rh_4(CO)_{12}$-$(n\text{-Bu})_3N$-γ-BL system because of the low concentration of the active species. The concentration of the active species in γ-BL solvent seems to be lower than that in THF, as will be described later.

Influence of Addition of Amine at a High Temperature. Table 5 shows the influence of addition of Et_3N on the $Rh_4(CO)_{12}$-tetraglyme (TGM) system at a high temperature. The $Rh_4(CO)_{12}$-TGM system produced Rh precipitates in the reaction solution after the reaction at 250 °C (No. 2). The catalytic activity in the reaction at 250 °C (No. 2) was lower than that at 230 °C (No. 1). However, an addition of Et_3N to the $Rh_4(CO)_{12}$-TGM system caused no Rh precipitation after the reaction at 250 °C and improved the activity for the EG formation remarkably (No. 3). The addition of Et_3N serves for a stabilization of the catalyst in addition to the improvement of the activity for the EG formation and of the EG selectivity.

IR Spectra of Reaction Solutions. As shown in Scheme 1 below, Vidal and Walker[8)] observed absorption bands of the cluster anion $[Rh_{13+x}(CO)_mH_y]^{n-}$ and the mononuclear species $[Rh(CO)_4]^-$ as a result of IR spectral measurement on a catalytic reaction solution of $Rh(CO)_2$acac-*N*-methylmorpholine-$CsPhCO_2$-sulfolane solvent system under condition (A) for the direct EG synthesis:

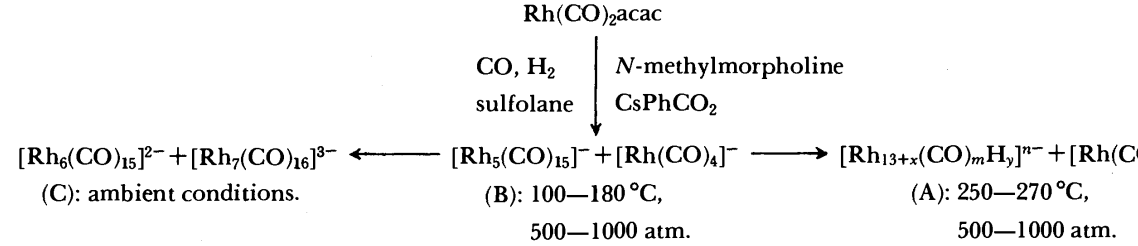

Scheme 1.

Under condition (B) of low temperature, absorption bands of $[Rh_5(CO)_{15}]^-$ and $[Rh(CO)_4]^-$ anions were observed. Similar results are obtained when solutions of rhodium carbonyl clusters such as $Rh_4(CO)_{12}$ and $Rh_6(CO)_{16}$ are treated in the same way. They also observed absorption bands of Rh cluster anions, $[Rh_6(CO)_{15}]^{2-}$ and $[Rh_7(CO)_{16}]^{3-}$, under condition (C) of ambient temperature and pressure.

On the other hand, we observed that the IR spectrum of the catalyst system of Fig. 6 obtained at the N/Rh ratio of 1, where the activity for the EG formation became maximum, gave an absorption band (I) at 1900 cm^{-1} under ambient IR measurement conditions as shown in Fig. 10-a. This absorption band (I) at 1900 cm^{-1} seems to be due to the mononuclear Rh species $[Rh(CO)_4]^-$.[9] This IR spectrum gave also a broad absorption band (II) at about 1960 cm^{-1}. The absorption intensity of (I) decreased remarkably over a short period of time (5—30 min) as shown in Fig. 10-b. Simultaneously with the decrease in absorption intensity of (I), the absorption band (II) had its breadth widened and its intensity increased relative to (I).

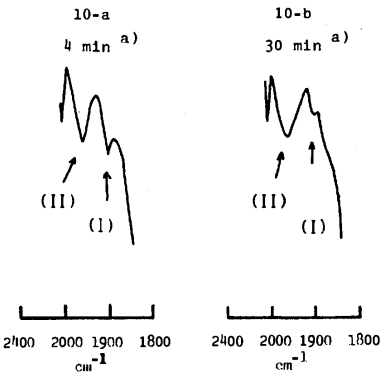

Fig. 10. IR spectra of the catalyst system of Fig. 6 obtained at the N/Rh ratio of 1. a) A time period from withdrawal of the reaction mixture from the autoclave to measurement for IR spectrum.

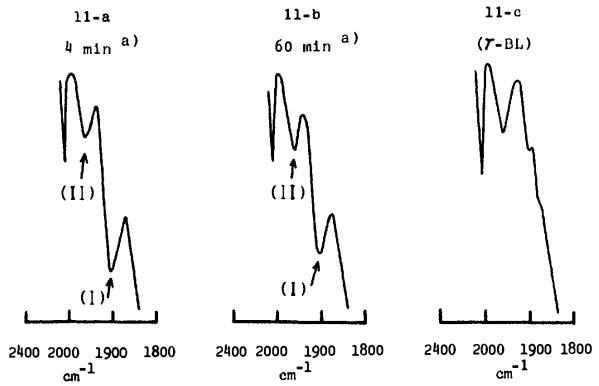

Fig. 11. IR spectra of the catalyst system of Fig. 6 obtained at the N/Rh ratio of 5.6. a) A time period from withdrawal of the reaction mixture from the autoclave to measurement for IR spectrum.

$[Rh_6(CO)_{15}]^{2-}$ has absorption bands at 1960 cm^{-1} and 1980 cm^{-1}.[9] Therefore, the above-mentioned variation of the absorption bands of (I) and (II) with time suggests a decrease in concentration of $[Rh(CO)_4]^-$ and an increase in concentration of $[Rh_6(CO)_{15}]^{2-}$.

On the other hand, in the case of the catalyst system of Fig. 6 obtained at the N/Rh ratio of 5.6, the absorption band of (I) was relatively stable as shown in Figs. 11-a and 11-b. Since γ-BL solvent has a shoulder at 1900 cm^{-1} (Fig. 11-c), the shoulder was removed from the IR spectra of Figs. 11-a and 11-b by the compensation method. Consequently, it was confirmed that the IR spectra of the catalyst system of Fig. 6 obtained at the N/Rh ratio of 5.6 have a strong absorption band due to $[Rh(CO)_4]^-$ at 1900 cm^{-1} as shown in Figs. 12-a and 12-b.

The catalyst system of Vidal and Walker[8] composed of $Rh(CO)_2acac$, *N*-methylmorpholine, and cesium carboxylate contains $[Rh(CO)_4]^-$ anion under conditions of catalytic reaction such as elevated temperature (250—270 °C) and high pressure (500—1000 atm). And this $[Rh(CO)_4]^-$ anion changes into a cluster anion under ambient temperature and pressure as shown in Scheme 1. Therefore, in the case of the catalyst systems of Fig. 6 obtained at N/Rh=1—5.6 where the absorption band of $[Rh(CO)_4]^-$ anion is observed under ambient temperature and pressure, it is suggested that a mononuclear Rh species is present in the reaction solution under the reaction conditions of 230 °C and 1800 $kg\,cm^{-2}$. It seems that the formation of the mononuclear Rh species at 1800 $kg\,cm^{-2}$ of synthesis

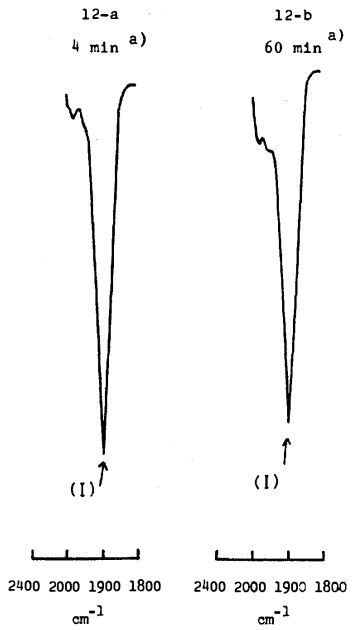

Fig. 12. IR spectra of the catalyst system of Fig. 6 obtained at the N/Rh ratio of 5.6. Absorption bands of γ-BL solvent were removed by compensation method. a) A time period from withdrawal of the reaction mixture from the autoclave to measurement for IR spectrum.

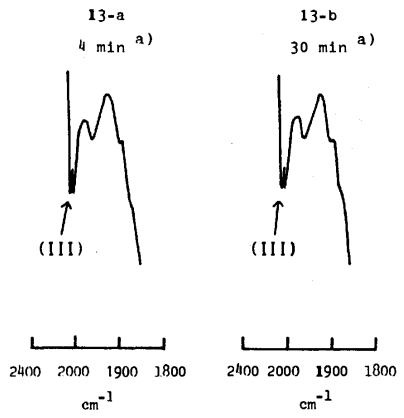

Fig. 13. IR spectra or the catalyst system of Fig. 6 obtained at the N/Rh ratio of zero. a) A time period from withdrawal of the reaction mixture from the autoclave to measurement for IR spectrum.

gas is easier than that at 500—1000 atm used by Vidal and Walker.[8]

The IR spectrum of the catalyst system of Fig. 6 obtained at the N/Rh ratio of zero showed an absorption band (III) assignable to $[Rh_{12}(CO)_{30}]^{2-}$ anion[9] at 2053 cm^{-1} (Fig. 13-a). The absorption band (III) is stable as shown in Figs. 13-a and 13-b. Further, it was confirmed by the compensation method that the shoulder[10] at 1900 cm^{-1} in Fig. 13-a was due to γ-BL.

Active Species. The above results of the IR spectra in Figs. 10—13 suggest that $(n\text{-Bu})_3N$ serves for the formation of mononuclear Rh species from the Rh catalyst precursor under the catalytic reaction conditions. Because the activity for the EG formation shows the maximum value at N/Rh=1 in Fig. 6, a mononuclear Rh species containing $(n\text{-Bu})_3N$ is suggested to be a species for the catalytic activity at N/Rh=1. Further, the main product of the catalyst systems of Fig. 6 obtained at N/Rh ratios ranging from 1 to 5.6 was also EG. From the results of Figs. 11 and 12, a mononuclear species of Rh containing $(n\text{-Bu})_3N$ is likewise suggested to be an active species of the catalyst systems of Fig. 6 obtained at N/Rh ratios ranging from 1 to 5.6.

The IR spectrum of the catalyst system of Fig. 8 obtained at N/Rh 2.5, where the yield of EG became maximum, showed also an absorption band of $[Rh(CO)_4]^-$ anion. A mononuclear Rh species containing $(i\text{-Bu})_3N$ is likewise considered as an active species of the catalyst system of Fig. 8 obtained at N/Rh=2.5.

The optimum amine/Rh ratios for the EG formation are 50—100 in THF solvent with a low polarity (Figs. 1 and 2) and 1—3 in γ-BL solvent with a high polarity (Figs. 6 and 8). And the addition of excess Et_3N (N/Rh=100) decreases remarkably the catalytic activity in γ-BL solvent (No. 6, Table 1). Further, in our previous paper, we reported that a high catalyst activity for the EG formation is observed in $(n\text{-Bu})_3N$ solvent with a low polarity at 1800 kg cm^{-2} of synthesis gas.[12] Considering these results, in γ-BL solvent with a high polarity, factors diminishing the catalyst activity are suggested to include the formation of $[Rh(CO)_4]^-$ anion by an excessive amine. Therefore, a mononuclear species of neutral Rh complex containing amine, $HRh(CO)_3(R_3N)$ (**2**), is suggested as an active species.[13] A possible reaction path for the formation of **2** may be written as the sequence

$$Rh_4(CO)_{12}+R_3N \xrightarrow{CO+H_2} [Rh(CO)_4]^- R_3NH^+,$$
$$[Rh(CO)_4]^- R_3NH^+ \rightleftharpoons \underset{\mathbf{1}}{HRh(CO)_4}+R_3N,$$
$$HRh(CO)_4+R_3N \rightleftharpoons \underset{\mathbf{2}}{HRh(CO)_3(R_3N)}+CO. \quad (5)$$

The concentration of the neutral active species **2** in γ-BL solvent seems to be lower than that in THF because of the higher polarity of γ-BL. The effect of amine on the EG formation by Eq. 2 can be explained in terms of the nucleophilic attack on the carbonyl C atom of formaldehyde by Rh whose electron density is increased by amine coordination.

However, $Rh_4(CO)_{12}$-$(n\text{-Bu})_3N$ catalyst system (Fig. 6) in γ-BL solvent with a high polarity seems to show high EG selectivities compared to those (Fig. 1 and Run Nos. 2—4, Table 2) in THF solvent with a low polarity. Therefore, there is a possibility that the proton of $[Rh(CO)_4]^- R_3NH^+$ contributes to the formation of Rh-CH_2OH complex, an intermediate in the EG formation, by an electrophilic attack on the carbonyl O atom of the coordinated formaldehyde shown by Eq. 2. Another possible reason for the high EG selectivity of the $Rh_4(CO)_{12}$-$(n\text{-Bu})_3N$-γ-BL system is that the diatomic reaction (Eq. 4) is relatively unlikely to proceed because of the low concentration of the active species.

The activity for the MeOH formation becomes maximum at N/Rh ratios ranging from 0.2 to 0.4 as shown in Fig. 8. Further, Tables 1 and 2 show that the catalyst systems without nitrogen-containing compounds form MeOH as the main product. $(i\text{-Bu})_3N$ is considered to be weaker in coordination ability than $(n\text{-Bu})_3N$ because of the bulkiness of $(i\text{-Bu})_3N$. From this and the above results and a related result,[10] a mononuclear Rh species, $HRh(CO)_4$ (**1**), shown in Eq. 5 is suggested as an active species for the MeOH formation of the catalyst system of Fig. 8 obtained at lower N/Rh ratios (0—0.5). $HRh(CO)_4$ is also suggested as an active species for the MF formation of the catalyst system of Fig. 9 obtained at lower N/Rh ratios (0—0.5).

The absorption band (I) of $[Rh(CO)_4]^-$ anion was observed also in the IR spectrum of the catalyst system of Fig. 1 obtained at Et_3N/Rh=100. But this catalyst system caused precipitaion of Rh species during the IR spectrum measurement at ambient conditions. This indicates that the stability of $[Rh(CO)_4]^-$ anion is low in THF solvent with a low polarity.

It is known[14] that alkyl manganese pentacarbonyls

react with amines producing amine acyl manganese tetracarbonyl complexes according to

$$RMn(CO)_5 + \text{amine} \longrightarrow [\text{amine} \rightarrow Mn(R)(CO)_5] \longrightarrow RCOMn(CO)_4(\text{amine}). \quad (6)$$

This study seems to provide a support for the C-C bond formation via a hydroxy acetyl Rh complex containing amine.

This work is a part of "C_1-Chemistry Project," a National Research and Development Program of the Agency of Industrial Science and Technology, the Ministry of International Trade and Industry (M.I.T.I.), Japan. The authors thank Dr. Haruo Takaya for his valuable suggestions.

References

1) For reviews, see: a) T. Deguchi, T. Takano, M. Ishino, and S. Nakamura, *Shokubai (Catalyst)*, **23**, 18 (1981); b) D. D. Dombek, *Advan. Catal.*, **32**, 325 (1983).

2) L. Kaplan (Union Carbide), U.S. Patent 4224237 (1980).

3) A. Deluzarche, R. Fonseca, G. Jenner, and A. Kiennemann, *Erdol und Kohle-Erdgas-Petrochemie Vereinigt mit Brennstoff-Chemie*, **32**, 313 (1979).

4) W. Keim, M. Anstock, M. Roper, and J. Schlupp, *C_1 Mol. Chem.*, **1**, 21 (1984).

5) D. R. Fahey, *J. Am. Chem. Soc.*, **103**, 136 (1981).

6) T. Masuda, K. Murata, T. Kobayashi, and A. Matsuda, *Nippon Kagaku Kaishi*, **1986**, 171.

7) T. Masuda, K. Murata, and A. Matsuda, The Fourth Symposium of C_1 Catalysis (in Tokyo, Japan), 1987, p. 70.

8) J. L. Vidal and W. E. Walker, *Inorg. Chem.*, **19**, 896 (1980).

9) P. Chini, G. Longoni, and V. G. Albano, *Adv. Organomet. Chem.*, **14**, 285 (1976).

10) A catalyst solution of $Rh_4(CO)_{12}$-γ-BL system obtained under a high temperature (275 °C) condition with a small amount of γ-BL solvent gave a relatively large proportion of MeOH to Rh complex and γ-BL. This solution showed an absorption band assignable to $[Rh(CO)_4]^-$ anion, although the absorption band was not stable under ambient conditions.[11] The large amount of MeOH obtained seems to stabilize[15] the $[Rh(CO)_4]^-$ anion.

11) T. Masuda, K, Murata, and A. Matsuda, to be published.

12) T. Masuda, K, Murata, T. Kobayashi, and A. Matsuda, *Bull. Chem. Soc. Jpn.*, **59**, 2349 (1986).

13) For the direct synthesis of EG with $Rh_4(CO)_{12}$/*N*-alkyl pyrrolidone solvent system, the active species has been proposed: a) E. Watanabe, K. Murayama, Y. Hara, Y. Kobayashi, K. Wada, and T. Onoda, *J. Chem. Soc., Chem. Commun.*, **1986**, 227; b) Y. Ohgomori, S. Mori, S. Yoshida, and Y. Watanabe, *Chem. Lett.*, **1986**, 1935.

14) K. A. Keblys and A. H. Filbey, *J. Am. Chem. Soc.*, **82**, 4204 (1960).

15) W. Reppe, *Justus Liebigs Ann. Chem.*, **582**, 116 (1953).

NMR Spectra of Organogermanium Compounds. VI.[1] NMR Spectra and Molecular Mechanics Calculations of 3-Methyl- and 3,3-Dimethylgermacyclohexanes

Yoshito TAKEUCHI,* Yasuko ICHIKAWA, Katsumi TANAKA, and Norihiro KAKIMOTO†
Department of Chemistry, The College of Arts & Sciences, The University of Tokyo, Komaba, Meguro-ku, Tokyo 153
†ASAI Germanium Research Institute, Komae-shi, Tokyo 201
(Received February 8,1988)

Several 3-methyl- or 3,3-dimethylgermacyclohexanes were prepared and their ^{13}C and ^{73}Ge NMR spectra were determined. Steric energies for all of stereoisomers of some of these germacyclohexanes were calculated by MM2 program. The effect of axial 3-methyl group of germacyclohexanes upon its C-5 is much the same with the corresponding effect in cyclohexanes, and is much smaller than the effect caused by axial methyl on germanium upon C-3,5. A large upfield shift is recorded for germanium nuclei when there is an axial methyl on C-3 of germacyclohexanes.

In the previous communication[2] we have reported the ^{13}C NMR spectra and molecular mechanics calculations of a variety of germacyclohexanes, i.e., germacyclohexane (**1G**) and such methyl-substituted germacyclohexanes as 1-methyl- (**2G**), 3-methyl- (**3G**), 1,1-dimethyl- (**4G**), 1,3-dimethyl- (**5G**) 1,4-dimethyl- (**6G**), and 1,1,3-trimethyl- (**9G**) germacyclohexanes. It revealed that (i) the ring is flattened around the germanium and that (ii) a methyl group on germanium has a slight preference to axial conformation to the equatorial, which is in line with the results for the corresponding silacyclohexanes.[3]

	R_1	R_2	R_3	R_4	R_5
1G	H	H	H	H	H
2G	Me	H	H	H	H
3G	H	H	Me	H	H
4G	Me	Me	H	H	H
5G	Me	H	Me	H	H
6G	Me	H	H	Me	H
7G	H	H	Me	Me	H
8G	H	H	Me	H	Me
9G	Me	Me	Me	H	H
10G	Me	H	Me	Me	H
11G	Me	Me	Me	Me	H

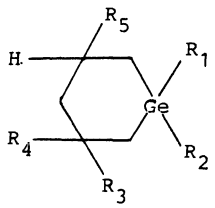

Furthermore, both ^{13}C and ^{73}Ge NMR data indicate that **2G** is a ca. 60:40 mixture of axial and equatorial conformers. Attempts to observe directly the two conformers by freezing the inversion on NMR timescale, however, failed because of the very low barrier for inversion. Instead, we prepared a mixture of *trans*-**6G** and *cis*-**6G** where the methyl group on germanium remains equatorial and axial, respectively. This pair of compounds is interesting as a model to estimate the magnitude of γ-gauche effect by an axial methyl group on germanium in germacyclohexanes. The chemical shift difference (1.30 ppm; the cis isomer gives the signal in a higher field) observed for C-3,5 resonances for the two compounds[4] is much smaller as compared with the corresponding difference for equatorial and axial methylcyclohexane (**2C**; 5.40 ppm).[5]

Qualitatively this is not unexpected in view of the prolonged distance between the axial methyl group on germanium and axial hydrogens on C-3,5. γ-gauche effect is also clear for the ^{13}C resonances of methyl carbon itself. Thus, the methyl groups on germanium of *trans*-**6G** and *cis*-**6G** resonate at −5.77 and −7.83 ppm, respectively.[4]

In the germacyclohexane derivatives with an axial methyl group on C-3 the axial methyl group and the germanium nuclei are in the γ-gauche relation. Hence it is expected that NMR data of such compounds will show us whether the germanium shift is also susceptible to γ-effect, and that, if ever it exists, whether the direction of this effect is upfield (as in the case of ^{13}C shifts) or not.

Study on the γ-effect in the system where a heteroatom is involved in the four-atom unit has been the target of continuing interests.[6,7] No attempt has, however, been done to observe γ-effect associated with germanium nuclei. Germanium should be very suitable for the probe of γ-effect since it does not have the lone-pair electrons which will bring in some new effect to obscure the analysis.

For this purpose we prepared 3,3-dimethyl- (**7G**), 3,5-dimethyl- (**8G**), 1,1,3-trimethyl- (**9G**), 1,3,3-trimethyl- (**10G**), and 1,1,3,3- tetramethyl-(**11G**) germacyclohexanes and determined their NMR spectra. The molecular mechanics calculation of these compounds were also carried out.

Results and Discussion

^{73}Ge Chemical Shifts. ^{73}Ge and ^{13}C NMR spectra of these germacyclohexanes were determined and the results together with the data of relevant compounds, such as **1G**, **2G**, **3G**, **4G**, *cis*-**5G**, *trans*-**5G**, and **9G**, which are necessary for comparison, were included in the Table 1.

In our previous communication,[2] we have shown that ^{73}Ge chemical shift (δ value) of germacyclohexanes without any methyl group on germanium is ca. −130 ppm, that with an axial methyl is ca. −70 ppm, that with an equatorial methyl is ca. −60 ppm and that

Table 1. $^{73}Ge^{a)}$ and $^{13}C^{b)}$ Chemical Shifts of Germacyclohexanes (**1**—**11**)

Number of compound	Position of Me	Ge-1	C-2	C-3	C-4	C-5	C-6	Me-1	Me-3
1G	None	−130.3	9.32	26.78	29.89	26.78	9.32		
2G	1	−65.3	12.10	25.58	29.61	25.58	12.10	−7.01	
3G	3	−131.2	17.55	33.18	37.90	25.71	8.10		27.09
4G	1,1	−11.3	15.33	25.90	30.50	25.90	15.33	−3.74	
cis-**5G**	1,3	−60.6	21.75	31.97	38.43	26.12	11.95	−5.28	27.60
trans-**5G**	1,3	−70.9	20.66	31.97	38.26	24.61	11.00	−7.58	27.29
7G	3,3	−142.1	23.17	32.60	42.67	22.04	8.22		32.23
trans-**8G**	3,5	−145.0	15.62	26.95	43.37	26.95	15.62		23.91
9G	1,1,3	−12.2	24.94	32.44	38.54	24.01	13.94	−4.75 −2.45	27.59
10G	1,3,3	−70.6	26.48	32.46	42.42	21.33	11.31		30.07 34.15
11G	1,1,3,3	−18.7	29.80	33.61	43.24	21.26	14.54	−0.80	30.98

a) In ppm relative to external $GeMe_4$ (δ=0). b) In ppm relative to internal $SiMe_4$ (δ=0).

with two methyl groups is ca. −15 ppm.[4]

The sample of **8G** is in fact a mixture of trans and cis isomers. The ^{13}C NMR spectrum gave two sets of signals corresponding to two isomers, the ratio of which is ca. 6 : 1. The signal due to C-2 of the major stereoisomer is in the highest field among ring carbon signals, and is in higher field than that of the minor isomer. Thus, the major compenent of **8G** is the trans isomer since the ax,ax conformer of *cis*-**8G** has much higher energy than the eq,eq isomer where there is no axial methyl group.

The ^{73}Ge chemical shift of the major component, i.e., *trans*-**8G**, is −145.0 ppm, about 15 ppm upfield as compared with that of **3G**. This upfield shift is to our knowledge the first example of γ-gauche shift associated with ^{73}Ge resonances.

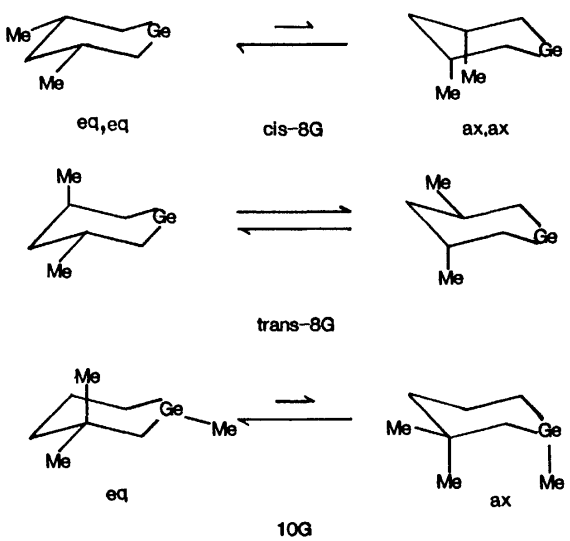

As compared with a very large upfield shift of ^{73}Ge caused by axial methyl group on C-3 of *trans*-**8G**, the effect caused by geminal 3,3-dimethyl group upon ^{73}Ge is somewhat smaller. Thus, **7G** resonates at −142.1 ppm, 10.9 ppm upfield as compared with **3G**, and **11G** resonates at −18.7 ppm, only 6.5 ppm upfield as compared with **9G**. As described later, this difference is likely due to the difference in the dihedral angle associated with the germanium atom. Thus, the upfield shift is smaller for compounds in which the ring is more flattened around the germanium. At any rate the existence of γ-effect upon ^{73}Ge chemical shifts in germacyclohexanes is now well-established.

It is worthwhile to mention that ^{73}Ge chemical shift of **10G** clearly indicates the predominance of equatorial conformation of methyl group on germanium. Otherwise, the ^{73}Ge nucleus should resonate at ca. −80 ppm. This in turn indicates that 1,3-diaxial dimethyl interaction is operative between *Ge*-methyl and *C*-methyl groups.

^{13}C Chemical Shifts. The ^{13}C chemical shifts of compounds **1G**—**6G** and **9G** were previously reported.[4] The assignments of ^{13}C signals of **7G**, **8G**, **10G**, and **11G** were carried out based on the conventional strategy. Where appropriate, SFORD (single-frequency off-resonance decoupling) and INEPT (insensitive nuclei enhancement by polarisation transfer) spectra were recorded for facilitating the assignments. The assignments based on the multiplicity and chemical shifts consideration are consistent with the additivity relations which have been established for the germacyclohexanes.[2,4]

The effect on the ^{13}C chemical shifts of germacyclohexanes caused by an axial methyl group on C-3 can be estimated by two ways. One way is the chemical shift difference between **7G** and **3G**, or between **11G** and **9G**. This difference can be compared with the case of carbon analog, i.e., the chemical shift difference between 1,1-dimethylcyclohexane (**4C**) and methylcyclohexane (**2C**). The differences estimated from the ^{13}C chemical shifts of these compounds are tabulated in Table 2.

The other way is the chemical shift difference between **8G** and **3G**, which can be compared with the corresponding difference in methylcyclohexanes, i.e., that between *trans*-1,3-dimethylcyclohexane (*trans*-**5C**) and **2C**. The results are also included in Table 2.

Table 2. Effects of an Axial Methyl Group at C-3 upon ^{13}C Chemical Shifts[a)]

A pair of compd. compared	C-2 β	C-3 α	C-4 β	C-5 γ	C-6 δ	Me-3	
7G−**3G**	5.62	−1.05	4.77	−3.67	0.12	5.14	
11G−**9G**	4.86	1.17	4.70	−3.25	0.60	5.50	
4C−**2C**	4.05	−2.95	4.05	−3.95	0.30	6.10	
(*trans*-**8G**)−**3G**[b)]	7.52		1.24	5.47	−6.23	−2.07	−3.18
(*trans*-**5C**)−**2C**[b)]	7.50		−0.50	5.65	−5.80	−1.90	−2.25

a) In ppm. b) In *trans*-**8G** and *trans*-**5C** the carbon with axial methyl group is numbered as C-3 for the sake of comparison.

Table 3. MM2 Component Steric Energies[a)] of Cyclohexanes and Germacyclohexanes (in kcal mol^{-1}; 1 cal=4.181 J)

Compound	Position of Me	Conformation	E_s	E_c	E_b	E_{sb}	E_t	$E_{1,4}$	E_{other}
4C	1,1		9.27	0.77	1.06	0.16	3.04	0.77	−1.55
trans-**5C**	1,3	eq,ax	9.02	0.59	1.08	0.18	3.08	5.85	−1.76
cis-**5C**	1,3	eq,eq	7.21	0.55	0.57	0.13	2.13	5.72	−1.90
		ax,ax	12.55	0.61	7.52	0.26	4.58	6.28	−1.71
4G	1,1		3.53	0.41	1.81	0.15	1.40	2.35	−2.59
trans-**5G**	1,3	eq,ax	6.63	0.60	2.63	0.23	1.85	3.30	−1.97
		ax,eq	5.05	0.58	1.91	0.16	1.38	3.39	−2.36
cis-**5G**	1,3	eq,eq	5.28	0.59	1.89	0.16	1.33	3.41	−2.11
		ax,ax	7.37	0.58	2.94	0.24	2.49	3.24	−2.11
7G	3,3		7.39	1.00	2.71	0.22	1.81	3.85	−2.22
trans-**8G**	3,5	eq,ax	8.01	0.77	2.74	0.25	1.82	4.36	−1.93
cis-**8G**	3,5	eq,eq	6.62	0.76	2.00	0.18	1.30	4.46	−2.07
		ax,ax	11.16	0.78	4.70	0.36	2.73	4.50	−1.91
10G	1,3,3	eq	7.39	1.00	2.71	0.22	1.81	3.85	−2.22
		ax	8.28	1.00	3.04	0.23	2.50	3.78	−2.27
11G	1,1,3,3		7.33	1.05	3.13	0.21	2.52	3.38	−2.97

a) For definition of each component steric energies, see text.

The effects of an axial methyl group at C-3 upon other carbon shifts of germacyclohexanes are, roughly speaking, similar with these for cyclohexanes. There are, however, some difference between the substituent parameters for cyclohexanes and germacyclohexanes. Thus, in geminal dimethyl compounds, germacyclohexanes exhibit a smaller β-effect, but its γ-effect is somewhat larger. α-Effects are scattering, and it is hard to draw any definite conclusion.

In *trans*-3,5-dimethyl series, the methyl substituent parameters are much the same for cyclohexanes and germacyclohexanes.

Molecular Mechanics Calculations. In Table 3, MM2[8)] steric energies of germacyclohexanes **4G**, **5G**, **7G**, **8G**, **10G**, and **11G** are listed together with relevant cyclohexanes **4C** and **5C**. For **5C**, **5G**, and **8G**, all stereoisomers associated with the orientation of methyl group are taken into consideration.

In MM2 calculations, total steric energies (E_s) are the sum of component energies, i.e., compression energy (E_c), bending energy (E_b), strech-bend energy (E_{sb}), tortional energy (E_t), and van der Waals energy which is subdivided into the energy associated with 1,4-interaction ($E_{1,4}$) and that with other interactions (E_{other}).

Two conclusions were drawn from the previous results.[2)] It has been shown that the axial and equatorial methyl group on germanium contributes to the steric energy to much the same extent. Though the change of C-5 chemical shifts caused by an axial methyl group at C-3 of germacyclohexanes is not so much different from the corresponding value of cyclohexanes, the difference in steric energy is large. Thus, the increment of steric energies caused by geminal dimethyl groups as estimated from the difference between **7G** (7.39 kcal mol^{-1}) and **1G** (5.72 kcal mol^{-1} [2)]) (i.e., 1.67 kcal mol^{-1} difference) is much smaller than that between **4C** (9.27 kcal mol^{-1}) and **1C** (6.55 kcal mol^{-1}) (i.e. 2.72 kcal mol^{-1} difference).

Next, we attempted to compare the magnitude of 1,3-diaxial dimethyl interaction under different steric environment from the difference of steric energies among 1,3 (or 3,5)-diequatorial conformer, 1,3 (or 3,5)-equatorial, axial conformer and 1,3 (or 3,5)-diaxial conformer of the identical geometrical isomers.

Thus, for **5C**, the steric energy difference between eq,eq isomer and eq,ax isomer is +1.81 kcal mol^{-1}, while that between eq,ax isomer and ax,ax isomer is +5.32 kcal mol^{-1}. When the ring is a germacyclohexane but two methyl groups are at C-3 and C-5 as is the case with **8G**, the corresponding differences are +1.39 and +3.15 kcal mol^{-1}, respectively. This is in line with

the results of the comparison given above.

When one of the methyl groups is at germanium, as is the case with **5G**,[4] the difference between 1-eq,3-eq and 1-ax,3-eq isomers is −0.23 kcal mol^{-1}, in line with the preference of axial conformation for this type of methyl group. The difference between 1-eq,3-eq and 1-eq,3-ax conformers is +1.35 kcal mol^{-1}, which is essentially identical with the value for **5C** and **8G**. The difference between 1-eq,3-eq and 1-ax,3-ax isomers of **5G** is only +2.09 kcal mol^{-1} in a sharp contrast with two previous cases, where the differences are +5.34 (*cis*-**5C**) and +4.54 kcal mol^{-1} (*cis*-**8G**), respectively. Thus, the 1,3-diaxial dimethyl interaction is smaller in germacyclohexane as compared with that in cyclohexane, and this is particularly so when one of the methyl is at germanium.

It is interesting to examine how the molecular mechanics calculations predict the structural change upon introduction of methyl groups on germanium and C-3. In Table 4, the predicted structures by MM2 for all the compounds discussed are summerized. Of all possible stereoisomers, high energy conformers are not taken into consideration.

It is clear from a glance of Table 4 that all the parameters, the bond lengths (r), the bond angles (θ), and the dihedral angles (ω) are not largely changed by the number and position of methyl groups introduced. It is slightly different from the case of methylcyclohexanes where a small change in bond length is invoked upon introduction of methyl groups.[2] A more relaxed structure of germacyclohexane as compared with cyclohexane is responsible for this phenomenon.

In one particular case where there exists a 1,3-diaxial dimethyl interaction with the buttress effect as is with **11G**, the change in dihedral angle caused by methyl groups is substantial. Thus, for germacyclohexanes without any 1,3-diaxial dimethyl interaction, the dihedral angle $\omega_{1,2}$ is in the range of 47°—49°. When there is a 1,3-diaxial dimethyl interaction present, the angle changes to 43°—44°, a substantial change. The ring is now further flattened around the germanium atom. This is also reflected in the dihedral angle $\omega_{2,3}$ which is nearly 50° for **11G**. A similar change is invoked when there is geminal 3,3-dimethyl group is present. The angle $\omega_{2,3}$ reduced to 54°.

That this change is associated with 1,3-diaxial di-

Table 4. Structures[a] of Methylgermacyclohexanes Optimized by Molecular Mechanics Calculations

Compound	$r_{1,2}$ nm	$r_{2,3}$ nm	$r_{3,4}$ nm	$r_{4,5}$ nm	$r_{5,6}$ nm	$r_{6,1}$ nm	θ_1 °	θ_2 °	θ_3 °
1G	0.1947	0.1530	0.1543	0.1543	0.1538	0.1947	101.6	109.9	113.5
3Geq	0.1947	0.1542	0.1546	0.1543	0.1537	0.1946	101.6	110.4	112.6
5Geq,eq	0.1947	0.1542	0.1547	0.1543	0.1537	0.1945	101.8	110.2	112.7
5Geq,ax	0.1947	0.1542	0.1547	0.1543	0.1537	0.1946	101.8	111.2	112.8
5Gax,eq	0.1947	0.1542	0.1547	0.1543	0.1537	0.1946	101.7	110.5	112.6
7G	0.1948	0.1548	0.1553	0.1543	0.1544	0.1945	101.7	112.3	111.8
8Geq,eq	0.1946	0.1541	0.1547	0.1547	0.1541	0.1946	101.6	110.2	112.7
8Geq,ax	0.1946	0.1541	0.1547	0.1547	0.1541	0.1946	101.6	110.4	112.3
9Geq	0.1946	0.1542	0.1547	0.1544	0.1538	0.1945	101.9	110.3	112.6
9Gax	0.1949	0.1542	0.1547	0.1544	0.1538	0.1945	102.3	112.7	113.2
10Geq	0.1947	0.1548	0.1553	0.1543	0.1537	0.1944	101.9	112.2	111.8
10Gax	0.1950	0.1548	0.1552	0.1537	0.1537	0.1945	102.3	113.9	112.1
11G	0.1949	0.1548	0.1533	0.1545	0.1537	0.1944	102.4	113.8	112.1

Compound	θ_4 °	θ_5 °	θ_6 °	$\omega_{1,2}$ °	$\omega_{2,3}$ °	$\omega_{3,4}$ °	$\omega_{4,5}$ °	$\omega_{5,6}$ °	$\omega_{6,1}$ °
1G	114.6	113.5	109.9	47.8	58.2	66.4	66.4	58.2	47.8
3Geq	115.1	113.5	109.6	48.0	57.7	66.0	66.9	58.3	47.7
5Geq,eq	115.1	113.5	109.6	48.0	57.7	66.1	66.8	58.2	47.8
5Geq,ax	116.5	113.5	109.8	47.3	55.5	63.7	65.6	57.7	47.7
5Gax,eq	115.1	113.5	109.7	47.8	57.6	66.0	66.8	58.1	47.5
7G	117.3	113.6	109.7	47.2	54.3	62.6	65.3	57.9	47.7
8Geq,eq	115.6	112.7	110.2	48.1	57.8	66.3	66.3	57.8	48.1
8Geq,ax	117.0	112.9	111.1	48.0	57.4	65.2	64.0	55.6	47.2
9Geq	115.0	113.4	109.6	47.6	57.6	66.4	67.3	58.3	47.5
9Gax	116.3	113.2	109.9	43.4	52.0	62.9	67.6	58.7	45.9
10Geq	117.4	113.6	109.6	47.1	54.2	62.7	66.0	57.8	47.5
10Gax	117.4	113.4	109.7	43.1	50.5	61.5	67.7	58.5	45.6
11G	117.2	113.2	109.7	43.2	50.7	61.8	67.9	58.6	45.7

a) The definition of the structural parameters is as follows: $r_{1,2}$ is the distance between Ge-1 and C-2 in nm, θ_1 is the bond angle C-6-Ge-1-C-2 in degrees and $\omega_{1,2}$ is the tortion angle in degrees defined by the C-6-Ge-1-C-2-C-3 moiety. The other parameters are defined analogously.

methyl group is evident since a similar change is invoked in $\omega_{5,6}$ and $\omega_{6,1}$ where there is a 1,5-diaxial dimethyl interaction.

Thus, an introduction of several methyl groups in germacyclohexane is calculated to cause no significant change in the bond length and bond angle of the ring. A substantial change in the dihedral angle is predicted instead. We are continuing efforts to demonstrate experimentally these characteristics of germacyclohexanes.

Experimental

Preparation of Germacyclohexanes. The necessary precursor for 3,3-dimethylgermacyclohexanes, 1,5-dibromo-2,2-dimethylpentane does not seem to have previously been described. This arises from the fact that the treatment of 2,2-dimethyl-1,5-pentanediol with the standard brominating reagents such as hydrogen bromide or phosphorus tribromide causes a migration of β-methyl group (a Wagner-Meerwein rearrangement) to result in the formation of unexpected compound. Hence we treated the diol with dibromotriphenylphosphorane[9] to end up with the desired dibromopentane.

The dibromopentane was converted to the bis-Grignard reagent, which was caused to react with tetrachlorogermane to give 1,1-dichlorogermacyclohexanes. Treatment of dichlorogermacyclohexanes with lithium aluminum hydride(LAH) afforded 1,1-dihydrogermacyclohexanes (**7G** and **8G**). 1,1-Dichlorogermacyclohexanes were treated with methylmagnesium bromide to give the 1,1-dimethylgermacyclohexanes (**9G** and **11G**). Treatment of bis-Grignard reagent with dichloromethylgermane gave **10G**. The details of these procedures were described in our previous communication.[2] 1,5-dibromo-2,2-dimethylpentane. 2,2-Dimethylglutaric acid was esterified with ethanol under an acidic condition, and the ester was reduced to 2,2-dimethyl-1,3-pentanediol by means of LAH in a conventional manner.

The diol (10.0 g; 0.075 mol) and triphenylphosphine (43.8 g; 0.167 mol) were dissolved in dry *N*,*N*-dimethylformamide (DMF; 80 ml), to which bromine (27.5 g; 0.169 mol) was added dropwise under the atmosphere of argon and ice-cooling. During the addition the temperature was kept at 10—20 °C. Stirring was further continued for another 20 h at 25 °C. The forerun of the distillation under the reduced pressure (fraction of bp 63—66 °C/30 mmHg (1 mmHg≈133.322 Pa)) was discarded and the second fraction (bp 60—68 °C/4 mmHg) was collected, and this was poured into the ice-water. The heavy oil was extracted with dichloromethane, which was washed with water, dried over anhydrous calcium carbonate, and the solvent evaporated. The residue was reduced in vacuo to afford yellow oil of 2,2-dimethyl-1,5-dibromopentane (10.32 g; 53% overall), bp 125—127 °C/29 mmHg. ^{1}H NMR (90.0 MHz; $CDCl_3$) δ=1.03 (6H, s), 3.26 (2H, s), 3.38 (2H, t. J=7 Hz).

Found: C, 32.48; H, 5.50%. Calcd for $C_7H_{14}Br_2$: C, 32.59, H, 5.47%.

3,5-Dimethylpiperidine (Tokyo Kasei Co.) and benzoyl chloride were caused to react in aqueous NaOH to give 1-benzoyl-3,5-dimethylpiperidine (91%), mp 95 °C. IR (KBr) 1615 (C=O).

Found: C, 77.44; H, 8.79; N, 6.40%. Calcd for $C_{14}H_{19}NO$: C, 77.37; H, 8.81; N, 6.44%.

The benzoyl derivative was treated with PBr_3/Br_2 to afford 1,5-dibromo-2,4-dimethylpentane, bp 105—107 °C/1.5 mmHg.

Preparation of germacyclohexanes has been carried out based on the procedure described in the previous report.[2] Thus, the reaction between the bis-Grignard reagent of 1,5-dibromo-2,2-dimethylpentane and tetrachlorogermane afforded 1,1-dichloro-3,3-dimethylgermacyclohexane which, without isolation, was converted to **7G** by means of LAH, or to **11G** by the reaction with methylmagnesium bromide. Treatment of the same dibromide with dichloromethylgermane afforded **10G**.

The reaction between the bis-Grignard reagent of 1,5-dibromo-2,4-dimethylpentane and tetrachlorogermane afforded 1,1-dichloro-3,5-dimethylgermacyclohexane which, without isolation, was converted to **8G** by means of LAH. The physical properties of these germacyclohexanes are summerized in Table 5.

Measurements of Spectra. Infrared spectra were obtained with a JASCO A102 grating infrared spectrophotometer as a liquid film.

The ^{1}H NMR spectra were recorded with a Varian EM-390 spectrometer as $CDCl_3$ solution containing a small amount of tetramethylsilane (TMS) as the internal standard.

The ^{13}C NMR spectra of germacyclohexanes were recorded as solutions of $CDCl_3$ or C_6D_6 on a JEOL FX-90Q spec-

Table 5. Physical Properties of Germacyclohexanes (**7G—11G**)

Compound (formula)	Yield[a] %	Bp θ_m °C/mmHg	IR(Ge-H) ν_H(neat)	^{1}H NMR δ_H(90MHz; $CDCl_3$)	MS m/z[b]
7G ($C_7H_{14}Ge$)	14	88—90/22	2040	1.00 (6H, s, 3,3-diMe) 3.60 (2H, m, 1-H)	
8G ($C_7H_{14}Ge$)	8	97—100/17	2045	1.00 (6H, d, J=7 Hz, 3,5-Me) 3.63 (2H, m, 1-H)	
9G ($C_8H_{16}Ge$)	7	85—87/26	—	0.13 (6H, s, 1,1-diMe) 0.93 (3H. d, J=7 Hz, 3-Me)	
10G ($C_6H_{16}Ge$)	6	90—93/13	2050	0.21 (3H, d, J=3 Hz, 1-Me) 0.98 (6H, s, 3,3-diMe) 3.88 (1H, m, 1-H)	160.1 (M^+), 145.2 (M^+-15) 132.2 (M^+-28)
11G ($C_9H_{18}Ge$)	12	98—100/18	—	0.15 (6H, s, 1,1-diMe) 0.95 (6H, s, 3,3-diMe)	160.1 (M^+), 132.2 (M^+-28)

a) Yield based on the immediate precursor. b) Of the peaks due to various isotomers, only the one due to ^{74}Ge is given.

trometer at 22.50 MHz in 10 mm tube at 30°C. The condition of measurements are the standard ones.

The ^{73}Ge NMR spectra of germacyclohexanes were recorded as solutions in $CDCl_3$ (1 : 1 v/v) on a JEOL FX-90Q spectrometer equipped with an NM-IT 10LF low-frequency insert, operating at 3.10 MHz, in a 10 mm tube at 30°C. Typical measurement conditions were as follows: pulse width, 150 μs (90°); spectral width, 2000 Hz: number of scans, 5000; pulse delay, 100 ms; data points, 4096. The ^{13}C NMR spectra were determined for the same solutions on the same instrument at 22.50 MHz. Typical measurement conditions were as follows: pulse width. 13 μs (40°): spectral width, 2000 Hz: number of scans, 500; pulse delay, 1 s; data points, 4096.

GC/MS spectra were obtained on a Hewlett-Packard 5995A instrument controlled by a Hewlett-Packard 9825 desktop computer system with a 25 m (ϕ 0.2 mm) cross-linked methyl silicone column.

Molecular Mechanics Calculations. The program used was Allinger's MM2. Since in MM2 the parameters for germanium are not available, we installed the parameters reported by Ouellette[10] in MM2. Since the parameters were prepared for the older force field of Allinger[11] (before MM1) based on the experimental values of methylgermane and dimethylgermane, there is some doubt as for the consistency between parameters for germanium and for other atoms. This point has been discussed in the previous communication[2] where it has been shown that the use of the combination of MM2 and germanium parameters of Ouellette[10] is acceptable, and this combination is used throughout this investigation.

For the sake of comparison, calculations were also carried out for the corresponding cyclohexanes, and the results were also included in Table 2.

The authors thank the Ministry of Education, Culture and Health for Grant-in-Aid.

References

1) Part V: T. Harazono, K. Tanaka, and Y. Takeuchi, *Inorg. Chem.*, **26**, 1894 (1987).

2) Y. Takeuchi, M. Shimoda, K. Tanaka, S. Tomoda, K. Ogawa, and H. Suzuki, *J. Chem. Soc., Perkin Trans. 2*, **1988**, 7.

3) R. J. Ouellette, *J. Am. Chem. Soc.*, **96**, 2421 (1974).

4) Y. Takeuchi, M. Shimoda, and S. Tomoda, *Magn. Reson. Chem.*, **23**, 580 (1985).

5) D. K. Dalling and D. M. Grant. *J. Am. Chem. Soc.*, **89**, 66 (1967).

6) E. L. Eliel, W. F. Bailey, L. D. Kopp. R. L. Willer, D. M. Grant, R. Bertrant, K. A. Christensen, D. K. Dalling, M. W. Duch, E. Wenkert. F. M. Schell, and D. W. Cochran, *J. Am. Chem. Soc.*, **97**, 322 (1975).

7) J. B. Lambert and A. R. Vagenas, *Org. Magn. Reson.*, **17**, 270 (1981).

8) N. L. Allinger and Y. H. Yuh, *QCPE* No. 395 (1977). The University of Tokyo Computer Center, Program Library Y4MM2.

9) G. A. Wiley, R. L. Hershkowitz, B. M. Rein, and B. C. Chung, *J. Am. Chem. Soc.*, **86**, 964 (1964).

10) R. J. Ouellette, *J. Am. Chem. Soc.*, **94**, 7674 (1972).

11) N. L. Allinger, J. A. Hirsch, M. A. Miller, I. J. Tyminsky, and F. A. Van-Catledge, *J. Am. Chem. Soc.*, **90**, 1199 (1968).

Formation of 4-Benzamidoisoxazole Derivatives[1)]

Shonosuke ZEN,* Kazuho HARADA, Hikaru NAKAMURA,† and Yoichi IITAKA†
School of Pharmaceutical Sciences, Kitasato University, Shirokane, Minato-ku, Tokyo 108
†Faculty of Pharmaceutical Sciences, University of Tokyo, Hongo, Bunkyo-ku, Tokyo 113
(Received February 10, 1988)

The titled compounds (**3**) were synthesized by the reaction of nitrile oxides with 1-azirines and also the reaction of aliphatic nitro compounds with dibenzoylmethane derivatives in the presence of acetyl chloride and sodium methoxide. The structure of **3** was established by single crystal X-ray analysis. A mechanism of the formation for **3** is proposed.

This is dealing with an one-pot synthesis of 4-benzamidoisoxazole derivatives **3** through the reaction of nitrile oxides **1**[2)] with 1-azirines **2**.[3,4)] **3** was synthesized by the two methods as follows: (I) Nitrile oxides **1a—1c**, which are isolated or generated in situ by the acylation[5)] of aliphatic nitro compounds **4a—4c** with acetyl chloride, are allowed to react with 2-benzoyl-1-azirines (**2a—2c**) in the presence of NaOMe. In this case furazan 2-oxides (**6**),[2)] dimers of **1**, were obtained as main products. (II) Dibenzoylmethanes (**5a, 5b**) are reacted with two molecular equivalents of **4a, b** in the presence of acetyl chloride and NaOMe also (Scheme 1). The results of these procedures are summarized in Table 1.

The structure of **3** was determined by single crystal X-ray analysis with **3e** (Fig. 1) and also by alternative preparations of **3c** and **3g** from **9f** and **9g**[6)] respectively (III) (Scheme 1). Compound **3c** obtained via (I) was identical to that obtained from the reaction (III).

The postulated mechanism of the formation of **3** was illustrated by Scheme 2: Nitrile oxide **1** generated from **4** reacts with dibenzoylmethane derivative **5** in an 1,3-dipolar cycloaddition to give an isoxazoline intermediate **10**. A fission of N-O bond[7)] of **10** in basic conditions followed by elimination of benzoic acid affords nitrene intermediate **11**, which isomerizes[8)] to 1-azirine **2**. Subsequently, nucleophilic attack of methoxide anion to **2** gives aziridine intermediate **12**. Furthermore a fission of C-C bond[9)] of **12** gives olefinic intermediate **13**, which cyclizes with another **1** to finally lead to **3**.

This mechanism was also supported by the following experimental results: i) Isolated nitrile oxide **1b** reacts with **5a** to give the corresponding 1-azirine **2b**.[10)] ii) Isoxazoles (**7** and **8**) were isolated as by-products in

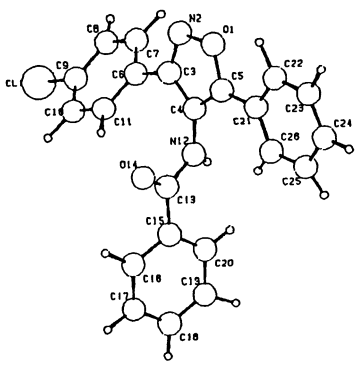

Fig. 1. Molecular structure of the compound **3e**.[15)]

Table 1. Yields and Spectral Data of the Derivatives of Benzamidoisoxazoles and Related Compounds

	R^1	R^2	R^3	Mp θ_m/°C	Yield/% I	II	III	IR cm^{-1}	MS, m/z	^{1}H NMR δ/ppm (NH and Me)
3a	H	H	H	202—203	20[b)]	16		3210, 1650	340(M^+)	7.60
3b	CH_3	H	H	188—190	13,[a)] 23[b)]			3240, 1640	354(M^+)	7.55, 2.37
3c	CH_3	CH_3	H	216—219	18[a)]	28	76	3240, 1650	368(M^+)	7.53, 2.33, 2.40
3d	CH_3	CH_3	CH_3	238—241	35[b)]	41		3260, 1650	382(M^+)	7.42, 2.40, 2.37(2Me)
3e	Cl	H	H	176—178	5[b)]			3260, 1660	374(M^+), 376(M^++2)	7.50
3g	CH_3	H	CH_3	223—224			91	3220, 1650	368(M^+)	7.45, 2.33(2Me)
14a	H	H	H	153—155		92		1660	354(M^+)	3.47
14b	CH_3	H	H	155—157		76		1660	368(M^+)	2.45, 3.47
14c	CH_3	CH_3	H	176—178		83		1660	382(M^+)	2.22, 2.45, 3.45
14d	CH_3	CH_3	CH_3	213—214		58		1660	396(M^+)	2.34(2Me), 2.43, 3.45
15a	—	—	—	222—224		64		3230, 1640	342(M^+)	7.50, 8.43, 8.80
15b	—	—	—	211—213		67		3370, 3300, 1630	356(M^+)	3.24, 6.63, 7.00
16a	—	—	—	173—175[c)]		14		—	—	—
16b	—	—	—	130—132		60		3440, 1720, 1690	357(M^+)	—
17	—	—	—	201—202		74		3260, 1630	324(M^+)	—

a) The yields of **3** by the reaction of (**1**+**2**→**3**). b) The yields of **3** by the reaction of (**4**+**2**→**3**). c) Lit. 173.5—174.5 °C (Ref. 14). All compounds had elemental analyses (C,H,N) within ±0.3% of theoretical values.

Table 2. The Positional Parameters and Equivalent Isotropic Thermal Parameters with Their Estimated Standard Deviation in Parentheses

Atom	x (×10⁴)	y (×10⁴)	z (×10⁴)	B_{eq}/Å²
O1	1679(1)	1789(4)	8110(2)	3.25(0.04)
N2	1978(1)	1606(5)	7109(3)	3.24(0.05)
C3	2560(2)	2069(6)	7470(3)	2.88(0.06)
C4	2657(2)	2564(6)	8681(3)	2.77(0.05)
C5	2095(2)	2389(6)	9048(3)	2.91(0.06)
C6	3013(2)	2080(6)	6642(3)	2.97(0.06)
C7	2854(2)	2795(7)	5502(4)	3.72(0.07)
C8	3289(2)	2858(7)	4742(4)	4.15(0.07)
C9	3881(2)	2222(7)	5135(4)	3.93(0.07)
C10	4050(2)	1468(7)	6243(4)	4.00(0.07)
C11	3610(2)	1409(6)	7006(4)	3.48(0.07)
C12	3217(1)	3230(5)	9339(3)	2.83(0.05)
C13	3615(2)	2077(6)	10035(3)	3.14(0.06)
C14	3510(1)	467(4)	10124(3)	4.86(0.06)
C15	4192(2)	2981(6)	10668(3)	3.06(0.06)
C16	4694(2)	1834(7)	11052(4)	4.07(0.07)
C17	5245(2)	2618(8)	11637(4)	4.96(0.08)
C18	5287(2)	4463(7)	11848(4)	4.10(0.07)
C19	4794(2)	5560(7)	11472(4)	3.97(0.07)
C20	4241(2)	4820(6)	10875(4)	3.64(0.07)
C21	1855(2)	2699(6)	10151(3)	3.24(0.06)
C22	1248(2)	2203(7)	10235(4)	4.41(0.08)
C23	1014(2)	2525(8)	11277(4)	5.34(0.09)
C24	1382(2)	3354(8)	12227(4)	5.24(0.09)
C25	1982(2)	3845(8)	12145(4)	4.88(0.09)
C26	2225(2)	3518(7)	11106(4)	4.30(0.08)
Cl	4433(1)	2391(2)	4191(1)	5.68(0.02)

the reaction (II). This result shows that the above mechanism includes intermediate **10**, for **7** is a dehydroxy compound of **10**, and **8** is considered to be formed from **11**.[8]

The reactivity of **3** was also studied as follows: i) *N*-Methylations of **3a—3d** were carried out with CH_3I to afford **14a—14d** in good yields as summarized in Table 1. ii) Hydrogenation of **3** with Raney Ni afforded *β*-aminoenone (**15**), which was hydrolyzed to give **16** and/or imidazole **17** (Scheme 3).

The authors (Z. and H.) reported[11] previously the reaction of **1** with **2** to give **3** and assigned the structure of **3** to 4*H*-1,2,4-oxadiazine derivative based on spectroscopic analysis and also a ring opening reaction mentioned above. However, the structure of **3** was established to be 4-benzamido-3,5-diarylisoxazole, as illustrated in Fig. 1 by X-ray analysis. Accordingly, the authors (Z. and H.) correct the structure of **3** herein.

Table 3. Bond Length and Torsional Angle for the Bond Connecting the Conjugated Groups

A-X-Y-B	Bond length (l/Å) X-Y	Torsional angle (ϕ/°) along X-Y
N2-C3-C6-C7	1.474 (6)	42.9 (5)
O1-C5-C21-C22	1.458 (6)	6.6 (5)
C3-C4-N12-C13	1.419 (4)	−97.6 (4)
N12-C13-C15-C20	1.506 (5)	20.8 (5)

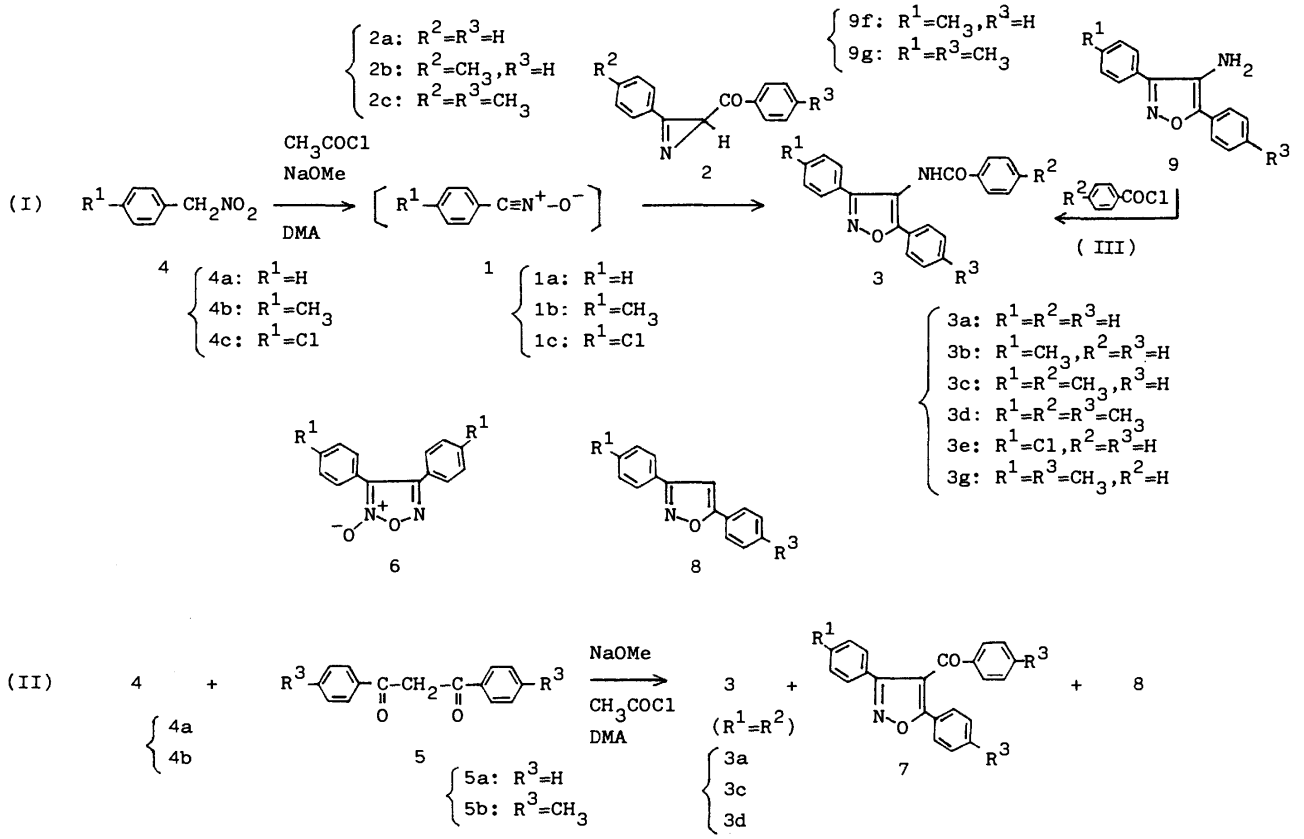

Scheme 1.

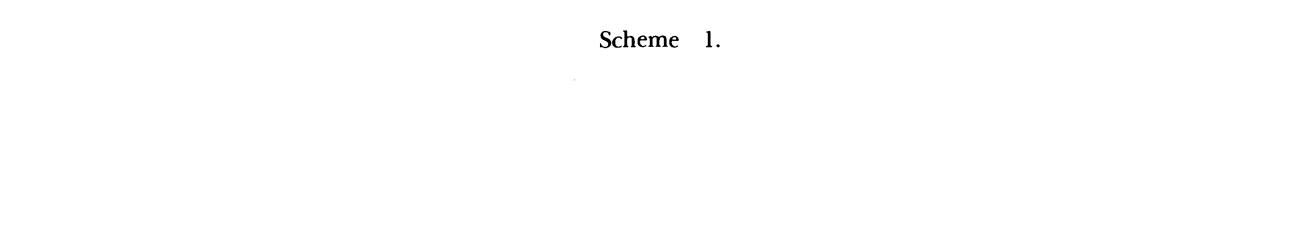

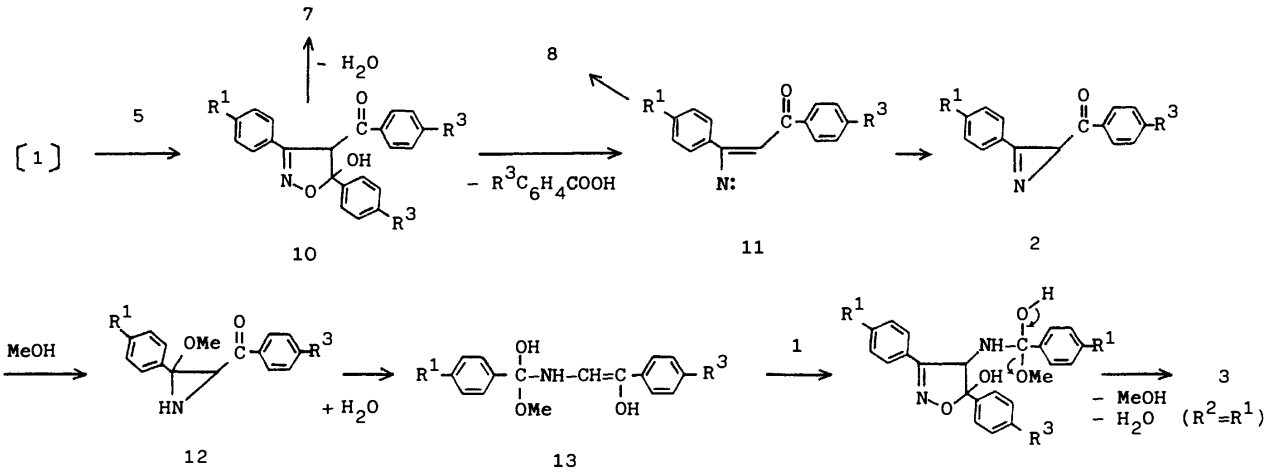

Scheme 2.

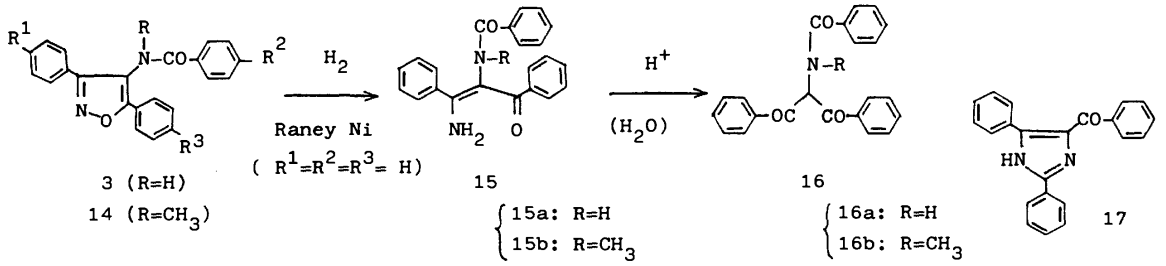

Scheme 3.

Experimental

Reaction of *p*-Tolunitrile Oxide (1b) with 3-Benzoyl-2-phenyl-1-azirine (2a). General Procedure for Method(I): To a solution of **2a**[12] (57.0 mg, 0.26 mmol) in anhydrous *N,N*-dimethylacetamide (DMA) (5 cm^3) was added freshly prepared **1b**[13] (37.0 mg, 0.26 mmol) and 1 mol dm^{-3} NaOMe in MeOH (0.52 cm^3) with ice-cooling. After stirring at room temperature overnight, the reaction mixture was partitioned between ice-water (20 cm^3) and benzene (10 cm^3). The aqueous phase was extracted with benzene (3×10 cm^3), dried (Na_2SO_4) and concentrated to dryness. The residue (46.2 mg) was separated by column chromatography on silica gel with AcOEt–hexane (5 : 1) as an eluent to afford 3,4-di-*p*-tolylfurazan 2-oxide (**6b**) (20.1 mg, 54%) and 4-benzamido-5-phenyl-3-(*p*-tolyl)isoxazole (**3b**) (11.9 mg, 13%): mp 188—190 °C (EtOAc–hexane).

Reaction of Phenylnitromethane (4a) with 3-Benzoyl-2-phenyl-1-azirine (2a): To a solution of **4a** (137 mg, 1.0 mmol) in anhydrous DMA (15 cm^3) was added 1 mol dm^{-3} NaOMe in MeOH (1.0 cm^3), acetyl chloride (0.70 cm^3, 1.0 mmol), **2a** (221.0 mg, 1.0 mmol) with ice-cooling. After further addition of 1 mol dm^{-3} NaOMe in MeOH (4.0 cm^3), the reaction mixture was stirred at room temperature overnight. Then, the reaction mixture was poured into ice-water (20 cm^3). After neutralization with 1 mol dm^{-3} HCl, the aqueous phase was extracted with benzene (3×15 cm^3), dried (Na_2SO_4) and concentrated to dryness. The residue (284 mg) was chromatographed on silica gel with EtOAc–hexane (5 : 1) as an eluent to give 3,5-diphenylisoxazole (**8a**) (79.0 mg, 35%), 3,4-di-*p*-tolylfurazan 2-oxide (**6a**) (13.0 mg, 54%), and 4-benzamido-3,5-diphenylisoxazole (**3a**) (68.0 mg, 20%): mp 202—203 °C (MeOH–H_2O).

Reaction of Phenylnitromethane (4a) with Dibenzoylmethane (5a). General Procedure for Method(II): To a solution of **4a** (548 mg, 4.0 mmol) in anhydrous DMA (20 cm^3) was added 1 mol dm^{-3} NaOMe in MeOH (4 cm^3), acetyl chloride (0.29 cm^3, 4.1 mmol), **5a** (448 mg, 2.0 mmol) with ice-cooling. After further addition of 1 mol dm^{-3} NaOMe in MeOH (16 cm^3), the reaction mixture was poured into ice-water (120 cm^3). After neutralization with 1 mol dm^{-3} HCl, the aqueous phase was extracted with benzene (3×40 cm^3), dried (Na_2SO_4) and concentrated to dryness. The residue (887.5 mg) was chromatographed on silica gel with benzene–EtOAc (20 : 1) as an eluent to give **8a** (140.5 mg, 32%), 4-benzoyl-3,5-diphenylisoxazole (**7a**) (195.3 mg, 30%), methyl benzoate (33.0 mg, 12%), acetophenone (28.0 mg, 12%) and **3a** (108.2 mg, 16%).

X-Ray Analysis of 4-Benzamido-3-(*p*-chlorophenyl)-5-phenylisoxazole (3e): X-Ray specimen of **3e** of approximate dimensions 0.35×0.1×0.06 mm was recrystallized from hexane–EtOAc. Diffraction intensities were measured using Cu $K\alpha$ radiation monochromated by a graphite plate. The crystal data are: 4-Benzamido-3-(*p*-chlorophenyl)isoxazole, $C_{22}H_{15}N_2O_2Cl$, MW=374.8. Monoclinic, space group $P2_1/n$, Z=4. Unit cell dimensions, a=21.833(10), b=7.339(5), c=11.448(7) Å, β=99.02(6)°, U=1812 Å^3. D_{cal}=1.374 g cm^{-3}, μ for Cu $K\alpha$=31 cm^{-1}. Number of observed reflections as above the 2δ(I) level was 2390 out of 3947 within the 2θ range of 6° through 156°. The crystal structure was determined by the direct method and refined by the method of block-diagonal matrix least-squares to an R value of 0.058 including 27 heavier atoms and 42 hydrogen atoms. The hydrogens were

located on the difference electron-density map and their positional and isotropic temperature factors were included in the least-squares refinement. The molecular structure of **3e** is shown in Fig. 1. The molecule consists of an isoxazole ring(A), two phenyl groups (B and C, B ring bears a chlorine atom at *p*-position), and a benzamido group (D). The dimensions of each part of the molecule are quite normal. The torsional angles along the bonds connecting each group are listed in Table 3.

***N*-Benzoylation of 4-Amino-5-phenyl-3-(*p*-tolyl)isoxazole (9f):** A mixture of **9f** (30 mg, 0.12 mmol), *p*-toluoyl chloride (19 mg, 0.12 mmol) and K_2CO_3 (18 mg, 0.12 mmol) in a ether–benzene–H_2O (1 : 3 : 1) mixed solution was stirred at 0—5 °C for 15 h. The mixture was poured into ice-water and extracted with toluene (5 $cm^3 \times 3$), dried (Na_2SO_4) and concentrated to dryness. The residue (47.4 mg) was chromatographed on silica gel with hexane–EtOAc (3 : 1) as an eluent to give **3c** (33.6 mg, 76%): mp 218—220 °C (MeOH–H_2O).

***N*-Methylation of 3a:** A mixture of **3a** (20 mg, 0.06 mmol), KOH (3.9 mg, 0.06 mmol), and 18-crown-6 (0.25 mg, 0.001 mmol) in benzene (2 cm^3) was refluxed for 2 h. After the addition of CH_3I (14 mg, 0.1 mmol) in benzene (1 cm^3), the reaction mixture was refluxed for 4 h and concentrated in vacuo. After washing with H_2O, the crude product was recrystallized from EtOAc–hexane to give 4-(*N*-methylbenzamido)-3,5-diphenylisoxazole (**14a**) (19.0 mg, 92%).

Reductive Ring Opening Reaction of 3a: A solution of **3a** (100 mg, 0.26 mmol) in MeOH (30 cm^3) was hydrogenated (1 atm, r.t.) for 3 h in the presence of activated Raney Ni-Tl. After the solution was filtered, the filtrate was concentrated to dryness. The residue (95.2 mg) was chromatographed on silica gel with hexane–EtOAc (3 : 1) as an eluent to furnish 3-amino-2-benzamido-1,3-diphenyl-2-propen-1-one (**15a**) (64.6 mg, 64%).

Hydrolysis of 15a: A mixture of **15a** (50 mg, 0.15 mmol) and 1 mol dm^{-3} HCl (1 cm^3) in MeOH (2 cm^3) was refluxed for 2h. After cooling, the reaction mixture was diluted with 5 cm^3 of cooled H_2O, and the resultant precipitates were collected. 2-Benzamido-1,3-diphenyl-1,3-propanedione (**16a**) (7.0 mg, 14%): mp 173—175 °C (MeOH) (lit,[14] 173.5—174.5 °C). The filtrate was neutrallized with 2 mol dm^{-3} NaOH and the resultant precipitates were collected. 2-Benzoyl-3,5-diphenylimidazole (**17**) (37.0 mg, 74%): mp 201—202 °C (MeOH).

References

1) The Synthetic Reactions of Aliphatic Nitro Compounds XXV. Presented at the 54th Annual Meeting of Chemical Society of Japan, Tokyo, April 1987. (Part XXIV: S. Zen, T. Nishino, K. Harada, H. Nakamura, and Y. Iitaka, *Chem. Pharm. Bull.*, **31**, 4181 (1983).

2) For reviews, a) P. Caramella and P. Grünanger, "1,3-Dipolar Cycloaddition Chemistry," ed by A. Padwa, John Wiley & Sons, New York (1984), Vol. 1, Chap. 3, pp. 291—392; b) R. Huisgen, *Angew. Chem., Int. Ed. Engl.*, **2**, 565 (1963); C. Grundmann, "The Chemistry of the Cyano Group," ed by Z. Rappoport, Interscience Publishers, New York (1970), pp. 832—846.

3) For reviews, a) V. Nair and K-H Kim, *Heterocycles*, **7**, 353 (1977); b) A. Hassner, *Heterocycles*, **14**, 1517 (1980).

4) V. Nair, *Tetrahedron Lett.*, **1971**, 4831.

5) K. Harada, E. Kaji, and S. Zen, *Chem. Pharm. Bull.*, **28**, 3296 (1980)

6) V. D. Piaz, S. Rinzauti, and P. Lacrimini, *Synth. Commun.*, **1975**, 664.

7) G. Bianchi, R. Gandolfi, and P. Grünanger, *J. Heterocycl. Chem.*, **5**, 49 (1968).

8) A. N. Nesmeyanov, M. I. Rybinskaya, and I. G. Kelekhsaeva, *Izvest. Akad. Nauk, SSSR*, **1969**, 866.

9) A. Padwa, O. Eastman, and L. Hamilton, *J. Org. Chem.*, **33**, 1317.

10) S. Zen and K. Harada, *Chem. Pharm. Bull.*, **30**, 366 (1982).

11) S. Zen and K. Harada, *Chem. Lett.*, **1982**, 1711.

12) E. F. Ullman and B. Singh, *J. Am. Chem. Soc.*, **88**, 1844 (1966).

13) G. Barbaro, G. Battaglia, and A. Dondoni, *J. Chem. Soc. B*, **1970**, 588; A. Quilico, "Five and Six-membered Compounds with Nitrogen and Oxygen," ed by R. H. Wiley, Intersciences, New York (1962), p. 21.

14) D. Y. Curtin and M. L. Poutsma, *J. Am. Chem. Soc.*, **84**, 4887 (1962).

15) Tables of anisotropic thermal parameters, coordinates of hydrogen atoms are deposited as Document No. 8817 at the Office of the Editor of Bull. Chem. Soc. Jpn.

Dual-Mode Behavior in Doping-Undoping of Polypyrrole with Alkanesulfonate

Takeo SHIMIDZU,* Akira OHTANI, and Kenichi HONDA
Division of Molecular Engineering, Graduate School of Engineering, Kyoto University, Sakyo-ku, Kyoto 606
(Received February 15, 1988)

Polypyrrole (PPy) films incorporated with a series of 1-alkanesulfonates, $R_nSO_3^-$ ($C_nH_{2n+1}SO_3^-$, n=3—10), were prepared by the electrochemical polymerization of pyrrole in H_2O containing sodium salt of $R_nSO_3^-$. The mass transfer in the PPy matrix of the $R_nSO_3^-$ incorporated PPy (PPy/$R_nSO_3^-$) films were investigated by electrochemical measurements. The electrochemical properties of PPy/$R_nSO_3^-$ were affected by the chain length of the incorporated $R_nSO_3^-$. The incorporation and release of cationic species into the PPy/$R_nSO_3^-$ matrix during an electrochemical oxidation-reduction of PPy were observed and the contribution of cationic species during the doping-undoping process was increased with the dopant size. The PPy/$R_nSO_3^-$ showed a dual-mode behavior during the electrochemical doping-undoping process.

Conducting PPy[1-6] has applications in such equipment as, electronic devices,[7,8] electrochromic displays,[9-11] polymer batteries,[12-15] polymer modified electrodes,[16] functional membranes,[17,18] etc. In these applications, the oxidation-reduction capability accompanying the incorporation-release of ions, which is called "doping-undoping," is an important feature of PPy.[19] Though PPy has been studied most widely, it has not provided any advantageous properties from a practical point of view. Many hybridization procedures of PPy with various functional molecules have been developed so as to improve the properties of PPy.[20-31] Especially, a hybridization procedure utilizing an anodic doping process during the electrochemical polymerization of pyrrole has been actively studied, and many kinds of PPy/functional anion composites were prepared. However, there is a question whether PPy/functional anion composites show stable properties under all redox states of PPy, because incorporated anions (dopants) are usually released from the PPy matrix when PPy is reduced. We reported that the size of the dopant affected the doping-undoping capability of PPy.[32] In recent years, studies of mass transfer in the PPy matrix on the oxidation-reduction of PPy have been reported.[33-36] Either anion releasing or cation incorporating was observed when PPy was electrochemically reduced. In this study, a series of 1-alkanesulfonates was chosen as the dopant[37] and the detailed electrochemical property of PPy/$R_nSO_3^-$ during the electrochemical oxidation-reduction process is discussed.

Experimental

Materials. Pyrrole (Aldrich Chemical Co.) was distilled and stored under an N_2 atmosphere. Potassium chloride (Wako Chemical Co.) and sodium 1-alkanesulfonates, such as sodium 1-propanesulfonate, 1-butanesulfonate, 1-pentanesulfonate, 1-hexanesulfonate, 1-heptanesulfonate, 1-octanesulfonate, 1-nonanesulfonate, and 1-decanesulfonate (Nakarai Chemicals), were used without further purification.

Preparation of PPy. PPy/$R_nSO_3^-$ films on an indium-tin oxide (ITO) electrode (7 cm^2) for elemental analyses, measurements of conductivity, and deionization experiments were prepared by the electrochemical polymerization of pyrrole (0.1 mol dm^{-3}) in H_2O containing sodium salt of $R_nSO_3^-$ (0.1 mol dm^{-3}) under 10 mA galvanostatic electrolysis for 1 h. The thicknesses of these films were estimated by an optical microscopic photograph of the cross section of the PPy/$R_nSO_3^-$. PPy/$R_nSO_3^-$ films on a Pt electrode (0.047 cm^2) for cyclic voltammetry were prepared by an electrochemical polymerization of pyrrole (0.1 mol dm^{-3}) in H_2O containing sodium salt of $R_nSO_3^-$ under potentiostatic electrolysis (1.0 V vs. SCE) for 4.9 mC. A chloride anion incorporated PPy (PPy/Cl^-) on an ITO electrode (7 cm^2) was prepared by the electrochemical polymerization of pyrrole (0.2 mol dm^{-3}) in 0.5 mol dm^{-3} KCl aqueous solution under 10 mA galvanostatic electrolysis for 1 h. The reduced PPy/Cl^- (PPy/Cl^-(red.)) for deionization experiments was prepared by a −2.0 mA galvanostatic electrolysis of the PPy/Cl^- anode in a 0.1 mol dm^{-3} KCl aqueous solution until the potential reached −1.0 V vs. SCE, at which point the incorporated Cl^- was quantitatively released.

Electrochemical Measurements. Cyclic voltammetries were carried out in H_2O containing a 0.1 mol dm^{-3} sodium salt of $R_nSO_3^-$ or KCl. Deionization experiments were carried out by potentiostatic electrolysis of the PPy/Cl^- (red.) anode and the PPy/$R_nSO_3^-$ cathode. The concentration of K^+ in a KCl aqueous solution was measured by an atomic absorption analysis (Shimadzu AA-670). All electrochemical experiments were carried out at room temperature under an N_2 atmosphere using a potentiogalvanostat (Nikko Keisoku NPGS- 301), a function generator (Nikko Keisoku NFG-3), and a coulomb/ampere-hour meter (Hokuto Denko Ltd. HF-201).

Results and Discussion

Electrochemical Properties of PPy/$R_nSO_3^-$. The dopant ratio and conductivity are indicative characteristics for the electrochemical properties of conducting polymers. Table 1 shows elementary analyses and film thickness of the PPy/$R_nSO_3^-$. The S/N ratio, which allowed us to estimate the ratio of incorporated anions to the pyrrole moiety (dopant ratio), increased with the dopant size. The resulting film thickness also increased with the dopant size. Figure 1 shows the conductivity of the PPy/$R_nSO_3^-$ films. The conduc-

Table 1. Elemental Analysis and Film Thickness of $PPy/R_nRO_3^-$ [a)]

Carbon number of dopant	Elemental analysis				Mole ratio S/N	Film thickness /μm
	C	H	N	S		
3	57.3	4.46	14.3	5.54	0.169	18
4	57.3	4.78	13.6	6.23	0.200	23
5	58.4	5.34	12.8	7.45	0.254	24
6	58.9	5.79	11.9	7.99	0.293	25
7	60.0	6.28	11.0	7.84	0.311	25
8	60.6	6.41	10.5	7.64	0.317	26
9	61.1	6.89	9.86	7.46	0.330	27
10	62.0	7.28	9.07	7.26	0.349	33

a) $PPy/R_nSO_3^-$ films were prepared by electrochemical polymerization for 4.7 C cm^{-2}.

Table 2. Peak Potentials[a)] of $PPy/R_nSO_3^-$ Electrodes

Carbon number of dopant	E_{Pa}	E_{Pc} /mV vs. SEC	$E_{1/2}$
3	−440	−600	−520
4	−450	−600	−525
5	−460	−610	−535
6	−475	−610	−543
7	−480	−720	−600
8	−520	−750	−635
9	−520	−765	−643
10	−510	−670	−590

a) Sweep rate was 50 mV s^{-1}.

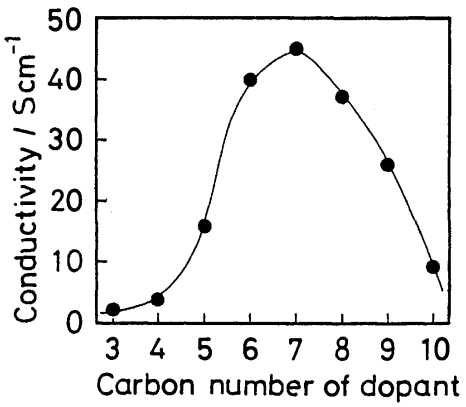

Fig. 1. Relationship between conductivity and carbon number of dopant for $PPy/R_nSO_3^-$.

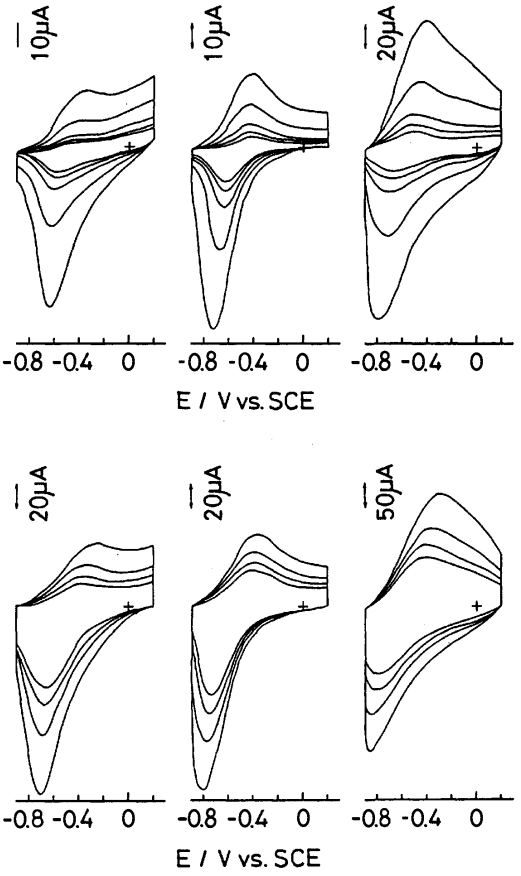

Fig. 2. Cyclic voltammograms of $PPy/R_3SO_3^-$ (left), $PPy/R_5SO_3^-$ (middle), and $PPy/R_{10}SO_3^-$ (right) in H_2O containing the incorporated anion (0.1 mol dm^{-3}) as a supporting electrolyte. Sweep rate was 20—100 mV s^{-1} (upper) and 200—500 mV s^{-1} (bottom).

tivity of the $PPy/R_nSO_3^-$ first increased with the dopant size (n=3—7) and then decreased (n=7—10). In general, the conductivity of the conducting polymer increases with the dopant ratio. However, the optimum conductivity was observed with $PPy/R_7SO_3^-$. The decrease of the conductivity was explained by the decrease of the electron carrier density, which was governed by the alkyl-chain length of the incorporated anion.

Cyclic voltammetry is one of the most important measurement techniques for investigating the electrochemical properties of PPy. Figure 2 shows typical cyclic voltammograms (sweep rates were 20—500 mV s^{-1}) of $PPy/R_nSO_3^-$ (n=3, 5, and 10) in H_2O containing the incorporated anion (0.1 mol dm^{-3}) as a supporting electrolyte. These cyclic voltammograms reflect the doping-undoping behavior of the incorporated anion, not involving any exchange reactions of incorporated anions (as stated below). Table 2 shows the redox potentials of $PPy/R_nSO_3^-$ at a sweep rate of 50 mV s^{-1}. The redox potentials of $PPy/R_nSO_3^-$ appeared in the range −520—−643 mV, and decreased with the dopant size. It has already been reported that the redox potential is affected by the properties of the incorporated anion.[33)]

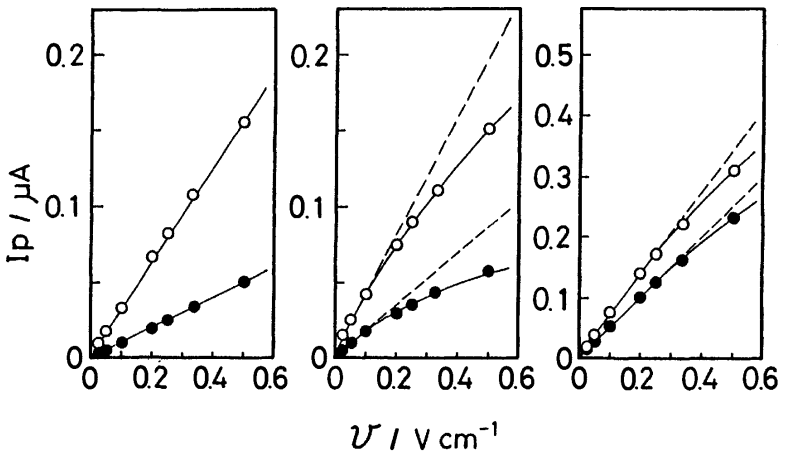

Fig. 3. Relationship between i_p and v for the cyclic voltammograms of $PPy/R_3SO_3^-$ (left), $PPy/R_5SO_3^-$ (middle), and $PPy/R_{10}SO_3^-$ (right). (●); anodic peak current, (○); cathodic peak current.

It is well-known that the relationship between the peak current (i_p) and the sweep rate (v) in a cyclic voltammogram shows the characteristics of mass transfer in the electroactive film on the electrode. The power number (X), the slope of the linear relationship between $\log(i_p)$ and $\log(v)$, is a convenient factor for estimating the mobility of the ionic species in the matrix. In general, $X=1$ shows that the mobility of the ionic species is higher than the electron-transfer rate, which is called "a surface wave;" $X=0.5$ shows that the mobility of the ionic species is lower than the electron-transfer rate, "a diffusion-controlled wave." In fact, X can have values from 0.5 to 1.0. Therefore, the contribution of the diffusion-controlled wave behavior is estimated by the X-value. It has been reported that the charge propagation mechanism, surface wave behavior or diffusion-controlled wave behavior, is affected by the properties of the counter ions in a polymer-modified electrode.[38] Figure 3 shows typical i_p-v relationships obtained from Fig. 2. In a surface wave ($X=1$) i_p is proportional to v, and in a diffusion-controlled wave ($X=0.5$) i_p is proportional to $v^{1/2}$. At $v<100$ mV s^{-1} all $PPy/R_nSO_3^-$ showed the surface-wave behavior, as in some previous studies on ordinary PPy. However, at $v>100$ mV s^{-1}, $PPy/R_3SO_3^-$ (small-size dopant) and $PPy/R_{10}SO_3^-$ (large-size dopant) showed almost the surface-wave behavior, and $PPy/R_5SO_3^-$ did not show the surface-wave behavior. Figure 4 shows the relationship between the X-value and the carbon number of the dopant (n). The X-value was estimated to be in the range 200—500 mV s^{-1}. The X-value decreased with the dopant size at $n<5$, and gradually increased with the dopant size at $n>6$. The X-value reflects the mobility of ionic species in the PPy matrix. In other words, when $X=1$, the mobility of ionic species is high, but when $X=0.5$, that of ionic species is low. Accordingly, it was concluded that the mobilities of the ionic species in $PPy/R_3SO_3^-$ and

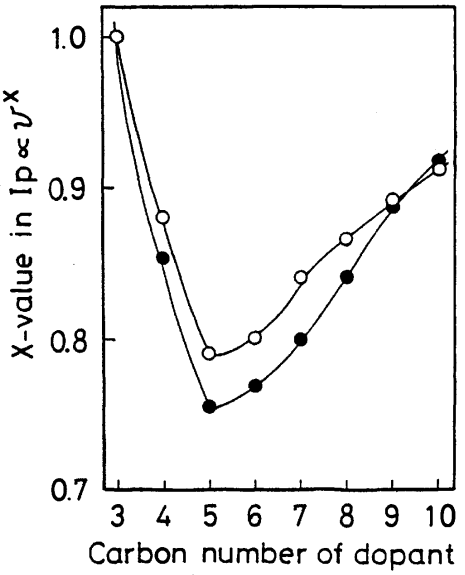

Fig. 4. Relationship between X and carbon number of dopant for $PPy/R_nSO_3^-$. X-Values were estimated from the slope between $\log(i_p)$ and $\log(v)$ (v were in the range 200—500 mV s^{-1}).

$PPy/R_{10}SO_3^-$ were high, and that in $PPy/R_5SO_3^-$ was low. Assuming only the anion can be transported in the PPy matrix, the mobility of $R_{10}SO_3^-$ was higher than that of $R_5SO_3^-$. Thus, the present observation can not be explained only by the dopant size. It was considered that other ionic species, an electrolyte cation, contributed to the electrochemical doping-undoping process. We had already reported that in the case that the polymer anion incorporated PPy (PPy/PA), the electrolyte cation was incorporated into the PPy matrix in lieu of the anion, when the PPy was electrochemically reduced.[32]

Cyclic voltammetry for $PPy/R_nSO_3^-$ in H_2O containing KCl was carried out in order to estimate only

the mobility of the anion. Figure 5 shows typical cyclic vltammograms of PPy/$R_nSO_3^-$ (n=3, 5, and 10) in H_2O containing 0.1 mol dm^{-3} KCl as a supporting electrolyte. We have already reported that the PPy/Cl^- had a more positive redox potential (>0 V vs. SCE) than the PPy/$R_5SO_3^-$, and that the potential sweeps in cyclic voltammetry for PPy/$R_5SO_3^-$ in a KCl aqueous solution induced an exchange reaction of the dopants (PPy/$R_5SO_3^-$ → PPy/Cl^-).[33] The rate of dopant exchange is controlled by the mobility of the original dopant in the PPy matrix, so that the diffusion rate of the original dopant can be estimated by the rate of the dopant-exchange reaction. Changes of the cyclic voltammograms during 5 sweeps can be observed in Fig. 5. The redox peaks at low and high potentials corresponded to the oxidation-reduction of PPy/$R_nSO_3^-$ and PPy/Cl^-, respectively. The redox peaks of PPy/$R_nSO_3^-$ decreased and those of PPy/Cl^- increased in all cyclic voltammograms. The cyclic voltammograms for PPy/$R_3SO_3^-$ and PPy/$R_5SO_3^-$ were profoundly changed. On the contrary, the cyclic voltammogram for PPy/$R_{10}SO_3^-$ was hardly changed. The rate of change of the peak currents decreased with the dopant size. Upon the first reduction of PPy, the original dopant, $R_nSO_3^-$, was partly released from the PPy matrix. On the successive oxidation, Cl^- in the electrolytic solution was partly incorporated into the PPy, since the concentration of Cl^- in the electrolytic solution was much higher than that of $R_nSO_3^-$. We defined a convenient dopant exchange rate as

$$\Phi = 1 + (i_{pc}(Cl^-)/i_{pc}(R_nSO_3^-)) \text{ at 5th cycle,} \quad (1)$$

Φ increased with the mobility of $R_nSO_3^-$. Figure 6 shows the relationship between Φ and the carbon number of the dopant. Φ decreased with the dopant size, which indicates that the mobility of the $R_nSO_3^-$ decreased with the dopant size. This conclusion could not explain the profile of Fig. 4, in which the mobility of the ionic species does not monotonously decrease with the dopant size. The increasing mobility observed for the longer alkyl dopants (n=5—10) in Fig. 4 should be explained by the incorporation of an electrolyte cation into the PPy matrix. We already reported that the electrolyte cation, e.g., K^+, was incorporated into the PPy matrix in order to conserve the electro-neutrality in the PPy matrix when the PPy/PA was electrochemically reduced. In this case, the polymer anion dopant was not released from the PPy matrix, owing to its macromolecularity. We called this observation "a pseudo-cathodic doping" and the polymer anion dopant "an immobilized dopant." It was suggested that the long alkyl dopants, such as $R_{10}SO_3^-$, were partly immobilized in the PPy matrix as a polymer anion dopant, so that the electrolyte cation was partly incorporated and released upon the oxidation and reduction of PPy. Because K^+ is much smaller than $R_nSO_3^-$, the increasing mobility observed for longer alkyl dopants in Fig. 4 could be explained by the incorporation of K^+ instead of the release of $R_nSO_3^-$.

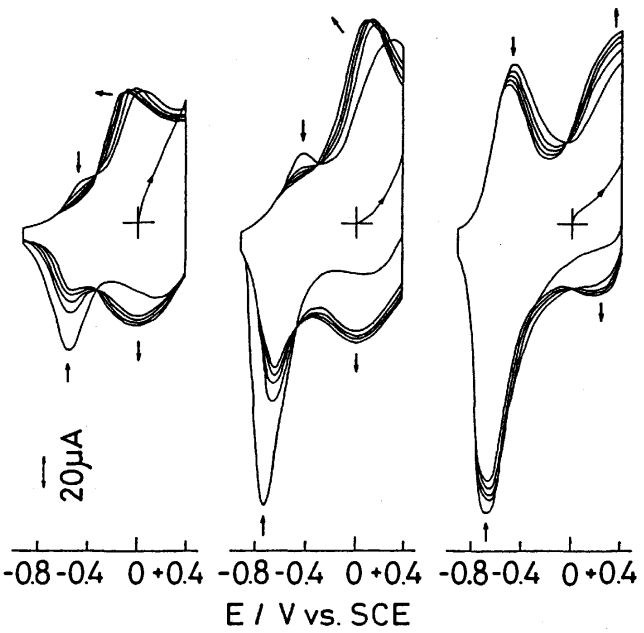

Fig. 5. Cyclic voltammograms of PPy/$R_3SO_3^-$ (left), PPy/$R_5SO_3^-$ (middle), and PPy/$R_{10}SO_3^-$ (right) in H_2O containing KCl (0.1 mol dm^{-3}) under potential sweep. Sweep rate was 200 mV s^{-1}.

Cation-Exchange Capability of PPy/$R_nSO_3^-$. We have reported that a novel type of electrochemical deionization system was constructed using a PPy/Cl^- (red.) anode and a PPy/PA cathode.[39,40] In this system an electrolyte anion was incorporated into the PPy/Cl^- by ordinary doping and an electrolytic cation was incorporated into PPy/PA by pseudo-cathodic doping. Thus, the PPy/Cl^- had an anion-exchange ability, and the PPy/PA had a cation-exchange ability. Electrochemical deionization experiments were carried out using an PPy/Cl^- (red.) anode and the present PPy/$R_nSO_3^-$ cathode in order to reveal a cation-

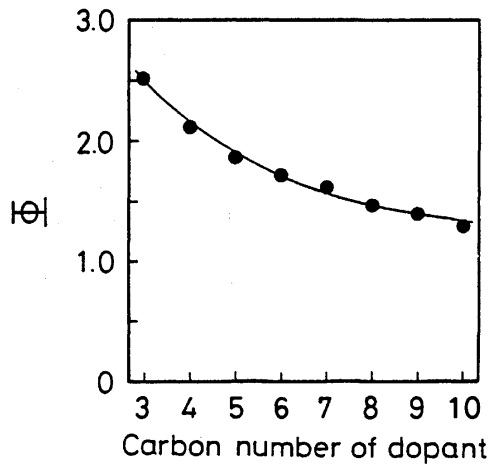

Fig. 6. Relationship between Φ and carbon number of dopant. Φ is defined by Eq. 1.

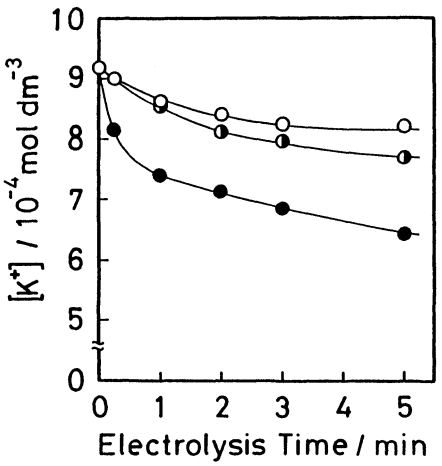

Fig. 7. Change of K^+ concentration in KCl aqueous solution with deionization time on 4 V potentiostatic electrolysis, using a PPy/Cl^- (red.) anode and a PPy/$R_nSO_3^-$ cathode. (○); PPy/$R_3SO_3^-$, (◑); PPy/$R_5SO_3^-$, and (●); PPy/$R_{10}SO_3^-$.

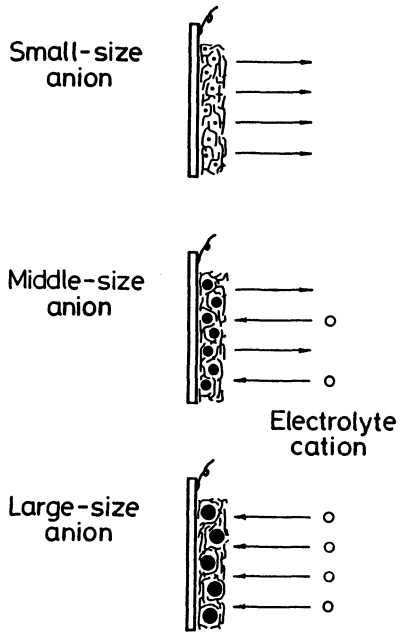

Fig. 8. A proposed model for the doping-undoping behavior of PPy/$R_nSO_3^-$.

exchange capability, i.e., the pseudo-cathodic doping, of the PPy/$R_nSO_3^-$. In these experiments the PPy/Cl^- (red.) was used as an anode in order to prevent any pH change in the solution and to promote the effective deionization of K^+.[40] Figure 7 shows the concentration change of K^+ in a KCl aqueous solution (original; 9.2×10^{-4} mol dm^{-3}) treated by the potentiostatic electrolysis (4 V) of the two electrodes. The concentration of K^+ decreased as a result of this treatment. The quantity of incorporated K^+ increased with the dopant size. This observation indicated that PPy/$R_nSO_3^-$ had a considerable capability of pseudo-cathodic doping. Moreover, the capability of pseudo-cathodic doping increased with the dopant size.

Figure 8 shows a proposed model for the doping-undoping behavior of PPy/$R_nSO_3^-$. Controlling such a dual-mode behavior, the release of an anion or the incorporation of a cation, of the present films will provide a prismatic electerochemical material.

This work was partly supported by a Grant-in-Aid from the Ministry of Education.

References

1) A. F. Diaz, K. K. Kanazawa, and G. P. Gardini, *J. Chem. Soc., Chem. Commun.*, **1979**, 635.
2) K. K. Kanazawa, A. F. Diaz, R. H. Geiss, W. D. Gill, J. F. Kwak, J. A. Logan, J. F. Rabolt, and G. B. Street, *J. Chem. Soc., Chem. Commun.*, **1979**, 854.
3) A. F. Diaz and J. I. Castillo, *J. Chem. Soc., Chem. Commun.*, **1980**, 397.
4) A. F. Diaz, J. I. Castillo, J. A. Logan, and W.-Y. Lee, *J. Electroanal. Chem.*, **129**, 115 (1981).
5) A. F. Diaz, A. Martinez, K. K. Kanazawa, and M. Salmon, *J. Electroanal. Chem.*, **130**, 181 (1981).
6) A. F. Diaz, J. I. Castillo, K. K. Kanazawa, J. A. Logan, M. Salmon, and O. Fajardo, *J. Electroanal. Chem.*, **133**, 233 (1981).
7) H. S. White, G. P. Kittlesen, and M. S. Wrighton, *J. Am. Chem. Soc.*, **106**, 5375 (1984).
8) G. P. Kittlesen, H. S. White, and M. S. Wrighton, *J. Am. Chem. Soc.*, **106**, 7389 (1984).
9) F. Garnier, G. Tourillon, M. Gazard, and J. C. Dubois, *J. Electroanal. Chem.*, **148**, 299 (1983).
10) R. Bjorklund, S. Andersson, S. Allenmark, and I. Lundström., *Mol. Cryst. Liq. Cryst.*, **121**, 263 (1985).
11) S. Kuwabata, H. Yoneyama, and H. Tamura, *Bull. Chem. Soc. Jpn.*, **57**, 2247 (1984).
12) K. Kaneto and Y. Yoshino, *Kino Zairyo (Jpn.)*, **4**, 8 (1984).
13) A. Mohammadi, O. Inganas, and I. Lundström, *J. Electrochem. Soc.*, **133**, 947 (1986).
14) N. Mermilliod, J. Tanguy, and F. Petiot, *J. Electrochem. Soc.*, **133**, 1073 (1986).
15) T. Osaka, K. Naoi, H. Sasaki, and S. Ogano, *J. Electrochem. Soc.*, **134**, 285 (1987).
16) A. F. Diaz, *Chemica Scripta.*, **17**, 145 (1981).
17) P. Burgmayer and R. W. Murray, *J. Am. Chem. Soc.*, **104**, 6139 (1982).
18) P. Burgmayer and R. W. Murray, *J. Phys. Chem.*, **88**, 2515 (1984).
19) A. F. Diaz, W.-Y. Lee, A. Logan, and D. C. Green, *J. Electroanal. Chem.*, **108**, 377 (1980).
20) R. A. Bull, F.-R. Fan, and A. J. Bard, *J. Electrochem. Soc.*, **130**, 1636 (1983).
21) R. Noufi, *J. Electrochem. Soc.*, **130**, 2126 (1983).
22) K. Okabayashi, O. Ikeda, and H. Tamura, *J. Chem. Soc., Chem. Commun.*, **1983**, 684.
23) R. B. Bjorklund and I. Lundström, *J. Electron. Mater.*, **13**, 211 (1984).
24) O. Niwa and T. Tamamura, *J. Chem. Soc., Chem. Commun.*, **1984**, 817.
25) S. E. Lindsey and G. B. Street, *Synth. Metals*, **10**, 67 (1984).

26) M-A. de Paoli, R. J. Waltman, A. F. Diaz, and J. Bargon, *J. Chem. Soc., Chem. Commun.*, **1984**, 1015.
27) N. Bates, M. Cross, R. Lines, and D. Walton, *J. Chem. Soc., Chem. Commun.*, **1985**, 871.
28) T. Ojio and S. Miyata, *Polym. J.*, **18**, 95 (1986).
29) F.-R. F. Fan and A. J. Bard, *J. Electrochem. Soc.*, **133**, 301 (1986).
30) H. Yoneyama, T. Hirai, S. Kuwabata, and O. Ikeda, *Chem. Lett.*, **1986**, 1243.
31) T. Iyoda, A. Ohtani, T. Shimidzu, and K. Honda, *Synth. Metals*, **18**, 725 (1987).
32) T. Iyoda, A. Ohtani, T. Shimidzu, and K. Honda, *Chem. Lett.*, **1986**, 687.
33) T. Shimidzu, A. Ohtani, T. Iyoda, and K. Honda, *J. Electroanal. Chem.*, **224**, 123 (1987).
34) J. H. Kaufmann, K. K. Kanazawa, and G. B. Street, *Phys. Rev. Lett.*, **53**, 2461 (1984).
35) E. M. Genies and J. M. Pernaut, *Synth. Metals*, **10**, 117 (1984).
36) G. Nagasubramanian, S. Di Stefano, and J. Moacanin, *J. Phys. Chem.*, **90**, 4447 (1986).
37) W. Wernet, M. Monkenbusch, and G. Wegner, *Makromol. Chem., Rapid Commun.*, **5**, 157 (1984).
38) N. Oyama and F. C. Anson, *J. Electrochem. Soc.*, **127**, 640 (1980).
39) T. Shimidzu, A. Ohtani, T. Iyoda, and K. Honda, *J. Chem. Soc., Chem. Commun.*, **1986**, 1415.
40) T. Shimidzu, A. Ohtani, and K. Honda, *J. Electroanal. Chem.*, in press.

The Reaction of 1-Amino-2,3-diphenylcyclopropenium Ions with 1,3-Diketones to Afford 2,4-Cyclopentadien-1-ols: The Regioselective Ring-Opening of 1-Amino-cyclopropene Intermediates

Hiroshi YOSHIDA,* Tomoji TAMAI, Tsuyoshi OGATA, and Kiyoshi MATSUMOTO†
Department of Applied Chemistry, Faculty of Engineering, Shizuoka University, Hamamatsu 432
†College of Liberal Arts and Sciences, Kyoto University, Kyoto 606
(Received February 20, 1988)

1-Amino-2,3-diphenylcyclopropenium tetrafluoroborates (**4**) reacted with cyclic or acyclic 1,3-dicarbonyl derivatives (**5**) such as 1,3-diketones, β-keto esters, or gem-diesters in the presence of triethylamine to give 2,4-cyclopentadien-1-ols in moderate to good yields. Some isolated cyclopropene intermediates were, upon heating, converted to the corresponding cyclopentadienols. The factors that influence on the reactivities of **4** and **5** (basicities of the amino groups of **4** and bulkiness of the substituents of **4** and **5**) are discussed qualitatively.

The chemistry of cyclopropene derivatives has attracted considerable interest because of the high strain energy associated with the unsaturated three-membered ring. A number of studies on the photochemical and thermal ring-opening reactions of cyclopropenes have appeared in recent years.[1,2]

We have recently reported the reaction of 1-(methylthio)-2,3-diphenylcyclopropenium ion (**1**) with 2,4-pentanedione and with 1,3-cyclohexanedione to yield cyclopentadienol (**2**)[3] and 2*H*-pyran derivative (**3**),[4] respectively (Scheme 1). In this connection we have been interested in the effect of heteroatom substituents (such as alkoxy, alkylthio, and amino groups) on the attacking position of cyclopropenium ions and ring opening of the resulting cyclopropenes.[2-4] This paper describes the reaction of 1-amino-2,3-diphenylcyclopropenium ions (**4**) with 1,3-dicarbonyl compounds **5** to afford cyclopropenes **6**, followed by regioselective ring opening to give cyclopentadienols **7**.

1-Amino-2,3-diphenylcyclopropenium tetrafluoroborates (**4**) were prepared by a reaction of 2,3-

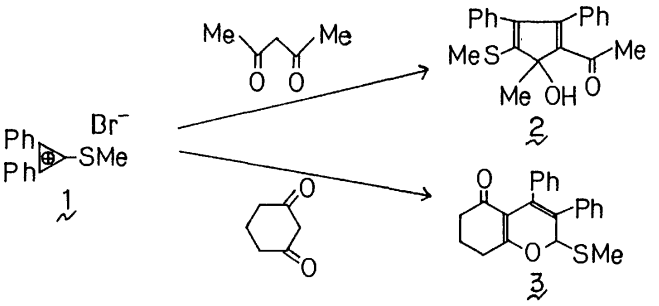

Scheme 1.

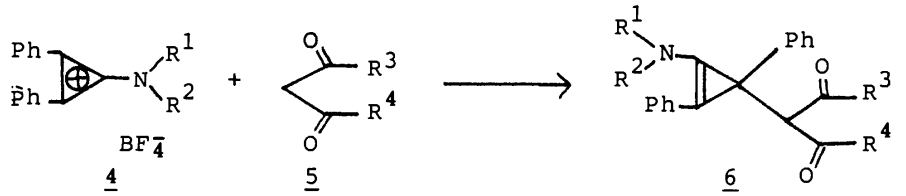

4	R^1	R^2
a	$(CH_2)_2O(CH_2)_2$	
b	$(CH_2)_5$	
c	$(CH_2)_4$	
d	C_2H_5	C_2H_5
e	CH_3	CH_3
f	CH_3	Ph

5	R^3	R^4
a	CH_3	CH_3
b	CH_3	Ph
c	Ph	Ph
d	$(CH_2)_3$	
e	$CH_2C(CH_3)_2CH_2$	
f	$(CH_2)_2$	
g	CH_3	OCH_3
h	CH_3	OC_2H_5
i	CH_3	OBu-t
j	OC_2H_5	OC_2H_5

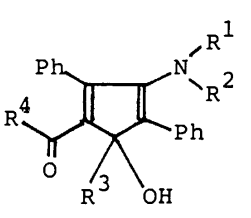

Scheme 2.

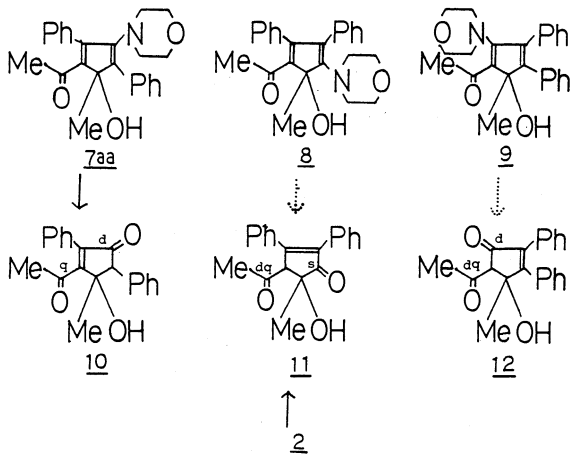

Scheme 3.

diphenylcyclopropenone with triethyloxonium tetrafluoroborate, followed by a treatment with secondary amines.[5-7] A mixture of 1-morpholino-2,3-diphenylcyclopropenium tetrafluoroborate (**4a**), 2,4-pentanedione (**5a**), and triethylamine in a mole ratio of 1 : 1.1 : 2 was stirred in dry benzene at room temperature for 1 h to yield the reaction product **X** as yellow needles. The ^{1}H and ^{13}C NMR, and mass spectra of **X** revealed the structure to be a cyclopentadienol derivative arising from a 1 : 1 adduct of **4a** and **5a**, but did not permit a clear choice among mechanistically possible isomers (**7aa**, **8**, and **9** in Scheme 3).

Upon hydrolysis **7aa**, **8**, and **9** might give cyclopentenones **10**, **11**, and **12** respectively (Scheme 3). Previously we have shown[3] that desulfurization of **2** yields 2-cyclopentenone **11** (mp 184—185 °C), whose ^{13}C NMR spectrum shows two carbonyl carbons at δ=204.9 (dq, $\underline{C}OCH_3$) and 206.8 (s, C_1). Cyclopentenone **12** might yield two carbonyl carbons as a dq ($\underline{C}OCH_3$ due to coupling with $COC\underline{H}_3$ and $C_5\underline{H}$) and a d (C_1 due to $C_5\underline{H}$). Hydrolysis of **X** under mild conditions (formic acid in benzene) afforded cyclopentenone as a colorless crystalline mass (mp 159—161 °C), whose ^{13}C NMR spectrum showed a d at 203.1 ($^{2}J_{CCH}$=6.8 Hz, C_1) and a q at 204.1 ($^{2}J_{CCH}$=6.0 Hz, $\underline{C}OCH_3$) due to carbonyl carbons, establishing the structure of the cyclopentenone to be **10**. Consequently, **X** was unambigously revealed to be 1-acetyl-2,4-diphenyl-5-hydroxy-5-methyl-3-morpholinocyclopentadiene (**7aa**).

Although stable under basic conditions (NaOH in ethanol) **7aa** upon being treated with trifluoroacetic acid produced complex mixtures. In a mixture of chloroform and ethanol containing a small amount of trifluoroacetic acid, **7aa** yielded the cyclopentadienone **13** in quantitative yield, which underwent a Diels-Alder addition with dimethyl acetylenedicarboxylate (DMAD) to give the hexasubstituted benzene **14** in a 28% yield.

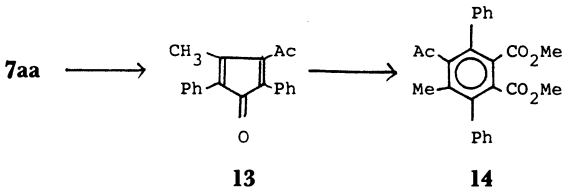

13 **14**

Table 1. The Reaction of **4** with **5** in the Presence of Triethylamine at Room Temperature

Reactant 4	Reactant 5	Reaction time /h	Product (yield/%)
4a	**5a**	1	**7aa** (71)
	5b	1	**7ab** (33)
	5c	24	**6ac** (28)
	5d	1	**7ad** (67)
	5e	1	**7ae** (82)
	5f	1	**7af** (43)
	5g	4	**6ag** (66)
	5h	4	**7ah** (63)
	5i	4	**6ai** (60)
	5j	4	**6aj** (65)
4b	**5a**	1	**7ba** (45)
	5b	1	**7bb** (7)
	5c	1	**7bc** (56)
	5d	1	**7bd** (79)
	5e	1	**7be** (76)
	5f	1	—
	5g	2	**7bg** (43)
	5h	2	**7bh** (51)
4c	**5a**	1	—
	5c	1	—
	5d	1	—
	5f	1	—
4d	**5a**	1	**7da** (74)
	5b	1	**7db** (4)
	5c	1	—
	5d	1	**7dd** (86)
	5g	4	**6dg** (71)
	5h	4	**6dh** (93)
4e	**5a**	1	**7ea** (38)
	5d	1	**7ed** (70)
4f	**5a**	1	—
	5d	1	**7fd** (45)

Table 2. Thermal Ring Opening of Cyclopropenes **6**

Reactant 6	Reaction condition: Solvent	Temp/°C	Time/h	Product (Yield/%)
6ac	Xylene	120	3	Recovery
6ag	Benzene	50	3	**7ag** (73)
6ai	Benzene	50	3	**7ai** (52)
6aj	Benzene	80	5	Unknown mixture
6dj	Benzene	80	3	**7dj** (84)
6dh	Benzene	80	3	**7dh** (76)

The results of the reaction of cyclopropenium ions possessing amino substituents **4a—4d** with acyclic and cyclic 1,3-diketones, -ketoesters, and diethyl malonates **5a—5j** are collected in Table 1. In certain cases, 1-aminocyclopropenes **6** were isolated, whose structure were elucidated on the basis of their IR (around 1840 cm^{-1}) and ^{13}C NMR (C_3, sp^3 carbon) spectroscopic studies. The cyclopropenes could be isolated when they were derived from either small enolizable[8-10] or bulky

diketones **5**, and/or bulky amines **4** (Table 1). The cyclopropenes **6** were converted to the corresponding cyclopentadienols **7** under the stronger conditions as listed in Table 2.

Six-membered cyclic ketones **5d** and **5e** showed high reactivities toward ions **4** yielding good crystalline products, whereas, a 5-membered ketone **5f** gave unstable mixtures from which no crystalline product could be isolated. The reaction of **4a** and **4b** with sterically hindered ketones **5c** afforded **6ac** and **7bc**, respectively, while **4d** gave no crystalline product with **5c**. Thus, the reactivities of the ions **4** seem to have been influenced by the basicities of the amines and bulkiness of the amino substituents. The pyrrolidinyl substituted **4c** reacted with diketones **5a**, **5c**, and **5d**, but gave unidentifiable tarry mixtures, probably because the enamine-type products would be hydrolyzed under the purification procedure.[11]

Finally, we propose a mechanism for the reaction of **4** with **5**, as illustrated in Scheme 4. The initial step involves a nucleophillic attack of the carbanion generated fron 1,3-diketones **5** on the C_2 or C_3 of **4** to yield 1-aminocyclopropene **6**, since the electron-releasing properties of the amino group would increase the electron density of C_1. Two routes are possible for the ring opening of the cyclopropenes. As we mentioned in an earlier paper,[3] 3-(1,2,3-triphenylcyclopropenyl)-2,4-pentadienone was stable at 100 °C in both the presence and absence of triethylamine. This observation indicates that the electron-attracting nature of the carbonyl

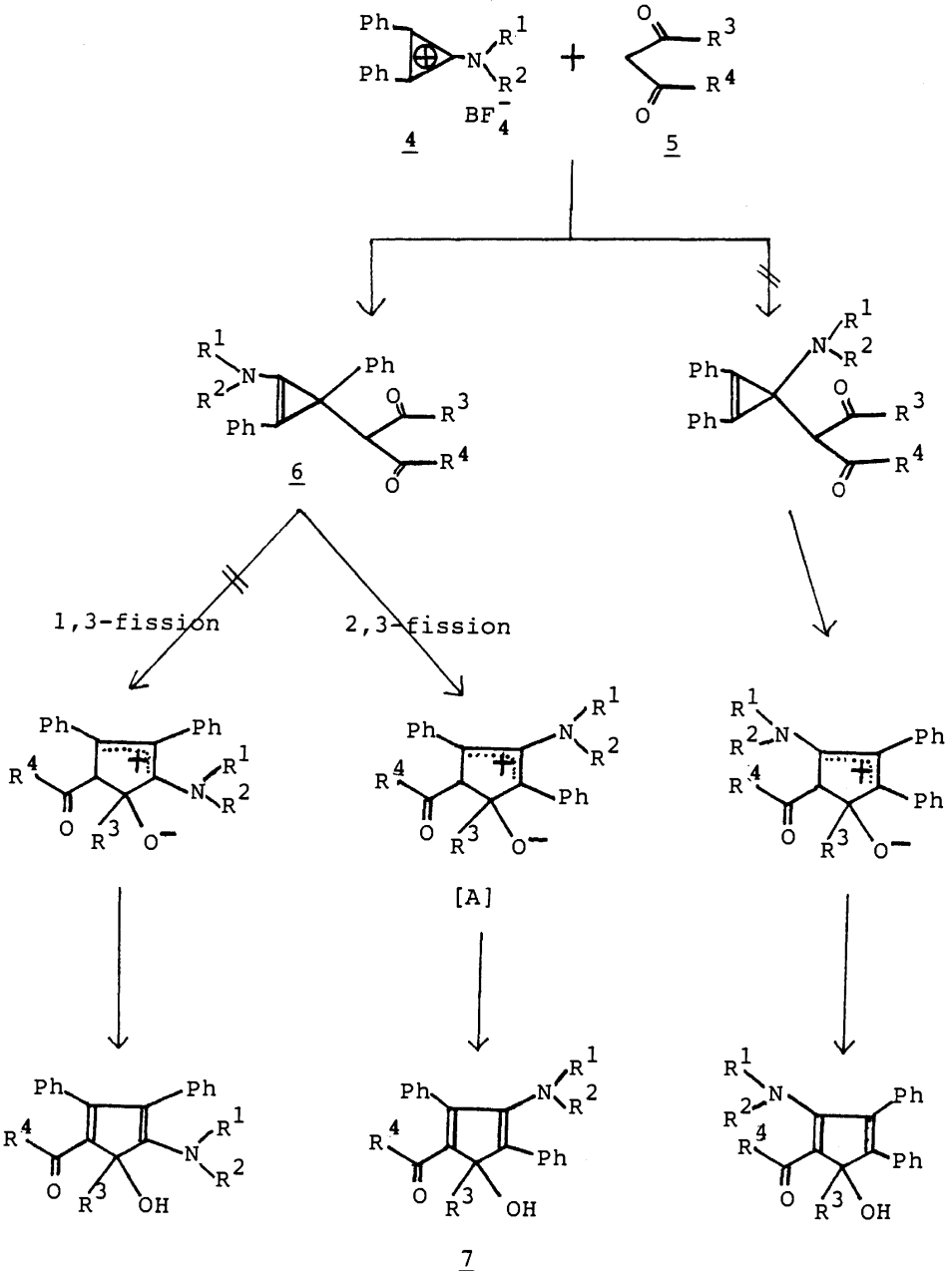

Scheme 4.

groups does not facilitate a ring opening of the cyclopropene. Considering the products obtained (**7**), a process involving a carbenium ion like **A** seems to be most stabilized by the adjacent amino group.

In the reaction of **1**, as shown in Scheme 1, acyclic and cyclic diketones gave two kinds of products, respectively (**2** and **3**). These results can be well-explained in terms of the electron-releasing and -accepting properties of the alkylthio group.[3] The electron-releasing nature of the amino substituent does not permit a formation of 2*H*-pyran derivatives (**3** analogues), yielding only cyclopropentadienol **7**(**2** analogues).

Experimental

General. Melting points were uncorrected. The ^{13}C NMR spectra were recorded either on a JEOL JMN FX-60 spectrometer (15.04 MHz) or JEOL JNM FX-90Q (22.49 MHz) and ^1H NMR spectra on a Hitachi R-24B (60 MHz). The IR spectra were recorded on a JASCO A-3 spectrometer.

Preparation of 1-Amino-2,3-diphenylcyclopropenium Tetrafluoroborates 4. The salts **4** were prepared by a known method.[5-7] Analytical and spectroscopic data for new derivatives are as follows. **4a** in 85% yield: mp 273—275 °C; IR(KBr) 1890 cm^{-1}; ^1H NMR ($CDCl_3$-CF_3CO_2H in 10:1) δ=4.04 (s, 8H, $2N(CH_2)_2O$) and 7.4—8.1 (m, 10H, 2Ph). Found: C, 62.53; H, 4.88; N, 3.69%. Calcd for $C_{19}H_{18}BF_4NO$: C, 62.84; H, 5.00; N, 3.86%. **4b** in 56% yield: mp 252—253 °C; IR(KBr) 1890 cm^{-1}; ^1H NMR ($CDCl_3$-CF_3CO_2H in 10:1) δ=1.88 (bs, 6H, $(CH_2)_3$), 3.8—4.2 (m, 4H, $N(CH_2)_2$), and 7.5—8.1 (m, 10H, 2Ph). Found: C, 66.62; H, 5.53; N, 3.99%. Calcd for $C_{20}H_{20}BF_4N$: C, 66.51; H, 5.58; N, 3.88%. **4c** in 15% yield: mp 275—278 °C; IR(KBr) 1900 cm^{-1}; ^1H NMR ($CDCl_3$-CF_3CO_2H in 10:1) δ=2.3—2.7 (m, 4H, $(CH_2)_2$), 4.0—4.4 (m, 4H, $N(CH_2)_2$), and 7.5—8.2 (m, 10H, 2Ph). Found: C, 65.47; H, 5.06; N, 4.12%. Calcd for $C_{19}H_{18}BF_4N$: C, 65.74; H, 5.23; N, 4.03%.

The Reaction of 4 with 1,3-Diketones 5. A general procedure. A mixture of **4** (1 mmol), **5** (1.1 mmol), and triethylamine (2 mmol) in 15 cm^3 of dry benzene was stirred at room temperature. After the reaction (no change of the precipitate and TLC of the reaction mixture) the solution was poured into cold water, and the organic layer was separated and dried over sodium carbonate. Recrystallization of the product from benzene-petroleum ether afforded faint-yellow crystals. Yields are listed in Table 1.

Thermal Reaction of 6. A solution of **6** (0.2 g) in an appropriate solvent (10 cm^3) was heated at reflux and the reaction was checked by TLC. After the reaction the mixture was condensed and the products which separated were recrystallized from benzene-petroleum ether (Table 2). The physical properties are as follows. **7aa:** mp 143—144 °C; IR(KBr) 3440 and 1620 cm^{-1}. ^1H NMR ($CDCl_3$) δ=1.41 (s, 3H, CH_3), 1.80 (s, 3H, $COCH_3$), 2.3—2.6 (m, 4H, $N(CH_2)_2$), 3.1—3.4 (m, 4H, $O(CH_2)_2$), 3.95 (s, 1H, OH), and 7.2—7.7 (m, 10H, 2Ph). ^{13}C NMR ($CDCl_3$) δ=25.4(q), 30.2(q), 50.9(t), 66.6(t), 83.4(s), 127.5(d), 128.6(d), 128.9(d), 130.2(d), 134.3(s), 134.4(s), 137.5(s), 144.1(s), 147.3(s), 153.5(s). and 196.1(s). Found: C, 76.57; H, 6.58; N, 3.83%; M^+, 375. Calcd for $C_{24}H_{25}NO_3$: C, 76.76; H, 6.72; N, 3.73%; M, 375. **7ab**: mp 164—165 °C; IR(KBr) 3350 and 1610 cm^{-1}; ^1H NMR ($CDCl_3$) δ=1.50 (s, 3H, CH_3), 2.2—2.5 (m, 4H, $N(CH_2)_2$), 3.1—3.4 (m, 4H, $O(CH_2)_2$), 3.57 (s, 1H, OH), and 6.8—7.8 (m, 15H, 3Ph). Found: C, 79.55; H, 6.21; H, 3.19%; M^+, 437. Calcd for $C_{29}H_{27}NO_3$: C, 79.61; H, 6.22; N, 3.20%; M, 437. **6ac**: mp 179—181 °C; IR (KBr) 1840, 1700, and 1670 cm^{-1}; ^1H NMR ($CDCl_3$) δ=2.66 (t, J=5Hz, 4H, $N(CH_2)_2$), 3.51 (t, J=5 Hz, 4H, $O(CH_2)_2$), 6.8—8.1 (m, 20H, 4Ph). ^{13}C NMR ($CDCl_3$) δ=51.0(t), 66.4(t), 87.5(s), 92.8(d), 124.7(s), 126.8(d), 127.2(d), 128.0(d), 128.2(d), 128.3(d), 128.6(d), 129.0(d), 129.6(d), 131.5(d), 132.2(d), 133.0(d), 133.9(d), 137.2(s), 139.7(s), 147.1(s), 150.8(s), 185.4(s), and 195.1(s). Found: C, 81.71; H, 5.61; N, 2.73%; M^+, 499. Calcd for $C_{34}H_{29}NO_3$: C, 81.74; H, 5.85; N, 2.80%; M, 499. **7ad**: mp 160—162 °C; IR(KBr) 3400 and 1660 cm^{-1}; ^1H NMR ($CDCl_3$) δ=1.5—2.2 (m, 6H, $(CH_2)_3$), 2.2—2.7 (m, 4H, $N(CH_2)_2$), 3.1—3.4 (m, 4H, $O(CH_2)_2$), and 7.0—7.8 (m, 10H, 2Ph). ^{13}C NMR ($CDCl_3$) δ=18.7(t), 34.6(t), 41.7(t), 50.9(t), 66.4(t), 85.9(s), 127.0(d), 127.3(d), 127.7(d), 128.4(d), 129.5(d), 130.4(d), 132.1(s), 134.9(d), 142.2(s), 145.2(s), 146.8(s), and 197.9(s). Found: C, 77.42; H, 6.60; N, 3.76%; M^+, 387. Calcd for $C_{25}H_{25}NO_3$: C, 77.48; H, 6.52; N, 3.62%; M, 387. **7ae**: mp 131—133 °C; IR (KBr) 3430 and 1650 cm^{-1}; ^1H NMR ($CDCl_3$) δ=0.82 (s, 3H, CH_3) 1.10 (s, 3H, CH_3), 1.9—2.4 (m, 4H, $(CH_3)_2C(C\underline{H}_2)_2$), 2.4—2.7 (m, 4H, $N(CH_2)_2$), 3.2—3.6 (m, 4H, $O(CH_2)_2$), 5.85 (s, 1H, OH), and 7.2—7.9 (m, 10H, 2Ph). Found: C, 77.73; H, 7.08; N, 3.65%; M^+, 415. Calcd for $C_{27}H_{29}NO_3$: C, 78.03; H, 7.05; N, 3.37%; M, 415. **7af**: mp 136—138 °C; IR (KBr) 3450 and 1690 cm^{-1}; ^1H NMR ($CDCl_3$) δ=1.82 (bs, 4H, $(CH_2)_2$), 2.1—2.5 (m, 4H, $N(CH_2)_2$), 2.8—3.3 (m, 4H, $O(CH_2)_2$), 5.65 (s, 1H, OH), and 6.7—7.6 (m, 10H, 2Ph). Found: C, 77.23; H, 6.18; N, 3.39%; M^+, 373. Calcd for $C_{24}H_{23}NO_3$: C, 77.19; H, 6.18; N, 3.75%; M, 373. **6ag**: oil; IR (KBr) 1850 and 1650 cm^{-1}; ^1H NMR ($CDCl_3$) δ=1.77 (s, 3H, CH_3), 2.7—2.9 (m, 4H, $(CH_2)_2$), 2.93 (s, 3H, OCH_3), 3.1—3.4 (m, 4H, $O(CH_2)_2$), 4.71 (s, 1H, OH), and 6.9—7.4 (m, 10H, 2Ph). Found: C, 73.53; H, 6.24; N, 3.51%; M^+, 391. Calcd for $C_{24}H_{25}NO_4$: C, 73.63; H, 6.44; N, 3.58%; M, 391. **7ag**: mp 168—170 °C; IR (KBr) 3350 and 1680; cm^{-1}. ^1H NMR ($CDCl_3$) δ=1.46 (s, 3H, CH_3), 2.48 (t, J=5 Hz, 4H, $O(CH_2)_2$), 3.28 (t, J=5 Hz, $O(CH_2)_2$), 3.53 (s, 3H, OMe), and 7.1—7.5 (m, 10H, 2Ph). Found: C, 73.22; H, 6.41; N, 3.46%; M^+, 391. Calcd for $C_{24}H_{25}NO_4$: C, 73.63; H, 6.44; N, 3.58%; M, 391. **7ah**: mp 148—149 °C; IR (KBr) 3500 and 1680 cm^{-1}; ^1H NMR ($CDCl_3$) δ=0.99 (t, J=8 Hz, 3H, $C\underline{H}_3CH_2$), 1.45 (s, 3H, CH_3), 2.3—2.7 (m, 4H, $N(CH_2)_2$), 3.1—3.5 (m, 4H, $O(CH_2)_2$), 3.70 (s, 1H, OH), 4.01 (q, 2H, $CH_3C\underline{H}_2$), and 7.1—7.6 (m, 10H, 2Ph). Found: C, 73.78; H, 6.64; N, 3.40%; M^+, 405. Calcd for $C_{25}H_{27}NO_4$: C, 74.04; H, 6.72; N, 3.45%; M, 405. **6ai** oil; IR (KBr) 1850, 1720, and 1640 cm^{-1}; ^1H NMR ($CDCl_3$) δ=0.90 (s, 6H, $C(CH_3)_2$), 1.11 (s, 3H, CCH_3), 2.88 (t, J=5Hz, 4H, $N(CH_2)_2$), 3.42 (t, J=5Hz, 4H, $O(CH_2)_2$), 4.73 (s, 1H, OH), and 6.9—7.5 (m, 10H, 2Ph). Found: C, 74.91; H, 7.01; N, 3.33%; M^+, 433. Calcd for $C_{27}H_{31}NO_4$: C, 74.80; H, 7.21; N, 3.23%; M, 433. **7ai**: mp 178—179 °C; IR (KBr) 3520 and 1670 cm^{-1}; ^1H NMR ($CDCl_3$) δ=1.21 (s, 9H, *t*-Bu), 1.45 (s, 3H, CH_3), 2.48 (t, J=5Hz, 4H, $N(CH_2)_2$), 3.24 (t, J=5Hz, 4H, $O(CH_2)_2$), 3.82 (s, 1H, OH), and 7.2—7.5 (m, 10H, 2Ph). Found: C, 74.82; H, 7.11; N, 3.20%; M^+, 433. Calcd for $C_{27}H_{31}NO_4$: C, 74.80; H, 7.21; N, 3.23%; M, 433. **6aj** oil; IR (KBr) 1850 and 1750 cm^{-1}; ^1H NMR ($CDCl_3$) δ=1.00 (s, J=9Hz, 6H, $2C\underline{H}_3CH_2$), 3.2—4.0 (m, 12H, $2CH_3C\underline{H}_2$ and $O(CH_2CH_2)_2$), and 7.0—8.2 (m, 10H, 2Ph). Found: C, 71.68; H, 6.90; N, 3.61%; M^+, 435. Calcd for $C_{26}H_{29}NO_5$: C, 71.70; H, 6.71; N, 3.22%; M, 435. **7ba**: mp 167—168 °C; IR (KBr)

3430 and 1620 cm^{-1}; ^1H NMR ($CDCl_3$) δ=1.0—1.3 (m, 6H, $(CH_2)_3$), 1.45 (s, 3H, CH_3), 2.3—2.6 (m, 4H, $N(CH_2)_2$), 4.00 (s, 1H, OH), and 7.2—7.5 (m, 10H, 2Ph). Found: C, 80.38; H, 7.40; N, 3.91%; M^+, 373. Calcd for $C_{25}H_{27}NO_2$: C, 80.38; H, 7.30; N, 3.75%; M, 373. **7bb**: mp 161—163 °C; IR (KBr) 3470 and 1620 cm^{-1}; ^1H NMR ($CDCl_3$) δ=1.1—1.4 (m, 6H, $(CH_2)_3$), 1.21 (s, 3H, CH_3), 2.4—2.7 (m, 4H, $N(CH_2)_2$), 4.75 (s, 1H, OH), and 6.8—7.6 (m, 10H, 2Ph). Found: C, 80.64; H, 8.79; N, 3.06%; M^+, 445. Calcd for $C_{30}H_{39}NO_2$: C, 80.85; H, 8.82; N, 3.14%; M, 445. **7bc**: mp 189—191 °C; IR (KBr) 3450 and 1620 cm^{-1}; ^1H NMR ($CDCl_3$) δ=0.7—1.5 (m, 6H, $(CH_2)_3$), 2.7—3.2 (m, 4H, $N(CH_2)_2$), and 6.5—7.9 (m, 20H, 4Ph). ^{13}C NMR ($CDCl_3$) δ=23.7(t), 25.1(t), 51.7(t), 118.6(s), 125.4(d), 126.4(d), 127.4(d), 127.9(d), 128.2(d), 128.5(d), 129.3(d), 129.8(d), 130.4(s), 132.5(s), 137.3(s), 139.0(s), 139.4(s), 140.9(s), 154.2(s), 160.1(s), and 192.8(s). Found: C, 84.21; H, 6.18; N, 2.93%; M^+, 497. Calcd for $C_{35}H_{31}NO_2$: C, 84.47; H, 6.28; N, 2.82%; M, 497. **7bd**: mp 163—165 °C; IR (KBr) 3330 and 1650 cm^{-1}; ^1H NMR ($CDCl_3$) δ=1.2—1.4 (m, 6H, $(CH_2)_3$), 1.4—2.3 (m, 6H, $CO(CH_2)_3$), 2.3—2.6 (m, 4H, $N(CH_2)_2$), and 7.2—7.6 (m, 10H, 2Ph). Found: C, 80.86; H, 7.12; N, 3.57%; M^+, 385. Calcd for $C_{26}H_{27}NO_2$: C, 81.00; H, 7.07; N, 3.57%; M, 385. **7be**: mp 155—157 °C; IR (KBr) 3340 and 1660 cm^{-1}; ^1H NMR ($CDCl_3$) δ=1.00 (s, 3H, CH_3), 1.17 (s, 3H, CH_3), 0.8—2.9 (m, 14H, $(CH_2)_5$ and $C(CH_2)_2$), and 7.1—7.8 (m, 10H, 2Ph). Found: C, 81.23; H, 7.62; N, 3.49%; M^+, 413. Calcd for $C_{28}H_{31}NO_2$: C, 81.31; H, 7.57; N, 3.39%; M, 413. **7bg**: mp 169—172 °C; IR (KBr) 3530 and 1670 cm^{-1}; ^1H NMR ($CDCl_3$) δ=1.0—1.4 (m, 6H, $(CH_2)_3$), 1.41 (s, 3H, CH_3), 2.3—2.6 (m, 4H, $N(CH_2)_2$), 3.51 (s, 3H, CO_2CH_3), and 7.2—7.6 (m, 10H, 2Ph). Found: C, 77.12; H, 6.98; N, 3.57%; M^+, 389. Calcd for $C_{25}H_{27}NO_3$: C, 77.08; H, 7.00; N, 3.57%; M, 389. **7bh**: mp 150—152 °C; IR (KBr) 3480 and 1670 cm^{-1}. ^1H NMR ($CDCl_3$) δ=1.00 (t, J=8 Hz, 3H, $C\underline{H}_3CH_2$), 1.1—1.4 (m, 6H, $(CH_2)_3$), 1.49 (s, 3H, CH_3), 2.3—2.7 (m, 4H, $N(CH_2)_2$), 4.09 (s, q, J=8Hz, 2H, $CH_3C\underline{H}_2$), and 7.2—7.5 (m, 10H, 2Ph). Found: C, 77.31; H, 7.19; N, 3.45%; M^+, 403. Calcd for $C_{26}H_{29}NO_3$: C, 77.39; H, 7.24; N, 3.47%; M, 403. **7da**: mp 103—105 °C; IR (KBr) 3480 and 1620 cm^{-1}; ^1H NMR ($CDCl_3$) δ=0.62 (t, J=7 Hz, 6H, $C\underline{H}_3CH_2$), 1.38 (s, 3H, CH_3), 1.69 (s, 3H, $COCH_3$), 2.43 (q, J=7 Hz, 4H, $2CH_3C\underline{H}_2$), 3.95 (s, 1H, OH), and 7.2—7.5 (m, 10H, 2Ph). Found: C, 79.55; H, 7.42; N, 3.59%; M^+, 361. Calcd for $C_{24}H_{27}NO_2$: C, 79.74; H, 7.53; N, 3.88%; M, 361. **7db**: mp 149—150 °C; IR (KBr) 3450 and 1610 cm^{-1}; ^1H NMR ($CDCl_3$) δ=0.70 (t, J=5Hz, 6H, $2CH_2C\underline{H}_3$), 1.41 (s, 3H, CH_3), 2.48 (q, J=5 Hz, 4H, $2CH_3C\underline{H}_2$), 4.59 (s, 1H, OH), and 6.7—7.4 (m, 15H, 3Ph). Found: C, 81.96; H, 6.77; N, 3.40%; M^+, 423. Calcd for $C_{29}H_{29}NO_2$: C, 81.96; H, 6.90; N, 3.31%; M, 423. **7dd**: mp 150—151 °C; IR (KBr) 3340 and 1660 cm^{-1}; ^1H NMR ($CDCl_3$) δ=0.75 (t, J=6 Hz, 6H, $2CH_3$), 1.5—2.2 (m, 6H, $(CH_2)_3$), 2.45 (q, J=6 Hz, 4H, $2CH_3C\underline{H}_2$), 5.40 (s, 3H, OH), and 6.9—7.5 (m, 10H, 2Ph). ^{13}C NMR ($CDCl_3$) δ=12.6(q), 18.9(t), 35.3(t), 41.8(t), 44.6(t), 81.6(s), 127.0(d), 127.9(d), 128.0(d), 128.2(d), 129.4(d), 129.8(d), 131.6(s), 133.2(s), 135.6(s), 142.3(s), 146.1(s), 147.2(s), and 198.1(s). Found: C, 80.65; H, 7.31; N, 3.91%; M^+, 373. Calcd for $C_{25}H_{27}NO_2$: C, 80.65; H, 7.30; N, 3.75%; M, 373. **7de**: mp 118—119 °C; IR (KBr) 3440 and 1650 cm^{-1}. ^1H NMR ($CDCl_3$) δ=0.80 (t, J=5 Hz, 6H, $2CH_2C\underline{H}_3$), 0.80 (s, 3H, CH_3), 1.11 (s, 3H, CH_3), 2.0—2.5 (m, 4H, $(CH_3)_2C(C\underline{H}_2)_2$), 2.65 (q, J=6 Hz, 4H, $2CH_3C\underline{H}_2$), 5.62 (s, 1H, OH), and 7.2—7.7 (m, 10H, 2Ph). Found: C, 80.82; H, 7.91; N, 3.55%; M^+, 401. Calcd for $C_{27}H_{31}NO_2$: C, 80.76; H, 7.22; N, 3.49%; M, 401. **6dg**: mp 103—105 °C; IR (KBr) 1750, 1700, and 1650 cm^{-1}; ^1H NMR ($CDCl_3$) δ=0.93 (t, J=7 Hz, 6H, $2C\underline{H}_3CH_2$), 1.90 (s, 3H, $COCH_3$), 3.00 (q, J=7 Hz, 4H, $2CH_3C\underline{H}_2$), 3.10 (s, 3H, CH_3), 4.84 (s, 1H, CH), and 7.1—7.5 (m, 10H, 2Ph). ^{13}C NMR (C_6D_6) δ=13.0(q), 28.2(q), 42.2(t), 50.4(d), 50.9(q), 70.8(s), 103.3(s), 126.1(d), 127.2(d), 127.8(d), 128.0(d), 129.1(d), 130.0(d), 136.3(s), 137.6(s), 171.1(s), and 201.5(s). Found: C, 76.38; H, 7.16; N, 3.65%; M^+, 377. Calcd for $C_{24}H_{27}NO_3$: C, 76.35; H, 7.22; N, 3.71%; M, 377. **7dg**: mp 124—125 °C; IR (KBr) 3490 and 1680 cm^{-1}; ^1H NMR ($CDCl_3$) δ=0.78 (t, J=7Hz, 6H, $2C\underline{H}_3CH_2$), 1.50 (s, 3H, CH_3), 2.51 (q, J=7 Hz, 4H, $2CH_3C\underline{H}_2$), 3.55 (s, 3H, CO_2CH_3), and 7.2—7.7 (m, 10H, 2Ph). ^{13}C NMR ($CDCl_3$) δ=13.0(q), 25.1(q), 44.8(t), 50.9(q), 82.8(s), 127.0(d), 127.5(d), 127.7(d), 128.9(d), 129.6(d), 134.4(s), 135.0(s), 135.2(s), 135.3(s), 145.9(s), 154.9(s), and 164.8(s). Found: C, 76.14; H, 7.09; N, 3.88%; M^+, 377. Calcd for $C_{24}H_{27}NO_3$: C, 76.35; H, 7.22; N, 3.71%; M, 377. **7dh**: mp 96—98 °C; IR (KBr) 3500 and 1670 cm^{-1}. ^1H NMR ($CDCl_3$) 0.79 (t, J=7 Hz, 6H, $2C\underline{H}_3CH_2$), 0.98 (t, J=8 Hz, 3H, $C\underline{H}_3CH_2CO_2$), 1.49 (s, 3H, CH_3), 2.51 (q, J=7 Hz, 4H, $2CH_3C\underline{H}_2$), 4.00 (q, J=8Hz, 2H, $CH_3C\underline{H}_2CO_2$), and 7.1—7.6 (m, 10H, 2Ph). Found: C, 76.58; H, 7.44; N, 3.62%; M^+, 391. Calcd for $C_{25}H_{29}NO_3$: C, 76.69; H, 7.47; N, 3.58%; M, 391. **7ea**: mp 121—122 °C; IR (KBr) 3500 and 1610 cm^{-1}; ^1H NMR ($CDCl_3$) δ=1.40 (s, 3H, CH_3), 1.75 (s, 3H, $COCH_3$), 2.18 (s, 6H, $N(CH_3)_2$), and 7.1—7.5 (m, 10H, 2Ph). Found: C, 79.09; H, 6.97; N, 4.34%; M^+, 333. Calcd for $C_{22}H_{23}NO_2$: C, 79.24; H, 6.97; N, 4.20%; M, 333. **7ed**: mp 146—148 °C; IR (KBr) 3350 and 1660 cm^{-1}; ^1H NMR ($CDCl_3$) δ=1.4—2.7 (m, 6H, $(CH_2)_3$), 2.15 (s, 6H, $2CH_3$), and 6.8—7.4 (m, 10H, 2Ph). Found: C, 79.82; H, 6.64; N, 4.13%; M^+, 345. Calcd for $C_{23}H_{23}NO_2$: C, 79.96; H, 6.72; N, 4.04%; M, 345. **7fd**: mp 118—120 °C; IR (KBr) 3340 and 1650 cm^{-1}; ^1H NMR ($CDCl_3$) δ=1.7—2.8 (m, 6H, $(CH_2)_3$), 2.40 (s, 3H, CH_3), and 6.8—7.5 (m, 15H, 3Ph). Found: C, 82.66; H, 6.42; N, 3.51%; M^+, 407. Calcd for $C_{28}H_{25}NO_2$: C, 82.52; H, 6.18; N, 3.44%; M, 407.

Hydrolysis of 7aa with Formic Acid in Benzene. A solution of **7aa** (200 mg) and formic acid (0.08 cm^3) in benzene (5 cm^3) was heated at 50 °C for 40 h. Evaporation of the solvent under the reduced pressure and TLC separation over aluminum oxide yielded 3-acetyl-4-hydroxy-4-methyl-2,5-diphenyl-2-cyclopentenone **10** in 27% yield. **10**: mp 159—161 °C; IR (KBr) 3450 and 1700 cm^{-1}; ^1H NMR ($CDCl_3$) δ=1.33 (s, 3H, CH_3), 2.13 (s, 3H, $COCH_3$), 3.35 (s, 1H, OH), 4.14 (s, 1H, CH), and 7.0—7.6 (m, 10H 2Ph). ^{13}C NMR ($CDCl_3$) δ=25.9(q), 31.3(q), 66.0(d), 80.0(s), 127.6(d), 128.3(d), 128.5(d), 128.7(d), 129.1(d), 129.5(d), 129.9(d), 134.7(s), 141.8(s), 163.4(s), 203.1(s), and 204.1(s). Found: C, 78.22; H, 5.61%; M^+, 306. Calcd for $C_{20}H_{18}O_3$: C, 78.41; H, 5.92%; M, 306.

Hydrolysis of 7aa with Trifluoroacetic Acid. Hydrolysis of **7aa** (0.3 g) in chloroform (10 cm^3) and ethanol (1 cm^3) catalyzed by trifluoroacetic acid (0.01 cm^3) was run for 40 h at room temperature. The reaction mixture was washed with water, dried over magnesium sulfate, chromatographed over aluminum oxide to yield a purple resinous mass, 3-acetyl-4-methyl-2,5-diphenyl-2,4-cyclopentadienone **13** in a quantitative yield. **13**: IR (Nujol) 1710 and 1690 cm^{-1}; ^1H NMR ($CDCl_3$) δ=1.50 (s, 3H, CH_3), 1.67 (s, 3H, $COCH_3$), and 6.5—7.2 (m, 10H, 2Ph). ^{13}C NMR ($CDCl_3$) δ=14.3 (q), 30.9(q), 127.7(d), 128.0(d), 128.1(d), 128.3(d), 128.4(d), 128.6(d), 129.2(s), 129.5(s), 130.0(s), 130.5(s), 149.7(s), 154.2(s), 199.7(s), and 201.8(s). Found: C, 83.05; H, 5.66%; M^+, 288. Calcd for

$C_{20}H_{16}O_2$: C, 83.31; H, 5.59%; M, 288.

The Reaction of 13 with DMAD. A mixture of **13** (0.1 g) and DMAD (3 times excess) in benzene (2 cm^3) was allowed to react at room temperature for 20 h. Condensation of the solution yielded colorless prisms of dimethyl 4-acetyl-5-methyl-3,6-diphenylphthalate **14**: mp 200—202 °C; IR (KBr) 1740 and 1700 cm^{-1}; ^1H NMR ($CDCl_3$) δ=1.90 (s, 3H, CH_3), 2.20 (s, 3H, $COCH_3$), 3.42 (s, 3H, CO_2CH_3), 3.47 (s, 3H, CO_2CH_3), and 7.1—7.6 (m, 10H, 2Ph). ^{13}C NMR ($CDCl_3$) δ=17.4(q), 31.9(q), 52.1(q), 127.7(d), 128.1(d), 129.0(d), 129.4(d), 133.9(s), 135.5(s), 136.9(s), 137.7(s), 140.2(s), 167.7(s), 167.8(s), and 205.7(s). Found: C, 74.54; H, 5.64%; M^+, 402. Calcd for $C_{25}H_{22}O_5$: C, 74.61; H, 5.51%; M, 402.

References

1) M. G. Steinmetz and R. T. Mayers, *J. Am. Chem. Soc.*, **107**, 2111 (1985).

2) H. Yoshida, H. Sano, M. Kato, T. Ogata, and K. Matsumoto, *Bull. Chem. Soc. Jpn.*, **59**, 2833 (1986) and references cited therein.

3) H. Yoshida, M. Nakajima, T. Ogata, R. M. Acheson, and J. D. Wallis, *Bull. Chem. Soc. Jpn.*, **56**, 3015 (1983).

4) H. Yoshida, M. Nakajima, T. Ogata, and K. Matsumoto, *Bull. Chem. Soc. Jpn.*, **57**, 734 (1984).

5) R. Breslow, T. Eicher, A. Krebs, R. A. Peterson, and J. Posner, *J. Am. Chem. Soc.*, **87**, 1320 (1965).

6) R. C. Kerber and C. Hsu, *J. Am. Chem Soc.*, **95**, 3239 (1973).

7) H. Yoshida, K. Yagi, T. Tamai, H. Sano, T. Ogata, and K. Matsumoto, *Bull. Chem. Soc. Jpn.*, **58**, 1073 (1985).

8) S. Forsen and M. Nilsson, "The Chemistry of the Carbonyl Group," ed. by J. Zabicky, Interscience Publishers, London (1970), Vol. 2, p. 157.

9) H. O. House, "Synthetic Organic Chemistry," 2nd ed., W. A. Benjamin Inc., Menlo Park (1972), p. 492.

10) J. Hine, "Structural Effects on Equilibria in Organic Chemistry," John Wiley & Sons, New York (1975), p. 276.

11) A. G. Cook, "Enamines: Synthesis, Structure, and Reactions," Marcel Dekker, New York (1969).

Synthesis and Acid-Catalyzed Ring Opening of 1-Alkenyl Cyclopropyl Ketones

Otohiko TSUGE,* Shuji KANEMASA, Tatsuya OTSUKA, and Toshiro SUZUKI
Institute of Advanced Material Study, and Department of Molecular Science and Technology, Interdisciplinary Graduate School of Engineering Sciences, Kyushu University, Kasugakoen, Kasuga 816
(Received February 26, 1988)

1-Alkenyl cyclopropyl ketones, when activated by cation-stabilizing substituents at the ring carbon or at the terminal carbon of the enone moiety, undergo polyphosphoric acid-catalyzed ring enlargement producing cyclopentanone or cyclohexenone derivatives. Similar acid-catalyzed ring opening of 1-alkenyl 2-phenoxycyclopropyl ketones offers a convenient and effective synthesis of 4-oxo-5-alkenals and their dioxolane-protected derivatives.

Our previous article described the simple synthesis of 1-alkenyl cyclopropyl ketones by a tandem cyclopropanation of 1-diazo-3-silyl-2-propanone and Peterson olefination sequence.[1] As a synthetic utilization and application of 1-alkenyl cyclopropyl ketones, homo-Nazarov type cyclization is expected since there are numerous examples known for ring opening reactions of cyclopropyl ketones[2] in the presence of acid catalysts such as protonic acids,[3] silylated acids,[4] Lewis acids,[5] and a pyridinium chloride.[6] Mostly the resulting carbonium ion intermediates are either quenched by nucleophiles present in the reaction mixture, e.g. conjugate bases arising from the acid catalysts or reaction solvents, or undergo β-elimination forming olefins.

To the best of our knowledge, no example of homo-Nazarov type ring enlargement of 1-alkenyl cyclopropyl ketones is known. Only a few examples for the related reactions have been reported previously. Aroyl cyclopropanes undergo acid-catalyzed ring enlargements to lead to tetralone derivatives,[7] or the cation intermediates involved in the acid-catalyzed ring opening were intramolecularly trapped by a separated aryl or olefin moiety.[8]

We wish to report here that 1-alkenyl cyclopropyl ketones undergo novel ring enlargements leading to cyclopentanones or cyclohexenones by action with polyphosphoric acid. Though the presence of an oxygen substituent on the cyclopropane ring of 1-alkenyl cyclopropyl ketones produces no ring-enlarged products, their ring openings are highly accelerated to furnish 4-oxo-5-alkenals or their dioxolane-protected derivatives.

Results and Discussion

1-Alkenyl cyclopropyl ketones **5a—h** used as substrates in the present work were previously prepared by a sequence of reactions including cyclopropanation of olefins with 1-diazo-3-trimethylsilyl-2-propanone (**1**), lithiation of the resulting cyclopropyl silylmethyl ketones **3**, and Peterson olefination using a variety of carbonyl compounds R^1COR^2 (Scheme 1).[1] Due to their susceptibility to moisture, silylmethyl ketones **3** were employed to the subsequent olefination without isolation and purification. As an additional example, the reaction of diazo ketone **1** with 2-(trimethylsilyl)-1,3-butadiene in the presence of a catalytic amount (1 mol%) of copper(II) acetylacetonate gave a mixture of two regioisomeric cyclopropanes. The mixture was then lithiated with lithium diisopropylamide (LDA) and allowed to react with benzaldehyde to afford **5i** and its regioisomer in 22% yield (2:1 by ^{1}H NMR, based on **1**).

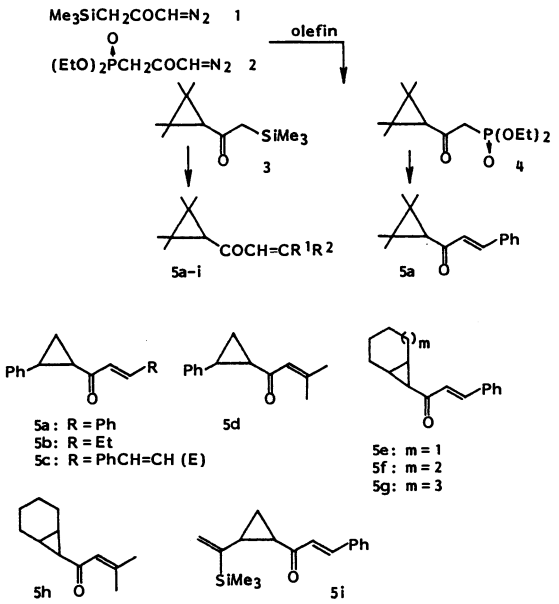

Scheme 1.

It was expected that 1-diazo-3-[(diethoxyphosphoryl)-methyl]-2-propanone (**2**) could serve as a new synthetic equivalent of **1** and would lead to less moisture-sensitive cyclopropyl ketones such as **4**.[9] However cyclopropanations using diazo ketone **2** resulted in the formation of complex products. Only styrene furnished the corresponding cyclopropyl ketone **4** in a fair yield (44%).

Stable ketone **4** was converted into 1-alkenyl cyclopropyl ketone **5a** in 85% yield by the reaction with benzaldehyde in the presence of triethylamine and lithium bromide.[10]

With an expectation of acid-catalysis for the ring opening, the 1-alkenyl cyclopropyl ketone **5a** was treated with a variety of Lewis or protonic acids. In many cases **5a** was either recovered intact ($Zn(OTf)_2$ in CH_2Cl_2, rt, 48 h; $Zn(OTf)_2$ in MeCN, rt, 48 h; $AlMe_3$ in CH_2Cl_2, rt, 19 h; LiOTf in CH_2Cl_2, rt, 9 d; $BF_3 \cdot OEt_2$ in CH_2Cl_2, rt, 7 h; PPSE[11] in $MeNO_2$, rt, 30 min) or decomposed into complex mixture ($TiCl_4$ in $MeNO_2$, rt, 10 min; $SnCl_4$ in CH_2Cl_2, rt, 22 h; PPSE in $MeNO_2$, reflux, 2 d; CF_3SO_3H in CH_2Cl_2, rt, 1 h).

Treatment of **5a** with trifluoromethanesulfonic acid in trifluoroacetic acid (TFA) at room temperature gave the expected ring-opened product **6** (Table 1, Entry 1). In this reaction water served as a nucleophile (Nu) to trap the resulting carbonium ion **A** (Scheme 2). Use of benzene as a solvent caused electrophilic substitution of **A** on the benzene to provide **7** (Entry 2). Boron trifluoride etherate also works as an effective catalyst (E^+) in a polar solvent, nitromethane which accelerates the ring opening of **5a**. Thus by action of boron trifluoride etherate and acetic anhydride, **5a** or **4** was readily converted into diacetate **8** or **9**, respectively (Entries 3 and 4). Polyphosphoric acid (PPA) is also able to open **5h** to give hydroxy ketone **10** (Entry 5).

Both diacetates **8** and **9** were obtained as single isomers. *Z*-Geometry of **8** with respect to the newly formed enol acetate was confirmed on the basis of the NOE difference ^1H NMR spectrum in which notable signal enhancement was observed between β-H of the enol acetate and the two styryl protons. Equally *Z*-selective formation of **8** was achieved regardless of the cis-trans ratio of the starting cyclopropyl ketones **5a**.

The above *Z*-selectivity seems to be a kinetical result on the basis of the following discussion: In the acid-

Table 1. Acid-Catalyzed Ring Opening of Cyclopropyl Ketones **4** and **5**

Entry	Ketone		Acid	Solvent	Condition	Product (yield/%)[a]	
1	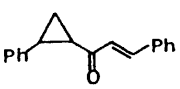	**5a**	CF_3SO_3H	CF_3COOH	rt, 3h	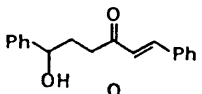	**6** (66)
2	**5a**		CF_3SO_3H	Benzene	rt, 1.5 h	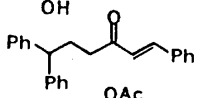	**7** (84)
3	**5a**		$BF_3 \cdot OEt_2/Ac_2O$	$MeNO_2$	rt, 10 min	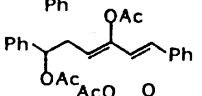	**8** (59)
4	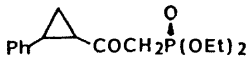	**4**	$BF_3 \cdot OEt_2/Ac_2O$	$MeNO_2$	rt, 18 h	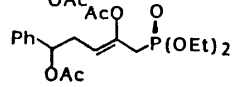	**9** (78)
5	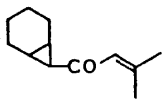	**5h**	PPA	Benzene	Reflux, 2.5 h	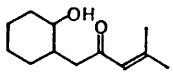	**10** (78)
6	**5a**		PPA	Benzene	Reflux, 40 h	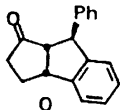	**11** (71)
7	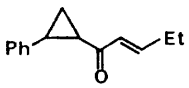	**5b**	PPA	Benzene	Reflux, 30 h	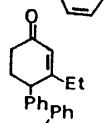	**12** (63)
8	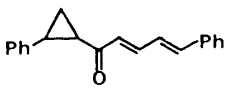	**5c**	PPA	Benzene	Reflux, 10 d	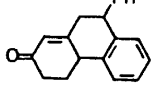	**13** (43)
9	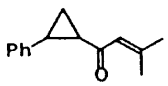	**5d**	PPA	Benzene	Reflux, 47 h	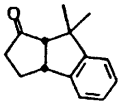	**14** (89)
	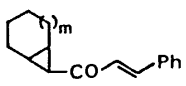					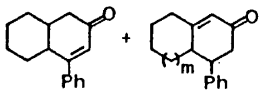	
10	**5e**: m=1		PPA	Benzene	Reflux, 55 h	**15** (57)	**16**: m=1 (18)
11	**5f**: m=2		PPA	Benzene	Reflux, 40 h		**17**: m=2 (15)
12	**5g**: m=3		PPA	Benzene	Reflux, 65 h		**18**: m=3 (26)
13	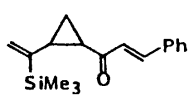	**5i**	PPA	Benzene	rt, 24 h	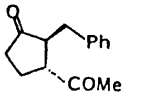	**19** (38)

a) Yield of isolated products.

catalyzed ring opening of cyclopropyl ketones, the σ-bond to be cleaved must interact effectively with the carbonyl π-orbital.[12] So a concerted ring opening would occur in a stereospecific fashion if the bond to be cleaved is nearly perpendicular to the plane of the carbonyl. As the most stable conformations for *trans*-**5a** and for *cis*-**5a** are expected to bear the bulkier substituent R far from the unsubstituted methylene carbon (**B** for *trans*-**5a** and **C** for *cis*-**5a**),[13] their concerted ring opening would lead to *Z*-isomer **8**. This is the result actually observed. Conformation **D** may be less stable due to some serious steric hindrance between R and one of the ring methylene hydrogens.[14]

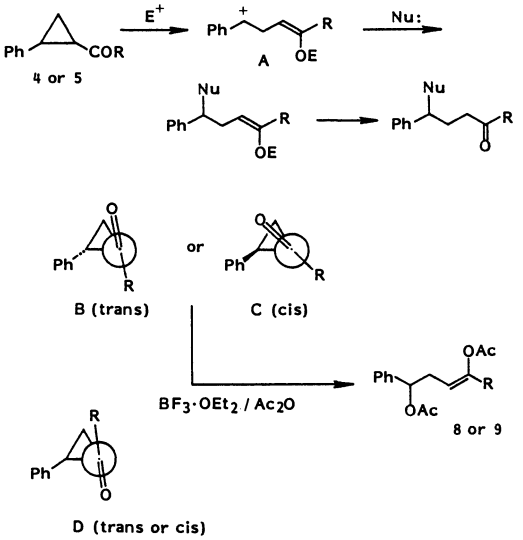

Scheme 2.

On treatment of cyclopropyl ketone **5a** with PPA under reflux in benzene in a two phase reaction, cyclopent[*a*]inden-1-one (**11**) was obtained in 71% yield as a single isomer (Table 1, Entry 6). The 3a,8a-cis-8,8a-trans stereochemistry was confirmed on the basis of the coupling constants ($J_{3a\text{-}8a}$=7.5 and $J_{8\text{-}8a}$=0.8 Hz).

Scheme 3 illustrates a possible mechanism for the stereoselective ring enlargement of 1-alkenyl cyclopropyl ketone **5a** leading to **11**. As discussed above (in Scheme 2), the acid-catalyzed ring opening of **5a** exclusively forms (*Z*)-enol cation intermediate **E** which can not undergo cyclization. Under the reaction conditions this enol **E** would equilibrate with (*E*)-enol cation **F** through a keto-enol tautomerization, presumably via a hydroxylated intermediate. Though olefin cyclization of **F** could lead to both cis benzyl cation intermediate **G** and its trans isomer, only **G** can undergo further cyclization. As a result, *cis*-selective cyclization into **G** takes place under equilibrating conditions. Intramolecular electrophilic substitution on the benzene ring as a substituent occurs again stereoselectively to give the isolated product **11**. As the cyclization of **G** should take place with the most stable

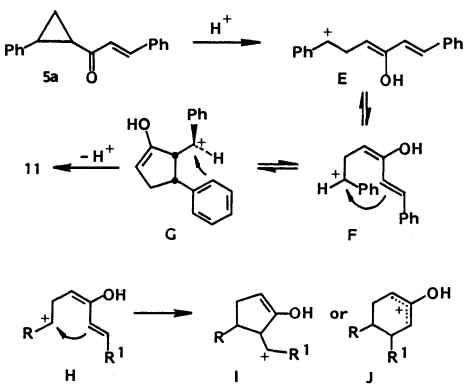

Scheme 3.

configuration where the bulkier phenyl group must be anti to the fused five-membered ring, it is now quite easy to understand the selective formation of **11**.

There are two possible cyclization patterns of intermediary cation **H** which is equivalent with the aforementioned intermediate **F**: One cyclization leads to five-membered ring **I** with an exo cation and the other six-membered ring **J** with an endo cation. It is expected that regiochemistry of the cyclization would depend upon the nature of cation stabilization by substituent R^1. Therefore some derivatives **5b—g** wearing a variety of substitution patterns were employed in PPA-catalyzed ring enlargement reactions.

Ketone **5d** bearing two methyl substituents on the β-carbon of enone showed a similar cyclization pattern, via intermediate **I**, to give **14** (Table 1, Entry 9). On the other hand, cyclizations of ketones **5b** and **5c** proceeded via six-membered intermediates **J** to furnish

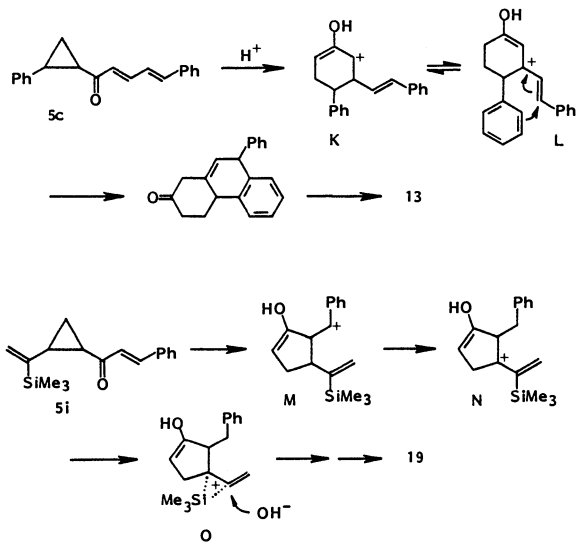

Scheme 4.

12 and **13** (Entries 7 and 8). Ring-fused cyclopropyl ketones **5e—g** are similarly isomerized into fused cyclohexenones **15—18** albeit in low yields (Entries 10—12).

In the isomerization of dienone **5c**, the direct cyclization of intermediate **K** is impossible due to the *E*-configuration of the styryl moiety (Scheme 4). This cation **K** can equilibrate with pentadienyl cation **L** through a deprotonation and reprotonation process, which is then transformed to the isolated product **13** via the step of making the second six-membered ring and the followed double-bond migration.

Ring enlargement of ketone **5i** bearing a 1-silylethenyl moiety on the cyclopropane ring occurred in a different way to produce desilylated cyclopentanone **19** as a single isomer. Structure of **19** was assigned to be *trans*-3-acetyl-2-benzylcyclopentanone mainly on the basis of the spectral data ($J_{2\text{-}3}$=9.7 Hz; ring CO: =210.03; MeCO: 1.88 and 200.70). This unusual reaction would involve the initial formation of intermediary benzyl cation **M** which then rearranges into equally stable tertiary 2-silyl-substituted allyl cation **N**. A 1,2-silyl migration[15] is followed by hydroxylation leading to the isolated product **19** after a spontaneous desilylation.

Though these PPA-catalyzed ring enlargements of 1-alkenyl cyclopropyl ketones are attractive as a new direct and stereoselective synthetic way to fused cyclopentanones and cyclohexenones, lack of the cation-stabilizing substituents in the substrates provides either only poor yields of ring-enlarged products or complex results.[16] An effective cation-stabilizing substituent is essential.

With an expectation that an alkoxy or aryloxy moiety would accelerate the ring enlargement, a variety of 1-alkenyl cyclopropyl ketones **21a—h** were prepared and their ring openings were studied.[17] Cyclopropanation of vinyl ethers with **1** in the presence of a catalytic amount (0.5—1 mol%) of copper(II) acetylacetonate or rhodium(II) acetate gives the corresponding cyclopropyl silylmethyl ketones **20a—d** in 46—79% yields (Scheme 5). As **20a—d** belong to moisture sensitive α-silyl ketones, vacuum distillation was the only practical separation method. Immediately after their separation **20a—d** were lithiated with LDA and then allowed to react with benzaldehyde to form 2-alkoxy enones **21a—d** in good yields (by ^{1}H NMR). Though in lower yields, these two steps of cyclopropanation and olefination can be performed in one flask (see Experimental).

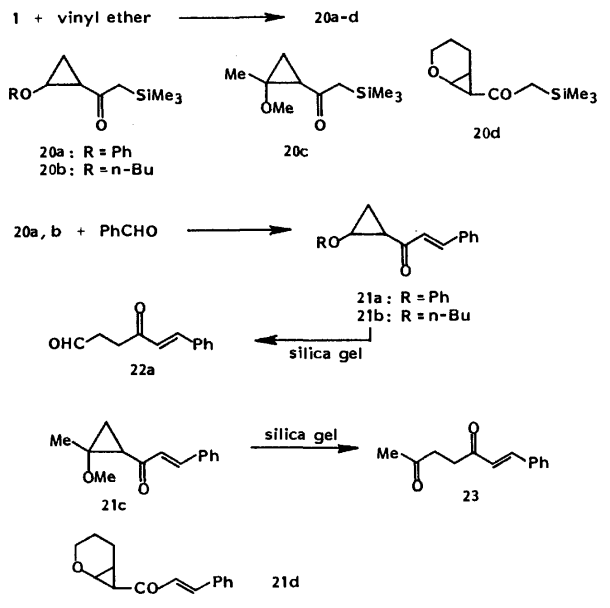

Scheme 5.

Compared with the sufficient stability of the phenoxy derivative **21a** which can be separated and purified through column chromatography, the other three **21b—d** are all labile. Though their formation can be confirmed on the basis of ^{1}H and/or ^{13}C NMR spectra of the crude reaction mixtures, all attempts to isolate them by column chromatography resulted in their ring opening or decomposition. Thus crude **21b** and **21c** were chromatographed over silica gel to give 4-oxo-5-alkenal **22a** (60%) and 5-alkene-1,4-dione **23** (23% based on **1**), respectively, both as *E*-isomers (Scheme 5). The ring-fused enone **21d** decomposed to complex mixture by a similar procedure.

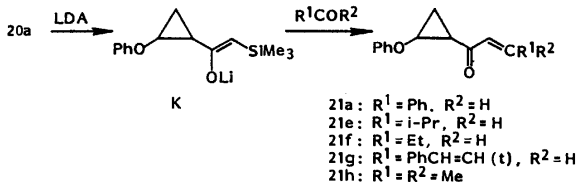

Scheme 6.

As the phenoxy-substituted enone **21a** proved to have higher stability, several derivatives **21e—h** were prepared from silylmethyl ketone **20a** by the same procedure applied for **21a** (Scheme 6). As a step-saving procedure, the following one-flask reactions can be employed: The reaction mixture containing crude **20a**, supplied from the cyclopropanation procedure using **1**, is immediately lithiated with LDA at −78 °C and then reacted with a variety of carbonyl compounds. The resulting mixtures are chromatographed over silica gel to give **21a** and **21e—h** in 20—40% total yields based upon **1**.

It was disappointing that treating **21a** with PPA under the same conditions applied in the conversion of **5a** into **11** gave no sign of formation of the expected cyclization product. However simple treatment of **5a** with TFA in aqueous tetrahydrofuran (THF) at room temperature gave (*E*)-4-oxo-6-phenyl-5-hexenal (**22a**) in 88% yield, which is identical with that obtained from **21b** (Scheme 7 and Table 2, Entry 1). Similarly a variety of 4-oxo-5-alkenals such as (*E*)-7-methyl-4-oxo-5-octenal (**22b**), (*E*)-4-oxo-5-octenal (**22c**), (*E*,*E*)-4-oxo-8-phenyl-5,7-octadienal (**22d**), and 6-methyl-4-oxo-5-heptenal (**22e**) were obtained in good yields (Entries 2—5). Although the ring opening of **21h** was so slug-

Table 2. Acid-Catalyzed Ring Opening of 1-Alkenyl 2-Phenyloxycyclopropyl Ketones **21a** and **21d—h**

Entry	Ketone	Reaction condition		Product (yield/%)[a]	
1	**21a**	TFA in wet THF	rt, 20.5 h	**22a** (88)	
2	**21e**	TFA in wet THF	rt, 24 h	**22b** (100)	
3	**21f**	TFA in wet THF	rt, 22 h	**22c** (71)	
4	**21g**	TFA in wet THF	rt, 63 h	**22d** (73)	
5	**21h**	TFA + LiCl[b] in wet THF	rt, 0.5 h	**22e** (71)	
6	**21a**	TFA + $HOCH_2CH_2OH$ in $MeNO_2$	0 °C, 20 min	**24a** (90)	
7	**21e**	TFA + $HOCH_2CH_2OH$ in $MeNO_2$	0 °C, 10 min	**24b** (58)	
8	**21f**	TFA + $HOCH_2CH_2OH$ in $MeNO_2$	0 °C, 10 min	**24c** (42)	
9	**21g**	TFA + $HOCH_2CH_2OH$ in $MeNO_2$	0 °C, 20 min	**24d** (58)	
10	**21h**	TFA + $HOCH_2CH_2OH$ in $MeNO_2$	0 °C, 30 min	**24e** (67)	
11	**21d**	TFA in wet THF	rt, 20 min	**25** (44)[c]	1 : 1[d]
12	**21d**	TFA + $HOCH_2CH_2OH$ in $MeNO_2$	0 °C, 1 h	**26** (60)[c]	8 : 52[e]
13	**21d**	TFA + EtOH in $MeNO_2$	0 °C, 15 min	**27** (46)[c]	13 : 33[e]

a) Yield of isolated products. b) Two equivalents of lithim chloride was used. c) Yield based on diazo ketone **1**. d) Inseparable mixture (NMR). e) Each isomer was isolated (cis : trans).

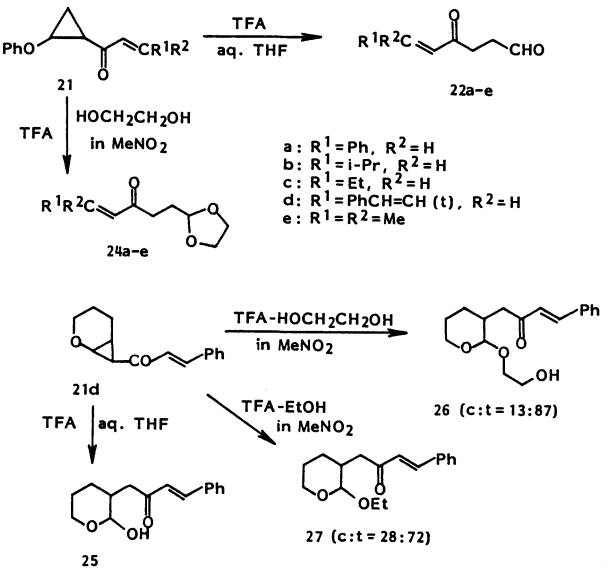

Scheme 7.

gish under these conditions that most of **21h** was recovered after a week at room temperature, the addition of lithium chloride accelerated this reaction to such an extent that the reaction was complete in 30 min to give 71% yield of **22e**.

When the ring opening reactions of **21** are carried out in the presence of 1,2-ethanediol in nitromethane, dioxolane-protected derivatives **24a—e** are directly obtained (Scheme 7 and Entries 6—10 in Table 2). The reactions proceed smoothly and are complete at 0 °C in less than 30 min.

The ring-fused cyclopropyl ketone **21d** is very susceptible to acid. Thus TFA in THF or nitromethane opens the cyclopropane ring of **21d** to give hemiacetals **25—27** through an addition of the nucleophiles employed (Scheme 7 and Entries 11—13 in Table 2).

Experimental

General. Melting points were determined on a Yanagimoto melting point apparatus and are uncorrected. IR spectra were taken with a JASCO IRA-1 or a JASCO A-702 spectrometer. ^1H NMR spectra were recorded on a Hitachi R-40 (90 MHz), a JEOL FX-100 (100 MHz), or a JEOL GSX-270 instrument (270 MHz), and ^{13}C NMR on a JEOL FX-100 (25.05 MHz) or a JEOL GSX-270 spectrometer (67.94 MHz). Chemical shifts are expressed in parts per million downfield from tetramethylsilane as an internal standard. Mass spectra were measured with a JEOL-01SG-2 spectrometer at 70 eV of ionization energy. High-resolution mass spectra were obtained on the same instrument. Elemental analyses were performed on a Hitachi 026 CHN analyzer. Thin-layer chromatography (TLC) was accomplished on 0.2 mm precoated plates of silica gel 60 F-254 (Merck). Visualization was made with ultraviolet light (254 and 365 nm), iodine, molybdophosphoric acid (5% in ethanol), or *p*-anisaldehyde (5% in ethanol containing 5% of sulfuric acid). For preparative column chromatography, Wakogel C-200, C-300 (Wako), and silica gel 60 (Merck) were employed. Flash chromatography was carried out on an EYELA EF-10 apparatus using a column (20×180 mm) packed with silica gel 60 (Merck, size: 0.04—0.063 mm). Preparative high-performance liquid chromatography (HPLC) was performed on a Kusano KHLC-201 apparatus with a UV-detector Uvilog-III using a column (22×300 mm) packed with silica gel (Wakogel LC-50H). Gas liquid chromatography (GLC) was accomplished on a Yanaco G-2800 gas chromatograph (Yanagimoto) with an ionization flame detector using a glass column (SE-30, 3×2000 mm) or a glass capillary column (Silicone GE, SE-30, 0.25×50000 mm). Micro vacuum distillation was carried out on a Sibata GTO-250R Kugelrohr distilling apparatus. Solvents were evaporated with a Tokyo Rikakikai rotary evaporator type-V at about 50 °C unless otherwise stated.

Materials. 1-Diazo-3-trimethylsilyl-2-propanone (**1**),[1] 1-diazo-3-(diethoxyphosphoryl)-2-propanone (**2**),[9] (diethoxyphosphoryl)methyl 2-phenylcyclopropyl ketone,[9] 2-trimethylsilyl-1,3-butadiene,[18] phenyl vinyl ether[19] were prepared according to the reported methods. Butyl vinyl ether, 2-methoxypropene, and 3,4-dihydro-2*H*-pyran are all commercially available and used without further purification. Trifluoromethanesulfonic acid and polyphosphoric acid (PPA, H_3PO_4 content; 105%, Katayanma Kagaku Co., Ltd.) are also commercially available. 1-Alkenyl cyclopropyl ketones **5a—h** were previously prepared by one-pot proce-

dure for a sequence of cyclopropanation using diazo ketone **1** and Peterson olefination with a variety of carbonyl compounds.[1,9]

(*E*)-2-Phenylethenyl 2-[(1-Trimethylsilyl)ethenyl]cyclopropyl Ketone (5i): To the mixture of copper(II) acetylacetonate (3 mg, 0.01 mmol) and 2-trimethylsilyl-1,3-butadiene (1 g, 8 mmol) preheated at 75 °C was added slowly under nitrogen 1-diazo-3-trimethylsilyl-2-propanone (**1**, 0.156 g, 1 mmol) in a period of 0.5 h. After cooled to room temperature, the reaction mixture was diluted with dry THF (1 ml). This solution was added dropwise at −78 °C to lithium diisopropylamide (LDA, 1.61 mmol) freshly prepared in THF (1.5 ml). After 45 min at the same temperature, benzaldehyde (0.16 ml, 1.61 mmol) was added. The resulting mixture was stirred at −78 °C for 2 h and then at room temperature for 0.5 h. Saturated aqueous ammonium chloride was added and extraction procedure with dichloromethane (20 ml×2) was followed. The combined extracts were dried over magnesium sulfate and evaporated in vacuo. The residue was chromatographed over silica gel by using hexane–ethyl acetate (20 : 1 v/v) to give **5i** (0.04 g, 15% based on **1**) and then (*E*)-2-phenylethenyl 2-trimethylsilyl-2-vinylcyclopropyl ketone (0.02 g, 7% based on **1**). **5i:** Colorless liquid; IR (neat) 1690, 1246, and 850 cm^{-1}; ^1H NMR ($CDCl_3$) δ=0.12 (9H, s, $SiMe_3$), 1.23 (1H, ddd, J=8.6, 8.0, and 3.8 Hz, ring CH_2), 1.55 (1H, ddd, J=8.6, 5.0, and 3.8 Hz, ring CH_2), 2.1—2.3 (2H, m, ring CH), 5.36 (1H, d, J=2.6 Hz, $=CH_2$), 5.49 (1H, dd, J=2.6 and 2.0 Hz, $=CH_2$), 6.88 (1H, d, J=16.1 Hz, =CH), 7.3—7.6 (5H, m, Ph), and 7.60 (1H, d, J=16.1 Hz, =CH); ^{13}C NMR ($CDCl_3$) δ=−1.71 ($SiMe_3$), 17.67 (ring CH_2), 29.43, 30.11 (ring CH), 121.97 ($=CH_2$), 126.55, 128.29, 128.91, 130.35, 134.35, 142.11, 150.97, and 198.45 (CO); MS m/z (rel intensity, %) 270 (M^+, 31), 139 (20), 131 (62), and 73 (base peak). HRMS Found: m/z 270.1444. Calcd for $C_{17}H_{23}OSi$: M, 270.1439.

(*E*)-6-Hydroxy-1,6-diphenyl-1-hexen-3-one (6). To a solution of **5a** (0.037 g, 0.15 mmol) in trifluoroacetic acid (TFA, 1 ml) was added trifluoromethanesulfonic acid (0.01 ml). After 3 h at room temperature, the mixture was poured into saturated aqueous sodium hydrogencarbonate and extracted with dichloromethane (20 ml×2). The combined extracts were dried over magnesium sulfate and evaporated in vacuo. The residue was chromatographed over silica gel with hexane–ethyl acetate (2 : 1 v/v) to provide **6** (0.026 g, 66%): Yellow liquid; IR (neat) 3430 and 1675 cm^{-1}; ^1H NMR ($CDCl_3$) δ=1.58 (1H, br s, OH), 2.14 (2H, dt, J=7.0 and 6.2 Hz, 5-H), 2.80 (2H, t, J=7.0 Hz, 4-H), 4.79 (1H, t, J=6.2 Hz, 6-H), 6.70 (1H, d, J=16.5 Hz, 2-H), 6.9—7.6 (10H, m, Ph), and 7.54 (1H, d, J=16.5 Hz, 1-H); ^{13}C NMR ($CDCl_3$) δ=33.36, 37.18 (each t, 4- and 5-C), 73.77 (d, 6-C), 126.13, 126.48, 127.83, 128.65, 128.83, 129.30, 130.89, 134.83, 143.24, 144.85, and 201.07 (s, CO); MS m/z (rel intensity, %) 266 (M^+, 15), 248 (82), 157 (22), 146 (44), 144 (20), 131 (base peak), 116 (33), 103 (58), 91 (24), and 77 (57). Found: C, 80.49; H, 6.81%. Calcd for $C_{18}H_{18}O_2$: C, 81.18; H, 6.81%.

(*E*)-1,6,6-Triphenyl-1-hexen-3-one (7). To a solution of **5a** (0.15 g, 0.6 mmol) in benzene (6 ml) was added trifluoromethanesulfonic acid (0.265 ml, 3 mmol). After stirred at room temperature for 1.5 h, the mixture was poured into aqueous sodium hydrogencarbonate and extracted with diethyl ether (20 ml×2). The combined extracts were dried over magnesium sulfate and evaporated in vacuo. The residue (0.197 g) was subjected to column chromatography over silica gel with hexane–ethyl acetate (9 : 1 v/v) to give **7** (0.165 g, 84%). Colorless needles; mp 124—125 °C (diethyl ether–hexane); IR (KBr) 1687 cm^{-1}; ^1H NMR ($CDCl_3$) δ=2.3—2.7 (4H, m, 4- and 5-H), 3.95 (1H, t, J=8.0 Hz, 6-H), 6.64 (1H, d, J=16.0 Hz, 2-H), 7.0—7.6 (15H, m, Ph), and 7.40 (1H, d, J=16.0 Hz, 1-H); ^{13}C NMR ($CDCl_3$) δ=29.77, 39.06 (each t, 4- and 5-C), 50.47 (d, 6-C), 126.42, 127.95, 128.30, 128.65, 128.95, 130.48, 134.54, 142.36, 144.54 (d, 1-C), and 199.89 (s, CO). Found: C, 88.43; H, 6.87%. Calcd for $C_{24}H_{22}O$: C, 88.31; H, 6.79%.

(*E*)-3,6-Diacetoxy-1,6-diphenyl-1,3-hexadiene (8). A mixture of **5a** (0.05 g, 0.2 mmol), boron trifluoride etherate (0.024 ml, 0.2 mmol), acetic anhydride (0.038 ml, 0.4 mmol), and nitromethane (1 ml) was stirred at room temperature for 10 min. Treatment with saturated aqueous sodium hydrogencarbonate was followed by extraction with dichloromethane (10 ml×2). The combined extracts were dried over magnesium sulfate and evaporated in vacuo. The residue (0.073 g) was subjected to column chromatography over silica gel by using hexane–ethyl acetate (4 : 1 v/v) to give **8** (0.042 g, 59%): Pale yellow liquid; IR (neat) 1760 and 1739 cm^{-1}; ^1H NMR ($CDCl_3$) δ=2.08, 2.30 (each 3H, s, COMe), 2.4—2.9 (2H, m, 5-H), 5.32 (1H, t, J=7.5 Hz, 4-H), 5.80 (1H, t, J=7.0 Hz, 6-H), 6.40 (1H, d, J=15.9 Hz, 2-H), 6.60 (1H, d, J=15.9 Hz, 1-H), and 7.2—7.4 (10H, m, Ph); ^{13}C NMR ($CDCl_3$) δ=20.47, 21.18 (each q, COMe), 33.18 (t, 5-H), 74.59 (d, 6-C), 117.12 (d, 4-C), 123.07 (d, 4-C), 126.60, 126.83, 128.13, 128.36, 128.71 (each d), 136.36, 139.89 (each s), 148.01 (d, 1-C), 168.30, and 170.37 (each s, COMe); MS m/z (rel intensity, %) 350 (M^+, 1), 290 (34), 248 (36), 159 (87), 131 (51), 107 (39), 103 (26), 91 (24), 77 (31), and 43 (base peak). HRMS Found: m/z 350.1518. Calcd for $C_{22}H_{22}O_4$: M, 350.1517.

(*E*)-2,5-Diacetoxy-1-(diethoxyphosphoryl)-5-phenyl-2-pentene (9). To a solution of **4** (0.101 g, 0.34 mmol) in dry nitromethane (2 ml) were added at 0°C boron trifluoride etherate (0.041 ml, 0.34 mmol) and acetic anhydride (0.065 ml, 0.68 mmol). The mixture was stirred at room temperature under nitrogen for 18 h, poured into saturated aqueous sodium hydrogencarbonate, and extracted with dichloromethane (15 ml×2). The combined extracts were dried over magnesium sulfate and evaporated in vacuo. The residue (0.18 g) was subjected to column chromatography over silica gel with ethyl acetate to give **9** (0.105 g, 78%): Pale yellow liquid; IR (neat) 1753, 1240, 1051, and 1025 cm^{-1}; ^1H NMR ($CDCl_3$) δ=1.29 (6H, t, J=7.0 Hz, OEt), 2.06, 2.16 (each 3H, s, COMe), 2.4—2.7 (2H, m, 4-H), 2.84 (2H, d, $J_{H\text{-}P}$=21.5 Hz, PCH_2), 4.07 (4H, qd, J=8.4 and 7.0 Hz, OEt), 5.11 (1H, td, J=7.0 and $J_{H\text{-}P}$=4.5 Hz, 3-H), 5.74 (1H, t, J=7.0 Hz, 5-H), and 7.31 (5H, s, Ph); MS m/z (rel intensity, %) 398 (M^+, 0.5), 296 (50), 207 (67), 179 (24), 151 (24), and 43 (base peak). HRMS Found: m/z 398.1500. Calcd for $C_{19}H_{27}O_7P$: M, 398.1493.

2-(3-Methyl-1-oxo-2-butenyl)cyclohexanol (10). A mixture of **5h** (0.13 g, 0.73 mmol), polyphosphoric acid (PPA, P_2O_5 content, 75%, 1.3 g) in benzene (1 ml) was heated under reflux for 2.5 h. The mixture was poured into saturated aqueous sodium hydrogencarbonate and extracted with diethyl ether (20 ml×2). The combined extracts were dried over magnesium sulfate and evaporated in vacuo. The residue was subjected to column chromatography over silica gel with hexane–ethyl acetate (20 : 1 v/v) to afford **10** (0.079 g, 55%) as a single isomer: Colorless liquid; IR (neat) 3440, 1680, and 1620 cm^{-1}; ^1H NMR ($CDCl_3$) δ=1.0—3.0 (11H, m,

CH_2 and CH), 1.84, 2.08 (each 3H, s, Me), 3.7—3.8 (1H, m, CHOH), and 6.00 (1H, s, =CH); ^{13}C NMR ($CDCl_3$) δ=20.82 (q and t, Me and CH_2), 24.65, 27.47 (each t), 27.76 (q, Me), 32.53 (t), 37.65 (d), 46.53 (t), 69.42 (d, CHOH), 124.48 (d, =CH), 155.83 (s, $=CMe_2$), and 201.95 (s, CO); MS *m/z* (rel intensity, %) 196 (M^+, 12), 178 (11), 99 (36), 98 (38), 83 (base peak), 82 (13), and 55 (49). HRMS Found: *m/z* 196.1462. Calcd for $C_{12}H_{20}O_2$: M, 196.1461.

3a,8a-*cis*-8,8a-*trans*-8-Phenyl-3,3a,8,8a-tetrahydrocyclopent[*a*]inden-1(2*H*)-one (11). A mixture of **5a** (0.15 g, 0.6 mmol) and PPA (P_2O_5 content, 75%, 1.5 g) in benzene (1.5 ml) was heated at 80—85 °C for 40 h during which time the reaction was monitored by GLC. The reaction mixture was poured into saturated aqueous sodium hydrogencarbonate and extracted with diethyl ether (20 ml×2). The combined extracts were dried over magnesium sulfate and evaporated in vacuo. The residue was chromatographed over silica gel by using hexane–ethyl acetate (50 : 1 v/v) to give **11** (0.106 g, 71%) as a single isomer: Colorless needles (ethyl acetate–hexane); mp 97—98 °C; IR (KBr) 1725, 1490, 1445, 1130, 795, 750 and 735 cm^{-1}; ^1H NMR ($CDCl_3$) δ=2.0—2.5 (4H, m, 2- and 3-H), 2.82 (1H, dd, *J*=7.5 and 0.8 Hz, 8a-H), 4.1—4.2 (1H, m, 3a-H), 4.75 (1H, d, *J*=0.8 Hz, 8-H), and 6.8—7.3 (9H, m, Ar); ^{13}C NMR ($CDCl_3$) δ=26.26 (t, 2-C), 36.74 (t, 3-C), 46.00, 54.36, 61.06 (each d, 3a-, 8-, and 8a-C), 124.07, 125.66, 126.60, 127.48, 127.78, 127.90, 128.01, 128.78, and 221.31 (s, CO); MS *m/z* (rel intensity, %) 248 (M^+, 31), 220 (26), 204 (52), 192 (base peak), 191 (66), 189 (38), 165 (42), 115 (39), and 42 (21); Found: C, 87.27; H, 6.57%. Calcd for $C_{18}H_{16}O$: C, 87.06, 6.49%.

3-Ethyl-4-phenyl-2-cyclohexen-1-one (12). A similar procedure using **5b** (0.105 g, 0.53 mmol), PPA (P_2O_5 content, 75%, 1 g), and benzene (1 ml) under reflux for 30 h and subsequent chromatographic operation (silica gel, hexane–ethyl acetate (50 : 1 v/v)) gave **12** (0.066 g, 63%): Colorless liquid; IR (neat) 1660, 1445, 1245, 880, 760, and 700 cm^{-1}; ^1H NMR ($CDCl_3$) δ=1.02 (3H, t, *J*=6.5 Hz, Et), 1.1—2.4 (4H, m, CH_2), 2.09 (2H, q, *J*=6.5 Hz, Et), 3.60 (1H, t, *J*=4.0 Hz, 4-H), 6.0—6.1 (1H, m, 2-H), and 7.0—7.3 (5H, m, Ph); ^{13}C NMR ($CDCl_3$) δ=11.35 (q, Et), 29.36, 31.65, 34.00 (each t, CH_2), 45.47 (d, 4-C), 126.48, 127.24, 128.36, 129.01 (each d), 140.95 (s), 167.95 (s, 3-C), and 200.13 (s, CO); MS *m/z* (rel intensity, %) 200 (M^+, 63), 172 (53), 158 (38), 157 (42), 143 (39), 129 (base peak), 128 (41), 115 (51), 91 (25), and 43 (28). HRMS Found: *m/z* 200.2794. Calcd for $C_{14}H_{16}O$: M, 200.2794.

9-Phenyl-4,4a,9,10-tetrahydro-2(3*H*)-phenanthrenone (13). A similar procedure using **5c** (0.14 g, 0.5 mmol), PPA (P_2O_5 content, 75%, 1.4 g), and benzene (1 m) at 80—85 °C for 10 d and subsequent chromatographic separation (silica gel, hexane–ethyl acetate (30 : 1 v/v)) afforded **13** (0.06 g, 43%) as a single isomer: Colorless prisms (ethyl acetate–hexane); mp 114—115 °C; IR (KBr) 1670, 1430, 1370, 1290, 750, and 695 cm^{-1}; ^1H NMR ($CDCl_3$) δ=2.0—3.2 (7H, m, CH_2 and CH), 4.2—4.4 (1H, m, 9-H), and 6.8—7.8 (10H, m, Ar and 1-H); ^{13}C NMR ($CDCl_3$) δ=23.35, 29.30, 31.00, 33.59 (each t, CH_2), 50.42 (d, 9-C), 126.48, 126.83, 128.13, 128.30, 128.60, 130.13, 130.48, (each d), 134.36 (d, 1-C), 141.42, 143.13, 145.71 (each s), 163.83 (s, 10a-C), and 209.72 (CO); MS *m/z* (rel intensity, %) 274 (M^+, base peak), 246 (53), 218 (71), 217 (42), 215 (28), 204 (20), and 202 (22). HRMS Found: *m/z* 274.1357. Calcd for $C_{20}H_{18}O$: M, 274.1368.

8,8-Dimethyl-3,3a,8,8a-tetrahydrocyclopent[*a*]inden-1(2*H*)-one (14). A similar procedure using **5d** (0.14 g, 0.62 mmol), PPA (P_2O_5 content, 75%, 1.4 g), and benzene (1.5 ml) at 80—85 °C for 47 h and subsequent chromatography (silica gel, hexane–ethyl acetate (50 : 1 v/v)) gave **14** (0.075 g, 89%): Colorless liquid; IR (neat) 1730, 1680, 1485, 1455, 1280, 1160, 805, and 765 cm^{-1}; ^1H NMR ($CDCl_3$) δ=1.27, 1.34 (each 3H, s, Me), 2.0—2.3 (4H, m, CH_2), 2.56 (1H, d, *J*=8.0 Hz, 8a-H), 3.9—4.1 (1H, m, 3a-H), and 7.0—7.2 (4H, m Ar); ^{13}C NMR ($CDCl_3$) δ=24.77 (q, Me), 27.07 (t, 3-C), 33.30 (q, Me), 38.71 (t, 2-C), 45.42 (d, 8a-C), 47.53 (s, 8-C), 61.95 (d, 3a-C), 122.18, 124.01, 127.54, 127.77 (each d), 143.36, 152.07 (each s), and 220.02 (s, CO); MS *m/z* (rel intensity, %) 200 (M^+, 17), 185 (56), 157 (39), 143 (52), 142 (23), 141 (28), 129 (base peak), 128 (87), 127 (30), and 115 (43). HRMS Found: *m/z* 200.1200. Calcd for $C_{14}H_{16}O$: M, 200.1213.

4-Phenyl-4a,5,6,7,8,8a-hexahydro-2(1*H*)-naphthalenone (15) and 4-Phenyl-4,4a,5,6,7,8-hexahydro-2(3*H*)-naphthalenone (16). A mixture of **5e** (0.14 g, 0.62 mmol), PPA (P_2O_5 content, 75%, 1.4 g), and benzene (1.5 ml) was heated at 80—85 °C for 55 h during which time the reaction was monitored by GLC. The mixture was poured into saturated aqueous sodium hydrogencarbonate and extracted with diethyl ether (15 ml×2). The combined extracts were dried over magnesium sulfate and evaporated in vacuo. The residue was chromatographed over silica gel; the elution with hexane–ethyl acetate (50 : 1 v/v) gave **15** (0.08 g, 57%) and with hexane–ethyl acetate (20 : 1 v/v) **16** (0.025 g, 18%), both as single isomers. **15**: Colorless viscous liquid; IR (neat) 1660 cm^{-1}; ^1H NMR ($CDCl_3$) δ=1.1—3.0 (12H, m, CH_2 and CH), 6.24 (1H, s, 6-H), and 7.1—7.6 (5H, m Ph); ^{13}C NMR ($CDCl_3$) δ=20.47, 25.83, 27.17, 30.41 (each t, CH_2), 33.77 (d, 8a-C), 37.77 (t, 8-C), 39.71 (d, 4a-C), 124.95, 126.83, 129.01 (each d), 130.07, 138.18 (each s), 165.36 (s, 5-C), and 200.89 (s, CO); MS *m/z* (rel intensity, %) 226 (M^+, 26), 184 (33), 169 (26), 157 (23), 156 (29), 155 (26), 142 (34), 141 (76), 131 (30), 129 (59), 128 (87), 127 (37), 116 (25), 115 (base peak), 103 (33), 102 (42), 91 (41), and 77 (55). HRMS Found: *m/z* 226.1357. Calcd for $C_{16}H_{18}O$: M, 226.1363. **16**: Colorless prisms (ethyl acetate–hexane); mp 61—63 °C; IR (KBr) 1660 cm^{-1}; ^1H NMR ($CDCl_3$) δ=1.1—3.1 (12H, m, CH_2 and CH), 5.90 (1H, s, 8-H), and 7.1—7.6 (5H, m, Ph); ^{13}C NMR ($CDCl_3$) δ=25.47, 26.59, 32.41, 35.71 (each t, CH_2), 44.06 (t, 2-C), 44.89, 47.77 (each d, 4a- and 5-C), 124.72, 127.13, 127.71, 128.89 (each d, Ph and 8-C), 142.83 (s, Ph), 166.30 (s, 8a-C), and 199.31 (s, CO); MS *m/z* (rel intensity, %) 226 (M^+, 16), 128 (24), 122 (base peak), 115 (41), 107 (21), 104 (60), 103 (34), 94 (65), 91 (65), 79 (63), 78 (59), and 77 (75). HRMS Found: *m/z* 226.1357. Calcd for $C_{16}H_{18}O$: M, 226.1351.

4-Phenyl-3,4,4a,5,6,7,8,9-octahydro-2*H*-benzocyclohepten-2-one (17). A similar procedure using **5f** (0.153 g, 0.64 mmol), PPA (P_2O_5 content, 75%, 0.85 g), and benzene (1.5 ml) at 80—85 °C for 40 h and subsequent chromatography over silica gel (hexane–ethyl acetate (50 : 1 v/v)) gave **17** (0.023 g, 15%) as a single isomer: Colorless viscous liquid; IR (neat) 1660 cm^{-1}; ^1H NMR ($CDCl_3$) δ=0.9—3.2 (14H, CH_2 and CH), 5.89 (1H, m, 4-H), and 7.0—7.4 (5H, m, Ph); ^{13}C NMR ($CDCl_3$) δ=26.18, 29.00, 29.18, 30.36, 37.06 (each t, CH_2), 44.42 (t, 2-C), 46.00, 47.53 (each d, CH), 127.07, 127.48, 127.71, 129.01 (each d), 143.42 (s), 171.07 (s, 4a-C), and 199.01 (s, CO); MS *m/z* (rel intensity, %) 240 (M^+, 31), 136 (base peak), 108 (52), 93 (24), 91 (34), 79 (37), 78 (21), 77 (35), 41 (25), and 39. HRMS Found: *m/z* 240.1513. Calcd for $C_{17}H_{20}O$: M, 240.1509.

4-Phenyl-3,4,4a,5,6,7,8,9,10-octahydrobenzocycloocten-2-(3*H*)-one (18). A similar procedure using **5g** (0.15 g, 0.6 mmol), PPA (P_2O_5 content, 75%, 1.5 g), and benzene (1.5 ml) at 80—85 °C for 65 h and subsequent chromatographic separation (silica gel, hexane–ethyl acetate (50:1 v/v)) gave **18** (0.039 g, 26%) as a single isomer: Colorless viscous liquid; IR (neat) 1660 cm^{-1}; ^1H NMR ($CDCl_3$) δ=1.1—3.4 (16H, m, CH_2 and CH), 5.93 (1H, m, 4-H), and 6.9—7.3 (5H, m, Ph); ^{13}C NMR ($CDCl_3$) δ=24.35, 24.83, 25.06, 26.65, 31.94, 34.36 (each t, CH_2), 44.42 (t, 2-C), 44.77, 45.47 (each d, 1- and 10a-C), 127.07, 127.48, 129.01 (each d), 143.24 (s), 172.83 (s, 4a-C), and 198.48 (s, CO); MS *m/z* (rel intensity, %) 254 (M^+, 40), 150 (86), 122 (base peak), 91 (33), 77 (27), and 43 (20). Found: C, 84.99; H, 2.54%. Calcd for $C_{18}H_{22}O$: C, 85.12; H, 8.85%.

***trans*-3-Acetyl-2-benzylcyclopentanone (19).** A mixture of **5i** (0.026 g, 0.1 mmol) and PPA (P_2O_5 content, 75%, 0.3 g) in benzene (1 ml) was stirred at room temperature for 23 h during which time the reaction was monitored by GLC. The mixture was poured into saturated aqueous sodium hydrogencarbonate and extracted with diethyl ether (15 ml×2). The combined extracts were dried over magnesium sulfate and evaporated in vacuo. The residue was chromatographed over silica gel with hexane–ethyl acetate (2:1 v/v) to give **19** as a single isomer: Yellow liquid; IR (neat) 1725 and 1715 cm^{-1}; ^1H NMR ($CDCl_3$) δ=1.88 (3H, s, COMe), 1.9—2.0 (1H, m, CH_2), 2.1—2.3 (1H, m, CH_2), 2.4—2.7 (4H, m, CH_2), 3.16 (1H, dt, *J*=9.7 and 3.8 Hz, CH), 3.27 (1H, dt, *J*=9.7 and 6.5 Hz, CH), and 7.2—7.4 (5H, m, Ph); ^{13}C NMR ($CDCl_3$) δ=28.11 (t, 4-C), 30.24 (q, COMe), 39.88 (t, 5-C), 46.41 (d, 3-C), 47.82 (t, $PhCH_2$), 55.35 (d, 2-C), 127.07, 127.32, 128.98 (each d, Ph), 141.81 (s, Ph), 200.70 (s, COMe), and 210.03 (s, CO); MS *m/z* (rel intensity, %) 216 (M^+, 48), 156 (28), 146 (22), 145 (20), 117 (27), 104 (27), 103 (21), 91 (48), 83 (28), 76 (23), 55 (24), and 43 (base peak). HRMS Found: *m/z* 216.1143. Calcd for $C_{14}H_{16}O_2$: M, 216.1149.

2-Phenoxycyclopropyl Trimethylsilylmethyl Ketone (20a). Under nitrogen, a mixture of phenyl vinyl ether (0.6 g, 5 mmol) and copper(II) acetylacetonate (0.006 g, 0.02 mmol) was heated at 75 °C. A solution of **1** (0.312 g, 2 mmol) in dry diethyl ether (0.5 ml) was added dropwise in a period of 1 h. The reaction mixture was subjected to micro vacuum distillation on a Kugelrohr distilling apparatus to provide **20a** (0.28 g, 46%): Pale yellow liquid; bp 130 °C/26 Pa (bulb-to-bulb); IR (neat) 1660, 1245, and 850 cm^{-1}; ^1H NMR ($CDCl_3$) δ=0.15 (9H, s, $SiMe_3$), 1.38 (1H, ddd, *J*=9.7, 5.4, and 3.8 Hz, ring CH_2), 1.54 (1H, dt, *J*=5.9 and 5.4 Hz, ring CH_2), 2.15 (1H, ddd, *J*=9.7, 5.4, and 2.2 Hz, ring CH), 2.37, 2.53 (each 1H, d, *J*=10.3 Hz, CH_2CO), 4.05 (1H, ddd, *J*=5.9, 3.8, and 2.2 Hz, ring CH), 6.9—7.1 (3H, m, Ph), and 7.2—7.4 (2H, m Ph); ^{13}C NMR ($CDCl_3$) δ=−0.07 ($SiMe_3$), 17.98 (ring CH_2), 30.17 (ring CH), 40.21 (CH_2CO), 59.23 (ring CH), 115.08, 121.63, 129.71, 158.26 (each Ph), and 206.55 (CO); MS *m/z* (rel intensity, %) 248 (M^+, 1), 155 (23), 153 (36), 94 (33), 82 (49), 81 (84), 76 (26), 72 (base peak), and 43(26). HRMS Found: *m/z* 248.1240. Calcd for $C_{14}H_{20}O_2Si$: M, 248.1231.

2-Butoxycyclopropyl Trimethylsilylmethyl Ketone (20b). Butyl vinyl ether (3 ml, 23 mmol) was heated at 75 °C under nitrogen together with copper(II) acetylacetonate (0.003 g, 0.01 mmol). Diazo ketone **1** (0.312 g, 2 mmol) was added dropwise in a period of 1 h. The reaction mixture was distilled under vacuum on a Kugelrohr distilling apparatus to give **20b** (0.29 g, 64%): Pale yellow liquid; bp 110 °C/106 Pa (bulb-to-bulb); IR (neat) 1670, 1250, and 850 cm^{-1}; ^1H NMR ($CDCl_3$) δ=0.15 (9H, s, $SiMe_3$), 0.91 (3H, t, *J*=7.3 Hz, *n*-Bu), 1.1—1.2 (1H, m, ring CH_2), 1.3—1.7 (4H, m, *n*-Bu), 1.9—2.0 (1H, m, ring CH_2), 2.2—2.5 (3H, m, ring CH and CH_2CO), and 3.3—3.6 (3H, m, *n*-Bu and ring CH); ^{13}C NMR ($CDCl_3$) δ=−0.83 (q, $SiMe_3$), 14.02 (q, *n*-Bu), 18.02 (t, ring CH_2), 19.46 (t, *n*-Bu), 30.41 (d, ring CH), 32.06 (t, *n*-Bu), 39.76 (t, CH_2CO), 63.29 (d, ring CH), 71.25 (t, *n*-Bu), and 206.97 (s, CO); MS *m/z* (rel intensity, %) 228 (M^+, 2), 80 (20), 73 (base peak), 57 (30), and 45 (25). HRMS Found: *m/z* 228.1542. Calcd for $C_{12}H_{24}O_2Si$: M, 228.1544.

2-Methoxy-2-methylcyclopropyl Trimethylsilylmethyl Ketone (20c). Under nitrogen, a mixture of 2-methoxypropene (2 ml, 20 mmol) and rhodium(II) acetate (0.002 g, 0.005 mmol) was heated at 75 °C. Diazo ketone **1** (0.312 g, 2 mmol) was added dropwise in a period of 1 h. The resulting mixture was distilled under vacuum on a Kugelrohr distilling apparatus to give **20c** (0.25 g, 63%) as a mixture of two stereoisomers: Colorless liquid; bp 80 °C/266 Pa (bulb-to-bulb); ^{13}C NMR ($CDCl_3$) δ=−1.28, −0.88 (each $SiMe_3$), 13.44, 18.39 (each ring CH_2), 22.54, 25.42 (each Me), 36.19 (ring CH), 40.45, 40.54 (each CH_2CO), 49.52, 54.22 (each MeO), 68.04 (ring CH), and 205.88 (CO). This mixture was directly used in the reaction with benzaldehyde leading to **21c**.

5-[(Trimethylsilyl)acetyl]perhydrocyclopropa[*b*]pyran (20d). A mixture of 3,4-dihydro-2*H*-pyran (3 ml, 33 mmol) and copper(II) acetylacetonate (0.003 g, 0.01 mmol) was heated under nitrogen at 75 °C. Diazo ketone **1** (0.312 g, 2 mmol) was added dropwise in a period of 1 h. The reaction mixture was distilled on a Kugelrohr distilling apparatus to give **20d** (0.335 g, 79%): Colorless liquid; bp 110 °C/80 Pa (bulb-to-bulb); IR (neat) 1665, 1250, and 850 cm^{-1}; ^1H NMR ($CDCl_3$) δ=0.08 (9H, s, $SiMe_3$), 1.3—1.5 (2H, m, 4-H), 1.7—2.0 (4H, m, 3-, 4a-, and 5-H), 2.28 (2H, s, CH_2CO), 3.2—3.4 (1H, m, 2-H), 3.5—3.6 (1H, m, 2-H), and 3.77 (1H, d, *J*=7.0 Hz, 5a-H); ^{13}C NMR ($CDCl_3$) δ=−0.90 (q, $SiMe_3$), 19.25 (t, 4-C), 22.17 (t, 3-C), 24.36 (d, 4a-C), 36.31 (t, 5-C), 40.01 (t, CH_2CO), 63.02 (d, 5a-C), 64.62 (t, 2-C), and 206.18 (s, CO); MS *m/z* (rel intensity, %) 212 (M^+, 42), 122 (47), 75 (38), and 73 (base peak). HRMS Found: *m/z* 212.1197. Calcd for $C_{11}H_{20}O_2Si$: M, 212.1231.

(*E*)-2-Phenoxycyclopropyl 2-Phenylethenyl Ketone (21a): Reaction of diazo ketone **1** (0.312 g, 2 mmol) with phenyl vinyl ether (1.2 g, 10 mmol) in the presence of a catalytic amount of copper(II) acetylacetonate (0.003 g, 0.01 mmol) was carried out according to the procedure mentioned above. The reaction mixture was diluted with dry THF (2 ml). This solution was added dropwise, at −78 °C under nitrogen, to LDA (1.8 mmol) freshly prepared in THF (2 ml). After 1 h, benzaldehyde (0.18 mmol) was added. The mixture was stirred at −78 °C for 1 h and at room temperature for 0.5 h. Quench with saturated aqueous ammonium chloride was followed by extraction with dichloromethane (15 ml×2). The combined extracts were dried over magnesium sulfate and evaporated in vacuo. The residue (1.02 g) was chromatographed over silica gel with hexane–ethyl acetate (50:1 v/v) to give **21a** (0.223 g, 42% based on **1**): Colorless needles (diethyl ether-hexane); mp 75—78 °C; IR (KBr) 1675, 1645, and 1600 cm^{-1}; ^1H NMR ($CDCl_3$) δ=1.58 (1H, ddd, *J*=9.5, 5.5, and 4.4 Hz, ring CH_2), 1.76 (1H, ddd, *J*=6.6, 6.2, and 5.5 Hz, ring CH_2), 2.57 (1H, ddd, *J*=9.5, 6.2, and 2.2 Hz, ring CH), 4.12 (1H, ddd, *J*=6.6, 4.4, and 2.2 Hz, ring CH), 6.92 (1H, d, *J*=16.1 Hz, =CHCO), 6.9—7.6 (10H, m, Ph), and 7.65

(1H, d, J=16.1 Hz, =CH); ^{13}C NMR ($CDCl_3$) δ=17.98 (ring CH_2), 28.08 (ring CH), 60.13 (ring CH), 114.80, 121.65, 126.27, 128.40, 128.95, 129.57, 130.62, 134.39, 143.19, 157.99 (=CH), and 197.07 (CO); MS m/z (rel intensity, %) 171 (34), 170 (base peak), 143 (24), 141 (23), 131 (27), 128 (40), 115 (22), 103 (32), and 77 (55). Found: C, 81.86; H: 6.13%. Calcd for $C_{18}H_{16}O_2$: C, 81:80; H, 6.10%.

(*E*)-2-Butoxycyclopropyl 2-Phenylethenyl Ketone (21b). A solution of silylmethyl ketone **20b** (0.272 g, 1.19 mmol) in dry THF (1 ml) was added dropwise at −78 °C to LDA (1.43 mmol) freshly prepared in THF (1 ml). After 1 h, benzaldehyde (0.12 ml, 1.19 mmol) was added and the mixture was stirred at −78 °C for 1 h and then at room temperature for 1 h. Quench with saturated aqueous ammonium chloride was followed by extraction with dichloromethane (20 ml×2). The combined extracts were dried over magnesium sulfate and evaporated in vacuo to give **20b** which decomposed to **22a** (0.134 g, 60% based on **20b**) on column chromatography over silica gel (hexane-ethyl acetate (9 : 1 v/v)). **20b**: Yellow liquid; ^{13}C NMR ($CDCl_3$) δ=13.92 (*n*-Bu), 19.37 (*n*-Bu), 28.65 (ring CH_2), 31.60 (ring CH), 64.45 (*n*-Bu), 71.30 (*n*-Bu), 126.53, 128.41, 129.44, 130.51, 134.75, 142.43 (=CH), and 197.57 (CO). Purification of **21b** by chromatography over silica gel gave **22a**.

(*E*)-2-Methyl-2-methoxycyclopropyl 2-Phenylethenyl Ketone (21c). A similar one-flask procedure using **1** (0.156 g, 1 mmol in dry diethyl ether (1 ml)), rhodium(II) acetate (0.002 g, 0.005 mmol), and 2-methoxypropene (0.48 ml, 5 mmol) for cyclopropanation (80 °C, 1 h) and then LDA (1.61 mmol in THF (1.5 ml)) and benzaldehyde (0.16 ml, 1.61 mmol) for olefination (1 h at −78 °C and 0.5 h at room temperature) gave **21c** as unstable product. Column chromatography of **21c** gave **23** in 23% yield based on **1**.

(*E*)-5-(1-Oxo-3-phenyl-2-propenyl)perhydrocyclopropa[*b*]pyran (21d). To freshly prepared LDA (1.74 mmol) in dry THF (1 ml) was added at −78 °C a solution of silylmethyl ketone **20d** (0.307 g, 1.45 mmol). After 1 h at −78 °C under nitrogen, benzaldehyde (0.14 ml, 1.45 mmol) was added. Stirring was continued at the same temperature for 1.5 h and at room temperature for 0.5 h. The mixture was poured into saturated aqueous ammonium chloride and extracted with dichloromethane (15 ml×2). The combined extracts were dried over magnesium sulfate and evaporated in vacuo to give **21d** as a labile product. This compound **21d** decomposed to complex mixture when chromatographed over silica gel. **21d**: ^{13}C NMR ($CDCl_3$) δ=19.19 (ring CH_2), 22.02 (ring CH_2), 25.72 (ring CH), 34.55 (ring CH), 64.09, 64.68 (ring CH_2 and CH), 126.75, 128.26, 128.91, 130.29, 134.74, 141.82 (=CH), and 196.95 (CO). Column chromatography of **21d** over silica gel led to complex mixture.

(*E*)-4-Methyl-1-oxo-2-pentenyl 2-Phenoxycyclopropyl Ketone (21e). A similar one-flask procedure using **1** (0.312 g, 2 mmol), copper(II) acetylacetonate (0.003 g, 0.01 mmol), and phenyl vinyl ether (1.2 g, 10 mmol) for cyclopropanation (1 h at 70 °C) and then LDA (3.2 mmol in THF (2 ml)) and 2-methylpropanal (0.3 g, 3.2 mmol) for olefination (1h at −78 °C and 0.5 h at room temperature) gave **21e** (0.179 g, 39% based on **1**) after column chromatography over silica gel with hexane-ethyl acetate (50 : 1 v/v). **21e**: Colorless liquid; IR (neat) 1677 and 1655 cm^{-1}; ^{1}H NMR ($CDCl_3$) δ=1.08 (6H, d, J=6.6 Hz, *i*-Pr), 1.46 (1H, ddd, J=9.5, 5.2, and 5.1 Hz, ring CH_2), 1.66 (1H, dt, J=6.2 and 5.2 Hz, ring CH_2), 2.4—2.6 (2H, m, ring CH and *i*-Pr), 4.02 (1H, ddd, J=6.2, 4.0, and 1.8 Hz, ring CH), 6.21 (1H, d, J=16.1 Hz, =CHCO), and 6.9—7.3 (6H, m, Ph and =CH); ^{13}C NMR ($CDCl_3$) δ=17.66 (ring CH_2), 21.42, 21.45 (each *i*-Pr), 27.25 (ring CH), 31.40 (*i*-Pr), 59.96 (ring CH), 114.95, 121.73, 127.93, 129.64, 154.52, 158.16 (=CH), and 197.67 (CO); MS m/z (rel intensity, %) 137 (20), 136 (45), 121 (40), 105 (20), 97 (42), 95 (20), 94 (31), 93 (20), 91 (29), 81 (30), 79 (28), 77 (96), 75 (19), and 73 (base peak). Found: C, 77.67; H, 8.01%. Calcd for $C_{15}H_{18}O_2$: C, 78.23; H, 7.88%.

(*E*)-1-Oxo-2-pentenyl 2-Phenoxycyclopropyl Ketone (21f). A similar one-flask procedure using **1** (0.312 g, 2 mmol), copper(II) acetylacetonate (0.003 g, 0.01 mmol), and phenyl vinyl ether (1.2 g, 10 mmol) for cyclopropanation (1 h at 70 °C) and then LDA (2 mmol in THF (2 ml)) and propanal (0.22 ml, 2.4 mmol) for olefination (1 h at −78 °C and 0.5 h at room temperature) gave **21f** (0.128 g, 29% based on **1**) after column chromatography over silica gel with hexane-ethyl acetate (50 : 1 v/v). **21f**: Colorless liquid; IR (neat) 1677 and 1655 cm^{-1}; ^{1}H NMR ($CDCl_3$) δ=1.09 (3H, t, J=7.7 Hz, Et), 1.48 (1H, ddd, J=9.1, 6.2, and 4.0 Hz, ring CH_2), 1.67 (1H, dt, J=6.2 and 5.8 Hz, ring CH_2), 2.2—2.4 (2H, m, Et), 2.45 (1H, ddd, J=9.1, 5.8, and 2.2 Hz, ring CH), 4.03 (1H, ddd, J=6.2, 4.0, and 2.2 Hz, ring CH), 6.25 (1H, d, J=16.1 Hz, =CHCO), and 6.9—7.3 (6H, m, Ph and =CH); ^{13}C NMR ($CDCl_3$) δ=12.45 (Et), 17.81 (ring CH_2), 25.27 (Et), 27.31 (ring CH), 60.01 (ring CH), 115.02, 121.81, 129.72, 149.93, 158.23 (=CH), and 197.60 (CO); MS m/z (rel intensity, %) 123 (38), 122 (base peak), 107 (36), 105 (19), 95 (46), 94 (18), 93 (15), 83 (40), 79 (27), and 77 (66). Found: C, 77.19; H, 7.48%. Calcd for $C_{14}H_{16}O_2$: C, 77.75; H, 7.46%.

(2*Z*,4*E*)-1-Oxo-5-phenyl-2,4-pentadienyl 2-Phenoxycyclopropyl Ketone ((*Z*,*E*)-21g) and (*E*,*E*)-1-Oxo-5-phenyl-2,4-pentadienyl 2-(Phenyloxy)cyclopropyl Ketone ((*E*,*E*)-21g). A similar one-flask procedure using **1** (0.312 g, 2 mmol), copper(II) acetylacetonate (0.003 g, 0.01 mmol), and phenyl vinyl ether (1.2 g, 10 mmol) for cyclopropanation (1 h at 70 °C) and then LDA (2 mmol in THF (2 ml)) and cinnamaldehyde (0.23 ml, 1.8 mmol) for olefination (1 h at −78 °C and 0.5 h at room temperature) gave (*Z*,*E*)-**21g** (0.051 g, 8% based on **1**) and then (*E*,*E*)-**21g** (0.288 g, 50% based on **1**) after column chromatography over silica gel with hexane-ethyl acetate (50 : 1 v/v). (*Z*,*E*)-**21g**: Yellow liquid; IR (neat) 1660, 1600, and 1580 cm^{-1}; ^{1}H NMR ($CDCl_3$) δ=1.52 (1H, ddd, J=8.6, 6.0, and 4.0 Hz, ring CH_2), 1.73 (1H, q, J=6.0 Hz, ring CH_2), 2.33 (1H, ddd, J=8.6, 6.0, and 2.0 Hz, ring CH), 4.07 (1H, ddd, J=6.0, 4.0, and 2.0 Hz, ring CH), 6.27 (1H, d, J=11.0 Hz, =CHCO), 6.66 (1H, t, J=11.0 Hz, =CH), 6.8—7.6 (11H, m, Ph and =CH), and 8.24 (1H, dd, J=15.8 and 12.5 Hz, =CH); MS m/z (rel intensity, %) 290 (M^+, 4), 225 (21), 205 (23), 94 (53), 76 (35), 75 (46), 73 (base peak), and 43 (27). (*E*,*E*)-**21g**: Colorless plates (hexane); mp 91—93 °C; IR (KBr) 1637 cm^{-1}; ^{1}H NMR ($CDCl_3$) δ=1.52 (1H, ddd, J=9.1, 5.1, and 4.0 Hz, ring CH_2), 1.72 (1H, dt, J=6.2 and 5.1 Hz, ring CH_2), 2.47 (1H, ddd, J=9.1, 6.2, and 2.2 Hz, ring CH), 4.08 (1H, ddd, J=6.2, 4.0, and 2.2 Hz, ring CH), 6.44 (1H, d, J=15.4 Hz, =CHCO), and 6.8—7.5 (13H, m, Ph and =CH); ^{13}C NMR ($CDCl_3$) δ=17.85 (ring CH_2), 28.01 (ring CH), 60.06 (ring CH), 114.83, 121.64, 126.62, 127.31, 128.86, 129.31, 129.56, 135.96, 141.94, 143.18, 158.04, and 197.03 (CO); MS m/z (rel intensity, %) 290 (M^+, 14), 196 (36), 94 (29), and 32 (base peak); Found: C, 82.91; H, 6.30%. Calcd for $C_{20}H_{18}O_2$: C, 82.73; H, 6.25%.

3-Methyl-1-oxo-2-butenyl 2-Phenoxycyclopropyl Ketone

(**21h**). A similar one-flask procedure using **1** (0.312 g, 2 mmol), copper(II) acetylacetonate (0.003 g, 0.01 mmol), and phenyl vinyl ether (1.2 g, 10 mmol) for cyclopropanation (1 h at 70 °C) and then LDA (1.8 mmol in THF (2 ml)) and acetone (0.15 ml, 2 mmol) for olefination (2 h at −78 °C and 1 h at room temperature) gave **21h** (0.082 g, 19% based on **1**) after column chromatography over silica gel with hexane–ethyl acetate (50 : 1 v/v): Colorless liquid; IR (neat) 1670 cm^{-1}; ^1H NMR ($CDCl_3$) δ=1.42 (1H, ddd, J=9.5, 5.1, and 4.0 Hz, ring CH_2), 1.62 (1H, dt, J=6.2 and 5.5 Hz, ring CH_2), 1.92, 2.18 (each 3H, d, J=1.1 Hz, Me), 2.2—2.3 (1H, m, ring CH), 4.00 (1H, ddd, J=6.2, 4.0, and 2.2 Hz, ring CH), 6.28 (1H, dd, J=2.6 and 1.1 Hz, =CHCO), and 7.0—7.3 (5H, m Ph); ^{13}C NMR ($CDCl_3$) δ=17.45 (ring CH_2), 20.94 (Me), 27.72 (ring CH), 30.71 (Me), 59.72 (ring CH), 114.80, 121.51, 124.16, 156.01, 158.12 (=CH), and 197.46 (CO); MS m/z (rel intensity, %) 123 (33), 122 (base peak), 95 (63), 93 (21), and 82 (52). Found: C, 77.11; H, 7.56%. Calcd for $C_{14}H_{16}O_2$: C, 77.75; H, 7.46%.

(*E*)-**4-Oxo-6-phenyl-5-hexenal (22a).** A mixture of **21a** (0.223 g, 0.84 mmol), water (0.03 ml, 1.68 mmol), and trifluoroacetic acid (TFA, 0.064 ml, 0.84 mmol) in dry THF (2 ml) was stirred at room temperature for 20.5 h. The mixture was poured into saturated aqueous sodium hydrogencarbonate and extracted with dichloromethane (20 ml×2). The combined extracts were dried over magnesium sulfate and evaporated in vacuo. The residue (0.195 g) was chromatographed over silica gel with hexane–ethyl acetate (9 : 1 v/v) to afford **22a** (0.139 g, 88%): Colorless liquid; IR (neat) 1715, 1680, 1653, and 1605 cm^{-1}; ^1H NMR ($CDCl_3$) δ=2.87 (2H, t, J=6.5 Hz, CH_2), 3.03 (2H, t, J=6.5 Hz, CH_2), 6.77 (1H, d, J=16.1 Hz, 5-H), 7.3—7.6 (5H, m, Ph), 7.60 (1H, d, J=16.1 Hz, 6-H), and 9.87 (1H, s, CHO); ^{13}C NMR ($CDCl_3$) δ=32.37, 37.58 (2- and 3-C), 125.74, 128.32, 128.97, 130.59 (each Ph), 135.17 (5-C), 143.06 (6-C), 197.45 (4-C), and 200.61 (CHO); MS m/z (rel intensity, %), 188 (M^+, 1), 160 (30), 131 (55), 103 (78), 102 (30), 91 (51), 76 (85), 51 (48), 42 (26), and 30 (base peak). HRMS Found: m/z 188.0838. Calcd for $C_{12}H_{12}O_2$: M, 188.0837.

(*E*)-**7-Methyl-4-oxo-5-octenal (22b).** A similar procedure using **21e** (0.044 g, 0.19 mmol), water (0.004 ml, 0.19 mmol), and TFA (0.015 ml, 0.19 mmol) in THF (0.5 ml) at room temperature for 24 h and subsequent silica-gel chromatography (hexane–ethyl acetate (9 : 1 v/v)) gave **22b** (0.029 g, 100%): Colorless liquid; IR (neat) 1720 and 1670 cm^{-1}; ^1H NMR ($CDCl_3$) δ=1.08 (6H, d, J=6.6 Hz, Me), 2.4—2.6 (1H, m, 7-H), 2.7—2.9 (4H, m, 2- and 3-H), 6.08 (1H, dd, J=16.1 and 1.5 Hz, 5-H), 6.86 (1H, dd, J=16.1 and 6.6 Hz, 6-H), and 9.84 (1H, s, CHO); MS m/z (rel intensity, %) 154 (M^+, 15), 126 (21), 97 (base peak), 84 (49), 82 (26), 69 (33), 41 (58), and 30 (22). HRMS Found: m/z 154.0990. Calcd for $C_9H_{14}O_2$: M, 154.0993.

(*E*)-**4-Oxo-5-octenal (22c).** A similar procedure employing **21f** (0.063 mg, 0.29 mmol), water (0.005 ml, 0.29 mmol), and TFA (0.022 ml, 0.29 mmol) in THF (1 ml) at room temperature for 22 h and subsequent column chromatography over silica gel with hexane–ethyl acetate (9 : 1 v/v) provided **22c** (0.029 g, 71%): Colorless liquid; IR (neat) 1725 and 1670 cm^{-1}; ^1H NMR ($CDCl_3$) δ=1.09 (3H, t, J=7.7 Hz, Et), 2.26 (2H, dq, J=7.7 and 1.4 Hz, 7-H), 2.79, 2.90 (each 2H, t, J=5.5 Hz, 2- and 3-H), 6.14 (1H, dt, J=16.1 and 1.4 Hz, 5-H), 6.95 (1H, dt, J=16.1 and 6.6 Hz, 6-H), and 9.83 (1H, s, CHO); MS m/z (rel intensity, %) 140 (M^+, 1), 82 (base peak), 55 (76), 41 (20), and 39 (38). HRMS Found: m/z 140.0794. Calcd for $C_8H_{12}O_2$: M, 140.0837.

(*E,E*)-**4-Oxo-8-phenyl-5,7-octadienal (22d).** A similar procedure using **21g** (0.045 g, 0.16 mmol), water (0.005 ml, 0.29 mmol), TFA (0.012 ml, 0.15 mmol) in THF (1 ml) at room temperature for 63 h and subsequent chromatography over silica gel with hexane–ethyl acetate (4 : 1 v/v)) gave **22d** (0.025 g, 73%): Colorless crystals; mp 71—73 °C; IR (KBr) 1718 and 1673 cm^{-1}; ^1H NMR ($CDCl_3$) δ=2.83, 2.96 (each 2H, t, J=6.6 Hz, 2- and 3-H), 6.31 (1H, d, J=15.4 Hz, 5-H), 6.8—7.0 (2H, m, 6- and 7-H), 7.3—7.5 (6H, m, Ph and 8-H), and 9.85 (1H, s, CHO); MS m/z (rel intensity, %) 214 (M^+, 31), 186 (20), 157 (41), 129 (25), 128 (35), and 32 (base peak). HRMS Found: m/z 214.0986. Calcd for $C_{14}H_{14}O_2$: M, 214.0993.

6-Methyl-4-oxo-5-heptenal (22e). To a mixture of **21h** (0.035 g, 0.16 mmol) and lithium chloride (0.013 g, 0.32 mmol) in THF (1 ml) were added water (0.006 ml, 0.32 mmol) and TFA (0.012 ml, 0.16 mmol). This mixture was stirred at room temperature for 30 min, poured into saturated aqueous sodium hydrogencarbonate, and extracted with dichloromethane (20 ml×2). The combined extracts were dried over magnesium sulfate and evaporated in vacuo. The residue (0.039 g) was chromatographed over silica gel with hexane–ethyl acetate (9 : 1 v/v) to give **22e** (0.016 g, 71%): Colorless liquid; IR (neat) 1720 and 1687 cm^{-1}; ^1H NMR ($CDCl_3$) δ=1.90, 2.14 (each 3H, s, Me), 2.76 (4H, s, 2- and 3-H), 6.12 (1H, s, 5-H), and 9.83 (1H, s, CHO); MS m/z (rel intensity, %) 140 (M^+, 12), 83 (base peak), 55 (50), and 39 (21). HRMS Found: m/z 140.0838. Calcd for $C_8H_{12}O_2$: M, 140.0837.

(*E*)-**7-Phenyl-6-heptene-2,5-dione (23).** Crude **21c** prepared from **1** (0.156 g, 1 mmol) according to the above method was chromatographed twice over silica gel with hexane–ethyl acetate (9 : 1 v/v) to give **23** (0.046 g, 23%): Yellow liquid; IR (neat) 1715, 1690, and 1665 cm^{-1}; ^1H NMR ($CDCl_3$) δ=2.22 (3H, s, COMe), 2.81, 2.97 (each 2H, t, J=5.9 Hz, CH_2), 6.75 (1H, d, J=16.5 Hz, =CHCO), 7.3—7.5 (5H, m, Ph), and 7.58 (1H, d, J=16.5 Hz, =CH); ^{13}C NMR ($CDCl_3$) δ=30.00 (MeCO), 34.24, 37.06 (each CH_2), 126.00, 128.30, 128.94, 130.49, 134.47, 142.82 (=CH), 198.48 (CO), and 207.32 (COMe); MS m/z (rel intensity, %) 202 (M^+, 13), 144 (22), 131 (base peak), 108 (37), 107 (34), 103 (41), 83 (29), 78 (48), and 76 (51). HRMS Found: m/z 202.0990. Calcd for $C_{13}H_{14}O_2$: M, 202.0993.

(*E*)-**2-(3-Oxo-5-phenyl-4-pentenyl)-1,3-dioxolane (24a).** To a solution of **21a** (0.1 g, 0.37 mmol) and 1,2-ethanediol (0.05 ml, 0.82 mmol) in nitromethane (2.5 ml) was added TFA (0.03 ml, 0.39 mmol) at 0 °C. After stirring at the same temperature for 20 min, the mixture was poured into saturated aqueous sodium hydrogencarbonate and extracted with diethyl ether (20 ml×2). The combined extracts were dried over magnesium sulfate and evaporated in vacuo. The residue (0.119 g) was chromatographed over silica gel with hexane–ethyl acetate (9 : 1 v/v) to give **24a** (0.078 g, 90%): Pale yellow liquid; IR (neat) 1685 and 1655 cm^{-1}; ^1H NMR ($CDCl_3$) δ=2.08 (2H, dt, J=7.3 and 4.4 Hz, CH_2), 2.82 (2H, t, J=7.3 Hz, CH_2), 3.8—4.0 (4H, m, OCH_2CH_2O), 4.97 (1H, t, J=4.4 Hz, CH), 6.74 (1H, d, J=16.1 Hz, =CHCO), and 7.3—7.6 (6H, m, Ph and =CH); ^{13}C NMR ($CDCl_3$) δ=27.98, 34.56 (each CH_2), 64.89 (OCH_2CH_2O), 103.44 (CH), 126.20, 128.25, 128.94, 130.42 (each Ph), 134.54, 142.52 (each =CH), and 199.32 (CO); MS m/z (rel intensity, %) 232 (M^+, 14), 146 (35), 131 (74), 103 (74), 103 (56), 99 (47), 87 (59), 77 (40), 73 (base peak), and 44 (28). HRMS Found: m/z 232.1096. Calcd for $C_{14}H_{16}O_3$: M, 232.1099.

(*E*)-2-(6-Methyl-3-oxo-4-heptenyl)-1,3-dioxolane (24b). A similar procedure using **21e** (0.12 g, 0.52 mmol), 1,2-ethanediol (0.05 ml, 1.04 mmol), TFA (0.04 ml, 0.52 mmol) in nitromethane (2 ml) at 0 °C for 10 min and subsequent column chromatography over silica gel with hexane–ethyl acetate (9 : 1 v/v) gave **24b** (0.06 g, 58%): Colorless liquid; IR (neat) 1695, 1670, and 1630 cm^{-1}; ^1H NMR ($CDCl_3$) δ=1.06 (6H, d, J=6.6 Hz, *i*-Pr), 2.00 (2H, dt, J=7.7 and 4.4 Hz, CH_2), 2.46 (1H, dq, J=6.6 and 1.5 Hz, *i*-Pr), 2.70 (2H, t, J=7.7 Hz, CH_2), 3.8—4.0 (4H, m, OCH_2CH_2O), 4.94 (1H, t, J=4.4 Hz, CH), 6.05 (1H, dd, J=16.1 and 1.5 Hz, =CHCO), and 6.81 (1H, dd, J=16.1 and 6.6 Hz, =CH); ^{13}C NMR ($CDCl_3$) δ=21.32 (*i*-Pr), 27.90 (CH_2), 31.13 (*i*-Pr), 33.84 (CH_2), 64.97 (OCH_2CH_2O), 103.52 (CH), 127.48, 153.56 (each =CH), and 199.92 (CO); MS m/z (rel intensity, %) 198 (M^+, 3), 155 (25), 97 (25), 85 (22), and 73 (base peak). HRMS Found: m/z 198.1253. Calcd for $C_{11}H_{18}O_3$: M, 198.1255.

(*E*)-2-(3-Oxo-4-heptenyl)-1,3-dioxolane (24c). A similar procedure using **21f** (0.12 g, 0.56 mmol), 1,2-ethanediol (0.06 ml, 1.12 mmol), TFA (0.042 ml, 0.56 mmol) in nitromethane (2 ml) at 0 °C for 10 min and subsequent column chromatography over silica gel with hexane–ethyl acetate (9 : 1 v/v) gave **24c** (0.043 g, 42%): Colorless liquid; IR (neat) 1670 and 1630 cm^{-1}; ^1H NMR ($CDCl_3$) δ=1.08 (3H, t, J=7.3 Hz, Et), 2.00 (2H, dt, J=7.3 and 4.4 Hz, CH_2), 2.24 (2H, m, Et), 2.69 (2H, t, J=7.3 Hz, CH_2), 3.8—4.0 (4H, m, OCH_2CH_2O), 4.93 (1H, t, J=4.4 Hz, CH), 6.09 (1H, dt, J=16.2 and 1.5 Hz, =CHCO), and 6.90 (1H, dt, J=16.2 and 6.2 Hz, =CH); ^{13}C NMR ($CDCl_3$) δ=12.27 (Et), 25.54, (Et), 27.92, 33.81 (each CH_2), 64.98 (OCH_2CH_2O), 103.52 (CH), 129.37, 148.79 (each =CH), and 199.65 (CO); MS m/z (rel intensity, %) 184 (M^+, 11), 85 (23), 82 (32), and 73 (base peak). HRMS Found: m/z 184.1104. Calcd for $C_{10}H_{16}O_3$: M, 184.1099.

(*E,E*)-2-(3-Oxo-7-phenyl-4,6-heptadienyl)-1,3-dioxolane (24d). A similar procedure using **21g** (0.089 g, 0.31 mmol), 1,2-ethanediol (0.033 ml, 0.6 mmol), TFA (0.023 ml, 0.3 mmol) in nitromethane (1.5 ml) at 0 °C for 20 min and subsequent column chromatography over silica gel with hexane–ethyl acetate (9 : 1 v/v) gave **24d** (0.046 g, 58%): Colorless crystals; mp 66—70 °C; IR (KBr) 1654 and 1621 cm^{-1}; ^1H NMR ($CDCl_3$) δ=2.05 (2H, dt, J=7.3 and 4.4 Hz, CH_2), 2.74 (2H, t, J=7.3 Hz, CH_2), 3.8—4.1 (4H, m, OCH_2CH_2O), 4.95 (1H, t, J=4.4 Hz, CH), 6.28 (1H, d, J=15.7 Hz, =CHCO), and 6.8—7.5 (8H, m, Ph and =CH); ^{13}C NMR ($CDCl_3$) δ=28.02, 34.41 (each CH_2), 64.97 (OCH_2CH_2O), 103.47 (CH), 126.72, 128.82, 129.14, 129.56, 136.02, 141.20, 142.52, and 199.33 (CO); MS m/z (rel intensity, %) 258 (M^+, 12) and 32 (base peak). HRMS Found: m/z 258.1254. Calcd for $C_{16}H_{18}O_3$: M, 258.1254.

2-(5-Methyl-3-oxo-4-hexenyl)-1,3-dioxolane (24e). A similar procedure employing **21h** (0.065 g, 0.3 mmol), 1,2-ethanediol (0.033 ml, 0.6 mmol), TFA (0.023 ml, 0.3 mmol) in nitromethane (1 ml) at 0 °C for 30 min and subsequent column chromatography over silica gel with hexane–ethyl acetate (9 : 1 v/v) provided **24e** (0.037 g, 67%): Colorless liquid; IR (neat) 1690 cm^{-1}; ^1H NMR ($CDCl_3$) δ=1.88 (3H, d, J=1.1 Hz, Me), 1.97 (2H, dt, J=7.7 and 4.4 Hz, CH_2), 2.14 (3H, d, J=1.1 Hz, Me), 2.55 (2H, t, J=7.7 Hz, CH_2), 3.8—4.0 (4H, m, OCH_2CH_2O), 4.92 (1H, t, J=4.4 Hz, CH), and 6.08 (1H, t, J=1.1 Hz, =CH); ^{13}C NMR ($CDCl_3$) δ=20.71, 27.65 (each Me), 27.98, 38.07 (each CH_2), 64.97 (OCH_2CH_2O), 103.63 (CH), 123.70 (=CH), 155.03 (=CMe_2), and 199.76 (CO); MS m/z (rel intensity, %) 184 (M^+, 8), 86 (23), 82 (base peak), 73 (78), 55 (60), and 53 (20). HRMS Found: m/z 184.1097. Calcd for $C_{10}H_{16}O_3$: M, 184.1099.

(*E*)-3-(2-Oxo-4-phenyl-3-butenyl)-3,4,5,6-tetrahydro-2*H*-pyran-2-ol (25). To a solution of crude **21d** (0.257 g), which had been prepared from **20d** (0.184 g, 0.87 mmol) according to the method mentioned above, were added water (0.031 ml, 1.74 mmol) and TFA (0.066 ml, 0.87 mmol). After 20 min at room temperature, this mixture was poured into saturated aqueous sodium hydrogencarbonate and extracted with dichloromethane (20 ml×2). The combined extracts were dried over magnesium sulfate and evaporated in vacuo. The residue (0.219 g) was subjected to column chromatography over silica gel with hexane–ethyl acetate (1 : 1 v/v) to provide **25** (0.095 g, 44% based on **20d**) as a 1 : 1 mixture of two inseparable stereoisomers: Colorless liquid; IR (neat) 3400 and 1675 cm^{-1}; ^1H NMR ($CDCl_3$) δ=1.3—1.9 (4H, m), 2.1—2.4 (1H m), 2.64 (1H, dd, J=17.8 and 6.5 Hz), 2.88 (1H, dd, J=17.3 and 6.5 Hz), 2.98 (1H, dd, J=17.3 and 6.5 Hz), 3.5—3.7 (1H, m), 3.9—4.1 (1H, m), 4.45 (0.5H, J=7.7 Hz), 5.11 (0.5H, d, J=2.6 Hz), 6.74 (1H, d, J=16.1 Hz), 6.75 (1H, d, J=16.1 Hz), and 7.2—7.6 (6H, m); ^{13}C NMR ($CDCl_3$) δ=24.42, 24.58, 24.97, 28.49 (each ring CH_2), 35.76, 38.44 (each ring CH), 41.93, 43.02 (each CH_2CO), 60.62, 65.84 (each ring CH_2), 93.77, 99.50 (each ring CH), 126.07, 126.56 (each =CHCO), 128.35, 128.39, 128.96, 130.55, 130.65, 134.35, 134.46, 143.02 (=CH), 143.28 (=CH), 200.06, and 200.12 (each CO); MS m/z (rel intensity, %) 246 (M^+, 23), 159 (28), 147 (41), 146 (20), 131 (base peak), 129 (21), 113 (31), 103 (61), 100 (32), 97 (27), 76 (41), 73 (74), and 43 (41). Found: C, 73.02; H, 7.45. Calcd for $C_{15}H_{18}O_3$: C, 73.15; H, 7.37%.

(*E*)-2-(2-Hydroxyethoxy)-3-(2-oxo-4-phenyl-3-butenyl)-3,4,5,6-tetrahydro-2*H*-pyran (26). A mixture of crude **21d**, which had been similarly prepared as above from **20d** (0.324 g, 1.52 mmol), 1,2-ethanediol (0.11 ml, 2.4 mmol), and TFA (0.09 ml, 1.2 mmol) in dry nitromethane (6 ml) was stirred at 0 °C for 1 h. This mixture was poured into saturated aqueous sodium hydrogencarbonate and extracted with dichloromethane (20 ml×2). The combined extracts were dried over magnesium sulfate and evaporated in vacuo. The residue (0.334 g) was chromatographed over silica gel with hexane–ethyl acetate (1 : 1 v/v) to provide *cis*-**26** (0.028 g, 8% based on **20d**) and then *trans*-**26** (0.182 g, 52% based on **20d**). *cis*-**26**: Pale yellow liquid; IR (neat) 3450 and 1680 cm^{-1}; ^1H NMR ($CDCl_3$) δ=1.5—1.8 (4H, m, ring CH_2), 2.3—2.4 (1H, m, ring CH), 2.58 (1H, dd, J=15.8 and 6.6 Hz, $COCH_2$), 2.79 (1H, dd, J=15.8 and 7.7 Hz, $COCH_2$), 2.89 (1H, br s, OH), 3.5—3.9 (6H, m, OCH_2), 4.71 (1H, d, J=3.3 Hz, ring CH), 6.75 (1H, d, J=16.5 Hz, =CHCO), and 7.3—7.6 (6H, m, Ph and =CH); ^{13}C NMR ($CDCl_3$) δ=24.79, 24.94 (each ring CH_2), 36.20 (ring CH), 42.71 (CH_2CO), 60.32, 62.14 (OCH_2), 70.16 (ring CH_2), 99.29 (ring CH), 126.30 (=CHCO), 128.36, 128.98, 130.61, 134.42, 143.02 (=CHPh), and 199.65 (CO); MS m/z (rel intensity, %) 290 (M^+, 3), 144 (35), 131 (base peak), 103 (83), 77 (56), and 73 (22). HRMS Found: m/z 290.1525. Calcd for $C_{17}H_{22}O_4$: M, 290.1517. *trans*-**26**: Pale yellow liquid; IR (neat) 3450 and 1675 cm^{-1}; ^1H NMR ($CDCl_3$) δ=1.2—2.3 (5H, m, ring CH_2 and CH), 2.54 (1H, dt, J=15.8 and 6.6 Hz, $COCH_2$), 2.87 (1H, dd, J=15.8 and 7.0 Hz, $COCH_2$), 3.12 (1H, br s, OH), 3.5—4.1 (6H, m, OCH_2 and ring CH_2), 4.25 (1H, d, J=7.0 Hz, ring CH), 6.76 (1H, d, J=16.1 Hz, =CHCO), and 7.4—7.6 (6H, Ph and =CH); ^{13}C NMR ($CDCl_3$) δ=24.43, 27.80 (each ring CH_2), 37.52 (ring CH), 43.27 (CH_2CO), 62.11, 65.17 (CH_2O), 71.66 (ring CH_2), 104.85 (ring

CH), 126.06, 128.33, 128.95, 130.54, 134.44, 142.77 (=CH), and 199.49 (CO); MS *m/z* (rel intensity, %) 290 (M^+, 5), 157 (24), 144 (59), 131 (base peak), 103 (52), 101 (25), and 77 (28). HRMS Found: *m/z* 290.1520. Calcd for $C_{17}H_{22}O_4$: M, 290.1517.

(*E*)-2-Ethoxy-3-(2-oxo-4-phenyl-3-butenyl)-3,4,5,6-tetrahydro-2*H*-pyran (27). To a solution of crude **21d**, which had been prepared from **20d** (0.286 g, 1.35 mmol) according to the method mentioned above, and ethanol (0.08 ml, 1.36 mmol) in nitromethane (3 ml) was added TFA (0.052 ml, 0.68 mmol) at 0 °C. After stirring at the same temperature for 15 min, the reaction mixture was poured into saturated aqueous sodium hydrogencarbonate and extracted with dichloromethane (20 ml×2). The combined extracts were dried over magnesium sulfate and evaporated in vacuo. The residue (0.134 g) was chromatographed over silica gel with hexane–ethyl acetate (20:1 v/v) to give *cis*-**27** (0.026 g, 13% based on **20d**) and *trans*-**27** (0.06 g, 33% based on **20d**). *cis*-**27**: Pale yellow crystals; mp 67—71 °C; IR (KBr) 1691 cm^{-1}; ^1H NMR ($CDCl_3$) δ=1.20 (3H, t, J=7.0 Hz, OEt), 1.5—1.8 (5H, m, ring CH_2 and CH), 2.53 (1H, dd, J=16.5 and 7.0 Hz, CH_2CO), 2.79 (1H, dd, J=16.5 and 7.0 Hz, CH_2CO), 3.3—3.6 (2H, m, OEt), 3.7—3.8 (2H, m, ring CH_2), 4.68 (1H, d, J=2.9 Hz, ring CH), 6.73 (1H, d, J=16.1 Hz, =CHCO), and 7.3—7.6 (6H, m, Ph and =CH); MS *m/z* (rel intensity, %) 274 (M^+, 8), 131 (base peak), 128 (91), 103 (53), and 77 (26). HRMS Found: *m/z* 274.1566. Calcd for $C_{17}H_{22}O_3$: M, 274.1568. *trans*-**27**: Pale yellow liquid; IR (neat) 1690 cm^{-1}; ^1H NMR ($CDCl_3$) δ=1.22 (3H, t, J=7.0 Hz, OEt), 1.2—2.2 (5H, m, ring CH_2 and CH), 2.48 (1H, dd, J=15.4 and 8.1 Hz, CH_2CO), 2.98 (1H, dd, J=15.4 and 5.5 Hz, CH_2CO), 3.4—3.6 (2H, m, OEt), 3.8—4.0 (2H, m, ring CH_2), 4.25 (1H, d, J=6.6 Hz, ring CH), 6.75 (1H, d, J=16.1 Hz, =CHCO), and 7.3—7.6 (6H, m, Ph and =CH); ^{13}C NMR ($CDCl_3$) δ=15.16 (OEt), 24.13, 27.03 (each ring CH_2), 36.89 (ring CH), 42.63 (CH_2CO), 63.86, 64.39 (each OCH_2), 103.35 (ring CH), 126.36 (=CHCO), 128.26, 128.92, 130.41, 134.57 (each Ph), 142.50 (=CH), and 199.22 (CO); MS *m/z* (rel intensity, %) 274 (M^+, 7), 141 (24), 131 (63), 128 (base peak), 103 (25), and 77 (25). HRMS Found: *m/z* 274.1564. Calcd for $C_{17}H_{22}O_3$: M, 274.1568.

References

1) O. Tsuge, S. Kanemasa, T. Suzuki, and K. Matsuda, *Bull. Chem. Soc. Jpn.*, **59**, 2851 (1986).

2) As reviews: M. Murakami and S. Nishida, *Yuki Gosei Kagaku Kyokai Shi*, **41**, 22 (1983); D. Tunemoto and K. Kondo, *ibid.*, **35**, 1070 (1977).

3) E. Wenkert and D. A. Berges, *J. Am. Chem. Soc.*, **89**, 2507 (1967); C. U. Pittman, Jr., *ibid.*, **91**, 5915 (1969); F. Sakan, H. Hashimoto, A. Ichihara, H. Shirahama, and T. Matsumoto, *Tetrahedron Lett.*, **1971**, 3703; T. Nakai, E. Wada, and M. Okawara, *ibid.*, **1975**, 1531; D. Caine, A. A. Boucugnani, and W. R. Pennington, *J. Org. Chem.*, **41**, 3632 (1976); J. Yovell, D. Hirsch, and S. Sarel, *ibid.*, **42**, 850 (1977); A. Murai, K. Kato, and T. Masamune, *Tetrahedron Lett.*, **23**, 2887 (1982); W. S. Murphy and K. Hantawong, *J. Chem. Soc., Perkin Trans. 1*, **1983**, 817.

4) T. Hiyama, H. Saimoto, K. Nishio, M. Shinoda, H. Yamamoto, and H. Nozaki, *Tetrahedron Lett.*, **1979**, 2043; Y. Morizawa, T. Hiyama, and H. Nozaki, *ibid.*, **22**, 2297 (1981); R. D. Miller and D. R. McKean, *J. Org. Chem.*, **46**, 2412 (1981); S. P. Brown, B. S. Bal, and H. W. Pinnick, *Tetrahedron Lett.*, **22**, 4891 (1981); R. K. Dieter and S. Pounds, *J. Org. Chem.*, **47**, 3174 (1982).

5) H. W. Pinnick, S. P. Brown, E. A. McLean, and L. W. Zoller, III, *J. Org. Chem.*, **46**, 3760 (1981); T. Nakajima, H. Miyaji, M. Segi, and S. Suga, *Chem. Lett.*, **1986**, 181.

6) L. Pellacani, P. A. Tardella, and M. A. Loreto, *J. Org. Chem.*, **41**, 1282 (1976).

7) W. S. Murphy and S. Wattanasin, *J. Chem. Soc., Perkin Trans. 1*, **1981**, 2920 and references cited therein.

8) P. A. Grieco and R. S. Finkelhor, *Tetrahedron Lett.*, **1974**, 527 and references cited therein.

9) Diazo ketone **2** was prepared in the reaction of (diethoxyphosphoryl) acetyl chloride with dry diazomethane in diethyl ether (O. Tsuge, S. Kanemasa, and T. Otsuka, unpublished results).

10) M. A. Blanchette, W. Choy, J. T. Davis, A. P. Essenfeld, S. Masamune, W. R. Roush, and T. Sakai, *Tetrahedron Lett.*, **25**, 2183 (1984); M. W. Rathke and M. Nowak, *J. Org. Chem.*, **50**, 2624 (1985); T. Rosen and C. H. Heathcock, *J. Am. Chem. Soc.*, **107**, 3731 (1985); O. Tsuge, S. Kanemasa, N. Nakagawa, and H. Suga, *Bull. Chem. Soc. Jpn.*, **60**, 4091 (1987).

11) Polyphosphoric acid trimethylsilyl ester (PPSE) has been used as a strong dehydrating agent which is soluble in most of organic solvent (S. Ogata, A. Mochizuki, M. Kakimoto, and Y. Imai, *Bull. Chem. Soc. Jpn.*, **59**, 2171 (1986) and references cited therein).

12) M. Julia, S. Julia, and R. Guegan, *Bull. Soc. Chim. Fr.*, **1960**, 1072; M. Julia, S. Julia, and S. Y. Tchen, *ibid.*, **1961**, 1849.

13) The MM2 calculation of 2-phenylcyclopropyl ethyl ketone as a model compound of **5a** shows the following total energy for each conformer (R=Et in all cases): For *trans*-2-phenylcyclopropyl ethyl ketone: conformer **B**: 114.2982 kcal mol^{-1} (1 cal=4.184 J); conformer D: 114.4617 kcal mol^{-1}. For *cis*-2-phenylcyclopropyl ethyl ketone: conformer C: 115.7168 kcal mol^{-1}; conformer **D**: 117.6096 kcal mol^{-1}.

14) Another explanation is possible with a bisected structure model preferred for the resulting cyclopropylcarbinyl cation (D. S. Kabakoff and E. Namanworth, *J. Am. Chem. Soc.*, **92**, 3234 (1970); L. Radom, J. A. Pople, V. Buss, and P. v. R. Schleyer, *ibid.*, **92**, 6380 (1970)).

15) As similar silyl migrations: R. L. Danheiser, D. J. Carini, and A. Basak, *J. Am. Chem. Soc.*, **103**, 1604 (1981); A. Jellal and M. Santelli, *Tetrahedron Lett.*, **21**, 4487 (1980); A. W. P. Jarvie, A. Holt, and J. Thompson, *J. Chem. Soc. B*, **1969**, 852.

16) Replacement of the phenyl group on the ring of **5a—d** with an alkyl substituent led to no ring-enlarged product, but mixture of complex products.

17) E. Wenkert, B. L. Buckwalter, A. A. Craveiro, E. L. Sanchez, and S. S. Sathe, *J. Am. Chem. Soc.*, **100**, 1267 (1978); Y. Morizawa, A. Kanakura, H. Yamamoto, T. Hiyama, and H. Nozaki, *Bull. Chem. Soc. Jpn.*, **57**, 1935 (1984).

18) S. Kyushin, A. Hosomi, Y. Nakadaira, and H. Sakurai, unpublished results (presented at the 7th International Symposium on Organo Silicon Chemistry (Kyoto), 1984, PT19, preprint p. 221).

19) U. L. Tweedie and B. G. Barron, *J. Org. Chem.*, **25**, 2027 (1960).

Synthesis of Homoiceane (Tetracyclo[6.3.1.$1^{2,7}$.$0^{4,10}$]tridecane) and 3,13-Dehydrohomoiceane (Pentacyclo[7.3.1.$0^{2,4}$.$0^{3,8}$.$0^{5,11}$]-tridecane) through Homo-Diels-Alder Reaction[1)]

Ryohei YAMAGUCHI,* Masakazu BAN, and Mituyosi KAWANISI
Department of Industrial Chemistry, Faculty of Engineering, Kyoto University, Yoshida, Kyoto 606
(Received May 3, 1988)

Homo-Diels-Alder reaction of tricyclo[5.3.1.$0^{4,9}$]undeca-2,5-diene with maleic anhydride proceeds very nicely in refluxed *o*-dichlorobenzene to give a single cycloadduct in 81% yield. The stereochemistry of the adduct is determined to be exo by leading to the *exo*-dimethyl ester and comparing it with the *endo*-dimethyl ester which is prepared by homo-Diels-Alder reaction of the above diene with dimethyl acetylenedicarboxylate followed by catalytic hydrogenation. Basic hydrolysis of the cycloadduct followed by oxidative decarboxylation with $Pb(OAc)_4$ in pyridine affords 3,13-dehydrohomoice-5-ene, catalytic hydrogenation of which gives 3,13-dehydrohomoiceane. Photoinduced intramolecular [$_\pi$2+$_\sigma$2] cycloaddition of 3,13-dehydrohomoice-5-ene produces the compound which contains two cyclopropane rings in its rigid structure. When this strained cage compound is treated with Pd-black under H_2, hydrogenolysis of the two cyclopropane rings takes place simultaneously to afford homoiceane.

Iceane (**1**, tetracyclo[5.3.1.$1^{2,6}$.$0^{4,9}$]dodecane) is named after its geometrical similarity to one of the crystalline structure of water[2)] and possesses a unique rigid structure that consists of two chair and three boat cyclohexane rings.[3-5)] In the course of our works on synthesis and reactions of strained cage compounds related iceane,[6,7)] we previously reported synthesis of a nor-analogue of iceane, i.e. noriceane (**2**) as well as its 3,5-dehydro derivative, i.e. 3,5-dehydronoriceane (**3**).[6)] Recently we have found that tricyclo[5.3.1.$0^{4,9}$]undeca-2,5-diene (**4**) reacts with tetracyanoethene faster than norbornadiene to give the homo-Diels-Alder adduct, providing the first example of a 1,4-cyclooctadiene system participating as a diene partner in the homo-Diels-Alder reaction.[8)] In addition to its mechanistic interest, the resulting adduct consists of a skeleton of homoiceane (a homologue of iceane). We now wish to report here the first synthesis of homoiceane (**5**) and its 3,13-dehydro derivative **6** by using this highly efficient one-step framework construction.[9)]

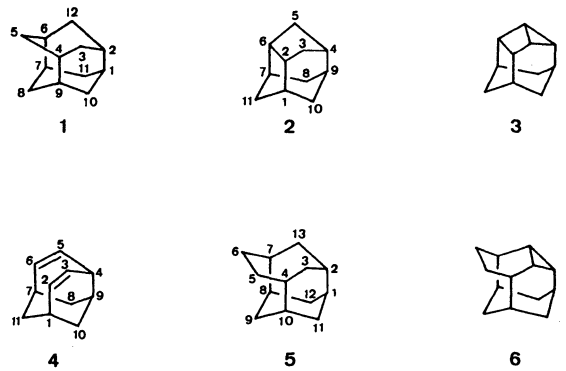

Scheme 1.

Results and Discussion

When a 2:3 mixture of **4** and maleic anhydride in *o*-dichlorobenzene was heated under reflux for 12 h, the homo-Diels-Alder reaction proceeded very nicely to give the [2+2+2] adduct **7** as the single stereoisomer in 81% yield (Scheme 2). The ^{13}C NMR spectrum of **7** showed 9 peaks, supporting the C_s symmetry of **7**. Furthermore, the ^{13}C-H coupling constants of two higher field signals (δ=5.5 and 15.4) were 167 and 169 Hz, respectively, clearly indicating the presence of a cyclopropane ring. Thus, **4** demonstrated the remarkably high homo-Diels-Alder reactivity as a 1,4-cyclooctadiene derivative.[8)]

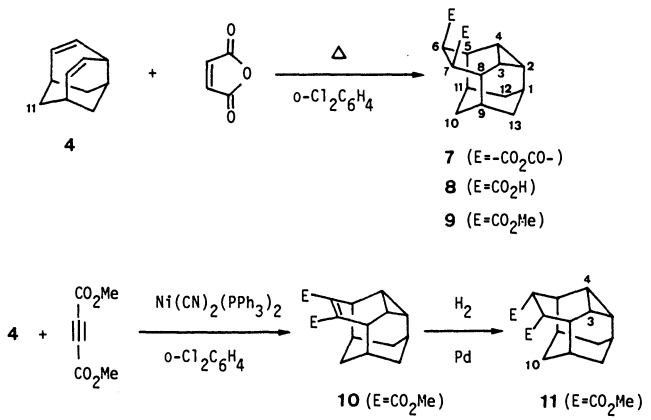

Scheme 2.

The stereochemistry of the adduct **7** was expected to be exo in consideration of the endo-selectivity of homo-Diels-Alder reaction and this expectation was further supported by the following experiments. Hydrolysis of **7** with potassium carbonate in H_2O gave the dicarboxylic acid **8**, which was esterified with diazomethane to afford the *exo*-dimethyl ester **9** in 86% yield (Scheme 2). On the other hand, the *endo*-dimethyl ester **11** was prepared as follows; cycloaddition of **4** with dimethyl acetylenedicarboxylate in the presence of catalytic amount of $Ni(CN)_2(PPh_3)_2$[10)] gave the cycloadduct **10** (45%), hydrogenation of which

over Pd-black took place from the exo-side, probably owing to steric hindrance by C^{10} methylene bridge, to give **11** (Scheme 2). The stereochemical assignments to **9** and **11** were compatible with a steric compression effect[11] observed in their ^{13}C NMR spectra: the signal due to C^3 (C^4) appears at higher field (δ=6.3) in **9** than in **11** (δ=10.6), whereas the signal due to C^{10} is at lower field (δ=32.2) in **9** than in **11** (δ=29.2). Thus, it is noteworthy that the present homo-Diels-Alder reaction proceeds exclusively in an endo-selective manner, since 67—79% endo-selectivity has been observed in the reaction of norbornadiene (**12**) with maleic anhydride.[12] The steric hindrance due to C^{11} methylene bridge of **4** may enhance the endo-selectivity in the present case.

In order to compare the homo-Diels-Alder reactivity of **4** with that of norbornadiene (**12**), we undertook a competitive reaction of **3** and **12** (Scheme 3). When a 1:1:1 mixture of **4**, **12**, and maleic anhydride in *o*-dichlorobenzene was heated at 180 °C in a sealed tube for 5 h, the cycloadducts, **7** and **13**,[13] were obtained in a ratio of 67:33 by ^1H NMR. This result suggested again the higher reactivity of **4** than that of **12**.[8]

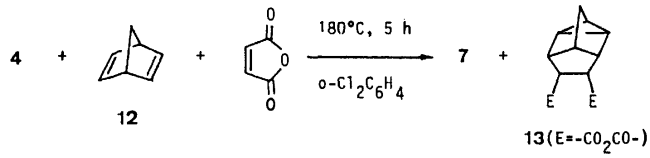

Scheme 3.

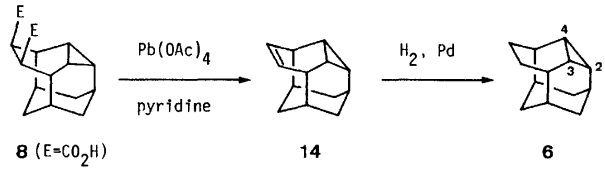

Scheme 4.

As the dehydrohomoiceane skeleton could be obtained in one step, we next examined transformation of **7** into **5** and **6**. Oxidative decarboxylation of **7** with lead tetraacetate in pyridine[14] gave the cage olefin **14** in 65% yield (Scheme 4). It should be noted that **14** contains a rigid chair bicyclo[4.1.0]hept-3-ene system, in which the π-σ interaction between the double bond and the cyclopropane ring has been of great interest.[15,16] Catalytic hydrogenation of **14** with Pd-black gave 3,13-dehydroiceane (**6**) in 97% yield.

On the other hand, transformation into homoiceane (**5**) was not so straightforward as above, because hydrogenolysis of the cyclopropane ring of **6** gave a unsymmetrical product which might be formed by hydrogenolysis of the side C-C bond (C^2-C^3 or C^2-C^4) of the cyclopropane ring: treatment of **6** with PtO_2 under H_2 in AcOH at 50 °C gave a compound, the ^{13}C NMR spectrum of which showed a lack of symmetry. In order to accomplish a regioselective cleavage of the central C-C bond (C^3-C^4), we have noticed an intramolecular [π2+σ2] cycloaddition[16] between the olefin and the cyclopropane moieties in **14**. Thus, irradiation of **14** in ether by a medium-pressure mercury lamp through a quartz filter afforded a 73:27 mixture of the [π2+σ2] cycloadduct **15** and unchanged **14** in 83% yield (Scheme 5). The ^1H NMR spectrum of **15** showed no olefinic protons and its ^{13}C NMR spectrum showed 8 peaks, suggesting C_s symmetry. The ratio of **15** to **14** was not changed after prolonged irradiation, suggesting a photostationary state between **14** and **15**.[17]

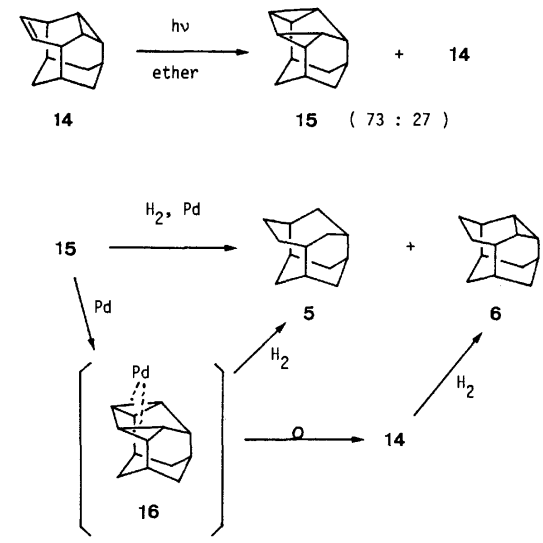

Scheme 5.

Since **15** contains two cyclopropane rings in its rigid cage structure, **15** is expected to be reactive toward transition metals.[18] When **15** was treated with Pd-black under H_2, hydrogenolysis of the two cyclopropane rings took place simultaneously to afford a 1:1 mixture of homoiceane (**5**) and **6**, along with a small amount of an unidentified compound (Scheme 5). The ^{13}C NMR spectrum of **5** clearly indicated C_s symmetry. The successful simultaneous hydrogenolysis of the two cyclopropane rings and the formation of **6** could be rationalized as follows (Scheme 5). The reaction would be probably initiated through complexation of Pd to the two cyclopropane rings, such as **16**. When **16** would undergo a valence isomerization to **14**, **6** would be produced after hydrogenation of the olefinic group. On the other hand, reaction of **16** with H_2 *before the isomerization* could afford **5**.

Experimental

All the temperatures were uncorrected. The IR spectra were obtained on a Hitachi 215 spectrometer. The mass spectra were taken by using a Hitachi RMS-4 mass spectrometer. The ^1H and ^{13}C NMR spectra were obtained on Varian EM-390 and CFT-20 or a JEOL FX-90Q spectrometer, Me_4Si being chosen as an internal standard. Analytical

GLC were carried out on a Shimadzu GC-4C gas chromatography with 10% SE-30 and 10% PEG-20M on Chromsorb W columns. Preparative GLC were performed on a Varian 920 gas chromatography with a 10% PEG-20M on Chromsorb W column. The microanalyses were carried out by Kyoto University Elemental Analysis Center.

Pentacyclo[7.3.1.$0^{2,4}$.$0^{2,8}$.$0^{5,11}$]tridecane-*exo,exo*-dicarboxylic Anhydride (7). A mixture of tricyclo[5.3.1.$0^{4,9}$]undeca-2,5-diene (146 mg, 1.0 mmol), maleic anhydride (147 mg, 1.5 mmol), and a small amount of hydroquinone in *o*-dichlorobenzene (15 mL) was heated at reflux under Ar for 12 h. The reaction mixture was chromatographed on silica gel. Elution by hexane and, then, a mixture of hexane and CH_2Cl_2 (1 : 1) gave **7** (198 mg, 81%): mp 153—155 °C; MS *m/z* (%) 244 (M^+, 100); IR (Nujol): 1845, 1780 cm^{-1}; ^1H NMR ($CDCl_3$) δ=3.09 (s, 2H), 2.80—3.05 (m, 2H), 1.84—2.30 (m, 3H), 1.10—1.73 (m, 7H), 0.67—1.04 (m, 2H); ^{13}C NMR ($CDCl_3$) δ=174.7 (s), 44.1 (d), 32.6 (t), 31.9 (t), 31.0 (d), 28.4 (d), 18.4 (d), 15.4 (d, $^1J_{C\text{-}H}$=169 Hz), 5.5 (d, $^1J_{C\text{-}H}$=167 Hz). Found: C, 73.60; H, 6.60%. Calcd for $C_{15}H_{16}O_3$: C, 73.75; H, 6.60%.

***Dimethyl* Pentacyclo[7.3.1.$0^{2,4}$.$0^{3,8}$.$0^{5,11}$]tridecane-*exo,exo*-6,7-dicarboxylate (9).** A mixture of **7** (305 mg, 1.3 mmol) in 5% aqueous K_2CO_3 (10 mL) was heated at reflux for 2 h. The reaction mixture was acidified by 10% aqueous HCl and extracted with AcOEt. The organic solution was washed with H_2O and dried (Na_2SO_4). Evaporation of the solvent gave pentacyclo[7.3.1.$0^{2,4}$.$0^{3,8}$.$0^{5,11}$]tridecane-*exo*-,*exo*-6,7-dicarboxylic acid (**8**, 317 mg, 97%). A solution of **8** (123 mg, 0.5 mmol) in diethyl ether (30 mL) was treated with CH_2N_2 generated from $C_7H_7SO_2N(NO)CH_3$ and KOH. Usual work-up and chromatography on silica gel gave **9** (117 mg, 86%): mp 98—101 °C; MS *m/z* (%) 290 (M^+, 30), 258 (100); IR (Nujol): 1760, 1740 cm^{-1}; ^1H NMR ($CDCl_3$) δ=3.61 (s, 6H), 2.94 (s, 2H), 2.53—2.80 (m, 2H), 1.57—2.20 (m, 4H), 0.93—1.53 (m, 7H); ^{13}C NMR ($CDCl_3$) δ=174.8 (s), 51.4 (q), 44.1 (d), 32.8 (t), 32.2 (t), 31.9 (d), 30.7 (d), 18.8 (d), 16.3 (d), 6.3 (d). Found: C, 70.07; H, 7.57%. Calcd for $C_{17}H_{22}O_4$: C, 70.32; H, 7.64%.

Dimethyl Pentacyclo[7.3.1.$0^{2,4}$.$0^{3,8}$.$0^{5,11}$]tridec-6-ene-6,7-dicarboxylate (10). A mixture of **4** (146 mg, 1.0 mmol), dimethyl acetylenedicarboxylate (710 mg, 5.0 mmol), $Ni(CN)_2(PPh_3)_2$ (12 mg, 0.02 mmol), and a small amount of hydroquinone in *o*-dichlorobenzene (5 mL) was heated at reflux under Ar for 4 h. The reaction mixture was chromatographed on silica gel. Elution by hexane, hexane-CH_2Cl_2 (1 : 1), and CH_2Cl_2 gave a mixture of **10** and some by-products, which was distilled (Kugelrohr, 130 °C/53 Pa) to give **10** (131 mg, 45%, 95% pure by ^1H NMR). Further purification by using a Lobar column (10% AcOEt-hexane) gave pure **10**: mp 63—4 °C; MS *m/z* (%) 288 (M^+, 28), 256 (83), 228 (100); IR (Nujol): 1720 cm^{-1}. ^1H NMR ($CDCl_3$) δ=3.77 (s, 6H), 3.07—3.33 (m, 2H), 2.00—2.33 (m, 1H), 1.43—1.97 (m, 3H), 0.73—1.37 (m, 8H); ^{13}C NMR ($CDCl_3$) δ=168.6 (s), 143.5 (s), 51.9 (q), 34.2 (d), 31.5 (t), 30.2 (t), 24.3 (d), 23.8 (d), 18.5 (d), 15.6 (d). Found: C, 70.86; H, 6.80%. Calcd for $C_{17}H_{20}O_4$: C, 70.81; H, 6.99%.

Dimethyl Pentacyclo[7.3.1.$0^{2,4}$.$0^{3,8}$.$0^{5,11}$]tridecane-*endo-endo*-6,7-dicarboxylate (11). A mixture of **10** (68 mg, 0.3 mmol) and Pd-black (27 mg) in MeOH (5 mL) was stirred under H_2 for 48 h and, after addition of Pd-black (20 mg), for 48 h. Pd-black was filtered off through Celite and the solvent was evaporated. The residue was chromatographed on silica gel and elution by CH_2Cl_2 gave **11** (35 mg, 51%): mp 80—82 °C; MS *m/z* 290 (M^+, 22), 258 (100); IR (Nujol): 1730 cm^{-1}; ^1H NMR ($CDCl_3$) δ=3.64 (s, 6H), 3.08 (br s, 2H), 2.45—2.83 (m, 2H), 1.57—2.27 (m, 4H), 0.63—1.53 (m, 8H); ^{13}C NMR ($CDCl_3$) δ=174.1 (s), 51.3 (q), 44.5 (d), 32.9 (t), 32.0 (d), 29.2 (t), 27.8 (d), 19.4 (d), 18.3 (d), 10.6 (d). Found: C, 69.93; H, 7.69%. Calcd for $C_{17}H_{22}O_4$: C, 70.32; H, 7.64%.

Competitive Reaction of 4 and Norbornadiene (12) with Maleic Anhydride. A mixture of **4** (73 mg, 0.5 mmol), **12** (46 mg, 0.5 mmol), maleic anhydride (49 mg, 0.5 mmol), and a small amount of hydroquinone in *o*-dichlorobenzene (3 mL) was heated at 180 °C in a sealed tube for 5 h. The similar work-up to the above gave a mixture of **7** and **13** (46 mg) in a ratio of 67 : 33 (by ^1H NMR). The endo : exo ratio of **13** was determined to be 67 : 33 by ^1H NMR.

Pentacyclo[7.3.1.$0^{2,4}$.$0^{3,8}$.$0^{5,11}$]tridec-6-ene (14). To dry pyridine (11 mL) saturated with O_2 was added **8** (733 mg, 2.8 mmol) and $Pb(OAc)_4$ (1880 mg, 4.2 mmol). The mixture was heated at 65—70 °C in a preheated oil bath for 3 min and immediately cooled to room temperature in an ice bath. The reaction mixture was poured into 10% aqueous HNO_3 and extracted with diethyl ether. The ether solution was washed with saturated $NaHCO_3$ and brine, and dried (Na_2SO_4). The solvent was evaporated and the residue was chromatographed on silica gel. Elution by pentane gave **14** (322 mg, 67%) and further elution by CH_2Cl_2 gave **7** (66 mg, 10%). **14**: mp 205 °C (decomp); MS *m/z* (%) 172 (M^+, 70), 129 (72), 91 (100); IR (Nujol): 1465 cm^{-1}; ^1H NMR ($CDCl_3$) δ=6.17 (dd, 2H, *J*=2, 5 Hz), 2.57—2.90 (m, 2H), 1.97—2.27 (m, 1H), 1.06—1.77 (m, 8H), 0.63—1.03 (m, 3H); ^{13}C NMR ($CDCl_3$) δ=135.4 (d), 32.8 (t), 31.5 (d), 30.9 (t), 24.3 (d), 23.7 (d), 19.2 (d), 15.8 (d). Found: C, 90.62; H, 9.51%. Calcd for $C_{13}H_{16}$: C, 90.64; H, 9.36%.

Pentacyclo[7.3.1.$0^{2,4}$.$0^{3,8}$.$0^{5,11}$]tridecane (6). A mixture of **14** (76 mg, 0.44 mmol) and Pd-black (7.6 mg) in MeOH (4 mL) was stirred under H_2 for 2h. The catalysts were removed by filtration through Celite and the solvent was evaporated. The residue was chromatographed on silica gel and elution by pentane gave **6** (75 mg, 97%): mp 207 °C (decomp); MS *m/z* (%) 174 (M^+, 100); ^1H NMR ($CDCl_3$) δ=0.50—2.50 (m, 18H); ^{13}C NMR ($CDCl_3$) δ=33.5 (t), 31.9 (t), 30.4 (d), 27.5 (d), 24.1 (t), 19.8 (d), 14.9 (d), 8.8 (d). Found: C, 89.30; H, 10.64%. Calcd for $C_{13}H_{18}$: C, 89.59; H, 10.41%.

Hexacyclo[7.3.1.$0^{2,7}$.$0^{3,5}$.$0^{4,11}$.$0^{6,8}$]tridecane (15). A solution of **14** (228 mg, 1.3 mmol) in diethyl ether (15 mL) was irradiated through quartz filter under Ar by medium-pressure mercury lamp for 12h. The solvent was evaporated and the residue was chromatographed on silica gel. Elution by pentane gave a mixture of **15** and **14** (198 mg) in a ratio of 73 : 27 (by GLC). Pure **15** was isolated by preparative GLC. **15**: mp 199 °C (decomp); MS *m/z* 172 (M^+, 29), 91 (100); ^1H NMR ($CDCl_3$) δ=0.60—3.00 (m, 16H); ^{13}C NMR ($CDCl_3$) δ=35.6 (d), 35.5 (t), 33.8 (d), 33.3 (d), 32.4 (t), 27.1 (d), 26.7 (d), 22.5 (d). Found: C, 90.47; H, 9.50%. Calcd for $C_{13}H_{16}$: C, 90.64; H, 9.36%.

Tetracyclo[6.3.1.$1^{2,7}$.$0^{4,10}$]tridecane (5). A mixture of **15** (70 mg, 0.41 mmol) and Pd-black (7 mg) in MeOH (5 mL) was stirred under H_2 for 6 h. The catalysts were removed by filtration through Celite and the residue was chromatographed on silica gel. Elution by pentane gave a mixture of **5**, **6**, and an additional product (57 mg) in a ratio of 2 : 2 : 1 (by GLC). Pure **5** was isolated by preparative GLC. **5**: mp 176 °C; MS *m/z* (%) 176 (M^+, 100); ^1H NMR ($CDCl_3$)

δ=0.65—2.70 (m, 20H); ^{13}C NMR ($CDCl_3$) δ=35.0 (t), 34.2 (t and d), 32.8 (t), 31.7 (d), 30.7 (t), 30.2 (d), 26.4 (d). Found: C, 88.72; H, 11.72%. Calcd for $C_{13}H_{20}$: C, 88.57; H, 11.43%.

We thank Dr. E. Ōsawa for valuable discussions. This work was partially supported by a Grant-in-Aid for Scientific Research from Ministry of Education, Science and Culture (Nos. 58470073 and 62303004).

References

1) Trivial nomenclatures are used for simplicity. The IUPAC names are described in Experimental Section.

2) L. F. Fieser, *J. Chem. Educ.*, **42**, 408 (1965).

3) A. Greenberg and J. F. Liebman, "Strained Organic Molecules," Academic Press, New York (1978), p. 197.

4) For synthesis of iceane and its derivatives: C. A. Cupas and L. Hodakowski, *J. Am. Chem. Soc.*, **96**, 4668 (1974); H. Tobler, R. O. Klaus, and C. Ganter, *Helv. Chim. Acta*, **58**, 1455 (1975); D. P. G. Hamon and G. F. Taylor, *Aust. J. Chem.*, **29**, 1721 (1976); P. R. Spurr and D. P. G. Hamon, *J. Am. Chem. Soc.*, **105**, 4734 (1983).

5) For synthesis of heteroiceanes: R. O. Klaus, H. Tobler, and C. Ganter, *Helv. Chim. Acta*, **57**, 2517 (1974); R. O. Klaus and C. Ganter, *ibid.*, **63**, 2559 (1980); D. P. G. Hamon, G. F. Taylor, and R. N. Young, *Aust. J. Chem.*, **30**, 589 (1979); A. T. Nielsen, S. L. Christian, D. W. Moore, R. D. Gilardi, and C. F. George, *J. Org. Chem.*, **52**, 1656 (1987).

6) T. Katsushima, R. Yamaguchi, and M. Kawanisi, *Bull. Chem. Soc. Jpn.*, **55**, 3245 (1982).

7) T. Katsushima, R. Yamaguchi, M. Kawanisi, and E. Ōsawa, *Bull. Chem. Soc. Jpn.*, **53**, 3133 (1980); T. Katsushima, R. Yamaguchi, S. Iemura, and M. Kawanisi, *ibid.*, **53**, 3318, 3324 (1980); R. Yamaguchi and M. Kawanisi, *J. Org. Chem.*, **49**, 4460 (1984); R. Yamaguchi, S. Tokita, Y. Takeda, and M. Kawanisi, *J. Chem. Soc., Chem. Commun.*, **1985**, 1285; R. Yamaguchi, K. Honda, and M. Kawanisi, *ibid.*, **1987**, 83.

8) R. Yamaguchi, M. Ban, M. Kawanisi, E. Ōsawa, C. Jaime, A. B. Buda, and S. Katsumata, *J. Am. Chem. Soc.*, **106**, 1512 (1984) and references on homo-Diels-Alder reactions are cited therein.

9) For a preliminary report: R. Yamaguchi, M. Ban, and M. Kawanisi, *J. Chem. Soc., Chem. Commun.*, **1984**, 826.

10) G. N. Schrauzer and P. Glockner, *Chem. Ber.*, **97**, 2451 (1964).

11) G. C. Levy and G. L. Nelson, "Carbon-13 Nuclear Magnetic Reasonance for Organic Chemists," Wiley-Interscience, New York (1972), p. 24.

12) I. Tabushi, K. Yamamura, Z. Yoshida, and A. Togashi, *Bull. Chem. Soc. Jpn.*, **48**, 2922 (1975).

13) The endo : exo ratio was 67 : 33 by ^{1}H NMR analysis.

14) C. M. Cimarusti and J. Wolinsky, *J. Am. Chem. Soc.*, **90**, 113 (1968).

15) For a review on transannular interactions: H.-D. Martin and B. Mayer, *Angew. Chem., Int. Ed. Engl.*, **22**, 283 (1983).

16) For [$_\pi$2+$_\sigma$2] photocycloadditions: H. Prinzbach, H.-P. Schal, and G. Fischer, *Tetrahedron Lett.*, **24**, 2147 (1983) and references cited therein.

17) Irradiation of **15** under the same conditions also gave a 73 : 27 mixture of **15** and **14**.

18) For a review on reactions of strained molecules with transition metals: K. C. Bishop III, *Chem. Rev.*, **76**, 461 (1976).

Novel Syntheses of Arylcarbamic Esters from Carbon Dioxide and Aromatic Amine via a Zinc Carbamate

Yasuhiko YOSHIDA,* Shigeru ISHII, Akinori KAWATO, Tadataka YAMASHITA, Masahiro YANO,† and Shohei INOUE†

Department of Applied Chemistry, Faculty of Engineering, Toyo University, Kawagoe, Saitama 350
†Department of Synthetic Chemistry, Faculty of Engineering, The University of Tokyo, Bunkyo-ku, Hongo, Tokyo 113

(Received March 12, 1988)

Arylcarbamic esters were synthesized directly from carbon dioxide and an aromatic amine via a zinc carbamate. The alkylation of the reaction mixture of carbon dioxide, an aromatic amine, and diethylzinc with dialkyl sulfate formed alkyl arylcarbamate in a high yield. Also, 2-hydroxycyclohexyl diphenylcarbamate was obtained selectively in a good yield by the reaction of carbon dioxide, epoxycyclohexane, and ethylzinc diphenylamide. Other arylcarbamates of 1,2-cyclohexanediol were obtained by the reactions of carbon dioxide, an aromatic amine, diethylzinc, and epoxycyclohexane.

The carbamic esters are used industrially as plasticizers for rubbers and melamine alkyd resins, fuel additives, and agricultural chemicals such as insecticide and herbicide. The process to synthesize carbamic esters uses isocyanate, carbamoyl chloride, or chloroformate, which are obtained by the reaction using phosgene as a starting material.[1] Since phosgene is toxic and corrosive, and its use produces a large quantity of HCl, it is of interest to develop the novel synthetic methods of carbamic ester without phosgene.

The interest in the fixation of carbon dioxide has led us to investigate the direct synthetic reaction of carbamic ester from carbon dioxide as a starting material.[2-6] Alkylcarbamic esters of 1,2-diol or hemiacetal can be synthesized directly by the reaction of carbon dioxide, primary or secondary aliphatic amines, and epoxides or vinyl ethers, respectively. An analogous reaction by using aromatic amines did not occur, since their basicities are evidently lower.

On the other hand, it is well-known that carbon dioxide inserts to the nitrogen-metal bond to form the salt of carbamic acid.[7-25]

$$R_2N\text{-}M + CO_2 \rightarrow R_2NCOO\text{-}M \quad (1)$$
(M: Ti,Zr,V,Nb,Ta,W,Sn,Si,Ge,P,As,Sb,Zn,Al)

Hydrolysis of the salt, however, forms metal hydroxide and releases amine with evolution of carbon dioxide. Since carbamic acid is unstable, the fixation of carbon dioxide may not be accomplished by this reaction only.

We reported that the reactions of carbon dioxide, epoxycyclohexane, and metal dimethylamides, such as $Ti(NMe_2)_4$, $TiCp_2(NMe_2)_2$, or $W(NMe_2)_6$+$W_2(NMe_2)_6$, proceeded to afford dimethylcarbamate of 1,2-cyclohexanediol in high yields.[5,6] Similar reaction using metal arylamide, however, has not been reported. This paper reports a novel synthesis of arylcarbamic esters by the reaction of carbon dioxide with zinc arylamides followed by alkylation with dialkyl sulfates or an epoxide.

Results and Discussion

Synthesis of Arylcarbamic Esters by the Reaction of Zinc Carbamate with Dialkyl Sulfate. The reaction of *N*-methylaniline, diethylzinc, and carbon dioxide at 120 °C for 5 h was confirmed to give the corresponding ethylzinc carbamate quantitatively, as observed by the NMR spectral analysis of the reaction mixture.

$$PhMeNH + Et_2Zn + CO_2 \rightarrow PhMeNCOO\text{-}Zn\text{-}Et \quad (2)$$

When the reaction of *N*-methylaniline, diethylzinc, and carbon dioxide was followed by the alkylation of the product with diethyl sulfate at 140—160 °C for 20 h, ethyl methylphenylcarbamate was obtained in 93—96% yield (Eq. 3).

$$PhMeNCOO\text{-}Zn\text{-}Et + Et_2SO_4 \rightarrow PhMeNCOOEt \quad (3)$$

Attempted alkylation of zinc carbamate with diethyl sulfate at a temperature below 100°C hardly occurred (Table 1, Runs 1—5). The results of the synthesis of carbamic esters using various aromatic amines are shown in Table 1. By this method, aromatic amines gave the corresponding alkyl arylcarbamates in good yields.

Synthesis of Arylcarbamic Esters by the Reaction of Zinc Carbamate with Epoxycyclohexane. 2-Hydroxycyclohexyl arylcarbamates were found to be obtained selectively in good yields by the reaction of epoxycyclohexane with zinc arylcarbamates.

Carbon dioxide (50 atm) was reacted with an equimolar mixture of epoxycyclohexane and ethylzinc diphenylamide ($EtZnNPh_2$) in benzene solution at 80 °C for 120 h, to give selectively *trans*-2-hydroxycyclohexyl diphenylcarbamate in 48% yield (Table 2, Run 10).

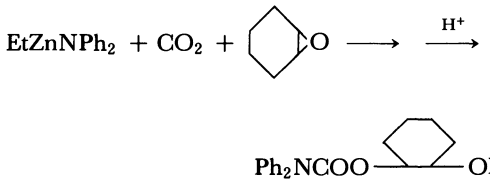

(4)

Table 1. Reaction of Aromatic Amine, Et_2Zn, and CO_2,[a] Followed by the Reaction of the Product with R_2SO_4[b]

Run	Aromatic amine	R_2SO_4	Temp °C	Product Carbamate	Yield/%[c]
1	PhMeNH	Et_2SO_4	100	PhMeNCOOEt	4[f]
2	PhMeNH	Et_2SO_4	110	PhMeNCOOEt	16[f]
3	PhMeNH	Et_2SO_4	120	PhMeNCOOEt	60[f]
4	PhMeNH	Et_2SO_4	140	PhMeNCOOEt	93[f]
5	PhMeNH	Et_2SO_4	160	PhMeNCOOEt	96[f]
6	Ph_2NH	Et_2SO_4	140	$Ph_2NCOOEt$	46[g]
7	PhNpNH[c]	Et_2SO_4	140	PhNpNCOOEt	26[g]
8	*p*-MeC_6H_4(Et)NH[d]	Et_2SO_4	140	*p*-MeC_6H_4(Et)NCOOEt	79[h]
9	*p*-MeC_6H_4(Et)NH[d]	Me_2SO_4	140	*p*-MeC_6H_4(Et)NCOOMe	50[h]

a) Aromatic amine; 50 mmol, $ZnEt_2$; 50 mmol, CO_2; 50 atm, benzene; 30 ml, 120 °C, 5 h. b) R_2SO_4; 110 mmol, 20 h. c) 2-Naphthylphenylamine. d) *N*-Ethyl-*p*-toluidine. e) The yields of carbamates were based on amine. f) Yield by GLC of the reaction mixture of Et_2SO_4 and zinc carbamate for 15 h. g) Isolated yield by recrystallization from 1-pentanol. h) Isolated yield by distillation.

Table 2. The Reaction of Aromatic Amine, Et_2Zn, CO_2, and Epoxycyclohexane[a]

Run	Aromatic amine	Time h	Temp °C	Product Arylcarbamate/%[b]
1	Ph_2NH	16	40	0
2	Ph_2NH	16	60	15
3	Ph_2NH	16	80	32
4	Fh_2NH	16	100	40
5	Ph_2NH	2	80	21
6	Ph_2NH	4	80	23
7	Ph_2NH	8	80	29
8	Ph_2NH	32	80	37
9	Ph_2NH	44	80	44
10	Ph_2NH	120	80	48
11	PhMeNH	68	80	65
12	PhEtNH	48	80	34
13	PhNpNH	72	80	27

a) Aromatic amine; 40 mmol, $ZnEt_2$; 40 mmol, CO_2; 50 atm, epoxycyclohexane; 40 mmol, benzene; 40 ml. For Runs 1—10, ethylzinc diphenylamide prepared from Ph_2NH and $ZnEt_2$, was reacted with CO_2 and epoxycyclohexane. b) The isolated yields of arylcarbamates based on amine.

Although arylcarbamic ester was not formed in the reaction for 16 h at 40 °C, the yields of arylcarbamic ester increased to 40% at a high temperature such as 100°C (Table 2, Runs 1—4). No side products, such as polyether (homopolymer of epoxide), polycarbonate (copolymer of carbon dioxide and epoxide), or cyclic carbonate (the equimolar reaction product of epoxide and carbon dioxide), could be detected even in the reaction at 100 °C.

The reactions of epoxycyclohexane with carbon dioxide, diethylzinc, and an aromatic amine, without isolation of the zinc aromatic amide, were found to give the corresponding 2-hydroxycyclohexyl arylcarbamate, as shown in Table 2. In the case of secondary aromatic amines (PhMeNH, PhEtNH, and PhNpNH), arylcarbamic esters were obtained in good yields (Table 2, Runs 11—13), but the yields of arylcarbamic ester from primary aromatic amines were low.

A similar reaction of carbon dioxide, epoxycyclohexane, and diethylaluminum diphenylamide (Et_2AlNPh_2)[26] instead of $EtZnNPh_2$ also gave diphenylcarbamic ester in a low yield (9%), and simultaneously yielded polycarbonate.

Experimental

General. Commercially available aromatic amines, epoxycyclohexane, benzene, diethylzinc, and triethylaluminium were purified by recrystallization or distillation, and stored in a nitrogen atmosphere. Dialkyl sulfates were used without further purification. Commercial high-purity carbon dioxide gas was introduced into an autoclave directly from a gas cylinder without further purification.

Measurements. IR spectra were recorded on a Hitachi EPI-G3 apparatus, and NMR spectra were measured by using Hitachi 24B spectrometer operating at 60 MHz and JEOL FX90Q at 90 MHz, using hexamethyldisiloxane (HMDS) as internal standard. GC-MS spectra were measured by using a Shimadzu QP-1000 GC-MS spectrometer, and gas liquid chromatogram (GLC) were recorded on a Shimadzu GC-4C apparatus with a thermal conductor.

Reaction of Carbon Dioxide with the Reaction Mixture of Diethylzinc and *N*-Methylaniline. A 100 cm^3 stainless autoclave was swept free of air by displacement with nitrogen. Into the autoclave was added a solution of Et_2Zn (10 cm^3, 100 mmol) and *N*-methylaniline (10.8 cm^3, 100 mmol) in 30 cm^3 of benzene, and CO_2 gas was introduced directly from gas cylinder until the pressure reached 50 atm (5.1×10^6 Pa). After the autoclave was allowed to stand in an oil bath controlled at 120 °C for 5 h, the excess of CO_2 gas was released, and IR and ^1H NMR of the reaction mixture was measured. The IR spectrum of the reaction mixture showed a new absorption at 1565 cm^{-1} to suggest the presence of carboxylate group. ^1H NMR spectrum of the reaction mixture in $CDCl_3$ showed signals at δ 0.2 (2H, q), 1.4 (3H, t), 3.1 (3H, s, $NC\underline{H}_3$), and 7.0 (5H, $C_6\underline{H}_5N$), while ethyl group bonded to zinc such as ethylzinc diethylamide is known to show signals at δ 0.4 (2H, q, $CH_3C\underline{H}_2Zn$) 1.4 (3H, t, $C\underline{H}_3CH_2Zn$).[27]

Synthesis of Arylcarbamate. Reaction of Et_2Zn, aromatic amine, and CO_2, followed by the reaction of the product with dialkyl sulfate: A typical example for the synthesis of

ethyl ethyl(4-methylphenyl)carbamate is as follows.

A 100 cm^3 stainless autoclave was swept free of air by displacement with nitrogen. Into the autoclave was added a solution of Et_2Zn (5.1 cm^3, 50 mmol) and *N*-ethyl-*p*-toluidine (7.2 cm^3, 50 mmol) in 30 cm^3 of benzene, and CO_2 gas was introduced directly from gas cylinder until the pressure reached 50 atm. After the autoclave was allowed to stand in an oil bath controlled at 120 °C for 5 h, the excess of CO_2 gas was released, and diethyl sulfate (14.4 cm^3, 110 mmol) was added into the reaction mixture in the autoclave. After the reaction mixture was heated at 140 °C for 20 h, the contents of the reaction mixture was washed with diluted hydrochloric acid, then with water, and subjected to distillation under a reduced pressure to give the product, ethyl ethyl(4-methylphenyl)carbamate, 100 °C/1.5 mmHg (1 mmHg=133.322 Pa), 8.15 g (79%).

Preparations of other alkyl arylcarbamates were carried out by a similar procedure.

Synthesis of 2-Hydroxycyclohexyl Arylcarbamate: A typical example for the synthesis of 2-hydroxycyclohexyl diphenylcarbamate is as follows.

A 100 cm^3 stainless autoclave was swept free of air by displacement with nitrogen. Into the autoclave was added a solution of $EtZnNPh_2$[24] (10 g, 40 mmol) and epoxycyclohexane (4.0 cm^3, 40 mmol) in 40 cm^3 of benzene, and CO_2 gas was introduced directly from gas cylinder until the pressure reached 50 atm. After the autoclave was allowed to stand in an oil bath controlled at 80 °C for 16 h, the excess of CO_2 gas was released and the contents of the reaction mixture was washed with diluted hydrochloric acid, then with water, and subjected to freeze drying to give a white powder. The white powder was recrystallized from hexane to yield 3.8 g (32%) of 2-hydroxycyclohexyl diphenylcarbamate, mp 133 °C. This carbamate was confirmed to be of trans form, since *trans*-1,2-cyclohexanediol was obtained quantitatively by the hydrolysis of the carbamic ester with methanolic sodium hydroxide.

Preparations of other 2-hydroxycyclohexyl arylcarbamates were carried out by using Et_2Zn and an aromatic amine instead of $EtZnNPh_2$.

Reaction of Et_2AlNPh_2, CO_2, and Epoxycyclohexane: Diethylaluminum diphenylamide (Et_2AlNPh_2)[26] (11 g) in benzene solution (40 cm^3) was heated with epoxycyclohexane (3.9 g) at 80 °C for 87 h under a carbon dioxide pressure (50 atm) in a 100 cm^3 stainless autoclave. The reaction mixture was washed with diluted hydrochloric acid, then with water, and poured to methanol (500 cm^3) to give a white powdery precipitate (polycarbonate; 1.4 g). Evaporation of the solvent from the filtrate left a white residue, which was recrystallized from hexane to give 1.1 g (9%) of 2-hydroxycyclohexyl diphenylcarbamate.

Identification of the Products. Ethyl Methylphenylcarbamate: Bp 79—80 °C/0.45 mmHg (lit,[28,29] 79—80 °C/1 mmHg); IR(neat) 1700 cm^{-1}; ^1H NMR ($CDCl_3$) δ=1.15 (3H, t, $OCH_2C\underline{H}_3$), 3.2 (3H, s, $NC\underline{H}_3$), 4.1 (2H, q, $OC\underline{H}_2CH_3$), 7.2 (5H, $NC_6\underline{H}_5$); MS (70 eV) m/z=179 (M^+).

Ethyl Diphenylcarbamate: Mp 69—70 °C (lit,[29] mp 72—73 °C); IR (KBr pellet) 1695 cm^{-1}; ^1H NMR ($CDCl_3$) δ=1.1 (3H, t, $OCH_2C\underline{H}_3$), 4.1 (2H, q, $OC\underline{H}_2CH_3$), 7.1 (10H, s, N($C_6\underline{H}_5$)$_2$); MS (70 eV) m/z=241 (M^+).

Ethyl (2-Naphthyl)phenylcarbamate: Mp 87—89 °C (lit,[30] mp 93 °C); IR (KBr pellet) 1708 cm^{-1}; ^1H NMR ($CDCl_3$) δ=1.4 (3H, t, $OCH_2C\underline{H}_3$), 4.1 (2H, q, $OC\underline{H}_2CH_3$), 7.2 (5H, s, $NC_6\underline{H}_5$), 7.1—7.8 (7H, m, naphthyl group); MS (70 eV) m/z=291 (M^+).

Ethyl Ethyl(4-methylphenyl)carbamate: Bp 100 °C/1.5 mmHg; IR (neat) 1710 cm^{-1}; ^1H NMR ($CDCl_3$) δ=0.9—1.2 (6H, methyl groups of NC_2H_5 and OC_2H_5), 2.1 (3H, s, CH_3 of 4-methylphenyl group), 3.6 (2H, q, $NC\underline{H}_2CH_3$), 4.0 (2H, q, $OC\underline{H}_2CH_3$), 7.0 (4H, aromatic ring); MS (70 eV) m/z=207 (M^+); EA,Found: C, 69.54; H, 8.26; N, 6.76%. Calcd for $C_{12}H_{17}NO_2$: C, 69.69; H, 8.34; N, 6.73%.

Methyl Ethyl(4-methylphenyl)carbamate: Bp 83.3—83.4 °C/0.5 mmHg; IR (neat) 1695 cm^{-1}; ^1H NMR ($CDCl_3$) δ=1.0 (3H, t, $NCH_2C\underline{H}_3$), 2.2 (3H, s, CH_3 of 4-methylphenyl group), 3.5 (3H, s, $OC\underline{H}_3$), 3.6 (2H, q, $NC\underline{H}_2CH_3$), 7.0 (4H, aromatic ring); MS (70 eV) m/z=193 (M^+); EA,Found: C, 68.37; H, 7.82; N, 7.25%. Calcd for $C_{11}H_{15}NO_2$: C, 68.35; H, 7.81; N, 7.21%.

2-Hydroxycyclohexyl Diphenylcarbamate: Mp 133 °C (recrystallized from hexane); IR (KBr pellet) 3500 and 1695 cm^{-1}; ^1H NMR ($CDCl_3$) δ=1.0—2.1 (8H, methylenes of cyclohexane ring), 2.6 (1H, O$\underline{H}$), 3.4 (1H, C$\underline{H}$-OH), 4.4 (1H, C$\underline{H}$-O(C=O)), 7.2 (10H, N($C_6\underline{H}_5$)$_2$); EA, Found: C, 72.93; H, 6.89; N, 4.48%. Calcd for $C_{19}H_{21}NO_3$: C, 73.29; H, 6.80; N, 4.50%.

2-Hydroxycyclohexyl Methylphenylcarbamate: Mp 100 °C (recrystallized from hexane); IR (KBr pellet) 3500 and 1695 cm^{-1}; ^1H NMR ($CDCl_3$) δ=1.0—2.1 (8H, methylenes of cyclohexane ring), 3.2 (4H, $NC\underline{H}_3$ and O$\underline{H}$), 3.5 (1H, C$\underline{H}$-OH), 4.4 (1H, C$\underline{H}$-O(C=O)), 7.2 (5H, $NC_6\underline{H}_5$); EA, Found: C, 67.35; H, 7.90; N, 5.61%. Calcd for $C_{14}H_{19}NO_3$: C, 67.45; H, 7.68; N, 5.62%.

2-Hydroxycyclohexyl Ethylphenylcarbamate: Bp 66 °C/7 mmHg; IR (neat) 3500 and 1695 cm^{-1}; ^1H NMR ($CDCl_3$) δ=0.9—2.1 (8H, methylenes of cyclohexane ring), 1.0 (3H, t, $NCH_2C\underline{H}_3$), 3.1—3.6 (2H, C$\underline{H}$-C$\underline{H}$), 3.6 (2H, q, $NC\underline{H}_2CH_3$), 4.4 (1H, m, C$\underline{H}$-O(C=O)), 7.2 (5H, $NC_6\underline{H}_5$); EA,Found: C, 68.19; H, 8.37; N, 5.15%. Calcd for $C_{15}H_{21}NO_3$: C, 68.41; H, 8.03; N, 5.31%.

2-Hydroxycyclohexyl (2-Naphthyl)phenylcarbamate: Mp 175 °C (recrystallized from hexane); IR(KBr pellet) 3500 and 1695 cm^{-1}; ^1H NMR ($CDCl_3$) δ=1.0—2.1 (8H, methylenes of cyclohexane ring), 2.6 (1H, O$\underline{H}$), 3.4 (1H, C$\underline{H}$-OH), 4.6 (1H, C$\underline{H}$-O(C=O)), 6.8—7.9 (12H, phenyl and 2-naphthyl groups); EA,Found: C, 76.61; H, 6.39; N, 3.91%. Calcd for $C_{23}H_{23}NO_3$: C, 76.43; H, 6.41; N, 3.87%.

References

1) P. Adams and F. A. Baron, *Chem. Rev.*, **65**, 567 (1965).
2) Y. Yoshida and S. Inoue, *Chem. Lett.*, **1977**, 1375.
3) Y. Yoshida and S. Inoue, *Chem. Lett.*, **1978**, 139.
4) Y. Yoshida and S. Inoue, *J. Chem. Soc., Perkin Trans. 1*, **1979**, 3146.
5) Y. Yoshida and S. Inoue, *Bull. Chem. Soc. Jpn.*, **51**, 559 (1978).
6) Y. Yoshida and S. Inoue, *Polym. J.*, **12**, 763 (1980).
7) J. Chandra, A. D. Jenkins, M. F. Lappert, and R. C. Srivastava, *J. Chem. Soc. A*, **1970**, 2550.
8) R. F. Dalton and K. Jones, *J. Chem. Soc. A.*, **1970**, 590.
9) M. H. Chisholm and M. W. Extine, *J. Am. Chem. Soc.*, **96**, 6214 (1974).
10) M. H. Chisholm and M. W. Extine, *J. Chem. Soc., Chem. Commun.*, **1975**, 438.
11) M. H. Chisholm and M. W. Extine, *J. Am. Chem. Soc.*, **97**, 1623 (1975).

12) M. H. Chisholm and M. W. Extine, *J. Am. Chem. Soc.*, **97**, 5625 (1975).
13) M. H. Chisholm and M. W. Extine, *J. Am. Chem. Soc.*, **99**, 782, 792 (1977).
14) H. Breederveld, *Rec. Trav. Chim.*, **81**, 276 (1962).
15) G. Oetel, H. Marz, and H. Holtschmidt, *Chem. Ber.*, **97**, 891 (1964).
16) R. H. Crag and M. F. Lappert, *J. Chem. Soc. A*, **1966**, 82.
17) L. K. Peterson and K. I. The, *Can. J. Chem.*, **50**, 562 (1972).
18) J. Satge, M. Lesbre, and M. Baudet, *Compt. Rend.*, **259**, 4733 (1964).
19) M. R. Baudet and J. Satge, *Bull. Soc. Chim. Fr.*, **1969**, 1356.
20) T. A. George, K. Jones, and M. F. Lappert, *J. Chem. Soc.*, **1965**, 2157.
21) A. J. Bloodworth, A. G. Davies, and S. C. Vasishtha, *J. Chem. Soc. C*, **1967**, 1309.
22) A. G. Davies and P. G. Harrison, *J. Chem. Soc. C*, **1967**, 1313.
23) J. Koketsu and Y. Ishii, *J. Chem. Soc. C*, **1971**, 511.
24) J. G. Noltes, *Rec. Trav. Chim.*, **84**, 126 (1965).
25) S. Inoue and Y. Yokoo, *Bull. Chem. Soc. Jpn.*, **45**, 3651 (1972).
26) S. Murahashi, T. Niki, T. Obokata, H. Yuki, and K. Hatada, *Kobunshi Kagaku*, **24**, 198 (1967); H. Yuki, K. Hatada, T. Ninomi, and Y. Kikuchi, *Polym. J.*, **1**, 36 (1970).
27) Y. Yoshida, S. Asano, and S. Inoue, *Chem. Lett.*, **1984**, 1073.
28) O. Schmidt, *Z. Physik. Chem.*, **58**, 513 (1907).
29) R. L. Dannley, M. Lukin, and J. Shapiro, *J. Org. Chem.*, **20**, 92 (1955).
30) V. Merz, *Ber. Bunzeneges. Physik. Chem.*, **24**, 2905 (1920).

 © 1988 The Chemical Society of Japan Bull. Chem. Soc. Jpn., 61, 2917—2922 (1988)

Retentive Solvolysis. 15. Salt Effect on the Retentive Phenolyses of 1-(*p*-Substituted phenyl)ethyl *p*-Nitrobenzoates. The Pattern of Salt Effect and the Number of Ion-Pair Intermediates in the S_N1 Solvolysis

Tomomi KINOSHITA,* Koichi SHIBAYAMA, Keizo IKAI, and Kunio OKAMOTO†
Department of Hydrocarbon Chemistry, Faculty of Engineering, Kyoto University, Kyoto 606
(Received March 14, 1988)

The salt effect of sodium phenoxide on the polarimetric (k_p) and titrimetric rate constants (k_t) has exhibited pattern B for the phenolysis of optically active 1-(*p*-methylphenyl)ethyl *p*-nitrobenzoate (ROPNB; (**1**)) in pure phenol. The other patterns A, C, and D were previously observed for the phenolyses of 1-phenylethyl *p*-nitrobenzoates with *p*-MeO- (**2**), *p*-H- (**3**), and *p*-NO_2-substituents (**4**), respectively. Thus, the k_p–k_t pattern changes in the order A → B → C → D as the stability of the intermediate decreases in the order of **2**>**1**>**3**>**4**. All the k_p–k_t patterns can be correlated with the ion-pair stage for product formation, i.e., the pattern A with the second ion-pair intermediate and the patterns B, C, and D with the first one. The pattern of salt effect on the product distribution (% of ROPh, *o*- and *p*-RC_6H_4OH, and *p*-$MeC_6H_4CH{=}CH_2$) for **1** is also compatible with the k_p–k_t pattern B.

The structure of ion-pair intermediates in the S_N1 solvolysis[2] should be discussed after confirmation of the ion-pair stage of nucleophilic attack, e.g., the first ion-pair intermediate (Int-**1**) or the second one (Int-**2**). For such confirmation, the pattern of salt effect of an added salt on the polarimetric and titrimetric rate constants (k_p and k_t, respectively) can serve as a useful tool.[2e,2i,3-8] The possible k_p–k_t diagrams in the S_N1 solvolysis can be generally classified into four patterns, A, B, C, and D,[8,9] provided no normal salt effect[10] was observed (Fig. 1).

On the basis of a stability-selectivity relationship for solvolysis intermediate,[11] it was anticipated that the k_p–k_t pattern should change in the order A → B → C → D with a decrease in the stability of ion-pair intermediate.[9] The retentive phenolyses of 1-(*p*-substituted phenyl)ethyl *p*-nitrobenzoates exhibited the patterns A, C, and D for the *p*-methoxy (**2**), *p*-H (**3**), and *p*-nitro derivatives (**4**), respectively, in the presence of sodium phenoxide.[7] However, the pattern B has not been known for any of 1-phenylethyl systems.

In this paper, we report that the k_p–k_t profile for the phenolysis of 1-(*p*-methylphenyl)ethyl *p*-nitrobenzoate (**1**) exhibited the pattern B, filling up the sequence and, as a consequence, we have confirmed a clear-cut correlation between the stability of phenolysis intermediates (*p*-MeO>*p*-Me>H>*p*-NO_2) and the k_p–k_t pattern, A → B → C → D.

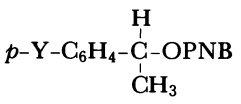

1: Y = CH_3
2: Y = CH_3O
3: Y = H
4: Y = NO_2

Results and Discussion

Phenolysis Rates and Stability of the Ion-Pair Intermediate. Racemic **1** was solvolyzed in pure phenol in the presence of NaOPh (0.106 M) (1M=1 mol dm^{-3}) at 125 °C. The phenolysis rate was determined by the titrimetric method. The k_t value is shown along with those for **2**, **3**, and **4**, which had been previously reported,[7] in Table 1.

The k_t value decreases in the sequence **2**>**1**>**3**>**4** (relative rate 220 : 14.1 : 1.00 : 0.0430 at 125 °C). The k_p value ($k_p/k_t < 1.32$) also decreases in the sequence **3**>**4** (relative rate 1.00 : 0.034). Thus, each of the phenolysis intermediates should become less stable in the order of the rate sequence.

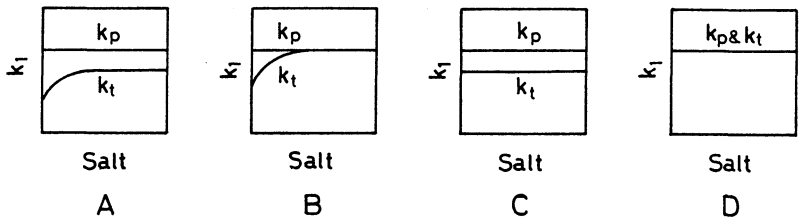

Fig. 1. Four patterns of salt effect on k_p and k_t in the S_N1 solvolysis (in the absence of normal salt effect; cited from Refs. 8 and 9).

† Current address: Meisei Chemical Works, Ltd., 1 Nakazawacho, Ukyo-ku, Kyoto 615.

Table 1. Phenolysis Rates of *p*-Substituted 1-Phenylethyl *p*-Nitrobenzoates **1**—**4** in the Presence of Sodium Phenoxide in Phenol at 125 °C

Substrate[a]	$[NaOPh]_0/M$[b]	k_t/s^{-1}[c]	$k_{t,rel.}$	k_p/s^{-1}[c]
2[d]	0.104	4.1×10^{-2}	220	
1	0.107	2.61×10^{-3}	14.1	
3[d]	0.103	1.85×10^{-4}	1.00	
	0.105			2.45×10^{-4}
4[d]	0.102	7.95×10^{-6}	0.0430	
	0.115			$(8.35\pm0.37)\times10^{-6}$

a) $[Substrate]_0$=0.10—0.11 M. b) Determined by titration. c) Accurate to within ±1.0% for k_t and ±3.0% for k_p, unless otherwise noted. d) Cited from Ref. 7.

Table 2. Phenolysis Rates of 1-(*p*-Methylphenyl)ethyl *p*-Nitrobenzoate (ROPNB) in the Presence of Sodium Phenoxide in Phenol at 75 °C

$[ROPNB]_0$	$[NaOPh]_0/M$[a]	k_t/s^{-1}[b]	k_p/s^{-1}[c]
0.0511	0.000	1.03×10^{-4}	
0.0999	0.000		1.25×10^{-4}
0.0502	0.0178	1.17×10^{-4}	
0.0496	0.0478	1.26×10^{-4}	
0.0499	0.0445		1.27×10^{-4}
0.0501	0.106	1.27×10^{-4}	
0.100	0.101		1.28×10^{-4}
0.0504	0.145	1.32×10^{-4}	

a) Determined by titration. b) Accurate to within ±1.0 %. c) Accurate to within ±3.0%.

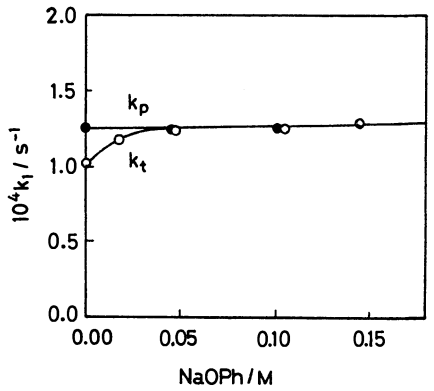

Fig. 2. Effect of added NaOPh concentration on the first-order rate constants (k_p and k_t) for the phenolysis of 1-(*p*-methylphenyl)ethyl *p*-nitrobenzoate in phenol at 75 °C.

Solvolysis rate constants for several aralkyl systems, including 1-phenylethyl acetates in aqueous ethanol,[12] are reported to be well correlated by the Brown-Okamoto equation.[13] In contrast, the σ^+ plot of log k_t shows definitely a curved line for the phenolyses of **1**—**4**, similarly to those of 2,2-dimethyl-1-phenylpropyl *p*-nitrobenzoates,[8] the hydrolyses of 1-phenylethyl chlorides,[14,15] and many other solvolyses.[16] However, a linear plot is given by the use of Yukawa-Tsuno equation,[16] $\log(k/k_0)=\rho[\sigma^0+r(\sigma^+-\sigma^0)]$ with $\rho=-1.78$ and $r=1.88$ (correlation coefficient 0.9939) for the phenolyses of **1**—**4**. Such a *r* value is comparable with that (2.05)[8] for the phenolyses of 2,2-dimethyl-1-phenylpropyl system and is larger than those (1.25 and 0.28) for the hydrolyses of 1-phenylethyl chlorides[14,15] and those (0.542—1.350) for the other solvolysis systems,[16] which may be attributed to the larger resonance effect for the phenolysis system than those for the other systems. Although the *r* value might be a parameter characteristic of the structure of the possible transition state model as well as a parameter measuring the availability of the transition state resonance, it could hardly describe the number and the detailed structure of ion-pair intermediate.

The phenolyses of **1**—**4** exhibit a reactivity parallel with that of the corresponding chlorides in aqueous ethanol[14] and in aqueous acetone;[15] there is a linear free-energy relationship (correlation coefficient 0.991 and 0.988) between the phenolysis and the hydrolysis rates, reflecting approximately similar transition states to each other.

Salt Effect on the Phenolysis Rates. The k_p and k_t for the optically active and racemic substrates **1** were measured in the presence of sodium phenoxide in phenol at 75 °C. Satisfactory first-order kinetic behavior, as expected for the S_N1 solvolysis, was observed at variable concentrations (0—0.145 M) of added sodium phenoxide. The k_p and k_t are summarized in Table 2, and are plotted against the salt concentrations (Fig. 2).

The salt effect of NaOPh on the k_p-k_t diagram for the phenolysis of **1** exhibits a pattern which belongs to the pattern B (Fig. 1) where the discrepancy between k_p and k_t virtually disappears, owing to the special salt effect[3,4,17] on k_t, at higher salt concentrations. We can characterize such salt effect using the parameters proposed by Winstein and his coworkers,[17a] i.e., $k^0_{t,ext}/k^0_t=k^0_p/k^0_t=1.21$ and $[salt]_{1/2}=0.012$ M and also using Winstein's equation[17a] $k_t=k^0_{t,ext}(1+0.0275\cdot[salt])$, where $k^0_{t,ext}$ is k_t value extrapolated at zero salt concentration from its linear part at higher salt concentrations, k^0_t and k^0_p are the k_t and k_p values at zero salt concentration, and $[salt]_{1/2}$ is the salt concentration corresponding to 1/2 $(k^0_{t,ext}+k^0_t)$.

Such k_p-k_t pattern indicates that the phenoxide ion attacks the first ion-pair intermediate (Int-**1**), not the second one (Int-**2**), to produce all the products and to result in neither ion-pair return nor racemization of the intermediate itself at higher NaOPh concentrations.[6,9]

Table 3. The Relative Rates and the Features[a] of Four k_p–k_t Patterns for the Phenolyses of 1-(*p*-Substituted phenyl)ethyl *p*-Nitrobenzoates (RX) **1**—**4** in the Presence of Sodium Phenoxide in Phenol

RX	$k_{t,rel.}$[b] (125 °C)	k_p–k_t pattern[c]	No. of intermediate	Nucleophile[d]	Ion-pair return	Ion-pair intermediate		
						Stability (Reactivity)	Life	Racemization
2	220	A	2	NaOPh	exists	higher (lower)	longer	more
1	14.1	B	1	NaOPh	exists[e]	↑	↑	less[f]
3	1.00	C	1	PhOH	exists	↓	↓	less
4	0.0430	D	1	PhOH	not exist	lower (higher)	shorter	no

a) Cited from Ref. 9. b) Cited from Table 1. c) See Fig. 1 for each profile. d) Reacting with ion-pair intermediate at higher salt concentrations. e) Does not exist at higher salt concentrations. f) No racemization at higher salt concentrations.

The other examples of this pattern have been observed for the phenolyses of 2,2-dimethyl-1-phenylpropyl *p*-nitrobenzoate,[8,9] 2,2-dimethyl-1-(*p*-methoxyphenyl)propyl trifluoroacetate,[8] 1,5-dimethyl-1-ethylhexyl chloride[8] and *p*-nitrobenzoate,[6] and 1-methylheptyl tosylate,[6] the acetolysis of 2-(*p*-methoxyphenyl)propyl tosylate,††[4] and the trifluoroacetolysis of 1-methylpropyl tosylate.[18]

Features of the k_p–k_t profiles for **1**—**4** are summarized in Table 3. These results distinctly show that the k_p–k_t pattern does change in the sequence A → B → C → D as the stability of phenolysis intermediate decreases.

Thus, by means of each of the four k_p–k_t patterns, we can unambiguously determine (i) the number of ion-pair intermediate, in other words, the ion-pair stage of product formation, in addition, (ii) the species of nucleophile reacting with the ion-pair intermediate, and (iii) the existence or absence of ion-pair return.

The kinetic features of each k_p–k_t pattern (Table 3) can be expressed by the following reaction Schemes 1 and 2 for the patterns A and B-D, respectively.

According to such schemes, the total rate expressions for k_p and k_t can be derived as the following equations (Eqs. 1—4).

For the pattern A:

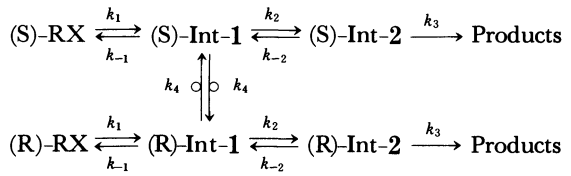

Scheme 1.

$$k_p = \frac{k_1}{1 + \dfrac{k_{-1}}{[k_2 k_3/(k_3 + k_{-2})] + 2k_4}} \quad (1)$$

$$k_t = \frac{k_1}{1 + \dfrac{k_{-1}}{k_2 k_3/(k_3 + k_{-2})}} \quad (2)$$

$$k_3 = k_3' + k_3''[\mathrm{PhOH}] + k_3'''[\mathrm{NaOPh}]$$

For the patterns B, C, and D:

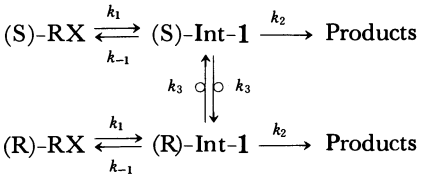

Scheme 2.

$$k_p = \frac{k_1}{1 + [k_{-1}/(k_2 + 2k_3)]} \quad (3)$$

$$k_t = \frac{k_1}{1 + k_{-1}/k_2} \quad (4)$$

$$k_2 = k_2' + k_2''[\mathrm{PhOH}] + k_2'''[\mathrm{NaOPh}]$$

where $k_2''' = 0$ for the pattern C
$k_2''' = 0$, and $k_3 = 0$ and/or $k_{-1} = 0$ for the pattern D

All solvolysis systems are summarized in Table 4, which have been unequivocally proved to proceed via multiple, e.g., two, and a single ion-pair intermediate on the basis of the k_p–k_t pattern. Table 4 suggests that, although S_N1 solvolysis has been generally recognized to proceed through multiple ion-pair intermediates,[2a-h] such a solvolysis system is rather exceptional and, in major ones, the first ion-pair intermediate (Int-1) is the product source.

Salt Effect on the Product Distribution. The product distribution was analyzed by the use of GLPC for the phenolysis of **1** (ROPNB) under identical conditions with those employed for the rate study. The

†† Although the pattern A was previously reported for this system,[4] reexamination of the pattern of salt effect has clarified that it does not follow pattern A, but B.[9]

Table 4. S_N1 Solvolysis Systems Proved Experimentally to Proceed via Multiple (e.g., two) and a Single Ion-Pair Intermediate

Number of intermediate	k_p–k_t pattern[a]	Substrate	Solvent	Added salt	Temp °C	Ref.
2	A	AnCH(Me)OPNB (**2**)	PhOH–benzene[b]	NaOPh	25	c
		AnCH(*t*-Bu)OPNB	PhOH	NaOPh	75	d
					125	e
		AnCH(Me)CH(Me)X (X=OBs,OTs)	AcOH	$LiClO_4$	25	f
1	B	TolCH(Me)OPNB (**1**)	PhOH	NaOPh	75	This work
		PhCH(*t*-Bu)OPNB	PhOH	NaOPh	75	d
		AnCH(*t*-Bu)OTFA	PhOH	NaOPh	75	e
		HexCH(Me)OTs	PhOH–benzene[b]	Et_3N	75	g
		i-HexCMe(Et)Cl	PhOH–toluene[b]	Et_3N	25	e
		i-HexCMe(Et)OPNB	PhOH–benzene[b]	Et_3N	100	g
		$AnCH(Me)CH_2OTs$	AcOH	$LiClO_4$	50	h
		EtCH(Me)OTs	CF_3COOH	$NaOCOCF_3$	25	i
	C	PhCH(Me)OPNB (**3**)	PhOH	NaOPh	125	c
		PhCH(Me)Cl	PhOH–benzene[b]	$PhNH_2$	25	j
		PhCH(Et)OPNB	PhOH	NaOPh	125	e
		PhCH(*i*-Pr)OPNB	PhOH	NaOPh	125	e
		PhCH(*t*-Bu)OPNB	PhOH	Bu_4NClO_4	75	d
		p-ClC_6H_4CH(Ph)OPNB	PhOH–benzene[b]	NaOPh	100	e
		PhCMe(Et)OPNB	PhOH–benzene[b]	Et_3N	50	e
		exo-2-NorbOBs	AcOH	KOAc	25	k
		PhCH(Me)Cl	60%aq.Dioxane	$LiClO_4$	40	l
	D	*p*-$O_2NC_6H_4CH$(Me)OPNB (**4**)	PhOH	NaOPh	125	c
		p-$O_2NC_6H_4CH$(*t*-Bu)OPNB	PhOH	NaOPh	125	e
		i-HexCMe(Et)OTFA	PhOH–toluene[d]	Et_3N	50	e
		endo-2-NorbOBs	AcOH	KOAc	75	k

a) The pattern of salt effect on k_p–k_t; see Fig. 1, Table 3, and the text for each profile. b) A composition of 1:1 (w/w). c) Ref. 7. d) Ref. 9. e) Ref. 8. f) Ref. 3. g) Ref. 6. h) Ref. 4; see a footnote in the text. i) Ref. 18. j) Ref. 5. k) Estimated by us (Ref. 9) from the rate data at one or two concentrations of added KOAc (S. Winstein and D. Trifan, *J. Am. Chem. Soc.*, **74**, 1147 and 1154 (1952)). l) P. B. D. de la Mare, D. M. Hall, and E. Mauger, *Rec. Trav. Chim. Pays-Bas*, **87**, 1394 (1968).

phenolysis produces a major amount of ROPh and small amounts of *o*- and *p*-RC_6H_4OH, and *p*-methylstyrene. Plots of the distribution (%) against the salt concentration exhibit patterns similar to the salt effect on k_t; the yield (%) of aralkyl phenyl ether decreases and those of *o*- and *p*-aralkylphenol and *p*-methylstyrene increase (Fig. 3). Analogous patterns of the salt effect on product distributions were observed for the phenolyses of 1-aryl-2,2-dimethylpropyl systems.[9] The constancy of the product distribution at higher salt concentrations gives an indication that all the products come from the reaction of the ion-pair intermediate (Int-**1**) with added NaOPh, not with the solvent phenol molecule, at higher salt concentrations. The product distribution, which is extrapolated at zero base concentration from curves for respective products, suggests ROPh as the single product (Fig. 3). In contrast to such extrapolated product distribution, the phenolysis actually gave no ROPh but *o*- and *p*-RC_6H_4OH in the absence of NaOPh. This is most probably due to the slow rearrangement of ROPh to RC_6H_4OH by the liberated acid.[19]

In conclusion, it has been clearly confirmed that we can determine the number of ion-pair intermediate, namely, the ion-pair stage of nucleophilic attack by means of each of the four k_p–k_t patterns.

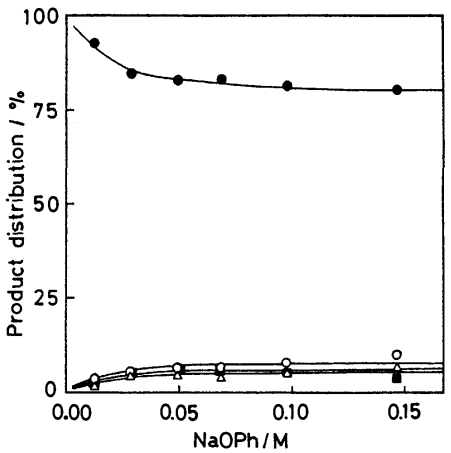

Fig. 3. Effect of added NaOPh concentration on the product distribution for the phenolysis of 1-(*p*-methylphenyl)ethyl *p*-nitrobenzoate in phenol at 75°C. ●: ROPh, ○: *o*-RC_6H_4OH, △: *p*-RC_6H_4OH, ■: *p*-$MeC_6H_4CH{=}CH_2$.

Table 5. Physical Constants, Spectral Data, and Elemental Compositions for 1-(*p*-Methyphenyl)ethyl Derivatives (RX) Relevant to the Phenolysis

RX	Mp(°C) (bp(°C/Pa))	Spectral data					Elemental composition/%			
		IR[a]	^{1}H NMR (δ)[b]				Found		Required	
		cm^{-1}	CH_3	-CH-	Ar	OH	C	H	C	H
ROPNB	69.8—70.5	1710(C=O)[c]	1.69 (d) 2.33 (s)	6.13 (q)	7.10 −7.40 (m) 8.21 (s)		67.29	5.12	67.36[d]	5.30[d]
ROPh	(140—142/370)	1240(C-O-C)	1.57 (d) 2.24 (s)	5.22 (q)	6.79 −7.27 (m)		84.89	7.51	84.87[c]	7.60[e]
RC_6H_4OH (*o*-)	(162—163/270)	3540(OH) 3610(OH)	1.54 (d) 2.23 (s)	4.30 (q)	6.52 −7.23 (m)	5.08 (s,broad)	85.16	7.69	84.87[c]	7.60[e]
RC_6H_4OH (*p*-)	(175—176/270)	3400(OH) 3610(OH)	1.52 (d) 2.24 (s)	3.98 (q)	6.60 −7.29 (m)	6.14 (s,broad)	84.74	7.62	84.87[c]	7.60[e]

a) In CCl_4, unless otherwise noted. b) In $CDCl_3$. c) KBr disk. d) For $C_{16}H_{15}NO_4$. e) For $C_{15}H_{16}O$.

The structure of ion-pair intermediate will be discussed in the following paper on the basis of the stereochemical outcomes for *O*- and *C*-alkylations in the phenolysis of **1**.

Experimental

^{13}C and ^{1}H NMR spectra were taken with a JEOL model JNM FX-90Q 22.5 MHz (FT) and a Hitachi R-24 60 MHz instruments, respectively. IR spectra were recorded with a Hitachi model 215 spectrophotometer. Optical rotations were measured with a JASCO model DIP-SL polarimeter. GLPC was performed with Hitachi model 163 and model 023-6003 instruments. MPLC was done with a chromatograph system composed of a FMI model RP-SY-2 pump and a Merck silica gel 60 column. Melting points were measured on a Yamato model MP-21 apparatus. Microanalyses were performed by the Elemental Analytical Center, Kyoto University.

Materials. Sodium phenoxide was synthesized in the usual way.[7] Racemic[14] and optically active ROH's[20] were synthesized by the literature method. Other organic reagents were of analytical grade, dried, and fractionated prior to use.

Synthesis of 1-(*p*-Methylphenyl)ethyl *p*-Nitrobenzoate. According to the usual method,[7] optically active ROPNB was synthesized. A solution of (*R*)-(+)-ROH (10.017 g, 0.0735 mol, $[\alpha]_D^{26.0}$ +20.5±0.03° (*c* 10.90, ethanol)) and *p*-nitrobenzoyl chloride (15.66 g, 0.08440 mol) in pyridine (40 ml) was stirred at room temperature for 3 h. After usual work-up,[21] (*R*)-(−)-ROPNB (12.29 g, 58.60% yield; mp 69.8—70.5 °C (uncorr.); $[\alpha]_D^{23.4}$ −8.27±0.05° (*c* 3.784, benzene) was obtained. Racemic ROPNB was obtained in a similar manner. The physical constants and spectral data for ROPNB are shown along with those for the phenolysis products in Tables 5 and 6.

Rate Measurements. The usual aliquot technique was employed for measurements of k_p and k_t as previously described.[21] In each run, the reaction was followed to at least 80% conversion; smooth first-order linear relationships were obtained (the correlation coefficients ≥ 0.999). The rate data against the added NaOPh concentration are shown in Tables 1 and 2 and Fig. 1.

Table 6. ^{13}C NMR Spectral Data for 1-(*p*-Methylphenyl)-ethyl Derivatives (RX) Relevant to the Phenolysis[a]

RX	CH_3	-CH-	Ar
ROPNB	21.01 (q) 21.95 (q)	73.97 (d)	123.29 (d) 135.79 (s) 125.99 (d) 137.85 (s) 129.16 (d) 150.29 (s) 130.51 (d) 163.68 (s)
ROPh	21.03 (q) 24.45 (q)	75.63 (d)	115.86 (d) 136.85 (s) 120.47 (d) 140.21 (s) 125.42 (d) 157.99 (s) 129.19 (d)[b]
o-RC_6H_4OH	20.83 (q) 20.93 (q)	38.02 (d)	115.81 (d) 132.19 (s) 120.69 (d) 135.65 (s) 127.22 (d) 142.24 (s) 127.29 (d) 153.06 (s) 127.75 (d) 129.19 (d)
p-RC_6H_4OH	20.83 (q) 22.00 (q)	43.41 (d)	115.15 (d) 135.24 (s) 127.29 (d) 138.87 (s) 128.56 (d) 143.68 (s) 128.93 (d) 153.21 (s)

a) δ; in $CDCl_3$. b) Corresponding to four carbon atoms.

Product Distribution Analysis. Each phenolysis of racemic **1** was carried out in the presence of diphenyl ether as an internal standard under the conditions identical with those adopted for the rate study. After usual work-up[22] with ether, each ethereal solution was concentrated by a distillation using a short column. Then product distributions were analyzed by GLPC in a manner similar to those reported earlier.[22] They are plotted against the added NaOPh concentration in Fig. 3.

Isolation of the Phenolysis Products. Residues of the reaction solutions used for the rate measurements were combined. After the usual work-up as described previously,[21] products were separated by MPLC, distilled in vacuo, and identified on the basis of their IR, ^{13}C and ^{1}H NMR spectral data, chromatographic data, and the elemental compositions. They are summarized along with those for ROPNB in Tables 5 and 6.

The authors thank the Ministry of Education, Science and Culture for a Grant-in-Aid for Scientific Research.

References

1) Part 14, T. Kinoshita, K. Komatsu, K. Ikai, T. Kashimura, S. Tanikawa, A. Hatanaka, and K. Okamoto, *J. Chem. Soc., Perkin Trans. 2*, in press.

2) For recent reviews, a) S. Winstein, B. Appel, R. Baker, and A. Diaz, *Chem. Soc., Spec. Pub.*, **19**, 109 (1965) and their many earlier papers cited therein; b) C. D. Ritchie, *Acc. Chem. Res.*, **5**, 348 (1972); c) F. G. Bordwell, *ibid.*, **5**, 374 (1972); d) R. A. Sneen, ibid., **6**, 46 (1973); e) D. J. Raber, J. M. Harris, and P. v. R. Schleyer, "Ions and Ion Pairs in Organic Reactions," ed. by M. Szwarc, John Wiley & Sons, New York, N. Y. (1974), Chap. 3; f) J. M. Harris, *Progr. Phys. Org. Chem.*, Vol. 11, pp. 88—174 (1974); g) T. W. Bentley and P. v. R. Schleyer, *Adv. Phys. Org. Chem.*, Vol. 14, pp. 1—67 (1977); h) D. Bethell, "Reactive Intermediates," Vol. 1, ed. by M. Jones, Jr., and R. A. Moss, John Wiley & Sons, New York, N. Y. (1978), Chap. 4; i) K. Okamoto, *Pure Appl. Chem.*, **56**, 1797 (1984).

3) S. Winstein and G. C. Robinson, *J. Am. Chem. Soc.*, **80**, 169 (1958).

4) S. Winstein and A. H. Fainberg, *J. Am. Chem. Soc.*, **80**, 459 (1958).

5) K. Okamoto, K. Takeuchi, and H. Shingu, *Bull. Chem. Soc. Jpn.*, **35**, 525 (1962); detailed reexamination for the salt effect on k_p-k_t will be described in a following paper (Part 16; T. Kinoshita, T. Ueno, K. Ikai, M. Fujiwara, and K. Okamoto, *Bull. Chem. Soc. Jpn.*, in press).

6) K. Okamoto and T. Kinoshita, *Bull. Chem. Soc. Jpn.*, **45**, 2802 (1972).

7) K. Okamoto, T. Kinoshita, Y. Takemura, and H. Yoneda, *J. Chem. Soc., Perkin Trans. 2*, **1975**, 1426.

8) K. Okamoto, T. Kinoshita, T. Oshida, T. Yamamoto, Y. Ito, and M. Dohi, *J. Chem. Soc., Perkin Trans. 2*, **1976**, 1617.

9) T. Kinoshita, K. Ikai, T. Kashimura, M. Fujiwara, and K. Okamoto, *Bull. Chem. Soc. Jpn.*, **59**, 2843 (1986).

10) A. H. Fainberg and S. Winstein, *J. Am. Chem. Soc.*, **78**, 2743 (1956).

11) K. Okamoto and T. Kinoshita, *Chem. Lett.*, **1974**, 1037 and references cited therein.

12) E. A. Hill, M. L. Gross, M. Stasiewicz, and M. Manion, *J. Am. Chem. Soc.*, **91**, 7381 (1969).

13) a) H. C. Brown and Y. Okamoto, *J. Am. Chem. Soc.*, **79**, 1913 (1957); b) Y. Okamoto and H. C. Brown, *J. Org. Chem.*, **22**, 485 (1957).

14) V. J. Shiner, Jr., W. E. Buddenbaum, P. L. Murr, and G. Lamaty, *J. Am. Chem. Soc.*, **90**, 418 (1968).

15) G. T. Bruce, A. R. Cooksey, and K. J. Morgan, *J. Chem. Soc., Perkin Trans. 2*, **1975**, 551.

16) Y. Yukawa and Y. Tsuno, *Bull. Chem. Soc. Jpn.*, **32**, 965 and 971 (1959).

17) a) S. Winstein, E. Clippinger, A. H. Fainberg, and G. C. Robinson, *J. Am. Chem. Soc.*, **76**, 2597 (1954); b) A. H. Fainberg and S. Winstein, *ibid.*, **78**, 2767 (1956); c) A. H. Fainberg, G. C. Robinson, and S. Winstein, *ibid.*, **78**, 2777 (1956); d) S. Winstein and E. Clippinger, *ibid.*, **78**, 2784 (1956); e) S. Winstein and J. Sonnenberg, *ibid.*, **83**, 3235 (1961).

18) A. D. Allen, I. C. Ambidge, and T. T. Tidwell, *J. Org. Chem.*, **48**, 4527 (1983).

19) K. Okamoto, T. Kinoshita, O. Makino, and H. Shingu, *Bull. Chem. Soc. Jpn.*, **47**, 1770 (1974).

20) O. Červinka and J. Fusek, *Z. Chem.*, **8**, 145 (1968).

21) K. Okamoto, T. Kinoshita, and Y. Osada, *J. Chem. Soc., Perkin Trans. 2*, **1975**, 253.

22) K. Okamoto, K. Matsubara, T. Kinoshita, and H. Shingu, *Bull. Chem. Soc. Jpn.*, **45**, 1191 (1972).

Radical Transport Reaction. Concurrent Transfer of Electron and Proton

Junji ICHIKAWA, Takaaki SONODA, and Hiroshi KOBAYASHI*
Institute of Advanced Material Study, Kyushu University, Kasuga, Fukuoka 816
(Received March 14, 1988)

Concurrent transport of electron and proton on the same molecule; formal hydrogen-transfer reaction, is successfully realized in aprotic media by using 1-butyl-4,4′-bipyridinium cation radical ($BuPPH^{+\cdot}$), which is prepared from 1-butyl-4-(4-pyridyl)pyridinium ion. Hydrogen reduction with $BuPPH^{+\cdot}$ was discriminated from electron reduction with octylviologen cation radical by the chemoselective reduction preferring enedione to *vic*-dibromide in aprotic media.

Alkylviologens (1,1′-dialkyl-4,4′-bipyridinium, RV^{2+}) are well-known to undergo one-electron reduction to give the resonance-stabilized cation radicals ($RV^{+\cdot}$), which in turn easily release an electron to regenerate RV^{2+}. On the merits of their reversible redox reactions with large negative potentials, they have been widely used as effective electron carriers in a variety of studies in photochemistry,[1] solar energy conversion and storage,[2] and organic synthesis,[3,4] In all cases, however, alkylviologen served as an electron-transfer agent, and the overall reactions were most frequently completed with protons which were supplied from a large excess of surrounding protic media.

Our interests had been focused on the functions of alkylviologens as a catalytic electron mediator across a liquid membrane and a cation transporter coupled therewith, which led us to explore the potentialities of viologen analogues to transport concurrently both an electron and a cationic species, formally equivalent to a radical species. In the first place, we examined the hydrogen-transfer reduction as the simplest example of this scheme. On the basis of the structure of alkylviologens, one of the two *N*-alkyl groups was replaced with a protic hydrogen, which was expected to be transferred along with an electron (Scheme 1). In this article, we report that 1-butyl-4,4′-bipyridinium cation radical ($BuPPH^{+\cdot}$) functions efficiently as a formal hydrogen-transfer agent in aprotic media, and the scheme is exemplified by the selective reduction preferring enedione to *vic*-dibromide.

Results and Discussion

1-Butyl-4-(4-pyridyl)pyridinium ion ($BuPP^+$) showed the lowest redox potential, −0.48 V vs. NHE, in a pH<3 region,[5] where it is in the form of 1-butyl-4,4′-bipyridinium ($BuPPH^{2+}$). The formation of $BuPPH^{+\cdot}$ X^-, where X denotes halogen, was effected by the reduction of $BuPP^+Br^-$[6] with zinc under acid conditions (Scheme 1), and was characterized by a strong sharp band at 400 nm and a weak broad one at 610 nm, resembling those of alkylviologen cation radicals (e.g. that of octylviologen, $C_8V^{+\cdot}$). The blue coloration lasted long enough stably under unaerobic conditions.

When prepared in the two-phase system of aqueous buffer and dichloromethane, $BuPPH^{+\cdot}$ X^- was partitioned only in the aqueous phase, but it could be incorporated into the dichloromethane phase by anion-exchanging the halide for highly lipophilic tetrakis-[3,5-bis(trifluoromethyl)phenyl]borate ($TFPB^-$)[7] (Eq. 1). $BuPPH^{+\cdot}$ was also prepared under anhydrous conditions by using anhydrous TsOH in DMF (Eq. 2). For comparison, other radical analogues having no protic hydrogens within each molecule were prepared according to Eqs. 3—5. In every case, an excess of zinc was filtered off before use.

In order to prove the efficacy of $BuPPH^{+\cdot}$ as a hydrogen-transfer agent, two types of model substrates were selected to be reduced. One is (*E*)-1,4-diphenyl-2-

Table 1. Reduction of Enedione **1** and *vic*-Dibromide **3**

Entry	Reductant	Additive	Yield/%[a]	
			2 in (A)	**4** in (B)
1	$BuPPH^{+\cdot}TFPB^-$[b] /CH_2Cl_2		97[c]	38
2	$BuPPH^{+\cdot}TsO^-$/DMF		99	97
3	$BuPP^{\cdot}$/DMF		7[d]	84[c]
4	$C_8V^{+\cdot}X^-$[e]/CH_2Cl_2		Trace[d]	Quant.
5	$C_8V^{+\cdot}Br^-$/DMF		Trace[d]	Quant.
6	$C_8V^{+\cdot}Br^-$/DMF	TsOH	27	64
7	$C_8V^{+\cdot}Br^-$/DMF	PyH^+TsO^-	34	70

a) Isolated yield. b) See the text. c) Molar ratio of substrate/reductant=1 : 3.3. d) **1** was recovered only in a small amount. e) X denotes halogen.

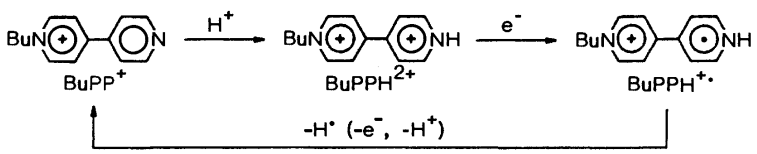

Scheme 1.

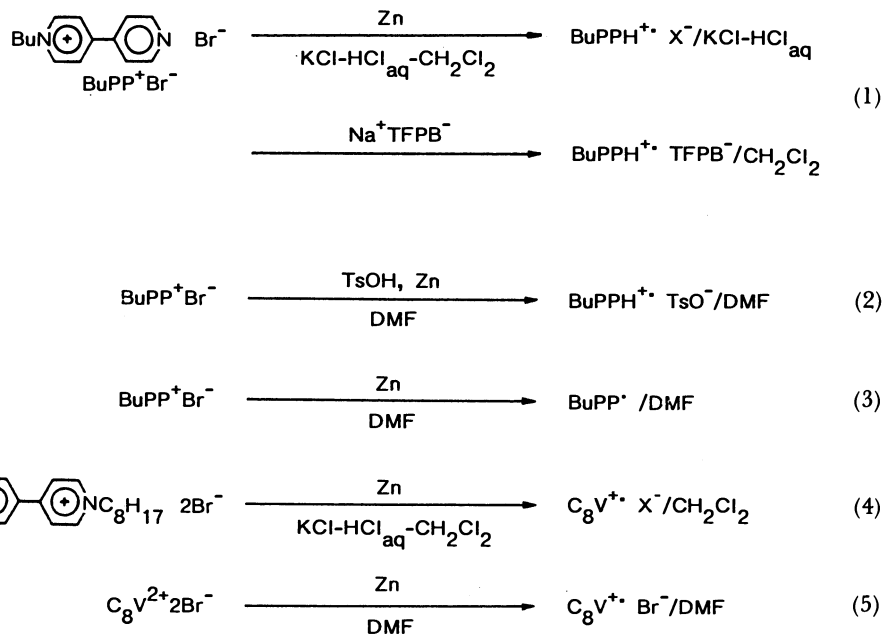

butene-1,4-dione (**1**), whose reduction to 1,4-diketone **2** requires proton source for its completion (System (A)), and the other is *meso*-1,2-dibromo-1,2-diphenylethane (**3**), which can be debrominated to olefin **4** by accepting electrons alone (System (B)). The reducing efficiencies of BuPPH‡ are summarized in Table 1, in comparisons with those of BuPP· and C$_8$V‡ in the two reaction systems (A) and (B).

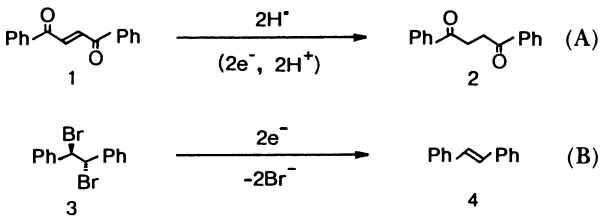

As shown in Table 1, BuPPH‡ worked dually as a hydrogen-reducing agent in the system (A),[8] as well as an electron-reducing agent in the system (B) both in dichloromethane and DMF (Entries 1 and 2), though seemed more favorable to the former system (A). By contrast, C$_8$V‡ served only as an electron-reducing agent in such aprotic media to afford the debrominated product in the system (B), and when applied to the system (A), afforded only a trace amount of the hydrogenated product (Entries 4 and 5). In the same reaction systems, BuPP· which had no protic hydrogens in the molecule showed similar chemoselectivities to those of C$_8$V‡ (Entry 3 vs. Entry 5). The highly efficient reduction of the system (A) in the presence of protic hydrogens may be explained as follows: Enedione **1** initially accepts an electron to give the anion radical **5**, which is difficult to accept an additional electron to the dianion **6**. However, if the anion radical **5** is protonated in situ to the radical **7**, then it is easily reduced further to yield the expected product **2** (Scheme 2). Therefore, when the separate proton source such as TsOH or pyridinium tosylate (PyH$^+$ TsO$^-$) was added, the reduction of the system (A) proceeded even with C$_8$V‡, though did to much less extent than the reaction with BuPPH. (Entries 6 and 7 vs. Entry 2). These results indicate that the protic hydrogen which is carried concurrently with an electron on the same molecule promoted the hydrogenation of the system (A) more efficiently than that carried separately from the electron, thus, the concurrent transport of an electron and a proton; formal hydrogen transfer, was successfully attained by BuPPH‡.

These observations forced us to examine the effica-

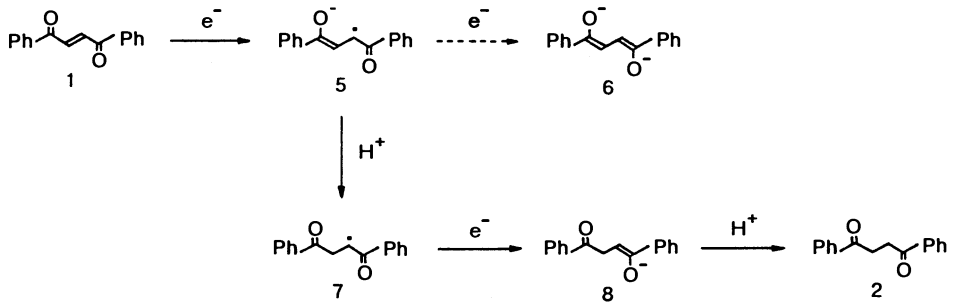

Scheme 2.

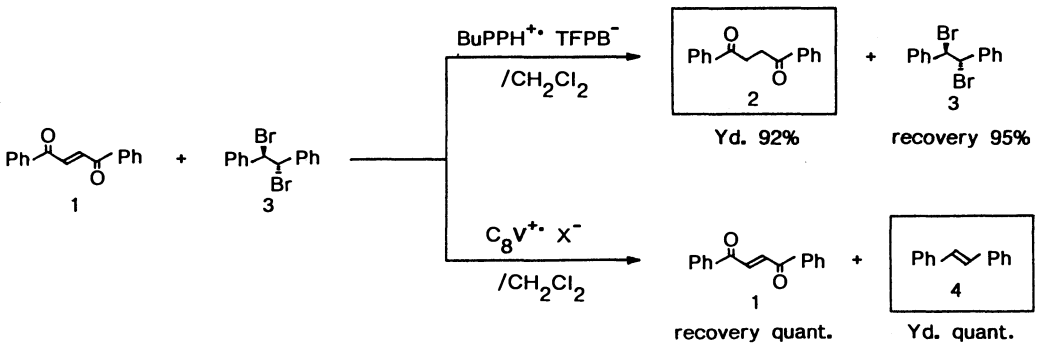

Scheme 3.

Table 2. Reduction of α,β-Unsaturated Ketones with $BuPPH^+$ in DMF

Substrate	Product	Temp	Time/h	Yield/%
p-Benzoquinone	Hydroquinone	r.t.	20	60
Diphenyl diketone	Benzoin	r.t.	10	83
Chalcone	1,3-Diphenyl-1-propanone	r.t.	4	11

cies of hydrogen and electron transfer in terms of chemoselectivities in the reduction of enedione **1** and *vic*-dibromide **3**. When the equimolar mixture of **1** and **3** was treated with $BuPPH^+$ or C_8V^+ in dichloromethane, the reduction of **1** or **3** proceeded selectively without affecting the other substrate which could be recovered in each case (Scheme 3). In these reactions it is noted that $BuPPH^+$ favors exclusively the hydrogen reduction and the chemoselective reduction between **1** and **3** can be achieved simply by the selection of the present two types of bipyridinium salts. $BuPPH^+$ could hydrogenate some analogous substrates, as shown in Table 2, though in the last line rather poor yield resulted.

This reagent would be also useful as hydrogen-transporting agent through a hydrophobic liquid membrane, combined with the photosensitized formation of 4,4′-bipyridinium cation radicals.[3b,4a)]

Experimental

Materials. $BuPP^+Br^-$ was prepared from the reaction of 4,4′-bipyridine with butyl bromide in acetonitrile according to the literature.[6,9)] When $BuPP^+Br^-$ was stirred with powdered zinc in DMF under an argon atmosphere, the blue coloration was rapidly developed due to the formation of $BuPP^{\cdot}$; VIS 736.2 (relative absorbance 0.05), 665 (sh, 0.16), 607.6 (0.31), 400.8 (1.00), 390 (0.67), and 375 nm (0.43). The absorption maxima of its protonated form, $BuPPH^+$, developed in the presence of an equimolar amount of TsOH were almost unchanged; VIS 736.4 (0.08), 666 (sh, 0.20), 609.6 (0.39), 400.4 (1.00), 388.6 (0.85), and 374.6 nm (0.72). These values corresponded to those of C_8V^+ in DMF; VIS 736.0 (relative absorbance 0.06), 660 (sh, 0.16), 608.8 (0.33), 400.8 (1.00), 390 (0.62), and 373 nm (0.37).

Procedures. Reductions of **1** or **3** with viologen analogues were carried out at room temperature, where the viologen analogue was used by 2.2 times molar amounts to the substrate, unless otherwise described, and reduced with powdered zinc to its radical form. The excess of zinc was removed before use by filtration through a disposable Teflon membrane filter (pore size of 0.5 μm) attached to the nozzle of a syringe. The product was isolated by column chromatography on silica gel, eluted with 9:1 mixture of hexane and ether.

Typical procedures of the reduction reaction were as follows:

Reduction of 1 with $BuPPH^+$ $TFPB^-$ in Dichloromethane: Into a two-phase mixture of dichloromethane (20 cm^3) and aqueous HCl-KCl buffer (pH 2.0, 20 cm^3) were added $BuPP^+Br^-$ (97 mg, 0.33 mmol) and Na^+TFPB^- $2.5H_2O$ (308 mg, 0.33 mmol). The mixture was stirred under argon atmosphere, and was added powdered zinc (106 mg, 16.2 mmol). Blue coloration of $BuPPH^+TFPB^-$ rapidly developed in the organic phase. After stirred for 1 min at room temperature, the organic phase was filtered. The filtrate was added to **1** (24 mg, 0.10 mmol) and the reaction mixture was stirred at room temperature for 20 h. After usual work-up, 1,4-diphenyl-1,4-butanedione (**2**) (23 mg, 97% yield) was isolated.

Reduction of 1 with $BuPPH^+TsO^-$ in DMF: To a DMF solution (4 cm^3) of $BuPP^+Br^-$ (78 mg, 0.27 mmol) and anhydrous TsOH (46 mg, 0.27 mmol) was added powdered zinc (183 mg, 2.8 mmol) under an argon atmosphere. After stirred for 1 min at room temperature, the mixture was filtered. To the filtrate, **1** (29 mg, 0.12 mmol) in DMF (1 cm^3) was added dropwise and the reaction mixture was stirred at room temperature for 11 h. After usual work-up, 1,4-diphenyl-1,4-butanedione (**2**) (29 mg, 99% yield) was isolated.

Reduction of 1 with $C_8V^+Br^-$ in the Presence of TsOH: $C_8V^+Br^-$ in DMF was prepared from $C_8V^{2+}2Br^-$ (106 mg, 0.20 mmol) and zinc (126 mg, 1.9 mmol). Anhydrous TsOH (34 mg, 0.20 mmol) was added to the filtrate before the addition of **1**. After usual work-up, **2** (5.6 mg, 27% yield) was isolated.

Reduction of 3 with $C_8V^+Br^-$ in the Presence of TsOH: $C_8V^+Br^-$ in DMF was prepared in a similar manner as above. The addition of the filtrate to a mixture of anhy-

drous TsOH and **3** resulted in **4** (8.8 mg, 64% yield).

Reduction of a Mixture of 1 and 3 with $BuPPH^+TFPB^-$ in Dichloromethane: $BuPPH^+TFPB^-$ was prepared in a two-phase mixture of dichloromethane and aqueous HCl-KCl buffer (pH 2) from $BuPP^+Br^-$ (38 mg, 0.13 mmol), $Na^+TFPB^- 2.5H_2O$ (133 mg, 0.14 mmol) and zinc (444 mg, 6.79 mmol) in a similar manner as above. $BuPPH^+TFPB^-$ in dichloromethane was added to a mixture of **1** (14 mg, 0.059 mmol) and **3** (20 mg, 0.059 mmol). After usual work-up, **2** (13 mg, 92% yield) and **3** (19 mg, 95% recovery) were isolated.

Reduction of a Mixture of 1 and 3 with $C_8V^+X^-$ in Dichloromethane: $C_8V^+X^-$ was prepared in dichloromethane from $C_8V^{2+}2Br^-$ (58 mg, 0.11 mmol) and zinc (350 mg, 5.35 mmol). The filtered solution of $C_8V^+X^-$ was added to a mixture of **1** (21 mg, 0.089 mmol) and **3** (30 mg, 0.089 mmol). After usual work-up, **4** (16 mg, quantitative yield) and **1** (21 mg, quantitative recovery) were isolated.

This work was supported by a Grant-in-Aid for Scientific Research No. 61550643 from the Ministry of Education, Science and Culture, to whom the authors are grateful.

References

1) T. W. Ebbeson, L. E. Manring, and K. S. Peters, *J. Am. Chem. Soc.*, **106**, 7400 (1984) and references therein.

2) "Photogeneration of Hydrogen," ed by A. Harriman and M. A. West, Academic Press, London (1982) and references therein.

3) a) T. Endo, K. Ageishi, and M. Okawara, *J. Org. Chem.*, **51**, 4309 (1986); I. Thanos and H. Simon, *Angew. Chem., Int. Ed. Engl.*, **25**, 462 (1986) and references therein; b) H. Tomioka, K. Ueda, H. Ohi, and Y. Izawa, *Chem. Lett.*, **1986**, 1359 and references therein.

4) The debromination of *vic*-dibromide with RV^+ has been already reported; a) R. Maidan and I. Willner, *J. Am. Chem. Soc.*, **108**, 1080 (1986); b) T. Endo, Y. Saotome, and M. Okawara, *J. Am. Chem. Soc.*, **106**, 1124 (1984).

5) T. Shimizu, K. Takuma, T. Sonoda, and H. Kobayashi, *Rep. Inst. Adv. Mat. Stud.*, **1**, 11 (1987).

6) B. A. Khaskin, I. V. Sablina, N. N. Mel'nikov, and G. S. Supin, *Zh. Obshch. Khim.*, **42**, 2061 (1972).

7) K. Takuma, T. Sonoda, and H. Kobayashi, *Chem. Lett.*, **1984**, 243 and references therein.

8) The $BuPPH^+$ reduction of the olefinic bond in the enedione was effected selectively enough without any detectable side reactions. For the reduction of enediones with other reductants, see: J. P. Schaefer, *J. Org. Chem.*, **25**, 2027 (1960); J. R. Hanson and E. Premuzic, *J. Chem. Soc. C*, **1969**, 1201; L. C. Blaszczak and J. E. McMurry, *J. Org. Chem.*, **39**, 258 (1974); J. M. McIntosh and P. Beaumier, *J. Org. Chem.*, **37**, 2905 (1972).

9) K. Kamogawa, H. Mizuno, Y. Todo, and M. Nanasawa, *J. Polym. Sci., Polym. Chem. Ed.*, **17**, 3149 (1979).

 © 1988 The Chemical Society of Japan Bull. Chem. Soc. Jpn., 61, 2927—2931 (1988)

Synthesis and Properties of Dinitromethylated Arenes. Reinvestigation of the Ponzio Reaction[1)]

Hitomi SUZUKI,* Hiroshi TAKAOKA, Hidetoshi YAMAMOTO, and Takuji OGAWA
Department of Chemistry, Faculty of Science, Ehime University, Bunkyo-cho, Matsuyama 790
(Received March 22, 1988)

Several title compounds have been prepared by the modified Ponzio procedure and their IR, ^{1}H and ^{13}C NMR data are presented. In some cases trinitromethylated arenes were obtained as a by-product. Oxidative cleavage to parent aldehydes and oxidation to carboxylic acids were the major competing reactions. 9-Anthracenecarbaldehyde oxime and 10-methyl-9-anthracenecarbaldehyde oxime reacted with nitrogen dioxide in an unexpected way, giving 10-nitro-9-anthracenecarbonitrile oxide and 10-methyl-10-nitro-9-anthrone as the respective main products. Nitration of (dinitromethyl)benzene has also been examined under various conditions.

In a previous paper,[2)] we reported that the action of concentrated nitric acid on 9-methyl-9-nitro-10-nitromethylene-9,10-dihydroanthracene led to 9-methyl-10-trinitromethylanthracene as one of the main products. Contrary to our expectation, 9-dinitromethyl-10-methylanthracene could not be detected in the product mixture. This unexpected result made us necessary to investigate the behavior of dinitromethylated arenes toward nitric acid. Search for relevant literature revealed that there are only several scattered papers which describe the preparation and properties of (dinitromethyl)arenes.[3-9)] The sole general method for the direct preparation of this type of compounds is that first reported by Ponzio, who converted benzaldehyde oxime (**1a**) into (dinitromethyl)benzene (**2a**) by the action of nitrogen dioxide in ether.[3,4)]

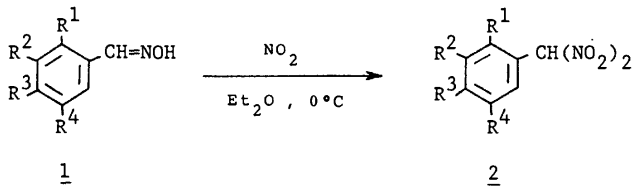

1 2

	R^1	R^2	R^3	R^4
a	H	H	H	H
b	H	H	Me	H
c	MeO	H	H	H
d	H	H	MeO	H
e	MeO	H	H	MeO
f	H	H	Cl	H
g	H	NO_2	H	H
h	H	H	NO_2	H
i	-(CH=CH)$_2$-		H	H
j	-(CH=CH)$_2$-		Me	H

In order to obtain **2a** in some quantity, we initially tried to carry out the Ponzio reaction of aldoxime **1a** according to the original conditions given in the literature. However, to our disappointment, duplication proved to be quite unsatisfactory; the yields of **2a** were always lower, the major product being benzoic acid. We have therefore undertook a systematic study to find the optimum conditions to obtain **2a** in acceptable yields.

Bubbling of nitrogen dioxide gas into an ice-cooled solution of **1a** in ether, followed by quenching with water and extraction with aqueous sodium hydrogencarbonate led to little or no dinitromethyl compound. Dropwise addition of an ethereal solution of **1a** to a solution of 2 equiv of nitrogen dioxide in the same solvent gave the desired product only in a low yield. Increase in amount of nitrogen dioxide from 2 to 5 equiv improved the yield of **2a** appreciably, but the benzoic acid was the main product as yet. To our satisfaction, acceptable results were obtained with good reproducibility when the reaction of **1a** was allowed to proceed in the presence of 10 equiv of nitrogen dioxide and the solvent was removed under reduced pressure immediately after complete disappearance of **1a** on TLC plate. Aqueous work-up of the reaction mixture as described in the literature led to poor results.

Using the optimized conditions defined above, a series of substituted benzaldehyde oximes **1b—1h** and 1-naphthaldehyde oximes **1i—1j** were converted into the corresponding dinitromethylated arenes **2b—2j**, the yields and physical properties of which are presented in Table 1. No spectral data of these appear to have been reported previously in the literature. (Dinitromethyl)arenes are colorless crystals which can be stored indefinitely under the exclusion of light and moisture. They are readily soluble in dichloromethane, chloroform, carbon tetrachloride, benzene, ethanol, and ether; fairly soluble in hot hexane, and slightly soluble in cold hexane. They melt without decomposition.

In some cases trinitromethylated compounds were obtained as the minor product. These compounds are thermally unstable and on heating readily decompose under the evolution of nitrogen oxides to afford arenecarboxylic anhydride.[10)] In contrast to (dinitromethyl)-arenes which appear as a yellow spot on TLC and

Table 1. (Dinitromethyl)arenes Obtained

	(Dinitromethyl)arene **2**				Mp	Yield	IR (KBr)	^{1}H NMR ($CDCl_3$/TMS)	^{13}C NMR ($CDCl_3$/TMS)	Elementary analysis/%	
	R^1	R^2	R^3	R^4	(θ_m/°C)	%	cm^{-1}	δ/ppm	δ/ppm	Found	Calcd
a	H	H	H	H	79—80 (lit,[6] 78—80)	41	1540, 1360, 1320, 1290, 805, 710, 680	7.10 (s, 1H), 7.48—7.61 (m, 5H)	133.0, 129.6, 129.5, 125.3, 112.4	—	—
b	H	H	Me	H	78—80	47	1590, 1560, 1375, 1330, 820, 755	2.38 (s, 3H), 7.07 (s, 1H), 7.29 (d, 2H; J=8.2 Hz), 7.44 (d, 2H; J=8.2 Hz)	143.9, 130.0, 129.5, 122.3, 112.5, 21.24	C: 49.27 H: 4.13 N: 13.99	48.98 4.11 14.28
c	MeO	H	H	H	48—50	36	1570, 1495, 1470, 1440, 1375, 1330, 1300, 1260, 1190, 1170, 1115, 1055, 1030, 825, 760, 715	3.90 (s, 3H), 7.00—7.13 (m, 2H), 7.39—7.41 (m, 1H), 7.54—7.58 (m, 1H), 7.60 (s, 1H)	158.1, 134.4, 128.8, 121.4, 114.3, 111.3, 108.1, 56.03	C: 45.16 H: 3.75 N: 12.76	45.29 3.80 13.20
d	H	H	MeO	H	30—32	39	1560, 1370, 1330, 1255, 1170, 1020, 815, 755	3.87 (s, 3H), 7.02 (d, 2H; J=8.9 Hz), 7.03 (s, 1H), 7.53 (d, 2H; J=8.9 Hz)	163.2, 131.5, 117.2, 114.9, 112.6, 55.55	C: 45.67 H: 3.89 N: 13.01	45.29 3.80 13.20
e	MeO	H	H	MeO	41—42	37	1570, 1505, 1460, 1330, 1235, 1040, 830, 800, 765	3.76 (s, 3H), 3.83 (s, 3H), 6.92 (d, 1H; J=3.0 Hz), 6.95 (d, 1H; J'=9.2 Hz), 7.10 (dd, 1H; J=3.0 Hz, J'=9.2 Hz) 7.61 (s, 1H)	153.7, 152.3, 119.8, 114.2, 113.6, 112.5, 107.8, 56.27, 56.23	C: 44.35 H: 4.20 N: 11.18	44.63 4.16 11.57
f	H	H	Cl	H	52—53	48	1575, 1550, 1480, 1360, 1320, 1080, 800, 740	7.08 (s, 1H), 7.53 (d, 2H; J=9.2 Hz), 7.55 (d, 2H; J=9.2 Hz)	139.9, 131.1, 129.9, 123.6, 111.7	C: 39.07 H: 2.16 N: 12.56	38.82 2.33 12.93
g	H	NO_2	H	H	122—124 (lit,[7] 127—129)	42	1595, 1565, 1530, 1345, 1330, 720	7.23 (s, 1H), 7.77—7.85 (m, 1H), 7.99—8.02 (m, 1H), 8.51—8.56 (m, 2H)	148.5, 135.3, 131.0, 127.8, 126.9, 125.3, 110.7	C: 37.20 H: 2.07 N: 18.47	37.02 2.22 18.50
h	H	H	NO_2	H	72—74	44	1565, 1525, 1345, 1325, 845, 815, 720	7.27 (s, 1H), 7.87 (d, 2H; J=8.7 Hz), 8.42 (d, 2H; J=8.7 Hz)	150.5, 131.2, 130.8, 124.6, 110.7	C: 37.23 H: 2.19 N: 17.98	37.02 2.22 18.50
i	-(CH=CH)$_2$-		H	H	84—85	50	1595, 1565, 1370, 1330, 1250, 780	7.53—7.70 (m, 4H), 7.78—7.81 (m, 1H), 7.92 (s, 1H), 7.93—7.97 (m, 1H), 8.06—8.09 (m, 1H)	133.7, 133.6, 130.7, 129.6, 128.7, 128.3, 127.1, 125.1, 121.3, 120.7, 110.6	C: 57.23 H: 3.33 N: 12.46	56.90 3.47 12.07
j	-(CH=CH)$_2$-		Me	H	107—110	28	1585, 1565, 1380, 1360, 1330, 1250, 805, 775, 755	2.75 (s, 3H), 7.43 (d, 1H; J=7.7 Hz), 7.58 (d, 1H; J=7.7 Hz), 7.61—7.68 (m, 2H), 7.77—7.82 (m, 1H), 7.89 (s, 1H), 8.11—8.14 (m, 1H)	141.0, 132.8, 130.7, 128.3, 128.1, 126.9, 126.1, 125.7, 121.2, 119.6, 110.9, 19.96	C: 58.30 H: 4.07 N: 10.88	58.54 4.09 11.38

move slowly, (trinitromethyl)arenes are colorless on TLC, run fast, and could be examined only in ultraviolet light. Trinitromethyl group is characterized by its very intense antisymmetric vibration of the nitro groups, which appears as split infrared bands at around 1600 cm^{-1}.

Quite perplexing results were obtained when 9-anthracenecarbaldehyde oxime (**3**; R=H) and 10-methyl-9-anthracenecarbaldehyde oxime (**3**; R=Me) were subjected to the conditions of the Ponzio reaction. The former compound gave 10-nitro-9-anthracenecarbonitrile oxide (**7**) as the major product together with 9-anthracenecarboxylic acid as a by-product, whereas the latter compound produced mainly 10-methyl-10-

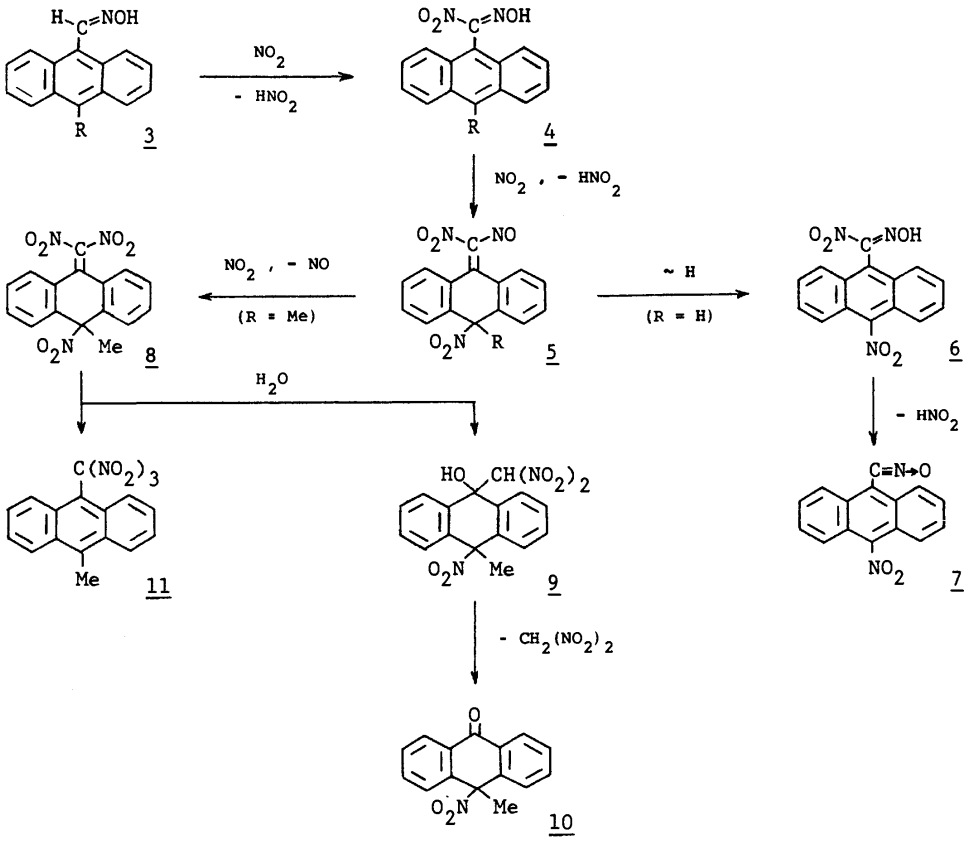

Scheme 1.

nitro-9-anthrone (**10**), 9-methyl-10-trinitromethylanthracene (**11**) being the minor product. Anomalous results observed in the anthracene system pose an interesting problem, a possible solution to which is outlined in Scheme 1.

Abstraction of the oxime hydrogen from **4** followed by attachment of nitrogen dioxide at the meso position leads to the triene intermediate **5**. When R in **5** is hydrogen atom, a facile aromatization would ensue to form the oxime **6**, which loses nitrous acid to give the nitrile oxide **7**.[11] When R in **5** is methyl group, oxidation of nitroso group to nitro group would occur in preference to aromatization to produce the triene **8**, which either undergoes hydration to form carbinol **9** or isomerizes to **11** possibly via homolytic fission of the carbon-nitrogen bond at the quaternary carbon atom. The carbinol **9** would suffer the retro nitro-aldol reaction to be cleaved into ketone **10** and dinitromethane.

When (dinitromethyl)benzene **2a** was treated with fuming nitric acid (d=1.5) or mixed acid at −20—−10 °C for a few hours, there was obtained *m*-nitrophenyldinitromethane (**2g**) as the sole product in accord with the literature report.[7] Neither the formation of trinitromethylated arenes nor the anomalous reaction similar to that observed during the nitration of (dicyanomethyl)arenes took place under the conditions employed.[12] However, when a mixture of **2a** and fuming nitric acid was allowed to stand for several days at room temperature, the initially formed **2g** slowly underwent further nitration on the alkyl side-chain to afford *m*-nitrophenyltrinitromethane (**12**) as the main product. *m*-Nitrobenzoic acid was a side product. In contrast to Titov's claim,[7] no para substitution products could be obtained.

Experimental

All melting points were determined on a hot stage apparatus and are uncorrected. Infrared spectra were run as KBr pellets on a Hitachi 260-10 spectrophotometer and only prominent peaks are recorded. ^{1}H and ^{13}C NMR spectra were obtained on Hitachi R-600 and JNM-FX-100 spectrometers using TMS as an internal standard. Unless otherwise stated, NMR data refer to deuteriochloroform solutions.

Aromatic aldoximes were prepared according to the conventional procedure.[13] Nitrogen dioxide was obtained from commercial source (Seitetsu Kagaku Co., Ltd., Osaka) and used without purification.

Preparation of (Dinitromethyl)arenes (2). To a solution of nitrogen dioxide (20 mmol) in ether (2 ml) chilled in ice was added a solution of aldoxime (2 mmol) in ether (10 ml). The blue reaction mixture immediately turned deep green and the liberation of gaseous product was observed. After standing for 30—60 min, when TLC monitoring showed completion of the reaction, the reaction mixture was evaporated under reduced pressure. The oily residue was taken up in ether, and the ethereal solution was extracted with 0.5 M aqueous potassium hydroxide (1 M = 1 mol dm^{-3}) until the initial yellow aqueous phase became almost colorless. The combined alkaline extracts were saturated with sodium chlo-

ride, made weakly acidic by the addition of hydrochloric acid, and extracted with ether. Evaporation of the former ethereal extract gave parent aldehyde and arenecarboxylic acid, while removal of the solvent from the latter ethereal extract afforded **2** and carboxylic acid. The product **2** was further purified by chromatography on silica gel using hexane–dichloromethane as the eluent.

Reaction of 9-Anthracenecarbaldehyde Oxime (3; R=H) with Nitrogen Dioxide. To a solution of nitrogen dioxide (2.6 mmol) in dry ether (1 ml) at 0 °C was added dropwise a solution of 9-anthracenecarbaldehyde oxime (0.058 g; 0.26 mmol) in the same solvent (15 ml). The resulting green mixture was stirred for 2 h, allowing gradually to attain room temperature. After this time TLC monitoring showed complete disappearance of aldoxime. The solvent was removed together with nitrogen dioxide under reduced pressure and a yellow residue was taken up in chloroform and chromatographed on a silica gel column. Elution with chloroform gave 10-nitro-9-anthracenecarbonitrile oxide (**7**) as yellow crystals, mp 212—215 °C. Yield, 0.038 g (55%). ^{1}H NMR: δ=7.6—8.0 (m, 6H) and 8.3—8.5 (m, 2H); IR: 2275, 1520, 1310, 1275, 1255, and 765 cm^{-1}. Found: C, 67.67; H, 3.21; N, 10.46%. Calcd for $C_{15}H_8N_2O_3$: C, 68.18; H, 3.05; N, 10.60%.

Further elution with methanol gave 9-anthracenecarboxylic acid as yellow crystals.[14] Yield, 0.020 g (35%).

Reaction of 10-Methyl-9-anthracenecarbaldehyde Oxime (3; R=Me) with Nitrogen Dioxide. A suspension of aldoxime (0.264 g; 1.12 mmol) in dry ether (20 ml) was stirred and a stream of nitrogen dioxide was slowly passed at 0—10 °C until the reaction mixture turned to a blue clean solution. After standing for 1 h at room temperature, the mixture was diluted with water (30 ml). Effervescence was followed by separation into two layers. The yellow organic phase was separated, dried with sodium sulfate, and evaporated under reduced pressure. A yellow oily residue was chromatographed on silica gel using hexane–dichloromethane (1 : 1) as the eluent to give 10-methyl-10-nitro-9-anthrone (**10**) as colorless crystals, mp 145—152 °C (decomposition under foaming).[15] Yield, 0.0753 g (27%). MS (70 eV) *m/z* (rel intensity) 253 (M^+, 1), 237 (13), and 207 (100); ^{1}H NMR: δ=2.33 (s, 3H) and 7.40—8.63 (m, 8H); ^{13}C NMR: δ=31.03 (q), 88.94 (s), 125.76 (s), 128.05 (d), 130.09 (d), 134.42 (d), and 139.68 (s); IR: 1680, 1600, 1550, 1340, 1300, and 940 cm^{-1}. Found: C, 70.83: H, 4.52; N, 5.14%. Calcd for $C_{15}H_{11}NO_3$: C, 71.14; H, 4.38; N, 5.53%.

The minor product was identified as 9-methyl-10-trinitromethylanthracene (**11**) by direct comparison with the authentic specimen obtained by the other route.[2]

Nitration of (Dinitromethyl)benzene (2a). The reaction was carried out under various conditions. The typical results are shown below:

a) Compound **2a** (0.614 g; 3.37 mmol) was dissolved into fuming nitric acid (10 ml, *d*=1.5) at −20 °C and the resulting mixture was left for 2 h at this temperature, then poured into brine (300 ml). The organic phase was extracted with ether and the extract was evaporated to leave a yellow solid, which was recrystallized from hexane–dichloromethane to give *m*-nitrophenyldinitromethane (**2g**) as nearly colorless plates, mp 122—124 °C (lit,[7] 127—129°C). Yield, 0.665 g (87%). Found: C, 37.20; H, 2.07; N, 18.47%. Calcd for $C_7H_5N_3O_6$: C, 37.02; H, 2.22; N, 18.50%.

Infrared and ^{1}H NMR spectral inspection of the crude product mixture showed the absence of other important products.

When the reaction mixture was allowed to stand for several days at room temperature, TLC monitoring revealed the gradual accumulation of the second nitration product, which was easily separated from **2g** by chromatography on silica gel and identified as *m*-nitrophenyltrinitromethane (**12**). Colorless prisms, mp 63—65 °C (lit,[7] 65 °C). ^{1}H NMR: δ=7.86—7.97 (m, 2H) and 8.58—8.72 (m, 2H); IR: 1610, 1575, 1530, 1350, 1290, 1225, 870, 840, 800, and 730 cm^{-1}. Found: C, 30.96; H, 1.51; N, 18.30%. Calcd for $C_7H_4N_4O_8$: C, 30.90; H, 1.48; N, 20.59%.

Attempted nitration of **2a** with fuming nitric acid in dichloromethane led to recovered substrate.

b) Compound **2a** (0.099 g, 0.054 mmol) was dissolved into concentrated sulfuric acid (5 ml) to yield a slightly yellow solution, to which fuming nitric acid (5 ml) was added and the resulting mixture was left to stand for 2 h at room temperature. Quenching with water followed by usual work-up gave the expected product **2g** in 78% yield. Mp 122—124 °C.

The authors thank Advanced Instrumentation Center for Chemical Analysis, Ehime University, for ^{13}C NMR determinations and elemental analyses.

References

1) The reaction of polysubstituted aromatics. Part LXIII; Part LXII: H. Suzuki, H. Koide, and T. Ogawa, *Bull. Chem. Soc. Jpn.*, **61**, 501 (1988).

2) H. Suzuki, E. Kimura, T. Katayama, and T. Ogawa, *Chem. Lett.*, **1987**, 979.

3) G. Ponzio, *J. Prakt. Chem.*, **73**, 494 (1906); *Gazz. Chim. Ital.*, **36**, **II**, 287 (1906).

4) Other preparative methods of limited scope include; a) Reaction of aryl halides with dinitromethanide ion: I. V. Tselinskii and G. I. Kolesetskaya, *Zh. Org. Khim.*, **9**, 2471 (1973). b) Reaction of arenes with iodonium dinitromethanide: V. V. Semenov, A. B. Bruskin, S. A. Shevelov, and A. A. Faizel'berg, *Izv. Akad. Nauk SSSR, Ser. Khim.*, **1982**, 2741. c) Electrolysis of tetraalkylammonium dinitromethanide in the presence of arenes: M. E. Niyazymbetov, V. A. Petrosyan, S. A. Shevelov, V. V. Semenov, and A. A. Faizel'berg, *Izv. Akad Nauk SSSR, Ser. Khim.*, **1982**, 2747.

5) M. Milone and A. Massa, *Gazz. Chim. Ital.*, **70**, 196 (1940).

6) L. F. Fieser and W. von E. Doering, *J. Am. Chem. Soc.*, **68**, 2252 (1946).

7) A. I. Titov and V. V. Smirnov, *Dokl. Akad. Nauk SSSR*, **83**, 243 (1952).

8) L. I. Khmel'nitskii, S. S. Novikov, and O. V. Lebedev, *Zh. Obshch. Khim.*, **28**, 2303 (1958).

9) S. S. Novikov, L. I. Khmel'nitskii, and O. V. Lebedev, *Zh. Obshch. Khim.*, **28**, 2296 (1958); *Izv. Akad. Nauk SSSR, Ser. Khim.*, **1960**, 1783.

10) For a review of the chemistry of trinitromethyl compounds, See L. A. Kaplan, "The Chemistry of the Nitro and Nitroso Groups," part 2, ed by H. Feuer, Interscience, New York (1970), p. 289.

11) H. Wieland and L. Semper, *Ber.*, **39**, 2522 (1906). See also C. Grundmann, "Methoden der Organischen Chemie," Vol. 10/3, ed by E. Müller, 4th ed., Georg Thieme,

Stuttgart (1965), p. 841.
12) H. Suzuki, H. Koide, and T. Ogawa, *Bull. Chem. Soc. Jpn.*, **61**, 501 (1988).
13) R. L. Shriner, R. C. Fuson, and D. Y. Curtin, "The Systematic Identification of Organic Compounds," 4 th ed., Maruzen, Tokyo (1957), p. 254.
14) P. D. Bartlett and F. D. Greene, *J. Am. Chem. Soc.*, **76**, 1088 (1954).
15) E. B. Barnett and J. W. Cook, *J. Chem. Soc.*, **123**, 2640 (1923).

Electron Spin Resonance Studies of Anion Radicals of Benzoylsilanes

Kunio MOCHIDA* and Keiji YAMAMOTO†
Department of Chemistry, Faculty of Science, Gakushuin University, 1-5-1 Mejiro, Tokyo 171
†Department of Chemical Engineering, Tokyo Institute of Technology, Meguro, Tokyo 152
(Received March 22, 1988)

ESR studies of anion radicals of seven substituted benzoylsilanes were investigated. ESR data of these anion radicals are discussed in comparison with those of aryl alkyl ketones. ESR spectra of secondary product derived from the anion radical of benzoylsilanes were also examined.

Metalloidal ketones have been of considerable interest as homologs of ketones; in this connection, their unusual chemical and spectroscopic properties have been compared with those of the common ketones.[1] The large bathochromic shifts observed in the electronic spectra of metalloidal ketones recently received attention.[2] Several quantitative theories have been presented to account for these shifts in lower energies.[3]

A variety of physical techniques have been employed in order to clarify the electronic spectra of metalloidal ketones. Electron spin resonance (ESR) is potentially useful to study this problem. An examination of the ESR spectra of anion radicals of benzoylsilanes gives quantitative information which is concerned with the unpaired electron occupying the π^* level.[3a]

Now we describe the ESR spectra of anion radicals of seven substituted benzoylsilanes. The ESR spectra of the secondary derived product derived from the anion radicals of benzoylsilanes are also reported.

Results and Discussion

ESR Spectra of Anion Radicals. Substituted benzoylsilanes (**1**) were reduced with potassium metal in 1,2-dimethoxyethane (DME) at −80 °C. These conditions were chosen so as to prevent any formation of secondary anion radicals derived from the anion radicals of **1**. The ESR spectra of the anion radicals of **1** are shown in Figs. 1—5. The g factors and hyperfine splitting constants (hfsc), determined by computer simulation, of anion radicals of **1** are summarized in Table 1 together with those of certain reported benzoylsilanes and two alkyl aryl ketones (**2**).

The ESR spectrum of an anion radical of benzoyltrimethylsilane (**1a**) obtained by potassium reduction in DME at −80 °C comprised about 15 lines, due to ring protons having g=2.0039. The experimental spectrum of the anion radical of **1a** was reproduced by computer simulation with the listed hfsc's. The ESR spectrum of the anion radical of **1a** observed in this study coincides exactly with that reported by Bock and co-workers.[4]

Each line splits further into a multiplet due to 9 equiv methyl protons (a_{SiMe}=0.14 G (1G=10^{-4} T)).

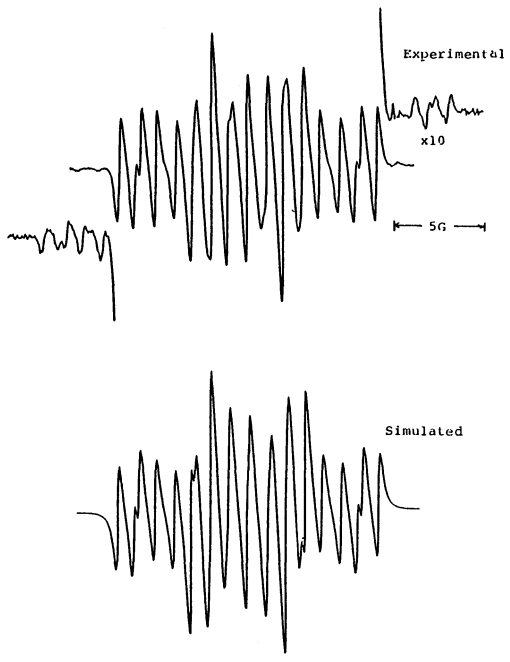

Fig. 1. ESR spectrum of anion radical of benzoylphenyldimethylsilane (**1b**) at −80 °C.

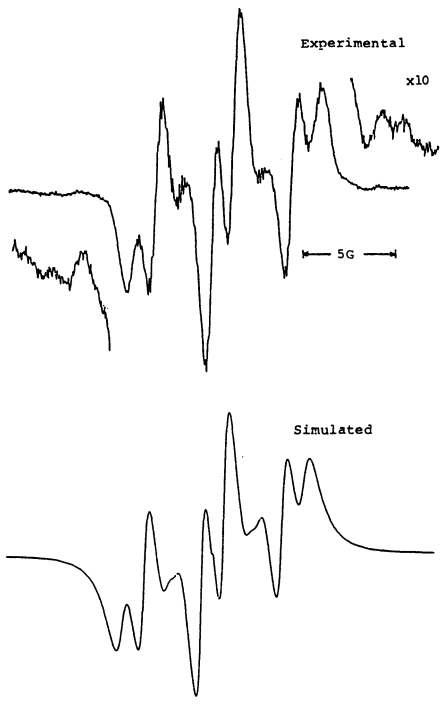

Fig. 2. ESR spectrum of anion radical of *p*-methoxylbenzoyltrimethylsilane (**1d**) at −80 °C.

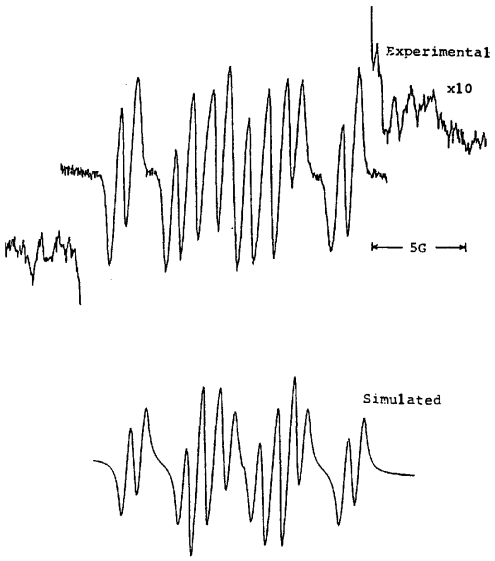

Fig. 3. ESR spectrum of anion radical of *m*-methoxylbenzoyltrimethylsilane (**1e**) at −80°C.

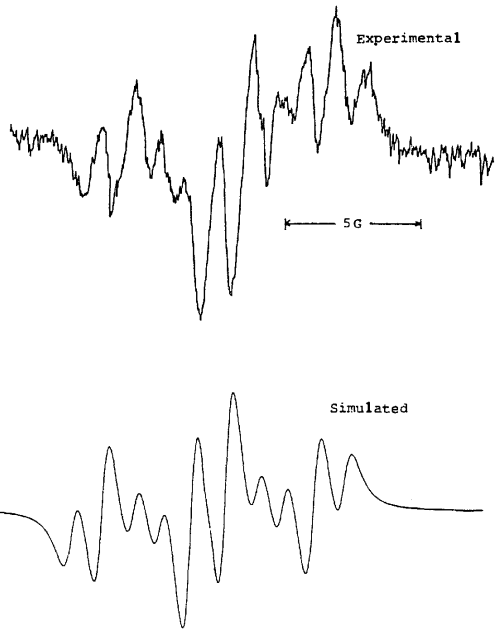

Fig. 4. ESR spectrum of anion radical of *p*-*t*-butylbenzoyltrimethylsilane (**1f**) at −80°C.

Under higher gain, the ^{29}Si splitting (natural abundance=4.7%, I=1/2) of the anion radical of **1a** (a_{Si}=8.86 G) was detected. The fact that the hyperfine coupling constants of two-protons are not equivalent indicates a restricted rotation of the phenyl group about the carbon-carbon bond.

The ESR spectrum of an anion radical of benzoyldimethylphenylsilane (**1b**), shown in Fig. 1, was interpreted in the same manner as described for **1a**. The ESR spectrum was reproduced by computer simulation with the hfsc's listed in Table 1. None of the hfsc's of both ortho- and meta-protons are equivalent.

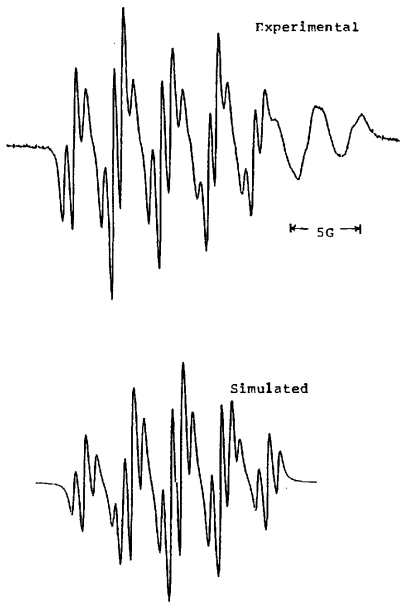

Fig. 5. ESR spectrum of anion radical of *p*-nitrobenzoyltrimethylsilane (**1g**) at −80°C.

This fact also indicates a restricted rotation of the phenyl ring. Attempts to determine the rotational barrier by studying the temperature dependence of the ESR spectrum of the anion radical of **1b** were unsuccesful, since the spectrum was essentially unchanged over a temperature range between 0 and −80 °C. Upon warming above 0 °C, the new spectra of certain species, derived from an anion radical of **1b**, gradually appeared. The secondary ESR spectrum will be discussed later.

The ESR spectrum of an anion radical of *p*-methoxylbenzoyltrimethylsilane (**1d**) in DME at −80 °C is shown in Fig. 2. About 8 lines due to ring protons, and g=2.0040, were observed. Under higher gain, ^{29}Si splitting of the anion radical of **1d** (a_{Si}=9.53 G) was detected. The coupling constants of two non-equivalent meta-protons could be determined by computer simulation.

The ESR spectra of anion radicals of *m*-methoxylbenzoyltrimethylsilane (**1e**) (g=2.0042) and *p*-*t*-butylbenzoyltrimethylsilane (**1f**) (g=2.0040) are shown in Figs. 3 and 4, respectively. The coupling constants of the anion radical of **1e**, shown in Table 1, were determined by computer simulation while taking the ESR data of the related silyl ketyls into consideration. The ESR spectrum of the anion radical of **1f** exhibits an essentially similar pattern to that of the anion radical of **1d**. The ESR spectra of **1e** and **1f** were also reproduced by computer simulation with the hfsc's listed in Table 1. Some of the line intensities of an anion radical of **1f** were not satisfactorily reproduced by computer simulation.

The ESR spectrum of an anion radical of *p*-nitrobenzoyltrimethylsilane (**1g**) (g=2.0051) and its computer simulation are shown in Fig. 5. At low field

Table 1. The g Factors and Hyperfine Coupling Constants of Anion Radicals of Benzoylsilanes and Aryl Ketones

Anion radical $R\text{-}C_6H_4\text{-}\dot{C}(O^-)\text{-}MR'_3$	g value	h.f.s. c/G $a_{o\text{-}H}$	$a_{m\text{-}H}$	$a_{p\text{-}H}$	others	Reference
M=Si						
R=H, R'_3=Me_3 (**1a**)	2.0039	4.20(1H), 3.17(1H)	1.03(2H),	5.25(1H),	a_{SiMe} 0.14, a_{Si} 8.86	This work
		4.28(1H), 3.15(1H)	1.02(2H),	5.25(1H),	a_{SiMe} 0.13	4
R=H, R'_3=$PhMe_2$ (**1b**)	2.0040	4.20(1H), 3.24(1H),	1.27(1H), 0.92(1H)	5.23(1H),	a_{Si} 8.67	This work
R=H, R'_3=Ph_3 (**1c**)	2.0040	3.97(1H), 3.09(1H),	1.18(1H), 0.88(1H)	4.86(1H),	a_{Si} 8.56	6
R=*p*-OMe, R'_3=Me_3 (**1d**)	2.0040	4.60(1H), 3.22(1H),	1.28(1H), 1.22(1H)		a_{SiMe} 0.15, a_{Si} 9.53	This work
R=*m*-OMe, R'_3=Me_3 (**1e**)	2.0042	4.01(1H), 3.22(1H)	0.80(1H),	4.98(1H)	a_{Si} 9.0	This work
R=*t*-Bu, R'_3=Me_3 (**1f**)	2.0040	4.34(1H), 3.18(1H)	1.12(2H)			This work
R=*p*-NO_2, R'_3=Me_3 (**1g**)	2.0051	0.76(2H),	3.36(1H) 2.84(1H)		a_N 3.40	This work
M=C						
R=H, R'_3=Me_3 (**2a**)	2.0037	3.67(2H),	0.90(1H), 1.57(1H)	6.67(1H)		13
R=H, R'_3=Ph_3 (**2b**)		3.69(2H),	0.98(2H),	5.78(1H)		5

various contaminant signals appeared as the result of another signals. The assignment of the coupling constants of ortho and meta-protons was determined while taking those of the anion radical of *p*-nitroacetophenone into consideration.[5]

Three ESR spectra of anion radicals of benzoylgermanes, $PhCOGeR_3$ (R_3=Me_3, **3a**; R_3=$PhMe_2$, **3b**; R_3=Ph_3, **3c**) were also examined. These spectra all exhibit similar patterns (**3a**; g=2.0032, $a_{o\text{-}H}$=4.63, 3.45 G, $a_{m\text{-}H}$=1.32, 0.92 G, $a_{p\text{-}H}$=5.65 G. **3b**; g=2.0032, $a_{o\text{-}H}$=4.32, 3.38 G, $a_{m\text{-}H}$=1.22, 0.90 G, $a_{p\text{-}H}$=5.52 G. **3c**; g=2.0030, $a_{o\text{-}H}$=4.24, 3.34 G, $a_{m\text{-}H}$=1.24, 0.88 G, $a_{p\text{-}H}$=5.54 G). It may well be that the ESR spectra obtained can be assigned to the germyl radical adducts of benzoylgermanes, $[PhC(OGeR_3)GeR_3]$.[6]

As shown in Table 1, the g factors of the anion radicals of **1** are larger than those of the carbon analogs **2**. It has been pointed out that the larger g factors of anion radicals of silylketyls reflect the lower energy of the carbonyl π^* orbital in these radical anions.[3b,7] The interaction of silicon's d orbital with the π^* orbital leads to a lowering of the energy of this orbital. Electron delocalization of $Si\leftarrow C_\pi$ in the radical anions of **1** can be shown form the ^{29}Si coupling constants.

Secondary Anion Radicals. When the anion radical of **1b** was allowed to warm to above 0 °C, a new ESR spectra of the secondary anion radical arising from the original radical of **1b** gradually appeared. The new anion radical was found to be a 1,4-bis(phenyldimethylsilyl)benzene anion radical ($a_{o,\ m\text{-}H}$=2.54 G and a_{SiMe}=0.31 G). The ESR the spectrum of the 1,4-bis(phenyldimethylsilyl)benzene anion radical was confirmed by computer simulation and by a comparison with an authentic anion radical. Then, the 1,4-bis(phenyldimethylsilyl)benzene anion radical changed to an unidentified paramagnetic species with time. The formation of 1,4-bis(phenyldimethylsilyl)-benzene is not easy to explain. In general, the formation of a trace of benzene is known in reactions of phenyl-substituted silyl compounds with alkali metals.[8] Silyl anions have been reported to react with benzene to give 1,4-bis(phenyldimethylsilyl)benzene.[9]

The radical anion of **1b** when warmed to 20 °C changed to either benzophenone ketyl ($a_{o\text{-}H}$=2.60 G, $a_{m\text{-}H}$=0.87 G, and $a_{p\text{-}H}$=3.45 G) or benzil anion radical ($a_{o\text{-}H}$=1.00 G, $a_{m\text{-}H}$=0.36 G, and $a_{p\text{-}H}$=1.10 G), the change being dependent upon the amounts of **1b** and potassium metal used. Benzophenone ketyl and benzil anion radical are stable under these conditions.

The formation of benzil from **1b** can be interpreted by a mechanism involving a coupling of the initially formed radical anion of **1b**, followed by an elimination of the phenyldimethylsilyl anion, as outlined below.

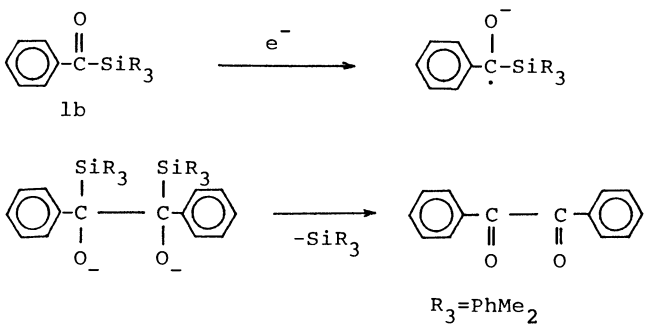

There may be an alternative mechanism which involves a dimerization of the benzoyl radical, first formed by an elimination of the silyl anion radical of **1b**.

The formation of benzophenone from **1b** might be explained by the work of Brook and co-workers.[10] Thus, an attack by a nucleophile must occur on the silicon atom of **1b**, followed by a 1,2-migration of a phenyl group to the adjacent carbonyl group, as shown below. The α-silyl alkoxide formed may

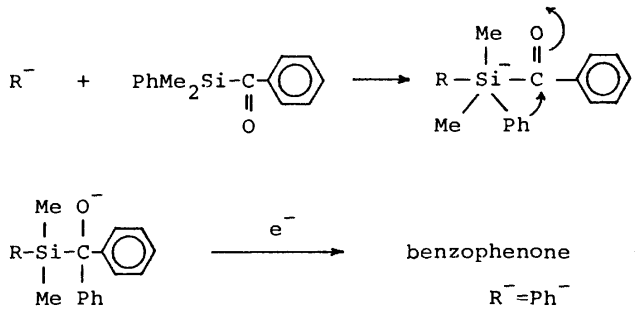

undergo homolysis of a silicon-carbon bond to give benzophenone. An analogous mechansim for the formation of benzil and benzophenone has been postulated by Arberti and co-workers.[6]

Experimental

ESR Measurements. All the ESR spectra were obtained using a Varian E-9 ESR spectrometer. The field sweep of the spectrometer was calibrated with an aqueous solution of Fremy's salt (a_N=13.07 G). The *g* factors were determined by reference to that of Fremy's salt (*g*=2.0055) using a dual cavity.

Materials. Benzoyltrimethylsilane,[3a] benzoylphenyldimethylsilane,[3a] *p*-methoxylbenzoyltrimethylsilane,[3a] *m*-methoxylbenzoyltrimethylsilane,[3a] *p*-nitrobenzoyltrimethylsilane,[3a] benzoyltrimethylgermane,[3a] benzoylphenyldimethylgermane,[11] and benzoyltriphenylgermane[12] were prepared according to the cited literatures. DME was dried over sodium-potassium alloy.

ESR Studies of Anion Radicals of Benzoylsilanes. The ESR samples were prepared in 3-mm Pyrex sample tubes which were sealed to an 8-mm tube having a side arm and an "O" ring fitting for attaching the sample preparation tube to the vacuum line. The desired potassium metal was placed in the side arm, a very small amount of the desired benzoylsilane was placed in the sample tube, and the entire apparatus was attached to a vacuum line. The sample was degassed and DME was transferred from the reservoir while filling the sample tube to a height of about 70—100 mm. The potassium was then distilled from the side arm into the upper portion of the Pyrex sample tube, and the tube was sealed off. The samples were kept frozen in liquid nitrogen until used. To develop the radical anion of benzoylsilane, the contents of the sample tube were allowed to warm to slightly above the melting point; the tube was then inverted in order to bring the sample into contact with the mirror, at which time the sample tube was immediately inserted into the variable-temperature probe of the spectrometer, which was cooled to about −80 °C.

The authors thank Prof. Tadashi Suehiro of Gakushuin University for making Varian E-9 ESR spectrometer available for our use. We also thank Toshiba Silicone Co. Ltd. for a gift of chlorosilane.

References

1) For example; D. A. Armitage, "Comprehensive Organometallic Chemistry," ed by G. A. Wilkinson, F. G. A. Sone, and E. W. Abel, Pergamon, New York (1982), Vol. 2, pp. 71—76; P. Riviere, M. R-Baudet, and J. Satgé, "Comprehensive Organometallic Chemistry," ed by G. Wilkinson, F. G. A. Stone, and E. W. Abel, Pergamon, New York (1982), Vol. 2, p. 474.

2) For recent example; K. Yamamoto, A. Hayashi, S. Suzuki, and J. Tsuji, *Organometallics*, **6**, 974 (1987) and reference cited therein; K. Yamamoto, A. Hayashi, S. Suzuki, and J. Tsuji, *Organometallics*, **6**, 979 (1987) and reference cited therein.

3) For example; a) A. G. Brook, *Acc. Chem. Res.*, **7**, 77 (1974) and reference cited therein. b) P. R. Jones and R. West, *J. Am. Chem. Soc.*, **90**, 6978 (1968) and reference cited therein. c) H. Bock and H. Seidal, *J. Am. Chem. Soc.*, **91**, 355 (1969) and reference cited therein. d) M. Kumada, M. Ishikawa, K. Yamamoto, and K. Tamao, "Yūki Keiso Kagōbutsu no Kagaku," Kagaku Dōjin, Kyoto (1972), pp. 78—79.

4) F. Gerson, U. Krynitz, and H. Bock, *Helv. Chim. Acta*, **52**, 252 (1969).

5) P. H. Rieger and G. K. Fraenkel, *J. Chem. Phys.*, **12**, 2811 (1962).

6) A. Alberti, G. Seconi, G. R. Redulli, and A. Degl'innocenti, *J. Organomet. Chem.*, **253**, 291 (1983).

7) A. J. Stone, *Mol. Phys.*, **6**, 509 (1963); **7**, 311 (1964).

8) K. Mochida, M. Wakasa, Y. Sakaguchi, and H. Hayashi, *J. Am. Chem. Soc.*, **109**, 7942 (1987).

9) A. Okada, Dr. Dissertation of Tohoku University (1973).

10) A. G. Brook, T. J. D. Vandersar, and W. Linburg, *Can. J. Chem.*, **56**, 2758 (1978).

11) K. Mochida, S. Okui, K. Ichikawa, O. Kanakubo, T. Tsuchiya, and K. Yamamoto, *Chem. Lett.*, **1986**, 805.

12) A. G. Brook, M. A. Quigley, G. J. D. Peddle, N. V. Schwartz, and C. M. Warner, *J. Am. Chem. Soc.*, **82**, 5102 (1960).

13) A. Cecceon, C. Corvaja, G. Giacometti, and A. Venzo, *J. Chim. Phys.*, **72**, 23 (1975).

 © 1988 The Chemical Society of Japan Bull. Chem. Soc. Jpn., 61, 2937—2942 (1988)

The Effect of the Wettability of the Injection Nozzle on the Size of Oil Droplets in Water

Keizo OGINO,* Hiroshi OHKI, Masahiko ABE, Jiro HIRANO,† and Tadashi FUNADA†
Faculty of Science and Technology, Science University of Tokyo, 2641, Yamazaki, Noda, Chiba 278
†Tsukuba Research Laboratory, Nippon Oil & Fats Co., Ltd., 5-10, Tokodai, Toyosato, Ibaraki 300-26
(Received December 11, 1987)

The effect of the wettability of an injection nozzle on the size of oil droplets in water has been studied. Dodecane as an oil was dispersed into a continuous water phase through various polymers attached to the top of each single nozzle. The polymer filters used were polyethylene (PE), poly(vinyl chloride) (PVC), poly(vinyl alcohol) (PVA), cellophane (CP), and cotton (CT). The hydrophilic cotton filter is found to be more effective as the injection nozzle than any other hydrophobic polymer filter tested to disperse smaller oil droplets of dodecane into the continuous water phase. The droplet size is reduced with an increase in the hydrogen-bonding force of the polymer-filter surfaces. This may be attributed to the strong adhesion tension between the water molecules and hydrophilic groups of the polymer surface.

The technique for the dispersion of one liquid into another immiscible liquid is of importance in various fields. Droplet formation in the dispersion (from single nozzles and/or orifices) of one liquid into another immiscible liquid will assure the homogeneous size of the droplets. Many studies have been carried out;[1-7] most have been concerned with the effect of flow conditions, nozzle shapes and diameters, and the physical properties of the dispersed phase and/or continuous phase on the droplet formation. The sizes of the droplets formed are fairly large. However, few studies have been made of the influence of the chemical properties of the polymer filters attached to the nozzle top on the droplet formation.

The wettability of a polymer surface is of importance in various fields and is also of great theoretical interest. The contact angle is very useful in the evaluation of wettability. The magnitude of the contact angle is determined by the balance of forces at the boundary line between a liquid, a solid, and a second fluid, which is normally air. This balance of forces is described by Young's equation:

$$\gamma_S = \gamma_{SL} + \gamma_L \cos\theta \quad (1)$$

where γ_{SL} is the interfacial tension between a solid and a liquid and where γ_S and γ_L are the surface tension of the solid and liquid phases.

Zisman[8,9] proposed the critical surface tension (γ_C) as a unifying concept, and it was found to be useful in correlating the wettability of many polymer surfaces. Since γ_L and θ are measured easily, we should then be able to obtain γ_L from Zisman plots.[8,9] Zisman and his co-workers observed that $\cos\theta$ is usually a monotonic function γ_C for a homogeneous series of liquids. Each line extrapolates to zero θ at a certain γ_L value, which Zisman[9] called the critical surface tension γ_C; since various series extrapolated to about the same value, he proposed that γ_C was a quantity characteristic of a given solid. The critical surface tension concept has provided a useful means of summarizing wetting behavior.

In recent years, many scientists, for example Fowkes,[10] Owens,[11] Kaeleble,[12] Wu,[13] and Kitazaki,[14] have developed equations for assuming the surface tension (γ_S) of a solid. Especially, Kitazaki et al.[14] reported that the surface free energy of an organic material was divided into three components: the dispersion force (non-polar γ^d), the interaction force of polar characters (γ^p), and the hydrogen-bonding force (γ^h). The surface tension of a solid and a liquid may, therefore, be described as follows:

$$\gamma_S = \gamma_S^d + \gamma_S^p + \gamma_S^h \quad (2)$$

$$\gamma_L = \gamma_L^d + \gamma_L^p + \gamma_L^h \quad (3)$$

The interfacial tension between solid and liquid phases (γ_{SL}) may be written by:

$$\gamma_{SL} = \gamma_S + \gamma_L - 2(\gamma_S^d \gamma_L^d)^{1/2} - 2(\gamma_S^p \gamma_L^p)^{1/2} - 2(\gamma_S^h \gamma_L^h)^{1/2} \quad (4)$$

One interesting variation is obtained by combining Eqs. 1 and 4:

$$\gamma_L(1+\cos\theta) = 2(\gamma_S^d \gamma_L^d)^{1/2} + 2(\gamma_S^p \gamma_L^p)^{1/2} + 2(\gamma_S^h \gamma_L^h)^{1/2} \quad (5)$$

When the critical surface tension can not be obtained from Zisman plots, the force components of a solid can be given from the contact angle measurements with Eq. 5.

In this study, we investigate the wetting behavior of polymers in terms of the force components. We discuss the effect of the wettability of the injection nozzle on the size of oil droplets in water.

Experimental

Material. Polymers: The polymer samples used are shown in Table 1. Films of PE and PVC were washed by the methods described by Tamai et al.,[15] while those of PVA and CP were washed by the method of Matsunaga et al.[16] Textile fibers of CT were purified by Soxhlet extraction with ethanol and diethyl ether; the fibers were dried by means of a through-flow of air and shaped into a sheet under pressure.

Dispersed and Continuous Phases: Dodecane as an oil was purchased from the Tokyo Kasei Co., Ltd. It was purified by conventional distillation and was chromatographi-

Table 1. Sample Polymer

Polymer		Manufacturer	Shape	Thickness /mm	Degree of polymerization
Polyethylene	(PE)	Sumitomo Chemical Co., Ltd.	Film	0.1	3000
Poly(vinyl chloride)	(PVC)	Shin-etsu Chemical Co., Ltd.	Film	0.1	1000
Poly(vinyl alcohol)	(PVA)	Mitsubishi Monsanto Chemical Co., Ltd.	Film	0.1	1800
Cellophane	(CP)	Tokyo Cellophane Co., Ltd.	Film	0.1	400
Cotton	(CT)	The Japan Oil Chemists' Society	Textile	—	—

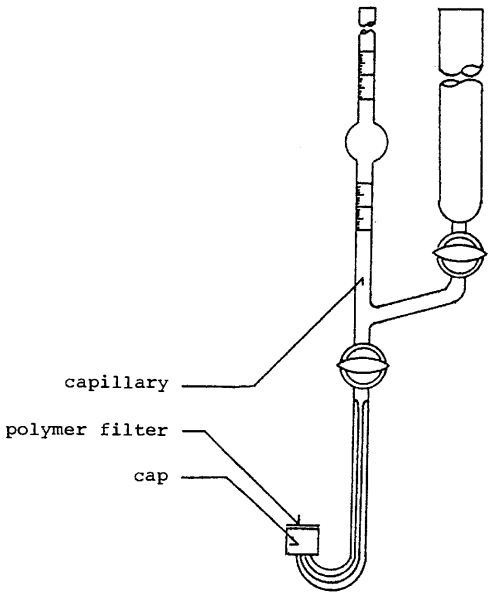

Fig. 1. Experimental instrument.

cally pure. The water employed for the continuous phase was twice-distilled water.

Standard Liquids: The series of standard liquids used here for measurements of the contact angle were chosen on the basis of the classification (three series of liquids; non-polar, polar, or hydrogen bonding liquids) proposed by Kitazaki et al.[14] The classification is as follows: **A** series (non-polar) liquids, $\gamma_L=\gamma_L^d$; **B** series(polar) liquids, $\gamma_L=\gamma_L^d+\gamma_L^p$;C series(hydrogen bonding) liquids, $\gamma_L=\gamma_L^d+\gamma_L^p+\gamma_L^h$. The standard liquids used here were obtained from the Tokyo Kasei Co., Ltd. Their purification by conventional distillation was found to be chromatographically satisfactory.

Apparatus and Procedure. Measurements of the Droplet Size: All the polymer filters were holed with glass rods of given diameters. The hole size of the polymer filters was changed by using glass rods with various diameters. The polymer filter was attached to the top of the single nozzle. The instrument, with each polymer filter, is depicted in Fig. 1. The single droplets were formed statically (velocity of the dispersed phase=0) through the polymer filter after the instrument has been immersed in water at 30 °C. Their diameters were determined from photographs.

Estimation of the Wettability of the Polymer Surface: The wettability of the polymer surface was estimated by measurements of the advancing contact angle (θ_a), using three series of liquids (**A**-series, **B**-series, and C-series liquids) as is shown in Table 2. The wettability was evaluated by means of the critical-surface tension and its components as obtained from a Zisman plot and Eq. 5. The advancing contact angles (θ_a) were measured by the sessile-drop (I) and inverted-bubble (II) methods, both shown in Fig. 2.[17] The measurements of the contact angles and the surface tension of standard liquids were performed with a Goniometer G-II (Erma Co., Ltd.) and a Wilhelmy-type Surface Tensiometer ST-1 (Shimadzu Co., Ltd.) at 30 °C.

Table 2. Surface Tension[a] of Standard Liquids

	γ_L	γ_L^d	γ_L^p	γ_L^h
A-series(non-polar) liquid				
Octane	21.0	21.0	0	0
Decane	23.2	23.2	0	0
Dodecane	25.0	25.0	0	0
Tetradecane	26.5	26.5	0	0
Hexadecane	27.4	27.4	0	0
B-series(polar) liquid				
1,1,2,2-Tetrachloroethane	34.4	31.5	2.9	0
1,1,2,3,4,4-Hexachloro-1,3-butadiene	35.5	35.3	0.2	0
Tritolyl phosphate	41.0	37.5	3.5	0
1-Bromonaphthalene	43.3	43.1	0.2	0
1,1,2,2-Tetrabromoethane	47.1	43.9	3.2	0
Diiodomethane	48.9	45.0	3.9	0
C-series(hydrogen bonding) liquid				
Diethylene glycol	44.4	31.7	0.0	12.7
Ethylene glycol	50.5	31.9	0.0	18.6
Thiodiglycol	53.3	38.7	1.4	13.2
Formamide	58.8	35.5	1.6	21.7
Glycerol	64.4	37.4	0.1	26.9
Water	71.2	27.5	1.5	42.2

a) Units in dyn cm^{-1}.

Results and Discussion

Observation of Oil-Droplet Formation. Figure 3 shows the results of the observation of oil droplets formed through a polymer filter with a constant hole size at 30 °C. As can be seen in Fig. 3, the droplets formed with a polymer filter vary considerably in size.

In general, for a stationary continuous phase, drop-

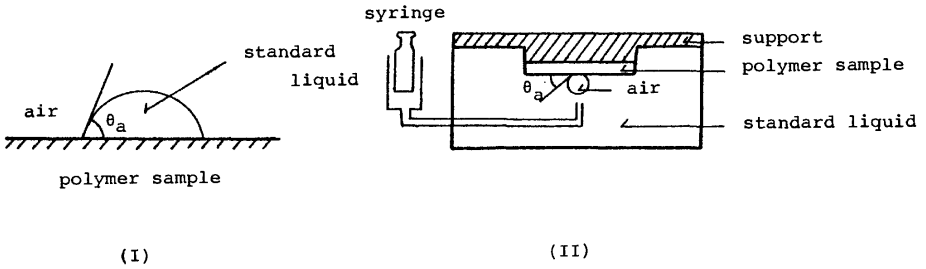

Fig. 2. Schematic diagram of an apparatus for measuring the contact angle by the sessile drop (I) and inverted bubble (II) methods.[17]

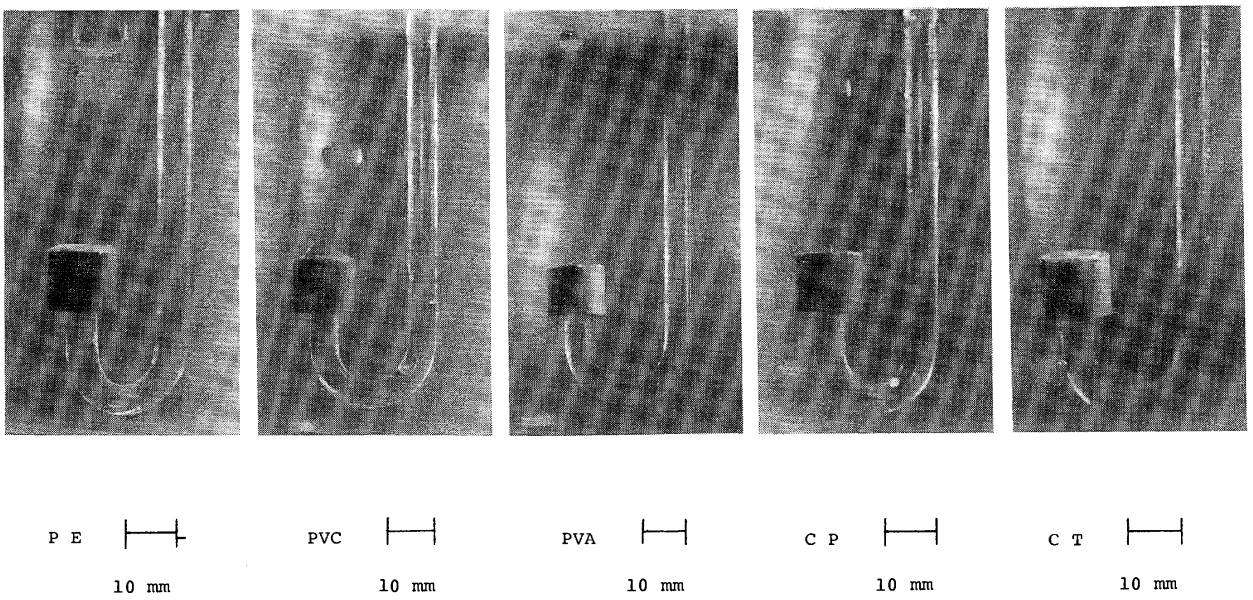

Fig. 3. Photographs of oil droplet formation.

let formation from a single nozzle is classified into several types in terms of the velocity (v) of the dispersed phase: (1) when the v is equal to zero, droplets are formed separately: (2) when the v is low, droplets are formed in a chainlike manner, and (3) when the v is high, droplets are sprayed out. If the velocity of the dispersed phase is markedly low (if, that is, the effect of the velocity is negligible), single droplets are formed "statically." Harkins and Brown[2] have reported that the droplet size is proportional to the interfacial tension between immiscible liquids, the radius of the nozzle, etc. At the same time the droplet size is inversely proportional to the local acceleration of gravity and the density difference between immiscible liquids. When the radii of nozzles with installed polymer filters are the same, droplets of the same size must be formed. It is, however, clear that the size of the oil droplets formed is greatly dependent on the chemical properties of the polymers (Fig. 3). The oil does not spread out over the filter surfaces of PVA, CP, and CT, while it does spread out over those of PE and PVC. It can, then, be postulated that the droplet size is closely related to the wettability of the polymer-filter surfaces.

The Size of Oil Droplets. Table 3 lists the size of the oil droplets obtained from a study of photographs (Fig. 3). By the replacement of one hydrogen atom of the ethylene group of polyethylene (PE) by a chlorine atom or a hydroxyl group, the size of the oil droplets formed is reduced (PE, 10.11 mm; PVC, 9.05 mm; PVA, 6.08 mm). It seems that a poor wettability of the polymer surface (the hydrophilic surface) by the oil would make the size of the droplet smaller. One should note that the size of the droplets formed through a cotton filter (1.34 mm) is the smallest, being about 1/8 of that of those formed through a PE filter.

Figure 4 exhibits the sizes of droplets against the change in the inner diameters of polymer filters (outer

Table 3. The Size of Oil Droplets[a]

		Droplet size[b] /mm
(a) Polyethylene	(PE)	10.11
(b) Poly(vinyl chloride)	(PVC)	9.05
(c) Poly(vinyl alcohol)	(PVA)	6.08
(d) Cellophane	(CP)	3.21
(e) Cotton	(CT)	1.34

a) Diameter of hole size=0.566 mm, at 30 °C.
b) Diameter of oil droplet.

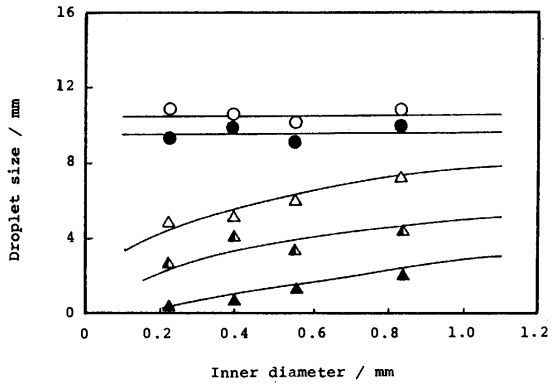

Fig. 4. The change of droplet size as a function of varying inner diameter of filter at 30 °C (outer diameter=constant). (○): PE, (●): PVC, (△): PVA, (△): CP, (▲): CT.

diameter=constant). The sizes of the oil droplets formed through PE and/or PVC filters do not change much with a decrease in the hole size of the filters. However, for the PVA, CP, and CT filters, the sizes of the oil droplets formed decrease with a decrease in the hole size of the polymers. Furthermore, for the CT filter, when a low pressure is exerted on the oil, the size of the oil droplets obtained is smaller than the hole size of the filters.

Effect of the Wettability of the Polymer Filter Surface on the Sizes of Oil Droplets. Let us now consider the effect of the surface-tension components on the sizes of the oil droplets.

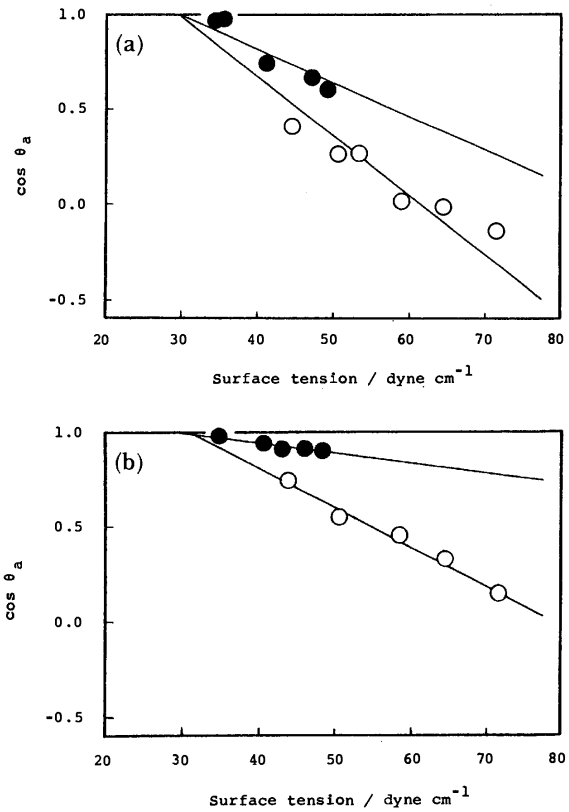

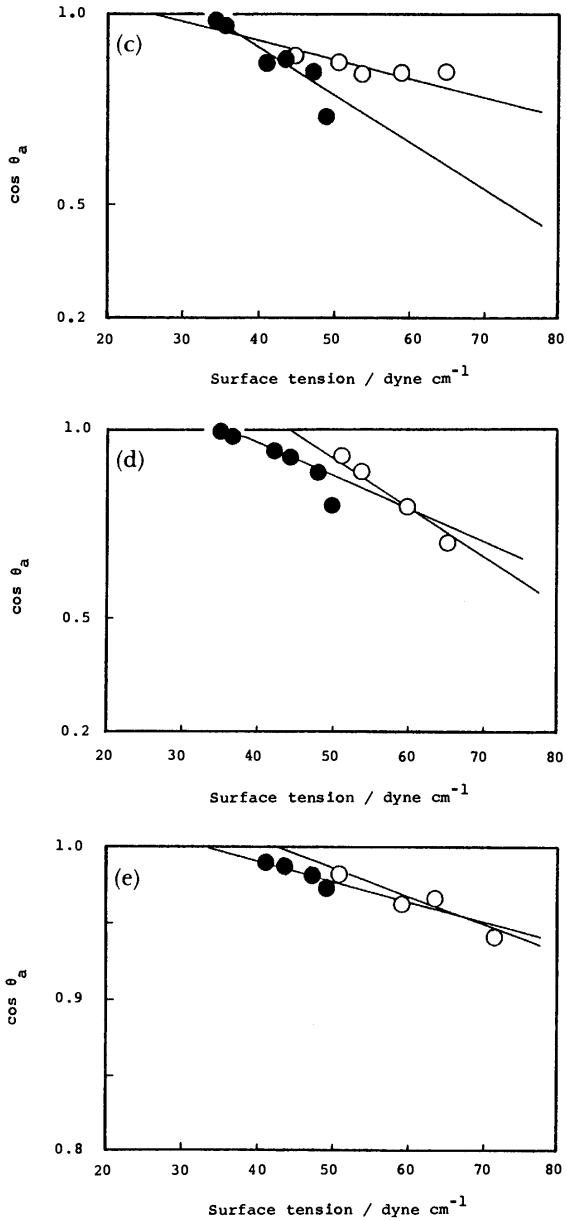

Fig. 5. Zisman plot for **B** series and C series liquids. (a) PE, (b) PVC, (c) PVA, (d) CP, (e) CT. (●): **B** series liquids, (○): C series liquids.

Figure 5(a—e) represent plots of cos θ_a versus γ_L for various series (**B** series and **C** series) on polymers. As can be seen in these figures, each cos θ_a is a monotonic function γ_L for **B**-series liquids and for **C**-series liquids. The value of γ_L, extrapolated to zero θ_a in these figures, corresponds to the γ_C obtained with **B**-series and **C**-series liquids, as has been mentioned above. The γ_S^h was obtained from the difference between the two values of γ_C. According to Kitazaki et al.,[14] the γ_S^d is the value of γ_L extrapolated to zero θ_a for **A**-series liquids, while the γ_S^p is the γ_C difference between **A**-series and **B**-series liquids. All **A**-series liquids, however, spread out over the polymer-filter surfaces used here, so the plots could not be measured. Therefore, the γ_S^d and γ_S^p were obtained from measurements of the con-

Table 4. Critical Surface Tension and Its Components for Polymer Surfaces at 30 °C

	Dispersion force		Non-dispersion force	
	γ_c	γ_s^d	γ_s^p	γ_s^h
	dyn cm^{-1}	dyn cm^{-1}	dyn cm^{-1}	dyn cm^{-1}
(a) Polyethylene (PE)	34.5	34.5	0.0	0.0
(b) Poly(vinyl chloride) (PVC)	42.8	34.4	8.1	0.3
(c) Poly(vinyl alcohol) (PVA)	41.4	34.1	0.8	6.5
(d) Cellophane (CP)	43.2	34.0	0.7	8.5
(e) Cotton[a] (CT)	52.2	42.5	0.2	9.5

a) Inverted bubble method.

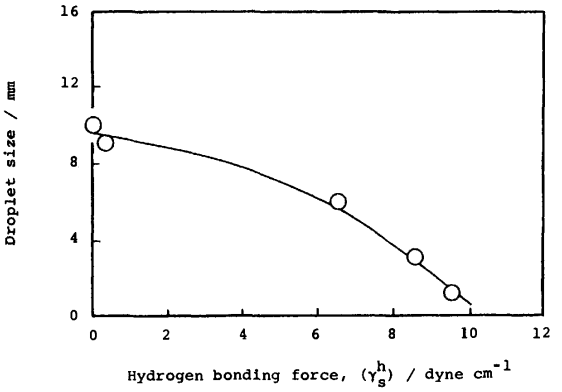

Fig. 6. Correlation between droplet size and hydrogen bonding force.

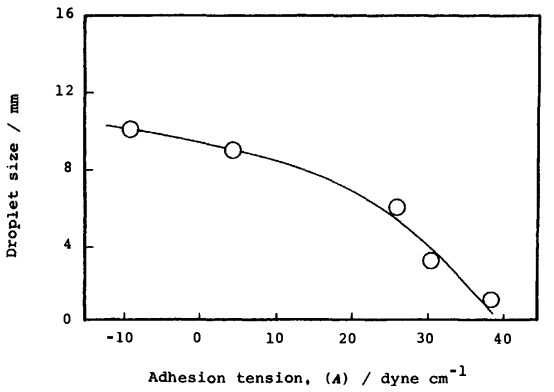

Fig. 7. Effect of adhesion tension on droplet size.

tact angles of two different liquids of the **B** series by using Eq. 5. The results of γ_s^d, γ_s^p, and γ_s^h are summarized in Table 4.

The dispersion force (γ_s^d) of the polymer surfaces, except for CT, are almost the same, while the non-dispersion forces (γ_s^p and γ_s^h) of polymer surfaces are dependent on the kind of polymer. Kitazaki et al.[19] have mentioned that γ_s^h correlates with the wettability of solids by liquids with hydrogen-bonding, like water, glycol, and formamide. The values of γ_s^h at 30 °C are plotted against the size of the oil droplets in Fig. 6. The size of the oil droplets is reduced with an increase in γ_s^h. This may indicate that the droplet size is reduced by using polymer filters, which are easily bonded to water molecules because of hydrogen bonding formation.

Interaction between Water Molecules and Polymer Surfaces. In general, the term "wetting" is taken to mean the phenomenon which occurs when a solid/air interface is replaced by a solid/liquid interface. In practice, we may distinguish three distinct types of wetting (adhesional, immersional, spreading) which are involved when a dry solid is placed into a liquid so that it is completely immersed within the liquid. Immersional wetting is the phenomenon whereby a unit area of surface is completely immersed in the liquid. In this phenomenon, a specific area of the solid/air interface is converted to a solid/liquid interface. The work involved, A, per unit area of the surface is given by:

$$A = \gamma_S - \gamma_{SL} = -\Delta G \quad (6)$$

From Eqs. 4 and 6, we obtain:

$$A = 2(\gamma_S^d \gamma_L^d)^{1/2} + 2(\gamma_S^p \gamma_L^p)^{1/2} + 2(\gamma_S^h + \gamma_L^h)^{1/2} - \gamma_L \quad (7)$$

The relationship between the adhesion tension and the size of the oil droplets obtained is shown in Fig. 7. The size of the oil droplets becomes smaller with an increase in the adhesion tension. As can be seen from Eq. 6, the adhesion tension also means a change in the surface free energy. If the free energy (negative) of a liquid/polymer interface is large, in other words, the interface is thermodynamically stable. This is reasonable if the wetting of the liquid is carried out spontaneously. Since a water/hydrophilic polymer such as a water/cotton interface is thermodynamically stabilized, a decrease in the droplet size results from the prevention of oil spreading. That is, the droplet size is dependent on the interaction between water molecules and polymer surfaces.

Formation Process of Oil Droplets. The above suggestion is illustrated by the schematic model of the formation process of oil droplets shown in Fig. 8. Figures 8(A) and (B) exhibit typical examples of a hydrophilic-surface polymer (PVA) and of a hydrophobic-surface polymer (PE). In the case of Fig. 8(B), as the γ_s^h of polymer surface and adhesion tension of polymer-water are small, the interaction between the water molecules and the polymer surface is weak (no water/polymer interface is stabilized); the oil which comes out from a hole is spread out over the surface of

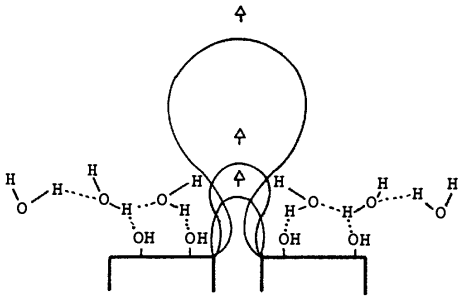

(A)

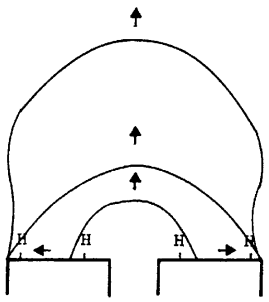

(B)

Fig. 8. Schematic model for formation process of oil droplets. (A) hydrophilic polymer (PVA, CP, CT), (B) hydrophobic polymer (PE, PVC).

the polymer filter (the arrow →), and then the droplet grows along the outer edge of the filter. Necking occurs over the surface of the polymer filters and results in the increase in the size of the oil droplets. In the case of Fig. 8(A), on the other hand, the interaction between the water molecules and the polymers is stronger because of hydrogen bonding (the water/polymer interface is stabilized by the large reduction in the surface free energy). As a result, water molecules are adsorbed strongly on the polymer surfaces. Therefore, the oil droplets which come out from a hole do not spread out over the surface of the polymer filter by the adsorption of water molecules (a droplet grows toward the arrow —▷); as a result, the necking which occurs in the vicinity of a hole brings about the decrease in the size of the oil droplets.

Conclusion

We conclude that the size of an oil droplet formed through a hole is dependent on the chemical property (wettability) of the polymer-filter surface. A cotton filter is most suitable for the formation of small-sized oil droplets. This may be attributed to the fact that the interaction between the continuous phase (water) and the hydrophilic polymer-filter surface, which has a large hydrogen-bonding force (γ_s^h), becomes strong; in other words, the adhesion tension between water molecules as a continuous phase and the polymer-filter surface becomes large.

References

1) F. Bashforth and J. C. Adams, "An Attempt to Test the Theory of Capillary Action," Univ. Press, Cambridge, England (1883).
2) W. D. Harkins and F. E. Brown, *J. Am. Chem. Soc.*, **41**, 999 (1919).
3) T. Otaka and S. Fujita, *Chem. Eng. Jpn.*, **13**, 199 (1949).
4) C. B. Harworth and R. E. Treybal, *Ind. Eng. Chem.*, **42**, 1174 (1950).
5) H. R. Null and H. F. Johnson, *AIChE J.*, **4**, 273 (1958).
6) J. F. Paddy, "Surface and Colloid Science," Wiley Interscience (1969), Vol. 1, p. 38.
7) M. Hozawa, T. Tsukada, N. Imaishi, and K. Fujinawa, *J. Chem. Eng. Jpn.*, **14**, 358 (1981).
8) W. A. Zisman, *J. Phys. Chem.*, **58**, 260 (1954).
9) W. A. Zisman, "Contact Angle, Wettability and Adhesive," Adv. Chem. Ser., 43, American Chemical Soc. (1964).
10) F. M. Fowkes, *Ind. Eng. Chem.*, **56**, 40 (1964).
11) D. K. Owens and R. C. Wendt, *J. Appl. Polym. Sci.*, **13**, 1741 (1964).
12) D. H. Kaelble and K. C. Uy, *J. Adhesion*, **2**, 50 (1970).
13) S. Wu, *J. Polym. Sci., Part C*, **34**, 19 (1971).
14) Y. Kitazaki and T. Hata, *Nippon Settyaku Kyokaishi*, **8**, 131 (1972).
15) Y. Tamai, K. Makuuchi, and M. Suzuki, *J. Phys. Chem.*, **71**, 4177 (1967).
16) T. Matsunaga and Y. Ikada, *J. Colloid Interface Sci.*, **81**, 9 (1981).
17) Y. Ikada, T. Matsunaga, and M. Suzuki, *Nippon Kagaku Kaishi*, **1985**, 1079.
18) E. R. Kaswell, "Textile Fibers, Yarns, and Fabrics," Reinhold Pub. Corp. N. Y. (1953), pp. 240—243.
19) Y. Kitazaki and T. Hata, *Nippon Settyaku Kyokaishi*, **8**, 126 (1972).

 © 1988 The Chemical Society of Japan Bull. Chem. Soc. Jpn., 61, 2943—2947 (1988)

Permeability Control of Polyelectrolyte Complex Membrane Including Chitosan Derivative as a Component

Yasuo KIKUCHI† and Naoji KUBOTA*,††
Department of Environmental Chemistry and Engineering, Faculty of Engineering,
Oita University, Dannoharu, Oita 870-11
(Received February 4, 1988)

The properties of polyelectrolyte complexes (PEC) and PEC membranes were investigated in the systems of glycol chitosan (GC)-poly(vinyl sulfate) (PVSK) and methyl glycol chitosan (MGC)-(carboxymethyl)dextran (CMD). The degree of dissociation and the conformation of GC and CMD depend upon pH, because GC and CMD are weak polybase and weak polyacid, respectively. On the basis of this knowledge, a research into the pH dependence of dissociation and viscosity of GC and CMD was carried out. PEC including chitosan derivative as a constituent was synthesized at the adequate pH, pH 3.0 in the GC-PVSK system and pH 7.0 in the MGC-CMD system. PEC membranes were prepared, and the permeability of KCl, urea, and sucrose through the GC-PVSK membrane was determined under various pH. It was revealed that the permeability of KCl, urea, and sucrose varies with the solution pH. The permeability in the neutral region was 2—10 times as high as that in acidic region. The increase of permeability in neutral region was considered from IR spectra of membranes to be due to swelling caused by a conformational change.

Polyelectrolyte complexes (PEC) are expected to find a great many applications because of diversity of their structures and properties.[1-3] In particular, membrane application was widely developed, and there have been many studies on the permeability of ions and low-molecular-weight solutes through PEC membranes.[1-5] The investigation on PEC membrane, however, is confined mostly to synthetic polymers, and only a few works on PEC membranes made up of polysaccharide are available.[6,7]

On the other hand, a large amount of chitin is biosynthesized every year and chitin and chitosan derivatives have aroused great interest in recent years.[8] Many-sided applications of them have been proposed as to occupy a field of functional materials. We have already reported about the transport of alkali metal ions through PEC membranes which consist of chitosan derivatives and/or dextran derivatives, methyl glycol chitosan (MGC)-glycol chitosan (GC)-poly(vinyl sulfate) (PVSK),[9] MGC-(carboxymethyl)dextran (CMD)-PVSK,[10] and [2-(diethylamino)ethyl]-dextran (EA)-CMD-PVSK[11] systems.

The present article describes the characterization of GC and CMD and the preparation of PEC and PEC membranes in the GC-PVSK and MGC-CMD systems. Further, the permeability of KCl, urea, and sucrose was determined under various pH conditions in the GC-PVSK membrane, and it is exhibited that the permeation is controlled by pH change. This investigation will support the drug delivery system, the release control capsule, and so on.

† Present address: Department of Industrial Chemistry, Faculty of Engineering, Nippon Bunri University, Ichigi, Oita 870-03.

†† Present address: Marine Science Laboratory, Faculty of Engineering, Oita University, Dannoharu, Oita 870-11.

Experimental

GC (D.P. 400; nitrogen content 5.51 wt%), PVSK (D.P. 1500; sulfur content 18.91 wt%), and MGC (D.P. 400; nitrogen content 3.33 wt%) were of reagent grade for the colloidal titration supplied by Wako Pure Chemical Industry, Ltd. CMD (mol wt 3×10^7; sodium content 7.38 wt%) was provided by Meito Sangyo Co., Ltd. Deionized water (0.3 $\mu S\,cm^{-1}$) which was degassed with boiling was used for all reagents.

Deionization of GC and CMD solution (0.02 base mol dm^{-3}) was performed by use of a mixture of cation and anion exchangers. After adding NaCl up to 0.1 mol dm^{-3}, 50 cm^3 of GC solution was neutralized by HCl, followed by the back titration with 0.5 mol dm^{-3} NaOH at 25 °C in nitrogen atmosphere. In the case of CMD, 50 cm^3 of CMD solution was directly titrated with 0.5 mol dm^{-3} NaOH after addition of NaCl. In order to estimate the degree of dissociation, hydrogen ion concentration was corrected by back titration of polyelectrolyte-free blank solution.[12] All titrations were carried out with a Hiranuma UCB-7 autoburet and a Horiba M-8 pH meter.

Intrinsic viscosity of GC, PVSK, MGC, and CMD was measured with an Ostwald viscometer in the presence of 1 mol dm^{-3} NaCl in a water bath controlled at 25±0.02 °C.

The preparation of PEC was achieved as described in the previous paper.[9] By the results of potentiometric titrations, GC solution was added dropwise to 100 cm^3 of PVSK solution at pH 3.0, and CMD solution was added dropwise to 100 cm^3 of MGC solution at pH 7.0. In the GC-PVSK system, the resulting precipitate of PEC was dried at 30 °C on a Petri dish. In the MGC-CMD system, the precipitate was interposed between silicone rubbers (50×50×0.5 mm), pressed with PMMA plates (50×50×5 mm) and dried at 30 °C. Thus the PEC membranes about 75 μm in thickness were obtained. The membranes were washed with methanol to remove micro ions prior to the permeation experiment. The measurement of permeability of KCl, urea, and sucrose was carried out with a diaphragm type cell which has 4.0 cm^2 of effective area. In the left-hand chamber of the cell 25 cm^3 of pH 3.0 solution was introduced, and 25 cm^3 of 0.05 mol dm^{-3} KCl, 0.01 mol dm^{-3} urea, or 0.02 mol dm^{-3} sucrose in the

right-hand chamber, of which pH value was adjusted as the same as that of the left-hand chamber. Similarly the measurement of permeability was performed under proper pH from 3.5 to 7.0. Each pH was adjusted by the citrate or 2-amino-2-hydroxymethyl-1,3-propanediol buffer solution. The cell was then placed in a thermostat controlled at 30 °C, and 0.1 cm^3 of samples were withdrawn from both sides of the membrane every 2 h. KCl was determined by measuring K^+ ion with a Shimadzu AA-640 atomic absorption spectrophotometer. Urea and sucrose were determined with a Hitachi 100-10 spectrophotometer by the biacetyl monoxime method and the phenol–sulfuric acid method, respectively. IR spectra of GC-PVSK membranes previously immersed for 4 h in the pH 3.0, 4.0, 5.0, 6.0, and 7.0 solutions were taken with a Hitachi 270-50 IR spectrophotometer.

Results and Discussion

The applications of chitin and chitosan derivatives have been energetically investigated recently, because they have been produced in a comparable amount to cellulose and have the specific structure of amino polysaccharide. GC is also a chitosan derivative which is hydroxyethylated at the 6-position. Water-insoluble chitosan results in a water-soluble chitosan derivative by this etherification to make GC a very useful reagent for the colloidal titration.[13] However, the degree of dissociation (protonation) varies with pH of the solution, because GC has a primary amino group at the 2-position.[14] The pH dependence of the degree of dissociation, α, of glycol chitosan hydrochloride (GCH) was examined by the potentiometric titration, and is shown in Fig. 1. Free primary amino group was dominant in the pH region above 6.63, and primary ammonium ion was dominant in the region below 6.63. Therefore, pH has to be kept below pH 6.63 in order to prepare the ion-bonded PEC which includes GC as a component.[15] Figure 1 also indicates the pH dependence of the degree of dissociation of CMD by the potentiometric titration. Free carboxyl group was preferential in the pH region below 3.64, and the carboxylate ion was preferential in the region above 3.64. Consequently, pH has to be kept above pH 3.64 for the purpose of preparing the ion-bonded PEC which contains CMD as a component.

Furthermore, $pK=pH-\log\{\alpha/(1-\alpha)\}$ vs. α plots are shown in Fig. 2. It is exhibited that intrinsic and apparent pK of GCH in 0.1 mol dm^{-3} NaCl solution are 6.35 and 6.63, respectively. It was already known that a break is observed in the pK-α curve when the conformational change of macromolecular chain occurs like a helix↔coil transition of poly(L-glutamic acid).[16] No conformational change seems to occur in the main chain of GC, as pK-α curve is linear. We could not observe the conformational change in GC by the potentiometric titration, while Rha et al. have reported that the conformational change occurs in chitosan by the measurement of intrinsic viscosity.[17] They have obtained the result that as the pH of solution was increased, the intrinsic viscosity or the hydrodynamic volume of chitosan was decreased. Our measurement of the intrinsic viscosity, $[\eta]$, of GC showed that the intrinsic viscosity at high pH is larger than that at low pH, on the contrary. These results are shown in Fig. 3. This effect seems to be due to the 2-hydroxyethyl group, but it is indefinite in detail. Further investigation should be performed on this point. Figure 2 also gives the pK-α plots of CMD. It is exhibited that intrinsic and apparent pK of

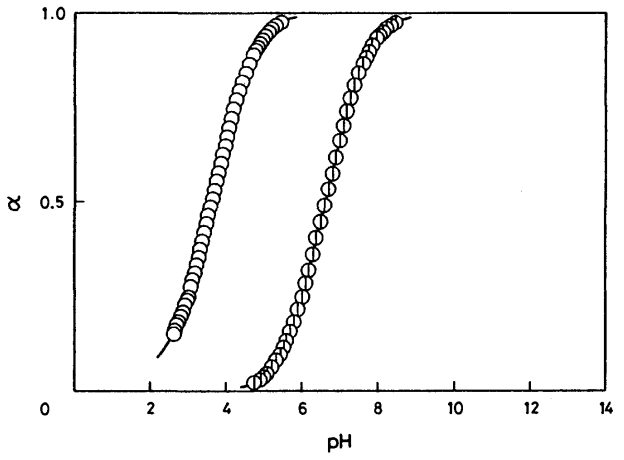

Fig. 1. pH dependence of the degree of dissociation of glycol chitosan hydrochloride and (carboxymethyl)dextran in the presence of 0.1 mol dm^{-3} NaCl at 25 °C. Polymer concentrations are 0.02 base mol dm^{-3}. ⊕: Glycol chitosan hydrochloride, ○: (carboxymethyl)dextran.

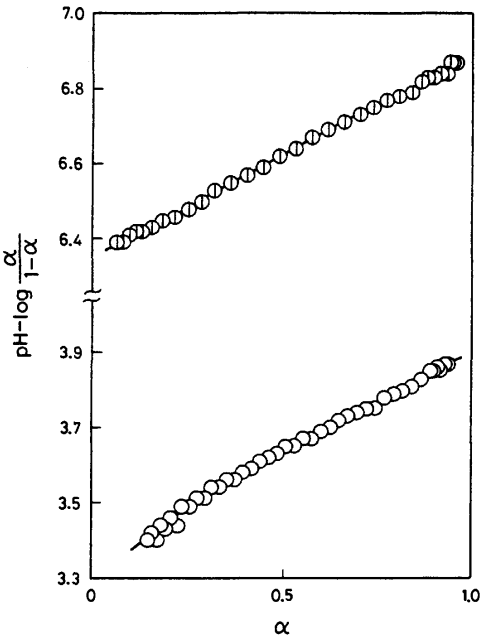

Fig. 2. pK vs. α plots of glycol chitosan hydrochloride and (carboxymethyl)dextran in the presence of 0.1 mol dm^{-3} NaCl at 25 °C. Polymer concentrations are 0.02 base mol dm^{-3}. ⊕: Glycol chitosan hydrochloride, ○: (carboxymethyl)dextran.

CMD in 0.1 mol dm^{-3} NaCl solution are 3.2 and 3.64, respectively. It appears that there is no conformational change in main chain of CMD similarly to GC, for the pK-α curve is continuous. These results of potentiometric titration of CMD were consistent with Gekko's results.[18] The pH dependence of [η] of CMD is shown in Fig. 3. The [η] of CMD changed at about pH 3, and this pH value was same as the inflection point in the α-pH curve in Fig. 1 which indicates the conditions of dissociation of CMD. The [η] of CMD is supposed to increase on account of a more bulky conformation caused by the inter- and intramolecular electrostatic repulsions between dissociable groups, -OCH_2COOH, in the pH region above 3.64.

In addition, Fig. 3 shows the relationship between [η] and pH of MGC and PVSK dealt in this paper, which are strong polybase and strong polyacid, respectively. Linear curves were obtained with respect to the [η]-pH plots of MGC and PVSK. It is apparent that [η] of these two polyelectrolytes is not influenced by pH, because the degree of dissociation of strong polyelectrolytes is constant over wide range of pH.

On the above conclusion, PEC was prepared. In the system of GC-PVSK, i.e., weak polybase-strong polyacid system, GC solution was added dropwise to PVSK solution at pH 3.0. In the system of MGC-CMD, i.e., strong polybase-weak polyacid system, CMD solution was added dropwise to MGC solution at pH 7.0. These synthetic conditions are summarized in Table 1 with the properties of membranes. It was thought that PEC has a ladder-like structure of ionic bond between ammonio groups in GC or MGC and -OSO_3^- group in PVSK or -OCH_2COO^- group in CMD, respectively. Further, inter- and intramolecular hydrogen bond seems to take place, because polysaccharides which are constituents of these PEC have many hydroxyl groups.

Transparent PEC membranes of 75 μm in thickness were obtained from both of the PEC. GC-PVSK membrane was very sturdy and similar to a cellophan membrane. MGC-CMD membrane was moisture-sensitive and extremely swollen in water. It has been reported that once PEC is prepared containing at least one strong polyelectrolyte component, ionic bond of PEC is maintained throughout wide pH range.[19] This concept, however, was not suitable for the MGC-CMD membrane. On the other hand, GC-PVSK membrane was stable over wide range of pH, and the stability of GC-PVSK seems to be due not only to the above reason but also to packing of GC. This fact manifests that PEC consisting of GC and PVSK is

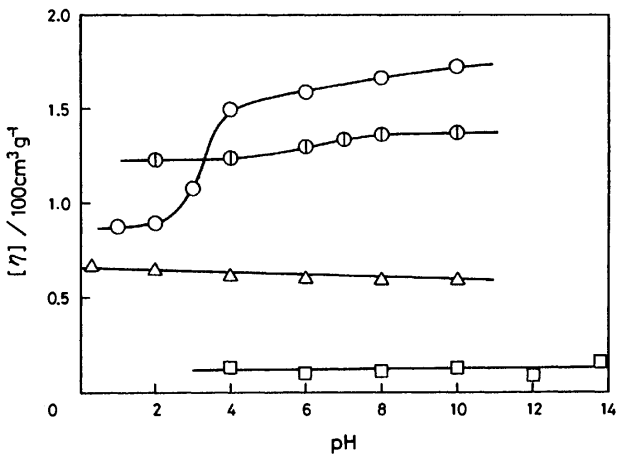

Fig. 3. pH dependence of the intrinsic viscosity of polyelectrolytes in the presence of 1 mol dm^{-3} NaCl at 25°C. ⦶: Glycol chitosan, △: poly(vinyl sulfate), □: methyl glycol chitosan, ○: (carboxymethyl)-dextran.

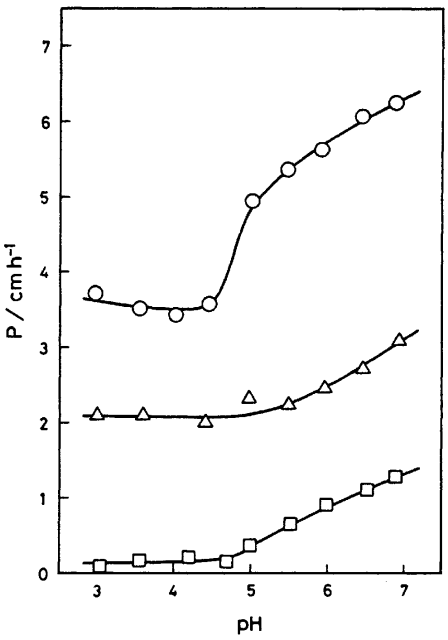

Fig. 4. Effect of pH on the permeability of solutes through polyelectrolyte complex membrane consisting of glycol chitosan and poly(vinyl sulfate) at 30°C. ○: 0.05 mol dm^{-3} KCl, △: 0.01 mol dm^{-3} urea, □: 0.02 mol dm^{-3} sucrose.

Table 1. Synthetic Conditions for Polyelectrolyte Complexes and Stability of Membranes in Water

Sample	Polycation	Polyanion	pH	Volume of polycation /cm^3	Volume of polyanion /cm^3	Molar ratio of cation site to anion site in the reaction mixture	Membrane
1	GC	PVSK	3.0	150	100	1.00	Stable
2	MGC	CMD	7.0	100	74	1.00	Swollen

Concentrations of polyelectrolytes were 2.0 g dm^{-3} each. Arrows represent the titration order.

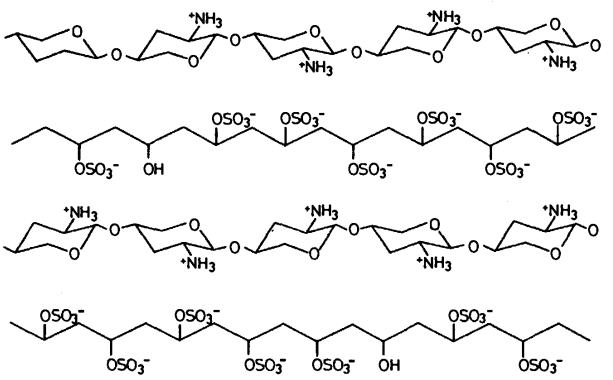

Fig. 5. Schematic model of polyelectrolyte complex in the system of glycol chitosan-poly(vinyl sulfate).

favorable for a membrane material.

Thus the permeability of KCl, urea, and sucrose through this membrane was investigated, and the results are shown in Fig. 4. Permeability, P, was evaluated by the following equation, which derived from the Fick's law of diffusion:[3]

$$Pt = -\frac{V}{2A} \ln \frac{\Delta C}{C_0},$$

where t is the time, V is the volume of each chamber of the cell, A is the area of membrane, C_0 is the initial concentration of solutes in the right-hand chamber, and ΔC is the difference of concentrations in the right- and left-hand chambers. Figure 4 shows that the permeability of KCl, urea, and sucrose depends on the molecular weight and pH. Each permeability decreased proportionally to the molecular weight in the order of KCl>urea>sucrose. GC-PVSK membrane has a cation-exchange ability, because GC is a rigid molecule and the density of cation site of GC is lower than that of anion site of PVSK, as described previously.[15] Schematic model of PEC consisting of GC and PVSK is represented in Fig. 5. Therefore, the electric potential on the left-hand chamber must be higher than that on the right-hand chamber when salt such as KCl was permeated. The electric potential difference between both sides of the membrane was actually 7—8 mV at pH 3.0 after 10 h. Furthermore, permeability increased at about pH 5 where the degree of dissociation and intrinsic viscosity change as shown in Figs. 1 and 3. IR spectra of the GC-PVSK membranes treated for 4 h with the buffer solutions of pH 3.0, 4.0, 5.0, 6.0, and 7.0 are shown in Fig. 6. The absorption band at 1530 cm^{-1} assigned to primary ammonium ion was present in all membranes, whereas 1600 cm^{-1} assigned to primary amino group of GC was absent. That is to say, the dissociation of GC in the membrane was not observed at pH from 3.0 to 7.0. It is clear that breaking of ionic bonds is not responsible for the increase in permeability. Considering that GC has a conformation swelling

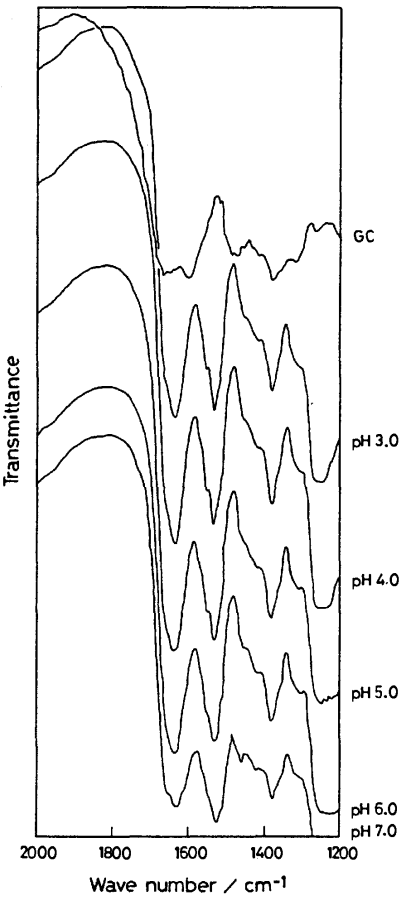

Fig. 6. IR spectra of glycol chitosan and treated polyelectrolyte complex membranes consisting of glycol chitosan and poly(vinyl sulfate).

as pH increases and PVSK has a flexible polymer chain, it is thought that GC-PVSK membrane becomes rather swollen to form a bulky conformation, and hence the permeability increases. Rha et al. have prepared micro capsule whose diffusion rate for γ-globulin and BSA was decreased by decrease in pH, where chitosan was gelified with alginate.[17] PEC membrane in the system of GC-PVSK has controllable permeability for KCl, urea, and sucrose to some extent, even though PEC is previously prepared at a constant pH value.

These investigations suggest a possibility of permeation control of PEC membrane consisting of GC, which is a amino polysaccharide, and PVSK, which has a flexible polymer chain, because it is possible to control the permeability by pH which controls the conformation and packing of PEC.

References

1) H. J. Bixler and A. S. Michaels, *Encycl. Polym. Sci. Technol.*, **10**, 765 (1969).
2) A. Nakajima, *Kagaku To Kogyo*, **27**, 750 (1974).
3) E. Tsuchida and K. Abe, *Adv. Polym. Sci.*, **45**, 18 (1982).
4) S. M. Ryu and I. F. Miller, *J. Biomed. Mater. Res.*, **5**, 287 (1971).

5) V. F. Smolen and D. E. Hahman, *J. Colloid Interface Sci.*, **42**, 70 (1973).
6) A. Nakajima and K. Shinoda, *J. Appl. Polym. Sci.*, **21**, 1249 (1977).
7) C. M. Berke, U. S. Patent 4501835 (1985); *Chem. Abstr.*, **102**, 168601v (1985).
8) K. Kurita, *Yuki Gosei Kagaku Kyokai Shi*, **42**, 567 (1984).
9) Y. Kikuchi, N. Kubota, and H. Mitsuishi, *J. Appl. Polym. Sci.*, **35**, 259 (1988).
10) Y. Kikuchi and N. Kubota, *Nippon Kagaku Kaishi*, **1986**, 1229.
11) Y. Kikuchi and N. Kubota, *Nippon Kagaku Kaishi*, **1985**, 111.
12) S. Sugai and K. Nitta, "Kobunshi-denkaishitsu," ed by Kobunshi Gakkai, Kyoritsu Shuppan, Tokyo (1978), Chap. 3.
13) R. Senju, *Bull. Chem. Soc. Jpn.*, **26**, 148 (1953).
14) E. Kokufuta, M. Hirata, and S. Iwai, *Shikizai Kyokaishi*, **48**, 493 (1975).
15) Y. Kikuchi and N. Kubota, *Bull. Chem. Soc. Jpn.*, **60**, 375 (1987).
16) M. Nagasawa and A. Holtzer, *J. Am. Chem. Soc.*, **86**, 538 (1964).
17) C. Hwang, C. K. Rha, and A. J. Sinskey, "Chitin in Nature and Technology," ed by R. A. A. Muzzarelli, C. Jeuniaux, and G. W. Gooday, Plenum Press, New York (1986), pp. 389—396.
18) K. Gekko, *ACS Symposium Ser.*, **150**, 415 (1981).
19) H. Sato, M. Maeda, and A. Nakajima, *J. Appl. Polym. Sci.*, **23**, 1759 (1979).

 © 1988 The Chemical Society of Japan Bull. Chem. Soc. Jpn., 61, 2949—2953 (1988)

Partial Oxidation of Isobutene to Methacrylic Acid on V_2O_5-P_2O_5 Catalysts

Mamoru Ai
Research Laboratory of Resources Utilization, Tokyo Institute of Technology,
4259 Nagatsuta, Midori-ku, Yokohama 227
(Received February 13, 1988)

The vapor-phase air oxidation of isobutene was studied with V_2O_5, V_2O_5-TiO_2, V_2O_5-MoO_3, V_2O_5-P_2O_5, V_2O_5-P_2O_5-TeO_2, and heteropoly compound catalysts, such as $H_3PMo_{12}O_{40}$, $Cs_2HPMo_{12}O_{40}$, $H_5PMo_{10}V_2O_{40}$, and $Cs_{2.5}H_{2.5}PMo_{10}V_2O_{40}$, in the presence of water vapor. On pure V_2O_5, the oxidation products were acetic acid and carbon oxides, plus small amounts of acetone and methacrylaldehyde. With the addition of TiO_2 to V_2O_5, the selectivity to acetic acid increased a little, but the formation of methacrylaldehyde disappeared. The addition of MoO_3 to V_2O_5 enhanced the formations of acetone and methacrylaldehyde, to a certain extent, but methacrylic acid was not obtained. With the V_2O_5-P_2O_5 catalysts, the yield of methacrylic acid attained 21 mol%, the sum of the yields of methacrylaldehyde and methacrylic acid attained 30 mol%, and the yield of acetic acid attained also 30 mol%. The P/V atomic ratio=1.6 catalyst was better than the P/V=1.06 catalyst in the formation of methacrylic acid. Further, the performance of the P/V=1.6 catalyst was better than that of the heteropoly compound catalysts. The results were discussed in the light of the acid-base properties of the catalysts.

Methacrylic acid is an important chemical as a raw material of so-called organic glass. It is currently produced by a two-step partial oxidation of isobutene. The first step, oxidation of isobutene to methacrylaldehyde, is performed with multicomponent oxide catalysts which are similar to those used in the oxidation of propylene to acrylaldehyde. A number of studies have been made of this reaction, as summarized in several review articles.[1-4] The second step, oxidation of methacrylaldehyde to methacrylic acid, is performed mostly with heteropoly compound catalysts based on molybdovanadophosphoric acid, $H_{3+x}PMo_{12-x}V_xO_{40}$ (x=1—2), and its salts. Besides the patent information,[2-4] several scientific works have been done on this reaction.[5-10] It is recognized that the effective catalytic performance of heteropoly compounds is ascribed to their eminent acidic property as well as their redox property. However, it is also known that these compounds are decomposed at around 400 °C and lose their catalytic activity.

On the other hand, the V_2O_5-P_2O_5 (P/V=1.0 to 1.2) system is a unique catalyst possessing a surprisingly high selectivity in the oxidation of butane to maleic anhydride and, moreover, it is stable enough at around 400 °C. Recently, it was found that the V_2O_5-P_2O_5 system possesses an enhanced acidic property.[11,12]

In view of the acid-base property of the reactant and product, the enhanced-acid catalyst is expected to be effective for "acid-formation-type" partial oxidations.[13-16] Indeed, the V_2O_5-P_2O_5 catalysts are found to be effective for the oxidation of acrylaldehyde to acrylic acid[17] and that of isobutyric acid to methacrylic acid.[18] Further, it was recently found that propylene is oxidized directly to acrylic acid.[19]

From these findings, we can predict that the V_2O_5-P_2O_5 catalysts are effective for the oxidation of isobutene to methacrylic acid, also. Therefore, in this study, we focused our attention on the oxidation of isobutene to form methacrylic acid, since no detailed information about this reaction has yet been reported.

Experimental

Oxidation Procedures. The reaction was carried out with a continuous-flow system using tertiary butyl alcohol (TBA) as the starting material for isobutene. It was confirmed that almost all of the TBA is converted promptly into isobutene and water over every catalyst tested. The reactor and the experimental procedures were the same as those employed in the previous works.[17-19] Air was fed in from the top of the reactor with a fixed rate of 400 ml (at 20 °C)/min and a mixture of TBA and water with a TBA/H_2O volumetric ratio of 1/4 was introduced into the preheating section of the reactor by means of a micro liquid-feeder. The feed rate was TBA/H_2O/Air=0.014/0.22/1.00 mol h^{-1} and the amount of catalyst used was 10 to 30 g.

The yield (mol%) is defined as (except for carbon oxides); 100·(moles of product)/(moles of TBA fed in). On the assumption that the formation of carbon oxides is accompanied with those of acetone and acetic acid; that is, C_4H_8 →acetone+CO_x and C_4H_8→acetic acid+2 CO_x, the yield of carbon oxides is calculated as follows; 100·([moles of CO_x]−[moles of acetone] −2[moles of acetic acid])/4 (moles of TBA fed in).

Catalysts. The catalysts used in this study were the same as those used in the previous works.[15-19]

Results

Performance of the V_2O_5 Catalyst. The oxidation of isobutene was conducted with a 10 g-portion of pure V_2O_5 catalyst under the conditions described in the Experimental section. The products were acetic acid and carbon oxides, plus small amounts of acetone and methacrylaldehyde. The methacrylic acid was not detected. The change in the yields of the partial oxidation products with the elevation of the reaction temperature is shown in Fig. 1.

Performance of the V_2O_5-TiO_2 Catalyst. The

results obtained with a 10 g-portion of the V_2O_5-TiO_2 (Ti/V atomic ratio=6/4) catalyst are shown in Fig. 2. This catalyst was a little more active than the pure V_2O_5 catalyst. The yield of acetone attained 12 mol% at the isobutene conversion of 50 to 70% and selectivity to acetic acid also increased. However, the formation of methacrylaldehyde was not observed.

Performance of the V_2O_5-MoO_3 Catalysts. Figure 3 shows the results obtained with a 10 g-portion of the V_2O_5-MoO_3 (Mo/V=2/8) catalyst. This catalyst was much less active than the pure V_2O_5 catalyst for the consumption of isobutene. A small amount of methacrylaldehyde was obtained, but methacrylic acid was not obtained. The main partial oxidation product was acetic acid. Figure 4 shows the results obtained with a 10 g-portion of the Mo/V=8/2 catalyst. The perfor-

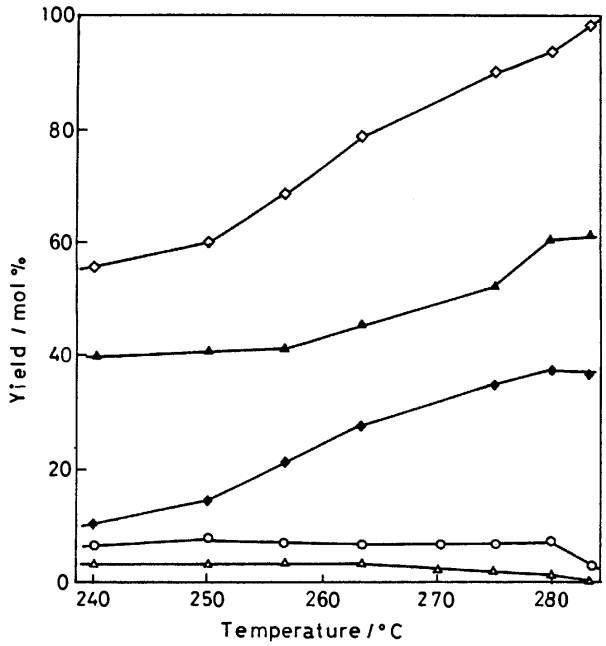

Fig. 1. Oxidation of isobutene with the pure V_2O_5 catalyst. (◇)=isobutene conversion. Yield: (●)=methacrylic acid, (○)=methacrylaldehyde, (▲)=acetic acid, (△)=acetone, (◆)=carbon oxides.

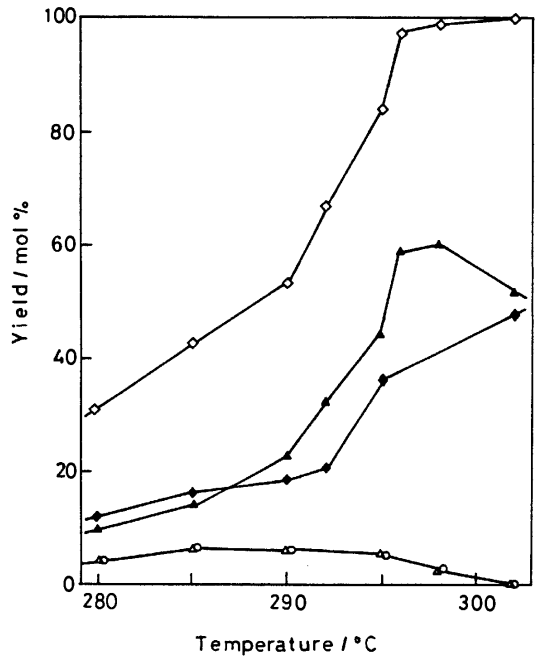

Fig. 3. Oxidation of isobutene with the V_2O_5-MoO_3 (Mo/V=2/8) catalyst. Symbols as in Fig. 1.

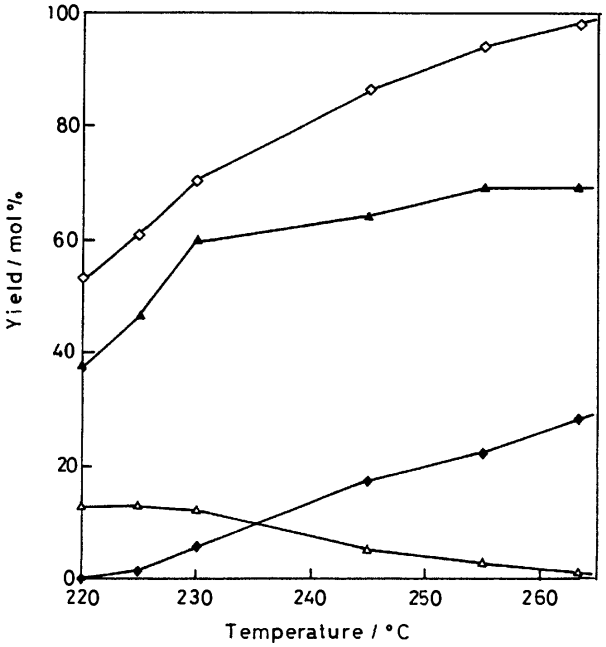

Fig. 2. Oxidation of isobutene with the V_2O_5-TiO_2 (Ti/V=6/4) catalyst. Symbols as in Fig. 1.

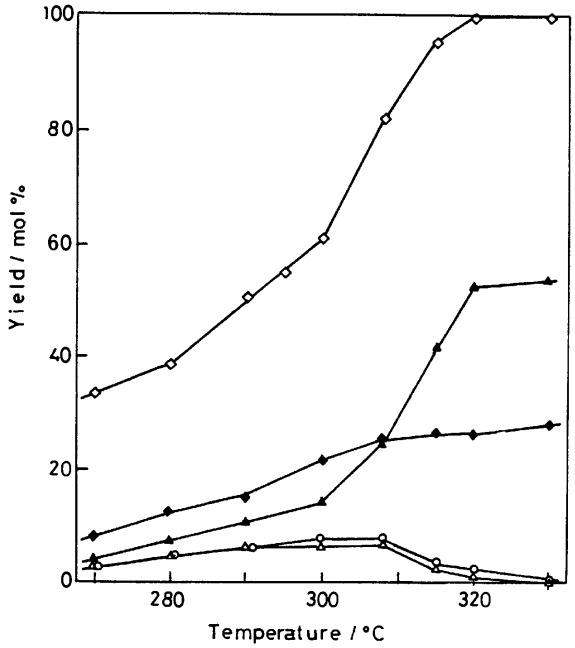

Fig. 4. Oxidation of isobutene with the V_2O_5-MoO_3 (Mo/V=8/2) catalyst. Symbols as in Fig. 1.

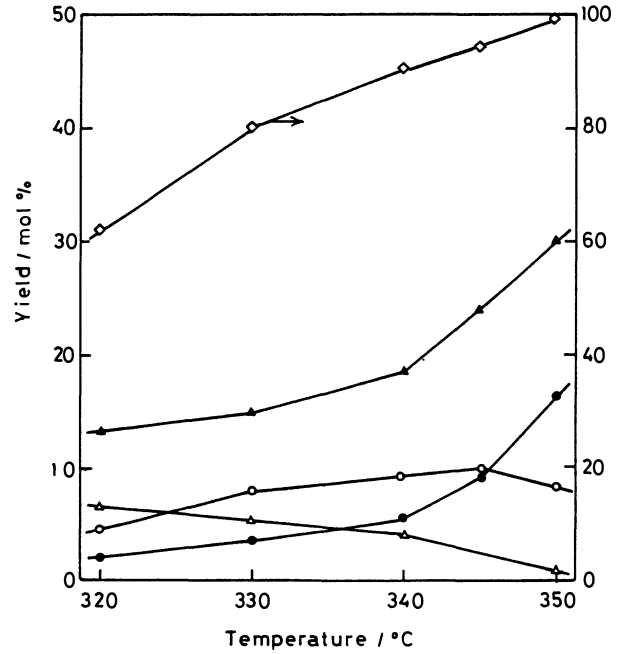

Fig. 5. Oxidation of isobutene with the V_2O_5-P_2O_5 (P/V=1.06) catalyst. Symbols as in Fig. 1.

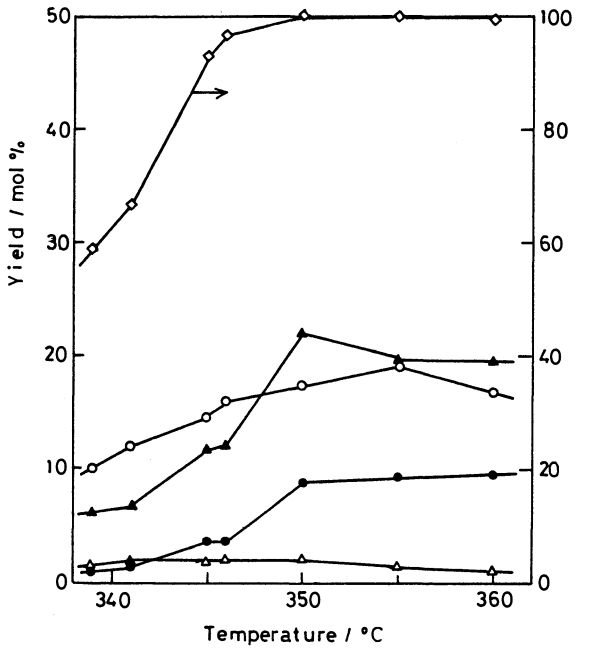

Fig. 7. Oxidation of isobutene with the $H_3PMo_{12}O_{40}$ catalyst. Symbols as in Fig. 1.

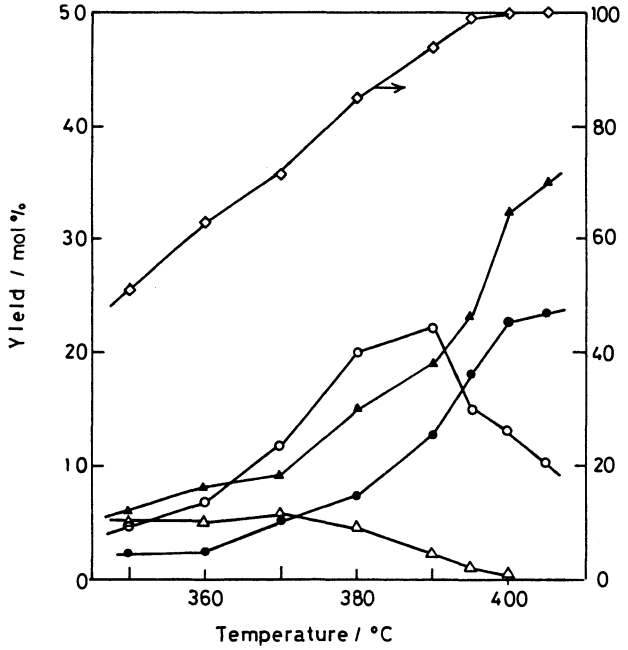

Fig. 6. Oxidation of isobutene with the V_2O_5-P_2O_5 (P/V=1.6) catalyst. Symbols as in Fig. 1.

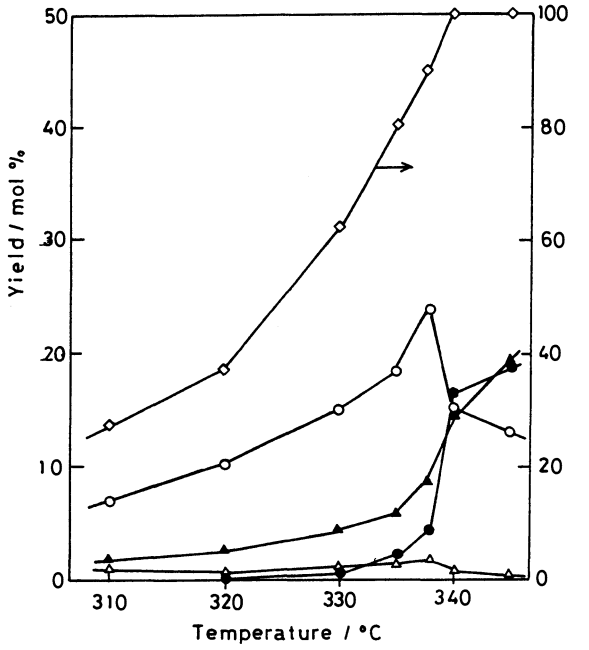

Fig. 8. Oxidation of isobutene with the $Cs_2HPMo_{12}O_{40}$ catalyst. Symbols as in Fig. 1.

mance of this catalyst was similar to that of the Mo/V=2/8 catalyst.

Performance of the V_2O_5-P_2O_5 Catalysts. Figure 5 shows the results obtained with a 20 g-portion of the V_2O_5-P_2O_5 (P/V=1.06) catalyst. The formation of methacrylic acid attained 15 mol% and that of methacrylaldehyde was much greater than in the reaction with the pure V_2O_5 catalyst.

Figure 6 shows the results obtained with a 20 g-portion of the V_2O_5-P_2O_5 (P/V=1.6) catalyst. This catalyst was markedly less active than the P/V=1.06 catalyst. However, the yields of methacrylic acid and methacrylaldehyde were greater. The yield of methacrylic acid attained 21 mol%, the sum of the yields of methacrylic acid and methacrylaldehyde attained about 30 mol%, and the yield of acetic acid attained also about 30 mol%.

Since it has been reported[19] that the V_2O_5-P_2O_5-

TeO_2 ternary system performs better than the V_2O_5-P_2O_5 binary system in the oxidation of propylene to acrylic acid, the Te/P/V=0.15/1.2/1 catalyst was tested in the oxidation of isobutene. It was found that the catalytic performance is not improved by the addition of TeO_2 to the V_2O_5-P_2O_5 system.

Performance of the Heteropoly Compound Catalysts. Since heteropoly compounds are known to be effective as catalysts for the oxidation of methacrylaldehyde to methacrylic acid, the performance of these catalysts was examined. The results obtained with a 30g-portion of $H_3PMo_{12}O_{40}$ and $Cs_2HPMo_{12}O_{40}$ catalysts are shown in Figs. 7 and 8, respectively. The sum of the yields of methacrylic acid and methacrylaldehyde attained about 30 mol% as in the reaction with the P/V=1.6 catalyst (Fig. 5), but the formation of acetic acid was lower.

The performance of the $H_5PMo_{10}V_2O_{40}$ and $Cs_{2.5}H_{2.5}PMo_{10}V_2O_{40}$ was also tested. It was found that the performances of these catalysts were comparable to that of the P/V=1.6 catalyst.

It should also be noted that the activity of these heteropoly compounds decreases gradually with the duration of the reaction time at temperatures above 350 °C.

Discussion

The character of the curves of methacrylic acid and methacrylaldehyde shown in Figs. 5 and 8 reveals that methacrylaldehyde is an intermediate in the oxidation of isobutene to methacrylic acid. Similarly, the shape of the curves of acetic acid and acetone shown in Figs. 1 to 8 also reveals that acetone is an intermediate in the oxidation of isobutene to acetic acid. Further, it appears that methacrylaldehyde, acetone, and a part of carbon oxides are formed by the following three parallel pathways.

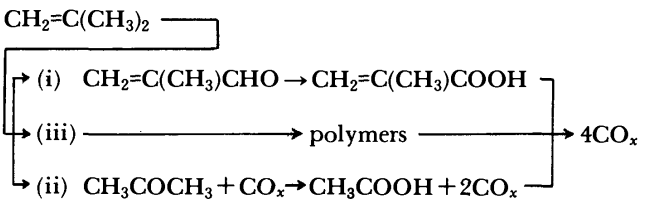

Reaction i is an allylic oxidation, Reaction ii is an oxidative C-C fission, and Reaction iii is a deep oxidation and/or polymerization.

Methacrylaldehyde was not obtained with the V_2O_5-TiO_2 catalyst. This indicates that the catalyst is lacking in the function to promote Reaction i. However, it promotes Reaction ii with a high selectivity than the pure V_2O_5 catalyst. This can easily be understood from the fact that V_2O_5-TiO_2 is very effective as a catalyst for the oxidative C-C fission of butene to form acetic acid.[20,21]

In the case of the pure V_2O_5 and V_2O_5-MoO_3 catalysts, a small amount of methacrylaldehyde was obtained, but methacrylic acid was not obtained. This finding suggests that these catalysts possess a catalytic function to promote Reaction i, to a certain extent, but they are lacking in the function to convert the methacrylaldehyde to methacrylic acid.

Appreciable amounts of methacrylic acid and methacrylaldehyde were obtained with the V_2O_5-P_2O_5 and heteropoly compound catalysts, indicating these catalysts possess both the function to promote Reaction i and that to promote the oxidation of methacrylaldehyde to methacrylic acid. As may be seen in Fig. 5 to 8, the yield of methacrylaldehyde passes through a maximum at the isobutene conversion of about 90%, indicating that methacrylaldehyde is more stable than isobutene under the conditions used.[22]

It has been pointed out[16] that the basic sites of catalyst promote the oxidative C-C fission rather than the allylic oxidation. In line with this thought, the results can be explained as follows. On the pure V_2O_5, about 60 to 70% of isobutene is directed to Reaction ii. The addition of a more basic oxide such as TiO_2 to V_2O_5 enhances the basic property of catalyst.[23] Therefore, the selectivity to Reaction ii increases to about 70 to 90%, but the function to promote Reaction i disappears. On the other hand, the addition of an acidic oxide such as MoO_3 to V_2O_5 induces an increase in the selectivity to Reaction i at the expense of a decrease in the selectivity to Reaction ii. This may be caused by an enhancement of the acidic property and/or a suppression of the basic property.

The addition of P_2O_5 to V_2O_5 induces a marked increase in the acidic property and, at the same time, a marked decrease in the basic property.[11] This may be the reason why a markedly higher selectivity to Reaction i can be obtained with the V_2O_5-P_2O_5 catalysts.

On the other hand, the possession of an enhanced acidic property seems to be required to promote selectively the oxidation of methacrylaldehyde to methacrylic acid.[8] This may be one of the reason why the V_2O_5-P_2O_5 catalysts are effective for the oxidation of isobutene to methacrylic acid.

It has been proposed[15] that heteropoly compounds are similar to V_2O_5-P_2O_5 system in their balance between acidic and basic properties. This may be the reason why similar catalytic performances are obtained in the oxidation of isobutene with the V_2O_5-P_2O_5 and heteropoly compounds.

However, it should be noted that a great extent of Reaction ii is accompanied with Reaction i even with the V_2O_5-P_2O_5 and heteropoly compound catalysts, that is, the suppression of Reaction ii is difficult. This may be a main disadvantage of this process.

It is interesting to note that the P/V=1.6 catalyst exhibits a higher yield of methacrylic acid than the P/V=1.06 catalyst, unlike the case of the oxidation of butane to maleic anhydride, and that the $Cs_2HPMo_{12}O_{40}$ catalyst shows a higher yield of methacrylic acid than the $H_3PMo_{12}O_{40}$ catalyst. At present, it is hard to

describe clearly the reason. Further study on the oxidation of methacrylaldehyde is necessary. This will be studied in forthcoming paper.

References

1) D.J. Hucnall, "Selective Oxidation of Hydrocarbons," Academic Press, London/New York, (1974), p. 105.
2) M. Kitahara, *Yuki Gosei Kagaku Kyokai Shi*, **33**, 710 (1975).
3) T. Ohara, *Shokubai (Catalyst)*, **19**, 157 (1977).
4) M. Kato, *Shokubai (Catalyst)*, **28**, 560 (1986).
5) M. Otake and T. Onoda, *Shokubai (Catalyst)*, **18**, 169 (1976).
6) A, G. Perrota, R. B. Bjorklund, J. T. Hoggins, and C. L. Kibby, *J. Catal.*, **61**, 285 (1980).
7) S. Nakamura and H. Ichihashi, Proc. 7th Intern. Congr. Catal., Tokyo, (1981), p. 755.
8) M. Ai, *J. Catal.*, **71**, 88 (1981).
9) M. Ai, *Appl. Catal.*, **4**, 245 (1982).
10) Y. Konishi, K. Sakata, M. Misono, and Y. Yoneda, *J. Catal.*, **77**, 169 (1982).
11) M. Ai, *J. Catal.*, **100**, 336 (1986).
12) G. Busca, G. Centi, F. Trifiró, and V. Lorenzelli, *J. Phys. Chem.*, **90**, 1337 (1986).
13) M. Ai and T. Ikawa, *J. Catal.*, **40**, 203 (1975).
14) M. Ai, Proc. 7th Intern. Congr. Catal., Tokyo, (1981), p. 1060.
15) M. Ai, Proc. 8th Intern. Congr. Catal., Berlin, (1984), V, p. 475.
16) M. Ai, *Polyhedron*, **5**, 103 (1986).
17) M. Ai, *Appl. Catal.*, **27**, 167 (1986).
18) M. Ai, *J. Catal.*, **98**, 401 (1986).
19) M. Ai, *J. Catal.*, **101**, 473 (1986).
20) R. Brockhaus, *Chem. Ind. Tech.*, **38**, 1039 (1966).
21) W. E. Slinkard and P. B. DeGroot, *J. Catal.*, **68**, 423 (1981).
22) J. C. Jungers, "Cinetique Chimique Applique," Technip, Paris, (1958), p. 176.
23) M. Ai, *Bull. Chem. Soc. Jpn.*, **49**, 1328 (1976).

Kinetic Studies of Fast Equilibrium by Means of High-Performance Liquid Chromatography. XVII. Separation of Tautomers of 1,3-Cyclohexanediones

Masataka MORIYASU,* Atsushi KATO, and Yohei HASHIMOTO
Kobe Women's College of Pharmacy, Motoyamakita-machi, Higashinada-ku, Kobe 658
(Received January 21, 1988)

Synopsis. Tautomers of 1,3-cyclohexanediones have been separated by means of low-temperature high-performance liquid chromatography (HPLC). The ratios of keto- and enol-forms have been found to be highly solvent dependent, which is explained in terms of solute-solvent and solute-solute hydrogen bonding.

We have already separated keto- and enol-forms of various β-dicarbonyl compounds[1-3] by means of low-temperature HPLC. However, the separation of tautomers of cyclic β-diketones has been unsuccessful, even though various column packings including narrow-pore silica gel, wide-pore silica gel, and narrow-pore diol-silica (chemically bonded silica-gel packings which contain alcoholic hydroxyl-groups) have been tried under various conditions. In the course of this study, we found that only wide-pore diol-silica achieved the separation. The nature of the keto-enol tautomerism of 1,3-cyclohexanediones was found to differ markedly from other β-dicarbonyl compounds, which is explained in terms of ring dimer formation of the enol-form in nonpolar media.

Experimental

1,3-Cyclohexanedione and 5,5-dimethyl-1,3-cyclohexanedione (dimedone) were obtained commercially. These were used without further purification because no peak attributable to the impurity appeared on the chromatograms.

The HPLC apparatus for low-temperature measurements have been detailed elsewhere.[1,2] In the present work it was necessary to cool the column to about −60 °C.

Wide-pore diol-silica (Nucleosil 4000-OH, 7 μm, from M. Nagel) was slurry packed into a stainless steel column (4.6 mm×10 cm). Various other column packings of different types were also tried, but no satisfactory results were obtained.

Results and Discussion

Among various column packings tested, only wide-pore diol-silica seems to separate tautomers. As shown in Fig. 1, the separation was attained on Nucleosil 4000-OH under the solvent system composed of hexane and ethyl acetate. For the complete separation in which the interconversion between tautomers during chromatography is negligible, a low column temperature (−60 °C) was necessary. The interconversion of 1,3-cyclohexanediones seems to be highly sensitive to the solvent. The solvent system composed of hexane and 1-propanol, which had given satisfactory separations of tautomers of various β-dicarbonyl compounds, did not give any separation even at −60 to −70 °C. Furthermore, addition of a minute amount of alcohols to the eluent (hexane-ethyl acetate) seriously depressed the separation. It seems that the interconversion was very fast in alcohols. The interconversion seems to be somewhat slower in less polar solvents, but still too fast to measure the rate constants at 0 °C or lower. The interconversion also seems to be activated on the surface of the adsorbent. On both narrow-pore and wide-pore silica gel, the interconversion seems to be fast, since no separation was attained. Acidic silanol group seems to drastically accelerate the interconversion. Although narrow-pore diol-silica did not, wide-pore diol-silica gave the separation, probably due to its low concentration of residual silanol group and less content of alcoholic -OH groups. In addition to 1,3-cyclohexanediones, separation of tautomers of 1,3-cycloheptanedione was also tried, but no separation was attained, even at −70 °C.

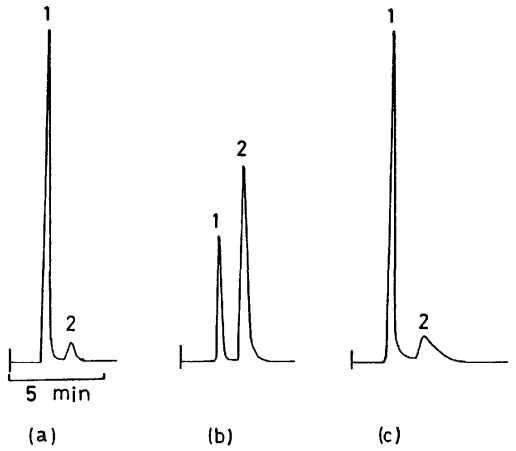

Fig. 1. HPLC separation of tautomers of 1,3-cyclohexanediones. Column: Nucleosil 4000-DIOL, 7 μm (4.6 mm×10 cm). Eluent: hexane:ethyl acetate=100:50. Flow rate: 2.5 $cm^3 min^{-1}$. Detector: UV 254 nm. Column temperature: −60 °C. Sample: (a) 10 mM dimedone in chloroform, (b) 10 mM dimedone in ethyl acetate, (c) 10 mM 1,3-cyclohexanedione in chloroform. 1: keto-form, 2: enol-form.

Table 1. Percentages of Enol-Form of 1,3-Cyclohexanedione and Dimedone in Different Solvents

Solvent	Enol-form/%	
	1,3-Cyclohexanedione	Dimedone
Carbon tetrachloride[a]	28	5
Chloroform	30	12
Dichloromethane	26	10
Diethyl ether	72	70
Ethyl acetate	78	69
Tetrahydrofuran	48	54
Acetonitrile	60	50
1-Propanol	92	95
Ethanol	93	97

10 mM solution, 25 °C. a) 1 mM solution.

Peak identification in Fig. 1 was done by comparing the present HPLC data with other data obtained by UV or NMR.[4] It is established that 1,3-cyclohexanediones are highly ketonic in dilute nonpolar media such as chloroform and cyclohexane[4] or in the gaseous phase.[5] With increasing concentration, the ratios of keto-form decrease. Since in chloroform the peak area with shorter retention time in Fig. 1 decreases with increasing concentration, the peak should be attributed to the keto-form. The percentages of enol-form were determined from peak area measurements for 1,3-cyclohexanedione in chloroform as follows: 89% (750 mM, 1 M=1 mol dm^{-3}), 85% (500 mM), 77% (250 mM), 58% (100 mM), 53% (70 mH), 33% (20 mM), 24% (5 mM), and 20% (2 mM). The reported values by means of NMR and UV[4] are as follows: 89% (770 mM, NMR), 82% (510 mM, NMR), 71% (240 mM, NMR), 52% (103 mM, NMR), 46% (68 mM, NMR), 25% (19 mM, UV), and 15% (4.2 mM, UV). Both results agree rather well. With similar procedures the percentages of enol-form of dimedone in chloroform were also determined, the results being as follows: Our results; 33% (100 mM), 23% (60 mM), 21% (40 mM), 15% (20 mM), and 10% (6 mM). NMR or UV data;[4] 28% (94 mM, NMR), 18% (63 mM, NMR), 5% (42 mM, NMR), 14% (39 mM, UV), and 4% (6.2 mM, UV). The ratios of keto- and enol-forms in different solvents at dilute concentration (10 mM) at 25 °C were also measured, and the results are summarized in Table 1.

The chromatographic behavior and the nature of the tautomerism of 1,3-cyclohexanediones differ markedly from other various β-dicarbonyl compounds

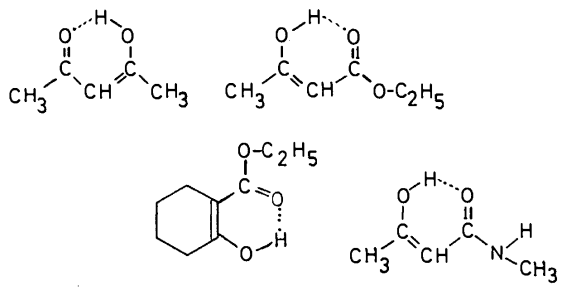

we investigated previously.[1-3] (1) For the separation of tautomers of 1,3-cyclohexanediones, a lower column temperature than for other β-dicarbonyl compounds is necessary. This suggests a faster interconversion of 1,3-cyclohexanediones. (2) The keto form is eluted faster than the enol-form for 1,3-cyclohexanediones on adsorption chromatography, which is the reverse to other β-dicarbonyl compounds. (3) For 1,3-cyclohexanediones, the percentages of enol-form are higher in polar solvents such as alcohols, which is also opposite in the case of other β-dicarbonyl compounds. These characteristic features can be explained in terms of the difference of structure between enol-forms of 1,3-cyclohexanediones and others. As shown above, enol-forms of most β-dicarbonyl compounds such as β-diketones, β-keto esters including cyclic ones, and β-keto amides form chelated intramolecular hydrogen bonds. Consequently, enol-forms are less polar chemically than keto-forms.[6] Since adsorption on silica gel (or diol-silica) surface will occur by intermolecular hydrogen bonding between polar groups of substances and -OH group of the stationary phase, strongly chelated enol-forms may not be easily adsorbed. Thus, the enol-forms are eluted faster than the keto-forms, although alcohols are usually more polar than ketones. Strongly chelated enol-forms also might be somewhat resistant to hydrogen abstraction by a solute molecule which is one of the fast steps of keto-enol conversion. The situation differs for 1,3-cyclohexanediones. The equilibrium of 1,3-cyclohexanediones is explained in terms of the following three labile species, ketone monomer, enol monomer, and enol dimer.[4,7] Due to geometrical restrictions, intra-

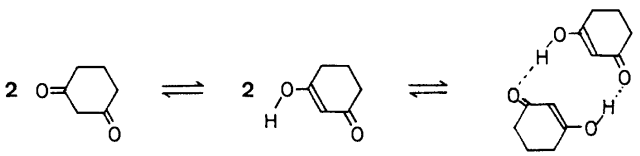

molecular hydrogen bonds cannot be formed for enol-forms. Thus, enol-forms should be more polar and eluted later than keto-forms. As shown above, in non-polar solvents such as cyclohexane and chloroform or in gaseous phase, the ketone monomer is predominant. With increasing concentration, the intermolecular hydrogen-bonded enol dimer begins to be formed. In protic solvents such as alcohols, enol monomer may be predominant due to strong solute-solvent intermolecular hydrogen bonds. Thus, the ratios of keto- and enol-forms of 1,3-cyclohexanediones differ markedly from other β-dicarbonyl compounds. The behavior rather resembles the case for the separation of rotamers of formanilide[8] in which the (*E*)-rotamer forms an intramolecular hydrogen-bonded ring dimer.

References

1) M. Moriyasu, A. Kato, and Y. Hashimoto, *J. Chem. Soc., Perkin Trans. 2*, **1986**, 515.

2) M. Moriyasu, A. Kato, and Y. Hashimoto, *J. Chromatogr.*, **400**, 143 (1987).

3) M. Moriyasu, A. Kato, and Y. Hashimoto, *J. Chromatogr.*, **411**, 466 (1987).

4) A. Yogev and Y. Mazur, *J. Org. Chem.*, **32**, 2162 (1967).

5) K. N. Houk, L. P. Davis, G. R. Newkome, R. E. Duke, Jr., and R. V. Nauman, *J. Am. Chem. Soc.*, **95**, 8364 (1973).

6) K. H. Meyer and V. Schoeller, *Chem. Ber.*, **53**, 1410 (1920).

7) N. Cyr and L. W. Reeves, *Can. J. Chem.*, **43**, 3057 (1965).

8) M. Moriyasu, K. Kawanishi, A. Kato, and Y. Hashimoto, *Bull. Chem. Soc. Jpn.*, **57**, 1766 (1984).

Proton NMR Spectra of Methyl Alkanoates in Aromatic Solvents

Takashi HOSHINO* and Yoshio IMAMURA
Department of Chemistry, Faculty of Science, Science University of Tokyo, Kagurazaka, Shinjuku-ku, Tokyo 162
(Received February 5, 1988)

Synopsis. The splitting of methylene peaks in ^{1}H NMR spectra was studied for long-chain methyl alkanoates in 1-chloronaphthalene as a function of the carbon number, n_c, of alkyls. With increase in n_c, the singlet peak of methylene is first split into a doublet and then into a triplet.

ASIS (Aromatic-Solvent-Induced Shift) phenomena in NMR have been widely accepted by organic chemists and applied successfully to conformational studies on organic molecules.

In 1967, a peculiar solvent effect by an aromatic solvent was reported by Liu.[1] He observed that methylene envelopes in ^{1}H NMR spectra of long-chain hydrocarbons (the number of carbons >16) were split into doublets in 1-chloronaphthalene. Similar observations have been reported for other solute molecules with long alkyl chains. For example, Gonzalez de la Campa et al. reported on a series of *N*-alkylmaleimides[2] and alkyl 11-maleimidoundecanoates in benzene solution,[3] and Winnik et al.[4] also reported on the octadecyl ester of benzophenone-4-carboxylic acid in 1-chloronaphthalene. In ^{1}H NMR spectra of these compounds, splittings of methylene signals were observed for shorter alkyl chains rather than for *n*-alkanes, and it was suggested that terminal substituted groups seemed to accentuate the splitting of methylene peaks of ^{1}H NMR spectra, observed in aromatic solvent.

The first theoretical investigation was carried out by Ando and Nishioka.[5] They concluded that the splitting of peaks in aromatic solvent arose from increase in the number of gauche forms for long chain hydrocarbons. On the other hand, Winnik et al. applied T_1 measurements[4] and used the heteronuclear (^{13}C-^{1}H) shift correlated two-dimensional NMR spectroscopy.[6] They concluded that the splitting was due to a solvent effect associated with the chain end, and conclusively ruled out the presence of slowly interconverting gauche and trans conformations for long alkyl chains. Furthermore, several papers have been published to discuss the origin of these phenomena, without setting the issue.

In this paper, we intend to present another example of similar phenomenon to add to information so as to facilitate insight into the reason for the splitting found for methylene peaks of substituted alkyl chains.

Experimental

Methyl alkanoate compounds with alkyl carbon (n_c=6 to 24) were used as solute substances. The compounds and solvents used were of the best available commercial grade. The samples were prepared in an about 0.5 M solution (1 M=1 mol dm^{-3}) of deuterated benzene or a mixed solvent of 90 vol% 1-chloronaphthalene/10 vol% deuterated benzene. NMR spectra were observed using a JEOL FX-100 NMR spectrometer operated at 100 MHz at ambient temperature, unless otherwise indicated.

Results and Discussion

100 MHz ^{1}H NMR spectra of a series of methyl alkanoates in 1-chloronaphthalene are shown in Fig. 1. The carbon number of alkyl chains, n_c, is in the range from 6 to 24. Triplet peaks at higher fields were assigned to their terminal methyl protons and the rest to methylene protons. The peaks which appeared in lower fields at about δ 3.4 and 2.2, were assigned to the methyl and methylene adjacent to the ester group, respectively, but they are not shown in Fig. 1. The small peaks at the lowest field were assigned to β methylene protons to the carbonyl. A singlet methylene peak was observed for the compounds with n_c ranging from 6 to 10. When n_c=12, one more partially resolved peak appeared in the spectrum as a shoulder. Then, there are two distinguishable peaks in the spec-

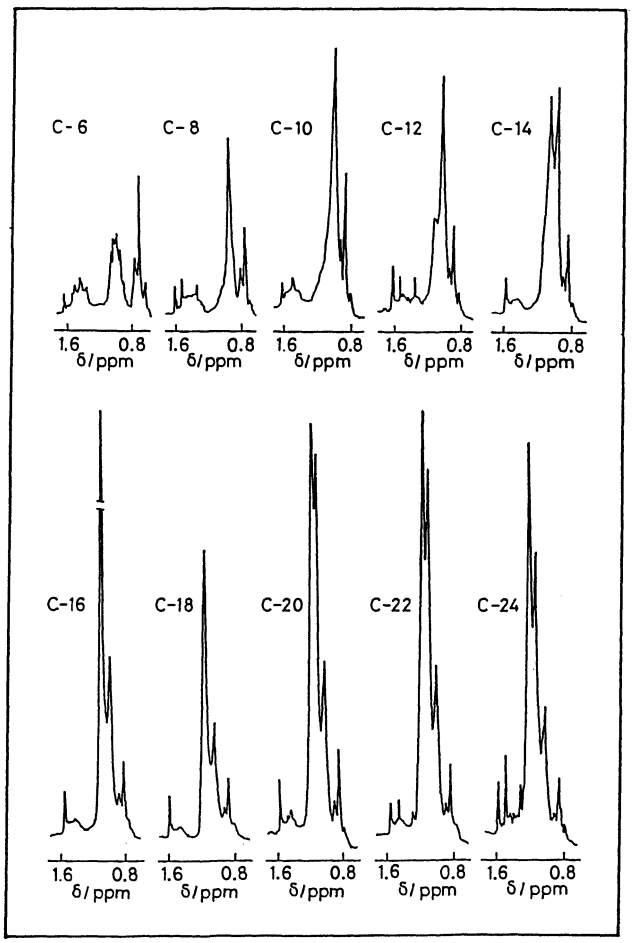

Fig. 1. The ^{1}H NMR spectra at 100 MHz of methyl alkanoates in 90 vol% 1-chloronaphthalene/10 vol% deuterated benzene.

Table 1. The Least Carbon Numbers of Alkyl Chains, n_c, at which the Splitting of Methylene Proton Signals is Observed

Solute	Solvent	Doublet	Triplet	Ref.
Normal alkanes	1-Clnap[a)]	17		1
	Benzene	None		7
N-Alkyl maleimides	Benzene	12		2
Alkyl 11-maleimido-undecanoates	Benzene	12		3
Methyl alkanoates	1-Clnap[a)]	12	20	b)
	Benzene	12		b)
1-Chloroalkanes	1-Clnap[a)]	18		b)
	Benzene	None		b)

a) 1-Chloronaphthalene. b) Present investigation.

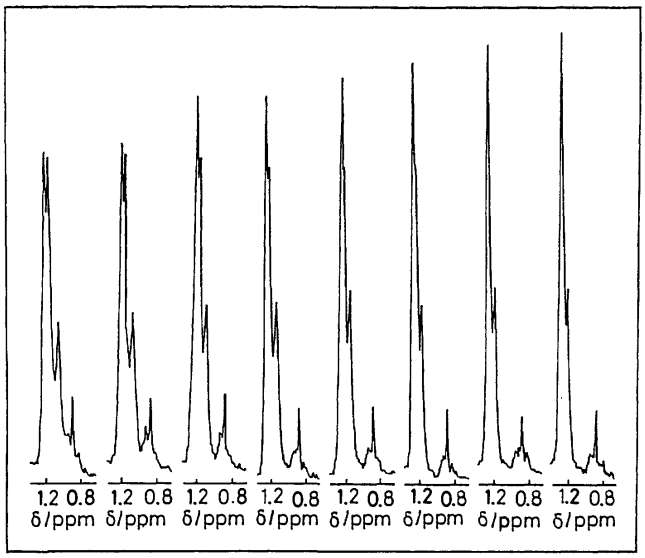

Fig. 2. The ^{1}H NMR spectra of methyl eicosanoate in 1-chloronaphthalene solution at various temperatures; 25, 38.8, 55.0, 70.3, 85.3, 99.7, 115.5, and 129.5 °C from left to right, respectively.

tra of the compounds for n_c=12 to 18. When $n_c \geqslant 20$, the lower field peak further split into a doublet, and a distinct triplet peak was recognized. A peak splitting at n_c=12 was also observed in benzene solutions but no splitting at n_c=20 in 1-chloronaphthalene was observed in benzene, as shown in Table 1, which shows a list of the splitting behavior for substituted alkanes in aromatic solvent. This splitting at n_c=12 has substantially the same character as observed in the case of a series of *N*-alkylmaleimides[2)] and alkyl 11-maleimidoundecanoates[3)] in benzene solutions. On the other hand, the second splitting of the lower field peak observed in 1-chloronaphthalene solutions for $n_c \geqslant 20$ was not observed in the case of benzene solutions. The splitting for $n_c \geqslant 20$ seems to be consistent with the results obtained by Liu[1,7)] for a series of alkanes. He reported that the splitting was observed only in 1-chloronaphthalene solutions[1)] but not in benzene solutions for alkanes.[7)] We considered that the nature of the origin of this splitting of the peak of the methylene envelope for $n_c \geqslant 12$ is different from that of the splitting effect in the case of alkanes.

The splitting for n_c=12 seems to be strongly dependent on the presence of the ester function. In the series of 1-chloroalkanes in 1-chloronaphthalene solutions, the splitting was not observed for n_c less than 18. This behavior is the same as in the case of alkanes.

^{1}H NMR spectra of methyl eicosanoate of n_c=20 in 1-chloronaphthalene solutions at various temperatures are shown in Fig. 2. The chemical shift differences among the three peaks in the methylene envelope decrease with temperature raise, and the two lower field peaks for the methylene coalesce at about 100 °C. This temperature is lower than that reported for *n*-alkanes. Winnik et al.[6)] calculated the energy barrier to be 120 kJ mol^{-1} for *n*-alkanes by assuming the two site exchange. They suggested that this value was too large for the constraint of the interconversion between gauche and trans conformers to account for the splitting phenomena.[5)] In this study, the energy barrier for methyl alkanoates was calculated to be about 80 kJ mol^{-1} using the coalesce temperature method.[8)] This value is less than the value reported for alkanes but still large for the ordinary interconversion energy. However, in order to make further discussion on the results of our observation, it may be desirable to establish a new molecular model for the solvent-solute interaction.

References

1) K. J. Liu, *J. Polym. Sci.*, Part A-2, **5**, 1209 (1967).
2) J. I. Gonzalez de la Campa, J. M. Barrales-Rienda, and J. Gonzalez Ramos, *Macromolecules*, **10**, 989 (1977).
3) J. I. Gonzalez de la Campa and J. M. Barrales-Rienda, *Polym. J.*, **13**, 679 (1981).
4) M. A. Winnik, A. Mar, W. F. Reynoldes, Ph. Dais, B. Clin, and B. Caussade, *Macromolecules*, **12**, 257 (1979).
5) I. Ando and A. Nishioka, *Makromol. Chem.*, **152**, 7 (1972); **160**, 145 (1972); **171**, 195 (1973); I. Ando and Y. Inoue, *Makromol. Chem., Rapid. Commun.*, **4**, 753 (1983).
6) W. F. Reynoldes, M. A. Winnik, and R. G. Enriquez, *Macromolecules*, **19**, 1105 (1986).
7) K. J. Liu, *Polymer*, **10**, 951 (1968).
8) J. Sandstrom, "Dynamic NMR Spectroscopy," Academic Press, London, New York (1982).

Photo-Excitable Membranes. Effects of pH of the Solution on the Photoresponse of Poly(vinyl chloride) Membrane Doped with a Spirobenzopyran Derivative

Jun-ichi ANZAI, Yasushi HASEBE, Akihiko UENO, and Tetsuo OSA*
Pharmaceutical Institute, Tohoku University, Aobayama, Sendai 980
(Received February 18, 1988)

Synopsis. The magnitude of the photoinduced membrane potential across a poly(vinyl chloride)/spirobenzopyran membrane depends considerably on the pH of the solution adjacent to the membrane surface which is exposed to light. The photoresponse is enhanced in the acidic region, while is depressed in the alkaline region. The results are explained in terms of the formation of the asymmetric membrane and of the charge density on the membrane surface.

Several reports have appeared on the photoinduced membrane potential across the polymer membranes modified with spirobenzopyran derivatives.[1-6] To improve the photoresponse of the membranes, we have employed a plasticized poly(vinyl chloride) membrane doped with spirobenzopyran derivative **1** and found followings; (1) UV irradiation induces membrane potential changes of more than 100 mV with a response time of 1—2 min, (2) the photoinduced potential changes arise from the change in charge density on the membrane surface (i.e., surface potential change), which stems from the photo-generated open form of **1**, and (3) the content of open form of **1** is higher on the UV-irradiated surface than that on the nonirradiated surface (i.e., formation of asymmetric membrane).[7-11]

The effects of pH of the solution on the photoresponse were also checked in the range of pH 5.3—8.0.[9] In this pH range, the photoresponse of the PVC/**1** membrane slightly depended on the pH of the solution. The present paper reports the pH-dependent photoresponse of the PVC/**1** membrane over the wide pH range of 3—12 under the condition that the pH values of both aqueous solutions separated with the membrane are not equal with each other. To our knowledge, such systematic study of the pH effect on the photoresponse of the spiropyran-doped membrane has not appeared.

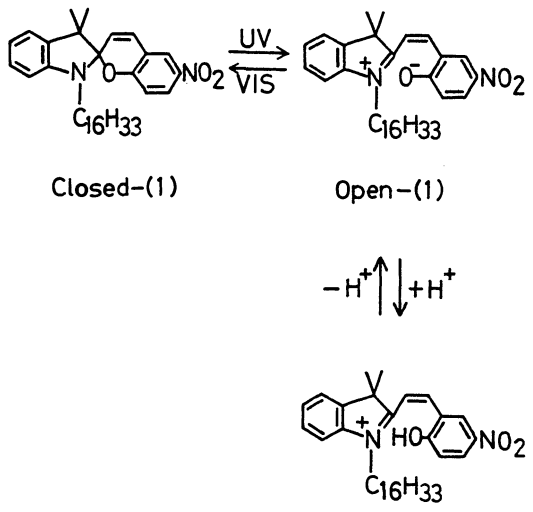

Experimental

Materials. PVC (molecular weight of ca. 70000) was purchased from Wako Co., Ltd. and used without further purification. Diisodecyl phthalate (DIDP) and tetrahydrofuran (THF) are of extra pure reagent grade. The synthetic procedure and analytical data of **1** were described previously.[9]

Membrane Preparation. PVC/**1** membrane of ca. 0.15 mm thickness was prepared by pouring the mixture of 250 mg of PVC, 0.5 ml of DIDP, 30 mg of **1**, and 20 ml of THF onto a flat Petri dish (8.5 cm diameter), and allowing the solution to evaporate at room temperature. The membrane was conditioned by soaking it in 5 mM ($M=mol\cdot dm^{-3}$) Britton-Robinson buffer for ca. 15 h before use.

Membrane Potential Measurement. All measurements were conducted at 25 °C using a U-shaped glass cell (Fig. 1). The composition of the electrochemical cell for the membrane potential measurements was as follows; Ag/AgCl|0.1 M $(CH_3)_4NCl$|electrolyte solution (c_1)|PVC/**1** membrane|electrolyte solution (c_2)|0.1 M $(CH_3)_4NCl$|Ag/AgCl. The electrode in the c_1 compartment was earthed. The pH value of the solutions were regulated with 5 mM Britton-Robinson buffer. Photoirradiation was carried out from the c_2 side with a 500 W xenon lamp using cut-off filters to isolate UV ($320\ nm<\lambda<400\ nm$) and visible ($490\ nm<\lambda$) light. Noise level in the potential was within 1 mV under the present experimental conditions.

Results and Discussion

Figure 2 shows the magnitude of photoinduced membrane potential, $\Delta(\Delta\phi)$, as a function of pH of the c_2 side solution. The pH value of the c_1 side solution was maintained constant at 3 or 12, and the membrane surface facing the c_2 solution was exposed to light. In the range of pH 3—7, the $\Delta(\Delta\phi)$ value scarcely depended on the pH of the c_2 solution, while, above pH 8, the $\Delta(\Delta\phi)$ value decreased almost linearly with increasing the pH. Such tendency was observed for both cases when the pH of the c_1 solution was maintained at 3 and 12.

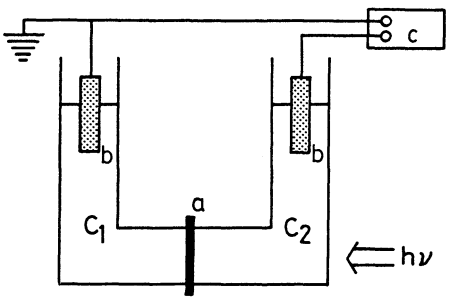

Fig. 1. Schematic representation of the cell for measuring membrane potential. a; Membrane, b; Ag/AgCl electrode, c; potentiometer.

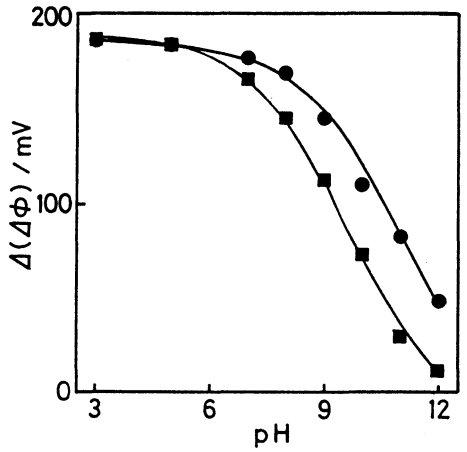

Fig. 2. Effects of pH of the c_2 solution on the photoresponse of the PVC/1 membrane. The pH value of the c_1 solution was constant at 3 (—■—) or 12 (—●—). The membrane surface facing the c_2 solution was exposed to light.

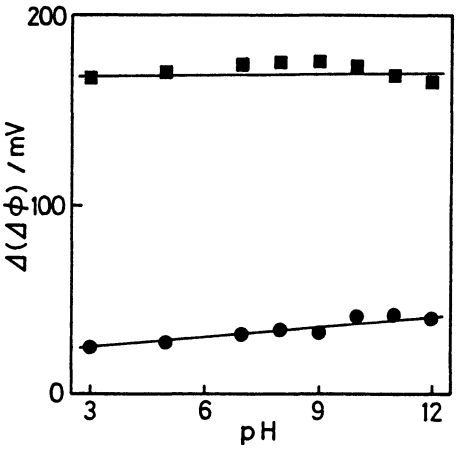

Fig. 3. Effects of pH of the c_1 solution on the photoresponse of the PVC/1 membrane. The pH value of the c_2 solution was constant at 3 (—■—) or 12 (—●—). The membrane surface facing the c_2 solution was exposed to light.

These results are compatible with our idea[7-11] that the photoinduced membrane potential stems from the change in charge density on the UV-irradiated surface of the membrane. In the case of the PVC/1 membrane, the charge density of the membrane surface is considered to depend on the amount of the protonated form of **1** which has an electrically positive net charge. It is envisaged that the pH of the c_2 side solution considerably affects the equilibrium of protonation to the open **1** on the irradiated surface.

Figure 3 shows the results obtained when the pH of the c_1 side solution was varied from 3 to 12 with keeping the pH of the opposite side solution constant at 3 or 12. The membrane surface facing c_2 solution was exposed to light. Contrary to the data shown in Fig. 2, the effects of pH of the c_1 solution was small. When the c_2 solution was maintained at pH 3, the photoinduced potential of 160—180 mV was observed irrespective of pH value of c_1 solution. This result consists with the fact that the photochemical reaction from the closed-**1** to the open form is severely depressed on the nonirradiated surface of the membrane (i.e., asymmetric membrane), as was previously shown spectrophotometrically.[11] On the other hand, the $\Delta(\Delta\phi)$ value decreased to 20—40 mV when the pH of the c_2 solution was 12. These observations also show that the photoresponse of the PVC/1 membrane depends on the change in charge density of the irradiated surface, not of the opposite surface, of the membrane. These findings should be important in relation to the mechanistic study on the pH-dependent photoresponse of the enzyme-modified PVC/1 membrane,[10] which can be used as a sensitive layer of a novel class of potentiometric enzyme sensors.[12]

The authors are grateful to the Ministry of Education, Science and Culture of Japan for support of this work through a Grant-in-Aid for Special Project Research (No. 62117003).

References

1) S. Kato, M. Aizawa, and S. Suzuki, *J. Membr. Sci.*, **1**, 289 (1976).

2) S. Kato, M. Aizawa, and S. Suzuki, *Kobunshi Ronbunshu.*, **34**, 793 (1977).

3) S. Kato, M. Aizawa, and S. Suzuki, *J. Membr. Sci.*, **2**, 39 (1977).

4) I. R. Bellobono, S. Giovanardi, B. Marcandalli, S. Calgari, and D. Nasari, *Polym. Photochem.*, **4**, 59 (1984).

5) I. R. Bellobono, B. Marcandalli, E. Selli, and S. Calgari, *Photogr. Sci. Eng.*, **28**, 162 (1984).

6) M. Irie, A. Menju, and K. Hayashi, *Nippon Kagaku Kaishi*, **1984**, 227.

7) J. Anzai, A. Ueno, and T. Osa, *J. Chem. Soc., Chem. Commun.*, **1984**, 688.

8) J. Anzai, H. Sasaki, A. Ueno, and T. Osa, *Chem. Lett.*, **1985**, 1443.

9) J. Anzai, Y. Hasebe, A. Ueno, and T. Osa, *Kobunshi Ronbunshu*, **43**, 693 (1986).

10) J. Anzai, Y. Hasebe, A. Ueno, and T. Osa, *Maku (Membrane)*, **12**, 165 (1987).

11) J. Anzai, Y. Hasaebe, A. Ueno, and T. Osa, *Bull. Chem. Soc. Jpn.*, **60**, 3169 (1987).

12) Y. Hasebe, J. Anzai, A. Ueno, and T. Osa, *J. Phys. Org. Chem.*, in press.

Effect of the Aggregation Number on Gel Chromatographic Patterns of Micellar Systems

Noriaki FUNASAKI,* Sakae HADA, and Saburo NEYA
Kyoto Pharmaceutical University, Yamashina, Kyoto 607
(Received March 18, 1988)

Synopsis. Gel chromatographic patterns and their derivatives of micellar systems are predicted as a function of the total surfactant concentration and the aggregation number m by plate theory and asymptotic theory. These predicted patterns provide the basis for estimation of monomer concentration and m from experimental chromatographic data.

Gel chromatography has provided important information about aqueous surfactant solution; e.g., micellar size,[1,2] monomer concentration,[2-4] and mixed micelle formation.[5] This technique has been also used for investigations of self-association of proteins,[6,7] but a wealth of knowledge obtained from such studies has not well been utilized for surfactants.

For quantitative analysis of self-associating systems, a large amount of sample is usually charged into a gel column so that a plateau region may appear on the elution curve.[2-7] For a nonassociable solute, asymptotic theory presumes the elution curve of a rectangle possessing the same concentration and volume with those of the charged sample.[3,4,6] For a self-associable solute with the aggregation number m, this theory predicts the equation[4,6]

$$V_c = C_1V_1/C_0 + (C_0 - C_1)V_m/C_0 \quad (1)$$

Here V_c is the centroid of elution profile defined as

$$V_c = \int_0^{C_0} V dC/C_0 \quad (2)$$

C_0 and C_1 denote the total concentration and the monomer concentration, and V_1 and V_m denote the elution volumes of monomer and m-mer, respectively. For proteins, first derivative of the elution curve often provides more detailed information than the original curve,[6,7] but has not yet been reported for surfactants.

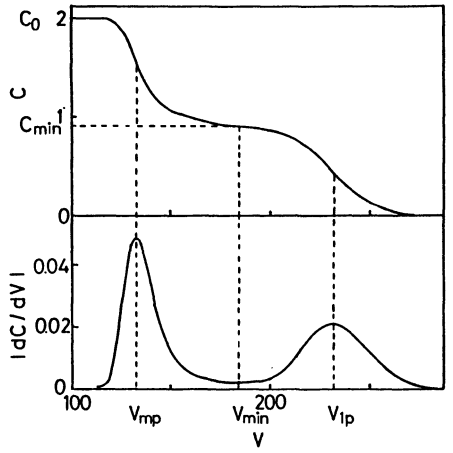

Fig. 1. Elution curve and its derivative simulated by using values of m=40 and C_0=2 and definitions of characteristic values.

Plate theory, based on phase separation model for micelle formation, was applied for simulation of gel chromatograms of surfactants.[5] This theory may predict a more realistic elution pattern than the above asymptotic theory, though no comparison has been reported for surfactants.

In this work, we develop plate theory based on mass action model for micellization of surfactants. This model is more rigorous than phase separation model and may also apply for proteins. Based on this theory, we investigate the effects of the total concentration and the aggregation number upon gel chromatographic patterns of self-associating systems. Derivative elution patterns are also simulated. These simulations make possible a better analysis of experimental results of gel chromatograms and reveal the scope and limitations of the asymptotic theory.

Methods

The procedure of computer simulation for plate theory developed by Nakagawa[5] was employed. It was assumed that the equilibrium of partition of solute between the mobile phase and the stationary phase is established instantaneously. At time zero, the column bed is saturated with surfactant solution of concentration C_0 and water as eluent begins to enter onto the gel bed. That is, the trailing boundary of frontal elution chromatography[6] is investigated.

For the monomer-m-mer equilibrium, the association constant K can be written as

$$K = (C_0 - C_1)/C_1^m \quad (3)$$

This reaction was assumed to be rapid. The value of C_1 was calculated by the Newton-Raphson method from Eq. 3.

To simulate a chromatogram, we must input the number N of plate, the void volume V_0, K, V_1, V_m, m, and C_0; N=100, K=1, V_1=230, V_m=130, and m=2, 3, 6, 10, 40, 80, 200, or ∞ were used together with a wide range of concentration C_0 Derivation of the elution curve was replaced by differentiation $\Delta C/\Delta V$.

Results and Discussion

Figure 1 shows a sample of simulation and definitions of C_{min}, V_{min}, V_{1p}, and V_{mp}. In general, derivative pattern has two peaks of V_{1p} and V_{mp} and a minimum of V_{min}. The C_{min} value is defined as the concentration at V_{min} on the elution curve. The V_c value can be calculated from the elution curve by using Eq. 2. For only cases of m=10, 40, and ∞, V_{1p}, V_c, and V_{mp} are shown as a function of C_0. Other cases are omitted, since we can infer such patterns from Fig. 2 roughly. For the case of m=2, derivative patterns had a single peak, regardless of C_0, whereas for cases of $m \geqq 3$, those patterns had two peaks. These results are consistent

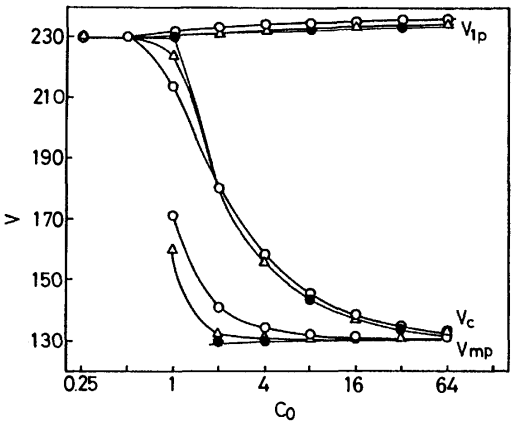

Fig. 2. Plots of V_{1p}, V_c, and V_{mp} against the logarithm of C_0 for cases of m=10 (○), m=40 (△), and m=∞ (●).

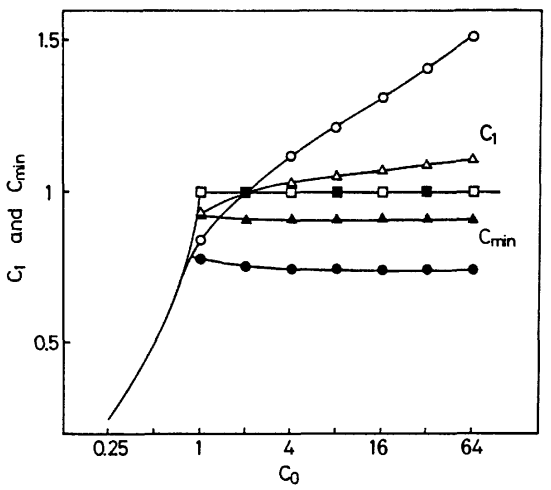

Fig. 3. Plots of C_1 (hollow symbols) and C_{min} (filled symbols) against the logarithm of C_0 for cases of m=10 (○,●), m=40 (△,▲), and m=∞ (□,■).

with predictions from asymptotic theory.[6] The V_c value simulated was in excellent agreement with that from Eq. 1: this equation, though obtained from asymptotic theory, holds rigorously for self-associating systems. As C_0 decreases, V_{1p} decreases and approaches V_1. This result indicates that V_1 should be evaluated at zero concentration. When m is small, V_{mp} decreases with increasing C_0 and approaches V_m. These results indicate that V_m should be evaluated at infinite concentration and that variation of V_{mp} with C_0 does not always reflect true size changes of the micelle. Concentration dependence of V_{mp} for hexamerization of α-chymotrypsin[7] is in qualitative agreement with the above prediction. Accurate estimation of micellar size of hexaethylene glycol dodecyl ether from V_{mp}[2] cannot be justified, though we do not deny micellar growth of this surfactant with C_0. According to asymptotic theory, V_{min} is expected to be $[(2m-1)V_1+(m-2)V_m]/(3m-3)$, regardless of C_0,[6] whereas the V_{min} value simulated increased with increasing C_0 (data are not shown). The latter prediction is in agreement with the experimental result.[8]

The C_1 value calculated from Eq. 3 is shown as a function of C_0 in Fig. 3. As is well known, the increase in C_1 decreased with increasing m above a concentration, called the critical micelle concentration. At $m \to \infty$, (phase separation model) C_1 was a constant of unity. As Fig. 3 shows, the C_{min} value simulated slightly decreased with increasing C_0 and increased with increasing m. According to asymptotic theory,

$$C_{min} = 2(m^2-1)[(m-2)/K]^{1/(m-1)}[m(2m-1)]^{m/(1-m)} \quad (4)$$

The C_{min} values calculated from Eq. 4 at m=10, 40, and ∞ were 0.733, 0.940, and 1, respectively. These values are close to the simulated values at large values of C_0 (see Fig. 3). Values of monomer concentration of hexaethylene glycol dodecyl ether were estimated from Eq. 1[4] and from C_{min}.[2] These values are different from each other, as expected.

The present results provide the basis for analysis of experimental chromatographic data. If V_1 and V_m can be estimated from the data, we can determine C_1 as a function of C_0. As we have shown herein, V_1 can be evaluated from V_{1p} or V_c at C_0=0 and V_m from V_{mp} or V_c at infinite concentration. Concentration dependence of C_1 changes with m, as shown in Fig. 3. This suggests the possibility for determination of m from the C_1 vs. C_0 relationship. In gel chromatography the elution volume of solute decreases with increasing size of the solute. For self-associating systems, however, the value of V_{mp} depends on C_0 as well as on size.[7] This must be taken into consideration, when we estimate micellar size from V_{mp}. Values of V_c and V_{mp} at infinite concentration correspond to correct micellar size. As m increases, the difference between C_{min} and C_1 decreases (Fig. 3). When $m>200$, C_{min} is practically equal to C_1 and then we can estimate C_1 from C_{min}, without use of Eq. 1. Asymptotic theory can predict a correct value of V_c and a rough value of C_{min}. Derivative elution patterns can provide useful information about micellar size and monomer concentration of surfactants. The above predictions based on plate theory are in agreement with experimental results, which will be published elsewhere.[8]

References

1) C. Tanford, Y. Nozaki, and M. F. Rohde, *J. Phys. Chem.*, **81**, 1555 (1977).
2) A. Goto, R. Sakura, and F. Endo, *J. Colloid Interface Sci.*, **67**, 491 (1978).
3) T. Sasaki, *Yukagaku*, **16**, 49 (1967).
4) T. Sasaki, M. Yasuoka, and H. Suzuki, *Bull. Chem. Soc. Jpn.*, **50**, 2538 (1977).
5) T. Nakagawa, *Yukagaku*, **20**, 277 (1971).
6) G. K. Ackers and T. E. Thompson, *Proc. Natl. Acad. Sci. U. S. A.*, **53**, 342 (1962).
7) D. J. Winzor and H. A. Scheraga, *Biochemistry*, **2**, 1263 (1963).
8) N. Funasaki, S. Hada, and S. Neya, *J. Phys. Chem.*, in press.

The CH-Surface Area of Sugar Molecules as a Measure of Their Potential Hydrophobicity

Yuki YANO,† Keiko TANAKA, Yukio DOI, and Masanobu JANADO*
Department of Food Science, Kyoto Women's University, Kyoto 605
(Received March 23, 1988)

Synopsis. Differential affinity of three groups of sugars (monosaccharides, glucodisaccharides and methyl glycosides) can reasonably be interpreted in terms of a molecular surface parameter, the ratio of the surface area of hydrophobic groups (CH, CH_2, and CH_3) to that of hydrophilic groups (OH and -O-) computed from the crystallographic data.

We reported several items of evidence indicating the potential hydrophobicity of sugars:[1-5] these include the configuration- and conformation-dependent affinity of sugars for polystyrene gel in aqueous solvents, which is also strongly affected by the type of salt (chaotropic or nonchaotropic) present, the cosolvent effect of sugars increasing the aqueous solubilities of hydrocarbons and 1-alkanols, and the strong affinity of *n*-aliphatic alcohols for dextran gel. In these studies, the hydrophobicity of sugars was measured in terms of their partition coefficients (K_{av}) between polystyrene gel (Bio-Beads SM-4, Bio-Rad Labs) and aqueous solvent. Inspection of the K_{av} spectrum of various sugars including monosaccharides, deoxy sugars, methyl glycosides and oligosaccharides led us to conclude that the hydrophobic behaviors of sugars are due to CH, CH_2, and CH_3 groups of the sugar molecules. Indeed, for monosaccharides, Miyajima et al.[6] showed that the polystyrene affinity ($\ln K_{av}$) is closely correlated with a CH-surface parameter, index A which is defined as the percent ratio of the total surface area of the hydrophobic groups (CH and CH_2) to that of the hydrophilic groups (OH and -O-). However, the CH index,[5] a CH-surface parameter defined on essentially the same basis as index A, totally fails to predict the order of the polystyrene affinity of glucodisaccharides and methyl glycosides where the effect of other molecular properties such as molecular planarity, rigidity and spatial segregation between OCH_3 and OH groups may become important.[5] Nevertheless, since the CH-surface effect seems to be the primary factor giving rise to the hydrophobic behaviors of sugars, it is of interest and profitable to examine the correlation between the polystyrene affinity and the CH index over a wide range of K_{av}.

The surface area is defined by the area of the surface traced out by the center of spherical water molecule of radius 1.4 Å sliding over the surface of sugar molecule.[7] The orthogonal atomic coordinates of sugar molecules were obtained from the Cambridge crystallographic data file (CAM), and the surface area was calculated using the computer program ASA written by H. Mizuno (Kyushu Univ.). The CH index was defined by

$$\text{CH Index} = \frac{\text{Total surface area of CH, } CH_2\text{, and } CH_3 \text{ groups}}{\text{Total surface area of OH, and -O- groups}}$$

which is formally identical to the Index A of Miyajima et al.[6] but differs in that, instead of assuming the free rotations of OH groups about the C-O linkages, the crystallographic atomic coordinates were used to calculate the surface area and that the parameters accounting for the 2α- and β- anomer equilibrium of glucodisaccharides were dropped out. Accordingly, the CH indexes of glucodisaccharides (Fig. 1) are those of β-anomers. The chromatographic partition coefficients (K_{av}) of sugars, obtained using a column of polystyrene beads (Bio-Beads SM-4) in 2 mol dm^{-3} NaCl,[2,5] can be correlated with the association constant (K) for sugar-polystyrene interaction by

$$K = \frac{1}{[B_o]}\left(\frac{K_{av} - K_{av}^{o}}{K_{av}^{o}}\right)$$

where $[B_o]$ is the total concentration of the independent and equivalent binding sites in the volume of the polystyrene gel phase accessible to sugar molecules,

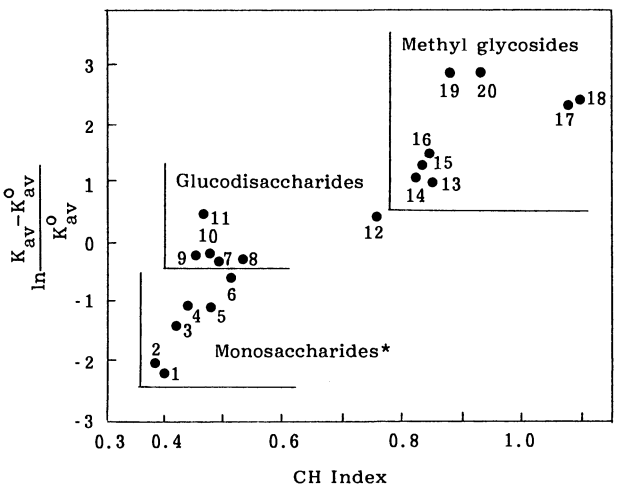

Fig. 1. Correlation between the polystyrene affinity and CH index. CH index=ratio of total surface area of CH, CH_2, and CH_3 groups to total surface area of OH and O groups. 1: galactose, 2: glucose, 3: mannose, 4: xylose, 5: arabinose, 6: ribose, 7: cellobiose, 8: maltose, 9: trehalose, 10: gentiobiose, 11: laminaribiose, 12: deoxyribose, 13: β-methyl D-galactoside, 14: α-methyl D-galactoside, 15: β-methyl D-glucoside, 16: α-methyl D-glucoside, 17: β-methyl D-xyloside, 18: β-methyl D-arabinoside, 19: α-methyl D-mannoside, 20: α-methyl D-xyloside. *: Data of CH-surface area from Miyajima et al. (Ref. 6).

† Present address: Department of Education, Kogakkan University, Ise-shi 516.

and K_{av}° is the partition coefficient in the absence of sugar-polystyrene interactions.[2] Accordingly, $\ln[(K_{av}-K_{av}^{\circ})/K_{av}^{\circ}]$ is a measure of the standard free energy of sugar-polystyrene interaction and hence it was taken as a measure of the polystyrene affinity of sugars in the present study.

Figure 1 shows the polystyrene affinity, $\ln[(K_{av}-K_{av}^{\circ})/K_{av}^{\circ}]$, of monosaccharides, glucodisaccharides and methyl glycosides plotted against the CH index. As previously noted,[5] the parallelism between the order of the polystyrene affinity and that of the CH index does not hold for glucodisaccharides and methyl glycosides. However, it is important to note that on the macroscale the CH index well correlates with the polystyrene affinity of sugars. Strictly, direct comparison of monosaccharides (methyl glycosides included) with disaccharides may not be valid as the multi-point interactions of sugar molecule with polystyrene will increase with increase of the molecular weight of sugars. (Note that the effect of the multi-point interactions, in which the hydrophobic surfaces on the glucose residues of the disaccharide molecules contribute cooperatively, but not additively, to the polystyrene affinity, is not taken into account in the formulation of K nor of the CH index.) Indeed, for monosaccharides and methyl glycosides an approximate linearity appears to exist between the two parameters. This strongly suggests that the hydrophobicity of sugars is primarily determined by the hydrophobic/hydrophilic surface balance. The failure of the CH index to predict the order of K_{av} of α and β-methyl D-mannosides ($\alpha(10.6) \gg \beta(4.3)$) indicates that the neglect of the anomeric equilibrium effect in the calculation of the CH index does not impose a serious limitaion on the validity of the CH index. Rather, more or less poor accuracy of the CH index compared with index A may be attributed to an increase in the conformational freedom of glucodisaccharides and methyl glycosides leading to an increased deviation from the crystalline state.

References

1) M. Janado and T. Nishida, *J. Solution Chem.*, **10**, 489 (1981).
2) M. Janado and Y. Yano, *J. Solution Chem.*, **14**, 891 (1985).
3) M. Janado and Y. Yano, *Bull. Chem. Soc. Jpn.*, **58**, 1913 (1985).
4) Y. Yano and M. Janado, *J. Chromatogr.*, **200**, 125 (1980).
5) Y. Yano, K. Tanaka, Y. Doi, and M. Janado, *J. Solution Chem.*, in press.
6) K. Miyajima, K. Machida, and M. Nakagaki, *Bull. Chem. Soc. Jpn.*, **58**, 2595 (1985).
7) R. B. Hermann, *J. Phys. Chem.*, **76**, 2754 (1972).

Preparation of Highly Pure Lithium and Sodium Fluorides Using Solvent Extraction

Kenji KOBAYASHI
NTT Opto-electronics Laboratories, Tokai-mura, Naka-gun, Ibaraki 319-11
(Received November 17, 1987)

Synopsis. LiF and NaF can be purified by solvent extraction. The impurity concentrations in the purified NaF are 2.5 ng g^{-1} for chromium, 60 ng g^{-1} for iron, 0.03 ng g^{-1} for cobalt, and 1.5 ng g^{-1} for copper. The concentrations in the purified LiF are 42 ng g^{-1} for nickel and 2.1 ng g^{-1} for copper.

For the fabrication of ultra-low-loss fluoride optical glass fibers (lower than 0.1 dB km^{-1}), it is necessary to decrease the amounts of impurities to a level of 1 ng g^{-1}. This is because the presence of more than 1 ng g^{-1} of a transition element in fluoride optical glass fibers causes transmission loss from the fibers.[1] LiF and NaF are used as raw materials in fiber production. Impurity concentrations of transition elements in LiF and NaF prepared by distillation and zone melting are at the 1 μg g^{-1} level.[2,3] Preparation of highly pure LiF and NaF in which transition elements are lower than 1 μg g^{-1} have not been reported yet.

In the determination of iron, copper, and nickel, chelate extractions of iron(III) with cupferron, copper(II) with dithizone, and nickel(II) with dimethylglyoxime have been used frequently.[4] The extraction technique can also be applied to the removal of iron(III), copper(II), and nickel(II) impurities from LiF and NaF, because lithium(I) and sodium(I) do not react with these reagents.

The determination of trace amounts of transition elements at 1 ng g^{-1} is difficult. Although ordinary analytical methods such as atomic absorption spectrometry and spark-source mass spectrometry, etc are sensitive to most elements, the application of these methods is limited when the concentrations of the transition elements are at a level of 1 ng g^{-1}. Neutron Activation Analysis(NAA) is a highly sensitive method for determining transition elements and the determination of chromium, cobalt, and copper of an order of ng g^{-1} in silica glass by NAA has been reported.[5] This paper describes the preparation of highly pure LiF and NaF by solvent extraction, and the NAA of transition elements in the purified LiF and NaF.

Experimental

Reagents and Apparatus. Reagent grade of LiCl and Na_2CO_3 were used as starting materials. Three chelate reagents (dithizone, cupferron, and dimethylglyoxime) were used without further purification. Highly pure 49% hydrofluoric, nitric, and hydrochloric acids, as well as ammonia, carbon tetrachloride, and chloroform were obtained commercially. Distilled water was produced by sub-boiling distillation. Radioactivity was measured by a Ge(Li) detector coupled with a 4096-channel pulse-height analyzer (4K-PHA), and a low-background gas-flow counter.

Tracer Experiment. $^{60}Co(T_{1/2}=5.27\ y)$, $^{65}Ni(T_{1/2}=2.52\ h)$, and $^{64}Cu(T_{1/2}=12.7\ h)$ tracers were prepared by irradiation of small amounts of cobalt nitrate, highly pure nickel and copper metals in the JRR-2 nuclear reactor and the product was dissolved in 1 mol dm^{-3} nitric acid. $^{59}Fe(T_{1/2}=44.6\ d)$ tracer($FeCl_3$ in 0.5 mol dm^{-3} hydrochloric acid solution; radiochemical purity=99%) was imported from USA and was diluted before use. Ten μg of each tracer was added to the solution containing 10 g of LiCl or Na_2CO_3. Then, ^{59}Fe(III), ^{60}Co(II) and ^{64}Cu(II), and ^{65}Ni(II) were extracted with cupferron into chloroform, dithizone into carbon tetrachloride, and dimethylglyoxime into chloroform, respectively. The radioactivity of the organic extract was measured and recovery for each element was calculated. Each recovery for extraction of iron(III) with cupferron at pH=0.4—6.1, cobalt(II) with dithizone at pH=4.0—6.5, nickel(II) with dimethylglyoxime at pH=9.0—10.0, and copper(II) with dithizone at pH=0.3—6.5 was more than 99%. Thus, iron(III), cobalt(II), and copper(II) can be extracted with the above chelate reagents at pH=4.0 and nickel(II) is extracted with dimethylglyoxime into chloroform at pH=9.0.

Preparation of LiF and NaF. LiCl (100 g) or Na_2CO_3 (100 g) was dissolved in 100 ml of distilled water. The LiCl solution was adjusted to pH=4.0, and extractions were carried out with cupferron into chloroform and dithizone into carbon tetrachloride. The residual aqueous solution was adjusted to pH=9.0, and the nickel impurity was extracted with dimethylglyoxime into chloroform. The impurities in the Na_2CO_3 solution were also extracted with the same reagents and at pH value as described above. A solution of 150 ml of 49% highly pure hydrofluoric acid was added to the residual aqueous solution and alkali metal fluoride was precipitated. The precipitate was aged for 1 d, washed with distilled water, dried in a vacuum oven at 100 °C for 2 d, and dehydrated at 400 °C for 5 h in argon atmosphere. The prepared LiF and NaF were identified by X-ray powder diffraction analysis.

Neutron Activation Analysis. LiF, LiCl, NaF, and Na_2CO_3 samples (0.2—2.0 g) and chromiun, iron, cobalt, nickel, and copper standards (1.0 μg—4.0 mg) were irradiated in the JRR-2 or JRR-4 nuclear reactor at a thermal neutron flux of $3—8\times10^{13}$ n cm^{-2} s^{-1}. In order to determine nickel and copper, the irradiation was carried out for 5—20 min, while for chromium, iron, and cobalt the irradiation time was 265 h. After irradiation for 265 h, the irradiated NaF was cooled 30 d until undesired radioactivities of $^{24}Na(T_{1/2}=15\ h)$ had almost decayed. The radioactivities of NaF and chromium, iron, and cobalt standards were measured by a Ge(Li) detector coupled with a 4K-PHA for $1\times10^4—3\times10^5$ s. The concentrations of chromium, iron, and cobalt were determined by the photopeaks from ^{51}Cr(320 keV), ^{59}Fe(1099 keV), and ^{60}Co(1332 keV). Trace amounts of nickel and copper were determined by the comparison method of substoichiometric radioactivation analysis. Carriers of nickel (0.5 mg) and copper (0.2 mg) were added to the irradiated samples, and the samples were dissolved in 0.1 mol dm^{-3} nitric acid. Substoichiometric extractions of copper with dithizone into carbon tetrachloride at pH 1.0 and nickel with sodium diethyldithiocarbamate into carbon tetrachloride at pH 9.0 were carried out.[6,7] The irradiated

Table 1. Impurity Concentrations in LiF, LiCl, NaF, and Na_2CO_3 by NAA

Element	Analytical result/ng g^{-1} a)						
	LiF-1	LiF-2-1	LiF-2-2	LiCl	NaF-1	NaF-2	Na_2CO_3
Cr	—	—	—	—	2.5±0.3	29±1.7	35±2.1
Fe	—	—	—	—	60±10	440±40	690±70
Co	—	—	—	—	0.03±0.01	9.6±1.0	0.31±0.03
Ni	42±4.5	190±9.5	570±29	150±7.5	<40	<40	<40
Cu	2.1±0.6	37±4.0	550±28	13±4.3	1.5±0.5	22±2.9	13±4.0

a) Mean value ± standard deviation for five determinations.

nickel and copper standards were treated with exactly the same substoichiometric extraction as was described for the sample. The radioactivities of the extracts for the samples and standards were measured by a low-background gas-flow counter for 20 min.

Results and Discussion

The analytical results for chromium, iron, cobalt, nickel, and copper in LiF, LiCl, NaF, and Na_2CO_3 are shown in Table 1.

Results for the elements are mean values for five determinations. LiF-1 and NaF-1 were prepared samples. LiF-2-1, LiF-2-2, and NaF-2 were analytical grade commercial samples. The impurity concentrations in LiF-1 and NaF-1 were lower than those in LiCl and Na_2CO_3, which were the starting materials for the preparation of LiF-1 and NaF-1, and purified LiF and NaF could be prepared by the solvent extraction method. The concentration in LiF-1 was 42 ng g^{-1} for nickel, and 2.1 ng g^{-1} for copper. These values were lower than those in LiF-2-1 and LiF-2-2 by a factor of 2.2×10^{-1} to 3.8×10^{-3}. The impurity concentrations in NaF-1 were 2.5 ng g^{-1} for chromium, 60 ng g^{-1} for iron, 0.03 ng g^{-1} for cobalt, and 1.5 ng g^{-1} for copper and these values were lower than those in NaF-2 by a factor of 3.0×10^{-3} to 8.6×10^{-1}. The 40 ng g^{-1} detection limit for nickel was due to the interference by the radioactivity of ^{24}Na.

It was found that solvent extraction is a useful method for the preparation of highly pure LiF and NaF.

References

1) Y. Ohishi, S. Mitachi, and T. Kanamori, *Jpn. J. Appl. Phys.*, **20**, L787 (1981).
2) A. J. Singth, *J. Appl. Phys.*, **36**, 1367 (1966).
3) F. Rosenberger, "Ultrapurity," ed by M. Zief and R. Speights, Marcel Dekker Inc., New York (1972), p. 3.
4) J. Stary, "The Solvent Extraction of Metal Chelates," Pergamon Press, Oxford (1964), p. 116.
5) K. Kobayashi and K. Kudo, *J. Radioanal. Chem.*, **53**, 233 (1979).
6) N. Suzuki and K. Kudo, *Anal. Chim. Acta*, **32**, 456 (1965).
7) K. Kudo and N. Hishinuma, *J. Radioanal. Chem.*, **5**, 331 (1970).

Solvatochromism of the Co(III) Complexes with Macrocyclic N_3O_3-Type Ligands

Mika FUJIWARA, Michiko YOSHITAKE,† Yutaka FUKUDA, and Kozo SONE*
Department of Chemistry, Faculty of Science, Ochanomizu University, Ohtsuka, Bunkyo-ku, Tokyo 112
(Received December 24,1987)

Synopsis. The color and visible spectrum of [Co(tacnta)] and [Co(tacntp)]·$3H_2O$ depend remarkably on the acceptor number of the solvent, as also do those of K[Co(edta)]·$2H_2O$ and related chelates. The changes are especially large in the case of [Co(tacntp)]·$3H_2O$, extending to solvents of high acidity. A plausible explanation is given for this solvatochromism.

Two types of solvatochromism are known to take place in solutions of metallic complexes.[1,2] They are: (i) the solvatochromism caused by structural changes in the first coordination sphere, for example, that of [Cu(acac)(tmen)]ClO_4 studied by Fukuda, Sone, and collaborators[1] which depends on the donor number (DN) of the solvent,[3] and (ii) the solvatochromism caused by the solute-solvent interactions in the second coordination sphere, for example, that of [Fe(bipy)$_2$-(CN)$_2$] studied by Schilt[4] which depends on the acceptor number (AN) of the solvent.[3]

Recently, we synthesized the Co(III) complexes of two macrocyclic N_3O_3-type ligands, 1,4,7-triazacyclononane-*N*,*N*′,*N*″-triacetate (tacnta) and 1,4,7-triazacyclononane-*N*,*N*′,*N*″-tripropionate (tacntp) (cf. Fig. 1). In the course of this work, we noticed that they show a characteristic solvatochromism in polar solvents, which seems to be related to that of K[Co(edta)]·$2H_2O$ and related complexes reported by Taura,[5] Ogino, and collaborators.[6] Since these are all inert 6-coordinated complexes, it seems that the observed solvatochromism is due to the solvent-solute interaction in the second coordination sphere. The outline of our spectral observations, and their plausible explanation, are given in this paper.

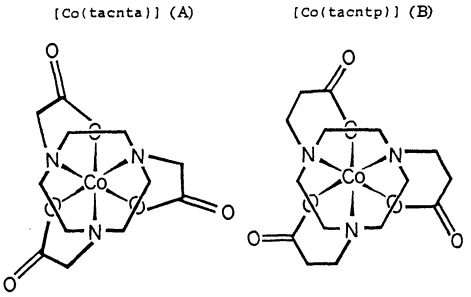

Fig. 1. Structures of the ligands and complexes.

Experimental

Preparation of Ligands. Tacnta was prepared according to the method described in the literature.[7] Tacntp was prepared similarly, but using 3-chloropropionic acid instead of chloroacetic acid. Because they were difficult to purify, the raw products obtained were directly converted to the Co(III) complexes.

Preparation of Complexes. [Co(tacnta)] was prepared according to the method described in the literature[7] (Found: C, 39.31; H, 5.12; N, 11.73%). To prepare [Co(tacntp)]·$3H_2O$, $CoCl_2 \cdot 6H_2O$ was added to the aqueous solution of tacntp. After adjusting the pH to ca. 5.5 with NaOH(aq), the mixture was stirred vigorously for several hours, and then evaporated to a small volume, and purified by passing into a column of Sephadex G-15. The eluent was evaporated to a small volume, and methanol was added to it to yield the complex as a violet powder. After washing twice with methanol, the residue was recrystallized from formamide-ethanol. Found: C, 38.78; H, 6.76; N, 9.14%. Calcd for $CoC_{15}H_{30}N_3O_9$: C, 39.57; H, 6.64; N, 9.23%.

Solvents. Methanol was purified by distillation over magnesium. Other solvents (Guaranteed Grade) were used without further purification.

Measurements. The electronic absorption spectra of the complexes were measured on a Hitachi 340 Recording Spectrophotometer using a 10-mm cell at room temperature (ca. 25 °C).

Results and Discussion

Some of the visible absorption spectra of [Co(tacnta)] (A) and [Co(tacntp)]·$3H_2O$ (B) obtained are shown in Fig. 2. Each of them shows two bands: the band I at ca. (19—20)×10^3 cm^{-1} and the band II at ca. (26—27)×10^3 cm^{-1}, as expected from their *fac*-N_3O_3-type structure.[8] Both bands shift slightly according to the solvent polarity, so that a remarkable color change from bluish violet to reddish violet comes about.

If the $\tilde{\nu}_{max}$ value of the band I is plotted against the Acceptor Number (AN) of the solvent, it can be seen that there is a good parallelism between these values,

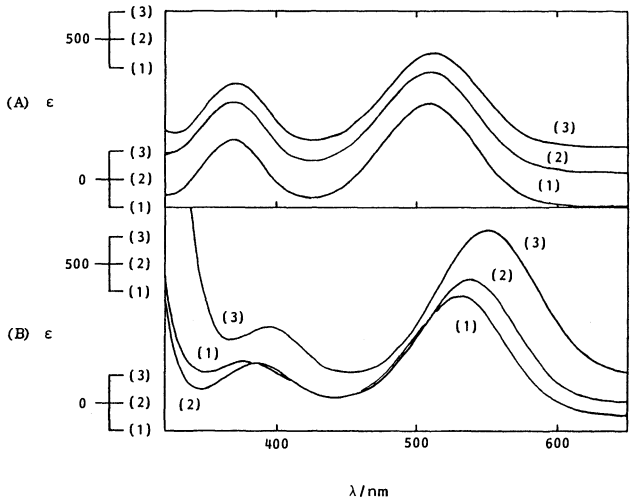

Fig. 2. Electronic spectra of the complexes. A: [Co(tacnta)]. Solvents: 1, HCOOH; 2, H_2O; 3, $HCONH_2$. B: [Co(tacntp)]·$3H_2O$. Solvents: 1, HCOOH; 2, H_2O; 3, $(CH_3)_2SO$.

† Present address: National Research Institute for Metals, 2-3-12 Nakameguro, Meguro-ku, Tokyo 153.

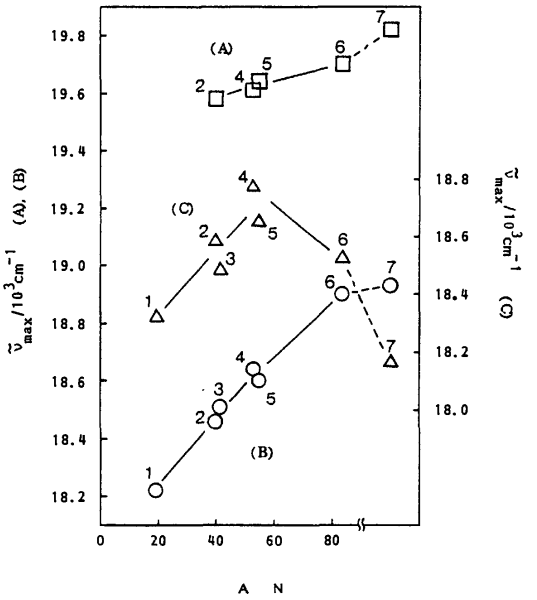

Fig. 3. Relation of $\tilde{\nu}_{max}$ with AN. A: [Co(tacnta)], B: [Co(tacntp)]·$3H_2O$, C: K[Co(edta)]·$2H_2O$.[a] Solvents: 1, $(CH_3)_2SO$; 2, $HCONH_2$; 3, CH_3OH; 4, CH_3COOH; 5, H_2O; 6, HCOOH; 7, H_3PO_4 (85%).[b] a) The AN of H_3PO_4 (85%) is expected to be higher than HCOOH, but is not exactly known. So the points 7 are given on a blank scale. b) The points 1, 2, and 3 on curve C were found to be slightly lower than those in the literature,[6] but the differences ($\Delta\tilde{\nu}$: $(0.03—0.06)\times10^3 cm^{-1}$) were mostly in the range of experimental error. The points 4, 6, and 7 on the same curve were newly obtained in the present study.

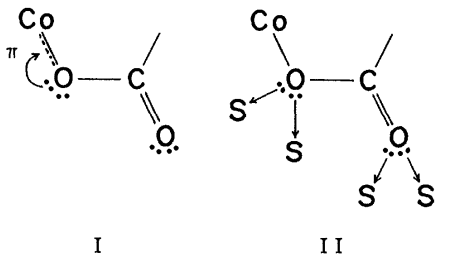

I II

Fig. 4. Effect of solvation by acceptor solvent molecules (S in II) on the structure of a coordinated COO^- group(I).

as that observed with K[Co(edta)]·$2H_2O$ and related complexes.[5,6] Figure 3 shows such a plot. It can be seen that the rise in $\tilde{\nu}_{max}$ with increasing AN is small with [Co(tacnta)], but with [Co(tacntp)]·$3H_2O$ it is much larger than with K[Co(edta)]·$2H_2O$, the curve of which tends to drop when the AN becomes very large.[9,10]

One can now explain the solvatochromism as follows. The COO^- groups of these complexes, which are most susceptible to outer influences, are solvated by the polar solvents which accept their lone-pair electrons. The strength of this solvation is governed by the AN of the solvent. This solvation weakens the (Co←O)σ and π bonds as shown in Fig. 4, by pulling out the lone-pair electrons on the O atoms toward the solvent molecules. The weakening of the σ bonds decreases the value of 10 Dq, but the weakening of the π bonds increases it.[11] Since the weaker π bonds will be more strongly affected by this kind of solvation, the value of the apparent 10 Dq tends to increase, shifting $\tilde{\nu}_{max}$ to a higher value.

It is also plausible that the large solvatochromism of [Co(tacntp)]·$3H_2O$ is related to the relative weakness of the COO^-–Co bonds in it which belong to the more deformable 6-membered chelate rings, as compared with those in the other complexes which belong to the rigid 5-membered chelate rings.

The authors are cordially grateful to Prof. Susumu Takamoto of Gakushuin University for his kind aid in the preparation of the macrocyclic ligands.

References

1) K. Sone and Y. Fukuda, "Ions and Molecules in Solution," ed by N. Tanaka, H. Ohtaki, and R. Tamamushi, Elsevier, Amsterdam (1983), p. 251.
2) R. W. Soukup and R. Schmid, *J. Chem. Educ.*, **62**, 459 (1985).
3) V. Gutmann, "The Donor-Acceptor Approach to Molecular Interactions," Plenum, New York (1978).
4) A. A. Schilt, *J. Am. Chem. Soc.*, **82**, 3000, 5779 (1960); **85**, 904 (1963).
5) T. Taura, *Chem. Lett.*, **1984**, 2011.
6) N. Miura, M. Shimura, and H. Ogino, *Bull. Chem. Soc. Jpn.*, **60**, 1349 (1987).
7) M. Takahashi and S. Takamoto, *Bull. Chem. Soc. Jpn.*, **50**, 3413 (1977).
8) N. Matsuoka, J. Hidaka, and Y. Shimura, *Bull. Chem. Soc. Jpn.*, **40**, 1868 (1967).
9) This drop which was found in the present study is probably caused by the notable weakening of the (Co←O)σ bonds in very strong acceptor solvents, which eventually will lead to a decrease in 10 Dq; the fact that the tacnta and tacntp complexes do not show such a drop may be taken as proof of their robustness in such acceptor solvents.
10) A set of curves which are similar in shape, and in the magnitude of the shifts in $\tilde{\nu}_{max}$, to those in Fig. 3 can also be observed with the $\tilde{\nu}_{max}$ values of the band II. Here, however, the accuracy of the curves A and B is lower, since band II is weaker than band I and is more difficult to locate exactly in some cases.
11) A. B. P. Lever, "Inorganic Electronic Spectroscopy," 2nd ed., Elsevier, Amsterdam (1984), p. 751.

Pheophytinization of Chlorophyll *a* and Chlorophyll *a'* in Aqueous Acetone

Hitoshi MAZAKI and Tadashi WATANABE*
Institute of Industrial Science, University of Tokyo, Roppongi, Minato-ku, Tokyo 106
(Received November 20, 1987)

Synopsis. Chlorophyll (Chl) *a* and its C-10 epimer, Chl *a'*, are compared for pheophytinization (demetallation) kinetics in aqueous acetone containing HCl. For each pigment the pheophytinization rate is of second order with respect to proton, and under identical conditions Chl *a'* is pheophytinized by roughly 50% faster than Chl *a*, due probably to weaker Mg-N bonds in Chl *a'*.

Our recent pigment composition analyses on higher plant chloroplasts, photosystem (PS) I and II particles, and several cyanobacteria showed for the first time that one molecule of Chl *a'*, or the C-10 epimer[1] of Chl *a*, is closely associated with the PS I reaction center (P700).[2,3] This has prompted us to carry out detailed physicochemical characterization of Chl *a'* against Chl *a*. In this Note we compare Chls *a* and *a'* for the kinetics of pheophytinization (replacement of the central Mg^{2+} ion with two protons), which would reflect the Mg-N bond strength in the chlorin macrocycle.

A few works have been reported on the pheophytinization of Chl derivatives. Following earlier observations by Mackinney and Joslyn,[4] Schanderl et al. compared Chl *a* and *b* pheophytinization rate constants in aqueous acetone at a single HCl concentration of 10^{-4} M (M=mol dm^{-3}).[5] A work of Berezin et al.[6] suggested indirectly that the Chl *a* pheophytinization rate is of second order with respect to proton in *t*-butyl alcohol containing trichloroacetic acid. The pheophytinization kinetics of Chl *a* in monomolecular films[7] and in heated green leaves[8] have been investigated. However, quantitative comparison between Chls *a* and *a'* with regard to pheophytinization kinetics has not been reported in the literature.

Experimental

Chls *a* and *a'*, with epimeric purity higher than 98%, were prepared by means of preparative scale high-performance liquid chromatography (HPLC) as described elsewhere.[9] Chl *a* or Chl *a'* was dissolved in an acetone/water (3/1, v/v) mixed solvent, and the solution was introduced in a temperature-controlled glass cell placed in a JASCO UVIDEC-650 spectrophotometer. The absorbance change due to the progress of pheophytinization was measured as a function of time at 430 nm [absorption peak for Chl *a*(*a'*)] or 409 nm [absorption peak for pheophytin (Pheo) *a*(*a'*)]. The concentration[10] of Chl *a*(*a'*) in aqueous acetone was 1.0×10^{-6} M, and that of HCl was varied in a range from 3×10^{-4} to 2×10^{-3} M. Thus the pheophytinization reaction

$$\text{Chl } a(a') + n\text{H}^+ \xrightarrow{k(k')} \text{Pheo } a(a') + \text{Mg}^{2+} \qquad (1)$$

can be regarded as pseudo-first-order with respect to Chl *a*(*a'*) concentration, with k and k' being the apparent rate constants for Chls *a* and *a'*, respectively. The k and k' values were obtained by fitting the time courses of Chl *a*(*a'*) concentration to the following kinetic formula:

$$\ln([\text{Chl}]_t/[\text{Chl}]_0) = -k(k')t \qquad (2)$$

where $[\text{Chl}]_0$ and $[\text{Chl}]_t$ are the concentrations of Chl *a*(*a'*) at the onset of measurement and at time t, respectively.

Results and Discussion

Figure 1 illustrates the temporal evolution of the relative concentration of Chl *a*(*a'*), observed at 430 nm, for different H^+ concentrations at 25 °C. The apparent rate constants are calculated from the slopes of the lines and Eq. 2. Under identical conditions, the k and k' values thus obtained were practically the same as those obtained by observing absorbance increase at 409 nm.

The rate constants from Fig. 1 are plotted in Fig. 2 against $-\log[H^+]$. The slope of −2.0 common for both Chl *a* and Chl *a'* indicates that the rate is indeed of second order with respect to proton (n=2 in Eq. 1). The pheophytinization rate of Chl *a'* is 1.4-fold higher than that of Chl *a* at a given $-\log[H^+]$ value; this is in contrast to a qualitative observation by Hynninen[11] that Chl *a'* was pheophytinized much more rapidly than Chl *a*. The higher tendency of Chl *a'* to be pheophytinized is due probably to its weaker Mg-N coordination bonds in the chlorin ring. A recent ^{13}C NMR

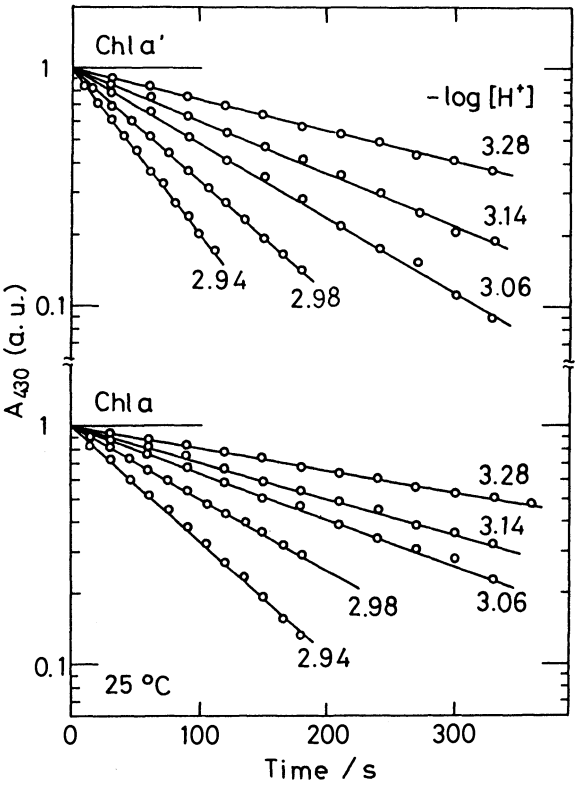

Fig. 1. Kinetic plots for the pheophytinization of Chls *a* and *a'* in aqueous acetone at different H^+ concentrations.

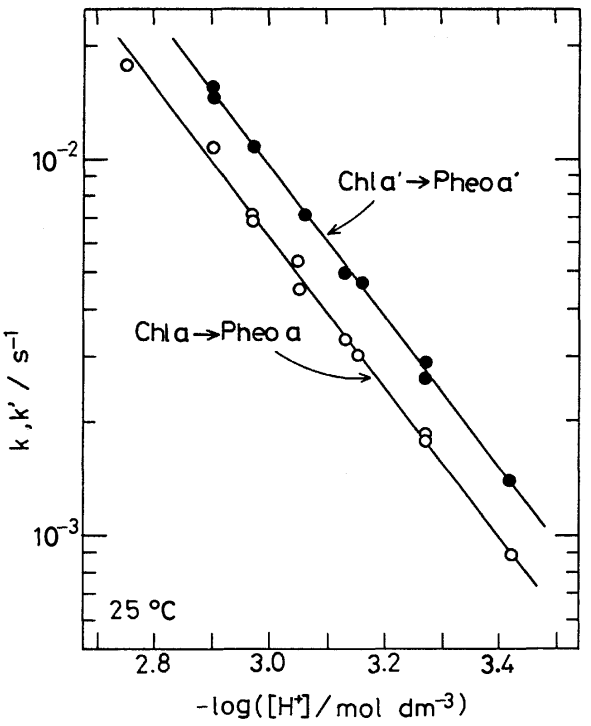

Fig. 2. Dependence of the pheophytinization rate constant k for Chl a (○) and k' for Chl a' (●) on H^+ concentration.

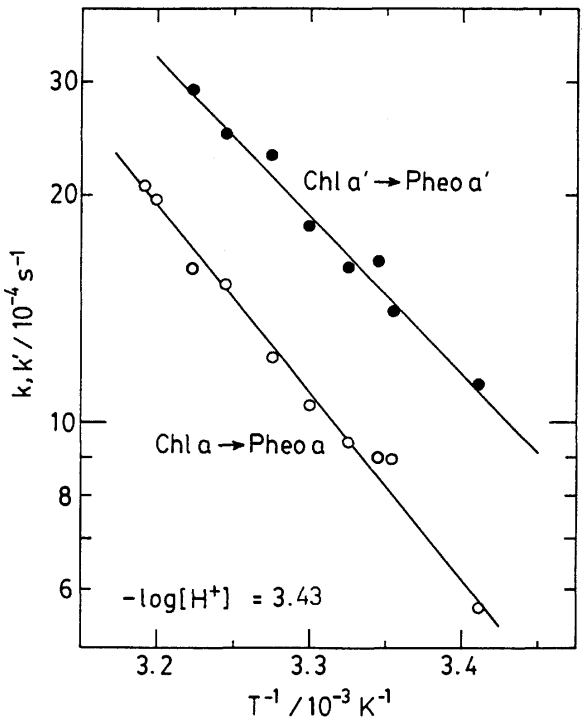

Fig. 3. Arrhenius plots over a temperature range 10—40 °C for the pheophytinization rate constants for Chl a (○) and Chl a' (●).

study on Chl derivatives[12] indicates that an enhanced steric hindrance between the bulky substituents (the C-7 phytyl chain and C-10 methoxycarbonyl group) in the Chl a' molecule induces a peripheral strain, especially in rings IV and V,[1] which in turn influences the conformation and stability of the whole macrocycle.

In aqueous acetone at 25 °C, though with a slightly different acetone/water volume ratio (4/1), Schanderl et al.[5] obtained a k value of 1.72×10^{-4} s^{-1} at $-\log[H^+]=4.0$. Extrapolation of our k vs. $-\log[H^+]$ plot in Fig. 2 to $-\log[H^+]=4.0$ yields $k=6.97\times10^{-5}$ s^{-1}. The 2.5-fold difference seen between these two values might reflect a difference in the solvent composition.[13]

The temperature dependence of the pheophytinization rates was examined in a range from 10 °C to 40 °C at a $-\log[H^+]$ value of 3.43. The Arrhenius plots in Fig. 3 gives the activation energies of 47.4 and 40.4 kJ mol^{-1} for Chls a and a', respectively. The former value compares well with a literature value[5] of 43.5 kJ mol^{-1}.

Based on the results presented above, the pseudo-first-order rate constants $k(k')$ for the Chl $a(a')$ pheophytinization in aqueous acetone are expressed as follows:

$$k\ /s^{-1} = 1.30\times10^{12}\,[H^+]^2\exp(-47400[J]/RT)$$
$$k'/s^{-1} = 1.20\times10^{11}\,[H^+]^2\exp(-40400[J]/RT)$$

The authors are grateful to Mr. M. Nakazato, Nampo Pharmaceutical Co., Ltd., for his help in preparing Chl a and a' samples. This work has been supported partially by a Grant-in-Aid from the Ministry of Education, Science and Culture (No. 62602508).

References

1) See Ref. 2 for the carbon numbering and structure of Chl derivatives.
2) T. Watanabe, M. Nakazato, H. Mazaki, A. Hongu, M. Konno, S. Saitoh, and K. Honda, *Biochim. Biophys. Acta*, **807**, 110 (1985).
3) T. Watanabe, M. Kobayashi, M. Nakazato, I. Ikegami, and T. Hiyama, "Progress in Photosynthesis Research," ed by J. Biggins, Martinus Nijhoff, Dordrecht, The Netherlands (1987), Vol. 1, pp. 303—306.
4) G. Mackinney and M. Joslyn, *J. Am. Chem. Soc.*, **62**, 231 (1940); **63**, 2530 (1941).
5) S. H. Schanderl, C. O. Chichiester, and G. L. Marsh, *J. Org. Chem.*, **27**, 3865 (1962).
6) B. D. Berezin, A. N. Drobysheva, and L. P. Karamanova, *Russ. J. Phys. Chem.*, **50**, 1194 (1976).
7) M. Rosoff and C. Aron, *J. Phys. Chem.*, **69**, 21 (1965).
8) D. R. Haisman and M. W. Clarke, *J. Sci. Fd. Agric.*, **26**, 1111 (1975).
9) T. Watanabe, M. Nakazato, M. Konno, S. Saitoh, and K. Honda, *Chem. Lett.*, **1984**, 1411.
10) The volume reduction by mixing acetone with water was taken into account in calculating concentrations.
11) P. Hynninen, *Acta Chem. Scand.*, **27**, 1487 (1973).
12) S. Lötjönen and H. Hynninen, *Org. Magn. Reson.*, **21**, 757 (1983).
13) However, by closely tracing the measurement described in Ref. 5, we obtained a k value of 5.4×10^{-5} s^{-1} at 25 °C and $-\log[H^+]=4.0$.

Sesquiterpene Lactones from Flowers of *Picris hieracioides* L

Takeshi KANAYAMA and Masahiro TADA*
Laboratory of Bio-organic Chemistry, Tokyo University of Agriculture and Technology, Fuchu, Tokyo 183
(Received February 17, 1988)

Synopsis. The isolation and structural elucidation of four guaianolides from the antimicrobial fractions of the flowers of *Picris hieracioides* L. (Compositae) are reported. Two of them are new compounds.

The flowers of *Picris hieracioides* L. var. *japonica* Regel (Compositae) are bitter and these cause a contact allergy for human skin. Schönbeck reported that the antibiotic activity of flowers of many higher plants is stronger than that of the other parts, leaves, roots and branches.[1] In the course of our investigation of antimicrobial compounds from flowers of higher plants,[2] we found that the extract of the flowers of *P. hieracioides* L. var. *japonica* Regel showed antimicrobial activity by the paper-disk method against *Bacillus subtilis*. Meanwhile, Nishimura et al. reported the isolation of some sesquiterpene lactone glycosides from whole plants of *P. hieracioides* L. var. *japonica* Regel.[3] We report here the isolation of two new sesquiterpene lactones, hieracin I and II with the known guaianolides, jacquilenin[4] and 8-deoxylactucin[5] from the antimicrobial fractions of methanol extract of the flowers of *P. hieracioides* L. var. *japonica* Regel.

The methanol extract of flowers (3.0 kg) of *P. hieracioides* L. var. *japonica* Regel. was concentrated in vacuo and the residue was partitioned with ethyl acetate and water. The antimicrobial activity [paper disk method against *B. subtilis* (IFO 3734)] was found in the ethyl acetate fraction. The residue of the ethyl acetate phase was chromatographed on silica gel with hexane-ethyl acetate. The active fractions were purified by HPLC to give an antimicrobial compound (**A**, 30 mg) and other compounds (**B**, 150 mg; **C**, 5.2 mg; and **D**, 0.5 mg).

8-Deoxylactucin (1). The spectroscopic properties (High resolution MS IR, ^{1}H NMR, and ^{13}C NMR) suggested that the compound **A** is a sesquiterpene lactone. The presumed structure from the ^{1}H-^{1}H COSY[6] and the J-resolved 2D[7] agreed with 8-deoxylactucin (**1**). The reported ^{1}H NMR data[5,8] of 8-deoxylactucin **1** corresponded with our data of the compound **A**.

Jacquilenin (2). The spectral data showed that compound **B** is very similar to 8-deoxylactucin (**1**) although one of the double bonds is saturated. Finally the structure of **B** was identified to be jacquilenin (**2**) by comparing the ^{1}H NMR (^{1}H-^{1}H COSY and NOESY[9]) and the ^{13}C NMR data with those of jacquilenin (**2**).[5,10]

Two new guaianolides, which were named hieracin I (**3**) and hieracin II (**4**), were isolated from a more polar fraction than 8-deoxylactucin (**1**).

Hieracin I (3). Compound **C** has a molecular formula $C_{15}H_{20}O_5$ (MS: *m/z* 280.1339, Calcd M, 280.1331). The IR [3450 (br), 1765, 1690, 1620 cm^{-1}] and ^{1}H NMR spectra suggested **C** should be a guaianolide similar to **1** and **2**. The MS (M^+-H_2O at *m/z* 262.1149, Calcd 262.1204), IR, ^{1}H NMR, and ^{13}C NMR spectra [δ 59.08 (d) and 71.90 (s)] proved that **C** has a tertiary hydroxyl group instead of a double bond (C1—C10) of jacquilenin **2**. The partial structure (**P**) was clearly revealed by the ^{1}H-^{1}H COSY spectrum of **C**. These observations led to the structure **3** for compound **C** which was named hieracin I. The chemical shift of H-13 (δ 1.24, d, J=7.0 Hz) and the coupling constant ($J_{7\alpha\text{-}11\beta}$=12.5

Table 1. NMR Data of 8-Deoxylactucin (**1**) and Jacqilenin (**2**)

C	8-Deoxylactucin (**1**)		Jacquilenin (**2**)	
	^{13}C NMR	^{1}H NMR[a]	^{13}C NMR	^{1}H NMR
1	131.0		131.1	
2	195.2		195.1	
3	133.2	6.44 (s)	133.2	6.43 (s)
4	171.7		171.6	
5	49.8	3.69 (d, 10.3)	49.5	3.59 (d, 10)
6	83.9	3.61 (dd, 10.3, 10.3)	83.7	3.61 (dd, 10, 10)
7	52.7	2.90 (dddd, 13, 10.3, 3.1, 3.1)	56.1	1.98 (m)
8	24.2	α 2.21 (ddd, 13, 5.7, 2.5)	25.8	α 1.99 (m)
		β 1.45 (dddd, 13, 13, 13, 2.6)		β 1.39 (m)
9	37.3	α 2.51 (ddd, 13, 13, 2.5)	37.7	α 2.40 (m)
		β 2.40 (ddd, 13, 5.7, 2.6)		β 2.42 (m)
10	153.3		153.5	
11	138.4		41.3	2.28 (dq, 12.4, 7.0)
12	172.0		177.2	
13	119.3	a 6.18 (d, 3.1)	12.2	1.25 (d, 7.0)
		b 5.49 (d, 3.1)		
14	21.9	2.45 (s)	21.8	2.43 (s)
15	62.4	a 4.89 (d, 17.8)	62.5	a 4.85 (d, 17.7)
		b 4.54 (d, 17.8)		b 4.48 (d, 17.7)

a) The coupling constants were estimated from the J-resolved 2D spectrum.

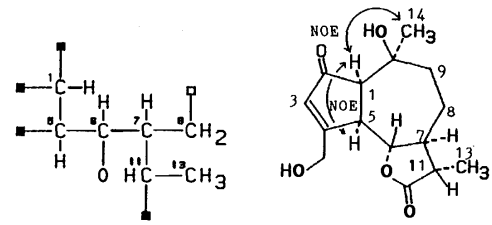

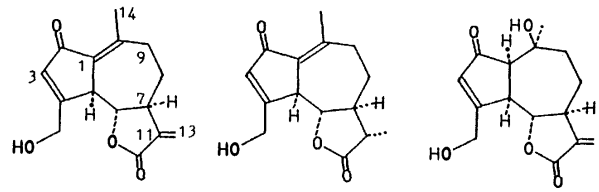

Table 2. NMR Data of Hieracin I (**3**) and II (**4**)

C	Hieracin I (**3**)		Hieracin II (**4**)
	^{13}C (DEPT)[11]	^{1}H[a]	^{1}H
1	59.2 (CH)	2.72 (d, 6.8)	2.74 (d, 6.6)
2	207.0		
3	129.8 (CH)	6.33 (s)	6.35 (s)
4	180.4		
5	50.7 (CH)	3.25 (dd, 9.6, 6.8)	3.35 (dd, 9.9, 6.6)
6	83.3 (CH)	4.34 (dd, 9.6, 9.6)	4.40 (dd, 9.9, 9.9)
7	52.7 (CH)	1.78 (m)	2.01 (m)
8	23.8 (CH_2)	a 1.95 (m)	
		b 1.60 (m)	
9	41.0 (CH_2)		
10	71.9		
11	41.7 (CH)	2.30 (dq, 12.5, 7.0)	
12	177.9		
13	12.7 (CH_3)	1.24 (d, 7.0)	a 6.23 (d, 3.7)
			b 5.55 (d, 3.7)
14	32.3 (CH_3)	1.63 (s)	1.50 (s)
15	63.1 (CH_2)	a 4.83 (d, 17.8)	a 4.87 (d, 17.8)
		b 4.51 (d, 17.8)	b 4.55 (d, 17.8)

a) The coupling constants were estimated from the *J*-resolved 2D spectrum.

Hz) indicated that the methyl group at C-11 is α-oriented.[10] The stereochemistry at C-1, C-5, C-6, C-7 and C-10 was clarified by comparing the coupling constants ($J_{5\alpha\text{-}6\beta}$=9.6 and $J_{6\beta\text{-}7\alpha}$=9.6 Hz) with those of jacquilenin (**2**) ($J_{5\alpha\text{-}6\beta}$=10 Hz and $J_{6\beta\text{-}7\alpha}$=10 Hz) and the NOESY spectrum of hieracin I (**3**). The NOE were observed between H-14 and H-1α and between H-1α and H-5α. Whereas no NOE were observed between H-5α and H-6β, between H-6β and H-7α, and between H-7α and H-11β (Fig. 1).

Hieracin II (4). The spectral deta: MS (Found: *m/z* 278.1144; 260.1082, Calcd for $C_{15}H_{18}O_5$: M, 278.1152; M−H_2O, 260.1047), IR, and ^{1}H NMR [δ 6.23 (1H, d, *J*=3.7 Hz) and 5.55 1H, d, *J*=3.7 Hz)] suggested that compound **D** has an *exo*-methylene group (C11-C13) instead of a methyl group at C-11 of hieracin I (**3**). The novel compound **D** was named hieracin II (**4**).

8-Doxylactucin (**1**) showed moderate activity against *Bacillus subtilis* whereas jacquilenin (**2**) showed no activity against *B. subtilis*. Clearly the antimicrobial activity of **1** should depends on the α-methylene γ-lactone moiety.

Experimental

NMR spectra were measured with a JEOL GX-270 spectrometer in $CDCl_3$ solution containing tetramethylsilane as internal standard. IR spectra were measured on Jasco IR-810 spectrometer. Mass spectra were recorded by JEOL JMS-D300. HPLC was performed by JASCO BIP-1 HPLC system with UV detector on a silica-gel column (Lichrosorb Si-60 10 μm, 7.5×500 mm), an Asahipak-310 column, or an ODS column (INERTSIL 10 μm, 7.5×300 mm). Thin-layer chromatography was carried out on Kieselgel GF_{254} (Merck) in 0.25 mm thickness. Wakogel C-200 (Wako Pure Chemical Industries) was used for column chromatography.

Isolation of Sesquiterpene Lactones. The flowers (3.0 kg) of *Picris hieracioides* were collected in Yamanashi prefecture, Japan in September 1985 and extracted with methanol. The extract was concentrated in vacuo and the residue was partitioned with ethyl acetate and water. The antimicrobial activity was tested by paper-disk method against *Bacillus subtilis* (IFO 3734) for each fraction. The activity was found in the ethyl acetate phase. The residue of the ethyl acetate phase was chromatographed on silica gel with hexane–ethyl acetate. The repeated purification by HPLC on a silica-gel column (Lichrosorb Si-60, 10 μm, 7.53×500 mm) eluted with hexane–ethyl acetate (3:5) and ethyl acetate, and on an ASAHIPAK-310 column eluted with 40%-methanol and on an ODS column (INERTSIL 10 μm, 7.53×300 mm) eluted with 35%-methanol to give 8-deoxylactucin (**1**, 30 mg), jacquilenin (**2**, 150 mg), hieracin I (**3**, 5.2 mg), and hieracin II (**4**, 0.5 mg).

8-Deoxylactucin (1). MS: Found: *m/z* 260.1033, Calcd for $C_{15}H_{16}O_4$: M, 260.1048; IR (film) 3420, 1770, 1690, 1620, 1250, 1130, and 990 cm^{-1}.

Jacquilenin (2). Mp 147—152 °C; MS: Found: *m/z* 262.1194, Calcd for $C_{15}H_{18}O_4$: M, 262.1204; IR (KBr) 3350, 1750, 1660, 1260, and 995 cm^{-1}.

Hieracin I (3). MS: Found: *m/z* 280.1339; 262.1149, Calcd for $C_{15}H_{20}O_5$: M, 280.1311; M^+-H_2O, 262.1204; IR (neat) 3450, 1765, 1690, 1620, and 985 cm^{-1}.

Hieracin II (4). MS: Found: *m/z* 278.1144; 260.1082, Calcd for $C_{15}H_{18}O_5$: M, 278.1152; M^+-H_2O, 260.1047; IR 3400, 1760, 1680, 1620, and 985 cm^{-1}.

We are grateful Dr. H. Hirota (Department of Chemistry, The University of Tokyo) for the measurement of the high resolution mass spectra.

References

1) F. Schönbeck, *Phytopathol. Z.*, **59**, 205 (1967).
2) M. Nagai and M. Tada, *Chem. Lett.*, **1987**, 1337.
3) K. Nishimura, T. Miyase, A. Ueno, T. Noro, M. Kuroyanagi, and S. Fukushima, *Chem. Pharm. Bull.*, **34**, 2518 (1986).
4) J. B. Barrera, J. L. B. Funes, and A. G. Gonzalez, *J. Chem. Soc.*, **1966**, 1298.
5) J. St. Pyrek, *Roczniki Chem.*, **51**, 2165 (1977).
6) W. O. Aue, E. Bartholdi, and R. R. Ernst, *J. Chem. Phys.*, **64**, 2229 (1976); A. Bax and R. Freeman, *J. Magn. Reson.*, **44**, 542 (1981).
7) K. Nagayama, P. Bachmann, K. Wuthrich, and R. R. Ernst, *J. Magn. Reson.*, **31**, 133 (1978).
8) G. Savona and M. Bruno, *J. Nat. Prod.*, **46**, 277 (1983).
9) S. Macura and R. R. Ernst, *Mol. Phys.*, **41**, 95 (1980).
10) F. Bohlmann, C. Zdero, H. Robinson, and R. M. King, *Phytochemistry*, **20**, 2029 (1981).
11) D. M. Doddrell, D. T. Pegg, and M. R. Bendall, *J. Magn, Reson.*, **48**, 323 (1982).

Synthesis of Bis[1,2-bis(methylseleno)vinylenedithio]-tetrathiafulvalene (TMSVT)

Hideyuki NAKANO, Takashi NOGAMI,* and Yasuhiko SHIROTA
Deparment of Applied Chemistry, Faculty of Engineering, Osaka University, Yamadaoka, Suita, Osaka 565
(Received March 12, 1988)

Synopsis. The title molecule was synthesized as an effective donor molecule for highly conductive organic complexes. It is a TTF dirivative possessing four selenium atoms and eight sulfur atoms. Its oxidation potential ($E_{1/2}$) is 0.86 V vs. SCE in THF,which is slightly higher than that of VT and TMTVT.

TTF derivatives possessing multi-chalcogen atoms have recently been found to give materials of interesting solid-state electrical properties. For example, the ion radical salt (BEDT-TTF)$_2$Cu(SCN)$_2$ gave organic superconductors of high T_c (10.4 K)[1] without applying pressure. The superconductivity of various BEDT-TTF salts is a subject of extensive study.[2] Other aspects of the multi-chalcogen TTF derivatives are a molecular fastener effect[3] of a series of TTC$_n$-TTF and high mobility of TTeC$_1$-TTF.[4] One of the important factors governing the electrical properties of these materials is the existence of a chalcogen-chalcogen network in the solid. The syntheses of various TTF derivatives were reviewed by Krief.[5] We have synthesized bis[1,2-bis(methylthio)vinylenedithio]-tetrathiafulvalene (TMTVT)[6] which has twelve sulfur atoms. This molecule has the largest number of chalcogen atoms in TTF derivatives known at present. This paper reports the synthesis of bis[1,2-bis(methylseleno)vinylenedithio]tetrathiafulvalene (TMSVT) which also has twelve chalcogen atoms in the molecule.

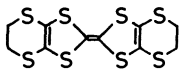
BEDT-TTF

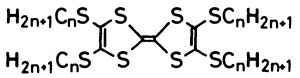
TTC$_n$-TTF

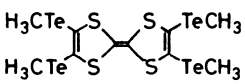
TTeC$_1$-TTF

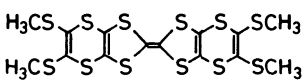
TMTVT

Results and Discussion

Synthesis of TMSVT. The synthetic route of TMSVT is shown in Scheme 1. 4,5-(Vinylenedithio)-1,3-dithiole-2-thione (**1**) was synthesized from 4,5-(ethoxyethylenedithio)-1,3-dithiole-2-thione as reported previously[7,8] with slight modifications.[9] It was lithiated by lithium diisopropylamide (LDA), followed by the selenium insertion reaction under supersonic wave irradiation for 2.5 h. Without supersonic wave irradiation, it took 4—5 h for the completion of the insertion reaction. The selenolate **3** was then reacted with methyl iodide to give 4,5-[1,2-bis(methylseleno)vinylenedithio]-1,3-dithiole-2-thione (**4**). The conversion of

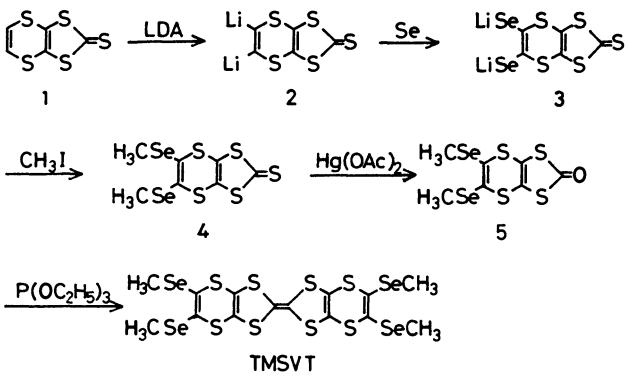

Scheme 1.

the thiocarbonyl group of **4** to a carbonyl group was made by mercury(II) acetate[10] to give 4,5-[1,2-bis-(methylseleno)vinylenedithio]-1,3-dithiol-2-one (**5**). The coupling reaction of **5** was made by heating it in neat triethyl phosphite to give TMSVT.

Two other synthetic routes of TMSVT are conceivable. One is a reaction starting with the lithiation of bis(vinylenedithio)tetrathiafulvalene (VT). However, the poor solubility of VT in THF hampered this route. The other is the reaction starting from the lithiation of 4,5-(vinylenedithio)-1,3-dithiol-2-one (**6**) followed by the selenium insertion reaction and the subsequent reaction with methyl iodide. However, the carbonyl group of **6** was found to be decomposed after the reaction.

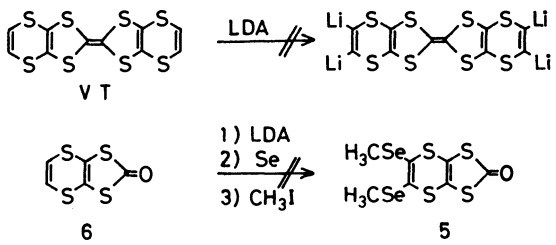

Cyclic voltammetry of TMSVT in THF gave a single and electrochemically irreversible wave. The separation of the redox peak positions was about 0.2 V, which is much larger than that of the reversible wave (0.059 V). In spite of this, if we define the oxidation potential as the mid-point of the redox peaks, $E_{1/2}$ was 0.86 V vs. SCE. This value was higher than those of TMTVT (0.83 V vs. SCE),[6] VT (0.83 V vs. SCE),[7] bis(methylvinylenedithio)tetrathiafulvalene (0.80 V vs. SCE),[7] bis(dimethylvinylenedithio)tetrathiafulvalene (0.80 V vs. SCE),[11] and BEDT-TTF ($E_{1/2}(1)$=0.69 V, $E_{1/2}(2)$=0.82 V vs. SCE). The order of the oxidation potential, TMSVT>TMTVT≈VT, seems to conflict with that reported for methylthio- and methylseleno-

derivatives of TTF or TSeF.[12] However, strict comparison can not be made, because VT, TMTVT, and TMSVT are electrochemically irreversible materials, and only one redox wave is observed for them unlike the cases of TTF, TTC_1-TTF, $TSeC_1$-TTF, TSeF, TTC_1-TSeF, and $TSeC_1$-TSeF;[12] all of the latter compounds gave two redox waves $E_{1/2}(1)$ and $E_{1/2}(2)$.

Experimental

All of the following reactions except the one from **4** to **5** were carried out in a nitrogen atmosphere. The mass spectra of the molecular ion peaks of the following products agreed with those calculated by computer simulation.

4,5-[1,2-Bis(methylseleno)vinylenedithio]-1,3-dithiole-2-thione (4). To the THF solution (150 ml) of diisopropylamine (0.94 g, 9.3 mmol) was added a hexane solution of butyllithium (9 mmol) at −78 °C, and the solution was stirred for 40 min at −78 °C. To this stirred solution was added **1** (1.00 g, 4.5 mmol) in one portion at −78 °C. The solution became dark red. The temperature of the solution was elevated gradually to 0 °C, and it was stirred for another 2 h at 0 °C to obtain the solution of **2**. It was then cooled to −78 °C, and well-ground selenium powder (0.711 g, 9.0 mmol) was added in one portion. The temperature of the stirred solution was elevated gradually to 0 °C under supersonic wave irradiation using a Bransonic 220 (Yamato Kagaku Co. Ltd). The solution was stirred for another 2.5 h at 0 °C to obtain a black solution. No selenium powder could be seen at this stage. The solution was then cooled to −78 °C, and methyl iodide (1.4 g, 9.9 mmol) was added with stirring. The temperature of the solution was then allowed to rise to room temperature, and the solution was stirred for another 1 h at this temperature to obtain a black solution. After evaporating the solvent, the residue was extracted with benzene, washed with water, and the benzene layer dried over Na_2SO_4. The crude product was chromatographed on silica gel using the mixed solvent of chloroform and hexane (1 : 4) as an eluent. The first pale yellow portion was discarded, and the second orange portion gave a yellow powder of **4** (0.338 g, 18.4%). It was recrystallized from the mixed solvent of THF and ethyl alcohol to obtain yellow needles. Mp: 126—127 °C. ^{1}H NMR δ=2.37 (s). MS m/z 410 (strongest M^+). Found: C, 21.03; H, 1.63%. Calcd for $C_7H_6S_5Se_2$: C, 20.59; H, 1.48%.

4,5-[1,2-Bis(methylseleno)vinylenedithio]-1,3-dithiol-2-one (5). The molecule **4** (0.2 g, 0.49 mmol) was dissolved in a mixed solvent of chloroform (40 ml) and acetic acid (40 ml), and mercury (II) acetate (0.312 g, 0.98 mmol) was added in one portion with stirring. The solution was stirred for 30 min at room temperature, and the pale yellow powder filtered off. The filtrate was washed with water, and the organic layer was dried over Na_2SO_4. After evaporating the solvent, the residue was chromatographed on silica gel using a mixed solvent of chloroform and hexane (1 : 1) as eluent, and the first pale yellow portion gave **5** (0.144 g, 75%). It was recrystallized from hexane or ethyl alcohol to obtain pale yellow needles. Mp: 96.5—97.5 °C. ^{1}H NMR δ=2.36 (s). MS m/z 394 (strongest M^+). Found C, 21.64; H, 1.72%. Calcd for $C_7H_6OS_4Se_2$: C, 21.44; H, 1.54%.

Bis[1,2-bis(methylseleno)vinylenedithio]tetrathiafulvalene (TMSVT). The reaction vessel containing **5** (0.204 g, 0.52 mmol) was purged with nitrogen gas, and triethyl phosphite (2.5 ml), which was distilled just before the reaction, was then added. The solution was stirred for a while to obtain a homogeneous solution. It was then heated with stirring, and red powder began to precipitate at around 100 °C. It was stirred at 110 °C for 2 h. After cooling to room temperature, the red powder was collected, washed with methyl alcohol, and dried in vacuum (0.155 g, 75.1%). The product was recrystallized from carbon tetrachloride to obtain red needles. Mp: 185 °C (decomp). ^{1}H NMR δ=2.31 (s). MS m/z 754 (strongest M^+). UV (THF): 338 nm (log ε 4.30) and 306 nm (log ε 4.37). Found: C, 22.24; H, 1.83%. Calcd for $C_{14}H_{12}S_8Se_4$: C, 22.35; H, 1.61%.

References

1) H. Urayama, H. Yamochi, G. Saito, K. Nozawa, T. Sugano, M. Kinoshita, S. Sato, K. Oshima, A. Kawamoto, and J. Tanaka, *Chem. Lett.*, **1988**, 55.

2) J. M. Williams and K. Carneiro, *Adv. Inorg. Chem. Radiochem.*, **29**, 249 (1985); J. M. Williams, M. A. Beno, H. H. Wang, P. C. W. Leung, T. J. Emge, U. Geiser, and K. D. Carlson, *Acc. Chem. Res.*, **18**, 261 (1985); for recent proceedings of International Conference of Synthetic Metals, see, *Synth. Metals*, Vols. 17—19 (1987).

3) K. Imaeda, T. Enoki, Z. Shi, P. Wu, N. Okada, H. Yamochi, G. Saito, and H. Inokuchi, *Bull. Chem. Soc. Jpn.*, **60**, 3163 (1987).

4) H. Inokuchi, K. Imaeda, T. Enoki, T. Mori, Y. Maruyama, G. Saito, N. Okada, H. Yamochi, K. Seki, Y. Higuchi, and N. Yasuoka, *Nature (London)*, **329**, 39 (1987).

5) A. Krief, *Tetrahedron*, **42**, 1209 (1986).

6) H. Nakano, T. Nakamura, T. Nogami, and Y. Shirota, *Chem. Lett.*, **1987**, 1317.

7) T. Nakamura, S. Iwasaka, H. Nakano, K. Inoue, T. Nogami, and H. Mikawa, *Bull. Chem. Soc. Jpn.*, **60**, 365 (1987).

8) T. Nakamura, T. Nogami, and Y. Shirota, *Bull. Chem. Soc. Jpn.*, **60**, 3447 (1987).

9) 4,5-(Ethoxyethylenedithio)-1,3-dithiole-2-thione was synthesized as reported in Ref. 8 except for the method of purification. The crude product was washed with acetonitrile, and then recrystallized from acetonitrile. The compound **1** was purified as follows. After the reaction described in Ref. 8, the black solid was extracted with a Soxhlet for 48 h by using ethyl alcohol, and the solid extracted was recrystallized from ethyl alcohol in the presence of active charcoal.

10) J. Ellis, R. D. Frier, and R. A. Schibeci, *Aust. J. Chem.*, **24**, 1527 (1971).

11) K. Inoue, Y. Tasaka, O. Yamazaki, T. Nogami, and H. Mikawa, *Chem. Lett.*, **1986**, 781.

12) N. Iwasawa, G. Saito, K. Imaeda, T. Mori, and H. Inokuchi, *Chem. Lett.*, **1987**, 2399. This paper reports the order of the oxidation potentials as follows; TTC_1-TTF>$TSeC_1$-TTF>TTF. TTC_1-TSeF>$TSeC_1$-TSeF>TSeF.

Efficient Synthesis of Sterically Hindered Chiral Binaphthol Derivatives

Keiji MARUOKA, Takayuki ITOH, Yoshitaka ARAKI, Tadashi SHIRASAKA, and Hisashi YAMAMOTO*
Department of Applied Chemistry, Faculty of Engineering, Nagoya University, Chikusa, Nagoya 464-01
(Received March 28, 1988)

Synopsis. A highly effective method for preparation of a variety of sterically hindered chiral binaphthol derivatives has been described which involves the intramolecular 1,3-rearrangement of bis(trialkylsilyl ether) of chiral 3,3′-dibromo-1,1′-bi-2-naphthol with *t*-BuLi.

In connection with our recent study on the enantioselective activation of carbonyl moiety by complexing with the exceptionally bulky, chiral organoaluminum reagents,[1,2] it was required to synthesize certain sterically hindered, chiral phenol derivatives. An attractive possibility for the synthesis appeared to be the effective introduction of bulky trialkylsilyl substituents adjacent to hydroxyl groups of chiral binaphthols in view of the readily availability of a wide variety of trialkylsilyl derivatives. Here we report a new and highly effective approach to the synthesis of such sterically hindered, chiral 3,3′-bis(trialkylsilyl)-1,1′-bi-2-naphthol (*R*)-**1** and (*S*)-**1** based on the remarkably facile 1,3-rearrangement of bis(trialkylsilyl ether) of chiral 3,3′-dibromo-1,1′-bi-2-naphthol with *t*-BuLi as illustrated in Scheme 1.[3]

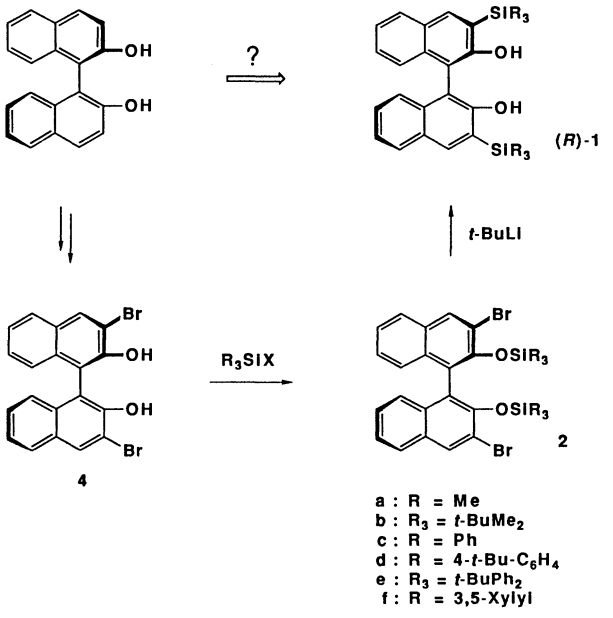

Scheme 1.

The requisite bis(silyl ether) **2** was readily obtainable from the known (*R*)-(+)-3,3′-dibromo-1,1′-bi-2-naphthol dimethyl ether (**3**)[4] in two steps. Thus, demethylation of **3** with BBr_3 (5.5 equiv) in CH_2Cl_2 at room temperature for 3 h afforded (*R*)-(+)-3,3′-dibromo-1,1′-bi-2-naphthol (**4**) quantitatively, which without purification was treated with trialkylsilyl halide (2.5—3 equiv) and imidazole (3—4 equiv) in DMF at 20—70 °C for several hours, producing the bis(silyl ether) **2** in 80—97% yield. Treatment of the bis(silyl ether) **2** with *t*-BuLi (3—3.5 equiv) under mild conditions furnished the corresponding (*R*)-(+)-3,3′-bis(trialkylsilyl)-1,1′-bi-2-naphthol (*R*)-**1** in 85—96% yield. The enantiomeric (*S*)-**1** can be prepared from (*S*)-(−)-1,1′-bi-2-naphthol in a same manner as described above. The readily obtainable, optically pure 3,3′-bis(silylated) binaphthol of type **1** should have vast synthetic potential as chiral bidentate ligands for designing of chiral metal catalyst or reagent as recently shown in our laboratory to be quite effective as a modified organoaluminum catalyst **5** (R=Ph or 3,5-Xylyl) for asymmetric hetero-Diels-Alder and ene reactions.[1]

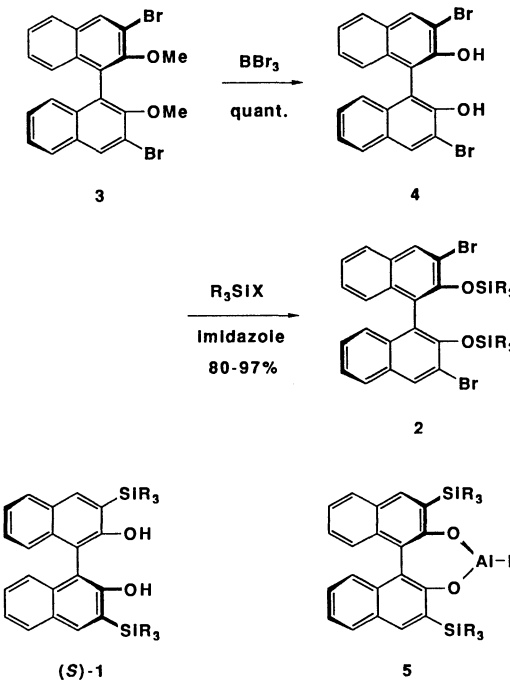

Since the present 1,3-rearrangement proceeds rigorously in an intramolecular fashion, introduction of different trialkylsilyl groups at the 3,3′-positions of chiral binaphthols appeared feasible, thereby further enhancing the synthetic utility of the present method as exemplified by the facile synthesis of (*R*)-(+)-3-(*t*-butyldiphenylsilyl)-3′-(trimethylsilyl)-1,1′-bi-2-naphthol (**6**) in 80% yield.

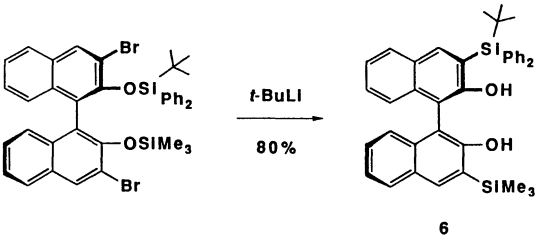

Experimental

The IR spectra were measured on a Hitachi 260-10 spectrometer. The ^{1}H NMR spectra were recorded on a JNM-PMX 60 spectrometer, using TMS (tetramethylsilane) as an internal standard. Splitting patterns are indicated as s, singlet; m, multiplet. Melting points are not corrected. The microanalysis was performed at the Institute of Applied Organic Chemistry, Faculty of Engineering, Nagoya University. Tetrahydrofuran (THF) was distilled from benzophenone ketyl. Dichloromethane (CH_2Cl_2) and *N*,*N*-dimethylformamide (DMF) were stored over 4-A Molecular Sieves. All experiments were carried out under an argon atmosphere. Purification of the product was carried out by column chromatography on silica gel Fuji-Davison BW-300.

Preparation of (*R*)-(+)-3,3′-Bis(triphenylsilyl)-1,1′-bi-2-naphthol ((*R*)-1c): To a solution of (*R*)-(+)-3,3′-dibromo-1,1′-bi-2-naphthol dimethyl ether (**3**)[4] (2.78 g, 5.9 mmol) in CH_2Cl_2 (180 mL) was added BBr_3 (3.13 mL, 33 mmol) at 0 °C. The mixture was stirred at room temperature for 5 h. Then excess BBr_3 was decomposed by adding water carefully at 0 °C. The mixture was washed with water, extracted with CH_2Cl_2, dried over Na_2SO_4, and evaporated. The crude (*R*)-(+)-3,3′-dibromo-1,1′-bi-2-naphthol (**4**), thus obtained, was dissolved in DMF (36 mL), and imidazole (1.22 g, 18 mmol) followed by triphenylsilyl chloride (4.42 g, 15 mmol) was added at room temperature. The resulting mixture was stirred at room temperature for 5 h, poured into saturated $NaHCO_3$, and extracted with CH_2Cl_2. The organic layers were washed again with saturated $NaHCO_3$, dried over Na_2SO_4, and concentrated. The crude solid was applied to short-path column chromatography on silica gel (CH_2Cl_2/hexane=1 : 2 as eluent) to furnish bis(triphenylsilyl ether) **2** (5.48 g, 5.7 mmol) in 97% yield. To a solution of **2** in dry THF (80 mL) was added dropwise a 2.67 M pentane solution (1M=1 mol dm^{-3}) of *t*-BuLi (6.4 mL, 17.1 mmol) over a period of 10 min at 0 °C. The mixture was stirred at room temperature for 30 min, poured into saturated NH_4Cl, and extracted with CH_2Cl_2. The combined extracts were dried over Na_2SO_4 and concentrated. The crude product was chromatographed on silica gel (benzene/hexane=1 : 2 to 1 : 1 as eluent) to give (*R*)-(+)-3,3′-bis(triphenylsilyl)-1,1′-bi-2-naphthol ((*R*)-**1c**) (3.89 g, 85% yield) as white solids: $[\alpha]_D$ +125° (*c* 1.11, THF); mp 165—167 °C; IR ($CHCl_3$) 3540, 3065, 3015, 1590, 1428, 1359, 1305, 1105, 988, 910 cm^{-1}; ^{1}H NMR (CCl_4) δ=7.87 (s, 2H, Ar-H), 6.93—7.85 (m, 38H, Ar-H), 5.24 (s, 2H, OH); Anal. ($C_{56}H_{42}O_2Si_2$) C, H. If necessary, this material was further recrystallized from CH_2Cl_2/hexane at low temperature to furnish white crystals.

Other chiral 3,3′-bis(trialkylsilyl)-1,1′-bi-2-naphthols were prepared in a similar manner as described above. Their analytical and physical data are listed below.

(*R*)-(+)-3,3′-Bis(trimethylsilyl)-1,1′-bi-2-naphthol ((*R*)-1a): Yield: 86%; mp 68—71 °C; $[\alpha]_D$ +143° (*c* 0.985, THF); IR (CCl_4) 3540, 1584, 1356, 1305, 1248, 1181, 1149, 840 cm^{-1}; ^{1}H NMR (CCl_4) δ=7.97 (s, 2H, Ar-H), 7.63—7.96 (m, 2H, Ar-H), 6.84—7.43 (m, 6H, Ar-H), 5.15 (s, 2H, OH), 0.40 (s, 18H, CH_3); Anal. ($C_{26}H_{30}O_2Si_2$) C, H.

(*R*)-(+)-3,3′-Bis(*t*-butyldimethylsilyl)-1,1′-bi-2-naphthol ((*R*)-1b): Yield: 87%; mp 63—66 °C; $[\alpha]_D$ +136° (*c* 1.02, THF); IR (CCl_4) 3535, 1584, 1355, 1250, 1194, 830 cm^{-1}; ^{1}H NMR (CCl_4) δ=7.93 (s, 2H, Ar-H), 7.56—7.84 (m, 2H, Ar-H), 6.78—7.37 (m, 6H, Ar-H), 5.10 (s, 2H, OH), 0.97 (s, 18H, *t*-Bu), 0.41 (s, 12H, CH_3); Anal. ($C_{32}H_{42}O_2Si_2$) C, H.

(*R*)-(+)-3,3′-Bis[tris(4-*t*-butylphenyl)silyl]-1,1′-bi-2-naphthol ((*R*)-1d): Yield: 96% (amorphous solid); $[\alpha]_D$ +91.4° (*c* 1.22, THF); IR (CCl_4) 3550, 2980, 1395, 1270, 1095 cm^{-1}; ^{1}H NMR (CCl_4) δ=7.90 (s, 2H, Ar-H), 7.10—7.70 (m, 32H, Ar-H), 5.23 (s, 2H, OH), 1.31 (s, 54H, *t*-Bu); Anal. ($C_{80}H_{90}O_2Si_2$) C, H.

(*R*)-(+)-3,3′-Bis(*t*-butyldiphenylsilyl)-1,1′-bi-2-naphthol ((*R*)-1e): Yield: 95%; mp 145—147 °C; $[\alpha]_D$ +111° (*c* 1.01, THF); IR (CCl_4) 3530, 1430, 1360, 1150, 1110 cm^{-1}; ^{1}H NMR (CCl_4) δ=7.93 (s, 2H, Ar-H), 7.15—7.80 (m, 28H, Ar-H), 5.32 (s, 2H, OH), 1.23 (s, 18H, *t*-Bu); Anal. ($C_{52}H_{50}O_2Si_2$) C, H.

(*R*)-(+)-3,3′-Bis(tri-3,5-xylylsilyl)-1,1′-bi-2-naphthol ((*R*)-1f): Yield: 90%; mp 285—286 °C; $[\alpha]_D$ +135° (*c* 1.02, THF); IR (CCl_4) 3550, 2930, 1590, 1420, 1400, 1145 cm^{-1}; ^{1}H NMR (CCl_4) δ=7.73 (s, 2H, Ar-H), 6.83—7.33 (m, 26H, Ar-H), 5.13 (s, 2H, OH), 2.22 (s, 36H, Me); Anal. ($C_{68}H_{66}O_2Si_2$) C, H.

(*R*)-(+)-3-(*t*-Butyldiphenylsilyl)-3′-(trimethylsilyl)-1,1′-bi-2-naphthol (6): Yield: 80% (amorphous solid); mp 107—116 °C; $[\alpha]_D$ +128° (*c* 1.16, THF); IR (CCl_4) 3530, 1435, 1365, 1250, 1155 cm^{-1}; ^{1}H NMR (CCl_4) δ=7.03—8.01 (m, 20H, Ar-H), 5.25 (s, 1H, OH), 5.18 (s, 1H, OH), 1.22 (s, 9H, *t*-Bu), 0.41 (s, 9H, SiMe); Anal. ($C_{39}H_{40}O_2Si_2$) C, H.

(*S*)-(−)-3,3′-Bis(triphenylsilyl)-1,1′-bi-2-naphthol ((*S*)-1c): $[\alpha]_D$ −125° (*c* 1.10, THF). The spectral data is in consonance with those of (*R*)-**1c**.

References

1) Enantioselective activation of carbonyl group: K. Maruoka, T. Itoh, T. Shirasaka, and H. Yamamoto, *J. Am. Chem. Soc.*, **110**, 310 (1988); K. Maruoka, Y. Hoshino, T. Shirasaka, and H. Yamamoto, *Tetrahedron Lett.*, in press.

2) For diastereoselective activation of carbonyl group, see: K. Maruoka, T. Itoh, and H. Yamamoto, *J. Am. Chem. Soc.*, **107**, 4573 (1985); K. Maruoka, M. Sakurai, and H. Yamamoto, *Tetrahedron Lett.*, **26**, 3853 (1985); K. Maruoka, T. Itoh, M. Sakurai, K. Nonoshita, and H. Yamamoto, *J. Am. Chem. Soc.*, **110**, 3588 (1988).

3) The anionic 1,3-rearrangements of sterically less hindered trimethylsilyl and triethylsilyl groups in trialkylsiloxybenzenes and trialkylsiloxypyridines have been advanced: G. Simchen and J. Pfletschinger, *Angew. Chem., Int. Ed. Engl.*, **15**, 428 (1976); D. Habich and F. Effenberger, *Synthesis*, 841 (1979); R. J. Billedeau, M. P. Sibi, and V. Snieckus, *Tetrahedron Lett.*, **24**, 4515 (1983).

4) D. S. Lingenfelter, R. S. Helgeson, and D. J. Cram, *J. Org. Chem.*, **46**, 393 (1981).

One-Step Conversion of Mesoionic Olate to Thiolate by Lawesson's Reagent

Shuki ARAKI,* Tetsuya GOTO, and Yasuo BUTSUGAN
Department of Applied Chemistry, Nagoya Institute of Technology, Gokiso-cho, Showa-ku, Nagoya 466
(Received March 29, 1988)

Synopsis. Treatment of mesoionic olates with Lawesson's reagent provides a convenient one-step conversion to mesoionic thiolates.

Mesoionic compounds, expressed by the general formula **1**, where a—f are suitably substituted carbons or heteroatoms, are an interesting family of heterocycles because of their unique structure, reaction behavior, and pharmaceutical activity.[1] Most of mesoions bear oxygen, sulfur, nitrogen, and carbon as the exocyclic group (f), and are called meso-ionic olate, thiolate, aminide, and methylide, respectively; and their interconversion is important from a synthetic standpoint. Mesoionic olates were hitherto converted to the corresponding thiolates via following two steps: alkylation with a trialkyloxonium salt and then replacement of the resulting alkylthio group by sulfide or hydrogensulfide anion (Eq. 1).[2]

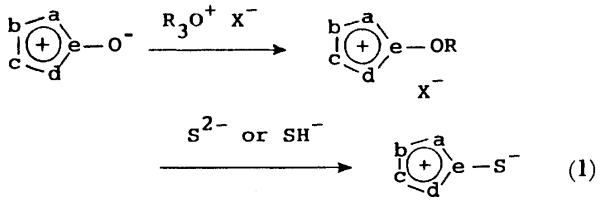

(1)

Lawesson's reagent (**2**), 2,4-bis(*p*-methoxyphenyl)-1,3-dithiadiphosphetane-2,4-disulfide, is known as an excellent reagent for the conversion of various types of carbonyl group to the corresponding thiocarbonyl group.[3] However, the reaction of **2** with mesoionic olates has not to our knowledge been reported so far. Here, we describe the reaction of **2** with several mesoionic olates which provides a convenient method for the one-pot conversion of mesoionic olates to thiolates.

A mixture of 1,3-diphenyltetrazolium-5-olate (**3**) and Lawesson's reagent (**2**) in toluene was heated at reflux for 18 h. Purification by column chromatography gave 93% yield of the thiolate **4**, identical with the authentic sample prepared according to the literature method.[2a] Table 1 summarizes the results for other mesoionic olates. 3-Phenyl-1,2,3-thiadiazolium- (**5**) and 3-phenyl-1,2,3,4-thiatriazolium-5-olates (**7**) were converted to the corresponding thiolates **6** and **8** in high yields, whereas 3-*p*-methoxyphenyl-1,2,3-thiadiazolium-4-thiolate (**10**) was obtained in only 16%. The yields of the thiolates **4**, **6**, **8**, and **10** are much higher than or at least equivalent to those obtained by the existing method (Eq. 1).[2]

Treatment of 3-phenyl-1,2,3-oxadiazolium-5-olate (3-phenylsydnone) (**11**) with **2** gave 1,4-diphenyl-1,4-dihydro-1,2,4,5-tetrazine (**12**) quantitatively, and the expected thiolate **13** could not be obtained at all. The tetrazine **12** has been obtained from the reaction of **11** with P_4S_{10} in a low yield.[4] The thiolate **13** prepared by an independent method[2b] also gave **12** in 88% yield upon the treatment with **2**, suggesting the intermedi-

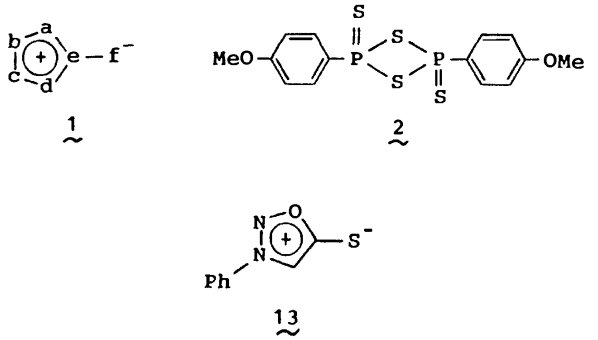

Table 1. Reaction of Mesoionic Olates with Lawesson's Reagent

Run	Olate	Product	Yield/%[a]
1	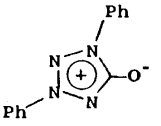 **3**	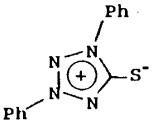 **4**	93 (59)[b]
2	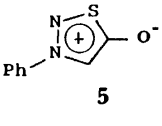 **5**	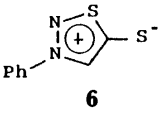 **6**	98 (63)[c]
3	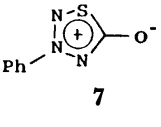 **7**	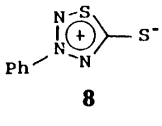 **8**	93 (25)[d]
4	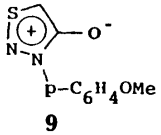 **9**	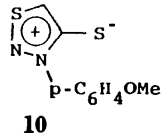 **10**	16 (19)[e]
5	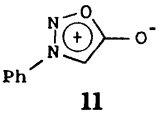 **11**	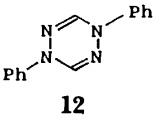 **12**	100
6	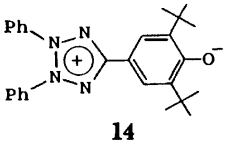 **14**	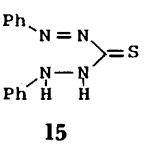 **15**	100

a) Numbers in parentheses refer to the reported yields of the existing two-step conversion (Eq. 1). b) Ref. 2a. c) Ref. 2b. d) Ref. 2c. e) Ref. 2d.

acy of **13** in the reaction of the olate **11** and **2**. Interestingly, the sulfur analog **5** of sydnone gave a high yield of the thiolate **6**. The reaction of a quinonoid mesoionic olate **14**[5] with **2** resulted in the cleavage of the pivotal carbon-carbon bond giving diphenylthiocarbazone (dithizone) **15** in a quantitative yield. Unfortunately, mesoionic olates of type B[1] such as 2,3-diphenyltetrazolium-5-olate and 3,5-diphenyl-1,2-dithiolium-4-olate gave complex mixtures of products on the treatment with **2**.

In summary, the thionation of mesoionic olates of type A by Lawesson's reagent (**2**) provides a convenient route to the corresponding mesoionic thiolates.

Experimental

Melting points were determined with a hot-stage apparatus and are uncorrected. Infrared spectra were recorded on a JASCO IRA-1 spectrophotometer. Mass spectra were recorded on a Hitachi M-52 instrument at 20 eV. ^{1}H and ^{13}C NMR spectra were recorded on a Hitachi R-24A spectrometer (60 MHz) and on a Varian XL-200 spectrometer (50 MHz), respectively, with Me_4Si as an internal standard.

Reaction of Mesoionic Olates with Lawesson's Reagent (2). Run 1. 1,3-Diphenyltetrazolium-5-olate (**3**) (103 mg, 0.43 mmol) and **2** (118 mg, 0.29 mmol) in toluene (5 cm^3) were heated at reflux for 18 h. The reaction mixture was cooled and adsorbed on a silica-gel column and eluted with dichloromethane. A yellow band was collected and the solvent was evaporated leaving yellow crystals of thiolate **4** (102 mg, 93%). Mp 151 °C (CH_2Cl_2) (lit,[2a] mp 155 °C); IR (KBr): 1494, 1374, 1302, 1266, 1190, 774, 764, 692, 686 cm^{-1}; MS m/z 254 (M^+).

Run 2. 3-Phenyl-1,2,3-thiadiazolium-5-olate (**5**) (100 mg, 0.56 mmol) and **2** (159 mg, 0.39 mmol) in toluene (6 cm^3) were warmed to 100 °C during the period of 30 min. The mixture was cooled and column chromatographed on silica gel (CH_2Cl_2) to give red crystals of thiolate **6** (107 mg, 98%). Mp 165 °C (CH_2Cl_2) (lit,[2b] mp 170—171 °C); IR (KBr): 1430, 1252, 1198, 1030, 898, 760 cm^{-1}; MS m/z 194 (M^+).

Run 3. 3-Phenyl-1,2,3,4-thiatriazolium-5-olate (**7**) (176 mg, 1.1 mmol) and **2** (300 mg, 0.74 mmol) in toluene (11 cm^3) were heated at reflux for 50 min. The mixture was cooled and column chromatographed on silica gel to give orange needles of thiolate **8** (178 mg, 93%). Mp 125 °C (CH_2Cl_2) (lit,[2c] mp 128 °C); IR (KBr): 1270, 1226, 1056, 922, 762, 660 cm^{-1}; MS m/z 195 (M^+).

Run 4. 3-*p*-Methoxyphenyl-1,2,3-thiadiazolium-4-olate (**9**) (121 mg, 0.58 mmol) and **2** (163 mg, 0.40 mmol) in toluene (6 cm^3) were heated at reflux for 16 h. Column chromatography on silica gel (ethyl acetate) gave red needles of thiolate **10** (20 mg, 16%). Mp 189 °C (MeOH) (lit,[2d] mp 193—194 °C); IR (KBr): 1512, 1394, 1306, 1254, 1176, 1152, 1078, 1022, 988, 834 cm^{-1}; MS m/z 224 (M^+).

Run 5. 3-Phenylsydnone (**11**) (110 mg, 0.68 mmol) and **2** (191 mg, 0.47 mmol) in toluene (6 cm^3) were refluxed for 3.5 h. The solvent was evaporated under reduced pressure and the residue was column chromatographed on silica gel (benzene) to give pale yellow plates of dihydrotetrazine (**12**) (80 mg, 100 %). Mp 191 °C (acetone) (lit,[4] mp 189—189.5 °C); IR (KBr): 1600, 1494, 1318, 1156, 906, 892, 754, 750, 700 cm^{-1}; MS: m/z 236 (M^+); ^{1}H NMR ($CDCl_3$): δ=6.90 (s, 2H, =CH–), 7.30 (m, 10H, Ph); ^{13}C NMR ($CDCl_3$): δ=115.3, 123.8, 129.4, 139.5, 142.3.

Run 6. 2,6-Di-*t*-butyl-4-(2,3-diphenyl-5-tetrazolio)phenolate (**14**)[5] (13 mg, 0.032 mmol) and **2** (9 mg, 0.022 mmol) in toluene (2 cm^3) were slowly heated to reflux during the period of 20 min. The solvent was removed under reduced pressure and the residue was purified by column chromatography on silica gel (benzene) to furnish dithizone **15** (8 mg, 100%). The melting point and spectral data were identical with those of a commercially obtained sample.

Reaction of 3-Phenyl-1,2,3-oxadiazolium-5-olate (13) with 2. A mixture of **13** (110 mg, 0.62 mmol) and **2** (177 mg, 0.44 mmol) in toluene (6 cm^3) was refluxed for 3.5 h. Column chromatography on silica gel (dichloromethane) gave dihydrotetrazine (**12**) (64 mg, 88%). The physical data were identical with those of the product of Run 5.

References

1) W. D. Ollis and C. A. Ramsden, *Adv. Heterocycl. Chem.*, **19**, 1 (1976); C. G. Newton and C. A. Ramsden, *Tetrahedron*, **38**, 2965 (1982).

2) a) R. N. Hanley, W. D. Ollis, and C. A. Ramsden, *J. Chem. Soc., Perkin Trans. 1*, **1979**, 741; b) K. Masuda, J. Adachi, and K. Nomura, *ibid.*, **1979**, 956; c) R. N. Hanley, W. D. Ollis, and C. A. Ramsden, *ibid.*, **1979**, 732; d) J. Adachi, H. Takahata, K. Nomura, and K. Masuda, *Chem. Pharm. Bull.*, **31**, 1746 (1983).

3) For a review, see: M. P. Cava and M. I. Levinson, *Tetrahedron*, **41**, 5061 (1985).

4) W. Baker, W. D. Ollis, and V. D. Poole, *J. Chem. Soc.*, **1950**, 3389; K. Sugimoto and M. Ohta, *Bull. Chem. Soc. Jpn.*, **46**, 2921 (1973).

5) S. Araki, N. Aoyama, and Y. Butsugan, unpublished work; see also: *idem*, *Tetrahedron Lett.*, **28**, 4289 (1987).

1,3,4-Thiadiazolines by a 1,5-Dipolar Ring Reconstruction of Mesoionic (2,3-Diphenyltetrazolio)thio Ylides

Shuki ARAKI,* Tetsuya GOTO, and Yasuo BUTSUGAN
Department of Applied Chemistry, Nagoya Institute of Technology, Gokiso-cho, Showa-ku, Nagoya 466
(Received March 29, 1988)

Synopsis. 4-Phenyl-2-phenylazo-2,3-dihydro-1,3,4-thiadiazoles were synthesized from 2,3-diphenyltetrazolium-5-thiolate by two methods. The formation of the thiadiazolines is rationalized by 1,5-dipolar ring closure of the intermediate mesoionic (tetrazolio)thio ylides.

We have recently reported[1] the synthesis of mesoionic thiocarbonyl ylides by the treatment of mesoionic thiolates with bromine followed by the reaction of the conjugate anions of active methylene compounds (Eq. 1). Now, we have examined the reaction of the bromine adduct of 2,3-diphenyltetrazolium-5-thiolate (**1**) with various conjugate anions of active methylene compounds and found that several anions gave thiadiazoline derivatives **2** exclusively, instead of the expected thiocarbonyl ylides. Furthermore, same thiadiazoline derivatives were also obtained from the reaction of **1** with the diazo compounds of active methylene compounds.

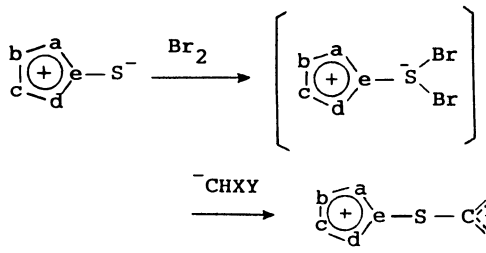

(1)

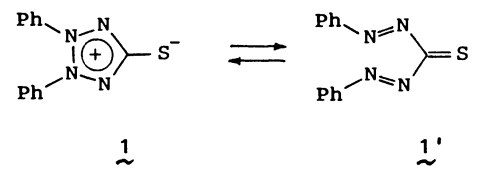

1 **1'**

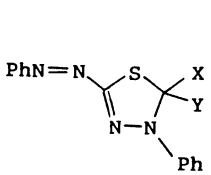

2a: X=Y=CO_2Et
b: X=CO_2Et, Y=CN
c: X=CO_2Et, Y=COMe
d: X,Y= 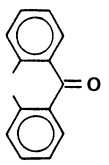

The reaction of the bromine adduct of **1** with ethyl sodio-*p*-tolylsulfonylacetate gave the expected (tetrazolio)thio ylide **3** as stable crystals in a high yield. On the other hand, the reaction with diethyl sodiomalonate led to the exclusive formation of 5,5-bis(ethoxycarbonyl)-4-phenyl-2-phenylazo-2,3-dihydro-1,3,4-thiadiazole (**2a**) as deep red crystals in 94% yield, and the corresponding (tetrazolio)thio ylide was not obtained at all. The structure of **2a** was deduced from its analytical and spectral properties. The ^{13}CNMR spectrum showed two sets of phenyl signals and the absorptions of the thiadiazoline ring carbons at δ 83.0 and 154.6 ppm. Its ^1HNMR revealed the nonequivalency of the two ethoxycarbonyl groups. An intense absorption at 470 nm in the electronic spectrum is consistent with the presence of a phenylazo chromophore. Similar reactions with the sodium salt of ethyl cyanoacetate or ethyl acetoacetate gave the respective thiadiazolines **2b** and **2c** in good yields.

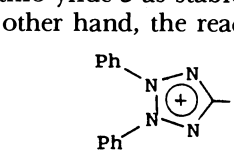

3

The thiadiazolines **2a** and **2c** were also prepared by refluxing of the thiolate **1** in chloroform with the diazo derivatives of diethyl malonate and ethyl acetoacetate, respectively.[2] A new thiadiazoline **2d** having a spirostructure was synthesized by the reaction of **1** with 10-diazo-9-anthrone.

Two syntheses of 4-phenyl-2-phenylazo-2,3-dihydro-1,3,4-thiadiazole derivatives from mesoionic thiolate **1** are so far reported; treatment of **1** with iron pentacarbonyl gave 1,3,4-thiadiazol-2(3*H*)-one (**4**)[3] and reaction with 2-alkylaminoindenes yielded products with the general structure **5**.[4] The formation of these products **4** and **5** is thought to occur via the acyclic valence tautomer **1'** of thiolate **1**. In our reactions, the formation of thiadiazolines **2** can also be rationalized in terms of participation of the acyclic valence tautomer **6'** of intermediate thiocarbonyl ylide **6**. The tautomer **6'** undergoes 1,5-dipolar ring closure to furnish thiadiazolines **2** (Eq. 2). The isolation of (tetrazolio)thio ylide **6** is depend upon the nature of the substituents (X and Y) on the carbanionoid carbon; only in the

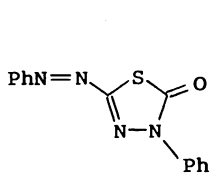

4

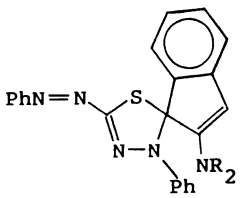

5

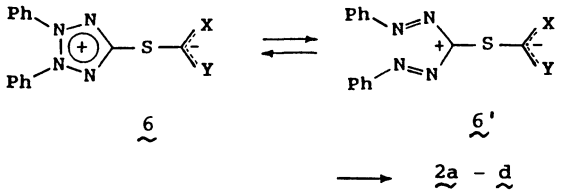

6 **6'**

(2)

cases of strongly electron-withdrawing substituents, the ylide **6** is thought to be isolated stably.

Experimental

General. Melting points were determined on a hot-stage apparatus and are uncorrected. Infrared spectra were taken for KBr discs with a JASCO IRA-1 spectrometer. Electronic spectra were run with a Hitachi 124 spectrophotometer. ^{1}H NMR spectra were recorded on a Hitachi R-24A spectrometer (60 MHz) or on a Varian XL-200 spectrometer (200 MHz) with Me_4Si as an internal standard. ^{13}C NMR spectra were determined on a Varian XL-200 spectrometer (50 MHz). Mass spectra were recorded on a Hitachi M-52 instrument at 20 eV or on an ESCO EMD-05B at 70 eV using a direct-inlet system. Elemental analyses were performed at the Elemental Analysis Center of Kyoto University.

Synthesis of Mesoionic (Tetrazolio)thio Ylide (3). To a stirred suspension of mesoionic thiolate **1** (127 mg, 0.5 mmol) in dry dichloromethane (1.5 cm^3) was added bromine (0.030 cm^3, 0.55 mmol) and the mixture was stirred at room temperature for 10 min. The sodium salt of ethyl *p*-tolylsulfonylacetate, prepared from ethyl *p*-tolylsulfonylacetate (242 mg, 1 mmol) and an equimolar amount of sodium hydride in tetrahydrofuran (THF) (1 cm^3), was added to the bromine adduct. After 5 min, the reaction was quenched by the addition of water (1 cm^3) and ether (20 cm^3) was added. Pale yellow precipitates were filtered and washed successively with ether, water, and THF, and then dried to give ylide **3** (220 mg, 89%), mp 125 °C (MeCN); IR: 1630, 1354, 1292, 1274, 1132, 1070, 764, 686, 662 cm^{-1}; UV (MeCN): λ_{max} 231 (log ε 4.34), 258 (sh) (4.12), and 343 nm (3.21); ^{1}H NMR (60 MHz, DMSO-d_6): δ=1.00 (t, J=7 Hz, $CH_2\underline{Me}$), 2.28 (s, 3H, Me), 3.80 (q, J=7 Hz, 2H, $C\underline{H}_2$Me), 7.10 (d, J=9 Hz, 2H, aryl H), 7.70 (m, 10H, Ph), 7.75 (d, J=9 Hz, 2H, aryl H); ^{13}C NMR (DMSO-d_6): δ=14.9 ($CH_2\underline{Me}$), 21.0 (Me), 57.6 ($\underline{C}H_2$Me), 60.4 (S-C$^-$), 126.5 (ortho), 127.2 (aryl), 128.0 (aryl), 130.1 (meta), 133.3 (ipso), 133.7 (para), 139.8 (C-Me), 145.0 (C-SO_2), 166.0 (C=O), 172.9 (S-C$^+$); Found: C, 56.38; H, 4.56; N, 10.79%. Calcd for $C_{24}H_{22}N_4S_2 \cdot H_2O$: C, 56.23; H, 4.71; N, 10.93%.

Reaction of the Bromine Adduct of 1 with the Conjugate Bases of Active Methylene Compounds. The following reaction with diethyl sodiomalonate is representative. To a suspension of the bromine adduct of **1**, prepared as above from **1** (127 mg, 0.5 mmol) and bromine (0.030 cm^3, 0.55 mmol) in dichloromethane (1.5 cm^3), was added diethyl sodiomalonate (1.5 mmol) in THF (1 cm^3). The mixture was stirred at room temperature for 10 min. Water was added and the product was extracted with dichloromethane. The extracts were dried over anhydrous sodium sulfate and the solvent was removed. The residue was chromatographed on silica gel (eluent: dichloromethane–hexane 1 : 1) to give thiadiazoline **2a** (198 mg, 96%) as red crystals, mp 91 °C (benzene–hexane); IR: 1772, 1554, 1490, 1250, 1234, 1150, 1130, 1038, 756, 682 cm^{-1}; UV-VIS (MeCN): λ_{max} 253 (log ε 4.08), 310 (4.03), and 470 nm (4.35), ^{1}H NMR (200 MHz, $CDCl_3$): δ=1.18 (t, J=7 Hz, 6H, Me), 4.30 (q, J=7 Hz, 2H, CH_2), 4.31 (q, J=7 Hz, 2H, CH_2), 7.13—7.52 (m, 8H, Ph), 7.92 (m, 2H, Ph); ^{13}C NMR ($CDCl_3$): δ=13.7 (Me), 63.5 (CH_2), 83.0 (C^5), 117.8 (ortho), 123.4 (ortho), 124.1 (para), 128.9 (meta), 129.2 (meta), 132.1 (para), 142.1 (ipso), 151.8 (ipso), 154.6 (C^2), 165.8 (C=O); MS (20 eV): m/z (rel intensity) 412 (M$^+$, 6), 77 (Ph, 100); Found: C, 58.43; H, 4.80; S, 7.79%. Calcd for $C_{20}H_{20}N_4O_4S$: C, 58.24; H, 4.89; S, 7.77%.

Similarly, thiadiazolines **2b** and **2c** were synthesized and obtained as red crystals.

2b: 62% yield; mp 98 °C (MeOH); IR: 1744, 1564, 1500, 1354, 1260, 1148, 748, 680 cm^{-1}; UV-VIS (MeCN): λ_{max} 245 (log ε 4.08), 315 (4.01), and 450 nm (4.36); ^{1}H NMR (60 MHz, $CDCl_3$): δ=1.23 (t, J=7 Hz, 3H, Me), 4.34 (q, J=7 Hz, 2H, CH_2), 7.40 (m, 8H, Ph), 7.85 (m, 2H, Ph); ^{13}C NMR ($CDCl_3$): δ=13.7 (Me), 65.1 (CH_2), 71.2 (C^5), 113.2 (CN), 116.3 (ortho), 123.7 (ortho), 124.6 (para), 129.6 (meta), 129.4 (meta), 133.0 (para), 140.5 (ipso), 151.5 (ipso), 155.0 (C^2), 163.4 (C=O); MS (20 eV): m/z (rel intensity) 365 (M$^+$, 34), 292 (M−CO_2Et, 100); Found: C, 59.23; H, 4.04; N, 19.37%. Calcd for $C_{18}H_{15}N_5O_2S$: C, 59.17; H, 4.14; N, 19.16%.

2c: 94% yield; mp 72 °C (hexane); IR: 1742, 1730, 1550, 1500, 1366, 1248, 1164, 1152, 774, 752, 686 cm^{-1}; UV-VIS (MeCN): λ_{max} 254 (log ε 4.06), 304 (4.02), and 477 nm (4.41); ^{1}H NMR (60 MHz, $CDCl_3$): δ=1.17 (t, J=7 Hz, 3H, $CH_2\underline{Me}$), 2.45 (s, 3H, COMe), 4.27 (q, J=7 Hz, 2H, CH_2), 7.35 (m, 8H, Ph), 7.80 (m, 2H, Ph); ^{13}C NMR ($CDCl_3$): δ=13.6 (Me), 25.5 (CO$\underline{Me}$), 63.2 ($\underline{C}H_2$Me), 86.7 (C^5), 116.5 (ortho), 123.3 (ortho), 123.7 (para), 129.0 (meta), 129.2 (meta), 132.2 (para), 141.8 (ipso), 151.7 (ipso), 153.5 (C^2), 166.5 ($\underline{C}O_2$Et), 196.0 ($\underline{C}$OMe); MS (70 eV): m/z (rel intensity) 382 (M$^+$, 2), 77 (Ph, 100); Found: C, 59.82; H, 4.66; N, 14.60%. Calcd for $C_{19}H_{18}N_4O_3S$: C, 59.67; H, 4.74; N, 14.65%.

Reaction of Thiolate 1 with Diazo Compounds. A solution of thiolate **1** (389 mg, 1.53 mmol) and diethyl diazomalonate[5] (549 mg, 2.95 mmol) in chloroform (12 cm^3) was heated at reflux for 24 h. The solvent was removed and the residue was column chromatographed on silica gel (eluent: chloroform) to afford red crystals of thiadiazoline **2a** (229 mg, 47%), identical with the compound obtained above. The reactions with ethyl diazoacetoacetate[5] and 10-diazo-9-anthrone[6] were similarly carried out and the corresponding thiadiazolines **2c** and **2d** were isolated in 5 and 65% yields, respectively.

2d: Mp 286 °C (benzene); IR: 1660, 1596, 1536, 1492, 1362, 1318, 1266, 1224, 1156, 930, 770, 746, 740, 710, 682 cm^{-1}; UV-VIS (MeCN): λ_{max} 253 (log ε 4.32), 279 (sh) (4.24), 302(sh) (4.11), and 476 nm (4.33); ^{1}H NMR (200 MHz, $CDCl_3$): δ=6.90—7.10 (m, 4H, aryl H), 7.50—7.70 (m, 8H, Ph and aryl H), 7.70—7.90 (m, 4H, Ph and aryl H), 8.41 (d, J=8 Hz, 2H, aryl H); ^{13}C NMR ($CDCl_3$): δ=81.1 (C^5), 116.9 (ortho), 122.9 (para), 123.3 (ortho), 127.5 (aryl CH), 127.8 (aryl CH), 129.0 (meta or aryl CH), 129.2 (meta or aryl CH), 129.4 (meta or aryl CH), 132.0 (para), 133.4 (aryl =$\underset{|}{C}$–), 134.9 (aryl CH), 140.5 (ipso or aryl =$\underset{|}{C}$–), 143.7 (ipso or aryl =$\underset{|}{C}$–), 151.9 (ipso), 154.8 (C^2), 181.8 (C=O); MS (20 eV): m/z (rel intensity) 446 (M$^+$, 100); Found: C, 72.62; H, 4.01; S, 7.24%. Calcd for $C_{27}H_{17}N_4OS$: C, 72.63; H, 4.06; S, 7.18%.

References

1) S. Araki and Y. Butsugan, *Chem. Lett.*, **1985**, 1639.

2) Syntheses of thiocarbonyl ylides by the reaction of thiones and diazo compounds are known: S. Tamagaki and S. Oae, *Tetrahedron Lett.*, **1972**, 1159; P. Gronski and K. Hartke, *ibid.*, **1976**, 4139.

3) P. N. Preston, N. J. Robinson, K. Turnbull, and T. J. King, *J. Chem. Soc., Chem. Commun.*, **1974**, 998; P. N. Preston and K. Turnbull, *J. Chem. Soc., Perkin Trans. 1*, **1977**, 1229.

4) G. V. Boyd, T. Norris, and P. F. Lindley, *J. Chem. Soc., Chem. Commun.*, **1975**, 100; *J. Chem. Soc., Perkin Trans. 1*, **1976**, 1673.

5) M. Regitz and A. Liedhegener, *Chem. Ber.*, **99**, 3128 (1966).

6) M. Regitz, *Chem. Ber.*, **97**, 2742 (1964).

Potentiometric Study of Cadmium(II) Halide and Thiocyanate Complexes in Methanol. Determination of Thermodynamic Stability Constants of Third and Fourth Complexation Step

Khin Nwe SOE, Hidekazu DOE, and Toyokichi KITAGAWA*
Department of Chemistry, Faculty of Science, Osaka City University, Sumiyoshi-ku, Osaka 558
(Received October 19, 1987)

Synopsis. The stability constants, K_3 and K_4, of $[Cd^{II}X_n]^{2-n}$ (X^-=Cl^-, Br^-, I^-, NCS^-) complexes in methanol have been determined by X^- ion measurements with Ag-AgX and NCS^- ion selective electrodes at 25 °C.

With the confirmation of the structural postulation, the formation of cadmium halide and thiocyanate complexes at any consecutive step accompanying the conformational change was earlier investigated by Ahrland and his co-workers in dimethyl sulfoxide.[1-3] Those investigations were performed at high ionic strength. We have previously studied the formation of mono- and dihalide and thiocyanate complexes in methanol at an ionic strength of 0.05 M (1 M=1 mol dm^{-3}).[4] The thermodynamic stability constants of mono- and dihalide and thiocyanate complexes, K_1 and K_2, have been studied. In this extended study, we aimed to determine the thermodynamic stability constants of tri- and tetrahalide and thiocyanate complexes, K_3 and K_4. In the present study, all potentiometric measurements were carried out at low ionic strength because it was extremely difficult to evaluate an ion activity coefficient at high ionic strength. The octahedral structure of both aquocadmium and solvated cadmium ion in dimethyl sulfoxide solution was postulated from an X-ray diffraction analysis.[5,6] Moreover, the tetrahedral structure postulation of cadmium tetrahalide complexes in aqueous solution were confirmed by X-ray diffraction studies.[5,7] Recently, the ambidentate coordination of N and S with cadmium at the formation of tri- and tetrathiocyanate complexes in aqueous solution has been postulated as $[Cd(SCN)(NCS)_2]^-$ and $[Cd(SCN)_2(NCS)_2]^{2-}$,[8,9] For these reasons, a conformational change will take place at any consecutive step of the formation of cadmium(II) halide and thiocyanate complexes.

Experimental

Materials. Cadmium(II) perchlorate hexahydrate was prepared by neutralizing cadmium carbonate (Nakarai, Guaranteed Grade) with perchloric acid.[10] This hexahydrate salt was purified by triple recrystallization from distilled water and was then dried on a vacuum line over diphosphorus pentaoxide for three days in order to obtain a dihydrate salt. The preparations of the other reagents were described in previous papers.[11,12]

Instrumentation. Outlines of the instrumentation and measurement procedure were described previously.[11,12] In the present study, the sensor for I^- was a Horiba iodide ion-selective electrode 8005-06T. All measurements were carried out in a closed cell thermostated at 25.0±0.1 °C. The cell contained 40 cm^3 of sample solution before titration.

Data Treatment and Results

In general, the following equilibria are established in methanol:

$$[CdX_{n-1}]^{3-n} + X^- \rightleftharpoons [CdX_n]^{2-n} \ (K_n;\ n=1—4) \quad (1)$$

$$Cd^{2+} + ClO_4^- \rightleftharpoons [CdClO_4]^+ \ (K_{1A}) \quad (2)$$

By considering these equilibria, a function, $\bar{n}$, defined as the average number of ligands, X^-, attached to the metal, M^{2+}, is written as:

$$\bar{n} = (C_X^\circ - [X^-])/C_M^\circ$$
$$= (y_1\beta_1[X^-] + 2y_2\beta_2[X^-]^2 + 3y_3\beta_3[X^-]^3 + 4y_4\beta_4[X^-]^4)/$$
$$(1 + y_1K_{1A}[ClO_4^-] + y_1\beta_1[X^-] + y_2\beta_2[X^-]^2 + y_3\beta_3[X^-]^3 + y_4\beta_4[X^-]^4). \quad (3)$$

C_M° and C_X° are the total concentrations of $Cd(ClO_4)_2$ and NaX respectively, and β_n is the overall stability constant ($\beta_n = \prod_{i=1}^{n} K_n$). It has been assumed that ions with an identical absolute value of charge have the same ion activity coefficient at I=0.05 M.[12] Thus, this assumption leads to $y_1=y_{2+}$, $y_2=y_3=y_{2+}y_\pm^2$, and $y_4=y_\pm^4$, where $y_\pm$ and y_{2+} are the ion activity coefficients of mono- and divalent ions, respectively. By rearranging Eq. 3, the following equation is obtained:

$$\bar{n}(1 + y_1K_{1A}[ClO_4^-]) = \beta_1(1-\bar{n})y_1[X^-] + \beta_2(2-\bar{n})y_2[X^-]^2 + \beta_3(3-\bar{n})y_3[X^-]^3 + \beta_4(4-\bar{n})y_4[X^-]^4. \quad (4)$$

Here, $\bar{n}$ and $[X^-]$ are measurable and K_{1A} has already been determined by conductometric measurements.[13]

Now, in consideration of the equilibria 1—3, the concentration of Cd^{2+} is:

$$[Cd^{2+}] = C_M^\circ/(1 + y_1K_{1A}[ClO_4^-] + y_1\beta_1[X^-] + y_2\beta_2[X^-]^2 + y_3\beta_3[X^-]^3 + y_4\beta_4[X^-]^4). \quad (5)$$

In order to calculate the y_1, y_2, y_3, and y_4 values, the Debye-Hückel second approximation has been used:

$$\ln y = -Az_i^2I^{1/2}/(1+BaI^{1/2}). \quad (6)$$

Data processing started with initial values of $[ClO_4^-] = 2C_M^\circ + C_I^\circ$ and of y_1, y_2, y_3, and y_4 values at I=0.05 M. By the use of these values, β_n were initially estimated by a multiple regression analysis with weighted terms according to Eq. 4. Those n values were used to calculate $[Cd^{2+}]$, $[CdX_n^{2-n}]$, and $[ClO_4^-]$. Then, I was calculated by the use of $[Cd^{2+}]$ and $[CdX_n^{2-n}]$. Since this calculated I value was slightly different from 0.05 M, $[X^-]$ was corrected by a $y_\pm$ value since the calibration

Table 1. Thermodynamic Stability Constants of Cadmium Halide and Thiocyanate Systems in Methanol at 25 °C

X^-	K_1/M^{-1}	K_2/M^{-1}	K_3/M^{-1}	K_4/M^{-1}	K_3K_4/M^{-2}	β_4/M^{-4}
Cl	$(1.83\pm0.01)\times10^6$	$(9.4\pm3.4)\times10^2$				
Br	$(3.5\pm0.2)\times10^6$	$(4.4\pm0.7)\times10^3$			$(7.9\pm3.5)\times10^3$	$(1.2\pm0.5)\times10^{14}$
I	$(7.8\pm0.2)\times10^6$	$(2.5\pm0.2)\times10^4$	$(1.1\pm0.2)\times10^3$	$(2.2\pm0.6)\times10^2$	$(2.3\pm0.5)\times10^5$	$(4.5\pm1.0)\times10^{16}$
NCS	$(7.2\pm0.1)\times10^5$	$(1.7\pm0.1)\times10^3$			$(5.3\pm3.2)\times10^3$	$(6.5\pm3.9)\times10^{12}$

Table 2. Concentration Stability Constants of Cadmium Halide and Thiocyanate Systems in Methanol at 25 °C: I=0.05 M

X^-	$y_{2+}K_1/M^{-1}$	$y_{\pm}^2K_2/M^{-1}$	K_3/M^{-1}	$(y_{\pm}^2/y_{2+})K_4/M^{-1}$	$(y_{\pm}^2/y_{2+})K_3K_4/M^{-2}$	$y_{\pm}^4\beta_4/M^{-4}$
Cl	$(1.5\pm0.01)\times10^5$	$(2.5\pm0.9)\times10^2$				
Br	$(2.9\pm0.2)\times10^5$	$(1.1\pm0.2)\times10^3$			$(2.5\pm1.1)\times10^4$	$(8.2\pm3.4)\times10^{12}$
I	$(6.5\pm0.2)\times10^5$	$(6.6\pm0.6)\times10^3$	$(1.1\pm0.2)\times10^3$	$(6.9\pm1.9)\times10^2$	$(7.2\pm1.6)\times10^5$	$(3.0\pm0.9)\times10^{14}$
NCS	$(5.94\pm0.05)\times10^4$	$(4.5\pm0.3)\times10^2$			$(1.7\pm1.0)\times10^4$	$(4.4\pm2.6)\times10^{11}$

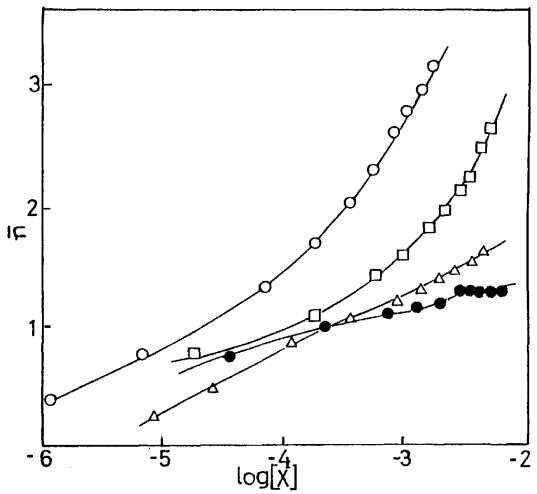

Fig. 1. Average coordination numbers, $\bar{n}$, as a function of log[X^-]: ● chloride; □ bromide; ○ iodide; △ thiocyanate. Dashed line: experimental line.

was made at I=0.05 M.[4] Here, we could return to Eq. 4 with new values of I, [ClO_4^-], and [X^-]. This series of processing was repeated until β_n values became constant.

Table 1 shows the stepwise stability constants, including K_1 and K_2. The y_{2+} and $y_{\pm}$ values at I=0.05 M are 0.08285 (a=5° A)[4] and 0.5110. The concentration stability constants are summarized in Table 2. The products of K_3K_4 are shown in Table 1.

Discussion

For the chloride system, K_3 and K_4 were so small that they could not be determined under this experimental conditions (Fig. 1), that $\bar{n}$ does not exceed 2. Similarly, in the bromide system, $\bar{n}$ does not exceed 3 due to the small values of K_3 and K_4. For the iodide system, the complex was formed up to tetraiodide under this experimental conditions and generally, thermodynamic stability constants decrease in the order $K_1>K_2>K_3>K_4$. Besides, the stabilities of halide complexes decrease in the order $I^->Br^->Cl^-$, as shown in Fig. 1, since cadmium(II) is a soft acid, preferring to coordinate with soft donor ligands.[14,15] In a protic solvent like water, the same sequence was found for cadmium(II) halides in various ionic media.[3]

The existence of $[Zn(MeOH)_6]^{2+}$ and $[Zn(MeOH)_5(ClO_4)]^+$ was postulated from a proton magnetic resonance investigation of the zinc-methanol system.[16] For this reason, the solvated cadmium ion probably has an octahedral $[Cd(MeOH)_6]^{2+}$ structure in this study. Additionally, according to the structural postulation described above (introduction), it can be obviously seen that the structural change of an octahedral coordination to tetrahedral coordination will certainly occur at any consecutive step of formation of cadmium(II) halide complexes in methanol.

According to the K_2 value, we have discussed earlier[4] how the steric hindrance of ligands in an octahedrally coordinated structure would suppress the formation of cadmium dihalide complexes; it would cause the value of K_2 to become small, making the ratio of K_1/K_2 extremely large. Therefore, it was impossible for a coordination change to take place at the second step. In other words, it will take place at the subsequent steps.

The coordination change at the subsequent steps was confirmed by a Raman study[17] on the C_{3v}, bent structure of $CdBr_3^-$ in an aqueous solution. For this reason, it is quite possible that $CdBr_3^-$ and CdI_3^- have a tetrahedral structure with a solvent molecule at an apex in methanol. Our results did not clearly indicate the step at which the conformational change occurs viz. the formation of a trihalide complex or the formation of a tetrahalide complex. However, an extremely small K_2 value may support a change at the third step. If data on enthalpy and entropy changes is available, they will be of great help in discussing the conformational change in greater detail.

K. N. S. thanks Professor Dr. Ko Ko Gyi of Rangoon University, Rangoon, Burma, for his kind permission to do research work in Japan.

References

1) S. Ahrland and N. O. Bjork, *Acta Chem. Scand.*, **30A**, 249 (1976).
2) S. Ahrland and N. O. Bjork, *Acta Chem. Scand.*, **30A**, 257 (1976).
3) S. Ahrland, *Pure Appl. Chem.*, **51**, 2019 (1979).
4) H. Doe, K. Wakamiya, C. Yoshida, H. Ozaki, K. N. Soe, and T. Kitagawa, *Inorg. Chem.*, **26**, 2244 (1987).
5) H. Ohtaki, H. Maeda, and S. Ito, *Bull. Chem. Soc. Jpn.*, **47**, 2217 (1974).
6) I. Persson, A. Iverfeldt, and S. Ahrland, *Acta Chem. Scand.*, **A35**, 295 (1981).
7) S. Pocev, R. Trido, and G. Johansson, *Acta Chem. Scand.*, **A33**, 179 (1979).
8) T. Yamaguchi. K. Yamamoto, and H. Ohtaki, *Bull. Chem. Soc. Jpn.*, **58**, 3235 (1985).
9) S. Isiguro, K. Yamamoto, and H. Ohtaki, *Bull. Chem. Soc. Jpn.*, **59**, 1009 (1986).
10) "Shin Jikken Kagaku Koza," Maruzen, Tokyo (1976), Vol.8, Chaps. 1—3.
11) H. Doe, A. Shibagaki, and T. Kitagawa, *Inorg. Chem.*, **22**, 1639 (1983).
12) H. Doe and T. Kitagawa, *Inorg. Chem.*, **21**, 2272 (1982).
13) H. Doe and T. Kitagawa, *Bull. Chem. Soc. Jpn.*, **58**, 2975 (1985).
14) R. G. Pearson, *J. Am. Chem. Soc.*, **85**, 3533 (1963).
15) R. G. Pearson, *J. Chem. Educ.*, **45**, 581 (1968).
16) S. A. Al. Baldawi and T. E. Gough, *Can. J. Chem.*, **47**, 1417 (1969).
17) J. W. Macklin and R. A. Plane, *Inorg. Chem.*, **9**, 821 (1970).

Crystal Structures of the Imidazole and the 1,4-Di(1-imidazolyl)butane Adducts of *N,N'*-Ethylenebis[salicylideneaminato]-manganese(III) Perchlorate

Naohide MATSUMOTO,* Naohiko TAKEMOTO, Akira OHYOSI, and Hisashi ŌKAWA†
Department of Applied Chemistry, Faculty of Engineering, Kumamoto University, Kurokami 2-39-1, Kumamoto 860
†Department of Chemistry, Faculty of Science, Kyushu University, Hakozaki, Higashi-ku, Fukuoka 812
(Received December 14, 1987)

Synopsis. Crystal structures of the titled compounds [Mn(Him)(salen)][ClO_4]CH_3OH (**1**) and [Mn(biim)(salen)][ClO_4] (**2**), have been determined by the single-crystal X-ray diffraction method. The molecular structure of the imidazole adduct (**1**) is a binuclear structure bridged by phenoxy oxygen atoms of salen ligand, while that of the 1,4-di(1-imidazolyl)butane adduct (**2**) is a polynuclear structure bridged by imidazole nitrogen atoms of 1,4-di(1-imidazolyl)-butane.

It is well-known that metal complexes with N,N'-ethylenebis[salicylideneamine] (well-known salen ligand) tend to assume a dimeric structure bridged by phenoxy oxygen atoms.[1] In this study the imidazole adduct and the 1,4-di(1-imidazolyl)butane adduct of [Mn(salen)][ClO_4] were prepared and their crystal structures were determined by a single-crystal X-ray diffraction technique in order to investigate their molecular structures.

Experimental

Synthesis. [Mn(Him)(salen)][ClO_4]CH_3OH (**1**). To a solution of [Mn(salen)][ClO_4]$2H_2O$ (2 mmol) in 30 cm^3 of methanol was added a solution of imidazole (3 mmol) in 10 cm^3 of methanol. The solution was gently warmed on a water bath for 10 min and cooled to room temperature. The solution was kept standing overnight. The dark-brown crystals precipitated were collected by suction filtration and dried. Found: C, 45.72; H, 4.31; N, 10.78%. Calcd for $MnClO_7N_4C_{20}H_{22}$: C, 46.13; H, 4.26; N, 10.76%. Mp >300 °C, Λ_M 88 S mol^{-1} cm^2 (methanol).

[Mn(biim)(salen)][ClO_4] (**2**). The complex (**2**) was prepared by a method similar to that of **1**, where 1,4-di(1-imidazoyl)butane instead of imidazole was used. Found: C, 51.07; H, 4.62; N, 13.75%. Calcd for $MnClO_6N_6C_{26}H_{28}$: C, 51.12; H, 4.62; N, 13.76%. Mp 253—257 °C, Λ_M 65 S mol^{-1} cm^2 (DMF).

Physical Measurements. Elemental analyses were performed by Mr. Shinichi Miyazaki at the Technical Service Center of Kumamoto University. Melting points were measured on a Yanagimoto micro-melting points apparatus and were uncorrected. Molar electrical conductivities were measured on a Denki Kagaku Keiki AOC-10 digital conductometer.

X-Ray Diffraction Study. Diffraction data for complexes **1** and **2** were obtained on a Rigaku Denki AFC-5 four-circle diffractometer at the Faculty of Science, Kyushu University, using graphite monochromatized Mo$K\alpha$ radiation at ambient temperature (20±1 °C). Pertinent crystallographic parameters are summarized below:

[Mn(Him)(salen)][ClO_4]CH_3OH (**1**). Formula=$MnClO_7N_4C_{20}H_{22}$, FW=520.8, triclinic, space group $P\bar{1}$, a=11.203(2) Å, b=11.565(2) Å, c=9.832(1) Å, α=112.25(1)°, β=107.50(1)°, γ=86.64(1)°, V=1119.9 Å^3, D_x=1.544 g cm^{-3} (Z=2), D_m=1.52 g cm^{-3}, crystal size 0.2×0.3×0.4 mm, scan mode θ-2θ, scan rate 6° min^{-1}, 2θ range 2.5°<2θ<48°, no. unique data used 2182, R=4.93%, R_w=5.16%.

[Mn(biim)(salen)][ClO_4] (**2**). Formula=$MnClO_6N_6C_{26}H_{28}$, FW=610.9, monoclinic, space group $P2_1/a$, a=16.566 (9) Å, b=16.141(4) Å, c=10.527(2) Å. β=102.81(2)°, V=2759.7 Å^3, D_x=1.470 g cm^{-3} (Z=4), D_m=1.46 g cm^{-3}, crystal size 0.2×0.2×0.4 mm, scan mode θ-2θ, scan rate 6° min^{-1}, 2θ range 2.5°<2θ<48°, no. unique data used 3204, R=5.62%, R_w=5.68%. One of two imidazole moieties of biim has been subjected to disorder. The occupancy factors for C(17) and C(18) atoms were assigned on the basis of the peak heights of the difference Fourier synthesis.

Reflection data were corrected for Lorentz-polarization effects but not for absorption. The structures were solved by the standard heavy-atom method and refined by a block-diagonal least-squares method using the Universal Crystallographic Computation Program System UNICS III.[2]

Table 1. Atomic Parameters of Non-Hydrogen Atoms for [Mn(Him)(salen)][ClO_4]MeOH (×10^4)

Atom	x	y	z	B_{eqv}
Mn	1418(1)	851(1)	659(1)	2.6
O(1)	1569(3)	324(3)	−1338(4)	2.6
O(2)	−252(3)	1315(3)	79(4)	2.6
N(1)	2962(4)	60(4)	1388(5)	2.5
N(2)	1297(4)	1154(4)	2735(5)	2.3
N(3)	2391(4)	2715(4)	1395(5)	2.7
N(4)	3564(5)	4128(5)	1302(6)	4.3
C(1)	2375(5)	−427(5)	−1927(6)	2.5
C(2)	2219(6)	−785(5)	−3509(6)	3.3
C(3)	3006(6)	−1581(6)	−4200(7)	4.0
C(4)	3990(6)	−2062(6)	−3362(7)	4.2
C(5)	4156(6)	−1715(6)	−1802(7)	3.9
C(6)	3381(5)	−900(5)	−1060(6)	2.7
C(7)	3632(5)	−618(5)	574(6)	2.8
C(8)	3323(5)	325(5)	3063(6)	3.2
C(9)	2133(6)	404(5)	3494(6)	2.9
C(10)	575(5)	1928(5)	3379(6)	2.7
C(11)	−323(5)	2613(5)	2646(6)	2.6
C(12)	−901(6)	3567(5)	3538(7)	3.8
C(13)	−1811(6)	4213(5)	2894(8)	4.4
C(14)	−2157(6)	3898(5)	1312(8)	4.1
C(15)	−1622(5)	2948(5)	381(7)	3.2
C(16)	−702(5)	2286(5)	1025(6)	2.5
C(17)	2728(7)	3690(6)	2798(7)	4.8
C(18)	3438(8)	4555(6)	2736(8)	5.6
C(19)	2917(6)	3019(5)	539(7)	3.3
Cl	4397(2)	2902(1)	−2726(2)	3.5
O(3)	4624(5)	3951(4)	−1340(5)	6.2
O(4)	5568(7)	2600(6)	−3010(9)	9.8
O(5)	3950(5)	1844(5)	−2621(6)	6.7
O(6)	3641(8)	3179(6)	−3938(6)	10.7
OS	194(6)	1837(7)	−3097(7)	9.7
CS	135(9)	3134(9)	−2292(10)	8.2

Table 2. Atomic Parameters of Non-Hydrogen Atoms for [Mn(biim)(salen)][ClO_4] ($\times 10^4$)

Atom	x	y	z	B_{eqv}
Mn	517(0)	1693(0)	2013(1)	3.2
O(1)	704(2)	1705(2)	315(3)	3.6
O(2)	−543(2)	1231(2)	1513(3)	3.7
N(1)	1670(2)	2220(2)	2738(4)	3.0
N(2)	456(2)	1708(3)	3879(4)	3.4
N(3)	43(3)	3023(3)	1730(5)	4.2
N(4)	−407(4)	4262(3)	1976(8)	8.2
N(5)	−3003(3)	5623(3)	2615(4)	3.4
N(6)	−3877(3)	4589(3)	2305(4)	3.5
C(1)	1418(3)	1765(3)	−19(5)	3.2
C(2)	1460(4)	1543(3)	−1289(5)	4.0
C(3)	2176(4)	1610(4)	−1707(5)	4.5
C(4)	2895(4)	1910(4)	−894(6)	4.4
C(5)	2877(3)	2139(3)	351(5)	3.8
C(6)	2148(3)	2060(3)	820(5)	3.1
C(7)	2185(3)	2316(3)	2135(5)	3.2
C(8)	1667(3)	2561(4)	4048(5)	4.0
C(9)	1226(3)	1972(4)	4770(5)	4.5
C(10)	−147(3)	1452(4)	4352(5)	4.0
C(11)	−904(3)	1111(3)	3594(5)	3.7
C(12)	−1491(4)	843(4)	4275(6)	5.3
C(13)	−2222(4)	500(4)	3631(7)	5.7
C(14)	−2378(4)	408(4)	2299(7)	5.0
C(15)	−1815(3)	664(3)	1590(6)	4.2
C(16)	−1059(3)	1012(3)	2225(5)	3.3
C(17A)[a]	81(15)	4385(13)	1233(23)	5.9
C(17B)[a]	−411(6)	4098(7)	395(11)	3.8
C(17C)[a]	287(13)	4426(14)	1629(21)	2.5
C(18A)[a]	444(13)	3625(12)	1126(22)	5.0
C(18B)[a]	−86(6)	3322(7)	356(11)	4.1
C(18C)[a]	−328(22)	3601(20)	1088(34)	6.3
C(19)	−296(3)	3518(3)	2440(5)	4.0
C(20)	−775(4)	4973(4)	2503(9)	7.1
C(21)	−1457(4)	5352(4)	1508(7)	5.1
C(22)	−1764(4)	6168(3)	1958(7)	4.7
C(23)	−2227(4)	6084(3)	3034(6)	4.4
C(24)	−3725(4)	5923(3)	1872(6)	4.3
C(25)	−4260(3)	5282(3)	1696(5)	4.1
C(26)	−3123(3)	4816(3)	2844(5)	3.4
Cl	3915(1)	1591(1)	5841(2)	5.4
O(3)	4722(3)	1697(4)	5685(5)	8.5
O(4)	3900(4)	995(5)	6780(8)	12.0
O(5)	3422(4)	1373(5)	4647(6)	12.0
O(6)	3580(4)	2339(4)	6237(7)	10.8

a) Occupancy factors: A 0.3; B 0.2; C 0.5.

The positions of hydrogen atoms were calculated. The hydrogen atoms were included in the structure factor calculation but not refined. The calculations were carried out on a FACOM M 200 computer at the Computer Center of Kyushu University. Positional parameters of non-hydrogen atoms for the complexes **1** and **2** are given in Tables 1 and 2, respectively. Tables of the anisotropic thermal parameters for non-hydrogen atoms, atomic parameters for hydrogen atoms, and F_o-F_c tables are given as supplementary data at the office of the Chemical Society of Japan as Document No. 8815.

Results and Discussion

Bond distances and angles with their estimated standard deviaitons of **1** and **2** are given in tables, which are deposited as supplementary data. Perspective drawings of the cations of **1** and **2** with the atom numbering scheme are shown in Figs. 1 and 2, respectively.

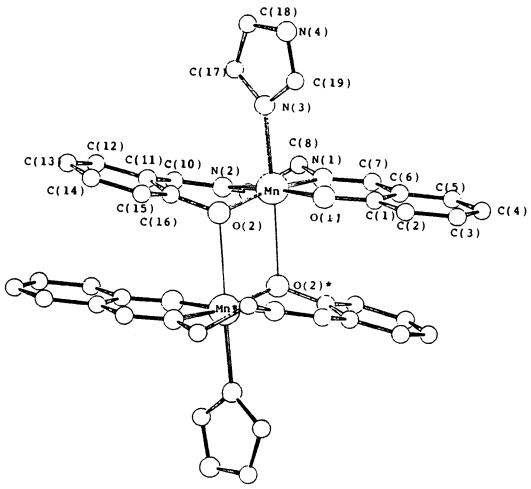

Fig. 1. Perspective drawing of **1** with the atom numbering scheme.

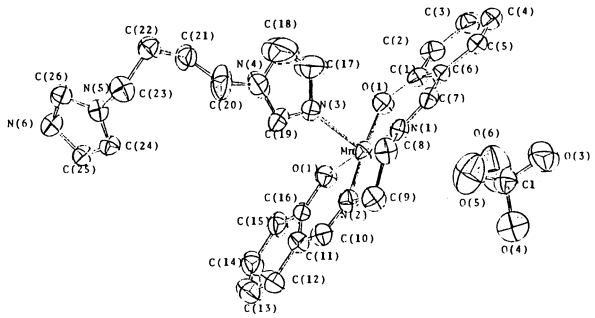

Fig. 2. Perspective drawing of unique molecule of [Mn(biim)(salen)][ClO_4] **2** with the atom numbering scheme.

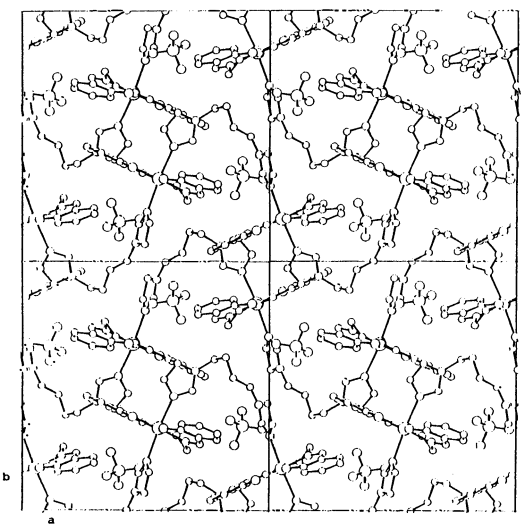

Fig. 3. Polynuclear structure of **2**.

Structural Description of [Mn(Him)(salen)][ClO_4] CH_3OH (1). As shown in Fig. 1, the structure of **1** is a binuclear structure bridged by phenoxy oxygen atoms

of salen ligands, in which two $[Mn(Him)(salen)]^+$ cations are related by an inversion center. The manganese(III) ion has a tetragonal bipyramidal coordination geometry, in which the basal coordination plane comprises N_2O_2 donors of quadridentate salen ligand; the two elongated axial positions are occupied by an imidazole nitrogen atom N(3) (Mn-N(3) 2.231(4) Å) and a phenoxy oxygen atom O(2)* of symmetry related salen ligand ($-x$, $-y$, $-z$) (Mn-O(2)* 2.635(3) Å). The imidazole plane lies on the Mn-O(1) and Mn-N(2) bonds.

Structural Description of [Mn(biim)(salen)][ClO_4] (2). The structure of **2** is a polymeric chain structure bridged by imidazole nitrogen atoms of 1,4-di(1-imidazolyl)-butane, as shown in Fig. 3. The manganese(III) ion has a tetragonal bipyramidal coordination geometry, in which the basl plane comprises N_2O_2 donors of the salen ligand; the two elongated axial positions are occupied by imidazole nitrogen atoms N(3) and N(6)* ($x+1$, $-y+1/2$, $z+1/2$) of biim ligands with the bond distances Mn-N(3) (2.278(5) Å) and Mn-N(6)* (2.283(4) Å).

References

1) M. Gerloch and F. E. Mabbs, *J. Chem. Soc. A*, **1967**, 1900; M. Calligaris, G. Nardin, and L. Randaccio, *Coord. Chem. Rev.*, **7**, 385 (1972).

2) T. Sakurai and K. Kobayashi, *Rikagaku Kenkyusho Houkoku*, **55**, 69 (1979); S. Kawano, *Rep. Compuut. Cent. Kyushu Univ.*, **13**, 39 (1980).

Preparation and Resolution of Bis[tris(2-aminoethaneselenolato)-cobalt(III)-μ-Se, μ-Se', μ-Se'']cobalt(III) Complex

Shin MIYANOWAKI, Takumi KONNO,* Ken-ichi OKAMOTO, and Jinsai HIDAKA
Department of Chemistry, University of Tsukuba, Tsukuba, Ibaraki 305
(Received January 30, 1988)

Synopsis. The title *Se*-bridged complex, $[Co^{III}\{Co^{III}(aese)_3\}_2]^{3+}$ (aese=2-aminoethaneselenolate), was newly prepared by the reaction of *fac*-[Co(aese)$_3$] with Co^{2+} and separated into three isomers, *ΔΔ*, *ΔΛ*, and *ΛΛ*, by the ion-exchange chromatographic method. The isomers were characterized from their absorption, CD, and ^{13}C NMR spectra.

Thiolate ligands tend to form polynuclear metal complexes with μ-thiolato structure and several trinuclear cobalt(III) complexes with 2-aminoethanethiolate (aet) and L-cysteinate (L-cys) have been investigated.[1-12] This tendency is also expected for the selenolate ligand such as 2-aminoethaneselenolate (aese). However, up to now no study has appeared on the *Se*-bridged polynuclear cobalt(III) complexes. This note describes the preparation and resolution of the *Se*-bridged tricobalt(III) complex with 2-aminoethaneselenolate $[Co\{Co(aese)_3\}_2]^{3+}$ (Fig. 1). The isomers obtained are characterized from their absorption, CD, and ^{13}C NMR spectra in comparison with those of the corresponding tricobalt(III) complexes with 2-aminoethanethiolate, $[Co\{Co(aet)_3\}_2]^{3+}$.[3,4,9] The redox properties of $[Co\{Co(aese)_3\}_2]^{3+}$ and $[Co\{Co(aet)_3\}_2]^{3+}$ are also reported.

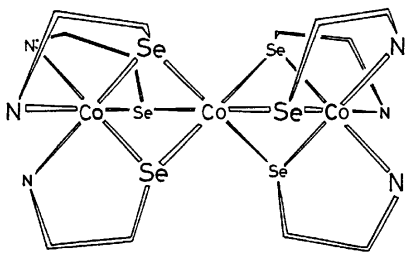

Fig. 1. The *ΔΔ* isomer of $[Co\{Co(aese)_3\}_2]^{3+}$.

Experimental

Preparation and Resolution of Complexes. 1) *fac*-[Co(aese)$_3$]: To a deoxygenated solution containing 0.7 g (18.2 mmol) of $NaBH_4$ in 45 cm^3 of water were successively added with stirring a deoxygenated solution containing 3.0 g (9.1 mmol) of $(NH_2CH_2CH_2Se-)_2\cdot 2HCl\cdot 0.5H_2O$[13] in 70 cm^3 of water and a deoxygenated solution containing 2.2 g (6.1 mmol) of $Na_3[Co(CO_3)_3]\cdot 3H_2O$ in 45 cm^3 of water. The mixture was continuously stirred at 60 °C for 5 h under nitrogen atmosphere. The resultant deep green complex was collected by filtration and washed with ethanol and ether. This complex is sparingly soluble in water. Found: C, 16.84; H, 4.24; N, 9.82%. Calcd for $[Co(aese)_3]=C_6H_{18}N_3Se_3Co$: C, 16.83; H, 4.21; N, 9.69%.

2) *meso*-$[Co\{Co(aese)_3\}_2]I_3$ and *rac*-$[Co\{Co(aese)_3\}_2]Cl_3\cdot 1.5H_2O\cdot NaCl$: To a suspension of 1.8 g (4.2 mmol) of *fac*-[Co(aese)$_3$] in 30 cm^3 of water was added a solution containing 0.5 g (2.1 mmol) of $CoCl_2\cdot 6H_2O$ in 10 cm^3 of water. The mixture was stirred at 40 °C for 1 h, whereupon the color of the solution became deep brownish green. Addition of a large amount of ethanol to the reaction solution in an ice bath yielded a deep green precipitate of $[Co\{Co(aese)_3\}_2]Cl_3$, which was collected by filtration.

One gram of $[Co\{Co(aese)_3\}_2]Cl_3$ was dissolved in a small amount of water and poured onto a column of SP-Sephadex C-25 (Na^+ form, 5.5 cm×45 cm). After the column had been swept with water, the adsorbed band was eluted with a 0.2 mol dm^{-3} aqueous solution of NaCl. A circulating-chromatographic technique was employed for the separation of the isomers. After circulating the eluate in the same column twice, two dark green bands, A-1 and A-2, were eluted in that order. It was found, from the result of the optical resolution procedure, that the A-1 and A-2 eluates contained *meso*- and *rac*-$[Co\{Co(aese)_3\}_2]^{3+}$, respectively. Each eluate was concentrated to a small volume with a rotary evaporator below 25 °C. On cooling the concentrated eluate in a refrigerator overnight, crystals of the A-2 isomer appeared and were collected by filtration. This isomer was recrystallized twice from water by adding ethanol in an ice bath. The crystals of the A-1 isomer were obtained as an iodide salt by adding a large amount of saturated NaI solution to the concentrated eluate. These aese tricobalt(III) isomers are unstable in aqueous solution in comparison with the aet tricobalt(III) ones. Found for A-1: C, 11.03; H, 2.78; N, 6.30%. Calcd for $[Co\{Co(aese)_3\}_2]I_3=C_{12}H_{36}N_6I_3Se_6Co_3$: C, 11.12; H, 2.80; N, 6.49%. Found for A-2: C, 13.11; H, 3.59; N, 7.64%. Calcd for $[Co\{Co(aese)_3\}_2]Cl_3\cdot 1.5H_2O\cdot NaCl=C_{12}H_{39}N_6O_{1.5}NaCl_4Se_6Co_3$: C, 13.02; H, 3.55; N, 7.59%.

3) Optical Resolution of $[Co\{Co(aese)_3\}_2]^{3+}$: The A-2 isomer was optically resolved by column chromatography, while the A-1 isomer could not be resolved. An aqueous solution of the A-2 isomer (0.2 g) was charged on the top of an SP-Sephadex C-25 column (Na^+ form, 4 cm×85 cm). Two bands were separated by eluting with a 0.2 mol dm^{-3} aqueous solution of $K_2[Sb_2(d\text{-tart})_2]\cdot 3H_2O$. After the separation into two bands, each adsorbed band was eluted with a 0.2 mol dm^{-3} aqueous solution of NaCl. It was found from the CD spectral measurements that the earlier moving band contained $(-)^{CD}_{680}$-$[Co\{Co(aese)_3\}_2]^{3+}$ and the later one contained $(+)^{CD}_{680}$-$[Co\{Co(aese)_3\}_2]^{3+}$. The $\Delta\varepsilon$ values of them were evaluated on the basis of the absorption spectrum of the racemic chloride salt.

4) Preparation and Resolution of $[Co\{Co(aet)_3\}_2](NO_3)_3$: This complex was prepared from *fac*-[Co(aet)$_3$] and $CoCl_2\cdot 6H_2O$ by the method of Busch et al.[3] Three isomers, *ΔΔ*, *ΔΛ*, and *ΛΛ*, were chromatographically separated according to the procedures described in 2) and 3).

Measurements. The electronic absorption spectra were recorded with a JASCO UVIDEC-610A spectrophotometer, the diffuse reflection spectra with a JASCO UVIDEC-1 spectrophotometer, and the CD spectra with a JASCO J-20 spectropolarimeter. The ^{13}C NMR spectra were recorded with a JEOL JNM-FX-90Q NMR spectrometer at the probe temperature in a D_2O solvent. Sodium 2,2-dimethyl-2-silapentane-5-sulfonate (DSS) was used as the internal reference. The cyclic voltammograms were recorded with a Hokuto Denko potentiogalvanostat, model HA-201, to which a linear potential scanner, model HB-103, was at-

tached. A grassy carbon electrode, a Pt wire counter electrode with a sufficiently large surface area, and a 3.33 mol dm^{-3} KCl calomel reference electrode were used for the potentiostatic measurements in a 0.01 mol dm^{-3} sodium nitrate solution at room temperature (20±1 °C). The electrode potential data were corrected to those for the standard hydrogen electrode (SHE).

Results and Discussion

Two geometrical isomers, *fac* and *mer*, are possible for the tris(2-aminoethaneselenolato)cobalt(III) complex, [Co(aese)$_3$]. The diffuse reflection spectrum of the selenolato complex which belongs to the [Co(N)$_3$(Se)$_3$] type is similar to that of the *fac* isomer of the corresponding thiolato complex, [Co(aet)$_3$] (Fig. 2). This suggests that the selenolato complex takes selectively the *fac* geometry as well as the corresponding thiolato complex.[3,14] The reflection spectrum of *fac*-[Co(aese)$_3$] shifts to lower energy than that of *fac*-[Co(aet)$_3$] in accordance with the fact that the ligand field strength is selenolate < thiolate.[15] Three isomers, *ΔΔ*, *ΔΛ*, and *ΛΛ*, are expected for [Co{Co(aese)$_3$}$_2$]$^{3+}$, considering the absolute configurations of two terminal *fac*-[Co(aese)$_3$] (Fig. 1), as in the case of [Co{Co(aet)$_3$}$_2$]$^{3+}$.[4] The A-1 and A-2 isomers exhibit similar absorption spectra, showing two intense d-d bands at ca. 17 and 21×10^3 cm^{-1} and more intense charge transfer bands at ca. 26 and 33×10^3 cm^{-1} (Fig. 3). This absorption spectral behavior coincides well with that of the tricobalt(III) complex with 2-aminoethanethiolate, [Co^{III}{Co^{III}(aet)$_3$}$_2$]$^{3+}$, whose molecular structure has been determined by single crystal X-ray analysis.[9] Therefore, both the A-1 and A-2 isomers can be assigned to the tricobalt(III) complex with 2-aminoethaneselenolate, [Co^{III}{Co^{III}-(aese)$_3$}$_2$]$^{3+}$. The absorption components of [Co{Co(aese)$_3$}$_2$]$^{3+}$ commonly shift to lower energy than those of [Co{Co(aet)$_3$}$_2$]$^{3+}$ (Fig. 3) and this behavior is consistent with that of the cobalt(III) complexes with selenium- or sulfur-containing ligands.[15-20]

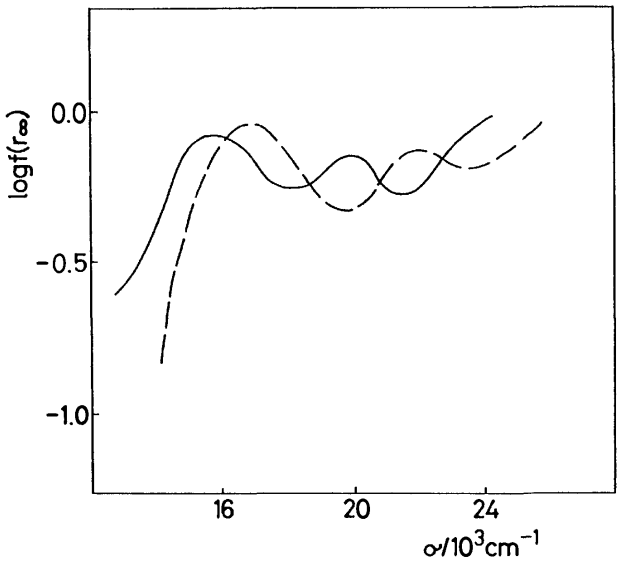

Fig. 2. Diffuse reflection spectra of *fac*-[Co(aese)$_3$] (——) and *fac*-[Co(aet)$_3$] (-----).

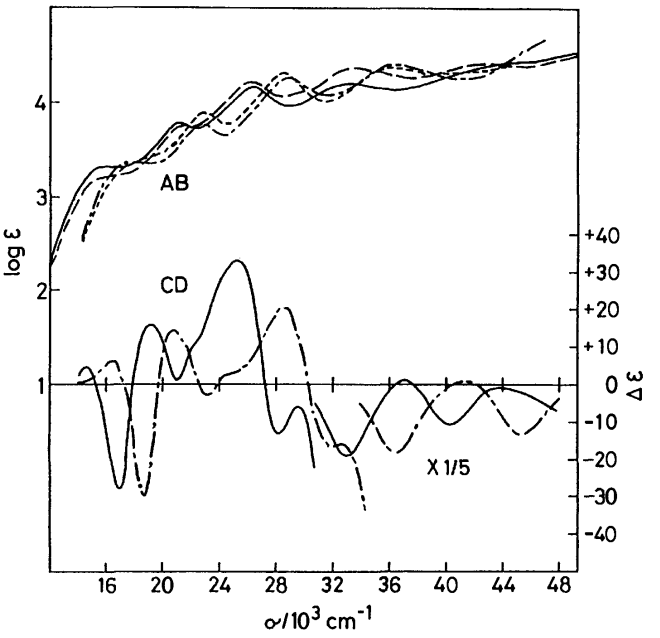

Fig. 3. Absorption and CD spectra of *ΔΔ*-[Co{Co(aese)$_3$}$_2$]$^{3+}$ (——), *ΔΛ*-[Co{Co(aese)$_3$}$_2$]$^{3+}$ (----), *ΔΛ*-[Co{Co(aet)$_3$}$_2$]$^{3+}$ (-·-·-), and *ΔΛ*-[Co{Co(aet)$_3$}$_2$]$^{3+}$ (------).

The A-2 isomer was optically resolved into the $(+)^{CD}_{680}$ and $(-)^{CD}_{680}$ ones, while the A-1 isomer could not. This result suggests that the A-1 and A-2 isomers take meso and racemic forms respectively, taking the similarity of their absorption spectra into consideration. This assignment is also supported by their ^{13}C NMR spectral behavior. Namely, both trinuclear isomers exhibit two ^{13}C NMR resonance lines due to two methylene carbons of the aese ligand; 27.09 and 49.68 ppm for the meso (A-1) isomer having S_6 symmetry, and 26.71 and 49.52 ppm for the racemic (A-2) isomer having D_3 symmetry. The $(+)^{CD}_{680}$ isomer exhibits the CD spectrum enantiomeric to the $(-)^{CD}_{680}$ one over the whole region. The CD spectral pattern of the $(+)^{CD}_{680}$ isomer agrees well with that of *ΔΛ*-[Co{Co(aet)$_3$}$_2$]$^{3+}$ (Fig. 3)[4] and furthermore, that of *Λ*$_{LLL}$*Λ*$_{LLL}$-[Co{Co(L-cys-*N*,*S*)$_3$}$_2$]$^{3-}$ whose absolute configuration has been determined by the single crystal X-ray analysis,[11] though the CD bands of the aese isomer shift significantly to lower energy than those of the aet isomer in parallel with their absorption spectral behavior. Accordingly, it is confidently assigned that the $(+)^{CD}_{680}$ isomer is *ΔΛ*-[Co{Co(aese)$_3$}$_2$]$^{3+}$ and the $(-)^{CD}_{680}$ isomer is the *ΔΔ* one.

The trinuclear complexes, [Co{Co(aese)$_3$}$_2$]$^{3+}$ and [Co{Co(aet)$_3$}$_2$]$^{3+}$, display a quasi-reversible cyclic response with $E_{1/2}$=−0.47 V for [Co{Co(aese)$_3$}$_2$]$^{3+}$ and $E_{1/2}$=−0.46 V for [Co{Co(aet)$_3$}$_2$]$^{3+}$, and no other redox process is observed in the potential range of −0.7—+0.5 V. The anodic and cathodic peaks separation, $E_{pa}-E_{pc}$, is 95 mV for [Co{Co(aese)$_3$}$_2$]$^{3+}$ and 65 mV for [Co{Co(aet)$_3$}$_2$]$^{3+}$, and the anodic peak current and the cathodic peak current are nearly equal for the two complexes. A similar redox reaction ($E_{1/2}$=−0.43 V, $E_{pa}-E_{pc}$=90 mV) was observed for the tricobaltate(III)

complex with L-cysteinate, $[Co\{Co(L\text{-}cys\text{-}N,S)_3\}_2]^{3-}$,[12] where the quasi-reversible redox reaction was assigned as the Co(III)/Co(II) redox process due to the central cobalt ion. Therefore, it is probable that the central cobalt ion is the active site of the redox reaction between Co(III) and Co(II) oxidation states for the present tricobalt(III) complexes with the aese and with the aet.

References

1) D. C. Jicha and D. H. Busch, *Inorg. Chem.*, **1**, 872 (1962).
2) D. C. Jicha and D. H. Busch, *Inorg. Chem.*, **1**, 878 (1962).
3) D. H. Busch and D. C. Jicha, *Inorg. Chem.*, **1**, 884 (1962).
4) G. R. Brubaker and B. E. Douglas, *Inorg. Chem.*, **6**, 1562 (1967).
5) C. H. Vei and L. F. Dahl, *Inorg. Chem.*, **9**, 1878 (1970).
6) R. E. DeSimone, T. Ontko, L. Wardman, and E. L. Blinn, *Inorg. Chem.*, **14**, 1313 (1975).
7) E. L. Blinn, P. Bulter, K. M. Chapman, and S. Harris, *Inorg. Chim. Acta*, **24**, 139 (1977).
8) P. R. Bulter and E. L. Blinn, *Inorg. Chem.*, **17**, 2037 (1978).
9) M. J. Heeg, E. L. Blinn, and E. Deutsch, *Inorg. Chem.*, **24**, 1118 (1985).
10) T. Konno, S. Aizawa, K. Okamoto, and J. Hidaka, *Chem. Lett.*, **1985**, 1017.
11) K. Okamoto, S. Aizawa, T. Konno, H. Einaga, and J. Hidaka, *Bull. Chem. Soc. Jpn.*, **59**, 3859 (1986).
12) S. Aizawa, K. Okamoto, H. Einaga, and J. Hidaka, *Bull. Chem. Soc. Jpn.*, **61**, 1601 (1988).
13) W. H. H. Gunther and H. G. Mautner, *J. Med. Sci.*, **7**, 229 (1964).
14) M. Kita, K. Yamanari, and Y. Shimura, *Bull. Chem. Soc. Jpn.*, **55**, 2873 (1982).
15) T. Konno, K. Okamoto, and J. Hidaka, *Bull. Chem. Soc. Jpn.*, **57**, 3104 (1984).
16) T. Konno, K. Okamoto, and J. Hidaka, *Chem. Lett.*, **1982**, 535.
17) T. Konno, K. Okamoto, H. Einaga, and J. Hidaka, *Chem. Lett.*, **1983**, 969.
18) K. Nakabayashi, K. Doi, M. Kojima, and J. Fujita, *Bull. Chem. Soc. Jpn.*, **57**, 989 (1984).
19) T. Konno, K. Okamoto, H. Einaga, and J. Hidaka, *Bull. Chem. Soc. Jpn.*, **58**, 1119 (1985).
20) H. Umehara, T. Konno, K. Okamoto, and J. Hidaka, *Bull. Chem. Soc. Jpn.*, **60**, 1367 (1987).

Ylide-Metal Complexes. XIV.[1] An X-Ray Photoelectron Spectroscopic Study on Tellurium Complexes of Methylenetriphenylphosphorane

Hidetaka KONNO† and Yoshihisa YAMAMOTO*
Faculty of Pharmaceutical Sciences, Higashi Nippon Gakuen University, Ishikari-Tobetsu, Hokkaido 061-02
†Faculty of Engineering, Hokkaido University, Sapporo 060
(Received February 4, 1988)

Synopsis. A series of new tellurium complexes of methylenetriphenylphosphorane, $(C_6H_5)_3P{=}CH_2$ (**L**), namely, dichlorobis(methylenetriphenylphosphorane)tellurium dichloride, $[L_2TeCl_2]Cl_2$, chlorotris(methylenetriphenylphosphorane)tellurium trichloride, $[L_3TeCl]Cl_3$, and tetrakis(methylenetriphenylphosphorane)tellurium tetrachloride, $[L_4Te]Cl_4$, were examined by XPS. Binding energies of Te 3d electrons for the complexes are considerably lower than those for common Te(IV) compounds such as $(C_6H_5)_2TeCl_2$, $TeCl_4$ (correctly Te_4Cl_{16}) and others, and they diminished with increasing number of **L**'s and decreasing number of bonded chlorine atoms, indicating that **L** is an electron donor. Bonded chlorine atoms and free chloride ions were clearly distinguished from the binding energy of Cl $2p_{3/2}$ electrons.

The preparation and properties of ylide metal complexes have been widely investigated in recent years. However, the electronic states of ylide metal complexes have not been reported except for the Cu and Au complexes.[1,2] In a previous paper,[3] we reported a series of new tellurium complexes of methylenetriphenylphosphorane, $(C_6H_5)_3P{=}CH_2$ (**L**), namely, dichlorobis(methylenetriphenylphosphorane)tellurium dichloride, $[L_2TeCl_2]Cl_2$, chlorotris(methylenetriphenylphosphorane)tellurium trichloride, $[L_3TeCl]Cl_3$, and tetrakis(methylenetriphenylphosphorane)tellurium tetrachloride, $[L_4Te]Cl_4$. The present paper deals with the electronic states of the above tellurium complexes by means of X-ray photoelectron spectroscopy (XPS).

Experimental

Preparation of dichlorobis(methylenetriphenylphosphorane)tellurium(IV) dichloride, $[\{(C_6H_5)_3P{=}CH_2\}_2TeCl_2]Cl_2$ (**1**), chlorotris(methylenetriphenylphosphorane)tellurium(IV) trichloride, $[\{(C_6H_5)_3P{=}CH_2\}_3TeCl]Cl_3$ (**2**), and tetrakis(methylenetriphenylphosphorane)tellurium(IV) tetrachloride, $[\{(C_6H_5)_3P{=}CH_2\}_4Te]Cl_4$ (**3**), were carried out as reported previously.[3]

For XPS measurements, samples were placed on a gold mesh holder and introduced into a spectrometer in a 99.9995% pure nitrogen atmosphere. After evacuating to a vacuum better than 2.7×10^{-5} Pa, the sample was cooled to 180—200 K. The instrument was a VG ESCA 3 electron spectrometer and Mg $K\alpha$ X-ray (50 W) was used. Peak separation was made by a nonlinear least squares method using a mixed Gaussian-Lorentzian curve shape. The background level was determined by a method proposed by Shirley,[4] in which the level was assumed to increase in proportion to the spectral intensity, and contributions by X-ray satellites were excluded. The electron-binding energies, E_B, were calibrated by assigning 285.0 eV to the C 1s peak of the phenyl carbons in methylenetriphenylphosphorane.[1,2]

Results and Discussion

Results of XPS Measurements: Binding energy, E_B, data for three complexes are summarized in Table 1. Apparently, no indication of decomposition of the complexes was observed in regard to the ligand ylide, since E_B values and relative peak widths for phosphorus were in a range comparable to those for the ylide or the ylide-gold complexes.[2] After peak separation, however, a second peak appeared in Te 3d spectra (peak (b) in Table 1) for complexes **1**—**3** and a third peak appeared in Cl 2p spectra (peak (c) in Table 1) for complexes **1** and **2**. This indicates that, in spite of

Table 1. Binding Energies for Ylide Tellurium Compounds in eV

	Complex	Te		5/2-3/2 Split	Cl	P		C
		$3d_{5/2}$	$3d_{3/2}$		$2p_{3/2}$	2p	2s	1s
1	$[L_2TeCl_2]Cl_2$	(a) 574.7(±0.4)	585.1(±0.3)	10.4	(a) 196.9(±0.5)	132.8(±0.2)	190.5(±0.2)	285.0
		(b) 576.7(±0.2)	586.5(±0.4)	10.4	(b) 198.3(±0.1)			
					(c) 200.4[a]			
		[1.03]	[0.98]		[0.95]	[1.08]	[1.30]	[1.00]
2	$[L_3TeCl]Cl_3$	(a) 574.5(±0.3)	584.9(±0.1)	10.4	(a) 196.8(±0.3)	132.9(±0.2)	190.3(±0.2)	285.0
		(b) 576.1(±0.1)	586.5(±0.1)	10.4	(b) 197.8(±0.5)			
					(c) 199.9[a]			
		[1.06]	[1.03]		[0.87]	[1.08]	[1.33]	[1.00]
3	$[L_4Te]Cl_4$	(a) 574.3(±0.3)	584.7(±0.3)	10.4	(a) 196.8(±0.3)	132.8(±0.2)	190.3(±0.4)	285.0
		(b) 576.0(±0.1)	586.5(±0.4)	10.5				
		[1.12]	[1.08]		[0.95]	[1.07]	[1.28]	[1.00]

L: $(C_6H_5)_3P{=}CH_2$.
Uncertainties shown in parentheses are 90% confidence limits in eV. Values in brackets are a mean FWHM ratio to C 1s peak. Scattering of the ratio was always less than ±0.15.
a) An average of two data.

careful sample handling and measuring procedures, partial decomposition of the complexes could not be avoided. As expected from its instability,[3] decomposition was considerable for **1** judging from the intensity of the second peak of Te 3d. It is probable that the decomposition was caused by a trace amount of oxygen or water vapor during handling. Damage by X-ray irradiation can be disregarded, because no appreciable change in Te 3d spectra was observed after irradiating with 440 W-h of Mg$K\alpha$ X-ray, which is about four times the irradiation for taking all the spectra. Since the samples were contaminated by decomposition products, we shall only consider the binding energy data of the complexes and avoided quantitative discussion. It was unfortunate that the validity of the peak separation could not be supported by relative peak intensities. However it is unlikely that the accuracy of peak separation is less than the case of gold complexes previously reported,[1] where the results were examined quantitatively.

Electronic States of Ylide and Tellurium Atom: The E_B[P 2p] and E_B[P 2s] for ligand ylide in complexes **1—3** are practically identical as shown in Table 1. Further, E_B[P 2p] agrees with the values for ylide (**L**) (132.6 eV), triphenylmethylphosphonium bromide, $[(C_6H_5)_3PCH_3]Br$ (**4**), (132.6±0.4 eV), and chlorobis(methylenetriphenylphosphorane)gold(I), $[(C_6H_5)_3P{=}CH_2]_2AuCl$ (**5**), (132.4±0.4 eV), reported previously.[1,2] The E_B[P 2s] for **1—3** is also in agreement with that[2] (190.1 eV) for **L**, but is slightly higher than that[2] (189.6—8 eV) for **5**. The lower E_B[P 2s] for **5** was found to be due to the interference by X-ray satellite peaks of Cl 2p orbitals. After correction for the interference, E_B[P 2s] for **5** agreed with that for **1—3**; with the previous calculation program,[2] contributions by X-ray satellites could not be excluded. These results indicate that the electronic state of phosphorus in complexes **1—3** is identical to that in **L** and complex **5**.

It was not possible to separate the ylide methylene carbon peak from the phenyl carbon peak in **1—3**, precisely.[2] According to the ^{1}H NMR spectra,[3] however, the electronic state of the ylide methylene group in **1—3** is considered to be similar to that of the methyl group in **4**, that is, the chemical shift[3] (δ=3.15—3.30) of CH_2P in **1—3** agrees with that[5] (δ=3.17) of PCH_3 in **4**, but differs from the values of CH_2P in **L**[6] (δ=0.13) and **5**[7] (δ=1.7). This suggests that the carbanion of the ylides in **1—3** is donating electrons to the tellurium atom and the density of the electrons on the tellurium may be higher than that in common Te(IV) compounds.

An example of a Te 3d spectrum for **3** is shown in Fig. 1. The E_B[Te 3d] of peak (a) for each complex is assigned to the Te(IV) in each complex, and peak (b) to decomposition products. Since, as mentioned above, a methylene carbon in a ligand ylide is anionic[1,2,8] and a donor of electrons, it is able to raise the density of electrons on the central tellurium atom and lower the E_B. The E_B[Te 3d] values for **1—3** are lower than those[9-11] for common Te(IV) compounds: usually, E_B[Te $3d_{5/2}$]=575.3 eV and E_B[Te $3d_{3/2}$]=585.7 eV and two examples, diphenyltellurium(IV) dichloride, $(C_6H_5)_2TeCl_2$ (**6**), and $TeCl_4$ (**7**) (correctly, Te_4Cl_{16})[12] are shown in Table 2. In addition, E_B[Te 3d] values for **1—3** decrease slightly with increasing number of bonded ylides. The fall of E_B[Te 3d] can be caused both by increasing the number of bonded ylides and decreasing the number of bonded chlorine atoms. Further, it is considered that the donation of electrons from the ylides to the tellurium atom in **1—3** may be larger than in the case in gold complex **5**.[2] The conjecture is parallel to the results of ^{1}H NMR for CH_2P in tellurium[3] and gold[7] complexes. As a first approximation, the chemical shifts, ΔE_B, can be explained by a ligand chemical shift,[9,13] in which ΔE_B is a sum of each ligand chemical shift of bonded ligands, ΔE(j), that is, $\Delta E_B=\sum\Delta E(j)$. The ligand chemical shift by

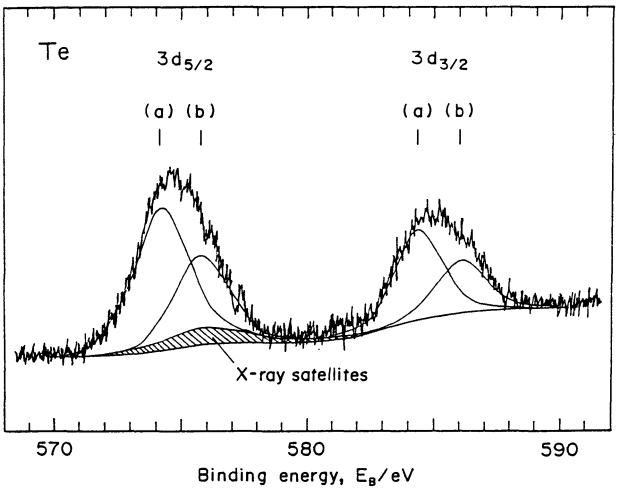

Fig. 1. The Te 3d spectrum of $[\{(C_6H_5)_3P{=}CH_2\}_4Te]$-$Cl_4$. (See Table 1 for (a) and (b).)

Table 2. Ligand Chemical Shifts, ΔE(j), Calculated by Using Binding Energy Data in Ref. 5

	Te $3d_{5/2}$			Te $3d_{3/2}$		
	E_B/eV	ΔE(Ph)/eV	ΔE(Cl)/eV	E_B/eV	ΔE(Ph)/eV	ΔE(Cl)/eV
Te metal	573.1			583.5		
Ph_2Te_2	573.9[a]	0.8		584.3[a]	0.8	
Ph_2TeCl_2	576.2[a]		0.75	586.6[a]		0.75
$TeCl_4$	576.9		0.63[b]	587.3		0.63[b]
$(NH_4)_2TeCl_6$	576.9[a]		0.63	587.4[a]		0.63

Ph: C_6H_5.
a) Cited from Ref. 7 where original data[5] were converted by using E_B[C 1s]=284.8 eV for adventitious hydrocarbon. b) An average of six coordinated chlorine atoms.

the ylide, $\Delta E(\mathbf{L})$, can be calculated from E_B[Te $3d_{5/2}$] for **3** as follows by using E_B[Te $3d_{5/2}$] for metal Te, the mean value of which is calculated at 573.0±0.2 eV from compiled data:[11]

$$\Delta E(\mathbf{L}) = (574.3 - 573.0)/4 = 0.33 \text{ eV}.$$

As described above, the electronic states of bonded ylides in **1**—**3** are equivalent. Then, the ligand chemical shift by chlorine atom can be calculated as follows:

from complex **1**,

$\Delta E(\text{Cl}) = (574.7 - 573.0 - 0.33 \times 2)/2 = 0.52$ eV, and

from complex **2**,

$\Delta E(\text{Cl}) = 574.5 - 573.0 - 0.33 \times 3 = 0.51$ eV.

This agreement implies that the chlorine atoms in **1** and **2** are also equivalent in bonding. The ΔE(Cl) values in **1** and **2** are a little smaller than that in $(NH_4)_2TeCl_6$ (**8**) as shown in Table 2. In the case of $TeCl_4$ (**7**), which is a tetramer and should be expressed as Te_4Cl_{16},[12] each tellurium forms three short bonds to chlorine atoms (bond length 0.2312—0.2317 nm[12] and bond order 1.18[9]) and three long bonds to bridging chlorine atoms (bond length 0.2898—0.2959 nm[12] and bond order 0.11[9]), so that the contribution from the former chlorine atoms may be larger than 0.63 eV in Table 2 and that from the bridging atoms may be smaller. The structures of complexes **1** and **6** are essentially the same as for diphenyltellurium(IV) dibromide, $(C_6H_5)_2TeBr_2$ (**9**), whose structure is a distorted tetrahedron having nearly linear Br-Te-Br bonds.[14] In consideration of a smaller ΔE(Cl) in complex **1**, the Te-Cl bond length in **1** may be longer than that in **6**. The bond in complex **2** will be similar to that in **1**, as ΔE(Cl) is nearly the same.

Electronic States of the Bonded Chlorine Atom and the Free Chloride Ion: Only one chlorine species was identified in complex **3** (Table 1) and E_B[Cl $2p_{3/2}$] was close to those for $[(CH_3)_4]N^+Cl^-$[1] and similar type chloride ions in others.[15] Therefore, it is clear that peak (a) of Cl $2p_{3/2}$ for each complex is assigned to the free chloride ion. The reproducibility of E_B[Cl $2p_{3/2}$] of peak (b) for **1** and **2** is poorer compared with that of peak (a), but this peak can be assigned to bonded chlorine atom, since E_B[Cl $2p_{3/2}$] values are in a similar range with that for bonded chlorine atom in **5**.[1,2] Then, peak (c) is attributed to decomposition products. The E_B[Cl $2p_{3/2}$] of peak (c) is close to that[16] (199.9 eV) for a type of bridging chlorine atom, e.g., $Mo_6Cl_{12}(phen)_2$, phen: 1,10-phenanthroline, but it will be imprudent to conclude this at present. Due to partial decomposition of the complexes, the intensity ratios between peak (a) and (b) for **1** and **2** do not correspond to the atomic ratios of 2 : 2 and 3 : 1.

As a conclusion, all the XPS data obtained in the present work support the structures of the complexes which were constructed from the NMR data and the elemental analysis.[3]

References

1) Part XIII. H. Konno and Y. Yamamoto, *Bull. Chem. Soc. Jpn.*, **60**, 2561 (1987).
2) Y. Yamamoto and H. Konno, *Bull. Chem. Soc. Jpn.*, **59**, 1327 (1986).
3) Y. Yamamoto, *Bull. Chem. Soc. Jpn.*, **59**, 3053 (1986).
4) D. A. Shirley, *Phys. Rev.*, **B5**, 4709 (1972).
5) Y. Yamamoto and H. Schmidbaur, *Chem. Commun.*, **1975**, 668.
6) H. Schmidbaur, H. Stühler, and W. Vornberger, *Chem. Ber.*, **105**, 1084 (1972).
7) Y. Yamamoto and Z. Kanda, *Bull. Chem. Soc. Jpn.*, **52**, 2560 (1979).
8) J. C. J. Bart, *J. Chem. Soc. B*, **1969**, 350.
9) M. K. Bahl, R. L. Watson, and K. J. Irgolic, *J. Chem. Phys.*, **66**, 5526 (1977).
10) F. Garbassi, J. C. J. Bart, and G. Petrini, *J. Electron Spectrosc. Relat. Phen.*, **22**, 95 (1981).
11) "Practical Surface Analysis," ed by D. Briggs and M. P. Seah, John Wiley & Sons, New York (1983), p. 506.
12) B. Buss and B. Krebs, *Inorg. Chem.*, **10**, 2795 (1971).
13) B. Lindberg and J. Hedman, *Chem. Scripta.*, **7**, 155 (1975).
14) G. D. Christofferson and J. D. McCullough, *Acta Crystallgr.*, **11**, 249 (1958).
15) J. Escard, G. Mavel, J. E. Guerchais, and R. Kergoat, *Inorg. Chem.*, **13**, 695 (1974).
16) A. D. Hamer and R. A. Walton, *Inorg. Chem.*, **13**, 1446 (1974).

Determination of Iodide Ion Using Alkali-Free Lead Phosphate Glasses as Potentiometric Detector Sensors in Nonsuppressed Ion Chromatography

Tsuyoshi NOMURA,* Yasuo HIKICHI, and Genkichi NAKAGAWA
Department of Materials Science and Engineering, Nagoya Institute of Technology, Gokiso-cho, Showa-ku, Nagoya 466
(Received February 8, 1988)

Synopsis. Alkali-free lead phosphate glasses containing silver oxide show a linear relationship with the Nernstian slope for iodide concentration. By using these glass membranes as potentiometric detector sensors for ion chromatography, the limit of detection for iodide ion was extended down to 0.05 $\mu g\,cm^{-3}$. The high sensitivity can be interpreted in terms of the strong interaction between iodide ion and the silver ion incorporated in the membrane material.

A wide variety of detectors are presently used for the determination of iodide ion in ion chromatography, and have been quantified by the conductimetric method[1] and the UV absorbsnce method,[2,3] in addition to the electrochemical detector methods such as the amperometric method[4] and the potentiometric method.[5] The potentiometric detector method, chiefly using ion-selective electrodes, has been reported by a number of workers.[6,7] Various types of ion-selective glass electrodes are available. However, most of those glasses respond to cationic species,[8,9] and no reports on anion-responsive glass electrodes have apparently been published to date. We have already investigated some alkali-free phosphate glasses as sensing materials for nitrate ion[10] and as potentiometric detector sensors for ion chromatography.[11]

This paper reports on properties of lead phosphate glass membranes containing silver oxide and on their application to the analysis of iodide ion as potentiometric detector sensors for ion chromatography.

Experimental

Apparatus. Alkali-free lead phosphate glasses were prepared as previously described.[11] Chemical compositions of some of the tested glasses, their potential changes per decade change in iodide ion activity, and their physical and chemical properties are listed in Table 1.

A schematic diagram for an ion-chromatographic system is shown in Fig. 1. It consists of a Toso Co. HLC-803D pump with a Rheodyne sample injector with a 100 mm^3 sample loop, a combination of a TSK IC-A guard column and duplicated TSK Gel IC anion SW anion separator columns, two valves (V1 and V2) of a column changing switch, and a DKK Co. ion-selective flow cell with some improvements. Under the ordinary circumstances, the guard column and only separator column SW 1 were used. However, when the iodide concentration in seawater was determined, most of chloride ion was eluted by column SW 1, valve 2 was switched back on the line after about an 8 min period, and the chromatogram of iodide ion was obtained by column SW 2.

Both of peak height (potential difference, mV) and peak area gave essentially straight lines against the logarithmic iodide concentration. Therefore, the peak height was routinely used for the determination of iodide concentration.

Solutions. Aqueous solutions of inorganic anions and sodium citrate eluent were prepared by the corresponding sodium salts of analytical reagent grade with twice distilled water. Before use, the eluent was degassed under vacuum with sonication. Artificial seawater was prepared as previously described.[12]

Recommended Procedure. A 10 cm^3 sample solution containing a 0.03 $\mu g\,cm^{-3}$ iodide species was taken in a 50 cm^3 beaker, and 1.0 cm^3 of 10^{-3} $mol\,dm^{-3}$ ascorbic acid was added to reduce the iodide species to iodide. Sodium citrate

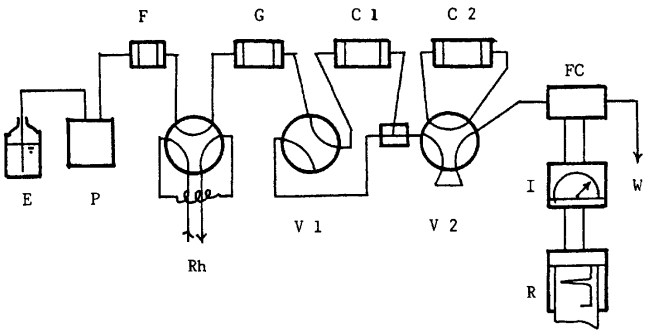

Fig. 1. The schematic diagram of the chromatographic system. E: eluent reservoir; P: pump; F: filter; RH: Rheodyne injector; G: guard column; V1: valve 1; C1: TSK Gel IC Anion SW 1 column; V2: valve 2; C2: SW 2 column; FC: flow cell; I: ion meter; R: recorder; W: waste.

Table 1. Chemical Compositions and Properties of Glasses

Glass no.	Chemical composition (Ag_2O : P_2O_5 : PbO : Al_2O_3, mol%)				Physical and chemical property: Transition temp	Softening temp	Thermal expansion	Membrane resist.	Chemical durability	Potential change
					°C	°C	$10^7/cm\,°C^{-1}$	$M\Omega\,cm^{-1}$	$10^4\,mg\,mm^{-2}$	mV/pI^-
1	—	55	35	10	433	506	102.4	37.6	8.96	35.2
2	5	55	30	10	447	536	118.1	24.4	7.78	52.3
3	10	55	25	10	506	567	113.4	29.6	16.5	58.2
4	15	55	20	10	493	552	120.6	39.2	14.6	48.9

eluent of 0.5 mmol dm^{-3} (pH about 5.0) was pumped at a flow rate of 1.0 cm^3 min^{-1}. For direct determination of iodide, a 100 mm^3 sample was injected and determined by comparison with the standard iodide concentration. Elution curves were obtained in the order: BrO_3^-, Cl^-, ClO_3^-, NO_2^-, Br^-, NO_3^- I^-, SCN^-, and ClO_4^-.

Results and Discussion

Properties of Glasses and Potential Response of Glass Electrodes. As is evident from Table 1, the values of physical and chemical properties of the lead phosphate glasses containing silver oxide are not so much different from those containing no silver oxide. The potential response for the glass number 3 in Table 1 is linear over the iodide ion activity range 10^{-1}—5×10^{-6} mol dm^{-3}, and it has a Nernstian response of about 58 mV per decade change in iodide activity at 25 °C. However, the glass electrode containing no silver oxide yields only a small unstable potential response for iodide.

Detection of Iodide Ion Using Lead Phosphate Glass Membrane Electrode in the Potentiometric Detector for Ion Chromatography. Figure 2 shows the chromatograms for 4 anions obtained with the potentiometric detectors for lead phosphate glass electrode No. 3(A) and No. 1(B) and with the conductivity detector (C), column SW 1 being used as the separator column and 0.5 mmol dm^{-3} sodium citrate (pH 4.96) as the eluent.

In measurement of peak heights for iodide ion, a negative dip peak is observed at the end of the iodide ion peak, and it increases with decreasing pH of the eluent and with increasing iodide ion concentration.

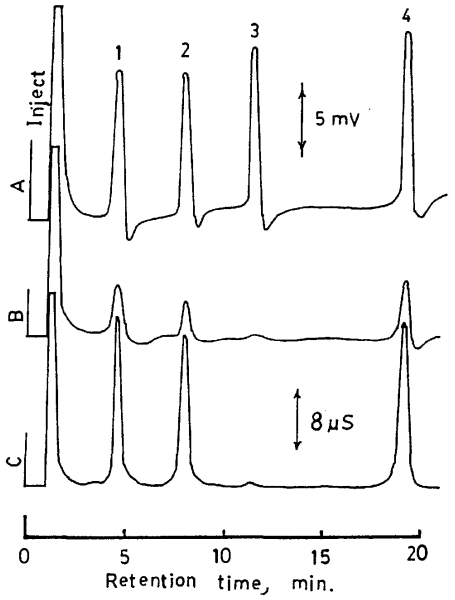

Fig. 2. Ion chromatograms of 4 anions with anion-exchange column. Eluent: 0.5 mol dm^{-3} sodium citrate (pH 4.96). Detector system: A: $10Ag_2O:55P_2O_5:25PbO:10Al_2O_3$ glass detector; B: $55P_2O_5:35PbO:10Al_2O_3$ glass detector; C: Conductivity detector. Anionic species: 1: 5 μg cm^{-3} Cl^-; 2: 10 μg cm^{-3} NO_3^-; 3: 0.4 μg cm^{-3} I^-; 4: 10 μg cm^{-3} ClO_4^-.

The glass number 3 detector is capable of detecting iodide ion with an extremely high sensitivity as compared with the other detectors. This suggests that the addition of silver ion in the glass material has led to the high sensitivity in potential response to iodide ion. Silver ion forms insoluble salts with anions such as Cl^-, Br^-, I^-, SCN^-, S^{2-}, and PO_4^{3-}, so that the insoluble silver iodide adsorbs strongly on the detector glass surface, resulting in the high sensitivity to iodide.

The sensitivity of UV absorbance method for the detection of iodide ion is as high as that of this method, but such anions as fluoride, chloride, and perchlorate ions will provide no sufficient absorbances for UV radiation.

Effect of Eluent pH on the Retention Time. Figure 3 shows the effect of eluent pH on the retention time of 5 anions. Decreasing the eluent pH produces good separation of peaks, but the accuracy for the measurement on these anions decreases due to the increase of the negative dip peak at the end of each peak. Therefore, the eluent pH around 5.0 yields only a small variation in the retention time for each anion, resulting in

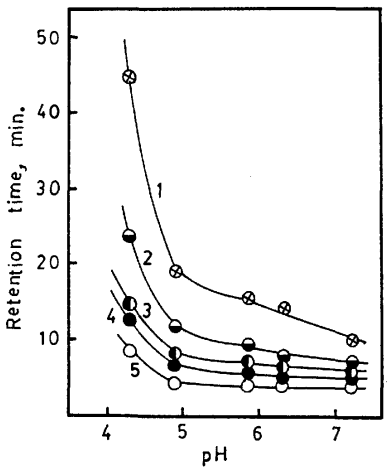

Fig. 3. Effect of pH on the retention time. Eluent: 0.5 mol dm^{-3} citric acid (pH 4.2—7.2). 1: ClO_4^-; 2: I^-; 3: NO_3^-; 4: Br^-; 5: Cl^-.

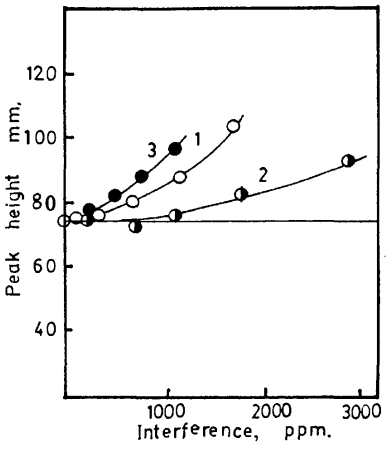

Fig. 4. Effect of diverse anions on the determination of 0.63 μg cm^{-3} iodide. Eluent: 0.5 mol dm^{-3} sodium citrate (pH≈5.0). 1: Br^-; 2: Cl^-; 3: NO_3^-.

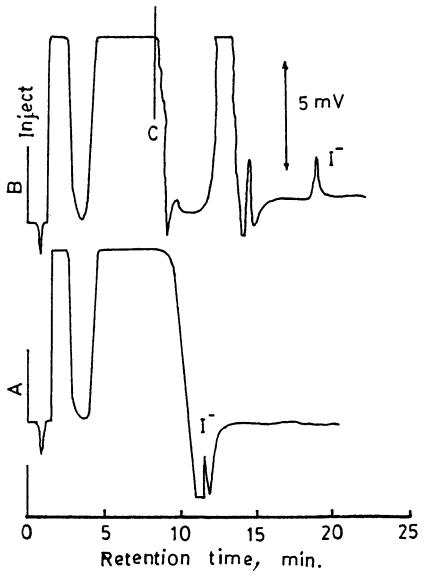

Fig. 5. Chromatograms of artificial seawater sample. Composition of artificial seawater: Cl^- 19 mg cm^{-3}, Br^- 65 μg cm^{-3}, I^- 0.06 μg cm^{-3} and IO_3^- 0.02 μg cm^{-3}. A: chromatogram of SW 1 column. B: chromatogram as similar to A when switched onto the line of SW 2 column after 8 minutes period. C: the place where the valve V 2 is switched onto the line of SW 2 column.

a favorable result will respect to the separation of each anion.

The peak height is considered to be proportional directly to the logarithmic concentration of iodide ion between 0.05 and 1.5 μg cm^{-3}. The relative standard deviation for five separate runs on 0.05 μg iodide ion in 100 mm^3 was about 4%. The detection limit of this procedure was estimated to be 3 ng for direct injection of 100 mm^3.

Interferences. Interferences of diverse ions, such as chloride, bromide, and nitrate ions, with the determination of 0.63 μg cm^{-3} of iodide ion are shown in Fig. 4. Of the anions examined, chloride, bromide, and nitrate ions cause interference if the specified amounts are exceeded (about 1500 for chloride, 400 for bromide, and 200 μg cm^{-3} for nitrate for the determination of 0.63 μg cm^{-3} of iodide). Iodate ion gives a small response and has a retention time different from that of iodide ion.

The amounts of the halogenic anions generally existing in seawater are about 0.05—0.06 μg cm^{-3} of total iodine, 65 μg cm^{-3} of bromide ion, and 19 mg cm^{-3} of chloride ion, so that the total iodine in seawater cannot be determined by the present procedure. When applying this procedure to the practical seawater, most of chloride ions must be removed by pretreatment.

The determination of total iodine in seawater is to be made as follows: (1) Ascorbic acid is added to reduce iodate to iodide, (2) a 200 mm^3 sample is injected, (3) chromatographic separation of anions is run with column SW 1 positioned as indicated in Fig. 1, (4) after most of chloride ions have passed through the detector (after 8 min), V2 valve is switched over to the line of column SW 2, and (5) the chromstogram of iodide ion is recorded with column SW 2.

Figure 5 shows typical chromatograms for the artificial seawater sample (Cl^- 19 mg cm^{-3} and Br^- 65, I^- 0.06, and IO_3^- 0.02 μg cm^{-3}) by both the ordinary method and the two column method. By the latter method, the large negative dip peak associated with chloride ion can be removed from the iodide peak, and the total iodide concentration can be determined accurately.

This work was supported by a Grant-in-Aid for General Scientific Research No. 62540433 from the Japanese Ministry of Education.

References

1) C-Yu Wang, S. D. Bunday, and J. G. Tartar, *Anal. Chem.*, **55**, 1617 (1983).
2) M. Miyashita, K. Kaji, Y. Seyama, and S. Yamashita, *Chem. Pharm. Bull.*, **32**, 2430 (1984).
3) A. Mangia and M. T. Lugari, *Anal. Chim. Acta*, **159**, 349 (1984).
4) W. J. Hurst, J. W. Stefovic, and W. J. White, *J. Liq. Chromatogr.*, **7**, 2021 (1984).
5) E. C. V. Butler and R. M. Gershey, *Anal. Chim. Acta*, **164**, 153 (1984).
6) P. R. Haddad and A. L. Heckenberg, *J. Chromatogr.*, **300**, 357 (1984).
7) K. Suzuki, H. Aruga, H. Ishiwada, T. Oshima, H. Inoue, and T. Shirai, *Bunseki Kagaku*, **32**, 585 (1983).
8) H. Freiser, "Ion-Selective Electrodes in Analytical Chemistry," Plenum Press, New York (1980), p. 213.
9) G. Eisenman, *Biophys. J. Part 2, Suppl.*, **1962**, 259.
10) T. Nomura and G. Nakagawa, *Bull. Chem. Soc. Jpn.*, **57**, 1491 (1984).
11) T. Nomura and G. Nakagawa, *Bull. Chem. Soc. Jpn.*, **60**, 2861 (1987).
12) J. Lyman and R. H. Fleming, *J. Marine Research*, **3**, 134 (1940).

The Determination of a Small Amount of Biological Constituent by the Use of Chemiluminescence. XIV. The Flow-Injection Analysis of Protein Using Ultrasonic Chemiluminescence of Luminol

Tadashi HARA,* Kazuhiro NAKATSU, Akihiro ARAI, Tatsunari YOSHIDA, and Kazuhiko TSUKAGOSHI
Department of Chemical Engineering, Faculty of Engineering, Doshisha University, Karasuma Imadegawa, Kamigyo-ku, Kyoto 602
(Received February 10, 1988)

Synopsis. A flow-injection analysis method for the determination of a small amount of protein has been established by the use of the ultrasonic chemiluminescence of luminol. The present method was based on the phenomenon that the catalytic activity of cobalt(II) for the ultrasonic chemiluminescence of luminol decreased in the presence of protein. The apparatus consisted of only a luminol solution line equipped with an ultrasonic irradiation bath and a cobalt(II) catalyst solution line equipped with a sample inlet. Under optimum conditions, similar calibration curves were obtained for bovine serum albumin, bovine serum γ-globulin, human serum albumin, and human serum γ-globulin. According to the present method, these proteins could be determined in the concentration range 5.0×10^{-6}—1.0×10^{-1} g dm^{-3}, with a detection limit of 200 pg (injected sample volume 40 mm^3, S/N=2) and a coefficient of variation of 2.9% (n=8) at a rate of about 60 samples per hour.

The authors have already reported the flow-injection analysis (FIA) method for the determination of a small amount of protein using a 5-animo-2,3-dihydro-1,4-phthalazinedione (luminol) or a 1,10-phenanthroline (phen)-hydrogen peroxide (H_2O_2)-copper(II) system.[1,2] These methods were about 10^2—10^6 times as sensitive as the conventional methods, such as colorimetry and fluorometry for the determination of protein.[3,4] However, an improvement of the analytical capabilities and a simplification of the flow system have also been desired in these methods.

A selective, sensitive method for the determination of cobalt(II) (Co(II)) was established by Suzuki et al., in which the ultrasonic chemiluminescence (CL) reaction of luminol was utilized.[5] This method was carried out using a simple flow-injection system without a H_2O_2 line. On the other hand, the phenomenon that the catalytic activity of the cobalt(III) complex compound for the CL reaction between luminol and H_2O_2 decreased in the presence of protein was found by the authors in the previous paper.[6]

In the present study, a new FIA method for the determination of protein was established by the use of an ultrasonic CL reaction by which Co(II) at sub-pg levels could be detected and the complex formation between Co(II) and protein. Some improvements were achieved compared with the previous study,[2] regarding the following points: detection limit, coefficient of variation, sampling rate, and simplification of a flow system.

Experimental

Reagents. All the reagents used were of a commercially available special grade. Ion-exchange water was distilled for use. A 5.0×10^{-9} mol dm^{-3} Co(II) catalyst solution was prepared by diluting a Co(II) stock solution containing 1.0×10^{-3} mol dm^{-3} cobalt(II) chloride, 1.0×10^{-3} mol dm^{-3} hexadecyltrimethylammonium bromide (HTAB), and 1.0×10^{-1} mol dm^{-3} hydrochloric acid with a buffer solution (pH 10.2) containing 1.0×10^{-1} mol dm^{-3} boric acid, 1.0×10^{-1} mol dm^{-3} potassium hydroxide, and 1.0×10^{-3} mol dm^{-3} HTAB. A 5.0×10^{-5} mol dm^{-3} luminol solution containing 1.0×10^{-1} mol dm^{-3} sodium hydroxide (NaOH) was prepared for use. All the sample solutions of bovine serum albumin (BAS) from Nakarai Chemical Ltd., human serum albumin (HSA) from Chemical Dynamics Corporation, and bovine serum γ-globulin (BγG) and human serum γ-gulobulin (HγG) from Sigma Chemical Co. were prepared by dissolving and diluting them with the above-mentioned buffer solution.

Apparatus and Procedure. A schematic diagram of the FIA apparatus was shown in Fig. 1. The luminol solution (a) was fed at a flow rate of 1.5 cm^3 min^{-1} by means of a pump (P_1) (PERISTA MINI PUMP SJ-1211) and passed through a cooling bath (k), followed by the exposure to the ultrasonic irradiation in sonication cell (m) (0.7 cm i.d., 1.4 cm^3 volume) made of poly-propylene by mean of an oscillator (Tomy Seiko Co., Handy Sonic Model UR-20P; 28 kHz, max. 20W) equipped with an exponential horn (1). Then, the luminol solution was fed into a flow cell at a flow rate

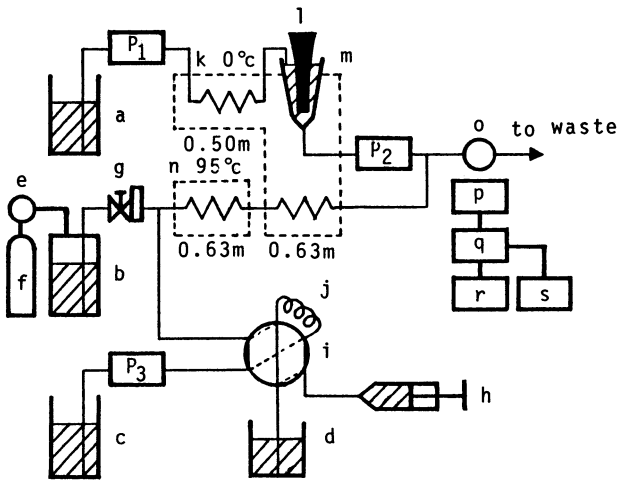

Fig. 1. Schematic diagram of the flow-injection system. a: Luminol solution, b: Co(II) catalyst solution, c: buffer solution, d: sample solution, e: regulator, f: N_2 cylinder, g: flowmeter equipped with a needle valve, h: syringe, i: six-way cock, j: sampling loop, k: cooling bath, l: exponential horn, m: sonication cell, n: heating bath, o: flow cell, p: photomultiplier, q: amplifier, r: recorder, s: integrator, and P_1, P_2, P_3: pump.

of 1.5 cm^3 min^{-1} by means of a pump (P_2) (PERISTA MINI PUMP SJ-1221).

The Co(II) catalyst solution (b) was fed at a flow rate of 1.0 cm^3 min^{-1} by means of an N_2 gas cylinder; the buffer solution (c) was fed at a rate of 1.5 cm^3 min^{-1} by means of a high-pressure pump (P_3) (Nishio kogyo Co., Ltd., SSP DM3M-2044). A definite volume (40 mm^3) of a protein sample solution (d) was injected into the buffer solution line through the sampling loop (j) and the six-way cock (i) (Reodyne). The injected protein sample solution was mixed with the Co(II) catalyst solution, passed through the heating bath (n) and the cooling bath, mixed with the luminol solution, and finally fed to the flow cell.

The CL intensity of the solution containing no sample was recorded as a base line, while the CL intensity of the solution containing protein was record as a negative peak because the catalytic activity of Co(II) decreased due to the formation of a complex compound between Co(II) and protein. The amount of protein was estimated from the peak area.

Results and Discussion

Optimization of Experimental Conditions. Prior to the determination of protein, the optimum concentrations of luminol, NaOH, Co(II), and HTAB were examined. Bovine serum albumin was used as a model protein.

The relationship between the luminol concentration and the peak area as well as the relationship between the NaOH concentration and the peak area were examined. Both the luminol concentration and the NaOH concentration did not affect the noise of the base line. From the experimental results, the optimum concentrations of luminol and NaOH were chosen as the concentrations which gave the maximum peak area. The relationship between the Co(II) concentration and the peak area or detection limit (S/N=2) are shown in Fig. 2. Both the peak area and the noise of the base line increased with increasing Co(II) the concentration; however, the optimum Co(II) concentration was chosen as the Co(II) concentration which gave a minimum detection limit.

In order to examine the catalytic effect of micelle on the CL intensity, HTAB (cationic surfactant), TritonX-100 (nonionic surfactant), and sodium dodecyl sulfate (SDS) (anionic surfactant) were used. The CL intensity in the presence of 1.0×10^{-3} mol dm^{-3} HTAB or 1.0×10^{-3} mol dm^{-3} TritonX-100 and in the absence of surfactant were 160, 27, and 75 mV respectively. Since SDS did not dissolve in the buffer solution (pH 10.2), HTAB was used in the present study. The relationship between the HTAB concentration and the peak area or detection limit (S/N=2) are shown in Fig. 3. Both the peak area and the noise of the base line increased with increasing HTAB concentration; however, the optimum HTAB concentration was chosen as the HTAB concentration which gave a minimum detection limit.

On the basis of these results, the following optimum

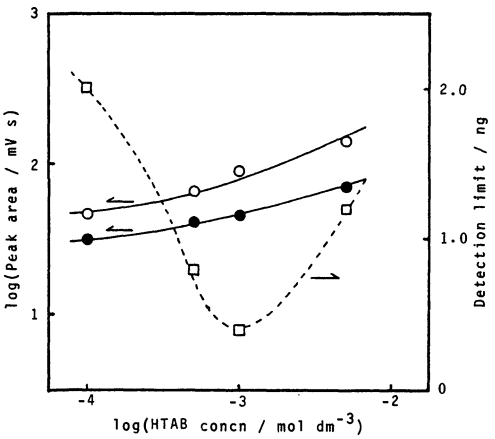

Fig. 3. Relationship between HATB concn and peak area or detection limit. ○: 1.0×10^{-3} g dm^{-3}- and ●: 1.0×10^{-4} g dm^{-3}-BSA. □: Detection limit (S/N=2). Conditions: 5.0×10^{-5} mol dm^{-3} luminol, 1.0×10^{-1} mol dm^{-3} NaOH, and 5.0×10^{-9} mol dm^{-3} Co(II).

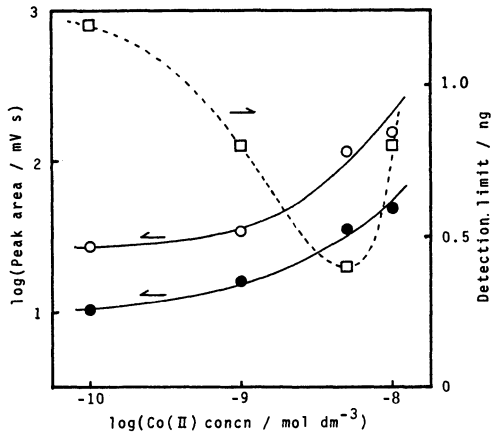

Fig. 2. Relationship between Co(II) concn and peak area or detection limit. ○: 1.0×10^{-3} g dm^{-3}- and ●: 1.0×10^{-4} g dm^{-3}-BSA. □: Detection limit (S/N=2). Conditions: 5.0×10^{-5} mol dm^{-3} luminol, 1.0×10^{-1} mol dm^{-3} NaOH, and 1.0×10^{-3} mol dm^{-3} HTAB.

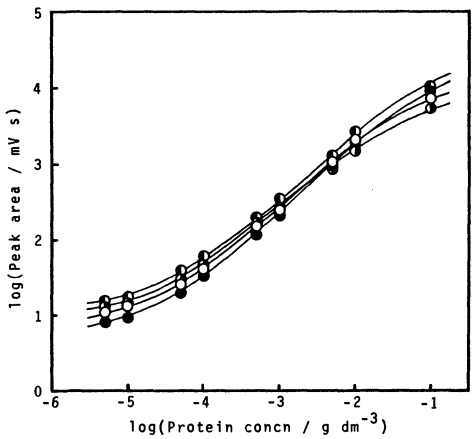

Fig. 4. Calibration curves of various proteins. ○: BSA, ●: BγG, ◑: HSA, and ◐: HγG. Conditions: 5.0×10^{-5} mol dm^{-3} luminol, 1.0×10^{-1} mol dm^{-3} NaOH, 5.0×10^{-9} mol dm^{-3} Co(II), and 1.0×10^{-3} mol dm^{-3} HTAB.

Table 1. Comparison of the Present Method with the Other FIA Methods

Method	Detection limit[a]	Determination range	Sampling volume	C.V.[b]	Sampling rate
	ng	g dm^{-3}	mm^3	%	sample h^{-1}
Present	0.2	5.0×10^{-6}—1.0×10^{-1}	40	2.9	60
Dyestuff-binding[7]	40	2.0×10^{-3}—5.0×10^{-1}	20	0.2	60
Electrode[8]	120	1.0×10^{-3}—2.0×10^{-1}	40	5	
Spectrophotometry[9]	1000	1.0×10^{-1}—1.0×10^{-1}	10	<1	60
Lowry[10]	1000	5.0×10^{-3}—2.0×10^{-2}	100	<2	90

a) As BSA. b) Coefficient of variation.

concentrations of various reagents were used in the study thereafter: 5.0×10^{-5} mol dm^{-3} luminol, 1.0×10^{-1} mol dm^{-3} NaOH, 5.0×10^{-9} mol dm^{-3} Co(II), and 1.0×10^{-3} mol dm^{-3} HTAB.

Determination of Various Proteins. The calibration curves shown in Fig. 4 were obtained under the optimized conditions for a determination of various proteins. The responses for BSA, BγG, HSA, and HγG were almost similar. These proteins could be determined in the concentration range of 5.0×10^{-6}—1.0×10^{-1} g dm^{-3} with a detection limit 200 pg (injected sample volume 40 mm^3, S/N=2).

Since H_2O_2 was unnecessary in the present method, the FIA apparatus used in the present study consisted only of the luminol solution line equipped with an ultrasonic irradiation bath and the Co(II) catalyst solution line equipped with a sample inlet. The peak shape obtained by the present method was much sharper than that obtained by the previous method.[2] This seemed to be due to a reduction in the dilution degree of the sample solution in the simplified FIA system, which had two lines different from the previous system having three lines. The detection limit (S/N=2), coefficient of variation, and sampling rate are as follows: 1 ng (injected sample volume 50 mm^3), 4.9% (1.0×10^{-3} g dm^{-3} BSA, n=10), and about 20 samples per hour (1.0×10^{-2} g dm^{-3} BSA) in the previous method; 200 pg (injected sample volume 40 mm^3), 2.9% (1.0×10^{-3} g dm^{-3} BSA, n=8), and about 60 samples per hour (1.0×10^{-2} g dm^{-3} BSA) in the present one. Protein up to 250 pg could be detected using the previous method; however, it can be obtained only by the use of the amplifying effect of an amino acid. As can be seen from the above-mentioned results, the present method was superior to the previous one regarding analytical capabilities and a simplification of the flow system.

Comparison of the Present Method with the Other FIA Methods. Several FIA methods for a determination of protein have recently been reported. As can be seen from Table 1, the present method was superior regarding the detection limit and the concentration range for a determination of protein to the other FIA methods.

References

1) T. Hara, M. Toriyama, and K. Tsukagoshi, *Bull. Chem. Soc. Jpn.*, **57**, 1551 (1984).
2) T. Hara, T. Ebuchi, A. Arai, and M. Imaki, *Bull. Chem. Soc. Jpn.*, **59**, 1833 (1986).
3) K. Sano, "Bunseki-library 3 Rinsho Kagaku Bunseki II," ed by the Japan Society for Analytical Chemistry, Tokyo Kagaku Dojin, Tokyo (1979).
4) K. Sugawara and M. Soejima, "Seibutsu Kagaku Jikken-ho 7 Tanpakushitsu No Teiryo-ho," Japan Scientific Societies Press, Tokyo (1981).
5) T. Komatsu, M. Ohira, M. Yamada, and S. Suzuki, *Bull. Chem. Soc. Jpn.*, **59**, 1849 (1986).
6) T. Hara, M. Toriyama, and K. Tsukagoshi, *Bull. Chem. Soc. Jpn.*, **57**, 289 (1984).
7) T. Shuto, M. Koga, I. Tanaka, T. Akiyama, and H. Igisu, *Bunseki Kagaku*, **36**, 256 (1987).
8) C. J. Yaun and C. O. Huber, *Anal. Chem.*, **57**, 180 (1985).
9) L. C. Davis and G. A. Radke, *Anal. Biochem.*, **161**, 152 (1987).
10) R. A. Salerno, C. Odell, N. Cyanovich, B. P. Bubnis, W. Morges, and A. Gray, *Anal. Biochem.*, **151**, 309 (1985).

Ligand-Substitution Reaction Kinetics of Tris(8-quinolinolato)- and Bis-(2-methyl-8-quinolinolato)(8-quinolinolato)aluminum(III) Complexes with Ethylenediamine-*N,N,N',N'*-tetraacetic Acid

Tomonori HORIHATA, Ken-ichi OKAMOTO,† Jinsai HIDAKA,† and Hisahiko EINAGA*
Institute of Materials Science, University of Tsukuba, Tsukuba, Ibaraki 305
†Department of Chemistry, University of Tsukuba, Tsukuba, Ibaraki 305
(Received February 22, 1988)

Synopsis. Ligand-substitution reactions of $[Al(hq)_3]$ and $[Al(hq)(mhq)_2]$ (H(m)hq: (2-methyl-)8-quinolinol) with H_4edta have been studied at 25 °C and 1.0 mol dm^{-3} NaCl by means of the stopped-flow spectrophotometric method. Three concurrent reaction pathways, a dissociative activation one and two parallel associative activation ones, to which H_2edta^{2-} and $Hedta^{3-}$ contribute, are elucidated.

Only one ligand-substitution reaction kinetics of aluminum(III) chelate complexes with multidentate ligands has been studied,[1] although they are of fundamental importance in the elucidation of the kinetic characteristics of aluminum(III). In our previous paper,[1] a ligand-substitution reaction of an aluminum(III) complex containing 7-[(2-carboxyphenyl)-azo]-8-hydroxy-5-quinolinesulfonic acid (H_3pqs) with 8-hydroxy-5-quinolinesulfonic acid was studied; it was found that the reaction proceeds with dissociative activation and with the liberation of one of the pqs^{3-} in $[Al(pqs)_2]^{3-}$ as the rate-determining step. In a subsequent investigation of the ligand-substitution reactions of an aluminum(III) complex containing 8-quinolinol (Hhq) and one containing Hhq and 2-methyl-8-quinolinol (Hmhq) with ethylenediamine-*N,N,N',N'*-tetraacetic acid (H_4edta); it was found, besides the dissociative activation process, which has been accepted as a general kinetic feature of aluminum-(III) (vide infra), that there exist processes in which the coordinating ligand participates and that these processes take place concurrently. This paper will be concerned with the ligand-substitution reaction kinetics and mechanisms of $[Al(hq)_3]$ and $[Al(hq)(mhq)_2]$ with H_4edta.

Experimental

Complexes. $[A(hq)_3]\cdot 1/2H_2O$. This complex was prepared from stoichiometric mixtures of aluminum(III) and Hhq in an ethanolic aqueous solution of pH 5—6.[2] Found: C, 69.75; H, 4.05; N, 8.80%. Calcd for $C_{27}H_{19}N_3O_{3.5}Al$: C, 69.22; H, 4.08; N, 8.97%.

$[Al(hq)(mhq)_2]\cdot 1/2H_2O$. Hmhq (3.2g, 0.020 mol) in 200 cm^3 ethanol was added to $AlK(SO_4)_2\cdot 12H_2O$ (4.7 g, 0.010 mol) in 200 cm^3 of an aqueous solution below pH 4. To the solution we then added Hhq (1.5 g, 0.010 mol) in 100 cm^3 of ethanol, and the resulting solution was adjusted to pH 5—6 with aqueous NH_3 to obtain a crystalline precipitate. The complex was recrystallized from acetone and was dried in vacuo at 140 °C for 7 h. Found: C, 70.38; H, 4.11; N, 8.87%. Calcd for $C_{29}H_{23}N_3O_{3.5}Al$: C, 70.15; H, 4.66; N, 8.46%.

Measurements. Kinetic runs were carried out in an ethanolic aqueous solution (ethanol, 10 vol%) of 1.0 mol dm^{-3} NaCl at 25.0±0.2 °C on a JASCO stopped-flow spectrophotometer[3] under pseudo-first-order kinetic conditions with respect to the H_4edta concentration. The change in the absorbance with the time was followed at 260 nm, where the aluminum(III) complexes of the 8-quinolinolate-type ligands (10^{-5}—10^{-3} mol dm^{-3}, λ_{max}: ca. 252 nm) showed a maximum absorbance against the free ligand. The rate constant, k_{obsd}, was calculated from Eq. 1:

$$\ln (A_0 - A_\infty)/(A_t - A_\infty) = k_{obsd}\, t \qquad (1)$$

Here, A_0, A_t, and A_∞ stand for absorbances at the initial state, at time t, and at equilibrium respectively. The hydrogen-ion concentration was measured, in principle, according to the literature procedure.[3] Analysis by the curve-fitting method (vide infra) was carried out with an NEC PC-9801VM2 personal computer.

Results and Discussion

The ligand-substitution reaction kinetics of $[Al(hq)_n(mhq)_{3-n}]$ (n=1 and 3) with H_4edta proceed in weakly acidic aqueous media (pH 3.0—4.5), where H_4edta is present mainly in the species of H_3edta^-, H_2edta^{2-}, $Hedta^{3-}$ and slightly in that of H_4edta.[4] The preliminary absorption spectral study gave evidence that $[Al(hq)_n(mhq)_{3-n}]$ turned quantitatively into $[Al(edta)]^-$ at equilibrium under the kinetic conditions specified in the experimental section. The dependence of the absorbance at a specified wavelength on the time

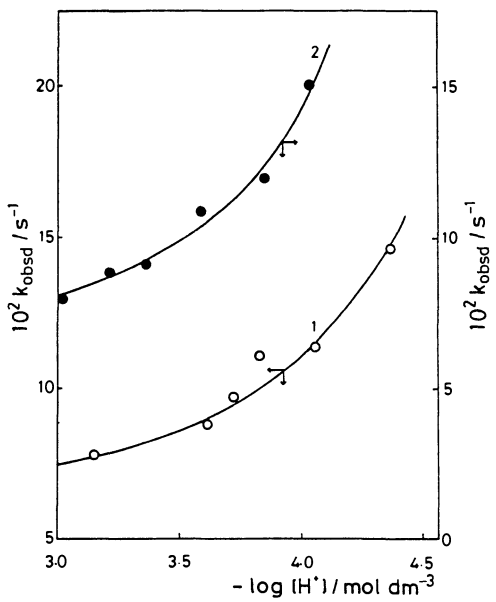

Fig. 1. Relation between k_{obsd} and $-\log[H^+]$. 1: $[Al(hq)_3]$, 1.49×10^{-5} mol dm^{-3}; and C_{edta}, 3.79×10^{-3} mol dm^{-3}. 2: $[Al(hq)(mhq)_2]$, 1.53×10^{-5} mol dm^{-3}; and C_{edta}, 3.78×10^{-3} mol dm^{-3}. 1.0 mol dm^{-3} NaCl (ethanol, 10 vol%), 25 °C.

conformed well to Eq. 1 for more than three half-life periods under a constant total H_4edta concentration, C_{edta}, and hydrogen-ion concentration, $-\log[H^+]$; this fact indicates that there is only one rate-determining step in the ligand-substitution reaction. The experimental data obtained under pseudo-first-order kinetic conditions with respect to C_{edta} are shown in Figs. 1 and 2. These data indicate that k_{obsd} depends not only on $-\log[H^+]$ but also on C_{edta}; k_{obsd} increases exponentially with the increases in $-\log[H^+]$ and in $\log C_{edta}$. The dependence of k_{obsd} on C_{edta} implies that H_4edta contributes to the ligand-substitution reaction. Hence, the rate equation can be given as follows (cf. Appendix):

$$-d[[Al(hq)_n(mhq)_{3-n}]]/dt = k_{obsd}[[Al(hq)_n(mhq)_{3-n}]]$$
$$k_{obsd} = \{k_d + [f_2([H^+]) + f_4([H^+])]C_{edta}/f_1([H^+])\}/[1 + f_3([H^+])]C_{edta}/f_1([H^+]) \quad (2)$$

Equation 2 indicates that the k_{obsd} vs. C_{edta} curve at a constant $-\log[H^+]$ should be asymptotic to a limiting line of:

$$k_{obsd,\infty} = [f_2([H^+]) + f_4([H^+])]/f_3([H^+]) \quad (2')$$

with an increase in C_{edta}. This is not the case for the present investigation, as is evident from Fig. 2 for $[Al(hq)_3]$. Therefore, the contribution of the $f_3([H^+])$ and $f_4([H^+])$ terms in Eq. 2 should be negligible; any possibilities can be excluded of the k_{osj} process and hence of any contribution of a mechanism in which a coordinated ligand is replaced by an entering ligand in the outer-sphere complex as the mechanistic rate-determining step. Accordingly, Eq. 2 can be simplified as follows:

$$k_{obsd} = k_d + [f_2([H^+])/f_1([H^+])]C_{edta} \quad (3)$$

It is reasonable to assume that the presence of H_4edta species and the contribution of the k_{i_4} pathway to the kinetics can be neglected above $-\log[H^+]$ of 3 (vide infra). Therefore, Eq. 3 can be modified to Eq. 4:

$$k_{obsd} = k_d + k_{i3}C_{edta} + \{(k_{i2} - k_{i3})K_{a2}[H^+] + (k_{i1} - k_{i3})\}C_{edta}/(K_{a3}K_{a2}[H^+]^2 + K_{a2}[H^+] + 1) \quad (4)$$

Equation 4 can be analyzed for the k_{obsd} vs. $-\log[H^+]$ relation by means of the curve-fitting method[5] with a normalized curve of:

$$Y = (av + b)/((K_{a3}/K_{a2})v^2 + v + 1\} + c,\ X = -\log v \quad (5)$$

with $a \equiv (k_{i2} - k_{i3})C_{edta}$, $b \equiv (k_{i1} - k_{i3})C_{edta}$, and $c \equiv k_d + k_{i3}C_{edta}$. Likewise, Eq. 4 can be analyzed for the k_{obsd} vs. $\log C_{edta}$ relation with a normalized curve of:

$$Y' = a'u + c',\ X' = \log u \quad (6)$$

with $a' \equiv f_2([H^+])/f_1([H^+])$ and $c' \equiv k_d$. Hence, the k_{ij}'s and k_d can be estimated from the a, b, c, and c' constants and the experimental parameter of C_{edta}. These rate constants can then be refined by using the a' constant, the K_{aj}'s, and the experimental parameter of $-\log[H^+]$. The k_{obsd} vs. $-\log[H^+]$ and the k_{obsd} vs. $\log C_{edta}$ relations in Figs. 1 and 2 were used for the analysis; the rate constants thus estimated are summarized in Table 1. The k_{i_3} rate constant was found to be negligibly smaller than k_d, which indicates that the k_{i_3} pathway, like the k_{i_4} one, does not contribute to the ligand-substitution processes. Hence, the substitution reaction of $[Al(hq)_n(mhq)_{3-n}]$ with H_4edta is concluded to proceed through the k_d and the k_{ij} (j: 1 and 2) pathways, to the latter of which H_2edta^{2-} and $Hedta^{3-}$ contribute, as the rate-determining steps.

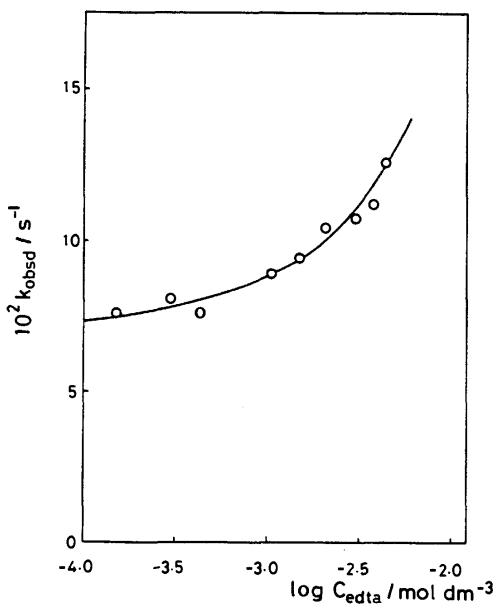

Fig. 2. Relation between k_{obsd} and $\log C_{edta}$. $[Al(hq)_3]$, 1.49×10^{-5} mol dm^{-3}; and $-\log[H^+]$, 3.83. 1.0 mol dm^{-3} NaCl (ethanol, 10 vol%), 25 °C.

It was found in the present investigation that the ligand-substitution reaction of $[Al(hq)_n(mhq)_{3-n}]$ with H_4edta proceeds through three reaction pathways, irrespective of the composition of the starting complex. The rate constants decrease in the following order: $k_{i1} > k_{i2} > k_d$ ($k_{i3} \fallingdotseq k_{i4} \fallingdotseq 0$). Each rate constant differs slightly with different compositions of the complex. Therefore, we would like to focus our attention first on the reaction kinetics of $[Al(hq)_3]$.

The dissociative activation pathway (k_d) of $[Al(hq)_3]$ is considered to originate from the nature of the aluminum(III) of an octahedral coordination.[6] In fact, the k_d of 7×10^{-2} s^{-1} of $[Al(hq)_3]$ is in fairly good agreement with that of 3×10^{-2} s^{-1} of $[Al(pqs)_2]^{3-}$,[1] when differen-

Table 1. Rate Constants for the Ligand-Substitution Reactions

Complex	k_d/s^{-1}	k_{i2}/mol^{-1} dm^3 s^{-1}	k_{i1}/mol^{-1} dm^3 s^{-1}	Remarks
$[Al(hq)_3]$	$(7.3\pm0.5)\times10^{-2}$	3.6±0.2	$(1.30\pm0.05)\times10^3$	This work[a]
$[Al(hq)(mhq)_2]$	$(7.5\pm0.5)\times10^{-2}$	4.0±0.2	$(2.38\pm0.05)\times10^3$	This work[a]
$[Al(pqs)_2]^{3-}$	$(3.00\pm0.43)\times10^{-2}$	—	—	Ref. No. 1[b]

a) 1.0 mol dm^{-3} NaCl (ethanol, 10 vol%), 25 °C. b) 0.1 mol dm^{-3} NaCl, 25 °C.

ces in the configuration and the chelate-ring structure of these two complexes are taken into consideration. The dissociative activation pathway may be initiated by a cleavage of the metal-oxygen bond of the coordinated quinolinolato ligand, for the Al-O bond of $[Al(hq)_3]$ has been estimated, by the ^1H NMR spectral[7] and the magnetic circular dichroism spectral[8] studies, to be dominantly ionic and highly labile.

There are two parallel associative activation pathways (k_{i1} and k_{i2}) in competition with the dissociative activation one (k_d). The k_{i1} rate constant, to which $Hedta^{3-}$ relates, is about three orders of magnitude larger than the k_{i2} rate constant, to which H_2edta^{2-} relates. This difference in the rate constants can not be ascribed simply to formation of the outer-sphere complex with the entering ligand by ionic or related interaction, because $[Al(hq)_3]$ has no formal charge and because no experimental evidence on the formation of the outer-sphere complex was obtained; the difference can, however, be ascribed to numbers of the protons blocking the coordination sites of the entering ligand.

Two associative activation mechanisms, the associative (A) and the associative interchange (I_a), can possibly explain the k_{i1} and k_{i2} pathways. However, the I_a mechanism may be more probable than the A one in view of the facts that aluminum(III) of a small ionic radius prefers intrinsically to take the dissociative interchange (I_d) mechanism[1,9] and that the k_{i1} and k_{i2} pathways do not become appreciable until the concentration of the entering ligand reaches a high point compared with that of the starting complex. These reaction pathways may be initiated by the substitutional interchange of the coordinated bulky quinolinolato ligand with the glycinate ligating group of H_4edta, probably to form an intermediate of the $[Al(hq)_2(Hedta\text{-}O,N)]^{2-}$ type.

No appreciable differences were noticed in the rate constants of $[Al(hq)_3]$ and $[Al(hq)(mhq)_2]$. These two ligands may take an equal opportunity to leave in the first step.

Appendix

The following general expression of k_{obsd} can be derived from the text:

$$k_{obsd} = \frac{k_d + \sum_{j=1}^{4} k_{ij}[H_j\,edta^{(4-j)-}] + \sum_{j=1}^{4} k_{osj}\,K_{osj}[H_j\,edta^{(4-j)-}]}{1+\sum_{j=1}^{4} K_{osj}[H_j\,edta^{(4-j)-}]}. \quad (A1)$$

Here, k_d, k_{ij}, and k_{osj} are the rate constants for the dissociative activation, the associative activation, and the outer-sphere complex related reaction processes, while K_{osj} is the formation constant for the outer-sphere complex. Equation A1 can, by using C_{edta} ($=\sum_{j=1}^{4}[H_jedta^{(4-j)-}]$), be rearranged to Eq. 2 with:

$$f_1([H^+]) \equiv (K_{a4}K_{a3}K_{a2}[H^+]^3 + K_{a3}K_{a2}[H^+]^2 + K_{a2}[H^+] + 1)K_{a1}[H^+], \quad (A2)$$

$$f_2([H^+]) \equiv (k_{i4}K_{a4}K_{a3}K_{a2}[H^+]^3 + k_{i3}K_{a3}K_{a2}[H^+]^2 + k_{i2}K_{a2}[H^+] + k_{i1})K_{a1}[H^+], \quad (A3)$$

$$f_3([H^+]) \equiv (K_{os4}K_{a4}K_{a3}K_{a2}[H^+]^3 + K_{os3}K_{a3}K_{a2}[H^+]^2 + K_{os2}K_{a2}[H^+] + K_{os1})K_{a1}[H^+], \quad (A4)$$

$$f_4([H^+]) \equiv (k_{os4}K_{os4}K_{a4}K_{a3}K_{a2}[H^+]^3 + k_{os3}K_{os3}K_{a3}K_{a2}[H^+]^2 + k_{os2}K_{os2}K_{a2}[H^+] + k_{os1}K_{os1})K_{a1}[H^+], \quad (A5)$$

where the K_{aj}'s are the protonation constants of H_4edta ($K_{aj}=[H_jedta^{(4-j)-}]/[H^+][H_{j-1}edta^{(5-j)-}]$, j: 1—4).[4]

References

1) I. Ohkura, K. Fujiwara, K. Okamoto, J. Hidaka, and H. Einaga, *J. Coord. Chem.*, **13**, 221 (1984).

2) R. G. W. Hollingshead, "Oxine and Its Derivatives," Butterworths London (1954), Vol. 1, Chap. 6.

3) Y. Hara, K. Okamoto, J. Hidaka, and H. Einaga, *Bull. Chem. Soc. Jpn.*, **57**, 1211 (1984).

4) The following data were used as the K_{aj} values of H_4edta at 25 °C and the ionic strength of 0.1 mol dm^{-3} (A. E. Martell and R. M. Smith, "Critical Stability Constants," Plenum, New York (1974), Vol. 1, p. 204): $\log K_{a1}=10.17$, $\log K_{a2}=6.11$, $\log K_{a3}=2.68$, and $\log K_{a4}=2.0$, because only small changes in magnitude are expected as a result of the differences in the ionic strength of 0.1 and 1.0 mol dm^{-3} (cf. L. G. Sillén and A. E. Martell, "Stability Constants of Metal-Ion Complexes," Chem. Soc., London(1971), Sp. Pub. No. 25, p. 63).

5) L. G. Sillén, *Acta Chem. Scand.*, **10**, 186 (1956).

6) Ref. No. 1 and the references cited therein.

7) B. C. Baker and D. T. Sawyer, *Anal. Chem.*, **40**, 1945 (1968).

8) N. Teramae, S. Tanaka, and S. Toda, *Bunko Kenkyu*, **27**, 29 (1978).

9) It has been widely accepted that aluminum(III) proceeds through the I_d mechanism, although it is difficult to exclude totally the possibility of the (limiting) dissociative (D) mechanism. See, for example, a) A. E. Merbach, *Pure Appl. Chem.*, **54**, 1479 (1982); b) D. Fiat and R. E. Connick, *J. Am. Chem. Soc.*, **90**, 608 (1968); c) L. S. Frankel and E. P. Danielson, *Inorg. Chem.*, **11**, 1964 (1972); d) C. Ammann, P. Moore, and A. E. Merbach, *Helv. Chim. Acta*, **63**, 268(1980); e) D. Hugi-Cleary, L. Helm, and A. E. Merbach, *Helv. Chim. Acta*, **68**, 545 (1985).

Chemistry of Germanium Atoms. IV. A New Method for Preparation of Organogermanium Halides by Co-condensation of Germanium Vapor with Tetrahydrofuran[1)]

Kunio MOCHIDA,* Yūko NAKAI, and Shigeru SHIOTA
Department of Chemistry, Faculty of Science, Gakushuin University, 1-5-1 Mejiro, Tokyo 171
(Received February 6, 1988)

Synopsis. Germanium vapor (atom) when co-condensated with THF at 77 K was found to be reactive toward organic halides. Several organogermanium halides were prepared by the addition of organic halides to the resultant germanium atom-THF slurry at ambient temperatures.

The co-condensation of metal vapor (atom) with certain solvents has been reported to make very reactive metal surfaces (slurries in solution).[2)] With this method it is becaming feasible to synthesize organometallic compounds, which would be difficult to prepare by other methods, at ambient conditions. However, there have been few reports on the reactivities of group 4B metal vapor-solvent slurries.[3)] Particularly no reports on silicon and germanium atoms-solvent slurries have appeared. In studying the reaction of germanium atoms in the condensed phase,[4-6)] we have found that germanium vapor (atom)-THF co-condensate is reactive toward organic halides. Here, we report on a new method for the preparation of organogermanium halides using germanium atom-THF co-condensate (slurry) at ambient temperatures.

Results and Discussion

A reactive germanium metal surface was conveniently produced by the co-condensation of germanium vapor with THF and by the use of essentially the same apparatus and conditions described previously (ca. 1200—1300 °C, 5×10^{-3} Torr, 1 Torr=133.322 Pa).[4)] Germanium metal was evaporated at a rate of ca. 10 mg min^{-1}, while an excess of THF was co-condensed on the wall of a quartz reaction flask containing the crucible and a perforated inlet tube through which THF was introduced. The reaction flask was immersed in liquid nitrogen during the germanium evaporation. Germanium atoms that co-condensed with THF were warmed to room temperature. The ensuing germanium atom-THF slurry was found to react with organic halides under argon. The size of particles in the germanium atom-THF slurry ranged from 0.7 to 18 μm as shown in Fig. 1.[7)]

Reactions of germanium atom-THF slurry with organic halides were examined. Germanium-containing products are summarized in Table 1. Bromotrichloromethane ($BrCCl_3$) reacted with this germanium atom-THF slurry at 50 °C for 5 h to give germanium tetrachloride ($GeCl_4$) (ca. 1.0%) and (trichloromethyl)-tribromogermane (CCl_3GeBr_3) The yields of germanium-containing products increased slightly at 50 °C for 20 h, as shown in Table 1. On the other hand, no reaction of $BrCCl_3$ took place with commercially available germanium powder (200 mesh) under these reaction conditions.

Reactions of germanium atom-solvent slurries with $BrCCl_3$ were also examined using various solvents. The yields of germanium-containing products were extremely low when a germanium atom-hexane slurry was used. No reaction of $BrCCl_3$ with germanium-benzene slurry occurred. The yields of germanium-containing products decreased roughly in the order: THF > DME ≃ hexane ≫ benzene. The differences of reactivities of solvents employed in this study might be attributed to the size and shape of particles in the germanium atom-solvent slurries. Similar results have been reported for nickel[1e)] and calcium atoms.[8)] Carbon tetrachloride (CCl_4) reacted with germanium atom-THF slurry to give $GeCl_4$ (ca. 1.0%) and (trichloromethyl)trichlorogermane (CCl_3GeCl_3) (3.0%). When $GeCl_4$ was used as a substrate, germanium atom-THF slurry produced hexachlorodigermane (Ge_2Cl_6) (10.0%) and octachlorotrigermane (Ge_3Cl_8) (3.0%). The reactions of germanium atom-THF slurry with sulfur monochloride (S_2Cl_2) and trichlorophophine (PCl_3) gave only $GeCl_4$ in 6.0 and 2.0% yields, respectively. No reaction of germanium atom-THF slurry with chloroform occurred.

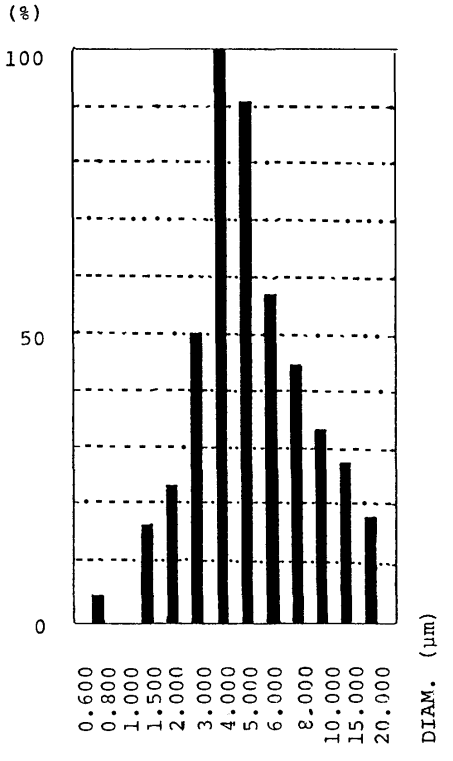

Fig. 1. Differential graph of germanium atom-THF slurry.

Table 1. Reactions of Germanium Atom-Solvent Slurries with Organic Halides

Halide (RX)	Solvent	Condition	Product (Yield/%)[a]
$BrCCl_3$	THF	50 °C, 5 h	$GeCl_4$ (ca. 1.0),[b] CCl_3GeBr_3 (2.5)
$BrCCl_3$	THF	50 °C, 20 h	$GeCl_4$ (ca. 1.0),[b] CCl_3GeBr_3 (3.5)
$BrCCl_3$	DME	50 °C, 5 h	$GeCl_4$ (trace), CCl_3GeBr_3 (1.5)
$BrCCl_3$	Hexane	50 °C, 5 h	$GeCl_4$ (trace), CCl_3GeBr_3 (1.0)
$BrCCl_3$	Hexane	50 °C, 20 h	$GeCl_4$ (trace), CCl_3GeBr_3 (1.5)
$BrCCl_3$	Benzene	50 °C, 20 h	No reaction
CCl_4	THF	50 °C, 5 h	$GeCl_4$ (ca. 1.0),[b] CCl_3GeCl_3 (3.0)
$GeCl_4$	THF	50 °C, 5 h	Ge_2Cl_6 (10.0), Ge_3Cl_8 (3.0)
S_2Cl_2	THF	50 °C, 5 h	$GeCl_4$ (6.0)
PCl_3	THF	50 °C, 5 h	$GeCl_4$ (2.0)
$CHCl_3$	THF	50 °C, 5 h	No reaction
MeI	THF	50 °C, 5 h	$MeGeI_3$ (1.0), Me_2GeI_2 (1.0)
EtI	THF	50 °C, 5 h	$EtGeI_3$ (1.0), Et_2GeI_2 (1.0)

a) Yields of products are based on the amount of germanium metal used. b) The retention time of $GeCl_4$ on GLC was partially overlapped with that of solvents.

Methyl iodide reacted with germanium atom-THF slurry to produce methyltriiodogermane ($MeGeI_3$) (1.0%) and dimethyldiiodogermane (Me_2GeI_2) (1.0%). With ethyl iodide, germanium atom-THF slurry produced ethyltriiodogermane ($EtGeI_3$) (0.5%) and diethyldiiodogermane (Et_2GeI_2) (0.5%).

The reactions of this germanium atom-THF slurry with organic halides proceed under milder conditions than a general direct synthesis of organogermanium halides,[9,10] although the yields of products are very low.

Experimental

GLC analyses were performed on a Shimazu GC-6A and 8A gas chromatograph equipped with a 2m×column packed with 20% SE-30 on celite 545. Infrared spectra were recorded on a Hitachi 260-10 spectrometer. GC-MASS spectra were obtained with a JEOL JMS-DX 303 mass spectrometer and data analyses were performed on a JMN-DA 5000 mass data system. ^1H NMR spectra were recorded on a Varian FT 80A, using tetramethylsilane as an internal standard.

Materials. The organic halides were commercially available products. THF and other solvents were dried over benzophenone ketyl and distilled before use. $MeGeI_3$,[11] Me_2GeI_2,[9] $EtGeI_3$,[11] and Et_2GeI_2[12] were prepared according to the cited literature.

Preparation of Gremanium Atom-Solvent Slurries. Germanium atom-solvent slurries were produced using essentially the same apparatus and conditions described previously.[4] A typical procedure is described below. Germanium metal (0.5 g, 6.9 mmol) was vaporized at a rate of ca. 10 mg min^{-1}, at a temperature of 1200—1300 °C using a resistence-heated, alumina-coated tungsten spiral crucible (5.0—6.0 V, 15 A) connected to copper electrodes, in vacuo (ca. 5×10^{-3} Torr). During the vaporization of germanium metal, a large excess of THF (20 cm^3) was introduced as a vapor through a perforated inlet tube. The THF was co-condensed onto the wall of a quartz reaction flask was immersed in liquid nitrogen during the entire operation. Then, the reaction flask was allowed to warm to room temperature and was left to stand for 1 h. The reaction flask was evacuated and then filled with argon.

Reactions of Germanium Atom-THF Slurry with Organic Halides. The reaction with $BrCCl_3$ is described as a typical example. The germanium atom-THF slurry was shaken vigorously and a given volume of the germanium atom-THF slurry was quickly placed in a two-necked 50-cm^3 flask equipped with a serum cap and a reflux condenser in an argon-filled glove box. Ten times molar amounts of $BrCCl_3$ were then syringed in. The reaction mixture was stirred at 50 °C for 5 h under argon. The products were identified by comparing their GC-MASS[4,5] and their retention times on GLC with those of authentic samples.

Identification of Products. The known compounds were identified by comparing their GC-MS and retention times on GLC with those of authentic samples. The unkown compounds were carefully identified by comparing their GC-MS with those of similar samples and by parent peaks and cleavage patterns considering natural abundance of germanium (ratio, $^{70}Ge/^{72}Ge/^{73}Ge/^{74}Ge/^{76}Ge=56/75/21/100/21$) and chlorine (ratio, $^{35}Cl/^{37}Cl=75.4/24.6$). $^{74}Ge_2{}^{35}Cl_6$[13] (parent ion peak at $m/z=358$), $m/z=323$ (6), 253 (12). $^{74}Ge_3{}^{35}Cl_8$ (parent ion peak at $m/z=502$), $m/z=327$ (21), 288 (7), and 253 (7).

The authors thank Dr. Kohji Ujiie, Messers. Hiroshi Yamashita and Hajime Takahashi of Ricoh Company Ltd., for measuring the size of germanium particles. We also thank Mitsubishi Metal Corporation for a gift of germanium metal. This work was supported in part by a Grant-in-Aid for Special Project Research (Nos. 61125004 and 62115003) provided by the Ministry of Education, Science and Culture.

References

1) Chemsitry of germanium atoms. III. See; Ref. 6.

2) For examples; a) R. D. Rieke and P. M. Hundnall, *J. Am. Chem. Soc.*, **94**, 7178 (1972); b) R. D. Rieke, S. J. Uhm, and P. M. Hundnall, *J. Chem. Soc., Chem. Commun.*, **1973**, 269; c) D. F. Stark and A. Streitwieser, *J. Am. Chem. Soc.*, **95**, 3423 (1973); d) K. J. Klabunde, H. F. Efner, T. O. Murdock, and W. Donley, *J. Organomet. Chem.*, **71**, 309 (1974); e) K. J. Klabunde, H. F. Efner, T. O. Murdock, and R. Ropple, *J. Am. Chem. Soc.*, **98**, 1021 (1976); f) K. J. Klabunde, "Chemistry of Free Atoms and Particles," Academic Press, New York (1980); g) Y. Imizu, *Shokubai*, **27**, 480 (1985).

3) K. J. Klabunde, "Reactive Intermediates," ed by R. A. Abramovitch, Plenum Press (1980), Vol. 1, Chap. 2, p. 140.

4) K. Mochida and K. Tashiro, *Nippon Kagaku Kaishi*, **1987**, 1168.

5) K. Mochida and K. Tashiro, *Chem. Lett.*, **1987**, 1105; K. Mochida, K. Tashiro, Y. Yoshida, and Y. Mizuno, *Bull. Chem. Soc. Jpn.*, **61**, 1247 (1988).

6) K. Mochida and Y. Yoshida, *Bull. Chem. Soc. Jpn.*, **61**, 1785 (1988).
7) The size of particles in the germanium atom-THF slurry was measured by a coulter method (Coulter Counter Model TA-II, Coulter Electronics Co., Ltd.,) and a centrifugal sedimentation method.
8) K. Mochida and T. Yamanishi, *J. Organomet. Chem.*, **332**, 247 (1987).
9) K. Moedritzer, *J. Organomet. Chem.*, **6**, 282 (1966).
10) K. Moedritzer and J. R. V. Wazer, *Inorg. Chem.*, **5**, 547 (1966).
11) E. A. Flood, *J. Am. Chem. Soc.*, **55**, 4935 (1933).
12) L. Horvitz znd F. A. Flood, *J. Am. Chem. Soc.*, **55**, 5055 (1933).
13) N. N. Kochanova and I. I. Lapidas, *Zh. Fiz. Khim.*, **47**, 2937 (1973); *Chem. Abstr.*, **80**, 41634e (1974).

Facile Photorearrangement of Some Crowded Azoxyarenes via Two Concurrent Pathways

Masao Ōkubo,* Hayato Hyakutake, and Naoki Taniguchi
Department of Chemistry, Faculty of Science and Engineering, Saga University, Honjō-machi, Saga 840
(Received February 12, 1988)

Synopsis. Naphthalene-1-*ONN*-azoxybenzenes and some unsymmetrically ortho-substituted *ONN*- and *NNO*-azoxybenzenes were prepared, and their photochemical behavior in ethanol was compared. The crowded azoxyarenes tend to undergo a facile Wallach rearrangement via the known *azoxy-ortho* oxygen mirgation and a concurrent pathway involving *ONN–NNO* isomerization. The relative contribution of the two pathways was affected by substituents.

The photo-Wallach rearrangement of azoxyarenes via azoxy-ortho migration of oxygen (Scheme 1) is established.[1] However, neither systematic study on the steric repulsion effect nor that on the electronic effect of unsymmetrical (*unsym*-) azoxyarenes has appeared because their *ONN* and *NNO* isomers have so far been difficultly accessible. The difficulty has recently been overcome by a convenient method for the independent preparation of *unsym*-azoxyarene isomers by the condensation of nitroarenes with aryliminodimagnesium reagent ($ArN(MgBr)_2$, aryl-IDMg, Scheme 2).[2]

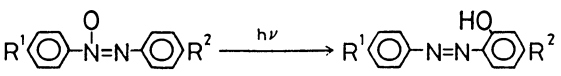

Scheme 1.

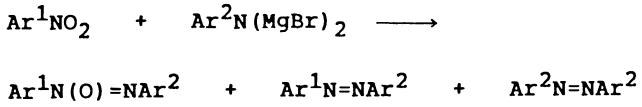

Scheme 2.

In this paper, the steric repulsion effect on the photoreactivity of crowded azoxyarenes and the directive effect of substituents on oxygen migration will be described. The azoxyarenes concerned are naphthalene-1-*NNO*-azoxybenzene ($\mathbf{1}^{H}_{NNO}$),[3] its more crowded *ONN*-isomer ($\mathbf{1}^{H}_{ONN}$), their *p*-Me and *p*-MeO derivatives ($\mathbf{1}^{Me}_{ONN}$ and $\mathbf{1}^{MeO}_{ONN}$), and some *o*-substituted *ONN*- and *NNO*-azoxybenzenes (**3** and **4**). The structure having an azoxy nitrogen combined to a bulky aryl group is indicated by *ONN*. Photochemical behavior was compared with one another and with that of non-crowded ones **2**. All the crowded and noncrowded azoxyarenes were prepared by the reaction of Scheme 2: $\mathbf{3}^{Et}_{NNO}$ was unavailable because of unsuccessful IDMg treatment (see Experimental).

The azoxyarenes were dissolved in ethanol, introduced into quartz cells, and irradiated for 30 min by a high-pressure mercury lamp. In addition to the azoxy isomers, two photo-Wallach products were isolated. The normal product has an *o*-OH group on the benzene ring nearer to the original "azo" nitrogen, and the isomeric one has an *o*-OH group on the ring nearer to

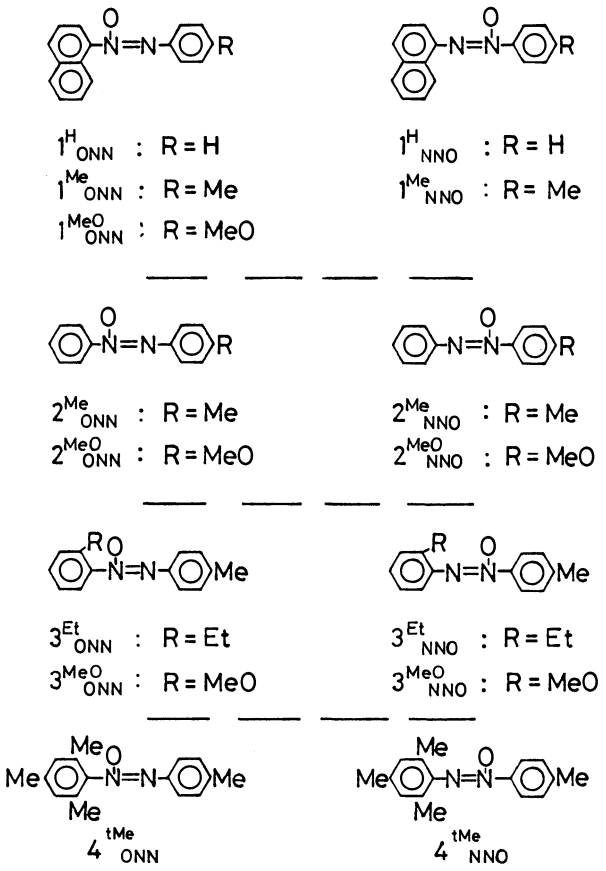

the original "azoxy" nitrogen (Scheme 1). Yields of isolated azoxy isomers, two Wallach products, and associated recoveries, based on amounts of azoxyarenes used, are given in Table 1 (Runs 1—11). When the azoxyarenes used in Runs 1—6 were irradiated in Pyrex glass cells of the same size, the yield of the normal Wallach product decreased by 4—11% and the recovery increased by 7—10%. By use of ordinary glass cells, additional decrease (1—5%) and increase (0—5%) were observed.

The higher reactivity of the crowded 1-naphthyl-*ONN* derivatives ($\mathbf{1}_{ONN}$), ascribable to the steric repulsion of *peri*-hydrogen, is shown by their recoveries (18 and 40%, Runs 1 and 2) lower than those of the non-crowded phenyl derivatives ($\mathbf{2}_{ONN}$ and $\mathbf{2}_{NNO}$, Runs 3—6). The latter are converted via the known pathway of Scheme 1. According to the "normal" pathway i) of Scheme 3, $\mathbf{1}^{Me}_{ONN}$ gave the normal Wallach product in higher yield (35%, Run 1) than $\mathbf{2}^{Me}_{ONN}$ (30%, Run 3). Participation of the other pathway ii) involving the *ONN–NNO* isomerization, probably via the oxadiaziridine intermediate **A**,[4,5] is shown by the isolation of an inseparable red oily mixture in 24% yield. The oil was composed of the less crowded $\mathbf{1}^{Me}_{NNO}$ and the "isomeric"

Table 1. Photochemical Rearrangement of Some Sterically Crowded Azoxyarenes

Run No.	Azoxyarenes $Ar^1N(O)=NAr^2$			Yield/%		
	No.	Ar^1	Ar^2	Wallach product	*NNO*-Isomer and/or isomeric Wallach product	Recovery/%
1	$\mathbf{1}^{Me}_{ONN}$	1-NaPh	*p*-MePh	35	24[a]	18
2	$\mathbf{1}^{MeO}_{ONN}$	1-NaPh	*p*-MeOPh	33	low[b]	40
3	$\mathbf{2}^{Me}_{ONN}$	Ph	*p*-MePh	30	0	54
4	$\mathbf{2}^{MeO}_{ONN}$	Ph	*p*-MeOPh	25	0	60
5	$\mathbf{2}^{Me}_{NNO}$	*p*-MePh	Ph	27	0	51
6	$\mathbf{2}^{MeO}_{NNO}$	*p*-Meph	Ph	17	0	77
7	$\mathbf{3}^{Et}_{ONN}$	*o*-EtPh	*p*-MePh	44	0	35
8	$\mathbf{3}^{MeO}_{ONN}$	*o*-MeOPh	*p*-MePh	37	15	37
9	$\mathbf{3}^{MeO}_{NNO}$	*p*-MePh	*o*-MeOPh	7[c]	5[c]	61[e]
10	$\mathbf{4}^{tMe}_{ONN}$	2,4,6-Me_3Ph	*p*-MePh	22	42	9
11	$\mathbf{4}^{tMe}_{ONN}$	*p*-MePh	2,4,6-Me_3Ph	0	29[d]	29[e]

a) An oily mixture composed of the *NNO*-isomer and the corresponding Wallach product (see text). b) No *NNO*-isomer was isolated, but the formation was suggested (see text). c) Two isomeric Wallach products were obtained as an inseparable mixture. The minor one (5%) is the same as that obtained in Run 8. d) The product is the same as the Wallach product obtained in Run 10. e) Smaller overall amount due to unidentified decomposition products.

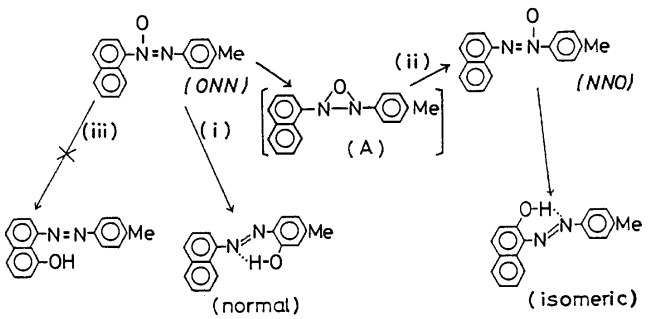

Scheme 3.

Wallach product (1-(4-methylphenylazo)-2-naphthol) in a molar ratio of 8 : 2 (see Experimental). Similarly, $\mathbf{1}^{MeO}_{ONN}$ gave the normal Wallach product in higher yield (33%, Run 2) than $\mathbf{2}^{MeO}_{ONN}$ (25%, Run 4). Neither the less crowded $\mathbf{1}^{MeO}_{NNO}$ nor the isomeric product was isolated from a small amount of complex mixture, but the second lowest amount of recovery among Runs 1—6 suggests a more or less participation of pathway ii). The conversion of *p*-MeO derivatives lower than that of the corresponding *p*-Me derivatives (Runs 1—6) is in accord with the electronic substituent effect of symmetrical azoxybenzenes.[6]

Also in solid state, $\mathbf{1}_{ONN}$'s are highly photosensitive as shown by color change of pure crystals from pale yellow into red even in an ordinary glass bottle placed under a fluorescent ceiling light. In the dark, their crystals or benzene solutions (even under refluxing) suffer no color change. All the other azoxyarenes used in this study were handled in the usual manner. Some effect of naphthalene ring sensitive to different wavelengths may also be responsible for the unique behavior of $\mathbf{1}_{ONN}$'s. No existence of the alternative pathway iii) (Scheme 3) via the *azoxy-peri* oxygen migration[7] was confirmed (see Experimental).

In the case of the *o*-substituted *ONN*-azoxybenzenes having a *p'*-Me group (Runs 7, 8, and 10) and their *NNO* isomers (Runs 9 and 11), the former are more reactive than the latter but the directive effects are somewhat complicated. Whereas $\mathbf{3}^{Et}_{ONN}$ reacts via the single pathway i), $\mathbf{3}^{MeO}_{ONN}$ reacts via the two pathways i) and ii). The highly crowded $\mathbf{4}^{tMe}_{ONN}$ was most easily converted, as shown by the lowest amount of recovery, to give the normal Wallach product and *NNO*-isomer via the two pathways. The lowest conversion of $\mathbf{1}^{MeO}_{NNO}$ is understandable because it may be electronically stabilized by the less hindered *o'*-MeO group[4] (vide infra), but the reaction proceeds via the two pathways. Since $\mathbf{4}^{tMe}_{NNO}$ has no ortho-hydrogen essential to the "normal" rearrangement, the exclusive formation of the "isomeric" product in lower yield is explicable. The lower combined yields and recovery in Runs 9 and 11 arise from the partial decomposition leading to some unidentified materials.

The primary conclusion is that the crowded azoxyarenes undergo the facile rearrangement via the two pathways, whereas the less crowded ones react sluggishly via the single and normal pathway. The conclusion is reasonable because the oxadiaziridine intermediate[4,5] is effective for the release of steric repulsion. With regard to the directive effect, the results of Runs 7 and 9 are exceptional to the conclusion, as seen from their contrast with those of Run 8. The comparably bulky *o*-Et and *o*-MeO groups exhibit the comparable reactivities but different directive effects. In conflict with no detection of the isomeric Wallach product from $\mathbf{2}^{MeO}_{NNO}$ (Run 6, vide supra), the normal and isomeric ones were previously isolated[4] probably due to different conditions of irradiation. The quite low reactivity of $\mathbf{2}^{MeO}_{NNO}$ suggests that the previous result arises from the electronic stabilization of oxadiaziridine by the *p'*-MeO group. The conversion of $\mathbf{1}^{MeO}_{ONN}$ lower than that of $\mathbf{1}^{Me}_{ONN}$ is similarly explaina-

Table 2. Melting Points and ^{1}H NMR Data of "Normal" Wallach Products (*o*-Hydroxyazoarenes)

Product formed from (Run No.)	Mp θ_m/°C	^{1}H NMR Data/δ
$\mathbf{1}^{Me}_{ONN}$(1)	112—113	12.88 (1H, s), 8.44—8.56 (1H, m), 7.45-8.04 (7H, m), 6.80—6.94 (2H, m), 2.40 (3H, s).
$\mathbf{2}^{MeO}_{ONN}$(2)	134—136	14.38 (1H, s), 8.50—8.62 (1H, m), 7.56—8.10 (7H, m), 6.56—6.78 (2H, m), 3.92 (3H, s).
$\mathbf{3}^{Et}_{ONN}$(7)	80.5—82	12.63 (1H, s), 7.80—7.66 (2H, m), 7.33—7.00 (3H, m), 6.80—6.56 (2H, m), 2.96 (2H, q), 2.33 (3H, s), 1.33 (3H, s).
$\mathbf{3}^{MeO}_{ONN}$(8)	128—128.5	13.13 (1H, s), 7.93—7.73 (2H, m), 7.63—6.60 (5H, m), 4.00 (3H, s), 2.36 (3H, s).
$\mathbf{3}^{MeO}_{NNO}$(9)[a]	—	Pairs of singlets at 13.53 and 13.13, 4.00 and 3.90, and 2.36 and 2.28 were observed.
$\mathbf{4}^{tMe}_{ONN}$(10)	104.5—105	12.30 (1H, s), 7.50 (2H, d), 6.70—6.43 (3H, m), 2.36 (6H, s), 2.33 (3H, s), 2.23 (3H, s).

a) The mixture gave three pairs of OH, OCH_3, and CH_3 singlets. Relative intensities are recognized as the composition of the mixture.

ble. The exceptions and conflict ascribable to the electronic directive effect on oxygen migration possibly involving the mutual conversion of *unsym*-azoxy isomers via oxadiaziridine[5] (see Scheme 3) remain to be studied.

Experimental

Azoxyarenes. The reactions of Scheme 2 were carried out as previously reported.[2] The azoxyarenes were separated from the reaction mixture by column chromatography, and purified by recrystallization. Attempts to prepare $\mathbf{3}^{Et}_{NNO}$ were unsuccessful because the treatment of *p*-$MeC_6H_4NO_2$ with *o*-EtC_6H_4-IDMg gave only a trace amount and the treatment of *o*-$EtC_6H_4NO_2$ with *p*-MeC_6H_4-IDMg afforded only $\mathbf{3}^{Et}_{ONN}$ (vide infra). The *NNO*-derivative, $\mathbf{1}^{tMe}_{NNO}$ (Run 11), was obtained by the photoreaction of Run 10; it was also obtained by a lucky *ONN-NNO* isomerization in the reaction of *p*-MeC_6H_4-IDMg with 2,4,6-$Me_3C_6H_2NO_2$.[8] The assignment of structures of *o*-substituted azoxyarenes and the product distributions in the reactions of Scheme 2 will be reported elsewhere.[8]

Procedures. The photoreactions were carried out using 0.002 M (1 M=1 mol dm^{-3}) solution in spectro-grade ethanol.[6] The quite low conversion in benzene and no effect of atmosphere were reported.[6] The solutions in quartz cells were placed at a distance of 4.5 cm from a water-jacketted mercury lamp of a merrygo-round UV-irradiation apparatus, and were irradiated for 30 min at room temperature (15—20 °C). The amounts of Wallach products and recovered and/or isomeric azoxyarenes were determined by chromatographic separation and/or by comparison of intensities of ^{1}H NMR signals with those of authentic samples.

Products. The authentic samples for photo-Wallach products, *o*-hydroxyazoarenes, were obtained as the minor products of coupling reactions of appropriate aryldiazonium salts with phenolates (except 2-naphthol derivatives, which were obtained as major products). They were isolated from the filtrates of crystallization of the major *p*-hydroxyazoarenes by column chromatography (Wako Gel C-200 and C-300), and were purified by recrystallization. The melting points (uncorrected) and ^{1}H NMR data of the "normal" products in Runs 1, 2, and 7—10 are summarized in Table 2. The elemental analyses gave satisfactory results. The minor isomeric product in Run 9 is the same as the normal one obtained in Run 8, and the product in Run 11 is the same as the normal one obtained in Run 10. The products obtained in Runs 3—6 are known.[4,9]

The composition of the inseparable mixture of $\mathbf{1}^{Me}_{NNO}$ and "isomeric" product (Run 1) was estimated from the relative intensities of two Me-proton ^{1}H NMR signals. The authentic sample of alternative *azoxy-peri* oxygen migration (cf. Run 1) was prepared in low yield by treating 8-nitro-1-naphthol[10] with a large excess of *p*-MeC_6H_4-IDMg.

The authors wish to thank Advanced Instrumentation Center for Chemical Analysis, Ehime University, for the elemental analyses. A part of this work is financially supported by a Grant-in-Aid for Scientific Research (60470026).

References

1) a) H. E. Bigelow, *Chem. Rev.*, **9**, 139 (1931); b) G. G. Spence, E. C. Taylor, and O. Buchardt, *ibid.*, **70**, 321 (1970).
2) M. Ōkubo and K. Koga, *Bull. Chem. Soc. Jpn.*, **56**, 203 (1983).
3) G. M. Badger, R. G. Butterby, and G. E. Lewis, *J. Chem. Soc*, **1953**, 2143; G. M. Badger and G. E. Lewis, *ibid.*, **1953**, 2147, 2151.
4) N. J. Bunce, *Can. J. Chem.*, **53**, 3477 (1975).
5) S. S. Hecht and F. D. Greene, *J. Am. Chem. Soc.*, **89**, 6761 (1968); H. G. Taylor, S. R. Isaac, and J. L. Swigert, *J. Org. Chem.*, **41**, 1146 (1976).
6) R. Tanikaga, *Bull. Chem. Soc. Jpn.*, **41**, 1664, 2151 (1968).
7) N. J. Bunce, D. J. W. Goon, and J. P. Schoch, *J. Chem. Soc., Perkin Trans. I*, **1976**, 688.
8) M. Ōkubo, Y. Inatomi, N. Taniguchi, and K. Imamura, *Bull. Chem. Soc. Jpn.*, in press.
9) E. Bamberger, *Chem. Ber.*, **33**, 3188 (1900).
10) H. H. Hodgson and J. Ratcliffe, *J. Chem. Soc.*, **1949**, 1314; H. Musso, *Chem. Ber.*, **105**, 1017 (1971).

Novel Synthesis of Isoflavones by the Palladium-Catalyzed Cross-Coupling Reaction of 3-Bromochromones with Arylboronic Acids or Its Esters

Yukio HOSHINO,* Norio MIYAURA,† and Akira SUZUKI†
Department of Natural Science, Muroran Institute of Technology, Mizumoto-cho, Muroran 050
†Department of Applied Chemistry, Faculty of Engineering, Hokkaido University, Sapporo 060
(Received February 26, 1988)

Synopsis. The synthesis of isoflavone derivatives by means of palladium-catalyzed cross-coupling reaction between 3-bromochromones and arylboronic acids or its butyl esters is described.

Isoflavones (3-phenyl-4*H*-1-benzopyran-4-ones) belong to the main categories of flavonoids, such as flavones (2-phenyl-4*H*-1-benzopyran-4-ones) and chalcones, which exist in plants, fruit, and flowers. Although many synthetic methods of isoflavones have been reported, including: (1) the oxidative rearrangement of chalcones with thallium(III) nitrate;[1] (2) the aryl migration of 2′-hydroxychalcone epoxides using $BF_3 \cdot OEt_2$;[2] and (3) the oxidation of products obtained by boiling *N*-styrylmorpholine and salicylaldehyde with CrO_3-pyridine in benzene;[3] no synthetic procedures of isoflavones have been presented hitherto using a direct arylation on a chromone framework. Recently, we have reported that the palladium-catalyzed cross-coupling reaction[4] of phenylboronic acids with haloarenes proceeds smoothly in the presence of bases to give corresponding biaryls. Thereafter, several articles[5] with respect to the application of this reaction have appeared. We report here the preparation of isoflavones (**3**) from 3-bromochromones (**1**) and arylboronic acids or its esters (**2**) by applying the above-mentioned cross-coupling reaction (Eq. 1).

Results and Discussion

The optimum conditions for carrying out the reaction of Eq. 1 were studied by using 3-bromochromone and phenylboronic acid or its butyl ester in the presence of 3 mol% of $Pd(PPh_3)_4$ and 2 equivs of various bases. The results are summarized in Table 1. From

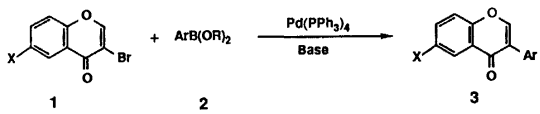

1 2 3 (1)

the table, it is shown that the best yield of isoflavone can be obtained by using aqueous Na_2CO_3 as a base. The reaction is also effected with aqueous Tl_2CO_3[6] and found to be complete in the shorter reaction time compared with other bases (Entry 4). A more interesting use of Tl_2CO_3 may be the reaction of dibutyl phenylboronate with **1** under nonaqueous conditions (Entry 5). The desired isoflavone was obtained in 91% yield, whereas the reaction time had to be increased to 6 h. When the coupling reaction was carried out in the presence of NaOH or NaOAc, the formation of *o*-hydroxyacetophenone was observed in the GLC analysis. It has been known that chromones are subject to ring fission[7] by a strong base such as NaOH to give the corresponding *o*-hydroxyacetophenones. Furthermore, it has also been reported that arylboronic acids are protonized[5a,b] with water in the presence of a base. The low yields of isoflavone in those cases may be due to such side reactions.

Table 1. Effects of Bases on the Cross-Coupling Reaction of 3-Bromochromone with Phenylboronic Acid or Its Butyl Ester[a]

Entry	$PhB(OR)_2$	Base	Reaction time/h	Yield/%[b]
1	OH	3 M $NaOH/H_2O$	3	49
2	OH	3 M $NaOAc/H_2O$	8[c]	25
3	OH	2 M Na_2CO_3/H_2O	6	94
4	OH	1 M Tl_2CO_3/H_2O	1.5	85
5	OBu	Tl_2CO_3[d]	6	91

a) All the reactions were conducted under reflux temperature of benzene, using 3-bromochromone (1 mmol), phenylboron compound (1.1 mmol), $Pd(PPh_3)_4$ (0.03 mmol), and base (2 mmol). b) Isolated yield beased on 3-bromochromone. c) Reaction was not complete. d) Powdered Tl_2CO_3 was suspended in benzene.

To establish a generality of this method as a synthetic procedure of **3**, eleven isoflavone derivatives were prepared from the corresponding 3-bromochromones and arylboronic acids. Representative results are summarized in Table 2. The conditions using aqueous Na_2CO_3 as a base (Entry 3 in Table 1) were found to work for the most of phenylboronic acids with ortho and para substituents, and for the 3-bromochromones substituted with 6-Cl and 6-MeO groups. The yields of **3** seem to largely depend upon the functional groups on **2** rather than those of **1**. Namely, the reaction of *p*-nitrophenylboronic acid with **1** gave only 23% of 4′-nitroisoflavone after refluxing for 4 h. Mesitylboronic acid reacted only slowly (completed after 26 h) and gave less than 5% of 2′,4′,6′-trimethylisoflavone together with a substantial amount of mesitylene. The results indicated that the protonolysis of phenylboronic acids is competitive with the coupling even under the conditions using aqueous Na_2CO_3. Thus, such aqueous conditions are not suitable for the phenylboronic acids with electron-withdrawing substituents which accelerate the rate of protonolysis or two ortho substituents which retard the transmetallation step in the mechanism[8] of cross-coupling reaction. For these boronic acids, an alternative procedure (Entry 5 in Table 1) using the esters of boronic acids and Tl_2CO_3 was developed. Under these

Table 2. Synthesis of Isoflavones (Eq. 1)

Entry	1, X=	$ArB(OR)_2$	Base	Reaction time/h	Yield %[a]
1	H	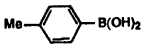	2 M Na_2CO_3/H_2O	10	84
2	H	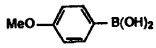	2 M Na_2CO_3/H_2O	3	94
3	H	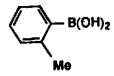	2 M Na_2CO_3/H_2O	6	94
4	Cl	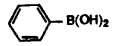	2 M Na_2CO_3/H_2O	23	71
5	MeO	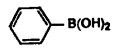	2 M Na_2CO_3/H_2O	7	87
6	H	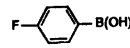	2 M Na_2CO_3/H_2O	6	80
7	H	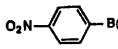	Tl_2CO_3	9	88[b]
8	H	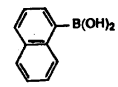	2 M Na_2CO_3/H_2O	7	90
9	H	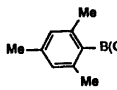	Tl_2CO_3	48	47[b]

a) Isolated yields based on 3-bromochromones. b) Reaction was carried out under the nonaqueous conditions (Entry 5 in Table 1).

nonaqueous conditions, the protonolysis of arylboronic acids can be prevented. Indeed, the reactions of dibutyl mesitylboronate and *p*-nitrophenylboronate with **1** gave the corresponding coupling products in yields of 47 and 88% (Entries 7 and 9 in Table 2). Although it is necessary to further define the scope and limitations of this nonaqueous procedure, the conditions should be more useful for the coupling reactions[5] of the arylboron compounds which are sensitive to protonolysis or sterically hindered.

Since, the 3-bromochromones are readily prepared from commercially available *o*-hydroxyacetophenone and the arylboronic acids are also conventionally prepared by the reaction of aryl-Grignard reagents with trialkylborates followed by hydrolysis, it can be concluded that the present procedure is a general and straightforward method for isoflavone synthesis.

Experimental

All melting points are uncorrected. IR spectra were recorded on a JASCO-IRA-1 spectrometer by means of KBr pellet. ^1H NMR spectra were obtained with a Hitachi-R-90H Fourier Transform NMR spectrometer (90 MHz) and are reported in δ units using tetramethylsilane as an internal standard. Mass spectra were taken on a JEOL JMS-D300. GLC analyses were performed on a Hitachi 163 instrument using silicon OV-17 (2 m) on Uniport B.

Materials and Reagents. Benzene was the commercially available grade, and was distilled and dried over sodium before use. Tetrakis(triphenylphosphine)palladium(0) was prepared by the literature procedure.[9] Phenylboronic acid,[10] *p*-tolylboronic acid,[10] *p*-methoxyphenylboronic acid,[10] *p*-fluorophenylboronic acid,[11] 1-naphthylboronic acid,[12] *p*-nitrophenylboronic acid,[10] and mesitylboronic acid[13] were prepared by the known procedures.[14] 3-Bromochromones were also synthesized by the method reported by Gammill.[15] All isoflavones isolated and 3-bromo-6-methoxychromone were identified by IR, ^1H NMR, and mass spectra, and these physical data are as follows.

3-Bromo-6-methoxychromone: Mp 122.0—122.5 °C; IR (KBr) 1660 cm^{-1} (C=O); ^1H NMR ($CDCl_3$) δ=3.90 (s, 3H, OCH_3), 7.20—7.48 (m, 2H, aromatic), 7.59 (d, 1H, J=2.6 Hz, C_5-H), and 8.20 (s, 1H, C_2-H); MS, Found: m/z 255.9566, Calcd for $C_{10}H_7BrO_3$: M, 255.9558.

Isoflavone: Mp 131.5—132.0 °C; IR (KBr) 1640 cm^{-1} (C=O); ^1H NMR ($CDCl_3$) δ=7.32—7.78 (m, 8H, aromatic), 8.01 (s, 1H, C_2-H), and 8.31 (dd, 1H, C_5-H, J=7.5 and 1.8 Hz); MS, Found: m/z 222.0682, Calcd for $C_{15}H_{10}O_2$: M, 222.0681.

4′-Methylisoflavone: Mp 153.5—154.5 °C; IR (KBr) 1635 cm^{-1} (C=O); ^1H NMR ($CDCl_3$) δ=2.38 (s, 3H, CH_3), 7.18—7.77 (m, 7H, aromatic), 7.99 (s, 1H, C_2-H), and 8.31 (dd, 1H, C_5-H, δ=8.4 and 1.8 Hz); MS, Found: m/z 236.0838, Calcd for $C_{16}H_{12}O_2$: M, 236.0838.

4′-Methoxyisoflavone: Mp 141—142 °C; IR (KBr) 1630 cm^{-1} (C=O); ^1H NMR ($CDCl_3$) δ=3.84 (s, 3H, OCH_3), 6.92—7.77 (m, 7H, aromatic), 7.99 (s, 1H, C_2-H), and 8.31 (dd, 1H, C_5-H, J=7.5 and 1.9 Hz); MS, Found: m/z 252.0782, Calcd for $C_{16}H_{12}O_3$: M, 252.0787.

2′-Methylisoflavone: Mp 113.5—114.0 °C; IR (KBr) 1640 cm^{-1} (C=O); ^1H NMR ($CDCl_3$) δ=2.26 (s, 3H, CH_3), 7.08—7.80 (m, 7H, aromatic), 7.87 (s, 1H, C_2-H), and 8.30 (dd, 1H, C_5-H, J=7.6 and 1.4 Hz); MS, Found: m/z 236.0821, Calcd for $C_{16}H_{12}O_2$: M, 236.0837.

6-Chloroisoflavone: Mp 186.0—186.5 °C; IR (KBr) 1635 cm^{-1} (C=O); ^1H NMR ($CDCl_3$) δ=7.37—7.69 (m, 7H, aromatic), 8.01 (s, 1H, C_2-H), and 8.26 (d, 1H, C_5-H, J=2.4 Hz); MS, Found m/z 256.0276. Calcd for $C_{15}H_9ClO_2$: M, 256.0292.

6-Methoxyisoflavone: Mp 172—173 °C; IR (KBr) 1625 cm^{-1} (C=O); ^1H NMR ($CDCl_3$) δ=3.91 (s, 3H, OCH_3), 7.19—7.64 (m, 7H, aromatic), 7.68 (d, 1H, C_5-H, δ=2.4 Hz), and 8.00 (s, 1H, C_2-H); MS, Found: m/z 252.0797, Calcd for $C_{16}H_{12}O_3$: M, 252.0787.

4′-Fluoroisoflavone: Mp 192.0—192.5 °C; IR (KBr) 1630 cm^{-1} (C=O); ^1H NMR ($CDCl_3$) δ=7.02—7.79 (m, 7H, aromatic), 7.99 (s, 1H, C_2-H), and 8.30 (dd, 1H, C_5-H, J=7.4 and 1.8 Hz); MS, Found: m/z 240.0583, Calcd for $C_{15}H_9FO_2$: M, 240.0587.

4′-Nitroisoflavone: Mp 202—204 °C; IR (KBr) 1640 cm^{-1} (C=O); ^1H NMR ($CDCl_3$) δ=7.38—8.46 (m, 8H, aromatic), and 8.13 (s, 1H, C_2-H); MS, Found: m/z 267.0533, Calcd for $C_{15}H_9NO_4$: M, 267.0532.

2′,3′-Benzoisoflavone: Mp 107.5—108.0 °C; IR (KBr) 1630 cm^{-1} (C=O); ^1H NMR ($CDCl_3$) δ=7.35—7.96 (m, 10H, aromatic), 8.00 (s, 1H, C_2-H), and 8.34 (dd, 1H, C_5-H, J=7.9 and 1.5 Hz); MS, Found: m/z 272.0818, Calcd for $C_{19}H_{12}O_2$: M, 272.0837.

2′,4′,6′-Trimethylisoflavone: Mp 105.5—106.0 °C; IR (KBr) 1635 cm^{-1} (C=O); ^1H NMR ($CDCl_3$) δ=2.13 (s, 6H, 2′-CH_3 and 6′-CH_3), 2.31 (s, 3H, 4′-CH_3), 6.94 (s, 2H, C_3-H, C_5-H), 7.24—7.80 (m, 3H, aromatic), 7.75 (s, 1H, C_2-H), and 8.28 (dd, 1H, C_5-H, J=7.8 and 1.8 Hz); MS, Found: m/z 264.1131, Calcd for $C_{18}H_{16}O_2$: M, 264.1151.

General Procedure. A 25 mL two-necked round-bottomed flask equipped with a reflux condenser, a septum inlet, and a magnetic stirring bar, was charged with 3-bromochromone (2.0 mmol), phenylboronic acid (2.2 mmol), and $Pd(PPh_3)_4$ (0.072 g, 0.06 mmol). The flask was flushed with nitrogen and filled with 4 ml of dry benzene and 2 ml of aqueous 2 M-Na_2CO_3 solution through the septum inlet with a syringe. For the reaction under nonaqueous conditions, dibutyl arylboronate (2.2 mmol) and powdered Tl_2CO_3 (2 mmol) were

used in place of phenylboronic acid and aqueous Na_2CO_3 solution. The mixture was refluxed in an oil bath with stirring. At suitable time intervals, a part of the reaction solution was sampled with a microsyringe and was subjected to GLC analysis. After the reaction was complete, the flask was cooled to room temperature. The product was extracted with benzene, washed with brine, and dried over anhydrous magnesium sulfate. Finally the product was isolated by silica gel column chromatography using a mixture of benzene, dichloromethane, and ether (2:2:1) as an eluent, followed by recrystallization from a mixture of hexane and a small amount of benzene.

References

1) A. McKillop, B. P. Swann, and E. C. Taylor, *Tetrahedron Lett.*, **1970**, 5281; W. D. Ollis, K. L. Ormand, B. T. Redman, R. J. Roberts, and T. O. Sutherland, *J. Chem. Soc.*, **1970**, 125; L. Farkas and A. Wolfner, *Magy. Kem. Foly.*, **81**, 357 (1975); *Chem. Abstr.*, **83**, 178725s (1975).

2) A. C. Jain, P. Lal, and T. R. Seshadri, *Indian J. Chem.*, **7**, 305 (1969).

3) L. A. Paquette and H. Stucki, *J. Org. Chem.*, **31**, 1232 (1966).

4) N. Miyaura, T. Yanagi, and A. Suzuki, *Synth. Commun.*, **11**, 513 (1981).

5) a) S. Gronowitz and K. Lawitz, *Chem. Scripta*, **22**, 265 (1983); b) W. J. Tompson and J. Gaudino, *J. Org, Chem.*, **49**, 5237 (1984); c) M. J. Sharp, W. Cheng, and V. Snieckus, *Tetrahedron Lett.*, **28**, 5093 (1987); d) R. B. Miller and S. Duger, *Organometallics*, **3**, 1261 (1984).

6) Very recently, Kishi and his co-workers reported that TlOH accelerates the cross-coupling reaction of 1-alkenylboronic acids in the presence of palladium catalyst; J. Uenishi, J-M. Beau, R. W. Armstrong, and Y. Kishi, *J. Am. Chem. Soc.*, **109**, 4759 (1987).

7) H. Simonis, *Ber.*, **50**, 779 (1915).

8) N. Miyaura, K. Yamada, H. Suginome, and A. Suzuki, *J. Am. Chem. Soc.*, **107**, 972 (1985).

9) D. R. Coulson, *Inorg. Synth.*, **13**, 121 (1972).

10) F. R. Bean and J. R. Johnson, *J. Am. Chem. Soc.*, **54**, 4415 (1932).

11) G. E. K. Branch, D. L. Yabroff, and B. Bettman, *J. Am. Chem. Soc.*, **56**, 1865 (1934).

12) K. Smith, "Organometallic Compounds of Boron," Chapman and Hall, London (1985), p. 118.

13) R. T. Hawkins, W. J. Lennarr, and H. R. Snyder, *J. Am. Chem. Soc.*, **82**, 3053 (1960).

14) T. Onak, "Organoborane Chemistry," Academic Press, New York (1975), p. 222.

15) R. B. Gammill, *Synthesis*, **1979**, 901.

Ruthenium Complex-Catalyzed Silylation of Olefins. Selective Synthesis of Allylsilanes

Yoji HORI, Take-aki MITSUDO,* and Yoshihisa WATANABE*
Department of Hydrocarbon Chemistry, Faculty of Engineering, Kyoto University, Kyoto 606
(Received March 11, 1988)

Synopsis. (1-2;5-6-η-Cyclooctadiene)(1-6-η-cyclooctatriene)ruthenium catalyzes the silylation of olefins at 60—140 °C to give allylsilanes with good selectivity in high yields. The reactions of trialkylsilane with 2-methyl-1-butene, 2-methyl-2-butene, and 3-methyl-1-butene give the same product, 3-methyl-1-trialkylsilyl-2-butene. Silylation of ethyl (*E*)-2-butenoate gives ethyl (*E*)-4-trialkylsilyl-2-butenoate in high yield.

Allylsilanes are highly versatile synthetic intermediates.[1] Allylsilanes are prepared by 1) the reaction of allyl chloride with copper-silicon powder at 250 °C,[2-4] 2) Ni or Pd complex-catalyzed reactions of dienes with disilanes,[5-7] 3) hydrosilylation of dienes,[8-11] 4) dissolving metal reductions of aromatic hydrocarbons,[12] 5) Wittig reactions,[13-16] 6) silylation of allylic organometallics.[17,18] Recently, Seki et al. reported the preparation of vinylsilanes and allylsilanes from olefins and triethylsilane catalyzed by $[Ru_3(CO)_{12}]$.[19] In the course of our study on the organic syntheses catalyzed by (1-2;5-6-η-cyclooctadiene)(1-6-η-cyclooctatriene)ruthenium(0) [Ru(cod)(cot)] and its derivatives,[20] we found that Ru(cod)(cot) catalyzes the selective silylation of olefins which provides a versatile method of the preparation of allylsilanes.

Results and Discussion

Triethylsilane and diethylmethylsilane readily reacted with 2-methyl-1-butene, 2-methyl-2-butene, 3-methyl-1-butene, 1-hexene, and ethyl (*E*)-2-butenoate in the presence of a catalytic amount of Ru(cod)(cot) at 60—140 °C to give the corresponding allylsilanes selectively. The results are summarized in Table 1.

The reactions of triethylsilane with 2-methyl-1-butene, 2-methyl-2-butene, or 3-methyl-1-butene gave 1-triethylsilyl-3-methyl-2-butene (**1**) as a major product in yields of 39—61% with 78—81% selectivity (Table 1, Runs 1—4). The minor products were regioisomers of **1**, (*E*)- and (*Z*)-1-trialkylsilyl-2-methyl-2-butene. Diethylmethylsilane also reacted with 2-methyl-2-butene to give 1-diethylmethylsilyl-3-methyl-2-butene (**2**) in a yield of 65% with 86% selectivity (Run 5). In all the reactions shown in Eq. 1, only small

Table 1. Selective Synthesis of Allylsilanes Catalyzed by Ru(cod) (cot)[a]

Run	Olefin	Silane	Temp °C	Time h	Total yield[b,c] %	Product yield of **1**,**2**,**4**,**6**, or **7**/%[c]
1		$HSiEt_3$	60	5	72	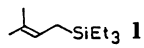 **1** 56
2		$HSiEt_3$	80	2	76	**1** 59
3		$HSiEt_3$	80	2	75	**1** 61
4		$HSiEt_3$	80	2	49	**1** 39
5		$HSiEt_2Me$	80	2	(76)	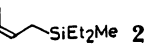 **2** 65
6		$HSiEt_3$	80	7	82	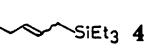 **4** 67(*E*/*Z*=65/35)
7		$HSiEt_3$	140	0.5	(81)	**4** 66(*E*/*Z*=65/35)
8		$HSiEt_3$	80	2	(74)	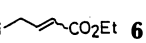 **6** 63(*E*/*Z*=91/9)
9		$HSiEt_2Me$	80	2	(74)	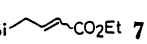 **7** 66(*E*/*Z*=92/8)

a) Silane (10 mmol), olefin (50 mmol), catalyst (0.1 mmol). b) Total yield of silylated olefins. c) GLC yield (isolated yield based on the amount of hydrosilane).

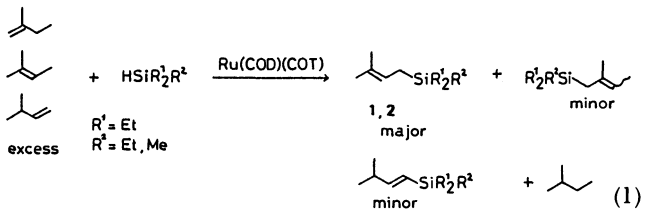

(1)

amounts of vinylsilanes were detected. Though Seki et al. reported that $[Ru_3(CO)_{12}]$ is an effective catalyst for the synthesis of vinylsilanes from olefins and hydrosilanes,[19] they did not mention the silylation of 2-methylbutenes. Several allylsilanes can be prepared by hydrosilylation catalyzed by Pd[8] and Rh[10] complexes. We confirmed that, in the presence of a catalytic amount of $[Ru_3(CO)_{12}]$, the reaction of triethylsilane with 3-methyl-1-butene gave (*E*)-1-triethylsilyl-3-methyl-1-butene (**3**) and **1** in yields of 60 and 30% respectively (Eq. 2). However, $[Ru_3(CO)_{12}]$ does not catalyze the reaction of triethylsilane with 2-methyl-1-butene and with 2-methyl-2-butene at 80 °C for 2 h; only the starting materials were recovered.

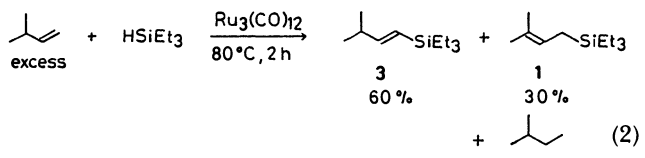

(2)

1-Hexene reacted with triethylsilane in the presence of Ru(cod)(cot) to give the product **4** in a yield of 67% (*E*/*Z*=65/35) with 82% selectivity (Run 6). (*E*)-1-Triethylsilyl-1-hexene (**5**) was also obtained in 15% yield. This result is almost the same as that of $[Ru_3(CO)_{12}]$-catalyzed reaction reported.[19] The reaction of triethylsilane with 1-hexene was rapid at 140 °C (Run 7). The yield and selectivity of products were the same as those in the reaction at 80 °C for 7 h (Runs 6, 7).

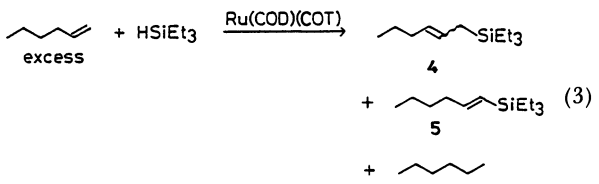

(3)

The reaction of ethyl (*E*)-2-butenoate with triethylsilane and with diethylmethylsilane gave the products **6** and **7** in yields of 63% (*E*/*Z*=91/9) and 66% (*E*/*Z*=92/8) with 85 and 89% selectivities (Runs 8, 9), respectively.

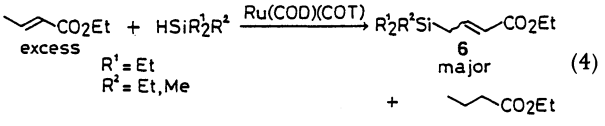

(4)

In these reactions, hydrogen did not evolve. In the reaction of ethyl (*E*)-2-butenoate, ethyl butanoate was formed in 92% yield based on triethylsilane.

When a catalytic amount of phosphorus ligands such as triphenylphosphine, tributylphosphine, triphenyl phosphite, and triethyl phosphite were added to the reaction mixture, no reaction occurred and starting materials, triethylsilane and olefins, were recovered. Dichlorotris(triphenylphosphine)ruthenium(II) $[RuCl_2(PPh_3)_3]$ was inactive in the reaction of triethylsilane with 2-methyl-2-butene. Silanes such as trimethoxysilane, triisopropylsilane, and dimethylphenylsilane, reacted with olefins. However, these reactions were very slow and only a trace amounts of the corresponding products were detected.

We consider the mechanism of the present reaction which is substantially the same as the $[Ru_3(CO)_{12}]$-catalyzed synthesis of vinylsilanes[19] except two features. The first one is a rapid equilibrium among three C_5 olefins, 2-methyl-1-butene, 2-methyl-2-butene, and 3-methyl-1-butene shown in Eq. 5. Probably a

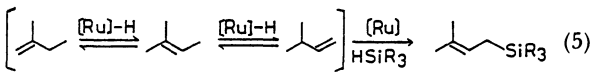

(5)

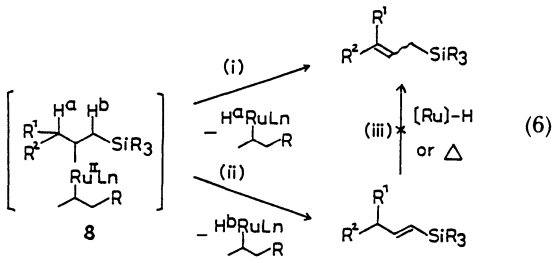

(6)

catalytic amount of ruthenium hydride causes the isomerization of the double bond, then the silylation would occur. The second concerns a β-elimination step from an intermediate **8**[19] (Eq. 6). When two possible paths of β-elimination are considered in the last step of the present reaction, the path (i) would occur predominantly. The possibility of the isomerization of **3** to **1** was investigated. The reaction of a mixture of **3** and **1** (ratio **3**/**1**=68/32) in hexane was carried out in the presence of a catalytic amount of Ru(cot)(cod) and $HSiEt_3$ at 80 °C for 2 h; slight isomerization occurred (ratio **3**/**1**=54/46); however, the rate of the isomerization of vinylsilane to allylsilane (path (iii)) was very slow. Thus the product distribution would be determined by the direction of the β-elimination of **8**.

Experimental

All boiling points were uncorrected. Infrared spectra were recorded on a NICOLET 5-MX FT-IR spectrometer as films. Proton nuclear magnetic resonance spectra were obtained on a JNM-FX-90 spectrometer as 5—10% solutions with tetramethylsilane as an internal reference. Carbon-13 nuclear magnetic resonance spectra were obtained on a JNM-FX-100 (25.05 MHz) spectrometer as 40—50% solutions with tetramethylsilane and $CDCl_3$ as internal references. Mass spectra were taken on a Shimadzu QP-1000 GC-Mass spectrometer. Microanalyses were performed by the Laboratory for Organic Elemental Microanalysis of Kyoto University. Gas chromatographic analysis (GLC) were carried out on a 3 m×3 mm diameter column with OV 17 or a 2.9 m×3 mm diameter column with DEGA. All olefins, hydrosilanes, phosphines, and $[Ru_3(CO)_{12}]$ were commercial samples and were purified by distillation or by recrystallization under an atmosphere of argon before use. The complexes, Ru(cot)(cot)[21] and $[RuCl_2(PPh_3)_3]$[22] were prepared by the reported

methods. All catalytic reactions were carried out under an atmosphere of argon.

General Reaction Procedure. The reaction of triethylsilane with ethyl (*E*)-2-butenoate is representative. A mixture of triethylsilane (1.16 g, 10 mmol), ethyl (*E*)-2-butenoate (5.71 g, 50 mmol), and Ru(cod)(cot) (0.032 g, 0.1 mmol) was heated in a 50 cm^3 autoclave at 80 °C for 2 h. Careful vacuum distillation of the reaction mixture afforded 1.69 g (yield 74%) of ethyl 4-triethylsilyl-2-butenoate (**5**). Other reactions were carried out in a similar manner. Allylsilanes (**4** and **5**) are known compounds.[19]

1-Triethylsilyl-3-methyl-2-butene (1). Colorless liquid, bp 95 °C (22 mmHg) (1 mmHg=133.322 Pa); IR (neat) 1665 cm^{-1}; ^1H NMR ($CDCl_3$) δ=5.14 (1H, tqq, J=8.4 and 1.4 Hz), 1.68 (3H, s), 1.58 (3H, s), 1.41 (2H, d, J=8.4 Hz), 0.85—1.05 (9H, m), and 0.43—0.68 (6H, m); ^{13}C NMR ($CDCl_3$) δ=128.2 (s), 120.1 (d), 25.7 (q), 17.4 (q), 13.4 (t), 7.3 (q), and 3.3 (t). MS m/z: 184 (M^+). Found: C, 71.38; H, 13.37%. Calcd for $C_{11}H_{24}Si$: C, 71.65; H, 13.12%.

1-Diethylmethylsilyl-3-methyl-2-butene (2). Colorless liquid, bp 77 °C (22 mmHg); IR (neat) 1667 cm^{-1}; ^1H NMR ($CDCl_3$) δ=5.13 (1H, thep, J=8.5 and 1.3 Hz), 1.68 (3H, s), 1.56 (3H, s), 1.40 (2H, J=8.5 Hz, d), 0.84—1.04 (6H, m), 0.34—0.62 (4H, m), and −0.08 (3H, s); ^{13}C NMR($CDCl_3$) δ=128.2 (s), 120.0 (d), 25.7 (q), 17.4 (q), 15.2 (t), 7.2 (q), 5.1 (t), and −6.3 (q). MS m/z: 170 (M^+). Found: C, 70.65; H, 13.31%. Calcd for $C_{10}H_{22}Si$: C, 70.50; H, 13.02%.

1-Triethylsilyl-3-methyl-1-butene (3). Colorless liquid, bp 80 °C (22 mmHg); IR (neat) 1615 cm^{-1}; ^1H NMR ($CDCl_3$) δ=6.03 (1H, dd, δ=18.9 and 5.8 Hz), 5.45 (1H, dd, J=18.9 and 1.1 Hz), 2.25 (1H, m), 0.99 (6H, d, J=6.8 Hz), 0.84—1.04 (9H, m), and 0.36—0.67 (6H, m); ^{13}C NMR($CDCl_3$) δ=155.3 (d), 121.4 (d), 34.8 (d), 22.1 (q), 7.5 (q), and 3.9 (t). MS m/z: 184 (M^+). Found: C, 71.37; H, 13.38%. Calcd for $C_{11}H_{24}Si$: C, 71.65; H, 13.12%.

Ethyl (*E*)-4-Triethylsilyl-2-butenoate (6). Colorless liquid, bp 97 °C (2 mmHg); IR (neat) 1722 and 1644 cm^{-1}; ^1H NMR ($CDCl_3$) δ=7.07 (1H, td, J=9.0 and 15.4 Hz), 5.67 (1H, dt, J=15.4 and 1.3 Hz), 4.16 (2H, q, J=7.0 Hz), 1.76 (2H, dd, J=9.0 and 1.3 Hz), 1.28 (3H, t, J=7.0 Hz), 0.86—1.07 (9H, m), and 0.41—0.69 (6H, m); ^{13}C NMR ($CDCl_3$) δ=166.3 (s), 147.6 (d), 118.9 (d), 59.7 (t), 19.8 (t), 14.4 (q), 7.3 (q), and 3.3 (t). MS m/z: 228 (M^+). Found: C, 63.24; H, 10.76%. Calcd for $C_{12}H_{24}O_2Si$: C, 63.10; H, 10.59%.

Ethyl (*E*)-4-Diethylmethylsilyl-2-butenoate (7). Colorless liquid, bp 94 °C (3 mmHg); IR (neat) 1721 and 1644 cm^{-1}; ^1H NMR ($CDCl_3$) δ=6.96 (1H, dt, J=15.4 and 9.0 Hz), 5.57 (1H, dt, J=15.4 and 1.3 Hz), 4.06 (2H, q, J=7.2 Hz), 1.64 (2H, dd, J=9.0 and 1.3 Hz), 1.17 (3H, t, J=7.2 Hz), 0.70—0.96 (6H, m), 0.30—0.64 (4H, m), −0.10 (3H, s); ^{13}C NMR ($CDCl_3$) δ=165.4 (s), 146.6 (d), 118.5 (d), 58.8 (t), 20.5 (t), 13.6 (q), 6.4 (q), 4.2 (t), −7.1 (q). MS m/z: 214 (M^+). Found: C, 61.35; H, 10.64%. Calcd for $C_{11}H_{22}O_2Si$: C, 61.63; H, 10.34%.

References

1) For review, see: W. P. Weber, "Silicon Reagents for Organic Synthesis," Springer-Verlag, Berlin (1983), p. 173.
2) D. T. Hurd, *J. Am. Chem. Soc.*, **67**, 1813 (1945).
3) Rhone-Poulenc, French Patent 2051903 (1969).
4) N. Furuya and T. Sukawa, *J. Organomet. Chem.*, **96**, C-1 (1975).
5) M. Lefort, C. Simmonet, M. Birot, G. Deleris, J. Dunogues, and R. Calas, *Tetrahedron Lett.*, **21**, 1857 (1980).
6) H. Matsumoto, T. Yako, S. Nagashima, T. Motegi, and Y. Nagai, *J. Organomet. Chem.*, **148**, 97 (1978).
7) H. Watanabe, M. Saito, N. Sutou, and Y. Nagai, *J. Chem. Soc., Chem. Commun.*, **1981**, 617.
8) J. Tsuji, M. Hara, and K. Ohno, *Tetrahedron*, **30**, 2143 (1974).
9) J. P. Pillot, G. Deleris, J. Dunogues, and R. Calas, *J. Org. Chem.*, **44**, 3397 (1979).
10) I. Ojima and M. Kumagai, *J. Organomet. Chem.*, **157**, 359 (1978); I. Ojima, M. Kumagai, and Y. Miyazawa, *Tetrahedron Lett.*, **21**, 1385 (1980).
11) H. Matsumoto, K. Shono, A. Wada, I. Matsubara, H. Watanabe, and Y. Nagai, *J. Organomet. Chem.*, **199**, 185 (1980).
12) M. Laguerre, J. Dunogues, R. Calas, and N. Duffaut, *J. Organomet. Chem.*, **112**, 49 (1976).
13) I. Fleming and I. Paterson, *Synthesis*, **1979**, 446.
14) D. Seyferth, K. R. Wursthorn, T. F. O. Lim, and D. J. Sepelak, *J. Organomet. Chem.*, **181**, 293 (1979).
15) G. D. Cooper and M. Prober, *J. Am. Chem. Soc.*, **76**, 3943 (1954).
16) A. Gopalan, R. Moerck, and P. Magnus, *J. Chem. Soc., Chem. Commun.*, **1979**, 548.
17) A. Hosomi and H. Sakurai, *Tetrahedron Lett.*, **1978**, 2589.
18) D. Seyferth, G. J. Murphy, and R. A. Woodruff, *J. Organomet. Chem.*, **141**, 71 (1977).
19) Y. Seki, K. Takeshita, K. Kawamoto, S. Murai, and N. Sonoda, *J. Org. Chem.*, **51**, 3890 (1986).
20) T. Mitsudo, Y. Hori, and Y. Watanabe, *J. Organomet. Chem.*, **334**, 157 (1987) and references cited therein; T. Mitsudo, Y. Hori, Y. Yamakawa, and Y. Watanabe, *J. Org. Chem.*, **52**, 2230 (1987); T. Mitsudo, Y. Hori, Y. Yamakawa, and Y. Watanabe, *Tetrahedron Lett.*, **28**, 4417 (1987).
21) K. Itoh, H. Nagashima, T. Ohshima, N. Ohshima, and H. Nishiyama, *J. Organomet. Chem.*, **272**, 179 (1984).
22) P. S. Hallman, T. A. Stephenson, and G. Wilkinson, *Inorg. Synth.*, **12**, 237 (1970).

Yeast-Mediated Reduction of *N*-Substituted Acetoacetamides. Improvement of Conversion by Immobilization

Masao KAWAI, Kenji TAJIMA, Satoko MIZUNO, Koichi NIIMI, Hiroaki SUGIOKA, Yasuo BUTSUGAN,* Akimasa KOZAWA,† Tsuneo ASANO,† and Yoshio IMAI†

Department of Applied Chemistry, Nagoya Institute of Technology, Gokiso-cho, Showa-ku, Nagoya 466
†Inoue MTP Co. Ltd., 3-1-36 Imaike-cho, Anjo-shi, Aichi 446

(Received March 24, 1988)

Synopsis. *N*-Ethylacetoacetamide and acetoacetanilide were enantioselectively converted into the corresponding (*S*)-3-hydroxy compounds by alginate- or polyurethane-immobilized bakers' yeasts, while without immobilization the yield of the yeast-mediated reaction was very low.

Microbial transformations of organic molecules are useful for the preparation of chiral compounds. One of the most intensively studied reactions is bakers' yeast-mediated conversion of β-keto esters into the corresponding optically active 3-hydroxy compounds. While ethyl acetoacetate (**1**) is reduced by bakers' yeast to afford ethyl (*S*)-3-hydroxybutanoate (**2**) possessing high optical purity,[1] chemical and optical yields of reactions of analogs of **1** fluctuate widely. Improvement of stereoselectivity of the microbial reduction of the analogs of **1** by chemical modification of the substrates[2] and stereochemical control of the reaction by the use of immobilized yeast[3,4] were described. In this note we will report microbial reduction of *N*-substituted acetoacetamides into the corresponding

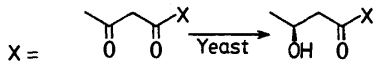

X =		
OEt	**1**	**2**
NHEt	**3**	**4**
NHPh	**5**	**6**

alcohols and marked enhancement of the conversion by immobilizing bakers' yeast.

Bakers' yeast is commercially available in the form either of dried granules or of freshly prepared cake. The former is more convenient since it is stable and can be stored without significant deterioration. Microbial reduction of *N*-ethylacetoacetamide (**3**), a nitrogen analog of **1** was attempted using granular bakers' yeast. Under the conditions which assured efficient conversion of **1** to **2**, however, the amide **3** failed to give the corresponding alcohol, *N*-ethyl-3-hydroxybutanamide (**4**). Acetoacetanilide (**5**) was then subject to examination as a substrate of yeast-mediated reduction because of the ease of detection by TLC and separation of the expected reduction product, 3-hydroxybutananilide (**6**), as well as the unchanged **5**. Incubation of **5** for 7 days with fermenting yeast derived from granular dry yeast did not give the reduction product **6** but resulted in the recovery of **5** in 90% yield. When fresh yeast was used instead of dry yeast, however, the hydroxy derivative **6** was obtained in 11% yield. Brewers' yeast was also able to reduce **5** though in low yield (2%). Cultivated suspension of a strain, *Saccharomyces cerevisiae* H-194, was found to convert **5** into **6** in higher yield (48%) as given in Table 1.

The results described above leads to the following suggestion. The apparent inability of the dry bakers'

Table 1. Chemical Yield and Optical Purity of Yeast-Mediated Reduction of *N*-Substituted Acetoacetamides

Method of microbial reduction	Yield of reduction product (%)	e.e. of product estimated by ^{1}H NMR (%)	Recovery of unchanged substrate (%)
Transformation of **3** to **4**			
bakers' yeast (dry), suspension	0		82
bakers' yeast (fresh), suspension	0		90
S. cerevisiae H-194, growing culture	0		90
bakers' yeast (dry), immobilized by alginate	9	90—95	54
brewers' yeast, immobilized by alginate	8		51
bakers' yeast (dry), immobilized by polyurethane	9		37
Transformation of **5** to **6**			
bakers' yeast (dry), suspension	0		90
bakers' yeast (fresh), suspension	11		55
brewers' yeast, suspension	2		90
S. cerevisiae H-194, growing culture	48	>90	44
bakers' yeast (dry), immobilized by alginate	36	>95	46
bakers' yeast (fresh), immobilized by alginate	21	>98	53
brewers' yeast, immobilized by alginate	8		75
bakers' yeast (dry), immobilized by polyurethane	28	84	45
bakers' yeast (dry), immobilized by polyurethane containing alginate as an additive	27	80	42
baker's yeast (dry), immobilized by polyurethane containing chitosan as an additive	31	79	46

yeast simply implies a low rate of the reaction and modification of the environment might improve the situation. Thus, attempts have been made to use the bakers' yeast in immobilized form. In fact, treatment of **5** with the dry yeast entrapped in calcium alginate gel[4,5] yielded **6** in 36% yield clearly demonstrating the effect of immobilization. The *N*-ethylamide **3** was also reduced by the alginate-immobilized yeast affording a 9% yield of **4**.

The optical purities of the reduction products, **4** and **6**, were determined by ^{1}H NMR spectral analysis using chiral shift reagents. The reduction was shown to proceed with considerably high stereoselectivity (>90% e.e.) as shown in Table 1. For the purpose of determining the absolute configuration of the hydroxyl group, **4** and **6** were converted into the *O*-benzoyl derivatives. The CD spectra of the benzoates showed the same sign of Cotton effects as those of the authentic compounds having *S*-configuration which were prepared from **2**, establishing the stereochemistry of **4** and **6**.

Microbial reduction of the acetoacetamides **3** and **5** was also studied using polyurethane-immobilized yeast.[6] Paste made of dry yeast and water was admixed with a prepolymer to yield the immobilized yeast entrapped in foaming polyurethane. The polyurethane-immobilized yeast was also found to convert **3** and **5** into the hydroxy compounds **4** and **6** in 9 and 28% yields, respectively. The optical purity of the product, however, was slightly lower than that using alginate-immobilized yeast. Modification of the nature of the polyurethane foams were attempted by the addition of acidic and basic polysaccharides, alginate and chitosan, respectively. But, essentially the same results were obtained as those without polysaccharide additives.

The results are all summarized in Table 1. The starting material, **3** or **5**, was recovered in 37 to 90% yield. Use of a larger amount of yeast can be expected to improve the chemical yield of the product, but was not undertaken in the present study. During the microbial reduction glucose was added daily, which may not be necessary when the reduction proceeded slowly.

In summary, acetoacetamides were enantioselectively reduced by bakers' yeast to the corresponding hydroxy derivatives in much lower yield than acetoacetic esters. However, improvement in conversion yield was attained by immobilization of the yeast with calcium alginate gel or polyurethane foam.

Experimental

^{1}H NMR spectra were recorded on a HITACHI R-24A (60 MHz) or on a Varian XL-200 (200 MHz) spectrometer. UV and CD spectra were measured in MeOH solutions with HITACHI 124 spectrophotometer and JASCO J-40C spectropolarimeter, respectively.

Dry granular yeast ("Active Dry Yeast", S. I. LeSaffre Co.) and fresh bakers' yeast (Oriental Yeast Co.) used in the study are commercially available. *S. cerevisiae* H-194 strain was provided by Professor N. Gunge of The Kumamoto Institute of Technology.

Preparation of Immobilized Yeast. Immobilization by calcium alginate gel was done following the reported procedure.[4] Polyurethane-immobilized bakers' yeast was prepared as follows: Prepolymer (20 g) containing ca. 2 mmol g^{-1} of free NCO group prepared from polyethylene oxide (mol wt ca. 1000) and methylphenylenediisocyanate was added to an intimate mixture of dry bakers' yeast (6.5 g) and H_2O (13 cm^3) and was stirred vigorously for 20 s. After standing for 1 h the resulting polyurethane foam (ca. 200 cm^3) was cut into pieces and washed with water. For the cases with polysaccharide additives, sodium alginate (83 mg) in H_2O (2.6 cm^3) or chitosan (86 mg) in 0.2 mol dm^{-3} AcOH aq (8 cm^3) was added to the yeast-H_2O mixture before the prepolymer addition.

Yeast-Mediated Reductions of Acetoacetamides. *N*-Ethyl-3-oxobutanamide (**3**) was prepared from diketene and ethylamine according to the literature.[7] Typical procedures for the microbial reductions of **3** and **5** are described below.

Reduction of 5 with Fresh Bakers' Yeast: A suspension of fresh bakers' yeast (20 g) in H_2O (125 cm^3) containing D-glucose (15 g) was preincubated at 30 °C for 1 h. A solution of **5** (708 mg) in EtOH (5 cm^3) was added to the suspension and the mixture was shaken at 30 °C for 7 d with daily addition of D-glucose (10 g).

Reduction of 3 with Alginate-Immobilized Bakers' Yeast: Calcium alginate-immobilized bakers' yeast, prepared from dry bakers' yeast (4.2 g) and sodium alginate (4.2 g),[4] and D-glucose (9 g) in H_2O (75 cm^3) were shaken at 30 °C for 1 h. A solution of **3** (774 mg) in EtOH (4 cm^3) was added to the mixture and shaking was continued at 30 °C for 7 d with daily addition of D-glucose (9 g).

Reduction of 5 with Polyurethane-Immobilized Bakers' Yeast: The immobilized yeast prepared from dry bakers' yeast (6.5 g) and prepolymer (20 g) was immersed in the mixture of **5** (992 mg) in EtOH (25 cm^3) and D-glucose (12 g) in H_2O (225 cm^3). The mixture was shaken at 30 °C for 7 d with daily addition of D-glucose (8 g).

Reduction of 5 with *S. cerevisiae* H-194: Sterilized culture medium (pH 5.5) comprising yeast extract (1.25 g), peptone (2.5 g), D-glucose (2.5 g), and H_2O (120 cm^3) was inoculated with *S. cerevisiae* H-194 and cultured at 30 °C for 2 d. The substrate **5** (124 mg) in EtOH (1 cm^3) was added to the culture and incubated further for 7 d with daily addition of D-glucose (7.5 g).

Extraction and Identification of the Products: The incubation mixture was filtered with the aid of celite when necessary, and the filtrate was extracted with Et_2O, AcOEt, and/or $CHCl_3$. The residue was washed with the same solvent and the washings were combined with the extract. The starting material and the reduction product were isolated by SiO_2 column chromatography ($CHCl_3$–MeOH) of the extract and were characterized by ^{1}H NMR spectra without further purification. The authentic samples of the racemic forms of **4** and **6** for the NMR and TLC comparisons were prepared from 3-butanolide by treatment with $EtNH_2$[8] and from **5** by $NaBH_4$ reduction,[9] respectively.

Determination of Optical Purity and Absolute Configuration. The optical purities of **4** and **6** were determined by 200 MHz ^{1}H NMR chiral shift studies using (+)-tris[bis-[perfluoro(2-propoxypropionyl)]methanate]europium(III) and tris[3-(heptafluoropropylhydroxymethylene)-*d*-camphorato]europium(III), respectively, in $CDCl_3$ solutions.

(*S*)-3-Benzoyloxy-*N*-ethylbutanamide: Ethyl (*S*)-3-hydroxybutanoate (**2**, 528 mg), prepared by the microbial reduction of **1** using fresh bakers' yeast, was benzoylated with benzoyl chloride (1 g) and pyridine (1 cm^3) at 0 °C for 1 h. Usual work-up and SiO_2 column chromatography ($CHCl_3$) afforded ethyl (*S*)-3-(benzoyloxy)butanoate (660 mg) as a colorless oil: ^{1}H NMR (CCl_4) δ=1.13 (3H, t, J=7 Hz), 1.36 (3H, d, J=6 Hz), 2.53 (1H, dd, J=15 and 6 Hz), 2.65 (1H, dd, J=15 and 6 Hz), 4.02 (2H, q, J=7 Hz), 5.36 (1H, hexad, J=6 Hz), 7.4 (3H, m), and 7.9 (2H, m). The benzoate (354 mg) in MeOH (4 cm^3) and 1 mol dm^{-3} NaOH aq (1.28 cm^3) was

stirred at 0 °C for 1 h. The mixture was acidified with HCl aq, evaporated, and extracted with $CHCl_3$ to afford crude (*S*)-3-(benzoyloxy)butanoic acid (200 mg). The free acid, without purification, was dissolved in $SOCl_2$ (1 cm^3) and stirred for 1 h. After evaporation of $SOCl_2$ the resulting acid chloride was dissolved in $CHCl_3$ and a solution of $EtNH_2$ in Et_2O was added until the mixture became alkaline towards moistened litmus paper. Usual work-up and preparative TLC (SiO_2, 5% MeOH/$CHCl_3$) gave (*S*)-3-benzolyoxy-*N*-ethylbutanamide (50 mg): mp 58 °C; ^1H NMR (CCl_4) δ=1.03 (3H, t, J=7 Hz), 1.35 (3H, d, J=6 Hz), 2.46 (1H, dd, J=13 and 6 Hz), 2.62 (1H, dd, J=13 and 6 Hz), 3.15 (2H, quint, J=6 Hz), 5.40 (1H, hexad, J=6 Hz), 7.3 (3H, m), 7.5 (1H, br s), and 7.9 (2H, m); UV 227 nm (ε 12500); CD $[\theta]_{225}$ −4300. Anal. ($C_{13}H_{17}NO_3$) C, H, N.

(*S*)-3-Benzoyloxy-*N*-phenylbutanamide: To an ice-cooled solution of (*S*)-3-(benzoyloxy)butanoic acid (100 mg) and aniline (137 mg) in $CHCl_3$ (4 cm^3) were added dicyclohexylcarbodiimide (206 mg) and 1-hydroxybenzotriazole (32 mg) and stirred for 1 h at 0 °C and for 1 d at room temperature. Usual work-up and SiO_2 column chromatography ($CHCl_3$) afforded (*S*)-3-benzolyoxy-*N*-phenylbutanamide (65 mg) as colorless crystals: mp 116 °C; ^1H NMR ($CDCl_3$) δ=1.38 (3H, d, J=7 Hz), 2.64 (1H, dd, J=14 and 7 Hz), 2.78 (1H, dd, J=14 and 7 Hz), 5.56 (1H, hexad, J=7 Hz), 7.1—7.9 (10H, m), and 8.6 (1H, br s); UV 232 nm (ε 25000); CD $[\theta]_{242}$ +22000, $[\theta]_{225}$ −17000. Anal. ($C_{17}H_{17}NO_3$) C, H, N.

***O*-Benzoyl Derivatives Derived from 4 and 6:** The microbial reduction products **4** and **6** were benzoylated with benzoyl chloride–pyridine and the benzoates were isolated by SiO_2 column chromatography ($CHCl_3$). The ^1H NMR spectra of the benzoyl derivatives and those of the corresponding authentic samples described above were indistinguishable and their CD spectra were also very similar having the same sign of the Cotton effects.

We are grateful to Professor Masanori Utaka of Okayama University for his advice on immobilization of bakers' yeast, to Professor Norio Gunge of The Kumamoto Institute of Technology for the gift of strains of yeast, and to Professor Ruka Nakashima of Tottori University for his helpful discussion and encouragement.

References

1) T. Sugai, M. Fujita, and K. Mori, *Nippon Kagaku Kaishi*, **1983**, 1315.

2) M. Hirama, M. Shimizu, and M. Iwashita, *J. Chem. Soc., Chem. Commun.*, **1983**, 599; B. Zhou, A. S. Gopalan, F. VanMiddlesworth, W. Shieh, and C. J. Sih, *J. Am. Chem. Soc.*, **105**, 5925 (1983); K. Nakamura, K. Ushio, S. Oka, A. Ohno, and S. Yasui, *Tetrahedron Lett.*, **25**, 3979 (1984); T. Fujisawa, T. Itoh, and T. Sato, *Tetrahedron Lett.*, **25**, 5083 (1984); C. Fuganti, P. Grasselli, P. Casati, and M. Carmeno, *Tetrahedron Lett.*, **26**, 101 (1985); M. Hirama, T. Nakamine, S. Itô, *Chem. Lett.*, **1986**, 1381.

3) K. Nakamura, M. Higaki, K. Ushio, S. Oka, and A. Ohno, *Tetrahedron Lett.*, **26**, 4213 (1985).

4) T. Sakai, T. Nakamura, K. Fukuda, E. Amano, M. Utaka, and A. Tanaka, *Bull. Chem. Soc. Jpn.*, **59**, 3185 (1986).

5) M. Kierstan and C. Bucke, *Biotechnol. Bioeng.*, **19**, 387 (1977).

6) S. Fukushima, T. Nagai, K. Fujita, A. Tanaka, and S. Fukui, *Biotechnol. Bioeng.*, **20**, 1645 (1978).

7) Z. Bukac and J. Sebenda, *Collect. Czech. Chem. Commun.*, **31**, 3315 (1966).

8) S. S. Simons, Jr., *J. Org. Chem.*, **38**, 414 (1973).

9) A. K. Bose, M. S. Manhas, D. P. Sahu, and V. R. Hegde, *Can. J. Chem.*, **1981**, 2498.

A Tin-Mediated One-Step Synthesis of (+)-Dicrotaline, an 11-Membered Dilactonic Pyrrolizidine Alkaloid

Haruki NIWA,* Osamu OKAMOTO, Hiroyuki ISHIWATA, Akio KURODA, Youichi UOSAKI, and Kiyoyuki YAMADA
Department of Chemistry, Faculty of Science, Nagoya University, Chikusa, Nagoya 464
(Received March 24, 1988)

Synopsis. A new synthesis of (+)-dicrotaline (**1**), an 11-membered dilactonic pyrrolizidine alkaloid of retronecine (**6**) type has been achieved in one step by utilizing a tin-mediated lactonization process.

Macrocyclic pyrrolizidine alkaloids are attractive synthetic targets owing to interesting biological activities such as marked hepatotoxicity and carcinogenicity as well as intriguing chemical structures characterized by the presence of a large-ring dilactone.[1] The final crucial step in the total synthesis of these alkaloids is the formation of the large-ring dilactone from a pyrrolizidine diol ["necine," the most commonly (+)-retronecine (**6**)] and a diacid ("necic acid"). Overcoming this synthetic hurdle, some of the macrocyclic pyrrolizidine alkaloids have been synthesized recently by several research groups including us.[2,4a] Herein we wish to disclose a new, single-step synthesis of (+)-dicrotaline (**1**),[2b] an 11-membered dilactonic pyrrolizidine alkaloid of retronecine (**6**) type by virtue of a tin-mediated lactonization reaction.[3]

Shanzer et al. have reported the novel synthesis of macrocyclic tetralactones by the reaction of various cyclic anhydrides with stannoxanes derived from diols and dibutyltin oxide (Bu_2SnO).[3a] We envisioned that this tinmediated "template-driven" macrocyclization process would be applicable to the construction of macrocyclic pyrrolizidine dilactones. In fact, treatment of the stannoxane intermediate **7**[4a] prepared from **6**[4b] and Bu_2SnO, with glutaric anhydride (**8**) in refluxing xylene provided in one step an 11-membered dilactone **3**[5] in 32% yield. We therefore applied this tin-mediated dilactone formation process to the synthesis of **1**. Thus, dicrotalic anhydride (**9**)[2b,6] prepared from dicrotalic acid (3-hydroxy-3-methylglutaric acid) (**11**)[6] was treated with **7** in refluxing xylene to give **1**[2b] and the diastereomer **2**[2b] in 10 and 12% yields, respectively. Spectral (^{1}H NMR, IR, and mass spectra) and chiroptical properties of synthetic **1** were identical with those of natural **1**. Although **1** could be synthesized in one step, the diastereoselectivity and the chemical yield were unsatisfactory, which may be explained by the presence of the free hydroxyl group in the anhydride **9**. Therefore, we next examined the lactonization using the protected cyclic anhydride **10** and **7**. The anhydride **10** was prepared from the the dimethyl ester **12**[6] as follows: (i) conversion of **12** into the methoxymethyl (MOM) ether **13**;[7] (ii) hydrolysis of **13** into the diacid **14**; (iii) conversion of **14** into **10**. Treatment of **10** with **7** under the conditions described above, however, provided a 1 : 1 mixture of the dilactones **4** and **5** in 19% yield. No improvement on the diastereoselectivity and the chemical yield in the dilactone formation could be achieved even employing **10**.

In summary, a one-step synthesis of (+)-dicrotaline (**1**) has been achieved by using the tin-mediated lactonization process although there has been a limitation in view of the diastereoselectivity and the chemical yield.

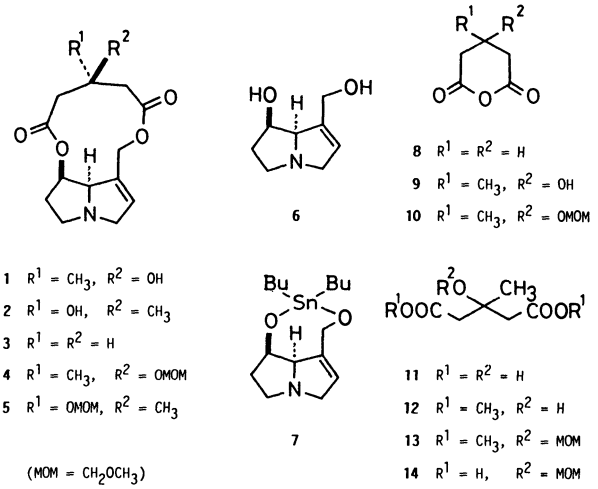

Experimental

Melting points are uncorrected. Infrared (IR) spectra were obtained on a JASCO Model IR-810 spectrophotometer. Proton nuclear magnetic resonance (^{1}H NMR) spectra were recorded on a JEOL JNM-C675 (270 MHz) or a JEOL 90QE (90 MHz) spectrometer in $CDCl_3$ using tetramethylsilane (TMS) as an internal standard. Chemical shifts were expressed in parts per million (ppm) downfield from TMS (δ=0.0) and coupling constants in Hz. Optical rotations were measured on a JASCO DIP-181 polarimeter. The low- (CIMS and EIMS) and high-resolution (HRCIMS and HREIMS) mass spectra were recorded on a JEOL JMS-LG2000 instrument. Fuji-Davison silica gel BW-820-MH was used for column chromatography. Merck precoated silica gel 60 F_{254} plates, 0.25 mm thickness, were used for analytical and preparative thin-layer chromatography (TLC). Xylene and benzene were distilled from Na under nitrogen. Dichloromethane was distilled from CaH_2 under nitrogen. Tetrahydrofuran (THF) was distilled from Na-benzophenone ketyl under nitrogen. Chloroform was distilled from phosphorus pentoxide (P_2O_5).

17,18,19,20-Tetranorcrotalanan-11,15-dione (3). A mixture of **6**[4b] (25.9 mg, 0.167 mmol) and Bu_2SnO (49.9 mg, 0.200 mmol) in benzene (5 ml) was heated under reflux for 23 h with continuous removal of water by use of Molecular Sieves 4A (ca. 1 g). After cooling, the mixture was concentrated under reduced pressure to leave **7** as a pale yellow oil, which was suspended in xylene (3 ml). To the stirred suspension cooled at −25 °C was added a solution of **8** (21.0 mg, 0.184 mmol) in xylene (2 ml). The mixture was gradually warmed to room temperature for 3 h with stirring and then heated under reflux for 18 h. After cooling, the reaction mixture was concentrated under reduced pressure. Purifica-

tion of the residual oil by column chromatography on silica gel (2.5 g) with acetone–MeOH (1/0→5/1 volume ratio) afforded 13.5 mg (32% from **6**) of **3** as a colorless oil; $[\alpha]_D^{13}$ +37.8° (*c* 1.28, $CHCl_3$); lit,[5] $[\alpha]_D^{13}$ +39.0° (*c* 1.0, $CHCl_3$). The chiroptical and spectral (IR, ^1H NMR, and MS) properties of synthetic **3** were identical with those reported for **3**.[5]

(+)-Dicrotaline (1) and (+)-Epidicrotaline (2). The stannoxane **7** prepared from 20.2 mg (0.130 mmol) of **6** and 37.0 mg (0.150 mmol) of Bu_2SnO as described above was suspended in xylene (4.3 ml). To the stirred suspension was added **9**[2b,6] (19.3 mg. 0.134 mmol) at room temperature. The mixture was heated under reflux for 19 h. After cooling, the reaction mixture was concentrated under reduced pressure. Separation and purification of the residual oil with column chromatography on silica gel (3 g) with $CHCl_3$–MeOH (4/1→0/1 volume ratio) gave a mixture of **1** and **2** (11.6 mg) along with the unreacted **6** (16 mg, 79%). Further separation of the mixture of **1** and **2** by preparative TLC on silica gel with $CHCl_3$–MeOH–28% NH_3 aq (70/10/1 volume ratio) provided 3.8 mg (10% from **6**) of **1** as a colorless oil[8] and 4.2 mg (12% from **6**) of **2** as a colorless oil, respectively. **1**: $[\alpha]_D^{22}$ +11° (*c* 0.38, $CHCl_3$); lit,[2b] $[\alpha]_D^{18}$ +8.1° (*c* 1.18, $CHCl_3$). The hydrochloride of **1**: mp 198—200 °C decomp (EtOH); lit, mp 200 °C decomp (EtOH),[9] mp 211—212 °C decomp (EtOH).[2b] **2**: $[\alpha]_D^{22}$ +44° (*c* 0.32, $CHCl_3$); lit,[2b] $[\alpha]_D^{18}$ +43.3° (*c* 0.72, $CHCl_3$). Spectral (IR, ^1H NMR, and MS) properties of synthetic **1** and **2** were identical with those of natural **1** and those reported to synthetic **2**, respectively.[2b]

Dimethyl 3-(Methoxymethoxy)-3-methylglutarate (13). Dimethyl 3-hydroxy-3-methylglutarate (**12**) was prepared from **11** by the reported procedure.[6] To a solution of **12** (93.2 mg, 0.491 mmol) in $CHCl_3$ (3 ml) was added dimethoxymethane (methylal) (3 ml) and P_2O_5 (1.5 g).[7] The mixture was vigorously stirred at room temperature for 30 min. The reaction mixture was poured into a precooled, saturated aqueous $NaHCO_3$ solution (3 ml) and extracted with ether (3×8 ml). The extracts were combined, dried, and concentrated. Purification of the residual oil by column chromatography on silica gel (2 g) with hexane–EtOAc (6/1 volume ratio) gave 87.2 mg (76%) of **13** as a pale yellow oil; IR ($CHCl_3$) 1740, 1440, 1230, 1150, 1035 cm^{-1}; ^1H NMR (90 MHz) δ=1.49 (3H, s), 2.84 (4H, s), 3.35 (3H, s), 3.68 (6H, s), 4.76 (2H, s); CIMS (200 eV) *m/z* (rel intensity) 235 (M^++1; 100), 205 (40), 204 (95), 203 (51), 201 (57), 174 (92), 173 (40), 161 (46), 147 (96), 142 (90), 117 (65), 113 (40). HRCIMS. Found: *m/z* 235.1176. Cacld for $C_{10}H_{19}O_6$: M+H, 235.1181.

3-(Methoxymethoxy)-3-methylglutaric Acid (14). To a solution of **13** (47.6 mg, 0.203 mmol) in THF (2 ml) was added 0.5 M LiOH (2 ml) (1 M=1 mol dm^{-3}). The mixture was vigorously stirred at 40 °C for 24 h. The reaction mixture was neutralized by the addition of Amberlite CG-50 (acid form, 0.5 g). After being stirred for 10 min, the mixture was filtered through a column packed with Amberlite CG-50 (0.5 g). The column was washed thoroughly with MeOH. The filtrate and the column washings were combined and concentrated under reduced pressure. Purification of the residual oil by column chromatography on silica gel (4 g) with hexane–EtOAc–AcOH (15/15/1 volume ratio) gave 30.1 mg (76%) of **14** as a colorless oil; IR ($CHCl_3$) 3700—2400 (broad), 1720, 1025 cm^{-1}; ^1H NMR (90 MHz) δ=1.51 (3H, s), 2.89 (4H, s), 3.38 (3H, s), 4.80 (2H, s); CIMS (200 eV) *m/z* (rel intensity) 207 (M^++1; 3), 175 (100), 159 (40), 155 (37), 145 (84), 141 (65), 128 (20), 103 (37), 85 (21). HRCIMS. Found: *m/z* 207.0863. Calcd for $C_8H_{15}O_6$: M+H, 207.0868.

3-(Methoxymethoxy)-3-methylglutaric Anhydride (10). To a solution of **14** (46.2 mg, 0.224 mmol) in CH_2Cl_2 (1 ml) was added a solution of dicyclohexylcarbodiimide (46.2 mg, 0.224 mmol) in CH_2Cl_2 (1 ml) under nitrogen. The mixture was stirred at room temperature for 45 min and concentrated under reduced pressure. The residue was diluted with anhydrous acetone (5 ml) and insoluble materials were removed by filtration through a cotton plug. The filtrate was concentrated to leave 42.6 mg of crude **10** as a colorless oil; IR ($CHCl_3$) 1820, 1770, 1065, 1030 cm^{-1}; ^1H NMR (270 MHz) δ=1.44 (3H, s), 2.62 (2H, d, *J*=16.5), 3.16 (2H, d, *J*=16.5), 3.33 (3H, s), 4.72 (2H, s); CIMS (200 eV) *m/z* (rel intensity) 189 (M^++1; 22), 159 (100), 141 (87), 127 (55), 115 (33), 99 (38), 85 (37). HRCIMS. Found: *m/z* 189.0744. Calcd for $C_8H_{13}O_5$: M+H, 189.0763. The crude **10** was used for the next reaction without further purification.

13-(Methoxymethoxy)-17,19,20-trinorcrotalanan-11,15-diones (4 and 5). The stannoxane **7** prepared from 12.0 mg (0.0774 mmol) of **6** and 22.4 mg (0.0914 mmol) of Bu_2SnO as described before was suspended in xylene (3 ml). To the stirred suspension cooled at 0 °C was added a solution of **10** (16.0 mg, 0.0851 mmol) in xylene (1.0 ml). The mixture was stirred at 0 °C for 30 min and then at room temperature for 2 h. To the reaction mixture was added an another solution of **10** (5.8 mg, 0.030 mmol) in xylene (0.36 ml). After being stirred at 35 °C for additional 7 h, the mixture was heated under reflux for 36 h. After cooling, the reaction mixture was concentrated under reduced pressure. Separation of the residual oil by column chromatography on silica gel (2 g) with acetone→MeOH afforded 4.9 mg (19%) of a 1:1 mixture of **4** and **5** as a colorless oil. **4** and **5**: IR ($CHCl_3$) 1740, 1260, 1150, 1030 cm^{-1}; ^1H NMR (270 MHz) δ=1.57 (1.5H, s), 1.61 (1.5H, s), 2.2—2.3 (2H, complex pattern), 2.4—2.9 (5H, complex pattern), 3.43 (1.5H, s), 3.45 (1.5H, s), 3.5—3.6 (2H, complex pattern), 4.0—4.2 (2H, complex pattern), 4.56 (1H, m), 4.81 (2H, m), 5.22 (0.5H, m), 5.28 (0.5H, m), 5.32 (0.5H, d, *J*=12.9), 5.37 (0.5H, d, *J*=12.5), 5.92 (0.5H, br s), 5.95 (0.5H, br s); EIMS (70 eV) *m/z* (rel intensity) 325 (M^+; 45), 310 (7), 294 (26), 280 (6), 265 (53), 242 (28), 220 (23), 138 (51), 137 (71), 136 (86), 121 (74), 120 (75), 95 (78), 94 (100), 93 (63), 80 (55). HREIMS. Found: *m/z* 325.1535. Calcd for $C_{16}H_{23}O_6N$: M, 325.1526.

We thank Professor D. J. Robins, University of Glasgow, UK for providing us with the copies of IR, ^1H NMR, and mass spectra of natural **1**. Financial support from the Ministry of Education, Science and Culture [Grant-in-Aid for Special Project Research No. 62114007, Chemical Syntheses for Elucidation of Biological Functions] is gratefully acknowledged.

References

1) A. R. Mattocks, "Chemistry and Toxicology of Pyrrolizidine Alkaloids," Academic Press Inc., Orlando (1986), Chaps. 1, 3, 7 and 11.

2) a) For the synthesis of crobarbatine acetate: J. Huang and J. Meinwald, *J. Am. Chem. Soc.*, **103**, 861 (1981); b) For the synthesis of (+)-dicrotaline (**1**): J. A. Devlin and D. J. Robins, *J. Chem. Soc., Chem. Commun.*, **1981**, 1272; K. Brown, J. A. Devlin, and D. J. Robins, *J. Chem. Soc., Perkin Trans. 1*, **1983**, 1819; c) For the synthesis of (±)-integerrimine: K. Narasaka, T. Sakakura, T. Uchimaru, K. Morimoto, and T. Mukaiyama, *Chem. Lett.*, **1982**, 455; K. Narasaka, T. Sakakura, T. Uchimaru, and D. Güedin-Vuong, *J. Am. Chem. Soc.*, **106**, 2954 (1984); d) For the synthesis of (−)-integerrimine: See Ref. 4a; J. D. White and S. Ohira, *J. Org. Chem.*, **51**, 5492 (1986); e) For the synthesis of (±)-fulvine and (±)-crispatine: E. Vedejs and S. D. Larsen, *J. Am. Chem. Soc.*, **106**, 3030 (1984); f) For the synthesis of (−)-monocrotaline: E. Vedejs, S. Ahmad, S. D. Larsen, and S. Westwood, *J. Org. Chem.*, **52**, 3937 (1987).

3) a) A. Shanzer and N. Mayer-Shochet, *J. Chem. Soc., Chem. Commun.*, **1980**, 176; A. Shanzer and E. Berman,

ibid., **1980**, 259; A. Shanzer, J. Libman, H. Gottlieb, and F. Frolow, *J. Am. Chem. Soc.*, **104**, 4220 (1982); A. Shanzer, J. Libman, and H. E. Gottlieb, *J. Org. Chem.*, **48**, 4612 (1983); b) See also: K. Steliou, A. Szczygielska-Nowosielska, A. Favre, M. A. Poupart, and S. Hanessian, *J. Am. Chem. Soc.*, **102**, 7578 (1980); K. Steliou and M.-A. Poupart, *J. Am. Chem. Soc.*, **105**, 7130 (1983).

4) a) H. Niwa, Y. Miyachi, Y. Uosaki, A. Kuroda, H. Ishiwata, and K. Yamada, *Tetrahedron Lett.*, **27**, 4609 (1986). b) H. Niwa, Y. Miyachi, O. Okamoto, Y. Uosaki, and K. Yamada, *Tetrahedron Lett.*, **27**, 4605 (1986); H. Niwa, O. Okamoto, Y. Miyachi, Y. Uosaki, and k. Yamada, *J. Org. Chem.*, **52**, 2941 (1987).

5) J. A. Devlin, D. J. Robins, and S. Sakdarat, *J. Chem. Soc., Perkin Trans. 1*, **1982**, 1117.

6) P. Lewer and J. MacMillan, *J. Chem. Soc., Perkin Trans. 1*, **1983**, 1417; H. J. Klosterman and F. Smith, *J. Am. Chem. Soc.*, **76**, 1229 (1954).

7) K. Fuji, S. Nakano, and E. Fujita, *Synthesis*, **1975**, 276.

8) Although the literature[2b] reported **1** as a crystalline material, we could not obtain crystalline **1**.

9) J. C. S. Marais, *Onderstepoort J. Vet. Sci. Anim. Ind.*, **20**, 61 (1944).

Selective Reduction of Carbon-Carbon Double Bonds with an NAD(P)H Model-Acetic Acid System

Yoshio INOUE,* Shin IMAIZUMI, Hiromitsu ITOH,† Takao SHINYA,†
Harukichi HASHIMOTO,† and Sotaro MIYANO*,†
Department of Engineering Science, Faculty of Engineering, Tohoku University, Aoba, Sendai 980
†Department of Applied Chemistry, Faculty of Engineering, Tohoku University, Aoba, Sendai 980
(Received April 15, 1988)

Synopsis. The carbon-carbon double bond in conjugated nitro and certain carbonyl compounds was reduced smoothly and selectively by Hantzsch ester (HEH), an NAD(P)H model, in the presence of a small amount of acetic acid.

Normally the reducing ability of NAD(P)H models is so modest that only strongly electron-deficient olefins are reduced[1] in contrast to certain enzymatic systems where NAD(P)H reduces smoothly the carbon-carbon double bond in a conjugated carbonyl compound with the aid of dehydrogenase.[2] In model systems, some cationic species such as proton,[3] Lewis acid,[4] or magnesium ion[5] have been used as an activator. For example, an NAD(P)H model, 3,5-bis-(ethoxycarbonyl)-1,4-dihydro-2,6-dimethylpyridine (Hantzsch ester: HEH) was demonstrated to reduce the carbon-carbon double bond in nitroalkenes smoothly with the aid of silica gel in benzene without any side reaction.[6]

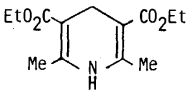

HEH

Nitroalkanes are useful intermediates because the nitro group can be easily converted to other functional groups, e.g., carbonyl,[7] nitrile oxide,[8] and amino group.[9] The synthetic method used widely for nitroalkanes is the reduction of conjugated nitroalkenes with $NaBH_4$.[10] The reaction proceeds smoothly for aliphatic nitroalkenes usually. However for aromatic nitroalkenes, side reactions such as dimerization take place affording low yields of the desired product.

In this paper we present another example of the selective reduction of conjugated aromatic nitroalkenes to nitroalkanes with HEH-acetic acid system[11] and also describe the extension of the scope to α,β-unsaturated carbonyl compounds.

Results and Discussion

The reduction of aromatic nitroalkene **1** to nitroalkane **2** was performed usually in benzene at 80 °C using 1.3 equivalent amounts of HEH under a nitrogen atmosphere. Other solvents such as ethanol and acetonitrile could be used in place of benzene.

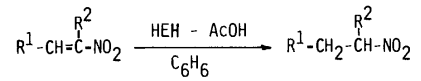

As shown in Table 1, even a catalytic amount of acetic acid is enough as an activator for the selective reduction of various nitroalkenes. Besides acetic acid (pK_a=4.76), several carboxylic acids such as benzoic (pK_a=4.21), formic (pK_a=3.75), and chloroacetic (pK_a=2.87) acids showed efficient activation effects in catalytic amounts whereas dichloroacetic (pK_a=1.26) and trifluoroacetic (pK_a=0.3) acids did not exert sufficient effects in the reduction of β-nitrostyrene.

Table 1. Reduction of Nitroalkene **1**

1		AcOH/HEH	Yield of 2[a]
R^1	R^2	molar ratio	%
C_6H_5	H	0	28
		0.04	73
		0.23	(100)[b]
		2.30	(90)[b]
p-$CH_3C_6H_4$	H	0.23	95
m-$CH_3OC_6H_4$	H	0.23	96
p-$CH_3OC_6H_4$	H	0.23	(95)[b]
p-ClC_6H_4	H	0.23	95
p-$NO_2C_6H_4$	H	0.23	97
C_6H_5	CH_3	0.23	70
m-$CH_3OC_6H_4$	CH_3	0.23	85

1; 1.0 mmol, HEH; 1.3 mmol: 80 °C, 15 h in benzene.
a) Isolated yield. b) GLC yield.

The products were obtained in excellent yields irrespective of the kind of the aromatic substituent in nitrostyrenes. In every case, no formation of dimer or other side products were observed.

To clarify the substituent effect, the reactions of substituted β-nitrostyrenes were carried out with HEH-trifluoroacetic acid system. Results are shown in Fig. 1. Apparently the yield of products increased with the increase in electron-withdrawing effect of the aromatic substituent.

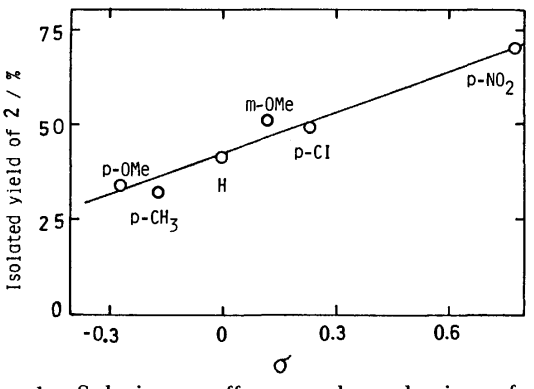

Fig. 1. Substituent effect on the reduction of β-nitrostyrenes **1**. **1**; 1.0 mmol, HEH; 1.3 mmol, CF_3COOH; 0.05 mmol: 80 °C for 15 h in benzene.

Reduction of α,β-unsaturated carbonyl compounds required more severe conditions than those of nitroalkene reduction in terms of reaction temperature and acid concentration. Thus the reactions were performed in toluene at 100 °C for 15 h using 2.3 equivalent amounts of acetic acid to HEH under a nitrogen atmosphere.

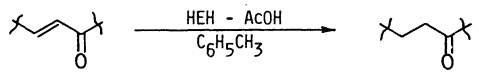

Table 2. Reduction of α,β-Unsaturated Carbonyl Compounds

Carbonyl compound	AcOH/HEH molar ratio	Yield[a] %
PhCH=CHCHO	0	9[b]
	0.3	32[b]
	2.3	61[b]
	2.3	76
$CH_3(CH_2)_2CH=CHCHO$	2.3	83
$PhCH=CHCOCH_3$	2.3	54
	(0.05)[c]	33
$(CH_3)_2C=CHCOCH_3$	(0.05)[c]	35
2-Cyclohexen-1-one	2.3	trace
2-Cyclopenten-1-one	2.3	13

Carbonyl compound; 1.0 mmol, HEH; 1.3 mmol: 100 °C for 15 h in toluene. a) GLC yield. b) The reaction was run in benzene at 80 °C. c) The reaction was performed in benzene at 80 °C for 5 h employing CF_3COOH instead of CH_3COOH.

Results are given in Table 2. α,β-Unsaturated aldehydes were reduced smoothly yielding saturated aldehydes. α,β-Unsaturated linear ketones were moderately reactive whereas cyclic ketones such as 2-cyclohexenone reacted only scantily. Esters like methyl cinnamate, butyl acrylate, dimethyl fumarate, dimethyl maleate, and coumarin did not take part in the reaction.

The chemoselectivity between nitroalkene and α,β-unsaturated aldehyde is noteworthy. Thus an equimolar mixture of β-nitrostyrene and cinnamaldehyde was allowed to react with 0.9 equivalent amounts of HEH in the presence of a small amount of acetic acid (acetic acid/HEH=0.3) at 80 °C in benzene for 15 h. The reduction of the β-nitrostyrene to (2-nitroethyl)benzene took place selectively in 82% yield while the cinnamaldehyde was recovered unchanged in 98%.

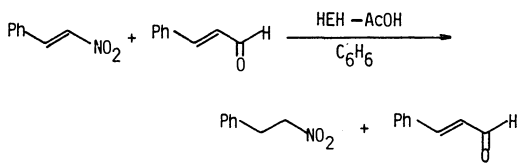

As a whole, the present HEH-acetic acid system exhibited somewhat weaker reducing ability than that of HEH-silica gel system[6] in the reduction of a carbon-carbon double bond. In terms of this mildness, HEH-acetic acid system revealed the marked difference in reactivity toward the linear and cyclic α,β-unsaturated ketones. Since HEH is stable and obtained easily the present method has synthetic utility.

Experimental

HEH[12] and nitrostyrene derivatives[13] were prepared according to the literature. Other materials were commercially obtained. The structures of the products were confirmed by ^1H NMR and IR spectra.

General Procedure for the Reduction of Nitrostyrenes. Into a 50 cm^3 flask containing nitroalkene (1.0 mmol) and HEH (1.3 mmol) were added benzene (5 cm^3) and acetic acid (0.3 mmol) under a nitrogen atmosphere. The mixture was agitated at 80 °C for 15 h. After cooling, the reaction mixture was submitted to column chromatography on silica gel eluting with hexane-ethyl acetate to afford the reduced product. The results are given in Table 1.

General Procedure for the Reduction of α,β-Unsaturated Carbonyl Compounds. Into a 50 cm^3 flask containing α,β-unsaturated carbonyl compound (1.0 mmol) and HEH (1.3 mmol) were added toluene (5 cm^3) and acetic acid (3.0 mmol) under a nitrogen atmosphere. The mixture was agitated at 100 °C for 15 h. The product was analyzed by GLC. On the employment of trifluoroacetic acid (0.05 mmol), the reaction was performed in benzene (10 cm^3) at 80 °C for 5 h. The results are shown in Table 2.

Competitive Reaction of β-Nitrostyrene and Cinnamaldehyde. β-Nitrostyrene (1.0 mmol) and cinnamaldehyde (1.0 mmol) were agitated in the presence of HEH (0.9 mmol) and acetic acid (0.27 mmol) in benzene (5 cm^3) at 80 °C for 15 h under a nitrogen atmosphere. GLC analysis revealed the formation of (2-nitroethyl)benzene in 82% yield (based on HEH). The formation of 3-phenylpropionaldehyde was negligible (ca. 2%) and the most of the cinnamaldehyde remained unchanged (ca. 98%).

References

1) B. E. Norcross, P. E. Klinedinst, Jr., and F. H. Westheimer, *J. Am. Chem. Soc.*, **84**, 797 (1962); Y. Ohnishi, M. Kagami, T. Numakunai, and A. Ohno, *Chem. lett.*, **1976**, 915; S. Fukuzumi, Y. Kondo, and T. Tanaka, *J. Chem. Soc., Perkin Trans. 2*, **1984**, 673.

2) For example: G. Weeks and S. J. Wakil, *Methods Enzymol.*, **14**, 66 (1969); C. C. Levy and G. D. Weinstein, *Biochemistry*, **3**, 1944 (1964); P. D. Show, *Biochemistry*, **6**, 2253 (1967).

3) S. Shinkai, H. Hamada, and O. Manabe, *Tetrahedron Lett.*, **1979**, 1397.

4) A. Ohno, Y. Ishihara, S. Ushida, and S. Oka, *Tetrahedron Lett.*, **23**, 3185 (1982).

5) A. Ohno, M. Ikeguchi, T. Kimura, and S. Oka, *J. Am. Chem. Soc.*, **101**, 7036 (1979).

6) K. Nakamura, M. Fujii, S. Oka, and A. Ohno, *Chem. Lett.*, **1985**, 523; K. Nakamura, M. Fujii, A. Ohno, and S. Oka, *Tetrahedron Lett.*, **25**, 3983 (1984); S. Yasui, M. Fujii, K. Nakamura, and A. Ohno, *Bull. Chem. Soc. Jpn.*, **60**, 963 (1987); M. Fujii, K. Nakamura, S. Yasui, S. Oka, and A. Ohno, *Bull. Chem. Soc. Jpn.*, **60**, 2423 (1987); S. Yasui, M. Fujii, and A. Ohno, *Bull. Chem. Soc. Jpn.*, **60**, 4019 (1987).

7) M. R. Galobardes and H. W. Pinnick, *Tetrahedron Lett.*, **22**, 5235 (1981), and references cited therein.

8) C. Grundman and P. Grunanger, "The Nitrile Oxides," Springer-Verlag, New York (1971), p. 51.

9) O. Von Schickh, G. Apel, H. G. Padeken, H. H. Schwarz, and A. Segnitz, "Houben-Weyl-Müller: Methoden der Organischen Chemie," Thieme, Stuttgart (1971), Vol. X/1.

10) H. Shechter, D. E. Ley, and E. B. Roberson, Jr., *J. Am.*

Chem. Soc., **78**, 4984 (1956); A. I. Meyers and J. C. Sircar, *J. Org. Chem.*, **32**, 4134 (1967).

11) Reduction of nitrostyrene by *N*-benzyl-1,4-dihydronicotinamide–acetic acid system has been described with unsatisfactory results; K. Wallenfels, W. Ertel, A. Hockendorf, J. Rieser, and K. H. Uberschar, *Naturwissenschaften*, **62**, 459 (1975).

12) V. Baliah, V. Gopalakrishnan, and T. S. Govindarajan, *J. Ind. Chem. Soc.*, **31**, 832 (1954).

13) D. E. Worrall, *Org. Synth.*, Coll. Vol., I, 413 (1941); H. B. Hass, A. G. Susie, and R. L. Herder, *J. Org. Chem.*, **15**, 8 (1950); S. Miyano, H. Hokari, and H. Hashimoto, *Bull. Chem. Soc. Jpn.*, **55**, 534 (1982); B. M. Vanderbilt and H. B. Hass, *Ind. Eng. Chem.*, **32**, 34 (1940).

Catalytic Oxygenation of Cholesterol with a Platinum Catalyst under Moderate Pressure of Oxygen

Hiroshi SAKAMAKI,* Masa-aki TAKE, Toshihiro AKIHISA,† Taro MATSUMOTO,† and Yoshiyuki ICHINOHE*
College of Science and Technology, Nihon University Narashino Campus, Narashinodai, Funabashi, Chiba 274
†College of Science and Technology, Nihon University Surugadai Campus, Kanda Surugadai, Chiyodaku, Tokyo 101
(Received November 25, 1987)

Synopsis. The catalytic oxygenation of cholesterol **1** with a platinum black catalyst under moderate pressure (20—25 atm) of oxygen yielded eleven oxidation products, **3**—**13a**. The reaction pathway of the catalytic oxygenation is discussed on the basis of the results for several reaction conditions.

Although the autoxidation of cholesterol (**1**) has been well-known for a long time, its mechanism has recently been clarified by Smith et al.[1a,b] On the other hand, Sneeden and Turner[2] performed the catalytic oxygenation of various steroidal alcohols with a platinum black catalyst (platinum catalyst) at ordinary pressures of oxygen and reported that the reaction proceeded easily, though their attempts concerning the catalytic oxygenation of **1** failed. However, in our previous paper[3] we reported success with the catalytic oxygenation of **1** with a platinum catalyst at room temperature under ordinary pressure of oxygen.

In this paper, we describe the structure of new products obtained by performing the catalytic oxygenation of **1** with a platinum catalyst at 80 °C under ordinary pressure and at 90 °C under moderate pressure (20—25 atm) of oxygen.

In the catalytic oxygenation of cholestanol with a platinum catalyst, the yield of cholestanone varied according to the method of preparing the platinum catalyst. Therefore, in order to investigate the catalyst activity, we performed the catalytic oxygenation of cholestanol using a platinum catalysts prepared under various conditions in ethyl acetate at room temperature for 24 h under ordinary pressures of oxygen, and obtained the results shown in Fig. 1. From the experimental results, it was found that the maximum yield (78%) of cholestanone was obtained when the platinum catalyst prepared by reducing platinum oxide (100 mg; 4.4×10^{-4} mol) with hydrogen (45 ml; 2.0×10^{-3} mol) was used.

For the catalytic oxygenation of **1** at moderate pressures of oxygen, we used the method of Sneeden and Turner.[2] The results of the catalytic oxygenation of **1** at ordinary pressure and at moderate pressure of oxygen performed using platinum catalyst under various conditions are given in Table 1. These oxidation products (**3**—**13a**) were directly identified by comparing them with the authentic samples by a known preparation method.[4-6]

The catalytic oxygenation of **1** with a platinum catalyst at 80 °C under ordinary pressure of oxygen gave oxidation products **3**—**9** with a good yield. In addition to the above products **3**—**9**, the reaction products **10**, **11**, and acidic substances **12a**, **13a** were newly isolated by the catalytic oxygenation of **1** using a catalytic amount of platinum catalyst under a moderate oxygen pressure. This was considered attributable to the effect of applying the moderate oxygen pressure, with the oxidation products **10**, **11**, and the acidic substances **12a**, **13a** being obtained only under a moderate pressure of oxygen.

According to the experimental results, the order on the oxidation position of cholesterol **1** is: hydroxyl group at C-3 > allylic hydrogen at C-7 > 5,6-double

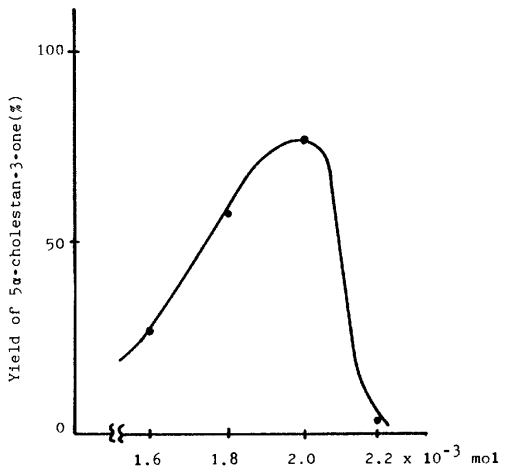

Fig. 1. Catalyst activity of platinum catalyst. Reaction conditions. Substrate: 5α-cholestane-3β-ol (100 mg, 2.5×10^{-4} mol); catalyst: PtO_2 (100 mg, 4.4×10^{-4} mol); O_2-absorption volume (10 ml, 4.5×10^{-4} mol); solvent: EtOAc (3 ml); temperature: room temp; reaction time: 24 h.

Table 1. Composition of the Catalytic Oxygenation Products

Substrate	Composition of the oxygenation products (%)											
	Recov.	Neutral products									Acidic products		Others
	1	**3**	**4**	**5**	**6**	**7**	**8**	**9**	**10**	**11**	**12a**	**13a**	
1[a]	24.7	3.8	16.4	24.9	7.7	3.9	4.9	8.9					4.8
1[b]	36.9	2.7	12.4	11.7	2.8	3.9	1.7	13.0	3.5	1.3	1.8	2.7	5.6

a) Ratio of **1**: Pt (1 : 1); temp 80 °C; O_2-pressure 1 atm; solvent EtOAc; time 24 h. b) Ratio of **1**: Pt (1 : 0.1); temp 90 °C; O_2-pressure 20—25 atm; solvent *t*-BuOH; time 24 h.

Table 2. Composition of the Catalytic Oxygenation Products for Some Steroids

Substrates	Recov. substrate	Composition of the oxygenation products (%)								
		6	**7**	**8**	**9**	**10**	**11**	**12a**	**21**	Others
6[a]		37.9						47.9		14.2
10[a]						11.0	79.9			9.1
16[c]			56.2	2.6	39.7					1.5
18[b]	29.2	5.0				59.6	4.5			1.7
20[c]			6.0						94.0	

a) Ratio of **1**: Pt (1 : 1); O_2-pressure 20—25 atm; solvent *t*-BuOH; temp 80 °C; time: 24 h.
b) Ratio of **1**: Pt (1 : 1); O_2-pressure 1 atm; solvent 2%-aq. Me_2CO; temp 80 °C; time 24 h.
c) Ratio of **1**: Pt (1 : 1); O_2-pressure 1 atm; solvent *t*-BuOH; temp: room temp; time 24 h.

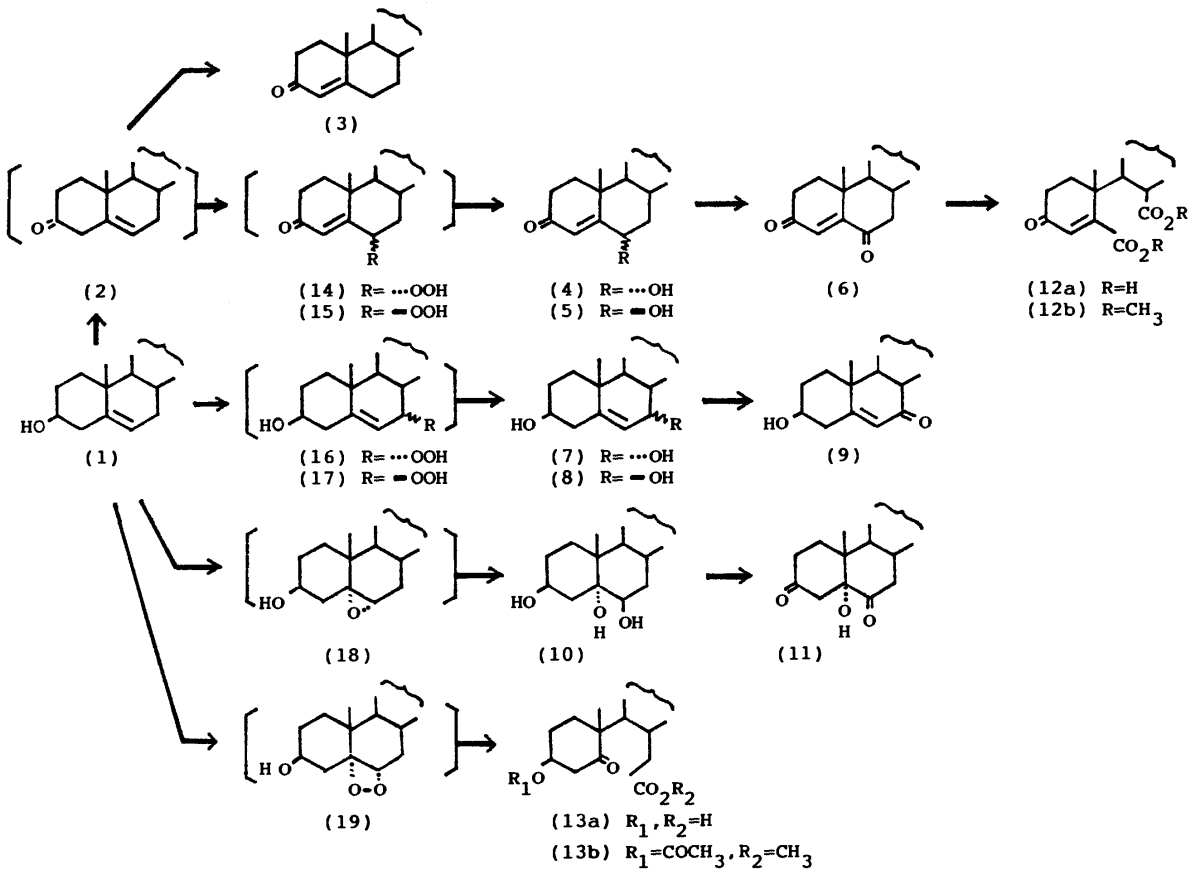

Fig. 2. Proposed pathways for the catalytic oxygenation of cholesterol (**1**).

bond.

The pathway of this catalytic oxygenation under moderate pressure of oxygen, presumed from the obtained oxidation product, is shown in Fig. 2. The courses of formation from **1** to **3** and **6** were shown in our previous paper.[3] In order to confirm the formation of the 6,7-seco acid **12a**, we performed catalytic oxygenation of diketone **6** with a platinum catalyst under a moderate pressure of oxygen with the result that **12a** was formed in a yield of 47%, as shown in Table 2. Therefore, **12a** was confirmed to be formed from **1** via **6**.

As for the formation of the 7-oxo compound **9**, it was assumed that there are two pathways: one is the pathway in which the 7α-hydroperoxide (**16**)[8] is directly formed and another is the course in which the 5α-hydroperoxide (**20**)[7a] is formed as is known to be formed by autoxidation[1a,b] and photoxidation.[7a,b] In order to confirm these pathways, the catalytic oxygenation of **16** with a platinum catalyst under ordinary pressure of oxygen was performed to give 3β,7α-diol **7** and **9** in yields of 56.2 and 39.7% respectively. On the other hand, 3β,5α-diol (**21**)[7a] was formed at a yield of 94% by catalytic oxygenation of **20** under these same conditions.

Therefore, in the catalytic oxygenation of **1**, it has become clear that the intermediate **16** is formed by the direct abstraction of the hydrogen of the allylic position at C-7 with the platinum catalyst, and an attack of oxygen; then **7** is formed with the reduction by hydrogen on the platinum catalyst and is further oxidized to give **9**.

In order to investigate the course of formation of hydroxy diketone **11**, catalytic oxygenation of 5,6α-epoxycholestan-3β-ol (**18**)[9] with a platinum catalyst in 2%-aqueous acetone at 80 °C under ordinary pressure of oxygen was performed to afford triol **10** with a yield of 59.6%. Furthermore, catalytic oxygenation of **10** with the platinum catalyst in *t*-butyl alcohol at room temperature under ordinary pressure of oxygen was performed to give **11** with a yield of 79.9%. These experimental results showed that the epoxide **18** was an intermediate in the formation of **11**.

Finally, regarding the pathway of the formation 5,6-seco acid **13a**, we have presumed that it is formed via the 5,6-dioxetane (**19**).[10a,b] We have inferred that the catalytic oxygenation of **1** with the platinum catalyst is considered a radical reaction, including the four pathways (Fig. 2).

Experimental

All melting points are uncorrected. IR spectra were obtained in KBr on a JASCO IR-G instrument. ^{1}H NMR were measured at 100 MHz using deuteriochloroform as the solvent. The chemical shift are given in ppm using tetramethylsilane (TMS) as an internal standard on a JNM-FX100 instrument. The mass spectra were recorded on a Hitachi RMU-7M system at 70 eV. GLC was performed on a Shimadzu GC-9A gas chromatography equipped 2%OV-17 (3 m×5 mm) at 300 °C and a SCOT OV-17 glass capillary column (30 m×0.3 mm).

Material and Authentic Specimens. Cholesterol (**1**) was a commercial source (Riken Vitamin Co. (Tokyo)) and purified by acetylation, hydrolysis and repeated recrystallization from methanol. The authentic specimens of cholest-4-en-3-one (**3**, mp 76—79 °C),[4a] 6α-hydroxycholest-4-en-3-one (**4**, mp 155—156 °C),[4b] 6β-hydroxycholest-4-en-3-one (**5**, mp 184—185 °C,[4b] cholest-4-ene-3,6-dione (**6**, mp 124—125 °C),[4b,c] cholest-5-ene-3β,7α-diol (**7**, mp 188—189 °C),[4d] cholest-5-ene-3β,7β-diol (**8**, mp 177—178 °C),[4d] 3β-hydroxycholest-5-en-7-one (**9**, mp 169—170 °C),[4d,e] cholestane-3β,5α,6β-triol (**10**, mp 236—238 °C),[4f] IR(KBr) ν 3400 cm^{-1} (OH); ^{1}H NMR ($CDCl_3$) (diacetate) δ=0.69 (3H, s, 18-CH_3), 1.15 (3H, s, 19-CH_3), 2.02 (3H, s, 6-OCOCH_3), 2.07 (3H, s, 3-OCOCH_3), 4.69 (1H, br.s *w*/2=6 Hz, 6-H), 5.15 (1H, m, *w*/2=24 Hz, 3-H); MS Found: *m*/*z* 420.3572. Calcd for $C_{27}H_{48}O_3$: M, 420.3591; 5α-hydroxycholestane-3,6-dione (**11**, mp 230—231 °C),[4b] IR(KBr) ν 3300 cm^{-1} (OH), 1710 cm^{-1} (C=O); ^{1}H NMR ($CDCl_3$) δ=0.68 (3H, s, 18-CH_3), 1.01 (3H, s, 19-CH_3); MS Found: *m*/*z* 416.3245. Calcd for $C_{27}H_{44}O_3$: M, 416.3279; dimethyl 3-oxo-6,7-seco-cholest-4-ene-6,7-dioate (**12b**, mp 137—139 °C),[5] IR(KBr) ν 1735, 1720 cm^{-1} (OAc), 1690 cm^{-1} (C=O), 1660 cm^{-1} (C=C); ^{1}H NMR ($CDCl_3$) δ=0.64 (3H, s, 18-CH_3), 1.37 (3H, s, 19-CH_3), 3.67 (3H, s, 7-CO_2CH_3), 3.81 (3H, s, 6-CO_2CH_3), 6.49 (1H, s, 4-H); MS Found: *m*/*z* 474.3293. Calcd for $C_{29}H_{46}O_5$: M, 474.3333; methyl 3β-acetoxy-5-oxo-5,6-seco-cholestan-6-oate (**13b**, amorphous),[6] IR(KBr) ν 1735 cm^{-1} (OAc), 1715 cm^{-1} (C=O); ^{1}H NMR ($CDCl_3$) δ=0.68 (3H, s, 18-CH_3), 1.04 (3H, s, 19-CH_3), 2.01 (3H, s, 3-OCOCH_3), 3.58 (3H, s, CO_2CH_3); MS Found: *m*/*z* 430.3429. Calcd for $C_{30}H_{50}O_5$: M, 490.3435, M−CH_3CO_2H, 430.3435; 7α-hydroperoxycholest-5-en-3β-ol (**16**, mp 150—152 °C),[8] 5α-hydroperoxycholest-6-en-3β-ol (**20**, mp 149—150 °C),[7a,b] 5,6α-epoxycholestan-3β-ol (**18**, mp 141—142 °C),[9] IR(KBr) ν 3380 cm^{-1} (OH); ^{1}H NMR ($CDCl_3$) δ=0.68 (3H, s, 18-CH_3), 1.18 (3H, s, 19-CH_3), 3.54 (1H, br.s *w*/2=6 Hz, 6-H); MS Found: *m*/*z* 402.3492. Calcd for $C_{27}H_{46}O_2$: M, 402.3486; cholest-6-ene-3β,5α-diol (**21**, mp 148—149 °C)[7a,b] IR(KBr) 3610, 3400, 3300 cm^{-1} (OH); ^{1}H NMR ($CDCl_3$) δ=0.70 (3H, s, 18-CH_3), 0.95 (3H, s, 19-CH_3), 4.07 (1H, m *w*/2=24 Hz, 3-H), 5.59 (2H, br.s, *w*/2=4.5 Hz, CH=CH); MS Found: *m*/*z* 402.3482. Calcd for $C_{27}H_{46}O_2$: M, 402.3486; were prepared and purified as reported in references.

Catalytic Oxygenation of Cholesterol with Platinum Catalyst under Moderate Pressure of Oxygen. Platinum oxide (200 mg) was reduced to platinum black with hydrogen (60 ml) in *t*-butyl alcohol (10 ml) and then hydrogen was carefully replaced with air. The system filled with oxygen and catalyst was absorbed with oxygen (10 ml).

A solution of *t*-butyl alcohol (100 ml), platinum catalyst (200 mg), and cholesterol (**1**, 2g) was added to autoclave and the system was filled with oxygen (20—25 atm) and stirred at 90 °C for 24 hours. After reaction ceased, catalyst was removed by filtration and then the filtrate was concentrated to dryness at 40 °C under reduced pressure. Resulting reaction products were poured into ether and a treatment with 5%-Na_2CO_3 solution gave an acidic portion (160 mg, 8%) and a neutral portion (1.8 g, 90%). A portion of neutral product was separated on alumina column chromatography, TLC, and HPLC, while the other portion was analyzed by GLC as TMSE derivative. Acidic product was methylated with diazomethane and then acetylated with acetic anhydride-pyridine. A portion of the acidic products were separated on silica gel column chromatography, while the other portion was analyzed by GLC. All of the above oxidation products were identified by comparing with authentic sample by a known method.[4-6]

The authors wish to thank professor A. Nickon, Johns Hopkins University, for his kind donation of authentic samples and Dr. T. Iwadare, Sakura Fine-technical Co., Ltd., for his useful suggestion.

References

1) a) J. E. van Lier and L. L. Smith, *J. Org., Chem.*, **35**, 2627 (1970); b) J. I. Teng, M. J. Kulig, L. L. Smith, G. Kan, and J. E. van Lier, *ibid*, **38**, 6658 (1973).

2) R. P. A. Sneeden and R. B. Turner, *J. Am. Chem. Soc.*, **77**, 190 (1955).

3) T. Akihisa, T. Matsumoto, H. Sakamaki, M. Take, and Y. Ichinohe, *Bull. Chem. Soc. Jpn.*, **59**, 680 (1986).

4) a) N. Rabjohn, *Org. Synth.*, Coll. Vol. 4, 192 (1962); b) L. F. Fieser, *J. Am. Chem. Soc.*, **75**, 4377 (1953); c) N. Rabjohn, *Org. Synth.*, Coll. Vol. 4, 189 (1962); d) C. W. Shoopee and B. C. Newman, *J. Chem. Soc. C*, **1968**, 981; e) O. Wintersteiner and W. L. Ruigh, *J. Am. Chem, Soc.*, **64**, 2453 (1942); f) L. F. Fieser and S. Rajagopalan, *J. Am. Chem. Soc.*, **71**, 3938 (1949).

5) L. F. Fieser, *J. Am. Chem. Soc.*, **75**, 4386 (1953).

6) F. Sǒrm, *Col. Czech.*, **12**, 437 (1947).

7) a) G. O. Schenck, O. A. Neumuller, and W. Eisfeld, *Justus Liebigs Ann. Chem.*, **618**, 202 (1958); b) A. Nickon and J. F. Bagli, *J. Am. Chem. Soc.*, **83**, 1498 (1961).

8) G. O. Schenck and O. A. Neumuller, *Justus Liebigs Ann. Chem.*, **618**, 194 (1958).

9) L. F. Fieser and M. Fieser, "Reagents for Organic Synthesis, "John Wiley & Sons Inc., (1967), Vol. 1, p. 136.

10) a) D. R. Kearns, *Chem. Revs.*, **71**, 395 (1971); b) F. McCapra, *Chem. Commun.*, **1968**, 155.

Synthesis of 1,4-Benzoquinone Derivatives Having Two Side-Armed Polyethers and Crown Ethers, and Their Electrochemical Study in the Presence of Alkali Metal Cations (Na^+ and K^+)

Hideo TOGO, Kiichi HASHIMOTO, Kenji MORIHASHI, and Osamu KIKUCHI*
Department of Chemistry, University of Tsukuba, Tsukuba, Ibaraki 305
(Received February 16, 1988)

Synopsis. Several crown ethers and two side-armed polyethers which have reducible quinonoid groups were prepared. Some of them, **7a**, **7b**, and **7d**, showed highly enhanced cation-binding properties for the Na^+ cation upon electrochemical reduction.

The design of redox-switched crown ethers and polyethers has been achieved by several researchers. The reducible functions involved in these compounds are disulfide,[1] quinone derivatives,[2] and nitrobenzene.[3] Their complexation abilities with metal cations are accelerated by the interaction of metal cations and polyether functions, and also by the ionic interaction of reduced functions with metal cations upon electrochemical reduction. In general, Li^+ has a large binding enhancement in most of the redox crowns or polyethers due to the strong affinity of Li^+ to heteroatoms, i.e. oxygen or nitrogen during electrochemical reduction.[2,3] In the case of Na^+ and K^+, the binding enhancements depend on the structures of the host compounds; it is a very interesting problem to determine the new redox-switched compounds which have large binding enhancements for Na^+ and K^+ cations. Here, we report on a series of crown ethers and two side-armed polyethers having quinonoid groups as well as their cyclic voltammetric studies, both in the presence and absence of metal cations (Na^+ and K^+).

Results and Discussion

We prepared the compounds **7a—d** and **8a—c**, which were obtained from 3,5-dimethylphenol by the following procedure.

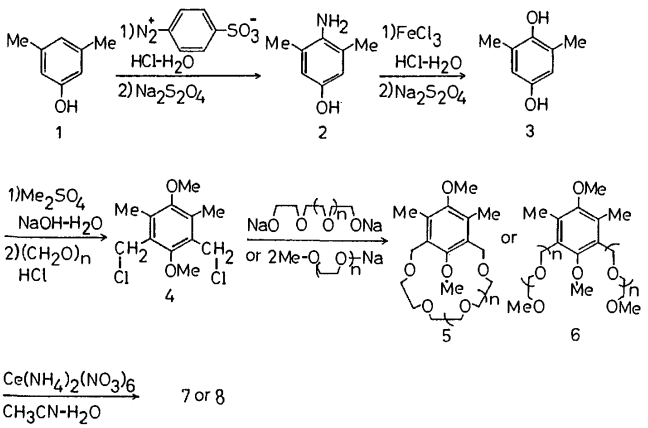

Cyclic voltammetric studies of **7** and **8** in acetonitrile were carried out in the presence of metal cations, Na^+ and K^+, in order to examine the relative complexing abilities of the neutral ligand and the reduced one with metal cations; the binding enhancement, K^2/K^1, upon a one-electron reduction was obtained from the shift values ($E^{o1}-E^{o2}$) by Eq. 1.[3]

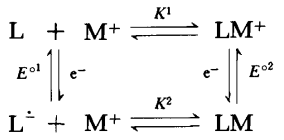

$$K^2/K^1 = \exp\left\{-\frac{F}{RT}(E^{o1}-E^{o2})\right\} \quad (1)$$

L : ligand, M^+: metal cation,
K^1 : binding constant for the neutral ligand,
K^2 : binding constant for the reduced ligand,
E^{o1} : redox potential for the free ligand,
E^{o2} : redox potential for the complex.

The binding enhancements and other electrochemical results are summarized in Table 1. In **7a**, the presence of Na^+ cation results in the observation of a new reduction peak, which corresponds to a one-electron reduction of the complex of crown **7a** and the Na^+ cation.

The cyclic voltammogram for the K^+ cation is reversible and the potential shift is small (0.10 V). Obviously, **7a** forms a 1-to-1 complex with Na^+ and K^+ cations during a one-electron reduction. Compounds **7b** and **7c** also form 1-to-1 complexes, both with Na^+ and K^+ cations, as shown in Table 1; compound **7b**, which has been reported by Cooper,[2a] exhibits large binding enhancements in both Na^+ and K^+ cations in acetonitrile, although Cooper used *N,N*-dimethylformamide as a solvent. Compound **7c** exhibits a small binding enhancement with both Na^+ and K^+ cations. Compound **7d** forms a 1-to-2 complex with the Na^+ cation, and its binding enhancement was the largest in the present ligands. On the other hand, **7d** forms a 1-to-1 complex with the K^+ cation and the binding enhancement was small. The binding enhancements of **8a—c** were found to be very small, though single-armed anthraquinone derivatives have large binding enhancements (ca. 10^2).[2c] We believe that one of the reasons is the result of a steric hindrance between two arms of **8** in the formation of a complex with metal cations during electrochemical reduction.

Experimental

Apparatus. ^1H NMR spectra were obtained on a JEOL FX-100 spectrometer. The chemical shifts are in ppm using TMS as an internal standard. IR spectra were measured on a

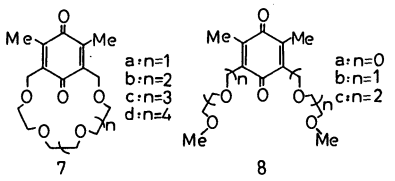

7 8

Table 1. Cation Dependance of Quinone Electrochemistry[a)]

Compound	M^+	Equiv	E^{c1}	E^{a1}	E^{o1}	E^{c2}	E^{a2}	E^{o2}	ΔE^{1-2}	Binding Enhancement (K^2/K^1)
7a[d)]	None	—	−0.67	−0.53	−0.60	—	—	—		
	Na^+	0.5	−0.64	−0.55	−0.60	−0.46	—	—	0.18[g)]	12×10^2
		1.0	—	—	—	−0.46	—	—		
	K^+	0.5	−0.63	−0.55	−0.59	−0.53	−0.45	−0.49	0.10	51
		1.0	—	—	—	−0.55	−0.43	−0.49		
7b[d)]	None	—	−-0.66	−0.56	−0.61	—	—	—		
	Na^+	0.5	−0.64	−0.56	−0.60	−0.46	−0.37	−0.42	0.18	12×10^2
		1.0	—	—	—	−0.46	−0.35	−0.41		
									0.12[c)]	
	K^+	0.5	−0.63	−0.57	−0.60	−0.46	−0.36	−0.41	0.19	18×10^2
		1.0	—	—	—	−0.46	−0.36	−0.41		
									0.13[c)]	
7c[d)]	None	—	−0.67	−0.55	−0.61	—	—	—		
	Na^+	0.5	−0.65	−0.57	−0.61	−0.52	−0.44	−0.48	0.13	166
		1.0	—	—	—	−0.54	−0.41	−0.48		
	K^+	0.5				−0.58[b)]	−0.45[b)]	−0.52		
		1.0	—	—	—	−0.55	−0.45	−0.50	0.11	76
7d[e)]	None	—	−0.65	−0.55	−0.60	—	—	—		
	Na^+	0.5	−0.65	−0.54	−0.60	−0.43	−0.35	−0.39	0.21	38×10^2
		1.0	−0.62	−0.55	−0.59	−0.43	−0.32	−0.38	0.21	
		1.5	−0.61	−0.55	−0.58	−0.43	−0.31	−0.37	0.21	
		2.0	—	—	—	−0.43	−0.30	−0.37		
	K^+	0.5				−0.63[b)]	−0.48[b)]	−0.56		
		1.0	—	—	—	−0.58	−0.46	−0.52	0.08	23
8a[f)]	None	—	−0.71	−0.61	−0.66	—	—	—		
	Na^+	1.0				−0.71	−0.58	−0.65	0.01[h)]	2
	K^+	1.0				−0.71	−0.61	−0.66	0.00[h)]	1
8b[f)]	None	—	−0.71	−0.61	−0.66	—	—	—		
	Na^+	1.0				−0.67	−0.53	−0.60	0.06[h)]	10
	K^+	1.0				−0.70	−0.60	−0.65	0.01[h)]	2
8c[f)]	None	—	−0.70	−0.60	−0.65	—	—	—		
	Na^+	1.0				−0.66	−0.50	−0.58	0.07[h)]	15
	K^+	1.0				−0.68	−0.57	−0.63	0.02[h)]	2

a) Quinone crown concentration 2 mM in CH_3CN containing 0.1 M Bu_4NClO_4 under Ar atmosphere. b) These peaks were broad. c) Quinone crown concentration 1 mM in DMF containing 0.1 M Et_4NClO_4 in the presence of 0.1 M $NaClO_4$ or KBF_4 (see to Ref. 2a). d) At 22 °C. e) At 23 °C. f) At 24 °C. g) Obtained from the difference between E^{c1} and E^{c2}. h) Obtained from the difference between E^{o1} (in the absence of metal cation) and E^{o2} (in the presence of metal cation).

Hitachi 260-50 spectrometer. Mass spectra were obtained with a Hitachi High MS M-80B mass spectrometer. Cyclic voltammograms were obtained by using a Hokuto Denko HB-104 and an HA-303.

Preparation of 1,4-Dimethoxy-2,6-bis(chloromethyl)-3,5-dimethylbenzene (4). Compound **4** was obtained by a known method from 3,5-dimethylphenol. 3,5-Dimethyl-4-aminophenol; mp 185—186 °C (lit,[4)] mp 181.5—182.5 °C). 2,6-Dimethylhydroquinone; mp 153—154 °C (lit,[4)] mp 150—151 °C). 1,4-Dimethoxy-2,6-dimethylbenzene; bp 90—93 °C/4 mmHg (lit,[5)] bp 80—82 °C/2 mmHg, 1 mmHg=133.322 Pa). 1,4-Dimethoxy-2,6-dimethylbenzene was treated with paraformaldehyde in concd hydrochloric acid solution under a closed system at about 60 °C overnight to give the desired chloromethylated compound **4** in 39% yield. 1,4-Dimethoxy-2,6-bis(chloromethyl)-3,5-dimethylbenzene; mp 143.0—143.5 °C (lit,[6)] mp 141.5—142.0 °C).

Preparation of Compounds 7 and 8. To the THF (100 ml) solution of 4506 mg (95%, 28.5 mmol) of triethylene glycol was added 3420 mg (60%, 85.5 mmol) of sodium hydride under cooling with an ice bath and stirred for 20 min. Then, both the above THF solution of disodium salt of triethylene glycol and the THF (100 ml) solution of 7500 mg (28.5 mmol) of 1,4-dimethoxy-2,6-bis(chloromethyl)-3,5-dimethylbenzene were added slowly with dropping funnels, respectively, to the THF (100 ml) solution in a three-necked flask which was cooled with an ice bath under an Ar atmosphere. After the addition, the reaction mixture was stirred at room temperature overnight. The solvent was removed and the residue was poured into water; the solution was then extracted with dichloromethane twice and the organic layer was dried over $MgSO_4$. After removing the solvent, the residue was chromatographed on silica gel (eluent; ethyl acetate) to give 2035 mg of **5a**.

5a; 21%; oil; ^{1}H NMR ($CDCl_3$) δ=2.35 (s, 6H, CH_3), 3.10—3.80 (m, 12H, $-CH_2CH_2-$), 3.67 (s, 3H, OCH_3), 3.68 (s, 3H, OCH_3), 4.58 (d, 2H, J=11.4 Hz, CH-H), and 4.76 (d, 2H, J=11.4 Hz, CH-H); IR (NaCl) 1080 and 1250 cm^{-1}; Found: C, 63.18; H, 8.30%. Calcd for $C_{18}H_{28}O_6$: C, 63.50; H, 8.29%.

5b; 30%; mp 97—99 °C; ^{1}H NMR ($CDCl_3$) δ=2.32 (s, 6H, CH_3), 3.40—3.70 (m, 20H, $-CH_2CH_2-$), 3.66 (s, 3H, OCH_3), 4.00 (s, 3H, OCH_3), and 4.60 (s, 4H, CH_2); IR (NaCl) 1115 cm^{-1}; Found: C, 62.21; H, 8.43%. Calcd for $C_{20}H_{32}O_7$: C, 62.48; H, 8.38%.

5c; 35%; mp 61—62 °C; ^{1}H NMR ($CDCl_3$) δ=2.32 (s, 6H, CH_3), 3.54 (s, 3H, OCH_3), 3.50—3.70 (m, 20H, $-CH_2CH_2-$), 3.93 (s, 3H, OCH_3), and 4.55 (s, 4H, CH_2); Found: C, 61.27; H, 8.49%. Calcd for $C_{22}H_{36}O_8$: C, 61.66; H, 8.46%; IR (NaCl) 1110 cm^{-1}.

5d; 10%; oil; ^{1}H NMR ($CDCl_3$) δ=2.32 (s, 6H, CH_3), 3.50—3.70 (m, 24H, $-CH_2CH_2-$), 3.66 (s, 3H, OCH_3), 3.86 (s, 3H, OCH_3), and 4.58 (s, 4H, CH_2); IR (NaCl) 1115 cm^{-1}; Found: C, 60.67; H, 8.65%. Calcd for $C_{24}H_{40}O_9$: C, 60.99; H, 8.53%.

Two side-armed polyethers were obtained by the same procedure.

6a; 100%; mp 142—143 °C: ^{1}H NMR ($CDCl_3$) δ=2.31 (s, 6H, CH_3), 3.41 (s, 6H, OCH_3), 3.66 (s, 3H, aromatic OCH_3), 3.77 (s, 3H, aromatic OCH_3), and 4.47 (s, 4H, CH_2); IR (NaCl) 1255 and 1080 cm^{-1}; Found: C, 66.14; H, 8.82%. Calcd for $C_{14}H_{22}O_4$: C, 66.11; H, 8.71%.

6b; 100%; oil; ^{1}H NMR ($CDCl_3$) δ=2.32 (s, 6H, CH_3), 3.37 (s, 6H, OCH_3), 3.50—3.70 (m, 8H, $-CH_2CH_2-$), 3.66 (s, 3H, aromatic OCH_3), 3.77 (s, 3H, aromatic OCH_3), and 4.58 (s, 4H, CH_2); IR (NaCl) 1090 cm^{-1}; Found: C, 63.07; H, 8.90%. Calcd for $C_{18}H_{30}O_6$: C, 63.13; H, 8.83%.

6c; 100%; oil; ^{1}H NMR ($CDCl_3$) δ=2.32 (s, 6H, CH_3), 3.37 (s, 6H, OCH_3), 3.77 (s, 3H, aromatic OCH_3), 3.66 (s, 3H, aromatic OCH_3), 3.50—3.70 (m, 16H, $-CH_2CH_2-$), and 4.57 (s, 4H, CH_2); IR (NaCl) 1110 cm^{-1}; Found: C, 61.32; H, 8.97%. Calcd for $C_{22}H_{38}O_8$: C, 61.37; H, 8.89%.

Dimethyl crown compound **5a**, 1.31 g (3.85 mmol), which was obtained above, was dissolved in 12 ml of acetonitrile; then, 12 ml of water solution of 5.30 g (9.63 mmol) of cerium (IV) diammonium nitrate was added to the solution and stirred for 45 min at room temperature. After the reaction, the reaction mixture was poured into dichloromethane and washed twice with water. The organic layer was dried over $MgSO_4$. After removing the solvent, the residue was chromatographed on silica gel (eluent: ethyl acetate) to give 0.94 g of **7a**. Compounds **7b—d** and **8a—c** were obtained by the same procedure.

7a; 79%; mp 56—59 °C; ^{1}H NMR ($CDCl_3$) δ=2.12 (s, 6H, CH_3), 3.50—3.70 (m, 12H, $-CH_2CH_2-$), and 4.53 (s, 4H, CH_2); IR (NaCl) 1655, 1135, and 1080 cm^{-1}; Found: C, 61.96; H, 7.13; MS (70 eV) m/z 310 (M^+). Calcd for $C_{16}H_{22}O_6$: C, 61.92; H, 7.14; M, 310.

7b; 31%; oil; ^{1}H NMR ($CDCl_3$) δ=2.13 (s, 6H, CH_3), 3.50—3.70 (m, 16H, $-CH_2CH_2-$), and 4.47 (s, 4H, CH_2); Found: C, 60.31; H, 7.43%; MS (70 eV) m/z 354 (M^+). Calcd for $C_{18}H_{26}O_7$: C, 61.00; H, 7.39%; M, 354; IR (NaCl) 1115 and 1650 cm^{-1}.

7c; 67%; oil; ^{1}H NMR ($CDCl_3$) δ=2.14 (s, 6H, CH_3), 3.60—3.70 (m, 20H, $-CH_2CH_2-$), and 4.48 (s, 4H, CH_2); IR (NaCl) 1650 and 1110 cm^{-1}; Found: C, 59.85; H, 7.64%; MS (70 eV) m/z 398 (M^+). Calcd for $C_{20}H_{30}O_8$: C, 60.28; H, 7.58%; M, 398.

7d; 60%; mp 48—51 °C; ^{1}H NMR ($CDCl_3$) δ=2.15 (s, 6H, CH_3), 3.50—3.70 (m, 24H, $-CH_2CH_2-$), and 4.49 (s, 4H, CH_2); IR (NaCl) 1650 and 1090 cm^{-1}; Found: C, 59.17; H, 7.69%; MS (70 eV) m/z 442 (M^+). Calcd for $C_{22}H_{34}O_9$: C, 59.71; H, 7.74%; M, 442.

8a; 94%; mp 47—48 °C; ^{1}H NMR ($CDCl_3$) δ=2.14 (s, 6H, CH_3), 3.38 (s, 6H, OCH_3), and 4.37 (s, 4H, CH_2); IR (NaCl) 1645 and 1095 cm^{-1}; Found: C, 64.11; H, 7.24%. Calcd for $C_{12}H_{16}O_4$: C, 64.27; H, 7.19%.

8b; 92%; oil; ^{1}H NMR ($CDCl_3$) δ=2.15 (s, 6H, CH_3), 3.36 (s, 6H, OCH_3), 3.50—3.70 (m, 8H, $-CH_2CH_2-$), and 4.47 (s, 4H, CH_2); IR (NaCl) 1640 and 1090 cm^{-1}; Found: C, 61.40; H, 7.77%. Calcd for $C_{16}H_{24}O_6$: C, 61.52; H, 7.74%.

8c; 84%; oil; ^{1}H NMR ($CDCl_3$) δ=2.15 (s, 6H, CH_3), 3.37 (s, 6H, OCH_3), 3.50—3.70 (m, 16H, $-CH_2CH_2-$), and 4.46 (s, 4H, CH_2); IR (NaCl) 1650 and 1110 cm^{-1}; Found: C, 59.82; H, 8.04%. Calcd for $C_{20}H_{32}O_8$: C, 59.98; H, 8.05%.

Reagents for Electrochemistry. Acetonitrile was distilled from CaH_2. Tetrabutylammonium perchlorate was twice recrystallized from ethyl acetate and alkali metal perchlorate salts were recrystallized from deionized water and dried over vacuum pumping at 100 °C. All these salts were stored in a desiccator, and samplings were carried out under an N_2 atmosphere in a dry box.

Cyclic Voltammetry Experiments. A 2 mM solution (1 M=1 mol dm^{-3}) of substrate was prepared by mixing of 0.1 mmol of quinone derivative, 1701 mg (5 mmol) of Bu_4NClO_4, and 50 ml of acetonitrile. Pt metallic working electrode (Beckman 39273) and Pt wire as the counter electrode were used. $E°$ values were reported vs. saturated calomel electrode (SCE). A scan rate of 200 mV s^{-1} was used. 25 ml of the solution was added to a cell equipped with a magnetic stirrer and an inlet for an Ar atmosphere. After 30 min of Ar purging and stirring, cyclic voltammograms were recorded under unstirred conditions. Also, 0.5, 1.0, 1.5, and 2.0 equiv metal perchlorate solutions were prepared by the same procedure with 0.1 mmol of quinone derivative, 5 mmol of Bu_4NClO_4, and 50 ml of acetonitrile.

The authors wish to express their thanks to Professor Naomichi Furukawa for his helpful advice and Professor Yasumasa Kuwabara for valuable help with MS measurements in University of Tsukuba.

References

1) S. Shinkai, K. Inuzuka, O. Miyazaki, and O. Manabe, *J. Am. Chem. Soc.*, **107**, 3950 (1985).

2) a) R. E. Wolf and S. R. Cooper, *J. Am. Chem. Soc.*, **106**, 4646 (1984); b) K. Maruyama, H. Sohmiya, and H. Tsukube, *Tetrahedron Lett.*, **26**, 3583 (1985); c) D. A. Gustowski, M. Delgado, V. J. Gatto, L. Echegoyen, and G. W. Gokel, *J. Am. Chem. Soc.*, **108**, 7553 (1986); d) K. Sugihara, H. Kamiya, M. Yamaguchi, T. Kaneda, and S. Misumi, *Tetrahedron Lett.*, **22**, 1619 (1981); e) T. Kaneda, K. Sugihara, H. Kamiya, and S. Misumi, *ibid.*, **22**, 4407 (1981); f) M. Delgado, D. A. Gustowski, H. K. Yoo, V. J. Gatto, G. W. Gokel, and L. Echegoyen, *J. Am. Chem. Soc.*, **110**, 119 (1988).

3) A. Kaifer, D. A. Gustowski, L. Echgoyen, V. J. Gatto, R. A. Schultz, T. P. Cleary, C. R. Morgan, D. M. Goli, A. M. Rios, and G. W. Gokel, *J. Am. Chem. Soc.*, **107**, 1958 (1985).

4) Y. Nomura, *Sci. Papers Coll. Gen. Educ. Univ. Tokyo*, **11**, 43 (1961).

5) J. L. G. Nilsson, H. Sievertsson, and H. Selander, *Acta Chem. Scand.*, **22**, 3160 (1968).

6) G. Manecke and H. J. Beyer, *Makromol. Chem.*, **105**, 59 (1967).

A Facile Syntehsis of 2-Substituted Azetidines[1)]

Tatsuya SHONO,* Yoshihiro MATSUMURA, Kenshi UCHIDA, and Fumihiko NAKATANI
Department of Synthetic Chemistry, Faculty of Engineering, Kyoto University, Yoshida Sakyo, Kyoto 606
(Received March 7, 1988)

Synopsis. A new method for the synthesis of 2-substituted azetidines has been exploited. The method consists of (1) anodic acetoxylation of 1-(*p*-tolylsulfonyl)azetidine at the 2-position and (2) subsequent nucleophilic substitution of the acetoxyl group with nucleophiles such as trimethylsilyl cyanide, allyltrimethylsilane, 2-acetoxyfuran, and trimethyl phosphite.

Although formation of 2-carbanions of azetidines followed by introduction of electrophiles to the 2-position has been recently reported,[2)] the opposite methods introducing nucleophiles (Nu^-) to the 2-position of azetidines have been unknown so far. We wish to report a new method for introducing Nu^- to the 2-position of azetidines. Our method consists of (1) anodic acetoxylation of 1-(*p*-tolylsulfonyl)azetidines **1** at the 2-position and (2) subsequent nucleophilic substitution of the acetoxyl group with a variety of Nu^- (Eq. 1).[3)]

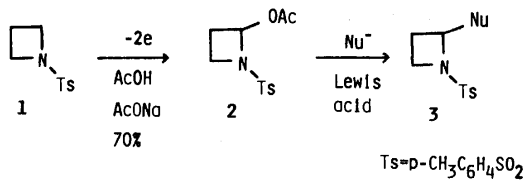

(1)

The advantages of this method are (i) the starting compound **1** is easily available, and (ii) a variety of substituents can be introduced to the 2-position of the azetidine skeleton.

The procedure of anodic oxidation is simple as described in the experimental section. The yield of **2** was 70%. The anodic oxidation of **4** under similar conditions gave **5** in 59% yield (Eq. 2).

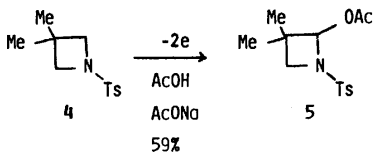

(2)

Although anodic oxidation of 1-formylazetidine and 1-(methoxycarbonyl)azetidine under similar conditions also gave the 2-acetoxylated products in 42 and 20% yields, respectively, compound **1** seems to be the most useful intermediate to the preparation of 2-substituted azetidines, since the synthesis of 1-formylazetidine and 1-(methoxycarbonyl)azetidine requires azetidine itself as the precursor, while **1** can easily be prepared from 3-amino-1-propanol.[6)] The anodic oxidation of **1** may proceed with direct electron transfer from **1** to anode, since the oxidation peak of **1**

Table 1. Reaction of **2** with Nucleophiles

Nucleophiles (equiv)		Lewis acid (equiv)		Condition	Product (Yield/%)
Me_3SiCN	(1.2)	$TiCl_4$	(1)	−70 °C, 2 h then r.t., 1 h	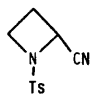 **3a** (68)
	(1.5)	$TiCl_4$	(1)	−70 °C to r.t., 2.5 h	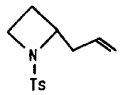 **3b** (62)
6[a)]	(1.2)	$TiCl_4$	(1)	−70 °C, 5 h	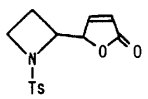 **3c** (38)
6[a)]	(1.2)	BF_3OEt_2	(1)	−18 °C, 15 min then r.t., 4 h	**3c** (36)
$P(OMe)_3$ **7**	(1.2)	$TiCl_4$	(1)	−70 °C, 2h	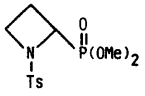 **3d** (34)
7	(1.2)	BF_3OEt_2	(1)	−18 °C, 10 min then r.t., 23 h	**3d** (43)

a) See Ref. 7.

was observed at 2.60 V vs. SCE in acetonitrile.

The reaction of **2** with various Nu^- in the presence of Lewis acid catalysts gave **3a—d** in the yields shown in Table 1. In conclusion, this method provides a new synthetic route to various 2-substituted azetidines.

Experimental

Proton nuclear magnetic resonance spectra were measured on a Varian Associates EM-360 or EM-390 spectrometer with chemical shifts given in parts per million (δ) downfield from tetramethylsilane as an internal standard. Infrared spectra were recorded on a Hitachi 260-10 spectrometer. Elemental analyses were determined by the Center for Instrumental Analysis of Kyoto University. Electrooxidation was carried out using a DC power supply (GD 050-2) of Takasago Seisakusho. Ltd. 1-(*p*-Tolylsulfonyl)azetizine (**1**)[6] and 1-formylazetidine[8] were synthesized according to the reported methods.

1-(Methoxycarbonyl)azetidine was prepared similarly to the synthesis of 1-(ethoxycarbonyl)azetidine[8] (73% yield): bp 80 °C (20 mmHg (1 mmHg≈133.322 Pa), bulb-to-bulb); IR(neat) 2970, 2900, 1715, 1455, 1392, 1200, 1145, 1000, 780 cm^{-1}; ^1H NMR ($CDCl_3$) δ=2.16 (quint, 2H, J=7.0 Hz), 3.55 (s, 3H), 3.89 (t, 4H, J=7.0 Hz); MS, m/z 115(M^+), 100, 59, 56, 41(base); Found: C, 52.01; H, 7.93; N, 11.97%. Calcd for $C_5H_9NO_2$: C, 52.16; H, 7.88; N, 12.17%.

1-(*p*-Tolylsulfonyl)-3,3-dimethylazetidine (4) was prepared from 2,2-dimethyl-3-amino-1-propanol similarly according to the synthesis of **1**[6] (77% yield in two steps): mp 60—62 °C; IR(KBr) 2950, 2860, 1595, 1453, 1340, 1232, 1168, 1090, 1060, 825 cm^{-1}; ^1H NMR ($CDCl_3$) δ=1.70 (s, 6H), 2.47 (s, 3H), 3.49 (s, 4H), 7.47 (d, 2H, J=9.0 Hz), 7.82 (d, 2H, J=9.0 Hz); Found: C, 60.25; H, 7.07; N, 5.71; S. 13.32%. Calcd for $C_{12}H_{17}NO_2S$: C, 60.22; H, 7.16; N, 5.85; S, 13.40%.

Anodic Oxidation of 1. Into a cell equipped with a carbon rod cathode (8 mmϕ) and a platinum anode (2 cm×2 cm) was placed a solution of **1** (422 mg, 2 mmol) and sodium acetate (1g, 12 mmol) in acetic acid (20 mL). After having been passed 40 F mol^{-1} of electricity at room temperature (current density; 50 mA cm^{-2}, terminal voltage; 40 V), the mixture was poured into water and the organic portion was extracted with CH_2Cl_2. The solvent was removed in vacuo and the residue was subjected to preparative TLC (silica gel, AcOEt : hexane=1 : 2) to yield **2** (376 mg, 1.4 mmol, 70% yield): IR (KBr) 2950 (br), 1745, 1605, 1360, 1240, 1175, 1160, 1115, 1060, 850, 680 cm^{-1}; ^1H NMR ($CDCl_3$) δ=1.93—2.67 (m, 2H), 2.10 (s, 3H), 2.48 (s, 3H), 3.22—4.00 (m, 2H), 6.16 (t, 1H, J=6.0 Hz), 7.41 (d, 2H, J=9.0 Hz), 7.86 (d, 2H, J=9.0 Hz); Found: C, 53.55; H, 5.57; N, 4.91; S, 11.87%. Calcd for $C_{12}H_{15}NO_4S$: C, 53.52; H, 5.61; N, 5.20; S, 11.90%.

Anodic oxidation of 4, 1-formylazetidine, and 1-(methoxycarbonyl)azetidine in a similar manner to the anodic oxidation of **1** gave the corresponding 2-acetoxylated products.

5: 59% yield at 180 F mol^{-1} of electricity; IR (KBr) 2980, 1750, 1604, 1360, 1228, 1169, 1062 cm^{-1}; ^1H NMR ($CDCl_3$) δ=0.94 (s, 3H),1.16 (s, 3H), 2.12 (s, 3H), 2.49 (s, 3H), 3.16 (d, 1H, J=7.0 Hz), 3.41 (d, 1H, J=7.0 Hz), 5.75 (s, 1H), 7.45 (d, 2H, J=9.0 Hz), 7.85 (d, 2H, J=9.0 Hz); Found: C, 56.60; H, 6.62; N, 4.71; S, 10.50%. Calcd for $C_{14}H_{19}NO_4S$: C, 56.55; H, 6.44; N, 4.71; S, 10.78%.

2-Acetoxy-1-formylazetidine: 42% yield at 200 F mol^{-1} of electricity; IR (neat) 2980, 2900, 1745, 1675, 1460, 1405, 1228, 1100, 859 cm^{-1}; ^1H NMR ($CDCl_3$) δ=2.17 (s, 3H), 2.20—3.00 (m, 2H), 3.80—4.20 (m, 2H), 6.31—6.51 (m, 1H), 8.33—8.56 (br, 1 H); Found: C, 50.71; H, 6.30; N, 9.60%. Calcd for $C_6H_9NO_3$: C, 50.34; H, 6.34; N, 9.79%.

2-Acetoxy-1-(methoxycarbonyl)azetidine; 20% yield at 180 F mol^{-1} of electricity; ^1H NMR ($CDCl_3$) δ=2.00—2.90 (m, 2H), 2.13 (s, 3H), 3.73 (s, 3H), 3.70—4.10 (m, 2H), 6.25—6.43 (m, 1H); Found: C, 48.90; H, 6.31; N, 8.01%. Calcd for $C_7H_{11}NO_4$: C, 48.55; H, 6.40; N, 8.09%.

Reaction of 2 with Nucleophiles. A typical procedure is exemplified by the synthesis of 2-cyano-1-(*p*-tolylsulfonyl)-azetidine (**3a**): To a stirred solution of **2** (200 mg, 1.86 mmol) and trimethylsilyl cyanide (222 mg, 2.24 mmol) in CH_2Cl_2 was added dropwise $TiCl_4$ (0.2 mL, 1.86 mmol) at −70 °C under an atmosphere of nitrogen. The mixture was stirred at the temperature for 2 h and warmed to room temperature. Then, the reaction mixture was poured into water, and extracted with CH_2Cl_2. Drying and evaporation of the solvent gave a residue, which was subjected to a silica-gel chromatography (AcOEt : hexane=1 : 5) to yield **3a** (299 mg, 1.265 mmol, 68% yield): mp 106—108 °C; IR (neat) 2250, 1600, 1350, 1165, 1100, 820, 675 cm^{-1}; ^1H NMR ($CDCl_3$) δ=1.87—2.97 (m, 2H), 2.50 (s, 3H), 3.64—4.15 (m, 2H), 4.69 (t, 1H, J=9.5 Hz), 7.43 (d, 2H, J=8.3 Hz), 7.86 (d, 2H, J=8.3 Hz); MS, m/z 236 (M^+), 155, 91 (base), 81; Found: C, 55.75; H, 5.14; N, 11.54; S, 13.33%. Calcd for $C_{11}H_{12}N_2O_2S$: C, 55.92; H, 5.13; N, 11.86; S, 13.57%.

Data for new compounds **3b—d** are shown below.

3b: IR (neat) 3080, 2985, 1645, 1600, 1500, 1455 (br), 1345, 1305, 1295, 1240, 1163, 1100, 1000, 925, 820, 780, 735, 715, 670 cm^{-1}; ^1H NMR ($CDCl_3$); δ=1.59—2.12 (m, 2H), 2.28—2.60 (m, 2H), 2.41 (s, 3H), 3.18—4.13 (m, 3H), 4.72—5.15 (m, 2H), 5.37—6.06 (m, 1H), 7.23 (d, 2H, J=8.3 Hz), 7.63 (d, 2H, J=8.3 Hz); MS, m/z 251 (M^+), 210 (base), 155, 91; Found: C, 62.24; H, 6.89; N, 5.65; S, 12.51%. Calcd for $C_{13}H_{17}NO_2S$: C, 62.12; H, 6.82; N, 5.57; S, 12.76%.

3c: Mp 130—133 °C; IR (KBr) 1795, 1760, 1610, 1600, 1343, 1315, 1252, 1168, 1101, 1028, 900, 823 cm^{-1}; ^1H NMR ($CDCl_3$) δ=1.90—2.41 (m, 2H), 2.51 (s, 3H), 3.67 (t, 2H, J=8.0 Hz), 4.48—4.73 (m, 1H), 5.29—5.44 (m, 1H), 6.29—6.43 (m, 1H), 7.57 (d, 2H, J=9.0 Hz), 7.81—7.96 (m, 1H), 7.92 (d, 2H, J=9.0 Hz); Found: C, 57.49; H, 5.33; N, 4.77; S, 10.70%. Calcd for $C_{14}H_{15}NO_4S$: C, 57.32; H, 5.15; N, 4.78; S, 10.93%.

3d: Isolated by alumina chromatography; mp 86—87 °C; IR (KBr) 2960 (br), 1600, 1460 (br), 1355, 1250, 1170, 1100, 1075, 1030, 850, 825, 775, 720, 670 cm^{-1}; ^1H NMR ($CDCl_3$) δ=1.86—2.97 (m, 2H), 2.48 (s, 3H), 3.70 and 3.76 (2s, 3H), 3.89 and 3.94 (2s, 3H), 3.57—4.53 (m, 3H), 7.44 (d, 2H, J=9.0 Hz), 7.85 (d, 2H, J=9.0 Hz); Found: C, 45.20; H, 5.67; N, 4.28; P, 9.41%. Calcd for $C_{12}H_{18}NO_5SP$: C, 45.14; H, 5.86; N, 4.39; P, 9.70%.

Oxidation Potentials. Oxidation peak potential of **1** was measured at room temperature by using an H-type cell, a potentiostat HA-104 and function generator HB-107A (Hokuto Denko Ltd.) under the following conditions; scan rate: 100 mV s^{-1}; electrordes: platinum anode and cathode; E_p, 2.60 V vs. SCE (4.74×10^{-3} M (1M=1 mol dm^{-3})), 2.70 V vs. SCE (9.50×10^{-3} M) in CH_3CN–0.1 M $LiClO_4$.

References

1) Electroorganic Chemistry 97.

2) W. Wykypiel, J. J. Lohmann, and D. Seebach, *Helv. Chim. Acta*, **64**, 1337 (1981).

3) Anodic α-methoxylation of *N*-protected amines and a variety of reactions of the α-methoxylated products with nucleophiles have already been reported by us.[4] However, anodic methoxylation of **1**, 1-formylazetidine, and 1-(methoxycarbonyl)azetidine under conditions of the α-methoxylation did not always give satisfactory results, though the anodic 2-methoxylation of 1-formyl-2,2-dimethylazetidine has been reported as the only example.[5]

4) T. Shono, Y. Matsumura, and K. Tsubata, *J. Am. Chem. Soc.*, **103**, 1172 (1981); T. Shono, Y. Matsumura, K.

Tsubata, K. Uchida, T. Kanazawa, and K. Tsuda, *J. Org. Chem.*, **49**, 3711 (1984); T. Shono, Y. Matsumura, and K. Tsubata, *Tetrahedron Lett.*, **22**, 2411 (1981); T. Shono, Y. Matsumura, and K. Tsubata, *ibid.*, **22**, 3249, (1981); T. Shono, Y. Matsumura, K. Tsubata, and J. Takata, *Chem. Lett.*, **1981**, 1121; T. Shono, Y. Matsumura, K. Uchida, and H. Kobayashi, *J. Org. Chem.*, **50**, 3243, (1985).

5) K. Warning, M. Mitzlaff, and H. Jensen, *Liebigs Ann. Chem.*, **1978**, 1713.

6) W. R. Vaughan, R. S. Klonowski, R. S. McElhinney, and B. B. Millward, *J. Org. Chem.*, **26**, 138 (1961).

7) The preparation of 2-acetoxyfuran: T. Shono, Y. Matsumura, and S. Yamane, *Tetrahedron Lett.*, **22**, 3269 (1981).

8) J. C. Sheehan, and R. W. Tulis, *J. Org. Chem.*, **39**, 2264 (1974).

 © 1988 The Chemical Society of Japan Bull. Chem. Soc. Jpn., 61, 3033—3036 (1988)

Molecular Structure of Trimethylphosphine-Borane as Determined from Electron Diffraction and Microwave Spectroscopic Data

Kinya IIJIMA,* Yumi HAKAMATA, Takashi NISHIKAWA, and Shuzo SHIBATA
Department of Chemistry, Faculty of Science, Shizuoka University,
Oya, Shizuoka 422
(Received January 13, 1988)

The molecular structure of trimethylphosphine-borane has been determined from gas electron diffraction and spectroscopic data. The molecular parameters and their uncertainties are r_g(B-H)=1.225±0.011 Å, r_g(P-B)=1.899±0.006 Å, r_g(C-P)=1.815±0.003 Å, r_g(C-H)=1.103±0.002 Å, ∠HBH=108.6±0.6°, and ∠CPC=104.6±0.3°. The P-B distance of this complex is about 0.04 Å shorter than those of trimethylphosphine-boron trihalides.

Molecular structures of trimethylamine-borane and trimethylamine-boron trifluoride have been sudied by electron diffraction and microwave spectroscopic methods in the gas phase.[1-6] The molecular structures determined from microwave spectroscopic data, however, were found to be significantly different from those determined from electron diffraction data. Since a trimethylamine complex with borane or boron trifluoride has C_{3v} symmetry, the number of the rotational constants used in the structural analysis was limited and some molecular parameters had to be assumed in the microwave spectroscopic method. These assumptions were not necessary in electron diffraction, though electron diffraction data were less precise than microwave spectroscopic data. Therefore the joint analysis of electron diffraction and microwave spectroscopic data yielded highly accurate molecular parameters.[2,3]

The structural parameters of trimethylphosphine-borane have also been determined from the rotational constants of $(CH_3)_3P\cdot{}^{11}BH_3$, $(CH_3)_3P\cdot{}^{10}BH_3$, $CD_3(CH_3)_2P\cdot{}^{11}BH_3$, and $(CH_3)_3P\cdot{}^{11}BDH_2$.[7] We have reported in the study of $(CH_3)_3N\cdot BH_3$ that the substitution of D for H causes shortening of the B-H distance and opening of the HBH angle.[3] The microwave spectroscopic study, where isotopic molecules were assumed to have the same molecular dimension as the normal species, might have given incorrect molecular parameters as shown in the studies on trimethylamine complexes. Thus we reinvestigated the molecular structure of gaseous trimethylphosphine-borane by using both electron diffraction and microwave spectroscopic data.

Experimental

Diborane was prepared by the reaction of orthophosphoric acid and potassium tetrahydroborate,[8] and trimethylphosphine was obtained by the decomposition of trimethylphosphine-silver iodide complex at 200 °C.[9] The diborane and trimethylphosphine were allowed to react in a glass tube cooled by Dry Ice-acetone. The crude complex was purified by sublimation under reduced pressure. The purity was checked from the IR absorption spectra.

Electron diffraction photographs were taken by the use of an r³-sector on Kodak Electron-Image plates at camera distances of 293.79 and 143.85 mm. The sample was sublimed at 349 K by a high temperature nozzle. The accelerating voltage was about 40 kV and the wavelength was determined from the diffraction patterns of thallium(I) chloride.[10] The exposure times were about 30 and 105 s for the long and the short camera-distance photographs, respectively, with an electron-beam current of 0.8 μA. The pressure in the diffraction chamber was 1.5×10^{-3} Pa during the experiment. Two photographic plates taken at the long camera distance and three plates taken at the short camera distance were selected for the intensity measurement by a digital microphotometer. The electron diffraction unit and the digital microphotometer used in the present study have been described elsewhere.[11]

Analysis and Results

The scattering intensities in the range of q=10.0—53.5 Å^{-1} were obtained from the long camera-distance plates and those in the range of q=20.0—107.0 Å^{-1} from the short camera-distance plates. Here q represents $(40/\lambda)\sin(\theta/2)$, where λ is the wavelength

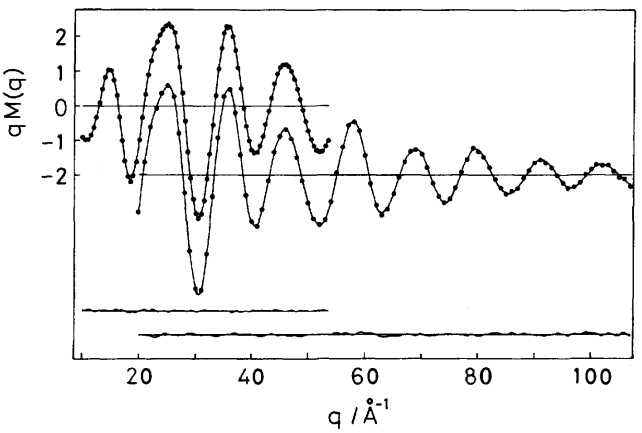

Fig. 1. Molecular intensities for trimethylphosphine-borane. The upper curve is the long camera-distance data and the lower the short camera-distance data. Dots represent the observed ones and solid curves the calculated ones. The residuals are shown at the lower part of the figure.

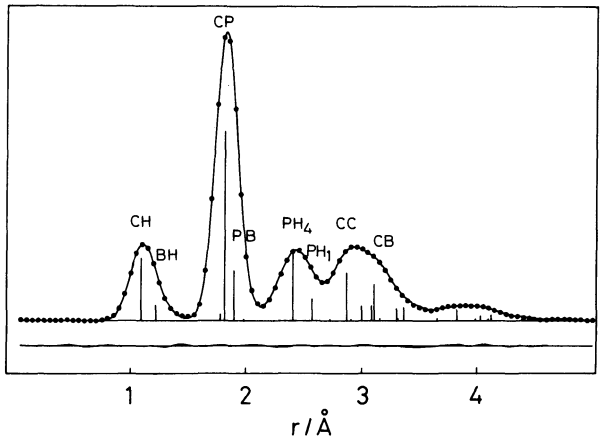

Fig. 2. Radial distribution curve for trimethylphosphine-borane. Dots represent the experimental one, solid curve the theoretical one, and the difference is shown below. The vertical bars represent bond distances and the scattering powers.

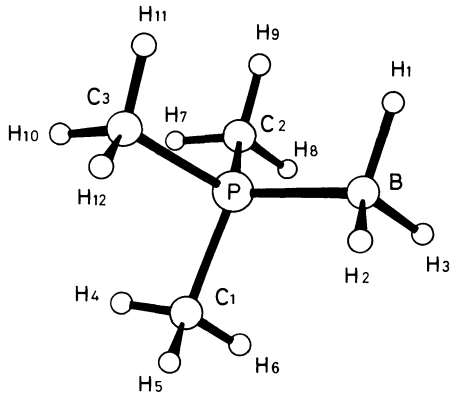

Fig. 3. Molecular model and numbering of atoms in trimethlphosphine-borane.

and θ is the scattering angle. They were leveled by using theoretical backgrounds, and the intensities for each camera distance were averaged. The elastic and inelastic scattering factors were taken from Refs. 12—14. The experimental molecular intensities obtained are shown in Fig. 1. Figure 2 shows the experimental radial distribution function. The molecular model of trimethylphosphine-borane and the numbering of the atoms are shown in Fig. 3.

It was assumed that the molecule of $(CH_3)_3P \cdot BH_3$ has C_{3v} symmetry in a staggered form and the methyl groups also have C_{3v} symmetry. The latter local C_3 axes were assumed to be coincident with the C-P bond. The r_α parameters[15] determined by least-squares analyses were r(B-H), r(P-B), r(C-P), r(C-H), r(C-C), r(H-(B)-H), and $\angle$PCH. Vibrational mean amplitudes and shrinkage corrections, $r_a - r_\alpha$,[15] were calculated from the reported force field,[16] where the force constants for the torsional vibration around the C-P and P-B bonds had not been estimated. The force

Table 1. Root-Mean-Square Amplitudes and Shrinkage Corrections for $(CH_3)_3P \cdot BH_3$ (in 10^{-4} Å unit)

	l	$r_a - r_\alpha$		l	$r_a - r_\alpha$
B-H_1	883	375	P-C_1	557	23
P-B	598	37	P-H_4	1110	164
B-C_1	1105	−12	C_1-C_2	1096	−10
B-H_4	1228	85	C_1-H_4	783	376
B-H_5	2067	1	C_1-H_7	2059	6
H_1-H_2	1419	572	C_1-H_8	2085	0
H_1-P	1265	176	C_1-H_9	1255	93
H_1-C_1	1394	86	H_4-H_5	1289	579
H_1-C_2	2062	24	H_4-H_7	2883	−23
H_1-H_4	1608	138	H_4-H_8	3187	−115
H_1-H_5	2117	103	H_4-H_9	2130	101
H_1-H_7	2087	110	H_5-H_8	2094	103
H_1-H_8	3190	−91	H_5-H_9	1474	148
H_1-H_9	2903	−3	H_5-H_{12}	2973	−47

The numbering of atoms is shown in Fig. 3.

constant for the C-P torsion was estimated to be 0.081×10^{-18} N m from the potential barrier height of 2.6 kcal mol^{-1} in trimethylphosphine.[17] From the preliminary analysis assuming a low potential barrier approximation[18] the potential barrier around the P-B bond was about 3 kcal mol^{-1}, though it might include a large error. The force constant for the torsional vibration around the P-B bond was 0.09×10^{-18} N m. Thus the torsional vibrations around the C-P and P-B bonds were treated in a high potential barrier approximation.[18] The calculated mean amplitudes and shrinkage corrections are listed in Table 1. The asymmetry parameters, κ, for the B-H, P-B, C-P, and C-H bonds were estimated to be 20, 4.3, 3.2, and 13×10^{-6} Å^3, respectively, by the diatomic approximation[19] and those for the other atomic pairs were ignored.

The results of the least-squares analysis from the electron diffraction data are listed in Table 2. The rotational constant of a normal species of trimethylphosphine-borane was calculated by using the r_α°[15] parameters transformed from the r_α parameters in Table 2. Although it was in good agreement with the observed one as shown in Table 3, the joint analysis of electron diffraction data and rotational constant was performed. The relative weight for the observed rotational constant in the least-squares calculation was estimated to be 1×10^7 in such a way that the standard deviation of the rotational constant obtained from the least-squares calculation is nearly equal to the uncertainty in B_z, which is a rotational constant corrected for the vibrational effect.[15] The geometrical parameters and the mean amplitudes obtained from the joint analysis are listed in Tables 2 and 4, respectively. The limits of error in the distances were taken to be the square root of the sum of the squares of the random and systematic errors, while those in the angles and the mean amplitudes were taken to be the

Table 2. Molecular Parameters Obtained from Least-Squares Analysis for $(CH_3)_3P \cdot BH_3$

	r_α[a]	r_g[b]	r_α°[c]	r_g[d]	r_o[e]
r(B–H)/Å	1.183(11)	1.227	1.201(11)	1.225	1.212(10)
r(P–B)/Å	1.892(7)	1.899	1.894(6)	1.899	1.901(7)
r(C–P)/Å	1.810(3)	1.815	1.811(3)	1.815	1.819(10)
r(C–H)/Å	1.059(2)	1.103	1.077(2)	1.103	1.08(2)
r(H–(B)–H)/Å	1.931(26)	1.999	1.957(23)	1.990	
r(C–C)/Å	2.868(4)	2.870	2.870(4)	2.870	
∠PCH/°	109.9(2)		109.7(2)		109.6(10)
∠HBH/°[f]	109.5(10)	109.1	109.2(6)	108.6	113.5(5)
∠CPC/°[f]	104.8(4)	104.5	104.8(3)	104.6	105.0(4)
∠PBH/°[f]	109.5(10)	109.8	109.8(7)	110.3	105.1(6)
∠BPC/°[f]	113.9(3)	114.1	113.8(3)	114.0	113.6(4)

Limits of error are in parentheses. Parameters r_α, r_α°, and r_g are defined in Ref. 15. a) Results from electron diffraction data. b) r_g parameters transformed from r_α parameters. The limits of error are equal to those in the r_α parameters. c) Results from the joint analysis of electron diffraction data and rotational constants of the normal species. d) r_g parameters transformed from r_α° parameters. The limits of error are equal to those in the r_α° parameters. e) Results from the microwave spectroscopic study. Ref. 7. f) Dependent parameters in the present analysis.

Table 3. Observed and Calculated Rotational Constants of $(CH_3)_3P \cdot {}^{11}BH_3$

B_o/MHz[a]	3215.63(3)
B_z/MHz[b]	3216.0(4)
B_α°/MHz[c]	3217(5)
B_{av}/MHz[d]	3216.1(3)

Uncertainties in parentheses are attached to the last digit of the values. a) Observed rotational constant for the ground vibrational state. Ref. 7. b) Rotational constant corrected for the vibrational effect. The uncertainty was assumed to be 100% the vibrational correction. c) Rotational constant calculated from the parameters obtained by the analysis of electron diffraction data. d) Best-fit rotational constant obtained from the joint analysis. The error means the standard deviation in the least-squares calculation.

Table 4. Observed Root-Mean-Square Amplitudes for $(CH_3)_3P \cdot BH_3$

	l_{obsd}/Å[a]	l_{calcd}/Å[b]
C_1–P	0.058(1)	0.056
C_1–C_2	0.094(3)	0.110
C_1–B	0.109(4)	0.111
C_1–H_4	0.084(2)	0.078
P–B	0.073(9)	0.060
P–H_9	0.112(2)	0.111

Limits of error are in parentheses. a) Results obtained from the joint analysis of electron diffraction data and rotational constant of the normal species. b) Values calculated from the force field.

random errors. The random errors were assumed to be 2.6 times as large as the standard errors in the least-squares calculation. The systematic errors in the distances were estimated from the errors in both the measurements of camera distance (0.03%) and wavelength (0.11%). The best-fit molecular intensities and the radial distribution function are shown in Figs. 1 and 2, respectively. The experimental intensities, the experimental smooth backgrounds, and the correlation matrix for the molecular parameters are deposited in Document No. 8825 at the Office of the Editor of the Bulletin of the Chemical Society of Japan. The least-squares calculations were carried out on a HITAC M-682H computer in the Computer Center of the University of Tokyo.

Discussion

The molecular parameters of gaseous trimethylphosphine–borane obtained from the present study are in agreement with those from the microwave spectroscopic study[7] except the parameters of r(B–H) and ∠HBH. The P–B bond distance of $(CH_3)_3P \cdot BH_3$, 1.90 Å, is greater than that of $F_3P \cdot BH_3$, 1.84 Å,[20] but the former complex is more stable than the latter. The unusually short but weak P–B bond of the latter complex has been discussed elsewhere.[7,21] The P–B bond distance of $(CH_3)_3P \cdot BH_3$ is about 0.04 Å shorter than those of $(CH_3)_3P \cdot BX_3$ (X=Cl,Br,I),[22–24] which are in the range of 1.94—1.95 Å, though the sequence of the stability of the complexes is $(CH_3)_3P \cdot BBr_3 > (CH_3)_3P \cdot BH_3 > (CH_3)_3P \cdot BCl_3$.[25] This close approach of boron to phosphorus in $(CH_3)_3P \cdot BH_3$ is probably achieved by a relatively small steric hindrance of borane to the donor molecule.

The magnitude of structural changes of donor molecules on the complex formation is one of the measures of the acid strength of acceptors. The structural parameters of trimethylamine and trimethylphosphine in the complexes with boron compounds are listed in Table 5 in decreasing order of the CNC or CPC angles. This order is almost the same as the increasing order of the C–N or C–P distances.

The order of trimethylamine boron trihalides is the same as that of trimethylphosphine boron trihalides in Table 5, but a free trimethylamine molecule is at the top of the corresponding series and a free

Table 5. Comparison of Molecular Parameters

Compound	r(C–N)/Å	∠CNC/°	Ref.	Compound	r(C–P)/Å	∠CPC/°	Ref.
$(CH_3)_3N$	1.461(2)	110.6(6)	26	$(CH_3)_3P \cdot BCl_3$	1.800(4)	109.3(3)	22
$(CH_3)_3N \cdot BH_3$	1.485(1)	109.2(2)	3	$(CH_3)_3P \cdot BBr_3$	1.804(4)	108.0(7)	23
$(CH_3)_3N \cdot BF_3$	1.485(2)	109.2(4)	2	$(CH_3)_3P \cdot BI_3$	1.809(3)	106.0(5)	24
$(CH_3)_3N \cdot BCl_3$	1.497(3)	108.1(3)	27	$(CH_3)_3P \cdot BH_3$	1.811(3)	104.8(3)	This work
$(CH_3)_3N \cdot BBr_3$	1.500(5)	107.8(5)	27	$(CH_3)_3P$	1.846(3)	98.6(3)	29
$(CH_3)_3N \cdot BI_3$	1.497(2)	106.0(8)	28				

The values represent r_g parameters.

trimethylphosphine molecule is at the bottom. The borane complexes are located at the position next to the free molecules. This fact means that both donor molecules require the least deformation energy on the complex formation with borane, and that the deformation energy of trimethylamine increases with the atomic number of halogens of the acceptor molecules while that of trimethylphosphine decreases. The different changes of the structures of trimethylamine and trimethylphosphine on the complex formation with boron trihalides will be explained by the ab initio molecular orbital calculation.

The authors express their thanks to Professor Teruhiko Ogata of Shizuoka University for his valuable discussion.

References

1) M. Hargittai and I. Hargittai, *J. Mol. Struct.*, **39**, 79 (1977).
2) K. Iijima and S. Shibata, *Bull. Chem. Soc. Jpn.*, **52**, 711 (1979).
3) K. Iijima, N. Adachi, and S. Shibata, *Bull. Chem. Soc. Jpn.*, **57**, 3269 (1984).
4) P. S. Bryan and R. L. Kuczkowski, *Inorg. Chem.*, **10**, 200 (1971); P. Cassoux, R. L. Kuczkowski, and A. Serafini, *ibid.*, **16**, 3005 (1977).
5) J. R. Durig, Y. S. Li, and J. D. Odom, *J. Mol. Struct.*, **16**, 443 (1973).
6) P. Cassoux, R. L. Kuczkowski, P. S. Bryan, and R. C. Taylor, *Inorg. Chem.*, **14**, 126 (1975).
7) P. S. Bryan and R. L. Kuczkowski, *Inorg. Chem.*, **11**, 553 (1972).
8) A. D. Norman and W. L. Jolly, *Inorg. Synth.*, **11**, 15 (1968).
9) R. T. Markham, E. A. Dietz, Jr., and D. R. Martin, *J. Inorg. Nucl. Chem.*, **35**, 2659 (1973).
10) W. Witt, *Z. Naturforsch., Teil A*, **19**, 1363 (1964).
11) S. Shibata, K. Iijima, R. Tani, and I. Nakamura, *Rep. Fac. Sci. Shizuoka Univ.*, **9**, 33 (1974).
12) L. Schäfer, A. C. Yates, and R. A. Bonham, *J. Chem. Phys.*, **55**, 3055 (1971).
13) D. T. Cromer and J. B. Mann, *J. Chem. Phys.*, **47**, 1892 (1967); D. T. Cromer, *ibid.*, **50**,4857 (1969).
14) C. Tavard, D. Nicolas, and M. Rouault, *J. Chim. Phys.*, **64**, 540 (1967).
15) K. Kuchitsu and S. J. Cyvin, "Molecular Structures and Vibrations," ed by S. J. Cyvin, Elsevier, Amsterdam (1972), Chap. 12.
16) J. D. Odom, B. A. Hudgens, and J. R. Durig, *J. Phys. Chem.*, **77**, 1972 (1973).
17) "Kagaku Binran," 2nd ed, ed by the Chemical Society of Japan, Maruzen, Tokyo (1975), p. 1330.
18) Y. Morino and E. Hirota, *J. Chem. Phys.*, **28**, 185 (1958).
19) K. Kuchitsu, *Bull. Chem. Soc. Jpn.*, **40**, 505 (1967).
20) R. L. Kuczkowski and D. R. Lide, Jr., *J. Chem. Phys.*, **46**, 357 (1967).
21) R. W. Rudolph and R. W. Parry, *J. Am. Chem. Soc.*, **89**, 1621 (1967).
22) K. Iijima and S. Shibata, *Bull. Chem. Soc. Jpn.*, **52**, 3204 (1979).
23) K. Iijima, E. Koshimizu, and S. Shibata, *Bull. Chem. Soc. Jpn.*, **54**, 2255 (1981).
24) K. Iijima, E. Koshimizu, and S. Shibata, *Bull. Chem. Soc. Jpn.*, **55**, 2551 (1982).
25) D. C. Mente and J. L. Mills, *Inorg. Chem.*, **14**, 1862 (1975).
26) B. Beagley and A. R. Medwid, *J. Mol. Struct.*, **38**, 229 (1977).
27) K. Iijima and S. Shibata, *Bull. Chem. Soc. Jpn.*, **53**, 1908 (1980).
28) K. Iijima and S. Shibata, *Bull. Chem. Soc. Jpn.*, **56**, 1891 (1983).
29) L. S. Bartell and L. O. Brockway, *J. Chem. Phys.*, **32**, 512 (1960).

The ^{19}F Solid-State High-Resolution Nuclear Magnetic Resonance Study of K_2SiF_6, K_2GeF_6, and K_2SnF_6

Yoshichika YOSHIOKA,† Nobuo NAKAMURA, and Hideaki CHIHARA*
Department of Chemistry, Faculty of Science, Osaka University,
Toyonaka, Osaka 560
(Received January 21, 1988)

High-resolution ^{19}F NMR experiments were carried out on K_2SiF_6, K_2GeF_6, and K_2SnF_6, and the chemical-shift shielding tensors were determined. In all three substances, the shielding tensors are axially symmetric, and the most shielded direction is parallel to the MF (M=Si, Ge, and Sn) bond. The values of the shielding tensor elements ($\sigma_{//}$ and $\sigma_{\perp}$) change systematically from K_2SiF_6 to K_2SnF_6, except for the $\sigma_{\perp}$ component of K_2SiF_6, which is very large compared with those in the Ge and Sn-complexes. The analysis of σ's by a simple MO treatment indicates that π-backbonding is the strongest in the Si-F bond, probably because of the extraordinarily low electronegativity of Si. At room temperature, the reorientation of MF_6^{2-} anions is rapid enough to average out the shielding tensor components in the Si and Sn-complexes.

High-resolution NMR spectroscopy is a very useful technique for examining the structures and the chemical reactivities of such inorganic complex ions as MF_6^{2-} and is widely used for those ions in solutions. However, usual high-resolution NMR in solution gives only an averaged value of the chemical shift. In order to study the electronic structure and the reactivity of complex ions more closely, it is desirable to measure the anisotropy in the chemical-shift tensor by using crystalline materials. The temperature dependence of the chemical shift also provides valuable information about the very slow anisotropic molecular motion in the crystalline state.

It has been recognized that various types of compounds of Group IV_b metals, i.e., Si, Ge, and Sn, show unusual properties in that they do not obey the so-called law of corresponding states: the halogen nuclear quadrupole resonance frequencies in MX_4 (M=Si, Ge, and Sn) do not vary in a regular manner.[1] Also the ^{19}F chemical shift in MF_6^{2-} in solution does not change systematically from Si to Sn, etc.[2] These and other unique aspects of the behavior of the Group IV_b compounds have not yet been fully understood, although it can be inferred that the nature of the chemical bond changes abruptly on going from Si to Ge.[3] It is, therefore, interesting to determine the chemical shielding tensor completely using crystalline materials of Group IV_b compounds. Here we applied the solid-state high-resolution NMR technique to a series of K_2MF_6, where M=Si, Ge, and Sn, in an attempt to obtain detailed information on the electronic structure of MF_6^{2-} anions.

At room temperature, K_2SiF_6 is cubic,[4] while the other substances are trigonal,[5] as is shown in Figs. 1 and 2. The site symmetry at Si in K_2SiF_6 is O_h, while that of the central atoms in the other compounds is D_{3d}, which reflects the slight distortion of the MF_6 polyhedra from the regular octahedron. All the

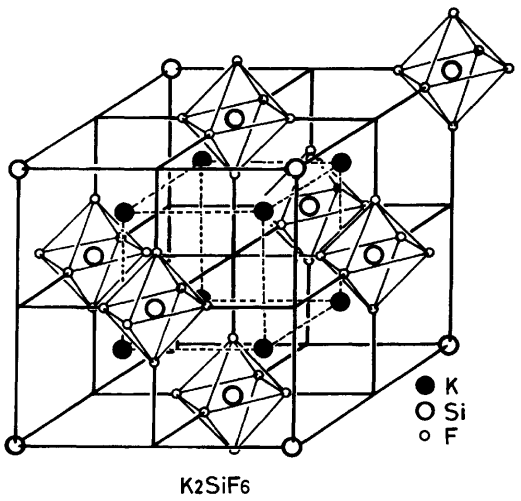

Fig. 1. Structure of K_2SiF_6. After Ref. 4.

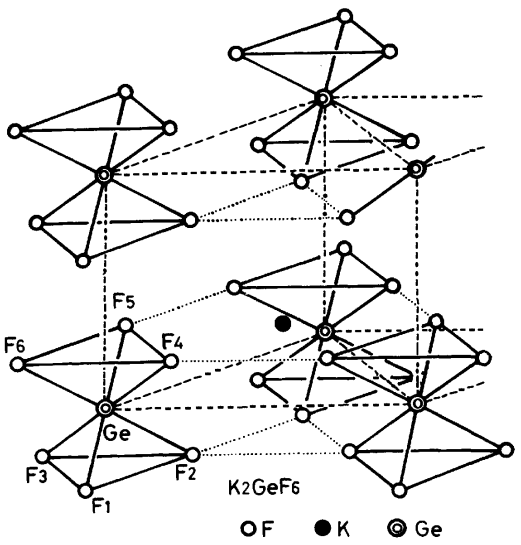

Fig. 2. Structure of K_2GeF_6 and K_2SnF_6. After Ref. 5.

† Present address: 2nd Department of Physiology, School of Medicine, Iwate Medical University, Morioka 020.

anions in these crystals are crystallographically equivalent. Since MF_6^{2-} ions form an approximately regular octahedron, the electron distribution in the M-F bond must be close to the axial symmetry. Therefore, axially symmetric chemical-shift tensors at the F atoms may be expected.

Experimental Results and Discussion

1. Spectrometer. Measurements were made by a home-built spectrometer which operates at 40 MHz (suitable for ^{19}F resonance at 1 T). The MREV-8[6] pulse sequence was employed to obtain the high-resolution spectrum in the solid. The shortest interval between pulses was chosen as 6.7 μs, and the optimum resolution of the spectrometer was about 8 ppm (300 Hz). The details of the spectrometer, its operation, and the data-processing procedure have been described elsewhere.[7]

2. Potassium Hexafluorosilicate, K_2SiF_6.

i) Preparation and Measurements: Powdered K_2SiF_6 as purchased from the Nakarai Chemical Co., Ltd., was used for multiple-pulse NMR measurements at 300 and 77 K. The time-domain signals were accumulated 20 times and then Fourier-transformed to obtain a spectrum. The spectra thus obtained are shown in Fig. 3. The spectrum at 300 K has the half-height-width of 30 ppm (1.2 kHz) and does not appear to have any anisotropy. The line-width at 77 K is larger than that at 300 K, and a small additional hump appears on the high-field side.

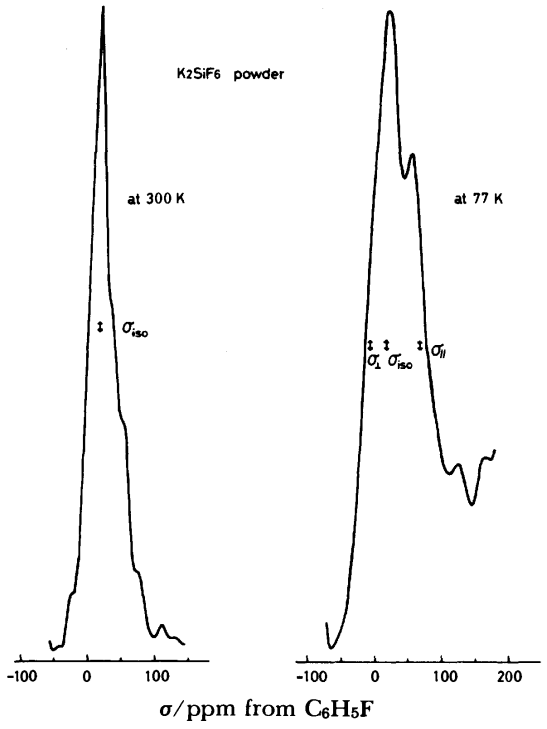

Fig. 3. High-resolution NMR spectra of ^{19}F in powdered K_2SiF_6 at 300 and 77 K. The reference material for the chemical shift is liquid C_6H_5F.

ii) Determination of Chemical-Shift Tensor: The spin-lattice relaxation time of ^{19}F was measured in the temperature range between 77 and 973 K by Moskvich et al.[8] According to them, the correlation time τ_c for the isotropic reorientation of SiF_6^{2-} is about 10^{-6} s at 300 K; therefore, it can be expected that this spherical reorientation will completely average the anisotropy of the chemical-shielding tensor of the ^{19}F nuclei. In fact, the spectrum at 300 K in the present work consists of a single, relatively narrow peak (shown in Fig. 3), which can be explained by such an averaging effect. The value of σ_{av} (isotropically averaged value) obtained is 16±5 ppm relative to the ^{19}F resonance in liquid C_6H_5F.

The spectrum at 77 K shown in Fig. 3 is different from the typical pattern for a rigid lattice: there is a small hump on the high-field side. The overall reorientation of SiF_6^{2-} will affect the line shape to some extent. Thus, Spiess[9] calculated the powder patterns for trigonal bipyramidal, tetrahedral, and octahedral molecules with an axially symmetric shielding tensor in the presence of a certain molecular reorientation in each case. He showed, based on the sudden-jump model, that a small hump may appear as the reorientational correlation time of the molecule approaches the inverse of the magnitude of the chemical-shift anisotropy. The powder pattern of K_2SiF_6 at 77 K was analysed according to the jump model; the chemical-shift anisotropy was estimated to be about 3 kHz, and the correlation time, to be about 3.3×10^{-3} s. The principal values of the shielding tensor were then determined as follows: $\sigma_{33}=66\pm5$ ppm and $\sigma_{22}=\sigma_{11}=-9\pm5$ ppm from liquid C_6H_5F ($\sigma_{33}\geqq\sigma_{22}\geqq\sigma_{11}$).

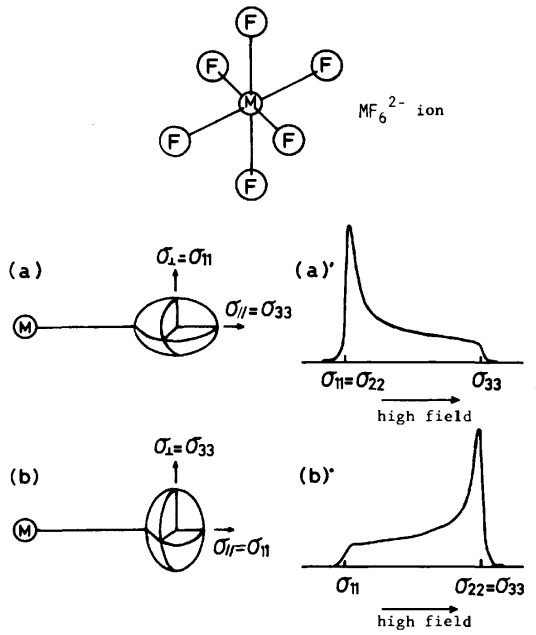

Fig. 4. Axially symmetric shielding tensor models and their powder patterns.

The SiF_6^{2-} ion forms a regular octahedron in the crystal;[4] therefore, the chemical-shielding tensor should be axially symmetric about the Si–F bond. In the case of an atom which forms a single bond, there are two possibilities of axially symmetric shielding tensors, as is shown in Fig. 4. In the **a** type, the maximum shielding direction is along the Si–F bond; in this case, the powder pattern of the **a′** type is obtained. In the case of the **b** type, the least shielded direction is along the Si–F bond, and so the powder pattern should be of the **b′** type. The analysis of the powder pattern of K_2SiF_6 indicates that the shielding tensor in this compound belongs to the **a** type. Therefore, its most shielded direction is along the Si–F bond, and the value of the chemical shift is 66 ppm. Its least shielded direction, on the other hand, is perpendicular to the Si–F bond, and its chemical shift is −9 ppm. The chemical shift of SiF_6^{2-} in a solution is 12 ppm,[2] slightly smaller than the isotropically averaged value in a solid (16 ppm) at room temperature.

3. Potassium Hexafluorogermanate, K_2GeF_6.

i) Preparation and Measurements: A colorless, transparent single crystal in the shape of a hexagonal plate was obtained by the slow evaporation at 30 °C of a solution of GeO_2 and KF in a stoichiometric ratio in 47% hydrofluoric acid. The crystal is of a trigonal symmetry, D_{3d}^3, with $Z=1$, and the C_3 axis of the GeF_6^{2-} ion is parallel to the crystallographic C axis[5] (see Fig. 2). The GeF_6^{2-} ion has the shape of a nearly regular octahedron, and so all the fluorines in the anion may be regarded as having nearly axially symmetric shielding tensors. Therefore, a pair of lines with the intensity ratio of 2:1 may be expected if the Zeeman field is rotated in the plane which is defined by the F_5, Ge, and F_1 atoms and the C_3 axis of the anion (see Fig. 2). A typical example of the spectrum at 300 K is shown in Fig. 5. The time-domain signals were accumulated 20 times at every 1800 s and then Fourier-transformed. When the Zeeman field was rotated in the above-mentioned plane of the crystal, the rotational patterns shown in Fig. 6 were obtained at 300 K. The line labelled by A is about twice as strong as the B line.

ii) Determination of the Chemical-Shift Tensor: From the ^{19}F second moment measured as a function of the temperature, Sergienko et al.[10] saw no sign of the reorientation of the GeF_6 anion, not even at 300 K. Therefore, we can use the rotational pattern of Fig. 6 to derive the rigid-lattice values of the shielding tensor components of ^{19}F. The dotted lines in Fig. 6 show the theoretical angular dependence of the shielding components on the assumption of the axially symmetric shielding tensor. The maximum point of the B curve (low-intensity line) corresponds to a Ge–F bond direction; that is, at this orientation the F_1–Ge–F_5 bond (see Fig. 2) is parallel to the Zeeman field. At the same orientation of the Zeeman field, the A curve (high intensity) has a minimum which indicates that the Zeeman field is perpendicular to both F_2–Ge–F_6 and F_3–Ge–F_4 bonds. Therefore, much as in the case of K_2SiF_6, the most shielded direction is along the Ge–F bond, while the least shielded direction is perpendicular to the Ge–F bond. The

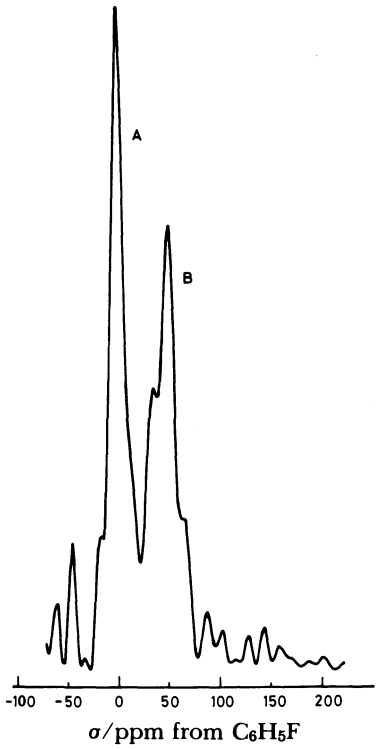

Fig. 5. ^{19}F NMR spectrum obtained by the Fourier transform of FID. The spectrum corresponds to the orientation, a* of Fig. 6.

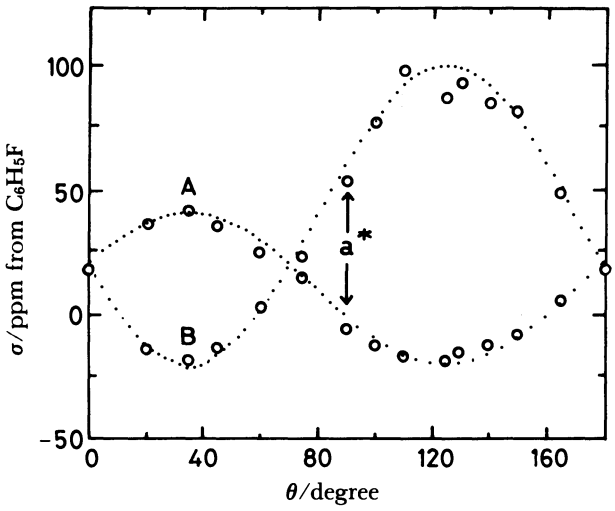

Fig. 6. Angular dependence of the ^{19}F chemical shifts of K_2GeF_6 single crystal. The pattern was obtained when the Zeeman field was rotated in the plane which is defined by F_5, Ge, and F_1 atoms and the C_3 axis (see Fig. 2). The angle θ is measured from the direction of the C_3 axis.

values of the shielding tensor components were thus determined as follows: $\sigma_{33}=99\pm3$ ppm and $\sigma_{22}=\sigma_{11}=-20\pm3$ ppm from liquid C_6H_5F. The isotropically averaged value is 19 ppm, significantly larger than that of ^{19}F in GeF_6^{2-} in solution (7 ppm).[2]

4. Potassium Hexafluorostannate, K_2SnF_6.

i) Preparation and Measurements: A K_2SnF_6 single crystal was obtained by the slow evaporation at 30 °C of a solution of $K_2Sn(OH)_6$ in 47% hydrofluoric acid. The crystal belongs to a trigonal system, and the site symmetry of Sn is D_{3d}.[5]

Multiple pulse measurements were made on the single crystal at 300 K in a manner similar to the case of K_2GeF_6. Contrary to the case of K_2GeF_6, no angular dependence of the shielding tensor was detected at 300 K, which indicates that the rapid molecular reorientation averages out the anisotropy in the shielding tensor, as in the case of K_2SiF_6. Then we carried out experiments on the powdered specimen at 300 and 77 K and reproduced the resulting spectra in Fig. 7. The spectrum at 300 K is a single, approximately symmetric peak, whereas the spectrum at 77 K corresponds to a typical powder pattern, involving some degree of anisotropy.

ii) Determination of the Chemical-Shift Tensor: The powder pattern at 300 K gives a motionally averaged, isotropic shielding with a σ_{av} value of 83 ± 5 ppm. The analysis of the powder pattern at 77 K, on the other hand, gives $\sigma_{33}=183\pm5$ ppm and $\sigma_{22}=\sigma_{11}=33\pm5$ ppm by assuming an axially symmetric shielding tensor. The most shielded direction is along the Sn–F bond, while the least shielded direction is perpendicular to the Sn–F bond. The averaged value, 83 ppm, is very different from that in SnF_6^{2-} in a solution (40 ppm).[2]

5. Discussion. Among the series of compounds of Group IV_b elements (C, Si, Ge, Sn, and Pb), silicon compounds show unusual behavior in several magnetic resonance properties, e.g., NMR chemical shifts[2,11] and NQR frequencies,[1] which reflect the electronic structures of atoms or molecules. The values of the chemical shielding of the compounds in this study are summarized in Fig. 8. To obtain some insight into the electronic structure of the molecules, the theory of Karplus and Das[12] will be used. The chemical-shift tensor consists of two contributions;

$$\sigma = \sigma^d + \sigma^p \tag{1}$$

where σ^d and σ^p are, respectively, the diamagnetic and paramagnetic parts of the chemical-shift tensor. Since it is the paramagnetic contribution that mainly gives rise to the experimentally observed variations in the chemical shifts of ^{13}C, ^{19}F, etc.,[12] only the paramagnetic part will be considered in investigating the electronic structure. According to the theory of Karplus and Das, the axially symmetric chemical-shift tensor for the atoms in this study can be given as follows:

$$\sigma_{//}^p = (3/2)\sigma_o(2\rho_\perp - \rho_\perp^2) \tag{2}$$

for the component along the M–F bond and

$$\sigma_\perp^p = (3/2)\sigma_o[\rho_\perp + (1-\rho_\perp)\varepsilon] \tag{3}$$

for the component perpendicular to the M–F bond, where σ_o is a semiempirical parameter, where $\rho_\perp$ is the π-bond character, and where

$$\varepsilon = 1 + IS - I - S. \tag{4}$$

I and S are the ionic character and the degree of sp hybridization respectively.

The $\sigma_{//}$ component increases regularly from K_2SiF_6 to K_2SnF_6, as is shown in Fig. 8. On the other hand, the $\sigma_\perp$ component of K_2SiF_6 seems to be anomalously large, presumably reflecting the anomalous character of the Si–F bond. Since $\sigma_{//}$ increases on going from K_2SiF_6 to K_2SnF_6, $|\sigma_{//}^p|$ must decrease in the same order. According to Eq. 2, it is concluded that the π-bond character, $\rho_\perp$, decreases regularly from K_2SiF_6 to K_2SnF_6. Such a tendency may be interpreted by

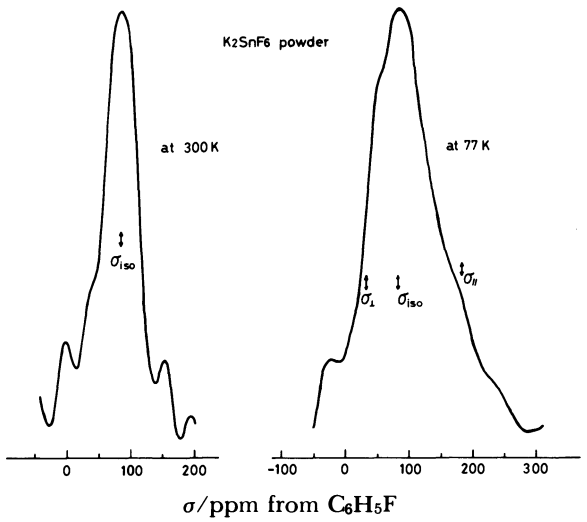

Fig. 7. Powder pattern of ^{19}F NMR in K_2SnF_6.

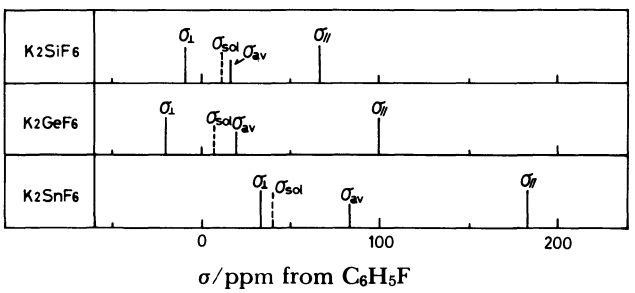

Fig. 8. Pictorial representation of the chemical shift tensor elements in K_2MF_6 (M=Si, Ge, and Sn) compounds. σ_{sol} is isotropic value in solution after Ref. 2.

introducing the concept of π-backbonding: the Group IV_b elements employ two d-orbitals in the octahedral d^2sp^3 hybridized orbitals for the framework of the MF_6^{2-} complex, and so the three remaining d-orbitals have the capability of forming π-bonding with orbitals of the ligand atoms. Through this π-bonding, partial electrons will be transferred from the ligands to the center atom. As $\rho_\perp$ is largest in the Si complex in the present series, we may consider that the π-backbonding is the strongest in K_2SiF_6.

An anomalously large $\sigma_\perp$ value was derived for SiF_6^{2-} compared with the other two compounds. According to Eq. 3, ε should be very small, so small as to cancel the effect of the large $\rho_\perp$ value in SiF_6^{2-}, which implies that the ionic or hybridyzation term in Eq. 4 should be large. Sanderson[13] and Hargittai and Bliefert[14] reexamined the electronegativity scale and showed that the electronegativity decreases in this order; C>Ge>Sn>Si. The anomalously large $\sigma_\perp$ value may be attributed to the high ionic character of the Si-F bond.

It may be noted in Fig. 8 that the difference between the trace of the chemical-shift tensor in the solid state, σ_{av}, and the isotropic chemical shift in a solution, σ_{sol}, is largest in K_2SnF_6. The large value shows that there is a large difference in the electronic structure of the MF_6^{2-} ion between the solid and liquid states. It is considered that the affinity of SnF_6^{2-} to water molecules in a solution is strongest, since the solubility of K_2SnF_6 is largest, and that this interaction causes a change in the electronic distribution in the SnF_6^{2-} anion.

References

1) R. Livingston, *J. Phys. Chem.*, **57**, 496 (1953); A. Schawlow, *J. Chem. Phys.*, **22**, 1211 (1954); H. Robinson, H. G. Dehmelt, and W. Gordy, *J. Chem. Phys.*, **22**, 511 (1954).

2) P. A. W. Dean and D. F. Evans, *J. Chem. Soc. A*, **1967**, 698.

3) E. A. C. Lucken, "Nuclear Quadrupole Coupling Constants," Chap. 12, Academic Press (1969).

4) J. A. A. Ketelaar, *Z. Kristallogr.*, **92**, 155 (1935).

5) J. L. Hoard and W. B. Vincent, *J. Am. Chem. Soc.*, **61**, 2849 (1939); A. Lari-Lavassani, G. Jourdan, C. Avinens, and L. Cot, *C. R. Hebd. Seances Acad. Sci., Ser. C*, **279**, 193 (1974).

6) P. Mansfield, *J. Phys. C*, **4**, 1444 (1971); W. K. Rhim, D. D. Elleman, and R. W. Vaughan, *J. Chem. Phys.*, **58**, 1772 (1973).

7) Y. Yoshioka, Doctoral Dissertation, Osaka University (1983).

8) Yu. N. Moskvich and B. I. Cherkasov, *Yader Magnit. Resonans v Kristallakh, Krasnoyarsk*, **1978**, 96.

9) H. W. Spiess, *Chem. Phys.*, **6**, 217 (1974).

10) V. I. Sergienko, L. N. Ignatieva, P. S. Gordienko, M. F. Eiberman, and S. F. Bogdan, *Spectrosc. Lett.*, **11**, 877 (1978).

11) K. J. Johnson, J. P. Hunt, and H. W. Dodgen, *J. Chem. Phys.*, **51**, 4493 (1969); H. S. Gtowsky and C. J. Hoffman, *J. Chem. Phys.*, **19**, 1259 (1951); P. C. Lauterbur, *Ann. N. Y. Acad. Sci.*, **70**, 841 (1958); H. W. Spiess and R. K. Sheline, *J. Chem. Phys.*, **53**, 3036 (1970).

12) M. Karplus and T. P. Das, *J. Chem. Phys.*, **34**, 1683 (1961).

13) R. T. Sanderson, *J. Am. Chem. Soc.*, **105**, 2259 (1983).

14) I. Hargittai and C. Bliefert, *Z. Naturforsch*, **38b**, 1304 (1983).

 © 1988 The Chemical Society of Japan Bull. Chem. Soc. Jpn., 61, 3043—3047 (1988)

Kinetics of the Denaturation of Ovalbumin and S-Ovalbumin by Alcohols

Kiyofumi MURAKAMI
Department of Chemistry, Faculty of Science, Yamaguchi University,
Yoshida 1677-1, Yamaguchi 753
(Received January 28, 1988)

The kinetics of denaturation of ovalbumin and S-ovalbumin by butyl alcohol isomers (butyl alcohol, isobutyl alcohol, *s*-butyl alcohol, and *t*-butyl alcohol) have been studied. The reactions were characterized as first order with respect to the protein and 11th order for the alcohols, irrespective of the kind of protein or alcohol. The rate constant was, however, significantly reduced by the branching of the alcohol structure and by the conversion of native ovalbumin to S-ovalbumin. The measurements were also performed on ovalbumin and S-ovalbumin whose SH groups were blocked from SH⇌S–S exchange reactions by modification with iodoacetamides. By the conversion to S-ovalbumin, the modified protein also exhibited a considerable resistivity against denaturation, suggesting that SH⇌S–S exchange reactions play no essential role in the formation of S-ovalbumin. On the basis of these results as well as determined activation parameters, the mechanism of the denaturation is discussed in the light of a combination of the hydrophobic interactions, between hydrophobic residues of the proteins and the alcohol molecules, and the fluctuations of the protein structures.

S-ovalbumin (stable ovalbumin) which is produced by a long-time storage of shell eggs[1] or by holding isolated ovalbumin in a warm and alkaline solution[2] is known to exhibit a considerable resistivity against various denaturation conditions, such as heat and urea.[2,3] Many attempts have been made in order to find some structural differences between ovalbumin and S-ovalbumin, which are very similar to each other.[2] (a) SH⇌S–S exchange reactions,[2-4] (b) an increase in the antiparallel β-sheet geometry with the expense of the same amount of the α-helical conformation,[5] (c) liberation of carboxyl groups,[6] (d) a reduced radias,[7] and (e) an increase in the surface hydrophobicity[7] have been suggested in explanation of the increased resistivity. However, it is still unclear that which of these plays an essential role for the conversion to S-ovalbumin.

Effects of alcohols on protein denaturation and as protein denaturants have extensively been studied for many proteins.[8-15] The main result of these studies is that the effectiveness of the alcohols increases with increase in the alkyl residue content while it reduces for branched alcohols. The result has been attributed to hydrophobic interactions between hydrophobic residues of the proteins and the alcohol molecules. On the other hand, it has also been pointed out that the effectiveness of the alcohols is highly correlated with their ability to disrupt water structure.[16,17] Furthermore, Bull and Breese[18] have recently studied the kinetics of the denaturation of many proteins by alcohols and reported an enhanced effect for alcohols having longer alkyl chains. However, the details of the kinetic aspects and the mechanism of the denaturation are still not fully elucidated.

The present paper describes the kinetics of the denaturation of ovalbumin and S-ovalbumin by butyl alcohol isomers and presents a possible denaturation mechanism as well as suggesting the difference between these proteins.

Experimental

Materials. The ovalbumin was prepared from fresh egg white by a method, essentially same with that of Kekwick and Cannan.[19] It was recrystallized three times from a $(NH_4)_2SO_4$ solution at pH=4.7 and stored at 4 °C. Before using, the preparation was exhaustively dialyzed against distilled water. The S-ovalbumin was prepared from the ovalbumin by the method of Smith and Back.[2]

The SH-blocked ovalbumin was prepared by the following method.[20] A stock solution of iodoacetamide was added dropwise to an aliquot of the dialyzed ovalbumin solution with stirring so as to make a final solution containing 10 moles of iodoacetamide per mole of SH group. The pH of the solution was then adjusted to 8.0 using a 0.2 M† NaOH solution. The solution was then kept at room temperature (about 18 °C) for 20 h, after which it was exhaustively dialyzed against water. This procedure was carried out in the dark. The SH group content of the preparation was determined according to the method of Boyer,[21,22] and it was found that two of the three SH groups which are exposed in the native ovalbumin[23] were blocked by the above method. For the conversion to the modified S-ovalbumin, this sample was also treated by the same method[2] as cited above.

The concentrations of the ovalbumin and S-ovalbumin solutions were determined spectrophotometrically, using the optical density $E^{1\%}_{1\,cm}=7.12$[24,25] at 280 nm.

p-Chloromercuribenzoic acid (guaranteed grade) was purchased from Katayama Chemicals. All other chemicals used were of reagent grade. Iodoacetamide, alcohols, sodium acetate and acetic acid were purchased from Wako Pure Chemical Industries and ammonium sulfate was from Katayama Chemicals.

Methods. The following procedure of the present kinetic measurements is similar to that of Bull and Breese.[18] All sample solutions were prepared in 0.2 M acetate buffer of pH=4.7. A 0.5 ml of ovalbumin solution (5×10^{-4} M) thermostated at 30 °C was rapidly mixed with 2 ml of an aqueous alcohol solution of an appropreate concentration,

† 1 M=1 mol dm^{-3}.

which was also thermostated at 30 °C: time=zero. It was found that the denatured protein began to precipitate in the course of time. After a time passage, the solution was diluted with 30 ml of the acetate buffer solution in order to stop the denaturation, and was kept at room temperature for 2 h for the full precipitation of the denatured protein. The solution was then centrifuged at 11000 rpm for 30 min, and an aliquot of the supernatant solution was subjected to the determination of the concentration of the remaining native protein. Blank measurements were also performed in the absence of the denaturants.

Analysis of Kinetic Data. Kinetics of the denaturation of the proteins by alcohols may be described by the equation:

$$P + m\,R\text{-}OH \longrightarrow D \qquad (1)$$

where R-OH, P, and D denote the alcohol molecule, the native protein, and the denatured one respectively and where m is the number of alcohol molecules required to denature one molecule of the protein. The rate of denaturation at any time can then be written by:

$$\frac{d\,[D]}{d\,t} = k\,[P]\,[R\text{-}OH]^m \qquad (2)$$

where [D], [P], and [R-OH] are the molar concentrations of the denatured and native proteins and alcohol, respectively and where k is the rate constant of the denaturation. The initial rate becomes in the logarithmic form as:

$$\log\left[\frac{d\,[D]}{d\,t}\right]_0 = m \log [R\text{-}OH]_0 + \log [P]_0 + \log k \qquad (3)$$

where the subscript 0 means the quantity at time zero: for instance $[P]_0$ is the initial concentration of the protein. According to this equation, m (the order of reaction) and k can be determined from the slope and the intercept of the plot of $\log[d[D]/dt]_0 - \log[P]_0$ vs. $\log[R\text{-}OH]_0$, respectively.

Results and Discussion

Kinetic Parameters. Figure 1 shows the time courses of the denaturation of ovalbumin and S-ovalbumin in the presence of *s*-butyl alcohol. As can be seen in this figure, S-ovalbumin is highly resistant to denaturation as compared to ovalbumin. In order to ensure the order of reaction with respect to the protein, the dependence of the initial rate of the denaturation on the concentration of ovalbumin was measured (see Eq. 3). The result shown in Fig. 2 yields the slope of 1.09, confirming that the reaction is first order with respect to the protein.

Figure 3 shows the plots of $\log[d[D]/dt]_0 - \log[P]_0$ vs. $\log[R\text{-}OH]_0$ for the denaturation of the four kinds of proteins by the butyl alcohol isomers. In accordance with Eq. 3, each plot exhibits a linear dependence; m and k determined from these plots are summarized in Table 1. The solubility of isobutyl alcohol is so small that the determination of the denaturation curve by the low alcohol concentration required an extremely long time (1 or 2 days) and the data were not collected.

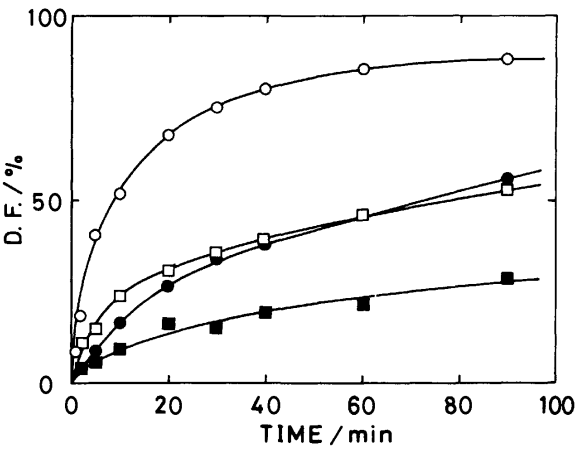

Fig. 1. Typical time courses of the denaturation of ovalbumin and S-ovalbumin by *s*-butyl alcohol. The ordinate shows the denatured fraction (D.F.) of the proteins. The initial concentrations of the alcohol are 1.1 M (○) and 0.95 M (●) for ovalbumin and 1.2 M (□) and 1.1 M (■) for S-ovalbumin.

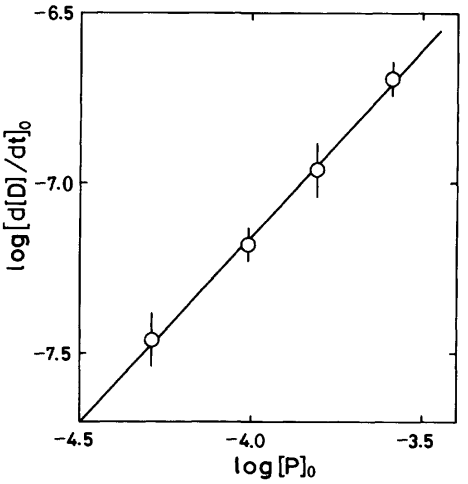

Fig. 2. Plot of $\log[d[D]/dt]_0$ vs. $\log[P]_0$ for ovalbumin in the presence of 1 M *s*-butyl alcohol. The solid line represents a least-square fit to the data, the slope of which is 1.09.

The following points can be seen from Table 1. At first, the order of reaction with respect to alcohols (m) is, within the experimental error, 11th, being irrespective of the kinds of protein or alcohol structure. The value of m for butyl alcohol is relatively in agreement with that reported by Bull and Breese.[18] They also reported that the order of the denaturation reaction by streight-chain alcohols decreases with the increase in the hydrocarbon content. Considering this together with the present results, it is suggestive for the denaturation mechanism that the number of alcohol molecules required for the denaturation depends on their hydrocarbon content

but is independent of the degree of branching.

Secondarily, k is, on the other hand, highly dependent on the structure of the denaturants and on the state of the protein. It progressively decreases with increase in the degree of branching of the denaturant's alkyl chain. Furthermore, it reduces by a factor from 3 to 10 on the conversion from ovalbumin to S-ovalbumin, that is, S-ovalbumin is highly resistant to the denaturation as compared to the native ovalbumin.

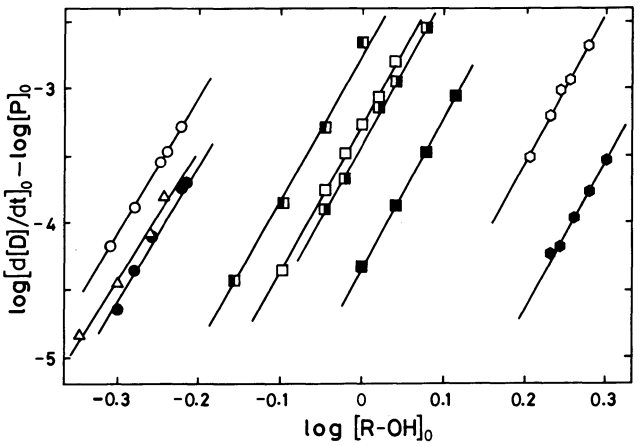

Fig. 3. Plot of $\log[d[D]/dt]_0-\log[P]_0$ vs. $\log[R\text{-}OH]_0$ for the denaturation of the proteins by butyl alcohol isomers. The denaturants are differentiated by the symbols as circle (butyl alcohol), triangle (isobutyl alcohol), square (*s*-butyl alcohol), and hexagon (*t*-butyl alcohol). Open symbols denote ovalbumin and filled ones S-ovalbumn. Half filled symbols ◧ and ◨ denote SH-modified native ovalbumin and S-ovalbumin produced from the SH-modified ovalumin respectively.

Table 1. Rate Constants and Orders of Reaction of the Denaturation by Butyl Alcohol Isomers at 30 °C[a)]

Alcohol	Ovalbumin	$k/M^{-m}S^{-1}$	m
n-BuOH	n-	2.14×10^{-1}	11.7
	S-	6.46×10^{-2}	11.5
i-BuOH	n-	2.95×10^{-2}	9.6
	S-	—	—
s-BuOH	n-	5.38×10^{-4}	11.1
	S-	4.68×10^{-5}	10.8
	n-mod.-	1.93×10^{-3}	11.3
	S-mod.-	3.89×10^{-4}	11.1
t-BuOH	n-	1.83×10^{-6}	11.0
	S-	2.36×10^{-7}	10.3

a) Abbreviations: *n*-BuOH=butyl alcohol, *i*-BuOH=isobutyl alcohol, *s*-BuOH=*s*-butyl alcohol, *t*-BuOH=*t*-butyl alcohol, n-=native ovalbumin, S-=S-ovalbumin, n-mod.-=SH-modified native ovalbumin, S-mod.-=S-ovalbumin produced from the SH-modified native ovalbumin. The error of m was estimated as ±1.

Activation Parameters. From the temperature dependence of k, the activation parameters of the denaturation of ovalbumin and S-ovalbumin by *s*-butyl alcohol were determined in the usual manner.[26)] Figure 4 shows the plot of $\ln[k/T]$ vs. T^{-1}. The slope and the intercept of the plot provide the activation enthalpy (ΔH^*) and the activation entropy

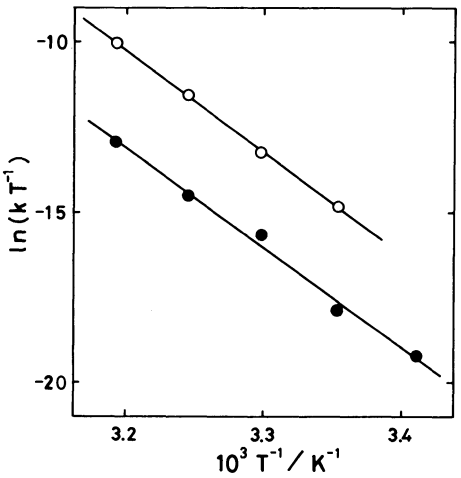

Fig. 4. Plots of $\ln(kT^{-1})$ vs. T^{-1} for the denaturation of ovalbumin and S-ovalbumin by *s*-butyl alcohol. Open circles denote ovalbumin and filled ones S-ovalbumin. The solid lines represent least-square fits to the data.

Table 2. Activation Parameters of the Denaturation by *s*-Butyl Alcohol[a)]

Protein	ΔG^*	ΔH^*	ΔS^*	$\Delta\Delta G^*$	$\Delta\Delta H^*$	$\Delta\Delta S^*$
	kJ mol^{-1}	kJ mol^{-1}	J K^{-1} mol^{-1}	kJ mol^{-1}	kJ mol^{-1}	J K^{-1} mol^{-1}
Ovalbumin	93	248	511			
S-ovalbumin	100	243	472	7	−5	−39

a) ΔΔ means the difference between the activation parameter for S-ovalbumin and that for native ovalbumin. The errors of ΔH^* and ΔS^* were estimated as 2—5% of those values.

(ΔS^*) of the denaturation respectively. The results are summarized in Table 2.

Denaturation Mechanism. The effects of alcohols on the protein denaturation and as the denaturants have been found to become pronounced with increasing alkyl residue content of the alcohols and to reduce with the increase in the degree of branching. They have been interpreted in terms of hydrophobic interactions:[8-15] bound alcohol molecules penetrate into the protein molecule, and interact with hydrophobic residues by replacing the native hydrophobic bonds between these residues and thereby destabilize the protein structures. These result have been derived from static information such as the effects on the transition temperature for thermal denaturation and on the denaturation midpoint, i.e., the concentration of a denaturant required to produce 50% change in the particular observable. The mechanism is, however, not sufficient to account for the present data for the effects of the branching of alcohol molecules on the kinetic parameters (Table 1).

It has been well-known that the structure of a globular protein is not rigid but fluctuates about its most stable conformation. The fluctuations may accompany an exposure of a part of hydrophobic regions to the solvent by openings of channels or crevices, the degree of which must necessarily depend on the degree of the spatial extent of the fluctuations. The so called "breathing"[27,28] motions may be involved in these fluctuations. A large fluctuation is expected to occur only rarely while small ones occur frequently. It is reasonable to assume that the alcohol molecules approach to the hydrophobic region by taking, among the possible conformations, the most fine-line-shape of the hydrophobic portion and by orienting along the channels or the crevices. Therefore, straight-chain molecules can easily approach the hydrophobic region through the frequently opening narrow channels or crevices. Thereby hydrophobic interactions between alcohol molecules and the hydrophobic residues will soon be achieved, resulting in the subsequent denaturation. This leads to large values of k for normal alcohols. On the other hand, branched alcohol molecules which have large diameters must, at the surface of the protein, wait for a wide channel or a wide crevice to open. Small values of k are, therefore, expected for the branched molecules. This mechanism seems to interpret well the observed correlation between the degree of branching of the alcohol molecules and the order of the value of k for these molecules, i. e., butyl alcohol > isobutyl alcohol > *s*-butyl alcohol > *t*-butyl alcohol (Table 1).

An alternative explanation for the effects of alcohols as protein denaturants is based on their ability to destabilize the structure of water.[16,17] Protein molecules, stabilized by hydration around their exposed hydrophobic residues, could be destabilized by the collapse of the hydrated water structure. It is likely that the collapse of the water structure enhances the fluctuations of the protein structure, and hence makes the alcohol molecules easily accesible to the hydrophobic region. The resultant hydrophobic interactions between alcohol molecules and the hydrophobic residues further destabilize the protein structure and amplify the structural fluctuations. Like this, the hydrophobic interactions and the collapse of the hydrated water structure may act cooperatively on the protein denaturation. Both the collapse of the water structure and the enhanced fluctuations will result in a large activation entropy. These considerations are consistent with the result of Segawa and Kume[29] that isopropyl alcohol enhances the fluctuations of the activated state of the thermal denaturation of lysozyme. A schematic illustration of the denaturation mechanism is shown in Fig. 5. Although it is well-known that alcohol molecules have, in general, the effect of increasing α-helix content of many proteins, the role of this fact on the potein denaturation is still unclear.[16] For the sake of simplicity, such a fact is not illustrated in Fig. 5.

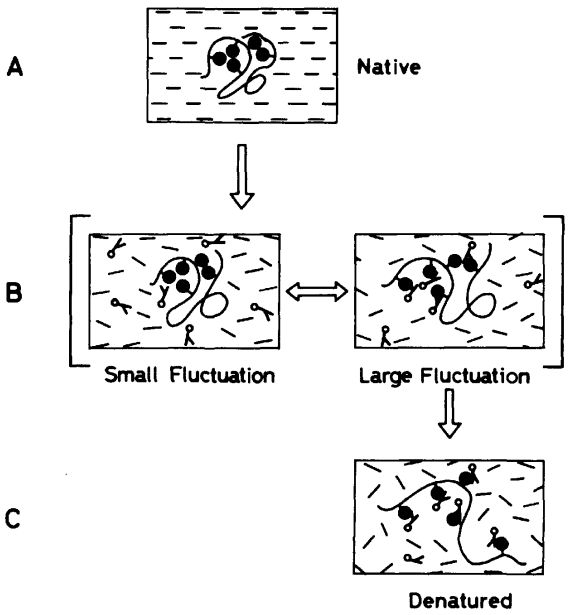

Fig. 5. A schematic illustration of the possible denaturation mechanism by alcohols. An addition of alcohol molecules (O—<) to the protein solution (A) destabilizes the structure of water, and hence enhances the fluctuations of the protein structure (B). When a large fluctuation takes place, alcohol molecules can approach so closely to the hydrophobic region of the protein that resultant hydrophobic interactions, between hydrophobic side chains (filled circles) and hydrophobic portions of alcohols, break the native hydrophobic bonds and thereby lead to the full denaturation of the protein structure (C).

According to the above mechanism, it may be concluded that S-ovalbumin is in a state in which the structural fluctuations are to some extent depressed as compared to the native ovalbumin. Nakamura and Ishimaru[7] reported that the Stokes radius of S-ovalbumin (25.5 Å) is smaller than that of ovalbumin (27.3 Å). The compact form of S-ovalbumin seem to be responsible for the depressed fluctuations. It can also be seen from Table 2 that the positive value of $\Delta\Delta G^*$ (7 kJ mol^{-1}) arises from the entropy term ($-T\Delta\Delta S^*$=12 kJ mol^{-1} at 30 °C) rather than the enthalpy term ($\Delta\Delta H^*$=−5 kJ mol^{-1}). This implies that the stability of S-ovalbumin is achieved by changes in the state of the structural fluctuations and/or in the hydration state of the protein rather than by any other strong bond formations. The increase in the surface hydrophobicity[7] and the change of a part (3—4%) of the protein from the α-helix to the antiparallel β-sheet conformation[5] in the conversion from ovalbumin to S-ovalbumin may also be closely related to the above changes. The fact that the number of alcohol molecules, required for the denaturation, decreases with the increase in the hydrocarbon content of the denaturant[18] but does not depend on the degree of branching for both of the ovalbumin and S-ovalbumin (Table 1) suggests that a definite amount of hydrophobic bonds must be broken in the activation process and it is not changed by the conversion of ovalbumin to S-ovalbumin. This is also supported by the small value of $\Delta\Delta H^*$ in Table 2.

The author wishes to thank Dr. Yasuo Fujisaki for his helpful discussion, and Mr. Tatsuhiro Sasaki for his support on the measurements.

References

1) M. B. Smith, *Aust. J. Biol. Sci.*, **17**, 261 (1964).
2) M. B. Smith and J. F. Back, *Aust. J. Biol. Sci.*, **18**, 365 (1965).
3) M. B. Smith and J. F. Back, *Aust. J. Biol. Sci.*, **21**, 539 (1968).
4) A. D. Nisbet, R. H. Saundry, A. J. G. Moir, L. A. Fothergill, and J. E. Fothergill, *Eur. J. Biochem.*, **115**, 335 (1981).
5) S. Kint and Y. Tomimatsu, *Biopolymers*, **18**, 1073 (1979).
6) R. Nakamura, Y. Takemori, and S. Shitamori, *Agric. Biol. Chem.*, **45**, 1653 (1981).
7) R. Nakamura and M. Ishimaru, *Agric. Biol. Chem.*, **45**, 2775 (1981).
8) A. Kurono and K. Hamaguchi, *J. Biochem. (Tokyo)*, **56**, 432 (1964).
9) E. E. Schrier, R. T. Ingwall, and H. A. Scheraga, *J. Phys. Chem.*, **69**, 298 (1965).
10) J. F. Brandts and L. Hunt, *J. Am. Chem. Soc.*, **89**, 4826 (1967).
11) T. T. Herskovits and H. Jaillet, *Science*, **163**, 282 (1969).
12) T. T. Herskovits, B. Gadegbeku, and H. Jaillet, *J. Biol. Chem.*, **245**, 2588 (1970).
13) S. Y. Gerlsma and E. R. Stuur, *Int. J. Pept. Protein Res.*, **4**, 377 (1972).
14) R. M. Parodi, E. Bianchi, and A. Ciferri, *J. Biol. Chem.*, **248**, 4047 (1973).
15) G. Velicelebi and J. M. Sturtevant, *Biochemistry*, **18**, 1180 (1979).
16) D. Eagland, in "Water—A Comprehensive Treatise, Vol. 4," ed by F. Franks, Plenum, New York (1975), pp. 305—518.
17) F. Franks and D. Eagland, *CRC Cr. Rev. Biochem.*, **3**, 165 (1975).
18) H. B. Bull and K. Breese, *Biopolymers*, **17**, 2121 (1978).
19) R. A. Kekwick and R. K. Cannan, *Biochem. J.*, **30**, 227 (1936).
20) W. E. Moore and J. F. Foster, *Biochemistry*, **7**, 3409 (1968).
21) P. D. Boyer, *J. Am. Chem. Soc.*, **76**, 4331 (1954).
22) R. Benesch and R. E. Benesch, *Methods Biochem. Anal.*, **10**, 43 (1962).
23) L. A. Fothergill and J. E. Fothergill, *Biochem. J.*, **116**, 555 (1970).
24) A. N. Glazer, H. A. McKenzie, and R. G. Wake, *Biochim. Biophys. Acta*, **69**, 240 (1963).
25) J. W. Donovan and C. J. Mapes, *J. Sci. Fd. Agric.*, **27**, 197 (1976).
26) S. Glasstone, K. J. Laidler, and H. Eyring, "The Theory of Rate Processes," McGraw-Hill, New York (1941), Chap. 4.
27) K. Linderstrom-Lang and J. A. Schellman, "The Enzymes," ed by P. D. Boyer, H. Lardy, and K. Myrback, Academic Press, New York (1959), pp. 443—510.
28) A. Hvidt and S. O. Nielsen, *Adv. Protein Chem.*, **21**, 287 (1966).
29) S. Segawa and K. Kume, *Biopolymers*, **25**, 1981 (1986).

 © 1988 The Chemical Society of Japan Bull. Chem. Soc. Jpn., 61, 3049—3053 (1988)

A Peculiar Conformation of Normal-Chain Dicarboxylic Acid Salts in Aqueous Solutions

Kunio FUKUSHIMA,* Koichi ADACHI, and Kiyohisa WATANABE
Department of Chemistry, Faculty of Science, Shizuoka University,
836, Oya, Shizuoka 422
(Received January 29, 1988)

The Raman spectra of adipic acid, pimelic acid, and their salts were observed for various states. The spectra of the acids in aqueous sodium hydroxide solutions were found to be very different from those of the acids in organic solvents. The difference was interpreted, on the basis of normal vibration calculations, as being due to the helix formation of molecules in the former solutions. This tendency toward helical coiling is consistent with the same tendency found for the salts of azelaic acid and suberic acid in our previous study.

In our recent paper[1] on the measurements of the Raman spectra of suberic acid ($HOOC(CH_2)_6COOH$), azelaic acid ($HOOC(CH_2)_7COOH$) and their salts in solutions, we reported a remarkable spectral difference between the acids and their salts, especially for the C–C stretching bands in the region of 850 to 1000 cm^{-1}. On the basis of the normal-vibration calculation of the molecules, we ascribed the difference to the helix formation of the molecular chains of the acid salts. However, these molecules are rather complicated for clear vibrational analyses; in addition, the spectral difference might be ascribed to other factors including the end group difference, COOH and COO^-. In the present study, smaller molecules, adipic acid ($HOOC(CH_2)_4COOH$), pimelic acid ($HOOC(CH_2)_5COOH$) and their salts, which are more suitable for clear vibrational analyses, were treated in order to ascertain if the tendency of forming a helix of molecular chain found in our previous study is also observed in these smaller molecules; the spectral change due to the end group change, COOH to COO^-, was studied.

Experimental

The samples, adipic acid and pimelic acid, were commercial products (GR grade) of the Tokyo Kasei Kogyo Co. The Raman spectra of these samples were recorded for a solid, for solutions of organic solvents, and for aqueous sodium hydroxide solutions. The spectra were obtained with an R-800T Raman Spectrometer (Japan Spectroscopic Co.), using a 514.5 nm line (250 mW) of an NEC argon ion laser. 0.3 ml liquid cells were used for the measurements. The results are shown in Tables 1 and 2 and in Fig. 1.

Normal-Vibration Calculation

The normal-vibration calculation was carried out for pimelic acid according to Wilson's GF matrix method.[2] The following molecular parameters were used: C–C 1.53 Å, C–O 1.49 Å, C=O 1.25 Å, C–H 1.09 Å, O–H 1.07 Å, ∠CC=O=113°, ∠CCO=113°, ∠C–CO–C=124°, the other bond angles were equal to the tetrahedral angle. First, the normal-vibration calculation of a molecular model with an all-*ap* molecular chain (point group, C_{2v}) was calculated using the same force field as in the previous report[1] for force constants transferred from related molecules (Set I in Table 3). The calculated frequencies were then fitted to the observed frequencies of the solid by the method of least squares.[3] The results are shown for the region from 200 to 1700 cm^{-1} in Fig. 2. Then, using the refined force constants (Set II in Table 3),

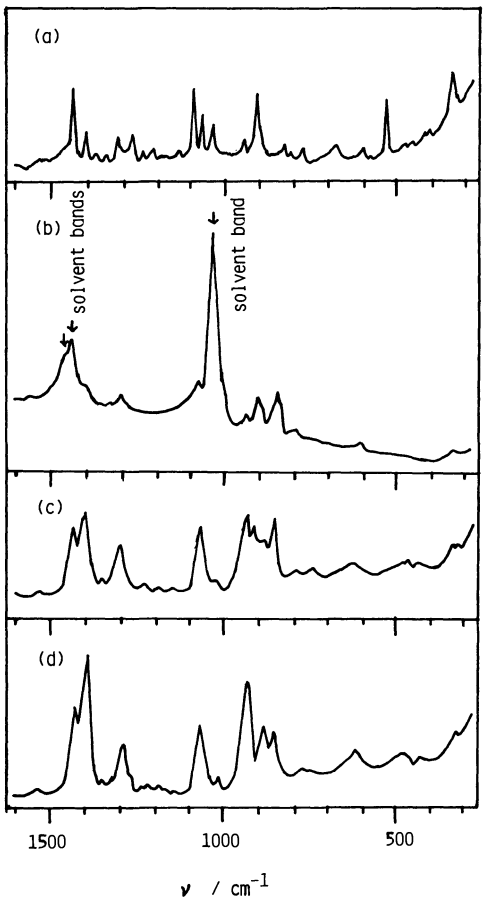

Fig. 1. Raman spectra of pimelic acid.
(a) Solid, (b) methanol solution (33.9 wt%), (c) aq. sodium hydroxide solution (mole ratio; NaOH: acid=1:1), (d) aq. sodium hydroxide solution (mole ratio; NaOH: acid=2.7:1).

normal-vibration calculations for various conformers were carried out. In Fig. 3, the results are compared with the observed C–C stretching bands.

Results and Discussion

Adipic acid was found to have an all-*ap* molecular chain in the crystalline state.[4] In addition, the infrared and Raman spectra were measured and analyzed based on the normal-vibration calculation by Suzuki and Shimanouchi.[5]

A pimelic acid is expected to assume an all-*ap* molecular chain in the solid state, a normal-vibration calculation was carried out for the model as has been described in the section of normal-vibration calculation. These calculations afford a basic information for the interpretation of the spectral difference of the solutions found in the present study; this information is shown in Tables 1 and 2 and in Fig. 1, in which the spectra of methanol solutions are shown as representatives of solutions of organic solvents (for adipic acid: methanol, pyridine, ethylacetate, 1,4-dioxane, dimethyl sulfoxide, acetic acid, formic acid; for pimelic acid: methanol, ethanol, pyridine, dimethyl sulfoxide, 1,4-dioxane).

The Spectra of Methanol Solutions. In Tables 1 and 2, the spectra in the regions from 1000 to 1080 cm^{-1} and from 1420 to 1500 cm^{-1} are not shown as the bands of the solvent overlap with the bands of the samples. Besides the bands corresponding to those of the solid conformer, new bands appear, showing that the conformer with an all-*ap* molecular chain and other conformer co-exist in methanol solutions. The prominent C–C stretching bands of pimelic acid at 807 and 854 cm^{-1} which are not ascribed to the all-*ap* conformation, correspond to the calculated frequencies of the TGTTGT, TTGGTT, TGGTGT conformers, as is shown in Fig. 3. Here, for example, TGTTGT represents the *ap-sc-ap-ap-sc-ap* conformation along the molecular chain of $CO-CH_2-CH_2-CH_2-CH_2-CH_2-CO$.

The Spectra of Aqueous Sodium Hydroxide Solutions. Even after excluding the spectral change arising from the end group change, COOH to COO^-, from the spectral changes shown in Tables 1 and 2 with reference to Table 4, the following spectral change still remains. Bands with frequency values entirely different from those of methanol solutions appear at 384, 775, 930, 1193, 1235, 1255, and 1275 cm^{-1} (adipic acid) and at 332, 434, 779, 864, 896, 1143, and 1194 cm^{-1} (pimelic acid). At the same time, the bands observed for methanol solutions, 372, 735, 790, 829, 895, 1106, and 1154 cm^{-1} (adipic acid) and 339, 755, 807, 854, 904, and 1211 cm^{-1} (pimelic acid) decrease in intensity. Although Table 4 suggests that the stretching frequency of the CC bond attached to the COOH group increases upon the group change from COOH to COO^-, the above-mentioned spectral change cannot be explained by the frequency change alone. These facts show that a peculiar molecular conformation which differs from those in methanol solutions and also in a solid becomes abundant in aqueous sodium hydroxide solutions. Therefore, in

Table 1. Raman Spectra of Adipic Acid (<2000 cm^{-1})[a]

Solid		CH_3OH soln			Aq. NaOH soln			Solid		CH_3OH soln			Aq. NaOH soln		
ν	I	ν	I	ρ	ν	I	ρ	ν	I	ν	I	ρ	ν	I	ρ
166	20							1051	46				1050	sh	?
246	9												1065	49	0.29
304	58												1080	sh	?
		372	8					1091	54						
					384	4	0.28			1106	33	0.69			
445	2	445	7	DP?						1154	15	0.75	1150	5	0.63
		475	8	DP									1193	8	0.50
					487	10	0.59	1224	4						
514	14												1235	8	?
575	11							1248	15						
		616	21	0.50									1255	8	?
					625	16	0.18			1265	8	P			
666	35	660	10	0.75	660	sh	?						1275	10	?
		735	13	P				1302	36	1307	19	0.75	1305	sh	?
					775	8	0.14						1315	38	0.38
		790	8	?									1360	16	0.21
800	3							1383	2						
		829	58	0.15				1413	76				1412	100	0.27
		850	sh	?	845	29	0.18	1436	33						
		895	100	0.15	890	38	0.13	1448	39				1443	48	0.54
		900	sh	?				1481	7						
920	100												1550	10	0.44
					930	95	0.09	1644	25				1635	7	0.50
					972	sh	?			1705	42	0.20			
					1020	sh	?								

a) ν, frequency in cm^{-1}; I, relative intensity; ρ, depolarization ratio; P, polarized; Dp, depolarized.

Table 2. Raman Spectra of Pimelic Acid (<2000 cm^{-1})[a]

Solid		CH_3OH soln			Aq. NaOH soln (1 : 1)			Aq. NaOH soln (2.7 : 1)		
ν	I	ν	I	ρ	ν	I	ρ	ν	I	ρ
271	57									
328	43									
								332	8	0.67
		339	25	0.33	345	18	0.50			
					436	sh	?	434	8	?
					489	14	0.75	482	11	0.75
525	43									
598	29	600	8	?						
					628	18	P	623	16	0.5
670	29									
		755	17	0.50	755	17	P			
								779	8	?
					800	17	P			
810	14	807	25	P						
		854	100	0.33						
					863	77	0.24	864	32	0.38
					889	sh	?	896	39	0.27
906	86	904	83	P						
					917	sh	?			
945	29	942	sh	?	941	86	0.21	944	74	0.29
1036	43									
1068	57				1077	82	0.56	1074	47	0.56
1091	50									
								1143	3	?
		1165	20	?				1165	3	?
								1194	7	?
1214	13	1211	17	?						
								1256	7	?
1277	43									
1321	36	1314	33	0.75	1313	59	0.75	1315	39	0.75
		1393	17	?						
1412	43				1417	100	0.50	1413	100	0.50
1454	100				1450	86	0.75	1446	67	0.75
								1558	12	0.75
1645	43	1712	67	0.50	1703	32	P			

a) Figures in parentheses represent the mole ratio, NaOH: acid. ν, frequency in cm^{-1}; I, relative intensity; ρ, depolarization ratio; P, polarized; DP, depolarized.

Table 3. Force Constants of Pimelic Acid (in mdyn/Å)

	Set I	Set II		Set I	Set II	
K(CH_2-CH_2)	2.137	2.134	H(CCO)	0.616	0.522	
K(CH)	4.026	4.229	F(CCO)	1.158	1.685	
K(C=O)	7.454	7.272	H(O=CO)	0.038	0.117	
K(C-O)	4.058	4.162	F(O=CO)	0.502	0.319	
K(OH)	4.994	4.945	H(COH)	0.450	0.401	
H(CH_2-CH_2-CH_2)	0.332	0.259	F(COH)	0.461	0.474	
F(CH_2-CH_2-CH_2)	0.353	0.336	π(C=O)	0.559	0.534	mdyn.Å
H(CCH)	0.198	0.191	Y(CH_2-CH_2)	0.08	0.154	mdyn.Å
F(CCH)	0.507	0.514	Y(CH_2-CO)	0.154	0.500	mdyn.Å
H(HCH)	0.412	0.389	Y(C-O)	0.087	0.087	mdyn.Å
F(HCH)	0.066	0.043	κ	0.056	0.034	mdyn.Å
H(CC=O)	1.168	1.368	t	0.159	0.180	mdyn.Å
F(CC=O)	0.970	0.833	g	−0.017	−0.059	mdyn.Å

aqueous sodium hydroxide solutions, most of the molecular chains have a conformation entirely different from those in methanol solutions.

Similarity of the Spectra of Adipic Acid and Pimelic Acid in Aqueous Sodium Hydroxide Solutions. As to the skeletal vibrations (<1000 cm^{-1}), which are sensitive to conformational changes, both acids have mutually corresponding observed frequencies: adipic acid (384, 775, 845, and 930 cm^{-1}); pimelic acid(332, 779, 864, and 944 cm^{-1}), although the increase of a

Table 4. Spectral Change Due to the Group Change, COOH to COO^-, for Acetic Acid and Its Salt

CH_3COOH Pure liquid	CH_3COONa Aq. soln (47.7%)	$CH_3COONa\ 3H_2O$ Solid	
453	480	490	CO_2 bend
610	621	635	CO_2 rock
627	655	670	CO_2 wag
900	922	935	CC str
1020	1018	1022	CH_3 rock
1280			CO str, COH bend
	1343	1360	CH_3 sym. def
1373		1377	CH_3 sym. def
	1409	1430	CO str
1425			COH bend, Co str
1435	1426	1450	CH_3asym. def
1673			C=O str (hydrogen-bonded)
1760			C=O str (free)

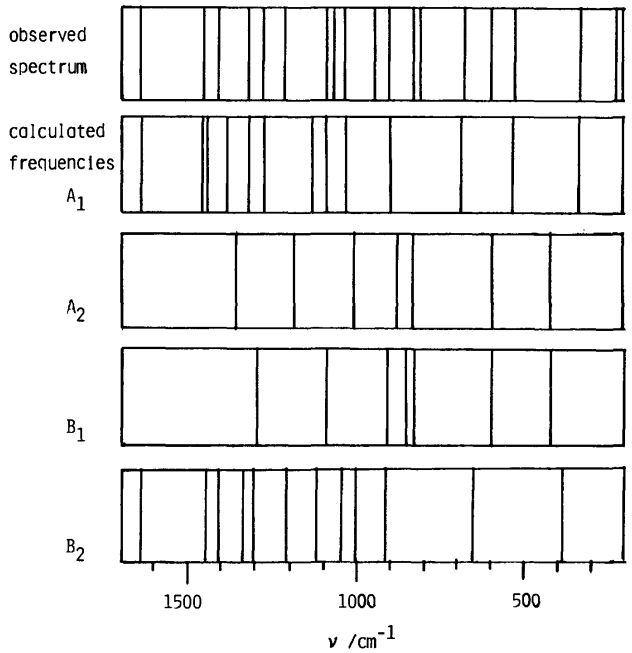

Fig. 2. Observed Raman spectrum of solid pimelic acid compared with calculated frequencies of the all-*ap* conformer.

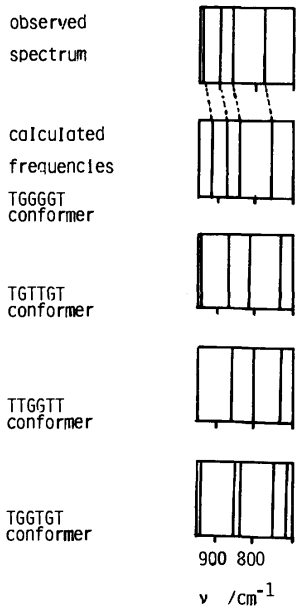

Fig. 3. Observed frequencies of C-C stretching bands of aq. hydroxide solution and calculated frequencies of various conformers for pimelic acid.

CH_2 group in pimelic acid compared with adipic acid shows an expected spectral difference between the acids. This correspondence suggests a similarity in the molecular conformations of the acids in aqueous sodium hydroxide solutions.

Molecular Conformation in Aqueous Sodium Hydroxide Solutions. Normal vibration calculations of various conformers were carried out using the refined force constants. For the C-C stretching vibrations, which give stronger bands in Raman spectra and which have remarkably different frequencies between methanol solutions and aqueous sodium hydroxide solutions, the calculated frequencies (Fig. 3) of various conformers are compared with the spectra of aqueous sodium hydroxide solutions. The bands of the spectrum of Fig. 1(c) correspond to the calculated frequencies of some conformers in Fig. 3; therefore, the solution corresponding to the figure might contain a mixture of those conformers. However, the pattern of the spectra (Fig. 1(d) and the top of Fig. 3) for a higher concentration of sodium hydroxide fits very well to the spectral pattern of the calculated frequencies of the TGGGGT conformer. Taking the similar situation found in the case of suberic acid and azelaic acid[1] into consideration, the conformer having the TGGGGT conformation of the skeleton is considerded to be abundant in aqueous sodium hydroxide solutions. This is in contrast to the case of some monocarboxylic acid salts, where the molecules may be supposed to gather to form micelles, taking an all-*ap* molecular chain.[6]

Interpretation of the Conformational Change. The remarkable conformational change from solutions of organic solvents to aqueous sodium hydroxide solutions may be interpreted as follows. In aqueous sodium hydroxide solutions, the carboxyl groups change to carboxylato groups, which are not capable of causing the intermolecular association of acid salt molecules. Therefore, the stabilization by hydrogen bonding, as in the case of the acids, is lost. Moreover, contact of the hydrophobic molecular chain of acid salt molecule with water molecules increases the instability of the molecular energy. In addition, the presence of a carboxylato group on each end of the molecular chain prevents the molecules from being stabilized by the formation of spherical micelles. These situations make the acid salt molecules take a conformation where the contact area of the hydrophobic molecular chain with water is minimized. The conformation with TGGGGT carbon-chain skeleton is a part of a helix in which the skeleton comes in contact with water molecules only at the outer surface of the helix; instability due to contact of the hydrophobic group and water is thus minimized. Therefore, this helical structure may be stable in aqueous solutions. This is consistent with the agreement of the observed frequencies for aqueous sodium hydroxide solutions with the calculated frequencies of the conformer with the helical structure.

References

1) K. Fukushima, T. Watanabe, and M. Umemura, *J. Mol. Struct.*, **146**, 61 (1986).

2) E. B. Wilson, Jr., *J. Chem. Phys.*, **7**, 1047 (1939); **9**, 76 (1941).

3) D. E. Mann, T. Shimanouchi, J. H. Meal, and L. Fano, *J. Chem. Phys.*, **27**, 43 (1957).

4) J. D. Morrison and J. M. Robertson, *J. Chem. Soc.*, **1949**, 987.

5) M. Suzuki and T. Shimanouchi, *J. Mol. Spectrosc.*, **29**, 415 (1969).

6) H. Okabayashi, M. Okuyama, and T. Kitagawa, *Bull. Chem. Soc. Jpn.*, **48**, 2264 (1975).

 © 1988 The Chemical Society of Japan Bull. Chem. Soc. Jpn., 61, 3055—3059 (1988)

Pulse Radiolysis Studies of Solvent Radical Cations in Liquid 1,2-Dichloroethane

Takashi SUMIYOSHI,* Naoki SUGITA, Kazuyuki WATANABE, and Meiseki KATAYAMA
Department of Atomic Science and Nuclear Engineering, Faculty of Engineering,
Hokkaido University, Sapporo 060
(Received February 20, 1988)

Transient absorption spectra with maxima at 270 and 550 nm were observed in liquid pure 1,2-dichloroethane by means of ps and ns pulse radiolysis. The broad absorption band with a maximum around 550 nm decayed according to a first-order reaction with $t_{1/2}$=0.2 ns in ps pulse radiolysis and $t_{1/2}$=200 ns in ns pulse radiolysis. These short lived species were attributed to solvent cations on the basis of scavenger experiments. The slowly decaying species with $t_{1/2}$=1.2 μs which absorbs around 400 nm superimposed on the 550 nm band, was tentatively assigned to carbocations. The 270 nm band formed during and after the electron pulse decayed over several microseconds by second-order kinetics. Those radicals which were produced by the dissociative electron attachment to the solvent and by the reaction of cations were responsible for this UV band.

Radiolysis of chlorinated hydrocarbonds such as carbon tetrachloride,[1] 1,2-dichloroethane (1,2-DCE),[2] and butyl chloride[3] has been applied to studies on solute cations by many workers. In these solvents electrons are dissociatively attached to solvent molecules to form stable chloride ions. The absorption spectra of solvent cations of carbon tetrachloride[4,5] and butyl chloride[6–8] have been observed and the rate constants of charge transfer with various solutes have been determined in pulse radiolysis experiments. However, it is reported that 1,2-DCE shows only a very weak absorption in the μs pulse radiolysis.[9] We initiated this study in order to obtain the spectral and kinetic information of 1,2-DCE cations. This paper reports the observation of radical cations of 1,2-DCE by means of ns and ps pulse radiolysis at room temperature and the rate constants of charge transfer for various cation scavengers.

Experimental

1,2-Dichloroethane was spectrograde of Wako Junyaku. The stroboscopic picosecond pulse radiolysis system[5] with a time resolution of 30 ps and the nanosecond pulse radiolysis system[10] with a time resolution of 10 ns were described earlier. Electron pulses of 45 MeV and 10 ns width from an S-band LINAC were used as a radiation source. The absorbed doses were determined with the KSCN dosimeter[11] for the 10 ns pulse and the hydrated electron dosimeter for the 30 ps fine-structure electron pulse applying $G(e_{aq}^-)$ at 30 ps as 4.8.[12] The detection system consisted of a monochromator (Bausch and Lomb, 33-86-25) and a photomultiplier (HTV, R928). The bandwidth of the monochromator was 10 nm. Samples were bubbled with argon in a quartz cell which has an optical path length of 1 or 2 cm and sealed with a teflon bulb for the ns pulse radiolysis. In the case of ps pulse radiolysis the solution was circulated through the 2 cm path length cell by a pump to prevent the deposition of radiation products. All experiments were carried out at 18 °C.

Results

Picosecond Pulse Radiolysis. Pure liquid 1,2-DCE was irradiated with a train of 30 ps fine structure electron pulses spacing at 350 ps each other. A typical kinetic trace observed at 550 nm is presented in Fig. 1. The solid line is the computer simulated first-order decay curve with parameters $G\varepsilon$=2.4×10^4 mol^{-1} dm^3 cm^{-1} and $t_{1/2}$=200 ps. The dose of the macro pulse whose time profile can be approximated as a gaussian with a half width of 10 ns was 38 Gy. Figure 2 shows the transient absorption spectra obtained immediately after the 30 ps pulse in the range of 350 to 700 nm. The spectrum exhibits a maximum at 550 nm.

Nanosecond Pulse Radiolysis. Figure 3 shows the

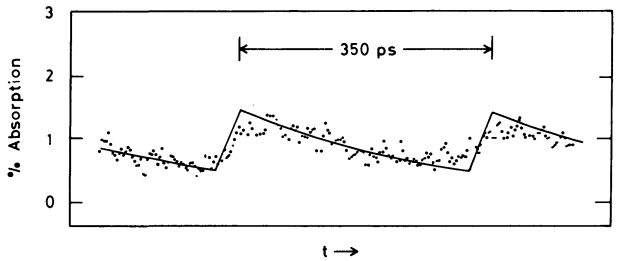

Fig. 1. The picosecond kinetic trace observed at 550 nm in pure 1,2-dichloroethane at 18 °C. The solid line is the simulated trace with $G\varepsilon$=2.4×10^4 mol^{-1} dm^3 cm^{-1} and $t_{1/2}$=200 ps.

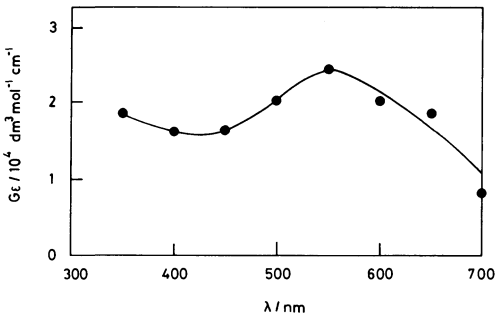

Fig. 2. The absorption spectrum obtained at the end of 30 ps electron pulse irradiation of pure 1,2-dichloroethane.

transient absorption spectra observed at the end of the 10 ns pulse, 120, 600 ns and 2 μs after the pulse in pure 1,2-DCE by the ns pulse radiolysis. Two distinguished transient absorption bands could be observed at 550 and 270 nm. However, the kinetic behavior is not identical for both absorption bands as shown in the insets of Fig. 3. The visible absorption spectrum immediately after pulse is quite similar to that was observed in the ps pulse radiolysis. The maximum of the visible band shifts from 550 to 500 nm in the first 120 ns then to 450 nm in 600 ns. This change can be also demonstrated by the different kinetic behavior observed at 400 and 650 nm as presented in Fig. 4. The decay trace at 650 nm consists two first-order components, i.e., $k_1=(2.5\pm0.5)\times10^7\ s^{-1}$ and $k_2=(3.5\pm0.5)\times10^6\ s^{-1}$. On the other hand, the kinetic trace at 400 nm is the superposition of these two components and a much slowly decaying component with $k_3=6\times10^5\ s^{-1}$. Therefore, the blue shift of the visible band is due to the rather long-lived species which absorbs near UV region.

The 270 nm band is formed during and after the pulse (Fig. 5a) and decays by a second-order reaction with $2k/\varepsilon=2\times10^7$ cm s^{-1}.

Typical electron scavengers such as N_2O, oxygen and CCl_4 have been added to the solution and it was found that they do neither reduce the initial absorbance of both 270 and 550 nm bands nor increase the decay rate. On the other hand, solutes which have a lower ionization potential than that of 1,2-DCE (11.41 eV)[14] increase the decay rate of 550 nm band and decrease the absorbance of the 270 nm band. Typical results obtained with cyclohexane (IP=10.32 eV)[14] as a cation scavenger are illustrated in Figs. 5a—c. The high concentration of cyclohexane ($>10^{-1}$ mol dm^{-3}) supresses the visible band almost completely

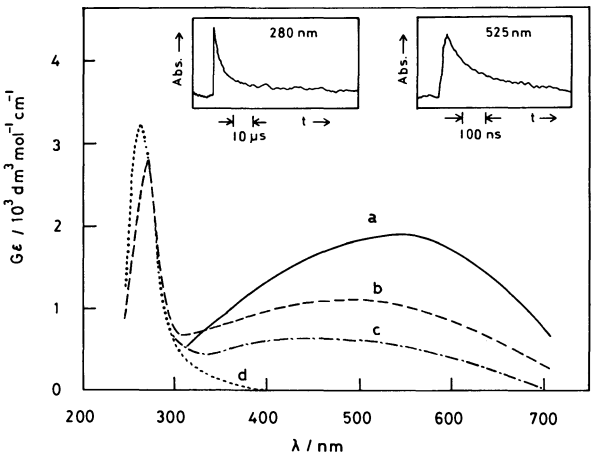

Fig. 3. Absorption spectra recorded at the end of the 10 ns electron pulse (a) and 120 ns (b), 600 ns (c) and 2 μs (d) after the pulse. Dose was 82 Gy and optical path length was 2 cm.
Insets: kinetic traces illustrating the decay of the absorbance at 280 and 525 nm.

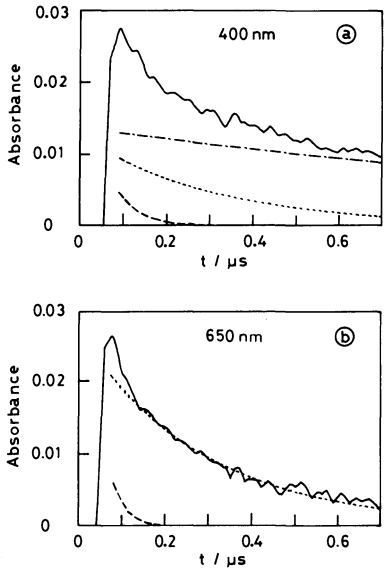

Fig. 4. Kinetic traces observed in pulse irradiated 1,2-DCE at 400 (a) and 650 nm (b). First-order components; (-----): $k_1=2.5\times10^7\ s^{-1}$, (------): $k_2=3.5\times10^6\ s^{-1}$, (—·—·—): $k_3=6\times10^5\ s^{-1}$.

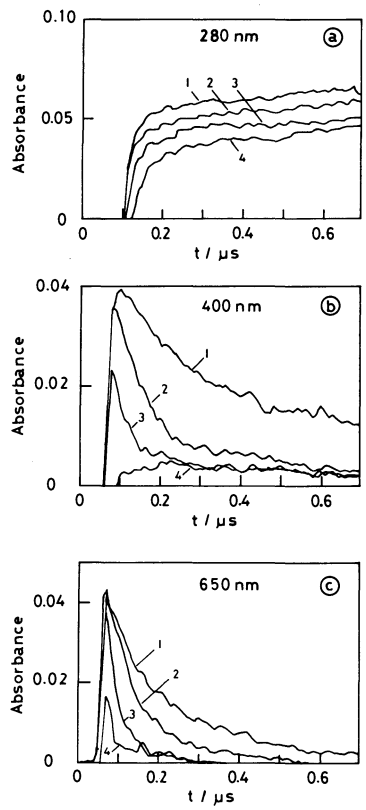

Fig. 5. Effects of cyclohexane on the transient absorption decay at 280 (a), 400 (b) and 650 nm (c). Dose was 110 Gy. Optical path length was 1 cm. Concentration of cyclohexane (in mol dm^{-3}); 1: 0; 2: 4.6×10^{-3}; 3: 1.8×10^{-2}; 4: 9.2×10^{-2}.

but the UV band to about a half. These results strongly indicate that the visible band is due to cationic species and reaction product of this primary cationic species contribute to the UV band to a certain extent. Obviously, the decay rate increases with increasing concentration of cyclohexane (Figs. 5b and 5c). Upon application of pseudo-first order kinetic treatment, the rate constant of positive charge transfer to cyclohexane was determined to be 1.5×10^{9} mol^{-1} dm^{3} s^{-1}.

In the case of pure 1,2-DCE, the absorbance vs. time profiles at 400 and 650 nm are different due to the contribution of the slowly decaying component as mentioned above. However, on addition of cyclohexane decay rate constants obtained at both wavelengths become same as shown in Figs. 5b and 5c. The initial signal intensity at 650 nm does not decrease significantly on addition of cyclohexane up to 2×10^{-2} mol dm^{-3}. On the contrary, the initial absorbance at 400 nm decreases with increasing cyclohexane concentration. These results suggest that the slowly decaying component at 400 nm reacts more rapidly with cation scavenger than the fast component or might be a secondary reaction product of cationic species.

The charge transfer rate constants have been obtained with 13 solutes. The rate constants determined are then correlated with the difference of ionization potential between 1,2-DCE and the added solute as shown in Fig. 6.

Aniline (IP=8.00 eV)[14] is well-known as a cation scavenger and the yield of the solvent cation can be estimated based on the maximum yield of aniline cation radicals.[15-17] The aniline cation radical exhibits an absorption maximum at 423 nm in aqueous solution[18] and at 385 nm in pure aniline.[19] Its extinction coefficient was established to be 2000 mol^{-1} dm^{3} cm^{-1}.[18] Figure 7 shows the typical transient absorption spectrum of the aniline cation radical observed in 2.75×10^{-2} mol dm^{-3} aniline solution. The spectral shape is the same with those observed in aqueous solution[18] and in pure aniline,[19] indicating that only one species is present. Figure 8 shows the decrease of the absorbance at 525 nm and the increase of 410 nm band with increasing aniline concentration. At higher concentration of aniline ($>10^{-2}$ mol dm^{-3}) the absorbance of aniline cation radical is too strong to determine the reduced absorbance of the solvent cations. In spite of this difficulty, the increase of aniline cation radical absorbance seems to correspond with the decrease of the absorbance at 525 nm. The yield of the aniline cation radical has been estimated to be G=2.8 based on the plateau yield of it (OD_{max}=0.088) at the concentration larger than 10^{-1} mol dm^{-3}.

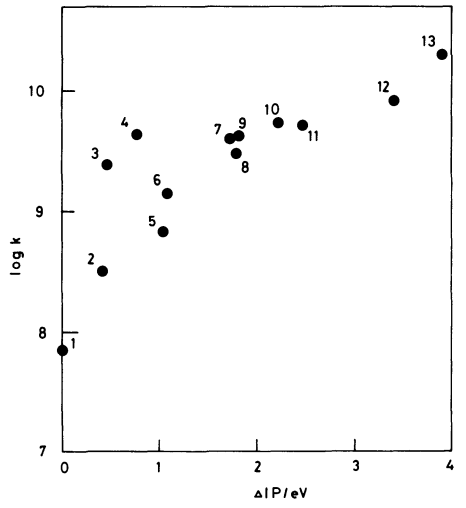

Fig. 6. Dependence of charge transfer rate constant on the ionization potential difference between 1,2-DCE and the solute.
Solutes; 1: dichloromethane; 2: cyclopentane; 3: methanol; 4: ethanol; 5: nonane; 6: cyclohexane; 7: 1-pentene; 8: diethyl ether; 9: 1-hexene; 10: cyclopentene; 11: cyclohexene; 12: aniline; 13: triethylamine.

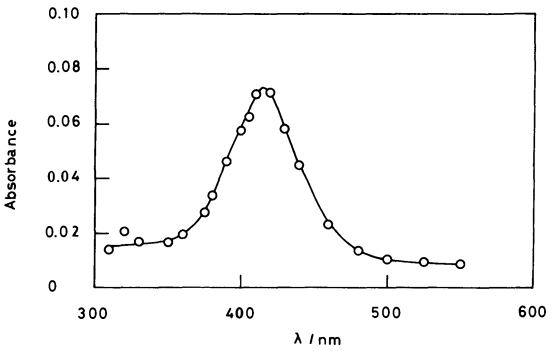

Fig. 7. The absorption spectrum obtained at 500 ns after the pulse in 2.75×10^{-2} mol dm^{-3} aniline in 1,2-DCE. Dose was 120 Gy.

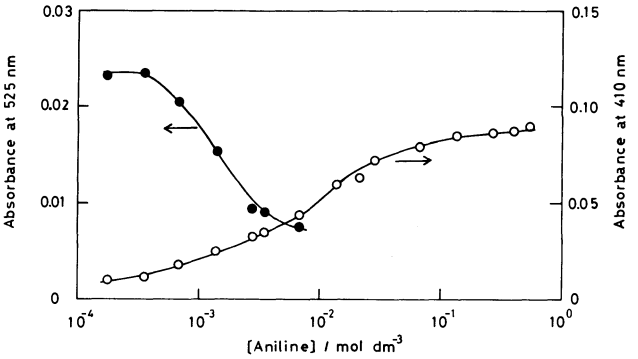

Fig. 8. Effect of aniline concentration on the absorbance at 525 nm of the 1,2-DCE radical cation and at 410 nm of the aniline cation. The absorbance was obtained at the end of pulse and 500 ns after the pulse, at 525 and 410 nm, respectively. Dose was 120 Gy. Optical path length was 1 cm.

Discussion

Assignment of the Transient Species. The transient absorbing species with a maximum at 550 nm has been observed in both ps and ns pulse radiolysis. This visible band can be assigned to 1,2-DCE radical cations based on the experimental evidence of the effects of the electron and cation scavengers on this band. This assignment is also supported by the relation between decay rate constants and the difference of ionization potential between 1,2-DCE and added solutes. The reaction rate constant of the added solute with the visible band increases with increasing difference of the ionization potential as illustrated in Fig. 6.

The $G\varepsilon$-value at 550 nm are 2.4×10^4 mol^{-1} dm^3 cm^{-1} at the end of 30 ps pulse and 1800 mol^{-1} dm^3 cm^{-1} at the end of 10 ns pulse. The higher G-value for ps pulse radiolysis and the short half lifetime of 200 ps indicate that more than 90% of primary 1,2-DCE radical cations disappears by geminate ion reactions. The faster decay observed at 400 and 650 nm during the first 120 ns is indicative of the tail of such geminate ion reactions.

The spectral shift from 550 to 500 nm in the first 120 ns can be due to the slowly decaying species with $k_3=6\times10^5$ s^{-1}. This species absorbs around 400 nm, and disappears almost completely by addition of cyclohexane larger than 5×10^{-3} mol dm^{-3}. These results show that the slow component is very reactive cationic species or has solvent cations as a precursor.

With respect to the spectral shift, it is interesting to note that the similar spectral change was observed in the case of butyl chloride cations.[6,7] Upon irradiation of butyl chloride the initial spectrum with a peak at 520 nm was obtained. However, the peak shifted to 450 nm within 80 μs at 133 K.[6] The short-lived species with a peak at 520 nm and the long-lived species with a peak at 450 nm were attributed to butyl chloride radical cations and butene radical cations, respectively. In that work, Arai et al. suggested that butene and butyl chloride cations must originate from a common precursor such as a vibrationally excited butyl chloride cations on the basis of cation scavenging experiments.

The formation of additional cationic species originating from the solvent was also suggested in the case of irradiated 1,2-DCE by Wang et al.[13] It was reported that there are two kinetically distinguishable cationic species of the 1,2-DCE solvent which react selectively with different solutes to form the phenylcarbenium ion. It was suggested that one is a 1,2-DCE radical cation and other a carbocation formed after C–Cl bond cleavage.

Therefore, we conclude that the fast decaying visible band with $k=(3.5\pm0.5)\times10^6$ s^{-1} is due to the 1,2-DCE radical cation and the slowly decaying visible band with $k=6\times10^5$ s^{-1} might due to cationic species such as $CH_2CHCl^{\ddagger}$ and $CH_2ClCH_2^+$ originates from 1,2-DCE.

The UV band with a peak at 270 nm was formed during and after pulse then decayed with a second-order reaction. This band can be ascribed to radicals which are produced by the dissociative electron attachment (reaction 1) and reactions of solvent cations such as deprotonation (reaction 2) and ion-molecular reactions (reaction 3).

$$CH_2ClCH_2Cl + e^- \longrightarrow CH_2ClCH_2\cdot + Cl^- \quad (1)$$

$$CH_2ClCH_2Cl^{\ddagger} \longrightarrow CH_2ClCHCl\cdot + H^+ \quad (2)$$

$$CH_2ClCH_2Cl^{\ddagger} + CH_2ClCH_2Cl \longrightarrow CH_2ClCH_2ClH^+ + CH_2ClCHCl\cdot \quad (3)$$

Yield of Solvent Cations. Wang et al.[13] estimated the yield of 1,2-DCE cations to be $G=0.87$ based on the yields of phenylcarbenium ions. The yield of solvent cations determined in the present experiment from the limiting absorbance of aniline cation radicals was $G=2.8$. Three times difference of cation yields can not be explained in the present situation. Since the extinction coefficient of the aniline cation radical was determined in water,[18] there might be a changing of the value depending on solvents. Also we have to consider the efficiency of cation scavenging. Since the yields of phenylcarbenium ion varies from $G=0.18$ to 0.87 depending on the solutes,[13] the solutes which were used by Wang et al. might be less effective than aniline to scavenge the solvent cation radical. Further experiments with various cation scavengers which have a well-defined extinction coefficient of cations are needed.

The authers wish to acknowledge Dr. Takeaki Enoto and Messrs. Hiroaki Tanida and Koichi Sato for their help in operating the LINAC.

References

1) T. Shida and W. H. Hamill, *J. Chem. Phys.*, **44**, 2369 (1966).

2) S. Arai, H. Ueda, R. F. Firestone, and L. M. Dorfman, *J. Chem. Phys.*, **50**, 1072 (1969).

3) T. Shida and W. H. Hamill, *J. Chem. Phys.*, **44**, 4372 (1966).

4) R. Mehnert, O. Brede, J. Bös, and W. Naumann, *Ber. Bunsenges. Phys. Chem.*, **83**, 992 (1979).

5) T. Sumiyoshi, S. Sawamura, Y. Koshikawa, and M. Katayama, *Bull. Chem. Soc. Jpn.*, **55**, 2341 (1982).

6) S. Arai, A. Kira, and M. Imamura, *J. Phys. Chem.*, **80**, 1968 (1976).

7) R. Mehnert, O. Brede, and W. Naumann, *Ber. Bunsenges. Phys. Chem.*, **86**, 525 (1982).

8) T. Sumiyoshi, T. Yamada, A. Ohtaka, K. Tsugaru, and M. Katayama, *Chem. Lett.*, **1986**, 307.

9) J. Mönig, K-D. Asmus, L. W. Robertson, and F. Oesch, *J. Chem. Soc., Perkin Trans. 2*, **1986**, 891.

10) Y. Kondo, M. Aikawa, T. Sumiyoshi, M. Katayama, and J. Kroh, *J. Phys. Chem.*, **84**, 2544 (1980).
11) E. M. Fielden and N. W. Holm, "Manual on Radiation Dosimetry," ed. by N. M. Holm and R. J. Berry, Marcel Dekker, New York (1970), p. 261.
12) T. Sumiyoshi, K. Tsugaru, T. Yamada, and M. Katayama, *Bull. Chem. Soc. Jpn.*, **58**, 3073 (1985).
13) Y. Wang, J. J. Tria, and L. M. Dorfman, *J. Phys. Chem.*, **83**, 1946 (1979).
14) K. Kimura, S. Katsumata, Y. Achiba, T. Yamazaki, and S. Iwata, "Handbook of HeI Photoelectron Spectra of Fundamental Organic Molecules," Japan Scientific Societies Press, Tokyo (1981), p. 92.
15) R. Cooper and J. K. Thomas, *Adv. Chem. Ser.*, **82**, 351 (1968).
16) R. E. Bühler and B. Hurni, *Helv. Chim. Acta*, **61**, 90 (1978).
17) H. D. Burrows, D. Greatorex, and T. J. Kemp, *J. Phys. Chem.*, **76**, 20 (1972).
18) E. J. Land and G. Porter, *Trans. Faraday Soc.*, **59**, 2027 (1963).
19) R. Cooper and J. K. Thomas, *J. Chem. Phys.*, **48**, 5103 (1968).

 © 1988 The Chemical Society of Japan Bull. Chem. Soc. Jpn., 61, 3061—3066 (1988)

Hopping Phenomena of [1-^{14}C]Octadecanoic Acid Molecules at the Surface of the Langmuir-Blodgett Film Regarded as an Extremely Thin Crystal

Makio Iwahashi,* Kiyoharu Itoh,† Katsumi Ohshima,†,†††† Tsutomu Seimiya,†
Akira Yoshida,†† Koichi Kobayashi,††† and Kei Takaoka†††
Department of Chemistry, School of Hygienic Sciences, Kitasato University, Sagamihara, Kanagawa-ken 228
†Department of Chemistry, Faculty of Sciences, Tokyo Metropolitan University, Setagaya-ku, Tokyo 158
††Instrumental Analysis Center, Musashi Institute of Technology, Setagaya-ku, Tokyo 158
†††Department of Chemistry, Faculty of Technology, Musashi Institute of Technology, Setagaya-ku, Tokyo 158
(Received February 29, 1988)

The desorption of [1-^{14}C]octadecanoic acid molecules in vacuo from a Langmuir-Blodgett film, which is regarded as an extremely thin crystal, was studied by using three kinds of radioactive samples containing ten molecular layers: The first sample was labeled at the tenth (the outermost) layer; the second one, at the ninth layer and the third one, at both the ninth and tenth layers. From the initial slopes in the desorption curves for these samples it is suggested that most of the acid molecules desorb from the tenth layer and some acid molecules desorb as a dimer consisting of a pair of molecules from the ninth and tenth layers. The scanning electron micrographic observations were carried out for nonradioactive samples stored for a week at 298.2 or 278.2 K under atmospheric pressure; it was concluded that the fatty acid molecules jump back and forth between a boundary (stagnant) layer and the surface of the LB multilayer and coagulate into micron-size crystals.

Vapor pressure and heat of sublimation of long-chain fatty acid crystals at room temperature have been measured by only a few investigators in spite of their thermodynamical and practical utilities. This is attributable to the experimental difficulty in measuring the extremely low vapor pressure of the crystals. Some attempts[1-4] have been made by Knudsen's method to determine the vapor pressure for the long-chain compounds but only near their melting points in which relatively high vapor pressures are available.

The highly oriented Langmuir-Blodgett (LB) multilayer of octadecanoic acid takes on a C-type (monoclinic) crystal structure in the upper monolayers other than the first monolayer.[5] This is the most stable crystal form at room temperature. X-Ray diffraction and IR spectrum measurements indicated that the LB multilayer of octadecanoic acid consisted of its extremely small three-dimensional crystallites which are oriented so that their c-axes align with an angle of ca. 30° to the normal axis of the substrate plate.[5,6] The desorption of the acid molecules from the LB film is therefore regarded as that from the extremely thin and small crystals. Accordingly, the measurement of the desorption for the acid molecules labeled radioactively from the LB multilayer will give us useful information about the mechanism of the desorption process from the crystal. In the present study the desorption from the surface of the fatty acid multilayer was investigated by using the ^{14}C-samples labeled at arbitrary layers; the desorption mechanism was estimated and confirmed also by scanning electron micrographic observations for the nonradioactive LB films.

Experimental

Materials. [1-^{14}C]Octadecanoic acid (specific activity of 59.0 Ci mol^{-1}) from New England Nuclear, Inc., and the purest grade sample of octadecanoic acid from Wako Chemical Industry were used for the built-up process. Ferrotype plates (20×15×0.5 mm) were used as the substrate plate. The plates were washed in aqueous ethanol solution (ethanol:water=1:1 in volume ratio) containing 5% of potassium hydroxide and rinsed in triple distilled water, and their surfaces were pretreated with iron (III) octadecanoate (the purest grade of Tokyo Kasei Industry Co., Tokyo) to be hydrophobic. The subphase solution was triple-distilled water[7] whose pH was adjusted to 2 with twice distilled HCl. Under this pH condition, the monolayers consisting of only salt-free octadecanoic acid molecules are transfered onto the substrate plate even if some metal ions existed in the subphase solution.[8,9]

Troughs and Movable Barriers. Two sizes of Teflon troughs were used: The small one had inside dimensions of 260 mm^{length}×25 mm^{width}×15 mm^{depth} and large one, 282×155×5 mm. The large trough had a pocket (40×20×15 mm) in its bottom for vertical dipping of the substrate plate. The inside of the small trough was hydrophilic by the glow discharge in an oxigen atmosphere and the rims remained hydrophobic by protective adhesion tapes for a smooth movement[10] of a thin glass plate (32×24×0.5 mm) coated with paraffin. For the large trough a paraffin-coated silk thread of ca.20 cm in length was used as a movable barrier for the compression of the monolayers.

Built-up Procedure. A benzene solution (1×10^{-3} mol dm^{-3}) of nonradioactive octadecanoic acid was used as spreading solution for the large trough and hexane solutions (1×10^{-4} mol dm^{-3}) of radioactive or nonradioac-

†††† Present address: Nippon Paint Co., Ltd., Minami-shinagawa, Shinagawa-ku, Tokyo 140.

tive sample, for the small trough. The purest grade ethyl tetradecanoate (Wako Chemical Industry) as used as a piston oil whose surface pressure was about 20.7 mN m^{-1}.

The samples of LB film containing eight monomolecular layers of the nonradioactive acid were prepared by the conventional vertical-dipping method, using the large Teflon trough, at 285—290 K. Let us term the samples thus obtained LB-8 plates.

The substrate plate as dipped to a depth of 15 mm in the subphase solution and withdrawn through the nonradioactive monolayer at a velocity of 0.1—0.5 cm s^{-1} by means of a synchronous motor. In order to know the transfer ratio of the monolayer onto the substrate plate, we used the small Teflon trough and the floating glass plate (movable barrier) coated with paraffin. From the movement of the glass plate in the transfer process we evaluated the transfer ratio of the monolayer. The ratios for both upward and downward strokes were almost unity (0.97—1.00).

A modified horizontal-lifting method[10] was employed for the transfer of the additional two radioactive and/or nonradioactive monolayers on the LB-8 plates by using the small Teflon trough. The transfer process by the method is schematically shown in Fig. 1. After the solution surface was swept with Teflon barriers, the surface was divided into two equal parts with a narrow glass barrier **A** which was made hydrophobic by treatment with dimethyldichlorosilane. In order to prepare a radioactive sample labeled at the tenth layer, a nonradioactive octadecanoic acid monolayer was spread on one part of the divided surface. The monolayer was compressed with the floating glass plate by piston oil pressure. Then, the LB-8 plate on the monolayer (Fig. 1-a) was touched almost horizontally. A new glass barrier **B** was then placed near the end of the plate (Fig. 1-b),

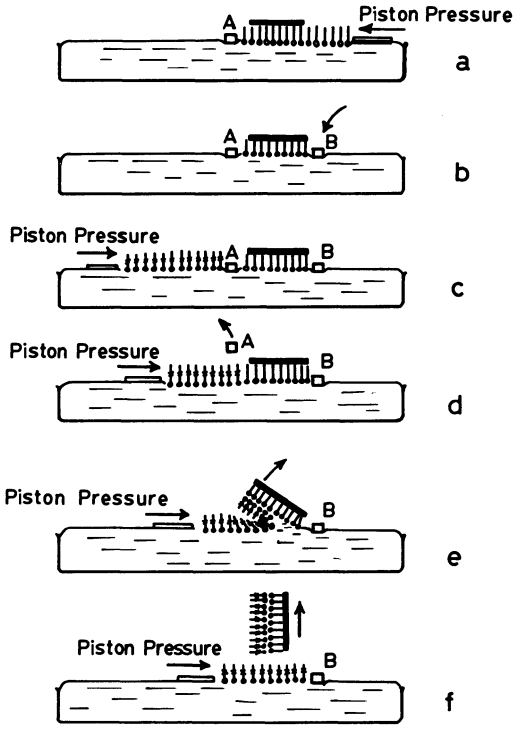

Fig. 1. Scheme of the transfer process of radioactive and/or nonradioactive monolayer onto LB-8 plate.

and the monolayer remaining around the plate was cleaned out with several hydrophobic glass barriers and an aspirator. Subsequently a [1-^{14}C]octadecanoic acid monolayer was spread on the other surface. The monolayer was also compressed with the second floating glass plate by a piston oil pressure. On removing the glass barrier **A** from the solution surface, the radioactive monolayer came from one part of the divided surface and spread around the plate (Fig. 1-d). The plate was then turned gradually by a mechanical operation controlled with a personal computer (NEC model PC-8001 MKII), lifted and finally removed from the surface (see Fig. 1-e and f). One molecular layer of the nonradioactive octadecanoic acid and an additional layer of [1-^{14}C]octadecanoic acid were transferred onto the LB-8 plate by this process. In order to prepare a sample labeled at the ninth layer, the LB-8 plate should be initially attached to the radioactive monolayer. For the preparation of a sample labeled simultaneously at both the ninth and tenth layer, the water surface should be occupied only by the radioactive monolayer: It is not necessary to use the glass barrier **A** to devide the solution surface into two parts. This depositing process gave Y-type films for the octadecanoic acid monolayer and the transfer ratios by this method were also almost unity.

The Measurement of the Desorption in Vacuo. The radioactive samples thus obtained were set in the vacuum chamber thermostated at ±0.1 K. After the samples had been set in the chamber, it took about 3 minutes to reach a pressure of 1×10^{-2} Pa with rotary and diffusion pumps. Isothermal desorption experiments were performed under this pressure and at a number of different temperatures (288—303.9 K). The radioactivity of each sample, being proportional to the remaining amount of [1-^{14}C]octadecanoic acid, was measured batchwise with a thin end-window Geiger-Müller tube, with a mica window of thickness 1.4 mg cm^{-2} at any given time.

Observation with Scanning Electron Micrographs. Scanning electron micrographic observation (SEM) of the nonradioactive samples containing ten monomolecular layers either freshly prepared or stored for a week under atmospheric pressure at 298.2 or 278.2 K were carried out with a JOEL JXA-840 scanning electron microscope.

Results and Discussion

Figure 2 shows the relative desorption profiles, $\ln(R/R_0)$-t, for the [1-^{14}C]octadecanoic acid from the LB films labeled at the tenth layer under the conditions of 1×10^{-2} Pa and various temperatures (288.6—303.8 K). R denotes the radioactivity due to the labeled molecules remaining in the LB film at time t and R_0, that at t=0. By assuming a first-order reaction for the desorption process, initial slopes in the curves were adopted to obtain the rate constants k_1 for the desorption of the acid molecules. Figure 3 show the Arrhenius plots for the rate constants. Five plots at lower temperatures (288.6—298.2 K) show good linearity, while a plot at 303.8 K deviates from this line. Not only desorption but also molecular exchange reactions most likely occur from and among

monolayers at the higher temperature. The apparent activation energy, 191.2 kJ mol^{-1}, for the desorption was obtained from the linear portion of the Arrheneus plots. This value is somewhat larger than the heat of sublimation for the octadecanoic acid crystal.[2] The heat of sublimation was calculated from the temperature dependence of its vapor pressure, which was obtained by Knudsen's method, near the melting point (342.2 K) of the crystal.

Figure 4 shows the desorption profiles for three kinds of samples in vacuo at 298.2 K. The first sample (▽) as labeled at the 9th layer, the second one (○), at the 10th layer, and the third one (□), at both the 9th and 10th layers. The desorption rate for the first sample is slower than that for the second one, but not zero. Some acid molecules seem to escape from the 9th layer as well as from the 10th layer even at the initial stage in spite of the existence of an additional monolayer on the 9th layer. The molecules is therefore thought to desorb as a dimer consisting of a pair of molecules across the 9th and 10th layers. One-half the sum (▲) of the relative radioactivities of the first and the second samples should be equal to the relative radioactivity of the third sample (□). However, the former was always larger than the latter.

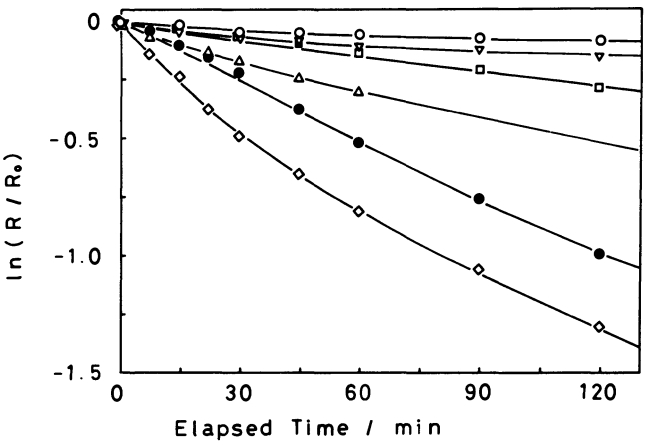

Fig. 2. Relationship between logarithm of relative radioactivity and evacuation time for the ^{14}C-sample labeled at the 10th layer under a pressure of 1× 10^{-2} Pa and various temperature. The mark ○ is at 288.7 K, ▽, at 290.7 K, □, at 293.4 K, △, at 296.3 K, ●, at 298.2 K, and ◇, at 303.9 K.

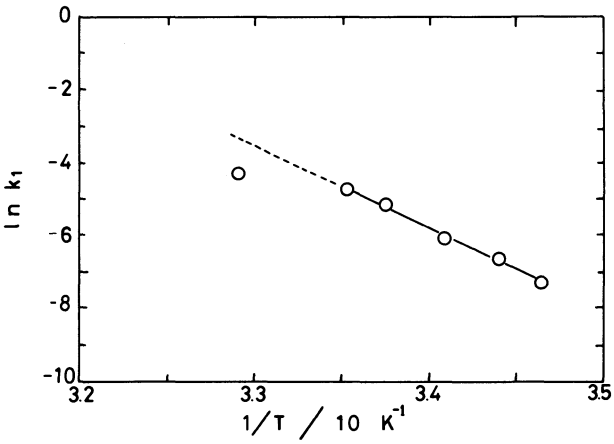

Fig. 3. The logarithm of the desorption rate for octadecanoic acid LB film labeled at the 10th layer vs. reciprocal temperature.

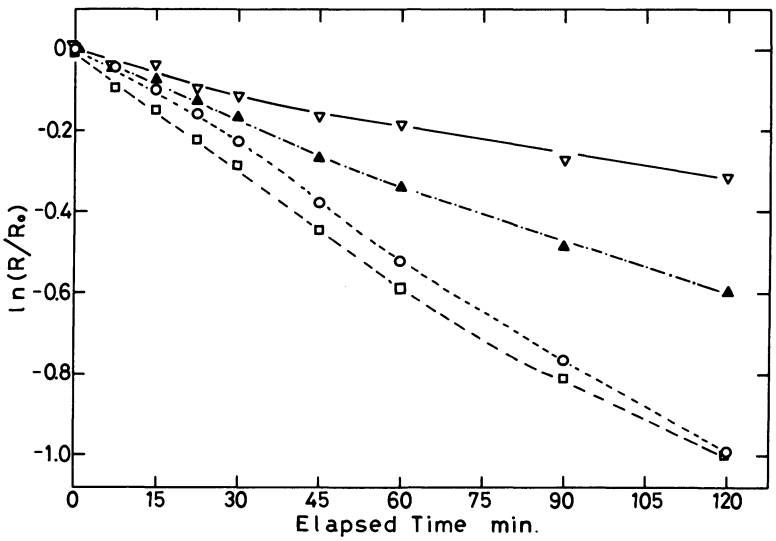

Fig. 4. Relationship between logarithm of relative radioactivity and evacuation time for various samples under a pressure of 1×10^{-2} Pa and at 298.2 K. ▽ denotes the sample labeled at the 9th layer, ○, the sample labeled at the 10th layer; □, the sample labeled simultaneously at the 9th and 10th layers; and ▲ one-half the sum of ▽ and ○.

Moreover, the relative radioactivity for the sample decreases significantly more than the relative radioactivities for the first and second samples. Consequently, the ^{14}C-labeled molecules appear to migrate among the layers even during the evacuation.

The radioactivity of another sample labeled at the 10 th layer was not altered after one-week storage under the conditions of atmospheric pressure and room temperature (298.2 K). The acid molecules, therefore, do not evaporate, but might migrate among and/or in layers under the above conditions. Fujihira et al.[11] observed the translayer diffusion in LB films by measuring the mobility of dyes. Such a translayer diffusion can be attributed to molecular exchange among the layers. To confirm the possibility of molecular exchange, four kinds of samples were prepared by the following procedure: Sample **a** was a LB film labeled at the 10 th layer; sample **b**, same as sample **a**, but stored for a week at 298.2 K and atmospheric pressure; sample **c**, a LB film labeled at the 9 th layer; sample **d**, same as sample **c**, but stored for a week at 298.2 K and atmospheric pressure. Desorption in vacuo for these four samples was observed. The $\ln(R/R_0)$-t relationship obtained is shown in Fig. 5. The desorption from sample **a** (◇) was faster than that from sample **b** (○), while the desorptions from the other samples **c** (□) and **d** (▽) were almost equal with that for sample **b** (○). Apparently, the acid molecules exchange their positions in and/or among monomolecular layers during the storage of the samples.

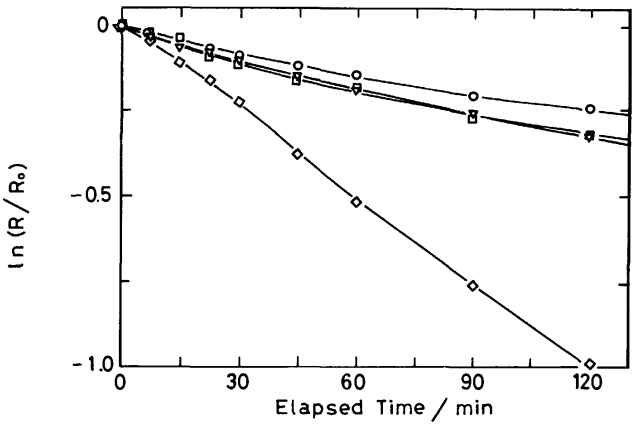

Fig. 5. Relationship between relative radioactivity and evacuation time for the various samples under a pressure of 10^{-2} Pa and 298.2 K. ◇ denotes sample **a** which is a LB film labeled at the 10th layer; ○, sample **b**, same as sample **a**, but stored for a week at 298.2 K and atmospheric pressure; □, sample c, LB film labeled at the 9th layer; ▽ sample **d**, same as sample c, but stored for a week at 298.2 K and atmospheric pressure.

The samples **b** and **d** stored for a week at 298.2 K and atmospheric pressure, showed a powdery appearance at their surfaces, while the sample just prepared or stored at lower temperature (278.2 K) did not have such an appearance. Figures 6-a and -b show the SEM pictures for two samples containing 10-monolayers of nonradioactive acid stored for a week at 278.2 K and at 298.2 K, respectively, under atmospheric pressure. The picture for the sample stored at 278.2 K (Fig.6-a) was as smooth as that for the sample just prepared, while that of the sample stored at 298.2 K (Fig. 6-b) had many white clusters having a diameter in the range of 0.2 to 3 μm. The clusters seem to be micron-

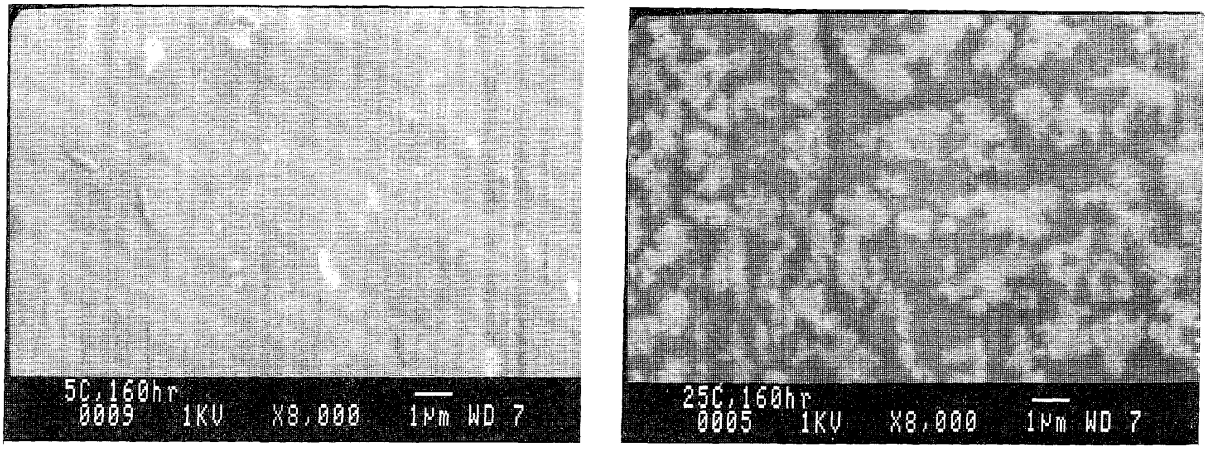

Fig. 6. Scanning electron micrographic (×5200) of the two samples containing 10 molecular layers of nonradioactive acid stored for a week under atmospheric pressure at 278.2 and 298.2 K. Photograph **a** is the sample stored at 278.2 K and photograph **b**, the sample stored at 298.2 K.

size crystals. The acid molecules in the LB film appear to migrate and aggregate to form the micron-size crystals during the storage at room temperature and under the atmospheric pressure. Let us examine the mechanism to produce such crystals.

The desorption of octadecanoic acid molecules in vacuo from its LB film is considerable:[12,13] Almost 90% of the [1-^{14}C]octadecanoic acid molecules in its monolayer on a quartz backing was evaporated after one hour evacuation at a pressure of 10^{-4} Pa.[12] Under atmospheric pressure, however, the radioactivity of the LB film of ^{14}C-labeled acid did not alter for a long time: There hardly occured any desorption of the acid molecules from the LB film under these conditions. The above two contradictory facts suggest the following for consideration: A thin boundary layer (stagnant layer) of the acid vapor occurs near the surface of the LB film as illustrated schematically in Fig. 7. In vacuo the molecules have a long mean-free path and can escape easily from the layer, while in air under the conditions of atmospheric pressure and room temperature the molecules, colliding frequently with air molecules or one another, have a short mean free path (10^{-7} m) and rarely escape (diffuse) from the layer into the air. Consequently, the desorption and adsorption of the molecules are continuously repeated between the LB film and the stagnant layer; the rates in the above two processes are in balance with one another. By repeated processes, an isothermal distillation[14] may occur from the extremely small crystallites (the LB film of multilayer of octadecanoic acid is, as mentioned before, an assembly of the extremely small crystallites),[6] to slightly larger crystallites. The extremely small crystallites would evaporate and disappear, while the slightly larger crystallites would become larger and larger during the one-week storage of the LB film. Thus film molecules can transfer over a long distance and coagulate into micron-size crystals. The "overturning" of octadecanoic acid molecules in monolayer[15,16] and the transference of ^{14}C-labeled acid from its LB film deposited on a solid surface onto other solid when the former solid was contacted with the latter one[17] might be due to the molecular migration by the desorption/adsorption process. Beischer,[18] and Rideal and Tadayon[19] reported the surface diffusion for the octadecanoic acid molecules in the monolayer deposited on mica surface the mobility of the molecules on the surface was found to be much greater than inside the bulk substance. The surface diffusion also seems to be attributed mainly to the desorption/adsorption process.

Estimation of Equilibrium Vapor Pressure. The desorption rate of an acid molecule from the LB film at time t is expressed as

$$-(d\Gamma/dt)_{des} = k_1\Gamma, \quad (1)$$

where Γ is the amount of radioactive octadecanoic acid in the LB film; k_1, the rate constant for the desorption. For the adsorption of molecules from the vapor layer onto a solid surface, the following equation is applicable,[20]

$$(d\Gamma/dt)_{ads} = k_2PS_o \quad (2)$$

where k_2 is the rate constant for the adsorption; P, the vapor pressure and S_o, the number of sites available for the adsorption of the film molecules.

From the constancy in the Γ-t relationship under atmospheric pressure it is concluded that the

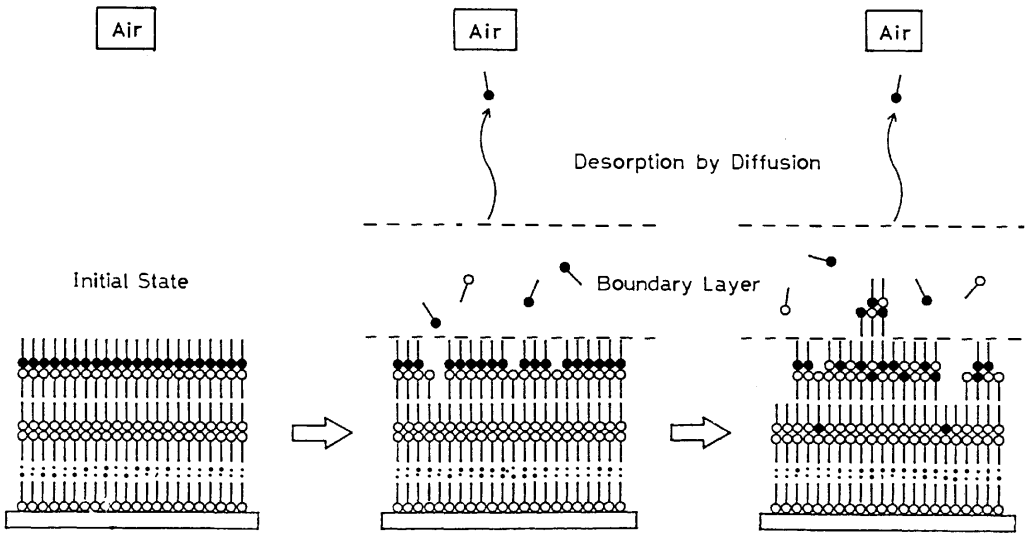

Fig. 7. Schematic drawing of molecular migration of the octadecanoic acid through the boundary (stagnant) layer near the surface of LB film.

adsorption and desorption rates are in balance with one another. Thus, we obtain

$$k_1\Gamma = k_2PS_o. \quad (3)$$

As Γ corresponds to the molecular density of octadecanoic acid at the outermost layer, S_o can be taken as equal to Γ, assuming that the adsorption occurs at any place in the outermost layer. According to the molecular kinetic theory, k_2 is proportional to the collision number of the molecules against the site having a definite area. Thus,

$$k_2 = N_aC\sigma_o\exp(-E_a^*/kT)/(2\pi MRT)^{1/2} \quad (4)$$

where N_a denotes the Avogadro number σ_o, the collision cross-section of octadecanoic acid molecule;[21] C, the sticking coefficient; M, the molar weight of octadecanoic acid and E_a^*, the apparent activation energy for the diffusion of the octadecanoic acid. Consequently, we obtain

$$P = k_1/k_2 = (2\pi MRT)^{1/2}k_1/N_aC\sigma_o\exp(-E_a^*/RT). \quad (5)$$

The average time τ which the molecule remains on the surface is calculated to be of the order of 10^{21} s.[20] from the apparent activation energy, 191.2 kJ mol^{-1}, for the desorption of octadecanoic acid. The sticking coefficient can therefore be taken as unity. By putting the experimental k_1 value, 1.51×10^{-4}s^{-1}, at 298.2 K into Eq. 5, P is expressed as the function of E_a^*,

$$P = 6.66 \times 10^{-8}\exp(-E_a^*/RT). \quad (6)$$

Unfortunately as there are no data about the activation energy for the diffusion of the octadecanoic acid molecule in air, we substituted, as a rough approximation, the E_a^* value, 3.83 kJ mol^{-1}, for the octadecane into Eq. 6. This E_a^* value was obtained from the temperature dependence of its the diffusion coefficient[21] in air. Equation 6 gives 3.12×10^{-7} Pa at 298.2 K as the vapor pressure of octadecanoic acid. On the other hand, 10.6×10^{-7} Pa is obtained as the vapor pressure of octadecanoic acid at room temperature by the extrapolation of the reference value[2] of its vapor pressure near its melting point to room temperature. The former value is smaller than the latter. However, the molecular arrangement in the solid near its melting point is thought to be more disordered than at room temperature; the molecules in the former solid appear to evaporate more easily than at room temperature.

References

1) M. Davies, A. H. Jones and G. H. Thomas, *Trans. Faraday Soc.*, **55**, 1100 (1959).
2) M. Davies and V. E. Malpass, *J. Chem. Soc.*, **1961**, 1048.
3) M. Davies and B. Kybett, *Trans. Faraday Soc.*, **61**, 1608 (1965).
4) M. Davies and B. Kybett, *Trans. Faraday Soc.*, **61**, 1893 (1965).
5) F. Kimura, J. Umemura, and T. Takenaka, *Langmuir*, **2**, 9 (1986).
6) T. Takenaka, "Kinousei Yuki Hakumaku" Gakkai Shuppan Center, (1984), p. 60; G. L. Clark and P. W. Leppla, *J. Am. Chem. Soc.*, **58**, 2199 (1936).
7) M. Iwahashi, K. Aruga, O. Hirata, T. Horiuchi, and M. Muramatsu, *J. Colloid Interface Sci.*, **42**, 349 (1973).
8) G. A. Wolstenholme and J. H. Schulman, *Trans. Faraday Soc.*, **46**, 475 (1950).
9) M. Iwahashi, Y. Yamaguchi, K. Kobayashi, and T. Seimiya, *Bull. Chem. Soc. Jpn.*, **60**, 3808 (1987).
10) M. Iwahashi, F. Naito, N. Watanabe, and T. Seimiya, *Chem. Lett.*, **1985**, 187; *Bull. Chem. Soc. Jpn.*, **58**, 2093 (1985).
11) M. Fujihira, K. Nishiyama, and Y. Hamaguchi, *J. Chem. Soc., Chem. Commun.*, **1968**, 823.
12) G. L. Gaines, Jr., and R. W. Roberts, *Nature*, **26**, 787 (1963).
13) J. A. Spink, *J. Colloid Interface Sci.*, **24**, 61 (1967).
14) P. C. Hiemenz,"Principle of Colloid and Surface Chemistry," Marcel Dekker Inc., (1977), p. 231.
15) G. L. Gaines, Jr., *Nature*, **186**, 384 (1960).
16) E. K. Rideal and J. Tadyon, *Proc. R. Soc. London, Ser. A*, **225**, 346 (1954).
17) J. E. Young, *Australian J. Chem.*, **8**, 173 (1955); D. E. Beischer, *J. Phys. Chem.*, **57**, 134 (1953).
18) D. E. Beischer, *Science*, **112**, 535 (1950).
19) E. K. Rideal and J. Tadayon, *Proc. R. Soc. London, Ser. A*, **225**, 357 (1954).
20) I. Langmuir, *J. Am. Chem. Soc.*, **38**, 2221 (1916).
21) A. W. Adamson, "Physical Chemistry of Surfaces" John Wiely & Sons Inc., (1976), p. 551.
22) R. S. Bradley and A. D. Shellard, *Proc. R. Soc. London, Ser. A*, **198**, 239 (1949).

 © 1988 The Chemical Society of Japan Bull. Chem. Soc. Jpn., 61, 3067—3072 (1988)

The Heat of Immersion in Water and the Nature of the Surface Hydroxyl Group of Maghemite and Hematite

Haruo WATANABE* and Jun'etsu SETO
Sony Corporation Research Center, 174 Fujitsuka-cho, Hodogaya-ku, Yokohama 240
(Received March 5, 1988)

The heats of immersion in water of maghemite (γ-Fe_2O_3) were measured in comparison to those of hematite (α-Fe_2O_3) prepared from the same maghemite by crystal transformation with heat treatment, and outgassing up to 200 °C. The heats of immersion and the heat of hydration of maghemite were lower than those of hematite throughout the measurement conditions. These differences were concluded to be due to the differences in bulk crystal structure, especially the density of the crystal. That is, the heat of hydration at the stage of physisorption depends on the surface hydroxyl group density, corresponding to the bulk crystal density. Also the surface hydroxyl groups are strongly affected by the polarization of the bonds in the bulk, this results in the difference of the heat of hydration at the stage of chemisorption (formation of the hydroxyl groups) and the acidity of the hydroxyl groups. This view is confirmed on the polymorphs of other metal oxides.

Maghemite is widely used as a magnetic material for magnetic recording tape, and hence information on the surface properties of maghemite is essential for controlling the manufacturing conditions. However, little work has been reported on the surface properties of maghemite, and no work has been reported on the heat of immersion in water, whereas there have been many reports on hematite.[2-10] Our previous work[1] looked at the IEP (Isoelectric point) and the PZC (Point of zero charge) of maghemite, and clarified that the difference in these characteristics for maghemite and hematite arose from differences in the crystal structure. In the present work, the interaction between water and the surface of maghemite and the nature of the surface hydroxyl groups are investigated through the measurement of the heat of immersion and the adsorption isotherm, with hematite as a reference.

Experimental

Materials. The maghemite sample used in the present work was prepared from the acicular synthetic α-FeOOH (goethite) by sequential dehydration, reduction and oxidation processes. The hematite sample was prepared by heat treatment of the above maghemite sample in air at 550 °C. Impurities of the sample surface influence the value of the heat of immersion.[3] So in all cases the samples were purified as follows: First, washing with an alkali solution then distilled water and finally by electrodialysis. The samples and the purification procedure are the same as reported previously.[1]

Surface Area Measurements. The specific surface area of the samples was measured by applying the BET theory[11] to the nitrogen adsorption data obtained at the temperature of liquid nitrogen, assuming the cross-sectional area of nitrogen molecule to be 16.2 Å^2.

Heat of Immersion Measurements. A twin type heat conduction calorimeter (Tokyo Rikou MPC-2) was used. The sample was treated in a Pyrex glass ampoule at the desired temperature for 5 h in a vacuum of 2×10^{-4} Pa before sealing. The heat of immersion measurements were carried out with doubly distilled water at 25.0±0.1 °C. The heat of breaking of the ampoule was found to be 0.26 J.

Water Content Measurements. The water desorbed from the sample by evacuating at a given temperature was condensed in a cold trap of liquid nitrogen, followed by reevaporation and recondensation in a cold trap of dry ice. The water content of the sample was determined by the measurement of the amount of reevaporated water volumetrically, by using an all glass apparatus equipped with Baratron pressure gauge, assuming the water content to be zero at 1000 °C.

Water Adsorption Measurements. The sample was first prepared by evacuating at 25 °C for 5 h in a vacuum of 2×10^{-4} Pa. The adsorption of water on the sample was then measured gravimetrically at 25.0±0.1 °C, using a Cahn 2000 electrobalance housed in an all glass apparatus. Water vapor pressure was measured by Baratron pressure gauge.

Results and Disccusion

Adsorption of Water on the Surface. Maghemite is a less stable form of iron oxide[12] than hematite and becomes reduced under vacuum at temperatures higher than 250 °C, releasing oxygen and turning dark. Therefore, to measure the intrinsic surface properties, the heat treatment was always carried out under 200 °C. The samples treated under this condition were confirmed to contain no detectable divalent iron ions by analysis.

The specific surface areas (S_{N_2}) of the samples by BET method of nitrogen adsorption are shown in Table 1. The smaller value for the comparative hematite sample can be explained by the shrinkage due to the increase in crystal density caused by the crystal transformation. The change of the shape can not be detected by electron microscopic observation,[1] and no substantial change in the values of the samples was detected following the heat treatment.

The water content of the samples is shown in Fig. 1, where the amount of water is expressed by the number of water molecules per unit of surface area. Almost perfect desorption of the physisorbed water is

Table 1. Specific Surface Area (S_{N_2}) and Surface Density of Adsorbed Water (V_p and V_c)

	S_{N_2}	V_p	V_c	V_p/V_c
	$m^2\ g^{-1}$	H_2O molecules nm^{-2}	OH groups nm^{-2}	
Maghemite	18.6	5.52	11.80	0.47
Hematite	16.0	5.85	12.82	0.46

Table 2. X-Ray Density (D_x), Unit Volume of Fe^{3+} ($V_{Fe^{3+}}$) and Surface Denity of Fe^{3+} ($S_{Fe^{3+}}$)

	D_x	$V_{Fe^{3+}}$	$S_{Fe^{3+}}$	
	$g\ cm^{-3}$	$Å^{-3}$	Fe^{3+} ions nm^{-2}	
Maghemite	4.907	27.03	11.10 (Dx)	8.73 (111)
Hematite	5.277	25.13	11.66 (Dx)	9.15 (0001)

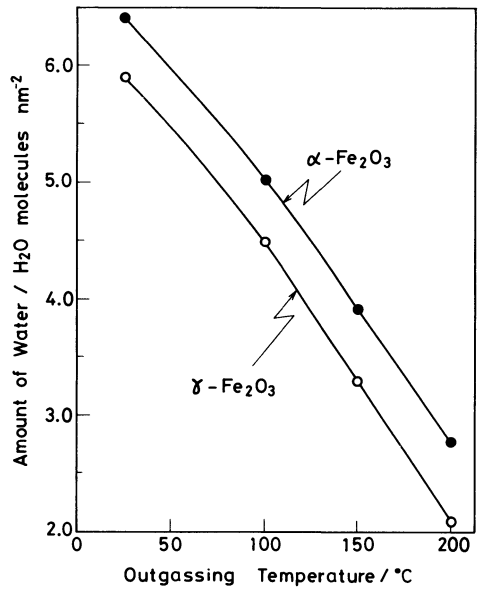

Fig. 1. Water content of maghemite (γ-Fe_2O_3) and hematite (α-Fe_2O_3) at various temperatures.

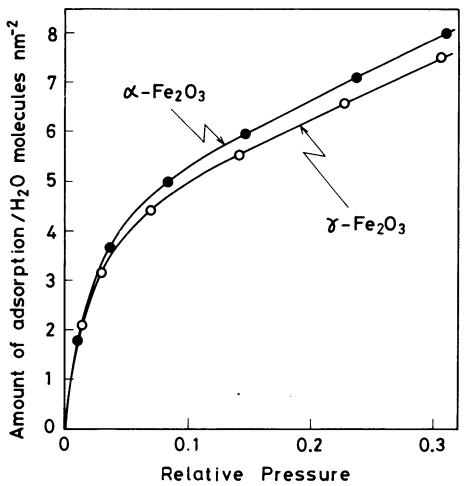

Fig. 2. Adsortion isotherms of water vapor on maghemite (γ-Fe_2O_3) and hematite (α-Fe_2O_3) at 25 °C.

attained by the evacuation at 25 °C in a vaccum of 2×10^{-4} Pa. The number of chemisorbed water molecules is shown as the hydroxyl groups per unit area (V_c) in Table 1.

The water adsorption isotherms of the samples are shown in Fig. 2. The ordinate in the figure represents the amount of water adsorbed per unit area. These isotherms indicate that the water is physically adsorbed on the hydroxyl groups formed on the surface. By applying the BET method[11] to the isotherm, the amount of water per unit area in the physisorbed monolayer (V_p) was calculated and are shown in Table 1.

The samples in the present work have an acicular shape inherited from the starting goethite, this series of solid phase reactions follow the topotaxial rule.[14] The cylindrical face of the particle forms the main part of the total surface area, and is mainly the (lll) plane in the case of maghemite, and the (0001) plane in the case of hematite. The number of the surface iron ions per unit area ($S_{Fe^{3+}}$) for the (lll) plane of maghemite and the (0001) plane of hematite calculated crystallographically[15] are shown in Table 2. The values for the real surfaces of the samples may be larger than these values, because of the incorporation of the higher indexed planes due to the curvature of the surface. A convenient method to approximate the values is to calculate the average number of surface iron ions per unit area ($S_{Fe^{3+}}$) from the volume of unit cell per iron ion ($V_{Fe^{3+}}$) which is derived from the X-ray density data.[13] Values for the average number of surface iron ions per unit area ($S_{Fe^{3+}}$) are shown in Table 2. They are almost equal in number to the number of surface hydroxyl groups (V_c) in Table 1. This numerical correspondence was reported by Morimoto et al.,[16] and that the ratio V_p:V_c is nearly 1:2, which led them to suggest the model where one physisorbed water connects two neighboring surface hydroxyl groups through hydrogen bonds. The V_p:V_c ratio for maghemite and hematite from our result supports the above model.

Heat of Immersion and Heat of Hydration. The relation between the heats of immersion and the

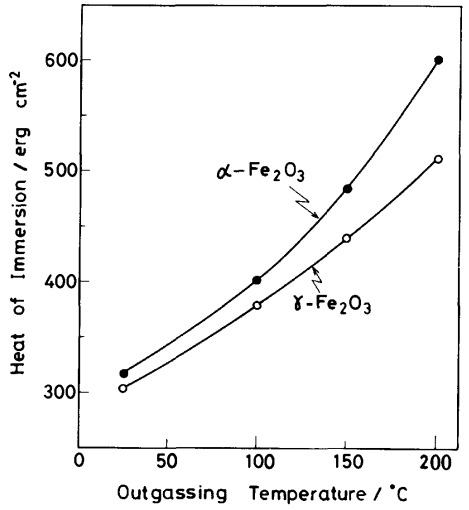

Fig. 3. Heat of immersion in water of maghemite (γ-Fe_2O_3) and hematite (α-Fe_2O_3) as a function of outgassing temperature.

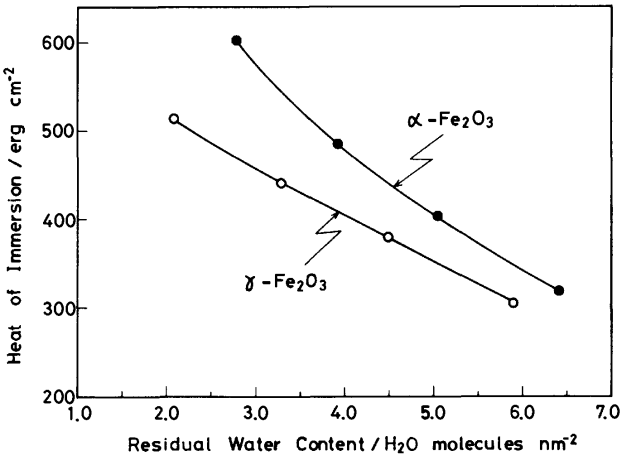

Fig. 4. Heat of immersion in water of maghemite (γ-Fe_2O_3) and hematite (α-Fe_2O_3) as a function of water content.

outgassing temperature for both samples is shown in Fig. 3. The amount of heat generated increased according to the outgassing temperature for both samples. Outgassing temperatures below 200 °C are low enough to allow complete rehydroxylation of the dehydrated sites.[6] The hematite sample shows a larger heat of immersion than the maghemite sample all through the temperature range of the measurement. The difference of the heat of immersion between the samples increased with increasing outgassing temperature.

The points for the highest water content of the samples corresponding to outgassing at 25 °C, indicate the heat of immersion for the completely hydroxylated state, that is, the surface is perfectly covered with chemisorbed water, as shown by the values of the $S_{Fe^{3+}}$, V_c and V_p. The value of the heat of immersion at this stage is 304 erg cm^{-2} for the maghemite, and 317 erg cm^{-2} for the hematite. The values of the heat of the immersion for hematite at this stage, are reported as 280 erg cm^{-2} by Jurinak and Burau,[3] 322 erg cm^{-2} by Furuichi et al.,[10] and 367 erg cm^{-2} by McCafferty and Zettlemoyer.[5] The present value for hematite compares favorably with other reported values, considering the differences of the samples and the conditions of measurement.

The heats of immersion for the lowest water content corresponding to outgassing at 200 °C, are 513 erg cm^{-2} for the maghemite and 602 erg cm^{-2} for the hematite. Healy and Fuerstenau[21] reported that the various metal oxides show a linear relation between the values of the heat of immersion (after outgassing at 200 °C) and the values of PZC. A metal oxide with a high value of PZC shows a large heat of immersion. The previous study[1] made it clear that the value of PZC of maghemite (pH 5.5) is lower than that of hematite (pH 6.7). The present results on the heats of immersion for samples outgassed at 200 °C fit the above relation.

Figure 4 shows the plots of the heat of immersion against the residual water content for both samples. The heat of surface hydration is calculated by the slope of these plots. At the stage of complete hydroxylation, shown in the below scheme [**II-III**], the heats of hydration are 32.2 kJ mol^{-1} for the maghemite and 37.6 kJ mol^{-1} for the hematite.

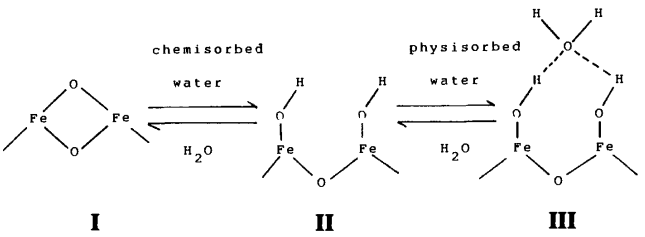

The heat of hydration at this stage corresponds to the physisorption of water, that is the construction of the hydrogen bonds, as in the above model **III**, between the oxygen atom of the physisorbed water and the two protons of the neighboring surface hydroxyl groups. The validity of this model in the present work is supported by the numerical correspondence of V_c and V_p in Table 1.

The average distance between the neighboring hydroxyl groups on the surface, relates to the density of hydroxyl groups on the surface (V_c), which is related to the average surface density of Fe^{3+} ($S_{Fe^{3+}}$) and the average bulk density of Fe^{3+} ($V_{Fe^{3+}}$) in Table 2. When the distance between the neighboring groups is long, the hydrogen bonds of the above model **III** are weak, and the heat of hydration is low. The average distance between the neighboring hydroxyl groups of maghemite is longer than that of hematite, as shown by the values of V_p and V_c. Thus, the heat of hydration

at the stage of physisorption of maghemite should be lower than that of hematite. This speculation is strongly supported by the experimental heats of hydration. The heat of the formation of the hydrogen bonds is given by halfing the value of the heat of hydration (one water molecule forms two hydrogen bonds). This gives values less than 20 kJ mol^{-1}, which is reasonable for hydrogen bond formation.

The heat of surface hydration for the stage when half of the surface is dehydrated, that is the heat of surface rehydration, is shown in the above scheme [I-II], and is 35.1 kJ mol^{-1} for the maghemite and 60.6 kJ mol^{-1} for the hematite. The maghemite shows the lower heat of hydration throughout the present study.

On the heat of hydration of the hematite, several different values have been reported, 101 kJ mol^{-1} by Healey et al.,[2] 66 kJ mol^{-1} by Furuichi et al.,[10] 47.2 kJ mol^{-1} by Morimoto et al.,[6] and 34.3 kJ mol^{-1} by Rossi et al.[9] These scattered values are caused by differing levels of ionic impurities, the difference of particle shape, differences in the preparation and outgassing conditions.

For comparing the intrinsic values of the heat of immersion and the heat of hydration for the maghemite and hematite, the above mentioned conditions were virtually identical. Consequently, the differences of the heat of immersion and the heat of hydration are due to the difference of the crystal structure.

The maghemite (γ-Fe_2O_3) has the spinel type crystal structure, and the hematite (α-Fe_2O_3) has the corundum type crystal structure.[17] These crystal structures correspond to γ-Al_2O_3 and α-Al_2O_3, respectively. In the comparative studies on the heat of immersion of γ- and α-Al_2O_3, γ-Al_2O_3 always shows a lower value for the heat of immersion than α-Al_2O_3.[18-20] These results are in good agreement with our results on maghemite and hematite.

The values for the heat of immersion of γ- and α-Al_2O_3 also follow the tendency described by Healy and Fuerstenau,[21] as the value of PZC for γ-Al_2O_3 is lower than that of α-Al_2O_3.[22]

Difference of the Nature of Surface Hydroxyl Groups Based on Difference of Crystal Structure. The average difference in the acidity of the surface hydroxyl groups between maghemite and hematite was reported as the difference of the IEP or the PZC of 1.1 to 1.2 pH units.[1]

The unit lattice of maghemite is expressed by the following formula:[23]

$$Fe^{3+}_8 \quad (Fe^{3+}_{40/3}\square_{8/3})\ O^{2-}_{32}$$

Coordination number = 4 Coordination number = 6

In the above formula a vacant lattice point of coordination number 6 is expressed by □, i.e. 6 oxygen ions adjacent to the Fe^{3+} ion site. Fe^{3+} ions are arranged at positions of coordination number 4 and 6 in a ratio of 3:5. On the other hand, hematite is a corundum-type oxide in which all of the Fe^{3+} ions have a coordination number of 6.

Parks[24] proposed a semiempirical equation for the PZC of metal oxides and metal hydroxides as follows:

$$PZC = A - 11.5(Z/R + 0.0029a)$$

where A is a constant depending on the coordination number of the metal ion and the hydration state of the surface. Z is the valency of the metal ion, R is the distance from the surface metal ion to the hydrogen ion in the surface hydroxyl group attached to the metal ion, and a is the crystal field stabilization energy of the metal ions by the hydroxide ions. The last term is zero when the metal ion is Fe^{3+} with a coordination number of 6 or 4.[25] The PZC value is more acidic by 2.4 pH units for four-coordinated than for six-coordinated metal ions, corresponding to the difference of the above constant A at the same hydration state. Thus the difference in the PZCs between maghemite and hematite is calculated to be 2.4×3/(3+5)=0.9, assuming that the additivity rule holds.[26]

Yoon et al.[27] has proposed improvements to Parks' equation: for complex oxides in which the correction of the crystal field stabilization energy is not required,

$$PZC = 18.43 - 53.12\sum f_i(v/L_s)_i - 0.5\sum f_i \log((2-v)/v)_i$$

where v is the bond valence, i.e., the valency of the metal ion per coordination number, and L_s ($=L+r$) is the sum of the mean M-O bond length (L) and the O-H distance (r), taken to be 1.01 Å. The f_i's are the ratio of the bonds to the total number of bonds. The value of PZC for maghemite is lower than that for hematite by 1.40 pH units as calculated by the above formula with the data for maghemite (γ-Fe_2O_3)[28] and hematite (α-Fe_2O_3).[17]

The above mentioned calculations support the proposition that the bonding energy between H^+ and O^{2-} of the surface hydroxyl groups of maghemite is lower than that of hematite, which is further supported by our experimental values.[1] As a matter of course, the difference in the heats of hydration at the [I-II] stage, shown in the previous scheme, further includes the difference in the bond formation energy of the Fe-O(-H) bonds for maghemite and hematite.

To discuss the Fe-O bond of the surface hydroxyl groups, it is necessary to examine the nature of this bond in the bulk. As aforementioned, the crystal density (D_x) of maghemite is lower than that of hematite, which means that the average bond length Fe-O of maghemite is longer than that of hematite. The ions are less ionic and the bonds are less polar[29] in maghemite than in hematite, which is supported by the lower electron density of the oxygen atoms of maghemite than of hematite as measured by XPS.[30]

(The same characteristics are also reported for γ- and α-Al_2O_3.[31]) The difference in the ionic characteristics of the bulk bonds should also be reflected in the surface hydroxyl groups.

From this point of the view, Healy et al.[32] introduced this ionic characteristics concept as "volume field strength", and successfully showed the linear relationship between the PZCs and the "volume field strength" for the polymorphs of manganese oxides. This electrostatic field is proportional to $(V_m)^{-2/3}$, where V_m is the volume of the unit cell per metal ion. And the value of PZC is given by the following formula:

$$PZC = A_1(V_m)^{-2/3} + B_1$$

This formula indicates that the value of PZC increases as V_m decreases, A_1 and B_1 are constants for the oxide series. The plots of this relation for maghemite and hematite are shown in Fig. 5. The plots of the polymorphs of manganese oxides from Healy et al.,[32] and of γ- and α-Al_2O_3 (PZC values[22] and V_m values from the crystal densities[33]) are also shown in Fig. 5. Almost the same slope can be found for the plot of each polymorph. This fact supports the view of Healy et al.[32] that the surface hydroxyl groups are strongly influenced by the electrostatic field within the lattice of the crystal. In other words, the surface hydroxyl groups are strongly affected by the polarization of the bonds in the bulk. The degree of the polarization becomes higher, as the bond length becomes shorter corresponding to an increasing the bulk crystal density. This increase in the polarization of the bonds in the bulk affects the surface hydroxyl groups, that is the acidity of the hydroxyl groups, which can be characterized by the parameter PZC, decreases.

In addition to this, it is suggested that the line of each metal ion has a different intercept, and this difference may be caused by the degree of the polarization of the bonds between the metal ion and the oxygen ion or the ionic characteristics of the metal ion, which is characterized by the electronegativity of the metal ion. The order of the intercept $Mn^{4+}>Fe^{3+}>Al^{3+}$ corresponds well to the electronegativity of the metal ion.[34]

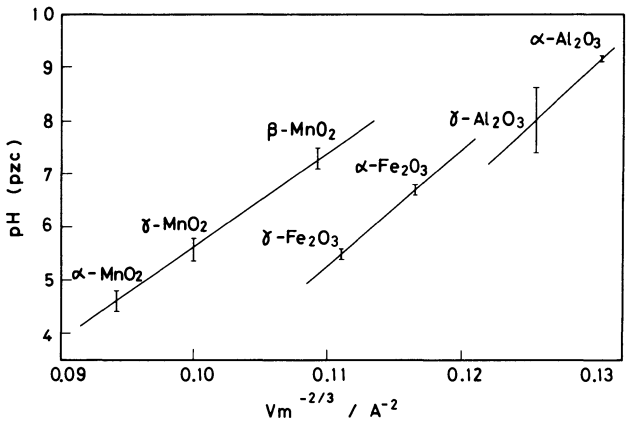

Fig. 5. Inter-relation of the values of the PZCs (pH_{pzc}) and the average volume of the unit cell per metal ion (V_m) for various metal oxides series.

Conclusion

(1) The surface density of hydroxyl groups for maghemite is lower than for hematite, corresponding to the difference in the density of the bulk crystal.

(2) The amount of the water physisorbed in a monolayer on maghemite is less than that for hematite, corresponding to the lower surface density of hydroxyl groups.

(3) The heat of the surface hydration at the stage of physisorption for maghemite is lower than for hematite, because the average distance between neighboring hydroxyl groups for maghemite is longer than for hematite.

(4) The heat of the surface hydration at the stage of chemisorption (the formation of the surface hydroxyl groups) for maghemite is lower than for hematite. This difference is caused by the different degree of the polarization of the bonds in the bulk which extends to the surface hydroxyl groups.

(5) The surface hydroxyl groups are strongly affected by the bulk, especially the polarization of the bonds in bulk. The degree of the polarization becomes higher, both as the bond length becomes shorter, corresponding to a higher bulk crystal density, and as the electronegativity of the metal ion becomes higher. This polarization of the bond in the bulk affects the surface hydroxyl groups, resulting in the dissociation of the hydroxyl groups, that is the acidity of the hydroxyl groups decreases.

The authors wish to thank Dr. Michael L. Hair of Xerox Research Centre of Canada for useful discussions, and Dr. Stephen Baker of Sony Corporation Research Center for reading the manuscript.

References

1) H. Watanabe and J. Seto, *Bull. Chem. Soc. Jpn.*, **59**, 2683 (1986).

2) F. H. Healey, J. J. Chessick, and A. V. Fraioli, *J. Phys. Chem.*, **60**, 1001 (1956).

3) J. J. Jurinak and R. G. Burau, *Soil Sci. Soc. Am. Proc.*, **31**, 732 (1967).

4) A. C. Zettlemoyer and E. McCafferty, *Z. Phys. Chem. Neue Folge*, **64**, 41 (1969).

5) E. McCafferty and A. C. Zettlemoyer, *Discuss. Faraday Soc.*, **52**, 239 (1972).

6) T. Morimoto, N. Katayama, H. Naono, and M. Nagao, *Bull. Chem. Soc. Jpn.*, **42**, 1490 (1969).

7) Y. Nakahara, *Kogyo Kagaku Zasshi*, **74**, 1061 (1971).

8) T. Ishikawa and K. Inouye, *Bull. Chem. Soc. Jpn.*, **46**, 2665 (1973).

9) P. F. Rossi and C. De Asmundis, *Annali di chimica*, **67**,

65 (1977).
10) R. Furuichi, T. Ishii, and Y. Oshima, *Thermochimica Acta.*, **56**, 31 (1982).
11) S. Brunauer, P. H. Emmett, and E. Teller, *J. Am. Chem. Soc.*, **60**, 309 (1938).
12) J. M. Trautmann, *Bull. Soc. Chim. Fr.*, **1966**, 992.
13) "Landolt-Börnstein, in Numerical data and functional relationships in science and technology, Neue Series, Group III, Band 4a," Springer-Verlag, Berlin (1970), pp. 9 and 18.
14) G. W. van Oosterhout, *Acta Crystallogr.*, **13**, 932 (1960).
15) S. Kachi, K. Moriyama, and S. Shimizu, *J. Phys. Soc. Jpn.*, **18**, 106 (1963).
16) T. Morimoto, M. Nagao, and F. Tokuda, *J. Phys. Chem.*, **73**, 243 (1969).
17) R. W. G. Wyckoff, "Crystal Structure," 2nd ed, Interscience, New York (1963).
18) T. Morimoto, K. Shiomi, and H. Tanaka, *Bull. Chem. Soc. Jpn.*, **37**, 392 (1964).
19) H. Cochrane and R. Rudham, *Trans. Faraday Soc.*, **61**, 2246 (1965).
20) H. Cochrane, B. A. Hendriksen, D. R. Pearce, and R. Rudham, *S. C. I. Monograph*, **25**, 370 (1967).
21) T. W. Healy and D. W. Fuerstenau, *J. Colloid Sci.*, **20**, 376 (1965).
22) Z. P. Kozmina, M. P. Belova, and V. A. Sannikov, *Kolloidn. Zh.*, **25**, 169 (1963).
23) R. Schrader and G. Bütter, *Z. Anorg. Allg. Chem.*, **320**, 205 (1963).
24) G. A. Parks, *Chem. Rev.*, **65**, 177 (1965).
25) F. Basolo and R. G. Pearson, "Mechanisms of Inorganic Reactions," 2nd ed, John Wiley and Sons Inc., New York (1969).
26) G. A. Parks, *Adv. Chem. Ser.*, **67**, 121 (1967).
27) R. H. Yoon, T. Salman, and G. Donnay, *J. Colloid Interface Sci.*, **70**, 483 (1979).
28) C. Greaves, *J. Solid State Chem.*, **49**, 325 (1983).
29) R. T. Sanderson, "Chemical Bonds and Bond Energy," 2nd ed, Academic Press, New York (1976).
30) N. S. McIntyre and D. G. Zetaruk, *Anal. Chem.*, **49**, 1521 (1977).
31) O. Pitton, C. K. Jorgensen, and H. Berthou, *Chimia*, **30**, 540 (1976).
32) T. W. Healy, A. P. Herring, and D. W. Fuerstenau, *J. Colloid Interface Sci.*, **21**, 435 (1966).
33) H. P. Rooksby, "Oxides and Hydroxides of Aluminium and Iron," in "The X-ray Identification and Crystal Structures of Clay Minerals," 2nd ed, ed by G. Brown, Jarrold and Sons Ltd., London (1961), p. 388.
34) K. Tanaka and A. Ozaki, *J. Catal.*, **8**, 1 (1967).

 © 1988 The Chemical Society of Japan Bull. Chem. Soc. Jpn., 61, 3073—3076 (1988)

The Temperature Dependence of the Conductivities and Ion-Association Constants of Potassium Nitrate and Potassium Perchlorate in Water

Haruhiko YOKOYAMA* and Tomoko OHTA
Department of Chemistry, Yokohama City University, 22-2 Seto, Kanazawa-ku, Yokohama 236
(Received March 19, 1988)

The electric conductivities of potassium nitrate and potassium perchlorate in water have been measured at eleven temperatures from 0 to 50 °C and analyzed in order to obtain the ion-association constants and the limiting molar conductivities of these salts. It was found that the observed ion-association constants have a minimum value at 30 °C for KNO_3 and at 36 °C for $KClO_4$. Such a characteristic temperature dependence was considered to be due to the presence of specific short-range interactions within contact ion pairs, although the weak hydration of the ions seemed to help the formation of the contact ion pairs. The experimental standard enthalpies and entropies of ion association were discussed in comparison with the theoretical ones. The limiting molar conductivities of NO_3^- and ClO_4^- at each temperature were also evaluated and expressed as cubic equations of the temperature.

Potassium nitrate and potassium perchlorate have been known to be slightly associated in water.[1-4] It is of interest what interactions are concerned with their ion associations, since, from the electrostatic ion-association theories,[5,6] 1:1 electrolytes can be predicted to be almost completely dissociated in water. The detailed knowledge of the temperature dependence of their ion-association constants (K) should be useful in clarifing such a problem. At the present stage, however, we have no available information about this.

The limiting molar conductivities (λ^∞) of alkali metal ions and halide ions in water have been measured in detail at temperatures between 0 and 55 °C and expressed as cubic equations of the temperature.[7,8] However, the λ^∞ values of the nitrate ion and the perchlorate ion are known only for a few temperatures, although information on their temperature dependence would be valuable for the analysis of the conductivities of unsymmetrical electrolytes involving these anions and also for the investigation of the ion-solvent interactions in water.[8] For these reasons we performed conductivity measurements on aqueous solutions of potassium nitrate and potassium perchlorate at eleven temperatures between 0 and 50 °C and obtained the ion-association constants of KNO_3 and $KClO_4$ and the limiting molar conductivities of NO_3^- and ClO_4^- as a function of the temperature. On the basis of these results, we will discuss the character of the interactions between the ions.

Experimental

Materials. The potassium nitrate and potassium perchlorate (Wako Pure Chemical Industries, reagent-grade) were recrystallized twice from conductivity water and then air-dried at room temperature. The potassium perchlorate was then further dried at about 150 °C and kept over diphosphorus pentaoxide in a desiccator under reduced pressure. Small quantities of adsorption water (0.21 wt% for KNO_3 and 0.01 wt% for $KClO_4$) were found by the Karl-Fischer method with an AQ-5 Aquacounter of the Hiranuma Sangyo Co. and were corrected in the calculation of the concentrations of solutions.

Solutions. All the solutions were made by weight, and the molar concentration at each temperature was calculated by the use of the solution densities, which had been themselves estimated from those at 25 °C in the manner described previously.[9] The density measurements at 25 °C were carried out by using a vibrating-tube SS-D-200 twin-type densimeter of the Shibayama Scientific Co. Water purified by the use of Milli-Q Reagent-grade Water Systems of Japan Millipore was used for the preparation of the solutions. Its conductivity was always lower than 1×10^{-7} S cm^{-1} at 25 °C after the dissolved carbon dioxide had been removed. Ten solutions (from 0.0007 to 0.010 mol dm^{-3}) were examined.

Conductivity Measurements. The conductivity measurements were made with a Fuso 360 linear-bridge conductometer in the manner described previously.[10] The cell constant of the cell used was 0.13720 cm^{-1} at 25 °C. For the other temperatures, the change in the cell constant due to the thermal expansion of platinum and glass was corrected; it was regarded as −0.0014% for the elevation of 1 °C, which was estimated in the manner described by Robinson and Stokes.[8] The reproducibility of the conductivity measurements was within 0.03%, and the precision of the temperature measurements was ±0.003 °C. The accuracy of the temperature was ±0.01 °C.

Results and Discussion

Analysis of Conductivity Data. The observed molar conductivities (Λ)[11] were analyzed by assuming the ion association(ion-pair formation) of the salts in terms of the 1970 Fuoss-Justice equation,[12,13] with $E=E_1\Lambda^\infty-2E_2$:

$$\Lambda = \alpha[\Lambda^\infty - S(\alpha c)^{1/2} + E\alpha c\log(\alpha c) + J_1\alpha c - J_2(\alpha c)^{3/2}],$$

where S, E_1, E_2, J_1, and J_2 have the usual meanings and where α is the fraction of free ions. The values of the

closest distance of approach of the ions(a) involved in J_1 and J_2 and the Debye-Hückel equation of the activity coefficient were assumed to be equal to 3.38 and 3.63 Å for KNO_3 and $KClO_4$ respectively. These values were estimated from the crystallographic radius of K^+ (1.33 Å)[8] and the effective radii of NO_3^- and ClO_4^- (2.05 and 2.30 Å respectively, estimated from the ionic partial molar volumes[14] by the use of Glueckauf's equation[10,15]). The ion-association constant (K) and the limiting molar conductivity (Λ^∞) were determined by the least-squares procedure, minimizing σ, where $\sigma^2=\sum[\Lambda(\text{obsd})-\Lambda(\text{calcd})]^2/(n-2)$. The details of the calculations have been described previously.[10]

Ion-Association Constants and Their Temperature Dependence. The values of K, Λ^∞, and σ obtained are summarized in Tables 1 and 2.[16] The values of K and Λ^∞ at 25 °C are in practical agreement with the following values reported by Carman[2]: K=1.2—1.3 dm³ mol⁻¹ and Λ^∞=145.05 S cm² mol⁻¹ (a=3.46—3.83 Å) for KNO_3 and K=1.6 dm³mol⁻¹ and Λ^∞=140.65 S cm²mol⁻¹ (a=4.21 Å) for $KClO_4$. The experimentally obtained ion-association constants are larger than those predicted from the electrostatic ion-association theory[6], K=0.52 and 0.48 dm³ mol⁻¹ at 25 °C for a=3.38 and 3.63 Å respectively. The temperature dependence of the ion-association constant can be well characterized when $\log(K/\text{dm}^3\,\text{mol}^{-1})$ values are plotted against t/°C, as shown in Fig. 1. That is, the experimental ion-association constant has a minimum value at a certain temperature, while the theoretical one[6] increases with an increase in the temperature: for example, K/dm³ mol⁻¹=0.46 (0 °C), 0.48 (10 °C), 0.50 (20 °C), 0.53 (30 °C), 0.56 (40 °C), and 0.59 (50 °C) for a=3.38 Å and 0.43 (0 °C), 0.45 (10 °C), 0.47 (20 °C), 0.49 (30 °C), 0.52 (40 °C), and 0.55 (50 °C) for a=3.63 Å.

The experimental $\log K$ values can be reproduced well by a full line shown in Fig. 1 using this equation:

$$\log K = p(t - t_{\min})^2 + \log K_{\min}, \quad (1)$$

where the values of p, $t_{\min}$, and $K_{\min}$ are as given in Table 3. This equation is similar to that used by Harned and Embree[17,18] for the temperature dependence of the dissociation constants of such weak acids as acetic acid. The p values in Table 3 are near to the usual one, 5×10^{-5} K⁻², for the acid-dissociation constants reported by Harned and Embree.[17,18] The standard enthalpy and entropy of ion association ($\Delta H°$ and $\Delta S°$), which can be estimated by the use of Eq. 1, are shown for several temperatures in Tables 4 and 5. These values are smaller than the theoretical ones,[6] as shown in the same tables. Their deviation becomes remarkable with a decrease in the tempera-

Table 1. Experimental Ion-Asssociation Constants and Limiting Molar Conductivities of KNO_3 Obtained by Assuming a=3.38 Å

t	K	Λ^∞	σ
°C	dm³ mol⁻¹	S cm² mol⁻¹	S cm² mol⁻¹
0	1.28±0.09	80.57±0.02	0.0121
5	1.26±0.11	92.52±0.02	0.0163
10	1.25±0.11	104.98±0.02	0.0195
15	1.26±0.12	117.94±0.03	0.0264
20	1.21±0.11	131.30±0.03	0.0241
25	1.21±0.10	145.10±0.02	0.0172
30	1.20±0.10	159.30±0.02	0.0193
35	1.22±0.10	173.85±0.03	0.0204
40	1.22±0.10	188.74±0.03	0.0211
45	1.22±0.14	203.94±0.03	0.0265
50	1.25±0.19	219.44±0.05	0.0460

Table 2. Experimental Ion-Asssociation Constants and Limiting Molar Conductivities of $KClO_4$ Obtained by Assuming a=3.63 Å

t	K	Λ^∞	σ
°C	dm³ mol⁻¹	S cm² mol⁻¹	S cm² mol⁻¹
0	1.80±0.12	77.52±0.02	0.0174
5	1.73±0.10	89.18±0.02	0.0164
10	1.68±0.10	101.36±0.02	0.0189
15	1.64±0.10	114.04±0.03	0.0207
20	1.61±0.10	127.17±0.03	0.0244
25	1.57±0.08	140.70±0.03	0.0235
30	1.56±0.08	154.64±0.03	0.0264
35	1.55±0.09	168.93±0.04	0.0301
40	1.56±0.10	183.56±0.04	0.0347
45	1.58±0.13	198.53±0.05	0.0413
50	1.59±0.11	213.75±0.05	0.0427

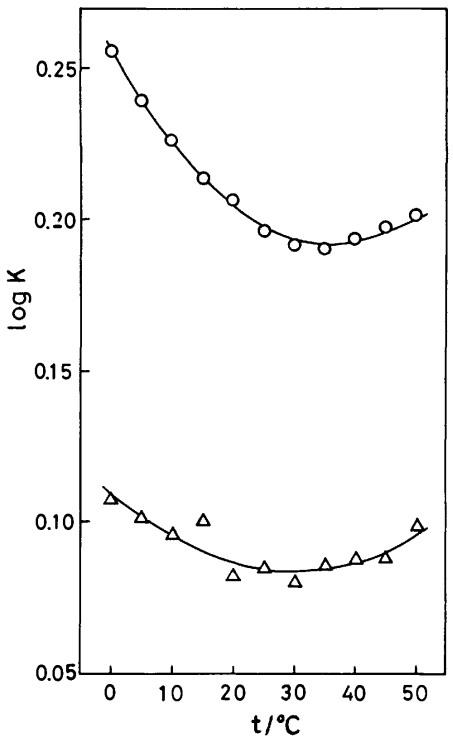

Fig. 1. Temperature dependence of ion-association constants of KNO_3 (△) and $KClO_4$ (○).

ture. Negative or small $\Delta H°$ values mean that exothermic interactions exist between the ions and become dominant at temperatures below t_{min}.

Although one may consider that the ion associations of KNO_3 and $KClO_4$ are due only to the weakness of the hydration of NO_3^- and ClO_4^-, this explanation is not necessarily adequate for the following reason. The hydration of I^- is supposed to be weaker than that of NO_3^- because of its more positive hydration free energy at 25 °C.[19] However, the ion-association constant between K^+ and I^- is 0.64 $dm^3\ mol^{-1}$ (a=4.5 Å, t=25 °C) smaller than that of KNO_3, and it decreases with the decrease in the temperature in the range from 5 to 55 °C.[20] This temperature dependence differs from that observed in the present study, although it is in agreement with the prediction from the electrostatic ion-association theory.[6]

Table 3. Values of Parameters in Eq. 1 Representing the Temperature Dependence of the Ion-Association Constants

Salt	$p\times10^5$ / K^{-2}	t_{min} / °C	$\log K_{min}$
KNO_3	2.88	29.9	0.084
$KClO_4$	5.10	35.6	0.192

Table 4. Experimental and Theoretical Values of Standard Enthalpy and Entropy of Ion Association Obtained for KNO_3 with a=3.38 Å

t	Experimental $\Delta H°$	Experimental $\Delta S°$	Theoretical[6] $\Delta H°$	Theoretical[6] $\Delta S°$
°C	kJ mol^{-1}	J K^{-1} mol^{-1}	kJ mol^{-1}	J K^{-1} mol^{-1}
5	−2.1±1.3	−5.7±4.8	2.54	2.9
15	−1.4±0.7	−3.0±2.5	3.06	4.7
25	−0.5±0.5	0.0±1.8	3.61	6.6
35	0.5±0.8	3.4±2.7	4.19	8.5
45	1.7±1.7	7.0±5.4	4.80	10.5

Table 5. Experimental and Theoretical Values of Standard Enthalpy and Entropy of Ion Association Obtained for $KClO_4$ with a=3.63 Å

t	Experimental $\Delta H°$	Experimental $\Delta S°$	Theoretical[6] $\Delta H°$	Theoretical[6] $\Delta S°$
°C	kJ mol^{-1}	J K^{-1} mol^{-1}	kJ mol^{-1}	J K^{-1} mol^{-1}
5	−4.6±0.5	−12.0±1.6	2.53	2.2
15	−3.3±0.3	−7.5±0.9	3.05	4.0
25	−1.8±0.2	−2.4±0.6	3.59	5.9
35	−0.1±0.3	3.3±0.9	4.17	7.8
45	1.9±0.6	9.6±1.9	4.78	9.8

The exothermic interactions between the ions are considered to be specific interactions within contact ion pairs, independent of the macroscopic properties of a solvent such as the dielectric constant. The negative $\Delta S°$ values at lower temperatures suggest that the specific interactions require steric restrictions for the formation of contact ion pairs. The local charges of oxygen atoms are presumed to play an important role in such interactions within the contact ion pairs. The slightly large values of K and t_{min} of $KClO_4$ compared with those of KNO_3 mean that the specific interactions of K^+ with ClO_4^- are stronger than those with NO_3^-. This may be due to the relatively weak hydration of ClO_4^-[19] and also to the difference in the number of oxygen atoms of the anions.

The nitrate and perchlorate ions have been known to associate also with the other alkali metal ions.[2] Their ion-association constants increase with the ionic radii of the cations in the following sequences: $K(NaNO_3)<K(KNO_3)K(CsNO_3)$ and $K(KClO_4)<K(RbClO_4)<K(CsClO_4)$.[21] This may indicate that the formation of the contact ion pairs depends also on the ease of the release of the hydration water molecules of the cations, since the ion-association constants increase with a decrease in the hydration power of the alkali metal ions.[19]

The Temperature Dependence of the Limiting Molar Conductivities of NO_3^- and ClO_4^-. Harned and Owen represented the temperature dependence of the limiting molar conductivities (λ^∞) of alkali metal ions and halide ions between 5 and 55 °C by means of this cubic equation:[7]

$$\lambda^\infty = \lambda^\infty(25\,°C) + a(t-25) + b(t-25)^2 + c(t-25)^3. \quad (2)$$

The values of $\lambda^\infty(K^+)$ were calculated with this equation and then used to evaluate those of $\lambda^\infty(NO_3^-)$ and $\lambda^\infty(ClO_4^-)$ at the temperatures between 0 and 50 °C from $\Lambda^\infty(KNO_3)$ and $\Lambda^\infty(KClO_4)$. By using the resulting values, the parameters, a, b, c, and λ^∞(25 °C), for NO_3^- and ClO_4^- were determined; they are summarized in Table 6. With these parameter values, the experimental values of $\lambda^\infty(NO_3^-)$ and $\lambda^\infty(ClO_4^-)$ can be reproduced by the use of Eq. 2 within an accuracy of 0.01 S cm^2 mol^{-1}.

Table 6. Values of Parameters in Eq. 2 Representing the Temperature Dependence of the Limiting Ionic Molar Conductivities

Ion	λ^∞(25 °C) / S cm^2 mol^{-1}	a / S cm^2 mol^{-1} K^{-1}	$b\times10^3$ / S cm^2 mol^{-1} K^{-2}	$c\times10^6$ / S cm^2 mol^{-1} K^{-3}
NO_3^-	71.60	1.3670	3.776	−3.5
ClO_4^-	67.20	1.3159	3.833	−5.9

References

1) A. D. Pethybridge and D. J. Spiers, *J. Chem. Soc., Chem. Commun.*, **1974**, 423.
2) P. C. Carman, *J. Solution Chem.*, **6**, 609 (1977).
3) A. E. Martell and L. G. Sillén, "Stability Constants," The Chemical Society, London (1964), pp. 168, 317; "Stability Constants," Supplement No.1, The Chemical Society, London (1971), p. 95.
4) E. Högfeldt, "Stablity Constants of Metal-Ion Complexes," Pergamon Press (1982), Part A, pp. 120, 246, 247.
5) N. Bjerrum, *Kgl. Danske Videnskab. Selskab.*, **7**, No.9 (1926).
6) H. Yokoyama and H. Yamatera, *Bull. Chem. Soc. Jpn.*, **48**, 1770, 3002 (1975).
7) H. S. Harned and B. B. Owen, "The Physical Chemistry of Electrolytic Solutions," 3rd ed, Reinhold, New York (1958), p. 233.
8) R. A. Robinson and R. H. Stokes, "Electrolyte Solutions," 2nd ed, Butterworths, London (1959), Chaps. 5—7 and Appendices.
9) H. Yokoyama and M. Nishimura, *Bull. Chem. Soc. Jpn.*, **58**, 1094 (1985).
10) H. Yokoyama, *Bull. Chem. Soc. Jpn.*, **57**, 1304 (1984).
11) The tables of the observed molar conductivities (Λ) are deposited as Document No.8820 at the Office of the Editor of the Bull. Chem. Soc. Jpn.
12) E. Renard and J-C. Justice, *J. Solution Chem.*, **3**, 633 (1974).
13) J. Quint and A. Viallard, *J. Solution Chem.*, **7**, 533 (1978).
14) F. J. Millero, "Water and Aqueous Solutions," ed by R. A. Horne, Wiley-Interscience, New York (1972), Chap. 13.
15) E. Glueckauf, *Trans. Faraday Soc.*, **61**, 914 (1965).
16) The values of K are somewhat dependent on a: for example, assuming values larger by 0.5 Å for a, those values are increased by about 0.2 $dm^3\ mol^{-1}$, while the t_{min} values in Table 3 are decreased by 3.8 °C for KNO_3 and 0.7 °C for $KClO_4$. The experimental ion-association constants are also dependent on the conductivity equation used and the manner of the analysis, as has been described in the literature.[1,2,22] However, the following discussion in the present study is qualitatively unaltered, even if somewhat different values of a are assumed and even if the other high-precision conductivity equations are used.
17) H. S. Harned and N. D. Embree, *J. Am. Chem. Soc.*, **56**, 1050 (1934).
18) R. W. Gurney, "Ionic Processes in Solution," Dover Publications, New York (1953), Chap. 7.
19) Y. Marcus, "Ion Solvation," John Wiley & Sons, New York (1985), Chap. 5.
20) E. Andalaft, R. P. T. Tomkins, and G. J. Janz, *Can. J. Chem.*, **46**, 2959 (1968).
21) Estimated from Ref. 2 by comparing the values of K with similar a values with one another.
22) C. B. Monk, "Electrolytic Dissociation," Academic Press, New York (1961), Chap. 8.

 © 1988 The Chemical Society of Japan Bull. Chem. Soc. Jpn., 61, 3077—3082 (1988)

Monolayers of Triple Long-Chain Salts on the Concentrated Sodium Chloride Solution

Osamu SHIBATA,* Shoji KANESHINA, and Ryohei MATUURA†
College of General Education, Kyushu University-01, Ropponmatsu, Fukuoka 810
†Department of Chemistry, Faculty of Science, Kyushu University-33, Higashi-ku, Fukuoka 812
(Received March 28, 1988)

The surface pressure–area (π–A) curves for monolayers of four kinds of cation-anion triple long-chain salts [dialkyldimethylammonium alkanesulfonates] on the aqueous solution of 4.4 M NaCl were measured at various temperatures by the Langmuir method. Some π–A curves of these salts showed two transition points. Judging from the apparent molar entropy change on the transition, the first was assigned to the transition from the expanded state (E phase) to the condensed state (C-I phase) and the second to the transition from the C-I phase to another condensed state (C-II phase). In this paper, another condensed phase (C-I′) was newly observed over a certain temperature range on the phase diagram, which is the intermediate phase between the C-I phase and the C-II phase. There exist two triple points on the phase diagram at which three phases (i.e., E, C-I, and C-I′, and C-I, C-I′, and C-II) coexist. From the apparent molar entropy change, limiting area, compressibility, and phase diagram, the orientation of (2-1) long-chain salts in the monolayer state was assumed.

Many papers have been published on the adsorbed film at the air/water interfaces from the mixtures of cationic and anionic surfactant solutions.[1–11] Some studies concerning the mixed monolayers of cationic and anionic surfactants have also been reported.[12–16] We have recently investigated the surface chemical properties of the insoluble monolayers of double long-chain salts, which are composed of a long-chain cation and a long-chain anion, on water and/or electrolyte solutions.[17–20] The monolayers of double long-chain salts on 4.4 M NaCl solution (1 M=1 mol dm^{-3}) showed such outstanding behavior as some surface pressure–area (π–A) curves had two transition points.[19–20] To investigate the phase transitions of monolayer more deeply, it is necessary to extend the study from the viewpoint of molecular structure and to compare the results with those of other types of long-chain salts at the same experimental conditions, i.e., on 4.4 M NaCl solution.

In the present study then, dialkyldimethylammonium alkanesulfonates [which is denoted as (2-1)long-chain salt or as 2CnNCnS, in which n is the number of carbon atoms in the long-chain cation and anion, while a customary double long-chain salt will be described as (1-1) long-chain salt or as CnNCnS] were prepared, and the surface pressures of monolayers of these salts have been measured as a function of molecular area at various temperatures. The NaCl concentration of the substrate was fixed at 4.4 M throughout the experiments. The phase type in the monolayer states of the (2-1) long-chain salts could be judged from both the phase diagrams and thermodynamic quantities on the phase transition.

Experimental

The (2-1) long-chain salts (2CnNCnS), dialkyldimethylammonium alkanesulfonates, were prepared by mixing equimolar solutions of dialkyldimetylammonium bromides from Prof. T. Kunitake of Kyushu University and sodium alkanesulfonates from Tokyo Kasei Kogyo. The precipitates were purified by recrystallization from an acetone/water mixture (7:3 in v/v). The four salts of different hydrocarbon chain length are shown in Table 1. The purity of these salts was confirmed by elemental analyses. Each (2-1) long-chain salt was spread from hexane–ethanol mixture (4:1 in v/v, the former from Merck, Uvasol, and the latter from Nacalai Tesque) at the air/water interface.

The substrate solution of 4.4 M sodium chloride (Nacalai Tesque) was prepared using thrice distilled water. Sodium chloride was roasted at 973 K to remove any surface active impurities.

The surface pressure was measured by an automated Langmuir film balance, which was the same used in the previous study.[17–20] The concentration of NaCl in the substrate was held constant at 4.4 M throughout the experiments in order to observe the reproducible π–A curve and to compare the phase diagrams from the viewpoint of the molecular structures of the two kinds of salts [CnNCnS and 2CnNCnS].

Other experimental conditions were the same as described in the previous paper.[20]

Results and Discussion

The π–A curves obtained of 2CnNCnS salts with equal number of carbon atoms in three long chains, at

Table 1. Materials

(2-1) Long-chain salt	Structure	Abbreviation
Dialkyldimethylammonium alkanesulfonate	$(C_nH_{2n+1})_2N^+(CH_3)_2\,C_nH_{2n+1}SO_3^-$ where n=12, 14, 16, 18	2CnNCnS

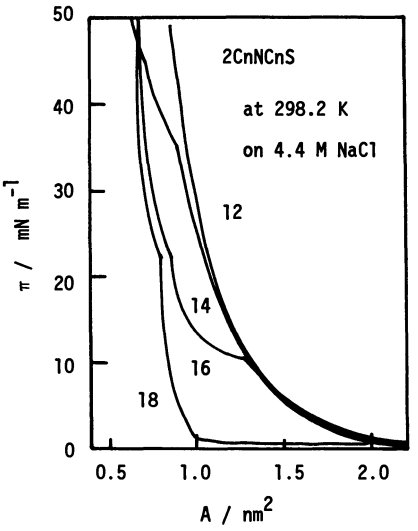

Fig. 1. The π–A curves of (2–1) long-chain salts on 4.4 M NaCl solution at 298.2 K. In the case of 2CnNCnS type; Curve 12, 2C12NC12S; 14, 2C14NC14S; 16, 2C16NC16S; 18, 2C18NC18S.

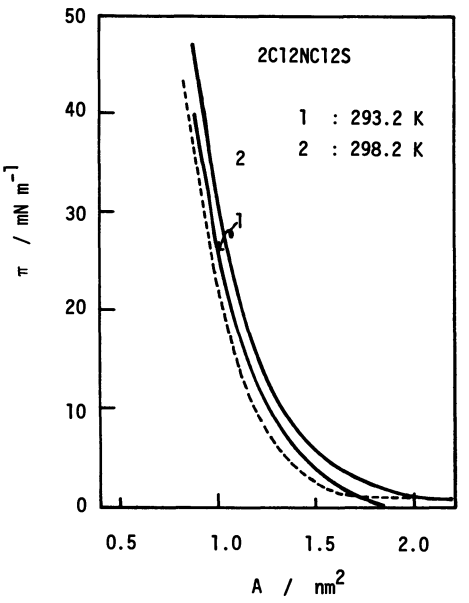

Fig. 2. The temperature dependence of π–A curves of 2C12NC12S salt. Substrate: 4.4 M NaCl solution. Dotted line: on pure water at 298.2 K.

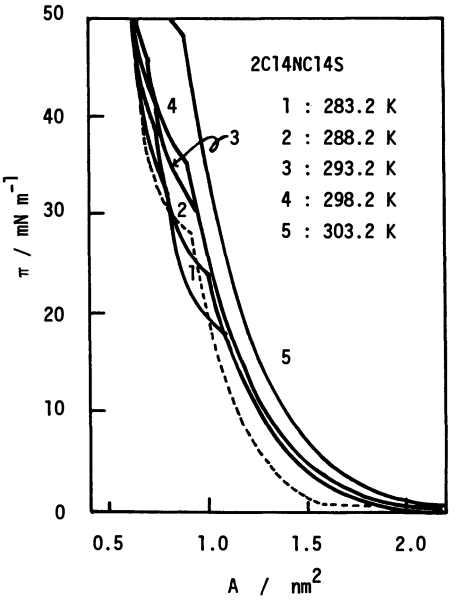

Fig. 3. The temperature dependence of π–A curves of 2C14NC14S salt. Substrate: 4.4 M NaCl solution. Dotted line: on pure water at 298.2 K.

298.2 K on 4.4 M NaCl are shown in Fig. 1. Numerical values in Fig. 1. refer to the number of carbon atoms in the long-chains. The longer the chain length of the salts, the smaller the value of the mean area per molecule at constant pressure. As seen from Fig. 1, all the π–A curves have one or two transition points at 298.2 K except for 2C12NC12S salt. Since the transition pressures remain constant irrespective of the compression rate,[19,20] all the transition points on the π–A curves can be regarded as the equilibrium point between two or three phases on the monolayer. The phase transition pressures (π^{eq}) change extensively with varying the chain length. Especially, both π–A curves of 2C14NC14S and 2C16NC16S revealed two distinct break points. The two transitions for these salts, however, have turned out to be different in phase; new intermediate phase appeared during the compression of the monolayer of 2C16NC16S. The first break point at a low surface pressure of the π–A curve for the 2C16NC16S salt indicates the transition from the expanded (E-phase) to the condensed film, and the second break point at a higher surface pressure is as the transition from a condensed film to another condensed film, as described in the previous papers.[19,20] These two condensed states are referred to the condensed phase I and the condensed phase II, respectively, in the same manner.[19,20] On the other hand, judging from the previous phase diagrams, the break point at a low surface pressure of 2C14NC14S can be assigned to the transition from the expanded phase (E-phase) to the condensed phase I′ (C-I′) which is different from the condensed phase I (C-I) on the monolayer phase diagram. The second break point at a higher surface pressure is regarded as the transition from the condensed phase I′ (C-I′) to the condensed phase II (C-II), which can be also assigned by the aid of thermodynamic quantities and the phase diagram as mentioned later.

On the other hand, the π–A isotherms of 2C18NC18S have only one transition point, which is the transition from one condensed state to another condensed state by the aid of thermodynamic quantities as mentioned later. The π–A curve of 2C12NC12S salt shows only an expanded film at 298.2 K.

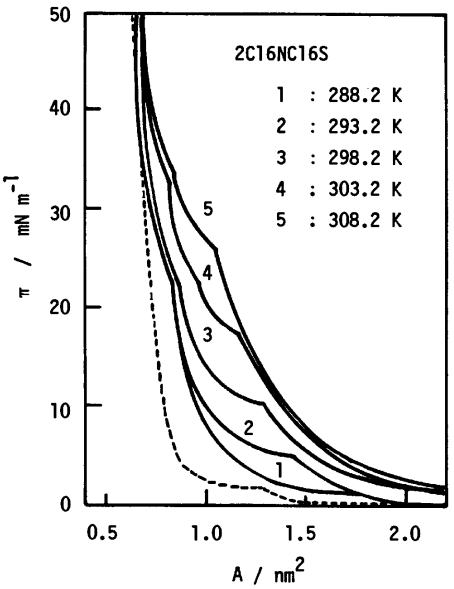

Fig. 4. The temperature dependence of π-A curves of 2C16NC16S salt. Substrate; 4.4 M NaCl solution. Dotted line: on pure water at 298.2 K.

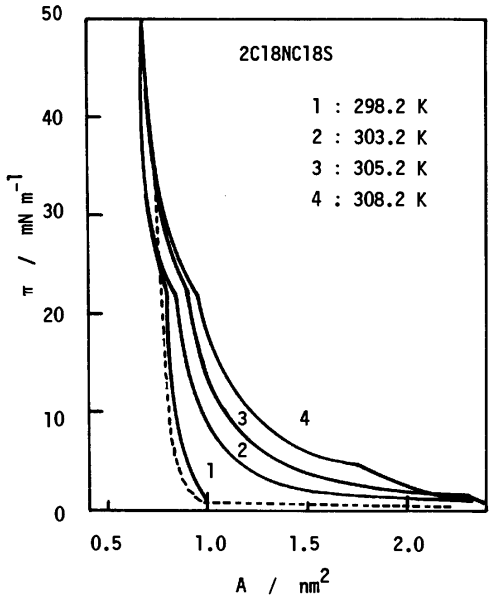

Fig. 5. The temperature dependence of π-A curves of 2C18NC18S salt. Substrate; 4.4 M NaCl solution. Dotted line: on pure water at 298.2 K.

In order to clarify the effect of the chain lengrh on the phase diagram, the π-A curves for the four (2-1) long-chain salts were compared at various temperatures in Figs. 2—5. The limiting area is found to be larger by about 0.6 nm² than threefold area of corresponding single long-chain fatty acids.[21] This is due to the bulky cationic head group. From these figures the π-A curves clearly have two or three transition points depending on the chain length of the cations and anions. In the previous experiments of (1-1) long-chain salt monolayer on 4.4 M NaCl solution, only two kinds transitions [E phase→C-I phase and C-I phase→C-II phase] have been observed. Therefore, the three kinds of transitions [E phase→C-I phase, C-I phase→C-I′ phase, and C-I′ phase→C-II phase] are characteristic of the present systems.

Table 2. Limiting Areas of (2-1) Long-Chain Salts and (1-1) Long-Chain Salts at 298.2 K (on 4.4 M NaCl)

Chain length (n) of salts	Limiting area (A/nm²)	
	C_nNC_nS	$2C_nNC_nS$
	Condensed phase I	
n=12	—	—
n=14	—	1.12(E→C-I′)[a]
n=16	0.728	1.06
n=18	0.700	—
	Condensed phase II	
n=12	—	—
n=14	—	0.910(C-I′→C-II)[b]
n=16	—	0.868
n=18	0.599	0.755

a) This value is the limiting area for the condensed phase I′(C-I′). b) This value is the limiting area for the condensed phase II(C-II).

In order to investigate the molecular orientation on the surface films, the limiting areas of the condensed film were estimated from the π-A curves by the same method described previously.[19,20] The values of the limiting area can be classified into two groups as shown in Table 2: one is the limiting area for the condensed phase I (for 2C14NC14S salt, the value is the limiting area for the condensed phase I′, this will be made clear later by the phase diagram), and the other is that for the condensed phase II. The π-A curves of 2C18NC18S (curve of n=18 in Fig. 1) and C16NC16S [curve of n=16 in Fig. 2 of Ref. 20], for example, have one transition point. As seen from Table 2, the limiting area (0.364 nm²) per alkyl chain for C16NC16S quite resembles the limiting area (0.350 nm²) per alkyl chain for the condensed phase I of the C18NC18S salt with two break points on the π-A curve, whereas the value of the limiting area (0.252 nm²) per alkyl chain for 2C18NC18S should be classified to another condensed phase, the condensed phase II of the $2C_nNC_nS$ salt.

As seen from Figs. 2 to 5, there exists evidently an appreciable difference in the limiting area of the π-A curves for (2-1) long-chain salt between on pure water and on the 4.4 M NaCl solution, which amounts to about 0.1 nm². The monolayer of the 2C18NC18S salt on pure water at 298.2 K exhibits a direct transition to condensed film and has no break point on the π-A curve. On the other hand, the monolayer on the 4.4 M NaCl solution is somewhat more loosely packed in the condensed state (C-I) than that on pure water and has a break point due to the transition from the condensed phase I to II at 298.2 K. The values of somewhat

expanded limiting area for the condensed phase I and the occurrence of the phase transition from the condensed phase I to II are attributable to the substrate of concentrated NaCl solution.

The film compressibilities of (2-1) long-chain salts are also useful for a discussion of the molecular interaction in the film. Compressibility is taken as $C_s=-1/A(\mathrm{d}A/\mathrm{d}\pi)\fallingdotseq(a_0-a_1)/a_0\pi_1$, where a_1 is the area at a certain surface pressure π_1, and a_0 is the area extrapolated to zero pressure. A suitable surface pressure was chosen 49 mN m^{-1} because above this surface pressure all the films are the state of the condensed phase II, as is clear from the π-A curves of Figs. 3 to 5. For the salts 2CnNCnS, the values of the compressibility decrease with increasing the chain length (n) of (2-1) long-chain salts (Table 3) and approach to that of octadecanoic acid. On the other hand, the condensed monolayer (C-II) of C18NC18S has twice the compressibility of the condensed films (C-II) of 2C18NC18S, and presents approximately similar compressibility to the 2C16NC16S monolayers (C-II), as seen in Table 3. This indicates that the cohesive interaction between the long chains increases with the number of alkyl chains, while decreasing with shortening of alkyl chain.

Table 3. Compressibilities of (2-1) Long-Chain Salts and (1-1) Long-Chain Salts in the Condensed Film at 298.2 K (on 4.4 M NaCl)

Chain length (n) of salts	Compressibility/m mN^{-1} [a]	
	CnNCnS	2CnNCnS
n=12	—	—
n=14	—	0.0056
n=16	—	0.0047
n=18	0.0039	0.0020

a) Octadecanoic acid, 0.0015 (m mN^{-1}); Dipalmitoyl phosphatidylcholine, 0.0064 (m mN^{-1}) at 298.2 K. Compressibility is taken as $(a_0-a_1)/a_0\pi_1$, where a_1 is the area at π_1=49 mN m^{-1}, and a_0 is the area extrapolated to zero pressure.

The studies of the temperature effect on the transition pressure are of much interest, since they provide us with thermodynamic information about the state of monolayers. Figures 3—5 show, the π-A isotherms of 2C14NC14S, 2C16NC16S, and 2C18NC18S at various temperatures, which have two break points. As for 2C16NC16S salt in particular, three break points are observed on the π-A isotherm. As was expected, the transitions pressures increased with an increase in the temperature.

In Fig. 6 are illustrated the three types of phase diagrams from the transition pressure (π^{eq}) and temperature for 2CnNCnS salts, where the slope of the π^{eq} against temperature is a key point to assign the phases.

The thermodynamic quantities on the phase transition of monolayers were calculated by the same method as described in our previous study.[17-20,22,23] The apparent molar entropy change (Δs^r) on the phase transition were evaluated by employing Eq. 29 of Ref. 22.

The apparent molar entropy changes on the various types of phase transition are given in Table 4 for (2-1) long-chain salts. As seen from in Table 4, the first

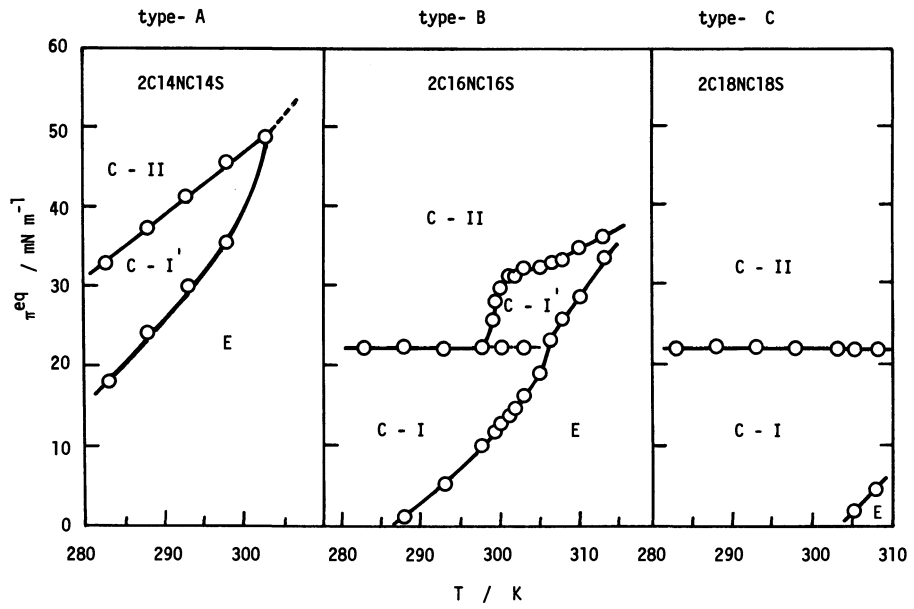

Fig. 6. The transition pressure (π^{eq}) as a function of the temperaure, and the transition pressure-temperature diagrams for the monolayers of 2C14NC14S, 2C16NC16S, and 2C18NC18S salts on the 4.4 M NaCl solution.

Table 4. The Apparent Molar Entropy Changes on the Phase Transition of (2-1) Long-Chain Salts at Various Temperature (on 4.4 M NaCl)

	Entropy change ($-10^{-2}\Delta s^{\gamma}$/J K^{-1} mol^{-1})					
	2C14NC14S	2C16NC16S			2C18NC18S	
Temp/K / Transition	298.2	298.2	303.2	308.2	298.2	305.4
E →C-I	—	2.9	5.0	—	—	9.6
E →C-I′	1.2	—	—	3.4	—	—
C-I →C-II	—	0.14	—	—	0.07	0.16
C-I →C-I′	—	—	0.2	—	—	—
C-I′→C-II	0.3	—	0.5	0.68	—	—

transition includes two kinds of transitions; one from the expanded phase (E) to the condensed phase I (C-I) and the other from the expanded phase (E) to the condensed phase I′ (C-I′). The values of the apparent molar entropy change of 2C16NC16S salt increases with the temperature. Normally, the value of the apparent molar entropy change increases with an increase in the temperature. The smaller value at 308.2 K than that at 303.2 K reflects the difference in type of the phase transition between the E→C-I and the E→C-I′. The phase transition for the 2C14NC14S salt at 298.2 K can be classified as the transition from the expanded phase (E) to the condensed phase I′ (C-I′) by the aid of the phase diagram (Fig. 6), and the slope of π^{eq} vs. T curves. The longer the chain length of the salt, the larger the apparent molar entropy on the transition from their expanded to their condensed states.

The apparent molar entropy changes on the other types of the phase transition are also given in Table 4. The second transition includes three kinds of transitions; C-I→C-II, C-I→C-I′, and C-I′→C-II. The apparent molar entropy change on the second phase transition decreased in magnitude by one order, compared with the apparent molar entropy change on the first phase transition (E→C-I, and E→C-I′). The column of 2C16NC16S salt at 303.2 K includes three numerical values. Especially in this case, the assignment of the type of phase transition is difficult only by the aid of the apparent molar entropy change. The values of the apparent molar entropy changes are too small to compare with those of other phase transitions. So, the phase transition for 2C16NC16S at 303.2 K was classified judging from the slope of π^{eq} vs. T curves in Fig. 6. The classification of the phase transitions on other salts were also done by the same method. The 2C18NC18S salt also has the transition from C-I to C-II on the π-A curve at 298.2 K. The longer the chain length of (2-1) long-chain salts, the smaller the apparent molar entropy change on the phase transition from C-I to C-II. The larger entropy change on the first transition (i.e.; E→C-I, and E→C-I′) suggests the considerable change of the molecular orientation in the monolayers, whereas the small entropy change on the second transition (i.e.; C-I→C-II, C-I→C-I′, and C-I′→C-II) suggests the slight change in the monolayer configuration. As a result, five types of classifications are possible for the phase transitions on the monolayers of (2-1) long-chain salts (2CnNCnS).

The monolayers of (2-1) long-chain salts turned out to have two or three transition points on their π-A curves. Figure 6 shows the phase diagrams of the monolayers of 2C14NC14S (type-A), 2C16NC16S (type-B) and 2C18NC18 (type-C) as expmples. Judging from the slope of the π^{eq} vs. T curve of the type B in Fig. 6, it is possible to distinguish between the phases of C-I and C-I′. But, there remains some question that the C-I and the C-I′ phases are distinguishable from the phase diagram of the types A and C in Fig. 6. This distinction may be made clearer by other techniques such as surface potential measurement and ellipsometric measurement. It is noteworthy that two triple points exist on the phase diagram of type-B and that three phase transitions, E→C-I, C-I→C-I′, and C-I′→C-II are possible depending on a particular temperature range. At higher temperature, the phase transition of E→C-II will be observed, which is a conventional phase transition in monolayer research. There are some studies on the polymorphism in monolayers of docosanoic acid and 1-octadecanol.[24,25] As for these compounds, the condensed phase I has not appeared on the 0.1 M NaCl solution or water, but it appears on the 4.4 M NaCl solution. Especially, in this (2-1) long-chain salt, another condensed phase I′ (C-I′) appears. The C-I′ phase is the intermediate phase between the C-I and C-II phases. In the condensed phase II, the (2-1) long-chain salts are probably aligned perpendicular to the water surface judging from the limiting area. From the small entropy change from the condensed phase I to II (Table 4), the hydrocarbon tail interaction in the condensed phase I might be similar to that in the condensed phase II. However, the limiting areas for the condensed phase I are considerably larger than those for the condensed phase II as shown in Table 2.

For the condensed phases I and I′, therefore, the elongated distance can be imagined between the ionic head groups, because Na^+ and Cl^- ions are probably incorporated into the two-dimensional ionic crystal structure, causing the pronounced cohesive interaction between the long chains. This model may be clarified by data from other techniques such as surface potential measurement and ellipsometric measurement, which will be reported in a separate paper.

In conclusion, the monolayer of a (2-1) long-chain salts on the concentrated NaCl solution was found to have two triple points in the phase diagram. From the phase transitions, the phase diagrams can be classified into three types: type-A is of two phase transitions, expanded phase (E) → the condensed phase II (C-II) via the condensed phase I′ (C-I′); type-B is of three phase transitions, namely the expanded phase (E) → the condensed phase I (C-I), the condensed phase I (C-I) → the condensed phase I′ (C-I′), and the condensed phase I′ → the condensed phase II (C-II); and type-C is two phase transitions, the expanded phase (E) → the condensed phase II (C-II) via the condensed phase I (C-I). New finding of this study is the appearance of the condensed phase I′ (C-I′) which wasn't present for the (1-1) long-chain salts.

One of authors (O. S.) wants to express his deep gratitude to Prof. Makoto Nakamura of College of General Education, Kyushu University and Dr. Akira Yamauchi of the Department of Chemistry, Kyushu University, for many valuable and most stimulating discussions during this work and would like to thank Dr. Yoshikiyo Moroi of the department of Chemistry, Kyushu University for help with preparation on this manuscript for publication.

This work has been financially supported in part by a Grant-in-Aid for Scientific Research No. 59540268 from the Ministry of Education, Science and Culture.

References

1) J. M. Corkill, J. F. Goodman, C. P. Ogden, and J. R. Tate, *Proc. R. Soc. London, Ser. A*, **273**, 84 (1963).
2) J. M. Corkill, J. F. Goodman, S. P. Harrold, and J. R. Tate, *Trans. Faraday Soc.*, **62**, 994 (1966).
3) M. J. Schwuger, *Kolloid Z. Z. Polym.*, **243**, 129 (1971).
4) E. H. Lucassen-Reynders, *Kolloid Z. Z. Polym.*, **250**, 356 (1972).
5) E. H. Lucassen-Reynders, J. Lucassen, and D. Giles, *J. Colloid Interface Sci.*, **81**, 150 (1981).
6) E. H. Lucassen-Reynders, *J. Colloid Interface Sci.*, **85**, 178 (1982).
7) D. Góralczyk, *J. Colloid Interface Sci.*, **77**, 68 (1980).
8) D. Góralczyk and B. Waligora, *J. Colloid Interface Sci.*, **82**, 1 (1981).
9) J. Rodakiewicz-Nowak, *J. Colloid Interface Sci.*, **85**, 586 (1982).
10) L. Sepúlveda and J. Pérez-cotapos, *J. Colloid Interface Sci.*, **109**, 21 (1986).
11) Y. Moroi, R. Matuura, T, Kuwamura, and S. Inokuma, *J. Colloid Interface Sci.*, **113**, 225 (1986).
12) J. M. Corkill, J. F. Goodman, S. P. Harrold, and J. R. Tate, *Trans. Faraday Soc.*, **63**, 247 (1967).
13) Y. Hendrix and L. Ter-Minassian-Saraga, "Advances in Chemistry Series. 144. Monolayers", ed by E. D. Goddard, American Chemical Soc., Washington, D. C., (1975), pp. 177—191.
14) M. A. McGregor and G. T. Barnes, *J. Colloid Interface Sci.*, **62**, 213 (1977).
15) Y. Hendrix, *J. Colloid Interface Sci.*, **69**, 493 (1979).
16) Y. Hendrix and D. Mari, *J. Colloid Interface Sci.*, **78**, 74 (1980).
17) O. Shibata, S. Kaneshina, M. Nakamura, and R. Matuura, *J. Colloid Interface Sci.*, **77**, 182 (1980).
18) O. Shibata, S. Kaneshina, M. Nakamura, and R. Matuura, *Bull. Chem. Soc. Jpn.*, **55**, 2243 (1982).
19) O. Shibata, S. Kaneshina, M. Nakamura, and R. Matuura, *J. Colloid Interface Sci.*, **95**, 87 (1983).
20) O. Shibata, *J. Colloid Interface Sci.*, **96**, 182 (1983).
21) K. Motomura, M. Ikematsu, Y. Hayami, H. Matuo, and R. Matuura, *Bull. Chem. Soc. Jpn.*, **53**, 2217 (1980).
22) K. Motomura, T. Yano, M. Ikematsu, H. Matuo, and R. Matuura, *J. Colloid Interface Sci.*, **69**, 209 (1979).
23) K. Motomura, *Adv. Colloid Interface Sci.*, **12**, 1 (1980).
24) S. Ställberg-Stenhagen and E. Stenhagen, *Nature (London)*, **156**, 239 (1945).
25) W. D. Harkins and L. E. Copeland, *J. Chem. Phys.*, **10**, 272 (1942).

 © 1988 The Chemical Society of Japan Bull. Chem. Soc. Jpn., 61, 3083—3085 (1988)

New Mesomorphic Compounds: *N,N'*-Dialkanoyl-2,4-bis(alkanoyloxy)-1,3-benzenediamines

Hiromitsu KAWADA and Yoshio MATSUNAGA*
Department of Chemistry, Faculty of Science, Hokkaido University, Sapporo 060
(Received March 31, 1988)

A series of *N,N'*-dialkanoyl-2,4-bis(alkanoyloxy)-1,3-benzenediamines has been synthesized. The high-temperature phases appearing in the heptanoyl to hexadecanoyl derivatives are viscous and are transformed into isotropic liquids with enthalpy changes of 20 kJ mol^{-1} or less. Their X-ray diffraction patterns are characteristic of the hexagonal disordered columnar phase. The second moment of the broad-line proton NMR spectrum measured in the mesophase region is 0.8 to 0.9 G^2 in the case of the octanoyl derivative and 0.04 G^2 in the case of the tetradecanoyl derivative, indicating the rather large difference in the motional behavior between these half-disk-shaped molecules.

As we reported earlier,[1] the mesomorphic behavior can be considerably enhanced by the replacement of the two $OCOC_nH_{2n+1}$ groups in the 1 and 4 positions of hexakis(alkanoyloxy)benzenes by $NHCOC_nH_{2n+1}$ groups; namely, the clearing point of discogenic *N,N'*-dialkanoyl-2,3,5,6-tetrakis(alkanoyloxy)-1,4-benzenediamine (**1**) is much higher than that of the corresponding hexakis(alkanoyloxy)benzene,[2,3] while the melting point of the former compound remains almost the same as that of the latter. These two compounds are composed of disk-like molecules in which the planar rigid core is densely surrounded by a planar ring of aliphatic chains. Although it is generally assumed that the distinctive feature common to all the mesomorphic compounds is the rod-like or disk-like shape of the molecule,[4-6] we have found that *N,N'*-dialkanoyl-2,4,6-trimethyl-1,3-benzenediamines are mesogenic.[7] These findings suggest that the presence of two $NHCOC_nH_{2n+1}$ groups per molecule is favorable to form stable mesophases and also that the molecule is not required to be rod-like or disk-like in order to form a mesophase. What is indispensable to the formation of mesophase is apparently the presence of a molecular core which keeps the molecules aligned up to relatively high temperatures and that of long flexible alkyl chains conformationally disordered at lower temperatures. Consequently, it seemed to us highly probable that *N,N'*-dialkanoyl-2,4-bis(alkanoyloxy)-1,3-benzenediamine (**2**), even though the molecule of which is half-disk-shaped, can produce some kind of mesophase.

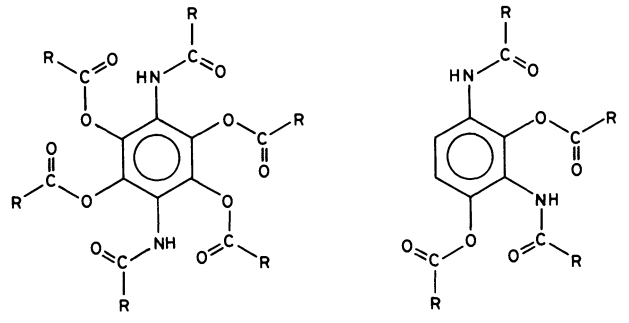

1 R=C_nH_{2n+1} **2**

Experimental

Materials. 2,4-Dinitrosoresorcinol was prepared following the method described by Fitz,[8] but the addition of sodium nitrite at lower temperatures, −2 to −4 °C, was found to be recommendable. The wet product was added in small portions to tin(II) chloride dissolved in concentrated hydrochloric acid avoiding excessive raising of the temperature by the heat of the reaction. The warm solution was filtered and the amine was precipitated by the addition of concentrated hydrochloric acid. The acylation was carried out at room temperature by adding acyl chloride drop by drop to a pyridine solution of the diamine. The desired compounds were recrystallized from acetone or mixtures of benzene and diethyl ether. Found: C, 73.03; H, 10.65; N, 3.71%. Calcd for $C_6H_2(NHCOC_9H_{19})_2(OCOC_9H_{19})_2$: C, 72.97; H, 10.65; N, 3.70%. Found: C, 75.82; H, 11.49; N, 2.86%. Calcd for $C_6H_2(NHCOC_{13}H_{27})_2(OCOC_{13}H_{27})_2$: C, 75.87; H, 11.50; N, 2.85%.

Measurements. Calorimetric, X-ray, and NMR measurements were made mostly as described in our previous papers.[1,7] As the endothermic peaks due to melting and clearing are closely located in some derivatives, a rather slow rate of heating, 150 K h^{-1}, was employed throughout the present work in order to improve the separation between the peaks.

Results and Discussion

The thermal properties of the eight derivatives carrying heptanoyl to hexadecanoyl groups are summarized in Table 1. Here, crystalline, discotic, and isotropic phases are denoted by K, D, and I respectively. No solid-solid transition is found above room temperature for any homologous member. It may be noted that the temperature range of the mesophase is narrowed as the series is ascended. The mesophase appears over 35 °C range in the case of the heptanoyl and octanoyl derivatives but only over 11 °C in the case of the hexadecanoyl derivative. Compared with the corresponding homologous member in the series **1**, the present compounds melt at higher temperatures and are transformed into isotropic liquids at much lower temperatures. While the enthalpy change at the clearing point (D–I transition temperature) is in a narrow range

Table 1. Transition Temperatures (°C) and Enthalpy Changes (kJ mol^{-1}) of Compounds **2**[a]

n[b]	K		D		I
6	·	89(9)	·	124(19)	·
7	·	87(10)	·	122(18)	·
8	·	90(16)	·	121(18)	·
9	·	93(18)	·	122(17)	·
10	·	95(23)	·	120(16)	·
11	·	97(26)	·	117(15)	·
13	·	101(41)	·	114(13)	·
15	·	103(60)	·	114(16)	·

a) The latter quantities are in parentheses. b) The number of carbon atoms in the alkyl group.

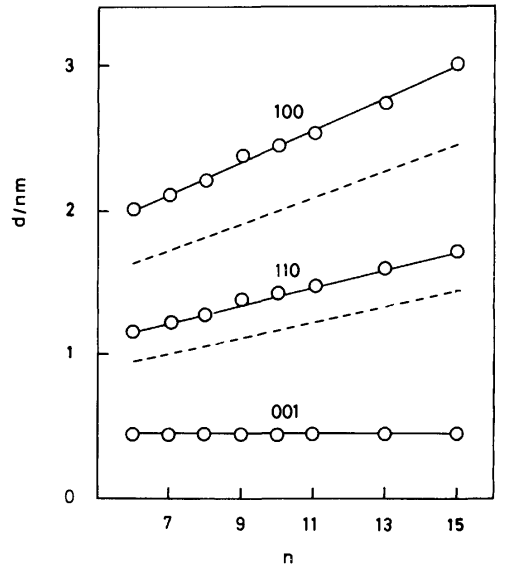

Fig. 1. Plots of spacings measured in the mesophases against the number of carbon atoms in the alkyl group for compounds **2**. Broken lines indicate the corresponding spacings of compounds **1**.

from 13 to 19 kJ mol^{-1}, that at the melting point (K-D transition temperature) increases rapidly with the increase of the alkyl chain length, from 9 to 60 kJ mol^{-1}. The entropy change at the clearing point is 83 J mol^{-1} K^{-1} for the heptanoyl derivative of the series **1** and 48 J mol^{-1} K^{-1} for the corresponding member of the series **2**. The value becomes smaller as both the series are ascended and 39 and 41 J mol^{-1} K^{-1} are obtained for the hexadecanoyl derivatives of the series **1** and **2** respectively. Thus, the entropy change in the present series is less dependent on the alkyl chain length than that in the hexasubstituted benzene series.

The isotropic liquid of all the derivatives may be supercooled as much as 20 °C. The mesophase of the heptanoyl to undecanoyl derivatives can be cooled to room temperature. No crystallization was observed even when the specimen was annealed at 5 °C below the melting point for four hours. On the other hand, three exothermic peaks are detected in the process of cooling for the dodecanoyl to hexadecanoyl derivatives. These metastable solid phases are easily transformed into the stable ones.

The X-ray diffraction pattern of the mesophase is essentially of the hexagonal disordered columnar structure; that is, there are two sharp inner peaks giving spacings in the ratio of $1:1/\sqrt{3}$ and one broad peak giving a spacing of 0.46 nm throughout the series. They may be assigned to 100, 110, and 001 reflections respectively. The innermost peak is accompanied in most cases by a weak peak assignable to the second order reflection. In addition, two weak extra peaks are detectable in the patterns given by the dodecanoyl derivative and the lower homologous members in the region between the sharp peaks and the broad one, indicating the appearance of some regularity in the molecular arrangement. The spacings d_{100} and d_{110} increase linearly with the alkyl chain length as shown in Fig. 1. For example, the heptanoyl derivative gives a d_{100} of 1.99 nm and the hexadecanoyl derivative 2.98 nm. They are much longer than those of the corresponding members in the series **1** represented by broken lines in the same figure. This suggests that the alkyl chains in compounds **2** are more extended and/or less interdigitated. In the mesophases formed by disk-like molecules, rotation of the whole molecule about the normal to the molecular plane and fluctuations of this axis around the preferred aromatic director are conceivable.[9] In order to achieve the hexagonal symmetry, the present half-disk-shaped molecule must be effectively disk-like in the mesophase. In other words, the molecules in a column must be oriented in various directions and rotating more freely than disk-like molecules do. Therefore, the interlocking of the alkyl chains must be less pronounced than that in the mesophase of compounds **1**. The supercooling of the mesophases of the heptanoyl to undecanoyl derivatives was confirmed by the X-ray measurements. The diffraction pattern recorded at room temperature for the once melted specimen is the same as that recorded in the temperature range of the stable existence.

The longest spacing in the crystalline phase is longer than that in the mesophase, d_{100} and changes linearly with the number of carbon atoms in the alkyl group; namely, 2.20 nm in the heptanoyl derivative and 4.70 nm in the hexadecanoyl derivative. The shrinkage at the melting point is only 0.21 nm in the former derivative and as much as 1.72 nm in the latter. This behavior is consistent with the remarkable increase in the enthalpy change as the series is ascended. The hexanoyl derivative is expected not to be mesomorphic because the shrinkage estimated by the linear relationship is nearly zero.

The liquid-like characteristics of alkyl chains in the mesophase are demonstrated by the small second moments of the broad-line proton NMR spectrum (the

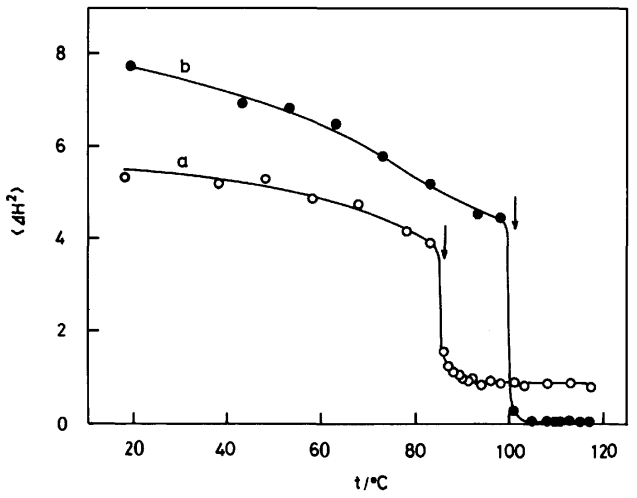

Fig. 2. Second moments of the broad-line proton NMR spectrum of compounds **2**, (a) n=7 and (b) n=13. The vertical arrows indicate the melting points determined by calorimetry.

mean-square width of the resonance line), $<\Delta H^2>$, measured above the melting point. As is shown in Fig. 2, the moment given by the octanoyl derivative is about 5.5 G^2 (1 G=10^{-4} T) at room temperature and about 4 G^2 just below the melting point which is indicated by a vertical arrow. An abrupt decrease of the moment occurs at the melting point and moments between 0.9 and 0.8 G^2 are shown by the mesophase. On the other hand, the tetradecanoyl derivative gives a moment of about 7.8 G^2 at room temperature and that of about 4.5 G^2 near the melting point. The moment observed above this temperature is only 0.04 G^2. Thus, the motional behavior in the hexagonal disordered columnar phase depends appreciably on the alkyl chain length. The similar but less pronounced tendency has been noted with compounds **1**; namely, the second moment observed for the mesophase of the octanoyl derivative was 0.3 G^2 and that of the hexadecanoyl derivative 0.03 G^2.[1] Judging from these values of the second moment, one may conclude that the alkyl chains in the lower homologous members are moving more slowly, in the time scale of NMR, than those in the higher members in both the series **1** and **2**. This conclusion is not incompatible with the entropy changes at the clearing point mentioned above.

According to the rule of selected miscibility of Sackmann and Demus,[10] an uninterrupted series of binary mixtures should be obtainable if the mesophases are of the same structural type. However, Dabrowski et al., employing a homologous series as one of the components, have shown that the smectic A phase in binary mixtures is more and more depressed and, in some extreme cases, separated by a gap as the layer spacing ratio is increased.[11,12] The mesophases given by the tetradecanoyl derivatives of series **1** and **2** were found not to be completely miscible by the contact method.[13] The d_{100} ratio of these two compounds is approximately 1.2. We also examined the combination of the hexadecanoyl derivative of series **1** and the decanoyl derivative of the series **2**. These two give the spacings similar to each other (see Fig. 1). In this combination too, the mesophases are not miscible. The results are apparently in contradiction to the above-mentioned rule and may be ascribed to the distinct difference in the shape of the molecules involved, disk-like and half-disk-like. We have examined the miscibility between the members in the present series. The mesophase of the tetradecanoyl derivative was found to be miscible in any ratio with those of the hexadecanoyl and dodecanoyl derivatives but not with those of undecanoyl derivative and the lower homologous members. The complete miscibility among the lower members is more severely restricted; that is, only the nearest neighboring members are miscible with each other. It may be too early to be certain of the situation, but these observations may imply that the similarity in the motional behavior is also of importance to provide complete miscibility.

The present work was supported by a Grant-in-Aid for Scientific Research No. 60470001 from the Ministry of Education, Science and Culture.

References

1) Y. Kobayashi and Y. Matsunaga, *Bull. Chem. Soc. Jpn.*, **60**, 3515 (1987).
2) S. Chandrasekhar, B. K. Sadashiva, and K. A. Suresh, *Pramana*, **9**, 471 (1977).
3) S. Chandrasekhar, B. K. Sadashiva, K. A. Suresh, N. V. Madhusudana, S. Kumar, R. Shashidar, and G. Venkatesh, *J. Phys. (Paris)*, **40**, C3-120 (1979).
4) G. W. Gray, "Advances in Liquid Crystals, Vol. 2," ed by G. H. Brown, Academic Press, New York (1976), pp. 1—72.
5) J. Billard, "Liquid Crystals of One- and Two-Dimensional Order," ed by W. Helfrich and G. Heppke, Springer-Verlag, Berlin (1980), pp. 385—395.
6) S. Chandrasekhar, "Advances in Liquid Crystals, Vol. 5," ed by G. H. Brown, Academic Press, New York (1982), pp. 47—78.
7) Y. Matsunaga and M. Terada, *Mol. Cryst. Liq. Cryst.*, **141**, 321 (1986).
8) A. Fitz, *Ber.*, **8**, 631 (1875).
9) V. Ruter, R. Blinc, M. Vilfan, A. Zann, and J. C. Dubois, *J. Phys. (Paris)*, **43**, 761 (1982).
10) H. Sackmann and D. Demus, *Mol. Cryst.*, **2**, 81 (1966).
11) R. Dabrowski, B. Wazynska, and B. Sosnowska, *Liq. Cryst.*, **1**, 415 (1986).
12) K. Czuprynski and R. Dabrowski, *Mol. Cryst. Liq. Cryst. Lett.*, **4**, 153 (1987).
13) H. Sackmann and D. Demus, *Z. Phys. Chem. Leipzig*, **222**, 143 (1963).

 © 1988 The Chemical Society of Japan Bull. Chem. Soc. Jpn., 61, 3087—3091 (1988)

The Brillouin Scattering of Highly Viscous Liquids-Triacetin and Propylene Glycol Diacetate

Ryuki HASHITANI, Hirohito MATSUI, Shinobu KODA, and Hiroyasu NOMURA*
Department of Chemical Engineering, School of Engineering, Nagoya University, Chikusa-ku, Nagoya-shi 464
(Received April 9, 1988)

The sound velocities of triacetin and propylene glycol diacetate were measured by means of Brillouin scattering in the temperature range from 200 to 350 K. The velocity dispersions due to the structural relaxation were observed in the gigahertz region. The relaxation behaviors could not be interpreted by the empirical equation proposed by Barlow et al., which holds in megahertz region and also the relaxation curves were located in higher frequency region than those predicted by the Maxwell model. The relaxation curves were well reproduced by single relaxation equation. In the temperature ranges of relaxation region, the temperature dependences of viscosity were expressed by Arrhenius' viscosity equation. The relaxation behaviors can be interpreted in terms of the weak cooperative motions of molecules.

Dynamic properties of liquids have been intuitively understood through observation of the viscous flow of liquids in an ordinary time scale. However, liquids behave as elastic media in a very short time scale, and so a definite time is needed for liquids to flow. The relaxation process is closely related to the collective translational motions and can occur in any liquids. The relaxation is called as viscoelastic and/or structural relaxation. In this sense, the relaxation process should reflect the dynamic nature of the local structure of liquid. In order to observe the relaxation process experimentally, one needs to measure the time- and frequency-dependences of viscosity and/or elastic modulus. The relaxation time in low-viscosity liquids is too short to measure by any experimental techniques available for us now. In this work we used highly viscous liquids or supercooled liquids as samples, because their relaxation times fall on the measurable frequency ranges.

The Brillouin scattering provides the sound velocity and the absorption coefficient of sound wave in the gigahertz region. In our previous papers, the structural relaxations of highly viscous liquids have been investigated by means of Brillouin scattering.[1-3] The relaxation behaviors in the GHz region have been discussed using the reduced variable method proposed by Lamb's school[4] which held very well in the MHz region and we pointed out that the distribution of relaxation times in GHz region was different from those in the MHz region, that is, Maxwellian relaxation curve reproduced our experimental results satisfactorily in the GHz region.

In this paper, the experimental results for two highly viscous liquids, triacetin (hereafter abbreviated as TAT) and propylene glycol diacetate (PGA), will be reported. Comparing with tri-*o*-tolyl phosphate (TOTP) and diisobutyl phthalate (DIBP) investigated before,[1-3] the molar volumes of TAT and PGA are small. In addition, the viscosity of PGA is much lower than that of TAT. The relaxation of PGA will appear in lower temperature region than those of TAT and the others.

Experimental

Samples. Triacetin(TAT), guaranteed grade, and propylene glycol diacetate (PGA), extra grade, were purchased from Kishida Chemical Co., Ltd. and Tokyo Chemical Industry Co., Ltd., respectively. They were purified by distillation under reduced pressure and were poured into scattering cells through a millipore filter with pore size of 0.2 μm.

Measurements. Rayleigh-Brillouin scattering spectra were observed by a pressure-scanning Fabry-Perot interferometer, using a He-Ne laser (NEC, GLG 5800, output 50 mW) as the light source. The detailes of experimental procedures were reported previously.[5] The range of scattering angle used was from 50° to 150°.

Refractive indexes were measured by an Abbe refractometer in the temperature range between 273 to 323 K. The values in the low temperature region were estimated by fitting the high temperature data to the Lorentz-Lorenz equation. The sound velocities at 5 MHz were measured by an ultrasonic interferometer in the temperature ranges from 268 to 318 K for TAT and from 248 to 318 K for PGA. The density and shear viscosity measurements were carried out by a buoyancy balance densitometer and rotational viscometer, respectively. These measurements were made in the temperature range from about 245 to 320 K for TAT and from 220 to 270 K for PGA.

Results

The sound velocity can be calculated from the Brillouin shift, Δf, which is the difference in the peak frequency between Rayleigh and Brillouin lines and is equal to the frequency of the sound wave, by following relation;

$$V=\frac{\lambda_i \Delta f}{2 n \sin(\theta/2)} \quad (1)$$

where λ_i is the wavelength of the incident light beam (632.8 nm). n is the refractive index of the sample, and θ is the scattering angle. The frequency dependences of sound velocity are shown in Fig. 1. The velocity dispersions are observed in the GHz region at 278, 298,

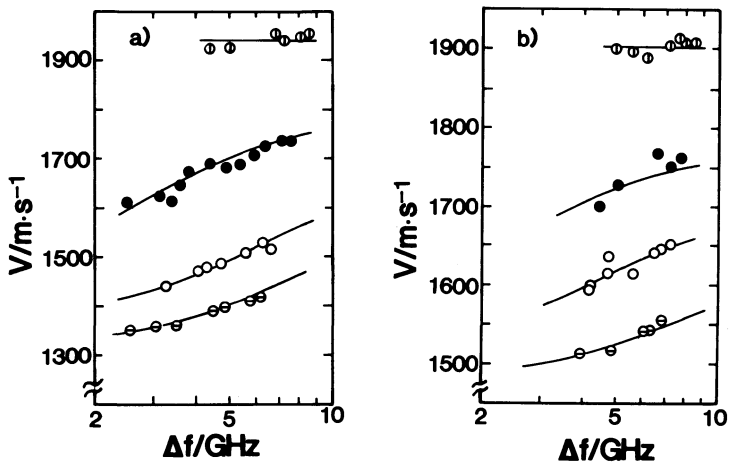

Fig. 1. Frequency dependence of sound velocity.
a) TAT; ⊕: 253 K, ●: 278 K, ○: 298 K, ⊖: 313 K.
b) PGA; ⊕: 218 K, ●: 233 K, ○: 243 K, ⊖: 253 K.

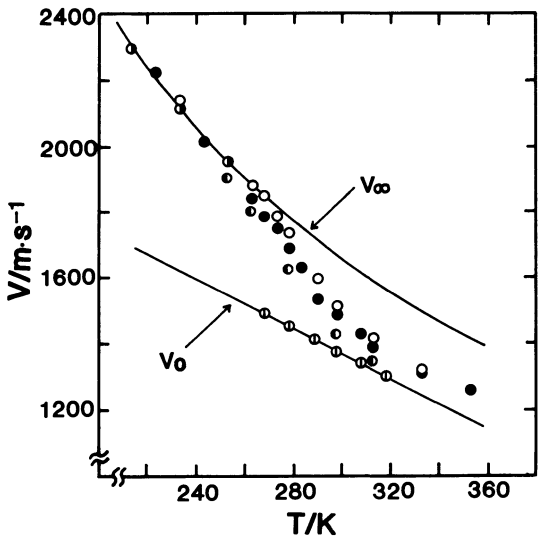

Fig. 2. Temperature dependence of sound velocity of TAT. Brillouin scattering; ◐: θ=50°, ●: θ=90°, ○: θ=100°, ◑: θ=150°. Ultrasonic interferometer (5 MHz); ⊕.

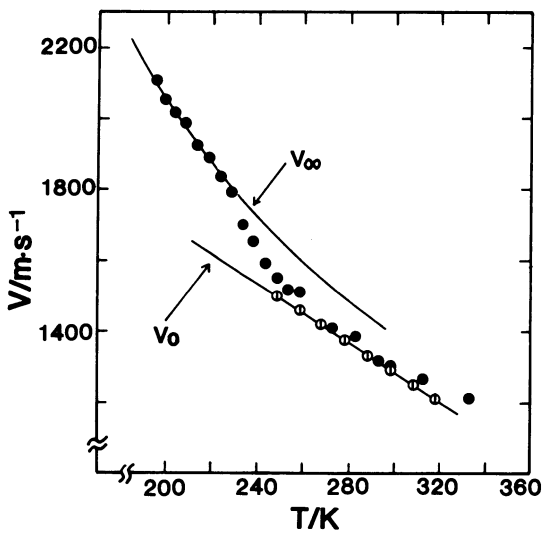

Fig. 3. Temperature dependence of sound velocity of PGA. Brillouin scattering (θ=90°); ●. Ultrasonic interferometer (5 MHz); ⊕.

and 313 K for TAT. In the case of PGA, the sound velocity dispersions appear in the lower temperature region than for TAT. Figures 2 and 3 show the temperature dependence of sound velocity for the TAT and PGA, respectively. The temperature dependence for TAT changes around at 250 K and for PGA around at 220 K. Besides, the velocities of TAT at 253 K and those of PGA at 218 K are independent of the frequency, as shown in Fig. 1. Therefore, the velocities of TAT below ca. 250 K and those of PGA below ca. 220 K may be considered to be the high-frequency limiting values. It has been assumed in our previous paper that the high-frequency limiting velocity, V_∞, has the following temperature dependence:

$$V_\infty = \frac{a}{T} + b \qquad (2)$$

where T is the absolute temperature and a and b are fitting parameters; a=4.80×10^5 m·s^{-1}·K, b=57 m·s^{-1} for the TAT and a=3.97×10^5 m·s^{-1}·K, b=61 m·s^{-1} for the PGA, respectively.

As is seen in Figs. 2 and 3, the relaxation strength, $\varepsilon=(V_\infty^2-V_0^2)/V_\infty^2$, decreases with increasing temperature in the temperature ranges where the sound velocity dispersions were observed (ε=0.34 (273 K)—0.31 (313 K) for TAT and ε=0.24 (233 K)—0.18 (253 K) for PGA). If the sound dispersions were due to the vibrational relaxation, the temperature dependence of the relaxation strength, ε, should increase with increasing temperature. Therefore, the sound velocity

dispersions we observed here may be due to structural relaxation, and not to vibrational one.

Discussion

The storage modulus, M', which is the real part of complex longitudinal modulus, M^*, can be calculated from $M'=\rho V^2$ under the assumption of $(\alpha V/\omega)^2 \ll 1$, where α is the absorption coefficient and $\omega=2\pi\Delta f$. In the reduced variable method proposed by Lamb, reduced modulus, $(M'-M_0)/M_2$, is plotted against reduced frequency, $\omega\eta_s/G_\infty$, where $M_2=M_\infty-M_0=\rho V_\infty^2-\rho V_0^2$, η_s is the shear viscosity, and G_∞ is the high-frequency limit of shear modulus. We have no experimental data for G_∞ of TAT and PGA. For this reason, we adopt $\omega\eta_s/M_2$ instead of $\omega\eta_s/G_\infty$. If G_∞/M_2 is assumed to be independent of temperature, as usually done,[4] the plots of reduced modulus against $\omega\eta_s/G_\infty$ and $\omega\eta_s/M_2$ become the same, although plots as a whole are shifted by an amount of $\log(G_\infty/M_2)$ along the abscissa. Figures 4 and 5 show the reduced plots of M' for TAT and PGA, respectively.

Assuming the B.E.L. (Barlow-Erginsav-Lamb) equation[4] for both complex shear and bulk moduli, one can obtain the following expression for M^*;

$$\frac{M^*-M_0}{M_2}=C\left[1+\frac{1}{i\zeta\omega\tau_s}+2K\left(\frac{1}{i\zeta\omega\tau_s}\right)^{1/2}\right]^{-1}+(1-C)\left[1+\frac{1}{i\omega\tau_s}+2K\left(\frac{1}{i\omega\tau_s}\right)^{1/2}\right]^{-1} \quad (3)$$

and

$$C=\frac{K_\infty-K_0}{M_\infty-M_0}=1-\frac{4}{3}\frac{G_\infty}{M_\infty-M_0},\quad \tau_s=\frac{\eta_s}{G_\infty}$$

$$\zeta=\frac{\tau_v}{\tau_s}=\frac{\eta_v}{\eta_s}\frac{G_\infty}{K_\infty-K_0}=\frac{3}{4}\frac{\eta_v}{\eta_s}\frac{1-C}{C}$$

where η_v is the bulk viscosity and K is an empirical parameter concerned with the distribution of the relaxation times. The values of K given by means of ultrasonic method were reported to be unity for highly viscous pure liquids. On the other hand, Eq. 3 with $K=0$ corresponds to the Maxwellian model. The solid and broken curves in Figs. 4 and 5 are those calculated from Eq. 3 by putting respectively $K=0$ and $K=1.0$, into the equation and taking account of the shift along the abscissa by $\log(G_\infty/M_2)$ as mentioned above. It has been reported that the value of C lies between 0.35 and 0.5 and that of η_v/η_s, does between 1 and 3.[2,4,6] The differences in C and η_v/η_s in the ranges mentioned above do not affect the relaxation curve largely. We used $C=0.5$ and $\eta_v/\eta_s=3$, in drawing the lines in Figs. 4 and 5.

As is clear in Figs. 4 and 5, the relaxation curves of TAT and PGA obtained from Brillouin scattering are quite different from those calculated from Eq. 3 with $K=1$ (broken lines). At first sight, it may seem that data at the different temperatures are well superimposed on a single curve for each case of TAT and PGA. However, the composed relaxation curves are similar to that calculated by Eq. 3 with $K=0$ (solid curve) and the positions of composed curves in all cases investigated here deviate clearly from the solid curves toward the higher frequency side. The positions and the shapes of curves obtained from Eq. 3 with $K=0$ depend on the choice of the values of C and η_v/η_s. For example in the case of TAT, if we use the values of $C=0.6$ and $\eta_v/\eta_s=0.32$, we can reproduce the composed curve. However, $\eta_v/\eta_s=0.32$ is too small in comparison with the values reported ($\eta_v/\eta_s=1$—3) in literature.[2,4,6] In the case of PGA, the deviation can not be fully interpreted by the variation of C and η_v/η_s. This result indicates that the reduced variable method does not hold well in such wide frequency ranges as covering from MHz to GHz region and that the relaxation

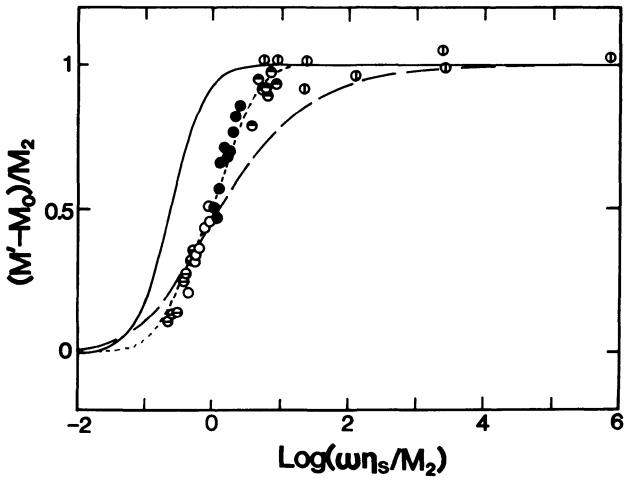

Fig. 4. Plots of $(M'-M_0)/M_2$ against $\log(\omega\eta_s/M_2)$ for TAT. ⊖: 263 K, ●: 278 K, ○: 298 K, ⊖: 313 K, ⊕: below 263 K. The dotted curve was calculated by Eq. 3 with $K=0$, $C=0.6$, and $\eta_v/\eta_s=0.32$.

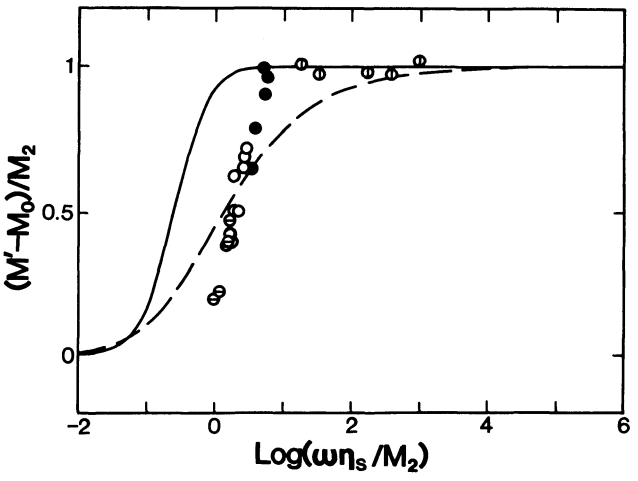

Fig. 5. Plots of $(M'-M_0)/M_2$ against $\log(\omega\eta_s/M_2)$ for PGA. ●: 233 K, ○: 243 K, ⊖: 253 K, ⊕: below 233 K.

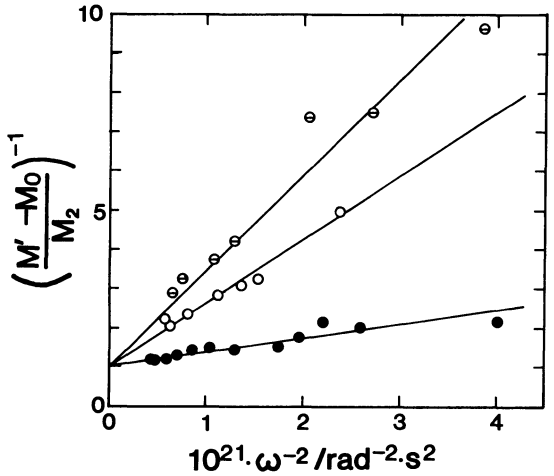

Fig. 6. Plots of $\{(M'-M_0)/M_2\}^{-1}$ against ω^{-2} for TAT.
●: 278 K, ○: 298 K, ⊖: 313 K.

behavior depends explicitly on the temperature in addition to the implicit temperature dependence involved in the reduced frequency. Thus it may be considered that the results obtained from Brillouin scattering reflect the high-temperature behavior, while those from ultrasonic method do the low-temperature one.

The shapes of relaxation curves obtained from Brillouin scattering are close to the Maxwellian model. If the reduced elastic modulus, $(M'-M_0)/M_2$, in the GHz region could be expressed by the following single (Maxwellian) relaxation equation:

$$\frac{M'-M_0}{M_2}=\frac{\omega^2\tau_M^2}{1+\omega^2\tau_M^2} \tag{4}$$

where τ_M is the relaxation time, the plot of $\{(M'-M_0)/M_2\}^{-1}$ against $1/\omega^2$ should be linear and its slope should be the square of the reciprocal relaxation time, $1/\tau_M$. As an example, Fig. 6 shows this relationship between $\{(M'-M_0)/M_2\}^{-1}$ and $1/\omega^2$ for the case of TAT at each temperature. As may be seen in Fig. 6, linear relationships are obtained within the limits of experimental error. Similar linear relationships are also obtained for the case of PGA at each temperature. If we use the relaxation times thus obtained, the reduced elastic moduli, $(M'-M_0)/M_2$, in the GHz region can be well expressed by a single relaxation equation (Eq. 4) within the frequency and temperature ranges investigated. This is shown in Fig. 7. The relaxation times of TAT obtained are 52, 25, and 20 ps at 278, 298, and 313 K, respectively and for PGA, 57, 33, and 20 ps at 233, 243, and 253 K, respectively.

It has been reported in some papers that single relaxation behavior or similar ones with narrow distribution of relaxation times appear when the temperature dependence of viscosity follows Arrhenius' viscosity equation.[1-3,7-9] At low temperature, where

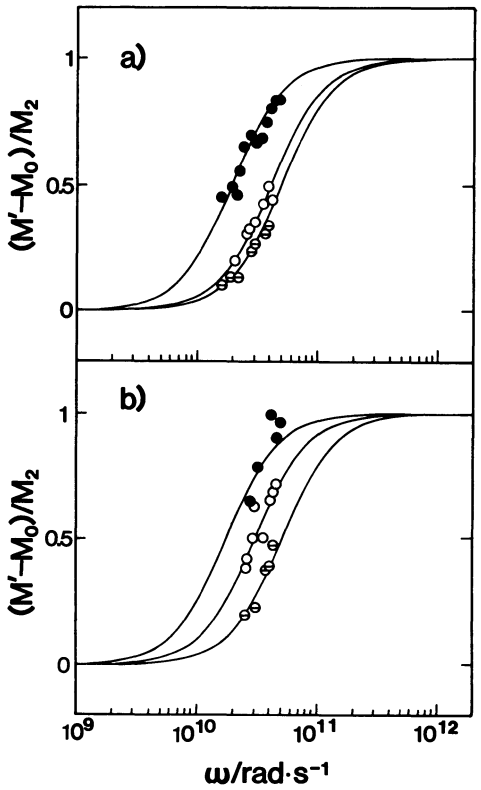

Fig. 7. Plots of $(M'-M_0)/M_2$ against angular frequency ω. a) TAT; ●: 278 K, ○: 298 K, ⊖: 313 K. b) PGA; ●: 233 K, ○: 243 K, ⊖: 253 K. Solid curves were drawn by single relaxation equation (Eq. 4).

relaxation behavior shows a broad distribution, the temperature dependence of viscosity can be understood in terms of the free volume theory. Litovitz and McDuffie suggest that if liquid viscosity obeys Arrhenius' equation, the cooperative character of molecular motions is weak in comparison with liquids which obey the free volume equation.[10] In the temperature region (278—313 K for TAT, and 233—253 for PGA). where the relaxation could be observed by the Brillouin scattering, the temperature dependence was close to the Arrhenius' equation, while in lower temperature, viscosity increased rapidly with decreasing temperature. Therefore, it is considered that the relaxation behavior investigated here is concerned with the weak cooperative motion of molecules, as well as in the cases of the samples we studied before.[1-3]

References

1) S. Koda, H. Nomura, M. Nakamura, and Y. Miyahara, *Bull. Chem. Soc. Jpn.*, **58**, 1484 (1985).

2) S. Koda, R. Hashitani, and H. Nomura, *Bull. Chem. Soc. Jpn.*, **58**, 3465 (1985).

3) R. Hashitani, S. Koda, and H. Nomura, *Bull. Chem. Soc. Jpn.*, **60**, 2705 (1987).

4) G. Harrison, "The Dynamic Properties of Supercooled Liquids," Academic Press, London (1976).

5) H. Nomura, H. Shimizu, Y. Tanaka, S. Koda, T. Okunishi, S. Kato, and Y. Miyahara, *Bull. Chem. Soc. Jpn.*, **55**, 3899 (1982).
6) A. J. Matheson, "Molecular Acoustics", John Wiley & Sons Ltd., London (1971).
7) J. Tauke, T. A. Litovitz, and P. B. Macedo, *J. Am. Ceram. Soc.*, **51**, 158 (1968).
8) G. J. Gruber and T. A. Litovitz, *J. Chem. Phys.*, **40**, 13 (1964).
9) W. M. Madigosky and R. W. Warfield, *J. Chem. Phys.*, **78**, 1912 (1983).
10) T. A. Litovitz and G. E. McDuffie, Jr., *J. Chem. Phys.*, **39**, 729 (1963).

 © 1988 The Chemical Society of Japan Bull. Chem. Soc. Jpn., 61, 3093—3102 (1988)

Topological Index and Thermodynamic Properties. IV.[3] Size Dependency of the Structure-Activity Correlation of Alkanes

Ying-duo GAO and Haruo HOSOYA*
Department of Chemistry, Ochanomizu University, Bunkyo-ku, Tokyo 112
(Received April 22, 1988)

Correlation coefficients between twelve thermodynamic properties (ΔS, ΔH_f, ΔG_f, bp, d, n_D, R_m, V_m, p_c, T_c, V_c, d_c) of 624 isomers of nonane through dodecane and five different topological indices (Z, p_3, w, p_2, A_3) were calculated, where the new index A_3 is proposed to be defined as the half sum of the off-diagonal elements of the cube of the adjacency matrix A. These properties can be classified into several types, according to the behavior of the two correlation coefficients, $\rho(Z)$ and $\rho(p_3)$, against the change of the size of molecules. ΔS and bp depend largely on Z, while d and n_D on p_3, irrespective of the size change of molecules. On the other hand, ΔH_f of smaller alkanes is largely dependent on Z, but for larger alkanes it turns out to be a p_3-dependent property. Various interesting behaviors of the structure-activity relationships including the "pentane effect" were observed and discussed.

There are two different standpoints in the study of structure-activity correlation for molecular properties, namely, application-oriented and theory-oriented, or in other words, practical and conceptual standpoints.[1,2] Choosing the latter road we showed, in paper III of this series,[3] that thermodynamic properties of the lower members ($N<9$) of alkanes can roughly be classified into a few types depending on their relative magnitudes of the correlation coefficients for the two different topological indices, Z and p_3. The former index Z[4] proposed by one of the present authors well reflect the dynamical topological features, such as rotational degree of freedom, while the latter index p_3,[5] Wiener's polarity number, represents the static topological factors governing the bulkiness of molecules. Boiling point and entropy are the typical quantities which depend largely on Z,[3,6] and density of liquid, refractive index, and some other properties form another type of thermodynamic properties whose topological characteristics are represented well by p_3.

However, it was observed in III that for several properties the correlation pattern fluctuates with the size of molecules. Do not these types of correlation of thermodynamic properties change all the way toward larger molecules? No systematic study for analyzing the size dependency of the structure-activity correlation patterns for alkanes has been reported. Further, correlations among the various topological indices for larger molecules have not yet been systematically analyzed. The purpose of the present paper is to study not only the behaviors of the thermodynamic properties of larger alkanes but also the size dependencies of these correlations and of the various topological indices of the corresponding graphs. The obtained results will be helpful both for further theoretical elucidation and quantitative prediction of the thermodynamic properties of molecular aggregates.

I. Definitions of Various Topological Indices

In this paper, only the topological indices of integer values will be considered. The Z index has been defined by one of the present authors.[4] Wiener's path number, (w), polarity number, (p_3),[5] and Gordon and Scantlebury's p_2[7] have been frequently introduced.[8-10] Besides them some new indices are introduced in this study. The quantity A_3 is the half sum of the cube of matrix A of a graph G. Namely,

$$A_3 = \sum_{i<j} (A^3)_{ij}.$$

The idea of Wiener's polarity number, p_3, can be extended to the definition of p_n as half the number of n in the off-diagonal elements of the distance matrix D of G.[11] However according to our experience, none of p_4, p_5, and p_6 was shown to be more effective than the above topological indices for analyzing the structure-activity relationship for alkanes. Thus in this paper, we will mainly deal with the five integral topological indices, Z, w, p_3, p_2, and A_3.

II. Thermodynamic Properties of Alkanes

In paper III of this series twenty-four different thermodynamic properties of lower members ($N<9$) of alkanes were classified into five types, A, B, C, W, and X, according to the relative magnitudes of the correlation coefficients for Z and p_3 parameters.[3] Namely, Type A properties, such as boiling point, are largely dependent on Z, whereas Type B (density of liquid etc.) and C (molar refraction etc.) properties have large positive and negative correlation with p_3, respectively. The correlation coefficients of Type W properties (critical temperature etc.) for both Z and p_3 are medium in value, and Type X properties such as melting point have really no correlation with either Z or p_3.

In this paper correlation coefficients of entropy (ΔS), heat of formation (ΔH_f), boiling point (bp),

liquid-state density (d), refractive index (n_D), molar refraction (R_m), molar volume (V_m), and free energy of formation (ΔG_f) with the above five indices for nonanes (35 isomers), decanes (75), undecanes (159), and dodecanes (355) were calculated. For critical pressure (p_c), critical temperature (T_c), critical volume (V_c), and critical density (d_c), analysis is not complete, because those data were available only up to decanes even in the up-dated version of the API Report.[12]

The data of the physical properties of isomers through nonane are almost all measured ones. For decane, the data of 42 isomers are the average of the independently calculated values obtained by Zwolinski,[13] Greenshields,[14] and Taylor, Pignocco, and Rossini.[15] By their methods, the calculated values of isomers are fairly in concordant with the measured ones, so that we think those calculated values are reliable. However, almost all the data of undecane and dodecane are calculated ones. Although we are doubtful about the reliability of those data, in order to analyze systematically, the correlation coefficients of twelve physical properties of the isomers of undecane and dodecane with the five indices are also calculated.

III. Liquid-State Density, Refractive Index and Related Properties

Correlation coefficients between each of the four properties (d, n_d, V_m, R_m) and various topological indices (Z, w, p_3, p_2, A_3) for the isomers of nonane, decane, undecane, and dodecane are given in Table 1.

Figure 1 shows the size dependency of the ρ values of d, n_D, V_m, and R_m. Although the majority of the data of undecane and dodecane are those calculated with a large set of structural parameters, the points of undecanes and dodecanes in Fig. 1 smoothly lie on the curves extended from the experimental ones for hexane through nonane. Thus we can conclude that there might be no large difference between the estimated and real values.

For these properties, correlation with Z and p_2 is too poor as compared with the case of smaller ($N<9$) alkanes. Actually liquid-state density and refractive

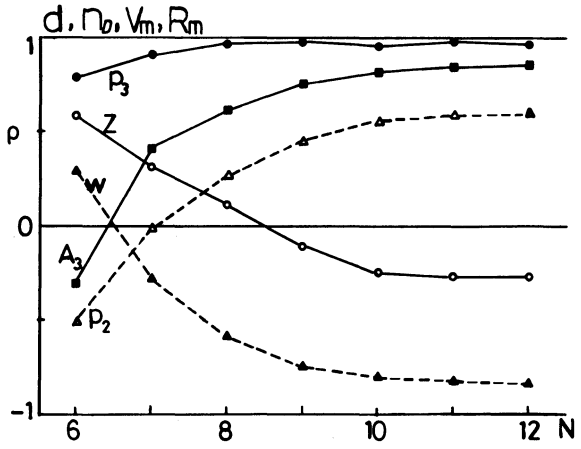

Fig. 1. The size dependency of the ρ values of d against the five topological indices for alkanes. The results for n_D, V_m, and R_m are identical to d.

Table 1. Correlation Coefficients between the Various Topological Indices and Several Thermodynamic Properties Depending Largely on p_3

Topological index	Property	C_9	C_{10}	C_{11}	C_{12}
p_3	d	0.980	0.963	0.978	0.980
	n_D	0.967	0.942	0.949	0.990
	V_m	−0.979	−0.963	−0.979	−0.981
	R_m	−0.986	−0.925	−0.967	−0.980
A_3	d	0.759	0.818	0.844	0.855
	n_D	0.734	0.813	0.837	0.873
	V_m	−0.754	−0.814	−0.842	−0.855
	R_m	−0.721	−0.731	−0.786	−0.828
w	d	−0.742	−0.802	−0.827	−0.834
	n_D	−0.733	−0.779	−0.809	−0.843
	V_m	0.741	0.804	0.831	0.840
	R_m	0.743	0.773	0.802	0.842
p_2	d	0.442	0.554	0.585	0.597
	n_D	0.451	0.563	0.590	0.618
	V_m	−0.436	−0.548	−0.581	−0.596
	R_m	−0.398	−0.455	−0.513	−0.552
Z	d	−0.104	−0.241	−0.263	−0.266
	n_D	−0.113	−0.255	−0.272	−0.269
	V_m	0.097	0.235	0.258	0.266
	R_m	0.069	0.165	0.209	0.236

d: liquid-state density (g ml^{-1}, 25 °C), n_D: refractive index (25 °C), V_m: molar volume (ml mol^{-1}, 25 °C), R_m: molar refraction (25 °C).

index were assigned to belong to B-type, while molar volume and molar refraction to C-type. All these properties have been known to be governed by the static topological features such as bulkiness of molecules.[3] Generally the absolute magnitudes of the $\rho(p_3)$ values for these properties increase quite similarly with the number of carbon atoms. It is surprizing to see that the absolute magnitudes of the linear correlation coefficients between p_3 and the four properties, d, n_D, V_m, and R_m, are all higher than 0.98 for the 355 isomers of dodecane. As seen in Fig. 1 for the size dependency of the $\rho(p_3)$ value for d, the Z index gradually loses its correlation with these Type properties with the increase of the molecular size. On the other hand, the ρ values for w and A_3 dramatically increase with the size of molecules but with opposite signs. The A_3 index was found to show remarkably good correlation with these properties when linearly combined with Z as aA_3+bZ, the ratio of b/a decreasing with the size of molecules. The results are listed in Table 2. It is interesting to see Fig. 2, where two randomly scattered correlation patterns of Z-p_3 and A_3-p_3 are seen to be merged into a fairly good linear plot when they are linearly combined with an appropriate ratio. If one carefully compares the $\rho(p_3)$ and the optimum $\rho(aA_3+bZ)$ values in Tables 1 and 2, no dramatic but fair improvement can be seen. So at this stage no merit is obtained by introducing the A_3 parameter for the QSAR analysis. However, as will be shown later the role of A_3 is highlighted for the correlation of A Type properties such as boiling point.

Table 2. Optimum Combinations of A_3 and Z Indices for Correlating the Four Topological Indices (A_3, w, p_2, Z)

Isomer	Property	Combination	ρ
C_9	d	A_3+0.39Z	*0.984*
	n_D	A_3+0.38Z	0.944
	V_m	A_3+0.38Z	*−0.983*
	R_m	A_3+0.38Z	−0.963
C_{10}	d	A_3+0.23Z	0.961
	n_D	A_3+0.22Z	*0.945*
	V_m	A_3+0.22Z	−0.958
	R_m	A_3+0.25Z	−0.897
C_{11}	d	A_3+0.15Z	*0.981*
	n_D	A_3+0.15Z	*0.964*
	V_m	A_3+0.15Z	*−0.981*
	R_m	A_3+0.16Z	−0.940
C_{12}	d	A_3+0.1Z	*0.983*
	n_D	A_3+0.1Z	*0.996*
	V_m	A_3+0.1Z	*−0.984*
	R_m	A_3+0.1Z	−0.967

The value in italic exceeds the corresponding correlation coefficients of p_3 parameter.

Now, let us take a closer look at the correlation between p_3 parameter and these four properties of B and C types. If we plot the values of d, n_D, V_m, and R_m of each group of isomers against p_3, most points are found to lie closely around a straight line, but a few points deviate from it, as exemplified in Figs. 3(a—d) for undecane isomers. For molar refraction the deviation is not obvious but can be detected from the correlation coefficients. The deviating points (the minority group) are represented with diamond marks.

Table 3. The Structures of Alkane Isomers (N=9—12) Deviating from the V_m-p_3 Plots. The Asterisks for Undecane and Dodecane Indicate that Except for Normal Alkanes the Data are Estimated Values

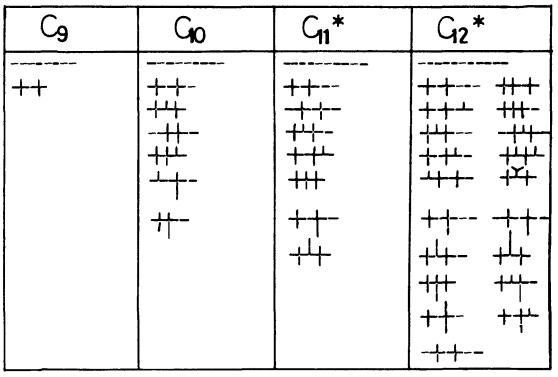

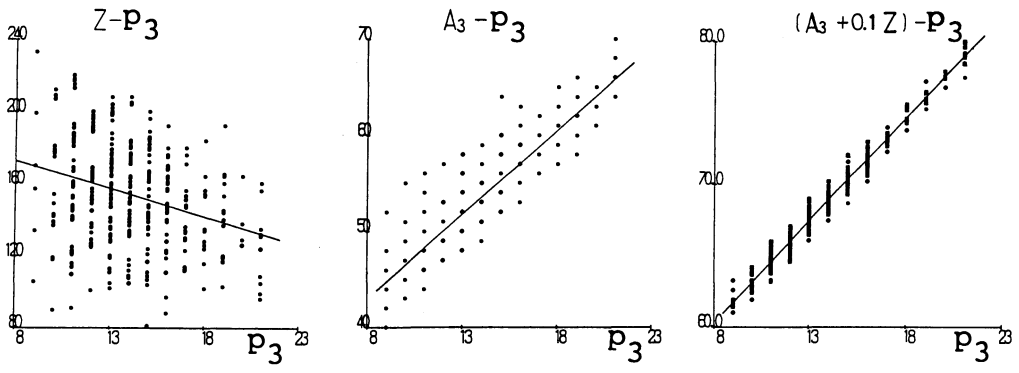

Fig. 2. The plots of Z—p_3, A_3—p_3, and (aA_3+bZ)—p_3, for dodecane isomers.

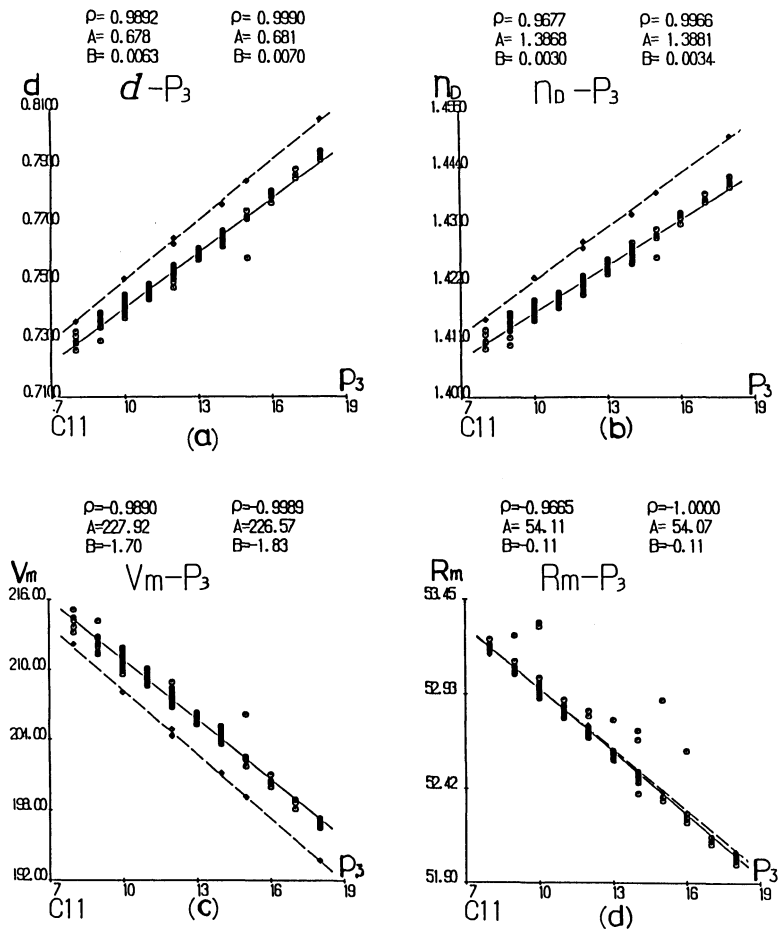

Fig. 3. The plots of d–p_3, n_D–p_3, V_m–p_3, and R_m–p_3 for undecane isomers. The ρ value and the coefficients A and B for $A+Bp_3$ corresponding to the majority and minority groups of undecane are, respectively, given in the top-left and right of each figrue.

The numerical results obtained from separate fittings are also given in the figures. For dodecane isomers quite a similar feature was found. We find that for these properties, except for R_m, all the deviating points correspond to a special group of compounds, whose structures are listed in Table 3.

It is remarkable that all the compounds but normal paraffins in Table 3 contain the common skeleton as ++. Further, among all the 624 alkanes studied, no compound other than those listed in Table 3 contains this skeleton. So we can safely assert that the ++ skeleton in alkanes works to decrease V_m, and increase d and n_D.†

IV. Pentane Effect

In general interactions between nonbonded pairs of alkane molecules in the liquid state are complicated enough to evade rigorous theoretical treatment. To simplify the question, we may consider only the dominant interactions. In calculating the conformational density of states of normal hydrocarbons, Terlin et al.,[16] proposed the so called "pentane effect". Namely, when four consecutive C–C bonds take the gauche–gauche conformation as those in cyclohexane, severe steric hindrance arises between the two methylene groups separated by four C–C bonds.

The measured volume of liquid compounds is interpreted to be composed of two factors. One is the volume which is really occupied by the component atoms, while the other is the spatial cavities, surrounded by either intra- or intermolecular group of atoms. The more efficient the molecules occupy the space, the smaller the cavities become. The skeleton of ++ is considered to decrease the V_m through the following two ways. First, a molecule with ++ skeleton generally tends to take a spherical shape compared to other isomers and is expected to expose

† In Table 3 those undecane and dodecane molecules are marked with asterisks whose thermodynamic properties are estimated. Even by omitting these data the present conclusion will not be changed.

lesser molecular surface than other molecules leading to smaller V_m value. Secondly, this is the most important, large steric hindrance within a molecule with a ++ skeleton causes the effective volume of the molecule to reduce considerably. As early as 1951, Platt[11] pointed out that steric hindrance reduces the effective volume of a molecule. Since under strong steric hindrance atoms are forced to get close to each other, the distance within nonbonding pair of atoms gets smaller than the van der Waals radii. Namely the so-called interpenetration occurs and the effective volume of a molecule is reduced.

Now, we can say without question that although the topological index p_3 is suitable for describing the "bulk" properties, such as liquid-state density molecular volume, and refractive index, etc., it fails in reflecting the effect of the ++ skeleton, or steric hindrance within a molecule.

The fact that normal paraffins belong to the minority group can be explained by the strong intermolecular interaction. Detailed discussion will be give in Section V.

We have attempted to get a single linear correlation for all the isomers. By assigning p_3+2 to the isomers with the ++ skeleton instead of p_3, all the isomers were found to lie on a straight line. The regression equations and correlation coefficients for d are obtained as follows:

For dodecane: $d = 0.68252 + 0.00600p_3'$
$\rho = 0.991$ (355 points)

For undecane: $d = 0.67790 + 0.00630p_3'$
$\rho = 0.990$ (159 points)

For decane : $d = 0.67754 + 0.00608p_3'$
$\rho = 0.973$ (75 points)

where

$$p_3' = \begin{cases} p_3+3 & \text{isomer which has ++ skeleton} \\ p_3 & \text{other} \end{cases}$$

All the correlations are of high quality including n_D and V_m, so that the p_3' index has a predictable power for these properties.

V. Entropy, Boiling Point, and Related Properties

The correlation coefficients between the topological indices and entropy (ΔS), boiling point (bp), heat of formation (ΔH_f), and free energy of formation (ΔG_f) of larger alkanes (N=9—12) are tabulated in Table 4. The size dependencies of these correlations are shown in Fig. 4(a—d).

For ΔS the $|\rho|$ values for Z, w, p_2, and A_3 do not change appreciably from hexanes to dodecanes. The discontinuous change at nonanes can be attributed to 3-methyl-4-ethylhexane, whose point deviates from the majority of their isomers. Although this molecule has no high symmetry, its entropy is extremely small compared with other isomers. So we deem that this data is erroneous. The recalculated ρ values by omitting this point are found to lie on more smoothed curves as marked with an asterisk in Fig. 4(a). Although the ρ value for p_3 gradually increases from hexane (0.1) to dodecane (0.7), one can safely conclude that entropy is governed by the dynamic feature of molecular topology and belongs essentially to A type.

For lower members of alkanes the correlation

Table 4. Correlation Coefficients between the Various Topological Indices and Several Thermodynamic Properties Depending Largely on Z

Topological index	Property	C_9	C_{10}	C_{11}	C_{12}
	bp	0.749	0.542	0.483	0.413
Z	ΔS	0.448	0.789	0.825	0.827
	ΔH_f	0.299	0.019	−0.111	−0.172
	ΔG_f	−0.373	−0.387	−0.425	−0.416
	bp	0.280	0.071	0.060	0.030
w	ΔS	0.674	0.841	0.807	0.778
	ΔH_f	−0.262	−0.503	−0.652	−0.695
	ΔG_f	−0.789	−0.775	−0.808	−0.794
	bp	−0.521	−0.292	−0.208	−0.136
p_2	ΔS	−0.610	−0.894	−0.937	−0.924
	ΔH_f	−0.463	0.212	0.350	0.419
	ΔG_f	0.632	0.603	0.645	0.642
	bp	−0.202	−0.007	0.063	0.137
A_3	ΔS	−0.665	−0.885	−0.914	−0.910
	ΔH_f	−0.088	0.483	0.602	0.657
	ΔG_f	0.801	0.786	0.817	0.814
	bp	0.355	0.407	0.400	0.408
p_3	ΔS	−0.518	−0.636	−0.664	−0.692
	ΔH_f	0.575	0.712	0.784	0.804
	ΔG_f	0.779	0.818	0.843	0.845

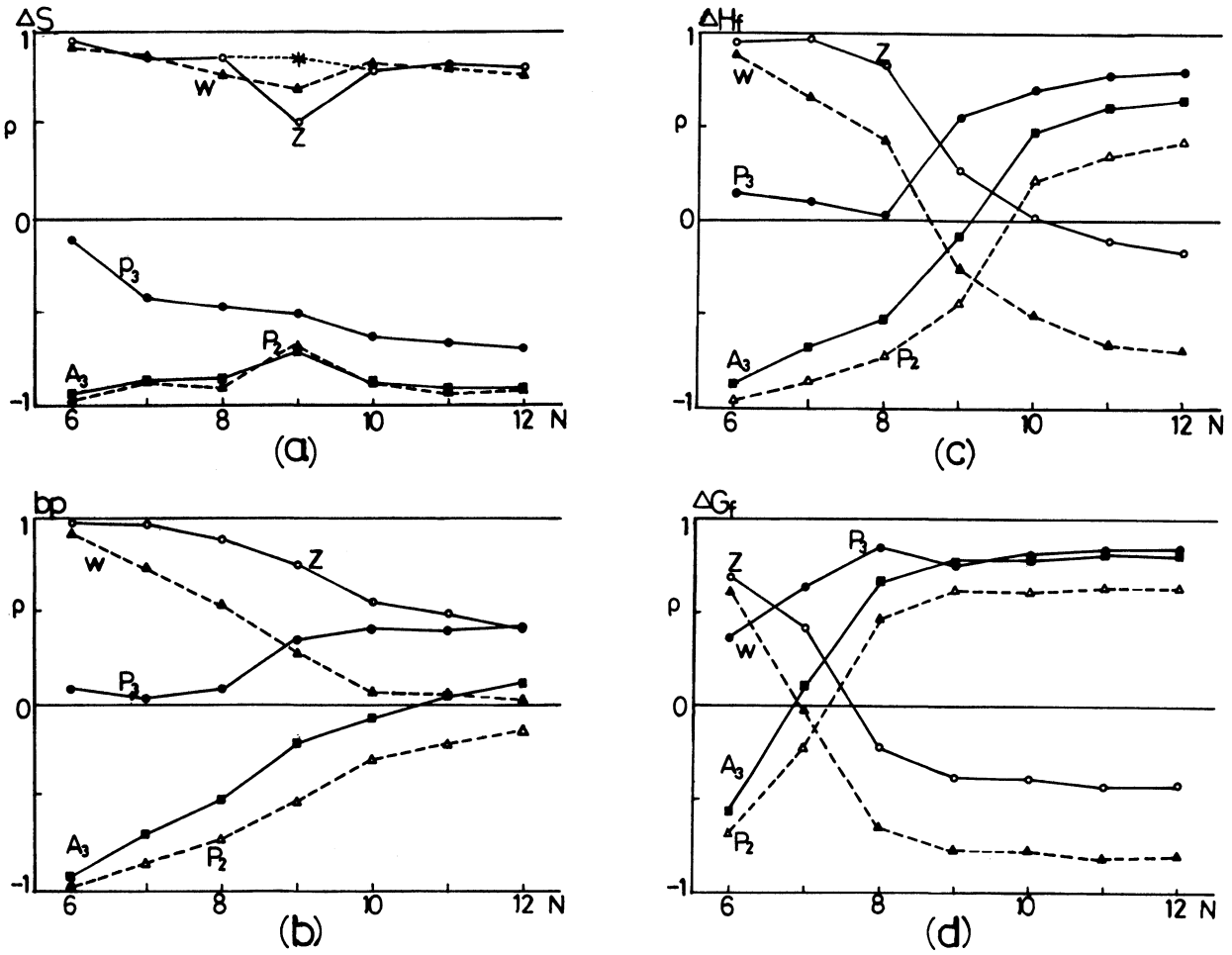

Fig. 4. The size dependency of the ρ values of ΔS, bp, ΔH_f, and ΔG_f against the five topological indices for alkanes. The asterisk for the Z curve in Fig. 4a was calculated by omitting one deviating point. The results for other topological indices are not shown.

pattern of boiling point, one of the typical A type properties, is very similar to that of entropy. However, as the size of molecules gets larger, the $|\rho|$ values of w and A_3 sharply drop down to zero while those of Z and p_2 slowly decrease. On the contrary $\rho(p_3)$ gradually increases but does not reach as high as 0.5. Thus boiling point of alkanes at least up to decane may well be classified into A-type. Although for dodecane isomers Z index still shows the largest $|\rho|$ value among all the indices studied, boiling point turns to belong to W-type, with medium $\rho(Z)$ and $\rho(p_3)$ values. It is to be noted that fairly large ρ value (>0.7) can be obtained by combining the Z and A_3 parameters as aA_3+bZ. (See Table 5 and Fig. 5). The ratio of b/a decreases with the size of molecules, whereas the $|\rho(A_3)|$ value decreases sharply down to zero.

Figure 5 shows that the deviant points correspond to the isomers with short branches. This is also the case with other properties, such as ΔS, ΔH_f, and ΔG_f. We have not found any appropriate topological index

Table 5. Optimum Combinations of A_3 and Z Indices for Boiling Point and Entropy, and Optimum Combination of p_3, p_4, p_5 for Heat and Free Energy of Formation

Isomer	Property	Combination	ρ
C_9	bp	$0.9A_3+Z$	0.886
	ΔS	$A_3+0.05Z$	−0.667
	ΔH_f	p_3+p_4	0.683
	ΔG_f	p_3-7p_5	0.958
C_{10}	bp	$1.8A_3+Z$	0.788
	ΔS	$A_3-0.20Z$	−0.912
	ΔH_f	$p_3-2.5p_5$	0.796
	ΔG_f	$p_3+0.7p_4$	0.763
C_{11}	bp	$2.7A_3+Z$	0.765
	ΔS	$A_3-0.15Z$	−0.945
	ΔH_f	$p_3+1.1p_4$	0.879
	ΔG_f	$p_3-1.2p_5$	0.915
C_{12}	dp	$4.2A_3+Z$	0.718
	ΔS	$A_3-0.10Z$	−0.942
	ΔH_f	$p_3+1.2p_4$	0.895
	ΔG_f	p_3+p_4	0.898

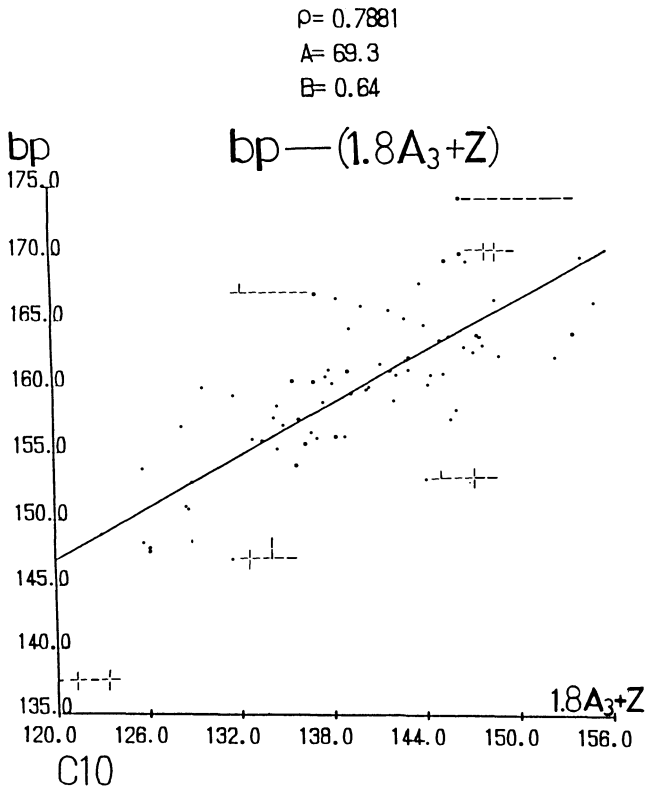

Fig. 5. The plots of bp-(aA_3+bZ) for decane isomers.

to discriminate those short-branched isomers from others. If we can find such a topological index that can effectively characterize those kinds of molecules, all these problem will be solved.

Heat of formation, ΔH_f, for lower members of alkanes also belongs to A-type. The ρ values for the five parameters exhibit "cross-over" patterns as shown in Fig. 4(c). Namely ΔH_f changes its character into B-type above decane.

Free energy of formation, ΔG_f, of W-type, also shows a similar crossover pattern. (See Fig. 4(d)). However, the "transition point" to B-type for ΔG_f is lower than that of ΔH_f but is higher than that of the majority of B-Type properties shown in Fig. 1.

VI. Properties at the Critical Point

The correlation coefficients among the various topological indices for the four properties at the critical point, T_c, p_c, V_c and d_c, of nonane and decane isomers are presented in Table 6. However, data are not available for the higher members of alkanes.

In Fig. 6(a—d) are shown the size dependency of the ρ values of p_c, d_c, V_c, and T_c. Obviously w is the best for the description of d_c, V_c, whereas p_3 is the best for d_c and T_c. However, if they are to be classified, p_c belongs to B-type for all N and the remaining three properties change from W-type to B-type at around heptane and octane.

From the van der Waals equation of state, we get the

Table 6. Correlation Coefficients between the Various Topological Indices and Critical Constants

Topological index	Property	C_9	C_{10}
p_3	d_c	0.921	0.927
	V_c	−0.910	−0.922
	p_c	0.947	0.963
	T_c	0.850	0.848
A_3	d_c	0.871	0.859
	V_c	−0.870	−0.835
	p_c	0.912	0.904
	T_c	0.499	0.630
w	d_c	−0.931	−0.945
	V_c	0.938	0.933
	p_c	−0.881	−0.877
	T_c	−0.415	−0.551
p_2	d_c	0.639	0.641
	V_c	−0.647	−0.608
	p_c	0.680	0.684
	T_c	0.155	0.551
Z	d_c	−0.356	−0.374
	V_c	0.376	0.347
	p_c	−0.376	−0.393
	T_c	0.189	0.165

relations, $p_c=a/(27b^2)$, $T_c=8a/(27Rb)$, $V_c=3b$, giving $a=9RT_cV_c/8$ and $b=V_c/3$. The parameters a and b can be interpreted respectively to reflect the intermolecular interaction and molecular volume.[3] The values of a can be calculated from the data of T_c and V_c, as shown in Table 7 for nonane isomers. From this table, one may notice that those compact molecules with large steric hindrance, such as 2244m-4, 22m3e-4 23m3e-4, 24m3e-4, and 33e-4 (m and e, respectively stand for methyl and ethyl) have rather smaller value of a. Same thing also happens in decane isomers.

The more compact the molecule is, the weaker the molecules interact with each other in the liquid state. Further, it is noticed that the normal paraffin has the largest a value among all the isomers. As has been discussed in Section IV, we can further say that, the intermolecular interaction of molecules with high steric hindrance is weaker than for other molecules. The reason why the volume of those compounds decreases is not because they interact with each other strongly, but just as we discussed in Section IV.

Since "critical state" is a kind of state in which liquid phase and gaseous phase not only coexist, but also have the same density without any phase boundary between them, molecules in this state do not approach each other as in the liquid state. This means that the intermolecular interaction is not so strong that the volume of the bulk is determined mainly by the molecular size, as implied in the relation, $V_c=3b$. As shown in Table 7, each normal paraffin has actually the largest size (or V_c value) of all the isomers.

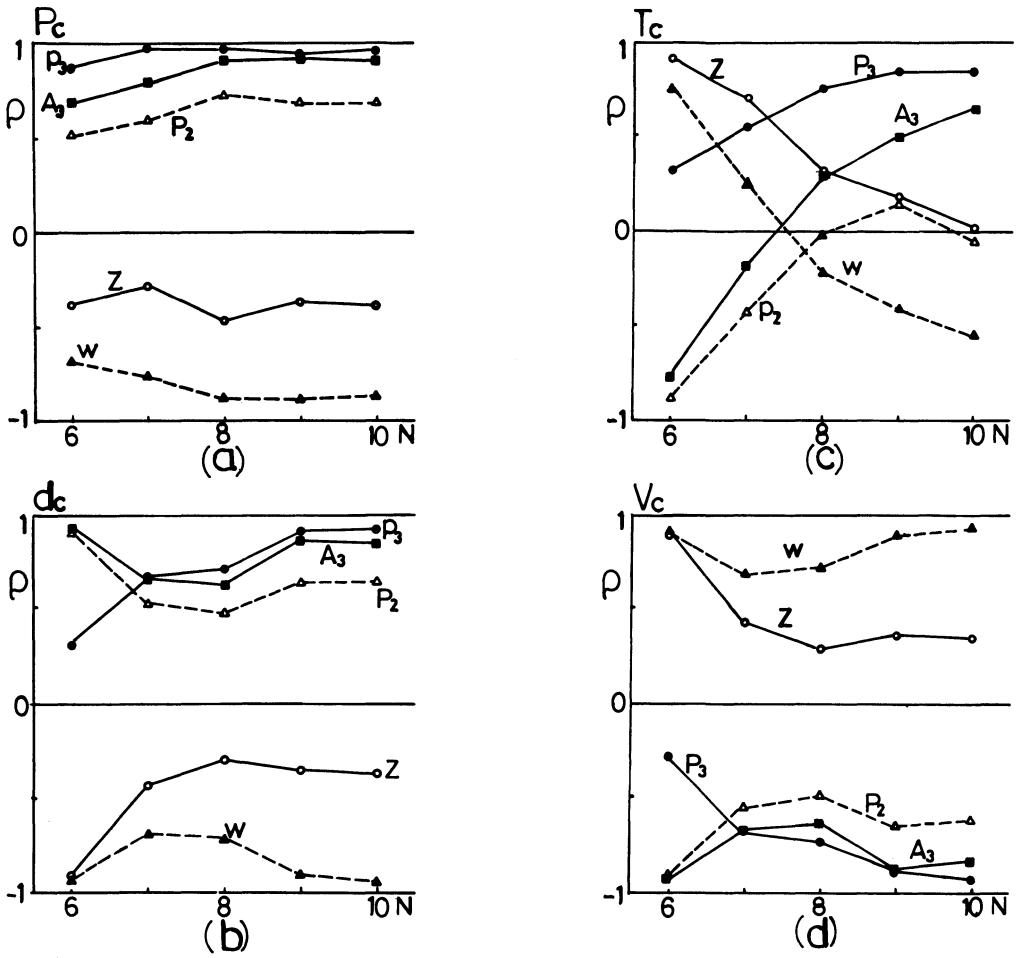

Fig. 6. The size dependency of the ρ values of p_c, d_c, T_c, and V_c against the five topological indices for alkanes.

But, liquid normal paraffin has the smallest volume among all the isomers having the same p_3 value. So it is clear that the decrease in volume of normal paraffins is due to the strong intermolecular interaction as to decrease the holes among molecules.

In liquid state, for alkanes, the most important intermolecular attraction is the London dispersion force, and its energy is proportional to the square of the polarizability and to inverse sixth power of the separation; i.e., $U_{\text{London}} \propto \alpha^2/\gamma^6$. Because of its loose structure, normal paraffin may have the largest polarizability and therefore it has the largest London dispersion force. We suppose this is the reason why the normal paraffins have the strongest intermolecular attraction.

VII. Concluding Remark

The size dependency of the correlations of twelve physical properties and topological types are summarized in Fig. 7. Since type C properties have large negative correlation with p_3, they can essentially be classified into type B. In Fig. 7, slant zebra indicates A-type, whose properties are largely dependent on Z index; stars indicate B-type, whose properties have large positive or negative correlations with p_3 index; checker and dots indicate W-type and X-type, respectively.

As seen from Fig. 7, the fact that entropy belongs essentially to A-type does not change even with the increase of molecular size. Boiling point can be classified into A-type up to decane, but it turns to belong to W-type above undecane. For heat of formation, as the number of cabon atoms in a molecule increases from six to twelve, its character changes from A-type to W-type for octane, and into B-type beyond decane. Liquid-state density, molar volume, refractive index, molar refraction and critical pressure are classified into B-type up to dodecane. Critical temperature, critical volume, and critical density turn to belong to B-type as the molecular size increases. Free energy of formation has almost no linear correlation both with Z and p_3 for lower members of alkanes, but it can be classified into B-type beyond undecane.

In paper III of this series, it has been pointed out that p_3 may be regarded as a kind of topological

Table 7. Critical Volume, Temperature and van der Waals' Constant a of Nonane Isomers

p_3	Compound	V_c	T_c	$8a/(9R)=T_cV_c$
6	n-9	0.548	594.6	325.84
	2m-8	0.541	586.6	317.35
	26m-7	0.535	577.9	309.18
	22m-7	0.526	577.6	303.82
	225m-6	0.519	567.9	294.74
	2244m-5	0.504	574.6	289.60
7	3m-8	0.529	590.0	312.11
	4m-8	0.523	587.6	307.31
	25m-7	0.522	581.1	303.33
	24m-7	0.517	576.8	298.21
	224m-6	0.507	573.5	290.76
8	3e-7	0.511	590.4	301.69
	4e-7	0.505	587.9	296.89
	35m-7	0.510	583.2	297.43
	23m-7	0.515	589.6	303.64
	2m4e-6	0.504	580.0	292.32
	33m-7	0.506	588.4	297.73
	44m-7	0.501	585.4	293.29
	235m-6	0.509	579.2	294.81
	244m-6	0.500	581.5	290.75
9	34m-7	0.503	591.9	297.73
	2m3e-6	0.497	588.1	292.29
	223m-6	0.498	588.0	292.82
10	3m4e-6	0.490	593.7	290.91
	3m3e-6	0.487	597.5	290.98
	234m-6	0.494	594.5	293.68
	24m3e-5	0.489	591.2	289.10
	233m-6	0.491	596.0	292.64
	22m3e-5	0.486	590.4	286.93
	2234m-5	0.490	592.6	290.37
11	334m-6	0.484	602.3	291.51
12	33e-5	0.473	610.0	288.53
	23m3e-5	0.477	606.8	289.44
	2334m-5	0.481	607.5	292.21
	2233m-5	0.478	607.5	292.39

bulkiness factor, or a static topological parameter, and Z may be regarded as a dynamical topological parameter. The present work confirms those inferences about Z and p_3 from the results of larger molecules.

We think p_3 is not a good parameter in reflecting the steric hindrance and complex interactions, and this conclusion is contrary to the results by some other authors.[11,17]

Boiling point, which is determined by the dynamical balance between the motion and interaction of molecules, has the best correlation with Z. This conclusion agrees with paper III. But for larger molecules, the correlation of Z with bp is not as good as that for smaller molecules. From Section V, it is revealed that the optimum linear combination among topological indices for bp is aA_3+bZ, and we have envisaged in Section III that aA_3+bZ has a certain

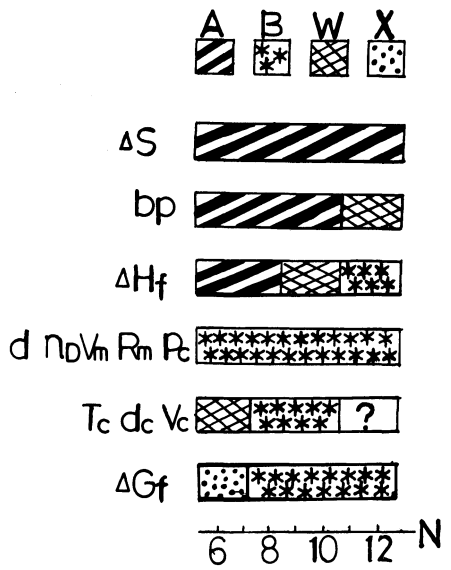

Fig. 7. Diagram showing the size dependency of the correlation types of physical properties and molecular topology for alkanes.

property close to p_3. Thus we may consider bp is also affected by bulkiness properties, and as the number of carbon atoms increases, the bulkiness properties become dominant. This is also the case with ΔH_f and ΔG_f.

The property of the parameter, A_3 is interesting, because when it is properly combined with Z, it will reflect various physical properties, whereas it has almost no correlation with any property by itself. It awaits further analysis.

References

1) R. Cramer, III, *J. Am. Chem. Soc.*, **102**, 1837, 1849 (1980).
2) M. Randić and C. L. Wilkins, *J. Phys. Chem.*, **83**, 1525 (1979).
3) Part III. H. Narumi and H. Hosoya, *Bull. Chem. Soc. Jpn.*, **58**, 1778 (1985).
4) H. Hosoya, *Bull. Chem. Soc. Jpn.*, **44**, 2332 (1971).
5) H. Wiener, *J. Am. Chem. Soc.*, **69**, 17, 2636 (1947); *J. Phys. Chem.*, **52**, 425, 1082 (1948).
6) H. Hosoya, K. Kawasaki, and K. Mizutani, *Bull. Chem. Soc. Jpn.*, **45**, 3415 (1972).
7) M. Gordon and G. R. Scantlebury, *Trans. Faraday Soc.*, **60**, 604 (1964).
8) L. B. Kier and L. H. Hall, "Molecular Connectivity in Chemistry and Drug Design," Academic Press, New York (1976).
9) A. T. Balaban, I. Motoc, C. Bonchev, and O. Mekenyan, *Topics in Current Chemistry*, **114**, 21 (1983).
10) N. Trinajstić, "Chemical Graph Theoty," CRC Press, Boca Raton, Florida (1983), Vol. II, p. 105.
11) J. R. Platt, *J. Phys. Chem.*, **56**, 328 (1952).
12) American Petroleum Institute Research Project 44 at the National Bureau of Standards, "Selected Values of Physical and Thermodynamic Properties of Hydrocarbons,"

Texas A & M Univ., 1945.
13) B. J. Zwolinski, *J. Res. Natl. Bur. Std.*, **38**, 365 (1947).
14) J. B. Greenshields and F. D. Rossini, *J. Phys. Chem.*, **62**, 271 (1958).
15) W. J. Taylor, J. M. Pignocco, and F. D. Rossini, *J. Res. Natl. Bur. Std.*, **34**, 413, (1945).
16) P. Terlin, F. P. Jones, S. Lafleur and L. E. H. Trainor, *J. Chem. Phys.*, **85**, 4052 (1986).
17) A. T. Balaban, *Theoret. Chim. Acta (Berl.).*, **53**, 355 (1979).

 © 1988 The Chemical Society of Japan Bull. Chem. Soc. Jpn., 61, 3103—3114 (1988)

Electrode Kinetics of Metal Complexes Confined in Perfluoro Polycarboxylate and Polysulfonate Coatings on Graphite Electrodes

Noboru OYAMA,* Takeo OHSAKA, Tooru USHIROGOUCHI, Sachiko SANPEI,† and Sadako NAKAMURA†

Department of Applied Chemistry for Resources, Tokyo University of Agriculture and Technology, Koganei, Tokyo 184

†Department of Chemistry, Japan Women's University, Mejirodai, Bunkyo-ku, Tokyo 112

(Received December 2, 1987)

A heterogeneous electron-transfer process of $[Os(bpy)_3]^{2+/3+}$ (bpy: 2,2′-bipyridine) and [(trimethylammonio)methyl]ferrocene/ferricinium ($TAF^{+/2+}$) redox couples, which were confined in perfluoro polycarboxylate and polysulfonate polyelectrolyte coatings on graphite electrodes, at the electrode/film interfaces as well as a homogeneous charge-transport process within the coating films were examined by means of potential-step chronoamperometry and chronocoulometry, normal pulse voltammetry and ac impedance measurements. The relevant kinetic parameters (i.e., the standard rate constant k° and the transfer coefficient of the heterogeneous electron-transfer process and the apparent diffusion coefficient D_{app} for the homogeneous charge-transport process) were determined at various concentrations of the redox species in the films at various pH's. The temperature dependences of D_{app}, k° and the formal potentials of the $[Os(bpy)_3]^{2+/3+}$ and $TAF^{+/2+}$ couples confined in the films were also examined and the relevant activation parameters for the heterogeneous electron-transfer and homogeneous charge-transport processes and the reaction entropies of these redox couples were evaluated. On the basis of the kinetic and thermodynamic data obtained, the mechanism of the charge-transport process within the films, the effects of polymer domain and pH on the rates of the heterogeneous electron-transfer and homogeneous charge-transport processes and on the incorporation of the redox species into the films, etc. are discussed.

Recently, much attention has been denoted to the electron-transfer processes at electroactive, thin polymer film-coated electrodes from the viewpoint of the fundamental studies on the mechanism and kinetics of electron transfer as well as the possible applications based on their interesting properties (e.g., electron-transfer catalysis (and mediation), redox conductivity and electrochromic property).[1] We have also been interested in this problem and have continued to conduct the kinetic and thermodynamic study of (i) the heterogeneous electron-transfer process between electrode and redox species (or sites) confined in polymeric domains and (ii) the homogeneous charge-transport process within polymer coatings for various types of redox polymer-coated electrode systems.[2-14] They involve (1) multiply-charged anionic metal complexes-electroinactive cationic polyelectrolyte film systems[2,4,7,8,11,13] (e.g., $[Mo(CN)_8]^{4-/3-}$, $[Fe(CN)_6]^{4-/3-}$ $[W(CN)_8]^{4-/3-}$ and $[IrCl_6]^{3-/2-}$-protonated poly(4-vinylpyridine) (PVP) systems and $[Fe(CN)_6]^{4-/3-}$, $[Mo(CN)_8]^{4-/3-}$, $[Fe(bp)_3]^{4-/3-}$ (bp: bathophenanthroline disulfonato) and $[W(CN)_8]^{4-/3-}$-electropolymerized poly(*N*,*N*-dialkylaniline) film systems), (2) polymer ligand-containing metal complex systems[2] (e.g., $[Fe(CN)_5]^{3-/2-}$-PVP system), (3) viologen polymer film systems[5,6,9] (e.g., *N*,*N*′-dimethyl-4,4′-bipyridinium-Nafion system, poly(xylylviologen) (PXV)-poly(*p*-styrenesulfonate) (PSS) system, poly(styrene-*co*-chloromethylstyrene) pendant viologen (PMV) film systems, and PMV-Nafion and -PSS systems) and (4) electropolymerized electroactive film systems[10,12,14] (e.g., poly(1-pyrenamine) and poly(*o*-phenylenediamine) film systems).

In the present report, we will describe the kinetic study concerning the electrode reactions ((i) and (ii)) of cationic redox couples (i.e., $[Os(bpy)_3]^{2+/3+}$ (bpy: 2,2′-bipyridine) and [(trimethylammonio)methyl] ferrocene/ferricinium ($TAF^{+/2+}$))-containing perfluoro polycarboxylate and polysulfonate polyelectrolyte coatings (Fig. 1) on graphite electrodes by means of potential-step chronoamperometry and chronocoulometry, normal pulse voltammetry and ac impedance measurements. Previously, Bard et al.[15] have examined the mechanism of charge transport through Nafion polymers (coated on glassy carbon electrodes)

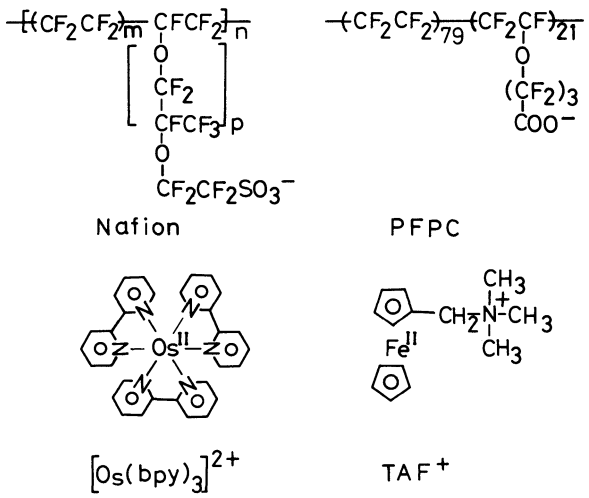

Fig. 1. Structures of the perfluoro polycarboxylate (PFPC) and polysulfonate (Nafion) polyelectrolytes, $[Os(bpy)_3]^{2+}$ and [(trimethylammonio)methyl]ferrocene (TAF^+) used in this study.

containing some redox species such as $[Os(bpy)_3]^{2+}$ and TAF^+ on the basis of the estimation of the apparent diffusion coefficient (D_{app}) for the charge-transport process within the films containing these redox species and the diffusion coefficients of actual mass transport of the same redox species through the polymer. Also, Anson et al.[16] have reported the shifts in formal redox potentials accompanying the incorporation of cationic complexes (including $[Os(bpy)_3]^{2+}$ and TAF^+) in perfluoro polycarboxylate and polysulfonate coatings on graphite electrodes. Our aim is to elucidate and understand the effect of polymer domain on the rates of both heterogeneous electron-transfer process and homogeneous charge-transport process and the dependences of the standard rate constant (k°) for the former process and the apparent diffusion coefficient (D_{app}) for the latter process upon concentration of redox species confined in the polymeric coatings. The temperature dependences of the formal redox potentials of the $[Os(bpy)_3]^{2+/3+}$ and $TAF^{+/2+}$ couples confined in the coatings, k° and D_{app} will be also examined in order to gain an additional insight into some possible factors controlling the rates of the heterogeneous electron-transfer and homogeneous charge-transport processes.

Experimental

Materials. Nafion membrane 125®, which is a perfluoro polysulfonate polyelectrolyte membrane, was obtained from E.I. du Pont de Nemours and Company (Wilmington, Delaware). According to a previous procedure,[5,6,17] the stock solution of Nafion was prepared from the membrane in order to facilitate the electrode coating. Then, an ethanol-dimethyl sulfoxide (EtOH-DMSO) mixture (50:50 volume percent) was used as a solvent and the concentration of Nafion was 3.6 mg ml^{-1}. Nafion coating films were prepared by evaporation of aliquots of the stock solution put on electrode surfaces. Perfluoro polycarboxylate polyelectrolyte (abbreviated as PFPC in this paper and shown in Fig. 1 together with Nafion) was obtained in the form of a fine suspension of the methyl ester from Asahi Glass Company (Tokyo). The suspension (15 mg) was dissolved in EtOH-DMSO (50:50 volume percent) mixture solution. The concentration of the prepared stock solution of PFPC (as the methyl ester form) was 3.6 mg ml^{-1}. To prepare the coating films on electrodes, aliquots (1—10 μl) of the stock solution were evaporated on freshly cleaved electrodes. The resulting deposite was exposed to 1 M (1 M=1 mol dm^{-3}) NaOH solution for 5 min to hydrolyze the ester to the carboxylate, and the electrode was then washed thoroughly with water. From the measurement of IR spectra of the PFPC film deposited on a glass slide, which was treated as mentioned above, it was confirmed that the extent of the hydrolysis under such a treatment is almost 100%.

$[Os(bpy)_3](ClO_4)_2$ (bpy: 2,2′-bipyridine) was synthesized according to the standard procedure.[18] [(Trimethylammonio)methyl] ferrocene bromide (abbreviated as TAF^+Br^-, see Fig. 1) was reagent grade (Tokyo Kasei Co.) and was used as received. The basal-plane pyrolytic graphite (BPG) (Union Carbide Co.) disk electrodes (area: 0.17 cm^2) were prepared and mounted into glass tube with heat-shrinkable polyolefin tube as previously described.[19] Aqueous solutions were prepared from doubly distilled water. The supporting electrolyte solution was 0.2 M CF_3COONa (Aldrich) adjust to pH 1.0, 2.0, and 3.0 with CF_3COOH and to pH 4.0 and 5.5 with 0.1 M CH_3COONa-CH_3COOH. Other chemicals were reagent grade and were used as received.

Apparatus and Procedures. A standard three-electrode electrochemical cell was used for all electrochemical experiments. The electrode assembly consisted of a film-coated BPG electrode as working electrode, a sodium chloride saturated calomel electrode (SSCE) as reference electrode and a spiral platinum as counter electrode. For cyclic voltammetry, potential-step chronoamperometry (and chronocoulometry), and normal pulse voltammetry, a home-made instrument was employed along with an X-Y recorder and a Nicolet digital oscilloscope (model 309).[2-14] Positive feed-back circuitry was employed to compensate the resistances (these were typically ca. 20—50 Ω) associated with the polymer coatings as much as possible. Potential-step chronoamperometric (and chronocoulometric) data (i.e., current-time and charge-time responses) were stored in the digital oscilloscope and then transferred via an interface (NEC, RSC-232C) to a microcomputer (NEC, PC-9801E) where an analysis of the data was performed. In normal pulse voltammetric experiments, the pulse width of 10—100 ms and the interval of 30—120 s between successive pulses were employed. Thus it can be safely considered that the depletion layer of reactants produced during the preceding pulse completely disappears before the following pulse starts. Normal pulse voltammetric measurements were confined to times (typically 1—10 ms) sufficiently short to ensure that semi-infinite linear diffusion prevailed. The ac impedance measurements were performed with a Frequency Response Analyzer (Solartron Model 1250) and a Potentiostat/Galvanostat 2000 (Toho Technical Research, Tokyo) as previously described.[7]

The Nafion or PFPC film-coated electrodes were soaked in 0.1—5.0 mM solutions (pH 1.0) (containing 0.2 M CF_3COONa) of metal complexes for 1—30 min in order to achieve the incorporation of desired quantities of metal complexes into the films. After that, the electrodes were replaced in a pure supporting electrolytic solution (0.2 M CF_3COONa, pH 1.0) and then the cyclic voltammograms were recorded. After the steady-state cyclic voltammograms were obtained, the quantity (Γ_p) of metal complexes incorporated into the films deposited on electrodes was estimated (in mol cm^{-2}) by measuring the charge required in a potential-step experiment to quantitatively oxidize or reduce the metal complexes and/or measuring the area of cyclic voltammograms (for the oxidation-reduction reactions of the incorporated metal complexes) obtained at slow potential scan rates. The Γ_p values estimated by the two procedures were the same within experimental error. The molar concentrations (C_p^0 in mol cm^{-3}) of the incorporated metal complexes were calculated from the Γ_p's thus obtained by using the thicknesses of the films which were estimated from their densities (mentioned below) under swelling state.

The film thicknesses under the "swelling" state were measured with a Surfcom 550 A (Surface Texture Measuring Instrument, Tokyo Seimitsu Co.). In this case, the samples

of wet Nafion films (thicknesses>2×10^{-5} cm) were produced by soaking the Pt-sputtered dry Nafion films coated on electrodes (the thickness of the Pt film coated<1×10^{-6} cm) in 0.2 M CF_3COONa solution (pH 1.0) for several hours and sorbing the water on the film surface by filter paper. The weight of the wet Nafion films (without Pt-sputtered films) coated on electrodes was also measured. The results indicated that the density of the wet Nafion film is 2.0 ± 0.3 g cm^{-3}, which is in good agreement with the previously reported value.[17,20] The wet thicknesses of the Nafion films incorporating various concentrations of the $[Os(bpy)_3]^{2+}$ (or TAF^+) complex were independent of the concentration of the incorporated $[Os(bpy)_3]^{2+}$ (or TAF^+) and were almost equal to those obtained for the swollen Nafion films containing no $[Os(bpy)_3]^{2+}$ (or TAF^+). With the PFPC film, at first by soaking the PFPC film-coated electrodes in 1 M NaOH for several tens of minutes for the hydrolysis of the methyl ester in the films and then by following the procedure similar to that used in the estimation of the densities of the swollen Nafion films, the density of the wet PFPC film was estimated to be 2.0 ± 0.4 g cm^{-3}, being independent of the incorporation of $[Os(bpy)_3]^{2+}$ (or TAF^+).

The experiments concerning temperature dependences of the formal potentials ($E^{0\prime}$), the apparent diffusion coefficients (D_{app}) for the diffusion-like charge-transport process within the films and the standard rate constant (k°) of the heterogeneous electron-transfer reaction at the electrode/film interfaces were carried out in a "non-isothermal electrochemical cell"[21-24] having a thermally jacketed compartment for the working and counter electrodes and a separate compartment for the reference electrode which was connected to the cell with a 3 M NH_4Cl salt bridge. The reference electrode was maintained at a fixed temperature (25 ± 0.2 °C). The temperature of the cell was varied in the range of 5—45 °C. The values of $E^{0\prime}$ were estimated as the average of the anodic and cathodic peak potentials of the cyclic voltammograms. The analysis of the data obtained was made according to the references[21-28] where the principles and assumption[21-24] involved in the use of such cells have been examined in detail and several recent experimental examples of their successful applications are available.[25-28]

Nitrogen gas was passed through the solutions to remove the dissolved oxygen before the experiments and over the solution during the experiments. Potentials were measured and are reported with respect to an SSCE. Experiments were conducted at ambient laboratory temperature (25 ± 1 °C), except for those concerning the temperature dependences of $E^{0\prime}$, D_{app}, and k°.

Results

Potential-Step Chronoamperometry and Chronocoulometry. Figure 2 shows the typical cyclic voltammograms for the $TAF^{+/2+}$ (or $[Os(bpy)_3]^{2+/3+}$) couple confined in the PFPC film on BPG electrodes in 0.2 M CF_3COONa solution (pH 5.5). The wave

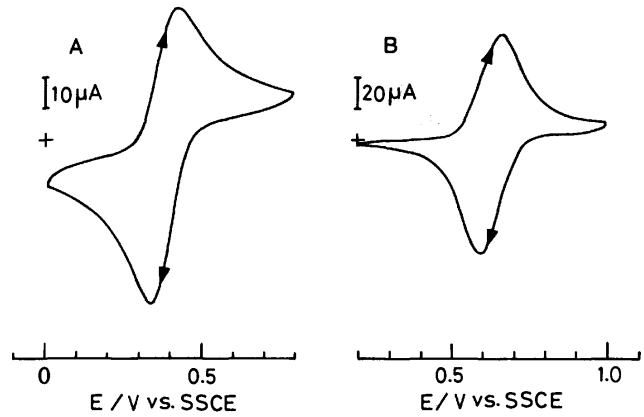

Fig. 2. Typical cyclic voltammograms for the redox reactions of (A) $TAF^{+/2+}$ and (B) $[Os(bpy)_3]^{2+/3+}$ couples confined in the PFPC films on BPG electrodes in 0.2 M CF_3COONa solution (pH 5.5) containing 0.1 M CH_3COONa/CH_3COOH buffer. Concentrations of redox species in the PFPC films (thickness: 2.1×10^{-5} cm): (A) 1.9×10^{-4} and (B) 2.3×10^{-4} mol cm^{-3}. Scan rate: 200 mV s^{-1}.

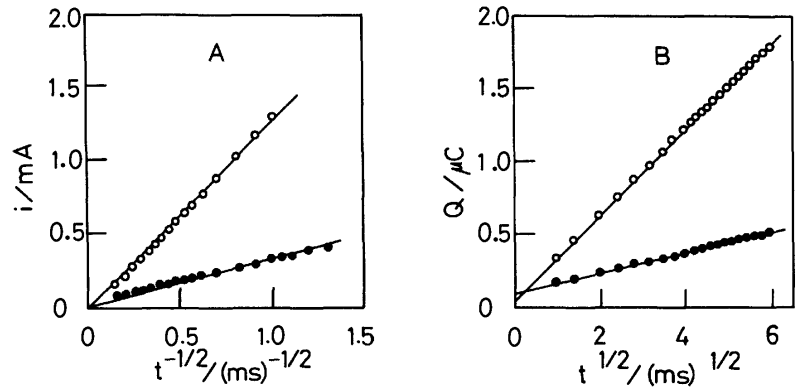

Fig. 3. Typical examples of the potential-step chronoamperometric and chronocoulometric Cottrell plots of (A) i vs. $t^{-1/2}$ and (B) Q vs. $t^{1/2}$ for the oxidation of the TAF^+ (●) and $[Os(bpy)_3]^{2+}$ (○) complexes confined in the PFPC film on BPG electrodes. Other experimental conditions are the same as in Fig. 2.

shapes are similar to those for the solution-phase $TAF^{+/2+}$ (or $[Os(bpy)_3]^{2+/3+}$) couple at a bare electrode, that is, the waves are diffusion-like, with broad peaks and diffusion tails. Typical examples of the potential-step chronoamperometric and chronocoulometric responses for the oxidation of the TAF^+ (or $[Os(bpy)_3]^{2+}$) complex confined in the PFPC film are shown in Fig. 3. These i vs. $t^{-1/2}$ and Q vs. $t^{1/2}$ plots (i: current Q: charge, t: time) are linear, indicating that the charge-transport processes within the films follow the Fick's diffusion laws.[2-14] Thus, the slopes of these plots yielded the values of the apparent diffusion coefficients (D_{app}) for the diffusional charge transport. The D_{app} values obtained from these both plots were almost the same. The linear i vs. $t^{-1/2}$ and Q vs. $t^{1/2}$ plots were also obtained at various concentrations of the $[Os(bpy)_3]^{2+}$ (or TAF^+) complex confined in the PFPC and Nafion films on electrodes in supporting electrolytic solutions of various pH's, and thus the relevant D_{app}'s were estimated from the slopes of these plots. The obtained data are summarized in Fig. 4.

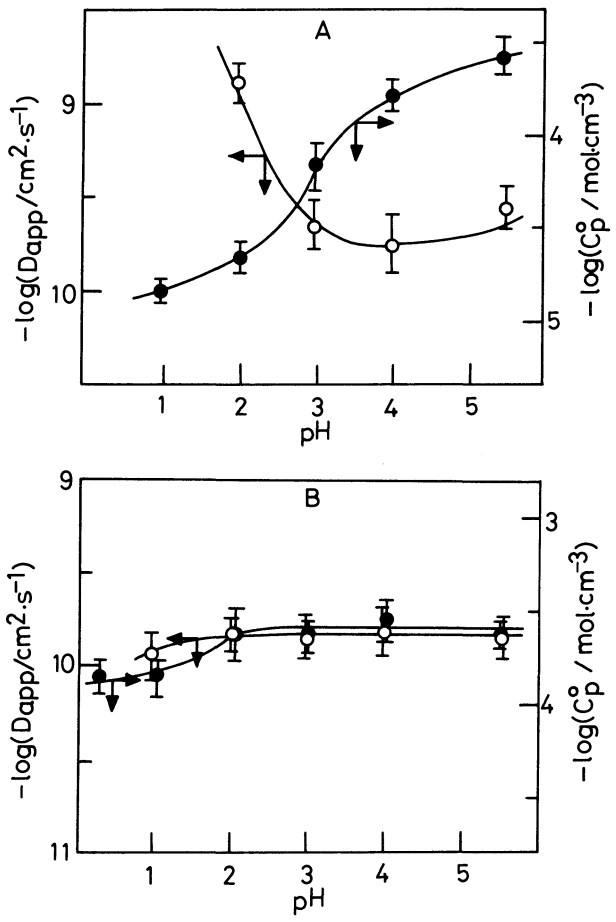

Fig. 4. pH dependences of C_p^0 and D_{app} for (A) $[Os(bpy)_3]^{2+}$-PFPC and (B) TAF^+-PFPC systems. The amount of the PFPC coatings: 4.2×10^{-5} g cm^{-2}. Supporting electrolyte: 0.2 M CF_3COONa. The values of D_{app} were estimated by potential-step chronoamperometry and chronocoulometry.

The D_{app}'s were found to depend on the incorporated redox species, their concentrations (C_p^0), the polymer films incorporating them, and the pH value of a solution.

Normal Pulse Voltammetry. Figure 5 shows the typical normal pulse voltammograms for the oxidation of the $[Os(bpy)_3]^{2+}$ (or TAF^+) complex confined in Nafion films on BPG electrodes in 0.2 M CF_3COONa solution (pH 5.5) at various sampling times (τ). These S-shaped waves are similar to those obtained for solution-phase redox species at an uncoated electrode[29,30] as well as for other redox compounds incorporated electrostatically into (or bound covalently to) polymer films on electrodes.[2-6,8-14] The half-wave potentials of the voltammograms shifted to more positive values with decreasing τ. Plots of the anodic limiting current (i_{lim}) of these

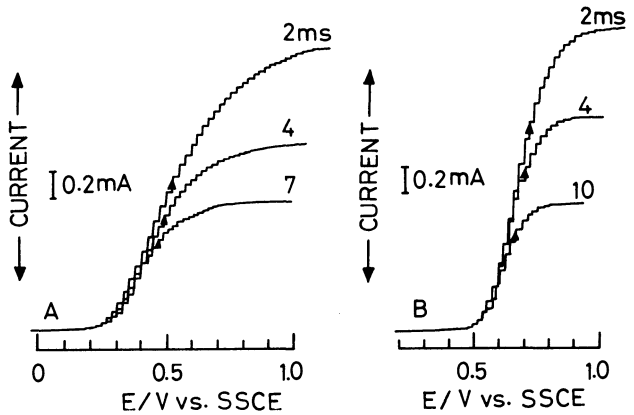

Fig. 5. Typical normal pulse voltammograms for the oxidation of (A) TAF^+ and (B) $[Os(bpy)_3]^{2+}$ complexes confined in the Nafion films on BPG electrodes at various sampling times. Concentration of SO_3^- group in Nafion films: 1.65×10^{-3} mol cm^{-3}. Film thickness: 4.3×10^{-5} cm. C_p^0: (A) 4.6×10^{-4}, (B) 3.2×10^{-4} mol cm^{-3}. Supporting electrolyte: 0.2 M CF_3COONa+0.1 M CH_3COONa/CH_3COOH (pH 5.5). Sampling times (ms) are given on each voltammogram.

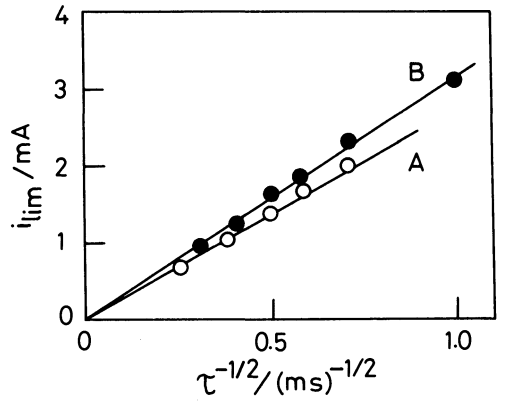

Fig. 6. Typical normal pulse voltammetric Cottrell plots of limiting current i_{lim} vs. $\tau^{-1/2}$ for the oxidation of (A) TAF^+ and (B) $[Os(bpy)_3]^{2+}$ confined in the Nafion film on BPG electrodes. Experimental conditions are the same as in Fig. 5.

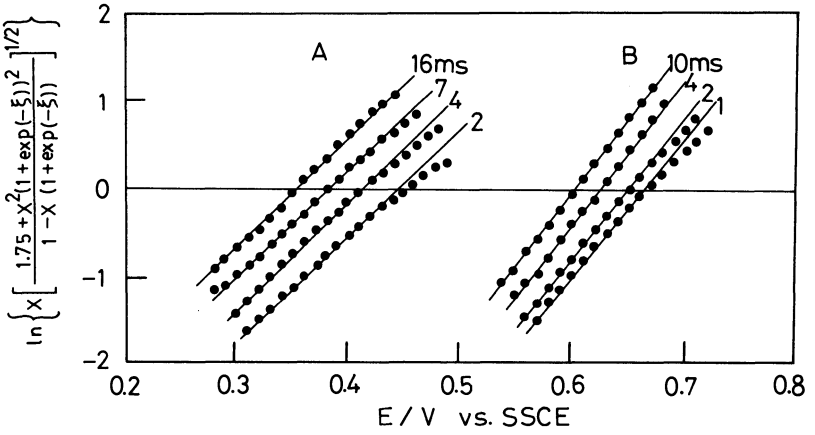

Fig. 7. Modified log plots of normal pulse voltammograms for the oxidation of (A) TFA^+ and (B) $[Os(bpy)_3]^{2+}$ complexes confined in the Nafion film. Sampling times (ms) are indicated on each straight line. other experimental conditions are the same as in Fig. 5.

normal pulse voltammograms against the inverse square root of τ were found to be linear as expected for a diffusion-controlled limiting current (Fig. 6).[2-6,8-14] Thus, the values of D_{app} were estimated from the slopes of the i_{lim} vs. $\tau^{-1/2}$ plots according to the normal pulse voltammetric Cottrell equation.[2-6,8-14,31] Further, the kinetic parameters (i.e., standard rate constant (k°) and transfer coefficient (α)) of the heterogeneous electron-transfer reaction at the electrode/film interfaces could be estimated from an analysis of the rising part of the current-potential curves shown in Fig. 5, as described previously.[2-6,8-14,29-31] The modified log plots for the normal pulse voltammograms of $\ln(x[\{1.75+x^2(1+\exp(-\xi))^2\}/\{1-x(1+\exp(-\xi))\}]^{1/2})$ vs. E were found to be linear (Fig. 7) and the slopes of the straight lines were constant at the different τ's in respective systems, where x is the ratio of the current at potential E to the anodic limiting diffusion current ($(i_d)_{Cott}$) expressed by the Cottrell equation and ξ is the dimensionless parameter expressed as $\{(nF/RT)(E-E^1_{1/2})\}$ ($E^1_{1/2}$: the reversible half-wave potential, n: the number of electrons involved in the heterogeneous electron-transfer reaction, F: the Faraday constant, R: the gas constant, T: the absolute temperature). Thus, according to the previously described procedures,[2-6,8-14,29-31] from the slopes of the straight lines and the intercepts of these lines with the axis, the values of k° and α were estimated. The values thus obtained of D_{app}, k°, and α are summarized in Fig. 9, together with those obtained by potential-step chronoamperometry (and chronocoulometry) and ac impedance measurements.

Alternating Current Impedance Measurements. In Fig. 8 are shown typical Cole-Cole plots (i.e., plots of the quadrature component of the ac impedance vs. its real component) for the redox reaction of the $[Os(bpy)_3]^{2+/3+}$ and $TAF^{+/2+}$ couples confined in the

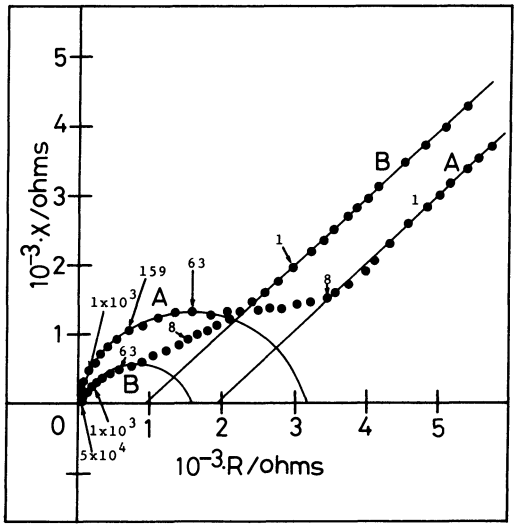

Fig. 8. Typical Cole-Cole plots for the redox reactions of (A) $TAF^{+/2+}$ and (B) $[Os(bpy)_3]^{2+/3+}$ couples confined in the PFPC film on BPG electrodes in a 0.2 M CF_3COONa solution (pH 5.5) containing 0.1 M CH_3COONa/CH_3COOH buffer. In both cases, the thicknesses of the PFPC films were 2.1×10^{-5} cm. C^0_P: (A) 2.9×10^{-5}, (B) 1.7×10^{-4} mol cm^{-3}. The dc potentials were set at (A) 0.328 and (B) 0.586 V vs. SSCE which are formal redox potentials in cases A and B, respectively. The amplitude of an imposed ac voltage was 5.0 mV. X and R show the quadrature and real components of the ac impedance, respectively. The numbers on each plot represent frequency in units of Hz.

PFPC films on BPG electrodes in a 0.2 M CF_3COONa solution (pH 5.5). The data in Fig. 8 show the complex plane impedance plots for the redox reactions of these couples at each formal redox potential. These plots are considered to consist of the semicircular part and the straight line which corresponds to the Warburg diffusional impedance.[32,34] It can be thus seen that the impedance loci of these

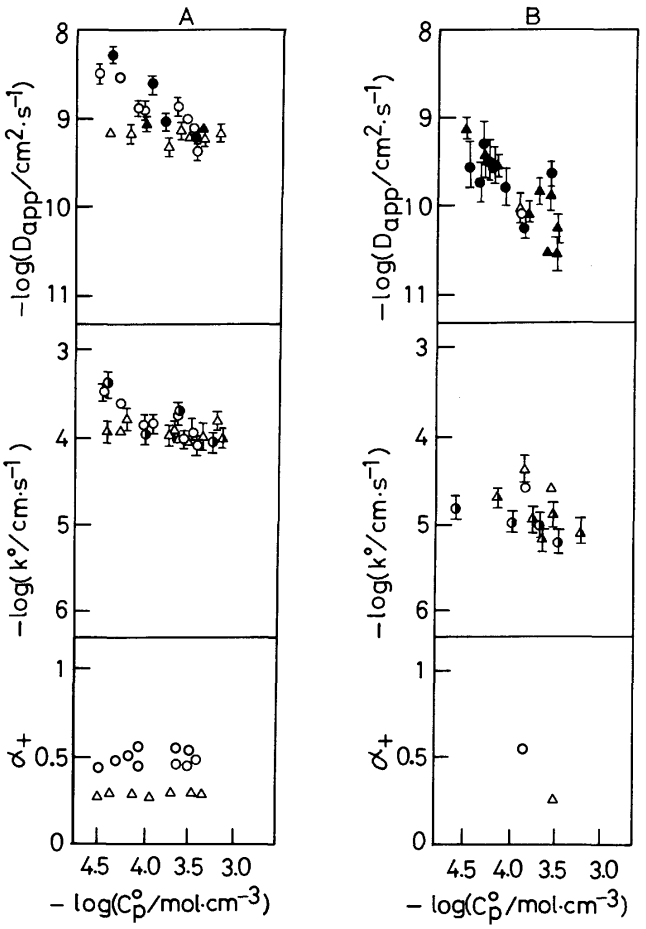

Fig. 9. Dependences of D_{app}, k°, and α_+ on C_p^0. Coating films: (A) Nafion (Thickness: 4.3×10^{-5} cm). (B) PFPC (Thickness: 2.1×10^{-5} cm). Supporting electrolyte: 0.2 M CF_3COONa+0.1 M CH_3COONa/CH_3COOH (pH 5.5). (●,◑,○): $[Os(bpy)_3]^{2+}$, (▲,▲,△): TAF^+. Methods used for the measurements: (●,▲) potential-step chronoamperometry and chronocoulometry; (◑,▲) ac impedance method; (○,△) normal pulse voltammetry.

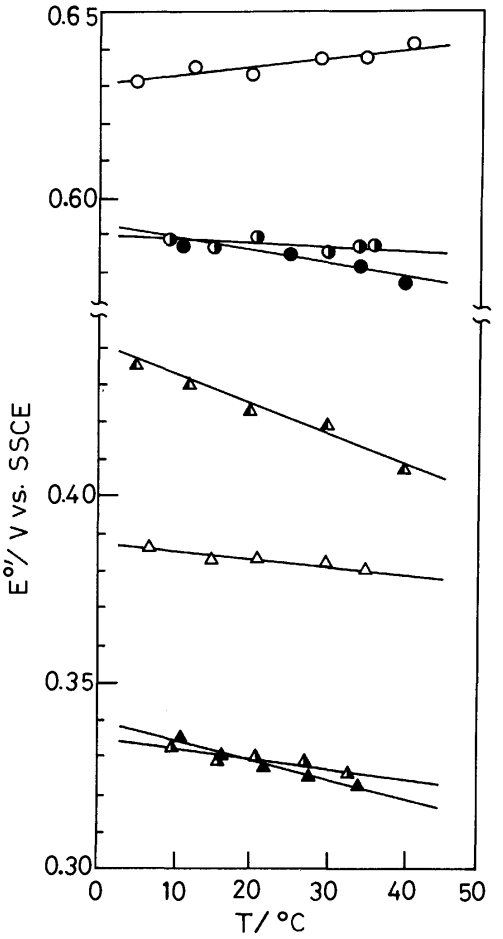

Fig. 10. Temperature dependences of the formal potentials ($E^{0\prime}$) of the $[Os(bpy)_3]^{2+/3+}$ and $TAF^{+/2+}$ couples confined in the films. Confined redox couples: (○,◑,●) $[Os(bpy)_3]^{2+/3+}$, (▲,▲,▲,▲) $TAF^{+/2+}$. Coating films: (○,▲,△) PFPC film (Thickness: 2.1×10^{-5} cm) (◑,●,▲,▲) Nafion film (Thickness: 4.3×10^{-5}). Supporting electrolyte: (▲) 0.2 M CF_3COONa (pH 1.0); (○,◑,●,△,▲,▲) 0.2 M CF_3COONa +0.1 M CH_3COONa/CH_3COOH (pH 5.5). C_p^0: (○) 1.4×10^{-4}; (◑) 6.6×10^{-5}; (●) 2.6×10^{-5}; (▲) 1.9×10^{-4}; (△) 1.3×10^{-4}; (▲) 6.6×10^{-4}; (▲) 6.6×10^{-5} mol cm^{-3}.

plots correspond approximately to those expected for the electrochemical impedance represented by the well-known "Randles's equivalent circuit".[33] Thus, the diameter of the semicircle enabled us to estimate the heterogeneous electron-transfer resistance and thus k°.[32-34] The k° values thus obtained for the redox reactions of the $TAF^{+/2+}$ and $[Os(bpy)_3]^{2+/3+}$ couples confined in the Nafion or PFPC films at various C_p^0 values are shown in Fig. 9. The film resistances involving the solution resistance, obtained from the high-frequency intercept with the real axis, were in the range of ca. 20—50 Ω in both redox systems.

Temperature Dependences of $E^{0\prime}$, D_{app}, and k°. Figure 10 shows the temperature (T) dependences of the formal redox potentials ($E^{0\prime}$) for the $TAF^{+/2+}$ and $[Os(bpy)_3]^{2+/3+}$ couples confined in the Nafion and PFPC films. The linear relationships between $E^{0\prime}$ and T were obtained and thus the reaction entropy differences (ΔS_{rc}^0) for these couples were estimated by using the equation:[23,25-28]

$$\Delta S_{rc}^0 = S_{red}^0 - S_{ox}^0 = F(dE^{0\prime}/dT) \quad (1)$$

where S_{red}^0 and S_{ox}^0 are absolute ionic entropies of the reduced and oxidized halves of the redox couple and F is the Faraday constant. The temperature coefficient (dE_f^{ni}/dT) of the overall potential (E_f^{ni}) across the non-isothermal electrochemical cell consists of those of the Galvani metal-solution potential difference (ϕ_f^m), the potential difference across the thermal liquid junction within the 3 M NH_4Cl salt bridge (ϕ_{tlj}) and the thermocouple potential difference between the hot and cold regions of the working electrode (ϕ_{tc}), which are expressed by $d\phi_f^m/dT$, $d\phi_{tlj}/dT$, and $d\phi_{tc}/dT$, respectively.[23] The value of $d\phi_{tlj}/dT$ has been

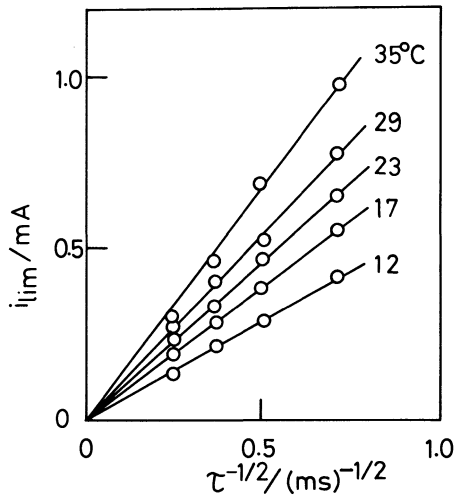

Fig. 11. Typical normal pulse voltammetric Cottrell plots of limiting current, i_{lim}, vs. (sampling time)$^{-1/2}$, $\tau^{-1/2}$, for the oxidation of the TAF$^+$ complex confined in the Nafion film on BPG electrodes at various temperatures. C_p^0; 1.56×10^{-4} mol cm^{-3}. Film thickness: 4.3×10^{-5} cm. Other experimental conditions are the same as in Fig. 5.

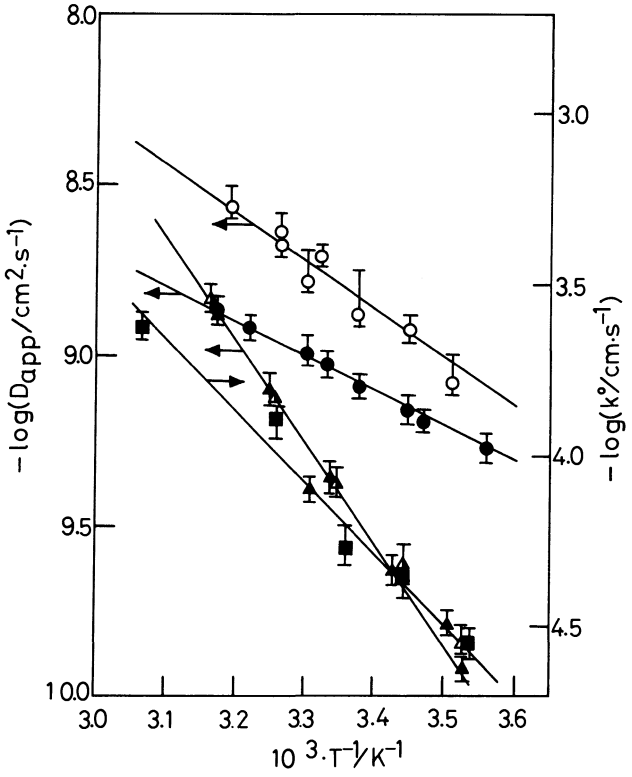

Fig. 12. Temperature dependences of D_{app} and $k°$ for the [Os(bpy)$_3$]$^{2+}$ and TAF$^+$ complexes confined in Nafion films. (○): [Os(bpy)$_3$]$^{2+}$ (C_p^0: 6.6×10^{-5} mol cm^{-3}), (●): [Os(bpy)$_3$]$^{2+}$ (C_p^0: 2.6×10^{-4} mol cm^{-3}), (▲,■): TAF$^+$ (C_p^0: 6.6×10^{-5} mol cm^{-3}), (▲): TAF$^+$ (C_p^0: 6.6×10^{-4} mol cm^{-3}). Film thicknesses: 4.3×10^{-5} cm. Supporting electrolyte: 0.2 M CF$_3$COONa+0.1 M CH$_3$COONa/CH$_3$COOH (pH 5.5). Widths of error bars indicate uncertainties in the measurements of D_{app} and $k°$.

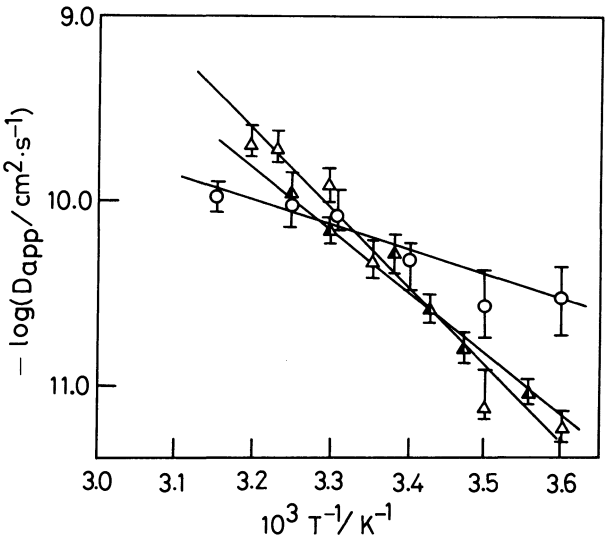

Fig. 13. Temperature dependences of D_{app} for the [Os(bpy)$_3$]$^{2+}$ and TAF$^+$ complexes confined in PFPC films. (○): [Os(bpy)$_3$]$^{2+}$ (C_p^0: 1.4×10^{-4} mol cm^{-3}), (▲): TAF$^+$ (C_p^0: 1.9×10^{-4} mol cm^{-3}), (△): TAF$^+$ (C_p^0: 1.3×10^{-4} mol cm^{-3}). Film thickness: 2.1×10^{-5} cm. Supporting electrolyte: (▲) 0.2 M CF$_3$COONa (pH 1.0); (○,△); 0.2 M CF$_3$COONa+CH$_3$COONa/CH$_3$COOH (pH 5.5). Widths of error bars indicate uncertainties in the measurements of D_{app}.

estimated to be less than 50 μV K^{-1}.[23,35] We have no data on the $d\phi_{tc}/dT$ for the BPG electrode, but it may be expected to be less than several tens of microvolts per degree from the $d\phi_{tc}/dT$ values for mercury and platinum which are 14 and 6 μV K^{-1}, respectively.[23,35] Thus we assumed that these temperature coefficients ($d\phi_{tlj}/dT$ and $d\phi_{tc}/dT$) can be negligible as compared with the experimental uncertainties (±2 cal mol^{-1} K^{-1} in ΔS_{rc}^0) in the present experiments.

In Fig. 11 is shown the typical dependence of the normal pulse voltammetric limiting current upon $\tau^{-1/2}$ for the oxidation of the TAF$^+$ confined in the Nafion film at different temperatures. From the slopes of such plots, the D_{app}'s at each temperature were obtained. Plots of the logarithm of D_{app} vs. T^{-1} were found to be linear over the temperature range 5—45 °C, indicating that the behaviors are of the Arrhenius type (see Figs. 12 and 13). Thus, according to Eyring et al.,[36,37] we can express the D_{app} as follows:

$$D_{app} = \lambda^2 \left(\frac{kT}{h}\right) \exp\left(\frac{\Delta S^{\ddagger}_{diffusion}}{R}\right) \exp\left(-\frac{\Delta H^{\ddagger}_{diffusion}}{RT}\right) \quad (2)$$

where $\Delta H^{\ddagger}_{diffusion}$ and $\Delta S^{\ddagger}_{diffusion}$ are the enthalpy and entropy, respectively, of activation for the homogeneous charge-transport process within the films, λ is the average distance between equilibrium positions in the process of diffusion, k is the Boltzmann constant, h is the Planck constant, and R is the gas constant. The values of λ have been unknown. Here, assuming that λ=1 and 10 Å, the values of $\Delta S^{\ddagger}_{diffusion}$ are estimated (Different investigators[37,38] have used values ranging

1 to 5 Å for λ). The obtained values of $\Delta H^{\neq}_{diffusion}$ and $\Delta S^{\neq}_{diffusion}$ are given in Table 2.

The temperature dependence of $k°$ for the $TAF^{+/2+}$ couple confined in the Nafion film is shown in Fig. 12, where the standard rate constants at the standard potential at each temperature are plotted against (temperature)$^{-1}$. According to Weaver et al.,[21-23] who have recently demonstrated in detail the possibility and significance of such measurements using a non-isothermal cell (see Experimental Section) for simple electrode reactions, the "real" enthalpy and entropy of activation of the heterogeneous electron-transfer reaction ($(\Delta H^0_{\neq})_{real}$ and $(\Delta S^0_{\neq})_{real}$) were estimated to be 9.6 ± 1.2 kcal mol^{-1} and -2 ± 1 cal mol^{-1} K^{-1}, respectively. In the estimation of $(\Delta S^0_{\neq})_{real}$, the transmission coefficient (κ) introduced in order to account for possible non-adiabaticity of the electrode reaction was assumed to be unity.[39]

Discussion

pH dependence of the Incorporation. From the data shown in Fig. 4, one can clearly see that the volume concentration (C^0_p) of the $[Os(bpy)_3]^{2+}$ incorporated into the PFPC film increases from 1.4×10^{-5} to 3.2×10^{-4} mol cm^{-3} with increasing pH from 1 to 5.5, while C^0_p of the incorporated TAF^+ is almost independent of pH in the range of pH ca. 2—5.5 and is ca. 2×10^{-4} mol cm^{-3}. This result for the $[Os(bpy)_3]^{2+}$ complex is explained by the equilibrium competition of protons and $[Os(bpy)_3]^{2+}$ ions for counterionic sites within the PFPC film. That is, at pH values as low as 1, protons compete quite successfully with $[Os(bpy)_3]^{2+}$ ions for counterionic sites within the PFPC, and with increasing pH $[Os(bpy)_3]^{2+}$ ions become dominantly trapped. The shape of the plot for the $[Os(bpy)_3]^{2+}$ resembles that of a typical pH titration curve. Thus, the effective pK_a of the carboxylic acid group in the PFPC is estimated to be ca. 2.9 from the pH at which the incorporation reaches one-half of its maximum value. This value is different from that (2,2) obtained from the incorporation experiments of $[Ru(NH_3)_6]^{3+}$ into the PFPC[16] and also from the pK_a of 1.9 measured directly for a similar perfluoro carboxylate polyelectrolyte.[40] As generally well-known, the effective pK_a of polyelectrolytes varies with the degree of protonation and with the ionic strength.[41] These are considered as main reasons for the different effective pK_a's.

On the other hand, the situation for the TAF^+ complex seems to be different from that for the above-mentioned $[Os(bpy)_3]^{2+}$ complex. The incorporation of TAF^+ complex changes slightly with pH, especially at pH<ca. 2. In this case, the effective pK_a, which is estimated from the C^0_p vs. pH curve by the same procedure as that used for the pK_a determination of the PFPC polyelectrolyte from the $[Os(bpy)_3]^{2+}$ incorporation experiments, is ca. 1, being clearly different from that obtained from the $[Os(bpy)_3]^{2+}$ incorporation experiments. The amount of the incorporation of the TAF^+ complex is comparable to the maximum value for the $[Os(bpy)_3]^{2+}$ complex, as seen from the C^0_p values for $[Os(bpy)_3]^{2+}$ and TAF^+ at pH 5.5.

These different pH-dependences of the incorporation of $[Os(bpy)_3]^{2+}$ and TAF^+ complexes into the PFPC film should be noted, because this result can be considered to suggest different interactions (between the complexes and the PFPC film) by which these complexes are incorporated into the film and confined in it. In the case of the Nafion (or poly(*p*-styrenesulfonate)) film, such a pH-dependence of the incorporation of the same complexes was not observed in the examined range of pH 1 to 5.5.[61] Thus, the observed pH-dependences of the incorporation are peculiar to the PFPC film. The feature to be noted on the basis of the above-mentioned incorporation experiments is that the morphology of the PFPC film changes from the non-ionic polymer film to the anionic polyelectrolyte film with cation-exchange properties with increasing pH from ca. 1 to 5.5. In the case of the $[Os(bpy)_3]^{2+}$ complex, the incorporation can be considered to be mainly due to "electrostatic interactions"[2-8,11,13,19,41-48,52] between anionic carboxylic sites in the PFPC and cationic $[Os(bpy)_3]^{2+}$ complexes. The C^0_p values were about 1.4×10^{-5} and 2.5×10^{-4} mol cm^{-3} at pH 1 and 5.5, respectively, where the PFPC films are in the nonionic and anionic states, respectively. Thus, the difference between the C^0_p values at pH 1 and 5.5 is considered to approximately correspond to the incorporation amount of $[Os(bpy)_3]^{2+}$ by electrostatic interactions. In addition, the C^0_p value of 1.4×10^{-5} mol cm^{-3} at pH 1 may be regarded as the amount of the $[Os(bpy)_3]^{2+}$ complex incorporated into the film by specific interactions other than such electrostatic interactions, for example, "hydrophobic interactions"[16,17,42] between the large fluorocarbon component of the polyelectrolyte coating and $[Os(bpy)_3]^{2+}$ complexes. On the other hand, in the case of the TAF^+ complex, the situation seems different. Unlike the $[Os(bpy)_3]^{2+}$ complex, there may be probably a minor contribution of electrostatic interactions to the incorporation. This is deducible from the fact that C^0_p scarcely depends on pH. In this case, the incorporation seems to be mainly due to "hydrophobic interaction".[16,17,42]

Apparent Diffusion Coefficients for Diffusion-Like Charge Transport within Nafion and PFPC Films. The data shown in Fig. 9 demonstrate the dependences of D_{app} on the redox complex confined in the film, its concentration (C^0_p) and the film confining it. For example, when C^0_p was increased from 3.2×10^{-5} to 3.2×10^{-4} mol cm^{-3}, D_{app} decreased from 4.7×10^{-9} to 4.5×10^{-10} cm^2 s^{-1} in the case of the Nafion-$[Os(bpy)_3]^{2+}$ system, while in the case of the Nafion-TAF^+ system D_{app} was found to slightly decrease. For the PFPC coatings, the dependences of D_{app} on C^0_p were

almost the same in both $[Os(bpy)_3]^{2+}$ and TAF^+ systems: D_{app} decreased from 8.3×10^{-10} to 5.1×10^{-11} $cm^2\,s^{-1}$ with an increase in C_p^0 from 3.2×10^{-5} to 3.2×10^{-4} mol cm^{-3}. These observed decreases of D_{app}'s with increasing C_p^0 may be understood by the same idea as that used to explain the concentration dependences of D_{app}'s found in the other previously reported redox polymer films:[2-14,42,46-48] These decreases are considered to be attributed to the effects of "electrostatic (or hydrophilic) cross linking"[2-8,11,13,16,17,19,41-48,52] of the films by the electrostatic (or hydrophilic) interactions between the redox ions and the polyelectrolytes containing them (as mentioned above) and/or of "single-file diffusion",[42,43,49] An increase of the electrostatic cross linking with increasing C_p^0 causes a decrease in the diffusion rate of redox ion itself as well as decreases in the rates of the charge-compensating counterion motion which is necessarily coupled to electron transfer, the motion of solvent and/or the segmental motion of the polymeric chain. Also, the diffusing species which must move between more or less fixed sites within a polymeric matrix are considered to have their rate of motion limited by the decreasing availability of sites as C_p^0 of the diffusing species increases. These result in the decrease of the overall rate of the charge transport with an increase in C_p^0 and thus the decreased D_{app}'s are observed. It is also apparent from Fig. 9 that at a given C_p^0 the values of D_{app} for the Nafion-TAF^+ and $[Os(bpy)_3]^{2+}$ systems are larger than those for the PFPC-TAF^+ and $[Os(bpy)_3]^{2+}$ systems. For example, at $C_p^0=1.0\times10^{-4}$ mol cm^{-3}, the values of D_{app} are 1.5×10^{-9} and 1.8×10^{-10} $cm^2\,s^{-1}$ for the Nafion-$[Os(bpy)_3]^{2+}$ and PFPC-$[Os(bpy)_3]^{2+}$ systems, respectively, and those are 6.2×10^{-10} and 1.0×10^{-10} $cm^2\,s^{-1}$ for the Nafion-TAF^+ and PFPC-TAF^+ systems, respectively.

The Dependence of D_{app} on pH is of interest in connection with the pH dependence of the incorporation of the $[Os(bpy)_3]^{2+}$ and TAF^+ complexes (Fig. 4). For the $[Os(bpy)_3]^{2+}$ system, the D_{app} decreased with increasing pH. This means that the decrease of D_{app} is owing to the increase of C_p^0, because C_p^0 increases with increasing pH as mentioned above. When pH was increased from 1 to 5.5, C_p^0 increased from 1.4×10^{-5} to 3.2×10^{-4} mol cm^{-3} and thus D_{app} decreased from 1.4×10^{-9} to 2.1×10^{-10} $cm^2\,s^{-1}$. For the TAF^+ system, on the other hand, D_{app}'s were almost independent of pH and were ca. 1.2×10^{-10} $cm^2\,s^{-1}$. Such a pH-independence of D_{app} can be expected, because C_p^0 rarely varies with pH in the examined range of pH.

Kinetic Parameters of Heterogeneous Electron-Transfer Reactions at Electrode/Film Interfaces. The k° values for a given system, estimated by normal pulse voltammetry and ac impedance method, were almost the same within experimental error as shown in Fig. 9.[55] It appears that k° depends, though slightly, on C_p^0. For example, when C_p^0 was increased from 3.2×10^{-5} to 3.2×10^{-4} mol cm^{-3}, k° decreased from ca. 3×10^{-4} to 7×10^{-5} cm s^{-1} in the case of the Nafion-$[Os(bpy)_3]^{2+}$ system and from ca. 2×10^{-5} to 7×10^{-6} cm s^{-1} in the case of the PFPC-$[Os(bpy)_3]^{2+}$ and TAF^+ systems. In the case of the Nafion-TAF^+ system, k° seemed almost independent of C_p^0. Further, the values of k° for the Nafion-$[Os(bpy)_3]^{2+}$ and TAF^+ systems are larger than those for the PFPC-$[Os(bpy)_3]^{2+}$ and TAF^+ systems, for example, at $C_p^0=1.0\times10^{-4}$ mol cm^{-3} the k° values (ca. 1×10^{-4} cm s^{-1}) for the former systems are about one order of the magnitude larger than those for the latter systems. The transfer coefficients were almost independent of the polymer films: The anodic transfer coefficients (α_+) for the oxidation of the $[Os(bpy)_3]^{2+}$ complex confined in the Nafion and PFPC films are 0.48 and 0.51, respectively, and those for the oxidation of the TAF^+ complex confined in the Nafion and PFPC films are 0.29 and 0.24, respectively.

Formal Potentials and Reaction Entropies for the $[Os(bpy)_3]^{2+/3+}$ and $TAF^{+/2+}$ Couples Confined in Films. The formal potentials ($E^{0\prime}$) of the $[Os(bpy)_3]^{2+/3+}$ and $TAF^{+/2+}$ couples largely varied with the films confining them (see Table 1), indicating that the relative equilibrium binding constants for two halves of a redox couple are not determined solely by the magnitudes of their positive charges. In the PFPC film, the less highly charged (i.e., reduced) form of each couple is stabilized larger, while in the Nafion film the more highly charged (i.e., oxidized) form is stabilized larger. As a result, the $E^{0\prime}$ values for the

Table 1. Formal Redox Potentials and Reaction Entropies for the $[Os(bpy)_3]^{2+/3+}$ and $TAF^{+/2+}$ Couples Confined in Nafion and PEPC Films

Film	Redox species	C_p^0/mol cm^{-3} [a]	$E^{0\prime}$/V vs. SSCE [b]	ΔS_{rc}°/cal $mol^{-1}\,K^{-1}$ [c]
Nafion	$[Os(bpy)_3]^{2+/3+}$ [d]	6.6×10^{-5}	0.587±0.003	−8±2
Nafion	$[Os(bpy)_3]^{2+/3+}$ [d]	2.6×10^{-4}	0.584±0.003	−9±2
Nafion	$TAF^{+/2+}$ [d]	6.0×10^{-5}	0.326±0.003	−11±2
Nafion	$TAF^{+/2+}$ [d]	6.0×10^{-4}	0.328±0.003	−7±2
PFPC	$[Os(bpy)_3]^{2+/3+}$ [d]	1.4×10^{-4}	0.637±0.003	5±2
PFPC	$TAF^{+/2+}$ [d]	1.9×10^{-4}	0.385±0.003	−5±2
PFPC	$TAF^{+/2+}$ [e]	1.3×10^{-4}	0.419±0.003	−19±2

a) Concentration of redox species confined in films. b) Formal redox potentials for the redox couples confined in films at 298 K. c) Reaction entropies for the redox couples confined in films (see text). d) Supporting electrolyte: 0.2 M CF_3COONa+0.1 M CH_3COONa/CH_3COOH (pH 5.5). e) Supporting electrolyte: 0.2 M CF_3COONa (pH 1.0).

$[Os(bpy)_3]^{2+/3+}$ and $TAF^{+/2+}$ couples confined in the PFPC film are more positive than those of these couples confined in the Nafion film. Further, in the PFPC film, the reduced form of the $TAF^{+/2+}$ couple is more stabilized at pH 1.0 than at pH 5.5. Thus, the values of $E^{0\prime}$ for these two couples indicate the more dominance of hydrophobic interactions for the $TAF^{+/2+}$ couple, compared with the $[Os(bpy)_3]^{2+/3+}$ couple where hydrophilic interactions are more dominant. This is also supported by the data of the incorporation of TAF^+ and $[Os(bpy)_3]^{2+}$ into the PFPC film (mentioned in the previous section). The present data seem to suggest that the hydrophobicity of the $TAF^{+/2+}$ couple is larger than that of the $[Os(bpy)_3]^{2+/3+}$ couple, in contrast to the previously reported results.[16]

The negative reaction entropy differences (ΔS^0_{rc}) were obtained except for the PFPC-$[Os(bpy)_3]^{2+}$ system. These negative ΔS^0_{rc} values may suggest that the net solvent ordering in the vicinity of the redox species is less extensive in the oxidized state than in the reduced state in qualitative disagreement with the expectations from an electrostatic treatment (e.g., by the Born model[50]). This is considered as a result of the hydrophobic interactions between the redox species and the surroundings (in the swollen Nafion and PFPC films) that are enhanced in the reduced state, leading to increased solvent ordering and a decrease in entropy compared with that for the oxidized state. Large negative values of ΔS^0_{rc} have been recently reported for the $[Ru(NH_3)_6]^{3+/2+}$ couple confined in the PFPC film on graphite electrodes[16] and the ferricinium-ferrocene couple attached to platinum electrodes.[28] Negative values of ΔS^0_{rc} have also been observed for the bulk-solution blue copper proteins[53] and ferricinium-ferrocene couple.[54]

On the other hand, the positive ΔS^0_{rc} value obtained for the PFPC-$[Os(bpy)_3]^{2+}$ system may be explained as follows: The increased polarization of water molecules adjacent to the aromatic rings of $[Os(bpy)_3]^{2+}$ ions occurs in the higher oxidation sate and, as a result, the positive ΔS^0_{rc} is obtained.

Activation Parameters for Homogeneous Charge-Transport Process and Heterogeneous Electron-Transfer Reaction. From the data in Table 2, some thermodynamic aspects on the homogeneous charge-transport process within the Nafion and PFPC films containing $[Os(bpy)_3]^{2+}$ or TAF^+ can be drawn as mentioned below. For a given film, the values of both $\Delta H^{\neq}_{diffusion}$ and $\Delta S^{\neq}_{diffusion}$ for the TAF^+ complex are larger than those for the $[Os(bpy)_3]^{2+}$ complex.[60] The values of D_{app} for the former complex are smaller than those for the latter complex. Thus, the charge-transport processes within the films containing TAF^+ are more favorable entropically and more unfavorable enthalpically, compared with those within the films containing $[Os(bpy)_3]^{2+}$ and as a whole the smaller values of D_{app} for the TAF^+ complex are due to the larger $\Delta H^{\neq}_{diffusion}$. In the case of the PFPC-TAF^+ system, the D_{app}'s obtained at pH 1.0 and pH 5.5 are almost the same. This results from the mutual compensation of the $\Delta H^{\neq}_{diffusion}$ and $\Delta S^{\neq}_{diffusion}$ terms, although the absolute values of $\Delta H^{\neq}_{diffusion}$ and $\Delta S^{\neq}_{diffusion}$ are largely different at these both pH's. As mentioned in the previous section, the incorporation of the TAF^+ complex into the PFPC film is due to mainly hydrophobic interactions, while in the case of the Nafion and PFPC-$[Os(bpy)_3]^{2+}$ systems an electrostatic interaction is the main force for the incorporation of the $[Os(bpy)_3]^{2+}$ (and $[Os(bpy)_3]^{3+}$) complexes

Table 2. Activation Parameters for Homogeneous Charge Transport in Nafion and PFPC Films

Film	Redox species	C°_p/mol cm^{-3} [a]	D_{app}/cm^2 s^{-1} [b]
Nafion	$[Os(bpy)_3]^{2+/3+}$ [g]	6.6×10^{-5}	21×10^{-10}
Nafion	$[Os(bpy)_3]^{2+/3+}$ [g]	2.6×10^{-4}	11×10^{-10}
Nafion	$TAF^{+/2+}$ [g]	6.0×10^{-5}	8.0×10^{-10}
Nafion	$TAF^{+/2+}$ [g]	6.0×10^{-4}	7.9×10^{-10}
PFPC	$[Os(bpy)_3]^{2+/3+}$ [g]	1.7×10^{-4}	7.9×10^{-10}
PFPC	$TAF^{+/2+}$ [g]	1.9×10^{-4}	0.9×10^{-10}
PFPC	$TAF^{+/2+}$ [h]	1.3×10^{-4}	1.7×10^{-10}

Film	$\Delta H^{\neq}_{diffusion}$/kcal mol^{-1} [c]	$\Delta S^{\neq}_{diffusion}$ cal mol^{-1} K^{-1} [d]	
Nafion	6.5±0.5	−13±2 [e]	−3±2 [f]
Nafion	4.9±0.6	−23±2 [e]	−13±2 [f]
Nafion	10 ±1.0	7±2 [e]	16±2 [f]
Nafion	10 ±1.0	7±2 [e]	16±2 [f]
PFPC	6.7±0.6	−19±2 [e]	−10±2 [f]
PFPC	12 ±1.2	−2±2 [e]	7±2 [f]
PFPC	18 ±3.0	7±3 [e]	16±3 [f]

a) Concentration of redox species confined in films. b) Values at 298 K. c) Activation enthalpies for homogeneous charge-transport in films. d) Activation entropies for homogeneous charge-transport in films. e) Calculated from Eq. 2 assuming $\lambda=10$ Å at 298 K. f) Calculated from Eq. 2 assuming $\lambda=1$ Å at 298 K. g) Supporting electrolyte: 0.2 M CF_3COONa+0.1 M CH_3COONa/CH_3COOH (pH 5.5). h) Supporting electrolyte: 0.2 M CF_3COONa (pH 1.0).

into these films. From the combination of these facts and the data in Table 2, it may be concluded that in the case of the incorporation by hydrophobic interactions both $\Delta H^{\neq}_{diffusion}$ and $\Delta S^{\neq}_{diffusion}$ are larger than those in the case of the incorporation by electrostatic interactions. In the latter case, an increase in C^0_p causes a decrease in D_{app}, and in this case the $\Delta S^{\neq}_{diffusion}$ values are negative and decrease with increasing C^0_p. Similar results have been previously obtained for protonated poly(4-vinylpyridine) film-$[W(CN)_8]^{4-}$ and $[IrCl_6]^{3-}$ systems.[4] Electrostatic cross linking and single-file diffusion effects seem to mainly be reflected as "negative" $\Delta S^{\neq}_{diffusion}$ values. In the case of the Nafion-TAF^+ system, the D_{app} values are almost independent of C^0_p and the $\Delta H^{\neq}_{diffusion}$ and $\Delta S^{\neq}_{diffusion}$ values are also independent of C^0_p.

The "real" entropy ($(\Delta S^0_{\neq})_{real}$)[21-23] of activation for the heterogeneous electron-transfer reaction of the $TAF^{+/2+}$ couple confined in the Nafion film is negative (close to zero)(-2 ± 1 cal mol^{-1} K^{-1}). This fact seems to be remarkable,[51] although at the present stage we have no satisfactory explanation for this. In the estimation of $(\Delta S^0_{\neq})_{real}$, the transmission coefficient (κ)[39] was assumed as unity. Thus, it may be also probable that if $(\Delta S^0_{\neq})_{real}$ has a "normal" positive value, κ should be smaller than 1 and thus the heterogeneous electron-transfer reaction would be nonadiabatic.[39,51]

The present work was partially supported by Grant-in-Aid for Scientific Research No. 62470071, for N. Oyama, from the Ministry of Education, Science and Culture.

References

1) See, for example, (a) R. W. Murray, "*Electroanal. Chem.*," ed by A. J. Bard, Marcel Dekker Inc., (1984), Vol. 13, p. 191. (b) A. R. Hillman, "Electrochemical Science & Technology 1," ed by R. G. Linford, Elsevier Applied Science Inc., (1987), p. 103.

2) N. Oyama, T. Ohsaka, M. Kaneko, K. Sato, and H. Matsuda, *J. Am. Chem. Soc.*, **105**, 6003 (1983).

3) K. Sato, S. Yamaguchi, H. Matsuda, T. Ohsaka, and N. Oyama, *Bull. Chem. Soc. Jpn.*, **56**, 2004 (1983).

4) N. Oyama, T. Ohsaka, and T. Ushirogouchi, *J. Phys. Chem.*, **88**, 5274 (1984).

5) T. Ohsaka, H. Yamamoto, M. Kaneko, A. Yamada, M. Nakamura, S. Nakamura, and N. Oyama, *Bull. Chem. Soc. Jpn.*, **57**, 1844 (1984).

6) T. Ohsaka, K. Sato, H. Matsuda, and N. Oyama, *J. Electrochem. Soc.*, **132**, 1871 (1985).

7) T. Ohsaka, T. Ushirogouchi, and N. Oyama, *Bull. Chem. Soc. Jpn.*, **58**, 3252 (1985).

8) N. Oyama, T. Ohsaka, and T. Shimizu, *Anal. Chem.*, **57**, 1526 (1985).

9) N. Oyama, T. Ohsaka, H. Yamamoto, and M. Kaneko, *J. Phys. Chem.*, **90**, 3850 (1986).

10) N. Oyama, K. Hirabayashi, and T. Ohsaka, *Bull. Chem. Soc. Jpn.*, **59**, 2071 (1986).

11) N. Oyama, T. Ohsaka, and M. Nakanishi, *J. Macromol. Sci.-Chem.*, **A24**, 375 (1987).

12) T. Ohsaka, K. Chiba, and N. Oyama, *Nippon Kagaku Kaishi*, **1986**, 457.

13) T. Ohsaka, T. Okajima, and N. Oyama, *J. Electroanal. Chem.*, **215**, 191 (1986).

14) K. Chiba, T. Ohsaka, and N. Oyama, *J. Electroanal. Chem.*, **217**, 239 (1987).

15) H. S. White, J. Leddy, and A. J. Bard, *J. Am. Chem. Soc.*, **104**, 4811 (1982).

16) Y.-M. Tsou and F. C. Anson, *J. Electrochem. Soc.*, **131**, 595 (1984).

17) N. Oyama, T. Ohsaka, K. Sato, and H. Yamamoto, *Anal. Chem.*, **55**, 1429 (1983).

18) C. Creutz, M. Chou, T. L. Netzel, M. Okumura, and N. J. Sutin, *J. Am. Chem. Soc.*, **102**, 1309 (1980).

19) N. Oyama and F. C. Anson, *Anal. Chem.*, **52**, 1192 (1980).

20) I. Rubinstein and A. J. Bard, *J. Am. Chem. Soc.*, **103**, 5007 (1981).

21) M. J. Weaver, *J. Phys. Chem.*, **83**, 1748 (1979).

22) M. J. Weaver, *J. Phys. Chem.*, **80**, 2645 (1976).

23) E. L. Yee, R. J. Cave, Y. L. Guyer, P. C. Tyme, and M. J. Weaver, *J. Am. Chem. Soc.*, **101**, 1131 (1979).

24) J. T. Hupp and M. J. Weaver, *J. Electroanal. Chem.*, **145**, 43 (1983).

25) M. J. Weaver and S. M. Nettles, *Inorg. Chem.*, **19**, 1641 (1980).

26) N. Sutin, M. J. Weaver, and E. L. Yee, *Inorg. Chem.*, **19**, 1096 (1980).

27) J. T. Hupp and M. J. Weaver, *Inorg. Chem.*, **23**, 3639 (1984).

28) J. T. Hupp and M. J. Weaver, *J. Electrochem. Soc.*, **131**, 619 (1984).

29) T. Ohsaka, N. Oyama, S. Yamaguchi, and H. Matsuda, *Bull. Chem. Soc. Jpn.*, **54**, 2475 (1981).

30) S. Yamaguchi, H. Matsuda, T. Ohsaka, and N. Oyama, *Bull. Chem. Soc. Jpn.*, **56**, 2952 (1983).

31) H. Matsuda, *Bull. Chem. Soc. Jpn.*, **53**, 3439 (1980).

32) M. Sluyters-Rehbach and J. H. Sluyters, "Electroanalytical Chemistry," Vol. 4, ed by A. J. Bard, Marcel Dekker, New York (1970), p. 1.

33) J. E. B. Randles, *Discuss. Faraday Soc.*, **1**, 11 (1947).

34) A. J. Bard and L. R. Faulkner. "Electrochemical Methods, Fundamentals and Applications," Wiley, New York (1980), p. 316.

35) J. N. Agar, *Adv. Electrochem. Electrochem. Eng.*, **3**, 31 (1963).

36) H. Eyring, *J. Chem. Phys.*, **4**, 283 (1936).

37) S. Glasstone, K. J. Laidler, and H. Eyring, "The Theory of Rate Processes," McGraw Hill, New York (1941), p. 525.

38) M. M. Berg, K. Ahmad, I. Altaf, and M. Arshad, *J. Mem. Sci.*, **9**, 303 (1981) and references therein.

39) R. A. Marcus, *J. Chem. Phys.*, **43**, 679 (1965) and references therein.

40) Z. Twardowski, H. L. Yeager, and B. O'Dell, *J. Electrochem. Soc.*, **129**, 328 (1982).

41) H. Zumbrunnen and F. C. Anson, *J. Electroanal. Chem.*, **152**, 111 (1983).

42) D. A. Buttry and F. C. Anson, *J. Am. Chem. Soc.*, **105**, 685 (1983).

43) Y.-M. Tsou and F. C. Anson, *J. Phys. Chem.*, **89**, 3818

(1985).
44) J. Facci and R. W. Murray, *J. Electroanal. Chem.*, **124**, 339 (1981).
45) K.-N. Kuo and R. W. Murray, *J. Electroanal. Chem.*, **131**, 37 (1982).
46) N. Oyama and F. C. Anson, *J. Electrochem. Soc.*, **127**, 640 (1980).
47) N. Oyama, T. Shimomura, K. Shigehara, and F. C. Anson, *J. Electroanal. Chem.*, **112**, 271 (1980).
48) F. C. Anson, T. Ohsaka, and J. M. Saveant, *J. Phys. Chem.*, **87**, 640 (1983).
49) K. Heckmann, "Biomembranes," ed by A. L. Manson, Plenum Press, New York (1972), Vol. 3, p. 127.
50) R. M. Noyes, *J. Am. Chem. Soc.*, **84**, 513 (1962).
51) T. Ohsaka, H. Yamamoto, and N. Oyama, *J. Phys. Chem.*, **91**, 3775 (1987).
52) N. Oyama, T. Ohsaka, and T. Okajima, *Anal. Chem.*, **58**, 979 (1986).
53) N. Sailasuta, F. C. Anson, and H. B. Gray, *J. Am. Chem. Soc.*, **101**, 455 (1979).
54) E. L. Yee and M. J. Weaver, *Inorg. Chem.*, **19**, 1077 (1980).
55) The conventional positive feedback techniques[56,57] were used to compensate the resistances associated with the polymer coatings as much as possible. That is, a normal pulse voltammetric experiment was carried out in a potential region preceding the wave corresponding to the oxidation of $[Os(bpy)_3]^{2+}$ (or TAF^+) confined in Nafion (or PFPC) films, where the current was due almost entirely to double-layer charging. The extent of compensation was increased until the onset of oscillation and then it was reduced slightly. Using these techniques, the residual uncompensated resistance can be, though not completely, decreased below typically ca. several ohms.[58,59] By comparing the uncompensated resistance with the heterogeneous electron-transfer resistances which were in the range of a few hundreds to thousands (in ohm) (as typically shown in Fig. 8), we conclude that uncompensated resistance is not a major contributor to error in the measurement.
56) A. J. Bard and L. R. Faulkner, "Electrochemical Methods, Fundamentals and Applications," Wiley, New York (1980), Chap. 13.
57) D. T. Sawyer and J. L. Robert, "Experimental Electrochemistry for Chemists," Wiley, New York (1974), Chap. 5.
58) P. E. Whitson, H. W. VandenBorn, and D. H. Evans, *Anal. Chem.*, **45**, 1298 (1973).
59) T. W. Ronsanske and D. H. Evans, *J. Electroanal. Chem.*, **72**, 277 (1976).
60) The differences between $\Delta S^{*}_{diffusion}$ values obtained for the $[Os(bpy)_3]^{2+}$ and TAF^+ complexes confined in Nafion films were 29—30 cal mol^{-1} K^{-1} and those obtained for the same complexes confined in PFPC films were 17—26 cal mol^{-1} K^{-1} (Table 2). These differences in $\Delta S^{*}_{diffusion}$ values are fairly larger than those (4—5 cal mol^{-1} K^{-1}) between the $\Delta S^{*}_{diffusion}$ values estimated using λ values ranging 1 to 5 Å[37,38] which have usually been used in a quantitative analysis of the process of diffusion.
61) The sulfonate ion-exchange sites of Nafion perfluorosulfonate and poly(*p*-styrenesulfonate) films show strong acid behavior ($pK_a<1$).[40]

 © 1988 The Chemical Society of Japan Bull. Chem. Soc. Jpn., 61, 3115—3120 (1988)

The α-Helical Conformation of the Aib-Containing Oligopeptide, Boc-(Leu$_3$-Aib)$_2$-OBzl

Kenji Okuyama,* Nobuo Tanaka, Masamitsu Doi, and Mitsuaki Narita
Faculty of Technology, Tokyo University of Agriculture and Technology, Koganei, Tokyo 184
(Received February 19, 1988)

The octapeptide Boc-(Leu$_3$-Aib)$_2$-OBzl crystallizes in the space group $P2_1$, with a=11.450(2), b=27.915(7), c=11.255(2) Å, β=116.95(1)°, and Z=2. The crystal structure has been solved by direct methods and refined to an R value of 0.08. The peptide back-bone, except for the C-terminal Aib residue, folds into a right-handed α-helical conformation, stabilized by four intramolecular (5→1) hydrogen bonds and two intermolecular hydrogen bonds between molecules related by the 2_1 symmetry along the b direction. In order to determine the helical conformation definitively, the helical parameters (unit height h and unit twist θ) at each amino-acid residue were derived from the bond lengths, bond angles, and torsional angles of the peptide main chain. The average values of these parameters for seven residues (h=1.57 Å and θ=99.0°) showed much better agreement with those for an α-helix (h=1.5 Å and θ=100°) rather than with those for a 3_{10}-helix (h=2.0 Å and θ=120°). Peptide helices are arranged in columns in head-to-tail fashion. These columns are packed in parallel with respect to their helical direction. Between neighbouring chains of helices only hydrophobic contacts are found.

The membrane-channel-forming polypeptides, alamethicin and suzukacillin, contain a high proportion of α-aminoisobutyric acid (Aib) residues. As a result of the steric hindrance of the two methyl moieties linked to a C_α atom, the torsional angles, ϕ and ψ, of an Aib residue are severely restricted to the values near those associated with either the right- or left-handed α-helix (ϕ=±57°, ψ=±47°) and the 3_{10}-helix (ϕ=±60°, ψ=±30°).[1] Therefore, Aib-containing oligopeptides have shown a high tendency to the above helical conformations,[1] especially the 3_{10}-helical conformation. At least, up to pentapeptides, they have all been shown to adopt the 3_{10}-helix with the exception of Boc-Aib-Pro-Val-Aib-Val-OMe, in which the helix is stabilized by two types of hydrogen bonds, 5→1 and 4→1, indicating an α-helix and a 3_{10}-helix respectively.[2] Although the difference in the torsional angles of ϕ and ψ between the α-helix and the 3_{10}-helix is very small, the type of helix is important in many aspects. For example, the helical type affects its length and radius and also the distribution of hydrophobic amino-acid residues on the surface of a helix. These factors are very important in any study of the design of three-dimensional structures of peptides using the Aib residues.

Recently, Narita and Doi succeeded in improving the solubility of protected peptide fragments by utilizing the nature of the Aib residue to promote helical folding in peptides.[3] Boc-(Leu$_3$-Aib)$_2$-OBzl is one of the oligopeptides they prepared to demonstrate the above usefulness of Aib residues. The IR absorption spectra of the peptide both in dichloromethane and in the single-crystal state showed strong intensity bands at 3340—3320 cm^{-1} (amide A) and 1665—1659 cm^{-1} (amide I). This indicated a helical conformation (3_{10}- or α-helix) in both the solution and the crystal state.[4]

In our preliminary single crystal study of Boc-(Leu$_3$-Aib)$_2$-OBzl, the α-helical conformation was deduced from the intensity distribution of the meridional ($0k0$) and near-meridional reflections with the spacing in the range of 1.4—2.2 Å and by comparison of the molecular size and the lattice dimensions.[4] In this paper, we will discuss in detail the molecular and crystal structure of this oligopeptide and will also discuss its helical type by using helical parameters calculated from the bond lengths, bond angles, and torsional angles of the peptide main chain for each residue.

Materials and Methods

The Boc-(Leu$_3$-Aib)$_2$-OBzl was prepared by the step-by-step elongation and fragment condensation methods. The procedures have been reported in detail elsewhere.[3] Boc-(Leu$_3$-Aib)$_2$-OBzl powder (40 mg) was dissolved in 30 ml of aqueous methanol (methanol:water=2:1 by volume) at 50 °C. Subsequently, the solution was cooled slowly to room temperature. After several days, transparent, plate-like single crystals were obtained. The lattice parameters and diffraction intensities were measured on a Rigaku four-circle diffractometer with Ni-filtered Cu $K\alpha$ radiation (λ=1.542 Å). The lattice parameters were refined by the least-squares fit using 20 reflections in the 2θ range of 40—50°. By using the ω-scan mode for reflections with 2θ values less than 30°, and by using the 2θ–ω-scan mode for the other reflections, the intensities of 3391 reflections were collected up to 100° in 2θ. The intensity measurements were carried out at scan speeds of 8° min^{-1} for reflections with $0<F_o^2<200$, 4° min^{-1} for $200<F_o^2<600$, and 2° min^{-1} for $600<F_o^2$. The scan width was $\Delta\omega=(1.2+0.45\tan\theta)°$. Three reference reflections, monitored every 100 reflections, showed no significant intensity deterioration during the data collection. Corrections were made for the

Table 1. Fractional Coordinates and Equivalent Isotropic Temperature Factors for Non-Hydrogen Atoms of Boc-(Leu$_3$-Aib)$_2$-OBzl, with Estimated Standard Deviations in Parentheses

	Atom	x	y	z	B_{eq}/Å^2
Boc					
	C_1	0.8522(26)	−0.3000(9)	1.3014(26)	14.36
	C_2	0.9702(26)	−0.3704(8)	1.4062(23)	13.00
	C_3	1.0681(27)	−0.2885(11)	1.4626(23)	16.58
	C_4	0.9800(22)	−0.3207(7)	1.3585(19)	10.22
	O_1	1.0229(13)	−0.3287(4)	1.2565(12)	9.30
	C_5	1.0526(17)	−0.2943(5)	1.1953(17)	7.34
	O_2	1.0348(12)	−0.2520(4)	1.1991(11)	8.10
Leul 1					
	N	1.1018(12)	−0.3125(4)	1.1127(12)	6.47
	C_α	1.1619(15)	−0.2803(5)	1.0538(16)	6.26
	C′	1.0668(15)	−0.2483(4)	0.9616(15)	6.22
	O	1.0986(11)	−0.2049(4)	0.9532(11)	7.36
	C_β	1.2308(15)	−0.3094(5)	0.9855(17)	7.22
	C_γ	1.3087(16)	−0.2835(6)	0.9321(20)	8.28
	C_{δ_1}	1.4221(21)	−0.2610(9)	1.0347(29)	14.25
	C_{δ_2}	1.3445(25)	−0.3139(8)	0.8486(26)	13.54
Leu 2					
	N	0.9455(11)	−0.2622(4)	0.8787(12)	6.06
	C_α	0.8467(16)	−0.2285(5)	0.7812(16)	6.97
	C′	0.8322(14)	−0.1847(5)	0.8462(16)	6.55
	O	0.8260(16)	−0.1441(3)	0.8012(11)	7.71
	C_β	0.7214(16)	−0.2532(6)	0.7017(20)	8.91
	C_γ	0.6142(17)	−0.2218(6)	0.5929(22)	11.54
	C_{δ_1}	0.4933(28)	−0.2226(13)	0.6054(29)	20.72
	C_{δ_2}	0.5543(32)	−0.2422(9)	0.4544(26)	17.60
Leu 3					
	N	0.8176(13)	−0.1905(5)	0.9632(14)	7.51
	C_α	0.8027(15)	−0.1490(5)	1.0307(17)	6.41
	C′	0.9254(15)	−0.1188(4)	1.0873(15)	5.64
	O	0.9205(10)	−0.0751(3)	1.0791(10)	6.38
	C_β	0.7661(18)	−0.1671(6)	1.1438(20)	8.39
	C_γ	0.7446(20)	−0.1265(7)	1.2217(22)	10.47
	C_{δ_1}	0.6279(20)	−0.0946(7)	1.1441(25)	11.45
	C_{δ_2}	0.7481(27)	−0.1483(10)	1.3453(26)	15.03
Aib 1					
	N	1.0468(12)	−0.1387(4)	1.1511(11)	6.29
	C_α	1.1716(13)	−0.1128(5)	1.2108(14)	5.61
	C′	1.1749(14)	−0.0793(4)	1.1038(15)	5.81
	O	1.2113(10)	−0.0386(4)	1.1294(10)	6.97
	C_{β_1}	1.1821(16)	−0.0850(6)	1.3319(16)	7.41
	C_{β_2}	1.2813(15)	−0.1490(6)	1.2511(17)	7.69
Leu 4					
	N	1.1389(12)	−0.0984(4)	0.9842(12)	6.26
	C_α	1.1473(14)	−0.0688(5)	0.8767(15)	5.75
	C′	1.0597(13)	−0.0286(5)	0.8374(14)	5.08
	O	1.0907(10)	0.0095(4)	0.8078(12)	8.28
	C_β	1.1191(16)	−0.1024(6)	0.7553(16)	6.92
	C_γ	1.2152(17)	−0.1392(7)	0.7714(17)	8.21
	C_{δ_1}	1.1662(22)	−0.1735(7)	0.6597(21)	11.25
	C_{δ_2}	1.3396(22)	−0.1161(9)	0.7776(27)	13.27
Leu 5					
	N	0.9433(10)	−0.0319(4)	0.8346(11)	5.39
	C_α	0.8423(12)	0.0070(5)	0.7935(14)	5.12
	C′	0.8729(14)	0.0439(4)	0.8956(15)	5.51
	O	0.8415(10)	0.0847(3)	0.8662(9)	6.95
	C_β	0.7086(13)	−0.0144(5)	0.7475(14)	5.37
	C_γ	0.6482(15)	−0.0455(6)	0.6203(17)	7.67

Table 1. (Continued)

	Atom	x	y	z	B_{eq}/Å^2
	C_{δ_1}	0.6145(21)	−0.0141(7)	0.4964(17)	10.61
	C_{δ_2}	0.5352(16)	−0.0740(7)	0.6088(22)	10.52
Leu 6					
	N	0.9368(11)	0.0301(4)	1.0266(11)	5.30
	C_α	0.9768(13)	0.0664(5)	1.1335(14)	5.17
	C′	1.0952(13)	0.0933(4)	1.1478(13)	5.07
	O	1.1139(10)	0.1349(4)	1.1859(11)	6.98
	C_β	1.0006(14)	0.0416(6)	1.2651(14)	5.93
	C_γ	0.8831(13)	0.0185(6)	1.2672(15)	6.44
	C_{δ_1}	0.7762(17)	0.0487(8)	1.2410(22)	10.23
	C_{δ_2}	0.9281(21)	−0.0045(7)	1.4126(19)	10.18
Aib 2					
	N	1.1900(12)	0.0705(4)	1.1296(12)	6.14
	C_α	1.3079(12)	0.0907(5)	1.1361(13)	5.28
	C′	1.3839(15)	0.1170(5)	1.2675(17)	6.90
	O	1.4490(12)	0.1497(4)	1.2850(12)	9.72
	C_{β_1}	1.3943(15)	0.0495(6)	1.1314(18)	7.75
	C_{β_2}	1.2713(16)	0.1262(6)	1.0219(16)	7.94
OBzl					
	O_1	1.3817(11)	0.0935(4)	1.3717(10)	7.69
	C_1	1.4527(18)	0.1178(7)	1.4960(17)	10.19
	C_2	1.4236(15)	0.0872(6)	1.5952(15)	7.38
	C_3	1.3321(16)	0.0552(6)	1.5676(17)	8.55
	C_4	1.3051(19)	0.0325(7)	1.6637(19)	10.10
	C_5	1.3840(20)	0.0426(7)	1.7921(19)	9.85
	C_6	1.4772(19)	0.0749(7)	1.8267(18)	9.66
	C_7	1.5044(16)	0.0994(6)	1.7327(17)	8.23

Lorentz and polarization factors, but not for the absorption effect. A total of 2863 reflections greater than $3\sigma(F_o)$ were used in the following analysis.

The density was measured by means of a flotation method using a solution of carbon tetrachloride and toluene. On the basis of the measured density and the unit cell volume, the unit cell can be said to contain two oligopeptide molecules.

Crystal Data: $C_{56}H_{96}N_8O_{11}$, F.W.=1057.4, monoclinic, space group $P2_1$, Z=2, a=11.450(2), b=27.915(7), c=11.255(2) Å, β=116.95(1)°, V=3207(1) Å^3, D_x=1.093, D_m=1.09 g cm^{-3}, ρ(Cu $K\alpha$)=5.7 cm^{-1}.

Determination and Refinement of the Structure

The direct method with the SAPI87[5] program based on MULTAN-80[6] was applied to the $P2_1$ space group. After several cycles of block-diagonal least-squares refinement starting from the coordinates of all the non-hydrogen atoms of the oligopeptide obtained by the direct method, difference Fourier syntheses revealed no significant peak. After an anisotropic refinement of the non-hydrogen atoms, the hydrogen atoms located on their calculated positions with isotropic temperature factors were included in the refinement. The quantity minimized was $\sum\omega(|F_o|-|F_c|)^2$, with w=1.0 for all reflections. After several cycles, some hydrogen atoms with unacceptable geometry were excluded from further calculations. The final R value was 0.083 (R_w=0.077) for all the non-hydrogen atoms and 28 hydrogen atoms. The final atomic parameters for the non-hydrogen atoms are given in Table 1.[7]

The atomic scattering factors were taken from International Tables for X-Ray Crystallography, Vol. IV.[8] Computations were done on a HITAC M-280H computer at the Computer Center, University of Tokyo, with the help of the programs in UNICS III.[9]

Results and Discussion

For the convenience of atom specification, all the residues are numbered in series from the N- to the C-terminus. Therefore, the molecule of Boc-(Leu$_3$ Aib)$_2$-OBzl is denoted as Boc-Leu1-Leu2-Leu3-Aib1-Leu4-Leu5-Leu6-Aib2-OBzl. The atomic names in the Leu and Aib residues are those given in the IUPAC-IUB recommendations,[10] while those in the protected groups at N- and C-termini are shown in Fig. 1.

Peptide-Backbone Conformation. A perspective view of the molecule is shown in Fig. 1, together with a part of the upper molecule related by the 2_1-symmetry. The bond distances, bond angles, and torsional angles (ϕ, ψ, ω) of the peptide main chain are given in Table 2. The bond lengths of C_i^α-C_i' in

Leu1 (1.43 Å), Leu2 (1.47 Å), Leu4 (1.43 Å), and Leu5 (1.46 Å) are slightly shorter, while those of C'_i–N_{i+1} in Leu2 (1.41 Å), Leu3 (1.36 Å), Leu5 (1.37 Å), and Leu6 (1.35 Å) are slightly longer, than the values of 1.53 Å and 1.32 Å respectively derived by Pauling et al.[11] Because of the contact between the two methyl moieties linked to the C^α_i atom and the carbonyl oxygen, the bond angles of C'_{i-1}–N_i–C^α_i (126° and 128°) and N_i–C^α_i–C'_i (108° and 108°) in the Aib residues are significantly different from those in the Leu residues.

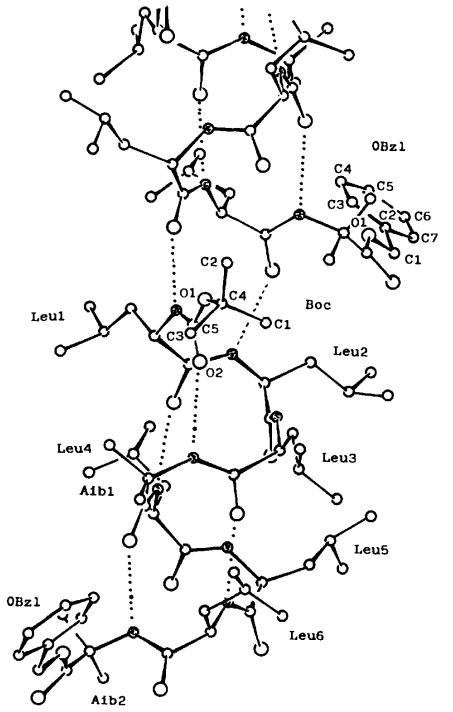

Fig. 1. Molecular structure of Boc-(Leu3-Aib)2-OBzl together with the atomic numbering in the terminal protected moieties (Boc and OBzl). The upper and lower side molecules are related to each other by a crystallographic 2_1 symmetry. Broken lines denote intra- and intermolecular hydrogen bonds.

All the peptide torsional angles, ω, showed a very good planarity. The values of the torsional angles, ϕ and ψ, showed that the octapeptide folds into a right-handed helix with the exception of the Aib2 residue at the C-terminus, in which the ϕ and ψ values belong to a left-handed helix. A change in the helical sense at the C-terminal Aib residue is usually observed in the oligopeptide helices with the protected moiety at the C-terminus.[12-14] This may be attributed to the bulky protected moiety linked to the Aib residue and the restricted conformation of the Aib residue. Since the ϕ and ψ values of an Aib residue are restricted to only two narrow regions, that is, near the right- or the left-handed α- (or 3_{10}-) helical regions, the helical sense of the C-terminus Aib residue has to be different from that of the preceding peptide region in order to avoid contact between the protected moiety and the rest of the molecule.

Since the allowed regions of torsional angles for the α-helix and the 3_{10}-helix almost entirely overlap in the ϕ–ψ map, it is not possible to decide a helical conformation on the basis of only the torsional angles in Table 2. Therefore, the helical conformation of Aib-containing oligopeptides have usually been determined by the intramolecular hydrogen bonding type, that is, the hydrogen bonds between the C=O group of Residue i and the N-H group of Residue i+3, which belong to the 3_{10}-helix, and those between Residue i and Residue i+4, which belong to the α-helix. However, even by the hydrogen-bonding type it is difficult to determine a helical structure definitively when the N-H groups of Residues i+3 and i+4 are both close to the C=O group of Residue i. In this study, therefore, the helical parameters were used as the criterion of the helical structure. They are the unit height (h) and the unit twist (θ), that is, the height per residue along the helical axis and the rotational angle per residue about the helical axis respectively. Assuming that each amino acid residue forms its own helix, the helical parameters are derived from its bond

Table 2. Bond Lengths, Bond Angles, and Torsional Angles of the Peptide Main Chain, together with Standard Deviations in Parentheses

	Leu 1	Leu 2	Leu 3	Leu 4	Leu 5	Leu 6	Aib 1	Aib 2
Bond length/Å								
N_i–C^α_i	1.46(2)	1.50(2)	1.44(2)	1.50(2)	1.50(2)	1.48(2)	1.46(2)	1.43(2)
C^α_i–C'_i	1.43(2)	1.47(2)	1.51(2)	1.43(2)	1.46(2)	1.49(2)	1.54(2)	1.52(2)
C'_i–N_{i+1}	1.33(2)	1.41(3)	1.36(2)	1.32(2)	1.37(2)	1.35(2)	1.33(2)	—
Bond angle/°								
C'_{i-1}–N_i–C^α_i	120(4)	122(1)	120(1)	119(1)	126(1)	120(1)	126(1)	128(1)
N_i–C^α_i–C'_i	111(1)	112(1)	111(2)	113(2)	113(1)	111(1)	108(1)	108(1)
C^α_i–C'_i–N_{i+1}	122(1)	117(1)	122(1)	121(1)	118(1)	120(1)	116(1)	—
Torsional angle/°								
$\phi(C'_{i-1}$–N_i–C^α_i–$C'_i)$	−66(2)	−53(2)	−66(2)	−65(2)	−76(2)	−76(2)	−53(2)	53(2)
$\psi(N_i$–C^α_i–C'_i–$N_{i+1})$	−40(2)	−47(2)	−43(2)	−35(2)	−33(2)	−36(2)	−46(2)	40(2)
$\omega(C^\alpha_i$–C'_i–N_{i+1}–$C^\alpha_{i+1})$	−179(1)	−180(1)	−179(1)	−179(1)	176(1)	178(1)	−176(1)	—

Table 3. Helical Parameters for Each Amino Acid in Boc-(Leu$_3$-Aib)$_2$-OBzl

	Leu 1	Leu 2	Leu 3	Aibl	Leu 4	Leu 5	Leu 6	Average
h/Å	1.55	1.64	1.51	1.69	1.74	1.48	1.39	1.57
θ/°	97.5	101.8	95.6	104.1	100.4	98.4	94.9	99.0

Table 4. Torsional Angles of Side Chains in Leu Residues, together with Estimated Standard Deviations in Parentheses

	χ_1	χ_2	χ_2'
Leu 1	−174(1)	66(2)	−168(2)
Leu 2	−177(1)	−127(2)	127(2)
Leu 3	−179(2)	66(2)	−165(2)
Leu 4	−68(2)	−71(2)	170(2)
Leu 5	−66(2)	−69(2)	164(1)
Leu 6	−64(2)	−58(2)	−179(1)

Table 5. Hydrogen-Bond Parameters

Hydrogen bond	Bond length/Å (N···O)	Bond angle/° (N-H···O)
Intermolecular		
N(Leu 1)···O(Leu 5)	2.93	172
N(Leu 2)···O(Leu 6)	2.97	154
Intramolecular		
N(Aib 1)···O2(Boc)	3.22	162
N(Leu 4)···O(Leu 1)	3.01	167
N(Leu 6)···O(Leu 3)	3.02	175
N(Aib 2)···O(Leu 4)	3.06	176

lengths, bond angles, and torsional angles by the method of Sugeta and Miyazawa.[15] These values for each residue except for the C-terminus Aib2 are shown in Table 3. The average values are h=1.57 Å and θ=99.0°. Since the helical parameters for the α-helix and the 3_{10}-helix are h=1.5 Å and θ=100°, and h=2.0 Å, and θ=120°, respectively, it is obvious that the molecular conformation of Boc-(Leu$_3$-Aib)$_2$-OBzl is not a 3_{10}-helix, but an α-helix. This finding agreed with our previous conclusion from the X-ray intensity distribution of the meridional reflections and the consideration of the lattice dimensions.[4]

Side-Chain Conformations. The torsional angles in the Leu side chains are given in Table 4. The torsional angle of χ_1 (N-C_α-C_β-C_γ) is trans (Leu1, Leu2, and Leu3) or gauche (Leu4, Leu5, and Leu6), while those of χ_2 and χ_2' (C_α-C_β-C_γ-C_{δ_1} and C_α-C_β-C_γ-C_{δ_2}) are also trans or gauche, except in the Leu2 residue. The C_{δ_1} and C_{δ_2} atoms in the Leu2 residue cannot adopt either the trans or gauche conformation because of the short contact with the carbonyl oxygen atom of the Aib2 residue in the neighbouring molecule.

Hydrogen Bonds. The right-handed α-helical conformation of the peptide is stabilized by four intramolecular and two intermolecular hydrogen bonds (Fig. 1). The hydrogen-bond parameters are given in Table 5. All the lengths of the intramolecular hydrogen bonds are significantly longer than the mean value (2.9±0.1 Å)[16] usually observed in the peptide structures in which no Aib residues are included. This fact is also observed in other Aib-containing oligopeptides, such as Boc-(Ala-Aib)$_2$-Aib-OMe,[12] Boc-Leu-Aib-Pro-Val-Aib-OMe,[13] *p*-BrBz-(Aib)$_8$-O-*t*-Bu,[14] Boc-(Ala-Aib)$_2$-Ala-Glu(OBzl)-(Ala-Aib)$_2$-Ala-OMe,[17] and Boc-Leu-Aib-Pro-Val-Aib-Aib-Glu(OBzl)-Gln-Phl monohydrate.[18] This marked tendency of the Aib-containing peptides is probably due to the fact that the molecular conformations of these peptides are mainly determined by the stereochemical restrictions of the Aib residues rather than by the stabilization by the intramolecular hydrogen bonds. All the intramolecular hydrogen bonds listed in Table 5 are between the C=O group of Residue i and the N-H group of Residue i+4, which indicates the α-helical conformation. There is no hydrogen bond associated with N(Leu3) and N(Leu5). In the case of N(Leu3), there is no acceptor oxygen in the upper-peptide molecule because of the opposite helical sense at the C-terminal Aib2 residue. On the other hand, in the case of N(Leu5), the distance of 3.36 Å to the carbonyl oxygen in the Leu2 residue is

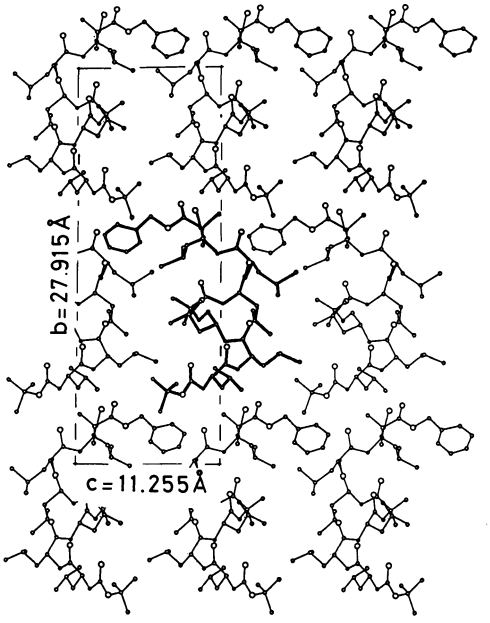

Fig. 2. Head-to-tail arrangement of Boc-(Leu$_3$-Aib)$_2$-OBzl molecules as viewed along the a direction. One molecule in a unit cell is drawn with bold lines.

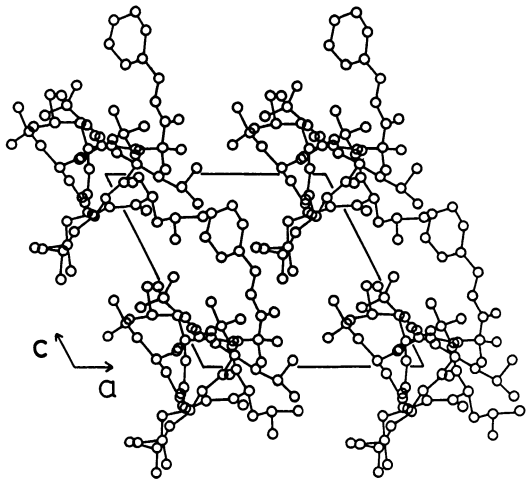

Fig. 3. Packing of octapeptide molecules in the crystal viewed along the *b* (helical) direction. For the sake of clarity only one molecule in the unit cell is shown.

fairly short, but too long as a hydrogen bond distance. In addition to the four intramolecular hydrogen bonds, two intermolecular hydrogen bonds, N(Leu1)···O(Leu5) of 2.93 Å and N(Leu2)···O(Leu6) of 2.97 Å, stabilize the helical conformation.

Crystal Structure of Boc-(Leu$_3$-Aib)$_2$-OBzl. Figure 2 shows the head-to-tail arrangement of the molecules as viewed along the *a* direction. The upper and lower molecules are related by the 2_1 symmetry along the *b*-axis and are linked head-to-tail by two intermolecular hydrogen bonds to form columns along this direction. These columns are arranged parallel with respect to their helical direction. The packing structure of Boc-(Leu$_3$-Aib)$_2$-OBzl molecules in the *ac*-plane is shown in Fig. 3. In this figure, only four equivalent molecules are illustrated; the molecules related by the 2_1 symmetry are omitted for the sake of clarity. Since the lattice dimensions of *a* and *c* are similar to each other, and since $\beta(=117°)$ is very close to 120°, the columns are packed pseudo-hexagonally. There is no hydrogen bond between laterally packed molecules, and only hydrophobic interactions stabilize the crystal structure. The benzyl moieties and the side chains of the Leu residues project from the helix core and interact with the neighbouring molecules (Figs. 2 and 3). The fairly short contacts between molecules are O(Leu5)···C7(OBzl) 3.47 Å, O(Leu5)···O1(Boc) 3.48 Å, O(Aib2)···C(Leu2) 3.39 Å, O(Aib2)···C(Leu1) 3.48 Å, and O(Leu6)···N(Leu1) 3.47 Å.

The authors wish to express their gratitude to Rigaku Corporation, for the permission to use a full-automatic X-ray structure analysis system (RASA-5RII) and to Mr. Toshihiko Hori, Rigaku Corporation, for his help with the intensity measurements.

References

1) Y. Paterson, S. M. Rumsey, E. Benedetti, G. Nemethy, and H. A. Sheraga, *J. Am. Chem. Soc.*, **103**, 2947 (1981), and the references cited therein.

2) A. K. Francis, M. Iqbal, P. Balaram, and M. Vijayan, *J. Chem. Soc., Perkin Trans. 2*, **1982**, 1235.

3) M. Narita, M. Doi, H. Sugasawa, and K. Ishikawa, *Bull. Chem. Soc. Jpn.*, **58**, 1473 (1985).

4) K. Okuyama, S. Nakanishi, N. Tanaka, M. Doi, M. Narita, and K. Imada, *Polym. J.*, **20**, 707 (1988).

5) J. Yao, C. Zheng, J. Qian, F. Han, Y. Gu, and H. Fan, (1987), SAPI87: A System of Computer Programs for the Automatic Solution of Crystal Structures from X-ray Diffraction Data. Academia Sinica, Beijing, China.

6) P. Main, S. J. Fiske, S. E. Hull, L. Lessinger, G. Germain, J. P. Declercq, and M. M. Woolfson, (1980), MULTAN-80: A System of Computer Programs for the Automatic Solution of Crystal Structures from X-ray Diffraction Data. Univers. of York, England, and Louvain, Belgium.

7) The tables of anisotropic thermal parameters, the coordinates of the hydrogen atoms, and the observed and calculated structure factors are kept at the Chemical Society of Japan, Document No. 8822.

8) International Tables for Crystallography, Vol. IV, Kynoch Press, Birmingham (1974), p. 71.

9) T. Sakurai and K. Kobayashi, *Rep. Inst. Phys. and Chem. Res.*, **55**, 69 (1978).

10) IUPAC-IUB Commission on Biochemical Nomenclature 1969, *Biochemistry*, **9**, 3471 (1970).

11) L. Pauling, R. B. Corey, and H. R. Branson, *Proc. Natl. Acad. Sci.*, **37**, 205 (1951).

12) A. K. Francis, M. Iqbal, P. Balaram, and M. Vijayan, *Biopolymers*, **22**, 1499 (1983).

13) C. P. Rao and P. Balaram, *Biopolymers*, **21**, 2461 (1982).

14) C. Toniolo, G. M. Bonosa, A. Bavoso, E. Benedetti, B. D. Blasio, V. Pavone, and C. Pedone, *Macromolecules*, **19**, 472 (1986).

15) H. Sugeta and T. Miyazawa, *Biopolymers*, **5**, 673 (1967).

16) G. E. Schulz and R. H. Schirmer, "Principle of Protein Structure," ed by C. R. Cantor, Springer, New York.

17) R. Bosh, G. Jung, H. Schmitt, and W. Winter, *Biopolymers*, **24**, 961 (1985).

18) R. Bosh, G. Jung, H. Schmitt, and W. Winter, *Biopolymers*, **24**, 979 (1985).

 © 1988 The Chemical Society of Japan Bull. Chem. Soc. Jpn., 61, 3121—3127 (1988)

Spectroscopic Studies on the Intramolecular Hydrogen Abstraction Reactions of *n*-Alkyl Anthraquinone-2-carboxylates

Yoshifumi TANIMOTO,* Megumu UEHARA, Masanobu TAKASHIMA, and Michiya ITOH
Faculty of Pharmaceutical Sciences, Kanazawa University, Takara-machi, Kanazawa 920
(Received March 30, 1988)

Chain length dependence of the intramolecular hydrogen abstraction reaction of *n*-alkyl anthraquinone-2-carboxylates (AQ-*n*, *n*=2—20) has been studied by steady-state photolysis, phosphorescence, laser flash photolysis, and two-step laser induced fluorescence spectroscopies. All the results indicate that the excited triplet of the anthraquinone chromophore abstracts a hydrogen atom from its methylene side chain, whose rate increases with increasing chain length. The rate constant of AQ-8 is 1×10^4 s^{-1} and the increase in the rate is about 1.5×10^4 s^{-1} per one additional methylene unit for $n\geqslant10$.

For many years chemistry and physics of bifunctional chain molecules have drawn much attention of polymer chemists, ESR and NMR spectroscopists, photochemists, photophysicists, and synthetic organic chemists, as reviewed in the literature.[1] It is because we can elucidate structural and energetic factors required in a reaction. Concerning with photochemistry, remote hydrogen abstraction of *n*-alkyl benzophenone-4-carboxylates, for example, have been extensively studied by Winnik and coworkers, to show how chain motion affects their photochemistry and photophysics.[2] In intramolecular excimer fluorescence of pyrene-$(CH_2)_n$-pyrene (*n*=2—22), fluorescence yields of the excimer were reported to be maximum at *n*=3 and minimum at *n*=7.[3] Switching of photochemical reaction pathways was found for redox reaction of a series of *N*-[ω-(*p*-nitrophenoxy)-alkyl]anilines.[4]

We have studied the magnetic field effects on the intermolecular hydrogen abstraction reaction of anthraquinones in aqueous sodium dodecyl sulfate (SDS) micellar solution, where a SDS surfactant acts itself as a hydrogen donor.[5] As intramolecular analogue of the reaction between excited triplet anthraquinone and SDS in a micelle, we designed a intramolecular reaction of anthraquinone with its methylene side chain. The excited triplet state is highly reactive compared with that of benzophenone so that the reaction processes may be followed precisely by time-resolved spectroscopic technique. This paper describes the effect of methylene chain lengths on photochemical and photophysical processes of *n*-alkyl anthraquinone-2-carboxylates, studied by steady-state photolysis, phosphorescence, laser flash photolysis, and two-step laser excitation fluorescence spectroscopies.[6]

Experimental

Chemicals. *n*-Alkyl anthraquinone-2-carboxylates (AQ-*n*, *n*=2—20) were synthesized by the condensation of anthraquinone-2-carboxylic acid sodium salt and *n*-alkyl bromides and purified by column chromatography and recrystallization. Typical analytical data of AQ-14 are as follows: mp 102 °C. IR(KBr) 2950—2840 (methylene), 1725 (aromatic ester), 1670 cm^{-1} (aromatic ketone). ^1H NMR (60 MHz, $CDCl_3$) δ=0.8—0.96 (t, 3H, CH_3-), 1.25 (s, 24H, $-CH_2-$), 4.23—4.45 (t, 2H, $-CO-O-CH_2-$), 7.63—8.80 (m, 7H, aromatic). Found: C, 77.64; H, 8.22%. Calcd for $C_{29}H_{36}O_4$: C, 77.64; H, 8.09%. Mass spectra; *m/z* 448 (M^+). Melting points of AQ-*n* are listed in Table 1.

EP Grade 1,1,2-trichloro-1,2,2-trifluoroethane (Freon 113) was purified by a column of basic aluminum oxide (1 m) and 3-methylpentane was distilled from $LiAlH_4$. Freon 113 was used in order to avoid intermolecular hydrogen abstraction reaction of AQ-*n* from solvent. Sample solutions were deaerated by several freeze-pump-thaw cycles, when necessary.

Apparatus. In steady-state photolysis, a 3 ml aliquote of the sample solution was irradiated with a 500 W xenon arc lamp filtered with a combination of a color glass (Toshiba UV-D33S) and a $NiSO_4$-$CoSO_4$ aqueous solution ($\lambda_{max}\approx330$ nm). The UV absorption spectral changes were recorded by a Hitachi U-3200 spectrophotometer.

Phosphorescence spectra were measured with a Hitachi MPF-4 spectrophotometer. The lifetimes were determined with an Ortec single photon counting system equipped with a PRA light pulser.

Transient absorption spectra were obtained by using an XeCl excimer laser (Lambda Physik EMG-50E, 308 nm) and a xenon arc lamp as an exciting and a probe light source, respectively. Transient signal on an Iwatsu TS-8123 storagescope was fed into a Fujitsu FM-11BS microcomputer for analysis.

Two-step laser induced fluorescence (TS-LIF) was measured by using an excimer laser (308 nm) and a N_2 laser-pumped dye laser (Molectron UV-12 and DL-14, 430 nm) as the first and the second laser. A homemade variable delay circuit was used for the timing of two lasers.

Table 1. Melting Points of *n*-Alkyl Anthraquinone-2-carboxylates (AQ-*n*)

n	Melting point/°C	*n*	Melting point/°C
2	149—150	12	97—98
3	101—102	14	102
4	122—123	16	104—105
6	83	18	107
8	86—87	20	107—108
10	93—94		

Results

Steady-State Photolysis. Figure 1 shows a typical UV absorption spectral change of AQ-14 in Freon 113 solution upon photoirradiation, indicating photoreaction of this molecule. After photolysis, the solution becomes fluorescent as shown in the figure. Photoproducts, whose absorption and fluorescence bands appear around 350—500 and 450—600 nm, respectively, may be attributable to the cyclization products, since cyclic photoproducts in the photoinduced intramolecular hydrogen abstraction of *n*-alkyl benzophenone-4-carboxylates[2] and a fluorescent photoadduct of anthrasemiquinone to a SDS surfactant in the photoreaction of anthraquinone[5,7] were reported (see bellow).

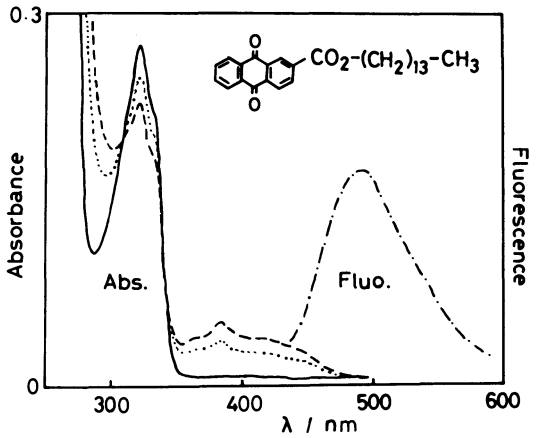

Fig. 1. Absorption and fluorescence spectra of AQ-14 in Freon 113 during photolysis. ——, before irradiation; -----, after 2 min irradiation, --- and —·—, after 4 min irradiation.

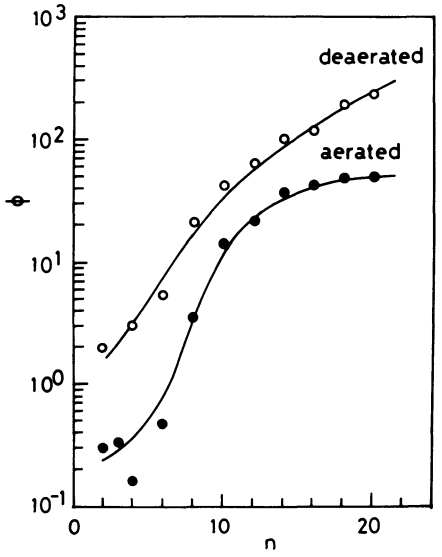

Fig. 2. Relative yields ϕ of disappearance of AQ-*n* in Freon 113.

Relative yield ϕ of disappearance of AQ-*n* were determined from the initial absorption intensity changes around 320 nm by the procedure described in a previous paper.[5] As shown in Fig. 2, ϕ is very small at shorter methylene chain length ($n<6$) and shows a sudden increase around $n=8$. Photolysis was also carried out in aerated Freon 113 solution of AQ-*n* (Fig. 2). The yields in aerated solutions are always smaller than those in deaerated solutions. The fact indicates that dissolved oxygen is also involved in the reaction though its mechanism is unknown at the present stage.

Phosphorescence. In order to clarify the primary step of the present photoreaction, we first examined the excited triplet of AQ-*n* by phosphorescence. Figure 3 shows phosphorescence spectra of AQ-*n* observed at room temperature and of AQ-2 at 77 K. In the spectra at room temperature, the band maxima appear at 435, 464, 502, 548, and 602 nm, and the shortest wavelength band at 435 nm disappears in the

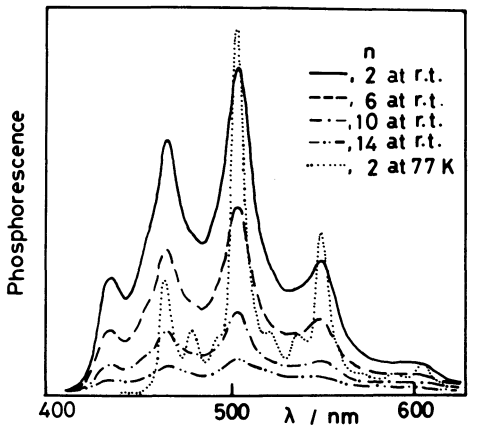

Fig. 3. Phosphorescence spectra of AQ-*n* at room temperature and 77 K.

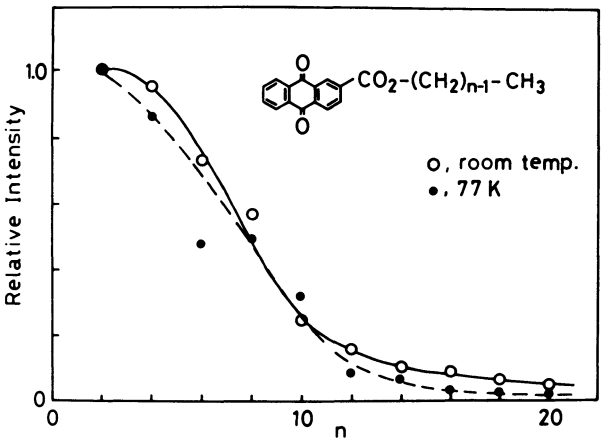

Fig. 4. Relative phosphorescence intensities of AQ-*n* at room temperature and 77 K. The intensities were normalized for that of AQ-2 at the respective temperature.

Table 2. Lifetimes (μs) of Excited Triplet State of AQ-n, Determined by Phosphorescence $\tau_P(n)$ and Laser Flash Photolysis $\tau_{LF}(n)$[a)]

n	τ_P	τ_{LF}	n	τ_P	τ_{LF}
2	75.8	48.7	12	11.9	10.0
4	70.4	42.9	14	7.9	7.3
6	52.3	38.1	16	6.8	6.0
8	40.7	30.4	18	5.5	5.2
10	19.0	12.6	20	4.3	4.5

Experimental errors are ±10 and ±20% for τ_P and τ_{LF}, respectively.

spectrum at 77 K. The energy difference between two successive bands are 1437, 1631, 1672, and 1637 cm^{-1}. Since the band progression from the second band is characteristic of the C=O stretching vibration, the 0–0 band of the phosphorescence is assigned to the one at 464 nm, and the lowest triplet state is of n,π^* nature. The assignment is compatible with the n,π^* nature of the lowest triplet state of anthraquinone.[8–11)] The shortest wavelength band at 435 nm, which disappears at 77 K, may be attributable to the emission from the thermally-populated higher triplet state. It is uncertain at the present stage whether it is the second triplet state or the vibronic state of the lowest one.[12)]

The relative phosphorescence intensities and lifetimes of AQ-n depend on the chain length n at room temperature as shown in Fig. 4 and Table 2, respectively. The lifetimes of AQ-n may be free from triplet-triplet (T–T) annihilation reaction, since they were obtained under low excitation density. Both phosphorescence intensities and lifetimes decrease with increasing the methylene chain length, n, suggesting that intramolecular reaction, i.e., hydrogen abstraction, is responsible for the lifetime of the excited triplet states. Furthermore, as shown in Fig. 4, the phosphorescence intensity dependence on the chain length observed at 77 K resembles that observed at room temperature. The facts may imply that the conformational distribution of the chain at room temperature is frozen at 77 K. Thus the phosphorescence lifetimes of AQ-n at 77 K may be determined by the intramolecular hydrogen abstraction. However, it is of interest that photoirradiation of AQ-14 in 3-methylpentane rigid matrix at 77 K did not show any appreciable change in its UV absorption spectrum. Probably, back reaction is fast in the rigid matrix because of conformational rigidity of the methylene chain in it.

Transient Absorption Spectra. Figure 5 shows transient absorption spectra of AQ-14 in Freon 113. As shown in the inset, decay of a transient absorption at 380 nm reaches a constant value around a 50 μs delay after laser excitation. In the transient absorption spectra at the present time scale (ca. 50 μs), there may be at least three species, i.e., excited triplet anthraquinone, semiquinone, and photoproducts. The absorption bands peaked around 380 and 500 nm, observed at a 1.2 μs delay, is mostly attributable to the T–T absorption of the anthraquinone chromophore. It is because similar spectra were observed for AQ-2, as shown in Fig. 5, and other molecules with n=3—20 in the μs time region, and the lifetime is comparable with its phosphorescence lifetime. On the other hand, the bands peaked around 380 and 450 nm, observed at a 33.5 μs delay, may be assigned to cyclization photoproducts, since they are similar to those of photoproducts observed in the steady-state photolysis (Fig. 1). The spectrum in the middle stage of the delay time might be attributable to the semiquinone radical, though its rigorous assignment is impossible. The decay of the semiquinone radical seems to be fast as observed in the reaction of the anthrasemiquinone radical in

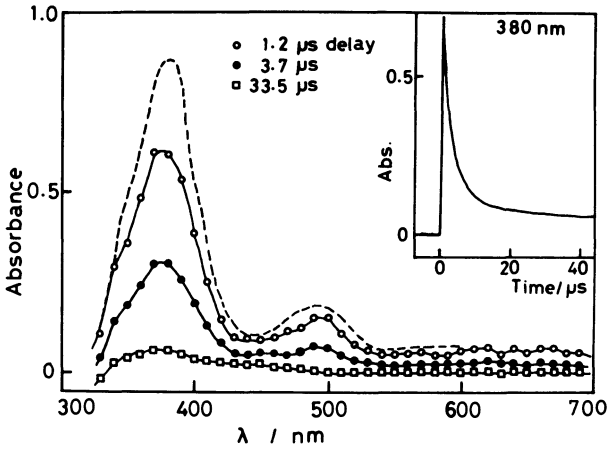

Fig. 5. Transient absorption spectra of AQ-14 in Freon 113. A broken line is the spectrum of AQ-2 at a 0.5 μs delay after laser excitation. Inset: A typical decay profile of transient absorption of AQ-14 monitored at 380 nm.

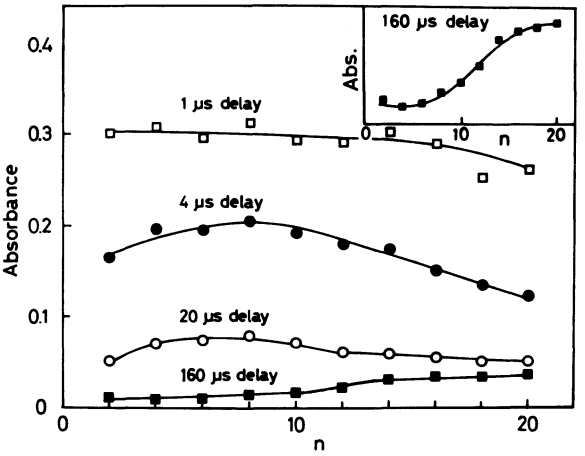

Fig. 6. Plots of transient absorption intensities at several delaytimes after laser excitation for AQ-n. Inset: Manification of the intensities at a 160 μs delay.

Table 3. Relative TS-LIF Intensities $I(n)$ and Risetimes $\tau_R(n)$ of AQ-n[a]

n	$I(n)$	$\tau_R(n)$ / μs
10	0.2	17.5
12	0.6	14.9
14	1.0	10.6
16	1.6	7.7
18	1.1	4.8
20	1.9	4.7

a) $I(n)$ are the intensities at a 70 μs delay after the first laser excitation. Experimental error is ±10—20%.

micellar solutions.[5]

In Fig. 6, transient absorption intensities at several delaytimes are shown as a function of n. The absorption intensities at a 4 μs delay decrease with increasing n, though those immediately after the laser excitation (1 μs delay) are almost independent of n. The n dependence of the absorption intensities at 4 and 20 μs delays is reflection of the lifetime shortening of the triplet states with increasing n. In contrast, the intensities at about 160 μs delay, which may be attributable to the photoproducts, gradually increases with increasing n, indicating the increase in the reaction yield with n.

The triplet lifetimes, estimated from the decay of the transient absorption at 380 nm, are listed in Table 2. The lifetimes estimated from the transient absorption are in good agreement with the phosphorescence lifetimes for longer methylene chain molecules (n=12—20). For the shorter chain molecules (n=2—6), triplet lifetimes estimated from the transient absorption is shorter than the phosphorescence lifetimes. This is mostly ascribed to the T–T annihilation due to the high excitation density in laser flash photolysis. Dependence of the lifetimes on n is almost the same as that of phosphorescence lifetimes. These observations present spectroscopic evidence that not physical but chemical quenching by methylene chain in the excited triplet determines its lifetime for long-chain molecules.

Two-Step Laser Induced Fluorescence. It was further attempted to monitor the initial yield of photoproducts with the aid of two-step laser induced fluorescence (TS-LIF) technique, since the cyclization products strongly fluoresce. This technique was proved to be effective to monitor the dynamics of fluorescent intermediates and products.[5,13] Figure 7 shows time-resolved TS-LIF spectra of AQ-14. The fluorescence band around 500 nm may be assigned to the photoproducts, since its spectrum and lifetime (22 ns) agree with those of photoproducts obtained from the steady-state photolysis (Fig. 1). As shown in the inset of Fig. 7, the fluorescence from photoproducts increases in intensity by increasing the delaytime between the first and second lasers, and

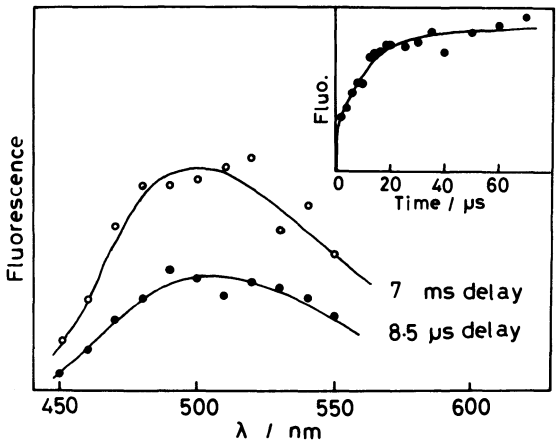

Fig. 7. Two-step laser induced fluorescence (TS-LIF) spectra of AQ-14 in Freon 113. Inset: Time profile of the TS-LIF intensity at 520 nm observed at several delaytimes.

reaches a plateau around 50 μs or so.

The relative yield and formation rate of the products were estimated from the relative TS-LIF intensities at a 70 μs delay and the growth curve of TS-LIF, respectively (Table 3). It is shown that the product yield determined by the TS-LIF increases with increasing n from 10 to 20, in accord with the increase in the formation rate (inverse of the risetime).

Discussion

A considerable effort has been made to elucidate photochemistry and photophysics of n-alkyl benzophenone-4-carboxylates (BP-n) by Winnik and coworkers.[2] According to their study, excited triplet benzophenone abstracts a hydrogen atom from its methylene side chain, leading to the cyclization products:

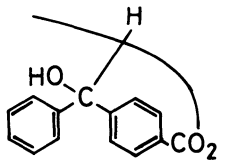

On the other hand, quite a few papers have been reported on the primary photochemical processes of quinones and benzophenones, in aqueous micellar solutions.[5,7,14–17] In micellar solution, their excited triplet states abstract a hydrogen atom from the methylene chain of a surfactant, resulting in the formation of an adduct of semiquinone (or ketyl radical) to the surfactant as a cage product. Upon photolysis of anthraquinone in micellar solution, the fluorescent products were obtained as the cage product:[7]

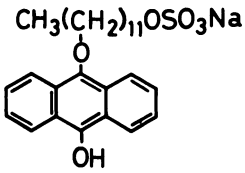

On analogy with the photoreactions mentioned above, photophysics and photochemistry of AQ-*n* may be described by the following scheme:

$$\text{AQ-}n \xrightarrow{h\nu} {}^1\text{AQ*-}n \quad (1)$$

$${}^1\text{AQ*-}n \longrightarrow {}^3\text{AQ*-}n \quad (2)$$

$${}^3\text{AQ*-}n \longrightarrow \text{AQ-}n + \text{phos.} \quad (3)$$

$${}^3\text{AQ*-}n \longrightarrow \text{AQ-}n \quad (4)$$

$${}^3\text{AQ*-}n \longrightarrow {}^3\text{BR} \quad (5)$$

$${}^3\text{BR} \rightleftharpoons {}^1\text{BR} \quad (6)$$

$${}^1\text{BR} \longrightarrow \text{P-}n. \quad (7)$$

The excited triplet state ^{3}AQ*-*n* of the anthraquinone chromophore is generated by the photoexcitation ((1) and (2)). While it phosphoresces (3), it abstracts a hydrogen atom from its methylene side chain, leading to a triplet biradical ^{3}BR. Triplet–singlet intersystem crossing of the biradical (6) results in the formation of a cage product P-*n*. Bimolecular reactions in the excited triplet ^{3}AQ*-*n* as well as those in triplet biradical might occur. A triplet biradical might be quenched by impurities. These reactions are not included in the scheme, though they might take place. In aerated solution, quenching of the excited triplet ^{3}AQ*-*n* as well as the biradical by dissolved oxygen may be responsible for the deactivation of the respective species.

As already shown for the reaction of *n*-alkyl benzophenone-4-carboxylates (BP-*n*),[2] the position of the hydrogen atom, which is abstracted by triplet anthraquinone, may spread over the polymethylenes, whose reaction probability seems proportional to the frequency of the collision of two sites. Further, in the present molecules, either one of two carbonyls at 9- and 10-positions, which are not equivalent with respect to the carboxyl group at 2-position, may abstract the hydrogen atom. Thus analysis of the reaction products is highly complicated. For example, in a thin-layer chromatogram of a photolyzed solution of AQ-14, at least four fluorescent products were detected, which may be isomers of different ring size, though chemical identification failed because of difficulty in isolation. These products change into nonfluorescent products upon aeration. This change is very similar to that described in the photoadduct of anthrasemiquinone to the surfactant in a SDS micellar solution, which may be attributable to the keto-enol isomerization.[7] Therefore, the main photoproducts are mostly ascribed to the coupling products at the two radical centers, i.e., cyclization products P-*n*:

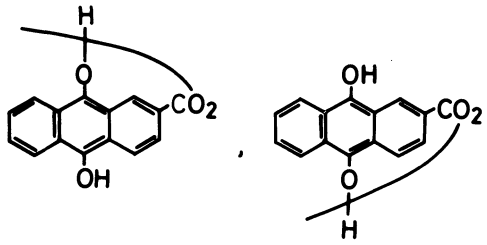

All the observations mentioned in the previous section can be now discussed how the methylene chain length affects the intramolecular reaction efficiency between the excited triplet anthraquinone and the methylene side chain. In steady-state photolysis, the relative yield of disappearance of AQ-*n* increases with increasing the methylene chain lengths (Fig. 2), suggesting that the hydrogen abstraction of the excited triplet anthraquinone chromophore from its methylene side chain is responsible for the net photoreaction. This conclusion is confirmed from the phosphorescence, transient absorption, and TS-LIF measurements. Dependence of the phosphorescence intensities and lifetimes on methylene chain length *n* (Figs. 3 and 4, and Table 2) indicates that the excited triplet is quenched by the collision with its methylene chain. It is further verified, by transient absorption (Fig. 6 and Table 2) and TS-LIF (Table 3), that the quenching is not physical but chemical one, which generates biradicals, followed by the formation of fluorescent products. Collision between the carbonyl carbon atom at the anthraquinone chromophore in the excited state and the hydrogen atom at the methylene chain is a rate controlling step, whose frequency depends on the length of the chain. In the short-chain molecules, e.g., AQ-2, the steric hindrance avoids its reaction. In the long-chain molecules ($n \geqslant 10$), the reaction rate increases in accord with the collision frequency between the carbonyl and the methylene groups.

Now let's estimate the rate of hydrogen abstraction reaction. The lifetime $\tau_T(n)$ of the excited triplet ^{3}AQ*-*n* is given by the following equation,

$$1/\tau_T(n) = k_3 + k_4 + k_5(n). \quad (8)$$

By assuming that lifetime $\tau_T(2)$ of AQ-2 is determined only by the physical processes (3) and (4), the rate constant $k_5(n)$ of intramolecular reaction of AQ-*n* can be estimated as follows;

$$k_5(n) = 1/\tau_T(n) - 1/\tau_T(2). \quad (9)$$

Experimentally, lifetimes of the triplet state were obtained as phosphorescence lifetimes $\tau_P(n)$ and lifetimes $\tau_{LF}(n)$ of T–T absorption. Thus we can

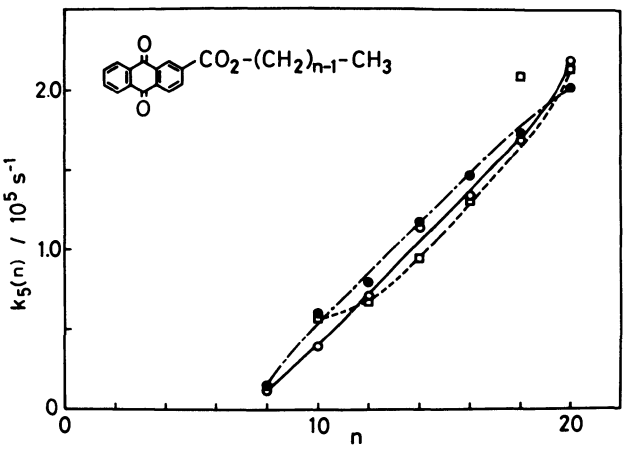

Fig. 8. Plots of the rate constant $k_5(n)$ of the intramolecular hydrogen abstraction against methylene chain length n. $k_5(n)$ were determined from phosphorescence lifetimes $\tau_P(n)$, ○, lifetimes $\tau_{LF}(n)$ of T–T absorption at 380 nm, ●, and risetimes $\tau_R(n)$ of photoproducts, □. See text.

determine $k_5(n)$ from the following equations:

$$k_5(n) = 1/\tau_P(n) - 1/\tau_P(2) \quad (10)$$

and

$$k_5(n) = 1/\tau_{LF}(n) = 1/\tau_{LF}(2). \quad (11)$$

The plots of Eqs. 10 and 11 against chain length n are given in Fig. 8. The $k_5(n)$ obtained by Eqs. 10 and 11 are in good agreement with each other as expected. In contrast with the phosphorescence lifetimes, triplet lifetimes of short-chain molecules ($n<8$) obtained from laser flash photolysis may be slightly shortened due to the T–T annihilation, which is not included in the above reaction scheme. For molecules with $n>8$, however, the triplet lifetimes are controlled predominantly by the rate $k_5(n)$ of intramolecular hydrogen abstraction.

In the TS-LIF measurements, the risetimes $\tau_R(n)$ of the fluorescence from the products may represent the formation rates. As discussed above, all the results indicate that the rate controlling step may be the reaction in the triplet state. If this is the case, the rate of product formation may be equal to the deactivation rate of the excited triplet,

$$1/\tau_R(n) = k_3 + k_4 + k_5(n). \quad (12)$$

Since $k_5(n) > k_3 + k_4$ for long-chain molecules as shown from the analysis of the excited triplet lifetimes, the following equation may approximately hold for $n \geqslant 10$:

$$k_5(n) \sim 1/\tau_R(n). \quad (13)$$

The plots of Eq. 13 against chain length n are also shown in Fig. 8. The k_5 values estimated from the risetimes of products (Eq. 13) coincide with those from lifetimes of the excited triplet states (Eqs. 10 and 11). The facts again demonstrate that the rate controlling step is the intramolecular hydrogen abstraction reaction in the excited state ^{3}AQ*-n for $n \geqslant 10$.

From the slope of the figure, we can conclude that the reaction rate of AQ-8 is 1×10^4 s^{-1} and the increase is 1.5×10^4 s^{-1} per one additional methylene unit for $n>8$.

Chain length dependence of intramolecular hydrogen abstraction of n-alkyl benzophenone-4-carboxylates (BP-n) has been studied by monitoring the disappearance yields and phosphorescence lifetimes of reactants.[2] BP-n shows methylene chain length dependence of the hydrogen abstraction rate in the triplet state similar to that of AQ-n mentioned above. In BP-n, the hydrogen abstraction rate of the benzophenone chromophore is 0.53×10^4 s^{-1} for $n=11$ and the increase is 0.46×10^4 s^{-1} per one additional methylene unit for $n>11$. When $n=14$, for example, the rates are 1×10^5 for AQ-14 and 0.18×10^5 s^{-1} for BP-14, respectively. Thus the rate constant of the former is about 5 times larger than that of the latter. The difference may be mainly attributable to the high reactivity of the anthraquinone triplet and partly to the existance of two reaction centers in the anthraquinone chromophore. Photochemical and photophysical similarity between AQ-n and BP-n implys that the photoreaction of AQ-n is conformationally controlled, in which conformational preequilibrium of the chain determines the reactivity, as theoretically analyzed for the latter.

The present work was partially supported by Grant-in-Aid for Sientific Research from the Ministry of Education, Science and Culture.

References

1) For reveiws, see: M. A. Winnik, *Acc. Chem. Res.*, **10**, 173 (1977); M. Sisido, *Kobunshi*, **26**, 260 (1977); M. A. Winnik, *Chem. Rev.*, **81**, 491 (1981); G. Illuminati and L. Mandolini, *Acc. Chem. Res.*, **14**, 95 (1981); K. Horie, *Kobunshi*, **32**, 196 (1983); P. J. Wagner, *Acc. Chem. Res.*, **16**, 461 (1983).

2) R. Breslow and M. A. Winnik, *J. Am. Chem. Soc.*, **91**, 3083 (1969); M. A. Winnik, A. Lemire, D. S. Saunders, and C. K. Lee, *ibid.*, **98**, 2000 (1976); M. A. Winnik, S. N. Basu, C. K. Lee, and D. S. Saunders, *ibid.*, **98**, 2928 (1976); M. A. Winnik and A. Lemire, *Chem. Phys. Lett.*, **46**, 283 (1977); D. S. Saunders and M. A. Winnik, *Macromolecules*, **11**, 25 (1978).

3) K. Zachariasse and W. Kuhnle, *Z. Phys. Chem. N.F.*, **101**, 267 (1976).

4) R. Nakagaki, M. Hiramatsu, K. Mutai, and S. Nagakura, *Chem. Phys. Lett.*, **121**, 262 (1985).

5) Y. Tanimoto, H. Udagawa, and M. Itoh, *J. Phys. Chem.*, **87**, 724 (1983); Y. Tanimoto, K. Shimizu, and M. Itoh, *Photochem. Photobiol.*, **39**, 511 (1984); *J. Am. Chem. Soc.*, **106**, 7257 (1984); *Chem. Phys. Lett.*, **112**, 217 (1984).

6) A preliminary report of this work has appeared: Y.

Tanimoto, M. Takashima, M. Uehara, M. Itoh, M. Hiramatsu, R. Nakagaki, T. Watanabe, and S. Nagakura, *Chem. Lett.*, **1985**, 15.

7) V. Swayambunathan and N. Periasamy, *J. Photochem.*, **13**, 325, (1980).

8) A. Kuboyama and S. Yabe, *Bull. Chem. Soc. Jpn.*, **40**, 2475 (1967).

9) T. Narisawa, M. Sano, and Y. J. I'haya, *Chem. Lett.*, **1975**, 1289; H. Murai, T. Hayashi, and Y. J. I'haya, *Chem. Phys. Lett.*, **106**, 139 (1984).

10) T. Murao and T. Azumi, *J. Chem. Phys.*, **70**, 4460 (1979).

11) K. Hamanoue, Y. Kajiwara, T. Miyake, T. Nakayama, S. Hirase, and H. Teranishi, *Chem. Phys. Lett.*, **94**, 276 (1983); K. Hamanoue, T. Nakayama, Y. Kajiwara, T. Yamaguchi, and H. Teranishi, *J. Chem. Phys.*, **86**, 6654 (1987).

12) K. Hamanoue, K. Yokoyama, Y. Kajiwara, K. Nakajima, T. Nakayama, and H. Teranishi, *Chem. Phys. Lett.*, **110**, 25 (1984); K. Hamanoue, K. Nakajima, Y. Kajiwara, T. Nakayama, and H. Teranishi, *ibid*, **110**, 178 (1984); K. Hamanoue, T. Nakayama, M. Shiozaki, Y. Funasaki, K. Nakajima, and H. Teranishi, *J. Chem. Phys.*, **85**, 5698 (1986).

13) M. Itoh, T. Adachi, and K. Tokumura, *J. Am. Chem. Soc.*, **105**, 4828 (1983); M. Itoh and Y. Fujiwara, *ibid.*, **107**, 1561 (1985); Y. Tanimoto, E. Shimada, and M. Itoh, *Bull. Chem. Soc. Jpn.*, **59**, 3039 (1986).

14) Y. Sakaguchi, S. Nagakura, and H. Hayashi, *Chem. Phys. Lett.*, **72**, 420 (1980); Y. Sakaguchi, H. Hayashi, and S. Nagakura, *J. Phys. Chem.*, **86**, 3177 (1982); Y. Sakaguchi and H. Hayashi, *ibid.*, **88**, 1437 (1984).

15) J. C. Scaiano and E. B. Abuin, *Chem. Phys. Lett.*, **81**, 209 (1981); J. C. Scaiano, E. B. Abuin, and L. C. Stewart, *J. Am. Chem. Soc.*, **104**, 5673 (1982).

16) Y. Tanimoto and M. Itoh, *Chem. Phys. Lett.*, **83**, 626 (1981): Y. Tanimoto, H. Udagawa, Y. Katsuda, and M. Itoh, *J. Phys. Chem.*, **87**, 3976 (1983).

17) M. Okazaki, S. Sakata, R. Konaka, and T. Shiga, *J. Am. Chem. Soc.*, **107**, 7214 (1985); M. Okazaki and T. Shiga, *Nature (London)*, **323**, 240 (1986); M. Okazaki, S. Sakata, R. Konaka, and T. Shiga, *J. Phys. Chem.*, **91**, 1131 (1987); *J. Chem. Phys.*, **86**, 6782 (1987).

 © 1988 The Chemical Society of Japan Bull. Chem. Soc. Jpn., 61, 3129—3139 (1988)

Biomolecules Conform to the Rule of Topological Charge Stabilization

Jun-ichi AIHARA
Department of Chemistry, Faculty of Science, Shizuoka University, Oya, Shizuoka 422
(Received April 12, 1988)

Almost all biomolecules conform to the rule of topological charge stabilization. Heteroatoms are placed at the right sites in proteins, nucleoside bases, porphyrins, and related metabolites. It is noteworthy that typical redox-mediating coenzymes obey this rule both in the oxidized and reduced states. Thus, it is very likely that the rule of topological charge stabilization has been one of the most important guiding principles not only in chemical evolution but also in general biosynthesis.

Molecules containing one or more heteroatoms occur widely in nature. Nitrogen, oxygen, and sulfur are typical heteroatoms commonly found in biomolecules. These atoms are more electronegative than carbon and hydrogen.[1] Nucleic acids, proteins, coenzymes, and porphyrins all contain one or more π-electron subsystems containing heteroatoms. Considering that these molecules are biologically indispensable, it is a very important matter in chemistry and biochemistry to seek for the reason why they were chosen to construct living organisms. Why do the biomolecules contain many heteroatoms? What factors stabilize these molecules? Of course, it is never easy to answer these questions. Even partial answers will mark an important progress in the study of biosynthesis and molecular evolution.

In 1983 Gimarc pointed out that the pattern of charge densities in a molecule is determined mainly by the connectivity or the topology of the molecule.[2] Nature tends to place heteroatoms of great electronegativity in those positions where the isostructural, iso-π-electronic hydrocarbon has large charge densities.[2-4] Gimarc called the effect the rule of topological charge stabilization or the TCS rule. He showed that generally a molecule conforming to this rule is stable in our chemical sense.[2-4] In previous papers[5,6] the TCS rule was successfully used to explain the stability of so-called quasi-aromatic molecules and various organic molecules formed in primitive-Earth-simulation experiments.

This paper aims at rationalizing the stability of nucleoside bases and other important biomolecules in terms of Gimarc's TCS rule. We will show below that very many biologically important molecules are stable owing to the presence of heteroatoms at the right sites. As will be seen, most heteroatoms in every biomolecule are situated in such a manner that they attain the maximum thermodynamic stability of the whole conjugated system. Ketone oxygen and imine nitrogen contriburte one π electron to the conjugated system, whereas amine nitrogen and alcohol (or ether) oxygen contribute two π electrons instead of one.

Results and Discussion

Charge densities calculated for a molecule containing heteroatoms depend on the choice of semiempirical parameters, but in the iso-π-electronic hydrocarbon all Coulomb integrals are uniform and charge densities are determined only by the topology of the molecule and the number of π electrons.[7] To emphasize this fact, Gimarc[2-4] referred to the isostructural, iso-π-electronic hydrocarbon as the uniform reference frame (URF). It is a (hypothetical) conjugated hydrocarbon obtained by replacing all the heteroatoms in a given molecule by sp^2 carbons and then by donating the same number of π electrons to the resulting conjugated system. The URF is, of course, not identical with a real molecule. It is charge densities in such URF's that the TCS rule adopts to estimate the stability of biomolecules containing heteroatoms. First-order perturbation theory has given a justification for the TCS rule.[3]

All charge densities given below will be those calculated for the π-electron systems of the URF's. We used the Hückel molecular orbital (HMO) model in its simplest form unless otherwise stated. The simple HMO model is known to yield exaggerated charges, but experience shows that they are adequate for the present purpose which requires only a qualitative pattern of charge distributions.[2] We assumed that the Coulomb integral has the same value for all carbons and that the resonance integral has the same value for all π bonds. All alkyl substituents will be disregarded for simplicity because they are scarcely conjugated with the parent π-electron framework.

Carboxylates and Peptides. Consider the allyl anion $C_3H_5^-$ (**1**), in which a central carbon is connected to two edge carbons. The conjugated system is composed of four π electrons moving through the three constituent carbons. The calculated charge density is greater at the edge carbons than at the central carbon. This anion represents the URF of the carboxyl group (**2**) not conjugated with the remainder of the molecule (R in **2**). Many carboxylic acids (**2**), carboxylic esters (**3**), and naturally occurring amino acids have this type of carboxyl groups. Here and hereafter R and R_i (i=1, 2, 3, ···) represent the substituents not conjugated with the π-electron system in question.

Topological charge stabilization says that electronegative heteroatoms prefer to occupy the sites where

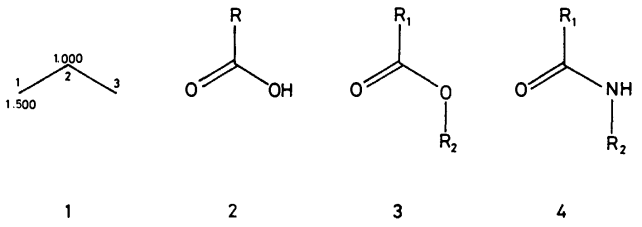

1 2 3 4

electron density is already very great in the iso-π-electronic URF.[2-4] Oxygen is much more electronegative than carbon.[1] Stability of carboxylic acids and carboxylates is attributable to the two constituent oxygens because these atoms occupy the two sites of greatest charge density in the URF. Individual peptide bonds in protein (**4**) are not conjugated with each other. They are also iso-π-electronic with the allyl anion (**1**). Stability of all proteins can thus be explained in terms of the TCS rule. This is possibly the primary reason why insulating methylenes intervene between adjacent peptide bonds.

Urea and Toxins. Gimarc considered the trimethylenemethane dianion $C(CH_2)_3^{2-}$ (**5**) as a URF of such common inorganic species as CO_3^{2-}, NO_3^- and SO_3.[2] The conjugated system of **5** is composed of six electrons moving through four carbons. The calculated charge density is greater at the peripheral carbons than at the central carbon. Naturally occurring CO_3^{2-}, NO_3^-, and SO_3 are very stable because all oxygens are located at the peripheral positions to achieve the maximum energy stabilization. Note that oxygen is more electronegative than nitrogen and sulfur.[1]

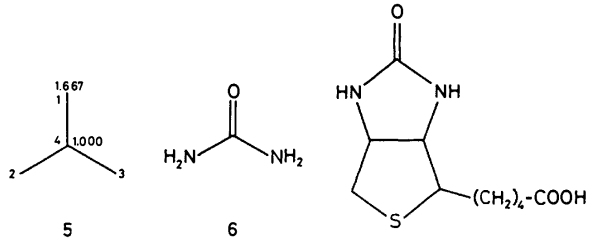

5 6 7

The trimethylenemethane dianion (**5**) also constitutes the URF's of urea (**6**) and biotin (**7**, growth factor). Analogous π-electron systems are found in many other biomolecules. For example, tetrodotoxin (**8**, swellfish toxin), saxitoxin (**9**, shellfish toxin), and streptomycin (**10**, antibiotic) have one, three, and two conjugated subsystems, respectively, which are all iso-π-electronic with urea. In these biomolecules nature puts oxygens and/or nitrogens at the peripheral positions of the trimethylenemethane framework where topology tends to distribute more charge density. These examples nicely illustrate the theory that the conformity to the TCS rule gives a stable molecular system.[2-4] Urea, biotin, tetrodotoxin, streptomycin, and saxitoxin are all Y-aromatic species.[8]

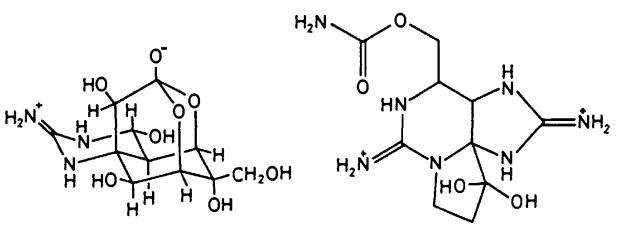

8 9

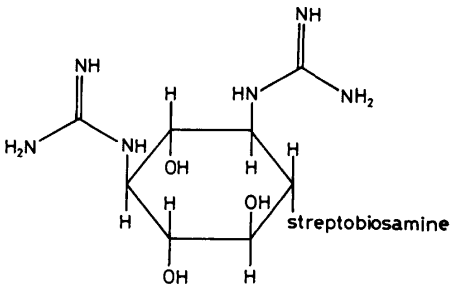

10

Nucleoside Bases. The purine and pyrimidine bases are key components of nucleic acids. Adenine (**11**), guanine (**12**), cytosine (**13**) thymine (**14**), and uracil (**15**) are principal nucleoside bases. The structural formulas **11**—**15** represent the bases in the tautomeric form which predominates according to spectroscopic analyses: the keto and amino form.[9,10] This form is favored in nucleic acids over the enol and imino form. In the present study, there is no need to discriminate between these two forms since both give the same URF. Even if a given base undergoes tautomerization, positions of the heteroatoms remain unchanged.

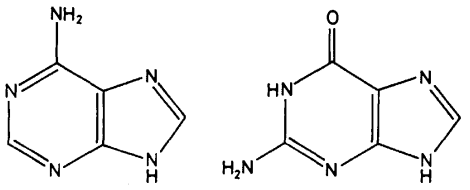

11 12

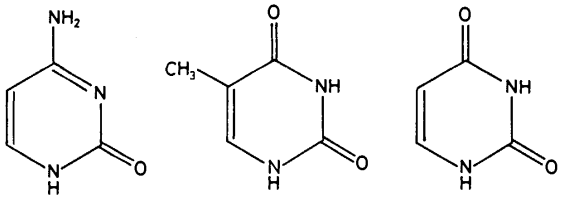

13 14 15

The URF's of two purine bases **11** and **12** are shown in **16** and **17**, respectively. Heteroatoms in these bases, without exceptions, are situated at the sites of large

charge density in the corresponding URF's. It is noteworthy that all exomethylene carbons in these URF's (i.e., carbon 10 in **16** and carbons 10 and 11 in **17**) have high charge density. All these sites are occupied by amine nitrogens or ketone oxygens in the purine bases. All positions of high charge density in the URF's are occupied by heteroatoms in the corresponding purine bases. Three pyrimidine bases **13**, **14**, and **15** happen to have the same URF (**18**) with ten π electrons. It is clear that heteroatoms in these bases occupy the sites of high charge density in their common URF. Therefore it seems very likely that nature selected these nucleoside bases as parts of gene because they are not only stable but also easy to form.

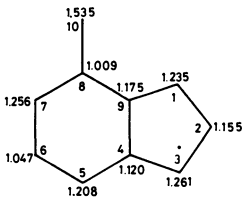

16

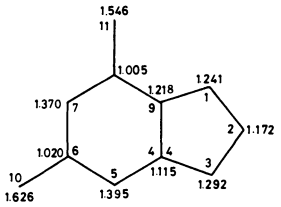

17

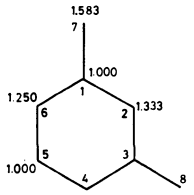

18

The nucleoside bases in the keto and amino form fit the base-pairing scheme of Watson and Crick for double-stranded DNA, whereas those in the enol and imino form do not. However, the charge density distribution in the URF of each base is not consistent with the keto and amino form. All exomethylene carbons in the URF are high in charge density as compared with ring carbons. The enol and imino form is favorable from this point of view since alcohol (or ether) oxygen attracts much more charge than ketone oxygen. This discrepancy might represent the limitation of the TCS rule.

There are many biomolecules which have either a purine or pyrimidine nucleus. Among purine bases and alkaloids are hypoxanthine (**19**), xanthine (**20**), caffeine (**21**), theophylline (**22**), theobromine (**23**), and uric acid (**24**). The URF of hypoxanthine is the same as that of adenine (**16**). The URF's of xanthine, caffeine, theophylline, and theobromine are all identical with that of guanine (**17**). The URF of uric acid is shown in **25**. Among biological pyrimidines are 5-methylcytosine (**26**), 5-(hydroxymethyl)cytosine (**27**), and orotic acid (**28**). The URF's of **26** and **27** are identical with that of cytosine. The URF of orotic acid is shown in **29**. All these molecules conform to the TCS rule.

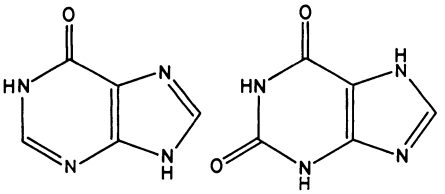

19 20

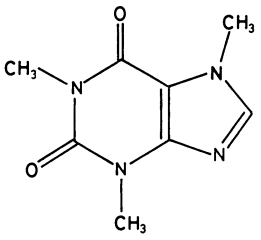

21

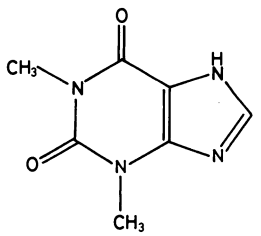

22

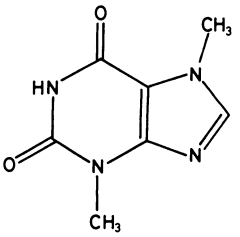

23

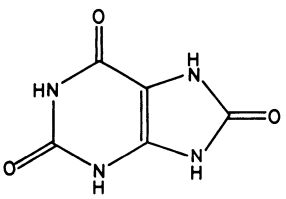

24

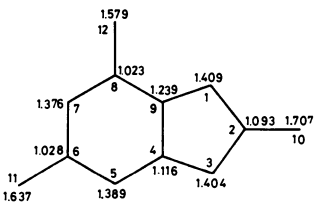

25

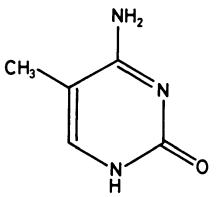

26

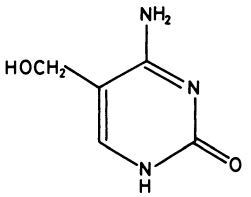

27

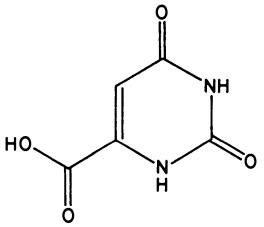

28

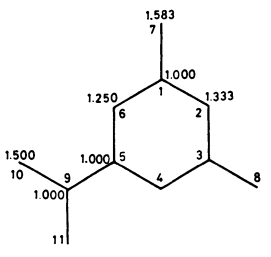

29

Unsubstituted purine and pyrimidine are not biomolecules. The calculated charge densities of the URF's of these molecules are not useful for rationalizing the positions of heteroatoms in nucleoside bases. The sites of high charge density in the URF's change by substitution. Furthermore, valence tautomerization sometimes occurs by substitution.[9,10] Unsubstituted purine (**30**) is iso-π-electronic with indole (**31**). Therefore, both have the same URF (**32**). A single indole nitrogen is located at one of the sites of greatest charge density in the URF. Thus, indole is stabilized by topological charge distribution, so are tryptophan (**33**) and many indole alkaloids. Indole is found in coal tar.

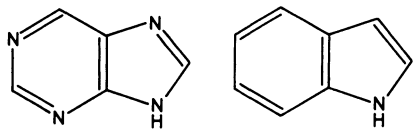

30 31

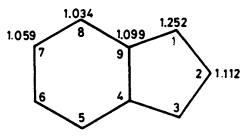

32

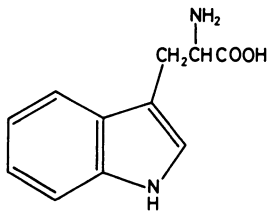

33

According to the original TCS rule,[2] one does not need to place heteroatoms at all sites of high charge density in the URF to stablize molecules. Indole indeed has one amine nitrogen at one of the sites of largest charge density in the URF. One nitrogen is enough to stabilize the indole conjugated system although there is one more site of largest charge density in the URF. Position 6 in the URF of pyrimidine bases (**18**) has high charge density, but these bases has no heteroatom there. In contrast, heteroatoms in **2**—**4**, **6**—**12**, and **19**—**24** are located at all sites of high charge density in the corresponding URF's. We might say that these biomolecules are extremely faithful to the TCS rule.

Coenzymes. Biological oxidation and reduction are catalyzed by enzymes, each of which functions in conjunction with a coenzyme which acts as an electron carrier. There are a number of oxidative enzymes but relatively few coenzymes.[11] These coenzymes are involved in many biological oxidation–reduction reactions. Biotin (**7**) acts as a coenzyme responsible for the transfer of carbon dioxide in carboxylation reactions.

There are two coenzymes which contain nicotinamide as an active center: namely, nicotinamide-adenine dinucleotide (NAD^+) and nicotinamide-adenine dinucleotide phosphate ($NADP^+$). NAD^+ ($NADP^+$) is reduced during the enzymatic reaction to give the dihydropyridine derivative NADH (NADPH). Their oxidized and reduced forms have the general formulas shown in **34** and **35**, respectively. The presence of a carbamoyl group ($-CONH_2$) in nicotinamide (**34**) is consistent with the charge density distribution in the URF (**36**, ten π electrons), whereas the ring nitrogen does not correspond to the site of high charge density in the URF. However, it seems unlikely that **34** is greatly destabilized by the ring nitrogen of the imine type.

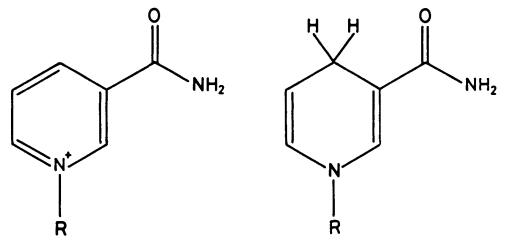

34 35

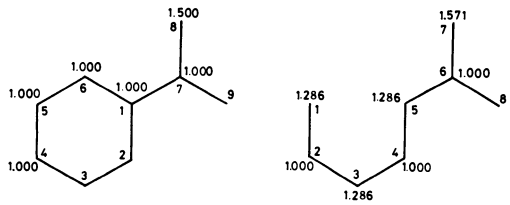

36 37

Let us consider the relative electron-attracting abilities of heteroatoms concerned. Amine nitrogen is a combination of N^{2+} and two π electrons, whereas imine nitrogen is a combination of N^+ and one π electron. Likewise, alcohol oxygen is a combination of O^{2+} and two π electrons, whereas ketone oxygen is a combination of O^+ and one π electron. The electron-attracting ability is then in the order: alcohol oxygen>amine nitrogen$\gg$ketone oxygen>imine nitrogen.[1] Considering that imine nitrogen is least electronegative, it seems unlikely that the imine nitrogen not situated at the right site destabilizes the π-electron system to a great extent. It is presumably for this reason that pyridine is as stable as benzene. The situation is essentially the same for nicotinamide (**34**). However, if alcohol oxygens and/or amine nitrogens are introduced into a given π-electron system, it is highly desirable for these atoms to occupy the sites of high charge density in the URF.

The URF of the reduced form of nicotinamide (**37**, ten π electrons) rationalizes the existence of three heteroatoms without any reservation. The ring nitrogen is now converted to amine nitrogen. It is then very desirable for this atom to occupy the site of high charge density in the URF. As shown in **37**, the amine nitrogen really occupys one of the sites of high charge density in the URF. Thus, three heteroatoms are required to stabilize both NAD^+ ($NADP^+$) and its reduced species.

There are two coenzymes which contain dimethylisoalloxazine as an active center: flavin mononucleotide (FMN) and flavin-adenine dinucleotide (FAD). These flavin coenzymes can be formulated as shown in **38**. They are formed in vivo from riboflavin (vitamin B_2), which can also be formulated as **38**. The isoalloxazine nucleus of a flavin coenzyme (oxidized form) is reduced during the enzymatic reaction to give the dihydro derivative or the reduced form (**39**). The yellow color of the flavin coenzyme disappears on reduction since the reduced form is colorless.

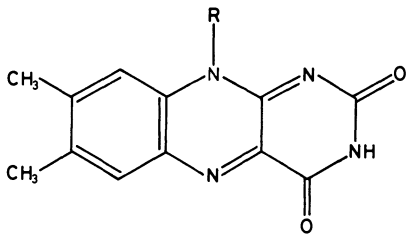

38

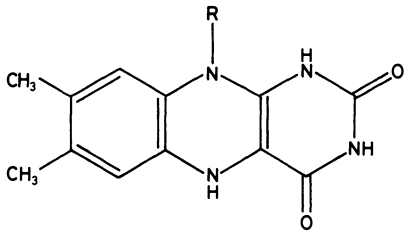

39

The URF of isoalloxazine (**40**, 18 π electrons) has large charge density at positions 1, 3, 13, 15, and 16. The corresponding positions in isoalloxazine are all occupied by electronegative heteroatoms. Position 6 in the URF is also occupied by a heteroatom (imine nitrogen) although it does not have very high charge density. This can again be rationalized by examining the charge density distribution in the URF of the reduced species (**41**, 20 π electrons). On reduction two imine nitrogens in isoalloxazine are converted into amine nitrogens. These amine nitrogens are assuredly placed at the sites of high charge density in the URF of the reduced form. Thus, imine nitrogen at position 6 in isoalloxazine is needed to stabilize its dihydro derivative. As mentioned above, imine nitrogens presumably influence the isoalloxazine conjugated system to a lesser extent. All sites of high charge density in **41** are occupied by heteroatoms in reduced isoalloxazine (**39**).

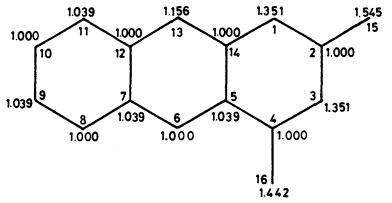

40

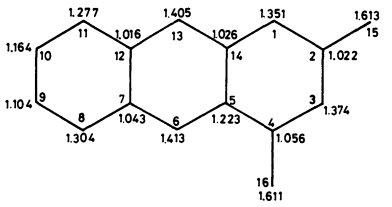

41

It is interesting to note that there are deazaflavin coenzymes,[12] which are structurally analogous to flavin coenzymes. It is a predominant cellular constituent in anaerobic methanogenic bacteria which biosynthesize methane. These bacteria are thought to be descendants of primordial organisms. Deazaflavin coenzymes (**42**) are likewise reduced during the enzymatic reaction to give the dihydro derivatives (**43**). The URF's of the oxidized and reduced forms are shown in **44** and **45**, respectively. Both forms have 20 π electrons each. All heteroatoms in **42** and **43** occupy the sites of high charge density in **44** and **45**, respectively. One carbon corresponding to position 6 in **44** is excluded from the conjugated system on

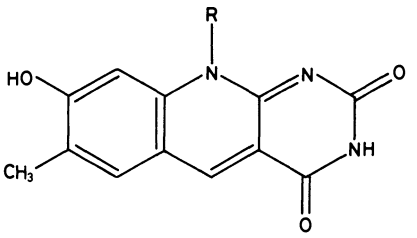

42

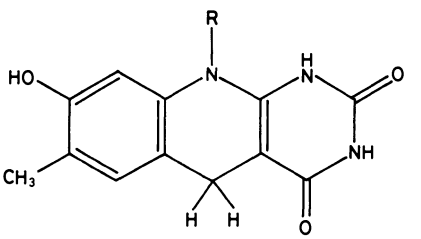

43

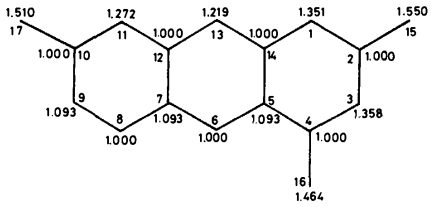

44

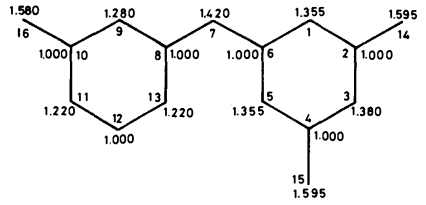

45

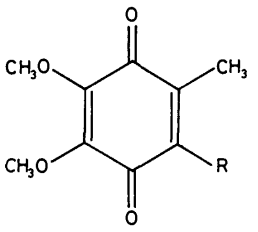

46

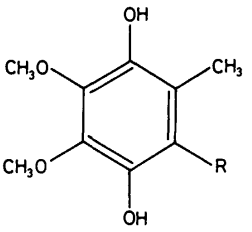

47

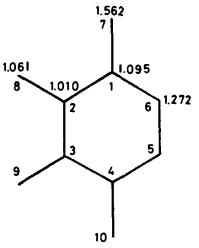

48

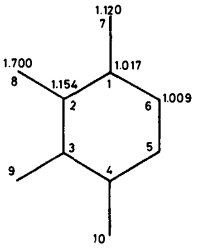

49

reduction. Therefore, there is no need to replace carbon 6 by nitrogen to stabilize the reduced form. Thus, the deazaflavin conjugated system is a functional hybrid between monocyclic nicotinamide and tricyclic flavin coenzymes.[12]

Mitochondria contain a quinone called ubiquinone which has the general structure **46**. The biological function of ubiquinone in redox reactions depends upon the reversible reduction to the corresponding hydroquinone (**47**). The URF of ubiquinone (**48**, 12 π electrons) has high charge density at positions 7 and 10. Two ketone oxygens are placed at the corresponding positions in the coenzyme. However, the positions of two methoxyl oxygens do not conform to the TCS rule. Charge density is not high at the corresponding positions (i.e, carbons 8 and 9) in the URF. Ubiquinone apparently constitutes an exceptional biomolecule, in the sense that highly electronegative methoxyl oxygens occupy the sites of low charge density in the URF.

This difficulty may be resolved in the following manner. Remember that carbons 8 and 9 in the URF of ubiquinone are to be replaced by methoxyl oxygens, but not by ketone oxygens. In general, a resonance integral between ether oxygen and carbon is relatively small.[7] Therefore, it might be meaningful to decrease the resonance integrals between carbons 2 and 8 and between carbons 3 and 9 in the URF of ubiquinone tentatively to 80% of the standard value. Such modification of the URF can be justified by the fact that ubiquinone has no possibility of valence tautomerization. The charge densities in the modified URF is shown in **49**. Then, we have largest charge density at carbons 8 and 9, which can now be replaced reasonably by methoxyl oxygens to give the ubiquinone conjugated system. Such a drastic change in charge densities was caused by the exchange of the sixth and seventh molecular orbitals. These two orbitals are accidentally very close in energy to each other in the unmodified URF.

Unfortunately, another diffuculty arises with the modified URF of ubiquinone (**49**). Charge densities at carbons 7 and 10 are greatly reduced in this URF, and it seems that the presence of two ketone oxygens is not so effective for stabilizing the conjugated system. In this context, it is well-known that exomethylene carbons in an organic molecule generally are very reactive with high reactivity indices. For example, 3,6-dimethylene-1,4-cyclohexadiene cannot be isolated, whereas *p*-benzoquinone is fairly stable and isolable. Ketone oxygens are obviously helpful for stabilizing exocyclic doube bonds. The presence of two ketone oxygens in ubiquinone can be rationalized in this manner.

Methoxyl oxygens in ubiquinone play an important role when it is converted to the reduced form. The URF of the reduced form (**50**, 14 π electrons) has high charge density at positions 7, 8, 9, and 10. Thus, the four alcohol (or ether) oxygens are placed at these positions to stabilize the reduced form. The modified URF of the reduced form (**51**) was defined using the same resonance integrals as those in the modified URF of ubiquinone (**49**). It has a charge density distribution similar to **50**.

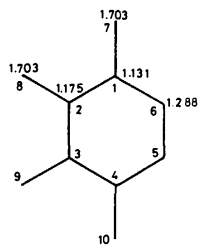

50

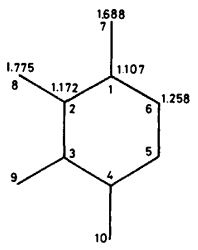

51

In photosynthesis plastoquinone (**52**) participates in reversible oxidation-reduction reactions. When plastoquinone is reduced during the reaction, the corresponding hydroquinone (**53**) is formed. Charge density is uniform over the URF of plastoquinone (**54**, eight π electrons). For the same reason as that given for ubiquinone, two exomethylene carbons in the URF are replaced by ketone oxygens in plastoquinone. The URF of hydroquinone (**55**, ten π electrons) has high charge density at positions 7 and 8. Two alcohol oxygens are placed at the corresponding positions in **53**. It follows that two oxygens are needed to stabilize both the oxidized and reduced forms of plastoquinone.

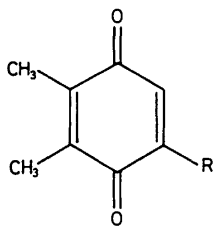

52

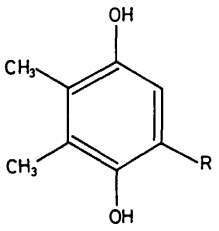

53

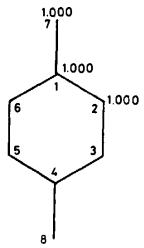

54

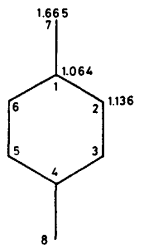

55

As has been seen above, it is very interesting that heteroatoms in representative redox-mediating coenzymes are arranged in such a manner that both the oxidized and reduced forms fulfill the TCS rule. Nature must have designed these molecular systems, taking into account the fact that amine nitrogen and alcohol (or ether) oxygen attract much more negative charge than imine nitrogen and ketone oxygen. The latter two atoms are sometimes introduced at sites of low charge density in the URF.

Porphyrins and Chlorophylls. All forms of life rely on the unique redox and electron-transfer abilities of hemoproteins and/or chlorophylls.[13,14] Active sites of hemoproteins and chlorophylls are the porphine (**56**) and chlorin (**57**) macrocycles, respectively, each acting as a ligand for a particular metal ion. Exactly speaking, chlorin represents a molecule formed by adding two hydrogens to the peripheral positions in the D-ring of any porphyrin. However, the term chlorin is here restricted to the unsubstituted chlorin nucleus (**57**). Although various substituents are usually attached to these molecules, we first disregard them all and evaluate the charge densities in metal-free porphine (**56**) and chlorin (**57**).

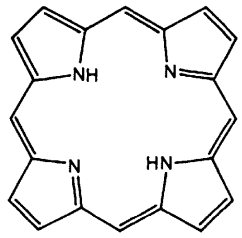

56

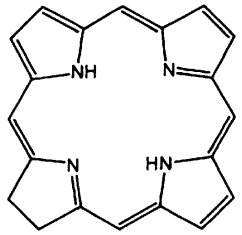

57

Pyrrole nitrogens in porphine (**56**) are located at those positions which have greatest charge density in the URF (**58**, 26 π electrons). Exactly the same observation was made over 35 years ago by Longuett-Higgins et al.[15] Historically, they were the first to introduce the idea of topological charge stabilization.[2] They noted that the great stability of porphine is largely due to the presence of nitrogens at positions in the skeleton where, for purely geometrical reasons, the π-electrons tend to congregate.[15] The TCS rule holds for **56**. Hemoproteins have an iron(II) ion at the center of every porphine nucleus. The metal ion is scarcely conjugated with the π-electron system of the porphine.[16] Therefore, there is no need to devise a different URF for the metal-porphine complex (**59**). In biosythesis the iron(II) ion is inserted after the formation of the porphine nucleus, and tightly bound to it.[13]

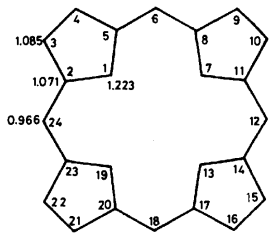

58

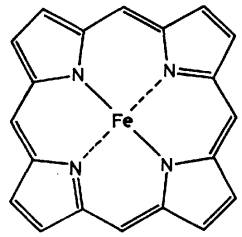

59

Substituted porphines have been referred to as porphyrins. All naturally occurring porphyrins have various substituents, most of which are not conjugated with the porphine nucleus. Heme (**60**) is an iron(II) complex of a porphyrin molecule called protoporphyrin. Human myoglobin and hemoglobin contain one and four heme molecules, respectively. The heme molecule not bound to protein has eight substituents, only two of which are conjugated with the porphine nucleus. As exemplified by **60**, vinyl and/or carbonyl groups in porphyrin are conjugated with the porphine nucleus. However, these substituents never displace the sites of large charge density in the URF. Compare the charge densities in the URF of porphine (**58**) with those in the URF of heme (**61**).

In generatal, a vinyl substituent is fairly reactive. Therefore, an alkyl group or the like is ofter attached to its β position. Otherwise, it is often replaced by the carbonyl substituent. When such a heme molecule is incorporated in protein, unsaturated substituents are used to bond the protein and become saturated ones.

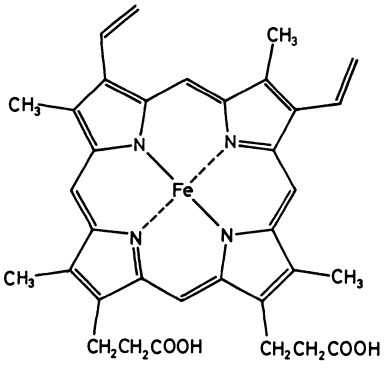

60

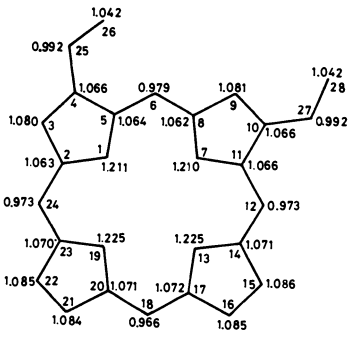

61

Chlorophylls have a magnesium-chlorin nucleus (**62**) with no carbon-carbon double bond in the D-ring. The calculated electron densities in the URF of chlorin (**63**, 24 π electrons) are highest at carbons 1, 7, and 13. There are nitrogens in the corresponding positions of chlorin. However, this molecule has one more nitrogen at position 20, the presence of which is not expectable from the URF (**63**). In the chlorophyll biosynthesis, the magnesium ion is inserted into the porphine nucleus in protoporphyrin.[13] After that, the reduction of the D-ring double bond occurs. Nitrogen at position 20 is thought to have been introduced to stabilize the metal-free porphine nucleus. After the reduction of the D-ring double bond all the four nitrogens are used to bind the magnesium ion tightly. If the magnesium ion is removed from chlorophyll, nitrogen at position 20 will be of the imine type. The magnesium ion is not conjugated with the π-electron system of chlorin.[17] Therefore, there is no need to devise a URF for the magnesium-chlorin complex (**62**).

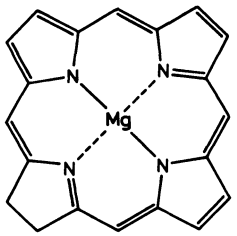

62

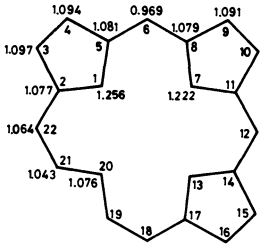

63

Naturally occurring chlorophylls have vinyl and/or formyl substituents in addition to alkyl substituents. Although photosynthetic organisms contain a variety of photosynthetic pigments, only chlorophyll *a* (**64**) performs a primary role in the photosynthetic act. This molecule has one vinyl and one carbonyl substituent attached to the chlorin nucleus. However, charge density is not large at all vinyl carbons of the URF (**65**). As in the case of porphyrins, vinyl substituents never change the sites of great charge density in the chlorin nucleus.

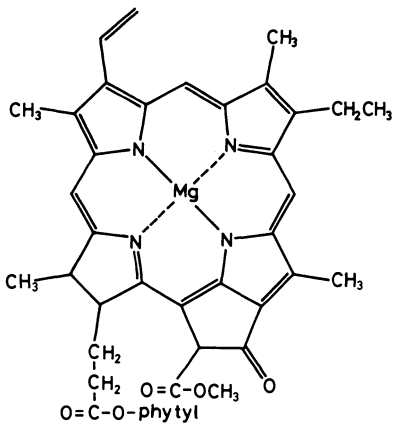

64

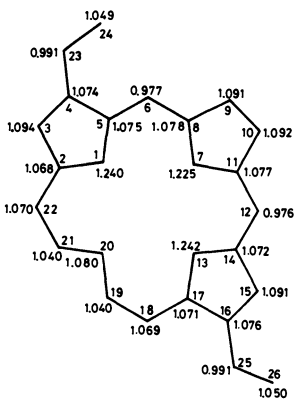

65

Photosynthetic bacteria produce a variety of photosynthetic pigments known collectively as bacte-

riochlorophylls.[13] Most bacteriochlorophylls have the same chlorin nucleus as those of chlorophylls. However, bacteriochlorophyll *a* (**66**) has a slightly different macrocycle (**67**), which has two additional hydrogens at the B-ring.[13] Two pyrrole nitrogens in **67** are located at sites of high charge density in the URF (**68**, 22 π electrons), but the other two are not. This again suggests that hydrogen addition at the B-ring must have occurred after the insertion of the magnesium ion. The URF of bacteriochlorophyll *a* itself is shown in **69**. The sites of high charge density in the URF are not displaced by the introduction of two unsaturated substituents. If the metal ion is removed from bacteriochlorophyll *a*, the two pyrrole nitrogens will be of the amine type, and the remaining two will be of the imine type.

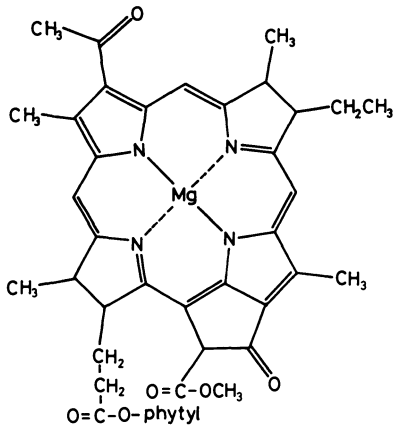

66

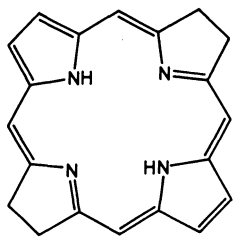

67

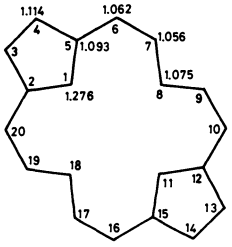

68

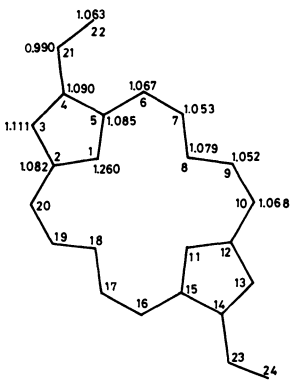

69

Porphyrins in geological samples[18] occur as complex mixtures of two major series: the etio and deoxophylloerythro types (**70** and **71**, respectively). In **70** and **71**, M represents an appropriate metal ion. These molecules are detectable in petroleum, shale, and coal. They have saturated substituents only, and the URF of porphine (**58**) applies. They were presumably derived from defunctionalization and full aromatization of naturally occurring chlorophylls.[18] This implies that unsaturated substituents attached to the original chlorophylls are not so stable as the porphine nucleus.

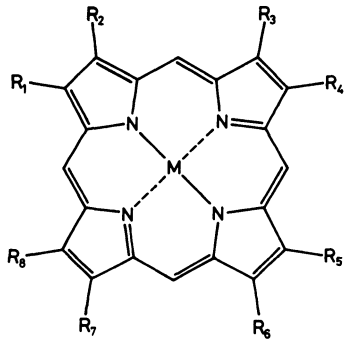

70

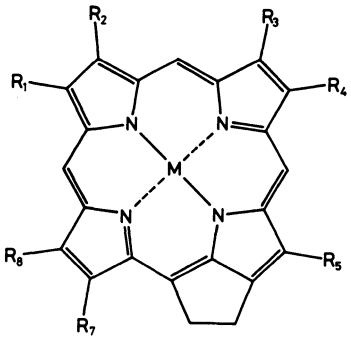

71

Phycobilins and bile pigments are formed in vivo by degradation of porphyrins.[14] Red and blue-green algae contain, in addition to chlorophyll *a*, blue or red pigments known as phycobilins, open-chain tetrapyrroles related to the chlorophylls but lacking the metal ion. These pigments absorb the sunlight effectively, and transfer its energy to chlorophyll *a*. Phycocyanobilin (**72**) is a phycobilin having the largest π-electron system. This blue compound has six heteroatoms except the isolated carboxyl groups. All heteroatoms occupy the sites of high charge density in the URF (**73**). Biliverdin (**74**) is one of the bile pigments, which is again an open-chain tetrapyrrole. A number of open tetrapyrroles are formed from biliverdin by reduction and oxidation reactions. The URF of biliverdin is shown in **75**. The locations of all heteroatoms in this molecule can be predicted from

the charge density distribution in the URF. Thus, it is noteworthy that not only porphyrins but also their metabolites conform to the TCS rule very faithfully although their molecular structures are far from being simple.

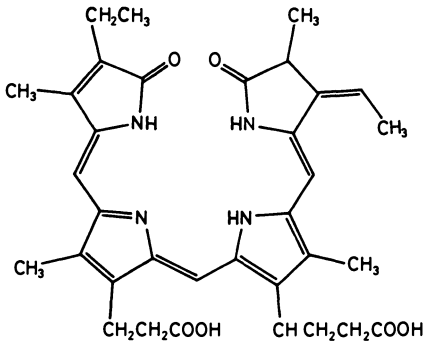

72

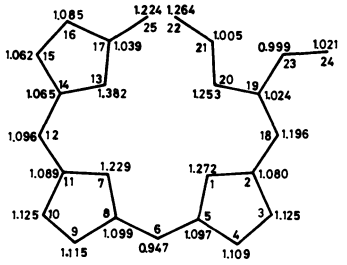

73

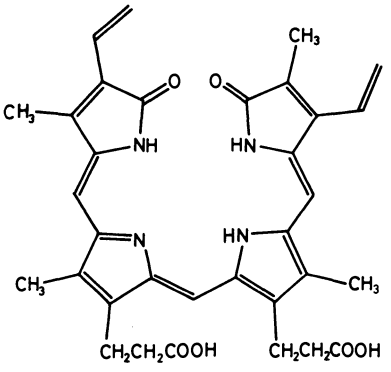

74

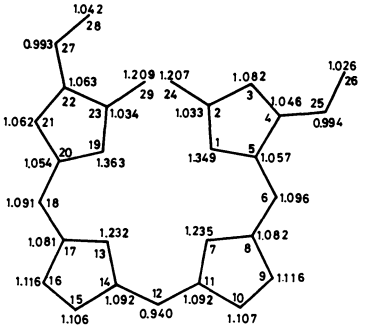

75

Concluding Remarks

Gimarc pointed out that the TCS rule has potential value as a guide for synthetic efforts to be made by organic chemists.[2] We have shown that many biologically important molecules conform to the TCS rule. Most heteroatoms in any biomolecule are placed at the sites of large charge density in its URF. In all examples shown above, highly electronegative alcohol (or ether) oxygens and amine nitrogens always occupy the sites of high charge density in the corresponding URF's. Nature obviously adopts the TCS rule as a general guide for biosynthesis. It should be noted that various coenzymes have been designed so that both the oxidized and reduced forms satisfy the TCS rule.

Chemical and biochemical evolution[19] must have occurred in harmony with the TCS rule.[6] As has been seen above, nucleoside bases, amino acids, and many other biomolecules are fully consistent with the TCS rule. This coincides with the fact that many of these molecules can be prepared by rather simple reactions intended to simulate chemical evolution.[17] Therefore, it is very probable that nature picked up molecules available readily in prebiotic chemistry to construct living organisms.[6] Some of the molecules must have exerted important functions incidentally in cellular systems. Conversely, nature has been so skillful as to choose biologically important molecules from the products of chemical evolution. For example, nucleoside bases are best suited for pairing in DNA and RNA. Such bases were chosen from a group of rather simple molecules which satisfy the TCS rule.

From a different point of view, we can say that living organisms adopted energetically very accessible ways of biosynthesis. In general, a stable molecule is associated with low activation energy of formation.[20] The resulting biomolecules are thermodynamically very stable as compared to their isomeric species. Many derivatives of indole (**31**) are prepared in vivo, but no structural isomers of indole, such as isoindole (**76**) and indolizine (**77**), are scarcely found in cellular systems. These isomers do not conform to the TCS rule, and are much less stable than indole. It is obvious that living organisms do not make much effort to prepare high-energy conjugated systems. Molecules with important biological functions must have been chosen from synthetically very accessible molecules. Thus, topological charge stabilization serves as a unifying principle for the systemization of biosynthesis.

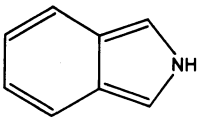

76

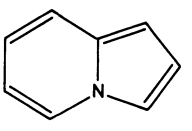

77

Helpful discussions with Prof. Yasuaki Okumura and Prof. Koichi Yoshinaga are gratefully acknowledged. This work was supported by the grant from the Ministry of Education, Science and Culture, administered by President of Shizuoka University.

References

1) L. Pauling, "The Nature of the Chemical Bond," Cornell University Press, Ithaca, NY (1960), Chap. 3.
2) B. M. Gimarc, *J. Am. Chem. Soc.*, **105**, 1979 (1983).
3) B. M. Gimarc and J. J. Ott, *J. Am. Chem. Soc.*, **108**, 4298 (1986).
4) J. J. Ott and B. M. Gimarc, *J. Am. Chem. Soc.*, **108**, 4303 (1986).
5) J. Aihara, *Bull. Chem. Soc. Jpn.*, **60**, 2268 (1987).
6) J. Aihara, *Bull. Chem. Soc. Jpn.*, **61**, 2309 (1988).
7) A. Streitwieser, Jr., "Molecular Orbital Theory for Organic Chemists," Wiley, New York (1961).
8) P. Gund, *J. Chem. Educ.*, **49**, 100 (1972).
9) J. Elguero, C. Marzin, A. R. Katritzky, and P. Linda, "The Tautomerism of Heterocycles (*Adv. Heterocycl. Chem., Suppl. 1*)," Academic Press, New York (1976), Chap. 5.
10) J. Elguero, C. Marzin, A. R. Katritzky, and P. Linda, "The Tautomerism of Heterocycles (*Adv. Heterocycl. Chem., Suppl. 1*)," Academic Press, New York (1976), Chap. 2.
11) H. C. S. Wood, "Comprehensive Organic Chemistry: The Synthesis and Reactions of Organic Compounds," ed by D. Barton and W. D. Ollis, Vol. 5, Pregamon, Oxford (1979), Part 24.3.
12) C. Walsh, *Acc. Chem. Res.*, **19**, 216 (1986).
13) H. Akhtar and P. M. Jordan, "Comprehensive Organic Chemistry: The Synthesis and Reactions of Organic Compounds," ed by D. Barton and W. D. Ollis, Vol. 5, Pregamon, Oxford (1979), Part 30.2.
14) K. M. Smith, "Rodd's Chemistry of Carbon Compounds: A Modern Comprehensive Treatise," ed by S. Coffey, Vol. IV, Part B, Elsevier, Amsterdam (1977), Chap. 12.
15) H. C. Longuet-Higgins, C. W. Rector, and J. R. Platt, *J. Chem. Phys.*, **18**, 1174 (1950).
16) H. Kashiwagi, personal communication.
17) F. Hirota, personal communication.
18) E. W. Baker and S. E. Palmer, "The Porphyrins," ed by D. Dorphin, Vol. 1, Academic Press, New York (1978), pp. 486—552.
19) S. L. Miller and L. E. Orgel, "The Origins of Life on the Earth," Prentice-Hall, Englewood Cliffs, NJ (1974).
20 W. J. le Noble, A. R. Miller, and S. D. Hamann, *J. Org. Chem.*, **42**, 338 (1977).

 © 1988 The Chemical Society of Japan Bull. Chem. Soc. Jpn., 61, 3141—3144 (1988)

Ab Initio Calculation for the Interaction Energy of He-H

Akira ICHIHARA,* Kohtoku SASAGANE, and Reikichi ITOH
Department of Chemistry, Faculty of Science and Engineering, Waseda University,
3-4-1 Ohkubo Shinjuku-ku, Tokyo 160
(Received April 25, 1988)

Using the help of an ab initio calculation with a configuration interaction (CI) treatment, the potential energies of a HeH system in the ground ($X^2\Sigma^+$) and the first three ($A^2\Sigma^+$, $B^2\Pi$, $C^2\Sigma^+$) excited electronic states were calculated, making due correction for the basis set superposition effect.

In recent years there have been several reports in which the radiative dissociation and predissociation of HeH were investigated.[1-8] Molecular calculations predict that the HeH system has a repulsive ground state, with only a van der Waals minimum,[9,10] and a series of bound Rydberg excited states.[11-13] Using a MRD-CI treatment, Theodorakopoulos et al.[11,12] calculated the potential energy curves of the ground and some excited electronic states of HeH. The theoretical radiative life times calculated by Petsalakis et al.[13] were in good agreement with the experimental values.[2,3]

In this paper we will report the results of full CI calculations of the potential energies of HeH in the ground ($X^2\Sigma^+$) and the first three ($A^2\Sigma^+$, $B^2\Pi$, $C^2\Sigma^+$) excited states, and the basis set superposition effect for these potential energies will be discussed. Then our results concerning the $A^2\Sigma^+ \rightarrow X^2\Sigma^+$ predissociation energy and the $B^2\Pi$ binding energy will be compared with the experimental values.[5-7]

In all the ab initio calculations, Gaussian basis sets [6S4P] for a H atom and [6S2P1D] for a He atom were employed. The hydrogen [6S4P] Gaussian basis set was composed of Schmidt (10s/4s) functions[14] augmented with the polarization and diffuse functions employed by Römelt et al.[15] and Theodorakopoulos et al.[11,12] The (10s/4s) contraction was performed so that the atomic energy with the contracted set came close to that with an uncontracted set. The Schmidt (10s) primitive functions were contracted to (6,2,1,1). The exponents of the polarization and diffuse functions were 0.025 and 0.01 for s-type orbitals and 0.7, 0.2, 0.035, and 0.01 for p-type orbitals. Moreover, the helium [6S2P1D] Gaussian basis set was composed of Schmidt (16s/6s) functions[14] augmented with the polarization functions employed by Römelt et al.[15] The Schmidt (16s) primitives were contracted to (6,5,2,1,1,1). The exponents of the polarization functions were 1.0 and 0.2 for p-type orbitals and 0.8 for the d-type orbital.

It has already been pointed out that the results of CI calculations for the interaction energy of the supermolecule system must be corrected in order to eliminate the type of error called a "basis set superposition error".[16-18] Boys et al. introduced the function counterpoise method[16] in order to overcome this error. In this method, the He–H interaction energy in the ground ($X^2\Sigma^+$) state ($E_{\rm int}^{X^2\Sigma^+}$) is calculated using the difference between the full CI energy of HeH ($E_{\rm HeH}^{X^2\Sigma^+}$) and an appropriate reference energy ($E_{\rm ref}$):

$$E_{\rm int}^{X^2\Sigma^+}(R) = E_{\rm HeH}^{X^2\Sigma^+}(R) - E_{\rm ref}(R), \tag{1}$$

where R is the internuclear distance of HeH. The reference energy is defined as the sum of the full CI energies of the ground H(1s) and ground He($1s^2$), with "ghost" orbitals at the expected location of the other atom:

$$E_{\rm ref}(R) = E_{\rm ghost}^{\rm H(1s)}(R) + E_{\rm ghost}^{\rm H(1s^2)}(R). \tag{2}$$

The term "ghost" represents an atom with a nuclear charge zero and without any electrons.

We also employed this method in the case of the $A^2\Sigma^+$, $B^2\Pi$, and $C^2\Sigma^+$ states of HeH in order to evaluate the "basis set superposition effect". As has been noted in the previous work by Theodorakopoulos et al.,[11,12] these three states are mainly described by a single configuration, the same one for the whole range of the internuclear distance, R, from 0.5 to 20.0 Bohr. These excited states have dissociation limits H(2s)+He($1s^2$) ($A^2\Sigma^+$) and H(2p)+He($1s^2$) ($B^2\Pi$ and $C^2\Sigma^+$) over R=20.0 Bohr. The interaction and reference energies may then be defined as:

$$\begin{aligned} E_{\rm int}^{\rm EXCITE}(R) &= E_{\rm HeH}^{\rm EXCITE}(R) - E_{\rm ref}(R), \text{ EXCITE} \\ &= A^2\Sigma^+, B^2\Pi, C^2\Sigma^+ \end{aligned} \tag{3}$$

$$\begin{aligned} E_{\rm ref}(R) &= E_{\rm ghost}^{\rm H(2s)}(R) + E_{\rm ghost}^{\rm H(1s^2)}(R) \quad \text{for } A^2\Sigma^+ \\ &= E_{\rm ghost}^{\rm H(2p\Pi)}(R) + E_{\rm ghost}^{\rm H(1s^2)}(R) \quad \text{for } B^2\Pi \\ &= E_{\rm ghost}^{\rm H(2p\Sigma)}(R) + E_{\rm ghost}^{\rm H(1s^2)}(R) \quad \text{for } C^2\Sigma^+ \end{aligned}$$

when there is the ghost He; the 2p orbitals of the H atom split into parallel ($2p\Sigma$) and perpendicular ($2p\Pi$) elements for the H—ghost He axis.

In the present work, the spatial symmetry considered in the CI treatment of the HeH system is $C_{\infty v}$. The CI calculations contain 6472 configurations for the $^2\Sigma$ symmetry and 7084 configurations for the $^2\Pi$ symmetry. These calculations were performed by using the graphical unitary group approach (GUGA) program of our group[19] and the HITAC M680H

system of the Computer Center of the Institute for Molecular Science (IMS).

Results and Discussion

Table 1 indicates the CI energies (E_H, E_{He}) of H(1s, 2s, 2p) and He($1s^2$), without ghost orbitals. These energies are equal to $E_{ghost}^{H(1s)}$, $E_{ghost}^{H(2s)}$, $E_{ghost}^{H(2p\Sigma,2p\Pi)}$, and $E_{ghost}^{He(1s^2)}$ at the internuclear distance of R=20.0 Bohr.

Tables 2—5 indicate the interaction energies of He–H in the ground $X^2\Sigma^+$ and excited $A^2\Sigma^+$, $B^2\Pi^+$, and $C^2\Sigma^+$ states, where the basis set superposition effect is evaluated by $E_{ref}-E_H-E_{He}$. It can be seen from Tables 2—5 that the basis set superposition effect grows with the electronic excitation level ($X^2\Sigma^+<A^2\Sigma^+<B^2\Pi^+<C^2\Sigma^+$). For the $X^2\Sigma^+$, $A^2\Sigma^+$, and $B^2\Pi$ states, the basis set superposition effect is less than 10^{-3} a.u. for the whole range of the R values

Table 1. Full CI Energies (E_H, E_{He}) of H(1s, 2s, 2p) and He($1s^2$)

		CI Energy/a.u.[a]
Hydrogen	(1s)	−0.4999954
	(2s)	−0.1249863
	(2p)	−0.1228372
Helium	($1s^2$)	−2.8965174

a) 1 a.u. = 4.359814×10^{-18} J.

Table 2. The He–H Interaction Energies ($E_{int}^{X^2\Sigma^+}$) for the $X^2\Sigma^+$ State

R/Bohr[a]	$E_{HeH}^{X^2\Sigma^+}$/a.u.[b]	E_{ref}/a.u.		$E_{int}^{X^2\Sigma^+}$/a.u.
		E_{ref}	$E_{ref}(R)-E_{H(1s)}-E_{He(1s^2)}$[c]	
1.0	−3.0917058	−3.3969760	−0.0004632	0.3052702
1.25	−3.2006385	−3.3968722	−0.0003594	0.1962337
1.5	−3.2632018	−3.3967590	−0.0002462	0.1335572
1.75	−3.3044846	−3.3966722	−0.0001594	0.0921876
2.0	−3.3330069	−3.3966110	−0.0000982	0.0636041
3.0	−3.3831444	−3.3965374	−0.0000246	0.0133930
4.0	−3.3941643	−3.3965274	−0.0000146	0.0023631
5.0	−3.3962007	−3.3965219	−0.0000091	0.0003212
6.0	−3.3965015	−3.3965181	−0.0000053	0.0000166

a) 1 Bohr = 0.529177×10^{-10} m. b) 1 a.u. = 4.359814×10^{-18} J. c) $E_{H(1s)}$ and $E_{He(1s^2)}$ are the CI energies of the H(1s) and He($1s^2$), without ghost orbitals. See Table 1.

Table 3. The He–H Interaction Energies ($E_{int}^{A^2\Sigma^+}$) for the $A^2\Sigma^+$ State

R/Bohr[a]	$E_{HeH}^{A^2\Sigma^+}$/a.u.[b]	E_{ref}/a.u.		$E_{int}^{A^2\Sigma^+}$/a.u.
		E_{ref}	$E_{ref}(R)-E_{H(2s)}-E_{He(1s^2)}$[c]	
1.0	−3.0440455	−3.0219687	−0.0004650	−0.0220768
1.25	−3.1066316	−3.0218640	−0.0003603	−0.0847676
1.5	−3.1124843	−3.0217504	−0.0002467	−0.0907339
1.75	−3.0994893	−3.0216635	−0.0001598	−0.0778258
2.0	−3.0819853	−3.0216022	−0.0000985	−0.0603831
3.0	−3.0355106	−3.0215285	−0.0000248	−0.0139821
4.0	−3.0242437	−3.0215184	−0.0000147	−0.0027253
5.0	−3.0219179	−3.0215129	−0.0000092	−0.0004050
6.0	−3.0212573	−3.0215091	−0.0000054	−0.0002518

a) 1 Bohr = 0.529177×10^{-10} m. b) 1 a.u. = 4.359814×10^{-18} J. c) $E_{H(2s)}$ and $E_{He(1s^2)}$ are the CI energies of the H(2s) and He($1s^2$), without ghost orbitals. See Table 1.

Table 4. The He–H Interaction Energies ($E_{int}^{B^2\Pi}$) for the $B^2\Pi$ State

R/Bohr[a]	$E_{HeH}^{B^2\Pi}$/a.u.[b]	E_{ref}/a.u.		$E_{int}^{B^2\Pi}$/a.u.
		E_{ref}	$E_{ref}(R)-E_{H(2p)}-E_{He(1s^2)}$[c]	
1.0	−3.0210546	−3.0198763	−0.0005217	−0.0011783
1.25	−3.0872280	−3.0197615	−0.0004069	−0.0674665
1.5	−3.0978919	−3.0196542	−0.0002996	−0.0782377
1.75	−3.0893517	−3.0195785	−0.0002239	−0.0697732
2.0	−3.0755452	−3.0195271	−0.0001725	−0.0560181
3.0	−3.0351654	−3.0194452	−0.0000906	−0.0157202
4.0	−3.0235834	−3.0193957	−0.0000411	−0.0041877
5.0	−3.0207334	−3.0193660	−0.0000114	−0.0013674
6.0	−3.0198897	−3.0193620	−0.0000074	−0.0005277

a) 1 Bohr = 0.529177×10^{-10} m. b) 1 a.u. = 4.359814×10^{-18} J. c) $E_{H(2p)}$ and $E_{He(1s^2)}$ are the CI energies of the H(2p) and He($1s^2$), without ghost orbitals. See Table 1.

Table 5. The He-H Interaction Energies ($E_{int}^{C^2\Sigma^+}$) for the $C^2\Sigma^+$ State

R/Bohr[a]	$E_{HeH}^{C^2\Sigma^+}$/a.u.[b]	E_{ref}/a.u.		$E_{int}^{C^2\Sigma^+}$/a.u.
		E_{ref}	$E_{ref}(R)-E_{H(2p)}-E_{He(1s^2)}$[c]	
1.0	−2.9656669	−3.0215125	−0.0021579	0.0558456
1.25	−3.0387007	−3.0213759	−0.0020213	−0.0173248
1.5	−3.0555992	−3.0211734	−0.0018188	−0.0344258
1.75	−3.0518279	−3.0209459	−0.0015913	−0.0308820
2.0	−3.0413713	−3.0207156	−0.0013610	−0.0206557
3.0	−3.0042729	−3.0200137	−0.0006591	0.0157408
4.0	−2.9939696	−3.0197653	−0.0004107	0.0257957
5.0	−2.9986434	−3.0197020	−0.0003474	0.0210586
6.0	−3.0066117	−3.0195035	−0.0001489	0.0128918
8.0	−3.0161292	−3.0194566	−0.0001020	0.0033274

a) 1 Bohr=0.529177×10^{-10} m. b) 1 a.u.=4.359814×10^{-18} J. c) $E_{H(2p)}$ and $E_{He(1s^2)}$ are the CI energies of the H(2p) and He($1s^2$), without ghost orbitals. See Table 1.

Table 6. $A^2\Sigma^+$ ($v'=0$) → $X^2\Sigma^+$ Predissociation and $B^2\Pi$ Binding Energies of HeH

	This work	Theodorakopoulos[a]	Experimental
		eV[b]	
$A^2\Sigma^+$ ($v'=0$) → $X^2\Sigma^+$ Predissociation	7.96[c]	7.91	7.9[d]
$B^2\Pi$ Binding	2.13	2.20	2.19±0.03[e]

a) From Ref. 12. b) 1 eV=1.6021892×10^{-19} J. c) The vibrational zero-point energy for the $A^2\Sigma^+$ state was estimated to be 0.2272 eV. d) Estimated from Fig. 3 in Ref. 5. e) From Ref. 7.

calculated and little effect on the shape of the interaction energy curves. This superposition effect changes the energy well depth by only 0.3—0.4 percent in the $A^2\Sigma^+$ and $B^2\Pi$ states. From these results, the basis set superposition effect can be said to be negligible for the $X^2\Sigma^+$, $A^2\Sigma^+$, and $B^2\Pi$ states. On the other hand, as may be seen in Table 5, the basis set superposition effect in the $C^2\Sigma^+$ state is about 0.002 a.u. in the energy minimum region and changes the well depth about 5 percent; therefore, it can not be neglected. The $C^2\Sigma^+$ state also has an upper boundary in the region of R=4.0 Bohr, where the basis set superposition effect is negligible.

Table 6 indicates the $A^2\Sigma^+(v'=0)\rightarrow X^2\Sigma^+$ predissociation and $B^2\Pi$ binding energies of HeH. In our calculation, the vibrational zero-point energy ($E_{vib}(v'=0)$) for the $A^2\Sigma^+$ state was estimated to be 0.2272 ev. The predissociation energy was calculated by the use of:

$$A^2\Sigma^+(v'=0) \rightarrow X^2\Sigma^+ \text{ predissociation energy}$$
$$= [\{E_{H(2s)} + E_{He(1s^2)} + E_{int}^{A^2\Sigma^+}(R = 1.5\,\text{Bohr}) + E_{vib}(v'=0)\} - \{E_{H(1s)} + E_{He(1s^2)}\}].$$

The results of the MRD-CI calculation by Theodorakopoulos et al.[11,12] and the experimental results reported by Peterson et al.[5] and by Möller et al.[7] are also listed in Table 6. Our calculated values are in good agreement with these other calculated and experimental values.

It may be concluded from the results of this investigation that our potential energies for the $X^2\Sigma^+$, $A^2\Sigma^+$, and $B^2\Pi$ states of the HeH system can give the $A^2\Sigma^+\rightarrow X^2\Sigma^+$ predissociation and $B^2\Pi$ binding energies. Moreover, the basis set superposition effect changes the interaction potential minimum about 5 percent for the $C^2\Sigma^+$ state.

We wish to thank professor Sigeru Huzinaga for suggesting this problem. Our study was based on the calculations by Giannoula Theodorakopoulos, Stavros C. Farantos, Ioannis D. Petsalakis, Cleanthes A. Nicolaides, Robert J. Buenker, and Sigrid D. Peyerimhoff.

References

1) T. Möller, M. Beland, and G. Zimmerer, *Phys. Rev. Lett.*, **55**, 2145 (1985).
2) W. Ketterle, H. Figger, and H. Walther, *Phys. Rev. Lett.*, **55**, 2941 (1985).
3) W. Ketterle, A. Dodhy, and H. Walther, *Chem. Phys. Lett.*, **129**, 76 (1986).
4) W. J. van der Zande, W. Koot, D. P. de Bruijn, and C. Kubach, *Phys. Rev. Lett.*, **57**, 1219 (1986).
5) J. R. Peterson and Y. K. Bae, *Phys. Rev. A*, **34**, 3517 (1986).
6) R. L. Brooks, J. L. Hunt, and J. J. Miller, *Phys. Rev. Lett.*, **58**, 199 (1987).
7) T. Möller, M. Beland, and G. Zimmerer, *Chem. Phys. Lett.*, **136**, 551 (1987).
8) C. Kubach, V. Sidis, D. Fussen, and W. J. van der Zande, *Chem. Phys.*, **117**, 439 (1987).
9) J. P. Toennies, W. Welz, and G. Wolf, *Chem. Phys. Lett.*, **44**, 5 (1976).
10) D. B. Knowles, J. N. Murrell, and J. P. Braga, *Chem. Phys. Lett.*, **110**, 40 (1984).

11) G. Theodorakopoulos, S. C. Farantos, R. J. Buenker, and S. D. Peyerimhoff, *J. Phys. B*, **17**, 1453 (1984).
12) G. Theodorakopoulos, I. D. Petsalakis, C. A. Nicolaides, and R. J. Buenker, *J. Phys. B*, **20**, 2339 (1987).
13) I. D. Petsalakis, G. Theodorakopoulos, C. A. Nicolaides, and R. J. Buenker, *J. Phys. B*, **20**, 5959 (1987).
14) M. W. Schmidt and K. Ruedenberg, *J. Chem. Phys.*, **71**, 3951 (1979).
15) J. Römelt, S. D. Peyerimhoff, and R. J. Buenker, *Chem. Phys.*, **34**, 403 (1978).
16) S. F. Boys and F. Bernardi, *Mol. Phys.*, **19**, 553 (1970).
17) J. R. Collins and G. A. Gallup, *Chem. Phys. Lett.*, **123**, 56 (1986).
18) J. H. van Lenthe, J. G. C. M. van Duijneveldt-van de Rijdt, and F. B. van Duijneveldt, "Weakly Bonded Systems," in "Advances in Chemical Physics, Volume LXIX, Ab Initio Methods in Quantum Chemistry, Part II," ed by K. P. Lawley, John Wiley & Sons, Chichester (1987), pp. 521—566.
19) A. Ichihara, K. Sasagane, T. Izaki, T. Miyazaki, and R. Itoh, *Bull. Chem. Soc. Jpn.*, **61**, 1014 (1988).

 © 1988 The Chemical Society of Japan Bull. Chem. Soc. Jpn., 61, 3145—3151 (1988)

Geometrical Isomers of Anionic Complexes Favorable to Chiral Discriminatory Ion-Pairing with Λ-$[Co(en)_3]^{3+}$ Ion and the Diastereomeric Ion-Pair Formation Constants in Solution[1)]

Akira TATEHATA* and Yasuyuki ASABA
Department of Chemistry, Faculty of Science, Shizuoka University, Ohya, Shizuoka 422
(Received September 5, 1987)

The stereoselectivities in the ion pairing of the geometrical isomers of anionic complexes, $[Co(ox)(gly)_2]^-$ and $[Co(ox)(edda)]^-$ (ox=oxalate dianion, gly=glycinate anion, and edda=ethylenediamine-*N*,*N*′-diacetate dianion) with $[Co(en)_3]^{3+}$ have been investigated by a chromatographic method. Only the C_1-*cis*(*N*) isomer of three geometrical isomers of $[Co(ox)(gly)_2]^-$ and the β-*cis* isomer of two of $[Co(ox)(edda)]^-$, in which three coordinated oxygen atoms are disposed triangularly along the pseudo C_3 axis, have been observed to interact more strongly with $[Co(en)_3]^{3+}$ than the other geometrical isomers. The diastereomeric ion-pair formation constants of C_1-*cis*(*N*)-$[Co(ox)(gly)_2]^-$ and β-*cis*-$[Co(ox)(edda)]^-$ with $[Co(en)_3]^{3+}$ in solution have been determined by a conductance method at 25 °C. The results were consistent with those of the chromatographic studies. An enhancement of the circular dichroism (CD) intensity of the A_2 component at the first d–d transition region of $[Co(en)_3]^{3+}$ has been observed upon the formation of ion pairing between the complex ions. Therefore, a favorable ion pair is considered to involve the hydrogen bonds between the coordinated oxygen atoms of the anionic complexes and the three N–H protons of $[Co(en)_3]^{3+}$ along the C_3 axis.

It is well-known that chromatography is an extremely valuable technique for the optical resolution of metal complexes.[2,3)] However, examples of a complete chromatographic resolution of anionic complexes are much fewer than those of cationic complexes because of a lack of effective eluting agents. We reported that the optically active $[Co(en)_3]^{3+}$ cation is an effective chiral discriminator for various complex anions and, hence, can serve as the highly promising eluting agent for the chromatographic resolution of many anionic complexes.[4,5)] It is thought that $[Co(en)_3]^{3+}$ can discriminate the chirality of anionic complexes by two different means: Λ-$[Co(en)_3]^{3+}$ prefers the Λ to the Δ isomer of $[Co(ox)_2(en)]^-$, whereas it prefers the Δ to the Λ isomer of $[Co(ox)_2(gly)]^{2-}$.[6–8)] The discrimination efficiency was shown to be largely different between the above two systems, though there is a difference in the electric charge on the anionic complexes. In order to explain why the absolute configurations of the favorable pairs of $[Co(ox)_2(en)]^-$ and $[Co(ox)_2(gly)]^{2-}$ with Λ-$[Co(en)_3]^{3+}$ are opposite to each other, our attention from an early stage was focused on the structural characteristics of the anionic complexes, especially on the difference in the spatial disposition of the coordinated oxygen atoms.[5,6)] It was therefore noted that $[Co(ox)_2(gly)]^{2-}$ has a triangular face comprising three coordinated oxygen atoms capable of forming three hydrogen bonds with N–H protons of Λ-$[Co(en)_3]^{3+}$ along its C_3 axis;[4)] however, $[Co(ox)_2(en)]^-$ has no such triangular face. It was then pointed out that the direction of the lone-pair electrons of coordinated oxygen atoms in Δ-$[Co(ox)_2(gly)]^{2-}$ is more favorable to the three hydrogen bonds with Λ-$[Co(en)_3]^{3+}$ than that in the antipode.[4,5)]

Subsequently, Miyoshi et al. investigated in detail the mechanism of chiral discrimination between metal complexes using a chromatographic method and proposed association models for the favorable pairs;[8,10)] chiral discrimination is effected along either the (pseudo) C_3 axis or the (pseudo) C_2 axis of the respective complexes. Thus, a homochiral (Λ–Λ or Δ–Δ) combination is favored when the cationic complex uses its C_3 axis, whereas a heterochiral (Λ–Δ or Δ–Λ) combination is favored when the cationic complex uses its C_2 axis, regardless of which axis (C_3 or C_2) of the anionic complex is directed to the cationic complex. Their proposal may explain the difference in the favorable association modes of $[Co(ox)_2(en)]^-$ and $[Co(ox)_2(gly)]^{2-}$. On the other hand, a crystal structure analysis of Δ-$[Co(l\text{-pn})_3]$ Λ-$[Cr(mal)_3]\cdot 3H_2O$ (*l*-pn=(R)-1,2-propanediamine, mal=malonate dianion) revealed that the cationic complex approaches the triangular face of Λ-$[Cr(mal)_3]^{3-}$ along the C_3 axis and makes face-to-face close contact through three hydrogen bonds.[9)] This indicates that the heterochiral combination mode can contribute effectively to chiral discrimination, even if the cationic complexes use the C_3 axis. Thus, their proposal may need to be tested further regarding many other metal complex systems.

In this paper the importance of the spatial disposition of coordinated atoms and the arrangement of chelate rings of anionic complexes are discussed in systems which involve the geometrical isomers of anionic complexes, $[Co(ox)(gly)_2]^-$ and $[Co(ox)(edda)]^-$. In order to obtain a measure of the discriminatory effect for strongly interacting ion pairs, the diastereomeric ion-pair formation constants are determined for $[Co(en)_3]^{3+}$–C_1-*cis*(*N*)-$[Co(ox)(gly)_2]^-$ and $[Co(en)_3]^{3+}$–β-*cis*-$[Co(ox)(edda)]^-$ systems. The favorable pair of these systems is Λ–Δ. It is then deduced from the CD change of Λ-$[Co(en)_3]^{3+}$ that the cationic complex uses its C_3 axis to discriminate the chirality of the anionic complexes, in disagreement with the proposal of Miyoshi et al. for the favorable pair containing the

heterochiral combination.

Experimental

Preparation of Complexes. The optically active $[Co(en)_3]I_3 \cdot H_2O$ was prepared by a method described in the literature[13] and converted to the chloride using an SP-Sephadex C-25 ion exchanger. Three geometrical isomers (*trans*(*N*), C_1-*cis*(*N*), and C_2-*cis*(*N*)) of $[Co(ox)(gly)_2]^-$ were prepared as described by Shimura and co-workers.[14] The C_1-*cis*(*N*) isomer for conductance measurements was resolved by a method described in the literature[15] (with a little modification) for obtaining the potassium salt.[16] Found for Λ-$(-)_{546}$ isomer ($[M]_{546}=-5530°$): C, 20.90; H, 2.64; N, 8.14%. Found for Λ-$(+)_{546}$ isomer ($[M]_{546}=+5540°$): C, 20.92; H, 2.63; N, 8.06%. Calcd for C_1-*cis*(*N*)-$K[Co(ox)(gly)_2] \cdot 0.5H_2O=C_6H_9N_2O_{8.5}KCo$: C, 21.00; H, 2.64; N, 8.16%. Two geometrical isomers (α-*cis* and β-*cis*) of $[Co(ox)(edda)]^-$ were prepared and separated by the method of Coleman et al.[17] Λ-$(-)_{589}$-β-*cis*-$K[Co(ox)(edda)] \cdot 2H_2O$ for conductance measurements was prepared according to the method of Jordan and Legg,[18] which was obtained as the dihydrate ($[M]_{589}=-3470°$, $\Delta\varepsilon_{544}=-2.22$ mol^{-1} dm^3 cm^{-1}) in this study though had been obtained as the monohydrate in Ref. 18 (The value of $\Delta\varepsilon_{544}$ reported for $(+)_{589}$ isomer was +2.05). Found: C, 24.35; H, 3.51; N, 7.04%. Calcd for β-*cis*-$K[Co(ox)(edda)] \cdot 2H_2O=C_8H_{14}N_2O_{10}KCo$: C, 24.25; H, 3.56; N, 7.07%.

Chromatographic Experiments. (*a*) Each sample of the racemic geometrical isomers of $[Co(ox)(gly)_2]^-$ and $[Co(ox)(edda)]^-$ was adsorbed on a column (1.9×60 cm) of DEAE-Sephadex A-25 anion exchanger and was eluted with an aqueous solution of NaCl (0.3 mol·dm^{-3}) or *rac*-$[Co(en)_3]Cl_3$ (0.1 mol·dm^{-3}) at a rate of 0.3—0.5 cm^{3}min^{-1}. The eluate was divided into fractions of 3-cm^3 portions and the concentration of the eluted isomer in each fraction was measured spectrophotometrically to obtain an elution curve.

(*b*) Each racemic isomer of the above anionic complexes was chromatographed in a similar manner as mentioned above, except for the length of the column (1.9×150 cm) and the use of an aqueous solution (0.05 mol·dm^{-3}) or 30% aqueous ethanol solution (0.05 mol·dm^{-3}) of Λ-$[Co(en)_3]Cl_3$ as the eluent.

(*c*) A column (1.9×60 cm) of SP-Sephadex C-25 cation exchanger which was converted completely to the Λ-$[Co(en)_3]^{3+}$ form was prepared. The bottom of the column was loaded with the cation exchanger in Na^+ form (10 cm long) in order to remove a small amount of Λ-$[Co(en)_3]^{3+}$ eluted from the upper part of the column. Each racemic anionic complex (5 ml of 20—30 mM; 1 M=1 mol dm^{-3}) was placed on the top of the column and eluted with water at a rate of 0.3 cm^3 min^{-1}. The concentration and the optical rotation of the partially resolved complex in each fraction (2.5 cm^3) were measured in order to determine percentage resolution.

Conductance Measurements. The complex anions of C_1-*cis*(*N*)-$[Co(ox)(gly)_2]^-$ and β-*cis*-$[Co(ox)(edda)]^-$, which were found to interact strongly with $[Co(en)_3]^{3+}$ by chromatographic studies, were selected for conductance measurements. The conductance of the mixed solutions containing various volume ratios of the chiral $[Co(en)_3]^{3+}$ and the chiral anionic complex (ionic strength, I=0.01 mol dm^{-3}) was measured at 25±0.01 °C using a conductometer (Type MY-8, Yanagimoto Mfg. Co. Ltd.) at a frequency of 800 Hz. The diastereomeric ion-pair formation constants were estimated according to the procedure described in various previous studies.[4,5,19]

CD Measurements. The CD spectra were measured on a Jasco J-500 spectropolarimeter using a 1-mm cell at room temperature. To an aqueous solution of Λ-$[Co(en)_3]I_3 \cdot H_2O$ (0.025 mol dm^{-3}) Λ- or *rac*-C_1-*cis*(*N*)-$K[Co(ox)(gly)_2]$ or *rac*-β-*cis*-$Na[Co(ox)(edda)] \cdot 2H_2O$ was added so as to prepare the solution of 0.025 (for Λ-complex) or 0.05 mol dm^{-3} (for *rac*-complex) with respect to the concentration of the anionic complex. Absorption spectra, absorbances of chromatographic fractions, and optical rotations were obtained on a Shimadzu MPS-50L recording spectrophotometer, a Jasco Uvidec-320 spectrophotometer, and a Union automatic polarimeter PM-101, respectively with 1 or 5 cm cells.

Results and Discussion

Chromatography of Geometrical Isomers of $[Co(ox)(gly)_2]^-$ and $[Co(ox)(edda)]^-$. Elution curves of geometrical isomers of $[Co(ox)(gly)_2]^-$ by anion-exchange chromatography are shown in Fig. 1. It can be seen that the C_1-*cis*(*N*)-isomer is eluted markedly faster when *rac*-$[Co(en)_3]Cl_3$ is used as an eluent than when sodium chloride is used, compared with *trans*(*N*)- and C_2-*cis*(*N*)-isomers.

By combining the ion-exchange equilibrium with the ion-pair formation equilibrium, the net retention volume, V, of the adsorbed anionic complex in the present anion-exchange chromatography can be

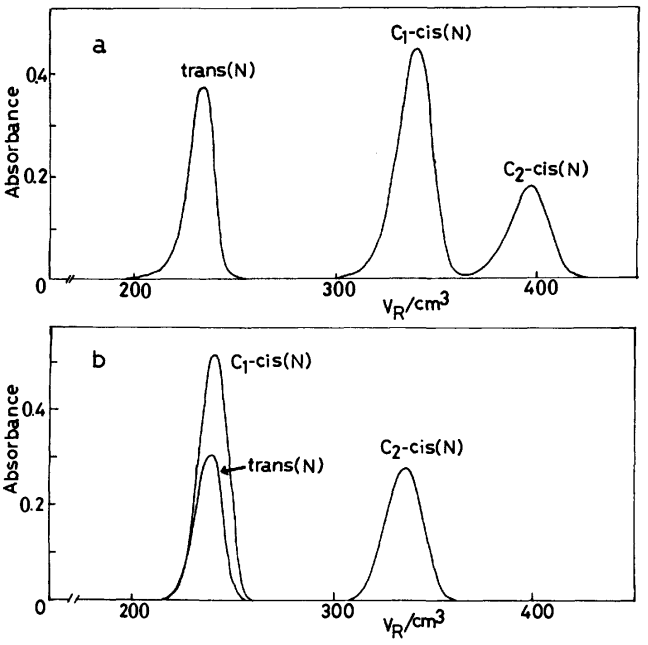

Fig. 1. Elution curves for geometrical isomers of $[Co(ox)(gly)_2]^-$ by chromatography using a column (1.9×60 cm) of DEAE-Sephadex A-25 and an aqueous solution of 0.3 mol dm^{-3} NaCl (a) and 0.1 mol dm^{-3} *rac*-$[Co(en)_3]Cl_3$ (b) as the eluent.

expressed by Eq. 1,[20]

$$V = V_s KQ/[Cl^-]\{1 + \beta[\text{cation}]\}, \quad (1)$$

where V_s is the volume of ion-exchange resin in the column, K the ion-exchange equilibrium constant for the reaction, $B^- + R\text{-}Cl \rightleftarrows Cl^- + R\text{-}B$ (B=anionic complex, R=ion-exchange group), Q the capacity of the ion-exchange resin, and β the ion-pair formation constant of the anionic complex with the cation contained in an eluting solution. We now consider the difference in the retention volumes of a certain anionic complex between elutions with sodium chloride and $[Co(en)_3]Cl_3$. The term $V_sKQ/[Cl^-]$ for a certain anionic complex is virtually identical in the two cases under the experimental conditions and the term β[cation] is expected to be negligibly small when the cation is sodium ion. Therefore, the ratio of the retention volumes is given by

$$V(Co(en)_3^{3+})/V(Na^+) = 1/\{1 + \beta[Co(en)_3^{3+}]\}, \quad (2)$$

where $V(Na^+)$ and $V(Co(en)_3^{3+})$ are the retention volumes observed when sodium chloride and $[Co(en)_3]Cl_3$ are used as an eluent, respectively. According to Eq. 2, the ratios of the retention volumes decrease with an increase in the value of the ion-pair formation constants between the anionic complexes and $[Co(en)_3]^{3+}$. This leads to the prediction that the anionic complex which forms a strong ion pair with $[Co(en)_3]^{3+}$ has a small value of the ratio, $V(Co(en)_3^{3+})/V(Na^+)$. Figure 1 indicates the decreasing order of the ratio for the three geometrical isomers of $[Co(ox)(gly)_2]^-$ to be *trans*(*N*)>C_2-*cis*(*N*)>C_1-*cis*(*N*)-isomer. Thus, it should be noted that C_1-*cis*(*N*)-$[Co(ox)(gly)_2]^-$ forms a stronger ion pair with $[Co(en)_3]^{3+}$ than do *trans*(*N*)- and C_2-*cis*(*N*)-isomers. This may be related to the observation that only a C_1-*cis*(*N*)-isomer is resolvable by usual anion-exchange chromatography using Λ-$[Co(en)_3]Cl_3$ as an eluent, as shown in Fig. 2. Figure 3 shows elution curves and percentage resolutions of three geometrical isomers in chromatography of which a column of SP-Sephadex C-25 in Λ-$[Co(en)_3]^{3+}$ form were employed (water: eluent). The complex anion of C_1-*cis*(*N*)-isomer was the last to be eluted, and a great degree of resolution was attained, being consistent with the results from the above-mentioned usual anion-exchange chromatography that C_1-*cis*(*N*)-isomer tends to form a strong ion pair with $[Co(en)_3]^{3+}$. The percentage resolution curve shows that the ion pair of Λ-$[Co(en)_3]^{3+}$-Λ-C_1-*cis*(*N*)-$[Co(ox)(gly)_2]^-$ is more favorable than Λ-$[Co(en)_3]^{3+}$-Λ-C_1-*cis*(*N*)-$[Co(ox)(gly)_2]^-$. Despite of the presence of an additional chelate ring between the coordinated nitrogen atoms in edda ligand, α-*cis* and β-*cis* isomers of $[Co(ox)(edda)]^-$ are the same as C_2-*cis*(*N*) and C_1-*cis*(*N*) isomers of $[Co(ox)(gly)_2]^-$, respectively, with respect to the spatial disposition of coordinated atoms around Co(III) (Scheme 1). Chromatograms of the geometrical isomers of $[Co(ox)(edda)]^-$ are shown in Fig.4.

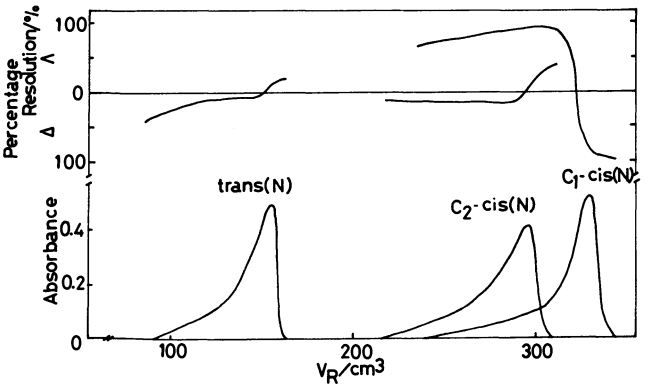

Fig. 3. Elution curves and percentage resolutions for geometrical isomers of $[Co(ox)(gly)_2]^-$ by chromatography using a column (1.9×60 cm) of SP-Sephadex C-25 in Λ-$[Co(en)_3]^{3+}$ form and water as an eluent.

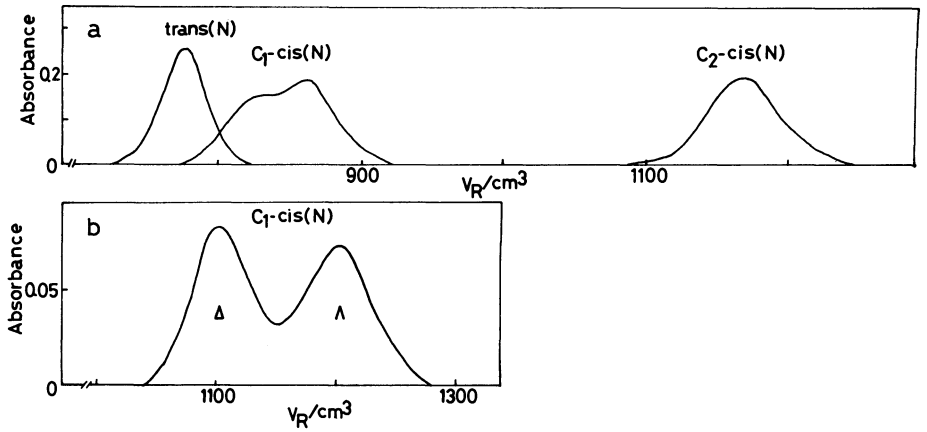

Fig. 2. Elution curves for geometrical isomers of $[Co(ox)(gly)_2]^-$ by chromatography using a column (1.9×150 cm) of DEAE-Sephadex A-25 and an aqueous solution (a) and a 30% ethanolic aqueous solution (b) of 0.05 mol dm^{-3} Λ-$[Co(en)_3]Cl_3$ as the eluent.

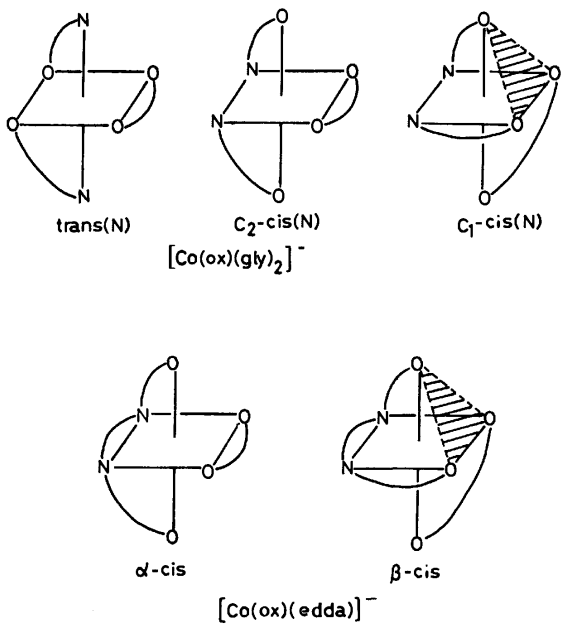

Scheme 1.

It can be seen that each chromatographic behavior of *α-cis* and *β-cis*-[Co(ox)(edda)]$^-$ is very similar to that of the corresponding geometrical isomer of [Co(ox)-(gly)$_2$]$^-$. The present observation suggests that the spatial disposition of the oxygen atoms in the complexes is important regarding both the ion pair formation and stereoselectivity. That is, *β-cis*-[Co(ox)(edda)]$^-$ and C$_1$-*cis*(*N*)-[Co(ox)(gly)$_2$]$^-$ are able to form a strong ion pair with [Co(en)$_3$]$^{3+}$ and to give a great degree of ion-pairing stereoselectivity since these isomers have a highly anionic triangular face consisting of three coordinated oxygen atoms (as shown by the shaded parts in Scheme 1). In order to obtain information about the structure of ion pair, especially about the direction of access of the complex anion to the complex cation, the CD changes of [Co(en)$_3$]$^{3+}$ in the first absorption band region were measured upon addition of C$_1$-*cis*(*N*)-[Co(ox)(gly)$_2$]$^-$ or *β-cis*-[Co(ox)(edda)]$^-$.

CD Changes and Ion Pair Structure. It is well-known that the addition of a chiral anion such as *d*-tartrate ion to such complexes as [Co(en)$_3$]$^{3+}$ and [Co(chxn)$_3$]$^{3+}$, which can form hydrogen bonds with the axial N-H protons along the C$_3$ axis, enhances the CD intensity of the A$_2$ component.[11,23] Yoneda and co-workers have shown by the CD studies of [Co-(sep)]$^{3+}$ (sep=1,3,6,8,10,13,16,19-octaazabicyclo[6.6.6]-icosane) and the related complexes that when the hydrogen bonds are formed by using equatorial N-H protons directed nearly along the C$_2$ axis, the effect leads to an enhancement of the E$_a$ rotational strength.[10-12] Therefore, we can determine the ion pair structure by observing which component (A$_2$ or E$_a$) of [Co(en)$_3$]$^{3+}$ is enhanced upon the addition of a chiral complex anion. Figure 5 shows the CD spectra

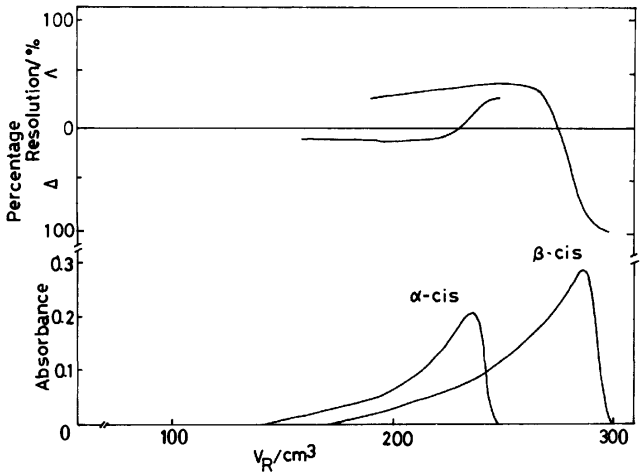

Fig. 4. Elution curves and percentage resolutions for geometrical isomers of [Co(ox)(edda)]$^-$ by chromatography using a column (1.9×60 cm) of SP-Sephadex C-25 in *Λ*-[Co(en)$_3$]$^{3+}$ form and water as an eluent.

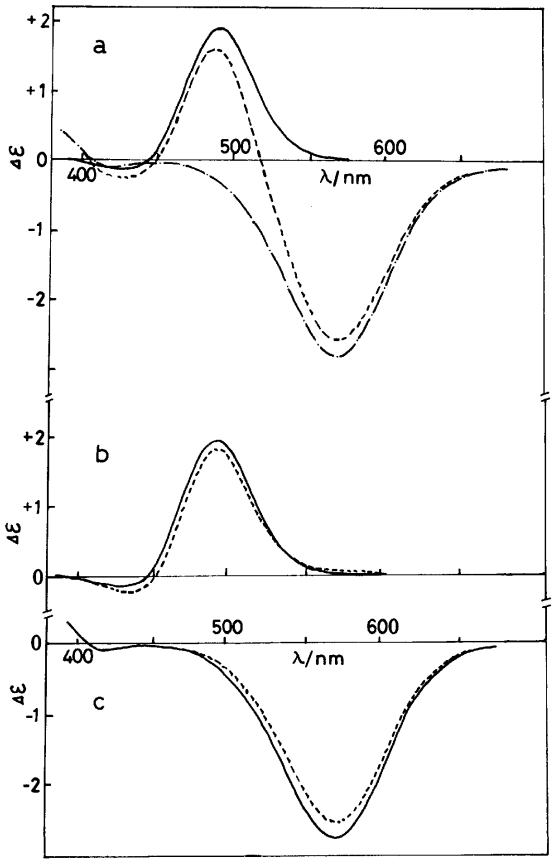

Fig. 5. (a) CD spectra of 0.025 mol dm^{-3} *Λ*-[Co-(en)$_3$]$^{3+}$ (——), 0.025 mol dm^{-3} *Λ*-C$_1$-*cis*(*N*)-[Co-(ox)(gly)$_2$]$^-$ (—·—), and the mixture (----). (b) CD spectra of 0.025 mol dm^{-3} *Λ*-[Co(en)$_3$]$^{3+}$ in the absence (——) and the presence (----) of 0.05 mol dm^{-3} *rac*-C$_1$-*cis*(*N*)-[Co(ox)(gly)$_2$]$^-$. (c) CD spectra of 0.025 mol dm^{-3} *Λ*-C$_1$-*cis*(*N*)-[Co(ox)(gly)$_2$]$^-$ in the absence (——) and the presence (----) of 0.05 mol dm^{-3} *rac*-[Co(en)$_3$]$^{3+}$. All the samples were measured using a 1 mm cell.

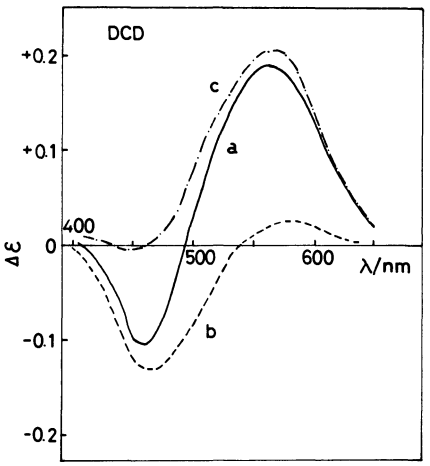

Fig. 6. The DCD spectra in the presence of *Λ*-$[Co(en)_3]^{3+}$ and *Δ*-C1-*cis*(*N*)-$[Co(ox)(gly)_2]^-$ (a), *Λ*-$[Co(en)_3]^{3+}$ and *rac*-C1-*cis*(*N*)-$[Co(ox)(gly)_2]^-$ (b), and *rac*-$[Co(en)_3]^{3+}$ and *Δ*-C1-*cis*(*N*)-$[Co(ox)(gly)_2]^-$ (c), respectively.

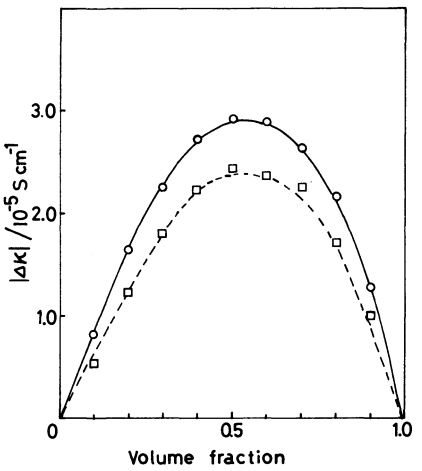

Fig. 7. The deviations, $|\Delta\kappa|$, of the measured conductivity from additivity as a function of the volume fraction, *x*, of *Λ*-$[Co(en)_3]I_3$ for the *Λ*-*Δ* (-O-) and the *Λ*-*Λ* (-□-) pairs in the $[Co(en)_3]^{3+}$-C1-*cis*(*N*)-$[Co(ox)(gly)_2]^-$ system at 25°C, I=0.01 mol dm^{-3}.

of aqueous *Λ*-$[Co(en)_3]^{3+}$ in the absence and the presence of *Δ*- or *rac*-C1-*cis*(*N*)-K$[Co(ox)(gly)_2]^-$ ion and the CD spectra of aqueous *Δ*-C1-*cis*(*N*)-$[Co(ox)(gly)_2]^-$ in the absence and the presence of *rac*-$[Co(en)_3]^{3+}$ ion. The difference CD (DCD) spectra, which are defined as the observed CD in the presence of both cationic and anionic complexes minus the simple sums of the component solution spectra, are shown in Fig. 6 in order to clarify the CD spectral changes due to ion pairing between these complex ions. The addition of *Δ*-C1-*cis*(*N*)-$[Co(ox)(gly)_2]^-$ to *Λ*-$[Co(en)_3]^{3+}$ not only enhances the CD intensity of the A_2 component at the first absorption band region of $[Co(en)_3]^{3+}$, but also produces a rather large decrease in the CD intensity of C1-*cis*(*N*)-$[Co(ox)(gly)_2]^-$ in the first d-d transition region ((*a*) in Figs. 5 and 6). Fortunately, the observed CD changes of $[Co(en)_3]^{3+}$ are not seriously disturbed by that of the anionic complex since the CD peaks of both the complex ions are very far apart from each other (at 430 nm(A_2) and 490 nm(E_a) for the cation, at 569 nm for the anion). The changes in the CD spectrum of *Λ*-$[Co(en)_3]^{3+}$ on addition of *Δ*- or *rac*-C1-*cis*(*N*)-$[Co(ox)(gly)_2]^-$ are remarkably similar to the case in which phosphate and *d*-tartrate ions are added. It has been established that three oxygen atoms of the phosphate[21,22] and *d*-tartrate ions[23,24] form hydrogen bonds with three N-H protons of the $[Co(en)_3]^{3+}$ along its C_3 axis, in solution as well as in crystal. The similarity in CD change detected in the present study suggests that the hydrogen bonds along the C_3 axis of the cation are formed between the three axial N-H protons of the $[Co(en)_3]^{3+}$ and the three coordinated oxygen atoms of the C1-*cis*(*N*)-$[Co(ox)(gly)_2]^-$. A similar existence of three N-H···O hydrogen bonds along the C_3 axis was reported for the diastereoisomer *Λ*-$[Co(l\text{-pn})_3]$*Λ*-$[Cr(mal)_3]\cdot 3H_2O$ in crystal.[9] The DCD spectrum for the solution involving *Λ*-$[Co(en)_3]^{3+}$ and *rac*-C1-*cis*-(*N*)-$[Co(ox)(gly)_2]^-$ has a small positive peak in the first d-d transition region of the complex anion ((*b*) in Fig.6). Since the ion-pairing interaction of the *Λ*-cation with the *Δ*-anion produces a large decrease in the CD intensity in the spectral region of the anion (a large positive DCD peak) ((*a*) in Figs. 5 and 6), the small positive DCD peak produced by the *Λ*-cation and the rac-anion indicates that the *Λ*-*Δ* interaction is stronger than the *Λ*-*Λ*; in other words, the favorable ion pair between $[Co(en)_3]^{3+}$ and C1-*cis*(*N*)-$[Co(ox)(gly)_2]^-$ is *Λ*-*Δ*.

Miyoshi et al. have reported that when the cationic complex uses its C_3 axis for hydrogen bonding to the anionic complex, a homochiral combination (*Λ*-*Λ* or *Δ*-*Δ*) is favored, whereas when the cationic complex uses its C_2 axis, a heterochiral combination (*Λ*-*Δ* or *Δ*-*Λ*) is favored.[8,10] However, in the present $[Co(en)_3]^{3+}$-C1-*cis*(*N*)-$[Co(ox)(gly)_2]^-$ system, it is strongly suggested from the CD spectral change (an enhancement of the A_2 component of $[Co(en)_3]^{3+}$) that the favorable pair is a heterochiral combination in which the cation uses its C_3 axis for hydrogen bonding. This is inconsistent with the discrimination mechanism proposed above by Miyoshi et al.

Diastereomeric Ion-Pair Formation Constants. We previously showed that the conductance method is useful for a determination of the diastereomeric ion-pair formation constants between chiral complex ions.[4,5] The conductance measurements were carried out for $[Co(en)_3]^{3+}$-C1-*cis*(*N*)-$[Co(ox)(gly)_2]^-$ and $[Co(en)_3]^{3+}$-*β*-*cis*-$[Co(ox)(edda)]^-$ systems. In Fig. 7 are shown the deviations ($\Delta\kappa$) of the measured conductivity from the additivity of the component conductivities at various volume fractions (*x*) of $[Co(en)_3]$-

$I_3 \cdot H_2O$ for the Λ-Δ and Λ-Λ pairs in the $[Co(en)_3]^{3+}$-C_1-*cis*(*N*)-$[Co(ox)(gly)_2]^-$ system at 25 °C, ionic strength I=0.01 mol dm^{-3}. The $\Delta\kappa$ value of the mixture, consisting of a solution of C_M mol dm^{-3} $[Co(en)_3]$-$I_3 \cdot H_2O$ and a solution of C_B mol dm^{-3} K-C_1-*cis*(*N*)-$[Co(ox)(gly)_2] \cdot 0.5H_2O$ at volume fractions of x and 1-x, respectively, is given by

$$10^3 \Delta\kappa = 10^3\kappa - C_M x \Lambda_m(MI_3) - C_B(1-x)\Lambda_m(KB), \quad (3)$$

where κ is the specific conductivity (S cm^{-1}) of the mixture and Λ_m is the molar conductivity (S cm^2 mol^{-1}) of the species specified in parentheses {M=$[Co(en)_3]^{3+}$, B=C_1-*cis*(*N*)-$[Co(ox)(gly)_2]^-$} at an ionic strength of 0.01 mol dm^{-3}. If a 1:1 ion pair, $M^{3+} \cdot B^-$, is assumed, $\Delta\kappa$ can be related to the molar concentration of the ion-pair by

$$[M^{3+} \cdot B^-] = 10^3 \Delta\kappa/\alpha \quad (4)$$

and

$$\alpha = 2\lambda(M^{3+} \cdot B^-) - 3\lambda(M^{3+}) - \lambda(B^-), \quad (5)$$

where λ is the ionic equivalent conductance at 25 °C, I=0.01 mol dm^{-3} of $M^{3+} \cdot B^-$, M^{3+}, and B^-, respectively. It can been seen in Fig. 7 that there exists a significant difference in the $|\Delta\kappa|$ values between the Λ-Δ and Λ-Λ pairs; that is, the $|\Delta\kappa|$ values for the Λ-Δ pair are invariably larger than those for the Λ-Λ pair at every volume fractions. The diastereomeric ion-pair formation constants, $K(\Lambda$-$\Delta)$ and $K(\Lambda$-$\Lambda)$, obtained by analyzing the $\Delta\kappa$ values according to procedures described in the literature[4,5,19] are given in Table 1 along with the relative formation constants (discrimination factors), $K(\Lambda$-$\Delta)/K(\Lambda$-$\Lambda)$, which is considered to be a measure of the stereoselectivity in ion pairing determined directly by conductance. The diastereomeric ion-pair formation constants and the discrimination factors for the $[Co(en)_3]^{3+}$-β-cis-$[Co(ox)(edda)]^-$ system are presented in Table 2. As can already be expected from the similarity of the chromatographic behavior to that of C_1-*cis*(*N*)-$[Co(ox)(gly)_2]^-$, the preference of the Λ-Δ combination was again observed in this system. However, it may be noteworthy that the discrimination factor for the $[Co(en)_3]^{3+}$-β-*cis*-$[Co(ox)(edda)]^-$ system is smaller than that for the $[Co(en)_3]^{3+}$-C_1-*cis*(*N*)-$[Co(ox)(gly)_2]^-$ system. In β-*cis*-$[Co(ox)(edda)]^-$ complex, the meridional acetate ring of the edda ligand is strained because of the presence of the "ethylenediamine" part of the edda, compared with the strain-free glycinate rings in C_1-*cis*(*N*)-$[Co(ox)(gly)_2]^-$. Consequently, both the anionic complexes are subtly different in the direction of the lone pair electrons on the coordinated oxygen atoms. Thus, as can be seen in Tables 1 and 2, this effect upon the ion-pair formation constants is more prominent for the favorable pairs ($K(\Lambda$-$\Delta)$=83.1 and 69.8 mol^{-1} dm^3 for $[Co(en)_3]^{3+}$-C_1-*cis*(*N*)-$[Co(ox)(gly)_2]^-$ and $[Co(en)_3]^{3+}$-β-*cis*-$[Co(ox)(edda)]^-$ systems, respectively) than for the unfavorable pairs ($K(\Lambda$-$\Lambda)$= 63.8 and $K(\Delta$-$\Delta)$=60.0 mol^{-1}dm^3 for the former and the latter systems, respectively) since the stabilization

Table 1. Ion-Pair Formation Constants and Discrimination Factors for $[Co(en)_3]^{3+}$-C_1-*cis*(*N*)-$[Co(ox)(gly)_2]^-$ System at 25 °C, I=0.01 mol dm^{-3}

Volume fraction x	Ion-pair formation constant/mol^{-1} dm^3 $K(\Lambda$-$\Delta)$	$K(\Lambda$-$\Lambda)$	Discrimination factor $K(\Lambda$-$\Delta)/K(\Lambda$-$\Lambda)$
0.2	85.9	58.7	1.46
0.3	83.9	62.0	1.35
0.4	85.6	66.2	1.29
0.5	82.0	66.3	1.24
0.6	80.8	64.3	1.26
0.7	80.7	67.8	1.19
0.8	82.6	61.4	1.35
	83.1±2.1[a]	63.8±3.2[a]	1.31±0.09[a]

a) Average and standard deviation.

Table 2. Ion-Pair Formation Constants and Discrimination Factors for $[Co(en)_3]^{3+}$-β-*cis*-$[Co(ox)(edda)]^-$ System at 25 °C, I=0.01 mol dm^{-3}

Volume fraction x	Ion-pair formation constant/mol^{-1} dm^3 $K(\Lambda$-$\Delta)$	$K(\Delta$-$\Delta)$	Discrimination factor $K(\Lambda$-$\Delta)/K(\Delta$-$\Delta)$
0.2	70.4	61.6	1.14
0.3	74.9	64.2	1.17
0.4	70.5	62.3	1.13
0.5	68.9	60.8	1.13
0.6	70.3	58.4	1.20
0.7	66.6	56.0	1.19
0.8	66.8	57.0	1.17
	69.8±2.8[a]	60.0±3.0[a]	1.16±0.03[a]

a) Average and standard deviation.

of a favorable pair should greatly depend on the fitness of the hydrogen bonding. The importance of the direction of lone pair electrons on the oxygen atom employed for hydrogen bonding was also observed in chromatographic ion-pairing investigations of C_1-*cis*(*N*)-$[Co(ox)(gly)_2]^-$ and C_1-*cis*(*N*)-$[Co(ox)(\beta\text{-ala})_2]^-$ with Λ-$[Co(en)_3]^{3+}$ [5]; that is, the separation factor for C_1-*cis*(*N*)-$[Co(ox)(\beta\text{-ala})_2]^-$ with six-membered chelate rings has been shown to be slightly greater than that for C_1-*cis*(*N*)-$[Co(ox)(gly)_2]^-$ with five-membered chelate rings, where the separation factor is defined as the value of the retention volume of the later eluted enantiomer devided by that of the faster eluted one. This enhanced stereoselectivity for C_1-*cis*(*N*)-$[Co(ox)(\beta\text{-ala})_2]^-$ suggests that the direction of lone pair electrons on the carboxyl oxygen atom in the six-membered chelate ring is more favorable to hydrogen bonding along the C_3 axis with the N-H groups on the Λ-$[Co(en)_3]^{3+}$ than that in the five-membered chelate ring. The stereoselectivity was observed to increase for chelate rings of the related anionic complexes in the following order: strained five-membered chelate ring<less strained five-membered chelate ring<six-membered chelate ring. Thus, β-*cis*-$[Co(ox)(edda)]^-$ with the strained meridional acetate ring can be understood to show reduced ion-pairing stereoselectivity. The observation that the CD change of Λ-$[Co(en)_3]^{3+}$ on addition of β-*cis*-$[Co(ox)(edda)]^-$ is quite similar to that on addition of C_1-*cis*(*N*)-$[Co(ox)(gly)_2]^-$ but is slightly smaller in magnitude also supports the reduced stereoselectivity in $[Co(en)_3]^{3+}$-β-*cis*-$[Co(ox)(edda)]^-$ system.

Concluding Remarks

It has been shown that C_1-*cis*(*N*)-$[Co(ox)(gly)_2]^-$ and β-*cis*-$[Co(ox)(edda)]^-$ associate more strongly with $[Co(en)_3]^{3+}$ than the respective other geometrical isomers. An important structural characteristic of the anionic complexes is that they have a triangular face consisting of three coordinated oxygen atoms along the pseudo C_3 axis. In both $[Co(en)_3]^{3+}$-C_1-*cis*(*N*)-$[Co(ox)(gly)_2]^-$ and $[Co(en)_3]^{3+}$-β-cis-$[Co(ox)(edda)]^-$ systems a Λ-Λ combination was preferred over a Λ-Λ combination. This has also been confirmed by the diastereomeric ion-pair formation constants determined by the conductance method. The effect of C_1-*cis*(*N*)-$[Co(ox)(gly)_2]^-$ and β-*cis*-$[Co(ox)(edda)]^-$ on the CD spectra of $[Co(en)_3]^{3+}$ was very similar to that of phosphate and *d*-tartrate ions; that is, the A_2 rotational strength of $[Co(en)_3]^{3+}$ was enhanced upon the formation of ion pairing. This result strongly suggests that the hydrogen bondings formed between the cationic and the anionic complexes play an important role in the ion-pairing stereoselectivity and, further, that the anionic complex approaches a triangular face of $[Co(en)_3]^{3+}$ along the C_3 axis and makes a face-to-face close contact through three hydrogen bonds. The ion-pair structure is disagreement with the discrimination mechanism proposed by Miyoshi et al.

References

1) A part of this paper was presented at the 33rd Symposium on Coordination Chemistry of the Chemical Society of Japan, Osaka, October 1983, Abstr. No. 1PA13.

2) Y. Yoshikawa and K. Yamasaki, *Coord. Chem. Rev.*, **28**, 205 (1979).

3) H. Yoneda, *J. Liq. Chromatogr.*, **2**, 1157 (1979).

4) A. Tatehata, M. Iiyoshi, and K. Kotsuji, *J. Am. Chem. Soc.*, **103**, 7391 (1981).

5) A. Tatehata, M. Fujita, K. Ando, and Y. Asaba, *J. Chem. Soc., Dalton Trans.*, **1987**, 1977.

6) A. Tatehata, Y. Ejima, and K. Kotsuji, 29th Symposium on Coordination Chemistry, Hamamatsu, October 1979, Abstr. No. 1B01.

7) U. Sakaguchi, I. Yamamoto, S. Izumoto, and H. Yoneda, *Bull. Chem. Soc. Jpn.*, **56**, 153 (1983).

8) K. Miyoshi, Y. Sakamoto, A. Ohguni, and H. Yoneda, *Bull. Chem. Soc. Jpn.*, **58**, 2239 (1985).

9) K. R. Butler and M. R. Snow, *J. Chem. Soc., Dalton Trans.*, **1976**, 251.

10) H. Yoneda, *J. Chromatogr.*, **313**, 59 (1984).

11) U. Sakaguchi, A. Tsuge, and H. Yoneda, *Inorg. Chem.*, **22**, 3745 (1983).

12) K. Miyoshi, S. Izumoto, K. Nakai, and H. Yoneda, *Inorg. Chem.*, **25**, 4654 (1986).

13) J. A. Broomhead, F. P. Dwyer, and J. W. Hogarth, *Inorg. Synth.*, **6**, 183 (1960).

14) N. Matsuoka, J. Hidaka, and Y. Shimura, *Bull. Chem. Soc. Jpn.*, **40**, 1868 (1967).

15) N. Matsuoka, J. Hidaka, and Y. Shimura, *Inorg. Chem.*, **9**, 719 (1970).

16) In Ref. 15 the optically active C_1-*cis*(*N*) isomer had not been isolated as crystal.

17) P. F. Coleman, J. I. Legg, and J. Steele, *Inorg. Chem.*, **9**, 937 (1970).

18) W. T. Jordan and J. I. Legg, *Inorg. Chem.*, **13**, 955 (1974).

19) S. Katayama and R. Tamamushi, *Bull. Chem. Soc. Jpn.*, **43**, 2354 (1970).

20) S. Yamazaki and H. Yoneda, 29th Symposium on Coordination Chemistry, Hamamatsu, October 1979, Abst. No. 2B04; G. Muto and K. Oikawa, "Ion Chromatography," Kodansha, (1983).

21) S. F. Mason and B. J. Norman, *Proc. Chem. Soc.*, **1964**, 339. *J. Chem. Soc. A*, **1966**, 307.

22) E. N. Duesler and K. N. Raymond, *Inorg. Chem.*, **10**, 1486 (1971).

23) M. Fujita and H. Yamatera, *Bull. Chem. Soc. Jpn.*, **49**, 1301 (1976).

24) Y. Kushi, M. Kuramoto, and H. Yoneda, *Chem. Lett.*, **1976**, 135.

 © 1988 The Chemical Society of Japan Bull. Chem. Soc. Jpn., 61, 3153—3158 (1988)

Seasonal Movements of Phosphorus and Iron Compounds, Dissolved Hydrogen Sulfide, and Others in Anoxic Seawater at Lake Hamana§

Norio Ichinose,* Kyoko Adachi, Mina Mitsui, Chiaki Shimizu,†
Ken Okamoto,† Hisashi Kurokura,†† Takuo Inui,†††
and Hisae Tamura†††
Department of Chemistry, Hamamatsu University School of Medicine, Handa-cho, Hamamatsu 431-31
†Fisheries Laboratory, Faculty of Agriculture, The University of Tokyo,
Maisaka, Hamana, Shizuoka 431-02
††Marine Biological Science Division, Faculty of Applied Biological Science,
Hiroshima University, Midori-cho, Fukuyama 720
†††Shizuoka Prefectural Industrial Research Institute, Makigaya, Shizuoka 421-21
(Received December 11, 1987)

The sea bottom in the vicinity of the center of Lake Hamana in Japan forms a sea basin, and anoxic seawater appears in this bottom layer in summer. We examined the seasonal movements of phosphorus and iron compounds, dissolved hydrogen sulfide, and others in this anoxic seawater with a view to investigating their elution processes from the sediments of the sea basin into the anoxic seawater. Some parts of the elution phenomena of these components from the sediments of the sea basin in Lake Hamana into the anoxic seawater in summer will be described in the present work.

The sea bottom in the vicinity of the center of Lake Hamana in Japan forms a sea basin. Anoxic seawater appears in this bottom layer in summer because the hydrosphere in the basin becomes a reducing atmosphere at a high temperature as a result of the small tidal currents and the decomposition of dead marine organisms such as plankton deposited on the sea floor. However, very little information is available in the literature on the seasonal movements of phosphorus and iron compounds, dissolved hydrogen sulfide (DHS), and others, in the anoxic seawater occurring in a sea basin such as Lake Hamana.

We ourselves have reported previously analytical methods for dissolved inorganic phosphorus (DIP) and organic phosphorus (DOP)[1-3] and DHS[4,5] eluted from the sediments of the sea basin in Lake Hamana into the anoxic seawater. By applying mainly our analytical methods, we have now examined the seasonal movements of DIP, DOP, iron(II) and iron(III) ions, DHS, and others in the anoxic seawater occurring in the sea basin, with a view to investigating geochemically their elution processes from the sediments.

Experimental

Analytical Procedure for DHS. Sample solutions (4-ml volume) from different water depths are introduced from Kitahara's bottle into a 10-ml syringe containing 4 ml of an acetone solution of hydroxylamine hydrochloride(0.2%). After the removal of an air bubble, the syringe is shaken gently, then most of the mixed sample solution is transferred into a 7-ml dark plastic bottle. The bottle is immediately sealed and stored at 0 °C. The DHS in the stored solution is determined by means of gas chromatography under the conditions shown in Table 1.

§ A part of this paper was presented at the Symposium of Environmental Science held in Tokyo, November, 1986.

Table 1. Analytical Conditions for the Determination of Dissolved Hydrogen Sulfide by Means of Gas Chromatography

Column temperature	110 °C
Injection temperature	150 °C
H_2 pressure	0.75 kg cm^{-2}
Air pressure	1.30 kg cm^{-2}
Carrier gas	Nitrogen, 90 ml min^{-1}
Injection volume	2 μl
Glass column	1.1×3.2 mm i.d.
Packing material	Porapak N (50—80 mesh)

The initial DHS concentration in anoxic seawater is determined by reference to previously prepared calibration and decay curves for DHS at a rate of about 0.5% per hour over a 24-h period after sampling. For further details, the reader should refer to Refs. 4 and 5.

Analytical Procedure for DIP and DOP, and for Fe(II) and Fe(III). The DIP and DOP and the Fe(II) and Fe(III) in anoxic seawater are determined by the heteropoly-blue method[1,3] and by 1,10-phenanthroline spectrophotometry[6] respectively.

Results and Discussion

The water samples were taken using Kitahara's bottle from different water depths (at intervals of about 1 m) at two Stations, A and B, in Lake Hamana.[5] The sea bottom of Station A, in the vicinity of the center in Lake Hamana, forms the deepest sea basin (about 12 m) in the lake, while Station B, used as a control for A, stands at one end of this sea basin.

Figure 1 shows the seasonal variations in the dissolved oxygen (DO), the salinity, the pH, and the temperature at different water depths of Stations A and B at roughly monthly intervals for the year in 1983. It may be observed from the results shown in Fig. 1 that DO decreased gradually with the increase

in the water depth from near 4 m of Station A in March to September, closely approaching zero at the deep water depths of 7 to 11 m in May to September; the pH in seawaters of Station A showed a decreasing

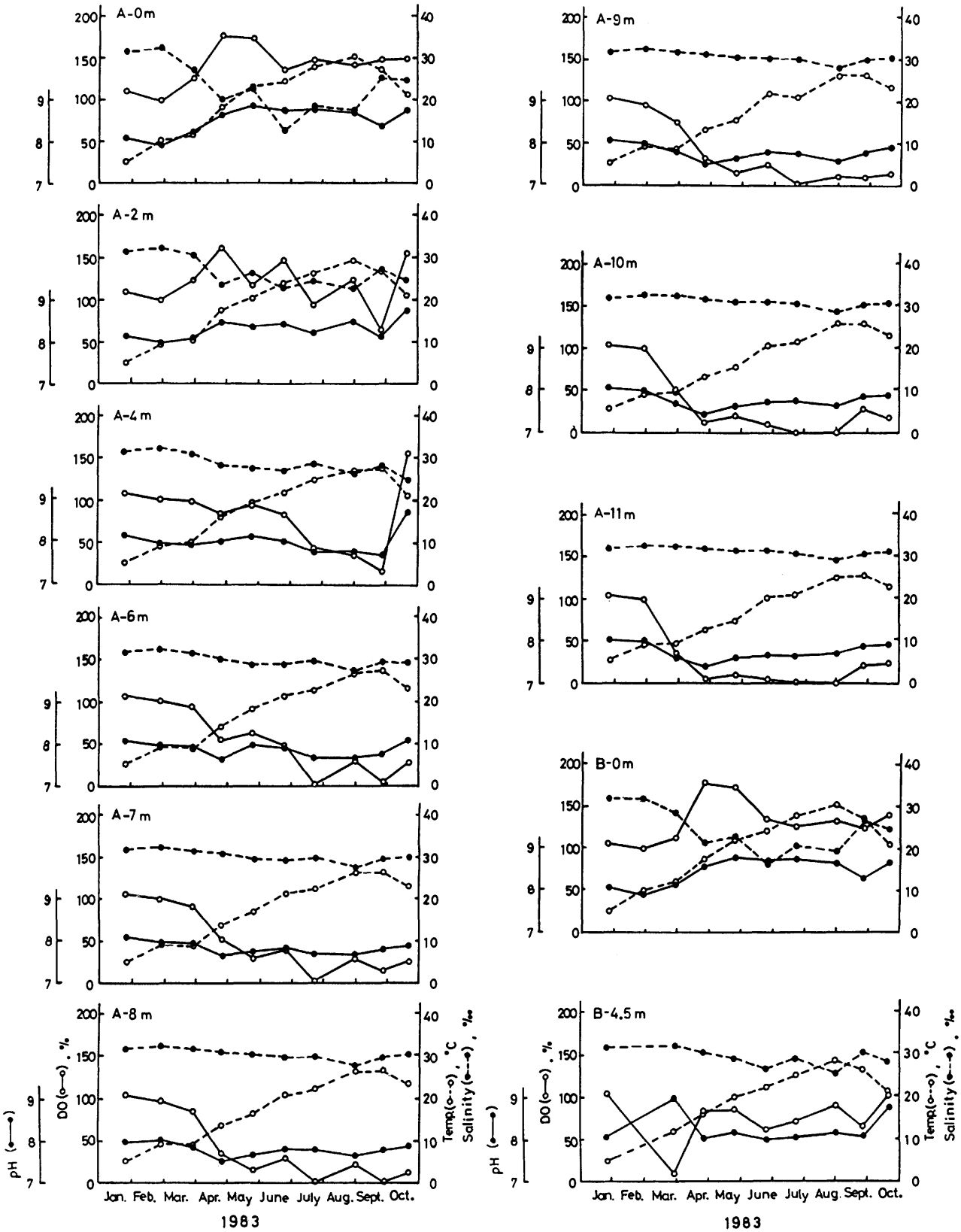

Fig. 1. Seasonal variations of dissolved oxygen, salinity, pH, and temperature in the seawater at different water depths of the stations A and B in 1983.

trend like DO with the increase in the water depth from near 4 m in March to September, while the water temperature reached a maximum near 30 °C at every water depth in August or September. From such changes in the DO and the pH, it can be estimated that the sea basin of Station A rises from a water depth of about 4 m and that its bottom layer presents a reducing atmosphere from March to September.

Figure 2 shows the seasonal variation in the contents of DIP, Fe(II), Fe(III), and DHS in the seawater at different water depths of Stations A and B at roughly monthly intervals for the year of 1983. The following points particularly attract attention among the results shown in Fig. 2:

(a) The DIP increased remarkably with the increase in water depth from near 3 m of Station A in roughly inverse interrelation to the DO and the pH in the summer season (June to September), while the DOP was 10 ppb or less at every water depth of both stations at all times. Therefore, the DOP was not

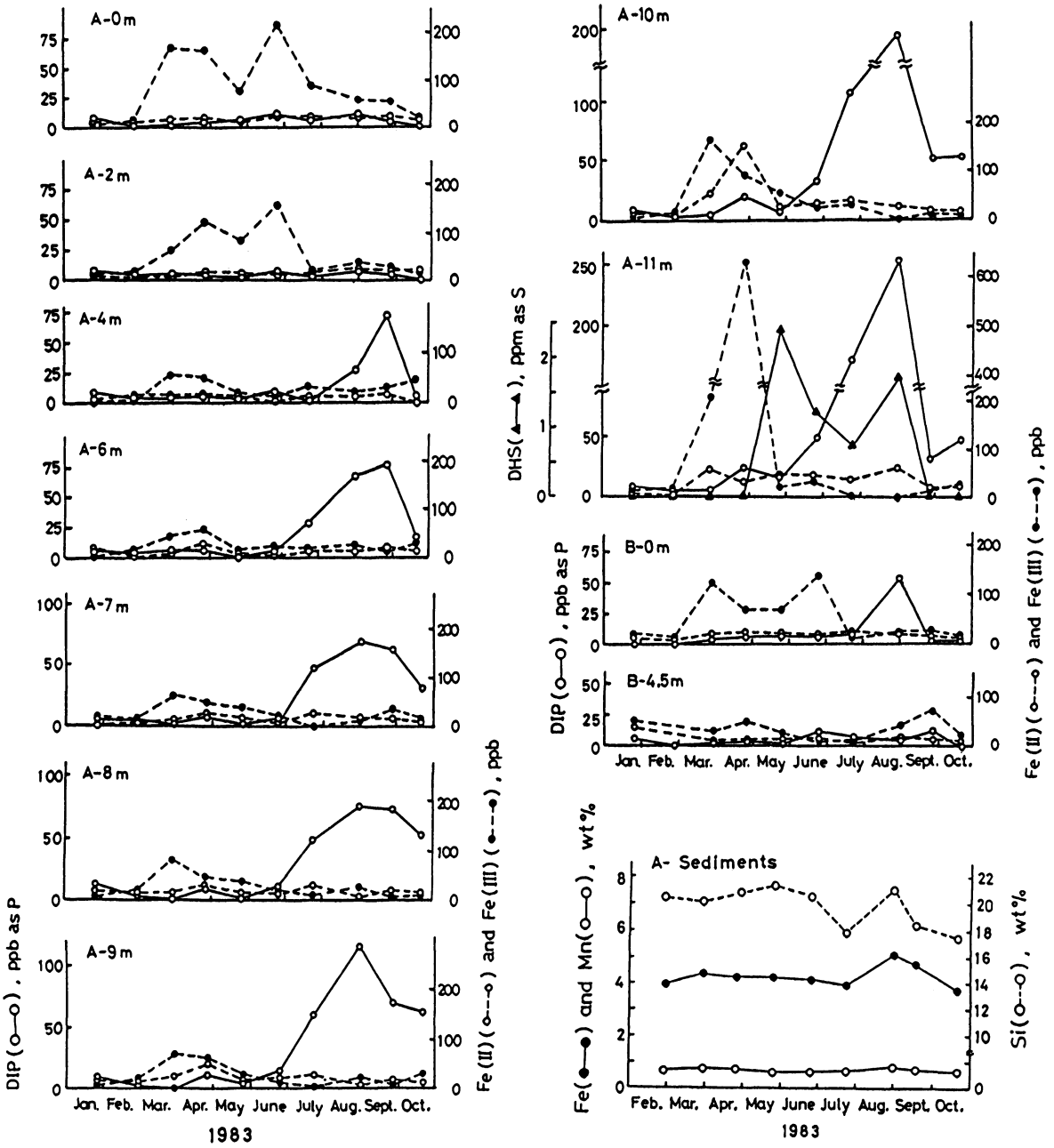

Fig. 2. Seasonal variations of dissolved inorganic phosphorus, Fe(II), Fe(III), and dissolved hydrogen sulfide in the seawater at different water depths of the stations A and B, and those of some elements in the sediments at the station A in 1983.

plotted in Fig. 2.

(b) The maxima of Fe(II) and DIP, even in a small peak, were simultaneously observed at the deep water depths from 7 to 11 m near the sediments of Station A around April.

(c) On the other hand, the peaks of Fe(III) at the same deep water depths appeared from March to April and had almost disappeared already when the DIP and a large amount of the DHS appeared in the anoxic seawater in the early summer season.

(d) However, the concentrations of Fe(III) in the seawater samples collected from the surface to a water depth of near 2 m of Stations A and B were higher than those in the anoxic seawater at the middle water depths of both stations from March to April, while they had the two maxima from March to the early summer season.

(e) The considerable amounts of DHS, which are several times as much as the DIP or Fe(II) contents, were detected at a water depth of 11 m of Station A in the summer season when the DIP appeared in the anoxic seawater.

(f) The seasonal variations of some elements in the surface layer of the sediments at the sea basin of Station A are shown in Fig. 2. It is evident from these results that considerable amounts of iron at least exist in the sediments, and that these seasonal curves of Fe and Si both have a miximum in summer. On the other hand, the Fe and Mn in plankton collected near the sea surface at Station A in August in 1983 constituted dry percentages of 3.5 and 0.05 respectively.

Figure 3 shows the vertical profiles of DIP, Fe(II),

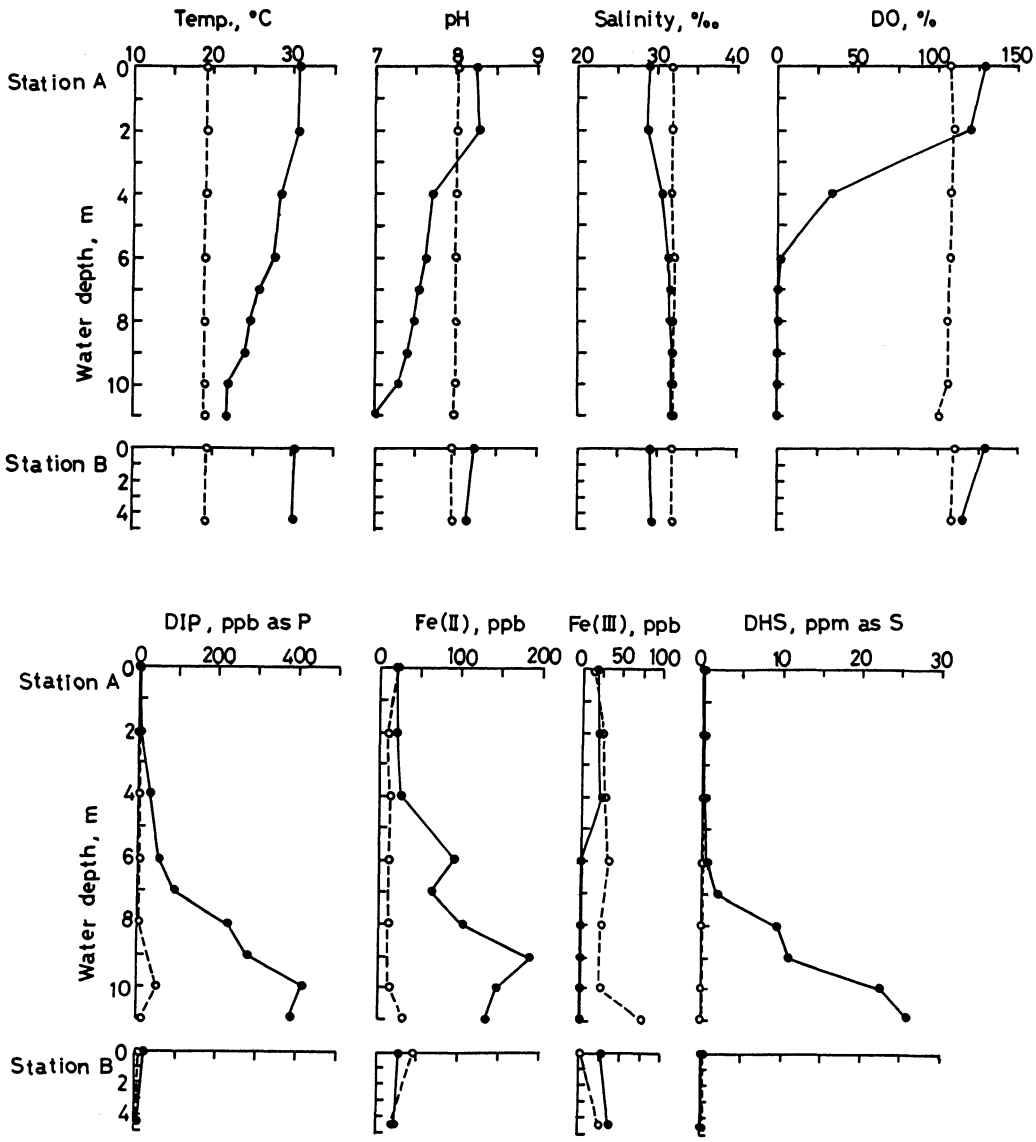

Fig. 3. Vertical profiles of dissolved inorganic phosphorus, Fe(II), Fe(III), dissolved hydrogen sulfide, and others in the seawater at the stations A and B in 1984. ●—●: in September, 1984, O---O in October, 1984.

Fe(III), DHS, and others in the anoxic seawater at Stations A and B in September and October in 1984. Since in Japan it was a relatively cold summer in 1984, and since, besides, some typhoons hit Lake Hamana in the summer, the anoxic seawater had not developed fully until the end of August that year. It is apparent from the vertical profiles shown in Fig. 3 that, in September at Station A, the DIP, Fe(II), and DHS were simultaneously eluted from the sediments of the sea basin into the anoxic seawater under the conditions at DO≈0, and that they then diffused gradually into the upper layer, whereas in October at Station A the DO has already reached saturation at every depth and so hardly any vertical changes with the water depth were observed. The variations shown in Fig. 3 correspond quite well to those shown in Fig. 2.

The molalities at each maximum in the seasonal-variation curves for DIP, Fe(II), Fe(III), and DHS at the water depth of A-11 m (Fig. 2) were 8.19, 1.07, 11.3, and 74.5 mmol m^{-3} respectively, while those for DIP, Fe(II), and DHS at the water depth of A-11 m in September (shown in Fig. 3) were 12.3, 2.38, and 754 mmol m^{-3} respectively.

Conclusion

On the basis of the above-mentioned experimental facts, we reached the following conclusions regarding the elution phenomena of DIP, Fe(II), Fe(III), and DHS from the sediments of the sea basin in Lake Hamana into the anoxic seawater in summer:

(1) The DIP is undoubtly eluted, together with a large amount of DHS and a small amount of Fe(II), from the sediments of the sea basin into anoxic seawater under the conditions of the water near the sediments at DO≈0 and at water temperatures≈20—30 °C in the summer season (see (a), (e) and Fig. 3 in Results and Discussion). The tendency for DIP to decrease with shallowing the water depth may be caused by the diffusion of the tidal current or by its being taken as nutrition by the plankton living in the shallow water layer. Such elutions of DIP and DHS from the sediments into the anoxic seawater in summer season might result mainly from the decomposition of dead plankton deposited on the surface of the sea basin according to a chemical reaction, represented by Richards,[7] which proceeds from the action of anaerobic bacteria in the sediments at the reducing atmosphere under the above-mentioned conditions.

Furthermore, the elutions of Fe(II) and DIP may occur by their changing chemically from very slightly soluble $FePO_4$ in water to hardly soluble $Fe_3(PO_4)_2$ in the sediments at the above-mentioned reducing state and by the dissociation of the $Fe_3(PO_4)_2$ with the drop in the pH(<7) of the interstitial water in the sediments according to the following Eqs. 1 and 2:[8]

$$FePO_4 \xrightarrow{\text{reducing state}} Fe_3(PO_4)_2 \quad (1)$$

$$Fe_3(PO_4)_2 \overset{pH<7}{\rightleftharpoons} 3Fe^{2+} + 2PO_4^{3-} \quad (2)$$

Such inference does not contradict the experimental fact that the maxima of Fe(II) and DIP at the deep water depths, even in a small peak accompanying the decrease in DO around April, appeared simultaneously in Fig. 2(see (b) and Fig. 3 in Results and Discussion).

(2) The Fe(II) appearing in the anoxic seawater from the sediments around April, as is shown in Fig. 2, and in August or September, as is shown in Figs. 2 and 3, may be rapidly oxidized to Fe(III) in the shallow water layer by the DO according to the following Eq. 3:

$$Fe(II) \xrightarrow{O_2(DO)} Fe(III) + e^- \quad (3)$$

(3) The peaks appearing in the seasonal-variation curves of Fe(III) at the deep water depths of Station A from March to April, as is shown in Fig. 2 (see (c) in Results and Discussion), may result from a slight dissociation of $Fe(OH)_3$ as a hardly soluble precipitate in water with the drop in the pH of the interstitial water in the sediments, as is shown in Fig. 1, and/or from the above-mentioned oxidation of Fe(II) by the DO (see (b) and (f)).

From the experimental findings that the concentrations of Fe(III) in the water near the surface of Stations A and B were higher than those in the anoxic seawater at the middle water depths of both stations for the above period, and that they had their two maxima in the season from March to early summer, as is shown in Fig. 2 (see to (d) in Results and Discussion), it can also be thought that some organic substances serving as chelators for Fe(III) which are produced from plankton living in the seawater near the sea surface may contain some Fe(III), or that on the occassion of sampling, a little plankton containing Fe(III) may be taken into the water samples (see (f) in Results and Discussion).

(4) The rapidly decaying phenomena, especially at the bottom layers, of Fe(II) and Fe(III) in the seasonal-variation curves at different water depths of Station A, as is shown in Fig. 2 (see (b), (c), and (d) in Results and Discussion) when the DIP and the large amounts of DHS appeared just in the anoxic seawater in the early summer season might be only an apparent decrease resulting from the formation[8] of FeS or FeS·S as a hardly soluble precipitate with the DHS, according to Eqs. 4 and 5:

$$2Fe^{3+} + H_2S \longrightarrow 2Fe^{2+} + S\downarrow + 2H^+ \quad (4)$$

$$Fe^{2+} + S^{2-} \longrightarrow FeS\downarrow \quad (5)$$

We wish to thank Professor Emeritus Dr. Hidehiro Gotô of Tohoku University, Professor Emeritus Dr. Michio Ôta of Yamanashi University, Professor Dr. Akira Murata of Shizuoka University, and Assistant Professor Dr. Mitsuru Sakamoto of Nagoya University for their kind and ever-continuing guidances.

References

1) N. Ichinose, C. Shimizu, H. Kurokura, T. Inui, and K. Kadohata, *Bunseki Kagaku*, **31**, 532 (1984).

2) N. Ichinose, C. Shimizu, H. Kurokura, and T. Inui, *F. Z. Anal. Chem.*, **316**, 791 (1983).

3) N. Ichinose, H. Kanai, and K. Nakamura, *Anal. Chim. Acta*, **156**, 345 (1984).

4) N. Ichinose, K. Adachi, and C. Shimizu, *J. Chromatogr.*, **292**, 393 (1984).

5) N. Ichinose, C. Shimizu, K. Okamoto, T. Inui, and K. Adachi, *Anal. Sci.*, **3**, 131 (1987).

6) E. B. Sandell, "Colorimetric Determination of Traces of Metals," Interscience Publishers, New York (1959).

7) F. A. Richards, in "Chemical Oceanography," Vol. 1, ed by J. P. Riley and G. Skirrow, Academic Press, London (1965), pp. 623—634.

8) K. Sugawara, T. Koyama, and E. Kamata, *J. Earth Sci., Nagoya Univ.*, **5**, 60 (1957).

 © 1988 The Chemical Society of Japan Bull. Chem. Soc. Jpn., 61, 3159—3167 (1988)

Study of Polarographic Anodic Wave in the Presence of Chloride Ions by a New Numerical Method

Kenji KIKUCHI and Teisuke MURAYAMA*
Shiga Prefectural Junior College, Hikone, Shiga 522
Department of Applied Chemistry, Faculty of Engineering, Shizuoka University, Johoku, Hamamatu 432
(Received January 7, 1988)

A new numerical method is applied to the simultaneous diffusion equations describing the anodic process of mercury in solutions in the presence of chloride ions. The terms corresponding to precipitation and dissolution of mercury(I) chloride are included in the differential equations. It is found that the differential equation for precipitate particles should be rewritten using the backward space difference method for successful computation.

Kolthoff and Miller studied the anodic wave of mercury in the presence of chloride ions.[1] They observed that the diffusion current corrected for residual current is proportional to the concentration of chloride ions. They assumed that the concentration of chloride ions at the surface of mercury electrode is determined by the solubility product and by the concentration of mercury(I) ions at the electrode surface which is controlled by the electrode potential. Based on this assumption they derived an equation of the current-potential curve accompanying with formation of slightly soluble mercury(I) chloride salt as

$$E = E^0 + \frac{RT}{2F} \ln \frac{K_{sp}\gamma_A}{C_{B0}^2} = E' + \frac{RT}{2F} \ln K_{sp} - \frac{RT}{F} \ln (\bar{i}_d - \bar{i}), \quad (1)$$

where E is the potential of dropping mercury electrode, C_{B0} the concentration of chloride ion at the electrode surface, γ_A the activity coefficient of mercury(I) ion, K_{sp} the solubility product of mercury(I) chloride, $\bar{i}$ the average current, $\bar{i}_d$ the average diffusion current, F the Faraday constant, and E^0 the standard electrode potential of Hg_2^{2+}-Hg couple. The plot of $\log(i_d - i)$ vs. E should be a straight line with a reciprocal slope of −59.2 mV/unit at 25 °C. Their plot produced a straight line, however, with a reciprocal slope of −54 mV/unit, which did not agree with Eq. 1.

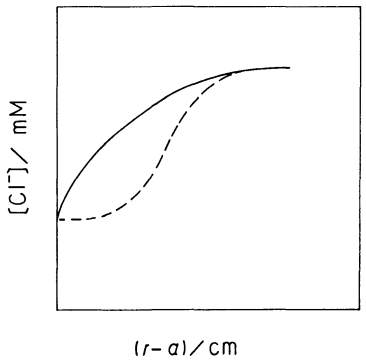

Fig. 1. Distance-concentration curves of chloride ions. A solid line represents a conception considered by Kolthoff and Miller. A dotted line represents a conception proposed by this paper.

After their study, the method and its variations have been generally used for analyzing anodic waves of electrode mercury in the presence of depolarizers which form slightly soluble mercury(I) compounds. The conception proposed by Kolthoff and Miller is that chloride ions are consumed only at the electrode surface and ionic concentration at the electrode surface can be determined by the solubility product and the electrode potential. Figure 1 schematically shows the concentration profile of chloride ions. A solid line was drawn according to their conception. However, chloride ions themselves do not receive any electrochemical change, but are consumed by the chemical reaction with mercury(I) ions produced through the electrochemical reaction. Hence the slope of concentration profile of chloride ions at the surface should be zero as illustrated by the dotted line in Fig. 1. These situations are not reflected in Eq. 1. The equation is a rather crude approximation to the phenomenon, which is waiting more detailed analysis.

This study has two purposes. One is application of a new numerical method,[2] and another is explicit consideration of formation and dissolution of precipitate particles in the process. No direct treatment of dissolution of precipitate particles has been found in literature.

Theory

In the anodic process, mercury is dissolved into solution as mercury(I) ions. When the concentration product of mercury(I) and chloride ions exceeds the solubility product, mercury(I) ions react with chloride ions producing mercury(I) chloride precipitate particles. These reactions are written as follows:

$$2Hg \rightleftharpoons Hg_2^{2+} + 2e^-, \quad (2)$$

and

$$Hg_2^{2+} + 2Cl^- \underset{k_b}{\overset{k_f}{\rightleftharpoons}} Hg_2Cl_2, \quad (3)$$

In Eq. 3, k_f and k_b are rate constants of formation and dissolution, respectively, of the precipitate particles. It is assumed that the effect of formation of mercury(II) ions on the anodic current is negligible in comparison with that of mercury(I) and chloride ions. Further it is assumed that Reaction 3 is rapid and in equilibrium. The solubility product is given by

$$K_{sp} = [Hg_2^{2+}][Cl^-]^2 = k_b[Hg_2Cl_2]/k_f = k_b^*/k_f. \quad (4)$$

Because the solubility of mercury(I) chloride is constant under experimental conditions, the product of the concentration and k_b is replaced by another constant k_b^* in Eq. 4.

In the following, subscripts A, B, and C denote, respectively, mercury(I) ion, chloride ion, and precipitate particle of mercury(I) chloride. Hence their concentrations are expressed as C_A, C_B, and C_C, respectively.

When precipitate particles exist in a volume element considered, or the condition that $C_AC_B^2 \geqq K_{sp}$ is satisfied in the volume element, the simultaneous equations governing concentrations of species appearing in Reactions 2 and 3 are

$$\frac{\partial C_A}{\partial t} = D_A\left(\frac{\partial^2 C_A}{\partial r^2}\right) + \left(\frac{2}{r}D_A - u\right)\frac{\partial C_A}{\partial r} - k_fC_AC_B^2 + k_b^*, \quad (5)$$

$$\frac{\partial C_B}{\partial t} = D_B\left(\frac{\partial^2 C_B}{\partial r^2}\right) + \left(\frac{2}{r}D_B - u\right)\frac{\partial C_B}{\partial r} - 2k_fC_AC_B^2 + 2k_b^*, \quad (6)$$

$$\frac{\partial C_C}{\partial t} = -u\frac{\partial C_C}{\partial r} + k_fC_AC_B - k_b^*, \quad (7)$$

and

$$u = m/(4\pi\rho r^2), \quad (8)$$

where D_h is the diffusion coefficient of species h, r the distance from the center of the electrode mercury drop, m the flow rate of mercury, and ρ the density of mercury. It is assumed that diffusion of the precipitate particles is negligible in comparison with that of ions. The precipitate concentration is expressed in formal concentration of the precipitate substance, which is assumed to be dispersed homogeneously in the volume element. As usually does, it is assumed that the center of mercury drop remains fixed.

When the precipitate does not exist in a volume element, that is $C_AC_B^2 < K_{sp}$, the simultaneous equations describing variation of concentrations are

$$\frac{\partial C_A}{\partial t} = D_A\left(\frac{\partial^2 C_A}{\partial r^2}\right) + \left(\frac{2}{r}D_A - u\right)\frac{\partial C_A}{\partial r}, \quad (9)$$

and

$$\frac{\partial C_B}{\partial t} = D_B\left(\frac{\partial^2 C_B}{\partial r^2}\right) + \left(\frac{2}{r}D_B - u\right)\frac{\partial C_B}{\partial r}. \quad (10)$$

Initial conditions are

$$C_A = 0,\ C_B = C^*_B, \text{ and } C_C = 0\ (t = 0, r > a). \quad (11)$$

Boundary conditions are as follows:

$$C_A = C_{A0},\ (\partial C_B/\partial r) = 0\ (t > 0, r = a), \quad (12)$$

and

$$C_A = 0,\ C_B = C^*_B,\ C_C = 0\ (t > 0, r = \infty). \quad (13)$$

In the above, a is the radius of mercury drop, C^*_B the concentration of chloride ions in bulk solution, and C_{A0} the concentration of mercury(I) ions at the surface of mercury electrode. The potential of mercury electrode dictates the value of C_{A0}. The instantaneous current, i, is given by

$$i = 2FD_AS(\partial C_A/\partial r)_{r=a}, \quad (14)$$

where S is the surface area of mercury drop.

Because the reaction proceeds in the neighborhood of electrode surface, numerical results most desired are those in the proximity of electrode surface. For this purpose, numerical integration of the differential equations is carried out more efficiently using a network, of which mesh is finer in near positions to the electrode surface and becomes coarser with the distance from the surface. Hence we introduce a parameter given by

$$s^P = 1 - 1/\{1 + (Hx)^P\}, \quad (15)$$

where H and P are constants. In the previous report,[2] the value of P is unity.

To facilitate calculation, we introduce the following transformations:[2]

$$y_A = C_A/C_{A0},\ y_B = C_B/C_{A0},$$
$$y_C = C_C/C_{A0},\ x = (r - a)/L,$$
$$d_A = D_A/D_A = 1,\ d_B = D_B/D_A,\ T = D_At/L^2,$$
$$U = Lur^2/(D_Aa^2),\ K_f = L^2k_fC_{A0}^2/D_A,$$

and

$$K_b = k_b^*L^2/C_{A0}D_A. \quad (16)$$

In the above, L is the representative length and H a constant. The maximum value of s is unity, where the value of r is infinite. With these transformations, Eq. 5 becomes

$$\frac{\partial y_A}{\partial T} = d_AH^2(1 - s^P)^{2(P+1)/P}\frac{\partial^2 y_A}{\partial s^2} + 2H(1 - s^P)^{(P+1)/P}\left\{\frac{2d_A}{x + a/L} + \frac{x(x + 2a/L)}{(x + a/L)^2}U - 2d_AH(P + 1)s^{P-1}(1 - s^P)^{1/P}\right\}\frac{\partial y_A}{\partial s} - K_fy_Ay_B^2 + K_b. \quad (17)$$

Derivation of Eq. 17 is carried out with the aid of the Crank-Nicolson's method[5] in a similar manner as the previous report. Space and time coordinates are expressed as

$$s_i = i\,\Delta s,\ T_j = j\Delta T,\ x_i = i\Delta s/H\{1 + (i\Delta s)^P\}^{1/P}, \quad (18)$$

and

$$y_A(s,T) = y_A(s_i, T_j) = y_{A,i,j}. \quad (19)$$

When the value of Δs is 0.01, the value of i ranges from 0, corresponding to the electrode surface, to 100, corresponding to infinite distance from the surface. The backward space difference method and the forward time difference method[2] are used in conversion of differential equations to difference equations.

In the case that $0<i<98$, the derivatives corresponding to both $\partial y_A(s,T)/\partial s$ and $\partial^2 y_A(s,T)/\partial s^2$ are expressed as

$$\left(\frac{\partial^2 y_A(s_i, T_{j+1})}{\partial s^2}\right) = \frac{1}{24(\Delta s)^2}\{(-y_{A,i+3,j+1} + 4y_{A,i+2,j+1} + 6y_{A,i+1,j+1} - 20y_{A,i,j+1} + 11y_{A,i-1,j+1}) + (-y_{A,i+3,j} + 4y_{A,i+2,j} + 6y_{A,i+1,j} - 20y_{A,i,j} + 11y_{A,i-1,j})\}, \quad (20)$$

and

$$\left(\frac{\partial y_A(s_i, T_{j+1})}{\partial s}\right) = \frac{1}{24\Delta s}\{(y_{A,i+3,j+1} - 6y_{A,i+2,j+1} + 18y_{A,i+1,j+1} - 10y_{A,i,j+1} - 3y_{A,i-1,j+1}) + (y_{A,i+3,j} - 6y_{A,i+2,j} + 18y_{A,i+1,j} - 10y_{A,i,j} - 3y_{A,i-1,j})\}, \quad (21)$$

with concentrations at the nodes $(i-1,j)$, (i,j), $(i+1,j)$, $(i+2,j)$, $(i+3,j)$, $(i-1,j+1)$, $(i,j+1)$, $(i+1,j+1)$, $(i+2,j+1)$, and $(i+3,j+1)$.

For the point that $i=98$, the outer nodes are ones with i of 99 and 100. Therefore, the backward space difference method was not applicable for conversion. The centered space difference method was used for this purpose. The derivatives are expressed as

$$\left(\frac{\partial^2 y_A(s_{98}, T_{j+1})}{\partial s^2}\right) = \frac{1}{24(\Delta s)^2}\{(-y_{A,100,j+1} + 16y_{A,99,j+1} - 30y_{A,98,j+1} + 16y_{A,97,j+1} - y_{A,96,j+1}) + (-y_{A,100,j} + 16y_{A,99,j} - 30y_{A,98,j} + 16y_{A,97,j} - y_{A,96,j})\}, \quad (22)$$

and

$$\left(\frac{\partial y_A(s_{98}, T_{j+1})}{\partial s}\right) = \frac{1}{24\Delta s}\{(-y_{A,100,j+1} + 8y_{A,99,j+1} - 8y_{A,97,j+1} + y_{A,96,j+1}) + (-y_{A,100,j} + 8y_{A,99,j} - 8y_{A,97,j} + y_{A,96,j})\}, \quad (23)$$

with concentrations at nodes $(96,j)$, $(97,j)$, $(98,j)$, $(99,j)$, $(100,j)$, $(96,j+1)$, $(97,j+1)$, $(98,j+1)$, $(99,j+1)$, and $(100,j+1)$.

For the point that $i=99$, the only outer node is a node with i of 100. Therefore, the forward space difference method was used for this purpose. The derivatives are expressed as

$$\left(\frac{\partial^2 y_A(s_{99}, T_{j+1})}{\partial s^2}\right) = \frac{1}{24(\Delta s)^2}\{(11y_{A,100,j+1} - 20y_{A,99,j+1} + 6y_{A,98,j+1} + 4y_{A,97,j+1} - y_{A,96,j+1}) + (11y_{A,100,j} - 20y_{A,99,j} + 6y_{A,98,j} + 4y_{A,97,j} - y_{A,96,j})\}, \quad (24)$$

and

$$\left(\frac{\partial y_A(s_{99}, T_{j+1})}{\partial s}\right) = \frac{1}{24\Delta s}\{(3y_{A,100,j+1} + 10y_{A,99,j+1} - 18y_{A,98,j+1} + 6y_{A,97,j+1} - y_{A,96,j+1}) + (3y_{A,100,j} + 10y_{A,99,j} - 18y_{A,98,j} + 6y_{A,97,j} - y_{A,96,j})\}. \quad (25)$$

with concentrations at the nodes $(96,j)$, $(97,j)$, $(98,j)$, $(99,j)$, $(100,j)$, $(96,j+1)$, $(97,j+1)$, $(98,j+1)$, $(99,j+1)$, and $(100,j+1)$.

By using the Crank-Nicolson method, the chemical kinetics term is reformulated as

$$K_f y_A y_b^2 = K_f(y_{A,i,j+1}y_{B,i,j+1}^2 + y_{A,i,j}y_{B,i,j}^2)/2. \quad (26)$$

Because the right-hand side of Eq. 26 contains square of $y_{B,i,j+1}$, the value of y_B at the next time coordinate, it is difficult to perform numerical computation without rewriting the term in linear form with respect to $y_{B,i,j+1}$. Linearization of the chemical kinetics term was treated in the previous report, where four methods were described. Larger reaction rate prevents computing by use of these methods because of truncation error. Considering large values of precipitation reaction rate constant (k_f) and dissolution rate constant (k_b) in the present system, the procedure proposed by Morihara and Cheng is applied to the present problem.[3]

By using the method of Morihara and Cheng, the chemical kinetics term is reformulated as follows:

$$K_f(y_{A,i,j+1}y_{B,i,j+1}^2 + y_{A,i,j}y_{B,i,j}^2)/2 = K_f y_{B,i,j+1}y_{B,i,j}(y_{A,i,j+1} + y_{A,i,j})/2. \quad (27)$$

When $0<i<98$, introduction of Eqs. 20, 21, and 27 to Eq. 17 gives

$$\begin{aligned}(1 &+ 20E_{A,i} + 10F_{A,i,j+1} + \Delta TK_f y_{B,i,j+1}y_{B,i,j}/2)y_{A,i,j+1}\\ &= (-E_{A,i} + F_{A,i,j+1})(y_{A,i+3,j+1} + y_{A,i+3,j})\\ &+ (4E_{A,i} - 6F_{A,i,j+1})(y_{A,i+2,j+1} + y_{A,i+2,j})\\ &+ (6E_{A,i} + 18F_{A,i,j+1})(y_{A,i+1,j+1} + y_{A,i+1,j})\\ &+ (11E_{A,i} - 3F_{A,i,j+1})(y_{A,i-1,j+1} + y_{A,i-1,j})\\ &+ (1 - 20E_{A,i} + 10F_{A,i,j+1}\\ &- \Delta TK_f y_{B,i,j+1}y_{B,i,j}/2)y_{A,i,j} + \Delta TK_b, \end{aligned} \quad (28)$$

$$E_{A,i} = \frac{\Delta T}{24\Delta s^2}\, d_A H^2\{1 - (s_i)^P\}^{2(P+1)/P}, \quad (29)$$

and

$$F_{A,i,j+1}=\frac{\Delta T}{12\Delta s}\left[H\{1-(s_i)^P\}^{(P+1)/P}+\frac{d_A}{x_i+a_{j+1}/L}\right.$$
$$\left.+\frac{x_i(x_i+2a_{j+1}/L)}{2(x_i+a_{j+1}/L)^2}U_{j+1}-\frac{d_A}{2}H(P+1)\{1-(s_i)^P\}^{1/P}\right]. \quad (30)$$

When i=98, introduction of Eqs. 22, 23, and 27 to Eq. 17 gives

$$\begin{aligned}&(1+30E_{A,98}+\Delta TK_f y_{B,98,j+1}y_{B,98,j}/2)y_{A,98,j+1}\\&=(-E_{A,98}-F_{A,98,j+1})(y_{A,100,j+1}+y_{A,100,j})\\&+(16E_{A,98}+8F_{A,98,j+1})(y_{A,99,j+1}+y_{A,99,j})\\&+(16E_{A,98}-8F_{A,98,j+1})(y_{A,97,j+1}+y_{A,97,j})\\&+(-E_{A,98}-3F_{A,98,j+1})(y_{A,96,j+1}+y_{A,96,j})\\&+(1-30E_{A,98}-\Delta TK_f y_{B,i,j+1}y_{B,i,j}/2)y_{A,i,j}\\&+\Delta TK_b. \quad (31)\end{aligned}$$

When i=99, introduction of Eqs. 24, 25, and 27 to Eq. 17 gives

$$\begin{aligned}&(1+20E_{A,99}-10F_{A,99,\,j+1}\\&+\Delta TK_f y_{B,99,j+1}y_{B,99,j}/2)y_{A,99,j+1}\\&=(11E_{A,99}+3F_{A,99,j+1})(y_{A,100,j+1}+y_{A,100,j})\\&+(6E_{A,99}-18F_{A,99,j+1})(y_{A,98,j+1}+y_{A,98,j})\\&+(4E_{A,98}+6F_{A,99,j+1})(y_{A,97,j+1}+y_{A,97,j})\\&+(-E_{A,99}-F_{A,99,j+1})(y_{A,96,j+1}+y_{A,96,j})\\&+(1-20E_{A,98}+10F_{A,99,j+1}\\&-\Delta TK_f y_{B,99,j+1}y_{B,99,j}/2)y_{A,99,j}+\Delta TK_b. \quad (32)\end{aligned}$$

The equation concerning species B is transformed as described below.

In the case that i=0, the boundary condition corresponding to $(\partial y_B/\partial s)_{r=a}$=0 is expressed as

$$\left(\frac{\partial C_B(s_0,T_{j+1})}{\partial s}\right)=\frac{1}{6(\Delta s)}(-11y_{B,0,j+1}+18y_{B,1,j+1}$$
$$-9y_{B,2,j+1}+2y_{B,3,j+1})=0, \quad (33)$$

with the concentration at nodes (0,j), (1,j), (2,j), (3,j), (0,j+1), (1,j+1), (2,j+1), and (3,j+1). The following equation is obtained from Eq. 33.

$$y_{B,0,j+1}=(18y_{B,1,j+1}-9y_{B,2,j+1}+2y_{B,3,j+1})/11 \quad (34)$$

In the case that i=1, the derivative corresponding to $\partial y_B/\partial s$ is expressed as

$$\begin{aligned}\left(\frac{\partial^2 y_B(s_1,T_{j+1})}{\partial s^2}\right)&=\frac{1}{276(\Delta s)^2}\{(-4y_{B,4,j+1}+6y_{B,3,j+1}\\&+159y_{B,2,j+1}-350y_{B,1,j+1}+189y_{B,0,j+1}\\&+30(\Delta s)y'_{B,0,j+1}+(-4y_{B,4,j}+6y_{B,3,j}\\&+159y_{B,2,j}-350y_{B,1,j}+189y_{B,0,j}\\&+30(\Delta s)y'_{B,0,j})\}, \quad (35)\end{aligned}$$

and

$$\begin{aligned}\left(\frac{\partial y_B(s_1,T_{j+1})}{\partial s}\right)&=\frac{1}{444(\Delta s)}\{(-4y_{B,4,j+1}+9y_{B,3,j+1}\\&+63y_{B,2,j+1}+175y_{B,1,j+1}-243y_{B,0,j+1}\\&-90(\Delta s)y'_{B,0,j+1})+(-4y_{B,4,j}+9y_{B,3,j}\\&+63y_{B,2,j}+175y_{B,1,j}-243y_{B,0,j}\\&-90(\Delta s)y'_{B,0,j})\}, \quad (36)\end{aligned}$$

with the first differential term at the mercury electrode surface ($y'_{B,0,j+1}$, $y'_{B,0,j}$) and with concentrations at nodes (0,j), (1,j), (2,j), (3,j), (4,j), (0,j+1), (1,j+1), (2,j+1), (3,j+1), and (4,j+1). Here values of $y'_{B,0,j+1}$ and $y'_{B,0,j}$ are zero because the chloride ions do not receive any electrochemical change. Introduction of Eqs. 27, 35, and 36 to Eq. 6 gives

$$\begin{aligned}&\{1+700E_{B,1}/23-350F_{B,1,j+1}/37\\&+\Delta TK_f y_{B,1,j}(y_{A,1,j+1}+y_{A,1,j})/2\}y_{B,1,j+1}\\&=(-8E_{B,1}/23-8F_{B,1,j+1}/37)(y_{B,4,j+1}+y_{B,4,j})\\&+(12E_{B,1}/23+18F_{B,1,j+1}/37)(y_{B,3,j+1}+y_{B,3,j})\\&+(318E_{B,1}/23+126F_{B,1,j+1}/37)(y_{B,2,j+1}+y_{B,2,j})\\&+(378E_{B,1}/23-486F_{B,1,j+1}/37)(y_{B,0,j+1}+y_{B,0,j})\\&+(1-700E_{B,1}/23+350F_{B,1,j+1})y_{B,1,j}+2\Delta TK_b. \quad (37)\end{aligned}$$

When 1<i, the equations concerning with species B are transformed in much the same way as species A. Equations correspoding to Eqs. 28, 31, and 32 are given as follows:

1<i<98,

$$\begin{aligned}&\{1+20E_{B,i}+10F_{B,i,j+1}\\&+\Delta TK_f y_{B,i,j}(y_{A,i,j+1}+y_{A,i,j})/2\}y_{B,i,j+1}\\&=(-E_{B,i}+F_{B,i,j+1})(y_{B,i+3,j+1}+y_{B,i+3,j})\\&+(4E_{B,i}-6F_{B,i,j+1})(y_{B,i+2,j+1}+y_{B,i+2,j})\\&+(6E_{B,i}+18F_{B,i,j+1})(y_{B,i+1,j+1}+y_{B,i+1,j})\\&+(11E_{B,i}-3F_{B,i,j+1})(y_{B,i-1,j+1}+y_{B,i-1,j})\\&+(1-20E_{B,i}-10F_{B,i,j+1})y_{B,i,j}+2\Delta TK_b. \quad (38)\end{aligned}$$

i=98,

$$\begin{aligned}&\{1+30E_{B,98}+\Delta TK_f y_{B,98,j}(y_{A,98,j+1}\\&+y_{A,98,j})/2\}y_{B,98,j+1}\\&=(-E_{B,98}-F_{B,98,j+1})(y_{B,100,j+1}+y_{B,100,j})\\&+(16E_{B,98}+8F_{B,98,j+1})(y_{B,99,j+1}+y_{B,99,j})\\&+(16E_{B,98}-8F_{B,98,j+1})(y_{B,97,j+1}+y_{B,97,j})\\&+(-E_{B,98}-3F_{B,98,j+1})(y_{B,96,j+1}+y_{B,96,j})\\&+(1-30E_{B,98})y_{B,i,j}+2\Delta TK_b. \quad (39)\end{aligned}$$

i=99,

$$\begin{aligned}&\{1+20E_{B,99}-10F_{B,99,j+1}+\Delta TK_f y_{B,99,j}(y_{A,99,j+1}\\&+y_{A,99,j})/2\}y_{B,99,j+1}\\&=(11E_{B,99}+3F_{B,99,j+1})(y_{A,100,j+1}+y_{B,100,j})\\&+(6E_{B,99}-18F_{B,99,j+1})(y_{B,98,j+1}+y_{B,98,j})\\&+(4E_{B,99}+6F_{B,99,j+1})(y_{B,97,j+1}+y_{B,97,j})\\&+(-E_{B,99}-F_{B,99,j+1})(y_{B,96,j+1}+y_{B,96,j})\\&+(1-20E_{B,98}+10F_{B,99,j+1})y_{A,i,j}+\Delta TK_b. \quad (40)\end{aligned}$$

In the volume element, where $C_A C_B^2 < K_{sp}$ is hold, Eqs. 5 and 6 are replaced by Eqs. 9 and 10, respectively. By neglecting chemical kinetics terms in Eqs. 28, 31, 32, 37, 38, 39, and 40, the finite difference equations are given as follows:

$0<i<98$,

$$\begin{aligned}(1 &+ 20E_{A,i} + 10F_{A,i,j+1})y_{A,i,j+1}\\ &= (-E_{A,i} + F_{A,i,j+1})(y_{A,i+3,j+1} + y_{A,i+3,j})\\ &+ (4E_{A,i} - 6F_{A,i,j+1})(y_{A,i+2,j+1} + y_{A,i+2,j})\\ &+ (6E_{A,i} + 18F_{A,i,j+1})(y_{A,i+1,j+1} + y_{A,i+1,j})\\ &+ (11E_{A,i} - 3F_{A,i,j+1})(y_{A,i-1,j+1} + y_{A,i-1,j})\\ &+ (1 + 20E_{A,i} + 19F_{A,i,j+1})y_{A,i,j}. \end{aligned} \quad (41)$$

$i=98$,

$$\begin{aligned}(1 &+ 30E_{A,98})y_{A,98,j+1}\\ &= (-E_{A,98} - F_{A,98,j+1})(y_{A,100,j+1} + y_{A,100,j})\\ &+ (16E_{A,98} + 8F_{A,98,j+1})(y_{A,99,j+1} + y_{A,99,j})\\ &+ (16E_{A,98} - 8F_{A,98,j+1})(y_{A,97,j+1} + y_{A,97,j})\\ &+ (-E_{A,98} - 3F_{A,98,j+1})(y_{A,96,j+1} + y_{A,96,j})\\ &+ (1 - 30E_{A,98})y_{A,98,j}. \end{aligned} \quad (42)$$

$i=99$,

$$\begin{aligned}(1 &+ 20E_{A,99} - 10F_{A,99,j+1})y_{A,99,j+1}\\ &= (11E_{A,99} + 3F_{A,99,j+1})(y_{A,100,j+1} + y_{A,100,j})\\ &+ (6E_{A,99} - 18F_{A,99,j+1})(y_{A,98,j+1} + y_{A,98,j})\\ &+ (4E_{A,99} + 6F_{A,99,j+1})(y_{A,97,j+1} + y_{A,97,j})\\ &+ (-E_{A,99} - F_{A,99,j+1})(y_{A,96,j+1} + y_{A,96,j})\\ &+ (1 - 20E_{A,98} + 10F_{A,99,j+1})y_{A,99,j}. \end{aligned} \quad (43)$$

$i=0$,

$$y_{B,0,j+1} = (18y_{B,1,j+1} - 9y_{B,2,j+1} + 2y_{B,3,j+1})/11. \quad (44)$$

$i=1$,

$$\begin{aligned}(1 &+ 700E_{B,1}/23 - 350F_{B,1,j+1}/37)y_{B,1,j}\\ &= (-8E_{B,1}/23 - 8F_{B,1,j+1}/37)(y_{B,4,j+1} + y_{B,4,j})\\ &+ (12E_{B,1}/23 + 18F_{B,1,j+1}/37)(y_{B,3,j+1} + y_{B,3,j})\\ &+ (318E_{B,1}/23 + 126F_{B,1,j+1}/37)(y_{B,2,j+1} + y_{B,2,j})\\ &+ (378E_{B,1}/23 - 486F_{B,1,j+1}/37)(y_{B,0,j+1} + y_{B,0,j})\\ &+ (1 - 700E_{B,1}/23 + 350F_{B,1,j+1})y_{B,1,j}. \end{aligned} \quad (45)$$

$1<i<98$,

$$\begin{aligned}(1 &+ 20E_{B,i} + 10F_{B,i,j+1})y_{B,i,j+1}\\ &= (-E_{B,i} + F_{B,i,j+1})(y_{B,i+3,j+1} + y_{B,i+3,j})\\ &+ (4E_{B,i} - 6F_{B,i,j+1})(y_{B,i+2,j+1} + y_{B,i+2,j})\\ &+ (6E_{B,i} + 18F_{B,i,j+1})(y_{B,i+1,j+1} + y_{B,i+1,j})\\ &+ (11E_{B,i} - 3F_{B,i,j+1})(y_{B,i-1,j+1} + y_{B,i-1,j})\\ &+ (1 - 20E_{B,i} - 10F_{B,i,j+1})y_{B,i,j}. \end{aligned} \quad (46)$$

$i=98$,

$$\begin{aligned}(1 &+ 30E_{B,98})y_{B,98,j+1}\\ &= (-E_{B,98} - F_{B,98,j+1})(y_{B,100,j+1} + y_{B,100,j})\\ &+ (16E_{B,98} + 8F_{B,98,j+1})(y_{B,99,j+1} + y_{B,99,j})\\ &+ (16E_{B,98} - 8F_{B,98,j+1})(y_{B,97,j+1} + y_{B,97,j})\\ &+ (-E_{B,98} - 3F_{B,98,j+1})(y_{B,96,j+1} + y_{B,96,j})\\ &+ (1 - 30E_{B,98})y_{B,98,j}. \end{aligned} \quad (47)$$

$i=99$,

$$\begin{aligned}(1 &+ 20E_{B,99} - 10F_{B,99,j+1})y_{B,99,j+1}\\ &= (11E_{B,99} + 3F_{B,99,j+1})(y_{B,100,j+1} + y_{B,100,j})\\ &+ (6E_{B,99} - 18F_{B,99,j+1})(y_{B,98,j+1} + y_{B,98,j})\\ &+ (4E_{B,99} + 6F_{B,99,j+1})(y_{B,97,j+1} + y_{B,97,j})\\ &+ (-E_{B,99} - F_{B,99,j+1})(y_{B,96,j+1} + y_{B,96,j})\\ &+ (1 - 20E_{B,98} + 10F_{B,99,j+1})y_{A,99,j}. \end{aligned} \quad (48)$$

In the above, the value of $y_{A,i,j+1}$ is calculated by Eqs. 28, 31, 32, and 41—43, and the value of $y_{B,i,j+1}$ by Eqs. 34, 37—40, and 45—48.

Equation 7 concerning species C contains a fluid flow term resulted from the growth of the mercury drop, but no diffusion term. The surface of electrode drop moves outward with time, and the solution around the drop flows from the outer regions to the surface of electrode. Hence concentrations at outer nodes control future concentrations at inner nodes. By this reason it is vital to use the backward space difference method for reformulation of the equation. This is contrary to other equations which contain diffusion terms. In diffusion, concentrations of both the inner and outer nodes are important factors determining their future concentrations. Hence, all the forward, centered, and backward space difference methods can be used for reformulation of an equation containing both the fluid flow and diffusion terms. In this paper, backward space difference method is used as shown in reformulation of Eqs. 5 and 6.

For transformation of Eq. 7 to difference equation, the derivatives are rewritten as shown below.

In the case that $i=1$, the derivative corresponding to $\partial C_C/\partial r$ is expressed as

$$\begin{aligned}\left(\frac{\partial y_C(s_1, T_{j+1})}{\partial s}\right) &= \frac{1}{24\Delta s}\{(-3y_{C,5,j+1} + 16y_{C,4,j+1}\\ &- 36y_{C,3,j+1} + 48y_{C,2,j+1} - 25y_{C,1,j+1}) + (-3y_{C,5,j+1}\\ &+ 16y_{C,4,j+1} - 36y_{C,3,j+1} + 48y_{C,2,j+1} - 25y_{C,1,j+1})\}, \end{aligned} \quad (49)$$

with the concentrations at the nodes $(1,j)$, $(2,j)$, $(3,j)$, $(4,j)$, $(5,j)$, $(1,j+1)$, $(2,j+1)$, $(3,j+1)$, $(4,j+1)$, and $(5,j+1)$.

When $1<i<98$, the derivative is expressed as

$$\begin{aligned}\left(\frac{\partial y_C(s_i, T_{j+1})}{\partial s}\right) &= \frac{1}{24\Delta s}\{(y_{C,i+3,j+1} - 6y_{C,i+2,j+1}\\ &+ 18y_{C,i+1,j+1} - 10y_{C,i,j+1} - 3y_{C,i-1,j+1})\\ &+ (-y_{C,i+3,j} - 6y_{C,i+2,j} + 18y_{C,i+1,j} - 10y_{C,i,j}\\ &- 3y_{C,i-1,j})\}, \end{aligned} \quad (50)$$

with the concentrations at the nodes $(i-1,j)$, (i,j), $(i+1,j)$, $(i+2,j)$, $(i+3,j)$, $(i-1,j+1)$, $(i,j+1)$, $(i+1,j+1)$,

$(i+2,j+1)$, and $(i+3,j+1)$.

When a point has i of 98, the outer nodes are those with i of 99 and 100. Therefore, application of the backward space difference method is impossible. The point is well distant from the electrode surface and the moment of the surface does not cause any significant effect. By this reason, the centered space difference method was used for transformation. The derivative is expressed with the concentrations at the nodes $(96,j)$, $(97,j)$, $(98,j)$, $(99,j)$, $(100,j)$, $(96,j+1)$, $(97,j+1)$, $(98,j+1)$, $(99,j+1)$, and $(100,j+1)$.

$$\left(\frac{\partial y_{C}(s_{98},T_{j+1})}{\partial s}\right)=\frac{1}{24\Delta s}\{(-y_{C,100,j+1}+8y_{C,99,j+1}-8y_{C,97,j+1}+y_{C,96,j+1})+(-y_{C,100,j}+8y_{C,99,j}-8y_{C,97,j}+y_{C,96,j})\}. \quad (51)$$

For the point that $i=99$, the only outer node is one with i of 100. Therefore, application of both the centered and backward space difference methods are impossible. The forward space difference method was used for this purpose. The derivative is expressed with the concentrations at the nodes $(96,j)$, $(97,j)$, $(98,j)$, $(99,j)$, $(100,j)$, $(96,j+1)$, $(97,j+1)$, $(98,j+1)$, $(99,j+1)$, and $(100,j+1)$.

$$\left(\frac{\partial y_{C}(s_{99},T_{j+1})}{\partial s}\right)=\frac{1}{24\Delta s}\{(3y_{C,100,j+1}+10y_{C,99,j+1}-18y_{C,98,j+1}+6y_{C,97,j+1}-y_{C,96,j})+(3y_{C,100,j}+10y_{C,99,j}-18y_{C,98,j}+6y_{C,97,j}-y_{C,96,j})\}. \quad (52)$$

Introducing Eqs. 49—52 into Eq. 7, we have the following equations:

$i=1$,

$$(1+25P_{C,1,j+1})y_{C,1,j+1}=P_{C,1,j+1}\{(-3y_{C,5,j+1}+16y_{C,4,j+1}-36y_{C,3,j+1}+48y_{C,2,j+1})+(-3y_{C,5,j}+16y_{C,4,j}-36y_{C,3,j}+48y_{C,2,j}-25y_{C,1,j})\}+y_{C,1,j}+\Delta TK_{f}y_{B,1,j+1}y_{B,1,j}(y_{A,1,j+1}+y_{A,1,j})/2-\Delta TK_{b}. \quad (53)$$

$1<i<98$,

$$(1+10P_{C,i,j+1})y_{C,i,j+1}=P_{C,i,j+1}\{(y_{C,i+3,j+1}-6y_{C,i+2,j+1}+18y_{C,i+1,j+1}-3y_{C,i-1,j+1})+(y_{C,i+3,j}-6y_{C,i+2,j}+18y_{C,i+1,j}-10y_{C,i,j}-3y_{C,i-1,j})\}+y_{C,i,j}+\Delta TK_{f}y_{B,i,j+1}y_{B,i,j}(y_{A,i,j+1}+y_{A,i,j})/2-\Delta TK_{b}. \quad (54)$$

$i=98$,

$$y_{C,98,j+1}=P_{C,98,j+1}\{(-y_{C,100,j+1}+8y_{C,99,j+1}-8y_{C,97,j+1}+y_{C,96,j+1})+(-y_{C,100,j}+8y_{C,99,j}-8y_{C,97,j}+y_{C,96,j})\}+y_{C,98,j}+\Delta TK_{f}y_{B,98,j+1}y_{B,98,j}(y_{A,98,j+1}+y_{A,98,j})/2-\Delta TK_{b}. \quad (55)$$

$i=99$,

$$(1-10P_{C,99,j+1})y_{C,99,j+1}=P_{C,99,j+1}\{(3y_{C,100,j+1}-18y_{C,98,j+1}+6y_{C,97,j+1}-y_{C,96,j+1})+(3y_{C,100,j}+10y_{C,99,j}-18y_{C,98,j}+6y_{C,97,j}-y_{C,96,j})\}+y_{C,99,j}+\Delta TK_{f}y_{B,99,j+1}y_{B,99,j}(y_{A,99,j+1}+y_{A,99,j})/2-\Delta TK_{b}. \quad (56)$$

$$P_{C,i,j+1}=\frac{\Delta TH(1-s_i)^2U_{j+1}x_i(x_i+2a_{j+1}/L)}{24\Delta s(x_i+a_{j+1}/L)^2}. \quad (57)$$

The value of $y_{C,i,j+1}$ is calculated with the aid of Eqs. 53—56.

The numerical computation described in the present method was programmed with the Gauss-Seidel method and the successive over relaxation method by using FORTRAN.

Converged values at $j\Delta T$ are usually used as initial values for computation of values at $(j+1)\Delta T$. This practice was successful when the concentration of chloride ions was lower than 1×10^{-4} mol dm^{-3}, where the difference between concentrations of mercury(I) and chloride ions was moderate. It produced, however, tremendous increase in the number of repetitions when the difference between concentrations of mercury(I) and chloride ions became large. It was nearly prohibitive. Therefore a new procedure was used instead of the practice described above. It was by use of estimated values at $(j+1)\Delta T$ as initial values for computation. The values at $(j+1)\Delta T$ are estimated roughly with the assumption that the converged values at $(j+1)\Delta T$ are situated on the extension of the line connecting two points, $y_{A,i,j-1}$ and $y_{A,i,j}$ The initial values at $(j+1)\Delta T$ are estimated with the following equations:

$$y_{A,i,j+1}=R(y_{A,i,j}-y_{A,i,j-1})+y_{A,i,j}, \quad (58)$$

where R is a constant ranging from 0.1 to 1.01.

Up to this point, consideration is confined solely to the current corresponding to the observed current. The residual current should be considered next. Because the residual current is the current in the absence of the chloride ion, the differential equation to be used for calculation of the residue current is Eq. 9, of which difference equation forms are Eqs. 41—43. Initial condition is

$$C_{A}=0 \quad (t=0,\quad r>a). \quad (59)$$

Boundary conditions are

$$C_{A}=C_{A0} \quad (t>0,\quad r=a), \quad (60)$$

$$C_{A}=0 \quad (t>0,\quad r=\infty). \quad (61)$$

The instantaneous anodic current in the absence of chloride ions, i_r, is given by

$$i_r=2FD_{A}S(\partial C_{A}/\partial r)_{r=a}. \quad (62)$$

Kolthoff and Miller corrected the observed current for residual current by

$$i_c=i-i_r. \quad (63)$$

The corrected current, i_c is the current mainly caused by precipitation reaction.

Results and Discussion

Any numerical method should be established by comparison of calculated results with observed data. The validity of the present method was examined under various experimental conditions. The anodic wave of mercury was measured in the presence of chloride ions of various concentrations.

The value of diffusion coefficient of mercury(I) ions for numerical computations was chosen so as to minimize difference between calculated and observed current.[2] This procedure produces a value of 0.847×10^{-5} cm^2 s^{-1}. The value of diffusion coefficient of chloride ions used is 2.03×10^{-5} cm^2 s^{-1}.[6]

Figure 2 shows the plots of $\log(i_d-i_c)$ vs. E constructed with observed data, where currents were measured at the end of life of mercury drop. The plots give straight lines. The slope of these lines ranges from −45 to −52 mV/unit. Experimental values of the reciprocal slope do not agree with Eq. 1. The half-wave potential shifts to anodic direction with increase of ionic strength. This shift is explained as follows: The concentration constant of the solubility product increases with ionic strength, because activity coefficients of ions decrease with ionic strength within the limit of the experimental conditions. The shift of half-wave potential is anodic direction as shown in Eq. 1. The value of anodic current corrected for residual current was proportional to the concentration of chloride ions.

Figure 3 shows the effect of concentration of ethanol added to the electrolyte. The concentration of ethanol does not influence on the value of reciprocal slope. However, the half-wave potential of anodic wave shifts to more negative by 52 mV with increase in the concentration of ethanol from 0 to 40 vol%, because the solubility product of mercury(I) chloride decrease with increase of ethanol concentration. The plots of $\log(i_d-i_c)$ vs. E produce straight lines with slopes ranging from −45 to −52 mV/unit.

Computation of the anodic current by the method described in Theory was successful when the concentration of chloride ions was within the range of 10^{-5} to 3×10^{-4} mol dm^{-3}. Values of parameters used are as follows: The value of L ranges from 10^{-5} to 10^{-2} cm and ΔT from 4.27×10^{-7} to 2.18×10^{-4} s. The rate constant of precipitate particle formation was chosen as the value of $C_AC_B^2$ in each volume element does not exceed the solubility product by as much as 10%. The computation failed, however, when the concentration of chloride ions was over 3×10^{-4} mol dm^{-3}. The reason of failure is as follows: The anodic wave caused by precipitation appears at the electrode potential ranging from 0.25 to 0.30 V vs. SCE. The concentration of mercury(I) ions in contact with mercury electrode at 0.30 V vs. SCE is 2.1×10^{-9} mol dm^{-3}, which is far lower than that of chloride ions. Remarkable imbalance between concentrations of mercury(I) and chloride ions prevents successful computation, even if it is performed with double precision.

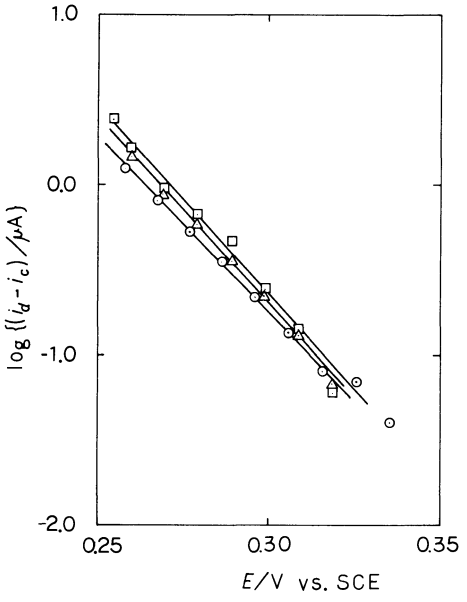

Fig. 2. Effect of ionic strength on the anodic wave in the solution of 0.5×10^{-3} mol dm^{-3} KCl and 0.005% gelatin. Value of ionic strength: ○, 0.05 M; △, 0.1 M; □, 0.2 M. The ionic strength is adjusted with potassium nitrate.

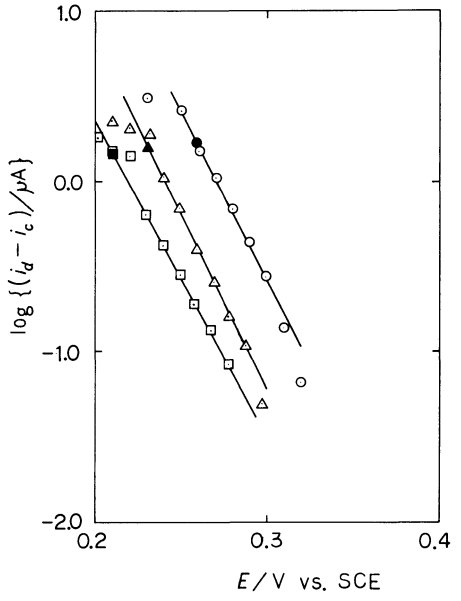

Fig. 3. Effect of the concentration of ethyl alcohol on the anodic wave in the solution containing 0.5×10^{-3} mol dm^{-3} KCl, 0.05 mol dm^{-3} KNO_3, and 0.005% gelatin. Concentration of ethyl alcohol: ○, 0 vol%; △, 20 vol%; □, 40 vol%. Filled symbols indicate the half-wave potentials.

Figure 4 shows the plots of $\log(i_d-i_c)$ vs. E constructed with calculated and observed data. The calculated data are consistent with the observed ones in the case that the concentration of chloride ions is 1×10^{-4} and 3×10^{-4} mol dm^{-3}.

Figure 5 shows the plot of the corrected limiting currents, i_l, vs. concentration of chloride ions. The current is proportional to the concentration. The points corresponding to calculated and observed limiting currents are on a straight line. The plot of observed half-wave potential against the logarithm of concentration of chloride ions produces another straight line. The value of slope of the straight line is -59 mV/unit, and this value agrees with the theoretical value given by Eq. 1. The calculated half-wave potential values are on this line. It indicates that the present method of the calculation reflects the phenomena going on in the vicinity of dropping mercury electrode. The value of the solubility product was chosen for the computed points to be on straight lines. A chosen value of solubility product of mercury(I) chloride is 2.0×10^{-17} mol^3 dm^{-9}. After making activity correction, the value of the activity product is given as 4.04×10^{-18} mol^3 dm^{-9}. This value is about three times as large as ones given in a standard literature.[4] It shows that the solubility of fresh precipitate, whose age is within the life of

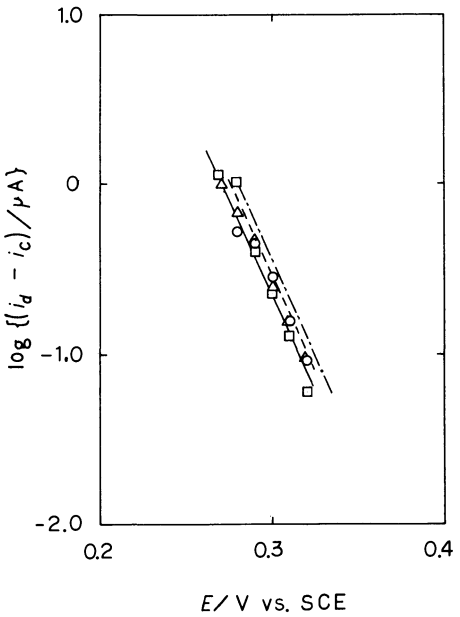

Fig. 4. Plots of E against $\log(i_d-i)$ in the solution of pH 1.93 containing 0.005% gelatin. Concentration of chloride ($\times10^{-3}$ mol dm^{-3}): (observed) O, 0.1; △, 0.2; □, 0.3; (computed), —·—, 0.1; ——, 0.2; ——, 0.3.

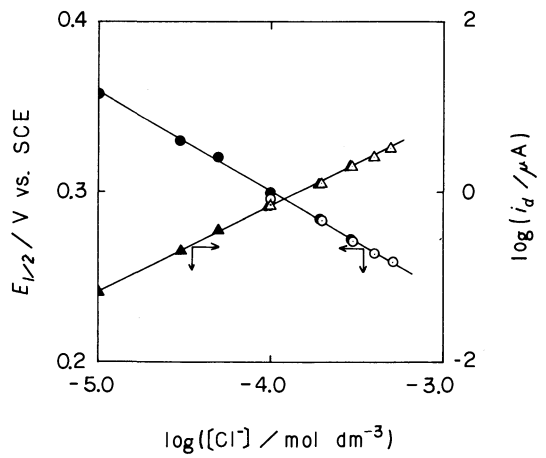

Fig. 5. Effect of chloride ions on the half-wave potential and the limiting current in the solution of pH 1.93 containing 0.01% gelatin. ●, half-wave potential computed; O, half-wave potential observed; ▲, limiting current computed; △, limiting current observed.

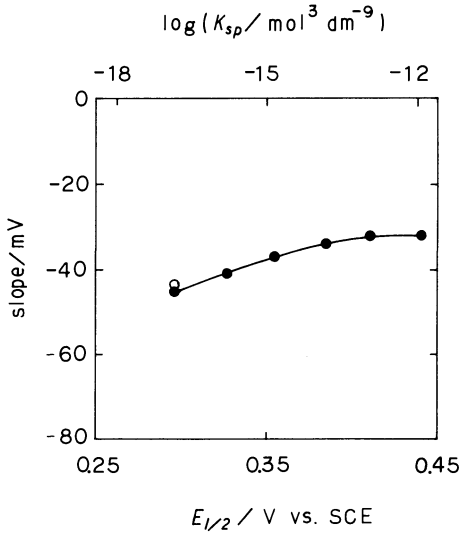

Fig. 6. Relation between the half-wave potential and the slope of logarithmic plot by the numerical method. pH 1.93 and 10^{-4} mol dm^{-3} sodium chloride. O, observed; ●, computed.

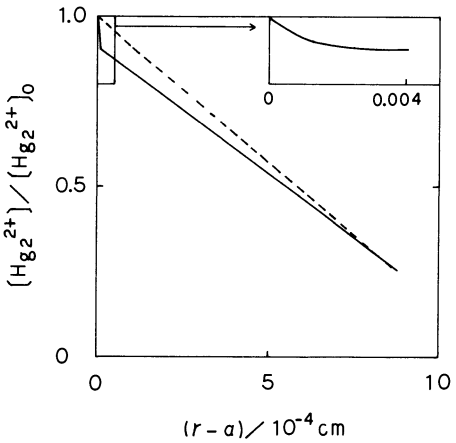

Fig. 7. Computed distance-concentration curves of mercury(I) ions at about the half-wave potential in the solution of 10^{-4} mol dm^{-3} chloride ions. The value of $\log(K_{sp})$: a solid line, -16.7; a dotted line, -11.7. The inset shows a graph with an enlarged abscissa.

electrode mercury drop, is larger than that of more aged precipitate.

Figure 6 shows the relation among the value of solubility product, the slope of logarithmic plot, and the half-wave potential of numerically-constructed polarograms. The concentration of chloride ions was kept at 10^{-4} mol dm^{-3}. The value of slope is almost constant when the half-wave potential is more positive than 0.40 V, whereas the slope decreases to approach to -59 mV/unit when the half-wave potential becomes more negative than 0.40 V vs. SCE.

Figure 7 shows numerically constructed concentration-distance curves of mercury(I) ions at about the half-wave potential. The concentration of mercury(I) ions at the surface of electrode is 5×10^{-4} mol dm^{-3} when a value of 2×10^{-12} mol^3 dm^{-9} is used for K_{sp}, and is 5×10^{-9} mol dm^{-3} when a value of 2×10^{-17} mol^3 dm^{-9} is used. The concentration of chloride ions is identical in the above two cases. It is found that the concentration-distance curve is divided into two parts. The interior and exterior curves correspond to the regions with and without mercury(I) chloride precipitate particles, respectively. The precipitation reaction proceeds in the interior region, but does not in the exterior one. It is found that the position of boundary between two regions approaches to the surface of electrode with decrease of K_{sp}. It indicates that the thickness of layer, in which the precipitation reaction proceeds, becomes small with decrease of K_{sp}. At the limit, it produces the concentration-distance curve of chloride ions by Kolthoff and Miller, who assumed that the precipitation reaction proceeds only at the surface of electrode. Therefore the value of slope becomes -59 mV/unit with the decrease of K_{sp} shown in Fig. 6.

Experimental

The chemicals used were of reagent grade. The concentration of chloride ion in stock solutions was calculated from amounts of sodium chloride or potassium chloride dissolved. The salts were dried at 110—120 °C for 2 h. Oxygen in test solutions were expelled by bubbling pure nitrogen for 50 min. The current of the anodic wave was measured just before the detachment of mercury drop. Measurements were carried out using a Hokuto Denko Model HA 104 Potentio-Galvanostat with three electrodes arrangement at 25 °C.

The dropping mercury electrode had the following characteristics (in 0.1 mol dm^{-3} sodium perchlorate at zero applied potential vs. SCE and at a mercury head of 80.0 cm): The flow rate of mercury (m), 2.08 mg s^{-1}; the drop time (t), 3.20 s; the capillary constant ($m^{2/3}t^{1/6}$), 1.978 mg$^{2/3}$ s$^{-1/2}$.

The numerical method described in the present paper was performed by an IBM 4361-L03 computer in Shiga Prefectural Junior College.

Conclusion

The anodic wave of mercury in the presence of chloride ions was studied by a new numerical method. The boundary condition, $(\partial C_B/\partial r)_{r=a}=0$, was used for computation, because chloride ions do not participate in the charge transfer at the electrode. The differential equation for precipitate particles was transformed to the difference equation with the backward space difference method which was chosen to reflect the relative motion of the solution around the electrode mercury drop. It was found that the transformation with the backward space difference method was vital for successful computation.

The results of numerical method indicate that the relations between the concentration of chloride ions and the half-wave potential, and those between the concentration of chloride ions and the limiting current corrected for residual current are in fair agreement with an equation derived by Kolthoff and Miller. However, the computed value of reciprocal slope of straight lines obtained by plotting $\log(i_d-i_c)$ against E does not agree with their theory but fairly agrees with observed data. Reason of this seems that the rate of production of mercury(I) ions is controlled both by the diffusion of chloride ions and by the potential of mercury electrode.

References

1) I. M. Kolthoff and C. S. Miller, *J. Am. Chem. Soc.*, **63**, 1405, (1941). Equation 1 corresponds to Eq. 16 in the original paper. The former differs from the latter in respect of inclusion of the activity coefficient and change of symbols.

2) K. Kikuchi, *Bull. Chem. Soc. Jpn.*, **60**, 903 (1987).

3) H. Morihara and R. T. Cheng, *J. Compu. Phys.*, **11**, 550 (1973).

4) "Stability Constant of Metal Complexes," ed by L. G. Sillén and A. E. Martell, Chemical Society (1964), p. 292.

5) G. D. Smith, "Numerical Solution of Partial Differential Equations," Oxford University Press (1965).

6) I. M. Kolthoff and J. J. Lingane, "Polarography," Interscience Publishers (1952), Vol. 1, p. 52.

 © 1988 The Chemical Society of Japan Bull. Chem. Soc. Jpn., 61, 3169—3174 (1988)

Mössbauer Spectroscopic Characterization of Iron Supported on Y Type Zeolites after Sulfiding

Setsuo HIDAKA,* Akira IINO, Kenji NITA, Kenji MORINAGA,† and Noboru YAMAZOE†

Central Research Laboratories of Idemitsu Kosan Co., Ltd., 1280 Kamiizumi, Sodegaura, Kimitsu, Chiba 299-02

†Graduate School of Engineering Science, Kyushu University, 6-1, Kasuga-Koen, Kasuga, Fukuoka 816

(Received January 9, 1988)

Iron supported on zeolite catalysts, prepared by treating NH_4Y with aqueous solutions containing Fe^{3+} or Fe^{2+} ions followed by calcination in air, were subjected to Mössbauer spectroscopic investigations before and after sulfiding treatments to elucidate the states and properties of Fe species supported. At least three types of Fe^{3+} species could be distinguished in the prepared samples. The first Fe^{3+} species were those located at the cation-exchange sites of zeolite. This type was reduced easily to Fe^{2+} species with the H_2S treatment, but was resistant to aggregation to form $Fe_{1-x}S$. The second Fe^{3+} species were those which had precipitated on the surface of zeolites as hydroxides. These were sulfided to crystalline $Fe_{1-x}S$ after H_2S treatment. Finally, the third Fe^{3+} species were those which were quite resistant to both reduction to Fe^{2+} and sulfiding to $Fe_{1-x}S$. These species were preferentially supported under the conditions where dealumination from zeolite framework took place simultaneously. Thus it was speculated that these species were bonded to zeolite framework to be stabilized. The distribution of the three Fe^{3+} species were quite different depending on the sample preparation. Comparison with the catalytic data clearly indicated that the third Fe^{3+} species acted as highly active sites for the toluene disproportionation reaction in the presence of H_2S.

Recently we reported that the iron supported on Y type zeolite (FeHY-1) prepared by treating NH_4Y with an aqueous $Fe(NO_3)_3$ solution showed high catalytic activity and low coke formation for the toluene disproportionation reaction in a flow of H_2S/H_2.[1] It was also shown that a FeHY-1 based catalyst was highly active for the hydrocracking of the atmospheric residual oil in the presence of H_2S.[2] There has been collected ample evidence to indicate that the iron species supported on FeHY-1 are clearly different from those on the other iron supported on zeolites prepared by conventional methods such as an ion-exchange method.[1,3] However, we still lack definite information as to the nature and state of iron species in FeHY-1.

It is known that Mössbauer spectroscopy is very useful to investigate the state of iron species on zeolites.[4] In this paper, we have studied the state of iron species after sulfiding treatment by using Mössbauer spectroscopy and the correlation between catalytic activity and the state of iron species supported on zeolite in the presence of H_2S.

Experimental

Preparation of Catalyst. To obtain FeHY-1-L, FeHY-1, FeHY-1-H, FeHY-2-L, and FeHY-2, ammonium-ion-exchanged Y type zeolite, NH_4Y (UCC; LZY-82), was mixed with the aqueous $Fe(NO_3)_3$ or $FeSO_4$ solution shown in Table 1 at room temperature, and stirred for 2 h at the specified temperatures. Then the suspension was filtered, washed with distilled water, dried in air at 363 K, and finally calcined in air at 773 K for 3 h.

For FeHY-3 and Fe/SiO_2, NH_4Y or silica gel(Fuji Davison) was suspended in water, to which aqueous $Fe(NO_3)_3$ solution was added as droplets while caution was paid to keep the pH of the suspension at 7 by adding droplets of aqueous ammonia solution simultaneously. This procedure was adopted in order to have Fe^{3+} ions precipitated as $Fe(OH)_3$. The subsequent procedures were the same as the above.

Measurements of Physicochemical and Catalytic Properties. The amount of supported Fe as well as the SiO_2/Al_2O_3 molar ratio of each sample were measured by Fluorescence spectrometer (Rigaku Denki; 3080E). The specific surface area was determined by BET method. The

Table 1. Preparation Methods of Catalysts

Catalyst	Starting Fe solution	Zeolite / Fe solution/g l^{-1}	Temp/K	Time/h
FeHY-1-L	0.10 M[b] $Fe(NO_3)_3$	8	323	2
FeHY-1	0.25 M $Fe(NO_3)_3$	8	323	2
FeHY-1-H	0.25 M $Fe(NO_3)_3$	8	373	2
FeHY-2-L	1.00 M $FeSO_4$	40	323	2
FeHY-2	1.00 M $FeSO_4$	40	363	2
FeHY-3	0.25 M $Fe(NO_3)_3$+NH_4OH	8	R.T.	1
Fe/SiO_2	0.25 M $Fe(NO_3)_3$+NH_4OH	8[a]	R.T.	1

a) SiO_2/Fe solution. b) 1 M=1 mol dm^{-3}.

unit cell dimension of zeolite lattice was determined by X-ray (Cu $K\alpha$) powder diffraction.

The toluene disproportionation reaction was carried out in a high-pressure fixed catalyst bed reactor. The loaded catalyst (1.8 g) was sulfided in a flow (60 $cm^3 m^{-1}$) of H_2S(0.2 vol%)/H_2 mixture at 523 K and 3 MPa for 16 h, before toluene was fed at a rate of 10 cm^3 (liquid) h^{-1} in a flow (200 $cm^3 m^{-1}$) of H_2S(0.2 vol%)/H_2 at 623 K and 6 MPa. The effluent, consisting mostly of unconverted toluene, xylene, and benzene was analyzed by FID gas chromatography. The amounts of coke deposition on spent catalysts were determined from increases in weight.

Mössbauer Measurement. Mössbauer spectroscopy was carried out by using a constant-acceleration spectrometer (Elscint, Inc.). Data were stored in a 1024-channel pulse height analyzer, TN-7200 (Tracor Northen, Inc.). A cobalt-57 source of 10 mCi diffused into a palladium foil (Amersham, Inc.) was used for the absorption measurement. Some of the spectra were fitted to the Lorentzian line shape by using a least-squares analysis. Isomer shift was referred to the center of the spectrum of metallic iron. In many cases samples were subjected to sulfiding treatments prior to the measurements: Samples were exposed to a flow of either H_2S(10 vol%)/He at 473 K or H_2S(10 vol%)/H_2 at 673 K for 2 h unless noted otherwise. The sulfied samples were measured in nitrogen atmosphere to prevent the reoxidation of sulfided iron species if any.

Results and Disscusion

Physicochemical Properties and Catalytic Activities. Some physicochemical and catalytic properties of the prepared samples as well as those of NH_4Y and HY are compared in Table 2. We have shown already that the treatment of NH_4Y with an aqueous solution of $Fe(NO_3)_3$ results in dealumination from zeolite framework.[1] The dealumination proceeds through

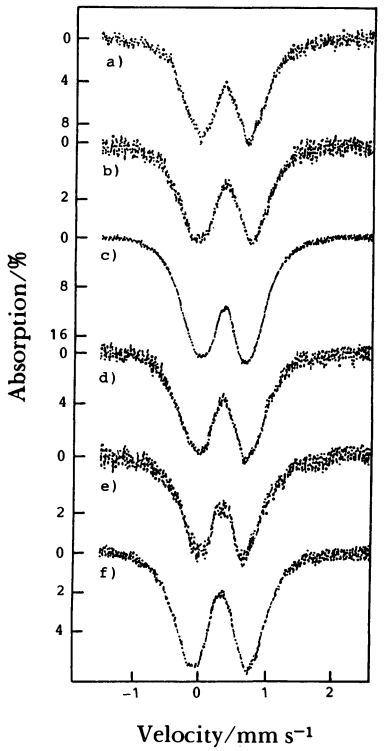

Fig. 1. Mössbauer spectra of iron supported on zeolites after calcination at 773 K.
a) FeHY-1-L, b) FeHY-1, c) FeHY-1-H, d) FeHY-2-L, e) FeHY-2, f) FeHY-3.

Table 2. Physicochemical Properties and Catalytic Activity

Catalyst	Physicochemical properties			
	Fe_2O_3/wt%	SiO_2/Al_2O_3 (molar ratio)	Surface area/$m^2 g^{-1}$	UD[a]/Å
NH_4Y	tr.	5.4	543	24.57
HY	tr.	5.4	427	24.51
FeHY-1L	4.8	6.6	463	24.50
FeHY-1	9.0	10.6	456	24.40
FeHY-1H	16.2	10.6	477	n[d]
FeHY-2L	4.1	5.7	443	24.51
FeHY-2	11.8	6.3	437	24.51
FeHY-3	10.0	5.9	451	24.51
Fe/SiO_2	9.2	—	96	—

Catalyst	Tol. dispro.[b]		
	Converted toluene/mol%	Sel.[c]/mol%	Coke deposited/wt%
NH_4Y	—	—	—
HY	5.5	100	14.6
FeHY-1L	12.9	76.0	11.6
FeHY-1	45.3	92.0	0.5
FeHY-1H	32.4	70.1	1.2
FeHY-2L	12.1	71.1	11.5
FeHY-2	18.2	72.5	8.0
FeHY-3	16.9	70.4	9.6
Fe/SiO_2	—	—	—

a) Unit cell dimension of zeolite lattice. b) Toluene disproportion. Sulfiding; H_2S(0.2 vol%)/H_2, 523 K, 3 MPa, 16 h. Reaction; H_2S(0.2 vol%)/H_2, 623 K, 6 MPa, LHSV: 4.0 h^{-1}. c) Selectivity to benzene and xylene. d) Not measured.

the attack of the protons which are produced from the hydrolysis of Fe^{3+} ions. As a result of the dealumination, SiO_2/Al_2O_3 molar ratio increases while the unit cell dimension of zeolite decreases. As seen from Table 2, FeHY-1 and FeHY-1-H showed larger SiO_2/Al_2O_3 ratios and smaller unit cell dimensions than the other samples, indicating the progress of significant degrees of dealumination. The amounts of supported Fe_2O_3 varied considerably with the samples, but these amounts were not directly related with the catalytic properties. As seen from the table, FeHY-1 and FeHY-1-H showed very high activities and very low coke depositions in a flow of H_2S(0.2 vol%)/H_2 compared with the other catalysts.

This clearly shows the importance of dealumination during the catalyst preparation. As stated previously, it is considered that the Fe species loaded on zeolite under the dealuminating conditions are present in a state significantly different from those loaded under the non-dealuminating conditions, and thus show unique acidic properties in the presence of H_2S.[1]

Mössbauer Spectra of Fresh Catalysts. Mössbauer spectra of prepared samples after calcination are shown in Fig. 1. The Mössbauer parameters estimated for the samples listed in Table 3. The spectra consisted of broad quadrupole doublets, denoted Type A hereafter. The doublets showed isomer shift (IS) 0.33—0.36 mm s^{-1} and quadrupole splitting (QS) 0.76—0.90 mm s^{-1}, which were in the anticipated ranges for octahedrally coordinated Fe^{3+} species.[5] However, the isomer shifts denied the existence of significant amounts of tetrahedrally coordinated Fe^{3+} ions in the samples. The absence of Zeeman splitting in the spectra assured that the particle sizes of the Fe^{3+} species were very fine, being 50—100 Å or less.[6]

As for the octahedrally coordinated Fe^{3+} species, several types are possible, such as Fe^{3+} ions located at the cation-exchange sites of zeolite,[4,7] oligomerized iron(III) oxide clusters located in supercages or on outer surface of zeolite, and fine Fe_2O_3 particles. The proportion of each type would depend on the sample preparation but more than a single type are likely to be loaded in each sample, as suggested from the broadness of the quadrupole doublet.

Mössbauer Spectra after H_2S/He Treatment at 473 K. The fresh samples were treated with H_2S(10 vol%)/He at 473 K (at 573 K for FeHY-1) and atmospheric pressure. Their Mössbauer spectra are

Table 3. Mössbauer Parameters of Quadrupole Doublets of Iron Supported on Zeolites

Catalyst	Treatment[a]	Isomer shift/mm s^{-1} (±0.02)	Quadrupole splitting/mm s^{-1} (±0.05)	Relative amount/%	
FeHY-1-L	Fresh	0.36	0.79	A	100
	I	0.30	0.74	A+C	32
		1.13	2.10	B	68
	II	0.35	0.85	A	27
		1.16	2.08	B	73
FeHY-1	Fresh	0.35	0.87	A	100
	I′	0.35	1.02	A	61
		1.17	2.17	B	39
	II	0.36	0.95	A	42
		1.12	1.99	B	58
FeHY-1-H	Fresh	0.34	0.76	A	100
	I	0.30	0.54	C	67
		0.39	1.00	A	19
		1.70	1.77	B	15
	II		Hyperfine splitting	D	—
FeHY-2-L	Fresh	0.35	0.83	A	100
	I	0.27	0.69	C	17
		1.15	2.11	B	83
	II	0.30	0.78	C	13
		1.14	2.10	B	87
FeHY-2	Fresh	0.34	0.77	A	100
	I	0.28	0.58	C	67
		1.13	2.05	B	33
	II		Hyperfine splitting	D	—
FeHY-3	Fresh	0.33	0.90	A	100
	I	0.28	0.42	C	93
		0.92	2.31	B	7
	II		Hyperfine splitting	D	—
Fe/SiO_2	I	0.30	0.61	C	100

a) Conditions I and I′: exposure to a flow of H_2S(10 vol%)/He at 473 K (I) or 573 K (I′) for 2 h. Conditions II: exposure to a flow of H_2S(10 vol%)/H_2 at 673 K for 2 h. b) A: Octahedrally coordinated Fe^{3+} ions. B: Fe^{2+} ions located at cation-exchange sites. C: $Fe_{1-x}S$ showing a quadrupole splitting. D: $Fe_{1-x}S$ showing a hyperfine structure.

shown in Fig. 2. The Mössbauer parameters are listed in Table 3. The spectra are all composed of two or three types of quadrupole doublets.

A type of quadrupole doublet (Type B), with large IS of 0.92—1.70 mm s^{-1} and large QS of 1.77—2.31 mm s^{-1}, was typically observed in FeHY-1-L and FeHY-2-L. These samples were prepared by treating NH_4Y with either a dilute Fe^{3+} solution or a Fe^{2+} solution, conditions where the ion exchange of NH_4^+ with Fe^{3+} or Fe^{2+} was favored over the other types of loading. It has also been reported that such Fe^{3+} ions are easily reduced.[8] Thus Type B doublet is likely to be assigned to Fe^{2+} ions located at the cation-exchange sites of zeolite. This doublet was far weaker in FeHY-1 and FeHY-2, almost unvisible in FeHY-1-H and FeHY-3, and not visible in Fe/SiO_2.

A quadrupole doublet (Type C), with IS of 0.27—0.30 mm s^{-1} and QS of 0.54—0.77 mm s^{-1} appeared typically in FeHY-1-H, FeHY-2, FeHY-3, and Fe/SiO_2, and was assigned to fine particles of nonstoichiometric iron sulfide ($Fe_{1-x}S$) according to literature.[9] These samples were prepared under such conditions that the precipitation of iron hydroxides on zeolite was facilitated more or less. It is inferred that the precipitate changed to fine particles of Fe(III) oxide with the calcination and then to ferric sulfide with the H_2S/H_2.

Quite remarkably, Type C doublet was hardly visible in FeHY-1. The spectrum was dominated by Type A doublet responsible for Fe^{3+} species, with a minor contribution of Type B. The survival of Fe^{3+} species is still more remarkable when it is taken into account that the H_2S/H_2 treatment was carried out at a higher temperature (573 K) than that for the other samples (473 K). This fact indicates that a prevailing part of the Fe^{3+} ions in FeHY-1 are situated in a form which is quite resistive to reduction. Type A doublet was also present, but far less visible, in FeHY-1-H. It is considered that the reduction-resistant property arises from a strong interaction of Fe^{3+} species with zeolite lattice, and that such Fe^{3+} species are formed when Fe^{3+} ions are loaded on zeolite under the dealuminating conditions. The relative intensities of the three types of quadrupole doublets were estimated from the areas under the doublets and are indicated in Table 3.

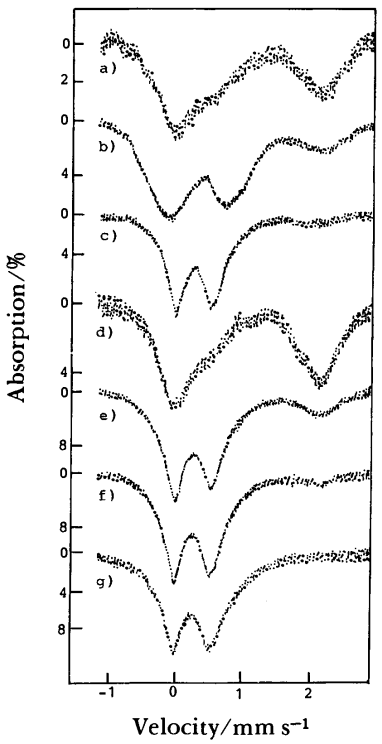

Fig. 2. Mössbauer spectra of iron supported on zeolites after sulfiding in H_2S(10 vol%)/He flow at 473 K or 573 K for 2 h.
a) FeHY-1-L, b) FeHY-1, c) FeHY-1-H, d) FeHY-2-L, e) FeHY-2, f) FeHY-3, g) Fe/SiO_2.

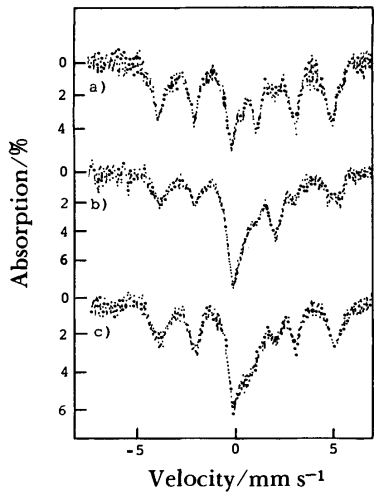

Fig. 3. Mössbauer spectra of iron supported on zeolites after sulfiding in H_2S(10 vol%)/H_2 flow at 673 K for 2 h.
a) FeHY-1-H, b) FeHY-2, c) FeHY-3.

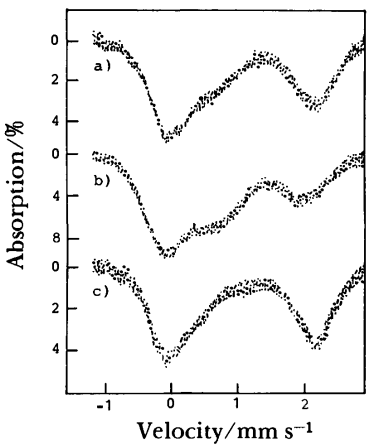

Fig. 4. Mössbauer spectra of iron supported on zeolites after sulfiding in H_2S(10 vol%)/H_2 flow at 673 K for 2 h.
a) FeHY-1-L, b) FeHY-1, c) FeHY-2-L.

Mössbauer Spectra after H_2S/H_2 Treatment at 673 K. Mössbauer spectra after H_2S(10 vol%)/H_2 treatment at 673 K are shown in Figs. 3 and 4, and Mössbauer parameters are listed in Table 3. Most of these spectra were drastically different from those described in the previous sections.

As shown in Fig. 3, the spectra of FeHY-1-H, FeHY-2, and FeHY-3 clearly showed a sextet of magnetic hyperfine structure with a paramagnetic doublet weakly superposing on it. The sextet was assigned to crystalline $Fe_{1-x}S$ of sufficiently large domains because the internal magnetic field (H_{int}) of about 28 T as well as the spectral shape coincided with those of commercially obtained $Fe_{1-x}S$ (Nippon Chikagaku Co., Ltd.).

As estimated from the area under the sextet, about 70% or more of iron species on these samples could be assigned to this kind of crystalline $Fe_{1-x}S$. It is considerd that fine particles $Fe_{1-x}S$, formed after sulfiding in H_2S(10 vol%)/He at 473 K, grew to large particles during sulfiding in H_2S(10 vol%)/H_2 at 673 K.

On the contrary, such a sextet magnetic hyperfine structure was not observed for FeHY-1-L, FeHY-1, and FeHY-2-L as shown in Fig. 4. This suggests that the crystal growth of $Fe_{1-x}S$ hardly proceeded. For FeHY-1-L and FeHY-2-L, a quadrupole doublet (Type B) due to Fe^{2+} ions at the cation-exchange sites of zeolite, remained predominant. While FeHY-1 exhibited not only this kind of quadrupole doublet (Type B) due to Fe^{2+} ions but also a quadrupole doublet (Type A) due to Fe^{3+} ions. As shown in Fig. 3, more than 40% of Fe^{3+} ions supported on FeHY-1 could survive after the treatment in H_2S(10%)/H_2 at 673 K. These results again indicate that the Fe^{3+} ions supported on FeHY-1 are resistant to reduction. This resistance should come from a strong interaction between the Fe^{3+} ions and zeolite lattice as described before.

States and Catalytic Activities of Supported Iron Species. The Mössbauer measurements mentioned above revealed that the states and properties of supported Fe^{3+} ions were largely different, depending on the preparation conditions.

When NH_4Y was treated with a dilute aqueous solution containing Fe^{3+} or Fe^{2+} at 323 K, as in the cases of FeHY-1-L and FeHY-2-L, most iron ions were loaded on zeolite by ion exchange and situated at the cationic sites. These Fe^{3+} ions were easily reduced to Fe^{2+} under the sulfiding conditions, but they were resistant to aggregation into crystalline $Fe_{1-x}S$.

When NH_4Y was treated with a Fe^{2+} or Fe^{3+} solution at higher temperature (363 or 373 K), as in the cases of FeHY-1-H and FeHY-2, a major part of Fe ions seemed to be loaded on zeolite by precipitation as hydroxides. Like FeHY-3 and Fe/SiO_2, the samples prepared in this way showed a superparamagnetic doublet due to finely dispersed $Fe_{1-x}S$ particles after the low temperature sulfiding (473 K) and a sextet hyperfine structure due to large particles of $Fe_{1-x}S$ after the high temperature sulfiding (673 K).

In contrast to these samples, FeHY-1 was shown to be very unique in the stability of Fe^{3+} ions loaded. In fact, more than 40% of the loaded Fe^{3+} ions could remain as Fe^{3+} even after the sulfiding treatment with H_2S(10%)/H_2 at 673 K. FeHY-1 was prepared under the conditions where dealumination from zeolite lattice took place. The hydrolysis of Fe^{3+} ions in the solution should produce protons and Fe^{3+} complexes. The released protons should attack zeolite lattice to dealuminate while the dealuminated sites would tend to be compensated by the Fe^{3+} complexes. In this way, Fe^{3+} complexes should be incorporated and partially bonded to zeolite lattice. It is assumed that such bonding should result in the remarkable resistivity of the Fe^{3+} ions to reduction.

It is interesting to compare these results with the catalytic activities for the toluene disproportionation reaction in the presence of H_2S. As already stated, FeHY-1 was the most active among the tested samples. This indicates the importance of the reduction-resistant Fe^{3+} species just mentioned. Moreover, the other two species dominating in the other samples, i.e., the ion-exchanged Fe^{3+} ions at the cation-exchange sites and the Fe species deposited on zeolite surface, which were easily reduced to Fe^{2+} or to crystalline $Fe_{1-x}S$ in the H_2S atmosphere, are judged to be not so active as the above one. A comment may be necessary for FeHY-1-H, which was active next to FeHY-1. Although the reduction-resistant Fe^{3+} could not be clealy revealed in this sample, probably due to the excessive amounts of the other species, one can expect its presence from the extent of dealumination of the sample. Therefore the high activity of FeHY-1-H can be assumed to result also from the reduction-resistant Fe^{3+} species.

Previously we estimated that the unique acidic properties of the Fe supported on zeolite in the toluene disproportionation reaction in the presence of H_2S were not associated with the formation of iron sulfide ($Fe_{1-x}S$) but with the adsorption of H_2S on a certain type of supported Fe^{3+} species.[1] This estimation has been confirmed with the above observation that the active sites are provided by the reduction-resistant Fe^{3+} species, although the mechanism for generating the unique acidity remains to be studied further.

Conclusion

Three types of Fe^{3+} species could be distinguished in the Fe supported on zeolite catalysts prepared. The Fe^{3+} located at cation-exchange sites of zeolite (the first type), dominating in FeHY-1-L and FeHY-2-L, are easily reduced to Fe^{2+} with the H_2S treatment, to give a characteristic quadrupole doublet with a large isomer shift. The second type, dominating in FeHY-

1-H, FeHY-2 and FeHY-3, consists of those which have precipitated on zeolite surface as iron hydroxides and have changed into Fe(III) oxide after calcination in air. This type is changed easily into well dispersed $Fe_{1-x}S$ with the H_2S treatment at 473 K, which further grows into sufficiently large particles of $Fe_{1-x}S$ to give a sextet hyperfine structure at higher temperature (673 K). The third type, typically formed in FeHY-1, is very resistant to chemical change, remaining almost intact even after the H_2S treatment at 673 K. The remarkable stability of this type is considered to arise from a strong interaction with the zeolite framework.

Comparison of these results with the catalytic performances, clearly indicates that it is the third type Fe^{3+} species which provide the highly active sites for the toluene disproportionation reaction in the presence of H_2S. The adsorption of H_2S on these Fe^{3+} species seems to produce the unique acidity required to the catalysis.

References

1) S. Hidaka, A. Iino, K. Nita, Y. Maeda, K. Morinaga, and N. Yamazoe, Proceedings of 7th International Zeolite Conference ed by Y. Murakami, A. Iijima, and J. W. Ward, Tokyo (1986), p. 329.

2) S. Hidaka, H. Shimakawa, A. Iino, T. Mibuchi, S. Nakay, and K. Nita, Ketjen Catalyst Symposium'86, H-9, 1986.

3) S. Hidaka, I. Iino, T. Mibuchi, K. Nita, and N. Yamazoe, *Chem. Lett.*, **1986**, 1213.

4) For example, R. L. Garten, W. N. Delgass, and M. Boudart, *J. Catal.*, **18**, 90 (1970).

5) H. Sano, "Mössbauer Spectroscopy," Koudan-sha Scientific (1972), p. 144.

6) W. N. Kundig, H. Bommel, G. Constabaris, and R. H. Lindquist, *Phys. Rev.*, **142**, 467 (1986).

7) K. Segawa, Y. Chen, J. E. Kubsh, W. N. Delgass. J. A. Dumesic, and W. K. Hall, *J. Catal.*, **76**, 112 (1982).

8) B. Wichterlova, *Zeolites*, **1**, 181 (1981).

9) P. P. Vaishnava, P. A. Montano, R. E. Tischer, and S. S. Pollack, *J. Catal.*, **78**, 454 (1982).

 © 1988 The Chemical Society of Japan Bull. Chem. Soc. Jpn., 61, 3175—3180 (1988)

Cobalt(III) Complexes with Quadridentate Ligands. VII.[1] The Preparation and Properties of the Salicylato or Dichloro[tris-(2-aminoethyl)amine]cobalt(III) Complexes and the Related Complexes

Eiko TOYOTA, Yutaka YAMAMOTO,† and Yoshihisa YAMAMOTO*
Faculty of Pharmaceutical Sciences, Higashi Nippon Gakuen University,
Ishikari-Tobetsu, Hokkaido 061-02
†Tohoku College of Pharmacy, Komatsushima, Sendai 983
(Received March 7, 1988)

Salicylato- or 3-methyl(or 4-methyl)salicylato[tris(2-aminoethyl)amine]cobalt(III) complexes, [Co(R-sal)tren]Cl·nH$_2$O (R: H, CH$_3$) have been prepared from a reaction mixture of dichloro[tris(2-aminoethyl)amine]cobalt(III) chloride hydrate, [CoCl$_2$(tren)]Cl·H$_2$O, Ag$_2$O, and salicylic acid or 3-methyl- or 4-methylsalicylic acid. Two geometrical isomers (*t*- and *p*-) of their complexes were separated by Dowex 50W-X2 column chromatography. Their *t*- and *p*-isomers have been established by their ^{1}H NMR and absorption spectra. The formation ratio of *t*- and *p*-isomers is ca. 3:1. The isomerization between *t*-isomer and *p*-isomer was not observed in water and methanol. In the absorption spectra, the first absorption band for the *t*- and *p*-isomers was observed at 535 nm and 515 nm, respectively. In the ^{1}H and ^{13}C NMR spectra of [CoCl$_2$(tren)]Cl·H$_2$O, the signals of the tertiary amine, $-\overset{|}{\underset{|}{N}}-$, side methylene protons and methylene carbons have been assigned to the individual methylene protons and methylene carbons of the coordinated tris(2-aminoethyl)amine ligand.

In this series, the previous papers[1,2] have been concerned with the preparation, properties, and NMR spectra of isomers such as the *cis*-β_1, β_2-salicylato- or salicylaldehydato(triethylenetetramine)cobalt(III) chloride hydrates. In the NMR spectra, the signals for center, NH$_2$- side, -NH- side, and =N- side methylene protons and carbons for the cobalt(III) complexes with quadridentate amine ligands have been assigned.[3,4] The signals for $-\overset{|}{\underset{|}{N}}-$ side methylene protons and carbons have, however, so far remained unsolved. Octahedral cobalt(III) complexes with a tris(2-aminoethyl)amine (abbreviation: tren) ligand are suitable for NMR studies. In addition, the coordinated tren ligand to a metal ion has a tripodal-type configuration, and is different from a linear-type configuration such as trien ligand. We are therefore interested in the difference between tren and trien complexes. Many tren cobalt(III) complexes have been reported with such aliphatic compounds as NH$_2$CH$_2$COOH,[5] CH$_3$SCH(CH$_3$)COOH,[6] CH$_3$SCH$_2$CH$_2$NH$_2$,[7] CH$_3$SeCH$_2$CH$_2$NH$_2$,[8] and their related compounds;[9,10] however, little is known about the preparation and properties of tren cobalt(III) complexes with the organic ligands such as salicylic acid,[2,3] salicylaldehyde,[1] 8-quinolinol,[11] and their related compounds.[12]

The present paper deals with the preparation and properties of *t*- and *p*-salicylato or 3-methyl(or 4-methyl)salicylato(tren)cobalt(III) complexes, [Co(R-sal)tren]Cl·nH$_2$O (R: H, CH$_3$); it deals with the assignments of the configuration of *t*- and *p*-isomers,[13] and of ^{1}H and ^{13}C chemical shifts of the $-\overset{|}{\underset{|}{N}}-$ side methylene protons and carbons for [CoCl$_2$(tren)]-Cl·H$_2$O and [Co(R-sal)tren]Cl·nH$_2$O (R: H, CH$_3$).

Experimental

Measurements. The ^{1}H and ^{13}C NMR spectra were recorded with an FX90Q apparatus (JEOL) and an FX-60 spectrometer (JEOL), respectively. The visible absorption spectra were recorded with a Shimadzu UV-210 recording spectrophotometer. The electric conductivities in aqueous solutions were determined by the use of a conductometric meter, CM-30 (Shimadzu), at room temperature. The melting points were measured on a MP-500D apparatus (Yanaco). The magnetic susceptibilities were measured at room temperature by Faraday's method using a magnetic balance (Shimadzu).

Preparation of Complexes. Dichloro[tris(2-aminoethyl)-amine]cobalt(III) Chloride Hydrate (1): This complex was prepared by the method of Kimura et al.[9]

Mixture of *t*- and *p*-Salicylato[tris(2-aminoethyl)-cobalt(III) Chloride Dihydrate: Complex **1** (10.0 g, 30.3 mmol) was added to moistend fresh Ag$_2$O, which was made from silver nitrate (10.4 g, 61.2 mmol) and potassium hydroxide (3.44 g, 61.3 mmol). The mixture was stirred for several minutes at room temperature, then 20 cm^3 of water was added to the mixture. The mixture was stirred for about 30 min at 60 °C. Thus the precipitated silver chloride was filtered off and washed with a small amount of water. To the reddish violet filtrate was added 4.2 g (30.4 mmol) of salicylic acid. The solution was stirred at 50 °C for 24 h, and concentrated on a rotary evaporator. The concentrated solution was injected into a column chromatograph on alumina. Upon elution with methanol–ethanol (1:1), the first reddish violet band was collected and concentrated on a rotary evaporator. Yield: 3.4 g (27.2%).

Separation of *t*-Salicylato[tris(2-aminoethyl)amine]cobalt-(III) Chloride Dihydrate (2) and *p*-Salicylato[tris(2-amino-ethyl)amine]cobalt(III) Chloride Dihydrate (3): The separation of complexes **2** and **3** from the mixture complex of 0.5 g was achieved by a column of ion-exchange resin (Dowex

50W-X2, Na^+ form, ϕ2.5×25 cm). Upon elution with 0.4 mol dm^{-3} NaCl, the effluent of the first reddish violet band (*t*-isomer) and that of the second red band (*p*-isomer) was collected and concentrated, respectively. The separated NaCl was removed. The purification for the *t*- and *p*-isomers was recrystallized from methanol-ether, respectively. Color: russet for **2**, red for **3**. Yields: 2.15 g (17.2%) for **2**, 0.8 g (6.4%) for **3**. Found **2**: C, 38.02; H, 6.51; N, 13.74; Cl, 8.88%. **3**: C, 38.11; H, 6.16; N, 13.71; Cl, 8.87%. Calcd for $CoC_{13}H_{26}N_4O_5Cl$ (MW 412.76) C, 37.83; H, 6.35; N, 13.57; Cl, 8.59%. Mp: 240 °C for **2**, 242 °C for **3**. Λ=130 for **2** and 110 S cm^2 mol^{-1} for **3** in water.

***t*-3-Methylsalicylato[tris(2-aminoethyl)amine]cobalt(III) Chloride Hydrate (4) and *p*-3-Methylsalicylato[tris(2-aminoethyl)amine]cobalt(III) Chloride Hydrate (5):** A mixture of complexes **4** and **5** has been prepared from a reaction mixture of **1** (10.0 g, 30.3 mmol), Ag_2O (7.02 g, 30.3 mmol) and 3-methylsalicylic acid (4.6 g, 30.2 mmol) according to the method used for complexes **2** and **3**. A separation for complexes **4** and **5** was achieved by using a column of ion-exchange resin (Dowex 50W-X2, Na^+ form, ϕ2.5×25 cm). Upon ellution with 0.2 mol dm^{-3} NaCl, the effluent of the first reddish violet band (complex **4**) and the second red band (complex **5**) was collected and concentrated on a rotary evaporator, respectively. The precipitated NaCl was removed by filtration. The purification for the *t*- and *p*-isomers was recrystallized from methanol-ether. Color: russet for **4**, red for **5**. Yields: 1.86 g (15.0%) for **4**, 0.58 g (4.7%) for **5**. Found **4**: C, 40.88; H, 6.52; N, 13.54; Cl, 8.91%. **5**: C, 40.92; H, 6.61; N, 13.84; Cl, 8.97%. Calcd for $CoC_{14}H_{26}N_4O_4Cl$ (MW 408.77) C, 41.14; H, 6.41; N, 13.71; Cl, 8.67%. Mp: 244 °C for **4**, 246 °C for **5**. Λ=125 for **4** and 113 S cm^2 mol^{-1} for **5** in water.

***t*-4-Methylsalicylato[tris(2-aminoethyl)amine]cobalt(III) Chloride Hydrate (6) and *p*-4-Methylsalicylato[tris(2-aminoethyl)amine]cobalt(III) Chloride Hydrate (7):** The preparation and separation for complexes **6** and **7** are attempted using the method for complexes **4** and **5**. Color: russet for **6**, red for **7**. Yields: 2.04 g (16.5%) for **6**, 0.45 g (3.6%) for **7**. Found **6**: C, 40.95; H, 6.62; N, 13.81; Cl, 8.82%. **7**: C, 40.85; H, 6.59; N, 13.66; Cl, 8.89%. Calcd for $CoC_{14}H_{26}N_4O_4Cl$ (MW 408.77) C, 41.14; H, 6.41; N, 13.71; Cl, 8.67%. Mp: 248 °C for **6**, 249 °C for **7**. Λ=115 for **6** and 110 S cm^2 mol^{-1} for **7** in water.

***t*-Salicylato[tris(2-aminoethyl)amine]cobalt(III) Nitrate Hydrate (8) and *p*-Salicylato[tris(2-aminoethyl)amine]cobalt(III) Nitrate (9):** Complexes **8** and **9** were prepared from the reaction mixture of silver nitrate (0.21 g, 1.24 mmol) and **2** or **3** (0.5 g, 1.21 mmol), respectively. They were recrystallized from methanol-acetone. Color: russet for **8**, red for **9**. Yields: 0.34 g (66.7%) for **8**, 0.36 g (73.8%) for **9**. Found **8**: C, 37.06; H, 6.02; N, 16.88%. Calcd for $CoC_{13}H_{24}N_5O_7$ (MW 421.30) C, 37.06; H, 5.74; N, 16.62%. Found **9**: C, 38.73; H, 5.45; N, 17.11%. Calcd for $CoC_{13}H_{22}N_5O_6$ (MW 403.29) C, 38.72; H, 5.50; N, 17.37%. Mp: 237 °C for **8**, 243 °C for **9**. Λ=106 for **8** and 114 S cm^2 mol^{-1} for **9** in water.

Solubility. Complexes **2**—**9** are very soluble in water and DMSO, and soluble in methanol but insoluble in the other common organic solvents such as acetone, ether, and benzene.

Results and Discussion

Dichloro[tris(2-aminoethyl)amine]cobalt(III) Chloride Hydrate (1): The ^1H NMR spectrum of **1** was measured in 1.8 mol dm^{-3} D_2SO_4. The signals at δ 2.5—3.9 and δ 4.6—5.7 of **1** were assigned to the methylene and amine protons of the coordinated tren ligand, respectively. The methylene protons of the coordinated tren ligand showed two signals at δ 2.50—3.03 (4H) and 3.03—3.90 (8H), as shown in Fig. 1. The signals at δ 2.50—3.03 at the highest field are assigned to the NH_2- side methylene protons[3] of the tren ligand. The signals at δ 3.03—3.90 have been assigned to the tertiary amine, $-\overset{|}{N}-$, side methylene protons. Two protons of the NH_2- side methylene protons at δ 2.50—3.03 overlapped with the $-\overset{|}{N}-$ side methylene protons of the tren ligand; this might be due to the electronic effect of the N(3)H_2 group, which is in a trans position for the Cl(1) ligand. Then, the

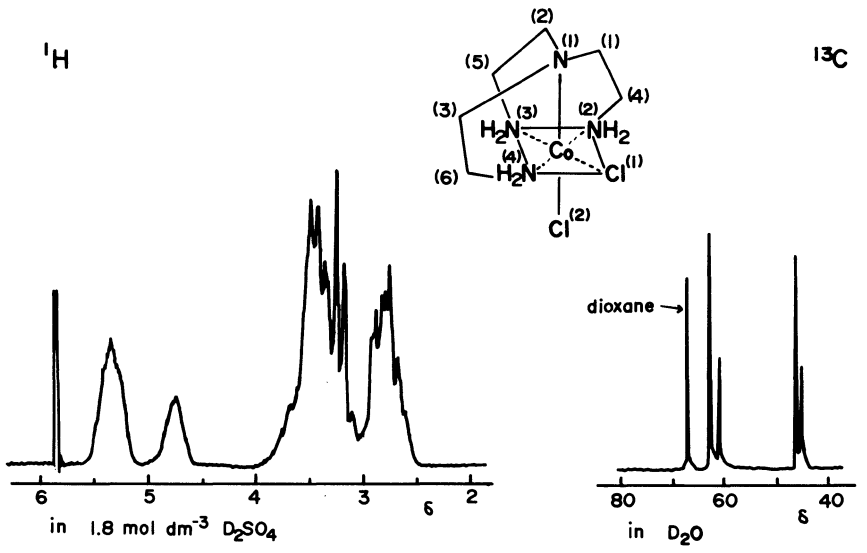

Fig. 1. The ^1H and ^{13}C NMR spectra of $[CoCl_2(tren)]Cl \cdot H_2O$.

methylene proton signals at δ 2.50—3.03 can be assigned to C(4)H_2 and C(6)H_2 protons, and those at δ 3.03—3.90 can be assigned to C(1)H_2, C(2)H_2, C(3)H_2, and C(5)H_2 protons.

The amine protons of the coordinated tren ligand showed two signals at δ 4.78 (2H) and 5.37 (4H), as shown in Fig. 1. The signal at δ 4.78 is assigned to the N(3)H_2 protons of the tren ligand in a position trans to the Cl(1) ligand. The signal at δ 5.37 is assigned to the N(2)H_2 and N(4)H_2 protons of the tren ligand in a position cis to the Cl(1) ligand. The above assignments were made in view of the following: studies of pentaammine(aniono)cobalt(III) ions, $[CoX(NH_3)_5]^{n+}$ (X: Cl, Br, OH···), have been reported by Buckingham,[14] Jolly,[15] Clifton,[16] who described that the chemical shift of the NH_3 group in a position trans to the electronegative atom (X) is at higher fields than those of NH_3 groups in a position cis to the electronegative atom.

The ^{13}C NMR spectrum of **1** was measured in D_2O. Both the signals at δ 45.4 and 46.6 are assigned to the NH_2- side methylene carbons[3] of the tren ligand, as shown in Fig. 1. The signals at δ 61.2 and 63.0 have been assigned to the -N< side methylene carbons. The methylene carbon signals at δ 45.4 and 61.2 are assigned to the C(5)H_2 and C(2)H_2 carbon, respectively, since both carbons are in a trans position for the Cl(1) ligand, and both carbon signals are smaller than those at δ 46.6 and 63.0. The signals at δ 46.6 and 63.0 are assigned to the C(4)H_2, C(6)H_2 and C(1)H_2, C(3)H_2, respectively.

Salicylato- or 3-Methyl(or 4-methyl)salicylato(tren)-cobalt(III) Chloride Hydrates (2—7): The abbreviations of the salicylato or 3-methyl(or 4-methyl)salicylato(tren)cobalt(III) complexes studied in this paper are listed in Table 1. The title complexes have *t*- and *p*-isomers, as shown in Fig. 2. A mixture of *t*- and *p*-salicylato(tren)cobalt(III) chloride dihydrate (**2**, **3**) or *t*- and *p*-3-methyl(or 4-methyl)salicylato(tren)-cobalt(III) chloride hydrate (**4**—**7**) has been isolated from a reaction mixture of complex **1**, Ag_2O, and salicylic acid or 3-methyl(or 4-methyl)salicylic acid. The separation of *t*- and *p*-isomers was attempted using an ion-exchange resin. The formation ratio of *t*- and *p*-isomers was ca. 3:1. The isomerization between *t*- and *p*-isomers is not observed in water and methanol. The corresponding nitrates (**8**, **9**) were prepared from the reaction mixture of complex **2** or **3** and silver nitrate, respectively. Complexes **2** and **3** were diamagnetic from the magnetic susceptibility. The electric conductivities for **2**—**9** in aqueous solutions were 106—130 S cm^2 mol^{-1}.

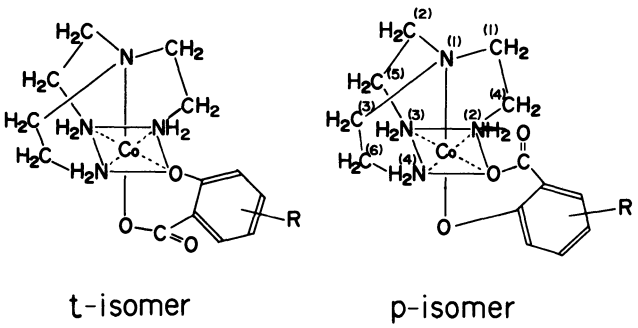

Fig. 2. Two geometrical isomers of [Co(R-sal)tren]-Cl·$n$$H_2O$ (R: H, CH_3).

In the ^1H NMR spectra, the signals at δ 2.5—4.0 and 4.6—5.3 of **2** and **3** were assigned to the methylene protons and the amine protons of the coordinated tren ligand, respectively, and the lowest field signals at δ 6.5—8.0 were assigned to the coordinated salicylato protons.[17] The methylene proton signals for the tren ligand in **2** are divided into two groups at the δ 2.6—3.1 and 3.1—4.0 regions. On the other hand, those for **3** are divided into three groups at the δ 2.5—2.8, 2.8—3.4, and 3.4—4.0 regions, as shown in Fig. 3. The methylene proton signals at δ 2.6—3.1 for **2** and at δ 2.5—2.8 for **3** are assigned to the NH_2- side methylene protons,[2,3] and those at δ 3.4—4.0 for **3** have been assigned to the -N< side methylene protons as shown in Table 2.

The amine protons for **2** showed one peak at δ 5.00, though those for **3** showed two peaks at δ 4.85 and 5.10 with an intensity ratio 2:1 as shown in Fig. 3. The signal at δ 4.85 of **3** is assigned to N(2)H_2 and N(3)H_2 protons, and that at δ 5.10 is assigned to the N(4)H_2 protons. The chemical shift (δ 4.85) of the proton signal of the NH_2 groups of **3** is at a higher field than that (δ 5.10) of **2**, i.e., the NH_2 group of **3** is considered to be at a position trans to the carboxyl oxygen of the coordinated salicylato ligand, which is more electronegative than the phenoxyl oxygen.[2,17] Thus, complexes **2** and **3** have been assigned to the *t*- and *p*-isomers, respectively. Also, the signals of the

Table 1. The Abbreviations of the (Methyl)salicylato(tren)cobalt(III) Complexes

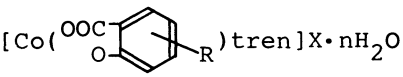

No.	2	3	4	5	6	7	8	9
Form	*t*	*p*	*t*	*p*	*t*	*p*	*t*	*p*
R	H	H	3-Me	3-Me	4-Me	4-Me	H	H
X	Cl	Cl	Cl	Cl	Cl	Cl	NO_3	NO_3
n	2	2	1	1	1	1	1	0

Table 2. ^1H and ^{13}C NMR Spectra of Complexes **2**—**9**

^1H Complex No. (isomer)	Tren δ			
	NH_2- side methylene protons	NH_2-+-N side methylene protons	-N side methylene protons	$N(3)H_2$ $N(2)H_2$ $N(4)H_2$
2 (*t*)	2.60—3.10(4H)	3.10—3.90(8H)		5.00(6H)
3 (*p*)	2.50—2.80(2H)	2.80—3.45(6H)	3.45—3.93(4H)	4.85(4H) 5.10(2H)
4 (*t*)	2.68—3.13(4H)	3.13—3.90(8H)		4.80(2H) 5.00(4H)
5 (*p*)	2.55—2.86(2H)	2.86—3.50(6H)	3.50—4.00(4H)	4.82(4H) 5.10(2H)
6 (*t*)	2.65—3.10(4H)	3.10—3.85(8H)		4.98(6H)
7 (*p*)	2.50—2.80(2H)	2.80—3.45(6H)	3.45—3.92(4H)	4.80(4H) 5.07(2H)
8 (*t*)	2.66—3.11(4H)	3.11—3.86(8H)		4.93(6H)
9 (*p*)	2.50—2.80(2H)	2.80—3.43(6H)	3.43—3.98(4H)	4.80(4H) 5.05(2H)

^1H Complex No. (isomer)	(Methyl)salicylato δ		Absorption band λ/nm (ε/cm^{-1} mol^{-1} dm^3)	
	ring protons	CH_3		
2 (*t*)	6.6—8.0(4H)	—	330(3000)	535(225)
3 (*p*)	6.6—7.9(4H)	—	332(3000)	515(210)
4 (*t*)	6.5—7.8(3H)	2.22(3H)	332(3200)	545(270)
5 (*p*)	6.5—7.8(3H)	2.34(3H)	335(3400)	515(230)
6 (*t*)	6.5—7.9(3H)	2.27(3H)	327(3300)	535(240)
7 (*p*)	6.5—7.8(3H)	2.30(3H)	330(3100)	515(220)
8 (*t*)	6.6—7.9(4H)	—	330(3000)	535(225)
9 (*p*)	6.5—7.9(4H)	—	332(3000)	515(210)

^{13}C Complex No.	Tren δ			
	NH_2- side methylene carbons		-N side methylene carbons	
	C(5)	[C(4), C(6)]	C(2)	[C(1), C(3)]
2	44.0	[45.4]	60.7	[61.4]
3	43.4	[45.2]	61.2	[61.5]
8	43.9	[45.4]	60.7	[61.3]
9	43.5	[45.4]	61.3	[61.6]

^{13}C Complex No.	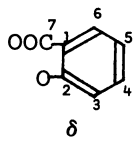 δ						
	C-1	C-2	C-3	C-4	C-5	C-6	C-7
2	118.8	167.9	117.3	134.6	123.6	132.6	174.0
3	117.4	167.7	117.0	134.6	124.7	132.4	174.6
8	118.7	167.9	117.3	134.6	123.6	132.6	174.0
9	117.5	167.7	117.0	134.6	124.8	132.5	174.6

Solvent and Standard: ^1H NMR spectra; 1.8 mol dm^{-3} D_2SO_4, internal DSS (δ=0), ^{13}C NMR spectra; D_2O, internal dioxane (δ=67.4), Absorption spectra; H_2O.

methylene protons of **3** are complicated signals compared with those of **2**. This can be due to the magnetic anisotropy between carbonyl oxygen of the coordinated salicylato ligand and methylene protons of the tren ligand, i.e., molecular models indicate that the carbonyl oxygen of the *p*-isomer has very near position for the methylene protons of the tren ligand, though that of the *t*-isomer has no such methylene protons around the carbonyl group. Also, the methylene protons for **3** showed two very sharp peaks in the δ 2.5—2.8 region, but those for **2** did not show the corresponding peaks. Thus, complexes **2** and **3** are assigned to the *t*- and *p*-isomers, respectively. In addition, a distinction between *t*- and *p*-isomers was found in the amine proton signals for **4** and **5**. The amine proton signal of **4** is different from those for **2** and **6**, but that for **5** is similar to those of **3** and **7** as shown in Fig. 3. This difference is attributed to the

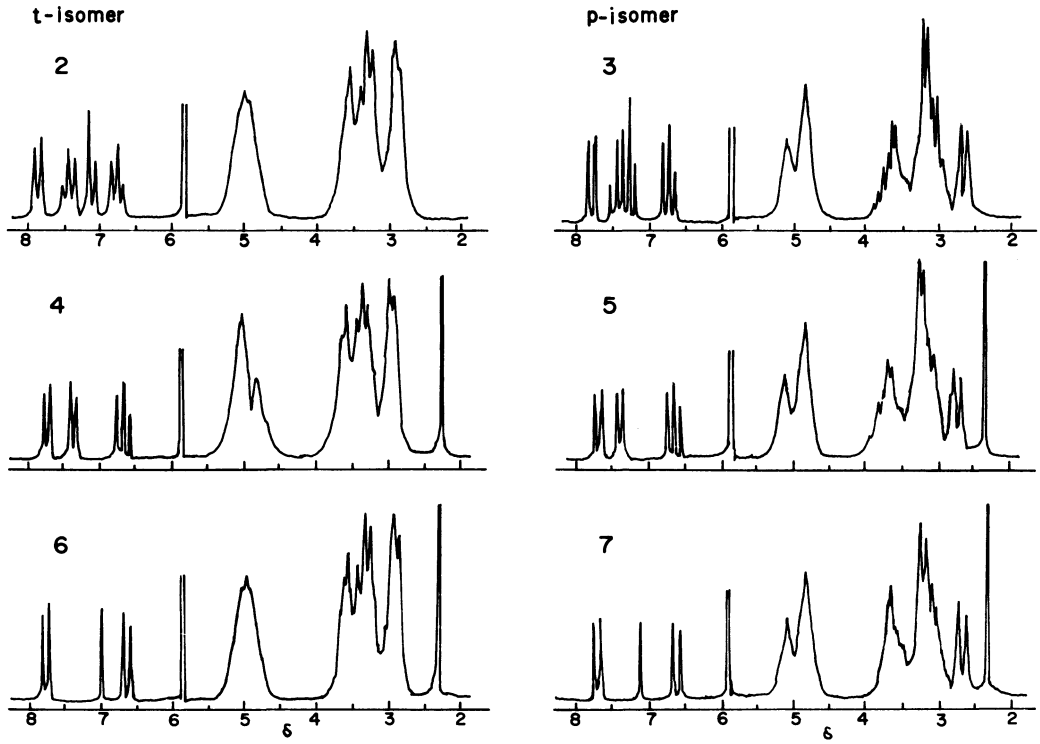

Fig. 3. The ^{1}H NMR spectra of complexes **2**—**7** in 1.8 mol dm^{-3} D_2SO_4.
2: *t*-[Co(sal)tren]Cl·2H_2O; **3**: *p*-[Co(sal)tren]Cl·2H_2O; **4**: *t*-[Co(3-Mesal)tren]Cl·H_2O; **5**: *p*-[Co(3-Mesal)tren]Cl·H_2O; **6**: *t*-[Co(4-Mesal)tren]Cl·H_2O; **7**: *p*-[Co(4-Mesal)tren]Cl·H_2O.

methyl group of the coordinated 3-methylsalicylato ligand. The methyl group of the 3-methylsalicylato ligand of **4** has the electronic effect to the phenoxyl oxygen, and the electronic state on the oxygen is a more electronegative, i.e., the amine protons split into two peaks. Accordingly, the N(3)H_2 group of **4** is considered to be at a position trans to the phenoxyl oxygen of the 3-methylsalicylato ligand. On the other hand, the N(3)H_2 group of **5** is considered to be at a position trans to the carboxyl oxygen from the results of the amine proton signals between **5** and **3**, **7**. Thus, complexes **4** and **5** have been assigned to the *t*- and *p*-isomers, respectively.

In the ^{13}C NMR spectra of complexes **2** and **3** in D_2O, there have been observed four signals for the coordinated tren ligand and seven signals for the coordinated salicylato ligand. The signals at δ 44.0, 45.4 for **2** are assigned to the NH_2– side methylene carbons. The signals at δ 60.7 and 61.4 for **2** have been assigned to the –N< side methylene carbons. The signals at δ 44.0 and 60.7 of **2** are assigned to the C(5) carbon and C(2) carbon, respectively, since both carbons are in the trans position for the phenoxyl oxygen, and their signals are smaller than those at δ 45.4 and 61.4. The signals at δ 45.4 and 61.4 are assigned to the C(4), C(6) and C(1), C(3) carbons, respectively. The distinction for *t*- and *p*-isomers is difficult from the results of the ^{13}C NMR spectra. The results of **3**, **8**, and **9** are collected in Table 2.

In the absorption spectra of complexes **2**—**7**, the absorption bands at ca. 330 nm for **2**—**7** were assigned to the specific absorption band.[3] The absorption bands at ca. 535 nm for **2**, **4**, and **6**, and those at 515 nm for **3**, **5**, and **7** were assigned to the first d–d absorption band ($^1T_{1g}\leftarrow{}^1A_{1g}$).[1] The first absorption bands of **2**, **4**, and **6** are at a longer wavelength than those of **3**, **5**, and **7**, respectively. This difference is agreement with that of the corresponding *cis*-β_1, β_2-salicylato- or 3-methyl(or 4-methyl)salicylato(trien)cobalt(III) complexes,[2,12] *cis*-β_1, β_2-[Co(R-sal)trien]Cl·*n*H_2O (R=H: β_1(**10**), β_2(**11**); R=3-CH_3: β_1(**12**), β_2(**13**); R=4-CH_3: β_1(**14**), β_2(**15**)). Thus, the NH_2 group of **3**, **5**, and **7** can be also considered to be at a position trans to the carboxyl oxygen of the coordinated salicylato ligand such as the *cis*-β_2 trien complexes (**11**, **13**, **15**). Also, the first absorption band (515 nm) of **5** is similar to those (515 nm) for **3** and **7**, but that (545 nm) of **4** is different from those (535 nm) for **2** and **6**, as is shown in Table 2. This can be due to the electronic effect of the methyl group of the coordinated 3-methylsalicylato ligand in complex **4** as previously described. Thus, complexes **2**, **4**, **6** and complexes **3**, **5**, **7** are assigned to *t*- and *p*-isomers, respectively.

The melting points, visible absorption spectra, colors of the solid state and solubilities of **2** and **3** are

almost similar to those of the trien complexes **10** and **11**. On the other hand, the isomerization between **2** and **3** is not observed, but complex **10** isomerizes to **11** in water at room temperature.

Some properties for complexes **2—9** are collected in Table 2 and the Experimental section.

References

1) Part VI: Y. Yamamoto, E. Toyota, and S. Tsukuda, *Bull. Chem. Soc. Jpn.*, **58**, 1595 (1985).
2) Y. Yamamoto and E. Toyota, *Bull. Chem. Soc. Jpn.*, **52**, 2540 (1979).
3) Y. Yamamoto, H. Kudo, and E. Toyota, *Bull. Chem. Soc. Jpn.*, **56**, 1051 (1983).
4) Y. Yamamoto and S. Tsukuda, *Bull. Chem. Soc. Jpn.*, **58**, 1509 (1985).
5) Y. Mitsui, J. Watanabe, Y. Harada, T. Sakamaki, Y. Iitaka, Y. Kushi, and E. Kimura, *J. Chem. Soc., Dalton Trans.*, **1976**, 2095.
6) M. Kojima and J. Fujita, *Bull. Chem. Soc. Jpn.*, **56**, 2958 (1983).
7) W. G. Jackson and A. M. Sargeson, *Inorg. Chem.*, **17**, 2165 (1978).
8) K. Nakajima, M. Kojima, and J. Fujita, *Chem. Lett.*, **1982**, 925.
9) E. Kimura, S. Young, and J. P. Collman, *Inorg. Chem.*, **9**, 1183 (1970).
10) M. Kojima and J. Fujita, *Bull. Chem. Soc. Jpn.*, **56**, 139 (1983).
11) Y. Yamamoto, E. Toyota, and Y. Yamamoto, *Bull. Chem. Soc. Jpn.*, **56**, 2721 (1983).
12) Y. Yamamoto, E. Toyota, and N. Mitsudera, *Bull. Chem. Soc. Jpn.*, **53**, 3517 (1980).
13) The designations *t* and *p* refer to the position of the carboxyl oxygen trans to a tertiary (*t*) or a primary (*p*) amine nitrogens of tren, respectively.
14) D. A. Buckingham, I. Olsen, and A. M. Sargeson, *Aust. J. Chem.*, **20**, 597 (1967).
15) W. L. Jolly, A. D. Jarris, and T. S. Briggs, *Inorg. Chem.*, **4**, 1064 (1965).
16) P. Clifton and L. Pratt, *Proc. Chem. Soc.*, **1963**, 339.
17) Y. Yamamoto, *Bull. Chem. Soc. Jpn.*, **51**, 2894 (1978).

 © 1988 The Chemical Society of Japan Bull. Chem. Soc. Jpn., 61, 3181—3186 (1988)

Voltammetric Study of Organic Metals. I. The Determination of the Electrochemical Conditions for Crystal Growth

Sachiko SAKURA, Hideo IMAI, Hiroyuki ANZAI,*,† and Tetsuo MORIYA†
Faculty of Pharmacy and Pharmaceutical Science, Fukuyama University,
Higashimura-cho, Sanzou 985, Fukuyama 729-02
†Electrotechnical Laboratory, 1-1-4 Umezono, Tsukuba, Ibaraki 305
(Received March 14, 1987)

The metallic crystals of organic charge-transfer complexes are grown by means of the electrolytic oxidation of tetrathiafulvalene (TTF) derivatives in the presence of trihalide anions in organic solvents. In order to obtain a crystal of good quality, the optimal conditions for the growth have been searched for based on the data on the cyclic voltammetry. In this paper, the electrochemical conditions, such as the oxidation potential, the stability of the donor monocation radicals, and the redox behavior of the anions under the oxidation potential of the donors, are discussed in relation to the chemical reactions proceeding in the solution during the crystal growth.

The metal-like crystals (organic metals) of organic charge-transfer complexes have various interesting characteristics, such as electrical[1] and optical[2] anisotropies and metal-insulator phase transitions.[3-5] Especially, some of the organic metals obtained from bis(ethylenedithio)tetrathiafulvalene (BEDT-TTF) and tetramethyltetraselenafulvalene (TMTSF) with several inorganic anions have been found to become superconductors at low temperatures,[6,7] so that numerous physicists and chemists have been concentrating their attention on the crystals of their organic charge-transfer complexes. Therefore, it is extremely important to establish a systematic way of growing crystals of good quality so as to explore their physical properties and develop a new category of electronic materials. There have appeared, hitherto, four methods of crystal growth; by means of slow cooling,[8] condensation,[9] diffusion,[10] and electrocrystallization.[11] The crystal growth of organic metals or superconductors, which are composed of organic donors and inorganic anions, has thus far been obtained mainly by the electrocrystallization. The electrocrystallization is carried out by the electrochemical oxidation of the donor in the presence of supporting electrolytes in various organic solvents.

There are many kinds of counter-anions used for the crystallization of organic metals. From among these, trihalide anions with a linear structure have now been investigated, because the chemical nature of the trihalides can be gradually changed from Cl_3^- to I_3^- depending on the combination of the components.

Usually, an electrolytic reaction in a solution has been controlled under constant-current conditions (not under constant voltage conditions). However, it has not yet been clarified whether or not the crystal growth has thereby been carried out under optimal conditions, since the chemical reactions occurring at the electrodes are complicated. This problem will be discussed in this paper based on the data obtained by the cyclic voltammetry (CV) of the donors (D) and the trihalide anions (X^-).

Experimental

Electrochemical Measurement. The measurement of CV was carried out with a Fuso 312 polarograph and a Hokuto HB-104 function generator. The working and counter electrodes were a platinum disk (2 mmϕ) and a platinum wire (0.5 mmϕ, 3 cm) respectively. The supporting electrolyte was 0.1 M (M=mol dm^{-3}) tetrabutylammonium perchlorate (Bu_4NClO_4). An aqueous SCE was used as a reference electrode with a salt bridge of 0.1 M Bu_4NClO_4 dissolved in organic solvents. The measuring temperature was controlled at 25±0.1 °C. Tetrahydrofuran (THF) and benzonitrile (BN) were chosen as convenient solvents for CV, because in them both the donors and the supporting electrolyte were easily dissolved. When THF was used as a solvent, nitrogen gas saturated beforehand with a THF vapor was bubbled in order to remove the dissolved oxygen.

Crystal Growth. All the crystal-growth procedures employed were similar to the following example. 0.13 mmol (BEDT-TTF) was electrolytically oxidized in a 60-ml THF solution, in which 0.52 mmol Bu_4NI_3 had been dissolved, under a controlled current of 1 μA at 20 °C. The electrolysis was performed under an atmosphere of nitrogen gas. The working electrode was separated with a porous glass plate from the counter electrode; both were of platinum. The period of crystal growth was about 1—1.5 months.

Reagents. The TMTSF was purchased from Japan Carlit Co., Ltd. The TTF, BEDT-TTF, tetrakismethylthiotetrathiafulvalene (TMT-TTF), and bis(trimethylenedithio)tetrathiafulvalene (BTDT-TTF) were obtained from Tokyo Kasei Co., Ltd. The tetramethyltetrathiafulvalene (TMTTF) was synthesized by the coupling of 4,5-dimethyl-1,3-dithiolium perchlorate.[12] The Bu_4NX (X=Br_2Cl, $BrCl_2$, and Cl_3) were obtained from Tokyo Kasei Co., Ltd. The other tetrabutylammonium trihalides were synthesized by the addition reaction of tetrabutylammonium halides and halogens.[13,14] The donors and the supporting electrolytes were purified by recrystallization. The THF was purified as follows: powdered iron(II) sulfate was added to the solvent, and the mixture was stirred; if the color of the powder turned from green to brown, the old powder was replaced with a new one. This treatment was repeated until the green coloring of iron(II) persisted. Then the powder was removed

by filtration. The solvent was dehydrated by adding NaOH pellets for 12 hours. The solvent was then filtered and distilled. BN was purified as follows: After the solvent had been dried by adding powdered phosphorous pentoxide for 12 hours, the desiccant was removed by decantation; powdered anhydrous sodium carbonate was then added to the solvent, and the mixture was stirred for 3 hours. The solvent was filtered and distilled under a reduced pressure.

Results and Discussion

In the electrolytic crystallization, organic metals can be grown from the de-electronated D^+ and the dissolved X^-. In this process, information on the oxidation potential of D to D^+, the stability of D^+, and the electronic state of X^- at the oxidation potential of D is essential in order to obtain good crystals. Therefore, the electrolytic oxidation and reduction behavior of D and X^- have been studied in detail with CV.

If the electron-transfer process at the electrode is reversible, the oxidation potential (E_p^o) obtained by means of CV is more positive by $28.5/n$ mV than the standard oxidation potential (E^o), where n is the number of participating electrons.[15] On the other hand, the E_p^o value of the irreversible process shifts toward more positive values than that of the reversible case, depending on degree of irreversibility. The E_p^o value for irreversible cases is, therefore, only a semi-quantitative measure of the oxidizability. If both the oxidation peak and the re-reduction peak are observable, the mean value of these two peaks, $E^{o'}$, can be conveniently used as the effective potential, which is near E^o.

Electrolytic Oxidation of D. Generally, the electrode reaction of TTF derivatives occurs as a two-step oxidation process; in the first step, one electron is transferred, and then the second electron is transferred. The corresponding reduction processes occur in the reversed way:[16]

$$D \underset{+e,\ E_p^{r1}}{\overset{-e,\ E_p^{o1}}{\rightleftharpoons}} D^+ \underset{+e,\ E_p^{r2}}{\overset{-e,\ E_p^{o2}}{\rightleftharpoons}} D^{2+} \quad (1)$$

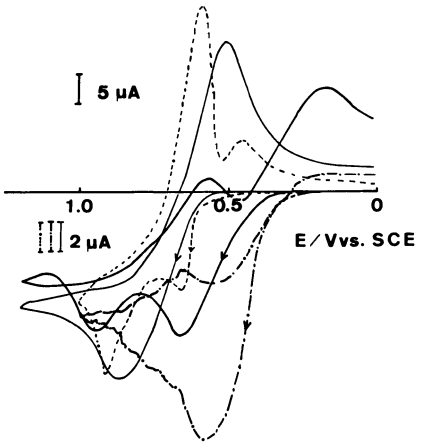

Fig. 1. Cyclic voltammograms of the donors in THF; 20 mV s^{-1}.
——: 5.88 mM TTF, —·—·—; 3.48 mM TMTTF, ——: 2.40 mM TMT-TTF, ·····: 2.20 mM BTDT-TTF.

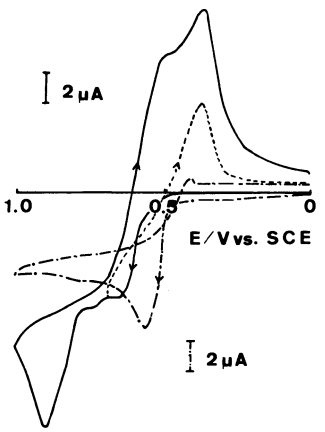

Fig. 2. Cyclic voltammograms of the donors in THF; 20 mV s^{-1}.
——: 1.13 mM BEDT-TTF, —·—·—: 1.26 mM TMTSF.

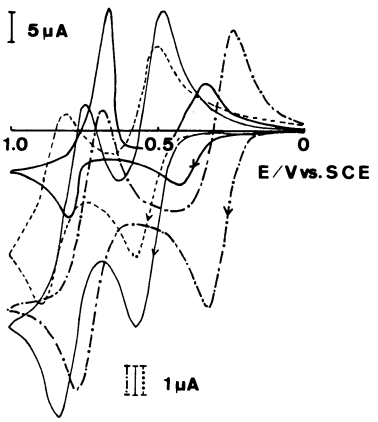

Fig. 3. Cyclic voltammograms of the donors in BN; 20 mV s^{-1}.
——: 2.77 mM TTF, —·—·—: 2.05 mM TMTTF, ——: 2.83 mM TMF-TTF, ·····: 1.62 mM BTDT-TTF.

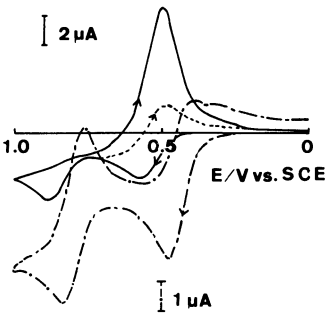

Fig. 4. Cyclic voltammograms of the donors in BN; 20 mV s^{-1}.
——: 1.25 mM BEDT-TTF, —·—·—: 1.41 mM TMTSF.

Table 1. Electrochemical Data of Various Donors (E/V vs. SCE, 20 mV s^{-1})

Solvent	Donor	E_p^{o1} $D \rightarrow D^+$	E_p^{o2} $D^+ \rightarrow D^{2+}$	$E^{o'}$	$\lvert E_p^{r1} - E_p^{o1} \rvert = \Delta E$	i_p^{r1}/i_p^{o1}	$\lvert E_p^{o1} - E_p^{o2} \rvert = \Delta E_p$
THF	TTF	0.67	0.95	0.44	0.47	0.79	0.28
	TMTTF	0.59	0.75[a]	0.40	0.39	b)	0.16
	TMT-TTF[c]	0.88	d)	0.71	0.35	0.86	—
	BEDT-TTF	0.65	0.90	0.51	0.29	0.63	0.25
	BTDT-TTF	0.66	0.91	0.58	0.16	0.09	0.25
	TMTSF	0.56	0.80	0.47	0.18	0.40	0.24
BN	TTF	0.43	0.79	0.39	0.09	1.00	0.36
	TMTTF	0.32	0.77	0.28	0.08	1.00	0.45
	TMT-TTF	0.57	0.83	0.53	0.08	0.88	0.26
	BEDT-TTF	0.57	0.84	0.51	0.13	0.63	0.27
	BTDT-TTF	0.58	0.89	0.54	0.08	0.79	0.31
	TMTSF	0.48	0.84	0.44	0.08	0.53	0.36

a) Shoulder. b) Very small value. c) The adsorption on the electrode was very strong. d) No wave was found until 1.2 V.

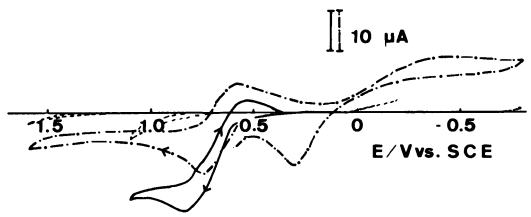

Fig. 5. Cyclic voltammograms of Bu_4NI_3; 20 mV s^{-1}. ——: 8.4 mM Bu_4NI_3 in THF, —·—·—: 6.5 mM Bu_4NI_4 in BN, ·····: blank.

Figures 1—4 show the CV measurements for TTF derivatives; the results are summarized in Table 1. It may be noted that the value of $\Delta E(=\lvert E_p^{o1} - E_p^{r1} \rvert)$ is the measure of the reversibility, which should be ≈60 mV for a reversible one-electron transfer process. In BN, the donors were oxidized quasi-reversibly to monocations ($\Delta E \approx 80$ mV). On the contrary, in THF, the donors were irreversibly oxidized; ΔE varies from 0.47 V to 0.16 V with an increase in the molecular weights of the donors. Though the irreversible reactions were carried out in THF, $E^{o'}$ can be obtained since re-reduction peaks were observed. It can be readily estimated whether or not the oxidation reaction really occurs under the applied potential from the E_p^{o1}, E_p^{o2}, and $E^{o'}$ values in Table 1. It seems that the pair of TMTTF and TMTSF, and the pair of BEDT-TTF and BTDT-TTF, which have very similar structures to each other, give similar CV profiles and similar oxidation potentials. No meaningful correlation of E_p^{o1} with the molecular weight of donors is found, however, as is plotted in Fig. 6.

In the electrolytic crystal growth, the applied potential should not exceed E_p^{o2} if only D^+ is to be generated in the solution.

The instability of D^+ can be judged from the CV data based on the following two viewpoints: i) If the ΔE value is large and the re-reduction peak is much distorted, or if the ratio of i_p^{r1}/i_p^{o1} is extremely small, then D^+ is chemically unstable and can easily be

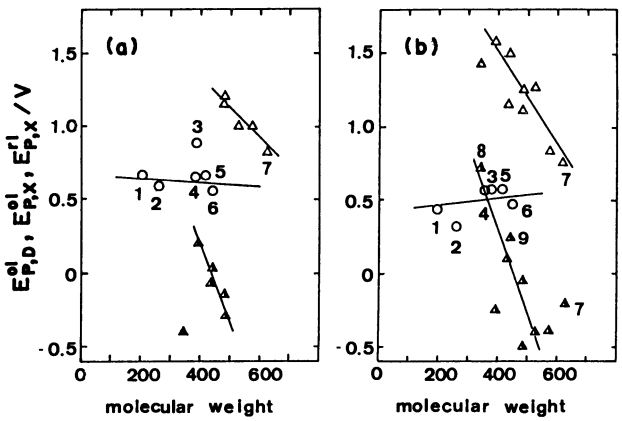

Fig. 6. Plots of E_p^{o1} of D, and $E_{p,X}^{o1}$ and $E_{p,X}^{r1}$ of X^- vs. the molecular weight. (a), in THF; (b), in BN. (○), $E_{p,D}^{o1}$; (△), $E_{p,X}^{o1}$; (▲), $E_{p,X}^{r1}$ 1: TTF, 2: TMTTF, 3: TMT-TTF, 4: BEDT-TTF, 5: BTDT-TTF, 6: TMTSF, 7: I_3^-, 8: Cl_3^-, 9: $BrCl_2^-$.

changed to other products. Therefore, most of the D^+ in BN are stable, while most of the D^+ in THF are unstable (Table 1). ii) D^+ is oxidized further to D^{2+} under relatively high potentials. If the value of $\Delta E_P(=\lvert E_p^{o1} - E_p^{o2} \rvert)$ is large, the proportionation reaction:

$$D^{2+} + D \rightarrow 2D^+ \qquad (2)$$

proceeds to the right and the D^{2+} will be transformed to D^+. Therefore, most of the D^{2+} in BN may be changed to D^+, while some of the D^{2+} in THF seem to persist in the solution and may become a cause of crystal defects or disorders.

Electronic State of Trihalide Anions in the Solution. As for the electrolytic crystal growth, the applied potential (E) must be an intermediate value between the oxidation peak potential ($E_{p,X}^{o1}$) and the reduction peak potential ($E_{p,X}^{r1}$) of X^- in order to keep X^- unchanged in the solution; of course, E should be more positive than the oxidation peak potential of D, $E_{p,D}^{o1}$, to generate D^+. Typical voltammograms for I_3^-

are shown in Fig. 5, while the results are summarized in Table 2. Figure 6 presents the plots of $E^{o1}_{p,X}$ and $E^{r1}_{p,X}$ vs. the molecular weight (MW) of the trihalide anions. The oxidation and reduction potentials of X^- decrease with an increase in the MW of trihalide anions; this can reasonably be understood by considering that the oxidation potential of halide anions decreases with an increase in MW, as $Cl^->Br^->I^-$ (Table 3). In Fig. 6 the plots of $E^{o1}_{p,D}$ vs. MW are also shown. Most trihalide anions were stable under the oxidation potential of D, except for the following cases.

Exception 1: When TMT-TTF is electrolytically oxidized in a THF solution containing I_3^-, the crystal growth is difficult, for such by-products from I_3^- as I_2 are produced[17]; the E_p^{o1} of TMT-TTF in THF is more positive than the E_p^{o1} of I_3^-. In a BN solution, Cl_3^- is reduced easily under the oxidation potential of the donors.

Exception 2: Generally, trihalide anions composed of lighter elements more easily decomposed in the organic solvent. Figure 7a shows the decomposition of $BrCl_2^-$ in THF. The reduction wave detected at 0.20 V in the first scan gradually decreased upon the repeated scanning, and eventually it disappeared. Moreover, a new oxidation wave appeared at 0.7 V on the disappearance of the yellow coloring in the solution; this new wave corresponds to the oxidation of Br^- (Table 3). These results suggest that $BrCl_2^-$ decomposes to other products containing Br^-. Since Cl_3^- is extremely unstable, the CV measurement in THF was difficult. Figure 7b shows such a situation; the CV peaks disappeared very rapidly on successive scannings. Figure 8 shows the change in the UV absorption spectra of Bu_4NCl_3 in THF after the dissolution of the reagent in the solution; the decrease in the absorption spectra may show the decomposition of Cl_3^- to Cl_2 and Cl^-, since the addition of Cl^- was found to suppress the change.

Table 2. Oxidation and Reduction Peak Potentials of Trihalide Anions (E/V vs. SCE, 20 mV s^{-1})

X^- of $Bu_4N^+X^-$	in THF		in BN	
	E_p^{o1}	E_p^{r1}	E_p^{o1}	E_p^{r1}
I_3^-	0.83	—	0.75	−0.20
I_2Br^-	1.00	—	0.83	−0.38
IBr_2^-	1.00	—	1.28	−0.40
$IBrCl^-$	1.20	−0.30	1.25	−0.50
ICl_2^-	b)	0.02	1.50	0.25
Br_3^-	1.15	−0.15	1.11	−0.05
Br_2Cl^- [a]	b)	−0.07	1.15	0.10
$BrCl_2^-$ [a]	b)	0.20[a]	1.58	−0.24
Cl_3^- [a]	b)	−0.40[a]	1.44	0.72

a) Very unstable and easily decomposed. b) More positive than 1.2 V.

Table 3. Oxidation Peak Potentials of Halide Anions (E/V vs. SCE, 20 mV s^{-1})

X^- of $Bu_4N^+X^-$	in THF E_p^{o1}	in BN E_p^{o1}
I^-	0.37	0.32
Br^-	1.00	0.72
Cl^- [a]	—	1.35

a) The adsorption on the electrode was very strong.

Crystal-Growth Conditions. As a typical case, we have carried out the electrocrystallization from BEDT-TTF and trihalide ions under constant current conditions; the results are summarized in Table 4.

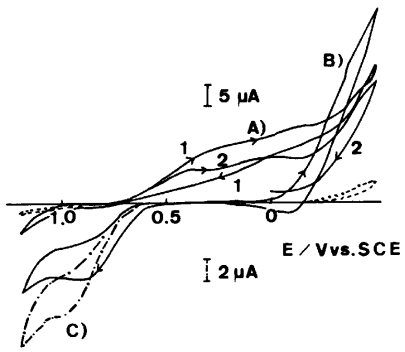

Fig. 7a. Cyclic voltammograms of 11.5 mM Bu_4NBrCl_2 in THF; 20 mV s^{-1}. (A), The yellow solution: the first scan 1) and the second scan 2); (B), after the color of the solution disappeared; (C), the voltammogram of 5.7 mM Bu_4NBr in THF.
·····: blank.

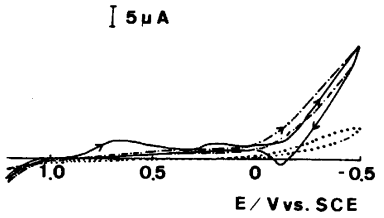

Fig. 7b. Cyclic voltammograms of 7.4 mM Bu_4NCl_3 in THF; 20 mV s^{-1}.
——: the first scan, —·—·—: the second scan, ·····: blank.

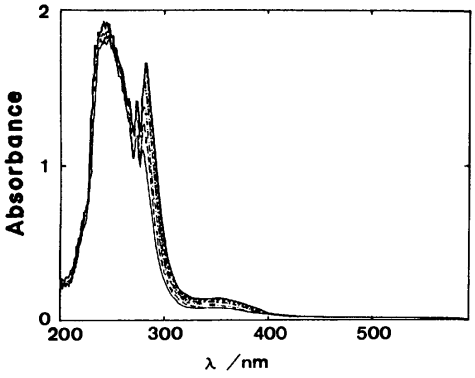

Fig. 8. UV absorption spectra of 0.76 mM Bu_4NCl_3 in THF (Time is in minute after dissolution of the salt).
——: 0 min, ·····: 1.65 min, —·—·—: 5.07 min, —·—·—: 10.07 min, ·····: 14.57 min, ——: 22.40 min.

Table 4. Results of the Electrocrystallization of BEDT-TTF with Trihalides[a]

X^- of $Bu_4N^+X^-$	In THF				In BN			
	day	i/μA	E/V	Size[b] /mm×mm	day	i/μA	E/V	Size[b] /mm×mm
I_3^-	29	1.0	1.0	3.5×1.5	40	1.0	1.2	2.0×2.0
I_2Br^-	44	1.0	1.0	3.0×2.5	33	1.0	0.2	3.3×2.0
IBr_2^-	44	2.0	1.0	4.0×1.1	45	1.0	0.3	8.9×1.9
$IBrCl^-$	54	1.0	0.3	Powder	32	1.0	0.2	1.4×0.1
ICl_2^-	49	1.0	0.3	1.9×0.3[c]	32	1.0	0.1	Powder
Br_3^-	17	1.0	0.2	Powder	—			d)
Br_2Cl^-	—			d)	—			d)
$BrCl_2^-$	—			d)	—			d)
Cl_3^-	—			d)	—			d)

a) The data are taken from *Synth. Met.*, **19**, 611 (1987). b) The thickness is not measured. c) Only at the bottom of the crystal-growth cell. d) No crystals were obtained.

When the current was set at 1 μA, the apparent voltage between the two electrodes[11] became 0.3—1.2 V, depending on the D, the X^-, and the solvents. Because our cells for the electrocrystallization had been prepared so as to obtain a crystal of the highest purity and to avoid any impurities such as water molecules diffused from the reference electrode, it is practically impossible to introduce a reference electrode to measure the rigorous potential at each electrode. In spite of such a restriction on the experimental system, from our experimental results we can derive some conclusions that are essential to the crystal growth of the BEDT-TTF complexes.

As is shown in Table 4, we could not obtain any trace of the crystal from BEDT-TTF with Cl_3^-, $BrCl_2^-$, and Br_2Cl^- in either THF or BN, or with Br_3^- in BN. This result is reasonably explained by the above-mentioned unstable nature of the trihalide anions composed of lighter halogens, which leads to the production of Cl_2 and Br_2 by their decomposition. Before BEDT-TTF is electrolytically oxidized, these dihalogen molecules react with BEDT-TTF and/or the solvent; moreover, unnecessary oxidation and reduction reactions occur in the solution, which prevent the formation of the aimed-at crystals.

In the case of a BEDT-TTF–I_3^- system in THF, crystals of a good quality and a proper size were obtained, whereas in the case of a TMT-TTF–I_3^- system, it was difficult to obtain crystals,[18] possibly because of the oxidation of I_3^- in THF under the oxidation potential of TMT-TTF. On the other hand, in the case of the TMT-TTF–I_3^- system in BN, the crystal growth was very difficult,[18] although I_3^- is electrolytically stable in BN. The reason for this must be left to a forthcoming study.

Summary

The electrolytic oxidation and reduction behavior of donors (D=TTF, TMTTF, TMT-TTF, BEDT-TTF, BTDT-TTF, and TMTSF) and trihalide anions (X^-=I_3^-, I_2Br^-, IBr_2^-, $IBrCl^-$, ICl_2^-, Br_3^-, Br_2Cl^-, $BrCl_2^-$, and Cl_3^-) in organic solvents (THF and BN) were clarified by means of cyclic voltammetry.

It was found that 1) radical cations (D^+) of most of the donors were stable in BN, but unstable in THF, and 2) most trihalide anions (X^-) were stable under the oxidation potential of D, with a few exceptions.

The authors gratefully acknowledge the help of Dr. Madoka Tokumoto for his critical reading of the manuscript. This work was supported by the "R and D Project of Basic Technology for Future Industries" of the Ministry of International Trade and Industry, Agency of Industrial Science and Technology.

References

1) T. Ishiguro, S. Kagoshima, and H. Anzai, *J. Phys. Soc. Jpn.*, **41**, 351 (1976).

2) D. B. Tanner, C. S. Jacobsen, A. F. Garito, and A. J. Heeger, *Phys. Rev. B*, **15**, 3381 (1976).

3) S. Kagoshima, T. Ishiguro, and H. Anzai, *J. Phys. Soc. Jpn.*, **41**, 2061 (1976).

4) C. Coulon, P. Delhaes, S. Flandrois, R. Lagnier, E. Bojour, and J. M. Fabre, *J. Phys.*, **43**, 1059 (1982).

5) R. Brusetti, R. Ribault, D. Jerome, and K. Bechgaard, *J. Phys.*, **43**, 801 (1982).

6) E. B. Yagubskii, I. F. Shchegolev, V. N. Laukhin, P. A. Kononovich, A. V. Kartsovnik, A. V. Zvarykina, and L. I. Buravov, *Pis'ma Zh. Eksp. Teor. Fiz.*, **39**, 12 (1984).

7) K. Bechgaard, K. Carneiro, M. Olsen, F. B. Rasmussen, and C. S. Jacobsen, *Phys. Rev. Lett.*, **46**, 852 (1981).

8) C. S. Jacobsen, J. R. Anderson, K. Bechgaard, and C. Berg, *Solid State Commun.*, **19**, 1209 (1976).

9) L. I. Buravov, O. N. Eremenko, R. B. Lyubovskii, L. P. Rosenberg, M. L. Khidekel, R. P. Shibaeva, I. F. Shchegolev, and E. B. Yagubskii, *JETP Lett.*, **20**, 208 (1974).

10) H. Anzai, *J. Cryst. Growth*, **33**, 185 (1976).

11) H. Anzai, T. Moriya, K. Nozaki, T. Ukachi, and G. Saito, *J. Phys.*, **44**, 1195 (1983).

12) J. P. Ferraris, T. O. Poehler, A. N. Bloch, and D. O. Cowen, *Tetrahedron Lett.*, **1973**, 2553.

13) A. I. Popov and R. F. Swensen, *J. Am. Chem. Soc.*, **77**, 3724 (1955).

14) H. Anzai, M. Tokumoto, T. Ishiguro, G. Saito, H. Kobayashi, R. Kato, and A. Kobayashi, *Synth. Met.*, **19**, 611

(1986).
15) H. Matsuda and Y. Ayabe, *Z. Electrochem.*, **59**, 495 (1955).
16) D. L. Coffen, J. Q. Chambers, D. R. Williams, P. E. Carrett, and N. D. Canfield, *J. Am. Chem. Soc.*, **93**, 2258 (1971).
17) C. K. Mann and K. K. Barnes, "Electrochemical Reactions in Nonaqueous Systems," Marcel Dekker, New York (1970), p. 498.
18) H. Anzai, unpublished results.

Molecular Structures of *cis*-[Co(CN)$_2$(acac)(dppe)] and *trans*(*C*,*N*)-[Co(CN)$_2$(acac)(edpp)]·H$_2$O and Trans Influence of Phosphine and Cyanide Ligands

Masakazu KITA, Kazuo KASHIWABARA, and Junnosuke FUJITA*
Department of Chemistry, Faculty of Science, Nagoya University, Chikusa-ku, Nagoya 464
(Received March 28, 1988)

Molecular structures of *cis*-[Co(CN)$_2$(acac)(dppe)] (**a**) and *trans*(*C*,*N*)-[Co(CN)$_2$(acac)(edpp)]·H$_2$O (**b**) have been determined by X-ray analysis, where acac, dppe, and edpp denote an acetylacetonate ion, 1,2-bis(diphenylphosphino)ethane and (2-aminoethyl)diphenylphosphine, respectively. Crystal data for **a**: monoclinic, $P2_1/a$, a=13.975(2), b=19.709(2), c=11.575(2) Å, β=109.71(1)°, V=3001.5(6) Å^3, Z=4, and R=0.049. Crystal data for **b**: monoclinic, $P2_1/c$, a=17.870(3), b=7.354(2), c=16.709(3) Å, β=105.45(2)°, V=2116.5(5) Å^3, Z=4, and R=0.056. The Co–O bonds trans to the phosphine and the cyanide ligands are longer, respectively, by ca. 0.06—0.08 Å and ca. 0.03—0.05 Å than those usually found in Co(III)-acac complexes such as [Co(acac)$_3$], indicating stronger trans influence of the former than the latter.

X-Ray structural studies of non-organocobalt(III)-phosphine complexes have been reported for [Co(O$_2$)-{(C$_6$H$_5$)$_2$PCHCHP(C$_6$H$_5$)$_2$}$_2$]$^+$,[1] [{P(CH$_3$)$_2$(C$_6$H$_5$)}$_2$(CN)-(O$_2$)Co(μ-CN)Co(CN)$_2${P(CH$_3$)$_2$(C$_6$H$_5$)}$_3$],[2] [Co(NCS)$_3$-{P(CH$_3$)$_3$}$_3$],[3] a number of bis(dimethylglyoximato)-cobalt(III) complexes containing unidentate phosphine ligands,[4] and a number of diphosphine-[5-8] and aminoalkylphosphine-cobalt(III) complexes[9-14] prepared in our laboratory. In this paper we have determined crystal structures of two cyanide-phosphine mixed ligand complexes of cobalt(III), [Co-(CN)$_2$(acac)(dppe)] and [Co(CN)$_2$(acac)(edpp)]. The complexes contain cyanide and phosphine ligands both of which give trans influence to many metal ions,[15] although the influence of the cyanide ligand in a cobalt(III) complex is not made clear.[15-21] The complexes studied here are suitable for examining trans influence of cyanide and phosphine ligands, since the magnitudes of influence can be compared within one complex molecule.

Experimental

X-Ray Analysis. ***cis*-[Co(CN)$_2$(acac)(dppe)].** The complex was prepared in a previous work.[22] Crystal data: monoclinic, $P2_1/a$, a=13.975(2), b=14.709(2), c=11.575(2) Å, β=109.71(1)°, V=3001.5(6) Å^3, Z=4, D_x=1.35 g cm^{-3}, D_m=1.36 g cm^{-3}, μ(Mo $K\alpha$)=7.055 cm^{-1}. An orange crystal of approximate dimensions 0.45×0.25×0.175 mm^3 was wrapped up in thin wax to protect it from moisture and used for X-ray work. Diffraction data were collected on a Rigaku AFC-5R diffractometer with graphite monochromatized Mo $K\alpha$ radiation (λ=0.71069 Å). Within the range $2\theta<60°$, 4006 independent reflections with $|F_o|>3\sigma(|F_o|)$ were obtained. No absorption correction was applied.

Calculations for the structure analysis were performed on a HITAC M-680H computer at the Computer Center of the Institute for Molecular Science with the Universal Crystallographic Computation Program System UNICS III.[23] Atomic scattering factors of neutral atoms were used.[24] The structure was solved by the usual heavy-atom method: The position of the cobalt atom was picked up by means of the

Table 1. Positional Parameters (×10^4) and Equivalent Isotropic Temperature Factors (Å^2) of [Co(CN)$_2$(acac)(dppe)] (**a**)

Atom	x	y	z	B_{eq}	Atom	x	y	z	B_{eq}
Co	1707.2(4)	1573.0(3)	9530.8(5)	2.8	C(124)	1925(4)	3689(3)	6325(5)	5.8
P(1)	2287(1)	1838(1)	8031(1)	2.8	C(125)	2344(4)	3146(2)	7113(4)	4.4
P(2)	3224(1)	1917(1)	10867(1)	2.9	C(21)	4062(3)	1223(2)	11605(4)	3.4
O(1)	1139(2)	1346(1)	10811(3)	3.5	C(22)	3263(3)	2466(2)	12149(4)	3.5
O(2)	2246(2)	669(1)	9515(3)	3.3	C(23)	3847(3)	2384(2)	9948(4)	3.4
N(1)	−364(3)	1202(2)	7659(4)	5.2	C(211)	3754(4)	813(2)	12378(4)	4.3
N(2)	1081(3)	3033(2)	9598(4)	4.3	C(212)	4318(4)	254(3)	12928(5)	5.8
C(1)	412(3)	1348(2)	8335(4)	3.5	C(213)	5188(5)	80(3)	12716(5)	6.8
C(2)	1299(3)	2482(2)	9557(4)	3.0	C(214)	5513(5)	493(4)	11973(6)	8.4
C(11)	2198(3)	1213(2)	6839(4)	3.6	C(215)	4952(4)	1062(3)	11398(5)	6.1
C(12)	1748(3)	2586(2)	7120(4)	3.1	C(221)	4120(4)	2843(3)	12722(4)	4.9
C(13)	3663(3)	1991(2)	8735(4)	3.5	C(222)	4180(5)	3243(3)	13738(5)	6.3
C(111)	1636(4)	618(3)	6729(5)	5.5	C(223)	3393(5)	3258(3)	14176(5)	6.0
C(112)	1576(5)	187(3)	5732(6)	7.7	C(224)	2539(4)	2884(3)	13623(5)	6.0
C(113)	2063(5)	345(3)	4925(5)	7.6	C(225)	2467(4)	2491(3)	12599(4)	5.2
C(114)	2622(5)	928(3)	5060(6)	7.7	C(31)	2517(4)	−498(2)	9891(5)	5.3
C(115)	2702(4)	1378(3)	6020(5)	5.9	C(32)	2018(3)	153(2)	10038(4)	3.6
C(121)	730(3)	2562(3)	6381(4)	4.6	C(33)	1374(3)	150(2)	10750(4)	3.7
C(122)	326(4)	3109(3)	5606(5)	5.7	C(34)	992(3)	735(2)	11092(4)	3.3
C(123)	920(5)	3656(3)	5581(5)	5.8	C(35)	360(4)	681(2)	11912(5)	4.7

Table 2. Positional Parameters ($\times 10^4$) and Equivalent Isotropic Temperature Factors(Å^2) of $[Co(CN)_2(acac)(dppe)]\cdot H_2O$ (**b**)

Atom	x	y	z	B_{eq}	Atom	x	y	z	B_{eq}
Co	8130.9(2)	2235.0(5)	4320.1(2)	2.3	C(16)	8483(2)	248(5)	5922(2)	3.4
P(2)	7158.9(4)	1325.8(9)	4805.6(4)	2.1	C(17)	7656(2)	−373(4)	5560(2)	3.1
O(3)	9041(1)	3073(3)	3973(1)	3.3	C(18)	6329(1)	162(4)	4130(2)	2.4
O(4)	8029(1)	95(3)	3633(1)	2.8	C(19)	6458(2)	−1331(4)	3668(2)	2.9
O(5)	386(2)	2325(4)	412(2)	6.0	C(20)	5835(2)	−2256(4)	3160(2)	3.5
N(6)	8436(2)	5510(4)	5451(2)	4.4	C(21)	5087(2)	−1728(5)	3118(2)	4.0
N(7)	7038(2)	4352(4)	2943(2)	4.0	C(22)	4952(2)	−295(4)	3591(2)	4.1
N(8)	8819(1)	741(4)	5229(2)	3.4	C(23)	5572(2)	665(3)	4102(2)	3.3
C(9)	8281(2)	4260(4)	5020(2)	2.8	C(24)	6754(1)	3055(4)	5335(2)	2.3
C(10)	7448(2)	3558(4)	3470(2)	2.6	C(25)	6377(2)	4536(4)	4886(2)	3.1
C(11)	9784(2)	3676(5)	3039(2)	3.9	C(26)	6036(2)	5851(5)	5266(2)	3.6
C(12)	9171(2)	2592(4)	3287(2)	2.8	C(27)	6094(2)	5719(5)	6105(2)	3.9
C(13)	8820(2)	1149(4)	2800(2)	3.1	C(28)	6483(2)	4285(4)	6558(2)	3.6
C(14)	8323(2)	−93(4)	3028(2)	2.7	C(29)	6809(2)	2946(4)	6180(2)	2.9
C(15)	8132(2)	−1826(5)	2542(3)	4.2					

Patterson synthesis, and all the non-hydrogen atoms were located by the subsequent Fourier synthesis. The positions of 22 among 31 hydrogen atoms were identified in the subsequent difference-Fourier maps and others were not located. The structure was refined by a block-diagonal least squares method with anisotropic thermal parameters for nonhydrogen atoms and isotropic for hydrogens. The function minimized was $\sum w||F_o|-|F_c||^2$. Final R was 0.049 and R_w 0.055 for 4006 observed unique reflections. The atomic parameters of the non-hydrogen atoms are listed in Table 1. Complete lists of observed and calculated structure factors, hydrogen atomic parameters, and anisotropic thermal parameters for non-hydrogen atoms are preserved by the Chemical Society of Japan (Document No. 8829).

***trans*(*C*,*N*)-[Co(CN)$_2$(acac)(edpp)]·H$_2$O.** The complex was prepared in a previous work.[25] An orange rhombic crystal of approximate dimensions 0.37×0.40×0.55 mm^3 was used for X-ray work. Crystal data: monoclinic, $P2_1/c$, a=17.870(3), b=7.354(2), c=16.709(3) Å, β=105.45(2)°, V=2116.5(5) Å^3, Z=4, D_x=1.396 g cm^{-3}, D_m=1.39 g cm^{-3}, μ(Mo $K\alpha$)=9.368 cm^{-1}. Diffraction data were collected on a Rigaku AFC-5A diffractometer with graphite monochromatized Mo $K\alpha$ radiation (λ=0.71069 Å). Within the range $2\theta<55°$, 3525 reflections were measured. No absorption correction was applied.

Calculations for the structure analysis were performed on a FACOM M-382 computer at the Computer Center, Nagoya University. Atomic scattering factors of neutral atoms were used.[24] The structure was solved by the Monte Carlo direct method[26] with the aid of MULTAN 78[27] using 3464 non-zero unique reflections with $|F_o|>3\sigma(|F_o|)$, and refined on F^2 by the full-matrix least-squares program. Non-hydrogen atoms were refined anisotropically. All hydrogen atoms were located from a difference Fourier synthesis and refined with isotropic temperature factors. Final R and R_w were 0.056 and 0.039, respectively. The atomic parameters of the non-hydrogen atoms are listed in Table 2. Complete lists of observed and calculated structure factors, hydrogen atomic parameters, and anisotropic thermal parameters for non-hydrogen atoms are preserved by the Chemical Society of Japan (Document No. 8829).

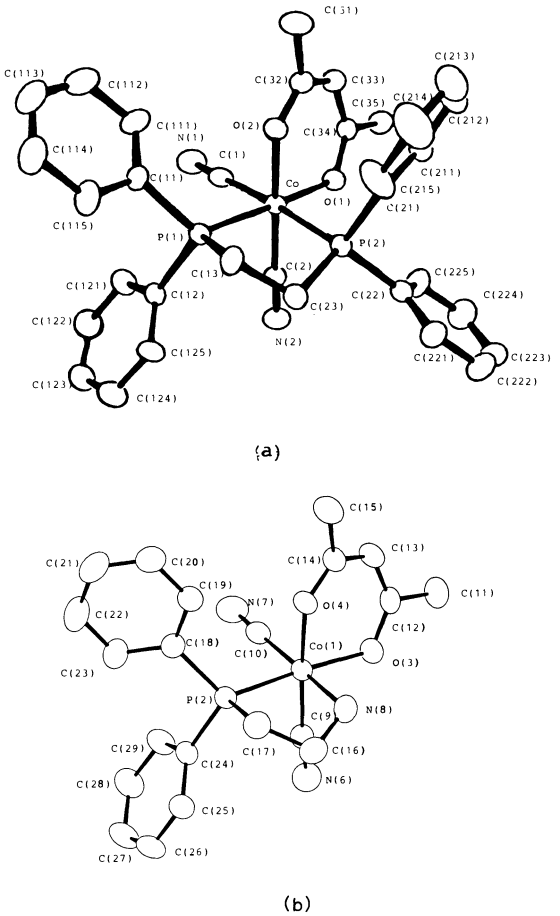

Fig. 1. ORTEP drawings[28] of **a** [Co(CN)$_2$(acac)(dppe)] and **b** [Co(CN)$_2$(acac)(edpp)].

Results and Discussion

Perspective drawings[28] of [Co(CN)$_2$(acac)(dppe)] and [Co(CN)$_2$(acac)(edpp)] with numbering schemes of the atoms are shown in Fig. 1. Selected bond distances and bond angles are listed in Tables 3 and 4. The cobalt atoms in both complexes are coordinated

Table 3. Selected Bond Distances (l/Å) and Angles (ϕ/°) for [Co(CN)2(acac)(dppe)] (**a**)

Co-P(1)	2.212(2)	Co-P(2)	2.265(1)
Co-O(1)	1.955(4)	Co-O(2)	1.937(3)
Co-C(1)	1.924(4)	Co-C(2)	1.884(4)
P(1)-C(11)	1.823(5)	P(1)-C(12)	1.820(4)
P(1)-C(13)	1.843(4)	P(2)-C(21)	1.816(4)
P(2)-C(22)	1.823(5)	P(2)-C(23)	1.834(5)
O(1)-C(34)	1.282(5)	O(2)-C(32)	1.278(6)
N(1)-C(1)	1.139(5)	N(2)-C(2)	1.133(6)
C(13)-C(23)	1.548(6)	C(31)-C(32)	1.496(7)
C(32)-C(33)	1.411(8)	C(33)-C(34)	1.382(7)
C(34)-C(35)	1.502(8)	C(11)-C(111)	1.393(7)
C(11)-C(115)	1.397(8)	C(111)-C(112)	1.414(9)
C(112)-C(113)	1.364(11)	C(113)-C(114)	1.369(10)
C(114)-C(115)	1.397(9)	C(12)-C(121)	1.391(6)
C(12)-C(125)	1.384(7)	C(121)-C(122)	1.394(7)
C(122)-C(123)	1.367(8)	C(123)-C(124)	1.380(8)
C(124)-C(125)	1.401(7)	C(21)-C(211)	1.379(7)
C(21)-C(215)	1.381(8)	C(211)-C(212)	1.378(7)
C(212)-C(213)	1.362(10)	C(213)-C(214)	1.369(10)
C(214)-C(215)	1.402(9)	C(22)-C(221)	1.375(6)
C(22)-C(225)	1.379(8)	C(221)-C(222)	1.395(8)
C(222)-C(223)	1.357(10)	C(223)-C(224)	1.365(8)
C(224)-C(225)	1.391(8)		
P(1)-Co-P(2)	87.66(5)	P(1)-Co-O(1)	177.67(8)
P(1)-Co-O(2)	87.9(1)	P(1)-Co-C(1)	89.7(2)
P(1)-Co-C(2)	88.9(2)	P(2)-Co-O(1)	94.39(8)
P(2)-Co-O(2)	90.24(8)	P(2)-Co-C(1)	175.6(1)
P(2)-Co-C(2)	85.6(1)	O(1)-Co-O(2)	93.2(1)
O(1)-Co-C(1)	88.2(2)	O(1)-Co-C(2)	90.1(2)
O(2)-Co-C(1)	93.2(2)	O(2)-Co-C(2)	174.9(2)
C(1)-Co-C(2)	90.8(2)	Co-P(1)-C(11)	119.0(2)
Co-P(1)-C(12)	117.1(2)	Co-P(1)-C(13)	107.2(2)
Co-P(2)-C(21)	113.7(1)	Co-P(2)-C(22)	119.9(2)
Co-P(2)-C(23)	105.8(1)	Co-O(1)-C(34)	123.2(3)
Co-O(2)-C(32)	124.6(3)	Co-C(1)-N(1)	177.6(5)
Co-C(2)-N(2)	178.0(3)	C(11)-P(1)-C(12)	101.5(2)
C(11)-P(1)-C(13)	103.9(2)	C(12)-P(1)-C(13)	106.9(2)
C(21)-P(2)-C(22)	103.1(2)	C(21)-P(2)-C(23)	107.1(2)
C(22)-P(2)-C(23)	106.5(2)	P(1)-C(11)-C(111)	122.0(4)
P(1)-C(11)-C(115)	115.8(4)	C(111)-C(11)-C(115)	122.2(5)
C(11)-C(111)-C(112)	117.2(6)	C(111)-C(112)-C(113)	121.0(6)
C(112)-C(113)-C(114)	120.8(6)	C(113)-C(114)-C(115)	120.9(7)
C(114)-C(115)-C(11)	117.9(6)	P(1)-C(12)-C(121)	117.8(3)
P(1)-C(12)-C(125)	121.1(3)	C(12)-C(121)-C(122)	118.6(5)
C(121)-C(122)-C(123)	120.4(5)	C(122)-C(123)-C(124)	121.5(5)
C(123)-C(124)-C(125)	118.9(5)	C(124)-C(125)-C(12)	119.6(4)
P(2)-C(21))-C(211)	117.0(4)	P(2)-C(21)-C(215)	124.6(4)
C(21)-C(211)-C(212)	120.8(5)	C(211)-C(212)-C(213)	121.7(6)
C(212)-C(213)-C(214)	118.0(6)	C(213)-C(214)-C(215)	121.6(6)
C(214)-C(215)-C(21)	119.6(6)	P(2)-C(22)-C(221)	119.7(4)
P(2)-C(22)-C(225)	121.4(3)	C(22)-C(221)-C(222)	120.4(6)
C(221)-C(222)-C(223)	120.5(5)	C(222)-C(223)-C(224)	120.2(6)
C(223)-C(224)-C(225)	120.0(6)	C(224)-C(225)-C(22)	120.4(5)
P(1)-C(13)-C(23)	108.2(3)	P(2)-C(23)-C(13)	108.0(3)
O(1)-C(34)-C(35)	113.9(4)	O(1)-C(34)-C(33)	126.9(5)
O(2)-C(32)-C(31)	115.3(5)	O(2)-C(32)-C(33)	126.2(4)
C(31)-C(32)-C(33)	118.5(4)	C(32)-C(33)-C(34)	123.3(4)
C(33)-C(34)-C(35)	119.2(4)		

nearly octahedrally. The dppe complex has a cis and the edpp one a trans(C,N) geometrical structure, as we have suggested by ^{1}H and ^{13}C NMR studies.[22,25] Other geometrical isomers were not yielded in the syntheses.[22,25]

Figure 2 shows schematic structures around the cobalt atoms of the dppe (**a**) and edpp (**b**) complexes, and a related complex, [Co(acac)(RR-chxn)(edpp)]$^{2+}$ (RR-chxn=(1*R*,2*R*)-1,2-cyclohexanediamine) (**c**)[13] with their bond distances. It is seen that both phosphine and cyanide ligands give remarkable trans influence to the cobalt-ligand bond. The Co–O bond distances of 1.955(3) Å in **a** and 1.968(2) Å in **b** both of which are trans to the phosphorus donor atom are longer by ca.

Table 4. Selected Bond Distances (l/Å) and Angles (ϕ/°) for $[Co(CN)_2(acac)(edpp)]\cdot H_2O$ (**b**)

Co-P(2)	2.211(1)	Co-O(3)	1.968(2)
Co-O(4)	1.933(2)	Co-N(8)	2.011(3)
Co-C(9)	1.874(3)	Co-C(10)	1.881(2)
P(2)-C(17)	1.832(3)	P(2)-C(18)	1.823(2)
P(2)-C(24)	1.811(3)	O(3)-C(12)	1.281(4)
O(4)-C(14)	1.266(4)	N(6)-C(9)	1.158(4)
N(7)-C(10)	1.147(3)	N(8)-C(16)	1.486(4)
C(11)-C(12)	1.503(5)	C(12)-C(13)	1.399(4)
C(14)-C(15)	1.505(5)	C(16)-C(17)	1.513(4)
C(18)-C(23)	1.394(4)	C(19)-C(20)	1.387(4)
C(20)-C(21)	1.378(5)	C(21)-C(22)	1.380(5)
C(22)-C(23)	1.398(4)	C(24)-C(25)	1.394(4)
C(24)-C(29)	1.391(4)	C(25)-C(26)	1.386(5)
C(26)-C(27)	1.383(5)	C(27)-C(28)	1.378(4)
P(2)-Co-N(8)	86.51(8)	P(2)-Co-O(3)	175.77(6)
P(2)-Co-O(4)	90.65(6)	P(2)-Co-C(9)	90.49(9)
P(2)-Co-C(10)	91.07(10)	O(3)-Co-O(4)	92.07(9)
O(3)-Co-N(8)	90.41(10)	O(3)-Co-C(9)	86.6(1)
O(4)-Co-N(8)	86.73(10)	O(4)-Co-C(9)	176.92(9)
O(4)-Co-C(10)	92.05(10)	C(9)-Co-C(10)	90.8(1)
Co-P(2)-C(17)	100.1(1)	Co-P(2)-C(18)	120.40(9)
Co-P(2)-C(24)	114.96(9)	C(17)-P(2)-C(18)	105.6(1)
C(17)-P(2)-C(24)	109.2(1)	C(18)-P(2)-C(24)	105.6(1)
Co-O(3)-C(12)	122.6(2)	Co-O(4)-C(14)	124.8(2)
Co-N(8)-C(16)	115.5(2)	Co-C(9)-N(6)	174.4(3)
Co-C(10)-N(7)	178.8(3)	O(3)-C(12)-C(11)	114.8(3)
O(3)-C(12)-C(13)	125.3(3)	C(11)-C(12)-C(13)	119.8(3)
C(12)-C(13)-C(14)	124.4(3)	O(4)-C(14)-C(13)	125.1(3)
O(4)-C(14)-C(15)	116.2(3)	C(13)-C(14)-C(15)	118.6(3)
N(8)-C(16)-C(17)	108.5(2)	P(2)-C(17)-C(16)	108.2(2)
P(2)-C(18)-C(19)	119.5(2)	P(2)-C(18)-C(23)	119.2(2)
C(19)-C(18)-C(23)	119.5(2)	C(18)-C(19)-C(20)	120.2(3)
C(19)-C(20)-C(21)	120.2(3)	C(20)-C(21)-C(22)	120.2(3)
C(21)-C(22)-C(23)	120.6(3)	C(22)-C(23)-C(18)	119.4(3)
P(2)-C(24)-C(25)	119.2(2)	P(2)-C(24)-C(29)	121.8(2)
C(25)-C(24)-C(29)	119.0(3)	C(24)-C(25)-C(26)	120.8(3)
C(25)-C(26)-C(27)	119.5(3)	C(26)-C(27)-C(28)	120.1(3)
C(27)-C(28)-C(29)	120.7(3)	C(24)-C(29)-C(28)	119.9(3)

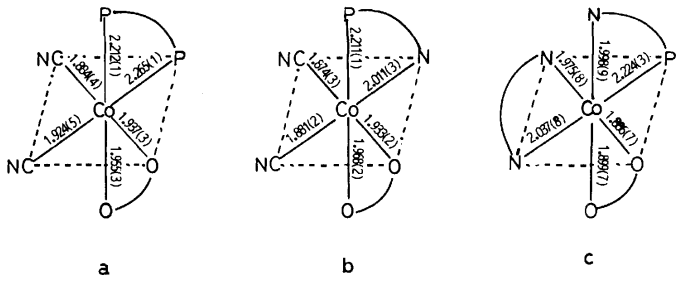

Fig. 2. Bond distances around the cobalt atom in the complexes, **a** $[Co(CN)_2(acac)(dppe)]$, **b** $[Co(CN)_2(acac)(edpp)]$, and c $[Co(acac)(RR\text{-}chxn)(edpp)]^{2+}$.[11]

0.06—0.08 Å than those in **c** (1.886(7) and 1.899(7) Å) and in $[Co(acac)_3]$ (1.883(4)—1.892(4) Å).[29] A similar elongation due to trans influence of phosphine ligands has been reported for Co-N bonds in a number of cobalt(III) phosphine-amine mixed ligand complexes.[5,6,9-14] The Co-O bond distances trans to the cyanide ligand in **a** (1.937(3) Å) and **b** (1.933(2) Å) are also longer by ca. 0.03—0.05 Å than those in **c** and $[Co(acac)_3]$, indicating trans influence of the cyanide ligand. However, the extent of elongation is somewhat small compared with that due to the phosphine ligand. The Co-N bond trans to the phosphine ligand in **c** (2.037(8) Å) is also longer than that trans to the cyanide ligand in **b** (2.011(3) Å). Although structural data are rather limited at present, a phosphine ligand seems to give stronger trans influence to cobalt(III)-ligand bonds than a cyanide ligand.

In complex **a** the Co-P bond distance of 2.265(1) Å and the Co-C bond distance of 1.924(5) Å, which are trans to each other, are fairly longer than the other Co-P and Co-C bond distances, respectively. The Co-C bond distances (1.927(2) and 1.930(2) Å) in *trans*-$[Co(CN)_2(tn)_2]^+$ (tn=trimethylenediamine)[30] are also longer than those (1.85(3) and 1.88(3) Å) in *cis*-$[Co(CN)_2(en)_2]^+$.[18] These results indicate that the two coordination bonds trans to each other are weakened by mutual trans influence of the phosphine and cyanide ligands. The results may also be related to the fact that the mixed cyano and

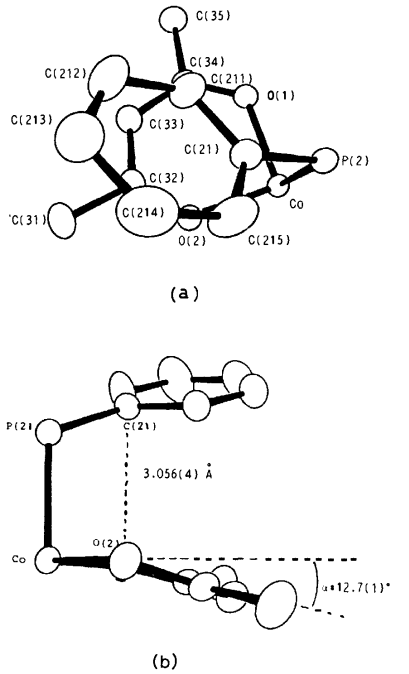

Fig. 3. A stacking structure of the acac and phenyl rings of [Co(CN)2(acac)(dppe)].

phosphine cobalt(III) complexes tend to form cis isomers for these ligands. The [Co(CN)2(acac)(edpp)] complex yielded selectively isomer **b**, in which two carbon and one phosphorus donor atoms are coordinated in a facial configuration. Two other possible isomers have these three donor atoms in a meridional configuration.

In complex **a** one of two phenyl groups is forced to be disposed over the acac chelate ring (Figs. 1(a) and 3). The O(2)···C(21) distance of 3.056(4) Å between two rings is shorter than the sum of their van der Waals radii (3.22 Å). A bent structure of the acac chelate ring with α=12.7(1)° as shown in Fig. 3(b) is probably attributable to such a stacking structure of these two rings. A similar bent structure has been observed in complex **c**.[13] On the other hand, complex **b** has no stacking structure of the phenyl and acac rings, and the acac chelate ring is nearly planar (α=4.1(5)°). All of the acac chelate rings in [Co(acac)3] are also nearly planar (α=1.6, 4.5, and 5.5°).[29] These results suggest that the interaction caused by stacking of the pseudo aromatic acac chelate and the phenyl rings is repulsive rather than attractive.

The dppe and edpp chelate rings in complexes **a** and **b** take a typical gauche conformation, and the tortion angle is 52.4(1)° (P(1)-C(13)-C(23)-P(2)) for the former and 49.9(1)° (P(2)-C(17)-C(16)-N(8)) for the latter.

The authors wish to thank the Ministry of Education for Science Reseach Grant-in Aid No. 61430013, and the Institute for Molecular Science (IMS), Okazaki National Reseach Institute for the use of X-ray and computation facilities. The authors are also grateful to Dr. Koshiro Toriumi (IMS) for his kind advice to X-ray structure analysis of [Co(CN)2-(acac)(dppe)].

References

1) N. W. Terry, E. L. Amma, and L. Vaska, *J. Am. Chem. Soc.*, **94**, 653 (1972).
2) J. Halpern, B. L. Goodall, G. P. Kahre, H. S. Lim, and J. J. Pluth, *J. Am. Chem. Soc.*, **97**, 2301 (1975).
3) O. Alnaji, Y. Peres, F. Dahan, M. Dartiguenave, and Y. Dartiguenave, *Inorg. Chem.*, **25**, 1383 (1986).
4) N. Bresciani-Pahor, M. Forcolin, L. G. Marzilli, L. Randaccio, M. F. Summers, and P. J. Toscano, *Coord. Chem. Rev.*, **63**, 1 (1985).
5) S. Ohba, Y. Saito, T. Ohishi, K. Kashiwabara, and J. Fujita, *Acta Crystallogr., Sect. C*, **39**, 49 (1983).
6) T. Ohishi, S. Ohba, K. Kashiwabara, Y. Saito, and J. Fujita, *Bull. Chem. Soc. Jpn.*, **57**, 877 (1984).
7) T. Ohishi, K. Kashiwabara, J. Fujita, S. Ohba, T. Ishii, and Y. Saito, *Bull. Chem. Soc. Jpn.*, **59**, 385 (1986).
8) S. Ohba, M. Ito, Y. Saito, and T. Ishii, *Acta Crystallogr., Sect. C*, **39**, 997 (1983).
9) I. Kinoshita, K. Kashiwabara, J. Fujita, K. Matsumoto, and S. Ooi, *Bull. Chem. Soc. Jpn.*, **54**, 2683 (1981).
10) I. Kinoshita, Y. Yokota, K. Matsumoto, S. Ooi, K. Kashiwabara, and J. Fujita, *Bull. Chem. Soc. Jpn.*, **56**, 1067 (1983).
11) T. Ohishi, K. Kashiwabara, H. Ito, T. Ito, and J. Fujita, *Bull. Chem. Soc. Jpn.*, **56**, 1551 (1983).
12) M. Atoh, K. Kashiwabara, H. Ito, T. Ito, and J. Fujita, *Bull. Chem. Soc. Jpn.*, **57**, 3139 (1984).
13) M. Takata, K. Kashiwabara, H. Ito, T. Ito, and J. Fujita, *Bull. Chem. Soc. Jpn.*, **58**, 2247 (1985). In Table 2 of this paper the numbering of the following atoms should be exchanged as follows: N(1)↔N(2), C(1)↔C(2), C(3)↔C(6), C(4)↔C(5).
14) M. Atoh, K. Kashiwabara, and J. Fujita, *Bull. Chem. Soc. Jpn.*, **58**, 3492 (1985).
15) T. G. Appleton, H. C. Clark, and L. E. Manzer, *Coord. Chem. Rev.*, **10**, 335 (1973).
16) R. Mason and A. D. C. Towl, *J. Chem. Soc. A*, **1970**, 1601.
17) R. Mason and D. R. Russell, *Chem. Commun.*, **1965**, 182.
18) K. Matsumoto, S. Ooi, and H. Kuroya, *Bull. Chem. Soc. Jpn.*, **44**, 2721 (1971).
19) M. Iwata and Y. Saito, *Acta Crystallogr., Sect. B*, **29**, 822 (1973).
20) K. Toriumi, S. Sato, and Y. Saito, *Acta Crystallogr., Sect. B*, **33**, 1378 (1977).
21) S. Alvarez and C. Lopez, *Inorg. Chim. Acta*, **64**, L99 (1982).
22) K. Kashiwabara, K. Katoh, T. Ohishi, J. Fujita, and M. Shibata, *Bull. Chem. Soc. Jpn.*, **55**, 149 (1982).
23) T. Sakurai and K. Kobayashi, *Rikagaku Kenkyusho Hokoku*, **55**, 69 (1979).
24) "International Tables for X-Ray Crystallography," Kynoch Press, Birmingham(1974), Vol. IV.

25) T. Ohishi, K. Kashiwabara, and J. Fujita, *Bull. Chem. Soc. Jpn.*, **56**, 1553 (1983).
26) A. Furusaki, *Acta Crystallogr., Sect. A*, **35**, 220 (1979).
27) P. Main, S. E. Hull, L. Lessinger, G. Germain, J. P. Declercq, and M. M. Woolfson (1978), MULTAN 78. "A System of Computer Programs for the Automatic Solution of Crystal Structures from X-Ray Diffraction Data," Univs. of York, England, and Louvain, Belgium.
28) C. K. Johnson, "ORTEP-II: A FORTRAN Thermal Ellipsoid Plot Program for Crystal Structure Illustrations, ORNL-5138, March 1976," Oak Ridge National Laboratory.
29) G. J. Kruger and E. C. Reynhardt, *Acta Crystallogr., Sect. B*, **30**, 822 (1974).
30) H. Kupka, J. Degen, A. Urushiyama, K. Angermund, and C. Kruger, *Inorg. Chem.*, **25**, 3294 (1986).

 © 1988 The Chemical Society of Japan Bull. Chem. Soc. Jpn., 61, 3193—3198 (1988)

Olefin Epoxidation Catalyzed by Sterically Bulky Metalloporphyrins (Metal=Fe,Mn) by Use of Sodium Hypochlorite as an Oxygen Source—A Kinetic Study

Hiroyuki AMATSU, T. Ken MIYAMOTO,* and Yukiyoshi SASAKI
Department of Chemistry, Faculty of Science, The University of Tokyo,
Hongo, Bunkyo-ku, Tokyo 113
(Received April 6, 1988)

Substituents around an active center give a variety of effects on metalloporphyrin catalyses. In order to examine the effects of a substituent on the kinetic parameters, several olefins (styrene derivatives, cyclooctene and 1-octene) have been epoxidized by iron(III) and manganese(III) complexes of *meso*-tetrakis(2,6-dimethylphenyl)porphyrin or *meso*-tetrakis(2,6-dichlorophenyl)porphyrin in the presence of sodium hypochrolite as an oxidant. As previously reported for a manganese porphyrin system, the rate-profile of an iron complex can be described by the Michaelis–Menten equation. Several examples of an anomalous rate dependence on the olefin concentration have been observed. The ortho substituents have little influence on the binding affinity of the oxo-iron complex to olefin, in contrast to the case of manganese complexes. It is additionally proposed that the *N*-alkylation of an iron porphyrin has some correlation to the kinetic parameters.

Metalloporphyrins, especially iron and manganese complexes, are capable of oxygenating hydrocarbons in a catalytic way, yielding alcohols from alkanes and epoxides from olefins. In these catalyses, several oxygen sources, either single oxygen donors such as iodosylbenzenes,[1–10] amine oxides,[11–13] and alkyl hydroperoxides,[14,15] or molecular oxygen in the presence of reducing agents such as sodium tetrahydroborate,[16] hydrogen and colloidal platinum,[17,18] or zinc powder and acetic acid[19] have been used. These reaction systems not only serve as models to cytochrome P-450 monooxygenase enzymes,[20] but have promising possibilities as catalysts. Several studies have been made to develop efficient metalloporphyrin catalysts for high-turnover oxygenation,[8,21,22] and to control the chemo-,[1,5,30,34] regio-,[1,23–26] and stereoselectivity.[27,28]

The use of manganese porphyrins with hypochlorite oxidant has recently been well-established for olefin epoxidation.[29–41] Nitrogen bases, such as pyridines and *N*-substituted imidazoles, enhance the reaction rate.[29,33,34,38] Kinetic studies have demonstrated that the rate can be described by the Michaelis–Menten equation and that the breakdown of an oxo-olefin intermediate (a proposed structure is a metallaoxetane **2**) is the rate-determining step of the catalytic cycle[35] (Fig. 1). The manganese–hypochlorite system has several advantages. First, sodium hypochrolite is a cheap oxidant and its concentration in solution can be determined by simple titration. Second, the rate is easy to measure since the reaction stops without adding a quencher when the aqueous and organic phases are separated. The observed kinetic parameters give information concerning catalyst-substrate interactions.

Although few iron porphyrins have been successful in oxygenation with hypochlorite, we found that a low catalytic activity results from an oxidative destruction of the catalysts and that the introduction of the electron-withdrawing substituents into the

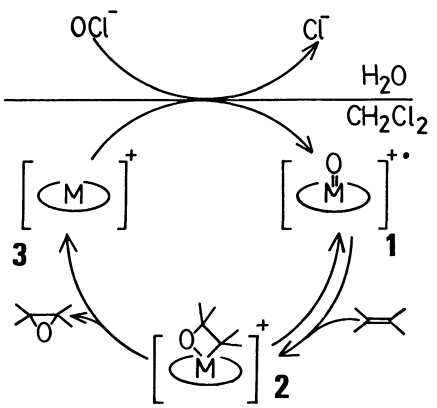

Fig. 1. Catalytic cycle of epoxidation by metalloporphyrin with hypochlorite oxidant.

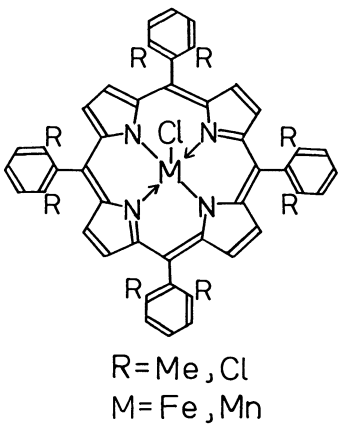

Fig. 2. The porphyrin complexes used as catalysts. Abbreviations: TPP=*meso*-tetraphenylporphyrin dianion; TMP=*meso*-tetramesitylporphyrin dianion; FeMe=[*meso*-tetrakis(2,6-dimethylphenyl)porphyrinato]iron(III) chloride; FeCl=[*meso*-tetrakis(2,6-dichlorophenyl)porphyrinato]iron(III) chloride; MnMe=[*meso*-tetrakis(2,6-dimethylphenyl)porphyrinato]manganese(III) chloride; MnCl=[*meso*-tetrakis(2,6-dichlorophenyl)porphyrinato]manganese(III) chloride.

ortho-position(s) of phenyl rings of TPP[42] reduces the catalyst decomposition; especially, an iron *meso*-tetrakis(2,6-difluorophenyl)porphyrin complex shows a sufficient epoxidation capability[39-41] (Fig. 2: R=F).

In order to obtain a greater undertstanding of olefin epoxidation by metalloporphyrin–hypochlorite systems, we used iron(III) and manganese(III) TPP derivatives carrying methyl- or chloro groups in the 2,6-positions of the phenyl rings (FeMe, FeCl, MnMe, and MnCl: Fig. 2).

Experimental

meso-Tetrakis(2,6-dimethylphenyl)porphyrin[42] and *meso*-tetrakis(2,6-dichlorophenyl)porphyrin[21] were prepared by methods described in the literature. The metals, iron(III) and manganese(III), were inserted by the procedure of Adler et al.[43]

Standard Conditions for Kinetics. A metalloporphyrin catalyst (4.6×10^{-5} M[44]), olefin (styrenes, cyclooctene, or 1-octene; 0.17 M), internal standard (*p*-dichlorobenzene; 0.014 M), phase-transfer reagent (benzyldimethyltetradecylammonium chloride; 0.010 M) were dissolved in 10 ml of dichloromethane. When manganese porphyrins were used, the addition of 4'-(1-imidazolyl)acetophenone was necessary; in the absence of the base, the reaction was too slow to obtain kinetic data. Sodium hypochlorite solution (20 ml, 0.42 M) was layered over the organic phase. The reaction was initiated by vigorous stirring. The temperature was maintained at 22 °C. The products were monitored periodically by gas chromatography.

Results and Discussion

Stabilities of Catalysts. When styrene was oxygenated catalytically by four metalloporphyrins (FeMe, FeCl, MnMe, and MnCl), phenylacetaldehyde could not be detected as a by-product. The same results were obtained in the styrene epoxidation, both by [(Mn(TMP)]$^+$–*N*-base–hypochlorite system[35] and by [Fe(TMP)]$^+$–iodosylbenzene system,[35] and by [Fe(TMP)]$^+$–iodosylbenzene system,[5] however, [Mn(TPP)]$^+$ produced a relatively large amount of phenylacetaldehyde (ca. 15%).[39-41] This tendency indicates that the steric hindrance of ortho substituents around the active site contributes to product selectivity.

In order to evaluate the ortho-substituent effect on the porphyrin catalyst stability, we measured the maximum yields of epoxides (Table 1). The reaction was continued until the catalyst was completely bleached or the epoxide formation stopped. (Both olefin and sodium hypochlorite were added, if necessary.) In Table 1, the yield of epoxide is expressed in turnovers (mol of produced epoxide per mol of catalyst). In styrene and cyclooctene epoxidation, all complexes, except for FeMe, showed quite high yields of the epoxidation compared with [Fe(TPP)]$^+$ and [Mn(TPP)]$^+$. In 1-octene epoxidation, all of the catalysts show low yields. In view of the fact that the TPP complexes have no reactivity, however, the R groups must contribute to the catalyst stability to a small extent.

It is well-known that metalloporphyrin, itself, suffers from oxidation at the meso-positions, followed by ring opening.[45] The ortho substituents of the meso-phenyl rings protect the meso-position from a bimolecular oxidative process, sterically or electronically (when the R is electron-withdrawing substituent). As far as iron porphyrin complexes are concerned, steric protection by the methyl groups is not efficient in stabilizing the catalyst against oxidative degradation.

Reaction Mechanism. The reaction rate was found to be first-order in the concentration of the iron or manganese porphyrin (0—1×10^{-4} M) and independent of the hypochlorite concentration (0.0043—0.42 M). With respect to the olefin concentration (0.002—2 M), the reaction order varied from zero to one. Plotting the reciprocal of the initial velocity vs. the reciprocal of the olefin concentration gave a straight line (Fig. 3). These results suggest that the mechanism of iron porphyrin-catalyzed epoxidation follows Michaelis–Menten kinetics, which has been proposed for the epoxidation by manganese complex-

Table 1. The Maximum Yields in Turnovers

M	R	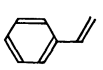		
	H	300[a]	300[a]	ca. 0
Fe	Me	450	2300	80
	Cl	9500	28000	350
Mn	H[b]	5000[a]	600[a]	20
+	Me	37000	8200	360
N-base	Cl	21000	10500	400

a) Ref. 41. b) Bromide complex was used. All the others are chlorides.

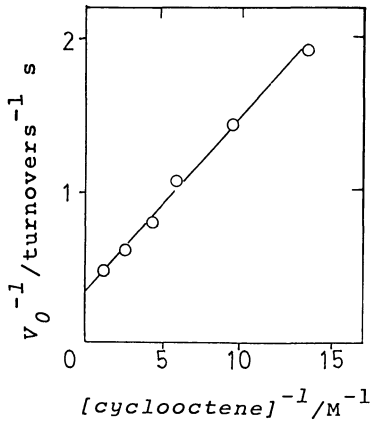

Fig. 3. Reciprocal plot of the initial velocity (V_0) vs. reciprocal of the cyclooctene concentration. catalysis by FeCl.

hypochlorite system,[35] i.e., the high valent oxo-iron complex and olefin reversibly interact to form an oxo-olefin intermediate. A breakdown of the intermediate to epoxide is the rate-determining step.

Since the ortho-substituents prevent μ-oxo dimerization, a by-pass mechanism can be avoided. During the catalytic cycle all porphyrin molecules serve as a single catalyst.[46]

Although the epoxidation rate essentialy fitted Michaelis-Menten kinetics, we observed two anomalies of the rate dependence on the olefin concentration. One is the case using FeMe as a catalyst. As shown in Fig. 4, rate saturation was not found, even in the concentration range [cyclooctene]>1 M. An analogous rate dependence on the substrate concentration was found for styrene and 1-octene epoxidation. The other is the case of a MnCl catalyst, particularly for cyclooctene epoxidation (Fig. 5). The rate remarkably decreased with an increase in the concentration of the olefin above 0.2 M. A similar behavior was observed for styrene or 1-octene epoxidation. In the presence of cyclooctene in large excess, the UV-vis spectra of organic aliquots from the reaction mixtures showed a Soret band at 437 nm. This band could not be assigned to a common high valent manganese porphyrin which usually has a Soret band at 420—425 nm.[47-50] The observed kinetic behavior would result from the formation of a low reactive unknown intermediate under conditions of excess olefin. At present, we can not characterize this intermediate.[51]

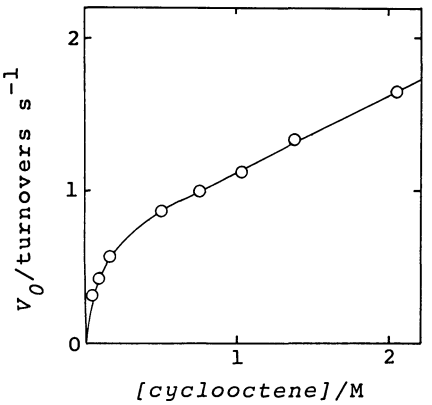

Fig. 4. Plot of initial velocity vs. cyclooctene concentration for FeMe-catalyzed epoxidation. The kinetic parameters were obtained from the linear part of double reciprocal plots at low cyclooctene concentration region.

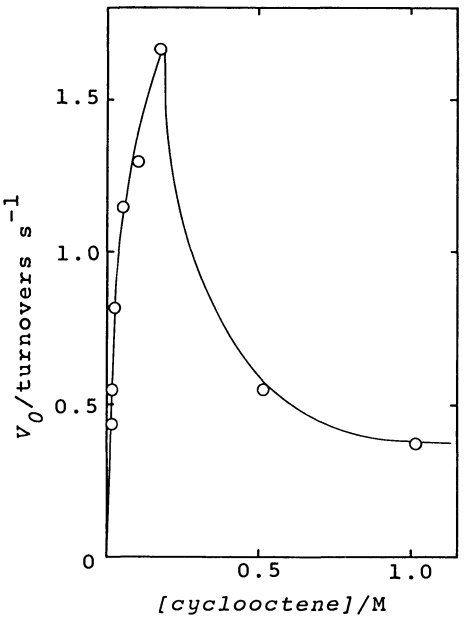

Fig. 5. Plot of initial velocity vs. cyclooctene concentration for MnCl-catalyzed epoxidation. The kinetic parameters were obtained from the linear part of double reciprocal plots at low cyclooctene concentration region.

Kinetic Parameters. In the Michaelis-Menten equation, the parameter V_{max} gives the rate-determining constant. The Michaelis constant K_m is a measure of the binding affinity of the olefin to a high valent metal-oxo complex: a large binding affinity corresponds to a low K_m value.

The values of V_{max} and K_m were calculated from the intercept and the slope of the straight line obtained by the Lineweaver-Burk plotting.[53]

In general, both the steric and electronic factors of porphyrin catalysts must govern the reactivity. On the assumption that both the methyl- and chloro-group would be nearly equal in steric hindrance, we expected to be able to obtain information concerning the electronic effect on the reaction. According to recent measurements of the CV redox potentials of iron porphyrin,[54] oxo $Fe^{IV}Cl^{+\cdot}$ is more oxidative than oxo $Fe^{IV}Me^{+\cdot}$ by 250 mV, reflecting the fact that the electron-withdrawing chloro groups might enhance the electrophilicity of the oxo-iron complex.

The above consideration encouraged us to examine the substituent effect on the binding affinity of the oxo-iron complex toward olefins. Table 2 gives the K_m values for the epoxidation of para-substituted styrenes(substituents: MeO-, Me-, H-, Cl-) by FeMe and FeCl. The K_m values decrease (i.e., the affinity toward the styrenes increases) as the styrene substituents become increasingly electron-donative, suggesting that the oxo-iron complexes are electrophilic.

Table 2. K_m Values for Para-Substituted Styrenes Epoxidation Catalyzed by Porphyrin Complexes

M	R	MeO-	Me-	H-	Cl-
		K_m/M	K_m/M	K_m/M	K_m/M
Fe	Me	0.0052	0.0095	0.40	0.5
	Cl	0.0077	0.017	0.065	0.6

The logarithm of the K_m values could be correlated with Hammett substituent constants σ_p (Fig. 6). The difference between the K_m values for FeMe and FeCl is small and the slopes of the two straight lines are almost equal; the difference in the ρ values is small. These results demonstrate that the difference between the methyl- and chloro-groups in the ortho-positions of TPP has little influence on the binding affinity of an oxo-iron complex to olefins. In other words, the electronic effect of oxo-iron complexes is not an important factor in epoxidation kinetics.

It is highly desirable that epoxidation by manganese catalyst should be carried out in the absence of an *N*-base, in comparison with that of iron catalysts. In all cases concerning our manganese system, the addition of an *N*-base was, however, required in order to monitor the reaction by gas chromatography. Moreover,in epoxidation by MnMe a determination of the initial velocity was very difficult because of the peculiar time course for epoxide production without any catalyst or *N*-base loss (Fig. 7). (The behavior has not yet been rationalized.) This prevented us from carrying out a manganese catalyzed epoxidation of a series of para substituted styrenes. In a calculation of the kinetic parameters for MnMe (Table 3), the initial velocities were obtained from the tangent slopes of the time course curves at time $T=0$.

The V_{max} and K_m values for the epoxidation of three different olefins to the four iron and manganese porphyrins are also listed in Table 3. Although large differences in the K_m values between the two different metals or between the two different subsituents to each olefin were not observed, a slight tendency is noticeable, as described below.

When iron porphyrins are used for olefin epoxidation, the difference in the K_m values between FeMe and FeCl to each olefin is not very large, compared with the difference obtained by using manganese complexes. This result indicates a small electronic effect

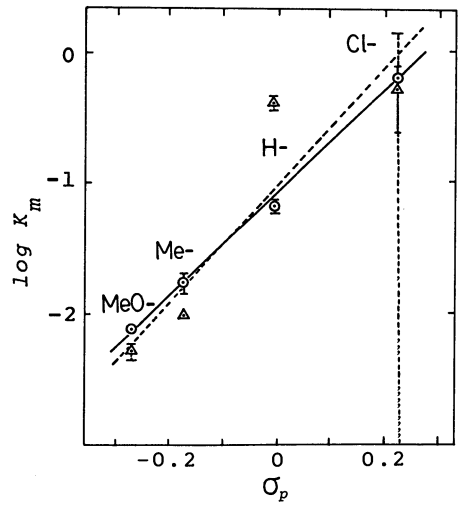

Fig. 6. Plot of log K_m for para-substituted styrenes vs. Hammett substituent constants σ_p for iron porphyrin-catalyzed epoxidation: —O— for FeCl catalyst; ---△— for FeMe catalyst. The two straight lines are drawn by the least squares method.

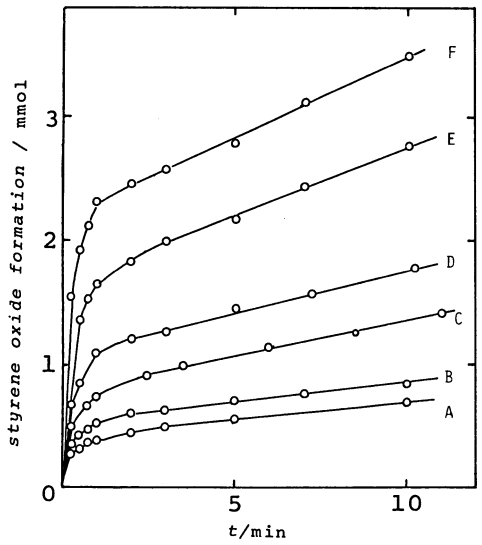

Fig. 7. Time course for styrene oxide production catalyzed by MnMe. [styrene]=A 0.21; B 0.31; C 0.75; D 1.3; E 2.7; F 3.9 M. By use of other complexes the plots of time course for epoxide production give straight lines.

Table 3. Kinetic Parameters for Epoxidation Catalyzed by Iron and Manganese Porphyrin Complexes

M	R	V_{max}[a]	K_m	V_{max}[a]	K_m	V_{max}[a]	K_m
		turnovers s^{-1}	M	turnovers s^{-1}	M	turnovers s^{-1}	M
Fe	Me	1.3	0.40	1.1	0.16	0.13	0.26
	Cl	1.4	0.065	2.8	0.30	0.37	0.06
Mn + *N*-base	Me	10.3	0.51	3.8	0.051	4	2
	Cl	2.8	0.06	1.9	0.036	2.1	0.09

a) V_{max} (in turnovers s^{-1}) here is identical to the rate-determining constant k_2.[35]

on the binding affinity of oxo-iron complex to olefin, as mentioned above. With respect to the manganese complexes, the K_m value for MnCl to each olefin is smaller than that of MnMe (by a factor of 8.5 for styrene; 22 for 1-octene). The electron-withdrawing chloro groups enhance the binding affinity of the oxo-manganese complex to olefin.

Taking all these facts together, we presently propose a speculative mechanism. One possible explanation for the difference between the iron and the manganese catalysts is that steric interactions between an ortho substituent and the olefin differ. According to previous EXAFS results regarding oxo-metal complexes, the distance Fe-O is 1.64 Å[55] and Mn-O is 1.84 Å.[56] Fe-O is shorter than Mn-O by 0.2 Å. Thus, when olefin approaches the oxygen atom of an oxo-metal complex, a relatively large steric interaction between the olefin and ortho substituents of oxo-iron complexes would be expected, compared with the case of manganese complexes. In iron complexes, owing to a large steric interaction, the electronic effect of the ortho-substituents has little influence on the binding affinity to the olefins. On the other hand, in manganese complexes, the steric interaction is not so large that the electronic effect reflects the binding affinity.

N-Alkylation of an Iron Porphyrin. Both cytochrome P-450 enzymes[57] and iron porphyrin-iodosylarene systems[58-62] undergo an *N*-alkylation of porphyrin in the epoxidation of 1-olefins. Although *N*-alkylation causes a "suicide" inactivation of P-450, a reduced activity is still retained in a model system.[59]

We observed an *N*-alkylaiton of FeCl in the course of the epoxidation of 1-octene. Under hypochlorite oxidant conditions FeCl and excess 1-octene were stirred for 4 min. The organic phase turned green. The UV-vis spectrum (λ_{max} 435, 578, 641 nm) was similar to that of the previously reported iron *N*-alkylporphyrins.[58,59]

For each of the two iron porphyrins the difference of K_m values among the three different olefins is small, as shown in Table 3. The V_{max} values for 1-octene are, however, about 1/10 of the V_{max} values for other two olefins. These kinetic data suggest that the oxo-1-octene intermediate has a relatively long lifetime. Therefore, a rearrangement of the intermediate may occur while affording *N*-alkylporphyrin.

Conclusively, we have demonstrated that: (1) the mechanism for the catalytic reaction by iron porphyrins is the Michaelis-Menten type as well as that by manganese complexes, (2) the differences of the metals or the ortho substituents give effects on oxidative catalyst destruction and on the Michaelis-Menten parameters, V_{max} and K_m, and (3) *N*-alkylation of an iron porphyrin has a relationship to the kinetic parameters.

This work was supported in part by a Grant-in-Aid for Scientific Research (No. 61470041) from the Ministry of Education, Science and Culture.

Refereces

1) J. T. Groves and T. E. Nemo, *J. Am. Chem. Soc*, **105**, 5786 (1983); **105**, 6243 (1983).
2) T. G. Traylor, J. C. Marsters, Jr., T. Nakano, and B. E. Dunlap, *J. Am. Chem. Soc.*, **107**, 5537 (1985).
3) T. G. Traylor and A. R. Miksztal, *J. Am. Chem. Soc.*, **109**, 2770 (1987).
4) J. P. Collman, T. Kodadek, S. A. Raybuck, J. I. Brauman, and L. M. Papazian, *J. Am. Chem. Soc.*, **107**, 4343 (1985).
5) D. Mansuy, J. Leclaire, M. Fontecave, and P. Dansette, *Tetrahedron*, **40**, 2847 (1984).
6) A. J. Castellino and T. C. Bruice, *J. Am. Chem. Soc.*, **110**, 158 (1988).
7) J. R. Lindsay Smith and P. R. Sleath, *J. Chem. Soc., Perkin Trans. 2*, **1982**, 1009.
8) C. K. Chang and F. Ebina, *J. Chem. Soc., Chem. Commun.*, **1981**, 778.
9) Y. Tatsuno, A. Sekiya, K. Tani, and T. Saito, *Chem. Lett.*, **1986**, 889.
10) J. A. Smegal and C. L. Hill, *J. Am. Chem. Soc.*, **105**, 3515 (1983).
11) T. C. Woon, C. M. Dicken, and T. C. Bruice, *J. Am. Chem. Soc.*, **108**, 7990 (1986).
12) W.-H. Wong, D. Ostović, and T. C. Bruice, *J. Am. Chem. Soc.*, **109**, 3428 (1987).
13) R. B. Brown, Jr., M. M. Williamson, and C. L. Hill, *Inorg. Chem.*, **26**, 1602 (1987).
14) D. Mansuy, P. Battioni, and J.-P. Renaud, *J. Chem. Soc., Chem. Commun.*, **1984**, 1255.
15) P. N. Balasubramanian, A. Sinha, and T. C. Bruice, *J. Am. Chem. Soc.*, **109**, 1456 (1987).
16) I. Tabushi and N. Koga, *J. Am. Chem. Soc.*, **101**, 6456 (1979).
17) I. Tabushi, M. Kodera, and M. Yokoyama, *J. Am. Chem. Soc.*, **107**, 4466 (1985).
18) J. van. Esch, M. F. M. Roks, and R. J. M. Nolte, *J. Am. Chem. Soc.*, **108**, 6093 (1986).
19) P. Battioni, J. F. Bartoli, P. Leduc, M. Fontecave, and D. Mansuy, *J. Chem. Soc., Chem. Commun.*, **1987**, 791.
20) F. P. Guengerich and T. L. Macdonald, *Acc. Chem. Res.*, **17**, 9 (1984).
21) P. S. Traylor, D. Dolphin, and T. G. Traylor, *J. Chem. Soc., Chem. Commun.*, **1984**, 279.
22) T. G. Traylor and S. Tsuchiya, *Inorg. Chem.*, **26**, 1338 (1987).
23) M. J. Nappa and C. A. Tolman, *Inorg. Chem.*, **24**, 4711 (1985).
24) B. R. Cook, T. J. Reinert, and K. S. Suslick, *J. Am. Chem. Soc.*, **108**, 7281 (1986).
25) K. S. Suslick and B. R. Cook, *J. Chem. Soc., Chem. Commun.*, **1987**, 200.
26) J. T. Groves and R. Neumann, *J. Am. Chem. Soc.*, **109**, 5045 (1987).
27) J. T. Groves and R. S. Myers, *J. Am. Chem. Soc.*, **105**, 5791 (1983).

28) D. Mansuy, P. Battioni, J.-P. Renaud, and P. Guerin, *J. Chem. Soc., Chem. Commun.*, **1985**, 155.
29) B. Meunier, E. Guilmet, M.-E. de Carvalho, and R. Poilblanc, *J. Am. Chem. Soc.*, **106**, 6668 (1984).
30) O. Bortolini and B. Meunier, *J. Chem. Soc., Perkin Trans. 2*, **1984**, 1967.
31) M.-E. de Carvalho and B. Meunier, *Nouv. J. Chim.*, **10**, 223 (1986).
32) B. Meunier, M.-E. de Carvalho, and A. Robert, *J. Mol. Catal.*, **41**, 185 (1987).
33) B. Meunier, M.-E. de Carvalho, O. Bortolini, and M. Momenteau, *Inorg. Chem.*, **27**, 161 (1988).
34) J. P. Collman, T. Kodadek, S. A. Raybuck, and B. Meunier, *Proc. Natl. Acad. Sci. U.S.A.*, **80**, 7039 (1983).
35) J. P. Collman, J. I. Brauman, B. Meunier, T. Hayashi, T. Kodadek, and S. A. Raybuck, *J. Am. Chem. Soc.*, **107**, 2000 (1985).
36) J. P. Collman, T. Kodadek, and J. I. Brauman, *J. Am. Chem. Soc.*, **108**, 2588 (1986).
37) R. J. M. Nolte, J. A. S. J. Razenberg, and R. Schuurman, *J. Am. Chem. Soc.*, **108**, 2751 (1986).
38) F. Montanari, M. Penso, S. Quici, and P. Viganó, *J. Org. Chem.*, **50**, 4888 (1985).
39) S. Takagi, E. Takahashi, T. K. Miyamoto, and Y. Sasaki, *Chem. Lett.*, **1986**, 1275.
40) T. K. Miyamoto, S. Takagi, T. Hasegawa, S. Tsuzuki, E. Takahashi, K. Okude, I. Banno, and Y. Sasaki, *Bull. Chem. Soc. Jpn.*, **60**, 1649 (1987).
41) E. Takahashi, H. Amatsu, T. K. Miyamoto, and Y. Sasaki, *Nippon Kagaku Kaishi*, **1988**, 480.
42) M. F. Zipplies, W. A. Lee, and T. C. Bruice, *J. Am. Chem. Soc.*, **108**, 4433 (1986).
43) A. D. Adler, F. R. Longo, F. Kampas, and J. Kim, *J. Inorg. Nucl. Chem.*, **32**, 2443 (1970).
44) 1 M=1 mol dm^{-3}.
45) J. A. S. Cavaleiro, M. J. E. Hewlins, A. H. Jackson, and G. P. M. S. Neves, *J. Chem. Soc., Chem. Commun.*, **1986**, 142.
46) Nolte et al. reported that μ-oxo dimerization complicates the epoxidation mechanism.[37]
47) N. Carnieri, A. Harriman, G. Porter, and K. Kalyanasundaram, *J. Chem. Soc., Dalton Trans.*, **1982**, 1231.
48) J. T. Groves and M. K. Stern, *J. Am. Chem. Soc.*, **109**, 3812 (1987).
49) J. T. Groves and Y. Watanabe, *Inorg. Chem.*, **25**, 4808 (1986).
50) O. Bortolini and B. Meunier, *J. Chem. Soc., Chem. Commun.*, **1983**, 1364.
51) Recent studies pointed out that more than one high-valent manganese intermediates presumably exist.[48,52] To our knowledge, however, the intermediate (λ_{max}=437 nm) has not been reported.
52) K. R. Rodgers and H. M. Goff, *J. Am. Chem. Soc.*, **109**, 611 (1987).
53) H. Lineweaver and D. Burk, *J. Am. Chem. Soc.*, **56**, 658 (1934).
54) W. A. Lee, T. S. Calderwood, and T. C. Bruice, *Proc. Natl. Acad. Sci. U.S.A.*, **82**, 4301 (1985).
55) J. E. Penner-Hahn, K. S. Eble, T. J. McMurry, M. Renner, A. L. Blach, J. T. Groves, J. H. Dawson, and K. O. Hodgson, *J. Am. Chem. Soc.*, **108**, 7819 (1986).
56) O. Bortolini, M. Ricci, B. Meunier, P. Friant, I. Ascone, and J. Goulon, *Nouv. J. Chim.*, **10**, 39 (1986).
57) O. R. Ortiz de Montellano, *Acc. Chem. Res.*, **20**, 289 (1987).
58) T. Mashiko, D. Dolphin, T. Nakano, and T. G. Traylor, *J. Am. Chem. Soc.*, **107**, 3735 (1985).
59) T. G. Traylor, T. Nakano, A. R. Miksztal, and B. E. Dunlap, *J. Am. Chem. Soc.*, **109**, 3625 (1987).
60) D. Mansuy, L. Devocelle, I. Artaud, and J.-P. Battioni, *Nouv. J. Chim.*, **9**, 711 (1985).
61) I. Artaud, L. Devocelle, J.-P. Battioni, J.-P. Girault, and D. Mansuy, *J. Am. Chem. Soc.*, **109**, 3782 (1987).
62) J. P. Collman, P. D. Hampton, and J. I. Brauman, *J. Am. Chem. Soc.*, **108**, 7861 (1986).

XANES of Aqua Complexes of 3d Transition Metals in Solid and Solution

Takafumi MIYANAGA, Iwao WATANABE,* Shigero IKEDA,† Kouji TASHIRO,†† and Takashi FUJIKAWA††
Department of Chemistry, Faculty of Science, Osaka University, Toyonaka, Osaka 560
†Institute of Science and Technology, Ryukoku University, Kyoto 612
††Faculty of Engineering, Yokohama National University, Yokohama 240
(Received April 13, 1988)

A characteristic second peak appears at about 10 eV from a main peak in the XANES (X-ray Absorption Near Edge Structure) spectrum of aqueous 3d transition metal complex of divalent state. This second peak is prominent in solid samples. The peak intensity depends on the kind of central metal or counter anion in solid. Theoretical calculations based on the full multiple scattering formalism provide the information regarding the origin and property of the second peak in XANES. The second peak can be reproduced by the multiple scattering calculation considering only six first coordinating oxygen atoms. The intensity and the position of the peak vary with the charge on the first coordinating oxygen atoms which is affected by the ions or solvent molecules contacting with the metal complex.

The coordination structures of hydrated complexes of 3d transition metals have been studied by X-ray diffraction technique[1] and EXAFS (Extended X-ray Absorption Fine Structure)[2,3] which investigate the pair correlation functions. Recently, it has been demonstrated that XANES spectroscopy directly provides higher order correlation function containing the information on geometries around the X-ray absorbing atom.[4] In the region of XANES are involved the electron transitions from a core level to unoccupied valence levels and multielectron effects (shake up and shake off). This complexity makes the XANES difficult to be applied to the characterization of materials.

We have found that there is a characteristic peak at about 10 eV higher from the main peak in the XANES spectra of hexaaqua 3d transition metal complexes of divalent state and the peak is stronger for solid samples than for aqueous solutions. Such a peak has also been reported in the XANES spectra of $MnCl_2$, $FeCl_2$, and $CoCl_2$, at about 5 eV higher from the main peak. Stern[5] explained it in terms of multielectron excitation such as shake up process by referring to the results of XPS. Sham[6] has observed an analogous peak at 6.8 eV higher from the main peak for L_{III}-edge of Pt in K_2PtCl_4 solid. This peak is not present in the spectrum of solution state. He concluded that this peak is most likely due to the density of state effects involving Pt–Pt interaction. In the XANES of Ge, a similar peak is more prominent in crystal state than in amorphous state. Proietti et al.[7] have attributed the peak to the multiple scattering effect by the second and the third coordination shell.

In this paper, we study the origin of the second peak in K-edge XANES of hexaaqua complexes of 3d transition metals by means of multiple scattering calculation. The XANES calculations are performed according to the scheme described in detail elsewhere[8] in which the full multiple scattering effect is taken into consideration. The scattering property of each atomic pair is described by a set of scattering phase shifts which depends on the electronic structure of the atom. Thus the charge distribution around the X-ray absorbing atom can be obtained by means of XANES analysis.

Experimental

$Mn(ClO_4)_2 \cdot 6H_2O$ and $Co(ClO_4)_2 \cdot 6H_2O$ were purchased from Kishida Chemicals, Ltd. and $Ni(NO_3)_2 \cdot 6H_2O$ and $Fe(ClO_4)_3 \cdot 6H_2O$ from Nakarai Chemicals, Ltd. $CrSO_4 \cdot 5H_2O$, $Cr(ClO_4)_3 \cdot 6H_2O$, $Fe(ClO_4)_2 \cdot 6H_2O$, $Cu(ClO_4)_2 \cdot 6H_2O$, and $Zn(ClO_4)_2 \cdot 6H_2O$ were prepared according to the text.[9] The solution of Ti^{3+}, Cr^{2+}, and Fe^{2+} were prepared by the electrolytic reductions of each sulphate (Ti^{4+}, Cr^{3+}) or perchlorate (Fe^{3+}) solutions. The solution of V^{3+} ion was prepared by mixing equal amounts of V^{4+} and V^{2+} sulphate solutions. Since these low valence state ions are very sensitive to air and are easily oxidized, all the procedures for the preparations as well as the X-ray absorption measurements were performed under a dry nitrogen gas atmosphere.

The solid powdered samples were held on adhesive tapes and the liquid samples were placed in airtight polyethylene pouches. The concentrations of metal ions in solution were 1.0 mol dm^{-3}.

All of the K-edge absorption spectra were recorded at BL-7C of the Photon Factory of National Laboratory for High Energy Physics (KEK) in Tsukuba. A Si(111) double crystal monochromator was used. The storage ring was operated at 2.5 GeV and the ring current was 150—200 mA.

Method of XANES Calculation

The XANES theory used in this paper is based on the short range order multiple scattering theory proposed by one of the present authors.[10] The $\chi(k)$ is calculated by the same method as the one for EXAFS. $\chi(k)$ is defined as

$$\chi(k) = (\sigma(k) - \sigma_o(k))/\sigma_o(k),$$

where $\sigma_o(k)$ is the photo-absorption cross section of the core orbital of a free atom, $\sigma(k)$ is the cross section in the presence of surrounding atoms, and k is the wave vector of the ejected photoelectron.

For semiconductors and insulators, the core holes

are not fully screened and the hole potential felt by a photoelectron is too large to be neglected.[11] One of the simplest models for the hole potential is a $Z+1$ potential. In this paper it is assumed that the system is fully relaxed in the final state and the photo-absorbing atom is replaced with a $Z+1$ atom.

The phase shifts are obtained under the Hartree-Fock approximation by using Pendry's program.[12] Practically it requires the charge densities of atoms calculated from the interatomic distances and the charges of atoms. Usually the distances are obtained from X-ray diffraction data and the charges are from Pauling's method.[13] In the present work, the charges are treated as the unknown parameters for the XANES calculations in order to clarify their contribution to the XANES.

Results and Discussion

XANES Spectra. The structures of the hexaaqua complexes of 3d transition metals are normally octahedral, except for Cr^{2+} and Cu^{2+} in which there are a Jahn-Teller distortion.

The K-edge XANES spectra for trivalent 3d metal complexes are shown in Fig. 1. There is a weak dipole-forbidden 1s–3d transition peak in the pre-edge region of each XANES spectrum. The energy scale refers to this pre-edge peak. The shapes of the XANES for trivalent hexaaqua complexes, especially Ti^{3+}, V^{3+}, and Cr^{3+}, resemble each other. Figure 2 shows the XANES spectra for divalent 3d metal complexes in solid and solution. It is interesting to note that the XANES spectra for hexaaqua complexes in solution (Fig. 2 right) are quite similar to each other, except for Cr^{2+} and Cu^{2+}. The shapes of XANES for Cr^{2+} and Cu^{2+} are different from those for other metal complexes possibly because of the Jahn-Teller distortion. Garcia et al.[14] reported that the theoretical calculation for a CuO_6 cluster, taking into account the Jahn-Teller distortion (>0.3 Å), predicted the presence of the peaks on both low- and high-energy sides of a main peak. In our spectra, there are two peaks on high-energy side of the main peak B in Fig. 2 for Cr^{2+} and Cu^{2+}, and there is a single peak on the edge for $CrSO_4 \cdot 5H_2O$ in which the difference in bond length between those for axial and equatrial amounts to 0.43 Å.[15] The distances between peaks in XANES are listed in Table 1. The main peak B shifts to high-energy side with the increase of atomic number of central metal.

Another characteristic spectral feature for aqua complexes of divalent metals is that the peak C at about 10 eV higher energy side from the main peak is stronger in solid than in solution. This peak is especially strong in the spectra of Zn^{2+} as shown in

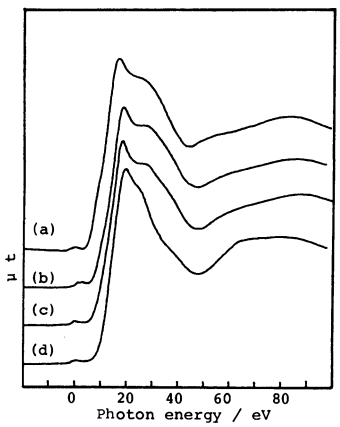

Fig. 1. K-edge XANES spectra for trivalent 3d metal complexes in aqueous solution of (a) Ti^{3+}, (b) V^{3+}, (c) Cr^{3+}, and (d) Fe^{3+} ions. The energy scale refers to the pre-edge peak.

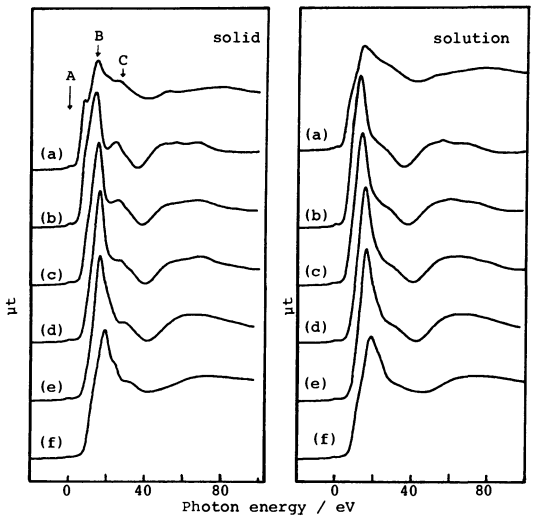

Fig. 2. K-edge XANES spectra for 3d metal complexes of (a) $CrSO_4 \cdot 5H_2O$, (b) $Mn(ClO_4)_2 \cdot 6H_2O$, (c) $Fe(ClO_4)_2 \cdot 6H_2O$, (d) $Co(ClO_4)_2 \cdot 6H_2O$, (e) $Ni(NO_3)_2 \cdot 6H_2O$, and (f) $Cu(ClO_4)_2 \cdot 6H_2O$ (left) and corresponding metal solutions (right).

Table 1. Intervals between Peaks in eV

	Cr^{2+}	Mn^{2+}	Fe^{2+}	Co^{2+}	Ni^{2+}	Cu^{2+}	Zn^{2+}
A–B (solid)	14.3	13.7	16.2	16.9	17.1	19.2	—
A–B (solution)	14.3	12.5	15.1	16.9	15.9	18.9	—
B–C (solid)	6.1 11.3	10.5	11.3	11.2	12.6	5.4 13.9	11.9

Fig. 3. The order of the intensities of this peak is $Zn^{2+}>Mn^{2+}>Fe^{2+}>Co^{2+}>Ni^{2+}$. Regarding the origin of the peak C, the possibility of the multielectron effect observed in XANES for 3d metal chlorides[5] can be ruled out because (1) the peak intensities are different in solids and solutions and (2) the peak appears remarkably in Zn^{2+} compounds in which 3d orbitals are filled with valence electrons exhibiting no shake up peak in XPS. It has also been reported[16] that the plasmon satellites are featureless and probably lost in the background in the low kinetic energy region in XPS and this would make the shake up phenomenon quite weak in XANES region. It is possible that the appearance of the peak C is caused by the multiple scattering effect of photoelectrons. The multiple scattering calculation for ZnSe by Matsuura,[17] reproduces the second peak at about 10 eV higher from the main peak when the second shell scattering is included for the calculation. In the case of Ge crystal,[7] the peak is caused presumably by the multiple scattering by the shell extending further than the second shell. The XANES spectra for Zn^{2+} crystals having various counter anions are shown in Fig. 3. The second peak is observed in each spectrum, with the intensity order of $ClO_4^->NO_3^->SO_4^{2-}$. The peak is also observed in solution though it is rather weak. The XANES spectra for Zn^{2+} solutions are the same regardless of the kind of the anion. From the results of solutions, it is inferable that the second shell is less important, and that the electron scattering by only nearest six coordinating oxygen atoms would make the peak appear.

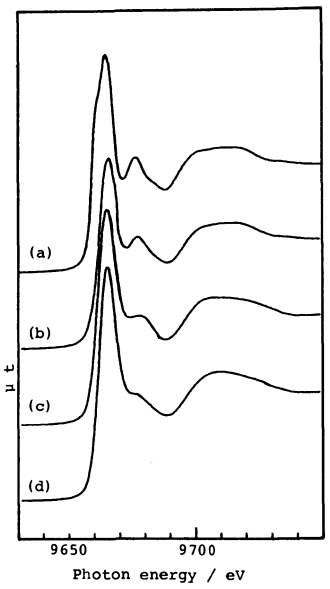

Fig. 3. K-edge XANES spectra for Zn^{2+} compounds, (a) $Zn(ClO_4)_2\cdot 6H_2O$, (b) $Zn(NO_3)_2\cdot 6H_2O$, (c) $ZnSO_4\cdot 7H_2O$, and (d) Zn^{2+} aqueous solution.

Multiple Scattering Calculation. $[Zn(OH_2)_6]^{2+}$ complex is chosen as a model in order to reveal the character of the second peak or the peak C in XANES, because the second peak for Zn^{2+} is the most prominent among the 3d transition metals and the calculation is expected to be the simplest owing to the fully occupied 3d orbitals.

First, the cluster consisting of 35 atoms having Zn at the center, $ZnO_{26}N_8$, is adopted as the model for solid $Zn(NO_3)_2\cdot 6H_2O$. The positions of the selected atoms are within 5 Å from Zn and fixed according to the X-ray diffraction results.[18] For the phase shift calculations of the central Zn atom and the first coordinating oxygen atoms, a diatomic molecule, Zn–O, is considered and its bond length is assumed to be 2.08 Å which is observed in solution.[1] The charges on Zn and O atoms are unknown parameters. They are determined by putting the trial values to get the best fit between the theoretical result and the experimental spectrum. Figure 4 (a) shows the

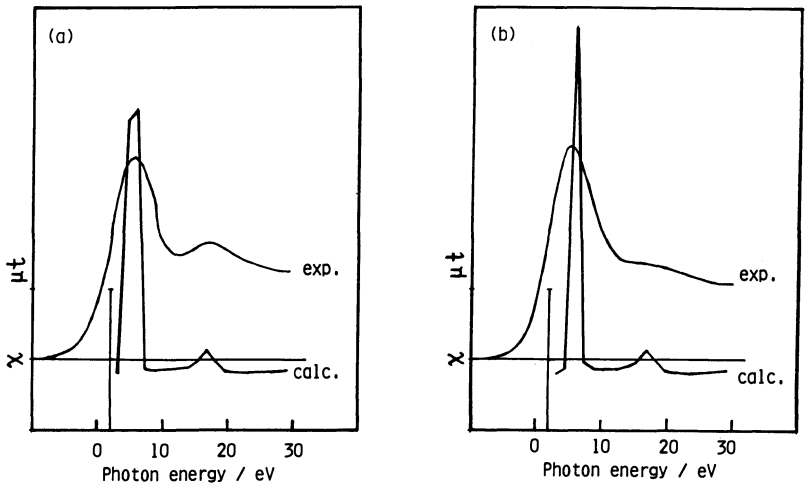

Fig. 4. Theoretical and experimental XANES spectra for (a) $Zn(NO_3)_2\cdot 6H_2O$ crystal and (b) Zn^{2+} aqueous solution.

XANES spectrum of $Zn(NO_3)_2 \cdot 6H_2O$ and the calculated XANES spectrum for the $ZnO_{26}N_8$ cluster model when the charge of Zn atom is 1.2 (that of O atom is −1.2). The charge of NO_3 is fixed as neutral. The charges of Zn and the first coordinating O atoms are determined so as to reproduce the positions of the main B and the second peak C of the experimental spectrum. In the present work, only the intensity and the position of the second peak are important. Therefore the theoretical XANES spectra are not corrected for the absolute intensity and the widths of the peaks, which can be estimated by considering the absorption cross section of free atom and the life time of the excited state.

Next, the calculation was performed on the model of a ZnO_6 cluster representing the complex present in aqueous solution. The second coordinating atoms are those in solvent molecules and they cannot contribute to produce the fine structure in XANES and EXAFS because their positions are randomly distributed. The shape of the cluster is octahedral and the distance of Zn–O is 2.08 Å.[1] The calculated XANES spectrum for the solution model is shown in Fig. 4 (b). This is a very important result which indicates that the multiple scattering effect confined only in the ZnO_6 moiety gives rise to the second peak. We had expected that the intensity of the second peak in the calculated spectrum for the solid model should be stronger than that for the aqueous solution model. The intensities and the positions of the second peaks are, however, almost the same.

Subsequently, the effect of solvent molecules in this calculation is studied just in case. Twelve oxygen atoms of water molecules are added to the ZnO_6 cluster. It is assumed that the water molecules bond to the complex through the hydrogen bonding and that the distance of O–O in Zn–O–H···O–H and the angle of Zn–O–H are 2.5 Å and 140° in this model. Further, the multiple scattering calculations are performed for the models having the water molecules at various places which simulate the distribution of the solvent molecules. However, the results are not different from those of the ZnO_6 cluster and the solid. We conclude that the second shell atoms and/or the atoms outside of the second coordination shell atoms should not contribute much to the appearance of the second peak in XANES for the 3d metal aqua complexes.

The Effect of the Charge on Oxygen. From the full multiple scattering calculation the following conclusions are derived. (1) In order to produce the second peak in XANES only the first coordination shell atoms are neccessary. (2) Addition of the second shell atoms results in no alteration in the strength or in the position of the second peak. (3) Thus it is impossible only by placing the scattering atoms around the central atom to reproduce the experimental facts that the second peak is lower for solution

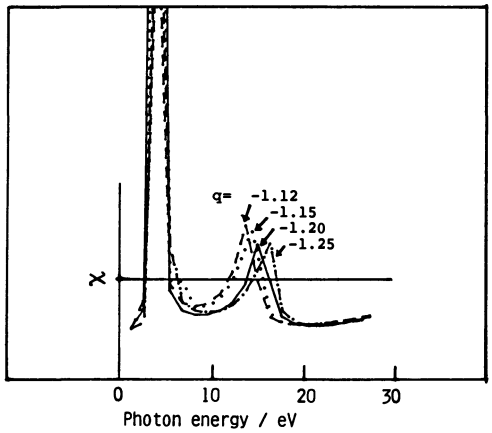

Fig. 5. Calculated XANES spectra for various charges (−1.12—−1.25) on the first coordinating oxygen atoms. The charge on Zn atom is fixed at 1.2.

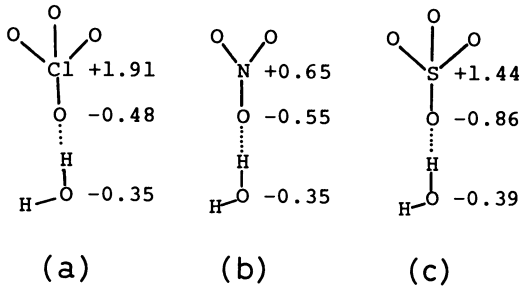

Fig. 6. Charge distributions on water molecule and counter anions determined by MNDO calculations: (a) ClO_4^-, (b) NO_3^-, and (c) SO_4^{2-}.

sample than that for solid sample and that the peak height for the solid sample is quite sensitive to the kind of counter anion.

In order to explain the effect of the counter anion on the second peak in XANES, the charge of the first coordinating oxygen atoms should be incorporated into the calculation. Figure 5 shows the calculated XANES spectra for the various charges (−1.12—−1.25) of the first coordinating oxygen atoms in ZnO_6 cluster model, where the charge of Zn is fixed to be 1.2. The intensities and positions of the second peak change according to the charge of the first coordinating oxygens. The more the negative charge on oxygens, the lower the second peak height and the lower the peak position in energy. Then, in order to estimate the charge on the oxygen atoms, or the alteration of the charge due to the anions, we perform MNDO calculations, which are recognized as the useful quantum chemical method to predict the charges of the atoms up to Cl atom in periodic table.[19,20] The calculations performed here consider only the counter anion and water molecule. The results of the calculations are shown in Fig. 6. The lengths of the hydrogen bondings between H_2O and counter anions are optimized by the calculations so

that they are not necessarily the same as those for the crystals. The calculations indicate that SO_4^{2-} ion induces more negative charge on the oxygen atom than ClO_4^- or NO_3^- does. The experimental result that the crystal with the ClO_4^- or NO_3^- counter ion gives the stronger second peak is in accordance with the theoretical prediction that these anions induced less negative charge on the oxygens, thus the intensities for these crystals are stronger. The peak shifts are also well-predicted with the present model calculation. In this way, the characteristics of the intensity and the position of the second peak can be explained qualitatively by taking into account the variation of the charge on the first coordinating oxygens.

In the case of solution sample, the second coordinating water molecules take various positions around the first coordinaing water molecules. Thus, the charge on the first coordinating oxygens fluctuates depending on the length of the hydrogen bonding between the first and the second water molecules. It may be concluded that the fluctuation of the charge on the first coordinating oxygen atoms would smooth out the second peak in XANES because the position of the peak shifts according to the charges of the first coordinating oxygens. In conformity with this view, the reason why the second peak for Mn^{2+} or Zn^{2+} having a larger ionic radius is stronger than the other complexes is understandable. That is, the negative charge induced by the central metal cation on the oxygen atoms of the first coordinating water molecules must be smaller for larger ionic radius cations.

In conclusion, we believe that the second peak in XANES of the aqueous 3d metal complex appears due to the multiple scattering effect in the system consisting of the central metal and only six first coordinating oxygen atoms, and that its intensity and position vary with the charge on the first-coordinating oxygen atoms which is affected by the second and/or further coordinating atoms. The feature at the higher energy region of several eV from the main peak in XANES seems to contain the information concerning the second coordinating atoms which are too far from the central atom to be studied by means of EXAFS.

The authors thank Drs. Tadashi Matsushita and Masaharu Nomura of the National Laboratory for High Energy Physics (KEK) for their help and suggestions on EXAFS measurements. This work was supported by the Grant-in-Aid for Special Project Research No. 62124039 from the Ministry of Education, Science and Culture.

References

1) H. Ohtaki, T. Yamaguchi, and M. Maeda, *Bull. Chem. Soc. Jpn.*, **49**, 701 (1976).
2) T. K. Sham, *Acc. Chem. Res.*, **19**, 99 (1986).
3) P. Lagarde, A. Fontaine, A. Sadoc, and D. Migliardo, *J. Chem. Phys.*, **72**, 3061 (1980).
4) M. Benfatto, C. R. Natoli, A. Bianconi, J. Garcia, A. Marcelli, M. Fanfoni, and I. Davoli, *Phys. Rev. B*, **34**, 5774 (1986).
5) E. A. Stern, *Phys. Rev. Lett.*, **49**, 1353 (1982).
6) T. K. Sham, *J. Chem. Phys.*, **84**, 7054 (1986).
7) M. G. Proietti, S. Mobilio, A. Gargano, L. Incoccia, and F. Evangelisti, "EXAFS and Near Edge Structure III," Springer, 26 (1985).
8) T. Fujikawa, T. Matsuura, and H. Kuroda, *J. Phys. Soc. Jpn.*, **52**, 905 (1983).
9) "Shin-Jikken Kagaku Koza," ed by M. Nakahara and M. Shibata, Maruzen, Tokyo (1977), Vol. 3.
10) T. Fujikawa, *J. Phys. Soc. Jpn.*, **50**, 1321 (1980).
11) R. V. Vedrinskii, L. A. Bugaev, I. I. Gegusin, V. L. Kraaizman, A. A. Novakovich, S. A. Prosandeev, R. E. Ruus, A. A. Maiste, and M. A. Elangs, *Solid State Commun.*, **44**, 1401 (1982); T. Fujikawa, *J. Phys. Soc. Jpn.*, **52**, 4001 (1983).
12) J. B. Pendry, "Low Energy Electron Diffraction," Academic Press, (1974).
13) L. Pauling, "The Nature of the Chemical Bond," Cornell University Press, (1960).
14) J. Garcia, A. Bianconi, M. Benfatto, and C. R. Natoli, *J. Phys. Paris*, **47** (C8), 49 (1986).
15) H. Ito, Y. Ito, F. Kanamaru, K. Koto, N. Matsubayashi, I. Watanabe, and S. Ikeda, *Z. Kristallogr.*, **181**, 99 (1987).
16) T. Fujikawa, *J. Phys. Soc. Jpn.*, **55**, 3244 (1986).
17) T. Matsuura, T. Fujikawa, and H. Oyanagi, *J. Phys. Soc. Jpn.*, **53**, 2837 (1984).
18) A. Ferrari, A. Branbanti, A. M. M. Lanfredi, and A. Tiripicchio, *Acta. Crystallgr.*, **22**, 240 (1967).
19) M. J. S. Dewar, H. S. Rzepa, and M. L. McKee, *J. Am. Chem. Soc.*, **100**, 3607 (1978).
20) T. Fujikawa, K. Tashiro, W. Krone, and G. Kaindl, *J. Phys. Soc. Jpn.*, **57**, 320 (1988).

Asymmetric Reduction of α-(Dimethylthiocarbamoylthio) Carbonyl Compounds with Bakers' Yeast

Sadao Tsuboi,* Noriyuki Kohara, Katsumi Doi, Masanori Utaka, and Akira Takeda
Department of Synthetic Chemistry, School of Engineering, Okayama University, Tsushima, Okayama 700
(Received February 15, 1988)

Treatment of α-(dimethylthiocarbamoylthio) ketones with bakers' yeast afforded the corresponding chiral alcohols in high yields with high enantiomeric excess (in most cases, more than 96% ee). α-(Dimethylthiocarbamoylthio) aldehydes were reduced to give chiral α-(dimethylthiocarbamoylthio) alcohols in 69—92% yields with 32—63% ee, which were converted to chiral 1,2-epithio derivatives.

Recently, asymmetric reduction of ketones with bakers' yeast (Saccharomyces cerevisiae) has been widely utilized for the preparation of chiral building blocks.[1] It is well-known that the reduction of β-keto esters by bakers' yeast affords optically active β-hydroxy esters.[1] Generally speaking, ketones α-substituted by an electron-withdrawing group are inclined to be reduced with bakers' yeast. Ketones α-substituted by sulfur atoms are also reduced to give chiral alcohols. For example, asymmetric reductions of compounds such as 1,3-dithians,[2] sulfides,[3] sulfones[4] with bakers' yeast are reported. Here, we describe an asymmetric reduction of α-(dimethylthiocarbamoylthio) ketones **1** with bakers' yeast, leading to chiral alcohols **2**. Ketones **1** can be obtained in high yield by the reaction of α-halo ketones with sodium dimethyldithiocarbamate, which is commercially available and can be easily prepared by the reaction of dimethylamine and carbon disulfide in the presence of sodium hydroxide.[5]

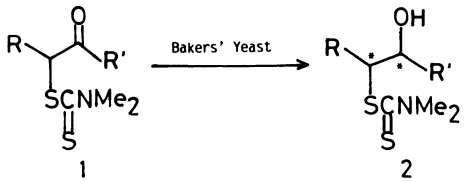

1 2

Various ketones **1** were prepared and treated with bakers' yeast in tap water in the presence of glucose. The reaction gave chiral alcohols **2** in good yield. Enantiomeric excess of the chiral alcohols obtained was determined by ^{1}H NMR analysis in the presence of chiral shift reagent (Eu(hfc)$_3$) and/or by HPLC analysis for the corresponding esters of (*S*)-(+)-α-methoxy-α-(trifluoromethyl)phenylacetic acid (MTPA).[6] These results are shown in Table 1.

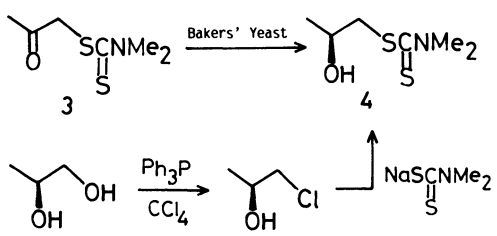

Treatment of α-(dimethylthiocarbamoylthio)acetone (**3**) with bakers' yeast gave the corresponding chiral alcohol **4** with more than 96% ee in unusually

Table 1. Asymmetric Reduction of α-(Dimethylthiocarbamoylthio)-Substituted Carbonyl Compounds with Bakers' Yeast

Ketone	Product	Reaction time/day	Yield[a] %	ee %
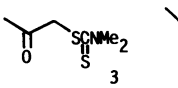 3	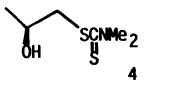 4	6	91	>96
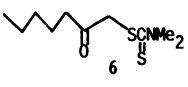 6	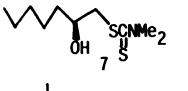 7	6	39	>96
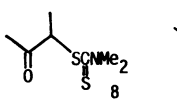 8	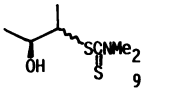 9	4	82[b]	>96[c]
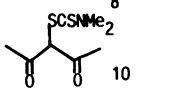 10	3	4	25	—
	4	4	39	77
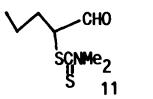 11	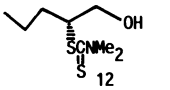 12	5	92	55
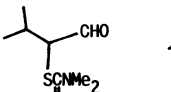 13	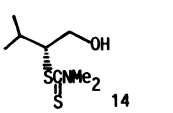 14	9	69	32
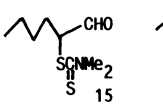 15	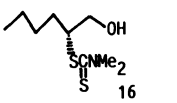 16	10	78	46
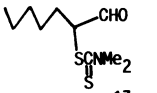 17	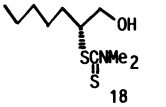 18	9	75	63

a) Isolated yield. b) Isolated as a diastereomeric mixture: erythro/threo=72/28. c) Both of erythro and threo.

high yield (91%). The absolute configuration was determined to be *S* by the independent synthesis of **4** via (*S*)-1-chloro-2-propanol from (*S*)-(+)-1,2-propanediol, as shown in experimental section. Reduction of **4** with $LiAlH_4$ gave 1-mercapto-2-propanol (**5**) in 83%

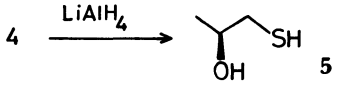

yield. Chiral reduction of 1-(dimethylthiocarbamoylthio)-2-heptanone (**6**) with bakers' yeast afforded optically pure (*S*)-(+)-1-(dimethylthiocarbamoylthio)-2-heptanol (**7**) in 39% yield. Treatment of 3-(dimethylthiocarbamoylthio)-2-butanone (**8**) with bakers' yeast yielded the diastereomeric mixture of the corresponding alcohols **9** with the ratio of erythro/threo (72/28) in 82% yield. Optical purities of each isomer separated by preparative HPLC were more than 96% ee. Treatment of 3-(dimethylthiocarbamoylthio)-2,4-pentanedione (**10**) with bakers' yeast gave a mixture of hydrolysis product **3** and its reduced product **4**. Absolute configuration of the chiral alcohols **7** and **9** was presumed to be *S* by comparison of the symbol of the optical rotation of **4**. This fact consists with the results obtained on the reduction of other sulfur-substituted ketones.[3,4]

Furthermore, α-(dimethylthiocarbamoylthio) aldehydes were also reduced with bakers' yeast to give chiral alcohols unexpectedly, although the optical purity was not high. For example, 2-(dimethylthiocarbamoylthio)pentanal (**11**) was reduced with bakers' yeast to give the corresponding alcohol **12** in 92% yield with 55% ee. As shown in the table, some aldehydes such as **13**, **15**, and **17** were also reduced with bakers' yeast to give the corresponding chiral alcohols **14**, **16**, and **18** in good yields.

Some optically active epithio compounds are synthesized because they are important for the preparation of chiral polymers containing sulfur.[7] The reduced products were converted to the thioepoxides and the absolute configuration was determined as *R* by comparison of the direction of the optical rotation with that of known epithio compounds.[7] Compound **12** was treated with sodium hydride to give (*R*)-(+)-1,2-epithiopentane (**19**) in 40% yield. Compound **14** was also treated with sodium hydride to give a known compound, (*R*)-(+)-3-methyl-1,2-epithiobutane (**20**).[7]

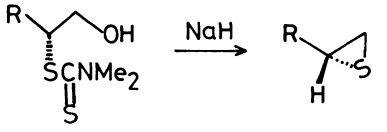

12, R=$CH_2CH_2CH_3$ **19**, R=$CH_2CH_2CH_3$
14, R=$CH(CH_3)_2$ **20**, R=$CH(CH_3)_2$

The present reduction with bakers' yeast afforded chiral (dimethylthiocarbamoylthio) alcohols in good yield, which would be useful for the synthesis of sulfur containing natural products[8] and chiral thiiranes[7] because the reaction conditions are mild and the procedures are simple and economically feasible.

Experimental

The melting points and boiling points are uncorrected. Elemental analyses were carried out by Eiichiro Amano in our laboratory. Analytical spectra were obtained with the following instruments: IR, Jasco Model A-102; ^1H NMR (60 MHz), JEOL JNM-PMX60SI apparatus; ^1H NMR (100 MHz) and ^{13}C NMR (25 MHz), JEOL JNM-FX100 apparatus. Optical rotations were measured on a Jasco DIP-4 spectrometer. HPLC analysis was performed with a Yanagimoto liquid chromatograph L-2000 fitted with a Yanapak SA-I (6-mm o.d.×250-mm length) and with a Sumipax OA-3000 (4-mm o.d.×250-mm length) for the determination of enantioselectivity.

Fermentation was carried out at 31—35 °C by using industrial bakers' yeast purchased from Oriental Yeast Co., Ltd. All glasswares were sterilized by boiling water before use. The amount of consumed glucose was checked by test paper for that of glucose in urine. During the fermentation, additional glucose was added when the concentration became less than 0.5%. α-Chloro aldehydes were prepared by the reaction of aldehydes with sulfuryl chloride.[9]

α-(Dimethylthiocarbamoylthio)acetone (3). To a solution of 5 g (35 mmol) of sodium dimethyldithiocarbamate in 30 ml of methanol was added dropwise 3.9 g (42 mmol) of chloroacetone with cooling. The mixture was stirred overnight at room temperature and then poured into water. After the mixture was concentrated in vacuo, the organic material was extracted with dichloromethane. The combined extracts were washed with water, dried over $MgSO_4$, and concentrated to give 5.46 g (88%) of **3**: mp 50—51 °C (from ethyl acetate); IR (KBr) 1715, 1498, 1355, 1255, 1155, and 980 cm^{-1}; ^1H NMR ($CDCl_3$) δ=2.33 (s, 3H, $COCH_3$), 3.49 (s, 6H, $N(CH_3)_2$), 4.18 (s, 2H, CH_2). Found: C, 40.78; H, 6.17; N, 7.68%. Calcd for $C_6H_{11}NOS_2$: C, 40.65; H, 6.26; N, 7.90%.

(*S*)-(+)-1-(Dimethylthiocarbamoylthio)-2-propanol (4). To a mixture of KH_2PO_4 (1 g), $NH_4H_2PO_4$ (1 g), $MgSO_4$ (0.5 g), $CaCO_3$ (2.5 g), glucose (90 g), and boiled water (450 ml) was added 9 g of bakers' yeast at 32 °C. After bubbles formed (ca. 20 min), 3 g (16.9 mmol) of **3** was added and then the mixture was stirred at 32 °C for 57 h. The organic layer was extracted with ethyl acetate. The combined extracts were washed with water, dried ($MgSO_4$), and concentrated to give 3.22 g of an oil, which was chromatographed on SiO_2 (hexane/CH_2Cl_2=5/1) to give 2.74 g (91%) of **4**: bp 240 °C (10 mm) (short-pass distillation); mp 50—51 °C (from ether); $[\alpha]_D^{13}$ +52.2° (*c* 0.20, $CHCl_3$); IR (neat) 3400, 2990, 2940, 1500, 1375, 1255, 1145, 1120, 980 cm^{-1}; ^1H NMR ($CDCl_3$) δ=1.28 (d, *J*=6 Hz, 3H, CH_3CHOH), 2.97 (s, 1H, OH), 3.43 (m, 8H, $(CH_3)_2N$, CH_2S), 4.00 (m, 1H, CH_3CHOH). Found: C, 39.78; H, 6.88; N, 7.20%. Calcd for $C_6H_{13}NOS_2$: C, 40.19; H, 7.31; N, 7.81%.

Independent Synthesis of 4. To 1.15 g (4.4 mmol) of triphenylphosphine was added a solution of 313 mg (4.12 mmol) of (*S*)-(+)-1,2-propanediol ($[\alpha]_D^{26}$ +16.9° (neat))

in 3 ml of CCl_4 under an atmosphere of nitrogen. The mixture was heated under reflux for 4 h and then cooled to room temperature. A mixed solvent of hexane and ether (3/1) was added and the mixture was filtered. After concentration of the filtrate, the residue was added dropwise into a solution of 630 mg (4.4 mmol) of sodium dimethyldithiocarbamate in 5 ml of methanol and then the mixture was heated under reflux for 4 h. After evaporation of the solvent, the residue was poured into water. The organic layer was extracted with ethyl acetate. The extracts were washed with water, and dried over $MgSO_4$. Evaporation of the solvent gave 256 mg of the crude product, which was purified by preparative TLC (hexane/ethyl acetate, 1/1) to give 43 mg (5.8%) of **4**: R_f 0.34—0.51; $[\alpha]_D^{27}$ +33.3° (*c* 0.96, $CHCl_3$). IR and ^1H NMR data were identical with those of an authentic sample prepared above.

(*S*)-(+)-1-Mercapto-2-propanol (5). To a stirred mixture of $LiAlH_4$ (150 mg, 3.95 mmol) and dry ether (5 ml) was added a solution of **4** (471 mg, 2.63 mmol) in 5 ml of dry ether at −20 °C. The mixture was stirred for 2 h at −20 °C and then quenched with dilute HCl. The organic layer was extracted with ether and the combined extracts were washed with water, dried over $MgSO_4$, and concentrated. Removal of the solvent gave 142 mg (59%) of **5**: $[\alpha]_D^{22}$ +86.1° (*c* 2.42, $CHCl_3$); IR (neat) 3400, 3000, 1260, 1125, 1070 cm^{-1}. ^1H NMR data were identical with those of the literature.[10]

1-(Dimethylthiocarbamoylthio)-2-heptanone (6). To a solution of 1.92 g (16.9 mmol) of 2-heptanone in 15 ml of ether was added 2.70 g (0.87 ml, 16.9 mmol) of bromine at 0 °C. After the brown color disappeared, the mixture was poured into water and the organic materials were extracted with ether. The combined extracts were washed with saturated $NaHCO_3$ and water, and dried over $MgSO_4$. Concentration of the solvent gave 3.17 g (97%) of a mixture of 3-bromo-2-heptanone and 1-bromo-2-heptanone (4/1): IR (neat) 1720, 1460, 1350, 1220 cm^{-1}; ^1H NMR (CCl_4) δ=0.91 (t, 3H, CH_3), 1.10—1.65 (m, 4H, $(CH_2)_2$), 1.70—2.20 (m, 2H, $C\underline{H}_2CHBr$), 2.27 (s, 3H, $C\underline{H}_3CO$), 4.17 (t, 1H, $C\underline{H}Br$). To a solution of 1.43 g (10.0 mmol) of sodium dimethyldithiocarbamate in 10 ml of methanol was added dropwise 1.50 g of the brominated 2-heptanone described above and the mixture was stirred overnight. After evaporation of the solvent, the residue was poured into water. The organic materials were extracted with CH_2Cl_2. The combined extracts were washed with water, dried over $MgSO_4$, and concentrated. The crude oil (2.55 g) was chromatographed on SiO_2 to give 1.06 g (74%) of 3-(dimethylthiocarbamoylthio)-2-heptanone: IR (neat) 1710, 1500, 1250, 1150, 1050, 980 cm^{-1}; ^1H NMR (CCl_4) δ=0.91 (t, 3H, CH_3), 1.10—2.00 (m, 6H, $(CH_2)_3$), 2.19 (s, 3H, $C\underline{H}_3CO$), 3.47 (s, 6H, $N(C\underline{H}_3)_2$), 4.82 (t, 1H, $C\underline{H}SCSN$). The last fraction gave 60 mg (16%) of **6**: ^1H NMR (CCl_4) δ=0.92 (t, 3H, CH_3), 1.1—2.0 (m, 6H, $(CH_2)_3$), 2.65 (t, 2H, $C\underline{H}_2CO$), 3.50 (s, 6H, $N(C\underline{H}_3)_2$), 4.20 (s, 2H, $C\underline{H}_2SCSN$). Found: C, 51.68; H, 7.94; N, 6.01%. Calcd for $C_{10}H_{19}NOS_2$: C, 51.46; H, 8.20; N, 6.00%.

(*S*)-(+)-1-(Dimethylthiocarbamoylthio)-2-heptanol (7). To a mixture of KH_2PO_4 (0.2 g), $NH_4H_2PO_4$ (0.2 g), $MgSO_4$ (0.1 g), $CaCO_3$ (0.5 g), glucose (10 g), and boiled water (100 ml) was added 1 g of bakers' yeast at 32 °C. After bubbles formed (ca. 15 min), 0.125 g (0.534 mmol) of **6** was added and then the mixture was stirred at 35 °C. After 84 h, 1 g of bakers' yeast was added. After 113 h, 2 g of glucose was added. After 5.5 h, the organic layer was extracted twice with ethyl acetate and CH_2Cl_2. The combined extracts were washed with water and dried over $MgSO_4$. Concentraion of the solvent gave 0.116 g of the crude product, which was purified with column chromatography to give 55 mg (39%) of **7**: ^1H NMR (CCl_4) δ=0.9 (t, 3H, CH_3), 1.1—1.8 (m, 8H, $(CH_2)_4$), 3.1—3.6 (m, 9H, $C\underline{H}_2C\underline{H}OH$, $N(C\underline{H}_3)_2$), 3.68 (d, 2H, $CHOHC\underline{H}_2$); $[\alpha]_D^{32}$ +12.0° (*c* 0.50, $CHCl_3$); >95% ee by ^1H NMR analysis in the presence of Eu(hfc)$_3$. Found: C, 51.07; H, 8.69; N, 5.83%. Calcd for $C_{10}H_{21}NOS_2$: C, 51.02; H, 8.99; N, 5.95%.

3-(Dimethylthiocarbamoylthio)-2-butanone (8). To a mixed solution of sodium dimethyldithiocarbamate in 10 ml of methanol was added 1.50 g of a mixture of 3-chloro-2-butanone and 3,3-dichloro-2-butanone (5/6)[9] with ice cooling. The mixture was stirred overnight and concentrated. The organic layer was extracted with CH_2Cl_2, washed with water, dried over $MgSO_4$, and concentrated. The residual oil (1.93 g) was purified with column chromatography (hexane/ethyl acetate, 10/1) to give 0.545 g (52%) of **8**: IR (neat) 1710, 1500, 1250, 1050, 980 cm^{-1}; ^1H NMR (CCl_4) δ=1.44 (d, *J*=8 Hz, 3H, CH_3), 2.25 (s, 3H, CH_3CO), 3.50 (s, 6H, $N(CH_3)_2$), 4.87 (q, 1H, $C\underline{H}SCSN$). Found: C, 43.85; H, 6.71; N, 7.24%. Calcd for $C_7H_{13}NOS_2$: C, 43.95; H, 6.85; N, 7.32%.

3-(Dimethylthiocarbamoylthio)-2-butanol (9). To a mixture of $NH_4H_2PO_4$ (0.6 g), KH_2PO_4 (0.6 g), $MgSO_4$ (0.3 g), $CaCO_3$ (1.28 g), glucose (30 g), and boiled water (300 ml) was added 3 g of bakers' yeast at 32 °C. After bubbles formed (ca. 20 min), 0.722 g (4.52 mmol) of **8** was added and then the mixture was stirred at 35 °C. After 64 h, 10 g of glucose was added. After 96 h, the organic layer was extracted twice with ethyl acetate and CH_2Cl_2. The combined extracts were washed with water, dried over $MgSO_4$, and concentrated. The residual oil (0.285 g) was chromatographed on SiO_2 to give 0.60 g (82%) of **9** as a mixture of erythro and threo (72/28): IR (neat) 3340, 1500, 1370, 1050, 980 cm^{-1}; ^1H NMR (CCl_4) δ=1.25 (m, 6H, $2CH_3$), 2.20 (s, 1H, OH), 3.43 (s, 6H, $N(CH_3)_2$), 4.03 (m, 2H, $C\underline{H}OHC\underline{H}SCS$). Found: C, 43.59; H, 7.96; N, 7.12%. Calcd for $C_7H_{15}NOS_2$: C, 43.49; H, 7.82; N, 7.25%. Each component was separated by preparative HPLC (column, SA-I(6ϕ×25 mm); eluent, hexane/ethyl acetate/ethanol (20/5/1)). *erythro*-**9**: $[\alpha]_D^{25}$ +109.4° (*c* 1.70, $CHCl_3$); IR (neat) 3430, 1500, 1381, 1260, 990, 980 cm^{-1}; ^1H NMR (CCl_4) δ=1.15 (d, *J*=6 Hz, 3H, $C\underline{H}_3CHOH$), 1.32 (d, *J*=6 Hz, 3H, $C\underline{H}_3CHSCS$), 2.55 (s, 1H, OH), 3.45 (s, 6H, $N(CH_3)_2$), 4.10 (m, 2H, $C\underline{H}C\underline{H}$); $J_{CH\text{-}CH}$=3.2 Hz, determined by ^1H NMR in the presence of 10% Eu(hfc)$_3$; >96% ee, no paired peaks in the presence of 40% Eu(hfc)$_3$. *threo*-**9**: $[\alpha]_D^{25}$ −51.4° (*c* 1.07, $CHCl_3$); IR (neat) 3420, 1500, 1372, 1250, 980, 962 cm^{-1}; ^1H NMR (CCl_4) δ=1.19 (d, *J*=6 Hz, 3H, $C\underline{H}_3CHOH$), 1.36 (d, *J*=6 Hz, 3H, $C\underline{H}_3CHSCS$), 2.40 (s, 1H, OH), 3.44 (s, 6H, $N(CH_3)_2$), 3.98 (m, 2H, >CH-CH<); $J_{CH\text{-}CH}$=4.8 Hz, determined by ^1H NMR in the presence of 10% Eu(hfc)$_3$; >96% ee, no paired peaks in the presence of 40% Eu(hfc)$_3$.

3-(Dimethylthiocarbamoylthio)-2,4-pentanedione (10). To a solution of 2.18 g (15.2 mmol) of sodium dimethyldithiocarbamate in 10 ml of methanol was added dropwise 2.01 g (15 mmol) of 3-chloro-2,4-pentanedione[11] with ice cooling. The mixture was stirred for 9 h at room temperature. After concentration of the solvent, the residue was poured into water and the organic layer was extracted with CH_2Cl_2. The combined extracts were washed with

water, dried over $MgSO_4$, and concentrated. The crude product (3.56 g) was purified with column chromatography (hexane/ethyl acetate, 20/1) to give 2.20 g (67%) of **10**: ^1H NMR (CCl_4) δ=2.06 (s, 6H, $2CH_3$), 3.50 (s, 6H, $N(CH_3)_2$), 17.32 (s, 1H, C=C-OH). Found: C, 43.49; H, 5.85; N, 6.12%. Calcd for $C_8H_{13}NO_2S_2$: C, 43.81; H, 5.97; N, 6.39%.

Reduction of 10 with Bakers' Yeast. Compound **10** (1.01 g, 4.59 mmol) was treated with bakers' yeast for 4 days, as described in the preparation of **9**. The crude product was chromatogaphed on SiO_2 (hexane/ethyl acetate, 20/1) to give 0.206 g (25%) of **3** as the first fraction. The second fraction gave 0.318 g (39%) of **4**: $[\alpha]_D^{25}$ +40.2 (*c* 2.56, $CHCl_3$): 77% ee. Spectral data were identical with those of the samples prepared above.

2-(Dimethylthiocarbamoylthio)pentanal (11). To a solution of 12.0 g (83.9 mmol) of sodium dimethyldithiocarbamate in 40 ml of methanol was added dropwise 9.57 g (79.4 mmol) of 2-chloropentanal with ice cooling. The mixture was stirred for 12 h at 25 °C and then for 1 h at 30—40 °C. After concentration of the solvent, the organic layer was extracted with CH_2Cl_2. The combined extracts were washed with water, dried over $MgSO_4$, and concentrated. The residue (14.9 g) was distilled to give 10.2 g (63%) of **11**: bp 127—129 °C (0.3 mm); IR (neat) 1720, 1500, 1380, 1250, 980 cm^{-1}; ^1H NMR (CCl_4) δ=1.00 (t, *J*=6 Hz, 3H, CH_3), 1.20—2.20 (m, 4H, $(CH_2)_2$), 3.50 (s, 6H, $N(CH_3)_2$), 4.75 (t, *J*=6 Hz, 1H, C<u>H</u>SCS), 9.37 (s, 1H, C<u>H</u>O). Found: C, 47.08; H, 7.34; N, 6.62%. Calcd for $C_8H_{15}ONS$: C, 46.79; H, 7.36; N, 6.82%.

Other aldehydes (**13**, **15**, **17**) were also prepared by the method described above.

2-(Dimethylthiocarbamoylthio)-3-methylbutanal (13): 53% yield; bp 133—135 °C (0.3 mm); IR (neat) 2950, 1720, 1500, 1470, 1250 cm^{-1}; ^1H NMR (CCl_4) δ=0.95 (d, *J*=6.5 Hz, 3H, CH_3), 1.10 (d, *J*=6.5 Hz, 3H, CH_3), 2.45 (m, 1H, $(CH_3)_2C\underline{H}$), 3.50 (s, 6H, $N(CH_3)_2$), 4.85 (d, *J*=5 Hz, 1H, C<u>H</u>CHO), 9.42 (s, 1H, CHO). Found: C, 46.72; H, 7.18; N, 7.03%. Calcd for $C_{18}H_{15}NOS_2$: C, 46.79; H, 7.36; N, 6.82%.

2-(Dimethylthiocarbamoylthio)hexanal (15): 63% yield; bp 80 °C (1.5 mm) (bath temperature); IR(neat) 2950, 1720, 1500, 1380, 1255, 980 cm^{-1}; ^1H NMR ($CDCl_3$) δ=0.89 (t, 3H), 1.11—2.13 (m, 6H), 3.46 (d, 6H), 4.75 (t, *J*=6.5 Hz, 1H), 9.50 (s, 1H). Found: C, 49.52; H, 7.80, N, 6.21%. Calcd for $C_9H_{17}NOS_2$: C, 49.28; H, 7.81; N, 6.39%.

2-(Dimethylthiocarbamoylthio)heptanal (17): 96% yield; IR (neat) 1720, 1500, 1380, 1250, 1150, 980 cm^{-1}; ^1H NMR ($CDCl_3$) δ=0.86 (t, *J*=6 Hz, 3H), 1.07—1.56 (m, 8H), 3.45 (s, 6H), 4.70 (t, *J*=6 Hz, 1H), 9.36 (s, 1H).

***(R)*-(+)-2-(Dimethylthiocarbamoylthio)-1-pentanol (12).** To a mixture of $NH_4H_2PO_4$ (1 g), KH_2PO_4 (1 g), $MgSO_4$ (0.5 g), $CaCO_3$ (2.5 g), glucose (40 g), and boiled water (500 ml) was added 5 g of bakers' yeast at 35 °C. After bubbles formed, 1.77 g (8.63 mmol) of **11** was added and then the mixture was stirred at 35 °C. After 21, 47, 69, 94, and 106 h, 5 g of bakers' yeast was added. After 5 days, the organic layer was extracted twice with ethyl acetate and CH_2Cl_2. The combined extracts were washed with water, dried over $MgSO_4$, and concentrated. The residual oil (1.85 g) was chromatographed on SiO_2 (hexane/ethyl acetate, 10/1) to give 1.64 g (92%) of **12**: $[\alpha]_D^{35}$ +30.3° (*c* 4.02, $CHCl_3$): IR (neat) 3300, 1500, 1362, 1240, 980 cm^{-1}; ^1H NMR (CCl_4) δ=1.10 (t, 3H, CH_3), 1.30—2.00 (m, 4H, $(CH_2)_2$), 3.50 (s, 6H, $N(CH_3)_2$), 3.61 (d, 2H, $C\underline{H}_2OH$), 4.10 (m, 1H, C<u>H</u>SCS). Found: C, 46.40; H, 8.15; N, 6.46%. Calcd for $C_8H_{17}ONS$: C, 46.34; H, 8.27; N, 6.76%.

MTPA Ester of 12. To a solution of **12** (0.248 g, 1.20 mmol), CCl_4 (5 ml), and pyridine (5 ml) was added 0.146 g (0.577 mmol) of (*S*)-(+)-α-methoxy-α-(trifluoromethyl)phenylacetyl chloride.[6] The mixture was stirred for 27 h at room temperature and then poured into water. The organic layer was extracted with ether and the combined extracts were washed with dilute HCl, saturated $NaHCO_3$, and water, and dried over $MgSO_4$. After removal of the solvent, the residue (0.34 g) was purified with preparative TLC (hexane/ethyl acetate, 2/1) to give 91 mg (39%) of MTPA ester of **12**: R_f 0.36—0.53; IR (neat) 1755, 1250, 1165, 1020, 980 cm^{-1}; ^1H NMR (CCl_4) δ=0.95 (t, *J*=6 Hz, 3H, CH_3), 1.1—1.9 (m, 4H, $(CH_2)_2$), 3.40 (s, 6H, $N(CH_3)_2$), 3.50 (s, 3H, OCH_3), 4.0—4.5 (m, 3H, OCH_2CHSCS), 7.3 (m, 5H); ^{13}C NMR ($CDCl_3$) δ=13.8 (q), 20.1 (t), 32.6 (t), 50.8 (d), 51.0 (d), 55.5 (q), 68.0 (t), 127.5 (d), 128.4 (d), 129.6 (d), 132.3 (s); 54.6% ee, determined by the peak ratio of δ 50.8 and 51.0 (<u>C</u>HSCS). Found: C, 51.18; H, 5.84; N, 3.28%. Calcd for $C_{18}H_{24}O_3NS_2F_3$: C, 51.04; H, 5.71; N, 3.31%.

***(R)*-(+)-2-(Dimethylthiocarbamoylthio)-3-methyl-1-butanol (14).** Compound **13** (4.09 g, 19.9 mmol) was treated with bakers' yeast as shown in the preparation of **12**. The crude product (3.76 g) was chromatographed on SiO_2 (hexane/ethyl acetate, 10/1—2/1) to give 1.58 g (39% yield, 69% yield based on the consumed **13**): TLC (hexane/ethyl acetate, 2/1), R_f 0.26; $[\alpha]_D^{26}$ +29.6° (*c* 1.34, $CHCl_3$); 32% ee, determined by ^1H NMR in the presence of Eu(hfc)$_3$; IR (neat) 3450, 1500, 1375, 1255, 980 cm^{-1}; ^1H NMR (CCl_4) δ=1.01 (d, *J*=6 Hz, 3H, CH_3), 1.05 (d, *J*=6 Hz, 3H, CH_3), 2.12 (s, 1H, OH), 2.30 (m, 1H, $C\underline{H}(CH_3)_2$), 3.44 (s, 6H, $N(CH_3)_2$), 3.69 (d, *J*=6 Hz, 2H, CH_2), 4.08 (m, 1H, CHSCS). Found: C, 46.41; H, 8.15; N, 7.02%. Calcd for $C_8H_{17}NOS_2$: C, 46.33; H, 8.27; N, 6.76%. The later fraction gave 1.80 g of **13**: TLC (hexane/ethyl acetate, 2/1), R_f 0.44.

***(R)*-(+)-2-(Dimethylthiocarbamoyl)-1-hexanol (16).** Aldehyde **15** (0.370 g, 1.69 mmol) was treated with bakers' yeast, as shown in the preparation of **12**. The crude product (2.9 g) was chromatographed on SiO_2 (hexane/ethyl acetate, 10/1) to give 0.29 g (78%) of **16**: $[\alpha]_D^{17}$ +39.6° (*c* 1.39, $CHCl_3$); IR (neat) 3400, 2940, 1500, 1250, 985 cm^{-1}; ^1H NMR ($CDCl_3$) δ=0.94 (t, *J*=6 Hz, 3H, CH_3), 1.14—2.00 (m, 6H), 2.41 (s, 1H), 3.50 (s, 6H), 3.66 (d, *J*=5.5 Hz, 2H), 4.00 (m, 1H); 46% ee, determined by ^{13}C NMR spectrum of the MTPA ester. Found: C, 48.79; H, 8.74; N, 6.44%. Calcd for $C_9H_{19}NOS_2$: C, 48.83; H, 8.65; N, 6.33%.

MTPA Ester of 16. To a mixture of **16** (0.1 g, 0.457 mmol), CCl_4 (5 ml), and pyridine (5 ml) was added 0.115 g (0.455 mmol) of (*S*)-(+)-α-methoxy-α-(trifluoromethyl)phenylacetyl chloride.[6] The mixture was stirred for 20 h at room temperature. After quenched with water, the organic layer was extracted with ether. The ethereal layer was washed with dil HCl, saturated $NaHCO_3$, and water, and then dried over $MgSO_4$. Concentration of the solvent gave the crude product, which was purified with preparative TLC (hexane/ethyl acetate, 2/1) to afford 68 mg (34%) of MTPA ester of **16**: R_f 0.45—0.55; IR (neat) 2950, 1750, 1500, 1250, 1165, 980 cm^{-1}; ^1H NMR (CCl_4) δ=0.89 (t, *J*=6 Hz, 3H), 1.1—2.0 (m, 6H), 3.40 (s, 6H), 3.51 (s, 3H), 3.9—4.6 (m, 3H), 7.32 (m, 5H); ^{13}C NMR ($CDCl_3$) δ=13.8 (q), 22.4 (t), 28.9 (t), 30.1 (t), 41.4 (q), 45.5 (q), 50.8 (d), 51.1 (d), 57.9 (t), 127.4 (d), 128.4 (d), 129.6 (d), 132.2 (s), 166.2 (s), 195.6 (s); 46% ee,

determined by the peak ratio of δ 50.8 and 51.1 (CHSCS). Found: C, 52.03; H, 6.12; N, 3.11%. Calcd for $C_{19}H_{26}F_3NO_3S_2$: C, 52.16; H, 5.99; N, 3.20%.

(*R*)-(+)-2-(Dimethylthiocarbamoylthio)-1-heptanol (18). Aldehyde **17** (2.23 g, 9.56 mmol) was treated with bakers' yeast for 9 days, as shown in the preparation of **12**. The crude product (2.2 g) was chromatographed on SiO_2 (hexane/ethyl acetate, 20/1) to give 1.69 g (75%) of **18**: $[\alpha]_D^{26}$ +39.6° (*c* 5.00, $CHCl_3$): IR (neat) 3425, 1500, 1375, 1255, 980 cm^{-1}; ^1H NMR (CCl_4) δ=0.95 (t, 3H), 1.13—1.90 (m, 8H), 2.82 (s, 1H), 3.50 (s, 6H), 3.70 (m, 2H), 4.00 (m, 1H). Found: C, 51.23; H, 8.89; N, 6.12%. Calcd for $C_{10}H_{21}NOS_2$: C, 51.02; H, 8.99; N, 5.95%.

MTPA ester of 18 was prepared by the reaction of **18** (116 mg, 0.498 mmol) with (*S*)-(+)-α-methoxy-α-(trifluoromethyl)phenylacetyl chloride[6] as described above. The crude product (0.25 g) was purified by preparative TLC (hexane/ethyl acetate, 2/1) to give 117 mg (52%) of MTPA ester of **18**: $[\alpha]_D^{26}$ +3.16° (*c* 3.16, $CHCl_3$); IR (neat) 2950, 1755, 1380, 1250, 1165 cm^{-1}; ^1H NMR ($CDCl_3$) δ=1.89 (t, *J*=5.5 Hz, 3H), 1.05—2.0 (m, 8H), 3.35 (s, 3H), 3.41 (s, 3H), 3.55 (s, 3H), 4.0—4.7 (m, 3H), 7.4 (broad S, 5H): ^{13}C NMR ($CDCl_3$) δ=13.9 (q), 22.3 (t), 26.4 (t), 30.4 (t), 31.5 (t), 41.4 (q), 45.3 (q), 50.9 (d), 51.1 (d), 55.5 (q), 68.0 (t), 127.5 (d), 128.3 (d), 129.5 (d), 132.2 (s), 166.2 (s), 195.5 (s); 63% ee, determined by the peak ratio of δ 50.9 and 51.1 (CHSCS). Found: C, 53.26; H, 6.17; N, 3.04%. Calcd for $C_{20}H_{28}F_3NO_3S_2$: C, 53.20; H, 6.25; N, 3.10%.

(*R*)-(+)-1,2-Epithiopentane (19). To a stirred mixture of NaH (0.661 g, 16.5 mmol) and THF (3 ml) was added a solution of 2.75 g (13.3 mmol) of **12** in 5 ml of THF at 0 °C during a period of 45 min. The mixture was stirred for 30 min at 0 °C and for 2 h at room temperature. After the mixture was poured into water, the organic layer was extracted with ether, washed with water, dried over $MgSO_4$, and concentrated. Short-pass distillation of the residue gave 0.523 g (40%) of **19**: $[\alpha]_D^{24}$ +8.0° (*c* 1.0, $CHCl_3$); IR (neat) 2890, 1460, 1261, 1040, 915 cm^{-1}; ^1H NMR (CCl_4) δ=0.98 (t, *J*=6 Hz, 3H, CH_3), 1.11 (m, 4H, CH_2CH_2), 2.04 (apparent d, *J*=5 Hz, 1H, CH_2S), 2.38 (apparent d, *J*=6 Hz, 1H, CH_2), 2.78 (m, 1H, CHS); ^{13}C NMR ($CDCl_3$) δ=13.7 (q), 22.5 (t), 25.8 (t), 35.7 (d), 38.6 (t); mass spectrum (70 eV) *m/z* 102 (M^+), 87, 74, 73, 70, 69, 64, 59. Found: C, 58.68; H, 9.57%. Calcd for $C_5H_{10}S$: C, 58.77; H, 9.86%.

(*R*)-(+)-3-Methyl-1,2-epithiobutane (20).[7] To a stirred mixture of 0.20 g (5.00 mmol) of NaH (60% in oil) and 1 ml of ether was added dropwise a solution of 1.03 g (4.98 mmol) of **14** in 3 ml of ether at 0 °C. The mixture was stirred for 2 days at 0 °C and then poured in ice water, and acidified with 10% HCl. The organic layer was extracted with ether, washed with water, dried over $MgSO_4$, and concentrated. Short-pass distillation of the residue afforded 18 mg (4%) of **20**: bp 70—90 °C (100 mm)(bath temperature); $[\alpha]_D^{26}$ +4.2° (*c* 3.52, $CDCl_3$); IR (neat) 2950, 1660, 1460, 1260, 1040 cm^{-1}: ^1H NMR ($CDCl_3$) δ=1.06 (d, *J*=6 Hz 6H, $2CH_3$), 1.22 (m, 1H, $CH(CH_3)_2$), 2.14 (apparent d, *J*=5 Hz, 1H, CH_2S), 2.42 (apparent d, *J*=5 Hz, 1H, CH_2S), 2.65 (m, 1H, CHS).

We thank Drs. Yoshitomo Yamamoto and Taizo Sako of Ouchi Shinko Chemical Industry Co., Ltd. for their generous gift of sodium dimethyldithiocarbamate.

References

1) For example, see: K. Mori and T. Sugai, *Yuki Gosei Kagaku Kyokai Shi*, **41**, 1044 (1983); T. Oishi and H. Akita, *ibid.*, **41**, 1031 (1983); R. F. Newton and S. M. Roberts, *Tetrahedron*, **36**, 2163 (1980); C. Le Drian and A. E. Greene, *J. Am. Chem. Soc.*, **104**, 5473 (1982); M. Hirama and M. Uei, *ibid.*, **104**, 4251 (1982); T. Fujisawa, T. Itoh, M. Nakai, and T. Sato, *Tetrahedron Lett.*, **26**, 771 (1985); S. Tsuboi, E. Nishiyama, H. Furutani, M. Utaka, and A. Takeda, *J. Org. Chem.*, **52**, 1359 (1987).

2) D. Ghiringhelli, *Tetrahedron Lett.*, **24**, 287 (1983); T. Fujisawa, E. Kojima, T. Itoh, and T. Sato, *Chem. Lett.*, **1985**, 1751.

3) T. Fujisawa, T. Itoh, and T. Sato, *Tetrahedron Lett.* **25**, 5083 (1984); T. Fujisawa, T. Itoh, M. Nakai,and T. Sato, *Tetrahedron Lett.* **26**, 771 (1985).

4) S. Iriuchijima and N. Kojima, *Agric. Biol. Chem.*, **42**, 451 (1978).

5) A. M. Clifford and J. G. Lichty, *J. Am. Chem. Soc.*, **54**, 1163 (1932).

6) J. A. Dale, D. L. Dull, and H. S. Mosher, *J. Org. Chem.*, **34**, 2548 (1969).

7) N. Spassky, P. Dumas, M. Sepulchre, and P. Sigwalt, *J. Polym. Sci., Polym. Symp.*, No. 52, 327 (1975).

8) W. Pickenhagen and H. Bronner-Schindler, *Helv. Chim. Acta*, **67**, 947 (1984).

9) C. L. Stevens, E. Farkas, and B. Gillis, *J. Am. Chem. Soc.*, **76**, 2695 (1954).

10) F. Alcudia, J. L. Garcia Ruano, and J. Ropdriguez, *Can. J. Chem.*, **57**, 2426 (1979).

11) S. Archer and M. G. Pratt, *J. Am. Chem. Soc.*, **66**, 1656 (1944).

Stereochemical Behavior of Intermediary Compounds in the Amine-Catalyzed Knoevenagel Reaction

Rikuhei TANIKAGA,* Naoto KONYA, Kazumasa HAMAMURA, and Aritsune KAJI
Department of Chemistry, Faculty of Science, Kyoto University,
Kitashirakawa, Sakyo-ku, Kyoto 606
(Received March 1, 1988)

Treatment of the active methylene compounds and aldehydes with a catalytic amount of a secondary amine produces thermodynamically stable alkenes, and the intermediary amino compounds are isolated. The reaction involves many reversible steps, and the stereochemistry of products is determined in the elimination step from the intermediary compounds via stable planar carbanions, in which the small difference in the steric requirements of two electron-withdrawing groups is effective. Steric and electronic effects in the intermediates sometimes bring about the carbon–carbon bond fission with recovery of active methylene compounds, and these effects prevent the Knoevenagel reaction from occurring.

Among a number of synthetic methods for carbon–carbon bond formation the amine-catalyzed Knoevenagel reaction is frequently employed because of its high reactivity under mildly basic conditions.[1-5] The main preparative application of the reaction has been condensation of aldehydes and ketones with easily enolizable compounds usually containing two electron-withdrawing groups. The reaction, though easy to operate, seems to involve a complicated mechanism. Previously we observed that simple treatment of methyl arylsulfinylacetate **1a** (X=CO_2Me, Y=S(O)Ar) and aldehydes **2** with a catalytic amount of a secondary amine **3** produced thermodynamically stable (*E*)-alkenes (*E*)-**4**, and assumed that the stereochemistry of the reaction was determined in the elimination step from intermediary amino compounds **5** via planar carbanions **6**[5] stabilized by both a sulfur atom and a carbonyl group (Scheme 1).

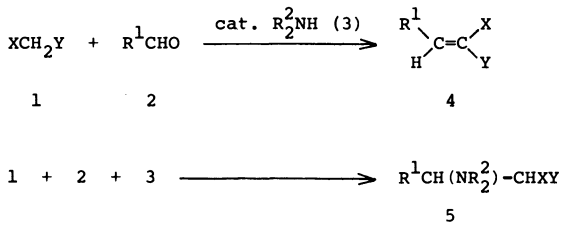

Scheme 1.

However, it remains obscure whether the presence of a sulfur atom is essential for stabilization of **6**. Here we wish further to clarify what factors influence the behaviors of the intermediate **5** in the amine-catalyzed Knoevenagel reaction starting from the active methylene compound **1** containing two electron-withdrawing groups (X and Y) in general.

Results and Discussion

The following amine-catalyzed reactions were carried out with the intention of examining the stereochemistry of products. Simple treatment of **1** (10 mmol) and **2** (12 mmol) with piperidine (0.5 mmol) in acetonitrile (50 ml) produced alkenes **4** as shown in Table 1.

Thermodynamically stable **4** were always obtained regardless of the absence of a sulfinyl group, and their formation was much influenced by the small difference in the steric requirements of X and Y groups, especially near a reaction center. Although such a selectivity was not observed in the presence of small X and Y groups (e.g., X=CO_2Me, Y=COMe), the *E*:Z ratio was slightly improved by using, instead of piperidine, larger 2,6-dimethylpiperidine or dicyclohexylamine (34:66, 36:64, respectively).

These findings can be rationalized by the explanation that the steric effects of X and Y groups are more

Table 1. Preparation of Alkenes **4**

X	Y	R^1	Temp	Time	Yield[a]	*E*:*Z*[b]
			°C	h	%	
COPh	S(O)Ph	Ph	60	6	71	99:1
CO_2Bu-*t*	$S(O)C_6H_4Cl$-*p*	*n*-Pr	0	24	68[c]	99:1
COPr-*i*	COPh	Ph	60	6	84	99:1
COPr-*i*	COPh	*n*-Pr	20	12	63	63:37
COMe	COPh	Ph	20	12	79	99:1
COMe	COPh	*i*-Pr	20	12	74	99:1
COMe	COPh	*n*-Pr	20	12	70	98:2
CO_2Me	COPh	Ph	60	6	85	1:99
CO_2Me	COMe	Ph	20	12	77	31:69
CO_2Me	COMe	*n*-Pr	20	12	74	45:55

a) Isolated yield. b) Determined by GLPC or HPLC. c) (R_S)-**4** was obtained in 100% e.e. from (R_S)-**1**.

Table 2. Formation of **4b** from **5b** in Acetonitrile or Acetic Acid

5b		MeCN[a]		AcOH[b]	
R^2	threo: erythro	Yield/%[c]	$E:Z$[d]	Yield/%[c]	$E:Z$[d]
$-(CH_2)_4-$	39:61	71	0:100	82	40:60
$-(CH_2)_5-$	29:71	90	0:100	90	45:55
$-(CH_2)_2CHMe(CH_2)_2-$	39:61	71	0:100	94	49:51
$-(CH_2)_6-$	32:68	82	0:100	90	38:62

a) 60 °C, 6 h. b) 20 °C, 10 min. c) Isolated yield. d) Determined by GLPC.

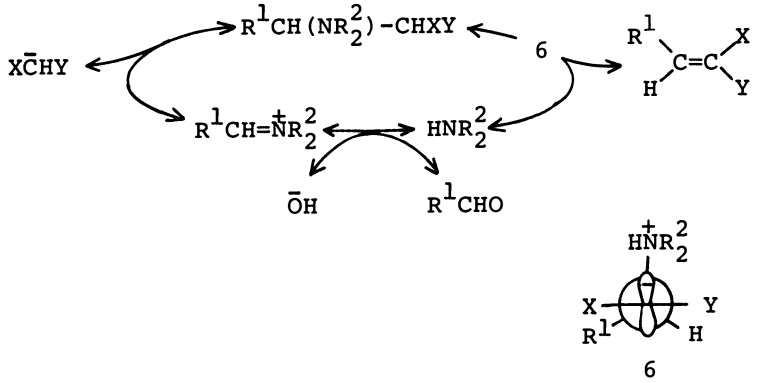

Scheme 2. Reaction mechanism (X<Y).

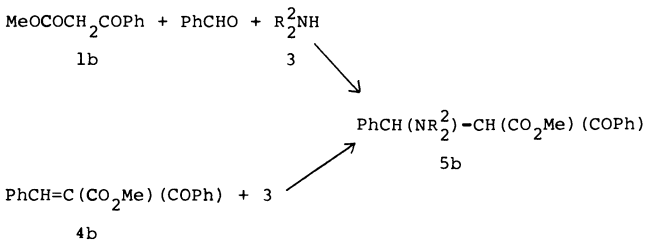

Scheme 3.

effective in planar carbanions **6**, in which two groups R^1 and X, or R^1 and Y are brought close together (Scheme 2).[5,6] Interestingly, the formation of **6** did not accompany loss of enantiomercal purity of a sulfinyl group (Y=(*R*)-S(O)C_6H_4Cl-*p*).

When a solution of methyl benzoylacetate (**1b**)(10 mmol), benzaldehyde (12 mmol), and secondary amine **3** (12 mmol) in a small quantity of acetonitrile was allowed to stand at 0 °C, the diastereoisomeric amino compounds *threo*- and *erythro*-**5b** crystallized directly with time in 70—92% yields. The amino compounds **5b** were also obtained with the same threo:erythro ratio from alkenes **4b** (10 mmol) and **3** (12 mmol) (Scheme 3).

Previously we reported that thermodynamically stable (*E*)-alkenes (*E*)-**4**, that is, the Knoevenagel reaction products were obtained simply by dissolving **5a** derived from **1a** in acetonitrile at 20—60 °C, whereas on treatment with acetic acid anti-elimination occurred to afford mixtures of (*E*)- and (*Z*)-**4a**.[5] Similar treatment of mixtures of *threo*- and *erythro*-**5b** lead to the results as listed in Table 2.

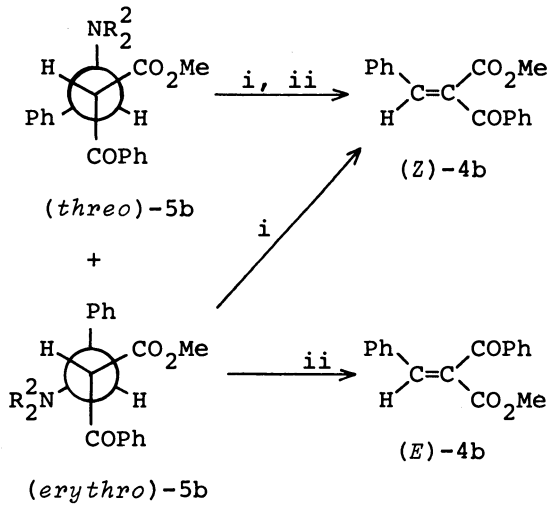

Scheme 4. Reaction conditions: i, MeCN; ii, AcOH

High selectivity in the Knoevenagel reaction was realized in an elimination step from **5b** rather than in its formation probably because steric repulsion between COPh and Ph groups is considerable in a planar carbanion **6** if R^1=Ph and Y=COPh in Scheme 2. Since the carbanion **6** is enolizable, the elimination may occur via an intermediate such as **6b′**. The stereochemistry in the elimination step can be interpreted essentially in the same way.

Similar treatment of 1-aryl-2-(arylsulfinyl)ethanone (**1c**) and an aldehyde (R^1=Ph or *i*-Pr) with a secondary amine **3** gave the amino compounds **5c**, **5c′** as crystalline solids, and interestingly **5c** or **5c′** appeared

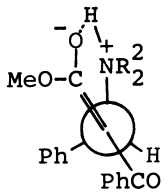

6b′

to be well suited for studies of the intermediate in the amine-catalyzed Knoevenagel reaction because both **1c** and (*E*)-alkenes (*E*)-**4c**, (*E*)-**4c′** were obtained by dissolving **5c** or **5c′** in a suitable solvent. Since a secondary amine is known to cause (*E*)-**4c′** to undergo further reactions yielding an allylic alcohol **7c′**,[7] it is important to neutralize the amine **3** formed as a by-product. Therefore, **5c′** was dissolved in dichloromethane containing aqueous ammonium chloride in which the Knoevenagel reaction proceeded as usual. These results are given in Table 3 (Scheme 5).

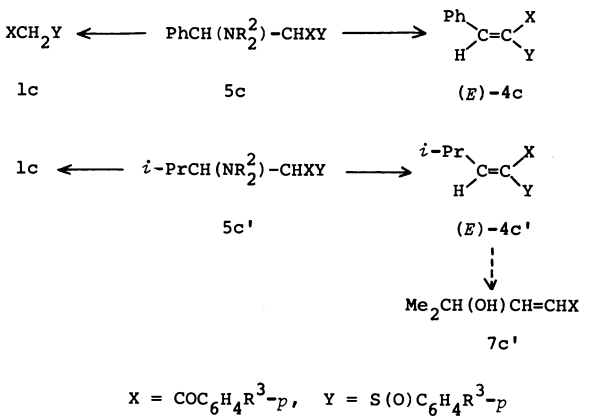

Scheme 5.

Table 3. Formation of **1c** and (*E*)-**4c**, **4c′** from **5c**, **5c′**[a,b]

R^1	R^2_2	R^3	Yield/%[c]	
			1c	(*E*)-**4c**, **4c′**[d]
Ph	Me, Me	H	39	49
Ph	$-(CH_2)_4-$	H	25	63
Ph	$-(CH_2)_5-$	H	42	58
Ph	$-CHMe(CH_2)_4-$	H	43	51
i-Pr	Me, Me	H	80	8
i-Pr	$-(CH_2)_5-$	H	94	3
i-Pr	$-(CH_2)_2CHMe(CH_2)_2-$	H	100	0
Ph	Me, Me	Me	98	0
Ph	$-(CH_2)_4-$	Me	69	17
Ph	$-(CH_2)_5-$	Me	78	14
Ph	$-(CH_2)_2CHMe(CH_2)_2-$	Me	80	19
i-Pr	Me, Me	Me	92	1
i-Pr	$-(CH_2)_4-$	Me	84	0
i-Pr	$-(CH_2)_5-$	Me	100	0
i-Pr	$-(CH_2)_2CHMe(CH_2)_2-$	Me	100	0

a) A mixture of threo- and erythro-isomers was used. b) Reaction conditions: **5c**; MeCN, 60 °C, 6 h; **5c′**; CH_2Cl_2, 20 °C, 12 h. c) Isolated yield. d) No (*Z*)-isomer was obtained.

The absence of (*Z*)-**4c**, (*Z*)-**4c′** means that the elimination is affected by the difference in the steric requirements of C=O and S→O groups [bond distance, 1.23 (C=O) and 1.44 Å (S→O);[8] van der Waals radius, 1.55 (C atom) and 1.85 Å (S atom)[9]]. Construction of a molecular model suggests considerable steric restraints for the formation of **5**, and actually preparation of **5** with bulky R^1 and R^2 [e.g., R^1=*i*-Pr, and R^2=$-CHMe(CH_2)_4-$] was impossible. This steric hindrance may also have contributed to weakening the linkage of both C–N and C–C bonds though the C–C bond fission mechanism has not yet been clarified (Scheme 7).

The **1c**/(*E*)-**4c** or **1c**/(*E*)-**4c′** ratio increased with the relative bulkiness of R^2_2 in the order; $-(CH_2)_4-$ < Me_2 ≈ $-(CH_2)_5-$ < $-(CH_2)_2CHMe(CH_2)_2-$, that is, a bulky R^2_2N group favored the C–C bond fission. Since the elimination reaction from **5** might be initiated by removal of the proton at the α-position of X and Y groups, the formation of the alkene **4** was depressed by the presence of an electron-donating group, e.g., R^1=*i*-Pr or R^3=Me, and accelarated by replacement of a sulfinyl group by a carbonyl group (Scheme 7).

The reversibility of the amine-catalyzed Knoevenagel reaction is supported by the findings that the intermediate **5** was obtained from both the starting compound **1** and the product **4** (Scheme 3), and at the same time, **5** produced **1** and **4** (Scheme 5). Solidification of **5** might make it possible to shift the equilibrium yielding **5**. In a solution, however, the equilibrium between **1c** and **5c** (or **5c′**) was sometimes found to be more in favor to **1c** (e.g., R^1=*i*-Pr in Table 3), and in fact the Knoevenagel reaction never occurred from **1c** and *i*-PrCHO. Neither usage of an equimolar

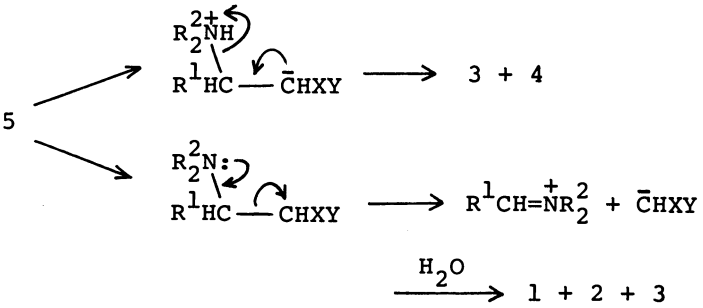

Scheme 6.

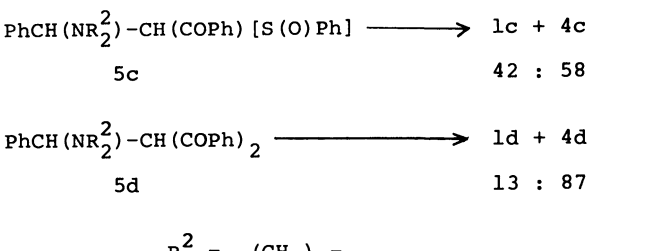

Scheme 7.

amount of an amine nor removal of water from the reaction mixture improved the yield of **4**.

In conclusion, the amine-catalyzed Knoevenagel reaction involves many reversible steps as shown in Scheme 2, the stereochemical behavior of an intermediary amino compound plays an important role, and the usage of a catalytic amount of a secondary amine forces this thermodynamically-controlled reaction to completion giving the most stable product.

Rappoport has studied the stereochemical behavior in vinylic substitution (via addition-elimination) of halosubstituted electrophilic olefins containing two electron-withdrawing groups by a nucleophile such as ArS^- and ArO^-, and interestingly proposed the planar carbanion similar to **6** in the elimination step.[10,11] Our present results may provide significant information concerning an addition-elimination reaction.

Experimental

^1H NMR spectra were determined at 100 MHz with a JEOL JNM-PS-100 or at 400 MHz with a JEOL JNM-GX-400 spectrometer, and refer to deuteriochloroform solution with tetramethylsilane as internal standard. IR spectra were recorded with a Hitachi 215 spectrometer, and MS with a JEOL JMX-DX-300 instrument. GLPC analysis was carried out with a Varian 920 instrument using a column packed with 20% silicone DS-550. Column chromatography and TLC were performed, using Wakogel 200 silica gel and Merck plastic sheets silica gel 60 F_{254} respectively. HPLC analysis was carried out with a Shimadzu LC-6A system containing a column packed with a commercially-available chiral cellulose derivative (Daicel Chemical Industry's CHIRALCEL-OC) or a ODS column.

Commercial 1-phenyl-1,3-butanedione, methyl benzoylacetate (**1b**), methyl acetoacetate, 1,3-diphenyl-1,3-propanedione (**1d**), aldehydes **2**, and amines **3** were purified before use. 4-Methyl-1-phenyl-1,3-pentanedione, 1-phenyl-2-(phenylsulfinyl)ethanone, and 1-(*p*-tolyl)-2-(*p*-tolylsulfinyl)ethanone were prepared by the reported methods.[12,13]

***t*-Butyl (*R*S)-*p*-Chlorophenylsulfinylacetate.** To a stirred solution of ethylmagnesium bromide [prepared from Mg (2.43 g, 0.1 mol) and bromoethane (10.9 g, 0.1 mol) in diethyl ether (50 ml)] under argon atmosphere was added diisopropylamine (14 ml, 0.1 mol). The resulting solution was refluxed for 30 min and cooled to −40 °C. To the solution was added successively a solution of *t*-butyl acetate (8.13 g, 0.07 mol) in tetrahydrofuran (THF) (5 ml) and a solution of menthyl (*S*S,*S*C)-*p*-chlorobenzenesulfinate[14] (9.45 g, 0.03 mol) in diethyl ether (80 ml)–THF (8 ml). The solution was stirred for further 10 h at −40 °C, and quenched with saturated aqueous ammonium chloride (50 ml). The aqueous layer was extracted with chloroform, and the combined organic phases were washed with water, and dried (anhydrous magnesium sulfate). After having removed the solvent column chromatography on silica gel eluting with hexane–ethyl acetate (3:1) and recrystallized from hexane–ethyl acetate (5:1) gave *t*-butyl (*R*S)-*p*-chlorophenylsulfinylacetate (6.26 g, 76%): mp 123.5 °C; $[\alpha]_D^{23.5}$ +169.7° (*c* 1.09, MeOH)(100% e.e. by HPLC); IR (KBr) 1720 (C=O) and 1040 cm^{-1} (S→O); ^1H NMR ($CDCl_3$) δ=1.40 (9H, s, Me), 3.57 (1H, d, *J*=13 Hz, CH_2), 3.81 (1H, d, *J*=13 Hz, CH_2), 7.51 (2H, d, *J*=7 Hz, Ar), and 7.67 (2H, d, *J*=7 Hz, Ar); Found: C, 52.25; H, 5.32%. Calcd for $C_{12}H_{15}ClO_3S$: C, 52.44; H, 5.50%.

Knoevenagel Reaction of Compounds 1 and Aldehydes 2. A solution of **1** (10 mmol), **2** (10 mmol), and an amine **3** (0.5 mmol) in acetonitrile (50 ml) was kept under the conditions given in Table 1. After having removed the solvent under the reduced pressure the residue was chromatographed on silica gel using hexane–ethyl acetate (4:1) to give the alkene **4** in the yield as shown in Table 1. A minimum quantity of the reaction mixture was withdrawn prior to isolation to determine the *E*:*Z* ratio of **4** by GLPC, HPLC, or ^1H NMR. The enantiomeric excess was determined by HPLC using a chiral derivative. By this route the following compounds were obtained.

(2*E*)-1,3-Diphenyl-2-phenylsulfinyl-2-propen-1-one [(*E*)-4c]: Mp 90 °C; IR (Nujol) 1640 (C=O) and 1060 cm^{-1} (S→O); ^1H NMR ($CDCl_3$) δ=6.9—7.8 (11H, m, Ph, CH=C); MS *m*/*z* 332 (M^+, 8%); Anal. ($C_{21}H_{16}O_2S$) C, H.

***t*-Butyl (*R*S, 2*E*)-2-(*p*-Chlorophenylsulfinyl)-2-hexenoate:** Liquid; $[\alpha]_D^{22}$=166.9° (*c* 1.10, MeOH)(100% e.e.); IR (neat) 1720 (C=O) and 1050 cm^{-1} (S→O); ^1H NMR ($CDCl_3$) δ=0.98 (3H, t, *J*=7 Hz, Me), 1.35 (9H, s, Me_3C), 1.6—2.7 (4H, m, CH_2), 7.11 (1H, t, *J*=8 Hz, CH=C), 7.48 (2H, d, *J*=8 Hz, Ar) and 7.69 (2H, d, *J*=8 Hz, Ar); MS *m*/*z* 328 (M^+, 10%); Anal. ($C_{16}H_{21}ClO_3S$) C, H.

(4*E*)-4-Benzoyl-2-methyl-5-phenyl-4-penten-3-one: Liquid; IR (neat) 1675 cm^{-1} (C=O); ^1H NMR ($CDCl_3$) δ=1.13 (6H, d, *J*=6 Hz, Me), 3.13 (1H, hept, CH), 7.76 (1H, s, CH=C), and 7.1—8.1 (10H, m, Ph); MS *m*/*z* 278 (M^+, 6%); Anal. ($C_{19}H_{18}O_2$) C,H.

4-Benzoyl-2-methyl-4-octen-3-one: Liquid; IR (neat) 1715 cm^{-1} (C=O); ^1H NMR ($CDCl_3$) δ=0.5—2.7 (7H, m, Me, CH_2), 1.08 (6H, d, *J*=7 Hz, Me_2C), 3.11 (1H, m, CH), 6.46 (1H, t, *J*=7 Hz, *Z* CH=C), 6.96 (1H, t, *J*=7 Hz, *E* CH=C), and 7.2—8.1 (5H, m, Ph); MS *m*/*z* 244 (M^+, 1%); Anal. ($C_{12}H_{20}O_2$) C, H.

(3*E*)-3-Benzoyl-4-phenyl-3-buten-2-one: Mp 98 °C (lit,[15] mp 98—99 °C).

(3*E*)-3-Benzoyl-5-methyl-3-hexen-2-one: Liquid; IR (neat) 1700 cm^{-1} (C=O); ^1H NMR ($CDCl_3$) δ=1.00 (6H, d, *J*=6 Hz, Me_2C), 2.32 (3H, s, MeCO), 3.10 (1H, hept, *J*=6 Hz, CH), 6.71 (1H, d, *J*=10 Hz, CH=C), and 7.2—8.1 (5H, m, Ph); MS *m*/*z* 216 (M^+, 12%); Anal. ($C_{14}H_{16}O_2$) C, H.

(3*E*)-3-Benzoyl-3-hepten-2-one: Liquid; IR (neat) 1720 cm^{-1}; (C=O); ^1H NMR ($CDCl_3$) δ=0.6—2.2 (7H, m, Me, CH_2), 2.31 (3H, s, MeCO), 6.96 (1H, t, *J*=7 Hz, CH=C), and 7.2—8.1 (5H, m, Ph); MS *m*/*z* 216 (M^+, 18%); Anal. ($C_{14}H_{16}O_2$) C, H.

Methyl (2*Z*)-2-Benzoyl-3-phenyl-2-propenoate [(*Z*)-4b]: Liquid; IR (neat) 1740(O-C=O) and 1680 cm^{-1} (C=O); ^1H NMR ($CDCl_3$) δ=3.68 (3H, s, MeO), 7.92 (1H, s, CH=C), and 6.9—8.1 (10H, m, Ph); MS *m*/*z* 266 (M^+, 7%); Anal. ($C_{17}H_{14}O_3$) C, H.

Methyl 2-Acetyl-3-phenyl-2-propenoate: Liquid; IR (neat) 1730 (O-C-O) and 1660 cm^{-1} (C=O); ^1H NMR ($CDCl_3$) (*E*)-isomer δ=2.30 (3H, s, MeCO), 3.81 (3H, s, MeO), 7.0—7.5 (5H, m, Ph), and 7.66 (1H, s, CH=C), (*Z*)-isomer δ=2.40 (3H, s, MeCO), 3.87 (3H, s, MeO), 7.2—7.6 (5H, m, Ph), and 7.57 (1H, s, CH=C).

Methyl 2-Acetyl-2-hexenoate: Liquid; IR (neat) 1730 (O-C=O) and 1690 cm^{-1} (C=O); ^1H NMR ($CDCl_3$) (*E*)-isomer δ=0.9—2.8 (7H, m, Me, CH_2), 1.16 (3H, s, MeCO), 3.80 (3H, s, MeO), and 6.68 (1H, d, J=11 Hz, CH=C), (*Z*)-isomer δ=0.9—2.8 (7H, m, Me, CH_2), 1.30 (3H, s, MeCO), 3.85 (3H, s, MeO), and 6.60 (1H, d, J=11 Hz, CH=C).

The elemental analyses found were in good agreement with the calculated values throughout.

Formation of the Amino Compounds 5. A solution of **1** (10 mmol), **2** (15 mmol), and **3** (15 mmol) in acetonitrile (20 ml) was kept at 0 °C for 24 h. The product precipitated was filtered off, washed several times with cold acetonitrile, and dried in vacuo. Almost pure diastereoisomeric **5** was obtained as a colorless solid. Further purification by recrystallization or column chromatography proved to be impossible owing to ready elimination reactions. The configuration of *threo*- and *erythro*-**5** were assigned on the basis of the results obtained by anti-elimination using acetic acid,[5] and their ratio was determined by ^1H NMR. Mass spectra of **5** indicated the absence of M^+ peaks.

By this route the following compounds were obtained.

Methyl 2-Benzoyl-3-pyrrolidino-3-phenylpropionate: Yield 70%; mp 128 °C; IR (Nujol) 1730 (O-C=O) and 1685 cm^{-1} (C=O); ^1H NMR ($CDCl_3$) δ=1.3—1.9 (4H, m, CH_2), 2.1—3.0 (4H, m, CH_2-N), 3.30/3.76 (3H, s, threo/erythro MeO), 4.71—4.81 (1H, d, J=12 Hz, CH-N), 5.15/5.27 (1H, d, J=12 Hz, threo/erythro CH-CO), and 7.0—8.2 (10H, m, Ph); Anal. ($C_{21}H_{23}O_3N$) C, H, N.

Methyl 2-Benzoyl-3-phenyl-3-piperidinopropionate: Yield 92%; mp 145—146 °C; IR (Nujol) 1730 (O-C=O) and 1685 cm^{-1} (C=O); ^1H NMR ($CDCl_3$) δ=0.9—1.8 (6H, m, CH_2), 1.8—2.9 (4H, m, CH_2-N), 3.51/3.79 (3H, s, threo/erythro MeO), 4.66/4.71 (1H, d, J=11 Hz, threo/erythro CH-N), 5.28/5.25 (1H, d, J=11 Hz, threo/erythro CH-CO), and 7.0—8.2 (10H, m, Ph); Anal. ($C_{22}H_{25}O_3N$) C, H, N.

Methyl 2-Benzoyl-3-(4-methylpiperidino)-3-phenylpropionate: Yield 78%; mp 130—132 °C; IR (Nujol) 1725 (O-C-O) and 1690 cm^{-1} (C=O); ^1H NMR ($CDCl_3$) δ=0.6—1.9 (8H, m, Me, CH, CH_2), 2.0—3.1 (4H, m, CH_2-N), 3.46/3.76 (3H, s, threo/erythro MeO), 4.47/4.73 (1H, d, J=11 Hz threo/erythro CH-N), 5.24/5.33 (1H, d, J=11 Hz, threo/erythro CH-CO), and 7.0—8.1 (10H, m, Ph); Anal. ($C_{23}H_{27}O_3N$) C, H, N.

Methyl 2-Benzoyl-3-(perhydro-1-azepinyl)-3-phenylpropionate: Yield 82%; mp 128—129 °C; IR (Nujol) 1730 (O-C-O) and 1685 cm^{-1} (C=O); ^1H NMR ($CDCl_3$) δ=0.9—1.8 (8H, m, CH_2), 2.1—3.1 (4H, m, CH_2-N), 3.46/3.77 (3H, s, threo/erythro MeO), 4.74/4.83 (1H, d, J=11 Hz, threo/erythro CH-N), 5.22/5.28 (1H, d, J=11 Hz, threo/erythro CH-CO), and 7.1—8.2 (10H, m, Ph); Anal. ($C_{23}H_{27}O_3N$) C, H, N.

3-Dimethylamino-1,3-diphenyl-2-phenylsulfinyl-1-propanone: Yield 84%; mp 139 °C; IR (Nujol) 1650 (C=O) and 1060 cm^{-1} (S→O); ^1H NMR ($CDCl_3$) δ=2.04 (3H, s, Me), 2.52 (3H, s, Me), 4.6—5.2 (2H, br, CH), and 6.8—7.7 (15H, m, Ph); very slightly soluble in $CDCl_3$; Anal. ($C_{23}H_{23}O_2NS$) C, H, N.

1,3-Diphenyl-2-phenylsulfinyl-3-(1-pyrrolidinyl)-1-propanone: Yield 94%; mp 139—140 °C; IR (Nujol) 1660 (C=O) and 1060 cm^{-1} (S→O); ^1H NMR ($CDCl_3$) δ=1.6—1.9 (4H, m, CH_2), 2.5—2.9 (4H, m, CH-N), 5.0—6.3 (2H, br, CH), and 6.9—7.8 (15H, m, Ph); very slightly soluble in $CDCl_3$; Anal. ($C_{25}H_{25}O_2NS$) C, H, N.

1,3-Diphenyl-2-phenylsulfinyl-3-piperidino-1-propanone: Yield 70%; mp 154—155 °C; IR (Nujol) 1660 (C=O) and 1055 cm^{-1} (S→O); ^1H NMR ($CDCl_3$) δ=1.0—2.0 (6H, m, CH_2), 2.0—3.0 (4H, m, CH_2-N), 4.21 (1H, d, J=11 Hz, CH-N), 5.90 (1H, d, J=11 Hz CH-SO), and 6.9—7.9 (15H, m, Ph); slightly soluble in $CDCl_3$; Anal. ($C_{26}H_{27}O_2NS$) C, H, N.

1,3-Diphenyl-3-(4-methylpiperidino)-2-phenylsulfinyl-1-propanone: Yield 91%; mp 147—149 °C; IR (Nujol) 1660 (C=O) and 1055 cm^{-1} (S→O); ^1H NMR ($CDCl_3$) δ=0.6—3.2 (12H, m, Me, CH, CH_2), 4.6—5.5 (2H, br, CH), and 6.8—7.9 (15H, m, Ph); very slightly soluble in $CDCl_3$; Anal. ($C_{27}H_{29}O_2NS$) C, H, N.

3-Dimethylamino-4-methyl-1-phenyl-2-phenylsulfinyl-1-pentanone: Yield 80%; mp 87—79 ° C; IR (Nujol) 1660 (C=O) and 1055 cm^{-1} (S→O); ^1H NMR ($CDCl_3$) δ=0.72—1.28 (6H, m, Me), 2.0 (1H, m, CH), 2.50/2.59 (6H, s, threo/erythro Me_2N), 3.22/3.61 (1H, d, J=11 Hz, threo/erythro CH-N), 4.82/5.26 (1H, d, J=11 Hz, threo/erythro CH-SO), and 6.8—7.9 (10H, m, Ph); Anal. ($C_{20}H_{25}O_2NS$) C, H, N.

4-Methyl-1-phenyl-2-phenylsulfinyl-3-piperidino-1-pentanone: Yield 94%; mp 99—101 °C; IR (Nujol) 1660 (C=O) and 1050 cm^{-1} (S→O); ^1H NMR ($CDCl_3$) δ=0.6—1.9 (6H m, CH_2), 2.1 (1H, m, CH), 2.4—3.1 (4H, m, CH_2-N), 3.23/3.57 (1H, dd, J=11, 6 Hz, threo/erythro CH-N), 4.71/5.21 (1H, d, J=11 Hz, threo/erythro CH-SO), and 6.9—7.9 (10H, m, Ph); Anal. ($C_{23}H_{29}O_2NS$) C, H, N.

4-Methyl-3-(4-methylpiperidino)-1-phenyl-2-phenylsulfinyl-1-pentanone: Yield 93%; mp 96—98 °C; IR (Nujol) 1660 (C=O) and 1055 cm^{-1} (S→O); ^1H NMR ($CDCl_3$) δ=0.5—1.8 (14H, m, Me, CH, CH_2), 2.0 (1H, m, CH), 2.2—3.3 (4H, m, CH_2-N), 3.30/3.62 (1H, dd, J=12, 7 Hz, threo/erythro CH-N), 4.72/5.21 (1H, d, J=12 Hz, threo/erythro CH-SO), and 6.9—7.9 (10H, m, Ph); Anal. ($C_{24}H_{31}O_2NS$) C, H, N.

3-Dimethylamino-3-phenyl-1-(*p*-tolyl)-2-(*p*-tolylsulfinyl)-1-propanone: Yield 77%; mp 148—149 °C; IR (Nujol) 1660 (C=O) and 1055 cm^{-1} (S→O); ^1H NMR ($CDCl_3$) δ=2.06/2.17 (3H, s, Me), 2.31 (1H, s, Me), 2.2—2.5 (6H, Me_2N), 4.1—5.1 (2H, CH), and 6.8—8.0 (13H, m, Ph, Ar); slightly soluble in $CDCl_3$; Anal. ($C_{25}H_{27}O_2NS$) C, H, N.

3-Phenyl-3-pyrrolidino-1-(*p*-tolyl)-2-(*p*-tolylsulfinyl)-1-propanone: Yield 99%; mp 145—147 °C; IR (Nujol) 1665 (C=O) and 1055 cm^{-1} (S→O); ^1H NMR ($CDCl_3$) δ=1.5—1.8 (4H, m, CH_2), 2.16/2.22 (3H, s, Me), 2.36 (3H, s, Me), 2.5—3.0 (4H, m, CH_2-N), 4.1—5.1 (2H, CH), and 6.8—7.9 (13H, m, Ph, Ar); slightly soluble in $CDCl_3$; Anal. ($C_{27}H_{29}O_2NS$) C, H, N.

3-Phenyl-3-piperidino-1-(*p*-tolyl)-2-(*p*-tolylsulfinyl)-1-propanone: Yield 66%; mp 165—166 °C; IR (Nujol) 1660 (C=O) and 1060 cm^{-1} (S→O); ^1H NMR ($CDCl_3$) δ=1.0—1.9 (6H, m, CH_2), 2.16/2.21 (3H, s, Me), 2.36 (3H, s, Me), 2.0—2.2 (4H, m, CH_2-N), 4.2—5.9 (2H, br, CH), and 6.7—8.0 (13H, m, Ph, Ar); very slightly soluble in $CDCl_3$; Anal. ($C_{28}H_{31}O_2NS$) C, H, N.

3-(4-Methylpiperidino)-3-phenyl-1-(*p*-tolyl)-2-(*p*-tolylsulfinyl)-1-propanone: Yield 68%; mp 167—168 °C; IR (Nujol) 1660 (C=O) and 1060 cm^{-1} (S→O); ^1H NMR ($CDCl_3$) δ=0.5—3.2 (18H, m, Me, CH, CH_2), 4.6—5.4 (2H, m, CH), and 6.7—8.0 (13H, m, Ph, Ar); very slightly soluble in $CDCl_3$; Anal. ($C_{29}H_{33}O_2NS$) C, H, N.

4-Methyl-3-dimethylamino-1-(*p*-tolyl)-2-(*p*-tolylsulfinyl)-

1-pentanone: Yield 68%; mp 104—105 °C; IR (Nujol) 1660 (C=O) and 1060 cm^{-1} (S→O); ^1H NMR ($CDCl_3$) δ=0.6—1.3 (6H, m, Me), 1.8—2.8 (13H, m, Me, CH), 3.17/3.61 (1H, dd, J=10, 5 Hz, CH-N), 4.69/5.22 (1H, d, J=10 Hz, CH-SO), and 6.8—7.9 (8H, m, Ar); slightly soluble in $CDCl_3$; Anal. ($C_{22}H_{29}O_2NS$) C, H, N.

4-Methyl-3-(1-pyrrolidinyl)-1-(*p*-tolyl)-2-(*p*-tolylsulfinyl)-1-pentanone: Yield 74%; mp 89—90 °C; IR (Nujol) 1660 (C=O) and 1060 cm^{-1} (S→O); ^1H NMR ($CDCl_3$) δ=0.7—3.2 (21H, m, Me, CH, CH_2), 4.0—4.8 (2H, m, CH), and 6.8—7.9 (8H, m, Ar); slightly soluble in $CDCl_3$; Anal. ($C_{24}H_{31}O_2NS$) C, H, N.

4-Methyl-3-piperidino-1-(*p*-tolyl)-2-(*p*-tolylsulfinyl)-1-pentanone: Yield 85%; mp 108—109 °C; IR (Nujol) 1660 (C=O) and 1060 cm^{-1} (S→O); ^1H NMR ($CDCl_3$) δ=0.7—3.1 (23H, m, Me, CH, CH_2), 3.20/3.58 (1H, dd, J=10, 4 Hz, CH-N), 4.65/5.26 (1H, d, J=10 Hz, CH-SO), and 6.8—7.4 (8H, m, Ar); slightly soluble in $CDCl_3$; Anal. ($C_{25}H_{33}O_2NS$) C, H, N.

4-Methyl-3-(4-methylpiperidino)-1-(*p*-tolyl)-2-(*p*-tolylsulfinyl)-1-pentanone: Yield 88%; mp 109—110 °C; IR (Nujol) 1655 (C=O) and 1060 cm^{-1} (S→O); ^1H NMR δ ($CDCl_3$) δ= 0.6—3.3 (25H, m, Me, CH, CH_2), 4.0—4.8 (2H, CH), and 6.8—7.9 (4H, m, Ar); slightly soluble in $CDCl_3$; Anal. ($C_{26}H_{35}O_2NS$) C, H, N.

2-Benzoyl-1,3-diphenyl-3-piperidino-1-propanone: Yield 90%; mp 150 °C; IR (Nujol) 1680 cm^{-1} (C=O); ^1H NMR ($CDCl_3$) δ=1.0—1.7 (6H, m, CH_2), 2.0—2.6 (4H, m, CH-N), 4.70 (1H, d, J=13 Hz, CH-N), 5.38 (1H, d, J=13 Hz, CH-CO), and 7.0—8.1 (15H, m, Ph); Anal. ($C_{27}H_{27}O_2N$) C, H, N.

The elemental analyses found were in good agreement with the calculated values throughout. Assignment between threo and erythro isomers sometimes was difficult because the compound **5** was slightly soluble in $CDCl_3$.

Reaction of Compounds 5b in Acetic Acid. A solution of **5b** (5 mmol) in acetic acid (10 ml) was stirred at 20 ° C for 10 min. Water (50 ml) was added and the mixture was extracted twice with diethyl ether (50 ml). The organic phase was washed with three portions of saturated aqueous $NaHCO_3$ and NaCl, and dried (anhydrous $MgSO_4$). After the solvent had been removed, the residue obtained was purified by column chromatography on silica gel eluting with hexane-ethyl acetate (4:1). The *E*:*Z* ratio was determined by GLPC using a diastereoisomeric mixture of **4b**.

Methyl (2*E*)-2-Benzoyl-3-phenyl-2-propenoate [(*E*)-4b]: Liquid; IR (neat) 1740 (O-C=O) and 1680 cm^{-1} (C=O); ^1H NMR ($CDCl_3$) δ=3.68 (3H, s, MeO), and 6.9—8.1 (11H, m, Ph, CH); MS *m/z* 266 (M^+, 5%); Anal. ($C_{17}H_{14}O_2$) C, H.

Reaction of Compounds 5b, 5c, 5c′ in Acetonitrile. A solution of **5b** or **5c** (5 mmol) in acetonitrile (100 ml) or **5c′** (5 mmol) in dichloromethane-saturated aqueous NH_4Cl (4:1, 50 ml) was kept under the reaction conditions given in Tables 2 and 3. Dichloromethane (100 ml) was added and the organic phase was washed with 10% hydrochloric acid (50 ml) and aqueous NaCl (50 ml). The aqueous layer was extracted with two portions of dichloromethane (50 ml), and the combined organic phases were again washed with aqueous NaCl before being dried (anhydrous $MgSO_4$). Removal of the solvent gave the residue which was chromatographed on a silica-gel column eluting hexane-ethyl acetate (4:1) to afford **1** and (*Z*)-**5b**, (*E*)-**5c**, or (*E*)-**5c′**. These results are given in Tables 2 and 3.

(2*E*)-3-Phenyl-2-(*p*-toluenesulfinyl)-1-(*p*-tolyl)-2-propen-1-one: Mp 83 °C; IR (Nujol) 1670 (C=O) and 1050 cm^{-1} (S→O); ^1H NMR ($CDCl_3$) δ=2.25 (6H, s, MeO) and 6.8—7.8 (14H, m, Ph, Ar, CH); MS *m/z* 360 (M^+, 2%); Anal. ($C_{23}H_{20}O_2S$) C, H.

We wish to thank the Ministry of Education, Science and Culture for a Grant-in-Aid for Scientific Research.

References

1) R. L. Reeves, "The Chemistry of the Carbonyl Group," ed by S. Patai, Interscience, London (1966), p. 593.
2) G. Jones, *Org. React.*, **15**, 204 (1967).
3) H. O. House, "Modern Synthetic Reactions," 2nd ed, W. A. Benjamin, Inc., Menlo Park (1972), p. 646.
4) J. Mathieu and J. Weill-Raynal, "Formation of C-C Bonds," G. Thieme Publishers, Stuttgart (1975), Vol. 2, p. 515.
5) R. Tanikaga, N. Konya, T. Tamura, and A. Kaji, *J. Chem. Soc., Perkin Trans. 1*, **1987**, 825, and references cited therein.
6) R. P. Redman, P. J. Thomas, and C. J. M. Stirling, *J. Chem. Soc., Perkin Trans. 2*, **1978**, 1135, and references cited therein.
7) R. Tanikaga, Y. Nozaki, T. Tamura, and A. Kaji, *Synthesis*, **1983**, 134.
8) G. Cilento, *Chem. Rev.*, **60**, 147 (1960).
9) L. Pauling, "The Nature of the Chemical Bond," 3rd ed, Cornell Univ. Press, (1960), p. 260.
10) Z. Rappoport, *Acc. Chem. Res.*, **14**, 7 (1981).
11) Z. Rappoport and A. Gazit, *J. Org. Chem.*, **51**, 4112 (1986).
12) N. Kunieda, A. Suzuki, and M. Kinoshita, *Bull. Chem. Soc. Jpn.*, **54**, 1143 (1981).
13) H. D. Murdoch and D. C. Nonhebel, *J. Chem. Soc.*, **1962**, 2153.
14) J. Nokami, T. Mandai, A. Nishimura, T. Takeda, and S. Wakabayashi, *Tetrahedron Lett.*, **27**, 5109 (1986).
15) M. Sekiya and K. Suzuki, *Chem. Pharm. Bull.*, **18**, 1530 (1970).

 © 1988 The Chemical Society of Japan Bull. Chem. Soc. Jpn., 61, 3217—3223 (1988)

Phosphonylation of Biomolecules with Inorganic Diphosphonate. II.[1] Phosphonylation of Phosphate Groups on Nucleoside 5′-Monophosphates, Deoxynucleoside 5′-Monophosphates, and Sugar Phosphates

Yoshisuke YAMAMOTO, Yoshinobu BABA,*,† Miwa MIZOKUCHI,† Mika ONOE,††
Tomoko SUMIYAMA,†† Mitsutomo TSUHAKO,†† Norimasa YOZA,*
and Shigeru OHASHI
Department of Chemistry, Faculty of Science, Kyushu University,
Hakozaki, Higashiku, Fukuoka 812
†Department of Chemistry, Faculty of Education, Oita University, Dannoharu, Oita 870-11
††Kobe Women's College of Pharmacy, Kitamachi, Motoyama, Higashinadaku, Kobe 658
(Received March 4, 1988)

Inorganic diphosphonate phosphonylated predominantly phosphate groups on nucleoside 5′-monophosphates (=NMP's: AMP, GMP, IMP, CMP, and UMP), deoxynucleoside 5′-monophosphates (=dNMP's: dAMP and dTMP), and sugar phosphates (=SP's: Glc1P, Glc6P, and Rib5P) in aqueous solutions under mild conditions (50—70 °C, pH 6). The chemical structures of phosphonylated products were discussed on their ^{31}P NMR spectra and high-performance liquid chromatograms. The main phosphonylated products from NMP's and dNMP's were analogous in structure to nucleoside 5′-diphosphates. The rate of phosphonylation of phosphate groups on NMP's, dNMP's, and SP's varied strongly depending on reaction conditions: pH, reaction temperature, and initial concentration of inorganic diphosphonate. The maximum yields of phosphonylated products were ca. 70% for all NMP's, dNMP's, and SP's under the following conditions: initial concentration of inorganic diphosphonate is 1.5 mol dm^{-3}; each initial concentration of NMP's, dNMP's, or SP's is 0.1 mol dm^{-3}; 70 °C; pH 6.

Blaser and Worms reported[2,3] that disodium inorganic diphosphonate (P^{III}–O–P^{III}), $Na_2P_2H_2O_5$, reacted with several nucleophiles (X) such as orthophosphate and fluoride to form new compounds (X–$\overset{\overset{O}{\|}}{\underset{\underset{O^-}{|}}{P}}$–H) and inorganic phosphonate (P^{III}) according to Eq. 1. Hypophosphate,[2,4] diphosphate,[3,5] triphosphate,[5,6] and ammonia[7] were also found to react

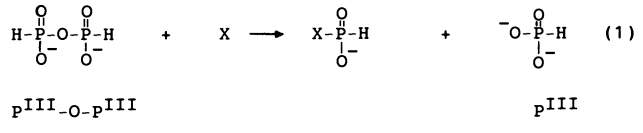

with inorganic diphosphonate to form new compounds. In such reactions a "phosphonyl" group ($\overset{\overset{O}{\|}}{\underset{\underset{O^-}{|}}{H\text{–}P}}$–) on P^{III}–O–P^{III} is transferred to a nucleophile to form a "phosphonylated" product. We called this type of reaction "phosphonyl transfer reaction" or "phosphonylation" rather than "transanhydrization" proposed by Blaser and Worms,[2,3] because of its similarity to phosphoryl transfer reaction or phosphorylation of biological importance.[8]

Much attention has recently been focused on phosphonylation of biomolecules in the field of nucleic acid syntheses and kinetic research of enzymatic reactions. Successful examples are the application of nucleoside H-phosphonate to automatic syntheses of DNA and RNA,[9,10] and the wide use of phosphonate analogues of biomolecules as a metabolic regulator.[11] On the other hand, no successful attempts with inorganic diphosphonate as a phosphonylating agent have been reported for the synthesis of phosphonylated analogues of "biophosphates" such as nucleotides and sugar phosphates. The main reason is the lack of analytical techniques for simultaneous determination of biophosphates and inorganic phosphonates. We have developed the HPLC system coupled with flow injection analysis for simultaneous determination of biophosphates and inorganic phosphonates.[12–16]

The purpose of our project in this series was to characterize the formation of phosphonylated analogues of biophosphates by means of the HPLC technique[12–16] and ^{31}P NMR spectroscopy. We have already reported[17] that adenosine 5′-monophosphate was phosphonylated by P^{III}–O–P^{III} to give an analogue of adenosine 5′-diphosphate as a main product, with some by-products phosphonylated at the 2′- or 3′-position of the ribose. We also reported in a preliminary paper that a phosphate group on glucose 1-monophosphate was phosphonylated selectively by P^{III}–O–P^{III}.[1] This paper deals mainly with phosphonylation of phosphate groups on nucleoside 5′-monophosphates (=NMP's: AMP, GMP, IMP, CMP, and UMP),[18] deoxynucleoside 5′-monophosphates (=dNMP's: dAMP and dTMP),[18] and sugar phosphates (=SP's: Glc1P, Glc6P, and Rib5P)[18] under various conditions.

Experimental

Chemicals. Disodium salt of AMP from Boehringer-Mannheim, disodium salts of GMP, IMP, CMP, UMP, dAMP, and dTMP from Yamasa Shoyu, and disodium salts

of Glc1P, Glc6P, and Rib5P from Sigma were commercially available.

Disodium inorganic diphosphonate, $Na_2P_2H_2O_5$, was prepared according to the literature[6] with a slight modification. In an Erlenmeyer flask with a glass stopper, 300 ml acetic anhydride, $(CH_3CO)_2O$, was added to a mixture of 18.5 g of phosphonic acid, H_2PHO_3, and 48.6 g of disodium phosphonate pentahydrate, $Na_2PHO_3 \cdot 5H_2O$. The resulting mixture was agitated for 1 h and allowed to be incubated in an ultrasonic cleaner for 3 h at room temperature to give a white precipitate. After the supernatant was removed, the precipitate was suspended in 300 ml acetone, filtered, and washed with acetone in order to remove acetic anhydride and acetic acid. The precipitate was dissolved in 150 ml of water and recrystallized by addition of 210 ml of ethanol. The precipitate was filtered, washed with acetone, and dried at 50 °C to get about 15 g of disodium inorganic diphosphonate. The purity of the disodium inorganic diphosphonate thus obtained was checked by HPLC[12] to be 97—99% (as P).

Reaction of NMP, dNMP, or SP with Inorganic Diphosphonate. Unless otherwise stated, initial concentration of inorganic diphosphonate varied form 0.5 to 1.5 mol dm^{-3}, keeping the initial concentration of NMP's, dNMP's, or SP's at 0.1 mol dm^{-3} constant. The reaction mixture was adjusted to the prescribed pH value (10, 8, 6, or 4) with a sodium hydroxide or hydrochloric acid solution and was allowed to react at 50, 60, 70, and 80 °C. The pH change during the reactions was not controlled strictly.

HPLC Measurement. The HPLC manifold and technique were described in previous papers.[12-16] An HLC-601 system (Toyo Soda) was used as a main pumping system. The separations were performed on a column (100×4.0 mm I.D.) packed with an anion exchanger (TSKgel SAX, 10 μm, Toyo Soda). Flow rate was 1.0 ml min^{-1} and column temperature was kept at 30, 40, or 50 °C. Separated NMP's or dNMP's were detected at 260 nm by use of UV spectrophotometer located at the outlet of the separation column. Phosphate and phosphonate groups on reactants and products were monitored by the on-line coupled flow injection system designed for the differential detection of phosphate and phosphonate groups.[12]

^{31}P NMR Measurement. Pulse FT ^{31}P NMR spectra were recorded at the room temperature by use of JEOL JNM-FX100 (40.25 MHz), VARIAN XL-300 (121 MHz), and JEOL JNM-GX400 (161 MHz) spectrometers. Chemical shifts were measured in comparison with the 85% orthophosphoric acid external standard.

Results and Discussion

Characterization of Phosphonylation by HPLC. An aqueous mixture of AMP and P^{III}-O-P^{III} was incubated at 80 °C. After 3 h incubation, aliquots of the reaction mixture were diluted and analyzed by an HPLC system designed for the simultaneous determination of nucleotides, sugar phosphates, and inorganic phosphonates.[12-16]

Figure 1 shows HPLC profiles for a 100-fold-diluted sample solution. With UV-detection at 260 nm (Fig. 1a), one main product (A) and two by-products (B and C) were observed in addition to a peak for AMP. A small peak for adenosine (Ado), probably as an impurity in AMP, was also recorded.

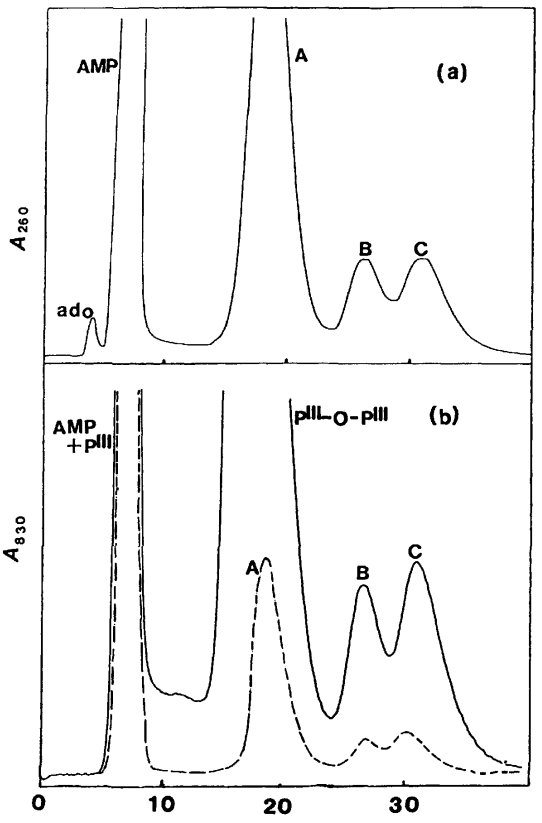

Fig. 1. HPLC profile for AMP (0.15 mol dm^{-3}) phosphonylated by inorganic diphosphonate (0.23 mol dm^{-3}) at 80 °C (pH 6) after 3 h incubation. The reaction mixture was diluted 100-fold. Eluent: 0.12 mol dm^{-3} KCl and 0.1% EDTA 4Na.

The solid lines in Figs. 1b and 2b indicate the sum of the absorbances (830 nm) due to phosphate and phosphonate groups measured in the presence of an oxidizing agent and the broken lines in Figs. 1b and 2b indicate the absorbance (830 nm) due to phosphate group measured in the absence of the oxidizing agent.

The peaks for P^{III} and P^{III}-O-P^{III} in Fig. 1b overlapped with those for AMP and a main product A, respectively. By lowering the sample concentration with 1000-fold dilution, the peaks for P^{III}-O-P^{III}, P^{III}, and A can well be resolved as shown in Fig. 2b. The results in Figs. 1 and 2 indicate that each of species A, B, and C is composed of phosphate, phosphonate, and adenosine, suggesting the formation of derivatives of AMP.

^{31}P NMR Spectra of Phosphonylated Products. No information was available from the HPLC profiles about the chemical structures of the products. To characterize the chemical structures of three phosphonylated products, ^{31}P NMR spectra of the reaction mixture were measured at room temperature on a JEOL JNM-FX100 spectrometer.

A proton-decoupled spectrum of the phosphonylated

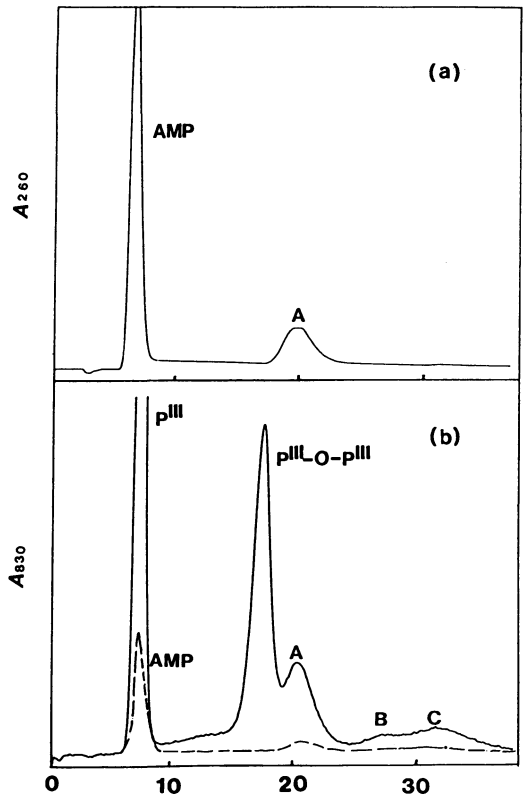

Fig. 2. HPLC profile for AMP (0.15 mol dm^{-3}) phosphonylated by inorganic diphosphonate (0.23 mol dm^{-3}) at 80 °C (pH 6) after 3 h incubation. The reaction mixture was diluted 1000-fold. Eluent: 0.12 mol dm^{-3} KCl and 0.1% EDTA 4Na.

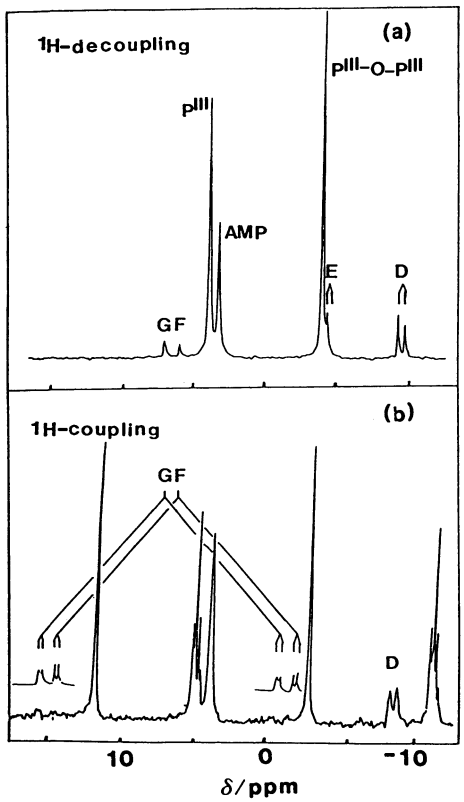

Fig. 3. ^{31}P NMR spectra for AMP (0.1 mol dm^{-3}) phosphonylated by inorganic diphosphonate (0.5 mol dm^{-3}) at 80 °C (pH 6) after 4 h incubation.

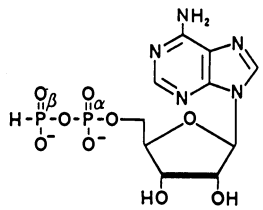

1

Chart 1.

product of AMP (Fig. 3a) shows five singlets and two doublets. Three singlets are assigned to P^{III} (3.93 ppm), AMP (3.30 ppm), and P^{III}-O-P^{III} (−3.93 ppm) on the basis of the chemical shifts for the authentic samples. Two unknown doublets (D and E, −9.55 and −4.00 ppm) and two unknown singlets (G and F, 7.10 and 5.90 ppm) are expected to be the signals for phosphonylated products. One of the signals for the doublet (E) overlapped with that of P^{III}-O-P^{III}. The doublet could be separated from the signal for P^{III}-O-P^{III} by the experiment using a high magnetic field NMR spectrometer (JEOL JNM-GX400). Since the intensities of NMR signals are proportional to phosphorus contents, the main peak (A) in Fig. 1 can be assigned to the doublet (D and E), and the other peaks (B and C) correspond to signals F and G.

The new POP bond is likely to be formed by phosphonylation of AMP because the doublets (D and E) have the same J value of 19.8 Hz and the magnitudes of these J values are approximately equal to the geminal coupling constant ($^2J_{PP}$=21.7 Hz)[19] in adenosine 5′-diphosphate (ADP). The POP bond formation and the intensities of the doublets (D and E) suggest that phosphate group on AMP is predominantly phosphonylated to form product **1** (Chart 1) similar in structure to ADP.

Further splitting of the doublet (E) into a double-doublet is shown in a proton-coupled spectrum (Fig. 3b), while the doublet (D) is not split. The double-doublet (E) is assigned to the phosphorus atom (P_β of **1**) of phosphonyl group (H-$\overset{\overset{O}{\|}}{\underset{\underset{O^-}{|}}{P}}$-) transferred from P^{III}-O-P^{III} to the phosphate group on AMP because the double-doublet (E) shows a splitting of 665.5 Hz for the hydrogen atom attached directly to a phosphorus atom.[20]

If the doublet (D) can be assigned to the signal of P_α of **1**, the doublet (D) is expected to be further split into double-triplets caused by spin-spin coupling with two 5′-hydrogen atoms. The doublet (D) is not split in Fig. 3b, however, the band widths are broadened

compared with the signal observed in the proton-decoupled spectrum. The magnitude of J value can be estimated to be 4 Hz from band broadening. This value is similar to the vicinal coupling constant ($^3J_{PH}$) in AMP (4.9 Hz).[21] Therefore, the doublet (D) is assigned to the signal of P_α of **1**. Phosphate groups on other NMP's (Chart 2), dNMP's (Chart 3), and SP's (Chart 4) were also confirmed to be phosphonylated predominantly. Table 1 lists NMR parameters for phosphonylated products.

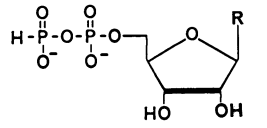

2~5

2: R=guanine
3: R=hypoxanthine
4: R=uracil
5: R=cytosine

Chart 2.

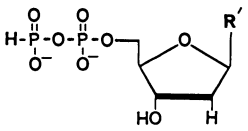

6~7

6: R′=adenine
7: R′=thymine

Chart 3.

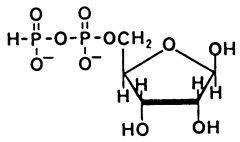

8

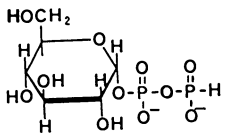

9

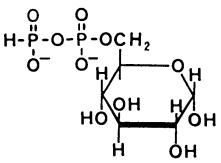

10

Chart 4.

The signals corresponding to G and F in Fig. 3a cannot be observed in a proton-coupled spectrum as shown in Fig. 3b, owing to a complex splitting and a low yield. Signals G and F are assigned to compounds **11** and **12** (Chart 5) produced by phosphonylation of

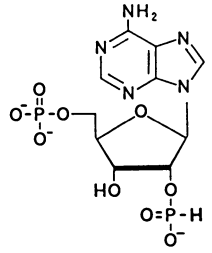

11

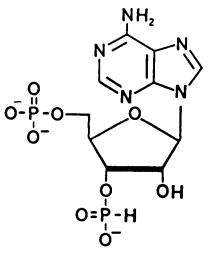

12

Chart 5.

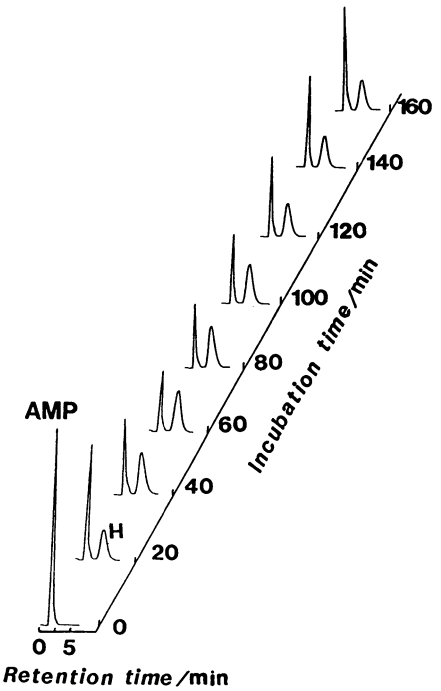

Fig. 4. Kinetic HPLC profile for phosphonylation of AMP (0.1 mol dm^{-3}) with inorganic diphosphonate (1.5 mol dm^{-3}) at 60 °C and pH 6. Eluent: 0.20 mol dm^{-3} KCl and 0.1% EDTA 4Na.

Table 1. ^{31}P NMR Parameters of Phosphonylated Products

Product	$\delta(P_\alpha)$	$\delta(P_\beta)$	$^1J_{P_\beta H}$/Hz	$^2J_{P_\alpha P_\beta}$/Hz	$^3J_{P_\alpha H}$/Hz
1	−9.51	−4.03	667	19.8	4[a]
2	−7.18	−1.30	665	18.8	4[a]
3	−9.35	−4.12	665	19.8	4[a]
4	−9.64	−4.19	666	19.8	4[a]
5	−9.67	−4.19	665	19.1	4[a]
6	−9.53	−4.11	665	19.8	4[a]
7	−10.4	−4.87	665	19.8	4[a]
8	−9.63	−4.29	663	19.6	6.5
9	−11.3	−4.18	666	19.5	7.26
10	−9.45	−4.19	664	19.8	5.81

a) Estimated from the band broadening.

2′- or 3′-OH group, because the double-doublets (+5.9 and +7.1 ppm, $^1J_{PH}$=650 Hz and $^3J_{PH}$=10 Hz each) are observed in a proton-coupled spectrum by other experiments under alkaline conditions (pH 10). Phosphonylation of AMP in an alkaline solution gave **11** and **12** predominantly, but in a neutral solution, **11** and **12** were formed in small amounts (<2%). Phosphonylation of OH groups will be described in detail in a subsequent paper of this series.

Kinetic Profiles for Phosphonylation. Figures 4 and 5 show kinetic HPLC profiles for phosphonylation of AMP and Rib5P. The reaction mixture (P^{III}–O–P^{III}; 1.5 mol dm^{-3}, AMP or Rib5P; 0.1 mol dm^{-3}) was incubated at 60 °C in the pH range from 6 (0 min) to 5.5 (after 100 min) without any buffer solution. Aliquots (0.1 ml) of mixed solutions were withdrawn at 10 or 20 min intervals and diluted with 100 ml of distilled water. An aliquot (0.1 ml) of diluted solutions was introduced into an HPLC system designed for determination of nucleotides and both phosphate and phosphonate groups on reactants and products.[12–16] In the reaction of NMP's and dNMP's, the reactant and the product were detected simultaneously at 260 nm as shown in Fig. 4. On the other hand, phosphate groups were detected in the reaction of SP's to determine SP's and a phosphonylated product simultaneously as shown in Fig. 5, since SP's and their products **8**, **9**, and **10** have no UV-absorption.

The HPLC profiles at time 0 in Figs. 4 and 5 showed the peaks of only AMP and Rib5P. The elution peaks (H and I) appearing after 10—20 min represent the peaks of the phosphonylated products **1** and **8**. The peak areas of the products increased with time at the expense of AMP and Rib5P. The yields of

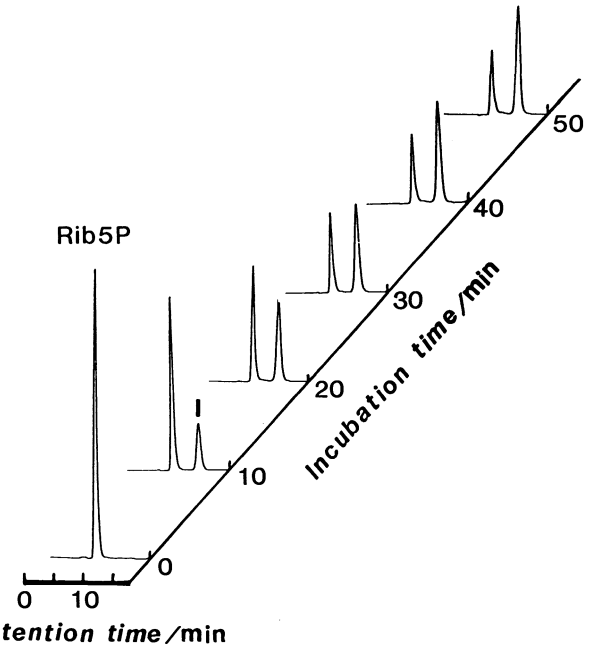

Fig. 5. Kinetic HPLC profile for phosphonylation of Rib5P (0.1 mol dm^{-3}) with inorganic diphosphonate (1.5 mol dm^{-3}) at 60 °C and pH 6. Eluent: 0.20 mol dm^{-3} KCl and 0.1% EDTA 4Na.

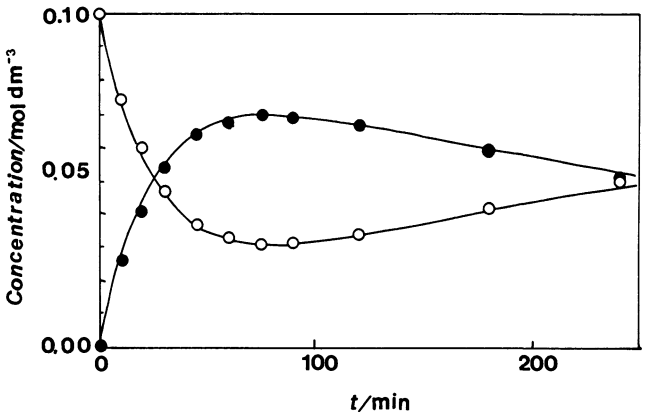

Fig. 6. Time dependence of the reaction components of phosphonylation for AMP with inorganic diphosphonate. Plot of the observed molar concentrations of AMP and product **1** vs. time/min in aqueous solution containing initially 0.1 mol dm^{-3} AMP and 1.0 mol dm^{-3} P^{III}–O–P^{III} at 60 °C and pH 6. (○): AMP, (●): product **1**. Eluent: 0.20 mol dm^{-3} KCl and 0.1% EDTA 4Na.

Table 2. Phosphonylation of AMP with P^{III}–O–P^{III}

Reaction condition					Yield/%
Molarity/mol dm^{-3}		pH	Temp/°C	Time/min	
P^{III}–O–P^{III}	AMP				
0.5	0.1	6	50	480	41
			60	300	43
			70	180	49
1.0	0.1	4	60	60	18
		6	50	300	59
			60	120	60
			70	60	62
		8	60	120	53
		10	60	0—120	0
1.5	0.1	6	50	180	69
			60	75	70
			70	30	69

the products reached a maximum after 50—60 min, and then gradually disappeared.

Effects of pH and Temperature on the Phosphonylation of NMP's. Figure 6 illustrates the time-dependent utilization of AMP and formation of product **1**. With the progress of the reaction, the amount of **1** increased gradually to a maximum (about 70% after 60 min), and then gradually decreased. Table 2 lists maximum yields and reaction times required to reach maximum yields under various reaction conditions.

The pH effect on the maximum yield was examined in the reaction of AMP at 60 °C and 1.0 mol dm^{-3} of initial concentration for P^{III}–O–P^{III}. In the pH range studied here, products were obtained in higher yields at neutral pH region, compared to a lower yield in both acidic and alkaline pH regions. The optimal pH was confirmed to be 6, because the reaction at pH ca. 6 gave a maximum yield, and the mixed solutions of P^{III}–O–P^{III} and NMP's, dNMP's, or SP's were kept at pH ca. 6 without any buffer solutions.

The maximum yield increased with increasing initial concentration of P^{III}–O–P^{III}: 50% at 0.5 mol dm^{-3}, 60% at 1.0 mol dm^{-3}, and 70% at 1.5 mol dm^{-3}. The increase in reaction temperature decreased the time required to reach a maximum yield, but did not contribute to an increase in a maximum yield. The optimal conditions for phosphonylation of AMP with P^{III}–O–P^{III} were found to be initial concentration of P^{III}–O–P^{III} 1.5 mol dm^{-3}, pH 6, and 60 °C.

Table 3. Yields/% of Phosphonylated Products of NMP's[a]

NMP[b]	[P^{III}–O–P^{III}]/mol dm^{-3}	Time/min		
		30	60	120
GMP	1.0	26	42	56
IMP	1.0	26	43	59
	1.5	43	61	66
UMP	1.0	25	42	57
	1.5	44	61	66
CMP	1.0	29	46	62
	1.5	50	68	73

a) Reaction temperature: 60 °C; pH: 6. b) Initial concentration of NMP is 0.1 mol dm^{-3}.

To examine effects of bases of NMP's on maximum yields, the maximum yields of GMP, IMP, UMP, and CMP were compiled in Table 3. The maximum yields and reaction times were almost the same as that obtained for the reaction of AMP. Therefore, we concluded that differences in bases on NMP's did not change the reactivity of NMP's even in the purine and pyrimidine nucleotides.

Effects of pH and Temperature on the Phosphonylation of dNMP's and SP's. Both dNMP's and SP's were also phosphonylated with P^{III}–O–P^{III} under various conditions and the maximum yields were listed in Tables 4 and 5.

dNMP was phosphonylated after 2 h in the yield of 59% at pH 6 and 60 °C when the initial concentration of P^{III}–O–P^{III} was 1.0 mol dm^{-3}. The yield increased and the reaction time decreased with an increase in initial concentration of P^{III}–O–P^{III} as well as in the reaction of NMP. In the reaction of dAMP the yield of **7** was found to be 57 and 70% at 1.0 and 1.5 mol dm^{-3} of P^{III}–O–P^{III}, respectively. The optimum conditions for the phosphonylation of dNMP's are at 1.5 mol dm^{-3} of P^{III}–O–P^{III}, pH 6, and 60 °C.

In the reaction of Rib5P, the yield of **8** at pH 6 was higher than that at pH 4 and 8 under the conditions of 1.0 mol dm^{-3} of P^{III}–O–P^{III} and 60 °C. At 1.5 mol dm^{-3} of P^{III}–O–P^{III}, Rib5P was phosphonylated in the yield of 70% at pH 6 and 60 °C, while the yields of **8** were 43 and 59% when the initial concentrations of P^{III}–O–P^{III} were 0.5 and 1.0 mol dm^{-3}, respectively. Initial concentration affected yields strongly, but reaction temperature did not contribute to changes in the yield in spite of decreasing reaction time. At pH 6 and 60 °C, other SP's were also phosphonylated by P^{III}–O–P^{III}. About 70% of Glc1P or Glc6P was phosphonylated after 1 h at 1.5 mol dm^{-3} of P^{III}–O–P^{III}. The optimal conditions for the phosphonylation of SP's are at 1.5 mol dm^{-3} of P^{III}–O–P^{III}, pH 6, and 60 °C as well as in the reaction of NMP's and dNMP's.

The results obtained in the reaction of dNMP's or SP's showed that the 2′-OH and bases on NMP's affected slightly the reactivity of phosphate groups on NMP's, dNMP's, and SP's.

Table 4. Phosphonylation of dNMP's with P^{III}–O–P^{III}

Reaction condition					Yield/%
Molarity/mol dm^{-3}		pH	Temp/°C	Time/min	
P^{III}–O–P^{III}	dTMP				
1.0	0.1	4	60	60	15
		6	60	120	59
		8	60	120	51
1.5	0.1	6	60	120	66
P^{III}–O–P^{III}	dAMP				
1.0	0.1	6	60	120	57
1.5	0.1	6	60	60	68

Table 5. Phosphonylation of SP's with P^{III}–O–P^{III}

Reaction condition					Yield/%
Molarity/mol dm^{-3}		pH	Temp/°C	Time/min	
P^{III}–O–P^{III}	Rib5P				
0.5	0.1	6	50	420	34
			60	270	43
		8	70	180	42
1.0	0.1	4	60	100	31
		6	50	240	61
			60	120	59
			70	60	57
		8	60	60	38
1.5	0.1	6	50	120	69
			60	60	70
			70	30	70
P^{III}–O–P^{III}	Glc1P				
1.0	0.1	6	60	120	60
1.5	0.1	6	60	60	70
P^{III}–O–P^{III}	Glc6P				
1.0	0.1	6	60	120	68
1.5	0.1	6	60	60	68

The authors wish to express their thanks to Dr. Tohru Miyajima and Dr. Eiichi Kuwano of Kyushu University for their help in measuring ^{31}P NMR spectra. The present work was partially supported by a Grant-in-Aid for Scientific Research No. 61790151 from the Ministry of Education, Science and Culture.

References

1) Part I of this series. Y. Baba, M. Onoe, T. Sumiyama, M. Tsuhako, N. Yoza, and S. Ohashi, *Chem. Lett.*, **1987**, 1389.

2) B. Blaser, K.-H. Worms, *Z. Anorg. Allg. Chem.*, **312**, 146 (1961).

3) B. Blaser and K.-H. Worms, O. Glemser, and A. von Bachmann, *Z. Anorg. Allg. Chem.*, **361**, 22 (1968).

4) N. Yoza, H. Yoshidome, and S. Ohashi, *J. Chromatogr.*, **150**, 393 (1978).

5) N. Yoza, M. Tokuda, T. Inoue, and S. Ohashi, *Inorg. Nucl. Chem. Lett.*, **9**, 385 (1973).

6) N. Yoza, K. Ishibashi, and S. Ohashi, *J. Chromatogr.*, **134**, 497 (1977).

7) R. E. Mesmer and R. L. Carroll, *J. Am. Chem. Soc.*, **88**, 1381 (1966).

8) J. R. Knowles, *Ann. Rev. Biochem.*, **4**, 877 (1980).

9) a) P. J. Garegg, T. Regberg, J. Stawinski, and R. Strömberg, *Chemica Screpta*, **25**, 280 (1985); **26** 59 (1986). b) P. J. Garegg, I. Lindh, T. Regberg, J. Stawinski, R. Strömberg, and C. Henrichson, *Tetrahedron Lett.*, **27**, 4051 (1986); **27**, 4055 (1986). c) P. J. Garegg, T. Regberg, J. Stawinski, and R. Strömberg, *Nuclesides and Nucleotides*, **6**, 283 (1987); **6**, 655 (1987). d) P. J. Garegg, T. Regberg, J. Stawinski, and R. Strömberg, *J. Chem. Soc., Perkin Trans. 1*, **1987**, 1269. e) P. J. Garegg, J. Stawinski, and R. Strömberg, *J. Org. Chem.*, **52**, 284 (1987). f) R. Strömberg and J. Stawinski, Nucleic Acids Res. Symp. Ser., No. 18, 185 (1987).

10) a) B. C. Froehler and M. D. Matteucci, *Tetrahedron Lett.*, **27**, 469 (1986). b) *Nucleosides and Nucleotides*, **6**, 287 (1987). c) B. C. Froehler, P. G. Ng, and M. D. Matteucci, *Nucleic Acids Res.*, **14**, 5399 (1986). d) B. C. Froehler, *Tetrahedron Lett.*, **27**, 5575 (1986).

11) R. Engel, *Chem. Rev.*, **77**, 349 (1977).

12) Y. Hirai, N. Yoza, and S. Ohashi, *J. Chromatogr.*, **206**, 501 (1981).

13) Y. Baba, N. Yoza, and S. Ohashi, *J. Chromatogr.*, **348**, 27 (1985).

14) Y. Baba, Y. Yamamoto, N. Yoza, and S. Ohashi, *Bunseki Kagaku*, **34**, 692 (1985).

15) H. Hirano, Y. Baba, N. Yoza, and S. Ohashi, *Chem. Lett.*, **1986**, 633.

16) N. Yoza, H. Hirano, Y. Baba, and S. Ohashi, *Phosphorus and Sulfur*, **30**, 605 (1987).

17) Y. Baba, M. Tsuhako, Y. Yamamoto, N. Yoza, and S. Ohashi, Nucleic Acids Res. Symp. Ser., No. 17, 69 (1986).

18) Abbreviations: NMP, nucleoside 5′-monophosphate; AMP, GMP, IMP, CMP, and UMP, adenosine, guanosine, inosine, cytidine, and uridine 5′-monophosphate; dNMP, deoxy-nucleoside 5′-monophosphate; dAMP and dTMP, deoxy-adenosine and thymidine 5′-monophosphate; SP, sugar phosphate; Glc1P, Glc6P, and Rib5P, glucose 1-monophosphate, glucose 6-monophosphate, and ribose 5-monophosphate.

19) H. J. Vogel and W. A. Bridger, *Biochemistry*, **21**, 394 (1982).

20) D. G. Gorenstein, "Phosphorus-31 NMR; Principles and Applications," Academic Press, Orlando (1984), Part 1—2, p. 39.

21) P. J. Cozzone and O. Jardetzky, *Biochemistry*, **15**, 4860 (1976).

 © 1988 The Chemical Society of Japan Bull. Chem. Soc. Jpn., 61, 3225—3229 (1988)

Skimmiarepin A and B, Two New Insect Growth Inhibitory Triterpenoids from *Skimmia japonica* Thunb. var. *intermedia* Komatsu f. *repens* (Nakai) Hara

Masamitsu Ochi,* Akira Tatsukawa, Naoki Seki, Hiyoshizo Kotsuki, and Kozo Shibata*,†

Faculty of Science, Kochi University, Akebono-cho, Kochi 780

†Faculty of Science, Osaka City University, Sumiyoshi-ku, Osaka 558

(Received March 7, 1988)

Two new triterpenoids, skimmiarepin A and B, which both exhibit an insect growth inhibitory activity against the silkworm, *Bombyx mori* L., have been isolated from the leaves and the fruit of *Skimmia japonica* Thunb. var. *intermedia* Komatsu f. *repens* (Nakai) Hara. Their structures have been determined by extensive 2D NMR studies and chemical methods.

The shrub *Skimmia japonica* Thunb. var. *intermedia* Komatsu f. *repens* (Nakai) Hara (Rutaceae)[1] is widely distributed in Japan and its leaves are relatively free from insect attack. In our preliminary screening for the biological activities of plant materials, the methanol extracts of the leaves and fruit of this plant exhibited an insect growth inhibitory activity against the silkworm, *Bombyx mori* L. Monitoring the fractionations of the methanol extracts by artificial diet feeding bioassay against silkworm larvae[2] led to the isolation of two new triterpenoids responsible to the observed activity.[3] This paper deals with the structures of these new compounds, named skimmiarepin A and B.

Skimmiarepin A (**1**), $C_{35}H_{56}O_6$, mp 164.5—165.5 °C, $[\alpha]_D^{20}$ −22.7° (*c* 0.20, EtOH), was isolated from the methanol extract of the leaves in 0.013% yield as colorless needles by conventional silica-gel column chromatography and preparative high-performance liquid chromatography. It had IR absorptions indicative of hydroxyl (3580 and 3320 cm^{-1}) and ester (1725 cm^{-1}) groups, and formed a couple of diacetates **3**, $C_{39}H_{60}O_8$, mp 79.0—80.0 °C, and **4**, $C_{39}H_{60}O_8$, mp 191.5—192.5 °C, on acetylation with 4-dimethylaminopyridine–acetic anhydride. The oxidation of **1** with pyridinium chlorochromate gave a keto lactone **5**, $C_{35}H_{52}O_6$, mp 135.0—136.0 °C, the IR spectrum of which showed the presence of the newly introduced γ-lactone (1780 cm^{-1}). These facts and the appearance of a pair of ^{13}C NMR signals due to a hemiacetal carbon atom in **1** (δ_C 98.12 and 102.00) suggested that **1** is an epimeric mixture with respect to the hemiacetal carbon atom which constitutes a five-membered cyclic ether. At first our attention was directed to the simplest compound **5**.

The 400 MHz ^1H NMR spectrum of **5** showed signals due to a cyclopropyl methylene group at δ 0.45 and 0.58 (1H each, d, *J*=5.6 Hz), six tertiary methyl groups at δ 0.84, 0.93, 1.09, 1.32, 1.34, and 1.37 (3H each, s), a trisubstituted epoxide at δ 2.80 (1H, d, *J*=7.3 Hz), and two oxygen-bearing methine groups at δ 4.17 (1H, ddd, *J*=10.5, 7.3, and 6.1 Hz) and 4.70 (1H, t, *J*=2.9 Hz). The presence of an isovaleric ester was also evident from the ^1H NMR signals at δ 0.96 (6H, d,

Table 1. ^1H NMR Spectrum of **5**[a]

Proton	δ	*J*/Hz	Proton	δ	*J*/Hz
1α-H	1.54 m#[b]		18a-H	0.45 d	5.6
1β-H	1.12 m#		18b-H	0.58 d	5.6
2α-H	1.93 m#		19- H_3	1.09 s	
2β-H	1.65 m#		20- H	2.89 ddd	12.7, 8.3, 4.4
3- H	4.70 t	2.9	22a-H	1.90 m#	
5- H	1.63 dd	14.0, 2.4	22b-H	2.22 m#	
6α-H	2.16 dd	14.0, 2.4	23- H	4.17 ddd	10.5, 7.3, 6.1
6β-H	2.56 t	14.0	24- H	2.80 d	7.3
9- H	1.15 m#		26- H_3	1.37 s	
11- H_2	1.40 m#		27- H_3	1.34 s	
12a-H	1.65 m#		28- H_3	0.84 s	
12b-H	1.92 m#		29- H_3	0.93 s	
15a-H	1.90 m#		30- H_3	1.32 s	
15b-H	2.00 m#		2′- H_2	2.17 d	6.6
16a-H	0.96 m#		3′- H	2.09 m#	
16b-H	1.57 m#		4′- H_3	0.96 d	6.6
17- H	2.47 ddd	11.5, 7.1, 4.4	5′- H_3		

a) The spectrum was determined at 25 °C in $CDCl_3$ solution, with TMS as the internal standard. Assignments were based on the ^1H–^1H and ^1H–^{13}C COSY, and NOESY experiments. b) m#: Overlapped multiplets.

J=6.6 Hz), 2.09 (1H, m), and 2.17 (2H, d, J=6.6 Hz), and the MS fragment at m/z 466 ($M^+-C_5H_{10}O_2$). In addition, an ^1H–^1H COSY analysis and simple homo-decoupling experiments, as summarized in Table 1, revealed the presence of four partial structures, **A**, **B**, **C**, and **D**, all suggesting a carbon framework analogous to those of glabretal (**6**)[4] and ailanthol (**7**)[5] for **5**. The ^1H–^{13}C COSY spectrum of **5** led to straightforward assignments of the ^{13}C NMR signals, except for those of the quaternary carbon atoms at δ_C 28.88, 34.02, 37.12, 37.23, and 50.53 (Table 2). Complete assignments of these quaternary carbon signals as well as ^1H NMR signals of tertiary methyl groups could be accomplished by NOE measurements and ^1H–^{13}C long-range COSY experiments. Namely, observations of NOEs between $H_{3\beta}$ and two methyl groups (δ_H 0.84 and 0.93; $C_{4\alpha}$- and $C_{4\beta}$-Me), between $H_{5\alpha}$ and one of the above methyl groups (δ_H 0.84), between the other one (δ_H 0.93) and $H_{6\beta}$ as well as the third methyl group at δ_H 1.09 (C_{10}-Me), and between the third (δ_H 1.09) and the fourth one at δ_H 1.32 (C_8-Me) defined the positions of all the tertiary methyl groups. The ^{13}C NMR signal at δ_C 37.23 (C_4) showed long-range correlations with methyl proton signals at δ_H 0.84 and 0.93, while the signal at δ_C 37.12 (C_{10}) showed a correlation with that at δ_H 1.09. Further, the methyl proton signal at δ_H 1.32 was long-range-coupled with the carbon signals at δ_C 50.53 (C_8) and

Table 2. ^{13}C Chemical Shifts of **1**—**5**[a]

Carbon	**1**	**2**	**3**	**4**	**5**
1	34.08	34.17	34.42	34.29	34.60
2	26.58	26.63	26.58	26.80	27.09
3	77.77	77.22	77.83	77.76	77.23
4	37.45 (37.18)	37.53 (37.18)	37.44	37.45	37.23
5	41.47 (41.53)	41.66 (41.74)	42.61	42.66	50.35
6	24.50	24.52	23.39	23.36	35.62
7	74.32 (74.20)	74.36 (74.24)	76.23	76.17	214.74
8	39.21 (39.28)	39.23 (39.28)	38.43	38.53	50.53
9	44.24 (44.02)	44.28 (44.18)	45.47	45.03	51.84
10	36.37	36.53	36.99	37.31	37.12
11	16.47 (16.34)	16.48 (16.35)	16.99	16.89	16.84
12	23.15	23.11	23.14	23.09	22.74
13	29.27 (28.92)	29.31 (28.85)	28.80	29.38	28.88
14	37.18	37.18	36.48	36.42	34.02
15	25.85 (26.17)	25.85 (26.23)	26.51	26.01	28.38
16	27.76 (26.48)	27.78 (26.43)	26.90	27.93	21.67
17	44.96 (48.50)	44.97 (48.41)	48.49	45.32	45.04
18	14.08 (13.90)	14.08 (13.93)	15.59	14.85	15.26
19	15.99 (15.87)	16.03 (15.92)	16.16	16.05	15.96
20	49.55 (51.00)	49.54 (50.87)	49.14	48.37	40.91
21	98.12 (102.00)	98.13 (102.01)	101.33	97.53	177.83
22	31.05 (33.28)	31.06 (33.13)	32.29	30.87	26.72
23	78.43 (77.77)	78.45 (77.70)	79.32	79.86	78.42
24	67.68 (65.36)	67.69 (65.39)	65.08	66.84	64.43
25	58.18 (57.36)	58.20 (58.53)	57.10	57.23	57.28
26	25.27 (25.18)	25.25 (25.17)	25.18	25.20	24.82
27	19.72 (19.83)	19.71 (19.81)	19.81	19.81	19.50
28	28.03	28.00	28.07	28.06	27.42
29	22.15	22.19	21.86	21.85	21.15
30	19.48 (19.83)	19.48 (19.71)	19.92	19.64	18.81
1′	172.44	166.02	171.93	172.00	172.40
2′	44.02	117.04	44.31	44.28	43.87
3′	26.03	144.09	26.04	26.04	25.80
4′	22.73	126.66	22.96	22.95	22.50
5′	22.73	139.65	22.86	22.86	22.46
6′		130.37			
7′		141.62			
8′		35.28			
9′		22.55			
10′		14.00			
$COCH_3$			21.66	21.65	
			21.85	21.85	
$COCH_3$			169.51	169.54	
			169.91	169.61	

a) The spectra were measured at 100 MHz in $CDCl_3$ solutions and the shifts are given in δ(ppm) relative to the internal TMS. Assignments were made by means of INEPT, ^1H–^{13}C COSY, and ^1H–^{13}C long-range COSY experiments. Values in parentheses are attributable to the $C_{21}\alpha$-OH epimer.

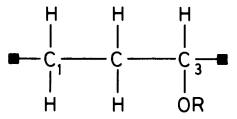

A

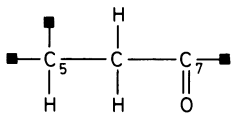

B

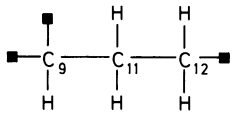

C

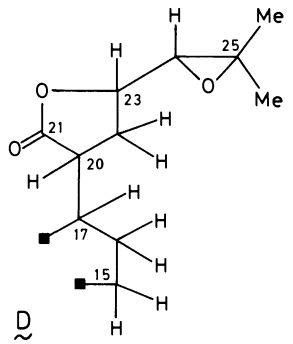

D

34.02 (C_{14}). The remaining quaternary carbon signal at δ_C 28.88 could, therefore, be assigned to C_{13}.

These facts inevitably led to an understanding of the gross structure of **5** for the keto lactone and, hence, structure **1** for skimmiarepin A. The locations of the isovaleric ester and the secondary hydroxyl group in **1** were apparently at $C_{3\alpha}$ and $C_{7\alpha}$, respectively, according to the chemical shifts and the coupling pattern of ^{1}H NMR signals due to their carbinyl protons [$H_{3\beta}$: δ 4.66 (t, J=2.8 Hz); $H_{7\beta}$: δ 3.76 (br s)].[4,6] The final confirmation of the assigned structure was achieved by a chemical correlation of **1** with **6**. Thus, a partial methanolysis of the diacetate **3** with triethylamine–methanol yielded an amorphous hemiacetal **8**, $C_{37}H_{58}O_7$. A treatment of **8** with ethyl vinyl ether–pyridinium *p*-toluenesulfonate and a selective methanolysis of the product with sodium methoxide–methanol, followed by a treatment with pyridinium *p*-toluenesulfonate, afforded a diol, the spectral data of which are identical with those of **6**. The stereochemistry at C_{21} of **3** and **4** was deduced from scrutinizing the ^{13}C NMR data for the carbon atoms on the side chains of both compounds.[6]

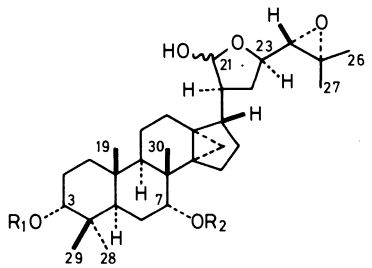

1 R_1 = $COCH_2CH(CH_3)_2$, R_2 = H

2 R_1 = $COCH\overset{Z}{=}CHCH\overset{E}{=}CHCH\overset{E}{=}CHCH_2CH_2CH_3$, R_2 = H

6 R_1 = H, R_2 = Ac

8 R_1 = $COCH_2CH(CH_3)_2$, R_2 = Ac

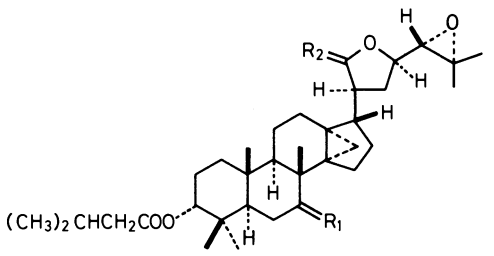

3 R_1 = α-OAc, β-H, R_2 = α-OAc, β-H

4 R_1 = α-OAc, β-H, R_2 = α-H, β-OAc

5 R_1 = R_2 = O

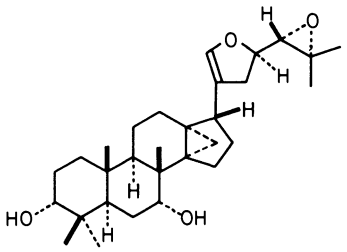

7

Skimmiarepin B (**2**) was obtained from a methanol extract of the fruit in 0.001% yield as fine needles, $C_{40}H_{60}O_6$, mp 168.0—169.0 °C, $[\alpha]_D^{18}$ −39.8° (*c* 0.11, $CHCl_3$), and exhibited spectral data quite similar to those of **1**, except for following observations. The IR and UV spectra of **2** showed the presence of an unsaturated carboxylic ester [ν_{max} 1705 and 1615 cm^{-1}; λ_{max} 303 nm (ε 21000)]. The ^{1}H NMR spectrum did not show any signal due to the isovaleric ester present in **1** but, instead, showed the presence of a 2,4,6-decatrienoic ester [δ 7.43 (1H, dd, J=14.6 and 11.4 Hz), 6.57 (1H, t, J=11.4 Hz), 6.46 (1H, dd, J=14.6 and 10.6 Hz), 6.27 (1H, dd, J=14.8 and 10.6 Hz), 5.91 (1H, dt, J=14.8 and 7.2 Hz), 5.69 (1H, d, J=11.4 Hz), 2.12 (2H, q, J=7.2 Hz), 1.46 (2H, sext, J=7.2 Hz), and 0.91 (3H, t, J=7.2 Hz)]. The relatively small coupling constant (11.4 Hz) between H_2' and H_3' and the appearance of the H_4' signal at a lower field (δ 7.43)[7] revealed the *Z*-geometry of the C_2' double bond. On the other hand, the *E*-configuration of the C_4' and C_6' double bonds was deduced from the trans ethylenic coupling constants between H_4' and H_5' (14.6 Hz) and between H_6' and H_7' (14.8 Hz), respectively. From this evidence and the pertinent ^{13}C NMR data (Table 2), the structure **2** was proposed for skimmiarepin B.

Experimental

All mps were determined on a Mitamura micro melting-point apparatus and are uncorrected. The IR and UV spectra were recorded on a JASCO model A-302 spectro-

photometer and a JASCO UVIDEC-670 spectrophotometer, respectively. The ^{1}H NMR (400 MHz) and ^{13}C NMR (100 MHz) spectra were taken on a JEOL JNM-GX400 instrument in $CDCl_3$ solutions, with TMS as the internal standard. Mass spectra as well as high-resolution mass spectra were measured with a JEOL JMS-D300 spectrometer at 70 eV of ionization energy. A Union Gikken apparatus, model PM-101, was used for measuring the rotations. High-performance liquid chromatographic separation was performed on a Waters Associates HPLC model 6000A, with a TSK-GEL LS-410KG (ODS) column.

Isolation. The leaves and the fruit of *Skimmia* japonica Thunb. var. *intermedia* Komatsu f. *repens* (Nakai) Hara were collected from Mt. Kuishi, Kochi Prefecture, in December 1985. Fresh leaves (1.82 kg) were chopped up and extracted with methanol (6 l) at room temperature for one week. The methanol solution was concentrated up to about 0.5 l, water (0.5 l) was added, and the resulting aqueous suspension was extracted with dichloromethane (3×0.3 l). The dichloromethane layer was washed with water, dried over sodium sulfate, and evaporated to dryness. The residue (65.1 g) was subjected to chromatography over silicic acid (800 g); upon eluting with hexane–ethyl acetate mixtures, ethyl acetate increased from 20 to 80%. Elution with 50% ethyl acetate in hexane gave a fraction (12.0 g) which was rechromatographed over neutral alumina (250 g), using 50% ether in hexane as the eluent, to yield skimmiarepin A (**1**) (347 mg). The fresh fruit (1.44 kg) was extracted in the same manner as described above and the dichloromethane extract (8.3 g) was subjected to chromatography over silicic acid (300 g); upon eluting with hexane–ethyl acetate mixtures, ethyl acetate increased from 20 to 80%. Elution with 50% ethyl acetate in hexane afforded a fraction (155 mg) which was further purified by high-performance liquid chromatography (TSK-GEL LS-410KG, 10% water in methanol) to give skimmiarepin B (**2**) (23 mg).

Skimmiarepin A (1). The crude material was recrystallized from ethanol to give colorless prisms (234 mg); mp 164.5—165.5 °C; $[\alpha]_D^{20}$ −22.7° (*c* 0.20, EtOH); IR (Nujol) 3580, 3320, 1725, 1270, and 1025 cm^{-1}; ^{1}H NMR ($CDCl_3$) δ=0.48 and 0.72 (1H each, d, *J*=4.7 Hz, 18-H_2), 0.96 and 0.97 (3H each, d, *J*=6.6 Hz, 4′- and 5′-H_3), 0.85, 0.88, 0.89, 1.05, 1.31, and 1.32 (3H each, s, 28-, 19-, 29-, 30-, 27-, and 26-H_3), 2.11 (1H, m, 3′-H), 2.23 (2H, d, *J*=6.6 Hz, 2′-H_2), 2.84 (1H, d, *J*=7.3 Hz, 24-H), 3.76 (1H, br s, 7-H), 3.88 (1H, ddd, *J*=9.5, 7.3, and 7.3 Hz, 23-H), 4.66 (1H, t, *J*=2.8 Hz, 3-H), and 5.44 (1H, t, *J*=3.2 Hz, 21-H); ^{13}C NMR (see Table 2); MS (70 eV) *m/z* (rel intensity) 572 (M^+, 3), 554 (M^+-H_2O, 22), 536 (M^+-2H_2O, 7), 470 ($M^+-C_5H_{10}O_2$, 11), 452 ($M^+-H_2O-C_5H_{10}O_2$, 32), 398 (45), 312 (78), 202 (87), and 187 (100). Found: *m/z* 572.4086. Calcd for $C_{35}H_{56}O_6$: M, 572.4077.

Skimmiarepin B (2). The crude substance was recrystallized from acetone to yield white needles (16 mg); mp 168.0—169.0 °C; $[\alpha]_D^{18}$ −39.8° (*c* 0.11, $CHCl_3$); IR (CCl_4) 3600, 3400, 1705, 1615, and 1170 cm^{-1}; UV (EtOH) 303 nm (ε 21000); ^{1}H NMR ($CDCl_3$) δ=0.45 and 0.71 (1H each, d, *J*=5.2 Hz, 18-H_2), 0.87, 1.05, 1.30, and 1.32 (3H each, s, 28-, 30-, 27-, and 26-H_3), 0.90 (6H, s, 19- and 29-H_3), 0.91 (3H, t, *J*=7.2 Hz, 10′-H_3), 1.46 (2H, sext, *J*=7.2 Hz, 9′-H_2), 2.12 (2H, q, *J*=7.2 Hz, 8′-H_2), 2.85 (1H, d, *J*=7.6 Hz, 24-H), 3.77 (1H, br t, *J*=3.2 Hz, 7-H), 3.88 (1H, ddd, *J*=9.5, 7.2, and 7.2 Hz, 23-H), 4.73 (1H, t, *J*=2.7 Hz, 3-H), 5.43 (1H, t, *J*=3.4 Hz, 21-H), 5.69 (1H, d, *J*=11.4 Hz, 2′-H), 5.91 (1H, dt, *J*=14.8 and 7.2 Hz, 7′-H), 6.27 (1H, dd, *J*=14.8 and 10.6 Hz, 6′-H), 6.46 (1H, dd, *J*=14.6 and 10.6 Hz, 5′-H), 6.57 (1H, t, *J*=11.4 Hz, 3′-H), and 7.43 (1H, dd, *J*=14.6 and 11.4 Hz, 4′-H); ^{13}C NMR (see Table 2). Found: C, 74.99; H, 9.51%. Calcd for $C_{40}H_{60}O_6 \cdot 1/4H_2O$: C, 74.90; H, 9.51%.

Acetylation of 1. To a solution of **1** (160 mg) in acetic anhydride (0.3 ml) and pyridine (0.6 ml) was added a catalytic amount of 4-dimethylaminopyridine. The mixture was stirred overnight at room temperature and then worked up in the usual way. The product was chromatographed over silicic acid (20 g), with 75% ether in hexane as the eluent, to give diacetates, **3** (72 mg) and **4** (105 mg).

Diacetate 3. The former fraction was recrystallized from hexane–ethyl acetate to yield colorless prisms (66 mg); mp 79.0—80.0 °C; IR (CCl_4) 1730 and 1250 cm^{-1}; ^{1}H NMR ($CDCl_3$) δ=0.37 and 0.74 (1H each, d, *J*=5.6 Hz, 18-H_2), 0.76, 0.87, 0.91, 1.10, 1.30, and 1.33 (3H each, s, 28-, 19-, 29-, 30-, 27-, and 26-H_3), 1.00 and 1.01 (3H each, d, *J*=6.4 Hz, 4′- and 5′-H_3), 2.04 and 2.06 (3H each, s, 2Ac), 2.12 (1H, m, 3′-H), 2.22 (2H, d, *J*=6.4 Hz, 2′-H_2), 2.75 (1H, d, *J*=7.6 Hz, 24-H), 3.90 (1H, ddd, *J*=10.2, 7.2, and 6.0 Hz, 23-H), 4.67 (1H, t, *J*=2.8 Hz, 3-H), 5.00 (1H, t, *J*=2.8 Hz, 7-H), and 6.29 (1H, d, *J*=3.4 Hz, 21-H); ^{13}C NMR (see Table 2); MS (70 eV) *m/z* (rel intensity) 596 (M^+-AcOH, 52), 536 (M^+-2AcOH, 29), 434 (M^+-2AcOH−$C_5H_{10}O_2$, 27), and 135 (100). Found: *m/z* 596.4049. Calcd for $C_{39}H_{60}O_8$−AcOH: M, 596.4076.

Diacetate 4. The latter fraction was recrystallized from aqueous methanol to afford white needles (89 mg); mp 191.5—192.5 °C; IR (CCl_4) 1730, 1250, and 1230 cm^{-1}; ^{1}H NMR ($CDCl_3$) δ=0.32 and 0.72 (1H each, d, *J*=5.7 Hz, 18-H_2), 0.76, 0.87, 0.91, 1.09, 1.27, and 1.32 (3H each, s, 28-, 19-, 29-, 30-, 27-, and 26-H_3), 1.00 (6H, d, *J*=6.4 Hz, 4′- and 5′-H_3), 2.04 and 2.08 (3H each, s, 2Ac), 2.12 (1H, m, 3′-H), 2.22 (2H, d, *J*=6.4 Hz, 2′-H_2), 2.67 (1H, d, *J*=7.6 Hz, 24-H), 3.88 (1H, ddd, *J*=10.0, 7.6, and 7.0 Hz, 23-H), 4.67 (1H, t, *J*=2.7 Hz, 3-H), 4.98 (1H, t, *J*=2.8 Hz, 7-H), and 6.27 (1H, d, *J*=3.4 Hz, 21-H); ^{13}C NMR (see Table 2); MS (70 eV) *m/z* (rel intensity) 596 (M^+-AcOH, 38), 536 (M^+-2AcOH, 21), 434 (M^+-2AcOH−$C_5H_{10}O_2$, 22), and 135 (100). Found: *m/z* 596.4095. Calcd for $C_{39}H_{60}O_8$−AcOH: M, 596.4076.

Oxidation of 1. To a suspension of pyridinium chlorochromate (50 mg) in dichloromethane (0.5 ml) was added a solution of **1** (30 mg) in dichloromethane (0.5 ml). The mixture was stirred for 6 h at room temperature and then worked up in the usual manner. The product was subjected to chromatography over silicic acid (3 g). Elution with 30% ethyl acetate in hexane gave a keto lactone **5** (22 mg) which was recrystallized from ether–hexane to yield white needles (15 mg); mp 135.0—136.0 °C; IR (CCl_4) 1780, 1738, and 1710 cm^{-1}; ^{1}H NMR (see Table 1); ^{13}C NMR (see Table 2); MS (70 eV) *m/z* (rel intensity) 568 (M^+, 8) and 413 (100). Found: *m/z* 568.3765. Calcd for $C_{35}H_{52}O_6$: M, 568.3764.

Partial Methanolysis of 3. A mixture of **3** (60 mg) and triethylamine (30 mg) in methanol (1.2 ml) was stirred under a nitrogen atmosphere at room temperature for 10 days and then evaporated to dryness. The residue was subjected to chromatography over silicic acid (5 g), with 30% ethyl acetate in hexane, to give a hemiacetal (**8**) as an amorphous solid (34 mg); IR (CCl_4) 3600, 3440, 1730, and 1255 cm^{-1}; ^{1}H NMR ($CDCl_3$) δ=0.35 and 0.65 (1H each, d, *J*=5.4 Hz, 18-H_2), 0.76, 0.87, 0.91, 1.10, 1.30, and 1.31 (3H each, s, 28-, 19-, 29-, 30-, 27-, and 26-H_3), 1.00 (6H d, *J*=6.6 Hz, 4′- and

5′-H_3), 2.04 (3H s, Ac), 2.12 (1H, m, 3′-H), 2.23 (2H, d, J=6.6 Hz, 2′-H_2), 2.83 (1H, d, J=7.6 Hz, 24-H), 3.87 (1H, ddd, J=9.5, 7.6, and 7.3 Hz, 23-H), 4.66 (1H, t, J=2.8 Hz, 3-H), 5.01 (1H, t, J=3.2 Hz, 7-H), and 5.41 (1H, t, J=3.4 Hz, 21-H); MS (70 eV) m/z (rel intensity) 596 (M^+-H_2O, 31), 536 ($M^+-H_2O-AcOH$, 17), 434($M^+-H_2O-AcOH-C_5H_{10}O_2$, 24), and 135 (100). Found: m/z 596.4093. Calcd for $C_{37}H_{58}O_7-H_2O$: M, 596.4077.

Conversion of 8 into Glabretal (6). A mixture of **8** (32 mg), ethyl vinyl ether (0.2 ml), and a catalytic amount of pyridinium *p*-toluenesulfonate was stirred overnight under a nitrogen atmosphere at room temperature. After dilution with dichloromethane (10 ml), the solution was washed with a saturated sodium hydrogencarbonate solution and saturated brine, successively, dried over magnesium sulfate, and evaporated to dryness. The residue, which no longer showed a hydroxylic band in the IR spectrum, was dissolved in methanol (0.5 ml); then, a 0.57 M sodium methoxide solution in methanol (1.0 ml) was added under a nitrogen atmosphere with ice cooling. The mixture was stirred at room temperature for 10 days and then worked up in the usual way. The resulting product was chromatographed over silicic acid (3 g), with 50% ethyl acetate in hexane, to afford a deisovaleryl compound (21 mg). A mixture of the product and a catalytic amount of pyridinium *p*-toluenesulfonate in methanol (0.5 ml) was stirred for 6 h at room temperature under a nitrogen atmosphere and then worked up in the usual manner. The product was chromatographed using a Lobar Column (Merck, LiChroprep Si 60, size B) and 50% ethyl acetate in benzene as the solvent to yield a diol (12 mg) which was identified by comparison of spectral data with those of **6** [IR ($CHCl_3$) 3500, 1715, and 1260 cm^{-1}; ^1H NMR ($CDCl_3$) δ=0.35 and 0.63 (1H each, d, J=5.6 Hz, 18-H_2), 2.04 (3H, s, Ac), 2.83 (1H, d, J=7.3 Hz, 24-H), 3.42 (1H, br s, 3-H), 3.84 (1H, ddd, J=9.5, 7.6, and 7.3 Hz, 23-H), 5.01 (1H, t, J=3.2 Hz, 7-H), and 5.42 (1H, d, J=3.2 Hz, 21-H)].

References

1) S. Kitamura and G. Murata, "Colored Illustrations of Woody Plants of Japan," Revised Ed, Hoikusha Publishing Co., Ltd., Osaka (1984), Vol. 1, p. 315. "Tsurushimi" in Japanese.

2) The second instar larvae of the silkworm were used as the test insects. The procedures for the diet preparation and bioassay were the same as those reported by Asano et al.: S. Asano, E. Kuwano, and M. Eto, *Appl. Entomol. Zool.*, **19**, 212 (1984).

3) The ED_{50}-values, the effective doses for 50% growth inhibition, of skimmiarepin A and B against *Bombyx mori* L. were 0.14 ppm and 0.10 ppm, respectively.

4) G. Ferguson, P. A. Gunn, W. C. Marsh, R. McCrindle, R. Restivo, J. D. Connolly, J. W. B. Fulke, and M. S. Henderson, *J. Chem. Soc., Perkin Trans. 1*, **1975**, 491.

5) B. S. Joshi, V. N. Kamat, S. W. Pelletier, K. Go, and K. Bhandary, *Tetrahedron Lett.*, **26**, 1273 (1985).

6) T. Nakanishi, A. Inada, M. Nishi, T. Miki, R. Hino, and T. Fujita, *Chem. Lett.*, **1986**, 69.

7) K. Ohkuma, F. T. Addicott, O. E. Smith, and W. E. Thiessen, *Tetrahedron Lett.*, **1965**, 2529.

 © 1988 The Chemical Society of Japan Bull. Chem. Soc. Jpn., 61, 3231—3237 (1988)

Synthetic Photochemistry. XLII.[1] Total Synthesis of Cycloaraneosene, a Fundamental Hydrocarbon of 5-8-5-Membered Tricyclic Diterpenoid from *Sordaria araneosa*[2]

Nobuo KATO,* Shinya TANAKA,† and Hitoshi TAKESHITA*
Institute of Advanced Material Study, 86, Kyushu University,
Kasuga-koen, Kasuga, Fukuoka 816
†Graduate School of Engineering Sciences, 39, Kyushu University,
Kasuga-koen, Kasuga, Fukuoka 816
(Received March 10, 1988)

A 5–8–5-membered tricyclic diterpene, cycloaraneosene, has been totally synthesized via a stereoselective condensation of two units of optically active iridoids, a Cope rearrangement, a chemical reduction of the tetrasubstituted double bond, and the formation of an eight-membered ring. The proposed structure of natural hydroxycycloaraneosene should be revised to 8β-hydroxycycloaraneosene, judging from the NMR spectral data.

In 1975, Borschberg reported the isolation and structure determination of a 5–8–5-membered tricyclic diterpene, cycloaraneosene (**1**),[3] from *Sordaria araneosa* Cain. Obviously, **1** is the biogenetic precursor of the congener diterpenoids of a fungus, such as sordaricin[4] and hydroxycycloaraneosene.[3] In this paper we describe the total synthesis of **1** using the condensation of two functionalized iridoids, in which the synthetic strategy is similar to our previous synthesis of fusicoccatriene.[5] Although several studies on this subject have been appeared, no total synthesis of natural 5–8–5-membered tricyclic compounds has been reported.[6]

Results and Discussion

Among the natural 5–8–5-membered compounds, the stereochemistry of **1** has two outstanding features: i) the syn-relation between the hydrogen at C-6 and the methyl group C-11 is reverse to that of cotylenins[7] and fusicoccins[8] and ii) the hydrogens at C-2 and C-3 of the saturated ring A have a cis-β-geometry (i.e., (2*R*,3*R*)-structure). The former arrangement can be created by a stereospecific Cope rearrangement of the dimeric condensate of appropriate iridoids.[9] Therefore, in order to synthesize **1**,[10] a stereoselective reduction of the tetrasubstituted double bond, which is indispensable for a Cope rearrangement, is crucial. This reduction must be performed prior to the formation of double bonds and the B-ring.

With the regard to those facts, the key compounds for a reduction must be the diol **2** or its equivalents, the stereochemical framework of which should be inherited from the condensation of (3*S*)-iridenals and (3*S*)-iridenyl chlorides.

In order to obtain **2**, we carried out further conversions of the Cope rearrangement product **3**, prepared from the chromium(II) chloride condensation[11] of (3*S*)-1-iriden-7-al and (3*S*,8*R*)-9-benzyloxy-7-chloro-1-iridene[5] as follows. The hydrolysis of **3** and the epimerization of the resulting aldehyde were consecutively performed with potassium fluoride on silica gel and on Florisil to give thermodynamically stable aldehyde **4** in good yield. The lithium aluminum hydride (LAH) reduction of **4** gave the corresponding primary alcohol **5**. The catalytic hydrogenolysis of **5** with palladium on carbon gave the desired **2**, which was further transformed to diacetate **6** and bis(tetrahydropyranyl) (THP) ether (**7**).

In order to generate the correct stereochemistry of the A-ring, the hydrogenation must occur from the β-side of **2**; this procedure was shown to be promising from observations of the Dreiding's Stereomodels; i.e., the α-side of the A-ring is more hindered than the β-side by substituents on the C-ring. However, all attempts to hydrogenate **2** failed, except for hydrogenation under Adam's conditions, platinum(IV) oxide in acetic acid, which gave a mixture of acetylated dihydro derivatives in low yields. This

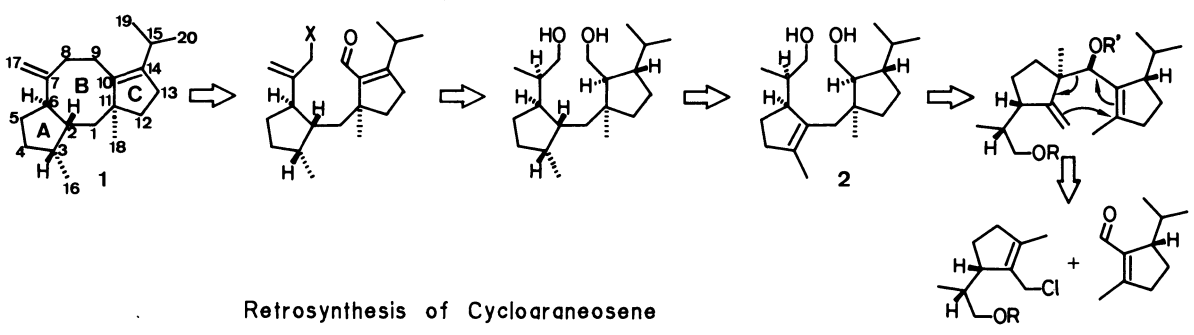

Retrosynthesis of Cycloaraneosene

Scheme 1.

should indicate that the hydrogenation of the acetate might be facile; indeed, when **6** was reduced in acetic acid at 70 °C, three dihydro derivatives were formed. Although this mixture was inseparable, hydrolyzed dihydro diols were fractionated through a silica-gel column chromatography; the yield (39%) of the major dihydro diol (**8a**) was still insufficient for a synthetic purpose. However, a ^{13}C NMR chemical shift comparison of the stereomers, **8b** and **8c** (27 and 16% yields, respectively), disclosed reliable information for selecting the correct isomer for the synthesis.

Interestingly, the catalytic deuteration of **6** under comparable conditions also afforded three products; these reduction products contained more than two deuterium atoms. This finding indicated that the hydrogen (deuterium) exchange via π-allyl complexation is very rapid. Furthermore, the complete disappearance of the signals due to C-2, C-3, and C-16 from the olefinic carbon region indicated the distributions of deuterium; the intactness of the C-6 signal for all isomers assured the original (6*R*)-configuration. According to the well-known relationship of the ^{13}C chemical shift and the stereochemistry, the configurations of the isomers were as follows: **8a** and **8c** having relatively higher secondary methyl signals suggested a cis-configuration between these methyls and the vicinal substituent.[12] The same criteria could be applied to deduce the geometries of C-2 and C-6 from the chemical shifts of C-1 methylene carbons to assign trans and cis, respectively, for **8a** and **8c**. Thus, the major diol, **8a**, is the required (2*R*,3*R*)-isomer, and **8c** is (2*S*,3*S*)-isomer. The remaining **8b**, exhibiting both methyl and methylene signals at a lower field, must be the (2*R*,3*S*)-isomer.

In order to improve the selectivity, an alkali metal reduction of the derivative of **2** in a polar aprotic media under forced conditions seems to be promising.[13] Thus, THP ether **9** prepared from **5** was hydrogenolyzed in order to furnish an alcohol **10**. A sodium metal reduction of **10** in hexamethylphosphoric triamide (HMPA) with added 1,1-dimethylethanol at room temperature yielded **8a** in moderate yield, accompanied by small amounts of **8b** and **8d** (**8a**:**8b**:**8d**=22:4:1). The absence of thermodynamically unstable **8c** was predictable from a mechanistic view point, and the ^{13}C NMR spectrum of **8d** is reasonable as a (2*S*,3*R*)-isomer based on the above-mentioned criteria.[12] These figures are found in illustrations **8a—d**. It is noteworthy that **7**, having no hydroxyl group, did not react under the above conditions. Therefore, a hydrogen-donating hydroxyl group is required in the molecule, and the direction of hydrogenation must be controlled by the orientation of the hydroxyl group. This must be an important factor for an improved selectivity. Further proof for this mechanistic assumption was obtained from a reduction of **11**, which was prepared from **5** in four steps: acetylation of **5** gave **12** which was hydrogeno-

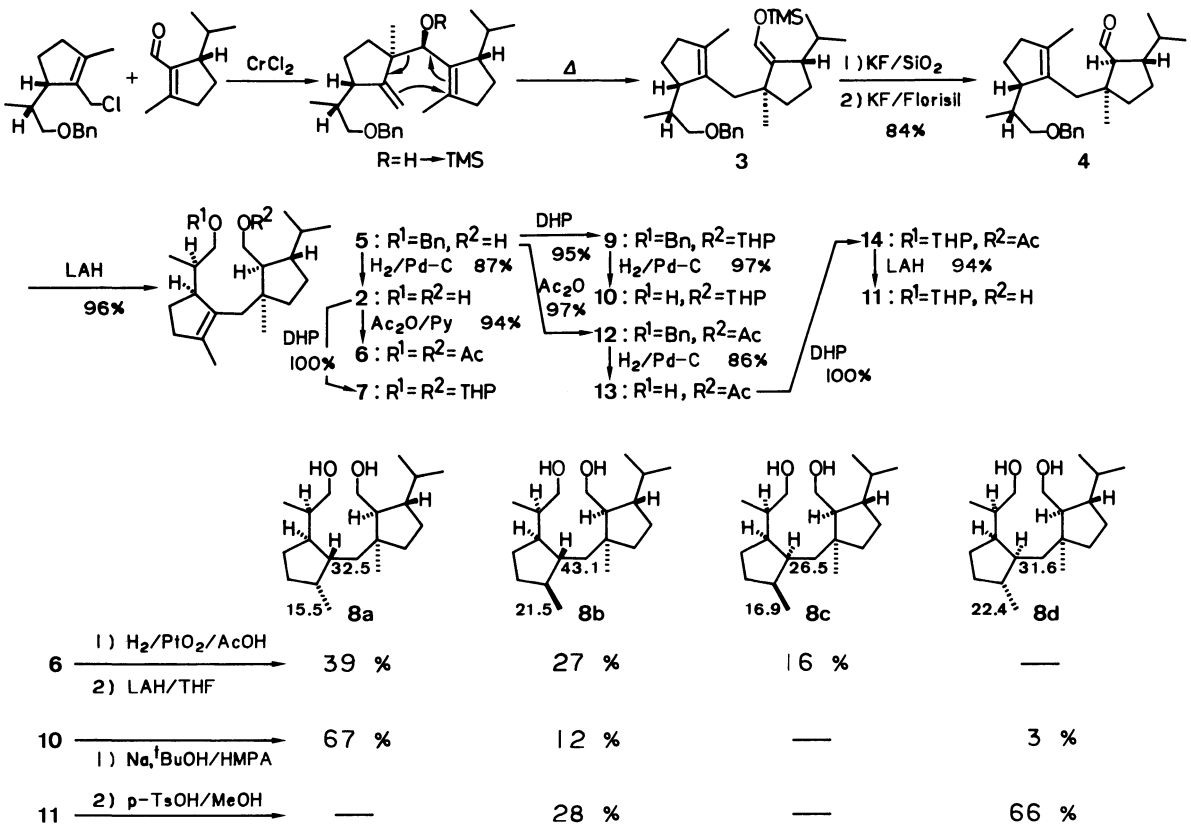

Scheme 2.

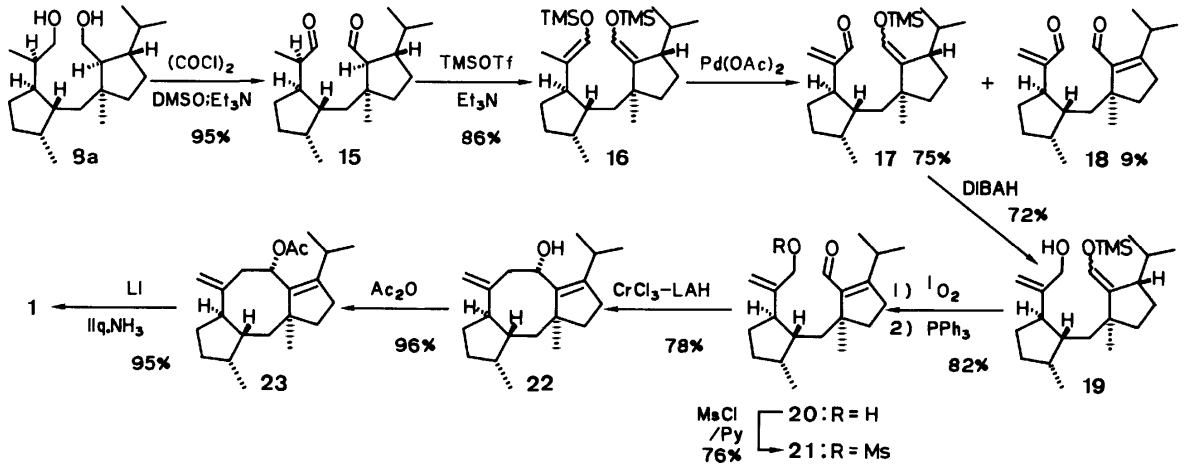

Scheme 3.

lyzed to **13**, and etherification of **13** by dihydropyran gave **14**. Finally, an LAH reduction of **14** yielded **11**. The product distributions of the sodium-1,1-dimethylethanol-HMPA reduction of **11** were completely different from the case of **10**. Namely, **8d** was produced as the major product accompanied by **8b** (**8d**:**8b**=7:3), and **8a** was not detected at all. This result can be explained in terms of the directional control of the hydroxyl group, which was conformationally oriented on the α-side of the A ring in **11**. Thus, the dissolving metal reduction of **10** provided the required stereochemistry for the present aim, while the reduction of a compound similar to **11** has been used in our recent synthesis of dictymal.[14]

Subsequently, to construct the tricyclic skeleton with proper functionalities for **1**, **8a** was oxidized to dialdehyde **15**, which was then converted to an isomeric mixture of bis(silyl enol ether)s **16**. Upon palladium(II) acetate-treatment,[15] the less-hindered enol ether of **16** was preferentially oxidized to give **17**; the yield of the accompanying dialdehyde **18** was only 9%. Diisobutylaluminum hydride (DIBAH) reduction gave an allyl alcohol **19**, and its sensitized photooxidation yielded a hydroxy aldehyde **20**. The mesylate **21** derived from **20** was treated with chromium(II) chloride to give a tricyclic compound **22**. The chemical shift of the singlet methyl, δ=1.20, indicated a syn-relationship with the allylic hydroxyl group.

The final transformation was achieved through a reductive elimination of the allylic hydroxyl group via the acetate **23**. The physical properties of **1**, thus obtained, were in accord to those of natural (−)-cycloaraneosene in all respects, including the optical rotation, ($[\alpha]_D$ −37.5° (lit,[3] −38.4°)), and the ^{13}C NMR chemical shifts.[3]

Incidentally, the structure of **22** is same as that proposed for a congener metabolite, hydroxycycloaraneosene (**22A**).[3] However, the physical data of **22** were clearly different from those recorded for the natural product or its epimer derived by chemical transformations.[3] Thus, our **22**, colorless scales, mp 64—65 °C, revealed a negative rotation ($[\alpha]_D$ −21.8°); however, **22A**, a colorless oil, was reported to be positive ($[\alpha]_D$ +7.5°). The reported ^1H NMR chemical shift for the singlet methyl of **22A** was δ=1.02. Presumably, **22A** is 8β-hydroxy derivative of **1**.

Syntheses of other members of terpenoids via this strategy is currently in progress.

Experimental

The elemental analyses were carried out by Miss S. Hirashima, of Institute of Advanced Material Study, Kyushu University. The NMR spectra were measured by a JEOL FX 100 Spectrometer in a $CDCl_3$ solution, unless otherwise specified, and the chemical shifts expressed were in δ units. The mass spectra were measured with a JEOL 01SG-2 Spectrometer. The IR spectra were taken as KBr disks or as a liquid film inserted between NaCl plates using a Jasco IR-A 102 Spectrometer. Optical rotations were measured with a Union Model PM-101 apparatus. The solvents for the reactions were carefully purified by distillation under an N_2 atmosphere immediately before use, and absolutely anhydrous unless otherwise specified. The stationary phase for the column chromatography was Wako Gel C 300 throughout, and elusion systems were mixtures of hexane and ethyl acetate (99:1 to 90:10).

Hydrolysis and Epimerization of 3 to 4. To a tetrahydrofuran (THF) solution (50 cm^3) of **3**[5] (1.69 g), silica gel (11 g), and KF (5.5 g) were added and stirred at 15—25 °C for 2 d. The mixture was then passed through a Florisil column and the residue, obtained by removing the solvent, was dissolved in MeOH (80 cm^3), to which Florisil (6 g) and KF (6 g) were added and kept at 15—25 °C for 1 d. The mixture was filtered on a Florisil column and the residue obtained by removing the solvent was chromatographed on a silica-gel column to give **4** [a colorless oil, 1.27 g; 84%. Found: C, 82.05; H, 10.40%. Calcd for $C_{27}H_{40}O_2$: C, 81.77, H, 10.12%. $[\alpha]_D^{24}$: −20.9° (*C* 2.29, $CHCl_3$). MS *m/z*, 396 (M^+). ^1H NMR δ=0.82 (3H, d, *J*=7 Hz), 0.87 (3H, d, *J*=7 Hz), 1.00 (3H, d, *J*=7 Hz), 1.18 (3H, s), 1.60 (3H, br s), 1.2—2.5 (13H, m), 2.5—2.9 (2H, m), 3.06 (1H, t, *J*=9 Hz), 3.21 (1H, dd, *J*=9, 4 Hz), 4.35 (1H, d, *J*=12 Hz), 4.40 (1H, d, *J*=12 Hz), 7.25 (5H,

br s), and 9.74 (1H, d, J=3 Hz). ^{13}C NMR δ=14.94 (q), 17.00 (q), 20.35 (q), 21.41 (q), 23.35 (t), 27.47 (t), 28.12 (q), 31.47 (t), 33.00 (d), 34.65 (d), 37.36 (t), 38.06 (t), 45.89 (d), 50.30 (s), 52.95 (d), 67.59 (d), 72.12 (t), 73.12 (t), 127.54 (d, 3C), 128.36 (d, 2C), 134.25 (s), 136.25 (s), 139.01 (s), and 205.72 (d). IR ν: 2950, 1715, 1455, 1370, 1100, 730, and 695 cm^{-1}].

LAH Reduction of 4 to 5. To a THF solution (20 cm^3) of **4** (1.18 g), added at 15—25 °C for 2 h was LAH (120 mg). The mixture was then treated with small portions of aq NH_4Cl and the resulting supernatant was dried on $MgSO_4$. After evaporation of the solvent, the residue was purified by silica-gel column chromatography to give **5** [a colorless oil, 1.15 g; 96%. Found: C, 81.24; H, 10.75%. Calcd for $C_{27}H_{42}O_2$: C, 81.35; H, 10.62%. $[\alpha]_D^{24}$: −39.3° (c 2.16, $CHCl_3$). MS m/z, 398 (M^+). ^{1}H NMR δ=0.84 (3H, d, J=7 Hz), 0.90 (3H, d, J=6 Hz), 1.02 (3H, d, J=7 Hz), 1.09 (3H, s), 1.60 (3H, br s), 1.2—2.0 (11H, m), 2.0—2.3 (4H, m), 2.75 (1H, m), 3.10 (1H, t, J=9 Hz). 3.29 (1H, dd, J=9, 4 Hz), 3.5—3.8 (2H, m), 4.40 (1H, d, J=12 Hz), 4.44 (1H, d, J=12 Hz), and 7.26 (5H, br s). ^{13}C NMR δ=14.94 (q), 17.06 (q), 17.71 (q), 22.30 (q), 23.47 (t), 24.41 (t), 28.53 (q), 29.88 (t), 31.00 (d), 34.71 (d), 37.36 (t), 37.53 (t), 46.53 (s), 47.83 (d), 53.18 (d), 56.24 (d), 63.95 (t), 72.48 (t), 73.18 (t), 127.48 (d), 127.66 (d, 2C), 128.42 (d, 2C), 135.30 (s, 2C), and 139.13 (s). IR ν: 2950, 1450, 1370, 1100, 1030, 730, and 695 cm^{-1}].

Catalytic Hydrogenolysis of 5 to 2. To an ethanol (EtOH) solution (6 cm^3) of **5** (310 mg), Pd/C (5%, 100 mg) was added and the mixture was stirred under an H_2 atmosphere at 15—25 °C for 24 h. After removing the catalyst and the solvent, the residue was chromatographed on a silica-gel column to give **2** [colorless crystals, mp 100—101.5 °C, 209 mg; 87%. Found: C, 77.96; H, 11.97%. Calcd for $C_{20}H_{36}O_2$: C, 77.87; H, 11.76%. $[\alpha]_D^{20}$: −30.8° (c 2.53, $CHCl_3$). ^{1}H NMR δ=0.83 (3H, d, J=6 Hz), 0.90 (3H, d, J=7 Hz), 0.95 (3H, d, J=7 Hz), 1.12 (3H, s), 1.61 (3H, br s), 1.2—2.4 (15H, m), 2.82 (2H, br s), 3.19 (1H, dd, J=11, 8 Hz), 3.48 (1H, dd, J=11, 5 Hz), and 3.6—3.8 (2H, m). ^{13}C NMR δ=15.06 (q), 16.71 (q), 17.82 (q), 22.18 (q), 23.00 (t), 24.47 (t), 28.83 (q), 29.36 (t), 30.83 (d), 36.47 (d), 37.36 (t), 37.71 (t), 46.59 (s), 47.18 (d), 53.24 (d), 56.30 (d), 63.18 (t), 64.36 (t), 135.48 (s), and 135.78 (s). IR ν: 3610, 2950, 1460, and 1010 cm^{-1}].

Diacetate 6 of 2. A pyridine solution (4 cm^3) of **2** (310 mg) was treated with Ac_2O (1 cm^3), and usual workup afforded a diacetate **6** [a colorless oil, 369 mg; 94%. Found: C, 73.36; H, 10.43%. Calcd for $C_{24}H_{40}O_4$: C, 73.43; H, 10.27%. MS m/z, 392 (M^+). ^{1}H NMR δ=0.84 (3H, d, J=6 Hz), 0.91 (3H, d, J=7 Hz), 0.97 (3H, d, J=7 Hz), 1.08 (3H, s), 1.61 (3H, br s), 1.3—1.9 (10H, m), 2.01 (3H, s), 2.04 (3H, s), 1.9—2.4 (4H, m), 2.75 (1H, m), 3.69 (1H, dd, J=10, 9 Hz), 3.85 (1H, dd, J=10, 5 Hz), and 4.0—4.2 (2H, m). ^{13}C NMR δ=14.88 (q), 16.65 (q), 17.59 (q), 20.88 (q, 2C), 22.00 (q), 22.88 (t), 24.41 (t), 28.12 (q), 29.59 (t), 30.65 (d), 33.36 (d), 37.24 (t, 2C), 46.47 (s), 47.94 (d), 52.47 (d), 53.00 (d), 65.59 (t), 66.30 (t), 134.36 (s), 136.01 (s), and 171.18 (s, 2C). IR ν: 2950, 1740, 1460, 1365, 1235, and 1030 cm^{-1}].

Bis(tetrahydropyranyl) Derivatives 7 of 2. A CH_2Cl_2 solution (4 cm^3) of **2** (209 mg) was treated with dihydropyran (0.2 cm^3) and pyridinium p-toluenesulfonate (PPTS, 20 mg) at 15—25 °C for 15 h. The mixture was then extracted with ether, washed with aq $NaHCO_3$, and dried over $MgSO_4$. After evaporation of the volatile material, the residue was chromatographed on a silica-gel column to give **7** [a colorless oil, 323 mg; 100%. Found: m/z, 476.3860 (M^+). Calcd for $C_{30}H_{52}O_4$: 476.3863. ^{1}H NMR δ=0.7—1.1 (9H, m), 1.09 (3H, s), 1.58 (3H, br s), 1.3—2.4 (26H, m), 2.75 (1H, m), 3.2—3.6 (4H, m), 3.6—4.0 (4H, m), and 4.4—4.6 (2H, m). IR ν: 2950, 1450, 1195, 1115, 1025, and 970 cm^{-1}].

Catalytic Reduction and Subsequent LAH-Reduction of 6 to 8a, 8b, and 8c. An AcOH solution (15 cm^3) of **6** (889 mg) was reduced with PtO_2 (95 mg) at 15—25 °C for 24 h under an H_2 atmosphere to give an oily stereoisomeric dihydro derivatives (866 mg; 97%), which was dissolved in a THF solution (10 cm^3) and reduced with LAH (250 mg) to give a stereoisomeric mixture. High-pressure liquid chromatography (Micropolasil, hexane-EtOAc (10:1)) of the mixture afforded **8a** [colorless crystals, mp 113—114 °C, 252 mg; 40%. Found:C, 77.31; H, 12.26%. Calcd for $C_{20}H_{38}O_2$: C, 77.36; H, 12.33%. MS m/z, 310 (M^+). ^{1}H NMR δ=0.82 (3H, d, J=7 Hz), 0.84 (3H, d, J=7 Hz), 0.89 (3H, d, J=7 Hz), 0.99 (3H, d, J=6 Hz), 1.05 (3H, s), 1.1—2.4 (19H, m), 3.35 (1H, dd, J=10, 8 Hz), and 3.5—3.8 (3H, m). ^{13}C NMR δ=15.53 (q), 17.06 (q), 18.06 (q), 22.35 (q), 24.18 (t), 24.88 (t), 27.71 (q), 31.47 (d), 32.47 (t), 33.24 (t), 36.83 (d), 37.41 (d), 38.00 (t), 41.65 (d), 44.89 (s), 47.00 (d), 47.89 (d), 56.06 (d), 64.12 (t), and 65.36 (t). IR ν: 3300, 2950, 1445, 1370, and 1020 cm^{-1}], **8b** [colorless crystals, mp 69—70.5 °C, 188 mg; 28%. Found: m/z, 310.2882 (M^+). Calcd for $C_{20}H_{38}O_2$: 310.2870. ^{1}H NMR δ=0.84 (3H, d, J=6 Hz), 0.90 (3H, d, J=6 Hz), 0.91 (3H, d, J=6 Hz), 1.00 (3H, d, J=6 Hz), 1.06 (3H, s), 1.1—2.2 (19H, m), 3.37 (1H, dd, J=10, 7 Hz), and 3.5—3.8 (3H, m). ^{13}C NMR δ=16.53 (q), 18.06 (q), 21.47 (q), 22.41 (q), 24.83 (t), 27.94 (t), 28.12 (q), 31.41 (d), 33.12 (t), 38.06 (t), 40.12 (d), 41.00 (d), 43.12 (t), 45.36 (s), 45.94 (d), 47.89 (d), 52.42 (d), 56.18 (d), 63.95 (t), and 66.42 (t). IR ν: 3250, 2950, 1460, 1370, and 1030 cm^{-1}], and **8c** [colorless crystals, mp 94—95.5 °C, 119 mg; 17%. Found: m/z, 310.2882 (M^+). ^{1}H NMR δ=0.85 (3H, d, J=6 Hz), 0.90 (3H, d, J=7 Hz), 0.94 (3H, d, J=7 Hz), 1.00 (3H, d, J=6 Hz), 1.04 (3H, s), 1.0—2.2 (19H, m), 3.39 (1H, br dd, J=10, 6 Hz), and 3.5—3.8 (3H, m). ^{13}C NMR δ=16.87 (q), 17.85 (q), 18.44 (q), 22.30 (q), 24.61 (t), 25.47 (t), 26.48 (t), 28.40 (q), 30.51 (t), 31.05 (d), 35.04 (d), 37.58 (t), 39.10 (d), 40.20 (d), 44.49 (s), 47.66 (d), 50.90 (d), 55.82 (d), 63.75 (t), and 67.38 (t)].

Catalytic Deuteration of 6. Similarly, **6** (207 mg) was reduced with deuterium gas in the presence of PtO_2 (20 mg) in AcOD (4 cm^3) and, without isolation, consecutively reduced with LAH to give the deuterio derivatives of **8a**, **8b**, and **8c** in similar product distributions. Silica-gel column chromatography of the mixture afforded analytically pure samples.

THP-Ether 9 from 5. As a manner similar to the formation of **7**, **5** (1.10 g) was treated with dihydropyran (0.5 cm^3) and PPTS (20 mg) to give **9** [a colorless oil, 1.24 g; 95%. Found: C, 79.82; H, 10.56%. Calcd for $C_{32}H_{50}O_3$: C, 79.62; H, 10.44%. MS m/z, 482 (M^+). ^{1}H NMR δ=0.83 (3H, d, J=7 Hz), 0.90 (3H, d, J=7 Hz), 1.02 (3H, d, J=7 Hz), 1.08 (3H, s), 1.58 (3H, br s), 1.2—2.0 (16H, m), 2.0—2.4 (4H, m), 2.75 (1H, m), 3.09 (1H, t, J=9Hz), 3.27 (1H, dd, J=9.4 Hz), 3.3—3.6 (2H, m), 3.6—4.0 (2H, m), 4.37 (1H, d, J=12 Hz), 4.43 (1H, d, J=12 Hz), 4.54 (1H, m), and 7.25 (5H, br s). IR ν: 2950, 1450, 1365, 1200, 1115, 1025, 730, and 695 cm^{-1}].

Catalytic Hydrogenolysis of 9 to 10. An EtOH solution (12 cm^3) of **9** (1.26 g) was hydrogenated with Pd/carbon (5%, 120 mg) at 15—25 °C for 23 h to give **10** [a colorless oil, 997 mg; 97%. Found: C, 76.29; H, 11.49%. Calcd for

$C_{25}H_{44}O_3$: C, 76.48; H, 11.30%. MS *m/z*, 392 (M^+). ^1H NMR δ=0.8—1.0 (9H, m), 1.08 (3H, s), 1.61 (3H, br s), 1.2—1.9 (16H, m), 1.9—2.4 (5H, m), 2.78 (1H, m), 3.1—3.7 (4H, m), 3.7—4.0 (2H, m), and 4.53 (1H, m). IR ν: 3450, 2950, 1460, 1370, 1200, 1120, 1030, and 980 cm^{-1}].

Na-*t*-BuOH-HMPA-Reduction of 10 to 8a, 8b, and 8d. To HMPA (60 cm^3), metallic Na (350 mg) was added under an N_2 atmosphere. To a blue solution, thus formed, *t*-BuOH (1 cm^3) was added with stirring. Then, **2** (1.30 g) was introduced at 15—25 °C under an N_2 atmosphere and stirring continued for further 15 h. The mixture was then extracted with ether, washed with water, and dried on $MgSO_4$. Silica-gel column chromatography of the organic material gave an oily mixture (1.24 g; 95%), which was subsequently dissolved in MeOH (12 cm^3) containing *p*-TsOH (120 mg) and refluxed for 3 h. The mixture was then extracted with EtOAc and chromatographed on a silica-gel column to give **8a** (660 mg; 70%), **8b** (126 mg; 13%), and **8d** [colorless crystals, mp 142—143 °C, 31.3 mg; 3%. Found: *m/z*, 310.1905 (M^+). Calcd for $C_{20}H_{38}O_2$: 310.2870. ^1H NMR δ=0.84 (3H, d, *J*=6 Hz), 0.91 (3H, d, *J*=7 Hz), 0.94 (3H, d, *J*=7 Hz), 0.97 (3H, d, *J*=6 Hz), 1.06 (3H, s), 2.02 (2H, br s), 1.2—2.2 (17H, m), 3.32 (1H, dd, *J*=10, 7 Hz), and 3.5—3.8 (3H, m). ^{13}C NMR δ=16.64 (q), 18.20 (q), 22.30 (q), 22.38 (q), 25.23 (t), 27.50 (t), 27.81 (q), 31.41 (d), 31.60 (t, 2C), 36.13 (d), 37.85 (t), 39.10 (d), 44.41 (d), 44.80 (s), 45.66 (d), 47.58 (d), 56.21 (d), 64.02 (t), and 67.62 (t). IR ν: 3250, 2950, 1450, 1365, and 1020 cm^{-1}], **8a**, and **8b** were identical with the sample prepared from **2**.

Acetate 12 of 5. A pyridine solution (3 cm^3) of **5** (296 mg) was treated with Ac_2O (0.5 cm^3) to give, after a usual workup, **12** [a colorless oil, 317 mg; 97%. Found: C, 79.15; H, 10.14%. Calcd for $C_{29}H_{44}O_3$: C, 79.04; H, 10.06%. MS *m/z*, 440 (M^+). ^1H NMR δ=0.83 (3H, d, *J*=7 Hz), 0.90 (3H, d, *J*=7 Hz), 1.02 (3H, d, *J*=7 Hz), 1.07 (3H, s), 1.56 (3H, br s), 1.2—1.9 (10H, m), 2.00 (3H, s), 1.9—2.3 (4H, m), 2.71 (1H, m), 3.08 (1H, t, *J*=9 Hz), 3.25 (1H, dd, *J*=9, 4 Hz), 4.10 (2H, br d, *J*=7 Hz), 4.36 (1H, d, *J*=12 Hz), 4.43 (1H, d, *J*=12 Hz), and 7.24 (5H, br s). IR ν: 2950, 1740, 1450, 1360, 1240, 1100, 1025, 730, and 695 cm^{-1}].

Catalytic Hydrogenolysis of 12 and 13. A mixture of **12** (303 mg) and Pd/C (5%, 30 mg) in EtOH (6 cm^3) was stirred under an H_2 atmosphere at 15—25 °C for 24 h. After removing the catalyst and the solvent, the residue was chromatographed on a silica-gel column to give **13** [a colorless oil, 208 mg; 86%. Found: C, 75.48; H, 11.19%. Calcd for $C_{22}H_{38}O_3$: C, 75.38; H, 10.93%. MS *m/z*, 350 (M^+). ^1H NMR δ=0.83 (3H, d, *J*=6 Hz), 0.90 (3H, d, *J*=7 Hz), 0.94 (3H, d, *J*=7 Hz), 1.07 (3H, s), 1.61 (3H, br s), 2.03 (3H, s), 1.2—2.3 (15H, m), 2.74 (1H, m), 3.23 (1H, dd, *J*=11, 8 Hz), 3.49 (1H, dd, *J*=11, 6 Hz), and 4.13 (2H, br d, *J*=6 Hz). IR ν: 3450, 2950, 1740, 1460, 1370, 1240, and 1030 cm^{-1}].

THP-Ether 14 of 13. A CH_2Cl_2 solution (4 cm^3) of **13** (208 mg) was treated with dihydropyran (0.1 cm^3) and PPTS (20 mg) to give **14** [a colorless oil, 257 mg; 100%. Found: C, 74.63; H, 10.83%. Calcd for $C_{27}H_{46}O_4$: C, 74.61; H, 10.67%. MS *m/z*, 434 (M^+). ^1H NMR δ=0.8—1.1 (9H, m), 1.09 (3H, s), 1.60 (3H, br s), 1.2—2.0 (16H, m), 2.03 (3H, s), 2.0—2.3 (4H, m), 2.74 (1H, m), 2.8—4.0 (4H, m), 4.11 (2H, br d, *J*=6 Hz), and 4.46 (1H, m). IR ν: 2950, 1745, 1460, 1370, 1240, 1125, 1035, and 970 cm^{-1}].

LAH-Reduction of 14 to 11. A THF solution (2 cm^3) of **14** (257 mg) was treated with LAH (23 mg) at 0 °C for 1 h. A small amount of aq NH_4Cl was added, and the resulting supernatant was dried on $MgSO_4$ and evaporated in vacuo. The residue was chromatographed on a silica-gel column to give **11** [a colorless oil, 220 mg; 94%. Found: *m/z*, 392.3288 (M^+). Calcd for $C_{25}H_{44}O_3$: 392.3288. ^1H NMR δ=0.8—1.1 (9H, m), 1.10 (3H, s), 1.56 (3H, br s), 1.1—2.0 (17H, m), 2.0—2.4 (4H, m), 2.76 (1H, m), 2.9—3.9 (6H, m), and 4.50 (1H, m). IR ν: 3450, 2950, 1460, 1370, 1120, 1030, 980, 905, 870, and 810 cm^{-1}].

Na-*t*-BuOH-HMPA-Reduction of 11 to 8b and 8d. Similar to the reduction of **10**, **11** (180 mg) was treated with Na (42 mg) and *t*-BuOH (0.14 cm^3) in an HMPA (6 cm^3). Successive treatments with *p*-TsOH (20 mg) in refluxing MeOH (4 cm^3) afforded a mixture of dihydro-diols. Silica-gel column chromatography of the mixture gave **8b** (40 mg; 28%) and **8d** (94 mg; 66%). Despite careful inspections of every chromatographic fraction, no **8a** was detected.

Swern's Oxidation of 8a to Dial (15). To a CH_2Cl_2 solution (16 cm^3) of $(COCl)_2$ (0.68 cm^3), DMSO (1.10 cm^3) was added drop by drop at −78 °C for 15 min. Then, a THF solution (5 cm^3) of **8a** (801 mg) was added and stirred for another 30 min; after the introduction of Et_3N (7.2 cm^3), the temperature was gradually raised to −10 °C, and treated with aq $NaHCO_3$. The mixture was extracted with EtOAc, and the organic extract was chromatographed on a silica-gel column to give **15** [a colorless oil, 747 mg; 95%. Found: *m/z*, 306.2561 (M^+). Calcd for $C_{20}H_{34}O_2$: 306.2557. ^1H NMR δ=0.80 (3H, d, *J*=7 Hz), 0.82 (3H, d, *J*=7 Hz), 0.87 (3H, d, *J*=7 Hz), 1.11 (3H, d, *J*=7 Hz), 1.17 (3H, s), 1.2—2.5 (17H, m), 9.67 (1H, d, *J*=2 Hz), and 9.70 (1H, br s). ^{13}C NMR δ=13.12 (q), 15.12 (q), 20.41 (q), 21.41 (q), 24.65 (t), 27.24 (q), 27.59 (t), 33.00 (t, 2C), 33.71 (d), 36.65 (d), 38.41 (t), 42.36 (d), 45.77 (d), 45.89 (d), 47.71 (d), 48.94 (s), 67.59 (d), 205.60 (d), and 205.83 (d). IR ν: 2950, 1720, 1460, and 1380 cm^{-1}].

Bis(TMS-Enol Ether) 16 of 15. To a CH_2Cl_2 solution (8 cm^3) of **15** (747 mg), Et_3N (1.7 cm^3) and trimethylsilyl triflate (2.26 cm^3) were added under an N_2 atmosphere, and stirred for 15 h. The mixture was then washed with aq K_2CO_3 and extracted with ether. Florisil-column chromatography of the organic material afforded **16** [a colorless oil, 942 mg; 86%. Found: *m/z*, 450.3368 (M^+). Calcd for $C_{26}H_{50}O_2Si_2$: 450.3338. ^1H NMR δ=0.16 (18H, s), 0.74 (3H, d, *J*=6 Hz), 0.80 (3H, d, *J*=7 Hz), 0.87 (3H, d, *J*=7 Hz), 0.97 (3H, s), 1.2—2.8 (18H, m), and 5.9—6.0 (2H, m). IR ν: 2950, 1665, 1445, 1250, 1155, 870, 840, and 750 cm^{-1}].

$Pd(OAc)_2$-Oxidation of 16. Formation of 17 and 18. To an acetonitrile solution (5 cm^3) of **16** (216 mg) was added $Pd(OAc)_2$ (160 mg) under N_2 atmosphere. After stirring at 15—25 °C for 6 h, the mixture was filtered on a Florisil column, and washed with ether. The residue obtained by removing the solvent was chromatographed on a silica-gel column to give **17** [a colorless oil, 136 mg; 75%. Found: C, 73.17; H, 10.91%. Calcd for $C_{23}H_{40}O_2Si$: C, 73.34; H, 10.70%. MS *m/z*, 376 (M^+). ^1H NMR δ=0.14 (9H, s), 0.73 (3H, d, *J*=7 Hz), 0.86 (6H, d, *J*=7 Hz), 0.96 (3H, s), 1.1—2.8 (15H, m), 5.9—5.95 (2H, m), 6.22 (1H, s), and 9.50 (1H, s). IR ν: 2950, 1690, 1660, 1250, 1150, 865, and 845 cm^{-1}] and **18** [a colorless oil, 13.2 mg; 9%].

DIBAH-Reduction of 17. Formation of 19. To a toluene solution (5 cm^3) of **17** (494 mg), DIBAH dissolved in hexane (1.8 M, 1 cm^3) was added under an N_2 atmosphere and kept at −78 °C for 30 min with stirring. The mixture was then diluted with aq NH_4Cl and extracted with ether. After

removing the solvent, the residue was chromatographed on a silica-gel column to give **19** [a colorless oil, 359 mg; 72%. Found: C, 72.91; H, 11.25%. Calcd for $C_{23}H_{42}O_2Si$: C, 72.95; H, 11.18%. MS *m/z*, 378 (M^+). ^1H NMR δ=0.15 (9H, s), 0.74 (3H, d, *J*=7 Hz), 0.83 (3H, d, *J*=7 Hz), 0.87 (3H, d, *J*=7 Hz), 0.99 (3H, s), 1.1—2.5 (15H, m), 2.65 (1H, br s), 4.04 (2H, br s), 4.86 (1H, br s), 5.04 (1H, q, *J*=1.5 Hz), and 5.98 (1H, d, *J*=2 Hz). IR ν: 3300, 2950, 1660, 1450, 1375, 1250, 1155, 1055, 870, 840, and 750 cm^{-1}].

$^1O_2$-Oxygenation of 19 to 20. An acetone solution (10 cm^3) of **19** (359 mg), pyridine (30 mg), and Rose Bengal (30 mg) was irradiated by means of 500-W tungsten lamp with an air stream at 0—5 °C. After 20 min, the mixture was treated with PPh_3 (373 mg) and kept at 15—25 °C for 15 h. The residue obtained by removing the solvent was then purified with silica-gel column chromatography to give **20** [a colorless oil, 236 mg; 82%. Found: *m/z*, 304.2399 (M^+). Calcd for $C_{20}H_{32}O_2$: 304.2401. $[\alpha]_D^{25}$: −57.8° (*c* 1.28, $CHCl_3$). ^1H NMR δ=0.86 (3H, d, *J*=7 Hz), 1.09 (3H, d, *J*=7 Hz), 1.10 (3H, d, *J*=7 Hz), 1.17 (3H, s), 1.2—2.4 (14H, m), 3.40 (1H, sept, *J*=7 Hz), 3.96 (2H, br s), 4.80 (1H, br s), 5.06 (1H, q, *J*=1.5 Hz), and 9.90 (1H, s). ^{13}C NMR δ=16.00 (q), 21.59 (q, 2C), 26.24 (t), 26.83 (d), 28.94 (q), 30.06 (t), 33.41 (t), 35.59 (t), 36.06 (t), 36.06 (d), 44.71 (d), 48.00 (d), 49.94 (s), 64.42 (t), 108.89 (t), 142.19 (s), 152.30 (s), 172.78 (s), and 188.96 (d). IR ν: 3450, 2950, 1660, 1650, 1450, 1050, 1020, and 890 cm^{-1}].

MsCl-Treatment of 20 to 21. A toluene solution (3 cm^3) of **20** (31.2 mg) was treated with MsCl (0.12 cm^3) and pyridine (0.24 cm^3) at 0 °C under an N_2 atmosphere for 15 h. The mixture was then diluted with aq $NaHCO_3$ and extracted with ether. The extract was chromatographed on a silica-gel column to give **21** [a colorless oil, 29 mg; 76%. Found: *m/z*, 382.2141 (M^+). Calcd for $C_{21}H_{34}O_4S$: 382.2176. ^1H NMR δ=0.88 (3H, d, *J*=7 Hz), 1.10 (6H, d, *J*=7 Hz), 1.19 (3H, s), 1.2—2.6 (13H, m), 3.00 (3H, s), 3.41 (1H, sept, *J*=7 Hz), 4.58 (2H, br s), 5.01 (1H, br s), 5.16 (1H, br s), and 9.94 (1H, s). IR ν: 2950, 1660, 1610, 1460, 1360, 1170, 830, and 730 cm^{-1}].

$CrCl_2$-Cyclization of 21. Formation of 22. A THF solution (5 cm^3) of $CrCl_2$ (prepared from $CrCl_3$, 158 mg, and LAH, 19 mg), was diluted with *N*,*N*-dimethylformamide (DMF, 30 cm^3) and then **21** (29 mg) in THF (2 cm^3) was added at 0 °C under N_2 atmosphere, and kept stirring for 15 h. The mixture was then diluted with water, extracted with ether, and dried on $MgSO_4$. Silica-gel column chromatography of the organic material gave **22** [colorless scales, mp 64—65 °C, 12.4 mg; 78%. Found: C, 83.27; H, 11.46%. Calcd for $C_{20}H_{32}O$: C, 83.27; H, 11.18%. $[\alpha]_D^{24}$: −21.8° (*c* 2.66, $CHCl_3$). MS *m/z*, 288 (M^+). ^1H NMR δ=0.84 (3H, d, *J*=7 Hz), 0.91 (3H, d, *J*=6 Hz), 0.96 (3H, d, *J*=7 Hz), 1.20 (3H, s), 1.2—2.6 (16H, m), 2.73 (1H, sept, *J*=7 Hz), 4.77 (1H, dd, *J*=8, 7 Hz), 4.79 (1H, br s), and 4.95 (1H, m). ^{13}C NMR δ=17.59 (q), 21.47 (q), 21.94 (q), 27.12 (d), 27.94 (t), 28.65 (t), 29.83 (q), 31.41 (t), 38.18 (d), 38.71 (t), 40.65 (t), 41.00 (d), 45.06 (d), 50.36 (d), 51.53 (s), 69.06 (d), 113.48 (t), 139.30 (s), 148.19 (s), and 148.72 (s). IR ν: 3350, 2950, 1640, 1455, 1380, 1000, 885, and 730 cm^{-1}].

Acetylation of 22 to 23. A pyridine solution (1 cm^3) of **22** (79.1 mg) was treated with Ac_2O (0.2 cm^3) at 15—25 °C to give **23** [a colorless oil, 80.8 mg; 96%. $[\alpha]_D^{26}$: −39.8° (*c* 2.31, $CHCl_3$). Found: C, 80.19; H, 10.39%. Calcd for $C_{22}H_{34}O_2$: C, 79.95; H, 10.34%. MS *m/z*, 330 (M^+). ^1H NMR δ=0.85 (3H, d, *J*=7 Hz), 0.89 (3H, d, *J*=7 Hz), 0.94 (3H, d, *J*=7 Hz), 1.17 (3H, s), 1.2—2.6 (16H, m), 2.85 (1H, sept, *J*=7 Hz), 1.97 (3H, s), 4.80 (1H, br s), 4.90 (1H, br s), and 5.84 (1H, dd, *J*=10, 7 Hz). ^{13}C NMR δ=17.35 (q), 21.06 (q), 21.47 (q, 2C), 27.30 (d), 27.94 (t, 2C), 30.00 (q), 31.00 (t), 38.36 (t), 38.71 (t), 38.71 (d), 42.77 (t), 45.36 (d), 49.83 (d), 51.12 (s), 71.83 (d), 112.24 (t), 133.60 (s), 147.31 (s), 151.31 (s), and 170.30 (s). IR ν: 2950, 1750, 1650, 1470, 1390, 1255, 1040, 975, and 910 cm^{-1}].

Li-NH_3 Reduction of 23. Formation of 1. At −78 °C, to liq NH_3 containing **23** (11.5 mg), an excess of Li metal, two drops of *t*-BuOH, and THF (1 cm^3) were added. After stirring for 30 min, the mixture was diluted with hexane, and sodium benzoate was added until the solution became yellow. Then, NH_4Cl was added and NH_3 was allowed to vaporize in a hood; the residue, thus obtained, was diluted with hexane, washed with aq $NaHCO_3$, and dried on $MgSO_4$. Silica-gel column chromatography of the organic material gave **1** [9.8 mg; 95%. Found: *m/z*, 272.2527 (M^+). Calcd for $C_{20}H_{32}$: 272.2502. $[\alpha]_D^{27}$: −37.5° (*c* 0.21, $CHCl_3$). ^1H NMR δ=0.82 (3H, d, *J*=7 Hz), 0.87 (3H, s), 0.89 (3H, d, *J*=7 Hz), 0.97 (3H, d, *J*=7 Hz), 1.1—2.5 (17H, m), 2.59 (1H, sept, *J*=7 Hz), 4.67 (1H, m), and 4.76 (1H, d, *J*=2 Hz). ^{13}C NMR δ=16.36 (q), 21.19 (q), 21.34 (q), 24.22 (t), 26.90 (q), 27.10 (t), 27.39 (d), 31.69 (t), 33.06 (t), 35.89 (t), 36.03 (t), 39.16 (d), 40.48 (t), 47.17 (d), 49.32 (d), 50.78 (s), 110.59 (t), 138.91 (s), 142.43 (s), and 155.95 (s). IR ν: 3070, 2955, 2860, 1635, 1450, 1375, 1360, 1330, 1100, and 880 cm^{-1}].

We are grateful to the Ministry of Education, Science and Culture for financial assistance through a Grant-in-Aid for Scientific Research to N. K. (No. 61740307) and H. T. (No. 61540401).

References

1) Part XLI: A. Mori, S. Kasai, and H. Takeshita, *Bull. Chem. Soc. Jpn.*, **61**, 547 (1988).

2) For the preliminary account of this paper, see N. Kato, S. Tanaka, and H. Takeshita, *Chem. Lett.*, **1986**, 1989.

3) H. J. Borschberg, Ph. D. Dissertation, Eidgenössischen Technischen Hochschule, Zurich, Switzerland, 1975. We thank Dr. Toshihide Hatsui, University of Geneve, for sending us a photo copy of this literature.

4) D. Hauser and H. P. Sigg, *Helv. Chim. Acta*, **54**, 1178 (1971); A. Vasella, Ph. D. Dissertation, Eidgenössischen Technischen Hochschule, Zurich, Switzerland, 1972.

5) N. Kato, K. Nakanishi, and H. Takeshita, *Bull. Chem. Soc. Jpn.*, **59**, 1109 (1986).

6) See references cited in a review article, H. Takeshita and N. Kato, *Yuki Gosei Kagaku Kyokai Shi*, **44**, 1081 (1986).

7) T. Sassa, *Agric. Biol. Chem.*, **36**, 2037 (1972).

8) A. Ballio, M. Brufani, C. G. Casinovi, S. Cerrini, W. Fedeli, R. Pellicciari, B. Santurbano, and A. Vaciago, *Experientia*, **24**, 631 (1968); K. D. Barrow, D. H. R. Barton, E. B. Chain, U. F. W. Ohnsorge, and R. Thomas, *Chem. Commun.*, **1968**, 1198.

9) H. Takeshita, T. Hatsui, N. Kato, T. Masuda, and H. Tagoshi, *Chem. Lett.*, **1982**, 1153; H. Takeshita, N. Kato, K. Nakanishi, H. Tagoshi, and T. Hatsui, *ibid.*, **1984**, 1495; N. Kato and H. Takeshita, *Bull. Chem. Soc. Jpn.*, **58**, 1574 (1985).

10) The positional numbers and ring letters shown in **1** are used throughout in this paper.

11) Y. Okude, S. Hirano, T. Hiyama, and H. Nozaki, *J.*

Am. Chem. Soc., **99**, 3179 (1977); For other examples of acyclic ring closure, see, W. C. Still and D. Mobilio, *J. Org. Chem.*, **48**, 4786 (1983); H. Shibuya, K. Ohashi, K. Kawashima, K. Hori, N. Murakami, and I. Kitagawa, *Chem. Lett.*, **1986**, 85.

12) H.-J. Schneider, N. Nguyen-Ba, and F. Thomas, *Tetrahedron*, **38**, 2327 (1982).

13) G. M. Whitesides and W. J. Ehman, *J. Org. Chem.*, **35**, 3565 (1970).

14) N. Kato, S. Tanaka, H. Kataoka, and H. Takeshita, *Chem. Lett.*, **1987**, 2295. For recent example of stereocontrolled dissolving metal reduction with internal hydroxyl groups as proton source, see J. K. Whitesell and M. A. Minton, *J. Am. Chem. Soc.*, **109**, 6403 (1987).

15) Y. Ito, T. Hirao, and T. Saegusa, *J. Org. Chem.*, **43**, 1011 (1978).

Reactivities of Stable Rotamers. XXII. Lewis Acid-Catalyzed Reactions of 3-(1,4-Disubstituted 9-Triptycyl)-3-methylbutanoyl Chloride: Isolation of Rotameric Ketones and Competition between Cyclizations to Substituted and to Unsubstituted Benzene Rings[1,2]

Toshimasa TANAKA, Katsumi YONEMOTO, Yasufumi NAKAI, Gaku YAMAMOTO, and Michinori ŌKI*,†
Department of Chemistry, Faculty of Science, The University of Tokyo, Bunkyo-ku, Tokyo 113
(Received March 18, 1988)

Rotational isomers of 3-(1,4-disubstituted 9-triptycyl)-3-methylbutanoic acid, where the substituent is either a methoxyl or a methyl, have been prepared, starting from 1,4-disubstituted 9-(1,1-dimethyl-3-butenyl)triptycene. Lewis acid-catalyzed reactions of the *ap*-acid chloride afforded corresponding ketones expected from the intramolecular Friedel–Crafts reaction. The *sc* form of the 1,4-dimethoxy compound gave a ketone that was formed by the reaction of the unsubstituted benzene ring and a lactone which was derived by the attack of the acylium ion on the methoxy-oxygen followed by demethylation. The *sc* form of the 1,4-dimethyl compound afforded a ketone which was expected from cyclization to the unsubstituted benzene ring and another ketone that was derived from the ipso attack of the acylium ion followed by 1,2-methide migration. In both cases, the ketone derived from the *ap* form of the acid chloride was different from that obtained from the *sc*. The barriers to isomerization of the *ap*-ketone to the *sc*-ketone was 29.6 kcal mol^{-1} at 100.5 °C and 25.6 kcal mol^{-1} at 56.0 °C for the methoxy and the methyl compounds, respectively. In both cases, the ketone derived from the *sc*-form was more stable than that from the *ap*, the *sc*/*ap* ratio at the equilibrium being 20.0 (56.0 °C) and 5.9 (100.5 °C), respectively, for the methyl and the methoxy compounds. In the reaction of the *sc* form, the competitive results between the cyclization toward the unsubstituted benzene ring and that toward the substituted vary according to the solvent and the Lewis acid used.

Since the isolation of rotational isomers in the triptycene and 9-arylfluorene series,[3] we have been interested in the study of reactivities of rotational isomers.[3] Due to the difficulty in the syntheses of the triptycene series, the examples that have been studied are rather limited: halogenation of a *t*-butyl group,[5] and some radical reactions[6] and cation-forming reactions[7] of the halogenated compounds. We now wish to report successful isolation of 3-(1,4-disubstituted 9-triptycyl)-3-methylbutanoic acid rotamers where the substituents are methyls or methoxyls and Lewis acid-catalyzed reactions of the corresponding acid chlorides.

Results

Syntheses of the compounds were carried out in the following ways. A Grignard reagent prepared from 4-chloro-4-methyl-1-pentene (**1**) was added to 9-anthrone and the adduct (**2**) was treated with phosphorus pentaoxide to form 9-(1,1-dimethyl-3-butenyl)anthracene (**3**). Addition of benzynes to the anthracene afforded the corresponding olefinic triptycenes (**4**), the *ap* isomer being the major product. Recrystallization of the product from hexane–dichloromethane afforded pure *ap*-form of **4**. The *ap*-olefins were oxidized with trimethylamine oxide in the presence of osmium tetraoxide[8] to the corresponding diols which were successively oxidized with periodic acid[9] and then with potassium permanganate to yield the desired *ap*-carboxylic acid (*ap*-**7**). Separation of the *sc*-isomers was tried at various stages of the synthesis of the carboxylic acid (**7**) but none of them was promising. Thus, although the number of steps required for the synthesis increased, we derived the corresponding diols to acetonides which were separated by chromatography. The best route to the prepartion of the *sc*-acid (*sc*-**7**) was the following. The

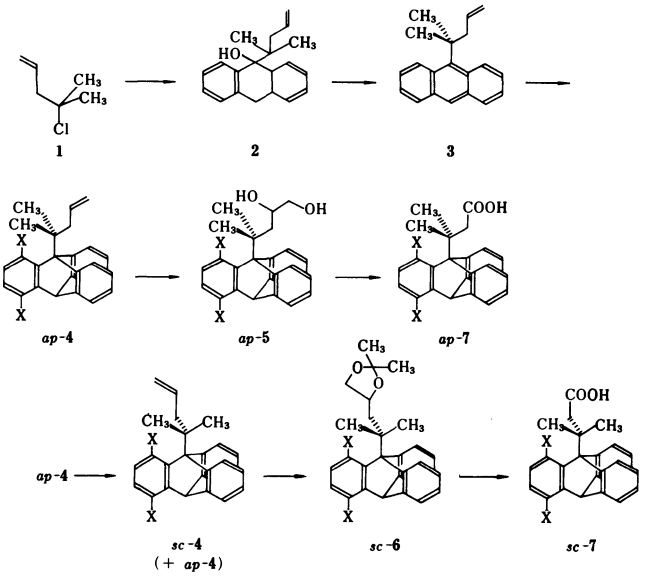

Scheme 1. Synthetic routes to 3-(1,4-disubstituted 9-triptycyl)-3-methylbutanoic acid rotamers: X is a methoxyl or a methyl. Only one form of the *sc* is shown.

† Present address: Department of Chemistry, Faculty of Science, Okayama University of Science, Ridaicho, Okayama 700.

olefin (**4**) was heated in 1-chloronaphthalene to isomerize and the *sc*-enriched olefin was oxidized with trimethylamine oxide as above and the resulted diols **5** were converted to acetonides in the presence of *p*-toluenesulfonic acid. The acetonides (**6**) were separated by medium-pressure chromatography on silica gel, the *sc* form giving two diastereomers (two pairs of enantiomers) due to the fact that a new chiral center was formed in addition to the chirality due to the frozen rotation about the C_9-to-substituent bond. The separated two forms of *sc*-acetonides were hydrolyzed to regenerate the diols (*sc*-**5**) which were similarly oxidized with periodic acid and then with potassium permanganate to yield the *sc*-carboxylic acid (*sc*-**7**).

3-(1,4-Dimethoxy-9-triptycyl)-3-methylbutanoic acid (**7a**) was treated with oxalyl dichloride to produce the corresponding chloride which was then treated with titanium(IV) chloride in benzene. *ap*-**7a** gave the corresponding ketone (*ap*-**8a**) in a good yield, whereas *sc*-**7a** afforded the corresponding ketone (*sc*-**8a**) and a lactone (**9**) which was formed by the reaction of intervening acylium ion on the methoxy-oxygen followed by demethylation. The formation ratio, *sc*-**8a**/**9**, varied when the solvent and/or the catalyst was varied and the results are shown in Table 1. *ap*-**8** and *sc*-**8** were definitely different, though they melted at the same temperature and their analytical data as well as the spectral data were all consistent with the proposed structure, 8,11-dimethoxy-1,1-dimethyl-1,2-dihydro-7*H*-7,11b-*o*-benzeno-3*H*-benz[*de*]anthracen-3-one.

The similar treatment of *ap*-3-(1,4-dimethyl-9-triptycyl)-3-methylbutanoic acid (*ap*-**7b**) afforded the corresponding ketone (*ap*-**8b**) as a sole product. By contrast, *sc*-**7b** yielded under the similar conditions a ketone (*sc*-**8b**) which was conformationally isomeric with *ap*-**8b** and another ketone to which we assign structure **10** from spectroscopic evidence and from consideration of reaction mechanisms. The formation ratio, *sc*-**8b**/**10**, was affected again by the reaction conditions, solvent and Lewis acid. The results are summarized in Table 2.

Heating *ap*-**7b** with thionyl chloride afforded *ap*-**8b** and a vinyl chloride type compound (**11**) which could be independently synthesized from *ap*-**8b** and thionyl chloride. Similarly *sc*-**7b** afforded **11** and another vinyl chloride type compound(**12**)in addition to *ap*-**8b** and **10**, when it was heated with thionyl chloride. **12** was independently synthesized from **10** and thionyl chloride.

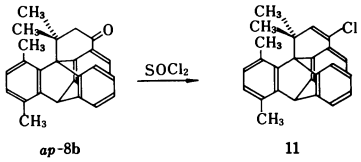

Table 1. The Effects of Solvent and Catalyst on the Formation Ratio, *sc*-**8a**/**9**, in the Reaction of *sc*-**7a** in the Presence of 2 Equivalents of the Lewis Acid

Solvent	Lewis acid	*sc*-**8a**/**9**
CH_2Cl_2	$TiCl_4$	42
C_6H_6	$TiCl_4$	6.0
C_6H_{12}[a)]	$TiCl_4$	1.3
CH_2Cl_2	$SnCl_4$	1.7
C_6H_6	$SnCl_4$	0.42
C_6H_{12}[a)]	$SnCl_4$	0.18
C_6H_6	$AlCl_3$	0.84
C_6H_{12}[a)]	$AlCl_3$	0.49

a) Cyclohexane.

Table 2. The Effects of Solvent and Catalyst on the Formation Ratio, *sc*-**8b**/**10**, in the Reaction of *sc*-**7b** in the Presence of 2 Equivalents of the Lewis Acid

Solvent	Lewis acid	*sc*-**8b**/**10**
CH_2Cl_2	$TiCl_4$	0.96
C_6H_6	$TiCl_4$	0.89
C_6H_{12}[a)]	$TiCl_4$	1.2
C_6H_6	$SnCl_4$	1.4

a) Cyclohexane.

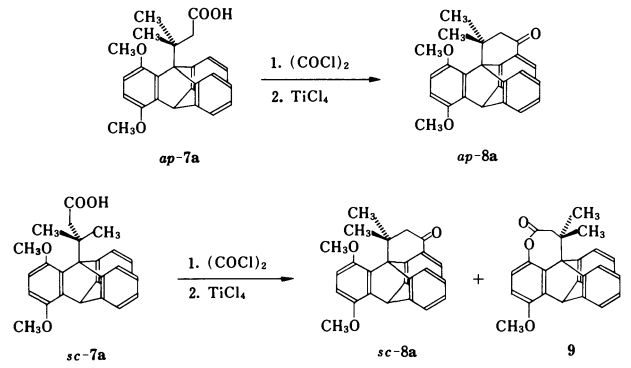

Scheme 2. Reaction of *ap*-**7a** and *sc*-**7a** under the Friedel-Crafts reaction conditions. Only one form of enantiomers is given.

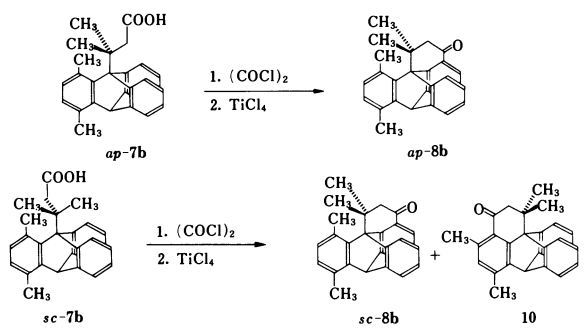

Scheme 3. Reaction of *ap*-**7b** and *sc*-**7b** under the Friedel-Crafts conditions. Only one enantiomeric form is shown.

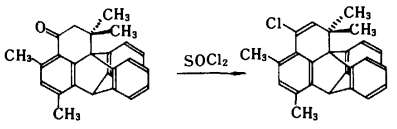

9 12

Further heating of the chloro compound (**12**) with thionyl chloride afforded further-chlorinated compounds, the main product being a dichloro compound to which we assign the structure of 2,3-dichloro-1,1,4,6-tetramethyl-7*H*-7,11b-*o*-benzeno-1*H*-benz[*de*]-anthracene (**13**). The reason for the assignment is the loss of the olefinic proton signal in its ^{1}H NMR spectra. However, the compound could not be purified to give the correct elemental analyses. Mass spectra of the enriched dichloro compound **13** showed that there were even trichlorinated and tetrachlorinated compounds as contaminants. Interestingly **11** did not give further-chlorinated compound on the same treatment as above.

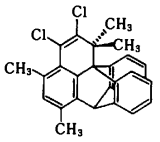

13

The ketone **8** obtained from the *ap*-form and the *sc* of the acids could be isomerized by heating. The rate constants for isomerization, thermodynamic parameters, and activation parameters are shown in Tables 3 and 4. Apparently, the barrier to rotation in the methyl series was lower than that of the methoxyl series and at the equilibrium the *sc*-ketone was favored over the *ap*, the preference being greater in the methyl series than in the methoxyl series.

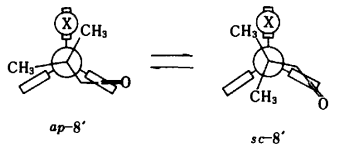

ap-8′ *sc*-8′

Scheme 4. Isomerization of ketones (**8**): X is either a methoxyl or a methyl.

Table 3. Rate Constants for Isomerization, *ap*-**8a** → *sc*-**8a**, Equilibrium Constants, Thermodynamic Parameters and Activation Parameters

Temperature/°C	$k\times10^5$/s^{-1}	K(*sc*-**8a**/*ap*-**8a**)
77.5	0.31±0.01	6.2
90.0	1.24±0.04	6.0
100.5	3.8 ±0.1	5.9
111.5	11.1 ±0.4	5.6

ΔH^*=27.6±0.6 kcal mol^{-1}; ΔS^*=−5±2 cal mol^{-1} K^{-1}; $\Delta H°$=−0.8±0.6 kcal mol^{-1}; $\Delta S°$=1±2 cal mol^{-1} K^{-1}.

The gem-dimethyl groups in **9**, **10**, and **12** were found to be diastereotopic in ^{1}H NMR spectra, suggesting that there are enantiomers. The barriers to racemization were investigated but are apparently higher than 26 kcal mol^{-1} (1 cal=4.184 J), because their ^{1}H NMR spectra did not change up to 130 °C.

Discussion

When one looks at the Newman-type projections of the *ap*-acid and the *sc*, it is clear why the *ap*-acid gives a ketone as a sole product, because the cyclization to one benzeno bridge gives an enantiomer of the one that is obtained by cyclization to another benzeno bridge. The carboxyl group in the *ap* is too far to have any significant interactions with the substituted benzeno bridge. By contrast,the carboxymethyl group in the *sc* isomer is flanked by an unsubstituted and a substituted benzeno bridge. If cyclization takes place to the unsubstituted benzeno bridge, the ketone (**8**) is formed, whereas the acid gives another product if it reacts with the other substituted benzeno bridge.

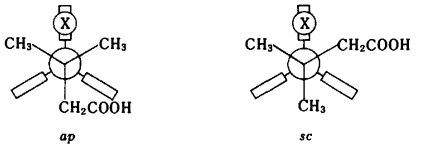

ap *sc*

The structures of the products other than the normal ketones were elucidated in the following ways. Compound **9** showed in its ^{1}H NMR spectra the loss of one methoxy-methyl group: that is consistent with the high resolution MS. Infrared spectrum showed an absorption at 1750 cm^{-1} to indicate the presence of an ester group. This is confirmed by ^{13}C NMR spectra. To accommodate these spectral information together with consideration of reaction mechanisms described below, we are compelled to assume the structure of the lactone (**9**). Although the IR absorption at 1750 cm^{-1} is a little low for phenolic esters,[10] we believe this is due to abnormal bond angles and conformations that are needed because of the congestedness of the molecular structure. The ketone other than that which can be isomerized to the ketone **8b**, both of which were obtained by the reaction of *sc*-**7b**, showed the presence of four methyl groups, two aromatic and two

Table 4. Rate Constants for Isomerization, *ap*-**8b** → *sc*-**8b**, Equilibrium Constants, Thermodynamic Parameters and Activation Parameters

Temperature/°C	$k\times10^5$/s^{-1}	K(*sc*-**8b**/*ap*-**8b**)
56.0	7.0±0.2	20.0
61.0	11.5±0.1	19.9
70.0	28.7±0.8	19.6
80.0	76 ±2	18.6

ΔH^*=22.4±0.9 kcal mol^{-1}; ΔS^*=−10±3 cal mol^{-1} K^{-1}; $\Delta H°$=−0.7±0.7 kcal mol^{-1}; $\Delta S°$=4±2 cal mol^{-1} K^{-1}.

aliphatic, and loss of an aromatic proton that shows absorption at high magnetic fields in its ^{1}H NMR spectra. It is most reasonable to assume that a proton on the dimethylbeneno bridge is lost, because these give absorptions at a high field among aromatic protons. The IR spectrum indicates the presence of a carbonyl group by the absorption at 1673 cm^{-1}. Although this absorption seems to be at a too low frequency for the normal noncoplanar aromatic carbonyl group,[11] this anomaly may again be attributed to abnormal molecular structure of this kind of congested molecules. Thus we assign structure **10** to this compound that accommodates all of spectroscopic, analytical, and mechanistic implications.

Formation of a lactone (**9**) from *sc*-**7a** is interesting because it is a reaction of an ether with an acyl chloride to form an ester in the presence of a Lewis acid. However, there are some literatures that reported this type of reactions.[12] The mechanism of the reaction must be the attack of the acylium ion produced from the acyl chloride in the presence of the Lewis acid on the 1-methoxy-oxygen atom followed by demethylation by a nucleophile. In *sc*-**7b**, the basicity of the methyl group at 1-position is too low to be attacked by the acylium ion, instead the π-system at the 1-position is attacked (ipso attack).[13] The benzenonium ion thus produced undergoes 1,2-methide shift to afford the product.

The results in Tables 1 and 2 reveal that, whereas the ratio of *sc*-**8b**/**10** is not much affected by the reaction conditions, that of *sc*-**8a**/**9** changes dramatically by the conditions. Therefore, we should like to discuss the results of *sc*-**7a** first.

The results in Table 1 indicate that the *sc*-**8a**/**9** ratio is generally small if the solvent is nonpolar: in dichloromethane with titanium(IV) chloride catalyst *sc*-**8a** is practically the sole product, whereas in cyclohexane *sc*-**8a** and **9** are almost equally produced. This tendency is again observed when tin(IV) chloride is used as a catalyst: this time, the lactone becomes an overwhelming product when cyclohexane is used as a solvent. The reaction rates, though it was not possible to determine exactly, were large in dichloromethane and small in benzene and further smaller in cyclohexane. Since titanium(IV) chloride is known to be a stronger Lewis acid than tin(IV) chloride,[14] we should like to propose the following mechanisms for the explanation of the results.

The acid chloride and the Lewis acid form a complex and then an ion pair, $RCO^+MCl_5^-$. The ion pair must be tighter, when the acidity of the Lewis acid is low and when the solvent polarity is low. When the ion pair is loose, the steric effects on the approach of the acylium ion to the reaction site will be small, whereas the steric effects will be great, when the ion pair is tight, because the acylium cation as well as the MCl_5^- anion must approach the reaction site. Thus the reaction with less steric hindrance will be favored when the ion pair is tight. In the Lewis acid-catalyzed reaction of *sc*-**7a**, there are two sites of reaction: though in principle it is possible to consider the ipso attack of the acylium ion to the 1-position where the methoxyl group is borne, the electron density at this position is too low[15] for the reaction. The reaction that occurs at the methoxy-oxygen suffers less steric hindrance than that occurring at the benzeno bridge, because the acylium cation must approach the peri-carbon, penetrating into the triptycene skeleton, if it reacts at the 8-position. The results with aluminium chloride are confusing in that aluminium chloride is a stronger Lewis acid than others. However, there is a possibility that the reaction with aluminium chloride is very complex and may even be taking place under heterogeneous conditions. We defer the discussion of the results until further information becomes available.

Examination of Table 2 reveals that, firstly, the ratio *sc*-**8b**/**10** is relatively insensitive to the conditions and, secondly, the attack to the 1-position is slightly favored in dichloromethane but, in cyclohexane, cyclization to the 8-position is slightly favored. We should like to attribute this difference between the methoxy compound and the methyl compound to the difference in the reaction sites. Namely, in the methyl compound, both reactions are occurring to the π-system of the triptycene skeleton. The steric effects given at the 1-position may not be much different from that given at the 8-position, although the methyl group at the 1-position gives additional steric effects on the attack. These steric effects together with the fact that the π-electron density at the 1-position must be slightly higher than at the 8-position where no substituent is present are reflected in the product ratio. However, the tendency seen in the methoxy compound, that is a less crowded site is more favorably attacked in nonpolar solvents and in the presence of less acidic Lewis acid is again reproduced.

As to the barriers to isomerization of the ketones **8**, we may compare them with those in similarly substituted 9-(1,1-dimethyl-2-phenylethyl)triptycenes (**14**),[16] because they are structurally similar and the substituent at the β-position of the 9-substituent is

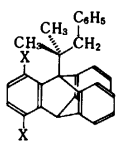

14

known to affect the barrier to rotation little, if any.[5] Table 5 compiles free energies of activation, calculated by using the reported activation parameters and the equilibrium constants, at 150 °C that is an interim point for the two series. The barriers are strikingly

reduced in the ketones (**8**) relative to the open chain analogs (**14**). This must reflect the instability of the ground state of the ketone. However, the order of the height of barriers is the same: in both series, the methyl compound gives a lower barrier to isomerization than the methoxy compound. According to our discussion previously made,[16] this is a reflection of the fact that the ground state of the methyl compound is more congested than the methoxy compound because of the steric size of the methyl and the methoxyl groups.

The congestedness of the methyl compound seems to be reflected as well in the population ratio: the *sc*-**8b**/*ap*-**8b** is 18.6 at 80 °C, whereas the *sc*-**8a**/*ap*-**8a** is 6.0 at 90 °C. As the first approximation, we would assume that the ketones are planar with the benzeno bridge to which it is attached and the gem-dimethyl groups would eclipse the benzeno bridges. However, it is not the case, because a pair of isomers is isolated for each compound, **8a** and **8b**. To the next approximation, one would think that the ketone moiety avoids coplanarity with the benzeno bridge and the carbonyl moiety taking the planar structure, as is seen in the Newman type projections (*ap*-**8′** and *sc*-**8′**). However, the dihedral angle made by the benzeno bridge and the carbonyl cannot be very large if one considers the carbonyl absorption in the IR spectra. This model also fails to show why *ap*-**8b** and *sc*-**8b** are so much different in their stabilities. Since good crystals of these compounds have not been obtained so far, we decided to carry out molecular mechanics calculations to find possible answers to these questions.

Since MM2 calculations with the parameters originally given gave far larger differences in the total energies of the *ap*- and *sc*-ketones than the observed,[2] we have modified some parameters which are concerned with the carbonyl-to-aromatic ring bond for the calculation here. The results are compiled in Table 6.

Table 5. Comparison of Free Energies of Activation for Rotation at 423 K in **8** and **14** (kcal mol^{-1})

X	Process	Compound **8**	Compound **14**
CH_3O	*ap* → *sc*	29.9	42.5
	sc → *ap*	31.2	42.0
CH_3	*ap* → *sc*	26.5	37.7
	sc → *ap*	28.8	36.1

The calculations predict that *sc*-**8a** is more stable than *ap*-**8a** by 2.74 kcal mol^{-1} and *sc*-**8b** more stable than *ap*-**8b** by 3.27 kcal mol^{-1}. Thus the calculations still overestimate the energy difference of the rotamers but the difference is smaller than the results using the standard parameters and the tendency is correctly predicted. Of particular interest in the calculated structures of the ketones is the large distorsion of the triptycene skeleton. The geometries are far different from those expected from molecular models. The dihedral angles about the bridgehead to substituent bond are about 45° at the smallest. The difference in the stabilities between *ap*-**8** and *sc*-**8** is mainly ascribed to the difference in the torsion term, suggesting that the distorsion of the triptycene skeleton is severer in *ap*-**8** than in *sc*-**8**.

This predicted distorsion of the triptycene skeleton by the calculation is supported by the ^{1}H NMR spectra. The most interesting feature in the ^{1}H NMR spectra of these ketones is that one of the aliphatic methyl groups gives its signal at a considerably high field of δ ca. 1.65, compared with the other methyl, as a doublet because of the long range coupling of ca. 1.5 Hz with one of the methylene protons. The molecular mechanics calculations show that the relevant methyl group (-*sc*-methyl in *ap*-**8′** and *ap*-methyl in *sc*-**8′** in Scheme 4) and one of the methylene hydrogens are exactly antiperiplanar, ideally located for the W-letter coupling. It further indicates that the methyl group is located in the shielding region of the highly distorted benzene ring and also in the shielding region of the carbonyl moiety, in conformity with the ^{1}H NMR spectra.

Although cyclization of the acid (**7b**) on heating with thionyl chloride might seem odd, there is a precedence of this type of reactions. Namely, 3-(9-triptycyl)propionic acid is known to cyclize when it is heated with thionyl chloride.[17] The proximity of the carbonyl

Table 6. Steric Energies and Their Components Calculated by MM2 Method

	8a		**8b**	
	ap	*sc*	*ap*	*sc*
Total steric energy	28.08	25.34	25.61	22.34
Compression	5.48	4.97	6.01	5.72
Bending	17.69	18.16	18.00	17.69
Stretch-Bend	−0.03	−0.07	−0.01	−0.07
van der Waals, 1,4-	26.20	26.03	22.62	22.76
other	−1.49	−1.82	−0.29	−1.01
Torsional	−19.50	−21.47	−21.14	−23.21
Dipole	−0.28	−0.46	0.42	0.45

Table 7. Modified Parameters for MM2 Calculations

Atom type[a]	Stretching l_0/Å	k/mdyn Å^{-1}
2-2	1.3925	8.0667
2-3	1.4950	4.40

Atom type[a]	Torsional/kcal mol^{-1} V_1	V_2	V_3
2-2-2-5	−0.93	9.0	−1.06
n-2-2-m[b]	−0.93	9.0	0.0
2-2-3-1	0.0	0.9	0.0
2-2-3-7	0.0	0.9	0.0

a) Atom type: 1=sp^3 carbon, 2=aromatic carbon, 3=carbonyl carbon, 5=hydrogen, 7=carbonyl oxygen. b) Any combination other than 2-2-2-5.

moiety to the triptycene skeleton must be the cause for this reaction. Easily enolizable ketones are known to afford vinyl chloride type compounds, when they are heated with thionyl chloride.[18,19] The formation of **11** and **12** can be rationalized by the analogies of this reaction, because acetophenone is known to undergo this reaction.[19]

Experimental

Spectral Measurements. The ^{1}H NMR spectra were recorded on a JEOL GX270 spectrometer which operates at 270 MHz. The infrared spectra were obtained on a Hitachi IR-260-30 spectrophotometer with KBr discs.

9-(1,1-Dimethyl-3-butenyl)-9,10-dihydro-9-anthracenol (2). A solution of 6.2 g (56.6 mmol) of 4-chloro-4-methyl-1-pentene (**1**)[20] and 5.15 mL (56.6 mmol) of 1,2-dibromoethane in 60 mL of tetrahydrofuran was added to 2.75 g (113 mmol) of magnesium covered with 10 mL of tetrahydrofuran in 2 h under a nitrogen atmosphere. After the formation of the Grignard reagent was completed, the mixture was diluted with 50 mL of tetrahydrofuran and 5.0 g (26 mmol) of 9-anthrone was added. The mixture was stirred for 1 h at room temperature and then heated under reflux for 1 h. After cooling, the mixture was decomposed with aqueous ammonium chloride. The mixture was extracted with benzene and the solvent was evaporated from the combined extract. After removal of the unreacted anthrone that deposited from the mixture, the products were submitted to medium-pressure chromatography on silica gel (hexane eluent) to give the desired material in 10% yield. The pure sample was obtained by recrystallization from hexane, mp 76.0 °C. Found: C, 86.01; H, 7.94%. Calcd for $C_{20}H_{22}O$: C, 86.29; H, 7.97%. ^{1}H NMR ($CDCl_3$) δ=0.83 (6H, s), 2.01 (1H, s), 2.11 (2H, d, J=7.3 Hz), 3.87 and 4.16 (2H, ABq, J=20 Hz), 4.86—4.98 (2H, m), 5.66—5.79 (1H, m), 7.23—7.34 (6H, m), 7.80—7.84 (2H, m).

9-(1,1-Dimethyl-3-butenyl)anthracene (3). A solution of 1.45 g (5.2 mmol) of the preceding alcohol (**2**) in 40 mL of carbon tetrachloride was heated under reflux with 11 g of phophorus pentaoxide for 15—20 min. The carbon tetrachloride solution was decanted and the residue was extracted several times with hot carbon tetrachloride. The solvent was evaporated from the carbon tetrachloride solution and the residue was chromatographed on silica gel (7:1 hexane-dichloromethane eluent) to give the desired product in 90% yield. The pure sample was obtained by recrystallization from hexane, mp 57.5—59.5 °C. Found: C, 92.11; H, 7.71%. Calcd for $C_{20}H_{20}$: C, 92.26; H, 7.74%. ^{1}H NMR ($CDCl_3$) δ=1.82 (6H, s), 3.13 (2H, d, J=7.3 Hz), 4.88—5.07 (2H, m), 5.54—5.67 (1H, m), 7.26—7.35 (4H, m), 7.88—7.92 (2H, m), 8.23 (1H, s), 8.48—8.52 (2H, m).

1,4-Dimethoxy-9-(1,1-dimethyl-3-butenyl)triptycene (4a). To a solution of 4.5 g (17 mmol) of **3** and 3.5 mL (26 mmol) of isopentyl nitrite in 300 mL of dichloromethane, were simultaneously added from two dropping funnels 7.0 g (34 mmol) of 3,6-dimethoxyanthranilic acid[21] in 130 mL of acetone and 5 mL (37 mmol) of isopentyl nitrite in 40 mL of dichloromethane in 6 h, with stirring and refluxing under a nitrogen atmosphere. After the addtion was over, the whole was refluxed for another hour and cooled. The solvents were evaporated and the residue was submitted to chromatography on silica gel (5:1 hexane-dichloromethane eluent) to afford 35% of the desired material as a ca. 5.5:1 mixture of *ap* and *sc* isomers. The pure *ap*-**4a** was obtained by recrystallization of the product from dichloromethane-hexane, mp 245.5—246.5 °C. Found: C, 84.64; H, 6.91%. Calcd for $C_{28}H_{28}O_2$: C, 84.81; H, 7.12%. ^{1}H NMR ($CDCl_3$) δ=2.04 (6H, s), 3.29 (2H, d, J=6.9 Hz), 3.71 (3H, s), 3.80 (3H, s), 5.20—5.29 (2H, m), 5.87 (1H, s), 6.22—6.38 (1H, m), 6.57 and 6.60 (2H, ABq, J=8.8 Hz), 6.92—7.00 (4H, m), 7.37—7.41 (2H, m), 7.83—7.87 (2H, m).

1,4-Dimethyl-9-(1,1-dimethyl-3-butenyl)triptycene (4b). This compound was similarly prepared as described above, starting from **3** and 3,6-dimethylanthranilic acid.[22] The yield of the crude product (ca. 5.5:1 mixture of *ap*-**4b** and *sc*-**4b**) was 96%. Recrystallization of the product from hexane-dichloromethane afforded pure *ap*-**4b**, mp 208.5—209.0 °C. Found: C, 92.10; H, 7.62%. Calcd for $C_{28}H_{28}$: C, 92.26; 7.74%. ^{1}H NMR ($CDCl_3$) δ=2.22 (6H, s), 2.49 (3H, s), 2.64 (3H, s), 3.31 (2H, d, J=7.0 Hz), 5.23—5.57 (2H, m), 5.58 (1H, s), 6.19—6.34 (1H, m), 6.73 (2H, s), 6.93—7.02 (4H, m), 7.24—7.38 (2H, m), 7.83—7.88 (2H, m).

***ap*-3-(1,4-Dimethoxy-9-triptycyl)-3-methylbutanoic Acid (*ap*-7a).** A solution of 20 mg of osmium tetraoxide in 1 mL of *t*-butyl alcohol was added to a solution of 1.0 g (2.5 mmol) of the olefin (*ap*-**4a**), 3.7 g (49 mmol) of trimethylamine oxide dihydrate and 2 mL of pyridine in 15 mL of water and 50 mL of *t*-butyl alcohol and the whole was refluxed for 12 h. The mixture was cooled and treated with 20 mL of 20% aqueous sodium sulfite. Most of the *t*-butyl alcohol was evaporated and the aqueous layer was extracted with dichloromethane after being saturated with sodium chloride. The extract was washed with dilute hydrochloric acid to remove pyridine. Evaporation of the solvent afforded practically pure *ap*-4-(1,4-dimethoxy-9-triptycyl)-4-methyl-1,2-pentanediol (*ap*-**5a**) in almost quantitative yield. ^{1}H NMR ($CDCl_3$) δ=2.10 (3H, s), 2.23 (3H, s), 2.55 (1H, dd, J=15 and 2.6 Hz), 2.68 (1H, dd, J=15 and 7.3 Hz), 3.52 (1H, m), 3.73 (3H, s), 3.75—3.80 (1H, m), 3.80 (3H, s), 4.30—4.47 (1H, m), 5.87 (1H, s), 6.58 and 6.61 (2H, ABq, J=9.2 Hz), 6.90—7.02 (4H, m), 7.38—7.42 (2H, m), 7.66—7.70 (1H, m), 7.98—8.01 (1H, m).

Periodic acid (750 mg or 3.5 mmol) was added to a solution of 400 mg (0.93 mmol) of the diol (*ap*-**5a**) in 15 mL of tetrahydrofuran and 3 mL of water and the whole was stirred for 1 h at room temprature. The mixture was poured into

water and extracted with dichloromethane. Evaporation of the solvent afforded *ap*-3-(1,4-dimethoxy-9-triptycyl)-3-methylbutanal in 75% yield. ^{1}H NMR ($CDCl_3$) δ=2.26 (6H, s), 3.65 (2H, d, J=2.6 Hz), 3.74 (3H, s), 3.80 (3H, s), 5.88 (1H, s), 6.58 and 6.62 (2H, ABq, J=9.1 Hz), 6.97—7.00 (4H, m), 7.40—7.44 (2H, m), 7.76—7.82 (2H, m), 10.25 (1H, t, J=2.6 Hz).

To a solution of 100 mg (0.25 mmol) of the *ap*-aldehyde in 4 mL of acetone were added 4 mg of sodium hydrogencarbonate and 40 mg (0.25 mmol) of potassium permanganate with ice-cooling and the mixture was stirred for 50 min. The mixture was treated with an aqueous solution of sodium hydrogensulfite to destroy the excess of potassium permanganate, acidified with hydrochloric acid, and extracted with dichloromethane. After evaporation of the solvent the residue was recrystallized from tetrahydrofuran-pentane to give pure *ap*-**7a**, mp 198.5 °C (decomp). The yield was 60%. Found: C, 77.98; H, 6.49%. Calcd for $C_{27}H_{26}O_4$: C, 78.24; H, 6.32%. ^{1}H NMR ($CDCl_3$) δ=2.25 (6H, s), 3.62 (2H, s), 3.73 (3H, s), 3.81 (3H, s), 5.89 (1H, s), 6.59 and 6.62 (2H, ABq, J=8.1 Hz), 6.99—7.03 (4H, m), 7.41—7.44 (2H, m), 7.86—7.90 (2H, m).

***ap*-3-(1,4-Dimethyl-9-triptycyl)-3-methylbutanoic Acid (*ap*-7b).** This compound was prepared similarly as described above from *ap*-**4b**. The NMR data and yield, where appropriate, are given. *ap*-4-(1,4-Dimethyl-9-triptycyl)-4-methyl-1,2-pentanediol (*ap*-**5b**): ^{1}H NMR ($CDCl_3$) δ=2.27 (3H, s), 2.42 (3H, s), 2.49 (3H, s), 2.67 (3H, s), 2.45—2.84 (2H, m), 3.48 (1H, dd, J=11 and 2.1 Hz), 3.69 (1H, dd, J=11 and 2.1 Hz), 4.3—4.5 (1H, m), 5.58 (1H, s), 6.74 (2H, s), 6.85—7.10 (4H, m), 7.29—7.41 (2H, m), 7.60—8.22 (2H, m); yield>95%. *ap*-3-(1,4-Dimethyl-9-triptycyl)-3-methylbutanal: ^{1}H NMR ($CDCl_3$) δ=2.43 (6H, s), 2.49 (3H, s), 2.67 (3H, s), 3.74 (2H, d, J=2.2 Hz), 5.60 (1H, s), 6.76 (2H, s), 6.90—7.01 (4H, m), 7.36—7.42 (2H, m), 7.78—7.81 (2H, m), 10.19 (1H, t, J=1.9 Hz); yield>95%. *ap*-**7b**: ^{1}H NMR ($CDCl_3$) δ=2.43 (6H, s), 2.50 (3H, s), 2.68 (3H, s), 3.67 (2H, s), 5.60 (1H, s), 6.76 (2H, s), 7.01—7.13 (4H, m), 7.37—7.40 (2H, m), 7.85—7.87 (2H, m); yield 95%. This compound did not give correct analyses of elements, the phenomenon being often observed in the compounds in triptycene series probably because of inclusion of solvent or other molecules. The methyl ester, mp 204—205 °C, however, gave correct analytical results. Found: C, 84.70; H, 7.00%. Calcd for $C_{28}H_{28}O_2$: C, 84.81; H, 7.12%. ^{1}H NMR ($CDCl_3$) δ=2.36 (6H, s), 2.48 (3H, s), 2.65 (3H, s), 3.59 (2H, s), 3.80 (3H, s), 5.58 (1H, s), 6.73 (2H, s), 6.97—7.00 (4H, m), 7.35—7.38 (2H, m), 7.84—7.88 (2H, m).

***sc*-3-(1,4-Dimethoxy-9-triptycyl)-3-methylbutanoic Acid (*sc*-7a).** Thermal isomerization of *ap*-**4** was accomplished by heating a solution of *ap*-**4** in 1-chloronaphthalene at 250 °C for 12 h under a nitrogen atmosphere. The solvent was removed by chromatography on silica gel. The residue showed the presence of isomers in *sc*/*ap*=1.4 ratio. It was possible to enrich the *sc*-isomer up to 95% by recrystallization from dichloromethane-hexane. ^{1}H NMR ($CDCl_3$) δ=1.97 (3H, s), 2.02 (3H, s), 3.31 and 3.54 (2H, AB of ABX, J=6.2 and 7.3 Hz), 3.74 (3H, s), 3.82 (3H, s), 5.17—5.24 (2H, m), 6.23—6.38 (1H, m), 6.55 and 6.63 (2H, ABq, J=8.8 Hz), 6.90—7.02 (4H, m), 7.38—7.42 (2H, m), 7.66—7.70 (1H, m), 7.98—8.01 (1H, m).

Dihydroxylation of the olefin mixture with osmium tetraoxide and trimethylamine oxide was carried out similarly as described for the *ap*-isomer. The *sc*-olefin gave two isomers (I and II) due to the fact that a new chiral center was formed, the ratio, I/II, being ca. 1.0. The yield was quantitative. ^{1}H NMR data ($CDCl_3$, δ) of *sc*-diols which were separated from the *ap* at the acetonide stage (see below): *sc*-**5a**(I) 2.09 (3H, s), 2.13 (3H, s), 2.67 (1H, dd, J=15 and 2.6 Hz), 2.68 (1H, dd, J=15 and 7.3 Hz), 3.52 (1H, m), 3.73 (3H, s), 3.75—3.87 (1H, m), 3.78 (3H, s), 3.82 (3H, s), 4.30—4.47 (1H, m), 5.87 (1H, s), 6.58 and 6.61 (2H, ABq, J=8.8 Hz), 6.90—7.02 (4H, m), 7.38—7.42 (2H, m), 7.66—7.70 (1H, m), 7.98—8.01 (1H, m); *sc*-**5a**(II) 2.06 (3H, s), 2.21 (3H, s), 2.64 (1H, dd, J=15 and 8.1 Hz), 2.69 (1H, dd, J=15 and 2.9 Hz), 3.49—3.56 (1H, m), 3.64—3.75 (1H, m), 3.70 (3H, s), 3.82 (3H, s), 4.37—4.45 (1H, m), 5.88 (1H, s), 6.57 and 6.64 (2H, ABq, J=9.2 Hz), 6.92—7.03 (4H, m), 7.35—7.42 (2H, m), 7.88—7.91 (1H, m), 8.01—8.04 (1H, m).

A solution of 300 mg of the mixture of diols **5a** in 15 mL of acetone was heated under reflux for 4 h with a catalytic amount of *p*-toluenesulfonic acid, the formed water being trapped by Molecular Sieves 5A. After cooling, the mixture was poured into aqueous sodium hydrogencarbonate and extracted with dichloromethane. After evaporation of the solvent, the residue was submitted to flash column or medium-pressure column chromatography on silica gel (9:1 hexane–ether eluent). The order of elution was *ap*-**6a**, *sc*-**6a**(I), and *sc*-**6a**(II). The separation of the two *sc* forms was not complete. The following ^{1}H NMR data ($CDCl_3$, δ) were recorded. *ap*-**6a**: 1.45 (3H, s), 1.49 (3H, s), 2.07 (3H, s), 2.18 (3H, s), 2.68 (1H, dd, J=15 and 6.8 Hz), 2.92 (1H, dd, J=15 and 3.6 Hz), 3.59 (1H, t, J=8.1 Hz), 3.72 (3H, s), 3.79 (3H, s), 4.26 (1H, dd, J=8.1 and 5.9 Hz), 4.64—4.74 (1H, m), 5.88 (1H, s), 6.57 and 6.60 (2H, ABq, J=9.2 Hz), 6.93—6.99 (4H, m), 7.38—7.41 (2H, m), 7.70—7.73 (1H, m), 8.00—8.03 (1H, m). *sc*-**6a**(I): 1.55 (6H, s), 2.04 (3H, s), 2.10 (3H, s), 2.70 (1H, dd, J=15 and 4.8 Hz), 3.24 (1H, dd, J=15 and 6.6 Hz), 3.64 (1H, dd, J=8.4 and 7.7 Hz), 3.77 (3H, s), 3.82 (3H, s), 4.27 (1H, dd, J=7.7 and 5.5 Hz), 4.67—4.73 (1H, m), 5.88 (1H, s), 6.59 and 6.64 (2H, ABq, J=8.8 Hz), 6.92—7.00 (4H, m), 7.35—7.41 (2H, m), 7.71—7.75 (1H, m), 7.84—7.87 (1H, m). *sc*-**6a**(II): 1.50 (3H, s), 1.51 (3H, s), 2.04 (3H, s), 2.16 (3H, s), 2.82 (1H, dd, J=11 and 8.1 Hz), 2.88 (1H, dd, J=11 and 2.6 Hz), 3.56 (1H, t, J=7.7 Hz), 3.70 (3H, s), 3.81 (3H, s), 4.16 (1H, dd, J=7.7 and 5.9 Hz), 4.68—4.72 (1H, m), 5.88 (1H, s), 6.63 and 6.65 (2H, ABq, J=8.8 Hz), 6.94—7.00 (4H, m), 7.36—7.40 (2H, m), 7.88—7.91 (1H, m) 8.06—8.10 (1H, m).

The mixture of *sc*-**6a**(I) and *sc*-**6a**(II) (1.0 g) in 25 mL of tetrahydrofuran was added to 25 mL of 1 M hydrochloric acid (1 M=1 mol L^{-1}) and the mixture was stirred at room temperature for 2.5 h. The mixture was poured into water and extracted with dichloromethane. Evaporation of the solvent afforded a mixture of two forms of *sc*-**5a**.

The oxidation of the mixture of *sc*-**5a** was carried out as described for the *ap*-form to afford the *sc*-aldehyde. ^{1}H NMR ($CDCl_3$) δ=2.19 (3H, s), 2.25 (3H, s), 3.57 and 3.97 (2H, ABdq, J=16 and 2.6 Hz), 3.72 (3H, s), 3.82 (3H, s), 5.90 (1H, s), 6.59 and 6.65 (2H, ABq, J=9.2 Hz), 6.94—7.02 (4H, m), 7.38—7.43 (2H, m), 7.74—7.82 (2H, m), 10.19 (1H, t, J=2.6 Hz).

The oxidation of the *sc*-aldehyde was caried out similarly as described for the *ap* form to afford 60% *sc*-**7a**, mp 270 °C (decomp). ^{1}H NMR ($CDCl_3$) δ=2.22 (3H, s), 2.24 (3H, s), 3.50 and 4.28 (2H, ABq, J=15 Hz), 3.79 (3H, s), 3.83 (3H, s), 5.90 (1H, s), 6.59 and 6.69 (2H, ABq, J=9.2 Hz), 6.96—7.03

(4H, m), 7.38—7.44 (2H, m), 7.81—7.85 (1H, m), 7.91—7.94 (1H, m). This compound did not give correct analyses but its methyl ester, mp 231—232 °C, did the correct data. Found: C, 78.38; H, 6.47%. Calcd for $C_{28}H_{28}O_4$: C, 78.48; H, 6.39%. ^{1}H NMR ($CDCl_3$) δ=2.14 (3H, s), 2.15 (3H, s), 3.60 (2H, ABq, J=15 Hz), 3.73 (3H, s), 3.79 (3H, s), 3.81 (3H, s), 5.89 (1H s), 6.56 and 6.62 (2H, ABq, J=9.2 Hz), 6.93—7.00 (4H, m), 7.36—7.42 (2H, m), 7.80—7.83 (1H, m), 7.90—7.94 (1H, m).

***sc*-3-(1,4-Dimethyl-9-triptycyl)-3-methylbutanoic Acid (*sc*-7b).** This compound was prepared as described for the preparation of *sc*-**7a**. The ^{1}H NMR data ($CDCl_3$, δ) and yield, where appropriate, are given. *sc*-**4b**: 2.07 (3H, s), 2.13 (3H, s), 2.52 (3H, s), 2.63 (3H, s), 3.21—3.70 (2H, m), 5.28 (2H, d, J=5.1 Hz), 5.68 (1H, s), 6.14—6.36 (1H, m), 6.78 (2H, s), 6.92—7.02 (4H, m), 7.32—7.41 (2H, m), 7.82—7.90 (2H, m); *sc*/*ap* ratio 0.69. *sc*-**5b (I)**: 2.12 (3H, s), 2.36 (3H, s), 2.52 (3H, s), 2.55 (3H, s), 2.65—2.97 (2H, m), 3.47—3.86 (2H, m), 4.3—4.4 (1H, m), 5.57 (1H, s), 6.73 and 6.77 (2H, ABq, J=6.1 Hz), 6.85—7.10 (4H, m), 7.29—7.41 (2H, m), 7.60—8.22 (2H, m). *sc*-**5b**(II): 2.12 (3H, s), 2.34 (3H, s), 2.52 (3H, s), 2.77 (3H, s), 2.65—2.97 (2H, m), 3.47—3.86 (2H, m), 4.3—4.4 (1H, m), 5.57 (1H, s), 6.73 and 6.77 (2H, ABq, J=6.1 Hz), 6.85—7.10 (4H, m), 7.29—7.41 (2H, m), 7.60—8.22 (2H, m). The ratio *sc*-**5b**(I)/*sc*-**5b**(II) was ca. 2:1. *ap*-**6b**: 1.45 (3H, s), 1.48 (3H, s), 2.25 (3H, s), 2.38 (3H, s), 2.48 (3H, s), 2.66 (3H, s), 2.60—3.01 (2H, m), 3.55 (1H, dd, J=10.0 and 7.1 Hz), 4.24 (1H, dd, J=10.0 and 7.1 Hz), 4.63—4.75 (1H, m), 5.55 (1H, s), 6.74 (2H, s), 6.91—7.20 (4H, m), 7.32—7.40 (2H, m), 7.68—7.75 (1H, m), 7.98—8.06 (1H, m). *sc*-**6b**(I): 1.53 (6H, s), 2.20 (6H, s), 2.51 (3H, s), 2.56 (3H, s), 2.65—3.16 (2H, m), 3.60 (1H, dd, J=7.9 and 5.9 Hz), 4.19 (1H, dd, J=7.9 and 5.9 Hz), 4.68—4.82 (1H, m), 5.58 (1H, s), 6.73 and 6.76 (2H, ABq, J=7.9 Hz), 6.90—7.10 (4H, m), 7.28—7.42 (2H, m), 7.76—8.20 (2H, m). *sc*-**6b**(II): 1.46 (3H, s), 1.48 (3H, s), 2.09 (3H, s), 2.31 (3H, s), 2.52 (3H, s), 2.77 (3H, s), 2.63—3.15 (2H, m), 3.58 (1H, dd, J=8.0 and 5.9 Hz), 4.19 (1H, dd, J=8.0 and 5.9 Hz), 4.68—4.82 (1H, m), 5.58 (1H, s), 6.60—6.70 (2H, m), 6.85—7.05 (4H, m), 7.30—7.42 (2H, m), 7.65—8.08 (2H, m). *sc*-Aldehyde: 2.31 (3H, s), 2.36 (3H, s), 2.53 (3H, s), 2.62 (3H, s), 3.79 (2H, m), 5.60 (1H, s), 6.78—6.79 (2H, m), 6.97—7.02 (4H, m), 7.35—7.40 (2H, m), 7.78—7.84 (2H, m), 10.24 (1H, m). *sc*-**7b**: mp 149—160 °C, yield>95%. Found: C, 84.51; H, 6.61%. Calcd for $C_{27}H_{26}O_2$: C, 84.78; H, 6.85%. ^{1}H NMR ($CDCl_3$) δ=2.30 (3H, s), 2.37 (3H, s), 2.53 (3H, s), 2.75 (3H, s), 3.75 and 3.94 (2H, ABq, J=16 Hz), 5.60 (1H, s), 6.80 (2H, s), 6.98—7.05 (4H, m), 7.35—7.41 (2H, m), 7.84—7.87 (1H, m), 7.91—7.94 (1H, m). *sc*-**7b** methyl ester: mp 210—211 °C. Found: C, 85.02; H, 7.00%. Calcd for $C_{28}H_{28}O_2$: C, 84.81; H, 7.12%. ^{1}H NMR ($CDCl_3$) δ=2.21 (3H, s), 2.28 (3H, s), 2.50 (3H, s), 2.70 (3H, s), 3.7—3.8 (2H, m), 3.81 (3H, s), 5.56 (1H, s), 6.75 (2H, s), 6.9—7.1 (4H, m), 7.2—7.5 (2H, m), 7.75—7.95 (2H, m) at 90 MHz.

Lewis Acid-Catalyzed Reaction of 3-(1,4-Dimethoxy-9-triptycyl)-3-methylbutanoic Acid (7a). The carboxylic acid (100 mg or 0.24 mmol) in 7.5 mL of benzene was stirred with 0.3 mL (3.5 mmol) of oxalyl dichloride at room temperature for 2 h and the solvent and the excess of oxalyl dichloride were evaporated in vacuo. The residue showed the following ^{1}H NMR spectra ($CDCl_3$, δ). *ap*: 2.22 (6H, s), 3.73 (3H, s), 3.80 (3H, s), 4.29 (2H, s), 5.89 (1H, s), 6.55 and 6.65 (2H, ABq, J=9.1 Hz), 6.98—7.05 (4H, m), 7.36—7.44 (2H, m), 7.73—7.77 (2H, m). *sc*: 2.17 (3H, s), 2.22 (3H, s), 3.79 (3H, s), 3.83 (3H, s), 4.32 and 4.82 (2H, ABq, J=19 Hz), 5.90 (1H, s), 6.60 and 6.70 (2H, ABq, J=10 Hz), 6.96—7.05 (4H, m), 7.35—7.46 (2H, m), 7.72—7.88 (2H, m).

The acid chloride produced in the above reaction was dissolved in 10 mL of benzene and 0.050 mL (2 equiv) of titanium(IV) chloride was added. The mixture was stirred for 4 h at room temperature and decomposed with water. The aqueous layer was extracted with dichlomethane and the solvents were evaporated from the combined organic layers.

The *ap*-acid afforded, after purification by recrystallization from tetrahydrofuran-pentane, 8,11-dimethoxy-1,1-dimethyl-1,2-dihydro-7*H*-7,11b-*o*-benzeno-3*H*-benz[*de*]-anthracen-3-one (*ap*-**8a**), mp 283.0—284.0 °C, in 70% yield. Found: C, 81.52; H, 5.85%. Calcd for $C_{27}H_{24}O_3$: C, 81.79; H, 6.10%. ^{1}H NMR ($CDCl_3$) δ=1.67 (3H, d, J=1.4 Hz), 2.10 (3H, s), 2.71 (1H, d, J=15 Hz), 3.37 (1H, app dd, J=15 and 1.4 Hz), 3.75 (3H, s), 3.87 (3H, s), 5.93 (1H, s), 6.62 and 6.71 (2H, ABq, J=9.0 Hz), 6.88—7.00 (2H, m), 7.06—7.13 (1H, m), 7.32—7.35 (1H, m), 7.56—7.62 (2H, m), 7.79—7.82 (1H, m), IR (KBr disc): 1690 cm^{-1}.

The *sc*-acid afforded a ketone (*sc*-**8a**) and a lactone (**9**) which were not easily separated. The pure ketone was obtained by recrystallization of the product, obtained with the use of dichloromethane or benzene as a solvent, from tetrahydrofuran-pentane. The pure lactone was obtained by chromatography on silica gel (1:2 hexane-dichloromethane) after conversion of the ketone into its oxime. The combined yields of the lactone and the ketone were ca. 70%.

sc-**8a**: mp 283.0—284.0 °C. Found: C, 81.54; H, 6.34%. Calcd for $C_{27}H_{24}O_3$: C, 81.79; H, 6.10%. ^{1}H NMR ($CDCl_3$) δ=1.63 (3H, d, J=1.5 Hz), 2.07 (3H, s), 2.62 (1H, d, J=16 Hz), 3.91 (1H, app dd, J=16 and 1.5 Hz), 3.75 (3H, s), 3.76 (3H, s), 5.94 (1H, s), 6.51 and 6.55 (2H, ABq, J=8.1 Hz), 7.09—7.25 (3H, m), 7.47—7.64 (3H, m), 7.86—7.89 (1H, m). IR (KBr disc): 1690 cm^{-1}.

9: mp 238.5—240.0 °C. This compound failed to give correct analysis, the phenomenon being often observed in the triptycene series as mentioned in the analysis of *ap*-**7b**. High resolution MS: M^+ 382.1549 (82.9%) and 383.1590 (25.6%) in accordance with the calculated values 382.1567 for $C_{26}H_{22}O_3$ and 383.1601 for $C_{25}{}^{13}CH_{22}O_3$. ^{1}H NMR ($CDCl_3$) δ=1.97 (3H, s), 2.19 (3H, s), 3.13 and 3.90 (2H, ABq, J=15 Hz), 3.87 (3H, s), 5.93 (1H, s), 6.69 and 6.82 (2H, ABq, J=9.2 Hz), 6.98—7.10 (4H, m), 7.39—7.58 (3H, m), 7.82—7.85 (1H, m). IR (KBr disc): 1750 cm^{-1}. ^{13}C NMR ($CDCl_3$): 170.6 ppm from TMS.

Lewis Acid-Catalyzed Reaction of 3-(1,4-Dimethyl-9-triptycyl)-3-methylbutanoic Acid (7b). The reaction was carried out as described for **7a**. The following ^{1}H NMR data ($CDCl_3$, δ) were recorded at 90 MHz.

***ap*-Acid Chloride:** 2.41 (6H, s), 2.47 (3H, s), 2.61 (3H, s), 4.30 (2H, s), 5.56 (1H, s), 6.72 (2H, s), 6.8—7.1 (4H, m), 7.2—7.5 (2H, m), 7.5—7.8 (2H, m).

***sc*-Acid Chloride:** 2.27 (3H, s), 2.34 (3H, s), 2.61 (3H, s), 2.70 (3H, s), 4.37 and 4.52 (2H, ABq, J=19.8 Hz), 5.56 (1H, s), 6.78 (2H, s), 6.8—7.2 (4H, m), 7.3—7.4 (2H, m), 7.6—7.9 (2H, m).

The *ap*-acid chloride afforded 1,1,8,11-tetramethyl-1,2-dihydro-7*H*-7,11b-*o*-benzeno-3*H*-benz[*de*]anthracen-3-one (**8b**), mp 192.0—192.5 °C, in 70% yield. Found: C, 88.64; H, 6.55%. Calcd for $C_{27}H_{24}O$: C, 88.97; H, 6.64%. ^{1}H NMR ($CDCl_3$) δ=1.70 (3H, d, J=1.8 Hz), 2.18 (3H, s), 2.52 (3H, s),

2.61 (3H, s), 2.72 (1H, d, J=15 Hz), 3.31 (1H, dd, J=15 and 1.8 Hz), 5.56 (1H, s), 6.76 and 6.81 (2H, ABq, J=8.1 Hz), 6.85—6.96 (2H, m), 7.02—7.08 (1H, m), 7.23—7.29 (1H, m), 7.46—7.57 (2H, m), 7.72—7.75 (1H, m). IR (KBr disc): 1678 cm^{-1}.

The *sc*-acid chloride gave two ketones which were separated by preparative TLC on silica gel (1:2 hexane–dichloromethane eluent).

1,1,8,11-Tetramethyl-1,2-dihydro-7*H*-7,11b-*o*-benzeno-3*H*-benz[*de*]anthracen-3-one (*sc*-8b): mp 247.0—248.0 °C. Yield 33%. Found: C, 88.75; H, 6.57%. Calcd for $C_{27}H_{24}O$: C, 88.97; H, 6.64%. ^1H NMR ($CDCl_3$) δ=1.65 (3H, d, J=1.5 Hz), 2.21 (3H, s), 2.43 (3H, s), 2.65 (3H, s), 2.73 (1H, d, J=15 Hz), 3.74 (1H, dd, J=15 and 1.5 Hz), 5.66 (1H, s), 6.66 and 6.67 (2H, ABq, J=8.1 Hz), 7.04—7.14 (3H, m), 7.43—7.46 (1H, m), 7.52—7.55 (1H, m), 7.63—7.67 (1H, m), 7.79—7.83 (1H, m). IR (KBr disc): 1692 cm^{-1}.

1,1,4,6-Tetramethyl-1,2-dihydro-7*H*-7,11b-*o*-benzeno-3*H*-benz[*de*]anthracen-3-one (10): mp 262.5—263.0 °C, yield 37%. Found: C, 88.85; H, 6.52%. Calcd for $C_{27}H_{24}O$: C, 88.97; H, 6.64%. ^1H NMR ($CDCl_3$) δ=1.69 (3H, s), 2.09 (3H, s), 2.51 (3H, s), 2.53 (3H, s), 2.60 and 3.55 (2H, ABq, J=16 Hz), 5.51 (1H, s), 6.75 (1H, s), 6.91—6.96 (2H, m), 7.04—7.08 (2H, m), 7.30 and 7.46 (2H, ABq, J=6.8 Hz), 7.75 and 7.83 (2H, ABq, J=7.3 Hz). IR (KBr disc): 1673 cm^{-1}.

Effects of Solvent and Catalyst. The reactions were carried out in essentially the same manner as described in the reaction of **7a**. Although the results were irregular when the amount of the catalyst was less than 1.0 equivalent to the acid chloride, they were essentially the same when the catalyst was 1.0—10 equivalents. When the solvent was cyclohexane, the reaction was slow. The results are given in Tables 1 and 2. The analysis of the products were caried out by ^1H NMR spectra using the signals due to the methyl or methoxyl protons.

3-Chloro-1,1,8,11-tetramethyl-7*H*-7,11b-*o*-benzeno-1*H*-benz[*de*]anthracene (11). A mixture of 100 mg of *sc*-**8b** and 5 mL of thionyl chloride, which was distilled over triphenylphospine, was heated under reflux for 2 h under a nitrogen atmosphere. The excessive thionyl chloride was evaporated in vacuo and the residue was treated with water. The mixture was extracted with dichloromethane, and the extract was washed with aqueous sodium hydrogencarbonate and dried over magnesium sulfate. After evaporation of the solvent, the residue was submitted to preparative TLC on silica gel with 2:1 hexane–dichloromethane as an eluent. **11** was obtained as crystals, mp 264.0—266.0 °C, in 50% yield. High resolution MS: M^+ 382.1480 and 384.1468. Calcd for $C_{27}H_{23}{}^{35}Cl$ and $C_{27}H_{23}{}^{37}Cl$: 382.1486 and 384.1458. ^1H NMR ($CDCl_3$) δ=1.72 (3H, s), 2.21 (3H, s), 2.34 (3H, s), 2.54 (3H, s), 5.54 (1H, s), 6.40 (1H, s), 6.49 and 6.62 (2H, ABq, J=8.1 Hz), 6.99—7.28 (5H, m), 7.47—7.50 (1H, m), 7.80—7.83 (1H, m).

3-Chloro-1,1,4,6-tetramethyl-7*H*-7,11b-*o*-benzeno-1*H*-benz[*de*]anthracene (12): mp 223.0—225.0 °C, was similarly obtained in ca. 50% yield from **10**. High resolution MS: M^+ 382.1468 and 384.1443. Calcd for $C_{27}H_{23}{}^{35}Cl$ and $C_{27}H_{23}{}^{37}Cl$: 382.1468 and 384.1458. ^1H NMR ($CDCl_3$) δ=1.74 (3H, s), 2.12 (3H, s), 2.44 (3H, s), 2.46 (3H, s), 5.43 (1H, s), 6.41 (1H, s), 6.64 (1H, s), 6.80—6.88 (2H, m), 7.02—7.24 (3H, m), 7.47—7.54 (2H, m), 7.76—7.82 (1H, m).

Further Heating of 11 and 12 with Thionyl Chloride. **12** and thionyl chloride for 12 h afforded a product which was almost pure on the ^1H NMR spectral ground. The structure of the product was assigned as 2,3-dichloro-1,1,4,6-tetramethyl-7*H*-7,11b-*o*-benzeno-1*H*-benz[*de*]anthracene (**13**). ^1H NMR ($CDCl_3$) δ=1.85 (3H, s), 2.28 (3H, s), 2.43 (3H, s), 2.46 (3H, s), 5.44 (1H, s), 6.65 (1H, s), 6.84—6.93 (2H, m), 7.05—7.25 (3H, m), 7.38—7.53 (2H, m), 7.84—7.87 (1H, m). High resolution MS: M^+ 416.1072 and 418.1049. Calcd for $C_{27}H_{22}{}^{35}Cl_2$ and $C_{27}H_{22}{}^{35}Cl^{37}Cl$: 416.1097 and 418.1067. The mass spectrum also showed the presence of peaks which indicated the contamination of **13** by trichloro and tetrachloro compounds.

11 did not react with thionyl chloride any more under the conditions.

Heating *ap*-7b and *sc*-7b with Thionyl Chloride. The *ap*-acid (100 mg) was heated with 5 mL of thionyl chloride similarly as mentioned above. The reaction afforded *sc*-**8b**, **11**, and *ap*-**8b** in 70, 11, and 3% yields, respectively.

sc-**7b**, on a similar treatment, afforded **10**, *sc*-**8b**, **12**, and **11** in 21, 42, 20, and 5% yields, respectively. In addition, **13** and *ap*-**8b** were detected by ^1H NMR spectra, the yields being ca. 1 and 2%, respectively.

Thermal Equilibration of Ketones 8. The *ap*-ketone was dissolved in toluene-d_8 to make up a ca. 25 mmol L^{-1} solution. The sample solution was heated in an appropriate boiling solvent bath except for the cases at 70 and 90 °C, when a thermostatted bath was used. The solvents used for the bath were toluene (111.5 °C), water (100.5 °C), and acetone (56.0 °C). The rates of isomerization were followed by ^1H NMR spectra by observing methyl signals. The rate constants were obtained by assuming the first order reaction which is reversible. The error limit in Tables 3 and 4 are given at the 95% confidence.

Calculation of the Data in Table 5. It was assumed that the thermodynamic parameters obtained at about or below 100 °C could be extrapolated to 150 °C for the ketones (**8**) and those obtained at 200 °C or higher temperatures for **14** could as well be extrapolated to 150 °C. Then the equilibrium contants at 150 °C could be calculated and were used for the calculation of the reverse reaction rates. Free energies of activation for the forward and backward reactions were thus calculated and listed.

Molecular Mechanics Calculations. Calculations were performed on Hitachi M-680H computer system at the Computer Center of the University of Tokyo (CCUT) using a modified version[23] of the MM2 program.[24] Some of the force field parameters were modified in order to properly reproduce deformations about the bond which connects a benzene ring with a carbonyl function attached to it and are listed in Table 7.

This work was supported by a Grant in Aid (No. 62124035) for Fundamental Scientific Research of Ministry of Education, Science and Culture, to which our thanks are due.

References

1) For Part XXI of this series, see M. Ōki, T. Tanaka, and G. Yamamoto, *Chem. Lett.*, **1987**, 1815.

2) Preliminary results have been published in two communications: K. Yonemoto, Y. Nakai, G. Yamamoto, and M. Ōki, *Chem. Lett.*, **1985**, 1739; Ref. 1.

3) M. Ōki, *Top. Stereochem.*, **14**, 1 (1983).

4) M. Ōki, *Acc. Chem. Res.*, **17**, 154 (1984).
5) S. Seki, T. Morinaga, H. Kikuchi, T. Mitsuhashi, G. Yamamoto, and M. Ōki, *Bull. Chem. Soc. Jpn.*, **54**, 1465 (1981).
6) K. Yonemoto, F. Kakizaki, G. Yamamoto, N. Nakamura, and M. Ōki, *Bull. Chem. Soc. Jpn.*, **58**, 3346 (1985).
7) H. Kikuchi, S. Seki, G. Yamamoto, T. Mitsuhashi, N. Nakamura, and M. Ōki, *Bull. Chem. Soc. Jpn.*, **55**, 1514 (1982).
8) R. Ray and D. S. Matteson, *Tetrahedron Lett.*, **21**, 449 (1980).
9) E. L. Jackson, *Org. React.*, **2**, 341 (1944).
10) E. J. Hartwell, R. E. Richards, and H. W. Thompson, *J. Chem. Soc.*, **1948**, 1436.
11) H. W. Thompson and P. Torkington, *J. Chem. Soc.*, **1945**, 640.
12) E. L. Gustus and P. G. Stevens, *J. Am. Chem. Soc.*, **55**, 378 (1933) and papers cited therein.
13) P. B. D. de la Mare, *Acc. Chem. Res.*, **7**, 361 (1974): R. B. Moodie and K. Schofield, *ibid.*, **9**, 287 (1976).
14) G. A. Olah, S. Kobayashi, and M. Tashiro, *J. Am. Chem. Soc.*, **94**, 7448 (1972): see also G. A. Olah, A. Germain, and A. M. White, "Acylium Ions," in "Carbonium Ions," ed by G. A. Olah and P. von R. Schleyer, Vol. V, John-Wiley, New York (1976), pp. 2049—2133.
15) P. Lazzeretti and F. Taddei, *Org. Magn. Reson.*, **3**, 283 (1971).
16) G. Yamamoto, M. Suzuki, and M. Ōki, *Bull. Chem. Soc. Jpn.*, **56**, 306 (1983).
17) E. C. Kornfeld, P. Barney, J. Blankley, and W. Faul, *J. Med. Chem.*, **8**, 342 (1965).
18) A. W. Crossley and H. R. Sueur, *J. Chem. Soc.*, **83**, 110 (1903): A. W. Crossley and N. Renouf, *ibid.*, **91**, 63 (1907): R. D. Clark and C. H. Heathcock, *J. Org. Chem.*, **41**, 636 (1976).
19) W. Taylor, *J. Chem. Soc.*, **1937**, 304.
20) J. Cologne and P. Garnier, *Bull. Soc. Chim. Fr.* **15**, 436 (1948).
21) M. Ōki, Y. Tanaka, G. Yamamoto, and N. Nakamura, *Bull. Chem. Soc. Jpn.*, **56**, 302 (1983).
22) S. Gronowitz and G. Hansen, *Ark. Kemi*, **27**, 145 (1967).
23) G. Yamamoto and M. Ōki, *Bull. Chem. Soc. Jpn.*, **58**, 1690 (1985).
24) N. L. Allinger and Y. H. Yuh, QCPE, No. 395.

 © 1988 The Chemical Society of Japan Bull. Chem. Soc. Jpn., 61, 3249—3254 (1988)

Asymmetric Synthesis of Axially Chiral, Unsymmetrical Diphenic Acids via Intramolecular Ullmann Coupling Reaction[1)]

Sotaro MIYANO,* Hiroshi FUKUSHIMA, Shigeru HANDA, Hiromitsu ITO, and Harukichi HASHIMOTO
Department of Applied Chemistry, Faculty of Engineering, Tohoku University, Aramaki-Aoba, Sendai 980
(Received March 22, 1988)

A practical route to unsymmetrical diphenic acids is described. Successive esterification of ethylene glycol with two different 2-halobenzoyl chlorides gave the corresponding mixed diester, which was treated with copper powder in boiling DMF under dilution conditions. Silica-gel column chromatography allowed ready separation of the intramolecularly coupled cyclic diester (30—60% yield) from other by-products accompanying the Ullmann reaction, and alkaline hydrolysis gave unsymmetrical diphenic acid. Axially chiral, unsymmetrical diphenic acids of more than 99% enantiomeric excess were obtained from the reaction of mixed diesters prepared from (*R*)-1,1′-bi-2-naphthol.

The formation of aryl–aryl bond continues to be an important problem in organic synthesis.[2)] Among a number of methods currently available, nucleophilic addition of aryl Grignard reagents to aryl halides in the presence of nickel–phosphine complex (Kumada-Tamao reaction)[3)] or 2-(*o*-alkoxyaryl)-2-oxazolines (Meyers reaction)[4)] has become widely utilized in the last decade. However, efforts have still been devoted to develop novel methodologies, because procedures are severely limited when one wants regioselective aryl–aryl bond formation between two differently substituted aromatic nuclei bearing substituents such as nitro or carbonyl which are incompatible with organomagnesium reagents.[5)] It is known that, for the aryl halides bearing such functionalities, the Ullmann coupling reaction is complementary to the organometallic routes.[6)] However, when applied to a mixture of two different aryl halides, the reaction rarely works well to give the unsymmetrical biaryl in good yield because of the inevitable formation of the symmetrically coupled products which are difficult to separate from the desired one.[7)]

In the course of our study on the asymmetric reaction by use of axially chiral biaryl auxiliaries, we encountered an occasion where unsymmetrical diphenic acids were needed.[8)] Herein we wish to report that the intramolecular Ullmann coupling reaction of mixed diester of 2-halobenzoic acids provides a convenient route to unsymmetrical diphenic acids, and if desired, with complete axial chirality.

Results and Discussion

Synthesis of Racemic Diphenic Acids. Newman and Cella had tried the synthesis of unsymmetrical diphenic acid via intramolecular Ullmann coupling of a mixed acid anhydride of 2-halobenzoic acids,[9)] but their attempt was not fully realized because of the rapid disproportionation of the anhydride before coupling, resulting in the formation of the corresponding symmetrical diphenic acids along with the unsymmetrical acid in a statistical ratio. Attempted intramolecular coupling of *N*-phenyl-2,2′-dibromodibenzimide or 2,2′-dibromobenzil also failed to cyclize to give *N*-phenyldiphenimide or phenanthrenequinone.

As we had succeeded in the intramolecular Ullmann coupling of diol diesters of 2-halobenzoic acids to give, after hydrolysis, symmetrical diphenic acids,[10)] we tried to extend the reaction to the unimolecular

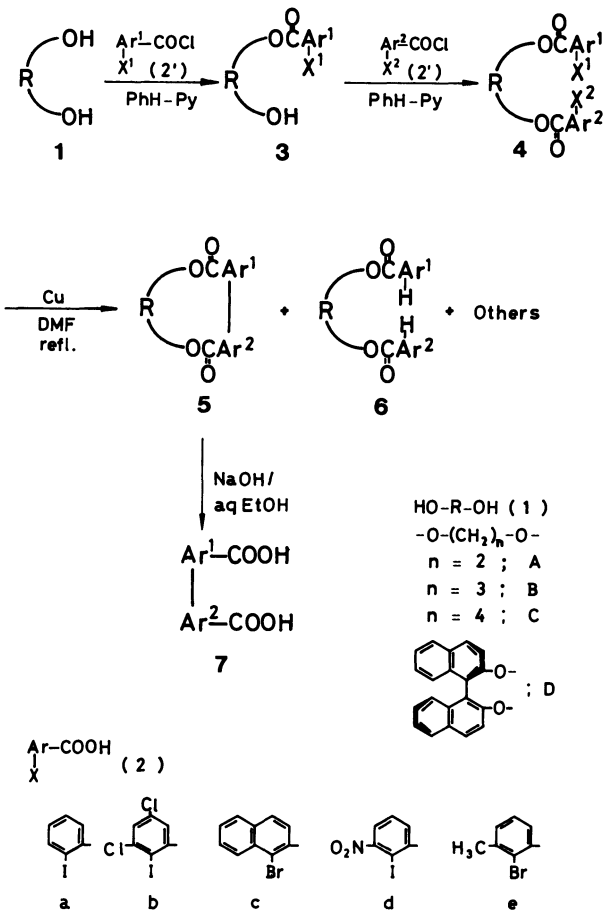

Scheme 1.

Table 1. Intramolecular Ullmann Coupling of Mixed Diesters of 2-Halobenzoic Acids[a]

	4					5		
	-O-R-O-	$Ar^1(X^1)$-	$Ar^2(X^2)$-	/mmol		Yield/%	IR(KBr)/cm^{-1}	Eluent[b]
4Aab	A	b	a	5.11	**5Aab**	51	1740	PhMe
4Aac	A	c	a	4.88	**5Aac**	43	1740	PhH
4Abc	A	b	c	3.57	**5Abc**	61	1750	PhH
4Abd	A	b	d	3.07	**5Abd**	56	1750	PhH
4Acd	A	c	d	3.77	**5Acd**	38	1745	PhH/EtOAC (4/1)
4Ace	A	e	c	2.24	**5Ace**	28	1740	PhH
4Bce	B	e	c	5.14	**5Bce**	31	1730	PhH
4Cce	C	e	c	3.33	**5Cce**	49	1730	PhH/EtOAc (20/1)
4Dbc	D	b	c	1.89	**5Dbc**	33	1750	Hexane/EtOAc (4/1)
4Dbd	D	b	d	1.92	**5Dbd**	80	1750	Hexane/PhMe (1/3)
4Dcd	D	c	d	1.83	**5Dcd**	44	1740	Hexane/EtOAc (4/1)

a) A solution of **4** in 40 ml of DMF was added to a vigorously stirred, gently refluxing suspension of Cu powder (20 equiv) in 60 ml of DMF during 6-h period. After the addition, the reaction was continued for 2 h. b) Eluent for the separation of **5** by silica-gel column chromatography; **5** was obtained as the first eluting component.

coupling of mixed diester of two different 2-halobenzoic acids for the synthesis of unsymmetrical diphenic acids (Scheme 1).

Treatment of a 2-halobenzoyl chloride **2′** with excess diol **1** in benzene–pyridine gave mono ester **3**. After purification by silica-gel column chromatography, **3** was in turn treated with a second 2-halobenzoyl chloride again in benzene–pyridine to give the corresponding unsymmetrical diester **4** in good yields.

The Ullmann reaction was carried out as before[10] by slowly adding a solution of **4** in *N,N*-dimethylformamide (DMF) to a vigorously stirred suspension of an activated copper powder in DMF heated at reflux. TLC analysis of the reaction mixture showed the presence of intramolecularly coupled cyclic diester **5** and of reduced, open chain diester **6** as the unimolecular reaction products accompanied by several oligomeric products originated from intermolecular coupling. It was shown that the monomeric cycle **5** was the first eluting component on silica-gel column, which enabled ready separation of **5** from the reduction product **6** and other by-products. Table 1 lists the results of the column-chromatographic separation of the intramolecularly coupled products, where yields refer to analytically pure samples.[11] This chromatographic behavior may reflect rather rigid, slightly strained cyclic structure of **5** as judged by higher IR absorption frequencies of the carbonyl function of **5** (1740—1750 cm^{-1}) than that of **6** (ca. 1720 cm^{-1}). CPK molecular models of **5** indicate that linking of two *o,o′*-positions of a biaryl by $-COO(CH_2)_2OCO-$ chain fixes the dihedral angle between the two phenyl rings to ca. 80°,[12] which disposes the $-OCH_2CH_2O-$ protons in diastereotopic positions, placing two of the vicinal protons near the shielding cones of the aromatic planes: ^1H NMR of **5** showed AA′BB′ pattern centered at around δ 4.1 and 5.1, while **6** showed a singlet at around δ 4.6 for these protons.

Hydrolytic removal of the bridging ethylenedioxy group from **5** was a trivial procedure, and afforded six unsymmetrical diphenic acids **7ab—7ce** listed.

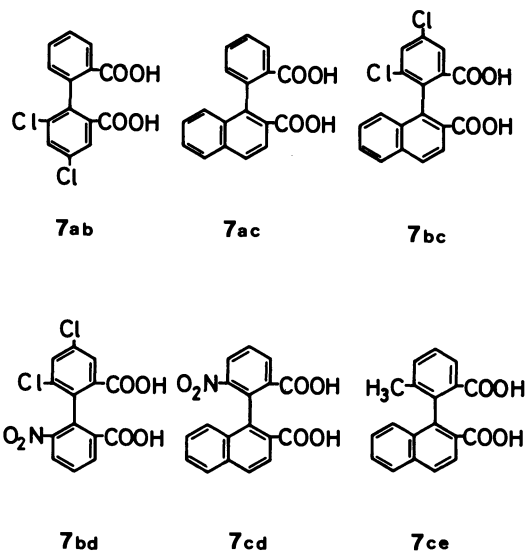

Steric bulk of the *o,o′*-substituents in biphenyl system is estimated by Adams to be in the order of $H<CH_3<Cl<NO_2$.[13] The inferior result of the reaction of **4Ace** should be ascribed to the electronic effects of the methyl substituent, as is known that electron-donating substituents disfavor the Ullmann coupling. The yield of the intramolecular coupling seems to be improved by the use of somewhat longer methylene chain, which will impose less steric constraints on the cycle (compare the reaction of **4Ace** with that of **4Bce** and **4Cce**). The advantage was offset by the reduced separability of **5Cce** from **6Cce** on silica-gel column; the enlargement of the bridging chain seemed to reduce the difference of the chromatographic behavior between the cycle **5** and the open chain diester **6**.

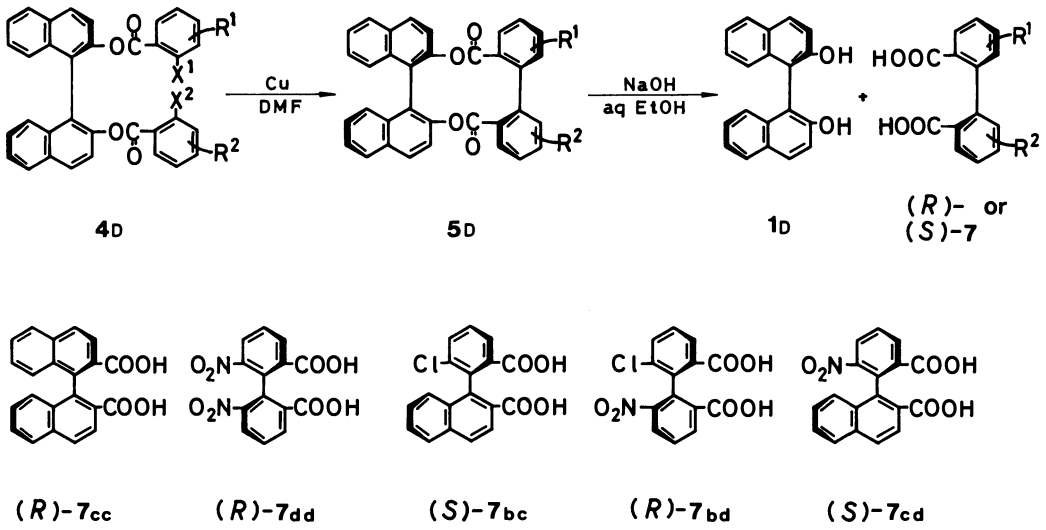

Scheme 2.

Asymmetric Synthesis of Axially Chiral, Unsymmetrical Diphenic Acids. We have reported virtually complete asymmetric synthesis of axially chiral, symmetrical diphenic acids ((*R*)-**7cc**[14] and (*R*)-**7dd**[10]) via the intramolecular Ullmann coupling of diesters (**4Dcc** and **4Ddd**, respectively) prepared from (*R*)-1,1′-bi-2-naphthol ((*R*)-binaphthol, **1D**) (Scheme 2). The remarkable stereoselectivity in the joining of two aryl rings has been explained on the basis of the steric requirements in assembling the 12-membered cyclic diester **5D** which contains two sets of biaryl skeletons connected each other by –COO– bridges on *o,o′*-positions.[15] This means that the sense of axial chirality of the one biaryl unit determines that of the other in such ring systems, which can be utilized for the determination of axial chirality of relevant biaryl skeletons.[16]

The high stereoselectivity and predictability of the axial chirality were utilized for the synthesis of axially chiral, unsymmetrical diphenic acids of known absolute configurations ((*S*)-**7bc**, (*R*)-**7bd**, and (*S*)-**7cd**) (Scheme 2 and Table 1). Enantiomeric purity of these acids (>99%) were readily confirmed by HPLC analyses carried out on chiral stationary phases prepared from axially chiral binaphthyl derivatives.[8] Further confirmation of the assignment of absolute configurations of these acids by use of ^{1}H NMR spectral studies will be presented elsewhere.

It is known that the Ullmann reaction is susceptible to the reaction conditions, especially the nature of the copper used and accidental moisture, which makes reproducibility difficult. Although we could not fully clarify at present the reason why the reaction of **4Dbd** gave exceptionally good results, we are inclined to say that it was not accidental considering the fact that duplicate runs in this work gave practically analogous results with the deviation range of around ±15%; the combination of two 2-halobenzoic acids as well as the choice of the linking bridge may play a significant role in the reaction.

Previous synthesis of unsymmetrical diphenic acids is only limited.[6] Meyers et al. reported the synthesis of 6-methoxydiphenic acid in high yield by the oxazoline route, which, however, needed somewhat troublesome transformation of the two carboxyl groups to oxazolines for protection and activation, and deprotection after aryl coupling to regenerate them.[17] Although the method disclosed herein needed chromatographic purification, it gave moderate to good yields in the key intramolecular coupling. The procedure is operationally rather simple, and seems to have synthetic utility, especially where the Meyers reaction can not be applied, or where axially chiral diphenic acids are needed.

Experimental

Measurements. IR spectra were measured on a Shimadzu IR-430 grating spectrophotometer. ^{1}H NMR spectra were recorded on a JEOL JNM-FX60 instrument using tetramethylsilane as internal standard and $CDCl_3$ as solvent. Optical rotations were recorded on a Union PM-101 automatic digital polarimeter in a 1-cm cell at 23—25 °C. HPLC was carried out on a JASCO TRIROTAR-III and/or a Shimadzu LC-5A, with UV detection at 254 nm. Melting points were uncorrected.

Materials. Analytical TLC was performed using Merck silica gel 60G or $60F_{254}$. Merck silica gel 60H was used for preparative TLC. Silica-gel columns were prepared by use of Wako Gel C-200, while alumina columns by Wako activated alumina (ca. 300 mesh). DMF was distilled from CaH_2 just prior to use under nitrogen. Solvents for experiments requiring anhydrous conditions were purified by the usual methods. Enantiomerically pure (*R*)-binaphthol was obtained as before;[14] $[\alpha]_D$+34.6 ° (*c* 0.905, THF). Copper powder (Junsei Chemical Co., 200 mesh) was

pretreated for activation before the Ullmann reaction.[14]

2-Halobenzoic Acids (2). **2a** was used as purchased. **2b** was prepared according to the literature;[18] mp 179—181 °C (lit,[18] 175—180 °C), IR(KBr) 1705 cm^{-1}. Preparation of **2c**,[19] **2d**,[10] and **2e**[20] were reported before. These acids were converted to acid chlorides **2'** by boiling in thionyl chloride for several hours. After the reaction, volatiles were removed in vacuo, and a small amount of benzene was added and distilled off in vacuo. The latter procedure was repeated two more times, and the remaining acid chlorides were used directly for esterification.

Monoesters 3A—3C of Glycols 1A—1C. The synthesis of 2-(3,5-dichloro-2-iodobenzoyloxy)ethanol (**3Ab**) is representative for the preparation of glycol monoesters. To a stirred mixture of ethylene glycol (**1A**) (30 ml), benzene (30 ml), and pyridine (10 ml) was added dropwise a solution of **2'b** (prepared from 4.50 g of **2b**, 14.2 mmol) in benzene (30 ml). The mixture was stirred overnight at ambient temperature, and then heated at reflux for 3 h. To the cool mixture were added 30 ml of benzene and 100 ml of 2 M† HCl, and phases were separated. Aqueous phase was extracted with portions of benzene. Combined organic phase was washed with 2 M HCl, 1M Na_2CO_3, and water, and then dried over Na_2SO_4. After volatiles were removed in vacuo, the residue was subjected to silica-gel column chromatography eluting with $CHCl_3$ to give 4.72 g of **3Ab** (92%); mp 85—86 °C; IR (KBr) 3250 (br) and 1720 cm^{-1}; ^1H NMR δ=1.9 (1H, s, OH), 3.8—4.2 (2H, m, $\underline{CH_2}$-OH), 4.2—4.6 (2H, m, COO-CH_2), and 7.2—7.9 (2H, m, Ar-H).

3Ac was obtained from **2c** in 87% yield using benzene as the eluent for silica-gel column chromatography; mp 74—76 °C; IR (KBr) 3500 (br) and 1710 cm^{-1}; ^1H NMR δ=2.2 (1H, s, OH), 3.7—4.1 (2H, m, $\underline{CH_2}$-OH), 4.3—4.6 (2H, m, COO-CH_2), and 7.3—8.6 (6H, m, Ar-H).

3Ae was obtained from **2e** as an oil in 82% yield, using chloroform as the eluent for silica-gel column chromatography; IR (liq. film) 3400 (br) and 1720 cm^{-1}; ^1H NMR δ=2.4 (4H, s, OH and CH_3), 3.6—3.9 (2H, m, $\underline{CH_2}$-OH), 4.4—4.7 (2H, m, COO-CH_2), and 7.1—7.6 (3H, m, Ar-H).

3Be was prepared from **2e** and 1,3-propanediol; 83% yield, benzene as the eluent; oil; IR (liq. film) 3400 (br) and 1720 cm^{-1}; ^1H NMR δ=2.0 (1H, s, OH), 2.0 (2H, tt, J_1=J_2=6.0 Hz, $CH_2\underline{CH_2}CH_2$), 2.4 (3H, s, CH_3), 3.77 (2H, t, J_1=6.0 Hz, $\underline{CH_2}$-OH), 4.46 (2H, t, J_2=6.0 Hz, $COOCH_2$), and 7.0—7.6 (3H, m, Ar-H).

3Ce was obtained from **2e** and 1,4-butanediol; 79% yield, benzene-ethyl acetate (3/1) as the eluent; oil; IR (liq. film) 3350 (br) and 1730 cm^{-1}; ^1H NMR δ=1.7 (1H, s, OH), 1.7—2.0 (4H, m, $CH_2(\underline{CH_2})_2CH_2$), 2.42 (3H, s, CH_3), 3.68 (2H, t, J_1=6.0 Hz, $\underline{CH_2}$-OH), 4.34 (2H, t, J_2=6.0 Hz), and 7.0—7.6 (3H, m, Ar-H).

Monoesters 3D of (*R*)-Binaphthol 1D. 3Db: **2b** (7.50 g, 23.7 mmol) was converted to **2'b**, which was treated with **1D** (5.75 g, 20.1 mmol) as above. The reaction mixture was chromatographed on alumina; after diester **4Dbb** had been eluted out with toluene (0.30 g, 1.7% based on **1D**), elution with toluene-ethanol (10/1) and crystallization from toluene gave **3Db**, 9.94 g (85% based on **1D**); mp 175—177 °C; $[\alpha]_D$ +86.8° (*c* 0.852, $CHCl_3$); IR (KBr) 3450 and 1730 cm^{-1}; ^1H NMR δ=5.0 (1H, s (br), OH) and 7.0—8.2 (14H, m, Ar-H). Found: C, 55.19; H, 2.61; halogen, 34.11%. Calcd for $C_{27}H_{15}Cl_2IO_3$: C, 55.42; H, 2.58; Cl+I, 33.80%.

3Dc was obtained from **2c** (3.60 g, 14.3 mmol) and **1D** (4.20 g, 14.7 mmol) as above; 6.03 g (81% based on **2c**); mp 192—193 °C (lit,[14] 179—180 °C); $[\alpha]_D$ +33.2° (*c* 0.918, acetone) (lit,[14] $[\alpha]$+ 34.1° (*c* 1.38, acetone)), $[\alpha]_D$ +140.9° (*c* 1.35, $CHCl_3$); IR (KBr) 3400 and 1730 cm^{-1}; ^1H NMR δ=5.4 (1H, s (br), OH) and 6.5—8.4 (18H, m, Ar-H). Found: C, 71.36; H, 3.96; Br, 15.11%. Calcd for $C_{31}H_{19}BrO_3$: C, 71.69; H, 3.69; Br, 15.38%.

Diesters 4. The synthesis of 1-(1-bromo-2-naphthoyloxy)-2-(3,5-dichloro-2-iodobenzoyloxy)ethane (**4Abc**) is representative. A mixture of **2'c** (prepared from 1.50 g (5.98 mmol) of **2c**) and **3Ab** (1.81 g, 5.01 mmol) in benzene (80 ml) and pyridine (10 ml) was stirred overnight at ambient temperature, and then heated at reflux for 3 h. The reaction was worked up as was stated for the synthesis of monoesters. Silica-gel column chromatography eluting with benzene gave 2.68 g of **4Abc** (90%); mp 105—106 °C; IR (KBr) 1720 cm^{-1}; ^1H NMR δ=4.6 (4H, s, $(CH_2)_2$) and 7.0—8.5 (8H, m, Ar-H). Found: C, 40.52; H, 2.38; halogen, 46.52%. Calcd for $C_{20}H_{12}BrCl_2IO_4$: C, 40.44; H, 2.04; Br+Cl+I, 46.75%.

Similar reactions gave the following diesters; silica-gel column was used for purification of the diester unless otherwise noted.

4Aab: 89% yield, toluene as the eluent; mp 52—54 °C; IR (KBr) 1730 and 1700 cm^{-1}; ^1H NMR δ=4.65 (4H, s, $(CH_2)_2$) and 6.9—8.2 (6H, m, Ar-H). Found: C, 32.88; H, 1.89; halogen, 54.72%. Calcd for $C_{16}H_{10}Cl_2I_2O_4$; C, 32.52; H, 1.71; Cl+I, 54.95%.

4Aac: 90% yield, benzene as the eluent; oil; IR (liq. film) 1720 cm^{-1}; ^1H NMR δ=4.65 (4H, s, $(CH_2)_2$) and 6.9—8.6 (10H, m, Ar-H). Found: C, 45.76; H, 3.08; halogen, 39.71%. Calcd for $C_{20}H_{14}BrIO_4$: C, 45.74; H, 2.69; Br+I, 39.38%.

4Abd: 83% yield, cyclohexane-ethyl acetate (20/1) as the eluent; mp 105—108 °C; IR (KBr) 1720 cm^{-1}, ^1H NMR δ=4.65 (4H, s, $(CH_2)_2$) and 7.0—7.8 (5H, m, Ar-H). Found: C, 30.83; H, 1.67; N, 2.20; halogen; 50.56%. Calcd for $C_{16}H_9Cl_2I_2NO_6$: C, 30.22; H, 1.43; N, 2.02; Cl+I, 51.06%. The discrepancy of the elemental analysis seemed to be caused by deiodination during the column chromatography as judged by coloring.

4Acd: 86% yield, benzene as the eluent; mp 110—112 °C; IR (KBr) 1720 cm^{-1}; ^1H NMR δ=4.65 (4H, s, $(CH_2)_2$) and 7.1—8.5 (9H, m, Ar-H). Found: C, 42.56; H, 2.46; N, 2.15; halogen, 36.66%. Calcd for $C_{20}H_{13}BrINO_6$: C, 42.13; H, 2.30; N, 2.46; Br+I, 36.27%.

4Ace: 90% yield, toluene-hexane (3/1) as the eluent; mp 72—73.5 °C; IR (KBr) 1720 cm^{-1}; ^1H NMR δ=2.4 (3H, s, CH_3), 4.6 (4H, s, $(CH_2)_2$), and 7.0—8.6 (9H, m, Ar-H). Found: C, 51.53; H, 3.36; Br, 32.31%. Calcd for $C_{21}H_{16}Br_2O_4$: C, 51.25; H, 3.28; Br, 32.47%.

4Bce: 87% yield, toluene as the eluent; oil; IR (liq. film) 1720 cm^{-1}; ^1H NMR δ=2.1—2.6 (2H, m, CH_2-$\underline{CH_2}$-CH_2), 2.40 (3H, s, CH_3), 4.4—4.7 (4H, m, O$\underline{CH_2}$-$CH_2\underline{CH_2}$O), and 7.0—8.6 (9H, m, Ar-H). Found: C, 52.03; H, 3.72; Br, 31.37%. Calcd for $C_{22}H_{18}Br_2O_4$: C, 52.20; H, 3.58; Br, 31.57%.

4Cce: 81% yield, benzene-hexane (4/1) as the eluent; mp 73—77 °C; IR (KBr) 1710 cm^{-1}; ^1H NMR δ=1.7—2.1 (4H, m, CH_2-$(\underline{CH_2})_2$-CH_2), 2.3 (3H, s, CH_3), 4.2—4.6 (4H, m, O$\underline{CH_2}$-$(CH_2)_2$-$\underline{CH_2}$O), and 7.0—8.6 (9H, m, Ar-H). Found:

† 1 M=1 mol dm^{-3}.

C, 53.34; H, 3.95; Br, 30.41%. Calcd for $C_{23}H_{20}Br_2O_4$: C, 53.10; H, 3.88; Br, 30.72%.

4Dbc: The monoester **3Dc** (2.50 g, 4.82 mmol) was treated with **2'b** (prepared from 1.90 g of **2b** (5.99 mmol)) in benzene–pyridine in the presence of 50 mg of 4-(dimethylamino)pyridine to give 2.68 g (68% yield) of **4Dbc**; toluene as the eluent on alumina column; mp 99—102 °C; IR (KBr) 1750 cm^{-1}; $[\alpha]_D$ +29.9° (*c* 0.735, $CHCl_3$). Found: C, 55.78; H, 2.38; halogen, 34.11%. Calcd for $C_{38}H_{20}BrCl_2IO_4$; C, 55.78; H, 2.46; Br+Cl+I, 33.94%.

4Dbd: 93% yield, toluene–hexane (3/1) as the eluent; mp 85-90 °C; IR (KBr) 1745 cm^{-1}; $[\alpha]_D$ +46.0 ° (*c* 0.891, $CHCl_3$). Found: C, 47.20; H, 2.08; N, 1.58; halogen, 37.94%. Calcd for $C_{34}H_{17}Cl_2I_2NO_6$:C, 47.47; H, 1.99; N, 1.63; Cl+I, 37.74%.

4Dcd: 86% yield, toluene as the eluent; mp 103—106 °C; IR (KBr) 1745 cm^{-1}; $[\alpha]_D$ +29.4 ° (*c* 0.782, $CHCl_3$). Found: C, 57.81; H, 2.45; N, 1.89; halogen, 25.67%. Calcd for $C_{38}H_{21}BrINO_6$: C, 57.46; H, 2.66; N, 1.76; Br+I, 26.03%.

Synthesis of Unsymmetrical Diphenic Acids 7. General procedure for the Ullmann reaction was the same as that described in the previous paper unless otherwise noted.[10] To a vigorously stirred suspension of the activated copper powder (40—100 mg-atom) in DMF (60 ml) heated at gentle reflux, was added a solution of **4** (2—5 mmol) in 40 ml of DMF over a 6-h period under a nitrogen atmosphere. After 2-h heating at reflux, the reaction was treated as before:[10] The reaction mixture was filtered, products were taken into benzene, worked up as usual, and solvents were removed in vacuo. Organic residue was chromatographed on silica-gel column with eluent depicted in Table 1 to isolate the intramolecularly coupled cycle **5**, which was obtained as the first eluting component. Alkaline hydrolysis of **5** (0.3—1.6 mmol) was performed by boiling with KOH (1—2 g) in ethanol(50 ml)–water(3 ml).

Synthesis of 7ab: The treatment of **4Aab** (3.02 g) with 6.5 g of copper powder gave, after usual workup, 1.60 g of organic residue, which was chromatographed on silica-gel column with toluene as the eluent to give 0.878 g of **5Aab** (R_f=0.41 on Merck 60G/toluene) and 50 mg of **6Aab** (R_f=0.31). **5Aab**; mp, 165—167 °C; ^1H NMR δ=3.8—4.3 (2H, m, CHH-CHH), 4.8—5.3 (2H, m, CHH-CHH), and 7.1—8.0 (6H, m, Ar-H). Found: C, 57.17; H, 3.22; Cl, 21.34%. Calcd for $C_{16}H_{10}Cl_2O_4$: C, 57.00; H, 2.99; Cl, 21.03%. **6Aab**: IR (KBr) 1720 cm^{-1}; ^1H NMR δ=4.6 (4H, s, $(CH_2)_2$) and 7.1—8.0 (8H, m, Ar-H).

After a sample of **5Aab** (0.50 g, 1.48 mmol) had been boiled with KOH (1 g) in aq ethanol for 4 h, the mixture was diluted with water, and most of the ethanol was removed under reduced pressure. The aqueous phase was extracted with ether, made acidic by adding concd HCl, and then extracted with ether. After the usual workup, evaporation of the solvent afforded **7ab** as white powder; 0.41 g, 89% yield; mp 204—205 °C; IR (KBr) 2900 (br), 1690, 1400, 1260, 1080, 1000, 800, and 700 cm^{-1}. Found: C, 53.91; H, 2.65; Cl, 23.03%. Calcd for $C_{14}H_8Cl_2O_4$: C, 54.05; H, 2.59; Cl, 22.79%.

Synthesis of 7ac: Treatment of 2.56 g of **4Aac** gave 0.667 g of **5Aac**; mp 58—59 °C; ^1H NMR δ=3.8—4.4 (2H, m, CHH-CHH), 4.8—5.4 (2H, m, CHH-CHH), and 7.1—8.2 (10H, m, Ar-H). Found: C, 75.31; H, 4.30%. Calcd for $C_{20}H_{14}O_4$: C, 75.46; H, 4.43%.

Hydrolysis of 0.50 g of **5Aac** gave 0.39 g of **7ac**; 85% yield; mp 228—230 °C; IR (KBr) 2900 (br), 1680, 1400, 1280, 1240, and 750 cm^{-1}. Found: C, 73.81; H, 4.20%. Calcd for $C_{18}H_{12}O_4$: C, 73.96; H, 4.14%.

Synthesis of 7bc: Treatment of 2.12 g of **4Abc** gave 0.843 g of **5Abc**; mp 60—61 °C; ^1H NMR δ=3.8—4.4 (2H, m, CHH-CHH), 4.9—5.3 (2H, m, CHH-CHH), and 7.1—8.1 (8H, m, Ar-H). Found: C, 61.66; H, 3.26; Cl, 17.98%. Calcd for $C_{20}H_{12}Cl_2O_4$: C, 62.04; H, 3.12; Cl, 18.31%.

Hydrolysis of 0.55 g of **5Abc** gave 0.46 g of **7bc**: 89% yield; mp 238—239 °C; IR (KBr) 2950 (br), 1690, 1280, 1250, 1080, 1010, and 790 cm^{-1}. Found: C, 59.57; H, 2.94; Cl, 19.34%. Calcd for $C_{18}H_{10}Cl_2O_4$: C, 59.86; H, 2.79; Cl, 19.63%.

Synthesis of 7bd: Treatment of 1.95 g of **4Abd** gave 0.661 g of **5Abd**; mp 172—173 °C; ^1H NMR δ=3.7—4.3 (2H, m, CHH-CHH), 4.7—5.4 (2H, m, CHH-CHH), and 7.0—8.3 (5H, m, Ar-H). Found: C, 50.58; H, 2.57; N, 3.45; Cl, 18.25%. Calcd for $C_{16}H_9Cl_2NO_6$: C, 50.29; H, 2.37; N, 3.67; Cl, 18.55%.

Hydrolysis of 0.50 g of **5Abd** gave 0.45 g of **7bd**; 96% yield; mp 276—277 °C; IR (KBr) 2900 (br), 1690, 1530, 1280, 1240, 820, and 690 cm^{-1}. Found: C, 47.63; H, 2.21; N, 3.65; Cl, 20.19%. Calcd for $C_{14}H_7Cl_2NO_6$: C, 47.22; H, 1.98; N, 3.93; Cl, 19.91%.

Synthesis of 7cd. Treatment of 2.15 g of **4Acd** gave 0.520 g of **5Acd**; 260—262 °C; ^1H NMR δ=3.8—4.4 (2H, m, CHH-CHH), 4.8—5.5 (2H, m, CHH-CHH), and 7.2—8.3 (9H, m, Ar-H). Found: C, 65.76; H, 3.66; N, 3.99%. Calcd for $C_{20}H_{13}NO_6$: C, 66.12; H, 3.61; N, 3.86%.

Hydrolysis of 0.35 g of **5Acd** gave 0.31 g of **7cd**: 95% yield, mp 249—250 °C; IR (KBr), 2950 (br), 1690, 1530, 1350, 1280, 1070, and 790 cm^{-1}. Found: C, 63.76; H, 3.63; N, 3.91%. Calcd for $C_{18}H_{11}NO_6$: C, 64.10; H, 3.29; N, 4.15%.

Synthesis of 7ce: Treatment of 1.10 g of **4Ace** gave 0.212 g of **5Ace**; mp, 196—199 °C; ^1H NMR δ=1.92 (3H, s, CH_3), 3.8—4.4 (2H, m, CHH-CHH), 4.7—5.4 (2H, m, CHH-CHH), and 7.1—8.0 (9H, m, Ar-H). Found: C, 76.10; H, 4.94%. Calcd for $C_{21}H_{16}O_4$: C, 75.89; H, 4.85%.

Hydrolysis of 0.15 g of **5Ace** gave 0.12 g of **7ce**; 87% yield; mp 211—215 °C; IR (KBr) 3000 (br), 1690, 1400, 1290, 1250, and 760 cm^{-1}. Found: C, 74.42; H, 4.81%. Calcd for $C_{19}H_{14}O_4$: C, 74.50; H, 4.61%.

From 2.60 g of **4Bce** was obtained 0.55 g of **5Bce**; mp, 180—182.5 °C; ^1H NMR δ=1.9 (3H, s, CH_3), 1.8—2.4 (2H, m, $CH_2CH_2CH_2$), 3.7—5.0 (4H, m, $OCH_2CH_2CH_2O$), and 7.2—8.0 (9H, m, Ar-H). Found: C, 76.53; H, 5.26%. Calcd for $C_{22}H_{18}O_4$: C, 76.29; H, 5.24%.

From 1.73 g of **4Cce** was obtained 0.59 g of **5Cce**; mp, 165—168.5 °C; ^1H NMR δ=1.6—2.0 (4H, m, $CH_2(CH_2)_2CH_2O$), 1.9 (3H, s, CH_3), 3.8—4.6 (4H, m, $OCH_2(CH_2)_2CH_2O$), and 7.1—8.0 (9H, m, Ar-H). Found: C, 76.23; H, 5.81%. Calcd for $C_{23}H_{20}O_4$: C, 76.65; H, 5.59%.

Synthesis of (*R*)-7bd: Treatment of 1.65 g of **4Dbd** gave 0.93 g of **5Dbd**; mp 195—198 °C; $[\alpha]_D$ +151.3 ° (*c* 0.840, $CHCl_3$). Found: C, 67.46; H, 2.81; N, 2.02; Cl, 11.95%. Calcd for $C_{34}H_{17}Cl_2NO_6$: C, 67.34; H, 2.83; N, 2.31; Cl, 11.69%.

A portion of the **5Dbd** (0.53 g, 0.875 mmol) was treated with KOH in aq ethanol as above. The reaction mixture was diluted with 50 ml of water, and most of ethanol was removed in vacuo. The residue was extracted with ether, and the aqueous phase was made acidic with concd HCl, followed by extraction with diethyl ether. Ether extracts were combined, and then extracted with 2 M sodium hydrogencarbonate solution, leaving binaphthol in ether

phase. The diphenic acid and binaphthol were recovered by the usual procedure. Recovered (*R*)-binaphthol (0.22 g, 88%) showed no sigh of racemization as judged by its optical rotation; $[\alpha]_D$ +35.0° (*c* 0.813, THF).

(*R*)-**7bd:** 0.28 g (90% yield); mp 237—238°C; $[\alpha]_D$ +35.0° (*c* 0.485, 95% EtOH); IR (KBr) 3000 (br), 1700, 1530, 1350, 1280, 1240, 820, and 790 cm^{-1}. Found: C, 47.63; H, 2.21; N, 3.65; Cl, 20.19%. The enantiomeric purity of the acid (>99% ee) was confirmed by HPLC analysis by comparing the corresponding racemic acid; the details of the experiment have been reported.[8]

Diphenic acids were converted to *N,N'*-dibutyldiphenamides for HPLC analysis as follows: A mixture of a diphenic acid (5—10 mg) in 0.5 ml of thionyl chloride in a screw-capped bottle was stirred under sonication for 1.5 h at 60 °C. Excess thionyl chloride was removed in vacuo, and then 0.5 ml of butylamine was added. After the mixture had been stirred for 1 h at ambient temperature, excess amine was removed in vacuo. The residue was purified by preparative TLC (ethyl acetate-hexane (2/1)).

Synthesis of (*S*)-7bc: Treatment of 1.55 g of **4Dbc** gave 0.38 g of **5Dbc**; mp 205—208 °C; $[\alpha]_D$+272° (*c* 2.22, $CHCl_3$). Found: C, 75.01; H, 2.94; Cl, 11.35%. Calcd for $C_{38}H_{20}Cl_2O_4$: C, 74.64; H, 3.30; Cl, 11.60%.

Hydrolysis of 0.20 g of **5Dbc** gave 0.11 g of (*S*)-**7bc**; 93% yield; mp 238—239 °C; $[\alpha]_D$ −1.3° (*c* 1.57, THF), −18.6° (*c* 1.02, $CHCl_3$); IR (KBr) 2900 (br), 1700, 1440, 1400, 1270, 1230, 790, and 760 cm^{-1}. Found: C, 59.41; H, 2.73; Cl, 19.26%.

Synthesis of (*S*)-7cd: Treatment of 1.45 g of **4Dcd** gave 0.47 g of **5Dcd**; mp 324—326 °C; $[\alpha]_D$ +201° (*c* 0.762, $CHCl_3$). Found: 78.04; H, 4.01; N,2.26%. Calcd for $C_{38}H_{21}NO_6$: C, 77.68; H, 3.60; N, 2.38%.

Hydrolysis of 0.25 g of **5Dcd** gave 0.13 g of (*S*)-**7cd**; 91% yield; mp 210—212 °C; $[\alpha]_D$ +42.0° (*c* 1.95, THF), +30.4° (*c* 0.520, 95% EtOH); IR (KBr) 2900 (br), 1690, 1530, 1345, 1300, 1070, 1010, 790, 770, and 750 cm^{-1}. Found: C, 64.10, H, 3.19; N, 4.09%.

This work was partly supported by a Grant-in-Aid for Scientific Research No. 62550539 from the Ministry of Education, Science and Culture.

References

1) Previous paper in this series of investigation: S. Miyano, S. Handa, M. Tobita, and H. Hashimoto, *Bull. Chem. Soc. Jpn.*, **59**, 235 (1986).

2) Review: M. Sainsbury, *Tetrahedron*, **36**, 3327 (1980).

3) K. Tamao, K. Sumitani, Y. Kiso, M. Zembayashi, A. Fujioka, S. Kodama, I. Nakajima, A. Minato, and M. Kumada, *Bull. Chem. Soc. Jpn.*, **49**, 1958 (1976).

4) M. Reuman and A. I. Meyers, *Tetrahedron*, **41**, 837 (1985).

5) For example, G. P. Stahly, *J. Org. Chem.* **50**, 3091 (1985); R. B. Miller and S. Dugar, *Organometallics*, **3**, 1261 (1984).

6) Review: P. E. Fanta, *Synthesis*, **1974**, 9.

7) Cf., For example, J. Cornforth, A. F. Sierakowski, and T. W. Wallace, *J. Chem. Soc., Chem. Commun.*, **1979**, 294; F. Effenberger, W. Agster, P. Fischer, K. H. Jogun, J. J. Stezowski, E. Daltrozzo, and G. K. Nell, *J. Org. Chem.*, **48**, 4649 (1983).

8) J. Yamashita, T. Numakura, H. Kita, T. Suzuki, S. Ōi, S. Miyano, H. Hashimoto, and N. Takai, *J. Chromatogr.*, **403**, 275 (1987).

9) M. S. Newman and J. A. Cella, *J. Org. Chem.*, **39**, 2084 (1974).

10) S. Miyano, S. Handa, K. Shimizu, K. Tagami, and H. Hashimoto, *Bull. Chem. Soc. Jpn.*, **57**, 1943 (1984).

11) Abbreviations for respective compounds imply that first digit stands for the type of compound, the second capital letter for the linking group, and the last two letters for the aromatic nuclei.

12) Cf., G. van Koten, J. W. Marsman, G. A. K. Breedijk, and A. L. Speck, *J. Chem. Soc., Perkin Trans. 2*, **1977**, 1942.

13) R. Adams, *Rec. Chem. Prog.*, **1949**, 91; M. Charton, *J. Org. Chem.*, **42**, 2528 (1977).

14) S. Miyano, M. Tobita, and H. Hashimoto, *Bull. Chem. Soc. Jpn.*, **54**, 3522 (1981).

15) S. Miyano, K. Shimizu, S. Sato, and H. Hashimoto, *Bull. Chem. Soc. Jpn.*, **58**, 1345 (1985).

16) For example, K. Yamamoto, H. Yumioka, Y. Okamoto, and H. Chikamatsu, *J. Chem. Soc., Chem. Commun.*, **1987**, 168; K. Yamamoto, K. Noda, and Y. Okamoto, *J. Chem. Soc., Chem. Commun.*, **1985**, 1065.

17) A. I. Meyers, R. Gabel, and E. D. Mihelich, *J. Org. Chem.*, **43**, 1372 (1978).

18) V. Valenta, A. Dlabać, and M. Protiva, *Collection Czech. Chem. Commun.*, **46**, 781 (1981).

19) S. Miyano, H. Inagawa, S. Handa, and H. Hashimoto, *Chem. Ind., (London)*, **1985**, 236.

20) S. Miyano, H. Fukushima, H. Inagawa, and H. Hashimoto, *Bull. Chem. Soc. Jpn.*, **59**, 3285 (1986).

 © 1988 The Chemical Society of Japan Bull. Chem. Soc. Jpn., 61, 3255—3264 (1988)

Regio- and Stereoselective Ring Opening of ω-Alkenyllactones Using Organocopper Reagents[1)]

Masatoshi KAWASHIMA, Toshio SATO, and Tamotsu FUJISAWA*
Chemistry Department of Resources, Mie University, Tsu, Mie 514
(Received April 2, 1988)

New synthetic methods are described for the preparation of (*E*)-3-, (*E*)-4-, and (*E*)-5-alkenoic acids by the regio- and stereoselective ring opening of β, γ, and δ-lactones with unsaturated substituents at the ω-position using organocopper reagents such as halomagnesium diorganocuprates or Grignard reagents in the presence of copper(I) iodide. Both the organocopper reagents with primary, secondary, tertiary alkyl, and phenyl groups gave the corresponding carbon homologated alkenoic acids in good yields. Alkadienoic acids were also obtained in good yields by the reactions of ω-alkenyllactones with divinyl- and diallylcuprates. Utilizing the ring opening of β-isopropenyl-β-propiolactone, homoterpenoid carboxylic acids were easily obtained in good yields. The ring opening of β-(1-chlorovinyl)-β-propiolactone afforded 4-chloro-3-alkenoic acids which were easily transformed to 4-oxoalkanoic acids and 4-oxo-2-alkenoic acids.

Nucleophilic displacement reactions of allylic compounds have received considerable attention[2)] because of their synthetic and mechanistic importance on the regio- and stereochemistry. Recently their attentions have been poured into the applications of organometallic reagents to selective carbon homologation with newly formed carbon–carbon double bond. Among organometallic reagents, organocopper reagents have been most widely used for the substitution reactions and applied to the synthesis of various kinds of alkenes. The regio- and stereoselective synthesis of alkenes is very important but not so easy since the selectivity is affected by many factors such as the structure of substrate, the nature of organocopper reagent, solvent, temperature and so on.[3,4)] On the other hand, there were many reports on the synthetic methods of alkenoic acids which are useful building blocks for the synthesis of natural products. The representative methods such as Ramberg-Bäcklund rearrangement of ω-halo-ω-(alkylsulfonyl)alkanoic acids,[5)] Knoevenagel condensation of malonic acid with aldehyde,[6)] and the reduction of the alkynoic acid[7)] are capable for disubstituted alkenes, but not for trisubstituted alkenes such as terpenoid carboxylic acid. Moreover, there is no sufficient method, to our knowledge, in all of aspects of stereoselectivity of carbon–carbon double bond, the product yield, the applicability, and the convenience of the synthetic procedure.

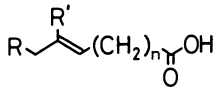

1

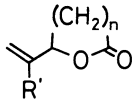

2

Previously the synthetic methods of 3-substituted propanoic acids by the reactions of β-propiolactones with organocopper reagents were reported.[8)] The high regioselectivity of the ring opening of the lactone was achieved by the attack of organocopper reagents, considered as "soft base", to the "soft" β-carbon atom of the lactone rather than the attack to the "hard" carbonyl carbon atom.[9)] Therefore, if β-propiolactone possesses a vinyl group at β-carbon, it is expected that the "softer" organocopper reagent attacks the "softer" terminal vinyl carbon of the lactone in the S_N2' manner to afford 4-substituted 3-alkenoic acid. Moreover, this concept seems to be capable for the new synthetic method of alkenoic acid **1** by the ring opening of ω-alkenyllactones **2** using organocopper reagents. Actually ring opening of γ- and δ-lactones possessing ω-unsaturated substituent with organocopper reagents have been reported.[10)] The present paper shows the detail on the regio- and stereoselective ring opening of ω-alkenyllactones such as β-vinyl-β-propiolactone, β-isopropenyl-β-propiolactone, β-(1-chlorovinyl)-β-propiolactone, γ-vinyl-γ-butyrolactone, and δ-vinyl-δ-valerolactone with organocopper reagents to afford various kinds of alkenoic acids.

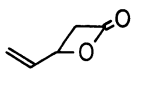

3

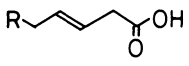

4

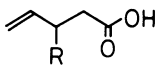

5

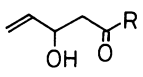

6

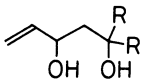

7

When β-vinyl-β-propiolactone (**3**), prepared by the cycloaddition of acrylaldehyde with ketene,[11)] was treated with butylmagnesium bromide in the presence of copper(I) iodide (2 mol%) in THF at −30 °C, two kinds of carboxylic acids, 3-nonenoic acid (**4b**) and 3-butyl-4-pentenoic acid (**5b**), formed by both S_N2' and S_N2 reactions respectively, were obtained in 91% yield

Table 1. Reactions of β-Vinyl-β-propiolactone with Butylmetallic Compounds

BuM	Solvent	Temp/°C	Time/min	Yield[a]/%	Product ratio[b]				
					4	((E)-:(Z)-)	5	6	7
BuMgBr	THF	−30	15	36	28	(81:19)	3	47	22
BuCu·PBu$_3$	Et$_2$O	−30	15	79	48	(56:44)	52	0	0
BuCu·BF$_3$	THF	−30	15	66	95	(85:15)	5	0	0
BuCu·SMe$_2$	THF-Me$_2$S[c]	−30	15	85	96	(84:16)	4	0	0
Bu$_2$CuLi	THF	−30	15	82	95	(83:17)	5	0	0
BuMgBr, 2 mol% CuI	THF-Me$_2$S[c]	0	15	94	87	(74:26)	13	0	0
BuMgBr, 2 mol% CuI	THF-Me$_2$S[c]	−30	15	96	98	(84:16)	2	0	0
BuMgBr, 2 mol% CuI	THF	−30	15	91	98	(83:17)	2	0	0
BuMgBr, 2 mol% CuI	Et$_2$O	−30	15	68	80	(83:17)	20	0	0
BuMgBr, 2 mol% CuI	THF-Me$_2$S[c]	−78	15	96	99	(87:13)	1	0	0
BuMgBr, 2 mol% CuI	THF-Me$_2$S[c]	−100	15	94	>99	(90:10)	<1	0	0

a) Isolated yield. b) Determined by GLC analysis. c) For the case of butylcopper-dimethyl sulfide and copper-catalyzed butyl Grignard reagent, the ratio of THF to Me$_2$S was 5:1 and 20:1, respectively.

without accompanying the products **6** and **7** by the attack to the carbonyl carbon. GLC analysis of the acids showed the ratio of **4b** to **5b** as 98:2, indicating that the reaction regioselectively proceeds through S_N2' pathway. Butyl Grignard reagent and other butylcopper reagents were used in this ring opening of the lactone **3**. It should be noted that the reaction of the lactone **3** with butylmagnesium bromide in the absence of copper catalyst in THF at −30 °C gave only 11% of **4b** along with **6** and **7**. Although three kinds of monoorganocopper complexes with tributylphosphine, trifluoroborane,[12] and dimethyl sulfide gave only carboxylic acids **4** and **5** in high yields, the ratio of the S_N2' product to the S_N2 product was somewhat inferior to that of the reaction of Grignard reagents in the presence of copper(I) iodide. Even lithium diorganocuprate which is commonly used in the allylic substitutions did not reveal the selectivity as high as copper-catalyzed Grignard reagent. Therefore optimum conditions were examined in the reaction of the lactone **3** with Grignard reagent in the presence of copper(I) iodide. The solvent and temperature effects on both the regioselectivity and the stereochemistry of the newly formed double bond of **4b** were examined. When homogeneous reaction was carried out by adding dimethyl sulfide as a co-solvent of THF to dissolve the copper catalyst, the yield of the acids increased from 91% to 96% with the same ratio of **4b** to **5b** (98:2). Ether, instead of THF, was employed as a solvent to result in decreasing both the yield (68%) and regioselectivity (**4b**:**5b**=80:20). High regio- and stereoselectivity by the S_N2' reaction was exhibited at a lower temperature. When the reaction was carried out at −100 °C, **4b** was obtained in a high yield of 94% along with only a trace amount of **5b** and the ratio of the *E*- to *Z*-isomer of **4b** was 90:10. These results are shown in Table 1. Since it was reported that the active species in copper-catalyzed Grignard reaction were halomagnesium cuprates,[3,13] the reaction of the lactone **3** with dibutylcuprate, prepared from one equivalent of copper(I) iodide and two equivalents of butylmagnesium bromide, was examined. Expectedly the reaction proceeded regio- and stereoselectively to afford the acid **4b** in a yield of 92% (E:Z=89:11) along with a small amount of **5b**. The reactions of several representative Grignard reagents in the presence of copper catalyst and diorganocuprates with the lactone **3** were examined. Both of the reactions of diorganocuprates and of Grignard reagents in the presence of a catalytic amount of copper(I) iodide proceeded with similar selectivity to afford the corresponding 3-alkenoic acids **4a—g** in similar good yields, when the organic groups of organocopper reagents are primary, secondary, and tertiary alkyl ones. In contrast to the poor result of the copper-catalyzed reaction of allylmagnesium bromide, the reaction using diallylcuprate proceeded with higher regio- and stereoselectivity to give the corresponding dienoic acid. The result was not improved in the case of divinylcuprate. These results are summarized in Table 2.

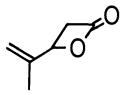

8

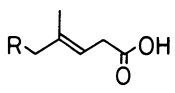

9

Synthesis of 4-methyl-5-substituted 3-pentenoic acids **9** was performed by using regio- and stereoselective ring opening of β-isopropenyl-β-propiolactone (**8**) prepared by the cycloaddition of methacrylaldehyde with ketene.[11b] Grignard reagents with primary, secondary, and tertiary alkyl groups, and with phenyl group furnished the acids **9a—e** in good yields, respectively. Although copper-catalyzed Grignard reagents with vinyl and allyl groups gave the acids **9f** and **9g** in poor yields, the use of divinyl- and diallylcuprate increased the yield of **9f** and **9g** in similar to the case of the lactone **3**. On the stereochemistry of the products, the ratio of *E*-isomer to *Z*-isomer was ranging from 82:18 to 66:34.

Table 2. Reactions of β-Alkenyl-β-propiolactone with Organocopper Reagents[a]

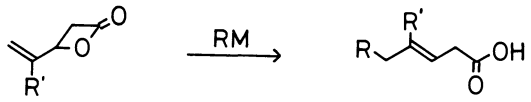

RM	R'=H **3**				
	Temp/°C	Time/min	Yield/%	(**4**:**5**)	(*E*)-:(*Z*)-**4**
MeMgBr, cat. CuI[b]	−100	15	**4a**, **5a** 70	(97: 3)	92: 8
Me_2CuMgX[c]	−78	60	**4a**, **5a** 70	(98: 2)	91: 9
BuMgBr, cat. CuI[b]	−100	15	**4b**, **5b** 94	(>99:<1)	90:10
Bu_2CuMgX[c]	−78	60	**4b**, **5b** 92	(99: 1)	89:11
s-BuMgCl, cat. CuI[b]	−100	15	**4c**, **5c** 96	(>99:<1)	88:12
s-Bu_2CuMgX[c]	−78	60	**4c**, **5c** 72	(>99:<1)	79:21
t-BuMgCl, cat. CuI[b]	−78	50	**4d** 84	—	86:14
t-Bu_2CuMgX[c]	−78	60	**4d**, **5d** 79	(>99:<1)	78:22
PhMgBr, cat. CuI[b]	−100	15	**4e**, **5e** 91	(91: 9)	83:17
Ph_2CuMgX[c]	−78	60	**4e**, **5e** 72	(89: 11)	91: 9
CH_2=CHMgBr, cat. CuI[b]	−78	30	**4f**, **5f** 61	(92: 8)	78:22
$(CH_2=CH)_2CuMgX$[c]	−50	60	**4f**, **5f** 64	(87: 13)	82:18
$CH_2=CHCH_2MgBr$, cat. CuI[b]	−50	120	**4g**, **5g** 25	(87: 13)	77:23
$(CH_2=CHCH_2)_2CuMgX$[c]	−50	60	**4g**, **5g** 88	(98: 2)	89:11

RM	R'=Me **8**			
	Temp/°C	Time/min	Yield/%	(*E*):(*Z*)
MeMgBr, cat. CuI[b]	−78	60	**9a** 80	66:34
Me_2CuMgX[c]	−78	60	**9a** 89	73:27
BuMgBr, cat. CuI[b]	−78	60	**9b** 92	73:27
Bu_2CuMgX[c]	−78	60	**9b** 83	82:18
s-BuMgCl, cat. CuI[b]	−78	60	**9c** 91	76:24
s-Bu_2CuMgX[c]	−78	60	**9c** 93	71:29
t-BuMgCl, cat. CuI[b]	−78	60	**9d** 88	72:28
t-Bu_2CuMgX[c]	−78	60	**9d** 98	66:34
PhMgBr, cat. CuI[b]	−78	60	**9e** 84	72:28
Ph_2CuMgX[c]	−78	60	**9e** 96	72:28
CH_2=CHMgBr, cat. CuI[b]	−78	60	**9f** 48	74:26
$(CH_2=CH)_2CuMgX$[c]	−78	60	**9f** 88	69:31
$CH_2=CHCH_2MgBr$, cat. CuI[b]	−78	60	**9g** 20	68:32
$(CH_2=CHCH_2)_2CuMgX$[c]	−78	60	**9g** 77	76:24

RM	R'=Cl **10**			
	Temp/°C	Time/min	Yield/%	(*Z*):(*E*)
MeMgBr, cat. CuI[b]	−78	50	**11a** 80	93: 7
Me_2CuMgX[c]	−50	50	**11a** 80	90:10
BuMgBr, cat. CuI[b]	−78	50	**11b** 81	89:11
Bu_2CuMgX[c]	−50	50	**11b** 85	89:11
s-BuMgCl, cat. CuI[b]	−78	50	**11c** 89	85:15
s-Bu_2CuMgX[c]	−50	50	**11c** 91	86:14
t-BuMgCl, cat. CuI[b]	−78	50	**11d** 91	80:20
t-Bu_2CuMgX[c]	−50	50	**11d** 80	86:14
PhMgBr, cat. CuI[b]	−78	50	**11e** 76	83:17
Ph_2CuMgX[c]	−50	50	**11e** 92	84:16
CH_2=CHMgBr, cat. CuI[b]	−78	50	**11f** 51	95: 5
$(CH_2=CH)_2CuMgX$[c]	−50	50	**11f** 71	91: 9
$CH_2=CHCH_2MgBr$, cat. CuI[b]	−78	50	**11g** 25	92: 8
$(CH_2=CHCH_2)_2CuMgX$[c]	−50	50	**11g** 77	91: 9

a) All products were isolated and the isomer ratios were determined by GLC analysis. b) Reactions were performed in THF-Me_2S (20:1). In the ring opening of **3** and **8**, 2 mol% of CuI was used. In the ring opening of **10**, 4 mol% of CuI was used. c) Reactions were performed in THF-Me_2S (10:1).

Compared with the ring opening of the vinyllactone **3**, the reaction of the isopropenyllactone **8** was found to give exclusively regioselective products by S_N2' reaction without any products through S_N2 pathway, but the stereoselectivity of newly formed carbon–carbon double bond somewhat decreased. These results are also summarized in Table 2.

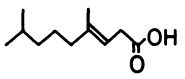

9h

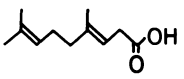

9i

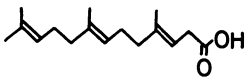

9j

Ring opening of the lactone **8** was applied to the synthesis of homoterpenoid carboxylic acids which were useful for the synthesis of terpenoid natural products.[14] 4,8-Dimethyl-3-nonenoic acid (**9h**) was obtained in 85% yield by the reaction of the lactone **8** with isopentylmagnesium bromide in the presence of copper(I) iodide (2 mol%). Homogeranic acid (**9i**) and homofarnesylic acid (**9j**) were obtained by the reaction of the lactone **8** with halomagnesium diprenylcuprate and digeranylcuprate in 89% and 68% yields, respectively. The isomer ratios of (*E*) to (*Z*) of newly formed carbon–carbon double bond of these acids **9h—j** were ca. 75:25.

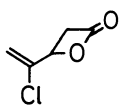

10

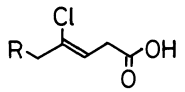

11

The synthesis of 4-chloro-3-alkenoic acid **11** was tried by the ring opening of β-(1-chlorovinyl)-β-propiolactone (**10**) prepared by the cycloaddition of α-chloroacrylaldehyde with ketene.[11b] When the lactone **10** was treated with various kinds of Grignard reagents in the presence of 4 mol% of copper(I) iodide, in THF–Me_2S at −78 °C, only S_N2' products, **11a—g** were formed in high yields. As the substituents of Grignard reagents, not only primary, secondary, and tertiary alkyl groups, but also phenyl and vinyl groups could be used to give good results. Diphenyl-, divinyl-, and diallylcuprates gave the corresponding acids **11e—g** in much higher yields than the corresponding Grignard reagents in the presence of copper(I) iodide. Stereochemistry of the newly formed carbon–carbon double bond of **11a—g** was determined to be predominant *Z* configuration in all cases, by comparing the NMR spectra with those of *E*- and *Z*-isomers of ethyl 4-chloro-3-pentenoate[15] and by capillary GLC analysis. Although the major isomer of obtained acid is named as *Z*-isomer in nomenclature, the relative configuration of the carbon–carbon double bond is same as that of (*E*)-3-alkenoic acid obtained by the ring opening reaction of the lactone **3**. These results are summarized also in Table 2.

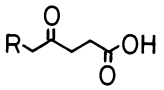

12

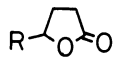

13

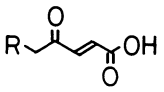

14

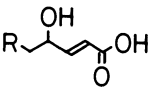

15

The utility of the acids **11** was demonstrated by the transformation to 4-oxoalkanoic acids **12** which are well-known as important precursors for γ-substituted γ-butyrolactones (**13**) as natural products.[16] According to the reported method of the hydrolysis of vinyl chloride to ketones,[17] treatment of **11b** with $TiCl_4$, MeOH, H_2O, and acetone in CH_2Cl_2 gave 4-oxononanoic acid (**12b**) in 82% accompanied with 8% yield of methyl 4-oxononanoate. The other acids **11** were also hydrolyzed to the corresponding keto acids **12** in good yields except for the cases of chlorodienoic acids such as **11f** and **11g**, which gave complex mixture. Moreover the transformation of **11** to 4-oxo-2-alkenoic acid **14**, which is incorporated in the macrolide antibiotics[18] such as A26771B, pyrenophorin, and vermiculine, was also achieved by the convenient method as follows. Hydrolysis of **11b** with refluxing 2 M NaOH (1 M=1 mol dm^{-3}) afforded 4-hydroxy-2-nonenoic acid (**15b**). Without any purification, **15b** was converted to 4-oxo-2-nonenoic acid (**14b**) by the Jones oxidation in a yield of 61% from **11b**. In this transformation, all of the other acids **11** were transformed to the corresponding keto alkenoic acids **14** in moderate yields. These results were summarized in Table 3.

γ-Butyrolactone and δ-valerolactone do not react with diorganocuprate and these lactones have been used for the synthesis of keto alcohol by the addition of alkyllithium to the carbonyl carbon of the lactones.[19] Nevertheless the ring opening of γ-vinyl-γ-butyrolactone and δ-vinyl-δ-valerolactone using organocopper reagents proceeded in S_N2' reaction leading to 4- and 5-alkenoic acids in a similar way to the case of four-membered lactones. Several papers concerning the reactions of the related γ-lactones

Table 3. Transformation of **11** to 4-Oxoalkanoic Acids (**12**) and 4-Oxo-2-alkenoic Acids (**14**)

R	Product yield/%	
	12[a,b]	**14**[c]
Me	**12a** 66 (10)	**14a** 44
Bu	**12b** 82 (8)	**14b** 61
s-Bu	**12c** 77 (17)	**14c** 52
t-Bu	**12d** 71 (23)	**14d** 37
Ph	**12e** 71 (12)	**14e** 62
CH_2=CH	**12f** 0	**14f** 16
CH_2=$CHCH_2$	**12g** trace	**14g** 47

a) All reactions were performed at room temperature for 64 h. b) The values in parentheses indicate the yields of methyl ester of **12**. c) Hydrolysis of **11** to **15** was carried out with refluxing 2 M NaOH for 20 min and the following Jones oxidation of **15** was carried out at 0 °C for 10 min. The yields were calculated from **11**.

possessing γ-unsaturated substituent with organocopper reagents have been reported.[20]

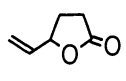

16

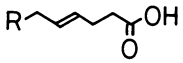

17

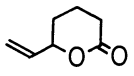

18

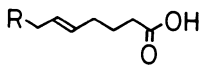

19

When γ-vinyl-γ-butyrolactone (**16**)[21] was treated with butylmagnesium bromide in THF–Me_2S in the presence of copper(I) iodide (2 mol%) at −30 °C, 4-decenoic acid (**17b**) was predominantly produced by

Table 4. Reactions of ω-Vinyllactones **16** and **18** with Organocopper Reagents[a]

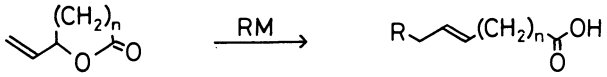

RM	*n*=2 **16**			
	Temp/°C	Time/min	Yield/%	(*E*):(*Z*)
MeMgBr, cat. CuI[b]	−30	60	**17a** 87	92: 8
Me_2CuMgX[c]	−30	60	**17a** 87	88:12
BuMgBr, cat. CuI[b]	−30	60	**17b** 93	86:14
Bu_2CuMgX[c]	−30	60	**17b** 88	85:15
s-BuMgCl, cat. CuI[b]	−30	60	**17c** 90	83:17
s-Bu_2CuMgX[c]	−30	60	**17c** 90	78:22
t-BuMgCl, cat. CuI[b]	−30	60	**17d** 91	78:22
t-Bu_2CuMgX[c]	−30	60	**17d** 91	79:21
PhMgBr, cat. CuI[b]	−30	60	**17e** 75	62:38
Ph_2CuMgX[c]	−30, 30 →	rt, 30	**17e** 91	82:18
CH_2=CHMgBr, cat. CuI[b]	−30	60	**17f** 59	57:43
$(CH_2$=$CH)_2CuMgX$[c]	−30, 30 →	rt, 30	**17f** 70	82:18
CH_2=$CHCH_2$MgBr, cat. CuI[b]	−30	60	**17g** 9	92: 8
$(CH_2$=$CHCH_2)_2CuMgX$[c]	−30, 30 →	rt, 30	**17g** 41	86:14

RM	*n*=3 **18**			
	Temp/°C	Time/min	Yield/%	(*E*):(*Z*)
MeMgBr, cat. CuI[b]	−45	60	**19a** 70	93: 7
Me_2CuMgX[c]	−45	60	**19a** 99	91: 9
BuMgBr, cat. CuI[b]	−45	60	**19b** 95	88:12
Bu_2CuMgX[c]	−45	60	**19b** 95	79:21
s-BuMgCl, cat. CuI[b]	−45	60	**19c** 94	83:17
s-Bu_2CuMgX[c]	−45	60	**19c** 89	72:28
t-BuMgCl, cat. CuI[b]	−45	60	**19d** 78	75:25
t-Bu_2CuMgX[c]	−45	60	**19d** 99	75:25
PhMgBr, cat. CuI[b]	−45	60	**19e** 56	67:33
Ph_2CuMgX[c]	−30	60	**19e** 57	71:29
CH_2=CHMgBr, cat. CuI[b]	−45	60	**19f** 28	67:33
$(CH_2$=$CH)_2CuMgX$[c]	−30	60	**19f** 67	78:22
CH_2=$CHCH_2$MgBr, cat. CuI[b]	−45	60	**19g** trace	—
$(CH_2$=$CHCH_2)_2CuMgX$[c]	−50	60	**19g** 51	92: 8

a) All products were isolated and the isomer ratios were determined by GLC analysis. b) Reactions were performed in THF–Me_2S (20:1). In the ring opening of **16** and **18**, 2 and 3 mol% of CuI were used, respectively. c) Reactions were performed in THF–Me_2S (10:1).

the S_N2' reaction. GLC analysis of the acid **17b** showed the predominance of the *E*-isomer (*E*:*Z*= 86:14). Both of copper-catalyzed Grignard reagents with primary, secondary, and tertiary alkyl groups and the corresponding dialkylcuprates attacked regioselectively the terminal vinyl carbon of the lactone to afford (*E*)-4-alkenoic acids **17a—d** in high yields. Diphenyl-, divinyl-, and diallylcuprates gave the acids **17e—g** in higher yields than the corresponding copper-catalyzed Grignard reagents. These results are summarized in Table 4.

δ-Vinyl-δ-valerolactone (**18**)[22] was also found to react regio- and stereoselectively with organocopper reagents as shown also in Table 4. In a similar way to the case of the reaction of vinylbutyrolactone **16**, (*E*)-5-alkenoic acids **19a—d** as the S_N2' products were predominantly obtained in the reaction of the lactone **18** with alkyl Grignard reagents in the presence of copper(I) iodide and with dialkylcuprates. The use of divinyl- and diallylcuprate resulted in increasing the yields and the geometrical purity of the dienoic acids **19f,g**.

In the synthetic methods of alkenoic acids described above, the cyclic structure of the lactones **3**, **8**, **10**, **16**, and **18** as the starting materials seems to be essential for high regio- and stereoselectivity as confirmed by the following control experiment. When methyl 5-acetoxy-6-heptenoate (**20**) was treated with butylmagnesium bromide in the presence of copper(I) iodide (3 mol%) in THF–Me_2S (20:1) at −45 °C for 1 h, methyl (*E*)- and (*Z*)-5-undecenoates (**21**) (S_N2' products) and methyl 5-vinylnonanoates (**22**) (S_N2 product) were obtained in 98% yield in the ratio of 52:40:8, while the reaction of the corresponding lactone **18** gave only S_N2' product with (*E*):(*Z*) ratio of 88:12. Anderson et al. reported that S_N2':S_N2 and (*E*)-S_N2':(*Z*)-S_N2' ratios of the substitution products of allylic esters were enhanced with leaving groups of lower acidity of the conjugate acid.[23] In also the above example, the acidity of the conjugate acids of ω-alkenyllactones is lower than that of methyl 5-acetoxy-6-heptenoate. Therefore the ring opening of three kinds of β-vinyllactones **3**, **16**, and **18** seemed to indicate almost similar selectivity regardless the number of the ring construction atoms, since it is thought that there is no large difference among the acidity of the conjugate acids of three kinds of β-vinyllactones **3**, **16**, and **18**.

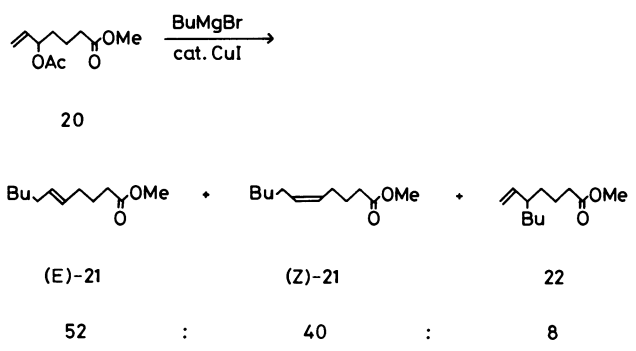

The above description defines a new convenient synthetic method of (*E*)-3-, (*E*)-4-, and (*E*)-5-alkenoic acids by the reactions of β-, γ-, and δ-lactones possessing ω-alkenyl group with organocopper reagents. Advantages of these C_5—C_7 carbon homologation methods are specified as follows: (1) starting materials are easily accessible, (2) the reaction procedure is simple, (3) the introduction of various kinds of organic groups to the alkenoic acid is possible because of the easy availability of Grignard reagent, (4) carboxyl group and carbon–carbon double bond are easily transformed to other functional groups. Synthetic utilities of these methods were represented in previous communications on the synthesis of natural products.[1b-d,24]

Experimental

General. Boiling points were measured at the pressure indicated and are uncorrected. Infrared spectra were recorded on a Hitachi EPI-G2 spectrometer. ^1H NMR spectra were recorded on a Varian A-60 spectrometer and on a Jeol JNM-PMX60SI spectrometer and are reported in parts per million (δ) from TMS. Samples were dissolved in CCl_4 containing TMS as an internal standard. GLC analysis were performed on a Yanaco G-180 Gas Chromatograph using a 0.25 mm×50 m FFAP column. Preparative thin-layer chromatography (TLC) was performed on 20×20 cm glass plates coated with 1.5 mm of silica gel (Wakogel B-5F). Distillation of reaction products was performed on a Kugelrohr apparatus.

All reactions were run under a positive pressure of dry argon. Reactions requiring anhydrous conditions were performed in a flame-dried glassware that was cooled under argon. Anhydrous solvents were transferred by an oven-dried syringe. Solvents were distilled before use: diethyl ether from lithium aluminium hydride; tetrahydrofuran (THF) from sodium benzophenone ketyl. Dimethyl sulfide (Me_2S) was used without purification. Grignard reagents and butyllithium were standardized by titration with 2-butanol using 1,10-phenanthroline as an indicator.[25] Copper(I) iodide was purified by a known method.[26] All ω-alkenyllactones were prepared by published procedures.[11,21,22]

Procedure for the Reaction of Butylmagnesium Bromide in the Presence of 2 mol% CuI with β-Vinyl-β-propiolactone (3). In a typical experiment a flask equipped with a magnetic stirring bar and a septum was charged 9.3 mg (0.04 mmol) of CuI. After flushing with dry argon, 6 ml of anhydrous THF and 0.5 ml of Me_2S were added and the solution was chilled to −100 °C. A THF solution (2 ml) of 200 mg (2.00 mmol) of **3** was added to the flask. After stirring the mixture for 10 min, a solution of 2.40 mmol of BuMgBr in 2 ml of THF was added over 5 min. The reaction mixture was stirred for 15 min at −100 °C and then quenched with 2 ml of 3 M HCl and extracted with ether. The separated organic layer was extracted with three 5 ml

portions of 3 M NaOH. The alkaline solution was acidified with 3 ml of 6 M HCl, and then extracted with ether. The ethereal extracts were washed with brine and dried ($MgSO_4$). Removal of the solvent followed by vacuum distillation gave 295 mg (94%) of clear oil. Regio- and stereoisomer ratios were determined by GLC analyses of the corresponding methyl ester using a FFAP 50 m column. Regioisomers were separated by TLC (hexane:AcOEt:AcOH=60:20:1).

The same procedure was used for the copper-catalyzed reactions of Grignard reagents with ω-alkenyllactones shown in Tables 2 and 4.

Procedure for the Reaction of Dibutylcuprate with the Lactone 3. In a typical experiment a flask equipped with a magnetic stirring bar and a septum was charged 420 mg (2.20 mmol) of CuI. After flushing with dry argon, 4 ml of anhydrous THF and 1 ml of Me_2S were added and the solution was chilled to −30 °C. A solution of 4.40 mmol of BuMgBr in 4 ml of THF was added. After stirring for 30 min at −30 °C, the mixture was chilled to −78 °C and a THF solution (2 ml) of 200 mg (2.00 mmol) of **3** was added to the flask. The reaction mixture was stirred for 60 min at −78 °C, worked up, purified, and analyzed as the case of copper-catalyzed reaction. The same procedure was used for the reactions of diorganocuprates with ω-alkenyllactones shown in Tables 2 and 4.

3-Hexenoic Acid (4a).[27] Bp 80 °C (bath temp)/1.5 mmHg (1 mmHg=133.322 Pa).

3-Nonenoic Acid (4b):[28] Bp 130 °C (bath temp)/1.5 mmHg; IR (neat) 1710 (s) and 965 (s) cm^{-1}; ^1H NMR δ=0.90 (t, J=6.5 Hz, 3 H), 1.07—1.80 (m, 6H), 1.80—2.30 (m, 2H), 2.83—3.17 (m, 2H), 5.33—5.68 (m, 2H), 10.84 (s, 1H).

3-Butyl-4-pentenoic Acid (5b). R_f=0.3 (Hexane:AcOEt:AcOH=60:20:1); IR (neat) 1710 (s), 995 (s), and 920 (s) cm^{-1}; ^1H NMR δ=0.87 (t, J=6.5 Hz, 3H), 1.05—1.52 (m, 6H), 2.13—2.76 (m, 3H), 4.69—5.84 (m, 3H), 10.83 (s, 1H); Anal. ($C_9H_{16}O_2$) C, H.

6-Methyl-3-octenoic Acid (4c). Bp 130 °C (bath temp)/1.5 mmHg; IR (neat) 1715 (s) and 970 (s) cm^{-1}; ^1H NMR δ=0.86 (d, J=6.5 Hz, 3H), 0.88 (t, J=6.5 Hz, 3H), 1.08—1.77 (m, 3H), 1.77—2.25 (m, 2H), 2.90—3.24 (m, 2H), 5.28—5.68 (m, 2H), 10.93 (s, 1H); Anal. ($C_9H_{16}O_2$) C, H.

6,6-Dimethyl-3-heptenoic Acid (4d). Bp 130 °C (bath temp)/1.5 mmHg; IR (neat) 1715 (s) and 970 (s) cm^{-1}; ^1H NMR δ=0.90 (s, 9H), 2.04—2.16 (m, 2H), 2.95—3.22 (m, 2H), 5.27—5.68 (m, 2H), 10.81 (s, 1H); Anal. ($C_9H_{16}O_2$) C, H.

5-Phenyl-3-pentenoic Acid (4e). Bp 200 °C (bath temp)/1.5 mmHg; IR (neat) 1710 (s), 965 (s), 740 (s), and 700 (s) cm^{-1}; ^1H NMR δ=2.85—3.15 (m, 2H), 3.15—3.50 (m, 2H), 5.44—5.70 (m, 2H), 7.08 (s, 5H), 11.30 (s, 1H); Anal. ($C_{11}H_{12}O_2$) C, H.

3,6-Heptadienoic Acid (4f). Bp 110 °C (bath temp)/1.5 mmHg; IR (neat) 1710 (s), 990 (s), 965 (s), and 910 (s) cm^{-1}; ^1H NMR δ=2.58—2.93 (m, 2H), 2.93—3.20 (m, 2H), 4.78—6.25 (m, 5H), 11.56 (s, 1H); Anal. ($C_7H_{10}O_2$) C, H.

3,7-Octadienoic Acid (4g). Bp 120 °C (bath temp)/1.5 mmHg; IR (neat) 1710 (s), 990 (s), 965 (s), and 915 (s) cm^{-1}; ^1H NMR δ=1.97—2.33 (m, 4H), 2.87—3.23 (m, 2H), 4.75—6.41 (m, 5H), 10.68 (s, 1H); Anal. ($C_8H_{12}O_2$) C, H.

4-Methyl-3-hexenoic Acid (9a). Bp 110 °C (bath temp)/1.5 mmHg; IR (neat) 1710 (s) and 835 (w) cm^{-1}; ^1H NMR δ=1.00 (t, J=7 Hz, 3H), 1.63 (s, 1.8H), 1.72 (s, 1.2H), 2.03 (q, J=7 Hz, 2H), 3.00 (d, J=7 Hz,, 2H), 5.22 (t, J=7 Hz, 1H), 10.87 (s, 1H).

4-Methyl-3-nonenoic Acid (9b). Bp 150 °C (bath temp)/1.5 mmHg; IR (neat) 1710 (s) and 830 (w) cm^{-1}; ^1H NMR δ=0.90 (t, J=6 Hz, 3H), 1.17—1.67 (m, 6H), 1.71 (s, 2.1H), 1.80 (s, 0.9H), 1.88—2.33 (m, 2H), 3.06 (d, J=7 Hz, 2H), 5.23 (t, J=7 Hz, 1H), 10.43 (s, 1H); Anal. ($C_{10}H_{18}O_2$) C, H.

4,6-Dimethyl-3-octenoic Acid (9c). Bp 150 °C (bath temp)/1.5 mmHg; IR (neat) 1710 (s) and 840 (w) cm^{-1}; ^1H NMR δ=0.85 (t, J=6 Hz, 3H), 0.90 (d, J=6 Hz, 3H), 1.14—1.55 (m, 3H), 1.60 (s, 2.1H), 1.69 (s, 0.9H), 1.79—2.09 (m, 2H), 3.00 (d, J=7 Hz, 2H), 5.27 (t, J=7 Hz, 1H), 10.90 (s, 1H); Anal. ($C_{10}H_{18}O_2$) C, H.

4,6,6-Trimethyl-3-heptenoic Acid (9d). Bp 150 °C (bath temp)/1.5 mmHg; IR (neat) 1710 (s) and 840 (w) cm^{-1}; ^1H NMR δ=0.90 (s, 6.3H), 0.93 (s, 2.7H), 1.67 (s, 2.1H), 1.76 (s, 0.9H), 1.94 (s, 2H), 3.00 (d, J=7 Hz, 2H), 5.23 (t, J=7 Hz, 0.7H), 5.42 (t, J=7 Hz, 0.3H), 11.30 (s, 1H); Anal. ($C_{10}H_{18}O_2$) C, H.

4-Methyl-5-phenyl-3-pentenoic Acid (9e). Bp 200 °C (bath temp)/1.5 mmHg; IR (neat) 1710 (s), 845 (w), 735 (s), and 700 (s) cm^{-1}; ^1H NMR δ=1.53 (s, 2.1H), 1.62 (s, 0.9H), 3.03 (d, J=7 Hz, 2H), 3.23 (s, 2H), 5.37 (t, J=7 Hz, 1H), 7.09 (s, 5H), 11.53 (s, 1H); Anal. ($C_{12}H_{14}O_2$) C, H.

4-Methyl-3,6-heptadienoic Acid (9f). Bp 120 °C (bath temp)/1.5 mmHg; IR (neat) 1710 (s), 990 (m), 910 (s), and 830 (w) cm^{-1}; ^1H NMR δ=1.60 (s, 2.1H), 1.69 (s, 0.9H), 2.82 (d, J=7 Hz, 2H), 3.14 (d, J=7 Hz, 2H), 4.77—6.27 (m, 4H), 11.42 (s, 1H); Anal. ($C_8H_{12}O_2$) C, H.

4-Methyl-3,7-octadienoic Acid (9g). Bp 130 °C (bath temp)/1.5 mmHg; IR (neat) 1710 (s), 990 (m), 910 (s), and 830 (w) cm^{-1}; ^1H NMR δ=1.70 (s, 2.1H), 1.79 (s, 0.9H), 2.20 (br s, 4H), 3.10 (d, J=7 Hz, 2H), 4.77—6.25 (m, 4H), 10.81 (s, 1H); Anal. ($C_9H_{14}O_2$) C, H.

4,8-Dimethyl-3-nonenoic Acid (9h).[28] R_f=0.6 (CH_2Cl_2:AcOEt:AcOH=200:20:1); IR (neat) 1710 (s) and 830 (w) cm^{-1}; ^1H NMR δ=0.87 (d, J=5.5 Hz, 6H), 1.11—1.55 (m, 4H), 1.63—1.86 (m, 3H), 3.03 (d, J=7 Hz, 2H), 5.35 (t, J=7 Hz, 1H); 11.21 (s, 1H).

4,8-Dimethyl-3,7-nonadienoic Acid (9i).[30] R_f=0.6 (CH_2Cl_2:AcOEt:AcOH=200:20:1)

4,8,12-Trimethyl-3,7,11-tridecatrienoic Acid (9j).[14b] R_f=0.4 (CH_2Cl_2:AcOEt:AcOH=200:20:1); ^1H NMR δ=1.60 (br s,3H), 1.67 (br s, 9H), 2.05 (br s, 8H), 3.00 (d, J=7 Hz, 2H), 4.65—5.30 (m, 3H), 10.85 (s, 1H).

4-Chloro-3-hexenoic Acid (11a). Bp 130 °C (bath temp)/1.5 mmHg; IR (neat) 1710 (s) and 820 (m) cm^{-1}; ^1H NMR δ=1.13 (t, J=7 Hz, 3H), 2.40 (q, J=7 Hz, 2H), 3.09 (d, J=6.5 Hz, 0.2H), 3.25 (d, J=6.5 Hz, 1.8H), 5.64 (t, J=6.5 Hz, 1H), 11.13 (s, 1H); Anal. ($C_6H_9ClO_2$) C, H.

4-Chloro-3-nonenoic Acid (11b). Bp 170 °C (bath temp)/1.5 mmHg; IR (neat) 1715 (s) 850 (m), and 810 (m) cm^{-1}; ^1H NMR δ=0.91 (t, J=6 Hz, 3H), 1.07—2.00 (m, 6H), 2.00—2.67 (m, 2H), 3.08 (d, J=7 Hz, 0.2 H), 3.24 (d, J=6.5 Hz, 1.8H), 5.62 (t, J=6.5 Hz, 0.9H), 5.69 (t, J=7 Hz, 0.1H), 11.22 (s, 1H); Anal. ($C_9H_{15}ClO_2$) C, H.

4-Chloro-6-methyl-3-octenoic Acid (11c). Bp 170 °C (bath temp)/1.5 mmHg; IR (neat) 1715 (s), 830 (m), and 800 (m) cm^{-1}; ^1H NMR δ=0.93 (t, J=6 Hz, 3H), 0.98 (d, J=6 Hz, 3H), 1.05—2.00 (m, 3H), 2.00—2.65 (m, 2H), 3.06 (d, J=7 Hz, 0.2H), 3.22 (d, J=6.5 Hz, 1.8H), 5.61 (t, J=6.5 Hz, 0.9H), 5.69 (t, J=7 Hz, 0.1H), 11.49 (s, 1H); Anal. ($C_9H_{15}ClO_2$) C, H.

4-Chloro-6,6-dimethyl-3-heptenoic Acid (11d). Bp 150 °C

(bath temp)/1.5 mmHg; IR (neat) 1715 (s) and 820 (m) cm^{-1}; ^1H NMR δ=0.98 (s, 9H), 2.27 (s, 2H), 3.07 (d, J=7 Hz, 0.2H), 3.26 (d, J=6.5 Hz, 1.8H), 5.57 (t, J=6.5 Hz, 0.9H), 5.85 (t, J=7 Hz, 0.1H), 11.32 (s, 1H); Anal. ($C_9H_{15}ClO_2$) C, H.

4-Chloro-5-phenyl-3-pentenoic Acid (11e). Bp 230 °C (bath temp)/1.5 mmHg; IR (neat) 1715 (s), 825 (m), 790 (m), 740 (s), and 700 (s) cm^{-1}; ^1H NMR δ=3.13 (d, J=7 Hz, 0.4H), 3.23 (d, J=6.5 Hz, 1.6H), 3.57 (s, 2H), 5.67 (t, J=6.5 Hz, 0.8H), 5.84 (t, J=7 Hz, 0.2H), 7.16 (s, 5H), 11.45 (s, 1H); Anal. ($C_{11}H_{11}COl_2$) C, H.

4-Chloro-3,6-heptadienoic Acid (11f). Bp 140 °C (bath temp)/1.5 mmHg; IR (neat) 1710 (s), 990 (s), and 810 (m) cm^{-1}; ^1H NMR δ=3.08 (d, J=6.5 Hz, 2H), 3.24 (d, J=6.5 Hz, 2H), 4.60—6.23 (m, 5H), 11.41 (s, 1H); Anal. ($C_7H_9ClO_2$) C, H.

4-Chloro-3,7-octadienoic Acid (11g). Bp 150 °C (bath temp)/1.5 mmHg; IR (neat) 1710 (s), 990 (s), and 845 (m) cm^{-1}; ^1H NMR δ=2.40 (s, 4H), 3.08 (d, J=7 Hz, 0.2H), 3.26 (d, J=6.5 Hz, 1.8H), 4.77—6.12 (m, 4H), 11.41 (s, 1H); Anal. ($C_8H_{11}ClO_2$) C, H.

4-Heptenoic Acid (17a).[7] Bp 110 °C (bath temp)/1.5 mmHg; IR (neat) 1715 (s) and 970 (s) cm^{-1}; ^1H NMR δ=0.94 (t, J=7 Hz, 3H), 1.68—2.17 (m, 2H), 2.17—2.45 (m, 4H), 5.40—5.74 (m, 2H), 11.01 (s, 1H).

4-Decenoic Acid (17b).[31] Bp 150 °C (bath temp)/1.5 mmHg.

7-Methyl-4-nonenoic Acid (17c). Bp 150 °C (bath temp)/1.5 mmHg; IR (neat) 1715 (s) and 970 (s) cm^{-1}; ^1H NMR δ=0.86 (t, J=6 Hz, 3H), 0.91 (d, J=6 Hz, 3H), 1.01—1.70 (m, 3H), 1.70—2.17 (m, 2H), 2.20—2.53 (m, 4H), 5.25—5.59 (m, 2H), 11.62 (s, 1H); Anal. ($C_{10}H_{18}O_2$) C, H.

7,7-Dimethyl-4-octenoic Acid (17d). Bp 150 °C (bath temp)/1.5 mmHg; IR (neat) 1715 (s) and 970 (s) cm^{-1}; ^1H NMR δ=0.84 (s, 9H), 1.73—2.05 (m, 2H), 2.23—2.43 (m, 4H), 5.26—5.52 (m, 2H), 11.53 (s, 1H); Anal. ($C_{10}H_{18}O_2$) C, H.

6-Phenyl-4-hexenoic Acid (17e).[32] Bp 200 °C (bath temp)/1.5 mmHg; IR (neat) 1715 (s), 970 (s), 740 (s), and 700 (s) cm^{-1}; ^1H NMR δ=2.20—2.50 (m, 4H), 3.04—3.43 (m, 2H), 5.23—5.59 (m, 2H), 7.02 (s, 5H), 11.49 (s, 1H).

4,7-Octadienoic Acid (17f). Bp 120 °C (bath temp)/1.5 mmHg; IR (neat) 1715 (s) 990 (s), 970 (s), and 915 (s) cm^{-1}; ^1H NMR δ=2.16—2.58 (m, 4H), 2.58—3.08 (m, 2H), 4.82—6.17 (m, 5H), 11.06 (s, 1H); Anal. ($C_8H_{12}O_2$) C, H.

4,8-Nonadienoic Acid (17g).[33] Bp 130 °C (bath temp)/1.5 mmHg.

5-Octenoic Acid (19a).[5b] Bp 120 °C (bath temp)/1.5 mmHg; IR (neat) 1715 (s) and 970 (s) cm^{-1}; ^1H NMR δ=0.96 (t, J=7 Hz, 3H), 1.42—2.50 (m, 8H), 5.20—5.50 (m, 2H), 10.21 (s, 1H).

5-Undecenoic Acid (19b).[34] Bp 170 °C (bath temp)/1.5 mmHg.

8-Methyl-5-decenoic Acid (19c). Bp 170 °C (bath temp)/1.5 mmHg; IR (neat) 1715 (s) and 970 (s) cm^{-1}; ^1H NMR δ=0.85 (t, J=6 Hz, 3H), 0.90 (d, J=6 Hz, 3H), 1.01—2.54 (m, 11H), 5.30—5.48 (m, 2H), 11.71 (s, 1H); Anal. ($C_{11}H_{20}O_2$) C, H.

8,8-Dimethyl-5-nonenoic Acid (19d). Bp 170 °C (bath temp)/1.5 mmHg; IR (neat) 1715 (s) and 970 (s) cm^{-1}; ^1H NMR δ=0.89 (s, 9H), 1.45—2.54 (m, 8H), 5.30—5.63 (m, 2H), 11.39 (s, 1H); Anal. ($C_{11}H_{20}O_2$) C, H.

7-Phenyl-5-heptenoic Acid (19e). Bp 220 °C (bath temp)/1.5 mmHg; IR (neat) 1715 (s), 970 (s), 740 (s), and 700 (s) cm^{-1}; ^1H NMR δ=1.45—2.57 (m, 6H), 3.12—3.41 (m, 2H), 5.21—5.64 (m, 2H), 7.08 (s, 5H), 9.97 (s, 1H); Anal. ($C_{13}H_{16}O_2$) C, H.

5,8-Nonadienoic Acid (19f). Bp 130 °C (bath temp)/1.5 mmHg; IR (neat) 1715 (s), 990 (s), 970 (s), and 915 (s) cm^{-1}; ^1H NMR δ=1.47—2.57 (m, 6H), 2.57—2.94 (m, 2H), 4.72—6.14 (m, 5H), 11.56 (s, 1H); Anal. ($C_9H_{14}O_2$) C, H.

5,9-Decadienoic Acid (19g). Bp 140 °C (bath temp)/1.5 mmHg; IR (neat) 1715 (s), 990 (s), 970 (s), and 910 (s) cm^{-1}; ^1H NMR δ=1.45—2.57 (m, 10H), 4.75—6.40 (m, 5H), 11.53 (s, 1H); Anal. ($C_{10}H_{16}O_2$) C, H.

Procedure for the Transformation of 4-Chloro-3-alkenoic Acids (11) to 4-Oxoalkanoic Acids (12). According to the reported method,[17] to a solution of $TiCl_4$ 1.95 g (10.3 mmol), MeOH 68.7 mg (2.14 mmol), H_2O 80.6 mg (4.47 mmol), and acetone 354 mg (6.09 mmol) in CH_2Cl_2 (4 ml), a solution of **11b** 385 mg (2.02 mmol) in 2 ml of CH_2Cl_2 was added at room temperature. The mixture was stirred at the same temperature for 64 h. Then the reaction was quenched by pouring into ice-water, and the organic layer was separated. The aqueous phase was washed twice with CH_2Cl_2 and the combined organic layers were washed with water and brine, dried with $MgSO_4$, and concentrated. The crude product was purified by preparative TLC (CH_2Cl_2:AcOH=20:1) to give 4-oxononanoic acid (**12b**) 285 mg (1.66 mmol) (82%) and methyl 4-oxononanoate 30.1 mg (0.162 mmol) (8%).

In the exactly same manner as above, the other 4-oxoalkanoic acids were obtained.

4-Oxohexanoic Acid (12a).[16] Mp 37—40 °C.

4-Oxononanoic Acid (12b).[16] Mp 68—70 °C.

4-Methyl-4-oxooctanoic Acid (12c).[35] IR (neat) 1740 (s), 1720 (s), and 1710 (s) cm^{-1}; ^1H NMR δ=0.86 (d, J=2.5 Hz, 3H), 0.92 (br s, 3H), 1.08—1.58 (m, 2H), 1.58—2.14 (m, 1H), 2.14—2.48 (m, 2H), 2.63 (br s, 4H), 11.10 (s, 1H).

6,6-Dimethyl-4-oxoheptanoic Acid (12d). IR (neat) 1735 (s), 1720 (s), and 1710 (s) cm^{-1}; ^1H NMR δ=1.00 (s, 9H), 2.32 (s, 2H), 2.40—2.92 (m, 4H), 13.17 (br s, 1H); Anal. ($C_9H_{16}O_3$) C, H.

4-Oxo-5-phenylpentanoic Acid (12e).[36] Mp 53—55 °C; IR (neat) 1720 (s), 1700 (s), 740 (m), and 700 (m) cm^{-1}; ^1H NMR δ=2.55 (br s, 4H), 3.58 (s, 2H), 7.15 (s, 5H), 10.68 (s, 1H).

Procedure for the Transformation of 11 to 4-Oxo-2-alkenoic Acid (14). A solution of **11b** 502 mg (2.63 mmol) in 13 ml of 2 M NaOH was refluxed with stirring for 20 min. After the mixture was cooled to room temperature and acidified with concd HCl, the mixture was extracted twice with ether. The extracts were washed with water and brine, dried with $MgSO_4$, and concentrated to give viscous oil. The crude 4-hydroxy-2-nonenoic acid was used for the following oxidation without any purification. To a solution of the hydroxy acid in acetone (5 ml) was added a solution of CrO_3 263 mg (2.63 mmol) in concd H_2SO_4 (0.3 ml) and water (1.0 ml) at 0 °C. After the mixture was stirred at the same temperature for 10 min, the products were extracted with ether. The extracts were washed with water and brine, dried with $MgSO_4$, and concentrated. Purification of the residue by preparative TLC (CH_2Cl_2:AcOH=20:1) gave 4-oxo-2-nonenoic acid (**14b**) 272 mg (1.60 mmol) (61%).

In the exactly same manner as above, the other 4-oxo-2-

alkenoic acids were obtained.

4-Oxo-2-hexenoic Acid (14a).[37] Mp 110—112 °C; IR (KBr) 1720 (s), 1690 (s), and 1670 (s) cm^{-1}; ^1H NMR δ=1.13 (t, J=7 Hz, 3H), 2.72 (q, J=7 Hz, 2H), 6.82 (AB, H_A=6.60, H_B=7.05, J=16 Hz, 2H), 11.55 (s, 1H).

4-Oxo-2-nonenoic Acid (14b). Mp 115—117 °C; IR (KBr) 1720 (s), 1680 (s), and 1660 (s) cm^{-1}; ^1H NMR δ=0.90 (t, J=5 Hz, 3H), 1.12—1.97 (m, 6H), 2.65 (t, J=6 Hz, 2H), 6.90 (AB, J=16 Hz, 2H), 11.62 (br s, 1H); Anal. ($C_9H_{14}O_3$) C, H.

6-Methyl-4-oxo-2-octenoic Acid (14c). Mp 78—80 °C; IR (KBr) 1710 (s), 1680 (s), and 1660 (s) cm^{-1}; ^1H NMR δ=0.87 (br s, 3H), 0.97 (br s, 3H), 1.13—1.63 (m, 2H), 1.63—2.30 (m, 1H), 2.30—2.88 (m, 2H), 6.87 (AB, J=16 Hz, 2H), 11.52 (br s, 1H); Anal. ($C_9H_{14}O_3$) C, H.

6,6-Dimethyl-4-oxo-2-heptenoic Acid (14d). Mp 91—93 °C; IR (KBr) 1710 (s), 1685 (s), and 1670 (s) cm^{-1}; ^1H NMR δ=1.06 (s, 9H), 2.55 (s, 2H), 6.88 (AB, H_A=6.60, H_B=7.17, J=16 Hz, 2H), 10.71 (br s, 1H); Anal. ($C_9H_{14}O_3$) C, H.

4-Oxo-5-phenyl-2-pentenoic Acid (14e). Mp 95—97 °C; IR (KBr) 1705 (s), 1680 (s), 1675 (s), 735 (m), and 695 (m) cm^{-1}; ^1H NMR δ=3.87 (s, 2H), 6.88 (AB, J=16 Hz, 2H), 11.03 (br s, 1H); Anal. ($C_{11}H_{10}O_3$) C, H.

4-Oxo-2,6-heptadienoic Acid (14f). Mp 80—82 °C; IR (neat) 1720 (s), 1685 (s), 1665 (s), 1000 (s), and 915 (s) cm^{-1}; ^1H NMR δ=3.40 (d, J=7 Hz, 2H), 4.93—6.30 (m, 3H), 6.88 (AB, J=16 Hz, 2H), 10.88 (br s, 1H); Anal. ($C_7H_8O_3$) C, H.

4-Oxo-2,7-octadienoic Acid (14g). Mp 100—102 °C; IR (neat) 1710 (s), 1685 (s), 1665 (s), 1005 (s), and 910 (s) cm^{-1}; ^1H NMR δ=2.43 (t, J=5.5 Hz, 2H), 2.63—3.03 (m, 2H), 4.80—6.23 (m, 3H), 6.85 (AB, J=16 Hz, 2H), 11.56 (s, 1H); Anal. ($C_8H_{10}O_3$) C, H.

We thank Messrs. Masashi Takeuchi, Toshiyuki Itoh, Masakuni Nakagawa, Kouichi Naruse, and Kouichi Tamai for their invaluable assistance in the experimental work. The present work was partially supported by a Grant-in-Aid for Scientific Research from the Ministry of Education, Science and Culture.

References

1) For preliminary reports on aspects of the present study, see: a) T. Sato, M. Takeuchi, T. Itoh, M. Kawashima, and T. Fujisawa, *Tetrahedron Lett.*, **22**, 1817 (1981); b) T. Fujisawa, T. Sato, M. Kawashima, and M. Nakagawa, *Chem. Lett.*, **1981**, 1307; c) T. Fujisawa, T. Sato, M. Kawashima, K. Naruse, and K. Tamai, *Tetrahedron Lett.*, **23**, 3583 (1982); d) M. Kawashima and T. Fujisawa, *Chem. Lett.*, **1984**, 1851; e) T. Fujisawa, T. Sato, and M. Takeuchi, *ibid.*, **1982**, 71.

2) R. M. Magid, *Tetrahedron*, **36**, 1901 (1980).

3) J. E. Bäckvall and M. Sellen, *J. Chem. Soc., Chem. Commun.*, **1987**, 827.

4) R. J. Anderson, C. A. Henrick, and J. B. Siddall, *J. Am. Chem. Soc.*, **92**, 735 (1970).

5) a) D. Scholz and P. Burtscher, *Justus Liebigs Ann. Chem.*, **1985**, 517; b) D. Scholz, *ibid.*, **1984**, 264.

6) S. E. Boxer and R. P. Linstead, *J. Chem. Soc.*, **1931**, 740.

7) M. F. Ansell, J. C. Emmett, and R. V. Coombs, *J. Chem. Soc. C*, **1968**, 217.

8) T. Fujisawa, T. Sato, T. Kawara, M. Kawashima, H. Shimizu, and Y. Ito, *Tetrahedron Lett.*, **21**, 2181 (1980); T. Sato, T. Kawara, M. Kawashima, and T. Fujisawa, *Chem. Lett.*, **1980**, 571; J. F. Normant, A. Alexakis, and G. Cahiez, *Tetrahedron Lett.*, **21**, 935 (1980).

9) K. Ito, Y. Kato, and Y. Ishii, *J. Org. Chem.*, **34**, 459 (1969); C. Couret, J. Escudié, and J. Satgé, *Recl. Trav. Chim. Pays-Bas*, **91**, 429 (1972).

10) E. J. Corey and J. Mann, *J. Am. Chem. Soc.*, **95**, 6832 (1973); B. M. Trost and T. P. Klun, *J. Org. Chem.*, **45**, 4256 (1980); C. B. Chapleo, M. A. W. Finch, S. M. Roberts, G. T. Woolley, R. F. Newton, and D. W. Selby, *J. Chem. Soc., Perkin Trans. 1*, **1980**, 1847; S. M. Ali, C. B. Chapleo, M. A. W. Finch, S. M. Roberts, G. T. Woolley, B. J. Care, and R. F. Newton, *ibid.*, **1980**, 2093; P. A. Grieco and C. V. Srinivasan, *J. Org. Chem.*, **46**, 2591 (1981).

11) a) J. H. McCain and E. Marcus, *J. Org. Chem.*, **35**, 2414 (1970); b) A. F. Noels, J. J. Herman, and P. Teyssie, *ibid.*, **41**, 2527 (1976).

12) Although 3-alkenoic acid is obtained by the conjugate addition of organocopper-trifluoroborane complex to 2,4-alkadienoic acid, the reaction has not so high regioselectivity of 1,4- and 1,6-adducts and excess organocopper reagent is needed to obtain the adducts in good yields: Y. Yamamoto and K. Maruyama, *J. Am. Chem. Soc.*, **100**, 3240 (1978).

13) C. C. Tseng, S. D. Paisley, and H. L. Goering, *J. Org. Chem.*, **51**, 2884 (1986).

14) a) S. Kumazawa, T. Kato, and Y. Kitahara, *Chem. Lett.*, **1973**, 633; R. Tschesche and J. Reden, *Justus Liebigs Ann. Chem.*, **1974**, 853; b) L. Ahlquist, B. Olsson, A. B. Stahl, and S. S. Ställberg, *Chem. Scr.*, **1**, 237 (1971).

15) S. Hosaka and J. Tsuji, *Tetrahedron*, **27**, 3821 (1971).

16) M. Utaka, H. Watabu, and A. Takeda, *J. Org. Chem.*, **52**, 4363 (1987) and references cited therein.

17) T. Mukaiyama, T. Imamoto, and S. Kobayashi, *Chem. Lett.*, **1973**, 715.

18) For example: M. Asaoka, N. Yanagida, and H. Takei, *Tetrahedron Lett.*, **21**, 4611 (1980); R. S. Mali, M. Pohmakotr, B. Weidmann, and D. Seebach, *Justus Liebigs Ann. Chem.*, **1981**, 2272.

19) For example: J. E. Hernandez, A. Cisneros, and S. Fernandez, *Synth. Commun.*, **13**, 191 (1983).

20) M. H. Beale, *J. Chem. Soc., Perkin Trans. 1*, **1985**, 1151; D. P. Curran, M. H. Chen, D. Leszczweski, R. L. Elliott, and D. M. Rakiewicz, *J. Org. Chem.*, **51**, 1612 (1986).

21) M. Kawashima and T. Fujisawa, *Bull. Chem. Soc. Jpn.*, **61**, 3377 (1988).

22) For the preparation of **18**, see: S. Danishefsky, R. L. Funk, and J. F. Kerwin, Jr., *J. Am. Chem. Soc.*, **102**, 6889 (1980).

23) R. J. Anderson, C. A. Henrick, J. B. Siddall, and R. Zurflüh, *J. Am. Chem. Soc.*, **94**, 5379 (1972).

24) T. Fujisawa, T. Sato, and T. Ito, *Chem. Lett.*, **1982**, 219; T. Fujisawa, M. Takeuchi, and T. Sato, *ibid.*, **1982**, 1795; T. Sato, K. Naruse, and T. Fujisawa, *Tetrahedron Lett.*, **23**, 3587 (1982).

25) S. C. Watson and J. F. Eastham, *J. Organomet. Chem.*, **9**, 165 (1967).

26) G. B. Kauffman and L. Y. Fang, *Inorg. Synth.*, **22**, 101 (1983).

27) Commercial (Aldrich).

28) W. Himmele, W. Hoffmann, and L. Janitschke, Ger.

Offen. DE 3345375 Al, (1985); *Chem. Abstr.*, **104**, 33773y (1986).
29) R. P. Linstead, J. Thomas, and W. Mann, *J. Chem. Soc.*, **1930**, 2064.
30) T. R. Hoye and M. J. Kurth, *J. Org. Chem.*, **43**, 3693 (1978).
31) R. E. Ireland, R. H. Mueller, and A. K. Willard, *J. Am. Chem. Soc.*, **98**, 2868 (1976).
32) M. J. Hoekman, G. L. Fagan, A. D. Webb, and R. E. Kepner, *J. Agric. Food Chem.*, **30**, 920 (1982).
33) R. Rossi, A. Carpita, and M. G. Quirici, *Gazz. Chim. Ital.*, **111**, 173 (1981).
34) B. Åkermark and A. Ljungqvist, *J. Org. Chem.*, **43**, 4387 (1978).
35) R. Menicagli, C. Botteghi, and M. Marchetti, *J. Heterocycl. Chem.*, **17**, 57 (1980).
36) "Dictionary of Organic Compounds," ed by I. Heilbron (1965), Vol. 4, p. 2594.
37) K. Haage and H. Reinheckel, Brit. Patent GB 1081234 (1966); *Chem. Abstr.*, **67**, 108235c (1967).

Dehydrooligopeptides. X. Useful Synthetic Method for (*E*)- and (*Z*)-Isomers of Dehydroaspartic Acids, and Their $\Delta^{1,2}$-Dehydrodipeptides by the Base-Catalyzed β-Elimination[1]

Chung-gi SHIN,* Takumi OBARA, Shigeru MORITA, and Yasuchika YONEZAWA
Laboratory of Organic Chemistry, Faculty of Technology, Kanagawa University, Rokkakubashi, Kanagawa-ku, Yokohama 221
(Received April 12, 1988)

Various kinds of *N*-benzyloxycarbonyl (*E*)- and (*Z*)-dehydroaspartic acid (Cbz-ΔAsp) derivatives were successfully synthesized by both a base-catalyzed β-elimination of β-hydroxyaspartic acid esters (HyAsp) via their β-mesyloxy Asp derivatives and several modes of the cleavages of α-(*N*-Cbz)-aminomaleic acid anhydride. Moreover, for high-yield synthesis of $\Delta^{1,2}$-dehydrodipeptides (DHP) containing a ΔAsp residue, a similar β-elimination was applied to Δ^{1}-DHP with a C-terminal HyAsp residue. The configuration of all the new ΔAsp derivatives and their $\Delta^{1,2}$-DHPs were confirmed mainly on the basis of ^{1}H NMR spectral data.

In the course of our work regarding the synthesis of α-dehydroamino acid (DHA; ΔAA) and dehydrooligopeptide (DHP), in particular, various kinds of DHA derivatives, which corresponded to the proteinic α-amino acid (AA), have so far been synthesized.[2-7] Recently, the reason why much attention has been directed on the synthesis and the chemical property of DHA is because the *N*-carboxy α-dehydroamino acid anhydride (ΔNCA), derived from *N*-benzyloxycarbonyl (Cbz)–DHA and thionyl chloride, has very effective and extensive coupling abilities with H–AA–OH and oligopeptide for the DHP synthesis, as already reported.[3,5,8-10]

A synthesis of the (*Z*)-isomer of *N*-protected dehydroaspartic acid dimethyl ester [ΔAsp(OMe)–OMe] has already been reported by Kolasa and Gross.[11] However, simple synthetic routes to the various kinds of (*E*)- and (*Z*)-ΔAsp derivatives have not yet appeared in the literature. Particularly, in order to synthesize the important partial skeleton of phomopsin A containing (*E*)-ΔAsp moiety (Fig. 1), isolated from the culture of *Phomopsis leptostromiformis*,[12] a high-yield syntheses of (*E*)-ΔAsp derivatives and their $\Delta^{1,2}$-dehydrodipeptides (DHP)[13] containing dehydroisoleucine (ΔIle) residue must be accomplished by all means.

In the present paper, we wish to report on a useful syntheses of (*E*)- and (*Z*)-ΔAsp derivatives from both β-hydroxyaspartic acids (HyAsp–OH) and α-(*N*-Cbz)-aminomaleic acid anhydride, and those of $\Delta^{1,2}$-DHP (ΔAA-ΔAsp) by the coupling of appropriate ΔNCA with HyAsp–OMe, followed by a base-catalyzed β-elimination. Moreover, based on ^{1}H NMR spectral data, the configurational structure of ΔAsp derivatives and the corresponding $\Delta^{1,2}$-DHPs could be clearly determined.

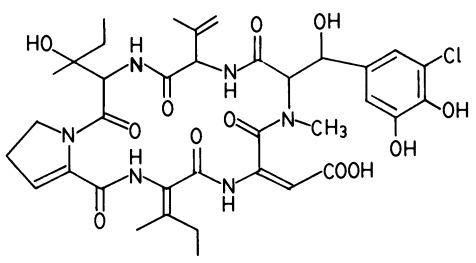

Fig. 1. Phomopsin A.

Results and Discussion

Syntheses of (*E*)- and (*Z*)-ΔAsp Derivatives. It has already been reported that the β-elimination of Cbz-β-(tosyloxy)aspartic acid dimethyl ester, derived from Cbz–β-(hydroxy)aspartic acid dimethyl ester [Cbz–HyAsp(OMe)–OMe] (**1a**) and *p*-toluenesulfonyl (tosyl) chloride, with organic base such as 1,4-diazabicyclo-[2.2.2]octane (Dabco) or 1,8-diazabicyclo[5.4.0]undec-5-ene (DBU) gave only the (*Z*)-isomer of Cbz-ΔAsp(OMe)-OMe [(*Z*)-**3a**].[11] In addition, detailed formation on the mechanism of (*Z*)-**3a** and its DHP was also discussed. However, syntheses of not only the (*E*)-isomer of **3a** but also its peptides have not been described.

At first, in order to investigate the synthesis of various (*E*)- and (*Z*)-isomers of ΔAsp derivatives **3**, instead of the above tosylation, the mesylation of **1a** was carried out, followed by a similar base-catalyzed β-elimination, by a previously reported method.[14]

The reaction of *threo*- and *erythro*-**1a**, respectively, which were freshly prepared (Table 1), with methanesulfonyl (mesyl; Ms) chloride in tetrahydrofuran (THF), was performed to yield the corresponding β-mesyloxy Asp derivatives (**2a**). Subsequently, the leaving mesyloxy group of **2a**, formed as an intermediate, was eliminated in situ with a base, such as triethylamine (TEA) or DBU, to give first an (*E*)-isomer of **3a** as a mixture with (*Z*)-**3a**. At the same time, the intermediate **2a** was also obtained purely. However, as can be seen in the summary given in Table 2, as long as the present method is used, the yield of (*E*)-**3a** was found to be less than 43%, although that of (*Z*)-**3a** was more than 72%. In any event, as a result, the expected (*E*)-**3a** was ultimately obtained, even though the yield was slightly low. Fortunately,

Table 1. β-Hydroxy- and β-Mesyloxyaspartic Acid Esters (**1** and **2**)

	Compound[a]	Yield %	Mp θ_m/°C	IR, ν/cm^{-1} in KBr -COO-	^{1}H NMR, δ in $CDCl_3$ (J/Hz) -NH-	-OH	α-H	β-H
1a	Threo[b]	77	129—130[c]	1760 1695	5.54d	3.44bs	4.44dd (9.0, 2.0)	4.55d (2.0)
	Erythro[b]	68	Syrup	1755 1740 1722	6.22d (9.0)	4.20d (4.5)	4.89dd (9.0, 2.5)	4.48dd (4.5, 2.5)
2a	Threo	70	Syrup	1760 1727	5.80—5.44m	—	5.08dd (9.5, 2.5)	5.50d (2.5)
	Erythro	73	98—99[d]	1775 1748 1690	5.76d (8.5)	—	4.96—5.24m	5.43d (3.0)
1b	Erythro	14	Syrup	1748 1740	6.08d (8.5)	3.91d (4.0)	4.80dd (8.0, 2.0)	4.40d (4.0, 2.0)
2b	Erythro	19	Syrup	1765 1730 1728	5.64d (8.0)	—	4.70dd (8.0, 2.0)	4.40d (2.0)
1c	Erythro	55	140—142[e]	1770 1745	7.52—7.12m (+Ph)		4.56dd (9.0, 4.0)	4.36d[f] (4.0)

a) All the compounds were analyzed for C, H, and N, and the results were within ±0.3% of theoretical values. b) Ref. 15. c) Colorless needles from benzene. d) Colorless needles from diisopropyl ether. e) Colorless needles from hexane-ethyl acetate. f) Measured in DMSO-d_6.

Table 2. Synthesis of **3** by the Base-Catalyzed β-Elimination of **1a** via **2a**

Substrate **1a**	Base	Time/h	Yield/% (*E*)-**3a**	(*Z*)-**3a**	**2a**	Recovery/% **1a**
Threo	TEA	2	2	27	70	—
	TEA	6	8	65	24	—
	TEA	16	12	72	15	—
	DBU	2	30	32	0	35
Erythro	TEA	1	1	2	73	—
	TEA	6	8	20	55	—
	TEA	24	11	49	34	3
	DBU	1	43	15	0	39
	DBU	2	29	29	0	38

according to the another method described later, various (*E*)-isomer of ⊿Asp derivatives could be successfully synthesized in good yields.

A subsequent ester hydrolysis of (*Z*)-**3a**, thus obtained, with an equimolar 1 M LiOH (1 M=1mol dm^{-3}) was carried out in dioxane under cooling to give three kinds of products. The three compounds could be readily isolated by a silica-gel column chromatogram method and were identified as being (*Z*)-Cbz-⊿Asp(OMe)-OH [(*Z*)-**4**] and (*Z*)-Cbz-⊿Asp-OH [(*Z*)-**5**] in 45 and 3% yields, respectively, along with a trace of a by-product, also identified as (*Z*)-Cbz-⊿Asp-OMe [(*Z*)-**6**], as was illustrated in Scheme 1.

Furthermore, when three moles of 1 M LiOH was used, compound (*Z*)-**5** alone was found to be obtained in 71% yield. In the above case, although it was difficult to confirm whether the structure of mono ester of ⊿Asp (**4** and **6**) is α-methyl or β-methyl ester, an independent preparation of (*Z*)-**4** was successfully tried in the following manner.

First, according to the method mentioned above, (*E*)- and (*Z*)-Cbz-⊿Asp(OMe)-OBu^t (**3b**) were synthesized in 35 and 40% yields, respectively, by the successive mesylation and β-elimination of Cbz-HyAsp(OMe)-OBu^t (**1b**), which was derived from Cbz-HyAsp(OMe)-OH (**1c**)[15] and isobutene. On the other hand, it was found that a small amount of the expected Cbz-β-(Bu^{t}O)-Asp(OMe)-OBu^t was also obtained. Subsequently, the *t*-butyl ester decomposition of both (*E*)- and (*Z*)-**3b**, respectively, with HCl was carried out in ethyl acetate to give only one chemical species almost quantitatively, which was in complete accord with (*Z*)-**4**.

From the above results, the structural determination of **4** was exactly accomplished; it can be seen that the

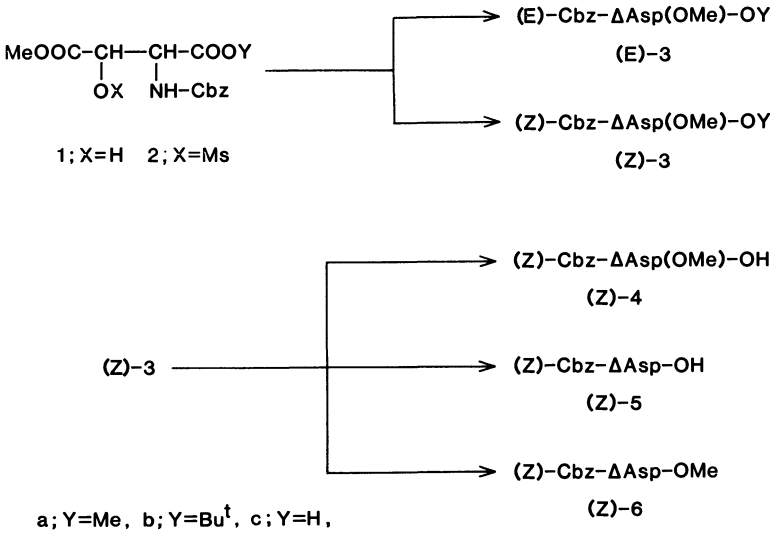

Scheme 1.

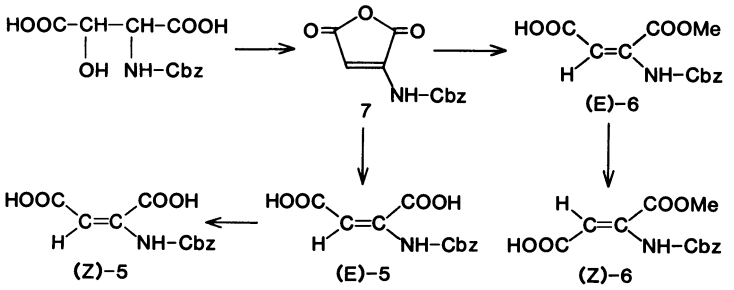

Scheme 2.

isomerization of (*E*)-**3b** took place during the ester decomposition.

Moreover, in order to obtain the (*E*)-isomers of **4**—**6** in high yields, the authentic 2-(*N*-Cbz)-aminomaleic acid anhydride (**7**)[16] was cleaved with 1 M LiOH in the absence of methanol to give (*Z*)-**5** in an almost quantitative yield, while the treatment of **7** with base such as dicyclohexylamine (DCA) or TEA was carried out in methanol to give a hitherto unknown kind. Concerning the configurational structure of the unknown compound, thus obtained, from both the spectral data (IR and ^{1}H NMR) and the satisfactory elemental analysis ($C_{13}H_{13}NO_6$), it was supposed that a kind of the possible total four regio and geometric isomers of the corresponding ⊿Asp monomethyl esters [(*Z*)-**4**, (*E*)-**4**, (*Z*)-**6**, and (*E*)-**6**] was formed. Furthermore, by a comparison with various ⊿Asp derivatives already obtained (see above), it could be concluded that the expected (*E*)-Cbz-⊿Asp-OMe [(*E*)-**6**] was first synthesized in 84% yield. Subsequent isomerization of (*E*)-**6** with HCl was completely performed in ethyl acetate to yield (*Z*)-**6**, which was in accord with the product derived by the hydrolysis of (*Z*)-**3a**. In addition, (*Z*)-**6** was also found to be obtainable quantitatively by a treatment of **7** with methanol in the presence of TEA. Accordingly, the configurational structure of (*E*)-**6** could be unambiguously determined.

On the other hand, more interestingly, it was also found that a treatment of **7** with a saturated $NaHCO_3$ aqueous solution gave (*E*)-Cbz-⊿Asp-OH [(*E*)-**5**] in 95% yield, which was readily isomerized with 1 M LiOH in dioxane to give (*Z*)-**5** quantitatively, according to Scheme 2. Consequently, as summarized in Table 3, all of the (*E*)- and (*Z*)-isomers of **3**—**6**, except for (*E*)-**4**, were obtained purely.

The yields, physical constants, and spectral data of ⊿Asp derivatives **3**—**6** are summarized in Table 3. Particularly, based on the fact that the olefin proton signal of (*E*)-isomer (δ 6.17) of DHA shifted always at lower magnetic field than that of (*Z*)-isomer (δ 5.54), similar to the results reported previously,[17] the configuration of all the ⊿Asp derivatives, thus obtained, could be clearly confirmed.

Synthesis of $\Delta^{1,2}$-DHP Containing ⊿Asp Residue. It has already been reported that the successive mesylation and base-catalyzed β-elimination of Δ^1- or Δ^2-DHP containing N- and C-terminal threonine residues respectively were carried out to give $\Delta^{1,2}$-

Table 3. (*E*)- and (*Z*)-Cbz-⊿Asp-OH Derivatives **3—6**

Compound[a]	Yield %	Mp θ_m/°C	IR, ν/cm^{-1} in KBr -NHCO-	-C=C-	^{1}H NMR, δ in $CDCl_3$ (DMSO-d_6) -NH-	-CH=
(*E*)-**3a**	30	Syrup	1715 1540	1630	7.49bs	6.40s
(*Z*)-**3a**	72	Syrup	1695 1485	1640	9.63bs	5.44s
(*E*)-**3b**	36	Syrup	1715 1535	1628	7.09bs	6.64s
(*Z*)-**3b**	40	Syrup	1685 1480	1635	9.62bs	5.40s
(*Z*)-**4**	91	121—122[b]	1692 1495	1632	(9.85bs	5.67s)
(*E*)-**5**	95	161—162[c]	1710 1500	1628	(10.10bs	5.78s)
(*Z*)-**5**	quant.	148—149[d]	1695 1518	1630	(9.78bs	5.53s)
(*E*)-**6**	94	146—147[c]	1682 1545	1625	(10.59bs	5.81s)
(*Z*)-**6**	quant.	84—85[b]	1630	1635	(9.95bs	5.58s)

a) All the compounds were analyzed for C, H, and N, and the results were within ±0.3% of theoretical values. b) Colorless needles from ethyl acetate. c) Colorless needles from diisopropyl ether-ethyl acetate. d) Colorless needles from hexane-ethyl acetate.

Table 4. The Yields and Melting Points of **10**

Compound	HyAsp	Yield %	Mp[c] θ_m/°C	Formula	Found (%) C	H	N	Calcd (%) (C	H	N)
10a	t[a]	30	92—93	$C_{15}H_{24}N_2O_8$	49.69	6.69	7.68	(49.99	6.71	7.77)
	e[b]	31	110—113		49.85	6.67	7.81	(49.99	6.71	7.77)
10b	t	42	132—136	$C_{16}H_{26}N_2O_8$	50.81	7.02	7.38	(51.33	7.00	7.48)
	e	30	136—137		50.95	7.04	7.42	(51.33	7.00	7.48)
10c	t	40	144—146	$C_{17}H_{28}N_2O_8$	52.40	7.25	7.18	(52.57	7.27	7.21)
	e	26	139—142		52.72	7.18	7.17	(52.57	7.27	7.21)
10d	t	53	128—129	$C_{20}H_{26}N_2O_8$	56.57	6.20	6.58	(56.86	6.20	6.63)
	e	38	146—147		56.77	6.24	6.59	(56.86	6.20	6.63)

a) Threo. b) Erythro. c) Threo=colorless prisms from hexane-ethyl acetate. Erythro=colorless needles from hexane-ethyl acetate.

DHP.[14] By taking advantage of the above-mentioned useful procedure, the desired various ⊿^{1,2}-dehydrodipeptides containing C-terminal ⊿Asp(OMe) residue were successfully synthesized as follows.

Firstly, for a high-yield synthesis of ⊿^{1}-DHP with a C-terminal HyAsp residue as the substrates, the so-called ⊿NCA method developed by us was carried out with very good results. Various (*Z*)-isomer of ⊿NCA derivatives (**8**: **a**; ⊿Abu,[18] **b**; ⊿Val, **c**; ⊿Ile)[2,3,5] were treated with di-*t*-butyl dicarbonate [$((CH_3)_3COCO)_2O$; $(Boc)_2O$] in the presence of pyridine and then with *threo*- or *erythro*-HyAsp(OMe)-OMe as an amine component in the presence of *N*-methylmorpholine (NMM) at pH 9 to give the corresponding (*Z*)-*t*-butoxycarbonyl (Boc)-⊿^{1}-dehydrodipeptide dimethyl ester [Boc-⊿AA-HyAsp(OMe)-OMe] (**10**) in ca. 36% overall yield.

From the above result, it is obvious that the acylation of **8** with $(Boc)_2O$ occurred at first to form Boc-⊿NCA (**9**) as an intermediate, which was immediately coupled with HyAsp(OMe)-OMe in one-pot to give **10**. Even though the overall yield of **10** was lower (at present) these procedures seem to be very useful for the synthesis of ⊿^{1}-dehydrodipeptide esters (**10**), as summarized in Tables 4 and 5.

Subsequently, the mesylation of **10** with mesyl chloride and then the β-elimination of the mesyloxy derivatives (**11**), formed as unstable intermediates, were carried out in situ in THF in the presence of TEA or DBU to give first the expected Boc-⊿^{1,2}-dehydrodipeptide dimethyl ester [Boc-⊿AA-⊿Asp(OMe)-OMe] (**12**). In the case of **10a—c** containing a *threo*-HyAsp

Table 5. The IR and ^{1}H NMR Spectral Data of **10**

Compound	HyAsp	IR, ν/cm^{-1} in KBr -NHCO-		^{1}H NMR, δ in $CDCl_3$ (J/Hz) -CH=	-OH	NH-CH-CO
10a	t[a]	1685,	1545	6.48q (7.0)	3.96bs	5.12dd (2.5, 9.5)
	e[b]	1665,	1550	6.52q (7.0)	4.10d	5.16dd (2.0, 8.0)
10b	t	1680,	1540	—	3.88bs	4.96dd (2.0, 8.2)
	e	1665,	1540	—	4.22bs	5.16dd (3.0, 8.0)
10c	t	1680,	1535	—	4.08bs	4.92dd (2.0, 8.0)
	e	1670,	1540	—	4.22bs	5.18dd (2.0, 10.0)
10d	t	1650,	1542	6.90s	4.26bs	5.00dd (2.0, 10.0)
	e	1674,	1548	7.11s	4.02d	5.12dd (2.5, 7.5)

a) Threo. b) Erythro.

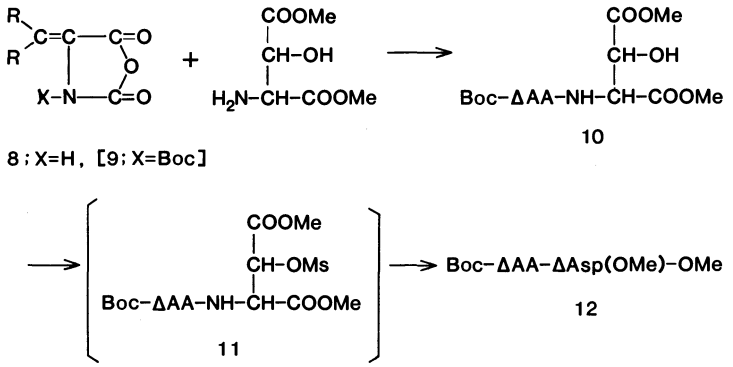

Scheme 3.

residue, the above-mentioned successive reactions were performed in the presence of TEA for 24 h to give only a (*Z,Z*)-isomer of **12a—c** in 51—92% yield, as summarized in Table 6. On the other hand, when compound **10b** containing *erythro*-HyAsp residue was similarly worked up in the presence of DBU for 4.5 h, Boc-⊿Val-(*E*)-⊿Asp(OMe)-OMe [(*E*)-**12b**] was obtained in a 20% yield, whereas the similar reaction of *erythro*-**10c** gave Boc-(*E*)- and (*Z*)-⊿Ile-(*Z*)-⊿Asp-(OMe)-OMe [(*E,Z*)- and (*Z,Z*)-**12c**] in a 23% yield. In this case, the N-terminal (*Z*)-⊿Ile of **10c** containing either *threo*- or *erythro*-HyAsp residue was found to be isomerized partially to give a mixture of (*E,Z*)- and (*Z,Z*)-**12** during β-elimination.

As Table 8 shows, the chemical shifts of the olefin proton of two isomers, (*Z,E*)- and (*Z,Z*)-**12**, are clearly distinguishable from each other; that is, the signal of (*E*)-⊿Asp (δ 6.72) shifts at a considerably lower magnetic field than that of (*Z*)-⊿Asp (δ 5.40) residue.[17] From this fact, the configurations of **12** could be readily confirmed. Furthermore, from the above results, it can be seen that the formation and yield of each geometric isomers of **12** results from differences between the structure of substrates, which contain *erythro*- or *threo*-HyAsp(OMe)-OMe residue, and the reaction conditions. Accordingly, if only product (*Z,Z*)-**12** is desired, the reaction time must necessarily to be prolonged in the presence of TEA, although only an example is shown. On the contrary, if an appropriate **12** containing (*E*)-⊿Asp residue is expected, it seems to be preferable to shorten the reaction time in the presence of DBU. Unfortunately, however, it is not understandable why the similar β-elimination of **10** containing *erythro*-HyAsp residue gave either (*Z, E*)- or (*Z,Z*)-**12**, as summarized in Tables 6, 7, and 8. Consequently, at present, it is difficult to

Table 6. Base-Catalyzed β-Elimination of **10**

Compound **10**		Reaction conditions		Yield of **12**/%	
⊿AA	HyAsp	Base	Time/h	(*E*)-⊿AsP	(*Z*)-⊿AsP
⊿Val	Threo	TEA	24	0	92
⊿Ile	Threo	TEA	24	0	67
⊿Abu	Threo	TEA	24	0	51
⊿Val	Erythro	DBU	4.5	20	0
⊿Ile	Erythro	DBU	4.5	0	23

Table 7. The Melting Points of **12**

Compound No.	⊿AA	Geometry	Mp θ_m/°C	Formula	Found (%)			Calcd (%)		
					C	H	N	(C	H	N)
12a	⊿Abu	(*Z*, *Z*)	Syrup	$C_{14}H_{20}N_2O_7$	51.82	6.25	8.39	(51.21	6.14	8.53)
12b	⊿Val	(*Z*)	120—122[b]	$C_{15}H_{22}N_2O_7$	52.80	6.61	7.91	(52.62	6.48	8.18)
		(*E*)	144—146[c]		52.59	6.53	7.95	(52.62	6.48	8.18)
12c	⊿Ile[a]	(*E*, *Z*) (*Z*, *Z*)	128—131[b]	$C_{16}H_{24}N_2O_7$	53.67	7.04	7.74	(53.92	6.79	7.86)

a) (*E*, *E*)- and (*Z*, *Z*)-**12** obtained as a mixture of 2:3 ratio. b) Colorless needles from hexane–ethyl acetate. c) Colorless prisms from hexane–ethyl acetate.

Table 8. The IR and ^{1}H NMR Spectral Data of **12**

Compound	Geometry	IR, ν/cm^{-1} in KBr -NHCO-		^{1}H NMR, δ in $CDCl_3$ (J/Hz) -CH=	-CH=	-NH-
12a	(*Z*, *Z*)	1635,	1480	6.54q (7.5)	5.39s	10.76bs
12b	(*Z*)	1630,	1480	—	5.40s	10.72bs
	(*E*)	1640,	1540	—	6.72s	8.62bs
12c	(*E*, *Z*)	1635,	1480	—	5.41s	10.74bs
	(*Z*, *Z*)				5.39s	10.69bs

obtain selectively and quantitatively only one of the geometric isomers.

In conclusion, it is noteworthy that various kinds of (*E*)- and (*Z*)-⊿Asp derivatives and their dehydrodipeptides were readily synthesized from several routes and that their configurations could be completely determined. Moreover, it is firmly believed that these obtained results will contribute to the synthesis of the important partial skeleton of phomopsin A.

Experimental

General. Melting points were determined with a Yamato micro melting-point apparatus MP-21 model and were uncorrected. The IR spectra were recorded with a Hitachi EPI-G2 grating spectrometer. The ^{1}H NMR spectra were measured with a JEOL JMN PS 100 spectrometer in a $CDCl_3$ solution with tetramethylsilane as the internal standard.

Preparation of 1c. To a solution of β-HyAsp(OMe)-OH (4.0 g, 24.5 mmol) in a saturated $NaHCO_3$ aqueous solution (61 ml) was added a solution of Cbz-Cl (5 ml, 29.4 mmol) in dry diethyl ether (20 ml), with vigorous stirring, drop by drop under cooling. After continuous stirring at room temperature for 1.5 h, Cbz-Cl (2.7 ml, 16.0 mmol) and $NaHCO_3$ (2.6 g, 30.0 mmol) were further added to the resultant solution at room temperature for 2 h. The reaction solution was poured into water (100 ml) and washed with ethyl acetate. The aqueous layer was made to pH 2 with 1 M HCl and then extracted three times with ethyl acetate (30 ml). The combined extracts were washed with saturated NaCl aqueous solution and then dried over anhydrous Na_2SO_4. After removing the solvent under reduced pressure, the residue was solidified with hexane and then the crude crystals were collected. Recrystallization from a mixture of hexane and ethyl acetate gave **1c** as colorless needles.

Reaction of 1c with Isobutene. Into a suspension of **1c** (3.56 g, 1.2 mmol) in dry CH_2Cl_2 (50 ml) was introduced isobutene gas below −40 °C, until the suspension volume increased to about 75 ml. After adding concentrated sulfuric acid (0.12 ml), the resulting suspension was put into a sealed tube and then allowed to stand at room temperature for 10 days until becoming homogeneous. The reaction solution was poured into a saturated $NaHCO_3$ aqueous solution (150 ml) and the resultant solution was extracted three times

with $CHCl_3$. The combined extracts were washed with water and then dried over anhydrous Na_2SO_4. After removing the solvent, the residue was purified on a silica-gel column using a mixture of benzene and acetone (30:1 v/v) as the eluent. The first fraction gave **1c** (0.6 g) and the second **2b** (0.9 g) in 19% yield.

Preparation of (*E*)- and (*Z*)-3a. To a solution of **1a** (2g, 6.43 mmol) and MsCl (1.1 g, 9.7 mmol) in dry THF (20 ml) was added drop by drop a solution of DBU or TEA (19.3 mmol) in dry THF (10 ml) at 0 °C. After stirring at 0 °C for 1 h, the resulting chilled solution was returned to room temperature and then allowed to stand. After removing the solvent, the residue was dissolved in ethyl acetate (100 ml) and the resultant solution was washed successively with 10% citric acid aqueous solution, saturated $NaHCO_3$ solution, water and finally dried over anhydrous $MgSO_4$. After concentrating the solution under reduced pressure, the residual syrup was chromatographed on a silica-gel column using a mixture of benzene and acetone (30:1 v/v) as the eluent. Three or four fractions were always obtained, as summarized in Table 2. The expected (*E*)- and (*Z*)-**3a** and intermediates Cbz-β-(MsO)Asp(OMe)-OMe (**2a**) are listed in Table 3.

Preparation of (*E*)- and (*Z*)-3b. In a similar manner, a treatment of **1b** with MsCl in the presence of DBU was worked up to give (*E*)- and (*Z*)-**3b**, no accompanying the corresponding β-mesyloxy derivative (**2b**). See Table 3.

Hydrolysis of 3a with LiOH. To a solution of (*Z*)-**3a** (4.26 g, 14.5 mmol) in dioxane (15 ml) was added 1 M LiOH (15 ml) drop by drop at 5—8 °C. The resulting solution was slowly returned to room temperature and then stirred continuously for 3.5 h. The reaction solution was poured into water (100 ml) and then washed with diethyl ether. The aqueous layer was acidified to pH 1 with 6 M HCl and extracted three times with ethyl acetate (50 ml). The combined extracts were washed with saturated NaCl aqueous solution and then dried over anhydrous Na_2SO_4. After removing the solvent under reduced pressure the residual crude crystals obtained were recrystallized from benzene to give (*Z*)-**4** as colorless needles. The filtrate was concentrated under reduced pressure to give a viscous syrup, which was chromatographed on a silica-gel column using a mixture of $CHCl_3$, methanol and ethyl acetate (200:1:1 v/v) to give three fractions. Compound (*Z*)-**4** was further obtained in a 45% yield from the first fraction and small amounts of (*Z*)-**5** and **6** were also obtained in 3 and 2% yields, respectively, from the second and the final fractions. On the other hand, from the ether layer (*Z*)-**3a** was recovered in 40% yield.

Similarly, the hydrolysis of (*Z*)-**3a** was worked up with 1 M LiOH (45 ml) at room temperature for 24 h to give (*Z*)-**5** in 71% yield. In addition, in a similar manner, treatment of (*E*)-**3a** was performed to give (*Z*)-**4**, **5**, and **6** in almost the same ratio obtained above.

Ester Decomposition of 3c. A solution of (*Z*)- or (*E*)-**3c** (1.0 g, 3.3 mmol) in ethyl acetate (30 ml) saturated with gaseous HCl was stirred at room temperature for 1.5 h. After removing the solvent and excess HCl under reduced pressure, the residue was dissolved in ethyl acetate (30 ml) and the resulting solution was again concentrated under reduced pressure. The residue,thus obtained, was crystallized by treating with hexane. The collected crystals were recrystallized from small quantity of ethyl acetate to give (*Z*)-**4** alone in 91% yield.

Preparation of (*E*)-5 from 7. a) Method A: A solution of **7** (2.47 g, 10.0 mmol) in saturated $NaHCO_3$ aqueous solution (50 ml) was stirred at room temperature for 1 h. The reaction solution was washed with diethyl ether and the aqueous layer was made to pH 2 with 1 M HCl and then extracted three times with ethyl acetate (50 ml). The combined extracts were washed with a saturated NaCl aqueous solution and then dried over anhydrous Na_2SO_4. After concentrating the solution under reduced pressure, the residue, thus obtained was crystallized by treating with diisopropyl ether. The collected crude crystals were recrystallized from a mixture of diisopropyl ether and ethyl acetate (5:2 v/v) to give (*E*)-**5** as colorless needles quantitatively.

b) Method B: To a solution of **7** (2.47 g, 10.0 mmol) in dioxane (30 ml) was added 1 M LiOH (13.5 ml) under cooling. After stirring for 1 h, ice-water (100 ml) was added to the reaction solution and the resulting solution was washed with chilled diethyl ether and then made to pH 2 with 1 M HCl. The acidified solution was similarly worked up to give (*E*)-**5**, according to Method A.

Preparation of (*Z*)-5. a) Method A: To a solution of **7** (2.47 g, 10.0 mmol) in dioxane (25 ml) was added 1 M LiOH (25 ml) at room temperature. After stirring for 1 h, the reaction solution was made to pH 2 with 1 M HCl and then extracted three times with ethyl acetate (50 ml). The combined extracts were washed with a saturated NaCl aqueous solution and dried over anhydrous Na_2SO_4. After removing the solvent under reduced pressure, the residue was crystallized by treating with hexane. Recrystallization from a mixture of ethyl acetate and hexane gave (*Z*)-**5** as colorless needles quantitatively.

b) Method B: The treatment of the solution of (*E*)-**5** (2.65 g, 10.0 mmol) in dioxane (30 ml) with 1 M LiOH (25 ml) was similarly worked up to give (*Z*)-**5** quantitatively by the isomerization.

Preparation of (*E*)-6. a) Method A: To a solution of **7** (1.0 g, 4.05 mmol) in dry methanol (10 ml) was added drop by drop a solution of DCA (0.8 ml, 4.05 mmol) in dry methanol (5 ml). After stirring for 30 min and then for 1.5 h at room temperature, the reaction solution was concentrated under reduced pressure. The crystalline residue, thus obtained, was dissolved successively in 10% citric acid (30 ml) and ethyl acetate (30 ml); then the resulting solution was vigorously shaken. The aqueous layer was extracted with ethyl acetate. The combined organic layers were dried over anhydrous Na_2SO_4. After removing the solvent under reduced pressure, the crude crystals collected by using diisopropyl ether were recrystallized from small amount of ethyl acetate to give (*E*)-**6** as colorless needles. 83% yield.

b) Method B: To a solution of **7** (1.0 g, 4.05 mmol) in dry methanol (10 ml) was added drop by drop a solution of TEA (0.57 ml, 4.05 mmol) in dry methanol (5 ml) under cooling. The resultant solution was stirred for 30 min and then at room temperature for 30 min. The treatment of the reaction solution was similarly worked up to give (*E*)-**6** almost quantitatively.

Preparation of (*Z*)-6. a) Method A: To a solution of **7** (1.0 g, 4.05 mmol) in dry methanol (10 ml) was added drop by drop TEA (0.86 ml, 6.08 mmol) under cooling. The

resulting solution was allowed to stand at room temperature and then stirred continuously for 12 h. After removing the solvent, the residue was dissolved in 10% citric acid (30 ml) and the resultant solution was extracted twice with ethyl acetate (30 ml). The combined extracts were washed with saturated NaCl aqueous solution and then dried over anhydrous Na_2SO_4. The concentration of the solution under reduced pressure gave crude crystals, which were collected by using hexane and then recrystallized from a mixture of hexane and ethyl acetate to give (*Z*)-**6** as colorless needles quantitatively.

b) Method B: A solution of (*E*)-**6** (1.0 g, 4.06 mmol) in ethyl acetate (30 ml) saturated with gaseous HCl was stirred at room temperature for 6 h. The reaction solution was concentrated under reduced pressure to give crude residue, which was again dissolved in ethyl acetate (30 ml). This procedure was repeated until HCl gas was completely taken off. The crude crystals collected by using hexane were similarly worked up to give (*Z*)-**6** quantitatively.

Preparation of 10. To a solution of ΔNCA (7.04 mmol) and $(Boc)_2O$ (8.45 g, 8.45 mmol) in THF (7 ml) was added drop by drop pyridine (0.15 ml, 1.85 mmol) under cooling. The resulting solution was slowly returned to room temperature and then stirred continuously overnight. To the solution,thus prepared, was further added a solution of HyAsp(OMe)-OMe·HCl (2.25 g, 10.6 mmol) and TEA (1.48 ml, 10.6 mmol) in dry THF (7 ml) at room temperature. After making the solution pH 9 with NMM (1.0 ml, 9.1 mmol), the resulting solution was stirred for more 2.5—4.0 h and then concentrated under reduced pressure to give a crude residue, which was dissolved in ethyl acetate (100 ml). This solution was successively washed with 10% citric acid, water, saturated aqueous $NaHCO_3$ solution and water and finally dried over anhydrous Na_2SO_4. After removing the solvent under reduced pressure, the crude residue obtained was crystallized and collected by using diisopropyl ether. In the case of a syrup, which did not crystallize, purification on a silica-gel column using a mixture of $CHCl_3$ and acetone (20:1 v/v) as the eluent was carried out to give crystals, which were recrystallized from a mixture of petroleum ether and ethyl acetate to give **10**. The dipeptide containing a *threo*-HyAsp residue, thus obtained, was colorless prisms; the one with an *erythro*-HyAsp residue was colorless needles.

Preparation of 12. To a solution of **10** (1.60 mmol) and MsCl (0.19 ml, 2.40 mmol) in dry THF (7 ml) below 0 °C. After stirring for 1 h and then at room temperature for 24 h in the case of TEA, or for 4.5 h in the case of DBU, the reaction solution was concentrated under reduced pressure. The residue, thus obtained, was dissolved in ethyl acetate (50 ml) and the resulting solution was washed successively with 10% citric acid, water, saturated aqueous $NaHCO_3$ solution, and then water and finally dried over anhydrous Na_2SO_4. After removing the solvent under reduced pressure, the obtained residual crystals were recrystallized from a mixture of petroleum ether and ethyl acetate to give **12** as colorless prisms [(*Z*)-isomer] or colorless needles [(*E*)-isomer].

The present work was partially supported by a Grant-in-Aid for Scientific Research No. 62540394 from the Ministry of Education, Science and Culture.

References

1) Part IX. Y. Yonezawa, N. Takefuji, N. Takahashi, and C. Shin, *Bull. Chem. Soc. Jpn.*, **61**, 2687 (1988).
2) C. Shin, Y. Yonezawa, and J. Yoshimura, *Chem. Lett.*, **1981**, 1635.
3) C. Shin, Y. Yonezawa, and T. Yamada, *Chem. Pharm. Bull.*, **32**, 3934 (1984).
4) C. Shin, Y. Yonezawa, and E. Watanabe, *Tetrahedron Lett.*, **26**, 851 (1985).
5) C. Shin, M. Ikeda, and Y. Yonezawa, *Agric. Biol. Chem.*, **49**, 2243 (1985).
6) C. Shin, Y. Yonezawa, and T. Obara, *Heterocycles*, **24**, 1561 (1986).
7) C. Shin, T. Obara, S. Segami, and Y. Yonezawa, *Tetrahedron Lett.*, **28**, 3827 (1987).
8) C. Shin, Y. Yonezawa, and M. Ikeda, *Bull. Chem. Soc. Jpn.*, **59**, 3573 (1986).
9) C. Shin, N. Takamatsu, and Y. Yonezawa, *Agric. Biol. Chem.*, **50**, 797 (1986).
10) C. Shin and Y. Yonezawa, *Chem. Lett.*, **1985**, 519.
11) T. Kolasa and E. Gross, *Int. J. Pept. Protein Res.*, **20**, 259 (1982).
12) C. C. J. Culvenor, P. A. Cockrum, J. A. Edgar, J. L. Frahn, C. P. Gorst-Allman, A. J. Jones, W. F. O. Marasa, K. E. Murry, L. W. Smith, P. S. Steyn, R. Vleggaar, and P. L. Wesseis, *J. Chem. Soc., Chem. Commun.*, **1983**, 1279.
13) In this paper, the symbols Δ^1 and $\Delta^{1,2}$ indicate the position number of double bond of DHA residue from the N-terminus in sequence.
14) C. Shin, Y. Yonezawa, M. Takahashi, and J. Yoshimura, *Bull. Chem. Soc. Jpn.*, **54**, 1132 (1981).
15) A. Singerman and Y. Liwschitz, *Tetrahedron Lett.*, **1968**, 4733.
16) Y. Liwschitz, A. Singerman, and S. Sokoloff, *J. Chem. Soc. C*, **1968**, 1843.
17) C. Shin, M. Hayakawa, T. Suzuki, A. Ohtsuka, and J. Yoshimura, *Bull. Chem. Soc. Jpn.*, **51**, 550 (1978).
18) 2-Amino-2-butenoic acid.

 © 1988 The Chemical Society of Japan Bull. Chem. Soc. Jpn., 61, 3273—3282 (1988)

Retentive Solvolysis. 16.[1] Reinvestigation of the Retentive Phenolysis of 1-Phenylethyl Chloride. The Mechanism and the Structure of Ion Pair Intermediate

Tomomi KINOSHITA,* Takuya UENO, Keizo IKAI, Masataka FUJIWARA, and Kunio OKAMOTO†

Department of Hydrocarbon Chemistry, Faculty of Engineering, Kyoto University, Kyoto 606

(Received April 12, 1988)

The effect of added aniline on the polarimetric (k_p) and titrimetric rate constants (k_t) has been reexamined for the phenolysis of 1-phenylethyl chloride (RCl) in phenol–benzene (1:1 w/w). The k_p–k_t plot against the aniline concentrations exhibited the pattern C, instead of A which was the previous results in our laboratory. It has been revealed that the previous rate constants at the lower aniline concentrations, including the case of absence of aniline, were underestimated due to overlooking the reverse reaction caused by the liberated hydrogen chloride. The pattern C indicates that the first ion pair intermediate, not the second one, is nucleophilically attacked by solvent phenol molecule. The major products were the partially retained *o*-RC_6H_4OH, the partially inverted *p*-RC_6H_4OH, together with the partially retained ROPh. The same k_p–k_t pattern C has been observed for the competitive solvolysis of RCl in phenol–methanol (85:15 w/w), which produced the partially retained ROMe and ROPh, the partially inverted *o*- and *p*-RC_6H_4OH, and styrene. Such stereochemical outcomes for both solvolyses demonstrate that the major first ion pair intermediate should be a rear-side-shielded ion pair intermediate.

On the basis of the pattern of salt effect of added aniline on the polarimetric and titrimetric rate constants (k_p and k_t, respectively),[2] the retentive phenolysis of 1-phenylethyl chloride[2–5] (RCl), the first example of the retentive phenolysis, has been hitherto recognized to be one of a few solvolysis systems,[1,6–9,††] which exhibited the pattern A[1,6,9] in the k_p–k_t plot against the concentration of added salt.

However, there have been left two problems for the phenolysis of 1-phenylethyl chloride. First, the pattern of k_p–k_t diagram, previously reported for the phenolysis of RCl,[2] exhibited an "unusually" steep slope of the special salt effect[7,10,11] on k_t. Although such a steep slope has been often reported for S_N1 solvolyses in some solvents[11] other than phenol, it has not been known for the phenolyses examined so far.[1,6,8,9,12,13]

The steep increase in the k_t is characterized by the use of the parameters proposed by Winstein and his co-workers.[11a] The parameters are: $k^0_{t,ext}/k^0_t$=5.0 and $[salt]_{1/2}$=0.0036 M (1 M=1 mol dm^{-3}) for RCl, whereas 1.09—2.69 and 0.01—0.03 M, respectively, for the other systems.[1,6,8,9,12,13] The $k^0_{t,ext}$ designates the k_t value extrapolated at zero salt concentration from the linear part at higher salt concentrations, k^0_t is the actual k_t value at zero salt concentration, and $[salt]_{1/2}$ is the salt concentration corresponding to $\frac{1}{2}\cdot(k^0_{t,ext}+k^0_t)$.

Secondly, it has been known that the phenolysis accompanies the reverse reaction in the absence of an added base,[14,15] which results in retardation of the apparent rate (k_t)[14] and rearrangement of ROPh to *o*- and *p*- RC_6H_4OH by the liberated strong acid such as hydrogen chloride.[15] Such an effect of reverse reaction was sometimes overlooked.[16]

We have therefore reinvestigated the k_p–k_t pattern for the phenolysis of 1-phenylethyl chloride with suspicions on the pattern A,[1,6,9] under the conditions where the effect of reverse reaction is completely eliminated.

Although we briefly mentioned the results in the footnotes of the preceding papers,[1,6,13] we now report in details that the k_p–k_t diagram for the phenolysis of RCl in the presence of $PhNH_2$, Et_3N, and NaOPh does exhibit the pattern C,[1,6] which specifies Int-1, not Int-2, for the ion pair stage of product formation. Furthermore, adding the stereochemical outcomes for the reinvestigated methanol-perturbed phenolysis of RCl,[17] we also report that the structure of the major Int-1 should be a rear-side-shielded ion pair intermediate.

Results and Discussion

Reexamination of Phenolysis Rates. Optically active 1-phenylethyl chloride (RCl) has been subjected to the phenolysis under the identical conditions with those employed previously,[2] i.e., in phenol–benzene (1:1 w/w) at variable concentrations (0—0.391 M) of added aniline at 25 °C, except the concentration of RCl, 0.10 M instead of previous 0.55 M[2] for the k_p measurements. The phenolysis rate has been reexamined both titrimetrically and polarimetrically. Titrimetric rate measurements have been carried out by the use of 0.05 M aqueous HCl (or NaOH) solution as a titrating reagent, cold acetone (ca. −15 °C) as a stop solution, and lacmoid as an indicator, instead of previous 0.1 M $HClO_4$ (or NaOAc) acetic acid

† Current address: Meisei Chemical Works, Ltd., 1 Nakazawacho, Ukyo-ku, Kyoto 615.

†† Although the acetolysis of 2-(*p*-methoxyphenyl)-propyl tosylate was previously reported to proceed via Int-2,[10] reexamination of the pattern of salt effect by us[6] has clarified that the product source is Int-1, not Int-2.

Table 1. The Titrimetric and Polarimetric Phenolysis Rates (k_t and k_p) of 1-Phenylethyl Chloride (RCl) in the Presence of a Base in Phenol-Benzene (1:1 w/w) at 25 °C

Added base/M		RCl	k_t	k_p
		M	s^{-1} [a]	s^{-1} [b]
None	0.000	0.050	3.20×10^{-4} [c]	
	0.000	0.100		3.82×10^{-4}
	0.000 [d]	0.050	5.95×10^{-5}	
	0.000 [d]	0.100	6.85×10^{-5}	
	0.000 [d]	0.550		3.48×10^{-4}
Hind.Py. [e]	0.0539	0.0501	3.33×10^{-4}	
$PhNH_2$	0.0051	0.050	3.23×10^{-4}	
	0.0075	0.050	3.17×10^{-4}	
	0.106	0.101	3.25×10^{-4}	
	0.169	0.104	3.22×10^{-4}	
	0.198	0.102	3.19×10^{-4}	3.79×10^{-4}
	0.391	0.103		3.75×10^{-4}
	0.0049 [d]	0.0500	2.30×10^{-4}	
	0.0095 [d]	0.0500	2.82×10^{-4}	
	0.0200 [d]	0.0500	3.02×10^{-4}	
	0.0402 [d]	0.100	3.03×10^{-4}	
	0.0500 [d]	0.0500	3.03×10^{-4}	
	0.10 [d]	0.100	3.00×10^{-4} [c]	
	0.265 [d]	0.100	2.83×10^{-4}	
	0.470 [d]	0.550		3.20×10^{-4}
	0.513 [d]	0.50		3.20×10^{-4} [c]
	0.523 [d]	0.500		3.20×10^{-4}
Et_3N	0.101	0.099	3.17×10^{-4}	3.80×10^{-4}
	0.201	0.103	3.00×10^{-4}	3.73×10^{-4}
	0.302	0.105	3.02×10^{-4}	3.71×10^{-4}
NaOPh	0.051	0.050	3.95×10^{-4}	4.87×10^{-4}
	0.102	0.100	5.25×10^{-4}	5.97×10^{-4}
	0.153	0.103	6.17×10^{-4}	7.04×10^{-4}
$LiClO_4$ [f]	0.010	0.0497	3.33×10^{-4}	
	0.020	0.0502	3.50×10^{-4}	
	0.030	0.0499	3.57×10^{-4}	

a) Accurate to within ±2%. b) Accurate to within ±3%. c) An average value for duplicate measurements. d) Cited from Ref. 2. e) 2,6-Di-*t*-butyl-4-methylpyridine (see the text). f) In the presence of 0.055 M 2,6-di-*t*-butyl-4-methylpyridine.

solution, acetic acid (ca. 10 °C), and Crystal Violet, respectively.[2] All the rate data are summarized along with those in the presence of Et_3N, NaOPh, lithium perchlorate, and a hindered pyridine in Table 1 and they are plotted against the concentration of aniline in Fig. 1 together with the previously-reported data.[2]

In the absence of aniline, the k_t^0 value had a tendency to decrease as the reaction proceeded at 1—25% conversion. After ca. 25% conversion, the reaction retarded much more. This phenomenon can be ascribed to the occurrence of competing reverse reaction, i.e., the cleavage reaction of the aralkyl phenyl ether by the liberated hydrogen chloride to give the starting RCl.[14,15] The initial k_t^0 value at zero % reaction, therefore, has been extrapolated from k_t^0 values at 1—13% reaction. The new k_t^0 value coincides within experimental errors with a k_t value (Table 1) in the presence of a hindered amine, 2,6-di-*t*-butyl-4-methylpyridine, which plays only as a neutralizer for the liberated acid, not as a phenoxide donor. The new k_t^0 value is 5.0 (±0.4) times larger than the previously-reported value,[2] which had been measured at 12—27% reaction. An approximately identical value with the previous one[2] could be obtained at such 10—25% reaction. The k_p^0 value, k_p value in the absence of the base, exhibited a little acceleration with an increase in the reaction %, most probably due to the cleavage reaction of the aralkyl phenyl ether.[14,15] The initial k_p^0 value was determined, therefore, by the extrapolation method similar to that described above. The new k_p values are 1.1 times larger than the previous ones over the whole range of $PhNH_2$ concentration (Fig. 1). The discrepancy can be mainly ascribed to the difference of the phenol concentration

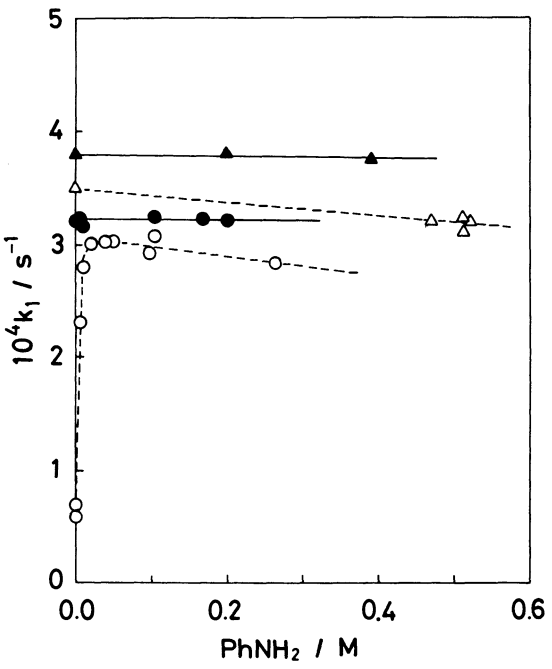

Fig. 1. Effect of added $PhNH_2$ concentration on the titrimetric and polarimetric rate constants (k_t and k_p) for the phenolysis of 1-phenylethyl chloride in phenol-benzene (1:1 w/w) at 25°C.
● k_t, ▲ k_p; this work. ○ k_t, △ k_p; cited from Ref. 2.

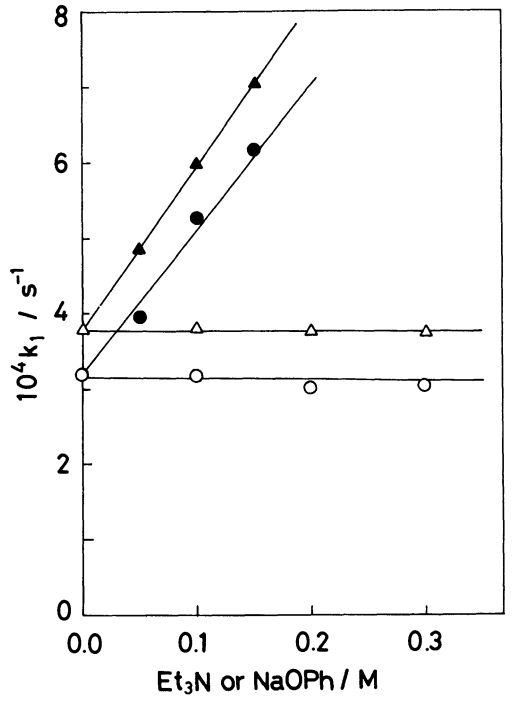

Fig. 2. Effect of added Et_3N and NaOPh concentration on the titrimetric and polarimetric rate constants (k_t and k_p) for the phenolysis of 1-phenylethyl chloride in phenol-benzene (1:1 w/w) at 25°C.
○ k_t, △ k_p; in the presence of Et_3N. ● k_t, ▲ k_p; in the presence of NaOPh.

in the respective solvents owing to that of the substrate concentrations between in this work (0.10 M) and in the previous work (0.55 M).[2]

The k_t value at 0.0050 M $PhNH_2$ (0.050 M RCl) was obtained from the data at 1—8% reactions. The new value is 1.4 times larger than the previously-reported value which had been estimated at 5.8% reaction.[2] For each run in the presence of 0.106—0.198 M $PhNH_2$, a smooth first-order linear relationship (correlation coefficient≧0.9997) has been obtained until at least 80% reaction and the new values are somewhat larger than the previous ones.[2] In view of the conditions and the accuracy of rate measurements, the new data are much more reliable than the previously-reported data.[2]

Reexamination of the k_p–k_t Pattern for Phenolysis. The new pattern of the salt effect of $PhNH_2$ on the k_p–k_t diagram exhibits no special salt effect on k_t, differently from the previous one[2] (Fig. 1). The k_p/k_t ratio is constant, 1.19, over the whole range of the concentration of $PhNH_2$. The analogous k_p–k_t patterns have been also observed in the presence of Et_3N and NaOPh (Fig. 2) instead of $PhNH_2$. Lithium perchlorate also exhibits no special salt effect on k_t[†††] (Table 1). Such patterns were classified as pattern C in one of our previous reports.[1,6]

Thus, the k_p–k_t patterns indicate that the first ion pair intermediate (Int-1), not the second one (Int-2), partially reacts with the solvent phenol molecule, partially returns to the substrate, and partially racemizes by itself,[1,6] whereas the previously-reported k_p–k_t profile[2] suggested that all the products derived from the reaction of Int-2 with the phenoxide at higher base concentrations.[1,6]

The same k_p–k_t pattern C[1,6] has been reported for the phenolyses of 1-phenylethyl,[8] 1-phenylpropyl,[9] 1-methyl-1-phenylpropyl,[9] 2-methyl-1-phenylpropyl,[9] and *p*-chlorobenzhydryl *p*-nitrobenzoates[9] in the presence of NaOPh or Et_3N, and 2,2-dimethyl-1-phenylpropyl *p*-nitrobenzoate in the presence of $(n\text{-}Bu)_4NClO_4$,[6] for the hydrolysis of RCl in 60% aqueous dioxane in the presence of $LiClO_4$,[18] and for the acetolysis of *exo*-2-norbornyl brosylate in the presence of KOAc.[19,§]

Product Distribution for the Phenolysis. Product distribution for the phenolysis of RCl was analyzed by the use of GLPC in the presence of $PhNH_2$ under the conditions identical with those employed in the

††† 2,6-Di-*t*-butyl-4-methylpyridine was added in order to neutralize the liberated acid which might cause the reverse reaction.

§ Although the rates for the acetolysis of *exo*-2-norbornyl brosylate were measured only at two concentrations of added KOAc,[19] the k_p–k_t pattern can be estimated to be the same as the corrected one for this system.[6]

Table 2. The Product Distribution for the Phenolysis of 1-Phenylethyl Chloride (RCl) in the Presence of Aniline in Phenol–Benzene (1:1 w/w) at 25 °C[a]

$PhNH_2$	Product distribution/%[b]						
	ROPh	o-RC_6H_4OH	p-RC_6H_4OH	RNHPh	o-$RC_6H_4NH_2$	p-$RC_6H_4NH_2$	Styrene
0.110	89.5	5.4	1.6	2.0	0.1	0.1	1.4
	(92.9)	(5.5)	(1.6)				
0.310	85.0	5.1	1.8	6.4	0.5	0.3	0.9
	(92.5)	(5.6)	(1.9)				
0.408[c]	69.0[d]	16.3[d]	14.7[d]	—	—	—	—

a) [RCl]=0.10 M. b) Determined by GLPC; (ROPh+o-RC_6H_4OH+p-RC_6H_4OH+RNHPh+o-$RC_6H_4NH_2$+p-$RC_6H_4NH_2$)%=100%: in parentheses; (ROPh+o-RC_6H_4OH+p-RC_6H_4OH)%=100%. c) In the presence of Et_3N instead of $PhNH_2$ at 40 °C; cited from Ref. 3. d) Isolated yield %.

kinetic measurements. Together with the usual phenolysis products, i.e., ROPh, o- and p-RC_6H_4OH, and styrene, the phenolysis produces minor amounts of RNHPh, o- and p-$RC_6H_4NH_2$ which were not previously detected[2] (Table 2). In the absence of aniline, no ROPh was obtained because of the rearrangement of ROPh to o- and p-RC_6H_4OH by the liberated acid.[15]

With an increase in the concentration of added $PhNH_2$, the yield% of the aniline derivatives increases, albeit still minor amounts. The yield% ratio of the phenol derivatives to the aniline ones in products can be regarded as approximately comparable with the composition of phenol and aniline in the solvolysis media. Furthermore, the ratio of ROPh to RC_6H_4OH (o- and p-) is almost invariable.§§

Such results of product analyses suggest that the added aniline in this system does not play a role of phenoxide donor, but roles of a scavenger of the liberated acid and of a competing nucleophile with an almost identical nucleophilicity with that of phenol. The effect of added $PhNH_2$ on the product distribution is compatible with the k_p–k_t profile.

Stereochemical Courses of the Phenolysis. All the substitution products for the phenolysis of optically active RCl in the presence of $PhNH_2$ (0.110 and 0.290 M) were isolated by MPLC and preparative TLC (silica gel), although ROPh alone had been isolated in the previous work.[2] The net stereochemical course was deduced for the formation of each substitution product from its optical rotation. The results are summarized along with the previously-reported ones[2] in Table 4. The absolute configurations and maximum rotations for the related 1-phenylethyl derivatives are shown in Table 3.

The configuration is partially retained for the ROPh formation and partially inverted for the p-RC_6H_4OH formation with predominant racemization, respectively, and highly inverted for the RNHPh[20] and o-$RC_6H_4NH_2$[21] formations with less racemization (Scheme 1).

Table 3. Maximum Rotations of 1-Phenylethyl Derivatives with (R)-Configuration Relevant to the Phenolysis

RX	$\alpha_{D,max}$ or $[\alpha]_{D,max}$/°
RCl	+125[a,b]
ROPh	−46.6[a,c]
o-RC_6H_4OH	+27.85[c,d]
p-RC_6H_4OH	−10.26[c,d]
RNHPh	−19.6,[e] −26.1,[f] −4.26,[a,g] −34.5[g,h]
o-$RC_6H_4NH_2$	−41.3[i]
ROMe	+135[a,j]
ROH	+45.7[a,k]

a) a) Neat, 1 dm. b) H. M. R. Hoffmann and E. D. Hughes, *J. Chem. Soc.*, **1964**, 1244. c) Ref. 3. d) In benzene. e) In methanol; the value extrapolated from data at 436, 546, and 578 nm by Wittig and Thiele (Ref. 20a) on the basis of the new value for maximum rotation of the starting RNH_2, 40.5° (A. P. Terent'ev, G. V. Pnova, G. N. Koval' and O. V. Toptygina, *Zh. Obshch. Khim.*, **40**, 1409 (1970)), from which RNHPh was synthesized. f) In ethanol; Ref. 20b. g) Ref. 20a. h) In cyclohexane. i) In chloroform; Ref. 21. j) Reported value, 120° (K. Mislow, *J. Am. Chem. Soc.*, **73**, 4043 (1951)), was recalculated on the basis of the above new value of maximum rotation for ROH, from which ROMe was synthesized. k) Ref. 8.

$$(R)\text{-}(+)\text{-RCl} + \text{PhOH} \xrightarrow{PhNH_2} (R)\text{-}(-)\text{-ROPh} + (R)\text{-}(+)\text{-}o\text{-}RC_6H_4OH + (S)\text{-}(+)\text{-}p\text{-}RC_6H_4OH + (S)\text{-}(+)\text{-RNHPh} + (S)\text{-}(+)\text{-}o\text{-}RC_6H_4NH_2 + (?)\text{-}p\text{-}RC_6H_4NH_2 + PhCH{=}CH_2$$

Scheme 1.

The retained ROPh formation (retentive phenolysis) has been confirmed in the presence of $PhNH_2$ in the phenolic solvent. For the retention % of ROPh formation, the previous[2] and new values coincide with each other within experimental errors. The retention % is somewhat smaller than that in the presence of Et_3N.[3] For 1-phenylethyl systems, some

§§ Although the isolated yield % of each product changed for the phenolysis of RCl in pure phenol at 50 °C with an increase in the NaOPh concentration,[15] direct GLPC analysis has shown that the product distribution is invariable (ROPh: o-RC_6H_4OH:p-RC_6H_4OH (%)=73:14:13) within experimental errors at variable NaOPh concentrations (0.05—0.3 M).

Table 4. The Stereochemical Courses for Products of the Phenolysis of 1-Phenylethyl Chloride (RCl) in the Presence of Aniline in Phenol–Benzene (1:1 w/w)[a]

Added base/M		Temp °C	RCl M {α_D/°}[b]	Net stereochemical course, α%, {$[\alpha]_D$/°}[c]				
				ROPh	*o*-RC_6H_4OH	*p*-RC_6H_4OH	RNHPh	*o*-$RC_6H_4NH_2$
$PhNH_2$	0.110	25	0.100 {+24.2}	17.2 Ret. (±0.9) {−1.55}[b]	7.4 Ret. (±0.7) {+0.398}	11.8 Inv. (±2.2) {+0.235}	64.0 Inv. (±3.6) {+2.43}[d]	55 Inv. (±28) {+4.4}[e]
	0.291	25	0.0970 {+24.0}	17.3 Ret. (±1.8) {−1.55}[b]	8.8 Ret. (±1.0) {+0.468}	12.2 Inv. (±2.4) {+0.241}	60.9 Inv. (±4.2) {+2.29}[d]	52 Inv. (±17) {+4.1}[e]
	0.550[f]	25	0.050	17.6 Ret.	—	—	—	—
Et_3N[g]	0.408	40	0.072	23.7 Ret.	38.1 Inv.	41.2 Inv.	—	—

a) The maximum rotations for relevant compounds in this table are shown in Table 3. b) Neat, 1 dm. c) In benzene unless otherwise noted. d) In methanol. e) In $CHCl_3$. f) Cited from Ref. 2. g) Cited from Ref. 3.

retentive solvolyses have been reported in 90% aqueous acetone,[22] 2,2,2-trifluoroethanol,[23] 97% aqueous 2,2,2-trifluoroethanol,[23] trifluoroacetic acid[24] other than in phenol solvents, whereas many inversive results have been observed.[18,23,25]

The partial retention for *o*-RC_6H_4OH formation in the presence of $PhNH_2$ is in marked contrast to the partial inversion for that in the presence of Et_3N. The direct and retentive ortho-alkylation have not been known in the phenolysis[16] except those for 1-phenylethyldiazonium salt[4] and for 2,2-dimethyl-1-(*p*-methoxyphenyl)propyl *p*-nitrobenzoate.[13] The inversion % for *p*-RC_6H_4OH formation is much lower in the presence of $PhNH_2$ than that in the presence of Et_3N. The inversion % for RNHPh and *o*-$RC_6H_4NH_2$ formation is higher than that for *p*-RC_6H_4OH and is somewhat smaller than that (87.9±9.1%) for the anilinolysis of RCl in aniline, although the reaction conditions are different from each other.§§§

The stereochemical courses for all substitution products are approximately constant within experimental errors with an increase in the concentration of added aniline (Table 4), which is consistent with the salt effects on k_p–k_t diagram and on the product distribution.

The extent of racemization is variable for each product, from 36.0% (for RNHPh) to 92.6% (for *o*-RC_6H_4OH), which indicates that the racemization can not be attributed to a simple reason.

Methanol-Perturbed Phenolysis. The competitive solvolysis of RCl has been carried out at 25 °C in phenol–methanol (85:15 w/w) solvent, which was one of binary mixture solvents adopted in the previous work.[17] The solvolysis, i.e., methanol-perturbed phenolysis, has been followed both titrimetrically and polarimetrically in the presence of Et_3N (0—0.30 M) and NaOPh (0—0.25 M), although the solvolysis was not kinetically examined before.[17]

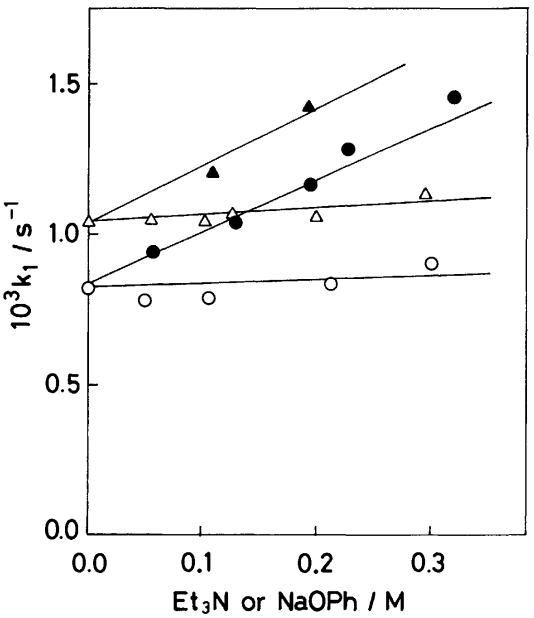

Fig. 3. Effect of added base concentration on the titrimetric and polarimetric rate constants (k_t and k_p) for the competitive solvolysis of 1-phenylethyl chloride in phenol–methanol (85:15 w/w) at 25 °C. ○ k_t, △ p_p; in the presence of Et_3N. ● k_t, ▲ k_p; in the presence of NaOPh.

The pattern of k_p–k_t diagram with k_p/k_t=1.24 (Fig. 3), analogous to that for the phenolysis in the phenol–benzene solvent (Figs. 1 and 2), indicates that all the products are derived from the reaction of Int-1 with solvent molecules, phenol and methanol, despite of the presence of the phenoxide.

The competitive solvolysis afforded ROMe together with the phenolysis products, ROPh, *o*- and *p*-R-C_6H_4OH, and styrene. The product distribution (Fig. 4) is similar to that at 50 ° C which was previously reported[17] and is invariable over the whole range of added base concentrations (0.05—0.3 M), which is consistent with the k_p–k_t profile.

§§§ Although the retentive nucleophilic substitution by aniline was recently mentioned for 1-phenylethyl benzenesulfonate in methanol,[26] the actual detailed data of stereochemical courses have not been reported.

The constancy of product distribution in the course of reaction (26.9—100%) has been confirmed at 0.110 M Et_3N concentration, showing that all the products were formed via a same reaction pathway.

Although RCl usually undergoes net inversion when solvolyzed in methanol–benzene[5] like in other common solvents,[18,23,25] the methanol-perturbation product, ROMe, and ROPh have the partially retained configurations, whereas *o*- and *p*-RC_6H_4OH's have the partially inverted ones (Table 5). These stereochemical results are approximately same as the previous results at 50 °C.[17] The stereochemical outcomes for the product formation in the presence of Et_3N (0.110 and 0.291 M) and NaOPh (0.13 M) are identical with each other within experimental errors.

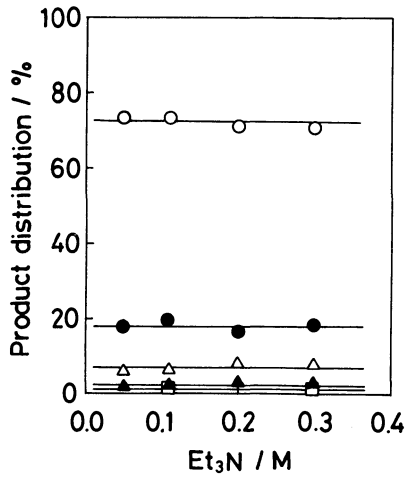

Fig. 4. Effect of added Et_3N concentration on the product distribution for the competitive solvolysis of 1-phenylethyl chloride in phenol–methanol (85:15 w/w) at 25 °C.
○ ROPh, ● ROMe, △ *o*-RC_6H_4OH, ▲ *p*-RC_6H_4OH, □ $C_6H_5CH{=}CH_2$.

That is consistent with the salt effect on the k_p–k_t diagram and on the product distribution.

For the formation of phenolysis products, ROPh, *o*- and *p*-RC_6H_4OH, the extents of racemization can be regarded as approximately identical with each other, suggesting that the phenolysis products might be derived from a single ion pair intermediate (Int-1).

Mechanism. The k_p–k_t profiles for the phenolysis and the methanol-perturbed phenolysis indicate that (i) all the products are derived from the first ion pair intermediate (Int-1), not from the second one (Int-2), (ii) the Int-1 is so reactive that it reacts with the solvent phenol or methanol molecule before it does with the added phenoxide, and (iii) the Int-1 partially returns to the substrate and partially racemizes by itself.[1,6] No contribution of phenoxide ion as a nucleophile has been confirmed by the constancy of product distribution for the phenol derivatives and that of the stereochemical course for each substitution product against an increase in added base concentration (vide supra).

These kinetic features can be expressed by the following reaction scheme, which contains a single ion pair intermediate.

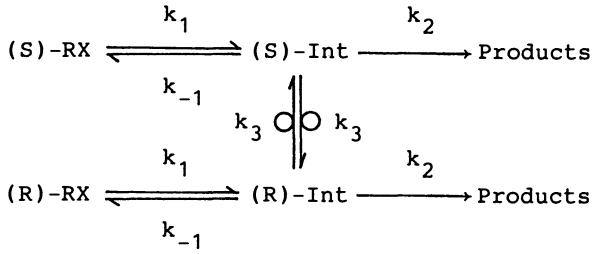

Scheme 2.

According to Scheme 1, the total rate expressions for k_p and k_t can be derived as following Eqs. 1 and 2.[1]

Table 5. The Stereochemical Courses for Products of the Competitive Solvolysis of 1-Phenylethyl Chloride (RCl) in Phenol–Methanol (85:15 w/w) in the Presence of Et_3N and NaOPh at 25 °C[a]

Added base/M		Temp	RCl	Net stereochemical course, α%, {$[\alpha]_D$/°}[c]			
		°C	M {α_D/°}[b]	ROPh	*o*-RC_6H_4OH	*p*-RC_6H_4OH	ROMe
Et_3N	0.109	25	0.102 {+19.4}	21.4 Ret. (±2.3) {−1.55}[b]	16.2 Inv. (±2.9) {−0.700}	18.3 Inv. (±8.4) {+0.291}	4.5 Ret. (±0.7) {+0.95}[b]
	0.201	25	0.102 {+19.4}	16.6 Ret. (±2.9) {−1.20}[b]	16.9 Inv. (±1.6) {−0.729}	15.1 Inv. (±10.3) {+0.241}	4.5 Ret. (±0.5) {+0.950}[b]
	0.11[d]	50	0.11	20.9 Ret.	9.4 Inv.	23 Inv.	2.5 Ret.
NaOPh	0.135	25	0.104 {+19.4}	13.9 Ret. (±2.4) {−1.21}[b]	17.1 Inv. (±2.4) {−0.878}	17.5 Inv. (±10.3) {+0.331}	5.5 Ret. (±1.7) {+1.37}[b]

a) The maximum rotations for relevant compounds in this table are shown in Table 3. b) Neat, 1 dm. c) In benzene unless otherwise noted. d) Cited from Ref. 14.

$$k_p = \frac{k_1}{1 + \{k_{-1}/(k_2 + 2k_3)\}} \quad (1)$$

$$k_t = \frac{k_1}{1 + (k_{-1}/k_2)} \quad (2)$$

where $k_2 = k_2' + k_2''[\mathrm{PhOH}] + k_2'''[\mathrm{MeOH}]$.

Structure of the Ion Pair Intermediate. For the retentive ROPh formation in the solvolysis systems, solvent-separated ion pair model (a),[7,11,27] four-center ion pair model (b),[3,4,28] and rear-side-shielded ion pair model (c)[5,13,27i] could provide reasonable explanations as a key intermediate. Althogh they were all proposed for Int-2, not for Int-1, the models (b) and (c) are also applicable to Int-1. However, the model (a) might be inapplicable to Int-1, because it should be generated only via a contact ion pair (d)[7,11,27] as Int-1 (Scheme 3).

The stereochemical courses for all the other products in the phenolysis and in the methanol-perturbed phenolysis could be explained by the use of the model (b) and its analogues, i.e., six-center ion pair models (e),[4,17] or the model (c) and its analogues, i.e., ion pairs shielded by aniline molecule from the rear-side.

Models for ion pair intermediate structure:

(a) solvent-separated ion pair model[7,11,27]

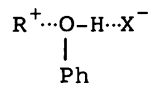

(b) four-center ion pair model[3,4,28]

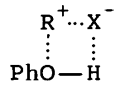

(c) rear-side-shielded ion pair model[5,13,27i]

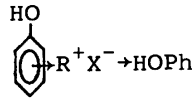

and its analogues

(d) contact ion pair model[7,11,27] $R^+X^- \rightarrow HOPh$

(e) six-center ion pair models[4,17]

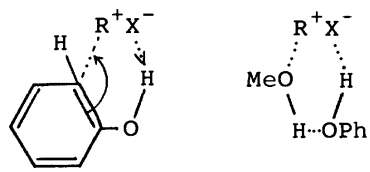

Scheme 3.

In view of the rear-side attack of phenol molecule toward R^+ of Int-1 which is predominantly occupied by the C-alkylation in the presence of Et_3N or NaOPh, the Int-1 should have an ion pair structure shielded by a phenol molecule from the rear-side. It is probable that the retentive methanolysis proceeds via models (c) ((iii) in Scheme 4).

In the presence of $PhNH_2$, the inversive alkylations of $PhNH_2$ give an indication that model (c) shielded by $PhNH_2$ might coexist with another model (c) shielded by PhOH ((iv) and (v) in Scheme 4). The aniline-shielded ion pair (c) could produce the retained alkylphenols ((vii) in Scheme 4); the *o*-isomer might be more easily formed via a six-center conformation (cf. (e) in Scheme 3) than the *p*-isomer. The formation of retained *o*-alkylphenol in the presence of $PhNH_2$ (Table 4) could suggest that the aniline-shielded ion pair (c) might be predominant. These are consistent with the other fact that the inverted *p*-alkylphenol accompanies more racemization in the presence of $PhNH_2$ than in the presence of Et_3N (Table 4). From such rear-side-shielded ion pair models, predominant formation pathway for each product may be expressed in Scheme 4.

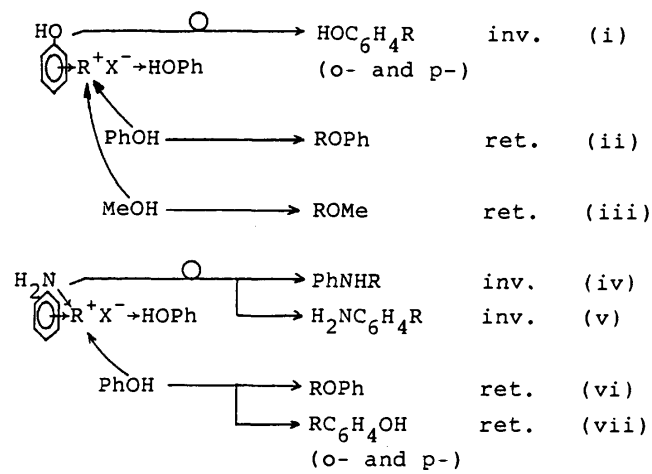

Scheme 4.

The Int-1 in this system, therefore, have an analogous ion pair structure to that for Int-2 in the phenolysis of 2,2-dimethyl-1-(*p*-methoxyphenyl)propyl *p*-nitrobenzoate.[13]

More racemization for ROMe than that for the other products suggests that a rear-side-open, not shielded, ion pair intermediate, e.g., a four-center ion pair (b) and/or a contact ion pair (d), might contribute as a minor Int-1 to the product formation.

In conclusion, (i) the reexamination of k_p–k_t profile for the phenolysis system has clarified that all the products are produced by the reaction of Int-1 with solvent phenol molecule, and (ii) the features of stereochemical outcomes for both solvolyses, the phenolysis in phenol-benzene (1:1 w/w) and the competitive solvolysis in phenol-methanol (85:15 w/w), indicate that the Int-1 might be composed of multiple ion pair intermediates with various types, not of a single one, but that the major Int-1 should be

a rear-side-shielded ion pair intermediate.

Experimental

^{13}C and ^{1}H NMR spectra were taken with a JEOL model JNM FX-100 25 MHz (FT) and Hitachi R-24 and R-600 (FT) 60 MHz instruments, respectively. IR spectra were recorded with a Hitachi model 215 spectrophotometer. Optical rotations were measured with a JASCO model DIP-SL polarimeter. GLPC was performed with a Hitachi model 163 instrument. MPLC was done with a chromatograph system composed of a FMI model RP-SY-2 pump system and a Merck silica gel 60 column. Melting points were measured on a Yamato model MP-21 apparatus.

Materials. Optically active 1-phenylethanol was obtained both by the resolution of the racemic alcohol according to the Pope-Peachey method[29] and by asymmetric reduction of acetophenone.[30] Optically active and racemic 1-phenylethyl chlorides were prepared by reactions of respective 1-phenylethanols with thionyl chloride as previously described.[2,3] Sodium phenoxide was prepared in the previously-reported manner.[31] 2,6-Di-*t*-butyl-4-methylpyridine was synthesized by a known method.[32] All the other organic reagents were of an analytical reagent grade, dried, and fractionated prior to use.

Titrimetric Rate Measurements. The usual aliquot technique[5] was employed, using cold acetone (ca. −15 °C) as a stop solution, 0.05 M NaOH (or HCl) solution as a titrating reagent, and lacmoid as an indicator. In the presence of a base, the reaction was followed to at least 80% reaction; smooth first-order linear relationships (correlation coefficient ≥0.9997) were obtained. In the absence of a base, the reaction was followed to ca. 30% completion; the initial rate constant was taken by extrapolation from rate constants at 1—13% reaction.

The rate data are shown along with polarimetric rate data in Table 1 and Figs. 1, 2, and 3.

Polarimetric Rate Measurements. (A) Phenolyses: The previous method[2] was followed. A reaction solution, prepared at the reaction temperature (25.0±0.1 °C), was immediately placed into a jacketed polarimeter tube (1 dm) maintained at 25 °C by circulation of water from a constant temperature bath kept at 25.0±0.1 °C. In each run, the reaction was followed to at least 80% conversion; a smooth first-order linear relationship was obtained (the correlation coefficients≥0.9997).

(B) Methanol-Perturbed Phenolyses: Each reaction solution ([RCl]=0.1 M, [Et_3N]=0—0.30 M; 10 ml) was kept at 25.0±0.1 °C. After a specified time, the solution was poured onto an ice-cooled mixture of 10% aq. NaOH solution (200 ml)–diethyl ether (400 ml) and immediately shaked. The ether layer was promptly separated, washed with cold 10% aq. NaCl solution, and dried. After subsequent removal of the solvent by rotary evaporation, the optical rotation of benzene solution (5 ml) of the concentrate was measured. Thus, the optical rotations at five or more specified times were graphically treated, and a smooth first-order linear relationship was obtained (the correlation coefficient≥ 0.9993).

The rate data are summarized in Table 1 and Figs. 1, 2, and 3 along with the titrimetric rate data.

Product Distribution Analysis. Product distributions for

Table 6. ^{13}C NMR Spectral Data for 1-Phenylethyl Derivatives (RX) Relevant to the Phenolysis[a]

RX	CH_3-	-C(H)-	Ar-		
ROPh	24.42(q)	75.80(d)	115.83(d)	120.53(d)	143.13(s)
			125.41(d)	127.28(d)	157.87(s)
			128.46(d)	129.22(d)	
o-RC_6H_4OH	20.96(q)	38.41(d)	115.83(d)	120.71(d)	131.98(s)
			126.72(d)	127.33(d)	145.31(s)
			127.46(d)	127.81(d)	153.17(s)
			128.52(d)		
p-RC_6H_4OH	22.02(q)	43.86(d)	115.13(d)	125.88(d)	138.67(s)
			127.46(d)	128.22(d)	146.60(s)
			128.63(d)		153.35(s)
RNHPh	24.95(q)	53.37(d)	113.25(d)	117.13(d)	145.13(s)
			125.76(d)	126.75(d)	147.19(s)
			128.52(d)	128.98(d)	
o-$RC_6H_4NH_2$	21.72(q)	40.22(d)	116.13(d)	118.65(d)	129.69(s)
			126.28(d)	127.17(d)	144.25(s)
			127.34(d)	128.63(d)	145.54(s)
p-$RC_6H_4NH_2$	21.96(q)	43.86(d)	115.07(d)	118.42(d)	136.44(s)
			125.70(d)	127.40(d)	144.25(s)
			128.28(d)		147.01(s)
ROMe	23.78(q)	79.55(d)	126.05(d)	127.28(d)	143.37(s)
			128.28(d)		

a) δ; in $CDCl_3$.

the phenolyses were analyzed by GLPC in a manner similar to that reported earlier.[1,33]

The data are shown for the phenolysis in Table 2 and for the methanol-perturbed phenolysis in Fig. 4.

Isolation of Phenolysis Products. The previous procedures[5] were followed. All substitution products were separated by MPLC and preparative TLC (silica gel). As a representative run, isolation of the products in the phenolysis of RCl in the presence of $PhNH_2$ (0.110 M) is described in the following. A solution (350 ml) of (*R*)-(+)-RCl (5.021 g, 0.03571 mol; $\alpha_D^{23.5}$ +24.2±0.1° (neat, 1 dm)), in phenol-benzene (1:1 w/w) containing aniline (0.110 M) was kept at 25.0±0.1 °C for 6 h. After usual working-up,[5] (*R*)-(−)-ROPh (4.994 g, $\alpha_D^{21.5}$ −1.55±0.08° (neat, 1 dm)), (*R*)-(+)-*o*-RC_6H_4OH (0.318 g, $[\alpha]_D^{25.8}$ +0.398±0.035° (*c* 5.773, benzene)), and (*S*)-(+)-*p*-RC_6H_4OH (0.339 g, $[\alpha]_D^{26.0}$ +0.235±0.043° (*c* 4.673, benzene)), were obtained from the organic solution. Simultaneously, (*S*)-(+)-RNHPh[20](0.132 g; mp 46.8—47.9 °C (lit,[20b] 47.5—48.1 °C); $[\alpha]_D^{31.0}$ +2.43±0.13° (*c* 2.391, methanol)), (*S*)-(+)-*o*-$RC_6H_4NH_2$[21] (0.0249 g; mp 57.0—58.2 °C (lit, 57.5—58.5 °C,[20b] 58—59 °C,[34] 58.5—59.0 °C[35]); $[\alpha]_D^{24.9}$ +4.4±0.6° (*c* 0.32, benzene)), and *p*-$RC_6H_4NH_2$(0.0073 g) were isolated from an aqueous acidic solution used for washing the organic solution.

The stereochemical data for products are tabulated along with those at 0.29 M $PhNH_2$ and the previously-reported ones in Table 4. Those for the methanol-perturbed phenolysis are summarized in Table 5.

Each solvolysis product was identified on the basis of ^1H and ^{13}C NMR and IR spectral data and chromatographic data. ^{13}C NMR spectral data for all substitution products are shown in Table 6.

Anilinolysis of 1-Phenylethyl Chloride. An aniline solution (100 ml) of (*S*)-(−)-RCl (1.505 g, 0.0107 mol; $\alpha_D^{21.2}$ −51.90±0.08° (neat, 1 dm)) was maintained at 50.0±0.1 °C for 4.5 h (ca. $t_{1/2}$×10). After removing the solvent by distillation at a reduced pressure and a usual work-up, (*R*)-(−)-RNHPh[20](1.853 g, 87.8% yield; mp 46.7—47.8 °C; $[\alpha]_D^{19.4}$ −12.6±1.3° (*c* 0.150, cyclohexane)) was isolated by chromatographic separation and distillation in vacuo.

The authors thank the Ministry of Education, Science, and Calture for a Grant-in-Aid for Scientific Research.

References

1) Part 15, T. Kinoshita, K. Shibayama, K. Ikai, and K. Okamoto, *Bull. Chem. Soc. Jpn.* **61**, 2917 (1988).

2) K. Okamoto, K. Takeuchi, and H. Shingu, *Bull. Chem. Soc. Jpn.*, **35**, 525 (1962).

3) K. Okamoto, H. Yamada, I. Nitta, and H. Shingu, *Bull. Chem. Soc. Jpn.*, **39**, 299 (1966).

4) K. Okamoto, T. Kinoshita, and H. Shingu, *Bull. Chem. Soc. Jpn.*, **43**, 1545 (1970).

5) K. Okamoto, T. Kinoshita, and Y. Osada, *J. Chem. Soc., Perkin Trans. 2*, **1975**, 253.

6) T. Kinoshita, K. Ikai, T. Kashimura, M. Fujiwara, and K. Okamoto, *Bull. Chem. Soc. Jpn.*, **59**, 2843 (1986).

7) S. Winstein and G. C. Robinson, *J. Am. Chem. Soc.*, **80**, 169 (1958).

8) K. Okamoto, T. Kinoshita, Y. Takemura, and H. Yoneda, *J. Chem. Soc., Perkin Trans. 2*, **1975**, 1426.

9) K. Okamoto, T. Kinoshita, T. Oshida, T. Yamamoto, Y. Ito, and M. Dohi, *J. Chem. Soc., Perkin Trans. 2*, **1976**, 1617.

10) S. Winstein and A. H. Fainberg, *J. Am. Chem. Soc.*, **80**, 459 (1958).

11) a) S. Winstein, E. Clippinger, A. H. Fainberg, and G. C. Robinson, *J. Am. Chem. Soc.*, **76**, 2597 (1954); b) A. H. Fainberg and S. Winstein, *ibid.*, **78**, 2767 (1956); c) A. H. Fainberg, G. C. Robinson, and S. Winstein, *ibid.*, **78**, 2777 (1956); d) S. Winstein and E. Clippinger, *ibid.*, **78**, 2784 (1956); e) S. Winstein and J. Sonnenberg, *ibid.*, **83**, 3235 (1961).

12) K. Okamoto and T. Kinoshita, *Bull. Chem. Soc. Jpn.*, **45**, 2802 (1972),

13) T. Kinoshita, K. Komatsu, K. Ikai, T. Kashimura, S. Tanikawa, A. Hatanaka, and K. Okamoto, *J. Chem. Soc., Perkin Trans. 2*, in press.

14) a) H. Hart and H. S. Eleuterio, *J. Am. Chem. Soc.*, **76**, 518 (1954); b) *ibid.*, **76**, 1379 (1954); c) H. Shingu and K. Okamoto, *Nippon Kagaku Zasshi*, **81**, 111 (1960); d) H. Hart and R. J. Elia, *ibid.*, **83**, 985 (1961); e) K. Okamoto, K. Takeuchi, and H. Shingu, *Bull. Chem. Soc. Jpn.*, **37**, 276 (1964).

15) K. Okamoto, T. Kinoshita, O. Makino, and H. Shingu, *Bull. Chem. Soc. Jpn.*, **47**, 1770 (1974).

16) H. Hart, W. L. Spliethoff, and H. S. Elueterio, *J. Am. Chem. Soc.*, **76**, 4547 (1954); although the direct retentive ortho-alkylation was reported for RCl in pure phenol, reexamination of the formation mechanism by us (Ref. 15) clarified that the retained *o*-alkylphenol is not produced by the direct alkylation, but by the rearrangement of ROPh which is caused by the liberated acid.

17) K. Okamoto, K. Komatsu, and H. Shingu, *Bull. Chem. Soc. Jpn.*, **40**, 1677 (1967).

18) P. B. D. de la Mare, D. M. Hall, and E. Mauger, *Rec. Trav. Chim. Pays-Bas*, **87**, 1394 (1968).

19) S. Winstein and D. Trifan, *J. Am. Chem. Soc.*, **74**, 1154 (1952).

20) a) G. Wittig and U. Thiele, *Justus Liebigs Ann. Chem.*, **726**, 1 (1969); b) Y. Ogata and K. Takagi, *J. Org. Chem.*, **35**, 1642 (1970).

21) M. Kawanishi, I. Otani, and H Nozaki, *Tetrahedron Lett.*, **1968**, 5575.

22) H. L. Goering, R. G. Briody, and G. Sandrock, *J. Am. Chem. Soc.*, **92**, 7401 (1970).

23) V. J. Shiner, Jr., S. R. Hartshorn, and P. C. Vogel, *J. Org. Chem.*, **38**, 3604 (1973).

24) A. D. Allen, V. M. Kanagasabapathy, and T. T. Tidwell, *J. Am. Chem. Soc.*, **107**, 4513 (1985).

25) a) J. Steigman and L. P. Hammett, *J. Am. Chem. Soc.*, **59**, 2536 (1937); b) E. D. Hughes, C. K. Ingold, and A. D. Scott, *J. Chem. Soc.*, **1937**, 1201; c) C. L. Arcus, M. P. Balfe, and J. Kenyon, *ibid.*, **1938**, 485; d) J. Hine, "Physical Organic Chemistry," McGraw-Hill Book Co., New York, (1953), p. 92; e) A. Streitwieser, Jr., *Chem. Rev.*, **56**, 571 (1956); f) K. Okamoto, N. Uchida, S. Saito, and H. Shingu, *Bull. Chem. Soc. Jpn.*, **39**, 307 (1966); g) C. K. Ingold, "Structure and Mechanism in Organic Chemistry," 2nd Ed., Cornell Univ., Ithaca, N. Y., (1969), p. 520.

26) I. Lee, H. Y. Kim, and H. K. Kang, *J. Chem. Soc., Chem. Commun.*, **1987**, 1216.

27) For recent reviews, a) S. Winstein, B. Appel, R. Baker,

and A. Diaz, *Chem. Soc., Spec. Pub.*, **19**, 109 (1965); b) C. D. Ritchie, *Acc. Chem. Res.*, **5**, 348 (1972); c) F. G. Bordwell, *ibid.*, **5**, 374 (1972); d) R. A. Sneen, *ibid.*, **6**, 46 (1973); e) D. J. Raber, J. M. Harris, and P. v. R. Schleyer "Ions and Ion Raber, J. M. Harris, and P. v. R. Schleyer "Ions and Ion Pairs in Organic Reactions," ed by M. Szwarc, John Wiley *Prog. Phys. Org. Chem.*, Vol. 11, pp. 88—174 (1974); g) T. W. Bentley and P. v. R. Schleyer, *Adv. Phys. Org. Chem.*, **14**, 1 (1977); h) D. Bethell "Reactive Intermediates," Vol. 1, ed by M. Jones, Jr., and R. A. Moss, John Wiley & Sons, New York, N. Y. (1978), Chap. 4; i) K. Okamoto, *Pure Appl. Chem.*, **56**, 1797 (1984).

28) K. Okamoto, K. Takeuchi, and T. Inoue, *J. Chem. Soc., Perkin Trans. 2*, **1980**, 842.

29) S. H. Wilen, R. Davidson, R. Spector, and H. Steffanou, *J. Chem. Soc., Chem. Commun.*, **1969**, 603.

30) S. Yamaguchi and H. S. Mosher, *J. Org. Chem.*, **38**, 1870 (1973).

31) K. Okamoto, T. Kinoshita, T. Oishi, and T. Moriyama, *J. Chem. Soc., Perkin Trans. 2*, **1978**, 453.

32) A. G. Anderson and P. J. Stang, *J. Org. Chem.*, **41**, 3034 (1976).

33) K. Okamoto, K. Matsubara, T. Kinoshita, and H. Shingu, *Bull. Chem. Soc. Jpn.*, **45**, 1191 (1972).

34) W. J. Hickinbottom, *J. Chem. Soc.*, **1934**, 319.

35) H. Hart and J. R. Kosak, *J. Org. Chem.*, **22**, 1752 (1957).

 © 1988 The Chemical Society of Japan Bull. Chem. Soc. Jpn., 61, 3283—3288 (1988)

The Catalytic Reduction of Aldehydes and Ketones with 2-Propanol over Hydrous Zirconium Oxide

Makoto SHIBAGAKI,* Kyoko TAKAHASHI, and Hajime MATSUSHITA
Life Science Research Laboratory, Japan Tobacco INC.,
6-2 Umegaoka, Midori-ku, Yokohama, Kanagawa 227
(Received April 20, 1988)

Reduction of aldehydes with 2-propanol proceeded efficiently by catalysis with hydrous zirconium oxide to give the corresponding alcohols. Most ketones also were reduced efficiently, but conjugated or sterically hindered ketones resisted the reduction. The reduction was carried out with primary, secondary, or tertiary alcohols, and only secondary alcohols served as hydrogen donors. Kinetic experiments have indicated that the reaction rate is of first-order dependence on each of the concentrations of the carbonyl compound, 2-propanol, and the catalyst. An observation of the primary isotope effect has suggested that a step of hydride transfer from absorbed 2-propanol to absorbed carbonyl compound constitutes the rate-determining step for the reduction.

The reduction of multiple bonds using an organic molecule as a hydrogen donor in place of hydrogen gas or metal hydride is known as hydrogen-transfer reaction.[1] One example is the reduction of aldehydes and ketones with metal alkoxide and alcohol. This is called the Meerwein-Ponndorf-Verley reduction. It was discovered in 1925 and has been used successfully in a number of instances.[2] Aluminium isopropoxide has been found to be the best reagent for this reduction. However, this method calls for both addition of at least 100 to 200% excess aluminium isopropoxide and neutralization of alkoxide salt with strong acid. As other catalysts for this reduction, complexes of cobalt,[3] iridium,[4,5] rhodium,[6-8] ruthenium,[8,9] indium,[10] molybdenum,[11] and zirconium[12] have been reported. Although these catalysts have many advantages over conventional metal alkoxides, the isolation of products is always attended by tedious workups.

Heterogeneous methods for the reduction are known, and zeolite[13] and oxides of aluminium,[14] magnesium,[15] silicon,[15] calcium[15,17] barium,[15] strontium,[15] zirconium,[16] titanium,[16] vanadium,[16] molybdenum,[16] zinc,[16] thorium,[16] and lanthanoid groups[18] have been reported to be successful catalysts. These methods have several advantages in the isolation of products. However, they need to be carried out in the vapor phase, and require high reaction temperatures and flow reactor systems.

Posner et al.[19] reported that dried chromatographic alumina served as a catalyst in the liquid phase. Several aldehydes and ketones could be reduced by use of this catalyst, and products were easily isolated by filtering-off of catalyst and subsequent evaporation of solvent. However, this reduction requires water-free conditions and a large amount of catalyst. In our previous paper,[20] we briefly reported that the reduction of aldehydes and ketones with 2-propanol proceeded efficiently over hydrous zirconium oxide in the liquid phase. The hydrous oxide is available in the form of hard and translucent granules, of which X-ray diffraction analysis has shown to be amorphous.

Reduction with hydrous zirconium oxide has the following advantages: 1) the reduction does not call for strong acid treatment; 2) the products are easily isolated by filtering-off of catalyst and subsequent evaporation of solvent, because this catalyst is insoluble in any solvents; 3) hydrous zirconium oxide is stable at room temperature in air for 7 years, and can be used for repeated reductions; 4) hydrous zirconium oxide is not sensitive to air or water, and the reduction does not require water-free conditions.

In this paper, we will report the scope and limitation of the reduction of carbonyl compounds with alcohols catalyzed by hydrous zirconium oxide. A proposition of the mechanism of this reaction also will be described.

Experimental

Materials. Commercial reagents were used for the reduction without further purification. 2-Propan-2-*d*-ol was prepared by the reduction of acetone with sodium borodeuteride.

Hydrous Zirconium Oxide. To a solution of zirconium(IV) dichloride oxide ($ZrOCl_2 \cdot 8H_2O$) (200 g of solid in 10 dm^3 deionized water) was slowly added an aqueous solution of sodium hydroxide (1 mol dm^{-3}) at room temperature. Constant gentle stirring was maintained and the addition was continued until the pH of the resulting solution reached 6.80. The solution was allowed to stand for 48 h at room temperature. The resulting product was filtered and washed free from chloride ions. The gel was spread on a glass plate and dried in air at room temperature for 10 h and at 80 °C for 2 h. Fifty four grams of hydrous zirconium oxide was obtained in the form of granules, and was heated at 300 °C for 5 h.

General Procedure for the Reduction of Aldehydes and Ketones with 2-Propanol. In a 25 cm^3 round-bottom flask equipped with a reflux condenser was placed hydrous zirconium oxide (24—60 mesh; 1.0 or 2.0 g), an aldehyde or ketone (5 mmol), 2-propanol (10 cm^3), and a hydrocarbon (0.5 mmol) as an internal standard. The contents were heated under gentle reflux. The reaction mixture was collected at appropriate times after refluxing, and the

concentration of the products were analyzed by GLC (a capillary column PEG 20M 30 m). The identification of the products was made by comparison of retention times in gas chromatography with those of authentic samples.

Reduction of Hexanal with Several Alcohols. In a 10 cm^3 round-bottom flask equipped with a reflux condenser was placed hydrous zirconium oxide (24—60 mesh; 0.2 g), hexanal (1.0 mmol), an alcohol (2.0 cm^3), and dodecane (0.1 mmol) as an internal standard. The contents were placed in an oil bath kept at 78.0 °C (±0.1 °C). The analysis of the products was performed in a simlar manner as described above.

Kinetic Experiment. All experiments are carried out in a 10 cm^3 round-bottom flask equipped with a reflux condenser. The concentrations of a carbonyl compound and a hydrocarbon as an internal standard were always 0.5 and 0.05 mol dm^{-3}, respectively, and 2 cm^3 of 2-propanol was used as both reductant and solvent. In the case of the reduction of hexanal, benzaldehyde, cyclohexanone, and acetophenone, the amount of catalyst was usually 0.2, 0.2, 0.1, 0.4 g, respectively. The reaction was performed in a similar manner as described above.

Results and Discussion

Reduction of Aldehydes. The reduction of aldehydes yielded the corresponding alcohols. Essentially no by-products could be detected. A linear correlation between the natural logarithm of the carbonyl concentration and the reaction time was obtained. This result indicates that the reduction rate is of pseudo-first-order in the carbonyl concentration. The rate of the reaction is represented by

$$r = k' \cdot [C], \quad (1)$$

where k' and [C] are the pseude-first-order rate constant and the concentration of carbonyl compound, respectively. The rate constants and yields are listed in Table 1. Generally, the reduction of aldehydes proceeds efficiently, and the steric hindrance around the carbonyl group does not interfere with the reduction. The reduction of conjugated aldehydes also proceeds efficiently to give allylic alcohols selectively.

Reduction of Ketones. Rate constants for the reduction of ketones were obtained in the similar manner as those for aldehydes and are listed in Table 2. Cyclohexanone and 4-methylcyclohexanone were reduced faster than 2-methylcyclohexanone. An α-substituted methyl group seems to interfere with the access of a carbonyl group to the active site of the catalyst. The slow reduction of camphor, 3-decanone, and benzophenone can be attributed to the steric

Table 1. Reduction of Several Aldehydes[a]

Entry	Reductant	Product	Yield/% (h)[b]	$k^{c}/10^{-4}$ s^{-1}
1			93 (6)	1.236
2			88 (6)	0.972
3	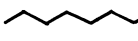	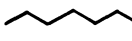	93 (6)	1.306
4			81 (6)	0.764
5		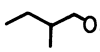	80 (6)	0.744
6		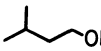	82 (6)	0.778
7	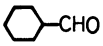		99 (6)	1.894
8	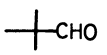		99 (4)	3.128
9	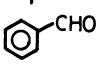		98 (6)	1.902
10	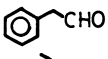		90 (6)	1.083
11	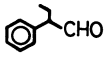		81 (6)	0.781
12	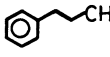		96 (6)	1.586
13	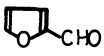		99 (6)	2.108
14	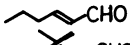		92 (6)	1.186
15	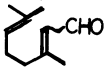		97 (6)	1.689

a) Aldehyde 5 mmol, 2-propanol 10 cm^3, cat. 1.0 g, reflux temperature of 2-propanol. b) Reaction time. c) Rate constant.

Table 2. Reduction of Several Ketones[a]

Entry	Reductant	Product	Yield/% (h)[b]	$k^{c)}/10^{-4}$ s^{-1}
1			99 (2)	7.188
2			91 (6)	1.110
3	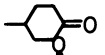	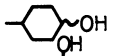	99 (2)	7.016
4			77 (6)	0.684
5			70 (10)	0.334
6			62 (20)	0.134
7			84 (6)	0.894
8			81 (10)	0.462
9	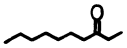	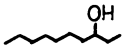	63 (20)	0.138
10			tr.	—[d]
11			68 (20)	0.156
12			98 (6)	1.816
13	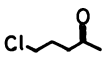	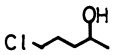	64 (10)	0.284
14			84 (10)	0.516
15			68 (20)	0.156
16		——	tr.	—[d]
17	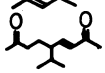	——	tr.	—[d]
18		——	tr.	—[d]
19		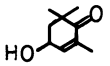	58 (10)	0.238
20		——	tr.	—[d]
21		——	tr.	—[d]

a) Ketone 5 mmol, 2-propanol 10 cm^3, cat. 1.0 g, reflux temperature of 2-propanol. b) Reaction time. c) Rate constant. d) Rate const. $<1\times10^{-6}$ s^{-1}.

hindrance. The presence of a double bond conjugated to the carbonyl group serves to slow down the rate of some reactions, although the reduction of 2-cyclohexen-1-one, 3-methyl-2-cyclohexen-1-one, and 2,6,6-trimethyl-2-cyclohexene-1,4-dione did proceed. The chloride substitution at the α-position increased the reduction rate, but at the γ-position it did not affect the rate. This suggests that electronic factors have some influence on the reaction.

Alcohols as Hydride Sources. The reduction of hexanal was carried out with some alcohols as well as with 2-propanol. The results are listed in Table 3. When primary alcohols were used, the acetalization proceeded faster than the reduction. Hexanal diethyl acetal and hexanal dimethyl acetal were obtained in 91 and 100% yields, respectively. Tertiary alcohol or methanol did not work as hydride donors. Basically, only secondary alcohols could be used.

Dependence on Catalyst Amount. For determining the order in catalyst amount, reduction rates of hexanal, cyclohexanone, and acetophenone were measured with 0.02—1.0 g of the catalyst. As shown in Fig. 1, the pseudo-first-order rate constants, k', were proportional directly to the amount of catalyst. Hence the specific rate constant, k, is to be introduced as

$$r = k'/[\text{cat.}], \quad (2)$$

where [cat.] is the concentration of catalyst.

Dependence on Reaction Temperature. In order to investigate the dependence on reaction temperature,

Table 3. Reduction of Hexanal with Several Alcohols[a]

Entry	Reductant	k[b]/10^{-4} s^{-1}
1	$(CH_3)_2CHOH$	0.514
2	Cyclohexanol	0.116
3	$C_6H_5CH(OH)CH_3$	0.447
4	CH_3CH_2OH	—[c]
5	CH_3OH	0[d]
6	$(CH_3)_3COH$	0

a) Hexanal 1 mmol, alcohol 2 cm^3, cat. 0.2 g, 78.0 °C. b) Rate constant. c) Reduction was slow ($<10^{-6}$ s^{-1}), and the main product was diethyl acetal (91% yield). d) Only dimethyl acetal was obtained (100% yield).

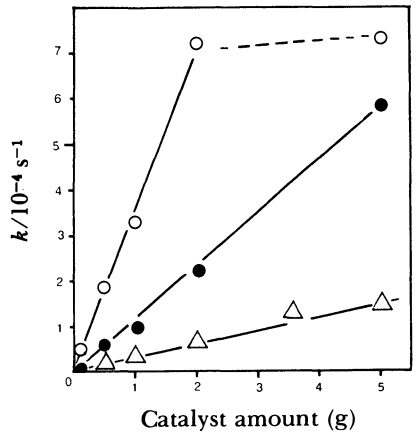

Fig. 1. The dependence of catalyst amount.
Carbonyl compound 5 mmol, 2-propanol 10 cm^3, reaction temperature 78.0 °C.
●; Hexanal. O; Cyclohexanone. △; Acetophenone.

the reduction of hexanal, benzaldehyde, cyclohexanone, or acetophenone was carried out at 59.0—82.5 °C. The natural logarithm of the specific rate constant, k, vs. the reciprocal of the absolute temperature, that is, the Arrhenius plot, is shown in Fig. 2. As can be seen from the figure, a good straight line is obtained. From the inclination of the line, the activation energies of these reductions were estimated, which are listed in Table 4.

Effect of Alcohol Concentration. The influence of the concentration of 2-propanol upon the reduction rate was investigated for the reduction of hexanal, benzaldehyde, cyclohexanone, and acetophenone under the following conditions: the amount of 2-propanol was changed in the range from 2 to 0.5 cm^3 and toluene as a diluent was added in order to keep the volume of reaction mixture constant. The correlation between the concentration of 2-propanol and the specific rate constant, k, is shown in Fig. 3. In all cases, similar rate constants were obtained, and the concentration of 2-propanol did not affect the reaction rate under the present experimental conditions. However, decreasing the ratio of 2-propanol to the carbonyl compound changed the reaction rate. When

Table 4. Activation Energies[a]

Carbonyl compound	Cat./g	ΔE^*/kcal mol^{-1}
Hexanal	0.2	13.7
Cyclohexanone	0.1	12.3
Benzaldehyde	0.2	10.5
Acetophenone	0.4	12.5

a) Carbonyl compound 1 mmol, 2-propanol 2 cm^3 reaction temperature 60.0—85.0 °C.

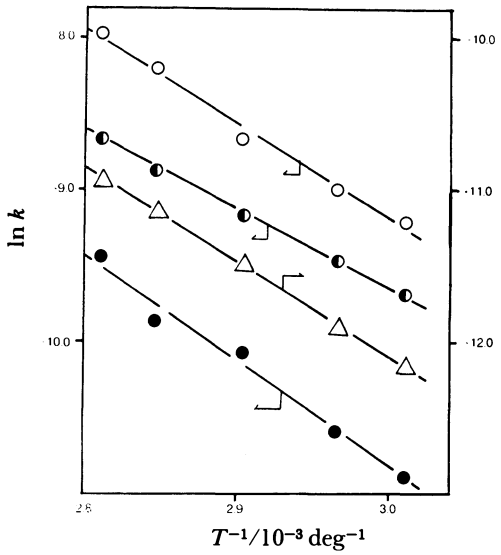

Fig. 2. Arrhenius plot.
Carbonyl compound 1 mmol, 2-propanol 2 cm^3.
●; Hexanal (cat. 0.2 g). O; Cyclohexanone (cat. 0.1 g). ◐; Benzaldehyde (cat. 0.2 g). △; Acetophenone (cat. 0.4 g).

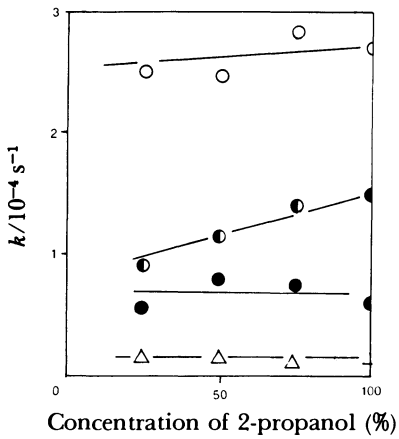

Fig. 3. The dependence of the concentration of 2-propanol.
Carbonyl compound 1 mmol, reaction temperature 78.0 °C. ●; Hexanal (cat. 0.2 g). O; Cyclohexanone (cat. 0.1 g). ◐; Benzaldehyde (cat. 0.2 g). △; Acetophenone (cat. 0.4 g).

the ratio of 2-propanol to hexanal, benzaldehyde, cyclohexanone, or acetophenone was 1 to 1, a linear correlation between the reciprocal of the concentra-

Table 5. Isotope Effect[a)]

Carbonyl compound	Cat./g	k_H/k_D
Hexanal	0.2	2.32
Cyclohexanone	0.1	2.16
Benzaldehyde	0.2	2.29
Acetophenone	0.4	2.46

a) Carbonyl compound 1 mmol, alcohol 2 cm^3 reaction temperature 78.0 °C.

tion of the carbonyl compound and the reaction time was observed in the early stage of reaction. This result indicates that the initial reaction rate is of second order under these conditions. Furthermore, when their ratio was 2 to 1, the following relationship was obtained:

$$\log_e\{([C_0]-[C])/(2\cdot[C_0]-[C])\} = k''\cdot[C_0]\cdot t, \quad (3)$$

where $[C_0]$, $[C]$, and k'' are the initial carbonyl concentration, the carbonyl concentration, and the pseude-second-order rate constant, respectively.

Isotope Effect. The reduction of hexanal, benzaldehyde, cyclohexanone, and acetophenone was performed with 2-propan-2-*d*-ol in place of 2-propanol. The primary isotope effects k_H/k_D of the reactions, which are listed in Table 5, are larger than 2, which indicates that the C–H bond at the 2-position in 2-propanol is broken in the transition state.

Kinetic Discussion. As described above, the reaction rate is of first-order dependence on each of the concentrations of the carbonyl compound, 2-propanol, and the catalyst, as represented by

$$r = k\cdot[C]\cdot[A]\cdot[\text{cat.}], \quad (4)$$

where k, [C], [A], and [cat.] are the rate constant and the concentrations of the carbonyl compound, 2-propanol, and the catalyst, respectively. These results suggest that the rate-determining step is to be assigned to the step subsequent to the adsorption of 2-propanol and carbonyl on the catalyst. Taking the mechanism into account, we should like to propose a scheme. Based on the proposed scheme, the reduction rate is expressed by

$$r = \frac{k_1\cdot k_2\cdot k_3\cdot[C]\cdot[A]\cdot[\text{cat.}]}{k_{-1}\cdot(k_2+k_{-2})+k_2\cdot k_3[C]}. \quad (5)$$

The observation of the primary isotope effect suggests that the step of the hydride transfer from 2-propanol to a carbonyl compound, that is, the third step in the scheme, constitutes the rate-determining step. Therefore, k_3 is far less than k_{-2}, and the rate equation is rewritten to

$$r = \frac{k_1\cdot k_3\cdot[C]\cdot[A]\cdot[\text{cat.}]}{k_{-1}/K_2+k_{-3}\cdot[C]}. \quad (6)$$

where $K_2=k_2/k_{-2}$. Furthermore, $k_{-1}/K_2 \gg k_3\cdot[C]$, hence the rate equation becomes

$$r = K_1\cdot K_2\cdot k_3\cdot[C]\cdot[A]\cdot[\text{cat.}], \quad (7)$$

where $K_1=k_1/k_{-1}$. This equation apparently corresponds to Eq. 4, and the proposed scheme may be concluded to be reasonable. A similar mechanism[17] has been proposed for the Meerwein–Ponndorf–Verley reduction with hydroapatite catalyst, leading to estimation of its activation energy as 12±2 kcal mol^{-1}, which is the same with our case (see Table 4).

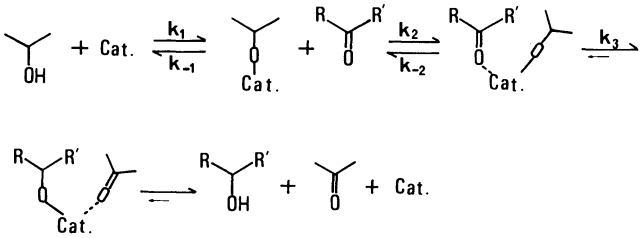

References

1) G. Brieger and T. J. Nestrick, Chem. Rev., **74**, 567 (1974).
2) A. L. Wilds, *Org. React.*, **2**, 178 (1944).
3) M. Onishi, M. Matsuda, and K. Hiraki, *Chem. Lett.*, **1984**, 1157.
4) F. Martinelli, G. Mestroni, A. Camus, and G. Zassinovich, *J. Organomet. Chem.*, **220**, 383 (1981).
5) E. Farnetti, F. Vinzi, and G. Mestroni, *J. Mol. Catal.*, **24**, 147 (1984).
6) G. Fragale, M. Gargano, and M. Rossi, *J. Mol. Catal.*, **5**, 65 (1979).
7) D. Beaupere, L. Nadjo, R. Uzan, and P. Bauer, *J. Mol. Catal.*, **14**, 129 (1982); **20**, 185 (1983); **20**, 195 (1983).
8) V. Z. Sharf, L. K. Freidlin, and V. N. Krutii, *Izv. Akad. Nauk SSSR, Ser. Khim.*, **1977**, 735.
9) J. Blum, S. Shtelzer, D. Albin, and Y. Sasson, *J. Mol. Catal.*, **16**, 167 (1982); M. Bianchi, U. Matteoli, P. Frediani, G. Menchi, and F. Piacenti, *J. Organomet. Chem.*, **236**, 375 (1982); *ibid.*, **240**, 59 (1982).
10) A. Miyamoto and Y. Ocino, *J. Catal.*, **43**, 143 (1976).
11) T. Tatsumi, M. Shibagaki, and H. Tominaga, *J. Mol. Catal.*, **13**, 331 (1981).
12) Y. Ishii, T. Nakano, A. Inada, Y. Kishigami, K. Sakurai, and M. Ogawa, *J. Org. Chem.*, **51**, 240 (1986).
13) Z. V. Gryaznova, G. V. Tsitsishvili, and T. M. Ramishvili, *Vestn. Mosk. Univ. Khim.*, **16**, 357 (1975); *Neftekhimiya*, **16**, 65 (1976).
14) L. H. Klemm and D. R. Taylor, *J. Org. Chem.*, **35**, 3216 (1970).
15) H. Niiyama, and E. Echigoya, *Bull. Jpn. Petrol. Inst.*, **14**, 83 (1972); *Bull. Chem. Soc. Jpn.*, **45**, 938 (1972).
16) L. K. Freidlin, V. Z. Sharf, E. N. German, N. K. Vorb'eva and S. I. Shcherbakova, *Izv. Akad. Nauk SSSR, Ser. Khim.*, **1970**, 2130.
17) C. L. Kibby and W. Keithhall, *J. Catal.*, **31**, 65 (1973).

18) K. M. Minachev, O. K. Atal'yan, and M. A. Markov, *Izv. Akad. Nauk SSSR, Ser. Khim.*, **1978**, 2737.
19) G. H. Posner, A. W. Runquist, and M. J. Chapdelaine, *J. Org. Chem.*, **42**, 1202 (1977).
20) H. Matsushita, S. Ishiguro, H. Ichinose, A. Izumi, and S. Mizusaki, *Chem. Lett.*, **1985**, 731.

 © 1988 The Chemical Society of Japan Bull. Chem. Soc. Jpn., 61, 3289—3293 (1988)

Reaction of 2-Hydroxyacetophenones with Thionyl Chloride in the Presence of a Catalytic Amount of Pyridine[1)]

Syed Mashhood ALI, Mohd ILYAS,† and Shigeo TANIMOTO
Institute for Chemical Research, Kyoto University, Uji, Kyoto 611
(Received April 22, 1988)

Reaction of 2-hydroxyacetophenone (**5**) with excess thionyl chloride in the presence of a catalytic amount of pyridine at room temperature afforded a thiirane **6**, while 2-hydroxy-4-methoxyacetophenone (**7**) furnished **8** when subjected to almost identical conditions. The products were characterized by microanalyses data and spectroscopic techniques including the mass spectroscopy. Plausible mechanisms for the conversions have been proposed in the light of available literature.

Thionyl chloride is routinely used as a chlorinating agent for many different substrate types.[2)] The course of the reaction of active methylene compounds with thionyl chloride seems unpredictable and so-called abnormal products have been reported in many cases[3)] often without further detailed investigations. The reaction of acetophenone (**1**) with $SOCl_2$ in the presence of a catalytic amount of pyridine furnishes **2** and **3**.[4,5)] The mechanism proposed for this reaction involves the intermediacy of α-oxobenzenethionyl chloride (**4**). However, the literature reveals that there is controversy over the existence of **4**[4,5)] and that little is known about the chemistry of related compounds with adjacent C=O and C=S functions.

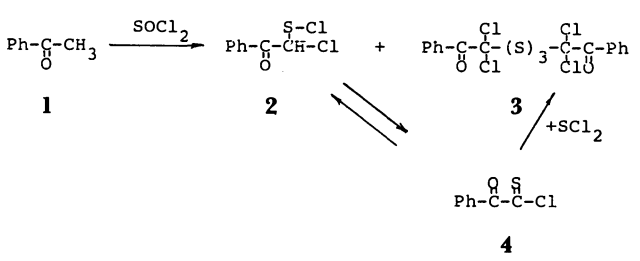

We have investigated the reaction of some 2-hydroxyacetophenones with excess of thionyl chloride in the presence of a catalytic amount of pyridine in an attempt to obtain cyclic α-oxothiocarboxylic esters with the aim to further the available information on the reaction intermediates and also to explore the synthetic potential of the products. We wish to report our results in this manuscript.

Results and Discussion

The reaction of 2-hydroxyacetophenone (**5**) with excess of thionyl chloride in the presence of a catalytic amount of pyridine at room temperature afforded a red gummy mass which was subjected to column chromatography. Elution with petroleum ether–benzene (1:1) yielded **6**. Further elution of the column with more polar solvents gave a gummy mixture which could not be resolved even on repeated column chromatography. When 2-hydroxy-4-methoxyacetophenone (**7**) was treated with excess $SOCl_2$, under almost identical conditions, also a red gummy mass was obtained which was subjected to column chromatography. Elution of the column with petroleum ether–benzene (4:1) furnished a white solid which was crystallized from petroleum ether–benzene to give white crystals of **8**. Attempts to resolve the complex tar obtained on further elution with more polar solvents were not successful. The structures of **6** and **8** were established with the help of microanalyses and spectroscopic data.

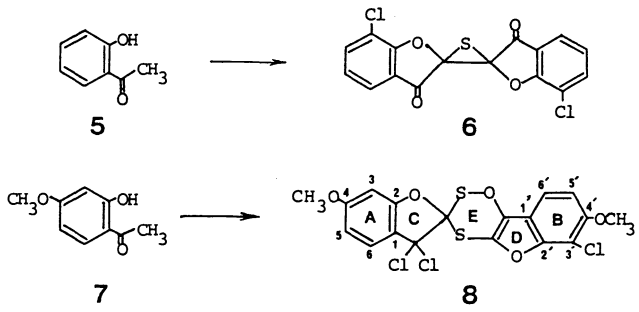

Compound **6** analyzing for $C_{16}H_6Cl_2O_4S$ gave a positive Beilstein test indicating the presence of halogen. The presence of chlorine in **6** was clearly shown by the isotopic clusters in the mass spectrum and confirmed by microanalysis. Its IR spectrum displayed bands at 1725 (five membered ketone) and 690 (C–Cl). The ^1H NMR spectrum exhibited only the signals for aromatic protons as a multiplet in the region δ 7.00—8.00 displaying the 1,2,3-trisubstituted nature of the aromatic rings. The actual structure could only be elucidated by taking into account the mass fragmentation pattern of **6**. The mass spectrum did not exhibit the molecular ion peak expected at *m/z* 364, however, the peak with the highest mass to charge ratio was recorded at *m/z* 332 along with the isotopic peaks at *m/z* 334 and 336 whose relative intensities supported the presence of two chlorine atoms in this fragment. The formation of this fragment can be explained by the elimination of sulfur from the molecular ion (Chart 1). The most

† Department of Chemistry, Aligarh Muslim University, Aligarh, India.

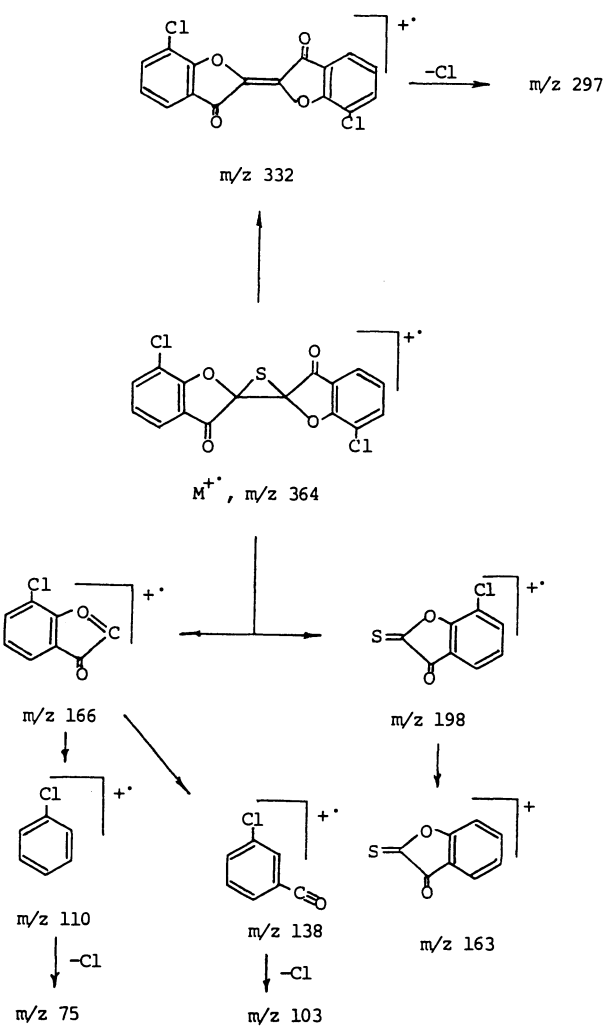

Chart 1.

diagnostic fragmentation was the fission of the molecule into two fragments recorded at *m/z* 166 (base peak) and 198 (11.52) accompanied by the isotopic peaks at *m/z* 168 (33.00) and 200 (3.84), respectively. The loss of chlorine from the ion at *m/z* 198 can give an ion at *m/z* 163, while the fragments at m/z 103, 110, and 138 can be derived either directly from the molecular ion or from the fragments with *m/z* 166 and 198. The position of the chlorine in the aromatic rings was located with the help of NMR data and taking into account the mechanistic considerations. On the basis of above discussion, two possibilities can be drawn, either a thiirane **6** or a 1,3-oxathiole **9**. The absence of an enol ether band in the IR spectrum, characteristic of 1,3-oxathiole skeleton,[6] helped in eliminating this possibility. The compound was, therefore, characterized as thiirane **6**.

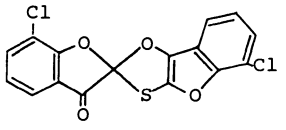

9

Compound **8** analyzing for $C_{18}H_{11}Cl_3O_5S_2$ also gave a positive Beilstein test. The presence of chlorine was confirmed by microanalysis and mass spectral data. Its IR spectrum displayed bands at 1610 (C=C), 1230 (enol ether), and 690 (C–Cl). The NMR spectrum proved comparatively more useful and clearly showed the presence of a chlorine in one of the aromatic rings. Two ortho-coupled doublets (J=9 Hz), each for one proton, at δ 7.44 and 7.80 were attributed to the protons at C-6 and C-6′, respectively. A high-field singlet at 6.54 ppm for one proton was due to C-3 proton. The signal for the C-5 and C-5′ protons merged and appeared as a multiplet centered at δ 6.75. Though the two methoxyl groups have slightly different environment, their signals appeared as a broad singlet at δ 3.80. The actual structure was, however, elucidated with the help of mass fragmentation pattern of **8** (Chart 2). The molecular ion peak could not be recorded in this case also and the peak at *m/z* 441 was the one with the highest mass to charge ratio accompanied by isotopic peaks at *m/z* 443 and 445, whose relative intensities showed the presence of two chlorine in this fragment. The formation of this fragment can be explained by the loss of a chlorine atom from the molecular ion. The most diagnostic peaks were those resulting by the retro-Diels–Alder fission of the ring E recorded at *m/z* 213 and 228. Another significant peak at *m/z* 214 was attributed to the doubly charged ion formed by the loss of sulfur monoxide from the $M^{+\cdot}$. The fragments derived from this ion were recorded at *m/z* 323, 358, 378, and 393. The above data grossly confirms the structure **8**. There are however few points which should be mentioned here. The assignment of chlorine on the ring A rather than on ring B is fully supported by the mass fragmentation pattern. Compound **10** was also taken into consideration. The possibility was however ruled out because there are few peaks which can only be explained by the loss of SO from the $M^{+\cdot}$ and this is not possible from **10**.

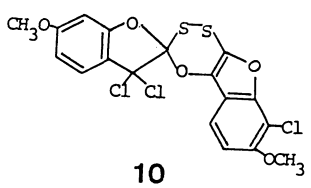

10

The reaction of active methylene compounds with $SOCl_2$ proceeds either by *O*- or *C*-sulfinylation. *O*-Sulfinylation of carbonyl compounds leads to either *gem*-dichlorides[7] or α-monochloro ketones, while *C*-sulfinylation gives rise to α-chlorosulfinyl ketones. These products may then undergo further transformations to give a variety of products. The formation of **6**

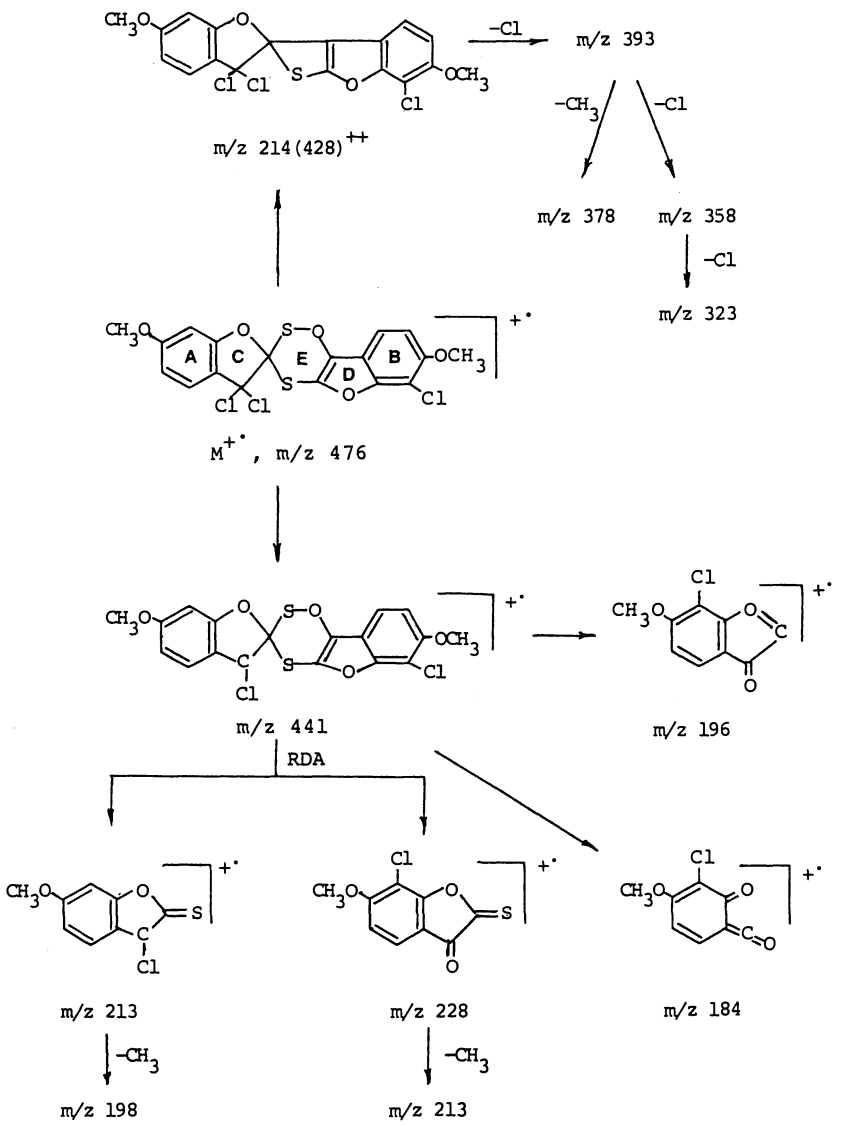

Chart 2.

and **8** can be explained by a combination of these processes.

There are some reports on the formation of thiirane from active methylene compounds by the reaction with $SOCl_2$.[8] A plausible mechanism for the formation of **6** from **5** can be outlined as in Scheme 1, in analogy to the precedent examples. *O*-Sulfinylation of both the hydroxyl as well as carbonyl functions of **5** can lead to **11** which can yield **12** by Cl migration accompanied by the loss of sulfur monoxide. Compound **13** can be obtained from **12** either by route (a) or (b). The loss of HCl from **13** followed by dimerization accompanied by the loss of SO_2 may furnish thiirane **6**.[8] It is important to mention here that the chlorination of phenol with $SOCl_2$ has never been observed and there is only one recent report which describes the chlorination of an aromatic compound with $SOCl_2$.[9]

The mechanism for the formation of **8** is not very clear, however, a probable mechanism can be outlined as in Scheme 2. α-Chlorosulfenyl chlorides **17** and **20** can be obtained from sulfinyl chlorides **16** and **19**, respectively, by the Pummerer rearrangement.[10] α-Oxo thiocarboxylic esters **18** and **21** can be obtained from **17** and **20**, respectively, by the loss of two molecules of HCl. [4+2]Cyclodimerization of **18** and **22** can lead to **8**. Though the probability of conversion of $\rangle C{=}O$ to $\rangle CCl_2$ after the dimerization also exists, we think that in such a case [4+4] addition would have been more preferable. It is not clear why the other mode of cyclization which could give compound **10** was not preferred. Though the mechanism proposed is purely speculative, it is most appropriate in the light of available data. It is clear that the two substrates show different behavior towards the reagent and since there are many factors such as nature of the substrate, amount and

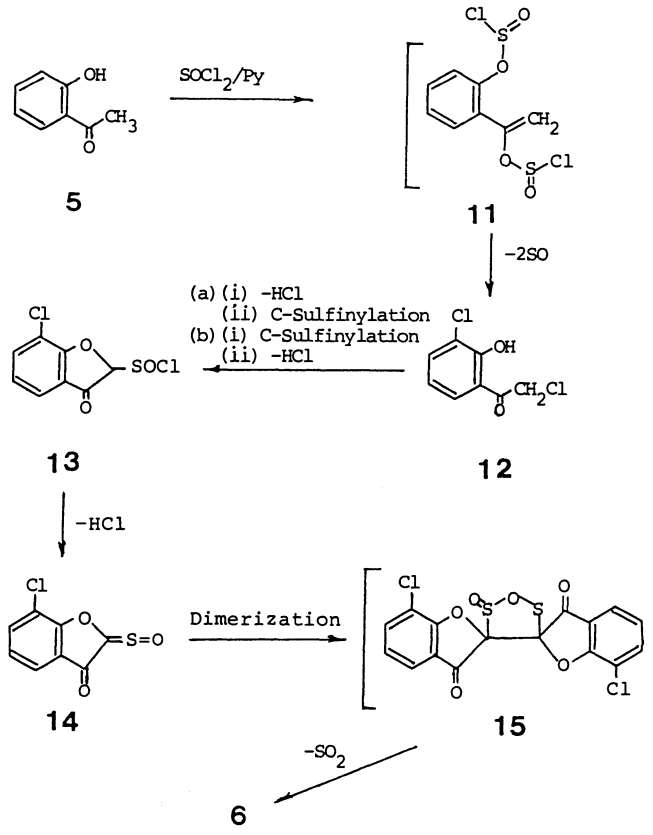

Scheme 1.

concentration of the reagent used, the order of addition, solvent and temperature, which affect the course of the reaction, it is difficult to explain the difference in their behavior at this stage.

In conclusion, the present manuscript describes the reaction of two 2-hydroxyacetophenones **5** and **6** with excess $SOCl_2$ in the presence of a catalytic amount of pyridine to furnish **6** and **8**, respectively. Though the yields are not high, the accomplishment of these complicated spiro skeleton in a single step from readily available starting materials is quite significant. The plausible mechanisms and their fragmentation patterns have been discussed. Nuclear chlorination with $SOCl_2$ of the aromatic systems has been observed which has only one precedence.

Experimental

All melting points were recorded on a Kofler microscopical hot stage and are uncorrected. Infrared spectra were obtained on a Pye Unicam SP3-100 spectrophotometer. Ultraviolet spectra measured on a Pye Unicam PU 8800 instrument. NMR spectra were recorded on a 60 MHz Varian A60D instrument using TMS as internal standard. Mass spectra were recorded with a JEOL JMS-D300 spectrometer at 70 eV.

Reaction of 2-Hydroxyacetophenone (5) with Thionyl Chloride in the Presence of a Catalytic Amount of Pyridine. 2-Hydroxyacetophenone (4.0 g, 29.4 mmol) was

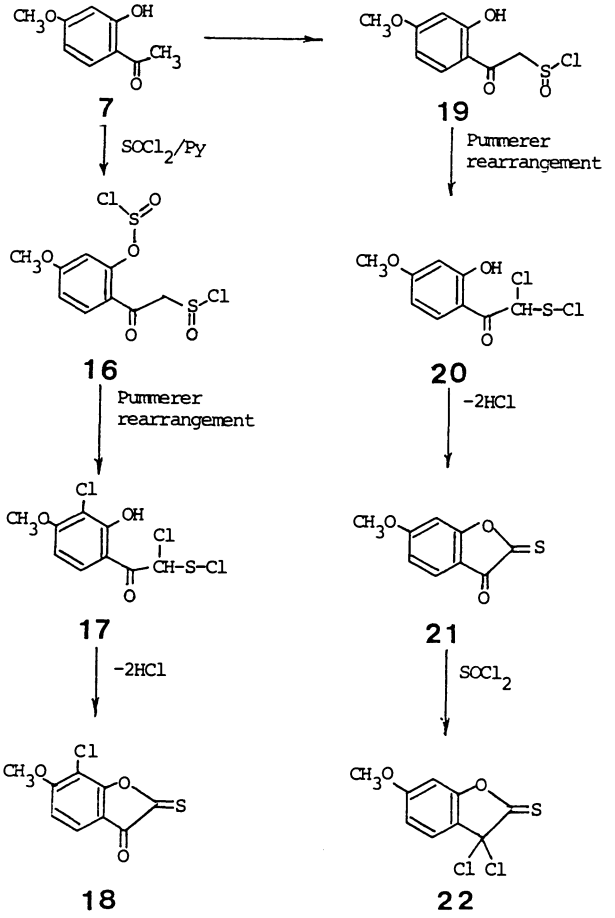

Scheme 2.

dissolved in thionyl chloride (52.5 g, 44.0 mmol) and a catalytic amount of pyridine (0.46 g, 0.58 mmol) was added. The contents were stirred at room temperature for 3 h. Excess $SOCl_2$ was removed at room temperature under reduced pressure to give a red gummy mass which was subjected to column chromatography over silica gel. Elution with petroleum ether–benzene (1:1) afforded a light pink solid, crystallized from $CHCl_3$–MeOH mixture to furnish white crystals of thiirane **6** (1.45 g, 27%), mp 160—162 °C; IR (KBr): ν_{max} 2940, 1725, 1610, 1590, 1470, 1450, 1320, 1295, 1215, 1190, 1140, 1100, 1060, 1000, 860, 830, 750, 730, 690, 640 cm^{-1}; UV (MeOH): λ_{max} 240, 290 nm; ^1H NMR ($CDCl_3$): δ=7.00—8.00 (m, Ar-H); MS (rel. int.): *m/z* 336 (4.01), 335 (3.68), 334 (21.76), 333 (3.05), 332 (33.27), 298 (1.94), 200 (3.84), 198 (11.52), 168 (33.00), 167 (2.50), 166 (100.00), 163 (18.21), 137 (10.30), 112 (8.90), 110 (35.32), 103 (18.45), 92 (15.00), 75 (40.35). Found: C, 52.52; H, 1.51; Cl, 19.18%. Calcd for $C_{16}H_6Cl_2O_4S$: C, 52.62; H, 1.66; Cl, 19.42%.

Reaction of 2-Hydroxy-4-methoxyacetophenone (7) with Thionyl Chloride in the Presence of a Catalytic Amount of Pyridine. To a solution of 2-hydroxy-4-methoxyacetophenone (3.0 g, 18 mmol) in thionyl chloride (32.26 g, 27.0 mmol) was added a small amount of pyridine (0.03 g,

0.36 mmol). The reaction mixture was stirred at room temperature for 3 h. Excess $SOCl_2$ was then removed at room temperature under reduced pressure to get a red gummy mass which was subjected to column chromatography over silica gel. Elution with petroleum ether–benzene (4:1) afforded a white solid which was crystallized from a mixture of petroleum ether–benzene to yield white crystals of **8** (1.46 g, 34%), mp 129—130 °C; IR (KBr): ν_{max} 2960, 1610, 1585, 1526, 1490, 1440, 1420, 1345, 1325, 1260, 1230, 1180, 1130, 1100, 1030, 1020, 975, 940, 930, 850, 830, 810, 785, 740, 690, 640, 620 cm^{-1}; ^1H NMR ($CDCl_3$): δ=3.80 (6H, s, 2×OMe), 6.54 (1H, s, H-3), 6.75 (2H, m, H-5,5′), 7.44 (1H, d, J=9 Hz, H-6), 7.80 (1H, d, J=9 Hz, H-6′); MS (rel. int.): m/z 445 (4.12), 443 (8.10), 441 (11.26), 397 (3.80), 395 (7.42), 394 (2.15), 393 (11.32), 382 (2.00), 380 (4.20), 378 (6.12), 360 (4.52), 359 (3.00), 358 (13.28), 324 (7.20), 323 (20.40), 230 (8.00), 229 (10.00), 228 (24.54), 216 (8.95), 215 (42.15), 214 (23.50), 213 (100.00), 198 (12.51), 196 (16.54), 184 (2.55), 150 (14.50). Found: C, 44.99; H, 2.17; Cl, 22.04%. Calcd for $C_{18}H_{11}Cl_3O_5S_2$: C, 45.25; H, 2.32; Cl, 22.26%.

References

1) Taken in Part from the Ph. D. Dissertation of S. M. A., Aligarh Muslim University, Aligarh, 1986.

2) For reviews of thionyl chloride, see a) K. Oka, *Synthesis*, **1981**, 661; b) S. S. Pizey, "Synthetic Reagents," Ellis Horwood, Chichester (1974), Vol. 1, Chap. 4; c) C. A. Gilberrad, *Chem. Ind. (London)*, **1926**, 36.

3) a) I. M. Goldman, *J. Org. Chem.*, **34**, 3285 (1969); b) K. Oka and S. Hara, *Tetrahedron Lett.*, **1977**, 3059; c) E. Wenkert, F. Haglid, and S. L. Mueller, *J. Org. Chem.*, **34**, 247 (1969); d) B. A. Dreikorn, A. F. Elsasser, and G. P. Jourdan, *ibid.*, **44**, 877 (1979); e) E. T. Tsankova, I. V. Ognyanov, and A. S. Orahovats, *Chem. Ind. (London)*, **1980**, 87.

4) K. Oka and S. Hara, *Tetrahedron Lett.*, **1976**, 2783.

5) V. G. Adiwidjaja, H. Gunther, and J. VoB, *Angew. Chem., Int. Ed. Engl.*, **19**, 563 (1980).

6) U. Jacobsson, T. Kempe, and T. Norin, *J. Org. Chem.*, **39**, 2722 (1974).

7) M. Davis, H. Szkuta, and A. J. Krubsack, *Mech. React. Sulfur Compds.*, **5**, 1 (1970); b) M. S. Newman and P. K. Sujeeth, *J. Org. Chem.*, **43**, 4367 (1978); c) K. Oka and S. Hara, *Tetrahedron Lett.*, **1977**, 2939.

8) W. A. Sheppard and J. Diekmann, *J. Am. Chem. Soc.*, **86**, 1891 (1964); b) T. Minami, F. Takimoto, and T. Agawa, *J. Org. Chem.*, **41**, 3811 (1976); c) K. Oka, A. Dobashi and S. Hara, *J. Am. Chem. Soc.*, **103**, 2757 (1981).

9) K. H. Bell, *Aust. J. Chem.*, **38**, 1209 (1985).

10) T. Higa and A. J. Krubsack, *J. Org. Chem.*, **40**, 3037 (1975).

 © 1988 The Chemical Society of Japan Bull. Chem. Soc. Jpn., 61, 3295—3300 (1988)

The Retardation of Methanol Oxidation at a Platinum Electrode in an Acid Solution

Hiroshi MATSUI
Department of Applied Chemistry, Faculty of Engineering, The University of Tokushima, Minami-josanjima-cho, Tokushima 770
(Received March 22, 1988)

The rate retardation of the oxidation of methanol at the potential range of about 0.65—0.8 V vs. a reversible hydrogen electrode on a platinum electrode in 0.5 mol dm^{-3} H_2SO_4 was studied. The rate retardation of the overall oxidation was caused by that of the oxidation, Reaction D, not via CO_{ad}. From the relationship among the rate of Reaction D, the CO_{ad} coverage, and the potentials, three types of rate retardation were found out: Type 1— Reaction D is not accelerated by the potential, and the rate of the reaction is determined by the CO_{ad} coverage and the methanol concentration. Type 2— the rate of Reaction D decreases at stationary CO_{ad} coverages as the oxidation is prolonged. Type 3— the rate decreases at CO_{ad} coverages close to the limiting value. It is proposed that Types 1 and 2 of the rate retardations take place when the adsorption of methanol molecules is rate-determining, and when the formaldehyde and formic acid formed from methanol are accumulated in the vicinity of the electrode, respectively. Type 3 of the rate retardation has been explained in a preceding paper in terms of the aggregate damaging effect of CO_{ad}.

It has been known[1-3] that a plot of log i vs. E gives a straight line for the oxidation of methanol at a platinum electrode in an acid solution in the potential range lower than about 0.6—0.7 V, but the downward deviation from the straight line takes place at higher potentials than about 0.65 V. Such a deviation for the rate of the methanol oxidation has been interpreted in terms of the formation of stably chemisorbed species (SCS),[2,4,5] the formation of platinum surface oxide,[6] and the accumulation of adsorbed impurities from a solution.[7,8] Furthermore, the rate deviation has been reported[1,9] to occur when the dissociative adsorption of methanol is rate determining. This information was based on the assumption that methanol was always oxidized to CO_2 via SCS. However, recent investigations[2,4,5] have revealed that methanol is oxidized via at least two parallel reactions; one via SCS (Reaction B), and the other not via SCS (Reaction D).

Two types of SCS are generally proposed: COH_{ad},[10,11] and CO_{ad}.[12,13] For example, mass spectroscopic measurements[10,11] gave results suggesting COH to be adsorbable. On the other hand, in situ IR spectroscopic investigations[12] gave strong evidence for the existence of CO_{ad}. Furthermore, our results[13] obtained by means of the electrochemical methods confirmed that SCS is CO_{ad}. In the present paper, therefore, the downward deviation of methanol oxidation is discussed by assuming CO_{ad} as SCS. Of course, the conclusions derived by the present investigation are not altered even when another chemical kind of SCS instead of CO_{ad} is assumed.

The present investigation was undertaken in order to determine the origin of such a downward deviation, i.e., the rate retardation in the electrooxidation of methanol to carbon dioxide at platinum in a 0.5 mol dm^{-3} H_2SO_4 solution in the potential range of 0.65—0.8 V vs. RHE. The upper limit of 0.80 V was taken in order to eliminate the rate retardation of methanol oxidation due to the formation of platinum oxide.

Experimental

The coverage θ, with CO_{ad} is expressed as:

$$\theta = (Q_H^0 - Q_H)/Q_H^0 \quad (1)$$

where Q_H^0 and Q_H are the charge required to cover fully the electrode surface with adsorbed hydrogen atoms in the absence and in the presence of CO_{ad} respectively. These charges were determined by the conventional hydrogen deposition method.

The rate of Reaction D was determined by the following procedure. As has been reported in a previous paper,[5] the overall rate, i_T, of the methanol oxidation can be expressed by:

$$\begin{aligned} i_T &= i_A + i_B + i_D \\ &= 2\,dQ^{ox}/dt + 3i_B + i_D \end{aligned} \quad (2)$$

where i_A and i_B are the rates of the formation and the further oxidation of CO_{ad} respectively. i_D is the rate of the methanol oxidation not via CO_{ad}, and Q^{ox} is the charge required to oxidize CO_{ad} to CO_2. When the methanol concentration is smaller than about 0.5 mol dm^{-3}, $i_B \ll i_T$ at potentials below about 0.8 V, as has been described in the previous work[5]. Consequently,

$$i_D \fallingdotseq i_T - 2\,dQ^{ox}/dt \quad (3)$$

Here, Q^{ox} can be approximated by $Q_H^0\,\theta$ (see Fig. 8 in Ref. 15). Thus,

$$i_D \fallingdotseq i_T - 2\,Q_H^0\,d\theta/dt \quad (4)$$

In the present investigation, i_D was determined under both potentiostatic and potentiodynamic conditions.

(A) Potentiostatic Conditions: The current and θ at a constant potential were measured by using the potential sequence of (a) in Fig. 1. i_T at the potential is equal to the observed current for the methanol oxidation, while $d\theta/dt$ was determined from the time-variation in θ. Then, i_D was

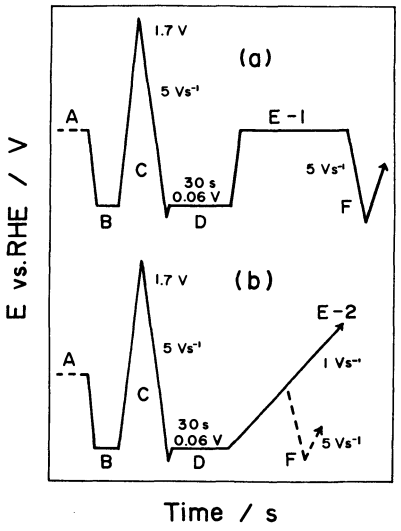

Fig. 1. Potential sequence for measurements of oxidation rate and surface coverage. Oxidation: (a) potentiostatic; (b) potentiodynamic. Steps: (A) introduction of deoxygenated solution; (B) reduction of remaining oxygen; (C) cleaning of electrode surface; (D) recovering equilibrium of concentrations; (E-1) measurement of oxidation rate at a constant potential; (E-2) potential scan; (F) measurement of surface coverage.

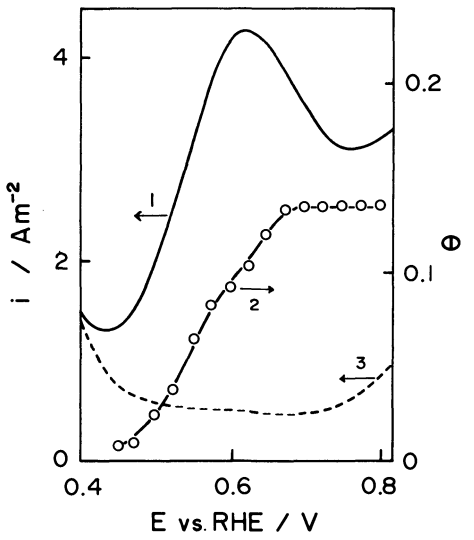

Fig. 2. Potentiodynamic i-E and θ-E curves for oxidation of methanol in 0.1 mol dm^{-3} CH_3OH +0.5 mol dm^{-3} H_2SO_4, scan rate 1 V s^{-1}. Curves: (1) currents; (2) surface coverages; (3) currents in the absence of CH_3OH and CO_{cd}. Platinized platinum (roughness factor=134).

calculated according to Eq. 4.

(B) Potentiodynamic Conditions: The i-E curves and θ values were obtained by using the potential sequence of (b) in Fig. 1. The potential was scanned after the preadsorbed CO species had been removed at Step C of the pretreatment in Fig. 1. Curves 1 and 3 in Fig. 2 show examples of i-E curves in the presence and the absence of methanol

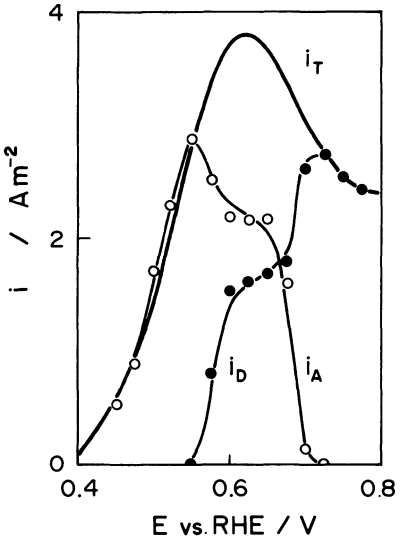

Fig. 3. Variation in i_A, i_D, and i_T with potential, 0.1 mol dm^{-3} CH_3OH+0.5 mol dm^{-3} H_2SO_4, scan rate 1 V s^{-1}. These values were obtained on the basis of Fig. 2.

respectively, when the scan rate is 1 V s^{-1} and the methanol concentration is 0.1 mol dm^{-3}. The values of i_T were determined from the differences in the current between Curves 1 and 3. Curve 2 in Fig. 2 is the θ-E curve obtained under the same experimental conditions as Curve 1. $d\theta/dt$ during the anodic scan is proportional to $d\theta/dE$, because the scan rate, s, is constant:

$$d\theta/dt = s\, d\theta/dE \quad (5)$$

Thus, $d\theta/dt$ was determinable from the slope of the θ-E curve, and then i_D was calculated from Eqs. 4 and 5. Figure 3 shows the potential dependence of the i_D value thus obtained. The i_D was approximately equal to i_T in the potential range of about 0.7—0.8 V, while $i_T \fallingdotseq i_A$ at potentials below about 0.55 V. Therefore, the order of Reaction D with respect to the methanol concentration was determined from the relationship between i_T at 0.7 V and the concentration.

The effects of the presence of formaldehyde and formic acid on the i-E curve and θ were also examined by using the potential sequence of (b) in Fig. 1. The other experimental conditions and procedures were almost the same as those used in the previous studies.[5,14] All the reaction rates and the charges were measured at 0 °C. The potentials were referred to a reversible hydrogen electrode (RHE) in 0.5 mol dm^{-3} H_2SO_4.

Results and Discussion

Figure 4 shows the relationship between the potential and i_D in the prolonged oxidation of methanol under potentiostatic conditions. Since the methanol oxidation, Reaction D, not via CO_{ad} does not occur at the electrode surface occupied by CO_{ad}, the rate of Reaction D was expressed by the current per the surface not occupied by CO_{ad}, $i_D/(1-\theta)$. As may be seen from Fig. 4, there is a linear relationship between

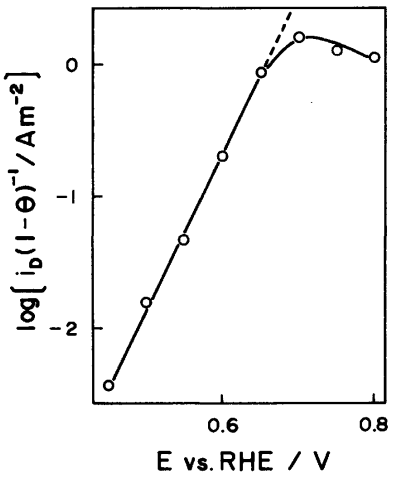

Fig. 4. Variation in stationary i_D with potential, oxidation time at a constant potential 300 s, 0.1 mol dm^{-3} CH_3OH+0.5 mol dm^{-3} H_2SO_4.

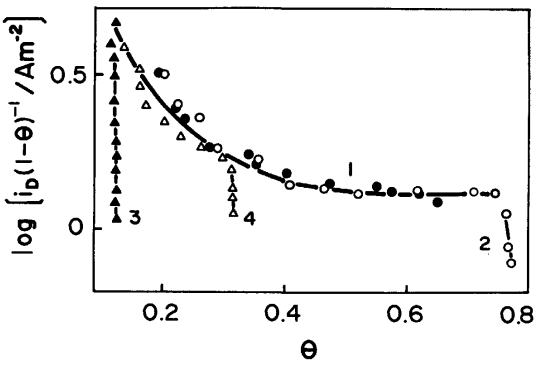

Fig. 5. Variation in $i_D/(1-\theta)$ with CO_{ad} coverage, 0.1 mol dm^{-3} CH_3OH+0.5 mol dm^{-3} H_2SO_4. Potential (V): ○ 0.65; ● 0.70; △ 0.75; ▲ 0.80. All of part of the rates at every potential belong to curve 1.

the potential and the logarithm of $i_D/(1-\theta)$ in the potential range of 0.45—0.65 V. The rate of Reaction D at the higher potentials, however, deviates downward from the straight line. In order to clarify the causes of this rate deviation, the relationship between $i_D/(1-\theta)$ and θ during the controlled potential oxidation of methanol at different potentials was examined. The results are presented in Fig. 5.

Figure 5 indicates three types of rate retardation: Type 1; $i_D/(1-\theta)$ directly deviates from the Tafel straight line without any other rate retardations at potentials above about 0.7 V. The resulting $i_D/(1-\theta)$ is at constant surface coverages, independent of the potential, as Curve 1 in Fig. 5 shows. Type 2: at potentials above about 0.75 V, the CO_{ad} coverage soon becomes stationary, although with small values, and then $i_D/(1-\theta)$ falls, as in indicated by Curves 3 and 4. Type 3: at a coverage close to about 0.8, $i_D/(1-\theta)$ begins to fall abruptly, as Curve 2 shows.

The rate retardation of Type 3 has already been presented in the preceding paper[15] as being due to the aggregate demaging effect on reaction sites indispensable for the methanol oxidation. The causes of the rate retardations of Types 1 and 2 will be discussed below.

Rate Retardation of Type 1. As Curve 1 in Fig. 5 shows, the rate retardation of Type 1 occurs at the same CO_{ad} coverage, although CO_{ad} has a retarding effect on Reaction D. Hence, the rate retardation of Type 1 is explicitly caused by some factor other than the formation of CO_{ad}.

Breiter et al.[7,8] reported that the rate of the oxidation of methanol at platinum electrodes could be retarded by the presence of not only CO_{ad}, but also easily desorbable surface substances, such as chloride anions. Although such desorbable adsorbates can not be detected by the conventional hydrogen-deposition method, the adsorbates are detectable by an anodic stripping method in which the potential scan is very rapid. In this method,[9] the hardly and easily oxidizable adsorbates are detected by the hindrance of the formation of the platinum oxide and the appearance of a new oxidation wave in the potentiodynamic *i-E* curve. In the present investigation, a potential scan of 718 V s^{-1} was applied to the electrode immediately after the methanol oxidation at 0.8 V in 0.01 mol dm^{-3} CH_3OH+0.5 mol dm^{-3} H_2SO_4. The wave of the dotted line 3 around 1.5 V is due to the formation of the platinum oxide, while the wave of the solid line 1 around 1.8 V is due to both the formation of the surface oxide and the oxidation of the CO_{ad} which was formed during the previous oxidation at a constant potential. The presence of methanol had little effect on the formation of the oxide; also, no appreciable wave for the oxidation of new adsorbates was detected. Hence, both hardly and easily oxidizable surface substances, even if these substances are easily desorbable, can be eliminated as possible causes of the rate retardation of Type 1. The remaining cause of the rate retardation is a change in the reaction mechanism.

In Fig. 5, $i_D/(1-\theta)$ goes down on Curves 2—4 as the oxidation time passed. Consequently, the extent of the rate retardations of Types 2 and 3 were slight at a short oxidation time. Hence, provided that the oxidation time is short, the reaction order with respect to the methanol concentration can be examined without any effect of rate retardations of Types 2 and 3. These experimental conditions were approximately satisfied by oxidizing methanol at a potential scan of a few V s^{-1} after the removal of CO_{ad}. That is, the oxidation time was short at this scan rate, and the retardation of Type 1 occurred at potentials of about 0.7—0.8 V, as is indicated by Fig. 3. Figure 7 shows the dependence of $i_D/(1-\theta)$ at 0.7 V on the methanol concentration obtained when the scan rate is 3 V s^{-1}. As may be seen from this figure, there was a

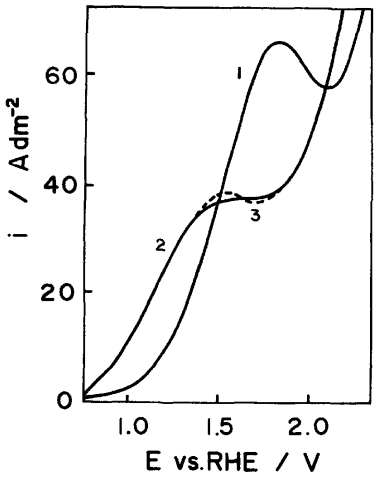

Fig. 6. i-E curves at rapid potential scan after 100 second oxidation of methanol at a constant potential, scan rate 718 V s^{-1}, 0.01 mol dm^{-3} CH_3OH +0.5 mol dm^{-3} H_2SO_4, smooth platinum. Potential (V): (1) 0.6; (2) 0.8; (3) in the absence of CH_3OH.

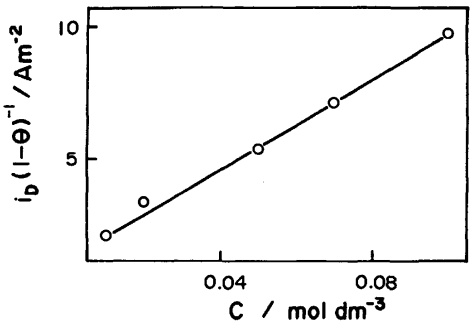

Fig. 7. Variation in i_D with methanol concentration, C. The rates were taken from potentiodynamic (3 V s^{-1}) i-E curves.

linear relationship between $i_D/(1-\theta)$ and the methanol concentration; i.e., the reaction order with respect to the methanol concentration was first.

An $i_D/(1-\theta)$ value independent of the potential and the first reaction order with respect to the methanol concentration would result, when one of the following nonelectrochemical processes of methanol molecules becomes rate-determining: (1) the diffusion to an electrode, (2) the adsorption on an electrode, and (3) a chemical reaction at the electrode surface, e.g., the dehydrogenation of methanol molecules. The maximum value of the observed rate of the methanol oxidation was smaller by a few orders of magnitude than the limiting diffusion rate previously estimated.[16] For example, the maximum value of i_D in Fig. 4 is less than about one hundredth of the estimate. Consequently, Process 1 can be rejected as a possible rate-determining step. Process 3 can also be ruled out as the rate-determining step, because no product of the surface reaction involved in Reaction D could be detected at the open circuit. Furthermore, the

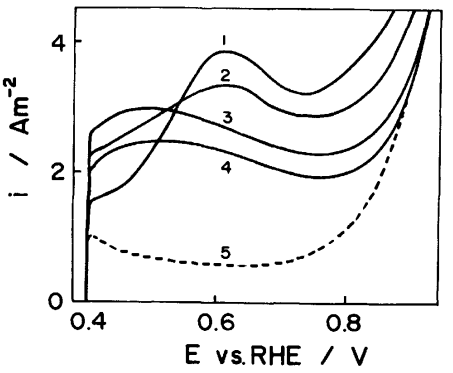

Fig. 8. Potentiodynamic i-E curves immediately after preoxidation at 0.8 V, 0.1 mol dm^{-3} CH_3OH +0.5 mol dm^{-3} H_2SO_4, scan rate 1 V s^{-1}. Preoxidation times (s): (1) 0; (2) 1; (3) 10; (4) 100; (5) in the absence of CH_3OH.

Table 1. Current Efficiencies for the Formation of Formaldehyde and Formic Acid in CH_3OH+ 0.5 mol dm^{-3} H_2SO_4; Oxidation Time, (300 s)

Potential	CH_3OH	HCHO	HCOOH
V	mol dm^{-3}	%	%
0.7	1.0	34	14
0.7	0.5	35	13
0.7	0.3	29	11
0.7	0.2	17	6
0.7	0.1	13	6
0.8	1.0	35	15
0.8	0.1	14	7

adsorption of methanol molecules has been proposed[2,4,17] as an elementary process in the electrooxidation. From these facts, it was concluded that the rate retardation of Type 1 is caused when the adsorption of methanol molecules is rate-determining.

Rate Retardation of Type 2. In order to clarify the cause of the rate retardation of Type 2, the effect of the preoxidation on i_D was examined by means of the potential scan of 1 V s^{-1}. Figure 8 shows the potentiodynamic i-E curves for the oxidation of methanol when a prolonged oxidation at 0.8 V is undertaken prior to the potential scan. By the preoxidation, i_T at 0.7—0.8 V, i.e., i_D decreased, and a new wave appeared at about 0.4—0.5 V. This finding suggests that some products retarding Reaction D are formed from methanol and are accumulated in the vicinity of the electrode.

Formaldehyde and formic acid are known[4,16] to be formed in the anodic oxidation of methanol. Under the present experimental conditions also, their formation was confirmed, as Table 1 shows. The effect of the presence of these substances on i_D was examined in mixed systems of methanol-formaldehyde and methanol-formic acid. As Table 1 shows, the current efficiencies for the production of these

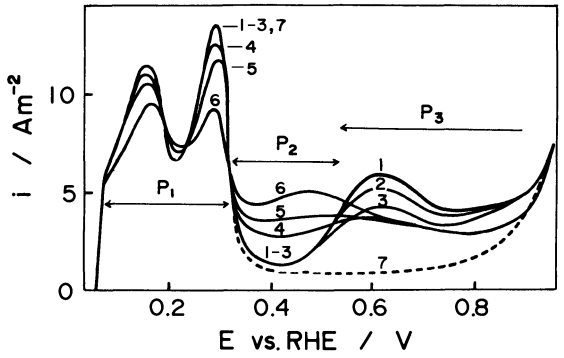

Fig. 9. Potentiodynamic i–E curves in the presence of formaldehyde added to solution, HCHO +0.1 mol dm^{-3} CH_3OH+0.5 mol dm^{-3} H_2SO_4, scan rate 1 V s^{-1}. HCHO (mol dm^{-3}): (1) 0; (2) 0.001; (3) 0.002; (4) 0.01; (5) 0.02; (6) 0.05; (7) in the absence of HCHO and CH_3OH.

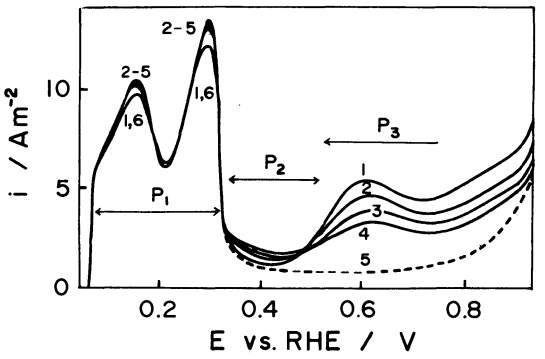

Fig. 10. Potentiodynamic i–E curves in the presence of formic acid added to solution, HCOOH +0.1 mol dm^{-3} CH_3OH+0.5 mol dm^{-3} H_2SO_4, scan 1 V s^{-1}. HCOOH (mol dm^{-3}): (1) 0; (2) 0.0005; (3) 0.002; (4) 0.005; (5) in the absence of HCOOH and CH_3OH.

substances are small at low methanol concentrations. Therefore, in order to reduce the accumulation of formaldehyde and formic acid from methanol, the methanol concentration of 0.1 mol dm^{-3} was used to examine the effect of the addition of formaldehyde and formic acid.

Figures 9 and 10 shows the potentiodynamic i–E curves in mixed systems of methanol–formaldehyde and methanol–formic acid. As these curves indicate, methanol was oxidized at potentials above about 0.45 V, while formaldehyde and formic acid were oxidized at potentials above 0.35 V, at the scan rate of 1 V s^{-1}. Consequently, the new wave observed around 0.4 V in Fig. 8 is ascribed to the oxidation of the formaldehyde and formic acid which are formed during the oxidation of methanol at 0.8 V. It is particularly interesting that, in the mixed system, the overall rate in the potential range of about 0.5—0.8 V decreased as the concentration of formaldehyde and formic acid increased up to about 0.02 mol dm^{-3}. As

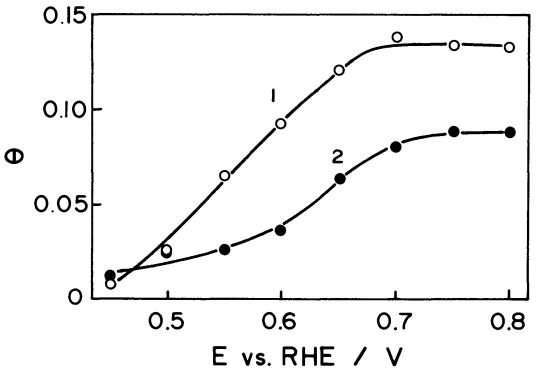

Fig. 11. Potentiodynamic θ–E curves for oxidation of methanol in (2) 0.02 mol dm^{-3} HCOOH +0.1 mol dm^{-3} CH_3OH; (1) in the absence of HCOOH, scan rate 1 V s^{-1}.

has been described in the Experimental section, the i_T values in the potential range of 0.7—0.8 V are approximately equal to i_D. Therefore, it seems certain that Reaction D is retarded by the formation of formaldehyde and formic acid. The effects of these substances are most remarkable in the concentrations of 0.02—0.03 mol dm^{-3}. At higher concentrations, the overall rate increased with an increase in the concentration. Since the oxidation of formaldehyde and formic acid was enhanced at high concentrations, the increase in the overall rate at the higher concentrations is probably due to the oxidation of these substances.

As has been described above, the adsorption of methanol molecules precedes both the CO_{ad} formation and Reaction D, and the accumulation of adsorbed molecules is very slight:

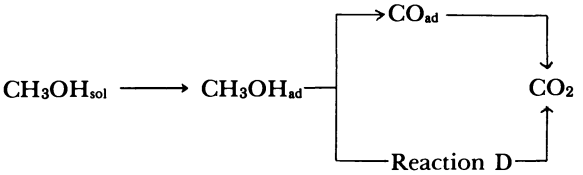

Consequently, the rate of the adsorption of methanol molecules, r_{ad} is the sum of the rates of the CO_{ad} formation and Reaction D, when each rate is expressed in mol s^{-1} m^{-2}:

$$r_{ad} = i_A/4F + i_D/6F \quad (6)$$

where i_A can be expressed in terms of $d\theta/dt$ by the same method as in the Experimental section:

$$i_A \fallingdotseq 2s Q_H{}^0 d\theta/dE \quad (7)$$

Figure 11 shows the relationship between the CO_{ad} coverage and the potential in the presence and in the absence of formic acid under potentiodynamic conditions. In the potential range of about 0.7—0.8 V, the slope of the θ–E curve, i.e., $d\theta/dE$ was little

influenced by the presence of formic acid, and i_D decreased, as may be seen from Fig. 9. Consequently, i_D and also r_{ad} are decreased by the presence of formic acid. A smilar decrease in r_{ad} was observed also in the case of formaldehyde, so long as the formaldehyde concentration was lower than about 0.05 mol dm^{-3}. At higher concentrations, however, the CO_{ad} formation from formaldehyde was remarkable at the pretreatment step D in Fig. 1b; therefore the effect of the presence of formaldehyde on i_D could not be examined.

To sum up, the rate retardation of Type 2 was related to the retardation of the adsorption of methanol molecules. The retardation occurred when small amounts of formaldehyde and formic acid were added to a solution of methanol, or when these substances were formed at the electrode by the preoxidation of methanol, although the adsorption of these substances was not confirmed by either the method of hydrogen deposition and by that of anodic stripping. From these results, it was concluded that the rate retardation of Type 2 was due to the accumulation of formaldehyde and formic acid in the vicinity of the electrode without adsorption.

References

1) V. S. Bagotzky and Yu. B. Vassilyev, *Electrochim. Acta*, **12**, 1323 (1967).

2) O. A. Petrii, "Adsorption of Organic Compounds on Electrodes," ed by B. B. Damaskin, O. A. Petrii, and V. V. Batrakov, Plenum Press, New York (1971) pp. 324, 457.

3) T. Biegler and D. F. A. Koch, *J. Electrochem. Soc.*, **114**, 904 (1967).

4) M. W. Breiter, *Discuss. Faraday Soc.*, **45**, 79 (1968).

5) H. Matsui and T. Hisano, *Bull. Chem. Soc. Jpn.*, **60**, 863 (1987).

6) V. S. Bagotzky and Yu. B. Vassilyev, *Electrochim. Acta*, **9**, 869 (1964).

7) M. W. Breiter, *Electrochim. Acta*, **9**, 827 (1964).

8) G. Belanger, *Can. J. Chem.*, **50**, 1891 (1972).

9) S. Gilman, "Electroanalytical Chemistry," ed by A. J. Bard, Marcel Dekker, New York (1967), Vol. 2, pp. 132, 137, 185.

10) J. Willsau, O. Wolter, and J. Heitbaum, *J. Electroanal. Chem.*, **185**, 163 (1985); J. Willsau and J. Heitbaum, *Electrochim. Acta*, **31**, 943 (1986).

11) H. W. Bushmann, S. Wilhelm, and W. Vielstich, *Electrochim. Acta*, **31**, 939 (1986); S. Wilhelm, W. Vielstich, H. W. Bushmann, and T. Iwasita, *J. Electroanal. Chem.*, **229**, 377 (1987).

12) B. Beden, C. Lamy, A. Bewick, and K. Kunimatsu, *J. Electroanal. Chem.*, **121**, 343 (1981); K. Kunimatsu, *ibid.*, **145**, 219 (1985); **213**, 149 (1986); A. Papoutsis, J. M. Leger, and C. Lamy, *ibid.*, **234**, 315 (1987).

13) H. Matsui, T. Hisano, and T. Terazawa, *Bull. Chem. Soc. Jpn.*, **58**, 911 (1985).

14) H. Matsui, T. Hisano, and T. Terazawa, 50th Meeting of the Electrochemical Society of Japan, Tokyo, May, 1983 Abstr., pp. 147.

15) H. Matsui and T. Hisano, *Bull. Chem. Soc. Jpn.*, **58**, 2298 (1985).

16) The limiting current density, i_L, for the linear diffusion was determined by means of the following equation:

$$i_L = nFDC/\delta$$

where each of the symbols represents its ordinary meaning. When n, D, C, and δ are 6, 1×10^{-9} m^2 s^{-1}, 0.1 mol dm^{-3}, and 5×10^{-4} m respectively, one obtains $i_L=1\times10^2$ A·m^{-2}. With a platinized platinum electrode, the limiting diffusion current per unit of apparent surface area would be equal to or a little larger than, this value* because of the roughened surface, though it appears that any exact estimation would be very complicated.

* G. Charlot, J. Badoz-Lambling, and B. Tremillon, "Electrochemical Reactions," Elsevier, New York (1962), pp. 117.

17) V. B. Hughes and R. Miles, *J. Electroanal. Chem.*, **145**, 87 (1983).

18) K. Ota, Y. Nakagawa, and M. Takahashi, *J. Electroanal. Chem.*, **179**, 179 (1984).

 © 1988 The Chemical Society of Japan Bull. Chem. Soc. Jpn., 61, 3301—3305 (1988)

Apparent Molal Volumes of Urea Derivatives in Water-Methanol Mixtures

Kiyoshi MIZUTANI and Motoo YASUDA*
Department of Chemistry, College of General Education, Nagoya University,
Chikusa-ku, Nagoya 464-01
(Received April 1, 1988)

Apparent molal volumes (ϕ_v) at 25 °C have been obtained for the following urea derivatives in water–methanol mixtures from measurements of the density using an Anton Paar digital densimeter: urea (U), methylurea (MU), ethylurea (EU), 1,1-dimethylurea (1,1-DMU), 1,3-dimethylurea (1,3-DMU), 1,1-diethylurea (1,1-DEU), and 1,3-diethylurea (1,3-DEU). The limiting values ϕ_v° were calculated by linear extrapolation using the least-squares method. A plot of ϕ_v° vs. X_2, the mole fraction of methanol, showed a minimum for each alkylurea studied at low methanol concentrations ($X_2 \simeq 0.1$), but none for unsubstituted urea: the more alkyl-substituted the urea was, the sharper the minimum. Inspection of the data shows that the assumption of independent solvation on both sides of the urea molecules also holds to a good approximation to the apparent molal volumes both in the pure solvents and in the mixtures.

It has long been known that alcohol–water mixtures often show abnormalities in their properties, such as the viscosity-composition and the ultrasonic velocity-composition maximum. Although they are not fully understood, such peculiarities are considered to be structural in origin. Thus, Franks and Ives postulated an enhancement of the structure of water by interactions between alkyl groups and water in the water-rich region; they therefore surveyed the properties of these systems with special reference to their structural implications.[1] Aqueous urea also has long been the subject of study, in particular the effect of urea on the water structure, and many biophysicochemical studies have been carried out on aqueous urea. The theoretical treatment of the mixture has been performed by Frank and Franks, who pictured dissolved urea as acting like a statistical water-structure breaker.[2] It is generally accepted that urea does not appreciably interact with either hydrophobic or hydrophilic molecules or groups, and so several thermodynamic and transport properties of aqueous urea solutions with added electrolytes or nonelectrolytes have been interpreted in terms of the nonspecific interaction of urea with the solute, as has been noted by Mathieson and Conway.[3] We feel that, in order to understand the effect of urea on the structure of water, it would now be useful to carry out the systematic study of urea solutions over the whole mole-fraction range of alcohol and water. Since the infinite-dilution apparent molal volumes are independent of solute–solute interactions, being determined only by the respective intrinsic value and solute–solvent interactions, they can be used to examine the solute–solvent interactions.

In the present work, densities were measured at 25 °C for the urea(or alkylurea)–methanol–water ternary system at various concentrations. The apparent molal volumes and their limiting values were obtained from these data.

Experimental

The density of the methanol, which was a guaranteed reagent from Wako Chemical Industries, Ltd., was 0.78663 g cm^{-3} at 25 °C; the reported densities are 0.78665[4] and 0.78660.[5] As will be seen later, the infinite apparent molal volume of urea in this solvent was 36.98 cm^3 mol^{-1}, which was in excellent agreement with the value (36.97) reported by Hamilton and Stokes.[5] The methanol, therefore, was used without further purification as a solvent or cosolvent. The urea (Wako Chemical Industries, Ltd.) and 1,1-dimethylurea (Sigma Chemical Company) were used as received. The methylurea (Wako Chemical), and the 1,1-diethylurea and 1,3-diethylurea, which have both been obtained from the Aldrich Chemical Company, Inc., were recrystallized from ethanol. The ethylurea and 1,3-dimethylurea, which were both from the Tokyo Kasei Kogyo Co., Ltd., were recrystallized from an ethanol–ethyl ether mixture.

Ternary systems are very complicated, and special interest is usually taken in their properties in the water-rich region. Thus, the densities of the urea solutions were measured at 25 °C in 0, 0.1, 0.2, 0.3, 0.4, 0.6, 0.8, and 1.0 by the use of mole-fraction methanol X_2 in water. All the solutions were prepared by weight in the concentration range of 0.2—0.9 mol kg^{-1} (the number of moles of urea per kg of the mixed solvent whenever the mixed solvent was used). The mixed solvent was prepared for each series of measurements, and its density was determined respectively. The densities were measured to $\pm 2 \times 10^{-6}$ g cm^{-3} with an Anton Paar DMA 02D Densimeter as before.[6] The temperature control of the thermostated bath system regulating the densimeter was better than ±0.005 °C.

Results

The apparent molal volumes were obtained using Eq. 1:

$$\phi_v = \frac{M}{d} + \frac{1000(d_o - d)}{m d_o d} \quad (1)$$

where M is the molecular weight of the urea; m, its molal concentration, and d_o and d, the densities of the solvent and the solution respectively. The apparent

molal volumes of a nonelectrolyte such as urea are usually expressed as in Eq. 2 below ca. 1 mol kg^{-1}:

$$\phi_v = \phi_v^\circ + S_v m \quad (2)$$

where ϕ_v° is the infinite-dilution apparent molal volume and where S_v is the experimental slope. At an infinite dilution, ϕ_v° is equal to $\overline{V}^\circ$ (the infinite-dilution partial molal volume). The ϕ_v° values were calculated by a linear extrapolation using the least-squares fit to Eq. 2. The derived values for ϕ_v° are summarized in Table 1. The standard deviations are less than 0.03 cm^3 mol^{-1}. Those for amino-acid–alkali-chloride–water ternary systems previously reported by the present authors were mostly less than 0.02 cm^3 mol^{-1};[6] the volatility of methanol probably makes the standard deviations a little larger in the present work. The ϕ_v° values in water for U, 1,1-DMU, and 1,3-DMU are reported by Philip et al. as 44.24, 78.88, and 80.04 cm^3 mol^{-1} respectively.[7] Our value for U is in excellent agreement, and for 1,1-DMU and 1,3-DMU our values are in good agreement, with the literature values. For the other alkylureas no accurate ϕ_v° values have yet been reported, although Herskovits and Kelly evaluated the partial specific volumes for the ureas using the density data;[8] their densities, however, were measured with 10-cm^3 pycnometers in order to obtain viscosity coefficients for the ureas and so can not be compared with our data. As has been mentioned earlier, the ϕ_v° value of urea in methanol was reported to be 36.97 cm^3 mol^{-1} by Hamilton and Stokes,[5] a value in excellent agreement with ours. As for the others, however, no comparable data have been reported.

Discussion

Apparent Molal Volume of Urea. First of all let us consider the results for the unsubstituted urea. The thermodynamic properties of aqueous urea solutions, including the volume, were intensively discussed by Stokes,[9] who reported apparent molal volumes of urea at 0, 40, and 50 °C to supplement the existing volume data. He showed that ϕ_v° is strongly temperature-dependent; 41.75 cm^3 mol^{-1} at 0 °C, 44.20 at 25, 44.55 at 30, 45.10 at 40, and 45.60 at 50. The estimated thermal expansion coefficient α of the limiting apparent molal volumes, defined by:

$$\alpha(\phi_v^\circ) = \mathrm{d} \ln \phi_v^\circ / \mathrm{d}T$$

is abnormally large at low temperatures, but decreases as the temperature is raised. The ϕ_v° values measured by Hamilton and Stokes[5] in various organic solvents, such as methanol, ethanol, and formamide, show a large variation in different solvents, though the temperature dependence of the limiting apparent molal volumes in nonaqueous solvents is slight, in marked contrast to the situation in water. Of the several properties of the solvents they examined, the compressibility of the solvent has the only clear correlation with the ϕ_v° values of urea; the ϕ_v° value increases as the compressibility of the solvent decreases. Regarding the compressibility as a measure of the void space in the liquid, they argued that the solute molecule does not have to create a hole for itself of the full dimensions demanded by its intrinsic size. Thus, methanol, with the largest compressibility of the solvents studied by them at 25 °C, gave the smallest ϕ_v° value of urea, 36.97 cm^3 mol^{-1}. As has been mentioned earlier, water–alcohol systems are well-known to enhance the structure of water considerably when alcohol is added to water in low mole fractions; as a result, the water–alcohol systems show often abnormalities in their properties. The isentropic compressibilities of water–methanol mixtures studied separately by Kiyohara and Benson[10] and by Lara and Desnoyers[11] show a minimum around X_2=0.13—0.14 at 25 °C. As is shown in Fig. 1, in which the volumes of the transfer of urea from water to the mixtures are plotted against X_2, U shows a volume maximum in the water-rich region. Though the maximum of the volume does not agree with that of its adiabatic compressibility, there is an indication that urea has a larger volume in the less compressibility solvents, as has been noted by Hamilton and Stokes.

Table 1. Limiting Apparent Molal Volumes ϕ_v° in Water-Methanol Mixtures

X_2	ϕ_v°/cm^3 mol^{-1}						
	U	MU	EU	1,1-DMU	1,3-DMU	1,1-DEU	1,3-DEU
0.0	44.24	62.40	79.26	78.53	80.32	111.63	113.74
0.1	44.34	61.64	77.86	77.11	78.53	109.33	110.86
0.2	44.89	62.18	78.84	77.77	79.18	110.48	112.34
0.3	45.16	62.45	79.64	78.06	79.73	111.80	114.20
0.4	44.65	62.51	80.26	78.10	80.02	112.42	115.47
0.6	43.36	61.75	79.88	77.48	80.03	112.17	116.64
0.8	40.98	60.44	78.67	76.10	79.64	111.20	116.76
1.0	36.98	57.38	76.15	73.26	77.57	109.55	115.47

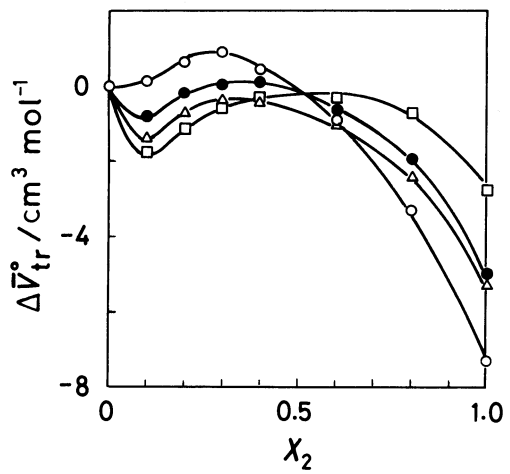

Fig. 1. Volumes of transfer for methylureas from H_2O to mixtures of MeOH+H_2O. ○: Urea, ●: methylurea, △: 1,1-dimethylurea, □: 1,3-dimethylurea.

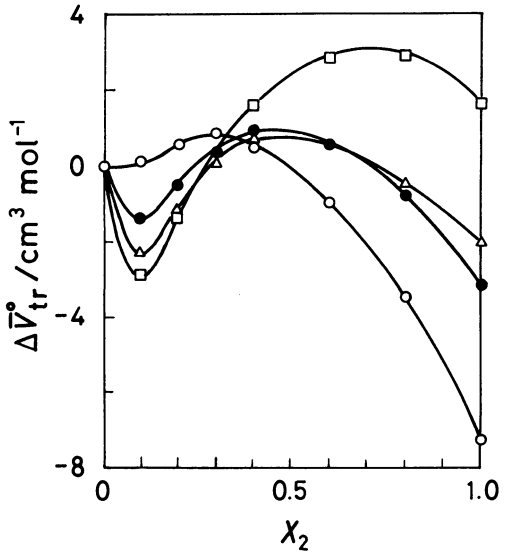

Fig. 2. Volumes of transfer for ethylureas from H_2O to mixtures of MeOH+H_2O. ○: Urea, ●: ethylurea, △: 1,1-diethylurea, □: 1,3-diethylurea.

ϕ_v° in Water. The ϕ_v° values of the six alkylsubstituted ureas studied here are listed in Table 1. The contribution of a methyl or ethyl group to the apparent molal volume can be thought of as the intrinsic volume of the group plus volume terms originating from interactions between the solute and solvent molecules. Thus, when a hydrogen atom bonded to a nitrogen of a urea molecule is replaced by a methyl group, which is hydrophobic in nature, the ϕ_v° values of the urea molecules are influenced by the following: (1) a contribution from the methyl group itself (intrinsic and hydrophobic), (2) a hindrance of the hydrogen-bonding ability of the substituted amino group, and (3) finally a decrease in the hydrogen-bonding ability of the carbonyl group.[7] By comparing the ϕ_v° values of two pairs of isomers, 1,1-DMU and 1,3-DMU, and 1,1-DEU and 1,3-DEU, the 1,3-isomers are seen to have definitely larger volumes than the corresponding 1,1-isomer, as Table 1 shows. In accounting for this difference the second effect mentioned above may be most important. The 1,1-isomer has one unsubstituted amino group, and so it has more hydrogen-bonding ability than the corresponding 1,3-isomer; that is, the former exhibits a greater volume decrease due to hydrogen-bonding. Next, half of the sum of the ϕ_v° values of U and 1,3-isomer is roughly equal to the value of the corresponding mono-substituted urea: (44.24+80.32)/2=62.28 and 62.40 for methylderivatives, (44.24+113.74)/2=78.99 and 79.26 for ethyl derivatives. This fact supports the assumption of independent solvation on both sides of the urea molecules, as reported by Rouw and Somsen from their measurements of the enthalpies of solutions.[12] From the additivity of the group contributions to the partial molar volumes for various kinds of organic analogues, such as carboxylic acids, alkylamines, amino acids, ketones, and alcohols, the group volume increment of CH_2 was calculated as 16.0±0.2 cm^3 mol^{-1} by Shahidi[13] except for cyclic compounds, for which the group volume increment is ca. 2 cm^3 mol^{-1} smaller than for acyclic compounds.[14] Thus, for open-chain compounds, a volume increment of 16 cm^3 mol^{-1} is usually brought about by the replacement of a hydrogen atom by a methyl group. As may be seen from Table 1, the volume difference between urea and methylurea in water is 18.16 cm^3 mol^{-1}, much larger than 16. In the case of alkylamines, this large volume increment may be due to the hindrance of hydrogen-bonding formation of the substituted amino group, as well as to the contribution from the methyl group itself, mentioned above: this brings about a smaller volume decrement. In this connection, it is very interesting to note the volume-change relationships of alkylamine compounds. The partial molal volumes at an infinite dilution reported by Verrall and Conway for the compounds are as follows:[15] CH_3NH_2 40.0, $(CH_3)_2NH$ 58.6, $(CH_3)_3N$ 77.9, and $(C_2H_5)_3N$ 119.7 cm^3 mol^{-1}. A value of 18.6 cm^3 mol^{-1}, much larger than 16, is observed in passing from CH_3NH_2 to $(CH_3)_2NH$, and one of 19.3, in passing from $(CH_3)_2NH$ to $(CH_3)_3N$.

ϕ_v° in Methanol. As may be seen from Table 1, the ϕ_v° values in methanol are smaller than the corresponding values in water except for 1,3-DEU. By comparing the transfer volumes from water to methanol, urea is found to have a more negative value than the other alkylureas studied. The transfer volumes at an infinite dilution from water to methanol $\Delta\bar{V}^\circ_{tr}$ increase in the following order:

U<1,1-DMU<MU<EU<1,3-DMU<1,1-DEU<1,3-DEU.

Thus, alkyl groups, methyl and ethyl, make a larger contribution to the volume in methanol than in water. In other words, a larger volume increment is observed in methanol than in water when urea is substituted by the methyl group, i.e., 20.40 $cm^3\,mol^{-1}$ from U to MU in methanol compared with 18.16 in water.

The assumption of the independent solvation of both sides of the urea molecules mentioned above can be applied also to the volume in methanol and in each water–methanol mixture studied as well.

Recently, Edward et al. have expressed volumes in CCl_4 and other organic solvents by using this equation:[16]

$$\bar{V}^\circ = V_c + \sum n_i I_i + \delta Z_g \qquad (3)$$

where V_c is independent of the solute and is defined as the co-volume, and where n_i and I_i are the number of and characteristic volume of group i. Z_g is the average number of gauche conformations of a molecule at a given temperature, and δ is the volume decrement associated with a gauche interaction. More recently, it has been demonstrated by French and Criss that the group-additive relationships can be expressed for volumes of organic nonelectrolyte solutes, such as alkanes, amines, ethers, and alkanols, in methanol also at 25 °C.[4,17] They obtained a V_c value of 15.8 $cm^3\,mol^{-1}$ and the I_i values by analyzing the volume data in methanol. Some of the I_i values in $cm^3\,mol^{-1}$ are as follows:

$$-CH_3\ 25.83;\ -CH_2-\ 17.72;\ -\underset{|}{\overset{|}{C}}H\ 10.44;\ -\underset{|}{\overset{|}{C}}-\ 3.4;\ -NH_2\ -0.8;$$
$$-OH\ -1.1;\ \diagdown\!\!\diagup C{=}O\ 3.8;\ -CONH-\ 6.4;\ -H\ 8.1.$$

As was pointed out by these authors, the group parameters for volumes are based upon the key assumption that each group contribution is independent of the location of the group and the nature of other groups in the molecule. As may be seen from the data, $I(NH_2)+I(CO)$ are not equal to $I(CONH)+I(H)$. This fact may suggest that amino and carbonyl groups adjacent each other do interact. In fact, as for U with no gauche interaction, the calculated values of the partial molal volume are 18.0 ($V_c+2I(NH_2)+I(CO)$) and 29.5 ($V_c+I(CONH)+I(H)+I(NH_2)$), compared with the experimental value of 36.98 $cm^3\,mol^{-1}$. Group additivity is apparently not applicable to the urea molecule, although the assumption of the independent solvation of both sides of the urea derivatives produced a good approximation of the molal volume.

ϕ_v° in the Mixed Solvents. In Figs. 1 and 2 volumes of the transfer from water to the methanol-water mixtures are plotted against the mole fraction of methanol in the mixture. As may be seen from these figures, each curve of $\Delta\bar{V}^\circ_{tr}$ in the water-rich region goes through a minimum and then turns upward except for the non-hydrophobic solute U. Upon the introduction of more or larger alkyl groups into the urea molecule, the curves gradually come to show deeper minima. The order of decreasing (more negative) $\Delta\bar{V}^\circ_{tr}$ values at $X_2=0.1$ is:

U<MU<1,1-DMU≃EU<1,3-DMU<1,1-DEU<1,3-DEU.

It is considered that this reflects the order of the hydrophobicity of the compounds. In this connection, it is interesting to note Rouw and Somsen's report concerning the enthalpies of transfer, $\Delta\bar{H}^\circ_{tr}$, from water to mixtures of DMF+H_2O for various alkyl-substituted ureas.[12] They show that the enthalpies of solution of these compounds (except for U) show an endothermic shift (i.e., $\Delta\bar{H}^\circ_{tr}>0$) upon the addition of small amounts of DMF to the water. The order of increasing $\Delta\bar{H}^\circ_{tr}$ values in the water-rich region is:

U<MU<1,1-DMU≃EU<1,3-DMU<TMU,

where TMU indicates tetramethylurea. These two sequences agree perfectly with each other, demonstrating that the 1,3-isomer is more hydrophobic than the 1,1-isomer and that 1,1-DMU has about the same hydrophobicity in nature as ethylurea. On the other hand, a volume increment is brought about upon the addition of a small amount of water to methanol. The volumes of transfer from CH_3OH to CH_3OH+H_2O increase in the following sequence:

1,3-DEU<1,1-DEU<1,3-DMU<EU<1,1-DMU<MU<U.

Here, the less hydrophobic the solute is, the more the volume increases. More studies will be necessary in order to elucidate further the behavior of the ternary water–methanol–urea system.

References

1) F. Franks and D. J. G. Ives, *Q. Rev. Chem. Soc.*, **20**, 1 (1966).
2) H. S. Frank and F. Franks, *J. Chem. Phys.*, **48**, 4764 (1968).
3) J. G. Mathieson and B. E. Conway, *J. Solution Chem.*, **3**, 781 (1974).
4) R. N. French and C. M. Criss, *J. Solution Chem.*, **10**, 231 (1981).
5) D. Hamilton and R. H. Stokes, *J. Solution Chem.*, **1**, 213 (1972).
6) T. Ogawa, K. Mizutani, and M. Yasuda, *Bull. Chem. Soc. Jpn.*, **57**, 2064 (1984).
7) P. R. Philip, G. Perron, and J. E. Desnoyers, *Can. J. Chem.*, **52**, 1709 (1974).
8) T. T. Herskovits and T. M. Kelly, *J. Phys. Chem.*, **77**, 381 (1973).
9) R. H. Stokes, *Aust. J. Chem.*, **20**, 2087 (1967).
10) O. Kiyohara and G. C. Benson, *J. Solution Chem.*, **10**, 281 (1981).
11) J. Lara and J. E. Desnoyers, *J. Solution Chem.*, **10**, 465

(1981).
12) A. Rouw and G. Somsen, *J. Chem. Soc., Faraday Trans. 1*, **78**, 3397 (1982).
13) F. Shahidi, *J. Solution Chem.*, **12**, 295 (1983).
14) S. Cabani, G. Conti, L. Lepori, and G. Leva, *J. Phys. Chem.*, **76**, 1343 (1972).
15) R. E. Verrall and B. E. Conway, *J. Phys. Chem.*, **70**, 3961 (1966).
16) J. T. Edward, P. G. Farrell, and F. Shahidi, *J. Phys. Chem.*, **82**, 2310 (1978); *Can. J. Chem.*, **57**, 2585 (1979).
17) R. N. French and C. M. Criss, *J. Solution Chem.*, **10**, 699, 713 (1981).

 © 1988 The Chemical Society of Japan Bull. Chem. Soc. Jpn., 61, 3307—3313 (1988)

The Addition Effect of CH_3Br and CH_3Cl on Ignition of CH_4 by Shock Wave

Kazuo TAKAHASHI, Tadaaki INOMATA,* Takao MORIWAKI, and Satiko OKAZAKI
Department of Chemistry, Faculty of Science and Technology, Sophia University,
Kioi-cho 7-1, Chiyoda-ku, Tokyo 102
(Received April 23, 1988)

Ignition delay times were measured in the CH_4–CH_3X (X: Cl or Br)–O_2 system diluted in Ar using a shock tube. The times were shorter than those without CH_3X, indicating that CH_3X accelerates the ignition of CH_4. A theoretical model including 8 elementary reactions concerning CH_3X, with a CH_4 oxidation mechanism consisting of 93 reactions, was used to examine the role of halogen for the ignition. The compounds containing Br formed a chain reaction with CH_4 and accelerated the decomposition of CH_4, while CH_3Cl acted only as a fuel which was easily decomposed.

Ignition delays in mixtures involving CH_4 and additives have been studied under various experimental conditions.[1–6] The results showed that additives generally promoted ignition in a CH_4–O_2 mixture, except for substances like N_2 which act as diluents only. The addition effect of some hydrocarbons or hydrocarbon derivatives can be attributed principally to a chemical reaction due to the alkyl radicals generated from the decomposition of the additives.

The ignition delay in CH_4–O_2 strongly depends on the rate of initiation reaction (R1) and the rate of CH_3 generation (R2 and R4), as reported previously.[7] The promotion of ignition by CH_3Br, well-known as an inhibitor for flame propagation, was caused by the additional production of the CH_3 radical, because the activation energy in CH_3Br decomposition (R94) was smaller than that in CH_4 decomposition. However, in addition to insufficient discussion for the role of Br atom, other problems remain, including how other halomethanes influence the ignition of CH_4 and what happens in the reaction mechanism due to the differences of kinds of halogen.

In this investigation, the measurements of ignition delay by using a shock tube and the analytical treatments are performed in the mixtures containing CH_3Br or CH_3Cl, to understand the reaction of halogenated compounds through the induction period. Although the CH_4–CH_3Br–O_2 system has already been studied,[7] CH_3Br had acted as a part of the main fuel, because the test mixture had involved a large amount of CH_3Br (about 30% of CH_4). So this system involving a small amount of CH_3Br was reexamined.

Experimental

The shock tube used in the experiment was made of 6.2 cm i.d. stainless steel pipe. The reaction and driver sections were 3.8 m and 1.7 m long, respectively, so dwell time above 1.5 ms could be obtained in all experimental regions. Other apparatus for measurements of shock velocity and of ignition delay time and the procedures were already reported in detail.[7] The composition of the gas mixtures in Table 1 was employed; the accuracy for preparation of gas mixture is below 0.01%, because silicone oil and mercury manometers were used. The pressure and temperature behind the reflected shock wave were 1.9—3.9 atm and 1500—2000 K, respectively.

Analytical Treatment

To clarify the role of halogen atoms for the ignition, ignition delay times were calculated based on the reaction mechanism presented in Table 2, under the constant pressure conditions.[8] Figure 5 shows that the OH concentration as a function of the time after the arrival of the shock wave increased gradually in the middle stage of the induction period, while the concentration in the last stage rose rapidly. These two sections are regarded as linear, and the ignition delay time was defined as the intersection of the two straight lines. When the profile between time and concentration of H atom, concentration of CH_4, or temperature was used, the ignition delay times were the same as that from the concentration profile of OH.

Rate constants for forward reactions accumulated by Westbrook[9] were used, except R94 and R102, which are not involved in Ref. 9. Most of these rate constants which had been used for the calculation of burning velocity are regarded as being reasonable at present. However, the rate constants of reactions involving CHCO, CH_2CO, or CH_2 are uncertain and more exact values need. In this calculation, reactions involving CHCO, CH_2CO, or CH_2 did not greatly affect an ignition delay time, so the values in Ref. 9 were used as presented. Rate constants for reverse reactions were calculated from forward ones and equilibrium constants.

R94 and R102 were estimated as calculated induction times so as to agree with experimental ones in 1500—2000 K. The rate constant of R94 in high pressure limit was expressed by

$$k_{94} = 1.58 \times 10^{14} \exp(-71700/RT).$$[10]

However, the agreement of experimental and calculated values could not be attained by using this expression. This experimental conditions are

correspond to the so called fall-off region for R94, so the ratio of k/k_∞ was estimated by unimolecular reaction theory. The ratio was 0.07—0.11; then the one-tenth of pre-exponential factor of the above expression was most suitable. Because the data for k_{102} could not be obtained, the expression in Table 2 was estimated. The estimated activation energy of R102 is located between the bond energy of CH_3–Cl and the activation energy of R94 and the pre-exponential factor is reasonable for a unimolecular reaction in fall-off region. Because the variation below 3% of k_{94} or k_{102} does not cause any important change to calculated ignition delay times, both estimated expressions include errors of ±3%.

Although most thermochemical and thermodynamic data which were needed to calculate induction time or reverse rate constants were obtained from Refs. 11 and 12, the data for nine compounds shown below, which were not published, were evaluated by the general statistical method.[11] From the moments of inertia and fundamental vibrational frequencies for C_2H_3 and C_2H_5,[12] C_2H_6,[13] CH_3O,[14] CH_3Cl and CH_3Br,[15] H_2O_2,[16] CHCO,[17] and CH_2CO,[18] we calculated the data for these compounds in the 0—4000 K range. The data in the 0—1500 K range was reported for the former seven compounds;[12–16] calculated values in the 0—1500 K range agree well with the data in the references, supporting the adequacy of calculated values for 1500—4000 K, because values in high temperature can be estimated more exactly. On the other hand, the calculated data for CHCO and CH_2CO may involve some error, because of using unreliable fundamental vibrational frequencies, but small changes of thermodynamic data for CHCO and CH_2CO do not affect calculations of ignition delay times.

Results and Discussion

Additives used in this study are a kind of fuel, so we must determine how a small additional amount of fuel changes the ignition delay. As shown in Fig. 1, ignition delay times are slightly longer in mixture 2 than that in mixture 1; namely, CH_4 acts as a self-inhibitive compound. Therefore, to discuss the role of halogen, we used the mixture containing only CH_4 as fuel and some mixtures in which a part of CH_4 was replaced by halomethane. For example, the concentrations of O_2 and Ar and the number of C atoms are constant in mixtures 2, 3, and 4 (Table 1) and it is proper to use them to examine the role of the halogen atom, as previously reported.[7]

Ignition delay times of mixtures including CH_3Br or CH_3Cl (in Fig. 1) are short in comparison with the times for the mixtures 1 and 2, indicating that these compounds accelerate an ignition of CH_4; the acceleration effect of CH_3Br is more predominant than CH_3Cl. The lines between $1/(10^{-4}\,T_5)$ and $\log(\tau/s)$

Table 1. Test Gas Mixture Composition (%)

No.	CH_4	CH_3Br	CH_3Cl	O_2	Ar
1	2.00	—	—	4.00	94.00
2	2.10	—	—	4.00	93.90
3	2.00	0.10	—	4.00	93.90
4	2.00	—	0.10	4.00	93.90

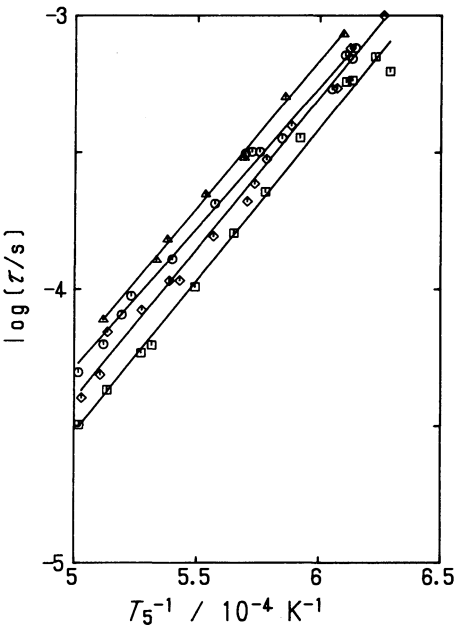

Fig. 1. Observed ignition delay times. ○, mixture 1; △, mixture 2; □, mixture 3; ◇, mixture 4.

are straight. The slopes are 1.04, 1.02, 1.08, and 1.09 K for the mixtures 1, 2, 3, and 4, respectively; namely, the addition effect is quite different absolutely each case but the dependence on temperature is almost identical in all mixtures. The fact that ignition delay times in mixtures 3 and 4 are shorter than that in mixtures 1 or 2 may be explained qualitatively by only the difference of bond energies of C–H and C–X. However it is hardly possible that only the initiation reactions (R1, R94, R102) control the ignition delay, even though they are the main factor.

We indicated[7] that the main reactions controlling the ignition of CH_4 are R1, R2, R4—R6, R8, R9, R13, R14, R22, and R69. CH_3, CH_3O, CH_2O, and CHO species participate in all these reactions, except for R69, which is the most important one to chain branching: These results suggest that the ignition reactions progress through the route of $CH_3 \rightarrow CH_3O \rightarrow CH_2O \rightarrow CHO$. When CH_3Br is added, the reaction scheme will differ; the initiation reaction is not R1 but R94, R1 does not contribute to ignition at all, and R95 and R98, known as inhibition ones, compete with R69 in the consumption of H atoms. Moreover, in CH_4–O_2, the behavior of CH_3 and of H atom made extremely important contribution to an ignition. CH_3, generated by the initiation reaction (R1), reacts

$CH_4 + M = CH_3 + H + M$ (R1)
$CH_4 + OH = CH_3 + H_2O$ (R2)
$CH_4 + O = CH_3 + OH$ (R4)
$CH_3 + HO_2 = CH_3O + OH$ (R5)
$CH_3 + O_2 = CH_3O + O$ (R6)
$CH_3 + O = CH_2O + H$ (R8)
$CH_3 + CH_3 = C_2H_6$ (R9)
$CH_3O + M = CH_2O + H + M$ (R13)
$CH_2O + OH = HCO + H_2O$ (R14)
$HCO + M = CO + H + M$ (R22)
$H + O_2 = O + OH$ (R69)
$CH_3Br = CH_3 + Br$ (R94)
$CH_3Br + H = CH_3 + HBr$ (R95)
$HBr + H = H_2 + Br$ (R98)

with O_2 or O atom. R6 is predominant in the early stage of the induction period and R8 becomes important later, while the concentration of H atom increased continuously. These facts are important in order to comprehend the role of halogen atoms.

Calculated induction times are in good agreement with the observed values, as shown in Fig. 2, indicating that the reaction mechanism in Table 2 is reasonable. Although a large number of reactions for halogen containing compounds have been reported, the set of R94—R109 for halogen containing compounds is enough to explain the ignition delay time. As is obvious from experimental results, additive effects are similar in all temperature regions; therefore, model calculations and various parametric analyses were performed in all mixtures at 1800 K. Calculated induction times are shown in Table 3. This includes the results which were calculated by the reaction mechanism in Table 2 and by deleting reactions concerning halogen species one by one from it.

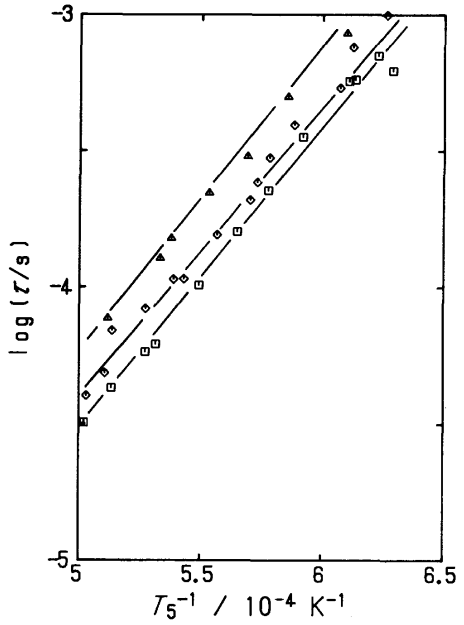

Fig. 2. Comparison of calculated and observed ignition delay times. △, mixtures 2; □, mixture 3; ◇, mixture 4. Straight lines are calculated ones.

In eight reactions involving bromine containing species, the reactions, R94, R95, R97, and R98 influence upon ignition delay time. When R94, R95, or R97 is deleted from the complete mechanism (Table 2), the ignition delay is longer than that in the complete mechanism, while deletion of R98 made it shorter, showing that R94, R95, and R97 promote an ignition and R98 inhibits an ignition.

The calculated ignition delay time without R94 is longer than that in mixture 2. This result is caused by R98, in addition, R95 can also inhibit an ignition, when R94 is deleted. R95 proceeds in the reverse direction in a greater part of the induction period, while R94, R97, and R98 proceed in the forward direction, in the complete mechanism. When R94 is deleted, R95 proceeds in the forward direction through the whole induction period, leading to the inhibition of ignition. Of course, the conditions in which R94 does not exist cannot occur in these experiments, but the result suggests that a reaction like R95 has some possibility to act as an inhibition one or as an acceleration one, depending on the rate of thermal decomposition of the halogenated hydrocarbons.

The initiation reaction is, of course, R94, because the rates of other initiation reactions (R1, R74, R92) did not contribute much to the ignition delay time. While CH_3 is consumed through R6 and R8, which are the main reactions for CH_3 consumption, Br atom consumed CH_4 through R97 and then CH_3Br was regenerated through the reverse reaction of R95. R97, including the same species as R95 on its right side, progresses forward, namely CH_4 is not regenerated by R97. Therefore, the next chain cycle is formed and promotes the decomposition of CH_4. Moreover, in the

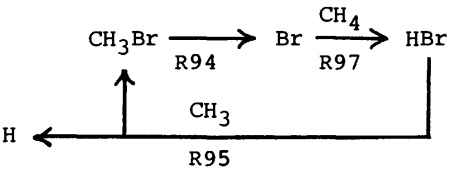

(I)

cycle, H atoms are produced, so that the chain branching reaction, R69, or the reaction of CH_4 consumption, R3, is accelerated catalytically. In brief, the net reaction of R94, R95, and R97 corresponds to a process having a fast rate in which CH_4 is decomposed to CH_3 and H atom instead of process R1 having a slow rate.

The effect of CH_3Cl as ignition promoter is low in comparison to that of CH_3Br; the effective reactions on ignition are R102, R103, R105, and R106. Al-

Table 2. Reaction Mechanism and Rate Constants

	Reaction	log A	n	E
R1	$CH_4+M=CH_3+H+M$	17.15	0.00	88.40
R2	$CH_4+OH=CH_3+H_2O$	3.54	3.08	2.00
R3	$CH_4+H=CH_3+H_2$	14.10	0.00	11.90
R4	$CH_4+O=CH_3+OH$	13.20	0.00	9.20
R5	$CH_4+HO_2=CH_3+H_2O_2$	13.30	0.00	18.00
R6	$CH_3+HO_2=CH_3O+OH$	13.51	0.00	0.00
R7	$CH_3+O_2=CH_3O+O$	13.68	0.00	29.00
R8	$CH_3+OH=CH_2O+H_2$	12.60	0.00	0.00
R9	$CH_3+O=CH_2O+H$	14.11	0.00	2.00
R10	$CH_3+CH_3=C_2H_6$	12.95	0.00	0.00
R11	$CH_3+CH_3=C_2H_5+H$	14.90	0.00	26.52
R12	$CH_3+CH_3=C_2H_4+H_2$	16.00	0.00	32.00
R13	$CH_3+CH_2O=CH_4+CHO$	10.00	0.50	6.00
R14	$CH_3+CHO=CH_4+CO$	11.48	0.50	0.00
R15	$CH_3+HO_2=CH_4+O_2$	12.00	0.00	0.40
R16	$CH_3O+O_2=CH_2O+HO_2$	12.00	0.00	6.00
R17	$CH_3O+M=CH_2O+H+M$	13.70	0.00	21.00
R18	$CH_2O+OH=CHO+H_2O$	12.88	0.00	0.17
R19	$CH_2O+H=CHO+H_2$	14.52	0.00	10.50
R20	$CH_2O+O=CHO+OH$	13.70	0.00	4.60
R21	$CH_2O+HO_2=CHO+H_2O_2$	12.00	0.00	8.00
R22	$CH_2O+M=CHO+H+M$	16.52	0.00	81.00
R23	$CHO+OH=CO+H_2O$	14.00	0.00	0.00
R24	$CHO+H=CO+H_2$	14.30	0.00	0.00
R25	$CHO+O=CO+OH$	14.00	0.00	0.00
R26	$CHO+O_2=CO+HO_2$	12.60	0.00	7.00
R27	$CHO+HO_2=CH_2O+O_2$	14.00	0.00	3.00
R28	$CHO+M=CO+H+M$	14.16	0.00	19.00
R29	$CO+OH=CO_2+H$	7.11	1.30	−0.77
R30	$CO+O+M=CO_2+M$	15.77	0.00	4.10
R31	$CO+HO_2=CO_2+OH$	14.18	0.00	23.65
R32	$CO+O_2=CO_2+O$	11.50	0.00	37.60
R33	$C_2H_6+OH=C_2H_5+H_2O$	13.05	0.00	2.45
R34	$C_2H_6+H=C_2H_5+H_2$	2.73	3.50	5.20
R35	$C_2H_6+O=C_2H_5+OH$	13.40	0.00	6.36
R36	$C_2H_6+CH_3=C_2H_5+CH_4$	−0.26	4.00	8.28
R37	$C_2H_5+O_2=C_2H_4+HO_2$	12.00	0.00	5.00
R38	$C_2H_5+M=C_2H_4+H+M$	15.30	0.00	30.00
R39	$C_2H_4+OH=C_2H_3+H_2O$	12.68	0.00	1.23
R40	$C_2H_4+H=C_2H_3+H_2$	7.18	2.00	6.00
R41	$C_2H_4+M=C_2H_3+H+M$	18.80	0.00	108.72
R42	$C_2H_4+M=C_2H_2+H_2+M$	16.97	0.00	77.20
R43	$C_2H_4+OH=CH_3+CH_2O$	12.30	0.00	0.96
R44	$C_2H_4+O=CH_3+CHO$	12.52	0.00	1.13
R45	$C_2H_4+O=CH_2O+CH_2$	13.40	0.00	5.00
R46	$C_2H_4+C_2H_4=C_2H_5+C_2H_3$	14.70	0.00	64.70
R47	$C_2H_3+H=C_2H_2+H_2$	13.30	0.00	2.50
R48	$C_2H_3+O_2=C_2H_2+HO_2$	12.00	0.00	10.00
R49	$C_2H_3+M=C_2H_2+H+M$	14.90	0.00	31.50
R50	$C_2H_2+OH=C_2H+H_2O$	12.78	0.00	7.00
R51	$C_2H_2+H=C_2H+H_2$	14.30	0.00	19.00
R52	$C_2H_2+O=C_2H+OH$	15.51	−0.60	17.00
R53	$C_2H_2+M=C_2H+H+M$	14.00	0.00	114.00
R54	$C_2H_2+OH=CH_2CO+H$	11.51	0.00	0.20
R55	$C_2H_2+O=CHCO+H$	4.55	2.70	1.39
R56	$C_2H_2+O=CH_2+CO$	13.83	0.00	4.00
R57	$C_2H_2+O_2=CHO+CHO$	12.60	0.00	28.00
R58	$C_2H+O_2=CHO+CO$	13.00	0.00	7.00
R59	$C_2H+O=CH+CO$	13.70	0.00	0.00
R60	$CH_2CO+OH=CHCO+H_2O$	13.00	0.00	0.00
R61	$CH_2CO+H=CHCO+H_2$	13.00	0.00	0.00
R62	$CH_2CO+O=CHCO+OH$	13.00	0.00	0.00
R63	$CH_2CO+OH=CH_2O+CHO$	13.45	0.00	0.00
R64	$CH_2CO+H=CH_3+CO$	13.04	0.00	3.40
R65	$CH_2CO+O=CHO+CHO$	13.00	0.00	2.40
R66	$CH_2CO+M=CH_2+CO+M$	16.30	0.00	60.00

Table 2. (Continued)

	Reaction	log A	n	E
R67	CHCO+OH=CHO+CHO	13.00	0.00	0.00
R68	CHCO+H=CH_2+CO	13.70	0.00	0.00
R69	CHCO+O=CO+CHO	13.53	0.00	2.00
R70	CH_2+OH=CH+H_2O	11.43	0.67	25.70
R71	CH_2+H=CH+H_2	11.43	0.67	25.70
R72	CH_2+O=CH+OH	11.28	0.68	25.00
R73	CH_2+O_2=CHO+OH	14.00	0.00	3.70
R74	CH+O_2=CHO+O	13.00	0.00	0.00
R75	CH+O_2=CO+OH	11.13	0.67	25.70
R76	H+O_2=OH+O	14.27	0.00	16.79
R77	O+H_2=OH+H	10.26	1.00	8.90
R78	OH+OH=O+H_2O	12.50	0.00	1.10
R79	OH+H_2=H+H_2O	13.34	0.00	5.15
R80	H+H+M=H_2+M	15.48	0.00	0.00
R81	O+O+M=O_2+M	15.67	−0.28	0.00
R82	H+O+M=OH+M	16.00	0.00	0.00
R83	OH+H+M=H_2O+M	23.15	−2.00	0.00
R84	H+O_2+M=HO_2+M	15.22	0.00	−1.00
R85	H+HO_2=H_2+O_2	13.40	0.00	0.70
R86	H+HO_2=OH+OH	14.40	0.00	1.90
R87	H+HO_2=O+H_2O	11.95	0.50	3.97
R88	OH+HO_2=H_2O+O_2	13.70	0.00	1.00
R89	O+HO_2=OH+O_2	13.70	0.00	1.00
R90	H_2O_2+OH=H_2O+HO_2	13.00	0.00	1.80
R91	H_2O_2+H=HO_2+H_2	12.23	0.00	3.75
R92	H_2O_2+O_2=HO_2+HO_2	13.60	0.00	42.64
R93	H_2O_2+M=OH+OH+M	17.08	0.00	45.50
R94	CH_3Br=CH_3+Br	13.20	0.00	71.70
R95	CH_3Br+H=CH_3+HBr	14.24	0.00	6.90
R96	CH_3Br+Br=CH_3+Br_2	13.70	0.00	22.90
R97	CH_4+Br=CH_3+HBr	14.00	0.00	18.30
R98	HBr+H=H_2+Br	11.88	0.50	1.11
R99	Br_2+H=HBr+Br	12.81	0.50	1.11
R100	Br+Br+M=Br_2+M	16.00	0.00	0.00
R101	Br+H+M=HBr+M	18.00	−0.71	0.00
R102	CH_3Cl=CH_3+Cl	13.90	0.00	79.80
R103	CH_3Cl+H=CH_3+HCl	14.54	0.00	9.00
R104	CH_3Cl+Cl=CH_3+Cl_2	14.00	0.00	25.00
R105	CH_4+Cl=CH_3+HCl	13.41	0.00	3.85
R106	HCl+H=H_2+Cl	13.36	0.00	3.50
R107	Cl_2+H=HCl+Cl	14.57	0.00	1.80
R108	Cl+Cl+M=Cl_2+M	14.30	0.00	−1.79
R109	Cl+H+M=HCl+M	8.78	1.00	−36.52

Rate constants in the form $AXT^n\exp(-E/RT)$, in cm^{-3}, mol, s, kcal, and K units.

Table 3. Calculated Induction Times

Reaction[a)]	Ignition delay time/10^{-6} s			
	Mixture 1	Mixture 2	Mixture 3	Mixture 4
None	215	221	119	154
CH_3X=CH_3+X(R94, R102)			233	236
CH_3X+H=CH_3+HX(R95, R103)			142	145
CH_3X+X=CH_3+X_2(R96, R104)			118	154
CH_4+X=CH_3+HX(R97, R105)			140	152
HX+H=H_2+X(R98, R106)			115	150
X_2+H=HX+X(R99, R107)			119	153
X+X+M=X_2+M(R100, R108)			119	154
X+H+M=HX+M(R101, R109)			118	153

a) Reaction which is delected from the complete mechanism. X is Br or Cl.

though the initiation reaction is changed from R1 to R102, the chain reaction like (I) does not exist. This is because R102 is 100 times faster than R1 and R105 proceeds in the forward direction and promotes the decomposition of CH_4, but R103 progresses forward (Fig. 4), so CH_3Cl could not be regenerated during the whole induction period. The difference of rates between R95 and R103 depends on the rate constant. The forward and net rates of R103 are about 1/10 of R95 and the reverse rate of R103 is about 1/500 of R95, while the concentration of HCl is two times that of HBr (Figs. 5 and 6).

$$CH_3Cl = CH_3 + Cl \quad (R102)$$
$$CH_3Cl + H = CH_3 + HCl \quad (R103)$$
$$CH_4 + Cl = CH_3 + HCl \quad (R105)$$
$$HCl + H = H_2 + Cl \quad (R106)$$

As R103 proceeds in the forward direction and the

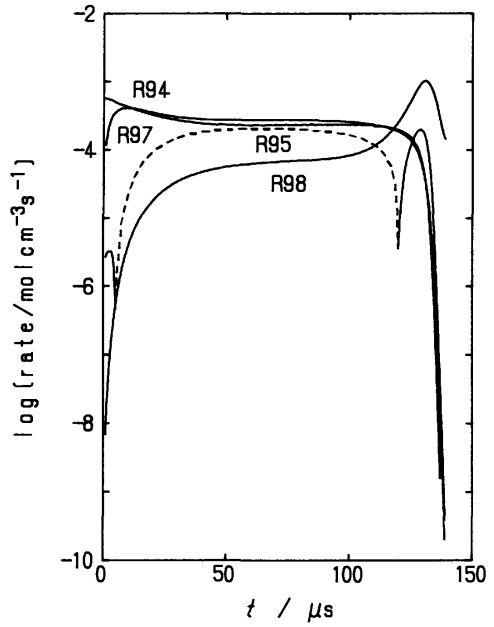

Fig. 3. Net reaction rates of R94, R95, R97, and R98 at 1800K in mixture 3. t is time after the arrival of shock wave. Solid line: net reaction proceeds in forward direction, dotted line: in reverse direction.

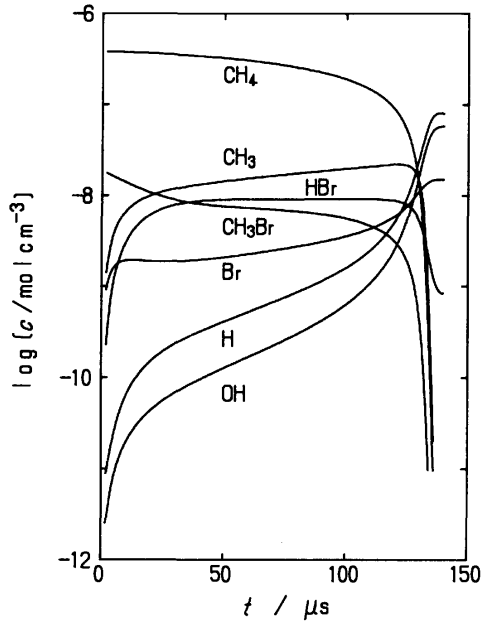

Fig. 5. Calculated concentration profiles of CH_4, CH_3, H, OH, CH_3Br, HBr, and Br at 1800K in mixture 3.

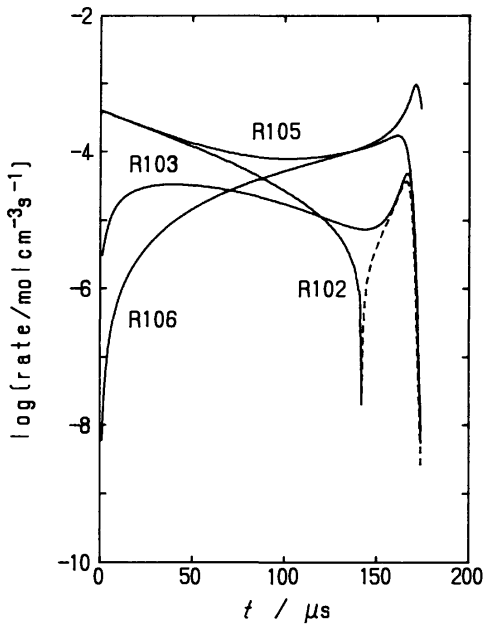

Fig. 4. Net reaction rates of R102, R103, R105, and R106 at 1800K in mixture 4.

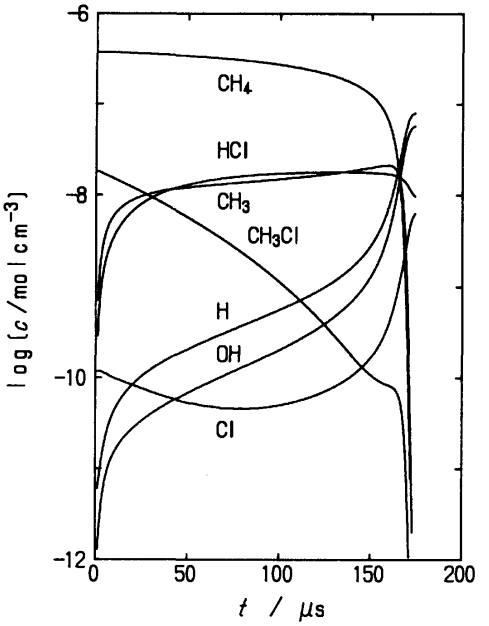

Fig. 6. Calculated concentration profiles of CH_4, CH_3, H, OH, CH_3Cl, HCl, and Cl at 1800 K in mixture 4.

reverse rate of R105 is very slow, HCl generated by R103 reacts through R106; as a result, R105 and R106, which have comparable rates, form chain (II). The

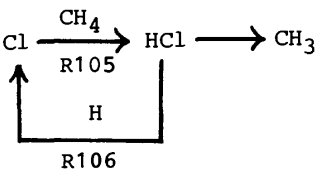

(II)

chain promotes the decomposition of CH_4, while consumes H simultaneously. H atom promotes R69 directly, while CH_3 needs two or more steps, which have low rate constants, to generate H atom, so the chain (II) inhibits the ignition. In CH_3Br, the chain like (II) is probably created too, but it contributes little to an ignition as the reverse rate of R96 is faster than that of forward rate of R98 through the whole induction period.

When R102 is deleted, the ignition delay is almost equal to that in mixture 3, as shown in Table 3. If R102 does not exist, it is predicted that CH_3Cl should consume H through R103; H is consumed furthermore by the chain (II), causing inhibition of an ignition. Exclusion of R103, R105, or R106 makes the ignition delay shorter by a few percent; this result indicates that these reactions certainly inhibit an ignition and that H atom has more effect on the ignition than CH_3 does.

The concentration profile of CH_3Br or of Br differ from that of CH_3Cl or of Cl, respectively. On the other hand, the profiles of CH_4, CH_3, OH, H, or HX (X: Br or Cl) are very similar in the mixtures 3 and 4. When the reaction is initiated, Br is first generated by R94 and then HBr rapidly increases, following Br, until it reaches a constant value at about 30 μs. The consumption of CH_3Br is retarded practically with increase of concentration of HBr. CH_3Cl is consumed gradually through the induction period and its concentration did not become constant. Moreover, Cl atom is produced in the early stages of induction period, but it generates HCl soon because of fast R105, resulting in the greater parts of Cl existing as HCl even in early stages. Although these profiles may be easily expected from Figs. 3 and 4, they express fully the difference of addition effect between CH_3Br and CH_3Cl. At the same time, they show that both additives change the rate of ignition reaction but not the main ignition mechanism.

In conclusion, the promotion mechanism by the addition of CH_3Br and CH_3Cl to methane is because of the relatively fast decomposition rates in both additives, which lead to easy generation of CH_3 radical; this is especially clear in CH_3Br, because of the existence of the chain reaction constructed by R94, R95, and R97. The fundamental discrepancy in CH_3Br and CH_3Cl depends on the relative rates of R95 or R103 and R98 or R106, in addition to the low rate in R102.

References

1) R. W. Crossley, E. A. Dorko, K. Scheller, and A. Burcat, *Combust. Flame*, **19**, 373 (1972).

2) E. A. Dorko, D. M. Bass, R. W. Crossley, and K. Scheller, *Combust. Flame*, **24**, 173 (1975).

3) A. Grillo and M. W. Slack, *Combust. Flame*, **27**, 377 (1976).

4) R. Ravikumar and K. A. Bhaskaran, *Combust. Flame*, **27**, 107 (1976).

5) E. K. Dabora, *Combust. Flame*, **24**, 181 (1975).

6) A. Burcat, *Combust. Flame*, **28**, 319 (1977).

7) T. Inomata, T. Moriwaki, and S. Okazaki, *Combust. Flame*, **62**, 183 (1985).

8) W. C. Gardiner, B. F. Walker, and C. B. Wakefield, "Mathematical Methods for Modeling Chemical reactions in Shock Waves," in "Shock Waves in Chemistry," ed by A. Lifshitz, Marcel Dekker Inc., New York (1981), p. 319.

9) C. K. Westbrook, F. L. Dryer, and K. P. Schug, "Nineteenth Symposium (International) on Combustion," The Combustion Institute, Pittsburgh (1982), p. 153; C. K. Westbrook and F. L. Dryer, *Proc. Energy Combust. Sci.*, **10**, 1 (1984); C. K. Westbrook, F. L. Dryer, and K. P. Schug, *Combust. Flame*, **52**, 299 (1983).

10) S. W. Benson, "Kinetic Data on Gas Phase Unimolecular Reactions," NSRDS-NBS 21, National Bureau of Standards, Washington D. C. (1970).

11) "JANAF Thermochemical Tables," 2nd ed, NSRDS-NBS 37, ed by D. R. Stull and H. Prophet, National Bureau of Standards, Washington D. C. (1971); and later supplements.

12) G. S. Bahn, NASA-CR-2178, NASA (1973).

13) K. M. Pamidimukkala, D. Rogers, and G. B. Skinner, *J. Phys. Chem. Ref. Data*, **11**, 83 (1982).

14) A. Burcat and S. Kudchadker, *Acta Acad. Sci. Hung.*, **101**, 249 (1979).

15) S. A. Kudchadker and A. P. Kudchadker, *J. Phys. Chem. Ref. Data*, **4**, 457 (1975).

16) P. A. Giguere and I. D. Liu, *J. Am. Chem. Soc.*, **77**, 6477 (1955).

17) M. J. S. Dewar and G. P. Ford, *J. Am. Chem. Soc.*, **99**, 1685 (1977); J. M. Oakes, M. E. Jones, V. M. Bierbaum, and G. B. Ellison, *J. Phys. Chem.*, **87**, 4810 (1983); G. Inoue and M. Suzuki, *J. Chem. Phys.*, **84**, 3708 (1986); Y. Endo and E. Hirota, 52nd National Meeting of the Chemical Society of Japan, Tokyo, April 1986, Abstr., No. 1D07; J. W. C. Jones and J. M. R. Stone, *J. Mol. Spectrosc.*, **42**, 523 (1972).

18) M. J. S. Dewar and G. P. Ford, *J. Am. Chem. Soc.*, **99**, 1685 (1977); D. D. Wagman, W. H. Evans, V. B. Parker, R. H. Schumm, I. Halow, S. M. Bailey, K. L. Chrney, and R. L. Nuttall, *J. Phys. Chem. Ref. Data*, **11**, Supplement No. 2, (1982).

Determination of Ionic Partial Molar Volumes of Bolaform Electrolytes by Means of Sedimentation Potential Measurements

Hiromitsu HIRAKAWA,* Hiroyasu NOMURA,† and Fumio KAWAIZUMI†
Department of Electronics, Faculty of Engineering, Kagoshima University, Kagoshima 890
†Department of Chemical Engineering, School of Engineering, Nagoya University, Nagoya 464
(Received March 31, 1988)

Synopsis. Sedimentation potentials (SP) and electrical conductivities have been measured in aqueous solutions of three kinds of bolaform electrolytes, $[R_3N-(CH_2)_n-NR_3]Br_2$ where R stands for ethyl group and n is equal to 4, 6, and 10. Using the SP and conductivity data the partial molar volumes of the bolaform salts were divided into cationic and anionic parts. Two ionic sites of the bolaform electrolytes behave independently.

Partial molar quantities of a dissolved electrolyte are known to give much information on various aspects of solute–solvent interactions. Among them, partial molar volumes V_2^0 is perhaps one of the most familiar and useful quantities, since its accurate values can be determined directly from density measurements. Inspection of the temperature dependence of partial molar volumes of electrolytes indicates that significant differences in ion–water interactions exist for cations and anions. For detailed discussion of V_2^0 data, ionic division of V_2^0 of electrolytes is indispensable. A number of workers have carried out the ionic division based on various theoretical and/or empirical criteria. The criteria or assumptions adopted and the results obtained are given in a review.[1)]

Method of ionic division founded on a firm theoretical ground has long been restricted to the ultrasonic vibration potential (UVP) measurement. Unfortunately, special techniques are needed to use this valuable method. An alternative to the UVP method is the sedimentation potential (SP) measurement. Recently a sedimentation potential generating apparatus (SPGA) was designed by one of the present authors (H.H) and the sedimentation potentials were measured with sufficient accuracy for aqueous solutions of ordinary inorganic electrolytes.[2)] In this note, we will report first the results of sedimentation potential measurement on bolaform electrolytes in aqueous solutions and then discuss the ionic partial molar volumes evaluated.

Bolaform electrolyte is a class of salts with general formula $[R_3N-(CH_2)_n-NR_3]Br_2$. Following the official nomenclature it is expressed as bis(tetraalkylammonio)alkaline dibromide. In this work three kinds of bolaform salts were used as samples for which R=ethyl, and n is equal to 4, 6, and 10. These samples will be abbreviated as J4, J6, and J10, respectively. Samples were prepared and purified as described elsewhere.[3)]

The experimental procedures of SP measurements are the same as those in our previous paper.[2)] For the ionic division of V_2^0 transference numbers are necessary. These values are not found in the literature. For this reason as part of this work, electric conductivities were measured using a Fuso 360 linear-bridge conductometer. The cell constant of the cell used in the present study was 0.1240 cm^{-1} and the concentration ranges were 10^{-4} to 10^{-3} mol dm^{-3}.

All measurements were done at 25 °C.

The concentration dependences of SP of bolaform electrolytes in aqueous solutions are shown in Fig. 1. Negative values of SP were observed for all samples investigated and the values decreased with increasing concentration. At lower concentrations, the SP values became independent of concentration of the salts. With increasing molecular weight, the absolute values of SP increased.

The limiting conductivities of bolaform electrolyte were evaluated from the least squares fitting of the following Debye–Hückel–Onsager equation;

$$\Lambda = \Lambda^\infty - (B_1\Lambda^\infty + B_2)c^{1/2} \quad (1)$$

where c is the concentration in mol dm^{-3} and B_1 and B_2 are the parameters given by the theory. For the sample J4, down ward deviation from Eq. 1 was observed, suggesting that ion-pairing occurs for this salt. But no further discussion on the conductivity will be done, since the conductivity data at infinite dilution are needed at this stage for the evaluation of the transference number only. The limiting values Λ^∞ obtained are summarized in the third column of Table 1.

The SP generated in aqueous electrolyte solutions

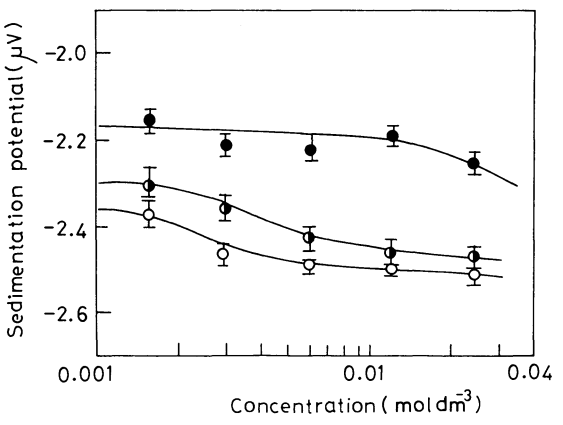

Fig. 1. Sedimentation potential for bolaform electrolytes as a function of concentration: ●J4; ◑J6; ○J10.

Table 1. Sedimentation Potential (SP) and Limiting Molar Conductivity of Bolaform Salts in Aqueous Solutions and Calculated Partial Molar Volumes for Cation and Anion

	SP	Λ^∞	V_2^0	V_+^0	V_-^0
	μV	S cm^2 mol^{-1}	cm^3 mol^{-1}	cm^3 mol^{-1}	cm^3 mol^{-1}
J4	−2.16	232.7	322.28[a]	267.0	27.5
J6	−2.30	237.6	356.50[a]	303.3	26.6
J10	−2.35	240.5	420.26[a]	365.3	27.5

a) Ref. 4.

using our apparatus is expressed as follows;[2]

$$V = 1.015 \times 10^{-6}\left[\frac{t_+}{z_+}(m_+ - V_+^0\rho) - \frac{t_-}{z_-}(m_- - V_-^0\rho)\right]x_0 \quad (2)$$

where t is the transference number, z is the charge, m is the molecular weight of the ion, ρ is the density of solvent, x_0 is the velocity amplitude, and the other symbols have their usual meanings. Since $V_2^0 = \nu_+V_+^0 + \nu_-V_-^0$, by combining the partial molar volume and the SP of an electrolyte, one can evaluate the partial molar volumes of the constituent ions without relaying on any kind of extra-thermodyamic or semiempirical assumptions. The partial molar volumes of J4, J6, and J10 are found in the literature.[4] The transference numbers t_+ and t_- were calculated from the limiting ionic conductivities given in Table 1 and the literature value[5] of $\Lambda^\infty(Br^-) = 78.14$ S cm^2 mol^{-1}. The estimated transference numbers of bolaform ions are 0.4944, 0.5100, and 0.5187, for J4, J6, and J10, respectively. The individual ionic partial molar volumes obtained are included in Table 1. The values of $V_-^0(Br^-)$ in Table 1 are all around 27.2 cm^{3}mol^{-1}. These values are a little smaller than those generally accepted; $V_-^0(Br^-) = 29.2$—30.9 cm^3 mol^{-1} according to the compilation of Millero.[1] However, in view of the precision of SP measurements[4] this difference has no significance. Rather, our work can serve as experimental evidence that ionic additivity of partial molar volume holds for these bolaform electrolytes. The ionic additivity corresponds to the independent behavior of the two separated ionic sites in the bolaform cations in aqueous solutions. The relationship for increment of partial molar volume and number of methylene groups in bolaform salts has been discussed elsewhere.[4]

References

1) F. J. Millero, "Water and Aqueous Solutions," Wiley-Interscience, New York (1972), p. 538.
2) H. Hirakawa, *J. Phys. Chem.*, **91**, 3452 (1987).
3) J. A. Burns and R. E. Verrall, *J. Solution Chem.*, **2**, 489 (1973); **4**, 369 (1975).
4) J. A. Burns and R. E. Verrall, *J. Solution Chem.*, **3**, 289 (1974).
5) R. A. Robinson and R. H. Stokes, "Electrolyte Solution," Butterworths, London (1959).

The Magnetic Properties of the Copper(II) Alkanoate Adducts with Benzimidazole and Related Nitrogen Donors

Shuji EMORI,* Hikari KURIHARA, and Yoneichiro MUTO
Department of Chemistry, Faculty of Science and Engineering, Saga University,
Honjo-machi, Saga 840
(Received February 10, 1988)

Synopsis. Various copper(II) alkanoate adducts with benzimidazole, *N*-acetylbenzimidazole, and benzoxazole have been prepared. The influence of the hydrogen bonded structure in the benzimidazole adducts on their magnetic properties are discussed.

A number of magnetic studies concerning dinuclear copper(II) carboxylates have revealed that the magnitude of the spin-exchange coupling between copper(II) ions is affected by the donor characteristics of both the bridging carboxylato and axial donor ligands.[1-3] For example, the room-temperature magnetic moments of the copper(II) alkanoate adducts with cyclic tertiary amines and cyclic ethers can be expressed according to

$$\mu_{eff} = -0.052(pK_a - 0.068pK_a' - 4.56) + \Delta\mu_\alpha + 1.38_5, \quad (1)$$

where pK_a and pK_a' are the acidities of the conjugate acids of alkanoate and axial ligands, respectively. $\Delta\mu_\alpha$ is the correction term for the substitution in the methyl group of acetic acid (-0.05_8 and -0.07_0 BM for the series of mono- and disubstituted acetates, respectively),[4] including the corrections for steric strain, field effect, and hyperconjugation.[4] Also, for the hydrates[1,5,6] and the ammonium chloride adducts,[7-9] a similar relationship can be demonstrated by plots of their corrected magnetic moments, $\mu_{eff}-\Delta\mu_\alpha$, against $pK_a-0.068pK_a'$, when -7.0 and -1.74 are used for the pK_a' values of chloride ion[10] and water molecule, respectively. However, the intercept obtained in this way (1.39_9 BM at $pK_a=4.56$ and $pK_a'=0$) is slightly larger than that in Eq. 1. This difference seems to be caused by the following two structural backgrounds: (1) the hydrogen bonding between the carboxylato oxygen atom and the neighboring proton donor, such as ammonium ion or water molecule,[11,12] decreases the electron density on the oxygen atom, and (2) the steric repulsion resulting from the bulky nature of the axial ligand, such as tertiary amines,[13] weakens its coordination bond. In order to clarify which factor plays a more important role in the above difference, we carried out preparations and magnetic susceptibility measurements of the copper(II) alkanoate adducts with benzimidazole, *N*-acetylbenzimidazole, and benzoxazole. These compounds are appropriate for studying the effect of hydrogen bonding on their magnetic properties, since all of these ligands have a similar bulkiness around their coordination sites, while only the benzimidazole adducts have hydrogen-bonded structures.[14,15]

Benzimidazole and benzoxazole are commercially available and were used without further purification.

Table 1. Analytical Data and Effective Magnetic Moments at 20°C

Compound	Found(Calcd)/%				μ_{eff}/BM
	Cu	C	H	N	
$Cu(C_2H_5COO)_2\cdot C_7H_6N_2$	19.63	47.02	4.93	8.05	1.33
	(19.38)	(47.63)	(4.92)	(8.55)	
$Cu(C_3H_7COO)_2\cdot C_7H_6N_2$	18.08	50.35	5.64	7.74	1.34
	(17.86)	(50.63)	(5.66)	(7.87)	
$Cu(ClCH_2CH_2COO)_2\cdot C_7H_6N_2$	15.79	39.13	3.63	6.81	1.37
	(16.02)	(39.36)	(3.56)	(7.06)	
$Cu(C_2H_5COO)_2\cdot C_7H_5NO$	19.41	47.14	4.63	4.08	1.31
	(19.33)	(47.49)	(4.60)	(4.26)	
$Cu(C_3H_7COO)_2\cdot C_7H_5NO$	17.69	50.37	5.35	3.87	1.30
	(17.81)	(50.49)	(5.37)	(3.92)	
$Cu(ClCH_2CH_2COO)_2\cdot C_7H_5NO$	15.95	39.14	3.27	3.51	1.35
	(15.98)	(39.26)	(3.29)	(3.52)	
$Cu(ClCH_2COO)_2\cdot C_7H_5NO$	17.23	35.16	2.48	3.68	1.42
	(17.19)	(35.74)	(2.45)	(3.79)	
$Cu(CH_3CHClCOO)_2\cdot C_7H_5NO$	16.23	39.07	3.18	3.47	1.41
	(15.98)	(39.26)	(3.29)	(3.52)	
$Cu(C_2H_5COO)_2\cdot C_9H_8N_2O$	17.12	48.42	4.90	7.62	1.31
	(17.18)	(48.71)	(4.91)	(7.57)	
$Cu(C_3H_7COO)_2\cdot C_9H_8N_2O$	15.98	51.28	5.55	7.05	1.30
	(15.97)	(51.31)	(5.57)	(7.04)	
$Cu(ClCH_2CH_2COO)_2\cdot C_9H_8N_2O$	14.43	40.99	3.71	6.36	1.34
	(14.48)	(41.06)	(3.68)	(6.38)	
$Cu[(CH_3)_2CHCOO]_2\cdot C_9H_8N_2O$	16.06	51.27	5.53	6.93	1.31
	(15.97)	(51.31)	(5.57)	(7.04)	
$Cu(CH_3CHClCOO)_2\cdot C_9H_8N_2O$	14.53	41.09	3.69	6.44	1.41
	(14.48)	(41.06)	(3.68)	(6.38)	

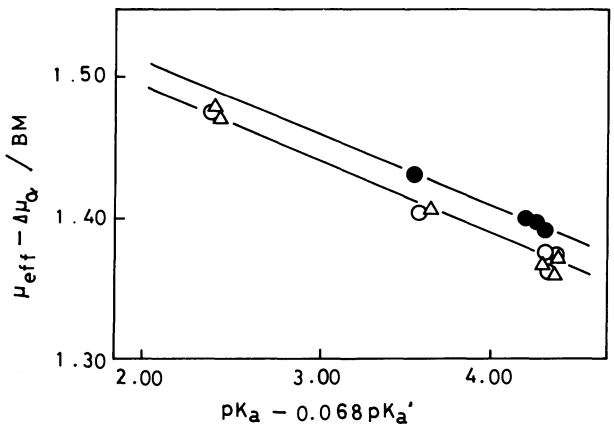

Fig. 1. The corrected magnetic moments at 20 °C plotted against the acidities of the ligands for the copper(II) alkanoate adducts with benzimidazole (●), *N*-acetylbenzimidazole (○), and benzoxazole (△).

N-Acetylbenzimidazole was prepared by the procedure of Reddy et al., mp 113 °C (lit, mp 113 °C).[17] Various copper(II) alkanoate adducts were obtained by a general procedure for synthesizing adducts with heterocyclic amines.[16,18]

The effective magnetic moments of these compounds (Table 1) were evaluated from the room-temperature magnetic susceptibilities, which were corrected for the diamagnetism of the ligands using Pascal constants,[19] and for $N\alpha$ using 60×10^{-6} emu mol^{-1} (1 emu=$4\pi\times10^{-6}$ m^3). The IR spectra of these compounds show characteristic bands in the ranges 1675—1615 and 1435—1405 cm^{-1} associated with unsymmetric and symmetric COO stretching vibrations of the carboxyl groups.[21] In the crystal of the copper(II) acetate adduct with benzimidazole, its dinuclear structure and the interdinuclear hydrogen-bond contact between the carboxylato oxygen atom and the benzimidazole ligand have been established by an X-ray analysis.[14] The magnetic and IR spectral data indicate that the present compounds also have bridged dinuclear structures similar to that of copper(II) acetate monohydrate.[11,12] In addition, the broad NH stretching bands[22] at about 3250—3200 cm^{-1} indicate that hydrogen bonding is involved in the benzimidazole adducts.

In order to confirm the linear correlation, the corrected magnetic moments, $\mu_{eff}-\Delta\mu_\alpha$, of the present compounds together with those of the corresponding acetates,[15,18] are plotted against $pK_a-0.068pK_a'$ in Fig. 1, using the pK_a' value of 5.46, 4.74, and 3.96, (the last two values are estimated by the Branch-Calvin equation[23]) for benzimidazole, *N*-acetylbenzimidazole, and benzoxazole, respectively. The error in the estimation of pK_a' values is practically permissible, since the coefficient of pK_a' in Eq. 1 is very small. As can be seen from Fig. 1, the points for the benzimidazole adducts and the rest are on different lines from each other, which have the same slope of −0.052 BM and intercepts of 1.37_9 and 1.36_3 BM, respectively. The intercepts obtained here are somewhat smaller than that of Eq. 1, and may be explained in terms of a steric hindrance for axial ligation. However, the present ligands have a similar bulkiness around the donor atoms. Thus, the difference in the intercepts apparently indicates the effect of hydrogen bonding in the benzimidazole adducts. The reported singlet-triplet separation values for the benzimidazole and benzoxazole adducts of copper(II) acetate (324 and 344 cm^{-1} respectively)[15,18] indicate that the hydrogen bonding weakens the intradinuclear antiferromagnetic interaction. The magnitude of the difference (ca. 0.01_5 BM) is comparable to that of the difference between the tertiary amine adducts and the ammonium chloride adducts of copper(II) alkanoate. Although both the strength and number of hydrogen bonds have been disregarded, this coincidence indicates that the difference between those of the tertiary amine and the ammonium chloride adducts is mainly attributable to hydrogen bonding and that the steric hindrance to an axial coordination of the tertiary amines is negligible, probably due to considerably long sp^3 hybridized orbitals at their coordination sites.

References

1) R. W. Jotham, S. F. A. Kettle, and J. A. Marks, *J. Chem. Soc., Dalton Trans.*, **1972**, 428.
2) M. Melnik, *Coord. Chem. Rev.*, **36**, 1 (1981).
3) V. Mohan Rao, D. N. Sathyanarayana, and H. Monohar, *Indian J. Chem.*, **24A**, 417 (1985).
4) S. Emori, H. Nonaka, N. Ikeda, and Y. Muto, *Bull. Chem. Soc. Jpn.*, **61**, 1812 (1988).
5) E. John, *J. Inorg. Nucl. Chem.*, **43**, 2735 (1981).
6) S. Emori, N. Morishita, and Y. Muto, *Bull. Chem. Soc. Jpn.*, **59**, 2893 (1986).
7) S. Emori and Y. Muto, *Bull. Chem. Soc. Jpn.*, **57**, 291 (1984).
8) S. Emori, N. Morishita, and Y. Muto, *Bull. Chem. Soc. Jpn.*, **60**, 1913 (1987).
9) S. Emori, Y. Tohyama, and Y. Muto, *Bull. Chem. Soc. Jpn.*, **60**, 4445 (1987).
10) F. A. Cotton and G. Wilkinson, "Advanced Inorganic Chemistry," 4th ed., John Wiley & Sons, New York (1980).
11) J. N. van Niekerk and F. R. L. Schoening, *Acta Crystallogr.*, **6**, 227 (1953).
12) G. M. Brown and R. Chidambaram, *Acta Crystallogr., Sect. B*, **29**, 2393 (1973).
13) V. Mohan Rao, D. N. Sathyanarayana, and H. Monohar, *J. Chem. Soc., Dalton Trans.*, **1983**, 2167.
14) M. Bukowska-Strzyzewska, J. Skoweranda, and A. Tosik, *Acta Crystallogr., Sect. B*, **38**, 2904 (1982).
15) J. Mrozinski and M. Bukowska-Strzyzewska, *J. Coord. Chem.*, **12**, 207 (1983).
16) G. J. Tennenhouse and J. C. Bailer, Jr., *J. Inorg. Nucl. Chem.*, **28**, 682 (1966).
17) G. S. Reddy, L. Mandell, and J. H. Goldstein, *J. Chem. Soc.*, **1963**, 1414.
18) T. Tokii and Y. Muto, *Bull. Chem. Soc. Jpn.*, **56**, 1549 (1983).
19) G. Foex, "Constants Sélectionées, Diamagnétisme et Paramagnétisme," Masson, Paris (1957).
20) J. Lewis, Y. C. Lin, L. K. Royston, and R. C. Thomson, *J. Chem. Soc.*, **1965**, 428.
21) S. Yamada, H. Nakamura, and R. Tsuchida, *Bull. Chem. Soc. Jpn.*, **31**, 303 (1958).
22) L. J. Bellamy, "The Infrared Spectra of Complex Molecules," 3rd ed., Chapman and Hall (1975).
23) G. E. K. Branch and M. Calvin, "The Theory of Organic Chemistry," Prentice-Hall, New York (1941).

Specific Binding of Substrates Containing Nitrogen and Oxygen Donor Groups to Copper(II)-Gadolinium(III) Hetero-Metal Center

Masatomi SAKAMOTO,* Tomitaro ISHIMORI, and Hisashi ŌKAWA†
Department of Industrial Chemistry, Faculty of Engineering, Ehime University, Bunkyo-cho, Matsuyama 790
†Department of Chemistry, Faculty of Science, Kyushu University, Hakozaki, Higashi-ku, Fukuoka 812
(Received April 15, 1988)

Synopsis. Substrate binding to the Cu(II)–Gd(III) hetero-metal complex of *N,N'*-bis(3-carboxysalicylidene)ethylenediamine was studied in *N,N*-dimethylformamide. It was suggested that substrates with a nitrogenous and an oxygenous groups (amino alcohols, 8-quinolinol, amino acids, and amino acid esters) were specifically bound to the Cu(II)-Gd(III) center, with the nitrogen to the copper and with the oxygen to the gadolinium.

Recently we have reported[1] that the copper(II)-lanthanoid(III) hetero-metal complexes (Fig. 1, I) of *N,N'*-bis(3-carboxysalicylidene)ethylenediamine (H_4-fsaen) show "solvation selectivity" associated with the copper or lanthanoid center depending upon the nature of solvents. That is, in pyridine solution the solvation occurs at the copper center to afford a pentacoordination around the metal, whereas in dimethyl sulfoxide or *N,N*-dimethylformamide solutions the solvation occurs exclusively at the lanthanoid center while maintaining the planar configuration around the copper ion. It should be emphasized that the mononuclear precursor complex (Fig. 1, II) takes a pentacoordination with a solvent molecule at an apical site in all of these solvents. The above findings prompted us to examine if the Cu(II)–Ln(III) center functions as a specific binding site for substrates containing both nitrogenous and oxygenous donating groups. In this study the Cu(II)–Gd(III) complex of H_4fsaen, in which gadolinium is located at the center of lanthanoid series, was adopted and the binding of various substrates (amino alcohols, 8-quinolinol, amino acids, and amino acid esters) to the complex was investigated in *N,N*-dimethylformamide (DMF).

Experimental

Materials. The Cu(II)-Gd(III) complex of H_4fsaen was synthesized according to the method reported previously.[1] 2-Amino-1-butanol was purchased from Tokyo Kasei Co. Other reagents used as substrates were purchased from Wako Pure Chemical Industries. Methyl esters of the amino acids were obtained as hydrochloride after the literature method[3] and used for the following experiments without neutralization.

Methods. A solution of the Cu(II)–Gd(III) complex in DMF (2.5×10^{-2} mol·dm^{-3}) was prepared. To 2 cm^3 of this solution was added a weighed amount of a substrate (except for amino acids), and the total volume was made up to 10 cm^3 with DMF. Visible spectra of the mixture were determined with a HP 8452A Spectrophotometer. For amino acids as substrates, a suspension of an amino acid in the complex solution was stirred for 2 h, and the supernatant solution was submitted to the spectral measurements. The CD spectra were determined with a JASCO J-20 Automatic Recording Spectropolarimeter.

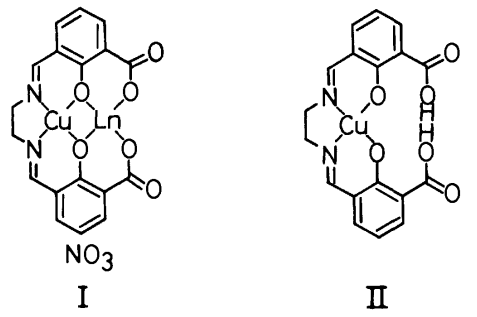

I II

Fig. 1. Chemical structures of copper(II)-lanthanoid(III) hetero-metal complexes(I) and copper(II) mononuclear complex(II) of *N,N'*-bis(3-carboxysalicylidene)ethylenediamine.

Results and Discussion

In general the axial coordination of a substrate to the copper center results in a red shift of the d–d band maximum, along with a color change from purple to green or blue. For example, when an amino alcohol (2-aminoethanol, 3-amino-1-propanol, 1-amino-2-propanol, 2-amino-1-butanol) was added as the substrate to the complex solution, the d–d band maximum shifted by 1×10^3—2×10^3 cm^{-1} to lower frequency.

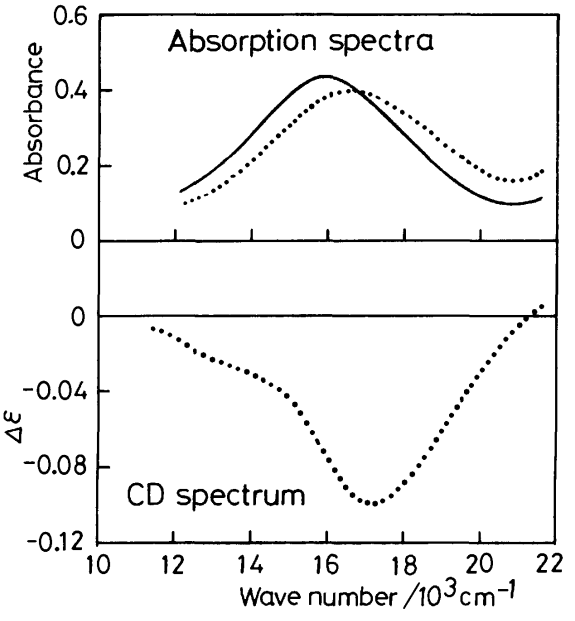

Fig. 2. Absorption and CD spectra in DMF. Concentration of the binuclear complex is 5×10^{-3} mol dm^{-3}. (——): with 2-aminoethanol (10 mol dm^{-3}); (……): with (*R*)-(−)-2-amino-1-butanol (10 mol dm^{-3}).

Table 1. The d–d Band Maxima of Cu(II)–Gd(III) Binuclear Complex in DMF Solution of Various Substrates[a]

Substrate	$\tilde{\nu}_{max}/10^3$ cm^{-1}
No substrate	17.86
1,2-Ethanediol[b]	18.08
1,3-Propanediol[b]	17.89
2-Aminoethanol[b]	15.97
3-Amino-1-propanol[b]	16.50
1-Amino-2-propanol[b]	16.19
(*R*)-(−)-2-Amino-1-butanol[b]	16.67
8-Quinolinol[c]	17.33
Glycine[d]	17.86
β-Alanine[d]	17.67
4-Aminobutyric acid[d]	17.48
Glycine methyl ester[e]	17.64
β-Alanine methyl ester[e]	17.73
Methyl 4-aminobutyrate[e]	17.67

a) Concentration of binuclear complex is 5×10^{-3} mol·dm^{-3}. b) Concentration is 10 mol·dm^{-3}. c) Concentration is 1 mol·dm^{-3}. d) Spectra were measured for the supernatant solution after these substrates were suspended with stirring for 2 h. e) Hydrochlorides were used. Concentration of glycinate, alaninate, and butyrate are 5.26×10^{-3}, 5.01×10^{-3}, and 5.40×10^{-3} mol·dm^{-3}, respectively.

Typical spectra are shown in Fig. 2 and the numerical data are given in Table 1. The largest red shift of the d–d band is observed for 2-aminoethanol and the shift tends to decrease when the alkane chain is lengthened or a substituent is introduced on the ethylene chain. When (*R*)-(−)-2-amino-1-butanol was added as the substrate, the solution showed significant circular dichroism at the d–d transitions of the copper(II) ion (Fig. 2). The addition of 1,2-ethanediol or 1,3-propanediol as the substrate, on the other hand, showed no indication of the coordination to the copper center (see Table 1). All these facts indicate that the amino alcohols coordinate to the copper center at the nitrogen atom. The coordination at the lanthanoid center, however, cannot be monitored spectroscopically, because electronic structures of lanthanoid ions are little affected by the change in the coordination geometry or the ligand field strength.[4] However, it is expected that oxygenous substrates such as alcohols, phenols, carboxylic acids, or esters have a high affinity towards lanthanoid ions compared with DMF (amide) used as the solvent. This is probably the case of 1,2-ethanediol and 1,3-propanediol; these substrates may exclusively coordinate to the gadolinium ion at both oxygen atoms. Therefore, we presumed that the amino alcohols are bound to the Cu(II)–Gd(III) center, with the nitrogen to the copper and with the oxygen to the gadolinium.

The addition of quinoline as the substrate showed no indication of the coordination to the copper(II) ion, whereas the addition of 8-quinolinol caused a significant red shift of the d–d band. This is rationalized in terms of that the binding of quinoline to the copper center is sterically hindered but the binding of 8-quinolinol to the Cu(II)–Gd(III) center is not subjected to any steric hindrance when the hydroxyl group is concerned with the coordination to the gadolinium(III) ion. This adds a support to our presumption that amino alcohols are bound as bidentate bridge to the Cu(II)–Gd(III) center.

Somewhat different feature of binding was recognized for amino acids. When glycine was added to the complex solution, no indication of the nitrogen coordination to the copper was observed from its electronic spectrum. When β-alanine was added, no apparent color change occurred but its electronic spectrum showed a slight red shift of the d–d band. When 4-aminobutyric acid was the substrate, apparent color change occurred and its spectrum showed a larger red shift of the d–d band. Therefore, the nitrogen coordination to the copper center becomes feasible on lengthening the alkane chain of amino acid. This trend differs from that found for amino alcohols. Conceivably carboxylate group of amino acids coordinate bidentately to the gadolinium center. Such bidentate carboxylates were reported for some lanthanoid(III) acetate hydrates.[5] If this is the case, the coordination of the terminal nitrogen to the copper should be difficult for glycine but is easier for amino acids with a longer methylene chain.

In order to gain an insight into the binding mode of amino acids, we also examined the binding of amino acid esters (methyl aminoacetate, methyl 3-aminopropionate, methyl 4-aminobutyrate) to the Cu(II)–Gd(III) center. As seen in Table 1, the substrate binding to the copper center was evidenced spectroscopically for all the cases. We assume that in these cases, the ester group functions as a unidentate donor so that the amino acid esters are bound to the Cu(II)–Gd(III) center in the essentially the same way as that of amino alcohols.

From the above discussions it is suggested that the substrates possessing a nitrogenous and an oxygenous donor groups are specifically bound to the Cu(II)–Gd(III) center, though their binding constants have not yet been determined.

References

1) M. Sakamoto, M. Takagi, T. Ishimori, and H. Ōkawa, *Bull. Chem. Soc. Jpn.*, **61**, 1613 (1988).

2) M. Tanaka, M. Kitaoka, H. Ōkawa, and S. Kida, *Bull. Chem. Soc. Jpn.*, **49**, 2469 (1976).

3) J. P. Greenstein and M. Winitz, "Chemistry of the Amino Acids," John Wiley & Sons, New York (1961), Vol. 2, pp. 925—928.

4) G. H. Dieke, "Spectra and Energy Levels of Rare Earth Ions in Crystals," Interscience, New York (1968), p. 249.

5) S. Ganapathy, V. P. Chacko, R. G. Bryant, and M. C. Etter, *J. Am. Chem. Soc.*, **108**, 3159 (1986).

Facile Conversion of Aldehydes into 1-Substituted 2-Chloro-3,3-difluoro-2-propen-1-ols with 1,1-Dibromo-1-chloro-2,2,2-trifluoroethane/Magnesium Reagent

Makoto FUJITA and Tamejiro HIYAMA*
Sagami Chemical Research Center, 4-4-1 Nishiohnuma, Sagamihara, Kanagawa 229
(Received May 13, 1988)

Synopsis. Aldehydes RCHO are converted in excellent yields into chlorodifluoroallyl alcohols $RCH(OH)CCl=CF_2$ upon treatment with $CClBr_2CF_3$ and magnesium in tetrahydrofuran at 0 °C.

Aldehyde adducts of halogenated ethenyl anions $^-CX=CF_2$ (X=Cl or F) have been shown to be useful intermediates for the synthesis of α-halo-α,β-unsaturated ketones and acid derivatives,[1] as well as artificial pyrethroids.[2] The aldehyde addition of $CX=CF_2$ anions was earlier realized at −130 °C with $LiCX=CF_2$,[1a-c] and recently achieved under milder conditions using $R_3SiCX=CF_2/F^-$,[3] $CF_3CCl_3/Zn/AlCl_3$(cat),[4] or CF_3CCl_3/Pb[1h] reagent. Even these reagents possess problems from practical viewpoints. For example, preparation of the fluorinated vinylsilanes is tedious;[5] the zinc and lead reagents seem to lack wide applicability.[6] Reported herein is an alternative facile way to 1-substituted 2-chloro-3,3-difluoro-2-propen-1-ols **2** through the reaction of aldehydes **1** with $CClBr_2CF_3$ and magnesium, both of which are commercially readily available and economical (Eq 1).

$$\underset{\mathbf{1}}{RCHO} + CClBr_2CF_3 \xrightarrow[THF]{Mg} \underset{\mathbf{2}}{RCH(OH)CCl=CF_2} \quad (1)$$

a: R = Ph-

b: R = 4-Cl-C_6H_4-

c: R = PhCH=CH-

d: R = $PhCH(CH_3)$-

e: R = *c*-C_6H_{11}-

f: R = 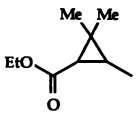

Results and Discussion

The adducts **2** were produced in excellent yields, when aldehydes were treated with 3 molar equivalents of 1,1-dibromo-1-chloro-2,2,2-trifluoroethane and 6 mol of magnesium chips in tetrahydrofuran (THF). Results are summarized in Table 1. In addition to common aliphatic and aromatic aldehydes, readily enolizable aldehydes (e.g. **1d** and **1f**) give the desired adducts. Cinnamaldehyde (**1c**) afforded a 1,2-adduct only. The adduct **2f** is a versatile intermediate for synthetic pyrethroids having a $CH=C(Cl)CF_3$ side chain.[2]

The reaction course of the transformation deserves particular comments. When 1:1 mole ratio of $CClBr_2CF_3$ and Mg was applied, any kinds of aldehyde adducts were not detected, but formation of $CClBr=CF_2$ was observed by ^{19}F NMR of the crude reaction mixture. Thus, the organomagnesium reagent responsible for the carbonyl addition is concluded to be a Grignard reagent $BrMgCCl=CF_2$ generated in situ by the reaction of magnesium metal and the $CClBr=CF_2$.[7] In this sense, the mechanism of the total transformation contrasts sharply to that of the $CF_3CCl_3/Zn/AlCl_3$ (cat) reagent, which first gives aldehyde adducts $RCH(OH)CCl_2CF_3$ and then reduces the adducts to give products of type **2**.

Although the Grignard reagent $BrMgCCl=CF_2$ is recorded by Stelin et al.,[7] its carbonyl addition has never been achieved due possibly to the instability of the reagent. Noteworthy is that the in situ prepared reagent can do the transformation at 0 °C as reported herein.

Experimental

Materials. Magnesium chips and 1,1-dibromo-1-chloro-2,2,2-trifluoroethane were purchased from Nakarai Chemicals Co. Ltd. and PCR Co. Ltd., respectively, and used directly. Aldehydes were purchased from Tokyo Kasei Kogyo Co. Ltd. Ethyl 2-formyl-3,3-dimethylcyclopropanecarboxylate was prepared by a procedure previously reported.[2b] Tetrahydrofuran was dried over benzophenone ketyl and freshly distilled before use.

Reaction of Aldehydes with $CClBr_2CF_3$/Mg Reagent. A Typical Procedure. Magnesium chips 144 mg (6.0 mmol) were suspended in THF 2 mL solution of benzaldehyde (**1a**) 106 mg (1.0 mmol). The whole was cooled at 0 °C, and THF 2 mL solution of 1,1-dibromo-1-chloro-2,2,2-trifluoroethane 825 mg (3.0 mmol) was added dropwise. After 3 h at 0 °C, sat ammonium chloride aq solution 15 mL was added, and the mixture was extracted with diethyl ether (10 mL×3). The ethereal extract was dried over anhydrous magnesium sulfate, concentrated under reduced pressure, and subjected to preparative TLC (silica gel, dichloromethane–hexane 1:1) to give 2-chloro-3,3-difluoro-1-phenyl-2-propen-1-ol 144 mg (**2a**) (70%) as a colorless oil. Spectral data are completely in accord with those of the authentic sample.[4b]

Table 1. Transformation of RCHO to $RCH(OH)CCl=CF_2$[a]

Run	Aldehyde	Conditions	Product	Yield/%
1	**1a**	0 °C, 3 h	**2a**	70
2	**1b**	0 °C, 3 h	**2b**	51
3	**1c**	0 °C, 4 h	**2c**	59
4	**1d**	0 °C, 4 h	**2d**	77
5	**1e**	0 °C, 4 h	**2e**	73
6	**1f**	0 °C, 4 h	**2f**	42

a) The molar ratio **1**:$CClBr_2CF_3$:Mg=1:3:6.

In a similar manner, **2b—f** were prepared. Physical data of **2d**, **2e**, and **2f** have been already reported.[4b]

2-Chloro-3,3-difluoro-1-(4-chlorophenyl)-2-propen-1-ol (2b): A colorless oil; ^{1}H NMR ($CDCl_3$) δ=2.20 (broad s, 1H), 5.72 (broad s, 1H), and 7.37 (s, 4H); ^{19}F NMR ($CDCl_3$-$CFCl_3$) δ=−87.0 (d, J=38 Hz, 1F) and −91.3 (d, J=38 Hz, 1F); IR (neat) 3400, 1746, 1500, 1296, 1096, 1012, 846, and 734 cm^{-1}; MS (70 eV) m/z (rel intensity) 240 (M^++2, 9), 238 (M^+, 10), 220 (64), 218 (100), 183 (45), 182 (29), 154 (20), 143 (41), 120 (43), 99 (21), 77 (20), 75 (30), 74 (21), and 50 (25).

Found: C, 45.09; H, 2.66%. Calcd for $C_9H_6Cl_2F_2O$: C, 45.22; H, 2.53%.

2-Chloro-1,1-difluoro-5-phenyl-1,4-pentadien-3-ol (2c): ^{1}H NMR ($CDCl_3$) δ=2.17 (broad s, 1H), 5.17 (broad s, 1H), 6.20 (dd, J=5.0, 16.0 Hz, 1H), 6.70 (d, J=16.0 Hz, 1H), and 7.20—7.45 (m, 5H). ^{19}F NMR ($CDCl_3$-$CFCl_3$) δ=−86.3 (d, J=40 Hz, 1F) and −90.0 (d, J=40 Hz, 1F); IR (neat) 3380, 1740, 1288, 1012, 993, 965, 753, and 693 cm^{-1}.

Found: m/z 230.0332. Calcd for $C_{11}H_9F_2ClO$: M, 230.0310.

References

1) a) J. F. Normant, J. P. Foulon, D. Masure, R. Sauvetre, and J. Villieras, *Synthesis*, **1975**, 122. b) D. Masure, R. Sauvetre, J. F. Normant, and J. Villieras, *Synthesis*, **1976**, 761. c) C. Chuit, R. Sauvetra, D. Masure, M. Baudry, J. F. Normant, and J. Villieras, *J. Chem. Res. (S)*, **1977**, 104. d) R. Sauvetre, D. Masure, C. Chet, and J. F. Normant, *Synthesis*, **1978**, 128. e) D. Masure, C. Chuit, R. Sauvetre, and J. F. Normant, *Synthesis*, **1978**, 458. f) J. P. Gillet, R. Sauvetre, and J. F. Normant, *Synthesis*, **1986**, 355. g) F. Tellier, R. Sauvetre, J. F. Normant, and C. Chutt, *Tetrahedron Lett.*, **29**, 3335 (1987). h) H. Tanaka, S. Yamashita, Y. Katayama, and S. Torii, *Chem. Express*, **2**, 751 (1987).

2) a) M. Fujita and T. Hiyama, *Tetrahedron Lett*, **27**, 3659 (1986). b) M. Fujita, K. Kondo, and T. Hiyama, *Bull. Chem. Soc. Jpn.*, **60**, 4385 (1987).

3) a) M. Fujita and T. Hiyama, *J. Am. Chem. Soc.*, **107**, 4085 (1985). b) M. Fujita, M. Obayashi, and T. Hiyama, *Tetrahedron*, in press.

4) a) M. Fujita and T. Hiyama, *Tetrahedron Lett.*, **27**, 3655 (1986). b) idem, *Bull. Chem. Soc. Jpn.*, **60**, 4377 (1987).

5) a) S. Martin, R. Sauvetre, and J. F. Normant, *Tetrahedron Lett.*, **24**, 5615 (1983); *Synthesis*, **1986**, 538. b) T. Hiyama, K. Nishide, and M. Obayashi, *Chem. Lett.*, **1984**, 1765.

6) We failed to obtain the $CCl{=}CF_2$ adducts of cyclopropanecarbaldehydes and α,β-unsaturated aldehydes with the CF_3CCl_3/Zn/$AlCl_3$ (cat) reagent.

7) $CF_2{=}CFMgBr$ from $CF_2{=}CFBr$: R. N. Stelin, R. D. Yatsenke, L. N. Pinkina, and I. L. Khunyants, *Khim. Nauka Prom.*, **4**, 810 (1959); *Chem. Abstr.*, **54**, 10838.

Helix Formation of Poly(L-ornithine) in Decyl and Dodecyl Sulfate Solutions

Kunio TAKEDA* and Kazuo YAMAMOTO
Department of Applied Chemistry, Okayama University of Science,
1-1 Ridai-cho, Okayama 700
(Received January 20, 1988)

Synopsis. Structural changes in poly(L-ornithine)[$(Orn)_n$] were studied in solutions of sodium decyl sulfate ($NaDecSO_4$) by the curve-fitting method of circular dichroism. In the $NaDecSO_4$ concentration range from 4 to 9 mmol dm^{-3}, only the β-structure was found. Below and above this concentration range, however, the α-helical structure was formed slightly, its fraction being less than 20%. The addition of 1-octanol enhanced the helix formation in the $(Orn)_n$–$NaDecSO_4$ complex.

Many investigations have been conducted in the past three decades that have dealt with the conformational changes in homopolypeptides such as poly(L-ornithine)[$(Orn)_n$] homologs in anionic surfactant solutions.[1-13] However, few attempts have been made to estimate quantitatively the presence of α-helix, β-structure, and random coil in these homologs in the surfactant solutions. Recently, we computed the fractions of α-helix, β-structure, and random coil of $(Orn)_n$ in a sodium dodecyl sulfate ($NaDodSO_4$) solution[12] using a simulation of the circular dichroism (CD) spectra similar to Greenfield and Fasman.[14] This method may make possible a quantitative study when a slight amount of helical structure in the polypeptide chain is induced by another surfactant solution. We now report proportional changes of α-helix, β-structure, and random coil in $(Orn)_n$ induced by sodium decyl sulfate ($NaDecSO_4$), together with the effect of added 1-octanol on the formation of helical structure in the same surfactant solution.

Experimental

The $(Orn)_n$ sample employed was described in a previous study.[12] The $NaDecSO_4$ was prepared from 1-decanol (purity: 99.8%), essentially according to the method of Dreger et al.[15] The critical micelle concentration of the surfactant, as determined by the electric conductivity method, was 31.5 mM (1 M=1 mol dm^{-3}) at 25 °C.

The CD measurements were carried out with a Jasco J-500A spectropolarimeter equipped with a Jasco DP-501 data processor. Details of the experimental procedures have been described elsewhere.[10,12] The CD measurements were made under the same conditions as have been described previously: temperature, 20 °C; pH, neutral; the residue concentration of $(Orn)_n$, 9.2×10^{-5} M.[12] The simulation of the CD spectrum was made over the wavelength region of 190—250 nm with the assumption that the $(Orn)_n$ assumes only three structures: α-helix, β-structure, and random coil. The relative proportions of these three structures were calculated by the same method as in a previous study.[12]

Results and Discussion

The CD spectra of $(Orn)_n$ at various $NaDecSO_4$ concentrations are shown in Fig. 1. Figure 1 also shows two CD spectra of the polypeptide in a 0.8 mM $NaDecSO_4$ solution containing slight amounts of 1-octanol. The addition of 1-octanol enhanced helix formation in $(Orn)_n$, as can be seen by the increase in the magnitude of the α-helical-type CD spectrum. In the $NaDecSO_4$ concentration range from 4 to 9 mM, the surfactant solution containing $(Orn)_n$ became slightly turbid, but this turbidity did not interfere in the CD measurements (the same phenomenon is observed in the $NaDodSO_4$.[12] In this concentration range, the CD spectra of $(Orn)_n$ were typically of β-structure (not shown, refer to Fig. 1 in Ref. 12). These CD spectra were analyzed using the same reference spectra as in the previous study.[12] The proportional

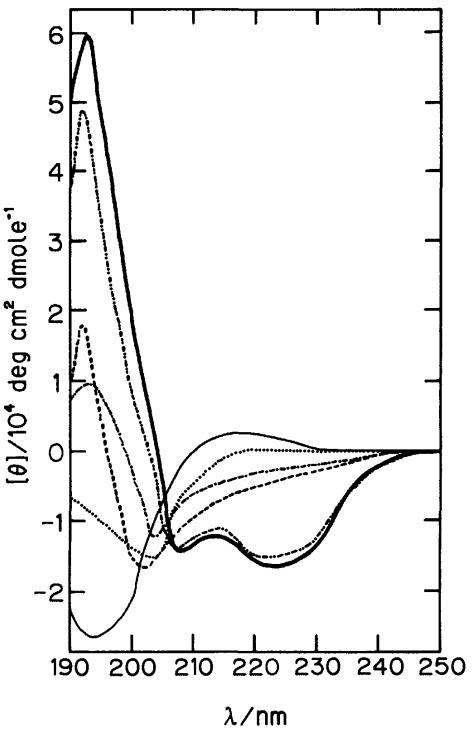

Fig. 1. CD spectra of $(Orn)_n$ in $NaDecSO_4$ solutions in the absence and the presence of 1-octanol. $NaDecSO_4$ concentrations in the absence of octanol: 0.3 (—); 0.4 (·····); 0.8 (-·-·-·) and 14 mM (-----). Added octanol concentrations to 0.8 mM $NaDecSO_4$ solution: 1.02 (-·-·-·-·-) and 1.28 mM (——). The polypeptide concentration: 9.2×10^{-5} M (residue). The CD spectra of $(Orn)_n$ were time-dependent in the order of hour in 0.4 and 0.8 mM $NaDecSO_4$ solutions without the octanol. All the measurements of spectra were carried out within 10 min after mixing the $(Orn)_n$ solution with the surfactant solution.

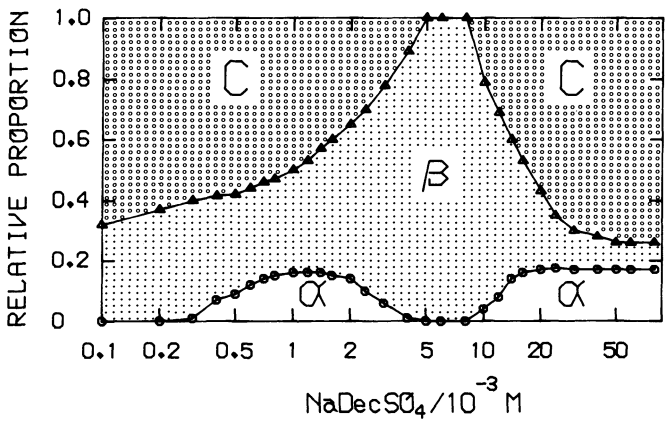

Fig. 2. Proportional changes of α-helix (α), β-structure (β), and random coil (C) in $(Orn)_n$ as a function of $NaDecSO_4$ concentration. The proportions were estimated using the CD spectra measured under the same conditions as mentioned in Fig. 1. The boundary between the α-helix and the β-structure is plotted (-⊖-) and that between the β-structure and the random coil done (-△-). Then, each area gives the fraction of the corresponding structure. The same method was used in the following figure.

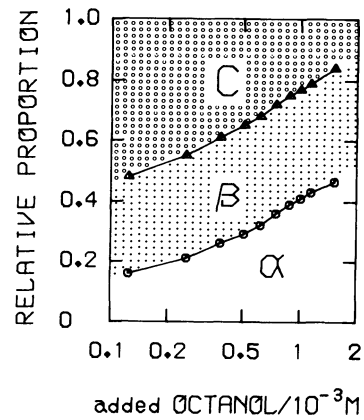

Fig. 3. Proportional changes of α-helix, (α), β-structure (β), and random coil (C) in $(Orn)_n$ as a function of added 1-octanol to 0.8 mM $NaDecSO_4$ solution.

changes in the secondary structure of $(Orn)_n$ as a function of concentration of $NaDecSO_4$ are presented in Fig. 2. As is seen, $(Orn)_n$ assumes a 100% β-structure in the $NaDecSO_4$ solutions of 5 to 9 mM. The data in this figure also show that the helical structure is assumed in two concentration ranges of $NaDecSO_4$; between 0.3 and 4 mM and above 9 mM $NaDecSO_4$. The $(Orn)_n$ assumes the helical structure also in two concentration ranges of $NaDodSO_4$.[12] However, higher concentrations of $NaDecSO_4$ were required than was the case with $NaDodSO_4$.[12] In the lower concentration range of $NaDodSO_4$, the polypeptide assumes an unstable helix. This unstable helix changes to β-structure within a matter of minutes.[12] The helical structure formed in the lower concentrations of $NaDecSO_4$ was also unstable, but not to the same extent; several hours were required for the change to the β-structure. The helical proportion was much lower in $NaDecSO_4$ than in $NaDodSO_4$; the proportion was less than 12 and 17% in the two $NaDecSO_4$ concentration ranges as seen in Fig. 2, whereas the maximal proportions of the unstable and the stable helical structures in $NaDodSO_4$ are 50 and 73% respectively.[12]

This difference between the helical proportions of $(Orn)_n$ formed in the two surfactant solutions must be necessarily due to the difference in the number of carbons in the hydrophobic portion of the two surfactants. As is seen in Fig. 1, the presence of slight amounts of octanol in 0.8 mM $NaDecSO_4$ greatly enhanced the double-minimum of the helical-type CD spectrum of $(Orn)_n$. The proportional changes in the three structures are plotted as a function of 1-octanol concentration in Fig. 3. The helical proportion increased to 46%, which is comparable with the maximal fraction of the unstabale helix in $NaDodSO_4$.[12] The increment of hydrophobicity due to 1-octanol (which probably leads to the formation of mixed micelle of $NaDecSO_4$ with 1-octanol) clearly correlates with the increase in helical proportion. The proportion of β-structure, however, was not affected by the addition of 1-octanol (Fig. 3). A similar increase in the helical proportion of $(Orn)_n$ was observed by the addition of 1-octanol to $NaDecSO_4$ solutions at other concentrations. For example, the addition of 2 mM 1-octanol increased helical proportion from 4 to 12% in 0.4 mM $NaDecSO_4$.

The positive charges in the side groups of $(Orn)_n$ or poly(L-lysine)[$(Lys)_n$] are generally considered to be eliminated by the electrostatic interaction with the hydrophilic groups of anionic surfactant ions such as alkyl sulfate ions.[4,7] The neutralization of the charges of polypeptide by the surfactant ions, however, is not enough to cause the formation of α-helix and β-structure, as is expected from the previous studies of the effect of the hydrocarbon chain length of a surfactant.[4,10,11] It is reasonable to speculate that the hydrocarbon chain may be involved in the formation of secondary structure in the surfactant-polypeptide complexes. Tseng and Yang have suggested that the hydrocarbon chains of surfactants bound to polypeptide might be juxstapositioned to other hydrocarbon chains of the excess surfactant molecules, thus forming a micelle-like structure.[7] In this regard, it is worth noting that the proportion of β-structure of $(Orn)_n$ reaches 100% in $NaDecSO_4$ as well as in $NaDodSO_4$.[12] $(Lys)_n$ also assumes 100% β-structure in $NaDodSO_4$.[13] In the antiparallel β-sheet structure, the polypeptide chains run in opposite directions, being hold together by hydrogen bonds of peptide linkage with the amino acid side groups alternatively sticking up and sticking down (see Fig. 6 in Ref. 16). This means that the alkyl sulfate ions bound to the side groups of β-structural polypeptide stretch out perpendicularly to both the polypeptide backbone and the hydrogen bonds. When such a β-sheet is formed, the alkyl chains of surfactants bound to the residues might stand close together on both sides of the sheet.

This might lead to the formation of the McBain lamellar micelle[17] with alkyl chains. These alkyl chains may belong to the excess surfactant molecules or to the surfactants bound to other β-structural polypeptides (or to other distant β-structural segments of the identical polypeptide). As mentioned above, when $(Orn)_n$ and $(Lys)_n$ predominantly assume the β-structure in these surfactant solutions, the solutions become slightly turbid. The turbidity might be due to the accumulation of the sheets through the formation of the lamellar micelle. On the other hand, when the polypeptide assumes the α-helical structure, the side groups of amino acids are considered to stretch out in every direction around the helical rod.[18] This feature suggests that alkyl sulfate ions bound to side groups of α-helical polypeptide might stretch out in every direction in a different manner from those bound to β-structural polypeptides. How these complexes assume the α-helical structure remains unknown.

References

1) M. J. Grourke and J. H. Gibbs, *Biopolymers*, **5**, 586 (1967).
2) L. K. Li and A. Spector, *J. Am. Chem. Soc.*, **91**, 220 (1969).
3) I. Satake and J. T. Yang, *Biochem. Biophys. Res. Commun.*, **54**, 930 (1973).
4) I. Satake and J. T. Yang, *Biopolymers*, **14**, 1841 (1975).
5) I. Satake and J. T. Yang, *Biopolymers*, **15**, 2263 (1976).
6) W. L. Mattice and W. H. Harrison, *Biopolymers*, **15**, 559 (1976).
7) Y. W. Tseng and J. T. Yang, *Biopolymers*, **16**, 921 (1977).
8) S. Kubota and J. T. Yang, *Biopolymers*, **18**, 743 (1979).
9) K. Hayakawa, K. Ohara, and I. Satake, *Chem. Lett.*, **1980**, 647.
10) K. Takeda, A. Iba, and K. Shirahama, *Bull. Chem. Soc. Jpn*, **54**, 1793 (1981).
11) K. Takeda, A. Iba, and K. Shirahama, *Bull. Chem. Soc. Jpn*, **55**, 1335 (1982).
12) K. Takeda, *Biopolymers*, **24**, 683 (1985).
13) K. Takeda, *Bull. Chem. Soc. Jpn.*, **58**, 1210 (1985).
14) N. Greenfield and G. D. Fasman, *Biochemistry*, **8**, 4108 (1969).
15) E. E. Dreger, G. I. Keim, G. D. Miles, L. Shedlovsky, and J. Ross, *Ind. Eng. Chem.*, **36**, 610 (1944).
16) L. Pauling and R. B. Corey, *Proc. Natl. Acad. Sci. U.S.A.*, **37**, 729 (1951).
17) K. Shinoda, T. Nakagawa, B. Tamamushi, and T. Isemura, "Colloidal Surfactants," Academic Press, New York (1963) pp, 16—25.
18) L. Pauling, R. B. Corey, and H. R. Branson, *Proc. Natl. Acad. Sci. U.S.A.*, **37**, 205 (1951).

Vapor Pressures of Diethyl, Diisopropyl, and Dibutyl Phthalates at Reduced Pressures

Hirotake KATAYAMA
Department of Mechanical Engineering, College of Engineering, Hosei University, Kajino-cho, Koganei, Tokyo 184
(Received January 26, 1988)

Synopsis. Vapor pressures of the three phthalates noted above were measured over the ranges 0.3—30, 0.3—10, and 0.3—9 kPa, respectively. The correlations of vapor pressures using the Cragoe equation with 4 constants give the percent root mean square deviations of 0.21, 0.33, and 0.28, respectively.

Few experimental data of vapor pressure for dialkyl phthalates have been published. Their accuracies are not good. Accordingly the vapor pressures of diethyl, diisopropyl, and dibutyl phthalates were measured over the ranges 0.3—30, 0.3—10, and 0.3—9 kPa, respectively. The results were checked by the Chebyshev polynomial[1] and the Cragoe,[2] Frost-Kalkwarf,[3] and Antoine[4] equations. The enthalpies of vaporization for the phthalates were also obtained from the slopes of the vapor pressure against the temperature (dP/dt).

Experimental

Special grade materials from Tokyo Kasei Co., Ltd., were used without further purification. The purity of each was determined by gas chromatographic analyses with a 3 mm I.D. and 2 m length column of 5% Silicone SE-52 on Celite. In all cases it exceeded 99%.

Table 1 shows the densities and refractive indices compared with published values.[5-8]

The experimental apparatus and procedure have already been described elsewhere.[9-11] The part of the equilibrium still unit with the Cottrell pump, which was of the vapor circulation type, was made of Pyrex glass. The measurement and the control of pressure were carried out with the Multi-Range Model 157/100 pressure standard from Texas Instruments Inc., which had a spiral quartz Bourdon guage and a servo controlled valve in a vacuum line. The accuracy of the gauge was ±0.002 kPa for 10—34 kPa range and ±0.001 kPa for 0.24—10 kPa. The variation of the pressure control on the operation was read from the attached deviation meter. It was found to be within ±0.00003 kPa for the 1—34 kPa, and within ±0.0004 kPa for the 0.3—1 kPa.

Four mercury thermometers with immersion lines marked at the 18 cm points from their bulb ends, i.e., the set of 40—100, 100—150, 150—200, and 200—250 °C graduations, were used for temperature measurements. They were calibrated at 5 °C intervals with accuracies of ±0.04 K by Watanabe Keiki Seisakusho Co., Ltd., Tokyo. The intermediate temperatures in the intervals were interpolated. After the circulation of vapor for one hour, no fluctuations of the thermometers were observed greater than 0.02 K.

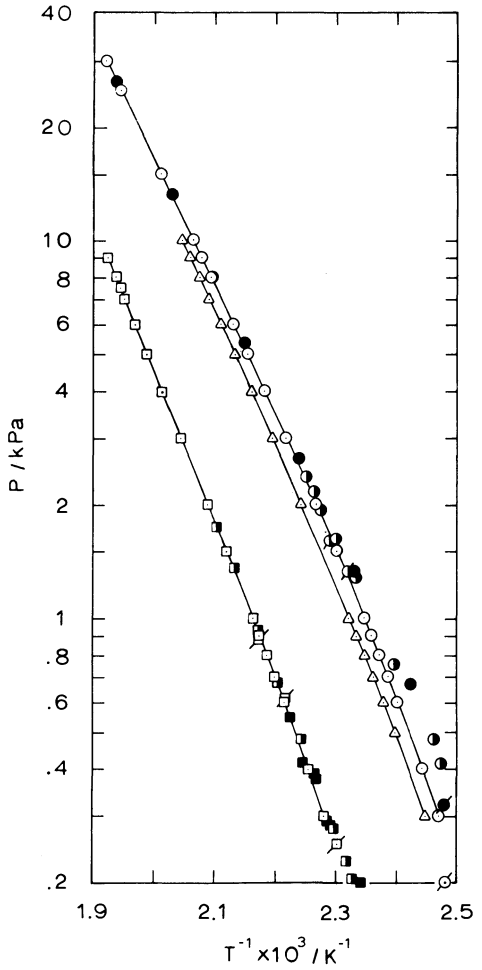

Fig. 1. Vapor pressures of three phthalates vs. T^{-1}. O, △, □: diethyl, diisopropyl and dibutyl phthalates, respectively, in this work. Diethyl phthalate (◑: Ishii and Nakayama,[12] ●: Stull,[13] ⌀: Matsuda and Kikkawa,[5] ◑: Wegscheider and Amann,[14] ◙: Hickman[15]). Dibutyl phthalate (◨: Hammer and Lydersen,[16] ■: Gardner and Brewer,[17] ⊏: Bonhorst et al.[18]).

Table 1. Densities ρ and Refractive Indices n_D of Three Phthalates

	T/K	ρ/g cm^{-3} Exptl	Lit	T/K	n_D Exptl	Lit
Diethyl phthalate	293.15	1.11881	1.1185[5]	287.45	1.50459	1.50490[6]
Diisopropyl phthalate	293.15	1.06286		293.15	1.49042	1.4900[7]
Dibutyl phthalate	293.15	1.04633	1.0474[5]	298.15	1.49122	1.4907[8]

Table 2. Vapor Pressure of Three Phthalates

Diethyl phthalate			Diisopropyl phthalate			Dibutyl phthalate		
P/kPa	T/K	ΔH_v / kJ mol^{-1}	P/kPa	T/K	ΔH_v / kJ mol^{-1}	P/kPa	T/K	ΔH_v / kJ mol^{-1}
30.000	520.81		10.000	489.00		9.000	520.09	
25.000	514.37		9.000	485.79		8.000	516.56	
15.000	497.17	63.3	8.000	482.27	66.4	7.500	514.74	
10.000	484.51	63.8	7.000	478.57	66.6	7.000	512.58	74.9
9.000	481.27	64.0	6.000	474.24	66.9	6.000	508.05	74.9
8.000	477.77	64.2	5.000	469.21	67.3	5.000	502.90	75.0
6.000	469.48	65.0	4.000	463.05	67.9	4.000	496.96	75.4
5.000	464.33	65.6	3.000	455.75	69.0	3.000	489.23	75.9
4.000	458.47	66.5	2.000	445.96	70.8	2.000	478.88	77.2
3.000	450.99	67.8	1.000	430.78	74.8	1.500	471.77	78.3
2.000	441.25	70.0	0.900	428.68	75.5	1.000	462.59	80.4
1.500	434.75	71.8	0.800	426.30	76.3	0.900	460.35	81.0
1.000	426.30	74.6	0.700	423.57	77.3	0.800	457.76	81.7
0.900	424.15	75.4	0.600	420.60	78.4	0.700	454.90	82.5
0.800	412.92	76.3	0.500	417.22	79.8	0.600	451.75	83.6
0.700	419.33	77.4	0.300	408.54	84.0	0.400	443.75	
0.600	416.52	78.7				0.300	438.55	
0.400	409.27							
0.300	404.53							

Results and Discussion

The experimental results are presented in Table 2. The results are also plotted in Fig. 1 including a comparison with values from the literature.[5,12–18]

The Chebyshev polynomial,[1] and the Cragoe,[2] Frost-Kalkwarf,[3] and Antoine[4] equations were used to fit the results.

The Chebyshev polynomial is :

$$t\ln(P) = a_0/2 + \sum a_i E_i(X). \quad (1)$$

where P kPa, $t(=T-273.15)$°C, T K, $E_1(x)=x$, $E_2(x)=2x^2-1$, $E_i(x)=2xE_{i-1}(x)-E_{i-2}(x)$, and x is a function of temperature defined as

$$x = \frac{2T - (T_{max} + T_{min})}{T_{max} + T_{min}} \quad (2)$$

where T_{max} and T_{min} are the maximum and minimum temperatures of the related substances, respectively. The polynomial with 4 parameters is identical to the Cragoe equation.

The Cragoe equation is:

$$\ln(P) = A_c + B_c/t + C_c t + D_c t^2 \quad (3)$$

or

$$t\ln(P) = A_c t + B_c + C_c t^2 + D_c t^3. \quad (4)$$

The Frost-Kalkwarf equation is:

$$\ln(P) = A_f + B_f/t + C_f \ln t + D_f P/t^2 \quad (5)$$

or

$$t\ln(P) = A_f t + B_f + C_f t \ln t + D_f P/t. \quad (6)$$

The Antoine equation is:

$$\ln(P) = A_a - B_a/(t + C_a) \quad (7)$$

or

$$t\ln(P) = A_a t + D_a - C_a \ln(P) \quad (8)$$

where $D_a=A_aC_a-B_a$.

All the constants of the expressions mentioned above were determined by least-square fits of $t\ln(P)$.

The percent root mean square deviations of pressure (prms) using Cragoe, Frost-Kalkwarf, and Antoine equations were estimated as 0.21, 0.21, and 1.25 for diethyl phthalate, respectively; 0.33, 0.33, and 1.88 for diisopropyl phthalate, respectively; and 0.28, 0.30, and 2.14 for dibutyl phthalate, respectively.

The prms using the Chebyshev polynomial for diethyl phthalate were taken as 0.33 with 3 parameters, 0.21 with 4 parameters, 0,20 with 5 parameters, 0.15 with 6 and 7 parameters, 0.14 with 8 and 9 parameters, and 0.11 with 10 parameters. The prms of diisopropyl phthalate were 0.34 with 3 parameters, 0.30 with 4 and 5 parameters, 0.24 with 6 parameters, 0.13 with 7 parameters, and 0.12 with 8—10 parameters. The prms of dibutyl phthalate were 0.37 with 3 parameters, 0.28 with 4 parameters, 0.26 with 5 and 6 parameters, 0.25 with 7 parameters, 0.18 with 8 parameters, and 0.15 with 9 and 10 parameters.

Conversely the temperatures were calculated from the pressures by using the Cragoe, Frost-Kalkwarf, and Antoine equations. The mean temperature differences of the Cragoe, Frost-Kalkwarf, and Antoine equations with the experimental values were taken as 0.04, 0.04, and 0.28 K for diethyl phthalate, respectively; 0.07, 0.06, and 0.32 K for diisopropyl phthalate, respectively; and 0.06, 0.06, and 0.46 K for dibutyl phthalate, respectively.

The constants of the Cragoe and Frost-Kalkwarf equations are listed in Table 3. The constants of the Antoine equation are not listed, because they give large errors. Those of the Chebyshev polynomial are omitted, because the polynomial with 4 parameters gives satisfactory fits.

The enthalpies of vaporization, ΔH_v, were calculated from the Clapeyron equation via the slopes of the

Table 3. Constants of Cragoe and Frost-Kalkwarf Equations

	Diethyl phthalate	Diisopropyl phthalate	Dibutyl phthalate
Constants of Cragoe equation			
A_c	4.55623	4.00826	7.50802
B_c	−903.1363	−892.0324	−1396.648
C_c	0.665139×10^{-2}	0.840047×10^{-2}	-0.769651×10^{-2}
D_c	0.137763×10^{-4}	0.131916×10^{-4}	0.368429×10^{-4}
prms[a]	0.21	0.33	0.28
ΔT_m[b]	0.04K	0.07K	0.06K
Constants of Frost-Kalkwarf equation			
A_f	−14.06478	−14.61002	−13.51560
B_f	−596.764	−606.515	−920.178
C_f	3.56600	3.64239	3.49727
D_f	452.28	687.37	1178.09
prms[a]	0.21	0.33	0.30
ΔT_m[b]	0.04K	0.06K	0.06K

a) Percent root mean square deviation defined by $100[\sum_i(P_{exptl}-P_{calcd})/P_{exptl})_i^2/n]^{1/2}$. n: number of data. b) Mean temperature difference defined by $\sum_i|T_{exptl}-T_{calcd}|_i/n$, K.

pressure against the temperature (dP/dt) using three expressions, the Chebyshev polynomial with 4 parameters (equivalent to the Cragoe equation), that with 5 parameters and the Frost-Kalkwarf equation. The ΔH_v values, of which the differences at their respective temperatures was less than 0.2 kJ mol^{-1}, are only listed in Table 2.

References

1) D. Ambrose, J. F. Counsell, and A. J. Davenport, *J. Chem. Thermodyn.*, **2**, 283 (1970).

2) C. S. Cragoe, "International Critical Tables of Numerical Data, Physics, Chemistry and Technology," 1st ed, ed by National Research Council of the United State of America, McGraw-Hill, New York (1928), Vol. 3, pp. 228—233.

3) A. A. Frost and D. R. Kalkwarf, *J. Chem. Phys.*, **21**, 264 (1953).

4) C. Antoine, *C. R. Acad. Sci., Paris*, **107**, 681, 836, 1143 (1888).

5) S. Matsuda and S. Kikkawa, *Kogyo Kagaku Zasshi*, **59**, 895 (1956).

6) J. W. Bruhl, *J. Prakt. Chem.*, **49**, 241 (1894).

7) J. A. Handy and L. F. Hoyt, *J. Am. Pharm. Assoc.*, **17**, 458 (1928).

8) M. A. Elliot, A. R. Jones, and L. B. Lockhart, *Anal. Chem.*, **19**, 10 (1947).

9) H. Katayama and Y. Harada, *J. Chem. Eng. Data*, **29**, 373 (1984).

10) H. Katayama, *J. Chem. Eng. Data.*, **33**, 75 (1988).

11) H. Katayama, *J. Chem. Eng. Jpn.*, **21**, 433 (1988).

12) H. Ishii and K. Nakayama, *Kogyo Kagaku Zasshi.*, **62**, 385 (1959).

13) D. R. Stull, *Ind. Eng. Chem.*, **39**, 517 (1947).

14) R. Wegscheider and W. v. Amann, *Monatsh. Chem.*, **36**, 549 (1915).

15) K. C. D. Hickman, *J. Phys. Chem.*, **34**, 627 (1930).

16) E. Hammer and A. L. Lydersen, *Chem. Eng. Sci.*, **7**, 66 (1957).

17) G. S. Gardner and J. E. Brewer, *Ind. Eng. Chem.*, **29**, 179 (1937).

18) C. W. Bonhorst, P. M. Althouse, and H. O. Triebold, *Ind. Eng. Chem.*, **40**, 2379 (1948).

The Cathodic Desulfonylation of 1-Ethoxycarbonyl- and 1-Cyano-1-(*p*-tolylsulfonyl)-2-phenylethenes at the Mercury Electrode in Nonaqueous Solvents

Akira KUNUGI* and Kyo ABE†
Department of Applied Chemistry, Faculty of Engineering, Tokushima University, Minamijosanjima-cho, Tokushima 770
†Department of Chemistry, Faculty of Science, Osaka City University, Sugimoto, Sumiyoshi-ku, Osaka 558
(Received March 25, 1988)

Synopsis. The cathodic reduction of 1-ethoxycarbonyl-1-(*p*-tolylsulfonyl)-2-phenylethene in MeCN and DMF is characterized by the selective elimination of the *p*-tolylsulfonyl group, resulting in the formation of ethyl (*E*)-cinnamate in good yields, in the presence of such efficient proton donors as benzoic acid and acetic acid. On the other hand, the cathodic desulfonylation of 1-cyano-1-(*p*-tolylsulfonyl)-2-phenylethene proceeds with low efficiencies, even in the presence of acetic acid and benzoic acid.

The cathodic desulfurization of organosulfur compounds has received considerable attention because most of them are valuable synthetic precursors. In general, α,β-unsaturated sulfides, sulfoxides, and sulfones are much more subject to cathodic desulfurization than to the hydrogenation of the double bond.[1-6] For example, the previous paper[6] showed that the cathodic reduction of 1-methylthio-1-(*p*-tolylsulfonyl)-2-arylethenes in nonaqueous solvents involves the selective cleavage of a carbon–sulfur bond, resulting in the formation of (*E*)-1-methylthio-2-arylethenes in moderate yields with the consumption of about 2 electrons per molecule, in the presence of such efficient proton donors as phenol and benzoic acid. The cathodic reduction of vinyl sulfones with the electron-withdrawing group at Position 1, such as the title compounds, 1-ethoxycarbonyl-1-(*p*-tolylsulfonyl)-2-phenylethene (**1**) and 1-cyano-1-(*p*-tolylsulfonyl)-2-phenylethene (**2**), is also of interest in connection with the reductive desulfonylation. Moreover, they may be expected to afford the corresponding desulfonylated compounds in a manner similar to the cathodic reduction of 1-methylthio-1-(*p*-tolylsulfonyl)-2-phenylethene.[6]

In the present work, the electrolytic reductions of **1** and **2** at a mercury electrode in nonaqueous media, such as acetonitrile (MeCN) and *N*,*N*-dimethylformamide (DMF), were studied by means of polarography, coulometry, and controlled-potential macroelectrolysis. The substrates, **1** and **2**, gave the corresponding desulfonylated compounds, (*E*)-ethyl cinnamate (**3**) and (*E*)-cinnamonitrile (**4**) respectively, but their yields were greatly dependent on the kind of electrolytic solution.

Experimental

The title compound, **1**, was synthesized by a condensation of benzaldehyde with ethyl (*p*-tolylsulfonyl)acetate according to a method described in the literature.[7] Ethyl (*p*-tolylsulfonyl)acetate was prepared starting from ethyl bromoacetate and sodium *p*-toluenesulfinate according to the published method:[8]

$$BrCH_2COOEt + p\text{-}TolSO_2Na \xrightarrow[\text{in DMF}]{} EtOOCCH_2SO_2\text{-}p\text{-}Tol$$

$$EtOOCCH_2SO_2\text{-}p\text{-}Tol + PhCHO \xrightarrow[\text{in benzene}]{\text{Piperidine}}$$

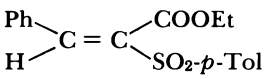

1

Similarly, **2** was synthesized from benzaldehyde and (*p*-tolylsulfonyl)acetonitrile,[7] which had itself been prepared starting from chloroacetonitrile and sodium *p*-toluenesulfinate according to the published method:[8]

$$ClCH_2CN + p\text{-}TolSO_2Na \xrightarrow[\text{in EtOH}]{} NCCH_2SO_2\text{-}p\text{-}Tol$$

$$NCCH_2SO_2\text{-}p\text{-}Tol + PhCHO \xrightarrow[\text{in DMF}]{\text{Triton B}}$$

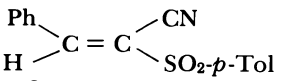

2

The substrates, **1** and **2**, were purified by recrystallization from a benzene–hexane mixture and from ethanol respectively; they were identified by means of their ^{1}H NMR spectra.

The nonaqueous acetonitrile solutions were prepared from predeoxygenated MeCN and tetrabutylammonium tetrafluoroborate (TBAB) or tetrabutylammonium perchlorate (TBAP), which had been purified and dried as has been described previously.[4] The nonaqueous *N*,*N*-dimethylformamide solutions were similarly prepared from the predeoxygenated DMF and TBAB or TBAP. DMF was purified in a manner similar to that described in the literature.[9] The concentration of the supporting electrolyte was 0.1 mol dm^{-3}. The phenol, acetic acid, and benzoic acid used as proton donors were purified by means of distillation or sublimation.

A Ag/0.1 mol dm^{-3} $AgNO_3$ in MeCN reference electrode (Ag/Ag^+) and a Ag/AgI, 0.1 mol dm^{-3} TBAI in DMF reference electrode (Ag/AgI) were used respectively, depending on the kind of solvent used. Polarography, coulometry, and controlled potential macroelectrolysis were carried out, using the same experimental set-up and procedure as were reported in the previous paper.[6]

Results and Discussion

Polarography. The influence of the proton donor on the dc polarograms of **1** and **2** at a dropping mercury electrode was examined in MeCN/TBAP and DMF/TBAP. Phenol, acetic acid, and benzoic acid were used as the proton donors. Among the media studied, the strongest influence on the polarogram was observed in the medium of MeCN/benzoic acid. Table 1 summarizes the half-wave potential ($E_{1/2}$) and the wave height (i_d) of the first reduction wave in various electrolytic solutions. As may be seen from Table 1, there is some difference among the proton donors used with respect to the influence of the proton donor on $E_{1/2}$ and i_d. That is, the $E_{1/2}$ of the first wave of **1** in MeCN was shifted to more positive values by the addition of acetic acid or benzoic acid, but $E_{1/2}$ in DMF was not changed. On the other hand, the $E_{1/2}$ of **2** was not influenced, not even in the medium of MeCN/benzoic acid. The influence of the proton donor on i_d was also observed; these results are also presented in Table 1.

Macroelectrolysis. A series of controlled potential macroelectrolyses of **1** and **2** at each plateau potential of the first reduction wave were carried out at the stirred mercury pool electrode in MeCN/TBAB and DMF/TBAB in the absence and in the presence of proton donors at room temperature. The results are summarized in Table 2. The coulometric n-values (electrons per molecule) were obtained from the amount of the substrate added and the quantity of electricity passed through before the termination of the electrolysis. Table 2 shows that the substrate with the COOEt group, **1**, affords the desulfonylated compound, **3**, and methyl p-tolyl sulfone (**5**) in good yields, in MeCN and DMF containing excess acetic acid and benzoic acid, whereas the yields of **3** and **5** were low in the absence of the proton donor and even

Table 1. Polarographic Data of the First Reduction Wave of **1** and **2** in MeCN and DMF Containing 0.1 mol dm^{-3} in the Absence and Presence of Proton Donors

Substrate	Solvent	Proton donor (equiv)	$-E_{1/2}$/V[a]	I_d/mA mol^{-1}
1	MeCN	None	1.71	3.2
		Phenol (4.0)	1.71	3.5
		Acetic acid (4.0)	1.66	6.5
		Benzoic acid (4.0)	1.64	7.2
	DMF	None	1.00	2.3
		Phenol (4.0)	1.00	2.3
		Acetic acid (4.0)	1.00	2.9
		Benzoic acid (4.0)	1.00	4.2
2	MeCN	None	1.46	3.7
		Phenol (4.0)	1.46	3.7
		Acetic acid (4.0)	1.46	3.7
		Benzoic acid (4.0)	1.46	4.5
	DMF	None	0.78	2.6
		Phenol (4.0)	0.78	2.6
		Acetic acid (4.0)	0.78	2.6
		Benzoic acid (4.0)	0.78	2.6

a) Against Ag/Ag$^+$ in MeCN and Ag/AgI in DMF.

Table 2. Controlled Potential Electrolysis of **1** and **2** at the First Reduction Potential on the Hg Pool Cathode in Nonaqueous Media Containing 0.1 mol dm^{-3} TBAB

Substrate	Solvent	Proton donor (equiv)	n-Value	Product[a]	(Yield/%)
1	MeCN	None	0.8	**3** (Trace)	**5** (Trace)
		Phenol (4.0)	1.3	**3** (30)	**5** (30)
		Acetic acid (4.0)	1.6	**3** (75)	**5** (69)
		Benzoic acid (4.0)	1.7	**3** (72)	**5** (62)
	DMF	None	0.7	**3** (Trace)	**5** (Trace)
		Phenol (4.0)	1.0	**3** (7)	**5** (Trace)
		Acetic acid (4.0)	1.5	**3** (74)	**5** (66)
		Benzoic acid (4.0)	1.6	**3** (70)	**5** (61)
2	MeCN	Phenol (4.0)	1.0	**4** (7)	**5** (Trace)
		Acetic acid (4.0)	1.2	**4** (13)	**5** (15)
		Benzoic acid (4.0)	1.5	**4** (29)	**5** (22)
	DMF	Phenol (4.0)	0.9	**4** (Trace)	**5** (Trace)
		Acetic acid (4.0)	1.0	**4** (4)	**5** (Trace)
		Benzoic acid (4.0)	1.1	**4** (8)	**5** (Trace)

a) **3**: 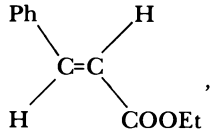 , **4**: 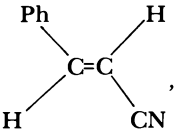 , **5**: p-TolSO$_2$Me.

in the presence of excess phenol. **5** was obtained as a product by a CH_3I methylation of the *p*-toluenesulfonyl anion formed upon electrolysis. It is worth noting that phenol is an effective proton donor in the cathodic desulfonylation of 1-methylsulfonyl-1-methylthio-2-phenylethene in both MeCN and DMF, but not in the case of **1**.

On the other hand, the electrolytic reduction of **2** afforded the desulfonylated compounds, **4** and **5**, in low yields, even in the presence of acetic acid. The yields of **4** and **5**, although still low, were increased to 29 and 22% respectively in the medium of MeCN/benzoic acid. Even though **2** was easier to reduce than **1**, the cathodic desulfonylation proceeded with a low efficiency compared with **1**. This seems to be not because the desulfonylated compound is subject to further reduction, but because the polymerization of a reduction intermediate of **2** proceeds in preference to the desulfonylation, although the polymeric products could not be characterized. This is supported by the evidence that coulometric *n*-values are low and that **4** is not easier to reduce than **2**. The stereochemical structures of **3** and **4** was determined on the basis of the NMR spectra of their olefinic protons. A perusal of the NMR spectra of the reaction mixtures indicated no formation of (*Z*)-isomers of **3** and **4** in any experiment.

The combination of Tables 1 and 2 indicates that the proton donor causing an increase in i_d by its addition has a tendency to bring about the cathodic desulfonylation with a high efficiency.

References

1) B. Lamm and J. Simonet, *Acta Chem. Scand., Ser. B,* **28**, 1147 (1974).
2) K. Anker, B. Lamm, and J. Simonet, *Acta Chem. Scand., Ser. B,* **31**, 747 (1977).
3) R. H. Ruttinger, W.-D. Rudorf, and H. Matschiner, *Electrochim. Acta,* **30**, 155 (1985).
4) A. Kunugi, T. Hagi, T. Hirai, and K. Abe, *Electrochim. Acta,* **30**, 1049 (1985).
5) A. Kunugi, K. Abe, T. Hagi, and T. Hirai, *Bull. Chem. Soc. Jpn.,* **59**, 2009 (1986).
6) A. Kunugi, T. Ikeda, T. Hirai, and K. Abe, *Electrochim. Acta,* **33**, 905 (1988).
7) R. Chodroff and W. F. Whitmore, *J. Am. Chem. Soc.,* **72**, 1073 (1950).
8) "Beilsteins Handbuck der Organishen Chemie," Springer-Verlag, Berlin (1923), H6, 423.
9) D. W. Leedy and D. L. Muck, *J. Am. Chem. Soc.,* **93**, 4264 (1971).

Electrical Properties of the Organic Conductor, (BEDT-TTF)$_3$(ClO$_4$)$_2$

Kenichi IMAEDA,* Toshiaki ENOKI,† Gunzi SAITO,†† and Hiroo INOKUCHI
Institute for Molecular Science, Okazaki 444
††The Institute for Solid State Physics, The University of Tokyo,
Roppongi, Minato-ku, Tokyo 106
(Received April 16, 1988)

Synopsis. Electrical conductivity and thermoelectric power have been measured for (BEDT-TTF)$_3$(ClO$_4$)$_2$. The electrical conduction is two-dimensional in the bc plane. The metal–insulator transition temperature is lowered by pressure at a rate of -8 K kbar^{-1}. The negligible thermopower at high-temperatures indicates that (BEDT-TTF)$_3$(ClO$_4$)$_2$ is the system with large on-site Coulomb repulsion.

Since our presentation on a two-dimensional metallic conductivity for (BEDT-TTF)$_2$ClO$_4$(C$_2$H$_3$Cl$_3$)$_{0.5}$ (BEDT-TTF: bis(ethylenedithio)tetrathiafulvalene),[1] BEDT-TTF radical salts have been actively investigated because they show a polymorphism and novel electronic properties due to the thermal vibrations of the ethylene groups. Interestingly, β-(BEDT-TTF)$_2$I$_3$ became a superconductor near 8 K.[2,3] Recently, Urayama et al. found a superconductivity at 10.4 K under ambient pressure in (BEDT-TTF)$_2$Cu(NCS)$_2$.[4] This transition temperature is the highest among organic superconductors hitherto known.

There are two crystalline phases in (BEDT-TTF)–ClO$_4$ salts, (BEDT-TTF)$_2$ClO$_4$(C$_2$H$_3$Cl$_3$)$_{0.5}$ and (BEDT-TTF)$_3$(ClO$_4$)$_2$. The former remaines metallic down to 0.8 K for a rapid cooling, while it shows a nesting transition at 25 K for a slow cooling, which is associated with the ordering of the C$_2$H$_3$Cl$_3$ molecules.[5,6] On the other hand, the latter shows a metal–insulator transition around 170 K.[7] As to (BEDT-TTF)$_3$(ClO$_4$)$_2$, the structural analysis presents that the BEDT-TTF molecules form a two-dimensional network with the face-to-face stacks along the [0$\bar{1}$1] direction and the side-by-side arrangements along not only the [012] direction but also the [021] direction.[7,8] The band calculation suggests the semimetallic band structure and the two-dimensional intermolecular interactions with a small anisotropy of transfer integral (t[012]/t[021]$\approx$3).[8] The polarized reflectance measurement gives the two-dimensional optical spectra.[9] ESR studies also suggest the two-dimensionality with large linewidth.[5] In this note, we report the experimental results of the anisotropy and pressure effect of electrical conductivity, and thermoelectric power for (BEDT-TTF)$_3$(ClO$_4$)$_2$.

Experimental

The black thin plate crystals of (BEDT-TTF)$_3$(ClO$_4$)$_2$ were prepared in C$_2$H$_3$Cl$_3$ solvent by a standard electrochemical technique. The anisotropy of electrical conductivity in the bc plane (see Ref. 7 for the definition of the crystal axes) was measured with a Montgomery method. Electrical conductivity under pressure up to 10 kbar along the c-axis was measured by a four-probe method in a BeCu clamp cell using Idemitsu Daphne oil #7373 as a pressure medium liquid. The pressure at room temperature was monitored with a manganin sensor. Thermoelectric power along the c-axis was measured with the method described by Chaikin and Kwak.[10]

Results and Discussion

Figure 1 shows the result of the anisotropy of the resistivity. The small anisotropy ($\rho_b/\rho_c\approx2$) at room temperature means that electrical conduction is two-dimensional in the bc plane, which is consistent with the results of X-ray analysis, band calculation, optical and ESR experiments. ρ_b/ρ_c is entirely independent of temperature in the metallic region. Below the metal–insulator (M–I) transition at 172 K, ρ_b/ρ_c increases gradually and then increases abruptly below 110 K. The ESR study has presented that the g-value for the applied field parallel to the b′-axis changes from 2.002 to 2.006 below the metal–insulator transition temperature (T_{MI}).[5] The shift of $g_{b'}$ suggests the displacement of the BEDT-TTF molecules. Therefore, the increase of ρ_b below T_{MI} is considered to be associated with such a displacement unfavorable for electron transport along the b direction.

Figure 2 shows the result of the thermoelectric power S. The value of S is almost zero in the high-temperature region. Then, S falls off sharply below 172 K. The thermopower for intrinsic semiconductors depends on temperature with the relation of $S\propto-(k/|e|)((b-1)/(b+1))(E_g/2kT)$, where b is mobility ratio μ_e/μ_h between electron and hole carriers and E_g is

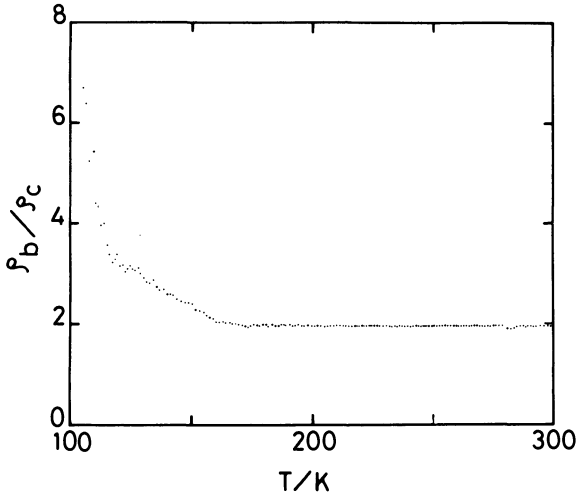

Fig. 1. Temperature dependence of the anisotropy ρ_b/ρ_c of the resistivity.

† Present address: Department of Chemistry, Faculty of Science, Tokyo Institute of Technology, Ookayama, Meguro-ku, Tokyo 152.

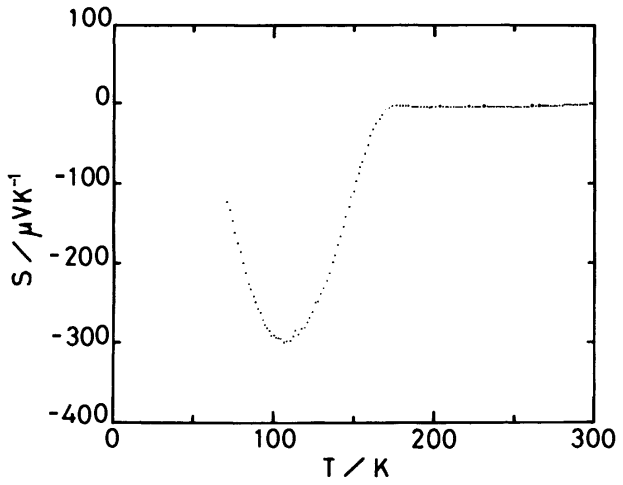

Fig. 2. Temperature dependence of the thermoelectric power.

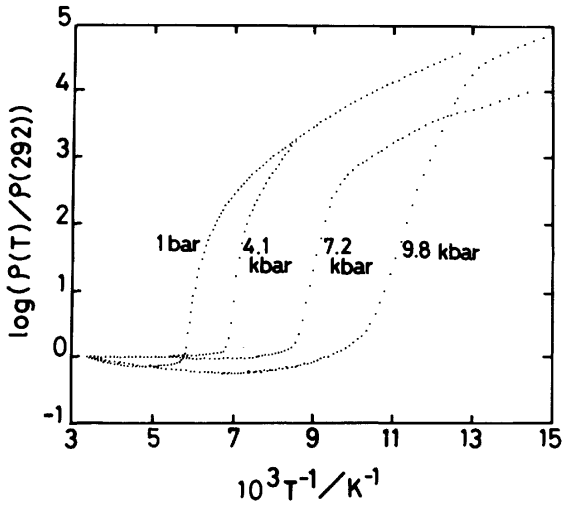

Fig. 3. Temperature dependence of the resistivities under 1 bar, 4.1 kbar, 7.2 kbar, and 9.8 kbar.

the energy band gap. The decrease proportional to T^{-1} below 172 K suggests that the M-I transition takes place at this temperature, which is just the same to T_{MI} observed in the resistivity. The constant thermopower in the metallic region and the sharp decrease below T_{MI} resemble those of α-(BEDT-TTF)$_2$I$_3$[11] and (BEDT-TTF)$_2$PF$_6$.[12] In the semiconducting region, S shows a minimum around 110 K with a large value of -300 μV K^{-1} and increases again with lowering temperature. The sign of the slope in the plot between S and T^{-1} depends on the magnitude of b (μ_e/μ_h). The negative slope above 110 K means that $b>1$, namely $\mu_e>\mu_h$, while the positive slope below 110 K means $\mu_e<\mu_h$. Therefore, the anomaly at 110 K, which corresponds to the temperature with a rapid increase in the anisotropy ρ_b/ρ_c, is considered to be caused by a some modulation in the electronic structure associated with the change in the magnitude of the mobility between electron and hole carriers.

Next, we present the result of the pressure effect on the M-I transition. Figure 3 shows the temperature

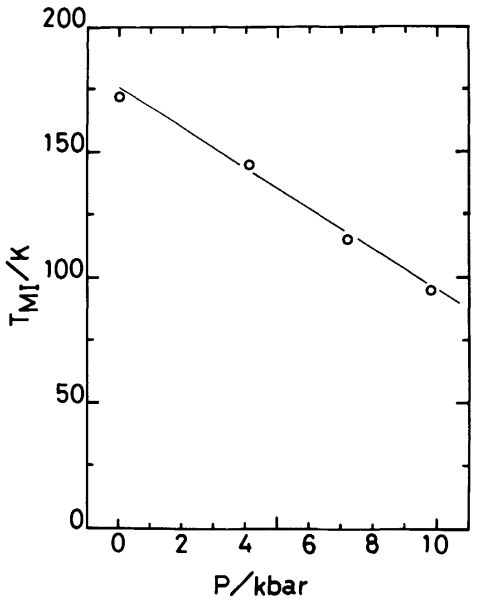

Fig. 4. Pressure dependence of the metal-insulator transition temperature (T_{MI}). The solid line corresponds to $dT_{MI}/dP=-8$ K kbar^{-1}.

dependence of the resistivities under several pressures. As the different samples are employed due to thin fragile crystals, the resistivity behaviors in the metallic region are somewhat different for each pressure. The M-I transition is suppressed as the pressure is increased. T_{MI} was determined to be the temperature with the maximum of $-d\log\rho/dT$. Figure 4 shows the correlation between T_{MI} and pressure. T_{MI} is lowered linearly with pressure at a rate of -8 K kbar^{-1}. This rate is approximately the same as those of other BEDT-TTF salts; $dT_{MI}/dP=-10$ K kbar^{-1} for (BEDT-TTF)$_2$ReO$_4$[13] and -11 K kbar^{-1} for α-(BEDT-TTF)$_2$I$_3$.[14] (BEDT-TTF)$_3$(ClO$_4$)$_2$ is expected to become a metal above ca. 22 kbar corresponding to the pressure at which T_{MI} is extrapolated to zero.

Finally, we mention the evidence of strong on-site Coulomb repulsion in the (BEDT-TTF)$_3$(ClO$_4$)$_2$ system. The thermopower in the high-temperature limit for a system with a strong on-site Coulomb repulsion U can be given by the following equation, according to the statistical-mechanical treatment by Chaikin and Beni;[15]

$$S=-\frac{k}{|e|}\ln(2(1-\gamma)/\gamma),$$

where γ is the degree of charge transfer. We obtain $S=0$ from the above equation using $\gamma=2/3$. The complete agreement of the magnitude of S with the experimental result suggests the importance of electron-electron Coulomb interactions in the present system. This fact is in good accordance with the result by Parkin et al.[16] They have reported that the spin susceptibility of (BEDT-TTF)$_3$(ClO$_4$)$_2$ is enhanced by Coulomb interactions beyond the Pauli paramagnetism expected for noninteracting electrons with $4t_{//}=0.75$ eV and U is estimated to be 3—4 eV according to the formalism presented by Torrance et al. for

$U \gg 4t$.[17]

The authors wish to thank Dr. Koichi Kikuchi of Tokyo Metropolitan University and Dr. Keizo Murata of Electrotechnical Laboratory for their advices about the conductivity measurement under pressure.

References

1) G. Saito, T. Enoki, K. Toriumi, and H. Inokuchi, *Solid State Commun.*, **42**, 557 (1982).

2) E. B. Yagubskii, I. F. Schegolev, V. N. Topnikov, S. I. Pesotskii, V. N. Laukhin, P. A. Kononovich, M. V. Karatsovnik, A. V. Zvarykina, S. G. Dedik, and L. I. Buravov, *Zh. Eksp. Teor. Fiz.*, **88**, 244 (1985).

3) K. Murata, M. Tokumoto, H. Anzai, H. Bando, G. Saito, K. Kajimura, and T. Ishiguro, *J. Phys. Soc. Jpn.*, **54**, 1236 (1985).

4) H. Urayama, H. Yamochi, G. Saito, K. Nozawa, T. Sugano, M. Kinoshita, S. Sato, K. Ohshima, A. Kawamoto, and J. Tanaka, *Chem. Lett.*, **1988**, 55.

5) T. Enoki, K. Imaeda, M. Kobayashi, H. Inokuchi, and G. Saito, *Phys. Rev. B*, **33**, 1553 (1986).

6) M. Kobayashi, T. Enoki, K. Imaeda, H. Inokuchi, and G. Saito, *Phys. Rev. B*, **36**, 1457 (1987).

7) H. Kobayashi, R. Kato, T. Mori, A. Kobayashi, Y. Sasaki, G. Saito, T. Enoki, and H. Inokuchi, *Chem. Lett.*, **1984**, 179.

8) T. Mori, Ph. D Thesis, The University of Tokyo, Tokyo, Japan (1985).

9) H. Tajima, Ph. D. Thesis, The University of Tokyo, Tokyo, Japan (1985).

10) P. M. Chaikin and J. F. Kwak, *Rev. Sci. Instrum.*, **46**, 218 (1975).

11) K. Bender, I. Hennig, D. Schweitzer, K. Dietz, H. Endres, and H. J. Keller, *Mol. Cryst. Liq. Cryst.*, **108**, 359 (1984).

12) H. Kobayashi, T. Mori, R. Kato, A. Kobayashi, Y. Sasaki, G. Saito, and H. Inokuchi, *Chem. Lett.*, **1983**, 581.

13) S. S. P. Parkin, E. M. Engler, R. R. Schumaker, R. Lagier, V. Y. Lee, J. C. Scott, and R. L. Greene, *Phys. Rev. Lett.*, **50**, 270 (1983).

14) H. Schwenk, F. Gross, C. P. Heidmann, K. Andres, D. Schweitzer, and H. Keller, *Mol. Cryst. Liq. Cryst.*, **119**, 329 (1985).

15) P. M. Chaikin and G. Beni, *Phys. Rev. B*, **13**, 647 (1976).

16) S. S. P. Parkin, M. Miljak, and J. R. Cooper, *Phys. Rev. B*, **34**, 1485 (1986).

17) J. B. Torrance, Y. Tomkiewicz, and B. D. Silverman, *Phys. Rev. B*, **15**, 4738 (1977).

Photosensitized Reduction of Methylviologen through the Energy Transfer from Triplet Dyes to 9-Anthracenecarboxylate Anion

Yoshiharu USUI,* Yoshimi SASAKI, Yukie ISHII, and Katsumi TOKUMARU†
Department of Chemistry, Faculty of Science, Ibaraki University, Mito 310
†Department of Chemistry, University of Tsukuba, Tsukuba 305
(Received April 30, 1988)

Synopsis. The reaction mechanism for photosensitized reduction of methylviologen, MV^{2+} through the triplet-triplet energy transfer from organic dyes to 9-anthracenecarboxylate, AC^- was investigated. From the kinetic analysis on MV^{+} formation, it was estimated that both efficiencies of the energy transfer and of the electron transfer from $^3AC^-$ to MV^{2+} were close to unity.

The mechanistic investigation of highly efficient photosensitized reactions has been required for the utilization of light energy and the application to the optical devices in technology. As for the ideal sensitizer in the reaction, there are three requirments; (a) a light absorption in the wide range of wavelength, (b) an efficient utilization of absorbed light energy and (c) the complete turnover of the light absorber. We have investigated the mechanism of electron-transfer reaction for sensitized formation of methylviologen radical by xanthene dyes, where the initial process is started through electron transfer from triplet dyes, ^{3}Dye to MV^{2+}. This is followed by electron transfer to the resulting semioxidized dyes from triethanolamine, TEOA (oxidation-cycle mechanism for three component system of Dye/MV^{2+}/TEOA).[1,2] The maximum yields for MV^{+} formation were equal to 0.16 and 0.045 in case of Eosine Y, $C_{20}H_6O_5Br_4Na_2$ and Erythrosine, Ery, $C_{20}H_6O_5I_4Na_2$ as the sensitizer, respectively. Although this sensitized reaction satisfied the requirement (c), much higher yield was expected by the excitation in the range of visible wavelength, i.e., requirements (a) and (b). In the present paper, attention is focused on the achievement of all requirements of (a)—(c) for the sensitized reaction mentioned above.

Experimental

Materials. Fluorescein, Eosine Y, Erythrosine, Proflavine and Acriflavine were recrystallized three times from ethanol. Methylviologen (Nakarai,G.R.) and triethanolamine (Tokyo kasei,G.R.) were used as received. Each sample was degassed by bubbling argon gas (99.9%) for at least 30 min or by repeating freezing and evacuation 5—7 times under vacuum.

Procedures. A degassed sample in a cell (1 cm×1 cm×4 cm) was irradiated at 25 °C in a steady-light illumination apparatus with a 300 W tungsten lamp. The quantum yield of MV^{+} formation was determined by the conventional actinometry using Eosine Y or potassium ferrioxalate solution.[2,3] Laser flash photolysis was carried out by using a pulsed dye laser (Phase R, 2100B; dye G4: excitation 500 nm and dye B1: excitation 440 nm; FWHM of pulse: 500 ns) and a usual monitoring system composed of a light source, a monochromator, and a transient recorder.

Results and Discussion

Using AC^- as a sensitizer instead of xanthene dyes, the steady light irradiation to three component system of AC^-/MV^{2+}/TEOA was carried out. The dependence of the quantum yield of MV^{+} formation, Φ^A on MV^{2+} concentration is shown in Fig. 1.
The maximum value of 0.9±0.1 was obtained at MV^{2+} concentration of ca. 1 mM (1 M=1 mol dm^{-3}) in aqueous solution (pH=8.3) and there was no decomposition of AC^- during the irradiation. Although the competitive reactions of $^3AC^-$ with MV^{2+} or with TEOA were considered, the decay rate of $^3AC^-$ was not affected by an addition of 3 mM TEOA in a laser-flash experiment. On the other hand, the rate constant of $^3AC^-$ reacting with MV^{2+} was obtained as 3.1×10^9 M^{-1} s^{-1}. Thus, at the concentrations of MV^{2+} in Fig. 1, the initial process occurred by the electron transfer from $^3AC^-$ to MV^{2+}, which leads to formation of MV^{+} and AC· followed by the electron transfer from TEOA (the oxidation cycle mechanism). The kinetical treatment for Φ^A could be performed in a similar manner to that reported in the case of Dye/MV^{2+}/TEOA system, since the linear relationships between $1/\Phi^A$ and $1/[MV^{2+}]$, and between $1/\Phi^A$ and 1/[TEOA] were held, respectively.[2] Then, Φ^A can be written in the following equation:

$$\Phi^A = \phi_{st}{}^A \frac{\alpha_2 k_{qA}^{r}[MV^{2+}]}{k_{dA} + k_{qA}[MV^{2+}]} \frac{k_2'[TEOA]}{k_2 + k_2'[TEOA]} \quad (1)$$

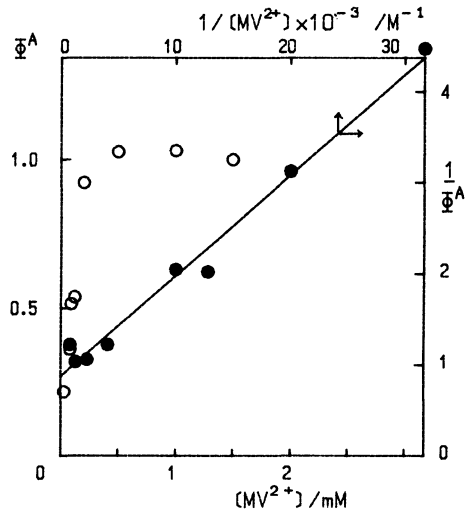

Fig. 1. MV^{2+} concentration effect on the quantum yield of MV^{+} formation, Φ^A. [AC^-]: 75 μM; [TEOA]: 3 μM; pH=8.5; μ=0.03.

where α_2 represents the formation efficiency of $MV^{+\cdot}$. k_{dA}, k^r_{qA} (k_{qA}), k_2 and k_2' are the rate constants for $^3AC^-$ decay, for the genuine (and total) reaction between $^3AC^-$ and MV^{2+}, for AC· decomposition and for the electron transfer reaction between AC· and TEOA, respectively. Maximum value of Φ^A was close to the values of an intersystem crossing probability to $^3AC^-$, ϕ_{st}^A. From the fact, it seems that the electron transfer from $^3AC^-$ to MV^{2+} occurred without any deactivation i.e., $k^r_{qA}=k_{qA}$ and that the production efficiency of radicals of $MV^{+\cdot}$ and AC· separated from its radical pair complex was unity, approximately i.e., $\alpha_2=1$.[4] The reaction system of AC^-/MV^{2+}/TEOA satisfies requirements, (b) and (c).

In order to achieve the requirement, (a), it is very useful to introduce the concept of an energy transfer from organic dyes. Many studies about triplet-triplet energy transfer have been carried out. Concerning the present system, the kinetical investigations on energy transfer from the triplet dyes to several anthracene derivatives have been reported.[5-7] The quantum yield of $MV^{+\cdot}$ formation through the energy transfer, Φ^T on

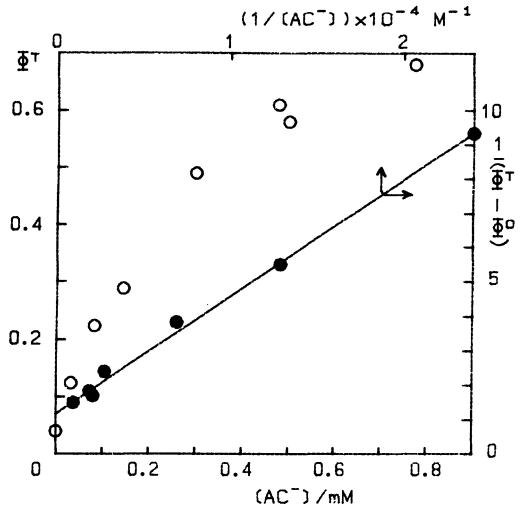

Fig. 2. AC^- concentration effect on the quantum yield of $MV^{+\cdot}$ formation through the energy transfer from $^3Ery^{2-}$ to AC^-, Φ^T. [Ery^{2-}]: 5 μM; [MV^{2+}]: 0.1 mM; [TEOA]: 3 mM; pH=8.5; μ=0.1.

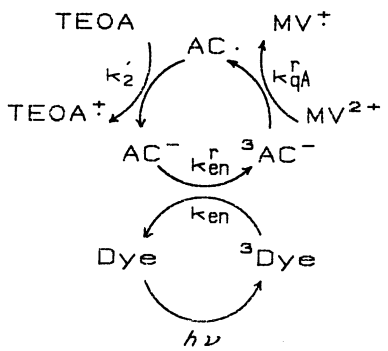

Fig. 3. The proposed reaction scheme for the sensitized reduction of MV^{2+} through the energy transfer from triplet dyes to AC^-.

four-component system of Dye/AC^-/MV^{2+}/TEOA by steady-light illumination increased both with MV^{2+} concentration and with AC^- concentration. For the AC^- concentration effect, an effective enhancement in about 16-fold on Φ^T was observed by the addition of 0.78 mM AC^- using Erythrosine as a sensitizer. The results on Φ^T are shown in Fig. 2 (Sens: Ery). The essential mechanism in Fig. 3 can be proposed which is applicable to the present system by referring to the results in Figs. 1 and 2. Depending on the concentrations of MV^{2+} and AC^-, the electron transfer from triplet dyes to MV^{2+} competes with the energy transfer.[1,2] Therefore, the quantum yield of free radical formation of $MV^{+\cdot}$ is given as follows:

$$\Phi^T = \phi_{st}^D \frac{1}{k_{dd} + k_q[MV^{2+}] + k_{en}[AC^-]} \left(\gamma_1 k^r_q[MV^{2+}] + \gamma_2 \frac{k^r_{qA}[MV^{2+}]}{k_{dA} + k_{qA}[MV^{2+}]} k^r_{en}[AC^-]\right) \quad (2)$$

and

$$\gamma_1 = \alpha_1 k_1'[TEOA]/(k_1 + k_1'[TEOA])$$

$$\gamma_2 = \alpha_2 k_2'[TEOA]/(k_2 + k_2'[TEOA])$$

where γ_1 and γ_2 refer to the reaction efficiency through the processes of dye-sensitized electron transfer and to that through the process of AC^- sensitized one, respectively. ϕ_{st}^D represents the intersystem crossing probability of dye. k_{dd}, k^r_q(k_q), k^r_{en} (k_{en}), k_1 and k_1' are the rate constants for ^{3}Dye decay, for the genuine (and total) reaction of electron transfer between ^{3}Dye and MV^{2+}, for the genuine (and total) reaction of energy transfer from ^{3}Dye to AC^-, for $Dye^{+\cdot}$ decomposition and for the electron transfer reaction between $Dye^{+\cdot}$ and TEOA, respectively. Putting Φ^T at $[AC^-]=0$ as Φ^0, the approximate equation, Eq. 3, is obtained under the condition of $k_{dd} \ll k_q[MV^{2+}]$, $k_{en}[AC^-]$ and $k_{dA} \ll k_{qA}[MV^{2+}]$ in Eq. 2:

$$\Phi^T - \Phi^0 = \phi_{st}^D \frac{(\gamma_2 k^r_{en} k^r_{qA}/k_{qA} - \gamma_1 k_{en} k^r_q/k_q)[AC^-]}{k_q[MV^{2+}] + k_{en}[AC^-]} \quad (3)$$

The linear relationship between $1/(\Phi^T - \Phi^0)$ and $1/[AC^-]$ is obtained as shown in Fig. 2. The values of interception are 1.7 and 1.1 for Eosine Y (ϕ_{st}^D=0.64) and Erythrosine ($\phi_{st}^D \approx 1$) sensitization, respectively. Since the interception equals to the value of $1/\phi_{st}^D$, the relation of $k^r_{en}=k_{en}$ is suggested. This means that the

Table 1. Maximum Quantum Yield of $MV^{+\cdot}$ Formation (Φ^T_{max}) through the Energy Transfer from Dyes to AC^- and the Rate Constants of the Energy Transfer (k_{en})

Dyes(concentration/μM)	Φ^T_{max}	$k_{en}/M^{-1}s^{-1}$
Fluorescein(10)	0.045	4.5×10^9
Eosine Y(10)	0.55	4.7×10^9
Erythrosine(10)	0.77	3.2×10^9
Proflavine(22)	0.23	2.7×10^9
Acriflavine(17)	0.28	7.4×10^9

energy transfer from triplet dye to AC^- occurs without any deactivation as is shown in Fig. 3.

Under the higher concentrations of AC^-, the following approximate equation can be derived from Eq. 2 and the effect of MV^{2+} concentration on Φ^T is analyzed.

$$\Phi^T = \phi_{st}^D \frac{k_{en}^r}{k_{en}} \frac{k_{qA}^r[MV^{2+}]}{k_{dA} + k_{qA}[MV^{2+}]} \quad (4)$$

From the interception of linear relationship between $1/\Phi^T$ and $1/[MV^{2+}]$, k_{en}^r/k_{en} values was also estimated to be unity using ϕ_{st}^D value of sensitizer. This result coincides with the fact ($k_{en}^r = k_{en}$) obtained from AC^- concentration effect on Φ^T.

Using xanthene dyes and acridine dyes as energy donors, the observed values of maximum yield of Φ^T_{max} and the values of the rate constant, k_{en} are summarised in Table 1. These reaction systems of Dye/AC^-/MV^{2+}/TEOA satisfy all requirements of (a), (b), and (c) since a light absorption extends in the range of wavelength from 370 nm to 550 nm.

This work was supported by a Grant-in-Aid for Special Project Research (No. 62113001 and 63104001) from the Ministry of Education, Science and Culture.

References

1) H. Misawa, H. Sakuragi, Y. Usui, and K. Tokumaru, *Chem. Lett.*, **1983**, 709.

2) Y. Usui, H. Misawa, H. Sakuragi and, K. Tokumaru, *Bull. Chem. Soc. Jpn.*, **60**, 1573 (1987). The quantum yield of Eosine Y photobleaching in aerated aqueous solution, 2.8×10^{-4} was used to determine the light intensity.

3) C. G. Hatchard and C. A. Parker, *Proc. R. Soc. London, Ser. A*, **235**, 518 (1956).

4) O. Johansen, A. W-H. Mau, and W. H. F. Sasse, *Chem. Phys. Lett.*, **94**, 107 (1983).

5) K. Kikuchi, H. Kokubun, and M. Koizumi, *Bull. Chem. Soc. Jpn.*, **43**, 2732 (1970).

6) K. Kikuchi, H. Kokubun, and M. Koizumi, *Bull. Chem. Soc. Jpn.*, **44**, 1527 (1971).

7) A. W-H. Mau, O. Johansen, and W. H. F. Sasse, *Photochem. Photobiol.*, **41**, 503 (1983).

Photochemical Generation of μ-Amido-μ-peroxo-bis[bis(ethylenediamine)-cobalt(III)] Complex from the Corresponding μ-Hyperoxo Complex in Neutral Aqueous Solution

Nobuyoshi SHINOHARA,* Emiko KOSE, and Wataru OHKUBO
Department of Chemistry, Yokohama City University,
Seto, Kanazawa-ku, Yokohama 236
(Received October 20, 1987)

Synopsis. A μ-amido-μ-hyperoxo complex, $[(en)_2Co(NH_2,O_2^-)Co(en)_2]^{4+}$, was found to generate the corresponding μ-peroxo complex, together with mononuclear cobalt(III) complexes upon irradiation with near-ultraviolet light in a neutral aqueous solution. The result is different from that obtained in an acidic aqueous solution, in which the products are $[Co(NH_3)(en)_2(H_2O)]^{3+}$ and Co_{aq}^{2+}. The photochemical reaction mechanisms are discussed.

The photosensitivity of the μ-hyperoxo-bis[pentaamminecobalt(III)] complex, $[(NH_3)_5Co(O_2^-)Co(NH_3)_5]^{5+}$, first observed by Sykes,[1] has been investigated by Barnes, et al.,[2] and by Valentine and Valentine.[3-5] The μ-hyperoxo cobalt(III) complexes are photosensitive, and photodecomposition occurs upon irradiation with near-ultraviolet light (i.e. light with wavelengths longer than 300 nm).

Photochemical reactions of μ-amido-μ-hyperoxo-bis[bis(ethylenediamine)cobalt(III)] complex, $[(en)_2Co(NH_2,O_2^-)Co(en)_2]^{4+}$, in acidic aqueous solutions were studied by Valentine and Valentine,[4] who established the stoichiometry of the reactions as follows:

$$[(en)_2Co(NH_2,\ O_2^-)Co(en)_2]^{4+} \xrightarrow[H^+,\ H_2O]{h\nu(>300\ nm)} cis\text{-}[Co(NH_3)(en)_2(H_2O)]^{3+} + O_2 + Co^{2+} + 2enH_2^{2+} \quad (1)$$

We have studied the photochemistry of the same complex in a neutral aqueous solution, and found that the corresponding μ-peroxo cobalt(III) complex is formed together with mononuclear cobalt(III) complexes, which is different from the result obtained in an acidic aqueous solution.

Experimental

$[(en)_2Co(NH_2,O_2^-)Co(en)_2](ClO_4)_4$ and $[(en)_2Co(NH_2,O_2^{2-})Co(en)_2](NO_3)_3\cdot 2.5H_2O$ were obtained by methods described in the literature,[4,6] and recrystallized. The deaerations of the solutions used for photolysis were carried out by bubbling with pure nitrogen. A sample solution containing the μ-amido-μ-hyperoxo complex was irradiated continuously in a 1-cm quartz cell using a high-pressure mercury lamp, UM-102 (100 W), or an ultrahigh-pressure mercury lamp, USH-500D (500 W) (Ushio Electric Co.), at room temperature. Monochromatic light (313, 365, and 436 nm) was obtained by a combination of solution and glass filters. The absorption spectra were recorded on a Shimadzu MPS-2000 spectrophotometer.

For investigating the reaction products, about 20 ml of the solution in a fused silica cell was irradiated with light. The number of components of the photochemical decomposition products and their identities were determined by spectrophotometric analyses of the photolyzed solutions and by ion-exchange chromatography on a cation-exchange resin (CM-Sephadex C-25 in the sodium form). A portion of the irradiated solution was passed through a cation-exchange column. The absorbed band was eluted with 1.2 mol dm^{-3} sodium perchlorate solution. The first group eluted consisted of two mononuclear complexes which could not be separated from each other for the acid-base equilibria in a neutral aqueous solution as described later. After removing mononuclear complexes, μ-peroxo and μ-hyperoxo complexes were successively eluted in this order. Another portion of the irradiated solution was passed through a column for the separation of two mononuclear complexes. The absorbed band was eluted with a 0.01 mol dm^{-3} sodium hydroxide solution containing 0.3 mol dm^{-3} sodium perchlorate. The first two bands corresponded to mononuclear complexes, *cis*-$[Co(OH)_2(en)_2]^+$ and *cis*-$[Co(OH)(NH_3)(en)_2]^{2+}$. The μ-peroxo complex was identified by comparing the absorption spectrum with that of an authentic sample synthesized by a method described in the literature.[6] The mononuclear products were identified spectrophotometrically.[7,8] Oxygen was determined by gas chromatography.

Results and Discussion

The absorption spectrum of $[(en)_2Co(NH_2,O_2^-)Co(en)_2]^{4+}$ in an aqueous solution has two peaks (466 and 686 nm) in visible region. The electronic structure was studied by Lever and Gray.[9] The absorption spectral changes are shown in Fig. 1 for irradiation of the deaerated aqueous solution at the $O_2^-\rightarrow Co(III)$ charge-transfer band (351 nm). The absorption at 466 and 686 nm decreased with an increase in the irradiation time. Valentine and Valentine[4] proposed Eq. 1 in order to account for the photodecomposition reaction by determining the photolyzed products chromatographically. We can suggest that more

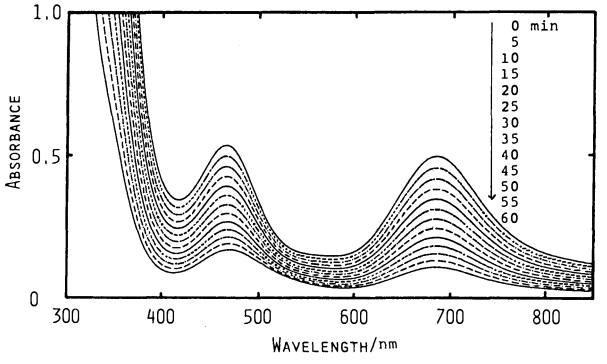

Fig. 1. Absorption spectral changes of 1.00×10^{-3} mol dm^{-3} $[(en)_2Co(NH_2,\ O_2^-)Co(en)]^{4+}$ in deaerated aqueous solution of 0.1 mol dm^{-3} $HClO_4$ upon irradiation at 365 nm light.

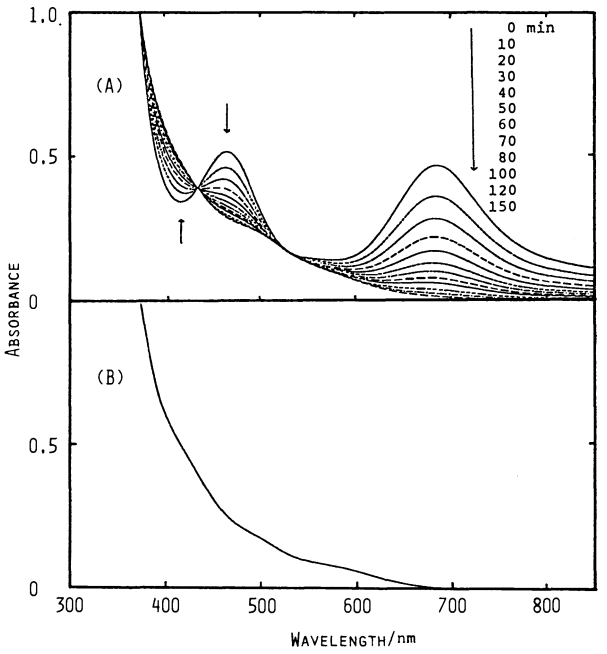

Fig. 2. UV and visible absorption spectra.
A: Absorption spectrtal changes of 1.00×10^{-3} mol dm^{-3} $[(en)_2Co(NH_2, O_2^-)Co(en)_2]^{4+}$ upon irradiation of the neutral deaerated solution at 365 nm light.
B: Absorption spectrum of 5.00×10^{-4} mol dm^{-3} $[(en)_2Co(NH_2, O_2^{2-})Co(en)_2]^{3+}$ in neutral aqueous solution.

detailed photodecomposition reactions in aqueous solutions are as follows. In the excited state that can be formulated as $*[(en)_2Co(III)(NH_2,O_2^0)Co(II)(en)_2]^{4+}$, the oxygen molecule should be released by a kinetically labile Co(II) species (Eq. 2), which then undergoes a very rapid aquation leading to the Co_{aq}^{2+} (Eq. 3) in an acidic aqueous solution. Since

$$[(en)_2Co(NH_2, O_2^-)Co(en)_2]^{4+} \xrightarrow{h\nu} *[(en)_2Co(NH_2, O_2^0)Co(en)_2]^{4+} \xrightarrow{H_2O} cis\text{-}[Co(OH)(NH_3)(en)_2]^{2+} + cis\text{-}[Co(en)_2(H_2O)_2]^{2+} + O_2 \quad (2)$$

$$cis\text{-}[Co(en)_2(H_2O)_2]^{2+} \xrightarrow{H^+} Co^{2+} + 2enH_2^{2+} + 2H_2O \quad (3)$$

the ligand dissociation reaction in Co(II)–polyamine complexes becomes slower as the pH is increased,[10,11] it appears that $[Co(en)_2(H_2O)_2]^{2+}$ reacts with μ-hyperoxo complex before the dissociation in neutral solution as stated below.

When the μ-amido-μ-hyperoxo complex was irradiated with light at 365 nm in a neutral aqueous solution, the absorption changes were different from those obtained in acidic aqueous solutions, as shown in Fig. 2A. The intensity of the absorption in the 432—850 nm range decreased with an isosbestic point at 432 nm. The absorbance at 686 nm disappeared after 150 min irradiation with a high-pressure mercury lamp under our experimental conditions. The spectrum in Fig. 2A changed with the irradiation time and approached a final form, which was very similar to the spectrum of the corresponding μ-peroxo complex (Fig. 2B). Similar results were obtained for 313 and 436 nm irradiation. Such an attainment of the limiting spectrum is due to the inertness of the resulting μ-peroxo complex, compared to the photosensitive μ-hyperoxo complex, upon irradiation in the range of the wavelength examined. The decomposition reaction was independent of the presence or absence of dissolved oxygen.

The number of components and their identities were determined by spectrophotometric analyses of photolyzed solutions and by ion-exchange chromatography. It was found that μ-amido-μ-peroxo complex and two kinds of mononuclear complexes could be generated in neutral solutions. The photodecomposition of μ-hyperoxo complex is also accompanied by the generation of oxygen. Accordingly, we concluded that Eq. 4 describes the stoichiometry for the photochemical decomposition of μ-amido-μ-hyperoxo complex in a neutral aqueous solution.

$$2[(en)_2Co(NH_2, O_2^-)Co(en)_2]^{4+} + 3H_2O \xrightarrow{h\nu} [(en)_2Co(NH_2, O_2^{2-})Co(en)_2]^{3+} + cis\text{-}[Co(OH)(NH_3)(en)_2]^{2+} + cis\text{-}[Co(OH)(en)_2(H_2O)]^{2+} + O_2 + H^+ \quad (4)$$

The resulting mononuclear hydroxo complexes in Eq. 4 are in equilibria with aqua complexes, *cis*-$[Co(NH_3)(en)_2(H_2O)]^{3+}$ and *cis*-$[Co(en)_2(H_2O)_2]^{3+}$, whose acid ionization constants are $pK=6.05$ (25 °C) and $pK=6.06$ (25 °C), respectively.[8,12]

The absorption near 500 nm of the final spectrum in Fig. 2A is a little larger than that in Fig. 2B, which is due to a contribution of the mononuclear complexes formed together with a μ-peroxo complex. The contribution is very small for the small molar extinction coefficient of the mononuclear cobalt(III) complexes, compared with that of the μ-peroxo complex.

We believe that in neutral aqueous solution the *cis*-$[Co(en)_2(H_2O)_2]^{2+}$, formed by the photodecomposition of the μ-hyperoxo complex (Eq. 2), reacts with the remaining μ-hyperoxo complex to give *cis*-$[Co(OH)(en)_2(H_2O)]^{2+}$ and μ-peroxo complex:

$$cis\text{-}[Co(en)_2(H_2O)_2]^{2+} + [(en)_2Co(NH_2, O_2^-)Co(en)_2]^{4+} \longrightarrow cis\text{-}[Co(OH)(en)_2(H_2O)]^{2+} + [(en)_2Co(NH_2, O_2^{2-})Co(en)_2]^{3+} + H^+ \quad (5)$$

The rate of the dissociation of en from $[Co(en)_2(H_2O)_2]^{2+}$ is slower in a neutral solution than in an acidic solution.[10,11] Therefore, it appears that the reaction shown by Eq. 5 occurs before the decomposition of $[Co(en)_2(H_2O)_2]^{2+}$ to $[Co(en)(H_2O)_4]^{2+}$ or Co_{aq}^{2+}.

References

1) A. G. Sykes, *Trans. Faraday Soc.*, **59**, 1325 (1963).
2) J. E. Barnes, J. Barrett, R. W. Brett, and J. Brown, *J. Inorg. Nucl. Chem.*, **30**, 2207 (1968).
3) J. S. Valentine and D. Valentine, Jr., *J. Am. Chem. Soc.*, **93**, 1111 (1971).
4) J. S. Valentine and D. Valentine, Jr., *Inorg. Chem.*, **10**, 393 (1971).
5) J. S. Valentine and D. Valentine, Jr., *Inorg. Chem.*, **12**, 1697 (1973).
6) M. Mori and J. A. Weil, *J. Am. Chem. Soc.*, **89**, 3732 (1967).
7) F. Basolo, *J. Am. Chem. Soc.*, **72**, 4393 (1950).
8) J. Bjerrum and S. E. Rasmussen, *Acta Chem. Scand.*, **6**, 1265 (1952).
9) A. B. P. Lever and H. B. Gray, *Acc. Chem. Res.*, **11**, 348 (1978).
10) J. Lilie, N. Shinohara, and M. G. Simic, *J. Am. Chem. Soc.*, **98**, 6516 (1976).
11) N. Shinohara, J. Lilie, and M. G. Simic, *Inorg. Chem.*, **16**, 2809 (1977).
12) R. D. Cannon and J. E. Earley, *J. Am. Chem. Soc.*, **88**, 1872 (1966).

The Preparation and Properties of an Enzyme Electrode for Creatine

Junko MOTONAKA,* Hisaaki TAKABAYASHI, Sanae IKEDA, and Nobuyuki TANAKA†
Technical College, The University of Tokushima, Minamijosanjima, Tokushima 770
†Nippon Jimuki Co., Ltd., 12, 3-Chome, Kanda Ogawa-cho, Chiyoda-ku, Tokyo 101
(Received December 17, 1987)

Synopsis. An enzyme electrode for creatine consisting of a single glass electrode and immobilized creatine kinase was prepared, and the effects of various conditions on the calibration curve obtained with this electrode were examined. Creatine in the range of 0.42—3.3 mmol dm^{-3} could be determined at 37 °C and pH 9.

Creatine is a nitrogenous compound produced by protein metabolism. It is found in muscle in combination with phosphoric acid as phosphocreatine and is intimately associated with the chemical changes which take place during muscle contraction. Creatine is not found in any appreciable amount in the urine. There is a little in the urine of women and children, but not normally in that of men.[1] It is increased by the destruction and denaturation of muscles. The creatine content in urine or serum can thus be used clinically.

There has been much recent progress in the study of enzyme electrodes,[2-8] but an enzyme electrode for creatine has not yet been developed. In this work, we prepared an enzyme electrode for the determination of creatine. The enzyme reaction is shown in Scheme 1.

Experimental

Apparatus and Reagents. A glass electrode, Model GST-155C (TOA Electronics, Ltd.), was employed to prepare the enzyme electrode. The pH was measured with a digital pH/mV meter, Model TSC-10A (TOA Electronics, Ltd.), connected with an electronic recorder, Model R-102 (Rikadenki Kogyo Co., Ltd.). All the measurements were carried out at 37±0.2 °C.

The creatine kinase (from rabbit muscle; specific activity, 800 units per mg at 38 °C) was obtained from Boehringer Mannheim Yamanouchi, and the adenosine 5′-triphosphate (ATP)(Purity is 98±3%), from the Oriental Yeast Co. The creatine (analytical-reagent grade), bovine serum albumin (BSA)(Fraction V powder; purity, 98.5±0.5%), and glutaraldehyde(25%) were obtained from Wako Pure Chemical Industries. The ATP(10^{-1} mol dm^{-3}), creatine (3×10^{-2} mol dm^{-3}), BSA(10 w/w%), and glutaraldehyde (12.5 v/v%) solutions were prepared with distilled water.

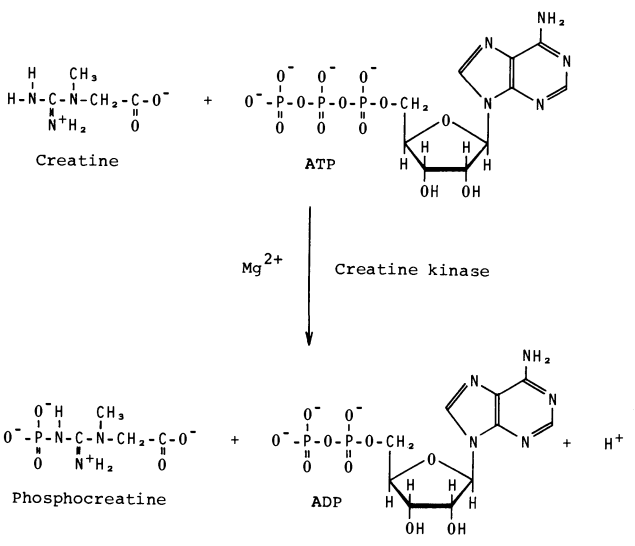

Scheme 1. Enzyme reaction of creatine.

Preparation of the Enzyme Electrode. The electrode consisted of a glass electrode with an immobilized creatine kinase membrane fitted to its detector end. A cross-linking method was used for the immobilization of the creatine kinase. That is, 30 µl of a 10 w/w% BSA solution was spread on a polycarbonate membrane (0.1 µm caliber), after which 5 mg of creatine kinase and 4 µl of 12.5 v/v% glutaraldehyde were added with prompt mixing. They were spread at a thickness of 0.05 mm. The membrane was then left to stand for at least 2 hours at 4 °C and then attached to the glass electrode by means of an O-ring.

Determination of Creatine. The enzyme electrode for creatine was immersed in 10 ml of a 2 mmol dm^{-3} ATP-0.1 mmol dm^{-3} magnesium sulfate (pH 9) solution in a thermostat-regulated cell. Then 2 ml of the creatine solution was injected into the cell, and the ion-production by the enzyme reaction during the first 10 minutes, unless otherwise indicated, was monitored as the change in the pH. The electrode was washed with distilled water in each measurement.

Results and Discussion

Immobilization of Enzyme. A cross-linking method and matrix-entrapping methods of enzyme immobilization were also examined. (A) Cross-linking method: The membrane was prepared as has been described in the experimental sections. (B) Matrix-entrapping method: On a glass plate, 10 µl of a 20 w/w% cellulose acetate–acetone solution and 30 µl of a creatine kinase aqueous solution (5 mg/30 µl) were mixed quickly and spread at a thickness of 0.05 mm. This immobilized enzyme membrane and a polycarbonate membrane with a caliber of 0.1 µm were attached to a single glass electrode by means of an O-ring.

The response curves of the two types of electrodes are shown in Fig. 1. The response curves of Electrodes A and B were similar. The ΔpH value (0.18) of Electrode A after 10 min was greater than that (0.11) of Electrode B. The caribration curve of Electrode A was also compared with that of Electrode B [Fig. 2, Curves (A) and (D)]. Both methods (cross-linking and matrix-entrapping) could be employed. Further studies were made on the cross-linking method with greater ΔpH values.

Effects of Alkaline Solutions. In the enzyme reaction shown in Scheme 1, the optimum pH of creatine kinase is pH 8—9.[9] The sample solution was adjusted to this pH with sodium hydroxide, aqueous

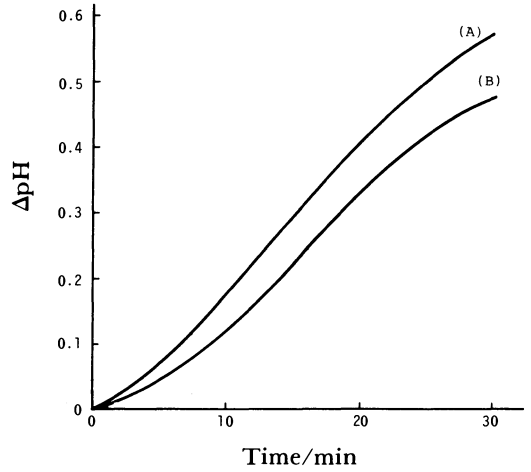

Fig. 1. Response curves of creatine enzyme electrode. (A) Cross-linking method. (B) Matrix-entrapping method. The sample (12 ml) contained 1.67 mmol dm^{-3} creatine, 1.67 mmol dm^{-3} ATP, and 8.33 mmol dm^{-3} magnesium sulfate. Temp 37 °C.

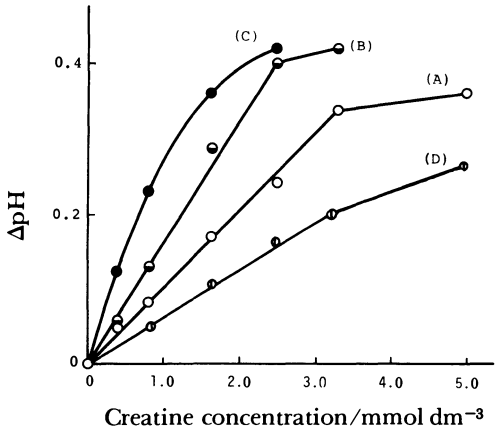

Fig. 2. Calibration curves of creatine. (A) Cross-linking method (after 10 min). (B) Cross-linking method (after 20 min). (C) Cross-linking method (after 30 min). (D) Matrix-entrapping method (after 10 min). The sample (12 ml) contained the indicated amount creatine, 1.67 mmol dm^{-3} ATP and 8.33 mmol dm^{-3} magnesium sulfate. Temp 37 °C.

ammonia, or potassium hydroxide. The response (ΔpH) was greatest with potassium hydroxide (0.18) and least with sodium hydroxide (0.03), because sodium hydroxide inactivated creatine kinase.[10] Potassium hydroxide was used in the subsequent experiments.

Effects of ATP and Magnesium Sulfate Concentrations. ATP plays an important part in energy metabolism, and the magnesium ion functions as a cofactor of creatine kinase.[11] The responses were measured with concentrations of 8.3×10^{-3}—8.33 mmol dm^{-3} ATP and 0.833—41.7 mmol dm^{-3} magnesium sulfate for 1.67 mmol dm^{-3} of creatine. The ΔpH values increased with the ATP concentration in the range of 8.33×10^{-3}—1.67 mmol dm^{-3} and was constant in the range of 1.67—8.33 mmol dm^{-3} (the amount required theoretically was 1.67 mmol dm^{-3} ATP), because at higher concentrations the amount of ATP passing through the membrane became constant. Similarly, the ΔpH increased with up to 8.33 mmol dm^{-3} magnesium sulfate, and then became constant because the magnesium-ion concentration was in excess of the amount required as a cofactor for the creatine kinase. Accordingly, 1.67 mmol dm^{-3} ATP and 8.33 mmol dm^{-3} magnesium sulfate were used.

Effect of the Temperature. The effect of the temperature on the ΔpH was also examined in the range of 20—40 °C. The ΔpH value (0.180 after 10 min) was the greatest at 37—38 °C. The creatine kinase was inactivated at 40 °C (ΔpH was 0.120). The optimum temperature for creatine kinase was 37—38 °C. Therefore, all subsequent measurements were done at 37 °C.

Effect of the Amount of Immobilized Creatine Kinase. The effects of the amount of immobilized enzyme will also be discussed. Creatine kinase in the range from 2000 units (2.5 mg) to 8000 units (10 mg) was immobilized with 6 μl of a 10 w/w% BSA solution and 0.8 μl of a 12.5 v/v% glutaraldehyde solution per 1 mg of enzyme. The value of ΔpH increased in the range of 2000—4000 units of the enzyme and remained constant with larger amounts. The enzyme activity was low with small amounts of enzyme because a part of the active site reacted with the cross-linking agent.[12] On the basis of these results, 5 mg (4000 units) of creatine kinase were immobilized with 30 μl of a 10 w/w% BSA solution and 4 μl of a 12.5 v/v% glutaraldehyde solution.

Calibration Curve. Linear plots of the creatine concentration vs. the ΔpH were obtained at concentrations of 0.42—3.3 mmol dm^{-3} at 10 min [Curve (A)], 0.42—2.5 mmol dm^{-3} at 20 min [Curve B)] and 0.42—1.6 mmol dm^{-3} at 30 min [Curve (C)], as is shown in Fig. 2. The plots fit these three equations; $Y=96.66X+0.006$ [Curve (A)], $Y=165.8X-0.006$ [Curve (B)], and $Y=183.3X-0.06$ [Curve (C)], where Y is ΔpH and X is the creatine concentration in mmol dm^{-3}. The correlation coefficients were 0.999, 0.998, and 0.991 respectively. The coefficients of variation were less than 7.2%.

Life-Time of the Electrode. The life-time of the prepared enzyme electrode for creatine was also considered. The stability of this electrode is good for 0—3 days (ΔpH was 0.18) after the preparation. However, the sensitivity of this electrode decreased after 4 days (the ΔpH values were 0.169, 0.150, 0.135, 0.117, 0.103, and 0.086 after 4, 5, 6, 7, 8, and 9 days respectively) because of the decrease in the activity of the enzyme. Just this electrode was used 10—20 times a day.

Effects of Concomitant Compounds. The creatine was determined in the presence of eight other compounds (creatinine, β-D-glucose, cholesterol, sodium chloride, urea, L-ascorbic acid, iodine, and citric acid), as is shown in Table 1. Creatinine, glucose, cholesterol, and sodium chloride were present in mole amounts about 10, 100, and 1000 times respectively

Table 1. Effects of Concomitant Compound on the Determination of Creatine

Concomitant compound	Molar ratio creatine : concomitant compound (mol : mol)	Relative error (%)
Creatinine	1 : 1	−1.0
	1 : 10	0.4
	1 : 100	0.9
β-D-Glucose	1 : 1	0.5
	1 : 10	0.3
	1 : 100	0.5
Cholesterol	1 : 0.01	−0.2
	1 : 0.05	−0.4
Sodium chloride	1 : 1	0.7
	1 : 100	−0.5
	1 : 1000	0.9
L-Ascorbic acid	1 : 1	0.6
	1 : 3	1.1
	1 : 5	−1.3
Iodine	1 : 0.1	−3.0
	1 : 0.5	−2.4
Citric acid	1 : 0.1	−2.2
	1 : 0.5	−3.0
Urea	1 : 1	−1.0
	1 : 10	−1.7
	1 : 100	2.9

Sample, 12 ml, of 1.67 mmol dm^{-3} creatine 1.67 mmol dm^{-3} ATP and 8.33 mmol dm^{-3} magnesium sulfate. Temp 37 °C.

that of creatine in human serum. Creatine could be determined with a relative error of less than ±1.7% in the presence of molar ratios of 1—100 creatinine, 1—100 β-D-glucose, 0.01—0.05 cholesterol, 1—1000 sodium chloride, 1—5 L-ascorbic acid, and 1—10 urea. The effect of cholesterol was examined at less than the presence ratio in human serum, because the solubility of cholesterol was small (0.2 mg/100 ml H_2O). Creatine could be determined with a relative error of less than −3% in the presence of molar ratios of 0.1—0.5 iodine as the SH reagent and 0.1—0.5 citric acid as the chelating agent.

References

1) I. Kanai, "Rinsho Kensaho Teiyo," ed by M. Kanai, Kodansha, Tokyo (1983), p. 428.
2) "Ion Denkyoku to Koso Denkyoku," ed by S. Suzuki, Kodansha, Tokyo (1981), pp. 65, 187.
3) M. Koyama and Y. Sato, *Anal. Chim. Acta*, **116**, 307 (1980).
4) D. P. Nikolelis and T. P. Hadjiioannou, *Anal. Chim. Acta.* **147**, 33 (1983).
5) G. G. Guilbault, S. P. Chena, and S. S. Kuan, *Anal. Lett.*, **13**, 1607 (1980).
6) G. G. Guilbault, B. Danielsson, C. F. Mandenius, and K. Mosbach, *Anal. Chem.*, **55**, 1582 (1983).
7) M. Meyerhoff and G. A. Rechnitz, *Anal. Chim. Acta*, **85**, 277 (1976).
8) G. J. Papariello, A. K. Mukherji, and C. M. Shearer, *Anal. Chem.*, **45**, 790 (1973).
9) "Koso Handbook," ed by Y. Kajiro, M. Tokushige, T. Yagi, and E. Ichishima, Asakura Shoten, Tokyo (1983), p. 372.
10) T. A. Mahowalb, E. A. Noltmann, and S. A. Koby, *J. Biol. Chem.*, **237**, 1535 (1962).
11) "Rinsyo Koso Handbook," ed by S. Baba, H. Wada, M. Kitamura, and J. Okuda, Kodansha, Tokyo (1982), p. 313.
12) "Ion Denkyoku to Koso Denkyoku," ed by S. Suzuki, Kodansha, Tokyo (1981), p. 67.

The Second Dissociation Constant of Sulfuric Acid at Elevated Temperatures from Potentiometric Measurements

Yoshiyuki MATSUSHIMA and Akitsugu OKUWAKI*
Department of Molecular Chemistry and Engineering, Faculty of Engineering, Tohoku University, Sendai 980
(Received December 28, 1987)

Synopsis. The second dissociation constant of sulfuric acid in 1 *m* KCl media has been determined from 25 to 200 °C using Debye-Hückel equation from the data on the electromotive force of a hydrogen ion-concentration cell. The thermodynamic values for the $HSO_4^-=H^++SO_4^{2-}$ reaction and the KSO_4^- ion-pair association constant are also presented.

The sulfate ion plays an important role in the equilibrium,[1,2] rate,[3] and morphology[4] of the precipitation of inorganic compounds at elevated temperatures through complex formation with metal ions. However, the formation constants for sulfate complexes are very limited except for the hydrogensulfate ion.

Cobble and Criss[5–7] developed a method of estimating the equilibrium constant applicable up to the critical temperature using the entropy-corresponding principle. Recently, Helgeson[8] has proposed another method applicable to 600 °C and 5 kbar for geological applications. Such an estimation, however, can be applied only for simple single ions. Consequently, the formation constants for many complexes must be known to understand the effect of chemical species on the nature of reactions in solutions at elevated temperatures.

The second dissociation constant for sulfuric acid at elevated temperatures has been determined by solubility measurements[9,10] and conductivity measurements,[11,12] but not yet by emf measurements. A hydrogen ion-concentration cell at an elevated temperature was first used to determine the pH of the buffer solutions by Le Peintre et al.[13] Mesmer and Baes have since reviewed the hydrolysis of metal ions at a high ionic strength.[14] MacDonald has also investigated this reaction using the electrochemical method.[15] In the present study, we have determined the second dissociation constant of sulfuric acid at elevated temperatures by using potentiometric measurements as the first step to determine the formation constants of multivalent metal ions with sulfate ions.

Experimental

Materials. A stock solution of 0.1 mol dm^{-3} HCl was prepared from reagent-grade hydrochloric acid diluted with doubly distilled water. Reagent-grade KCl and K_2SO_4 were used without further purification. Ultrapure hydrogen (99.99999%) was used for the hydrogen electrode.

Hydrogen Ion-Concentration Cell.[16] The hydrogen ion-concentration cell consisted of a 300-cm^{-3} titanium autoclave containing a 180-cm^{-3} outer quartz beaker and an inner PTFE compartment, the two being joined by a liquid junction and each containing a platinized platinum hydrogen electrode. Figure 1 shows a cross-sectional view of the inner compartment. The porous PTFE disk (pore size, 0.2 μm; thickness, 1 mm) provides a liquid junction between the two compartments. The side of this compartment has a pin hole 0.7 mm in diameter which allows a rapid pressure-equilibration of hydrogen gas. Thus, the cell may be represented as:

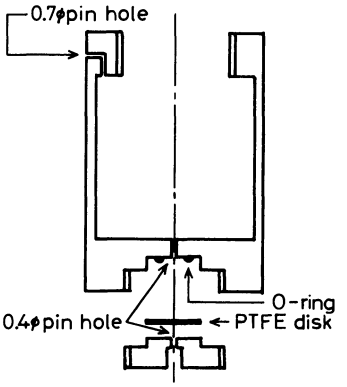

Fig. 1. Schematic of PTFE inner compartment.

$$\mathrm{Pt,H_2}\left|\begin{array}{l}\mathrm{HCl}(m_1)\\ \mathrm{K_2SO_4}(m_2)\\ \mathrm{KCl}(m_3=1)\end{array}\right\|\begin{array}{l}\mathrm{HCl}(m_4=0.001)\\ \mathrm{KCl}(m_5=1)\end{array}\left|\right.\mathrm{H_2,Pt} \qquad \text{(I)}$$

where m represents the molalities. The HCl concentration in the reference solution was 0.001 *m* in each experiment. The emf measurement was carried out for the 14 sets of composition as follows: m_1=0.0100—0.0240 and m_2= 0.0100—0.0250. In order to minimize the liquid junction potential and keep the ionic strength constant, KCl was added as a supporting electrolyte in both solutions (1 *m*). Because the PTFE is not wetted, the saturated KCl solution does not permeate the porous disk. We treated the disk using the following procedure: 1) wetting the porous disk with acetone and expelling air from the pores in the disk; 2) replacing the acetone with distilled water for a few days; 3) exchanging the water with a saturated KCl solution for two weeks. The cell was degassed after assembly by alternately pressurizing it with hydrogen and by venting it to atmospheric pressure several times. Finally, the cell was pressurized to about 0.5 MPa with hydrogen. The potential of the cell was measured over the temperature range from 25 to 200 °C at 25 °C intervals with a digital voltmeter. The voltage was recorded after a values had remained constant for several minutes (≧±1 mV).

Results and Discussion

Since the pressure of hydrogen is equal in the two compartments, the potential of the cell (I) is given by Eq. 1:

$$E=(RT/F)\ln(a_{\mathrm{H^+},t}/a_{\mathrm{H^+},r})+E_j \qquad (1)$$

where a_{H^+} is the activity of the hydrogen ion and where the subscripts t and r refer to the test solution and the reference solution respectively. E_j is the liquid junction potential, which can be estimated using the Henderson equation:[17]

$$E_j = -\sum D_i([i]_t - [i]_r) \quad (2)$$

$$D_i = RT|Z_i|\lambda_i/(Z_iF\sum(|Z_i|[\bar{i}]\lambda_i) \quad (3)$$

where $[i]$ denotes the molality of the species i and λ_i is the limiting equivalent conductance of the i th ion. The values of λ_i are available over the above temperature range.[18]

The Debye-Hückel equation was used to calculate the activity coefficient:

$$\log\gamma_i = -Z_i^2S\sqrt{I}/(1 + A\sqrt{I}) \quad (4)$$

where S is the Debye-Hückel limiting slope, Z_i is the charge of the ionic species, and A is the adjustable parameter experimentally determined from the solubilities of various $M_m(SO_4)_n$ at elevated temperatures.[19,20] In the test solution, the major equilibrium reactions are as follows:

$$HSO_4^- \rightleftarrows H^+ + SO_4^{2-} \quad (5)$$

$$K^+ + SO_4^{2-} \rightleftarrows KSO_4^- \quad (6)$$

The equilibrium constants of the above reactions, expressed in logarithmic form, and combined with Eq. 4 are thus related to the concentrations and ionic strength respectively:

$$\log K_2 = \log([H^+][SO_4^{2-}]/[HSO_4^-]) - 4S\sqrt{I}/(1 + A\sqrt{I}) \quad (7)$$

$$\log K_K = \log([KSO_4^-]/[K^+][SO_4^{2-}]) + 4S\sqrt{I}/(1 + A\sqrt{I}) \quad (8)$$

The total analytical concentrations of H^+, SO_4^{2-}, and K^+ are expressed as $[H^+]+[HSO_4^-]=m_1$ (9), $[SO_4^{2-}]+[HSO_4^-]+[KSO_4^-]=m_2$ (10), and $[K^+]+[KSO_4^-]=2m_2+m_3$ (11). From Eqs. 7—11 we obtain the calculated concentration of $[H^+]_{cal}$ by the Newton-Raphson method. Combining $[H^+]_{cal}$ with Eq. 1 produces the calculated values of the potential at each temperature. Then we employed a computer program to analyze the equilibrium constants of sulfate complexes, i.e., the pair of K_2 and K_K which best account for all the observed potential data. The values obtained in this work are listed and compared with the literature values in Table 1, while they are illustrated in Fig. 2. Except for 298 K, the standard deviation between E_{obsd} and E_{calcd} increased with the increase in the temperature as follows: 298 K ±1.2%; 323 K ±0.6%; 348 K ±0.5%; 373 K ±0.6%; 398 K ±0.8; 423 K ±1.6%; 448 K ±2.3%; 473K ±3.1%.

Assuming that ΔC_p° varied as a quadratic function of the temperature, the values of log K_2 and log K_K obtained as functions of temperature were fitted by the least-squares method to give a five-parameter equation:

Table 1. Values of log K_2 and log K_K as a Function of the Temperature

T/K	$-\log K_2$	$-\log K_2$[a]	$\log K_K$	$\log K_K$[b]
298	1.99	1.988	0.27	0.28
323	2.35	2.246	0.32	0.31
348	2.72	2.539	0.35	0.38
373	3.08	2.855	0.45	0.45
398	3.44	3.189	0.52	0.52
423	3.81	3.534	0.61	0.60
448	4.18	3.887	0.71	0.73
473	4.58	4.246	0.94	0.94

a) Marshall and Jones.[10] b) Calculated from Eq. 12.

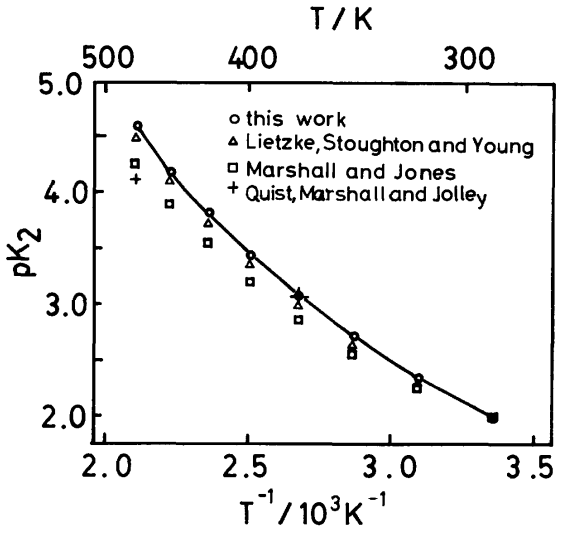

Fig. 2. pK_2 vs. T^{-1} for the second dissociation of sulfuric acid. Solid line is from Eq. 12.

$$\log K = a + b\log T + c/T + dT + eT^2 \quad (12)$$

where T is the absolute temperature. For log K_2, the parameters a, b, c, d, and e are:

a=577.214, b=−246.01, c=−12717, d=0.283133, e=−1.37566×10^{-4} and for log K_k their values are:

a=−3072, b=1310.68, c=68881, d=−1.56182, e= 7.1513×10^{-4}.

Usually, it is necessary to evaluate the A parameter as well as log K_2 to extrapolate the plots of log K_{app} vs. $\sqrt{I}/(1+A\sqrt{I})$ into an infinite dilution at each temperature. In the present study, however, the ionic strength in the test solution was fixed at 1 m in order that a liquid-junction potential should not exceed 1 mV. Thus, we used the literature value of the A parameter.[19,20] Nevertheless, the pK_2 values are substantially in agreement with the values determined by the solubility measurement at elevated temperatures[10] as well as with those reported by other investigators,[9-11] at 25 °C. In one earlier paper[10] the association of the calcium ion with sulfate was not assumed, but the existence of the $CaSO_4$ ion pair was pointed out later.[21] If the ion pair is present in the solution, it seems that the pK_2 values become higher,

Table 2. Thermodynamic Values for the $HSO_4^- \rightleftharpoons H^+ + SO_4^{2-}$ Reaction

T	$\Delta G°$	$\Delta H°$	$\Delta S°$	ΔC_p
K	kJ mol^{-1}	kJ mol^{-1}	J mol^{-1} K^{-1}	J mol^{-1} K^{-1}
298	11.4	−24.1	−119	−218
323	14.6	−29.2	−136	−192
348	18.1	−33.9	−149	−187
373	22.0	−38.7	−163	−200
398	26.3	−43.9	−176	−234
423	30.9	−50.6	−192	−287
448	35.9	−58.6	−211	−361
473	41.5	−68.6	−233	−452

as in the present work, than when without association.

The ion-pair association constant of KSO_4^- in the present study was somewhat lower than that determined by conductivity measurements.[22,23] There was some difficulty in obtaining a log K_K value for the present system. The log K values for the association of the univalent metal ion with the sulfate ion are considerably smaller than those of bi- and tervalent metal ions.[24] Thus, a weak complex of KSO_4^- results in a small contribution to the potential.

From the treatment of Eq. 12, the standard thermodynamic functions for changes in free energy ($\Delta G°$), enthalpy ($\Delta H°$), entropy ($\Delta S°$), and heat capacity ($\Delta C_p°$) were obtained for the temperature range from 25 to 200 °C. The values are given in Table 2. These values depend on the assumption of the dependency of $\Delta C_p°$ on the temperature. It is generally known that the standard heat capacities of ionic species in an aqueous solution show maximum values near 100 °C;[8] the $\Delta C_p°$ value in the present study indeed showed a maximum value at approximately 80 °C, in accordance with the maxima for $\Delta C_p°$ obtained for other ionization reactions.

The authors wish to thank Sumitomo Electric Industries, Ltd., for providing the porous PTFE membranes.

References

1) A. Okuwaki, O. Kanome, and T. Okabe, *Metal. Trans.*, **15B**, 609 (1984).
2) Y. Umetsu, K. Tozawa, and K. Sasaki, *J. Min. Met. Inst. Jpn.*, **89**, 1028 (1973).
3) H. Kubo, M. Kawahara, and Y. Shirane, *J. Min. Met. Inst. Jpn.*, **98**, 1257 (1982).
4) E. Matijević, M. Budnik, and L. Meites, *J. Colloid Interface Sci.*, **61**, 302 (1977).
5) C. M. Criss and J. W. Cobble, *J. Am. Chem. Soc.*, **86**, 5385 (1964).
6) C. M. Criss and J. W. Cobble, *J. Am. Chem. Soc.*, **86**, 5390 (1964).
7) J. W. Cobble, *J. Am. Chem. Soc.*, **86**, 5396 (1964).
8) H. C. Helgeson, "Chemistry and Geochemistry of Solutions at High Temperatures and Pressures" ed. by D. T. Rickard and F. E. Wickman, Pergamon Press, Oxford (1981), p. 133.
9) M. H. Lietzke, R. W. Stoughton, and T. F. Young, *J. Phys. Chem.*, **65**, 2247 (1961).
10) W. L. Marshall and E. V. Jones, *J. Phys. Chem.*, **70**, 4028 (1966).
11) A. A. Noyes, "The Electrical Conductivity of Aqueous Solutions", The Carnegie Institution of Washington, Washington, D. C. (1907).
12) A. S. Quist, W. L. Marshall, and H. R. Jolley, *J. Phys. Chem.*, **69**, 2726 (1965).
13) M. Le Peintre, C. Mahieu, and R. Fournie, Comm. energie at. (France), Rappt. No. 1951, 9pp (1961).
14) C. F. Baes, Jr., and R. E. Mesmer, "The Hydrolysis of Cations," Wiley, New York (1976).
15) D. D. MacDonald and D. Owen, "High Temperature High Pressure Electrochemistry in Aqueous Solution," NACE4 (1973), p. 513.
16) D. D. MacDonald, P. Butler, and D. Owen, *J. Phys. Chem.*, **77**, 2474 (1973).
17) C. F. Baes, Jr., and N. J. Meyer, *Inorg. Chem.*, **1**, 780 (1962).
18) A. S. Quist and W. L. Marshall, *J. Phys. Chem.*, **69**, 2984 (1965).
19) W. L. Marshall and R. Slusher, *J. Phys. Chem.*, **70**, 4015 (1966).
20) W. L. Marshall and R. Slusher, *J. Inorg. Nucl. Chem.*, **37**, 2171 (1975).
21) L. B. Yeatts and W. L. Marshall, *J. Phys. Chem.*, **73**, 81 (1969).
22) E. C. Righellato and C. W. Davies, *Trans. Faraday Soc.*, **26**, 592 (1930).
23) I. L. Jenkns and C. B. Monk, *J. Am. Chem. Soc.*, **72**, 2695 (1950).
24) R. M. Izatt, D. Eatough, J. J. Christensen, and C. H. Bartholomew, *J. Chem. Soc. A*, **1969**, 47.

Synthesis, and Crystal and Molecular Structure of Bis(benzylamine)bis-(thiocyanato)cadmium(II), $[Cd(SCN)_2(C_6H_5CH_2NH_2)_2]$, in Planar Polymeric Form: Allotrope of the Linear Polymeric Complex

Akira OUCHI* and Masahiro TANIGUCHI
Department of Chemistry, College of Arts and Sciences, The University of Tokyo, Komaba, Meguro-ku, Tokyo 153
(Received February 25, 1988)

Synopsis. The title complex (**1**), which is two-dimensional polymeric and an allotrope of the previously reported linear polymeric complex (**2**), was obtained and its crystal and molecular structure was determined by means of a single-crystal X-ray diffraction method. Since **1** is more soluble in organic solvents, **1** and **2** could be prepared, separately. The crystal of $CdC_{16}H_{18}N_4S_2$, F. W. 442.9, is monoclinic, space group $P2_1/c$, a=13.958(2), b=5.759(1), c=11.466(2) Å, β=99.24(1)°, U=909.8(3) Å^3, Z=2, D_m=1.61(3), D_x=1.62 g cm^{-3}, μ(Mo $K\alpha$)=14.2 cm^{-1}. The cadmium atom is in a trans-2*S*4*N*-hexa-coordinated octahedral geometry. Each cadmium atom is at the center of symmetry, and it is bridged to four cadmium atoms by an thiocyanate ion, respectively, and the complex network is extended on the bc-plane.

There have aleady been several structural reports concerning the one-, two-, and three-dimensional polymeric thiocyanato (SCN) complexes of metals.[1-4] In the case of thiocyanato complexes of cadmium, Cs[Cd(SCN)$_3$] has a three-dimensional,[5] Rb[Cd(SCN)$_3$] a two-dimensional,[5] and [(CH$_3$)$_4$N][Cd(SCN)$_3$] a one-dimensional network,[6] respectively. However, in the Lewis base adducts of cadmium(II) thiocyanates, they are in a double-SCN-ion-bridging one-dimensional polymeric form,[7-10] like cobalt thiocyanate.[4]

Recently, we found that other types of crystals were mixed in the sample of the benzylamine adduct of cadmium(II) thiocyanate, previously reported,[10] which gave the same chemical analysis and almost the same infrared spectrum, though they were found to have a different unit-cell.

Therefore, we investigated how to separated the previously reported adduct **2** and this new compound **1**; moreover, the crystal and molecular structure of **1** was determined by a single-crystal X-ray diffraction method.

Experimental

Syntheses of Both Types of Bis(benzylamine)bis(thiocyanato)cadmium(II), (1,2). The product obtained by mixing cadmium thiocyanate and benzylamine in the stoichiometric ratio in methanolic medium was always a mixture of **1** and **2**. Although the crystals of **2** were almost insoluble in methanol and ethanol after once precipitated, while the solubility of the crystals of **1** was also very low, the yield of **1** after recrystallization from methanol was poor. The process to obtain **1**, found empirically, is as follows.

Cadmium(II) thiocyanate (0.9 g, 4 mmol) and benzylamine (0.9 g, 8.4 mmol) were dissolved into 30 and 10 cm^3 of methanol–ethanol mixture (2:1=v/v), separately (the mixing of ethanol lowers the solubility of deposited **2**). They were warmed to about 80 °C and mixed. After the mixture was refluxed about 2 h, it was filtered off while hot in order to remove **2** (a part of **1** was also removed). The filtrate was slowly cooled to 6 °C, and deposited crystals of **1** were separated, washed with a little portion of the ethanol–methanol mixture, and dried in open air. Yield: 0.80 g, 1.8 mmol, 45%. Found: Cd, 25.30; C, 42.99; H, 4.00; N, 12.55%. Calcd for ($CdC_{16}H_{18}N_4S_2$) Cd, 25.38; C, 43.39; H, 4.10; N, 12.65%.

On the other hand, the precipitated crystals were almost pure **2**, when being added benzylamine a little less than the calculated quantity, using methanol–water mixture as the solvent (98:2=v/v) to increase the solubility of **1**, and being left standing the mixed solution overnight at room temperature. Yield: 0.48 g, 1.1 mmol (59%) from 2 mmol of Cd(SCN)$_2$ and 3.7 mmol of benzylamine in 40 cm^3 of the solvent.

Although both crystals of **1** and **2** appear commonly in a spatula-like plate form (as shown in Fig. 1**A**) relatively large crystals of **1** and **2** appear in the forms shown by Figs. 1**B** and 1**C**, respectively: this is the best simple method for distinguishing both types of the crystals. From an X-ray photographic study, the respective unit-cell axes of **1** and **2** are found to be in the directions shown in the figure captions.

Single Crystal X-Ray Structure Analysis. The crystal used for the structural analysis was colorless, and parallelepiped in shape (0.3×0.3×0.15 mm^3). The intensities in the range of $3<2\theta<67°$ (2θ) were collected on a Rigaku AFC-6A automated four-circle X-ray diffractometer using graphite monochromated Mo $K\alpha$ radiation (λ= 0.71073 Å) by means of ω–2θ scan technique (scan speed 4° min^{-1}; scan width 1.25+0.5 tanθ (°/θ)). The intensities were corrected for Lorentz and polarization factors, but not for absorption and extinction. Of 3891 independent intensities collected, 2457 reflections with $|F_o|>3\sigma(|F_o|)$ were used for the structure determination.

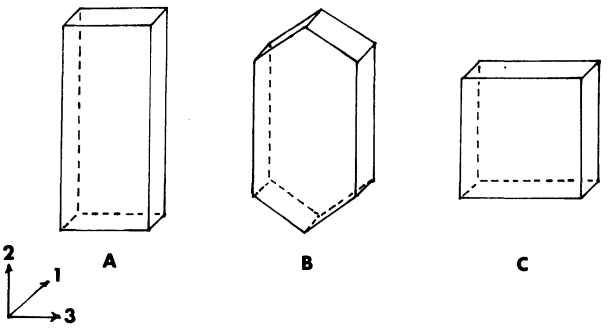

Fig. 1. The apparent features of the complexes **1** and **2** crystals. The directions of the unit-cell axes of **1** and **2** are as follows, respectively. **1**: 1, a; 2, b; 3, c. **2**: 1, a; 2, −c; 3, b.

All the calculations were carried out on a HITAC M-682H computer at the Computer Center of the University of Tokyo, using a local version of the UNICS program.[11] The scattering factors were taken from Ref. 12.

The structure was solved by the heavy-atom method (positional, and thermal parameters were refined by a block diagonal least-squares method). The final R value applying an anisotropic temperature factors was 0.057 (all the hydrogen atoms were not included into the structure factor calculations).

Results and Discussion

The selected bond lengths and bond angles are shown in Table 1. A perspective drawing of the complex including the four SCN ions bridging to the neighboring four metal atoms, together with the numbering scheme of the atoms, is shown in Fig. 2, and a packing diagram of a unit cell in Fig. 3.[13] Each cadmium atom is at the center of symmetry (0,0,0 and 0,0.5,0.5), and is bridged to four neighboring metal atoms with a SCN ion, respectively, and the two-dimensional network of the complex is expanded on the bc-plane. This type of the planar-polymeric structure is the first example found in a Lewis base adduct of cadmium(II) thiocyanates.

Table 1. Selected Bond Lengths and Bond Angles of the Complex **1**

Bond length	(l/Å)	Bond length	(l/Å)
Cd-S^{iii}	2.753(2)	Cd-N(1)	2.339(8)
Cd-N(2)	2.322(5)	S-C(1)	1.637(10)
N(1)-C(1)	1.157(13)	N(2)-C(2)	1.477(7)
Cd$\cdots$Cd^{ii}	6.416(1)		
Bond angle	**(ϕ/°)**	**Bond angle**	**(ϕ/°)**
N(1)-Cd-N(2)	86.8(2)	N(1)-Cd-S^{iii}	90.8(2)
N(2)-Cd-S^{iii}	89.20(14)	Cd-N(1)-C(1)	146.3(7)
Cd^{ii}-S-C(1)	98.39(16)	S-C(1)-N(1)	179.3(9)
Cd-N(2)-C(2)	117.0(4)	N(2)-C(2)-C(3)	113.9(6)

Key to the symmetry operations: ii, x, 0.5−y, 0.5+z; iii, −x, −0.5+y, 0.5−z.

As shown in Fig. 2, around a cadmium(II) atom, two SCN sulfur, two SCN nitrogen, and two benzylamine nitrogen atoms are coordinated, where each pair of the same kind of the ligating atoms are in a trans-configuration. The configuration of the complex, as well as the respective bond lengths around the metal atom (Cd-S(SCN), 2.753(2); Cd-N-(SCN), 2.339(8); Cd-N(benzylamine), 2.322(5) Å) are not much different from those of **2**. The Cd-N-C-(SCN) angle of **1**, 146.3(7)°, is much smaller than the other common thiocyanato complexes (160—180°), while the angles Cd-S-C (98.39(16)°) and S-C-N (179.3(4)°) are in the common range of the other

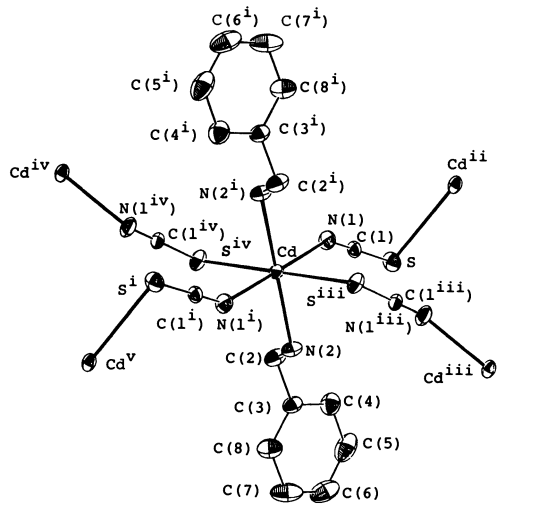

Fig. 2. The perspective drawing of the complex **1** around the central metal atom and thiocyanate ion bridgings: the numbering scheme of the atoms are shown in the figure. The key to the symmetry operations: i, −x, −y, −z; ii, x, 0.5−y, 0.5+z; iii, −x, −0.5+y, 0.5−z; iv, x, 0.5−y, −0.5+z; v, x, −0.5−y, −0.5+z.

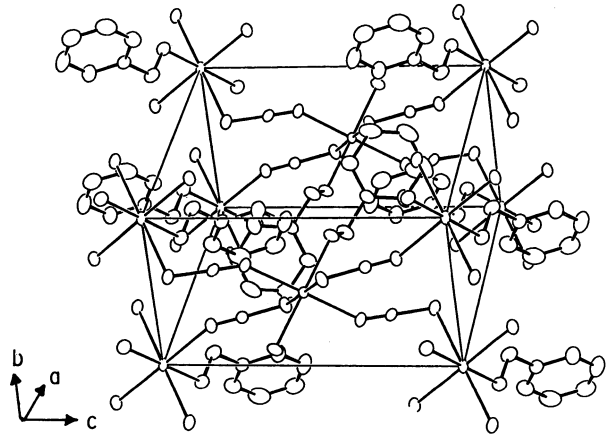

Fig. 3. Crystal packing diagram of the complex **1**.

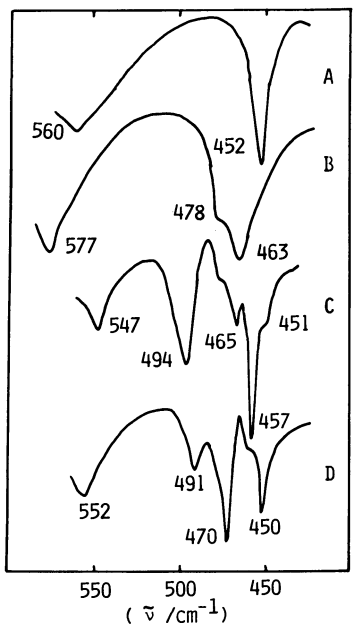

Fig. 4. Infrared absorption spectra of the complexes **1** and **2** near their δ(SCN) peak together with the spectra of some related compounds. (A) Benzylamine, (B) cadmium thiocyanate, (C) complexes **2**, (D) complexes **1**.

cadmium thiocyante complexes.[7-10] These data are the same for the cases of **2**. The inter-bridging-metal-atomic-distance of **1**, 6.416(1) Å, is much longer than that of **2**, 5.873(1) Å.

The infrared absorption spectra of **1** and **2** were found to be aproximately the same: ν(CN), 2080; ν(CS), 752(s), and 720(sh) cm^{-1}. However, as shown in Fig. 4, the features of the δ(SCN) bands of **1** and **2** are a little different from each other: the former peak is more clearly separated. This is another way to distinguish crystals of **1** and **2**.

References

1) J. W. Jeffery and K. M. Rose, *Acta Crystallogr., Sect. B*, **24**, 653 (1968).
2) H. Kinoshita and A. Ouchi, *Bull. Chem. Soc. Jpn.*, **59**, 3495 (1986).
3) N. K. Mills and A. H. White, *J. Chem. Soc., Dalton Trans.*, **1984**, 229.
4) F. H. Cano, S. Garcia-Blanco, and A. G. Laverat, *Acta Crystallogr., Sect. B*, **32**, 1526 (1976).
5) G. Thiele and D. Messer, *Z. Anorg. Allg. Chem.*, **464**, 255 (1980).
6) Y. Kuniyasu, Y. Sugita, M. Taniguchi, and A. Ouchi, *Bull. Chem. Soc. Jpn.*, **60**, 179 (1987).
7) M. Taniguchi, M. Shimoi, and A. Ouchi, *Bull. Chem. Soc. Jpn.*, **59**, 2299 (1986).
8) M. Taniguch, Y. Sugita, and A. Ouchi, *Bull. Chem. Soc. Jpn.*, **60**, 1321 (1987).
9) M. Taniguchi and A. Ouchi, *Bull. Chem. Soc. Jpn.*, **60**, 1192 (1987).
10) M. Taniguchi and A. Ouchi, *Bull. Chem. Soc. Jpn.*, **60**, 4172 (1987).
11) "Universal Crystallographic Computation Program System (UNICS)," ed by T. Sakurai, Crystallographic Society of Japan, Tokyo (1967).
12) "International Tables for X-Ray Crystallography," Kynoch Press, Birmingham, U. K. (1974), Vol. IV, pp. 72, 150.
13) The final atomic positional and thermal parameters, the final F_o-F_c table, and some additional bond length and bond angle data are deposited as Document No. 8821, at the Editor of the Office of Bull. Chem. Soc. Jpn.

The Synthesis and the Crystal and Molecular Structure of Tris(*N*-ethyl-2-pyrrolidone)tetrakis(thiocyanato)cobalt(II)mercury(II), $[CoHg(SCN)_4(C_6H_{11}NO)_3]$

Hisashi KINOSHITA* and Akira OUCHI†
Department of Chemistry, Faculty of Liberal Arts, Shizuoka University, Ohya, Shizuoka 422
†Department of Chemistry, College of Arts and Sciences, The University of Tokyo, Komaba, Meguro-ku, Tokyo 153
(Received March 1, 1988)

Synopsis. The title complex, which has a new-type layer structure, has been obtained, and its crystal and molecular structure has been determined by the X-ray diffraction technique. The crystallographic data are: monoclinic, space group $P2_1/n$, a=18.264(7), b=16.223(7), c=10.623(5) Å, β=92.77(5)° and Z=4. The final R value was 0.059. The cobalt atoms are in an octahedral geometry, ligated by three thiocyanato(SCN) nitrogen atoms and three oxygen atoms (*N*-methyl-2-pyrrolidone) in a meridional configuration; these cobalt atoms are cross-linked to adjacent mercury atoms by SCN ions, forming a characteristic layer structure which consists of twenty-four-membered rings of the $[Co_3Hg_3(SCN)_6]$ unit. The mercury atoms are in the tetrahedral geometry, ligated by four sulfur atoms of SCN ions, three bridging and one unidentate. The complex layers in parallel are piled up in the a-axis direction, and there are no bridgings or hydrogen bondings between them.

Previously, the present authors[1-3] have reported the crystal structures of some Lewis base adducts of tetrakis(thiocyanato)cobalt(II)mercury(II), $CoHg(SCN)_4$ (**1**), with the general formula of $CoHg(SCN)_4L_2$ (L= *N*-methyl-2-piperidone(mpp) (**2**)[1] or dimethyl sulfoxide(dmso) (**3**)[1]) and of $CoHg(SCN)_4(H_2O)_2\cdot 2L$ (L= *N*,*N*-dimethylacetamide(dma) (**4**)[2] or *N*-methyl-2-pyrrolidone(mpd) (**5**)[3]). These complexes were found to have two-dimensional planar networks consisting of sixteen-membered rings of the $Co_2Hg_2(SCN)_4$ unit. By continuing this line of research using *N*-ethyl-2-pyrrolidone(abbr.; epd) as the Lewis base, the title complex was obtained. From the preliminary test, its chemical composition ($CoHg(SCN)_4L_3$), its crystal system, and its unit cell size were found to be different from those of **2**—**5**. Therefore, we have investigated the crystal and molecular structure of this complex by means of the X-ray diffraction method.

Experimental

Synthesis of Tris(*N*-ethyl-2-pyrrolidone)tetrakis(thiocyanato)cobalt(II)mercury(II) (6). The crystalline powder of **1** (1.0 g, 2.0 mmol) was dissolved into epd (10 cm³), and 10 cm³ of tetrahydrofuran was added to the solution. The mixture was then left standing for several days; thereby red-purple crystals of **6** were deposited. They were filtered off and dried over silica gel. Yield: 0.6 g, 28%. Found: Co, 7.07; C, 31.68; H, 3.81; N, 11.82%. Calcd for $CoHgC_{22}H_{33}N_7O_3S_4$: Co, 7.09; C, 31.79; H, 4.00; N, 11.79%.

X-Ray Structure Analysis. A crystal of **6**, red-purple in color and in the shape of a parallelepiped (0.3×0.3×0.2 mm³), was used for the intensity measurement. Crystallographic data: $CoHgC_{22}H_{33}N_7O_3S_4$ $F.W.$=831.33, monoclinic, with the space group of $P2_1/n$, a=18.264(7), b=16.223(7), c=10.623(5) Å, β=92.77(5) ,U=3144.0(9) Å³, Z=4, D_m=1.75(3) g cm⁻³, D_x=1.76 g cm⁻³, μ(Mo $K\alpha$)=5.75 mm⁻¹. Reflections within the range of $3°<2\theta<60°$ were collected on a Rigaku AFC-6A automated four-circle X-ray diffractometer with graphite-monochromatd Mo $K\alpha$ radiation (λ=0.71073 Å): the $\omega-2\theta$ scan technique was employed (scan speed, 4° min⁻¹ (θ); scan width, 1.12+0.5 tan θ(θ/°)). Of the 3841 independent reflections measured, 3023 $|F_o|>3\sigma(|F_o|)$ reflections were used for the structure determination. The intensities were corrected for the Lorentz and polarization factors as well as for the absorption. The last correction was made using a numerical Gaussian integration.[4] The structure was solved by the heavy atom method. The positional and thermal parameters were refined by the block-diagonal least-squares method. Hydrogen atoms were not included in the structure factor calculation. The final R value obtained by applying the anisotropic temperature parameters was 0.059.[5]

All the calculations were carried out on a HITAC M-682H computer apparatus at the Computer Center of the University of Tokyo, using the local version of the UNICS program system.[6] The atomic scattering factors were taken from Ref. 7.

Results and Discussion

The selected bond lengths and bond angles, and also some interatomic distances, are shown in Table 1.[8] A perspective drawing of the complex around a cobalt atom is sown Fig. 1. The projection of the structure along the a axis is shown in Fig. 2.

Each mercury atom is coordinated tetrahedrally by four SCN sulfur atoms. The cobalt atom is six-coordinated and is in an octahedral geometry, where three SCN nitrogen atoms and three carbonyl-oxygen atoms of the *N*-ethyl-2-pyrrolidone molecule are ligated in a meridional configuration. Therefore, one of the four SCN ions, which are ligated to each mercury atom with their sulfur atom, has a free nitrogen terminal. The bond lengths of Co–O and Co–N (on the average, 2.080 and 2.131 Å respectively) are not very different from the respective sums of Shannon's ionic radii (Co–O: 2.00, and Co–N: 2.11 Å).[9] The Hg–S bond lengths (2.531 Å, on the average) are shorter than the sum of the Shannon ionic radii, 2.80 Å; especially, the bond length Hg–S(4) of the unidentate SCN ion, 2.455(7) Å, is a little shorter than the other three Hg–S bonds.

The bond angles, Co–N–C (160.5° on the average), deviate a little from 180°, while the N–C–S angles (177° on the average) are almost 180°. In this complex, three mercury(II), three cobalt(II), and six SCN ions make a twenty-four-membered ring unit which forms a two-dimensional polymeric network which is quite different from those of **2**, **3**, **4**, and **5**. In

Table 1. Selected Bond Lengths and Bond Angles, with Estimated Standard Deviations in Parentheses

Bond length	l/Å	Bond length	l/Å
Hg-S(1)	2.562(5)	Hg-S(2)	2.550(5)
Hg-S(3)	2.557(5)	Hg-S(4)	2.455(7)
Co-N(1)	2.137(16)	Co-N(2^{i})	2.125(12)
Co-N(3^{ii})	2.130(15)	Co-O(11)	2.064(10)
Co-O(21)	2.096(10)	Co-O(31)	2.081(10)
S(1)-C(1)	1.660(18)	C(1)-N(1)	1.12(2)
S(2)-C(2)	1.631(15)	C(2)-N(2)	1.146(19)
S(3)-C(3)	1.612(18)	C(3)-N(3)	1.15(2)
S(4)-C(4)	1.66(2)	C(4)-N(4)	1.14(3)
O(11)-C(11)	1.230(17)	O(21)-C(21)	1.25(2)
O(31)-C(31)	1.256(19)		
Bond angle	**ϕ/°**	**Bond angle**	**ϕ/°**
S(1)-Hg-S(2)	105.84(16)	S(1)-Hg-S(3)	104.49(15)
S(1)-Hg-S(4)	113.78(19)	S(2)-Hg-S(3)	102.04(15)
N(1)-Co-N(2^{i})	87.8(5)	N(1)-Co-N(3^{ii})	175.4(6)
N(1)-Co-O(11)	90.0(5)	N(1)-Co-O(21)	83.9(5)
N(1)-Co-O(31)	94.7(5)	O(11)-Co-O(21)	94.7(4)
O(11)-Co-O(31)	90.8(4)	O(21)-Co-O(31)	174.3(4)
Hg-S(1)-C(1)	95.7(6)	Hg-S(2)-C(2)	96.4(6)
Hg-S(3)-C(3)	98.3(6)	Hg-S(4)-C(4)	97.0(7)
Co-N(1)-C(1)	161.9(15)	Co-N(2^{i})-C(2^{i})	154.4(11)
Co-N(3^{ii})-C(3^{ii})	165.2(14)	S(1)-C(1)-N(1)	179.2(17)
S(2)-C(2)-N(2)	175.8(14)	S(3)-C(3)-N(3)	178.8(18)
S(4)-C(4)-N(4)	175.4(19)	Co-O(11)-C(11)	139.6(9)
Co-O(21)-C(21)	136.9(10)	Co-O(31)-C(31)	137.7(10)

a) Key to the symmetry operations: i, 1.5−x, 0.5+y, 0.5−z; ii, x, y, −1+z.

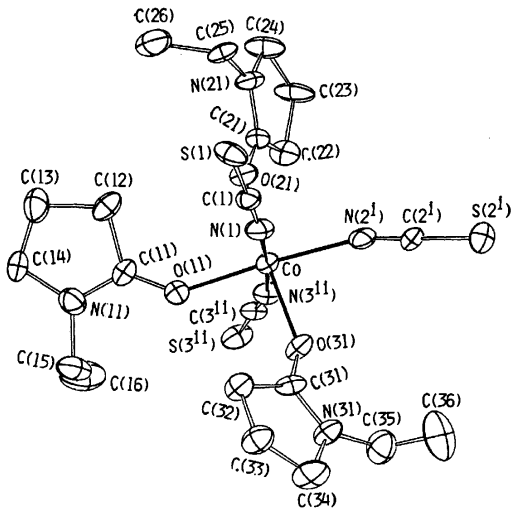

Fig. 1. The perspective drawing of the complex around a cobalt atom.

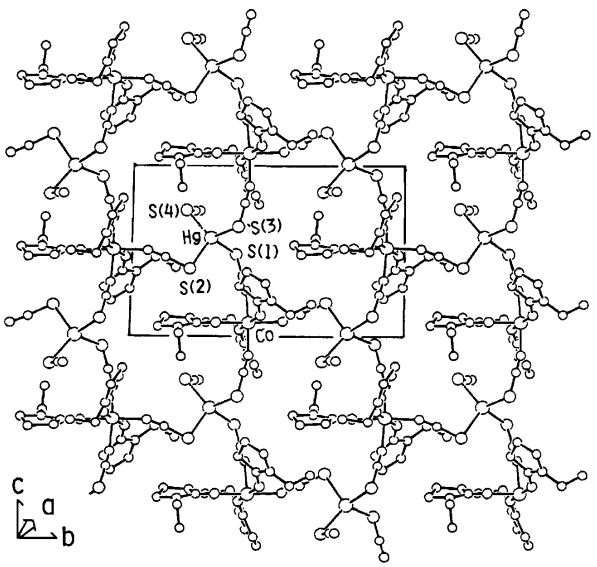

Fig. 2. The projection of the unit cell of the complex to the (100) plane.

the latter four complexes, the planar networks are composed of sixteen-membered ring units, including two mercury, two cobalt and four SCN^- ions.[1,2] Therefore, the present complex was found to have a new type of layer structure. In a unit cell there are two layers which spread out parallel to the (1 0 0) plane. The interlayer distance is 9.12 Å, which is much longer than those of **2** and **3**, where the distances are 8.21 and 6.85 Å respectively.[1] The ethyl group of epd may cause the steric hindrance, resulting in the bulky structure with the relatively small specific gravity of 1.76 g cm^{-3}; the specific gravities of **2**, **3**, **4**, and **5** are 2.03, 2.22, 1.99, and 2.04 g cm^{-3} respectively.

Regarding the metal atoms only, this complex layer has an obvious structural feature; it is of the so-called "graphite" type, consisting of the six-membered ring

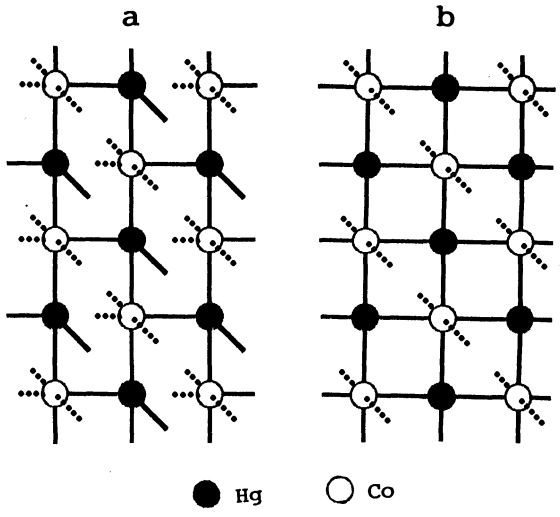

Fig. 3. The schematic presentation of the projection of the metal atomic arrangements of the complexes. a. $CoHg(SCN)_4(epd)_3$ projected to (100) plane. b. $CoHg(SCN)_4L_2$-type[1] or $CoHg(SCN)_4(H_2O)_2$·L-type[2,3] complexes projected to an appropriate plane. Each solid line indicates the thiocyanate ion. The dotted lines indicate the Lewis base (or water) molecules.

unit shown in Fig. 3(a), which is deduced from the "diamond" type structure of $CoHg(SCN)_4$, the starting material. On the other hand, in all of the layer structures of **2—5**, the units of the positions of the metal atoms are the four-membered ring units of Co_2Hg_2, as is shown in Fig. 3(b).

References

1) H. Kinoshita and A. Ouchi, *Bull. Chem. Soc. Jpn.*, **61**, 1169 (1988).

2) H. Kinoshita, M. Shimoi, A. Ouchi, and S. Sato, *Bull. Chem. Soc. Jpn.*, **58**, 2782 (1985).

3) H. Kinoshita, M. Shimoi, and A. Ouchi, *Bull. Chem. Soc. Jpn.*, **59**, 1253 (1986).

4) W. R. Busing and H. A. Levy, *Acta Crystallogr.*, **10**, 180 (1957).

5) $R=\Sigma||F_o|-|F_c||/\Sigma|F_o|$

6) "The Universal Crystallographic Computation Program-System (UNICS)," ed by T. Sakurai, Crystallographic Society of Japan, Tokyo (1967).

7) "International Tables for X-ray Crystallography," Kynoch Press, Birmingham (1974), Vol. IV, pp. 72, 150.

8) The final atomic positional and thermal parameters, and the final F_o-F_c table are deposited as Document No. 8824 at the Office of the Editor of Bull. Chem. Soc. Jpn.

9) R. D. Shannon, *Acta Crystallorgr., Sect. A*, **32**, 751 (1976). Shannon's Ionic Radii: Hg(Val=2+, CN=4) 0.96, Co(Val=2+, CN=6) 0.65, O(Val=2−, CN=2) 1.35, N(Val=3−, CN=4) 1.46, S(Val=2−, CN=6) 1.84 Å.

Dinuclear Cobalt(II), Iron(II), and Manganese(II), and Trinuclear Manganese(II) Complexes with Tridentate Ligands of NNS-Donor Set Derived from 2-Aminoethanethiol

Makoto HANDA, Hisashi ŌKAWA,* and Sigeo KIDA
Department of Chemistry, Faculty of Science, Kyushu University,
Hakozaki, Higashiku, Fukuoka 812
(Received April 16, 1988)

Synopsis. Thiolate-bridged dinuclear cobalt(II), iron(II), and Manganese(II) complexes and trinuclear manganese(II) complexes of thiolic ligands, 2-[(2-aminoethyl)amino]ethanethiol, 2-[(3-aminopropyl)amino]ethanethiol, 2-[(2-pyridylmethyl)amino]ethanethiol, and 2-[[(2-pyridylethyl]amino]ethanethiol, were prepared and their magnetic properties were examined in the temperature range 80—300 K. The results indicated a significant antiferromagnetic spin-exchange interactions through the bridging sulfur atom for all the complexes.

Sulfur-bridged polynuclear metal complexes are of interest in view of magnetic spin-exchange interaction through the sulfur bridge. Some thiolate-bridged polynuclear metal complexes have been synthesized.[1] However, magnetic investigations on thiolate-bridged polynuclear metal complexes are still limited. In this study we have obtained two types of thiolate-bridged complexes of cobalt(II), iron(II), and manganese(II) ions using tridentate thiolic ligands with an NNS-donor set, 2-[(2-aminoethyl)amino]ethanethiol (HL^1), 2-[(3-aminopropyl)amino]ethanethiol (HL^2), 2-[(2-pyridylmethyl)amino]ethanethiol (HL^3), and 2-[[(2-pyridyl)ethyl]amino]ethanethiol (HL^4). This paper reports the magnetic study of dinuclear complexes $[M_2(L)_2X_2]$ ($M=Co^{2+}$, Fe^{2+}, Mn^{2+}; X=Cl, NO_3) and trinuclear complexes $[Mn_3(L)_4]X_2$ ($X=ClO_4$, NO_3).

Experimental

Preparations. The thiolic ligands were obtained by the methods described previously.[2]

$[M_2(L)_2X_2]$ (M=Co, Fe, Mn; $L=L^1$—L^4; X=Cl, NO_3). A methanolic solution of equimolar amounts of a metal salt and a ligand was stirred overnight at room temperature under nitrogen atmosphere. Microcrystals separated were collected by filter suction, washed with methanol, and dried in vacuo. The cobalt, iron, and manganese complexes are violet, yellow, and colorless, respectively.

$[Mn_3(L)_4]X_2$ ($L=L^1$, L^2; $X=ClO_4$, NO_3). The complexes were obtained as almost colorless microcrystals in nearly the same way as described above, except for the use of an excess of a ligand (about 1.5 times).

Elemental analyses of the complexes are given in Table 1.

Measurements. IR spectra were recorded on a JASCO IR-800 spectrometer on KBr disks or Nujol mulls. Electronic spectra were recorded on powder samples by the use of a Simadzu MPS-5000 spectrometer. Magnetic susceptibilities were determined by the Faraday method over the temperature range 80—300 K.

Results and Discussion

$[M_2(L)_2X_2]$. The complexes have the stoichiometry of M:L:X=1:1:1 and are presumed to be dinuclear bridged by the thiolate group, because such a dimeric structure has been shown for the nickel(II) complexes with HL^4 [3] and 3-[[(2-pyridyl)ethyl]amino]-propanethiol (HL′)[4] by single-crystal X-ray analysis. Further, similar alkoxo-bridged dinuclear structures are known for the copper(II) complexes of tridentate alcoholic ligands.[5]

In the case of $[Co_2(L^4)_2(NO_3)_2]$ the unidentate coordination of the nitrate ion to the metal was evidenced by the split NO_3^- vibrations (1460, 1380, 1290, and 1030 cm^{-1}).[6] Further, the diffuse reflectance

Table 1. Elemental Analyses of the Complexes

Complex	Found(%)			Calcd(%)		
	C	H	N	C	H	N
$[Co_2(L^3)_2Cl_2]$	36.31	4.13	10.54	36.73	4.24	10.71
$[Co_2(L^4)_2Cl_2]\frac{1}{2}H_2O$	38.48	4.80	9.74	38.58	4.86	10.00
$[Fe_2(L^1)_2Cl_2]$	23.20	5.56	13.23	22.82	5.56	13.31
$[Fe_2(L^3)_2Cl_2]$	36.96	4.32	10.72	37.16	4.29	10.83
$[Fe_2(L^4)_2Cl_2]\frac{1}{2}H_2O$	39.16	4.92	9.86	39.01	4.91	10.11
$[Mn_2(L^1)_2Cl_2]$	23.07	5.36	13.15	22.92	5.29	13.37
$[Mn_2(L^2)_2Cl_2]$	26.50	5.81	12.23	26.85	5.86	12.53
$[Mn_2(L^3)_2Cl_2]$	37.25	4.33	10.71	37.30	4.30	10.87
$[Mn_2(L^4)_2Cl_2]\frac{1}{2}H_2O$	39.16	5.00	10.10	39.14	4.93	10.14
$[Mn_2(L^4)_2(NO_3)_2]$	36.21	4.53	13.89	36.25	4.39	14.09
$[Mn_3(L^1)_4](ClO_4)_2$	22.72	5.26	13.25	22.86	5.28	13.33
$[Mn_3(L^2)_4](ClO_4)_2$	26.48	5.84	12.46	26.79	5.85	12.50
$[Mn_3(L^2)_4](NO_3)_2$	28.90	6.41	16.66	29.38	6.38	17.05

spectra of the cobalt(II) complexes showed three d–d bands in the region 10000—20000 cm^{-1} (e.g., $[Co_2(L^4)_2Cl_2]$: 13000, 15800, and 18200 cm^{-1}), indicating a pentacoordination around the metal.[7] The manganese(II) complexes showed no spin-allowed d–d transition and any reliable spectra could not be obtained for the iron(II) complexes because of their sensitivity toward dioxygen. However, we believe that in both the manganese(II) and iron(II) complexes the chloride ion coordinates to the metal ion to complete a penta-coordination around the metal.

The magnetic moment (per metal ion) of each complex is subnormal at room temperature for high-spin metal ion (Table 2), and the cryomagnetic susceptibility determined in the range 80—300 K did not obey the Curie-Weiss law below 150 K. This is probably due to an intramolecular antiferromagnetic spin-exchange interaction. Typical examples of the temperature-variation of magnetic susceptibility are given in Figs. 1 and 2.

The χ_A vs. T curve of $[Co_2(L^3)_2Cl_2]$ shows a maximum at 160 K. Based on the isotropic exchange Hamiltonian (Heisenberg model) for a dimer ($\mathscr{H} = -2J\hat{S}_1 \cdot \hat{S}_2$), the maganetic susceptibility for the (S_1=3/2)–(S_2=3/2) dimer is given by the equation,[8]

$$\chi_A = (Ng^2\beta^2/kT)[14 + 5\exp(-6J/kT) + \exp(-10J/kT)]/[7 + 3\exp(-10J/kT) + \exp(-12J/kT)] + N\alpha \quad (1)$$

In this equation J is the exchange integral, N the Avogadro number, g the Lande g-factor, β the Bohr magneton, T absolute temperature, and $N\alpha$ the temperature-independent paramagnetism. As is seen

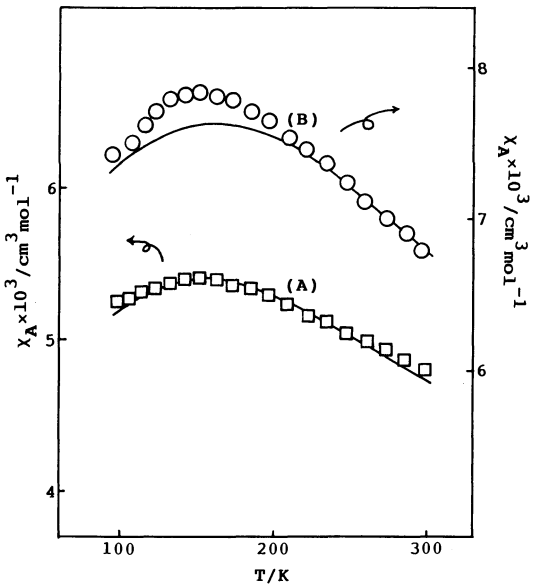

Fig. 1. Temperature variations of magnetic susceptibility of (A) $[Co_2(L^4)_2Cl_2]$ and (B) $[Fe_2(L^4)_2Cl_2]$. The solid curves are drawn based on the susceptibility equations based on the Heisenberg model (J=−35.1 cm^{-1}, g=2.20, $N\alpha$=220×10^{-6} cm^3mol^{-1} for (A) and J=−25.0 cm^{-1}, g=2.20, $N\alpha$=0 for (B)). The discrepancy in the case (B) is presumed to be due to an orbital contribution to the susceptibility.

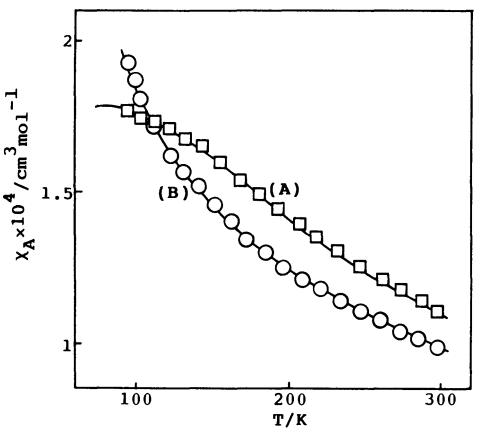

Fig. 2. Temperature variations of magnetic susceptibility of (A) $[Mn_2(L^4)_2Cl]$ and (B) $[Mn_3(L^2)_4](NO_3)_2$. The solid curves are drawn in terms of the Heisenberg model (Eqs. 2 and 3, respectively) using the magnetic parameters given in Table 2.

Table 2. Magnetic Data of the Complexes

Complex	g	J/cm^{-1}	$N\alpha$×10^6/cm^3 mol^{-1}	$\mu_{eff}/\mu_B(T/K)$
$[Co_2(L^3)_2Cl_2]$	2.20	−36.5	200	3.33(297.8)
$[Co_2(L^4)_2Cl_2]\frac{1}{2}H_2O$	2.20	−35.1	220	3.39(297.8)
$[Fe_2(L^1)_2Cl_2]$	—	—	—	3.58(299.0)
$[Fe_2(L^3)_2Cl_2]$	—	—	—	4.02(297.8)
$[Fe_2(L^4)_2Cl_2]\frac{1}{2}H_2O$	—	—	—	4.02(297.8)
$[Mn_2(L^1)_2Cl_2]$	2.00	−11.8	0	4.88(297.8)
$[Mn_2(L^2)_2Cl_2]$	2.00	−9.8	0	5.01(297.8)
$[Mn_2(L^3)_2Cl_2]$	2.00	−10.4	0	4.94(297.8)
$[Mn_2(L^4)_2Cl_2]\frac{1}{2}H_2O$	2.00	−9.0	0	5.14(297.8)
$[Mn_2(L^4)_2(NO_3)_2]$	2.00	−8.5	0	5.21(297.8)
$[Mn_3(L^1)_4](ClO_4)_2$	2.06	−14.7	0	4.71(297.8)
$[Mn_3(L^2)_4](ClO_4)_2$	2.05	−8.9	0	5.16(295.4)
$[Mn_3(L^2)_4](NO_3)_2$	2.03	−11.1	0	4.85(297.8)

in Fig. 1(A), the cryomagnetic behavior of this complex can be well simulated with the Eq. 1 using magnetic parameters given in Table 2, clearly demonstrating the dinuclear structure of this complex. Similarly, the magnetism of $[Co_2(L^4)_2Cl_2]$ obeyed the Eq. 1 in the temperature range 80—300 K.

The χ_A vs. T curves for the manganese(II) complexes show no maximum in the range 80—300 K but show an apparent decrease at lower temperature (Fig. 2(A)). The magnetic susceptibility for the $(S_1=5/2)$-$(S_2=5/2)$ system based on the Heisenberg model is given by the equation,[9]

$$\chi_A = (Ng^2\beta^2/kT)[55 + 30\exp(-10J/kT) + 14\exp(-18J/kT) + 5\exp(-24J/kT) + \exp(-28J/kT)]/[11 + 9\exp(-10J/kT) + 7\exp(-18J/kT) + 5\exp(-24J/kT) + 3\exp(-28J/kT) + \exp(-30J/kT)] + N\alpha, \quad (2)$$

where each simbol has the same meaning as in the Eq. 1. The magnetism of the manganese(II) complexes can be well explained with this equation, as exemplified in Fig. 2(A), using reasonable magnetic parameters given in Table 2. Thus, cryomagnetic investigations add a support for the dinuclear structure of the manganese(II) complexes.

Each χ_A vs. T curve of the iron(II) complexes shows a maximum near 120 K as seen in Fig. 1(B). Such a cryomagnetic behavior seemed to be characteristic of dimeric iron(II), but the exact magnetic simulation with the susceptibility equation for the $(S_1=2)$-$(S_2=2)$ system based on the Heisenberg model could not be attained as shown in Fig. 1(B). We believe that the complexes are indeed dinuclear but the magnetic simulation in terms of the Heisenberg model is not valid because of a significant orbital contribution, as suggested for related dinuclear iron(II) complexes.[10]

$[Mn_3(L)_4]X_2$. This type of complexes was obtained only with manganese(II) ions. The magnetic moment (per metal ion) of those complexes is also subnormal for high-spin manganese(II) ion and decreased with lowering of temperature. The most plausible structure for those complexes is trinuclear where each terminal metal is sixcoordinated with the two ligands, and the central metal is tetrahedrally coordinated with bridging thiolate sulfurs. Such a linear, trinuclear structure is known for nickel(II) complexes of amino thiolic ligands.[11] The evidence supporting this structure has been obtained by cryomagnetic investigations. The magnetic susceptibility equations for the $(S_1=5/2)$-$(S_2=5/2)$-$(S_3=5/2)$ system was derived Kambe's method[12] on assuming $J_{12}=J_{23}=J$ and $J_{13}=0$ and is expressed as follows:

$$\chi_A = (Ng^2\beta^2/36kT)[A/B] + N\alpha \quad (4)$$

where A=2040exp(55J/kT)+1365exp(50J/kT)+858exp(45J/kT)+1860exp(40J/kT)+858exp(37J/kT)+252exp(35J/kT)+495exp(34J/kT)+252exp(31J/kT)+105exp(30J/kT)+105exp(28J/kT)+858exp(27J/kT)+495exp(26J/kT)+252exp(25J/kT)+105exp(24J/kT)+30exp(23J/kT)+30exp(19J/kT)+105exp(18J/kT)+252exp(17J/kT)+498exp(16J/kT)+30exp(13J/kT)+108exp(10J/kT)+252exp(7J/kT)+30exp(5J/kT)+105

and B=8exp(55J/kT)+7exp(50J/kT)+6exp(45J/kT)+12exp(40J/kT)+6exp(37J/kT)+4exp(35J/kT)+5exp(34/kT)+4exp(31J/kT)+3exp(30J/kT)+3exp(28J/kT)+6exp(27J/kT)+5exp(26J/kT)+4exp(25J/kT)+3exp(24J/kT)+2exp(23J/kT)+2exp(19J/kT)+3exp(18J/kT)+4exp(17J/kT)+6exp(16J/kT)+2exp(13J/kT)+4exp(10J/kT)+4exp(7J/kT)+2exp(5J/kT)+3.

As shown in Fig. 2(B) good agreements were obtained between the experimental and theoretical magnetic susceptibilities. To our knowledge these are the first example of linear trinuclear manganese(II) complexes bridged by thiolate sulfurs.

In conclusion it was revealed that the thiolate bridge mediates a significant antiferromagnetic spin-exchange interaction between cobalt(II), iron(II), or manganese(II) ions.

References

1) e.g., J. R. Dorfman, C. P. Rao, and R. H. Holm, *Inorg. Chem.*, **24**, 453 (1985); J. P. Fackler, Jr., *Prog. Inorg. Chem.*, **21**, 55 (1976); I. Murase, S. Ueno, and S. Kida, *Bull. Chem. Soc. Jpn.*, **56**, 2748 (1983); S. L. Rose, R. E. Hoskin, J. E. Cavanaugh, C. J. Smith, and E. L. Blinn, *Inorg. Chim. Acta*, **40**, 7 (1980); K. D. Karlin and S. J. Lippard, *J. Am. Chem. Soc.*, **98**, 6951 (1976).

2) H. R. Snyder, J. M. Stewart, and J. B. Ziegler, *J. Am. Chem. Soc.*, **69**, 2672 (1947).

3) T. B. Vance, Jr., L. G. Warner, and K. Seff, *Inorg. Chem.*, **16**, 2106 (1977).

4) M. Handa, M. Mikuriya, Z. J. Zohng, H. Ōkawa, and S. Kida, submitted for publication.

5) M. Aihara, Y. Kubo, Y. Nishida, and S. Kida, *Bull. Chem. Soc. Jpn.*, **54**, 3207 (1981); M. Mikuriya, M. Nakamura, H. Ōkawa, and S. Kida, *Inorg. Chim. Acta*, **68**, 111 (1983); M. Mikuriya, M. Nakamura, H. Ōkawa, and S. Kida, *Inorg. Chim. Acta*, **70**, 223 (1983) and references therein.

6) N. F. Curtis and Y. M. Curtis, *Inorg. Chem.*, **4**, 804 (1965).

7) J. S. Wood, *Inorg. Chem.*, **7**, 852 (1968).

8) J. A. Andrew, P. W. Ball, and A. B. Blake, *J. Chem. Soc., Chem. Commun.*, **1969**, 143.

9) A. Earnshaw, E. A. King, and L. F. Larkworthy, *J. Chem. Soc. A*, **1968**, 1048.

10) A. P. Ginsberg, M. E. Lines, K. D. Karlin, S. J. Lippard, and F. J. DiSalvo, *J. Am. Chem. Soc.*, **98**, 6958 (1976).

11) D. H. Busch, D. C. Jicha, M. C. Thompson, J. W. Wrathall, and E. Blinn, *J. Am. Chem. Soc.*, **86**, 3642 (1964); C. H. Wei and L. F. Dahl, *Inorg. Chem.*, **9**, 1878 (1970); H. Barrera, J. Suades, M. C. Perucaud, and J. L. Brianso, *Polyhedron*, **3**, 839 (1984).

12) K. Kambe, *J. Phys. Soc. Jpn.*, **5**, 48 (1950).

A Short Step Synthesis of 3-Deoxy-D-*manno*-2-octulosonic Acid (KDO)

Hiroshi ITOH,* Tuyoshi KANEKO, Kazuhiro TANAMI, and Kazue YODA
The Noguchi Institute, 1-8-1 Kaga, Itabashi-ku, Tokyo 173
(Received October 16, 1987)

Synopsis. 3-Deoxy-D-*manno*-2-octulosonic acid (KDO) 1,4-lactone was synthesized from *aldehydo*-D-mannose derivatives by Horner–Emmons reaction in two steps.

3-Deoxy-D-*manno*-2-octulosonic acid (2-keto-3-deoxy-octonic acid; KDO) is an integral component of the lipopolysaccharides (LPS) of gram-negative bacteria and connects the lipophilic part of LPS, lipid A, to the core region of polysaccharide through its ketosidic bonds.[1]

Following an identification of the important and unique function of KDO and a determination of its structure, several partial syntheses from simpler sugars could be accomplished. The published methods regarding the synthesis of KDO involve a Wittig reaction of D-mannose derivatives[2] or a reaction of D-arabinose derivatives with di-*t*-butyl oxalacetate.[3] However, these methods required either many steps for the completion of the structure of KDO or a separation of KDO and its isomers.

We now wish to describe a synthesis of KDO involving fewer steps by a Horner–Emmons reaction. The condensation of Horne's phosphonate **1**[4] with aldehydes afforded a carboxymethyl enol ether derivative **2**. We attempted to convert this enol ethers **2** into a keto carboxymethyl derivative **3**, which corresponds to the C-1—C-3 part of KDO.

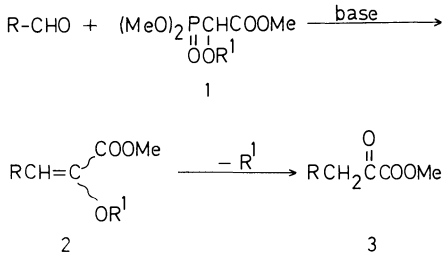

Reactions of acetylated or benzylated *aldehydo*-D-mannose derivatives **4** with **1** using lithium bis(trimethylsilyl)amide as a base in tetrahydrofuran (THF) afforded the expected methyl 3-deoxy-D-*manno*-oct-2-enoate derivatives **5** in reasonable yields; the results are summarized in Table 1. In most cases, the *E*-isomers were formed, predominantly, as judged from the ^{1}H NMR spectra.[6]

In contrast, the reaction of 3,4:5,6-di-*O*-isopropylidene-*aldehydo*-D-mannose, which was not purified after a dethioacetal reaction, with **1** (R^1=–$SiMe_2CMe_3$) did not afford the corresponding **5**, resulting in a complex mixture. 2-*O*-Acetyl-3,4:5,6-di-*O*-isopropylidene-*aldehydo*-D-mannose afforded **5**, though in low yield (25%). When butyllithium or DBU–$LiClO_4$[5] was used as a base, **5** was also obtained, but the yield was lower.

The deprotection step from **5** to KDO 1,4-lactone (**6**) was first investigated by using methyl 4,5,6,7,8-penta-*O*-acetyl-2-*O*-(*t*-butyldimethylsilyl)-3-deoxy-D-*manno*-oct-2-enoate (**5a**). When **5a** was treated with tetrabutylammonium fluoride, the solution immediately became dark brown, indicating a complex mixture. A treatment of **5a** with sodium methoxide in methanol and a subsequent addition of a cation-exchange resin afforded the expected **6**, though in low yield.

Table 1. Yields of 3-Deoxy-D-*manno*-oct-2-enoate Derivatives (**5**)

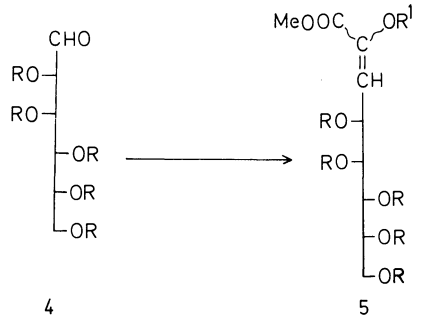

R	R^1	5 (%)
-Ac	$-SiMe_2Bu^t$	68 (**5a**)
	-Ac	29 (**5b**)
	$-COOCMe_2CCl_3$	56 (**5c**)
-Bn	$-SiMe_2Bu^t$	70 (**5d**)
	$-COOCMe_2CCl_3$	56 (**5e**)
	-Bn	77 (**5f**)

Bn=benzyl.

To improve the yield of **6**, other alkoxides or other methods[7] were investigated. The results are summarized in Table 2. Among these results, the best yield (45%) was obtained with sodium ethoxide in ethanol at −20 °C. The product **6** was readily separated from the reaction mixture by crystallization.

Conversions of other enoates **5b—f** to **6** were also examined, but proved to be unsatisfactory. A trace amount of **6** was obtained from **5c** upon a similar treatment with alkoxide, but not at all from **5b**. Attempts to convert **5d—f** into **6**, involving various methods reported for the removal of benzyl protecting groups (i.e., catalytic hydrogenolysis,[8] reductive cleavage with sodium in ethanol,[9] iodotrimethylsilane,[10] or ethanethiol–boron trifluoride etherate[11]) failed, always resulting in the formation of complex mixtures. When **5d** was first treated with tetrabutylammonium fluoride, the desired 4,5,6,7,8-penta-*O*-benzyl-3-deoxy-D-*manno*-octulosonic acid (66%) was obtained. However, it could not be converted into **6** by catalytic hydrogenolysis, a complex mixture being formed.

One method already described in the literature was used to give an ammonium salt of KDO from **6**[3]

Table 2. Conversion of **5a** into **6**

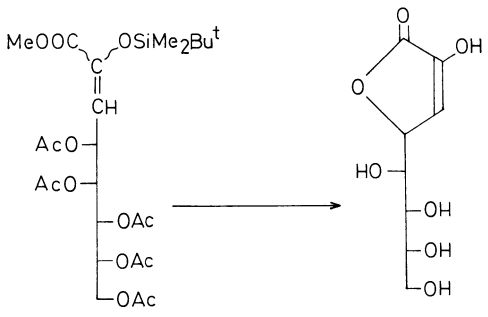

5a 6

Reagent	Temp	Time/h	Yield/%
KCN-MeOH	RT	5	7
K_2CO_3-MeOH	RT	5	0
MeONa-MeOH (2equiv, 0.03 M)	RT	5.5	28
MeONa-MeOH (0.2equiv, 0.003 M)	RT	5.5	0
MeONa-MeOH (10equiv, 0.15 M)	RT	5.5	0
MeONa-MeOH (2equiv, 0.03 M)	−20 °C	20	37
MeONa-MeOH (2equiv, 0.03 M)	−36 °C	40	26
MeONa-MeOH (0.2equiv, 0.03 M)	−20 °C	20	0
EtONa-EtOH (2equiv, 0.03 M)	−20 °C	20	45
PrONa-PrOH (2equiv, 0.03 M)	−20 °C	20	29

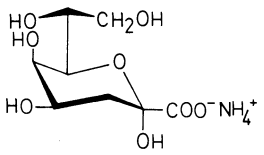

ammonium salt of KDO

Experimental

General Procedure. Melting points are uncorrected. NMR spectra were recorded in the solvents noted (Me_4Si, 0.00 ppm) with a JEOL FX 90A spectrometer. Column chromatography was performed by flash chromatography with silica gel. Specific rotations were measured with a JASCO DIP-360 polarimeter. IR spectra were recorded with a JASCO A-102 spectrometer.

2,3,4,5,6-Penta-*O*-acetyl-*aldehydo*-D-mannose. This compound was prepared as described by Miljikovic's method[12] from 2,3,4,5,6-penta-*O*-acetyl-*aldehydo*-D-mannose diethyl dithioacetal. The product was purified by column chromatography (ethyl acetate: hexane 1:5) as oil (it gradually crystallized). This compound could not be stored after purification, since it decomposed rapidly while in storage. ^1H NMR ($CDCl_3$) δ=2.00 (3H, s), 2.05 (3H, s), 2.10 (3H, s), 2.12 (3H, s), 2.17 (3H, s), 4.00—4.30 (2H, m), 4.90—5.25 (2H, m), 5.40—5.55 (2H, m), 9.42 (1H, d, J=1.0 Hz); IR (KBr) 1750, 1710 cm^{-1}.

Methyl α-(Dimethoxyphosphinyl)glycolate *t*-Butyldimethylsilyl Ether (1, R¹=*t*-butyldimethylsilyl). To a solution of methyl α-(dimethoxyphosphinyl)glycolate (0.198 g, 1.00 mmol) in DMF (1 ml) were added *t*-butyldimethylsilyl chloride (0.181 g, 1.20 mmol) and imidazole (0.082 g, 1.20 mmol) at room temperature. After stirring for 17 h at room temperature, the resulting mixture was extracted with diethyl ether; the product was purified by column chromatography (ethyl acetate: hexane 1:4) to give 0.255 g (82%) as oil; ^1H NMR ($CDCl_3$) δ=0.13 (6H, s), 0.93 (9H, s), 3.70 (3H, s), 3.77 (3H, s), 3.88 (3H, s), 4.58 (1H, d, J=18.0 Hz).

Methyl α-(Dimethoxyphosphinyl)glycolate Benzyl Ether (1, R¹=benzyl). To a solution of methyl α-(dimethoxyphosphinyl)glycolate (1.98 g, 10.0 mmol) in cyclohexane (60 ml) and dichloromethane (30 ml) were added benzyl trichloroacetimidate[13] (5.10 g, 20 mmol) and trifluoromethanesulfonic acid (0.44 ml, 5.0 mmol) at room temperature; the mixture was stirred for 23 h. The resulting mixture was extracted with dichloromethane and the product was purified by column chromatography (ethyl acetate:hexane 3:2) to give 2.73 g (95%) as oil; ^1H NMR ($CDCl_3$) δ=3.67 (3H, s), 3.73 (3H, s), 3.83 (3H, s), 4.37 (1H, d, J=18.4 Hz), 4.75 (1H, d, J=9.0 Hz), 4.83 (1H, d, J=9.0 Hz), 7.25 (5H, s).

Methyl 2-*O*-Acetyl-α-(dimethoxyphosphinyl)glycolate (1, R¹=acetyl). ^1H NMR ($CDCl_3$) δ=2.18 (3H, s), 3.73 (3H, s), 3.75 (3H, s), 3.92 (3H, s), 5.38 (1H, d, J=17.2 Hz).

Methyl 4,5,6,7,8-Penta-*O*-acetyl-2-*O*-(*t*-butyldimethylsilyl)-3-deoxy-D-*manno*-oct-2-enoate (5a). To a solution of methyl α-(dimethoxyphosphinyl)glycolate *t*-butyldimethylsilyl ether (0.225 g, 0.720 mmol) in THF (3 ml) was added 1 M lithium bis(trimethylsilyl)amide (1 M=1 mol dm^{-3}) in THF solution (0.660 ml) at −78 °C under an argon atmosphere. After 10 min, 2,3,4,5,6-penta-*O*-acetyl-*aldehydo*-D-mannose (0.234 g, 0.600 mmol) in THF (25 ml) solution was added dropwise over 20 min at −78 °C; the mixture was stirred for 2 h at −78 °C. The resulting mixture was extracted with diethyl ether and the products were separated by column chromatography (ethyl acetate:hexane 1:8). The faster moving compound was (*Z*)-**5a** (0.005 g, 1%) obtained as oil; ^1H NMR ($CDCl_3$) δ=0.20 (6H, s), 1.00 (9H, s), 1.99 (3H, s), 2.02 (3H, s), 2.04 (6H, s), 2.07 (3H, s), 3.72 (3H, s), 4.07—4.18 (1H, m), 5.00—5.22 (1H, m), 5.28—5.95 (5H, m); ^{13}C NMR ($CDCl_3$) δ=−4.2, 18.7, 20.4, 20.6, 20.7, 25.8, 52.3, 62.0, 65.5, 67.5, 68.1, 69.8, 114.1, 144.0, 169.4,

169.5, 169.8, 170.4. The slower moving compound was (*E*)-**5a** (0.231 g, 67%) obtained as colorless crystals; mp 56—59 °C. ^{1}H NMR ($CDCl_3$) δ=0.14 (6H, s), 0.92 (9H, s), 2.00 (3H, s), 2.04 (6H, s), 2.12 (3H, s), 2.16 (3H, s), 3.82 (3H, s), 4.06—4.21 (2H, m), 5.00—5.20 (1H, m), 5.28 (1H, d, J=9.8 Hz), 5.34 (1H, dd, J=2.1, 7.5 Hz), 5.50 (1H, dd, J=2.1, 9.0 Hz), 6.23 (1H, dd, J=7.5, 9.8 Hz); ^{13}C NMR ($CDCl_3$) δ=−5.0, 18.2, 20.6, 20.8, 20.9, 25.5, 52.0, 62.0, 67.7, 68.3, 69.9, 115.0, 145.6, 164.0, 169.4, 169.6, 169.7, 169.9, 170.5. IR (KBr) 1750, 1640, 1220 cm^{-1}; $[\alpha]_D^{28}$=31.2° (*c* 1.67, acetone); Found: C, 52.45, H, 7.11%. Calcd for $C_{25}H_{40}O_{13}Si$: C, 52.07, H. 6.99%. Other methyl 3-deoxy-D-*manno*-oct-2-enoate derivatives (**5**) were also obtained in a similar manner. ^{1}H NMR data of the main products are listed as follows.

Methyl 2,4,5,6,7,8-Hexa-*O*-acetyl-3-deoxy-D-*manno*-oct-2-enoate (5b); ^{1}H NMR ($CDCl_3$) δ=2.02 (12H, s), 2.08 (6H, s), 3.76 (3H, s), 3.73—4.18 (2H, m), 4.93—5.50 (1H, d, J=10.0 Hz), 6.22 (1H, dd, J=8.0, 10.0 Hz).

Methyl 4,5,6,7,8-Penta-*O*-acetyl-2-*O*-(2,2,2-trichloro-1,1-dimethylethoxycarbonyl)-3-deoxy-D-*manno*-oct-2-enoate (5c); ^{1}H NMR ($CDCl_3$) δ=2.02 (12H, s), 2.12 (3H, s), 3.82 (3H, s), 4.00—4.30 (2H, m), 5.00—5.60 (3H, m), 5.81 (1H, d, J=9.6 Hz), 6.23 (1H, dd, J=6.6, 9.6 Hz).

Methyl 4,5,6,7,8-Penta-*O*-benzyl-2-*O*-(*t*-butyldimethylsilyl)-3-deoxy-D-*manno*-oct-2-enoate (5d); ^{1}H NMR ($CDCl_3$) δ=0.13 (6H, s), 0.93 (9H, s), 3.58 (3H, s), 3.60—4.00 (5H, m), 4.20—4.70 (10H, m), 5.13 (1H, dd, J=2.4, 9.2 Hz), 5.58 (1H, d, J=9.2 Hz).

Methyl 4,5,6,7,8-Penta-*O*-benzyl-2-*O*-(2,2,2-trichloro-1,1-dimethylethoxycarbonyl)-3-deoxy-D-*manno*-oct-2-enoate (5e); ^{1}H NMR ($CDCl_3$) δ=3.66 (3H, s), 3.72—4.24 (5H, m), 4.40—4.82 (10H, m), 5.32 (1H, dd, J=5.0, 10.0 Hz), 6.15 (1H, d, J=10.0 Hz).

Methyl 4-*O*-Acetyl-2-*O*-(*t*-butyldimethylsilyl)-5,6:7,8-di-2-enoate (5f); ^{1}H NMR ($CDCl_3$) δ=3.68 (3H, s), 3.68—3.95 (5H, m), 4.25—4.78 (10H, m), 5.12 (1H, dd, J=2.5, 9.5 Hz), 5.32 (1H, d, J=9.5 Hz).

Methyl 4-*O*-acetyl-2-*O*-(*t*-butyldimethylsilyl)-5,6:7,8-di-*O*-isopropylidene-3-deoxy-D-*manno*-oct-2-enoate; ^{1}H NMR ($CDCl_3$) δ=0.17 (6H, s), 0.93 (9H, s), 1.35 (3H, s). 1.40 (9H, s), 2.03 (3H, s), 3.75 (3H, s), 3.75—4.33 (5H, m), 5.40 (1H, d, J=5.0 Hz), 6.22 (1H, dd, J=3.0, 5.0 Hz).

KDO 1,4-Lactone (6). To a solution of sodium ethoxide (0.106 g, 1.55 mmol) in ethanol (20 ml) was added **5a** (0.447 g, 0.775 mmol) in ethanol (32 ml) at −20 °C. This solution was stirred for 20 h at −20 °C. Then, Dowex 50 WX (H^+) was added at room temperature and the mixture stirred for 2.5 h. After filtration, the filtrate was evaporated under reduced pressure and ethanol–diethyl ether was added. Compound **6** was collected by filtration and dried to give 0.077 g (45%) of colorless crystals, mp 191—194 °C (lit,[3b] 192—194 °C). $[\alpha]_D^{28}$ +34.3° (*c* 1.4 water) (lit,[3b] $[\alpha]_D^{24}$ +31.8° (*c* 1.4, water).

References

1) F. M. Unger, *Adv. Carbohydr. Chem. Biochem.*, **38**, 323 (1981).

2) R. R. Schmidt and R. Betz, *Angew. Chem., Int. Ed. Eng.*, **23**, 430 (1984); P. M. Collins, W. G. Overend, and T. Shing, *J. Chem. Soc., Chem. Commun.*, **1981**, 1139; M. B. Perry and D. T. Williams, *Methods Carbohydr. Chem.*, **7**, 44 (1966).

3) N. K. Kochetkov, B. A. Dmitriev, and L. V. Backinowsky, *Carbohydr. Res.*, **5**, 399 (1967); C. Hershberger, M. Davis, and S. B. Binkley, *J. Biol. Chem.*, **243**, 1585 (1968).

4) D. Horne, J. Gaudino, and J. Thompson, *Tetrahedron Lett.*, **25**, 3529 (1984).

5) M. A. Blanchette, W. Choy, J. T. Davis, A. P. Escenteld, S. Masamune, W. R. Roush, and T. Sakai, *Tetrahedron Lett.*, **25**, 2183 (1984).

6) R. E. Ireland, R. H. Mueller, and A. K. Willard, *J. Am. Chem. Soc.*, **98**, 2868 (1976).

7) J. J. Plattner, R. D. Glass, and H. Rapoport, *J. Am. Chem. Soc.*, **94**, 8613 (1972); J. Harzig, *J. Org. Chem.*, **51**, 727 (1986).

8) C. H. Heathcock and R. Ratcliffe, *J. Am. Chem. Soc.*, **93**, 1746 (1971); G. M. Anantharamaiah and K. M. Sivanandaiah, *J. Chem. Soc., Parkin Trans. 1*, **1977**, 490.

9) C. M. McCloskey, *Adv. Carbohydr. Chem. Biochem.*, **12**, 137 (1957).

10) M. E. Jung and M. A. Lyster, *J. Org. Chem.*, **42**, 3761 (1977).

11) K. Fuji, K. Ichikawa, M. Node, and E. Fujita, *J. Org. Chem.*, **44**, 1661 (1979).

12) M. Miljkovic, D. Dropkin, P. Hagel, and M. Habash-Marino, *Carbohydr. Res.*, **128**, 11 (1984).

13) T. Iverser and D. R. Bundle, *J. Chem. Soc., Chem. Commun.*, **1981**, 1240.

Synthesis of Mixed Trialkyl Phosphates: Oxidative Phosphorylation of Alcohols with Dialkyl Phosphonates in the Presence of Copper(II) Chloride

Yoshiki OKAMOTO,* Tetuya KUSANO, and Setsuo TAKAMUKU
The Institute of Scientific and Industrial Research, Osaka University,
Ibaraki, Osaka 567
(Received January 13, 1988)

Synopsis. Mixed trialkyl phosphates were synthesized by oxidative phosphorylation of alcohols with dialkyl phosphonates and oxygen in the presence of copper(II) chloride in fairly good yields.

Various methods for the phosphorylation of alcohol have been reported.[1] The most frequently used method to prepare mixed trialkyl phosphate (**1**) involves the phosphorylation of alcohol with dialkyl phosphorochloridate (**2**), which is generally prepared by the chlorination of dialkyl phosphonate (**3**) with chlorine. Some modifications have been designed so as to avoid handling potentially hazardous chlorine gas. One is the reaction of alcohol with **3** in carbon tetrachloride and tertiary amine.[2] The other is an anodic phosphorylation of alcohol with **3** in the presence of lithium chloride.[3] In these reactions, **2** is presumed to be involved as an intermediate.

In the present paper, we report a more convenient procedure for preparation of **1** by the oxidation of **3** with oxygen by coupling with oxidation-reduction cycle of Cu(II) and Cu(I) chlorides in alcohol. This procedure possesses several advantages over the known methods: (1) handling potentially hazardous substances can be avoided, (2) water is the sole by-product, and (3) expensive reagents and special apparatus are unnecessary. Therefore, this method could be satisfactorily employed for the technical production of **1**. This procedure probably consists of three unit processes: (1) the chlorination of **3** with copper(II) chloride to give **2** and hydrogen chloride,[4] (2) the phosphorylation of alcohol with **2** to afford **1** and hydrogen chloride, and (3) the oxidation of hydrogen chloride and copper(I) chloride with oxygen to reproduce copper(II) chloride.[5] Consequently, in the presence of a catalytic amount of copper(II) chloride and by bubbling oxygen, alcohol is phosphorylated with **3** to give the corresponding **1**.

$$\underset{\mathbf{3}}{(RO)_2P(O)H} + 2CuCl_2 \longrightarrow \underset{\mathbf{2}}{(RO)_2P(O)Cl} + HCl + 2CuCl \quad (1)$$

$$\mathbf{2} + R'OH \longrightarrow \underset{\mathbf{1}}{(RO)_2P(O)OR'} + HCl \quad (2)$$

$$4CuCl + 4HCl + O_2 \longrightarrow 4CuCl_2 + 2H_2O \quad (3)$$

Table 1. Results of Oxidative Phosphorylation of Ethanol with **3b**[a]

EtOH/**3b**	$CuCl_2$[b]	Temp	Conv.[c]	Yield[c]
mole ratio	mol%	°C	%	%
1.2	10	5	84	19
1.2	10	17	86	44
1.2	10	50	98	97
1.2	10	70	95	34
3.0	10	50	98	95
10.0	10	50	98	78
1.2	2	50	33	32
1.2	3	50	90	88
1.2	5	50	98	97
1.2	7	50	98	82

a) Conditions; 10 ml of mixture EtOH/**3b** was charged in a reaction tube (ϕ=10 mm) and oxygen was bubbled through it at flow rate 30 ml min^{-1} for 5 h. b) Based on **3b** used. c) Conversion and yield based on **3b** were determined by GLC using biphenyl as an internal standard.

The results obtained on the reaction of ethanol with diethyl phosphonate (**3b**) under several conditions are shown in Table 1. At a lower temperature (5 °C), the yield of triethyl phosphate (**1b-Et**) was low, despite the large conversion of **3b**. The intermediate, diethyl phosphorochloridate (**2b**), remained almost unreacted. The yield of **1b-Et** increased remarkably upon raising the temperature, and reached a maximum at 50 °C. At a higher temperature (70 °C), the yield was again reduced due to the formation of tetraethyl pyrophosphate (**4**), which may have been formed by a reaction between **1b-Et** and **2b** (Eq. 4).

$$\underset{\mathbf{1b\text{-}Et}}{(EtO)_2P(O)OEt} + \underset{\mathbf{2b}}{(EtO)_2P(O)Cl} \longrightarrow (EtO)_2P(O)OP(O)(OEt)_2 + EtCl \quad (4)$$

It has been reported that Eq. 4 may be catalyzed with a small amount of copper.[6] Figure 1 shows the conversion of **3b** and the yield of **1b-Et** under optimum conditions as the function of the reaction time. The consumption of **3b** was completed within 5 h, and the yield of **1b-Et** became quantitative. Table 2 shows the obtained results regarding reactions of the other **3** with alcohols. With an increasing number of carbons of the alkyl group, the conversion of **3** decreased slightly; however, the yield of **1** decreased to

a great extent. This result suggests that an increase in the bulkiness of alkyl groups affected the phosphorylation rate of **2** (Eq. 2) more than the chlorination rate of **3** (Eq. 1). When isopropyl or *t*-butyl alcohol was used, the yield of **1** became reduced and **4** was yielded in substantial quantity. The phosphates (**1**) of these alcohols may particularly tend to dimerize while easily liberating the corresponding alkyl chlorides, according to the reaction similar to Eq. 4. The phosphorylation of phenol with **3b** gave only a 3% yield of diethyl phenyl phosphate. In this case, the reaction mixture became turbid and a white precipitate was observed. Since phenol is more acidic than aliphatic alcohol, this precipitate may be the copper salt of phenol. The formation of the salt impaired the catalytc activity of copper. However, diphenyl phosphonate (**3e**) reacted with ethyl alcohol to give a similar result as in the cases of dipropyl phosphonate (**3c**) or dibutyl phosphonate (**3d**). Reactions using other copper(II) salts, such as bromide, acetate, and sulfate, failed. This suggests that chloride is necessary in order to propagate the reaction. The reaction (Eq. 1) can be explained by using the following radical mechanism:

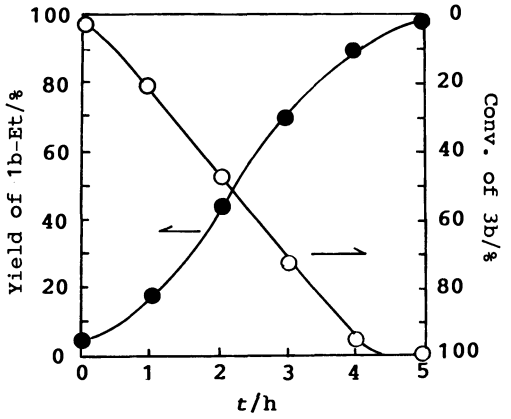

Fig. 1. Yield of **1b-Et** and conversion of **3b** as a function of reaction time.
Conditions: Ten ml of reaction mixture (EtOH/**3b** mole ratio=1.2 and $CuCl_2$ 10% based on **3b**) was bubbled with oxygen gas (flow rate 50 ml min^{-1}) at 50 °C. ●; Yield of **1b-Et**, ○; conversion of **3b**.

$$CuCl_2 \longrightarrow CuCl + Cl\cdot \quad (5)$$

$$Cl\cdot + \mathbf{3} \longrightarrow HCl + \cdot P(O)(OR)_2 \quad (6)$$

$$CuCl_2 + \cdot P(O)(OR)_2 \longrightarrow CuCl + \mathbf{2} \quad (7)$$

An electron transfer from the chloride to copper(II) occurs (Eq. 5), and the hydrogen atom of **3** is abstracted by the chlorine atom (Eq. 6). Since the oxidation potentials of the sulfate and acetate ions are higher than that of the chloride ion (oxidation of these ions are more difficult), consequently, the reactions using copper(II) sulfate and acetate did not occur. When copper(II) bromide is used, the resulting dialkyl phosphorobromidate (**5**) gives dialkyl hydrogenphosphate (**6**) and

$$\underset{\mathbf{5}}{(RO)_2P(O)Br} + ROH \longrightarrow \underset{\mathbf{6}}{(RO)_2P(O)OH} + RBr \quad (8)$$

alkyl bromide in place of **1** and hydrogen bromide (Eq. 8).

Upon the addition of triethylamine, the reaction was interrupted. Since hydrogen chloride may be consumed while binding the triethylamine, the progress of the reaction (Eq. 3) finally stopped. When acetonitrile was used as a solvent, **3** did not react, probably because of the extremely low solubility of

Table 2. Yields of Mixed Trialkyl Phosphates (**1**)[a]

Substrate		Conversion	Product	
$(RO)_2P(O)H$ (**3**) R	R'OH R'	%	$(RO)_2P(O)OR'$ (**1**)	Yield %[b]
Me (**3a**)	Et	99	$(MeO)_2P(O)OEt$	90
Me	*n*-Pr	99	$(MeO)_2P(O)OPr^n$	72
Me	*n*-Bu	98	$(MeO)_2P(O)OBu^n$	62
Et (**3b**)	Et	98	$(EtO)_2P(O)OEt$ (**1b-Et**)	95(87)
Et	*n*-Pr	99	$(EtO)_2P(O)OPr^n$ (**1b-Pr**)	85(78)
Et	*n*-Bu	86	$(EtO)_2P(O)OBu^n$ (**1b-Bu**)	73(69)
Et	*i*-Pr	83	$(EtO)_2P(O)OPr^i$	31[c]
Et	*t*-Bu	99	$(EtO)_2P(O)OBu^t$	25[d]
Et	Ph	5	$(EtO)_2P(O)OPh$	3
n-Pr (**3c**)	Et	92	$(Pr^nO)_2P(O)OEt$ (**1c-Et**)	65(52)
n-Bu (**3d**)	Et	95	$(Bu^nO)_2P(O)OEt$	63
Ph (**3e**)	Et	92	$(PhO)_2P(O)OEt$	61

a) Conditions: R'OH/**3** mole ratio; 1.3, $CuCl_2$; 10% based on **3**, oxygen flow rate; 30 ml min^{-1}, 50 °C, 5 h. b) Yields and conversion based on **3** were determined by GLC. Yields indicated in parentheses were for isolated product by distillation (**1b-Et**; bp 92—94 °C/12 mmHg, **1b-Bu**; bp 123—124 °C/15 mmHg, **1c-Et**; bp 110—112 °C/23 mmHg). In all cases, the phosphates were identified by comparison with authentic samples.[1] c) Tetraethyl pyrophosphate (**4**, 45%), which was assigned by comparison with an authentic sample[1] by means of GLC, yielded. d) The yield of **4** was 48%.

copper(I) chloride.

Experimental

Typical Procedure: A mixture of diethyl phosphonate (**3b**, 13.8 g, 0.1 mmol), propyl alcohol (7.2 g, 0.12 mmol), and copper(II) chloride (1.3 g, 0.01 mmol) was placed in a cylindrical reaction vessel (ϕ=10 mm). Copper(II) chloride was easily soluble in the mixture; however, after some time, white copper(I) chloride gradually precipitated due to its poor solubility. With bubbling of oxygen (flow rate 30 ml min^{-1}) at 50 °C, the precipitates soon disappeared and the solution became blue. The progress of the reaction was monitored by GLC (a 1-m glass column packed with Silicone OV 17 (2%) on Chromosorb W AW DMCS) at prescribed time intervals. After the conversion of **3 b** was complete, the reaction mixture was distilled in vacuo to afford diethyl propyl phosphate (**1b-Pr**, 78%, 100—101 °C/0.1 mmHg (1 mm Hg=133.322 Pa)).

References

1) K. Sasse, "Organische Phosphorverbindungen, Teil 2," in "Methoden der Organischen Chemie, Band XII," ed by E. Muller, Georg Thieme Verlag, Stuttgart (1967), p. 145; B. Gallenkamp, W. Hofer, B.-W. Kruger, F. Maurer, and T. Pfister, "Organische Phosphoverbindungen II," in "Methoden der Organischen Chemie," ed by M. Regitz, Georg Thieme Verlag, Stuttgart (1982), p. 485; E. Cherbuliez, "Organic Derivatives of Phosphoric Acid" in "Organic Phosphorus Compounds, Vol. 6, Chap 15," ed by G. M. Kosolapoff and L. Maier, Wiley Interscience, New York (1973), p. 211; L. A. Soltin, *Synthesis*, **1977**, 737.

2) G. M. Steinberg, *J. Org. Chem.*, **15**, 637 (1950).

3) H. Ohmori, S. Nakai, M. Sekiguchi, and M. Masui, *Chem. Pharm. Bull.*, **27**, 1700 (1979).

4) T. D. Smith, *J. Chem. Soc.*, **1962**, 1122.

5) "Gmelins Handbuch der Anorganischen Chemie", 8, Kupfer Teil B-1, Verlag Chemie, GMBH, Weinheim (1958), p. 226.

6) S. A. Hall and M. Jacobson, *Ind. Eng. Chem.*, **40**, 694 (1948).

One-Step Synthesis of 1,4-Diketones by Nucleophilic Reaction to Tricarbonyl Complexes of α,β-Unsaturated Ketones

Haruo KITAHARA,* Yasuyuki TOZAWA, Seikou FUJITA, Akio TAJIRI,†
Noboru MORITA,†† and Toyonobu ASAO*,††
Department of Chemistry, Faculty of Education, Hirosaki University,
Bunkyo-cho, Hirosaki 036
†Department of Chemistry, College of General Education, Hirosaki University,
Bunkyo-cho, Hirosaki 036
††Department of Chemistry, College of General Education, Tohoku University,
Kawauchi, Sendai 980
(Received February 5, 1988)

Synopsis. Tricarbonyliron complexes of 3-buten-2-one, 3-penten-2-one, and 4-phenyl-3-buten-2-one reacted with organolithium and Grignard reagents to afford 1,4-diketones in one step, some of the products are amenable to convertion to natural products.

Much attention has been devoted in recent years to the chemistry of iron carbonyl complexes of dienes and polyenes.[1] Recently, the reaction of tricarbonyl-(4-phenyl-3-buten-2-one)iron and its derivatives with organolithium and Grignard reagents to give the corresponding 1,4-diketones has been reported.[2] This has prompted us to report our similar results and their application to the synthesis of some natural products.[3]

(3-Buten-2-one)tricarbonyliron (**1**)[4] was reacted with 2.5 molar equivalents of butyllithium in THF at −78 °C for 25 min. The reaction mixture was quenched with diluted H_2SO_4 or with saturated NH_4Cl aqueous solution to give 2,5-nonanedione **2** (R^1=*n*-Bu) in 62% yield. The reaction of **1** with *t*-BuLi and PhLi afforded the corresponding 1,4-diketones in 29% and 75% yields, respectively.

The similar reaction of (3-penten-2-one)tricarbonyliron (**3**)[5] and tricarbonyl(4-phenyl-3-buten-2-one)iron (**5**)[6] with organolithium and Grignard reagents also yielded the corresponding 1,4-diketones **4** and **5**, respectively; the results are shown in Table 1. The reaction of **5** with allylmagnesium bromide, however, afforded a 1,2-addition product **7** in 80% yield.

The structures of these products were determined by spectroscopic analyses or by the comparison of their ^1H NMR and/or IR spectra with those of authentic samples.

As has already been reported,[2] the reactions probably proceed by acyl transfer from a metal acyl intermediate to the, α,β-unsaturated ketone followed by protonation. Therefore, we attempted a quenching of a reaction mixture of **1** and *n*-BuLi with excess MeI instead of NH_4Cl aqueous solution, however, no methylated product could be obtained, only **2** (R^1=*n*-Bu) was produced.

The reaction of **1** with hexyl- and *p*-methylbenzylmagnesium bromide afforded the corresponding 1,4-diketones **8** and **9** in 82% and 19% yields, respectively, as shown in Table 1. The compound **8** was then

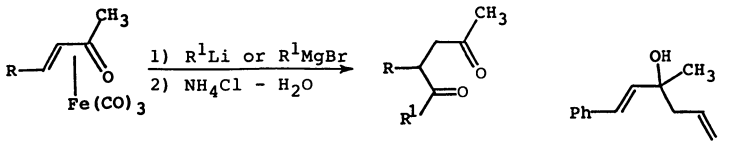

1 R = H 2 R = H 7

3 R = CH_3 4 R = CH_3

5 R = Ph 6 R = Ph

Table 1. Synthesis of 1,4-Diketones (in THF, −78 °C)

Complex	Reagent	Reaction time/min	Product (yield/%[a])
1	*n*-BuLi	25	**2** R^1=*n*-Bu[b] (62)
1	*t*-BuLi	40	**2** R^1=*t*-Bu[c] (29)
1	*n*-$C_6H_{13}MgBr$	20	**8** (**2** R^1=*n*-C_6H_{13}[d]) (82)
1	PhLi	25	**2** R^1=Ph[b] (75)
1	*p*-$MeC_6H_4CH_2MgBr$	65	**9** (**2** R^1=*p*-$MeC_6H_4CH_2$[e]) (19)
3	*n*-BuLi	10	**4** R_1=*n*-Bu[f] (53)
3	*t*-BuLi	10	**4** R^1=*t*-Bu[d] (32)
3	PhLi	10	**4** R_1=Ph[d] (29)
5	*n*-BuLi	60	**6** R_1=*n*-Bu[d] (61)
5	*s*-BuLi	20	**6** R^1=*s*-Bu (45)[g]
5	*t*-BuLi	110	**6** R^1=*t*-Bu[c] (17)
5	PhLi	60	**6** R^1=Ph[f] (19)
5	CH_2=CHMgBr	80	**6** R^1=CH=CH_2 (64)

a) Isolated yield. b) Ref. 7. c) Ref. 8. d) Ref. 9. e) Ref. 10. f) Ref. 11. g) Contaminated with an unidentified product.

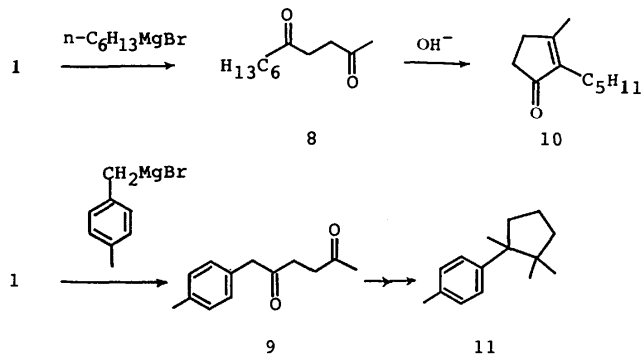

transformed by cyclization in basic medium conditions to dihydrojasmone **10**.[9] The compound **9** was reported to be converted to cuparene **11**.[10]

Thus it is found that this one-step synthesis of 1,4-diketones by nucleophilic reaction to tricarbonyliron complexes of α,β-unsaturated ketones will be widely useful to natural product syntheses. However, from these limited examples, we can not conclude which of the two reagents, alkyllithium and Grignard reagent, is the better in this 1,4-diketone synthesis.

In the course of the synthesis of **1** and **3** by the reaction of 3-buten-2-one and 3-penten-2-one with $Fe_2(CO)_9$ in benzene, we isolated new complexes [3-4-η-(3-buten-2-one)]tetracarbonyliron (**12**) and [3-4-η-(3-penten-2-one)]tetracarbonyliron (**13**) as orange oils along with tricarbonyl complexes **1** and **3**, respectively. The yield of **12** was dependent on the reaction temperature, thus, **1** and **12** were obtained in 7% and 47% yields, respectively at 60 °C and in 53% and 3% yields at 80 °C. Furthermore, **12** was gradually

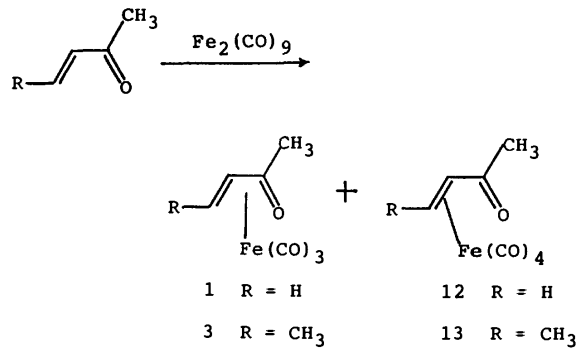

changed to **1** by heating in benzene. The structures of **12** and **13** were determined by the above fact as well as the analyses of ^{1}H NMR, IR and/or mass spectra (see Experimental).

Experimntal

General. The IR spectra were obtained with a Hitachi 260-50 spectrophotometer, ^{1}H NMR spectra were recorded with JEOL JNM-270 (270 MHz) or JNM-H60 (60 MHz) spectrometer in $CDCl_3$ solutions, and mass spectra were measured with JEOL JMS D-200 spectrometer.

Syntheses of (3-Buten-2-one)tricarbonyliron (1) and [3-4-η-(3-Buten-2-one)]tetracarbonyliron (12). A solution of 3-buten-2-one (0.41 ml, 5.0 mmol) and $Fe_2(CO)_9$ (2.728 g, 7.5 mmol) in anhydrous benzene (25 ml) was heated at 80 °C overnight. The precipitate was filtered off, solvent was removed under reduced pressure, the residue was purified by column chromatography on silica gel (45 g) using benzene as eluent to give complexes **1** (554 mg, 53% yield) and **12** (40 mg, 3% yield) as orange oils.

When the same reaction was carried out at 60 °C, **1** and **12** were obtained in 7% and 47% yields, respectively.

1:[4] IR (neat), 2080, 2010, 1990 cm^{-1}; MS *m/z* 210 (M^+), 182, 154; ^{1}H NMR ($CDCl_3$) δ=1.36 (d, d, J=2, 12 Hz, H-4(Z)), 2.07 (d, d, J=2, 7 Hz, H-4(E)), 2.48 (s, CH_3), 5.54 (d, d, J=7, 12 Hz, H-3).

12: IR (neat), 2110, 2030, 1960 cm^{-1}; MS *m/z* 238 (M^+), 210, 182, 154; ^{1}H NMR ($CDCl_3$) δ=2.35 (s, CH_3), 2.56 (d, d, J=2, 7 Hz, H-4(E)), 2.98 (d, d, J=2, 12 Hz, H-4(Z)), 3.53 (d, d, J=7, 12 Hz, H-3).

The patterns of the C=O stretching region in the IR spectra of **1** and **12** are very similar to those of tricarbonyliron and tetracarbonyliron complexes of styrene, respectively.[12]

Similarly, complexes **3** and **13** were obtained by the reaction of 3-penten-2-one and $Fe_2(CO)_9$ as orange oils.

3:[5] IR (neat), 2065, 1990, 1972 cm^{-1}; ^{1}H NMR ($CDCl_3$) δ=1.52 (d, J=6 Hz, CH_3), 1.9—2.4 (m, H-4), 2.48 (s, CH_3), 5.47 (d, J=9 Hz, H-3).

13: unstable orange oil; IR (neat), 2105, 2030, 1980 cm^{-1}; ^{1}H NMR ($CDCl_3$) δ=1.81 (d, J=6 Hz, CH_3), 2.33 (s, CH_3), 3.5—4.2 (m, 2H).

General Procedure of the Reaction of Complexes with Organolithium and Grignard Reagents. The general procedure will be illustrated below by using the reactions of (3-buten-2-one)tricarbonyliron (**1**) and *n*-BuLi, and tricarbonyl(4-phenyl-3-buten-2-one)iron (**5**) and vinylmagnesium bromide as example.

A stirred solution of **1** (106.6 mg, 0.5 mmol) in anhydrous THF (2 ml) was cooled at −78 °C under N_2 atmosphere and was added dropwise 2.34 M hexane solution (1 M=1 mol dm^{-3}) of *n*-BuLi (0.54 ml, 1.25 mmol). After 25 min, the reaction mixture was quenched with saturated aqueous solution of NH_4Cl (5 ml), extracted with CH_2Cl_2 three times, the extract was dried over anhydrous Na_2SO_4, the solvent was removed, and the residue was purified by preparative TLC on silica gel using a mixture of hexane and AcOEt (3:1) as eluent to give 2,5-nonanedione **2** (R^1=*n*-Bu) (49.1 mg, 62% yield) as colorless oil.

A stirred solution of **5** (143.1 mg, 0.5 mmol) in anhydrous THF (2 ml) was cooled at −78 °C under N_2 atmosphere and was added dropwise 0.9 M ethereal solution of vinylmagnesium bromide (1.5 ml, 1.25 mmol). After 80 min, the reaction mixture was quenched with saturated NH_4Cl (5 ml) and extracted with CH_2Cl_2. The extract was dried over anhydrous Na_2SO_4, the solvent removed, and the residue purified by preparative TLC using a mixture of hexane and AcOEt (5: 1) to give 4-phenyl-1-heptene-3,6-dione (**6**) (R^1=CH=CH_2) (66.7 mg, 64% yield) as colorless oil.

IR (neat), 1708, 1675 cm^{-1}; ^{1}H NMR ($CDCl_3$) δ=2.15 (s, CH_3), 2.63 (1H, d, d, J=4, 19 Hz, H-5), 3.58 (1H, d, d, J=11 19 Hz, H-5), 4.46 (d, d, J=4, 11 Hz, H-4), 5.68 (d, d, J=3, 10 Hz, H-2), 6.23—6.42 (2H, m, H-1), 7.10—7.40 (m, Ph).

References

1) Cf: "The Organic Chemistry of Iron", ed. by E. A. K. von Gustorf, F.-W. Grevels, and I. Fischer, Academic Press, New York (1978 and 1981) Vols. 1 and 2; A. J. Pearson, *Acc. Chem. Res.*, **13**, 463 (1980).

2) S. E. Thomas, *J. Chem. Soc., Chem. Commun.*, **1987**, 226.

3) Presented in part at the 54th Annual Meeting of Chemical Society of Japan, April 3, 1987, Tokyo, Abstract, II, p 1226.

4) A. N. Nesmeyanov, L. V. Rybin, N. T. Gubenko, M. I. Rybinskaya, and P. V. Petrovskii, *J. Organomet. Chem.*, **71**, 271 (1974).
5) M. Brookhart, G. W. Koszalka, G. O. Nelson, G. Scholes, and R. A. Watson, *J. Am. Chem. Soc.*, **98**, 8155 (1976).
6) J. A. S. Howell, B. F. G. Johnson, P. L. Josty, and J. Lewis, *J. Organomet. Chem.*, **39**, 329 (1972).
7) T. Hirao, D. Misu, K. Yao, and T. Agawa, *Tetrahedron Lett.*, **27**, 929 (1986).
8) D. Seyferth and R. C. Hui, *Tetrahedron Lett.*, **27**, 1473 (1986).
9) M. Kosugi, I. Takano, M. Sakurai, H. Sano, and T. Migita, *Chem. Lett.*, **1984**, 1221 and references cited therein.
10) T. Kametani, M. Tsubuki, and H. Nemoto, *J. Chem. Soc., Perkin Trans. 1*, **1980** 759.
11) L. S. Hegedus and R. J. Perry, *J. Org. Chem.*, **50**, 4955 (1985).
12) R. Victor, R. Ben-Shoshan, and S. Sarel, *J. Org. Chem.*, **37**, 1930 (1972).

Oxidative Formation of a Blue Pigment from a Dihydropyrrolo[2,1-*a*]-isoquinolin-3(2*H*)-one Derivative

Hajime IRIKAWA,* Sumio OOE, and Yasuaki OKUMURA
Department of Chemistry, Faculty of Science, Shizuoka University,
Oya, Shizuoka 422
(Received March 8, 1988)

Synopsis. A dimeric blue pigment was formed by the autoxidation of a dihydropyrrolo[2,1-*a*]isoquinolin-3(2*H*)-one derivative.

A blue pigment, trichotomine (**1a**, R=H), was isolated from *Clerodendron trichotomum* Thunb.[1] It was suggested that the biosynthesis of **1a** involved an oxidative dimerization of **2a** (R=H) formed from L-tryptophan and 2-oxoglutaric acid.[1,2] In the synthesis of **1a**, **1b** (R=Me) was obtained by the autoxidation of **2b** (R=Me).[3] We examined the extracts of the above plant, and isolated **3a** (R=α-H), **3b** (R=β-H), **3c** (R=α-COOH), and **3d** (R=β-COOH), which were other plausible precursors of **1a**.[4] Kapadia et al. reported the isolation of **4a** (R=H) and **4b** (R=Me); these formations were proposed to result from the condensation of 2-oxoglutaric acid with 3-demethylmescaline and mescaline, respectively.[2,5] The biosynthesis of **1a** caused us to anticipate the occurrence of natural dimeric pigments derived from such compounds as **4a,b**. In this paper, we wish to report on the oxidative dimerization of a dihydropyrrolo[2,1-*a*-]isoquinolin-3(2*H*)-one derivative **5** as a model compound.

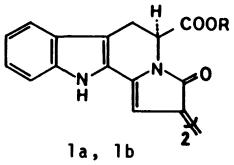

1a, 1b

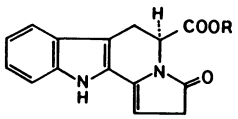

2a, 2b

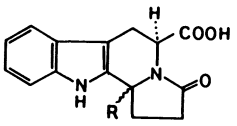

3a–3d

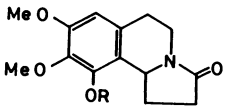

4a, 4b

The known compound, **6**[6], prepared from dopamine hydrochloride and 2-oxoglutaric acid, was acetylated with acetic anhydride and pyridine to an acetate **7**. Upon electrolysis in methanol containing $(n\text{-Bu})_4$NCl as a supporting electrolyte, **7** underwent decarboxylative methoxylation[7] to a methoxy lactam **8**. The ^{1}H NMR spectrum of **8** showed a singlet (δ=3.16) of the methoxyl group on C-10b and an octet (δ=4.18) of the equatorial C_5-proton deshielded by the carbonyl group at C-3.[8] On electrolysis in methanol containing Et_4NOTs as an electrolyte, **7** yielded **8** and a methoxy α,β-unsaturated lactam **9** in a ratio of 5:2. The structure of **9** was in line with the ^{1}H NMR spectrum [a singlet at δ=3.17 (OCH_3), two doublets at δ=6.23 (C_2–H) and 7.13 (C_1–H), and a characteristic octet at δ=4.29 (equatorial C_5–H)]; **9** seemed to be formed via an intermediate **5**. Using a large excess of lead tetraacetate in the presence of methanol, **9** was also obtained from **7**; **9** may be similarly formed by an oxidative decarboxylation of **7** to **5**, followed by further oxidation. Upon heating at 85—90 °C for 7 h, **8** was converted to a β,γ-unsaturated lactam **5** after a loss of methanol [^{1}H NMR δ=3.25 (d, J=2.9 Hz, C_2–2H) and 5.57 (t, J=2.9 Hz, C_1–H)].

The oxidative dimerization of **5** was achieved by heating a solution of **5** in 1,1,2,2-tetrachloroethane under an oxygen atmosphere at 123—127 °C for 3 h to give a blue pigment **10**. The described structure of **10** is in agreement with the spectral data; UV 634 nm, SIMS m/z 599 $(M+H)^+$, ^{1}H NMR δ=3.04 (t, J=6.4 Hz, C_6–2H×2) and 3.83 (t, J=6.4 Hz, C_5–2H×2). Under similar conditions to those used for **5**, **9** also afforded **10**, which might be formed by an initial homolytic fission of the C_{10b}-oxygen bond in **9**, followed by coupling at C-2 of the resulting allylic radical **11** and dehydrogenation. The coloration of **5** and **9** upon heating at their melting points was due to the formation of **10**, respectively, as confirmed by the TLC R_f values.

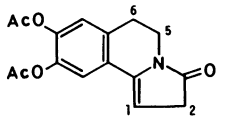

5

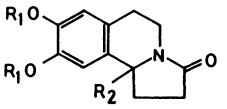

6 R_1=H R_2=COOH
7 R_1=Ac R_2=COOH
8 R_1=Ac R_2=OMe

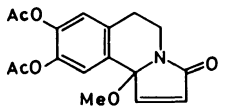

9

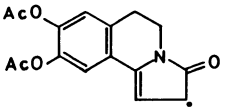

11

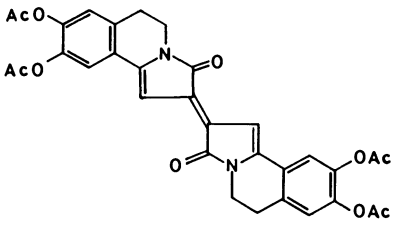

10

The formation of **10** from **5** may also proceed via **11**; this is another type of well-known oxidative dimerization of indoxyl to indigo.[9]

Experimental

All melting points were determined on a Yanagimoto micro melting point apparatus and are uncorrected. IR spectra were recorded on a Hitachi EPI-G_3 using Nujol. ^{1}H NMR spectra were obtained on a JNM-GSX-400 (400 MHz) and ^{13}C NMR spectra on a JNM-PFT-60 (15 MHz) or a JNM-GSX-400 (100 MHz). UV spectra were measured on a JASCO-UVIDEC-510. Mass spectra were obtained on a Hitach M-52 or M-80 mass spectrometer at an ionization energy of 70 eV. Analytical TLC was carried out on silica-gel plates (Kieselgel 60 F_{254}, E. Merk).

Preparation of 7. According to the literature,[6] a solution of dopamine hydrochloride (5.70 g) and 2-oxoglutaric acid (5.84 g) in water (50 ml) was refluxed for 9 h, and cooled to room temperature to give **6** (4.03 g, 51%). A solution of **6** (2.26 g) in acetic anhydride (20 ml) and pyridine (20 ml) was allowed to stand at 20 °C for 23 h, and concentrated under reduced pressure. The residue was crystallized from $CHCl_3$–CH_3OH to afford **7** (2.77 g, 93%); mp (in a sealed tube) 239—241 °C; UV (CH_3OH) 205 (ε 28400), 269 (1150), and 275 nm (1150); IR 1760, 1720, and 1632 cm^{-1}; ^{1}H NMR (DMSO-d_6) δ=2.06 (1H, m), 2.26 (3H, s), 2.27 (3H, s), 2.30—2.50 (2H, m), 2.77—2.88 (3H, m), 3.22 (1H, m), 4.02 (1H, ddd, J=12.9, 5.5, and 4.0 Hz), 7.10 (1H, s), and 7.31 (1H, s); ^{13}C NMR (DMSO-d_6) δ=20.1, 26.8, 30.0, 32.1, 35.1, 66.1, 121.5, 123.2, 132.2, 134.6, 140.3, 141.1, 168.0, 172.1, and 173.2. Anal. ($C_{17}H_{17}NO_7$) C, H, N.

Anodic Oxidation of 7. 1) A mixture of **7** (150 mg, 0.43 mmol), (n-Bu)$_4$NCl (0.50 g), and CH_3OH (50 ml) was placed in a beaker-type undivided cell, and glassy carbon rods were used as an anode and a cathode, respectively.[10] After ca. 3.6 F mol^{-1} (1F=96480 C) of electicity (the voltage between the anode and cathode=2.1 V), the electrolytic solution was concentrated under reduced pressure to give a residue which was dissolved in benzene (80 ml). The solution was washed with water, and brine, and then dried over Na_2SO_4. Evaporation of the solvent and crystallization from CH_3OH gave **8** (67 mg, 47%); UV (CH_3OH) 205 (ε 26400), 268 (1220), and 274 nm (1230); IR 1780 and 1701 cm^{-1}; ^{1}H NMR (CD_3OD) δ=2.21 (1H, m), 2.26 (3H, s), 2.27 (3H, s), 2.42 (1H, m), 2.63—2.90 (4H, m), 3.16 (3H, s), 3.23 (1H, dddd, J=13.0, 10.0, 6.2, and 1.1 Hz), 4.18 (1H, ddd, J=13.0, 5.5, and 3.3 Hz), 7.08 (1H, s), and 7.27 (1H, s); ^{13}C NMR ($CDCl_3$) δ=20.6, 28.1, 30.7, 32.3, 35.2, 50.5, 90.7, 121.2, 123.5, 132.8, 135.8, 141.1, 141.8, 168.2, and 174.7; MS m/z 301 (M^+−32). Anal. ($C_{17}H_{19}NO_6$) C, H, N.

Compound **8** melted at 160—168 °C with decomposition and changed into **5**.

2) Using Et_4NOTs (0.48 g) as a supporting electrolyte, **7** (138 mg, 0.40 mmol) was electrolyzed under similar conditions to those described above (electricity: ca. 3 F mol^{-1}). The work-up mentioned above and crystallization from CH_3OH afforded a mixture of **8** and **9** (76 mg) in a ratio of 5:2, which was separated after column chromatography (SiO_2–$CHCl_3$). **9**; mp 138—140 °C; UV (CH_3OH) 212 (ε 18300) and 277 nm (sh, 2170); IR 1779 and 1713 cm^{-1}; ^{1}H NMR ($CDCl_3$) δ=2.27 (3H, s), 2.29 (3H, s), 2.72 (1H, ddd, J=16.6, 4.2, and 1.5 Hz), 2.92 (1H, ddd, J=16.6, 11.9, and 6.1 Hz), 3.17 (3H, s), 3.23 (1H, ddd, J=13.0, 11.9, and 4.2 Hz), 4.29 (1H, ddd, J=13.0, 6.1, and 1.5 Hz), 6.23 (1H, d, J=5.9 Hz), 7.01 (1H, s), 7.13 (1H, d, J=5.9 Hz), and 7.33 (1H, s); ^{13}C NMR ($CDCl_3$) δ=20.6, 28.6, 34.5, 50.4, 90.8, 122.9, 123.9, 128.3, 132.5, 133.2, 140.7, 142.1, 147.9, 168.0, and 170.0. Found: m/z 331.1065. Calcd for $C_{17}H_{17}NO_6$: M, 331.1055.

Upon heating at the mp, **9** gave a colored oil, which showed a blue spot of **10** (R_f 0.55) and a spot of **9** (R_f 0.41) on TLC (CH_3OH:CH_2Cl_2=1:30).

Oxidation of 7 with Lead Tetraacetate (LTA). LTA (0.41 g, 0.93 mmol) was added to a solution of **7** (50 mg, 0.14 mmol) in benzene (20 ml), CH_3OH (0.5 ml), and pyridine (0.1 ml). The reaction mixture was stirred at 26 °C for 15 min, and washed successively with 0.5 wt% HCl, water, and brine, and then dried over Na_2SO_4. Evaporation of the solvent and crystallization from CH_3OH afforded **9** (18 mg, 38%), which was identical with that obtained as described above by spectroscopic (^{1}H NMR, IR) and TLC comparisons.

Preparation of 5. The crystals of **8** (58 mg, 0.17 mmol) were heated at 85—90 °C for 7 h under reduced pressure to give **5** almost quantitatively. Recrystallization from CH_3OH gave needles of **5**; mp 170—174 °C; UV (CH_3OH) 205 (ε 35700), 237 (21300), and 293 nm (5250); IR 1767, 1711, and 1626 cm^{-1}; ^{1}H NMR ($CDCl_3$) δ=2.30 (3H, s), 2.31 (3H, s), 2.95 (2H, t, J=6.2 Hz), 3.25 (2H, d, J=2.9 Hz), 3.75 (2H, t, J=6.2 Hz), 5.57 (1H, t, J=2.9 Hz), 7.08 (1H, s), and 7.40 (1H, s); ^{13}C NMR ($CDCl_3$) δ=20.6, 20.7, 28.5, 36.6, 38.2, 97.8, 119.1, 123.5, 125.7, 132.3, 138.5, 141.2, 142.2, 168.2, 168.3, and 176.3. Found: m/z 301.0913. Calcd for $C_{16}H_{15}NO_5$: M, 301.0948.

Upon heating at the mp, **5** gave a colored oil, which showed a blue spot of **10** (R_f 0.55) and a spot of **5** (R_f 0.35) on TLC (CH_3OH:CH_2Cl_2=1:30).

Dimerization of 5. A solution of **5** (30 mg, 0.10 mmol) in 1,1,2,2-tetrachloroethane (20 ml) was stirred at 123—127 °C for 3 h under oxygen atmosphere. The resulting blue solution was concentrated under reduced pressure. The residue was washed with CH_3OH and purified with column chromatography (SiO_2, 1 vol% CH_3OH–$CHCl_3$) to give **10** (5 mg, 17%) as amorphous powder; UV ($CHCl_3$) 316 (ε 28500), 590 (29900), and 634 nm (26500); IR 1767 and 1668 cm^{-1}; ^{1}H NMR ($CDCl_3$) δ=2.31 (3H×2, s), 2.34 (3H×2, s), 3.04 (2H×2, t, J=6.4 Hz), 3.83 (2H×2, t, J=6.4 Hz), 7.13 (1H×2, s), 7.19 (1H×2, s), and 7.60 (1H×2, s); MS (SIMS) m/z 599 $(M+H)^+$. Found: C, 63.87; H, 4.31; N, 4.60%. Calcd for $(C_{16}H_{13}NO_5)_2$: C, 64.21, H, 4.38, N, 4.68%.

Dimerization of 9. A solution of **9** (40 mg, 0.12 mmol) in 1,1,2,2-tetrachloroethane (20 ml) was stirred at 121—123 °C for 1 h. The resulting blue solution was worked up as described above to afford **10** (15 mg, 42%), which was identical to that obtained from **5** by spectroscopic (^{1}H NMR, IR) and TLC comparisons.

We would like to thank Dr. Hiroshi Sakurai of Meijo University for obtaining the mass spectra.

References

1) S. Iwadare, Y. Shizuri, K. Sasaki, and Y. Hirata, *Tetrahedron*, **30**, 4105 (1974).

2) G. J. Kapadia and R. E. Rao, *Tetrahedron Lett.*, **1977**, 975.

3) S. Iwadare, Y. Shizuri, K. Yamada, and Y. Hirata, *Tetrahedron*, **34**, 1457 (1978).

4) Y. Toyoda, H. Kumagai, H. Irikawa, and Y. Okumura, *Chem. Lett.*, **1982**, 903.

5) G. J. Kapadia and H. M. Fales, *J. Chem. Soc., Chem. Commun.*, **1968**, 1688.

6) J. R. Merchant, *J. Sci. Ind. Res.*, **16B**, 373 (1957); *Chem. Abstr.*, **52**, 5414b (1958).

7) T. Iwasaki, H. Horikawa, K. Matsumoto, and M.

Miyoshi, *J. Org. Chem.*, **44**, 1552 (1979).
8) B. E. Maryanoff, D. F. McComsey, and B. A. Duhl-Emswiler, *J. Org. Chem.*, **48**, 5062 (1983).
9) G. A. Russell and G. Kaupp, *J. Am. Chem. Soc.*, **91**, 3851 (1969).
10) T. Shono, Y. Matsumura, and K. Tsubata, *Org. Synth.*, Vol. 63, 206 (1984).

Simple Synthesis of (*Z*)-12-Nonadecen-9-one, (*Z*)-13-Icosen-10-one, the Sex Pheromone of Peach Fruit Moth, and (*Z*)-5-Undecen-2-one, a Biologically Active Molecule from the Pedal Gland of the Bontebok[1)]

Masakazu YAMASHITA,* Kaoru MATSUMIYA, Kotomi MURAKAMI, and Rikisaku SUEMITSU
Department of Applied Chemistry, Doshisha University, Kamikyo-ku, Kyoto 602
(Received March 26, 1988)

Synopsis. A simple and convenient synthesis of (*Z*)-12-nonadecen-9-one, (*Z*)-13-icosen-10-one, the sex pheromone of the peach fruit moth, and (*Z*)-5-undecen-2-one, the pheromone from the pedal gland of the bontebok, is described. These pheromones were readily synthesized using successive alkylation of acetone dimethylhydrazone in one-pot.

(*Z*)-12-Nonadecen-9-one (**2a**) and (*Z*)-13-icosen-10-one (**2b**) are the sex pheromones of the Japanese peach fruit moth (*Carposina niponensis* Walsingham), and have been isolated and identified by Tamaki et al. in 1977.[2)] Since these pheromones have attracted practical interest, several syntheses of these compounds have been reported.[2,3)]

On the other hand, we have previously reported a facile synthetic method of unsymmetrical ketones using acetone dimethylhydrazone (**1**) and the application of this method to the synthesis of jasmones.[4)]

In this paper, we wish to report on a simple and convenient synthesis of the pheromones **2a** and **2b** via acetone dimethylhydrazone (**1**). Using this method, (*Z*)-5-undecen-2-one (**3**), which is known as a principal volatile component contained in the pedal gland exudate of the bontebok, *Damaliscus dorcas dorcas*,[5)] could also be synthesized.

The synthetic route of (*Z*)-12-nonadecen-9-one (**2a**) and (*Z*)-13-icosen-10-one (**2b**) from acetone as a starting material is described in Scheme 1. Acetone dimethylhydrazone (**1**), easily prepared from acetone and *N*,*N*-dimethylhydrazine in 80% yield, was allowed to react with 1 equiv. of butyllithium in tetrahydrofuran (THF) at −5 °C and then with (*Z*)-1-bromo-2-nonene to give the α-monoalkylated hydrazone. The hydrazone was then alkylated regioselectively at the α′ methyl carbon using 1 equiv. of butyllithium and 1-bromoheptane to afford the corresponding α,α′-dialkylated hydrazone, which was readily converted to the desired pheromone **2a** by hydrolysis under an acidic condition. These reactions were carried out successively in one-pot and the overall yield of the product **2a** was 70% from **1**. Similarly, after successive alkylation of the hydrazone **1** and hydrolysis of the product, (*Z*)-13-icosen-10-one (**2b**) was obtained in 62% overall yield from **1**.

The synthesis of (*Z*)-5-undecen-2-one (**3**) was carried out as follows. Acetone dimethylhydrazone (**1**) was treated successively with 1 equiv. of butyllithium and (*Z*)-1-bromo-2-octene, and the product was hydrolyzed to give the desired compound **3** in 98% yield (Scheme 2).[6)] The alternative synthetic route is also shown in Scheme 2, although the yield was low. Treatment of the hydrazone (**1**) with 1 equiv. of butyllithium at −5 °C, followed by the addition of 3-bromopropyne,

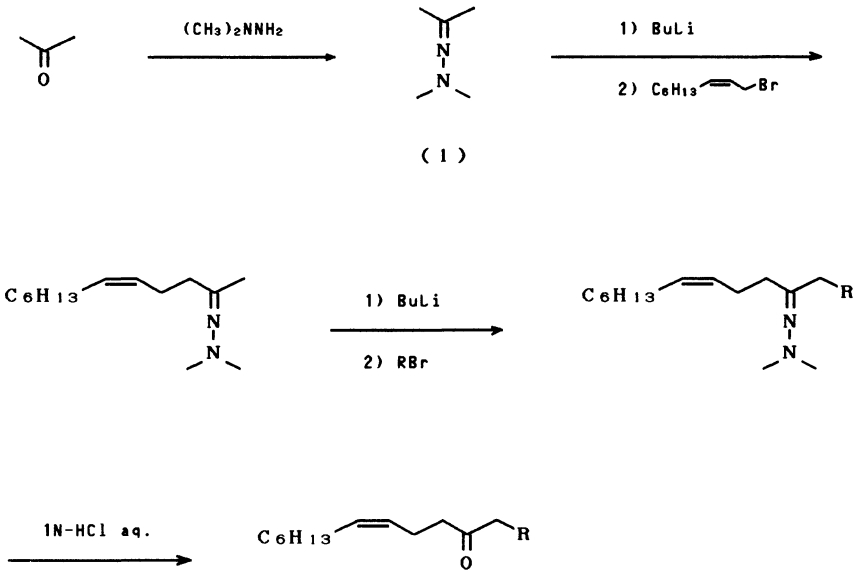

Scheme 1.

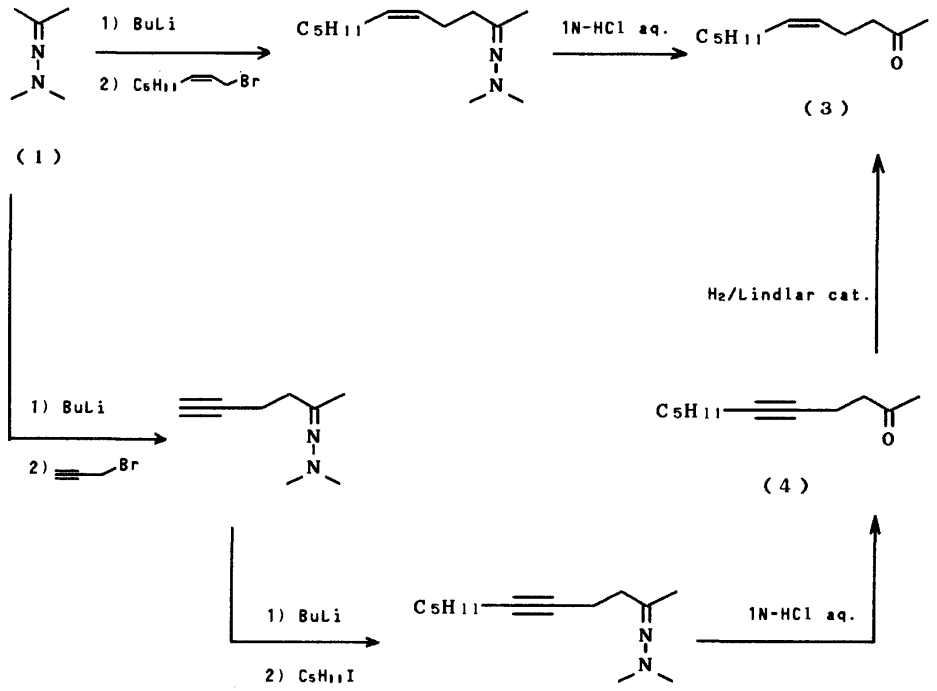

Scheme 2.

gave a monoalkylated hydrazone. To the hydrazone, without isolation, 1 equiv. of butyllithium was again added, followed by 1-iodopentane. The product was readily hydrolyzed by hydrochloric acid to afford 5-undecyn-2-one (**4**) in 14% yield from **1**. By partial hydrogenation of **4** over Lindlar catalyst, the expected pheromone **3** was obtained in 36% yield.

The corresponding (*E*)-isomers of **2a**, **2b**, and **3** were not detected by GC.

Experimental

The IR spectra were recorded on a Hitachi 260-10 Infrared Spectrophotometer. The NMR spectra were measured on a Hitachi R-600 FT-NMR Spectrometer at 60 MHz, using tetramethylsilane (δ=0.00) as an internal standard, and chemical shifts are given in ppm. The mass spectra (MS) were determined on a Hitachi RM-50 GC-MS spectrometer. The analytical gas chromatography was carried out on a Yanagimoto G-8 gas chromatograph with a column of 10% Silicone gum SE-30 on Chromosorb, and the column chromatography was performed on Merck silica gel 60 (230—400 mesh). All the boiling points were uncorrected, and all the yields were isolated ones.

Materials. Tetrahydrofuran (THF) was dried over potassium-benzophenone under argon and distilled just before use. Benzene was also purified by distillation over sodium-benzophenone under argon, and stored over 4A Molecular Sieves. 3-Bromopropyne, 1-bromoheptane, 1-bromooctane, 1-iodopentane, acetone, *N*,*N*-dimethylhydrazine, and Lindlar catalyst were commercial products of the highest available purity, and were used without further purification. Butyllithium in hexane, also a commercial product, was titrated with *s*-butyl alcohol using 1,10-phenanthroline as an indicator just before use. (*Z*)-1-Bromo-2-octene was prepared by the hydrogenation of 2-octyn-1-ol[7] over Lindlar catalyst[8] followed by bromination. By the same procedure, (*Z*)-1-bromo-2-nonene was obtained from 2-nonyn-1-ol.[7]

Acetone Dimethylhydrazone (1). The hydrazone **1** was prepared by refluxing of acetone and *N*,*N*-dimethylhydrazine in 80% yield. IR (neat): 1660, 1170, 1090 cm^{-1}; ^{1}H NMR ($CDCl_3$) δ=1.93 (3H, s, CCH_3), 1.97 (3H, s, CCH_3), 2.04 (6H, s, $N(CH_3)_2$); MS *m*/*z* (%): 100 (M^+, 8), 44 (90), 42 (83), 28 (100).

(*Z*)-12-Nonadecen-9-one (2a). Butyllithium (3.0 mmol) was added via syringe at −5 °C with stirring under argon to a solution of acetone dimethylhydrazone (**1**) (0.30 g, 3.0 mmol) in THF (10 ml). After standing for 1 h, (*Z*)-1-bromo-2-nonene (0.61 g, 3.0 mmol) was added; the mixture was stirred for 20 h at room temperature. After cooling the mixture at −5 °C again, butyllithium (3.0 mmol) was added dropwise; 1 h later, 1-bromoheptane (0.47 ml, 3.0 mmol) was added, and the reaction mixture was stirred for 20 h at room temperature. After 1 mol dm^{-3} hydrochloric acid was added, the mixture was refluxed at 80 °C for 2 h, cooled to the room temperature, and extracted with ethyl acetate. The organic layer was washed with brine, dried over anhydrous magnesium sulfate, filtered and concentrated. The residual liquid was distilled by Kugelrohr to give (*Z*)-12-nonadecen-9-one (**2a**) (0.59 g) in 70% yield, bp 210 °C/2 Torr (bath temp; Torr≈133.322 Pa). IR (neat): 2850, 1720, 1470 cm^{-1}; ^{1}H NMR ($CDCl_3$) δ=0.87 (6H, t, CH_3), 1.08—2.18 (20H, m, CH_2), 2.20—2.60 (8H, m, CH_2), 5.20—5.48 (2H, m, CH=CH); MS *m*/*z* (%): 280 (M^+, 6), 195 (7), 141 (100), 125 (15).

(*Z*)-13-Icosen-10-one (2b). In a manner similar to the above, (*Z*)-13-icosen-10-one (**2b**) was prepared by the successive alkylations of acetone dimethylhydrazone (**1**) using (*Z*)-1-bromo-2-nonene and 1-bromooctane and the hydrolysis in 62% yield. IR (neat): 2900, 1725, 1480 cm^{-1}; ^{1}H NMR ($CDCl_3$) δ=0.87 (6H, t, CH_3), 1.05—2.20 (22H, m, CH_2), 2.20—2.70 (8H, m, CH_2), 5.20—5.48 (2H, m, CH=CH) MS *m*/*z* (%): 294 (M^+, 10), 157 (100), 125 (22), 85 (18).

5-Undecyn-2-one (4). By the same procedure, using 3-bromopropyne and 1-iodopentane, successive alkylations of acetone dimethylhydrazone (**1**) and the hydrolysis were carried out. After the usual work up, column chromatography (hexane:ethyl acetate=9:1) gave 5-undecyn-2-one (**4**) in 14% yield. IR (neat): 1725 cm^{-1}; ^{1}H NMR ($CDCl_3$) δ=0.89

(3H, t, CH_3), 1.08—1.72 (6H, m, CH_2), 1.80—2.82 (6H, m, CH_2), 2.16 (3H, s, CH_3); MS *m/z*: 166 (M^+).

(*Z*)-5-Undecen-2-one (3). According to a manner similar to that described above, (*Z*)-5-undecyn-2-one (**3**) was obtained by the monoalkylation of acetone dimethylhydrazone (**1**) with (*Z*)-1-bromo-2-octene and the hydrolysis in 98% yield. On the other hand, the ketone **3** was also prepared by hydrogenation of 5-undecyn-2-one (**4**) over Lindlar catalyst[8] in 36% yield. IR (neat): 2930, 1735, 1360, 1160 cm^{-1}; ^1H NMR ($CDCl_3$) δ=0.90 (3H, t, CH_3), 1.06—1.70 (6H, m, CH_2), 2.14 (3H, s, CH_3), 1.80—2.75 (6H, m, CH_2), 5.20—5.50 (2H, m, CH=CH); MS *m/z* (%): 168 (M^+, 13), 109 (38), 81 (33), 43 (100).

References

1) Organic synthesis via dialkylhydrazones. 5. Part 4: M. Yamashita, K. Matsumiya, K. Nakano, and R. Suemitsu, *Chem. Lett.*, **1988**, 1215.

2) Y. Tamaki, K. Honma, and K. Kawasaki, *Appl. Entomol. Zool.*, **12**, 60 (1977).

3) S. Tamada, K. Mori, and M. Matsui, *Agric. Biol. Chem.*, **42**, 191 (1978); Y. Naoshima, M. Kawakubo, S. Wakabayashi, and S. Hayashi, *ibid.*, **45**, 439 (1981); O. P. Vig, M. L. Sharma, K. C. Taneja, and N. Malik, *Indian J. Chem.*, **20B**, 863 (1981); M. Liu, X. Zeng, and Z. Yan, *Huaxue Xuebao*, **39**, 475 (1981); T. Yoshida and S. Saito, *Bull. Chem. Soc. Jpn.*, **55**, 3047 (1982); J. E. Hernandez, A. Cisneros, and S. Fernandez, *Synth. Commun.*, **13**, 191 (1983); P. Yadagiri and J. S. Yadav, *ibid.*, **13**, 1067 (1983); S. Ito, N. Saito, K. Hatakeda, T. Goto, Y. Ikushima, and T. Asano, *Bull. Chem. Soc. Jpn.*, **57**, 2015 (1984); E. Wenkert, V. F. Ferreira, E. L. Michelotti, and M. Tingoli, *J. Org. Chem.*, **50**, 719 (1985); H. J. Bestmann and M. Schmidt, *Tetrahedron Lett.*, **26**, 6171 (1985); T. Miyakoshi, *J. Jpn. Oil Chem. Soc.*, **35**, 157 (1986).

4) M. Yamashita, K. Matsumiya, M. Tanabe, and R. Suemitsu, *Bull. Chem. Soc. Jpn.*, **58**, 407 (1985).

5) B. V. Burger, M. Le Roux, C. F. GarBers, H. S. C. Spies, R. G. Bigalke, K. G. R. Pachler, P. L. Wessels, V. Christ, and K. H. Maurer, *Naturforsch*, **31C**, 21 (1976); K. Mori, T. Ara, and M. Matsui, *Agric. Biol. Chem.*, **41**, 2295 (1977); H. C. Brown, U. S. Racherla, and D. Basavaiah, *Synthesis*, **1984**, 303; P. S. Reddy and J. S. Yadav, *Synth. Commun.*, **14**, 327 (1984); G. Rosini, R. Ballini, and M. Petrini, *Synthesis*, **1986**, 46; B. G. Kovalev, A. M. Sorochinskaya, and L. A. Avdeeva, *Khim. Prir. Soedin.*, **1986**, 123.

6) Synthesis of **3** according to this route has been reported: see I. R. Trehan, G. L. Kad, N. Varma, and L. Singh, *Indian J. Chem.*, **24B**, 1273 (1985).

7) H. H. Guest, *J. Am. Chem. Soc.*, **47**, 862 (1925); J. A. Toussaint and H. H. Wenzke, *ibid.*, **57**, 668 (1935).

8) H. Lindlar, *Helv. Chim. Acta*, **35**, 446 (1952).

The Structure and Absolute Stereochemistry of a Halogenated Chamigrene Derivative from the Red Alga *Laurencia* Species[1)]

Minoru SUZUKI,* Etsuro KUROSAWA, and Akio FURUSAKI*
Department of Chemistry, Faculty of Science, Hokkaido University, Sapporo 060
(Received April 13, 1988)

Synopsis. The structure of a halochamigrene derivative, 2,10-dibromo-3-chlorochamigran-7-en-9-ol, isolated from the red alga *Laurencia* species has been determined by spectral and chemical methods as well as X-ray crystallographic analysis of the ketone derivative. Furthermore, the conformations of this compound and its derivatives are briefly discussed.

During the course of our continuing search for the constituents of the red alga *Laurencia nipponica* Yamada, we have isolated a halogenated chamigrene derivative **1** from the specimens collected at Hamamasu[2)] and other locations[3)] in Hokkaido. In this paper, we report the structural determination of this compound.

Compound **1** was analyzed for $C_{15}H_{23}OBr_2Cl$ by elemental analysis together with low and high resolution mass spectrometry. The ^1H NMR spectrum of **1** presented signals at δ=0.99 (3H, s), 1.22 (3H, s), 1.70 (3H, s), and 2.05 (3H, dd, J=1.5, 1.5 Hz) due to four methyl groups and at δ=4.27 (1H, br d, J=9 Hz), 4.37 (1H, d, J=9 Hz), 4.90 (1H, dd, J=10, 8 Hz), and 5.44 (1H, dddd, J=3, 1.5, 1.5, 1.5 Hz) due to three methine protons and an olefinic proton. Acetylation of **1** with acetic anhydride and pyridine gave the corresponding acetate **2**, $C_{17}H_{25}O_2Br_2Cl$. Double resonance experiments on the ^1H NMR spectrum of the acetate **2** indicated the presence of ■–C(CH_3)=CH–CH(OAc)–CH(Br or Cl)–■ (■; quaternary carbon) grouping in the molecule. Oxidation of **1** with Jones reagent yielded an α,β-unsaturated ketone **3**, $C_{15}H_{21}OBr_2Cl$. In view of the above-mentioned data coupled with the coexistence of **1** with many other halochamigrenes in the same alga,[2,3)] it was strongly suggested that compound **1** would be a halochamigrene derivative. Comparison of the physical properties of **1** with those of previously reported halochamigrene derivatives suggested that compound **1** is 2,10-dibromo-3-chlorochamigran-7-en-9-ol,[4)] which has been obtained as the major metabolite from *Laurencia pacifica* Kylin collected at near Ensenada, Mexico. The IR and ^1H NMR spectra of both compounds along with their derivatives were identical. The proposed structure **1** for 2,10-dibromo-3-chlorochamigran-7-en-9-ol, however, has been deduced mainly from spectral analysis.[4)] Therefore, in order to confirm the structure of **1** including the absolute configuration, a single crystal of the ketone **3** was subjected to X-ray crystallographic analysis.

The crystal data for **3** were as follows: $C_{15}H_{21}OBr_2Cl$, mol wt 412.59, monoclinic, space group $P2_1$, a=9.773(4), b=10.897(5), c=7.616(2) Å, β=92.40(3)°, Z=2, D_c=1.691 g cm^{-3}. The structure was solved by the Monte Carlo direct method,[5)] and refined by the block-diagonal least-square method with anisotropic thermal parameters. The absolute configuration was determined by Hamilton's method;[6)] the R-factor ratio for the two enantiomeric structures, 1.037, excluded one of them at the 99.5% confidence level. After all the hydrogen atoms had been located in a difference Fourier map, further full-matrix least-squares refinements were carried out including the hydrogen atoms with the same fixed isotropic temperature factors of 2.5 Å^2. The final R-value was 0.054.[7)] The molecular framework obtained is shown

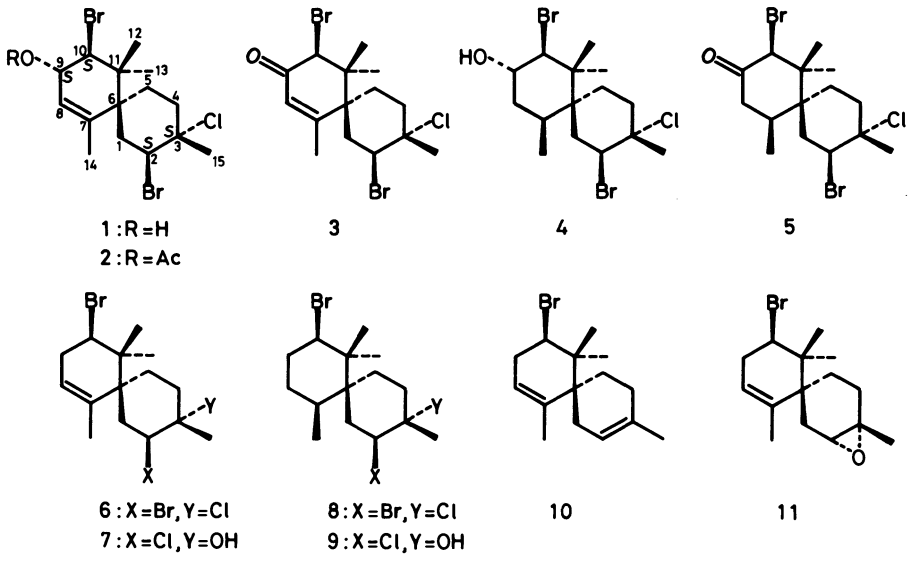

Fig. 1.

in Fig. 2. Thus, the molecular structure has been established as formula **3**.[8]

The C-9 configuration in **1** could be established on the basis of the coupling constant of the pertinent proton at C-9 in the ^{1}H NMR spectrum of the hydrogenated product **4**.[9] The J-value, J=11 Hz, between the protons at C-9 and C-10 indicated that the stereochemistry of the substituents at C-9 and C-10 is trans diequatorial to each other, thus showing that the absolute configuration at C-9 is *S*. Consequently, the absolute structure of 2,10-dibromo-3-chlorochamigran-7-en-9-ol is represented by formula **1**.

In the previous paper,[10] we have reported that the conformations of the B-ring in the halochamigrene derivatives, such as **6** and **7**, are not chair form (formulae **6C** and **7C**) (Fig. 3) but rather twist boat form (formulae **6B** and **7B**). Compound **1**, which has the same structural feature as **6** except for the hydroxyl group at C-9, seemed to adopt a conformation, formula **1B**, very similar to those of **6** and **7** (**6B** and **7B**). In fact, in the ^{1}H NMR spectra the signals of the methyl group at C-7 in **1** and **2** were shifted downfield compared with those[10] of compounds **10** and **11**. Furthermore, the coupling constants of the protons at C-2 in **1** and **2** indicated that these protons are neither axial nor equatorial proton on the cyclohexane ring with the normal chair conformation as observed in the case of **6** and **7**. Since the situation was almost same for the ketone **3**, the ketone **3** seemed to take conformation **3B**. However, as described above, the X-ray analysis of the ketone **3** showed that the B-ring conformation is a somewhat deformed chair form (Fig. 2). Detailed analysis of the ^{1}H NMR spectra of the ketone **3** and its dihydro derivative **5** gave the following information. In the ^{1}H NMR spectrum of **3**, some signals were rather broad at room temperature, whereas measuring at −30 °C sharpened the signals. In the spectrum measured at −30 °C, the signal due to the C_2–H was observed at δ=4.89, whose coupling constant, J=11 and 7 Hz, was compatible with those of **1** and **2**. This indicates that the ketone **3** exists in solution at room temperature as a mixture of interconverting conformers, reflecting the broad signals in the ^{1}H NMR spectrum. On the other hand, the ^{1}H NMR spectrum of **5** showed the signal due to the C_2–H at δ=4.43 (J=13 and 4 Hz), thus indicating that the B-ring conformation of the dihydro derivative **5** is represented by formula **5C** which is very similar to the conformations **8C** and **9C** of the compounds **8** and **9**.[10] Above results suggest that, although the B-ring conformation of the ketone **3** took the chair form (**3C**) in the solid state, a preferred conformation in solution would be twist boat form (**3B**).

2,10-Dibromo-3-chlorochamigran-7-en-9-ol (**1**) is the first example of the halochamigrene derivatives from *Laurencia* species with a trans-diequatorial bromohydrin moiety at C-9 and C-10 instead of cis-bromohydrin at C-9 and C-10 which have unexceptionally been encountered in a number of halogenated chamigrane-type sesquiterpenoids.[11]

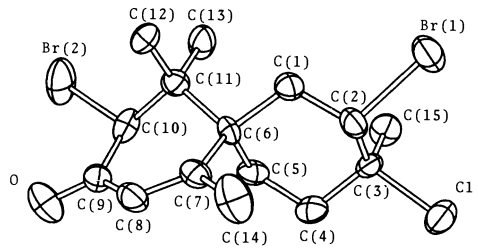

Fig. 2. A perspective view of the **3** molecule.

Experimental

All the mps were uncorrecterd. The IR spectra were recorded on a JASCO A-102 spectrophotometer and the UV spectrum on a Shimadzu UV-240 spectrophotometer. The ^{1}H and ^{13}C NMR spectra were measured on a JEOL JNM-FX 200 or a JEOL JNM-FX 100 spectrometer, using tetramethylsilane as an internal reference in $CDCl_3$. The low and high resolution mass spectra were taken at 70 eV with a JEOL JMS-D300 spectrometer. Optical rotations were determined on a JASCO DIP-140 polarimeter in $CHCl_3$. Silica gel (Merck, Kieselgel 60, 70—230 mesh) and silica gel (Merck, Kieselgel GF_{254} (Type 60)) were used for column and thin-layer chromatography, respectively.

1: Mp 119—120 °C (diisopropyl ether); $[\alpha]_D^{19}$ +25.3° (*c* 1.39); IR (Nujol), ν_{max} 3330, 1310, 1220, 1143, 1112, 1079, 1041, 1018, 999, 985, 850, and 810 cm^{-1}; ^{1}H NMR, in the text; ^{13}C NMR (25.0 MHz), δ=17.8 (q), 24.1 (q), 25.1 (q), 25.7 (q), 31.5 (t), 39.1 (t), 40.1 (t), 45.5 (s), 47.9 (s), 62.4 (d), 70.6 (s), 70.9 (d), 73.0 (d), 124.0 (d), and 143.0 (s); MS, *m/z* (rel intensity) 337, 335, 333 (0.3:0.9:0.7; M^+−Br), 319, 317, 315 (0.3:0.9:0.7; M^+−Br−H_2O), 164, 162 (3:3), 157 (2), 145 (2), 135 (3), 133 (2), 119 (23), 107 (3), 105 (4), 93 (3), 91 (5), 83 (100), 81 (2), 79 (3), 77 (3), 69 (3), 67 (2), 65 (2), 55 (5), 53 (3), 43 (2), and 41 (6). Found: *m/z* 393.9699. Calcd for

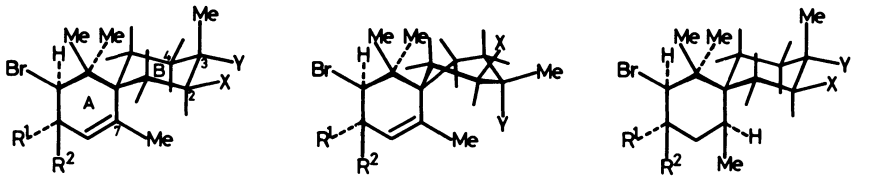

Fig. 3. B-ring conformations (H in the B-ring are omitted).

$C_{15}H_{21}{}^{79}Br^{79}Br^{35}Cl$: M−$H_2O$, 393.9699.

Found: C, 43.34; H, 5.63%. Calcd for $C_{15}H_{23}OBr_2Cl$: C, 43.45; H, 5.59%.

Acetylation of 1. Acetylation of **1** (17 mg) was carried out with acetic anhydride and pyridine by the usual method. The acetylated product was purified by column chromatography over silica gel to yield **2** (22 mg); colorless gum; $[\alpha]_D^{19}$ +75.6° (*c* 1.75); IR ($CHCl_3$), ν_{max} 1732, 1310, 1237, 1162, 1142, 1115, 1081, 1021, 991, 966, 957, 850, and 813 cm^{-1}; ^1H NMR, δ=1.03 (3H, s), 1.25 (3H, s), 1.71 (3H, s), 2.04 (3H, dd, *J*=1.5, 1.5 Hz), 4.42 (1H, d, *J*=9 Hz), 4.88 (1H, dd, *J*=11, 7 Hz), 5.36 (1H, dq, *J*=3, 1.5 Hz), and 5.44 (1H, ddq, *J*=9, 3, 1.5 Hz); MS, *m/z* 400, 398, 396, 394 (0.1:0.3:0.4:0.2; M^+−CH_3COOH), 378, 376, 374 (2:14:6; M^+−Br), 336, 334 332 (15:100:62; M^+−Br−CH_2CO), 119 (25), 105 (15), 91 (23), 83 (91), 55 (15), 43 (94), and 41 (24). Found: *m/z* 393.9701. Calcd for $C_{15}H_{21}{}^{79}Br^{79}Br^{35}Cl$: M−$CH_3COOH$, 393.9700.

Saponification of 2. A solution of **2** (9 mg) and potassium carbonate (15 mg) in methanol (1 ml) was stirred at room temperature for 50 min and then worked up in the usual way to give **1** (8 mg); The spectral data were identical with those of natural alcohol (**1**).

Oxidation of 1. To a solution of **1** (14 mg) in acetone (3 ml) was added Jones reagent dropwise with swirling at room temperature. After the usual work-up, the oily product was chromatographed on a silica-gel plate to give **3** (11 mg); crystals; mp 133—134 °C (diisopropyl ether); $[\alpha]_D^{17}$ −3.28° (*c* 1.54); UV (EtOH), λ_{max} 244 nm (ε 11800); IR (CCl_4), ν_{max} 1680, 1620, 1215, 1172, 1080, 970, 880, and 860 cm^{-1}; ^1H NMR, δ=1.02 (3H, br s), 1.35 (3H, br s), 1.74 (3H, s), 2.30 (3H, d, *J*=1.5 Hz), 4.85 (1H, m), 4.93 (1H, br s), and 6.01 (1H, br s); ^1H NMR (100 MHz, at −30 °C), δ=1.02 (3H, s), 1.37 (3H, s), 1.75 (3H, s), 2.34 (3H, br s), 4.89 (1H, dd, *J*=11, 7 Hz), 5.00 (1H, s), and 6.05 (1H, br s); MS, *m/z* 416, 414, 412, 410 (0.02:0.09:0.12:0.06; M^+), 335, 333, 331 (1:9:4; M^+−Br), 280 (13), 278 (76), 276 (60), 199 (28), 197 (100), 161 (58), 119 (12), 105 (16), 91 (31), 83 (19), 79 (14), 77 (18), 69 (18), 55 (33), 53 (27), 41 (27), and 39 (23). Found: *m/z* 409.9646. Calcd for $C_{15}H_{21}O^{79}Br^{79}Br^{35}Cl$: M, 409.9652.

Hydrogenation of 1. Hydrogenation of **1** (8 mg) was performed in ethyl acetate over PtO_2-catalyst. After the usual work-up, the residual oil was chromatographed on a silica-gel plate to afford **4** (7 mg); colorless oil; $[\alpha]_D^{19}$ +46.3° (*c* 0.72); IR ($CHCl_3$), ν_{max} 3550, 1300, 1120, 1095, 1047, 905, 890, 880, 873, 861, 838, and 810 cm^{-1}; ^1H NMR, δ=1.10 (3H, s), 1.16 (3H, s), 1.22 (3H, d, *J*=7.5 Hz), 1.71 (3H, s), 3.93 (1H, ddd, *J*=11, 11, 5 Hz), 4.17 (1H, d, *J*=11 Hz), and 4.41 (1H, dd, *J*=13, 4 Hz); MS, *m/z* 339, 337, 335 (1:5:4; M^+−Br), 321, 319, 317 (2:7:5; M^+−Br−H_2O), 149 (7), 121 (7), 109 (6), 105 (7), 93 (9), 91 (9), 85 (100), 83 (7), 81 (7), 79 (6), 77 (6), 69 (6), 67 (7), 57 (8), 55 (25), 53 (6), 43 (9), and 41 (40). Found: *m/z* 335.0776. Calcd for $C_{15}H_{25}O^{79}Br^{35}Cl$: M−Br, 335.0776.

Oxidation of 4. Oxidation of **4** (10 mg) was carried out with Jones reagent in acetone in the usual manner to give **5** (9 mg); crystals; mp 181—183 °C (diisopropyl ether); IR ($CHCl_3$), ν_{max} 1730, 1305, 1280, 1147, 1095, 867, and 859 cm^{-1}; ^1H NMR, δ=1.05 (3H, s), 1.16 (3H, d, *J*=7 Hz), 1.23 (3H, s), 1.75 (3H, s), 4.43 (1H, dd, *J*=13, 4 Hz), and 4.81 (1H, s); MS, *m/z* 337, 335, 333 (1:5:4; M^+−Br), 121 (14), 119 (55), 105 (9), 93 (13), 91 (13), 87 (11), 83 (100), 79 (12), 77 (11), 69 (12), 67 (10), 55 (30), 53 (19), 45 (13), 43 (9), 41 (36), and 39 (16). Found: *m/z* 333.0619. Calcd for $C_{15}H_{23}O^{-79}Br^{35}Cl$: M−Br, 333.0620.

X-Ray Experiment. A single crystal with dimensions of ca. 0.2×0.3×0.5 mm^3 was used for the X-ray measurement. The cell dimensions and diffraction intensities were measured on a Rigaku four-circle diffractometer at the High Brilliance X-Ray Diffraction Laboratory of Hokkaido University, using graphite-monochromated Mo $K\alpha$ radiation (λ=0.71073 Å). The θ–2θ scan technique was applied at a θ scan speed of 4° min^{-1}; the background was counted for 10 s at each end of the scan range. The intensities of three standard reflections, measured at intervals of every 100 reflections, decreased gradually during the course of data collection; the final-intensity/initial-intensity ratios were ca. 0.988—0.994. The intensities were corrected for this damage to the sample as well as for the Lorentz and polarization factors, but not for the absorption or the extinction effect. In the range of 2θ values up to 50°, 1274 independent structure factors above the 3σ(F) level were selected for the structure determination.

We are grateful to Professor William Fenical, University of California, Scripps Institution of Oceanography, for providing us with copies of the IR and ^1H NMR spectra of 2,10-dibromo-3-chlorochamigran-7-en-9-ol and its derivatives; the acetate, the ketone, and the dihydro derivative.

References

1) Part 73 of "Constituents of Marine Plants". Part 72; M. Suzuki, E. Kurosawa, M. Ikura, and K. Hikichi, *Phytochemistry*, in preparation.

2) H. Kikuchi, T. Suzuki, M. Suzuki, and E. Kurosawa, *Bull. Chem. Soc. Jpn.*, **58**, 2437 (1985).

3) Unpublished result.

4) W. Fenical, *Phytochemistry*, **15**, 511 (1976).

5) A. Furusaki, *Acta Crystallogr., Sect. A*, **35**, 220 (1979).

6) W. C. Hamilton, *Acta Crystallogr.*, **18**, 502 (1965).

7) The calculations for the X-ray study were performed on a HITAC M-280H computer at the Hokkaido University Computing Center, using our own programs.

8) The tables of the atomic parameters and bond distances and angles and the F_o–F_c table are kept at the Chemical Society Japan (Document No. 8823).

9) Oxidation of 2,10-dibromo-3-chlorochamigran-7-ene (**6**) with *m*-chloroperbenzoic acid gave the α-epoxide.[12,13] If hydrogenation follows the same course (attack from the less-hindered α-side) as oxidation, the secondary methyl group at C-7 of the hydrogenated product must be β-configuration.

10) M. Suzuki, A. Furusaki, and E. Kurosawa, *Tetrahedron*, **35**, 823 (1979).

11) "Marine Natural Products," ed by P. J. Scheuer, Academic Press, New York; J. D. Martin and J. Darias, (1978), Vol. 1, pp. 138—152; K. L. Erickson, (1983), Vol. 5, pp. 164—173.

12) B. M. Howard and W. Fenical, *Tetrahedron Lett.*, **1975**, 1687; M. Ojika, Y. Shizuri, and K. Yamada, *Phytochemistry*, **21**, 2410 (1982); T. Suzuki, H. Kikuchi, and E. Kurosawa, *Bull. Chem. Soc. Jpn.*, **55**, 1561 (1982).

13) A. Furusaki, C. Katayama, T. Matsumoto, M. Suzuki, T. Suzuki, H. Kikuchi, and E. Kurosawa, *Bull. Chem. Soc. Jpn.*, **55**, 3398 (1982).

Solid-Phase Synthesis of C-Terminal Hexapeptide Analogs of Substance P[1)]

Shosuke SOFUKU,* Atsushi ISHIKAWA, Ichiro MURAMATSU, and Kensuke SHIBATA†
Department of Chemistry, College of Science, Rikkyo University, Nishi-Ikebukuro, Toshima-ku, Tokyo 171
†Medicinal Research Laboratory, Toyo Jozo Co., Ohito-cho, Shizuoka 410-23
(Received April 19, 1988)

Synopsis. C-Terminal hexapeptide analogs of substance P (SP) were synthesized by a solid-phase method. These analogs, [Dab^6]-SP(6-11), [Orn^6]-SP(6-11), and [Lys^6]-SP(6-11), showed a contractile activity on an isolated guinea-pig ileum.

Substance P (SP) is a smooth muscle-contracting peptide having a sequence H–Arg–Pro–Lys–Pro–Gln–Gln–Phe–Phe–Gly–Leu–Met–NH_2. In studies of the relationships between chain length and activity of SP,[2,3)] it was found that the potency of the C-terminal hexapeptide of SP was similar to that of SP. We reported the relative potencies of C-terminal hexapeptide analogs of SP each having either Gly, γAbu (4-aminobutyric acid), δAva (5-aminovaleric acid), or εAcp (6-aminocaproic acid) at the N-terminus.[4)] In this paper,[5)] we would like to report the synthesis and structure-activity relationships of the other C-terminal hexapeptide analogs, **1**, **2**, and **3**, N-terminus of which is Dab, Orn,[6)] or Lys, respectively. These analogs were synthesized by a solid-phase method according to Merrifield's procedure.[7)]

H-Dab-Phe-Phe-Gly-Leu-Met-NH_2 **1**
H-Orn-Phe-Phe-Gly-Leu-Met-NH_2 **2**
H-Lys-Phe-Phe-Gly-Leu-Met-NH_2 **3**

For the synthesis, one of the present authors[8)] designed a manually operated apparatus with a Diflon vessel. The coupling was performed on a 2% cross-linked benzhydrylamine (BHA) resin support[9)] using Boc-amino acids. First of all, Boc–Met–OH was coupled with the BHA group on the resin by DCC. The resulting resin was treated with Ac_2O and Et_3N in CH_2Cl_2 in order to mask the residual free BHA groups. Then, the Boc-group was removed with 30% TFA/CH_2Cl_2 containing anisole as a scavenger. Boc–Leu–OH, Boc–Gly–OH, Boc–Phe–OH, and Boc–Phe–OH were coupled to the N-terminus on the resin, successively. In each case, for the first coupling a 2.5-fold excess of Boc-amino acid was used and for the second a 1.25-fold excess. The Boc–Phe–Phe–Gly–Leu–Met–BHA resin was divided into several parts. After deprotection of the N-terminus of the peptide-resin, Boc–Dab(Boc)–OH, Boc–Orn(Boc)–OH, and Boc–Lys(Boc)–OH were coupled with each. The peptide-resin bond of H–Dab–Phe–Phe–Gly–Leu–Met–BHA resin derived from Boc–Dab(Boc)-derivative by treatment with TFA was cleaved with liquid HF containing anisole and methionine.[10)] Column chromatography on Bio-Gel P-2 was used to separate the methionine from analog **1**. For further purification, partition chromatography was performed by using the upper phase of the mixture of *n*-BuOH and 0.1% AcOH (1 : 1) as an eluent on a column of Sephadex G-25. The other two analogs, **2** and **3**, were prepared from Boc–Orn(Boc)–Phe–Phe–Gly–Leu–Met–BHA resin and Boc–Lys(Boc)–Phe–Phe–Gly–Leu–Met–BHA resin by the same procedure respectively. The homogeneities of the analogs (**1**, **2**, and **3**) were confirmed by HPLC on an ODS column. The analogs were highly soluble in water and showed that the CD spectra had one peak at 220 nm and one trough at 235 nm. Their molar ellipticity values are summarized in Table 1. These CD spectra are referred to as an "unordered structure" by Mehlis et al.[11)] Their contractile activities, as measured on an isolated guinea-pig ileum, showed the relative potencies compared with the authentic SP in Table 2. Among them, [Orn^6]-SP(6-11) had the highest potency, though it was still less than that of SP. These results suggest that Dab, Orn, and Lys at the N-terminus of these analogs have a capability to increase the activity of H–Phe–Phe–Gly–Leu–Met–NH_2;[2)] and that the potency of each depends upon the length of the side chain of each basic amino acid.

Table 1. Circular Dichroism of SP(6–11) Analogs

Compound	[θ] (10^3 deg cm^2/dmol)[a)]	
	Peak (220 nm)	Trough (235 nm)
[Dab^6]-SP$^{6-11}$ (**1**)	+10.8	−1.4
[Orn^6]-SP$^{6-11}$ (**2**)	+10.8	−1.4
[Lys^6]-SP$^{6-11}$ (**3**)	+15.4	−1.5

a) Molar ellipticity value in water at room temp.

Table 2. Contractile Activities of SP and SP(6–11) Analogs on an Isolated Guinea-Pig Ileum

Compound	EC_{50}(M)[a)]	Relative Potencies
SP	4.4×10^{-9}	100
1	2.0×10^{-8}	22
2	9.7×10^{-9}	45
3	1.1×10^{-8}	40

a) EC_{50}: effective concentration (half maximal contraction).

Experimental

All coupling steps were carried out with a manual peptide synthesizer (TSP-D type, Taiatsu Scientific Glass Co., Ltd.). The cleavage of the peptide-resin was achieved with a HF reaction apparatus (Type II, Peptide Institute, Inc. and

Toho Kasei Co., Ltd.). The melting points were determined on a Mel-Temp apparatus and are uncorrected. The homogenity of the synthetic peptides was confirmed by TLC on Merck silica gel F_{254} plates and HPLC. HPLC was performed with 4.6 mm×25 cm Finepak SIL ODS column with UV detection at 215 nm. The following solvent system was used for HPLC: *n*-PrOH-10% $NaClO_4$aq (1:4) at a flow rate of 1.5 ml min^{-1}. TLC was developed in the following solvent system: *n*-BuOH-AcOH-pyridine-water (4:1:1:2). Ninhydrin and Rydon[12] reagents were used for detection on TLC plates. Amino acid analyses were performed with a JEOL automatic amino acid analyzer, after the samples had been hydrolyzed with constant-boiling HCl in evacuated sealed ampoules for 20 h at 110 °C. The CD spectrum was measured with a JASCO model J-20 spectrometer.

Preparation of Boc-Met-BHA Resin. BHA resin hydrochloride[13] (5 g, 0.4 mequiv of NH_2 group/g) was placed in the Daiflon vessel of a peptide synthesizer, and operations were carried out as shown in Table 3.

Preparation of Boc-Phe-Phe-Gly-Leu-Met-BHA Resin. According to the series of operations outlined in Table 4, the above Boc-Met-BHA resin was treated in the vessel succesively. The pentapeptide resin, thus derived, was dried in a vacuum desiccator; it weighed 6.45 g.

[Dab^6]-SP(6-11). Boc-Phe-Phe-Gly-Leu-Met-BHA resin (1.63 g, 0.5 mequiv) was placed in the vessel, and the coupling of Boc-Dab(Boc)-OH (1.25 mmol)[14] was carried out, as shown in Table 4. After the second coupling (steps 12—15 in Table 4) used 0.625 mmol of Boc-Dab(Boc)-OH, the Boc groups on Dab were removed by steps 1—3. H-Dab-Phe-Phe-Gly-Leu-Met-BHA resin was treated with anhydrous liquid HF (ca. 15 ml) containing anisole (2 ml) and D,L-methionine (171 mg) at 0 °C for 1 h. After evaporation of HF in vacuo, the mixture of peptide and

Table 3. Program for Preparation of Boc-Met-BHA-resin

Step	Reagents[a]	Vol/ml	Mixing time (min)×repeated times
1	CH_2Cl_2	50	5×2
2	0.5 M Et_3N/CH_2Cl_2	20	15×2
3	CH_2Cl_2	30	5×3
4	Boc-Met-OH/CH_2Cl_2	4 mmol/40	15 h
	0.5 M DCC/CH_2Cl_2	8	
5	CH_2Cl_2	30	5×3
6	DMF	30	5×2
7	CH_2Cl_2	30	5×2
8	0.5 M Et_3N/CH_2Cl_2	10	10×2
9	CH_2Cl_2	30	5×2
10	Boc-Met-OH/CH_2Cl_2	2 mmol/20	15 h
	0.5 M DCC/CH_2Cl_2	4	
11	CH_2Cl_2	30	5×2
12	DMF	30	15×2
13	CH_2Cl_2	30	5×2
14	25% Ac_2O/CH_2Cl_2	10	2 h
	0.5 M Et_3N/CH_2Cl_2	50	
15	CH_2Cl_2	30	5×2

a) 1 M=1 mol dm^{-3}.

Table 4. Program for Coupling of Boc-Amino Acid

Step	Reagents	Vol/ml	Mixing time (min)×repeated times
1	30% TFA/CH_2Cl_2	40	3
	anisole	a few drops	
2	30% TFA/CH_2Cl_2	40	1 h
	anisole	a few drops	
3	CH_2Cl_2	30	5×3
4	0.5 M Et_3N/CH_2Cl_2	30	5×2
5	CH_2Cl_2	30	5×2
6	Boc-amino acid/CH_2Cl_2	5 mmol/40	5—20 h[a]
	0.5 M DCC/CH_2Cl_2	10	
7	CH_2Cl_2	30	5×2
8	DMF	30	5×2
9	CH_2Cl_2	30	5×2
10	0.5 M Et_3N/CH_2Cl_2	30	5×2
11	CH_2Cl_2	30	5×2
12	Boc-amino acid/CH_2Cl_2	2.5 mmol/20	5—20 h[a]
	0.5 M DCC/CH_2Cl_2	5	
13	CH_2Cl_2	30	5×2
14	DMF	30	5×2
15	CH_2Cl_2	30	5×2

a) Boc-Leu-OH 15 h, Boc-Gly-OH 5 h, Boc-Phe-OH 10 h; Boc-Dab(Boc)-OH, Boc-Lys(Boc)-OH, and Boc-Orn(Boc)-OH 20 h.

resin was washed with ethyl ether. The peptide was extracted with 30% AcOH and the extract was concentrated by lyophilization. The crude peptide was charged on a column (2×100 cm) of Bio-Gel P-2 and eluted with 2% AcOH. The main fractions (132 mg) were further chromatographed on a column (2×35 cm) of Sephadex G-25 eluted with the upper phase of the system 0.5% AcOH-*n*-BuOH (1:1). The fractions collected were evaporated in vacuo. The aqueous solution of the residue was lyophilized and a white crystalline peptide was obtained. Yield, 67 mg (15%); mp 177—178 °C; amino acid ratio: Dab 1.06, Phe 1.93, Gly 0.97, Leu 1.01, Met 1.03; TLC: R_f 0.69; HPLC: t_R(min) 11.4.

Found: C, 53.01; H, 6.95; N, 12.50%. Calcd for $C_{35}H_{52}N_8SO_6 \cdot 2AcOH \cdot 3H_2O$: C, 52.81; H, 7.50; N, 12.63%.

[Lys^6]-SP(6-11). This peptide was synthesized by the same procedure as described for the preparation of [Dab^6]-SP(6-11). Boc-Phe-Phe-Gly-Leu-Met-BHA resin (1.63 g, 0.5 mequiv) and Boc-Lys(Boc)-OH (1.25 mmol for the first coupling and 0.625 mmol for the second) were used and the yield was 18% (93 mg). Mp 188—191 °C; amino acid ratio: Lys 0.99, Phe 1.82, Gly 1.06, Leu 1.08, Met 1.05; TLC: R_f 0.63; HPLC: t_R(min) 9.8.

Found: C, 53.37; H, 7.05; N, 11.19%. Calcd for $C_{37}H_{56}N_8SO_6 \cdot 4AcOH \cdot 1.5H_2O$: C, 53.61; H, 7.50; N, 11.11%.

[Orn^6]-SP(6-11). Another Boc-Phe-Phe-Gly-Leu-Met-BHA resin (1.3 g, 0.61 mequiv) was used for the coupling with Boc-Orn(Boc)-OH (the first, 1.83 mmol and the second, 0.92 mmol). The procedure used was the same as that for the cases of the above two analogs. The purified analog weighed 38 mg (7%) and the mp was 168—171 °C. Amino acid ratio: Orn 0.96, Phe 1.98, Gly 1.01, Leu 1.01, Met 1.04; TLC: R_f 0.66; HPLC: t_R(min) 10.4.

Found: C, 54.55; H, 7.17; N, 12.41%. Calcd for $C_{36}H_{54}N_8SO_6 \cdot 2AcOH \cdot 2H_2O$: C, 54.41; H, 7.53; N, 12.69%.

Bioassay. Isolated ileum preparations from male guinea pigs (430—480 g) were suspended in a bath containing Tyrode's solution, bubbled with air and maintained at 37 °C. Contractions were recorded isotonically. The relative potencies of the test peptides were calculated from the EC_{50}(M) values.

References

1) Preliminary account of this work was presented at the 52nd Annual Meeting of the Chemical Society of Japan, Kyoto, April 1—4, 1986.

2) H. Yajima, K. Kitagawa, and T. Segawa, *Chem. Pharm. Bull.*, **21**, 2500 (1973).

3) K. Kitagawa, K. Ujita, Y. Kiso, T. Akita, Y. Nakata, N. Nakamoto, T. Segawa, and H. Yajima, *Chem. Pharm. Bull.*, **27**, 48 (1979).

4) K. Torigoe, S. Sofuku, H. Sato, and I. Muramatsu, "Peptide Chemistry 1981", ed by T. Shioiri, Peptide Research Foundation, Osaka, pp. 71—74 (1982).

5) Amino acids used are of the L-configuration. Abbreviations for amino acids and peptides follow the IUPAC-IUB nomenclature described in *Eur. J. Biochem.*, **138**, 9 (1984). Abbreviations used are: Dab, 2,4-diaminobutyric acid; Boc, *t*-butoxycarbonyl; DCC, dicyclohexylcarbodiimide; TFA, trifluoroacetic acid; DMF, dimethylformamide.

6) C. Poulos, J. R. Brown, and C. C. Jordan, *J. Med. Chem.*, **29**, 1281 (1986).

7) G. Barany and R. B. Merrifield, "The Peptides," ed by E. Gross and J. Meienhoffer, Academic Press, New York, pp. 1—284, Vol. 2 (1980).

8) S. Sofuku, *Kagaku To Kogyo*, **36**, 247 (1983).

9) P. G. Pietta and G. R. Marshall, *J. Chem. Soc., Chem. Commun.*, **1970**, 650.

10) A. Fournier, R. Couture, D. Regoli, M. Gendreau, and S. St-Pierre, *J. Med. Chem.*, **25**, 64 (1982).

11) B. Mehlis, S. Böhm, M. Becker, and M. Bienert, *Biochem. Biophys. Res. Commun.*, **66**, 1447 (1975).

12) H. N. Rydon and P. W. Smith, *Nature (London)*, **169**, 922 (1952).

13) This resin was purchased from Peptide Institute, Inc., Osaka.

14) This derivative was prepared by the method of L. Morder, A. Hallett, E. Wünsch, O. Keller, and G. Wersin, *Hoppe-Seyler's Z. Physiol. Chem.*, **357**, 1651 (1976). L-2,4-Diaminobutyric acid dihydrochloride was purchased from Fluka AG, Switzerland and Boc-Dab(Boc)-OH·DCHA (DCHA=dicyclohexylamine) was obtained in a 62% yield; mp 118—120 °C. Anal. ($C_{26}H_{49}N_3O_6$) C, H, N.

A Facile Method for the Preparation of γ-Alkenyl-γ-butyrolactones

Masatoshi KAWASHIMA and Tamotsu FUJISAWA*
Chemistry Department of Resources, Mie University, Tsu, Mie 514
(Received April 28, 1988)

Synopsis. Methyl substituted γ-alkenyl-γ-butyrolactones were prepared from easily available α,β-unsaturated aldehydes such as acrylaldehyde, methacrylaldehyde, crotonaldehyde, and 3-methyl-2-butenal.

The structure of γ-alkenyl-γ-butyrolactones belongs to a kind of allylic esters and the lactones have been utilized to many synthetic reactions. For example, allylic substitutions of the lactones with organocopper reagents,[1] with ester enolate,[2] and with allylsilanes[3] leading to 4-alkenoic acids and 4,8-alkadienoic acid esters have been developed. Moreover γ-alkenyl-γ-butyrolactones have been incorporated in important key compounds for the synthesis of natural products such as ipsdienol,[4] biotin,[5] urinary metabolites of retinoic acid,[6] chrysanthemic acid,[7] avenaciolide,[8] marmelo oxide,[9] and dihydromevinolin.[10] The lactones have been prepared by many methods[11] such as condensation of vinyl epoxide with ethyl cyanoacetate and with diethyl malonate, decarboxylation of 2-vinyl-1,1-cyclopropanedicarboxylic acid prepared from 1,4-dibromo-2-butene and diethyl malonate, and reaction of 1,3-diene with carboxylic acid in the presence of metal oxide, however, these methods seem to have a limitation at the point of generality in which the kinds of applicable starting materials are confined. Here we wish to report the convenient method for the synthesis of methyl-substituted γ-alkenyl-γ-butyrolactones by the combination of easily available starting materials, two molecules of α,β-unsaturated aldehydes such as acrylaldehyde, methacrylaldehyde, crotonaldehyde, and 3-methyl-2-butenal.[12] General synthetic route was outlined in Scheme 1.

Although all of the aldehydes **1** are easily converted to the corresponding bromo acetal according to the published method for the preparation of 2-(2-bromoethyl)-1,3-dioxane (**2a**) from acrylaldehyde, 1,3-propanediol, and anhydrous hydrogen bromide,[13] crotonaldehyde and 3-methyl-2-butenal were transformed into the corresponding chloro acetals, which are preferable in the preparation of secondary and tertiary Grignard reagents rather than the corresponding bromo acetal. In the acetalization of 3-methyl-2-butenal, hydrochlorination was carried out in the presence of tetrabutylammonium chloride and Molecular Sieves 3A to improve the yields. These bromo and chloro acetals **2** were converted into the corresponding Grignard reagents **3** by the usual method.[13] Then the reactions of Grignard reagents **3** with aldehydes **4** gave the allylic alcohols **5** in high or moderate yields. An attempt of direct hydrolysis of **5** to lactol **7** in aqueous media unfortunately did not succeed even in a mixed solvent such as acetone–water because of the poor solubility in water except for the case of **5a**. Therefore the alcohols **5** were converted to lactol ether **6** in acidic methanol followed by hydrolysis of **6** in acidic aqueous acetone to give lactol **7** in moderate yields without accompanying a tautomer of the lactol, γ-hydroxy aldehyde. In the last oxidation step of **7** to **8**, silver oxide, prepared in situ from silver nitrate and sodium hydroxide, was used as the suitable oxidant which did not oxidize carbon–carbon double bond. The diastereomer ratios of the lactones **8b** and **8c** were determined by GLC analysis as 43:57 and 79:21, respectively. Unfortunately, assignment of the configurations of these lactones did not succeed. To reveal the utility of this method for the preparation of γ-alkenyl-γ-butyrolactone, a precursor **8e**[7] of chrysanthemic acid was synthesized from 3-methyl-2-butenal as the starting material.

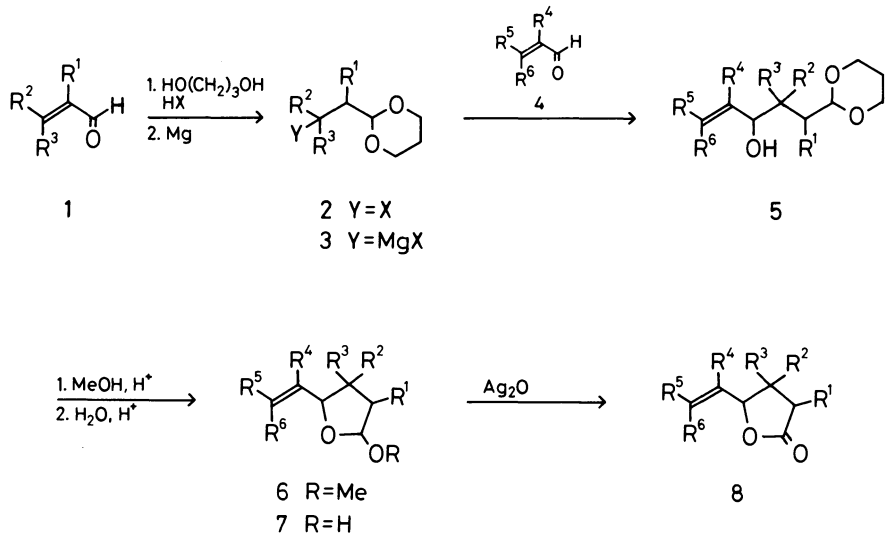

1 2 Y=X 3 Y=MgX 5 6 R=Me 7 R=H 8

Scheme 1.

Table 1. Preparation of γ-Alkenyl-γ-butyrolactones

Run	R^1	R^2	R^3	R^4	R^5	R^6	Yield/% 2	3	5	6	7	8
a	H	H	H	H	H	H	—	—	46[a]	—	53[b]	90
b	Me	H	H	Me	H	H	60(X=Br)	74	91	71	75	47
c	H	Me	H	Me	H	H	100(X=Cl)	68	74	65	52	41
d	H	H	H	Me	H	H	—	—	70[a]	68	69	83
e	H	Me	Me	H	Me	Me	68(X=Cl)	41	61	66	68	43

a) The yields were calculated from **1a**. b) The yield was calculated from **5a**.

Results for the synthesis of **8** were summarized in Table 1.

As described above, this method for the preparation of γ-alkenyl-γ-butyrolactone has the following advantages; (i) easy availabilities of starting materials and the other reagents, (ii) simple procedure and operations, (iii) generality for the preparation of various substituted γ-alkenyl-γ-butyrolactones.

Experimental

General. Boiling points were measured at the pressure indicated and are uncorrected. Infrared spectra (neat) were recorded on a Hitachi EPI-G2 spectrometer. ^{1}H NMR spectra were recorded on a JEOL JNM-PMX60SI spectrometer with Me_4Si as an internal standard in CCl_4. GLC analysis was performed on a Yanaco G-180 Gas Chromatograph.

Materials. Acrylaldehyde, methacrylaldehyde, crotonaldehyde, 3-methyl-2-butenal, 2-(2-bromoethyl)-1,3-dioxane, and the other reagents were commercially available.

Acetalization of Aldehydes 1b,c,e to 2b,c,e. According to the reported procedure[13] for the preparation of **2a**, 2-(2-bromo-1-methylethyl)-1,3-dioxane (**2b**) was prepared from methacrylaldehyde, 1,3-propanediol, and anhydrous HBr. In the similar manner as the preparation of **2b**, the other chloro acetals **2c** and **2e** were prepared from crotonaldehyde and 3-methyl-2-butenal, respectively, by the treatment with 1,3-propanediol saturated with anhydrous HCl in the presence of a half mole of tetrabutylammonium chloride. **2b**: bp 61—62 °C/0.5 mmHg (1 mmHg=133.322 Pa); ^{1}H NMR δ=1.02 (d, J=7 Hz, 3H), 0.83—2.43 (m, 3H), 3.08—4.28 (m, 6H), and 4.39 (d, J=5 Hz, 1H); IR 1145 (s), 1110 (s), and 1015 (s) cm^{-1}; Found: C, 40.46; H, 6.48%. Calcd for $C_7H_{13}BrO_2$: C, 40.21; H, 6.27%. **2c**: bp 63—64 °C/5 mmHg; ^{1}H NMR δ=1.05—2.53 (m, 2H), 1.48 (d, J=7 Hz, 3H), 1.93 (dd, J=5 Hz, 6 Hz, 2H), 3.47—4.50 (m, 5H), and 4.68 (t, J=5 Hz, 1H); IR 1140 (s), 1105 (s), 1080 (s), 1030 (s), 1000 (s), and 620 (s) cm^{-1}; Found: C, 50.94; H, 8.00%. Calcd for $C_7H_{13}ClO_2$: C, 51.07; H, 7.96%. **2e**: bp 68—70 °C/1.5 mmHg; ^{1}H NMR δ=0.82—2.43 (m, 2H), 1.55 (s, 6H), 1.96 (d, J=4.5 Hz, 2H), 3.40—4.21 (m, 4H), and 4.65 (t, J=4.5 Hz, 1H); IR 1145 (s), 1130 (s), 1115 (s), 1085 (s), and 990 (s) cm^{-1}; Found: C, 53.84; H, 8.46%. Calcd for $C_8H_{15}ClO_2$: C, 53.78; H, 8.46%.

Preparation of Grignard Reagents 3a—e. Grignard reagents **3a—e** were prepared from **2a—e**, respectively, by the treatment with magnesium turning in gently refluxing THF in the similar manner to the published procedure[13] and standardized by titration with 2-butanol using 1,10-phenanthroline as an indicator.[14]

Preparation of the Allylic Alcohols 5a—e. To the THF solution of **3a** (145 ml, 170 mmol) was added a solution of **1a** (10.0 g, 178 mmol) in THF (50 ml) at 0 °C and stirred at the same temperature for 3 h. Then the mixture was quenched by pouring into saturated aq. NH_4Cl and the layer were separated. The aqueous phase was washed three times with ether and the combined organic layers were washed with brine, dried with anhydrous $MgSO_4$, and concentrated. Distillation of the residue under a reduced pressure gave 2-(3-hydroxy-4-pentenyl)-1,3-dioxane (**5a**) (18.6 g, 108 mmol): bp 100—102 °C/1.5 mmHg; ^{1}H NMR δ=1.00—2.48 (m, 6H), 3.17 (s, 1H), 3.40—4.30 (m, 5H), 4.30—4.73 (m, 1H), and 4.85—6.14 (m, 3H); IR 3450 (s), 1145 (s), 1090 (s), 990 (s), and 925 (s) cm^{-1}; Found: C, 62.92; H, 9.48%. Calcd for $C_9H_{16}O_3$: C, 62.77; H, 9.36%.

In exactly the same manner as above, methyl-substituted analogues **5b—e** were prepared. **5b**: bp 125—127 °C/1.5 mmHg; ^{1}H NMR δ=0.75—2.47 (m, 5H), 0.93 (d, J=6 Hz, 3H), 1.70 (br s, 3H), 3.10 (s, 1H), 3.40—4.56 (m, 6H), 4.75 (br s, 1H), and 4.88 (br s, 1H); IR 3450 (s), 1145 (s), 1120 (s), 1100 (s), 1050 (s), 1000 (s), and 890 (s) cm^{-1}; Found: C, 65.68; H, 10.17%. Calcd for $C_{11}H_{20}O_3$: C, 65.97; H, 10.07%. **5c**: bp 102—104 °C/0.4 mmHg; ^{1}H NMR δ=0.83 (d, J=6 Hz, 3H), 1.05—2.45 (m, 5H), 1.63 (s, 3H), 3.04 (s, 1H), 3.28—4.25 (m, 5H), 4.51 (t, J=5 Hz, 1H), and 4.65—5.00 (m, 2H); IR 3425 (s), 1140 (s), 1105 (s), 1070 (s), 1015 (s), 990 (s), and 890 (s) cm^{-1}; Found: C, 65.70; H, 10.17%. Calcd for $C_{11}H_{20}O_3$: C, 65.97; H, 10.07%. **5d**: bp 116—118 °C/1 mmHg; ^{1}H NMR δ=0.77—2.47 (m, 9H), 2.83 (s, 1H), 3.30—4.30 (m, 5H), 4.33—4.63 (m, 1H), 4.76 (d, J=1.5 Hz, 1H), and 4.88 (d, J=1.5 Hz, 1H); IR 3450 (s), 1140 (s), 1085 (s), 990 (s), and 890 (s) cm^{-1}; Found: C, 64.56; H, 9.90%. Calcd for $C_{10}H_{18}O_3$: C, 64.49; H, 9.74%. **5e**: bp 135—138 °C/1.5 mmHg; ^{1}H NMR δ=0.75—2.47 (m, 4H), 0.90 (s, 3H), 0.93 (s, 3H), 1.67 (s, 3H), 1.75 (s, 3H), 2.91 (s, 1H), 3.47—4.33 (m, 5H), 4.67 (t, J=5 Hz, 1H), and 5.25 (d, J=9 Hz, 1H); IR 3500 (s), 1140 (s), 1085 (s), 1035 (s), 1000 (s), 985 (s), and 820 (m) cm^{-1}; Found: C, 68.08; H, 10.66%. Calcd for $C_{13}H_{24}O_3$: C, 68.38; H, 10.60%.

Preparation of Lactol Ether 6b—e. A solution of **5b** (1.70 g, 8.49 mmol) in MeOH (40 ml) was acidified with 2 drops of 6 M HCl (1 M=1 mol dm^{-3}) and stirred at room temperature for 12 h. After neutralization with saturated aq. $NaHCO_3$, ether was added to the mixture. The organic layer was separated and the aqueous layer was washed three times with ether. The combined extracts were washed with water. After the solution was dried with anhydrous $MgSO_4$ and concentrated, distillation of the residue under the reduced pressure afforded 2-methoxy-3-methyl-5-isopropenyltetrahydrofuran (**6b**) (940 mg, 6.01 mmol): bp 69—71 °C/24 mmHg; ^{1}H NMR δ=1.01 (br d, J=7 Hz, 3H), 1.23—2.37 (m, 3H), 1.69 (br s, 3H), 3.27 (s, 3H), 4.13—4.63 (m, 2H), 4.70 (br s, 1H), and 4.90 (br s, 1H); IR 1100 (s), 1070 (s), 1010 (s), and 895 (s) cm^{-1}; Found: C, 69.11; H, 10.48%. Calcd for $C_9H_{16}O_2$: C, 69.19; H, 10.32%.

In the same manner as above, methyl-substituted analogues **6c—e** were prepared. **6c**: bp 75—78 °C/22 mmHg; ^{1}H NMR δ=0.63—1.17 (m, 3H), 1.33—2.63 (m, 6H), 3.23 (s, 3H), 3.67—3.97 (m, 0.6H), 4.18—4.45 (m, 0.6H), and 4.67—5.10 (m, 2.8H); IR 1100 (s), 1070 (s), 1030 (s), and 895 (s) cm^{-1}; Found: C, 68.91; H, 10.37%. Calcd for $C_9H_{16}O_2$: C, 69.19; H, 10.32%. **6d**: bp 73—75 °C/30 mmHg; ^{1}H NMR δ=1.42—2.33 (m, 7H), 3.32 (s, 3H), 4.42 (br t, J=7 Hz, 1H), 4.77 (br s, 1H), and 4.85—5.13 (m, 2H); IR 1205 (s), 1105 (s), 1050 (s), 1035 (s), and 895 (s) cm^{-1}; Found: C, 67.33; H,

10.06%. Calcd for $C_8H_{14}O_2$: C, 67.57; H, 9.92%. **6e**: bp 105—110 °C/33 mmHg; ^{1}H NMR δ=0.85 (s, 3H), 0.98 (s, 3H), 1.47—2.17 (m, 2H), 1.70 (s, 3H), 1.77 (s, 3H), 3.25 (s, 3H), 4.07—4.40 (m, 1H), 4.82 (t, J=5 Hz, 1H), and 5.05 (d, J=8 Hz, 1H); IR 1100 (s), 1050 (s), 1030 (s), 1000 (s), 980 (s), and 840 (s) cm^{-1}; Found: C, 71.98; H, 11.00%. Calcd for $C_{11}H_{20}O_2$: C, 71.70; H, 10.94%.

Hydrolysis of 5a and 6b—e to Lactol 7a—e. A solution of **5a** (1.34 g, 7.77 mmol) in 10% H_2SO_4 (45 ml) and stirred at room temperature for 12 h. The mixture was extracted three times with ether. After the extracts were washed with brine, dried with anhydrous $MgSO_4$, and concentrated, distillation of the residue under a reduced pressure afforded 2-hydroxy-5-vinyltetrahydrofuran (**7a**) (474 mg, 4.15 mmol): bp 80—100 °C/1.5 mmHg (Kugelrohr); ^{1}H NMR δ=1.00—2.65 (m, 4H), 3.75 (br s, 1H), 4.17—4.80 (m, 1H), and 4.83—6.25 (m, 4H); IR 3420 (s), 1050 (s), 1020 (s), 990 (s), and 925 (s) cm^{-1}; Found: C, 63.37; H, 9.02%. Calcd for $C_6H_{10}O_2$: C, 63.14; H, 8.83%.

In the same manner as above, methyl-substituted analogues **7b—e** were prepared. **7b**: bp 60—70 °C/1.5 mmHg (Kugelrohr); ^{1}H NMR δ=1.05 (br d, J=6 Hz, 3H), 1.23—2.57 (m, 3H), 1.70 (br s, 3H), and 4.05—5.43 (m, 5H); IR 3425 (s), 1075 (s), 1040 (s), 1000 (s), 990 (s), and 895 (s) cm^{-1}; Found: C, 67.47; H, 9.96%. Calcd for $C_8H_{14}O_2$: C, 67.57; H, 9.92%. **7c**: bp 65—70 °C/1.5 mmHg; ^{1}H NMR δ=0.73—1.17 (m, 3H), 1.17—2.76 (m, 6H), and 3.65—5.75 (m, 5H); IR 3425 (s), 1090 (s), 1070 (s), 1050 (s), 1010 (s), 980 (s), and 895 (s) cm^{-1}; Found: C, 67.37; H, 9.97%. Calcd for $C_8H_{14}O_2$: C, 67.57; H, 9.92%. **7d**: bp 100—120 °C/1.5 mmHg (Kugelrohr); ^{1}H NMR δ=1.50—2.17 (m, 7H), 4.10—5.13 (m, 4H), and 5.17—5.73 (m, 1H); IR 3425 (s), 1060 (s), 1045 (s), 1000 (s), 980 (s), and 895 (s) cm^{-1}; Found: C, 65.55; H, 9.47%. Calcd for $C_7H_{12}O_2$: C, 65.60; H, 9.44%. **7e**: mp 65—70 °C; bp 70-85 °C/1.5 mmHg; ^{1}H NMR δ=0.87 (s, 3H), 1.00 (s, 3H), 1.50—2.07 (m, 2H), 1.70 (s, 3H), 1.77 (s, 3H), and 4.12—5.67 (m, 4H); IR 3375 (s), 1095 (s), 1050 (s), 1025 (s), 1000 (s), 985 (s), and 840 (s) cm^{-1}; Found: C, 70.39; H, 10.72%. Calcd for $C_{10}H_{18}O_2$: C, 70.55; H, 10.66%.

Oxidation of 7a—e to γ-Alkenyl-γ-butyrolactone 8a—e. To a solution of silver nitrate (780 mg, 4.59 mmol) in water (1 ml), 6.51 M NaOH solution (1.80 ml, 11.7 mmol) was added at room temperature. The mixture was heated to 50 °C and methanol (1 ml) was added. After being cooled to 0 °C, a solution of **7a** (262 mg, 2.29 mmol) in MeOH (2 ml) was added to the suspension of silver oxide. The reaction mixture was stirred at 40 °C for 12 h. After being cooled to room temperature and acidified with 10% H_2SO_4, the mixture was extracted with $CHCl_3$. The extracts were washed with water and brine, dried with anhydrous $MgSO_4$, and concentrated. Distillation of the residue gave 5-vinyltetrahydro-2-furanone (**8a**)[11b] (232 mg, 2.07 mmol): bp 100—120 °C/1.5 mmHg (Kugelrohr); ^{1}H NMR δ=1.78—3.15 (m, 4H), 4.78—6.20 (m, 4H); IR 1775 (s) and 980 (s) cm^{-1}.

In the same manner as above, methyl-substituted analogues **8b—e** were prepared. Determination of the diastereomer ratios of the lactones **8b** and **8c** was performed by analytical GLC (0.25 mm×50 m FFAP column, 120 °C, relative retention time was 1.00:1.01 and 1.00:1.07, respectively. **8b**: bp 120—130 °C/1.5 mmHg (Kugelrohr); ^{1}H NMR δ=1.25 (d, J=7 Hz, 3H), 1.50—3.05 (m, 3H), 1.75 (s, 3H), 4.54—5.20 (m, 3H); IR 1775 (s) and 900 (s) cm^{-1}; Found: C, 68.77; H, 8.55%. Calcd for $C_8H_{12}O_2$: C, 68.55; H, 8.63%. **8c**: bp 120—130 °C/1.5 mmHg (Kugelrohr); ^{1}H NMR δ=0.79—1.27 (m, 3H), 1.75 (s, 3H), 1.80—2.93 (m, 3H), 4.25—4.60 (m, 1H), 4.98 (br s, 2H); IR 1780 (s) and 910 (s) cm^{-1}; Found: C, 68.36; H, 8.74%. Calcd for $C_8H_{12}O_2$: C, 68.55; H, 8.63%. **8d**: bp 110—130 °C/1.5 mmHg (Kugelrohr); ^{1}H NMR δ=1.76 (s, 3H), 1.80—2.77 (m, 4H), 4.70—5.18 (m, 3H); IR 1770 (s) and 900 (s) cm^{-1}; Found: C, 66.54; H, 8.11%. Calcd for $C_7H_{10}O_2$: C, 66.65; H, 7.99%. **8e**:[7] mp 45—50 °C; bp 130—150 °C/1.5 mmHg (Kugelrohr); ^{1}H NMR δ=1.00 (s, 3H), 1.12 (s, 3H), 1.73 (s, 3H), 1.80 (s, 3H), 2.31 (s, 1H), 2.34 (s, 1H), 4.78 (d, J=9 Hz, 1H), 5.19 (br d, J=9 Hz, 1H); IR 1775 (s) and 850 (m) cm^{-1}.

References

1) T. Fujisawa, T. Sato, M. Kawashima, K. Naruse, and K. Tamai, *Tetrahedron Lett.*, **23**, 3583 (1982); B. M. Trost and T. P. Klun, *J. Org. Chem.*, **45**, 4256 (1980); b) idem, *J. Am. Chem. Soc.*, **101**, 6756 (1979).

2) B. M. Trost and T. P. Klun, *J. Am. Chem. Soc.*, **103**, 1864 (1981).

3) T. Fujisawa, M. Kawashima, and S. Ando, *Tetrahedron Lett.*, **25**, 3213 (1984).

4) K. Mori, T. Takigawa, and T. Matsuo, *Tetrahedron*, **35**, 933 (1979).

5) T. Ravindranathan, S. V. Hiremath, D. R. Reddy, and A. V. R. Rao, *Carbohydr. Res.*, **134**, 332 (1984).

6) T. H. Kim, K. Kon, and S. Isoe, *Helv. Chim. Acta*, **66**, 1936 (1983).

7) M. Julia, S. Julia, and B. Cochet, *Bull. Soc. Chim. Fr.*, **1964**, 1476 and 1487.

8) J. Kallmerten and T. J. Gould, *J. Org. Chem.*, **50**, 1128 (1985).

9) Y. Nishida, Y. Fukushima, H. Ohrui, and H. Meguro, *Agric. Biol. Chem.*, **48**, 1217 (1984).

10) A. H. Davidson, C. D. Floyd, A. J. Jones, and P. L. Myers, *J. Chem. Soc., Chem. Commun.*, **1985**, 1662.

11) a) G. D. Zuidema, P. L. Cook, and G. Van Zyl, *J. Am. Chem. Soc.*, **75**, 294 (1953); G. Van Zyl, E. E. van Tamelen, *ibid.*, **72**, 1357 (1950); O. R. Kreimeier, U. S. Patent 2122719 (1938); *Chem. Abstr.*, **33**, 6669 (1938); J. O. Jiiek and M. Protiva, *Coll. Czech. Comm.*, **23**, 692 (1980); R. Rusell and C. A. V. Werf, *J. Am. Chem. Soc.*, **69**, 11 (1947); idem., *ibid.*, **92**, 735 (1978); E. I. Heiba, R. M. Dessau, and P. G. Rodewald, *ibid.*, **96**, 7977 (1974); b) S. F. Birch, R. A. Dean, and N. J. Hunter, *J. Org. Chem.*, **23**, 1390 (1958).

12) Analogous methods for the preparation of γ-alkenyl-γ-butyrolactones and δ-alkenyl-δ-valerolactones were reported in following papers, but the detailed data were not described: Ref. 1b and S. Danishefsky, R. L. Funk, and J. F. Kerwin, Jr., *J. Am. Chem. Soc.*, **102**, 6889 (1980); and see also Ref. 6.

13) J. C. Stowell, *J. Org. Chem.*, **41**, 560 (1976).

14) S. C. Watson and J. F. Eastham, *J. Organomet. Chem.*, **9**, 165 (1967).

Asymmetric Addition of Organometallic Reagents to Homochiral β-Ketoacetals

Takahiro HOSOKAWA,* Tetsushi YAGI, Yoshiharu ATAKA, and Shun-Ichi MURAHASHI*
Department of Chemistry, Faculty of Engineering Science, Osaka University,
Machikaneyama, Toyonaka, Osaka 560
(Received May 9, 1988)

Synopsis. The diastereoselectivity of the carbonyl addition of organolithium reagents to β-keto acetals was examined. Addition of MeLi to β-keto acetal derived from Pd(II)-catalyzed acetalization of phenyl vinyl ketone with (*R*,*R*)-2,4-pentanediol gave (4*R*,6*R*)-4,6-dimethyl-2-[(2*R*)-2-hydroxy-2-phenylpropyl]-1,3-dioxane in 75%de.

We have recently found that terminal olefins bearing electron-withdrawing substituents such as COR, COOR, and CN are regioselectively acetalized at the terminal olefinic carbon with diols by using a catalyst system of $PdCl_2$–CuCl–O_2.[1] The reaction with readily available (*R*,*R*)-2,4-pentanediol gives homochiral acetals having functional groups at the side chain.

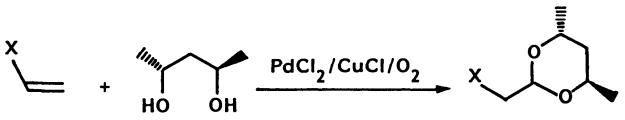

X= electron-withdrawing group

Homochiral cyclic acetals derived from (*R*,*R*)-2,4-pentanediol may be regarded as one of the useful precursors for the synthesis of homochiral alcohols. This stems from the basic finding that one of the diastereotopic acetal bonds is stereoselectively cleaved by nucleophiles in the presence of Lewis acids.[2] Described herein is a fundamental reaction using the acetal moiety as the chiral auxiliary, that is the diastereofacial differenciating addition[3] of alkyllithium reagents to β-keto acetal **1** leading to β-hydroxy acetal **2**.

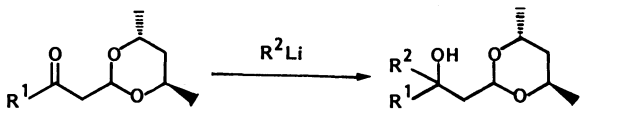

1

a: R^1=Ph
b: R^1=Me
c: R^1=H

2

a: R^1=Ph R^2=Me
b: R^1=Ph R^2=Bu^n
c: R^1=Me R^2=Bu^n
d: R^1=H R^2=Me

Results and Discussion

The keto acetals **1a** and **1b** were prepared by the Pd(II)-catalyzed acetalization of the corresponding vinyl ketones with (*R*,*R*)-2,4-pentanediol. Acetalization of vinyl acetal **3** with ethanol led to bis-acetal **4**, which upon hydrolysis gave the homochiral acetal **1c**.[4] The bis-acetal **4** can be also prepared by partial acetal-exchange reaction of 1,1,3,3-tetraethoxypropane with (*R*,*R*)-2,4-pentanediol.

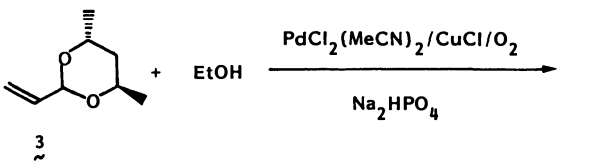

3

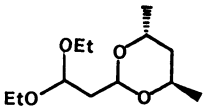

4

Commonyl used organometallic reagents such as RLi and RMgX were allowed to react with the carbonyl group of **1** under various conditions. In contrast to the carbonyl addition to α-keto acetals derived from (+)-tartaric acid,[5] RLi was found to react more selectively than RMgX. Thus, the reaction of **1a** (R=Ph)(5×10^{-2} M, 1 M=1 mol dm^{-3}) with 2 equiv of MeLi at −78 °C in ether gives **2a** as crystals in a relatively high diastereomeric excess (75% de), while the selectivity is extremely low with MeMgI (Table 1, Entries 1 and 2). The alcohol **2a** obtained was purified by recrystallizations to give a single diastereomer. Although the differenciation is significantly dependent on the nature of substituent R at β-carbon and reagents (Table 1, Entries 4—7), it is remarkable that a 75% differenciation is attained with **2a**, in spite of the reaction site being far from the chiral center.

The configuration of newly created chiral center in **2a** was determined to be (*R*) by the following transformations. The acetal exchange of recrystallized **2a** ($[\alpha]_D^{27}$ +22.0°) with methanol followed by hydrolysis (Amberlyst 15, acetone–H_2O) gave β-hydroxy aldehyde **6**, which upon reduction with $LiAlH_4$ afforded *R*-(+)-diol **7** ($[\alpha]_D^{26}$ +65.2°, 97.7% ee) of the known configuration.[6] Of note is that direct hydrolysis of **2a** to **6** by using HCl and *p*-TsOH was unsuccessful.

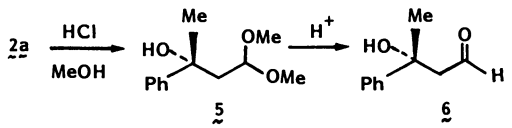

5 **6**

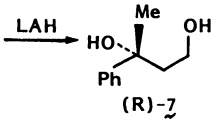

(R)-**7**

There is no doubt that the 1,3-dioxane **1** is conformationally most stable when the $RCOCH_2$ group at the C-2 carbon is in equatorial. If the C=O group in this moiety occupies the conformation as depicted

Table 1. Addition Reaction of Organometallic Reagents to Keto Acetals **1**

Entry	Acetal **1** R¹		Reagent (equiv)	Product **2** R¹	R²		Isolated yield/%	de[a]/%
1	Ph	**1a**	MeLi (2.0)	Ph	Me	**2a**	72	75
2	Ph	**1a**	MeMgI (2.0)	Ph	Me	**2a**	82[b]	7
3	Ph	**1a**	MeLi (2.0)/$TiCl_4$ (1.3)	Ph	Me	**2a**	34[b]	42[c]
4	Ph	**1a**	*n*-BuLi (2.5)	Ph	*n*-Bu	**2b**	42	3[d]
5	Me	**1b**	PhLi (2.5)	Me	Ph	**2a**	99	6
6	Me	**1b**	*n*-BuLi (2.8)	Me	*n*-Bu	**2c**	65	3
7	H	**1c**	MeLi (2.5)	H	Me	**2d**	83	55

a) Determined by capillary column GLC analysis. b) Determined by GLC analysis. c) In contrast to Entry 1, the formation of predominant diastereomer was reversed. d) Determined by NMR (FX-100).

in Scheme 1, the backside (*si*-face) of the diastereoplane of **1a** (R=Ph) is obviously less hindered. Coordination of Li to the oxygen atoms and subsequent attack of the methyl anion to the C=O bond from the *si*-face creates (*R*)-chiral carbon in **2a**. If this is the case, the conformational preference of $RCOCH_2$ group is determined by the nature of the substituent R and reagent.

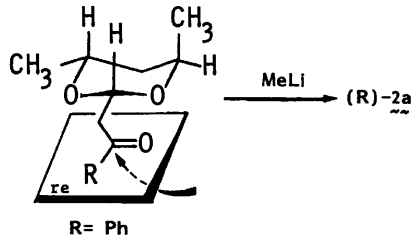

Scheme 1.

Experimental

Preparation of **1a** and **1b** was reported previously.[1] The keto acetal **1b** is also obtained by the reaction of 4-methoxy-3-butene-2-one with (*R,R*)-2,4-pentanediol.[7] Preparation of **1c** was described below.

(4*R*,6*R*)-4,6-Dimethyl-2-ethenyl-1,3-dioxane (3). Into a solution of (*R,R*)-2,4-pentanediol (Wako Pure Chemical Ind.) (1.00 g, 9.60 mmol), acrylaldehyde (1.30 mL, 19.4 mol), and *p*-TsOH (190 mg, 1.0 mmol) in anhydrous ether (20 mL) was added Molecular Sieves 4A (1.0 g). The mixture was stirred for 17 h at room temperature, and filtered. After addition of saturated aqueous $NaHCO_3$ (5 mL), the mixture was extracted with ether and dried ($MgSO_4$). Kugelrohr distillation gave **3** (1.14 g, 84% yield): bp 76—83 °C (64 mmHg); ^1H NMR (60 MHz, $CDCl_3$) δ=1.22 (3H, d, J=6.2 Hz, CH_3), 1.39 (3H, d, J=6.8 Hz, CH_3), 1.57—2.20 (m, 2H, C_5-H), 3.72—4.60 (2H, m, C_4- and C_6-H), 5.05—5.42 (2H, m, H_2C=C), and 5.45—6.20 (2H, m, C=CH and C_2-H); MS *m/z* 141 (M^+-1).

Found: C, 67.40; H, 9.91%. Calcd for $C_8H_{14}O_2$: C, 67.57; H, 9.92%.

(4*R*,6*R*)-4,6-Dimethyl-2-(2,2-diethoxyethyl)-1,3-dioxane (4). i) Pd(II)-Catalyzed Acetalization of 3 with Ethanol. To a test tube were placed a magnetic stirring bar, CuCl (10 mg, 0.10 mmol), Na_2HPO_4 (71 mg, 0.50 mmol), and ethanol (0.36 mL, 6.13 mmol), and there was added a solution of acrylaldehyde acetal **3** (143 mg, 1.00 mmol) and triethyl orthoformate (296 mg, 2.00 mmol) in DME (1 mL) and then $PdCl_2(CH_3CN)_2$ (26 mg, 0.10 mmol). The test tube was placed into an autoclave (10 mL) into which a 10 kg cm^{-2} pressure of O_2 was introduced. After stirring for 24 h at 50 °C, the resulting solution was cooled to room temperature, diluted with ether, and filtered. Florisil column chromatography (2.0 g, 1.5×1 cm) with ether (60 mL) gave oily material (221 mg), from which the product **4** (103 mg, 44%) was isolated by preparative TLC (SiO_2, hexane-EtOAc=7:3). **4**: R_f 0.64; ^1H NMR (500 MHz, $CDCl_3$) δ=1.19 (3H, d, J=6.3 Hz, C_4-Me_{eq}), 1.20 (6H, t, J=7.0 Hz, -$CH_2\underline{CH_3}$), 1.31—1.43 (1H, m, C_5-H), 1.35 (3H, d, J=6.9 Hz, C_6-Me_{ax}), 1.83 (1H, ddd, J=6.3, 11.4, and 13.4 Hz, C_5-H), 1.87 (1H, dt, J=14.1 and 6.7 Hz, $C_{1'}$-H), 1.94 (1H, dt, J=14.1 and 6.7 Hz, $C_{1'}$-H), 3.51 (1H, dq, J=9.7 and 7.0 Hz, -$OC\underline{H_2}CH_3$), 3.53 (1H, dq, J=9.7 and 7.0 Hz, -$OC\underline{H_2}CH_3$), 3.63 (1H, dq, J=9.3 and 7.0 Hz, -$OC\underline{H_2}CH_3$), 3.68 (1H, dq, J=9.3 and 7.0 Hz, -$OC\underline{H_2}CH_3$), 3.95 (1H, ddq, J=2.7, 6.3, and 11.4 Hz, C_6-H_{ax}), 4.28 (1H, dq, J=6.3 and 6.3 Hz, C_4-H_{eq}), 4.67 (1H, t, J=6.7 Hz, $C_{2'}$-H), and 4.96 (1H, t, J=6.7 Hz, -OCHO-); MS *m/z* 231 (M^+-1).

Found: C, 61.81; H, 10.19%. Calcd for $C_{12}H_{24}O_4$: C, 62.04; H, 10.41%.

ii) Partial Acetal Exchange of 1,1,3,3-Tetraethoxypropane with (*R,R*)-2,4-Pentanediol. To a solution of 1,1,3,3-tetraethoxypropane (Nakarai Kagaku) (1.43 g, 6.49 mol) and (*R,R*)-2,4-pentanediol (320 mg, 3.07 mmol) dissolved in THF (6 mL) was slowly added concd H_2SO_4 (10 µl), and the acidic solution was stirred for 4 h at 50 °C. The resulting mixture was neutralized with saturated aqueous $NaHCO_3$ (10 mL×2), and the aqueous layer was extracted with ether. The extract was dried ($MgSO_4$) and evaporated to give oily material (1.351 g), which was subjected into SiO_2 column chromatography (45 g, 17×0.9 cm). Unreacted 1,1,3,3-tetraethoxypropane (0.478 g) was recovered from 210 mL of elution with a 9:1 solution of hexane-EtOAc. Further elution (80 mL) gave **4** (0.520 g, 73%).

In this reaction 2,2'-methylene bis[(4*R*,6*R*)-4,6-dimethyl-1,3-dioxane] was formed as the byproduct.

(4*R*,6*R*)-4,6-Dimethyl-2-(2-oxoethyl)-1,3-dioxane (1c). Into a solution of the acetal **4** (200 mg, 0.86 mmol) in acetone (5 mL) and water (40 µL, 2.2 mmol) was added Amberlyst 15 (10 mg), and the mixture was stirred for 24 h at room temperature and filtered. The product was extracted with ether, dried ($MgSO_4$), and concentrated to give **1c** (75 mg, 55%): ^1H NMR (500 MHz, $CDCl_3$) δ=1.20 (3H, J=6.2 Hz, C_6-Me_{eq}), 1.38 (3H, d, J=6.9 Hz, C_4-Me_{ax}), 1.34—1.38 (1H, m, C_5-H_{eq}), 1.85 (1H, ddd, J=6.2, 11.9, and 13.3 Hz, C_5-H_{ax}), 2.62 (2H, dd, J=2.3 and 4.7 Hz, $C_{1'}$-H), 4.00 (1H, ddq, J=2.3, 11.9, and 6.2 Hz, C_6-H_{ax}), 4.31 (1H, dq, J=6.2 and 6.9 Hz, C_4-H_{eq}), 5.32 (1H, t, J=4.7 Hz, 1H, C_2-H), and 9.79 (1H, t, J=2.3 Hz, HC(O)-); Found: *m/z* 158.0953. Calcd for $C_8H_{14}O_3$: M, 158.0943.

General Procedure for Addition of Organometallic Reagents to Keto Acetal 1. Into a solution of ketoacetal **1** in

ether (5×10^{-2} M) was added organolithium or magnesium reagent (2.0—2.8 equiv) at −78 °C. The concentration of reagent used is as follows; MeLi (1.1 M in ether), Bu^{n}Li (1.5 M in ether), PhLi (0.6 M in ether), and MeMgI (2.3 M in ether). After the above mixture was stirred at −78 °C for 4 h, it was allowed to warm to room temperature, and the product was extracted by usual manner. The diastereomeric excess of crude product was determined by capillary column GLC analysis (base line separation) using SCOT OV-17 capillary column (30 m×0.3 mm, Wako Pure Chemical Ind.) or PEG-20M Bonded (25 m×0.25 mm, Chemical Bonded Column, GASUKURO KOGYO Inc.) with a Shimadzu Model GC-MINI 2, or 100 MHz NMR spectrometer. The results were shown in Table 1, and the spectral and analytical data of products are as follows.

(4*R*,6*R*)-4,6-Dimethyl-2-(2-hydroxy-2-phenylpropyl)-1,3-dioxane (2a). Recrystallization of the product from hexane gave a single diastereomer of **2a** (45% recovery): mp 97—98 °C; IR (neat) 3500 cm^{-1}; ^{1}H NMR (500 MHz, $CDCl_3$) δ=1.08 (3H, d, J=6.9 Hz, C_4-Me_{ax}), 1.16 (3H, d, J=6.0 Hz, C_6-Me_{eq}), 1.27 (1H, ddd, J=1.2, 2.4, and 13.3 Hz, C_5-H_{eq}), 1,15 (3H, s, $C_{2'}$-Me), 1.84 (1H, ddd, J=6.2, 11.8, and 13.3 Hz, C_5-H_{ax}), 2.12 (1H, J=8.3 and 14.2 Hz, $C_{1'}$-H), 2.25 (1H, dd, J=3.2 and 14.2 Hz, $C_{1'}$-H), 3.79 (1H, ddq, J=2.4, 11.8, and 6.0 Hz, C_6-H_{ax}), 4.29 (1H, ddq, J=1.2, 6.19, and 6.9 Hz, C_4-H_{eq}), 4.41 (1H, br s, -OH), 4.60 (1H, dd, J=3.2, and 8.3 Hz, C_2-H), 7.22—7.37 (3H, m, ArH), and 7.44—7.47 (2H, m, ArH); $[\alpha]_D^{27}$ +22.0° (*c* 0.528, $CHCl_3$).

Found: C, 71.75; H, 8.72%. Calcd for $C_{15}H_{22}O_3$: C, 71.97; H, 8.86%.

(4*R*,6*R*)-4,6-Dimethyl-2-(2-hydroxy-2-phenylhexyl)-1,3-dioxane (2b). R_f 0.47 (SiO_2, hexane-EtOAc=8:2); IR (neat) 3500 and 1140 cm^{-1}; ^{1}H NMR (60 MHz, CCl_4) δ=0.52—1.53 (17H, m, *n*-Bu, C_5-H, and Me), 2.14 (5H, d, J=5 Hz, $C_{1'}$-H), 3.33—4.03 (1H, m, C<u>H</u>CH$_3$), 4.03—4.53 (1H, m, C<u>H</u>CH$_3$), 4.30 (1H, s, OH), 4.70 (1H, t, J=5 Hz, C_2-H), 6.90—7.86 (5H, m, ArH).

Found: C, 73.68; H, 9.61%. Calcd for $C_{18}H_{28}O_3$: C, 73.93; H, 9.65%.

(4*R*,6*R*)-4,6-Dimethyl-2-(2-hydroxy-2-methylhexyl)-1,3-dioxane (2c). Bp 110 °C (3 mmHg); IR (neat) 3550 and 1140 cm^{-1}; ^{1}H NMR (60 MHz, $CDCl_3$) δ=0.87 (3H, m, C<u>H</u>$_3$-CH$_2$CH$_2$C<u>H</u>$_2$), 1.1—1.6 (12H, m, C<u>H</u>$_3$CH and CH$_3$C<u>H</u>$_2$C<u>H</u>$_2$-C<u>H</u>$_2$), 1.17 (3H, s, -CH$_2$C<u>H</u>$_3$), 1.5—2.0 (2H, m, C_5-H), 1.75 (2H, d, J=6.0 Hz, $C_{1'}$-H), 3.12—3.66 (1H, s, O<u>H</u>), 3.76—4.09 (1H, m, CH$_3$C<u>H</u>), 4.09—4.46 (1H, m, CH$_3$C<u>H</u>), 5.14 (1H, t, J=6.0 Hz, C_2-H).

(4*R*,6*R*)-4,6-Dimethyl-2-(2-hydroxypropyl)-1,3-dioxane (2d). R_f 0.63 (SiO_2, hexane-EtOAc=2:8); IR (neat) 3430 and 1140 cm^{-1}; ^{1}H NMR (100 MHz, $CDCl_3$) δ=1.17 (3H, 1d, J=6.0 Hz, CHC<u>H</u>$_3$), 1.21 (3H, d, J=6.0 Hz, CHC<u>H</u>$_3$), 1.38 (3H, d, J=7.0 Hz, CH(OH)C<u>H</u>$_3$), 1.60—2.02 (4H, m, C_5-H and $C_{1'}$-H), 3.24 (1H, br s, O<u>H</u>), 3.80—4.46 (3H, m, -C<u>H</u>CH$_3$ and $C_{1'}$-H), 5.08 (1H, t, J=6.0 Hz, C_2-H); MS *m/z* 173 (M^+-1).

Transformation of 2a into 7. Into a solution of **2a** ($[\alpha]_D^{27}$ +22.0°, 0.250 g, 1.00 mmol) in anhydrous methanol (5 mL) was added a solution (10 mL) of methanol saturated with dry HCl. After the solution was stirred for 3.5 h at 50 °C, the acidic solution was neutralized to pH ≈8.5 with 5% aqueous $NaHCO_3$ solution. Usual workup followed by a short path column chromatography (SiO_2, 0.1 g, hexane) gave a mixture (169 mg) of **5**, the starting material **2a**, and 2-phenyl-2,4,4-trimethoxybutane in a ratio of 7:1:1 by NMR. **5**: R_f 0.44 (SiO_2, hexane-EtOAc=7:3); IR (neat) 3450 and 1110 cm^{-1}; ^{1}H NMR (60 MHz, $CDCl_3$) δ=1.50 (3H, s, Me), 1.80 (1H, s, OH), 2.17 (2H, d, J=5.5 Hz, C_3-H), 3.19 (3H, s, OMe), 3.22 (3H, s, OMe), 4.12 (1H, t, J=5.5 Hz, C_4-H), 7.07—7.57 (5H, m, ArH). The above mixture was then dissolved in acetone (3 mL) and water (0.3 mL), into which Amberlyst 15 (30 mg) was added. After stirring for 3 h at 50 °C, the mixture was filtered, extracted with ether, and dried (Na_2SO_4) to give oily material (144 mg) containing **6** in 61% purity (NMR). **6**: ^{1}H NMR (60 MHz, $CDCl_3$) δ=1.67 (3H, s, Me), 2.40 (1H, s, OH), 2.75 (2H, d, J=3 Hz, CH_2), 6.60—7.90 (5H, m, ArH), 9.63 (1H, t, J=3 Hz, CHO); MS *m/z* 163 (M^+-1). The oily material was then dissolved in ether (1.5 mL), into which was added a suspended solution of $LiAlH_4$ (99 mg, 2.6 mmol) in ether (1.5 mL) at 0 °C. The mixture was stirred for 1 h at 0 °C and 3 h at room temperature. Usual workup followed by preparative TLC (SiO_2, chloroform) gave (3*R*)-3-phenyl-1,3-butanediol (**7**) (75 mg, 28% yield from **2a**). The compound **7** was further purified by preparative TLC (SiO_2, chloroform-ether=8:2, R_f=0.39) to give **7** (47 mg) of $[\alpha]_D^{26}$ +65.2° (*c* 0.406, benzene). The $[\alpha]_D$ value corresponds to be 97.7% ee based on the reported maximum rotation ($[\alpha]_D^{26}$ −66.7°).[6] **7**: ^{1}H NMR (100 MHz, $CDCl_3$) δ=1.54 (3H, s, Me), 2.01 (1H, dd, J=4.8 and 0.8 Hz, C_2-H), 2.42 (1H, br s, OH), 3.60 (3H, m, C_1-H and OH), and 7.9—7.4 (5H, m, ArH); IR (neat) 3500 cm^{-1}; MS *m/z* 166 (M^+).

References

1) T. Hosokawa, T. Ohta, S. Kanayama, and S.-I. Murahashi, *J. Org. Chem.*, **52**, 1758 (1987).

2) a) P. A. Bartlett, W. S. Johnson, and J. D. Elliott, *J. Am. Chem. Soc.*, **105**, 2088 (1983); A. Mori, J. Fujiwara, K. Maruoka, and H. Yamamoto, *Tetrahedron Lett.*, **24**, 4581 (1983); b) A. Alexakis, P. Mangeney, A. Ghribi, I. Marek, R. Sedrani, C. Guir, and J. Normant, *Pure Appl. Chem.*, **60**, 49 (1988) and references cited therein.

3) Conjugate addition of phenylcopper reagent to α,β-ethylenic acetal derived from (*R*,*R*)-2,4-pentanediol is also a diastereofacial differenciating reaction, see: P. Mageney, A. Alexakis, and J. Normant, *Tetrahedron Lett.*, **27**, 3134 (1986).

4) Attempts to obtain **1c** by the Pd(II)-catalyzed acetalization of acrolein with (*R*,*R*)-2,4-pentanediol resulted in the formation of **3**.

5) Y. Tamura, H. Kondo, H. Annoura, R. Takeuchi, and H. Fujioka, *Tetrahedron Lett.*, **27**, 81 (1986); Y. Tamura, T. Ko, H. Kondo, H. Annoura, M. Fuji, R. Takeuchi, and H. Fujioka, *ibid.*, **27**, 2117 (1986); M. P. Heitz, F. Gellibert, and C. Mioskowski, *ibid.*, **27**, 3143 (1986).

6) S. Mitsui, S. Imaizumi, Y. Senda, and J. Konno, *Chem. Ind.*, **1964**, 233.

7) For a related reation, see; W. F. Baile and D. L. Zartun, *J. Chem. Soc., Chem. Commun.*, **1984**, 34.

The Long-Term Testing of ZSM-5-Type Zeolite Containing Strontium for the High-Temperature Conversion of Methanol to Olefin

Hideo OKADO,* Tsuneji SANO,† Kunio SUZUKI,† Kiyomi OKABE,† and Haruo TAKAYA†
Maruzen Petrochemical Co., Ltd., Goi, Ichihara-shi, Chiba 290
†National Chemical Laboratory for Industry, Higashi, Tsukuba-shi, Ibaraki 304
(Received January 14, 1988)

Synopsis. Using ZSM-5-type zeolites containing alkaline earth metals (Mg, Ca, Sr), long-term tests for methanol conversion were carried out for up to 1000 h at 550 °C under a methanol LHSV of 2.3 h^{-1}. Strontium-containing zeolite showed the most stable activity. This was attributed to the effect of strontium on the acidity of the zeolite.

ZSM-5-type zeolites are excellent for the conversion of methanol to light olefins and gasoline.[1-7] It is well-known that a high selectivity to light olefins has been attained at high temperatures over highly siliceous zeolites.[8,9] However, catalyst deactivation is a serious problem under high reaction temperatures. The deactivation occurs predominantly for two causes; one is the poisoning of active sites due to the accumulation of carbonaceous deposits, and the other is the structure degradation of the zeolites by dealumination from the framework. In the former case, the deactivated catalyst can be regenerated by burning off the carbonaceous deposits, while in the latter case a practical method for regeneration has not yet been established. The deactivation due to the dealumination is, therefore, more serious than the coke deposition. Furthermore, it is known that the dealumination is accelerated in a moisture-rich atmosphere such as methanol conversion. In order to improve the catalyst life under high temperatures, the resistance against steaming must be much improved.

Recently, we reported that the ZSM-5-type zeolites containing alkaline earth metals (AE-ZSM-5, AE= Mg, Ca, Sr) showed an increased selectivity to olefins at temperatures above 500 °C.[10-12] Hence, we carried out a long-term life test of AE-ZSM-5, and compared the results of Sr-ZSM-5 with those of Mg-ZSM-5 and Ca-ZSM-5.

Experimental

The protonated zeolite catalysts (AE-ZSM-5, AE= Mg, Ca, Sr) with a SiO_2/Al_2O_3 ratio of 200 were prepared by the method described in our previous papers.[10,12]

Methanol-conversion runs were carried out under atmospheric pressure over a fixed bed in a quartz tube reactor (10 mm i.d.), and the product gas was analyzed by the use of TCD- and FID-type Yanaco AG-1000TFH auto gas chromatographs.[10] The reactant gas consisted of methanol/argon (1/1 mol/mol), while the argon served as a diluent as well as an internal standard for analysis. The products obtained will be abbreviated in the present paper as follows: ethylene=$C_2^=$; propylene=$C_3^=$;C_4-olefins=$C_4^=$; C_5-olefins=$C_5^=$; dimethyl ether=DME.

The catalyst regeneration was performed by burning off carbonaceous deposits under a stream of air/argon (0.8/1.0 v/v), just after DME appeared in the products. The temperature was maintained at 400 °C for the first 2 h, then raised to 550 °C, and finally maintained at 550 °C for 2 h.

The elemental composition, the ^{27}Al-MAS NMR spectra, and the diffuse reflectance FT-IR spectra of the hydroxyl groups of the zeolites were measured according to the methods described in our previous papers.[10,12]

Results and Discussion.

A long-term life test for the methanol conversion was carried out at a temperature of 550 °C and at a methanol LHSV value of 2.3 h^{-1}. For Sr-ZSM-5, a long-term life test was carried out for 1000 h, as is shown in Fig. 1. The catalyst was regenerated 12 times with intervals of from 74 to 79 h, while the methanol conversion was kept nearly constant (ca. 100%). The total yield of $C_2^=$ to $C_5^=$, the maximum value of which was 80 to 83%, decreased with time on-stream, but it was almost completely recovered by regeneration. Thus, the Sr-ZSM-5 catalyst was found to be stable and

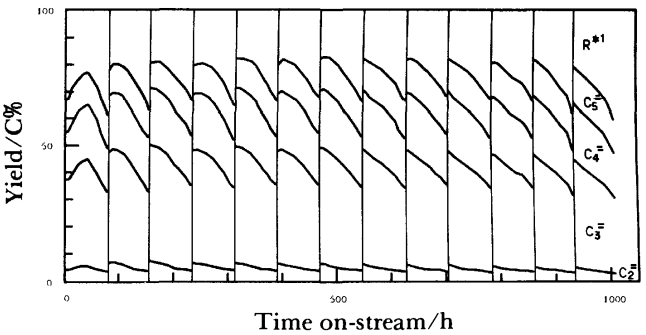

Fig. 1. Long-term life test over Sr-ZSM-5.
Reaction conditions: MeOH LHSV=2.3 h^{-1}, MeOH/Ar=1/1 mol/mol, temp=550 °C. *1) R is composed of paraffins, C_6^+-olefins, benzene, toluene, xylene, CO, and CO_2.

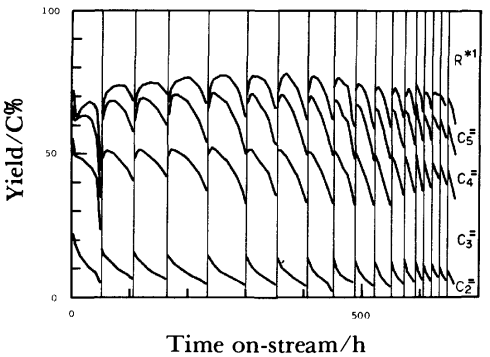

Fig. 2. Long-term life test over Mg-ZSM-5.
Reaction conditions: MeOH LHSV=2.3 h^{-1}, MeOH/Ar=1/1 mol/mol, temp=550 °C. *1) R is composed of paraffins, C_6^+-olefins, benzene, toluene, xylene, CO, and CO_2.

to show a high selectivity to light olefins.

On the other hand, for Mg-ZSM-5, a long-term life test was terminated at 660 h; the catalyst should be regenerated at shorter intervals because of the ease of deactivation, as is shown in Fig. 2. The maximum total yield of $C_2^=$ to $C_5^=$ during the regeneration interval ranged from 68 to 77% during the first 400 h time on-stream and decreased slightly after that. It is, therefore, concluded that the Mg-ZSM-5 catalyst is less stable and shows a lower selectivity to light olefins than that of Sr-ZSM-5.

For Ca-ZSM-5, a long-term life test was carried out for 1000 h, as is shown in Fig. 3. The total yield of $C_2^=$ to $C_5^=$ changed in a manner similar to that of Sr-ZSM-5. The number of regenerations, 10 times, was less than that of Sr-ZSM-5. The maximum total yield of $C_2^=$ to $C_5^=$ was 83 to 86%, higher than that of Sr-ZSM-5. However, the regeneration interval should be gradually shortened from 120 to 75 h along with the time on-stream. This implies that the active sites are rather unstable for Ca-ZSM-5 and that the life time for Ca-ZSM-5 is shorter than that of Sr-ZSM-5.

The three catalysts used in the long-term life tests were characterized by means of ^{27}Al-MAS NMR spectroscopy. The intensities of the peak at about 53 ppm assigned to tetrahedrally coordinated aluminium[13] were also measured. The intensity ratios, which means the percentage of a 53 ppm peak intensity of the used catalysts relative to that of the corresponding fresh catalysts, are listed in Table 1.

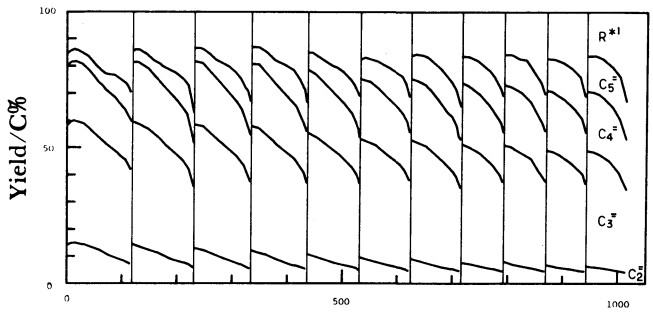

Fig. 3. Long-term life test over Ca-ZSM-5.
Reaction conditions: MeOH LHSV=2.3 h^{-1}, MeOH/Ar=1/1 mol/mol, temp=550 °C. *1) R is composed of paraffins, C_6^+-olefins, benzene, toluene, xylene, CO, and CO_2.

The ratio for Sr-ZSM-5 is 94%, distinctly higher than those of both Mg-ZSM-5 (18 to 19%) and Ca-ZSM-5 (32 to 56%). This implies that Sr-ZSM-5 has a higher resistance against the dealumination of the framework. It is considered that the acidity of zeolites originates from tetrahedrally coordinated aluminium, so that the long catalytic life of Sr-ZSM-5 (Fig. 1) is based on the greater resistance against the dealumination of the aluminosilicate framework.

Figure 4 shows the diffuse reflectance FT-IR spectra of hydroxyl groups for the three catalysts before and after the life tests. As has previously been reported,[14] each of the spectra is characterized by two well-defined peaks at 3605 and 3730—40 cm^{-1}. The low-frequency peak is assigned to an acidic bridged OH of Si(OH)Al, and the high-frequency one, to a terminal Si–OH or OH of the extra-framework silica. The broad peak near 3500 cm^{-1} is attributed to hydrogen bonding

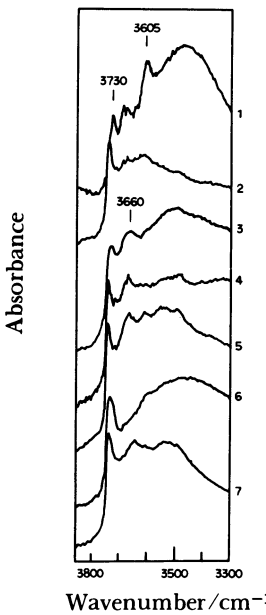

Fig. 4. IR spectra of AE-ZSM-5 before and after the life test.
1: Fresh Mg-ZSM-5. 2: Mg-ZSM-5 after the life test (660 h). 3: Fresh Ca-ZSM-5. 4: Upper-layer catalyst of Ca-ZSM-5 after the life test (1000 h). 5: Lower-layer catalyst of Ca-ZSM-5 after the life test (1000 h). 6: Fresh Sr-ZSM-5. 7: Sr-ZSM-5 after the life test (1000 h).

Table 1. Characteristics of AE-ZSM-5 before and after the Long-Term Life Test

Catalyst	Chemical composition[a] (Molar ratio)		Particle size (μm)	Relative intensity of the 53 ppm peak[b] after life test[c] (%)	
	SiO_2/Al_2O_3	AE/Al_2		Upper-layer[d]	Lower-layer[d]
Mg-ZSM-5	212	0.25	3—4	18	19
Ca-ZSM-5	200	2.63	4—6	32	56
Sr-ZSM-5	218	2.81	4—6	94	94

a) After proton ion-exchange. AE=Mg, Ca, and Sr. b) The intensity ratio (×100) of the 53 ppm peak of the used zeolite to the corresponding fresh one was determined by means of ^{27}Al-MAS NMR. c) The life tests were carried out at 550 °C under a MeOH LHSV of 2.3 h^{-1}, diluted with argon (MeOH/Ar=1/1 mol/mol). The total life times are 660 h for Mg-ZSM-5, 1000 h for Ca-ZSM-5 and 1000 h for Sr-ZSM-5. d) The upper-layer is 25% of the total volume of the catalyst, while the lower-layer is 75%.

between adjacent hydroxyl groups.[14] For Mg-ZSM-5, the peak at 3605 cm^{-1}, which was clearly observed in the fresh catalyst, disappeared nearly completely after the life test for 660 h, as is shown by Curves 1 and 2. This disappearance seems to be consistent with the release of a large number of aluminium atoms from the framework.

For the fresh Ca-ZSM-5 (Curve 3), the intensity of the peak at 3605 cm^{-1} was very low. We ourselves have previously reported[11] that the addition of calcium or strontium to the starting materials in the zeolite synthesis decreases the strong acid sites, corresponding to the peak at 3605 cm^{-1}, observed for the as-made zeolite catalyst because of the partial replacement of the H^+-acid sites for the calcium or strontium ions. On the other hand, the strong acid sites of the working catalyst gradually increase with the time on-stream in the methanol-conversion run because of the migration of the calcium ions from the initial sites. As compared to the 3605 cm^{-1} peak intensity of the fresh catalyst, that of the upper-layer catalyst of the reactor (Curve 4) remained almost unchanged, while that of the lower-layer one (Curve 5) increased. It is plausible that the deterioration of the catalyst, its dealumination, would take place in a greater degree at the upper-layer catalyst, since methanol was fed from the top of the reactor. The results for ^{27}Al-MAS NMR (Table 1) clearly support this possibility; that is to say, the relative intensity of the 53 ppm peak at the upper-layer catalyst (32%) is lower than that of the lower-layer one (56%). It is concluded, therefore, that the very low intensity for the upper-layer part is due to dealumination, while the increase in the intensity for the lower-layer part is due to the release of calcium ions from the strong acid sites, as has been mentioned above. This conclusion is also supported by the previous report that steam produced by methanol conversion accelerated the release of calcium ions from the acid sites.[15]

On the other hand, the peak at 3605 cm^{-1} was not observed for either the fresh Sr-ZSM-5 or the used one, as is shown by Curves 6 and 7. These observations of the FT-IR and ^{27}Al-MAS NMR spectra indicate that Sr-ZSM-5 is a remarkably stable catalyst for methanol conversion. From these results, it was confirmed that among AE-ZSM-5 Sr-ZSM-5 was the best catalyst in both the yield of light olefins and the catalyst life.

This work is a part of the "C_1 Chemistry Project," a National Research and Development program of the Agency of Industrial Science and Technology, Ministry of International Trade and Industry (M.I.T.I), Japan.

We wish to thank Dr. S. Shin (National Chemical Laboratory for Industry) for his helpful discussion.

References

1) R. J. Argauer and G. R. Landolt, U.S. Patent 3702886.
2) K. F. M. G. J. Scholle, W. S. Veeman, P. Frenken, and G. P. M. van der Velden, *Appl. Catal.*, **17**, 233 (1985).
3) C. D. Chang, *Catal. Rev-Sci. Eng.*, **26**, 323 (1984).
4) Y. Ono and T. Mori, *J. Chem. Soc., Faraday Trans. 1*, **77**, 2209 (1981).
5) C. D. Chang, W. H. Lang, and A. J. Silvestri, U.S. Patent 4052479.
6) R. J. McIntosh and D. Seddon, *Appl. Catal.*, **6**, 307 (1983).
7) M. Niwa, M. Kato, T. Hattori, and Y. Murakami, *J. Phys. Chem.*, **90**, 6233 (1986).
8) C. D. Chang, C. T-W. Chu, and R. F. Socha, *J. Catal.*, **86**, 289 (1984).
9) W. Hoelderich, H. Eichhorn, R. Lehnert, L. Marosi, W. Mross, R. Reinke, W. Ruppel, and H. Schlimper, Proceed. 6 th Intern. Zeol. Conf., ed by D. Olson and A. Bisio, Butterworths, London (1984) 545.
10) H. Okado, H. Shoji, K. Kawamura, Y. Kohtoku, Y. Yamazaki, T. Sano, and H. Takaya, *Nippon Kagaku Kaishi*, **1987**, 25.
11) H. Okado, T. Sano, K. Matsuzaki, K. Kawamura, Y. Shiomi, H. Watanabe, and H. Takaya, *Nippon Kagaku Kaishi*, **1987**, 791.
12) K. Fujisawa, T. Sano, K. Suzuki, H. Okado, K. Kawamura, Y. Kohtoku, S. Shin, H. Hagiwara, and H. Takaya, *Bull. Chem. Soc. Jpn.*, **60**, 791 (1987).
13) C. A. Fyfe, J. M. Thomas, J. Klinowski, and G. C. Gobbi, *Angew. Chem., Int. Ed. Engl.*, **22**, 259 (1983).
14) P. A. Jacobs and R. von Ballmoos, *J. Phys. Chem.*, **86**, 3050 (1979).
15) H. Okado, H. Shoji, T. Sano, K. Suzuki, Y. Kiyozumi, H. Hagiwara, and H. Takaya, *Nippon Kagaku Kaishi*, **1987**, 1654.

 © 1988 The Chemical Society of Japan Bull. Chem. Soc. Jpn., 61, 3387—3391 (1988)

An MO Study of Fragmentation Mechanism of Ethane and Propane Radical Cations

Yoshihiro OSAMURA,† Takae TAKEUCHI,†† and Kichisuke NISHIMOTO*
Department of Chemistry, Faculty of Science, Osaka City University, Sugimoto-cho, Sumiyoshi-ku, Osaka 558
†Department of Chemistry, Faculty of Science and Technology, Keio University, 3-14-1 Hiyoshi, Kohoku-ku, Yokohama 223
††Department of Chemistry, Faculty of Science, Nara Women's University, Kita-uoyanishimachi, Nara 630
(Received December 3, 1987)

The decomposition mechanisms were studied for ionized species of ethane and propane in the low-energy region by using an ab initio molecular orbital method. Calculations show that rather complex fragmentation processes may occur in addition to a simple cleavage of C-C and C-H bonds. In order to examine the possibility of an elimination of H_2 or CH_4 from the radical cation of saturated hydrocarbons, the potential energy curves were calculated for both 1,1- and 1,2-eliminations. An energy barrier of 1,2-elimination was estimated to be small, but a 1,1-elimination can also possibly occur. It was also found that a single C-H bond scission of the parent radical cation may occur with the same order of energy for the H_2 loss. The present results are qualitatively in a good agreement with the experiments.

The mass spectra of saturated hydrocarbons give a complex pattern for the fragment species caused by ionization under electron bombardment,[1] although there are only two different kinds of bonds: C-C and C-H. Since saturated hydrocarbon molecules are fundamental organic molecules constructed with σ-frameworks, it is important to investigate the behavior of the ionized species produced by removing a σ-bonding electron in order to understand the fragmentation pattern of the mass spectra.

The unimolecular decomposition processes of radical cation species are strongly related to the electronic structure of the parent molecules. When molecules have a double bond or heteroatoms, a characteristic mass spectrum can be observed; this result can be effectively used for a molecular identification. In the case of saturated hydrocarbon, however, mechanistic studies have been very few, since various types of fragment ions are observed. In this respect, we carried out a quantum chemical investigation and theoretically explored the mechanism of the fragmentation processes for saturated hydrocarbon. In this paper, we look at for ethane and propane as the simplest system.

Theoretical Procedure

The molecular geometries of radical cations are calculated by using an analytical gradient method based on an unrestricted Hartree-Fock (UHF) method with STO-3G and 6-31G basis sets.[2] In order to determine whether the structures obtained by geometry optimization are located at equilibrium or a transition state, we carried out vibrational analysis by using an analytical second derivative method.[3]

Results and Discussion

Experimental data resulting from electron impact and photoionization studies for propane and butane show that cation species are mainly produced by a simple cleavage of the C-C bond in the high-energy region. In the low-energy region, however, it seems that there are rather complex processes, such as H_2 or CH_4 loss, or isomerization.[4,5] Before discussing the fragmentation mechanisms of propane, we consider the potential energy surfaces for the fragmentation processes of the ethane radical cation, especially in the lowest electronic state.

$C_2H_6^{+\cdot}$. The experimental data for ethane by electron impact shows that various kinds of fragment ions are produced and $C_2H_5^+$, $C_2H_4^{+\cdot}$, $C_2H_3^+$, $C_2H_2^{+\cdot}$, and CH_3^+ are observed in the electron energy from 10 to 23 eV.[6] It should be noted that the appearance potential of $C_2H_5^+$ (12.5 eV) is nearly the same as that of $C_2H_4^{+\cdot}$ (12.1 eV). This evidence is also shown by photoionization,[7] and suggests that the H_2 elimination competes with the hydrogen atom loss from an ethane radical cation.

Unimolecular fragmentation takes place by breaking two C-H bonds which can be distinguished as 1,2-elimination and 1,1-elimination. The products are an ethylene radical cation CH_2=$CH_2^{+\cdot}$ and a methylcarbene radical cation CH_3-$CH^{+\cdot}$, respectively. Table 1 summarizes the energies of the parent ion $C_2H_6^{+\cdot}$ and fragments $C_2H_5^+$, $C_2H_4^{+\cdot}$, CH_3^+, etc. calculated at their equilibrium structures. Since the electron correlation effect is important for estimating the energy barrier, we also calculated the energies by using the MP3 method, as shown in Table 1. However, the qualitative feature of the product distribution for ionized species may be read from the SCF results.

Table 1 shows that the most stable fragments are CH_2=$CH_2^{+\cdot}$+H_2 and that the energy is 0.8 eV lower than that of $CH_3CH_2^+$+H·. This result seems to be consistent with the fact that the appearance potential of $C_2H_4^{+\cdot}$ is lower than that of $C_2H_5^+$. However, we must consider the barrier height to dissociate two hydrogens from ethane radical cation.

Let us discuss the energy barrier for the H_2 loss via a 1,2-elimination:[8]

$$C_2H_6^{+\cdot} \rightarrow C_2H_4^{+\cdot} + H_2. \quad (1)$$

Table 1. Total Energies (in Hartree) of Various Species Generated from the Ionization of Ethane and Propane[a)]

Method Basis set	HF STO-3G	MP3 STO-3G	HF 6-31G
C_3H_8 neutral ground state	−116.88642	−117.08059	−118.21617
$C_3H_8^{+\cdot}$ vertical ionized state			
C-C σ cation radical	−116.49155	—	−117.79739
π type C-H cation radical	−116.46667	—	−117.78382
CH_3-CH_2-$CH_3^{+\cdot}$	−116.54206	−116.72690	−117.85933
CH_3-CH_2-CH_2^{+}	−115.99633	−116.18340	−117.30797
CH_3-CH-CH_3^{+}	−116.02765	−116.21168	−117.33564
CH_3-CH=$CH_2^{+\cdot}$	−115.40747	−115.58188	−116.72748
CH_3-CH_2-$CH^{+\cdot}$	−115.34682	−115.51503	−116.65761
CH_3-C-$CH_3^{+\cdot}$	−115.38648	−115.55241	−116.69427
cyclo-$C_3H_6^{+\cdot}$	−115.38241	−115.56121	−116.69718
Tranisition state 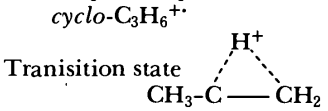	−115.33808	−115.51734	−116.65693
C_2H_6 neutral ground state	−78.30618	−78.43054	−79.19757
$C_3H_6^{+\cdot}$ vertical ionized state			
C-C σ cation radical	−77.88165	—	−78.75330
π type C-H cation radical	−77.86100	—	−78.74363
CH_3-$CH_3^{+\cdot}$	−77.94048	−78.06046	−78.82031
CH_3-CH_2^{+}	−77.40806	−77.52825	−78.28072
CH_3-CH_2·	−77.66300	−77.77419	−78.56873
CH_2=$CH_2^{+\cdot}$	−76.79755	−76.90882	−77.68118
CH_3-$CH^{+\cdot}$	−76.75790	−76.86099	−77.62983
Transition state[b)] 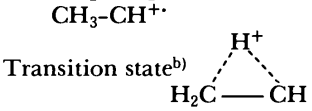	−76.73129	−76.84920	−77.61239
CH_4	−39.72686	−39.79712	−40.18055
CH_3^{+}	−38.77948	−38.83436	−39.21621
CH_3·	−39.07701	−39.12706	−39.54666
$CH_2^{+\cdot}$	−38.11894	−38.15645	−38.55390
H_2	−1.11751	−1.13452	−1.12683
H·	−0.46658	−0.46658	−0.49823

a) Equilibrium geometries are obtained by Hartree-Fock method (UHF method for radicals and RHF method for closed-shell molecules). The energies by MP3 method (third-order Møller-Plesset perturbation theory) are calculated at the geometries optimized by HF method with STO-3G basis set. b) Ref. 15.

In the case of a neutral ethane molecule, a reaction in which two hydrogens synchronously dissociate is known to be symmetry forbidden in the sense of the Woodward-Hoffmann rule. On the other hand, if one electron is removed from the system, one may expect that the barrier height of the 1,2-H_2 elimination for the ethane radical cation would be less than that in the case of a neutral molecule. Since an ethane radical cation is a potentially high energy species, the energy of a C-H bond dissociation of $C_2H_6^{+\cdot}$ has been calculated to be only 1.1 eV (6-31G). When we calculate the potential energy curve for a hydrogen abstraction reaction,

$$C_2H_5^{+} + H\cdot \rightarrow C_2H_4^{+\cdot} + H_2, \quad (2)$$

the reaction is found to be exothermic and to proceeds without an energy barrier. Therefore, we could estimate that the barrier height of a 1,2-H_2 elimination process,

$$C_2H_6^{+\cdot} \rightarrow [CH_3\text{-}CH_2\cdots H]^{+\cdot} \rightarrow [CH_2\text{=}CH_2]^{+\cdot} + H_2 \quad (3)$$

should not be greater than that of a two-step 1,2-H_2 elimination process:

$$C_2H_6^{+\cdot} \rightarrow [CH_3\text{-}CH_2]^{+} + H\cdot \rightarrow [CH_2\text{=}CH_2]^{+\cdot} + H_2. \quad (4)$$

Such an energy relation may explain why the appearance potential of $C_2H_4^{+\cdot}$ is slightly lower than that of $C_2H_5^{+}$ (see the dashed line in Fig. 2).

The other possibility of H_2 loss is a 1,1-elimination in which two hydrogens are removed from one carbon atom of ethane. Although a methylcarbene radical cation, being a product, seems to be a very unstable species, the energy of $CH_3CH^{+\cdot}+H_2$ is calculated to be only 0.6 eV higher than that of $CH_3CH_2^{+}+H\cdot$. This means that a 1,1-elimination can also occur. While electron-impact experiments for CH_3CD_3 at 70 eV show that $C_2H_2D_2^{+\cdot}$, $C_2H_3D^{+\cdot}$, and $C_2D_3H^{+\cdot}$ are all observed,[9)] experimental evidence for such mechanisms has not been reported in the low-energy region. The present calculation strongly suggests evidence for the formation of a carbene radical cation due to a H_2 or D_2 loss from $CH_3CD_3^{+\cdot}$. Such species have been men-

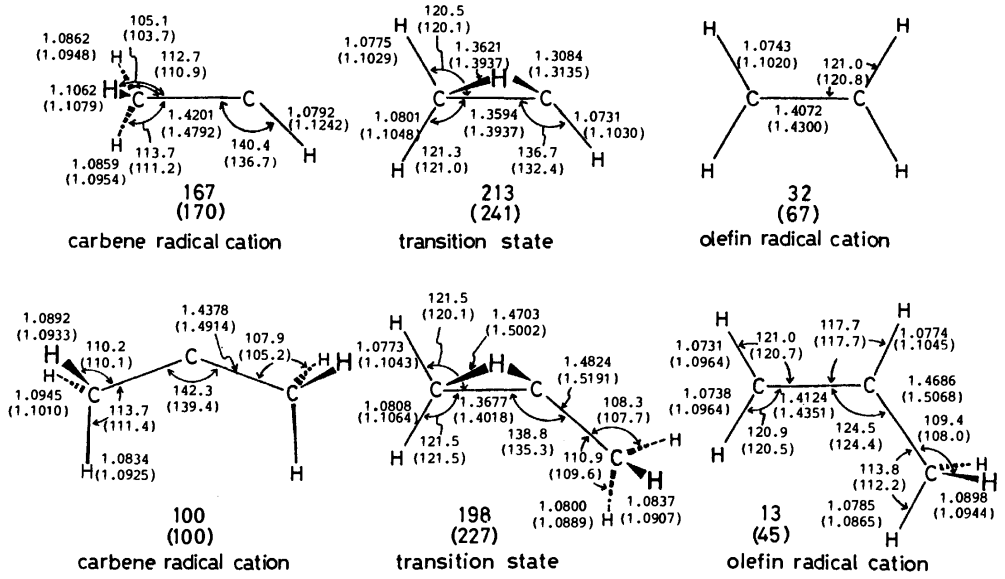

Fig. 1. The structures of methylcarbene radical cation and dimethylcarbene radical cation and their transition states of hydrogen migration calculated by using the UHF method with 6-31G (STO-3G) basis set. The units of bond lengths and bond angles are in Angstrom and degrees. The values shown in each geometry are the relative energies ($kJ\,mol^{-1}$) from the energy of the radical cation of ethane or propane at equilibrium structure. The values in parentheses are obtained with STO-3G basis set.

tioned as non-symmetric ethylene ions by von Koch[10] as the major precursor of acetylene ions. The methylcarbene radical cation may isomerize to a more stable ethylene radical cation; this energy barrier has been calculated to be ca. 0.5 eV. Figure 1 shows the geometries of the carbene radical cation and its transition state to an ethylene radical cation. The energy profile of this isomerization is shown by the curved line in Fig. 2. Most of the structures of other species have already been published elsewhere.[11,12,15]

Figure 2 summarizes the energy relations of the species formed by the ionization of ethane, as is discussed in this section. The ground state of an ethane radical cation was calculated to be a C-C σ-type radical cation which diabatically correlates to the cleavage of a C-C bond. The dissociation reaction of a C-C bond, however, requires more energy than the loss of H· or H_2. Since the energy of a C-C σ-type radical cation is very close to that of a C-H pseudo π-type radical cation, it would be expected that internal energy dispensation should rapidly occur during decomposition reactions.

$C_3H_8^{+\cdot}$. We have shown that there are two possibilities for removing two hydrogens from an ethane radical cation: 1,1- and 1,2-eliminations. In the case of propane, there are CH_3· and CH_4 losses as well as H· and H_2 losses. Table 1 also summarizes the energies of the possible fragments generated from propane. The potential energy surfaces are illustrated for H· and H_2 losses from $C_3H_8^{+\cdot}$ in Fig. 3(a) and for CH_3· and CH_4 losses in Fig. 3(b).

The experiment by Chupka and Berkowitz[7] shows that $C_3H_7^+$, $C_3H_6^{+\cdot}$, $C_2H_5^+$, and $C_2H_4^{+\cdot}$ are observed

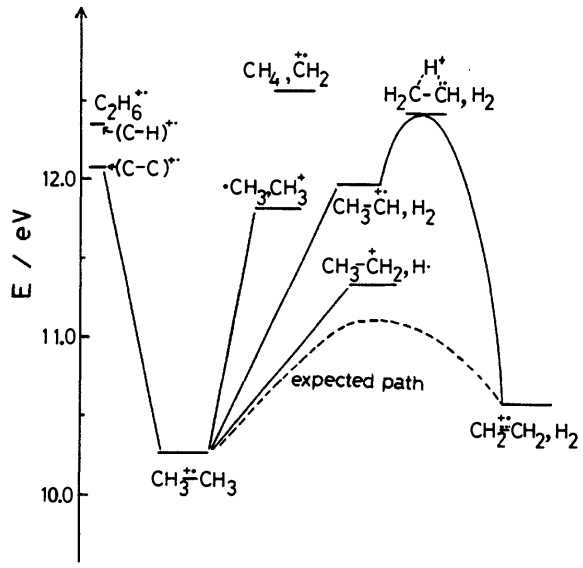

Fig. 2. The energy relations of the radical cation species caused by the ionization of ethane in the lowest state. The energies are calculated by UHF method at the optimized geometries with 6-31G basis set relative to the neutral ethane molecule.

over a narrow range: 11.3—11.9 eV. This means that losses of H·, H_2, CH_3·, and CH_4 from $C_3H_8^{+\cdot}$ occur at almost the same energy.[13]

As demonstrated in Fig. 3, the most stable product is an isopropyl cation. Due to the strong hyperconjugation by two methyl groups, the cation center prefers the central carbon to the terminal one. From Table 1, the dissociation of the central C-H bond in $C_3H_8^{+\cdot}$ is

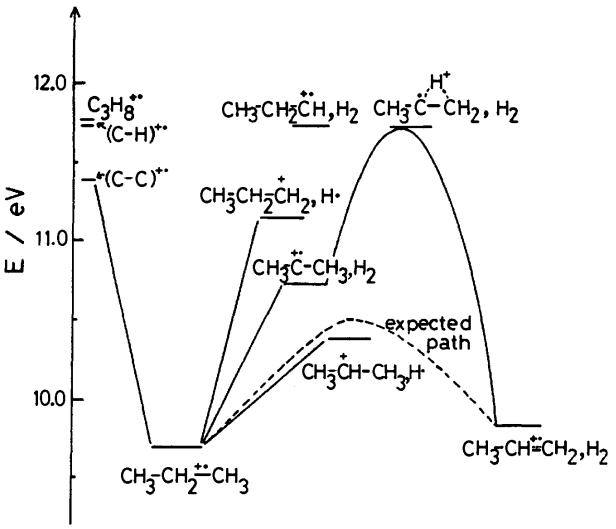

Fig. 3(a). The energy relations for H· and H_2 elimination from propane radical cation.

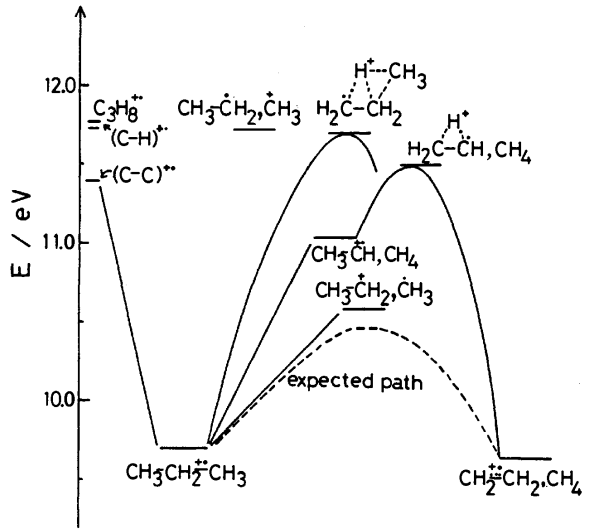

Fig. 3(b). The energy relations for CH_3· and CH_4 elimination from propane radical cation.

calculated to be only 0.7 eV (6-31G), while 1.4 eV is obtained for a terminal C-H bond dissociation.

Although an olefin π radical cation is energetically more stable, there is an energy barrier to be formed from a saturated hydrocarbon radical cation. It should be noted that the energy of the hydrogen atom loss of an ethane radical cation (1.1 eV) is in the middle of those of the central and terminal H· losses of $C_3H_8^{+\cdot}$ (0.7 eV and 1.4 eV). When the energy barrier of the H_2 loss of $C_3H_8^{+\cdot}$ is comparable to that in the case of $C_2H_6^{+\cdot}$, one can expect that the H· loss occurs more easily than the H_2 loss for $C_3H_8^{+\cdot}$. This expectation is in accord with the experimental results.[7]

Moreover, one can not neglect the two processes in which CH_4 or H_2 eliminates from the same carbon atom (1,1-elimination) and a different carbon atom (1,2-elimination). It is interesting that the energy of a dimethylcarbene radical cation is located between the energies of an isopropyl cation and a propyl cation. The molecular structure of a dimethylcarbene radical cation is illustrated in Fig. 1. Although the equilibrium geometry takes a C_2 symmetry, two methyl groups almost freely rotate internally. Since the carbene radical cation center is stabilized by two methyl groups, the energy barrier of the 1,2-hydrogen shift is calculated to be much higher than in the case of a methylcarbene radical cation. The dimethylcarbene radical cation is one of the strong candidates for a H_2 loss of the propane radical cation.

Molecular Orbitals and Ionization Potentials. The I.P. (ionization potential) from the high-lying occupied molecular orbitals of ethane is observed at 12.0—13.5 eV.[14] The degenerate C-H pseudo π-type bonding orbital ($1e_g$) and the C-C σ-type bond orbital ($3a_g$) are included in this energy region; these orbitals are energetically very close. Similar patterns of I.P. were measured at 11.5—12.6 eV in the case of propane. Although the highest occupied molecular orbitals of ethane and propane were assigned to be a C-H π-type molecular orbital through an RHF calculation,[14] a UHF calculation shows that the energy of a C-C σ-type radical cation is slightly lower than that of a C-H pseudo π-type radical cation. The energies of the vertical ionized states of ethane were estimated to be 12.1 eV for the C-C σ orbital and 12.4 eV for C-H π-type MO with the present UHF calculation.

As a result of geometry optimization, the lowest state of the ionized parent molecule was found to be a C-C σ-type radical cation for both ethane and propane. Since the energy difference is very small between C-C σ and C-H pseudo π-type radical cations, the electronic coupling between them becomes large through a geometrical relaxation. This fact would lead to the complex fragmentation profiles of ethane and propane radical cations.

Concluding Remarks

The fragmentation mechanisms of the saturated hydrocarbon in the low-energy region may be summarized as follows:

1) Hydrogen or alkyl radical (R·) elimination

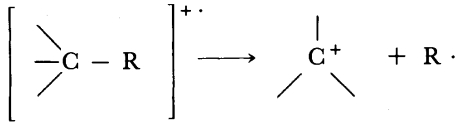

2) 1,2-HR elimination

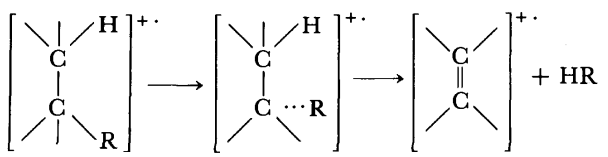

3) 1,1-HR elimination

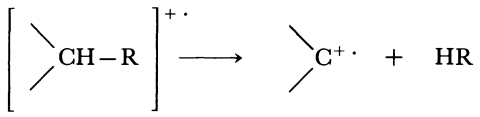

where R=H or CH_3. Mechanism 1 is a simple bond cleavage process. Mechanism 2 proceeds with a small energy barrier. Although a reverse 2+2 type reaction is symmetry forbidden in the case of a neutral system, the energy barrier is substantially reduced for the HR loss of a radical cation. The 1,2-HR elimination process is expected to compete with a simple C-R bond scission, since the expected transition-state energy of mechanism 2 is very close to the energy of the product by mechanism 1 (see Figs. 2 and 3). Our calculation also shows that a carbene radical cation could be produced via HR loss by 1,1-elimination in the low-energy region.

This research was carried out by using an HITAC M680-H at the computer center of Institute for Molecular Science. This work was supported by Grant-in-Aid for Scientific Research (No. 62470013).

References

1) H. Budzikiewicz, C. Djerassi, and D. H. Williams "Mass Spectrometry of Organic Compounds," Holdem-Day Inc., San Francisco, C. A. (1967).

2) J. S. Binkley and J. A. Pople, *J. Chem. Phys.*, **66**, 879 (1977).

3) J. S. Binkley, M. Frish, K. Raghavachari, D. DeFrees, H. B. Schaegel, R. Whiteside, E. Fluder, R. Seeger, and J. A. Pople, "GAUSSIAN-82," Carnegie-Mellon University.

4) T. Takeuchi, M. Yamamoto, K. Nishimoto, H. Tanaka, and K. Hirota, *Int. J. Mass Spectrom. Ion Phys.*, **52**, 139 (1983).

5) S. Meyerson, *J. Chem. Phys.*, **42**, 2181 (1965).

6) I. H. Suzuki and K. Maeda, *Int. J. Mass Spectrom. Ion Phys.*, **24**, 147 (1977).

7) W. A. Chupka and J. Berkowitz, *J. Chem. Phys.*, **47**, 2921 (1967).

8) We can exclude two-step elimination of hydrogen atoms

$$C_2H_6^{+\cdot} \rightarrow C_2H_5^+ + H\cdot \rightarrow C_2H_4^{+\cdot} + 2H\cdot \quad \text{(A1)}$$

because this process needs high energy (3.9 eV from $C_2H_6^{+\cdot}$ with 6-31G basis set).

9) C. Lifshitz and R. Sternberg, *Int. J. Mass Spectrom. Ion phys.*, **2**, 303 (1969).

10) H. von Koch, *Arkiv Fysik*, **28**, 559 (1968).

11) D. J. Bellville and N. L. Bauld, *J. Am. Chem. Soc.*, **104**, 5700 (1982).

12) R. A. Whiteside, M. J. Frisch, J. S. Binkley, D. J. DeFrees, H. B. Schlegel, K. Raghavachari, and J. A. Pople, *Carnegie-Mellon Quantum Chemistry Archive*, Department of Chemistry, Carnegie-Mellon University, Pittsburgh, PA.

13) M. L. Vestel, *J. Chem. Phys.*, **43**, 1356 (1965).

14) K. Kimura, S. Katsumata, Y. Achiba, T. Yamazaki, and S. Iwata, "Handbook of He I Photoelectron Spectra of Fundamental Organic Molecules," Halsted Press, New York (1981).

15) C. Sannen, G. Raseev. C. Galloy, G. Fauville, and J. C. Lorquet, *J. Chem. Phys.*, **74**, 2402 (1981).

 © 1988 The Chemical Society of Japan Bull. Chem. Soc. Jpn., 61, 3393—3397 (1988)

Kinetic Studies by Means of the NMR Techniques. I. Acid-Catalyzed Proton-Exchange Reactions of Some Substituted Phenols

Akihiro YOSHINO, Yasuki NAKASHIMA, and Kensuke TAKAHASHI*
Department of Applied Chemistry, Nagoya Institute of Technology, Gokiso-cho, Showa-ku, Nagoya 466
(Received March 11, 1988)

A kinetic study was conducted on the acid-catalyzed proton-deuteron-exchange reactions of several substituted phenols. The rates of the exchange were determined by using the two-bond isotope shifts ($^2\Delta$) on the carbons and the pattern-fitting analyses for the ^{13}C NMR signals. The observed reaction rates can be expressed additively with substituent parameters. The parameters of the para positions are linearly correlated to the σ_p^+ with ρ=−3.6.

The proton-deuteron-exchange reaction is a typical ionic reaction. Therefore, its study can provide useful indices for various ionic reactions. In the cases of the title reactions, the reactions proceed through the σ-complex, whose formation is a rate-determining step. Katritzky et al. reviewed such acid-catalyzed hydrogen-exchange reactions.[1]

In studies of hydrogen-exchange reactions, knowledge of the isotopic fractionation (D in %) is necessary. This fractionation can be obtained by various methods, such as IR,[2] ^{1}H NMR,[3] ^{2}H NMR,[4] MS,[4] and ^{13}C NMR.[4-8] The organic reaction rates have been discussed in terms of the substituent parameters presented by Hammett[9] and extended by Brown-Okamoto,[10] Taft,[11] and Yukawa-Tsuno.[12] The Hammett equation has been applied to many reaction rates of the meta- and para-substituted benzenes.[13] However, its application is limited in the cases of multiply substituted benzenes. Therefore, the parameters must be considered with regard to steric or mutual interactions between substituents.

In the present article, we present a method to evaluate simultaneously the title reaction rates for different sites of the substituted benzenes. The rates were obtained for thirty-eight sites of twenty unsubstituted and substituted phenols.

Experimental

The materials used were commercially available and were used without further purification. The reaction vessels were hand-made Pyrex ampules. A sample consisting of 0.01 mol of phenol was added to 1 g of a HCl/D_2O (0.1 wt%) solution, and the mixture was sealed into the Pyrex ampule with a stirring bar. The ampule was then kept at 80±1 °C in a DN-42 oven (Yamato Scientific Co.,Ltd.). The solution was stirred to produce the reaction. After the reaction had reached an extent of about 5—50 D%, the sample was cooled by immersing it in water; the contents were then separated into aqueous and oily (or solid) phases. The latter phase was used for the NMR measurement. The concentration of the NMR sample solution was neat for the liquid sample and ca. 50 wt% in dioxane for the solid sample. The samples were not degassed, since the presence of oxygen made T_1 short, which reduced the time needed to repeat its NMR measurement. The ^{13}C and ^{2}H NMR spectra were obtained with a Varian XL-200 FT-NMR spectrometer operating at 50.31 and 30.71 MHz respectively. The ^{13}C NMR spectra were measured by using the gated decoupling technique with no NOE pulse sequence. Data acquisition was carried out under the following conditions: flip angle of pulse, 45°: number of transients, 24—128: data points, 32000: delay time, 40 s, and spectral width, 2600—3500 Hz. The isotopic fractionation was obtained by the use of the Lorentzian lineshape-fitting procedure within an accuracy of ±0.5%. The computer-assisted lineshape simulations were run on a Sharp personal computer MZ-80B with a BASIC program, while the linear regressions were run on a Hitachi M-260H computer in our Institute using a FORTRAN program with double precision.

Results and Discussion

NMR Spectra. The NMR signal intensities of the deuterons meta to the hydroxyl or within the methyl group(s) did not change: that is, the natural abundance intensities remained even after the title reactions had been carried out for 200 h under the experimental conditions used. Those of the deuterium at the ortho and para positions were clearly observed with an increased intensity, but not separately, because of the broadening caused by the quadrupole interactions. In this system especially, the large solvent signal of D_2O sometimes interferes with the signals of the products. Therefore, the ^{2}H NMR signals of the products were not convenient for the product analyses. The NMR observation in the present study was, then, carried out only for the ^{13}C NMR spectra in the region of the aromatic carbons.

Figure 1 shows a typical ^{13}C NMR spectrum, which was observed for a solution obtained for 2-methylphenol. In this case, there are two reactive sites, C_4 and C_6, whose labeled carbon signals overlap with the unlabeled ones. The signal of the labeled carbon splits into three lines with coupling to deuterium, as may be seen in Fig. 1. It is also more shielded than that of the unlabeled carbon because of the so-called one-bond isotope shift, $^1\Delta$. The carbon atoms adjacent to the labeled one also suffer a high-field shift from the two-

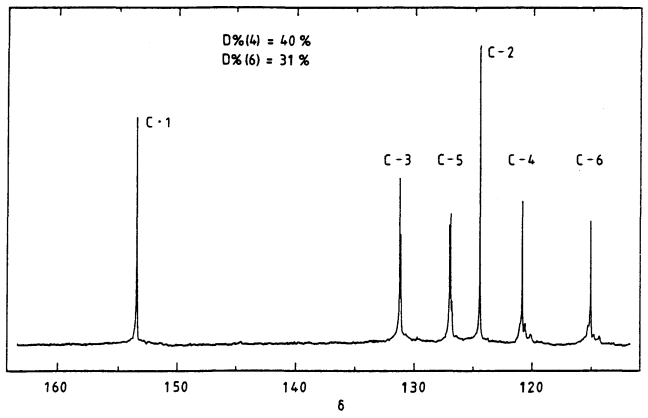

Fig. 1. The aromatic carbon regions of the 50.3 MHz ^{13}C NMR spectrum of the reaction mixtures of 2-methylphenol in the D_2O-HCl system. The spectrum was measured with the parameters of SW= 2600 Hz, 32 k data points, AT=6.154s, D1=40s, and 64 aquisitions (NT).

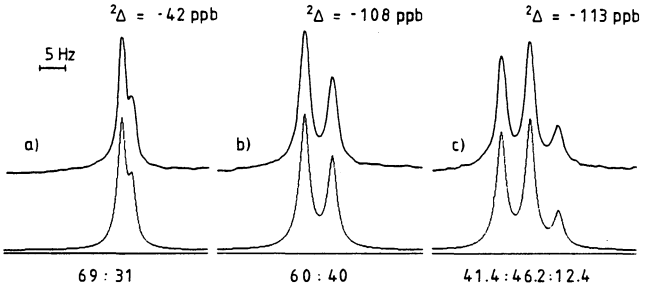

Fig. 2. ^{13}C NMR Spectra of (a) the C_1, (b) the C_3, and (c) the C_5 regions partly expanded from the spectrum of Fig. 1. The upper value gives the two-bond isotope shift and the lower one gives the intensity ratio of the signals. Data points were 427 points and half-height widths were 1.8, 2.3, and 2.4 Hz for a, b, and c, respectively.

bond isotope shift ($^2\Delta$). Therefore, both the C_1 and C_3 signals appear as two lines, and the C_5 signal, as three lines, as is shown in Fig. 2, though the C_2 signal does not split because it has no adjacent labeled carbon. The intensities of the signals are consistent with those obtained in each site, within an error of 1%.

Determination of *D* (%). In this article, the deuterium atom% is expressed as *D* (%). Reuben has reported a method of evaluating the deuterium/protium ratio by using the two-bond isotope shifts ($^2\Delta$).[6] His examples contain several equivalent labeled sites. However, in our cases, where the site in question has two nonequivalent adjacent site, its ^{13}C signal appears as three lines. This phenomenon may be ascribed to similar contributions from the two labeled deuterium atoms. In the cases of the method described here, the signals were sharp enough for the line separation to be observed and the *D*(%) could be determined accurately. As only the ortho and para protons of a phenol derivative undergo exchange reaction, the ^{13}C signals of C_1, C_3, and C_5 split into three or two lines only by means of adjacent labeled carbons. Thus, when the *D* (%) on the C_2, C_4, and C_6 of a phenol derivative are expressed as *p*, *q*, and *r*, the C_1, C_3, and C_5 signals split as follows:

$$C_1;\ (100-p)(100-r):(100-p)r+p(100-r):pr$$
$$C_3;\ (100-p)(100-q):(100-p)q+p(100-q):pq$$
$$C_5;\ (100-q)(100-r):(100-q)r+q(100-r):qr$$

If any one of C_2, C_4, or C_6 has a substituent, the *D*(%) of the substituted carbon is defined as zero. Then, in the case of 2-methylphenol, the *D*(%) of C_2 is equal to zero. Therefore, the two C_1 singlets have an intensity ratio of $(100-r):r$, while the two C_3 singlets have a ratio of $(100-q):q$. The three C_5 singlets have a ratio of $(100-q)(100-r):(100-q)r+q(100-r):qr$. Using these theoretical ratios, the pattern-fitting analyses were made for the experimental pattern, as is shown in Fig.2, by assuming that each signal fits the Lorentzian lineshape. The analyses need a parameter concerned with line widths. This is determined by a visual fitting of the calculated and observed spectra. The deuterium isotope shifts were determined from the spectra without any window function. As these parameters were determined independently, the *D*(%) of the sample can be obtained within an error of ±0.5% by means of the pattern-fitting analyses used. The values of *p*, *q*, and *r* can be determined by this method.

Evaluation of Reaction-Rate Constants. The exchange reaction between two reactants, AX and BX*, can be expressed as follows:

$$AX + BX^* \underset{k_{-1}}{\overset{k_1}{\rightleftharpoons}} AX^* + BX, \qquad (1)$$

where X* represents a labeled X atom. The reaction is first-order with respect to the concentration of the isotope X*. Let the concentrations be: [AX]+[AX*]=*a*, [AX*]=*x*, [BX]+[BX*]=*b*, [BX*]=*y*, and *x*+*y*=*z* (constant). Then, the rate will be expressed as:

$$\ln(x_0-x_e)-\ln(x-x_e)=kt((a+b)/ab) \qquad (2)$$

where x_0 and x_e are the values of *x* at $t=0$ and ∞ respectively and where

$$x_e=az/(a+b). \qquad (3)$$

The total exchange rate *k* is equal to the sum of k_1 and k_{-1}. Equation 2 has been named McKay's equation.[14] In this article, the hydrogen-deuterium-exchange reactions of the substituted phenols proceed as follows (Scheme 1):

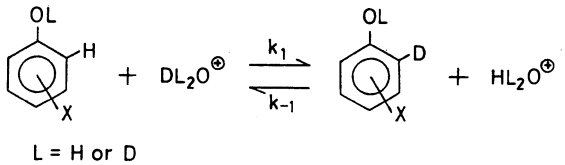

L = H or D

Scheme 1.

Table 1. ^2H Distributions and Reaction Rates as Calculated from ^{13}C NMR Lineshape Analyses of 3-Methoxyphenol in HCl-D_2O at 80 °C

Run No.	Time	HCl	D/%			D_e/%
	h	mmol dm^{-3}	C-2	C-4	C-6	
1	2.00	8.85	7	29	32	71.6
			(1.61)[a)]	(8.14)	(9.31)	
2	3.00	15.9	18	57	59	74.9
			(1.60)	(8.33)	(9.03)	

a) The values in parentheses are the reaction rates (k) calculated from Eq. 4 in the text: they are divided by the concentration of HCl and are given in units of 10^{-3} s^{-1} dm^3 mol^{-1}.

Table 2. Exchange Rate Constants (k_1) Observed for the Reactions in HCl-D_2O at 80 °C in Units of 10^{-6} dm^3 mol^{-1} s^{-1}

Compd. No.	Substituent	Site of exchange		
		H-2	H-4	H-6
1	H	8.97	16.7	8.97
2	2-CH_3	—	7.51	5.83
3	3-CH_3	53.5	156	77.0
4	4-CH_3	7.94	—	7.94
5	2-OCH_3	—	0.250	0.153
6	3-OCH_3	823	4120	4580
7	4-OCH_3	2.65	—	2.65
8	2-t-C_4H_9	—	1.23	2.12
9	3-t-C_4H_9	13.6	43.7	32.2
10	4-t-C_4H_9	1.60	—	1.60
11	2-Cl	—	0.019	0.019
12	3-Cl	1.56	2.64	2.43
13	4-Cl	0.235	—	0.235
14	2,3-$(CH_3)_2$	—	133	94.3
15	2,4-$(CH_3)_2$	—	—	6.45
16	2,5-$(CH_3)_2$	—	77.1	38.2
17	2,6-$(CH_3)_2$	—	0.668	—
18	3,4-$(CH_3)_2$	53.7	—	61.3
19	3,5-$(CH_3)_2$	546	1370	546
20	2,3-$(OCH_3)_2$	—	132	87.6

When the concentrations of the reactants are expressed by D(%), 0, D_e, and D can be substituted for x_0, x_e, and x in Eq. 2. Then, it is shown as follows:

$$((a+b)/ab)kt = \ln(D_e/(D_e-D)) = -\ln(1-(D/D_e)). \quad (4)$$

If k_1 is equal to k_{-1}, D_e can be calculated from the initial concentrations of the reactants. However, if k_1 is not equal to k_{-1}, where the reaction has the kinetic isotope effect (KIE), K ($=k_1/k_{-1}$) and D_e must be observed directly. In this case,

$$k_1 = k/(1+1/K),\ k_{-1} = k_1/K. \quad (5)$$

In the reactions studied for the 19 substituted phenols, no kinetic isotope effects (KIE) were observed except for that of 3-t-butylphenol. One reason seems to be the high reaction temperature used (80 °C). Two examples of evaluations of D(%) and the reaction rates are shown in Table 1. The error of log k is considered to be within ±0.03. The first-order rate constants evaluated for thirty-eight different sites of twenty phenols are given in Table 2. From the data in Table 2, it must be said that the rates of all the 3-substituted phenols are larger than those of the corresponding 2- or 4-substituted ones and that of the unsubstituted one. However, the rates of the 2- or 4-substituted phenols are smaller than that of phenol. These trends are to be expected from the electronic properties of the substituents. KIE was observed for the case of 3-t-butylphenol (**9**: hereafter compounds will be referred to using the numbers given in Table 2), and the K's were determined to be 0.0671, 0.206, and 0.119 for the 2-, 4-, and 6-positions respectively.

Substituent Parameters. The reaction rates for the substituted phenols are assumed to be expressed as the sum of the substituent parameters as follows:

$$\log k_x = \log k_H + \sum n_i S_i + \sum n_{jab} S_{jab}, \quad (6)$$

where k_x's are the observed rate constants k_1's for unsubstituted or substituted phenols. The value of log k_H on the right hand side of Eq. 6 can be determined as a parameter in a regression analysis of the parameters in Eq. 6. S_i(X) (for example, S_o, S_m, or S_p) is a substituent parameter for the i-position with respect to the substituent X. The notation of S_{jab}(X,Y) is used to express an interaction effect of the a- and b-positioned substituents, X and Y, to the j-positioned rate. These are correction terms for the interactions between the substituents, and n_i or n_{jab} is a weight factor for S_i or S_{jab}. For example, in the case of 3,5-dimethylphenol, the rates for two different sites can be calculated from Eq. 6 as follows:

2-position; $\log k_1 = \log k_H(\text{ortho}) + S_o + S_p + S_{213}$;
4-position; $\log k_1 = \log k_H(\text{para}) + 2S_o + S_{435}$.

A correction term, S_{213} or S_{435}, appears in the case where the observed site is sandwiched with two substituents, OH and X, or X and X, as in the present example. In the case of 3-methylphenol, the rates can be expressed as follows:

2-position; $\log k_1 = \log k_H(\text{ortho}) + S_o + S_{213}$;
4-position; $\log k_1 = \log k_H(\text{para}) + S_o$;
6-position; $\log k_1 = \log k_H(\text{ortho}) + S_p$.

In the case of 4-methylphenol, the rates can be expressed as follows:

2-(or 6-)position; $\log k_1 = \log k_H(\text{ortho}) + S_m$.

The observed data in Table 2 were analyzed except for those of Compounds **14**, **17**, and **20**, where three sub-

Table 3. Substituion Parameters of Eq. 6 Evaluated for the Reactions in HCl-D_2O

Parameter	Substituent			
	CH_3	CH_3O	t-C_4H_9	Cl
$S_o(X)$	0.991	2.403	0.429	−0.791
$S_m(X)$	−0.031	−0.510	−0.730	−1.563
$S_p(X)$	0.941	2.727	0.574	−0.549
$S_{213}(OH,X)$	−0.171	−0.421	−0.228	0.052
$S_{435}(X,X)$	−0.055	—	—	—
$S_{412}(OH,X)$	−0.295	−1.303	−0.393	−1.382
$S_{612}(OH,X)$	−0.113	−1.239	0.124	−1.103

log k_H(ortho)=−5.066. log k_H(para)=−4.788. Standard deviation=0.096. Probable error=0.011. Calculated from 33 data with 27 parameters.

stituents are adjacent to each other. Corrections for such three adjacent substituents can not be determined at the present stage. The $S_i(X)$ and $S_{jab}(X,Y)$ parameters thus obtained are given in Table 3. The parameters of log k_H in Eq. 6 were evaluated to be −5.066 and −4.788 for the two sites, ortho and para respectively. The values of log k_H(ortho) and log k_H(para) are in good agreement with the experimentally observed rates of phenol, within the limits of probable error. These parameters express S_o and S_p for the OH group. This group's k_H(ortho):k_H(para) ratio was obtained as 0.527:1. Thirty-three experimental data in Table 2 were correlated with 27 parameters with a standard deviation of 0.096. The reaction rates, log k_1, can be calculated within an error of ±0.03. S_o contains three contributions from the mesomeric, inductive, and steric effects of the substituents. S_m is evaluated from the data of the *p*-substituted phenols; it contains two contributions from the mesomeric and inductive effects of the substituents. S_p is essentially similar to Hammett's σ_p^+ and contains two contributions from the mesomeric and the inductive effects of the substituent. S_{213} appears in the cases of the meta-substituted phenols in which the two substituents interact sterically with each other in their activated states. As has been shown before in the example of 3-methylphenol (**3**), the log k_1's of the 2- and 4-positions of 3-substituted phenols are the same if S_{213} is not taken into consideration. The k_1's of phenol (**1**) are different for the two sites, the 2- and 4-positions. Therefore, the k_1's of 3-substituted phenols must be compared with each other after they have been divided by the corresponding k_1's of **1**. As a matter of fact, the k_1's of the 2-position are smaller than those of the 4-position except for one example. The ratios are, then, 0.579, 0.372, 0.639, and 1.100 for the 3-substituents of t-C_4H_9, CH_3O, CH_3, and Cl respectively. The bulkiness of the substituents is considered to be t-C_4H_9>CH_3O>CH_3>Cl, but the S_{213} of a methoxyl group shows a larger negative value than that of the t-C_4H_9 group. However, no details are known at present. The S_{435} appears in the case of the 4-position of **19**, much as with S_{213}. However, the S_{435} values of the two methyl groups are

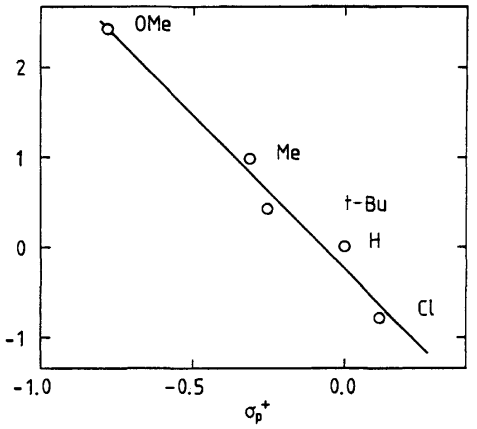

Fig. 3. Plot of S_o based on the σ_p^+ constants.

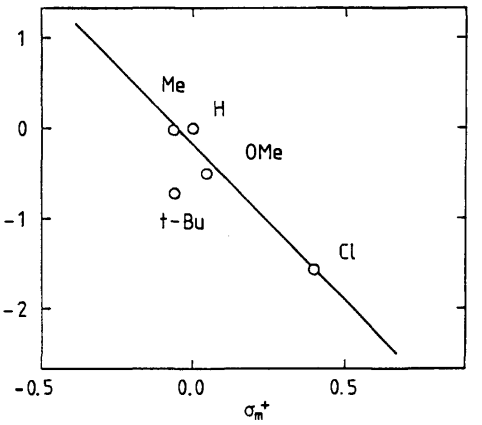

Fig. 4. Plot of S_m based on the σ_m^+ constants.

nearly zero. This shows that the hydoxyl group is more sterically effective than the methyl group in the present reaction. This is consistent with the fact that the methoxyl group is more effective than the *t*-butyl group for S_{213}. It is also considered that the presence of oxygen atom in the group has some effect. S_{412} and S_{612} appear in the cases of 2-substituted phenols. The two k_1's of the 4- and 6-positions of 2-substituted phenols must be compared with each other after the k_1's are divided by those of **1**. Their ratios are 0.692, 0.878, 0.312, and 0.537 for CH_3, CH_3O, t-C_4H_9, and Cl respectively. The k_1's at the 4-positions are affected more than those at the 6-positions by the introduction of 2-substituents. As may be seen in Table 3, the S_{412} and S_{612} values are especially large for the CH_3O and Cl groups. This contribution is probably due to the interference of the resonance effect of the hydroxyl group with the 2-substituents.

Correlation between Substituent Parameters and Hammett's Constants. The substituent parameters, S_o, S_m, and S_p, can be correlated with Hammett's constants, as is shown in Figs. 3—5. The S_o's are, however, plotted on a straight line with the σ_p^+ in Fig. 3, because no σ_o's are given in the Hammett relation. The straight line shows S_o=−3.4 σ_p^+−0.2, (r=0.986). In

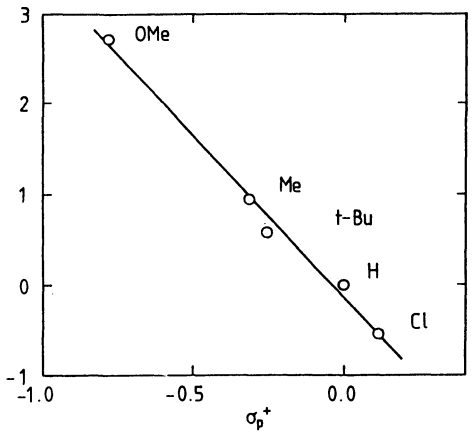

Fig. 5. Plot of S_p based on the σ_p^+ constants.

Fig. 4, the S_m of the *t*-butyl group is beneath the straight line. The straight line shows $S_m=-3.4\ \sigma_m^+-0.2$ ($r=0.979$) except for the point of the *t*-butyl group. In the case of S_p, all the values are correlated well with σ_p^+ by the use of the relation $S_p=-3.6\ \sigma_p^+-0.1$ ($r=0.995$), as is shown in Fig. 5. These values may be compared with that of $\rho=-3.51$ observed for similar reactions of 4-substituted anilines.[15]

It may be concluded that the method used in this article can be applied to ascertain the reaction rates in similar hydrogen-deuterium-exchange reactions with a good precision and with simplicity.

The substituent parameters can be expressed with the Hammett relation. Especially, it must be said that the additive relation can be applied even to ortho-substituted phenols with small deviations. This may be ascribed to the small size of the reagent, that is, a proton or deuteron, in the hydrogen-deuterium exchange reaction.

References

1) A. R. Katritzky and C. D. Johnson, *Angew. Chem., Int. Ed. Engl.*, **6**, 608 (1967).
2) V. K. Schwetlick and K. Unverferth, *J. Prakt. Chem.*, **314**, 603 (1972).
3) R. M. Kellogg, A. P. Schaap, E. T. Harper, and H. Wynberg, *J. Org. Chem.*, **33**, 2902 (1968).
4) J. L. Jurlina, H. A. Patel, S. Peiris, and J. B. Stothers, *Magn. Reson. Chem.*, **25**, 109 (1987).
5) a) J. B. Stothers, C. T. Tan, A. Nickon, F. Huang, R. Sridhar, and R. Weglein, *J. Am. Chem. Soc.*, **94**, 8581 (1972); b) D. H. Hunter, A. L. Johnson, J. B. Stothers, A. Nickon, J. L. Lambert, and D. F. Covey, *J. Am. Chem. Soc.*, **94**, 8582 (1972).
6) J. Reuben, *J. Am. Chem. Soc.*, **108**, 1082 (1986).
7) T. E. Walker and W. E. Wageman, *Magn. Reson. Chem.*, **24**, 157 (1986).
8) R. M. Jarrett and M. Saunders, *J. Am. Chem. Soc.*, **107**, 2648 (1985).
9) L. P. Hammett, *J. Am. Chem. Soc.*, **59**, 96 (1937).
10) H. C. Brown and Y. Okamoto, *J. Am. Chem. Soc.*, **80**, 4979 (1958).
11) R. W. Taft, Jr., and I. C. Lewis , *J. Am. Chem. Soc.*, **80**, 2436 (1958).
12) Y. Yukawa and Y. Tsuno, *Bull. Chem. Soc. Jpn.*, **32**, 960 (1959); **32**, 965 (1959); **32**, 971 (1959).
13) H. H. Jaffe, *Chem. Rev.*, **53**, 191 (1953).
14) H. A. C. McKay, *Nature (London)*, **142**, 997 (1983).
15) G. P. Bean and A. R. Katritzky, *J. Chem. Soc. B*, **1968**, 864.

 © 1988 The Chemical Society of Japan Bull. Chem. Soc. Jpn., 61, 3399—3402 (1988)

ESR Studies on Mn(II) Ions in Japanese Marine Pearls

Yong Li, Kunihiko Tajima, Kazuhiko Ishizu,* Nagao Azuma,† and Kiyonori Miyoshi††
Department of Chemistry, Faculty of Science, Ehime University, Matsuyama 790
†Faculty of General Education, Ehime University, Matsuyama 790
††Department of Metallurgical Engineering, Niihama National College of Technology, Niihama 792
(Received March 14, 1988)

X-band and Q-band ESR measurements of Mn(II) ions contained in Japanese cultured marine pearls and pearl oyster (*Pinctada fucata*) were carried out at room temperature. The ESR spectra observed for the powdered samples of nacreous and prismatic layers revealed the ESR hyperfine structures typical to Mn(II) in an aragonite lattice and a calcite lattice, respectively. The ESR spectra were interpreted with the following spin Hamiltonian.

$$\mathcal{H} = g\beta \boldsymbol{H}\cdot\boldsymbol{S} + a\boldsymbol{S}\cdot\boldsymbol{I} - g_n\beta_n\boldsymbol{H}\cdot\boldsymbol{I} + D[S_z^2 - S(S+1)/3] + E(S_x^2 - S_y^2)$$

The resonance fields for all the $M=+1/2 \leftrightarrow M=-1/2$ ESR transitions were derived, with the third-order corrections all taken into account. The zero-field splitting parameters D and E for Mn(II) ions in these biominerals were estimated by computer simulations of the ESR line shapes. The estimated parameters for the nacreous Mn(II) ion (D=20.8 mT, E=6.9 mT) are apparently different from those for the prismatic Mn(II) ion (D=8.5 mT, E=1.4 mT).

First observation of the ESR of marine seed pearls was recently reported by Ishizu et al.[1] They found that pearls containing the blackish materials gave a more intense ESR signal of an organic free radical assignable to that of melanin, as justified from the isotropic g-factor, line width, and microwave saturation behavior. It has also been reported that the blackish pearls revealed ESR spectra resemblant to those of the Mn(II) ion in the calcite lattice, whereas the ESR spectra of the Mn(II) ion in satin white and pale yellow pearls resemble those of Mn(II) ion in the aragonite lattice. Accordingly one will expect that a detailed analysis of the Mn(II) ESR spectrum will provide useful information to characterize the crystal structure of the calcification phase in terms of the ESR crystal field parameters. In this paper, the ESR spectra of the Mn(II) ion contained in typical Japanese marine pearls have been analyzed and their detailed parameters have been discussed. Those of pearl oyster (*Pinctada fucata*) have also been examined, as typical ESR spectra of the Mn(II) ion in the calcite lattice.

The crystal field characters of the Mn(II) ion are discussed based on a spin Hamiltonian involving an isotropic g-factor, isotropic hyperfine structure term a, and zero-field splitting parameters D and E, where the third-order perturbation corrections were all calculated. The D and E values have been obtained by computer simulation of the observed ESR line shapes.

Experimental

The pearls and pearl oyster (*Pinctada fucata*) were respectively cultured and collected at Uwa Sea, Ehime Prefecture, Japan. The pearls were pulverized after removal of their artificial nuclei. The shells were washed to remove the sludge and scales of acorn barnacles that covered them, then the powdered sample was collected from the outer surface, i.e. the prismatic layer, of the shell. Satin white and blackish pearls were used as typical reference materials.

X-band and Q-band ESR spectra were respectively recorded by a JEOL-FE-2XG X-band spectrometer and by a JEOL-ES-SQ4 Q-band spectrometer operating with 100 kHz magnetic-field modulation. Li-TCNQ (g=2.0025) and Cr(III) in MgO (g=1.9800) were used as standard g markers. The magnetic fields were calibrated with the hyperfine splitting of Mn(II) in MgO (8.69 mT).

The computer program used for simulation of the observed ESR spectra of the powdered samples is similar to those of Pilbrow et al. and Belford et al.[2] The calculations were carried out on a FACOM M-180II AD computer at the Data Processing Center of this University.

Results and Discussion

The spin Hamiltonian appropriate for Mn(II) ion (S=5/2, I=5/2) can be written by

$$\mathcal{H} = g\beta\boldsymbol{H}\cdot\boldsymbol{S} + a\boldsymbol{S}\cdot\boldsymbol{I} - g_n\beta_n\boldsymbol{H}\cdot\boldsymbol{I} + D[S_z^2 - S(S+1)/3] + E(S_x^2 - S_y^2) \quad (1)$$

where all symbols have their usual meaning, and we assume that g and a are both isotropic, which is a good approximation for an S state ion.

Approximate solutions of the spin Hamiltonian have been reported by various authors. In the ESR spectra of Mn(II) ions, forbidden transitions ($\Delta M=\pm1$, $\Delta m=\pm1$) have been usually observed in addition to the allowed transitions ($\Delta M=\pm1$, $\Delta m=0$). Bleaney et al.[3] previously explained the positions of the forbidden lines and their remarkably large intensity relative to the allowed transition, with application of the perturbation procedure, where they have restricted their third-order corrections to the terms of aD^2. Later, although the theoretical calculations have been reviewed by several authors. Their results were obtained by assuming some third-order corrections to be zero but these were not suitable for the simulation of the present spectra.[4] Therefore, we have derived the general solution which includes all the third-order corrections.

Theoretically, the spectrum of Mn(II) ion with D, $a \ll g\beta H_0$ exhibits fine structure due to five transitions with transition probability ratio of 5 : 8 : 9 : 8 : 5, each of which splits into six hyperfine lines and five pairs of forbidden hyperfine lines. However, we have not observed any clear fine structure due to the transition other than the strongest central fine structure transition ($M=1/2 \leftrightarrow M=-1/2$). One of the reasons for this may be that the concentrations of Mn(II) ions in the samples were too low to observe all the transitions. In fact, the contents of manganese ions in marine pearls and shells are one order less than those in fresh water ones.[5]

When the angle between the magnetic field direction and the z axis, and the angle between the projection of the magnetic field direction on the x-y plane and the x axis (θ and φ) are employed, the resonance fields concerned with the central fine structure transition are given for the allowed transitions $[(+1/2, m) \leftrightarrow (-1/2, m)]$ by,

$$H = H_0 - am/g\beta + [8(16v-2w)+a^2(4m^2-35)]/8g^2\beta^2H_0 - am[a^2(4m^2-65)+16(72v-w+2au)]/8g^3\beta^3H_0^2 \quad (2)$$

for the forbidden transitions $[(+1/2, m-1) \leftrightarrow (-1/2, m)]$,

$$H = H_0 - a(2m+1)/2g\beta - g_n\beta_nH_0/g\beta + [8(16v-2w)+a^2(4m^2+4m-67)]/8g^2\beta^2H_0 - a(2m+1)[a^2(4m^2+4m-195) + 16(72v-w+4au)]/16g^3\beta^3H_0^2 \quad (3)$$

and for the forbidden transitions $[(+1/2, m) \leftrightarrow (-1/2, m-1)]$,

$$H = H_0 - a(2m+1)/2g\beta + g_n\beta_nH_0/g\beta + [8(16v-2w)+a^2(2m+1)^2]/8g^2\beta^2H_0 - a(2m+1)[a^2(4m^2+4m+73) + 16(72v-w)]/16g^3\beta^3H_0^2 \quad (4)$$

where

$$H_0 = h\nu/g\beta \quad (5)$$

$$u = D(3\cos^2\theta-1)+3E\sin^2\theta\cos2\varphi \quad (6)$$

$$v = (D-E\cos2\varphi)^2\sin^2\theta\cos^2\theta+E^2\sin^2\theta\sin^22\varphi \quad (7)$$

$$w = [D\sin^2\theta+E\cos2\varphi(\cos^2\theta+1)]^2+4E^2\cos^2\theta\sin^22\varphi \quad (8)$$

The transition probabilities of the above forbidden transitions relative to the allowed transitions are given by

$$I = 64v[35-4m(m+1)]/g^2\beta^2H_0^2 \quad (9)$$

It has been well documented that the prismatic layer, or the outer surface, of the shell has the form of calcite. The calcite lattice has a symmetry octahedral unit. This reflects to the typical ESR spectrum with relatively high axial symmetry of the zero-field splitting as shown in Fig. 1(a). The six main lines arise from the allowed transitions, and five weak pairs of lines between the main lines are ascribed to the forbidden transitions. This spectrum is the same as that of the shell (*Balanus balanoides*) but some difference can be seen in the line width of the shell (*Mytilus edulis*), both reported by Chasteen et al.[6,7] In the case of the marine shell (*Mytilus edulis*) reported so far, the ESR line width is sharp because of the longer spin-lattice relaxation. The zero-field splitting parameters can therefore be determined from the observed spectrum. However, in the present case, those parameters have been estimated by computer simulation of the ESR line shape, since the fine structures are poorly observed. The apparent ESR intensities for the allowed transitions are decreased on the higher magnetic field side, as the D value is increased. For convenience, the E value is usually taken to be zero in the calcite case. However, the line shape of the spectrum simulated by taking account of the E term is similar to the observed one, Fig. 1(b), in comparison with that which is simulated by omitting the E term, Fig. 1(c).

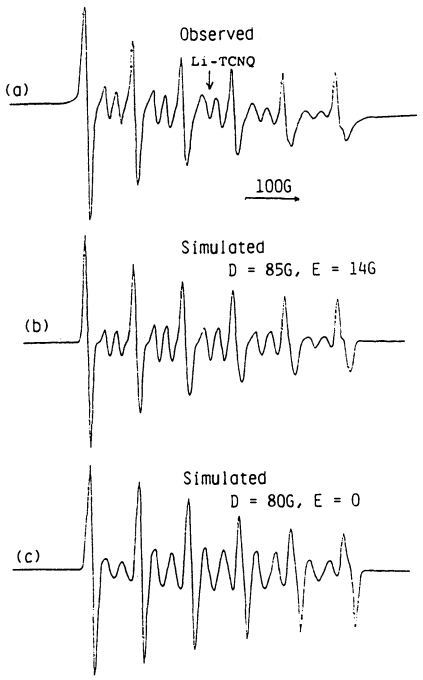

Fig. 1. (a): The X-band ESR spectrum observed at room temperature for Mn(II) ion in the prismatic layer of shell (*Pinctada fucata*). (b) and (c): The computer simulated ESR spectra for (a).

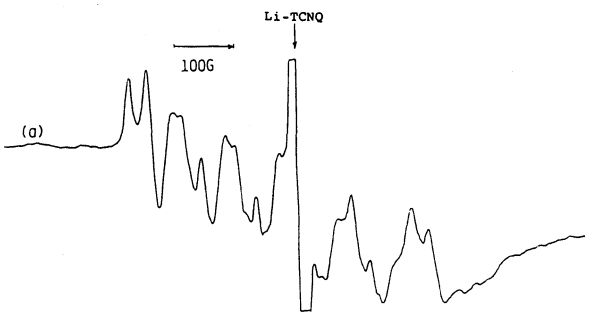

Fig. 2. The X-band ESR spectrum observed at room temperature for Mn(II) ion in the nacreous layer of the cultured marine pearl.

In contrast to the ESR spectrum of the prismatic layer, the X-band ESR spectrum of the nacreous layer of the cultured pearls appears to be very complicated, as shown in Fig. 2. The nacreous layer is composed of calcium carbonate in the form of aragonite. Because a metal ion in the aragonite lattice takes an unusual lower symmetrical nine-coordinate geometry,[8] the Mn(II) ion possesses the large zero-field interaction which brings the strong forbidden transition on the observed ESR spectrum. Consequently, the allowed and forbidden transition absorptions are overlapped each other; thus the Mn(II) ESR spectra become complicated with high anisotropy. According to Eq. 9, the forbidden transition intensity will be effectively reduced and the ESR hyperfine structure much simplified when the magnetic field increases. Actually, the Q-band ESR spectrum observed for the powdered sample of the nacreous layer is less complex and an effective reduction in the forbidden transition absorptions can be observed, Fig. 3(a). A similar Q-band ESR spectrum was reported for clam shell (*Mya arenaria*) by Chasteen et al.,[9] where the zero-field splitting parameters were determined from the hyperfine lines due to the second- and third-order terms in the perturbation equations. The spectrum for the pearl is less resolved than that for the clam shell. Therefore, the computer simulation of the Q-band ESR line shape has also been carried out to estimate the D and E values, as summarized in Table 1.

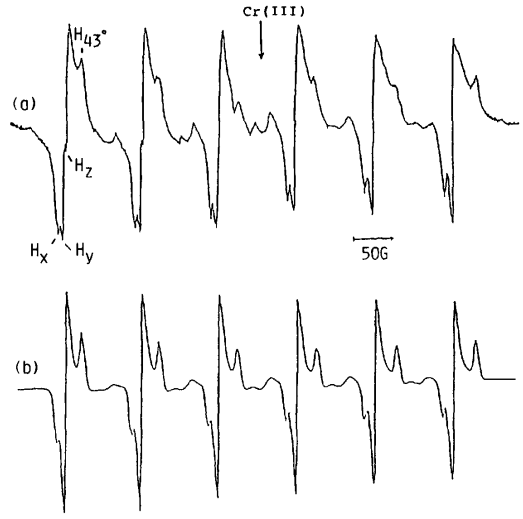

Fig. 3. (a): The Q-band ESR spectrum observed at room temperature for Mn(II) ion in the nacreous layer of the cultured marine pearl. (b): The computer simulated ESR spectrum for (a).

Table 1. ESR Parameters for Mn(II) Ions in the Calcite Lattice in the Prismatic Layer of Marine Shell (*Pinctada fucata*) and in the Aragonite Matrix in Nacreous Layer of the Marine Pearl

	g	a/mT	D/mT	E/mT	E/D	
Calcite	2.006	9.40	8.50	1.40	0.16	This work
	2.001	9.38	8.63	—	—	Ref. 7
Aragonite	2.004	9.60	20.80	6.90	0.33	This work
	2.006	9.40	25.00	4.20	0.17	Ref. 9

In the case of calcite, the present D value is similar to that reported by Chasteen et al.,[9] although the method used to determine the zero-field splitting parameters are different. The contribution of the E value was found to be larger than what we had expected from the usual approximation of setting the same term to zero. Thus the importance of the E term is demonstrated for the metal ion doped in a calcite lattice. The estimated D and E values for the Mn(II) ion in the aragonite phase of the marine pearl are different from those reported for the same phase in clam shell (*Mya arenaria*) by Chasteen et al.[9] The present D and E values for the marine pearl are respectively less and larger than the values for their shell, as shown in Table 1.

The range of ratio $r(=E/D)$ is distributed from 0 to 1/3, and it is taken to be a parameter which indicates a degree of ligand field symmetry. When the r value is zero, the ligand field has perfect axial symmetry, and if the r value is 1/3, that means perfect rhombic symmetry. It is interesting that the r value of the Mn(II) ion determined for the marine pearl is about 1/3. This means that the nacreous layer of the marine pearl is composed of aragonite which is highly distorted by the metal coordination geometry.

As described earlier, the satin white and the pale yellow pearls revealed ESR hyperfine structure ascribed to the Mn(II) ion contained in the aragonite matrix of the nacreous layer. The pearls containing blackish materials usually gave a mixed hyperfine splitting of prismatic Mn(II) and that of Mn(II) ascribed to the species in the aragonite matrix. In this case, the detailed analysis of the line shape is difficult, because the line shape analysis of the X-band ESR of Mn(II) in the aragonite lattice is much more complicated due to the overlapping of the multi-forbidden transition. The further calculation of the line shape in this case is now under way.

The authors wish to express their sincere thanks to Mr. Terumi Kobata who provided the valuable samples of pearls and shells, we also gratefully acknowledge Professors Noboru Hirota and Hiroaki Ohya-Nishiguchi of Kyoto University for their measurement of Q-band ESR spectra. This work was partially supported by the Grant-in-Aid for Scientific Research (No. 63540491) from the Ministry of Education, Science and Culture. The X-band ESR measurements were carried out at the Advanced Instrumentation Center for Chemical Analysis of this University.

References

1) K. Ishizu, *SHINJU*, No. **189**, 4 (1985); K. Ishizu, R. Ikeda, K. Tajima, and K. Miyoshi, *Nippon Kagaku Kaishi*, **1986**, 93.

2) A. D. Toy, S. H. H. Chaston, J. R. Pilbrow, and T. D.

Smith, *Inorg. Chem.*, **10**, 2219 (1971); J. R. Pilbrow and M. E. Winfield, *Mol. Phys.*, **25**, 1073 (1973); L. K. White and R. L. Belford, *J. Am. Chem. Soc.*, **98**, 4428 (1976).

3) B. Bleaney and R. S. Rubins, *Proc. Phys. Soc. (London)*, **77**, 103 (1961); corrigendum, *ibid.*, **78**, 778 (1961).

4) L. M. Matarresse, *J. Chem. Phys.*, **34**, 336 (1962); V. J. Folen, *Phys. Rev.*, **125**, 1581 (1962); B. C. Cavenett, *Proc. Phys. Soc. (London)*, **84**, 1 (1964); H. W. de Wijn and R. F. van Balderen, *J. Chem. Phys.*, **46**, 1381 (1967).

5) K. Wada, *Housekigaku Kaishi*, **2**, 3 (1975); **8**, 151 (1981).

6) S. C. Blanchard and N. D. Chasteen, *Anal. Chim. Acta*, **82**, 113 (1976).

7) S. C. Blanchard and N. D. Chasteen, *J. Phys. Chem.*, **80**, 1362 (1976).

8) J. P. R. De Villiers, *Am. Mineral.*, **56**, 758 (1971).

9) L. K. White, A. Szabo, P. Carkner, and N. D. Chasteen, *J. Phys. Chem.*, **81**, 1420 (1977).

 © 1988 The Chemical Society of Japan Bull. Chem. Soc. Jpn., 61, 3403—3407 (1988)

XRD Characteristics of Na-ZSM-5 Synthesized from an Organic-Free System

Feng-Yuen DAI,* Minoru SUZUKI, (the late) Hiroshi TAKAHASHI, and Yasukazu SAITO
Institute of Industrial Science, University of Tokyo, 7-22-1 Roppongi, Minato-ku, Tokyo 106
(Received March 15, 1988)

XRD profiles of as-synthesized Na- and TPA-ZSM-5 were not identical. They became similar to each other, however, when both zeolites were converted into organic-free or organic-contained forms. In terms of the framework topology, Na-ZSM-5 resembled TPA-ZSM-5 but differed from so-called ZSM-8. SEM images revealed the Na-ZSM-5 crystal to exhibit a hexagonal-lath-shaped morphology. Due to the preferred orientations, the intensities of (0k0) and (h0l) reflections were intensified and diminished, respectively. The hexagonal flat plane of the Na-ZSM-5 crystal was (010). Therefore, the 10-membered-ring straight channels were strongly indicated to penetrate perpendicularly to the hexagonal flat plane of the as-synthesized Na-ZSM-5 crystal.

Powder X-ray diffraction (XRD) is commonly used for identifying the structure of as-synthesized zeolites, because this technique is very simple and suitable for the small crystals of synthetic zeolites (ca. 0.5—15 μm).

Care should be taken on XRD characterization, since certain zeolites with different frameworks exhibit similar profiles, as has been pointed out previously by Breck[1] for phillipsite, harmotome and gismondine. Lechert[2] gave another example recently for structurally related zeolites of ZSM-5, ZSM-8, and ZSM-11, and stated that a splitting of the highest peak (2θ=23.0—23.5°; Cu $K\alpha$ radiation) was observed for ZSM-8 only.

ZSM-5 zeolite has been synthesized generally from the tetrapropylammonium (TPA)-contained aluminosilicate gel;[3] nevertheless, it is possible to obtain ZSM-5 without adopting expensive and toxic TPA components.[4-8] Grose et al.[5] mentioned that the XRD pattern and adsorption property of a novel zeolite synthesized from an organic-free system (designated as Na-ZSM-5 hereafter) resembled those of typical TPA-ZSM-5. According to our preliminary examinations, however, as-synthesized Na-ZSM-5 gave a splitting similar to ZSM-8 in the main peak region (2θ=23.0—23.5°). A new question arises therefore whether as-synthesized Na-ZSM-5 belongs to TPA-ZSM-5 or so-called ZSM-8.

XRD profiles of zeolites are well-known to be affected easily without changing the framework topology. For example, dehydration of chabazite brought about framework distortion.[10] According to Baerlocher and Meier,[11] synthetic tetramethylammonium gismondine with tetragonal crystal symmetry changed continuously to a pseudocubic form upon thermal decomposition of the organic cation. Wu et al.[12] showed that conversion of as-synthesized TPA-ZSM-5 into its ammonium or hydrogen form caused a symmetry change from orthorhombic to monoclinic, whereas the orthorhombic symmetry was regenerated by ammonia adsorption on the hydrogen form. The XRD profiles of zeolites are thus affected by guest substances in the skeleton, such as water or organic species.

The present study is an attempt to attribute the structure of as-synthesized Na-ZSM-5 zeolite to TPA-ZSM-5 or ZSM-8 and also to elucidate the correlation between its characteristic morphology and the crystal structure.

Experimental

Sample Preparation. TPA-ZSM-5 zeolite (designated sample A_1 hereafter) was synthesized from a starting composition of 2.0 TPA_2O-4.0 Na_2O-1.0 Al_2O_3-65 SiO_2-3000 H_2O under hydrothermal conditions of 170 °C for 48 h with stirring. Tetrapropylammonium bromide (TPABr) was adopted as the TPA source. The sample A_1 was calcined in air at 620 °C for 3 h to give a calcined (TPA)-ZSM-5 (sample B_1). The sample B_1 was then treated with 1 M NH_4Cl aqueous solution (1 M=1 mol dm^{-3}) at room temperature for 12 h, followed by calcination at 540 °C for 4 h to convert it into a hydrogen form. After this hydrogen form was degassed in vacuo at 150 °C for 1 h in a glass tube, an excess amount of prepurified diethylamine (DEA) was vacuum-transferred into the glass tube to immerse the zeolite at 15 °C for 12 h, producing a DEA-contained zeolite (sample A_1').

As-synthesized Na-ZSM-5 was prepared from a composition of 8.75 Na_2O-1.0 Al_2O_3-70 SiO_2-3150 H_2O by following the procedure reported previously.[8] Conversion of as-synthesized Na-ZSM-5 into its hydrogen form (sample B_2) was carried out by ion-exchange with 1 M NH_4Cl aqueous solution, followed by calcination at 540 °C for 4 h. Immersion with DEA changed the sample B_2 into another DEA-contained zeolite (sample A_2). The other organic-free ZSM-5 (sample B_2') was prepared by calcining the sample A_2 at 620 °C for 3 h.

Characterization. The XRD profiles of zeolites were measured by an X-ray diffractometer (Rigaku Denki Co. Ltd., D-9 C, equipped with a scintillation counter) under the conditions: Cu $K\alpha$ radiation (Ni-filter) at the intensity of 30 kV-10 mA with the slit system of RS=0.15 mm and DS=SS=1/2°; the 2θ scanning rate of 1/4 or 1/8° min^{-1}.

Silicon powder (300 mesh-pass) was adopted as the internal standard for adjusting 2θ values (22—25°) accurately with reference to the Si(111) reflection.

Crystal morphologies of zeolites were observed by means of scanning electron microscopy (SEM) (Akashi Co., Ltd., Alpha-10).

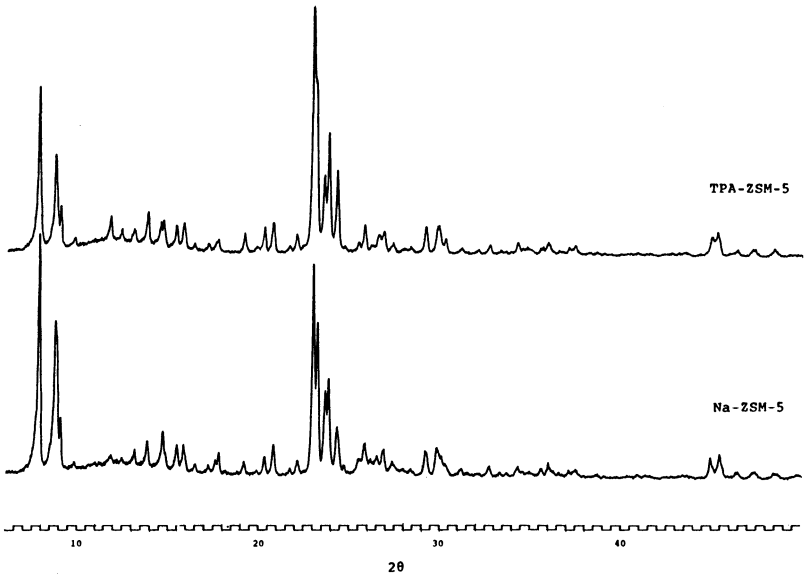

Fig. 1. XRD profiles of Na-ZSM-5 and TPA-ZSM-5 synthesized from organic-free and TPABr systems, respectively; XRD 2θ scanning rate of $1/4°\ min^{-1}$.

Results and Discussion

Effects of Organic Species on XRD Profiles. Typical XRD profiles of as-synthesized TPA-ZSM-5 and Na-ZSM-5 are contrasted in Fig. 1. Although it was once stated that almost all the diffraction peaks of as-synthesized Na-ZSM-5 coincided with those of typical TPA-ZSM-5,[5] these XRD profiles were not exactly identical. Firstly, peak intensity differences were apparent at 2θ=7.94, 8.87, 11.90, 12.50, 13.19, 14.70—14.88 (doublet), 20.34, 23.68, and 23.91°. Secondly, the splitting in the main peak region (2θ=23.0—23.5°) was much clearer for Na-ZSM-5 than for TPA-ZSM-5. Calcination of as-synthesized TPA-ZSM-5, however, resulted in a well-resolved profile of the main peak splitting,[13] accompanying the intensified peaks at 2θ=7.94, 8.87, 13.19, and 14.82°, and the diminished ones at 11.90, 12.50, 20.34, 23.68, and 23.91°.[14] Consequently, the XRD profile of calcined-(TPA)-ZSM-5 (B_1) well resembles that of as-synthesized Na-ZSM-5.

Readsorption of organic species onto either calcined-(TPA)-ZSM-5 or as-synthesized Na-ZSM-5 was attemped therefore to clarify the effect of organic guest substances on XRD profiles.

The XRD region of 2θ=22—25° was enlarged and shown in Figs. 2 and 3. Hydrogen forms of both kinds of as-synthesized ZSM-5 were prepared in order to minimize the steric hindrances for the adsorption of organic species. Diethylamine (DEA) was adopted as absorbate, because its molecule size is small enough to diffuse freely into the zeolite channel (size of ZSM-5 window: 5—6 Å).[15]

The XRD profile of five significant peaks of as-synthesized TPA-ZSM-5 was varied by sequential treatments of $A_1 \rightarrow B_1 \rightarrow A_1'$ (Fig. 2).

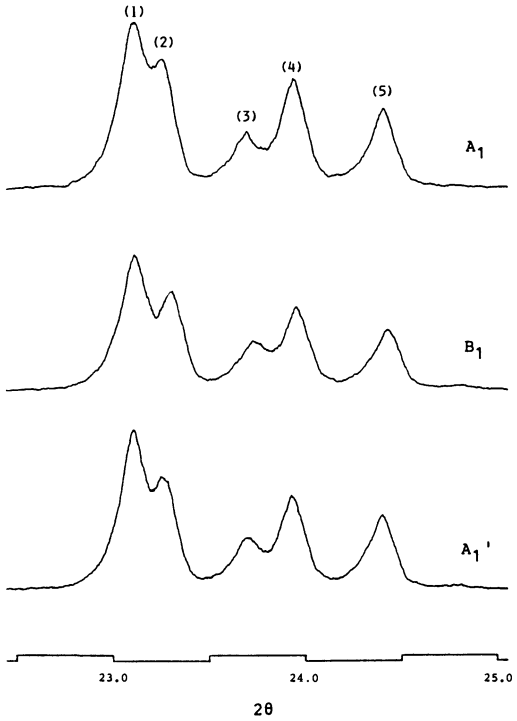

Fig. 2. Variation of XRD profiles: as-synthesized TPA-ZSM-5 (A_1) changed to calcined-TPA-ZSM-5 (B_1) by calcination at 620°C for 3 h, and finally to DEA-ZSM-5 (A_1') by loading diethylamine (DEA) at 15°C for 12 h; XRD 2θ scanning rate of $1/8°\ min^{-1}$.

As converting A_1 into B_1, the position of the strongest peak (marked as (1)) remained unchanged, whereas the others of (2)—(5) were shifted slightly toward high angles. As the peak (2) shifted to higher angle, the profile became well-resolved, which was accepted as grounds for the ZSM-8 assignment. On the contrary,

incorporation of DEA into H-ZSM-5 (B_1) induced peak shifts again toward lower angles, as shown for the (2)—(5) peaks of DEA-ZSM-5 (A_1'). The XRD profile was thus changed reversibly between as-synthesized TPA-ZSM-5 (A_1) and DEA-ZSM-5 (A_1').

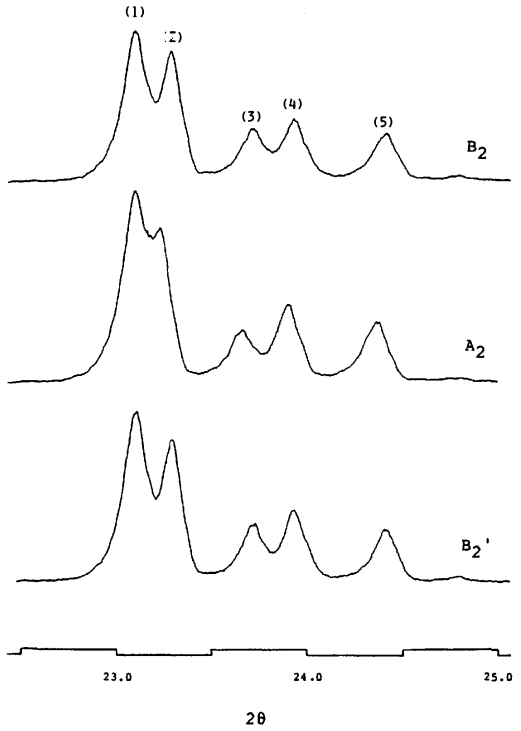

Fig. 3. Variation of XRD profiles: H-ZSM-5 (B_2), ion-exchanged from as-synthesized Na-ZSM-5, changed to DEA-ZSM-5 (A_2) by loading diethylamine (DEA) and finally to calcined-DEA-ZSM-5 (B_2') by calcination at 540°C for 4 h; XRD measurement conditions are the same as those of Fig. 2.

The hydrogen form of Na-ZSM-5 was loaded with DEA, then calcined to reproduce the organic-free form. These treatments brought the changes of XRD profiles as $B_2 \rightarrow A_2 \rightarrow B_2'$ (Fig. 3).

Conversion of H-ZSM-5(B_2) to DEA-ZSM-5(A_2) induced peak shifts toward lower angles except foi the main peak (1). The splitting profiles due to the main peaks of (1) and (2) were similar between DEA-ZSM-5 (A_2) and as-synthesized TPA-ZSM-5 (A_1 in Fig. 2). Thermal decomposition of guest organic substances contained in the sample A_2 yielded the sample B_2', which gave again the XRD profile similar to H-ZSM-5 (B_2).

The following aspects are deduced from Figs. 2 and 3.

(1) Either occluded during hydrothermal synthesis or absorbed by ammine immersion, organic species inside the zeolite skeleton exert an influence upon XRD profiles, irrespective of the ZSM-5 zeolite synthesized from the system with or without using organic templates.

(2) The adsorption and decomposition of guest organic subtances induce XRD profiles to change reversibly, as apparent from the resemblance between A_1' and A_1 (Fig. 2) or between B_2 and B_2' (Fig. 3).

(3) The shape of the main peaks around $2\theta = 23.0—23.5°$ is sensitive to the involvement of organic species in the zeolite skeleton; the well-resolved profile of the organic-free form (B_1, B_2, and B_2') is in sharp contrast to the poorly-resolved profile of those incorporated with organic species (A_1, A_1', and A_2).

(4) Certain diffraction peaks are induced to shift by the incorporation of organic species into both kinds of ZSM-5 skeletons.

Since both kinds of silicious zeolites exhibit high

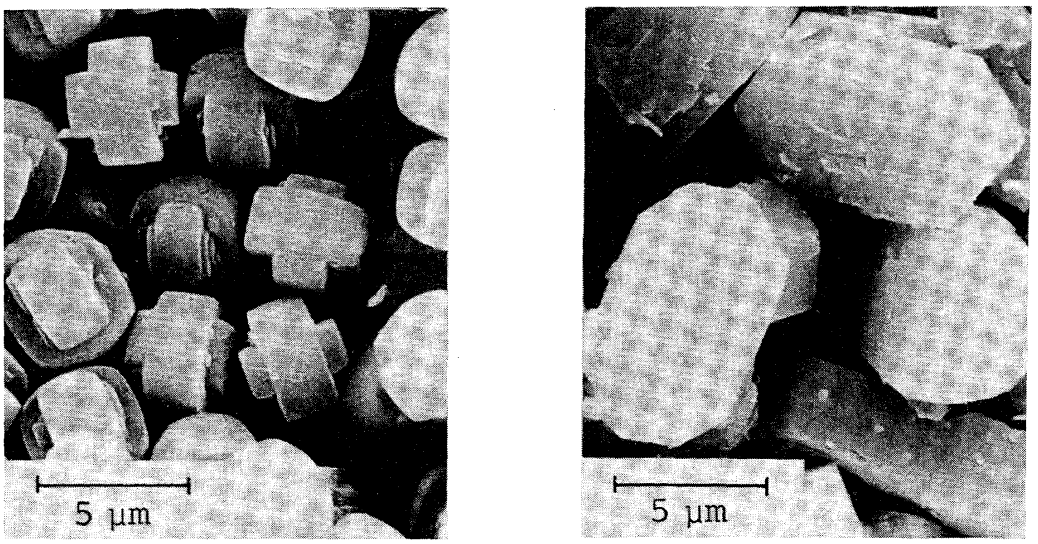

Fig. 4. Typical SEM morphologies of ZSM-5 zeolites synthesized from TPABr (B_1) and organic-free (B_2) systems; notations are common to those of Figs. 2 and 3.

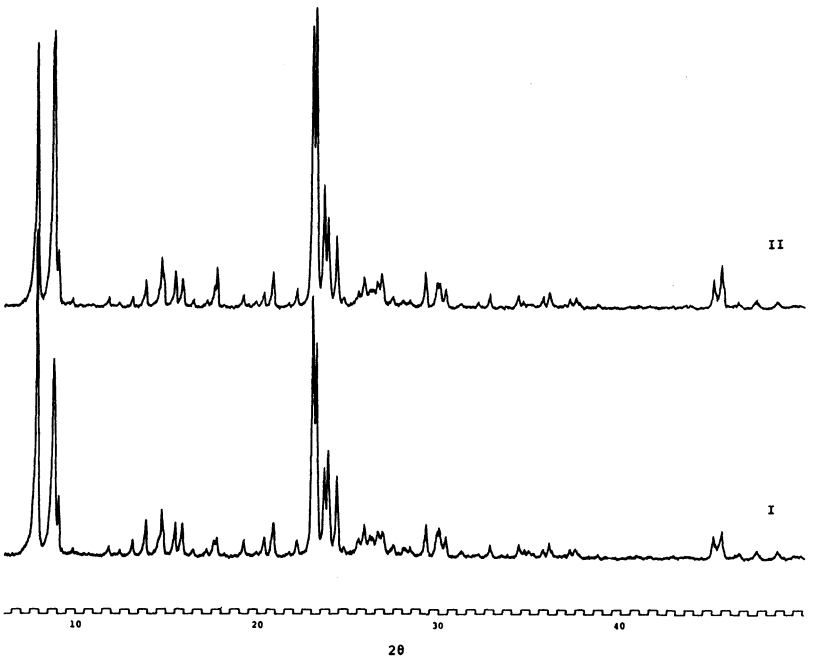

Fig. 5. Variation of XRD profiles for H-ZSM-5, ion-exchanged from as-synthesized Na-ZSM-5: specimen set with the normal manner (I) and extremely pressurized manner (II); XRD 2θ scanning rate of $1/4°\ min^{-1}$.

thermal stability against calcination (620 °C for 3 h), as evident from the reversible changes of those XRD profiles (point (2)), no topological changes occur throughout these conversion processes. These XRD profile changes (Figs. 2 and 3) can therefore be attributed to lattice expansion induced by the guest organic amine.

Throughout the XRD region of 2θ=5—50°, all the peak positions of calcined-(TPA)-ZSM-5 (B_1) coincided well (within an error of ±0.02°) with those of H-ZSM-5 (B_2). No doublet peaks were observed at the regions around 24.4, 29.2, and 48.6° for either Na-ZSM-5 or TPA-ZSM-5 during the conversion processes, suggesting both of them to belong commonly to the orthorhombic symmetry.[12] On these grounds, as-synthesized Na-ZSM-5 is concluded to possess an isostructure with TPA-ZSM-5, different from the so-called ZSM-8[9] in framework topology.

Crystal Characteristics of Na-ZSM-5 Synthesized from Organic Free System. Crystal Morphology. Typical SEM morphologies of Na- and TPA-ZSM-5 zeolites are shown in Fig. 4. Spherical-like or crossed-discus crystals (B_1) were easily formed with use of TPABr, whereas hexagonal-lath-shaped crystals (B_2) were always obtained from the organic-free system. Each crystal morphology remained unchanged throughout sequential treatments of ammonium ion exchange, calcination and DEA adsorption.

Effect of Preferred Orientation on XRD Profiles. Characteristic to the hexagonal-lath-shaped ZSM-5 crystals (B_2) synthesized from the organic-free system, certain XRD peak intensities were sensitive to the manner of mounting the specimen onto an X-ray sample holder. With regard to the spherical-like ZSM-5 zeolite (B_1), such changes of XRD spectra have never been experienced previously.

Table 1. Specific XRD Peak Intensities of Hexagonal-Lath-Shaped Na-ZSM-5 Crystals Sensitive to Specimen Setting Manner

$(h$	k	$l)$[a]	2θ[b]	(I/I_0)[c] Normal setting	(I/I_0)[c] Extreme pressing
1	0	2	13.90	76	47
2	0	2	15.86	69	49
1	0	3	20.34	40	28
3	0	3	23.91	219	156
0	4	0	17.79	38	69
0	5	1	23.25	436	526
1	5	1	23.68	186	213
0	10	0	45.46	57	73

a) See Ref. 18. b) Cu $K\alpha$ radiation ±0.02°. c) The intensity of isotropic (111) reflection (2θ=9.08°) was adopted as I_0, because this was the strongest peak insensitive to the preferred orientation.

Figure 5 illustrated the XRD profiles of hexagonal-lath-shaped ZSM-5 (B_2) measured in different conditions; one of the specimen was set by a standard procedure[16] (I) and the other was set in excess amount with extra pressure(II). The peaks located at 2θ=8.85, 17.79, 23.25, 23.68, 26.85, and 45.46° were intensified, whereas those of 7.92, 13.90, 15.86, 20.34, 23.01, and 23.91° were diminished, by pressing. Extra pressure induced the change of the total peak area within the region of 2θ=22.0—25.0°. Improper specimen pressing must be

avoided, since the peak area is often adopted for estimating the degree of crystallization.[17]

The diffraction peaks sensitive to the specimen pressing were specified (Table 1), together with the corresponding Miller Indices of ZSM-5.[18]

As evident from Table 1, the peaks diminished in intensity were classified to the group of ($h0l$) reflection, whereas the peaks intensified belonged to the ($0k0$) group.

Since the lath-shaped crystals were apt to deviate from random orientation, it is conceivable that the orientation of hexagonal-flat planes become parallel to the plane of the XRD sample holder. The XRD peaks of the diffraction planes parallel to the hexagonal-flat surface would therefore be intensified. This supports the view that the hexagonal-flat plane of Na-ZSM-5 crystal belong to the (010) plane.

In the ZSM-5 skeleton, the straight 10-membered-ring channel elongates along the 'b' axis, whereas the zigzag channel extends toward the 'a' axis.[15] Since the diffraction planes with ($0k0$) Miller Indices intersect perpendicularly with the 'b' axis, the straight channels are concluded to penetrate perpendicularly to the flat plane of the hexagonal-lath-shaped crystals.

Conclusion

(1) Na-ZSM-5 possesses an isostructure with TPA-ZSM-5 but differs from the so-called ZSM-8 in framework topology. XRD profiles of Na- and TPA-ZSM-5 were controlled by incorporation or decomposition of organic amine in the ZSM-5 skeleton.

(2) XRD intensities of ($0k0$) and ($h0l$) reflections for hexagonal-lath-shaped Na-ZSM-5 are sensitive to the preferred orientation. The hexagonal-flat plane of Na-ZSM-5 crystal is (010). Therefore, the 10-membered-ring straight channels of ZSM-5 are strongly indicated to penetrate perpendicularly to the hexagonal-flat plane of the crystal.

We are grateful to Mr. Hiromi Nakamoto (Catalysts & Chemical Industry, Co., Ltd.) for helpful advice on zeolite syntheses and to Mr. Shigeji Hagiwara (Institute of Industrial Science, University of Tokyo) for valuable comments on the XRD characterization.

References

1) D. W. Breck, "Zeolite Molecular Sieves: Structure, Chemistry and Use," John Wiley & Sons, New York (1974), pp. 205—207.

2) H. Lechert, *NATO ASI Ser., Ser. E, No. 80,* "Zeolite: Science and Technology," **1984**, pp. 158—161.

3) R. J. Argauer and G. R. Landolt, U. S. Patent 3702886 (1972).

4) K.-J. Chao, *Proc. Nat. Sci. Conc., Taiwan,* **3**, 233 (1979).

5) R. W. Grose and E.M. Flanigen, U. S. Patent 4257885 (1981).

6) A. Nastro, C. Colella, and R. Aiello, "Studies in Surface Science and Catalysis 24—zeolites: Synthesis, Structure, Technology, and Application," Elsevier, Amsterdam (1985), pp. 39—46; R. Aiello, F. Crea, A. Nastro, and C. Pellergrino, *Zeolites,* **7**, 549 (1987).

7) J. M. Berak and R. Mostowicz, "Studies in Surface Science and Catalysis 24—Zeolites: Synthesis, Structure, Technology, and Application," Elsevier, Amsterdam (1985), pp. 47—54.

8) F.-Y. Dai, M. Suzuki, H. Takahashi, and Y. Saito, "New Developments in Zeolite Science and Technology: Proc. 7th Int. Zeolite Confer.," Kodansha-Elsevier, Tokyo (1986), pp. 223—230.

9) The structure of ZSM-8 remains uncertain due to lacking of the single crystal analysis. It is suggested, however on the basis of ^{29}Si-MAS NMR study that "ZSM-8 crystal could be a mixture of ZSM-5 and ZSM-11 or an intergrowth of these two kinds of structure. See, for example, Z. Gabelica, J. B. Nagy, P. Bodart, G. Debras, E. G. Derouane, and P.A. Jacobs, *NATO ASI Ser., Ser. E, No. 80,* "Zeolite: Science and Technology," **1984**, pp. 193—210.

10) J. V. Smith, *Acta Crystallogr.,* **15**, 835 (1962).

11) Ch. Baerlocher and W. M. Meier, *Helv. Chim. Acta,* **53**, 1285 (1970).

12) E. L. Wu, S. L. Lawton, D. H. Olson, A. C. Rohrman, and G. T. Kokotailo, *J. Phys. Chem.,* **83**, 2777 (1979).

13) The splitting profile of the main peaks is also observed for hydrated ZSM-5, as shown in 18, and for NH_3-loaded H-ZSM-5 in 12.

14) Peak intensity changes were pointed out previously by Wu et al., when a highly silicious, as-synthesized TPA-ZSM-5 was converted to its ammonium-exchanged form.[12]

15) G. T. Kokotailo, S. L. Lawton, D. H. Olson, and W. M. Meier, *Nature (London),* **272**, 437 (1978); *J. Phys. Chem.,* **85**, 2238 (1981).

16) H. P. Klug and L. E. Alexander, "X-Ray Diffraction Procedures," John Wiley & Sons, New York (1954), pp. 290—305.

17) K.-J. Chao, T. C. Tsai, M.-S. Chen, and I. K. Wang, *J. Chem. Soc., Faraday Trans. 1,* **77**, 547 (1981).

18) R. Ballmoos, "Collection of Simulated XRD Powder Patterns for Zeolites," Butterworth, UK (1982), pp. 74—75.

 © 1988 The Chemical Society of Japan Bull. Chem. Soc. Jpn., 61, 3409—3415 (1988)

^{1}H NMR Study of the Regioisomers of Primary *O*-Di- and Trisubstituted α-Cyclodextrins

Yoshihisa MATSUI,* Masahiko FUJIE, and Hiroshi SAKATE
Faculty of Agriculture, Shimane University, Nishikawatsu, Matsue 690
(Received March 24, 1988)

The regioisomers of bis- and tris[C(6)-*O*-sulfonylated] α-cyclodextrins were converted in satisfactory yields to the corresponding C(6)-pyridinio derivatives, which afforded the characteristic splitting patterns of ^{1}H NMR signals available for a regioisomer determination. Electrostatic repulsive interactions between the positively charged pyridinio groups play an important role in the remarkable splitting of the ^{1}H NMR signals observed for some regioisomers.

O-Arylsulfonylated cyclodextrins are the key intermediates from which a number of other cyclodextrin derivatives have been prepared.[1] In particular, primary *O*-bis- or poly(arylsulfonylated) cyclodextrins have attracted much attention regarding the construction of refined artificial enzymes[2] or artificial receptors.[3] Polysubstituted cyclodextrins generally involve a fair number of regioisomers. For example, bis- and tris[C(6)-*O*-sulfonylated] α-cyclodextrins involve three and four regioisomers, respectively. They are designated as 6A,6B-, 6A,6C-, and 6A,6D-isomers for disubstituted α-cyclodextrins and 6A,6B,6C-, 6A,6B,6D-, 6A,6B,6E-, and 6A,6C,6E-isomers for trisubstituted α-cyclodextrins. Recently, Fujita et al.[4] have succeeded in separating a mixture of the regioisomers of C(6) polysulfonylated α-cyclodextrins from one another and determining the position of the substituents in them. In this regioisomer determination, however, ^{1}H NMR spectroscopy played only a minor role, owing to the similarity and/or complexity of the spectra.

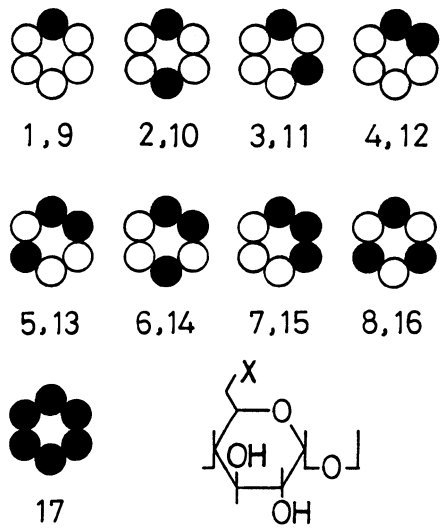

Fig. 1. α-Cyclodextrin derivatives examined.
○: X=-OH (**1**—**16**)
●: X= -OSO$_2$-(Me, Me) (**1**—**8**)
●: X= -N$^+$ (**9**—**17**)

In the course of an investigation of charged cyclodextrins,[5] we recently found that the regioisomers of bis- and tris[C(6)-*O*-arylsulfonylated] α-cyclodextrins are converted in satisfactory yields to the corresponding pyridinio derivatives, the ^{1}H NMR spectra of which afford more abundant structural information than those of the *O*-arylsulfonylated α-cyclodextrins. The present article deals with the structural information obtained from the ^{1}H NMR spectra of the hydrogencarbonate salts of mono-, bis-, and tris[6-(1-pyridinio)-6-deoxy]-α-cyclodextrins (**9**—**16**) as well as the ^{1}H NMR spectra of mono-, bis-, and tris(6-*O*-mesitylsulfonyl)-α-cyclodextrins (**1**—**8**), as shown in Fig. 1. The ^{1}H NMR spectra of the hydrogencarbonate salts of hexakis[6-(1-pyridinio)-6-deoxy]-α-cyclodextrins (**17**) and methyl 6-(1-pyridinio)-6-deoxy-α-D-glucopyranoside (**18**) were also examined for the sake of comparison. Brief ^{1}H and ^{13}C NMR data for **2**—**8** have been reported by Fujita et al.[4b]

Experimental

Materials. α-Cyclodextrin was kindly supplied by Nihon Shokuhin Kako Co., Ltd., and was dried overnight in vacuo at 110 °C. Reagent-grade pyridine was dried over calcium hydride and distilled in the presence of fresh calcium hydride just before use. Reagent-grade mesitylenesulfonyl chloride was used without further purification. Deuterium oxide (Merck, 99.75%), dimethyl-d_6 sulfoxide (DMSO-d_6, CEA, 99.8%), tetramethylsilane (TMS), and sodium 2,2-dimethyl-2-silapentane-5-sulfonate (DSS) were available for NMR use.

Apparatus. ^{1}H NMR spectra were recorded using a JEOL Model JNM-GX270 FT NMR spectrometer (270 MHz). Absorption spectra and optical rotation were measured with a Hitachi Model 220 spectrophotometer and a Union Giken Model PM-101 polarimeter, respectively. High-performance liquid chromatography (HPLC) was performed on a Hitachi Model 683-56 chromatograph.

Preparation of 1—8. *O*-Mesitylsulfonylated α-cyclodextrins **1**—**8** were prepared and separated from one another according to the method of Fujita et al.[4] A prepacked column (Merck, Lober column LiChroprep RP-8, 25×310 mm) was used for reversed-phase column chromatography to separate

a mixture of **1**—**8** from one another. Aqueous methanol solutions were used as eluents. A silica-gel column (Wako, C-200, 50×350 mm) was used for a further separation of **8** from **7**.[4b] The eluates of these column chromatographies were assayed by UV spectrophotometry at 275 nm. In addition, the main fractions were analyzed by HPLC with a LiChrosorb RP-18 column (Merck, 4×250 mm) and aqueous acetonitrile solutions as eluents. Typical chromatograms are shown in Fig. 2. All the peaks, except peaks 5 and 6, have been assigned in terms of their regiochemistries:[4] Peak 1 corresponds to monosulfonylated α-cyclodextrin **1**, peaks 2, 3, and 4 to disulfonates **2**, **3**, and **4** respectively, and peaks 7 and 8 to trisulfonates **7** and **8**, respectively. Peaks 5 and 6 have been attributed to the trisulfonylated regioisomers, **5** and **6**, but a discrimination between them has not been accomplished. As will be mentioned later, the ^{1}H NMR spectra of tripyridinio-α-cyclodextrins **13** and **14** derived from **5** and **6**, respectively, suggested that **5** is a 6A,6B,6E-isomer and **6** is a 6A,6B,6D-isomer. Here, we tentatively assume that peak 5 corresponds to regioisomer **5** and peak 6 to **6**. Purified samples of **5**—**8** were obtained by a repeated collection of the main peak fractions in the HPLC, followed by an evaporation of the fractions to dryness.

Preparation of 9—16. A typical run was as follows: A purified sample of **2** (140 mg, 0.105 mmol) was dissolved in dry pyridine (10 cm^3) and the resulting solution was refluxed with stirring for 5 h. After removing pyridine by evaporation in vacuo at 40 °C, a mixed solvent of acetone-water [9 : 1 (v/v)] was added to the residue. A resulting precipitate (156 mg) was separated by filtration, dissolved in water (2 cm^3), and chromatographed on a 15×130 mm CM-cellulose (Serva) column with the stepwise elution of 0.05, 0.10, 0.25, and 0.50 mol dm^{-3} aqueous ammonium hydrogencarbonate solutions. The elution was followed by UV-spectrophotometry at 270 nm and polarimetry at 589 nm. The eluates of 0.10 mol dm^{-3} ammonium hydrogencarbonate were combined and evaporated to dryness at 40 °C to give **10** (113 mg, 0.093 mmol, 89% yield). Likewise, **9** was obtained from the eluates of 0.05 mol dm^{-3} ammonium hydrogencarbonate in 80% yield, **11** and **12** from the eluates of 0.10 mol dm^{-3} ammonium hydrogencarbonate in 88 and 86% yields, respectively, and **13**, **14**, **15**, and **16** from the eluates of 0.25 mol dm^{-3} ammonium hydrogencarbonate in 82, 85, 73, and 23% yields, respectively. Each product gave a virtually single peak in HPLC on a TSKgel CM-5PW column (Toyo Soda, 7.5×75 mm) with 0.40 or 0.50 mol dm^{-3} ammonium hydrogencarbonate as an eluent.

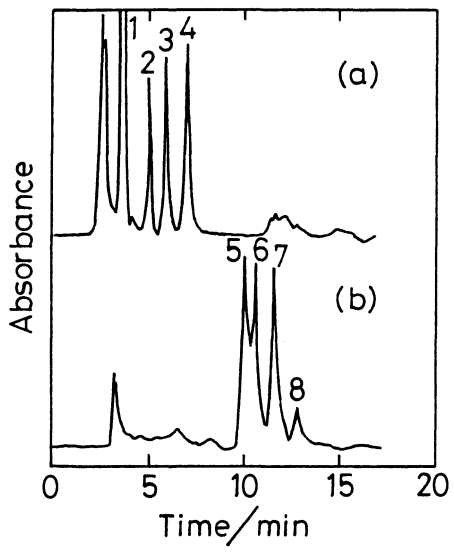

Fig. 2. The HPLC of **1**—**8** with a LiChrosorb RP-18 column and 40% (a) or 50% (b) aqueous acetonitrile as an eluent. The eluates were assayed by UV spectrophotometer at 275 nm.

Preparation of 17. Hexakis(2,3-di-*O*-acetyl-6-bromo-6-deoxy)-α-cyclodextrin (**19**) was prepared by the method of Takeo et al.[6] A solution of **19** (5.00 g, 2.7 mmol) in dry pyridine (50 cm^3) was refluxed with stirring for 30 h. A tar-like material was separated out from the solution during refluxing and was solidified upon cooling to room temperature. The solid was separated by filtration, dissolved in 25% aqueous ammonia solution, and allowed to stand for 0.5 h at room temperature to complete deacetylation. The solution was evaporated to dryness in vacuo to give a dark-brown residue (4.47 g). An aliquot (1.20 g) of the residue was chromatographed on a 20×280 mm Toyopearl CM 650S column (Toyo Soda). A stepwise elution was applied with 0.05, 0.10, 0.15, 0.20, 0.25, 0.30, and 0.50 mol dm^{-3} aqueous ammonium hydrogencarbonate solutions. Each fraction (10 cm^3) was assayed by UV spectrophotometry at 270 nm and polarimetry at 589 nm. Eluates given by 0.20 mol dm^{-3} ammonium hydrogencarbonate were combined and evaporated to dryness in vacuo at 40 °C to afford crude **17** (0.92 g, 0.54 mmol, 74% yield based on **19**). The HPLC of the product with a TSKgel CM-5PW column and 0.40 mol dm^{-3} hydrogencarbonate as an eluent gave a high main peak, though a few additional low peaks were also observed before and after the main peak. A purified sample of **17** was obtained by a repeated collection of a main peak fraction in the HPLC; then, the fraction was evaporated to dryness.

Preparation of 18. Methyl 6-*O*-(*p*-tolylsulfonyl)-α-D-glucopyranoside (5.00 g, 14.4 mmol) was dissolved in dry pyridine (100 cm^3) and heated at 100 °C for 5 h. After removal of pyridine by evaporation in vacuo at 40 °C, the residue was dissolved in 50 cm^3 of distilled water. To the solution was added Amberlite IR-120B (Na form, 15 cm^3); the mixture was stirred overnight at room temperature. The ion-exchange resin was separated by filtration, washed well with distilled water, and then added to 0.5 mol dm^{-3} aqueous ammonium hydrogencarbonate solution (100 cm^3). The mixture was stirred overnight at room temperature. After removal of the ion-exchange resin by filtration, the filtrate was evaporated to dryness in vacuo at 40 °C to give a crude product (4.23 g, 92% yield) of **18**. A purified sample of **18** was obtained by column chromatography with a 45×430 mm CM-cellulose (Serva) column and 0.05 mol dm^{-3} ammonium hydrogencarbonate as an eluent.

Results and Discussion

^{1}H NMR Spectra of 1—8. The ^{1}H NMR spectrum of the 6A,6B,6C-trisulfonylated isomer **7** (43 mmol dm^{-3}) in DMSO-d_6 at 50 °C is shown in Fig. 3 as being typical. In the spectrum, the absorptions at about δ=7.1, 2.5, and 2.3 were assigned to the meta-H's, ortho-methyl-H's, and para-methyl-H's, respectively, of the mesityl groups on the basis of a comparison with the spectrum of sodium mesitylenesulfonate.

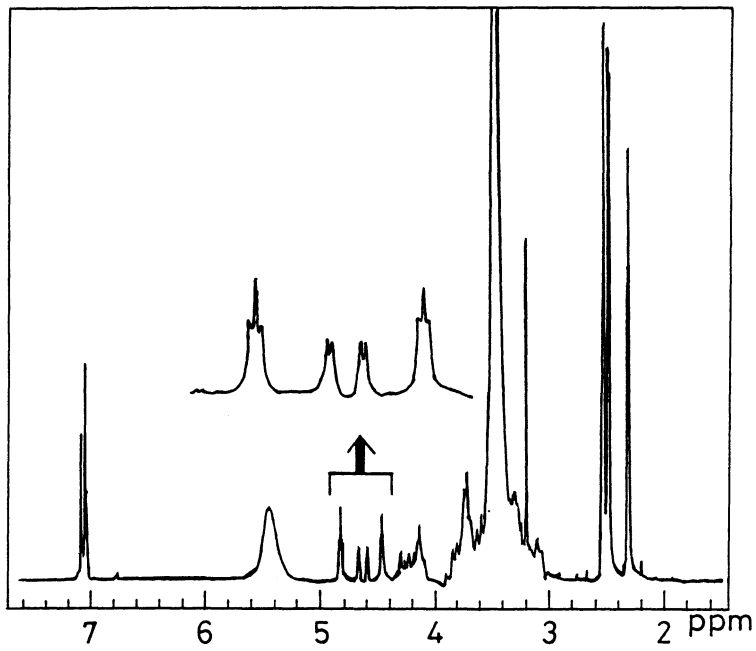

Fig. 3. 270 MHz ^{1}H NMR spectrum of **7** in DMSO-d_6 at 50 °C.

Table 1. ^{1}H NMR Data for **1**—**8**[a)]

Comound	meta-H[b)]	para-Me[b)]	C(1)-H[c)]		
			Region 1[d)]	Region 2[e)]	Region 3[f)]
1	7.09(2H)	2.29(3H)		4.64(1H)	4.79(2H)
				4.68(1H)	4.81(2H)
2	7.07(4H)	2.29(6H)		4.67(2H)	4.81(2H)
				4.70(2H)	
3	7.05(2H)	2.29(3H)		4.65(1H)	4.80(1H)
	7.09(2H)	2.30(3H)		4.66(1H)	4.82(1H)
				4.68(1H)	
				4.70(1H)	
4	7.07(2H)	2.29(6H)	4.48(1H)	4.57(1H)	4.81(3H)
	7.09(2H)			4.64(1H)	
5	7.01(2H)	2.28(6H)	4.52(1H)	4.64(1H)	4.83(1H)
	7.02(2H)	2.30(3H)		4.69(1H)	
	7.09(2H)			4.72(1H)	
				4.74(1H)	
6	7.05(4H)	2.29(9H)	4.51(1H)	4.63(1H)	4.82(1H)
	7.06(2H)			4.68(1H)	
				4.70(1H)	
				4.73(1H)	
7	7.04(4H)	2.29(6H)	4.45(1H)	4.58(1H)	4.81(1H)
	7.07(2H)	2.30(3H)	4.46(1H)	4.66(1H)	4.82(1H)
8	7.08(6H)	2.30(9H)		4.64(3H)	
				4.70(3H)	

a) Chemical shift (δ/ppm from TMS) in DMSO-d_6 at 50 °C. The number of protons in a molecule were evaluated by the integration of peak area and were shown in parentheses. b) Singlet signal. c) Doublet signal with J=3.20±0.03 Hz. d) Higher field than δ=4.55. e) δ=4.55—4.75. f) Lower field than δ=4.75.

Protons involved in the glucopyranose (GP) moieties gave complex signals at δ=3—5. Among them, doublet signals at δ=4.4—4.9 (J=2.8—3.4 Hz) were relatively distinct and were assigned to anomeric C(1)-H's.

Table 1 shows the chemical shifts (δ) and the numbers of protons for the singlets of meta-H's and para-Me-H's, together with those for the doublets of C(1)-H's, in **1**—**8**. The δ values for ortho-Me-H's were ambiguous in some cases, owing to an overlapping of the signals with solvent signals; thus, data for the signals are omitted from the table. The effect of sample concentrations on the NMR spectra, examined for **1**—**4**, indicated that the δ values shown in the table were virtually independent, within a standard error of 0.01 ppm, of sample concentrations ranging from 10 to 44 mol dm^{-3}.[7)] The A,D-isomer **2** or A,C,E-isomer **8** gave

only a singlet at δ=ca. 7.1 for meta-H's and a singlet at δ=ca. 2.3 for para-Me-H's, suggesting that two mesityl groups of **2** or three mesityl groups of **8** are equivalent (isochronous). On the ^{1}H NMR time scale, the molecular structures of **2** and **8** in solution are regarded as being symmetrical, as would be expected from their structural formula. On the other hand, essentially asymmetrical molecules, such as **3**—**7**, gave two or three signals for meta-H's and one or two signals for para-Me-H's (within the resolution limit of the apparatus). The splitting of the signals indicates that the mesityl groups in the compounds are not equivalent. However, the width of the splitting was too narrow to obtain more information regarding their regiochemistries.

More detailed information was available from the splitting patterns of the doublets due to C(1)-H's. All the C(1)-H's of **1**—**8** gave doublets in the region of δ=4.45—4.85, which could be subdivided into three regions, i.e., higher field than δ=4.55 (Region 1), δ=4.55—4.75 (Region 2), and lower field than δ=4.75 (Region 3). It was found that the numbers (m) of C(1)-H's giving doublets in Regions 1—3 reflect the structural characteristics of **1**—**8**: Thus, the ratio of the m's in Regions 1, 2, and 3 was equal to 0 : 2 : 4 for the monosulfonate **1**, 0 : 4 : 2 for the disulfonates **2** and **3**, 1 : 2 : 3 for another disulfonate **4**, 1 : 4 : 1 for the trisulfonates **5** and **6**, 2 : 2 : 2 for **7**, and 0 : 6 : 0 for **8**. These characteristic splitting patterns are well explained on the basis of the following assumptions:

1) The C(1)-H's of unsubstituted GP rings generally give doublets in Region 3.[8]

2) If the A ring [GP(A)] of the GP's in α-cyclodextrin is sulfonylated at C(6)-OH, the C(1)-H of GP(A) is subject to significant shielding by the sulfonylation to give a doublet in Region 2. Furthermore, one of the C(1)-H's involved in GP's adjacent to GP(A) is also significantly shielded by a remote substituent effect to give another doublet in Region 2. The C(1)-H, thus shielded, may belong to GP(B), but not to GP(F), since the substituent is favorably oriented to GP(B) and not to GP(F).[9]

3) If both of vicinal GP(A) and GP(B) are sulfonylated, the C(1)-H of GP(B) is subject to strong shielding by both of the substituents in GP(A) and GP(B) to give a doublet in Region 1. The C(1)-H of GP(A) is significantly shielded by the substituent of GP(A), but little by that of GP(B), and give a doublet in Region 2.

Based on these assumptions, we estimated the number (n) of C(1)-H's belonging to each δ region for **1**—**8** (Table 2). For example, the GP's of A,C,E-isomer **8** are alternatingly sulfonylated, so that all the C(1)-H's should give doublets in Region 2. The A,B,C-isomer **7** bears three sulfonylated-GP's which are bound in series. Then, two C(1)-H's of GP(B) and GP(C) should give doublets in Region 1, those of GP(A) and GP(D) in Region 2, and those of GP(E) and GP(F) in Region 3. The n values, thus estimated, agreed entirely with those observed (Table 1), indicating that the above assumptions are reliable. These results also mean that the regioisomer determination by Fujita et al.[4] is substantiated by ^{1}H NMR spectroscopy, though a distinction between A,B,E-isomer **5** and A,B,D-isomer **6** still remained impossible owing to the similarity of their splitting patterns.

^{1}H NMR Spectra of 9—18. Upon refluxing pyridine solutions containing **1**—**8**, the mesitylenesulfo-

Table 2. The Estimated Number (n) of C(1)-H's Giving Doublets in Regions 1—3

Compound	Region 1[a]	Region 2[b]	Region 3[a]
1	0	2	4
2	0	4	2
3	0	4	2
4	1	2	3
5	1	4	1
6	1	4	1
7	2	2	2
8	0	6	0

a) Higher field than δ=4.55. b) δ=4.55—4.75. c) Lower field than δ=4.75.

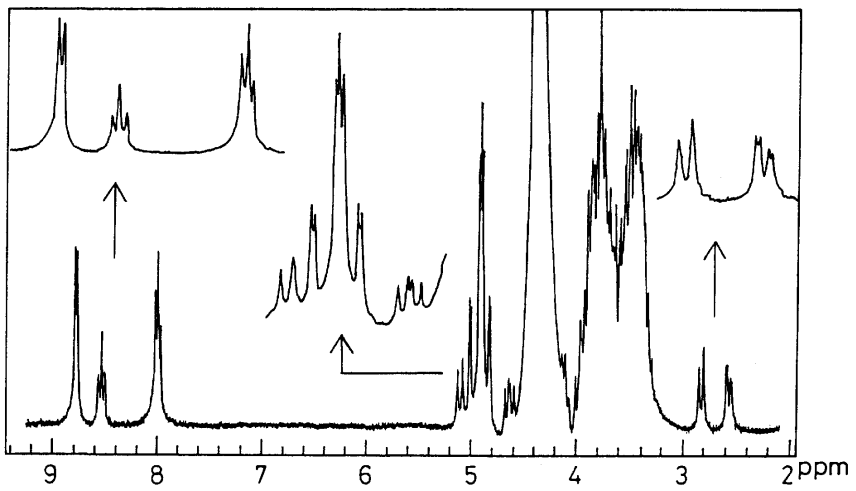

Fig. 4. 270 MHz ^{1}H NMR spectrum of **9** in D_2O at 50 °C.

Table 3. ^{1}H NMR Data for **17**, **18**, and Unsubstituted α-Cyclodextrin (**20**)[a)]

Proton	17	18	20
C(1)-H	5.16 (6H, d, J=3.2)	4.77 (1H, d, J=3.7)	4.94(1H, d, J=3.2)
C(2)-H	3.59 (6H, dd, J=10.0, 3.2)	3.55 (1H, dd, J=9.8, 3.9)	3.51(1H, dd, J=9.9, 3.3)
C(3)-H	4.01 (6H, t, J=9.2)	3.69 (1H, t, J=9.3)	3.87(6H, t, J=9.3)
C(4)-H	3.44 (6H, t, J=9.0)	3.30 (1H, dd, J=10.0, 8.8)	3.48 (6H, t, J=9.5)
C(5)-H	4.82 (6H, m)	4.00 (1H, m)	ca. 3.8 (6H, m)
C(6)-H(a)	4.70 (6H, d, J=13.9)	5.06 (1H, dd, J=13.9, 2.7)	3.7—3.9 (6H, m)
C(6)-H(b)	4.23 (6H, dd, J=13.9, 6.6)	4.78 (1H, dd, J=13.8, 8.2)	3.7—3.9 (6H, m)
ortho-H	8.73 (12H, d, J=5.9)	8.89 (2H, d, J=5.4)	
meta-H	8.09 (12H, t, J=7.0)	8.12 (2H, t, J=7.2)	
para-H	8.46 (6H, t, J=7.7)	8.63 (1H, t, J=7.9)	
OMe-H		3.05 (3H, s)	

a) Chemical shift (δ/ppm from DSS) in D_2O at 50 °C. The unit of J is Hz.

nyloxy groups were replaced by the positively charged pyridinio groups to give **9**—**16** in satisfactory yields. Figure 4 illustrates the ^{1}H NMR spectrum of the monopyridinio derivative **9** (14 mmol dm^{-3}) in D_2O at 50 °C.[10] The ortho-, meta-, and para-protons of the pyridinio group gave a doublet at δ=8.76 (2H, J=5.6 Hz), a triplet at δ=7.99 (2H, J=7.0 Hz), and a triplet at δ=8.52 (1H, J=7.4 Hz), respectively. The protons of the GP moieties gave complex absorptions at δ=2.5—5.1. Among them, the following absorptions were relatively distinct: Doublets at δ=4.8—5.0 (6H, J=ca. 3.2 Hz) due to anomeric C(1)-H's, a pair of a double doublet signal (dd-signal) (1H, δ=4.64, J=13.3 and 9.6 Hz) and an apparently doublet signal (1H, δ=5.12, J=12.9 Hz) due to diastereotopic geminal C(6)-H's, and a pair of a dd-signal (1H, δ=2.54, J=12.0 and 2.9 Hz) and an apparently doublet signal (1H, δ=2.81, J=12.0 Hz) due to another diastereotopic geminal C(6)-H's. The pairing of the absorptions was confirmed by spin-spin decoupling experiments. The dd-signals reflect spin-spin coupling between the geminal C(6)-H's (J=12—13 Hz), together with that between vicinal C(5)-H and C(6)-H(trans) (J=3—10 Hz). The magnitude of coupling constants between vicinal C(5)-H and C(6)-H(gauche) is too small to be detected with the apparatus used, so that another C(6)-H apparently gives a doublet signal. Upon assigning the GP rings involving these C(6)-H's, the ^{1}H NMR spectra of **17**, **18**, and unsubstituted α-cyclodextrin (**20**) were instructive. They gave clear signals, most of which could be assigned (Table 3).[10] The geminal C(6)-H's of **20** gave signals around δ=3.7—3.9, whereas those of **17** or **18** gave a pair of signals in the lower-field region of δ=4—5, but no signal in the higher-field region of δ=2.5—2.8. Based on these data, we assigned the lower-field pair of **9** to the C(6)-H's of the substituted GP ring [GP(A)] and the higher-field pair to those of the unsubstituted GP [GP(B)] adjacent to GP(A). A molecular model study showed that the pyridinium ring is located in the close vicinity of the C(6)-H's of GP(B), when the C(5)-C(6) bond of GP(A) is held in the gauche-trans conformation, as illustrated in Fig. 5.[11] The striking upfield shift of the absorptions for

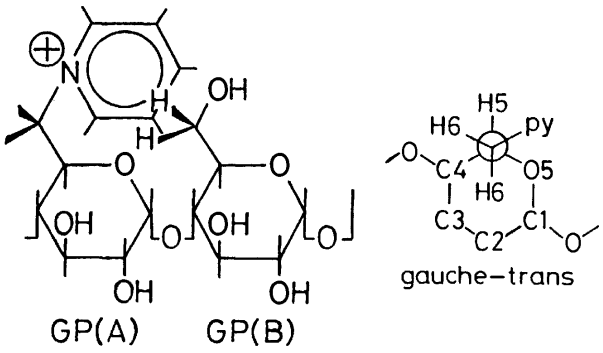

Fig. 5. The schematic diagram for the orientation of the pyridinio group in **9**.

the C(6)-H's of GP(B) in **9** compared with those for the C(6)-H's of **20** is attributable to the strong shielding by the ring current of the adjacent pyridinio group. On the other hand, the remarkable downfield shift observed for the C(6)-H's of GP(A) in **9** may be due to the deshielding effect of the positively charged pyridinio group directly bound to the C(6)-carbon. The vicinal coupling constant between C(5)-H and C(6)-H (trans) is larger in GP(A) (J=9.6 Hz) than in GP(B) (J=2.9 Hz), indicating that the rotation about the C(5)-C(6) bond is significantly restricted to a gauche-trans conformation in GP(A), but little in GP(B).[11]

Characteristic splitting patterns were observed for ^{1}H NMR signals due to the protons involved in the pyridinio groups of the di- and trisubstituted regioisomers of **10**—**16** (Table 4).[10] The A,D-isomer **10** gave the signals similar to those of **9**: A doublet at δ=8.75 for ortho-H's, a triplet at δ=7.97 for meta-H's, and a triplet at δ=8.49 for para-H's. The A,C-isomer **11** and A,B-isomers **12** gave more complex signals than **10**. Signals for ortho- and para-H's of **11** were split into two doublets at δ=8.79 and 8.70 ($\Delta\delta$=0.09) and two triplets at δ=8.49 and 8.46 ($\Delta\delta$=0.03) respectively, though meta-H's gave only a triplet at δ=7.96. The splittings of the signals for ortho- and para-H's were markedly enlarged in **12** to give two doublets at δ=8.79 and 8.46 ($\Delta\delta$=0.33) and two triplets at δ=8.47 and 8.12 ($\Delta\delta$=0.35). Furthermore, signals for meta-H's were

Table 4. ^{1}H NMR Data for Ortho-, Meta-, and Para-H's of the Pyridinio Groups in **9**—**17**[a)]

Compound	Ortho-H	Meta-H	Para-H
9	8.76 (2H, d, J=5.6)	7.99 (2H, t, J=7.0)	8.52 (1H, t, J=7.4)
10	8.75 (4H, d, J=6.1)	7.97 (4H, t, J=6.8)	8.49 (2H, t, J=7.8)
11	8.79 (2H, d, J=6.1)	7.96 (4H, t, J=6.3)	8.49 (1H, t, J=8.3)
	8.70 (2H, d, J=6.1)		8.46 (1H, t, J=8.1)
12	8.79 (2H, d, J=6.1)	7.94 (2H, t, J=6.2)	8.47 (1H, t, J=7.7)
	8.46 (2H, d, J=7.1)	7.80 (2H, t, J=6.4)	8.12 (1H, t, J=7.6)
13	8.92 (2H, d, J=6.4)	8.11 (4H, t, J=6.8)	8.63 (1H, t, J=7.8)
	8.90 (2H, d, J=7.8)	7.96 (2H, t, J=6.5)	8.60 (1H, t, J=7.6)
	8.70 (2H, d, J=5.9)		8.27 (1H, t, J=7.8)
14	9.01 (2H, d, J=5.6)	8.16 (2H, t, J=6.7)	8.66 (1H, t, J=7.3)
	8.97 (2H, d, J=5.6)	8.11 (2H, t, J=7.2)	8.62 (1H, t, J=7.9)
	8.75 (2H, d, J=5.6)	8.01 (2H, t, J=7.2)	8.29 (1H, t, J=7.8)
15	9.05 (2H, d, J=6.1)	8.12 (2H, t, J=7.0)	8.64 (1H, t, J=7.7)
	8.66 (4H, d, J=5.4)	8.05 (2H, t, J=8.1)	8.40 (1H, t, J=6.8)
		7.99 (2H, t, J=7.2)	8.30 (1H, t, J=6.8)
16	8.94 (6H, d, J=6.1)	8.13 (6H, t, J=6.5)	8.62 (3H, t, J=7.7)
17	8.73 (12H, d, J=5.9)	8.09 (12H, t, J=7.0)	8.46 (6H, t, J=7.7)

a) Chemical shift (δ/ppm from DSS) in D_2O at 50 °C. The unit of J is Hz.

also split into two triplets at δ=7.94 and 7.80 ($\Delta\delta$=0.14) in **12**. Somewhat similar splittings of signals have been observed for the regioisomers of disulfonylated α-cyclodextrins **2**—**4**, as described above. However, there is a large difference in the splitting mode of the signals between the pyridinio and mesitylsulfonyl derivatives. Thus, the splitting in **11** and **12** are much larger than those in **3** and **4** ($\Delta\delta$ less than 0.04), indicating that interactions between two pyridinio groups are much stronger than those between two mesitylsulfonyl groups. Moreover, the width of the splitting in the pyridinio derivatives increased with decreasing distance between the substituents, whereas that in the mesitylsulfonyl derivatives was not parallel to the distance. The splitting in the former may be caused mainly by strong electrostatic repulsive interactions between the positively charged pyridinio groups, which enlarge differences in the electronic and/or stereochemical structures between two pyridinio groups in a molecule.

The splitting patterns of the signals due to the protons involved in the pyridinio groups of trisubstituted regioisomers **13**—**16** were also characteristic. For example, the para-H's of A,C,E-isomer **16** gave only a triplet at δ=8.62, those of A,B,E-isomer **13** and A,B,D-isomer **14**, two triplets at δ=8.6—8.7 and one triplet at δ=8.3, and those of A,B,C-isomer **15**, one triplet at δ=8.64 and two triplets at δ=8.3—8.4. These results indicate that, if the C(6)-OH's of vicinal GP's [GP(A) and GP(B)] are displaced by the pyridinio groups, one of the para-H's of the pyridinio groups is subject to significant shielding to give a triplet in the higher-field region of δ=8.3—8.4, though another para-H is little affected to give a triplet at δ=8.6—8.7. In A,B,C-isomer **15**, two para-H's of the pyridinio groups are significantly shielded to give two triplets at the higher field-region. Similar splittings of the signals were also observed for the ortho-H's of **13**—**16**. These characteristic splitting patterns serve to distinguish the regioisomers from one another, though the distinction between A,B,E- and A,B,D-isomers are still impossible.

Table 5. ^{1}H NMR Data for the C(6)-H's of **9**—**17** Giving Double Doublet Signals in the High-Field Region of δ=2.4—2.7

Compound	δ[a)]
9	2.54 (1H, dd, J=12.0 and 2.9 Hz)
10	2.63 (2H, dd, J=13.0 and 4.6 Hz)
11	2.60 (1H, dd, J=12.9 and 4.7 Hz)[b)]
12	2.42 (1H, dd, J=11.6 and 4.3 Hz)
13	2.50 (1H, dd, J=12.4 and 4.3 Hz)[c)]
14	2.73 (1H, dd, J=13.2 and 4.6 Hz)[b)]
15	2.63 (1H, dd, J=12.6 and 4.1 Hz)
16	No Signal[d)]
17	No Signal

a) Chemical shift (ppm from DSS) in D_2O at 50 °C. b) Another C(6)-H gave a double doublet signal at δ=ca. 2.9. Details were ambiguous owing to overlapping with the other signals. c) Another C(6)-H gave a signal at δ=2.99 (1H, dd, J=11.7 and 5.3 Hz). d) The C(6)-H gave a signal at δ=2.99 (3H, dd, J=12.8 and 6.1 Hz).

There are another signals which are available for a regioisomer determination. They are the dd-signals appearing in the upfield region of δ=2.4—2.7 (Table 5). As described above, the dd-signal for **9** is attributable to one of the geminal C(6)-H's involved in an unsubstituted GP [GP(B)] adjacent to a substituted GP [GP(A)]. Similar dd-signals were observed for **10**—**15**, but not for **16** and **17**. It is reasonable that **17** gives no such dd-signal, since **17** has no unsubstituted GP. The A,C,E-isomer **16** gave no dd-signal in this region, though a dd-signal was found at a significantly lower field (δ=2.99). The A,C-isomer **11** also gave a dd-signal in the lower-field region (δ=ca. 2.9), together with a dd-signal in the higher-field region (δ=2.60). On the other hand, either A,D-isomer **10** or A,B-isomer **12** gave a dd-signal only in the higher-field region and

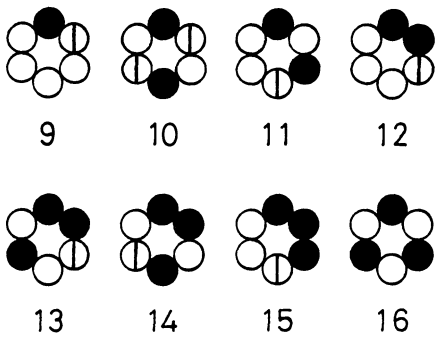

Fig. 6. Assigned glucopyranose rings (Ⓓ) which involve the C(6)-H's affording the high-field dd-signals at δ=2.4—2.7.

no dd-signal in the lower-field region. These facts indicate that the dd-signal of **11** in the lower-field region is due to the C(6)-H of GP(B) which is interposed between two substituted GP's [GP(A) and GP(C)]. The downfield shift of the dd-signal may be caused by electrostatic repulsive interactions between the pyridinio groups in GP(A) and GP(C) which compel the pyridinium ring of GP(A) to move away from the C(6)-H's of GP(B) and to weaken the ring current shielding effect. Upon this assumption, we assigned the GP rings which involve the C(6)-H's affording the upfield dd-signals (Fig. 6). The number of the GP's assigned was two for **10**, one for **9** and **11**—**15**, and zero for **16** and **17**, which agreed well with those observed (Table 5). This assignment also affords a clue to the distinction between regioisomers **13** and **14**. As Fig. 6 shows, GP(C) in **13** and GP(E) in **14** are responsible for the dd-signals in the higher-field region. It is worthwhile to point out that the intramolecular environments of GP(C) in **13** and GP(E) in **14** are significantly different from each other: The former is adjacent to two vicinal substituted-GP's [GP(A) and GP(B)] and the intramolecular environment is very similar to the GP(C) in A,B-isomer **12**. On the other hand, the latter is linked to an isolated substituted-GP [GP(D)] similar to the GP(E) in A,D-isomer **10**. If the intramolecular environments of GP(C) in **13** is similar to those of GP(C) in **12** and those of GP(E) in **14** to those of GP(E) in **10**, it is anticipated that the GP(C) of **13** gives the dd-signal at higher field than that for the GP(E) of **14**, since the dd-signal for the GP(C) of **12** was found at higher field by 0.21 ppm than that for the GP(E) of **10**. The upfield shift of the dd-signal for **12** compared with that for **10** may be attributed to strong electrostatic repulsive interactions between the pyridinio groups of the vicinal GP's [GP(A) and GP(B)], which force the pyridinium ring of GP(B) to come close to the C(6)-H's of GP(C) and strengthen the shielding by the ring current of the pyridinio group. Thus, the regioisomers which gave dd-signals at δ=2.50 (**13**) and δ=2.78 (**14**) are ascribable to the A,B,E- and A,B,D-isomers, respectively. The basis of the assignment described here is not necessarily rigid for a definite regioisomer determination. However, it must be one clue in solving this puzzling problem.

All the pyridinio derivatives **9**—**17** also gave distinct doublet signals at δ=4.7—5.3 due to C(1)-H's. The splitting patterns of the doublets reflected the structural features of the derivatives. However, details are omitted here, since they offer no further information concerning the regiochemistries than that which is described above.

References

1) A. P. Croft and R. A. Bartsch, *Tetrahedron*, **39**, 1417 (1983).

2) R. Breslow, J. B. Doherty, G. Guillot, and C. Lipsey, *J. Am. Chem. Soc.*, **100**, 3227 (1978); R. Breslow, P. Bovy, and C. L. Hersh, *ibid.*, **102**, 2115 (1980); I. Tabushi, Y. Kuroda, and A. Mochizuki, *ibid.*, **102**, 1152 (1980); I. Tabushi and Y. Kuroda, *ibid.*, **106**, 4580 (1984); I. Tabushi, Y. Kuroda, M. Yamada, H. Higashimura, and R. Breslow, *ibid.*, **107**, 5545 (1985).

3) I. Tabushi, Y. Kuroda, and K. Shimokawa, *J. Am. Chem. Soc.*, **101**, 1614 (1979); I. Tabushi, Y. Kuroda, and T. Mizutani, *Tetrahedron*, **40**, 545 (1984); I. Tabushi, Y. Kuroda, and T. Mizutani, *J. Am. Chem. Soc.*, **108**, 4514 (1986); A. Ueno, F. Moriwaki, T. Osa, F. Hamada, and K. Murai, *Tetrahedron Lett.*, **26**, 3339 (1985); A. Ueno, F. Moriwaki, T. Osa, F. Hamada, and K. Murai, *Bull. Chem. Soc. Jpn.*, **59**, 465 (1986).

4) a) K. Fujita, A. Matsunaga, and T. Imoto, *J. Am. Chem. Soc.*, **106**, 5740 (1984); b) K. Fujita, H. Yamamura, A. Matsunaga, T. Imoto, K. Mihashi, and T. Fujioka, *ibid.*, **108**, 4509 (1986).

5) Y. Matsui, K. Ogawa, S. Mikami, M. Yoshimoto, and K. Mochida, *Bull. Chem. Soc. Jpn.*, **60**, 1219 (1987).

6) K. Takeo, T. Sumimoto, and T. Kuge, *Stärke*, **26**, 111 (1974).

7) This fact suggests that no aggregation of host molecules occurs in solution. The size of the mesityl group may be too large to be deeply included in a cavity of another host molecule. The relatively apolar solvent DMSO-d_6 may also contribute to weakening the hydrophobic interactions between the host molecules.

8) The unsubstituted α-cyclodextrin gives a doublet at δ=4.81 (J=3.0 Hz) due to C(1)-H's in DMSO-d_6: B. Casu and M. Reggiani, *Tetrahedron*, **22**, 3061 (1966).

9) A study with the CPK molecular model suggested that the orientation of the mesitylsulfonyl group to GP(F) is unfavorable due to steric hindrance from the C(5)-oxygen of GP(F).

10) The effect of sample concentrations on the NMR spectra was examined for **9**—**12**. The δ values obtained were virtually independent, within the standard error of 0.02 ppm, of the sample concentrations ranging from 10 to 60 mmol dm^{-3}. This fact indicates that no aggregation of the host molecules occurs in solution. Electrostatic repulsive interactions between positively charged host molecules may be responsible for the repression of aggregation. The δ values for **13**—**17** were determined in dilute solutions of 2—3 mmol dm^{-3}, where the aggregation hardly occurs.

11) D. J. Wood, E. F. Hruska, and W. Saenger, *J. Am. Chem. Soc.*, **99**, 1735 (1977).

 © 1988 The Chemical Society of Japan Bull. Chem. Soc. Jpn., 61, 3417—3420 (1988)

Evaluation of Kinetic Parameters from Steady-State Voltammograms at Ultramicrodisk Electrodes

Takayuki ABE, Kingo ITAYA,* Isamu UCHIDA, Koichi AOKI,† and Koichi TOKUDA†
Department of Applied Chemistry, Faculty of Engineering, Tohoku University, Aoba, Aramaki, Sendai 980
†Department of Electronic Chemistry, Graduate School at Nagatsuta, Tokyo Institute of Technology, Nagatsuta, Midori-ku, Yokohama 227
(Received March 29, 1988)

Platinum ultramicrodisk electrodes 0.8 μm in radius were constructed by anodic electropolishing of a platinum wire followed by sealing it with soft glass. Voltammograms for oxidation of $[Mo(CN)_8]^{4-}$, Fe^{2-}, and $[Fe(CN)_6]^{4-}$, being of a sigmoidal form, were measured at these electrodes and microdisk electrodes with 7.5 μm in radius under the essentially steady-state condition. A voltammogram of Fe^{2+} at 7.5 μm electrode was drawn out, exhibiting a halfwave potential shifted from the formal potential. This trend was more distinctive for a wave at 0.8 μm electrode. Radii of the electrodes and diffusion coefficients of the electroactive species were determined consistently from the limiting currents. The conventional log-plot showed that electrode reactions of Fe^{2+} and $[Fe(CN)_6]^{4-}$ were, respectively, totally irreversible and almost reversible at these electrodes. Application of the modified log-plot to the voltammograms yielded straight line, of which slope allowed us to evaluate the transfer coefficient and of which intercept gave values of the charge-transfer rate constant. Simulated voltammograms at these values were in good agreement with experimental ones.

Since mass transport at ultramicroelectrodes is caused by two- or three-dimensional diffusion rather than linear diffusion, the diffusional flux at ultramicroelectrodes is larger than that at electrodes on a conventional scale. This trend becomes remarkable as electrolysis time is long. For example, the ratio of the diffusional flux at a microdisk electrode 10 μm in diameter to that at conventional electrodes is 5.3, 11, and 46, respectively, at 0.1, 1, and 10 s.[1] Thus overall electrode reactions at ultramicroelectrodes are often complicated by charge-transfer kinetics even at a long time electrolysis. Investigations on the charge-transfer kinetics have been undertaken at very small mercury droplets on a vitreous carbon electrode,[2] microring electrodes,[3-5] microdisk electrodes,[6-10] microcylinder electrodes[11-16] and at microband electrodes.[17,18] Since measurements of voltammograms at these electrodes can be made under the quasi-steady state or the steady-state conditions, they are free from complication associated with current transient.

The microdisk electrode makes the kinetic effect most distinctive of the ultramicroelectrodes currently employed. This intriguing feature encouraged derivation of analytical equations for stationary voltammograms complicated by the electrode kinetics at the microdisk electrode.[9] According to the theory,[9] the voltammogram can be transformed into a linear curve through a modified log-plot, of which slope and intercept provide kinetic parameters. In order to apply the modified log-plot to experimental curves, it is required to confirm the establishment of the steady state, to establish a method of residual current elimination or correction and to determine consistently the radius of the electrode and diffusion coefficients. In the paper, we construct platinum ultramicrodisk electrodes by anodic electropolishing[19,20] and measure stationary voltammograms for oxidation of Fe^{2+} and $[Fe(CN)_6]^{4-}$. From these curves, we evaluate the kinetic parameters by use of the modified log-plot, aiming at verification of the theory.

Experimental

Microdisk Electrodes. Two kinds of microdisk electrodes were constructed, one being ca. 7.5 μm in radius and the other being less than 1 μm. A platinum wire 7.5 μm in radius and 2 mm in length (Tanaka Noble Metal Ltd., Tokyo) was connected electrically to a copper wire with mercury contact. It was sealed with soft glass. The surface of the electrode was polished with 1200 mesh carbon powder on a glass plate until the disk-shaped electrode was exposed. It was polished with 0.05 μm alumina powder, followed by ultrasonication in distilled water for 5 minutes. A view of the exposed electrode through a SEM was a well-defined disk rather than a deformed circle.

An ultramicro filament with a radius less than 1 μm was constructed by anodic electropolishing of a platinum wire 32.5 μm in radius, according to a technique described previously.[19,20] The polished filament tapered off to a top. It was dipped into fused soft glass in a small furnace at 320 °C to yield a surface coating of soft glass with a few μm in thickness. This coating ensures high quality of the sealing. The coated filament was cured with epoxy resin (Quetol 812, Nisshin EM, Tokyo) and kept at 60 °C for 24 h. The epoxied block was cut with a diamond knife (Diatome) mounted with an ultramicrotome (Porter-BLUM Model MT2-B). It was difficult to discern quality of a circle through a SEM photograph. The shape was assumed to be a disk for the data analysis. Prior to each electrochemical msasurement, the electrode surface was renewed by the cutting; polished with 0.05 μm alumina powder, dipped into concentrated nitric acid for 2 min and rinsed with distilled water.

Electrochemical Measurements. Since Faradaic currents were as small as 10 nA, a two-electrode system was employed for current measurements, in which a saturated calomel electrode (SCE) was served as a counter electrode. Currents were measured with a high speed current amplifier (Keithley Model 427) in an electrically sealed box. An electrochemical cell was thermostated at 25 °C in a water bath. Before mea-

surements, the solution was deaerated with nitrogen gas for 20 min. All chemicals were of analytical grade.

Results and Discussion

We used oxidation of $[Fe(CN)_6]^{4-}$ and Fe^{2+} as a model reaction associated with electrode kinetics because these two species have well investigated electrochemically. Figure 1 shows three examples of background-corrected voltammograms for oxidation of $[Fe(CN)_6]^{4-}$ (Flg. 1A) and Fe^{2+} (Figs. 1B and 1C) at the potential sweep rate of 10 mV s^{-1}. Residual currents were almost a straight line, of which slope was ca. 0.8 nA V^{-1} for curves in Figs. 1A and 1B and 0.05 nA V^{-1} in Fig. 1C. Since they traced the same path at the forward and the reverse potential scan, they do not result from a capacitive factor. Thus, these electrodes are successful in excluding fully the capacitive current which frequently degrades voltammograms at microdisk electrodes. Hysteresis of the voltammogram was slight but sometimes detectable (in Fig. 1C). The current at the reverse scan was always smaller than the forward one. Two reasons for the hysteresis can be considered: One is unreached steady state and the other is deterioration of the electrode surface during electrolysis. We examined theoretically the extent of the unreached steady state through use of a geometrical parameter, $p=(nFa^2v/RTD)^{1/2}$, in linear sweep voltammetry, where a is a radius of the disk electrode, v the potential sweep rate, n the number of electrons transferred, F the faraday constant, R the gas constant, T the temperature, and D the diffusion coefficient.[21] Values of p were less than 0.21 for $a \leqq 7.5$ μm at $n=1$, $v=10$ mV s^{-1} and $D=0.5\times10^{-5}$ cm^2 s^{-1}, suggesting that the deviation from the steady-state current would be less than 3%[21] if the voltammogram were reversible. Thus the hysteresis is ascribed to deterioration of the electrode. When hysteresis was observed, voltammograms only at the forward scan were employed for the following data analysis.

Radii of the two kinds of microdisk electrodes were evaluated from measurements of the stationary diffusion-controlled limiting current, I_d, for oxidation of 5 mmol dm^{-3} $[Mo(CN)_8]^{4-}$ in 0.5 mol dm^{-3} Na_2SO_4 through the following equation:[22]

$$I_d=4nFc^*Da \qquad (1)$$

where c^* is the bulk concentration of the electroactive species. It was assumed that $D=4.6\times10^{-6}$ cm^2 s^{-1} for $[Mo(CN)_8]^{4-}$.[19] The calculated value of the radius of the large electrode was identical with a nominal value; 7.5 μm. The evaluated radius of the electropolished electrode was 0.70 μm.

We attempted to evaluate the radii from the limiting currents in Fig. 1 by use of $D=4.7\times10^{-6}$ cm^2 s^{-1} for Fe^{2+}[23] and $D=6.32\times10^{-6}$ cm^2 s^{-1} for $[Fe(CN)_6]^{4-}$.[24] The radii were 7.5 and 7.1 μm, respectively, for curves in Figs. 1A ($[Fe(CN)_6]^{4-}$) and 1B (Fe^{2+}). The former is in good agreement with both the nominal value and

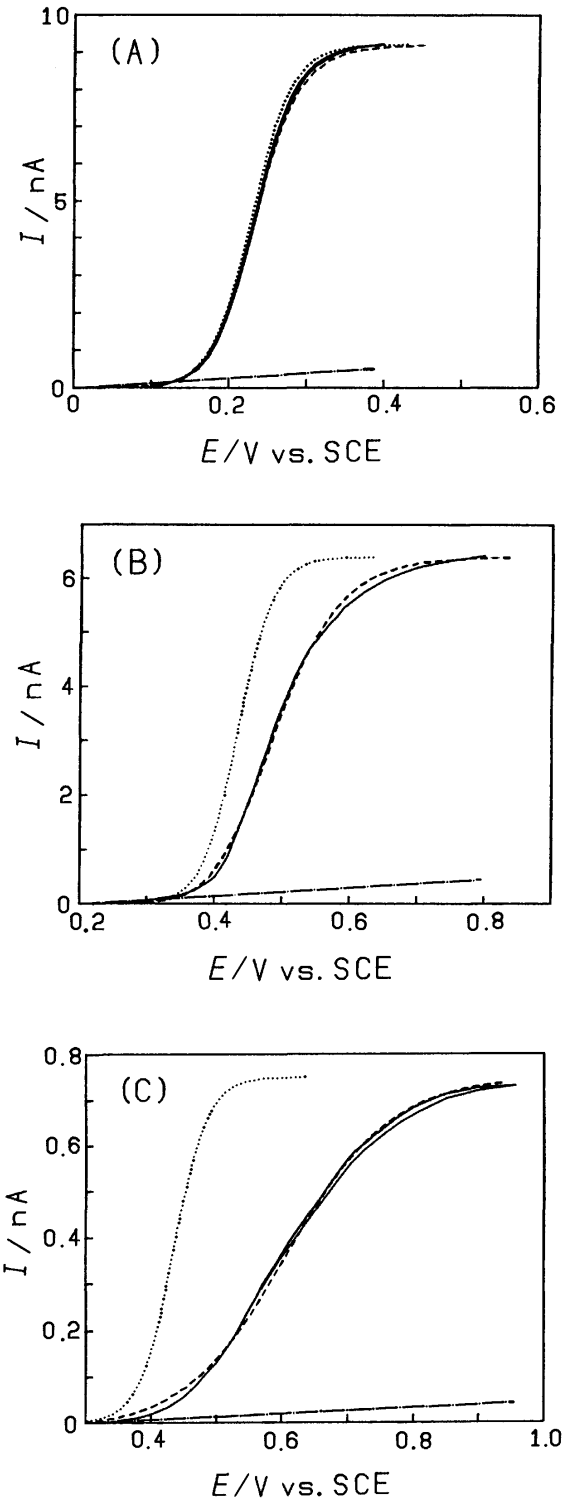

Fig. 1. Cyclic voltammogram (——) for 5 mmol dm^{-3} $[Fe(CN)_6]^{4-}$ in 1 mol dm^{-3} HCl solution at the electrode of $a=7.5$ μm (Fig. 1A), that (——) for 5 mmol dm^{-3} Fe^{2+} in 1 mol dm^{-3} H_2SO_4 solution at the electrode of $a=7.5$ μm (Fig. 1B) and that (——) for 5 mmol dm^{-3} Fe^{2+} in 1 mol dm^{-3} H_2SO_4 solution at the electrode of $a=0.88$ μm (Fig. 1C) when measure at $v=10$ mV s^{-1}. Curves (-·-·-) are residual currents. Dashed curves are simulated waves calculated from Eq. 5 at kinetic parameters evaluated from the modified log-plot. Reversible voltammograms might be expressed by dotted curves.

the value evaluated from the current of $[Mo(CN)_8]^{4-}$. Slight discrepancy for the latter may be due to an incomplete plateau of the limiting current. An expedient of satisfying Eq. 1 so as to make no influence on the log-plot is to determine the diffusion coefficient of Fe^{2+} specific to this electrochemical system. The value of D thus determined is 4.4×10^{-6} cm^2s^{-1}. This value will be used for D of Fe^{2+} in the discussion below. On the other hand, the radius evaluated from the limiting current in Fig. 1C by use of the above value of D was 0.88 μm, which was larger than 0.70 μm evaluated for $[Mo(CN)_8]^{4-}$. Such difference was frequently observed when the electrode surface was renewed by cutting at each measurement. The discrepancy may not be ascribed to difference in electroactive species but may be attributed to poor reproducibility of the renewal. Thus, for the analysis of a voltammetric waveform, it is desirable to use a radius determined from a limiting current at each renewed electrode.

According to the theory of the stationary voltammogram involving electrode kinetics at microdisk electrodes, the current-potential curves for the quasi-reversible and the totally irreversible waves are expressed by the following modified log-plot:[9]

$$E=E^*-2.3\frac{RT}{(1-\alpha)nF}\log\frac{[1-(I/I_d)\{1+\exp(-nF(E-E^{\circ\prime})/RT)\}]^{1.11}}{I/I_d} \quad (2)$$

with

$$E^*=E^{\circ\prime}-2.3[RT/\{(1-\alpha)nF\}]\log[(\pi/4)k^{\circ\prime}a/D] \quad (3)$$

where the Butler-Volmer equation has been used for the kinetic equation. Here I is the current at electrode potential E, α the cathodic transfer coefficient, $k^{\circ\prime}$ is the formal electrode reaction rate constant, and $E^{\circ\prime}$ the formal potential. On the other hand, the reversible wave can simply be expressed by

$$E=E^{\circ\prime}+2.3(RT/nF)\log[I/(I_d-I)] \quad (4)$$

We temporarily assume that the voltammograms in Fig. 1 are reversible. The conventional log-plots given by Eq. 4 are shown in Fig. 2. Plot A for $[Fe(CN)_6]^{4-}$ falls on a straight line of which inverse slope is 62 mV. The half-wave potential is shifted positively by 3 mV from the middle value (0.230 V vs. SCE) of the anodic and the cathodic peak potential measured at a platinum disk electrode 2 mm in diameter. Thus the reaction is very close to the reversible one although there appears slight kinetic effects. On the other hand; plots B and C for Fe^{2+} are curved and half-wave potentials are positively shifted by 55 and 171 mV, respectively, from the middle value (0.435 V vs. SCE) of the anodic and the cathodic peak potential measured at the large electrode. Thus the oxidation of Fe^{2+} belongs to the totally irreversible group. The difference in the radius is obviously responsible for the difference in the partic-

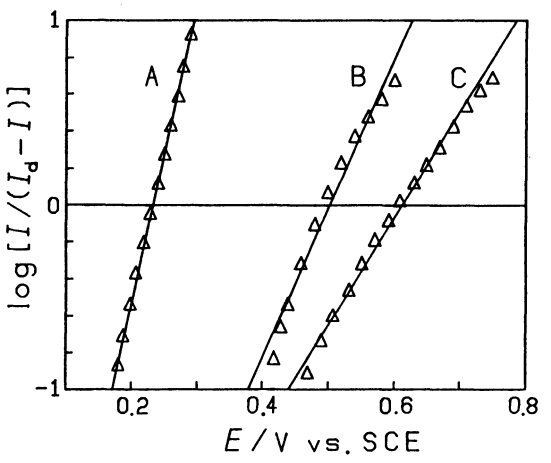

Fig. 2. Conventional log-plots for stationary voltammograms of (A) $[Fe(CN)_6]^{4-}$ at the electrode of a=7.5 μm, (B) Fe^{2+} at a=7.5 μm and (C) Fe^{2+} at a=0.88 μm. These three plots correspond to voltammograms in Fig. 1.

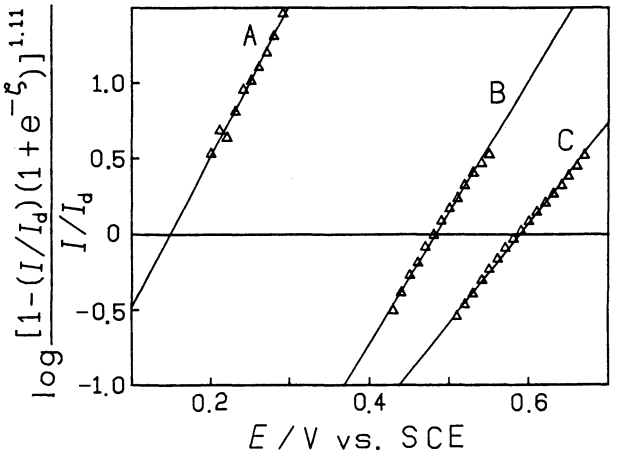

Fig. 3. Modified log-plots for voltammograms in Fig. 1. Plots A, B, and C correspond to waves in Fig. 1.

ipation of electrode kinetics. From the empirical concept on the electrode kinetics, logarithm of the reduced rate constant, $k^{\circ\prime}a/D$, has linear relation with $(1-\alpha)(nFE/RT)$. Thus the difference in the half-wave potential may be equivalent to $[RT/\{(1-\alpha)nF\}]\ln(a_B/a_C)$, where a_B and a_C are radii of electrodes for curves B and C, respectively. The difference in the measured half-wave potential was 0.116 V while the differences calculated from $\ln(a_B/a_C)$ were 0.110 and 0.117 V for α=0.5 and α=0.53, respectively. Agreement is good for reasonable values of α, demonstrating that miniaturizing electrodes causes the potential shift by the amount of $[RT/\{(1-\alpha)nF\}]\ln(a_0/a)$, where a_0 is the reference radius of a microdisk electrode.

It is possible to evaluate $k^{\circ\prime}$ and α from the modified log-plot through Eqs. 2 and 3. In Fig. 3, values of E are plotted against the logarithmic term involving Eq. 2 for the three voltammograms. Although plots B and C are slightly curved, the points fall on a straight line.

Equation 2 shows that the slope of the plot is $2.3RT/\{(1-\alpha)nF\}$, from which α can be evaluated. The slope was evaluated by the method of linear least squares. Values of α are 0.48 and 0.65 for plots B and C, respectively. The literature value is 0.58.[25] The intercept with the E-axis gives E^*, which determines $k^{o\prime}$ through Eq. 1 at known values of $E^{o\prime}$, α, and D. Values of $k^{o\prime}$ thus obtained are 3.0×10^{-3} (α=0.48, $D=4.4\times10^{-6}$ cm^2 s^{-1}, a=7.5 μm) and 6.5×10^{-3} cm s^{-1} (α=0.65, $D=4.4\times10^{-6}$ cm^2 s^{-1}, a=0.88 μm) for plots B and C, respectively. The discrepancy of $k^{o\prime}$ is ascribed to the difference in α because it has been demonstrated in the above that the difference in the half-wave potential was equivalent quantitatively to $\ln(k^{o\prime}a/D)$ at a common value of α. The difference in α may result in edge effects other than those due to diffusion, e.g., activation at the edge, selective adsorption at the edge, and deformation of the disk form of the electrode. If we take a common value of α to be 0.55 retaining values of E^*, values of $k^{o\prime}$ become common, being 3×10^{-3} cm s^{-1}.

Plot A in Fig. 3 falls on a straight line although the line is sensitive to errors in $E^{o\prime}$. The kinetic parameters from this straight line are α=0.43 and $k^{o\prime}$=0.07 cm s^{-1}. We attempted to measure voltammograms of $[Fe(CN)_6]^{4-}$ at an electrode with a radius less than 1 μm. Voltammograms were almost the same as in Fig. 1A, suggesting that the kinetic effect is vague. Consequently, $[Fe(CN)_6]^{4-}$ belongs to the reversible group rather than the quasi-reversible one at microelectrodes employed here. The kinetic values determined above may involve large errors.

We simulated the voltammograms through use of Eq. 2 for kinetic parameters obtained from the modified log-plot. Since Eq. 2 is non-linear with respect to both E and I, we valuated I/I_d at a given value of E through the following algorithm based on the Newton method:

$$x_{k+1}=x_k-f(x_k)/f'(x_k) \tag{5}$$

with

$$x_k=(I/I_d)_k$$
$$f(x)=[1-x\{1+\exp(-\zeta)\}]^{1.11}/x - \exp[-(1-\alpha)(nF/RT)(E-E^*)]$$
$$f'(x)=[1-x\{1+\exp(-\zeta)\}]^{0.11}[0.11\{1+\exp(-\zeta)\}x]/x^2$$
$$\zeta=(nF/RT)(E-E^{o\prime})$$

Starting at an initial value, x_0, less than $\exp[(1-\alpha)(nF/RT)(E-E^*)]$, we could successfully computed converged values of I/I_d. Values for the parameters employed for the simulation are $k^{o\prime}$=0.07 cm s^{-1}, α=0.43, $D=6.32\times10^{-6}$ cm^2 s^{-1}, a=7.5 μm for curve A, $k^{o\prime}=3.0\times10^{-3}$ cm s^{-1}, α=0.48, $D=4.4\times10^{-6}$ cm^2 s^{-1}, a=7.5 μm for curve B, $k^{o\prime}=6.5\times10^{-3}$ cm s^{-1}, α=0.65, $D=4.4\times10^{-6}$ cm^2 s^{-1}, a=0.88 μm for curve C. In Fig 1, simulated curves (---) are drawn, in good agreement with experimental waves. This fact indicates that the kinetic parameters obtained here are reasonable although there is no consistency in the kinetic parameters for curves B and C.

References

1) K. Aoki and J. Osteryoung, *J. Electroanal. Chem.*, **169**, 335 (1984).
2) P. Bindra, A. P. Brown, M. Fleischmann, and D. Pletcher, *J. Electroanal. Chem.*, **58**, 31 (1975); **58**, 39 (1975).
3) M. Fleischmann, J. Ghoroghchian, and S. Pons, *J. Phys. Chem.*, **89**, 5530 (1985).
4) A. Russell, K. Repka, T. Dibble, J. Ghoroghchian, J. J. Smith, M. Fleischmann, C. H. Pitt, and S. Pons, *Anal. Chem.*, **58**, 2961 (1986).
5) A. Szabo, *J. Phys. Chem.*, **91**, 3108 (1987).
6) B. Scharifker and G. Hills, *J. Electroanal. Chem.*, **130**, 81 (1981).
7) G. Hills, A. K. Pour, and B. Scharifker, *Electrochim. Acta*, **28**, 891 (1983).
8) J. O. Howell and R. M. Wightman, *Anal. Chem.*, **56**, 524 (1984).
9) K. Aoki, K. Tokuda, and H. Matsuda, *J. Electroanal. Chem.*, **235**, 87 (1987).
10) M. I. Montenegro and D. Pletcher, *J. Electroanal. Chem.*, **200**, 371 (1986).
11) K. Aoki, K. Tokuda, and H. Matsuda, *J. Electroanal. Chem.*, **206**, 47 (1986).
12) K. Aoki, K. Tokuda, and H. Matsuda, *J. Electroanal. Chem.*, **175**, 1 (1984).
13) M. R. Deakin, *J. Electrochem. Soc.*, **132**, 496C (1985).
14) C. A. Amatore, M. R. Deakin, and R. M. Wightman, *J. Electroanal. Chem*, **206**, 23 (1986).
15) K. Aoki and H. Kaneko, *J. Electroanal. Chem.*, **247**, 17 (1988).
16) K. Aoki, H. Kaneko, and K. Nozaki, *J. Electroanal. Chem.*, **247**, 29 (1988).
17) M. R. Reakin, R. M. Wightman, and C. A. Amatore, *J. Electroanal. Chem.*, **215**, 49 (1986).
18) C. A. Amatore, B. Fosset, M. R. Deakin, and R. M. Wightman, *J. Electroanal. Chem.*, **225**, 33 (1987).
19) K. Itaya, T. Abe, and I. Uchida, *J. Electrochem. Soc.*, **134**, 1191 (1987).
20) T. Abe, K. Itaya, and I. Uchida, *Chem. Lett.*, in press.
21) K. Aoki, K. Akimoto, K. Tokuda, H. Matsuda, and J. Osteryoung, *J. Electroanal. Chem.*, **171**, 219 (1984).
22) K. Aoki and J. Osteryoung, *J. Electroanal. Chem.*, **215**, 49 (1986).
23) H. P. Agarwal and S. Qureshi, *Electrochim. Acta*, **19**, 607 (1974).
24) M. V. Stackelberg and V. Toome, *Z. Elektrochem.*, **58**, 226 (1954).
25) H. P. Agarwal, *J. Electroanal. Chem.*, **5**, 236 (1963).

 © 1988 The Chemical Society of Japan Bull. Chem. Soc. Jpn., 61, 3421—3423 (1988)

Structure Images of a Nickel Fine-Particle Catalyst and Analysis of a Moiré Pattern

Michio NODA,* Hideki ICHINOSE, Yasukazu SAITO, and Yoichi ISHIDA
Institute of Industrial Science, University of Tokyo, 7-22-1 Roppongi, Minato-ku, Tokyo 106
(Received March 29, 1988)

Conventional HR-TEM was applied to a nickel fine-particle catalyst that had been prepared by means of a gas-evaporation method. A structure image of the nickel fine particle showed that the particle consisted of an fcc nickel crystal and thin oxide layers of the surfaces. A platinum-deposited nickel fine particle exhibited a moiré pattern, which was analyzed by the use of the Cowley-Moodie dynamical theory of diffraction. An accurate solution of the equations showed that a platinum lattice obliquely piled on a surface lattice of the particle.

High-resolution transmission-electron microscopy (HR-TEM) enables one to see a crystal lattice as it is in real space, though the interplanar spacing cannot be exactly measured.[1] The technology for HR-TEM has been sufficiently developed.[2] If a particle has a diameter of some ten nm, it can be observed without any slicing procedure. For example, γ-alumina particles were prepared by means of a gas-evaporation method, and photographs of them were taken with a high resolution.[3]

Nickel fine particles were produced using the same method. They had a spherical shape and a sharp distribution of size.[4] These nickel fine particles catalyzed liquid-phase dehydrogenation of 2-propanol.[5] Further, platinum-deposited nickel fine particles were more active than nickel alone.[6] In the present study, the two catalysts were observed by means of HR-TEM after a reaction, and their structure was analyzed.

Experimental

1. Materials. Nickel fine particles were supplied by Vacuum Metallurgical Co., Ltd. (Chiba Pref., Japan). They were black and light powder that had been prepared by evaporating molten nickel metal under argon at a low pressure. Their surfaces had been slowly oxidized before taking them out of the reactor. The oxide layers prevented the particles from burning in air. The oxygen content was about 10 wt%, that is, about 30 mol%. The average diameter of the nickel fine particles was 19.7 nm, and their BET surface area was 43.8 $m^2 g^{-1}$.

Bis(acetylacetonato)platinum(II) ($Pt(acac)_2$) was purchased from Nippon Engelhard Ltd.

2. Procedure. The nickel fine particles were heated under hydrogen in order to reduce the surface oxide partly, and then they were used as a catalyst of the liquid-phase dehydrogenation of 2-propanol. The technique was described in previous papers.[5,6] The nickel fine particles were collected by filtration after a reaction and preserved in air.

Platinum was deposited on a nickel fine-particle catalyst by reducing the divalent platinum in $Pt(acac)_2$ before the catalysis. Though 9 mg of $Pt(acac)_2$ revealed a sufficient promoter effect for 200 mg of nickel fine particles,[6] 100 mg of $Pt(acac)_2$ was used for a sample of HR-TEM.

3. Measurement. Nickel fine particles were suspended in ethanol and then scooped up with a micromesh. The particles on a micromesh were dried under a vacuum and then used as a specimen.

Samples were observed with a JEM-200CX HR-TEM apparatus, with the aberrations of C_s=0.7 mm and C_c=1.2 mm. The accelerating voltage was 200 kV, and the aperture of the electron beam was 5×10^{-4} rad. The error in the length was some ten %.

Results and Discussion

1. An Electron Micrograph of Nickel Fine Particles. Nickel fine particles were observed by means of HR-TEM after a catalytic reaction. Although TEM does not give an accurate value of the length, the ratio of the length is correct. Since nickel fine particles gathered and formed secondary particles, it was necessary to look for an isolated particle on the periphery of

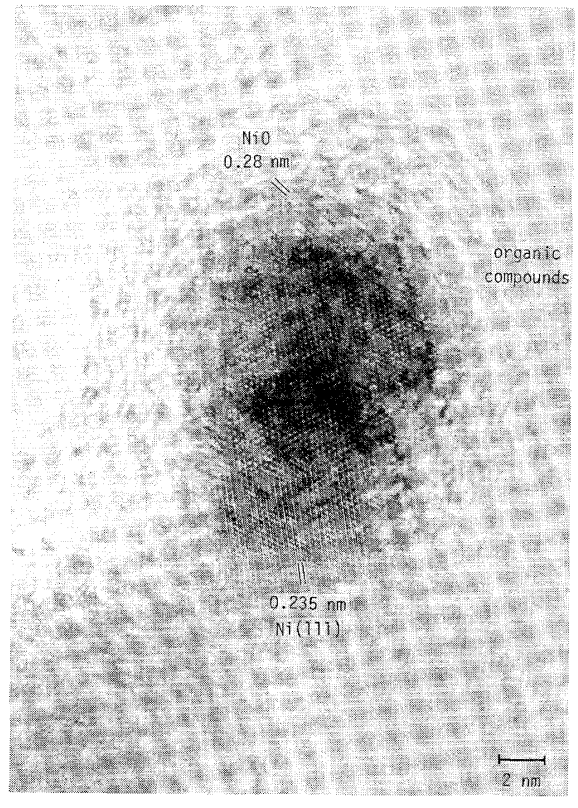

Fig. 1. A structure image of nickel fine particles by HR-TEM.

Table 1. Interplanar Spacings of Index (111)

Substance	Bravais' lattice of metal	d/nm		Obs./Ref.
		Ref.[a]	Obs.[b]	
Ni	fcc	0.203	0.235	1.16
NiO	fc trigonal	0.241	0.28	1.16
	fcc	0.240		1.17
Pt	fcc	0.226	0.275	1.22

a) X-Ray crystal-structure analysis.[7] b) HR-TEM. The present work.

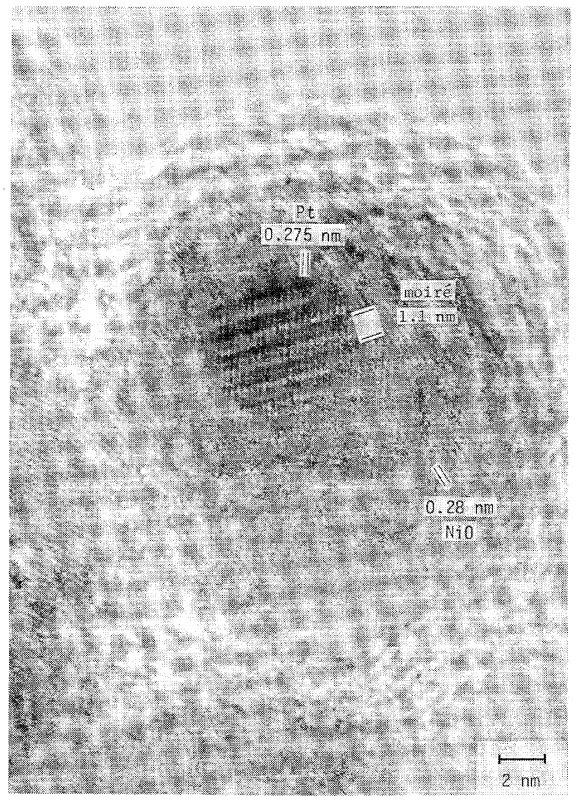

Fig. 2. A structure image of platinum-deposited nickel fine particles by HR-TEM.

a lump in order to obtain a clear picture.

Figure 1 is a tomogram of nickel fine particles. The Miller index of a lattice plane was identified by the comparison of an observed interplanar spacing with one in the literature of X-ray crystal-structure analysis.[7] The observed and cited spacings are summarized in Table 1.

A lattice of fcc Ni(111) appeared in the middle of a particle in Fig. 1. Thin layers of NiO(111) enclosed the nickel metal. The thickness of NiO was consistent with the oxygen content. Catalytically active sites on the surfaces of a particle were oxidized again, since the particle was preserved in air after a reaction.

Thick amorphous layers surrounded a particle. Probably they were organic compounds, because those amorphous layers were not found in a micrograph of the particle that was not used for a catalytic reaction.

2. Platinum-Deposited Nickel Fine Particles. When 9 mg of $Pt(acac)_2$ was reduced on 200 mg of nickel fine particles, the platinum was deposited on the active sites of the particles. This was because the number of active sites of a platinum-deposited nickel catalyst equaled that of a nickel-alone catalyst.[6] Since no image of platinum was observed in micrographs of those platinum-deposited particles, the amount of $Pt(acac)_2$ was increased to 100 mg. Thick layers of platinum were produced on a nickel fine particle and could be observed by means of HR-TEM, though excessive platinum coagulated to make a characteristic peak in the X-ray diffraction pattern.

These platinum-deposited nickel fine particles exhibited a moiré pattern, as shown in the middle of Fig. 2. The TEM was focused on a particle surface on this occasion. The lattice with an interplanar spacing of 0.275 nm was a Pt(111) lattice, judging from a comparison in Table 1. The observed interplanar spacing of Pt(111) was slightly larger than the value to be expected from a bulk crystal, because the observed platinum lattice was influenced by the layers under it.

The moiré crossed the Pt(111) lattice obliquely. This shows that another lattice was obliquely superposed on or under the Pt(111) lattice. On the basis of the analysis to be described below, a lattice of NiO(111) piled at an angle of 14° to the platinum. Probably surface nickel metal was oxidized again in spite of the covering of platinum.

When the amount of $Pt(acac)_2$ was 9 mg, platinum probably formed thin layers on the active sites of a nickel fine particle. In this case, the platinum layers were so thin that neither a platinum lattice nor a moiré pattern was observed.

3. Analysis of a Moiré Pattern. A micrograph of lattices is often analyzed using the Cowley-Moodie dynamical theory, because a beam of electrons is scattered many times.[8,9] Here, crystals were assumed to be set exactly at the Braggs angle. Further, a two-wave approximation dealing with only one incident beam and one diffracted beam was adopted in order to simplify the derivation of formulae.

According to the theory, the intensity distribution of a thick crystal with an interplanar spacing of d_1 is given by

$$\psi^*\psi = 1 - C_1 \cos \frac{2\pi}{d_1}\left(x - \frac{d_1}{4}\right),$$

where ψ is a wave function and x is a position. The coefficient C_1 can be regarded as a constant. When another thin crystal with an interplanar spacing of d_2 is superposed on or under the thick crystal in parallel near a focus, the reflection from the thin crystal causes a moiré pattern by interference. The intensity distribution of the moiré is given by

$$\psi^*\psi = C_2 - C_3 \cos \frac{2\pi x}{A}, \qquad (1)$$

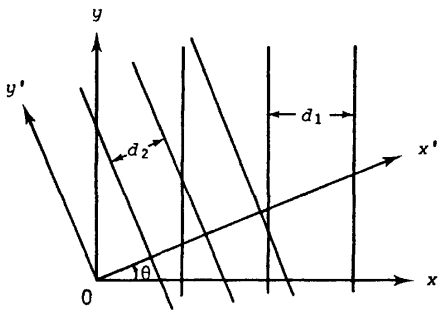

Fig. 3. Definition of the coordinates of crystal lattices.

where $1/A=1/d_1-1/d_2$. The coefficients of C_2 and C_3 are similar to C_1, and C_3 is in proportion to the thickness of the thin crystal.[9] If C_3 is very small, no moiré pattern appears.

In the present study, the theory was extended to a case in which the two crystals were obliquely superposed. The coordinates of the two crystals were defined as illustrated in Fig. 3. When θ was the angle from the x axis of a thick crystal to the x' axis of a thin crystal, the relation between the coordinates was given by

$$x'=x\cos\theta+y\sin\theta.$$

Thus, Eq. 1 was changed as follows:

$$\psi^*\psi=C_2-C_3\cos 2\pi\left(\frac{x}{d_1}-\frac{x\cos\theta+y\sin\theta}{d_2}\right)$$

$$=C_2-C_3\cos 2\pi\left\{\left(\frac{1}{d_1}-\frac{\cos\theta}{d_2}\right)x-\frac{\sin\theta}{d_2}y\right\}$$

$$=C_2-C_3\cos\frac{2\pi}{A}(x\cos\Theta+y\sin\Theta),$$

where

$$\frac{1}{A}=\sqrt{\left(\frac{1}{d_1}-\frac{\cos\theta}{d_2}\right)^2+\left(\frac{\sin\theta}{d_2}\right)^2},$$

$$\cos\theta=A\left(\frac{1}{d_1}-\frac{\cos\theta}{d_2}\right) \tag{2a}$$

and

$$\sin\theta=A\left(-\frac{\sin\theta}{d_2}\right). \tag{2b}$$

The variable Θ was the angle from the x axis to the X axis of a moiré. Since

$$X=x\cos\Theta+y\sin\Theta,$$

the intensity distribution of the moiré was given by

$$\psi^*\psi=C_2-C_3\cos\frac{2\pi X}{A},$$

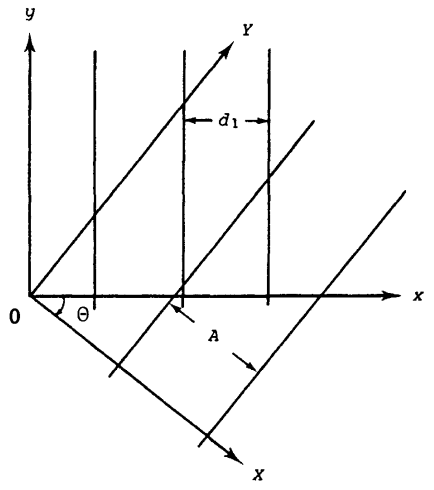

Fig. 4. Definition of the coordinates of lattice images.

as shown in Fig. 4. If θ was positive, Θ became negative. Transforming Eqs. 2 brought the solutions:

$$\theta=\arctan\left(\frac{d_1\sin\theta}{d_1\cos\theta-A}\right) \tag{3a}$$

and

$$d_2=\frac{Ad_1}{\sqrt{(A-d_1\cos\theta)^2+(d_1\sin\theta)^2}}. \tag{3b}$$

The values of d_1, A, and Θ in Fig. 2 were 0.275 nm, 1.1 nm, and $-74°$ respectively. Substituting these values into Eqs. 3 led to

$$\theta=14° \text{ and } d_2=0.28 \text{ nm}.$$

These results showed that NiO, with an interplanar spacing of 0.28 nm, was superposed under Pt at the angle of 14°.

References

1) O. Scherzer, *J. Appl. Phys.*, **20**, 20 (1949).
2) L. Reimer, "Transmission Electron Microscopy," Springer-Verlag, Berlin (1984); F. E. Fujita and M. Hirabayashi, "Microscopic Methods in Metals," ed by U. Gonser, Springer-Verlag, Berlin (1986), pp. 29—74.
3) S. Iijima, *Jpn. J. Appl. Phys.*, **23**, L347 (1984); S. Iijima and M. Ichikawa, *J. Catal.*, **94**, 313 (1985).
4) S. Kashu, M. Nagase, C. Hayashi, R. Uyeda, N. Wada, and A. Tasaki, *Jpn. J. Appl. Phys.*, Suppl. 2, Part 1, 491 (1974).
5) M. Noda, S. Shinoda, and Y. Saito, *Nippon Kagaku Kaishi*, **1984**, 1017; *Bull. Chem. Soc. Jpn.*, **61**, 961 (1988).
6) M. Noda, S. Shinoda, and Y. Saito, *Bull. Chem. Soc. Jpn.*, **61**, 2541 (1988).
7) "Kagaku Binran Kisohen," ed by Chem. Soc. Jpn., 3rd ed, Maruzen, Tokyo (1984), Part 2, pp. 695, 697; "Jikken Kagaku Guide Book," Maruzen, Tokyo (1984), pp. 459, 566.
8) J. M. Cowley and A. F. Moodie, *Acta Crystallogr.*, **10**, 609 (1957).
9) J. M. Cowley, *Acta Crystallogr.*, **12**, 367 (1959).

 © 1988 The Chemical Society of Japan Bull. Chem. Soc. Jpn., 61, 3425—3428 (1988)

Time-Dependent Metastable Fragmentations. The $\dot{C}H_2OH$ Loss from Methyl Acetate Ions

Ryuichi ARAKAWA
Institute of Chemistry, College of General Education, Osaka University, Toyonaka 560
(Received April 2, 1988)

The metastable ion intensity for the loss of $\dot{C}H_2OH$ from ionized methyl acetate has been measured as a function of the ion-source residence time up to 100 μs by means of the ion-trapping technique. The decay of the metastable ion intensity was adequately interpreted by the use of a prior isomerization mechanism on the basis of RRKM calculations. It was suggested that the intermediate precursor for the generation of CH_3CO^+ and $\dot{C}H_2OH$ from ionized methyl acetate is not a hydrogen-bridged complex structure, $CH_3CO\text{-}H\text{-}OCH_2^{+\cdot}$, but a distonic ion structure, $CH_3\overset{+}{C}(OH)O\dot{C}H_2$.

The unimolecular gas-phase chemistry of ionized methyl acetate has been the subject of a number of studies.[1-6]

$$CH_3COOCH_3^{+\cdot} \rightarrow CH_3CO^+ + COH_3^{\cdot} \quad (1)$$

This interest has been directed toward determining what configuration is a reacting precursor in the complexity of isomerization/dissociation paths, and also the structure of the neutral product, $COH_3^{\cdot}$. A variety of experimental techniques[1-3] have suggested that the structure of the neutral product is a hydroxymethyl $\dot{C}H_2OH$ radical rather than the methoxyl $CH_3\dot{O}$ which would be expected from a simple bond cleavage. However, recent studies[3,4] have shown that the neutral product is a mixture of these radicals. Moreover, the rearrangement of the $CH_3\dot{O}$ radical into $\dot{C}H_2OH$ is a possible process. Thus, the structure of the neutral product is still an unresolved question.

Extensive labeling experiments[3,5] on methyl acetate and its enol isomer have led to the proposal that the distonic ion $CH_3\overset{+}{C}(OH)O\dot{C}H_2$, in which the charge and radical site are separated by more than one atom, is the key intermediate. This intermediate accounts for the considerable, but incomplete, loss of the positional identity of H and D atoms in the labeled isomers. Moreover, ^{18}O-labeling and collisional activation experiments by Burgers et al.[5] have led to the similar conclusion that the distonic ion is the intermediate precursor for Reaction (1). However, their time-resolved mass spectra of ionized methyl acetate indicated that the isomerization of methyl acetate ions into other isomers is a rate-determining step in a microsecond time-frame. On the other hand, ab initio calculations at a sufficiently high level of theory were used for resolving the ionized methyl acetate problem of a multistep isomerization/dissociation pattern.[6] The theoretical analysis showed that the hydrogen-bridged radical ion/dipole complex, $CH_3CO\text{-}H\text{-}OCH_2^{+}$, is probably a precursor ion decomposing to the observed $CH_3CO^+ + \dot{C}H_2OH$.

There is, therefore, an unsettled problem regarding the isomerization/dissociation paths of ionized methyl acetate. The apparent activation energy (appearance energy—ionization energy) is as small as ca. 0.7 eV; RRKM theory predicts a minimum rate of ca. 10^7 s^{-1}. Thus, such a rate yields no metastable peak for the dissociation of ionized methyl acetate. One way of accounting for the unusual characteristics of Reaction (1) is to assume a mechanism in which the reaction path involves isomerization to a more stable structure prior to dissociation. This idea of a prior isomerization has been applied by Baer to explain the complex dissociation of several molecular ions.[7] We have investigated which isomer serves as the intermediate precursor by assuming a prior isomerization mechanism, based on RRKM calculations, so as to explain the experimental time-resolved metastable fragmentation. The decay of metastable ions is principally dependent on the rate vs. energy curve; thus, it is affected by the reaction mechanism.

Experimental

The ion-trapping technique has been described in detail elsewhere.[8] Briefly, the space charge formed by a continuous 5 eV electron beam was used to trap the ions produced when a negative pulse was applied to a filament. At a known delay time after the ionizing pulse, a positive pulse, 4 μs in duration and 5 eV in height, was applied to a repeller electrode to remove ions for mass analysis. The ionizing pulse was applied to the filament at 0.5 ms intervals. The delay time was successively varied at 3.6-μs steps. These pulse-sequence and data-acquisition systems were both computer-controlled. The measurement of the metastable-ion intensities was performed with a home-made tandem-type mass spectrometer. The temperature of the ion source was 423 K. The ion-source pressure was kept at 2×10^{-6} Torr (1 Torr≈133.322 Pa). A collision-induced reaction in the field-free region was negligible, because the pressure was maintained at less than 5×10^{-7} Torr.

Results and Discussion

The production of CH_3CO^+ was the predominant process in the metastable fragmentation of ionized methyl acetate. Figure 1 shows the metastable-to-main-beam intensity ratio against the delay time at the

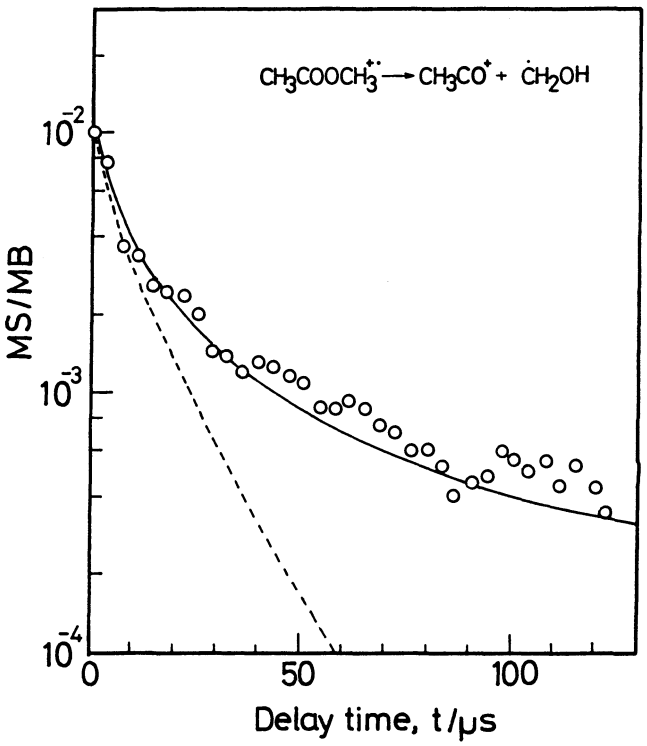

Fig. 1. A plot of the metastable to main beam intensity ratios, MS/MB, vs. the delay time for CH_3CO^+ from ionized methyl acetate: experiment (O) and calculated with the distonic precursor model (——), and the hydrogen-bridged complex model (----).

electron-impact energy of 40 eV. The metastable-ion intensity at the delay time of t is given by:[9]

$$m^*(t) \propto \int_0^\infty f(E)\, w(E)\, dE.$$

Here, $f(E)$ is the internal energy distribution, $w(E)=\exp(-t_1k(E))-\exp(-t_2k(E))$ is the time window in the present experiment ($t_1=6.5+t$ and $t_2=11.7+t$ μs), and $k(E)$ is the unimolecular rate constant. According to the threshold behavior of ionization,[10] $f(E)$ was approximated by the photoelectron spectrum of methyl acetate.[11]

The lowest energy path for ionized methyl acetate to CH_3CO^+ and $\dot{C}H_2OH$ was obtained by Heinrich et al.[6] using a high level of ab initio calculations. In the first step, methyl acetate ions isomerize into the distonic ion $CH_3\overset{+}{C}(OH)O\dot{C}H_2$, followed by rearrangement to the hydrogen-bridged complex, $CH_3CO\text{-}H\text{-}OCH_2^+$. Along their potential energy profile and the previous result[3] regarding barrier height (Fig. 2), we suppose two prior isomerization models for calculating $k(E)$ by the use of the RRKM theory: the distonic ion and the hydrogen-bridged complex serve as precursor ions, whose activation energies of E_0 for the generation of $CH_3CO^+ + \dot{C}H_2OH$ are assumed to be 1.27 and 0.64 eV respectively. The RRKM calculation was carried out by a direct counting method of the state and sum densities.[12]

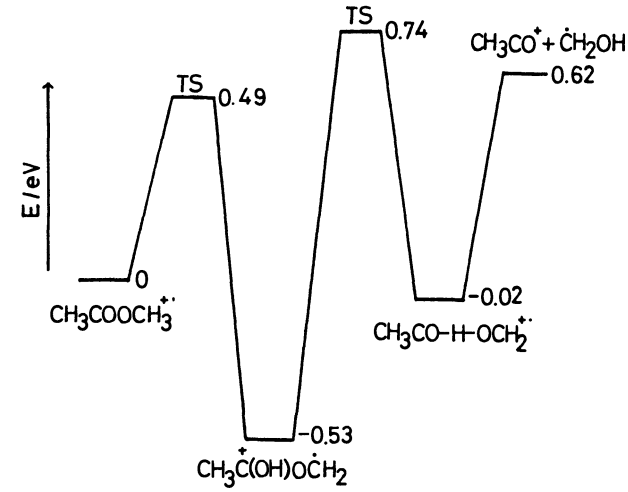

Fig. 2. A potential energy diagram of ionized methyl acetate and its isomers for the prior isomerization. This indicates a part of results previously determined from ab initio calculation by Heinrich et al.[6]

Another adjustable parameter is the set of vibrational frequencies for the reactant and transition states. Their vibrational frequencies are obtained by a vibrational analysis[13] for the assumed geometries and approximate simple-valence force fields (Appendix 1). For the distonic precursor model, the H atom of the OH bond migrates to another oxygen, and at the same time the bond order of C-OCH_2 decreases b 0.5. The hydrogen-bridged precursor model is described as a simple C-$HOCH_2$ bond cleavage for the H bridged bond. The bond orders of the hydrogen-bridged C-H and H-O bonds are assumed to be 0.5 in the reactant state. In both cases, the bond cleavage for the O-H stretching mode is employed as the reaction coordinate for the transition state; its bond order was taken as $n=0.1$. The vibrational frequencies obtained from the vibrational analysis are given in Appendix 2. The activation entropy, ΔS^*, is calculated from the set of vibrational frequencies for the reactant and transition state, and it is related to the Arrhenius preexponential factor.

The experimental results are well reproduced by the distonic-ion model (Fig. 1). The activation entropy is $\Delta S^*_{1000}=4.0$ e.u. (cal/mol/deg) if we adopt $T=1000$ K. This seems a reasonable value for the "tight" transition model, which involves a four-center cyclic moiety. For example, the loss of a halogen atom from a halobenzene ion proceeds via a simple bond cleavage and a "loose" transition state. Its activation entropy is known to be $\Delta S^*_{1000}=7—10$ e.u.[14] As may be seen in Fig. 3, the rate constants obtained by the prior isomerization models are metastably slow ($\leqq 10^5$ s^{-1}), but if the isomerization of methyl acetate ions is a rate-determining step, its rate is much greater than those obtained by the prior isomerization models. This is mainly because the distonic-ion model exhibits a high activation energy and because the hydrogen-bridged

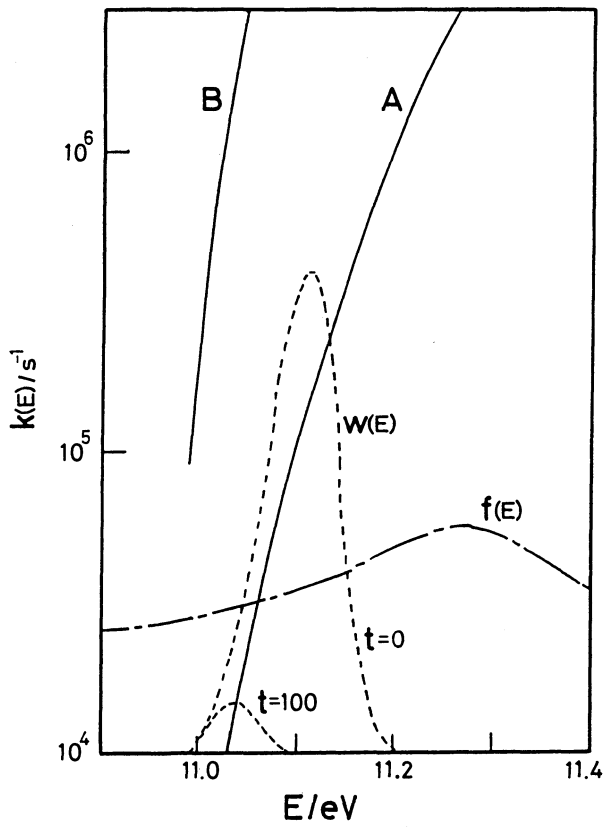

Fig. 3. The dissociation rate, $k(E)$, vs. energy, E; the rates derived from the distonic precursor model (A) and the hydrogen-bridged complex model B). $w(E)$ indicates the metastable time windows at t=0 and 100 μs. $f(E)$ represents the internal energy distribution. $w(E)$ and $f(E)$ are plotted on a linear scale.

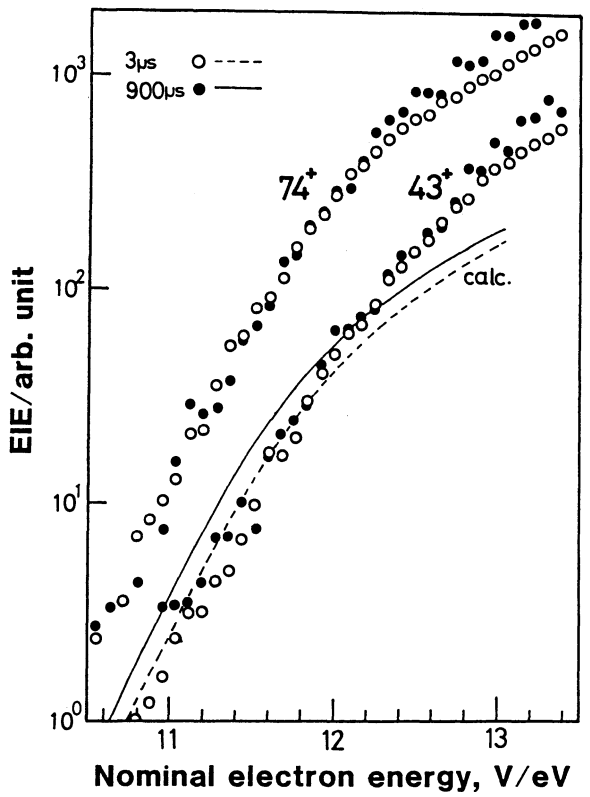

Fig. 4. The time-dependent electron ionization efficiency (EIE) curve vs. nominal electron energy, V, for methyl acetate ion (74^+) and CH_3CO^+ (43^+): experiment (O, ●) and calculated (----, ——) at the ion-source-residence time of t=3 and 900 μs.

complex model has a loose structure, e.g., small vibrational frequencies, in spite of the low activation energy. The prior isomerization models cause the higher state density of the reactant state at the threshold energy. The decay of metastable ions depends upon the two adjustable parameters of E_0 and ΔS^*. However, from actual calculations, the decay was found to be much more dependent on E_0 than ΔS^*. The activation entropy increases with the decrease in the bond order of the reaction coordinate.

The "kinetic shift," which is called the excess energy required to produce a detectable dissociation, usually in several μs, is attributable to a slope of $k(E)$ vs. the energy; a steeply-rising slope gives a less kinetic shift. In order to determine the kinetic shift, the time-dependent electron ionization efficiency (EIE) curves were measured for t=3 and 900 μs; they are shown on a semilogarithmic plot in Fig. 4. The EIE curves for the parent ion were used for normalization. There is no shift observed in the time-resolved EIEs of the CH_3CO^+ fragments. It can be reproduced, within the limits of experimental error, by use of the distonic-ion model. Naturally, the EIE shift decreases with the steepness of the $k(E)$ vs. energy plot. The energy distribution of electron impact should be considered for the EIE calculation.[9] Its distribution, as estimated from the second derivative of the helium EIE curve,[15] was found to be 0.8 eV at a half-maximum. Because of the poor energy resolution, the most significant result is not the EIE curve itself, but only its shift. The appearance energy of 10.9±0.1 eV obtained from the EIE difference near the threshold agrees with the previous result.[16]

In a system of ionized methyl acetate, the prior isomerization mechanism was examined in order to explain the present results of time-resolved metastable fragmentations and EIEs. It is suggested that the distonic structure among several isomers is the plausible precursor decomposing metastably to $CH_3CO^+ + \dot{C}H_2OH$.

Appendix

1. The geometry of the reactant state is most conveniently specified in terms of the bond orders and bond angles. The reacting bond length for the transition state is modified from the standard length, r_0, and adjusted by Pauling's expression, $r=r_0-0.31$ n (n), where n is the bond order. The stretching and angle bending force constants for the transition state are modified by $F_r=nF_r^0$ and $F_a=g(\theta)n_in_jF_a^0$, where F^0 is the standard force constant, n_i and n_j are the bond orders in the bending mode, and $g(\theta)=1.39+1.17\cos(\theta)$ is the hybridization factor for the bond angle θ. The torsional and

out-of-plain bending force constants are not modified from the reactant force constants. For a simple bond cleavage, the force constant for the stretching mode of the reacting bond in the reaction coordinate is negative. This provides an imaginary frequency because of a negative curvature at barrier.

2. The following vibrational frequencies (cm^{-1}) for the reactant and the transition state were obtained by means of vibrational analysis using a simple vibrational force field; they were used in the RRKM calculations.

1) Distonic-ion model(ΔS^*_{1000}=4.0 e.u.)

3750	3080	3080	3080	3000	2960	1530	1520	1480	1380
1260	1150	1130	1080	1010	960	900	800	630	560
480	430	360	240	230	200	100			
3080	3080	3080	3000	2960	1530	1520	1480	1380	1250
1140	1130	1080	970	900	800	630	560	470	440
260	240	220	200	180	100				

2) Hydrogen-bridged complex model(ΔS^*_{1000}=2.0 e.u.)

3290	3090	3080	3070	3010	2960	2010	1990	1760	1620
1530	1510	1320	1230	1070	980	820	680	520	500
380	290	260	230	190	100	50			
3090	3080	3070	3010	2960	2550	1990	1800	1730	1610
1530	1500	1230	1060	940	820	650	500	480	360
350	260	230	110	100	20				

References

1) H. Schwarz and C. Wesdemiotis, *Org. Mass Spectrom.*, **14**, 25 (1979).

2) J. K. Terlouw, J. L. Holmes, and P. C. Burgers, *Int. J. Mass Spectrom. Ion Processes*, **66**, 239 (1985).

3) C. Wesdemiotis, R. Csenscits, and F. W. McLafferty, *Org. Mass Spectrom.*, **20**, 98 (1985); H. Schwarz and C. Wesdemiotis, *Org. Mass Spectrom.*, **14**, 25 (1979); J. L. Holmes and F. P. Lossing, *Org. Mass Spectrom.*, **14**, 512 (1979).

4) J. L. Holmes, C. E. C. A. Hop, and J. K. Terlouw, *Org. Mass Spectrom.*, **21**, 776 (1986).

5) P. C. Burgers, J. L. Holmes, C. E. C. A. Hop, and J. K. Terlouw, *Org. Mass Spectrom.*, **21**, 549 (1986).

6) N. Heinrich, J. Schmidt, H. Schwarz, and Y. Apeloig, *J. Am. Chem. Soc.*, **109**, 1317 (1987).

7) L. F. Monterio, M. L. F. Monterio, J. J. Butler, and T. Baer, *J. Phys. Chem.*, **86**, 752 (1982); T. Baer, W. A. Brand, T. L. Bunn, and J. J. Butler, *Faraday Disc. Chem. Soc.*, **75**, 45 (1983); M. Panczel and T. Baer, *Int. J. Mass Spectrom. Ion Proc.*, **58**, 43 (1984); T. Baer and J. R. Hass, *J. Phys. Chem.*, **90**, 451 (1986).

8) A. A. Herod and A. G. Harrison, *Int. J. Mass Spectrom. Ion Phys.*, **4**, 415 (1970); C. Lifshitz, *Mass Spectrom. Rev.*, **1**, 309 (1982).

9) R. Arakawa and Y. Yoshikawa, *Bull. Chem. Soc. Jpn.*, **60**, 49 (1987).

10) From the threshold behavior of ionization,[17] the internal energy distribution is given by $f(E)=p(E)(V-E)^{k-1}\sim p(E)$, where $p(E)$ is the energy deposition function, V is the ionizing energy ($V\gg E$), and K is the number of electrons leaving the collision complex (K=2). In the present case, the photoelectron spectrum is assumed to represent the $p(E)$ function upon ionization by electron impact.

11) I. Watanabe, Y. Yokoyama, and S. Ikeda, *Bull. Chem. Soc. Jpn.*, **46**, 1959 (1973); D. A. Sweigart and D. W. Turner, *J. Am. Chem. Soc.*, **94**, 5592 (1972).

12) S. E. Stein and B. S. Rabinovitch, *J. Chem. Phys.*, **58**, 2438 (1973).

13) A frequency program in BEVOBIV-IV was used for the frequency calculations. L. B. Sims, G. W. Burton, and D. F. Lewis, BEVOBIV-IV, Quantum Chemistry Program Exchange No. 337 (1977); C. W. Burton, L. B. Sims, J. C. Wilson, and A. Fry, *J. Am. Chem. Soc.*, **99**, 3371 (1977).

14) H. M. Rosenstock, R. Stockbauer, and A. C. Parr, *J. Chem. Phys.*, **71**, 3708 (1979) and **73**, 773 (1980); G. Bouchoux, *Org. Mass Spectrom.*, **12**, 681 (1977); S. T. Pratt and W. A. Chupka, *Chem. Phys.*, **62**, 153 (1981).

15) J. D. Morrison, *J. Chem. Phys.*, **21**, 1767 (1953).

16) F. M. Benoit, A. G. Harrison, and F. P. Lossing, *Org. Mass Spectrom.*, **12**, 78 (1977).

17) W. Forst, "Theory of Unimolecular Reactions," Academic Press (1973); M. R. H. Rudge and M. J. Seaton, *Proc. R. Soc. London, Ser. A*, **283**, 262 (1965); M. R. H. Rudge, *Rev. Mod. Phys.*, **40**, 564 (1968).

 © 1988 The Chemical Society of Japan Bull. Chem. Soc. Jpn., 61, 3429—3434 (1988)

Photocatalytic Oxidation of Alcohols on TiO_2

Sadamu YAMAGATA,* Seiichiro NAKABAYASHI,† Kenneth M. SANCIER,†† and Akira FUJISHIMA
Department of Synthetic Chemistry, Faculty of Engineering, University of Tokyo, Hongo, Bunkyo-ku, Tokyo 113
†The Institute of Physical and Chemical Research, Wako-shi 351-01
††Materials Research Lab., SRI International, 333 Ravenswood Avenue, Menlo Park, C.A. 94025, U.S.A.
(Received April 8, 1988)

The reaction mechanisms of the photocatalytic oxidation of several different alcohols on TiO_2 were investigated by three experimental techniques: spin trapping, photocurrent measurement, and product analysis. The results are interpreted according to the band model of a semiconductor and current doubling. It was found that alcohols with α-hydrogens gave low concentrations of spin adducts since their photoproduced radicals have short lifetimes on TiO_2 due to a current-doubling process. Also, it was found that oxygen participated in a radical chain mechanism in the photocatalytic oxidation of ethanol to acetaldehyde.

The application of photoelectrochemistry and photocatalysis to organic synthesis has been recently reviewed.[1-3] In these reviews many kinds of organic reactions on photocatalysts have been introduced. Principally, reactions on photocatalyst are understood to be short-circuited electrolytic reactions. However, there are some reactions which afford different products from those obtained in electrolysis on metal electrodes or in chemical reactions with redox reagents. For example, the photocatalytic oxidation of diphenylethylene on TiO_2 gives diphenylketone, while the electrolysis on Pt attains oxidative dimerization.[4] Many attractive reactions, such as phenol formation from benzene[5] and N-alkylation of amines,[6] have also been reported. In some cases alcohols are involved in these reactions. Therefore, it is necessary to understand how alcohols react on a photocatalyst. In this work we investigated the reaction mechanism of the photocatalytic oxidation of several different alcohols on TiO_2 by correlating the results from three experimental techniques: spin trapping, photocurrent measurement, and product analysis.

In the current study, TiO_2 was used as the semiconductor since it is stable; a wealth of information has been developed concerning photocatalysis on its surface. Different alcohols were chosen for the reactants in order to obtain information on the effect of the molecular structure on the reaction mechanism.

Information on the reaction of organic substances on the irradiated surface of semiconductors was obtained by the spin-trapping technique.[7,8] This technique involves the reaction of a diamagnetic spin-trapping reagent with short-lived radicals to produce relatively stable paramagnetic spin adducts which can be detected and identified by electron spin resonance (ESR). For example, a spin-trapping reagent such as 5,5-dimethyl-4,5-dihydro-3*H*-pyrrole *N*-oxide (DMPO) reacts with various radicals to give spin adducts whose ESR spectra have hyperfine structures. From the hyperfine structure, information concerning the structure of the trapped radical can be deduced. In this way, we can obtain information about the kind of radicals involved in the reactions. Recent investigations concerning photocatalytic oxidations of alcohols on semiconductor powder using the spin-trapping method were reported by this laboratory[9] and Leaustic et al.[10]

Photocurrent doubling is another important technique[11] for investigating photocatalytic reaction mechanisms on semiconductors. This type of reaction on an n-type semiconductor is illustrated as follows. A photon ($h\nu$) whose energy is equal or larger than that of the band gap of semiconductor produces an electron-hole pair. The current-doubling reagent (R_{cd}) donates an electron to the valence band and the resultant radical species($R_{cd}^{\cdot}$) is then converted into species ($R_{cd}^{\cdot}$*), which has a sufficiently high electronic potential that another electron is injected from $R_{cd}^{\cdot}$* into the conduction band. The whole reaction is that R_{cd} donates two electrons to the semiconductor electrode; as a result, the photocurrent is theoretically double that which is usually observed when only the first electron is injected. Current-doubling reactions have been investigated using many different semiconductors and substances.[11-18] For alcohols on TiO_2, Miyake et al. reported that alcohols with α-hydrogens react as current-doubling reagents, but those without α-hydrogens do not.[13]

Since oxygen may play a significant role in photocatalytic reactions, we studied this effect under air and nitrogen.

Experimental

Spin Trapping Experiment. Slurries of TiO_2 were prepared in pure alcohols since the presence of water, even at a 50% level, causes losses in the ESR sensitivity and, hence, very weak ESR spectra result. Titanium dioxide powder (10 mg; P-25 Nippon Aerosil, 30 nm diameter) was dispersed in one of six alcohols (1 ml), and mixed ultrasonically for more than 20 min in order to produce a slurry that was stable during the course of the experiments. To remove dissolved oxygen, the slurry was freeze-pumped at least three times and back-filled with dry nitrogen. A spin-trapping reagent (DMPO 5 μl, Sigma, used as-received) was added to the slurry, an aliquot of which was introduced into a quartz ESR flat cell (volume 0.52 cm^3, spacing 0.3 mm) by means of a rubber squeeze bulb. To prevent oxygen from entering the

slurry, preparations were made under flowing nitrogen gas. The cell was placed in a TM_{110} cavity of an X-band electron spin resonance spectrometer (JEOL, JES-PE-1X). The microwave power was 10 mW and the modulation amplitude was 1.0 Gauss for all experiments. ESR measurements were made immediately after irradiation for 30 s and 1 min was required to scan the spectrum. Ultraviolet irradiation was directed to the window of the cavity using a 500 W high-pressure mercury lamp with a glass filter which cut off wavelengths shorter than 390 nm and a water filter which absorbed infrared radiation. Light with wavelengths <390 nm caused a decomposition of DMPO or its spin adducts to give a complicated ESR spectra. All alcohols used in these experiments were at least of 98% purity.

Current Doubling Experiment. The photocurrent was measured in a solution containing 0.05 M HCl in an alcohol-water mixture (1:1 in volume). The usual three-electrodes method[13] was employed, where a single crystal of TiO_2 was the working electrode, Pt was the counter electrode, and a saturated calomel electrode (S.C.E.) was the reference electrode, respectively. The light source was a 500 W Xe-lamp with a water filter to decrease infrared radiation.

Photoelectrochemical Oxidation of Ethanol and Product Analysis. The electrolyte for the photoelectrolysis was a mixture of aqueous HCl solution (0.1 M, 2 ml) and ethanol (2 ml). The working electrode (W.E.) was thin-layer TiO_2, deposited on tin oxide-coated glass by spray pyrolysis using titaniumoxy acetylacetonate. A Pt counter electrode and an S.C.E. reference electrode were incorporated in the cell. Irradiation to the TiO_2 was performed through the glass and the tin oxide. Quantitative analyses of a small aliquot of the solution were performed periodically by gas chromatography (Hitachi 163; column: PEG 4000). Qualitative analyses were performed using a GC-MS (Shimazu QP-1000; column: PEG 1500) after distillations of the electrolyte in order to condense the oxidation products. The amount of oxygen in solution was controlled by bubbling nitrogen or oxygen into the solution.

Results and Discussion

The role of oxygen in the mechanism of the photocatalytic oxidation of alcohols was studied by controlling the relative amount of oxygen in solution. Two main sets of experiments were performed: 1) in the "absence" of oxygen by prior purging the solution with nitrogen and 2) in the "presence" of oxygen by bubbling of the solution with oxygen or air. The four lower alcohols were investigated in the absence of oxygen, but only ethanol was studied in the presence of oxygen.

1. Photocatalytic Oxidation of Alcohols in the Absence of O_2. A. Spin Trapping Reaction: Prior to irradiation, the intensity of the ESR spectrum was insignificant. UV irradiation to the slurry of TiO_2 containing 2-methyl-2-propanol and DMPO gave the ESR spectrum shown in Fig. 1(a). The peak-to-peak values (indicated by the arrows in the figure) were used as a measure of the relative concentration of the spin adducts. Methanol, ethanol, and 2-propanol gave similar ESR spectra, but their adduct concentrations were much smaller than that of 2-methyl-2-propanol, as shown in Table 1. Slurries of C_5 alcohols, such as 2-methyl-2-butanol and 3-methyl-2-butanol, also gave concentrations of spin adducts about equal to that of 2-methyl-2-propanol. However, in the case of these higher alcohols, the ESR spectra were more complicated, suggesting that several kinds of radicals were formed and subsequently trapped by DMPO. The hyperfine splitting constants of the spectra of the alcohol-TiO_2-DMPO slurries in the absence of oxygen (Fig. 1, curve a) indicate that the radical trapped by DMPO is a carbon-centered radical.[19] The production of carbon-centered radicals in photocatalytic reaction

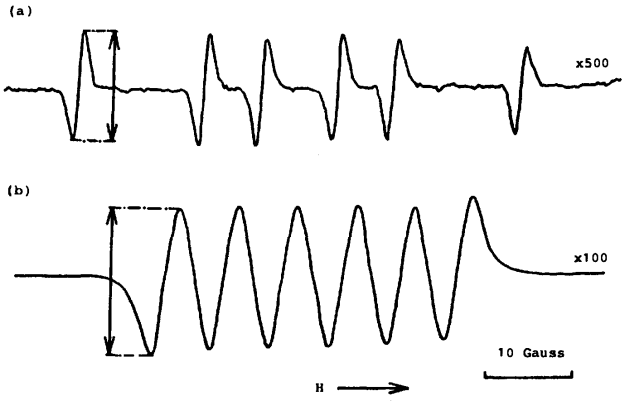

Fig. 1. ESR spectra observed after illumination of a slurry of 2-Me-2-PrOH, TiO_2, and DMPO; (a) spectrum in the absence of oxygen; (b) spectrum in the presence of oxygen.

Table 1. Comparison of Results of Spin Trapping and Current Doubling Experiments. The Relative Spin Adduct Concentrations were Determined from the Peak to Peak Values of ESR Spectra, and the Percent of the Photocurrent Increase Due to the Addition of an Alcohol was Determined from the Photocurrent Increase with Respect to Photocurrent in the Absence of Alcohol

Alcohol	Experimental method	
	Spin adduct concn. (a.u.)	Photocurrent increase (%)
MeOH	<1	25
EtOH	<1	27
2-PrOH	<1	30
2-Me-2PrOH	8	0

has also been suggested from product analyses of the slurries of 2-methyl-2-propanol and Pt-loaded TiO_2 by Nishimoto et al.[20]

Our results suggest that the radical species produced from 2-methyl-2-propanol have a sufficiently long lifetime to be trapped by DMPO, whereas those produced from methanol, ethanol, and 2-propanol had much shorter lifetimes and, hence, were not trapped. The fact that the latter three alcohols gave low concentrations of spin adducts suggests that the photocatalytically produced radicals were involved in another process whose reaction rate is faster than that of the spin-trapping reaction. The other process will be discussed in the section on current doubling. The significant difference among these alcohols is due to the fact that 2-methyl-2-propanol does not have an α-hydrogen, whereas the other three alcohols do. The results concerning the two C_5 alcohols, one of which has an α-hydrogen, can propably be explained by a rapid fragmentation of the photocatalytically produced radicals.

B. Current Doubling Reactions: We made current doubling measurements on the four lower alcohols in order to comfirm the work of Miyake et al.,[13] and also on the two higher C_5-alcohols. The results of the current-doubling experiments with the four lower alcohols in the absence of oxygen are shown in Table 1. The photocurrent was not increased by the addition of 2-methyl-2-propanol; however, upon by the addition of the other three alcohols the photocurrent increased within a range of 25 to 30%. Incidentally, the increase in current doubling was not as large with TiO_2 as with ZnO.[13-15] Our results with the six alcohols agree with the conclusions of Miyake et al.,[13] namely that an alcohol with an α-hydrogen reacts as a current-doubling reagent, but that an alcohol without α-hydrogen does not.

The results of the current-doubling experiments can be interpreted according to the band model theory, as shown in Fig. 2. This figure shows two mechanisms for oxidation, one for an alcohol with an α-hydrogen and the other for an alcohol without an α-hydrogen. The redox potentials of all alcohols are sufficiently low to be oxidized by the hole in the valence band of TiO_2. Therefore, regardless of whether the alcohols have an α-hydrogen or not, photoproduced holes oxidize the alcohols by electron transfer to the valence band of TiO_2, and an initial radical is produced. The redox potential of the produced radical determines whether the radical species can inject another electron into the conduction band of TiO_2 or not. An alcohol with α-hydrogen affords a radical which can inject another electron, while an alcohol without α-hydrogen does not.[21]

The results of spin trapping and current doubling shown in Table 1 (that is, current doubling reagents do not give a high concentration of spin adducts) suggest that the rate of second-electron injection into the conduction band is faster than that of spin trapping by DMPO under our conditions.

2. Photocatalytic Oxidation of Ethanol in the Presence of O_2. A. Spin Trapping Reactions: The introduction of oxygen into a spin-trapping slurry system containing 2-methyl-2-propanol changed both the hyperfine splitting (h.f.s.) constants and the intensities of the ESR spectra. The ESR spectrum is shown in Fig. 1 (curve b), where it is compared with the spectrum (curve a) observed when nitrogen was introduced into the slurry. In the presence of oxy en the hyperfine structures of the ESR spectra observed for all four alcohols were similar, and the h.f.s. constants indicated that oxygen-centered radicals were traped.[21] The concentrations of the spin adducts from all four alcohols could be increased by oxygen bubbling, and the intensity of the spectrum was significantly greater for 2-methyl-2-propanol than the other alcohols, as was the case in the absence of oxygen (Table 2).

There are two possible mechanisms for the formation of oxygen-centered radicals: (1) molecular oxygen reacts with the photocatalytically produced C-centered

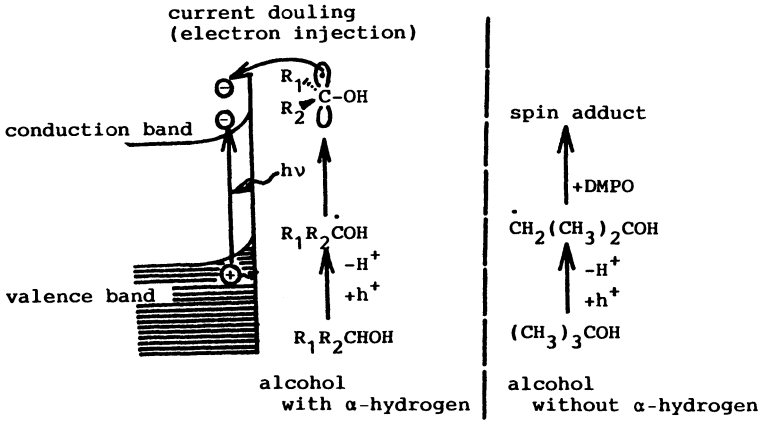

Fig. 2. Reaction mechanism of the current doubling and the spin trapping reactions of alcohols with and without α-hydrogens on TiO_2.

Table 2. Relative Spin Adduct Concentrations of Slurries of Alcohols TiO_2, and DMPO upon Irradiation in the Presence of Oxygen or Nitrogen. Spin Adduct Results under Nitrogen Were Taken from Table 1

Alcohol	Spin adduct concentration (a.u.)			
	MeOH	EtOH	2-PrOH	2-Me-2-PrOH
Under N_2	<1	<1	<1	8
Under O_2	4	4	4	56

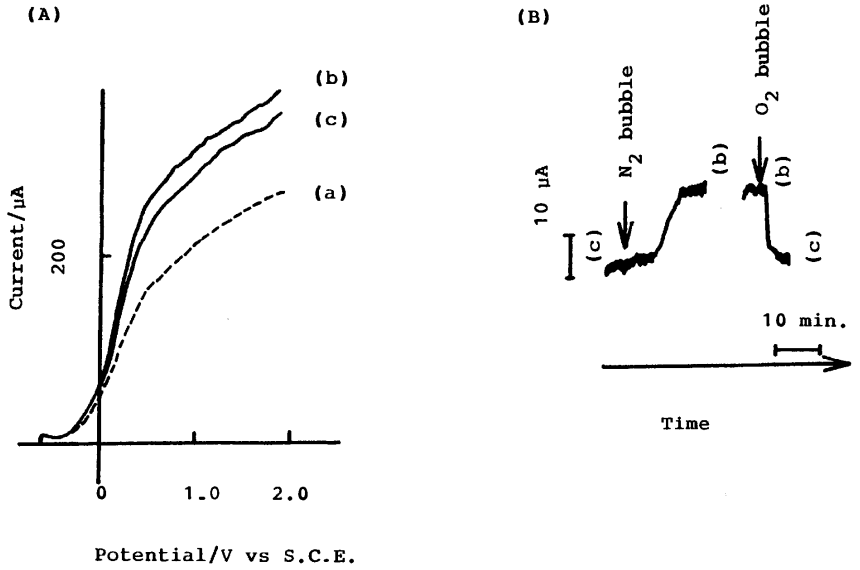

Fig. 3. Oxygen effect on the current doubling reaction of ethanol. (A) current-potential curves under illumination (a) without ethanol under nitrogen or oxygen, (b) with ethanol under nitrogen, and (c) with ethanol under oxygen; (B) time profile of photocurrent under oxygen or nitrogen in the presence of ethanol measured at 0.0 V vs S.C.E.

radicals, and (2) an oxygen anion radical, which is produced through the reduction of molecular oxygen by electrons from the conduction band, reacts with an alcohol molecule to produce a radical species. However, hydrogen atom abstraction from alcohol by a superoxide ($O_2^{\cdot-}$) is unlikely.[22] In this case a hydroperoxyl radical ($HO_2^{\cdot}$) or a hydroxyl radical ($\cdot OH$) produced by a cathodic reaction from oxygen molecule[5] may play a significant role. In both cases the formation of a C-centered radical is the first step and the reaction of this radical with oxygen molecule may give an O-centered radical.

The fact that oxygen increased the concentrations of the spin adducts for all alcohols, even for alcohols with an α-hydrogen, suggests that the rate of a second-electron injection step (i.e., current doubling) is not much faster than that of the reaction of the radicals with oxygen species. In this study we were not able to specify the reason why the concentrations of the spin adducts were increased by oxygen. However, we can propose several mechanisms, as follows, which may account for these results. First, an oxygen adsorbed on TiO_2 accepts a photoexcited electron from the conduction band and this results in a decrease of the recombination of the photoproduced hole with the electron. The resulting larger concentration of holes react with an alcohol to produce radicals more efficiently than the holes in the absence of oxygen. Secondly, an oxygen reacts with a photoproduced radical by a radical chain mechanism which is discussed later. By means of this chain mechanism the concentration of radicals increased and, hence, a higher concentration of spin adducts resulted. Thirdly, the reduction of an oxygen molecule leads to the formation of radical species which abstract a hydrogen atom from ethanol to give more radical species. Lastly, the trapping rate constant of DMPO differs according to the type of radical. For example, DMPO traps O-centered radicals more efficiently than C-centered radicals, which suggests even at the same concentration O-centered radicals give more spin adducts than C-centered radicals do.[23]

B. Current Doubling Reactions: The introduction of oxygen gas into the electrolyte containing ethanol partially reduced the current increase due to the addition of alcohol, as shown in Fig. 3 (A). The difference in the photocurrent increase under nitrogen and oxygen is small but significant. It was further substantiated by the time profile of the photocurrent

with ethanol under nitrogen or oxygen bubbling into an electrolyte, as shown in Fig. 3(B). In this experiment, when oxygen gas was replaced with nitrogen, the photocurrent increased slowly. Later, when the nitrogen was replaced with oxygen, the photocurrent decreased rapidly. Both these changes were reversible. The difference in the time profile between the photocurrent increase and decrease can be attributed to the oxygen adsorbed on the TiO_2. The radical species which injects another electron is adsorbed on the TiO_2. Therefore, effective oxygen should also be found on the TiO_2. It takes more time to remove the oxygen from the surface of TiO_2 by nitrogen gas bubbling than to provide adsorbed oxygen by oxygen gas bubbling. Consequently, the photocurrent increased slowly and decreased rapidly.

The reduction of the photocurrent by introducing oxygen into the photoelectrochemical system suggests that oxygen or an oxygen radical species reacted with the initial radical species. To account for the fact that oxygen did not completely eliminate the photocurrent increase, we propose that the reaction rate of electron injection from the alcohol radical species is comparable to that of the reaction of the radicals with oxygen species. Since these results were obtained with an electrode system in which most of the electrons in the conduction band were collected by the counter electrode and consumed to produce hydrogen, we conclude that the active species at the TiO_2 surface is probably molecular oxygen and not an oxygen anion radical.

C. Photoelectrochemical Oxidation of Ethanol and Product Analysis: A photoelectrolysis of an ethanol-HCl solution under nitrogen or oxygen led to a product with the same retention time in gas chromatograms. GC-MS revealed that the only product was acetaldehyde, the amount of which was about ten-times greater in the presence of oxygen, as shown in Fig. 4. The current efficiency for the production of acetaldehyde under nitrogen is about 20%. The low efficiency may be attributed to a competitive oxidation of water.

Acetaldehyde is reported to be produced by the current-doubling reaction with ethanol.[13] Moreover, our results show that acetaldehyde formation is enhanced by the presence of oxygen. This result and the discussions in the previous section lead us to conclude that molecular oxygen is the active species for the enhanced production of acetaldehyde compared to that in the absence of oxygen. To account for the photoelectrochemical oxidation of ethanol we propose the reaction mechanism shown in Fig. 5. Molecular oxygen reacts with a C-centered radical(I), which is produced photocatalytically to give a peroxyl radical (II), which in turn decomposes by an autoxidation step to produce acetaldehyde and hydroperoxyl radical(III). This radical(III) abstracts hydrogen from ethanol and leads to the production of another C-centered radical(I). According to this reaction mechanism, one photon results in the formation of several acetaldehyde

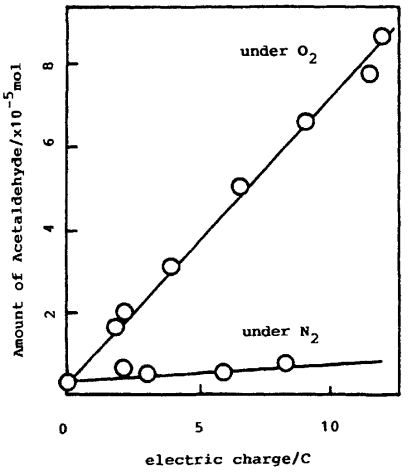

Fig. 4. The effect of oxygen on the amount of acetaldehyde produced by photoelectrolysis of ethanol in aqueous 0.1 M HCl (1:1). W.E.:TiO_2 on SnO_2 coated glass; C.E.:Pt; R.E.:S.C.E.; photoelectrolysis at 2.5 V vs. S.C.E.

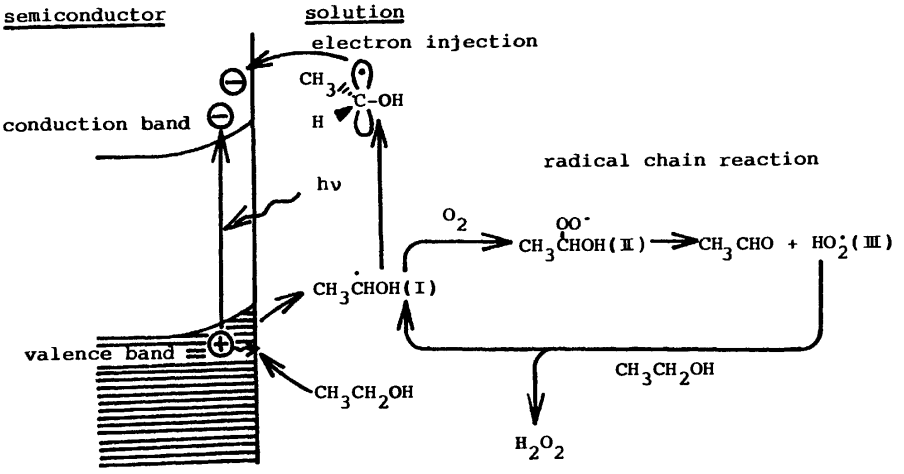

Fig. 5. Reaction mechanism of ethanol oxidation on illuminated TiO_2 in the presence of oxygen. The reduction processes are omitted.

molecules. This increase in the amount of acetaldehyde results from a free radical chain reaction mechanism involving molecular oxygen. Such a free radical chain mechanism has been suggested for photoirradiated slurries containing olefins and TiO_2 or CdS.[1] The formation of another product, H_2O_2, was also reported on photoexcited TiO_2, although it has only a transient existence in aqueous dispersion of TiO_2.[24]

Conclusion

In this article, we compared the photocatalytic reactions in slurries and on photoelectrodes and obtained a good correlation between the results from both systems. An alcohol with an α-hydorgen is oxidized to the radical species which can inject another electron into the conduction band of TiO_2. The rate of electron injection is faster than that of a spin-trapping reaction by DMPO and is comparable with that of the reaction with oxygen. The reaction process becomes a radical chain process under oxygen. An alcohol without an α-hydrogen is oxidized to the radical species which can not inject another electron. Therefore, this radical is trapped by DMPO. These results indicate a criterion for the application of photocatalytic reactions of alcohols to organic syntheses. Alcohols with α-hydrogen can be used for the in situ preparation of carbonyl compound for the *N*-alkylation of amines[6] since they are subjected to a rapid two-electron oxidation. On the other hand, alcohols without α-hydrogen can be used for the generation of radical species for the radical coupling reactions[20] because the produced radicals are relatively stable. The oxidation of 2-methyl-2-propanol on Pt electrode does not produce a new C-C bond like on photocatalyst, but gives acetone and 2-methylpropane.[25]

In our discussions of the photooxidation of alcohols we have stated that oxidation starts from direct reaction with the photoproduced holes in the valence band of TiO_2. However, it is equally possible that the oxidation occurs by an indirect process involving hydroxy radicals produced by oxidation of surface OH groups by holes, which we do not distinguish from the direct reaction with a hole.

We acknowledge valuable discussoins with Dr. Yorihiro Yamamoto of the Faculty of Engineering, University of Tokyo.

References

1) K. Tokumaru et. al., *Am. Chem. Soc. Symposium Series*, **278**, 43 (1985).
2) P. Pichat, *Am. Chem. Soc. Symposium Series*, **278**, 21 (1985).
3) M. A. Fox, *Acc. Chem. Res.*, **16**, 314 (1983).
4) M. A. Fox, C-C. Chen, K-H. Park, and J. N. Younathan, *Am. Chem. Soc. Symposium Series*, **278**, 69 (1985).
5) M. Fujihira, Y. Satoh, and T. Osa, *Nature (London)*, **293**, 206 (1981).
6) B. Ohtani, H. Osaki, S. Nishimoto, T. Kagiya, *J. Am. Chem. Soc.*, **108**, 308 (1986).
7) B. Kraeuter, C.D. Jaeger, and A. J. Bard, *J. Am. Chem. Soc.*, **100**, 4903 (1978).
8) J. R. Harbour and M. L. Hair, *Can. J. Chem.*, **57**, 1150 (1979).
9) S. Yamagata and A. Fujishima, Proc. 1st Int'l Symp. Electroorganic Syn., S. Torii (Ed.) Kodansha, Tokyo, Elsevier, Amsterdam, (1987), 401.
10) A. Leaustic, F. Babonneau, and J. Livage, *J. Phys. Chem.*, **90**, 4193 (1986).
11) W. P. Gomes, T. Freund, and S. R. Morrison, *J. Electrochem. Soc.*, **115**, 818 (1968).
12) J. Lee, T. Kato, A. Fujishima, and K. Honda, *Bull. Chem. Soc. Jpn.*, **57**, 1179 (1984).
13) M. Miyake, H. Yoneyama, and H. Tamura, *Chem. Lett.*, **1976**, 635.
14) K. Hirano, K. Inagaki, Y. Asami, and R. Takagi, *Denki Kagaku*, **51**, 893 (1983).
15) E. C. Dutoit, F. Cardon, and W. P. Gomes, *Ber. Bunsenges. Physik. Chem.*, **80**, 1285 (1976).
16) W. M. Seas and S. R. Morrison, *J. Phys. Chem.*, **88**, 976 (1984).
17) J. Li and L. M. Peter, *J. Electroanal. Chem.*, **182**, 399 (1985).
18) J. Li, R. Peat, and L. M. Peter, *J. Electroanal. Chem.*, **200**, 333 (1986).
19) E. G. Janzen and J. I-P. Liu, *J. Mag. Res.*, **9**, 510 (1973).
20) S. Nisimoto, B. Ohtani, H. Shirai, and T. Kagiya, *J. Chem. Soc., Perkin Trans. 2*, **1986**, 661.
21) J. Lilie, G. Beck, and A. Henglein, *Ber. Bunsenges. Physik. Chem.*, **75**, 458 (1971).
22) J. M. Gebicki and B. H. J. Bielski, *J. Am. Chem. Soc.*, **103**, 7020 (1981).
23) B. Kalyanaraman, "Reviews in Biochemical Toxicology," ed by E. Hodooson, J. R. Bend, and R. M. Philpot, Elsevier, N.Y., (1982), IV, 76.
24) J. R. Harbour, J. Tromp, and M. L. Hair, *Can. J. Chem.*, **63**, 204 (1985).
25) F. Sundholm, G. Sundholm, and K. Suontama, *Suomen Kemistilehti*, **B45**, 383 (1972).

 © 1988 The Chemical Society of Japan Bull. Chem. Soc. Jpn., 61, 3435—3437 (1988)

Thermotropic Liquid Crystal Properties of Alkylammonium Alkanesulfonates

Yoshio MATSUNAGA* and Kiyoshi NISHIDA

Department of Chemistry, Faculty of Science, Hokkaido University, Sapporo 060

(Received April 15, 1988)

Alkylammonium methane-, ethane-, 1-propane-, and 1-butanesulfonates exhibit a smectic A phase when the cation carries a dodecyl or longer alkyl group. The temperature range of the existence decreases in the following order: methanesulfonates > 1-propanesulfonates > ethanesulfonates > 1-butanesulfonates. In the last series, the mesophase is entirely metastable. The layer spacing in the 1-propanesulfonate is shorter by about 0.30 nm than that of the corresponding methanesulfonate, even though the alkyl chain length in the anion is increased by 0.25 nm.

Several series of long-chain alkylammonium salts have been known to exhibit mesophases. For example, alkylammonium tetrahalometallates, $(RNH_3)_2MX_4$, in which the alkylammonium ions form a double layer between MX_4 sheets, have been extensively examined and often considered as crystalline models of lipid bilayers.[1] Furthermore, the isotropic liquid of some alkylammonium chlorides is known to be preceded by a smectic A phase.[2] Since the role of a counter ion in the liquid crystal formation must be important in a system as simple as the above-mentioned salts, we have undertaken studies regarding the influence of the range of anions on the thermal properties of alkylammonium salts. Various sulfonic acids are readily available and form mesomorphic salts when combined with many long-chain alkylamines; therefore, these salts seemed to be particularly suitable for our purpose. This paper, the first of this series, reports on the properties of four series of alkanesulfonates.

Experimental

Materials. Equimolar amounts of an alkylamine and an alkanesulfonic acid dissolved in boiling alcohol were mixed. The precipitated salt was purified by recrystallization and kept in a vacuum desiccator. For example, Found: C, 59.40; H, 11.59; N, 4.33%. Calcd for $C_{15}H_{31}NH_3^+CH_3SO_3^-$: C, 59.40; H, 11.53; N, 4.33%.

Measurements. Calorimetric curves were recorded on a Rigaku Thermoflex differential scanning calorimeter at a heating or cooling rate of 5 K min^{-1}. The mesomorphic-isotropic transition was well defined on the curve; its reversal at the same temperature assured us of the purity of our salts. Enthalpy changes were estimated by comparing the peak areas with that due to the melting of indium, 3.26 kJ mol^{-1}. Phase diagrams were determined by the calorimetric curves of mixtures. X-Ray diffractions were measured with a Rigaku auto-diffractometer, model RAD IVB, using filtered copper radiation. The temperature of the sample holder was regulated as described in our earlier paper.[3]

Results and Discussion

The melting and clearing points and the associated enthalpies are summarized for alkylammonium methane-, ethane-, 1-propane-, and 1-butanesulfonates in Table 1. In the case of the methanesulfonates, the melting point decreases according to the sequence from dodecyl to tetradecylammonium and, then, remains at 143 °C. A plot of the clearing point against the number of carbon atoms (n) in the cation produces a curve which is slightly convex upwards. Conse-

Table 1. Transition Temperatures (°C), Enthalpy Changes (kJ mol^{-1}) and Layer Spacings (nm) of Alkylammonium Salts[a]

n[b]	Melting	Clearing	Layer Spacing
	Methanesulfonates		
12	150(25)	—	—
13	147(24)	150(1.1)	—
14	142(21)	157(0.9)	2.76
15	143(24)	159(1.0)	2.85
16	143(25)	159(0.9)	3.05
17	143(26)	159(0.9)	3.12
18	143(25)	156(1.0)	3.26
	Ethanesulfonates		
13	84(23)	—	—
14	85(24)	82(0.9)	—
15	89(29)	88(1.1)	—
16	88(31)	93(1.1)	2.75
17	95(33)	97(1.1)	2.89
18	95(35)	98(1.0)	3.00
	1-Propanesulfonates		
11	77(18)	—	—
12	76(22)	71(1.8)	—
13	73(21)	80(1.8)	2.39
14	77(21)	81(1.7)	2.50
15	79(22)	87(1.8)	2.59
16	85(25)	88(1.7)	2.75
17	88(27)	93(1.7)	2.83
18	90(34)	92(1.7)	2.96
	1-Butanesulfonates		
11	74(21)	—	—
12	76(21)	65(2.3)	—
13	73(23)	68(2.3)	2.31
14	80(24)	74(2.2)	2.41
15	85(28)	75(2.2)	—
16	85(29)	77(2.2)	2.68
17	90(34)	79(2.0)	—
18	88(37)	—	—

a) The second quantities are in parentheses. b) The number of carbon atoms in the alkyl group.

quently, the widest temperature range of stable existence is achieved when the cation carries pentadecyl to heptadecyl groups. The clearing point of the ethanesulfonate is lower by 58 to 75 °C than that of the corresponding methanesulfonate and increases smoothly with the number of carbon atoms in the alkyl group; the melting point is lower by 48 to 63 °C. As a result, the mesophase is metastable when n is fifteen or less. Even when the phase is stable the temperature range of stable existence is no more than 5 °C. Both the melting and clearing points of the 1-propanesulfonates are located at temperatures several degrees lower than those of the ethanesulfonates. The mesophase given by the 1-propanesulfonate is stable when n is thirteen or more but the existence range is merely two to eight degrees. It may be noted that the clearing point of this series shows a marked even-odd alternation which provides an additional check on the purity. The transition temperatures are further lowered in the 1-butanesulfonates. As the depression of the clearing point is more pronounced than that of the melting point, all the mesophases observed for this series are metastable. The enthalpy change at the clearing point increases slightly with the number of carbon atoms in the sulfonate ion, but not with that in the ammonium ion.

The X-ray diffraction pattern recorded for the mesophases of the methane- and 1-propanesulfonates within or a little below the temperature range of the stable existence consists of a sharp inner peak and a diffuse outer one, indicating that the phase is of the smectic A- or C-type. The inner peak is sometimes accompanied by weak peaks assignable to second- and third-order reflections, since the specimen spread in the form of a thin layer over an aluminum holder is not free from orientation. The layer spacing measured for the methanesulfonates (see Table 1) agrees well with the sum of lengths of the cation and anion. For example, Found: 3.26 nm. Calcd for $C_{18}H_{37}NH_3^+ + CH_3SO_3^-$: 2.59+0.64=3.23 nm. The former length is estimated for an all-trans conformation of the alkyl group, employing a C-C bond length of 0.154 nm, a C-N bond length of 0.147 nm, a tetrahedral angle, a van der Waals radius of methyl group of 0.20 nm, and a thermochemical radius of ammonium ion of 0.14 nm (the latter employing a C-S bond length of 0.182 nm and a thermochemical radius of sulfate ion of 0.26 nm). The thermochemical radii were taken from a table compiled by Jenkins and Thakur.[4] Therefore, one may conclude that the mesophase given by the methanesulfonates is of the smectic A-type and that the schematic representation given in Fig. 1a may be a reasonable model. Here, the large circle represents the ionic end of methanesulfonate ion, the small circle that of the alkylammonium ion, and the wavy line the alkyl chain. This conclusion is consistent with the strong tendency shown by the mesophase to be homeotropic. The smectic phases of 4-alkylpyridinium

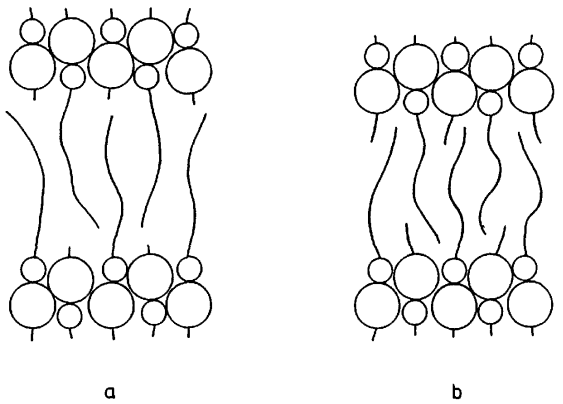

Fig. 1. Schematic representation of the proposed structure for (a) the smectic A phase of the methanesulfonate and (b) that of the 1-propanesulfonate. Large circle: the ionic end of the anion; small circle: the ionic end of the cation; wavy line: alkyl chain.

hydrochloride and 1-alkyl-4-methylpyridinium halides have been proposed to be represented by similar models by Sudhölter et al. and by Bazuin et al. respectively.[5,6] A plot of the layer spacing in the mesophase of the methanesulfonates against the number of carbon atoms in the alkylammonium ion can be fit to a slope of 0.125 nm, agreeing with the value calculated for a fully-extended configuration. The same slope appears to be applicable to a plot for the 1-propanesulfonates; however, the layer spacings, themselves, are shorter by about 0.30 nm than those of the corresponding methanesulfonates. Since the observed slope, and also the tendency to be homeotropic, strongly indicate that the mesophases are of the smectic A-type, the alkyl group attached to this anion (the whole length of which is estimated to be about 0.89 nm) must be dissolved into the layer formed by the paraffinic parts of the cations as sketched in Fig. 1b. The stable or metastable mesophases of the remaining alkanesulfonates also exhibit diffraction patterns of the same type. Although the data are scanty, the spacing seemingly decreases as the alkyl group on the anion becomes longer. The lateral spacing shrinks from about 0.47 nm for the methanesulfonates to about 0.45 nm for the 1-propanesulfonates. This change may indicate a crowding of the alkyl chains in the latter series.

The identification of the mesophases given by the ethane- and 1-butanesulfonates was supplemented by a demonstration of complete miscibility with the smectic A phase of hexadecylammonium methanesulfonate. Phase diagrams of the binary systems, consisting of hexadecylammnium ethane- and 1-butanesulfonates and a reference compound, are presented in Figs. 2a and b, respectively. In these diagrams, K, M, and I stand for crystalline, mesomorphic, and isotropic phases, respectively, and the reference compound is placed on the left-hand side. The complete miscibility between the two mesophases in the former system is

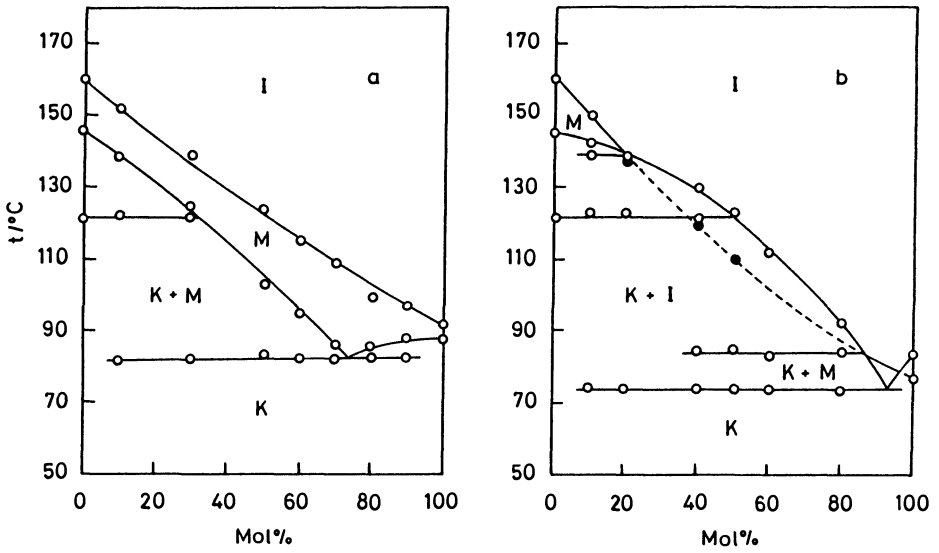

Fig. 2. Phase diagrams of (a) the hexadecylammonium methanesulfonate–ethanesulfonate and (b) the hexadecylammonium methanesulfonate–1-butanesulfonate systems. The reference compound is located on the left-hand side. The open and shaded circles are transitions observed in the processes of heating and cooling respectively.

shown by the fact that the curve smoothly connects the two clearing points. The eutectic is located at 82 °C and 73 mol% of the ethanesulfonate. The horizontal line at 121 °C on the left-hand side is due to the solid-solid transition of the reference compound. The mesophase of the 1-butanesulfonate in Fig. 2b is metastable and the major part of the M–I transition point curve is beneath the freezing-point curve of the reference compound. The shaded circles are the I–M transitions observed during the process of cooling. The intersections between these transition point curves give rise to the appearance of horizontal lines at 84 and 138 °C. The eutectic in this system is located at 73 °C and 93 mol% of the 1-butanesulfonate. The mesophase is stable only in two small regions near the melting point of the reference compound and above the eutectic point. The crystalline phase of the methanesulfonate coexists with the mesophase in the temperature range from 73 to 84 °C, with the isotropic melt in the range from 84 to 138 °C, and again with the mesophase in the range from 138 °C to the melting point (143 °C).

The present work was supported by a Grant-in-Aid for Scientific Research No. 60470001 from the Ministry of Education, Science and Culture.

References

1) G. F. Needham, R. D. Willett, and H. F. Franzen, *J. Phys. Chem.*, **88**, 674 (1984) and references cited therein.

2) J. D. Gault, H. A. Gallardo, and H. J. Müller, *Mol. Cryst. Liq. Cryst.*, **130**, 163 (1985).

3) N. Inoue and Y. Matsunaga, *Bull. Chem. Soc. Jpn.*, **51**, 90 (1978).

4) H. D. B. Jenkins and K. P. Thakur, *J. Chem. Educ.*, **56**, 576 (1979).

5) E. J. R. Sudhölter, J. B. F. N. Engberts, and W. H. de Jeu, *J. Phys. Chem.*, **86**, 1908 (1982).

6) C. G. Bazuin, D. Guillon, A. Skoulios, and J. F. Nicoud, *Liq. Cryst.*, **1**, 181 (1986).

 © 1988 The Chemical Society of Japan Bull. Chem. Soc. Jpn., 61, 3439—3443 (1988)

The Zinc-Photosensitized Reaction of Propane

Shunzo YAMAMOTO,* Mitsuru KOZASA, Yoshimi SUEISHI, and Norio NISHIMURA
Department of Chemistry, Faculty of Science, Okayama University, 3-1-1, Tsushima-naka, Okayama 700
(Received April 25, 1988)

The zinc-photosensitized reaction of propane has been studied at a wavelength of 307.6 nm, a temperature of 633 K and pressures from about 67 to 40000 Pa. The major products were hydrogen, methane, ethylene, and dimethylbutane, while minor products detected were propylene, isobutane, ethane, butane, and hexane. The yield of hydrogen fell off with time. The quantum yield calculated from the initial rates is about unity and almost independent of the propane pressure, while the quantum yield obtained at 20 min increased with increasing propane pressure and approached about unity at higher pressures. The methane/hydrogen ratio was always smaller than unity and was independent of the propane pressure. The yield of ethylene increased linearly with an increase in that of methane. It has been concluded that the decomposition of propane is initiated through a hydrogen atom abstraction by an excited zinc atom from both the primary and secondary hydrogen of propane. Possible mechanisms are discussed.

Although there has been a considerable amount of work carried out on the mercury-[1-6] and cadmium-photosensitized decomposition[7,8] of propane, almost no attention has been paid to the zinc-photosensitized reaction of alkanes.

In a previous paper,[9] a remarkable dependence of the quenching cross section of 307.6-nm zinc resonance line by alkanes on the C–H bond strength was reported. It was pointed out that the quenching cross section of a certain alkane can be estimated as the sum of the quenching cross section for each individual quenching site (C–H bond). These findings show that the excited zinc atoms attack all kinds of C–H bonds with efficiencies which depend on the bond strength.

Recently, we have further pointed out that the differences of activation energies for the quenching for primary, secondary, and tertiary C–H bond can be well interpreted in terms of a modified bond energy-bond order method by assuming the following reaction:[10]

$$Zn^* + RH \rightarrow Zn \cdots H \cdots R \rightarrow ZnH + R.$$

These results strongly suggest that hydrogen atom abstraction from alkanes by excited zinc atoms plays an important role in the quenching of $Zn(^3P_J)$.

We have examined the products from a zinc-photosensitized reaction of propane. Here, we report on the details of analytical results.

Experimental

A zinc-photosensitized reaction of propane was carried out in a cylindrical quartz cell. A spiral Pyrex zinc-discharge lamp filled with 2000-Pa argon was used as the source of the 307.6-nm resonance line. The cell and the lamp were inserted in an electric furnace kept at 360±2 °C in order to obtain a sufficient vapor pressure of zinc.

The zinc metal used was high-purity zinc (99.9999%) manufactured by the Osaka Asahi Metal Co. Research-grade propane (Tokyo Kasei K.K. 99.5%) was used after degassing at liquid-nitrogen temperature. The impurities detected by gas chromatography were ethane and propylene; the amount of propylene was below 0.1% of that of propane. Zinc metal was heated in vacumm and the zinc vapor was sealed into capillaries. The capillary and a known amount of propane were enclosed in the cell, and the capillary was broken just before each run.

Product analyses were carried out by fractionation at −196 °C, gas burette measures, and gas chromatography. The gases non-condensable at −196 °C (hydrogen and methane) were collected by a Toepler pump, and were analyzed by combustion over copper(II) oxide at 260 °C. The products which were condensable at −196 °C, were analyzed by gas chromatography, using a 6 m column of vz-7 (Gasukuro Kogyo Co., Ltd.) at 0 °C and a 2 m column of Gasukuro-pack 55 (Gasukuro Kogyo Co., Ltd.) at 30 °C.

The light intensity at 307.6 nm from the lamp was determined by diethyl ketone actinometry,[11] by assuming that the quantum yield of carbon monoxide production at 360 °C and 307.6 nm was unity, and by correcting for any contribution from photolysis by the 328.2- and 330.2-nm lines from the lamp.

Results and Discussion

The major products from the zinc-photosensitized decomposition of propane were hydrogen, methane, ethylene, and 2,3-dimethylbutane (DMB). The minor products detected were propylene, isobutane, ethane,

Table 1. Product Ratios in Zinc-Photosensitized Decomposition of Propane

P	H_2	CH_4	C_2H_4	DMB	C_3H_6	*iso*-C_4H_{10}	C_2H_6	*n*-C_4H_{10}	*n*-C_6H_{14}
Pa	10^{-6} mol	H_2	H_2	H_2	H_2	H_2	H_2	H_2	H_2
1790	0.653	0.58	0.59	0.10	0.08	0.05	0.04	0.01	0.01
6530	0.772	0.74	0.78	0.15	—	0.07	0.07	0.01	0.01
14300	0.843	0.65	0.70	0.21	—	0.09	0.03	0.03	—
25600	0.792	0.68	0.82	—	—	—	—	—	—
33300	1.049	0.72	0.80	—	—	—	—	—	—

butane, and hexane. Their yields were less than 10% of that of hydrogen (Table 1). Some products such as hydrogen, methane, and ethylene were detected when 6700-Pa propane was kept at 360 °C for 2 hours with zinc vapor in the dark; however, their yields were less than 2% of those from zinc-photosensitized reaction. Therefore, the thermal decomposition of propane and its reaction with zinc at 360 °C could be neglected.

The yields of hydrogen, methane, and ethylene increased linearly with the light intensity, while that of DMB showed a second-order dependence on the light intensity (Fig. 1). As Fig. 2 shows, the yield of hydrogen falls off with the reaction time, and the decrease in the yield is larger at lower pressures. This suggests that the influence of the products on hydrogen production is important at lower pressures.

The quantum yield of hydrogen production calculated from the initial rates is about unity and almost independent of the propane pressure, while the quantum yield obtained at a reaction time of 20 min increases asymptotically with increasing propane pressure to unity at high pressures (Fig. 3).

Appreciable amounts of methane are formed. The ratio of Φ_{CH_4}/Φ_{H_2} is almost independent of the propane pressure (Fig. 4). A roughly equal amount of ethylene to that of methane was produced. As Fig. 5 shows, the yield of ethylene increases linealy with an increase in methane.

As mentioned above, the quantum yield of hydrogen is about unity during the initial stage of the reaction and, as Fig. 3 shows, the quantum yield of hydrogen obtained at 20 min is close to unity at higher pressures and decreases with decreasing propane pressure. The experimental results obtained in the case of high propane pressures are very similar to those of mercury-

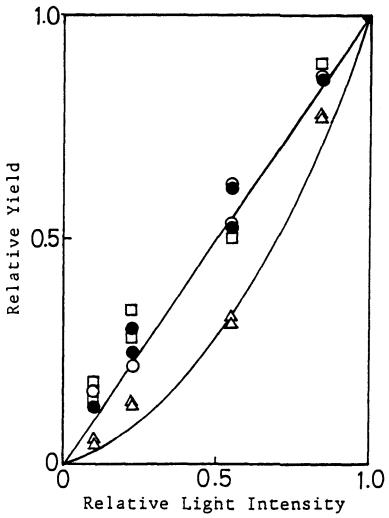

Fig. 1 Dependence of yields of hydrogen (●), methane (○), ethylene (□), and DMB (△) on light intensity in the zinc-photosensitized reaction of propane. ($P_{propane}$ is 30000 Pa and reaction time is 10min.)

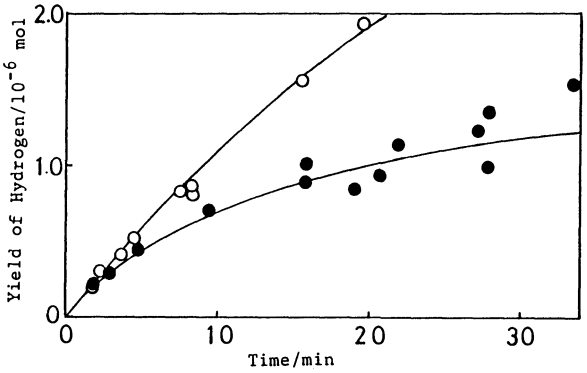

Fig. 2. Time dependence of yield of hydrogen. ○: 30000 Pa, ●: 1700 Pa.

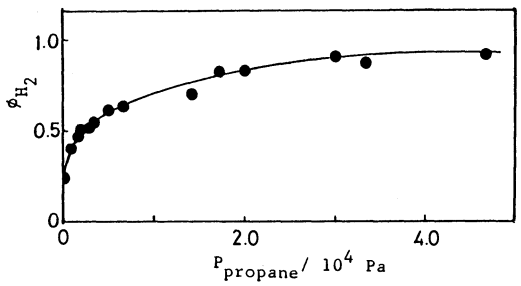

Fig. 3. Pressure dependence of quantum yield of hydrogen.

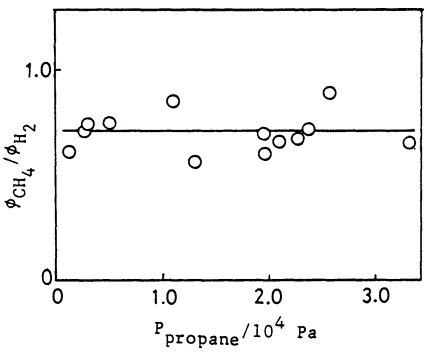

Fig. 4. Pressure dependence of Φ_{CH_4}/Φ_{H_2} ratio.

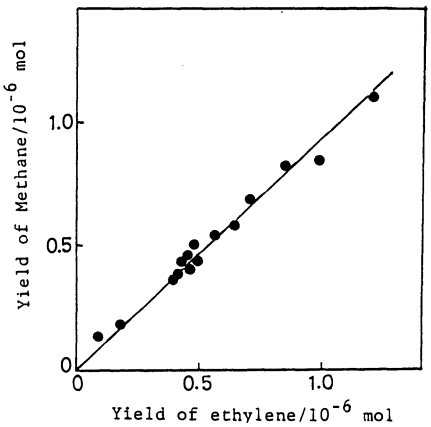

Fig. 5. Relation between yield of methane and that of ethylene.

photosensitized decomposition of propane at high temperatures,[1] and also to those of cadmium-photosensitized decomposition of propane obtained at the initial stage of reaction.[8] By following the mechanisms of $Hg(^3P_1)$-C_3H_8 and $Cd(^3P_1)$-C_3H_8 reactions, the zinc-photosensitized decomposition of propane could be discussed in terms of the following reactions:

$$Zn(^1S_0) + h\nu(307.6\ nm) \rightarrow Zn(^3P_1) \quad (1)$$
$$Zn(^3P_1) \rightarrow Zn(^1S_0) + h\nu(307.6\ nm) \quad (2)$$
$$Zn(^3P_1) + C_3H_8 \rightarrow ZnH + \alpha 1\text{-}C_3H_7 + (1-\alpha)2\text{-}C_3H_7 \quad (3)$$
$$ZnH \rightarrow Zn(^1S_0) + H \quad (4)$$
$$H + C_3H_8 \rightarrow H_2 + \beta 1\text{-}C_3H_7 + (1-\beta)2\text{-}C_3H_7 \quad (5)$$
$$1\text{-}C_3H_7 \rightarrow CH_3 + C_2H_4 \quad (6)$$
$$CH_3 + C_3H_8 \rightarrow CH_4 + \gamma 1\text{-}C_3H_7 + (1-\gamma)2\text{-}C_3H_7 \quad (7)$$
$$(H, CH_3, 1\text{-}C_3H_7, 2\text{-}C_3H_7) \rightarrow \text{recombination and disproportionation products} \quad (8)$$

Production of DMB and minor products is explained by Reactions (8).

From the above mechanism, the following relationships can be derived by neglecting Reactions (8):

$$\Phi_{H_2} = \frac{k_3[C_3H_8]}{k_2 + k_3[C_3H_8]} \quad (9)$$

and

$$\frac{\Phi_{CH_4}}{\Phi_{H_2}} = \frac{\Phi_{C_2H_4}}{\Phi_{H_2}} = (\alpha+\beta)(1+\gamma+\gamma^2+\cdots). \quad (10)$$

The quenching cross section of $Zn(^3P_J)$ by propane at 578 K was reported to be 6.94×10^{-16} cm^2.[9] This shows that k_2 in Eq. 9 can be neglected at all pressures examined here. This indicates that Φ_{H_2} is unity and is independent of the pressure. These findings are in agreement with observations during the initial stage of the reaction. As Fig. 3 shows, Φ_{H_2} is almost unity and is hardly dependent on the propane pressure at pressures higher than 20000 Pa. At lower pressures, however, Φ_{H_2} is considerably smaller than unity and depends on the propane pressure. This anomalous behavior at lower pressures and the nonlinear dependence of the hydrogen yield on time (espetially at lower pressures) shown in Fig. 2 seems to be due to the influence of the products. This point will be discussed later.

As Fig. 5 shows, the yield of ethylene is almost equal to that of methane under all conditions examined; this is in agreement with the prediction from Eq. 10. This shows that Reactions (8) can be neglected concerning the formation of methane and ethylene.

From the quenching cross sections of $Zn(^3P_J)$ by various hydrocarbons, the effective cross sections per primary C-H bond and secondary C-H bond were found to be 0.62×10^{-16} and 2.4×10^{-16} cm^2 at 578 K respectively.[9] As has been described previously,[10] the quenching rate of $Zn(^3P_1)$ by alkanes depends on the temperature. From the activation energies reported for the quenching of $Zn(^3P_1)$ by primary and secondary C-H bonds,[10] the cross sections per primary and secondary C-H bond at 633 K were estimated to be 1.1×10^{-16} and 3.9×10^{-16} cm^2, respectively. Using these values the value of α can be calculated as follows:

$$\frac{\alpha}{1-\alpha} = \frac{1.1\times6}{3.9\times2}, \text{ then } \alpha = 0.46.$$

Gunning et al.[12] gave a ratio of $\beta/(1-\beta)$ as 1.29 $\exp(-2000/1.987T)$, which is equal to 0.26 at 633 K. This value gives β=0.21. By assuming that γ is also equal to 0.21, we obtained $\Phi_{CH_4}/\Phi_{H_2}=\Phi_{C_2H_4}/\Phi_{H_2}=0.84$ from Eq. 10. This value is in fair agreement with the experimental values (0.72 for Φ_{CH_4}/Φ_{H_2} and 0.78 for $\Phi_{C_2H_4}/\Phi_{H_2}$). DMB is formed from a recombination of isopropyl radical and the steady-state concentration of this radical is probably proportional to the light intensity. This is in agreement with the tendency shown in Fig. 1.

Table 2 shows a comparison of the product formation in zinc-, cadmium-, and mercury-photosensitized decompositions of propane. The dependences of product formation on the time and propane pressure in the zinc-photosensitized decomposition of propane is different from those in the cadmium-photosensitized decomposition, but is similar to those in the mercury-photosensitized decomposition at high temperature. The dissimilarity of the cadmium-photosensitized decomposition to two other photosensitized decompositions can be ascribed to the large difference in the quenching cross section of propane and hydrogen in the case of cadmium ($\sigma_Q(H_2)/\sigma_Q(C_3H_8)$=6.2, 1500, and 3.7, for Zn,[9] Cd,[13] and Hg[14]). It was pointed out that the effect of hydrogen on the decomposition of propane must be important in the cadmium-photosensitized decomposition.[8]

We examined the effect on the product formation of the addition of *cis*-2-butene as a radical scavenger, of which the zinc-photosensitized reaction was studied in detail.[15] When *cis*-2-butene was added to propane, the quantum yields of hydrogen, methane, and ethylene

Table 2. Comparison of Product Formation in Zinc-, Cadmium-, and Mercury-Photosensitized Decomposition of Propane

Dependence on	R_{H_2}			R_{CH_4}/R_{H_2}			$R_{C_2H_4}/R_{H_2}$		
	Zn	Cd[a]	Hg[b]	Zn	Cd[a]	Hg[b]	Zn	Cd[a]	Hg[b]
Time	C(D[c])	I	C	C	D	C	C	D	—
Pressure	I(C[d])	I	I	C	C	—	C	—	—

C; constant, I; increase, D; decrease. a) At 265 °C, Ref. 8. b) At 300 °C, Ref. 1. c) At lower pressures. d) At shorter reaction times.

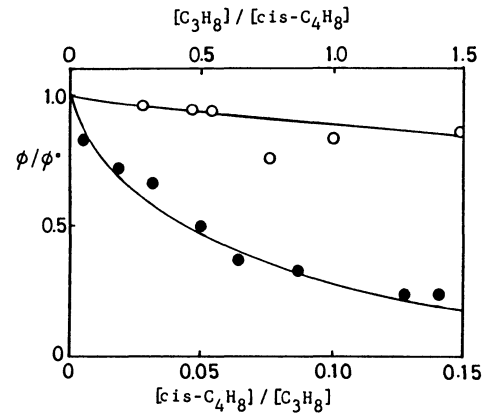

Fig. 6. Plots of $\Phi_{t\text{-}C_4H_8}/\Phi^{\circ}_{t\text{-}C_4H_8}$ against $[C_3H_8]/[cis\text{-}C_4H_8]$ (○), and of $\Phi_{H_2}/\Phi^{\circ}_{H_2}$ against $[cis\text{-}C_4H_8]/[C_3H_8]$ (●).

decreased as the quantum yield of *trans*-2-butene formation increased with an increase in the *cis*-2-butene pressure. Figure 6 shows the effect of *cis*-2-butene on the yield of hydrogen and the effect of propane on the yield of *trans*-2-butene. The following reactions are proposed to explain these effects:

$$Zn(^1S_0) + h\nu(307.6\ nm) \rightarrow Zn(^3P_1) \quad (1)$$
$$Zn(^3P_1) + C_3H_8 \rightarrow ZnH + \alpha 1\text{-}C_3H_7 + (1-\alpha)2\text{-}C_3H_7 \quad (3)$$
$$ZnH \rightarrow Zn(^1S_0) + H \quad (4)$$
$$Zn(^3P_1) + cis\text{-}C_4H_8 \rightarrow Zn\text{-}C_4H_8^* \quad (11)$$
$$H + C_3H_8 \rightarrow H_2 + \beta 1\text{-}C_3H_7 + (1-\beta)2\text{-}C_3H_7 \quad (5)$$
$$H + cis\text{-}C_4H_8 \rightarrow C_4H_9 \quad (12)$$
$$1\text{-}C_3H_7 \rightarrow CH_3 + C_2H_4 \quad (6)$$
$$CH_3 + C_3H_8 \rightarrow CH_4 + \gamma 1\text{-}C_3H_7 + (1-\gamma)2\text{-}C_3H_7 \quad (7)$$
$$Zn\text{-}C_4H_8^* \rightarrow Zn(^1S_0) + \delta trans\text{-}C_4H_8 + (1-\delta)cis\text{-}C_4H_8 \quad (13)$$

In the above, $Zn\text{-}C_4H_8^*$ is a transient triplet addition complex formed between an excited zinc atom and a *cis*-2-butene molecule. The value of δ has been reported to be 0.6 at 633 K.[15] From the above reactions, the quantum yields of *trans*-2-butene and hydrogen can be expressed as follows:

$$\Phi_{t\text{-}C_4H_8} = \delta \frac{k_{11}[cis\text{-}C_4H_8]}{k_3[C_3H_8] + k_{11}[cis\text{-}C_4H_8]} \quad (14)$$

and

$$\Phi_{H_2} = \frac{k_3[C_3H_8]}{k_3[C_3H_8] + k_{11}[cis\text{-}C_4H_8]} \cdot \frac{k_5[C_3H_8]}{k_5[C_3H_8] + k_{12}[cis\text{-}C_4H_8]} \quad (15)$$

Therefore,

$$\frac{\Phi_{t\text{-}C_4H_8}}{\Phi^{\circ}_{t\text{-}C_4H_8}} = \frac{1}{1 + \dfrac{k_3[C_3H_8]}{k_{11}[cis\text{-}C_4H_8]}} \quad (16)$$

and

$$\frac{\Phi_{H_2}}{\Phi^{\circ}_{H_2}} = \frac{1}{1 + \dfrac{k_{11}[cis\text{-}C_4H_8]}{k_3[C_3H_8]}} \cdot \frac{1}{1 + \dfrac{k_{12}[cis\text{-}C_4H_8]}{k_5[C_3H_8]}} \quad (17)$$

Here, $\Phi^{\circ}_{t\text{-}C_4H_8}$ is the quantum yield of *trans*-2-butene in the absence of propane and $\Phi^{\circ}_{H_2}$ is the quantum yield of hydrogen in the absence of *cis*-2-butene.

As has been described previously,[10] the quenching rate of $Zn(^3P_J)$ by alkane depends on the temperature. The values of k_3 and k_{11} at 578 K were reported to be 4.74×10^{-11}[9] and 8.58×10^{-10} ml molecule^{-1} s^{-1}.[15] From the activation energies for the quenching of $Zn(^3P_J)$ by primary and secondary C-H bonds, the k_3-value at 633 K was estimated to be 1.0×10^{-10} ml molecule^{-1} s^{-1}. By assuming that k_{11} is not temperature dependent, the value of k_{11}/k_3 at 633 K can be obtained (k_{11}/k_3=8.58). The upper solid line in Fig. 6 shows the value of $\Phi_{t\text{-}C_4H_8}/\Phi^{\circ}_{t\text{-}C_4H_8}$ calculated by using the above value for k_{11}/k_3. The agreement between the observed and calculated values is fair.

The value of k_5 at 633 K has been estimated to be 2.86×10^{-10} ml molecule^{-1} s^{-1} from the equation $k_5=10^{14.16}\exp(-8350/1.987T)$ ml mol^{-1} s^{-1} reported by Baker et al.[16] Unfortunately, the value of k_{12} at 633 K has not been obtained. We estimated this value as follows: The rate constant at 633 K for the $H + C_2H_4 \rightarrow C_2H_5$ reaction has been estimated to be 3.65×10^{-12} ml molecule^{-1} s^{-1} from the equation $10^{12.9}\exp(-1500/1.987T)$ ml mol^{-1} s^{-1} obtained by Penzhonn and Darwent.[17] If we assume that the ratio of $k_{12}(c\text{-}C_4H_8)/k_{12}(C_2H_4)$ obtained at 298 K by Cvetanovic[18] is independent of temperature, we obtain k_{12}/k_5=10.5. By using this value, we calculated $\Phi_{H_2}/\Phi^{\circ}_{H_2}$ as a function of $[c\text{-}C_4H_8]/[C_3H_8]$. This is shown in Fig. 6 by a solid line. The calculated value of $\Phi_{H_2}/\Phi^{\circ}_{H_2}$ is in fair agreement with the observed one.

Figure 7 shows the pressure dependence of the quantum yield for hydrogen production obtained at irradiation time of 20 min, and Fig. 8 shows the time dependence of the quantum yield obtained at 1700 and 30000 Pa. As mentioned above, the influence of products on the hydrogen yield can not be neglected. Of the products formed, hydrogen and ethylene seem to have large effects because of their large amounts compared with those of other products, their large cross sections for quenching of excited zinc atoms, and their high reactivities to hydrogen atom produced in the initial stage of reaction. The following reactions are considered to explain the pressure and time dependences of the hydrogen yield:

$$Zn(^3P_1) + C_3H_8 \rightarrow ZnH + \alpha 1\text{-}C_3H_7 + (1-\alpha)2\text{-}C_3H_7 \quad (3)$$

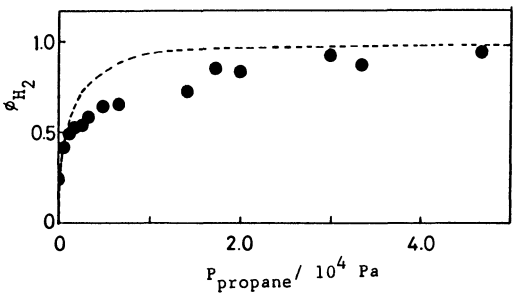

Fig. 7. Pressure dependence of quantum yield of hydrogen.

$$Zn(^3P_1) + H_2 \rightarrow ZnH + H \quad (18)$$
$$Zn(^3P_1) + C_2H_4 \rightarrow Zn\text{-}C_2H_4^* \quad (19)$$
$$ZnH \rightarrow Zn(^1S_0) + H \quad (4)$$
$$H + C_3H_8 \rightarrow H_2 + \beta 1\text{-}C_3H_7 + (1-\beta)2\text{-}C_3H_7 \quad (5)$$
$$H + C_2H_4 \rightarrow C_2H_5 \quad (20)$$

From the above reactions, the rate of hydrogen production can be expressed as follows:

$$R_{H_2} = I_0 \frac{k_3[C_3H_8] + 2k_{18}[H_2]}{k_3[C_3H_8] + k_{18}[H_2] + k_{19}[C_2H_4]} \cdot \frac{k_5[C_3H_8]}{k_5[C_3H_8] + k_{20}[C_2H_4]} \quad (21)$$

Here, we assume that hydrogen and ethylene are produced linearly with time and that their rates are independent of the initial propane pressure as a first approximation (at 20 min 1.8×10^{-6} mol of ethylene and 2.0×10^{-6} mol of hydrogen were obtained, therefore, at 633 K and in the 57 ml reaction cell at irradiation time of t min, $[C_2H_4]=6.3\times10^{14}\ t$ molecule/ml and $[H_2]=7.0\times10^{14}\ t$ molecule/ml). At 633 K and p Pa of propane $[C_3H_8]=1.14\times10^{14}\ p$ molecule/ml. By using following rate constants,

$k_3 = 10.0\times10^{-11}$ ml molecule^{-1} s^{-1},
$k_{18} = 106.6\times10^{-11}$ ml molecule^{-1} s^{-1},
$k_{19} = 121.7\times10^{-11}$ ml molecule^{-1} s^{-1},
$k_5 = 2.86\times10^{-13}$ ml molecule^{-1} s^{-1},

and

$k_{20} = 3.65\times10^{-12}$ ml molecule^{-1} s^{-1},

the rate for hydrogen formation can be rewritten as

$$R_{H_2} = I_0 \frac{1.14p + 14.9t}{1.14p + 15.1t} \cdot \frac{3.26p}{3.26p + 23.0t} \cdot \quad (22)$$

The value of $(1.14p+14.9t)/(1.14p+15.1t)$ is close to unity in the region of the pressure (67—40000 Pa) and time (0—40 min) examined here. Therefore, the quantum yield for hydrogen production can be expressed approximately by

$$\Phi_{H_2} = \frac{\int_0^t R_{H_2}\,dt}{I_0 t} = \frac{\int_0^t \frac{3.26p}{3.26p + 230t}\,dt}{t} = \frac{3.26p}{t} \frac{1}{230} \ln\left(1 + \frac{230t}{3.26p}\right) = \frac{0.0141p}{t} \ln(1 + 70.8\frac{t}{p}). \quad (23)$$

In Figs. 7 and 8, the dashed lines indicate the pressure dependence and the time dependence of the quantum yield of hydrogen calculated according to the above equation. The agreement between the observed and the calculated values is not very good, but the decrease in the quantum yield with decreasing propane pressure and with increasing reaction time could be explained qualitatively by the above treatment regarding the influence of the products.

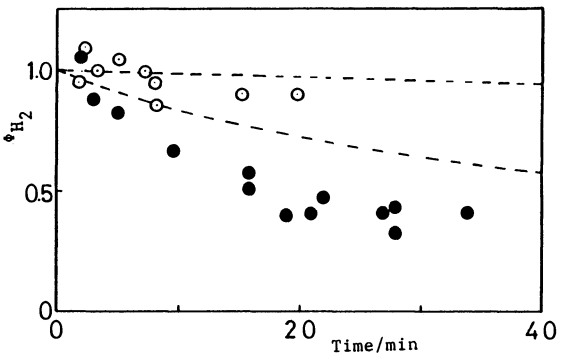

Fig. 8. Time dependence of quantum yield of hydrogen. ○: 30000 Pa, ●: 1700 Pa.

The quantum yield of hydrogen is somewhat smaller than the value predicted from the correlation mentioned above. In this manner, the decrease in the quantum yield of hydrogen must be mainly explained by the influence of ethylene on the production of hydrogen, but partly by other factors. The additional factors may include the influence of propylene and other products which react easily with hydrogen atom. We tried to identify these factors, were not successful. The origin of these factors remains an open question.

References

1) S. Bywater and E. W. R. Steacie, *J. Chem. Phys.*, **19**, 320 (1951).
2) R. A. Back, *Can. J. Chem.*, **37**, 1834 (1959).
3) P. Kebarle and M. Avrahami, *Can. J. Chem.*, **41**, 335 (1963).
4) M. Avrahami and P. Kebarle, *Can. J. Chem.*, **41**, 347 (1963).
5) J. M. Campbell, H. E. Gunning, and O. P. Strausz, *Can. J. Chem.*, **47**, 3763 (1969).
6) J. M. Campbell, O. P. Strausz, and H. E. Gunning, *J. Am. Chem. Soc.*, **95**, 740 (1973).
7) P. Agius and B. de B. Darwent, *J. Chem. Phys.*, **20**, 1679 (1952).
8) R. S. Konar and B. de B. Darwent, *J. Chem. Soc., Faraday Trans. 1*, **74**, 1545 (1978).
9) S. Yamamoto and N. Nishimura, *Bull. Chem. Soc. Jpn.*, **55**, 1395 (1982).
10) S. Yamamoto, *Bull. Chem. Soc. Jpn.*, **61**, 769 (1988).
11) K. O. Kutschike, M. H. J. Wijnen, and E. W. R. Steacie, *J. Am. Chem. Soc.*, **74**, 714 (1952).
12) J. M. Campbell, O. P. Strausz, and H. E. Gunning, *Can. J. Chem.*, **47**, 3759 (1969).
13) W. H. Breckenridge and A. M. Renlund, *J. Phys. Chem.*, **83**, 303 (1979).
14) R. J. Cvetanovic, *Prog. React. Kinet.*, **2**, 39 (1964).
15) S. Yamamoto, N. Nobusada, Y. Sueishi, and N. Nishimura, *J. Photochem.*, **38**, 55 (1987).
16) R. R. Baker, R. R. Baldwin, and R. W. Walker, *Trans. Faraday Soc.*, **66**, 2812 (1970).
17) R. D. Penzhorn and B. de B. Darwent, *J. Chem. Phys.*, **55**, 1508 (1971).
18) K. R. Jennings and R. J. Cvetanovic, *J. Chem. Phys.*, **35**, 1233 (1961).

Molar Volumes and Electrostriction Behavior of Dicarboxylate, Disulfonate, Tartrate, and Bis(ethylenediamine)-glycinatocobalt(III) Ions in Water

Haruhiko YOKOYAMA,* Midori MOCHIDA, and Yuko KOYAMA
Department of Chemistry, Yokohama City University, 22-2 Seto, Kanazawa-ku, Yokohama 236
(Received April 30, 1988)

The ionic partial molar volumes at infinite dilution, V^{∞}(ion), were determined for several dicarboxylate ions, disulfonate ions, tartrate ions, and $[Co(gly)(en)_2]^{2+}$ (gly=glycinate ion and en=ethylenediamine) from density measurements at 25°C. The values of V^{∞}(ion) obtained for the divalent anions generally increased with their van der Waals volumes. Significant differences in V^{∞}(ion) were observed between geometrical isomers with dicarboxylate and disulfonate ions and were attributed to those in both of electrostriction volume and the void space volume around the anions. The former volume was decreased and the latter was increased with increasing distance between two negatively charged groups in the anions. A relatively strong electrostriction behavior of the tartrate ions, compared to the dicarboxylate ions, suggested the presence of an extra electrostriction caused by hydroxyl groups. The electrostriction strength of $[Co(gly)(en)_2]^{2+}$ was significantly large compared to that of $[Ni(en)_3]^{2+}$, rather close to those of $[Cr(en)_3]^{3+}$ and $[Co(en)_3]^{3+}$, and was attributed to the dissymmetrically localized charge distribution in the $[Co(gly)(en)_2]^{2+}$ ion. The effective ionic radii and apparent van der Waals volumes were estimated by using Glueckauf's equation from the ionic partial molar volume and were discussed in comparison with those calculated from the van der Waals increments of atoms.

The ionic partial molar volumes at infinite dilution, V^{∞}(ion), provide useful information about ion-solvent interactions and the effective volumes of ions in solutions,[1] and are helpful for an estimation of the ion-size parameter in the theoretical equations regarding the activity coefficient and molar conductivity of ions.[2] The partial molar volumes of a series of dicarboxylate ions or disulfonate ions are of interest in connection with how the effective ionic volumes and ion-solvent interactions depend on the configuration and conformation of the ions in aqueous solutions. In the present study we measured the densities of aqueous solutions of sodium, potassium, or bis(ethylenediamine)-glycinatocobalt(III) complex salts of the several divalent anions in order to obtain the ionic partial molar volumes at 25 °C. The anions investigated were as follows: oxalate^{2-}, malonate^{2-}, succinate^{2-}, fumarate^{2-}, maleate^{2-}, phthalate^{2-}, 2,6-naphthalenedicarboxylate^{2-} (2,6-NDC^{2-}), (*R*,*R*)-tartrate^{2-}, *meso*-tartrate^{2-}, *o*-benzenedisulfonate^{2-} (*o*-BDS^{2-}), *m*-benzenedisulfonate^{2-} (*m*-BDS^{2-}), 2,6-naphthalenedisulfonate^{2-} (2,6-NDS^{2-}), and 2,7-naphthalenedisulfonate^{2-} (2,7-NDS^{2-}). We discuss the electrostriction volume and the void space (or dead space) around the ion through the effective ionic radius, or the apparent van der Waals volume, estimated from the observed ionic partial molar volume, in connection with the configuration and conformation of the ions in aqueous solutions. The adequacy of using the effective ionic radii for an estimation of the ion-size parameter is also examined.

Experimental

Materials. Chloride, sulfate, malonate, succinate, fumarate, maleate, phthalate, and *meso*-tartrate of $[Co(gly)(en)_2]^{2+}$ were prepared by a double decomposition between the silver salt of anions and the iodide of the complex obtained according a method described in the literature.[3] The oxalate was prepared similarly from the chloride. These salts[4] were recrystallized twice from a water-ethanol mixture and air-dried at room temperature. The numbers of water of crystallization, $n(H_2O)$, were 1.0, 3.0, 0.1, 2.0, 2.0, 2.0, 3.0, 3.7, and 4.9 for chloride, sulfate, oxalate, malonate, succinate, fumarate, maleate, phthalate, and *meso*-tartrate, respectively. The molar extinction coefficients of these complex salts at λ=488 nm were confirmed to be in agreement with one another by studies using a Hitachi 340 spectrophotometer: their average was 97.7±0.2 mol^{-1} dm^{3}cm^{-1}. Potassium oxalate (reagent grade), sodium malonate, sodium succinate, sodium fumarate, and sodium maleate (extra pure grade) were obtained from Wako Pure Chemical Industries, Ltd. and used without further purification; $n(H_2O)$ were 1.0, 0.0, 5.8, 0.0, and 0.2, respectively. Sodium (*R*,*R*)-tartrate (reagent grade) and sodium salts of *m*-BDS^{2-}, 2,6-NDS^{2-}, and 2,7-NDS^{2-} (obtained from the same company) were recrystallized twice from water and air-dried; $n(H_2O)$ were 2.0, 1.6, 0.2, and 3.5, respectively. Potassium salts of *o*-BDS^{2-} and 2,6-NDC^{2-} (obtained from Aldrich Chemical Company, Inc.) were similarly purified and dried; $n(H_2O)$ were 1.0 and 0.0, respectively. The determination of $n(H_2O)$ values was carried out by the dehydration at ca. 150 °C under reduced pressure with an Abderhalden dryer and by the Karl-Fischer method with an AQ-5 Aquacounter of Hiranuma Sangyo Co., Ltd.

Measurements. All aqueous solutions were made by weight. The concentrations of solutions were as follows: 0.0008—0.0045 mol dm^{-3} with sodium and potassium salts of the divalent anions and 0.0003—0.0040 mol dm^{-3} with the salts of $[Co(gly)(en)_2]^{3+}$. The density measurements were carried out at 25 °C by using a vibrating-tube SS-D-200 twin-type densimeter of Shibayama Scientific Co., Ltd. with two external measuring cells immersed in a water bath controlled to 25.00±0.01 °C. The apparatus constants were determined by using water and dry air as standard substances. The errors in the density measurements were usually within 2×10^{-6} g cm^{-3}.

Results and Discussion

The density of a solution, d, can be expressed by the equation:[1]

$$d = d_0 + 10^{-3}[M - d_0 V^\infty(\text{salt})]\, c - 10^{-3} S_v d_0 c^{3/2} - 10^{-3} b_v d_0 c^2, \quad (1)$$

where M is the molecular weight of the solute, c is the molar concentration, d_0 is the density of the solvent, V^∞(salt) is the partial molar volume of the salt at infinite dilution, S_v and b_v are constants. The values of S_v are theoretically given as 9.706 and 14.944 $cm^3 dm^{3/2} mol^{-3/2}$ in water at 25 °C for 2 : 1 or 1 : 2 and 2 : 2 electrolytes, respectively.[1] The values of b_v are usually in the range of −40 to 10 $cm^3 dm^3 mol^{-2}$.[1] The last term including b_v in Eq. 1 can be neglected in this study, since its values are considered to be smaller than 1×10^{-6} $g\,cm^{-3}$ for solutions of concentrations below 0.005 mol dm^{-3}. Thus, we can use the following approximate equation:

$$d + 10^{-3} S_v d_0 c^{3/2} = 10^{-3}[M - d_0 V^\infty(\text{salt})]\, c + d_0. \quad (2)$$

This equation indicates a linear relationship between the left side and the concentration. Using Eq. 2, we analyzed the observed densities.[5] The values of V^∞(salt) were obtained from the linear slope, $10^{-3}[M - d_0 V^\infty(\text{salt})]$, by a least-squares calculation,[8] and are shown in Table 1.[7]

The ionic partial molar volumes of the anions, V^∞(anion), were evaluated in the following way, and are shown in Table 1. The V^∞(anion) values from sodium or potassium salts were obtained by taking $V^\infty(Na^+)$ and $V^\infty(K^+)$ as −6.6 and 3.6 $cm^3 mol^{-1}$, respectively.[1] By subtracting these V^∞(anion) values from V^∞(salt) of the complex salts, the ionic partial molar volumes of $[Co(gly)(en)_2]^{2+}$ were obtained to be 126.7±0.6 $cm^3 mol^{-1}$ (on the average). Subtracting this value from V^∞(salt) with each complex salt, we also obtained the V^∞(anion) values. Significant differences in V^∞(anion) were observed between the geometrical isomers: fumarate^{2-} and maleate^{2-}; o-BDS^{2-} and m-BDS^{2-}; 2,6-NDS^{2-} and 2,7-NDS^{2-}. The V^∞(anion) of an isomer possessing two negatively charged groups (two carboxylato groups or two sulfonato groups) situated more distantly from each other is larger than that of another isomer. We discuss later why such differences arise.

Table 1. Partial Molar Volumes, V^∞(salt) and V^∞(anion), in Water at 25 °C

Salt	(cation)[a]	V^∞(salt) / $cm^3 mol^{-1}$	V^∞(anion) / $cm^3 mol^{-1}$
Chloride	(M^{2+})	172.2±0.4	23.2[b]
Sulfate	(M^{2+})	152.1±0.6	24.8[b]
Oxalate	(K^+)	42.6±0.4	35.4
	(M^{2+})	161.3±0.4	34.6
Malonate	(Na^+)	35.4±0.4	48.6
	(M^{2+})	176.1±0.5	49.4
Succinate	(Na^+)	53.6±0.4	66.8
	(M^{2+})	194.4±0.6	67.7
Fumarte	(Na^+)	54.0±0.4	67.2
	(M^{2+})	192.8±0.4	66.1
Maleate	(Na^+)	46.8±0.4	60.0
	(M^{2+})	187.5±0.5	60.8
Phthalate	(M^{3+})	225.0±0.4	98.3
2,6-NDC	(K^+)	146.9±0.5	139.7
(*R*,*R*)-Tartrate	(Na^+)	55.9±0.4	69.1
meso-Tartrate	(M^{2+})	194.7±0.5	68.0
o-BDS	(K^+)	127.5±0.5	120.3
m-BDS	(Na^+)	113.7±0.8	126.9
2,6-NDS	(Na^+)	160.9±0.5	174.1
2,7-NDS	(Na^+)	159.3±0.4	172.5

a) M^{2+} denotes the $[Co(gly)(en)_2]^{2+}$ ion. b) Ref. 1.

Glueckauf[8] expressed the partial molar volume of a spherical monoatomic ion by

$$V^\infty(\text{ion}) = V^\infty(\text{int}) + V^\infty(\text{el}) = 2.52(r+0.55)^3 - 33 z_i^2/(r+1.38), \quad (3)$$

where r is the crystallographic radius in Å and z_i is the charge number of the ion. V^∞(int) is the molar intrinsic volume of an ion involving a void space (or dead space) around it, and V^∞(el) is the molar electrostriction volume. Assuming that polyatomic anions are approximately spherical, we applied Eq. 3 in order to estimate radius r, which refers (here) to the effective ionic one (represented as r_{ef}(obsd)). The r_{ef}(obsd) values obtained from V^∞(anion) (from their average when plural values are given in Table 1) are shown in Table 2. The differences in V^∞(anion) between the geometrical isomers result in those in r_{ef}(obsd). An isomer that shows a greater deviation from the spherical approximation has a larger r_{ef}(obsd) than that of another isomer. According to Eq. 3, this means that the former isomer has a relatively large V^∞(int) and a small negative V^∞(el), compared to the latter; the V^∞(el) values estimated from Eq.3 are shown in Table 3. The differences in V^∞(el) between the isomers are slight compared to those in V^∞(anion). This indicates that the differences in V^∞(anion) can largely be attributed to those in V^∞(int). The increase of V^∞(int) with a deviation from the spherical shape of the ion is due to that of the effective ionic surface, which results in an increase in the void space volume around the ion.

By using the values of the van der Waals increments of atoms, v_0(atom), given by Edward,[9] we calculated the molar van der Waals volumes of the polyatomic anions, which are shown in Table 2 as V_0(calcd).[10] By assuming

$$V_0(\text{calcd}) = 4\pi N_A r_{ef}(\text{calcd})^3/3,$$

the effective ionic radii, r_{ef}(calcd), were calculated and are shown in Table 2. The r_{ef}(obsd) values are in agreement with those of r_{ef}(calcd) within about 0.1 Å. The apparent molar van der Waals volumes, V_0(app), were estimated from r_{ef}(obsd) by assuming

$$V_0(\text{app}) = 4\pi N_A r_{ef}(\text{obsd})^3/3$$

Table 2. Effective Ionic Radii, r_{ef}(calcd), and r_{ef}(calcd),and Molar van der Waals Volumes, V_0(app) and V_0(calcd), of the Divalent Anions[a)]

Anion		r_{ef}(obsd) Å	r_{ef}(calcd) Å	V_0(app) $cm^3\,mol^{-1}$	V_0(calcd) $cm^3\,mol^{-1}$
Oxalate^{2-}	$(COO^-)_2$	2.46_8	2.41_5	$37._9$	35.5
Malonate^{2-}	$CH_2(COO^-)_2$	2.64_0	2.62_8	$46._4$	45.8
Succinate^{2-}	$(CH_2COO^-)_2$	2.84_4	2.81_1	$58._1$	56.0
Fumarate^{2-}	*trans*-$(CHCOO^-)_2$	2.83_8	2.73_6	$57._6$	51.7
Maleate^{2-}	*cis*-$(CHCOO^-)_2$	2.77_0	2.73_6	$53._6$	51.7
Phthalate^{2-}	*o*-$C_6H_4(COO^-)_2$	3.14_8	3.13_3	$78._7$	77.6
2,6-NDC^{2-}	2,6-$C_{10}H_6(COO^-)_2$	3.49_5	$3.44._9$	$107._7$	103.5
(*R,R*)-Tartrate^{2-}	(*R,R*)-$(CH(OH)COO^-)_2$	2.86_3	2.95_8	$59._2$	65.3
meso-Tartrate^{2-}	*meso*-$(CH(OH)COO^-)_2$	2.85_2	2.95_8	$58._5$	65.3
o-BDS^{2-}	*o*-$C_6H_4(SO_3^-)_2$	3.33_9	(3.33_9)	$93._8$	(93.9)
m-BDS^{2-}	*m*-$C_6H_4(SO_3^-)_2$	3.39_4	(3.33_9)	$98._6$	(93.9)
2,6-NDS^{2-}	2,6-$C_{10}H_6(SO_3^-)_2$	3.74_6	(3.62_1)	$132._6$	(119.8)
2,7-NDS^{2-}	2,7-$C_{10}H_6(SO_3^-)_2$	3.73_5	(3.62_1)	$131._5$	(119.8)

a) Values in the parentheses were obtained by assuming V_0(calcd)=V_0(app) for *o*-BDS^{2-}.

and are shown in Table 2. Although the V_0(app) is not so much different from that of V_0(calcd), the former is, more or less, larger than the latter in each case of the dicarboxylate and disulfonate ions. The positive deviations of V_0(app) from V_0(calcd) generally increase with increasing distance between two negatively charged groups in the anions, due to the expansion of the void space around the ion (as described above). The negative deviation of V_0(app) from V_0(calcd) for the tartrate ions are attributed to the presence of an extra electrostriction volume caused by the hydroxyl groups (not considered by the second term of Eq. 3, which is expressed as a function of the formal charge). This phenomenon is similar to that observed for neutral compounds containing such hydroxyl groups as glucose.[9)]

We assumed the void space volume, V^∞(void), can be expressed by

$$V^\infty(\text{void}) = V^\infty(\text{int}) - V_0(\text{calcd}), \quad (4)$$

and showed the values of V^∞(void) in Table 3. Considerably smaller V^∞(void) of the tartrate ions (derivatives of succinate^{2-}) than that of succinate^{2-}, fumarate^{2-}, or maleate^{2-} supports the presence of an extra electrostriction (as described above). The relatively small V^∞(void) of succinate^{2-}, compared to fumarate^{2-}, are consistent with the fact that the succinate ion exists partly in gauche form about two carboxylato groups in aqueous solutions.[11)] The slightly small V^∞(void) of *meso*-tartrate^{2-}, compared to (*R,R*)-tartrate^{2-}, may be due to the fact that the *meso*-tartrate ion exists predominantly in gauche form.[12)] In order to estimate the overall electrostriction volume for the tartrate ions, we assumed the following equation:

$$V^\infty(\text{el}) = V^\infty(\text{ion}) - 2.52[r_{ef}(\text{calcd}) + 0.55]^3, \quad (5)$$

and obtained the values of $-39._7$ and $-40._8$ $cm^3\,mol^{-1}$ for V^∞(el) of (*R,R*)-tartrate^{2-} and *meso*-tartrate^{2-}, respectively. These values are more negative than V^∞(el) given in Table 3 and by $-9._3$ and $-10._4$ $cm^3\,mol^{-1}$ than $-30._4$ $cm^3\,mol^{-1}$ obtained from V^∞(el) in Eq. 3 by putting r_{ef}(calcd) into r. The procedure concerning Eq. 5 is identical to taking the void space volume of the tartrate ions as $43._5$ $cm^3\,mol^{-1}$, slightly larger than V^∞(void) of succinate^{2-}. Consequently, the above differences in the volumes correspond to extra electrostriction volumes caused by the hydroxyl groups.

Table 3. Elecrostriction Volumes, V^∞(el), and Void Space Volumes, V^∞(void), of the Divalent Anions Obtained by Use of Eqs. 3 and 4[a)]

Anion	V^∞(el) $cm^3\,mol^{-1}$	V^∞(void) $cm^3\,mol^{-1}$
Oxalate^{2-}	$-34._3$	$33._8$
Malonate^{2-}	$-32._8$	$36._0$
Succinate^{2-}	$-31._3$	$42._5$
Fumarate^{2-}	$-31._3$	$46._3$
Maleate^{2-}	$-31._8$	$40._5$
Phthalate^{2-}	$-29._2$	$49._9$
2,6-NDC^{2-}	$-27._1$	$63._3$
(*R,R*)-Tartrate^{2-}	$-31._1(-39._7)$	$34._9(43._5)$
meso-Tartrate^{2-}	$-31._2(-40._8)$	$33._9(43._5)$
o-BDS^{2-}	$-28._0$	$54._4$
m-BDS^{2-}	$-27._7$	$60._7$
2,6-NDS^{2-}	$-25._8$	$80._1$
2,7-NDS^{2-}	$-25._8$	$78._5$

a) Values in the Parentheses were obtained by assuming Eq. 5.

In the same manner as for the divalent anions, we estimated r_{ef}(obsd) and V_0(app) for $[Co(gly)(en)_2]^{2+}$ from its ionic partial molar volume by use of Eq.3. The obtained values are shown in Table 4 and are compared with those estimated for $[Ni(en)_3]^{2+}$, $[Cr(en)_3]^{3+}$, $[Co(en)_3]^{3+}$, and $[Co(NH_3)_6]^{3+}$. Although of the ionic partial molar volume of $[Ni(en)_3]^{2+}$ is considerably larger than those of $[Co(en)_3]^{3+}$ and $[Cr(en)_3]^{3+}$, the r_{ef}(obsd) values of these complex ions are very near to one another (within 0.1 Å). This is consistent with that the crystallographic metal-nitrogen bond lengths are not so largely different from one

Table 4. Partial Molar Volumes, V^{∞}(cation), Effective Ionic Radii, r_{ef}(obsd), Apparent Molar van der Waals Volumes, V_0(app), Difference Volumes, V_0(dif), and Crystallographic Metal-Ligand Bond Lengths, r_c(M-N) and r_c(M-O), of the Complex Ions[a]

Complex Ion	V^{∞}(cation)	r_{ef}(obsd)	V_0(app)	V_0(dif)	r_c(M-N)	r_c(M-O)
	$cm^3\,mol^{-1}$	Å	$cm^3\,mol^{-1}$	$cm^3\,mol^{-1}$	Å	Å
$[Co(gly)(en)_2]^{2+}$	$126._7$	3.39_2	$98._4$	$-9._7$	1.96[d]	1.916[e]
$[Ni(en)_3]^{2+}$	160.3[b]	3.64_9	$122._5$	$12._7$	2.11[f]	
$[Cr(en)_3]^{3+}$	123.1[b]	3.62_3	$120._2$	$10._2$	2.081[g]	
	124.5[c]					
$[Co(en)_3]^{3+}$	119.9[b]	3.58_8	$116._5$	$6._7$	1.978[h]	
	117.6[c]					
$[Co(NH_3)_6]^{3+}$	55.3[b]	3.09_6	$74._9$	$12._5$	1.972[h]	
	56.3[c]					

a) The reference values of V^{∞}(cation) were obtained from V^{∞}(salt) of the chlorides by using V^{∞}(anion) given in Table 1; The values of r_{ef}(obsd), V_0(app), and V_0(dif) for $[Cr(en)_3]^{3+}$, $[Co(en)_3]^{3+}$, and $[Co(NH_3)_6]^{3+}$ were obtained by using the averaged values of V^{∞}(cation). b) Ref. 19 and the value cited therein. c) Ref. 20. d) An average of the values given by Ref. 21. e) Ref. 21. f) An average of the values given by Ref. 22. g) Ref. 23. h) Ref. 16.

another as shown in Table 4. Such agreement suggests that the V^{∞}(el) in Eq. 3 is a good approximate expression of electrostriction for the tris(en) complexes.

The ionic partial molar volume of $[Co(gly)(en)_2]^{2+}$ is significantly smaller than that of $[Ni(en)_3]^{2+}$, rather close to those of $[Cr(en)_3]^{3+}$ and $[Co(en)_3]^{2+}$, the value of r_{ef}(obsd) is considerably smaller than those of the tris(en) complex ions. Accordingly, the value of V_0(app) of $[Co(gly)(en)_2]^{2+}$ becomes smaller by 24 $cm^3\,mol^{-1}$ than that of $[Ni(en)_3]^{2+}$. This difference in V_0(app) is too large to be explained by their molar van der Waals volumes. That is, an extra electrostriction is considered to be present in the case of $[Co(gly)(en)_2]^{2+}$. If the effective ionic radius of $[Co(gly)(en)_2]^{2+}$ can be approximated to be 3.59 Å (obtained for r_{ef}(obsd) of $[Co(en)_3]^{3+}$) the value of V^{∞}(el) is estimated to be -52 $cm^3\,mol^{-1}$ by using Eq. 5; the values of V^{∞}(el) for $[Ni(en)_3]^{2+}$, $[Cr(en)_3]^{3+}$, and $[Co(en)_3]^{3+}$ are calculated to be -26, -59, and -60 $cm^3\,mol^{-1}$, respectively. This means that the V^{∞}(el) value of $[Co(gly)(en)_2]^{2+}$, though a divalent ion, is close to that of $[Cr(en)_3]^{3+}$ or $[Co(en)_3]^{3+}$ rather than $[Ni(en)_3]^{2+}$. The such strong electrostriction is considered to be related to the dissymmetrically localized charge distribution in the $[Co(gly)(en)_2]^{2+}$ ion: the negative charge is on the carboxylato group of glycinato ligand and the positive charge is on the amino groups of ethylenediamine and glycinato ligands. If the $[Co(gly)(en)_2]^{2+}$ ion is regarded as being a dipolar ion (such as an ion pair formed between a trivalent cation and a monovalent anion), we can understand that the ion-solvent interaction of $[Co(gly)(en)_2]^{2+}$ is similar to that of $[Cr(en)_3]^{3+}$ or $[Co(en)_3]^{3+}$ rather than $[Ni(en)_3]^{2+}$. Such a strong interaction of $[Co(gly)(en)_2]^{2+}$ with the solvent is supported by its relatively large Stokes radius, 3.73 Å,[13] compared to 3.13 Å for $[Ni(en)_3]^{2+}$; the former value is in good agreement with 3.73 Å for $[Cr(en)_3]^{3+}$ and 3.72 Å for $[Co(en)_3]^{3+}$.[14]

By using the van der Waals increments of atoms,[9] the molar van der Waals volumes of free ligands can be calculated to be 41.7, 38.6, and 13.7 $cm^3\,mol^{-1}$ for ethylenediamine, glycinate ion, and ammonia, respectively.[15] However, the total volume of ligands constituting the complex ion exceeds the V_0(app) value in each case. This disagreement is due to a neglect of the effective charges on the ligands. It has been known that the central metal atom is largely neutralized by the donation of electrons from the ligating atoms, according to Pauling's electroneutrality rule and the formal charge of the complex ions is largely distributed on the ligand atoms.[16] Thus, assuming the ionicity of each metal-ligand bond to be about 50%, we obtained 36.6, 34.9, and 10.4 $cm^3\,mol^{-1}$ for the molar van der Waals volumes of ethylenediamine, glycinato, and ammine ligands coordinated to the metal atoms, respectively.[17] In Table 4, we show the volume differences, V_0(dif), obtained by subtracting the total volume of the ligands from V_0(app). The negative V_0(dif) for $[Co(gly)(en)_2]^{2+}$ is due to the extra electrostriction described above. The V_0(dif) values for the tris(en) complex ions are $6._7$ to $12._7$ $cm^3\,mol^{-1}$, somewhat larger than 4.9 $cm^3\,mol^{-1}$ for a sphere estimated from 1.25 Å for the metallic bond radii of Cr, Co, and Ni.[18] Such results are thought to be satisfactory, considering that the calculation process involves various assumptions.

Glueckauf's equation (Eq. 3) is valid as a standard expression for the partial molar volume of the ions examined in this study, and is useful for an estimation of their effective ionic radii; the values of r_{ef}(obsd) usually obtained are in agreement with those of r_{ef}(calcd) within about 0.1 Å, though for $[Co(gly)(en)_2]^{2+}$ the former is smaller by about 0.2 Å than the latter. This means that Eq. 3 can be satisfactorily used for an estimation of the ion-size parameter in the theoretical equations of the activity coefficient and molar conductivity of ions.

The authors are gratefully indebted to Professor Kunio Tamaki of Yokohama City University for his helpful advice and suggestions. We would also like to thank Mr. Kiyoshi Yamamoto and Mr. Hiroyuki Kon for their assistance.

References

1) F. J. Millero, *Chem. Rev.*, **71**, 147 (1971); "Water and Aqueous Solutions," ed by R. A. Horne, Wiely-Interscience, New York (1972), Chap. 13.

2) H. Yokoyama, *Bull. Chem. Soc. Jpn.*, **57**, 1304 (1984); H. Yokoyama and M. Nishimura, *ibid.*, **58**, 1094 (1985).

3) C. T. Liu and B. E. Douglas, *Inorg. Chem.*, **3**, 1356 (1964).

4) The $[Co(gly)(en)_2]^{2+}$ ion has been known to be a stable and inert complex in aqueous solutions under usual conditions.[3,21]

5) The tables of the observed densities (d) are deposited as Document No. 8832 at the Office of the Editor of Bull. Chem. Soc. Jpn.

6) The least squares calculation was carried out, including the density of water (d_0=0.997047 g cm^{-3} at 25.0 °C).

7) The effect of hydrolysis of the dicarboxylate ions on V^∞(anion) can be neglected for the following reason. Considering the hydrolysis, the V^∞(anion) can be approximately expressed by:

$V^\infty(\text{anion}) = V^\infty(A^{2-}) + \alpha[V^\infty(HA^-) + V^\infty(OH^-) - V^\infty(A^{2-}) - V^\infty(H_2O)]$,

where A^{2-} is the divalent anion, HA^- is the monoprotonated anion, and α is the fraction of HA^-. The second term in the right side does not exceed 0.1 cm^{3}mol^{-1} since the sum of the values in the brackets is presumed to be 3.2 to 9.5 cm^{3}mol^{-1} from the $V^\infty(OH^-)$ and $V^\infty(H_2O)$ values[1] and the difference between $V^\infty(HA^-)$ and $V^\infty(A^{2-})$ estimated by Eq. 3 and the value of α is considered to be smaller than 0.01 under present conditions from the protonation constants of the dicarboxylate ions.[24]

8) E. Glueckauf, *Trans. Faraday Soc.*, **61**, 914 (1965).

9) J. T. Edward, *J. Chem. Educ.*, **47**, 261 (1970).

10) The values of v_0(atom) in Å^3 used are as follows: 5.6 and 8.1 for the sp^3 and sp^2 carbon atoms, respectively; 5.7, 5.3, and 7.2 for the hydrogen atoms attached to aliphatic and aromatic carbon atoms and oxygen atom, respectively; 6.2, 11.3, and 10.1 for the oxygen atoms, [-O-], [=O] and [-O$^-$], respectively.[9] By using these v_0(atom), the molar van der Waals volume of [-COO$^-$] was estimated to be 17.8 cm^{3}mol^{-1}. That of [-SO$_3^-$] were taken as 26.0 cm^{3}mol^{-1} on the assumption of V_0(calcd)=V_0(app) for o-BDS^{2-} by considering that the V_0(calcd) and V_0(app) values of phthalate^{2-} were close to each other as shown in Table 2, since we had no available v_0(atom) data for the sulfur and oxygen atoms of this group.[9]

11) M. T. Nunes, V. M. S. Gil, and J. Ascenso, *Tetrahedron*, **37**, 611 (1981).

12) J. Ascenso and V. M. S. Gil, *Can. J. Chem.*, **58**, 1376 (1980).

13) H. Yokoyama, K. Yamamoto, and M. Mochida, to be published.

14) Calculated from the ionic molar conductivities given by the literatures: Ref. 25 for $[Ni(en)_3]^{2+}$; Ref. 26 for $[Cr(en)_3]^{3+}$ and $[Co(en)_3]^{3+}$.

15) The values of v_0(atom) for the nitrogen and hydrogen atoms of amino group were taken to be 7.2 and 5.2 Å^3, respectively.[9]

16) Y. Saito, "Inorganic Molecular Dissymmetry," Springer-Verlag, Berlin Heidelberg New York (1979), Chaps. 4 and 5.

17) The values of v_0(atom) for the nitrogen and hydrogen atoms of amino group and the ligating oxygen atom of carboxylato group were assumed to be 5.9, 3.8, and 8.2 Å^3, respectively. These values are the middle ones between those of 7.2, 5.2, and 10.1 Å^3 for the corresponding atoms in free ligands given in Refs. 10 and 15 and those of 4.6, 2.3, and 6.2 Å^3 for the atoms in the ligands of 100% covalent metal-ligand bonding.[9]

18) "CRC Handbook of Chemistry and Physics," 62nd ed, ed by R. C. Weast, CRC Press, Florida (1981).

19) F. Kawaizumi, F. Nakao, and H. Nomura, *J. Solution Chem.*, **14**, 687 (1985).

20) K. Kurotaki and S. Kawamura, *J. Chem. Soc., Faraday Trans. 1*, **77**, 217 (1981).

21) M. Gajhede and S. Larsen, *Acta Crystallogr., Sect. B*, **42**, 172 (1986).

22) Y. I. Smolin, *Soviet Phys. Crystallogr.*, **15**, 23 (1970).

23) K. N. Raymond and J. A. Ibers, *Inorg. Chem.*, **7**, 2333 (1968).

24) A. E. Martell and L. G. Sillén, "Stability Constants," The Chemical Society, London (1964); "Stability Constants," Supplement No. 1, The Chemical Society, London (1971).

25) M. Yokoi, Y. Mori, E. Kubota, and K. Murata, *Nippon Kagaku Zasshi*, **89**, 1192 (1968).

26) T. Takahashi and T. Koiso, *Bull. Chem. Soc. Jpn.*, **49**, 2784 (1976); **51**, 1307 (1978).

 © 1988 The Chemical Society of Japan Bull. Chem. Soc. Jpn., 61, 3451—3454 (1988)

Surface Potential of Mixed Micelles Composed of Prostaglandin B_2 and Heptaethylene Glycol Dodecyl Ether by the Fluorescence Method

Shoko YOKOYAMA,* Akiko KANEKO, and Tadao FUJIE
Kyoritsu College of Pharmacy, 1-5-30, Shibakoen, Minato-ku, Tokyo 105
(Received May 10, 1988)

The surface state of negatively charged mixed micelles prepared by addition of prostaglandin B_2 (PGB_2) to nonionic heptaethylene glycol dodecyl ether (HED) has been investigated and the surface potential ($\Delta\psi$) of the micelles has been estimated by measuring the fluorescence intensity of ammonium 8-anilino-1-naphthalenesulfonate (ANS) as a fluorescent probe. Since the binding constant of ANS, k, is dependent on the surface potential of the micelle, the value of $\Delta\psi$ was determined according to the equation $\Delta\psi=-59.16\log(k_0/k)$ at 25°C, where k_0 is the k of HED micelle. The value of $|-\Delta\psi|$ increases with increasing mole fraction of PGB_2 (X_{PGB_2}) and decreases with increasing ionic strength (J). These changes are due to the effects of the negative charge of PGB_2 and of ionic atmosphere of Na^+, respectively. Surface charge density (σ) was, therefore, determined from $\Delta\psi$ according to the Gouy-Chapman theory, with a result that σ is nearly independent of J and proportional to X_{PGB_2}. These results have led to a conclusion that the state of the diffuse layer surrounding the Stern layer on the micelle surface is represented well by the Gouy-Chapman theory as well as a previous result for the system of sodium dodecyl sulfate (SDS) and HED. The value of $|-\sigma|$ for PGB_2 micelle is less than that for SDS micelle, which suggests that PGB_2 forms a loosely packed micelle.

Regarding physicochemical properties of prostaglandins, critical micelle concentration, tilting angle, the area occupied by a molecule at air-water interface, solubility behavior, and ionization constant have been studied.[1-3] No surface potential of prostaglandin micelle has been determined, except a value[2] of −41 mV for prostaglandin $F_{2\alpha}$ as the maximum surface potential of micelle.

We have been studying the degradation of prostaglandins under such a condition that prostaglandins may form mixed micelles with a nonionic surfactant, heptaethylene glycol dodecyl ether. For accurate analysis of data in relation to catalysis in micellar systems, it is absolutely necessary to know the surface potential of mixed micelles composed of prostaglandins and heptaethylene glycol dodecyl ether.

From these points of view, we have studied the surface potential of mixed micelles composed of prostaglandin B_2 and heptaethylene glycol dodecyl ether, and compared with previous results[4] obtained for mixed micelles composed of sodium dodecyl sulfate and heptaethylene glycol dodecyl ether.

Experimental

Materials. Prostaglandin B_2 (PGB_2) of 99% purity was purchased from Sigma Chemical Company. Heptaethylene glycol dodecyl ether (HED) as a nonionic surfactant and ammonium 8-anilino-1-naphthalenesulfonate (ANS) as a fluorescent probe were the same as those used for a previous study.[4] Mixed micelles composed of PGB_2 and HED were prepared as previously described,[4] and dissolved in a phosphate buffer containing NaH_2PO_4 and Na_2HPO_4 (pH 7.0 with ionic strength 0.02 mol dm^{-3}) when fluorescence intensity was measured. All PGB_2 molecules were considered form mixed micelles with HED, on the basis of a previous result[4] that all sodium dodecyl sulfate (SDS) molecules formed mixed micelles with HED and of the less solubility of PGB_2 than that of SDS in phosphate buffer.

The degradation of PGB_2 at pH 7.0 and 25 °C in course of measurement was considered to be negligible because of its stability described in a previous paper.[1]

Measurement of Fluorescence Intensity. Mixed micelles were dissolved in a phosphate buffer (pH 7.0 with ionic strength 0.02 mol dm^{-3}). The total concentration of PGB_2 and HED was kept constant at 1 mmol dm^{-3}. A solution of ANS as a fluorescent probe was added to solutions of PGB_2 and HED up to 5×10^{-5} mol dm^{-3}. The fluorescence intensity was measured by use of a Hitachi F-4000 spectrofluorometer equipped with a pump-circulating water at a constant temperature through an outer tube. The temperature of the thermostat was maintained at 25±0.2 °C. The wavelength of excitation and emission are 360 and 480 nm, respectively. The measured fluorescence intensity was corrected as described in a previous paper.[4] Sodium chloride was used to control the ionic strength of buffer solution.

Results

Fluorescence Intensity. The relationship between the corrected fluorescence intensity, F, and the concentration of ANS, D, is shown in Fig. 1. As can be seen in Fig. 1, the plot of F vs. D is linear.

Adsorption of ANS on Micelle Surface. It is considered that fluorescence intensity is proportional to the amount of ANS adsorbed on micelle surface, because ANS fluoresces when adsorbed on micelle surface. The Langmuir adsorption isotherm can, therefore, be applied. The equation may be written as

$$\Gamma = \frac{D_m}{C} = \frac{\Gamma_s k D_f}{1+kD_f}\ , \qquad (1)$$

where Γ is the adsorbed amount of ANS per mole of micelle, Γ_s is the saturated adsorbed amount, k is the association constant related to the strength of adsorption, C is the total concentration of PGB_2 and HED which are in the form of micelle, D_m is the concentration of bound ANS, and D_f is the concentration of free

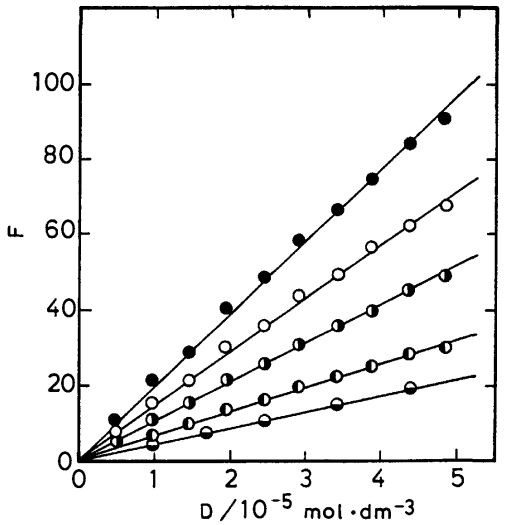

Fig. 1. Relationship between fluorescence intensity with correction and concentration of ANS. Mole fraction of PGB_2: ●; 0 (HED only), ○; 0.2, ◑; 0.4, ◐; 0.6, ◒; 0.8. Total concentration of PGB_2 and HED: 1 mmol dm^{-3}. Ionic strength: 0.02 mol dm^{-3}.

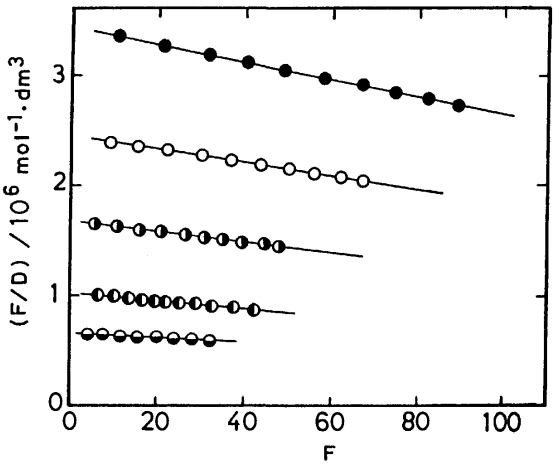

Fig. 2. Langmuir plots of F/D vs. F. Mole fraction of PGB_2: ●; 0 (HED only), ○; 0.2, ◑; 0.4, ◐; 0.6, ◒; 0.8. Total concentration of PGB_2 and HED: 1 mmol dm^{-3}. Ionic strength: 0.02 mol dm^{-3}.

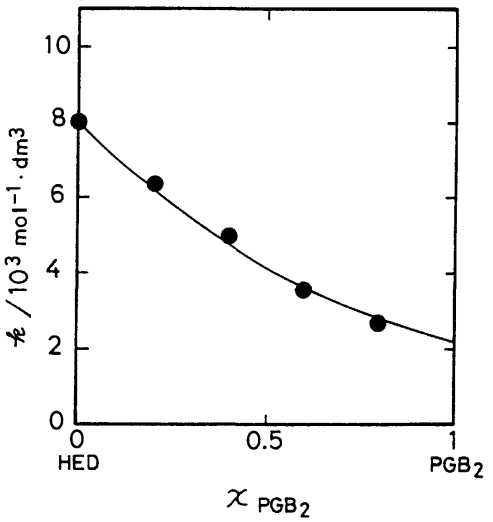

Fig. 3. Relationship between k and mole fraction of PGB_2. Total concentration of PGB_2 and HED: 1 mmol dm^{-3}. Ionic strength: 0.02 mol dm^{-3}.

ANS; $D=D_m+D_f$. Fluorescence intensity F is related to D_m by

$$F=fD_m, \tag{2}$$

where f is the fluorescence coefficient of ANS.

F_∞ is defined by

$$F_\infty=\lim_{D\to\infty} F=Cf\Gamma_s. \tag{3}$$

Equation 4 is, therefore, derived from Eqs. 1—3:

$$\frac{1}{F_\infty-F}=k\left(\frac{D}{F}-\frac{1}{f}\right). \tag{4}$$

Under our experimental conditions, D is sufficiently large. Therefore, Eq. 4 is reduced to

$$\frac{F}{D}=k(F_\infty-F). \tag{5}$$

Plots of F/D against F are presented in Fig. 2, which show a good linear relationship in accord with Eq. 5. From the values of slope and intercept, k and F_∞ are evaluated.

Values of F_∞ and k. The values of F_∞ are 439, 400, 351, 306, and 270 for the samples whose mole fractions of PGB_2 are 0 (HED alone), 0.2, 0.4, 0.6, and 0.8, respectively. The value of F_∞ decreased with increasing mole fraction of PGB_2. This is because the value of F_∞ depends on the concentration of HED, as described in a previous paper.[4]

Values of k are shown in Fig. 3 against the mole fraction of PGB_2. The value of k decreased with increasing mole fraction of PGB_2. This is due to the electrostatic repulsion between PGB_2 and ANS on the micelle surface. The value of k for HED obtained in this paper is consistent well with the value for HED obtained in a previous paper[4] at the same ionic strength, so that the results obtained in this paper may be taken to be reasonable.

Discussion

Surface Potential of Micelles. On the assumption described in a previous paper,[4] the binding constant of ANS to HED-PGB_2 mixed micelles, k, depends on the surface potential of the micelle, $\Delta\psi$. The relation is, therefore, written as

$$k=k_0\exp(-zF_A\Delta\psi/RT), \tag{6}$$

where z is the valency of ANS, F_A is the Faraday constant, R is the gas constant, and k_0 is the k for nonionic HED micelle. By substituting $z=-1$, $F_A=e\cdot N_A=9.648\times10^4$ (C mol^{-1}), $R=k_BN_A=8.314$ (J mol^{-1}K^{-1}), and $T=298.15$ K at 25 °C, we obtain

$$\Delta\psi = -59.16 \cdot \log \frac{k_0}{k} \quad (7)$$

The surface potential of the micelle, $\Delta\psi$, as calculated from the values of k shown in Fig. 3 by using Eq. 7, is plotted with closed circles against the mole fraction of PGB_2 in Fig. 4. To investigate the effect of ionic strength on the surface potential of the micelle, experiments were carried out with buffer solutions containing sodium chloride so that their ionic strengths are 0.06 and 0.20 mol dm^{-3} as well as 0.02 mol dm^{-3}, plots of $\Delta\psi$ against the mole fraction of PGB_2 being shown by symbols ◑ and ○ in Fig. 4.

No micelles composed of PGB_2 molecules alone are formed under these experimental conditions that the total concentration of PGB_2 and HED is 1 mmol dm^{-3}. The critical micelle concentration of PGB_2 is about 6 mmol dm^{-3}.[1] The surface potential of PGB_2 micelle is, therefore, obtained by extrapolation of the theoretical curve based on the Gouy-Chapman equation, which will be described in a later section. The surface potential of PGB_2 micelle thus obtained at ionic strength 0.02 mol dm^{-3} is −33 mV. This value |−33 mV| for PGB_2 micelle is less than the value[4] |−73 mV| for SDS micelle at the same ionic strength, which suggests that PGB_2 forms a loosely packed micelle.

The surface potential of the micelle becomes more negative with increasing mole fraction of PGB_2. On the other hand, the surface potential of the micelle, $|-\Delta\psi|$, becomes smaller as the ionic strength is increased by adding sodium chloride. These changes may be considered due to the effects of the negative charge of PGB_2 and of ionic atmosphere of Na^+, respectively.

Surface Charge Density of Micelles. According to the Gouy-Chapman theory, the relation between surface potential, $\Delta\psi$, and surface charge density, σ, is expressed as

$$\frac{\sigma}{\mathrm{C \cdot cm^{-2}}} = -5.8673 \times 10^{-6} \sqrt{\sum_i \left[\left(\frac{C_i}{\mathrm{mol \cdot dm^{-3}}} \right) \left\{ \exp\left(-0.03892\, z_i \frac{\Delta\psi}{\mathrm{mV}} \right) - 1 \right\} \right]}, \quad (8)$$

where 78.54[5] is used as the value for the relative dielectric constant of water at 25 °C. The relationship between surface charge density and the mole fraction of PGB_2 is shown in Fig. 5, The value of σ was found proportional to X_{PGB_2}, and thus the relation can be written as

$$\sigma = -1.044 \times 10^{-6} \cdot X_{PGB_2}. \quad (9)$$

By using this relation and Eqs. 7 and 8, theoretical values of the surface potential of the micelles and the binding constant were calculated, the results being shown in Figs. 3 and 4 by solid lines, respectively.

On the other hand, the surface charge density, σ, was found nearly independent of ionic strength.

These results indicate that the state of the diffuse layer surrounding the Stern layer on the micelle surface is represented well by the Gouy-Chapman theory as well as a previous result[4] obtained for the system of sodium dodecyl sulfate and HED.

Dissociation Degree of Micelles. The relationship

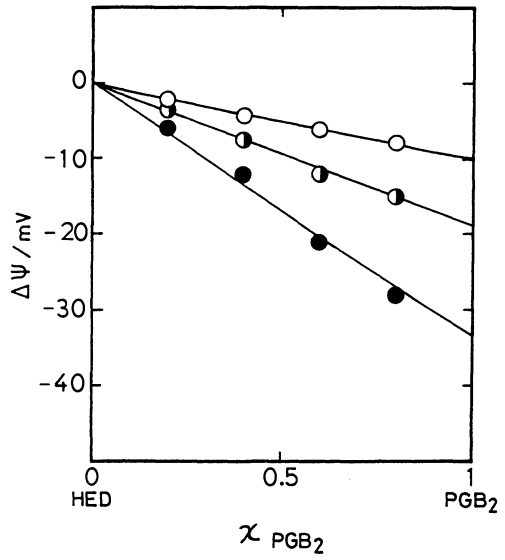

Fig. 4. Effect of ionic strength on the plots of surface potential of micelle, $\Delta\psi$, vs. mole fraction of PGB_2. Ionic strength: ●; 0.02, ◑; 0.06, ○; 0.20 mol dm^{-3}. Total concentration of PGB_2 and HED: 1 mmol dm^{-3}. Solid lines: theoretical curves by the Gouy-Chapman equation for $\sigma = -1.044 \times 10^{-6} \cdot X_{PGB_2}$ C cm^{-2}.

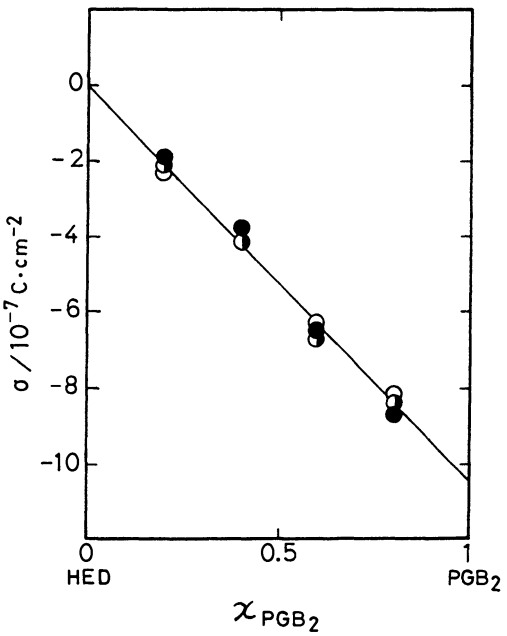

Fig. 5. Effect of ionic strength on the plots of surface charge density of micelle, σ, vs. mole fraction of PGB_2. Ionic strength: ●; 0.02, ◑; 0.06, ○; 0.20 mol dm^{-3}. Total concentration of PGB_2 and HED: 1 mmol dm^{-3}.

between surface charge density, $|\sigma|$, and dissociation degree, α, of micelles can be expressed by

$$\alpha = \frac{|\sigma| \cdot A}{X_{PGB_2} \cdot e}, \quad (10)$$

where A is the area occupied by a PGB_2 molecule, and $e=1.6021\times10^{-19}$ C. The area occupied by a PGB_2 molecule has been reported to be 54 Å^2 [1] as a value for maximum compression. A value of 80 Å^2 has been derived from a 3-dimensional model of prostaglandin molecule.[2,3] If a calculation is developed for the system of PGB_2 and HED in terms of these values (54—80 Å^2), the dissociation degree of PGB_2 in HED micelle is approximately 4—5%. The value of dissociation degree is found nearly independent of the mole fraction of PGB_2. This value ($\alpha\fallingdotseq4.5\%$) is a bit smaller than those obtained for sodium dodecyl sulfate in HED micelle (α=10%,[4] 8%[6]), so that the results obtained in this paper may be taken to be quite reasonable.

Effect of Electrolyte on the Surface Potential of Micelles. To investigate the effect of electrolyte on the surface potential of the micelle in a little more detail, experiments at various ionic strengths were carried out for a mixed micelle composed of PGB_2 and HED at X_{PGB_2}=0.6, the results being shown in Fig. 6. As shown in Fig. 6, the surface potential of the micelle, $|-\Delta\psi|$, becomes smaller as the ionic strength is increased by adding sodium chloride. By using the value of σ defined by Eq. 9 and the equation of Gouy-Chapman, theoretical values of the micellar surface potential are calculated, and represented by the solid line in Fig. 6. Thus, the relationship between ionic strength and micellar surface potential was found to be represented well by the Gouy-Chapman theory.

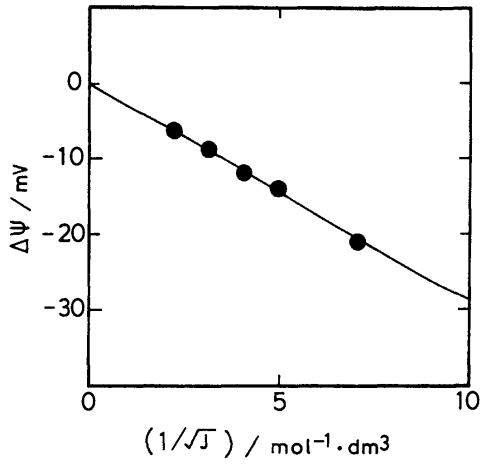

Fig. 6. Effect of ionic strength on surface potential of micelle composed of PGB_2 and HED at X_{PGB_2}=0.6. Total concentration of PGB_2 and HED: 1 mmol dm^{-3}. Solid line: theoretical curve by the Gouy-Chapman equation for $\sigma=-6.263\times10^{-7}$ C cm^{-2}.

Conclusion

The surface potential of mixed micelles composed of PGB_2 and HED has been determined by the fluorescence method.

The surface potential of the micelle, $|-\Delta\psi|$, increases with increasing mole fraction of PGB_2 (X_{PGB_2}), and decreases with increasing ionic strength. The surface state of the micelles is, therefore, represented well by the Gouy-Chapman theory. The value of $|-\Delta\psi|$ for PGB_2 micelle is less than that for sodium dodecyl sulfate micelle at the same ionic strength, which suggests that PGB_2 forms a loosely packed micelle.

References

1) S. Yokoyama, T. Kimura, M. Nakagaki, O. Hayaishi, and K. Inaba, *Chem. Pharm. Bull.*, **34**, 455 (1986).

2) T. J. Roseman and S. H. Yalkowsky, *J. Pharm. Sci.*, **62**, 1680 (1973).

3) M. C. R. Johnson and L. Saunders, *Biochim. Biophys. Acta*, **218**, 543 (1970).

4) M. Nakagaki, S. Yokoyama, and I. Yamamoto, *Nippon Kagaku Kaishi*, **1982**, 1865.

5) "Kagaku Binran," ed by Nippon Kagaku Kai, Maruzen, Tokyo (1966), p. 1005.

6) M. Nakagaki and S. Yokoyama, *Chem. Pharm. Bull.*, **33**, 2654 (1985).

 © 1988 The Chemical Society of Japan Bull. Chem. Soc. Jpn., 61, 3455—3459 (1988)

Crystal Structures and Electrical Properties of $TSeC_n$-TTF (n=2 and 4)

Ping WANG, Takehiko MORI, Chikako NAKANO, Yusei MARUYAMA, Hiroo INOKUCHI,* Naoko IWASAWA,† Hideki YAMOCHI,† Hatsumi URAYAMA,† and Gunzi SAITO†

Institute for Molecular Science, Myodaiji, Okazaki 444

†The Institute for Solid State Physics, The University of Tokyo, Roppongi, Tokyo 106

(Received May 16, 1988)

An organic compound $TSeC_n$-TTF [tetrakis(alkylseleno) tetrathiafulvalenes] with n=2, crystallizes in the monoclinic space group $P2_1/a$, a=23.218(5), b=8.960(3), c=10.489(3) Å, β=96.61(2)°, V=2168(1) Å^3, and Z=4; the compound with n=4 crystallizes in the triclinic space group $P\bar{1}$, a=9.198(1), b=10.539(2), c=8.248(2) Å, α=113.16(2), β=96.02(2), γ=90.61(2)°, V=729.9(3) Å^3 and Z=1. The molecule with n=2 has a bent structure, like a boat; and the molecule with n=4 has a structure in which each of the four alkyl chains is stretched towards different directions. The temperature dependence of electrical resistivity and the charge-carrier mobility have been measured, and the resistivities at room temperature are $\rho_a/\rho_b/\rho_c$=3.3×10^9/2.0×10^9/6.0×10^{11} and 2.2×10^{11}/1.0×10^{11}/1.3×10^{11} (Ω cm) for $TSeC_2$-TTF and $TSeC_4$-TTF, respectively. The quite isotropic character in the resistivities of a $TSeC_4$-TTF crystal may originate from its rather strange molecular structure.

Nowadays relatively high conductivities have been realized even in one-component organic materials under the presence of the columnar structures with the effective overlaps of π orbitals between molecules.[1] The physicochemical studies on the organic materials with long alkyl chains, such as TTC_n-TTF, $TTeC_n$-TTF, and $TSeC_n$-TTF (n=1—18)[2-4] have been widely carried out. A new function named as "molecular fastener effect" has been found. Comparing with TTC_n-TTF and $TTeC_n$-TTF, the electrical and thermal properties of $TSeC_n$-TTF series for large n ($n\geqq 8$) are similar to those of TTC_n-TTF and $TTeC_n$-TTF, in which the intermolecular interactions associated with alkyl chains play an important role. For the compounds with small n ($n\leqq 7$), the electrical and thermal properties of $TSeC_n$-TTF series are just in between TTC_n-TTF and $TTeC_n$-TTF series, in which the intermolecular interactions between chalcogen atoms and between C_6S_4 parts play an important role. In the present paper, we report the results of the single crystal X-ray structure analysis, the electrical conductivities and the charge-carrier mobilities of $TSeC_n$-TTF with n=2 and 4.

Experimental

Single crystals of $TSeC_2$-TTF and $TSeC_4$-TTF were prepared by a slow cooling method in a hexane solution. Dark yellow $TSeC_2$-TTF crystals were grown in a plate-like form after several days. For $TSeC_4$-TTF keeping the solution in a refrigerator for several days, dark red crystals were obtained in a block-like form.

The crystal structure analysis was carried out with a Rigaku automated four-circle X-ray diffractometer AFC-5R and AFC-5 for $TSeC_2$-TTF and $TSeC_4$-TTF, respectively. For the compound of $TSeC_2$-TTF the crystal data is: $C_{14}H_{20}S_4Se_4$, F.W. 631.84, monoclinic, space group $P2_1/a$, a=23.218(5), b=8.960(3), c=10.489(3)Å, β=96.61(2)°, V=2168(1)Å^3, Z=4, D_x=1.937 g cm^{-3} and μ(Mo $K\alpha$)=70.671 cm^{-1}. Intensity data were measured by the θ-2θ scan technique on the diffractometer with graphite monochromatized Mo $K\alpha$ radiation ($2\theta<60°$). The structure was solved by the direct method using MULTAN 78 program system[5] and refined by the block-diagonal least-squares procedure using 1354 independent reflections $|F_o|>3\sigma(|F_o|)$. After absorption correction the refinement was limited to a final R value of 0.079. Anisotropic thermal parameters were adopted for all nonhydrogen atoms, and the hydrogen atoms were refined isotropically. For the compound of $TSeC_4$-TTF, the crystal data is: $C_{22}H_{36}S_4Se_4$, F.W. 743.84, triclinic, space group $P\bar{1}$, a=9.198(1), b=10.539(2), c=8.248(2) Å, α=113.16(2), β=96.02(2), γ=90.61(2)°, V=729.9(3)Å^3, Z=1, D_x=1.69 g cm^{-3}, μ(Mo $K\alpha$)=52.609 cm^{-1}. Intensity data were measured by the θ-2θ scan technique on the diffractometer with graphite monochromatized Mo $K\alpha$ radiation ($2\theta<60°$). The structure was solved also by the direct method using MULTAN 78 program system[5] and refined by the block-diagonal least-squares procedure using 2743 independent reflections $|F_o|>3\sigma(|F_o|)$. The refinement was limited to a final R value of 0.065. Anisotropic thermal parameters were adopted for all nonhydrogen atoms, and the hydrogen atoms were refined isotropically.[10]

The electrical resistivities were measured by a two probe method from room temperature to just above the each melting point under a vacuum of 10^{-4} Pa to avoid an oxidation effect. The electrical contacts to the specimen crystals were made with gold paint. The mobilities were measured by a time-of-flight method for charge carriers generated by irradiation from a pulsed nitrogen laser.

Results and Discussion

$TSeC_2$-TTF. The atomic coordinates are listed in Table 1. The crystal structure is shown in Figs. 1 and 2. Along the a axis, the $TSeC_2$-TTF molecules are stacked with overlapping as shown in Fig. 2(b), where the distance between the two C_2S_4 molecular planes is 3.41 Å. The shortest intermolecular S-S contact is 3.72(1) Å (Fig. 1b) which is a little longer than the sum of the van der Waals radii (3.70 Å). The shortest intermolecular S-Se contact is 3.804(8) Å, which is a little shorter than the sum of the van der Waals radii (3.85 Å). Along the c axis the shortest intermolecular Se-Se distance between the neighboring two molecules is 3.618(5) Å, which is much shorter than the sum of the van der Waals radii (4.00 Å) (Fig. 1). The molecule has a bent structure like a boat (Figs. 3(a) and(b)), and

Table 1. Positional Parameters and Equivalent Isotropic Thermal Parameters of $TSeC_2$-TTF

Positional parameters (×10**4) and equivalent isotropic temperature factors (HAMILTON, 1959).

	X	Y	Z	B_{eq}(Å**2)
Se1	9937(1)	1810(1)	8555(1)	4.6
Se2	7411(1)	4346(1)	9888(1)	4.6
S3	5178(2)	2146(1)	6995(2)	4.0
S4	7266(2)	−74(1)	6068(2)	3.8
C5	7921(6)	1566(5)	7623(7)	3.1
C6	5507(5)	441(5)	5641(7)	3.2
C7	6997(6)	2549(5)	8026(7)	3.3
C8	10488(6)	−89(6)	7636(8)	3.8
C9	12062(6)	−167(7)	8327(8)	4.0
C10	12546(7)	−1643(7)	7538(10)	5.1
C11	6875(7)	5454(6)	8516(9)	4.8
C12	7923(8)	5531(7)	7161(10)	5.7
C13	14124(8)	−1777(9)	8139(11)	6.5
C14	7466(10)	6258(8)	6212(11)	7.5
C15	8458(9)	6208(9)	4839(12)	7.1

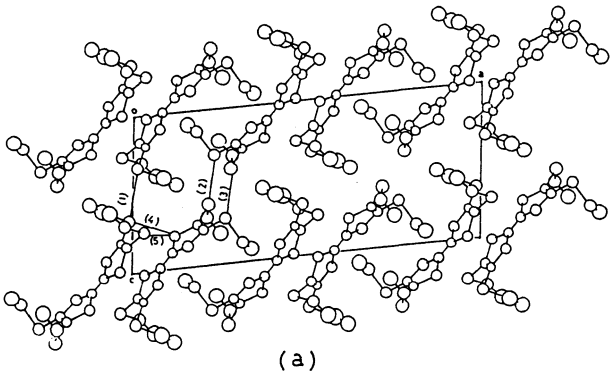

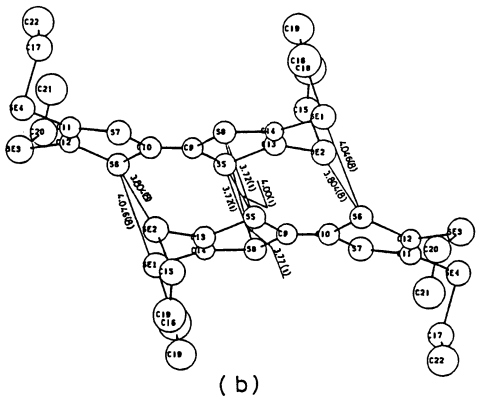

Fig. 1. Crystal structure of $TSeC_2$-TTF projected along the b axis (a) and the intermolecular interactions between two molecules along the a axis (b). [(1) 3.618(5), (2) 3.618(5), (3) 3.618(5), (4) 4.046(5), (5) 3.804(5)].

the dihedral angles between the optimal plane of the central C_2S_4 part and the planes of the two C_2Se_2 part are 8.5(2) and 12.0(2)°, respectively. The terminal Se-C-C bonds are strongly bent towards the central

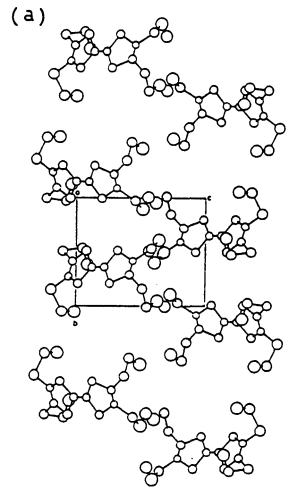

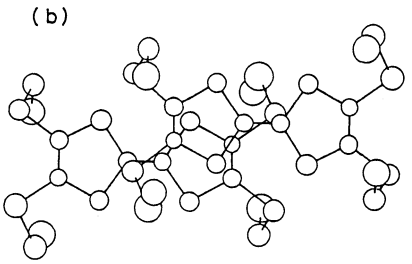

Fig. 2. Crystal structure of $TSeC_2$-TTF projected along the a axis(a) and the mode of overlaps of $TSeC_2$-TTF along the a axis (b).

plane and the molecules are overlapped along the stacking axis a.

The resistivities at room temperature are 3.3×10^9, 2.0×10^9, and 6.0×10^{11} (Ω cm) along the a, b, and c axis, respectively. The resistivity along the a axis is the same order as that along the b axis. The anisotropy between a or b and c directions is not so large, about 10^2, because of the absence of a special direction for easy electrical conduction. According to the crystal structure, it can be understood clearly. The easier axis for electrical conduction (ρ_a) corresponds to the stacking direction of C_6S_4 moiety (parallel to the a-axis), while the harder axis corresponds to the c-axis, where is almost no stacking but exist short Se-Se contacts (3.618(5)Å). These two factors give rise to the rather small anisotropy of about 10^2. Along the b-axis, adjacent $TSeC_2$-TTF molecules are arranged side by side which leads to about the same magnitude of ρ_b as ρ_a. The temperature dependence of the electrical resistivity along the a axis is shown in Fig. 4, in which the resistivity decreases with the temperature increase until the melting point, with an activation energy $E_a=3.7\times10^{-1}$ (eV).

Mobility measurements for single crystals at room temperature have indicated that the electron and hole mobilities along the c axis are $\mu_c^e=1.7$ cm^2 V^{-1} s^{-1} and

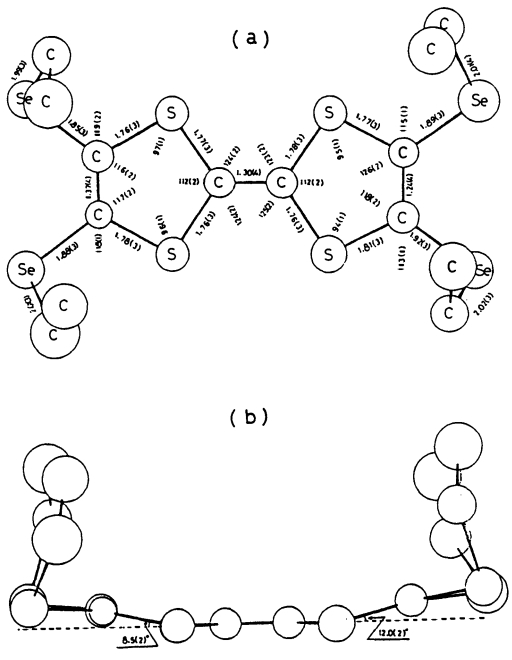

Fig. 3. Molecular structure of $TSeC_2$-TTF (a) and the side view (b).

μ_c^h=1.4 $cm^2 V^{-1} s^{-1}$, respectively. Taking into account of the resistivity data, we can estimate fairly high mobilities along the a or b axis. The charge-carrier mobilities in an anthracene crystal are 0.3 and 1.5 $cm^2 V^{-1} s^{-1}$ along the c and a or b axis, respectively. Comparing these values with the present data, we can conclude that the effect of chalcogen atoms is still important in $TSeC_2$-TTF crystals.

$TSeC_4$-TTF. The atomic coordinates are listed in Table 2. The crystal structure is shown in Fig. 5. The stacking axis with respect to the central molecular planes is c axis, along which the distance between the two molecular planes is as far as 4.82 Å, because the two isobutyl chains, which are just between the two molecular planes, are directed up and down from the optimal plane of the central S_4C_6 part, as shown in Figs. 5(b) and 6(b). The intermolecular interactions between adjacent C_6S_4 moieties are weak and can be described in terms of the van der Waals interactions because of the absence of discernible intermolecular overlaps between adjacent π systems. Therefore, the high resistivity along the stacking c axis can be understood by taking account of this fact. Along the b and a axis the interaction between two molecules is still rather weak, Fig. 5(c), so that no good conducting path can be formed in any direction. The distances between Se-Se, Se-S, Se-C, S-S, S-C, and C-C are all longer than the sum of van der Waals radii.

In the TYC_n-TTF family the $TSeC_4$-TTF molecule gives a quite special structure, neither of the chair nor boat form, in which the four isobutyl chains are almost perpendicular to each other. Such kind of molecular shape may lead to three dimensionally isotropic molecular packing form. Actually the electrical

Table 2. Posional Parameters and Equivalent Isotropic Thermal Parameters of $TSeC_4$-TTF

Positional parameters (X10**4)and equivalent isotropic temperature factors (HAMILTON, 1959).

	X	Y	Z	B_{eq}(Å**2)
Se1	115(1)	4730(3)	3332(3)	5.0
Se2	−327(1)	8455(3)	2516(3)	4.8
Se3	2188(1)	8526(3)	−3900(3)	6.0
Se4	2667(1)	4954(3)	−2918(3)	4.9
S5	359(3)	7979(7)	175(6)	3.7
S6	1234(3)	7994(7)	−2086(7)	4.3
S7	1602(3)	4960(7)	−1375(7)	4.2
S8	741(3)	4920(6)	861(6)	3.9
C9	830(8)	6457(22)	−83(20)	2.5
C10	1167(8)	6482(22)	−1006(23)	3.2
C11	2050(10)	5968(24)	−2280(19)	3.1
C12	1817(10)	7323(28)	−2645(21)	3.9
C13	169(9)	7220(25)	1649(25)	3.8
C14	337(8)	5885(25)	1984(21)	2.8
C15	246(10)	10096(28)	2987(28)	5.0
C16	895(14)	4049(40)	4140(32)	8.2
C17	3203(13)	4745(27)	−1230(28)	5.7
C18	730(16)	9613(32)	3919(34)	8.4
C19	1258(13)	5144(40)	4571(30)	8.4
C20	2128(11)	10596(29)	−3162(28)	5.8
C21	2554(16)	10670(42)	−2007(30)	9.3
C22	3418(14)	6219(32)	−725(34)	8.1

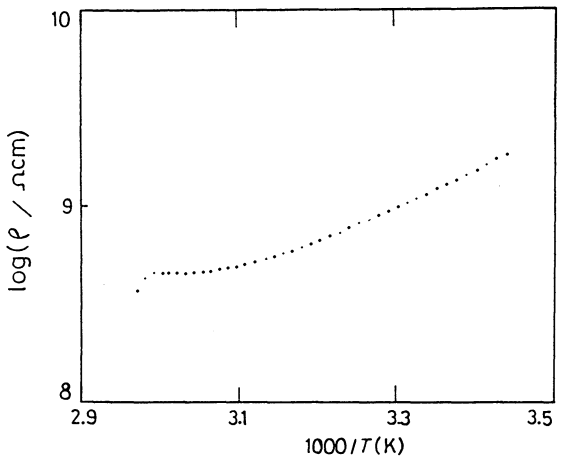

Fig. 4. The temperature dependence of electrical resistivity along the a axis for $TSeC_2$-TTF.

resistivities appear as 2.2×10^{11}, 1.0×10^{11}, and 1.3×10^{11} Ω cm along the a, b, and c axis, respectively, which clearly shows the isotropic character.

Therefore, in $TSeC_n$-TTF system both the physical properties[4] and the molecular packing form have been much influenced by the length of alkyl chains and the chalcogen atoms. The higher resistivity of $TSeC_4$-TTF can be understood with the crystal structure. The shortest Se-Se distance, 4.03 Å, is considerably longer as compared with 3.618(5) Å in $TSeC_2$-TTF and the interplanar distance (4.82 Å) between C_6S_4 parts is also much longer than 3.41 Å in $TSeC_2$-TTF. The quite different physical properties between $TSeC_2$-TTF and $TSeC_4$-TTF can be ascribed to the different molecular

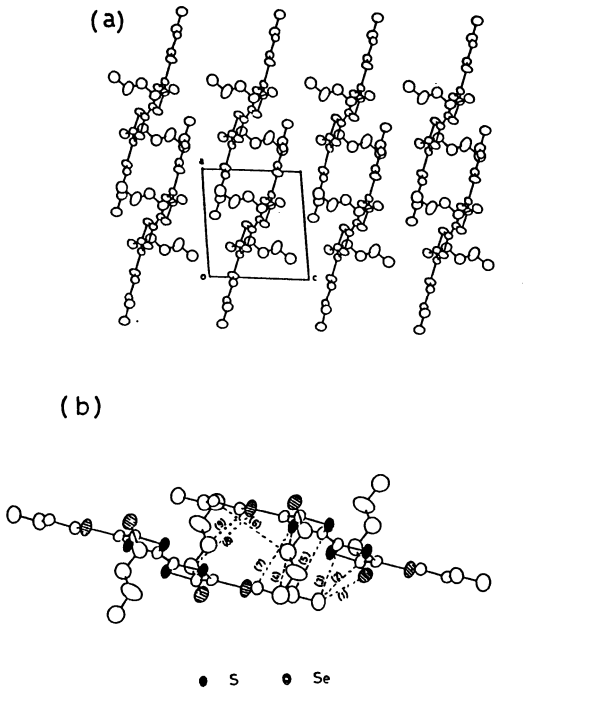

(1) C-Se 3.98(1) (4) C-S 3.844(7) (7) C-S 3.918(7)
(2) C-C 3.80(1) (5) C-C 3.90(1) (8) C-Se 3.947(6)
(3) C-C 3.93(1) (6) C-C 3.95(1) (8) C-Se 3.931(6)

Fig. 5. Crystal structure of $TSeC_4$-TTF projected along the b axis (a), the intermolecular interactions between two molecules along the c axis (b) and the crystal structure of $TSeC_4$-TTF projected along the c axis (c).

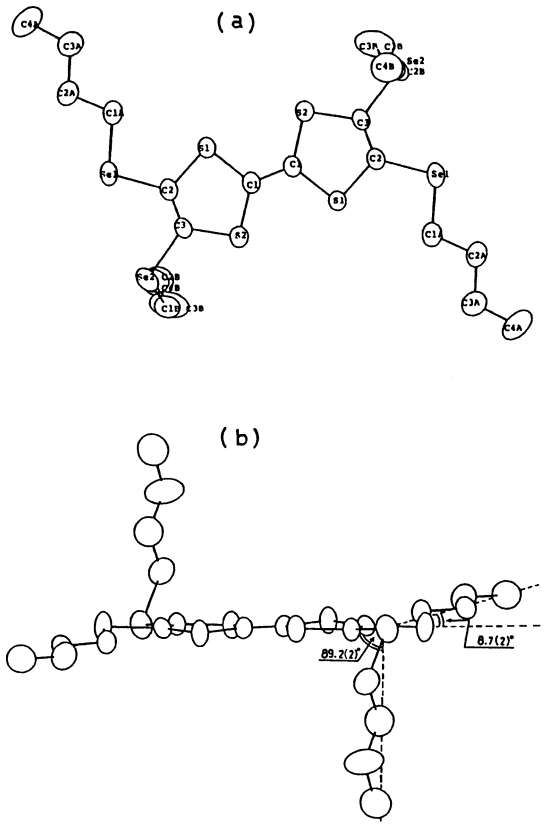

Fig. 6. Molecular structure of $TSeC_4$-TTF (a) and the side view (b). The interatomic distances and angles are shown in Table 3.

Table 3. The Interatomic Distances and Angles in the $TSeC_4$-TTF Compound

Distance (Å)			
C1-C1	1.362(6)	C1-S2	1.753(6)
S2-C3	1.761(6)	C3-C2	1.309(8)
C1-S1	1.757(6)	S1-C2	1.752(6)
C2-Se1	1.905(6)	Se1-C1A	1.944(6)
C1A-C2A	1.516(9)	C2A-C3A	1.52(9)
C3A-C4A	1.52(1)	C3-Se2	1.915(6)
Se2-C1B	1.955(8)	C1B-C2B	1.52(1)
C2B-C3B	1.51(1)	C3B-C4B	1.52(1)
Angle (°)			
S1-C1-S2	114.8(3)	C1-S1-C2	94.8(2)
C1-S2-C3	94.1(2)	S1-C2-C3	117.5(4)
S2-C3-C2	118.5(4)	S2-C3-Se2	116.7(3)
S1-C2-Se1	118.1(3)	C3-C2-Se1	124.4(4)
C2-C3-Se2	124.3(4)	C2-Se1-C1A	100.2(2)
Se1-C1A-C2A	110.1(4)	C1A-C2A-C3A	111.0(5)
C2A-C3A-C4A	113.3(5)	C3-Se2-C1B	98.5(3)
Se2-C1B-C2B	112.5(3)	C1B-C2B-C3B	109.1(7)
C2B-C3B-C4B	112.8(8)		

structure; one is in a boat form, and another is in the form in which each of the four alkyl chains are stretched towards different directions. The molecular structure of $TSeC_2$-TTF is similar to that of TTC_2-TTF,[6] both in boat form, and different from the chair form of $TTeC_2$-TTF.[7] The molecular structure of $TSeC_4$-TTF is not only different from that of TTC_4-TTF,[8] which is in a chair form, but also different from any other of the TYC_n-TTF family. It means that the selenium atoms play an important role to determine their crystal structures. Furthermore, although the intermolecular interactions in a $TSeC_4$-TTF crystal are rather weak just as stated above, it should be noted that they are almost isotropic. The three dimensionally isotropic character is rather unusual in the family of organic semiconductors or conductors, and in the history of developing organic conductors much efforts for increasing the dimensionality have been pursued. In this sense the molecular structure of $TSeC_4$-TTF may give a key to solve this problem, and the preparation of charge transfer complexes based on $TSeC_4$-TTF could give rise to a new type of organic conduc-

tors.

So far, three kinds of molecular structure, chair form, boat form and $TSeC_4$-TTF-like form, have been realized in TYC_n-TTF family. The chair form structure is favorable to decrease the distance between two molecular planes and build up a good conducting path along the stacking axis. The intermolecular overlaps between adjacent π systems are effectively large because there exists a columnar stacking consisting of the conjugated π systems, which can not be found in the crystals which have molecules of other structure forms. The compounds, such as TTC_n-TTF for n=4, 5, 7, 9, 10[6,8,9] and $TTeC_1$-TTF,[7] are in chair form structures and have relatively low resistivities in each own series. On the other hand, the boat form structure usually leads to a large interplane distance, in such compounds as $TSeC_2$-TTF, TTC_1-TTF, and TTC_2-TTF of which crystals have relatively high resistivities. In the case of $TSeC_4$-TTF-like form having rather weak intermolecular interactions, however, it is a good form to obtain a three dimensionally isotropic structure. If we can introduce much stronger intermolecular interactions to this system with keeping its isotropic character, for example, by applying a high pressure, we could obtain a new type of organic semiconductor. In the sense, the $TSeC_4$-TTF-like form has an unique significance.

In summary, we have analyzed the crystal structures of $TSeC_n$-TTF (n=2 and 4), and found out some specific factors to understand their properties. We have measured the electrical properties of both crystals and discussed them in correlation with their crystal structures. We are now proceeding with the preparation of charge-transfer complexes based on $TSeC_2$-TTF and $TSeC_4$-TTF.

References

1) H. Inokuchi, K. Imaeda, T. Enoki, T. Mori, Y. Maruyama, G. Saito, N. Okada, H, Yamochi, K.Seki, Y. Higuchi, and N. Yasuoka, *Nature (London)*, **329**, 39 (1987).

2) H. Inokuchi, G. Saito, P. Wu, K. Seki, T. B. Tang, T. Mori, K. Imaeda, T. Enoki, Y. Higuchi, K. Inaka, and N. Yasuoka, *Chem. Lett.*, **1986**, 1263.

3) K. Imaeda, T. Enoki, Z. Shi, P. Wu, N. Okada, H. Yamochi, G. Saito, and H. Inokuchi, *Bull. Chem. Soc. Jpn.*, **60**, 3163 (1987).

4) P. Wang, T. Enoki, K. Imaeda, H. Inokuchi, N. Iwasawa, H. Yamochi, H. Urayama, and G. Saito, to be published.

5) P. Main, S. E. Hull, L. Lessinger, G. Germain, J. P. Declercq, and M. M. Woolfson. MULTAN 78, (1978), Univs. of York, England, and Louvain, Belgium.

6) Y. Higuchi, K. Inaka, and N. Yasuoka, private communication; TTC_2-TTF, monoclinic, $P2_1/c$, a=10.220(2), b=8.759(2), c=22.950(4) Å, β=96.69°, boat form; TTC_5-TTF, triclinic, $P\bar{1}$, a=9.031(3), b=17.604(3), c=5.367(4)Å, α=90.26 (2), β=105.90(4), γ=90.85(2)°, chair form; TTC_9-TTF, monoclinic, $P2_1/a$, a=8.707(2), b=55.498(8), c=5.171(2) Å, β=103.45(2)°, chair form; TTC_{10}-TTF, triclinic, $P\bar{1}$, a=7.850 (3), b=32.960(9), c=5.115(4)Å, α=92.46(3), β=101.16(3), γ= 88.18(3)°.

7) Y. Higuchi and N. Yasuoka, private communication, $TTeC_1$-TTF, monoclinic, $P2_1/n$, a=13.769(3), b=5.480(3), c=9.239(5) Å, β=90.49(1)°, chair form; $TTeC_2$-TTF, monoclinic, $P2_1/a$, a=14.017(4), b=9.021(2), c=9.239(5)Å, β= 104.34 (3)°, chair form.

8) C. Nakano, unpublished results, TTC_4-TTF triclinic $P\bar{1}$, a=9.029(7), b=14.658(9), c=5.397(4) Å, α=97.98(5), β=94.05(6), γ=92.63(6)°, chair form; TTC_7-TTF, monoclinic, $P2_1/a$, a=8.797(2), b=46.90(1), c=5.141(1) Å, β=103.89 (2)°, chair form.

9) C. Katayama, M. Honda, H. Kumagai, J. Tanaka, G. Saito, and H. Inokuchi, *Bull. Chem. Soc. Jpn.*, **58**, 2272 (1985).

10) Tables of equations of the plane, anisotropic thermal parameters, F_o-F_c, coordinates of hydrogen atoms for the compounds of $TSeC_2$-TTF and $TSeC_4$-TTF, respectively, are deposited as Document No. 8834 at the Office of the Editor of Bull. Chem. Soc. Jpn. The atomic numbering in these Reference Tables ($TSeC_4$-TTF) is corresponding to that in the Fig. 6 of this paper as shown below: This Paper-Reference Table, C1-C6, C2-C5, C3-C7, S1-S4, S2-S3, Sel-Sel, Se2-Se2, C1A-C8, C2A-C9, C3A-C10, C4A-C13, C1B-C11, C2B-C12, C3B-C14, C4B-C15.

 © 1988 The Chemical Society of Japan Bull. Chem. Soc. Jpn., 61, 3461—3466 (1988)

Phosphorescence Properties of Pyridine and Its Methyl Derivatives in the Vapor Phase

Masayuki SUZUKI, Masahisa FUJITA, Takeshi TAKEMURA,* and Hiroaki BABA
Division of Chemistry, Research Institute of Applied Electricity, Hokkaido University, Sapporo 060
(Received June 3, 1988)

The phosphorescence spectra, lifetimes, and quantum yields of pyridine and its methyl derivatives, 2-picoline, 3-picoline, and 2,6-lutidine in the vapor phase have been measured with the aid of a specially designed circuit by means of control of the voltage imposed on the photomultiplier. The phosphorescence spectrum shifts to shorter wavelengths with increasing methylation. The phosphorescence lifetimes and quantum yields of pyridine and the picolines are of the order of 1 μs and 10^{-7} both values being one order of magnitude smaller than the corresponding values for the lutidine. These observations are explained by assuming that (1) the lowest triplet state (T_1) and the next lowest triplet (T_2) are of $^3(\pi,\pi^*)$ and $^3(n,\pi^*)$ types respectively, (2) the energy gap between T_1 and T_2 is small, especially in the unsubstituted pyridine, and (3) the potential energy curve for T_1 is distorted according to the energy gap, as the result of a pseudo-Jahn-Teller type of interaction between T_1 and T_2.

The phosphorescence spectrum from the pyridine molecule was first observed in the vapor phase by the present authors in 1983.[1,2] The phosphorescence properties of pyridine vapor are as follows: (a) In spite of the high intersystem crossing quantum yield,[3] the phosphorescence quantum yield is as anomalously low as 10^{-6}; (b) the phosphorescence spectrum has an onset near 350 nm, which is similar in position to the one of the benzene phosphorescence, but shows an anomalously red-shifted intensity maximum near 450 nm; and (c) the phosphorescence lifetime is anomalously short (1.2 μs) compared with those for vapors of other azines such as pyrazine (63 μs) and pyrimidine (50 μs).

These anomalous characteristics of the phosphorescence of pyridine were attributed to strong vibronic coupling between the lowest triplet state (T_1) of $^3(\pi, \pi^*)$ type and a close-lying $^3(n, \pi^*)$ state which is assigned to the second lowest triplet state (T_2).[4,5] It was supposed that the coupling may be strong enough to give rise to a pseudo-Jahn-Teller type of interaction between the two states.[2,6,7] Such an interaction would cause distortion of the potential surface of the $T_1(\pi, \pi^*)$ state and enhance the radiationless decay from T_1,[8,9] resulting in the extremely weak phosphorescence of pyridine.

Weisman et al.[10,11] have reported recently the decay of the triplet-triplet absorption in pyridine vapor at various pressures and explained the nonradiative behavior of the triplet pyridine in terms of the strong pseudo-Jahn-Teller interaction between the $T_1(\pi,\pi^*)$ and $T_2(n, \pi^*)$ states.

With pyridine in the vapor phase, the lowest triplet state, thus, is supposed to be of a (π, π^*) type. This assignment has received further supports from the experimental results of absorption measurements on pyridine.[12,13]

On the other hand, Schmidt et al.[14,15] have studied the lowest triplet state of pyridine in a single crystal of benzene by using electron-spin-echo spectroscopy, and reached the conclusion that the pyridine molecule is nonplanar in this state owing to the pseudo-Jahn-Teller coupling between the $T_1(n, \pi^*)$ state and a close-lying $^3(\pi, \pi^*)$ state. Thus, although the properties of the lowest triplet state of pyridine could be interpreted in terms of a pseudo-Jahn-Teller interaction, there is still a controversy about the character of the lowest triplet state.

For understanding fully the phosphorescence properties of pyridine, we attempted in this study to investigate the changes of the phosphorescence properties caused by introduction of the methyl group into pyridine; that is, the phosphorescence and excitation spectra, phosphorescence lifetimes, and quantum yields were measured for pyridine (**1**), 2-picoline (**2**), 3-picoline (**3**), and 2,6-lutidine (**4**) in the vapor phase.

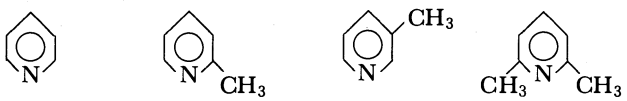

1 **2** **3** **4**

In order to obtain extremely weak phosphorescence emission of pyridine and its methyl derivatives, special care was directed to the purification of these compounds. Furthermore, a new circuit was employed which made it possible to measure time-resolved spectra in the microsecond or submicrosecond region of extremely weak emission by means of control of the voltage imposed on the photomultiplier; from now on this circuit will be called CVIPM circuit.

Experimental

Pyridine first treated after a method described in a previous paper[2] was purified by gas chromatography, and then distilled under reduced pressure. 2-Picoline, 3-picoline, and 2,6-lutidine were purified by fractional distillation under reduced pressure and were further purified by gas chromatography.

The optical experiments were carried out in the tempera-

ture range 0—40 °C and in the pressure range 2—20 Torr† with the sample vapor sealed into a 3.5 cm square quartz cell.

Absorption, emission, and excitation spectra were measured with a laser spectrophotometric system, which is essentially the same as the one described in a previous paper[16] except that a pulsed tunable dye laser (Lambda Physik FL 2002E) pumped by a XeCl excimer laser (Lambda Physik EMG 103 MSC) was used as the exciting light source in the present study. The frequency of the dye laser was doubled by a KDP crystal. The resulting UV laser pulses had an output energy of 1 mJ/pulse, a repetition rate of 20 pulses/s, a spectral bandwidth of 0.2 cm^{-1}, and a duration of 10 ns. The energy density of the pulsed UV laser beam was so high that the sample vapor was subject to chemical changes. Therefore, before reaching the sample cell, the laser beam was expanded in one direction by the use of a cylindrical lens.[17] The emission was dispersed by a Nikon G-250 monochromator and then detected by a Hamamatsu R106 photomultiplier.

Actually, the emission and excitation spectra were obtained in the form of time-resolved spectra by applying the CVIPM circuit to the laser spectrophotometric system. In the CVIPM circuit,[17] a part of the voltage imposed on the photomultiplier (PM) is pulsed so that the PM may operate (i.e., the PM may be sensitive to the incident light) only in a certain time range, e.g., 0.5—5 μs, after photoexcitation of the sample. Note that, with the present CVIPM circuit, the shorter limit of time is 0.5 μs. Under the ordinary conditions of the PM, owing to an after-effect of the irradiation of the PM by the fluorescence of pyridine, the lifetime of which is of the order of 10 ps, delayed output pulses emerge from the PM to yield a false delayed fluorescence with a lifetime of about 0.5 μs and a quantum yield comparable to that of the pyridine phosphorescence.[2] When the CVIPM circuit is used, such a delayed fluorescence does not occur. This is one of the advantages of the CVIPM circuit over the delay-and-gate circuit.[2] Thus, by measuring a time-resolved phosphorescence spectrum with the aid of the CVIPM circuit, one can eliminate the original and delayed fluorescence as well as the emissions from the cell and impurities.

Emission decays (or lifetimes) were measured by attaching a single photon counting lifetime apparatus,[16] equipped with a time-to-amplitude converter, to the laser spectrophotometric system. In this study, the delay-and-gate circuit[2] or the above-mentioned CVIPM circuit was applied to the original lifetime apparatus. For emission with a lifetime longer than 10 μs, the decay measurement was made by means of a phosphorimetric system using a circuit of a digital boxcar type.[18]

Results

Phosphorescence and Excitation Spectra. Figure 1 shows time-resolved phosphorescence spectra of pyridine and its methyl derivatives. These spectra were obtained with 6 nm emission bandwidth in the time range 0.5—5 μs for pyridine and the picolines and in the range 0.5—40 μs for 2,6-lutidine. The excitation of the sample vapors was carried out at the 0-0 band of the $S_1 \leftarrow S_0$ absorption for all compounds except 2,6-lutidine. With 2,6-lutidine, since the 0-0 band is not resolved, the excitation was carried out at 285 nm near the onset of the absorption.[3] The phosphorescence spectra have onsets near 350 nm for all the compounds concerned, but the intensity maximum is shifted to the blue with the increase in number of the methyl groups: The wavelengths of the phosphorescence maxima, λ^{P}_{max} are 450 nm for the unsubstituted pyridine, 420 and 430 nm for the monomethyl derivatives 2-picoline and 3-picoline, respectively, and 415 nm for the dimethyl derivative 2,6-lutidine. These values of λ^{P}_{max} are given in Table 1.

It should be noted here that the phosphorescence spectra of all the compounds concerned remain essentially unchanged in position and in shape upon changing the excitation wavelength and the sample vapor pressure.

† 1 Torr≈133.322 Pa.

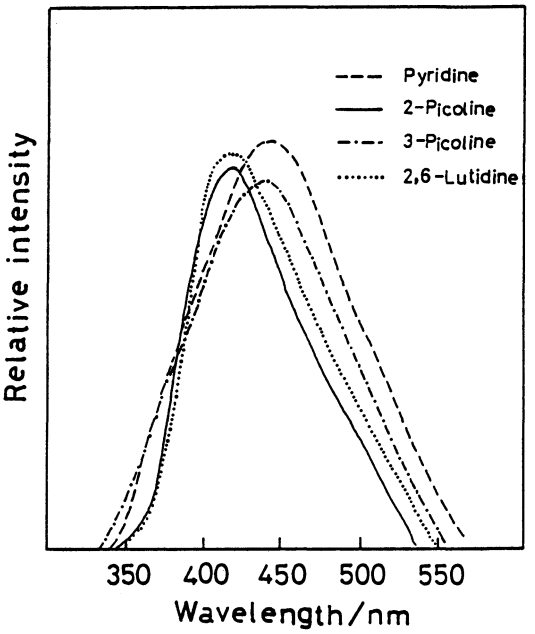

Fig. 1. Time-resolved phosphorescence spectra of pyridine and its methyl derivatives in the vapor phase. The spectra for 2 Torr of pyridine (----), 15 Torr of 2-picoline (——), and 8 Torr of 3-picoline (-·-·-) were obtained by excitation at the 0-0 band of the $S_1 \leftarrow S_0$ absorption and by observation in the time range 0.5—5 μs after pulse excitation; the spectrum for 8 Torr of 2,6-lutidine (------) was obtained by excitation at 285 nm near the onset of the $S_1 \leftarrow S_0$ absorption and by observation in the range 0.5—40 μs. The emission bandwidth is 6 nm in every case.

Table 1. Phosphorescence Characteristics of Pyridine and Its Methyl Derivatives in the Vapor Phase

Compound	λ^{P}_{max} / nm	τ_P / μs	Φ_P
Pyridine	450	1.2	4.4×10^{-7}
2-Picoline	420	4.2	2.4×10^{-7}
3-Picoline	430	1.4	
2,6-Lutidine	415	37	2.0×10^{-6}

It was already shown that the absorption and time-resolved phosphorescence-excitation spectra for pyridine agree reasonably well with each other.[1,2] In Figs. 2 and 3 are shown the absorption and time-resolved phosphorescence-excitation spectra in the region near the 0-0 band of the S_1-S_0 transition of 2-picoline and 3-picoline, respectively. The excitation spectrum of each of the compounds agrees very well with the corresponding absorption. This confirms that the observed phosphorescence spectra are attributable to the ones originating from the picolines. For 2,6-lutidine vapor also, the absorption and time-resolved phosphorescence-excitation spectra were measured and found to be in agreement with each other, though both spectra were completely structureless.

Figure 4 shows the phosphorescence spectrum of 2,6-lutidine in a rigid glass of 2-methylpentane (2-MP) at 77 K, together with the same spectrum in the vapor phase for the sake of comparison. The onset of the spectrum in the rigid glass is not very different from the one in the vapor phase, but the spectral maximum is shifted to the blue by about 15 nm in passing from the vapor phase to the rigid glass.

Phosphorescence Lifetimes. Figure 5 shows the phosphorescence decay curves for pyridine, 2-picoline, 3-picoline, and 2,6-lutidine vapors. The decay measurements were carried out using the delay-and-gate circuit for pyridine and 2-picoline, the CVIPM circuit for 3-picoline, and the digital boxcar type of circuit for 2,6-lutidine. The observed lifetimes τ_P are given in Table 1. The lifetime seems to become longer with increasing number of the methyl groups; i.e., the values of τ_P are 1.2 μs for pyridine, 4.2 μs for 2-picoline, 1.4 μs for 3-picoline, and 37 μs for 2,6-lutidine.

Phosphorescence Quantum Yields. Since there is a

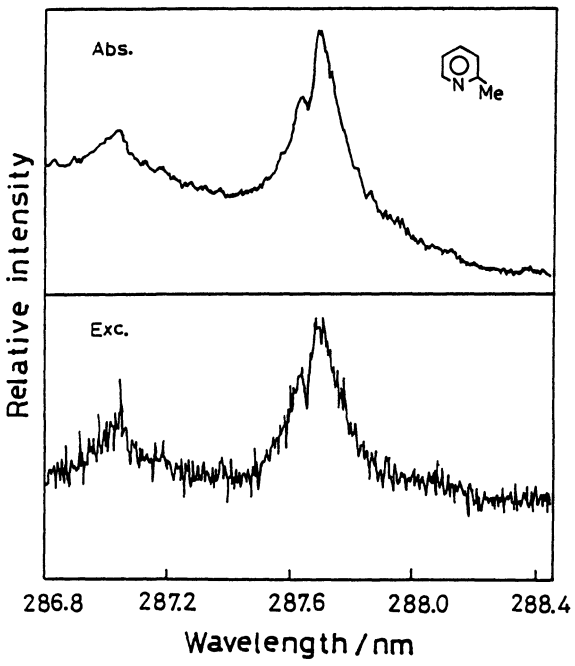

Fig. 2. Spectra near the 0-0 band of the $S_1 \leftarrow S_0$ absorption of 2-picoline vapor. (Abs.), absorption spectrum with the relative intensity representing the relative absorbance. (Exc.), time-resolved phosphorescence-excitation spectrum in the time range 0.5—5 μs after pulse excitation, obtained by monitoring the total emission.

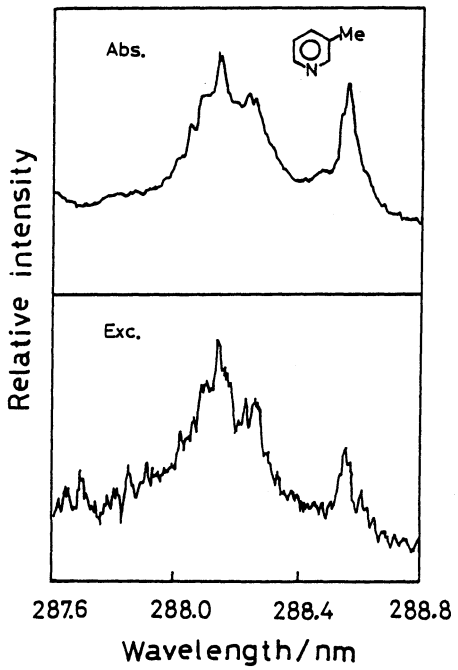

Fig. 3. Spectra near the 0-0 band of the $S_1 \leftarrow S_0$ absorption of 3-picoline vapor. (Abs.), absorption spectrum with the relative intensity representing the relative absorbance. (Exc.), time-resolved phosphorescence-excitation spectrum in the time range 0.5—5 μs after pulse excitation, obtained by monitoring the emission at 430 nm with 12 nm band width.

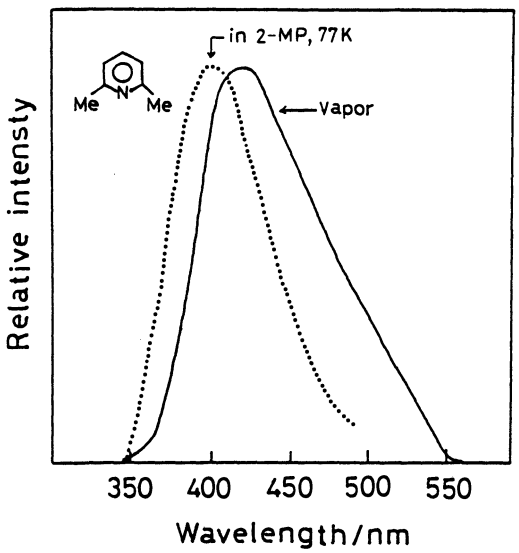

Fig. 4. Phosphorescence spectra of 2,6-lutidine in 2-methylpentane (2-MP) at 77 K and in the vapor phase. The vapor spectrum is the same as that in Fig. 1.

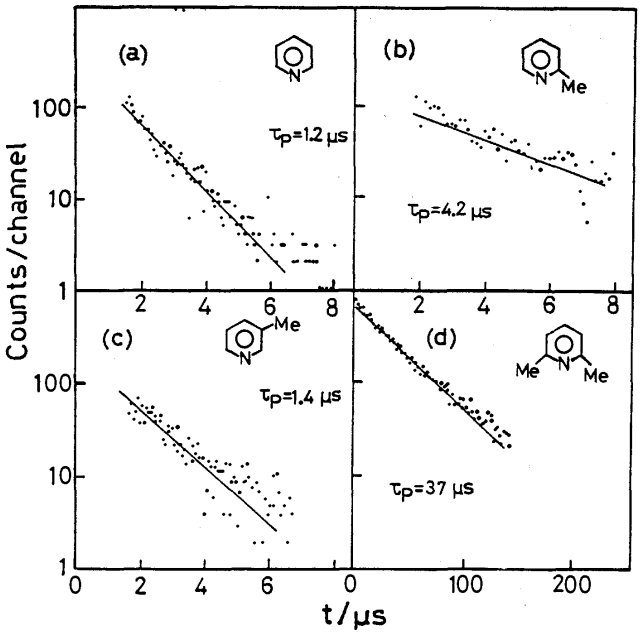

Fig. 5. Phosphorescence decays of pyridine and its methyl derivatives in the vapor phase obtained by monitoring the emission at the intensity maxima. (a) Pyridine; (b) 2-picoline; (c) 3-picoline; (d) 2,6-lutidine. For each compound, the excitation position is the same as that in Fig. 1.

little excitation-wavelength dependence of the fluorescence quantum yield for 2,6-lutidine compared with pyridine and picolines, the phosphorescence quantum yield (Φ_P) of 2,6-lutidine was first determined in the same way as that described in Ref. 2, by combining the known value of its fluorescence quantum yield (Φ_F) and the ratio of Φ_P to Φ_F. The resulting value of Φ_P for 2,6-lutidine along with the relative Φ_P values that were obtained for pyridine, 2-picoline, and 2,6-lutidine enabled us to determine the absolute values of Φ_P for pyridine and 2-picoline. In these experiments, to obtain desirable absorbance values, the pyridine vapor was cooled to 0 °C (pressure, 2 Torr), while the 2-picoline and 2,6-lutidine vapors were warmed to 40 °C (pressures, 15 and 8 Torr, respectively). The Φ_P values thus determined are shown in Table 1. It may be noted that Φ_P of pyridine given in Table 1 is about one third of that reported in our previous paper.[2]

Discussion

As is seen in Fig. 1, the phosphorescence spectra of pyridine and its methyl derivatives are similar in shape to each other. Further, it is seen from Fig. 4 that the phosphorescence spectrum of 2,6-lutidine vapor is also similar to the one in 2-MP at 77 K, which has been confirmed to originate from the $^3(\pi, \pi^*)$ state.[19] In addition, roughly speaking, all the spectra given in Figs. 1 and 4 are located in the same wavelength region. These observations suggest that the phosphorescent states for these four compounds, the unsubstituted, monomethyl-substituted, and dimethyl-substituted pyridines, are of $^3(\pi, \pi^*)$ type; in other words, T_1 is the $^3(\pi, \pi^*)$ state and T_2 is the $^3(n, \pi^*)$ in these pyridines.

The radiative phosphorescence lifetime (τ_P^R) of a molecule is given by $\tau_P^R = \Phi_{ISC}\tau_P/\Phi_P$, where Φ_{ISC} is the $S_1 \rightsquigarrow T$ intersystem crossing quantum yield. The experimental values of Φ_{ISC} are 0.30 and 0.6 for pyridine[20] and 2-picoline,[3] respectively. Although Φ_{ISC} for 2,6-lutidine has not been determined, one may tentatively assume it to be about 0.5. Then τ_P^R is 0.82 s for pyridine, 10 s for 2-picoline, and about 10 s for 2,6-lutidine. These values are one to two orders of magnitude larger than the values of τ_P^R for other azabenzenes the T_1 state of which is known to be of (n, π^*) character. In fact, $\tau_P^R \approx 70$ ms for pyrazine and pyrimidine in rigid-glass solution,[21] and $\tau_P^R = 30$ ms for pyrazine vapor;[22] in any of these three cases, it has been established that T_1 is of $^3(n, \pi^*)$ type. Thus, the data concerning τ_P^R support the view described above that the T_1 states in pyridine and its derivatives under study are $^3(\pi, \pi^*)$ states.

It is known, on the other hand, that the excitation energies of singlet and triplet (π, π^*) states in aromatic compounds are generally lowered by methyl substitution. We then have to explain the reason why the methyl substitution shifts the pyridine phosphorescence, which has been assigned to $T_1(\pi, \pi^*) \rightarrow S_0$, toward the blue (see Table 1). We shall discuss this problem in terms of the pseudo-Jahn-Teller interaction which is likely to occur between the two nearby triplet states, $T_1(\pi, \pi^*)$ and $T_2(n, \pi^*)$.

If T_1 in pyridine is essentially of $^3(\pi, \pi^*)$ nature, it is to be assigned to ^3L_a in Platt's notation.[23] It is here desirable to know effects of the methyl substitution on the zero-order $^3L_a(\pi, \pi^*)$ state which is hypothetically supposed to be free from the pseudo-Jahn-Teller interaction. For aromatic hydrocarbons, there is correlation between molecular-size dependence of the energy of the ^1L_a state and that of the ^3L_a state. Thus, as the molecular size increases the ^1L_a-^3L_a interval monotonically decreases and approaches a limiting value; the interval seems to be primarily size-dependent and virtually structure-independent.[23]

In view of the above fact, we examined the effects of methyl substitution on the excitation energies of the

Table 2. Data on the Energies of the ^1L_a and ^3L_a states of Benzene and Its Methyl Derivatives

Compound	^1L_a		^3L_a	
	$\tilde{\nu}_{max}$ [a]	ΔE	$\tilde{\nu}_{0\text{-}0}$ [b]	ΔE
	cm^{-1}	cm^{-1}	cm^{-1}	cm^{-1}
Benzene	49000	0	29500	0
Toluene	48100	−900	28900	−600
m-Xylene	47300	−1700	28700	−800

a) From absorption spectra in hexane. b) From phosphorescence spectra in cyclohexane at 77 K.

Table 3. Data on the Energies of the $^1(n,\pi^*)$, ^1L_a, and ^3L_a states of Pyridine and Its Methyl Derivatives in the Vapor Phase

Compound	$^1(n,\pi^*)$	^1L_a		^3L_a[c]
	$\tilde{\nu}_{0\text{-}0}$[a]	$\tilde{\nu}_{max}$	ΔE	ΔE[d]
	cm^{-1}	cm^{-1}	cm^{-1}	cm^{-1}
Pyridine	34769	51900	0	0
2-Picoline	34753	50400	−1500	−1000
3-Picoline	34684	50400	−1500	−1000
2,6-Lutidine	35100[b]	49100	−2800	−1300

a) Taken from Ref. 3. b) The position at which the absorption intensity is comparable to that of the 0-0 band of the $^1(n,\pi^*)\leftarrow S_0$ absorption spectrum of 2-picoline; the same absorption spctrum of 2,6-lutidine is structureless. c) Zero-order state. b) Estimated energy shift.

^1L_a and ^3L_a states of benzenes, i.e., the parent hydrocarbon of pyridine, to guess the energies of the zero-order ^3L_a states of the substituted pyridines. The results are summarized in Table 2, where ΔE denotes the energy shift caused by methyl substitution. In Table 3 are shown the observed excitation energies of the $^1(n, \pi^*)$ and ^1L_a states of pyridine and its mono- and dimethyl-derivatives. The values of ΔE for the zero-order ^3L_a states were estimated by comparing the data given in Tables 2 and 3; the results are also shown in Table 3.

As is seen in Table 3, on introducing the methyl group(s) into pyridine, the energy of the $^1(n, \pi^*)$ state remains almost unchanged. It may then be assumed that practically no change is produced in the $^3(n, \pi^*)$ state energy by the methyl substitution.

The $^3L_a(\pi, \pi^*)$ and $^3(n, \pi^*)$ states in pyridine (and also in 2,6-lutidine) belong to the irreducible representations A_1 and B_1 of the symmetry group C_{2v}, respectively, so that the vibronic coupling will be induced by a non-totally symmetric, out-of-plane bending vibration of b_1 symmetry, such as ν_{16b}.[11] The potential energy curves distorted by the vibronic coupling of the pseudo-Jahn-Teller type are illustrated schematically in Fig. 6, with pyridine and 2,6-lutidine taken as examples. Here, Q represents the cordinate of the coupling vibrational mode. It is assumed that, especially in the case of pyridine, the coupling is so strong that the potential curve for the T_1 state takes the form of a distinct double minimum. The phosphorescence is considered to be emitted, with the highest probability, from the potential minimum that corresponds to a nonplanar structure of the molecule concerned. It should be noted that the energy of the zero-order ^3L_a state corresponds to the energy of T_1 at Q=0 in Fig. 6.

Inspection of Fig. 6 will reveal the following: The T_2-T_1 energy gap at Q=0 is larger and the energy of T_1 at Q=0 is lower, but the $T_1\rightarrow S_0$ transition energy is larger, in 2,6-lutidine than in pyridine. The situation in 2- and 3-picolines may be understood in a similar way, though the molecular symmetry deviates from C_{2v} owing to the presence of the methyl group. Thus, the

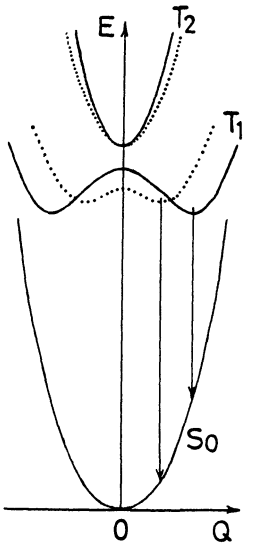

Fig. 6. Schematic potential energy curves resulting from the pseudo-Jahn-Teller interaction between T_1 and T_2: ——, pyridine; ·····, 2,6-lutidine.

potential curve for T_1 (and also for T_2) of the picolines would become intermediate, with respect to the form and location, between the corresponding curves of pyridine and 2,6-lutidine. To sum up, the $T_1\rightarrow S_0$ transition energy increases, and hence the phosphorescence spectrum shifts toward shorter wavelengths, in going from pyridine to 2- or 3-picoline and then to 2,6-lutidine, in general agreement with the experimental results.

The experimental results shown in Fig. 4 can also be explained by the same reasoning. On account of the general solvent effect, the $^3L_a(\pi, \pi^*)$ state energy (relative to the ground state energy) of 2,6-lutidine in the rigid glass is expected to be lower than that in the vapor phase. At the same time, however, this lowering of the state energy will give rise to an additional increase in the T_2-T_1 energy gap as measured at Q=0, so that little distortion will occur in the potential energy curve in the rigid glass. This explains the observation that the phosphorescence spectrum of 2,6-lutidine shifts further toward shorter wavelengths on changing the phase from the vapor to the rigid glass solution.

The observed phosphorescence lifetimes τ_P of pyridine and its derivatives, shown in Table 1, are only 10^{-6} times the radiative lifetimes τ_P^R mentioned previously. This means that in each case the rate constant for the decay of the phosphorescent triplet state, given by $1/\tau_P$, is practically equal to the rate constant for the nonradiative decay of that triplet state. In the case of pyridine, owing to the great distortion of the potential curve (Fig. 6), the frequency of the coupling vibration and the equilibrium nuclear configuration should be changed considerably on changing the electronic state from $T_1(\pi, \pi^*)$ to S_0.[6,9] As a result, the vibrational factor[9] for the $T_1 \rightsquigarrow S_0$ radiationless transition

increases to reach an extent that $1/\tau_P$ for pyridine is exceptionally large, and hence Φ_P as well as τ_P is exceptionally small.[2] As has been mentioned, the methyl substitution will reduce the degree of the potential distortion, resulting in an increase in τ_P in conformity with the experimental results (Table 1). This is particularly true of 2,6-lutidine, the τ_P value of which is 30 times as large as that of pyridine.

In the foregoing descriptions, the triplet states T_1 and T_2 have been expressed simply as $T_1(\pi, \pi^*)$ and $T_2(n, \pi^*)$. However, owing to the vibronic coupling, the $^3(\pi, \pi^*)$ and $^3(n, \pi^*)$ states are to be mixed with each other. Actually, therefore, the T_1 state partly has the character of $^3(n, \pi^*)$. This accounts for the observation that the values of τ_P^R for the pyridines given in Table 1 are smaller than τ_P^R for aromatic hydrocarbons,[24] the T_1 state of which can be regarded as a pure $^3(\pi, \pi^*)$ state. Furthermore, since the vibronic coupling should be strongest in the unsubstituted pyridine, one may readily understand the fact that the value of τ_P^R is smallest in pyridine.

We should here refer to recent reports by Schmidt and his co-workers,[14,15] who performed an electron paramagnetic resonance study of the triplet state of pyridine present as a guest in a single crystal of benzene at 1.2 K by using electron-spin-echo spectroscopy. According to these authors, the lowest triplet state (T_1 in our notation) of pyridine is the $^3B_1(n, \pi^*)$ state considerably admixed with the close-lying $^3A_1(\pi, \pi^*)$ state, the lifetime of T_1 being of the order of 1 ms, and the pyridine molecule is nonplanar in T_1 owing to the pseudo-Jahn-Teller coupling between the two triplet states mentioned above. Obviously their assignment of T_1 as the $^3B_1(n, \pi^*)$ state disagrees with our assignment of T_1 in pyridine vapor as $^3A_1(\pi, \pi^*)$; the latter assignment is supported by some other authors.[10-13] We are here not in a position to explain the reasons for the disagreement between the two assignments. Probably, however, one of the reasons would be that there is a large difference between the experimental conditions adopted. We used pyridine vapor at room temperature for our phosphorescence study, while Schmidt et al. used pyridine in a crystal at 1.2 K for their magnetic resonance study. The relative positions of the close-lying $^3(\pi, \pi^*)$ and $^3(n, \pi^*)$ levels in question will vary, depending upon the environment in which the pyridine molecule is placed.

In connection with the above problem, mention should be made of a very recent theoretical study by Kitao and Nakatsuji.[25] These authors have applied the SAC (symmetry-adapted cluster) and SAC-CI theories to ab initio calculations of the valence excitations and ionizations of pyridine. The results of their calculations indicate that (1) the lowest triplet state of pyridine is the $^3A_1(\pi, \pi^*)$ state, and (2) the second lowest is the $^3B_1(n, \pi^*)$ state, which exists higher by 0.15 eV than the $^3A_1(\pi, \pi^*)$ state.

References

1) K. Sushida, M. Fujita, T. Takemura, and H. Baba, *J. Chem. Phys.*, **78**, 588 (1983).
2) K. Sushida, M. Fujita, T. Takemura, and H. Baba, *Chem. Phys.*, **88**, 221 (1984).
3) I. Yamazaki, K. Sushida, and H. Baba, *J. Chem. Phys.*, **71**, 381 (1979).
4) H. Baba and T. Takemura, *Bull. Chem. Soc. Jpn.*, **40**, 2215 (1967).
5) H. Baba, I. Yamazaki, and T. Takemura, *Spectrochim. Acta*, **27A**, 1271 (1971).
6) R. M. Hochstrasser and C. A. Marzzacco, "Molecular Luminescence," ed by E. C. Lim, Benjamin, New York (1969), p. 631.
7) A. J. Duben, L. Goodman, and M. Koyanagi, "Excited States," Vol. 1, ed by E. C. Lim, Academic Press, New York (1974), p. 295.
8) W. A. Wassam, Jr. and E. C. Lim, *J. Chem. Phys.*, **68**, 433 (1978).
9) E. C. Lim, "Excited States," Vol. 3, ed by E. C. Lim, Academic Press, New York (1977), p. 305.
10) R. B. Weisman, P. L. Holt, and J. I. Selco, *J. Chem. Phys.*, **77**, 1600 (1982).
11) J. I. Selco, P. L. Holt, and R. B. Weisman, *J. Chem. Phys.*, **79**, 3269 (1983).
12) D. F. Evans, *J. Chem. Soc.*, **1957**, 3885.
13) S. Japar and D. A. Ramsay, *J. Chem. Phys.*, **58**, 5832 (1973).
14) F. C. Bos, W. J. Buma, and J. Schmidt, *Chem. Phys. Lett.*, **117**, 203 (1985).
15) W. J. Buma, E. J. J. Groenen, and J. Schmidt, *Chem. Phys. Lett.*, **127**, 189 (1986).
16) H. Baba, M. Fujita, N. Ohta, and Y. Shindo, *J. Spectrosc. Soc. Jpn.*, **29**, 387 (1980).
17) M. Fujita, T. Takemura, and H. Baba, *Tech. Rep. Res. Inst. Appl. Elec. Hokkaido Univ.*, No 8, 1 (1987).
18) T. Takemura, K. Uchida, M. Fujita, Y. Shindo, N. Suzuki, and H. Baba, *Chem. Phys. Lett.*, **73**, 12 (1980).
19) A. G. Motten and A. L. Kwiram, *J. Chem. Phys.*, **75**, 2608 (1981).
20) K. Sushida, M. Fujita, I. Yamazaki, and H. Baba, *Bull. Chem. Soc. Jpn.*, **56**, 2228 (1983).
21) R. S. Becker, "Theory and Interpretation of Fluorescence and Phosphorescence," Wiley-Interscience, New York (1969), p. 168; the values of Φ_{ISC} are assumed to be unity.
22) I. Yamazaki, M. Fujita, and H. Baba, *Chem. Phys.*, **57**, 431 (1981).
23) S. P. McGlynn, T. Azumi, and M. Kinishita, "Molecular Spectroscopy of the Triplet State," Prentice-Hall, Englewood Cliffs (1969), Chap. 3.
24) S. K. Lower and M. A. El-Sayed, *Chem. Revs.*, **66**, 199 (1966).
25) O. Kitao and H. Nakatsuji, *J. Chem. Phys.*, in press (private communication).

 © 1988 The Chemical Society of Japan Bull. Chem. Soc. Jpn., 61, 3467—3470 (1988)

A New Permanganate-Nitrite-Formic Acid-Methanol Oscillator

Makoto MORITA, Kazutoshi IWAMOTO, and Manabu SENŌ*
Contribution from the Institute of Industrial Science, University of Tokyo, 7-22-1, Roppongi, Minato-ku, Tokyo 106
(Received June 3, 1988)

Sustained oscillation and birhythmicity have been observed when aqueous solutions of potassium permanganate, potassium nitrite, formic acid, and methanol were mixed in a continuous-flow stirred tank reactor. A detailed phase diagram is shown. This new oscillator is composed of non-halogen compounds and the first example of the nitrogen-based oscillator.

In recent years much attention has been attracted to oscillators in chemical reactions,[1] and a number of examples of oscillations and related phenomena, e. g., multiple stationary states,[2-4] simple and complex oscillations,[5,6] aperiodic oscillation (chaos),[6,7] and the growth of traveling waves,[8,9] suggest that these dynamical phenomena are not exceptional but universal behavior sufficiently far from equilibrium. The majority of known oscillators are based on the reactions of oxohalogenate anions, which have been studied mainly by Epstein and co-workers.[10] Examples are the chlorite-bromate-iodide reaction,[11] the bromate-iodide reaction,[12] the arsenite-iodate reaction,[2,3] and the chlorite-thiosulfate reaction.[6]

On the other hand, there are some oscillators without oxohalogenate compounds, examples of which are the oxidation of benzaldehyde by oxygen in glacial acetic acid with $CoBr_2$ catalyst,[13] the oxidation of Methylene Blue by oxygen in a strongly alkaline medium in the presence of sulfite and sulfide,[14] the oxidation of sulfide ion by hydrogen peroxide in nearly neutral solutions,[15] the reduction of permanganate by hydrogen peroxide in phosphoric acid,[16] and the oxidation of oxalate[17,18] or ninhydrin[19] by permanganate. Many efforts have been made to find new oscillators, because discovery of a new chemical oscillator brings further understanding of the mechanism of chemical oscillation.

We have checked the reaction mechanisms of known chemical oscillators and noticed that these oscillators are composed of reducing and oxidizing reagents which include atoms with multiple oxidation states available. This suggests a possibility that a new oscillator could be made from reducing and oxidizing reagents suitably selected. Along these considerations, we have found a new halogen-free redox reaction which exhibits oscillatory behavior in a continuous flow stirred tank reactor (CSTR). Permanganate and nitrite ions were selected for the oxidizing and the reducing reagents, respectively, because manganese and nitrogen atoms have multiple oxidation states available. It was found that the addition of formic acid and methanol is needed to produce oscillations. Without them only vague and noisy oscillations with small amplitudes appear. The oscillations were monitored as changes in Pt-electrode potential. To our knowledge, the nitrite-permanganate oscillatory system is the first example of nitrogen-based oscillator. It exhibits not only complex periodic oscillations but also birhythmicity.[12,20,21]

Experimental

All experiments were carried out in a thermally regulated CSTR with a reaction cell of 9.5 cm^3 volume. Each of stock solutions of $KMnO_4$ (10^{-4}—10^{-2} mol dm^{-3}), KNO_2(10^{-4}—10^{-2} mol dm^{-3}), HCOOH (1.05 mol dm^{-3}) or CH_3OH (1.24 mol dm^{-3}) was prepared by dissolving the highest-purity-grade chemicals (Wako Chemicals) in doubly distilled water. Four syringe pumps (Micro Feeder, Furue Science) were used to feed simultaneously the respective stock solutions into the CSTR at controlled flow rates. In all experiments, the flow rate was set to be equal for the four pumps. The solution in the CSTR was mixed well with a magnetic stirrer at a constant stirring rate. The redox potential of the solution was monitored on an electrometer (Takeda Riken, TR-8651) as a potential difference between a standard Ag/AgCl reference electrode (TOA Electonics) and a platinum electrode. The temperature of the CSTR was kept constant at 25.0±0.1 °C throughout the experiments.

Results and Discussion

The system shows a stable stationary state and an oscillatory state, depending on the feed rate of the reagent solutions. Figure 1 shows typical behavior of the system. In this figure, the reciprocal residence time k_0 is used instead of the feed rate. The value of k_0 was calculated from $k_0=4J/V$, where J is the flow rate of the stock solution and V is the volume of the cell. When k_0 is lower than 6×10^{-3} s^{-1}, the potential difference is low (ca. 250 mV vs. Ag/AgCl). In this case, manganese is mainly in its reduced form (Mn^{2+}) and the solution is colorless in the CSTR. On increasing k_0 beyond 6×10^{-4} s^{-1}, the system enters into an oscillatory region. The amplitude of the oscillations is shown with bars in Fig. 1. With an increase in k_0 from 6×10^{-4} s^{-1} to 2×10^{-3} s^{-1}, the amplitude and the period of oscillations become large. It should be noted that the minimum potential in each cycle is almost constant, but the maximum potential tends to increase gradually. On the contrary, when k_0 increases beyond 2×10^{-3} s^{-1}, the maximum potential is nearly unchanged and the minimum potential increases.

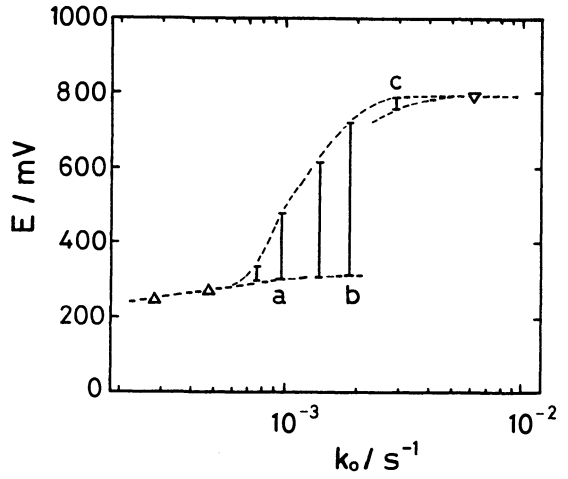

Fig. 1. Plots of the redox potential E vs. the reciprocal residence time k_0. Amplitudes of oscillations are shown with bars. The amplitude varies abruptly at about $k_0=2.3\times10^{-3}\,s^{-1}$. Fixed conditions; $[KMnO_4]_0=6.0\times10^{-4}\,mol\cdot dm^{-3}$, $[KNO_2]_0=1.0\times10^{-3}\,mol\cdot dm^{-3}$, $[HCOOH]_0=1.05\,mol\cdot dm^{-3}$, $[CH_3OH]_0=1.24\,mol\cdot dm^{-3}$, and the temperature in the CSTR is 25.0°C. The notation $[A]_0$ is used to show the concentration of a reagent A in the stock solution hereafter.

Finally the system falls into a stable steady state with a high redox potential (ca. 800 mV) when k_0 reaches $5\times10^{-3}\,s^{-1}$. In this steady state the manganese is in the form of MnO_4^-.

Characteristics of these oscillations is strongly dependent of the experimental conditions such as concentrations of the reagent solutions and k_0. The period of oscillation ranges from 30 s to 15 min, and the amplitude changes from 50 mV to 450 mV. Typical oscillatory traces are shown in Fig. 2. At lower values of k_0, a simple oscillation with a short period is exhibited, as illustrated in Fig. 2(a). Figure 2(b) shows a complicated periodic oscillation consisting of small and large period oscillations. Interestingly, the small period oscillation diminishes as k_0 increases. For example, when $k_0=2\times10^{-3}\,s^{-1}$, a simple oscillation with a large period continues stably, as shown in right-hand part of Fig. 3. At higher values of k_0, the system exhibits a simple high-potential-based oscillation of small amplitude (Fig. 2(c)).

When $k_0=2.3\times10^{-3}\,s^{-1}$, the amplitude of oscillation changes drastically and the presence of birhythmicity is suggested in this region. Detailed experiments show that either of two oscillations having different amplitudes appears depending on the initial state. These results are shown in Fig. 3, where k_0 is $2.3\times10^{-3}\,s^{-1}$. The concentrations of the reagent solutions were the same with those of Fig. 1. Initially, the potential of the Pt electrode oscillates with a small amplitude. At the time denoted by an asterisk in the figure, all the pumps were stopped for a few seconds and then turned on again. The potential then began to oscillate with a

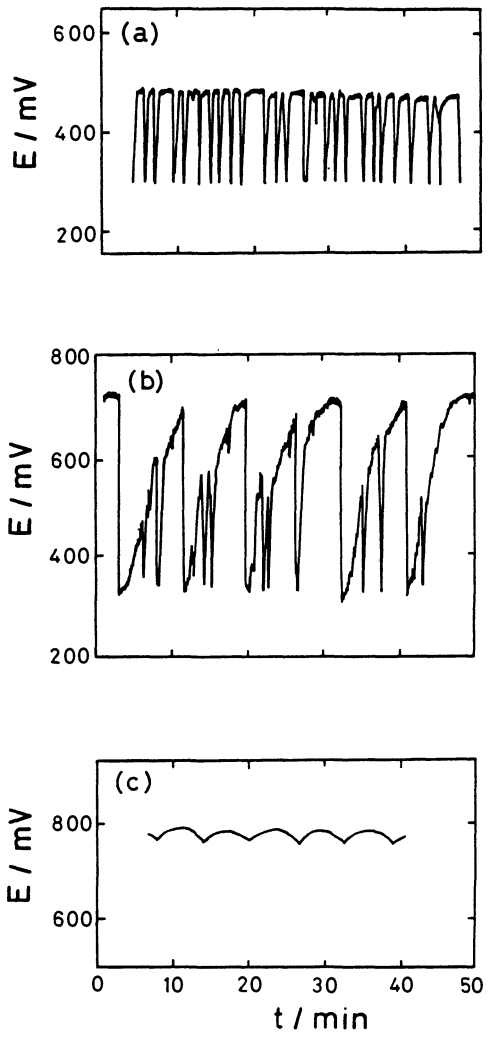

Fig. 2. Modes of oscillations vs. time t at **a**, **b**, and **c** marked in Fig. 1. The reciprocal residence time k_0; (a) $9.6\times10^{-4}\,s^{-1}$, (b) $1.7\times10^{-3}\,s^{-1}$, and (c) $2.9\times10^{-3}\,s^{-1}$.

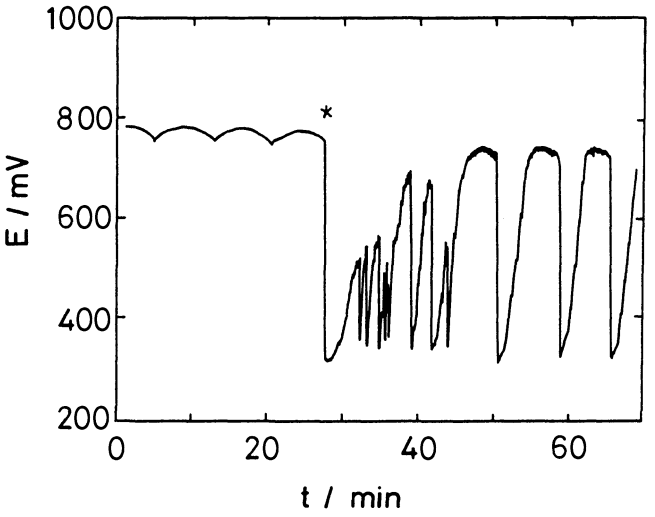

Fig. 3. Birhythmicity observed at $k_0=2.3\times10^{-3}\,s^{-1}$ in Fig. 1: All the pumps were stopped at (*) for a few second. Both two different oscillatory states are stable under the same conditions.

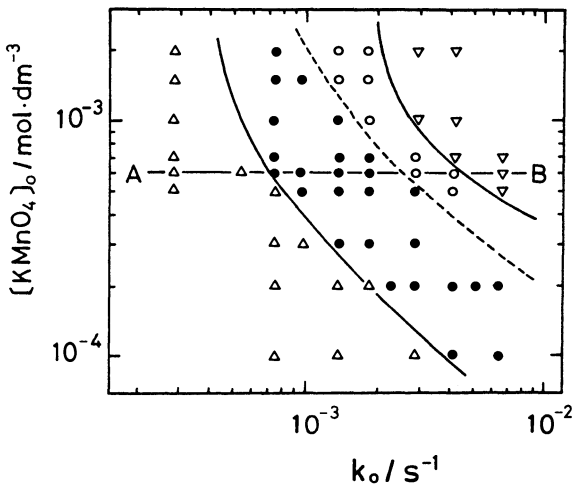

Fig. 4. Phase diagram in the reciprocal residence time k_0–$[KMnO_4]_0$ plane with $[KNO_2]_0=1.0\times10^{-3}$ mol·dm^{-3}, $[HCOOH]_0=1.05$ mol·dm^{-3}, $[CH_3OH]_0=1.24$ mol·dm^{-3}, and the temperature in the CSTR is 25.0 °C. Symbols; (△) lower potential steady state, (▽) higher potential steady state, (●) lower potential-based oscillations, (○) higher potential-based oscillations. Figure 1 shows the behavior of the system along the broken line A-B in this figure.

large amplitude, even though the conditions including the flow rate were exactly the same as before. Thus, this is birhythmicity.

Figure 4 shows a phase diagram of the system obtained by changing the concentration of the stock solution of potassium permanganate and k_0. The concentrations of other stock solutions were fixed. The phase diagram is divided into three regions; a region of oscillation and two regions of stable steady states. In the lower left-hand corner of Fig. 4, the system is in a reduced and stable steady state of lower potential. In the upper right-hand corner, it is in an oxidized and stable steady state of higher potential. Large amplitude oscillations are observed in the center of the oscillatory region. Lower potential-based oscillations are observed in the left part of the oscillatory region, and higher potential-based osillations appear in the right-hand region of the broken line in Fig. 4. In the region around the broken line, the system exhibits birhythmicity.

Without continuous supply of the reagent solutions, no oscillation takes place, probably because permanganate ions are reduced rapidly and an equilibrium state is attained immediately. By introducing constant flow of reactants, the system is kept far from equilibrium and a bifurcation takes place, producing oscillation.

Both manganese and nitrogen atoms have several oxidation states, and it is supposed that there exists a positive feedback mechanism between different oxidation states. According to the literature of inorganic chemistry,[22,23] we could give an example of the key mechanism of the system by the following process of reactions. In the first stage of the process, permanganate ions are reduced to manganese dioxide by formic acid:

$$2MnO_4^- + 3HCOOH + 2H^+ \rightarrow 2MnO_2 + 3CO_2 + 4H_2O. \quad (R1)$$

The second step is the reduction of manganese dioxide by nitrite ions:

$$MnO_2 + NO_2^- + 2H^+ \rightarrow Mn^{2+} + NO_3^- + H_2O. \quad (R2)$$

At the third step the oxidation of manganous ions by permanganate ions is followed:

$$2MnO_4^- + 3Mn^{2+} + 2H_2O \rightarrow 5MnO_2 + 4H^+. \quad (R3)$$

Then, 3(R2)+(R3) gives

$$3MnO_2 + 2MnO_4^- + 3NO_2^- + 2H^+ \rightarrow 5MnO_2 + 3NO_3^- + H_2O.$$

Therefore, three molucules of MnO_2 yield five molecules of MnO_2 in the process. This autocatalytic process may be the key mechanism of our system, because an autocatalytic reaction plays an essential role in chemical oscillation. Further studies are under way on the detailed mechanism and behavior of this chemical oscillator.

References

1) "Oscillations and Traveling Waves in Chemical Systems," ed by R. J. Field and M. Burger, Wiley, New York (1985).
2) P. De Kepper, I. R. Epstein, and K. Kustin, *J. Am. Chem. Soc.*, **103**, 6121 (1981).
3) G. A. Papsin, A. Hanna, and K. Showalter, *J. Phys. Chem.*, **85**, 2575 (1981).
4) M. Orban and I. R. Epstein, *J. Am. Chem. Soc.*, **104**, 5918 (1982).
5) J. L. Hudson, M. Hart, and D. Marinko, *J. Chem. Phys.*, **67**, 1601 (1979).
6) M. Orban and I. R. Epstein, *J. Phys. Chem.*, **86**, 3907 (1982).
7) J. L. Hudson and J. C. Markin, *J. Chem. Phys.*, **74**, 6171 (1981).
8) A. Hanna, A. Saul, and K. Showalter, *J. Am. Chem. Soc.*, **104**, 3838 (1982).
9) A. T. Winfree and S. H. Strogatz, *Nature(London)*, **311**, 611 (1984).
10) I. R. Epstein, *J. Phys. Chem.*, **88**, 187 (1984).
11) M. Alamgir, P. De Kepper, M. Orban, and I. R. Epstein, *J. Am. Chem. Soc.*, **105**, 2641 (1983).
12) M. Alamgir and I. R. Epstein, *J. Am. Chem. Soc.*, **105**, 2500 (1983).
13) J. H. Jensen, *J. Am. Chem. Soc.*, **105**, 2639 (1983).
14) M. Burger and R. J. Field, *Nature(London)*, **307**, 720 (1984).
15) M. Orban and I. R. Epstein, *J. Am. Chem. Soc.*, **107**, 2302 (1985).
16) A. Nagy and L. Treindl, *Nature(London)*, **320**, 344 (1986).
17) J. S. Reckley and K. Showalter, *J. Am. Chem. Soc.*, **103**, 7012 (1981).
18) N. Ganapathisubramanian, *J. Phys. Chem.*, **92**, 414 (1988).

19) L Treindl and A. Nagy, *Chem. Phys. Lett.*, **138**, 327 (1987).
20) J. C. Roux, *Physica*, **7D**, 57 (1983).
21) P. Lamba and J. L. Hudson, *Chem. Eng. Commun.*, **32**, 369 (1985).
22) W. M. Latimer, "Oxidation Potentials," 2nd ed., Prentice-Hall, N. J., (1952).
23) F. A. Cotton and G. Wilkinson, "Advanced Inorganic Chemistry," 2nd ed., Wiley, New York (1966).

 © 1988 The Chemical Society of Japan Bull. Chem. Soc. Jpn., 61, 3471—3477 (1988)

The Contents and Distributions of Arsenic, Antimony, and Mercury in Geothermal Waters

Hayao SAKAMOTO,* Masaakira KAMADA, and Norinobu YONEHARA
Department of Chemistry, Faculty of Science, Kagoshima University, Koorimoto, Kagoshima-shi, Kagoshima 890
(Received September 9, 1987)

The contents and distributions of arsenic, antimony, and mercury in geothermal water samples taken from various geothermal areas in Japan were investigated. Since the existing forms of arsenic, antimony, and mercury in geothermal waters are complex and can change during sample storage, it is difficult to determine all of the chemical forms. In this study, therefore, the arsenic(III+V), antimony(III+V), and total mercury contents were determined. In geothermal water, there is a high positive correlation between the contents of arsenic and antimony. However, there is no correlation at all between the contents of mercury and arsenic, or between those of mercury and antimony. It can be assumed that mercury behaves differently from either arsenic or antimony in geothermal water.

In keeping pace with the development of geothermal energy, attention has been paid to the various components of geothermal water, such as that of thermal water or hot spring water. Arsenic, antimony and mercury are included in these components. However, information on the contents, existing forms and distributions of these elements are insufficient. Investigations concerning arsenic have been continuing in view of the environmental contamination caused by the drainage of hot spring water[1] and the use of hot spring water for drinking.[2,3] In some sources of thermal well water obtained for geothermal power generation, there are high concentrations of arsenic; such thermal water is being recharged into underground regions as a counterplan. Investigations into the exclusion treatment of arsenic have also begun.[4]

Since antimony, the homologous element of arsenic, is found in relatively low content, compared to arsenic, and is difficult to analyze, there have not been many reports on antimony in geothermal water compared to those on arsenic. After Holak[5] developed atomic absorption spectrometry for arsenic hydroguret in 1969, determinations of arsenic and antimony in ppb-ppt levels became possible through the work of Fernandedz et al.[6] and Yamamoto et al.[7]

To determine the mercury content, cold vapor atomic absorption spectrometry has been widely employed.[8,9]

Nakagawa[10] and Awaya et al.[11] produced data concerning the mercury content in hot spring water at various locations in Japan.

There have been many reports concerning the arsenic and antimony contents in hot spring water at various specific areas.[12-18] There have also been reports by Watanuki et al.[19] and Sato[20] concerning the arsenic and antimony contents in acidic thermal water. However, there have been no reports concerning measurements of the contents of arsenic, antimony and mercury in the geothermal water found over a wide range of geothermal areas. In this study, we determined the contents of arsenic, antimony and mercury in geothermal water (thermal water, hot spring water and condensed water) sampled at various geothermal areas in Japan. We discuss their existing forms, mutual relations and distributions.

Experimental

Preservation of Sample. Geothermal water samples used for determining arsenic and antimony contents were kept in polyethylene bottles(1 l), which were exuded beforehand by approximately 3 mol dm^{-3} nitric acid for two weeks and then washed thoroughly with water. 10 ml of 35% hydrochloric acid was added to each 1 l of sample at the sampling place as quickly as possible. Samples were then brought back to the laboratory and analyzed.

The samples used in determinations of the mercury content were taken in hard glass bottles, which had been washed in a manner similar to that of the polyethylene bottles used for arsenic and antimony, equipped with Teflon packing. For every 1 l of sample, 10 ml of (1 : 1) (97%) sulfuric acid was added. Samples were then brought back to the laboratory and analyzed. When a sample containing much chloride, such as geothermal water, was preserved at less than pH 1, the loss of mercury was hardly observable. However, for samples containing much sulfide, the loss of arsenic, antimony, and mercury could be observed. In this case, the sulfide and its related compounds were oxidized by a sulfuric acid-potassium permanganate solution and determinations of arsenic, antimony, and mercury were quickly undertaken.

The acids(hydrochloric acid, sulfuric acid) and the potassium permanganate, which were used for measurements of arsenic, antimony and mercury were all analytical, special-reagent grade.

The present investigation aimed to provide a practical method for determining the contents of arsenic and antimony. Regarding arsenic and antimony determination we used the method of Yamamoto et al.,[7] and applied a differential determination of arsenic and antimony to geothermal waters. The procedures are as follows.

Determination of Arsenic. One method for a differential determination of arsenic(III+V) and arsenic(III) is described.

A sample solution (≦40 ml), containing less than 0.5 μg of arsenic(III+V), was placed in a reaction vessel and diluted with water, bringing it to 40 ml. Into this solution, 10 ml of

35% hydrochloric acid and 5 ml of 40% potassium iodide solution were added and the reaction vessel was then put into a hydroguret generator. Then, 1 ml of 3% sodium borohydride in 0.01 mol dm^{-3} sodium hydroxide solution was injected with a syringe over a period of 20 s while stirring with a bar. Arsine was evolved by passing nitrogen through the reaction vessel 70 s after injecting 3% sodium borohydride. The arsine was atomized in a hydrogen-nitrogen flame of an atomic absorption spectrometer and the arsenic(III+V) was determined at a wavelength of 193.7 nm. By using a calibration curve prepared in the same way as the sample, the arsenic(III+V) content could be determined.

In order to determine the content of arsenic(III), the sample solution was diluted with water, bringing it to 40 ml, in a reaction vessel. This solution was adjusted to pH 5—6 by the addition of 1 ml of 40% citric acid and 5 ml of 1 mol dm^{-3} sodium citrate tribasic, set into the hydroguret generator, and treated in the same way as in the procedure for arsenic(III+V).

Determination of Antimony. One method for a differential determination of antimony(III+V) and antimony(III) is described. A sample solution (≦40 ml), containing less than 0.5 μg of antimony(III+V), was placed in a reaction vessel and diluted with water, bringing it to 40 ml. Then, 5 ml of 35% hydrochloric acid and 2.5 ml of 40% potassium iodide solution were added. The vessel was then put into a hydroguret generator and the antimony(III+V) was treated in the same way as during the determination of arsenic(III+V). The amount of antimony(III+V) was determined by a hydrogen-nitrogen flame. The atomic absorption was done at a wavelength of 217.6 nm.

In order to determine the content of antimony(III), a 40 ml sample solution containing less than 0.5 μg was placed in a reaction vessel as in the determination of antimony(III+V). The sample solution was then adjusted to pH 2 by the addition of 2.5 ml of 40% citric acid solution; the antimony(III) was treated in the same way as treating antimony(III+V).

Determination of Mercury. The determination of mercury was achieved according to the method described previously.[9]

Results and Discussion

Existing Forms of Arsenic and Antimony in Geothermal Waters. Geothermal water was sampled and brought back to the laboratory. Then, the change in the arsenic(III) and arsenic(III+V) contents were examined during storage.

The analytical results are shown in Table 1. The contents of arsenic(III) in some samples decreased rapidly while standing after sampling; however, the contents of arsenic(III+V) remained almost constant. A similar result was obtained for antimony.

The underground regions where geothermal water exists are strongly reductive and the abundance ratios of arsenic(III) to arsenic(III+V) and antimony(III) to antimony(III+V) are higher than those of surface

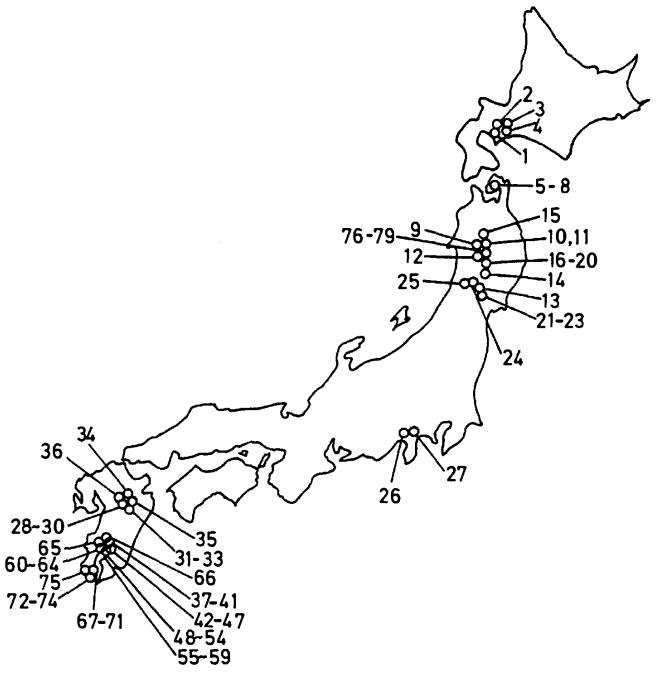

Fig. 1. Map of sampling locations for geothermal waters. 1: Usu, 2, 3: Tōya, 4: Noboribetsu, 5—8: Osorezan, 9: Tamagawa, 10, 11: Ōnuma, 12: Kuroyu, 13: Doroyu, 14: Oyasukyō, 15: Sumikawa, 16—20: Kakkonda, 21—23: Onikoube, 24: Onikoube Arayu, 25: Katayamajigoku, 26: Ōwakudani, 27: Miyanoshita, 28—30: Sujiyu, 31—33: Hattyoubaru, 34: Mizuwaketōge, 35: Takigami, 36: Ōtake, 37—41: Ebino rotenburo, 42—47: Ebino iwōyamashita, 48—54: Iwōdani, 55—59: Maruo, 60—64: Tearai, 65: Kurino, 66: Kurinodake onsen, 67—71: Ibusuki, 72—74: Yamagawa, 75: Kaimon, 76—79: Matsukawa.

Table 1. Change of Arsenic(III) and Arsenic(III+V) Concentration in Hot Spring Waters

Sample[f]	Standing after sampling					
	1 days Content/μg l^{-1}		10 days Content/μg l^{-1}		30 days Content/μg l^{-1}	
	As(III)	As(III+V)	As(III)	As(III+V)	As(III)	As(III+V)
A[a]	0.0	$12._4$	0.0	$12._6$	0.0	$12._4$
B[b]	$80._4$	225	7.0	224	5.0	218
C[c]	$31._4$	$60._8$	2.4	$60._4$	2.0	$59._4$
D[d]	0.9	1.8	1.0	2.0	0.9	1.7
E[e]	5.6	6.3	4.4	6.2	3.8	6.3

a) Ebino rotenburo. b) Iwōdani miyōban onsen. c) Ebino iwōyamashita (1). d) Kirishima kokusaihoteru. e) Ebino iwōyamashita (2). f) 10ml of 35% hydrochloric acid was added to each 1 liter of sample.

Table 2. Analytical Results of Mercury in Various Geothermal Waters

Sampling station	Inorg. Hg	Inorg. Hg+Org. Hg	Total Hg	Remarks
	ng l^{-1}	ng l^{-1}	ng l^{-1}	
Unagionsen(Yamagawa)	3.7	6.3	6.3	Hot spring water
Miyōban(Iwōdani)	0.7	5.0	4.7	Hot spring water
Rotenburo(Ebino)	2.9	4.9	5.0	Hot spring water
Iwōyamashita(Ebino)	1.7	2.2	$18._5$	Hot spring water
Kankyō-chōsasei(Tearai)	2.9	3.2	$10._5$	Thermal water
Fushime(Yamagawa)	8.7	9.9	$11._0$	Thermal water
Ōtake(Ōita)	$10._6$	$13._3$	$14._7$	Thermal water
Matsukawa No. 6 (Matsukawa)	0.1	9910	13700	Condensed water
Matsukawa No. 7 (Matsukawa)	0.1	9020	11400	Condensed water
Kankyō-chōsasei(Tearai)	2.3	4640	4600	Condensed water

Table 3. Analytical Results of Arsenic, Antimony, and Mercury in Geothermal Waters

No.	Sampling location	Date	Temp	pH	As(III+V)	Sb(III+V)	Hg(Total)
			°C		μg l^{-1}	μg l^{-1}	ng l^{-1}
1	Usu(Ginnumakakō)	Nov. 13. '82	90	3.0_6	1.7	0.0_5	$89._8$[a)]
2	Tōya(Soubetsu onsen) (1)	Nov. 14. '82	59.7	6.5_9	910	0.3_8	$10._8$
3	Tōya(Soubetsu onsen) (2)	Nov. 14. '82	67.0	6.4_9	1160	0.2_5	$10._2$
4	Noboribetsu onsen	Oct. 25. '83	87.5	2.5_4	$23._2$	0.8_6	$10._1$
5	Osorezan (1)	Nov. 15. '82	58.0	2.1_6	$16._0$	0.2_0	7.5
6	Osorezan (2)	Nov. 15. '82	59.6	2.0_5	1.4	0.0_5	$37._0$
7	Osorezan (3)	Nov. 15. '82	62.6	2.0_2	1430	0.1_5	$30._8$
8	Osorezan (4)	Nov. 15. '82	61.5	2.0_0	$20._0$	0.0_5	$10._2$
9	Tamagawa onsen Ōubuki	Sept. 8. '82	98.0	1.2_0	3050	7.8	$22._6$
10	Ōnuma (1)	Sept. 8. '82	—	7.9_1	9500	163	$18._7$
11	Ōnuma (2)	Sept. 8. '82	—	7.8_2	8050	153	$19._1$
12	Kuroyu	Sept. 9. '82	86.0	2.9_9	0.3_5	0.0_8	—
13	Doroyu	Sept. 10. '82	97.2	8.1_3	7.0	0.7_5	—
14	Oyasukyō Ōubukiyu	Sept. 10. '82	—	8.3_8	160	$14._7$	$26._5$
15	Dowa kōgyō(Sumikawa)	Sept. 10. '82	93.5	9.3_8	211	$22._6$	$21._1$
16	Kakkonda (1)	Oct. 30. '81	—	8.3_5	3350	146	$43._0$
17	Kakkonda (2)	Oct. 30. '81	87.5	8.6_0	2610	119	$16._6$
18	Kakkonda (3)	Oct. 15. '82	—	8.4_4	4500	147	$13._6$
19	Kakkonda (4)	Oct. 15. '82	—	8.7_8	2100	111	$15._2$
20	Kakkonda(Damushita onsen)	Oct. 30. '81	98.1	8.8_3	435	$26._7$	—
21	Onikoube (1)	Jun. 19. '82	93.0	4.7_0	1310	$17._2$	$21._3$
22	Onikoube (2)	Jun. 19. '82	97.3	7.1_8	1610	$55._2$	$19._0$
23	Onikoube (3)	Jun. 19. '82	97.4	3.4_6	1540	$26._2$	$14._8$
24	Onikoube Arayu	Jun. 19. '82	91.0	1.9_9	215	0.5_1	—
25	Katayamajigoku	Jun. 19. '82	92.1	2.5_0	8.6	1.4_7	—
26	Hakone(Owakudani)	Jul. 15. '83	—	2.3_9	1.8_6	0.0_4	$65._5$
27	Hakone(Miyanoshita-jakotsu)	Jul. 15. '83	86.0	8.0_6	1150	9.6_6	$12._7$
28	Sujiyu(Utaseyu)	Aug. 5. '83	55.3	3.4_9	306	5.1_0	$19._2$
29	Sujiyu(Yakushiyu)	Aug. 5. '83	55.0	3.5_1	330	5.9_0	$4._5$
30	Sujiyu(Oyu)	Aug. 5. '83	44.0	3.8_7	288	5.9_0	$6._3$
31	Hattyoubaru (1)	Aug. 5. '83	97.0	7.3_0	3660	119	$6._8$
32	Hattyoubaru (2)	Aug. 5. '83	96.5	7.1_7	4290	244	$31._6$
33	Hattyoubaru (3)	Aug. 5. '83	92.0	7.4_5	3670	$70._5$	$4._6$
34	Mizuwaketōge	Aug. 6. '83	96.2	8.9_8	480	$21._8$	$2._6$
35	Takigami	Aug. 3. '83	—	9.0_8	332	$13._6$	—
36	Ōtake	Nov. 9. '81	90	8.3_3	2590	$88._8$	$14._7$
37	Ebino rotenburo	Nov. 1. '81	40.5	2.2_3	$15._4$	0.1_5	9.7
38	Ebino rotenburo	Mar. 14. '82	39.0	2.2_5	$41._5$	0.7_0	5.0
39	Ebino rotenburo	Sept. 12. '82	40.5	2.3_1	$10._4$	0.1_5	$11._7$
40	Ebino rotenburo	Aug. 26. '83	39.5	2.3_5	$12._4$	0.3_4	$13._5$
41	Ebino rotenburo	Nov. 25. '83	37.5	2.3_9	7.3	0.2_0	7.1
42	Ebino iwōyamashita	Nov. 1. '81	56.0	1.8_5	$60._5$	0.9_7	$12._2$
43	Ebino iwōyamashita	Jan. 27. '82	45.8	1.8_5	$47._3$	1.0_3	9.8
44	Ebino iwōyamashita	Mar. 14. '82	49.0	1.7_0	$45._7$	1.4_2	9.2
45	Ebino iwōyamashita	Sept. 12. '82	58.5	1.8_4	$60._8$	0.9_3	9.4
46	Ebino iwōyamashita	Aug. 26. '83	57.8	1.8_8	$73._7$	1.0_1	9.7
47	Ebino iwōyamashita	Nov. 25. '83	46.0	1.9_7	$75._6$	0.8_0	6.8

Table 3. (Continued)

No.	Sampling location	Date	Temp °C	pH	As(III+V) $\mu g\,l^{-1}$	Sb(III+V) $\mu g\,l^{-1}$	Hg(Total) $ng\,l^{-1}$
48	Iwōdani miyouban	Jan. 27. '82	58.3	3.0_0	$86._3$	0.0_8	8.5
49	Iwōdani miyouban	Mar. 13. '82	58.5	3.1_2	$88._2$	0.4_5	4.7
50	Iwōdani miyouban	Sept. 12. '82	60.0	3.1_5	225	0.1_3	3.6
51	Iwōdani miyouban(Iwōsen)	Aug. 26. '83	45.8	3.3_3	$77._7$	0.3_8	$10._8$
52	Iwōdani miyouban(Iwōsen)	Nov. 25. '83	50.7	3.3_0	$43._2$	0.0_8	3.4
53	Iwōdani miyouban(Tetsusen)	Aug. 26. '83	61.6	3.1_6	154	0.4_1	8.4
54	Iwōdani miyouban(Tetsusen)	Nov. 25. '83	61.3	3.1_8	104	0.1_3	9.6
55	Maruo 3 gōsen	Dec. 6. '81	76.0	6.4_5	3.8	0.1_8	7.7
56	Maruo 3 gōsen	Jan. 27. '82	77.2	6.5_8	1.7	0.0_5	$54._6$
57	Maruo 3 gōsen	Mar. 13. '82	73.8	6.9_1	2.3	0.0_8	$72._5$
58	Maruo 3 gōsen	Apr. 14. '82	75.5	6.7_1	2.0	0.1_5	$51._7$
59	Maruo 3 gōsen	Sept. 12. '82	76.8	7.7_0	1.3	0.1_0	$61._3$
60	Tearai (1)	Feb. 17. '82	92.5	8.6_8	4410	193	$37._4$
61	Tearai (2)	Feb. 25. '82	93.0	8.3_7	5800	205	$65._5$
62	Tearai (3)	Mar. 10. '82	94.0	8.1_7	7150	231	$10._5$
63	Tearai (4)	Oct. 6. '82	94.2	2.9_4	4450	$92._3$	8.4
64	Tearai (5)	Oct. 23. '82	96.5	2.7_2	5350	$81._0$	$12._9$
65	Kurino KEI-3	Jan. 27. '82	93.5	8.5_4	2650	145	$21._7$
66	Kurinodake onsen	Mar. 13. '82	64.1	1.9_5	1.7	0.1_5	$17._0$
67	Sunaburo(Ibusuki)	Jul. 9. '82	51.8	6.8_1	$77._4$	4.2_0	$11._6$
68	Shokubutsushikenjō(Ibusuki)	Jul. 9. '82	52.0	6.6_2	$32._6$	0.3_0	$16._4$
69	Nigatsuden(Ibusuki)	Jul. 9. '82	59.5	7.0_8	$46._4$	0.3_3	$11._8$
70	Hakusuikan(Ibusuki)	Jul. 9. '82	69.0	6.8_7	155	4.5_0	$13._7$
71	Kokuritsubyōin(Ibusuki)	Jul. 9. '82	78.0	7.8_0	$62._4$	3.6_0	$11._7$
72	Okachogamizu(Yamagawa)	Jul. 9. '82	52.5	7.0_6	$74._0$	1.8_3	9.8
73	Masuda onsen(Yamagawa)	Jul. 9. '82	76.0	8.0_8	109	7.5_8	3.8
74	Fushime(Yamagawa)	Jul. 9. '82	89.5	6.5_7	1540	$73._6$	$27._9$
75	Kaimonsou(Kaimon)	Jul. 9. '82	39.2	7.7_1	$30._6$	1.1_0	$10._7$
76	Matsukawa (1)[b]	Oct. 28. '81	—	—	121	0.4_8	15900
77	Matsukawa (2)[c]	Oct. 28. '81	—	—	$97._3$	0.5_3	13700
78	Matsukawa (3)[d]	Oct. 28. '81	—	—	320	0.4_2	11400
79	Matsukawa (4)[e]	Oct. 29. '81	—	—	114	0.3_5	—

a) Stored in a polyethylene bottle. b), c), d), e): Condensed water.

water. After sampling, the arsenic(III) and antimony(III) were exposed to an oxidative atmosphere and may have been converted to arsenic(V) and antimony(V), respectively.

Since arsenic(III) and antimony(III) in geothermal water can change, depending on the storage conditions of the sample, any determination of arsenic(III) and antimony(III) must be carried out in as short a time as possible after sampling.

Existing Forms of Mercury in Geothermal Waters. The analytical results of the existing chemical forms are shown in Table 2.

In thermal water and hot spring water, there is no great difference in the contents of soluble inorganic mercury, soluble inorganic plus organic mercury, and total mercury. It may be noted that mercury in thermal water and hot spring water exists in almost soluble inorganic mercury. However, for volcanic gas condensed water, which contains much hydrogen sulfide, the amount of soluble inorganic plus organic mercury and the total amount of mercury is more than that of soluble inorganic mercury. This does not suggest that there is not much soluble inorganic mercury in volcanic gas condensed water, but implies that the reduction of soluble inorganic mercury is difficult because of the interference of sulfide ion. Therefore, it is difficult to determine the amount of soluble inorganic mercury and organic mercury in geothermal water samples which contain much sulfide ion.

Table 4. Arsenic, Antimony, and Mercury Contents in Geothermal Waters

Element	Range[a]	n[b]	$\bar{X}_A$[c]	$\bar{X}_G$[d]
As	0.35—9500	75	1230	141
Sb	0.05— 244	75	$35._4$	2.5_0
Hg	2.6 — $89._8$	69	$19._1$	$13._8$

a—c) in $\mu g\,l^{-1}$ for As, Sb and $ng\,l^{-1}$ for Hg. b) Number of samples. c) Arithmetic mean. d) Geometric mean.

The Arsenic, Antimony, and Mercury Contents in Geothermal Waters. The arsenic(III+V), antimony(III+V), and total contents of mercury were determined for geothermal water sampled from various geothermal areas in Japan. The sampling stations are illustrated in Fig. 1 and analytical results are tabulated in Table 3. Below, we discuss the data listed in Table 3.

The range, arithmetic and geometric mean of the arsenic, antimony, and mercury contents and the

number of samples measured, except for gas condensed water, are shown in Table 4.

Using the mean content of arsenic, antimony, and mercury in igneous rocks, accepted to be 1.5,[21] 0.2,[22] and 0.08[23] ppm, respectively, the gravimetric ratios of As/Sb, Sb/Hg, and As/Hg can be calculated as being 7.5, 2.5, and 19, respectively. From the values listed in Table 4, the gravimetric ratios of As/Sb, Sb/Hg, and As/Hg in geothermal water were calculated to be 56, 179 and 10000, respectively. Watanuki et al.[19] have reported that the gravimetric ratio of As/Sb in the Tamagawa and Kusatsu hot springs to be 100 and 50, respectively.

The antimony and mercury contents in geothermal water are smaller compared to the arsenic content. The reasons involve (assuming the differences of the composition of thermal water which comes into contact with igneous rock) the ease of sulfide precipitation and gas scattering in the atmosphere.

Mutual Relation of Arsenic, Antimony, and Mercury in Geothermal Waters. The mutual relation among arsenic, antimony and mercury contents in geothermal waters is shown in Figs. 2—4.

In geothermal water, there is a high positive correlation between the arsenic and antimony contents (correlation coefficient, 0.87). However, the correlation coefficients between the contents of arsenic and mercury or between that of antimony and mercury were 0.065 and 0.15, respectively, showing no correlation between arsenic and mercury or between antimony and mercury. This suggests that mercury behaves differently from arsenic and antimony in geothermal water.

Distributions of Arsenic, Antimony, and Mercury in Geothermal Waters. The frequency distributions of the arsenic, antimony, and mercury contents in geothermal water are shown in Figs. 5—7.

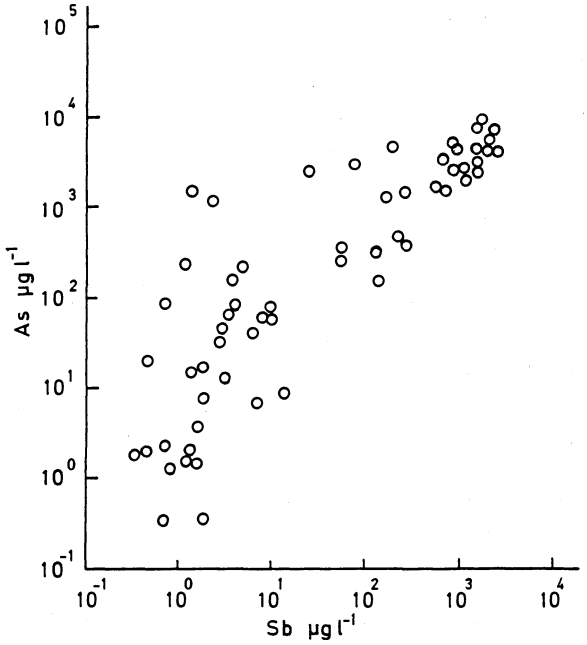

Fig. 2. Relation between arsenic and antimony in geothermal waters.

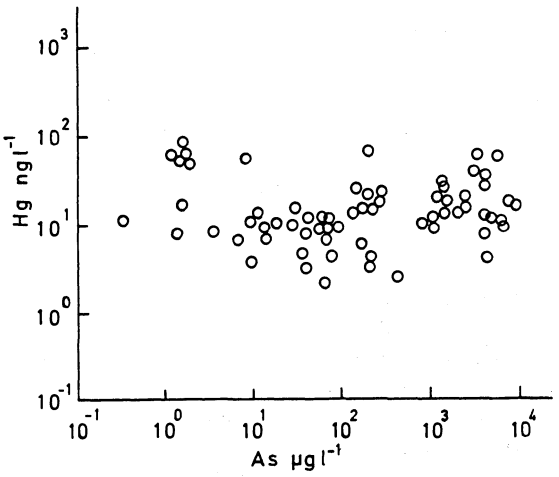

Fig. 3. Relation between mercury and arsenic in geothermal waters.

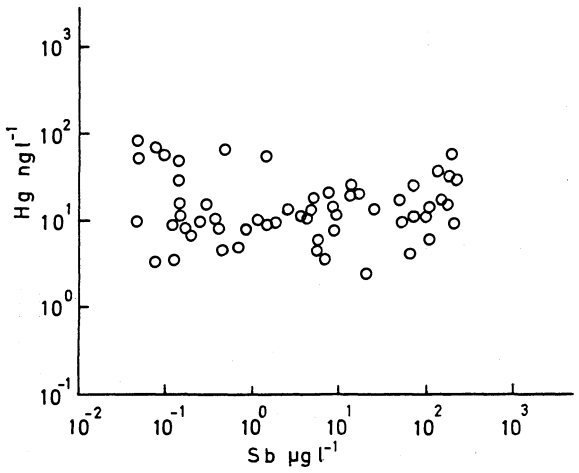

Fig. 4. Relation between mercury and antimony in geothermal waters.

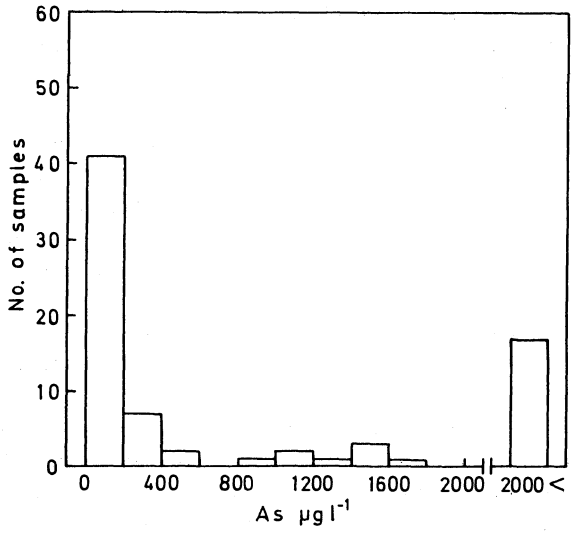

Fig. 5. Frequency for arsenic content distributions of geothermal waters.

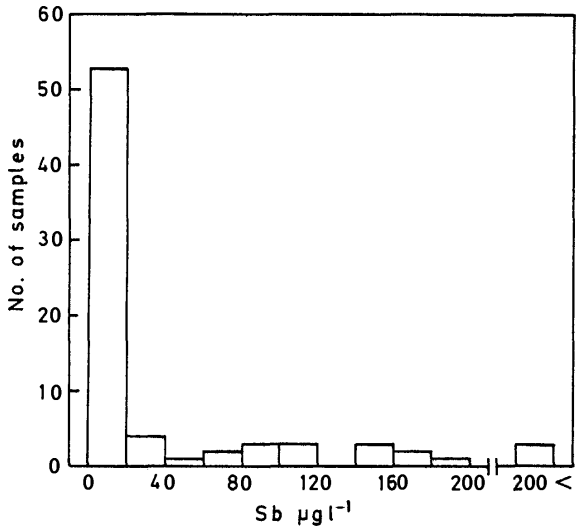

Fig. 6. Frequency for antimony content distributions of geothermal waters.

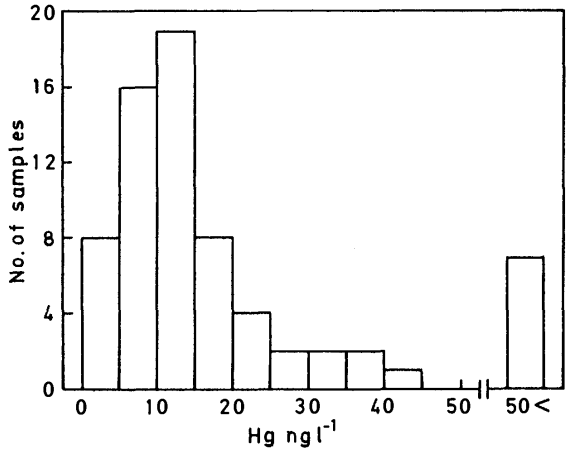

Fig. 7. Frequency for mercury content distributions of geothermal waters.

The distributions of arsenic and antimony are similar in the sense that they are spread over wide concentration range. On the other hand, except for a few of the samples, the mercury is limited to an extremely narrow concentration range.

One of the specificities of arsenic and antimony contents (cf. Table 3) in geothermal water is that the arsenic and antimony contents in a thermal water system (Ōnuma, Kakkonda, Onikoube, Ōtake, and others) tend to be larger than those in a vapor dominated system (Matsukawa).

The arithmetic and geometric means of the total mercury content in geothermal water for 69 samples, except for gas condensed water, are $19._1$ ng l^{-1} and $13._8$ ng l^{-1} respectively. Except for a few samples, there was no great difference in the mercury content from different geothermal areas; the mercury content in geothermal water was smaller than that of the arsenic and antimony contents. The range of the mercury content in the gas condensed water at Matsukawa was 11400—15900 ng l^{-1}; this concentration in gas condensed water is as much as a 1000 times higher than that found in general thermal waters. This seems to correlate with the fact that mercury is a component which changes easily to the gas phase.

No correlation between pH and the content of arsenic, antimony or mercury in geothermal water could be observed.

Conclusion

We have determined the arsenic, antimony, and mercury contents in geothermal water. The range of arsenic(III+V), antimony(III+V), and the total contents of mercury in geothermal water were 0.35—9500 μg l^{-1}, 0.05—244 μg l^{-1}, 2.6—$89._8$ ng l^{-1}, respectively, their arithmetic means were 1230 μg l^{-1}, 35.4 μg l^{-1}, and $19._1$ ng l^{-1}, respectively, and their geometric means were 141 μg l^{-1}, 2.5_0 μg l^{-1}, and $13._8$ ng l^{-1}, respectively.

There is a high positive correlation between the arsenic and antimony contents in geothermal water, but there is no correlation between the mercury and arsenic contents or between the mercury and antimony contents. It is assumed that mercury behaves differently from arsenic or antimony in geothermal water.

The arsenic and antimony contents in geothermal water tend to be larger in the thermal water of thermal water systems compared to the thermal water (condensed water) of vapor dominated systems.

On the other hand, except for a few cases, there is not much difference in the total mercury content of geothermal water in different geothermal areas. Mercury is thought to be a component which can not exit in high concentrations in geothermal water (thermal water and hot spring water).

The authors wish to express their thanks to Professor Yuroku Yamamoto of Fukui Institute of Technology (previously Hiroshima University) and Professor Takejiro Ozawa of Saitama University for their helpful advice.

Thanks are also due to my many colleagues with whom we have discussed the problems of analytical methodology. The present work was partially supported by a Grant-in-Aid for Scientific Research Nos. 56030070, 57030066, and 58030061 from the Ministry of Education, Science and Culture.

References

1) H. Numata and M. Kawanishi, *Yamanashi Eiken Houkoku*, **22**, 40 (1978).

2) Ooitaken kougaieisei senta-, Ooitaken kankyoukanrika, *Ooitaken onsen chousa houkoku*, **28**, 53 (1977).

3) N. Mizoguchi and Y. Ninomiya, *Ooitaken onsen chousa houkoku*, **22**, 90 (1971).

4) K. Yanagase, T. Yoshinaga, and K. Kawano, *Bunseki Kagaku*, **32**, T111 (1983).

5) W. Holak, *Anal. Chem.*, **41**, 1712 (1969).

6) F. J. Fernandez and D. C. Manning, *At. Abs. News Lett.*, **10**, 86 (1971).
7) M. Yamamoto, K. Urata, K. Murashige, and Y. Yamamoto, *Spectrochim. Acta*, **36B**, 671 (1981).
8) R. Nakagawa, *Nippon Kagaku Kaishi*, **1974**, 71 (1974).
9) H. Sakamoto and M. Kamada, *Nippon Kagaku Kaishi*, **1981**, 32 (1981).
10) R. Nakagawa, *Nippon Kagaku Kaishi*, **1982**, 1909 (1982).
11) T. Awaya, T. Hirano and Y. Oki *Kanagawaken Onsen Houkoku*, **7**, 43 (1976).
12) K. Watanuki, *Sci. Pap. Coll. Gen. Educ. Univ. Tokyo*, **11**, 205 (1961).
13) K. Watanuki, *Sci. Pap. Coll. Gen. Educ. Univ. Tokyo*, **13**, 191 (1963).
14) Y. Sakai and T. Takishima, *Onsenkagaku*, **26**, 13 (1975).
15) N. Mutou, T. Nakayama, S. Katumata, and T. Kitabayashi, *Akitaken Eiken Houkoku*, **23**, 157 (1980).
16) E. Minami, G. Sato, and K. Watanuki, *Nippon Kagaku Zasshi*, **78**, 1096 (1957).
17) E. Minami, G. Sato, and K. Watanuki, *Nippon Kagaku Zasshi*, **79**, 860 (1958).
18) Y. Sakai, Y. Hara, and T. Takishima, *Onsenkagaku*, **27**, 127 (1977).
19) K. Watanuki, B. Takano, T. Kiriyama, Y. Sakai, Y. Hara, and T. Takishima, *Jinetu*, **13**, 207 (1976).
20) A. Sato, *Onsenkougakukaishi*, **10**, 89 (1975).
21) "Handbook of Geochemistry," Springer (1969), Vol. II-4, 33-E-4.
22) "Handbook of Geochemistry," Springer (1969), Vol. II-4, 51-E-3.
23) "Handbook of Geochemistry," Springer (1969), Vol. II-5, 80-E-1.

 © 1988 The Chemical Society of Japan Bull. Chem. Soc. Jpn., 61, 3479—3484 (1988)

^{57}Fe-Mössbauer and ^{13}C-CP-MAS NMR Spectroscopic Studies of the Reaction Products of Ferrocene Derivatives with Mercury(II) Salts

Masanobu WATANABE, Yuichi MASUDA, Izumi MOTOYAMA, and Hirotoshi SANO*
Department of Chemistry, Faculty of Science, Tokyo Metropolitan University, Fukasawa, Setagaya-ku, Tokyo
(Received January 26, 1988)

The unstable adducts of ferrocene and methylferrocene and the stable adducts of biferrocene, diferrocenylmethane, 1,2-diferrocenylethane, and [*n*]ferrocenophane (*n*=2, 3) with HgX_2 (X=Cl, Br, I, and BF_4) were studied by means of ^{57}Fe-Mössbauer and high-resolution solid-state ^{13}C NMR spectroscopies. The large quadrupole splitting (Q. S.) values in the ^{57}Fe-Mössbauer and the large low-field shifts in the ^{13}C-CP-MAS NMR, spectroscopy suggest the presence of a direct chemical bond between the Fe and Hg atoms.

All attempts to prepare a stable $HgCl_2$ adduct of ferrocene have been unsuccessful and have given green-colored paramagnetic ferrocenium-type salts after standing for a day. However, stable light-colored diamagnetic adducts of biferrocene, diferrocenylmethane, and 1,2-diferrocenylethane with $HgCl_2$ could be prepared.[1,2] It was shown in our previous reports that [2]ferrocenophane derivatives give much more stable adducts in reactions with Lewis acids, $SnCl_4$, $HgCl_2$, $CdCl_2$, and I_2,[3-6] whereas binuclear ferrocene derivatives could be oxidized to their ferrocenium-type salts in reactions with Lewis acids other than $HgCl_2$. These results can be explained by assuming that [2]ferrocenophanes have less steric hindrance in donating e_{2g} electrons than ferrocene and binuclear ferrocene derivatives, on the basis of ^{57}Fe- and ^{119}Sn-Mössbauer spectroscopics, which provide direct information concerning the iron and tin atoms concerned with bond formation. X-Ray diffraction studies of the I_2 adduct with 1,1,2,2-tetramethyl[2]ferrocenophane show that the Fe atoms squeezed out of the tilted cyclopentadienyl (Cp) structure have I atoms at a short distance (2.675 Å),[6] much shorter than the sum of the van der Waals radii of the Fe and I atoms. Applications of ^{13}C-CP-MAS NMR spectroscopy to the reaction products of ferrocene and ruthenocene derivatives with various Lewis acid adducts have proved its sensitivity to the changes in structural distortion caused by adduct formation and have provided additional information; e.g., the large low-field shift of peaks ascribed to Cp rings of the ruthenocene suggests the formation of direct chemical bonds between the Ru atom and the Lewis acids (I^+, Hg^{2+}, and Sn^{4+}) in the adducts, as has already been verified by means of X-ray diffraction[8,9] and ^{119}Sn-Mössbauer spectroscopic studies.[10] The present studies were carried out in order to cross-examine the bond formation between the metal atoms in ferrocene derivative adducts with HgX_2 and the structural distortion associated with adduct formation by using both ^{57}Fe-Mössbauer spectroscopy and high-resolution ^{13}C-CP-MAS NMR spectroscopy.

Experimental

Materials: The reaction products of ferrocene,[8] biferrocene,[1] diferrocenylmethane,[2] 1,2-diferrocenylethane,[2] and [2]ferrocenophane[4] with $HgCl_2$ were prepared by the previously reported methods. The $HgCl_2$ adducts of methylferrocene and [3]ferrocenophane were first prepared by a method similar to that used in the case of ferrocene-7$HgCl_2$ adduct.[8] The purities of the adducts were confirmed by elemental analysis. Found: C, 7.03; H, 0.75%. Calcd for methylferrocene-6$HgCl_2$, $C_{11}H_{12}FeHg_6Cl_{12}$: C, 7.22; H, 0.66%. Found: C, 8.54; H, 0.84%. Calcd for [3]ferrocenophane-6$HgCl_2$, $C_{13}H_{14}FeHg_6Cl_{12}$: C, 8.42; H, 0.76%. Adducts of [2]ferrocenophane with $HgBr_2$ and HgI_2 were prepared in diethyl ether and benzene solution, respectively, by a method similar to that used in the preparation of [2]ferrocenophane-3$HgCl_2$ adduct.[4] A red-orange precipitate was filtered, washed with diethyl ether, and dried under vacuum. Found: C, 12.57; H, 1.16%. Calcd for [2]ferrocenophane-2.5$HgBr_2$, $C_{12}H_{12}FeHg_{2.5}Br_5$: C, 12.93; H,1.08%. Found: C, 11.86; H, 1.02%. Calcd for [2]ferrocenophane-2.2HgI_2, $C_{12}H_{12}FeHg_{2.2}I_{4.4}$: C, 11.89; H, 0.99%.

Measurements: ^{57}Fe-Mössbauer spectroscopic measurements were carried out by using a ^{57}Co(Rh) source moving in a constant acceleration mode. The isomer shift (I. S.) value for the ^{57}Fe-Mössbauer spectroscopic measurements was taken with respect to metallic iron; the experimental error of the I. S. and Q. S. values was estimated to be within ±0.02 mm s^{-1}.

The ^{13}C-CP-MAS NMR spectra were obtained under the same conditions as in the case of our previous reports.[7] The chemical-shift values were measured with respect to external adamantane and then converted to the shift values from TMS. Both the ^{1}H and ^{13}C NMR spectra in solution were measured by using a JEOL FX-200 spectrometer at 200.0 and 50.1 MHz, respectively, using TMS as a standard. The assignment of the ^{13}C signals of the metallocenes was carried out by selective proton decoupling experiments.

Results and Discussion

It has already been known that ferrocene gives an unstable orange-yellow diamagnetic ferrocene-7$HgCl_2$ adduct in a reaction with $HgCl_2$ in diethyl ether.[9] No ^{1}H NMR signals of the ferrocene-7$HgCl_2$ adduct could be obtained in acetonitrile solution because of oxida-

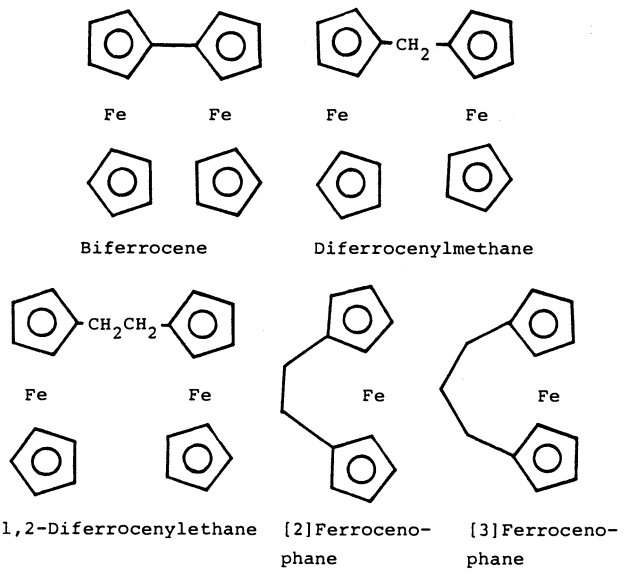

tion to the ferrocenium salt of the adduct. This smaller stability of the adduct in solution is one of the large differences from that of ruthenocene-3$HgCl_2$ adduct (i.e., the $HgCl_2$ adduct of ruthenocene is stable in the acetonitrile, giving a large low-field shift ($\Delta\delta$; 0.84 ppm)[7] caused by the direct chemical bond between the Ru and Hg atoms as already verified from X-ray diffraction studies[8]). In order to avoid the experimental difficulties associated with the lower stability of the ferrocene-7$HgCl_2$ adduct in solution, ^{13}C-CP-MAS NMR spectroscopic measurements of the solid adduct were carried out in the present studies.

A π-C_5H_5 ring carbon signal (δ) in the ferrocene appears at δ=69.8, while a broader signal of the $HgCl_2$ adduct appears at δ=79.7, as shown in Figs. 1-a, and b and Table 1. A large low-field shift ($\Delta\delta$; 9.9 ppm) has

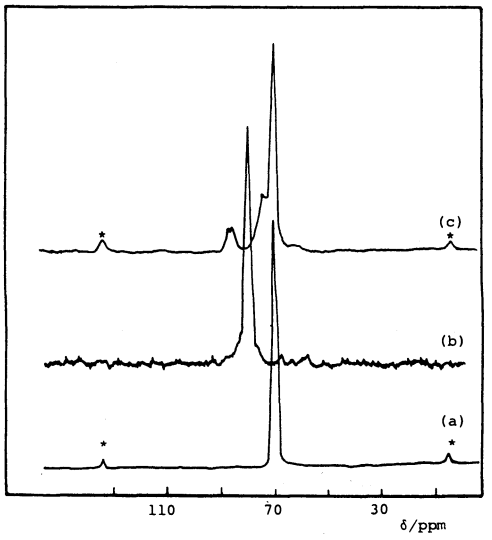

Fig. 1. ^{13}C-CP-MAS NMR spectra of ferrocene(a), its 7$HgCl_2$(b) adduct, and chloromercurioferrocene(c). The sample spinning side band (SSB) is represented by * in the Figure.

Table 1. ^{13}C-Chemical Shift Values of Ferrocene Derivatives and Their Mercury(II) Halides Adducts

Compound	Chemical shift value δ/ppm
Ferrocene	69.8(C_5H_5)
Ferrocene-7$HgCl_2$	79.7(C_5H_5)
Biferrocene	84.8(C_1)
	70.7(C_5H_5)
	67.1($C_{2,5}$, $C_{3,4}$)
Biferrocene-2$HgCl_2$	79.7(C_5H_5)
	71.4($C_{2,5}$, $C_{3,4}$)
Diferrocenylmethane	91.3, 86.6(C_1)
	70.1(C_5H_5)
	31.3(CH_2)
Diferroceneylmethane-6$HgCl_2$	91.4(C_1)
	78.9(C_5H_5, $C_{2,5}$, $C_{3,4}$)
	31.0(CH_2)
1,2-Diferrocenylethane	90.1(C_1)
	70.0(C_5H_5, $C_{2,5}$, $C_{3,4}$)
	36.6(CH_2CH_2)
1,2-Diferrocenylethane-6$HgCl_2$	91.9(C_1)
	78.4(C_5H_5, $C_{2,5}$, $C_{3,4}$)
	31.7(CH_2CH_2)
[2]Ferrocenophane	92.6(C_1)
	75.0($C_{2,5}$)
	70.8($C_{3,4}$)
	35.3(CH_2CH_2)
[2]Ferrocenophane-3$HgCl_2$	114.2(C_1)
	78.6($C_{2,5}$, $C_{3,4}$)
	35.1(CH_2CH_2)
[2]Ferrocenophane-2.5$HgBr_2$	119.6(C_1)
	83.0($C_{2,5}$)
	77.2($C_{3,4}$)
	35.6(CH_2CH_2)
[2]Ferrocenophane-2.2HgI_2	116.7(C_1)
	81.8($C_{2,5}$,$C_{3,4}$)
	36.3(CH_2CH_2)
[2]Ferrocenophane-0.5$Hg(BF_4)_2$	118.8, 117.3(C_1)
	81.8, 75.0($C_{2,5}$, $C_{3,4}$)
	34.1(CH_2CH_2)
[3]Ferrocenophane	86.6(C_1)
	70.5($C_{2,5}$, $C_{3,4}$)
	36.0(CH_2CH_2*CH_2)
	25.4(CH_2*CH_2CH_2*)
[3]Ferrocenophane-6$HgCl_2$	110.7(C_1)
	78.8—72.6($C_{2,5}$, $C_{3,4}$)
	35.7(CH_2CH_2*CH_2)
	24.6(CH_2*CH_2CH_2*)

been found in ferrocene-7$HgCl_2$ adduct, as in the case of ruthenocene-3$HgCl_2$ adduct ($\Delta\delta$; 8.0 ppm).[7] On the other hand, no low-field shift has been observed for the chloromercurioferrocene, (C_5H_5)(C_5H_4HgCl)Fe, in which a chloromercurio group (HgCl) is attached to the Cp-ring.[11] The ^{13}C chemical-shift value of the Cp-ring in the chloromercurioferrocene (δ=70.5) is very similar to that of ferrocene itself (δ=69.8) in the solid state, as can be seen in Figs. 1-a and c. These facts clearly indicate that the large low-field shift observed in the ferrocene-7$HgCl_2$ adduct can be ascribed to a chemical bond formed between the Fe and Hg atoms, as previously indicated on the basis of the anomalously large Q. S. value (3.09 mm s^{-1} at 80 K) in the

^{57}Fe-Mössbauer spectrum of the $HgCl_2$ adduct.[12]

It is suggested that an enhanced ligand-to-metal donation of the electrons from the Cp-ring associated with the Fe-Hg or Ru-Hg bond formation should result in a decreased in the electron density around Cp-ring carbons in the adducts, giving the large low-field shift of the Cp-ring observed in the adducts.

Similar Fe-Hg bond formation has also been found for the $HgCl_2$ adduct of methylferrocene. Methylferrocene reacts with $HgCl_2$ in diethyl ether and gives an orange-yellow $HgCl_2$ adduct, expressed as methylferrocene-6$HgCl_2$ on the basis of an elemental analysis. The $HgCl_2$ adduct is less stable than the ferrocene-7$HgCl_2$ adduct; i.e., its color changes to green for a few hours at room temperature, suggesting the oxidation of methylferrocene, while the color of the ferrocene-7$HgCl_2$ remains unchanged for a slightly longer period than that of methylferrocene-6$HgCl_2$. Attempts to obtain a clear ^{13}C-CP-MAS NMR spectrum of the methylferrocene-6$HgCl_2$ adduct have been unsuccessful, probably because of the formation of paramagnetic oxidized species. However, an anomalously large Q. S. value (3.02 mm s^{-1} at 78 K) is actually found in the ^{57}Fe-Mössbauer spectroscopy of the methylferrocene- 6$HgCl_2$ adduct. These facts indicate the presence of a less-stable bond formed between the Fe and Hg atoms in the adduct.

The $HgCl_2$ adduct of biferrocene has been found to be much more stable than the ferrocene-7$HgCl_2$ adduct; i.e., its color remains unchanged for more than 200 days upon standing at room temperature.[1] The ^{13}C chemical-shift values of the biferrocene in $CDCl_3$ solution have been found to be δ=83.9 (C_1), 69.2 (C_5H_5), 67.6 ($C_{3,4}$), and 66.4 ($C_{2,5}$), as illustrated in Fig. 2-c. Relatively sharp signals are observed for the biferrocene in the solid state and broader signals for the $HgCl_2$ adduct, as shown in Fig. 2-b. The signals of $C_{2,5}$, $C_{3,4}$, and C_1 of the $HgCl_2$ adduct cannot be well-resolved, being superimposed on the main C_5H_5-ring signal. Therefore, only the low-field shift values of π-C_5H_5 will be discussed. The large low-field shift of the main C_5H_5-ring signal ($\Delta\delta$; 9.0 ppm) is observed and the value is a little smaller than that of ferrocene-7$HgCl_2$ ($\Delta\delta$; 9.9 ppm). The result of ^{13}C-CP-MAS NMR spectroscopy is in line with that of the ^{57}Fe-Mössbauer study; i.e., the Q. S. value of the biferrocene-2$HgCl_2$ adduct (2.93 mm s^{-1} at 78 K) is a little smaller than that of the ferrocene-7$HgCl_2$ adduct (3.09 mm s^{-1} at 80 K).[12] Both results indicate that the chemical bond between the Fe and Hg atoms in the biferrocene-2$HgCl_2$ adduct is slightly weaker than that of

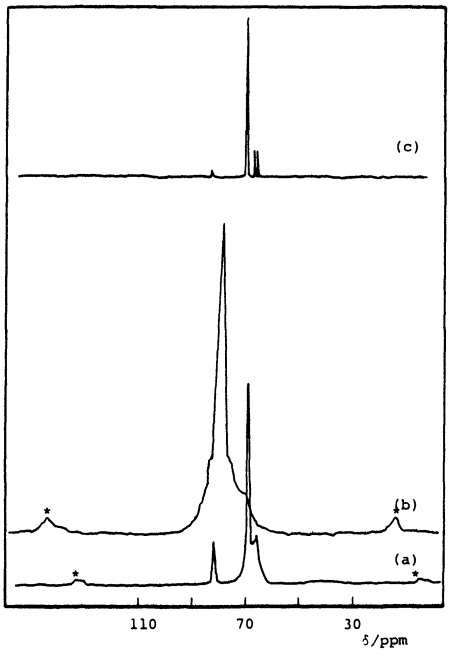

Fig. 2. ^{13}C-CP-MAS NMR spectra of biferrocene(a), its 2$HgCl_2$(b) adduct, and ^{13}C NMR spectrum of biferrocene(c) in chloroform solution.

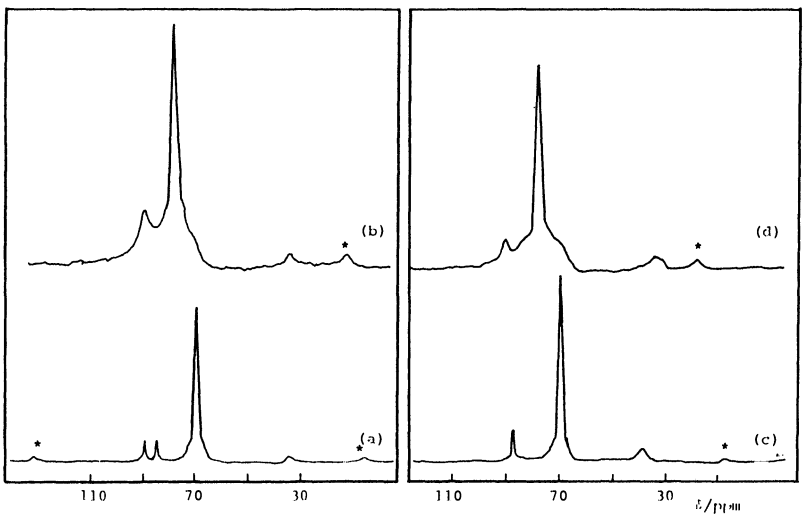

Fig. 3. ^{13}C-CP-MAS NMR spectra of diferrocenylmethane(a), its 6$HgCl_2$(b), 1,2-diferrocenylethane(c), and its 6$HgCl_2$(d) adduct.

the ferrocene-7$HgCl_2$ adduct. One of the possible explanations for the much larger stability of the biferrocene-2$HgCl_2$ adduct, than the ferrocene-7$HgCl_2$ adduct, can be given by assuming that biferrocene reacts with a mercury(II) atom as a chelating agent, such as $[(C_5H_5)(\overline{C_5H_4})Fe\rightarrow HgCl_2\leftarrow Fe(\overline{C_5H_4})(C_5H_5)]$.

Similar large Q. S. components (3.02 and 3.00 mm s^{-1} both at 78 K) have been observed for diferrocenylmethane-6$HgCl_2$ and 1,2-diferrocenylethane-6$HgCl_2$ adducts, respectively,[2] suggesting a chemical bond formation between the Fe and Hg atoms in the adducts. Slightly smaller but similar $\Delta\delta$ values of the Cp-rings have been observed ($\Delta\delta$; 8.8 and 8.4 ppm for the $HgCl_2$ adducts of diferrocenylmethane and 1,2-diferrocenylethane, respectively) compared with the value for biferrocene-2$HgCl_2$ adduct ($\Delta\delta$; 9.0 ppm). The slightly smaller $\Delta\delta$ values of these Cp-rings may be expected for a slightly weaker bond between the Fe and Hg atoms in the adducts. Changes in the color of the diferrocenylmethane and 1,2-diferrocenylethane-6$HgCl_2$ adducts from orange-yellow to blue-green within several days at room temperature after preparation also suggest a less-stable Fe-Hg bond formation.

All of the above-mentioned results lead us to the conclusion that there is a direct interaction between the Fe and Hg atoms in the $HgCl_2$ adducts of ferrocene, methylferrocene, biferrocene, diferrocenylmethane, and 1,2-diferrocenylethane. The smaller stability of the adducts of diferrocenylmethane and 1,2-diferrocenylethane, compared with that of biferrocene-2$HgCl_2$ adduct, may be ascribed to a larger distance between the Fe-Fe atoms for chelation in the adducts.

Table 2. ^{57}Fe-Mössbauer Parameters of Ferrocene Derivatives and Their Mercury(II) Salt Adducts

Compound	Temperature K	Q. S. mm s^{-1}	I. S. mm s^{-1}
Ferrocene	78	2.41	0.52
Ferrocene-7$HgCl_2$[a]	80	3.09	0.53
Methylferrocene	78	2.42	0.52
Methylferrocene-6$HgCl_2$	78	3.02	0.50
Biferrocene	78	2.33	0.53
Biferrocene-2$HgCl_2$	78	2.93	0.55
Diferrocenylmethane	78	2.38	0.52
Diferrocenylmethane-6$HgCl_2$	78	3.02	0.53
1,2-Diferrocenylethane	78	2.40	0.50
1,2-Diferrocenylethane-6$HgCl_2$	78	3.00	0.50
[2]Ferrocenophane	78	2.41	0.49
	300	2.34	0.42
[2]Ferrocenophane-3$HgCl_2$	78	3.29	0.49
[2]Ferrocenophane-2.5$HgBr_2$	78	3.08	0.52
[2]Ferrocenophane-2.2HgI_2	78	3.12	0.52
[2]Ferrocenophane-0.5$Hg(BF_4)$	78	3.11	0.53
	300	3.10	0.46
[3]Ferrocenophane	78	2.29	0.52
[3]Ferrocenophane-6$HgCl_2$	78	2.93	0.53

a) Date was taken from Ref. 12.

As mentioned in the introduction, [2]ferrocenophane gives stable adducts with some Lewis acids. The adducts were investigated by means of the same methods used for the binuclear ferrocene derivative-Lewis acid adducts for the sake of comparison. Slightly smaller Q. S. values for [2]ferrocenophane-HgX_2 (3.08 and 3.12 mm s^{-1} at 78 K for $HgBr_2$ and HgI_2, respectively) than the value of the $HgCl_2$ adduct (3.29 mm s^{-1} at 78 K) were found, but these values are much larger than the value of [2]ferrocenophane itself (2.41 mm s^{-1} at 78 K), as can be seen in Table 2. These facts indicate the presence of a stable bond between the Fe and Hg atoms in the $HgBr_2$ and HgI_2 adducts, as in the case of the $HgCl_2$ adduct.

The ^{13}C chemical shift values of [2]ferrocenophane in $CDCl_3$ were found to be δ=91.2 (C_1), 72.2 ($C_{2,5}$), 67.9 ($C_{3,4}$), and 33.7 (CH_2CH_2). The assignment of the carbon signals was made by using the same method as that in the case of biferrocene on the basis of the results of [n]ferrocenophane (n=1,2) derivatives.[13] Relatively sharp signals have been found for [2]ferrocenophane and broader signals for the HgX_2 adducts in the solid state. The ^{13}C chemical-shift values of $C_{2,5}$ and $C_{3,4}$ for the $HgCl_2$ adduct (δ=78.6) are almost the same as those of the $HgCl_2$ adducts of ferrocene (δ=79.7) and biferrocene (δ=79.7). One of the most striking features is the low-field shift value of the C_1 signal (about $\Delta\delta$; 21.6) in the adduct. This value is anomalously large in com-

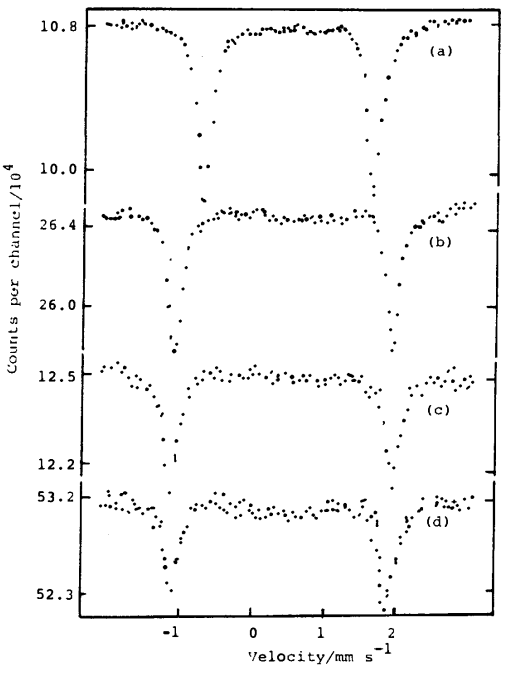

Fig. 4. ^{57}Fe-Mössbauer spectra of [2]ferrocenophane(a), its 2.5$HgBr_2$(b), 2.2HgI_2(c) adducts, and [3]ferrocenophane-6$HgCl_2$(d) adducts.

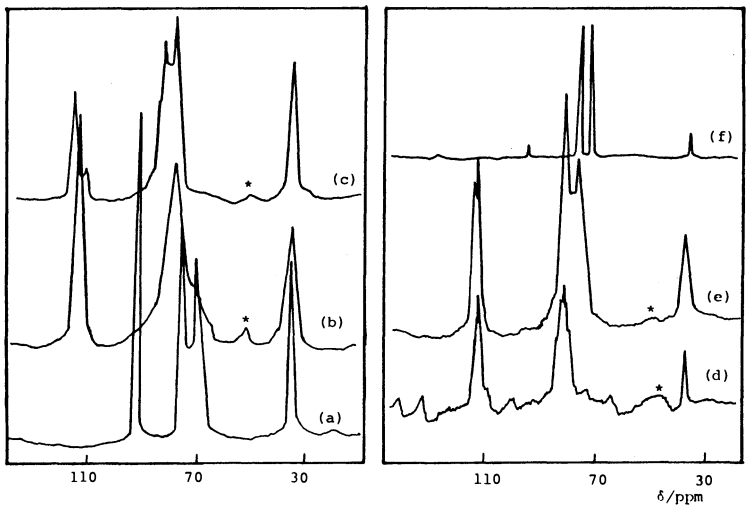

Fig. 5. ^{13}C-CP-MAS NMR spectra of [2]ferrocenophane(a), its $3HgCl_2$(b), $2.5HgBr_2$(c), $2.2HgI_2$(d), $0.5Hg(BF_4)_2$(e) adducts, and ^{13}C NMR spectrum of [2]ferrocenophane(f) in chloroform solution.

parison with the values of most adducts of ferrocene and ruthenocene derivative; i.e., most low-field shift values of the $HgCl_2$ adducts of ferrocene and ruthenocene derivatives are within the range 8.0 to 10.0 ppm.[7] Anomalously large low-field shifts of the C_1 signal were also observed for other [2]ferrocenophane-$2.5HgBr_2$ and -$2.2HgI_2$ adducts ($\Delta\delta$; 27.0 and 24.1 ppm, respectively). Moreover, the splittings (δ=118.8 and 117.3) and large low-field shifts of the C_1 signal ($\Delta\delta$; 26.2 and 24.7 ppm), shown in Fig. 5-f for a [2]ferrocenophane-$0.5Hg(BF_4)_2$ adduct, suggest the presence of two kinds of conformations of the Cp rings in the $Hg(BF_4)_2$ solid adduct.

A large low-field shift of the C_1 signal was also observed in the [3]ferrocenophane-$6HgCl_2$ adduct. [3]Ferrocenophane gives a less stable $HgCl_2$ adduct than the adduct of [2]ferrocenophane in a reaction with $HgCl_2$ in diethyl ether; i.e., the color of the [3]ferrocenophane-$6HgCl_2$ adduct was found to change to green within several days at room temperature. A slightly smaller Q. S. value of the $HgCl_2$ adduct (2.93 mm s^{-1} at 78 K) than the value of the [2]ferrocenophane-$3HgCl_2$ adduct (3.29 mm s^{-1} at 78 K) was found using ^{57}Fe-Mössbauer spectroscopy; however, this value (2.93 mm s^{-1}) is much larger than the value for [3]ferrocenophane, itself (2.29 mm s^{-1}). This fact suggests that the bond formed between the Fe and Hg atoms is weaker than the bond of the [2]ferrocenophane-$3HgCl_2$ adduct, as in the case of the ferrocenophane-$7HgCl_2$ adduct. The reason why [3]ferrocenophane forms a less-stable adduct with $HgCl_2$ has been interpreted on the basis of the fact that the Cp-rings in [3]ferrocenophane are only slightly inclined (ca. 9°) from each other;[14] i.e., the Fe-Hg bond is less stabilized by an increased steric hindrance of Cp-rings, while the Cp-rings in [2]ferrocenophane are greatly tilted (22.2°) from each other.[15] Relatively sharp signals (δ=86.6, 70.5, 36.0, and 25.4) have been found for [3]ferrocenophane and three broader signals (δ=78.8—72.6 for $C_{2,5}$ and $C_{3,4}$; δ=35.7 and 24.6 for methylene group's carbon) and a relatively strong, sharp signal (δ=110.7 for C_1) have been observed in the $HgCl_2$ adduct, as illustrated in Fig. 6. The spectral line shape and position of the methylene group in the [3]ferrocenophane-$6HgCl_2$ adduct correspond to those of [3]ferrocenophane, itself; however, those of the Cp-rings are much different from those of [3]ferrocenophane.

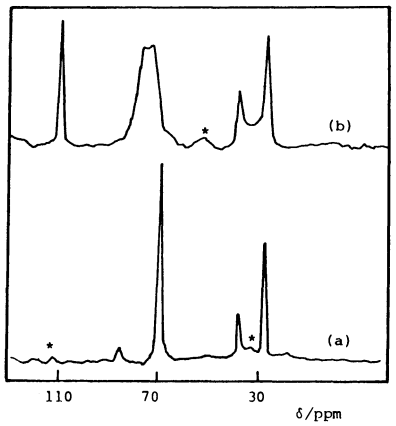

Fig. 6. ^{13}C-CP-MAS NMR spectra of [3]ferrocenophane(a) and its $6HgCl_2$(b) adduct.

The $\Delta\delta$ values (26.0—24.0) of the C_1 signal in [n]ferrocenophane (n=2,3) adducts with Hg(II) are much larger than the values of the ferrocenylmethane and 1,2-diferrocenylethane adducts with Hg(II). The structural distortion at the C_1 atoms of the [2]ferrocenophane-$n HgX_2$ (X=Cl, Br, I, and BF_4) and [3]ferrocenophane-$6HgCl_2$ adducts, caused by Fe-Hg bond formation, may be responsible for the large $\Delta\delta$ values in the C_1 signal in the [n]ferrocenophane adducts,

although further structural investigations are required in order to confirm these conclusions.

This work was partly supported by a Grant-in-Aid from the Ministry of Education, Scientific and Culture (No. 60430014).

References

1) M. Watanabe, K. Suto, I. Motoyama, and H. Sano, *Chem. Lett.*, **1984**, 1317.
2) M. Watanabe, I. Motoyama, and H. Sano, *Bull. Chem. Soc. Jpn.*, **59**, 2103 (1986).
3) M. Watanabe, H. Ichikawa, I. Motoyama, and H. Sano, *Chem. Lett.*, **1983**, 1009.
4) M. Watanabe, H. Ichikawa, I. Motoyama, and H. Sano, *Bull. Chem. Soc. Jpn.*, **56**, 3291 (1983).
5) H. Sano, M. Watanabe, and I. Motoyama, *Hyperfine Interactions*, **28**, 833 (1986).
6) M. Watanabe, K. Sato, I. Motoyama, and H. Sano, *Chem. Lett.*, **1983**, 1775.
7) M. Watanabe, Y. Masuda, I. Motoyama, and H. Sano, *Chem. Lett.*, **1987**, 1669; M. Watanabe, Y. Masuda, I. Motoyama, and H. Sano, *Bull. Chem. Soc. Jpn.*, **61**, 827 (1988).
8) A. I. Gusev and U. T. Struchkov, *Zh. Struckt. Khim.*, **6**, 1121 (1972); W. H. Morrison, Jr. and D. N. Hendrickson, *Inorg. Chem.*, **11**, 2912 (1972).
9) Y. S. Sohn, A. W. Schlueter, D. N. Hendrickson, and H. B. Gray, *Inorg. Chem.*, **13**, 301 (1974).
10) M. Watanabe, I. Motoyama, and H. Sano, *Bull. Chem. Soc. Jpn.*, **59**, 2109 (1986).
11) M. Rausch, M. Vogel, and H. Rosenberg, *J. Org. Chem.*, **22**, 900 (1957).
12) R. M. G. Roberts, J. Silver, and I. E. G. Morrison, *Organomet. Chem.*, **209**, 385 (1981).
13) A. G. Osborne, R. H. Whitely, and Meads, *Organomet. Chem.*, **193**, 345 (1980); T. H. Barr and W. E. Watts, *Tetrahedron*, **24**, 6111 (1968).
14) N. D. Jones, R. E. Marsh, and J. H. Richards, *Acta Crystallogr.*, **19**, 330 (1965).
15) T. Ito, private communication.

 © 1988 The Chemical Society of Japan Bull. Chem. Soc. Jpn., 61, 3485—3489 (1988)

Seasonal Changes in Eicosapentaenoic and Arachidonic Acid Contents in Bivalves and Plankton Collected from Lake Hamana†

Kyoko ADACHI, Norio ICHINOSE,* Chiaki SHIMIZU,†† and Ken OKAMOTO††
Department of Chemistry, Hamamatsu University School of Medicine, Handa-cho, Hamamatsu 431-31
††Fisheries Laboratory, Faculty of Agriculture, the University of Tokyo, Maisaka, Hamana, Shizuoka 431-02
(Received February 22, 1988)

Bivalves and plankton samples were collected monthly for one year from brackish Lake Hamana in Japan, and contents of 5,8,11,14,17-eicosapentaenoic acid (EPA) and 5,8,11,14-eicosatetraenoic acid (arachidonic acid, AA) and their weight percentage to total fatty acids were determined by fluorescence high-performance liquid chromatography. The results regarding bivalves showed that the EPA and AA levels are approximately ten-times higher in liver than in adductor on the average for one year, and are remarkably dependent upon the season. The seasonal changes of EPA and AA contents in bivalve liver are seemingly related to those of plankton, which are the diet of bivalves. From these facts, it can be seen that plankton is the main origin of EPA and AA in bivalve bodies and supply these fatty acids all the way up to humans through a food chain.

Fatty acids are one of the important substances constituting living cells; especially, 5,8,11,14,17-eicosapentaenoic acid (EPA) and 5,8,11,14-eicosatetraenoic acid (arachidonic acid, AA) of C_{20} serve as precursors of prostaglandins (PG) and thromboxanes (TX). In human blood vessels, EPA changes to PGI_3 and TXA_3, and AA to PGI_2 and TXA_2. Both PGI_2 and PGI_3 have the ability to suppress platelet aggregation and vascular smooth muscle contraction; whereas TXA_2 has a strong action on platelet aggregation and vascular smooth muscle contraction, TXA_3 shows almost no such action.[1-3] In addition, EPA can block TXA_2 synthesis;[4] thus, EPA is effective in preventing thrombosis and myocardial infraction.

The fatty acid content or composition in a human body depends upon both nutritional and physiological conditions. The EPA contents in human blood and plasma are much lower than AA contents, and the relative content of EPA can be increased by dieting on fish rich in EPA.[5,6] Thus, it is suggested that the main source of EPA in humans is marine organisms such as fish.

The food chain in marine environments has been an interesting subject: e.g., since fish cannot biosynthesize linoleic acid ($C_{18}^{2=}$) and linolenic acid ($C_{18}^{3=}$),[7] they obtain these fatty acids from phytoplankton or algae. In addition, a freshwater fish can produce long-chain fatty acids of C_{20} and C_{22} from the shorter chain precursors, C_{18} fatty acids, contained in diets, whereas marine fish cannot.[8-10] In contrast, bivalves cannot biosynthesize such long-chain fatty acids as EPA and AA.[11,12]

Thus, in a marine system, plankton plays a role of primary producer for long-chain fatty acids. The fatty acid content or composition in plankton varies in relation to such environmental conditions as temperature and light intensity.[13,14] Therefore, an investigation on the behavior of these long-chain fatty acids in plankton and the other marine organisms under the natural conditions is important for a better understanding of the food chain in marine environments.

The present authors have already established a fluorescence high-performance liquid chromatographic (HPLC) method using 9-anthryldiazomethane(ADAM) as a pre-labeling reagent,[15] and have determined the fatty acids of C_{18} and C_{20} in various marine organisms.[16,17] Although the free fatty acid level is much lower than the esterified fatty acid level, a highly sensitive and selective determination is possible by using this method. These studies have shown that the EPA contents and the EPA/AA ratios in plankton and Mollusca, such as cuttlefish, are higher than those in marine fishes.

We have studied C_{18} and C_{20} fatty acids in bivalves, a kind of Mollusca, and plankton collected monthly from brackish Lake Hamana, Japan, during 1985. Here, we present data on seasonal changes of the fatty acid contents and discuss the relationship between the EPA and AA contents in bivalves and those in plankton from the viewpoint of a food chain.

Experimental

Standards and Reagents. All standard fatty acids of $C_{18}^{0-3=}$ and $C_{20}^{0-5=}$ were purchased from Sigma (St. Louis, MO, USA), and ADAM was purchased from Funakoshi Chemical (Tokyo, Japan). All other reagents were of commercially analytical grade. The preparation techniques of a standard solution of fatty acids and an ADAM solution have been previously described in detail.[15-17]

Samples. Clam(*Tapes (Amygdala) japonica*) (3.5—4 cm long) and oyster (*Crassostrea gigas*) (8—12 cm long) were collected monthly during the year of 1985 from the southern inshore part (water depth: about 1 m) of brackish Lake Hamana. On the same sampling date, plankton samples of different size were collected by horizontal hauls (0.5—1 m layer from the surface) with 20, 40, and 94 μm mesh-sized nets from the same area, and separated into plankton A (20 μm), B (40 μm), and C (94 μm). These plankton samples were filtrated on a Millipore filter (pore size: 0.45 μm). All samples were stored in a freezer (−10 °C) before use.

† A part of this paper was presented at the 36th Annual Meeting of the Analytical Chemical Society of Japan, October, 1987.

As the representative organs to be examined in bivalve body, liver and adductor were selected from parts of viscera and muscle, respectively. Bivalve liver acts as a digestive organ, different from that of Vertebrate. Moreover, whole bodies were examined.

Analytical Procedure. Bivalve liver and adductor were isolated from bodies with a small knife. The homogenate of a whole body was obtained by grinding in a mortar. The liver, adductor and homogenate of a whole body of bivalve samples (10—20 mg) were weighed as wet weight in a glass homogenizer (volume: 1 ml). One ml of a mixture of chloroform and methanol (2:1) was added, and the sample was homogenized. The homogenate was transferred into a graduated centrifugal tube with a stopper, and diluted to 1 ml with the above-mentioned solvent since some part of the solvent evaporated during the homogenization. After centrifuging at 3000 rpm for 5 min, the supernatant was filtrated through a disposable filter (pore size: 0.45 μm).

An aliquot of the sample filtrates was derivatized with an ADAM and analyzed by the HPLC method using a Shimadzu Model LC-4A liquid chromatograph (Zorbax C_8 column) equipped with a Shimadzu Model RF-510LC fluorescence spectromonitor and a Shimadzu Model C-R1A(S) chromatopac as described in the previous papers.[16,17] In the determination of EPA and AA in living-body samples, the recovery was 90—100% and the coefficient of variation by repeated experiments was about 7%. The detection limit was 1—2 ng for $C_{18}{}^{0-3=}$ and $C_{20}{}^{0-5=}$ fatty acids.

Plankton samples (10—50 mg), which remained on the filter were homogenized after adding about 1 ml of the mixture of chloroform and methanol (2:1). The homogenates were transferred into the centrifugal tube, diluted with the same solvent up to 3 ml and then vortexed for 3 min. The procedure from centrifugation was the same as that mentioned above. The contents of fatty acids in plankton were obtained on a dry-weight basis, by determining the moisture in the sample.

Measurements of Chlorophylls, Carbon and Nitrogen in Plankton. For the extraction of pigments, the plankton together with the filter was ground in a mortar with 3—5 ml of acetone and water (9:1) and then transferred into a graduated centrifugal tube. After centrifugation at 3000 rpm for 5 min, the absorbance of the supernatant was measured at 630, 647, 664, and 750 nm. The contents of chlorophyll *a*, *b*, and *c* were calculated, without standards, according to the equation of Jeffrey and Humphrey.[18]

The carbon and nitrogen contents were measured using a Yanagimoto Model MT-500 CN corder with hippuric acid as a standard.

Results and Discussion

Figure 1 shows the seasonal changes of the EPA and AA contents in bivalves. In both clam and oyster, the EPA and AA contents in the liver are higher than those in the adductor and homogenate of a whole body; the ratio of EPA or AA content in the liver to that of the adductor was approximately ten on the average for one year. The contents of EPA and AA show seasonal fluctuations. In the case of liver, the EPA and AA contents remarkably increase in the late spring when bivalves breed, and again in the early winter. In the adductor and homogenate of a whole body, the variations of these fatty acid levels are not significant. Differences between clam and oyster were not significant regarding these results.

On the other hand, the EPA and AA contents in plankton increase during midsummer and early winter for plankton A or B, and in the above-mensioned seasons and late spring for plankton C as shown in Fig. 2(a). Since sand and mud in water may have been collected together with plankton by the plankton net, the fatty acid content per carbon weight was calculated in order to exclude any error due to sand or mud contamination. The peaks during midsummer (Fig. 2(b))

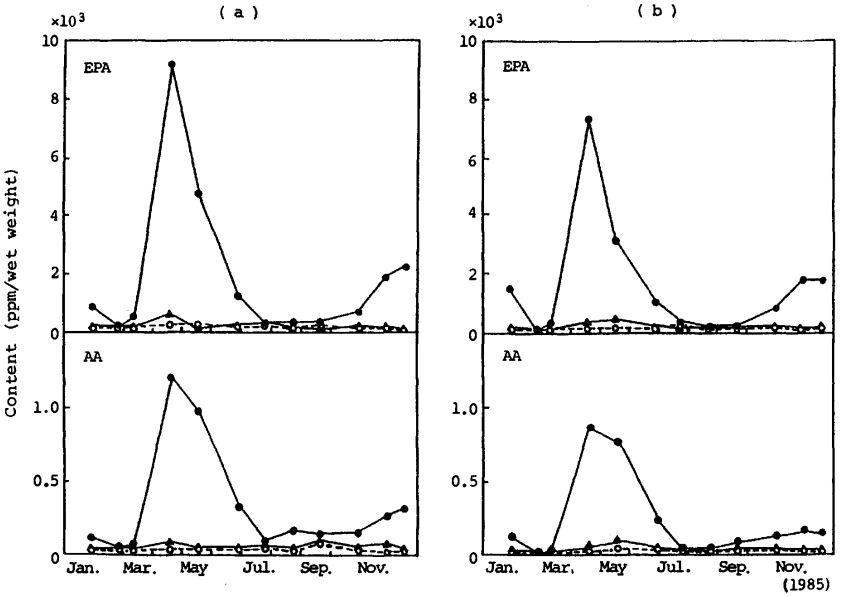

Fig. 1. Seasonal changes of EPA and AA contents in (a) clam and (b) oyster. ●—●: liver, ○···○: adductor, ▲—▲: whole body.

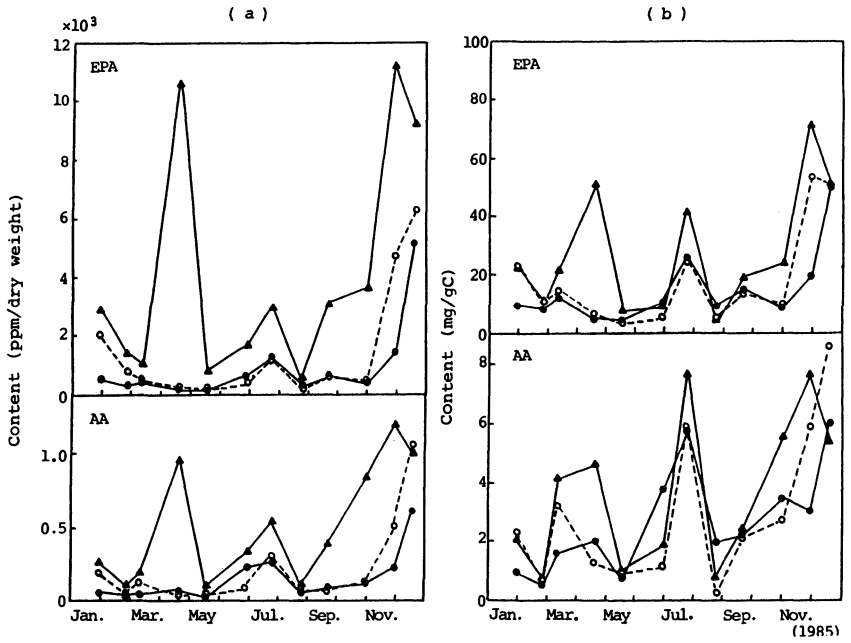

Fig. 2. Seasonal changes of EPA and AA contents per (a) dry weight and (b) carbon weight in plankton. ●—●: plankton A (mesh size of the used plankton net: 20 μm), ○--○: plankton B (40 μm), ▲—▲: plankton C (94 μm).

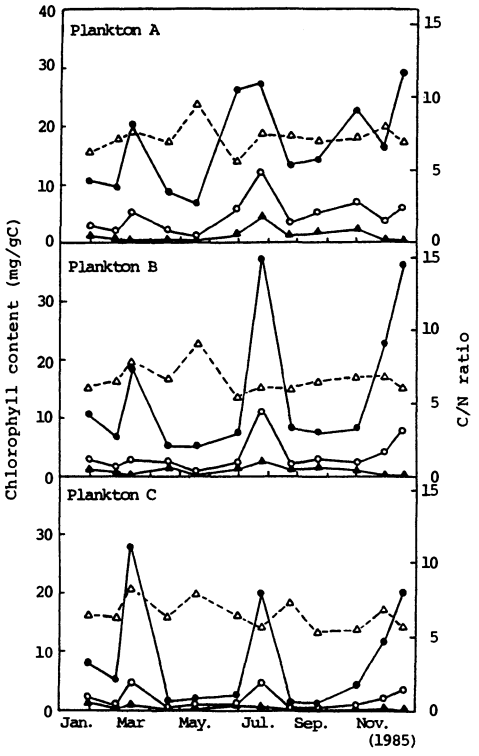

Fig. 3. Characteristics of plankton A, B, C and their seasonal changes. ●—●: chlorophyll *a*, ▲—▲: chlorophyll *b*, ○—○: chlorophyll *c*, △-△: C/N ratio.

are clear in comparison with those of Fig. 2(a).

Since collected plankton consists of various species, plankton A, B, and C were characterized by the chlorophyll content and C/N ratio (Fig. 3). On the average, the chlorophyll content, which is an index of

Table 1. Relation of Chlorophyll Contents to EPA and AA Contents in Plankton

Combination	Correlation coefficient		
	Plankton A	Plankton B	Plankton C[a)]
Chlorophyll *a*-EPA	0.687	0.764	0.527
Chlorophyll *b*-EPA	0.056	−0.386	−0.285
Chlorophyll *c*-EPA	0.484	0.590	0.556
Chlorophyll *a*-AA	0.893	0.927	0.611
Chlorophyll *b*-AA	0.512	0.249	−0.157
Chlorophyll *c*-AA	0.814	0.813	0.673

a) The correlation coefficients for the data except for April were calculated, since the data in April for plankton C were apparently predicted to deviate from the relationship of the data in other months.

phytoplankton, becomes higher in the order plankton C<B<A; thus, the size becomes smaller, since the size of phytoplankton is generally smaller than zooplankton.

The C/N ratio corresponds to adipose/protein ratio in the body. As can be seen in Fig. 3, the C/N ratio in plankton A and B in May is approximately 9, which is significantly high for a plankton value. This high C/N ratio could be due to the resuspension of bottom sediments (C/N ratios of which are higher than those of plankton) into overlying water. Lower EPA and AA contents in the sample of May (Fig. 2) seem to be consistent with higher C/N ratios.

In a comparison between Fig. 2(b) and Fig. 3, the peaks in the seasonal changes of the chlorophyll contents of plankton appear in roughly the same months as the peaks of EPA or AA contents. Then, their corre-

lation coefficients were calculated (Table 1). The seasonal changes of chlorophyll *a* and *c* contents were considerably related to that of the EPA and AA contents in Fig. 2(b), except that the EPA and AA contents in plankton C increase in April. This increase of EPA and AA is probably attributable to zooplankton, since the chlorophyll content in plankton C (94 μm) was very low during April. It is likely that zooplankton breeds by feeding on phytoplankton, which proliferates in March, as suggested from the significant increase in chlorophyll *a* and *c* contents (Fig. 3); consequently, zooplankton accumulates EPA and AA in its body.

When considering plankton as a diet of bivalve, the unit (ppm/dry weight) for fatty acid content in Fig. 2(a) is more adequate, rather than the unit (mg/gC) in Fig. 2(b) since bivalve cannot selectively feed on only plankton. Comparing Fig. 1 with Fig. 2(a), it is evident that when the EPA and AA contents increase in the bivalve liver, those in plankton C, which is the main diet for bivalve, also increase. This suggests that EPA and AA in bivalves are obtained from relatively large phytoplankton, zooplankton and their fecal pellets.

The averaged fatty acid composition and its degree of variation during one year, as a coefficient of the variation (the percentage of standard deviation to average), are given in Table 2 for the bivalve liver and plankton. The fatty acid compositions of clam and oyster were almost the same and the degree of year-round variation in the composition of the bivalve liver was smaller than that of plankton. This result can be explained by the fact that the dominant plankton species change depending on the season and that these plankton are different regarding fatty acid composition. In each plankton sample the variation of the $C_{18}^{1=}$ weight percentage was remarkable. Consequently, in Lake Hamana, it is considered that some plankton species, of which populations vary during the year, show $C_{18}^{1=}$ weight percentages different from

Table 2. Averaged Fatty Acid Composition in Bivalves and Plankton for a Year (1985)

Sample	Weight percentage[a] (Coefficient of variation(%))								
	$C_{18}^{0=}$	$C_{18}^{1=}$	$C_{18}^{2=}$	$C_{18}^{3=}$	$C_{20}^{1=}$	$C_{20}^{2=}$	$C_{20}^{3=}+C_{16}^{0=}$	$C_{20}^{4=}$ (AA)	$C_{20}^{5=}$ (EPA)
Clam liver	13.4	18.0	8.2	9.5	4.1	1.4	20.4	4.3	20.7
	(21.7)	(28.0)	(31.1)	(23.8)	(21.7)	(26.1)	(19.5)	(30.6)	(38.8)
Oyster liver	8.6	20.7	10.1	10.9	7.3	0.8	17.0	3.3	21.3
	(25.5)	(12.3)	(16.4)	(20.2)	(24.2)	(28.8)	(19.2)	(35.6)	(36.0)
Plankton A	13.1	13.6	3.4	24.7	ND	ND	20.1	3.5	21.6
	(52.5)	(115.7)	(73.1)	(37.3)			(19.6)	(31.9)	(49.3)
Plankton B	10.6	19.7	4.2	20.9	0.7	ND	18.6	3.4	21.9
	(43.0)	(89.9)	(76.7)	(40.4)	(47.5)		(20.9)	(34.3)	(49.5)
Plankton C	9.5	12.7	4.2	21.1	0.9	0.4	19.0	3.8	28.4
	(35.0)	(60.4)	(46.2)	(37.6)	(74.2)	(76.4)	(16.8)	(27.1)	(30.7)

a) Weight percentage to total fatty acids($C_{16}^{0=}$, $C_{18}^{0-3=}$, and $C_{20}^{0-5=}$)
$C_{20}^{0=}$ was not detected in all samples.

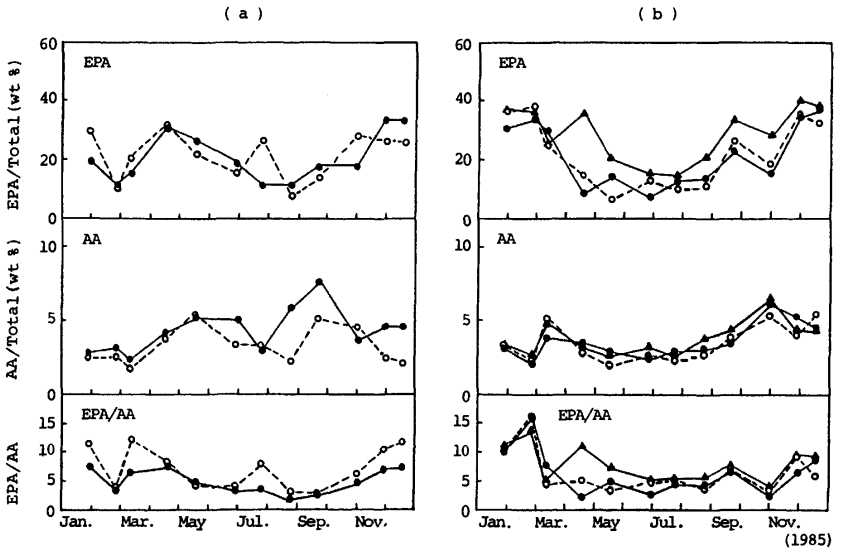

Fig. 4. Seasonal changes of EPA and AA weight percentage to total fatty acids ($C_{16}^{0=}$, $C_{18}^{0-3=}$, and $C_{20}^{0-5=}$) and EPA/AA ratio in (a) bivalve liver and (b) plankton. (a) ●—●: clam, ○--○: oyster, (b) ●—●: plankton A, ○--○: plankton B, ▲—▲: plankton C.

each other. In the bivalve liver, the variations of the EPA and AA weight percentages were larger than those of the other fatty acids.

Figure 4 shows the seasonal changes of the EPA and AA weight percentage to the total fatty acids ($C_{16}^{0=}$, $C_{18}^{0-3=}$, and $C_{20}^{0-5=}$) and the EPA/AA ratio for bivalve liver and plankton. The seasonal changes of the EPA weight percentage in individual samples were different from those of AA, whereas there was no significant difference in the behavior between clam and oyster, or among plankton A, B, and C. Between bivalve liver and plankton, a clear relationship was not found for the each seasonal change of the EPA and AA weight percentage.

Since all trends regarding the fatty acids for clam and oyster in this experiment were closely similar to each other, they are considered to be just as adequate for discussion as the typical data of bivalves.

We wish to thank late Emeritus Professor Dr. Hidehiro Gotô of Tôhoku University for his kind and ever continuing guidance.

References

1) P. Needleman, A. Raz, M. S. Minkes, J. A. Ferrendelli, and H. Sprecher, *Proc. Natl. Acad. Sci. U. S. A.*, **76**, 944 (1979).

2) P. Needleman, M. S. Minkes, and A. Raz, *Science*, **193**, 163 (1976).

3) P. Needleman, P. S. Kulkarni, and A. Raz, *Science*, **195**, 409 (1977).

4) I. Morita, R. Takahashi, Y. Saito, and S. Murota, *Throm. Res.*, **31**, 211 (1983).

5) T. O. von Lossonczy, A. Ruiter, H. C. Bronsgeest-Schoute, C. M. van Gent, and R. J. Hermus, *Am. J. Clin. Nutr.*, **31**, 1340 (1978).

6) J. Skorepa, H. Todorovicova, and P. Mares, *Lancet*, **26**, 717 (1983).

7) J. F. Mead, M. Kayama, and R. Reiser, *J. Am. Oil Chem. Soc.*, **37**, 438 (1960).

8) J. M. Owen, J. W. Adron, C. Middleton, and C. B. Cowey, *Lipids*, **10**, 528 (1975).

9) K. Kanazawa, S. Teshima, and K. Ono, *Comp. Biochem. Physiol.*, **63B**, 295 (1979).

10) K. Yamada, K. Kobayashi, and Y. Yone, *Bull. Jpn. Soc. Sci. Fish*, **46**, 1231 (1980).

11) J. E. A. de Moreno, V. J. Moreno, and R. R. Brenner, *Lipids*, **11**, 561 (1976).

12) J. E. A. de Moreno, V. J. Moreno, and R. R. Brenner, *Lipids*, **12**, 804 (1977).

13) H. P. Jeffries, *Limnol. Oceanogr.*, **15**, 419 (1970).

14) A. E. Smith and I. Morris, *Science*, **207**, 197 (1980).

15) N. Ichinose, K. Nakamura, C. Shimizu, H. Kurokura, and K. Okamoto, *J. Chromatogr.*, **295**, 463 (1984).

16) N. Ichinose, K. Nakamura, C. Shimizu, H. Kurokura, and K. Okamoto, *Bunseki Kagaku*, **33**, E271 (1984).

17) N. Ichinose, S. Abe, K. Adachi, and R. Kato, *Nippon Kagaku Kaishi*, **1986**, 1011.

18) S. W. Jeffrey and G. F. Humphrey, *Biochem. Physiol. Pflanzen*, **167**, 191 (1975).

X-Ray Crystal Structures of *cis*- and *trans*-Dinitrobis(1,4-butanediamine)cobalt(III) Nitrates. Conformation of Seven-Membered Chelate Rings

Mamoru SHIMOI, Yuki FUJINAWA, Hiroshi OGINO,* Kan KANAMORI,† and Kiyoyasu KAWAI†
Department of Chemistry, Faculty of Science, Tohoku University, Aoba, Sendai 980
†Department of Chemistry, Faculty of Science, Toyama University, Gofuku 3190, Toyama 930
(Received May 16, 1988)

The structures of *cis*- and *trans*-dinitrobis(1,4-butanediamine)cobalt(III) nitrates were determined by the single-crystal X-ray diffraction method. *cis*-$[Co(NO_2)_2(tmd)_2]NO_3$ (tmd=$H_2N(CH_2)_4NH_2$) is monoclinic with the space group $P2_1/a$; the cell constants are a=23.878(4), b=8.403(1), c=16.675(3) Å, β=103.24(1)°; Z=8, and the final R value was 0.051. *trans*-$[Co(NO_2)_2(tmd)_2]NO_3 \cdot H_2O$ is triclinic with the space group $P\bar{1}$; the cell constants are a=9.753(3), b=13.909(4), c=6.327(1) Å, α=102.07(2), β=91.05(2), γ=87.83(3)°; Z=2, and the final R value was 0.058. Both complexes have a slightly distorted octahedral geometry around the cobalt center. The conformations of the seven-membered chelate rings have twist-chair and chair forms for the cis and trans complexes, respectively.

Chelate rings containing more than six atoms have been scarce until recently, whereas numerous examples of five- and six-membered chelate rings have been known.[1] The stability of a chelate ring depends on its size. Thus, reactions between $[CoCl_2(en)_2]Cl$[2] and α,ω-alkanediamines in dimethyl sulfoxide gave no monomeric $[Co(en)_2(H_2N(CH_2)_nNH_2)]^{3+}$ for n=5—8, whereas the corresponding complexes were obtained for n=2—4 and 9—14.[1,3] Similar results were also obtained for the reaction of $[Co(H_2O)(NH_3)_5]^{3+}$ with α,ω-alkanediamines.[4] 1,4-Butanediamine (tetramethylenediamine) has the longest chain in the smaller chelate ring family.[2] Therefore the conformations of tmd chelate rings are of great interest. Only the structure of $(+)_{589}$-$[Co(tmd)_3]^{3+}$ was reported.[5,6] The conformation is 'lel$_3$' and the seven-membered rings take twist-chair forms. Preliminary reports on the crystal structures of *trans*-$[CoCl_2(tmd)_2]Cl \cdot H_2O$[7] and Δ-$[Co(en)(tn)(tmd)][Co(CN)_6] \cdot H_2O$[8] do exist but the full report is still lacking.

We have succeeded in the preparation of both *cis*- and *trans*-$[Co(NO_2)_2(tmd)_2]^+$ complexes using dimethyl sulfoxide as a solvent. The geometrical configurations were determined on the basis of their electronic and Raman spectra.[9] To elucidate the conformation of the seven-membered chelate rings we have determined the crystal structures of *cis*- and *trans*-$[Co(NO_2)_2(tmd)_2]NO_3 \cdot nH_2O$ (n is 0 for the cis and 1 for the trans complex).

Experimental

The compounds were prepared by the method reported in a previous paper,[9] and recrystallized from water. The reflections were collected on a Rigaku AFC-6A automated four-circle X-ray diffractometer with graphite-monochromated Mo $K\alpha$ radiation (the scan speed was 4° min^{-1}). The crystal data and the conditions of data collection are shown in Table 1.

The structures were solved by the heavy-atom method. For the trans complex, the reflections with odd $h+k$ indexes were very weak. Two models were therefore taken into consideration for this pseudo C lattice. In the first model the two crystallographically independent molecules were situated at the centers of symmetry: (0, 0, 0) and (1/2, 1/2, 0). In the second model the complex was situated in the general position, the two molecules being separated by about (0.5, 0.5, 0) and related through the center of symmetry. The second model gave a satisfactory result.

The positions of the central metal atoms and some coordinated atoms were deduced from the three-dimentional Patterson maps. The positional and thermal parameters were refined by the block-diagonal least-squares method. The positions of the hydrogen atoms, except for the amine and

Table 1. Crystal Data for *cis*- and *trans*-$[Co(NO_2)_2(tmd)_2]NO_3 \cdot nH_2O$

	cis-$[Co(NO_2)_2(tmd)_2]NO_3$	*trans*-$[Co(NO_2)_2(tmd)_2]NO_3 \cdot H_2O$
Formula	$C_8H_{24}CoN_7O_7$	$C_8H_{26}CoN_7O_8$
F. W.	389.25	407.27
C. S.	Monoclinic	Triclinic
S. G.	$P2_1/a$	$P\bar{1}$
a(*l*/Å)	23.878(4)	9.753(3)
b(*l*/Å)	8.403(1)	13.909(4)
c(*l*/Å)	16.675(3)	6.327(1)
α(ϕ/°)		102.07(2)
β(ϕ/°)	103.24(1)	91.05(2)
γ(ϕ/°)		87.83(3)
U(v/Å^3)	3256.9(8)	838.6(4)
D_m(d/g cm^{-3})	1.57	1.62
D_c(d/g cm^{-3})	1.59	1.61
Z	8	2
μ(Mo $K\alpha$)(n/cm^{-1})	1.15	1.12
Crystal size(*l*/mm)	0.35×0.35×0.45	0.16×0.08×0.26
Scan Mode	ω	ω-2θ
Scan width(ω/°)	1.3+0.5 tanθ	1.2+0.5 tanθ
$2\theta_{max}$(ϕ/°)	65	65
Refls. measured	$\pm h$, k, l	$\pm h$, $\pm k$,l
No. of refls. measured	12595	6108
No. of unique data used for calc. ($\|F_o\|>3\sigma(F_o)$)	7153	3884
R[a]	0.051	0.058
R_w[b]	0.063	0.053

a) $R=\sum\|\|F_o\|-\|F_c\|\|/\sum|F_o|$ b) $R_w=[\sum w(\|F_o\|-\|F_c\|)^2/\sum w|F_o|^2]^{1/2}$; $w=[\sigma^2(|F_o|)+aF_o^2]^{-1}$, where a=0.015.

the water hydrogens in the trans complex, were deduced from difference Fourier synthesis, and refined with isotropic thermal parameters. The positions of the amine hydrogens in the trans complex were calculated and fixed; they were included in the calculation of structure factors.

All the calculations were carried out on a Nippon Electric Co. ACOS-1000 computer at the computer center of Tohoku University, using the Universal Crystallographic Computation Program System UNICS III.[10] The atomic-scattering factors were taken from Ref. 11 for non-hydrogen atoms and from Ref. 12 for hydrogen atom.

Table 2. Final Atomic Coordinates ($\times 10^4$) and Equivalent Isotropic Temperature Factors for *cis*-$[Co(NO_2)_2(tmd)_2]NO_3$

Atom	x	y	z	B_{eq}/Å^{2} a)
Co(1)	1568.6(1)	1573.7(4)	609.7(2)	2.3
Co(2)	1635.0(1)	4647.1(4)	5676.0(2)	2.3
N(11)	1695(1)	2827(3)	1615(2)	3.6
N(12)	2230(1)	2737(3)	415(2)	3.5
N(13)	2090(1)	−84(3)	1183(1)	3.0
N(14)	894(1)	558(3)	899(1)	2.9
N(15)	1045(1)	3223(3)	28(2)	3.3
N(16)	1507(1)	320(3)	−419(1)	2.8
N(21)	1835(1)	3405(3)	6684(2)	3.3
N(22)	2388(1)	4052(4)	5498(2)	3.8
N(23)	1988(1)	6530(3)	6280(2)	3.1
N(24)	876(1)	5134(3)	5907(1)	2.5
N(25)	1287(1)	2720(3)	5094(2)	3.6
N(26)	1488(1)	5951(3)	4657(1)	2.9
O(11)	1428(1)	4056(4)	1622(2)	6.5
O(12)	2044(1)	2410(4)	2239(1)	6.0
O(13)	2720(1)	2246(4)	679(2)	6.2
O(14)	2166(1)	4013(4)	46(2)	6.0
O(21)	1840(1)	1956(3)	6657(2)	6.3
O(22)	1978(1)	4052(3)	7359(1)	4.8
O(23)	2823(1)	4755(4)	5834(2)	6.6
O(24)	2433(1)	2900(4)	5065(2)	6.9
C(11)	1927(1)	−1787(4)	1232(2)	3.4
C(12)	1676(1)	−2149(4)	1962(2)	4.1
C(13)	1042(2)	−1784(5)	1858(2)	4.5
C(14)	878(1)	−54(4)	1731(2)	3.5
C(15)	534(1)	2894(4)	−660(2)	3.4
C(16)	667(2)	2943(5)	−1492(2)	4.3
C(17)	951(2)	1488(5)	−1754(2)	4.4
C(18)	1535(1)	1065(4)	−1224(2)	3.6
C(21)	1718(1)	8130(4)	6268(2)	4.0
C(22)	1381(2)	8335(4)	6918(2)	4.6
C(23)	792(2)	7551(4)	6753(2)	4.5
C(24)	781(1)	5776(4)	6703(2)	3.4
C(25)	774(1)	2694(4)	4389(2)	4.0
C(26)	906(2)	2916(5)	3558(2)	4.9
C(27)	1016(2)	4606(5)	3331(2)	5.0
C(28)	1550(1)	5374(5)	3834(2)	4.4
N(3)	4610(1)	2333(3)	800(2)	4.6
O(31)	4642(1)	3690(3)	552(2)	5.1
O(32)	4131(1)	1775(4)	719(4)	12.9
O(33)	5057(1)	1585(3)	1088(2)	6.5
N(4)	4893(1)	3068(3)	5900(2)	4.5
O(41)	4791(1)	1770(3)	5546(2)	4.7
O(42)	5400(1)	3467(4)	6112(2)	7.6
O(43)	4498(2)	3806(5)	6034(4)	13.2

a) The equivalent isotropic temperature factors for non-hydrogen atoms were computed using the following expression: $B_{eq}=4/3(B_{11}a^2+B_{22}b^2+B_{33}c^2+B_{12}ab\cos\gamma+B_{13}ac\cos\beta+B_{23}bc\cos\alpha)$. The B_{ij}'s are defined by: $\exp[-(h^2B_{11}+k^2B_{22}+l^2B_{33}+2hkB_{12}+2hlB_{13}+2klB_{23})]$.

Results and Discussion

Final atomic parameters for the cis and trans complexes are listed in Tables 2 and 3, respectively. Relevant interatomic distances and angles are summarized in Tables 4 and 5.[13] The structures of complex cations with atom numbering scheme are depicted in Figs. 1 and 2. The configurations of the complexes agree with those proposed previously.[9]

The crystal of *cis*-$[Co(NO_2)_2(tmd)_2]NO_3$ consists of two crystallographically independent complex cations and nitrate ions. The structures of both cations were essentially the same as shown in Fig. 1 and Table 4. The coordination geometry around the cobalt atom is a slightly deformed octahedron and resembles the structure of $[Co(tmd)_3]^{3+}$ [5,6] except for the nitro groups. The Co-N(NO_2) bond lengths range from 1.943(3) to 1.953(3) Å, and are a little longer than the values for *cis*-$[Co(NO_2)_2(en)_2]^+$ complexes (1.887—1.936 Å)[14-16] and *cis*-$[Co(NO_2)_2(tn)_2]^+$ (1.924 and 1.936 Å).[17] The Co-N(amine) bond lengths span the range between 1.959(3) and 1.990(3) Å and are normal, although the Co-N(amine) bond lengths trans to NO_2 ligands are longer than those cis to NO_2 ligands by 0.014—0.023 Å. These differences are attributable to trans-influence of NO_2 as observed for the *cis*-

Table 3. Final Atomic Coordinates ($\times 10^4$) and Equivalent Isotropic Temperature Factors for *trans*-$[Co(NO_2)_2(tmd)_2]NO_3\cdot H_2O$

Atom	x	y	z	B_{eq}/Å^{2} a)
Co	2454.5(6)	2456.0(5)	4890.7(9)	1.4
N(1)	1987(3)	3184(2)	2668(5)	2.1
N(2)	2911(4)	1753(2)	7152(5)	2.2
N(3)	4166(4)	3173(3)	5543(5)	2.3
N(4)	1414(4)	3398(2)	7145(5)	2.1
N(5)	758(3)	1720(2)	4230(5)	2.0
N(6)	3502(3)	1530(2)	2604(5)	2.0
O(1)	796(3)	3333(3)	2166(6)	3.6
O(2)	2919(3)	3476(3)	1675(5)	3.5
O(3)	4108(3)	1599(3)	7680(5)	3.4
O(4)	1970(3)	1472(3)	8157(5)	3.3
C(1)	1125(5)	4459(4)	7087(8)	3.3
C(2)	2230(7)	5117(4)	8148(9)	4.4
C(3)	3648(7)	4951(4)	7137(9)	4.5
C(4)	4418(5)	4008(4)	7346(7)	3.2
C(5)	3925(4)	507(3)	2757(7)	2.6
C(6)	2860(5)	−237(3)	1849(7)	2.9
C(7)	1465(5)	−71(3)	2940(8)	3.1
C(8)	604(4)	802(3)	2559(7)	2.4
N(7)	6999(4)	2260(3)	2583(7)	3.1
O(5)	6790(4)	1957(4)	4285(7)	5.6
O(6)	6043(3)	2483(3)	1502(6)	4.0
O(7)	8201(3)	2331(3)	1996(7)	4.8
O(8)	8640(4)	2708(3)	7717(7)	5.2

a) The equivalent isotropic temperature factors for non-hydrogen atoms were computed using the following expression: $B_{eq}=4/3(B_{11}a^2+B_{22}b^2+B_{33}c^2+B_{12}ab\cos\gamma+B_{13}ac\cos\beta+B_{23}bc\cos\alpha)$. The B_{ij}'s are defined by: $\exp[-(h^2B_{11}+k^2B_{22}+l^2B_{33}+2hkB_{12}+2hlB_{13}+2klB_{23})]$.

Table 4. Selected Interatomic Distances and Angles for *cis*-$[Co(NO_2)_2(tmd)_2]NO_3$

Bond length	*l*/Å	Bond length	*l*/Å
Co(1)-N(11)	1.944(3)	Co(2)-N(21)	1.943(3)
Co(1)-N(12)	1.946(3)	Co(2)-N(22)	1.953(3)
Co(1)-N(13)	1.964(2)	Co(2)-N(23)	1.959(2)
Co(1)-N(14)	1.979(3)	Co(2)-N(24)	1.980(2)
Co(1)-N(15)	1.967(2)	Co(2)-N(25)	1.971(3)
Co(1)-N(16)	1.990(2)	Co(2)-N(26)	1.985(3)
N(13)-C(11)	1.490(4)	N(23)-C(21)	1.489(4)
N(14)-C(14)	1.487(4)	N(24)-C(24)	1.497(4)
N(15)-C(15)	1.496(4)	N(25)-C(25)	1.490(4)
N(16)-C(18)	1.496(4)	N(26)-C(28)	1.494(5)
C(11)-C(12)	1.505(5)	C(21)-C(22)	1.501(6)
C(12)-C(13)	1.515(5)	C(22)-C(23)	1.520(5)
C(13)-C(14)	1.509(5)	C(23)-C(24)	1.494(5)
C(15)-C(16)	1.494(5)	C(25)-C(26)	1.501(5)
C(16)-C(17)	1.510(6)	C(26)-C(27)	1.508(6)
C(17)-C(18)	1.513(5)	C(27)-C(28)	1.503(5)
O(11)···H(N15A)	2.00(3)	O(11)···N(15)	2.697(4)
O(12)···H(N13B)	2.08(4)	O(12)···N(13)	2.757(4)
O(13)···H(N13A)	2.11(4)	O(13)···N(13)	2.718(4)
O(14)···H(N15B)	1.94(5)	O(14)···N(15)	2.752(4)
O(21)···H(N25A)	2.25(3)	O(21)···N(25)	2.715(4)
O(22)···H(N23B)	2.08(3)	O(22)···N(23)	2.755(4)
O(23)···H(N23A)	2.13(3)	O(23)···N(23)	2.726(4)
O(24)···H(N25B)	2.16(3)	O(24)···N(25)	2.753(4)

Bond angle	*φ*/°	Bond angle	*φ*/°
N(11)-Co(1)-N(12)	84.3(1)	N(21)-Co(2)-N(22)	86.6(1)
N(11)-Co(1)-N(13)	90.5(1)	N(21)-Co(2)-N(23)	89.8(1)
N(11)-Co(1)-N(14)	89.9(1)	N(21)-Co(2)-N(24)	89.9(1)
N(11)-Co(1)-N(15)	90.0(1)	N(21)-Co(2)-N(25)	88.7(1)
N(12)-Co(1)-N(13)	89.4(1)	N(22)-Co(2)-N(23)	89.0(1)
N(12)-Co(1)-N(15)	90.7(1)	N(22)-Co(2)-N(25)	90.8(1)
N(12)-Co(1)-N(16)	91.4(1)	N(22)-Co(2)-N(26)	90.0(1)
N(13)-Co(1)-N(14)	92.1(1)	N(23)-Co(2)-N(24)	92.2(1)
N(13)-Co(1)-N(16)	87.5(1)	N(23)-Co(2)-N(26)	88.0(1)
N(14)-Co(1)-N(15)	87.9(1)	N(24)-Co(2)-N(25)	88.0(1)
N(14)-Co(1)-N(16)	94.5(1)	N(24)-Co(2)-N(26)	93.6(1)
N(15)-Co(1)-N(16)	92.0(1)	N(25)-Co(2)-N(26)	93.4(1)
Co(1)-N(13)-C(11)	124.3(2)	Co(2)-N(23)-C(21)	126.1(2)
Co(1)-N(14)-C(14)	124.9(2)	Co(2)-N(24)-C(24)	125.3(2)
Co(1)-N(15)-C(15)	124.2(2)	Co(2)-N(25)-C(25)	125.3(2)
Co(1)-N(16)-C(18)	122.8(2)	Co(2)-N(26)-C(28)	124.9(2)
N(13)-C(11)-C(12)	113.3(3)	N(23)-C(21)-C(22)	113.3(3)
N(14)-C(14)-C(13)	113.8(3)	N(24)-C(24)-C(23)	113.9(3)
N(15)-C(15)-C(16)	113.4(3)	N(25)-C(25)-C(26)	114.7(3)
N(16)-C(18)-C(17)	113.4(3)	N(26)-C(28)-C(27)	113.7(3)
C(11)-C(12)-C(13)	116.1(3)	C(21)-C(22)-C(23)	116.5(3)
C(12)-C(13)-C(14)	115.6(3)	C(22)-C(23)-C(24)	116.6(3)
C(15)-C(16)-C(17)	116.9(3)	C(25)-C(26)-C(27)	115.7(3)
C(16)-C(17)-C(18)	115.9(3)	C(26)-C(27)-C(28)	116.0(3)

Table 5. Interatomic Distances and Angles for *trans*-$[Co(NO_2)_2(tmd)_2]NO_3 \cdot H_2O$

Bond length	*l*/Å	Bond length	*l*/Å
Co-N(1)	1.936(4)	Co-N(2)	1.931(4)
Co-N(3)	1.970(4)	Co-N(4)	1.988(3)
Co-N(5)	1.971(3)	Co-N(6)	1.992(3)
N(3)-C(4)	1.473(5)	N(4)-C(1)	1.500(6)
N(5)-C(8)	1.489(5)	N(6)-C(5)	1.490(6)
C(1)-C(2)	1.497(8)	C(2)-C(3)	1.524(9)
C(3)-C(4)	1.515(8)	C(5)-C(6)	1.514(6)
C(6)-C(7)	1.525(7)	C(7)-C(8)	1.508(7)
O(1)···H(N5A)	2.208(4)	O(1)···N(5)	2.824(6)
O(2)···H(N3A)	2.109(3)	O(2)···N(3)	2.816(5)
O(3)···H(N3B)	2.268(4)	O(3)···N(3)	2.806(6)
O(4)···H(N5B)	2.129(3)	O(4)···N(5)	2.812(5)

Bond angle	*φ*/°	Bond angle	*φ*/°
N(1)-Co-N(2)	178.9(2)	N(1)-Co-N(3)	90.5(2)
N(1)-Co-N(4)	93.1(1)	N(1)-Co-N(5)	90.0(1)
N(1)-Co-N(6)	86.0(1)	N(2)-Co-N(3)	89.2(2)
N(2)-Co-N(4)	85.8(1)	N(2)-Co-N(5)	90.4(2)
N(2)-Co-N(6)	95.1(1)	N(3)-Co-N(4)	92.9(1)
N(3)-Co-N(5)	179.2(1)	N(3)-Co-N(6)	86.6(2)
N(4)-Co-N(5)	87.8(1)	N(4)-Co-N(6)	179.0(2)
N(5)-Co-N(6)	92.7(1)		
Co-N(3)-C(4)	127.1(3)	Co-N(4)-C(1)	124.2(3)
Co-N(5)-C(8)	125.7(3)	Co-N(6)-C(5)	123.6(3)
N(3)-C(4)-C(3)	113.9(4)	N(4)-C(1)-C(2)	113.0(4)
N(5)-C(8)-C(7)	115.0(4)	N(6)-C(5)-C(6)	113.1(4)
C(1)-C(2)-C(3)	117.1(4)	C(2)-C(3)-C(4)	116.2(5)
C(5)-C(6)-C(7)	115.6(4)	C(6)-C(7)-C(8)	116.6(4)

$[Co(NO_2)_2(en)_2]^{2+}$ complexes.[14,15]

As shown in Fig. 2, the complex cation in the crystal of *trans*-$[Co(NO_2)_2(tmd)_2]NO_3 \cdot H_2O$ is pseudo-centrosymmetric and the coordination geometry is also a slightly distorted octahedron. Co-N(NO_2) bond lengths, 1.931(4) and 1.936(4) Å, are normal and a little shorter than in the cis-isomer. Both NO_2 ligands are almost in a plane containing the cobalt atom: The deviations from the least-squares plane are Co −0.016, N(1) 0.015, N(2) −0.013, O(1) −0.002, O(2) −0.002, O(3) 0.009, and O(4) 0.009 Å. Such coplanarity is a common feature of trans-dinitro cobalt complexes.[15,18—21] Co-N(amine) bond lengths range between 1.970(4) and 1.992(3) Å.

Figures 3 and 4 show the packing diagrams for the two complexes. Some hydrogen bonding was observed between the amine nitrogens, nitrate ions, and water

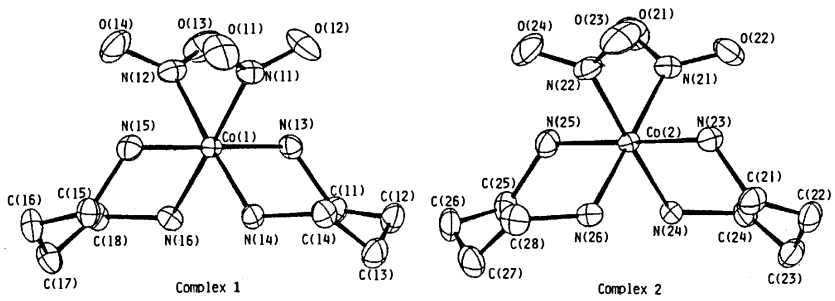

Fig. 1. ORTEP drawing of *cis*-$[Co(NO_2)_2(tmd)_2]^+$ ions.

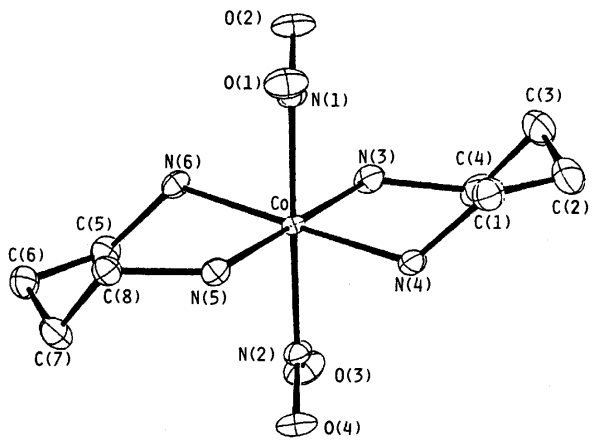

Fig. 2. ORTEP drawing of *trans*-$[Co(NO_2)_2(tmd)_2]^+$ ion.

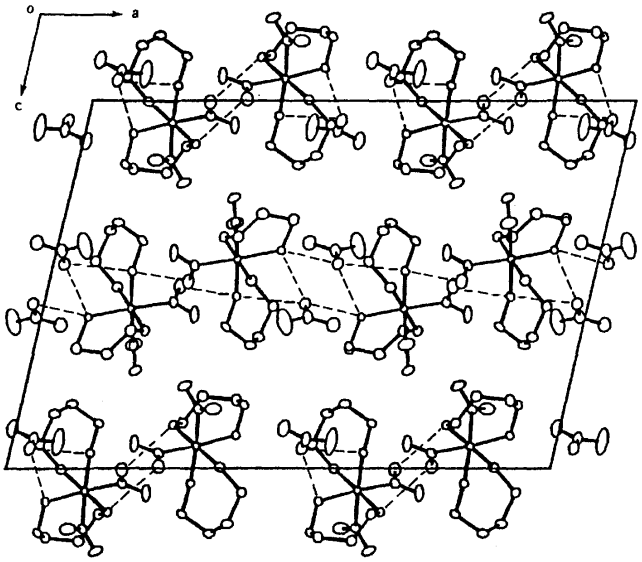

Fig. 3. Projection of the unit cell of *cis*-$[Co(NO_2)_2(tmd)_2]NO_3$ along b axis. Complex 1's and 2's are lying almost in the (0 0 1) and (0 0 2) plane, respectively. Interionic hydrogen bonds are indicated with broken lines.

molecules. Interatomic distances for hydrogen bonded atoms are listed as the supplementary data.[13]

Conformations of Chelate Rings. Bond lengths and angles in the chelate rings are almost the same for the cis and trans complexes, as shown in Tables 4 and 5. All the chelate rings in the cis complexes have a similar conformation. The two chelate rings in the trans complex are also similar to each other, but different from those in the cis complex. Figure 5 shows the projections of the chelate rings along the bisectors of the N-Co-N angle and the atom deviations from the N-Co-N plane.

The conformations of the chelate rings in the cis complex are quite similar to those in $[Co(tmd)_3]^{3+}$ [5,6]: The carbon atoms next to the nitrogens are displaced by 0.73—0.88 Å on the opposite sides of the plane formed by the cobalt and two nitrogen atoms, and the remaining carbon atoms are nearly in this plane. The deviations from the plane are 0.03 to 0.25 Å. This conformation corresponds to the twist-chair form of the cycloheptane ring.[22] The torsion angles shown in Table 6 indicate that only the central C-C bonds take gauche conformation. In contrast to the cis complex, the chelate rings of the trans complex take the chair form. One of the carbon atoms next to the nitrogen lies almost on the N-Co-N plane, and the other three carbon atoms deviate from the plane by more than 0.97 Å.

A conformation analysis of cycloheptane revealed that the chair form is less stable than the twist-chair form for seven-membered alkane ring, although the energy difference is quite small (2.16 kcal mol^{-1}).[22] Repulsion between hydrogen atoms across the ring is serious, especially in the chair-form.

However, such transannular interaction is not important in the chelate rings, because the corresponding H···H interatomic distances in the trans complex are only slightly shorter than the sum of the van der Waals radii: H(C4A)···H(N4A) 2.32(4) and H(C8A)···H(N6A) 2.18(5) Å. The difference in the conformations of the chelate rings in cis and trans complexes

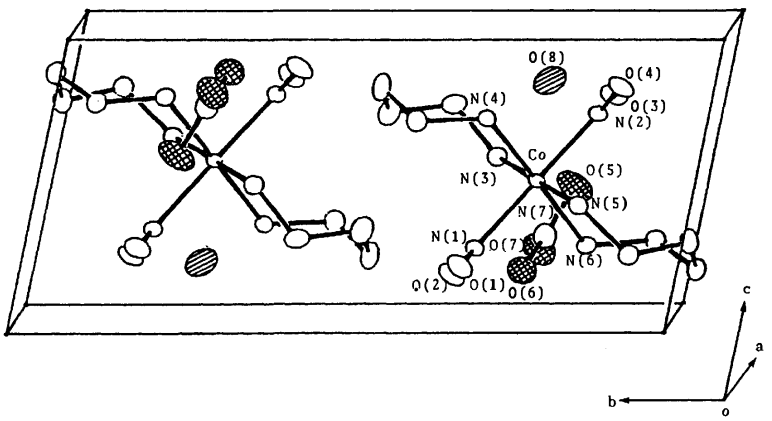

Fig. 4. Perspective of the unit cell of *trans*-$[Co(NO_2)_2(tmd)_2]$-$NO_3 \cdot H_2O$. The water oxygens are hatched and the nitrate oxygens are cross-hatched.

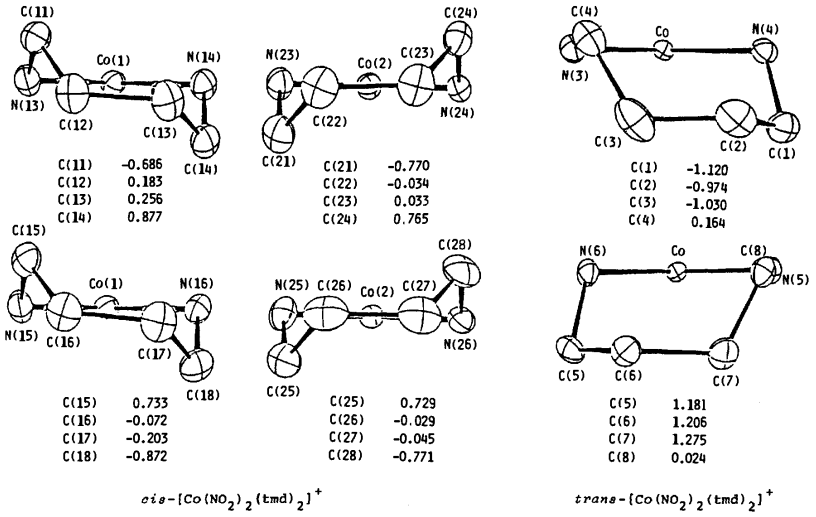

Fig. 5. Projections of tmd chelate rings along the bisector of the N-Co-N angle and the atom deviations (l/Å) from the N-Co-N plane.

Table 6. Torsion Angles in the Chelate Rings

Torsion angle[a]	ϕ/°	Torsion angle	ϕ/°
cis-$[Co(NO_2)_2(tmd)_2]NO_3$			
N(14)-Co(1)-N(13)-C(11)	33.8(2)	N(16)-Co(1)-N(15)-C(15)	36.5(2)
N(13)-Co(1)-N(14)-C(14)	45.9(2)	N(15)-Co(1)-N(16)-C(18)	44.2(2)
Co(1)-N(13)-C(11)-C(12)	−89.1(3)	Co(1)-N(15)-C(15)-C(16)	−90.6(3)
Co(1)-N(14)-C(14)-C(13)	−91.5(3)	Co(1)-N(16)-C(18)-C(17)	−93.0(3)
N(13)-C(11)-C(12)-C(13)	82.5(4)	N(15)-C(15)-C(16)-C(17)	79.4(4)
N(14)-C(14)-C(13)-C(12)	73.4(4)	N(16)-C(18)-C(17)-C(16)	75.3(4)
C(11)-C(12)-C(13)-C(14)	−63.6(4)	C(15)-C(16)-C(17)-C(18)	−61.5(4)
N(24)-Co(2)-N(23)-C(21)	−40.1(3)	N(26)-Co(2)-N(25)-C(25)	−36.6(3)
N(23)-Co(2)-N(24)-C(24)	−39.0(2)	N(25)-Co(2)-N(26)-C(28)	−39.3(3)
Co(2)-N(23)-C(21)-C(22)	89.5(3)	Co(2)-N(25)-C(25)-C(26)	86.6(3)
Co(2)-N(24)-C(24)-C(23)	88.3(3)	Co(2)-N(26)-C(28)-C(27)	87.8(3)
N(23)-C(21)-C(22)-C(23)	−76.9(4)	N(25)-C(25)-C(26)-C(27)	−79.0(4)
N(24)-C(24)-C(23)-C(22)	−76.9(4)	N(26)-C(28)-C(27)-C(26)	−78.7(4)
C(21)-C(22)-C(23)-C(24)	64.1(4)	C(25)-C(26)-C(27)-C(28)	66.6(5)
trans-$[Co(NO_2)_2(tmd)_2]NO_3 \cdot H_2O$			
N(4)-Co-N(3)-C(4)	7.9(3)	N(6)-Co-N(5)-C(8)	1.1(3)
N(3)-Co-N(4)-C(1)	65.2(3)	N(5)-Co-N(6)-C(5)	−71.6(3)
Co-N(3)-C(4)-C(3)	−70.5(5)	Co-N(5)-C(8)-C(7)	63.6(4)
Co-N(4)-C(1)-C(2)	−88.9(4)	Co-N(6)-C(5)-C(6)	89.8(4)
N(3)-C(4)-C(3)-C(2)	90.9(5)	N(5)-C(8)-C(7)-C(6)	−93.8(4)
N(4)-C(1)-C(2)-C(3)	63.7(6)	N(6)-C(5)-C(6)-C(7)	−60.7(5)
C(1)-C(2)-C(3)-C(4)	−69.8(7)	C(5)-C(6)-C(7)-C(8)	−70.9(5)

a) Looking from atom 2 to atom 3, the clockwise rotation of bond 3-4 with reference to bond 2-1 is given.

may be due to the interaction of the NO_2 ligands and the chelate rings. The oxygen atoms of the NO_2 ligands form intramolecular hydrogen bonds to amine groups of the chelate rings as shown in Tables 4 and 5. Such hydrogen bonds have been observed for *trans*-$[Co(NO_2)_2(en)_2]NO_3$,[15] *cis*-$[Co(NO_2)_2(en)_2]Cl$,[16] and *cis*-$[Co(NO_2)_2(tn)_2]Cl \cdot H_2O$.[17] Furthermore, the oxygen atoms of the nitro groups interact with the methylene groups adjacent to the tmd-nitrogens. Figure 6 shows the projection of the trans complex along the Co-N(NO_2) axis. The two nitro groups lie in a plane containing the cobalt atom, and the angle between Co-N(3) and the plane is 30.0°. Broken lines show the hypothetical structure with the twist-chair form for the chelate rings. To minimize the repulsion between the oxygen atoms of the nitro groups and the carbon atoms adjacent to the tmd-nitrogens in the hypothetical structure, the NO_2 ligands should lie in the plane bisecting the angle N(3)-Co-N(6). Even for this conformation, four O···C interatomic distances

Table 7. Comparison of Bond Angles between 5-, 6-, and 7-Membered Chelate Rings

Complex	ϕ/°			
	N-Co-N	Co-N-C	N-C-C	C-C-C
$[Co(en)_3]^{3+}$ a)	85.4	108.4	105.8	
$[Co(tn)_3]^{3+}$ b)	91.0	122.0	112.3	113.6
$[Co(tmd)_3]^{3+}$ c)	89.8	122.3	113.5	115.2
cis-$[Co(NO_2)_2(tmd)_2]^+$ d)	92.4(6)	124.7(9)	113.7(4)	116.2(4)
trans-$[Co(NO_2)_2(tmd)_2]^+$ d)	92.8(1)	125.2(14)	113.8(8)	116.4(5)

a) M. Iwata, K. Nakatzu, and Y. Saito, *Acta Crystallogr.,Sect. B*, **25**, 2562 (1969). b) R. Nagao, F. Marumo, and Y. Saito, *Acta Crystallogr., Sect. B*, **29**, 2438 (1973). c) Ref. 5. d) This work.

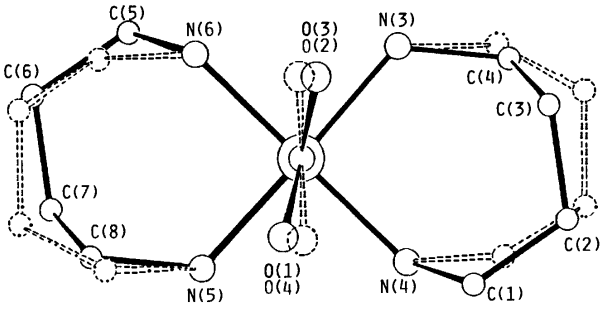

Fig. 6. Projection of the *trans*-$[Co(NO_2)_2(tmd)_2]^+$ ion along the Co-N(NO_2) axis. Broken lines show the hypothetical molecular structure with the chelate rings in the twist-chair form.

(O(1)···C(1), O(1)···C(8), O(3)···C(4), and O(3)···C(5)) are about 3.19 Å, i.e. shorter than the sum of the van der Waals radii, 3.40 Å. The adopted chair form and the inclination of the nitro groups help with alleviating this repulsion: Only two O···C distances in the real complex are shorter than the sum of the van der Waals radii, O(1)···C(1) 3.196(6) and O(3)···C(5) 3.172(5) Å.

There exists only one such O···C interatomic distance in the cis complex (O(22)···C(24) 3.167(4) Å).

Table 7 compares the bond angles for the five-, six-, and seven-membered chelate rings. The larger deviations from the tetrahedral angle for nitrogen and carbon atoms in tmd complexes clearly show the instability of seven-membered chelate rings.

References

1) H. Ogino, *J. Coord. Chem.*, **15**, 187 (1987).
2) Abbreviation used in this paper: en=$H_2N(CH_2)_2NH_2$, tn=$H_2N(CH_2)_3NH_2$, and tmd=$H_2N(CH_2)_4NH_2$.
3) H. Ogino and J. Fujita, *Bull. Chem. Soc. Jpn.*, **48**, 1836 (1975).
4) H. Ogino, *Bull. Chem. Soc. Jpn.*, **50**, 2459 (1977).
5) S. Sato, Y. Saito, J. Fujita, and H. Ogino, *Inorg. Nucl. Chem. Lett.*, **10**, 669 (1974).
6) S. Sato and Y. Saito, *Acta Crystallogr., Sect. B*, **31**, 1378 (1975).
7) Y. Nakayama, S. Ooi, and H. Kuroya, 30th National Meeting of the Chemical Society of Japan, Osaka, April 1974, Abstr., No. 3D36.
8) H. Ichida, S. Sato, and Y. Saito, 27th Symposium on Coordination Chemistry, Matsumoto, September 1977, Abstr., No. 1B04.
9) K. Nagata, K. Kanamori, K. Kawai, and H. Ogino, *Chem. Lett.*, **1985**, 1507.
10) T. Sakurai and K. Kobayashi, *Rikagaku Kenkyusho Hokoku*, **55**, 69 (1979).
11) International Tables for X-ray Crystalography, Kynoch, Birmingham, England, Vol. IV, Tables 2.2A and 2.3.1 (1974).
12) R. F. Stewart, E. R. Davidson, and W. T. Simpson, *J. Chem. Phys.*, **42**, 3175 (1965).
13) Some additional bond lengths and angles, the positional and thermal parameters of hydrogen atoms, the final anisotropic thermal parameters, and the F_o—F_c tables are deposited as Document No. 8833 at the Office of the Editor of the Bull. Chem. Soc. Jpn.
14) H. Shintani, S. Sato, and Y. Saito, *Acta Crystallogr., Sect. B*, **32**, 1184 (1984).
15) O. Börtin, *Acta Chem. Scand., Ser. A*, **30**, 657 (1976).
16) I. Bernal, *Inorg. Chim. Acta*, **96**, 99 (1985).
17) G. Srdanov, R. Herak, and B. Prelesnik, *Inorg. Chim. Acta*, **33**, 23 (1979).
18) P. C. Cagnon, J. R. Matalon, and A. L. Beauchamp, *Acta Crystallogr., Sect. B*, **34**, 1128 (1978).
19) I. Oonishi, F. Muto, and Y. Komiyama, *Bull. Chem. Soc. Jpn.*, **42**, 2791 (1969).
20) N. Yoshida, M. Fujimoto, A. Furusaki, and T. Matsumoto, *Chem. Lett.*, **1986**, 1091.
21) N. Bresciani-Pahor, M. Calligaris, and L. Randaccio, *Inorg. Chim. Acta*, **27**, 47 (1978).
22) J. B. Hendrickson, *J. Am. Chem. Soc.*, **83**, 4537 (1961).

 © 1988 The Chemical Society of Japan Bull. Chem. Soc. Jpn., 61, 3497—3501 (1988)

Cobalt(III) Complexes Containing an Aldonic Acid

Taro TSUBOMURA,† Shigenobu YANO,*,†† and Sadao YOSHIKAWA†††
Department of Synthetic Chemistry, Faculty of Engineering, The University of Tokyo,
Hongo, Bunkyo-ku, Tokyo 113
(Received June 11, 1988)

Stable complexes of the type $[Co(aldonato)(en)_2]^+$, where en is ethylenediamine and aldonato is the diacid anion of D-gluconic acid or L-mannonic acid, were prepared by the reaction of aldonic acid lactones with *rac*-$[Co(CO_3)(en)_2]^+$. Two diastereomers (Δ and Λ) have been separated by ion-exchange chromatography from each of the aldonato complexes. These complexes were characterized by NMR, electronic absorption, and circular dichroism spectra. The structures of all four complexes were found to have an aldonato ligand which coordinates bidentately through an oxygen atom of the carboxylato group and an oxygen atom of the deprotonated hydroxyl group on C(2).

It has been widely known for a long time that aldonic acids form stable complexes with metal ions.[1] Especially, gluconic acid and its salts have been used extensively as sequestering agents for metal ions in alkaline media. Numerous industrial applications have been reported.[2] These ligands have many functional groups which can bind to metal ions. However little has been reported on the coordination chemistry of aldonic acid complexes. Several crystal structures of aldonic acid salts have been reported,[3] but only two of the transition metal aldonic acid complexes, those are lead gluconate[4] and manganese gluconate,[5] have been clarified. Both complexes are polymer, in which the gluconato ligands bridge two metals. Because of the lability of these metal complexes, it seems that these complexes have no fixed chelate in solution.

Accordingly, substitution inert cobalt(III) complexes are suitable to study the coordination behavior of these ligands. It is interesting to examine the coordination behavior of metal complexes of the C-2 epimers, gluconic acid and mannonic acid, since the chelate ring formation via hydroxyl group on C(2) atom is expected.

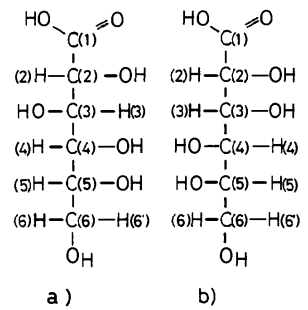

Fig. 1. Structure of (a) D-gluconic and (b) L-mannonic acid.

We report the first successful isolation of several Co(III) complexes of D-gluconic acid and L-mannonic acid (Fig. 1), and the coordination geometry of the complexes were studied by visible-UV absorption, CD, and NMR spectra as a part of our study to investigate sugar transition metal complexes.[6]

Experimental

Materials, Measurements and Analyses. D-Glucono-1,5-lactone and L-manno-1,4-lactone were purchased from Tokyo Kasei Kogyo and Sigma Co., respectively.

^1H NMR spectra were recorded on a JEOL GX-400 spectrometer using 2,2-dimethyl-1-propanol as an internal reference. ^{13}C NMR spectra were obtained on this instrument or JNM-PFT-100 spectrometer using tetramethylsilane as an external reference.

Visible-UV absorption spectra were obtained with a HITACHI model 340 spectrophotometer. Circular dichroism spectra were measured with a JASCO J-500 spectropolarimeter.

Preparation of Δ and Λ-$[Co(D\text{-gluconato})(en)_2]ClO_4 \cdot H_2O$. *Caution!* These perchlorate salts are stable under the experimental conditions as described below. However these complexes are potentially explosive, so that these materials should be handled with great care.

Aldonic acid complexes were prepared by a method analogous to that reported for the lactic acid complexes.[7,8] 1.38 g of $[Co(CO_3)(en)_2]Cl$[9] was dissolved in 10 mL of water, 0.89 g of D-glucono-1,5-lactone was added. The solution was heated to 90 °C and refluxed on a steam bath for 4 h. After cooling, the solution was diluted with water (500 mL) and poured onto a column of SP-Sephadex C25 gel (Na^+ form; 4×30 cm). The column was washed with water (1 L), and the adsorbed products were eluted with 0.05 M sodium perchlorate solution (1 M=1 mol dm^{-3}). A red band of unipositive charged complexes was eluted, this was made of a mixture of two isomers. Sodium perchlorate was partially removed from the red eluted solution by a Sephadex G-10 gel permiation chromatography, then the solution collected were separated again by Dowex 50W X-8 resin (Na^+ form; 3×60 cm) with 0.25 M NaH_2PO_4-0.25 M Na_2HPO_4 buffer solution. It was impossible to separate two isomers with one pass through the column, so that the isomers were separated by recycled elution using a peristaltic tube pump. After the complete separation in the resin, each band was eluted with 0.1 M sodium perchlorate. Sodium perchlorate was removed

† Present address: Department of Industrial Chemistry, Faculty of Engineering, Seikei University, Musashino-city, Tokyo 180.
†† Present address: Chemistry Department, Faculty of Science, Nara Women's University, Nara 630.
††† Present address: Department of Applied Chemistry, Faculty of Science and Technology, Keio University, Kouhoku-ku, Yokohama 223.

from each of the separated red solution by passing three times through a Sephadex G-10 gel column (3.5×50 cm). Each red liquor was evaporated under reduced pressure to a syrup, this was dissolved in a small amount of water, then ethanol was added to incipient turbidity. The solution was kept in a refrigerator. *Λ*-[Co(D-gluconato)(en)$_2$]ClO$_4$·H$_2$O (**1**) was obtained as a little hygroscopic reddish powder (100 mg) from the latter fractions of the Dowex eluents, and *Δ*-[Co(D-gluconato)(en)$_2$]ClO$_4$·H$_2$O (**2**) was obtained as red needles (180 mg) from the former fractions. Anal. Found for *Λ*-isomer: **1**: C, 24.61; H, 5.73; N, 11.48; Cl, 7.27%, for *Δ*-isomer **2**: C, 24.48; H, 5.50; N, 11.08; Cl, 6.97%. Calcd for $CoC_{10}H_{28}O_{12}N_4Cl$: C, 24.47; H, 5.75; N, 11.42; Cl, 7.22%.

Preparation of *Δ* and *Λ*-[Co(L-mannonato)(en)$_2$]ClO$_4$·H$_2$O. These complexes were prepared from [Co(CO$_3$)(en)$_2$]Cl and L-manno-1,4-lactone by the above mentioned procedure. The *Λ*-isomer **3** (160 mg) was also obtained from the latter fractions separated by a Dowex 50W X-8 cation-exchange column chromatography, and the *Δ* isomer **4** (130 mg) was obtained from the former fractions. Both of the isomers were isolated as somewhat hygroscopic red powder. Anal. Found for *Λ*-isomer **3**: C, 24.05; H, 5.35; N, 10.94; Cl, 7.83%, for *Δ*-isomer **4**: C, 23.63; H, 5.08; N, 10.59; Cl, 6.29%. Calcd. for $CoC_{10}H_{28}O_{12}N_4Cl$: C, 24.47; H, 5.75; N, 11.42; Cl, 7.22%.

Results and Discussions

Isolation of Aldonic Acid Complexes. Aldonic acid complexes were prepared by the reaction of [Co(CO$_3$)-(en)$_2$]Cl complex with aldonic acid lactones. In an aqueous solution, D-glucono-1,5-lactone and L-manno-1,4-lactone, which were used in this study, were known to have the equilibrium between the lactones and acid forms.[10] When D-glucono-1,5-lactone was used, two +1 charged red complexes (complex **1** and **2**) were separated from the reaction mixture by ion exchange chromatography, both of these complexes were isolated as perchlorate salts. When L-manno-1,4-lactone was used, two red complexes **3** and **4** were also obtained.

Analytical results indicated that all these complexes obtained have one dinegative charged aldonato ligand, two ethylenediamine ligands, a perchlorate counter anion, and a solvated water molecule. Two isomers were obtained for both the aldonic acid complexes. These isomers are found to be *Δ* and *Λ* isomers whose absolute configurations were determined by CD spectra as described later.

UV-Visible Absorption Spectra. The absorption and CD spectra for the series of complexes are shown in Fig. 2, and their spectral data are presented in Table 1. These absorption spectra all show two peaks in the d-d transition region. The band positions and the intensities of the absorption spectra for these complexes are nearly identical. Each lowest energy peak shows a symmetrical curve without any shoulder in the first absorption region, which is characteristic for

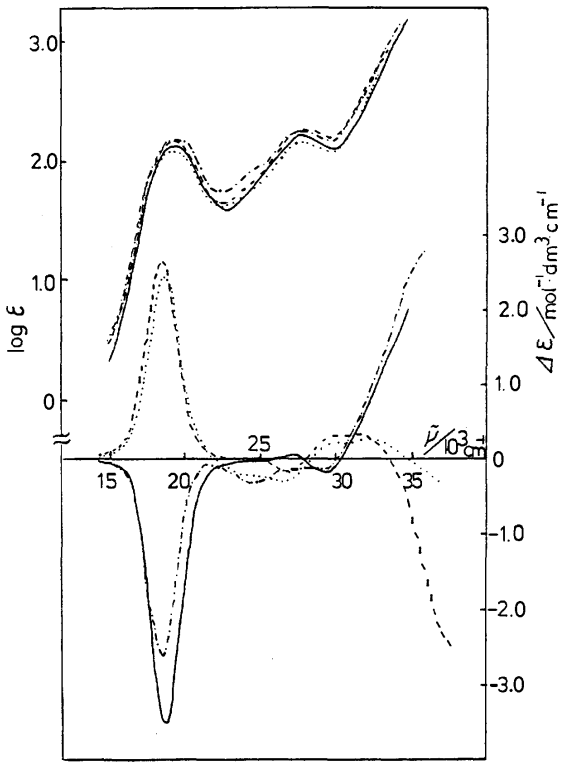

Fig. 2. Electronic absorption and circular dichroism spectra of aldonato complexes. (——) *Λ*-[Co(D-gluconato)(en)$_2$]$^+$, (----) *Λ*-[Co(D-gluconato)(en)$_2$]$^+$, (-·-·-) *Δ*-[Co(L-mannonato)(en)$_2$]$^+$, and (------) *Λ*-[Co(L-mannonato)(en)$_2$]$^+$.

Table 1. Electronic Absorption and CD Spectra

Complex	Abs max/10^{3}cm^{-1} (log ε)	CD max/10^{3}cm^{-1} (Δε/mol^{-1}dm^{3}cm^{-1})	
Λ-[Co(D-gluconato)(en)$_2$]ClO$_4$·H$_2$O	19.4(2.13)	18.6(+2.64)	
	28.1(2.24)	27.0(−0.19)	31.6(+0.30)
Δ-[Co(D-gluconato)(en)$_2$]ClO$_4$·H$_2$O	19.4(2.11)	18.7(−3.53)	
	28.0(2.20)	26.9(+0.075)	29.2(−0.21)
Λ-[Co(L-mannonato)(en)$_2$]ClO$_4$·H$_2$O	19.4(2.05)	18.7(+2.42)	
	28.0(2.12)	26.7(−0.30)	32.9(+0.24)
Δ-[Co(L-mannonato)(en)$_2$]ClO$_4$·H$_2$O	19.4(2.19)	18.5(−2.61)	
	28.0(2.24)	24.8(−0.30)	28.6(−0.12)
Λ-[Co((*R*)-lactato)(en)$_2$]Cl$_2$·H$_2$O[a]	19.4(2.12)	19.2(+2.37)	
	27.8(2.14)	24.7(−0.67)	30.0(+0.064)
Λ-[Co(D-tartrato)(en)$_2$]Cl[b]	19.7(2.07)	19.0(+1.79)	
	28.3(2.14)	27.5(−0.13)	

a) From Ref. 7. b) From Ref. 12.

Table 2. ^{13}C NMR Data for Aldonato Complexes. (ppm from TMS ext.)

Complex	Carbon atom of aldonato				Carbon atom of diamine	
	C1	C2	C3-5	C6		
Λ-[Co(D-gluconato)(en)$_2$]$^{2+}$	191.5	82.5	75.3	63.9	46.4	46.1
			72.2		44.3	43.9
			70.8			
Δ-[Co(D-gluconato)(en)$_2$]$^{2+}$	191.1	82.6	75.6	63.8	46.6	46.1
			72.2		44.6	44.5
			70.4			
Λ-[Co(L-mannonato)(en)$_2$]$^{2+}$	192.0	81.7	74.6	64.3	46.5	46.4
			73.4		44.7	44.6
			72.6			
Δ-[Co(L-mannonato)(en)$_2$]$^{2+}$	191.6	81.2	74.5	64.0	46.4	46.2
			72.8		44.9	44.5
			72.5			

the *cis*(*O*-*O*)-[CoN_4O_2] type.[11] The spectral results for Λ-[Co((*R*)-lactato)(en)$_2$]$^{+}$[7] and Λ-[Co(L-tartrato)(en)$_2$]$^{+}$[12] are also shown in Table 1. The similarity of band maxima and molar absorption coefficients of these aldonato complexes to those of lactato or tartrato complexes supports that the aldonic acids coordinate to cobalt atom through a carboxylato group and a deprotonated hydroxyl group of the aldonato ligand.

NMR Spectra and Coordination Structures. The ^{13}C NMR spectral data of these complexes together with those of sodium aldonate are given in Table 2. Because ^{1}H and ^{13}C NMR spectra of these complexes resemble each other, the following discussion applies equally to all of the complexes. The ^{13}C NMR spectra of these complexes show ten signals. The higher-field four signals and the lower-field six signals can be ascribed to the two ethylenediamine units and to the aldonic acid unit, respectively. The coordination points of the aldonato ligand were determined from these NMR data.

As a typical example, we deal with Λ-[Co(D-gluconato)(en)$_2$]$ClO_4 \cdot H_2O$ (**1**). The complete ^{1}H decoupled ^{13}C NMR spectrum of **1** in the range of 60—200 ppm is shown in Fig. 3. The C(1) and C(6) carbons of aldonato ligands were easily assigned by using non ^{1}H decoupling with NOE measurement. The C(2) carbon centered at about δ 82 was assigned by using selective decoupling methods as described below.

The ^{1}H NMR spectral data of the gluconato units of these complexes are tabulated in Table 3. A doublet at about δ 4.2 could be assigned to the H2 proton on C(2) atom. All other peaks were assigned by using double resonance techniques. In the ^{13}C NMR spectra, a selective irradiation of the proton resonance at about δ 4.2 gave one singlet peak at about δ 82. Accordingly, the ^{13}C signal at about δ 82 was assigned to C(2) atom.

Both C(1) and C(2) carbons shift clearly to the lower-field in comparison with those of sodium gluconate (Fig. 3). These low-field shift of the carbon nuclei may be caused by the coordination of the adjacent oxygen atom to the cobalt atom. In fact, we observed the similar low-field shift of ^{13}C signal for cobalt(III) complexes.[13]

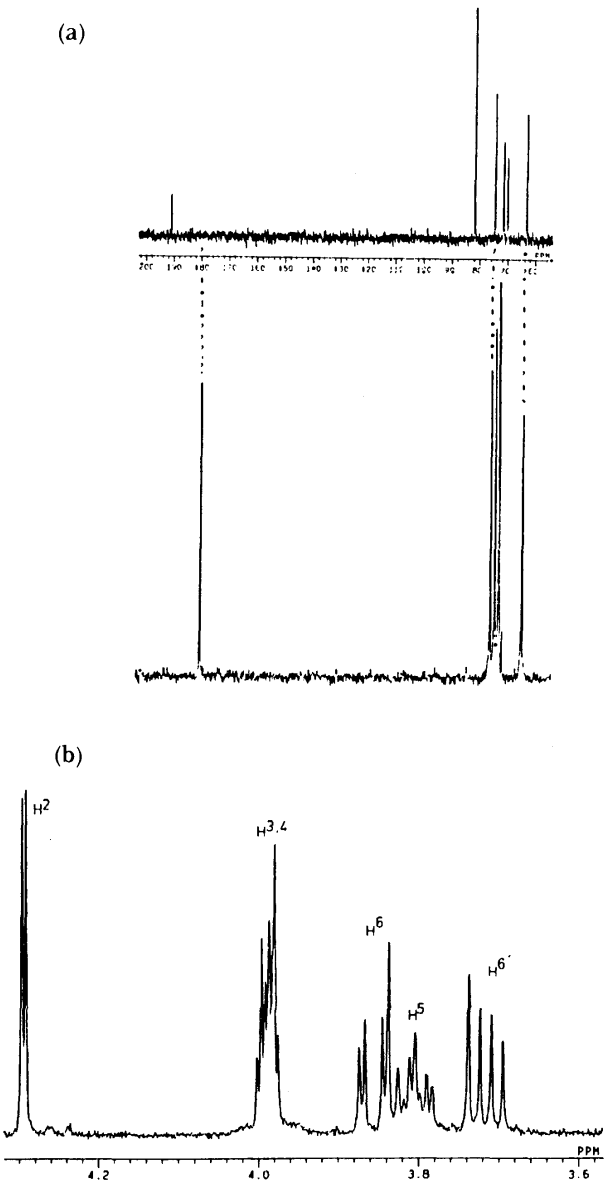

Fig. 3. (a) Upper, ^{13}C NMR spectrum of Λ-[Co(D-gluconato)(en)$_2$]$^{+}$ (60—200 ppm region). Lower, ^{13}C NMR spectrum of sodium D-gluconate. (b) ^{1}H NMR of Λ-[Co(D-gluconato)(en)$_2$]$^{+}$ (3.7—4.3 ppm). All spectra were obtained in D_2O solution.

Table 3. ^{1}H NMR Data for Aldonato Complexes

Complex	Chemical shift values (ppm)					
	H2	H3	H4	H5	H6	H6′
Λ-[Co(D-gluconato)(en)$_2$]$^{2+}$	4.30	3.98	4.00	3.80	3.72	3.86
Δ-[Co(D-gluconato)(en)$_2$]$^{2+}$	4.24	3.97	4.00	3.82	3.72	3.85
Λ-[Co(L-mannonato)(en)$_2$]$^{2+}$	4.21	4.06	3.93	3.78	3.71	3.86
Δ-[Co(L-mannonato)(en)$_2$]$^{2+}$	4.27	4.02	3.89	3.78	3.71	3.86
	Coupling constant/Hz					
	$J_{H2,3}$	$J_{H3,4}$	$J_{H4,5}$	$J_{H5,6}$	$J_{H5,6'}$	$J_{H6,6'}$
Λ-[Co(D-gluconato)(en)$_2$]$^{2+}$	1.8	2.0	a)	5.8	2.8	11.5
Δ-[Co(D-gluconato)(en)$_2$]$^{2+}$	1.5	2.4	7.6	5.8	2.8	11.3
Λ-[Co(L-mannonato)(en)$_2$]$^{2+}$	3.0	2.4	7.6	6.3	2.7	11.6
Δ-[Co(L-mannonato)(en)$_2$]$^{2+}$	3.0	2.6	6.4	6.1	2.5	9.0

a) Cannot determined due to the overlapping of the peaks.

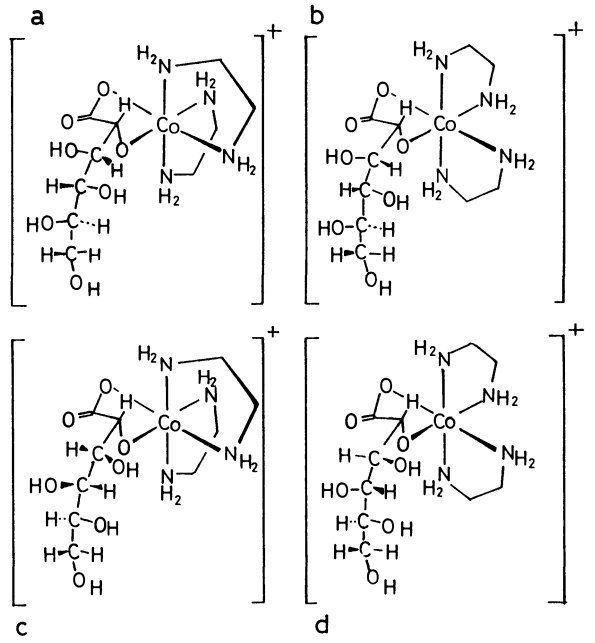

Fig. 4. Structures of (a) *Λ*-[Co(D-gluconato)(en)$_2$]$^+$, (b) *Δ*-[Co(D-gluconato)(en)$_2$]$^+$, (c) *Λ*-[Co(L-mannonato)(en)$_2$]$^+$, and (d) *Δ*-[Co(L-mannonato)-(en)$_2$]$^+$ ions.

From the above arguments we concluded that aldonato ligands coordinate to the cobalt at two points through the carboxylato oxygen atom and through the deprotonated hydroxyl oxygen atom on C(2) forming a five-membered chelate ring. The same discussions can be done for all of the other aldonato complexes (**2**, **3**, and **4**), their structures are shown in Fig. 4. No other complexes except these complexes containing five-membered aldonato chelate were detectable on the +1 charged reaction products. This fact points out that five-membered chelate formation is the most favorable coordination of the aldonato ligands.

Some interesting information concerning the conformation of the aldonato ligands can be drawn from the NMR J_{HH} coupling constant values. The values $J_{H4,5}$ and $J_{H5,6}$ are comparatively large, but $J_{H2,3}$ and $J_{H3,4}$ are small, so that it is deduced that the conformation of the carbon skeleton of aldonato ligands is not completely flexible, but it is somewhat fixed even in aqueous solution. There are no significant differences between the coupling constants of the gluconato complexes and the mannonato complexes except some differences in $J_{H2,3}$ values. This difference is reasonable because gluconato and mannonato ligands can originally be regarded as C(2) epimer, and only H2-H3 relative configuration is different between those ligands (see Fig. 1).

Circular Dichroism Spectra and Stereochemistry of the Complexes. Two diastereomers can be obtained from each of these aldonato complexes. The CD spectra in the first d-d absorption region of the two isomers give nearly mirror image curves. For both the D-gluconato and L-mannonato complexes, the compounds in the former eluted fractions from the Dowex cation exchange column are assigned to *Δ* isomers because these complexes have a minus CD peak in the region, on the other hand, those in the latter eluted fractions are assigned to *Λ* isomers.[14]

It is well-known that the contributions to the optical activity from the configurational and vicinal effects are essentially additive in considering the CD spectra of the octahedral metal complexes.[15] The vicinal effect ($\Delta\varepsilon(R)$ or $\Delta\varepsilon(S)$) includes the conformational effect of the chelate rings (δ or λ) and the effect induced from the asymmetric centers (R or S) in the ligand. The following relationships will then hold: $\Delta\varepsilon(\Lambda)=1/2[\Delta\varepsilon(\Lambda R)-\Delta\varepsilon(\Delta R)]$ and $\Delta\varepsilon(R)=1/2[\Delta\varepsilon(\Lambda R)+\Delta\varepsilon(\Delta R)]$, where $\Lambda\varepsilon(R)$ is the CD contribution due to the vicinal effect of the coordinated (R) chelate such as (R)-amino acids, (R)-hydroxy acids, or (R)-aldonic acids and $\Delta\varepsilon(\Lambda)$ is the contribution of *Λ* configuration. In general, the configurational effect is much greater than the vicinal effect in cobalt complexes. But, Kipp and Haines, however, reported that the CD spectra of *Λ*-[Co((R)-lactato)(en)$_2$]$^+$ and its *Δ* isomer are not mirror image, so the vicinal effect of the hydroxy acid ligand is more intense than would be expected from

comparison with similar amino acid complexes.[7]

In our aldonato complexes, however, the calculated configurational contribution to the circular dichroism $\Delta\varepsilon(\Lambda)$ is much greater than the vicinal contribution, $\Delta\varepsilon(R)$. In fact, $\Delta\varepsilon(\Lambda)$ are 3.1 for D-gluconato complexes and 2.5 for L-mannonato complexes and $\Delta\varepsilon(R)$ are 0.4 for D-gluconato complexes and 0.1 for L-mannonato complexes, respectively. Accordingly, the configurational effect is the main effect in these aldonato complexes as observed for other related complexes containing amino acids.

The formation ratio of Δ and Λ diastereomers of these aldonato complexes was determined on the basis of their absorption strength.

Λ: Δ (complex **1**: complex **2**), was determined to 52:48 for D-gluconato complexes and complex **3**: complex **4** was 67:33 for L-mannonato complexes. It is well-known that only a small stereoselectivity was observed in the preparation of $[Co(en)_2$(L-amino acidato)$]^{2+}$ in comparison with $[Co(en)_2$(chiral diamine)$]^{3+}$.[16] The hydroxy acid ligand seems to give a nearly planer five membered chelate ring as well as the amino acid. Therefore, the stereoselectivity of the aldonato complexes due to the conformational preferences is not expected so much. The isomers ratio (Λ:Δ) for the gluconato complexes is, indeed, nearly 50:50. However, small stereoselectivity was observed in the formation of the mannonato complexes. Accordingly, it is suspected that small stereoselectivity is given by the interaction between the hydroxylmethylene chain of the mannonato ligand and diamine ligands.

It is well-known that chiral amino acid ligands in the complex such as $[Co(ala)(en)_2]^+$ (ala=L- or D-alaninato) are easily epimerized in mild alkaline solution (pH 9—10).[17] The stability of these aldonato complexes in alkaline solution were monitored by CD measurement. The CD spectral curves of all these complexes do not change after heating at 40 °C even in 0.1 M Na_2CO_3 solution (pH 12). Thus, α-proton of aldonato chelate is found to be remarkably inactive in comparison with that of amino acid chelate. Since in the first stage of base catalyzed epimerization OH^- ions would smoothly attack to complexes which have large positive charges, one of the reasons of the stability is suspected to be more negative charge of the aldonato ligands than amino acid ligands.

Conclusion

Both Δ and Λ-$[Co(aldonato)(en)_2]^{2+}$ complexes containing five-membered aldonato chelate were obtained from the reaction between aldonic acid lactones and *rac*-$[Co(CO_3)(en)_2]^+$. Some stereoselectivity between the diastereomers (Δ and Λ) is observed although it is relatively low. α-Protons of these aldonato chelates are remarkably inactive in alkaline solution in comparison with the $[Co(\text{amino acidato})(en)_2]^{2+}$ complexes.

This work is partially supported by a Grant-in-Aid for Scientific Research from the Ministry of Education.

References

1) a) J. T. Spence and G. Kallos., *Inorg. Chem.*, **2**, 710 (1963). b) H. A. Tajmir-Riahi, *Inorg. Chim. Acta*, **136**, 93 (1987).

2) D. T. Sawyer, *Chem. Rev.*, **64**, 633 (1964).

3) C. D. Littleton, *Acta Crystallogr.*, **6**, 775 (1953); N. C. Panagiotopoulos and G. A. Jeffrey, *Acta Crystallogr., Sect. B*, **30**, 1421 (1974).

4) T. Lis, *Acta Crystallogr., Sect. C*, **40**, 374 (1984).

5) T. Lis, *Acta Crystallogr., Sect. B*, **35**, 1699 (1979).

6) S. Yano, S. Takizawa, H. Sugita, K. Takahashi, T. Tsubomura, H. Shioi, and S. Yoshikawa, *Carbohydr. Res.*, **142**, 180 (1985); H. Shioi, S. Yano, K. Toriumi, T. Ito, and S. Yoshikawa, *J. Chem. Soc., Chem. Commun.*, **1983**, 201; T. Tsubomura, S. Yano, K. Toriumi, T. Ito, and S. Yoshikawa, *Polyhedron*, **2**, 123 (1983); T. Tsubomura, S. Yano, K. Toriumi, T. Ito, and S. Yoshikawa, *Bull. Chem. Soc. Jpn.*, **57**, 1833 (1984); T. Tsubomura, S. Yano, K. Toriumi, T. Ito, and S. Yoshikawa, *Inorg. Chem.*, **25**, 392 (1986); T. Tsubomura, S. Yano, K. Kobayashi, T. Sakurai, and S. Yoshikawa, *J. Chem. Soc., Chem. Commun.*, **1986**, 459.

7) E. B. Kipp and R. A. Haines, *Inorg. Chem.*, **11**, 271 (1972).

8) R. A. Haines and A. A. Smith, *Inorg. Chem.*, **12**, 1426 (1973).

9) P. Pfeifer and O. Angern, *Ber. Deut. Chem. Ges.*, **60**, 308 (1927).

10) "The Carbohydrates. Chemistry and Biochemistry," ed by W. Pigman and D. Horton, Academic Press, New York (1980), Vol. IB, p. 883.

11) H. Yamatera, *Bull. Chem. Soc. Jpn.*, **31**, 95 (1958); N. Matsuoka, J. Hidaka, and Y. Shimura, *Bull. Chem. Soc. Jpn.*, **40**, 1868 (1967).

12) R. A. Haines, E. B. Kipp, and M. Reimer, *Inorg. Chem.*, **13**, 2473 (1974).

13) M. Yamaguchi, S. Yamamatsu, H. Oikawa, M. Saburi and S. Yoshikawa, *Inorg. Chem.*, **20**, 3179 (1981).

14) Y. Saito, "Inorganic Molecular Dissymmetry," Springer-Verlag: Berlin, (1979).

15) S. K. Hall and B. E. Douglas, *Inorg. Chem.*, **8**, 372 (1969).

16) C. T. Liu and B. E. Douglas, *Inorg. Chem.*, **3**, 1356 (1964).

17) D. A. Buckingham, L. G. Marzilli, and A. M. Sargeson, *J. Am. Chem. Soc.*, **89**, 5133 (1967).

 © 1988 The Chemical Society of Japan Bull. Chem. Soc. Jpn., 61, 3503—3509 (1988)

Preparation and Stereochemistry of Cobalt(III) Complexes Containing 1,1,11,11-Tetraphenyl-4,8-diaza-1,11-diphosphaundecane or (3*S*,9*S*)-3,9-Dimethyl-1,1,11,11-tetraphenyl-4,8-diaza-1,11-diphosphaundecane, $(C_6H_5)_2PCH_2CHRNHCH_2CH_2CH_2NHCHRCH_2P(C_6H_5)_2$ (R=H or CH_3)

Min-Ho JUNG, Masamichi ATOH,† Kazuo KASHIWABARA, and Junnosuke FUJITA*
Department of Chemistry, Faculty of Science, Nagoya University, Chikusa-ku, Nagoya 464
(Received June 11, 1988)

Two new quadridentate phosphine ligands 1,1,11,11-tetraphenyl-4,8-diaza-1,11-diphosphaundecane (pp-232PNNP) and (3*S*,9*S*)-3,9-dimethyl-1,1,11,11-tetraphenyl-4,8-diaza-1,11-diphosphaundecane (*SS*(*C*)-pp-232PNNP), and several their cobalt(III) complexes were prepared and characterized. The *RS*(*N*) isomers of *trans*-$[CoCl_2$(pp- or *SS*(*C*)-pp-232PNNP)$]^+$ were formed by oxidation of cobalt(II) complexes of these ligands in dichloromethane with chlorine, while the *RR*,*SS*(*N*), and *RR*(*N*) isomers of the pp-232PNNP and *SS*(*C*)-pp-232PNNP complexes, respectively, were derived from the corresponding carbonato complexes and hydrochloric acid. The $[Co(O\text{-}O)$(pp- or SS(C)-pp-232PNNP)$]^{n+}$ (O-O= CO_3^{2-}, $C_2O_4^{2-}$, $C_5H_7O_2^-$) complexes yielded only a cisβ isomer. The stereochemistry of the complexes was discussed on the basis of the absorption, circular dichroism and NMR spectra.

In our previous papers, we have reported a number of new cobalt(III) complexes containing the following quadridentate aminoalkylphosphine ligands; pp- and mm-222PNNP=$R_2PCH_2CH_2NHCH_2CH_2NHCH_2CH_2PR_2$ (R=C_6H_5 and CH_3),[1] *SS*(*C*)-pp- and SS(C)-mm-222PNNP= (*S*,*S*)-$R_2PCH_2CH(CH_3)NHCH_2CH_2NHCH(CH_3)CH_2PR_2$ (R=C_6H_5 and CH_3),[2] mp- and SS(C)-mp-222PNNP=$(C_6H_5)(CH_3)PCH_2CHRNHCH_2CH_2NHCHRCH_2P(CH_3)(C_6H_5)$ (R=H and CH_3),[3] and 222NPPN and SS(C)-222NPPN=$NH_2CHRCH_2P(C_6H_5)CH_2CH_2P(C_6H_5)CH_2CHRNH_2$ (R=H and CH_3).[4] The properties such as stereoselectivity and the relation between circular dichroism spectra and the absolute configuration observed for these complexes have often been found to differ from those reported for complexes containing the corresponding tetramine ligand $NH_2CH_2CH_2NHCH_2CH_2NHCH_2CH_2NH_2$ (trien) and its derivatives.[5] To elucidate properties of cobalt(III)-polydentate phosphine complexes in more detail, further preparative studies will be necessary on related complexes. This paper deals with the preparation and characterization of cobalt(III) complexes formed with two new ligands of the PNNP type, 1,1,11,11-tetraphenyl-4,8-diaza-1,11-diphosphaundecane (pp-232PNNP) and (3*S*, 9*S*)-3,9-dimethyl-1,1,11,11-tetraphenyl-4,8-diaza-1,11-diphosphaundecane (*SS*(*C*)-pp-232PNNP), which form two five-and one six-membered chelate rings upon coordination.

Experimental

Quadridentate phosphine ligands pp-232PNNP and SS(C)-pp-232PNNP were prepared and handled under an atmosphere of nitrogen until they formed cobalt(III) complexes. All solvents used for the preparation were made oxygen-free by bubbling nitrogen for 20 min immediately before use. 1,9-Dichloro-3,7-diazanonane dihydrochloride,[6] diphenylphosphine[7] and (*S*)-alaninol (2-amino-1-propanol)[8] were prepared according to the literature methods. Absorption, circular dichroism (CD), and ^1H and ^{13}C NMR spectra were recorded on Hitachi 323 and U3400 spectrometers, a Jasco J-40CS spectropolarimeter, and Jeol JNM PMX-60 and Hitachi R-90HS spectrometers, respectively.

Preparation of Ligands. 1,1,11,11-Tetraphenyl-4,8-diaza-1,11-diphosphaundecane (pp-232PNNP). To liquid ammonia (150 cm^3) containing metallic sodium (1.7 g, 74 mmol) in a 500 cm^3 round-bottom flask was added dropwise diphenylphosphine (12.1 g, 65 mmol) at −78 °C. After stirring for 20 min, 1,9-dichloro-3,7-diazanonane dihydrochloride (4.0 g, 14.7 mmol) was added in small portions with stirring. After 1 h, liquid ammonia was evaporated. To the residue were added water (50 cm^3) and then diethyl ether (60 cm^3) with stirring. The ethereal layer was separated and dried over $MgSO_4$ (ca. 10 g) overnight. A viscous liquid was obtained by removing the solvent and unreacted diphenylphosphine under vacuum. The oily product (ca. 4 g) thus obtained was used for the preparation of cobalt(III) complexes without further purification.

(2*S*,8*S*)-2,8-Dimethyl-3,7-diaza-1,9-nonanediol Dihydrochloride. To an ethanol solution (130 cm^3) of (*S*)-alaninol (31 g, 0.41 mol) in a 500 cm^3 round-bottom flask was added a solution of 1,3-dibromopropane (21 g, 0.106 mol) in ethanol (10 cm^3) over 30 min at 70 °C with stirring. Stirring was continued for 4 h. The solution was cooled to 0 °C and then was mixed with KOH (11.9 g, 0.212 mol) in ethanol (200 cm^3). After 1 h precipitated KBr was filtered off, and ethanol was removed under reduced pressure. The oily residue was distilled at ca. 130 Pa, giving unreacted (*S*)-alaninol (bp 68 °C, 17.95 g) and the desired material (bp 168 °C). Yield: 8.85 g (49.1 mmol, 46.5%). Since the product was very hygroscopic, it was converted into the dihydrochloride. A methanol solution (150 cm^3) of the product was mixed with concd HCl (15 cm^3) at 0 °C, and then the solvent was removed under reduced pressure. On addition of isopropyl alcohol the oily residue gave white crystals, which were filtered and recrystallized from isopropyl alcohol containing a

† Present address: Department of General Education, School of Commerce, Senshu University, Higashi-mita 2-1-1, Tama-ku, Kawasaki 214.

small amount of water. Yield: 7.6 g. Found: C, 40.88; H, 9.09; N, 10.89%. Calcd for $C_9H_{24}N_2Cl_2O_2$: C, 41.07; H, 9.19; N, 10.64%.

(2*S*,8*S*)-2,8-Dimethyl-1,9-dichloro-3,7-diazanonane Dihydrochloride. To a mixture of (2*S*,8*S*)-2,8-dimethyl-3,7-diaza-1,9-nonanediol dihydrochloride (7.6 g, 29 mmol) and chloroform (30 cm^3) was added $SOCl_2$ (22 cm^3) dropwise over 20 min at 0 °C. The mixture was stirred for 30 min at 0 °C, and then refluxed for 2 h at 70 °C. Excess $SOCl_2$ and chloroform were removed by distillation, and the residue was dissolved in hot methanol (50 cm^3). The solution was filtered and the filtrate was cooled in ice to give colorless crystals, which were filtered, washed with diethyl ether, and dried in vacuum. Yield: 1.85 g. An additional amount of products (4.85 g) was obtained from the filtrate by adding excess diethyl ether. Total yield: 6.7 g (77%). Found: C, 36.57; H, 7.22; N, 9.62%. Calcd for $C_9H_{22}N_2Cl_4$: C, 36.02; H, 7.39; N, 9.33%. The compound is very hygroscopic.

(3*S*,9*S*)-3,9-Dimethyl-1,1,11,11-tetraphenyl-4,8-diaza-1,11-diphosphaundecane (*SS*(*C*)-pp-232PNNP). To liquid ammonia (150 cm^3) containing metallic sodium (2.4 g, 104 mmol) in a 500 cm^3 round-bottom flask was added dropwise diphenylphosphine (18 g, 97 mmol), and the mixture was stirred for 1 h at −78 °C. To the resulting orange solution was added (2*S*,8*S*)-2,8-dimethyl-1,9-dichloro-3,7-diazanonane dihydrochloride (6.7 g, 22 mmol) in small portions with stirring. Stirring was continued for 2.5 h. Liquid ammonia was evaporated, and water (33 cm^3) and then diethyl ether (30 cm^3) were added to the residue with stirring. The ethereal layer was separated from the aqueous layer and dried over $MgSO_4$ (ca. 2.0 g) overnight. The solvent and unreacted diphenylphosphine were removed by distillation under vacuum. The oily residue (4.3 g) thus obtained was used for the preparation of cobalt(III) complexes without further purification.

Preparation of Cobalt(III) Complexes.[††] ***RS*(*N*)-*trans*-[$CoCl_2$(pp-232PNNP)]X(Isomer A, X=Cl, ClO_4). Method 1.** To $[CoCl(NH_3)_5]Cl_2$ (500 mg, 2.0 mmol) in a mixture of methanol (100 cm^3) and water (100 cm^3) was added pp-232PNNP (1.0 g, 2.0 mmol) in methanol (10 cm^3) with stirring. After 30 min concd HCl (2 cm^3) was added to the mixture, and stirring was continued overnight. The resulting green solution was filtered and the filtrate was evaporated to dryness under reduced pressure. The green residue was dissolved in water (300 cm^3), the solution was shaken with diethyl ether (300 cm^3), and the aqueous layer was separated and evaporated to dryness under reduced pressure. From the residue the green complex was extracted with a small amount of methanol, and the extract was evaporated again to dryness under reduced pressure to give the complex. Yield: 680 mg (51%). Found: C, 56.06; H, 5.94; N, 3.93%. Calcd for $C_{31}H_{36}N_2Cl_3P_2Co$: C, 56.09; H, 5.47; N, 4.22%. The complex is soluble in water, methanol, ethanol, acetone and dichloromethane, but insoluble in diethyl ether and benzene.

Method 2. To a methanol solution (10 cm^3) of $Co(ClO_4)_2 \cdot 6H_2O$ (470 mg, 1.28 mmol) was added pp-232PNNP (636 mg, 1.28 mmol) in methanol (10 cm^3). After a while the resulting orange-brown solution was evaporated to dryness under reduced pressure, and the residue was dissolved in dichloromethane (50 cm^3). Chlorine gas was bubbled into the solution for 10 min, and then excess chlorine was removed by bubbling nitrogen for 20 min. The solution was filtered, mixed with methanol (30 cm^3), evaporated to a small volume (ca. 20 cm^3) under reduced pressure, then mixed with $NaClO_4 \cdot H_2O$ (7.0 g), and concentrated again to ca. 10 cm^3 under reduced pressure. (The solution should not be evaporated to dryness.) On addition of water (10 cm^3) the solution gave a green precipitate, which was filtered, washed with water and air dried. Yield: 676 mg (72.5%). Absorption and NMR spectra of this [$CoCl_2$(pp-232PNNP)]ClO_4 complex coincide with those of the above chloride salt. The solubility of the complex is similar to that of the chloride salt except insoluble property in water.

***RR,SS*(*N*)-*trans*-[$CoCl_2$(pp-232PNNP)]Cl (Isomer B).** A solution of [Co(C_2O_4 or CO_3)(pp-232PNNP)]X (X=PF_6, $B(C_6H_5)_4$) (0.13 mmol) (see below) in a mixture of methanol (25 cm^3), water (25 cm^3) and concd HCl (5 cm^3) was warmed at 40 °C for 15 min. The resulting green solution was diluted with a mixture of methanol (500 cm^3) and water (500 cm^3), and applied on a column (ϕ 3 cm×10 cm) of SP-Sephadex C-25. The column was washed with water, and the adsorbed product was eluted with 1 mol dm^{-3} HCl in a mixture of methanol and water (1 : 1). The green eluate was evaporated to dryness under reduced pressure to give the complex, which was collected, washed with a small amount of water and then diethyl ether. Yield: 82 mg (97%). Found: C, 56.04; H, 5.75; N, 4.20%. Calcd for $C_{31}H_{36}N_2Cl_3P_2Co$: C, 56.09; H, 5.47; N, 4.22%. The solubility of the complex is similar to that of the corresponding RS(N) isomer.

***cis*β-[Co(C_2O_4)(pp-232PNNP)]PF_6.** To $K_3[Co(C_2O_4)_3] \cdot 3H_2O$ (500 mg, 1.0 mmol) in a mixture of water (50 cm^3) and methanol (5 cm^3) was added pp-232PNNP (500 mg, 1 mmol) in methanol (2 cm^3), and the mixture was stirred overnight. The resulting red solution was evaporated under reduced pressure to remove methanol, and then shaken with diethyl ether (100 cm^3). The separated aqueous layer was diluted with water (1 dm^3) and applied on a column (ϕ 3cm×30 cm) of SP-Sephadex C-25. The adsorbed product was eluted with 0.05 mol dm^{-3} NaCl, and the eluate of the main red band was concentrated to 20 cm^3 and filtered. The filtrate was mixed with NH_4PF_6 (200 mg) in water (5 cm^3), yielding a red precipitate, which was filtered, washed with a small amount of cold water, and air dried. Yield: 410 mg (52%). Found: C, 50.07; H, 4.74; N, 3.61%. Calcd for $C_{33}H_{36}N_2O_4F_6P_3Co$: C, 50.14; H, 4.59; N, 3.54%. The complex is soluble in methanol, ethanol, acetone, dichloromethane, and acetonitrile, slightly soluble in water, but insoluble in diethyl ether.

***cis*β-[Co(CO_3)(pp-232PNNP)]$B(C_6H_5)_4$.** To $K[Co(CO_3)_2(C_5H_5N)_2]$[9] (400 mg, 1.0 mmol) in methanol (50 cm^3) was added pp-232PNNP (500 mg, 1.0 mmol) in methanol (5 cm^3), and the mixture was stirred for 6 h. The resulting red solution was diluted with water (1.5 dm^3), filtered, and the filtrate was applied on a column (ϕ 3 cm×30 cm) of SP-Sephadex C-25. The adsorbed product was eluted with 0.1 mol dm^{-3} NaCl, and the eluate of the main red band was concentrated to ca. 20 cm^3 under reduced pressure. The concentrate was filtered, and the filtrate was mixed with $NaB(C_6H_5)_4$ (350 mg) in water (5 cm^3), yielding a red precipitate, which was filtered, washed with water, and air dried. Yield: 470 mg (50%). Found: C, 71.84; H, 6.25; N, 2.55%. Calcd for $C_{56}H_{56}N_2O_3BP_2Co$: C, 71.80; H, 6.03; N, 2.99%. The complex is soluble in acetone and acetonitrile, slightly soluble in methanol and dichloromethane, but insoluble in water.

[††] Caution; All of the perchlorate salts of cobalt(III)-phosphine complexes are potentially explosive, and should be handled carefully.

***cisβ*-[Co(acac)(pp-232PNNP)]$(ClO_4)_2 \cdot 4.5H_2O$ (acac=Acetylacetonate Ion).** An ethanol solution (60 cm^3) containing *RS(N)*- or *RR,SS(N)-trans*-[$CoCl_2$(pp-232PNNP)]X (X=Cl, ClO_4) (0.28 mmol) and Li(acac) (35 mg, 0.33 mmol) was warmed at 30 °C for 1 h. The resulting red solution was diluted with water (300 cm^3) and applied on a column (ϕ 2 cm×40 cm) of SP-Sephadex C-25. By elution with 0.2 mol dm^{-3} NaCl, the eluate of the main red band was collected , evaporated to dryness under reduced pressure, mixed with ethanol (50 cm^3), and the mixture was filtered. The filtrate was again evaporated to dryness under reduced pressure, and the residue was dissolved in water (50 cm^3). On addition of $NaClO_4 \cdot H_2O$ (0.5 g) in water (5 cm^3) the solution gave a red precipitate, which was filtered, washed with cold water then a small amount of ethanol, and air dried. Yield: 55 mg (23%). Found: C, 49.52; H, 5.78; N, 3.28%. Calcd for $C_{36}H_{52}N_2Cl_2O_{10.5}P_2Co$: C, 49.55; H, 6.01; N, 3.21%. The complex is soluble in methanol, ethanol and dichloromethane, slightly soluble in water, but insoluble in diethyl ether and benzene.

The hexafluorophosphate *cisβ*-[Co(acac)(pp-232PNNP)]-$(PF_6)_2$ was obtained by addition of NH_4PF_6 instead of $NaClO_4 \cdot H_2O$. Found: C, 45.77; H, 4.63; N, 2.97%. Calcd for $C_{36}H_{43}N_2O_2F_{12}P_4Co$: C, 45.68; H, 4.58; N, 2.96%. The solubility of this complex is similar to that of the perchlorate.

***RS(N)-trans*-[$CoCl_2$(SS(C)-pp-232PNNP)]$ClO_4 \cdot 1.5H_2O$ (Isomer C).** This complex was prepared from $Co(ClO_4)_2 \cdot 6H_2O$ (410 mg, 1.12 mmol) and *SS(C)*-pp-232PNNP (590 mg, 1.12 mmol) by a method similar to Method 2 for the corresponding pp-232PNNP complex. Yield: 250 mg (29%). Found: C, 50.47; H, 5.16; N, 3.45%. Calcd for $C_{33}H_{43}N_2O_{5.5}P_2Co$: C, 50.62; H, 5.54; N, 3.58%. The solubility of the complex is similar to that of the corresponding pp-232PNNP complex.

***RR(N)-trans*-[$CoCl_2$(SS(C)-pp-232PNNP)]$ClO_4 \cdot 1.5H_2O$ (Isomer D).** A solution of *Λ-cisβ*-[$Co(CO_3)$(SS(C)-pp-232PNNP)]$ClO_4 \cdot 0.5(NaClO_4)$ (50 mg, 0.062 mmol) (see below) in a mixture of methanol (20 cm^3) and concd HCl (2.5 cm^3) was warmed at 50 °C for 5 min to give a green solution. On addition of $NaClO_4 \cdot H_2O$ (5g) in water (20 cm^3) the solution gave a green precipitate, which was filtered, washed with cold water, and air dried. Yield: 44 mg (91%). Found: C, 50.74; H, 5.26; N, 3.69%. Calcd for $C_{33}H_{43}N_2Cl_3O_{5.5}P_2Co$: C, 50.62; H, 5.54; N, 3.58%. The solubility of the complex is similar to that for the corresponding *RS(N)* isomer.

***Λ-cisβ*-[$Co(CO_3)$(SS(C)-pp-232PNNP)]$ClO_4 \cdot 0.5(NaClO_4)$.** A mixture of *RS(N)-trans*-[$CoCl_2$(*SS(C)*-pp-232PNNP)]$ClO_4 \cdot 1.5H_2O$ (200 mg, 0.26 mmol), $(NH_4)_2CO_3$ (133 mg, 1.4 mmol) and active charcoal (ca. 50 mg) in methanol (40 cm^3) was stirred for 2 h at room temperature. Active charcoal was filtered off, the filtrate was diluted with water (1 dm^3) and applied on a column (ϕ 2.5 cm×100 cm) of SP-Sephadex C-25. By elution with 0.05 mol dm^{-3} NaCl the eluate of the main red band was collected and concentrated to ca. 40 cm^3 under reduced pressure. The concentrate was filtered, and the filtrate was mixed with $NaClO_4 \cdot H_2O$ (3.0 g) to yield a pink precipitate, which was filtered, washed with cold water, and air dried. Yield: 55 mg (27%). Found: C, 51.00; H, 5.14; N, 3.68%. Calcd for $C_{34}H_{40}N_2Cl_{1.5}O_9P_2Na_{0.5}Co$: C, 50.65; H, 5.00; N, 3.47%. The complex is soluble in water, methanol, ethanol and acetone, but insoluble in diethyl ether and benzene. The complex can also be prepared from $K[Co(CO_3)_2(C_5H_5N)_2]$ and the ligand by a method similar to that for the corresponding pp-232PNNP complex.

***Λ-cisβ*-[Co(acac)(SS(C)-pp-232PNNP)]$(PF_6)_2 \cdot 2(NaPF_6) \cdot 2H_2O$.** A methanol solution (50 cm^3) containing *RS(N)*-trans-[$CoCl_2$(*SS(C)*-pp-232PNNP)]$ClO_4 \cdot 1.5H_2O$ (200 mg, 0.26 mmol) and Li(acac) (30 mg, 0.28 mmol) was stirred for 1 h at room temperature. The resulting red solution was diluted with water (1 dm^3) and applied on a column (ϕ 2.5 cm×100 cm) of SP-Sephadex C-25. The adsorbed product was eluted with 0.4 mol dm^{-3} NaCl, the main red eluate was collected, concentrated to nearly dryness under reduced pressure, and the residue was mixed with methanol (ca. 100 cm^3) to extract the complex. The extract was evaporated again to dryness under reduced pressure, and the residue was dissolved in a small amount of water. On addition of NH_4PF_6 (ca. 100 mg) the solution gave a red precipitate, which was filtered, washed with a small amount of cold water and air dried. Yield: 174 mg (50.6%). Found: C, 33.85; H, 3.53; N, 2.20%. Calcd for $C_{38}H_{51}N_2F_{24}O_4P_6Na_2Co$: C, 33.89; H, 3.52; N, 2.08%. The complex is soluble in water, methanol, ethanol, acetone and dichloromethane, but insoluble in diethyl ether and benzene.

Results and Discussion

Preparation of Ligands. The quadridentate ligands pp-232PNNP and *SS(C)*-pp-232PNNP were prepared by methods similar to those for pp-222PNNP[1] and *SS(C)*-pp-222PNNP,[2] respectively. The yields of these ligands seem to depend largely on the purity of reactants and the presence of moisture.[1] The lower yield of *SS(C)*-pp-232PNNP may be attributable to moisture contained in the very hygroscopic starting material

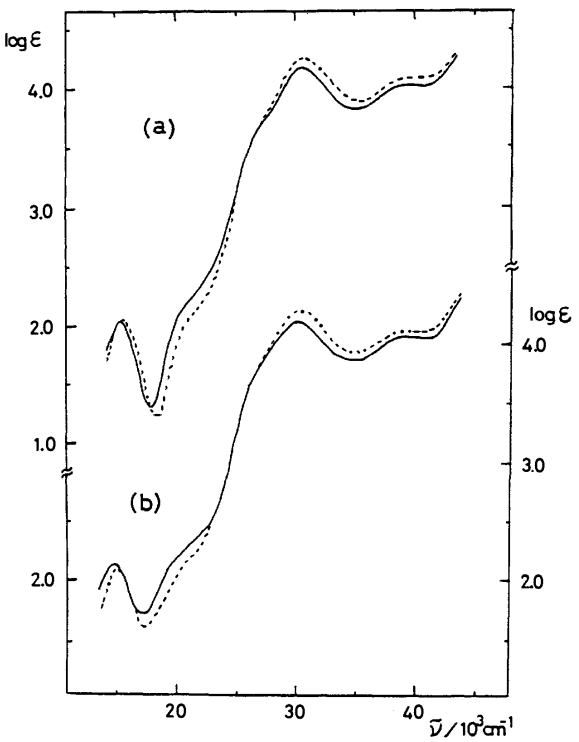

Fig. 1. Absorption spectra, (a) *RS(N)* (——) and *RR,SS(N)* (------) isomers of *trans*-[$CoCl_2$(pp-232PNNP)]$^+$, (b) *RS(N)* (——) and *RR(N)* (------) isomers of *trans*-[$CoCl_2$(SS(C)-pp-232PNNP)]$^+$.

Table 1. Absorption and CD Spectral Data for pp-232PNNP or SS(C)-pp-232PNNP Complexes (Solvent: CH_3OH)

Complex	AB $\tilde{\nu}/10^3$ cm^{-1} (log ε)	CD $\tilde{\nu}/10^3$ cm^{-1} ($\Delta\varepsilon$)
RS(N)-trans-[$CoCl_2$(pp-232PNNP)]$^+$	15.4(2.05), 21(2.2)*, 26(3.5) 30.7(4.25), 39.5(4.08)	
RR,SS(N)-trans-[$CoCl_2$(pp-232PNNP)]$^+$	15.6(2.06), 21(2.0)*, 26.8(3.6)*, 30.8(4.28)	
cis β-[Co(C_2O_4)(pp-232PNNP)]$^+$	19.50(2.60), 24.6(2.8)*, 31.6(4.36)	
cis β-[Co(acac)(pp-232PNNP)]$^{2+}$	19.23(2.78), 24(3.0)*, 28(4.1)*, 31.44(4.38)	
RS(N)-trans-[$CoCl_2$(SS(C)-pp-232PNNP)]$^+$	15.5(2.16), 20.5(2.2)*, 27(3.8)*, 30.5(4.21), 39.5(4.07)	15.0(+1.69), 16.5(−0.78), 20.6(−2.41), 26.3(−1.01), 28.6(−2.15), 31.0(+6.60), 33.8(−7.60), 39.3(−10.4), 42.3(+1.0), 44.3(−4.4)
RR(N)-trans-[$CoCl_2$(SS(C)-pp-232PNNP)]$^+$	15.5(2.11), 21(2.1)*, 23(3.6)*, 30.5(4.29), 39.5(4.13)	16.0(+1.00), 20.8(−2.32), 26.3(−2.09), 31.0(+12.8), 34.0(−8.85), 39.5(−11.4)
A-cis β-[Co(CO_3)(SS(C)-pp-232PNNP)]$^+$	19.5(2.55), 24.5(2.5)*, 31.5(4.20)	18.3(+3.28), 20.8(−2.98), 26.3(−0.39), 30.5(−2.28), 33.3(+2.56), 40.0(−7.31), 44.5(+14.6)
A-cis β-[Co(acac)(SS(C)-pp-232PNNP)]$^{2+}$	19.5(2.75), 27.5(3.9)*, 31.4(4.33)	18.0(+5.59), 21.0(−4.18), 27.8(−10.5), 31.0(+31.9), 35.0(−8.84), 38.5(−19.1), 45.0(+27.8)

*: Shoulder absorption.

(2*S*,8*S*)-2,8-dimethyl-1,9-dichloro-3,7-diazanonane dihydrochloride. The ligands could not be purified by distillation because of their high boiling points.

trans-Dichloro Complexes. For each quadridentate ligand, two kinds of green [$CoCl_2$(L)]$^+$ (L= pp-232PNNP or SS(C)-pp-232PNNP) were obtained by different preparative methods; one is oxidation of the Co(II)-L complex in CH_2Cl_2 with chlorine, and the other is reaction of [Co(CO_3 or C_2O_4)L]$^+$ with hydrochloric acid. Each method yielded only one kind of green complex. Absorption spectra of these complexes shown in Fig. 1 are very similar to that of *trans*(*Cl,Cl*),*cis*(*P,P*)-[$CoCl_2$(edpp)$_2$]$^+$ (edpp=NH_2CH_2-$CH_2P(C_6H_5)_2$) whose structure has been determined by X-ray analysis.[10,11] Thus the two complexes of each pp-232PNNP and *SS*(*C*)-pp-232PNNP can be assigned to isomers of the *trans*(*Cl,Cl*) complex. Table 1 lists the data of absorption and CD spectra. For *trans*-[$CoCl_2$(pp-232PNNP)]$^+$, a small difference in absorption spectra is observed between one isomer (A) obtained from oxidation with chlorine and the other isomer (B) derived from the CO_3^{2-} or $C_2O_4^{2-}$ complex. The ^{13}C NMR spectra show a more clear difference for these two isomers. Isomer A in CD_3CN shows signals at δ 28.5 (-CH_2-$\underline{C}H_2$-CH_2-), δ 30.7 (P-CH_2-: triplet), and δ 49.6 and 52.4 (-$\underline{C}H_2$-NH-$\underline{C}H_2$-), while isomer B in the same solvent gives the corresponding signals at δ 23.8, 28.3, and 45.5 and 51.5. The chemical shifts of signals due to the phenyl groups are also different between the isomers. In *trans*-[$CoCl_2$(pp-232PNNP)]$^+$ there are three possible isomers arising from the absolute configuration of the nitrogen atoms, the *RS*(*N*), *RR*(*N*) and *SS*(*N*) isomers, the latter two being a pair of enantiomers (Fig. 2). Thus two isomers A and B will be the *RS*(*N*) and *RR,SS*(*N*) isomers, although the assignment for the isomers can not be made from the

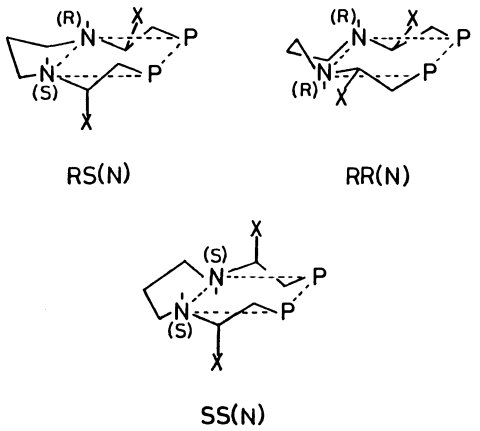

Fig. 2. Three possible isomers for *trans*-[$CoCl_2$(pp-232PNNP)]$^+$ (X=H) and *trans*-[$CoCl_2$(SS(C)-pp-232PNNP)]$^+$ (X=CH_3).

absorption and NMR spectra. However, it is assumed that isomer B which was prepared from *cis*β-[Co(CO_3 or C_2O_4)L]$^+$ (see below) and hydrochloric acid is the *RR,SS*(*N*)isomer, since molecular models suggest that the cisβ complex is more stable in the *RR,SS*(*N*) isomer than the *RS*(*N*) one, and the configuration of the nitrogen atom will be retained in strongly acidic solution. Thus the other isomer A can be assigned to the *RS*(*N*) isomer. The *trans*-[$CoCl_2$(232tet)]$^+$ complex (232tet=3,7-diazanonane-1,9-diamine) which has the same skeletal structure as the pp-232PNNP complex yields the same *RR,SS*(*N*) and *RS*(*N*) isomers, and the former is obtained from *cis*β-[Co(CO_3)(232tet)]$^+$.[12] All *cis*-[CoX_2 (232tet)]$^{n+}$ complexes so far known have a *RR,SS*(*N*) structure, no *RS*(*N*)-*cis*β and *cis*α isomers being reported. The pp-232PNNP complex seems to show the same stereoselectivity as the 232tet complex.

Possible isomers of *trans*-[$CoCl_2$(*SS*(*C*)-pp-

232PNNP)]$^+$ are three diastereomers with the *RS(N)*, *RR(N)*, and *SS(N)* configurations (Fig. 2). The *RR(N)* and *SS(N)* isomers have a C_2 axis, while the *RS(N)* isomer belongs to C_1 symmetry. Isomer C prepared by oxidation with chlorine shows two kinds of the methyl signal at δ 1.47 and 1.83 in the ^{1}H NMR spectrum in $CDCl_3$. On the other hand, the other isomer D derived from *cisβ*-[$Co(CO_3)$(*SS(C)*-pp-232PNNP)]$^+$ exhibits only one methyl signal at δ 1.83. Thus isomer C can be assigned to the *RS(N)* isomer, and isomer D to either *RR(N)* or *SS(N)* isomer. In the *RS(N)* isomer one of the two methyl groups is equatorial to the chelate ring, while the other is axial (Fig. 2). The axial methyl group comes fairly close to the phenyl ring and will receive its shielding effect. The methyl signal at the high field (δ 1.47) can be assigned to this axial methyl group, and the signal at δ 1.83 to the equatorial methyl group. Isomer D which shows the methyl signal at δ 1.83 should be the *RR(N)* isomer in which two methyl groups have an equatorial disposition. The *SS(N)* isomer has two axial methyl groups and will be less stable than the *RR(N)* isomer.[13] The assinment of *RR(N)* for isomer D indicates that its starting [$Co(CO_3)$(*SS(C)*-pp-232PNNP)]$^+$ complex has a *Λ-cisβ-RR(N)* configuration. As shown later this carbonate complex exhibits CD spectrum typical of a *Λ* configuration. Similar *RR(N)* and *RS(N)* isomers have been obtained for a structurally related tetramine complex *trans*-[$CoCl_2$((2*S*,10*S*)-Me_2-232tet)]$^+$ ((2*S*,10*S*)-Me_2-232tet= (2*S*,10*S*)-4,8-diazaundecane-2,10-diamine).[14]

As described before, the two isomers (A and B, or C and D) of each pp-232PNNP or *SS(C)*-pp-232PNNP dichloro complex show a small difference in absorption spectra, but the differences between the isomers

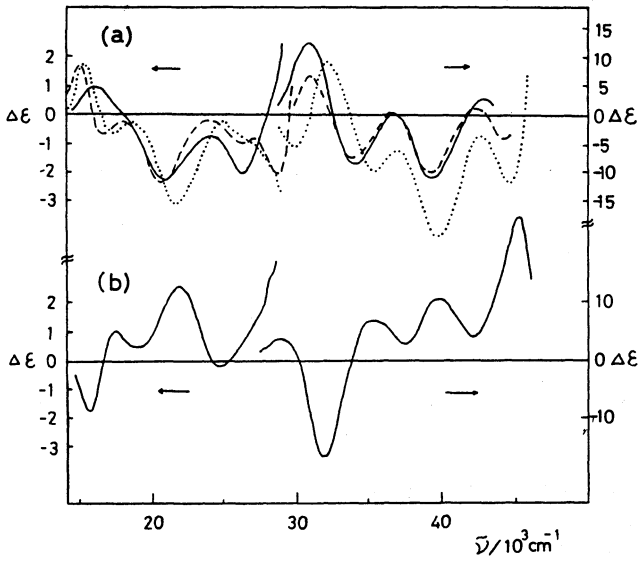

Fig. 3. CD spectra, (a) *RS(N)* (----) and *RR(N)* (——) isomers of *trans*-[$CoCl_2$(SS(C)-pp-232PNNP)]$^+$, and *trans*-[$CoCl_2$(S-pdpp)$_2$]$^+$ (·····), (b) *RR(N)-trans*-[$CoCl_2$(SS(C)-pp-222PNNP)]$^+$.

are very similar for both pp-232PNNP and *SS(C)*-pp-232PNNP complexes as seen in Fig. 1. This result supports the assignments of *RR,SS(N)* and *RS(N)* configurations for two pp-232PNNP complexes based on only stereochemical consideration.

Figure 3(a) shows CD spectra of *RR(N)* and *RS(N)* isomers of *trans*-[$CoCl_2$(*SS(C)*-pp-232PNNP)]$^+$. The spectra are rather similar except the region around 15000 cm^{-1} (the I_a absorption band region). The chiral sources of the isomers indicated by molecular models are as follows; the *RR(N)* isomer has two (*R*)-nitrogen and two (*S*)-carbon atoms, and δ-gauche, λ-skew and δ-gauche conformations for the five-, six-, and five-membered chelate rings, respectively, while the *RS(N)* isomer has one (*R*)- and one (*S*)-nitrogen and two (*S*)-carbon atoms, and δ-gauche, chair and λ-gauche conformations. The chiral sources are thus different between the isomers, but their CD spectra are similar and quite resemble that of *trans(Cl,Cl)cis(P,P)*-[$CoCl_2$-(S-pdpp)$_2$]$^+$ (*S*-pdpp=(*S*)-$NH_2CH(CH_3)CH_2P(C_6H_5)_2$) shown in Fig. 3(a) whose chiral sources are two (*S*)-carbon and two δ-gauche chelate rings.[11] On the other hand, the CD spectrum of a related complex *RR(N)-trans*-[$CoCl_2$(*SS(C)*-pp-222PNNP)]$^+$ [2] is nearly enantiomeric to those of the present isomers as shown in Fig. 3(b), although the chiral sources of this complex (two(*R*)-nitrogen and two (*S*)-carbon atoms, and δ-, λ- and δ-gauche conformations) are similar to those of the *RR(N)* isomer of the *SS(C)*-pp-232PNNP complex. No reasonable explanation can be given for these CD spectra at present. The complexes of the *trans(Cl,Cl)*-type have no chirality in the arrangement (*Δ,Λ*) of chelate rings around the metal ion, and their CD will be induced by a chiral field produced by chiral atoms and/or chiral conformations of ligands (vicinal effect). Little CD work has been reported for the vicinal effect of polydentate ligands.

O-O Chelate Complexes. All the complexes of [Co(O-O)(pp- or *SS(C)*-pp-232PNP)]$^{n+}$ were assigned to the cisβ isomer from the ^{1}H NMR spectra. For example, [Co(acac)(pp-232PNNP)]$^{2+}$ shows two kinds of methyl signals of acac at δ 1.84 and 2.29 in D_2O, indicating the cisβ structure (C_1 symmetry). Each of [Co(CO_3 or acac)(*SS(C)*-pp-232PNNP)]$^{n+}$ yielded only one optical isomer stereoselectively. These isomers

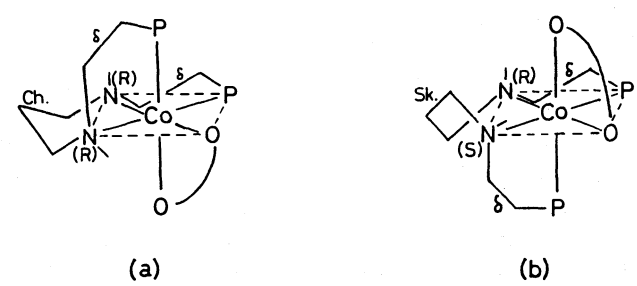

(a) (b)

Fig. 4. Two possible isomers, (a) *Λ-RR(N)* and (b) *Λ-RS(N)*, for *cisβ*-[$Co(CO_3$ or acac)(SS(C)-pp-232PNNP)]$^{n+}$

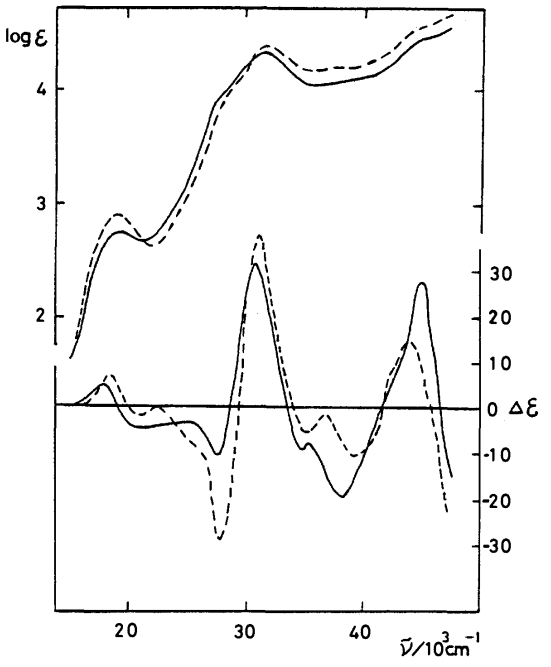

Fig. 5. Absorption and CD spectra of $(+)_{589}$-*Λ-cisβ*-[Co(acac)(SS(C)-pp-232PNNP)]$^{2+}$ (——) and $(+)_{589}$-*Λ-cisβ*-[Co(acac)(SS(C)-pp-222PNNP)]$^{2+}$ (------).

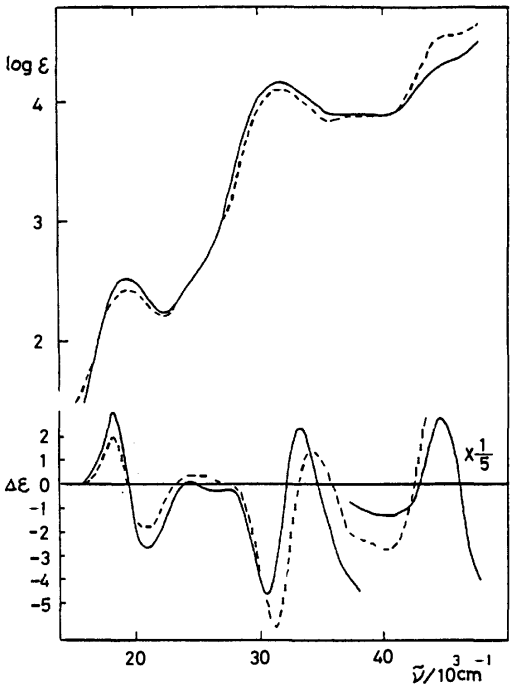

Fig. 6. Absorption and CD spectra of $(+)_{589}$-*Λ-cisβ*-[Co(CO_3)(SS(C)-pp-232PNNP)]$^{+}$ (——) and $(+)_{589}$-*Λ-cisβ*-[Co(CO_3)(SS(C)-pp-222PNNP)]$^{+}$ (------).

give two doublet methyl signals of the phosphine ligand at δ 1.67 ($^4J_{PH}$= 5 Hz) and at a fairly high field δ 0.85 ($^4J_{PH}$= 5 Hz).

Figure 4 shows structures of two probable cisβ isomers in which both methyl groups of the phosphine ligand have an equatorial disposition. The other two cisβ isomers will be unstable because of two axial methyl groups. Of the two probable isomers, the *Λ-cisβ-RR(N)* one has one methyl group disposed very close to one phenyl ring on the phosphorus atom. The signal at δ 0.85 can be assigned to the methyl group shielded by the phenyl group, and both carbonato and acac complexes can be assigned to the *Λ-cisβ-RR(N)* isomer. The *Λ* configuration of the isomers is confirmed by the CD spectra. Figures 5 and 6 compare CD spectra of the acac and carbonato complexes, respectively with those of the corresponding *Λ-cisβ-RR(N)* isomers of the *SS(C)*-pp-222PNNP complexes.[2] The absolute configurations of the latter complexes have been assigned from a comparison of CD spectra with that of *Λ-cisβ-RR(N)*-[Co(acac)(SS(C)-Me_2-mm-222PNNP)]$^{2+}$ (*SS(C)*-Me_2-mm-222PNNP=(4*S*,9*S*)-2,4,9,11-tetramethyl-5,8-diaza-2,11-diphosphadodecane) whose absolute configuration has been determined by the X-ray method.[2] In contrast to CD spectra of the *trans(Cl,Cl)*-type complexes, the *SS(C)*-pp-232PNNP and *SS(C)*-pp-222PNNP complexes show CD spectra very similar to each other over the whole region and give CD patterns characteristic of a *Λ* configuration in the first absorption band region. From *Λ-cisβ-RR(N)*-[Co(CO_3)(*SS(C)*-pp-232PNNP)]$^{+}$ the *RR(N)-trans(Cl,Cl)* complex was derived by reaction with hydrochloric acid. The [Co(CO_3)(pp-232PNNP)]$^{+}$ complex should also have the *cisβ-RR,SS(N)* structure, since it affords the *RR,SS(N)-trans(Cl,Cl)* complex by the same reaction. Thus cis-complexes containing the pp-232PNNP-type ligand yield selectively the cisβ-isomer with (*R,R*)- or (*S,S*)-nitrogen atoms and the six-membered chelate ring of a chair conformation. The same selectivity has been observed for the corresponding 232-tetramine complexes.[14]

The authors wish to thank the Ministry of Education for Scientific Research Grant-in-Aid No. 61430013.

References

1) M. Atoh, K. Kashiwabara, and J. Fujita, *Bull. Chem. Soc. Jpn.*, **58**, 2793 (1985).

2) M. Atoh, K. Kashiwabara, and J. Fujita, *Bull. Chem. Soc. Jpn.*, **58**, 3492 (1985).

3) M. Atoh, K. Kashiwabara, and J. Fujita, *Bull. Chem. Soc. Jpn.*, **59**, 1001 (1986).

4) M. Atoh, H. Sugiura, Y. Seki, K. Kashiwabara, and J. Fujita, *Bull. Chem. Soc. Jpn.*, **60**, 1699 (1987).

5) a) M. Saburi and S. Yoshikawa, "Kagaku Sosetu," Tokyo Univ. Press (1976), No. 13, Chap. 7, pp. 109—130: M. Saburi and S. Yoshikawa, *Bull. Chem. Soc. Jpn.*, **45**, 806, 1086 (1972) and references therein. b) G. R. Brubaker, D. P. Schaefer, J. H. Worrell, and J. I. Legg, *Coord. Chem. Rev.*, **7**, 161 (1971): A. M. Sargeson and G. H. Searle, *Inorg. Chem.*, **6**, 787 (1967).

6) W. W. Lee, B. J. Berridge, L. O. Ross, and L. Goodman, *J. Med. Chem.*, **6**, 567 (1963).

7) L. Horner, B. Beck, and H. Hoffman, *Chem. Ber.*, **92**, 2092 (1959).

8) O. Vogl and M. Pohm, *Monatsh. Chem.*, **83**, 541

(1952).
9) Y. Ida, K. Kobayashi, and M. Shibata, *Chem. Lett.* **1974**, 1299.
10) M. Atoh, K. Kashiwabara, and J. Fujita, *Bull. Chem. Soc. Jpn.*, **55**, 3179 (1982).
11) I. Kinoshita, Y. Yokota, K. Matsumoto, S. Ooi, K. Kashiwabara, and J. Fujita, *Bull. Chem. Soc. Jpn.*, **56**, 1067 (1983).
12) H. G. Hamilton, Jr, and M. D. Alexander, *J. Am. Chem. Soc.*, **89**, 5065 (1967).
13) E. J. Corey and J. C. Bailar, Jr., *J. Am. Chem. Soc.*, **81**, 2620 (1959).
14) M. Goto, T. Makino, M. Saburi, and S. Yoshikawa, *Bull. Chem. Soc. Jpn.*, **49**, 1879 (1976).

 © 1988 The Chemical Society of Japan Bull. Chem. Soc. Jpn., 61, 3511—3517 (1988)

Inversion of Stereoselectivity by Hydrophobic Interligand Interactions. Preparation, Structure, and Stereoselectivity of {*N*,*N*′-Ethylenebis(1,1,1-trifluoro-4-amino-2-pentanonato)}(L-amino acidato)cobalt(III)

Yuki FUJII,* Homare SHINOHARA, Masahiro MIKURIYA,†,†† Shigeo KIDA,† and Yoshie KONISHI
Department of Chemistry, Ibaraki University, Bunkyo, Mito 310
†Institute for Molecular Science, Myodaiji, Okazaki 444
(Received March 7, 1988)

Ternary cobalt(III) complexes with a general formula β_2-[Co(tfac$_2$en)(L-aa)], where tfac$_2$en is the titled Schiff base ligand and L-aa denotes L-ala, L-leu, L-phe, L-tyr, and L-trp, were synthesized and separated into two diastereoisomers. On the bases of X-ray crystal analysis of the L-phe complex, CD, and ^{1}H and ^{19}F NMR spectra, the structure of $(-)_{435}$- and $(+)_{435}$-isomers was determined to be *Λ*- and *Δ*-cis-β_2-forms, respectively, and preferred conformation of the coordinated L-amino acidates was assummed to be *h*-form in solution. All the complexes showed stereoselectivity for the *Λ*-isomer in acetone and methanol, but the selectivity decreased or reversed with addition of water. The solvent-dependent stereoselectivity was explained in terms of steric repulsion and hydrophobic interligand interactions between CF_3 group of tfac$_2$en and side chain of L-aa.

Of various interligand interactions in metal complexes, hydrophobic intramolecular ligand-ligand interactions had been regarded as extremely weak. However, it has recently been proved that this kind of interaction plays an important role in molecular recognition and/or chiral recognition in some metal chelates.[1-7] For instances, Sigel and his co-workers,[3] and Yamauchi and his co-workers[4] found that the ternary metal(II) complexes with diamines such as 1,10-phenanthroline and amino acidates show a high ligand selectivity due to intramolecular hydrophobic interligand interaction between the diamine chelate ring and the side chain of amino acidates. Okawa et al.[6] demonstrated that metal(III) chelates with *l*-menthol derivatives exhibit a high stereoselectivity for *Λ*-configuration on the basis of intramolecular interligand CH-π interactions.

In order to elucidate the effect of hydrophobic interligand interactions on the stereoselectivity of metal complexes with chiral amino acidates, we prepared the cobalt(III) complexes described in the title containing Schiff base ligand with hydrophobic CF_3 groups (tfac$_2$en) and L-amino acidates (L-aa) with hydrophobic side chains as shown in Fig. 4, and investigated their steric structure and solvent dependency of stereoselectivity.

Experimental

Preparation of Complexes. Complexes were prepared from [Co(tfac$_2$en)] (0.01 mol) and amino acids (0.011 mol) by air oxidation in methanol-water by means of a similar method to that for β_2-[Co(tfac$_2$en) (L-met)].[8] The crude reaction products were purified and/or separated into pure diastereoisomers by the following methods. The data of elemental analysis and the optical rotation of all the complexes are summarized in Tables 1 and 2, respectively.

1) β_2-[Co(tfac$_2$en)(L-phe)], β_2-[Co(tfac$_2$en)(L-leu)], and β_2-[Co(tfac$_2$en)(L-met)]. The crude reaction product (3.0 g) was dissolved in methanol (100 cm^3) and filtered. The filtrate was slowly concentrated to a small volume at room temperature in 3—5 days to give massive dark green crystals ($(-)_{435}$-isomer, about 2.5 g). A single crystal of L-phe complex, thus obtained, was used for X-ray diffraction study.

The $(-)_{435}$-isomer (2.0 g) was dissolved in hot methanol (100 cm^3) and water (10 cm^3) was added to it. The solution was slowly concentrated to almost dryness at room temperature to give a large amount of massive crystals ($(-)_{435}$-isomer) and a small amount of needle-shaped crystals ($(+)_{435}$-isomer). The needle-shaped crystals were sorted by hand. Yield of $(+)_{435}$-isomer; 0.05—0.1 g for L-phe and L-met complexes, 0.3—0.5 g for L-leu complex.

2) β_2-[Co(tfac$_2$en)(L-tyr)]. The crude reaction product was recrystallized from methanol to give light green needle-shaped crystals ($(+)_{435}$-isomer) in about 90% yield.

The recrystallization of the $(+)_{435}$-isomer from methanol-water (15 : 1 in volume) produced a large amount of $(+)_{435}$-isomer and a small amount of massive crystals ($(-)_{435}$-isomer, 0.05 g).

3) β_2-[Co(tfac$_2$en)(L-ala)] and β_2-[Co(tfac$_2$en)(L-trp)]. Recrystallization of the crude reaction product from methanol gave a 1 : 1 mixture of $(-)_{435}$- and $(+)_{435}$-isomers in about 90% yield. Acetone solution of the 1 : 1 mixture (0.2 g) was charged on a silica-gel column (Wakogel C-200, 15(ϕ)×120 mm), and was eluted with acetone at a flow rate of ca. 0.1 cm^3 s^{-1}. The first green fraction (40 cm^3) was collected and concentrated to dryness. In the case of L-trp complex, pure $(-)_{435}$-isomer was obtained by this procedure, but in the case of L-ala complex, a 4 : 1 mixture of $(-)_{435}$- and $(+)_{435}$-isomers of 70 mg was obtained.

Crystal Structure Determination. A Rigaku AFC-5 automated four-circle diffractometer was used at 25±1 °C. Crystal data and details of the data collection are given in Table 4. Lattice constants were determined by the least-squares refinement based on 40 reflections with $20 < 2\theta < 30°$.

†† Present address: Department of Chemistry, Faculty of Science, Kwansei Gakuin University, Uegahara, Nishinomiya 662.

The intensity data were corrected for Lorentz-polarization effects and for absorption. The structure was solved by the direct method. Refinements were carried out by the block-diagonal least-squares method. The absolute configuration was determined on the basis of the known configuration of L-phenylalanine. The absolute structure was further checked by performing cycles on two possible configurations, of which lower R factor was considered as the correct one. Hydrogen atoms were inserted in their calculated positions and fixed at their positions with B of 7Å^2. The final discrepancy factors are R(F) 0.054 and R_w(F) 0.059 for 2294 unique reflections.

The atomic scattering factors and anomalous dispersion corrections were taken from Ref. 9. All the calculations were carried out on HITACHI M-680H computer at the Computer Center of the Institute for Molecular Science using a local version of MULTAN 78,[10] UNIX-III,[11] and ORTEP[12] programs. Atomic coordinates are listed in Table 5. The anisotropic thermal parameters of non-hydrogen atoms, the atomic coordinates and thermal parameters of hydrogen atoms, and the F_o—F_c tables have been deposited as a Document No. 8827 at the office of Editor.

Measurements. The ^{1}H and ^{19}F NMR spectra were measured with Hitachi R-20 (60MHz), JEOL GSX-400 (400MHz), and Varian CFT-20 (80MHz) spectrometers at an ambient probe temperature using TMS or fluorobenzene as internal references. The electronic absorption spectra and CD spectra were recorded with JASCO UBIDEC-1 spectrometer and JASCO J-20 spectropolarimeter, respectively, at room temperature. The optical rotations at 435 nm were measured with a JASCO DIP-140 polarimeter with 1 cm cell by the use of a thermostated cell-holder (the deviation of the solution temperature $=\pm 0.1$ °C). When the mutarotation was slow, the solutions were placed in a thermostated bath, and picked up one by one at proper intervals. The observed isomerization rate constant was calculated from the slope of plots for $\ln(\alpha_\infty-\alpha_t)$ vs. time, where α_∞ and α_t denote the optical rotations under the equilibrium conditions and time t, respectively. The isomeric ratio, K=[$(-)_{435}$-isomer]/[$(+)_{435}$-isomer], under the equilibrium conditions was calculated from the equation, $K=([M]^T_\Delta-[M]^T_\infty)/([M]^T_\infty-[M]^T_\Lambda)$, where $[M]^T_\Delta$, $[M]^T_\Lambda$, and $[M]^T_\infty$ represent the molar rotations at a temperature T of $(+)_{435}$-isomer, $(-)_{435}$-isomer, and under equilibrium conditions, respectively. In the cases of L-ala and L-trp complexes, the K values were estimated by assuming $[M]^T_\Delta=-[M]^T_\Lambda$. The isomeric composition of all the isolated diastereoisomers was determined on the basis of their ^{1}H NMR spectra in CD_3OD.

Table 1. Elemental Analyses Data and Isomeric Composition of Complexes

Number of complex	Composition of isomer	Formula	Found(Calcd)		
			C(%)	H(%)	N(%)
1	a)	[Co(tfac$_2$en)(L-ala)]	38.03(37.75)	3.60(3.80)	8.92(8.81)
2	b)	[Co(tfac$_2$en)(L-ala)]	38.42(37.75)	3.91(3.80)	8.85(8.81)
3	$(-)_{435}$-ΛL-β_2	[Co(tfac$_2$en)(L-leu)]	41.69(41.63)	4.38(4.66)	8.01(8.06)
4	$(+)_{435}$-ΛL-β_2	[Co(tfac$_2$en)(L-leu)]	41.74(41.63)	4.41(4.66)	7.86(8.06)
5	$(-)_{435}$-ΛL-β_2	[Co(tfac$_2$en)(L-met)]	38.01(38.00)	3.90(4.13)	7.91(7.82)
6	$(+)_{435}$-ΛL-β_2	[Co(tfac$_2$en)(L-met)]	38.09(38.00)	4.05(4.13)	7.86(7.82)
7	$(-)_{435}$-ΛL-β_2	[Co(tfac$_2$en)(L-phe)]	45.55(45.58)	3.87(4.01)	7.61(7.59)
8	$(+)_{435}$-ΛL-β_2	[Co(tfac$_2$en)(L-phe)]	45.65(45.58)	3.85(4.01)	7.49(7.59)
9	$(-)_{435}$-ΛL-β_2	[Co(tfac$_2$en)(L-tyr)]·H_2O	42.78(42.94)	4.10(4.12)	7.22(7.15)
10	$(+)_{435}$-ΛL-β_2	[Co(tfac$_2$en)(L-tyr)]	44.46(44.30)	3.65(3.89)	7.51(7.38)
11	$(-)_{435}$-ΛL-β_2	[Co(tfac$_2$en)(L-trp)]	46.03(45.41)	3.91(3.81)	7.15(7.21)
12	a)	[Co(tfac$_2$en)(L-trp)]	45.37(45.41)	3.70(3.81)	9.33(9.21)

a) 1:1 mixture of $(-)_{435}$-ΛL- and $(+)_{435}$-ΛL-β_2-isomers. b) 4:1 mixture of $(-)_{435}$- and $(+)_{435}$-isomers.

Table 2. Molar Rotation and Stereoselectivity of β_2-[Co(tfac$_2$en)(L-aa)] in Methanol

L-aa	Number of complex	$[M]^{25}_{435}$ soon after dissolution	$[M]^{25}_{435}$ equilibrium condition	Observed isomerization rate constant $k_{obsd}/10^{-5}s^{-1}$	Isomeric ratio [Λ]/[Δ]
L-ala	**1**	−100[a]	−5200	13.4	1.2
	2	−29600[b]			
L-leu	**3**	−51200	−650	6.97	1.01
	4	+50500			
L-met	**5**	−47000	−3500	9.52	1.15
	6	+46800			
L-phe	**7**	−56300	−10500	7.45	1.41
	8	+54200			
L-tyr	**9**	−55000	−20200	5.50	2.14
	10	+54300			
L-trp	**11**	−54000	−28400	8.95	3.2
	12	0[a]			

a) 1:1 mixture. b) 4:1 mixture.

Table 3. ^{1}H and ^{19}F NMR Sapectral Data of β_2-[Co(tfac$_2$en)(L-aa)][a)]

L-aa	Number of complex and isomer form		tfac$_2$en				R-group of L-aa
			CH=C	CH_2CH_2	CH_3	CF_3	
L-ala	**2**[c)]	*Λ*	5.74	3.86	2.46	−11.93	1.37 CH_3(doublet)
			5.79			−12.31	1.49
	1[b)]	*ΔΔ*[e)]	5.72	3.86	2.46	−11.97	1.49 CH_3(doublet)
			5.84			−12.41	1.61
L-leu	**3**	*Λ*	5.74	3.84	2.46	−11.95	0.95 CH_3(doublet)
			5.80			−12.22	1.05
	4	*Λ*	5.74	3.85	2.46	−11.99	0.95 CH_3(doubet)
			5.84			−12.54	1.05
L-met	**5**	*Λ*	5.70	3.84	2.48	−11.78	2.14 S-CH_3
			5.74			−12.13	
	6	*Λ*	5.70	3.84	2.48	−11.92	2.14 S-CH_3
			5.78			−12.49	
L-phe	**7**	*Λ*	5.58	3.60	2.11	−11.93	7.32 ϕ(multiplet)
			5.71		2.43	−12.46	
	8	*Λ*	5.71	3.85	2.41	−11.88	7.38 ϕ(multiplet)
			5.76		2.49	−13.01	
L-tyr	**9**	*Λ*	5.56	3.61	2.18	d)	6.7—7.4 ϕ(multiplet)
			5.68		2.48		
	10	*Λ*	5.70	3.85	2.46	d)	6.7—7.4 ϕ(multiplet)
			5.75		2.54		
L-trp	**11**	*Λ*	5.05	3.84	1.71	−11.97	7.0—7.7 Indol group
			5.62		2.39	−12.59	
	12[b)]	*ΔΔ*[e)]	5.60	3.84	2.39	−11.85	7.0—7.7 Indol group
			5.73		2.49	−12.94	

a) ^{1}H: Soon after dissolution in CD_3OD; ^{19}F: in CD_3COCD_3 (Ref.=Fluorobenzene). b) 1 : 1 mixture of *Λ*- and *Δ*-isomers. c) 4 : 1 mixture of *Λ*- and *Δ*-isomers. d) Scarecely soluble in CD_3COCD_3. e) NMR data for *Δ*-isomer is cited.

Results and Discussion

Properties of Complexes. All the complexes exhibited a mutarotation in methanol to show a minus rotation under equilibrium conditions (Table 2). For each amino acidato complex, the rotation in the equilibrium conditions of $(-)_{435}$-isomer was the same as that of $(+)_{435}$-isomer, and the plots of $\ln(\alpha_\infty-\alpha_t)$ vs. time gave a linear relation in which the slope for $(-)_{435}$-isomer was identical as that for $(+)_{435}$-isomer. Hence, the observed mutarotation corresponds to the isomerization between two species of isomer, and the following equilibrium is established for each complex in methanol:[13)]

$$(+)_{435}\text{-isomer} \rightleftharpoons (-)_{435}\text{-isomer}.$$

The isomerization occurred readily in methanol, ethanol, 1-propanol, and a mixed solvent of acetone and water, but was very slow in pure acetone, chloroform, *N*,*N*-dimethylformamide, and dimethyl sulfoxide.

The ^{1}H NMR spectra (Table 3) of complexes **3**—**11** soon after dissolution in methanol correspond to the spectra of only one species of isomer, indicating that the complexes **3**—**11** were isolated as pure isomer. On the other hand, the ^{1}H NMR of complexes **1** and **12** soon after dissolution correspond to the spectra of a 1 : 1 mixture of two isomeric species, and the ^{1}H NMR of complex **2** to that of a 4 : 1 mixture. The isomeric compositions for all the complexes are listed in Table 1.

As the complexes are labile for isomerization in methanol, the ^{1}H NMR of all the complexes exhibited a time dependence in CD_3OD. The ^{1}H NMR under the equilibrium conditions corresponded to those for a mixture of two species of isomer, and the isomeric ratio of each amino acidato complex coincided with that determined from the optical rotation (Table 2). The isomeric ratios in Table 2 indicate that all the complexes show a stereoselectivity for *Λ*-isomer in methanol and the selectivity increases in the order of L-leu < L-met < L-ala < L-phe < L-tyr < L-trp. This order is almost parallel with the increasing order of steric bulkiness of the side chain of L-amino acidates, hence the steric repulsion between the side chain and Schiff base ligand seems to be responsible mainly to the stereoselectivity, as has been seen in β_2-[Co(α-Me-sal$_2$en) (L-aa)].[14-17)] However, the stereoselectivity of β_2-[Co(tfac$_2$en)(L-aa)] is much lower than that of β_2-[Co(α-Me-sal$_2$en)(L-aa)]. This lower selectivity is due to the presence of CF_3 groups on the tfac$_2$en skelton, and will be discussed later in detail.

The complexes readily isomerize in methanol, and when they are recrystallized from methanol, only one diastereoisomer or the 1 : 1 mixture of two isomers crystallized preferentially, as mentioned in Experimental section. Since the solubility of the preferentially crystallizing isomer in methanol was clearly

lower than that of the other isomer, the observed preferential crystallization corresponds to the second-order asymmetric transformation. Thus, in order to isolate more soluble isomer, we used a mixed solvent of methanol and water to lower the solubility. L-Ala and L-trp complexes were subjected to silica-gel column chromatography by use of acetone as an eluent to separate two isomers. However, silica-gel promoted isomerization of the complexes in acetone, so that only the $(-)_{435}$-isomer was separated.

Structure of Complexes. The results of X-ray structual analysis for $(-)_{435}$-[Co(tfac$_2$en)(L-phe)] are shown in Fig. 1 and numerical data are summarized in Tables 4, 5, and 6. The tfac$_2$en ligand takes cis-β- configuration and L-phenylalaninate coordinates as a bidentate ligand in forming a meridional N_3O_3 structure (cis-β_2 structure). The absolute configuration was determined to be Λ on the basis of the known absolute configuration, *S*(C), of the asymmetric carbon atom of L-phenylalaninate. The Λ-β_2-structure has been observed also for the $(-)_{435}$-isomer of [Co(tfac$_2$en)(L-met)][8] and [Co(α-Me-sal$_2$en) (L-ile)].[15] The bond lengths (Co-N and Co-O) and angles (N-Co-O, N-Co-N, and O-Co-O) of $(-)_{435}$-[Co(tfac$_2$en)(L-phe)] are close to those of $(-)_{435}$-[Co(tfac$_2$en)(L-met)], indicating that the steric structures of both complexes are essentially the same. In fact, not only they take the Λ-β_2-structure but also they take *t* conformation for coordinated amino acidates.[17,18] However, the bond length of Co-O(3), 1.891(4) Å, of L-phe complex is longer than that of L-met complex, 1.849(9) Å. Since the phenyl group of L-phe seems to approach to some extent to the π-conjugation system of β-diketone-iminate part of tfac$_2$en (the closest interatomic distances; C(17)···C(7)=3.617 (9) Å, C(17)···C(11)=4.050(9) Å, C(16)···C(8)=4.624(9) Å, and C(18)···F(6)=5.030(10) Å), the elongation of Co-O(3) bond length in L-phe complex may come from weak stacking between phenyl group and π-conjugation system of tfac$_2$en, although the dihedral angle between them is 132.5°.

The data for electronic absorption and CD spectra of the complexes are summarized in Table 7, and the representative spectra are shown in Fig. 2, together with the vicinal CD curves. Since the AB and CD spectra of $(-)_{435}$-isomers are very similar to those of $(-)_{435}$-Λ-β_2-isomer of L-phe complex whose structure

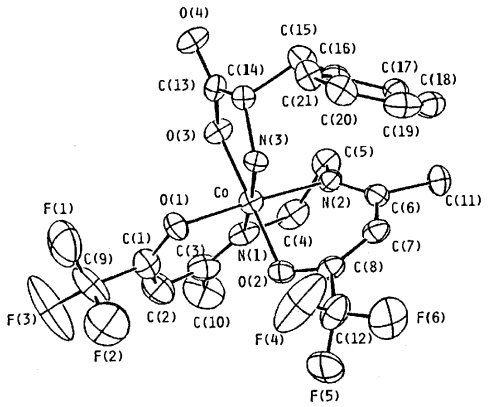

Fig. 1. A perspective drawing of $(-)_{435}$-Λ-β_2-[Co(tfac$_2$en)(L-phe)] with the numbering of atoms.

Table 4. Crystal Data and Data Collection Details

Compound $CoC_{21}H_{22}N_3O_4F_6$, Formula Weight 553.35, Crystal system orthorhombic, Space group $P2_12_12_1$, *a*/Å 12.628(1), *b*/Å 21.490(2), *c*/Å 8.959(1) *V*/Å^3 2431.3(4), *Z* 4, D_c/g cm^{-3} 1.51, D_m/g cm^{-3} 1.52 F(000) 1128, Radiation graphite-monochromated Mo $K\alpha$ (λ=0.71073 Å), Crystal size/mm 0.33×0.33×0.57, μ(Mo $K\alpha$)/cm^{-1} 7.78, Scan type θ-2θ, Scan Speed/deg min^{-1} 3, Scan width/deg 1.1+0.5 tan θ, 2θ Range/deg 1.5—64, Total No. of obsd reflecns 4740, No. of unique reflecns with $|F_o|>3\sigma(|F_o|)$ 2294, Final No. of variables 317, Final residuals[a] R=0.054, R_w=0.059, Weighting scheme $w=[\sigma^2_{count}+(0.015|F_o|)^2]^{-1}$, Goodness of fit[b] 2.011, Largest peak on final difference Map 0.58 e Å^{-3}

a) $R=\sum||F_o|-|F_c||/\sum|F_o|$; $R_w=[\sum W(|F_o|-|F_c|)^2/\sum W|F_o|^2]^{1/2}$. b) GOF$=[\sum W(|F_o|-|F_c|)^2/(N_{observns}-N_{params})]^{1/2}$.

Table 5. Atomic Coordinates (×10^4) and Thermal Parameters

Atom	*X*	*Y*	*Z*	B_{eq}/Å^2
Co	4353(1)	596(1)	4299(1)	3.6
F1	4898(6)	−1222(3)	6741(7)	12.8
F2	6263(6)	−738(3)	7197(7)	15.6
F3	6194(8)	−1473(3)	5592(8)	18.3
F4	5671(7)	1401(3)	8305(5)	16.6
F5	6992(4)	1564(2)	6998(8)	11.6
F6	6004(5)	2284(2)	7517(6)	10.7
O1	4700(3)	−130(2)	5353(5)	4.8
O2	5495(3)	995(2)	5346(4)	4.3
O3	3178(3)	185(2)	3437(4)	4.0
O4	1486(3)	−52(2)	3767(4)	5.0
N1	5174(4)	382(2)	2553(6)	4.6
N2	4075(4)	1367(2)	3261(5)	4.0
N3	3392(4)	764(2)	5967(5)	3.3
C1	5457(6)	−478(3)	4938(8)	5.4
C2	6033(6)	−459(3)	3638(9)	6.8
C3	5817(6)	−60(3)	2424(8)	5.5
C4	4955(6)	818(4)	1286(7)	5.9
C5	3971(6)	1204(3)	1636(7)	5.1
C6	4258(5)	1905(3)	3729(7)	4.4
C7	4731(5)	1989(3)	5184(7)	4.4
C8	5344(5)	1566(3)	5775(7)	4.4
C9	5732(8)	−990(4)	6099(9)	8.8
C10	6425(7)	−165(4)	999(10)	8.5
C11	4075(6)	2480(3)	2780(10)	6.5
C12	5962(8)	1694(3)	7168(9)	7.2
C13	2277(5)	205(2)	4158(6)	3.7
C14	2278(4)	607(3)	5558(6)	3.5
C15	1634(5)	1234(3)	5260(7)	4.7
C16	1726(5)	1677(3)	6527(7)	3.8
C17	2004(5)	2277(3)	6211(7)	5.0
C18	2092(6)	2724(3)	7368(10)	6.2
C19	1940(6)	2545(4)	8806(8)	6.9
C20	1670(6)	1927(3)	9123(8)	5.8
C21	1544(6)	1498(3)	7999(8)	5.0

Table 6. Interatomic Distances (Å) and Bond Angles (deg)

(a) Cobalt coordination spheres

	Distance		
Co-O(1)	1.876(4)	Co-N(1)	1.932(5)
Co-O(2)	1.921(4)	Co-N(2)	1.933(5)
Co-O(3)	1.891(4)	Co-N(3)	1.959(4)

	Angle		
O(1)-Co-O(2)	87.2(2)	O(2)-Co-N(3)	90.6(2)
O(1)-Co-O(3)	90.0(2)	O(3)-Co-N(1)	88.8(2)
O(1)-Co-N(1)	94.9(2)	O(3)-Co-N(2)	93.5(2)
O(1)-Co-N(2)	176.5(2)	O(3)-Co-N(3)	84.9(2)
O(1)-Co-N(3)	85.1(2)	N(1)-Co-N(2)	84.9(2)
O(2)-Co-O(3)	174.9(2)	N(1)-Co-N(3)	173.7(2)
O(2)-Co-N(1)	95.7(2)	N(2)-Co-N(3)	95.5(2)
O(2)-Co-N(2)	89.4(2)		

(b) tfac$_2$en moiety

	Distance		
O(1)-C(1)	1.269(8)	C(6)-C(11)	1.518(10)
C(1)-C(2)	1.374(11)	C(7)-C(8)	1.307(9)
C(1)-C(9)	1.555(11)	C(8)-O(2)	1.300(7)
C(2)-C(3)	1.411(11)	C(8)-C(12)	1.499(11)
C(3)-N(1)	1.255(9)	C(9)-F(1)	1.299(12)
C(3)-C(10)	1.507(12)	C(9)-F(2)	1.307(11)
N(1)-C(4)	1.496(9)	C(9)-F(3)	1.274(12)
C(4)-C(5)	1.527(10)	C(12)-F(4)	1.253(10)
C(5)-N(2)	1.503(8)	C(12)-F(5)	1.339(11)
N(2)-C(6)	1.251(8)	C(l2)-F(6)	1.307(9)
C(6)-C(7)	1.445(9)		

	Angle		
Co-O(1)-C(1)	121.2(4)	C(7)-C(6)-C(11)	117.8(6)
O(1)-C(1)-C(2)	129.1(7)	C(6)-C(7)-C(8)	121.5(6)
O(1)-C(1)-C(9)	112.9(6)	C(7)-C(8)-O(2)	128.7(6)
C(9)-C(1)-C(2)	118.1(7)	O(2)-C(8)-C(12)	110.1(5)
C(1)-C(2)-C(3)	124.7(7)	C(7)-C(8)-C(12)	121.2(6)
C(2)-C(3)-N(1)	121.0(7)	Co-O(2)-C(8)	117.1(4)
C(2)-C(3)-C(10)	117.6(7)	C(1)-C(9)-F(1)	112.7(8)
C(10)-C(3)-N(1)	121.4(7)	C(1)-C(9)-F(2)	108.9(7)
Co-N(1)-C(3)	126.9(5)	C(1)-C(9)-F(3)	116.1(7)
Co-N(1)-C(4)	111.5(4)	F(1)-C(9)-F(2)	104.0(7)
C(3)-N(1)-C(4)	121.6(6)	F(1)-C(9)-F(3)	102.6(8)
N(1)-C(4)-C(5)	109.6(5)	F(2)-C(9)-F(3)	111.8(9)
C(4)-C(5)-N(2)	104.7(5)	C(8)-C(12)-F(4)	115.5(8)
Co-N(2)-C(5)	106.4(4)	C(8)-C(12)-F(5)	111.9(7)
Co-N(2)-C(6)	126.7(4)	C(8)-C(12)-F(6)	113.5(7)
C(5)-N(2)-C(6)	123.8(5)	F(4)-C(12)-F(5)	105.8(8)
N(2)-C(6)-C(7)	119.7(6)	F(4)-C(12)-F(6)	107.8(7)
N(2)-C(6)-C(11)	122.4(6)	F(5)-C(12)-F(6)	101.1(7)

(c) L-Phenylalaninate moiety

	Distance		
O(3)-C(13)	1.309(7)	C(16)-C(17)	1.366(9)
O(4)-C(13)	1.194(7)	C(17)-C(18)	1.418(11)
C(13)-C(14)	1.523(8)	C(18)-C(19)	1.358(12)
N(3)-C(14)	1.492(7)	C(19)-C(20)	1.402(11)
C(14)-C(15)	1.597(9)	C(20)-C(21)	1.374(10)
C(15)-C(16)	1.486(9)	C(21)-C(16)	1.393(9)

	Angle		
Co-O(3)-C[13)	117.7(4)	C(14)-C(15)-C(16)	111.9(5)
O(3)-C(13)-O(4)	124.6(5)	C(15)-C(16)-C(17)	117.8(6)
O(3)-C(13)-C(14)	115.1(5)	C(15)-C(16)-C(21)	122.2(6)
O(4)-C(13)-C(14)	120.3(5)	C(16)-C(17)-C(18)	120.6(6)
Co-N(3)-C(14)	110.8(3)	C(17)-C(18)-C(19)	119.4(7)
N(3)-C(14)-C(13)	109.3(4)	C(18)-C(19)-C(20)	119.7(7)
N(3)-C(14)-C(15)	109.3(5)	C(19)-C(20)-C(21)	121.0(7)
C(13)-C(14)-C(15)	109.9(4)	C(20)-C(21)-C(16)	119.4(6)

Table 7. AB and CD Spectral Data for β_2-[Co(tfac$_2$en)(L-aa)][a)]

L-aa and No. of complex	AB (log ε)	CD ($\Delta\varepsilon$)	L-aa and No. of complex	AB (log ε)	CD ($\Delta\varepsilon$)
L-leu (**3**)	17.24(2.34)	17.54(+9.02)	L-tyr (**9**)	17.24(2.31)	17.54(+8.84)
	21.28(2.23, sh)	20.83(+4.96)		21.74(2.24, sh)	20.41(+5.12)
	24.39(2.78, sh)	25.00(−12.89)		24.79(2.72, sh)	25.00(−12.34)
	29.59(3.72)	30.86(−22.14)		29.59(3.71)	31.06(−20.70)
L-leu (**4**)	17.24(2.39)	17.54(−9.25)	L-tyr (**10**)	17.24(2.34)	17.54(−9.93)
	21.74(2.32, sh)	20.83(−6.11)		21.74(2.30, sh)	20.41(−5.57)
	24.39(2.80, sh)	25.00(+13.12)		24.39(2.76, sh)	25.00(+13.35)
	29.41(3.76)	30.70(+21.38)		29.76(3.71)	30.86(+22.24)
L-phe (**7**)	17.24(2.31)	17.54(+8.86)	L-trp (**11**)	17.24(2.30)	17.54(+9.95)
	21.74(2.24, sh)	20.41(+5.12)		21.28(2.25)	20.62(+5.76)
	24.39(2.73, sh)	25.00(−12.46)		24.39(2.77)	24.39(−12.94)
	29.41(3.70)	30.77(−20.37)		29.41(3.75)	30.30(−20.95)
L-phe (**8**)	17.24(2.34)	17.24(−8.94)	L-ala (**2**)[b)]	17.24(2.29)	17.54(+5.40)
	21.74(2.29, sh)	20.41(−5.06)		21.28(2.19)	18.18(+1.69)
	24.39(2.75, sh)	24.69(+12.36)		24.39(2.74)	24.21(+6.28)
	29.41(3.70)	30.86(+19.53)		29.41(3.70)	30.58(−11.61)

a) Solvent: DMF+$CHCl_3$(1 : 4 in volume). Wavenumbers are given in 10^3 cm^{-1}. The data of L-met complexes have been published in Ref. 8. b) 4 : 1 mixture of Λ- and Δ-β_2-isomers.

has been verified by X-ray analysis, the Λ-β_2-structure can safely be assigned to all the $(-)_{435}$-isomers. The AB spectra of $(+)_{435}$-isomers are also nearly identical with those of $(-)_{435}$-isomers, and the CD spectra of $(+)_{435}$-isomers are almost the mirror image of those of $(-)_{435}$-isomers. Accordingly, Δ-β_2-structure can be assigned to the $(+)_{435}$-isomers. Since the vicinal CD's of coordinated L-amino acidates show similar patterns with (−),

(+), and (−), signs from lower to higher energy in the first absorption region (16—23 kcm^{-1}), the coordinated amino acidates are assumed to take a very similar coordination structure to each other.

Generally, amino acids can take three conformations, *t*, *g*, and *h*, around the C(α)-C(β) bond.[17,18] In the cases of coordinated L-amino acidates in β_2-[Co(Schiff base)(L-aa)], they take the *t* conformation exclusively in the solid state.[8,15] Thus, the *t* rotamer seems to be very stable in this system. However, this is not the case in solution. In solution, the Λ-β_2-isomers of L-phe , L-tyr, and L-trp complexes show NMR spectra in which one of CH_3 and one of CH=C signals for $tfac_2en$ shift to a higher field due to the ring current effect of aromatic ring of amino acidates (Table 3). In the case of Δ-β_2-isomers, one of CF_3 signals shifts to a higher field. These high-field shifts are expected only when the conformation of coordinated amino acidates is *h* form, and in fact 400 MHz ^{1}H NMR spectral analysis of the L-phe complex indicates that the *h* conformer is predominant in acetone (Table 8). Therefore, we assume that all the complexes prepared here prefer the *h* conformation for the coordinated amino acidates in solution.

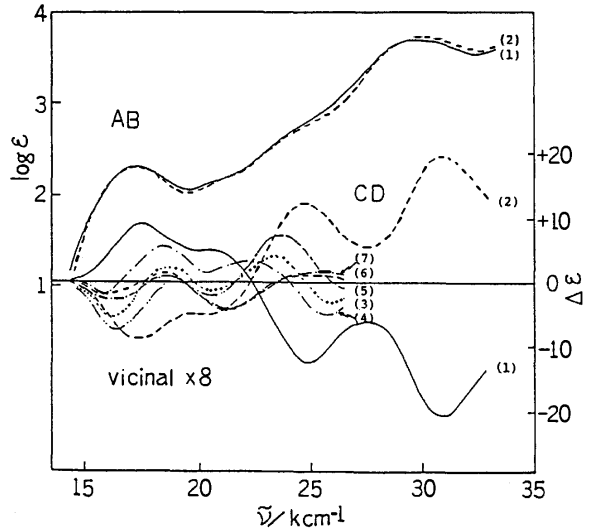

Fig. 2. Absorption (AB) and CD spectra of complexes in DMF-$CHCl_3$ (1:4) mixture. (1): (−)$_{435}$-Λ-β_2-[Co($tfac_2en$)(L-phe)], (2): (+)$_{435}$-Λ-β_2-[Co($tfac_2en$)-(L-phe)], (3): vicinal CD of L-phe, (4), (5), (6), and (7) are vicinal CD's of L-trp, L-tyr, L-ala, and L-leu, respectively.

Stereoselectivity of Complexes. When the coordinated amino acidates take the *h* conformation, the side chain of amino acidates approaches to CH_3 group of chelate ring **A** (Fig. 3) in the case of Λ-β_2-isomer. Whereas, in the case of Δ-β_2-isomer, the side chain approaches to CF_3 group of chelate ring **A'**. Since the approach is closer in Δ-β_2-isomer than in Λ-β_2-isomer in the model consideration, the main reason why the complexes prefer the Λ-configuration rather than the Δ will be that the steric repulsion between the side chain of amino acidates and $tfac_2en$ ligand is stronger in Δ-isomer than in Λ.

On the other hand, both the side chain of amino acidates and CF_3 group of $tfac_2en$ ligand are hydrophobic. Thus, when we use a hydrophilic solvent, hydrophobic interaction, especially solvophobic interaction, may occur between side chain and CF_3. In order to confirm the above assumption, the solvent effect on the stereoselectivity was investigated. The results are shown in Fig. 4. Here, we selected acetone

Table 8. Rotamer Populations about C_α-C_β Bond of Coordinated L-Phenylalaninate[19]

Complex	J_{AC}	J_{BC}	Rotamer/%		
			t	*g*	*h*
Λ-L-Phe	4.8	5.6	29.4	22.0	48.6
Δ-L-phe	4.4	6.8	18.3	40.4	41.3

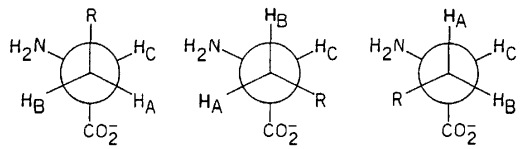

t *g* *h*

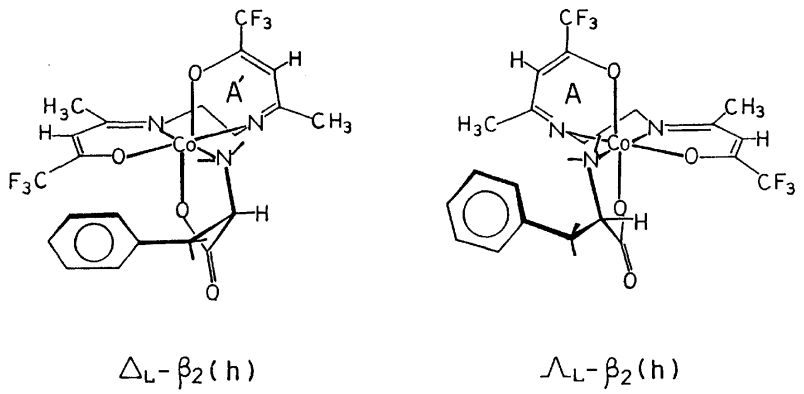

Δ_L-β_2(h) Λ_L-β_2(h)

Fig. 3. Stereochemical relation between side chain of coordinated L-amino acidate (*h*-conformation) and $tfac_2en$ ligand of Δ- and Λ-β_2-isomers in solution.

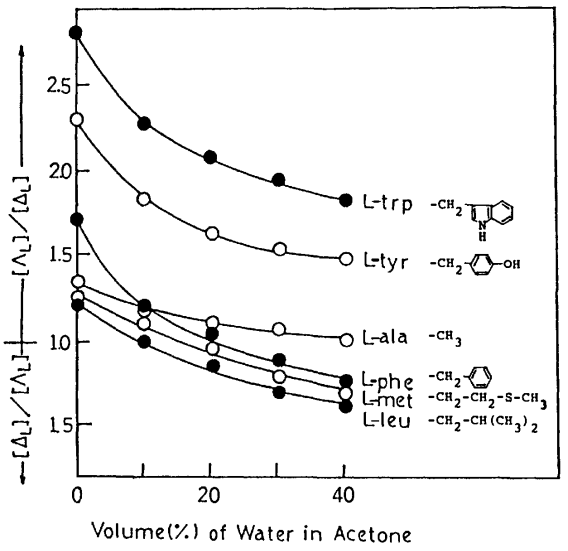

Fig. 4. Solvent dependence of stereoselectivity of β_2-[Co(tfac$_2$en)(L-aa)] at 25°C.

as a relatively hydrophobic solvent and investigated the effect of addition of water. Figure 4 indicates that 1) all the complexes prefer Λ-isomer in acetone, and the degree of the stereoselectivity is higher than that in methanol, and 2) the stereoselectivity decreases with addition of water and changes from Λ to Δ for L-leu, L-met, and L-phe complexes. The effect of addition of water is sensitive in the hydrophobic order of side chain of amino acidates, ala<met<leu<tyr<phe<trp, and the stereoselectivity for Λ-isomer increases in the hydrophilic order of solvents, acetone<methanol<water. Accordingly, hydrophobic interactions clearly contribute to the stereoselectivity of the employed complexes in water-acetone mixtures. The variation of the stereoselectivity with addition of water is the smallest for L-ala complex of all the complexes. This is due to the CH_3 group of L-alaninate, which is too small to cause hydrophobic interaction with CF_3 group of tfac$_2$en. In comparison with L-ala, L-leu, and L-met complexes, the variation of stereoselectivity with addition of water is much larger in L-phe, L-tyr, and L-trp complexes. This fact indicates that the hydrophobic interactions with CF_3 group are stronger for aromatic side chains than for aliphatic ones. The stereoselectivity of L-tyr and L-trp complexes remains in favor of Λ-isomer even at 40% water content. This may be due to the fact that the side chain of L-tyr and L-trp have electronegative OH and NH groups, respectively, near aromatic rings, so that the electrostatic repulsion between CF_3 group and OH and NH groups reduces hydrophobic interactions.

From the above results and discussion, we conclude that 1) the complexes investigated here prefer Λ-isomer in acetone and methanol, and the selectivity is based mainly on the steric repulsion between the side chain of coordinated L-amino acidates and CF_3 group of tfac$_2$en ligand in Λ-isomer, the counterpart of isomerization equilibrium, 2) in more hydrophilic solvents, the hydrophobic interactions occur between the above mentioned groups so as to increase the stereoselectivity for Λ-isomer, and 3) the hydrophobic interactions with CF_3 group is more effective when the side chain of amino acidates is aromatic group than aliphatic one.

References

1) H. Okawa and S. Kida, *Kagaku no Ryoiki*, **37**, 276 (1983).

2) R. M. Milburn, M. Gautam-Basak, R. Tribolet, and H. Sigel, *J. Am. Chem. Soc.*, **107**, 3315 (1985); R. Tribolet, R. Malini-Balakrishnan, and H. Sigel, *J. Chem. Soc., Dalton Trans.*, **1985**, 2291.

3) H. Sigel, R. Malini-Balakrishnan, and U. K. Häring, *J. Am. Chem. Soc.*, **107**, 5137 (1985); H. Sigel, R. Tribolet, and K. H. Scheller, *Inorg. Chim. Acta*, **100**, 151 (1985).

4) O. Yamauchi and A. Odani, *J. Am. Chem. Soc.*, **107**, 5938 (1985); A. Odani, S. Deguchi, and O. Yamauchi, *Inorg. Chem.*, **25**, 62 (1986).

5) Y. Numata, H. Okawa, and S. Kida, *Bull. Chem. Soc. Jpn.*, **53**, 2248 (1980).

6) M. Nakamura, H. Okawa, T. Inazu, and S. Kida, *Bull. Chem. Soc. Jpn.*, **55**, 2400 (1982); H. Okawa, K. Ueda, and S. Kida, *Inorg. Chem.*, **21**, 1594 (1982); M. Nakamura, H. Okawa, T. Ito, M. Kato, and S. Kida, *Bull. Chem. Soc. Jpn.*, **60**, 539 (1987).

7) K. Kashiwabara, I. Kinoshita, T. Ito, and J. Fujita, *Bull. Chem. Soc. Jpn.*, **54**, 725 (1981); M. Atoh, I. Kinoshita, K. Kashiwabara, and J. Fujita, *ibid.*, **55**, 3179 (1982).

8) K. Okamoto, K. Matsutani, and Y. Fujii, *Bull. Chem. Soc. Jpn.*, **58**, 3486 (1985).

9) "International Tables for X-Ray Crystallography," Kynoch Press, Birmingham (1974), Vol. 4.

10) P. Mani, S. E. Hull, L. Lessinger, G. Germain, J. P. Declercq, and M. M. Woolfson, MULTAN 78, A System of Computer Programs for the Automatic Solution of Crystal Structures from X-Ray Diffraction Data, University of York (1978).

11) T. Sakurai and K. Kobayashi, *Rikagaku Kenkyusho Hokoku*, **55**, 69 (1979).

12) C. K. Johnson, Report No. ORNL 3794, Oak Ridge National Laboratory, Oak Ridge, Tenessee (1965).

13) Y. Fujii, T. Kobayashi, M. Matsufuru, and S. Takahashi, *Bull. Chem. Soc. Jpn.*, **56**, 3608 (1983).

14) Y. Fujii, T. Isago, M. Sano, N. Yanagibashi, S. Hirasawa, and S. Takahashi, *Bull. Chem. Soc. Jpn.*, **49**, 3509 (1976).

15) Y. Kushi, R. Tamura, M. Kuramoto, T. Yoshizawa, H. Yoneda, and Y. Fujii, *J. Chem. Soc., Chem. Commun.*, **1978**, 266.

16) Y. Kushi, T. Tada, Y. Fujii, and H. Yoneda, *Bull. Chem. Soc. Jpn.*, **55**, 1834 (1982).

17) P. I. Vestues and R. B. Martin, *J. Am. Chem. Soc.*, **102**, 7906 (1980).

18) R. O. Gould, A. M. Gray, P. Taylor, and M. D. Walkinshaw, *J. Am. Chem. Soc.*, **107**, 5921 (1985).

19) The population was calculated from the coupling constants of ABX pattern for -CH_2-CH- group of L-phe complex in acetone-d_6 by the use of method in Ref. 17.

 © 1988 The Chemical Society of Japan Bull. Chem. Soc. Jpn., 61, 3519—3523 (1988)

The X-Ray Structure of Sodium *trans*-1,2-Cyclohexanediamine-*N,N,N',N'*-tetraacetatochromate(III) 4.5-Hydrate, Na[Cr(cydta)]·4.5H_2O

Sumio KAIZAKI,*,† Mariko HAYASHI, Keisuke UMAKOSHI,†† and Shun-ichiro OOI††
Department of Chemistry, Faculty of Science, Nara Women's University, Nara 630
†† Department of Chemistry, Faculty of Science, Osaka City University, Sumiyoshi-ku, Osaka 558
(Received March 22, 1988)

The crystal structure of the title compound has been determined from the X-ray diffraction data. This complex crystallizes in the monoclinic space group with unit-cell parameters of a=17.724(2), b=8.084(1), c=14.025(2) Å, β=95.06(1)°, and Z=4, and with a space group of $P2/c$. The structure converged to R=0.043 for 2898 reflections. In the complex anion, the chromium is coordinated by the sexadentate cydta ligand, producing a distorted octahedral CrN_2O_4 geometry. The glycinate chelates of the in-plane G(girdling) rings in the CrN_2O_2 plane are more distorted with respect to the Cr-O bond lengths and internal bond angles than are those of the out-of-plane R(relaxed) rings in the $CrNO_3$ plane. This may be responsible for the lability to dissociation of the G-ring acetate chelates. A close proximity of non-bonded hydrogen atoms (ca. 1.90 Å) is found between the methylene groups in the R ring and the cyclohexane ring. There are two nonequivalent sodium ions in the unit cell, which link the cydta complex anions to form an anion layer along the c axis.

Only two X-ray structure studies have been reported for six-coordinated sexadentate *trans*-1,2-cylcohexanediamine-*N,N,N',N'*-tetraacetatometallate ([M(cydta)]$^{n-}$); Manganate(III)[1] and cupurate(II), [2] both of which are severely distorted from a regular octahedron, though in opposite direction from each other, as a result of the Jahn-Teller effect. For non Jahn-Teller distorted cydta complexes, the X-ray structure data will make it possible to understand some characteristics of the thermodynamic, kinetic, and NMR and chiroptical spectroscopic behavior, which has suggested that the G-ring chelates are more labile to dissociation than the R-ring ones and that the sexadentate coordination of the cydta ligand in metal complexes is more favorable than that of the ethylenediamine-*N,N,N',N'*-tetraacetate (edta) one.[3-10] For such a study, the cydta Cr(III) complex is appropriate, because there have been reported some X-ray structure data of edta-like Cr(III) complexes[11-15] including K[Cr(edta)]·2H_2O, the solution structure of which has been well investigated, though there has long remained a controversy over whether it has a sexa- or quiquedentate edta coordination.[7-10]

This paper will report the determination of the crystal and molecular structure of Na[Cr(*rac*-cydta)]·4.5H_2O by means of X-ray structure analysis.

Experimental

X-Ray Analaysis of Na[Cr(cydta)]·4.5H_2O. Violet crystals of this complex suitable for X-ray analysis were obtained by the literature method[16] and then grown from a concentrated aqueous solution in a refrigerator for a few days. The elemental analysis showed 4.5 hydrate of this complex, in accord with the crystallographic result, though Tanaka et al. reported 4 hydrate.[16] Anal Calcd for Na[Cr(cydta)]·4.5H_2O: C, 33.74; H, 5.46; N, 5.62%. Found: C, 33.64; H, 5.44; N, 5.62%.

† Present address: Department of Chemistry, Faculty of Science, Osaka University, Toyonaka, Osaka 560.

The crystal data and experimental details are shown in Table 1. Weissenberg photography was used for the determination of the space group. The unit-cell parameters were derived by a least-squares analysis of 2θ values of the reflections in the $14<2\theta<23°$ range, measured on a Philips PW1100 diffractometer by the use of Mo$K\alpha$ radiation (λ=0.7107 Å). The intensity data were collected on the diffractometer by using graphite-monochromated Mo$K\alpha$ radiation at room temperature. The intensities of three standard reflections (600, 010, 004), monitored every 4h, showed no appreciable decay during the data collection. Of the 4814 unique reflections measured in the h, k, $\pm l$ region, 2898 with $F_o^2>3\sigma(F_o^2)$ were used for the structural analysis. No correction was made for absorption.

The crystal structure was solved by the direct method

Table 1. Crystallographic Data for Na[Cr(*rac*-cydta)]·4.5H_2O

Formula	$C_{14}H_{27}N_2O_{12.5}NaCr$
Space group	$P2/c$
a/Å	17.724(1)
b/Å	8.084(1)
c/Å	14.025(2)
β/deg	95.060
V/Å^3	2002.6(4)
Z	4
D_m/g cm^{-3}	1.65
D_c/g cm^{-3}	1.654
Cryst size/mm	0.095×0.2×0.19
Cryst color	blue violet
Cryst faces	(001) (00$\bar{1}$) (010) (0$\bar{1}$0) (100) ($\bar{1}$00)
μ(Mo$K\alpha$)/cm^{-1}	6.438
Scan method	ω
Scan speed/deg s^{-1}	0.033
Scan width/deg	1.0+ 0.4 tan θ
Data colln range(2θ)/deg	4—46
No. of observed reflections [$F_o^2>3\sigma(F_o^2)$]	2898
R_F[a]	0.0430
R_{WF}[b]	0.0504

a) $R_F=\sum||F_o|-|F_c||/\sum|F_o|$.
b) $R_{WF}=[\sum w(|F_o|-|F_c|)^2/\sum w|F_o|^2]^{1/2}$; $w=\sigma(|F_o|)^{-2}$.

(MULTAN).[17] The positional and thermal parameters were refined by the block-diagonal least-squares method. The minimized function was $\sum w(|F_o|-|F_c|)^2$, where $w=\sigma(F_o)^{-2}$. Hydrogen atoms were introduced in the calculated positions (C-H=0.97 Å), but those of the water molecules were located on a difference synthesis map except for one of the H atoms bonded to O(W1). These H atoms were included in the least-squares calculation, but their parameters were not refined. Each H atom was assigned an isotropic temperature factor equal to that of the atom to which it is bonded. The convergence was attained with the R_F and R_{WF} values listed in Table 1. All the parameter shifts in the final cycle of the refinement were $<0.2\sigma$. The final difference synthesis showed no peak greater than 0.7 e Å^{-3}. The atomic scattering factors, with correction for the real part of the anomalous dispersion effect for Cr and Na^+, were taken from Ref. 18. Tables of the observed and calculated structure factors, thermal parameters, and hydrogen-atom coordinates are deposited as Document No. 8828 at the Office of the Editor of the Bull. Chem. Soc. Jpn. The computational work was carried out by using standard programs.[19] The atomic coordinates are given in Table 2.

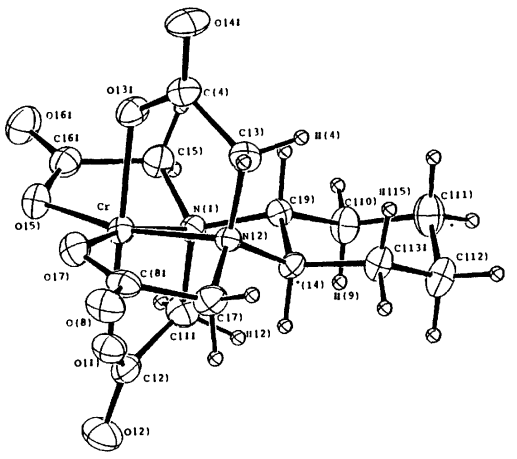

Fig. 1. The molecular structure of $[Cr(cydta)]^-$ ion in its sodium 4.5-hydrate. Thermal elipsoids are drawn at 50% probability level. Hydrogen atoms are represented as spheres of arbitrary radius. Besides Cr, C, N, and O atoms, only four hydrogen atoms which exhibit the close contact are numbered for clarity (see Text).

Results and Discussion

The Complex Anion $[Cr(cydta)]^-$. A perspective drawing of $[Cr(cydta)]^-$ is shown in Figure. 1. The bond lengths and angles are summarized in Table 3. The average bond lengths and angles, together with the torsion angles, are listed in Tables 4 and 5. The crystal structure analysis confirmed the sexadentate six-coordination mode of *trans*-1,2-cyclohexanediaminetetraacetate in this chromium(III) complex, as evidenced by our recent chiroptical study[8] and as found in $K[Cr(edta)]\cdot 2H_2O$.[11] The bond lengths and angles of the edta sub-unit in $[Cr(cydta)]^-$ are almost identical with those of the edta complex. The coordination geometry of the present complex anion is a distorted octahedron, with N-Cr-O and O-Cr-O angles of 81.2 and 112.9° respectively in the CrN_2O_2 plane. The Cr-N bond distances (2.058 Å) are as long as those of the edta complex[11] and the 1,3-propanediaminetetraacetato chromate(III) ($[Cr(1,3-pdta)]^-$)[12] and *cis*(*N*)-bis(iminodiacetato)chromate(III)-($[Cr(ida)]^-$)[13] complexes, but are shorter than those (average 2.085 Å) of *trans*(O_5)-(ethylenediamine-*N*,*N*′-diacetato-*N*,*N*′-dipropionato) chromate(III) ($[Cr(eddda)]^-$)[14] and *trans*(O_6)-(1,3-propanediamine-*N*,*N*′-diacetato-*N*,*N*′-dipropionato)chromate(III) ($[Cr(1,3-pddda)]^-$).[15] The Cr-O bonds fall into two classes with a mean bond length of 1.97 Å. The Cr-O bonds in G-ring chelates (average 1.992 Å) are longer than those (1.95—1.97 Å) usually found for the 1,3-pdta, bis(ida), and 1,3-pddda complexes,[12-15] whereas those in the R-ring chelates (average 1.953 Å) are almost the same. In other words, the differences between the Cr-O(R) and Cr-O(G) bond lengths for the edta and cydta complexes are larger than those for the bis(ida)[13] and 1,3-pdta[12] complexes, though these differences are smaller than those for the corresponding Mn(III) and Cu(II) complexes, the structures of which are susceptible to Jahn-Teller distortion[1,2] The sums of the G-ring bond angles in the cydta complex (average 524.0°) are samller than those of the R-ring ones (average 536.4°). The torsion anlges for the Cr-N-C-C chains

Table 2. Atomic Coordinates and Thermal Parameters

Atom	*X*	*Y*	*Z*	*U*(EQ) or *U*
Cr	0.30612(3)	0.0458(1)	0.1319(4)	0.0163(2)
Na(1)	0.5	0	0.5	0.028(1)
Na(2)	0.5	0.5	0.5	0.030(1)
O(1)	0.2673(1)	0.1773(3)	0.0215(2)	0.025(1)
O(2)	0.1680(2)	0.1891(4)	−0.0870(2)	0.039(2)
O(3)	0.3416(1)	−0.0911(3)	0.2414(2)	0.028(1)
O(4)	0.4062(2)	−0.0757(3)	0.3846(2)	0.039(2)
O(5)	0.2830(1)	−0.1648(3)	0.0607(2)	0.025(1)
O(6)	0.2139(2)	−0.3934(3)	0.0719(2)	0.048(2)
O(7)	0.4099(1)	0.1289(3)	0.1177(2)	0.018(1)
O(8)	0.4805(1)	0.3559(4)	0.1381(2)	0.022(1)
O(W1)	0.0109(2)	−0.2262(4)	0.3489(3)	0.037(2)
O(W2)	0.4408(2)	−0.2546(4)	0.0590(2)	0.036(2)
O(W3)	0.3775(2)	−0.4086(4)	0.4274(2)	0.043(2)
O(W4)	0.0595(2)	−0.5041(4)	0.0778(2)	0.060(2)
O(W5)	0.5	−0.3122(6)	0.25	0.145(2)
N(1)	0.1935(1)	0.0226(4)	0.1548(2)	0.020(1)
N(2)	0.3093(1)	0.2344(4)	0.2310(2)	0.016(1)
C(1)	0.1478(2)	0.0897(5)	0.0675(3)	0.021(2)
C(2)	0.1969(2)	0.1546(5)	−0.0069(3)	0.028(2)
C(3)	0.3490(2)	0.1698(5)	0.3223(3)	0.023(2)
C(4)	0.3680(2)	−0.0122(5)	0.3165(3)	0.017(2)
C(5)	0.1819(2)	−0.1596(5)	0.1642(3)	0.026(2)
C(6)	0.2285(2)	−0.2492(5)	0.0934(3)	0.025(2)
C(7)	0.3561(2)	0.3644(5)	0.1908(3)	0.024(2)
C(8)	0.4219(2)	0.2792(5)	0.1460(3)	0.019(2)
C(9)	0.1836(2)	0.1193(4)	0.2454(2)	0.020(2)
C(10)	0.1008(2)	0.1464(5)	0.2656(3)	0.018(2)
C(11)	0.0975(2)	0.2573(5)	0.3533(3)	0.026(2)
C(12)	0.1326(2)	0.4239(5)	0.3354(3)	0.029(2)
C(13)	0.2164(2)	0.4026(5)	0.3206(3)	0.024(2)
C(14)	0.2276(2)	0.2818(4)	0.2391(3)	0.017(2)

Table 3. Bond Distances and Bond Angles around the Complex Anion and Cation

Bond distance/Å							
Cr-O(1)	1.954(3)	O(8)-C(8)	1.224(4)	O(4)-C(4)	1.233(4)	C(5)-C(6)	1.528(5)
Cr-O(3)	1.951(3)	N(1)-C(1)	1.508(4)	O(5)-C(6)	1.299(4)	C(7)-C(8)	1.535(5)
Cr-O(5)	1.998(3)	N(1)-C(5)	1.495(5)	O(6)-C(6)	1.290(5)	C(9)-C(14)	1.534(5)
Cr-O(7)	1.985(2)	N(1)-C(9)	1.515(5)	C(8)-O(7)	1.290(5)	C(10)-C(11)	1.527(6)
Cr-N(1)	2.058(3)	N(2)-C(3)	1.499(4)	C(9)-C(10)	1.534(5)	C(12)-C(13)	1.527(5)
Cr-N(2)	2.060(3)	N(2)-C(7)	1.481(5)	C(11)-C(12)	1.514(6)	C(13)-C(14)	1.529(5)
O(1)-C(2)	1.289(4)	N(2)-C(14)	1.512(4)	Na(1)-O(7)[a]	2.617(3)	Na(1)-O(4)	2.298(3)
O(2)-C(2)	1.226(4)	C(1)-C(2)	1.511(5)	Na(1)-O(W2)[a]	2.485(3)	Na(2)-O(8)[a]	2.312(3)
O(3)-C(4)	1.284(4)	C(3)-C(4)	1.514(5)	Na(2)-O(W3)[b]	2.430(3)	Na(2)-O(W2)[c]	2.424(3)
Bond angle/deg							
O(1)-Cr-O(3)	177.9(1)	Cr-O(1)-C(2)	115.5(2)	C(3)-N(2)-C(14)	113.9(3)	N(2)-C(7)-C(8)	108.0(3)
O(1)-Cr-O(5)	91.4(1)	Cr-O(3)-C(4)	115.6(2)	C(7)-N(2)-C(14)	113.9(3)	O(7)-C(8)-O(8)	124.5(3)
O(1)-Cr-O(7)	90.0(1)	Cr-O(5)-C(6)	113.4(2)	N(1)-C(1)-C(2)	112.6(3)	O(7)-C(8)-C(7)	116.0(3)
O(1)-Cr-N(1)	84.0(1)	Cr-O(7)-C(8)	114.6(2)	O(1)-C(2)-O(2)	124.5(4)	O(8)-C(8)-C(7)	119.5(3)
O(1)-Cr-N(2)	96.8(1)	Cr-N(1)-C(1)	107.4(2)	O(1)-C(2)-C(1)	115.9(3)	N(1)-C(9)-C(10)	114.3(3)
O(3)-Cr-O(5)	87.0(1)	Cr-N(1)-C(5)	104.3(2)	O(2)-C(2)-C(1)	119.5(3)	N(1)-C(9)-C(14)	197.3(3)
O(3)-Cr-O(7)	91.9(1)	Cr-N(1)-C(9)	105.6(2)	N(2)-C(3)-C(4)	112.5(3)	C(10)-C(9)-C(14)	112.8(3)
O(3)-Cr-N(1)	94.4(1)	C(1)-N(1)-C(5)	111.0(3)	O(3)-C(4)-O(4)	124.4(3)	C(9)-C(10)-C(11)	109.8(3)
O(3)-Cr-N(2)	84.4(1)	C(1)-N(1)-C(9)	113.7(3)	O(3)-C(4)-C(3)	117.4(3)	C(10)-C(11)-C(12)	110.0(3)
O(5)-Cr-O(7)	112.9(1)	C(5)-N(1)-C(9)	114.1(3)	O(4)-C(4)-C(3)	118.3(3)	C(11)-C(12)-C(13)	110.0(3)
O(5)-Cr-N(1)	80.9(1)	Cr-N(2)-C(3)	107.5(2)	N(1)-C(5)-C(6)	108.9(3)	C(12)-C(13)-C(14)	111.4(3)
O(5)-Cr-N(2)	163.7(1)	Cr-N(2)-C(7)	104.5(2)	O(5)-C(6)-O(6)	124.0(4)	N(2)-C(14)-C(9)	106.4(3)
O(7)-Cr-N(1)	165.2(1)	Cr-N(2)-C(14)	105.6(2)	O(5)-C(6)-C(5)	116.2(3)	N(2)-C(14)-C(13)	114.0(3)
O(7)-Cr-N(2)	81.2(1)	C(3)-N(2)-C(7)	109.6(3)	O(6)-C(6)-C(5)	119.7(3)	C(9)-C(14)-C(13)	113.8(3)
N(1)-Cr-N(2)	86.1(1)						

a) At $1-x$, y, $1/2-z$. b) At x, $1+y$, z. c) At $1-x$, $1+y$, $1/2-z$.

in the G rings are considerably different from those in the R rin s(average 38.73° for the G rings and average 4.21° for the R rings, as shown in Table 5). These facts indicate that the G-ring chelates are more strained than the R ones, since the ring strain may be evaluated in terms of the torsion anlges as well as the deviation from the sum of the ideal chelate bond angles for five-membered rings.[20] On the other hand, the quinquedentate edta-type Cr(III) complexes such as [Cr(H_2O)-(Hedta)] exhibit a sum of the G-ring chelate bond angles similar to that for the cydta complex, but the Cr-O(G) bond (1.935—1.959 Å) is found to be shorter than that (1.99 Å) in the sexadentate edta complex.[21] There seems to be no correspondence between the G-ring strain and the Cr-O(G)-bond lengthening. Hence, it is probable that the cooperation of the chelate-ring strain and the Cr-O(G)-bond lengthening results in the lability to the dissociation of the G-ring chelates in the sexadentate edta and cydta Cr(III) complexes.

In general, the sexadentate edta complexes are less stable than the cydta complexes, forming the quinquedentate edta complexes with an uncoordinated G-ring acetate and one coordinated water molecule more readily than the cydta complexes.[3-5,7-14] This difference in stability of the G-ring chelates between these complexes may be brought about by a small change in the structure of the edta sub-unit around the Cr(III) ions; e.g., the O(G)-Cr-O(G) angles of the cydta Cr(III) complex is smaller by 1.4° than that of the edta complex. Another possible explanation for it is a steric interaction between the R rings and the cyclohexane backbone, a stereochemical requirement or steric compression responsible for the increased ring-closure rates of the cydta complexes over those of the edta ones, as has been discussed in connection with the kinetic differences between the cydta and edta complexes.[4a,5b,22] The present X-ray analaysis substantiates this possibility; short intramolecular nonbonding H-H distances (1.90 Å) are found betweeen the glycinate methylene groups in the R ring and the

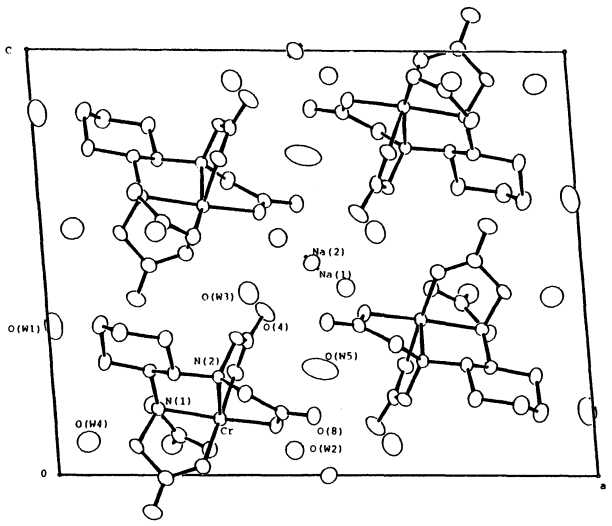

Fig. 2. Crystal structure of Na[Cr(cydta)]·4.5H_2O viewed down the b-axis. All hydrogen atoms are omitted for clarity. Na(2) at (1/2, 1/2, 1/2) overlaps just above Na(1) at (1/2, 0, 1/2) in this plane.

Table 4. Averaged Bond Lengths and Angles within the Complex Anion

Bond type	No. of bonds	Ring type	Av. length/Å	R.m.s. deviation/Å
C_9-C_{14}	1	E, CH	1.534	0.005
C_{11}-C_{12}	1	CH	1.514	0.006
C-C	4	CH	1.529	0.005
C-C	4	G, R	1.522	0.004
C-N	6	E,G,R	1.502	0.005
C-O_c	2	R	1.287	0.004
C-O_c	2	G	1.295	0.004
C-O_u	2	R	1.229	0.004
C-O_u	2	G	1.225	0.004
Cr-O	2	R	1.951	0.003
Cr-O	2	G	1.992	0.003
Cr-N	2	E	2.058	0.003

Ring type	Bond angle	Mean values (degree)	R.m.s devation (degree)
CH	C-C-C(C_{14}-C_9)	113.3	0.3
	C-C-C(C_{10}-C_{13})	110.6	0.3
	C-C-C(C_{11}-C_{12})	110.0	0.3
E	Cr-N-C	105.6	0.2
	N-C-C	106.9	0.3
	N-Cr-N	86.1	0.1
R	Cr-O-C	115.6	0.2
	O-C-C	116.7	0.3
	C-C-N	112.6	0.2
	C-N-Cr	107.5	0.2
	N-Cr-O	84.2	0.1
	C-C-O_u	118.9	0.3
	O-C-O_u	124.1	0.3
G	Cr-O-C	114.0	0.3
	O-C-C	116.1	0.3
	C-C-N	108.5	0.3
	C-N-Cr	104.4	0.3
	N-Cr-O	81.1	0.1
	C-C-O_u	119.6	0.3
	O-C-O_u	124.3	0.4
E-R	C-N-C	114.5	0.3
E-G	C-N-C	113.8	0.3
R-G	C-N-C	110.3	0.3

CH, E, R, and G stand for cyclohexane, diamine chelate, and the R and G rings of the acetate chelates, respectively. The subscripts c and u refer to coordinated and uncoordinated oxygen atoms respectively.

methylene groups in the 3 and 6 positions of the cyclohexane ring: C(1)-H(2) and C(10)-H(9) or C(3)-H(4) and C(13)-H(15), as is shown in Fig. 1.

The cyclohexane ring takes the chair conformation, and its bond lengths and angles agree with those found for cydta complexes of six-coordinate Mn(III), Cu(II), and seven-coordinate Fe(III).[1,2,23] The torsion angles for the C-C-C-C chains in the cyclohexane ring range from 47 to 63° in absolute value, with a mean magnitude of 54.28°, approximating those of other cydta complexes.[1,2]

The Crystal Structure. A projection of the structure of Na[Cr(cydta)]·4.5H_2O down the b-axis is shown in Fig. 2. There are two inequivalent sodium ions in the unit cell. Each sodium ion is surrounded by six oxygens in an octahedral configuration; for Na(1) at

Table 5. Selected Torsion Angles (/°)

Cr-N(1)-C(1)-C(2)	1.1(4)
Cr-N(2)-C(3)-C(4)	4.8(3)
Cr-N(1)-C(5)-C(6)	37.8(4)
Cr-N(2)-C(7)-C(8)	39.7(3)
C(1)-C(2)-O(1)-Cr	24.0(4)
C(3)-C(4)-O(3)-Cr	16.7(4)
C(5)-C(6)-O(5)-Cr	12.1(4)
C(7)-C(8)-O(7)-Cr	3.3(4)
N(1)-C(1)-C(2)-O(1)	14.5(5)
N(1)-C(5)-C(6)-O(5)	18.8(4)
N(2)-C(3)-C(4)-O(3)	7.3(4)
N(2)-C(7)-C(8)-O(7)	26.0(4)
Cr-N(1)-C(9)-C(14)	43.1(3)
C(9)-C(14)-N(2)-Cr	44.9(3)
N(1)-C(9)-C(14)-N(2)	59.9(3)

(1/2, 0, 1/2), four from uncoordinated oxygens of carboxylates in the anions and two from water molecules, and for Na(2) at (1/2, 1/2, 1/2), two from uncoordinated carboxylates and four from water molecules. The octahedral environment around the Na(2) is more deformed than that around the Na(1). The average Na(1)-O and Na(2)-O distances are 2.389 and 2.467 Å respectively. The values of the former bond are shorter than the range observed for the other $Na(O)_6$ polyhedra, but the latter one is within this range. The interbond angles of the $Na(O)_6$ polyhedra have mean deviations from the ideal octahedral values of 0.887° and 9.62° for Na(1) and Na(2) ions respectively. A cationic layer at around 1/2 with the Na(1) and Na(2) polyhedra, linking four and two complex anions respectively, is formed by hydrogen bonds between two crystalline water molecules, O(W5) and O(W2), the oxygen-oxygen distance of which is 2.892 Å. Consequently, this array of sodium ions combines two layers of the complex anions by forcing the hydrophilic moieties of the anions to be directed toward the cations. Hence, it seems to minimize contacts between the hydrophobic cyclohexane rings of the anions in the unit cell. Similar cationic arrangements in the unit cells are observed for K[Mn(cydta)]·H_2O[1] and Ca[Fe(H_2O)(cydta)]$_2$·8H_2O.[23]

References

1) S. J. Rettig and J. Trotter, *Can. J. Chem.*, **51**, 1303 (1972).

2) A. Fuertes, C. Miravitlles, E. Escriva, E. Coronado, and D. Beltran, *J. Chem. Soc., Dalton Trans.*, **1986**, 1795.

3) E. Erickson, D. C. Young, F. F.-L. Ho, S. R. Watkins, J. B. Terrill, and C. N. Reilley, *Inorg. Chem.*, **10**, 441 (1971).

4) a) D. S. Everhart and R. F. Evilia, *Inorg. Chem.*, **16**, 120 (1977); b) R. F. Evilia, *ibid.*, **24**, 2076 (1985).

5) a) O. W. Howarth, P. Moore, and N. Winterton, *J. Chem. Soc., Dalton Trans.*, **1974**, 2271; b) O. W. Howarth, P. Moore, and N. Winterton, *ibid.*, **1975**, 360.

6) J. Stein, J. P. Fackler, Jr., G. J. McClune, J. A. Fee, and L. T. Chan, *Inorg. Chem.*, **18**, 3511 (1979).

7) W. D. Wheeler and J. I. Legg, *Inorg. Chem.*, **23**, 3798 (1984); W. D. Wheeler and J. I. Legg, *ibid.*, **24**, 1292 (1985).

8) S. Kaizaki and H. Mizu-uchi, *Inorg. Chem.*, **25**, 2732 (1986).

9) N. Miura, M. Shimura, and H. Ogino, *Bull. Chem. Soc., Jpn.*, **60**, 1349 (1987).

10) H. Ogino and M. Shimura, *Adv. Inorg. Bioinorg. Mech.*, **4**, 107 (1986); K. Kanamori and K. Kawai, *Inorg. Chem.*, **25**, 3711 (1986).

11) Y. Kushi, K. Morimasa, and H. Yoneda, Presented at the 49th Annual Meeting of the Chemical Society of Japan, Tokyo, April 1984; Abstract 1N31.

12) R. Herak, G. Srdanov, M. I. Djuran, D. J. Radanović, and M. Bruvo, *Inorg. Chim. Acta*, **83**, 55 (1984).

13) D. Mootz and H. Wunderlich, *Acta Crystallogr., Sect. B*, **36**, 445 (1980).

14) R. T. Helm, W. H. Watson, R. D. Radanović, and B. E. Douglas, *Inorg. Chem.*, **16**, 2351 (1977).

15) S. Kaizaki, M. Byakuno, M. Hayashi, J. I. Legg, K. Umakoshi, and S. Ooi, *Inorg. Chem.* **26**, 2395 (1987).

16) N. Tanaka, K. Kanno, T. Tomita, and A. Yamada, *Inorg. Nucl. Chem. Lett.*, **7**, 953 (1971).

17) P. Main, S. E. Hull, L. Lessinger, G. Germain, J. P. Declercq, and M. M. Woolfson (1978). MULTAN 78. A System of Computer Programs for the Automatic Solution of Crystal Structures from X-Ray Diffraction Data. University of York, England, and Louvain, Belgium.

18) "International Tables for X-ray Crystallography," Kynoch Press: Birmingham, England, 1974, Vol. IV.

19) "UNICS,", Crystallographic Society of Japan, 1969, C. K. Johnson, "ORTEP II," Report ORNL-5138; Oak Ridge National Laboratory: Oak Ridge, TN, 1976.

20) a) H. A, Weakliem and J. L. Hoard, *J. Am. Chem. Soc.*, **81**, 549 (1959); b) F. Pavelcik, *J. Coord. Chem.*, **13**, 299 (1984).

21) a) G. D. Falton and B. M. Gatehouse, *Acta Crystallogr., Sect. B*, **30**, 1987 (1974); b) L. E. Gerdom, N. A. Baebzinger, and H. M. Goff, *Inorg. Chem.*, **20**, 106 (1980).

22) W. H. Woodruff, B. A. Burke, and D. W. Margerum, *Inorg. Chem.*, **13**, 2573 (1974).

23) G. H. Cohen and J. L. Hoard, *J. Am. Chem. Soc.*, **88**, 3228 (1966).

High Performance Micro-Enzyme Sensor Using Platinized Microelectrode

Yoshihito IKARIYAMA,*,† Shigeru YAMAUCHI, Masuo AIZAWA,†† Tomoaki YUKIASHI,††† and Hiroo USHIODA†††
Research Institute of National Rehabilitation Center, Namiki 4-1, Tokorozawa, Saitama 359
††Department of Bioengineering, Tokyo Institute of Technology, O-okayama 2-12-1, Meguro-ku, Tokyo 152
†††Central Research Laboratory, Sumitomo Cemment Co., Ltd., Toyotomi 5-8-5, Funabashi, Chiba 274
(Received June 10, 1988)

A unique micro-enzyme sensor for the determination of glucose has been prepared by incorporating glucose oxidase into the micropores of a platinized microelectrode. The electrode diameter is in the range from 10 μm to 200 μm. The detection limit is 5×10^{-7} mol L^{-1} for glucose, and an excellent linearity is obtained in the concentration range from 5×10^{-7} to 10^{-2} mol L^{-1} in the case of micro-enzyme electrode whose diameter is larger than 50 μm. In the case of micro-enzyme electrode whose diameter is 10 μm, the detection limit for glucose is 10^{-5} mol L^{-1}, and the linearity is observed in the concentration range from 10^{-5} to 5×10^{-2} mol L^{-1}. The sensor responds to every glucose sample of different concentration in 3 s or less, and the coefficients of variation for glucose (1 mM) determination were within 2%. The sensor output was stable over 4 weeks. This unique microfabrication approach to micro-enzyme electrodes enables the immobilization of intact enzyme molecules by a simple procedure.

Since the introduction of the enzyme electrode by Clark and Updike,[1,2] a wide variety of biosensors have been developed. In the early stage of biosensor research many enzyme-immobilized membranes have been attached to a Clark-type oxygen electrode.[3-5] In addition, antibodies,[6-9] organelles,[10,11] plant tissues,[12] animal tissues,[13] and microorganisms[14,15] have been immobilized for the preparation of a wide variety of Clark-type oxygen electrode-based biosensors.

The further practical application of enzyme electrodes has been extended by the microfabrication of electrode-based biosensors, since multifunctional biosensors can be developed by taking advantage of silicon technology.[16-18] Disposable biosensors can also be constructed.

In almost all areas of chemical measurement the philosophy "the smaller, the better" seems to be prevailing. Well-known examples are capillary columns for gas and liquid chromatography, and microelectrodes for in vivo neurochemical sensors.[19,20] These microinstruments have been gradually replacing the conventional ones because of their increased resolution, sensitivity, and saving in running cost. Miniaturization of biosensors is particularly important for the realization of not only high performance autoanalyzing systems with compactness in clinical laboratory but sensing devices for artificial organs.

Microelectrodes the size of which are less than 10 μm radius have been investigated and employed to obtain neurochemical information.[19,20] Small size also has many advantages in electrochemical analysis particularly with biosensors by virtue of specific reaction of an enzyme, and specific binding between an antigen and its corresponding antibody. Microfabrication of enzyme sensors has been mainly pursued by employing field effect transistors as potentiometric transducers.[16-18] This semiconductor-based approach is promising, since disposable enzyme electrodes are prepared by covering the gate of a field effect transistor with an enzyme-immobilized membrane by employing the conventional immobilization techniques. However, as long as the conventional immobilization techniques of enzymes are employed, enzyme electrodes with sizes in the μm range are beyond realization. By the conventional techniques the authors mean the polymer matrix-supported enzyme membranes. In our previous rapid communication,[21] we have reported fundamental properties of an enzyme electrode (diameter=200 μm) prepared by incorporating enzyme molecules on a platinized surface of platinum electrode.

Here we describe the details and further information on micro-enzyme sensors (diameter=10—200 μm) based on platinized microplatinum electrode, especially with the additional information of our world-smallest enzyme electrode which can be applied as an in vivo micro-enzyme sensor for glucose sensitive neurons. The relationship between the porosity of platinized microelectrode and the sensor output as well as long term stability are also described. Enzyme molecules are intactly inmobilized in the micropores of a transducer electrode. It is the platinization technique that enables the microfabrication of the biosensor. It is a well-known fact that platinized platinum, porous microparticles of platinum, possesses very huge surface and high catalytic activities for electrolytic processes. By employing a microelectrode as a base electrode for platinization and enzyme immobilization, a micro-enzyme sensor can be easily fabricated. Therefore, the size of the micro-enzyme sensor is directly related to that of the base electrode. Enzyme molecules are stably retained in the porous platinum particles with active surface. In other words, the platinum particles play the dual roles of transducing material and matrix for enzyme immobilization.

† Present address: Department of Bioengineering, Tokyo Institute of Technology, O-okayama 2-12-1, Meguro-ku, Tokyo 152.

Experimental

Reagents and Materials. Hexachloroplatinic acid and lead acetate were purchased from Wako Chem. Co. (Osaka). Glucose was the product of Nakarai Chem. Co. (Kyoto), and glucose oxidase (110 u mg^{-1}) was purchased from Toyobo Co. (Osaka). Bovine serum albumin and glutaraldehyde were obtained from Tokyo Kasei (Tokyo). All the chemicals were analytical reagent grade, and all solutions were prepared with glass-distilled water.

Platinum wires (diameter=10—200 μm) were the products of Sanwa Metal Co. (Tokyo). Imperial™ wrapping films of alumina powders of different particle sizes were obtained from Sumitomo 3M Co. (Tokyo).

Preparation of Glucose Oxidase-Immobilized Platinized Microelectrode. Platinum wire whose diameter is in the range from 50 μm to 200 μm was sealed by heating a platinum wire-inserted small soda glass tubing and then polished with the polishing films to prepare a flat surface. In the case of 10 μm platinum electrode, a 10 μm platinum wire was placed in a glass capillary tubing and then sealed at a mild heating temperature. The glass tubing was pulled gently by creeping for several minutes. This was performed by a glass microelectrode puller for patch-clamp pipet (type PP-83) of Narishige Scientific Instrument Laboratory (Tokyo). After sufficient encapsulation of the platinum wire in the capillary tubing, the wire-encapsulating tubing was cut into two microelectrodes. The tip of every platinum electrode was polished with a film of 30 μm alumina powder and then with a film of 9 μm alumina powder. At the last stage, the tip was polished with alumina powder of 1 μm diameter with the exception of the 10 μm microplatinum electrodes, which are polished carefully with 0.1 μm alumina powder. After the smoothing of the surface of the platinum microelectrode, platinization was carried out by reducing hexachloroplatinate (33 mg mL^{-1}) in the presence of lead acetate (0.6 mg mL^{-1}). The electrode potential is referred to a Ag/AgCl reference electrode in the following description. A platinum wire (d=200 μm, l=5 mm) was employed as an auxiliary electrode. The electrolytic reduction of the platinum complex was performed either potentiostatically or galvanostatically. In the potentiostatic preparation, the potential was varied from −0.15 to −0.20 V, and the deposition time was 10 min. On the other hand, in the case of galvanostatic preparation, the deposition current was changed in the range from −0.5 to −60 μA, and the deposition time was 5 min. After the reductive deposition of platinum particles, the platinized electrode was thoroughly washed in 0.1 M phosphate buffer (pH 6.8; 1 M=1 mol dm^{-3}). Enzyme incorporation was then carried out by immersing the electrode in a phosphate-buffered solution (pH 6.8) containing 50 mg glucose oxidase for 10 min. The enzyme-incorporated platinized microelectrode was rinsed thoroughly in 0.1 M phosphate buffer (pH 6.8) for over 12 hours. The electrode, if necessary, was then immersed in a bovine serum albumin solution (20 mg in 1 mL of 0.1 M phosphate buffer of pH 6.8) for 10 min. The albumin-incorporated platinized surface was then immersed in a glutaraldehyde solution (2% in 0.1 M phosphate buffer) for 10 min to form a thin albumin film over the platinized surface. The electrochemical microfabrication technique is schematically shown in Fig. 1.

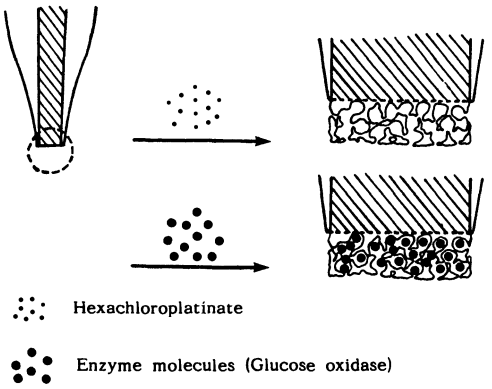

Fig. 1. Schematic illustration of the fabrication technique for the preparation of micro-enzyme sensor. After the encapsulation of micro-platinum wire, platinization is performed by electrochemical reduction of hexachloroplatinate, which is followed by the incorporation of enzyme molecules. The electrode was immersed in an albumin solution and then treated with glutaraldehyde.

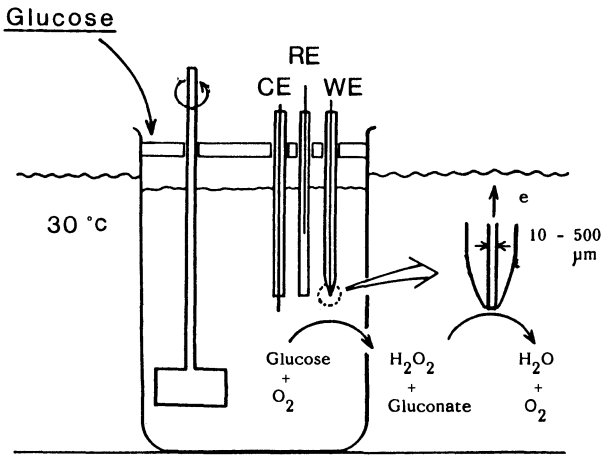

Fig. 2. Measuring apparatus for glucose determination with a micro-enzyme electrode. Glucose oxidase generates hydrogen peroxide from glucose, and the peroxide is oxidized by the transducer electrode of which potential is kept at 0.6 V vs. Ag/AgCl reference electrode. The anodic current is the sensor output.

Observation of Enzyme-Immobilized Microelectrode. A typical micro-enzyme electrode was observed by a SZH optical microscope of Olympus Co. (Tokyo). The surface of the platinized electrode was observed by a Hitachi S-450 scanning microscopy before and after enzyme incorporation. Each electrode was coated with gold by a Eiko IB-3 ion coater after the lyophylization of the electrodes. All the electrodes were kept at −60 °C overnight and then lyophylized with a freeze dryer (Model DC-55A) of Yamato Scientific Co., Ltd. (Tokyo). The gold coating (5 min) was repeated three times to keep the coating at moderate temperature.

Glucose Determination by Micro-Enzyme Electrode. Glucose was determined with a three electrode system by applying 0.6 V to the working micro-enzyme electrode. At the applied potential the hydrogen peroxide generated by glucose oxidase is oxidized to give anodic current. Figure 2

shows the measuring apparatus for glucose determination with micro-enzyme electrodes. A series of glucose samples were injected into the measuring buffer solution (0.1 M phosphate of pH 6.8) under the stirring with a motor-driven screw mixer. The mixing with a motor-driven screw was required to obtain a good signal to noise ratio especially in the case of an enzyme electrode of 10 μm diameter. The glucose determination was performed at 30 °C.

Results

Evaluation of Platinized Platinum Surface. After platinization the microelectrode was cleaned by sweeping the electrode potential repeatedly in 0.5 M sulfuric acid for the estimation of electrode surface area. A oxygen and hydrogen adsorption/desorption curve for a platinized electrode (diameter=10 μm) was investigated and compared with the curve for a flat electrode of the same diameter. From the two voltammograms the surface area of a platinized electrode is estimated to be about 5000 times that of a plain electrode. The surface area of a platinum electrode is easily controllable by changing the deposition time. The platinization is also controlled by choosing the applied potential in the case of potentiostatic preparation and by choosing the reducing current in the case of galvanostatic prepartation.

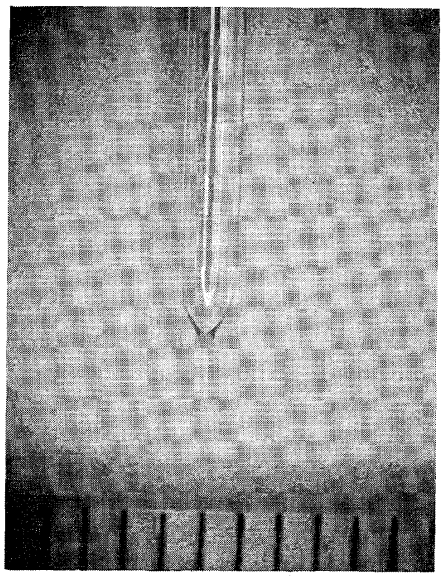

Fig. 3. A typical micro-enzyme electrode (diameter=10 μm) encapsulated in a soda glass tubing. The graduation lines of the scale is 1 mm.

Observation of Enzyme-Immobilized Microelectrode. A typical micro-enzyme electrode (10 μm) was observed by the microscope. Figure 3 shows that a 10 μm platinum wire is encapsulated in a capillary tubing. The surfaces of three different electrodes were observed by the scanning electron microscope. Figure 4 shows the surface of a platinized electrode before enzyme incorporation. Microparticles of platinum were seen on the surface. A photograph of a glucose oxidase-incorporated platinized electrode is shown in Fig. 4(B). Despite considerable enzyme activity in the porous electrode surface, no membrane-like structure was observed on the platinized surface. The last photograph, Fig.4(C), shows the surface of the enzyme-incorporated platinized electrode treated in the albumin solution and in the glutaraldehyde solution. A very thin protein layer was observed over the electrode surface after the crosslinking of albumin molecules by the bifunctional aldehyde.

The thickness of the albumin film was estimated to be a few hundred A from the cross section of the broken protein film during lyophylization.

Determination of Glucose by the Micro-Enzyme Electrode. The micro-enzyme electrode (diameter: 50 μm) was immersed in 0.1 M phosphate buffer (pH 6.8). After the residual current became a constant value, each glucose sample was injected. The output current increased promptly after the injection of a glucose

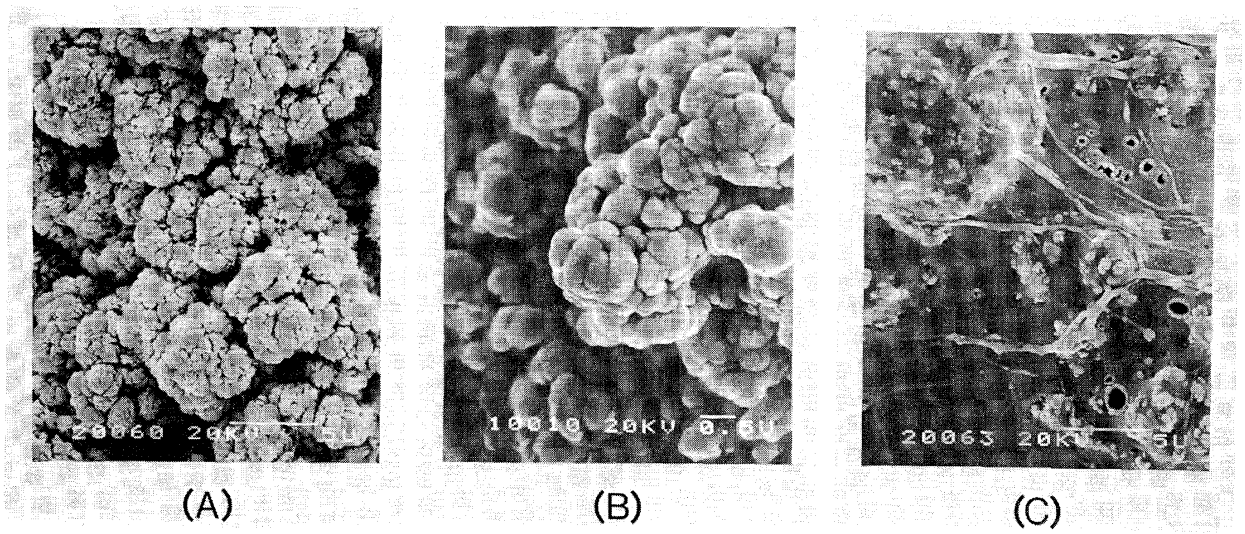

Fig. 4. SEM photographs of a platinized microelectrode (A), an enzyme-incorporated platinized microelectrode (B), and an enzyme-incorporated platinized microelectrode treated with albumin and glutaraldehyde (C).

sample as illustrated in Fig. 5. The output of a micro-enzyme electrode reached a steady state current in 3 s or less. The increase in the oxidizing current was caused by the oxidation of the hydrogen peroxide generated by immobilized glucose oxidase molecules. The response in Fig. 5 was measured repeatedly by changing the glucose concentration.

The change in sensor output was plotted versus glucose concentration to give a calibration curve for glucose as shown in Fig. 6. The lowest and highest detectable glucose concentrations were 0.5 μM and 10 mM,

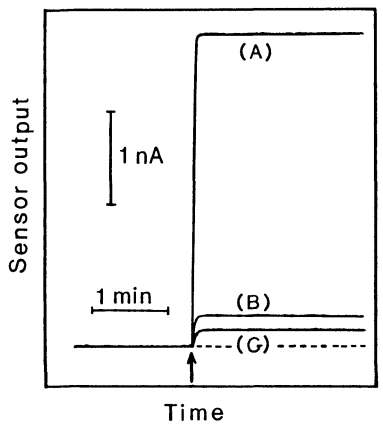

Fig. 5. Typical responses of a micro-enzyme electrode (diameter=50 μm). Glucose concentrations were 100 μM (A), 10 μM (B), and 5 μM (C).

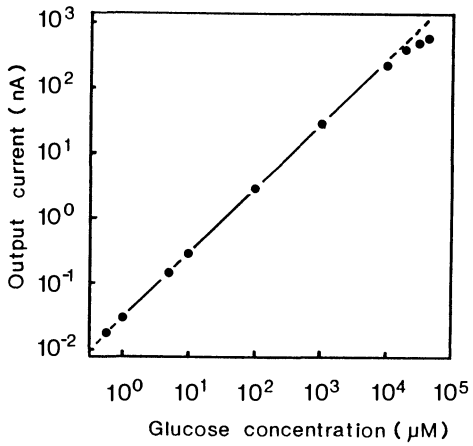

Fig. 6. Calibration curve for glucose with a micro-enzyme electrode (diameter=50 μm).

respectively. When the microenzyme electrode diameter is larger than 50 μm, the calibration curve and dynamic range of a given micro-enzyme electrode were not influenced by the size of a base platinum micro-electrode.

However, the 10 μm enzyme electrode showed a narrower dynamic range between 5 μM and 10 mM, although good linearity and rapid-response was observed within this range. Since the determination of 5 μM glucose sample caused a sensor output of only a few pA, the authors believe that a more sensitive recorder could make the 10 μm enzyme electrode more sensitive because of the high signal to noise ratio of the 10 μm enzyme electrode.

Three different enzyme electrodes (diameter: 10, 50, 200, 500 μm) prepared under different conditions were studied for the comparison of sensor characteristics such as response to 1 mM glucose and the Michelis-Menten constant with respect to the porosity of the platinized electrode and the electrode diameter. The calibration curves obtained by four enzyme electrodes allow the calculation of apparent Michaelis-Menten constants. These values are listed in Table 1. All the enzyme electrodes were prepared by following the galvanostatic conditions described in the experimental section. The charge, i.e., the product of reducing current and reducing time, needed for the platinization is also listed in Table 1. The relation between the peak current for hydrogen adsorption wave and the response to 1 mM glucose was compared for every enzyme electrode. One can understand that the electrode response to 1 mM glucose is related to the porosity of the platinized electrode where the enzyme molecules are immobilized. The relation was more clearly investigated by using three platinum electrodes of the same diameter (200 μm). Figure 7 shows the relation between the sensor response to 1 mM glucose and the total charge required for platinization.

The coefficients of variation for glucose analysis are also shown in Table 1. Here micro-enzyme electrodes prepared by using four different diameter electrodes were employed to evaluate the precision of the micro-enzyme sensors. The sensor response to 1 mM glucose was repeated studied. A micro-enzyme electrode prepared by greater reducing current for platinization showed greater response to 1 mM glucose. However,

Table 1. Relation between the Fabrication Conditions and the Characteristics of Micro-Enzyme Electrode

Fabrication condition		Characteristics of micro-enzyme electrode			
Electrode diameter	Peak height of H_2 adsorption wave/μA	Mean response to 1 mM glucose/nA	Detectable range	K_m	CV(N)
μm			M	mM	%
10	7	5.0	10^{-5}—5×10^{-2}	60	2.5(10)
50	20	29.2	5×10^{-7}— 10^{-2}	45	1.5(20)
200	65	166	5×10^{-7}— 10^{-2}	35	0.8(20)
500	105	278	5×10^{-7}— 10^{-2}	30	0.6(20)

The deposition currents for the platinization were −0.5 μA, −3 μA, −15 μA, and −60 μA for 10 μm, 50 μm, 200 μm, and 500 μm platinum electrode, respectively. And the deposition time was 5 min in every electrode.

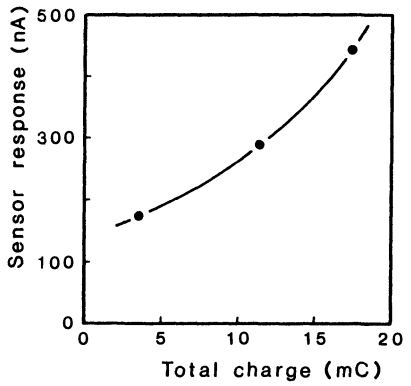

Fig. 7. The relation between the sensor response to 1 mM glucose and total charge required for the platinization. The diameter of the enzyme sensors is 200 μm, and the total current is shown in Coulomb.

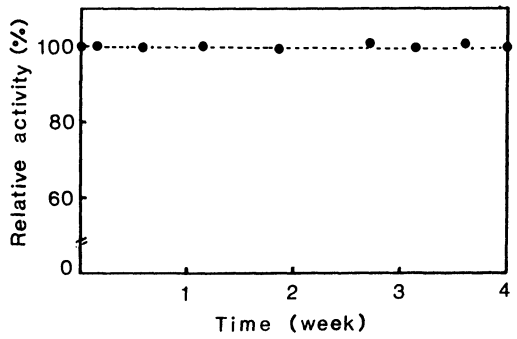

Fig. 8. Time stability of a typical micro-enzyme electrode (diameter=50 μm). The response of the micro-enzyme electrode (diameter=50 μm) was studied by the two injections of 1 mM glucose.

the microelectrodes which have greater output showed greater residual current. The mean response in Table 1 corresponds to the mean current increase when the same glucose sample (1 mM) was repeatedly determined, and the number of repeated analysis is shown in parenthesis.

Time Stability of Micro-Enzyme Electrode. The stability of the micro-enzyme electrode (diameter: 50 μm) was studied by measuring the sensor response to 1 mM glucose. The measuring conditions were the same as described in the above description. The enzyme electrode was kept in the refrigerator when not in use. The storage buffer was 0.1 M phosphate of pH 6.8. The sensor output on the first day was normalized to 100%.

Figure 8 is the time stability of one of the typical micro-enzyme electrode that was mainly stood in a refrigerator. On the 28th day the sensor output still demonstrated nearly 100% response, of which detailed reason is now being investigated. The time stability for an enzyme electrode that was repeatedly used was also studied. All the electrodes tested showed almost same response to the same glucose samples after six hundred injections.

The time-stability of the micro-enzyme electrode was improved by the crosslinking of the incorporated enzyme molecules by glutaraldehyde. The stability of the albumin membrane-coated enzyme electrode was almost the same as that of the glutaraldehyde-treated one. That fact suggests that the enzyme molecules after crosslinking are effectively retained on the microparticles because of the formation of conglomerate enzyme within the porous transducer matrix. On the other hand, without the glutaraldehyde treatment, the enzyme-incorporated electrode lost its activity gradually. The enzyme electrodes without glutaraldehyde treatment retained their activity of approximately 80% on the 28th day when they were kept in a refrigerator when not in use.

Discussion

The microfabrication technique described here is a unique approach by which method micro-enzyme electrodes are easily prepared in a simplified manner. The miniaturized enzyme electrode can be applied to the fabrication of a micro-biosensing device by which stationary trace glucose can be determined in 2 ms.[22] By micro-enzyme electrode the authors do not necessarily mean that the micro-enzyme electrode behaves as a conventional microvoltammetric electrode where the steady-state current is observed when the electrolysis rate is approximately equal to the rate of diffusion of molecules to the electrode surface.[20] Although the size of the electrode is in the range of a microelectrode (diameter=10 μm), the platinized electrode smaller than 10 μm in diameter is shown to behave as a macroelectrode as is shown in Fig. 2. The high sensitivity of the present enzyme electrodes can be explained by the behaviors as macroelectrodes. The smallest size of the enzyme electrode the authors have ever tried to fabricate is 10 μm, because of the difficulty in the preparation of the platinum wire. However, smaller enzyme electrode can be fabricated by either using a carbon fiber electrode or an electropolished platinum microelectrode on which surfaces platinization can also be easily carried out.

The main reason for the remarkable improvement of the long term stability by the bifunctional aldehyde treatment seems to have been caused by the crosslinking of the enzyme molecules, by which the polymerized enzyme can be retained stably in the micropores of the transducer electrode.

One of the advantages of the present fabrication technique is that the sensor response is easily controllable by selecting the current for platinization. Another advantage is the efficient transduction of biochemical signal to electric signal, since the porous surface provides efficient mass transfer from bulk solution to the electrode itself and the hydrogen peroxide generated within the electrode is efficiently oxidized to give sensor response, since the enzyme is embodied

with the porous matrix electrode. These can be the reasons of the fast response and the high sensitivity of the enzyme electrode.

The authors express their gratitude to Prof. William R. Heineman of the Department of Chemistry, University of Cincinnati, for his review of this manuscript and helpful suggestions throughout the course of this study.

References

1) L. C. Clark and Jr., C. Lyons, *Ann. N. Y. Acad.* **102**, 29 (1962).
2) S. J. Updike and G. P. Hicks, *Nature (London)*, **214**, 986 (1967).
3) M. Aizawa, I. Karube, and S. Suzuki, *Anal. Chim. Acta*, **69**, 431 (1974).
4) M. Nanjo and G. G. Guilbault, *Anal. Chim. Acta*, **73**, 367 (1974).
5) M. Koyama, Y. Sato, M. Aizawa, and S. Suzuki, *Anal. Chim. Acta*, **116**, 307 (1980).
6) M. Aizawa, S. Katoh, and S. Suzuki, *J. Membr. Sci.*, **2**, 125 (1977).
7) M. Aizawa, A. Morioka, S. Suzuki, and Y. Nagamura, *Anal. Biochem.*, **94**, 22 (1979).
8) H. Itagaki, Y. Hakoda, Y. Suzuki, and M. Haga, *Chem. Pharm. Bull.*, **31**, 1283 (1983).
9) Y. Ikariyama, M. Furuki, and M. Aizawa, *Anal. Chem.*, **57**, 496 (1985).
10) M. A. Arnold and G. A. Rechnitz, *Anal. Chem.*, **52**, 1170 (1980).
11) I. Karube, S. Sogabe, T. Matsunaga, and S. Suzuki, *J. Appl. Microbiol. Biotechnol.*, **17**, 216 (1983).
12) S. Kuriyama, M. A. Arnold, and G. A. Rechnitz, *Anal. Chim. Acta*, **131**, 91 (1981).
13) M. A. Arnold and G. A. Rechnitz, *Anal. Chem.*, **53**, 1837 (1981).
14) M. Hikuma, T. Kubo, T. Yasuda, I. Karube, and S. Suzuki, *Biotechnol. Bioeng.*, **21**, 1845 (1979).
15) M. Hikuma, H. Obana, T. Yasuda, I. Karube, and S. Suzuki, *Anal. Chim. Acta*, **116**, 61 (1980).
16) S. Caras and J. Janata, *Anal. Chem.*, **52**, 1935 (1980).
17) Y. Miyahara, T. Moriizumi, and K. Ichimura, *Sensors and Actuators*, **7**, 1 (1985).
18) Y. Hanazato, M. Nakako, and S. Shiono, *IEEE Trans. Electron Devices*, **ED-33**, 47 (1986).
19) J. O. Howell and R. M. Wightman, *Anal. Chem.*, **58**, 2321 (1986).
20) E. W. Kristensen, W. G. Kuhr, and R. M. Wightman, *Anal. Chem.*, **59**,1752 (1987).
21) Y. Ikariyama, S. Yamauchi, T. Yukiashi, and H. Ushioda, *Anal. Lett.*, **20**, 1407 (1987).
22) Y. Ikariyama, N. Shimada, S. Yamauchi, T. Yukiashi, and H. Ushioda, *Anal. Lett.*, **21**, 953 (1988).

 © 1988 The Chemical Society of Japan Bull. Chem. Soc. Jpn., 61, 3531—3537 (1988)

Photochemical Trifluoromethylation of Some Aromatic and Heteroaromatic Compounds with Trifluoromethyl Bromide

Takeo AKIYAMA,* Kohji KATO, Masatsugu KAJITANI, Yoshio SAKAGUCHI,† Junko NAKAMURA,† Hisaharu HAYASHI,† and Akira SUGIMORI

Department of Chemistry, Faculty of Science and Technology, Sophia University, Kioi-cho 7-1, Chiyoda-ku, Tokyo 102
†The Institute of Physical and Chemical Research, Hirosawa 2-1, Wako-shi, Saitama 351

(Received May 11, 1987)

The photochemical introduction of trifluoromethyl group with CF_3Br in aromatic and heteroaromatic rings was investigated for 9 compounds. Naphthalene, anthracene, anisole, *N*,*N*-dimethylaniline, ferrocene, benzo[*b*]thiophene, isoquinoline, and *N*-methylpyrrole gave trifluoromethylated products in 6.5—100% yields. In one step from uracil, a pharmacologically important 5-trifluoromethyluracil can be synthesized by this method in 11% yield. Based on the mechanistic study carried out for the naphthalene-CF_3Br-CH_3CN system, the reaction is found to proceed via the electron transfer from an excited singlet state of naphthalene to CF_3Br.

The introduction of trifluoromethyl group into aromatic and heteroaromatic compounds has been of recent interest,[1,2] because the strong electron-withdrawing ability and the high lipophilicity of the trifluoromethyl group will enhance the biological activity of the molecule. Several synthetic methods[3-16] including coupling reactions in the presence[3-8] and in the absence[9] of metal catalysts and several photochemical reactions[10-16] have been reported.

The photochemical trifluoromethylation hitherto reported requires expensive CF_3I[11,12,15,16] or hazardous[13,14] reagents so that a simple trifluoromethylation with a cheap, less hazardous and easy to handle reagent is needed. In view of this interest, we have undertaken a direct trifluoromethylation of aromatic and heteroaromatic compounds by a photochemical method using trifluoromethyl bromide, a cheap and easily available reagent.

We wish to report here the results of a one step photochemical trifluoromethylation of some aromatic and heteroaromatic compounds, together with the results of a mechanistic study of the excited states involved in the phototrifluoromethylation of these compounds.

Experimental

Materials. Bromotrifluoromethane was used as received from Japan Halon Co. Naphthalene (Wako Junyaku Co., G.R.) was recrystallized from ethanol. Anthracene (BDH Chemical Co., microanalytical reagent), *N*-methylpyrrole (Tokyo Kasei Co., G.R.), benzo[*b*]thiophene (Tokyo Kasei Co., G.R.), and ferrocene (Tokyo Kasei Co., G.R.) were used as purchased. Anisole (Wako Junyaku Co., G.R.), *N*,*N*-dimethylaniline (Junsei Yakuhin Co., G.R.), isoquinoline (Wako Junyaku Co., G.R.) were distilled under reduced pressure just before use. Uracil and 5-trifluoromethyluracil were supplied from Japan Halon Co. and were used as received. Acetonitrile (Wako Junyaku Co., G.R.) was dried over calcium hydride (Wako Junyaku Co., G.R.) and distilled twice in the presence of a small amount of phosphorus pentaoxide (Wako Junyaku Co., G.R.). Then the distillate was redistilled just before use with a 1 m Widmer distilling column in the presence of potassium carbonate (Junsei Yakuhin Co., G.R.). This distillate was used for photoreactions and measurements.

Measurements. IR-spectra were obtained by use of a Hitachi 260-50 grating spectrophotometer. ^1H NMR spectra were taken on a Hitachi R-22 (90 MHz) spectrometer or a JEOL-FX-200 (200 MHz) spectrometer. ^{19}F NMR spectra were obtained by using a Varian XL-100A spectrometer. GC-MS spectra were obtained by using JEOL JMA D-300 GC-MS spectrometer. Quantitative gas chromatography was performed on a Shimadzu GC-6A gas chromatograph, and preparative gas chromatography was done on a Shimadzu GC-5A gas chromatograph. UV-spectra were obtained on a Hitachi 228 spectrophotometer.

For the measurement of the fluorescence spectra, two sample solutions were prepared: one is the hexane solution of naphthalene (4.0×10^{-4} mol dm^{-3} deaerated with Ar by bubbling for 10 min), and the other is the similarly prepared hexane solution (4.0×10^{-3} mol dm^{-3}, deaerated with Ar) into which CF_3Br was bubbled for 10 min. The fluorescence spectra were recorded for these two solutions (excitation: 310 nm; recording wavelength range: 315—440 nm) on a Hitachi 650-60 fluorescence spectrophotometer.

Continuous Irradiation. An acetonitrile solution (170 cm^3) of aromatic or heteroaromatic compound (0.4—6.1 mmol) was irradiated in an immersion type photoreactor with a high pressure mercury lamp (a 100 W lamp of Taika Kogyo Co., with a pyrex jacket for water cooling) for 6 h under bubbling of CF_3Br (equipped with a cooling trap using Dry Ice-acetone at the outlet of the photoreactor).

In the cases of *N*-methylpyrrole and uracil the acetonitrile solutions of the substrates in a quartz tube (50 cm^3, equipped with a septum to introduce CF_3Br) was irradiated from outside of the tube with a low pressure mercury lamp (Riko-sha, UVL-160LA, 160 W) for 3 h.

Work-up Procedure. After the irradiation, water (ca. 300 cm^3) was added to the reaction mixture and the products were extracted with diethyl ether. The etherial solution was washed well with water to remove acetonitrile, then ether was removed under reduced pressure. The residual solid or liquid was dissolved in a small amount of diethyl ether and the etherial solution was submitted to preparative gas chromatography (for the photoproducts from naphthalene, 1-bromonaphthalene, anthracene, anisole, *N*-methylpyrrole, benzo[*b*]thiophene, and isoquinoline), or to column chromatography (for the photoproducts from ferrocene and *N*,*N*-dimethylaniline), or to thin-layer chromatography (for the photoproducts from uracil).

Isolation of the Products. Except for the photoproducts from uracil, the isolation of the trifluoromethylated products were all done by means of gas chromatography using a Shimadzu GC-5A (column, PEG-20M, 20%, 2 m, temp, 190 °C, for the photoproducts from naphthalene; PEG-20M, 5%, 2 m, temp, 230 °C, for the photoproducts from anthracene; PEG-20M, 20%, 2 m, temp, 130 °C, for the photoproducts from anisole; PEG-20M, 5%, 2 m, temp, 120 °C, for the photoproducts from *N,N*-dimethylaniline; OV-1, 5%, 2 m, temp, 160 °C, for the photoproducts from ferrocene; PEG-20M, 20%, 2 m, temp, 80 °C, for the photoproducts from *N*-methylpyrrole; PEG-20M, 20%, 2 m, temp, 190 °C, for the photoproducts from isoquinoline; and PEG-20M, 20%, 2 m, temp, 160 °C, for the photoproducts from benzo[*b*]thiophene). In the case of uracil the photoproduct was isolated by means of TLC (Merck, RP-18 F_{254}) and the quantitative analysis was done by using HPLC (Hitachi 655 liquid chromatograph, column: RP-18, solvent, CH_3CN-H_2O=3:7; monitoring wavelength, 254 nm; pressure, 3.5 kg cm^2) with 4-cyanopyridine as an internal standard.

Identification of the Photoproducts. Trifluoromethylnaphthalenes: 1- and 2-Trifluoromethylnaphthalene were obtained as a mixture (colorless oil, 153.5 mg, 0.78 mmol). ^{19}F NMR spectra of the mixture show one singlet ($CDCl_3$/$CFCl_3$, ϕ=−62.64) and one doublet peak ($CDCl_3$/$CFCl_3$, ϕ=−60.19, $J_{F\text{-}H}$=2 Hz). The latter peak is identical with that observed for 1-trifluoromethylnaphthalene by Matsui[7] (ϕ=−60.40, $J_{F\text{-}H^8}$=2 Hz). The chemical shifts of the two peaks were in nearly the same region as the reported ones[5] (ϕ=−60.6 for 2-CF_3, and −58.5 for 1-CF_3). The isomer ratio, 1-CF_3: 2-CF_3, calculated based on the peak area of ^{19}F NMR spectra was 78:22. Found: *m/z* 196.0492.

Trifluoromethylanthracenes: 9-, 1-, and 2-Trifluoromethylanthracene were obtained as a mixture (pale yellow oil, 19.6 mg, 0.08 mmol): ^{1}H NMR (200 MHz, $CDCl_3$) δ=7.45 (m, 4H, H^2, H^7, H^3, and H^6), 8.01 (d, J=8.0 Hz, 2H, H^5 and H^4), 8.51 (d, J=10 Hz, 2H, H^1 and H^8) and 8.59 (s, 1H, H^{10}); ^{19}F NMR ($CDCl_3$/$CFCl_3$) ϕ=−48.91 (t, $J_{F\text{-}H}$=1.5 Hz, 9-CF_3), −60.73 (d, $J_{F\text{-}H}$=2.0 Hz, 1-CF_3), and −63.20 (s, 2-CF_3). The ratio of the isomer, 9-CF_3: 1-CF_3: 2-CF_3, calculated based on the peak area of ^{19}F NMR spectra is 85:12:3. GC-MS (PEG-20M, 5%, 1 m, 200 °C, 70 eV) (rel intensity) 246 (M^+, 100), 227 ($(M-F)^+$, 7.4), 196 ($(M-CF_2)^+$, 21.4), and 177 ($(M-CF_3)^+$, 1.8). Found: *m/z* 246.0656. Calcd for $C_{15}H_9F_3$: M, 246.0657. Based on the GC-MS data a small amount of bis(trifluoromethyl)anthracene was also found.

Trifluoromethylanisole: 2-Trifluoromethylanisole was obtained as a colorless liquid substance (70 mg, 0.40 mmol): IR (neat) 3080, 2960, 2940, and 2840 cm^{-1} ($\nu_{C\text{-}H}$), 1320, 1170, and 1120 cm^{-1} ($\nu_{C\text{-}F}$); 1060 and 1040 ($\nu_{C\text{-}O\text{-}C}$), and 808, 760, and 740 cm^{-1} (out of plane C-H stretching); ^{1}H NMR (90 MHz, $CDCl_3$) δ=3.89 (s, 3H, -OCH_3), 6.96—7.03 (m, 2H, H^3 and H^5), and 7.57 (m, 2H, H^4 and H^6); GC-MS (PEG-20M, 20%, 1 m, 110 °C, 70 eV) (*m/z*, rel intensity) 176 (M^+, 100), 157 ($(M-F)^+$, 4.4), 145 ($(M-OCH_3)^+$, 17.0), 126 ($(M-CF_2)^+$, 5.6), and 107 ($(M-CF_3)^+$, 3.6). Found: *m/z* 176.0453. Calcd for $C_8H_7OF_3$: M, 176.0448.

3-Trifluoromethylanisole was obtained as a colorless liquid substance (27.5 mg, 0.156 mmol): IR (neat) 3080, 3020, 2970, and 2850 cm^{-1} ($\nu_{C\text{-}H}$), 1300, 1170, and 1130 cm^{-1} ($\nu_{C\text{-}F}$), 1070 and 1040 cm^{-1} ($\nu_{C\text{-}O\text{-}C}$), 880, 860, and 755 cm^{-1} (out of plane C-H stretching); ^{1}H NMR (90 MHz, $CDCl_3$) δ=3.80 (s, 3H, -OCH_3), 7.08—7.43 (m, 4H, H^2, H^4, H^5, and H^6); GC-MS (PEG-20M, 20%, 1 m, 110 °C, 70 eV) (*m/z*, rel intensity) 176 (M^+, 100), 157 ($(M-F)^+$, 8.3), 145 ($(M-OCH_3)^+$, 23.0), 126 ($(M-CF_2)^+$, 4.1), and 107 ($(M-CF_3)^+$, 2.4). Found: *m/z* 176.0452. Calcd for $C_8H_7OF_3$: M, 176.0448.

Trifluoromethyl-*N,N*-dimethylanilines: 2-Trifluoromethyl-*N,N*-dimethylaniline was obtained as a colorless liquid substance (47.6 mg, 0.252 mmol): IR (neat) 3100, 2950, and 2850 cm^{-1} ($\nu_{C\text{-}H}$), 1320, 1180, and 1110 cm^{-1} ($\nu_{C\text{-}F}$), 770 cm^{-1} (out of plane C-H stretching of 1,2-disubstituted benzene); ^{1}H NMR (90 MHz, $CDCl_3$) δ=2.73 (s, 6H, -$N(CH_3)_2$), 7.02—7.79 (m, 4H, H^3, H^4, H^5, and H^6); GC-MS (PEG-20M, 5%, 1 m, 100 °C, 70 eV) (*m/z*, rel intensity) 189 (M^+, 63), 188 ($(M-H)^+$, 100), 170 ($(M-F)^+$, 3.2), 145 ($(M-N(CH_3)_2)^+$, 10.6), 138 ($(M-CF_2)^+$, 3.5), 127 ($(M-N(CH_3)_2-F+H)^+$, 14), 120 ($(M-CF_3)^+$, 2.2), and 95 ($(M-N(CH_3)_2-CF_2)^+$, 3.2). Found: *m/z* 189.0764. Calcd for $C_9H_{10}NF_3$: M, 189.0766.

4-Trifluoromethyl-*N,N*-dimethylaniline was obtained as a white crystalline solid (92.4 mg, 0.489 mmol): mp 69.0—69.4 °C (lit.[18] 70.3—70.8 °C). Found: *m/z* 189.0763.

Bis(4-dimethylaminophenyl)methane was obtained as a white crystalline solid (142 mg, 0.559 mmol): mp 86.5—87 °C (lit.[19] 88.5—89.5 °C). ^{1}H NMR spectra of this compound are identical with the reported spectra.[19]

Trifluoromethylferrocene: This compound was obtained as a yellow liquid substance (115.6 mg, 0.455 mmol): IR (KBr) 3100, 2950, 2930, and 2860 cm^{-1} ($\nu_{C\text{-}H}$), 1310, 1145, and 1120 cm^{-1} ($\nu_{C\text{-}F}$), 1100, 1020, and 1000 cm^{-1} (monosubstituted ferrocene); ^{1}H NMR (90 MHz, $CDCl_3$) δ=4.15 (m, 7H, H_β to -CF_3, and unsubstituted ring 5H), and 4.37 (t, 2H, H_α to -CF_3); GC-MS (PEG-20M, 5%, 1 m, 140 °C, 70 eV) (*m/z*, rel intensity) 254 (M^+, 54), 235 ($(M-F)^+$, 3.6), 189 ($(M-C_5H_5)^+$, 4.8), 140 ($(M-C_5H_4CF_2)^+$, 75), and 121 ($(M-C_5H_4CF_3)^+$, 3.0). Found: *m/z* 254.0001. Calcd for $C_{11}H_9F_3Fe$: M, 254.0005.

2-Trifluoromethyl-*N*-methylpyrrole: The compound was obtained as a colorless oily substance (51 mg, 0.34 mmol). The ^{1}H NMR spectral data of this compound are consistent with those reported by Kobayashi.[12]

2-Trifluoromethylbenzo[*b*]thiophenes: 2-Trifluoromethylbenzo[*b*]thiophene was obtained as a white crystalline solid (18.2 mg, 0.09 mmol): mp 49.2—49.8 °C; IR (KBr) 3080, 2940, and 2870 cm^{-1} ($\nu_{C\text{-}H}$), 1310, 1170, and 1120 cm^{-1} ($\nu_{C\text{-}F}$), 880, 860, 760, and 740 cm^{-1} (out of plane C-H bending); ^{1}H NMR (200 MHz, $CDCl_3$) δ=7.43—7.48 (m, 2H, H^5 and H^6), 7.70 (s, 1H, H^3), and 7.85—7.91 (m, 2H, H^4 and H^7); GC-MS (PEG-20M, 5%, 1 m, 90 °C, 70 eV) (*m/z*, rel intensity) 202 (M^+, 100), 201 ($(M-H)^+$, 7.4), 183 ($(M-F)^+$, 29.2), 152 ($(M-CF_2)^+$, 20.0), and 101 ($(M-S-CF_3)^+$, 7.6). Found: *m/z* 202.0058. Calcd for $C_9H_5SF_3$: M, 202.0063.

3-Trifluoromethylbenzo[*b*]thiophene was obtained as a colorless oil (6 mg, 0.03 mmol): IR (neat) 3120, 3080, 2930, and 2870 cm^{-1} ($\nu_{C\text{-}H}$), 1320, 1170, and 1120 cm^{-1} ($\nu_{C\text{-}F}$), 850, 810, 760 and 740 cm^{-1} (out of plane C-H bending); ^{1}H NMR (200 MHz, $CDCl_3$) δ=7.43—7.49 (m, 2H, H^5 and H^6), 7.87—7.94 (m, 2H, H^4 and H^7), and 7.91 (s, 1H, H^2); GC-MS (PEG-20M, 5%, 1 m, 90 °C, 70 eV) (*m/z*, rel intensity) 202 (M^+, 100), 201 ($(M-H)^+$, 10.4), 183 ($(M-F)^+$, 28.6), 152 ($(M-CF_2)^+$, 17.0), and 101 ($(M-S-CF_3)^+$, 6.4). Found: *m/z* 202.0060. Calcd for $C_9H_5SF_3$: M, 202.0063.

4-Trifluoromethylbenzo[*b*]thiophene was obtained as a colorless oil (17 mg, 0.084 mmol): IR (neat) 3100 and 2940 cm^{-1} ($\nu_{C\text{-}H}$), 1310, 1170, and 1120 cm^{-1} ($\nu_{C\text{-}F}$), 870, 840, 780, and 710 cm^{-1} (out of plane C-H bending); ^{1}H NMR (200 MHz, $CDCl_3$) δ=7.38—7.70 (m, 4H, H^2, H^3, H^5, and H^6), and

8.06 (d, J=8 Hz, 1H, H^7); GC-MS (PEG-20M, 5%, 1 m, 90 °C, 70 eV) (m/z, rel intensity) 202 (M^+, 100), 183 ($(M-F)^+$, 22.4), 152 ($(M-CF_2)^+$, 20.6), 133 ($(M-CF_3)^+$, 3.4), 101 ($(M-S-CF_3)^+$, 7.1), and 89 ($C_6H_4CH^+$, 7.7). Found: m/z 202.0064. Calcd for $C_9H_5SF_3$: M, 202.0063.

7-Trifluoromethylbenzo[b]thiophene was obtained as a colorless oil (34 mg, 0.168 mmol): IR (neat) 3100 and 2940 cm^{-1} (ν_{C-H}), 1310, 1170, and 1120 cm^{-1} (ν_{C-H}), 870, 840, 800, 780, and 710 cm^{-1} (out of plane C-H bendiing); ^1H NMR (200 MHz, $CDCl_3$) δ=7.33—7.67 (m, 4H, H^2, H^3, H^5, and H^6), and 7.94 (d, J=8 Hz, 1H, H^4); GC-MS (PEG-20M, 10%, 2 m, 120 °C, 70 eV) (m/z, rel intensity) 202 (M^+, 100), 183 ($(M-F)^+$, 22.6), 152 ($(M-CF_2)^+$, 15.8), 133 ($(M-CF_3)^+$, 3.4), 101 ($(M-S-CF_3)^+$, 6.1), and 89 ($C_6H_4CH^+$, 6.6). Found: m/z 202.0049. Calcd for $C_9H_5SF_3$: M, 202.0063.

Trifluoromethylisoquinolines: The compounds were obtained by means of repeated preparative gas chromatography.

1-Trifluoromethylisoquinoline was obtained as a colorless liquid substance (3.1 mg, 0.015 mmol): IR (neat) 3040 cm^{-1} (ν_{C-H}), 1310, 1170, and 1120 cm^{-1} (ν_{C-F}), 980, 940, 820, 790, and 740 cm^{-1} (out of plane C-H bending); ^1H NMR (200 MHz, $CDCl_3$) δ=7.58—8.20 (m, 5H, H^4, H^5 H^6 and H^8), and 8.60 (d, J=5.5 Hz, 1H, H^3); GC-MS (PEG-20M, 5%, 1 m, 130 °C, 70 eV) (m/z, rel intensity) 197 (M^+, 100), 196 ($(M-H)^+$, 9.9), 178 ($(M-F)^+$, 11.7), 147 ($(M-CF_2)^+$, 25.4), and 128 ($(M-CF_3)^+$, 7.2). Found: m/z 197.0451. Calcd for $C_{10}H_6NF_3$: M, 197.0452.

4-Trifluoromethylisoquinoline was obtained as a colorless liquid substance (3.4 mg, 0.017 mmol): IR (neat) 3040 cm^{-1} (ν_{C-H}), 1320, 1170, and 1120 cm^{-1} (ν_{C-F}), 980, 930, 900, 820, 780, and 730 cm^{-1} (out of plane C-H bending); GC-MS (PEG-20M, 5%, 1 m, 130 °C, 70 eV) (m/z, rel intensity) 197 (M^+, 100), 196 ($(M-H)^+$, 10.2), 178 ($(M-F)^+$, 12.7), 147 ($(M-CF_2)^+$, 27.1), and 128 ($(M-CF_3)^+$, 23.3). Found: m/z 197.0449. Calcd for $C_{10}H_6NF_3$: M, 197.0452.

5-Trifluoromethylisoquinoline was obtained as a colorless liquid substance (17.4 mg, 0.088 mmol): ^1H NMR (200 MHz, $CDCl_3$) δ=7.39—8.20 (m, 5H, H^3, H^4, H^6, H^7, and H^8), and 8.94 (d, J=3.1 Hz, 1H, H^1). The compound readily converted to an unknown product in air.

8-Trifluoromethylisoquinoline was obtained as a colorless liquid substance (4.5 mg, 0.023 mmol): IR (neat) 3050 cm^{-1} (ν_{C-H}), 1310, 1180, and 1120 cm^{-1} (ν_{C-F}), 980, 940, 830, 810, 790, and 740 cm^{-1} (out of plane C-H bending); ^1H NMR (200 MHz, $CDCl_3$) δ=7.38—8.19 (m, 5H, H^3 H^4, H^5, H^6, and H^7), and 8.93 (dd, $J_{H^1H^3}$=4.3 Hz, J_{F-H^1}=1.5 Hz, 1H, H^1); GC-MS (PEG-20M, 5%, 1 m, 130 °C, 70 eV) (m/z, rel intensity) 197 (M^+, 100), 196 ($(M-H)^+$, 5.1), 178 ($(M-F)^+$, 11.7), 147 ($(M-CF_2)^+$, 17.5), and 128 ($(M-CF_3)^+$, 33.0). Found: m/z 197.0452. Calcd for $C_{10}H_6NF_3$: M, 197.0452.

5-Trifluoromethyluracil: The compound was isolated from the second fraction of TLC (Merck, RP-18 F_{254}, developing solvent: CH_3CN-H_2O=4:6). ^1H NMR spectra ($CDCl_3$, δ=7.78, s, H^6) and mass spectra (70 eV, m/z 180 (M^+)) are identical with those of the authentic sample.

Flash Photolysis. An acetonitrile solution of naphthalene (1.0×10^{-3} mol dm^{-3}, 5 cm^3) in a quartz cell (1 cm×1 cm, equipped with a solvent reservoir) was degassed by repeated (4 times) freeze-pump-thaw cycles, and the glass neck was sealed. The sample solution containing CF_3Br was prepared by introduction of CF_3Br into the degassed solution prepared as described above using needle and septum. These sample solutions were irradiated with a pulse of 266 nm light from a Nd-YAG laser and the transient absorption was monitored in the wavelength region of 360—670 nm.

Calculations by means of CNDO/2. Th CNDO/2 calculations of naphthalene, benzo[b]thiophene, and isoquinoline were carried out at Tokyo University Computer Center according to the Tokyo University Computer Center Library Program YT/TC/CB03 prepared by J.A. Pople, D.L. Beveridge, and P.A. Dobosh (Q.C.P.E. 141) arranged by H. Kihara, T. Fujikawa, and T. Aoyama.

Results and Discussion

Photo-Trifluoromethylation of Aromatic Compounds. The acetonitrile solution of aromatic compound was irradiated with a high-pressure mercury lamp for 1.5—6 h under bubbling of CF_3Br. Naphthalene, anthracene, anisole, N,N-dimethylaniline, and ferrocene gave trifluoromethylated products in 6.5—100% yields (Table 1).

The photo-trifluoromethylation of naphthalene occurs quantitatively and the ratio of the 1- and 2-trifluoromethylnaphthalene is 78:22.

In the case of anisole, 2- and 3-trifluoromethylanisole were obtained in 20 and 8% yields, respectively. Although 4-trifluoromethylanisole was detected by

Table 1. Photo-Trifluoromethylation of Some Aromatic Compounds with CF_3Br

Aromatic compound		Solvent[b]	Irrad. time	Conversion	Substituent introduced	Yield[c]
10^{-3} mol			h	%		%
Naphthalene	(6.0)	CH_3CN	6	13	1-CF_3	78[d]
					2-CF_3	22[d]
Anthracene	(0.6)	CH_3CN	1.5	16	9-CF_3	70[d]
					1-CF_3	10[d]
					2-CF_3	3[d]
Anisole	(6.1)	CH_3CN[a]	6	32	2-CF_3	20
					3-CF_3	8
N,N-Dimethylaniline	(6.1)	CH_3CN[a]	1.5	77	2-CF_3	5.5
					4-CF_3	11
					(p-Me_2N-C_6H_4)$_2$-CH_2	12
Ferrocene	(5.4)	CH_3CN	6	19	1-CF_3	43

a) Sodium acetate (2.4 mmol) was added. b) 170 cm^3. c) Yields are calculated based on the consumed aromatic compounds. d) Calculated based on the peak area of ^{19}F NMR spectra.

Table 2. Photo-Trifluoromethylation of Some Heteroaromatic Compounds with CF_3Br

Heteroaromatic compound		Solvent[b]	Irrad. time	Conversion	Substituent introduced	Yield[c]
10^{-3} mol			h	%		%
N-Methylpyrrole	(6.0)	CH_3CN[a]	3	85	2-CF_3	6.5
Benzo[*b*]thiophene	(6.0)	CH_3CN	6	20	2-CF_3	7.5
					3-CF_3	2.5
					4-CF_3	7.0
					7-CF_3	14
Isoquinoline	(6.0)	CH_3CN	6	18	1-CF_3	1.5
					4-CF_3	1.6
					5-CF_3	8.2
					8-CF_3	2.1
Uracil	(0.1)	CH_3CN	6	56	5-CF_3	11

a) Sodium acetate (2.4 mmol) was added. b) 170 cm^3. c) Yields are calculate based on the consumed starting material.

GC-MS analysis, the isolation of this isomer was not possible because of the contamination of the recovered anisole.

The photo-trifluoromethylation of *N,N*-dimethylaniline afforded 2- and 4-trifluoromethyl-*N,N*-dimethylaniline in 5.5 and 11% yields, respectively. Together with the trifluoromethylated products bis(4-dimethylaminophenyl)methane[19] was obtained in 12% yield.

The photo-trifluoromethylation of ferrocene gave selectively 1-trifluoromethylferrocene in 43% yield.

Photo-Trifluoromethylation of Heteroaromatic Compounds. In Table 2 are shown the results of the photo-trifluoromethylation of three heteroaromatic compounds and uracil.

In the case of *N*-methylpyrrole, only 2-trifluoromethyl-*N*-methylpyrrole was obtained in 6.5% yield.

In the case of benzo[*b*]thiophene and isoquinoline, the photo-trifluoromethylation occurs both in the heteroaromatic ring and benzene ring. The site reactivity of these compounds will be discussed later.

5-Fluorouracil has attracted much attention because of its significant tumor-inhibition activity and one-step fluorination of uracil has been developed.[1] However, little has been investigated about the biological activities of 5-trifluoromethyluracil, which is similar to 5-fluorouracil, because of difficulties of preparation of the compound.[20] Recently a convenient synthetic method of 5-trifluoromethyluracil has been reported by Fuchikami.[21] The convenient one-step trifluoromethylation of uracil might be possible if this photochemical trifluoromethylation can be applied for uracil. The photo-trifluoromethylation of uracil gave 5-trifluoromethyluracil in 11% yield.

Mechanistic Study on the Photo-Trifluoromethylation of Naphthalene. The excited state involved in the photo-trifluoromethylation of the aromatic compounds was examined using the naphthalene-CF_3Br-CH_3CN system, since the emission and T-T absorption spectra of naphthalene have been well-investigated.[22]

On the basis of the fact that the photoreaction proceeds under the irradiation with the light of wavelength longer than 300 nm, which is not absorbed by CF_3Br, the excited states which initiate the reaction can be considered as follows: (1) an excited state of a CT complex which is formed between naphthalene and CF_3Br in the ground state, and (2) the excited singlet state or the excited triplet state of naphthalene.

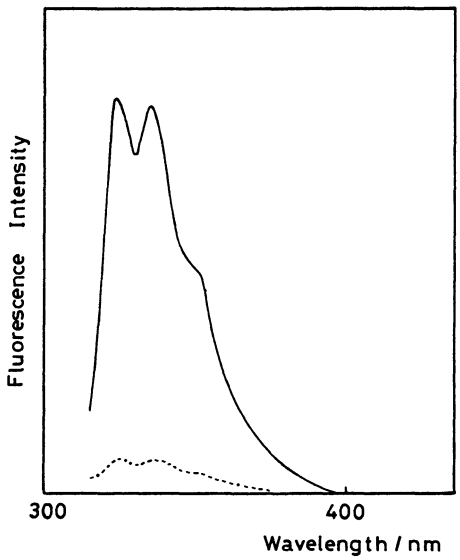

Fig. 1. Fluorescence spectra of naphthalene (4×10^{-4} mol dm^{-3} in CH_3CN) (excitation: 310 nm). (——): in the absence of CF_3Br, (------): in the presence of CF_3Br.

The first possibility can be excluded on the basis of the following results: the careful examination of the independently measured UV-spectra of naphthalene and CF_3Br in acetonitrile and those of the mixture of them in the same solvent shows no indication of the formation of CT complex between the two components in the ground state. In the cases of other aromatic and heteroaromatic compounds used in this photo-trifluoromethylation, except for uracil and *N*-methylpyrrole, similar results were obtained.

One of the second possibilities, in which the excited triplet state is involved, can also be excluded, based on

the following results: (1) the fluorescence intensity of naphthalene is strongly lowered by addition of CF_3Br (Fig. 1), (2) no increment of T-T absorption intensity was observed in the system containing CF_3Br (Fig. 2, —●—) compared to the system without CF_3Br (Fig. 2, ···●···), (3) the energy required for cleaving C-Br bond of CF_3Br (289 kJ mol^{-1})[23] is higher than the triplet energy of naphthalene (E_T=254 kJ mol^{-1}).[24]

In order to obtain further evidence for the excited states and reactive intermediates involved in this reaction, flash photolysis experiments (with 266 nm light from Nd-YAG laser) were carried out for the naphthalene-CF_3Br system.

The transient absorption spectra at 50—100 ns after a flash and their assignments[25d] are shown in Fig. 2. The lifetimes of fluorescence and $S_n \leftarrow S_1$ absorption are also shown in Table 3. The results obtained from flash photolysis experiments are as follows: (1) in the presence of CF_3Br, the lifetimes of fluorescence are

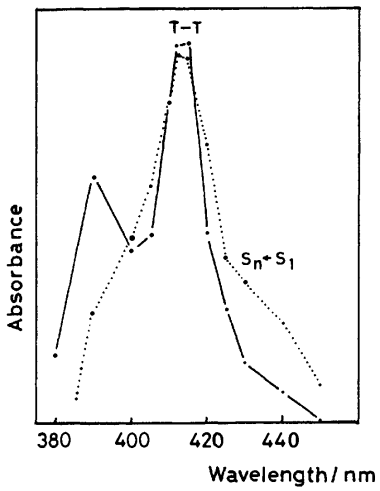

Fig. 2. Transient absorption spectra of naphthalene (1×10^{-3} mol dm^{-3} in CH_3CN). Irradiation: 266 nm light from Nd-YAG laser. (····●····): in the absence of CF_3Br, (—●—): in the presence of CF_3Br. 405—420 nm: T-T absorption; 420—450 nm: $S_n \leftarrow S_1$ absorption.[25d]

agreed with those of $S_n \leftarrow S_1$ absorption, (2) no new absorption which rises with the same rate as that of fluorescence decay was observed under this flash photolysis conditions, and (3) the intensity of T-T absorption was unchanged when CF_3Br was introduced and the T-T absorption decays with a second order rate constant (T-T annihilation: $k/\varepsilon l=(1.0\pm0.1)\times10^{-5}$ s^{-1}) both in the presence and in the absence of CF_3Br.

These results indicate that excited singlet state of naphthalene initiates the reaction. No new absorption which can be ascribed to an exciplex of naphthalene and CF_3Br, a cation radical of naphthalene,[25a-c] or to the CF_3 adduct to naphthalene formed by the addition of $\cdot CF_3$ to the cation radical of naphthalene was observed. These facts indicate that the process between the interaction of the singlet state of naphthalene with the ground state of CF_3Br and the product formation are so rapid that transient spectra of intermediates are not observed under our experimental conditions. However, an electron-transfer process from the excited singlet state of naphthalene to CF_3Br can be postulated based on the approximate oxidation potential of the excited singlet state of naphthalene (−2.45 V vs. SCE)[26] and the reduction potential of CF_3Br (−0.92 V vs. SCE) estimated from the reported values of CF_2BrCF_2Br,[27] since this process is an exothermic one from an energetic point of view ($\Delta G_{et}=E^{ox}(D^+/D)-E^{red}(A/A^-)-E_{0\text{-}0}-C<0$).[28]

As the oxidation potentials of excited singlet state of anthracene,[26] anisole,[26] isoquinoline,[27] and aniline[26] are all lower than −2.0 V (vs. SCE), the similar energetic relations can be considered for these compounds. On the basis of the results described above, the most probable reaction pathway for the photo-trifluoromethylation of naphthalene can be considered as illustrated in Scheme 1.

Site Reactivities of Naphthalene, Benzo[*b*]thiophene, and Isoquinoline. As discussed in the reaction mechanism, the photo-trifluoromethylation of naphthalene proceeds via the electron transfer from the excited singlet state of naphthalene to the ground state-CF_3Br to give a cation radical of substrate and

Table 3. The Lifetimes of Fluorescence and $S_n \leftarrow S_1$ Absorption of Naphthalene in the Absence and in the Presence of CF_3Br in Acetonitrile Solutions[a]

[Naphthalene]	Fluorescence		Absorption		Atmosphere
	Wavelength	Lifetime	Wavelength	Lifetime	
10^{-4} mol dm^{-3}	nm	ns	nm	ns	
5	330	73.02	—	—	N_2
10	330	67.98	—	—	degasesd
5	330	21.98	—	—	CF_3Br
10	330	20.99	—	—	CF_3Br
5	350	72.11	—	—	N_2
5	350	20.95	—	—	CF_3Br
5	—	—	435 ($S_n \leftarrow S_1$)	61.19	N_2
5	—	—	435 ($S_n \leftarrow S_1$)	25.41	CF_3Br

a) Excitation with 266 nm light from Nd-YAG laser.

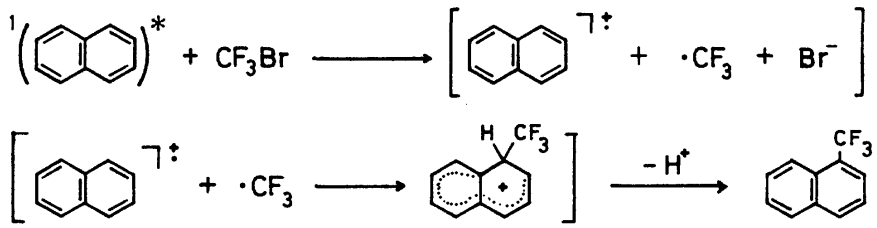

Scheme 1.

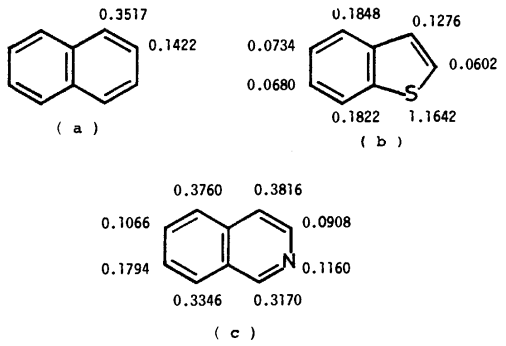

Fig. 3. HOMO Electron densities of naphthalene(a), benzo[*b*]thiophene(b), and isoquinoline(c).

a trifluoromethyl radical. The orientation of the trifluoromethylation should be determined by the succeeding process: the combination of the radical cation and $\cdot CF_3$. Thus, the site reactivities of the trifluoromethylation would be correlated with the densities of unpaired electron in HOMO orbital of the substrate. The HOMO electron densities of naphthalene, benzo[*b*]thiophene, and isoquinoline calculated by CNDO/2 method are shown in Fig. 3. In the case of benzo[*b*]-thiophene, a good correlation between the site selectivity and the electron densities in HOMO was obtained: the 4- and 7-positions which are in the benzene ring and 3-position in the heteroaromatic ring with higher electron densities are trifluoromethylated.

In the case of isoquinoline, a similar tendency is found: The sites where the higher electron density in HOMO orbital is found(1-, 4-, 5-, and 8-positions) are preferentially trifluoromethylated.

In the case of naphthalene, 1-position where the higher electron density in HOMO orbital was found is preferentially trifluoromethylated. These results also support the reaction mechanism in which an electron transfers from the excited singlet state of substrate to CF_3Br and then forms a cation radical of the substrate and a $\cdot CF_3$ radical.

Mechanistic Study on the Photo-Trifluoromethylation of *N*-Methylpyrrole and Uracil. In the cases of *N*-methylpyrrole and uracil, on the other hand, the excitation of the charge transfer complexes between the substrates and CF_3Br initiates the reaction. The UV-spectra of *N*-methylpyrrole and uracil in acetonitrile solutions to which CF_3Br was introduced showed increments of absorptions in the wavelength region of 300—500 nm. These absorptions could not be observed in the spectra measured independently for each of the components. When the photo-trifluoromethylation of *N*-methylpyrrole was carried out using a low pressure mercury lamp (16 W, 3 h) only a trace of trifluoromethylated product was obtained (conversion: 99%) and the decomposition of the substrate occurred, whereas the irradiation of the *N*-methylpyrrole-CF_3Br-CH_3CN system with a high pressure mercury lamp afforded 6.5% of 2-trifluoromethyl-*N*-methylpyrrole (conversion: 85%). In the case of uracil, the similar effect was also observed. In contrast to the irradiation with a high pressure mercury lamp (5-trifluoromethyluracil: 11%, conversion: 56%), the irradiation of the uracil-CF_3Br-CH_3CN system with a low pressure mercury lamp (16 W, 3 h) brought about the lowering of the yield of trifluoromethylated product (6.4%, conversion: 56%) accompanied by the decomposition of uracil. These results indicate that the direct excitation of *N*-methylpyrrole and uracil using 254 nm light brings about decomposition, whereas the excitation of the charge transfer complexes between the substrate and CF_3Br using the light of wavelength longer than 300 nm affords the trifluoromethylated products. The results described above seemed to suggest that in these two cases the reaction proceeds via the mechanism different from that considered for naphthalene. However, the reason for the difference of these mechanisms in the same type of reactions is not clear.

We thank Dr. Masao Onda of Sophia University for the assistance for the CNDO/2 calculation and Professor Sumio Tokita of Saitama University for sending us the geometrical data of benzo[*b*]thiophene and isoquinoline. We also thank Dr. Hiromichi Kono of Japan Halon Co. for supplying CF_3Br, uracil, and 5-trifluoromethyluracil and Dr. Mitsutoshi Tanimoto of Sagami Chemical Research Center for the measurement of ^{19}F NMR.

A part of this work is supported by Grant-in-Aid for Scientific Research No. 60470028 from the Ministry of Education, Science and Culture, to which acknowledgement is made.

References

1) F. A. Smith, *CHEMTECH*, Jul., 422 (1973); R. Filler, *ibid.*, Dec., 752 (1974).

2) T. Umemoto, *Yuki Gosei Kagaku Kyokai Shi*, **41**, 251 (1983).

3) Y. Kobayashi and I. Kumadaki, *Tetrahedron Lett.*, **1969**, 4095.
4) V. C. R. McLoughlin and J. Thrower, *Tetrahedron*, **25**, 5921 (1969).
5) K. Hosokawa and K. Inukai, *Nippon Kagaku Kaishi*, **1976**, 1792.
6) K. Matsui, E. Tobita, M. Ando, and K. Kondo, *Chem. Lett.*, **1981**, 1719.
7) T. Kitazume and N. Ishikawa, *Chem. Lett.*, **1982**, 137.
8) D. J. Burton and D. M. Wiemers, *J. Am. Chem. Soc.*, **107**, 5014 (1985); D. M. Wiemers and D. J. Burton, *J. Am. Chem. Soc.*, **108**, 832 (1986), and references cited therein.
9) A. B. Cowell and C. Tambolski, *J. Fluorine Chem.*, **17**, 345 (1981).
10) E. S. Huyser and E. Bedard, *J. Org. Chem.*, **29**, 1588 (1969).
11) J. M. Birchall, G. P. Irvin, and R. A. Boyson, *J. Chem. Soc., Perkin Trans. 2*, **1975**, 435.
12) Y. Kobayashi, I. Kumadaki, A. Ohsawa, S. Murakami, and T. Nakano, *Chem. Pharm. Bull.*, **26**, 1247 (1978).
13) T. Umemoto and O. Miyano, *Tetrahedron Lett.*, **23**, 3029 (1982).
14) A. Ando and T. Umemoto, *The 49th Annual Meeting of the Japan Chemical Society, Tokyo, Abstr.* 1478 (1984).
15) H. Kimoto, S. Fujii, and L. A. Cohen, *J. Org. Chem.*, **49**, 1060 (1984); H. Kimoto, S. Fujii, and L. A. Cohen, *ibid.*, **47**, 2867 (1982).
16) D. Naumann, B. Wilkes, and K. Kischkewitz, *J. Fluorine Chem.*, **30**, 73 (1985).
17) K. Matsui, private communication.
18) J. D. Roberts, R. L. Webb, and E. A. McElhill, *J. Am. Chem. Soc.*, **72**, 408 (1950).
19) C. Pac and H. Sakurai, *Kogyo Kagaku Zasshi*, **72**, 230 (1969).
A mechanism similar to that described in the reference above can be considered for the formation of bis(4-dimethylaminophenyl)methane:

$$[^1(\text{Ph-NMe}_2)^* + \text{Ph-}\overset{+}{\text{N}}\text{H(Me)}_2] \rightarrow [(\text{Ph-}\overset{+}{\text{N}}\text{Me}_2) + \text{Ph-NH(Me)}_2]_{\text{cage}}$$

$$[\text{Ph-}\overset{+}{\text{N}}\text{Me}_2 + \text{Ph-NH(Me)}_2]_{\text{cage}} \rightarrow \text{PhH} + \text{HN(Me)}_2 + \text{PhN(Me)}\overset{+}{\text{C}}\text{H}_2$$

$$\text{Ph-N(Me)}\overset{+}{\text{C}}\text{H}_2 + \text{Br}^- \rightarrow \text{Ph-N(Me)CH}_2\text{Br}$$

$$\text{Ph-N(Me)CH}_2\text{Br} + \text{H}_3\text{O}^+ \rightarrow \text{Ph-NHMe} + \text{CH}_2\text{O} + \text{HBr}$$

$$2\ \text{Ph-NMe}_2 + \text{CH}_2\text{O} + \text{H}^+ \rightarrow (\text{Me}_2\text{-C}_6\text{H}_4)_2\text{CH}_2 + \overset{+}{\text{H}}_3\text{O}$$

20) C. Heidelberger, D. G. Persons, and D. C. Remy, *J. Med. Chem.*, **7**, 1 (1964).
21) T. Fuchikami and I. Ojima, *Tetrahedron Lett.*, **23**, 4099 (1982); T. Fuchikami and A. Yamanouchi, *Chem. Lett.*, **1984**, 1595; T. Fuchikami, A. Yamanouchi, and I. Ojima, *Synthesis*, **1984**, 766.
22) N. J. Turro, "Modern Molecular Photochemistry," The Benjamin/ Cummings Publishing Co. Inc., California, (1978), pp. 111 and 131.
23) K. W. Egger and A. T. Cooks, *Helv. Chim. Acta*, **56**, 1516 (1973).
24) A. A. Lamola, W. G. Herkstroeter, J. C. Dalton, and G. S. Hammond, *J. Chem. Phys.*, **42**, 1715 (1965).
25) a) T. Shida and S. Iwata, *J. Am. Chem. Soc.*, **95**, 3473 (1982); b) A. Kira, T. Nakamura, and M. Imamura, *J. Phys. Chem.*, **81**, 511 (1977); c) R. Gschwind and E. Haselbach, *Helv. Chim. Acta*, **62**, 941 (1979); d) R. Bonneau, J. Faure, and J. Joussot-Dubien, *Chem. Phys. Lett.*, **2**, 65 (1968).
26) M. Julliard and M. Chanon, *Chem. Rev.*, **83**, 445 (1983).
27) M. D. Hawley, "Reduction of gem-Polyhaloalkanes," in "Encyclopedia of Electrochemistry of the Elements," ed by A. J. Bard and H. Lund, Marcel Dekker, Inc., New York, N. Y. (1980), Vol. 14, pp. 24—41.
28) M. O. Delcourt and M. J. Rossi, *J. Phys. Chem.*, **86**, 3233 (1982).
29) The oxidation potential of the isoquinoline in the excited singlet state was calculated based on the ground state oxidation potential of isoquinoline as Ref. 26.

 © 1988 The Chemical Society of Japan Bull. Chem. Soc. Jpn., 61, 3539—3547 (1988)

Preparation of Mesoverdohemochrome IXα Dimethyl Ester and Mössbauer Spectra of Related Porphyrins

Setsuo SAITO,* Shigeya SUMITA, Kumiko IWAI,† and Hirotoshi SANO†
Faculty of Pharmaceutical Sciences, Josai University, Keyakidai 1-1, Sakado, Saitama 350-02
†Department of Chemistry, Tokyo Metropolitan University, 2-1-1 Fukazawa, Setagaya, Tokyo 158
(Received January 20, 1988)

Mesobiliverdin IXα dimethyl ester (**7**) was obtained by hydrogenation of protobiliverdin IXα dimethyl ester (**8**). Zinc 5-oxamesoporphyrin IX dimethyl ester tetrafluoroborate (**6**) was prepared by the cyclization of **7** with zinc acetate in acetic anhydride followed by a treatment with aqueous sodium tetrafluoroborate. Bis(pyridine) mesoverdohemochrome IXα dimethyl ester (**4**) was obtained by the cyclization of **7** with both iron(II) sulfate and iron(III) chloride in acetic anhydride containing a small amount of pyridine. Bis(tosylmethyl isocyanide) mesoverdohemochrome IXα dimethyl ester (**5**) was prepared by the addition of excess tosylmethyl isocyanide ($TsCH_2NC$) to **4**. Both **4** and **5** reacted with ammonia to give iron(III) 5-azamesoporphyrin IX dimethyl ester (**10**). The Mössbauer spectra of bis(pyridine) verdohemochromes (**4**, **13**, and **14**) showed doublet peaks having parameters of δ=0.41—0.43 mm s^{-1} and ΔE_Q=1.24—1.26 mm s^{-1}, indicating that the oxidation states of the central irons of these complexes are iron(II). Bis($TsCH_2NC$) verdohemochromes (**5**, **15**, and **17**) showed single peaks having parameters of δ=0.21—0.28 mm s^{-1}. Unstable intermediate and stable final bis($TsCH_2NC$) octaethyl verdohemochromes, obtained by the addition of $TsCH_2NC$ to **4**, were compared with the ^{1}H NMR and Mössbauer spectra.

Heme oxygenase catalyzes the oxidative cleavage of the endogenous heme (protoheme IX) to give a blue pigment, biliverdin IXα, in both humans and many animals;[1] the latter is ultimately reduced enzymatically to bilirubin IXα.[2] Verdohemochrome IX (5-oxaprotoporphyriniron(II) complex) was posturated as being an intermediate in the reaction process.[1b,3,4] Verdohemochromes are obtained by a coupled oxidation, termed by Lemberg et al.,[3] of the corresponding hemes with oxygen in the presence of ascorbate in pyridine solution.[5] Because of having no labile vinyl group, mesohemin IX dimethyl ester (**1**) is used as a model compound for the elucidation of the reaction mechanism; a coupled oxidation of **1** with ascorbic acid in aqueous pyridine solution under air gives a mixture of mesoverdohemochromes (α, β, γ, and δ) [bis(pyridine)iron(II) 5-, 10-, 15-, and 20-oxamesoporphyrin complexes]. The mixture gives four mesobiliverdin IX isomers (α, β, γ, and δ)[6] after successive treatments with KOH–MeOH and mineral acid. Many attempts to isolate the four verdohemochrome isomers from the mixture obtained by the coupled oxidation were unsuccessful.

The oxidation state of the central iron of verdohemochromes obtained by a coupled oxidation of the corresponding hemins has been assigned to be iron(II).[7] Jackson et al.[8] obtained mesoverdohemin IXα dimethyl ester (**2**) (iron(III) 15-oxamesoporphyrin IX chloride dimethyl ester) by a reaction of β-hydroxymesohemin IX dimethyl ester (**3**) with oxygen in pyridine. The absorption spectrum of (**2**) was, however, similar to that of a mixture of mesoverdohemochrome IX isomers obtained by a coupled oxidation of mesohemin IX dimethyl ester.[9]

In this paper, we report on the preparation of bis(pyridine)-(**4**), and bis(tosylmethyl isocyanide) mesoverdohemochrome IXα dimethyl ester (**5**). The preparation of zinc 5-oxamesoporphyrin IX dimethyl ester (**6**) is also reported for a comparison of its ^{1}H NMR and FAB mass spectra with those of **4** and **5**. Furthermore, the oxidation state of the central iron of mesoverdohemochrome IXα and related porphyrins will be discussed in more detail in terms of Mössbauer, ^{1}H NMR, and electronic absorption spectroscopies.

Results and Discussion

Preparations of Zinc 5-Oxamesoporphyrin IX Dimethyl Ester (6) and Bis(pyridine)- (4) and Bis(tosylmethyl isocyanide) Mesoverdohemochrome IXα Dimethyl Ester (5). Metal porphyrins **4**, **5**, and **6** were prepared by a ring closure of mesobiliverdin IXα dimethyl ester (**7**) with corresponding metal ions. Previously, mesobiliverdin IXα was obtained by the oxidation of *d*-urobilin IXα under air[10] and by the oxidation of mesobilirubin IXα with iron(III) chloride.[11] In this study, compound **7** was obtained by the hydrogenation of biliverdin IXα dimethyl ester (**8**) according to a method of Muir and Neuberger;[12] this method was used for the preparation of mesoporphyrin IX from protoporphyrin IX.

Hydrogenation of biliverdin IXα dimethyl ester (**8**) gave compound **7**; the ^{1}H NMR spectrum of compound **7** showed the proton signals of two ethyl groups and three *meso*-methine groups (Table 1). The EI mass spectrum of **7** showed a molecular ion peak at *m/z* 614 (base peak). Compound **7** was heated together with $Zn(OAc)_2$ in acetic anhydride at 120 °C under argon, followed by a treatment with an aqueous $NaBF_4$ solution to give zinc 5-oxamesoporphyrin IX dimethyl ester tetrafluoroborate (**6**). The oxamesoporphyrin structure of **6** was supported by the peaks at *m/z* 659 (60.3% of base peak at *m/z* 140), 661 (26.7%), and 663 (24.7%) in FAB mass spectrum, which corre-

Table 1. ^{1}H NMR Data (δ in $CDCl_3$, Multiplicity and J/Hz in Parentheses)

	7	6	4	5
meso-H	6.70, 5.86, 5.82	9.25, 9.00, 8.96	8.98, 8.96, 8.64	9.04, 9.03, 9.02
$\gtrless$-CH_2	2.90(4H, t, 7.3)	3.80(4H)	3.84(4H)	3.80(4H)
$COCH_2$-	2.54(4H, t, 7.3)	2.94(4H)	2.86(4H, t, 6.9)	2.99(4H)
-CH_2CH_3	2.50(2H, q, 7.7)	3.46(2H, q, 7.7)	3.54(2H, q, 7.7)	3.52(2H, q, 7.3)
	2.23(2H, q, 7.7)	3.35(2H, q, 7.7)	3.52(2H, q, 7.7)	3.43(2H, q, 7.3)
-CH_2CH_3	1.20(3H, t, 7.7)	1.62(3H, t, 7.7)	1.61(3H, t, 7.7)	1.66(3H, t, 7.3)
	1.03(3H, t, 7.7)	1.59(3H, t, 7.7)	1.60(3H, t, 7.7)	1.64(3H, t, 7.3)
OMe	3.62, 3.62	3.59, 3.58	3.45, 3.45	3.63, 3.62
CH_3	2.07, 2.06, 2.06, 1.75	3.04, 3.00, 2.99, 2.93	3.45, 3.44, 3.44, 3.38	3.21, 3.09, 3.06, 3.03
Others			6.44(2H, γ-HX2 on pyridines)	7.04(4H, d, 8.1, ortho-H on $TsCH_2NC$)
			5.82(4H, β-HX4 on pyridines)	6.53(4H, d, 8.1, meta-H on $TsCH_2NC$)
			3.22(4H, α-HX4 on pyridines)	2.38(6H, s, CH_3X2 on $TsCH_2NC$)
				2.17(4H, s, CH_2X2 on $TsCH_2NC$)

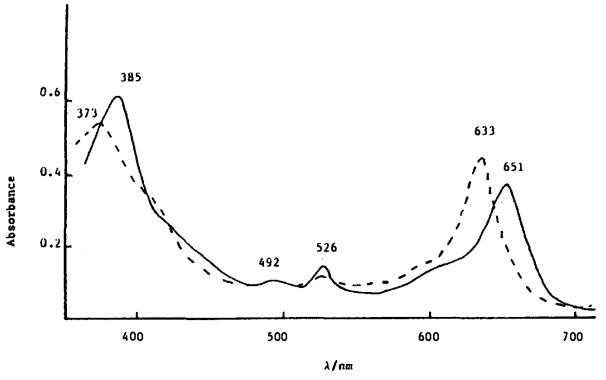

Fig. 1. Absorption spectra (CH_2Cl_2) of the (——) bis(pyridine) (**4**) (1.4×10^{-5} M) and (----) bis($TsCH_2NC$)iron(II) 5-oxamesoporphyrin IX dimethyl ester (**5**).

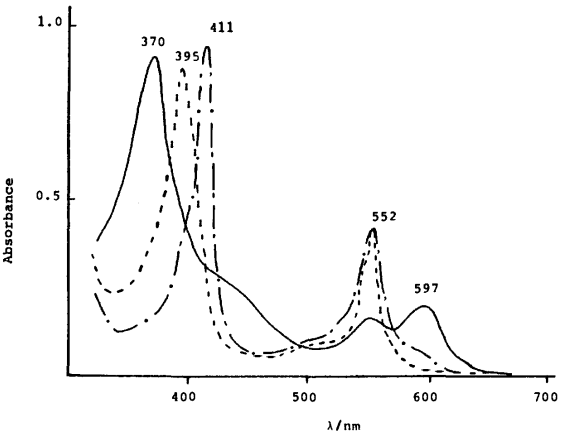

Fig. 2. Absorption spectra (1% pyridine-CH_2Cl_2, v/v) of 5-azamesoporphyrin IX iron(III) (**10**) (——) (2.5×10^{-5} M) and bis(pyridine) (**11**) (----) and bis($TsCH_2NC$)iron(II) 5-azamesoporphyrin IX dimethyl ester (**12**) (-·-·-).

spond to the cations $C_{35}H_{39}N_4O_5{}^{64}Zn^+$, $C_{35}H_{39}N_4O_5{}^{66}Zn^+$, and $C_{35}H_{39}N_4O_5{}^{68}Zn^+$, respectively, and the diamagnetic ring-current shifts of the *meso*-protons (δ 9.25, 9.00, and 8.96) in its ^{1}H NMR spectrum (Table 1). The cyclization of **7** with iron(II) sulfate in acetic anhydride containing a small amount of pyridine at 120 °C under argon, followed by treatment with aqueous $NaBF_4$, gave a green pigment **4**. The FAB mass spectrum of **4** showed a fragment ion peak at m/z 651 (19.2% of the base peak at m/z 140), which corresponds to the unliganded cation $C_{35}H_{39}N_4O_5Fe^+$ of **4**. The absorption spectrum of **4** showed the peaks at 385, 492, 526, and 651 nm (Fig. 1); this spectrum was similar to that of mesoverdohemin IXβ dimethyl ester (**2**) obtained by Jackson et al. These results indicated that the green pigment was mesoverdohemin IXα dimethyl ester (**9**). However, its ^{1}H NMR spectrum was similar to that of the zinc complex **6**, except for the presence of the signals of pyridine ligands; the spectrum showed diamagnetic ring-current shifts of the *meso*-protons (δ 8.98, 8.96, and 8.64) and the proton signals assigned to the pyridine ligands (δ 6.44, γ; 5.82, β; 3.33, α). In analogy with compound **14**,[14] the pyridine complex **4** was easily hydrolyzed to open the tetrapyrrole ring to obtain **7** and was susceptible to oxidation at the *meso*-methine group to give tripyrrins which showed pink spots on TLC (data were not shown). The pyridine ligands of compound **4** easily exchange with tosylmethyl isocyanide ($TsCH_2NC$), which is known to bind to iron(II), but not to iron(III), porophyrins;[13] addition of $TsCH_2NC$ to the solution of **4** resulted in the spectrum of bis($TsCH_2NC$) mesoverdohemochrome IXα dimethyl ester (**5**) with maxima at 373, 492, 526, and 633 nm (Fig. 1). The FAB mass spectrum of **5** showed a base peak at m/z 651 and a fragment ion peak at m/z 1041 (2.7% of the base peak), which correspond to the unliganded cation $C_{35}H_{39}N_4O_5Fe^+$ and to the cation of the bis($TsCH_2$-NC) complex of **5**, respectively. These results suggest that the oxidation state of the central iron of **4** is iron(II), not iron(III). The ^{1}H NMR spectrum of **5** showed the diamagnetic ring-current shifts of *meso*-methine protons (δ 9.04, 9.03,

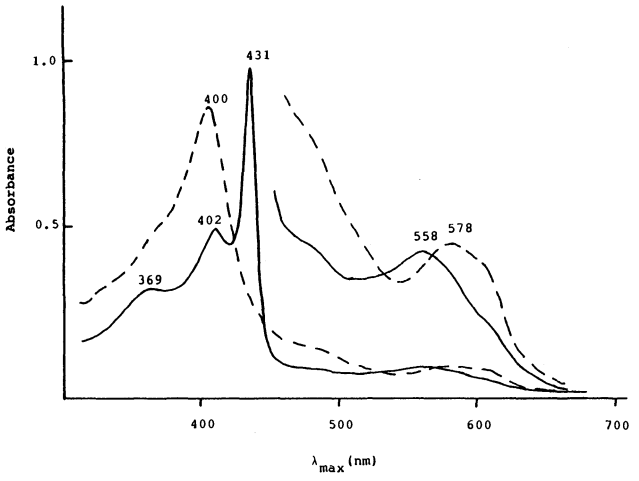

Fig. 3. Absorption spectra (CH_2Cl_2) in the reaction of bis($TsCH_2NC$)iron(II) protoporphyrin IX dimethyl ester: —— (16) (1.8×10^{-5} M); ---- after addition of an excess $K_3[Fe(CN)_6]$ dissolved in 18-crown ether in CH_2Cl_2.

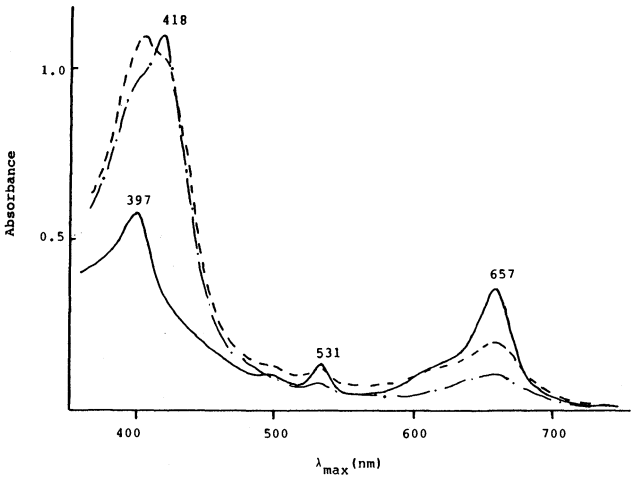

Fig. 4. Absorption spectra (1% pyridine-CH_2Cl_2, v/v) in the reaction of bis(pyridine)iron(II) 5-oxaprotoporphyrin IX dimethyl ester (**14**) with $K_3[Fe(CN)_6]$: —— (**14**) (1.4×10^{-5} M); ---- 1 min after addition of an excess $K_3[Fe(CN)_6]$; -·-·- 10 min after addition of $K_3[Fe(CN)_6]$.

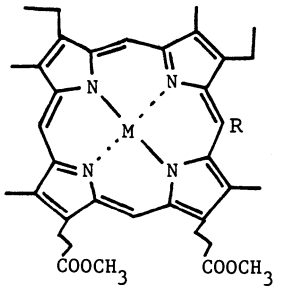

(1) M = Fe(III)·Cl
R = H

(3) M = Fe(III)·Cl
R = OH

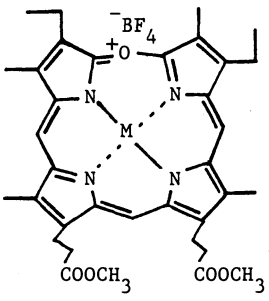

(4) M = Fe(II)•Py_2

(5) M = Fe(II)·$(TsCH_2NC)_2$

(6) M = Zn

(9) M = Fe(III)·Cl

(20) M = 2H

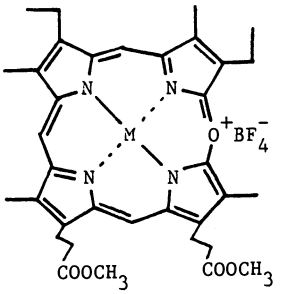

(2) M = Fe(III)·Cl

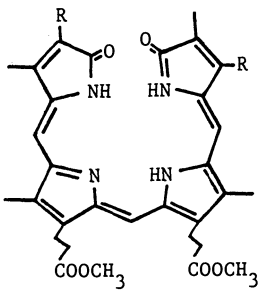

(7) R = $-CH_2CH_3$

(8) R = $-CH{=}CH_2$

Py = pyridine, $TsCH_2NC$ = CH_3-C$_6$H$_4$-SO_2CH_2NC

and 9.02) and of the protons of two $TsCH_2NC$ ligands (Table 1). Both oxaporphyrins **4** and **5** reacted with ammonia to give, after methylation, iron(III) 5-azamesoporphyrin IX dimethyl ester (**10**). The electronic absorption spectrum of compound **10** in 1% pyridine-CH_2Cl_2 showed peaks at 370, 553, and 579 nm (Fig. 2). Addition of sodium dithionite to the solution of **10** resulted in the spectrum of bis(pyridine)iron(II) 5-azamesoporphyrin IX dimethyl ester (**11**) with maxima at 395 and 552 nm. Compound **11** gave, upon an addition of excess $TsCH_2NC$, bis($TsCH_2NC$)iron(II) 5-azamesoporphyrin IX dimethyl ester (**12**), which was identified by FAB mass spectrum data and elemental analysis, as well as the ^1H NMR spectral data (Table 1). Thus, both products obtained by the cyclization of mesobiliverdin IXα dimethyl ester (**7**) with iron(II) sulfate and by a coupled oxidation of mesohemin IX dimethyl ester (**1**) showed the same absorption spectra and had the same oxidation state of the central iron.

Attempts to Obtain Iron(III) 5-Oxaporphyrin Derivatives. We tried to obtain iron(III) 5-oxamesoporphyrin complex by ring closure of mesobiliverdin IXα dimethyl ester (**7**) with iron(III) chloride instead of iron(II) sulfate; compound **7** was reacted with iron(III) chloride in acetic anhydride containing a small amount of pyridine to give a green pigment. The ^1H NMR and absorption spectra of the pigment, however, were the same as those of iron(II) 5-oxamesoporphyrin IX (**4**) obtained by the cyclization of **7** with iron(II) sulfate. Previously, we obtained 5-azamesoporphyrin (**20**) by the treatment of 5-azaprotoporphyrin-iron(III) chloride (**10**) with iron(II) sulfate in acetic acid which contained a small amount of concd HCl; in this reaction, the vinyl groups of **10** was reduced to give **20**. In the cyclization of **7**, iron(III) chloride was dissolved in a small amount of methanol, this mixture then was dissolved in acetic anhydride. Under these conditions, hydrogen might have evolved to reduce iron(III) to iron(II).

It is known that $K_3[Fe(CN)_6]$ oxidizes iron(II) porphyrin to give iron(III) porphyrin. The electronic absorption spectrum of bis($TsCH_2NC$)iron(II) protoporphyrin IX dimethyl ester (**16**) in CH_2Cl_2 showed peaks at 369, 406, 431, 558, and 606 nm (Fig. 3). The addition of $K_3[Fe(CN)_6]$ to the solution of **16** resulted in the spectrum of iron(III) protoporphyrin IX complex with maxima at 404, 578, and 602 nm. The absorption spectrum of bis(pyridine)iron(II) 5-oxaprotoporphyrin IX dimethyl ester (**14**) in pyridine showed peaks at 397, 495, 531, and 657 nm (Fig. 4). The addition of $K_3[Fe(CN)_6]$ to the solution of **14** resulted in a new spectrum with maxima at 418 and 658 nm. The large-scaled reaction of **14** with $K_3[Fe(CN)_6]$ was performed, and the mixture was worked-up according to the procedure for **4**. Most of the products of this reaction were tripyrrin derivatives,[14,15] and the starting material was found as a minor component; however, no iron(III) oxaporphyrin complex. Thus, attempts to obtain iron(III) oxaporphyrin were unsuccessful.

Mössbauer Spectra of Oxa- and Azaporphyriniron Complexes. Since the reactions of **7** with both iron(II) sulfate and iron(III) chloride gave the same product, the oxidation state of the central iron of mesoverdohemochrome IXα was reinvestigated by a comparison of the Mössbauer spectra with those of related porphyrins. Mössbauer parameters, isomer shifts (δ) and quadrupole splittings (ΔE_Q), of normal porphyrins and oxa- and azaporphyrins are listed in Tables 2 and 3, respectively. Figures 5a and 5b show typical Mössbauer spectra of bis(pyridine)iron(II)- (**13**) and bis($TsCH_2NC$)iron(II) octaethyl-5-oxaporphyrin (**17**), respectively. The parameters (δ and ΔE_Q) of **13** and bis(pyridine)iron(II) 5-oxaprotoporphyrin IX dimethyl ester (**14**) were close to those of bis(pyridine)iron(II) protoporphyrin IX ($Fe(pp)py_2$) and bis(pyridine)-iron(II) tetraphenylporphyrin ($Fe(tpp)py_2$). These results, together with the ^1H NMR spectra[9] of **13** and

Table 2. Mössbauer Parameters[16]

i) For low-spin iron(II) porphyrin complexes (S=0)

Compound	Temperature / K	δ[a] / mm s^{-1}	ΔE_Q[b] / mm s^{-1}
$Fe(pp)py_2$[c]	77	0.45	1.21
$Fe(oep)py_2$	85	0.46	1.14
$Fe(tpp)py_2$	77	0.40	1.15
ii) For high-spin iron(III) porphyrin complexes (S=5/2)			
Fe(pp)Cl	4.2	0.35	0.83
Fe(oep)Cl	4.2	0.41	0.93
iii) For diamagnetic carbonyl complexes			
Fe(tpp)(pip)(CO)	115	0.25	0.47
	295	0.18	0.53
Fe(pp)(pip)(CO)	115	0.26	0.57
	295	0.18	0.62

a) δ= isomer shift. b) ΔE_Q=quadrupole splitting. c) Porphyrin and ligand abbreviations: pp, protoporphyrin IX; oep, octaethylporphyrin; tpp, tetraphenylporphyrin; py, pyridine; pip, piperidine.

Table 3. Mössbauer Parameters for Oxo- and Azaporphyriniron Complexes and Protoheme Complex at 78 K

Compound	δ / mm s^{-1}	ΔE_Q / mm s^{-1}
i) Bis(pyridine)iron(II) complexes		
4	0.41	1.26
13	0.43	1.25
14	0.41	1.24
ii) Bis($TsCH_2NC$)iron(II) complexes		
5	0.26	0
17	0.28	0
15	0.21	0
iii) Azaporphyriniron(III) complexes		
18	0.40	0.50
19	0.39	0.49

14, were consistent with the idea that the oxidation state of the central iron of compounds **13** and **14** is low-spin iron(II). The parameters (δ and ΔE_Q) of bis(pyridine)iron(II) 5-oxamesoporphyrin dimethyl ester (**4**) under consideration were also close to those of **13**, **14**, Fe(pp)py_2, and Fe(tpp)py_2. These results indicate that the product obtained by the cyclization of mesobiliverdin IXα dimethyl ester (**7**) with both iron(II) sulfate and iron(III) chloride, are low-spin iron(II) but not high-spin iron(III), 5-oxamesoporphyrin IX complex.

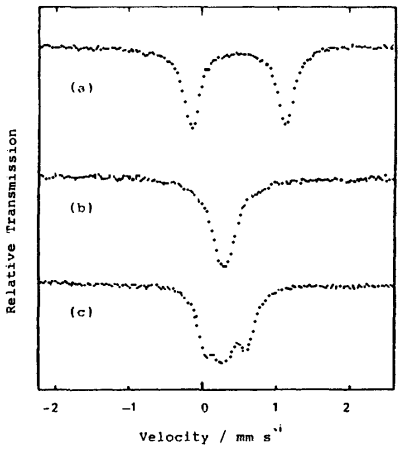

Fig. 5. Mössbauer spectra of bis(pyridine) and bis($TsCH_2NC$)iron(II) octaethyl-5-oxaporphyrins.

The Mössbauer spectra of bis($TsCH_2NC$)iron(II) protoporphyrin IX dimethyl ester (**15**) and bis($TsCH_2NC$)iron(II) 5-oxaporphyrins (**5**, **16**, and **17**) showed a singlet peak having parameters of ΔE_Q=0 mm s^{-1} and δ=0.21—0.28 mm s^{-1} (Table 3). These parameters differed completely from those of the corresponding bis(pyridine) complexes (ΔE_Q=1.24—1.26 mm s^{-1} and δ=0.41—0.43 mm s^{-1}). In general, in going from an Fe(por)L_2 complex (por=porphyrinate dianion, L=amine base) to the corresponding Fe(por)L(CO) derivative, δ decreases by about 0.2 mm s^{-1} and ΔE_Q by about 0.8—1.0 mm s^{-1}. Sams and Tsin[16] explained these phenomena as follows: the quadrupole splitting is small with a decrease in the *d*-electron density on the iron, arising from a strong Fe→CO π back bonding; an increase in the CO→Fe σ bonding decrease δ. Our experiments on the Mössbauer spectra showed that both parameters (δ and ΔE_Q) of the bis($TsCH_2NC$) complexes (**5**, **15**, **17**) decreased compared with those of the corresponding bis(pyridine) complexes (**4**, **14**, and **13**); δ decreases by 0.13—0.22 mm s^{-1} and ΔE_Q by 1.24—1.26 mm s^{-1}. These results seemed to coincide with the explanation for carbon monoxide heme complexes and indicate that bis-

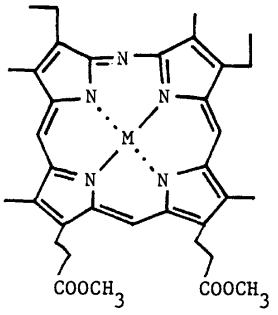

(10) M = Fe(III)·Cl

(11) M = Fe(II)·Py_2

(12) M = Fe(II)·$(TsCH_2NC)_2$

(20) M = 2H

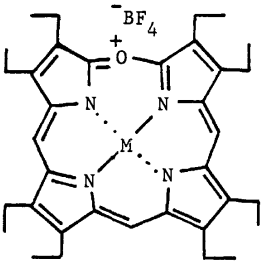

(13) M = Fe(II)·Py_2

(17) M = Fe(II)·$(TsCH_2NC)_2$

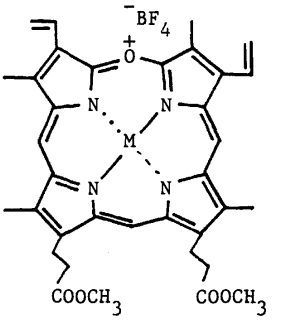

(14) M = Fe(II)·Py_2

(15) M = Fe(II)·$(TsCH_2NC)_2$

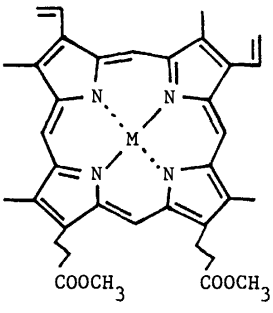

(16) M = Fe(II)·$(TsCH_2NC)_2$

(21) M = Fe(III)·Cl

Table 4. Chemical Shifts of Bis($TsCH_2NC$)iron(II) Octaethyl-5-oxaporphyrins[a)]

Compound	*meso*-H	$-C\underline{H}_2CH_3$	$-CH_2C\underline{H}_3$	CH_3	SO_2CH_2-	Aromatic protons
Mixture (**A**+**B**)	9.15(s) 8.81(s) 9.05(s) 8.89(s)	3.62—3.40	1.76—1.56	2.35(s) 2.33(s)	3.03(s) 3.16(s)	7.04(d, 8) 6.50(d, 8)
17	9.05(s, 2H) 8.89(s, 1H)	3.58—3.44	1.73—1.57	2.33(s, 6H)	3.16(s, 4H)	7.03(d, 8) 6.54(d, 8)

a) δ in $CDCl_3$, multiplicity and J/Hz in parentheses.

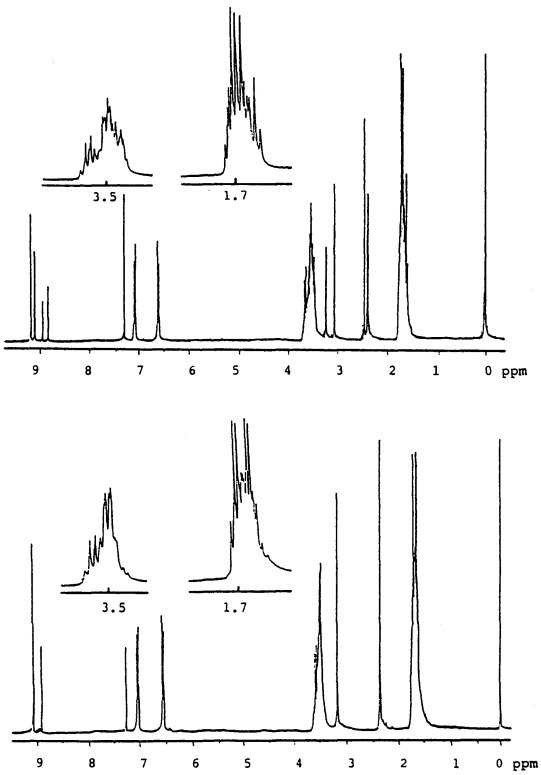

Fig. 6. ^{1}H NMR (270 MHz) spectra of bis($TsCH_2$-NC)iron(II) octaethyl-5-oxaporphyrin complexes.

($TsCH_2NC$) complexes have strong Fe→CN π back bonding and Fe←CN σ bonding.

In the course of an investigation of the ^{1}H NMR spectra of bis($TsCH_2NC$)iron(II) octaethyl-5-oxaporphyrin, we found that two kinds of bis($TsCH_2NC$)iron-(II) complexes existed. Bis(pyridine) complex **13** was reacted with excess $TsCH_2NC$, and the reaction mixture was evaporated at lower temperature (<10 °C) according to the method for **4** to give a blue mixture whose ^{1}H NMR spectrum showed two pairs of *meso*-protons due to compounds A and B (ca. 3 : 1, respectively) (δ 9.15 and 8.81 for compound A, 9.05 and 8.89 for compound B) (Table 4 and Fig. 6). Although compound A was not isolated (because of an easy conversion into compound B), compound B was isolated; in the ^{1}H NMR spectrum, the *meso*-proton at δ 9.15 and 8.81 for compound A disappeared after the mixture (A+B) was heated at 50 °C in benzene, and the intensity of two peaks at δ 9.05 and 8.89 of *meso*-protons of compound B increased. The FAB mass spectra of both products (the mixture of A and B and compound B) showed the similar spectra showing a base peak at m/z 591, which corresponds to the cation of $C_{35}H_{43}FeN_4O^+$. Furthermore, the absorption spectra of the mixture and compound B were not appreciably different (see experiment section). These results suggest that both compounds A and B have the same oxaporphyrin ring structure. Compound B was identified with **17** by FAB mass, ^{1}H NMR, and absorption spectra.

The Mössbauer spectrum of compound **17** showed a single peak (δ=0.28 mm s^{-1}). On the other hand, the spectrum of the mixture (A and B) showed a triplet peak which consisted of a singlet peak (δ=0.28 mm s^{-1}) and a doublet peak (δ=0.31 mm s^{-1} and ΔE_Q=0.55 mm s^{-1}) (Fig. 5c). These results suggest that an unstable intermediate (compound A) is first produced by binding $TsCH_2NC$ to iron(II), then the compound A converts to the stable compound B (**17**). The resonating structures of bis($TsCH_2NC$) complex were thought as follows: $Fe{=}C{-}\ddot{N}{-}R \leftrightarrow Fe{-}\bar{C}{\equiv}\overset{+}{N}{-}R$.[17] The Mössbauer parameters for the stable compound B indicate that the electronic structure of the bonding between iron(II) and isocyanide ligand can be assigned as a double-bonded structure, due to the strong Fe→CN π and Fe←CN σ bonding. On the other hand, the fact that the Mössbauer parameters of the unstable compound A are larger than those of the stable compound B suggests a decrease in the Fe→CN π back donation for compound A. Though the electronic structure of the bonding between iron(II) and isocyanide ligands for the unstable intermediate A has not yet been confirmed, we may presume that $TsCH_2NC$ binds to iron-(II) to initially form an unstable bonding, such as Fe←CN σ or $Fe{\leftarrow}\overset{C}{\underset{N}{|||}}$ bonding. In this case the bonding is formed between the π electrons of CN group and Fe; these unstable structures then convert to the stable double-bonded structure, resulting in the formation of compound B.

The Mössbauer spectra of (octaethyl-5-azaporphyrinato)iron(III) chloride (**18**) and 5-azaprotoporphyrin IX iron(III) chloride dimethyl ester (**19**) were obtained at 78 K. The parameters of the spectra are listed in

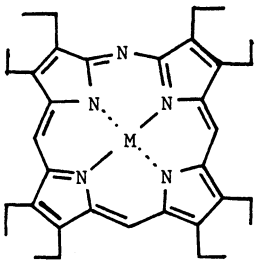

(18) M = Fe(III)·Cl

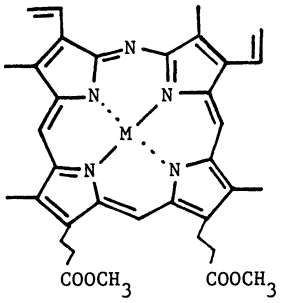

(19) M = Fe(III)·Cl

Table 3-iii. It is generally said that because of a second-order Doppler shift, the isomer shift decreases with an increase in the temperature, while the quadrupole splitting does not appreciably change upon a variation of the temperature in complexes of this type. From this suggestion, our experiments showed that the δ values of **18** and **19** were larger than that of Fe(III)(oep)Cl, and ΔE_Q values of **18** and **19** were smaller than that of Fe(III)(oep)Cl.[18] These effects seem to be due to the substitution of a nitrogen atom for a carbon atom of the porphyrin moiety. These effects will be discussed later in further detail.

Experimental

Materials. Protohemin IX dimethyl ester was prepared by methylation of protohemin IX, purchased from Aldrich. Biliverdin IXα was prepared by oxidation of bilirubin IXα, purchased from Aldrich, with 2,3-dichloro-5,6-dicyano-*p*-benzoquinone. Bis(pyridine) octaethylverdohemochrome was prepared according to a published procedure. Tosylmethyl isocyanide ($TsCH_2NC$), purchased from Aldrich, was recrystallized from ethanol after treatment with active carbon in ethanol. The solvents for analyses were of analytical grade. All other solvents and chemicals were of reagent grade. Analytical thin-layer chromatography (TLC) was performed on DC-Alufolien Kieselgel 60 HF254 (Merck). Wacogel C-200 was used for column chromatograph.

Measurements. Melting points were determined with a Yanoko micro melting-point apparatus. Electronic absorption spectra were recorded with a Hitach U-3200 Spectrophotometer. EI and FAB mass spectra were obtained with a JEOL JMS 300 mass spectrometer. ^1H NMR spectra at 270 MHz of samples in $CDCl_3$ solution containing Me_4Si were recorded with a JEOL JNM-GX 270 FT NMR spectormeter. The Mössbauer spectra were recorded with an Austin Science Associated Mössbauer Spectrometer Controller. A 20 mCi single-line ^{57}Co source in Rh matrix was used. The velocity scale of the spectrometer was calibrated by using the spectra of the metallic iron. Isomer shifts are reported relative to metallic iron at room temperature. By fitting the resonance line-shape to a Lorentzian function, the obtained Mössbauer parameters are within ± 0.002 mm s^{-1} for isomer shifts and ± 0.005 mm s^{-1} for quadrupole splittings. Low-temperature measurements were performed using a CA thermocouple embedded in a copper sample holder with an Air Products and Chemicals Model LT-3-110 Liquid Transter Helitran. The precision of the temperature measurement was with approximately ± 0.1 K over a period of several hours.

Preparation of Mesobiliverdin IXα Dimethyl Ester (7). In 50 ml of anhydrous formic acid, methyl methacrylate (400 mg) was dissolved, and 10% Pd-charcoal (75 mg) was added. The mixture was added with biliverdin IXα dimethyl ester (**8**) (350 mg) and passed with H_2 at 50 °C for 50 min. The mixture was filtered. The filtrate was diluted with H_2O (50 ml) and extracted with CH_2Cl_2 (50 ml×3). The combined organic extracts were washed with H_2O, dried over Na_2SO_4, and filtered. The filtrate was evaporated to give a residue which was subjected to column chromatography (benzene-acetone, gradient up to 10%) to isolate mesobiliverdin IXα dimethyl ester (**7**) (220 mg, 62.5%). EI MS *m/z* (rel intensity) 614 (M^+, 100), 598 (19.5), 583 (23.8), 555 (26.2), 541 (47.6), 527 (17.1), 467 (85.7), 454 (47.6). Found: C, 68.30; H, 6.89; N, 9.03%. Calcd for $C_{35}H_{42}N_4O_6$: C, 68.38; H, 6.89; N, 9.11%.

Zinc 5-Oxamesoporphyrin IX Dimethyl Ester Tetrafluoroborate (6). To a solution of mesobiliverdin IXα dimethyl ester (**7**) (150 mg), a solution of zinc acetate dihydrate (185 mg) in MeOH (5 ml) was added. The mixture was warmed at 60 °C for 30 min and filtered. The filtrate was evaporated and the residue was dissolved in CH_2Cl_2 (5 ml) and acetic anhydride (30 ml). After the mixture had been heated at 120 °C for 30 min under argon, the solvent was removed with a vigorous stream of argon at 140 °C. The resulting residue was chromatographed on silica gel with CH_2Cl_2-MeOH (gradient up to 5%) to give the major green pigment. The pigment was dissolved in CH_2Cl_2, washed with saturated aqueous $NaBF_4$ and water, dried, and evaporated to give a residue, which was subjected to column chromatography to isolate compound **6** (125.2 mg, 68.5%), mp 300 °C. Found: C, 56.03; H, 5.29; N, 7.35%. Calcd for $C_{35}H_{39}N_4O_5ZnBF_4$: C, 56.21; H, 5.26; N, 7.49%. FAB MS *m/z* (rel intensity) 659 (60.3), 661 (26.7), 663 (24.7), 406 (40.0), 252 (38.5), 140 (100).

Cyclization of 7 with Iron(III) Sulfate. To a solution of compound **7** (110 mg) in acetic anhydride (50 ml) and pyridine (5 ml), a solution of iron(II) sulfate heptahydrate (100 mg) in methanol (7 ml) was added under argon. The reaction mixture was heated for 30 min at 120 °C under argon, and the solvent was removed by a vigorous flow of argon at 140 °C to give a residue. The residue was extracted with 2% pyridine-CH_2Cl_2 (50 ml×3) and the combined organic extracts were washed succesively with saturated aqueous $NaBF_4$ and water, dried, and evaporated to give a green residue. The residue was chromatographed on silica gel with CH_2Cl_2 containing 1% pyridine-MeOH (gradient up to 5%) to give bis(pyridine)iron(II) mesoverdohemochrome IXα dimethyl ester (**4**) (94.1 mg, 58.6%). FAB MS *m/z* (rel intensity) 651 (17.8), 252 (56.2), 235 (28.8), 140 (100). Calcd

for $C_{45}H_{49}N_6O_5FeBF_4$: C, 60.28; H, 5.51; N, 9.37%. Found: C, 59.90; H, 5.60; N, 9.22%.

Cyclization of 7 with Iron(III) Chloride. To a solution of **7** (50 mg) in acetic anhydride (50 ml) and pyridine (5 ml), a solution of iron(III) chloride monohydrate (100 mg) in methanol (3 ml) was added. The reaction mixture was treated and worked-up according to the procedure just described above for **4**. The resulting green pigment (36.3 mg, 47.7%) was identified with **4** by TLC and ^{1}H NMR spectroscopy.

Bis($TsCH_2NC$)iron(II) Complex (5). Compound **4** (102 mg) was dissolved together with $TsCH_2NC$ (350 mg) in CH_2Cl_2 (5 ml). The solution was subjected to column chromatography (CH_2Cl_2-MeOH, gradient up to 5%) to give compound **5** (98.4 mg, 76.6%), mp>300 °C (after recrystallization from benzene-peteroleum ether). Found: C, 56.11; H, 5.12; N, 7.15%. Calcd for $C_{53}H_{57}N_6O_9S_2FeBF_4$: C, 56.39; H, 5.09; N, 7.44%. FAB MS *m/z* (rel intensity) 1041 (2.7, M^+-BF_4), 651 (100, $M^+-2\times TsCH_2NC-BF_4$).

Iron(III) 5-Azamesoporphyrin IX Dimethyl Ester (10). a) To a solution of compound **4** (53 mg) in pyridine (15 ml) and concd aqueous ammonia (10 ml) was added. The reaction mixture was stirred overnight at room temperature. The mixture was diluted with water (50 ml) and extracted with CH_2Cl_2 (50 ml×3). The combined organic extracts were washed with saturated aqueous NaCl and water, dried, and evaporated to give a residue. The residue was dissolved in 5% H_2SO_4-MeOH (100 ml) and allowed to stand overnight at room temperature. The reaction mixture was extracted with CH_2Cl_2 (100 ml×3). The extract was worked-up in the usual way. After recrystallization from CH_2Cl_2-peteroleum ether, compound **10** (32 mg, 39.5%) was obtained, mp>300 °C. Found: C, 61.43; H, 5.44; N, 9.93%. Calcd for $C_{35}H_{39}N_5O_4$-FeCl: C, 61.37; H, 5.34; N, 10.22%. b) To a solution of **5** (30 mg) in pyridine (1 ml) and concd aqueous ammonia (10 ml) was added. The reaction mixture was stirred overnight at room temperature. The reaction mixture was worked-up according to the procedure of a). The compound **10** (6 mg, 33%) was obtained.

Bis($TsCH_2NC$)iron(II) Complex (12). The solution of compound **10** (100 mg) in CH_2Cl_2 (50 ml) containing pyridine (5 ml) was washed with aqueous $Na_2S_2O_4$ and water. The organic solution was added with $TsCH_2NC$ (30 mg) and subjected to column chromatography (CH_2Cl_2-acetone, gradient up to 5%) to give **12** (103 mg, 67.8%). FAB MS *m/z* 649 (base peak, $M^+-2\times TsCH_2NC$) Found: C, 61.17; H, 5.53; N, 9.40%. Calcd for $C_{53}H_{57}N_7O_8S_2Fe$: C, 61.21; H, 5.52; N, 9.43%.

5-Azamesoporphyrin IX Dimethyl Ester (20). To a solution of compound **12** (40 mg) in pyridine (0.5 ml) and acetic acid (15 ml), a solution of iron(II) sulfate heptahydrate (40 mg) in concd HCl (1 ml) was added under argon, and the reaction mixture was poured into ice water (30 ml) and extracted with CH_2Cl_2 (25 ml×3). The combined organic extracts were washed with water, dried over Na_2SO_4, and filtered. The filtrate was evaporated to give a residue. The residue was dissolved in 5% H_2SO_4-MeOH (50 ml) and allowed to stand overnight. The mixture was poured into ice water (100 ml) and extracted with CH_2Cl_2 (50 ml×3). The combined organic extracts were washed successively with saturated aqueous sodium hydrogencarbonate and water, dried over Na_2SO_4, and filtered. The filtrate was evaporated to give a residue which was subjected to column chromatography (CH_2Cl_2) to obtain azaporphyrin (**20**) (15 mg, 52.4%). Compound **20** was identified with authentic sample[14] by TLC, ^{1}H NMR and mass spectra.

Bis($TsCH_2NC$)iron(II) Protoporphyrin IX Dimethyl Ester (16). To a solution of protohemin IX dimethyl ester (**21**) (100 mg) in pyridine (10 ml), a solution of $Na_2S_2O_4$ (50 mg) in water (1 ml) was added. The mixture was poured into ice water (50 ml) and extracted with CH_2Cl_2 (50 ml×3). The combined organic extracts were washed with H_2O, dried over Na_2SO_4, and filtered. The filtrate was evaporated to give a residue. The residue was dissolved in CH_2Cl_2 (2 ml) and was added with $TsCH_2NC$ (80 mg). The mixture was subjected to column chromatography (CH_2Cl_2-MeOH, gradient up to 5%) to obtain compound **16** (115.4 mg, 75.8%). Compound **16** was recrystallized from benzene-light peteroleum ether (1 : 1). Found: C, 62.63; H, 5.26; N, 8.07%. Calcd for $C_{54}H_{54}N_6O_8S_2Fe$: C, 62.66; H, 5.26; N, 8.12%. ^{1}H NMR ($CDCl_3$) δ=9.77, 9.73, 9.66, and 9.55 (each, 1H, s, *meso*-H), 8.25 (2H, dd, J=17.6, 11.7 Hz, H_C and H_F), 6.92 (4H, broad s, *ortho*-protons on $TsCH_2NC$×2), 6.23 (2H, d, J=17.8 Hz, H_A and H_D), 6.00 (2H, dd, J=11.7, 1.5 Hz, H_B and H_E), 5.69 (4H, broad s, *meta*-protons on $TsCH_2NC$×2), 4.27 (4H, t, J=7.2 Hz, $-CH_2-$×2), 3.63, 3.60, 3.54, and 3.52 (each 3H, s, CH_3), 3.22 (4H, t, J=7.2 Hz, $-CH_2CO-$×2), 2.40 (6H, s, CH_3×2 on $TsCH_2NC$×2), 2.23 (4H, s, CH_2×2 on $TsCH_2NC$×2).

Bis($TsCH_2NC$)iron(II) Octaethyl-5-oxaporphyrin (17). Bis(pyridine)iron(II) octaethyl-5-oxaporphyrin (**13**, 50 mg) was dissolved in CH_2Cl_2 (2 ml) and added with $TsCH_2NC$ (50 mg). The mixture was subjected to column chromatography (CH_2Cl_2-acetone, gradient up to 10%). The blue coloured eluant was evaporated at below 10 °C to give a blue oil (48.4 mg, 76%) which showed one spot on TLC (R_f 0.37; benzene-acetone 85 : 15). UV λ_{max} (CH_2Cl_2) nm (ε_{mM}) 628 (45.2), 583sh (13.1), 529 (11.5), 494 (10.5), 402sh (35.5), 372 (54.5). FAB MS *m/z* 591 ($M^+-2\times TsCH_2NC-BF_4$, 100%). IR ($CHCl_3$) 2960, 2930, 2860. 2140, 1708, 1610, 1595, 1560, 1450, 1400, 1380, 1340, 1260, 1145, 1095, 1060, 1005, 980, 960 cm^{-1}. The blue oil was dissolved in benzene and warmed at 50 °C for 30 min. The solution was evaporated to give a residue which showed the same R_f value and FAB mass spectrum as those of the blue oil obtained at the lower temperature. UV λ_{max} (CH_2Cl_2) nm (ε_{mM}) 627 (46.3), 582sh (13.0), 530 (12.4), 496 (12.1), 404 (37.0), 372 (56.3). IR ($CHCl_3$) 3080, 3000, 2960, 2950, 2860, 2140, 1960, 1817, 1605, 1595, 1480, 1380, 1340, 1263, 1150, 1480, 1060, 1030, 980, 960 cm^{-1}.

We thank Dr. Ronald L. Cerny, Assistant Director of the Midwest center for Mass Spectrometry at University of Nebraska, Lincoln, for several FAB mass spectra.

References

1) R. Schmid and A. F. McDonaph, "The porphyrins," ed by D. Dolphin, Academic press, New York (1979), Vol. VI, p. 257; E. C. Foulkes, R. Lemberg, and P. Purdom, *Proc. Roy. Soc. London Ser. B*, **138**, 368 (1951); R. Lemberg, B. Cortis-Jones and, M. Norrie, *Biochem. J.*, **32**, 149 (1938).

2) R. Tenhunen, H. S. Marver, N. R. Pimstone, W. F. Trager, D. Y. Cooper, and R. Schmid, *Biochemistry*, **11**, 1716 (1972).

3) R. Lemberg, B. Cortis-Jones, and M. Norrie, *Bio-*

chem. J., **32**, 149 (1938).

4) S. Saito and H. A. Itano, *Proc. Natl. Acad. Sci. U.S.A.* **79**, 1393 (1982).

5) R. Lemberg, *Biochem. J.*, **29**, 2322 (1935); E. Y. Levin, *Biochemistry*, **5**, 2845 (1966).

6) R. Lemberg, *Rev. Pure Appl. Chem.*, **6**, 1 (1956); P. O'Carra, "Porphyrins and Metalloporphyrins," ed by K. M. Smith, Elsevier Scientific Publishing Company, Amsterdam (1975), p. 123; R. Schmid and A. F. McDonaph, *Ann. N. Y. Acad. Sci.*, **244**, 533 (1975).

7) J. C. Lagarias, *Biochem. Biophys. Acta*, **717**, 12 (1982); T. Hirota and H. A. Itano, *Tetrahedron Lett.*, **24**, 995 (1983); S. Sano, Y. Sugiura, Y. Maeda, S. Ogawa, and I. Morishima, *J. Am. Chem. Soc.*, **103**, 2888 (1981).

8) A. H. Jackson, G. W. Kenner, and K. M. Smith, *J. Chem. Soc. C*, **1968**, 302.

9) S. Saito and H. A. Itano, *J. Chem. Soc., Perkin Trans. 1*, **1986**, 1.

10) C. J. Watoson, *J. Clin. Pathol.*, **16**, 1 (1963).

11) H. Fischer, H. Baumgarter, and R. Hess, *Z. Physiol. Chem.*, **206**, 201 (1932).

12) H. Muir and A. Neuberger, *Biochem. J.*, **45**, 163 (1949).

13) L. Pauling, "Haemoglobin," ed. F. J. W. Roughton and J. C. Kendrew, Butterworths Scientific Publications, London (1949), p. 57.

14) S. Saito and N. Tamura, *Bull. Chem. Soc. Jpn.*, **60**, 4037 (1987).

15) S. Saito and H. A. Itano, *J. Chem. Soc., Perkin Trans. 1*, **1987**, 1183.

16) J. R. Sams and T. B. Tsin, "The Porphyrins," ed by D. Dolphin, Academic press, New York (1979), Vol. IV, p. 425.

17) L. Pauling, *Stanford Medical Bull.*, **6**, 215 (1948).

18) B. W. Fitzsimmons, J. R. Sams, and T. B. Tsin, *Chem. Phys. Lett.*, **38**, 588 (1976).

 © 1988 The Chemical Society of Japan Bull. Chem. Soc. Jpn., 61, 3549—3552 (1988)

Heptafluoropropylation of Various Substituted Thiophenes with Bis(heptafluorobutyryl) Peroxide. Preparation of 3-Heptafluoropropylthiophene

Masato YOSHIDA,* Tatsuro YOSHIDA, Nobumasa KAMIGATA, and Michio KOBAYASHI
Department of Chemistry, Faculty of Science, Tokyo Metropolitan University, Fukazawa, Setagaya-ku, Tokyo 158
(Received February 24, 1988)

The heptafluoropropylations of several substituted thiophenes with bis(heptafluorobutyryl) peroxide were studied. The orientations of the heptafluoropropylation were examined and compared with those of usual electrophilic substitution. The method for the preparation of 3-heptafluoropropylthiophene was also explored.

The introduction of perfluoroalkyl groups has been the subject of much research in organofluorine chemistry, since the usual methods for alkylation cannot be applied to perfluoroalkylation. We have been studying perfluoroalkylation with bis(perfluoroalkanoyl) peroxide and have succeeded in introducing a heptafluoropropyl group into electron-rich compounds such as electron-rich benzenes, naphthalene, anthracene,[1] electron-rich olefins,[2] furan, and thiophene,[3] with bis(heptafluorobutyryl) peroxide (**1**). In this paper, we report on the orientation of the heptafluoropropylation in several substituted thiophenes with **1** as well as the method for the preparation of 3-heptafluoropropylthiophene.[4]

As described in our previous paper, a heptafluoropropyl group was introduced into the 2-position of thiophene regioselectively, with 98% yield.[3] The decomposition of bis(heptafluorobutyryl) peroxide **1** was accelerated in the presence of thiophene and the activation entropy for the decomposition of **1** in the presence of thiophene showed a negative value. From these results we propose the mechanism shown in Scheme 1.[3] The reaction is initiated by electron transfer from thiophene to the peroxide. The radical anion of the peroxide decomposes to the heptafluoropropyl radical, heptafluorobutyrate, and carbon dioxide. The heptafluoropropyl radical is coupled with the radical cation of thiophene to give heptafluoropropylthiophene. The reaction proceeds in a solvent cage, so the heptafluoropropyl group is introduced in good yield. Due to the high electronegativity of a perfluoroalkyl group, perfluoroalkylation involving a perfluoroalkyl cation as an intermediate are limited,[5] and the development of cationic perfluoroalkylation is very valuable. The method described in Scheme 1 is superficially equivalent to cationic perfluoroalkylation.

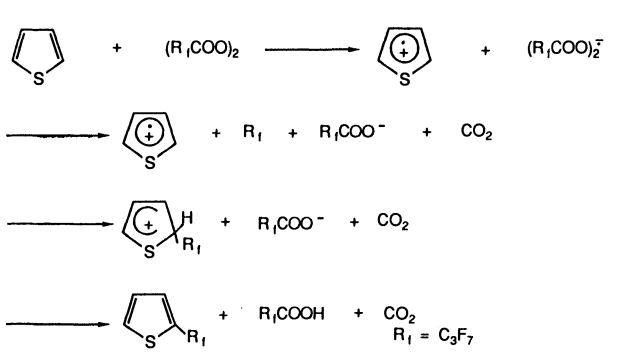

Scheme 1.

The factor for determining the orientation of the heptafluoropropylation with **1** should be the spin density distribution of a radical cation of thiophene[6] or the stability of cationic Wheland intermediates.[7] Thus, we were interested in examining the orientation of the heptafluoropropylation of various substituted thiophenes with peroxide **1** and compared with those of the usual electrophilic substitution.

3-Substituted thiophenes are important for polymeric materials and the exploitation in the preparation of 3-substituted thiophenes is valuable.[8] From results concerning the orientation of the heptafluoropropylation with **1**, we also explored the method for the preparation of 3-heptafluoropropylthiophene.

Results and Discussion

The reactions of **1** and several thiophenes were performed in Freon-113; results are summarized in Table 1. Generally, in electrophilic substitution reactions with thiophenes, an orienting effect is common for both substituents; +I and +M effect such as a methyl group and −I and +M effect such as a bromine group. Thus, for 2-substituted thiophenes further substitution occurs at position 5; for the 3-substituted type, substitution occurs preferentially at 2, unless a steric requirement forces an incoming substituent at position 5.[7] In the heptafluoropropylation of both 2-methylthiophene and 2-bromothiophene with peroxide **1**, heptafluoropropyl group was introduced into the 5-position. In a reaction of 3-bromothiophene and **1**, a heptafluoropropyl group was introduced into both the 2 and 5 positions in yields of 49% and 30%, respectively. When a substituent, such as a formyl group with −I and −M effect, are present at position 2, a further substitution occurs at the 4- or 5-position;[7] sulfur of thiophene activates the 5-position, while the 4-position is the least deactivated by an electron-withdrawing 2-substituent. However, in a reaction of 2-formylthiophene and **1**, a heptafluoropropyl group

Table 1. Heptafluoropropylation of Thiophenes with Bis(heptafluorobutyryl) Peroxide

Run	Substrate	Products (Yields/%)[a]
1		(98)[b] $R_f=C_3F_7$
2	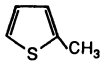	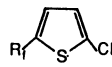 (92)[b]
3	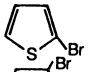	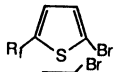 (44)[b]
4	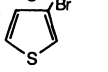	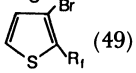 (49) 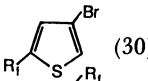 (30)
5	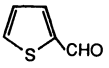	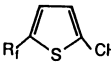 (25) 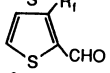 (24)
6		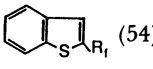 (54) 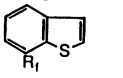 (20)
7	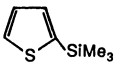	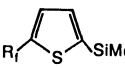 (68)
8	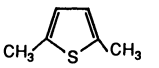	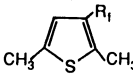 (48) 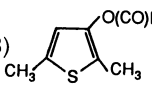 (9)[c]

a) The yields were determined by GC based on peroxide. b) The data from Ref. 3. c) This product was not isolated and its structure was estimated by GC-MS.

was introduced into the 3- and 5-position in a ratio of about 1 : 1; heptafluoropropylation at the 4-position did not occur. An electron-withdrawing formyl group decreases the electron-transfer tendency; thus, on the whole, the yield of the heptafluoropropylation was low in 2-formylthiophene. An electrophilic attack on benzothiophene occurs at the β-position of the thiophene ring prior to the α-position.[7] However, in a reaction of benzothiophene and **1**, 2-heptafluoropropylbenzothiophene and 7-heptafluoropropylbenzothiophene were formed, with no 3-heptafluoropropylbenzothiophene.

As described in our previous paper, heptafluoropropylations of benzenes, especially electron-rich benzenes, were achieved with **1**; the orientations and partial rate factors were much different from those for the usual free radical substitutions, but similar to those for electrophilic aromatic substitutions. We therefore proposed an electron-transfer mechanism for the heptafluoropropylation, but not a free radical aromatic substitution mechanism by a heptafluoropropyl radical produced by a homolytic cleavage of **1**.[1] In this study, we found that a heptafluoropropyl group was introduced into substituted thiophenes with **1** regioselectively. The orientations were similar to those expected from the usual electrophilic substitutions in 2-methylthiophene, 2- or 3-bromothiophenes. However, some differences were found in the orientations for the heptafluoropropylation of 2-formylthiophene and benzothiophene with **1** from those for the usual electrophilic substitutions; the orientations for the heptafluoropropylation cannot be explained in terms of the stabilities of cationic intermediates, and may be characteristic for an electron-transfer reaction.

Electrophilic ipso-substitutions of arylsilanes are well known.[9] Thus, it is interesting to examine whether ipso-substitution occurs in a reaction of 2-trimethylsilylthiophene and **1**. Regarding this reaction, however, the heptafluoropropyl group was found to enter into a 5-position (Table 1, run 7).

There are three expected products in the reaction of **1** and 2,5-dimethylthiophene, as shown in Scheme 2. It is known that the radical cation of 2,5-dimethylthiophene electrochemically produced gives those three types of compounds.[10] As a result, a heptafluoropropyl group was solely introduced into the 3-position of the thiophene to give 2,5-dimethyl-3-heptafluoropropylthiophene (Table 1, run 8), although the spin density of the radical cation of 2,5-dimethylthiophene is higher at the α-position than at the β-position.[6] These results suggested that we should use 2,5-disubstituted thiophene in order to prepare 3-heptafluoropropylthiophene: 2,5-disubstituted thiophenes are fluoroalkylated with **1**; then, substituents at the 2 and 5 positions are removed to give

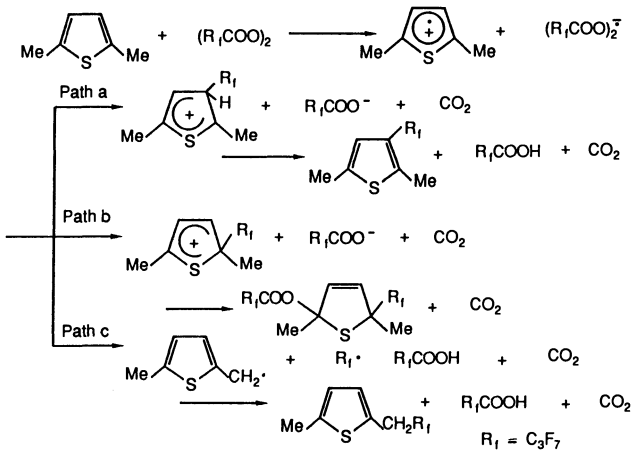

Scheme 2.

Table 2. Heptafluoropropylation of 2,5-Disubstituted Thiophenes with Bis(heptafluorobutyryl) Peroxide[a]

Substrate (mmol)	Products (Yields/%)[b]	
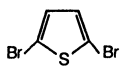	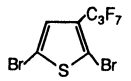	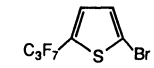
1.5	37	6
5.0	35	13
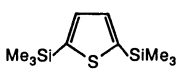	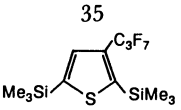	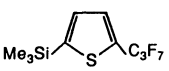
1.5	15	35
5.0	27	30
1.5[c]	47	5
5.0[c]	55	13

a) One mmol of the peroxide was used. b) The yields were determined by GC based on the peroxide. c) Ten mmol of MgO was added.

3-heptafluoropropylthiophene. At first, the reaction of commercially available 2,5-dibromothiophene was examined. The yield of 2,5-dibromo-3-heptafluoropropylthiophene was less than 40% (Table 2). Regarding electron transfer, it may not be adequate to use a bromine group as a protecting group of the 2,5-position. We also examined a reaction of 2,5-bis(trimethylsilyl)thiophene and peroxide **1**. In this reaction, the main product was 2-trimethylsilyl-5-heptafluoropropylthiophene; the yield of the desired 2,5-bis(trimethysilyl)-3-heptafluoropropylthiophene was low. There are two plausible reaction mechanisms for the formation of 2-trimethylsilyl-3-heptafluoropropylthiophene. One is an ipso-substitution of trimethylsilyl group, as shown in Scheme 3 (1). The other is shown in Scheme 3 (2). The acid-promoted desilylation of 2,5-bis(trimethylsilyl)thiophene occurred first. Since 2-trimethylsilylthiophene is more reactive than 2,5-bis(trimethylsilyl)thiophene in a reaction with **1**, 2-trimethylsilyl-5-heptafluoropropylthiophene is formed preferentially.

In order to trap the produced heptafluorobutyric acid, MgO was added. The yield of 2,5-bis(trimethylsilyl)-3-heptafluoropropylthiophene was improved in the presence of MgO, as shown in Table 2. This may imply the acid-promoted desilylation.

Bromine atoms of 2,5-dibromo-3-heptafluoropropylthiophene were reduced by $LiAlH_4$ in THF and 3-heptafluoropropylthiophene was obtained in 60% yield. Trimethylsilyl groups were removed from 2,5-bis(trimethylsilyl)-3-heptafluoropropylthiophene with KF in DMSO in the presence of water almost quantitatively.

It is known that, in a direct heptafluoroalkylation of thiophenes, 2-isomers are obtained as the main products.[11] Only one example is known for the preparation of 3-perfluoroalkylthiophene; the reaction of 3-halogenothiophene, perfluoroalkyl iodide and copper-bronze in DMF gave 3-perfluoroalkylthiophene in the yield of 17—50%.[12] We have so far explored novel methods for the introduction of a heptafluoropropyl group into the 3-position of thiophene.

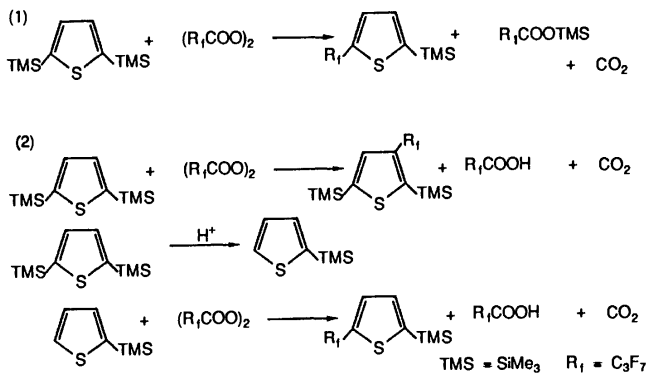

Scheme 3.

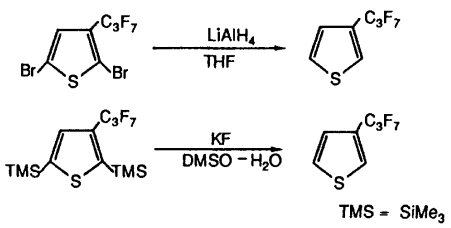

Scheme 4.

Experimental

^{1}H NMR spectra were taken with a JEOL JNM PMX 60Si (60MHz) spectrometer. ^{13}C NMR and ^{19}F NMR spectra were taken with a JEOL JNM FX90Q FTNMR spectrometer. IR spectra were recorded on a Hitachi 260-10 spectrometer. Gas chromatography was performed by using a Hitachi 163 or 263-30 gas chromatograph with SE-30 (10%) 1- or 2-m stainless columns. Gel permeation chromatography was performed by means of a JAI Model LC-08 liquid chromatograph equipped with two JAIGEL-1H columns and using chloroform as an eluent. MS spectra were obtained with JEOL JMS D-300 spectrometer by an electron-impact (EI) ionizing technique at 70 eV.

Materials. Thiophenes, except for 2-trimethylsilylthiophene and 2,5-bis(trimethylsilyl)thiophene, were commercially available and used after purification. 2-Trimethylsilylthiophene and 2,5-bis(trimethylsilyl)thiophene were synthesized from 2-lithiothiophene and 2,5-dilithiothiophene with trimethylsilyl chloride. The lithiothiophenes were synthesized according to methods described in the literature.[13] Bis(heptafluorobutyryl) peroxide was prepared from heptafluorobutyryl chloride and hydrogen peroxide in Freon-113 and water according to the literature.[14] The peroxide was not isolated and used as a solution of Freon-113.

General Procedure for Reactions of 1 and Thiophenes. A solution of **1** (1.0 mmol) and thiophenes (1.5 mmol) in 10 ml Freon-113 was degassed by a freeze-thaw cycle, sealed in an ampoule and kept at 40 °C for adequate time (until the peroxide was consumed). The reaction mixture was washed two times with 5% aq NaOH or $NaHCO_3$ and then with water. An organic layer was separated and dried over $MgSO_4$. The yields of the products were determined by GC using chlorobenzene as an internal standard. The products were isolated from the reaction mixture by the use of gel permeation chromatography and/or column chromatography over silica gel (Wakogel C-60), and identified by IR, NMR, and MS.

2-Heptafluoropropyl-3-bromothiophene: ^{1}H NMR ($CDCl_3$) δ=7.03, 7.42 (ABq, J=6.3 Hz); ^{13}C NMR ($CDCl_3$) δ=113.9 (C_3, t, J_{CCCF}=4.3 Hz), 129.1 (C_5), 133.2 (C_4); IR (cm^{-1}) 1350 (CF_3), 1230 (CF_2); MS m/z 332 (M^++2), 330 (M^+); Exact MS: m/z 329.8928. Calcd for $C_7H_2F_7SBr$: M, 329.8949.

2-Heptafluoropropyl-4-bromothiophene: ^{1}H NMR ($CDCl_3$) δ=7.21 (1H, s), 7.33 (1H, s); ^{13}C NMR ($CDCl_3$) δ=110.6 (C_4), 127.5 (C_5), 132.9 (C_3, t, J_{CCCF}=6.1 Hz); IR (cm^{-1}) 1350 (CF_3), 1230 (CF_2); MS m/z 332 (M^++2), 330 (M^+); Exact MS: m/z 329.8897. Calcd for $C_7H_2F_7SBr$: M, 329.8949.

2-Formyl-3-heptafluoropropylthiophene: ^{1}H NMR ($CDCl_3$) δ=7.22, 7.69 (ABq, J=5.4 Hz), 9.94 (1H, br); ^{13}C NMR ($CDCl_3$) δ=128.6 (C_4, t, J_{CCCF}=5.5 Hz), 134.1 (C_5), 181.8 (CHO, t, $J_{C\text{-}F}$=3.7 Hz);[15] ^{19}F NMR ($CDCl_3$, ppm from ext. CF_3COOH) −4.0, −27.6, −50.2; IR (cm^{-1}) 1340 (CF_3), 1230

(CF_2); MS m/z 280 (M^+); Exact MS: m/z 279.9830. Calcd for $C_8H_3F_7OS$: M, 279.9792.

2-Formyl-5-heptafluoropropylthiophene: ^1H NMR ($CDCl_3$) δ=7.44, 7.67 (ABq, J=4.2 Hz), 9.85 (1H, s); ^{13}C NMR ($CDCl_3$) δ=130.7 (C_4, t, J_{CCCF}=5.5 Hz), 134.6 (C_3), 147.4 (C_2), 182.5 (CHO); ^{19}F NMR ($CDCl_3$) −4.1, −27.7, −50.2; IR (cm^{-1}) 1350 (CF_3), 1230 (CF_2); MS m/z 280 (M^+); Exact MS: m/z, 279.9832. Calcd for $C_8H_3F_7OS$: M, 279.9792.

2-Heptafluoropropylbenzothiophene: ^1H NMR ($CDCl_3$) δ=7.2—7.9 (5H, m), ^{13}C NMR ($CDCl_3$) δ=122.5 (C_7), 125.2 (C_4), 125.3 (C_5), 126.7 (C_6), 127.6 (C_3, t, J_{CCCF}=6.1 Hz), 138.3 (C_8), 141.0 (C_9); IR (cm^{-1}) 1350 (CF_3), 1230 (CF_2); MS m/z 302 (M^+); Exact MS: m/z 301.9992. Calcd for $C_{11}H_5F_7S$: M, 302.0000.

7-Heptafluoropropylbenzothiophene: One of the possible isomers heptafluoropropylated at the benzene ring of benzothiophene was isolated and tentatively identified as 7-heptafluoropropylbenzothiophene, the possibility of 4-heptafluoropropylbenzothiophene cannot be denied. ^1H NMR ($CDCl_3$) δ=7.4—8.2 (5H, m); ^{13}C NMR ($CDCl_3$) δ=122.9 (C_5), 123.4 (C_3), 124.4 (C_6, t, J_{CCCF}=8.5 Hz), 126.5 (C_2), 128.7 (C_4), 141.7 (C_8); IR (cm^{-1}) 1350 (CF_3), 1230 (CF_2); MS: m/z 302 (M^+); Exact MS: m/z 301.9971. Calcd for $C_{11}H_5F_7S$: M, 302.0000.

2-Heptafluoropropyl-5-trimethylsilylthiophene: ^1H NMR ($CDCl_3$) δ=0.39 (9H, s), 7.17,* 7.41 (ABq, J=3.6 Hz, $*J_{HF}$=1.2 Hz); ^{13}C NMR ($CDCl_3$) δ=−0.4 ($SiCH_3$), 131.2 (C_3, t, J_{CCCF}= 4.9 Hz), 133.9 (C_4), 140.8 (C_5); IR (cm^{-1}) 1350 (CF_3), 1230 (CF_2); MS m/z 324 (M^+); Exact MS: m/z 324.0278. Calcd for $C_{10}H_{11}F_7SiS$: M, 324.0239.

2,5-Dimethyl-3-heptafluoropropylthiophene: ^1H NMR ($CDCl_3$) δ=2.36 (3H, s), 2.44 (3H, t, J_{HF}=2.4 Hz),[15] 6.58 (1H, s); ^{13}C NMR ($CDCl_3$) δ=13.7 (2-CH_3), 14.9 (5-CH_3), 124.7 (C_2, t, J_{CCCF}=3.0 Hz), 127.3 (C_5), 137.0 (C_4); ^{19}F NMR ($CDCl_3$) −4.3, −30.8 (J_{HF}=2.4 Hz), −50.8; IR (cm^{-1}) 1340 (CF_3), 1230 (CF_2); MS m/z 280 (M^+); Exact MS: m/z 280.0119 Calcd for $C_9H_7F_7S$: M, 280.0156.

2,5-Dibromo-3-heptafluoropropylthiophene: ^1H NMR ($CDCl_3$) δ=6.97 (s); ^{13}C NMR ($CDCl_3$) δ=113.0 (C_5), 115.1 (C_2, t, J_{CCCF}=4.9 Hz), 130.1 (C_4); IR (cm^{-1}), 1360 (CF_3), 1230 (CF_2); MS m/z 408 (M^+); Exact MS: m/z 407.8067. Calcd for $C_7HF_7SBr_2$: M, 407.8055.

2,5-Bis(trimethylsilyl)-3-heptafluoropropylthiophene: ^1H NMR ($CDCl_3$) δ=0.3 (18H, br), 7.31 (1H, t, J_{HF}=1.5 Hz); ^{13}C NMR ($CDCl_3$) δ=−0.2 (5-$SiCH_3$), 0.4 (2-$SiCH_3$, t),[15] 135.1 (C_4, m for CF coupling), 147.3 (C_5), 150.1 (C_2, t, J_{CCCF}=4.3 Hz); IR (cm^{-1}) 1370 (CF_3), 1230 (CF_2); MS m/z 396 (M^+); Exact MS: m/z 396.0642. Calcd for $C_{13}H_{19}F_7Si_2S$: M, 396.0635.

The Removal of Trimethylsilyl Group from 2,5-Bis-(trimethylsilyl)-3-heptafluoropropylthiophene. 2,5-Bis-(trimethylsilyl)-3-heptafluoropropylthiophene (120 mg), KF (175 mg), and water (0.1 ml) were dissolved in 5 ml DMSO, and the solution was heated at 100 °C for 24 h. From the DMSO solution the resulting 3-heptafluoropropylthiophene was extracted with Freon-113; the Freon-113 solution was washed with 20 ml of water two times in order to completely remove any DMSO. Freon-113 was carefully removed and almost pure 3-heptafluoropropylthiophene was obtained.

3-Heptafluoropropylthiophene: ^1H NMR ($CDCl_3$) δ= 7.1—7.2 (2H, m), 7.6 (1H); ^{13}C NMR ($CDCl_3$) δ=125.5 (C_4, t, J_{CCCF}=3.7 Hz), 127.4 (C_5), 128.1 (C_2, t, J_{CCCF}=6.7 Hz); IR (cm^{-1}), 1350 (CF_3), 1230 (CF_2); MS m/z 252 (M^+); Exact MS: m/z 251.9871. Calcd for $C_7H_3F_7S$: M, 251.9844.

The Removal of a Bromo Group from 2,5-Dibromo-3-heptafluoropropylthiophene. A standard solution of lithium aluminum hydride in THF (1.5 mol l^{-1}) was prepared according to a method described in the literature.[16] A standard solution (0.77 ml) and then 2,5-dibromo-3-heptafluoropropylthiophene were added to THF; the resulting solution was refluxed for 24 h. The reaction flask was cooled in an ice bath; then a 1 : 1 mixture of water and THF 20 ml was added slowly, drop by drop. Then, a 0.1 g NaOH pellet was added. The aqueous phase was extracted five times with 20 ml portions of ether. The formation of 3-heptafluoropropylthiophene was confirmed by GC-MS.

References

1) M. Yoshida, H. Amemiya, M. Kobayashi, H. Sawada, H. Hagii, and K. Aoshima, *J. Chem. Soc., Chem. Commun.*, **1985**, 234.

2) M. Yoshida, K. Moriya, H. Sawada, and M. Kobayashi, *Chem. Lett.*, **1985**, 755.

3) H. Sawada, M. Yoshida, H. Hagii, K. Aoshima, and M. Kobayashi, *Bull. Chem. Soc. Jpn.*, **59**, 215 (1986).

4) In this study, we used bis(heptafluorobutyryl) peroxide as a diacyl peroxide, because it is most convenient for the preparation. The comparison of the reactivity of some diacyl peroxides containing fluoroalkyl groups such as CF_3, C_3F_7, or C_7F_{15}, will be reported in another paper.

5) T. Umemoto, *Yuki Gosei Kagaku Kyokai Shi*, **41**, 251 (1983).

6) A. G. Davies, L. Julia, and S. N. Yazdi, *J. Chem. Soc., Chem. Commun.*, **1987**, 929; M. Shiotani, Y. Nagata, M. Tasaki, J. Sohma, and T. Shida, *J. Phys. Chem.*, **87**, 1170 (1983).

7) S. Rajappa, "Comprehensive Heterocyclic Chemistry," ed by C. W. Bird and C. W. H. Cheesmen, Pergamon Press (1984).

8) A. J. Carpenter and D. J. Chadwick, *J. Chem. Soc., Perkin Trans. 1*, **1985**, 173.

9) E. W. Colvin, "Silicon in Organic Synthesis," Chap. 10, Butterworth and Co. Ltd., (1981).

10) K. Yoshida, T. Saeki, and T. Fueno, *J. Org. Chem.*, **36**, 3673 (1971).

11) A. B. Cowell and C. Tamborski, *J. Fluorine Chem.*, **17**, 345 (1981); T. Umemoto, Y. Kuriu, and H. Shuyama, *Chem. Lett.*, **1981**, 1633.

12) J. Leroy, M. Rubinstein, and C. Wakselman, *J. Fluorine Chem.*, **27**, 291 (1985).

13) D. J. Chadwick and C. Willbe, *J. Chem. Soc., Perkin Trans. 1*, **1977**, 887.

14) C. Zhao, R. Zhou, H. Pan, X. Jin, Y. Qu, C. Wu, and X. Jiang, *J. Org. Chem.*, **47**, 2009 (1982).

15) CF or HF coupling was observed in the carbon or proton of the substituents adjacent to the heptafluoropropyl group, probably due to through space interaction.

16) H. C. Brown and S. Krishnamurty, *J. Org. Chem.*, **34**, 3918 (1969).

 © 1988 The Chemical Society of Japan Bull. Chem. Soc. Jpn., 61, 3553—3557 (1988)

Crystal and Molecular Structures of Tetraisopropyl 1,1′-(1,8-Naphthylene)-bis[1*H*-1,2,3-triazole-4,5-dicarboxylate] and Diisopropyl 1-(1-Naphthyl)-1*H*-1,2,3-triazole-4,5-dicarboxylate

Yoshinobu NAGAWA,* Midori GOTO, Koichi HONDA, and Hiroshi NAKANISHI
National Chemical Laboratory for Industry, 1-1, Higashi, Tsukuba, Ibaraki 305
(Received March 2, 1988)

Molecular structures of the title compounds, which belong to the class of peri-substituted naphthalenes, have been determined by means of X-ray diffraction. Tetraisopropyl 1,1′-(1,8-naphthylene)bis[1*H*-1,2,3-triazole-4,5-dicarboxylate] (**1**), monoclinic, space group $C2/c$, a=35.034(3), b=9.717(1), c=18.504(1) Å, β=96.43(1)°, Z=8; Diisopropyl 1-(1-naphthyl)-1*H*-1,2,3-triazole-4,5-dicarboxylate (**2**), monoclinic, space group $P2_1/n$, a=16.246(2), b=10.115(1), c=12.390(1) Å, β=96.67(1)°, Z=4. The dihedral angles between the mean plane of the naphthalene ring and that of the triazole ring are 88° and 85° for **1** and **2**, respectively. The naphthalene framework of **1** is much more distorted than that of **2** because of a steric repulsion between the two triazole rings with bulky ester groups of **1**.

Owing to a steric repulsion between two substituents, the naphthalene framework is distorted to some degree from a planar structure in 1,8-disubstituted naphthalenes. Among them, such a distorsion of 1,8-bis(trimethylelement) naphthalenes has been shown to be very large by an X-ray diffraction study.[1] However, there have been few X-ray analyses of compounds having aromatic rings in the 1 and 8 positions of the naphthalene moiety.[2]

Recently, we synthesized novel 1,8-bis(heteroaromatic substituted)naphthalenes, 1,1′-(1,8-naphthylene)bis[1*H*-1,2,3-triazoles], and investigated their spectroscopic properties.[3] A structure determination of the parent compound, 1,1′-(1,8-naphthylene)bis[1*H*-1,2,3-triazole], showed that the naphthalene framework in this molecule is very distorted because of a steric repulsion between the two triazole rings.[4]

In this paper, we report on the crystal and molecular structures of more overcrowding compounds, tetraisopropyl 1,1′-(1,8-naphthylene)bis[1*H*-1,2,3-triazole-4,5-dicarboxylate] (**1**), and the corresponding monotriazolylnaphthalene, diisopropyl 1-(1-naphthyl)-1*H*-1,2,3-triazole-4,5-dicarboxylate (**2**).

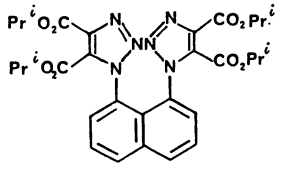

1

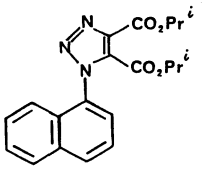

2

Experimental

Compounds **1** and **2** were prepared and purified according to a previous report.[3] Colorless needle-like crystals of **1** and **2** were obtained by a slow evaporation from diethyl ether-hexane solution at room temperature.

Crystal Data. 1; $C_{30}H_{34}N_6O_8$, M=606.6, monoclinic, space group $C2/c$, a=35.034(3), b=9.717(1), c=18.504(1) Å, β=96.43(1)°, V=6259.7(6) Å^3, D_m=1.28 g cm^{-3} (by floatation in carbon tetrachloride and hexane), D_c=1.29 g cm^{-3} for Z=8, μ(Mo $K\alpha$)=1.02 cm^{-1}. **2**; $C_{20}H_{21}N_3O_4$, M=367.4, monoclinic, space group $P2_1/n$, a=16.246(2), b=10.115(1), c=12.390(1) Å, β=96.67(1)°, V=2022.2(3) Å^3, D_m=1.20 g cm^{-3} (by floatation in carbon tetrachloride and hexane), D_c=1.21 g cm^{-3} for Z=4, μ(Mo $K\alpha$)=0.92 cm^{-1}.

Crystallographic Measurements. The cell dimensions and diffraction intensities of both crystals were measured on a Rigaku AFC-4 four-circle diffractometer with graphite-monochromated Mo $K\alpha$ radiation (λ=0.71069 Å) at room temperature. The crystals, approximate dimensions of 0.8×0.3×0.1 and 0.7×0.3×0.2 mm for **1** and **2**, were used for intensity data measurements. Unit-cell dimensions of both crystals were determined by least-squares fits using 25 reflections in the range $20°<2\theta<30°$. Intensity data were collected by the ω-2θ scan mode at a rate of $2°(2\theta)$ min^{-1}. The scan range (2θ) was from 2° to 55° for both crystals. Three standard reflections were measured after every 50 reflections, showing no significant intensity decay throughout the data collection for both crystals. Totals of 7793 and 5080 (including systematically absent) reflections were measured, of which 3024 and 2303 were observed ($|F_o| > 3\sigma(|F_o|)$) for **1** and **2**, respectively. The usual Lorentz and polarization corrections were applied, but no absorption corrections were made.

Structure Determination of 1. The structure was solved by direct methods using MULTAN 78.[5] An E-map using 276 ($|E| > 1.2$) revealed all the non-hydrogen atoms. Hydrogen atoms were placed at the calculated positions. The structure was refined by a block-diagonal least-squares method, using the UNICS III system.[6] Anisotropic thermal parameters were assumed for the non-hydrogen atoms, and isotropic parameters, for the hydrogen atoms. The final refinement, employing a weighting scheme of $w=(0.0024|F_o|^2-0.0156|F_o|+6.413)^{-1}$, led to R and R_w values of 0.058 and 0.056, respectively. The final atomic parameters are listed in Table 1.

Strucure Determination of 2. The solution and refinement of the structure of **2** was accomplished in the same way as that of **1**. The weighting scheme used in the final cycle of the refinement was $w=(0.0024|F_o|^2+0.054|F_o|+0.313)^{-1}$. The final R and R_w value was 0.069 and 0.067, respectively; the final atomic parameters are listed in Table 2.

Atomic scattering factors were taken from International Tables for X-Ray Crystallography.[7] All the calculations were carried out on a FACOM M-380 computer at Tsukuba Research Center.

Table 1. Final Atomic Coordinates ($\times 10^4$) and Equivalent Isotropic Temperature Factors of the Compound **1** with Estimated Standard Deviations in Parentheses $B_{eq}=4/3\sum_i\sum_j\beta_{ij}a_ia_j$

	x	y	z	B_{eq}/Å^2		x	y	z	B_{eq}/Å^2
O(1)	4807(1)	2494(4)	1382(2)	8.1(1)	C(9)	3837(1)	4144(4)	4117(2)	3.8(1)
O(2)	4283(1)	1207(4)	1190(2)	5.9(1)	C(10)	3808(1)	4873(4)	4784(2)	4.5(1)
O(3)	4523(1)	5128(3)	1966(2)	8.3(1)	C(11)	4417(1)	2151(4)	2334(2)	4.2(1)
O(4)	4358(1)	5604(3)	3063(1)	6.1(1)	C(12)	4386(1)	3322(4)	2733(2)	4.0(1)
O(5)	3060(1)	1532(4)	807(2)	8.8(1)	C(13)	4531(1)	1980(4)	1586(2)	4.7(1)
O(6)	3310(1)	−125(3)	1552(2)	5.3(1)	C(14)	4367(2)	871(6)	441(3)	6.7(1)
O(7)	3367(1)	1202(4)	3898(2)	7.2(1)	C(15)	3998(2)	728(9)	−1(3)	10.6(1)
O(8)	2995(1)	222(3)	2978(1)	5.3(1)	C(16)	4608(3)	−334(11)	483(4)	15.7(1)
N(1)	4267(1)	2859(3)	3371(2)	4.0(1)	C(17)	4433(1)	4788(4)	2540(2)	4.8(1)
N(2)	4240(1)	1470(3)	3360(2)	5.0(1)	C(18)	4353(2)	7112(4)	2938(3)	6.4(2)
N(3)	4326(1)	1051(3)	2728(2)	5.1(1)	C(19)	3969(2)	7604(5)	3157(4)	9.1(1)
N(4)	3478(1)	3411(3)	2921(1)	4.0(1)	C(20)	4689(2)	7668(6)	3412(4)	10.3(2)
N(5)	3535(1)	4180(4)	2336(2)	5.1(1)	C(21)	3337(1)	2163(4)	1970(2)	4.1(2)
N(6)	3451(1)	3413(4)	1763(2)	5.0(1)	C(22)	3349(1)	2139(4)	2719(2)	3.9(2)
C(1)	4201(1)	3599(4)	4025(2)	4.0(1)	C(23)	3215(1)	1151(5)	1386(2)	5.2(2)
C(2)	4508(1)	3713(5)	4540(2)	5.3(1)	C(24)	3240(2)	−1156(5)	968(3)	6.9(2)
C(3)	4471(1)	4425(5)	5196(2)	6.0(1)	C(25)	3510(3)	−2310(8)	1201(5)	13.1(3)
C(4)	4134(2)	4968(5)	5307(2)	5.5(1)	C(26)	2821(2)	−1558(8)	888(4)	10.8(3)
C(5)	3456(2)	5477(5)	4917(2)	6.0(1)	C(27)	3243(1)	1143(4)	3270(2)	4.7(3)
C(6)	3141(2)	5404(6)	4432(3)	6.9(1)	C(28)	2868(1)	−841(5)	3463(3)	6.1(3)
C(7)	3162(1)	4692(6)	3767(2)	6.0(1)	C(29)	2733(2)	−2045(6)	2962(4)	8.4(3)
C(8)	3494(1)	4090(4)	3629(2)	4.3(1)	C(30)	2554(2)	−289(7)	3848(4)	10.4(4)

Table 2. Final Atomic Coordinates ($\times 10^4$) and Equivalent Isotropic Temperature Factors of the Compound **2** with Estimated Standard Deviations in Parentheses $B_{eq}=4/3\sum_i\sum_j\beta_{ij}a_ia_j$

	x	y	z	B_{eq}/Å^2		x	y	z	B_{eq}/Å^2
O(1)	−2016(2)	440(3)	5826(3)	7.5(1)	C(8)	582(2)	−1276(4)	9174(3)	4.9(1)
O(2)	−1803(2)	2549(3)	6264(3)	6.1(1)	C(9)	1233(2)	−1229(3)	8534(3)	4.0(1)
O(3)	−702(2)	−1507(3)	5208(2)	6.3(1)	C(10)	1975(2)	−1954(4)	8870(3)	5.0(1)
O(4)	−185(2)	−2284(2)	6840(2)	5.9(1)	C(11)	−699(2)	1112(3)	6618(3)	3.8(1)
N(1)	490(2)	291(3)	7225(2)	3.7(1)	C(12)	−238(2)	−29(3)	6641(3)	3.5(1)
N(2)	486(2)	1582(3)	7522(3)	4.4(1)	C(13)	−1575(2)	1308(4)	6184(3)	4.4(1)
N(3)	−235(2)	2072(3)	7161(3)	4.4(1)	C(14)	−2683(3)	2860(5)	5943(4)	7.2(2)
C(1)	1218(2)	−497(3)	7558(3)	3.9(1)	C(15)	−2740(5)	3613(10)	4941(7)	14.0(1)
C(2)	1855(2)	−458(4)	6945(3)	5.0(1)	C(16)	−2963(5)	3667(13)	6839(7)	16.4(2)
C(3)	2582(3)	−1175(5)	7308(4)	6.5(1)	C(17)	−408(2)	−1360(3)	6126(3)	4.1(3)
C(4)	2634(2)	−1883(4)	8232(4)	6.2(1)	C(18)	−226(4)	−3673(4)	6467(5)	8.1(5)
C(5)	2003(3)	−2704(5)	9836(4)	6.9(1)	C(19)	587(5)	−4056(8)	6232(10)	15.1(4)
C(6)	1366(4)	−2732(5)	10429(4)	7.7(2)	C(20)	−410(10)	−4390(7)	7472(10)	19.9(6)
C(7)	637(3)	−2014(5)	10098(4)	6.6(1)					

Results and Discussion

Molecular Structure. The molecular structures and the atom labelings of **1** and **2** are presented by an ORTEP[8] drawing in Fig. 1. The selected bond distances and angles of **1** and **2** are given in Tables 3 and 4, respectively.[9]

The deviations of the each atom of the triazole rings from the mean plane are within 0.01 Å in both **1** and **2**, which suggests that they are almost planar due to an aromatic ring system. The dihedral angles between the mean plane of the naphthalene ring and those of two triazole rings in **1** are 87.1(1)° for the one triazole ring and 89.3(1)° for the other. In the case of **2**, the angle is 85.1(1)°, which is slightly smaller than that in **1**. The angles are nearly ninety degrees while in the parent compounds, 1,1′-(1,8-naphthylene)bis[1*H*-1,2,3-

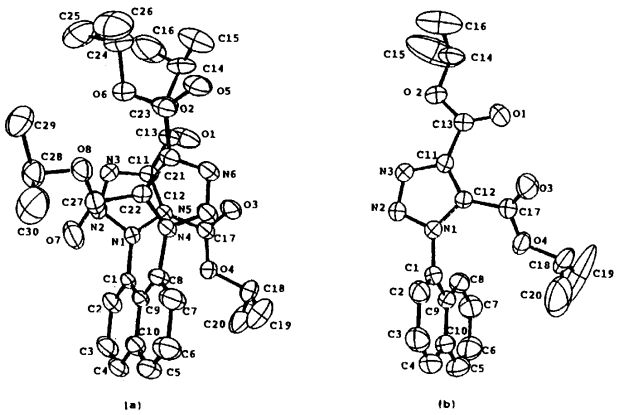

Fig. 1. Molecular structures. Non-hydrogen atoms are expressed as thermal ellipsoids with 40% probability level. Hydrogen atoms are omitted for clarity. (a) Compound **1**. (b) Compound **2**.

Table 3. Selected Bond Lengths and Bond Angles in **1** with Estimated Standard Deviations in Parentheses

Bond length l/Å				Bond angle ϕ/°			
C(1)-C(2)	1.361(5)	C(1)-C(9)	1.407(6)	C(2)-C(1)-C(9)	122.8(3)	C(2)-C(1)-N(1)	115.9(4)
C(1)-N(1)	1.449(5)	C(2)-C(3)	1.415(6)	C(9)-C(1)-N(1)	121.3(3)	C(1)-C(2)-C(3)	119.9(4)
C(3)-C(4)	1.332(7)	C(4)-C(10)	1.416(6)	C(2)-C(3)-C(4)	119.6(4)	C(3)-C(4)-C(10)	122.1(4)
C(5)-C(6)	1.345(7)	C(5)-C(10)	1.410(7)	C(6)-C(5)-C(10)	122.0(4)	C(5)-C(6)-C(7)	119.0(5)
C(6)-C(7)	1.421(7)	C(7)-C(8)	1.350(7)	C(6)-C(7)-C(8)	120.3(4)	C(7)-C(8)-C(9)	123.2(3)
C(8)-C(9)	1.423(5)	C(8)-N(4)	1.462(4)	C(7)-C(8)-N(4)	114.7(3)	C(9)-C(8)-N(4)	122.0(4)
C(9)-C(10)	1.437(5)	C(11)-C(12)	1.367(5)	C(1)-C(9)-C(8)	128.5(3)	C(1)-C(9)-C(10)	116.3(3)
C(11)-C(13)	1.491(5)	C(11)-N(3)	1.352(5)	C(8)-C(9)-C(10)	115.2(4)	C(4)-C(10)-C(5)	120.5(4)
C(12)-C(17)	1.482(5)	C(12)-N(1)	1.371(5)	C(4)-C(10)-C(9)	119.3(4)	C(5)-C(10)-C(9)	120.2(4)
C(13)-O(1)	1.188(6)	C(13)-O(2)	1.310(5)	C(12)-C(11)-C(13)	129.8(4)	C(12)-C(11)-N(3)	109.2(3)
C(17)-O(3)	1.190(5)	C(17)-O(4)	1.300(5)	C(13)-C(11)-N(3)	121.0(3)	C(11)-C(12)-C(17)	130.7(3)
C(21)-C(22)	1.382(5)	C(21)-C(23)	1.488(6)	C(11)-C(12)-N(1)	104.0(3)	C(17)-C(12)-N(1)	125.1(3)
C(21)-N(6)	1.348(5)	C(22)-C(27)	1.483(5)	C(11)-C(13)-O(1)	124.1(4)	C(11)-C(13)-O(2)	110.8(4)
C(22)-N(4)	1.355(5)	C(23)-O(5)	1.204(5)	O(1)-C(13)-O(2)	125.1(4)	C(12)-C(17)-O(3)	122.0(4)
C(23)-O(6)	1.312(5)	C(27)-O(7)	1.197(5)	C(12)-C(17)-O(4)	111.8(3)	O(3)-C(17)-O(4)	126.2(4)
C(27)-O(8)	1.320(5)	N(1)-N(2)	1.353(4)	C(22)-C(21)-C(23)	133.8(4)	C(22)-C(21)-N(6)	108.9(3)
N(2)-N(3)	1.306(5)	N(4)-N(5)	1.349(4)	C(23)-C(21)-N(6)	117.3(3)	C(21)-C(22)-C(27)	135.9(4)
N(5)-N(6)	1.303(4)			C(21)-C(22)-N(4)	103.5(3)	C(27)-C(22)-N(4)	120.5(3)
				C(21)-C(23)-O(5)	120.5(4)	C(21)-C(23)-O(6)	114.3(3)
				O(5)-C(23)-O(6)	125.1(4)	C(22)-C(27)-O(7)	123.0(4)
				C(22)-C(27)-O(8)	111.5(3)	O(7)-C(27)-O(8)	125.6(4)

Table 4. Selected Bond Lengths and Bond Angles in **2** with Estimated Standard Deviations in Parentheses

Bond length l/Å				Bond angle ϕ/°			
C(1)-C(2)	1.355(5)	C(1)-C(9)	1.416(5)	C(2)-C(1)-C(9)	123.8(3)	C(2)-C(1)-N(1)	118.5(3)
C(1)-N(1)	1.445(4)	C(2)-C(3)	1.415(6)	C(9)-C(1)-N(1)	117.8(3)	C(1)-C(2)-C(3)	118.2(4)
C(3)-C(4)	1.345(7)	C(4)-C(10)	1.405(6)	C(2)-C(3)-C(4)	120.7(4)	C(3)-C(4)-C(10)	122.1(4)
C(5)-C(6)	1.338(8)	C(5)-C(10)	1.413(6)	C(6)-C(5)-C(10)	121.8(4)	C(5)-C(6)-C(7)	120.5(5)
C(6)-C(7)	1.409(8)	C(7)-C(8)	1.361(6)	C(6)-C(7)-C(8)	119.9(5)	C(7)-C(8)-C(9)	121.1(4)
C(8)-C(9)	1.394(5)	C(9)-C(10)	1.431(5)	C(1)-C(9)-C(8)	124.3(3)	C(1)-C(9)-C(10)	116.6(3)
C(11)-C(12)	1.374(4)	C(11)-C(13)	1.475(5)	C(8)-C(9)-C(10)	119.1(3)	C(4)-C(10)-C(5)	123.6(4)
C(11)-N(3)	1.358(4)	C(12)-C(17)	1.502(5)	C(4)-C(10)-C(9)	118.8(4)	C(5)-C(10)-C(9)	117.7(4)
C(12)-N(1)	1.352(4)	C(13)-O(1)	1.186(5)	C(12)-C(11)-C(13)	128.4(3)	C(12)-C(11)-N(3)	108.7(3)
C(13)-O(2)	1.316(5)	C(17)-O(3)	1.191(4)	C(13)-C(11)-N(3)	122.8(3)	C(11)-C(12)-C(17)	132.2(3)
C(17)-O(4)	1.309(4)			C(11)-C(12)-N(1)	104.6(3)	C(17)-C(12)-N(1)	123.2(3)
				C(11)-C(13)-O(1)	123.5(3)	C(11)-C(13)-O(2)	111.6(3)
				O(1)-C(13)-O(2)	124.8(3)	C(12)-C(17)-O(3)	123.4(3)
				C(12)-C(17)-O(4)	109.3(3)	O(3)-C(17)-O(4)	127.4(3)

triazole] and 1-(1-naphthyl)-1*H*-1,2,3-triazole, the corresponding angles are 50.6(2)° and 56.8(2)°, respectively.[10] These results indicate that the repulsion between the isopropoxycarbonyl group in the 5-position of the triazole ring and the hydrogen in the 2′-position of the naphthalene ring is very large. The two triazole rings of **1** face each other with a dihedral angle of 33.1(2)°, and assume a trans conformation.

The fusion angle, Cl-C9-C8, is 129.0(4)° in **1**, while the angle in **2** is 124.3(3)°. The enlargement of this angle in **1** indicates that a severe steric strain is caused by a repulsion between two triazole rings with bulky ester groups. The angles C9-Cl-N1 and C9-C8-N4 in **1**, which are related to the pivot bond between the triazole ring and the naphthalene ring, are 121.3(3)° and 122.0(4)°, respectively. These are large compared with that in **2** (117.8(3)°), also suggesting a large repulsion between the two triazole rings of **1**. Similar relationships have been observed for the parent compounds.[10]

The equations of the least-squares planes of the naphthalene ring and the deviations of the atoms are listed in Table 5. The planarity of the naphthalene ring in **1** is as good as that in **2**.

Table 5. The Equations of the Naphthalene Least Squares Planes and the Deviations of the Atoms for the Compounds **1** and **2** (l/Å)

Compound **1**	$-0.3093X-0.8509Y+0.4566Z+4.1135=0$
Compound **2**	$-0.3158X-0.7927Y-0.4814Z+4.7353=0$

	Compound **1**	Compound **2**
C(1)	−0.012	0.002
C(2)	−0.005	0.009
C(3)	0.000	−0.005
C(4)	0.011	−0.015
C(5)	−0.005	0.012
C(6)	−0.013	0.007
C(7)	−0.009	0.002
C(8)	0.013	−0.010
C(9)	0.009	0.000
C(10)	0.001	−0.001

In **2**, the torsion angles C12-C11-C13-O1, 3.6(6)°, and C11-C12-C17-O3, 44.5(6)°, show that the carbonyl

Table 6. Distortions of the Naphthalene Framework in 1,8-Disubstituted Naphthalenes

	Distance (Å)		Bond angle (°)		Torsion angle (°)		Ref.
	C1-C8	Z1-Z8	C1-C9-C8	C9-C1-Z1	C10-C9-C1-Z1	C1-C9-C10-C4	
1	2.55	2.85	128.5	121.7	179.0	0.9	a)
1,1′-(1,8-Naphthylene)-bis[1*H*-1,2,3-triazole]	2.56	2.91	129.0	120.6	165.9	7.7	b)
1,8-Diphenylnaphthalene	2.56	2.99	126.2	125.2	178.0	6.3	c)
1,8-Dipiperidinonaphthalene	2.60	2.89	126.8	120.6	167.5	9.9	d)
1,8-Bis(dimethylamino)naphthalene	2.56	2.79	125.8	120.5	168.2	9.7	e)
1,8-Di-*t*-butylnaphthalene	2.62	3.86	129.9	125.7	138.1	19.3	f)

a) This work. b) Ref. 4. c) Calculated with Ref. 11. d) Calculated with Ref. 12. e) Calculated with Ref. 13. f) Calculated with Ref. 14.

group at the 4-position exists in the triazole plane, but that at the 5-position it twists from the triazole plane. Because the latter group is situated between the ester group at the 4-position and the naphthalene ring, coplanarity cannot be maintained owing to severe steric overcrowding. In the case of **1**, the arrangements of four carbonyl groups and two triazole rings are more complicated than those of **2**. The torsion angles C12-C11-C13-O1, C11-C12-C17-O3, C22-C21-C23-O5, and C21-C22-C27-O7 are 49.1(7)°, −2.4(7)°, 144.8(4)°, and 160.5(5)°, respectively. Although the results reflect the requirements of intramolecular contacts, the influence of intermolecular packing can not be ignored.

Comparison with Other Peri-Substituted Naphthalenes. Typical data regarding the effects of the distorsion on the naphthalene ring in **1** are listed in Table 6 along with data for the other peri-substituted naphthalenes. In this Table, Z1 and Z8 are the atoms in substituents and there bound to C1 and C8, respectively. In order to avoid any steric overcrowding of two bulky peri-substituents, the nonbonding distance between C1 and C8 as well as that between Z1 and Z8 is enlarged. Accordingly, fused angle C1-C9-C8 expands more than 120°, and C1 and C8 are displaced in opposite directions from the naphthalene ring with torsion angle C1-C9-C10-C4 not equal to 0°. In order to lengthen the distance between Z1 and Z8, angle C9-C1-Z1 expands more than 120°, and torsion angle C10-C9-C1-Z1 becomes less than 180°.

Considering the data in Table 6, there are various modes in which the strain of bulky substituents affect the naphthalene framework. The distorsion of the naphthalene ring in 1,3,6,8-tetra-*t*-butylnaphthalene is remarkably large because of severe steric overcrowding. Compared with other peri-substituted naphthalenes, the displacement of C1 and C8 from the naphthalene ring of **1** is very small. However, the two angles, C1-C9-C8 and C9-C1-Z1, are significantly large. Therefore, it may be pointed out that the above-described distorsions in **1** relieve the severe steric repulsion between the two triazole rings with bulky ester groups.

Crystal Structure. The packing modes of molecules in both crystals are shown in Fig. 2. The crystal structures are stabilized mainly by van der Waals forces; the shortest intermolecular distances are 3.209(5) Å for O(1) (*x*,*y*,*z*)-C(12) (1−*x*,*y*,0.5−*z*) and 3.286(4) Å for O(3) (*x*,*y*,*z*)-C(12) (−*x*,−*y*,1−*z*) in **1** and **2**, respectively.

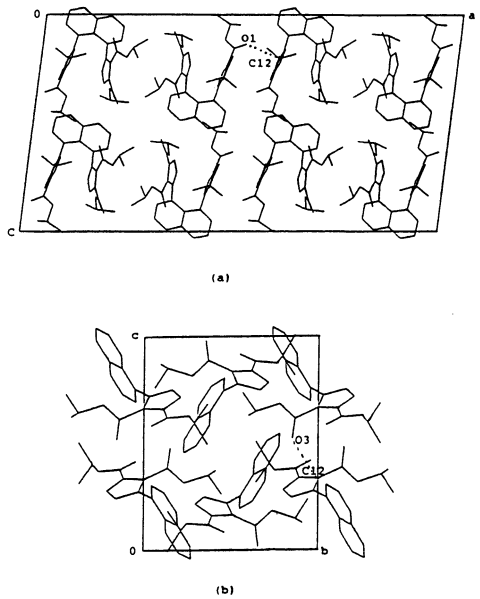

Fig. 2. Crystal structures. Hydrogen atoms are omitted for clarity. (a) Compound **1**, projected along the b axis. (b) Compound **2**, projected along the a* axis.

References

1) R. Sooriyakumaran, P. Boudjouk, and R. G. Garvey, *Acta Crystallogr., Sect. C*, **41**, 1348 (1985); J. F. Blout, F. Cozzi, J. R. Damewood, Jr., L. D. Iroff, U. Sjostrand, and K. Mislow, *J. Am. Chem. Soc.*, **102**, 99 (1980).

2) R. L. Clough, W. J. Kung, R. E. Marsh, and J. D. Roberts, *J. Org. Chem.*, **41**, 3603 (1976).

3) Y. Nagawa, K. Honda, and H. Nakanishi, *Bull. Chem. Soc. Jpn.*, **60**, 2931 (1987).

4) Y. Nagawa, M. Goto, K. Honda, and H. Nakanishi, *Acta Crystallogr., Sect. C*, **42**, 478 (1986).

5) P. Main, S. E. Hull, L. Lessinger, G. Germain, J. P. Declercq, and M. M. Woolfson, MULTAN 78, "A System of Computer Programs for the Automatic Solution of Crystal Structures from X-Ray Diffraction Data," University of York, England, and Louvain, Belgium (1978).

6) T. Sakurai and K. Kobayashi, *Rep. Inst. Phys. Chem. Res.*, **55**, 69 (1979).

7) International Tables for X-Ray Crystallography, Vol. IV, Kynoch Press, Birmingham (1974).

8) C. K. Johnson, ORTEP II, Report ORNL-5138, Oak Ridge National Laboratory, Tennessee (1976).

9) The lists of observed and calculated structure factors, the atomic parameters for the hydrogen atoms, and the anisotropic thermal parameters for the non-hydrogen atoms are deposited at the Chemical Society of Japan as Document No. 8826.

10) Y. Nagawa, M. Goto, K. Honda, and H. Nakanishi, *Acta Crystallogr., Sect. C*, **43**, 147 (1987).

11) R. A. Ogilvie, Ph. D. Thesis, Massachusetts Institute of Technology, Massachusetts (1971).

12) W. Wong-Ng, S. C. Nyburg, A. Awwal, R. Jankie, and A. J. Kresge, *Acta Crystallogr., Sect. B*, **38**, 559 (1982).

13) H. Einspahr, J. B. Robert, R. E. Marsh, and J. D. Roberts, *Acta Crystallogr., Sect B*, **29**, 1611 (1973).

14) J. Handal, J. G. White, R. W. Franck, Y. H. Yuh, and N. L. Allinger, *J. Am. Chem. Soc.*, **99**, 3345 (1977).

 © 1988 The Chemical Society of Japan Bull. Chem. Soc. Jpn., 61, 3559—3564 (1988)

Preparation and Complex Formation of Polymers Anchoring 2-Oxazolidinone

Tomomichi Ishikawa,* Hidehiko Nishizuka, and Tadashi Kawai
Department of Industrial Chemistry, Faculty of Technology, Tokyo Metropolitan University, Fukasawa, Setagaya-ku, Tokyo 158
(Received March 18, 1988)

Polymers anchoring 3-unsubstituted 2-oxazolidinone were prepared and their complex formation with phenol and mercury(II) acetate were investigated. Preformed poly(4-hydroxystyrene) was treated with tris(2,3-epoxypropyl) isocyanurate to give a polymer containing 2-oxazolidinone residues within the limits of 57.7 mol%. Polymers carrying 2-oxazolidinone were also prepared through the homopolymerization and copolymerization of 4-(2-oxo-5-oxazolidinylmethoxy)phenyl acrylate. The effective concentration of 2-oxazolidinone residue in the polymers, which is accessible to phenol, was determined on the assumption that the polymer-bound 2-oxazolidinone and phenol formed a 1 : 1 complex. 2-Oxazolidinone and a mercury atom formed a 2 : 1 complex; this relation on the molar ratio applies to all forms of complexes between the mercury atom and the 2-oxazolidinone residue in the polymers.

2-Oxazolidinone has a reactive carbamoyl group, and its reactions lead to the formation of various useful compounds such as biocides,[1] surface active agents,[2] reactive reagents,[3] and reaction intermediates.[4] Polymers containing 2-oxazolidinone residues have also been reported. Walls and co-worker[5] previously noted that poly(3-vinyl-5-methyl-2-oxazolidinone) absorbed phenol, alkyl halides, and halogens. The complexes between 5-alkyl-3-vinyl-2-oxazolidinones and chlorine are useful as bactericides, fungicides, and bleaches.[6] Further, we have reported that a polymer containing 2-oxazolidinone rings in the main chain, prepared from 2,4-diisocyanatotoluene and 1,4-bis(2-oxo-5-oxazolidinylmethoxy)benzene, formed complexes with phenol and halogens.[7] Okawara and co-workers[8] have reported on a complex formation between tin(II) chloride and 2-oxazolidinone or 3-glycidyl-2-oxazolidinone; however, a complex of the salt with the polymer obtained from the latter compound is not examined in its paper. We have discovered the fact that a precipitate is formed when treating 2-oxazolidinone with mercury(II) acetate in methanol. This is, presumably, a complex between 2-oxazolidinone and mercury(II) acetate; its structure has been confirmed in this present work. Most of the polymers anchoring 2-oxazolidinone studied until now were of polymer type **1**:[5,8-12] almost no polymers in which a nitrogen atom adjacent to a carbonyl group holds a reactive hydrogen, such as polymer **2**, has been reported, except for poly(5-vinyl-2-oxazolidinone).[13] Polymer **2** must be capable of a complex formation with phenol and mercury(II) acetate. In this paper, therefore, we also report on the syntheses and complex formations of new polymers, poly[4-(2-oxo-5-oxazolidinylmethoxy)styrene](POS) and poly[4-(2-oxo-5-oxazolidinylmethoxy)phenyl acrylate](POPA), owing to interest in the characteristic properties of polymer-bound 3-unsubstituted 2-oxazolidinone (polymer **2** type). This work gives fundamental information on the use as carriers for biocides, as ligands for a polymer-metal complex catalyst, and as agents for heavy metal ions recovery in solutions.

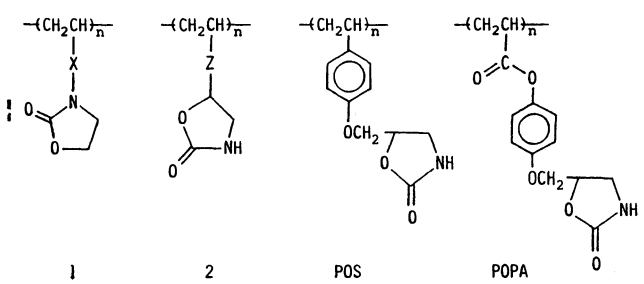

Experimental

Materials. Poly(4-hydroxystyrene)(PHS) was purchased from the Maruzen Petrochemical Corp., $\overline{M}_w$ 5850, $\overline{DP}$ 49, hydroxyl equivalent 120, and $[\eta]$ 0.0906 dl g^{-1} (at 30 °C in DMSO). Tris (2,3-epoxypropyl) isocyanurate (TEPIC) was offered by the Nissan Chemical Corp. and was recrystallized from methanol, mp 102—104 °C (lit,[14] 103—104.5 °C). Acryloyl chloride was distilled prior to use. 5-(4-Hydroxyphenoxymethyl)-2-oxazolidinone was prepared from hydroquinone and TEPIC in a way similar to that mentioned in a previous paper.[6] 3-Phenylcarbamoyl-2-oxazolidinone was prepared from 2-oxazolidinone and phenyl isocyanate according to a previously published report.[15] 3,5-Diphenyl-2-oxazolidinone was prepared from styrene oxide and phenyl isocyanate.[16] 5-Phenoxymethyl-2-oxazolidinone (2-oxo-5-oxazolidinylmethoxybenzene, abbreviated to OMB), was prepared from phenol and TEPIC.[17] Solvents were dried and distilled before use. Other chemicals of reagent grade were used without further purification.

General Procedure for Reaction of PHS with TEPIC. A 300 cm^3, four-necked round-bottomed flask equipped with a stirrer, reflux condenser, and thermometer was charged with the desired amount of PHS, TEPIC, sodium hydroxide, and DMF. The reaction mixture was stirred at 158 °C for 7 h, followed by treating with phenol for 5 h. After evaporation of the solvent under reduced pressure, the residue was poured into water. The precipitate was washed with ethyl acetate, followed by reprecipitation from an acetone solution with water. The reprecipitate was washed with diethyl ether and dried under reduced pressure. The obtained content in 2-oxazolidinone residue in the polymers was determined by an

IR absorption analysis at 1740 cm^{-1}.

Synthesis of 4-(2-Oxo-5-oxazolidinylmethoxy)phenyl Acrylate (OPA). A 300-cm^3, round-bottomed flask equipped with a stirrer, reflux condenser, thermometer, and a inlet tube for nitrogen gas was charged with 3.5 g (0.017 mol) of 5-(4-hydroxyphenoxymethyl)-2-oxazolidinone and 150 cm^3 of tetrahydrofuran; then 1.5 g (0.17 mol) of acryloyl chloride and 2.4 g (0.023 mol) of triethylamine were added. After stirring under nitrogen for 3 h, the precipitate was removed by filtration. The filtrate was treated first with a 5% aqueous solution of sodium hydrogencarbonate, followed by two extractions using diethyl ether. The ether-layer was washed with water, and dried over anhydrous sodium sulfate, followed by distillation. The residue was recrystallized from ethanol. Yield 31.8%; mp 141—142 °C (colorless needle). Found: N, 5.18%. Calcd for $C_{13}H_{13}NO_5$: N, 5.32%. IR(KBr) 3270 (NH), 1750 (C=O), 1730 (C=O), 1630 (C=C), 1500, 1405, 1300, 1250, 1200, 1165, 1150, 825, and 805 cm^{-1}.

Procedure for Polymerization of OPA. OPA 0.8 g, 1,4-dioxane 6 cm^3 and 1 mol% AIBN were charged into a reaction tube. The mixture was treated at 50 °C under nitrogen in a sealed tube. After 24 h, the contents of the tube had gelled. The obtained polymer was washed with 1,4-dioxane and diethyl ether, followed by vacuum drying. Yield 86%.

Copolymerization with styrene was carried out in a way similar to the homopolymerization method. Yield 48.3%. The composition of the copolymer was determined by an elementary analysis. Found: C, 59.51; H, 5.32; N, 4.91%.

General Procedure for the Complex Formation between 2-Oxazolidinones and Phenol. The 2-oxazolidinones (200 mg) were added to 5 cm^3 of an aqueous solution of phenol; the specimens were kept at 30 °C with shaking. After 2 days, the solids were separated by filtration, and the concentration of phenol in the liquid phase was evaluated by measuring the absorption at 280 nm.

General Procedure for the Complex Formation between 2-Oxazolidinones and Mercury(II) Acetate. The 2-oxazolidinones (200 mg) were added to 10 cm^3 of 0.08×10^{-3} mol dm^{-3} aqueous solution of mercury(II) acetate, and the specimens were kept at 30 °C with shaking. After 2 days, the solids were separated by filtration; then, the amount of mercury(II) acetate in the liquid phase was determined by atomic absorption analysis.

Reaction of 2-Oxazolidinone with Mercury(II) Acetate in Methanol. 2-Oxazolidinone (1.51 g, 1.74×10^{-3} mol) was dissolved in 20 cm^3 of methanol. The solution was poured into a solution containing mercury(II) acetate (2.82 g, 8.84×10^{-3} mol) in 30 cm^3 of methanol. The mixture was permitted to stand overnight. The precipitate was collected by filtration. The filtrate was washed with methanol, and dried under reduced pressure. Yield 2.05 g (colorless needle); Atomic absorption analysis Hg 48.6%; ^1H NMR (DMSO-d_6) δ=4.30 (2H, t, CH_2) and 3.60 (2H, t, CH_2); For IR(KBr) see Fig. 5.

Results and Discussion

Preparation of POS and POPA. It has been reported that OMB[17] was obtained by treating phenol with TEPIC in the presence of sodium hydroxide. Previously, we had also succeeded in synthesizing 5-(4-hydroxyphenoxymethyl)-2-oxazolidinone[6] from hydroquinone and TEPIC. Therefore, the reaction of PHS with TEPIC was studied in order to prepare POS. PHS is prepared through a polymerization of 4-hydroxystyrene; however, the proportion of the side reaction, such as chain-transfer and termination, becomes higher with an increase in the degree of polymerization, and an insoluble polymer is finally formed. It was attributed to forming a cross-linked polymer caused by a chain-transfer to phenolic hydroxyl groups.[18] Therefore, though its molecular weight is low, a linear soluble PHS was used for the reaction with TEPIC, since the number of phenolic hydroxyl groups in the polymer can be accurately measured. The reaction was carried out under homogeneous conditions in DMF in the presence of sodium hydroxide. Unreacted TEPIC was transformed into OMB by treating with phenol; the produced OMB was removed from the reaction products through washing with ethyl acetate and reprecipitation. The IR spectra of the reaction products show two characteristic absorption bands at 3400 (O-H of phenol) and 1740 cm^{-1} (C=O of 2-oxazolidinone). If the reaction was completed, the absorption attributed to the O-H bond should disappear. The results of the IR spectra are, thus, indicative of the presence of unreacted phenolic hydroxyl groups. The content in 2-oxazolidinone residue in the polymers was determined spectrophotometrically by using the absorbance at 1740 cm^{-1} with 5-phenoxymethyl-2-oxazolidinone as a standard.

The results are summarized in Table 1. It was confirmed that the 2-oxazolidinone content for POS 3 is nearly equal to that determined by elementary analysis. In stoichiometric reactions between TEPIC and phenolic hydroxyl groups in the polymer, the 2-oxazolidinone content was a maximum value, and could not rise beyond 58%, despite long reaction times (14 hours) and the use of excess TEPIC. These results can be explained by suggesting that the polymer-bound 2-oxazolidinones surrounding fresh active phenolic oxygens hinder, to some extent, a further reaction of TEPIC with these phenolic active sites. However, the results shown in Table 1 suggest that the use of a smaller amount of TEPIC than the stoichiometric molar ratio allows the 2-oxazolidinone content in the polymer to be controlled. All these polymers were soluble in acetone, benzene, THF, DMF, and DMSO.

As previously described, significant amounts of the unreacted phenolic hydroxyl groups are present in the polymers anchoring 2-oxazolidinone, prepared from the preformed PHS. Therefore, a vinyl monomer containing a 2-oxazolidinone moiety, OPA, was preformed from 5-(4-hydroxyphenoxymethyl-2-oxazolidinone and acryloyl chloride, and was homo- and copolymerized in 1,4-dioxane by using AIBN as initiator. Little and Pickens[7] have reported that homopolymerization of 5-vinyl-2-oxazolidinone for a type-2 polymer should be impossible, except for a copolymerization

Table 1. Preparation of the Polymers Anchoring 2-Oxazolidnone

Abbreviation[a]	Material[b] mole ratio	Reaction condition[c]			Product		
		Solvent	Time h	Temp °C	Yield %	$[\eta]$[d] dl g^{-1}	2-Oxazolidinone residue in the polymers/mole fraction
PHS	HSU=1	—	—	—	—	0.0906	0.000
POS 1	HSU/TEPIC=3.0	DMF	7	158	72.9	0.0710	0.577
POS 2	HSU/TEPIC=4.5	DMF	7	158	82.3	0.0814	0.506
POS 3	HSU/TEPIC=9.0	DMF	7	158	83.8	0.0849	0.282
POPA	OPA=1	Dioxane	24	50	76.7	insoluble[e]	1.000
OPA-St	OPA/St=1	Dioxane	24	50	48.3	soluble[e]	0.850

a) PHS: Poly(4-hydroxystyrene); POS: Poly[4-(2-oxo-5-oxazolidinylmethoxy)styrene] prepared from PHS; POPA: Homopolymer of 4-(2-oxo-5-oxazolidinylmethoxy)phenyl acrylate(OPA); OPA-St: Copolymer of OPA and styrene (St). b) HSU: Constitutional repeating unit in PHS; TEPIC: tris(2,3-epoxypropyl) isocyanurate. c) In the presence of ca. 4 mol% NaOH for POS 1, 2, and 3; used AIBN as an initiator for POPA, and OPA-St. d) Measured at 30 °C in DMSO. e) In DMF, DMSO, and NMP.

with methyl methacrylate. However, the monomer OPA obtained in this paper did homopolymerize, and gel. Homopolymerization gave a 86% conversion. The OPA-homopolymer (POPA) was swollen by, but insoluble in, pyridine, *m*-cresol, DMF, DMSO, and NMP, in contrast to water soluble poly(3-vinyl-2-oxazolidinone).[10] On the other hand, the equimolar reaction between OPA and styrene gave a copolymer (OPA-St) containing 15 mol% styrene, and it can be seen that the reactivity for OPA was higher than that for styrene. However, this should be judged more exactly on the basis of a reactivity ratio determination for OPA and styrene. The obtained copolymer was soluble in the solvents mentioned above.

Complex Formation of the Polymer-Bound 2-Oxazolidinone with Phenol. Several types of polymer-bound 2-oxazolidinone were incubated with an aqueous solution of phenol at 30 °C for 2 days. In confirmation of the attainment of equilibrium, several phenol determinations were performed after 2 and 7 days incubation: both values were identical.

The results were analyzed by applying an equation which Komiyama and co-workers[19] proposed for the complex formation between a β-cyclodextrin residue in immobilized catalysts and phenol. Namely, if the 2-oxazolidinone residue in the polymers and phenol formed a 1 : 1 complex, the following equation could be effective:

$$[\text{Phenol}]=[\text{OX}]_{\text{eff}}\,[\text{Phenol}]/[\text{Complex}]-K_{\text{d}}. \quad (1)$$

Here, [Phenol] and [Complex] are the equilibrium concentrations of phenol and the 1 : 1 complex between the 2-oxazolidinone residue and phenol, respectively. K_{d} is the equilibrium constant for the dissociation of the complex between the 2-oxazolidinone residue in the polymers and phenol. $[\text{OX}]_{\text{eff}}$ is the effective concentration of the 2-oxazolidinone residue in the polymers, which is accessible to phenol. Thus, the values of K_{d} and $[\text{OX}]_{\text{eff}}$ were determined from the intercepts and the slopes, respectively, for the straight lines in the plots of [Phenol] vs. [Phenol]/[Complex].

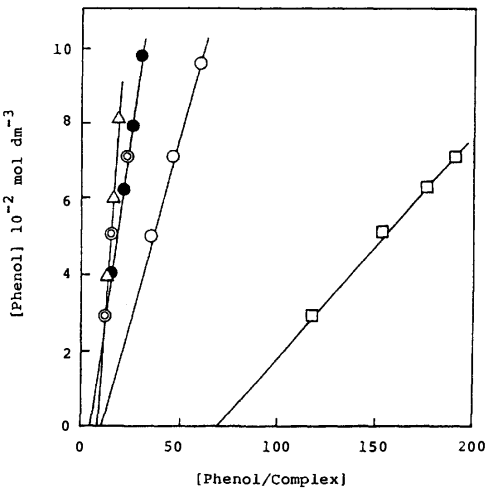

Fig. 1. Plots of [Phenol] vs. [Phenol]/[Complex] according to Eq. 1. △, data for POPA; ○, data for POS 1; ◎, data for POS 2; ●, data for POS 3; □, data for PHS.

Table 2. Complex Formation between the Polymer-Bound 2-Oxazolidinones and Phenol[a]

Substrate	K_{d} 10^{-2} mol dm^{-3}	Concentration of 2-oxazolidinone residue/10^{-3} mol dm^{-3}	
		$[\text{OX}]_{\text{eff}}$	$[\text{OX}]_{\text{charged}}$
PHS	3.83	0.564[b]	33.3[b]
POS 1	1.62	3.79	13.0
POS 2	1.60	3.77	11.9
POS 3	2.12	1.90	7.71
POPA	8.27	8.61	15.2

a) Reacted at 30 °C by using 200 mg of substrate. b) Showed as an amount of repeating unit in poly(4-hydroxystyrene).

The plots of [Phenol] vs. [Phenol]/[Complex] according to Eq. 1 for the polymers anchoring 2-oxazolidinone are shown in Fig. 1. As can be seen from this figure, a definitely linear correlation between [Phenol] and [Phenol]/[Complex] was observed for all the samples. These facts indicate that the 2-oxazolidinones generate a 1 : 1 complex with phenol.

The values of K_{d} and $[\text{OX}]_{\text{eff}}$ evaluated from the

plots in Fig. 1 are summarized in Table 2. It appears that the amount of complex generated between PHS and phenol is sufficiently low to be neglected. The $[OX]_{eff}$ value for POPA containing the OMB moiety indicates that about 57% of 2-oxazolidinone residues in the polymer generated the complex with phenol, while in the case of POS-polymers the amount of reacted phenol increased with an increase in the content of the 2-oxazolidinone residue in the polymers; however, only 20—30% of the polymer-bond 2-oxazolidinones were effectively complexed with phenol. Moreover, the K_d values for POS-polymers decreased with an increase in the content of the 2-oxazolidinone moieties. The variations of the K_d value and the low efficiency for the POS-polymers might be explained as follows: since, as previously described, the 2-oxazolidinone and phenol residues coexist in the POS-poymers, they interact with each other through inter- and intramolecular hydrogen bonding between carbonyl group in 2-oxazolidinone ring and phenolic hydrogen in the polymers; the number of free 2-oxazolidinone moieties decreases pronouncedly, and further complex formation between the previously coordinated 2-oxazolidinone moiety and fresh phenol becomes more difficult; i.e., this difficulty increases with an increase in the number of phenolic hydroxyl groups in the POS-polymer molecule. This explanation also supports the fact that 3-phenycarbamoyl-2-oxazolidinone gave only a small amount of the complex with phenol,[2] because of the intramolecular hydrogen bonding (Fig. 2). On the other hand, the reaction of POPA with phenol gave the highest K_d values of the series. POPA swells in organic solvents, but shrinks in water. The shrinkage of the polymer molecules prevents any effective segregation of the 2-oxazolidinone residues, and enhances the steric repulsion between two bulky phenolic substituents. This logical analysis allows us to conclude that K_d for POPA reaches large values. These results also suggest that the stability of the complexes is associated with the environmental conditions in the vicinity of the 2-oxazolidinone residue, rather than the 2-oxazolidinone content in the polymers.

As described above, the complex formation between polymer-bound 2-oxazolidinone and phenol has been reported only concerning *N*-substituted derivatives, such as polymer **1**. The polymer-phenol complexes were formed through hydrogen bonding between the carbonyl group in the 2-oxazolidinone ring and phenolic hydrogen. In these cases, 41—67% of the polymer-bound 2-oxazolidinones were effectively interacting with phenol.[6,12] However, since the reaction of 3-phenylcarbamoyl-2-oxazolidinone with phenol yielded only a small amount of the complex,[2] and no complex was formed by treating 3,5-diphenyl-2-oxazolidinone with phenol, 3-substituted 2-oxazolidinones are not, necessarily, effective ligands for phenol. On the other hand, the polymer-bound 2-oxazolidinone in this work has a hydrogen on a nitrogen atom adjacent to a carbonyl group in the 2-oxazolidinone ring. In this case, there is a possibility of forming an intramolecular hydrogen bonding between phenolic hydrogen and both N-H and C=O groups in the 2-oxazolidinone ring, as shown in Fig. 3. The IR spectra of the original OMB and the OMB-phenol complex are shown in Fig. 4. Several characteristic shifts observed near 3300 cm^{-1} and in the region 1800—1200 cm^{-1} support the idea that the complex was, indeed, formed through hydrogen bonding (Fig. 3).

Complex Formation of the Polymer-Bound 2-Oxazolidinone with Mercury(II) Acetate. When methanol was used as a solvent for mixing mercury(II) acetate and 2-oxazolidinone, a white precipitate was obtained. The mercury content (48.6%) for the precipitate suggests that one mercury atom formed a 1:2 complex with two moelcules of 2-oxazolidinone (see Table 3). The IR spectra of the starting 2-oxazolidinone and complex are shown in Fig. 5. The

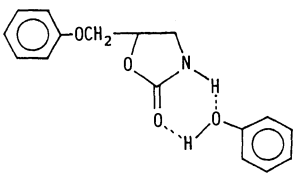

Fig. 3. Structure of the complex between PMO and phenol.

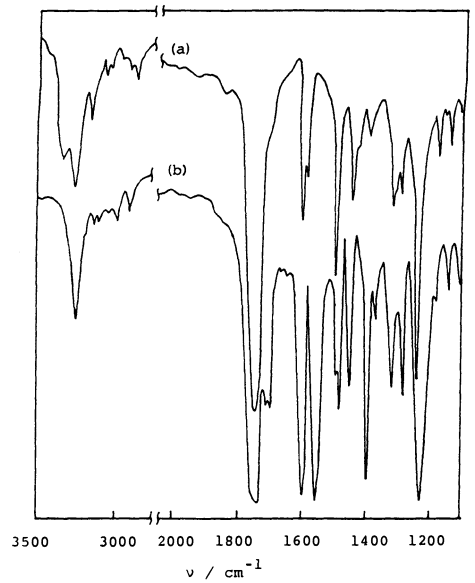

Fig. 4. IR spectra of PMO (chart a) and the complex between PMO and phenol (chart b).

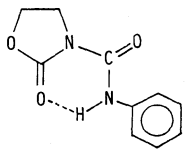

Fig. 2. Intramolecular hydrogen bonding in 3-carbamoyl-2-oxazolidinone.

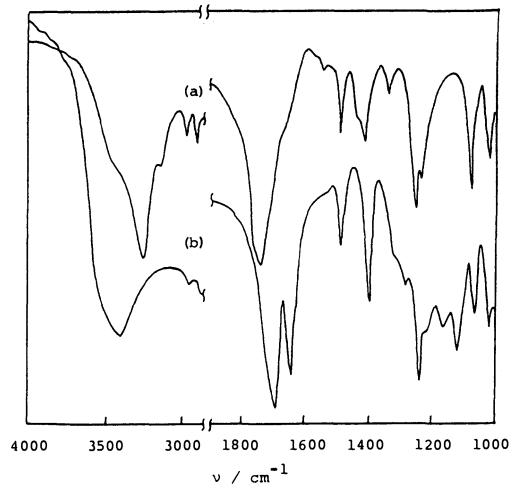

Fig. 5. IR spectra of 2-oxazolidinone (chart a) and the complex obtained from 2-oxazolidinone and mercury(II) acetate (chart b).

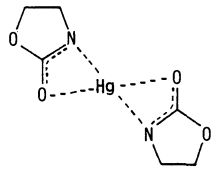

Fig. 6. Structure of the complex obtained from 2-oxazolidinone and mercury(II) acetate.

1740 cm^{-1} absorption band corresponds to the carbonyl stretching of 2-oxazolidinone shifted to 1705 cm^{-1} for the complex. In the case of the complex, furthermore, the 3280 cm^{-1} (N-H of 2-oxazolidinone) absorption band for the 2-oxazolidinone disappeared, and new absorption bands appeared at 1660 cm^{-1} and in the region 1200—1100 cm^{-1}. These two bands correspond to the C=N and C-O stretching vibration in the enol-type form of 2-oxazolidinone, respectively. Endo and co-workers[10] have reported on the formation of a 2 : 1 complex between 2-oxazolidinone and tin(II) chloride, with shifts of the IR absorption bands similar to those for the complex mentioned in this work.

In an ^1H NMR analysis, the chemical shifts of the pertinent protons in 2-oxazolidinone were observed at δ=3.45(t), 4.31(t), and 7.47(s). These signals have been assigned to the protons (H_a) attached to the ring carbon linked to nitrogen, to the protons (H_b) on a carbon atom attached to ring oxygen, and to the proton on the nitrogen atom, respectively.[20] However, the chemical shifts of the pertinent protons in the complex were observed at δ=3.60(t), and 4.30(t). The shift of the signal assigned to protons H_a and the disappearance of the signal assigned to proton on the nitrogen atom suggest that there is a considerable interaction between the mercury atom and the nitrogen atom adjacent to the protons H_a. Since no signal assigned to the pertinent protons in mercury(II) acetate was observed in the ^1H NMR spectrum of the complex, it is evident that the complex does not contain acetate ions.

Table 3. Complex Formation between the Polymer-Bound 2-Oxazolidinones and Mercury(II) Acetate[a]

Substrate	Amount of charged 2-oxazolidinone residue	Amount of mercury forming the complex	
	mmol	mmol[b]	mmol[c]
POS 1	0.328	0.007	0.164
POPA	0.381	0.160	0.191
OPA-St	0.359	0.079	0.180
OMB	0.262	0.095	0.131
2-Oxazolidinone	0.500[d]	0.226	0.250

a) Reacted at room temp in 10 cm^{-3} of 0.08 mol dm^{-3} mercury(II) acetate aq. solution. b) Determined by the change of absorbance in atomic absorption analysis. c) Calculated on the basis of assumption that the 2-oxazolidinone residue in the polymers and mercury atom formed a 2 : 1 complex. d) Reacted in methanol.

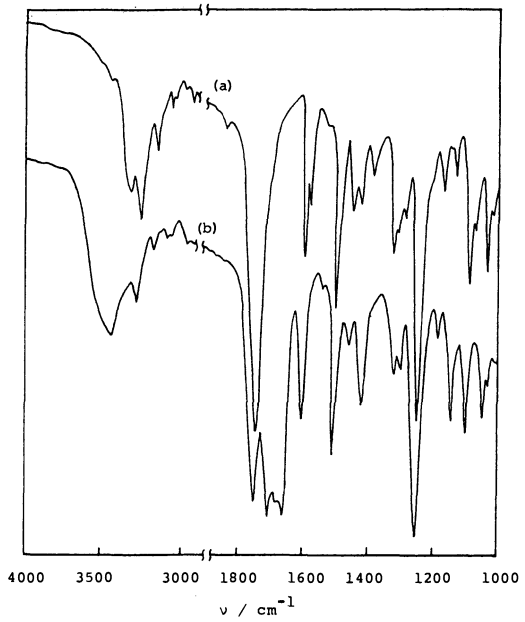

Fig. 7. IR spectra of PMO (chart a) and the complex obtained from PMO and mercury(II) acetate (chart b).

From these results, the reaction of 2-oxazolidinone (OxH) with mercury(II) acetate may be expressed in the form of Eq. 2; it seems reasonable to imagine that the structure of the resulting mercury compound is represented by the formula shown in Fig. 6.

$$2\,OxH + Hg(CH_3COO)_2 \rightarrow Hg(Ox)_2 + 2\,CH_3COOH \quad (2)$$

However, no precipitate was observed in the solution upon treating 2-oxazolidinone with several metal salts, which was tested by other means than mercury(II) acetate in this work. Spectrophotometrical evidence for the complex formation was not obtained.

On the other hand, OMB, POS 1, POPA, and OPA-St were treated with mercury(II) acetate under heterogeneous conditions in water, respectively. The results are listed in Table 3. The mercury content for the

OMB complex was only about 70% of the expected amount on the basis of an assumption that the polymer-bound 2-oxazolidinone and mercury atom formed a 2 : 1 complex. The IR spectra of the original OMB and OMB complex are shown in Fig. 7. As can be seen from the figure, the variations of absorption in both the 3500—3200 and 1740—1660 cm^{-1} regions indicate that the product obtained from OMB and mercury(II) acetate is a mixture of the original OMB and OMB complex, in comparison with Fig. 4. This is believed to be due to the formation of a complex on the solid surface of OMB.

The mercury content for the POPA complex reaches the highest value of the series, except for 2-oxazolidinone, and POPA absorbed about 80% of the amount originally expected. However, the mercury content was larger than that estimated on the basis of the $[OX]_{eff}$ value for complex formation between POPA and phenol. This result suggests that all the mercury atoms absorbed do not necessarily form a 2:1 complex, as shown in Fig. 6. It is thought that a mercury atom that chemically binds one mole of 2-oxazolidinone residue or/and is physically absorbed into polymer networks is present in the POPA-mercury complex. However, in the case of the polymer-mercury complexes, the IR-shifts were not so clearly observed. POS 1 and OPA-St, in spite of 58 and 85 mol% 2-oxazolidinone content, respectively, were not as absorptively effective as we had expected. The mercury contents for the polymers are in the order POPA->OPA-St->POS-complex; this order agrees with the 2-oxazolidinone content in the polymers. As can be seen in Table 3, a slight decrease in the 2-oxazolidinone content in the polymers affects the complex formation in a striking manner. The large discrepancies between the values calculated and determined for POS 1 and OPA-St can be explained on the basis of the assumption that, even if the polymers were used, two 2-oxazolidinone moieties in the polymers are consumed for binding one mercury atom. Since two 2-oxazolidinone moieties in the polymer are very far apart (as a function of the decrease in the 2-oxazolidinone content), their mutual cooperation in forming a 2 : 1 complex is effectively nil. In the case of POPA, therefore, the presumed 1 : 1 complex between the mercury atom and the 2-oxazolidinone residue may be neglected. As described above, POPA is insoluble and swelling in organic solvents and appears to be composed of networks of cross-linked polymers. Mercury(II) acetate which has permeated into the cross-linked POPA would be very difficult to remove, even by repeated washing with water, in comparison with soluble POS 1 and OPA-St.

It is, finally, concluded that one mercury atom forms a 1 : 2 complex with two molecules of 2-oxazolidinone. This relation concerning the molar ratio must apply to all forms of complexes between the mercury atom and the 2-oxazolidinone residue in polymers.

References

1) M. Echstein and W. Dymek, *Diss., Pharm. Pharmacol.*, **22**, 297 (1970).
2) R. A. Hickner and D. W. Bolme, U. S. Patent 3242187 (1966).
3) C. Palomo, *Synthesis*, **1981**, 809.
4) R. A. Hickner, *J. Chem. Eng. Data*, **12**, 413 (1967); T. Ishikawa and Y. Yamazaki, *Nippon Kagaku Kaishi*, **1974**, 1592.
5) W. E. Walls and W. F. Tousignant, *Ind. Eng. Chem.*, **52**, 12 (1960); U. S. Patent 2872321 (1959); 2941907 (1960).
6) W. E. Walls, U. S. Patent 3065130 (1962).
7) T. Ishikawa and N. Watanabe, *Nippon Kagaku Kaishi*, **1980**, 852.
8) T. Endo, R. Numazawa, and M. Okawara, *Bull. Chem. Soc. Jpn.*, **42**, 1101 (1969).
9) E. T. Drechsel, *J. Org. Chem.*, **22**, 849 (1957).
10) A. Kutner, *J. Org. Chem.*, **26**, 3495 (1961).
11) T. Endo and M. Okawara, *Makromol. Chem.*, **112**, 49 (1968).
12) T. Endo, R. Numazawa, and M. Okawara, *Makromol. Chem.*, **123**, 46 (1969).
13) E. D. Little and D. Pickens, U. S. Patent 3157668 (1964).
14) H. P. Price and G. E. Schroll, *J. Org. Chem.*, **32**, 2005 (1967).
15) R. C. Sovish, U. S. Patent 3119833 (1964).
16) J. I. Jones, *J. Chem. Soc.*, **1957**, 2735.
17) Henkel & Cie. G. m. b. H., Fr. Patent 1487641 (1967).
18) A. Hirao, K. Takenaka, S. Packirisamy, K. Yamaguchi, and S. Nakahama, *Makromol. Chem.*, **186**, 1157 (1985).
19) M. Komiyama, I. Sugiura, and H. Hirai, *J. Mol. Catal.*, **36**, 271 (1986).
20) J. E. Herweh, T. A. Foglia, and D. Swern, *J. Org. Chem.*, **33**, 4029 (1968).

 © 1988 The Chemical Society of Japan Bull. Chem. Soc. Jpn., 61, 3565—3568 (1988)

Synthesis and Cation-Complexing Ability of Ferrocene or Ruthenocene Functionalized Crown Ethers Possessing 2,6-Pyridino Moieties

Taeko IZUMI,* Satoshi MURAKAMI, and Akira KASAHARA
Department of Applied Chemistry, Faculty of Engineering, Yamagata University, Yonezawa 992
(Received March 26, 1988)

Keto crown ethers that contain ferrocene or ruthenocene and 2,6-disubstituted pyridine unit as part of the major ring have been reported. These keto crown ethers were synthesized by a reaction of 1,1′-metallocenedicarbonyl dichloride (ferrocene or ruthenocene) with 2,6-bis[ω-hydroxyoligo(oxyethylene)-α-ylmethyl]pyridine by using a high-dilution method. Their complexing ability with metal cations was measured by a solvent-extraction method, and was found to be poor with alkali metal cations but excellent with Ag^+, In^{3+}, and Zr^{4+} cations.

In view of the current interest in the functionality of crown ethers, many research groups have attempted investigations of new-type crown ethers[1] which contain sulfur or nitrogen atoms as well as heterocyclic or metallocene compounds and so on. We have previously described the synthesis and properties of ferrocene-incorporated keto crown ethers;[2] collected information indicates that the pyridyl unit in their crown ethers can be expected to be very efficient regarding cation extraction. Concerning macrocycles possessing subheterocyclic units, it has only been recently that these compounds have been shown to possess unique chemical and biochemical properties.[3] Furthermore, for the purpose of synthesizing crown compounds possessing specific properties, a number of ferrocene-incorporated crown ethers have already been reported; however, a crown ether containing a ruthenocene unit is rare.[4] We herein describe the preparation of multiheteromacrocycles that contain, as part of the major ring, metallocene (ferrocene or ruthenocene) and 2,6-disubstituted pyridine units combined with diester and $-OCH_2CH_2O-$ units, and their ability for forming complexes with various metal cations, including transition metals. In this work we considered (1) the influence of the pyridine unit depending on the ring size, and (2) the difference between ferrocene and ruthenocene on the complexing ability as a macrocycle.

Results and Discussion

Synthesis. Most of the hitherto reported macrocyclic diester compounds have been prepared by reactions between bis(acid chloride)s and diols in various yields, depending upon the ease of cyclization of substrates. In the present study, syntheses of **3** and **3′** were carried out in the presence of triethylamine by a modification of Bradshaw's method.[5]

Compounds **3a—d**, shown in Fig. 1, were prepared from 1,1′-ferrocenedicarbonyl dichloride **1** and an appropriate diol, **2a—d**. The dichloride (**1**) was generated from dicarboxylic acid with oxalyl dichloride in dichloromethane, and used immediately after extraction with hot hexane. Compound **3b**, for example,

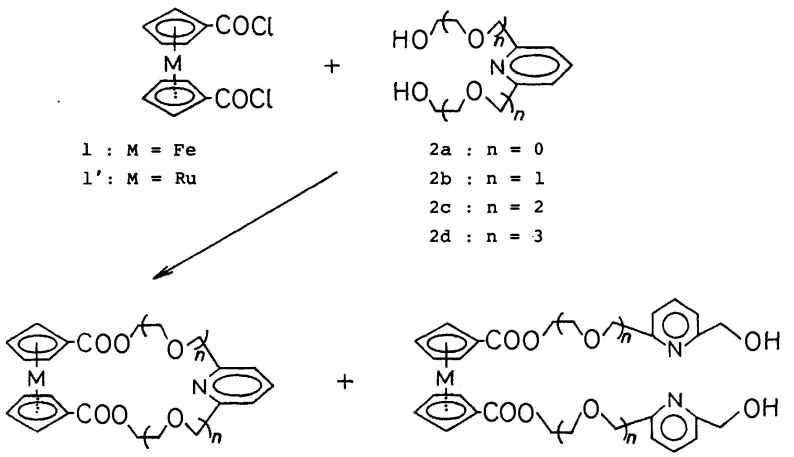

Fig. 1.

was prepared as follows: the reaction was run under high-dilution techniques; **1** was added dropwise to 1.7 equivalents of **2b** at 80 °C for 15 hours then stirred for 24 hours to generate the crown ester compound **3b** (16%) together with 1,1′-ferrocenedicarbonyl-linked bis(pyridinemethanol) **4b** (34%). Furthermore, we initially intended a synthesis to binuclear ferrocenophane[2] using this **4b**; thus, this reaction mole ratio was not optimum for mononuclear ferrocenophane **3b**. An equimolar reaction and prolonged reaction times (36 h) at this esterification stage resulted in a yield of **3b** that approached 30%. The structural assignments for **3a—d** were based on spectral evidence and elemental analyses. The IR spectra of **3a—d** exhibit the characteristic absorption of an ester carbonyl (1715—1725 cm^{-1}), a pyridine ring (1590—1600, 1570—1585 cm^{-1}), and a 1,1′-disubstituted ferrocene ring (3100, 815—840 cm^{-1}).

In the ^1H NMR spectra, all of the pyridinoferrocenophanes (**3a—3d**) showed a similar pattern: ether OCH_2 groups at δ 3.99—3.70, ester $COOCH_2$ groups at δ 4.62—4.36, α-methylene protons of pyridine as sharp singlet at δ 5.36—4.62, α and β ring protons of the ferrocene as the A_2B_2 pattern at δ 4.92—4.77 and 4.43—4.38, and pyridine protons at δ 7.76—7.06. For example, the ^1H NMR spectrum of **3b** has seven signals: doublet of doublets at δ 4.40 and 3.99 for the methylene protons of bridges, two triplets centered at δ 4.77 and 4.43 for the ferrocene ring protons, a singlet at δ 4.86 for α-methylene protons of pyridine, a double doublet at δ 7.76 for γ-protons, and a doublet at δ 7.38 for β-protons of the pyridine ring, respectively. A distinct downfield shift for α-methylene protons of a pyridine ring, could be explained by a deshielding effect by the pyridine π face. The mass spectra and elemental analyses also confirmed the structures.

The case of pyridinoruthenocenophane (**3′a—3′d**) also afforded a similar result (see Table 1). The general procedure was conducted in an analogous manner to the synthesis of pyridinoferrocenophane, except for the substitution of 1,1′-ruthenocenedicarbonyl dichloride (**1′**) for 1,1′-ferrocenedicarbonyl dichloride (**1**). In the ^1H NMR spectral data for **3′a—3′d**, very little change in the chemical shifts for the β-protons and α-methylene protons of pyridine ring were observed.

Table 1. Reaction of 1,1′-Metallocenedicarbonyl Dichloride(M=Fe, Ru) with 2,6-Bis(ω-hydroxy substituted)pyridines(**2**)

Metallocene-dicarbonyl dichloride	Diol **2**		Product	Yield/%	Mp θ_m/°C
M=Fe	**1**	n=0	**3a**	9	240—242 (decomp)
			4a	19	Oil
	1	n=1	**3b**	16	114—115
			4b	34	Oil
	1	n=2	**3c**	18	76—77
			4c	30	Oil
	1	n=3	**3d**	12	Oil
			4d	21	Oil
M=Ru	**1′**	n=0	**3′a**	8	233—234
			4′a	45	Oil
	1′	n=1	**3′b**	20	124—125
			4′b	45	Oil
	1′	n=2	**3′c**	22	84—85
			4,c	40	Oil
	1′	n=3	**3′d**	12	Oil
			4′d	47	Oil

Extraction Ability. Concerning the influence of the functional parts of crown ethers toward the complexing ability, we already know the following. The introduction of carbonyl to crown ethers produces a product that is different from a simple crown ether. The characteristics include: 1) a destabilizing effect on the complex and/or 2) a reversal of the K^+-Ba^{2+} selectivity sequence, distinguishing features of naturally occurring antibiotic macrocycles.[6] Furthermore, complexes of a pyridine-incorporated cyclic polyether compound with Na^+, K^+, Ag^+, and Ba^{2+} showed unusual stabilities,[7] even though nitrogen-incorporated crown ethers caused a considerable drop in the stability of the K^+ complexes.[8] The complexing ability of the synthesized pyridinometallocenophanes were assessed by a solvent extraction of alkali, alkaline earth, and heavy-metal picrates with dichloromethane solutions of the ligands. The data are summarized in

Table 2. Extraction Data (Water-Dichloromethane)[a]

Compound	Extracted/%																
	Li^+	Na^+	K^+	Rb^+	Cs^+	Mg^{2+}	Ca^{2+}	Sr^{2+}	Ba^{2+}	Al^{3+}	In^{3+}	Tl^+	Ce^{3+}	Ag^+	Hg^{2+}	Pb^{2+}	Zr^{4+}
3a	1.4	10.1	11.4	5.5	2.1	2.9	3.6	2.1	5.7	5.0	72.8	2.1	1.4	14.3	3.6	6.4	85.4
3b	4.0	4.6	5.4	9.9	3.7	3.6	3.1	3.1	5.1	24.5	85.7	5.6	7.7	84.0	4.3	8.9	90.1
3c	6.7	17.7	19.0	15.4	3.0	9.7	9.7	10.7	11.4	47.5	93.4	52.3	15.7	95.6	19.1	63.2	93.4
3d	11.5	11.5	44.6	26.6	2.1	10.3	9.3	24.5	14.1	10.4	88.1	74.9	2.6	96.0	22.1	43.1	88.1
3′a	1.4	0	1.4	1.0	1.1	1.4	1.0	0.7	1.0	5.0	60.7	1.4	1.4	17.9	4.3	1.0	69.3
3′b	1.4	0	0	1.4	1.0	1.4	1.4	1.4	0	5.0	61.4	2.8	1.0	59.0	4.3	2.9	72.0
3′c	1.4	1.4	2.1	2.9	2.9	4.3	4.3	3.6	1.4	11.4	81.4	21.0	3.9	91.0	6.4	40.0	84.3
3′d	1.4	1.4	4.2	2.9	1.0	1.4	2.6	1.4	0	11.7	80.4	17.8	1.4	86.4	7.1	30.7	84.3

a) Equal volumes of water and dichloromethane, and picric acid at 7.0×10^{-5} M(1M=1 mol dm^{-3}). Concentration of ferrocenophane: 7.0×10^{-4} M. Concentration of metal nitrate: 0.1 M.

Table 2. These two groups of pyridinometallocenophanes (M=Fe and Ru) showed a similar tendency regarding a low extractability toward alkali metal and alkaline earth metal cations, and a high extractability toward heavy-metal cations, in particular for Ag^+. Ferrocenophane, as a whole, however, showed a higher cation-binding ability compared to ruthenocenophane. For example, regarding the extractability toward a K^+ cation, **3a**, **3c**, and **3d** (M=Fe), expect **3b**, showed a moderate extractability and a similar K^+-Ba^{2+} selectivity sequence as was described above (due to an ester carbonyl); however, **3'a—3'd** (M=Ru) showed almost no extractability. These results indicate the distinction between ruthenium and iron(II) as the central metal of metallocene, as well as the cavity size. It is also interesting that the extraction ability of almost all pyridinometallocenophanes showed a remarkable dependence on the cavity size in the macrocycle of **3a—3d** and **3'a—3'd**; especially **3d** (n=3) and **3'c** (n=2) showed the best ability for Ag^+.

Furthermore, our original intention to introduce a pyridine moiety to metallocenophane in order to enhance the cation binding ability and selectivity has been accomplished. The effects of this pyridine are clear, compared with the results of the 1,1'-ferrocenyl keto crown ether, which we reported before.[2] A similar trend of affinity toward transition metal cations has been observed regarding hitherto reported "crowned" ferrocenophane as well as synthesized pyridinometallocenophanes; this suggests that the metal atom of the metallocene nucleus participates in the complexation process. It should be emphasized that all synthesized pyridinometallocenophanes are capable of forming stable complexes with silver (not an oxidative decomposition).

Experimental

Materials and Measurements. All melting points are uncorrected. 2,6-Bis(hydroxymethyl)pyridine, diethylene glycol, triethylene glycol were commercial products.

1,1'-Ferrocenedicarboxylic acid[9] and 1,1'-ruthenocenedicarboxylic acid[10] were prepared by methods described in the literature. The other reagents employed were commercial materials or were prepared by the usual methods. All inorganic compounds were reagents grade. The IR, ^{1}H NMR, and mass spectra were recorded on Hitachi 260-10, Hitachi R-22, and Hitachi RMU-6M spectrometers, respectively.

Synthesis of 2,6-Bis(ω-hydroxy substituted)pyridine (2) (n=1—3). Sodium 2-hydroxyethoxide was prepared from sodium methoxide (0.02 mol, 1.1 g) and dry ethylene glycol (0.05 mol, 3.1 g) in 20 cm^3 of ether with stirring at 40 °C for 4 h. Ether was removed in vacuo, and the residue was dissolved in 50 cm^3 of dry THF. To the solution, 2,6-bis(chloromethyl)pyridine (0.01 mol, 1.76 g) in 150 cm^3 of dry THF was added dropwise for 12 h at 55 °C; additional refluxing took place for 8 h. Sodium chloride salt was filtered off; the filtrate was then concentrated in vacuo, and the residue purified by silica-gel column chromatography. The first fraction yielded unreacted ethylene glycol; the second fraction gave 1.8 g (80%) of diol **2b** (n=1) as a pale-yellow viscous oil.

Diols **2c** (n=2) and **2d** (n=3) were also prepared by the above-mentioned procedure, except that diethylene glycol and triethylene glycol were used as a substitute for ethylene glycol, respectively. Along with unreacted diethylene glycol and triethylene glycol, the major isolated fraction was diol **2c** (74%) and **2d** (75%) as a pale-yellow viscous oil, respectively.

2,6-Bis[(2-hydroxy)methyl]pyridine (2b).[11] **2,6-Bis[[2-(2-hydroxyethoxy)ethoxy]methyl]pyridine (2c).** IR (neat) 3430—3350, 2930—2860, 1600, 1580 cm^{-1}. ^{1}H NMR ($CDCl_3$): δ=3.63—3.72 (m, -C<u>H</u>$_2$-C<u>H</u>$_2$-, 16H), 3.83 (s, -O<u>H</u>, 2H), 4.66 (s, Py-C<u>H</u>$_2$-, 4H), 7.35 (d, 3,5-Py<u>H</u>, 2H, J=8 Hz), 7.72 (d-d, 4-Py<u>H</u>, 1H, J=8 and 9 Hz). MS (70 eV) m/z 315 [M$^+$].

2,6-Bis[[[2-(2-hydroxyethoxy)ethoxy]ethoxy]methyl]pyridine (2d). IR (neat) 3400, 2900—2850, 1570, 1590 cm^{-1}. ^{1}H NMR ($CDCl_3$) δ=2.85 (br-s, -O<u>H</u>, 2H), 3.70—3.75 (m, -C<u>H</u>$_2$C<u>H</u>$_2$-, 24H), 4.68 (s, Py-C<u>H</u>$_2$-, 4H), 7.37 (d, Py-<u>H</u>, 2H, J=8 Hz), 7.73 (d-d, Py-<u>H</u>, 1H, J=8 and 9 Hz). MS (70 eV) m/z 403 [M$^+$].

Synthesis of 3a—d and 3'a—d. General Procedure. 1 was prepared from 1,1'-ferrocenedicarboxylic acid and oxalyl dichloride by a method described in the literature.[12] Under an atmosphere of nitrogen, to a solution of **1** (2.2 g, 7 mmol) and triethylamine (1.2 g, 12 mmol) in dry benzene (150 cm^3), diol **2** (n=0—3) (12 mmol) diluted with dry benzene (100 cm^3) and dry THF (50 cm^3) was added dropwise over 15 h with stirring. An additional 24 h period of gentle refluxing followed. After removing the solvent under reduced pressure, the residue was purified by silica-gel column chromatography. The first fraction eluted with benzene or chloroform gave pyridinoferrocenophane (**3a—d**); the second fraction eluted with chloroform-methanol (20 : 1) gave 1,1'-ferrocene dialcohol (**4a—d**) as a reddish oil. The crude product was recrystallized from benzene-hexane.

Pyridinoruthenocenophane (**3'a—d**) was also prepared by a reaction of **1'** (1.1 g, 3.1 mmol) and diol **2** (n=0—3) (6.2 mmol) through the above-mentioned method. The results are summarized in Table 1.

2,11-Dioxa[3](2,6)pyridino[3](1,1')ferrocenophane-1,12-dione(3a).[2] **2,5,14,17-Tetraoxa[6](2,6)pyridino[6](1,1')ferrocenophane-1,18-dione (3b).** IR(KBr) 3105, 2990, 2850, 1715, 1600, 1580 cm^{-1}. ^{1}H NMR ($CDCl_3$) δ=3.99 (d-d, 4H, -C<u>H</u>$_2$C<u>H</u>$_2$- J=4 and 7 Hz), 4.40 (m, 4H, -COOC<u>H</u>$_2$-), 4.43 (t, 4H, Fc-<u>H</u>$_\beta$, J=4.5 Hz), 4.77 (t, 4H, Fc-<u>H</u>$_\alpha$, J=4.5 Hz), 4.86 (s, 4H, Py-C<u>H</u>$_2$-), 7.38 (d, 2H, 3,5-Py<u>H</u>, J=8 Hz), 7.76 (d-d, 1H, 4-Py<u>H</u>, J=8 and 9 Hz). MS (70 eV) m/z 465 [M$^+$]. Found: C, 59.31; H, 4.93%. Calcd for $C_{23}H_{23}FeNO_6$: C, 59.37; H, 4.98%; M, 465.29.

2,5,8,17,20,23-Hexaoxa[9](2,6)pyridino[9](1,1')ferrocenophane-1,24-dione (3c). IR(KBr) 3105, 2960—2870, 1725, 1600, 1580 cm^{-1}. ^{1}H NMR ($CDCl_3$) δ=3.77 (br-s, 12H, -C<u>H</u>$_2$OC<u>H</u>$_2$C<u>H</u>$_2$-), 4.30—4.42 (m, 8H, -COOC<u>H</u>$_2$-+Fc-<u>H</u>$_\beta$), 4.67 (s, 4H, Py-C<u>H</u>$_2$-), 4.77 (t, 4H, Fc-<u>H</u>$_\alpha$, J=4.5 Hz), 7.35 (d, 2H, 3,5-Py<u>H</u>, J=8 Hz), 7.68 (d-d, 1H, 4-Py<u>H</u>, J=8 and 9 Hz). MS (70 eV) m/z 553 [M$^+$]. Found: C, 58.64; H, 5.61%. Calcd for $C_{27}H_{31}FeNO_8$: C, 59.60; H, 5.64%; M, 553.39.

2,5,8,11,20,23,26,29-Octaoxa[12](2,6)pyridino[12](1,1')-ferrocenophane-1,30-dione (3d). IR (neat) 3100, 2970—2880, 1720, 1600, 1585 cm^{-1}. ^{1}H NMR ($CDCl_3$) δ=3.70 (br-s, 20H, -C<u>H</u>$_2$OC<u>H</u>$_2$C<u>H</u>$_2$OC<u>H</u>$_2$C<u>H</u>$_2$-), 4.36 (m, 8H, -COOC<u>H</u>$_2$-+Fc-<u>H</u>$_\beta$), 4.62 (s, 4H, Py-C<u>H</u>$_2$-), 4.79 (t, 4H, Fc-<u>H</u>$_\alpha$, J=4.5 Hz), 7.35 (d, 2H, 3,5-Py<u>H</u>, J=8 Hz), 7.65 (d-d, 1H, 4-Py<u>H</u>, J=8

and 9 Hz). MS (70 eV) m/z 641 [M^+]. Found: C, 58.10; H, 6.09%. Calcd for $C_{31}H_{39}FeNO_{10}$: C, 58.04; H, 6.13%; M, 641.50.

2,11-Dioxa[3](2,6)pyridino[3](1,1')ruthenocenophane-1,12-dione (3'a). IR (KBr) 3100, 2930, 1720, 1600, 1585, 1295, 1150 cm^{-1}. ^1H NMR ($CDCl_3$) δ=4.72 (t, 4H, Rc-H$_\beta$, J=4.5 Hz), 5.32 (s, 8H, Rc-H$_\alpha$+Py-CH$_2$-), 7.04 (d, 2H, 3,5-PyH, J=8 Hz), 7.63 (d-d, 1H, 4-PyH, J=8 and 9 Hz). MS (70 eV) m/z 422 [M^+]. Found: C, 54.07; H, 3.61%. Calcd for $C_{19}H_{15}RuNO_4$: C, 54.03; H, 3.58%; M, 422.40.

2,5,14,17-Tetraoxa[6](2,6)pyridino[6](1,1')ruthenocenophane-1,18-dione (3'b). IR (KBr) 3100, 2950—2860, 1715, 1590, 1570, 1275, 1145 cm^{-1}. ^1H NMR ($CDCl_3$) δ=3.85 (d-d, 4H, -CH$_2$O-, J=5 and 8Hz), 4.28 (d-d, 4H, -COOCH$_2$-, J=5 and 8 Hz), 4.70 (t, 4H, Rc-H$_\beta$, J=4.5 Hz), 4.76 (s, 4H, Py-CH$_2$-), 5.08 (t, 4H, Rc-H$_\alpha$, J=4.5 Hz), 7.34 (d, 2H, 3,5-PyH, J=8 Hz), 7.74 (d-d, 1H, 4-PyH, J=8 and 9 Hz). MS (70 eV) m/z 510 [M^+]. Found: C, 54.06; H, 4.57%. Calcd for $C_{23}H_{23}RuNO_6$: C, 54.11; H, 4.54%; M, 510.51.

2,5,8,17,20,23-Hexaoxa[9](2,6)pyridino[9](1,1')ruthenocenophane-1,24-dione (3'c). IR (KBr) 3070, 2940—2840, 1715, 1590, 1570, 1275, 1135 cm^{-1}. ^1H NMR ($CDCl_3$) δ=3.65—3.80 (br-s, 12H, -CH$_2$OCH$_2$CH$_2$O-), 4.28 (d-d, 4H, -COOCH$_2$-, J=5 and 6 Hz), 4.66 (t, 4H, Rc-H$_\beta$, J=4.5 Hz), 4.69 (s, 4H, Py-CH$_2$-), 5.06 (t, 4H, Rc-H$_\alpha$, J=4.5 Hz), 7.35 (d, 2H, 3,5-PyH, J=8 and 9 Hz), 7.69 (d-d, 1H, 4-PyH, J=8 and 9 Hz). MS (70 eV) m/z 598 [M^+]. Found: C, 54.15; H, 5.27%. Calcd for $C_{27}H_{31}RuNO_3$: C, 54.17; H, 5.21%; M, 598.62.

2,5,8,11,20,23,26,29-Octaoxa[12](2,6)pyridino[12](1,1')-ruthenocenophane-1,30-dione (3'd). IR (neat) 3100, 2950—2850, 1720, 1595, 1580, 1280, 1150 cm^{-1}. ^1H NMR ($CDCl_3$) δ=3.74 (br-s, 20H, -CH$_2$OCH$_2$CH$_2$OCH$_2$CH$_2$O-), 4.30 (d-d, 4H, -COOCH$_2$-, J=5 and 6 Hz), 4.66 (s, 4H, Py-CH$_2$-), 4.70 (t, 4H, Rc-H$_\beta$, J=4.5 Hz), 5.14 (t, 4H, Rc-H$_\alpha$, J=4.5 Hz), 7.34 (d, 2H, 3,5-PyH, J=8 Hz), 7.71 (d-d, 1H, 4-PyH, J=8 and 9 Hz). MS (70 eV) m/z 686 [M^+]. Found: C, 54.19; H, 5.71%. Calcd for $C_{31}H_{39}RuNO_{10}$: C, 54.22; H, 5.72%; M, 686.72.

Solvent Extraction Experiments of Metal Ions. The extraction ability of synthesized polyoxapyridinometallocenophanes with metal picrates was examined by a method described in a previous paper.[2)]

References

1) J. S. Bradshaw, "Syntheses of Multidentate Compounds. In Synthetic Multidentate Macrocyclic Compounds," ed by R. M. Izatt and J. J. Christensen, Academic Press, New York (1977).

2) T. Izumi, T. Tezuka, S. Yusa, and A. Kasahara, *Bull. Chem. Soc. Jpn.*, **57**, 2435 (1984).

3) G. R. Newkome, J. D. Sauer, J. M. Roper, and D. C. Hager, *Chem. Rev.*, **77**, 513 (1977).

4) S. Akabori, H. Munegumi, Y. Habata, S. Sato, K. Kawazoe, C. Tamura, and M. Sato, *Bull. Chem. Soc. Jpn.*, **58**, 2185 (1985); Y. Habata, S. Akabori, and M. Sato, *Bull. Chem. Soc. Jpn.*, **58**, 3540 (1985); S. Akabori, S. Sato, T. Tokuda, Y. Habata, K. Kawazoe, C. Tamura, and M. Sato, *Bull. Chem. Soc. Jpn.*, **59**, 3189 (1986); P. J. Hammond, P. D. Beer, C. Dudman, I. P. Danks, C. D. Hall, J. Knychla, and M. C. Grossel, *J. Organomet. Chem.*, **306**, 367 (1986).

5) J. S. Bradshaw and M. D. Thompson, *J. Org. Chem.*, **43**, 2456 (1978).

6) R. M. Izatt, J. D. Lamb, G. E. Maas, R. E. Asay, J. S. Bradshaw, and J. J. Christensen, *J. Am. Chem. Soc.*, **99**, 365 (1977).

7) R. M. Izatt, J. D. Lamb, R. E. Asay, G. E. Maas, J. S. Bradshaw, and J. J. Christensen, *J. Am. Chem. Soc.*, **99**, 6134 (1977).

8) H. K. Frensdorff, *J. Am. Chem. Soc.*, **93**, 600 (1971).

9) M. Okawara, Y. Takemoto, H. Kitaoka, H. Haruki, and E. Imoto, *Kogyo Kagaku Zasshi*, **65**, 685 (1962).

10) M. D. Pausch, E. O. Fischer, and H. Grubert, *J. Am. Chem. Soc.*, **82**, 76 (1960).

11) T. W. Bell, P. G. Cheng, M. Newcomb, and D. J. Cram, *J. Am. Chem. Soc.*, **104**, 5185 (1982).

12) F. W. Knobloch and W. H. Rauscher, *J. Polymer Sci.*, **54**, 651 (1961).

 © 1988 The Chemical Society of Japan Bull. Chem. Soc. Jpn., 61, 3569—3573 (1988)

Photochemical Fatigue Resistances and Thermal Stabilities of Heterocyclic Fulgides in PMMA Film[1)]

Akira KANEKO, Akihiko TOMODA, Mitsuo ISHIZUKA, Hisao SUZUKI, and Ryoka MATSUSHIMA*,†
Polymer Science Department, Basic Research Development Laboratory, Toyooka Plant, Yamaha Co., Toyooka-mura, Iwata-gun, Shizuoka-ken 438-01
†Department of Applied Chemistry, Faculty of Engineering, Shizuoka University, Hamamatsu 432
(Received April 14, 1988)

Thermal stabilities of the colored forms at 80 °C and photochemical fatigue resistances against coloration-discoloration cycles were measured in PMMA thin film, using 14 derivatives of fulgide with different heterocyclic structures. The indolyl (**12**), oxazolyl (**13**), and thiazolyl (**14**) derivatives showed very low thermal degradabilities (TD≦1.5%/day) while **12** and pyrazolyl derivative (**9**) showed low photochemical fatigues (PF≦0.2%/cycle), as compared with the furyl (**1**), thienyl (**2**), and pyrrolyl (**3**) derivatives. However, many of them featured low photo-responsiveness and low absorptivities for coloration on UV irradiation.

Molecular-structural modifications are powerful and interesting methods for research and development of photochromic materials, e.g., thermally stable and photochemically fatigue-resistant 1,2-diarylethenes,[2)] spiropyrans,[3)] and highly photoresponsive heterocyclic fulgides[4-6)] and spiropyrans.[7)]

Though furyl (**1**),[8)] thienyl (**2**),[9,10)] and pyrrolyl (**3**)[4)] derivatives have been studied in some detail in solution as well as in polymeric media,[5,10)] other heterocyclic fulgides seem to have been scarcely studied. Nor has been the relationship between the heteroaromatic ring structure and the photochromic properties clarified. In order to realize the potential utility of photochromic organic compounds in optical memory devices, extensive studies in solid polymers are needed,[11)] clarifying the medium effects as well as the structure-activity relationships.

This work has been undertaken to investigate the effects of the heteroaromatic ring structure (Ar) on the photochromic properties, particularly thermal stabilities and photochemical fatigue resistances, in PMMA†† thin film as compared in dilute solution, using a wide variety of fulgides **1**—**14** (Scheme 1).

Results and Discussion

Absorption Spectra and Photochromic Properties. Figure 1 illustrates the spectra of **1** and their changes on alternative irradiations of UV and visible light in dilute toluene solution (a) and PMMA thin film (b). A photostationary state (pss) of coloration was attained by irradiation of **1E** (curve 0) with UV light in 30—60 s, hereafter the absorbance value in the visible band (A_0, curve 1) was no more increased on further UV irradiation. Subsequent irradiation with visible light led to rapid discoloration (in ca. 60 s). Similar colora-

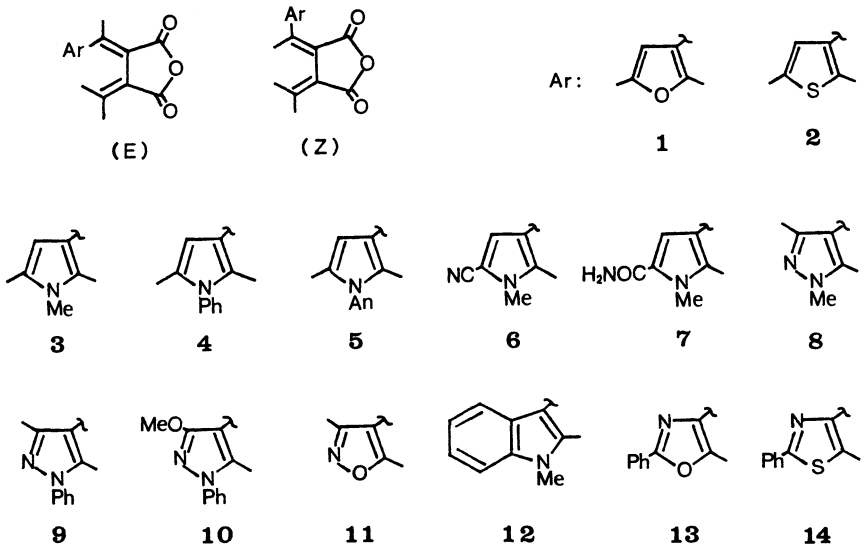

Scheme 1.

Heterocyclic fulgides. Methyl substituents on carbon atoms are denoted by bars for simplification.

†† PMMA=poly(methyl methacrylate).

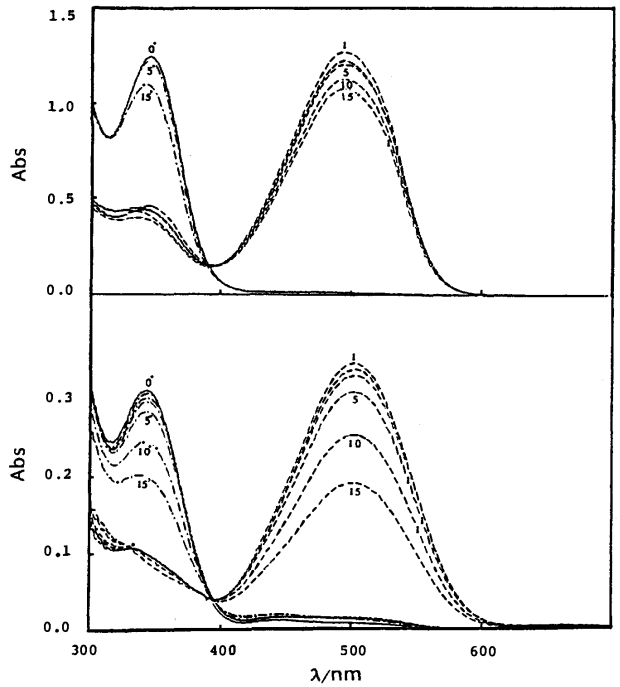

Fig. 1. Reversible changes in the absorption spectra of **1** on alternative irradiations with UV and visible light. (a) 2.0×10^{-4} mol dm^{-3} solution in toluene, (b) 15 wt% in PMMA film of 1.0 μm thickness. Curve 0: **1E** before irradiation, curve 1: after UV irradiation for 30 s. Absorption curves around 500 nm refer (from the top) to the colored forms after 2, 3, 5, 10, and 15 cycles of repeated coloration-discoloration reaction, while curves around 340 nm refer to the uncolored forms.

Table 1. Absorption Properties of Fulgides in PMMA Film[a)]

Fulgide	Uncolored form[b)]		Colored form[c)]	
	λ_E/nm	A_E	λ_C/nm	A_0
1	344	0.31	503	0.40
2[d)]	335(Z340)	0.31(Z0.33)	526	0.20
3	370 sh	0.26	662	0.10
4	379	0.32	635	0.20
5	380	0.14	636	0.10
6	345	0.50	579	0.16
7	355	0.10	629	0.05
8[e)]	336	0.35	546	0.04
9[e)]	336	0.38	539	0.04
10			545	0.06
11[e)]	304	0.27	435	0.04
12[e)]	392	0.35	589	0.07
13	338	0.52	462	0.45
14[d)]	305(Z310)	0.55(Z0.70)	486	0.29

a) PMMA film of 1.0 μm thickness containing 15 wt% of fulgide. b) Values in parentheses refer to *Z*-isomers. c) A_0 refers to the absorbance value at photostationary state attained on UV irradiation. d) Initial form was *Z*-isomer, which rapidly isomerized into *E*-isomer on UV irradiation. e) Initially a mixture of *E*/*Z* isomers, which rapidly changed into *E*-isomer on UV irradiation.

tion-discoloration cycles were repeated a number of times (curves *n*). The absorption properties of the colored forms (λ_C and A_0), obtained at the initial pss of coloration, are summarized in Table 1 together with those of the uncolored (*E*)-isomers (λ_E and A_E). The absorption maxima of the colored forms tend to red shift with the electron-donating ability of the heterocyclic groups, e.g., the λ_C increases in the order **1C**<**2C**<**3C**, **6C**<**7C**<**3C**, and **9C**<**8C**≪**4C**<**3C**, respectively. This suggests that the electronic transitions of the colored forms involve intramolecular electron migration from the heteroatoms to the carbonyl groups.

The absorbance values (A_0) attained at pss for coloration are low with **7**—**12**. The ^{1}H NMR spectra of the photolyzed mixtures (pss) of **9**, **12**, and **14** in $CDCl_3$ implied that the mole fractions of the colored forms were in the range of 15—40%. Also, a molecular model suggests that the steric repulsions between the 4-methyl groups and the 3-substituents of **8**—**12C** should hinder the coplanar configuration. Such poor coplanarity would lead to a poor overlapping of the pertinent orbitals and lower the transition probability (or extinction coefficient) for light absorption.[12] Further, **9**, **12**, and **14** featured rather low photo-responsiveness for coloration, thus their quantum yields (below 0.1) were significantly lower compared with 0.20 of **1**.[5,8]

It is speculated that the steric hindrance of the substituents (**9**, **12**) and/or the higher stabilities of the heteroaromatic groups depress the rate of the cyclization reaction as well as the C/E ratio at pss.

Photochemical Fatigues. As illustrated in Fig. 1 the reversibilities of the absorption spectra of **1**, on repeated coloration-discoloration cycles, are rather poor in PMMA film (b) while moderate in dilute toluene solution (a). This implies a significant effect of the medium and/or concentration of the solute on the photochemical fatigue. As a numerical measure for relative photochemical fatigue, a quantity PF=$(A_0-A)/nA_0$ was evaluated where A_0 and A are the absorbance values at pss attained on the lst and nth cycles of coloration, respectively. Table 2 lists the PF values of various fulgides obtained within half-lives, while Fig. 2 illustrates the plots of the fatigue resistance A/A_0 over a wide range of cycles. Fulgides **8**, **9**, and **12** show excellent fatigue resistances compared with **1**—**3**. The PF values of **4**—**12** are little affected by the medium and/or concentration. The high fatigue resistances and low medium dependences of **8**—**10**, **12**, and **13** are attributable to the high chemical stabilities of the heterocyclic groups.

Thermal Stabilities of the Colored Forms. Figure 3 illustrates thermal degradations of the colored forms in PMMA film at 80 °C in the dark. Similar tendence was obtained at 50 °C though more stable. As a measure for relative thermal degradability of the colored forms, a quantity TD=$(A_0-A)/dA_0$ has been evaluated, where A_0 refers to the initial absorbance value of the colored form and A is that measured after d days of

Table 2. Photochemical Fatigues and Thermal Degradabilities of Fulgides in PMMA Film[a)]

Fulgide	Photochemical fatigue[b)]			Thermal degradability[c)]		
	Cycle	$(A_0-A)/A_0$	PF/%	Time/day	$(A_0-A)/A_0$	TD/%
1	18(15)	0.50(0.10)	2.8(0.7)	1	0.90	90
2	16(15)	0.50(0.22)	3.1(1.4)	10	0.35	3.5
3	12(15)	0.50(0.42)	4.2(2.8)	1	0.70	70
4	20(15)	0.42(0.38)	2.1(2.6)	1	0.55	55
5	17(15)	0.50(0.36)	3.0(2.4)	1	0.60	60
6	6(8)	0.50(0.50)	8.3(6.2)	5	0.50	10
7	10(9)	0.50(0.50)	5.0(5.5)	1	0.50	50
8	20(15)	0.03(0.02)	0.2(0.2)	6	0.50	8.3
9	20(15)	0.03(0.03)	0.2(0.2)	10	0.35	3.5
10	(15)	(0.05)	(0.3)	10	0.45	4.5
11	15(15)	0.20(0.10)	1.3(0.7)	1	0.95	95
12	20(15)	0.02(0.02)	0.1(0.1)	10	0.13	1.3
13	50	0.40	0.8	10	0.07	0.7
14	10(10)	0.25(0.10)	2.5(1.0)	10	0.05	0.5

a) Experimental conditions are shown in the legends of Figs. 2 and 3. b) $PF=(A_0-A)/n\,A_0$, as a measure for photochemical fatigue, where n is the number of repeated cycles. Values in parentheses refer to the data in dilute toluene solution (2×10^{-4} mol dm^{-3}). c) $TD=(A_0-A)/d\,A_0$, as a measure for thermal degradability of colored forms, where d refers to the heating time (day) at 80 °C in the dark.

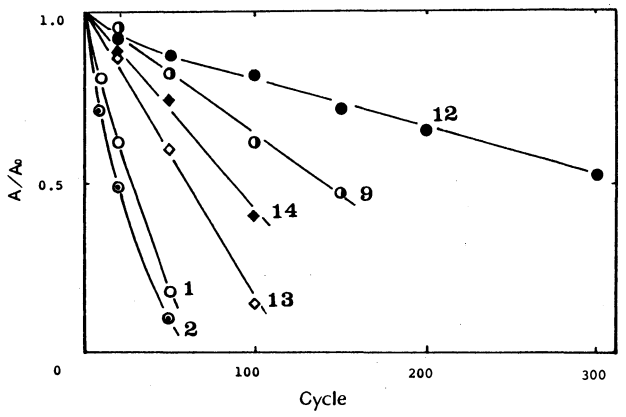

Fig. 2. Photochemical fatigues of fulgides by repeated coloration-discoloration cycles in PMMA film. PMMA film was of 1.0 μm thickness containing 15—20 wt% of fulgide.

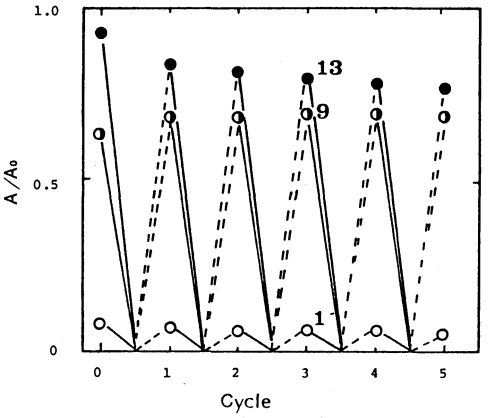

Fig. 4. Photochromic properties of the fulgides which had previously been heated at 80 °C for 10 days in PMMA film. Irradiated with visible (——) and UV (----) light at room temperature; **1** (○), **9** (◑), **13** (●).

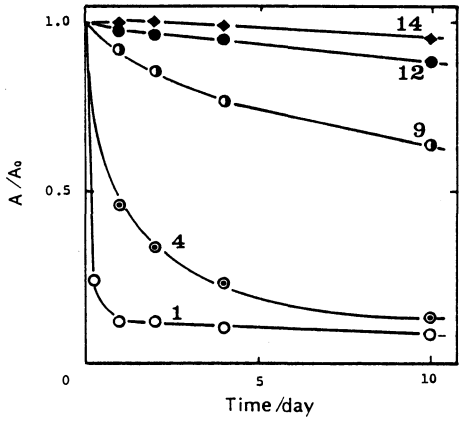

Fig. 3. Thermal degradations of the colored forms in PMMA film at 80 °C. PMMA film containing fulgide (15—20 wt%) had been previously irradiated with UV light leading to the photostationary state for coloration.

heating at 80 °C. The TD values of different fulgides are listed in Table 2. Figure 3 and Table 2 show a wide variation in the thermal stability: excellent stabilities with **12—14C**, fairly good with **2C** and **8—10C**, but poor with **1C** and **3—5C**.

Figure 4 shows the photochromic properties of the colored forms which had been heated at 80°C for 10 days in PMMA film. While **1** show little, **9** and **13** show substantial retainments of their photochromic properties, demonstrating their excellent thermal and photochemical fatigue resistances. With the fused benzene ring (**12**) or electronegative heteroatoms (**9**, **13**, **14**), the heterocyclic double bonds (both in the colored and uncolored forms) are considered to be stabilized and resistant to photochemical and thermal side reactions such as bimolecular cycloadditions[6)] and oxida-

Table 3. Physical Constants and Analytical Data of Heterocyclic Fulgide[a)]

Fulgide	Mp	^{1}H NMR, δ in $CDCl_3$				Found (Calcd)/%				*m/z*
	θ_m/°C	-CH_3(3H, s)			-CH= and others	C	H	O	N	M^+
5E	120—123	1.32	1.65	1.97	5.90(1H, s)	72.02	6.46	17.75	3.77	
		2.28	2.60	3.85	7.00(4H, s)	(72.30	6.36	17.51	3.83)	
6E	172—176	0.93	1.08	2.23	6.92(1H, s)	67.44	5.78	17.05	9.73	
		2.57	3.67			(67.58	5.68	16.89	9.85)	
7E	208—222	1.22	2.02	2.22	6.31—6.72(2H, br. s)	60.90	5.98	24.51	8.61	
	(decomp)	2.53	3.80		6.78(1H, s)	(63.59	6.02	21.12	9.27)	
8E[b)]	106—110	1.21	2.04	2.15		63.83	6.71	18.52	10.58	274
		2.26	2.56	3.21		(65.68	6.61	17.50	10.21)	
9E[b)]	164—166	1.32	2.08	2.20	7.20—7.40(5H, m)	70.70	6.03	14.61	8.19	336
		2.32	2.65			(71.41	5.99	14.27	8.33)	
10Z	188—192	1.95	2.15	2.25	7.20—7.23(5H, m)	67.94	5.97	18.50	7.59	
		2.40	3.95			(68.14	5.73	18.18	7.95)	
12E[b)]	154—158	0.92	2.18	2.78	7.17—7.28(4H, m)	74.13	6.28	15.13	4.56	309
		3.65	3.65			(73.77	6.19	15.52	4.53)	
13E	157—160	1.40	2.13	2.37	7.38—8.07(5H, m)	70.56	5.34	19.99	4.31	323
		2.73				(70.57	5.30	19.79	4.33)	
14E[c)]	166—168	1.32	2.15	2.30	7.30—7.93(5H, s)	66.68	5.09	14.26	4.02	339
		2.73				(67.24	5.06	14.14	4.13)	

a) Melting points and ^{1}H NMR spectra of **1E—4E** were consistent with those reported in the literature. **11** was out-of-stock. b) *E*-isomers were obtained by UV irradiation of the *E/Z* isomeric mixtures. c) *E*-isomer was obtained by photochemical isomerization of the *Z*-isomer with UV light.

tions. The higher chemical stabilities of the heterocyclic groups, however, would inevitably feature lower photochemical responsiveness as described above. Thus we are now put into a dilemma in molecular architecturing of *highly-responsive and highly-resistant* photochromic compounds.

Contrary to the high thermal stability in PMMA film, **14** (both colored and uncolored forms) underwent substantial degradations in hydroxylic solvents at room temperature in the dark, as readily as **1**. A major degradation product of **14C** in ethanol solution, isolated on silica gel, showed UV spectrum and R_f value (TLC on silica gel) different from those of **14E** or **Z**. From its UV (λ_{max}410, $\varepsilon\approx$5500) and ^{1}H NMR spectra (e.g., methylene protons of the ethyl ester group at 3.6 ppm), the half-ester of the colored form was implied. Thus, it is assumed that the anhydride groups of both colored and uncolored forms are subject to rapid solvolysis in hydroxylic solvents, regardless of the structure of the heterocyclic groups.

Experimental

Melting points were uncorrected. UV and ^{1}H NMR spectra were recorded on a Hitachi U-3200 spectrophotometer and a JEOL JNM-PMX 60 NMR spectrometer, respectively. Solvents were freshly distilled before use. PMMA film (ca. 1.0 μm thickness) was prepared on a glass plate by spin-coating of a deaerated cyclohexanone solution containing fulgide and PMMA (15—20:85—80 by weight). For the measurement of the thermal stability, the surface of the PMMA film was coated with acrylic polymer (SD-17 Dainihon-Inki) in 4—5 μm thickness to protect from sublimation. This treatment did not affect the photochromic properties, except that some intermixing appeared to take place and the absorbances of fulgides were somewhat reduced. The UV light beams of 310—380 nm isolated through a glass filter (Toshiba UV-D36C), were irradiated at a 50-cm distance from a 80-W cm^{-1} metal halide lamp (Ushio Electric). Visible light beams were irradiated at a 15-cm distance from a 50-W halogen lamp (Philips) through a glass filter (Toshiba Y-50, Y-45, or L-39). The incident light intensities were in the range of 10—40 mJ cm^{-2} s^{-1} both with UV and visible lights. Absorption spectra were measured at 10-s intervals during coloration and discoloration reactions.

Materials. Heterocyclic fulgides were prepared by the Stobbe condensation reaction of diethyl isopropylidenesuccinate with 3-(or 4-)acetyl derivatives of heteroaromatic compounds, according to the methods described in the literature.[8,9] The analytical data and other physical constants are summarized in Table 3.

References

1) Partially reported in the 56th National Meeting of the Chemical Society of Japan, Tokyo, April 1988, Abstr., p. 1839.

2) M. Irie and M. Mori, *J. Org. Chem.*, **53**, 803 (1988).

3) S. Arakawa, H. Kondou, and N. Seto, Jpn. Patent 60-54388 (1985); M. Irie and K. Hayashi, *Polymer Preprints*, **34**, 459 (1985).

4) H. G. Heller, U.S. Patent 4220708 (1980); H. G. Heller, *Fine Chem. Electronic Ind.*, **60**, 120 (1986).

5) H. Hayata, T. Inoue, I. Hitomi, Y. Yokoyama, and Y. Kurita, 54th National Meeting of the Chemical Society of Japan, Tokyo, April 1987, Abstr., p. 356.

6) J. Hibino, E. Andou, K. Morimoto, 53th National Meeting of the Chemical Society of Japan, Nagoya, October 1986, Abstr., p. 455.

7) S. Tazuke, S. Kurihara, H. Yamaguchi, and T. Ikeda, *J. Phys. Chem.*, **91**, 249 (1987).

8) P. J. Darcy, H. G. Heller, P. J. Strydom, and J. Whittall, *J. Chem. Soc., Perkin Trans. 1*, **1981**, 202; H. G. Heller and J. R. Langan, *J. Chem. Soc., Perkin Trans. 2*,

1981, 341.

9) A. P. Glaze, S. A. Harris, H. G. Heller, W. Johncock, S. N. Oliver, P. J. Strydom, and J. Whittall, *J. Chem. Soc., Perkin Trans. 1*, **1985**, 957.

10) Y. Suzuki, K. Ichimura, and N. Tamaoki, 54th National Meeting of the Chemical Society of Japan, Tokyo, April 1987, Abstr., p. 704.

11) G. H. Brown, "Photochromism," Wiley-Interscience, New York, N. Y. (1971); H. G. Heller, *Chem. Ind.*, **1978**, 193; C. D. Eisenbach, *Photographic Sci. Eng.*, **23**, 183 (1979); J. Guillet, "Polymer Photophysics and Photochemistry," Cambridge University Press, London (1985).

12) M. J. S. Dewar and R. C. Dougherty, "The PMO Theory of Organic Chemistry," Plenum Press, New York, N. Y. (1975), Chapter 6; H. D. Ilge, *J. Photochem.*, **33**, 333 (1986); K. Ogawa, H. Suzuki, and M. Futakami. *J. Chem. Soc., Perkin Trans. 2*, **1988**, 39.

Arylation of Olefins by Arylazo Aryl Sulfones under Palladium(0) Catalysis[1)]

Nobumasa KAMIGATA,* Akira SATOH, Tetsuya KONDOH, and Masayuki KAMEYAMA
Department of Chemistry, Faculty of Science, Tokyo Metropolitan University, Fukazawa, Setagaya-ku, Tokyo 158
(Received April 19, 1988)

The palladium(0)-catalyzed reaction of arylazo aryl sulfones with olefins in benzene at 80 °C gave aryl-substituted olefins in good yield. Diarylpalladium(II) species was proposed as an intermediate in this reaction.

The arylation of unsaturated compounds by arenediazonium salts with copper salt catalysis was first disclosed by Meerwein et al.[2)] The Meerwein arylation is a useful synthetic procedure, because of the availability of a variety of arylamines and good product yield. However, it generally requires the olefins to be activated by an electron-withdrawing group, such as carbonyl, cyano, aryl, vinyl, ethynyl or chloro group. Doyle et al. reported a modified Meerwein arylation with significant yield improvement by the use of free arylamines and alkyl nitrite in place of arenediazonium salts.[3)] However, the limitation of olefinic compounds still remains. Arylpalladium reagents obtained from aryl halides or arylmercurials have been utilized extensively for arylation of olefins,[4)] and the arylation is known to be free from the requirement for activation in the olefinic substance. Recently, Kikukawa et al. reported a novel arylation of olefins by arenediazonium salts[5)] or *N*-nitroso-*N*-arylacetamides[6)] in the presence of a catalytic amount of palladium(0). In a preliminary paper we reported that arylazo aryl sulfones react with styrene in the presence of tetrakis(triphenylphosphine)palladium(0) as a catalyst under mild conditions to give (*E*)-1-aryl-2-phenylethene and 1-aryl-1-phenylethene in good yields.[7)] We give here a full account for the palladium(0)-catalyzed arylation of olefins by arylazo aryl sulfones.

Results and Discussion

Dropwise addition of phenylazo *p*-tolyl sulfone (**1a**) in benzene to a stirred solution of styrene and tetrakis(triphenylphosphine)palladium(0) in benzene resulted in evolution of nitrogen. TLC analysis showed that the crude products are separated in roughly two spots, and these components were separated by column chromatography. The products of the former fraction were determined as 1,1-diphenylethylene (**2**) 10%, 1-phenyl-1-(*p*-tolyl)ethylene (**3**) 10%, (*E*)-stilbene (**4**) 32%, (*E*)-1-phenyl-2-(*p*-tolyl)ethylene (**5**) 32%, biphenyl 1%, and 4-methylbiphenyl 1%. The latter fraction was recrystallized from ethanol to give pale yellow crystals which were identified as 2-phenyl-2-(phenylazo)ethyl *p*-tolyl sulfone (**6a**) (yield, 21%). The products **2**—**6** seem to be formed by the catalytic reaction of **1a** by the palladium(0) complex since the thermal reaction of **1** with styrene without catalyst is known not to form such arylated compounds **2**—**6** but to form an aryl radical as an intermediate which acts as an initiator for the polymerization of styrene.[8)] The other transition metal catalysts such as $Pd(OAc)_2$, $Pd(dba)_2$, $PdCl_2$, $RhCl(PPh_3)_3$, and $RuCl_2(PPh_3)_3$ have showed little catalytic effect for the arylation of styrene by **1a**. It is interesting to note that both phenyl and *p*-tolyl groups of **1a** are arylated at the α- and β-position of styrene in almost equal amount to give **2** or **3**, and **4** or **5**, respectively.

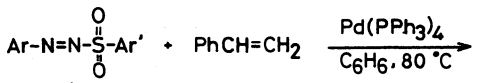

1

(1a: Ar=Ph, Ar'=p-$CH_3C_6H_4$)

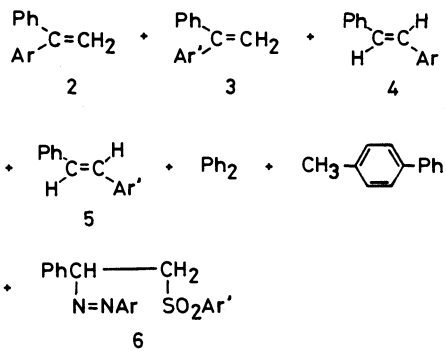

Similarly, the reactions of *p*-tolylazo phenyl sulfone (**1b**), phenylazo phenyl sulfone (**1c**), and *p*-tolylazo *p*-tolyl sulfone (**1d**) with styrene were carried out in the presence of tetrakis(triphenylphosphine)palladium(0) in benzene solution under nitrogen at 80 °C. The results are summarized in Table 1. It is noteworthy that the yields of the products **2**, **3**, **4**, and **5** were almost the same both in the reactions of **1a** and **1b**, respectively. The result suggests that a common reactive intermediate is formed from either reaction of **1a** and **1b** by the palladium(0) catalysis, and the Ar and Ar' groups of the intermediate have the same reactivity. When the Ar and Ar' groups of the azosulfone **1** are the same (Entries 3 and 4), the products are simplified.

These reactions may be accounted for by the oxidative addition of arylazo aryl sulfone to palladium(0) catalyst giving Ar-N=N-Pd(II)-SO_2-Ar' (**7**), which splits off nitrogen and sulfur dioxide to form a diarylpalladium(II) complex, Ar-Pd(II)-Ar' (**8**). The reactive intermediate **8** adds to an olefin giving adducts **9a** and **9b** which afford arylated olefin **2**—**5** and Ar'-Pd(II)-H (**10a**) or Ar-Pd(II)-H (**10b**). The reductive elimination of arenes (ArH and Ar'H) from **10** follows,

Table 1. Reaction of Arylazo Aryl Sulfones with Styrene Catalyzed by Tetrakis(triphenylphosphine)palladium(0) in Benzene at 80 °C[a)]

	Ar and Ar′ in **1**		Product, Yield[b)]/%					
	Ar	Ar′	**2**	**3**	**4**	**5**	**6**	Biaryls
1a	C_6H_5	*p*-$CH_3C_6H_4$	10	10	32	32	21	c
1b	*p*-$CH_3C_6H_4$	C_6H_5	11	12	33	32	22	c
1c	C_6H_5	C_6H_5	17	—	56	—	32	d
1d	*p*-$CH_3C_6H_4$	*p*-$CH_3C_6H_4$	—	15	—	49	35	e

a) The reactions were performed by addition of arylazo aryl sulfone (2.0 mmol) in benzene (8.0 cm^3) to a stirred solution of styrene (10 mmol) and $Pd(PPh_3)_4$ (0.02 mmol) in benzene (2.0 cm^3) under nitrogen at 80 °C for 2 h. b) The yield was determined by GC analysis based on the arylazo aryl sulfone used. c) Biphenyl (1%) and 4-methylbiphenyl (1%) were formed. d) Biphenyl (2%) was formed. e) 4-Methylbiphenyl (2%) and 4,4′-dimethylbiphenyl (4%) were formed.

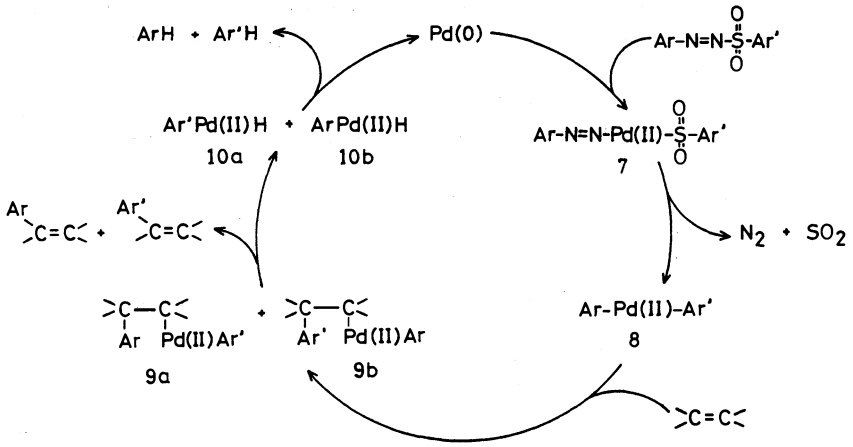

Scheme 1.

and Pd(0) is regenerated (Scheme 1).

The diarylpalladium(II) species **8** successfully interprets the product ratio 2/3=1 and 4/5=1 both in the reaction of **1a** and **1b** since Ar and Ar′ groups in **8** are expected to have the same reactivity toward olefin and it is also to be expected that **10a** and **10b** will eliminate from **9a** and **9b** in the same rate, respectively. The formation of the diarylpalladium(II) species was supported by detection of biphenyl, 4-methylbiphenyl, and 4,4′-dimethylbiphenyl (Table 1) since these products are considered to be formed by the reductive elimination from **8** accompanying with regeneration of Pd(0) (Scheme 2).

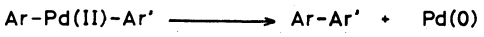

Scheme 2.

The formation of arene (ArH and Ar′H) by the reductive elimination from **10** is difficult to detect when the aryl group of **1** is phenyl. Next, the reaction of *p*-methoxyphenylazo *p*-tolyl sulfone with styrene was carried out in the presence of the palladium(0) catalyst in benzene, and the formation of both anisole and toluene was found by GC-MS.

The formation of **6** is accounted for by the addition of arylazo(arylsulfonyl)palladium(II) species **7** (shown in Scheme 1) to olefin to give the adduct **11a** or **11b** which followed by the reductive elimination of **6** accompanying with regeneration of Pd(0) species (Scheme 3).

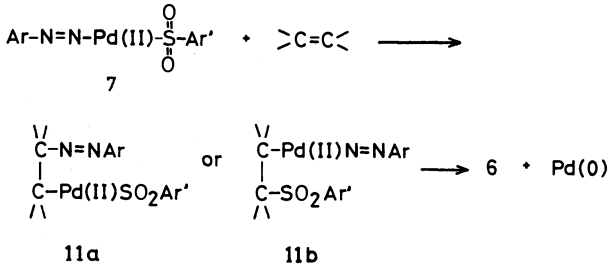

Scheme 3.

The regioselectivity for the arylation of styrene by **1** is different from that of the related arylation of styrene by *N*-nitroso-*N*-arylacetamide under palladium(0) reported by Kikukawa et al.[6)] They obtained the arylation products at the α- and β-position of styrene in the ratio of 5 : 95. On the other hand, in our case, the ratio of the arylation at the α- and β-position of styrene is 1 : 3. These differences may be attributed to the difference of the reductive-eliminating group from the adduct.

The reactions of **1c** with (*E*)-stilbene, 2-phenylpro-

pene, and (*E*)-1-phenylpropene in the presence of a catalytic amount of the palladium(0) catalyst in benzene were also carried out at 80 °C for 2 h. The reaction of **1c** with (*E*)-stilbene gave biphenyl 6% and triphenylethylene 44%. The reaction of **1c** with 2-phenylpropene afforded biphenyl 7%, (*Z*)-1,2-diphenylpropene (**12**) 6%, (*E*)-1,2-diphenylpropene (**13**) 30%, and 2,3-diphenylpropene (**14**) 35%. The reaction of **1c** with (*E*)-1-phenylpropene formed biphenyl 11%, **12** 4%, **13** 25%, 1,1-diphenylpropene (**15**) 20%, and 3,3-diphenylpropene (**16**) 7%.

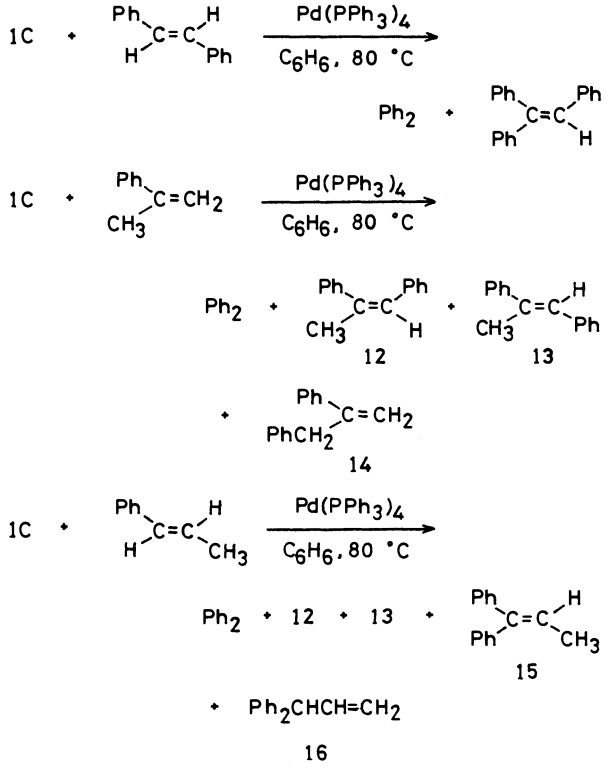

The formation of the compounds **12**—**16** is accounted for by the reaction of the diphenylpalladium(II) species, formed from **1c** and Pd(0), with 2-phenylpropene or (*E*)-1-phenylpropene giving the adduct **17** and **18** or **19**, respectively. The PhPd group can eliminate with all possible β-hydrogen from this intermediate: **17** affords **12**, **13**, and **14**; similarly, **18** affords **12** and **13**; and **19** affords **15** and **16**.

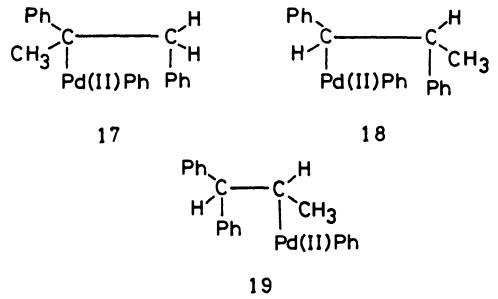

The palladium(0)-catalyzed arylation of cycloalkenes with **1** is also carried out under similar conditions. The results are summarized in Table 2. In this case, 3-arylcycloalkene **20** and 1-arylcycloalkene **21** were obtained in good yield with minor by-products, biaryls; although alicyclic olefins are known to be poor substrates in the Meerwein arylation.[2] It is of interest that 1-arylcyclopentene was formed in a little higher yield than 3-arylcyclopentene in each of the reactions of arylazo aryl sulfone with cyclopentene. The isomer distribution of the arylation products obtained here were considerably different from those of related phenylation of cyclopentene by aniline and *t*-butyl nitrite catalyzed by bis(dibenzylideneacetone)-palladium(0).[5e] Whereas, the reaction of arylazo aryl sulfone with cyclohexene, cycloheptene, and cyclooctene afforded 3-arylcyclohexene, 3-arylcycloheptene,

Table 2. Reaction of Arylazo Aryl Sulfones with Cycloalkenes Catalyzed by Tetrakis(triphenylphosphine)palladium(0) in Benzene at 80 °C[a]

n in cycloalkene	Ar in ArN_2SO_2Ar	Product, Yield[b]/%					
		3-Aryl-cycloalkene		1-Aryl-cycloalkene		ArPh	ArAr
1	C_6H_5	**20a**	18	**21a**	26	—	9
1	*p*-$CH_3C_6H_4$	**20b**	23	**21a**	41	5	4
1	*p*-$CH_3OC_6H_4$	**20c**	20	**21c**	23	3	2
2	C_6H_5	**20d**	61	**21d**	4	—	8
2	*p*-$CH_3C_6H_4$	**20e**	42	**21e**	2	8	0
2	*p*-$CH_3OC_6H_4$	**20f**	33	**21f**	1	7	1
3	C_6H_5	**20g**	62	**21g**	1	—	11
3	*p*-$CH_3C_6H_4$	**20h**	89	**21h**	0	0	10
3	*p*-$CH_3OC_6H_4$	**20i**	41	**21i**	Trace	9	1
3	*p*-ClC_6H_4	**20j**	37	**21j**	1	11	0
4	C_6H_5	**20k**	67	**21k**	6	—	8
4	*p*-$CH_3C_6H_4$	**20l**	66	**21l**	Trace	3	8
4	*p*-$CH_3OC_6H_4$	**20m**	76	**21m**	5	3	1
4	*p*-ClC_6H_4	**20n**	78	**21n**	0	5	0

a) The reactions were carried out by addition of arylazo aryl sulfone (2.0 mmol) in benzene (8.0 cm^3) to a stirred solution of cycloalkene (10.0 mmol) and $Pd(PPh_3)_4$ (0.02 mmol) in benzene (2.0 cm^3) under nitrogen at 80 °C for 24 h. b) The yield was determined by GC analysis based on the arylazo aryl sulfone employed.

and 3-arylcyclooctene, respectively, as the major arylation product, the corresponding 1-arylcycloalkene was obtained in much lower yield to zero, although the reason is not clear at the present time.

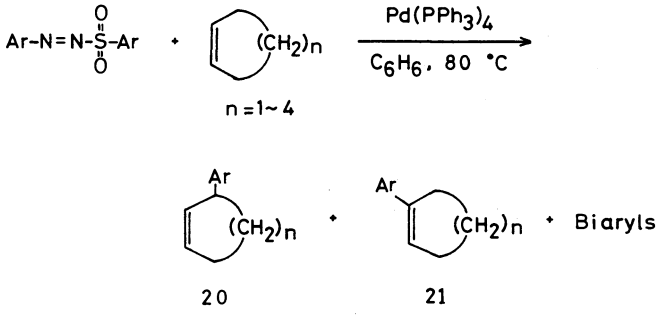

Experimental

Measurement. Melting points and boiling points are uncorrected. The infrared absorption spectra were determined on a Hitachi Model 260-10 spectrophotometer with samples as either neat liquids or in KBr disks. ^{1}H NMR spectra were recorded at 60 MHz by using a JNM-PMX 60 SI spectrometer with Me_4Si as an internal standard in $CDCl_3$. Mass spectra were determined with a JEOL JMS-DX300 mass spectrometer with JEOL JMA-5000 Mass Data System at an ionizing voltage of 20—70 eV. Gas chromatography was carried out with Hitachi Models 163 and 263-30 gas chromatographs (FID) using a 1 m column packed with 10% SE-30. The gel permeation chromatography was performed by using a JAI LC-08 liquid chromatograph with a JAIGEL-1H column (20 ϕ×600 mm×2, chloroform as eluent).

Materials. All solvents were distilled and stored under nitrogen. Palladium chloride of Wako Chemicals was used without further purification. Tetrakis(triphenylphosphine)-palladium(0),[9] palladium acetate(II),[10] bis(dibenzylideneacetone)palladium(0),[11] chlorotris(triphenylphosphine)rhodium(I),[12] and dichlorotris(triphenylphosphine)rutheniumm-(II),[13] were prepared by the method described in the literature. Phenylazo *p*-tolyl sulfone (**1a**), *p*-tolylazo phenyl sulfone (**1b**), phenylazo phenyl sulfone (**1c**), *p*-tolylazo *p*-tolyl sulfone (**1d**), *p*-methoxyphenylazo *p*-methoxyphenyl sulfone (**1e**), and *p*-chlorophenylazo *p*-chlorophenyl sulfone (**1f**) were prepared by the published procedures.[14] Styrene, 2-phenylpropene, (*E*)-1-phenylpropene, cyclopentene, cyclohexene, cycloheptene, cyclooctene of Tokyo Kasei Chemicals were purified by distillation under nitrogen prior to use.

General Procedure for the Reaction of Arylazo Aryl Sulfone with Styrenes. A solution containing arylazo aryl sulfone (2.0 mmol) in benzene (5.0 cm^3) was added dropwise to a stirred solution containing styrene or a styrene derivative (10 mmol) and tetrakis(triphenylphosphine)palladium(0) (0.02 mmol) in benzene (2.0 cm^3) heated at 80 °C under nitrogen over a period of 30 min, and the mixture was further stirred for 2 h. The crude reaction mixture was chromatographed on silica gel using hexane-ethyl acetate as eluent. The stereo- and regioisomers of the arylation products were isolated by GC. The structure of biphenyl, 4-methylbiphenyl, 4,4′-dimethylbiphenyl, 1,1-diphenylethylene (**2**), 1-phenyl-1-(*p*-tolyl)ethylene (**3**), (*E*)-stilbene (**4**), (*E*)-1-phenyl-2-(*p*-tolyl)ethylene (**5**), triphenylethylene (**11**), (*Z*)-1,2-diphenylpropene (**12**), (*E*)-1,2-diphenylpropene (**13**), 2,3-diphenylpropene (**14**), 1,1-diphenylpropene (**15**), and 3,3-diphenylpropene (**16**) were identified by comparison of their retention times of GC; IR, ^{1}H NMR, and GC mass spectra with those of authentic samples. The adducts **6** were isolated as the corresponding [1,3]sigmatropic hydrogen shifted isomer, and the structure was determined by the following spectroscopic data.

2-Phenyl-2-(phenylhydrazono)ethyl *p*-Tolyl Sulfone: Mp 179—180 °C; IR (KBr) 3340, 1310, and 1145 cm^{-1}; ^{1}H NMR ($CDCl_3$) δ=2.35 (3H, s), 4.58 (2H, s), 7.21 (2H, d, J=7.8 Hz), 7.24 (10H, s), 7.75 (2H, d, J=7.8 Hz), and 9.35 (1H, s); MS, m/z 364 (M^+); HRMS, m/z 364.1258 ($C_{21}H_{20}O_2N_2S$ requires 364.1245). This compound is easily converted to **6a** by treating with an acid. 2-Phenyl-2-(phenylazo)ethyl *p*-tolyl sulfone (**6a**): mp 139—140 °C; IR (KBr) 1450, 1310, and 1150 cm^{-1}; ^{1}H NMR ($CDCl_3$) δ=2.25 (3H, s), 3.5—3.9 (1H, m), 4.2—4.6 (1H, m), 5.3—5.6 (1H, m), 7.10 (2H, d, J=7.8 Hz), 7.25 (5H, s), 7.38 (5H, s), and 7.64 (2H, d, J=7.8 Hz); MS, m/z 364 (M^+); HRMS, m/z 364.1242 ($C_{21}H_{20}O_2N_2S$ requires 364.1245).

2-Phenyl-2-(*p*-tolylhydrazono)ethyl Phenyl Sulfone (Isomer of 6b): Mp 170—171 °C; IR (KBr) 3340, 1300, and 1150 cm^{-1}; ^{1}H NMR ($CDCl_3$) δ=2.31 (3H, s), 4.61 (2H, s), 7.2—7.8 (14H, m), and 9.36 (1H, s); MS, m/z 364 (M^+); HRMS, m/z 364.1239 ($C_{21}H_{20}O_2N_2S$ requires 364.1245).

2-Phenyl-2-(phenylhydrazono)ethyl Phenyl Sulfone (Isomer of 6c): Mp 153—154 °C; IR (KBr) 3350, 1300, and 1160 cm^{-1}; ^{1}H NMR ($CDCl_3$) δ=4.65 (2H, s), 7.2—8.0 (15H, m), and 9.40 (1H, s); MS, m/z 350 (M^+); HRMS, m/z 350.1119 ($C_{20}H_{18}O_2N_2S$ requires 350.1089).

2-Phenyl-2-(*p*-tolylhydrazono)ethyl *p*-Tolyl Sulfone (Isomer of 6d): Mp 172—173 °C; IR (KBr) 3340, 1300, and 1140 cm^{-1}; ^{1}H NMR ($CDCl_3$) δ=2.31 (3H, s), 2.37 (3H, s), 4.60 (2H, s), 7.1—7.8 (13H, m), and 9.38 (1H, s); MS, m/z 378 (M^+); HRMS, m/z 378.1409 ($C_{22}H_{22}O_2N_2S$ requires 378.1402).

Arylation of Cycloalkenes. General Procedure. All procedures were carried out under nitrogen, although aerobic conditions also gave satisfactory results. To a stirred solution containing cycloalkene (10 mmol), tetrakis(triphenylphosphine)palladium(0) (0.02 mmol) in benzene (2.0 cm^3) heated at 80 °C was added dropwise a solution containing of arylazo aryl sulfone (2.0 mmol) in benzene (5.0 cm^3) over a period of 30 min, and the solution was further stirred for 24 h. The crude reaction mixture was subjected to elution chromatography on silica gel using hexane-ethyl acetate as eluent. The regioisomers of the arylation products **20** and **21** were isolated by gel permeation chromatography, and the structures were determined on the basis of their spectroscopic data.

3-Phenylcyclopentene[15] (20a): IR(neat) 2940, 2850, 1605, 1495, 1450, 755, and 695 cm^{-1}; ^{1}H NMR ($CDCl_3$) δ=1.53—2.90 (4H, m), 3.63—4.10 (1H, m), 5.63—6.02 (2H, m), and 7.12 (5H, m); MS, m/z 144 (M^+), 129, and 115.

3-(*p*-Tolyl)cyclopentene (20b): A colorless oil; IR (neat) 3060, 2930, 2855, 1615, 1515, 820, and 715 cm^{-1}; ^{1}H NMR ($CDCl_3$) δ=1.52—2.85 (4H, m), 2.28 (3H, s), 3.62—4.08 (1H, m), 5.58—6.08 (2H, m), 6.82—7.23 (4H, m); MS, m/z 158 (M^+), 143, and 128; HRMS, m/z 158.1098 ($C_{12}H_{14}$ requires 158.1095).

3-(*p*-Methoxyphenyl)cyclopentene (20c): A colorless oil; IR (neat) 2960, 2910, 2850, 1615, 1515, 1250, 830, and 720 cm^{-1}; ^{1}H NMR ($CDCl_3$) δ=1.45—2.87 (4H, m), 3.30—4.98 (1H, m), 3.65 (3H, s), 5.43—5.97 (2H, m), 6.65 (2H, d, J=9.0

Hz), and 6.95 (2H, d, J=9.0 Hz); MS, m/z 174 (M^+) and 159; HRMS, m/z 174.1046 ($C_{12}H_{14}O$ requires 174.1044).

3-Phenylcyclohexene[16] **(20d):** IR (neat) 3030, 2930, 1610, 1500, 1460, 765, and 700 cm^{-1}; ^1H NMR ($CDCl_3$) δ=0.70—3.05 (6H, m), 3.13—3.60 (1H, m), 5.40—6.30 (2H, m), and 7.13 (5H, s); MS, m/z 158 (M^+), 143, and 129.

3-(*p*-Tolyl)cyclohexene (20e): A colorless oil; IR(neat) 3030, 2920, 1515, 1435, and 825 cm^{-1}; ^1H NMR ($CDCl_3$) δ= 1.22—3.02 (6H, m), 2.27 (3H, s), 3.10—3.50 (1H, m), 5.43—5.83 (2H, m), and 6.83—7.23 (4H, m); MS, m/z 172 (M^+), 157, and 144; HRMS, m/z 172.1250 ($C_{13}H_{16}$ requires 172.1252).

3-(*p*-Methoxyphenyl)cyclohexene (20f): A colorless oil; IR (neat) 3060, 2970, 1635, 1530, 1260, and 845 cm^{-1}; ^1H NMR ($CDCl_3$) δ=0.90—3.03 (6H, m), 3.27 (1H, m), 3.72 (3H, m), 5.35—5.98 (2H, m), 6.72 (2H, d, J=9.0 Hz), and 7.05 (2H, d, J=9.0 Hz); MS, m/z 188 (M^+), 173, and 160; HRMS, m/z 188.1208 ($C_{13}H_{16}O$ requires 188.1201).

3-Phenylcycloheptene[17] **(20g):** IR (neat) 3040, 2940, 2860, 1610, 1500, 1450, 760, and 705 cm^{-1}; ^1H NMR ($CDCl_3$) δ= 1.10—3.00 (8H, m), 3.23—3.77 (1H, m), 5.50—6.15 (2H, m), and 7.17 (5H, s); MS, m/z 172 (M^+), 157, 144, and 130.

3-(*p*-Tolyl)cycloheptene (20h): A colorless oil; IR (neat) 3010, 2925, 2855, 1510, 1440 and 810 cm^{-1}; ^1H NMR ($CDCl_3$) δ=0.87—2.95 (8H, m), 2.25 (3H, s), 3.17—3.72 (1H, m), 5.47—6.05 (2H, m), and 6.98 (4H, m); MS, m/z 186 (M^+), 171, and 158; HRMS, m/z 186.1417 ($C_{14}H_{18}$ requires 186.1408).

3-(*p*-Methoxyphenyl)cycloheptene (20i): A colorless oil; IR(neat) 2930, 1615, 1520, 1245, 1040, and 825 cm^{-1}; ^1H NMR ($CDCl_3$) δ=0.83—3.03 (8H, m), 3.42 (1H, m), 3.70 (3H, s), 5.60—5.93 (2H, m), 6.68 (2H, d, J=9.0 Hz), and 7.02 (2H, d, J=9.0 Hz); MS, m/z 202 (M^+), 187, and 173; HRMS, m/z 202.1336 ($C_{14}H_{18}O$ requires 202.1357).

3-(*p*-Chlorophenyl)cycloheptene (20j): A colorless oil; IR (neat) 2925, 1600, 1495, 1095, and 820 cm^{-1}; ^1H NMR ($CDCl_3$) δ=0.82—3.00 (8H, m), 3.25—3.65 (1H, m), 5.63—5.93 (2H, m), and 6.90—7.35 (4H, m); MS, m/z 206 (M^+) 191, 178, and 171; HRMS, m/z 206.0845 ($C_{13}H_{15}Cl$ requires 206.0862).

3-Phenylcyclooctene[15b,18] **(20k):** IR (neat) 3030, 2940, 2870, 1605, 1490, 1440, 750, and 695 cm^{-1}; ^1H NMR ($CDCl_3$) δ=1.00—3.05 (10H, m), 3.47—4.03 (1H, m), 5.35—6.17 (2H, m), and 7.17 (5H, s); MS, m/z 186 (M^+), 171, and 158.

3-(*p*-Tolyl)cyclooctene (20l): A colorless oil; IR (neat) 3020, 2940, 2870, 1520, 1470, and 810 cm^{-1}; ^1H NMR ($CDCl_3$) δ=0.92—2.95 (10H, m), 2.25 (3H, s), 3.23—3.95 (1H, m), 5.30—6.05 (1H, m), and 6.67—7.40 (4H, m); MS, m/z 200 (M^+), 185, and 172; HRMS, m/z 200.1568 ($C_{15}H_{20}$ requires 200.1565).

3-(*p*-Methoxyphenyl)cyclooctene (20m): A colorless oil; IR (neat) 2950, 1620, 1520, 1260, and 830 cm^{-1}; ^1H NMR ($CDCl_3$) δ=1.13—2.93 (11H, m), 3.68 (3H, s), 5.33—5.92 (2H, m), 6.70 (2H, d, J=9.0 Hz), and 7.00 (2H, d, J=9.0 Hz); MS, m/z 216 (M^+), 201, and 188; HRMS, m/z 216.1515 ($C_{15}H_{20}O$ requires 216.1514).

3-(*p*-Chlorophenyl)cyclooctene (20n): A colorless oil; IR (neat) 2930, 1490, 1095, and 820 cm^{-1}; ^1H NMR ($CDCl_3$) δ= 0.73—3.00 (10H, m), 3.38—3.97 (1H, m), 5.25—6.07 (2H, m), and 6.85—7.37 (4H, m); MS, m/z 220 (M^+), 192, and 185; HRMS, m/z 220.1017 ($C_{14}H_{17}Cl$ requires 220.1019).

1-Phenylcyclopentene[19] **(21a):** IR (neat) 2940, 2850, 1605, 1495, 1450, 755, and 695 cm^{-1}; ^1H NMR ($CDCl_3$) δ=1.53—2.90 (6H, m), 6.02—6.28 (2H, m), and 7.12—7.57 (5H, m); MS, m/z 144 (M^+), 129, and 115.

1-(*p*-Tolyl)cyclopentene[17,19] **(21b):** IR(neat) 2970, 2940, 2870, 1510, and 805 cm^{-1}; ^1H NMR ($CDCl_3$) δ=1.62—2.93 (6H, m), 2.28 (3H, s), 5.92—6.23 (1H, m), 7.02 (2H, d, J=8.0 Hz), and 7.25 (2H, d, J=8.0 Hz); MS, m/z 158 (M^+), 143, and 128.

1-(*p*-Methoxyphenyl)cyclopentene (21c): Mp 84.5—85.5 °C (lit, mp 81 °C):[19] IR (KBr) 2960, 2850, 1610, 1515, 1260, 840, and 805 cm^{-1}; ^1H NMR ($CDCl_3$) δ=1.50—2.28 (6H, m), 3.78 (3H, s), 5.88—6.07 (1H, m), 6.73 (2H, d, J=9.0 Hz), and 7.27 (2H, d, J=9.0 Hz); MS, m/z 174 (M^+), and 159.

The following 1-arylcycloalkenes **21d—g** and **21i—m** were determined only by the retention times of GC and GC mass spectra comparing with those authentic samples since these products were formed in very low yield.

1-Phenylcyclohexene[16,18] **(21d):** MS, m/z 158 (M^+), 143, and 128.

1-(*p*-Tolyl)cyclohexene[20] **(21e):** MS, m/z 172 (M^+), 157, and 144.

1-(*p*-Methoxyphenyl)cyclohexene[20] **(21f):** MS, m/z 188 (M^+), 173, and 158.

1-Phenylcycloheptene[21] **(21g):** MS, m/z 172 (M^+), 157, 144, and 129.

1-(*p*-Methoxyphenyl)cycloheptene[17] **(21i):** MS, m/z 202 (M^+), 187, and 174.

1-(*p*-Chlorophenyl)cycloheptene (21j): A colorless oil; MS, m/z 206 (M^+), 191, 178, and 171; HRMS, m/z 206.0802 ($C_{13}H_{15}Cl$ requires 206.0862).

1-Phenylcyclooctene[15b,18] **(21k):** MS, m/z 186 (M^+), 171, and 158.

1-(*p*-Tolyl)cyclooctene[22] **(21l):** MS, m/z 200 (M^+), 185, and 172.

1-(*p*-Methoxyphenyl)cyclooctene[23] **(21m):** MS, m/z 216 (M^+) and 188.

References

1) Reaction of Azo- and Azoxysulfones with Transition Metal Complexes. 2., Part 1: N. Kamigata, T. Kondoh, M. Kameyama, and M. Kobayashi, *Chem. Lett.*, **1987**, 347.

2) H. Meerwein, E. Buchner, and K. v. Emster, *J. Prakt. Chem.*, [2], **152**, 239 (1939); C. S. Rondestvedt, "Organic Reactions," Wiley, New York (1960), Vol. 11, p. 189; *ibid.*, (1977), Vol. 24, p. 225.

3) M. P. Doyle, B. Siegfreid, R. C. Ellicott, and J. F. Dellaria, *J. Org. Chem.*, **42**, 2431 (1977).

4) R. F. Heck, *Pure Appl. Chem.*, **50**, 691 (1978); R. F. Heck, *Acc. Chem. Res.*, **12**, 146 (1979); R. F. Heck, "Palladium Reagents in Organic Syntheses," Academic Press, New York (1985), Chap. 6.

5) a) K. Kikukawa and T. Matsuda, *Chem. Lett.*, **1977**, 159; b) K. Kikukawa, K. Nagira, and T. Matsuda, *Bull. Chem. Soc. Jpn.*, **50**, 2207 (1979); c) K. Nagira, K. Kikukawa, F. Wada, and T. Matsuda, *J. Org. Chem.*, **45**, 2365 (1980); d) K. Kikukawa, K. Kono, K. Nagira, F. Wada, and T. Matsuda, *J. Org. Chem.*, **46**, 4413 (1981); e) K. Kikukawa, K. Maemura, Y. Kiseki, F. Wada, and T. Matsuda, *J. Org. Chem.*, **46**, 4885 (1981); f) K. Kikukawa, K. Nagira, F. Wada, and T. Matsuda, *Tetrahedron*, **37**, 31 (1981); g) K. Kikukawa, K. Kono, F. Wada, and T. Matsuda, *Chem. Lett.*, **1982**, 35; h) K. Kikukawa, K. Kono, F. Wada, and T. Matsuda, *J. Org. Chem.*, **47**, 1333 (1983); i) K. Kikukawa, K. Ikenaga, F. Wada, and T. Matsuda, *Chem. Lett.*, **1983**, 1337; j) K. Ikenaga, K. Kikukawa, and T. Matsuda, *J. Org. Chem.*, **52**, 1276 (1987).

6) K. Kikukawa, M. Naritomi, G.-X. He, F. Wada, and T. Matsuda, *J. Org. Chem.*, **50**, 299 (1985).
7) N. Kamigata, T. Kondoh, M. Kameyama, T. Satoh, and M. Kobayashi, *Chem. Lett.*, **1987**, 347.
8) A. J. Rosenthal and C. G. Overberger, *J. Am. Chem. Soc.*, **82**, 108 (1960).
9) D. R. Coulson, *Inorg. Synth.*, Coll. Vol. 13, 121 (1972).
10) T. A. Stephenson, S. M. Morehouse, A. R. Powell, J. P. Heffer, and G. Wilkinson, *J. Chem. Soc.*, **1965**, 3632.
11) T. Uraki, H. Kawazura, Y. Ishii, J. J. Bonnet, and J. A. Ibers, *J. Organomet. Chem.*, **65**, 253 (1974).
12) J. A. Osborn and G. Wilkinson, *Inorg. Synth.*, Coll. Vol. 10, 67 (1967).
13) P. S. Hallman, J. A. Stephenson, and G. Wilkinson, *Inorg. Synth.*, Coll. Vol. 12, 238 (1972).
14) a) A. Hantzsch and M. Singer, *Ber.*, **30**, 312 (1897); **31**, 636 (1898); b) M. Kojima, H. Minato, and M. Kobayashi, *Bull. Chem. Soc. Jpn.*, **45**, 2032 (1972).
15) a) F. Winternitz, M. Mausseron, and E. Trebillon, *Bull. Soc. Chim. Fr.*, **1947**, 713; b) M. Yamamura, I. Moritani, A. Sonada, S. Teranishi, and Y. Fujiwara, *J. Chem. Soc., Perkin Trans. 1*, **1973**, 203.
16) E. L. Eliel, J. W. McCoy, and C. C. Price, *J. Org. Chem.*, **22**, 1533 (1958).
17) K. M. Davies, and W. J. Hickinbottom, *J. Chem. Soc.*, **1963**, 373.
18) R. Y. Mixer and W. G. Young, *J. Am. Chem. Soc.*, **78**, 3379 (1956).
19) A. D. Ketley and J. L. McClanahan, *J. Org. Chem.*, **30**, 942 (1965).
20) M. T. Davies, D. F. Dobson, D. F. Hayman, G. B. Jackman, M. G. Lester, V. Petrow, O. Stephenson, and A. A. Webb, *Tetrahedron*, **18**, 751 (1962).
21) A. C. Cope and S. S. Hecht, *J. Am. Chem. Soc.*, **89**, 6290 (1967).
22) W. F. Mooney, III, P. E. Brown, J. C. Russell, L. G. Pedersen, and D. G. Whitten, *J. Am. Chem. Soc.*, **106**, 5659 (1984).
23) P. J. Stang and A. G. Anderson, *Tetrahedron Lett.*, **1977**, 1485.

Aryliminodimagnesium Reagents. XIV.[1] Reactions with Nitrobenzenes Having Electronegative *ortho*-Substituents. Effects of Reaction Conditions on Condensation, Replacement, and Substitution

Masao Ōkubo,* Yoshito Inatomi, Naoki Taniguchi, and Kaori Imamura
Department of Chemistry, Faculty of Science and Engineering, Saga University, Honjō-machi, Saga 840
(Received April 25, 1988)

In reactions of $ArN(MgBr)_2$ with *o*-MeO- and *o*-halo-substituted nitrobenzenes, types and yields of products were different from those in its reactions with *m*- and *p*-substituted substrates. Condensation (leading to unsymmetrical azoxy- and azobenzenes), *o*-substituent replacement, and nuclear substitution took place. Relative yields of products were greatly affected by substituents and reaction conditions. *o*-MeO and *o*-F favor replacement, while *o*-Cl, *o*-Br, and *o*-I favor substitution. Replacement and/or substitution predominate when small molar excess of reagent and low concentration are used, while condensation predominates when large molar excess of reagent and high concentration are used, which phenomenon is mechanistically discussed.

The aryliminodimagnesium ($ArN(MgBr)_2$, aryl-IDMg) derived from aniline and EtMgBr condenses with *m*- and *p*-substituted nitrobenzenes (cf. Scheme 1),[2] and provides a convenient method for the independent preparation of *ONN* and *NNO* isomers of unsymmetrical (*unsym*-) azoxybenzenes (**1**).[3] **1** undergoes simple deoxygenation by molar excess of IDMg to give the corresponding *unsym*-azobenzene (**2**).[2] IDMg molecules are oxidatively dimerized, via single electron transfer (SET), to afford symmetrical (*sym*-) azobenzene (**3**).[2,4] The relative yield of **1**—**3** depends mainly on the relative efficiency of SET.[5,6]

The first purpose of the present study is to examine the formation of *o*-substituted azoxybenzene isomers which have so far been difficultly accessible. The second purpose is to examine the replacement of electronegative *o*-substituents on nitrobenzene via SET. 1-MeO and 1-Br substituents on the 9-fluorenylidene system are replaced by Grignard and IDMg reagents,[7] but no similar examples have been reported in reactions of nitroarenes with magnesium reagents. In IDMg reactions with *o*-MeO- and *o*-halo-nitrobenzenes, the expected azoxy formation and replacement as well as nuclear substitution took place, and relative yields of products depended greatly on reaction conditions. The results obtained will be summarized and discussed.

Results and Discussion

The results obtained by use of small and large molar excesses of IDMg will be separately described.

Relative Yields of Replacement, Substitution, and Condensation Products from *o*-MeO- and *o*-Halo-Nitrobenzenes in the Reaction with Small Molar Excess of Noncrowded IDMg. Effects of *o*-Substituted IDMg. The four products **4**—**7** in addition to **1**—**3** were obtained by the treatment of *o*-MeO- and *o*-halo-nitrobenzenes with small molar excess of *p*-MeC_6H_4-IDMg in tetrahydrofuran (THF, 50 ml). The product **4** is formed via replacement, **5** via substitution, **6** via

Table 1. Product Distribution in the Reaction with Small Excess of *p*-MeC_6H_4-IDMg

Run *o*-$XC_6H_4NO_2$		Addn. manner[a]	Molar ratio	Yield/%							Recov.
No.	X			**1**	**2**	**3**	**4**	**5**	**6**	**7**	
S1	MeO	N	1.2	35	14	4	27	3	0	0	14
S2	MeO	R	1.5	29	10	3	50	3	0	0	3
S3	F	R	1.5	44	9	7	19	4	4	2	0
S4	F	R	2.0	66	18	6	2	0	3	4	0
S5	Cl	R	1.5	8	17	7	1	29	2	0	36
S6	Cl	R	2.0	17	21	11	Trace	36	2	0	13
S7	Br	R	1.5	15	10	10	Trace	31	2	0	20
S8	Br	R	2.0	41	21	12	0	27	2	0	0
S9	I	R	1.5	14	9	7	0	27	3	0	39
S10	Cl	N	2.0	38	28	16	0	14	3	0	0
S11	Cl	N	5.0	28	36	36	0	0	0	0	0
S12	Cl[b]	R	2.0	12	13	12	0	35	1	0	27
S13	Me(*p*)[c]	N	1.5	46	18	1	0	0	0	0	13
S14	Et	N	1.2	28	12	13	0	0	0	0	18
S15	Me(*p*)[d]	N	1.5	14	13	14	0	0	0	0	4

a) N: "Normal" addition of substrate to reagent at 0 °C, followed by heating at 55 °C for 3 h. R: "Reverse" addition of reagent to substrate at room temp (12—15 °C) for 0.5 h, followed by heating at 55 °C for 1.5 h. b) 250 ml of THF was used. c) *o*-$MeOC_6H_4$-IDMg was used. d) *o*-EtC_6H_4-IDMg was used.

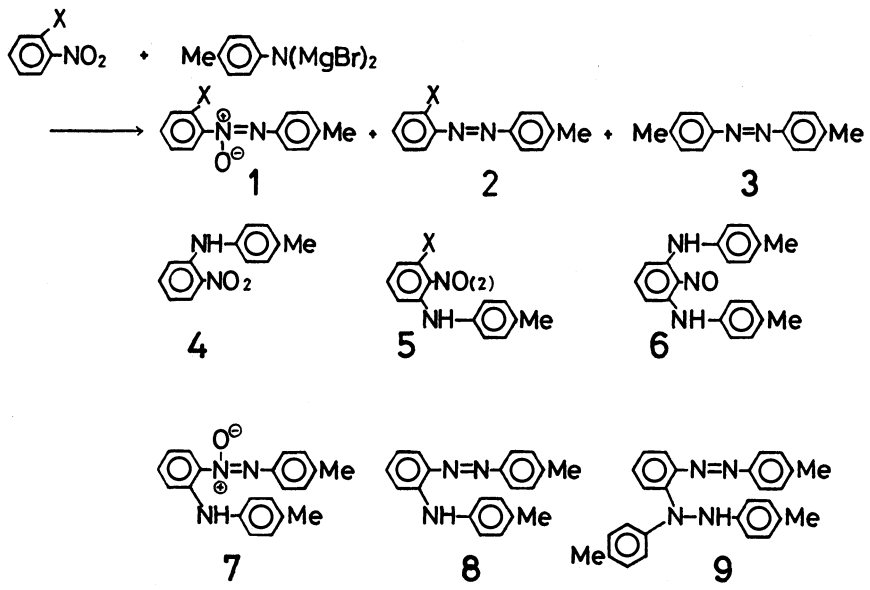

Scheme 1.

substitution-replacement, and **7** via substitution-condensation (limited to *o*-F substrate). $\mathbf{5}^{MeO}$ and $\mathbf{5}^{F}$ are nitro compounds, while $\mathbf{5}^{Cl}$, $\mathbf{5}^{Br}$, and $\mathbf{5}^{I}$ are nitroso compounds. The yields of **1**—**7** are summarized in Table 1 (Runs S1—S12).

By the "reverse" addition of slight molar excess of IDMg to substrate at room temperature (12—15 °C) for 30 min (S2—S9), the products **4** and **5** become predominant, while **6** and **7** remain as minor. The replacement is almost completely limited to *o*-MeO and *o*-F (S2—S4), while the substitution is limited to *o*-Cl, *o*-Br, and *o*-I (S5—S9). This cannot be explained in terms of the redox potentials (MeO, −1.540; F, −1.324; Cl, −1.321; Br, −1.348; I, −1.377 V),[6] but is probably due to the different leaving abilities of these substituents as anions (as their Mg salts) from the radical anion of substrate.[8] The replacement requires 1.2—1.5 mol of reagent and the substitution requires 1.5—2.0 mol (S1—S4 and S5—S9). The reason for the almost no replacement of *o*-Br on nitrobenzene (S7 and S8), in contrast to the facile replacement of 1-Br on 9-fluorenylidene system,[7] is equivocal. The replacement and substitution solely at ortho positions arise from tight coordination of the nitro group to the Mg atom of reagent.

In Runs S6 and S10—S12, the effect of reaction conditions on the conversion of *o*-Cl substrate is made disclosed. By the "normal" addition of substrate to 2.0 mol of IDMg (S10), the yields of **1** and **2** increase, while that of **5** decreases (cf. S6). By use of 5.0 mol of IDMg (S11), **1**—**3** become predominant at the expense of **5**. The use of 250 ml of THF (S12) causes a decrease in yield of **1** and **2**, but almost no effect on that of **5** (cf. S6).

The results of S1—S12 indicate that, under an ideal condition,[9] the replacement requires one molecule of IDMg, whereas the substitution requires two molecules; the second one may be consumed for eliminating the nitro-oxygen and ortho-hydrogen (Scheme 2). For the condensation, two or more IDMg molecules may cooperate via a complicated pathway and not via a simple addition-elimination. Since larger moles and/or higher concentrations of reagent favor also the deoxygenation of **1** (S11),[2,3] the optimum condition for the preparation of *o*-substituted **1** must be carefully explored.

The comparably bulky *o*-Et and *o*-MeO groups "on reagent" affect noticeably the yield of **1** and **2** in comparison with the same groups "on substrate" (S1 and S13—S15). In the "on substrate" cases (S1 and S14), the two groups lead to comparable yields of **1** and **2** lower than those in S13 (**4** is also formed in S1). In the "on reagent" cases, the *o*-MeO group (S13) favors the condensation, while the *o*-Et group (S15) leads to a poor combined amount of **1** and **2** and a poor recovery. The *o*-MeO group on reagent, probably chelating with its Mg atom, assists the IDMg nitrogen to access to the nitro group. The *o*-Et group on reagent causes interference with the access, resulting in self-decomposition of substrate via SET.[10]

Relative Yields of Condensation Products in the Reaction with Large Molar Excess of IDMg. By use of 8.0 mol of *p*-Me-C_6H_4-IDMg (L1—L7, Table 2), the other minor products **7**—**9** appeared at the expense of **4**—**6**. The products **7** and **8** are formed from **4** via condensation and deoxygenation, and **9** having a hydrazino group via replacement, probably by a dimeric salt ((ArN(MgBr)-)$_2$). Their formation in yields lower than 10% only in the case of *o*-MeO and *o*-F substrates (L1, L5, and L6) is in accord with the results of S1—S4. The products **1**—**3** are major ones (L1—L6), and the yields differ from those in the case of the *p*-substituted substrates (L8—L12), as specified by the following two features.

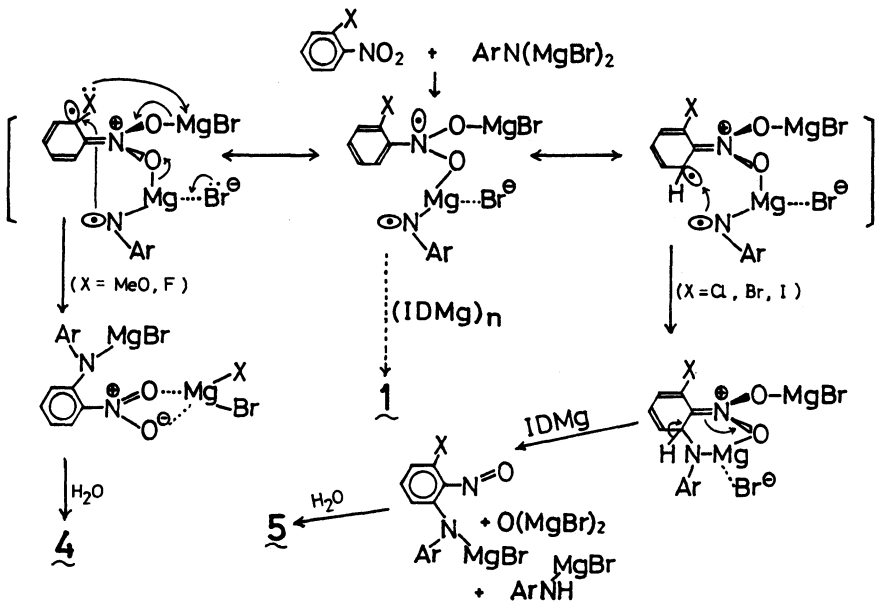

Scheme 2.

Table 2. Product Distribution in the Reaction with Large Excess (8.0 mol) of *p*-MeC_6H_4-IDMg

Run No.	$XC_6H_4NO_2$ X	Yields/%					
		1	**2**	**3**	**7**	**8**	**9**
L1	*o*-F	7	48	38	8	0	0
L2	*o*-Cl	16	35	40	0	0	0
L3	*o*-Br	7	36	39	0	0	0
L4	*o*-I	16	25	59	0	0	0
L5	*o*-MeO	0	57	33	6	0	3
L6	2,5-$(MeO)_2$	0	62	25	3	7	3
L7	*o*-Me	28	48	24	0	0	0
L8	*p*-F	27	39	22	0	0	0
L9	*p*-Cl	28	45	12	0	0	0
L10	*p*-Br	33	42	19	0	0	0
L11	*p*-I	36	39	19	0	0	0
L12	*p*-MeO	24	52	14	0	0	0
L13	2,4,6-Me_3	0[a] 16[b]	39	23	0	0	0
L14[c]	2,4,6-Me_3	36[a] 16[b]	23	20	0	0	0
L15[d]	2,4,6-Me_3	11[a] 2[b]	18	5	0	0	0

a) *ONN*-Isomer. b) *NNO*-Isomer. c) 4.0 mol of *p*-MeC_6H_4-IDMg was used. d) 1.2 mol of *p*-MeC_6H_4-IDMg was used. Product **4** was isolated in 29% yield.

The first feature is that shift of substituents from the para to ortho position causes decrease in combined yield of **1** and **2** from 66—76% (L8—L12) to 41—57% (L1—L5) and increase in that of **3** from 12—22% to 33—59%. The feature arises from the effect of lone-pair electrons of *o*-substituents favorable for the dimerization and not from that of steric repulsion against condensation, as indicated by the comparable yields caused by *o*-Me- (L7) and *p*-substituents (L8—L12). The formation of **3** is observed in IDMg reaction with ortho-quinones, but not with para-quinones.[11] According to the mechanism of two-electron oxidation of IDMg molecules,[4] all the adjacent halogeno, methoxyl, carbonyl, and nitro groups may coordinate to the Mg atoms of IDMg molecules to assist the arylaminyl radicals (Ar(MgBr)N·) to be produced in the proximity of each other in favor of the dimerization.

The second feature is the evidently lower yields of **1** in L1—L6 (0—16%) than those in L7—L12 (24—36%). The feature arises also from the effect of lone-pair electrons of *o*-substituents of **1** favoring its deoxygenation. The reciprocal of λ_{max}'s of *m*- and *p*-substituted azoxybenzenes are correlated with their reactivity in IDNg deoxygenation.[3] Thus the reduced electron-repelling resonance effect of *o*-substituent by steric hindrance causes the enhancement of positive charge on azoxy nitrogen to facilitate the attack of anionic IDMg nitrogen.[3]

Determination of *ONN* and *NNO* Structures of Azoxybenzenes, and Unique *ONN-NNO* Isomerization Caused by 2,6-Me_2 Groups. The *ONN*-structure of *o*-substituted *unsym*-azoxyarenes, having azoxy oxygen combined to the original "nitro" nitrogen, was confirmed by means of ^1H NMR spectra different from those of the known *NNO*-isomer obtained by the reaction of *o*-substituted phenyl-IDMg with *p*-Me-nitrobenzene. Comparison of photo-Wallach rearrangement products with authentic *o*-hydroxyazobenzenes[12,13] was also useful. X-Ray crystallography was not used because almost all the azoxyarenes are oil. A solid one having 2,6-Me_2 groups tends to form fluffy needles, and no single crystals of sufficient size with clean surface were obtained.

Similarly to *p*- and *m*-substituted azoxybenzenes,[3] the *o*-monosubstituted ones undergo no *ONN-NNO* isomerization even by being heated with large molar excess of IDMg. A unique *ONN-NNO* isomerization under the same conditions was observed in the case of the most crowded 2,4,6-Me_3-nitrobenzene (L13, Table 2). The less crowded azoxy product $\mathbf{1}^{3Me}_{NNO}$ is formed via isomerization of the much crowded "normal" isomer $\mathbf{1}^{3Me}_{ONN}$ by an interaction with IDMg. Even by use of 4.0 or 1.2 mol of IDMg (L14 and L15), both $\mathbf{1}^{3Me}_{ONN}$ and $\mathbf{1}^{3Me}_{NNO}$ were isolated.

Conclusion

The various effects of coordination proposed are in line with those given for modifying relative efficiency of SET estimated by oxidation and reduction potentials.[6] The reasons given for yield variations with leaving abilities and positional change of substituents are still equivocal, but the cooperation of reagent molecules for condensation is possibly an important clue to the mechanism of the essential reaction pathway of Scheme 1. Though optimum conditions remain to be studied, the IDMg method has proved to be useful for the preparation of crowded azoxyarenes available for studying the photoinduced[12,13] and acid-catalyzed[14] rearrangements as well as the deoxygenation by PX_3-type reagents.[15]

Table 3. Melting Points and ^1H NMR Data of Products Including Some Crowded Azoxybenzenes

No.	Run No.	Mp θ_m/°C	^1H NMR Data δ
$\mathbf{1}^{F}$	S3, S4, L1	Oil	8.12 and 7.22 (4H, ABq, J=15Hz), 7.96—7.78 (1H, m), 7.50—7.10 (3H, m), 2.42 (3H, s).
$\mathbf{1}^{Cl}$	S10, S11, L2	Oil	8.12 and 7.24 (4H, ABq, J=20Hz), 7.72—7.24 (4H, m), 2.40 (3H, s).
$\mathbf{1}^{Br}$	S7, S8, L3	Oil	8.12 and 7.24 (4H, ABq, J=20Hz), 7.84—7.20 (4H, m), 2.40 (3H, s).
$\mathbf{1}^{I}$	S9, L4	Oil	8.24 and 7.36 (4H, ABq, J=15Hz), 8.10 (1H, d), 7.80—7.15 (3H, m), 2.45 (3H, s).
$\mathbf{1}^{Me}$	L7	Oil	8.12 (2H, d), 7.77—7.58 (1H, m), 7.37—7.04 (5H, m), 2.44 (3H, s), 2.38 (3H, s).
$\mathbf{1}^{MeO}_{ONN}$	S1, S2, L5	Oil	8.00 and 7.17 (4H, ABq, J=27Hz), 7.66—6.76 (6H, m), 3.87 (3H, s), 2.40 (3H, s).
$\mathbf{1}^{MeO}_{NNO}$	S13	54.5—55	8.10 and 7.10 (4H, ABq, J=25Hz), 7.95—7.73 (1H, m), 7.73—6.66 (3H, m), 3.80 (3H, s), 2.43 (3H, s).
$\mathbf{1}^{3Me}_{ONN}$	L14	121—123	7.00 and 6.67 (4H, ABq, J=27Hz), 6.73 (2H, s), 2.27 (6H, s), 2.17 (6H, s).
$\mathbf{1}^{3Me}_{NNO}$	L13, L14	74.5—76.5	8.00 and 7.23 (4H, ABq, J=27Hz), 6.76 (2H, s), 2.44 (3H, s), 2.33 (3H, s), 2.23 (6H, s).
$\mathbf{1}^{Et}$	S14	Oil	8.00 and 7.13 (4H, ABq, J=27Hz), 8.16—7.87 (1H, m), 7.66—6.76 (3H, m), 2.66 (2H, q), 2.40 (3H, s), 1.26 (3H, t).
4	S1—S3	66.5—67	9.47 (1H, s), 8.22—6.71 (8H, m), 2.38 (3H, s).
$\mathbf{5}^{F}$	S3, S4	Oil	7.41—6.79 (8H, m), 2.25 (3H, s).
$\mathbf{5}^{Cl}$	S5, S6	Oil	7.33—6.82 (8H, m), 2.22 (3H, s).
$\mathbf{5}^{Br}$	S7, S8	Oil	7.67—6.93 (8H, m), 2.19 (3H, s).
$\mathbf{5}^{I}$	S9	Oil	7.70—6.76 (8H, m), 2.19 (3H, s).
$\mathbf{5}^{MeO}$	S1, S2	Oil	7.30—6.76 (8H, m), 3.67 (3H, s), 2.22 (3H, s).
6	S3—S10	147—149	13.39 (1H, s), 8.95 (1H, s), 7.29—6.20 (11H, m), 2.37 (6H, s).
7	S3, S4, L1, L5	Oil	9.50 (1H, s), 8.20—8.00 (3H, m), 7.79 (1H, d), 7.36—7.04 (7H, m), 6.86—6.64 (1H, m), 2.40 (3H, s), 2.24 (3H, s).
$\mathbf{7}^{MeO}$	L6	Oil	9.50 (1H, s), 8.38 (2H, d), 8.10—7.98 (1H, m), 7.64—7.00 (8H, m), 4.00 (3H, s), 2.50 (3H, s) 2.40 (3H, s).
$\mathbf{8}^{MeO}$	L6	Oil	9.42 (1H, s), 8.10—7.95 (2H, m), 7.64—7.00 (9H, m), 3.98 (3H, s), 2.46 (3H, s), 2.38 (3H, s).
9	L5	Oil	7.80—7.62 (3H, m), 7.34—7.02 (10H, m), 6.70—6.40 (3H, m), 5.76 (1H, s), 2.40 (3H, s), 2.36 (3H, s), 2.32 (3H, s).
$\mathbf{9}^{MeO}$	L6	Oil	9.50 (1H, s), 7.60—7.20 (2H, m), 7.08—6.80 (12H, m), 6.28 (1H, s), 3.80 (3H, s), 2.32 (3H, s), 2.22 (6H, s).

Experimental

Materials and Procedures. The reactions of Scheme 1 were carried out using 3—5 mmol of nitroarenes and calculated amounts of IDMg reagent in 50 ml of THF,[2,3] except in Run S12 where 250 ml of THF was used. The reaction conditions applied to the individual runs are given in Tables 1 and 2. Products were separated by column and preparative thin-layer chromatographies on silica gel and then recrystallized. Physical data of products **1** and **4—9** are summarized in Table 3, melting points being uncorrected. Elemental analyses gave satisfactory results. An identification of *ONN* and *NNO* structures of azoxyarenes by indirect means using photoreactions was carried out by comparison with authentic samples of *o*-hydroxyazoarenes.[13]

The authors wish to thank the Advanced Instrumentation Center for Chemical Analysis, Ehime University, for the elemental analyses. A part of this work was financially supported by a Grant-in-Aid for Scientific Research (No. 60470026).

References

1) Part XIII: T. Tsutsumi, M. Ōkubo, N. Yasuoka, and Y. Katsube, *Bull. Chem. Soc. Jpn.*, **61**, 237 (1988).
2) M. Ōkubo, T. Takahashi, and K. Koga, *Bull. Chem. Soc. Jpn.*, **56**, 199 (1983).
3) M. Ōkubo and K. Koga, *Bull. Chem. Soc. Jpn.*, **56**, 203 (1983).
4) M. Ōkubo, S. Yoshida, Y. Egami, K. Matsuo, and Y. Nagase, *Bull. Chem. Soc. Jpn.*, **60**, 1741 (1987).
5) M. Ōkubo, T. Tsutsumi, A. Ichimura, and T. Kitagawa, *Bull. Chem. Soc. Jpn.*, **57**, 2679 (1984).
6) M. Ōkubo, T. Tsutsumi, and K. Matsuo, *Bull. Chem. Soc. Jpn.*, **60**, 2085 (1987).
7) M. Ōkubo and Y. Uematsu, *Bull. Chem. Soc. Jpn.*, **55**, 1121 (1982).
8) E. G. Janzen, *Acc. Chem. Res.*, **2**, 279 (1969); J. F. Bunnett, *ibid.*, **11**, 413 (1978).
9) For example under an "ideal reverse addition" of reagent, its solution should be added in infinitely small drops.
10) G. A. Russell, E. G. Janzen, and E. T. Strom, *J. Am. Chem. Soc.*, **86**, 1807 (1964).
11) M. Ōkubo, M. Yoshida, K. Horinouchi, H. Nishida, and Y. Fukuyama, *Bull. Chem. Soc. Jpn.*, **56**, 1196 (1983).
12) G. G. Spence, E. C. Taylor, and O. Buchardt, *Chem. Rev.*,**70**, 321 (1970).
13) M. Ōkubo, H. Hyakutake, and N. Taniguchi, *Bull. Chem. Soc. Jpn.*, **61**, 3005 (1988).
14) H. E. Bigelow, *Chem. Rev.*, **9**, 139 (1931).
15) J. I. G. Cadogan and R. K. Mackie, *Chem. Soc. Rev.*, **1974**, 87.

Synthesis of Skeleton of Antitumor Quassinoid

Makoto SASAKI, Tatsushi MURAE,* Hisaaki MATSUO, Toshiyuki KONOSU, Naoko TANAKA, Kiyoshi YAGI, Yoshinosuke USUKI, and Takeyoshi TAKAHASHI†

Department of Chemistry, Faculty of Science, The University of Tokyo, Hongo, Bunkyo-ku, Tokyo 113

(Received April 27, 1988)

A compound having a skeleton of an antitumor quassinoid, bruceantin, was prepared according to the following strategy; 1) construction of ring ABC from ring AB by cyclization of a hindered 1,5-diketone; 2) construction of ring E (ether ring) by opening of a 12,13-epoxide ring followed by attack of oxygen at C-20 toward C-13; 3) formation of ring D (hemiacetal ring) by treatment of a 7α-hydroxy-16-al dimethyl acetal with PPTS.

Quassinoids, highly degraded triterpenes which are isolated from Simaroubaceae plants specifically, have a wide spectrum of biological properties.[1] Among a large number of quassinoids,[1,2] bruceantin (**1**) and bruceantinol (**2**) which have a skeletal structure **A** exhibit remarkable antileukemic activity.[3] Although a large number of efforts for syntheses of antitumor quassinoids have been reported,[4] none of them accomplished the total synthesis. The first synthesis of a compound having the skeletal structure **A** has been achieved by the authors.[4] The synthetic plan was based on AB → ABC → ABCE → ABCDE ring strategy. The details of the synthesis of compound **3** which has the skeletal structure **A** bearing functional groups at suitable positions for syntheses of antitumor quassinoids are described in this paper.

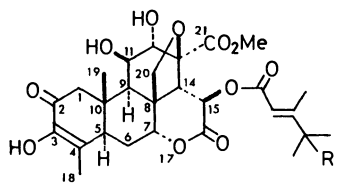

1: R=H
2: R=OH

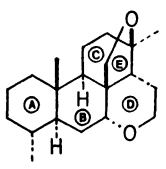

A

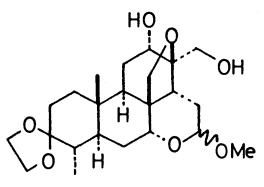

3

The first problem of our strategy was the construction of ABC ring from AB ring. It has been reported by Snitman et al.[5] that on Robinson annulation the hindered 1,5-diketone **4** did not yield **5** giving the retro-Michael product as the principal one and the similar compound **6** afforded cyclized compound **7** in only 15% yield. It was eventually found that a 1,5-diketone bearing a conjugated diene system at C-3 through C-6[6] gave a cyclized product in better yield than that of **7** from **6**. Steric compression around the carbonyl group at C-9 may have been decreased by the introduction of the diene system. The conjugated double bond is also useful for further syntheses because the diene system is stable on treatments with acid and base and introduction of oxygen functional groups into suitable positions in rings **A** and **B** (C-3 and C-7) utilizing the diene system is possible.

The retro-Michael reaction occurs hardly when 1,5-diketones having a methyl group instead of the methoxycarbonyl group are used for the cyclization reaction. Therefore, reaction of 1,5-diketone **11** was examined first to check the feasibility of the cyclization reaction. The tricyclic compound **12** was smoothly obtained from **11** which was prepared by the following sequences. Reduction of the known monoacetal **8**[7] with sodium borohydride was followed by an acid treatment to yield a diene **9** in a quantitative yield. The diene **9** was monomethylated by the treatment with methyl iodide in the presence of lithium diisopropylamide (LDA) to give **10** in 85% yield. The Michael addition reaction of methyl vinyl ketone to **10** proceeded in the presence of 0.3 equivalent of sodium methoxide in methanol at room temperature to afford **11**. The cyclization of the adduct **11** was accomplished to give tricyclic compound **12** by heating at reflux in methanol with 1 equivalent of sodium methoxide. The reactions to obtain **12** from **10** were carried out in one pot and the yield was 89%.

As the cyclization reaction of the 1,5-diketone **11** proceeded in high yield, the 1,5-diketone **14** having a methoxycarbonyl group and the diene system was examined next. The 1,5-diketone **14** was prepared by addition of methyl vinyl ketone to the β-keto ester **13** which was obtained by the methoxycarbonylation of the ketone **9**. The diketone **14** gave retro-Michael reaction product as major one on heating with sodium methoxide in methanol or on heating with pyrrolidine in benzene. However, on treatment with the same reaction conditions (a combination of pyrrolidine and benzoic acid) as those with which **6** afforded the cyclization product **7** in 15% yield,[5] **14** yielded the cyclization product **15** in 52% yield.

Several combinations of benzoic acid derivatives and

† Present address: Department of Agricultural Chemistry, Faculty of Agriculture and Veterinary Medicine, Nihon University, Shimouma, Setagaya-ku, Tokyo 154.

amines were examined to obtain **15** from **14** in better yield. Although couples of benzoic acid and secondary amines (pK_a) [pyrrolidine (11.3), piperidine (11.1), diethylamine (10.9), and morpholine (8.3)] did not show any remarkable change of the yield of **15**, couples of pyrrolidine and benzoic acid derivatives (pK_a) [*m*-toluic acid (4.94), *o*-toluic acid (4.79), benzoic acid (4.21), *m*-hydroxybenzoic acid (4.08), salicylic acid (3.00), and 3,5-dinitrobenzoic acid (2.82)] exhibited serious change of the yield of **15**. The weaker acid coupled with the amine gave **15** in the better yield. When salicylic and 3,5-dinitrobenzoic acids were used, only retro-Michael reaction occurred. The reason why the couple of pyrrolidine with the weaker benzoic acid gives **15** in better yield is not clear, but we consider that the weaker acid makes more tight complex with amines in benzene and suppresses base-catalyzed retro-Michael reaction.[8] It was also found that the use of excess amount of the acid made the yield better. And the treatment of **14** with 1.2 equivalent of *m*-toluic acid and 0.2 equivalent of pyrrolidine in benzene heated at reflux through Molecular Sieves 4A to remove water gave **15** in good yield (80—90%). By these reaction conditions, cyclization of **11** was accomplished in 6 h to give **12** in almost quantitative yield.

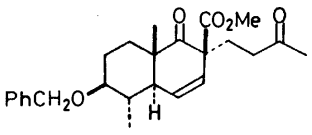

4

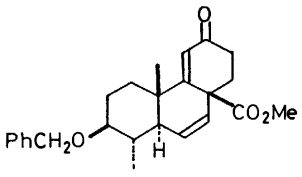

5

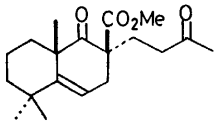

6

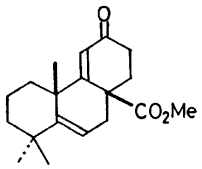

7

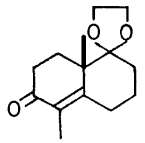

8

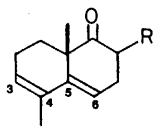

9: R=H
10: R=Me
13: R=CO_2Me

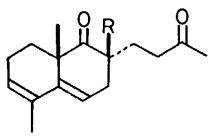

11: R=Me
14: R=CO_2Me

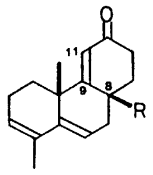

12: R=Me
15: R=CO_2Me

The stereochemistry of the methoxycarbonyl group of **15** was supposed to be β, because the Michael addition of methyl vinyl ketone to **13** was considered to proceed from less hindered opposite side to the angular methyl group. This was confirmed by conversion of the methoxycarbonyl group at C-8 of **15** into methyl group to give **12** and conversion of **12** into the α,β-unsaturated ketone **21**. The authentic specimen of **21** was derived from the known tricyclic compound **16**[9] via conjugated diene **17**, ketone **18**, tosylhydrazone **19**, and the enol thioether **20** according with the method developed by Nakai and Mimura.[10] The tricyclic compound **16** has been used for the construction of picrasane skeleton (skeletal structure **A** without ring E) by the authors.[9]

The UV absorption maximum at 302 nm indicates the presence of a conjugated enol thioether structure in **20**. This means that 1,3-shift of the proton at C-12 to C-14 occurred on the reaction of the tosylhydrazone **19** into the enol thioether **20**. Although hydrolysis of the enol thioether **20** using mercury(II) chloride gave the product in very poor yield and treatment of the thioether with titanium tetrachloride in acetic acid[11] afforded a complex mixture, on treatment with titanium tetrachloride in THF followed by addition of aqueous acetic acid **20** yielded the conjugated ketone **21** as a major product.

The transformations of **15** into **21** via **12** were carried out by the following reactions. Protection of the carbonyl group of **15** to give acetal **22**, whose methoxycarbonyl group was reduced with lithium alminium hydride (LAH) to yield alcohol **23**, which was oxidized with Collins' reagent to give aldehyde **24**. Wolff-Kishner reduction of **24** followed by treatment with

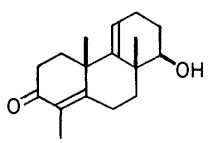

16

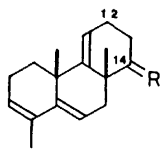

17: R=α-H, β-OH
18: R=O
19: R=NNHTs

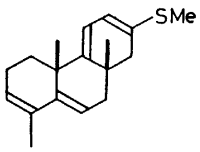

20

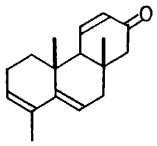

21

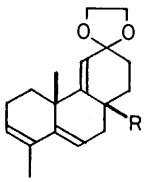

22: R=CO_2Me
23: R=CH_2OH
24: R=CHO

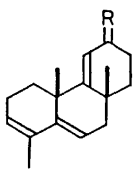

25: R=NNHTs

dilute hydrochloric acid gave the tricyclic compound **12**. The tricyclic compound **12** was converted into the conjugated ketone **21** via tosylhydrazone **25** and the enol thioether **20** using similar methods as those used for the conversion of **18** into **21**.

Although the diene system at C-3 through C-6 was very effective for the construction of the ring ABC, efficient methods for introduction of oxygen functions into C-3 and C-7 utilizing the diene system remained to be developed. A selective introduction of an oxygen function in a protected form into C-3 was desirable and it was performed by epoxidation with *m*-chloroperbenzoic acid (MCPBA) followed by a treatment under acetalization conditions. Hydrolysis of the acetal **23** gave ketone **26**, whose hydroxyl group was acetylated by the usual method to give acetate **27**. The acetate **27** afforded a 3 : 1 mixture of the α-epoxide **28**α and β-epoxide **28**β on epoxidation with MCPBA. The proton at C-3 was observed as a broad singlet ($W_{1/2}$=4.5 Hz) and a doublet (J=3.6 Hz) for **28**α and **28**β, respectively. Although **28**α afforded the acetal **29** in 90% yield by the treatment with ethylene glycol and boron trifluoride etherate ($BF_3 \cdot Et_2O$) in benzene at room temperature, **28**β gave a complex mixture by the same treatment. The fact suggests that the acetal at C-3 can be derived only from the α-epoxide and the use of a compound which gives α-epoxide in high selectivity is desirable.

On epoxidation with MCPBA the monoacetal **22** afforded a 5 : 1 mixture of α- and β-epoxides (**30**α and **30**β). On treatment with ethylene glycol and $BF_3 \cdot Et_2O$ in benzene, the mixture yielded a 6 : 1 mixture of monoacetal **31** and diketone **32**. On acetalization under standard conditions the mixture of **31** and **32** afforded diacetal **33**. The overall yield of **33** from **22** was 64%. The diacetal **33** was obtainable from **15** by two steps (epoxidation and acetalization), but the ratio of the α- and β-epoxides (**34**α and **34**β) obtained by epoxidation of **15** with MCPBA was 2 : 1 and the final yield of **33** was low.

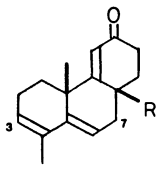

26: R=CH_2OH
27: R=CH_2OAc

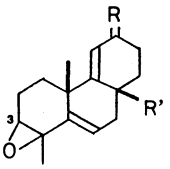

28: R=O, R'=CH_2OAc
30: R=-O(CH_2)$_2$O-, R'=CO_2Me
34: R=O, R'=CO_2Me

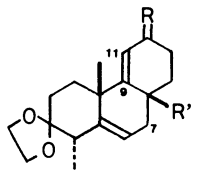

29: R=O, R'=CH_2OAc
31: R=O, R'=CO_2Me
33: R=-O(CH_2)$_2$O-, R'=CO_2Me

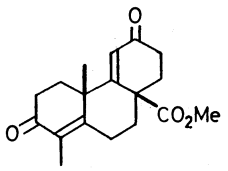

32

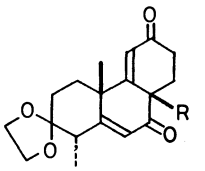

35: R=CO_2Me
36: R=CH_2OAc

Allylic oxidation of some tricyclic compounds obtained so far was tried to introduce an oxygen function into C-7. Oxidation of diacetal **33** yielded diketone **35**, but the yield (27%) was too low to continue the further syntheses. Oxidation of the acetate **29** afforded ketone **36** in poor yield. In our previous synthetic studies of quassinoids, it has been experienced that the yield of allylic oxidation at C-7 was seriously affected by the substituents of ring C. Therefore, we decided to examine the introduction of oxygen function into C-7 at the later stage.

Introduction of two carbon appendage into C-14 position through 1,4-addition was our strategy and so the presence of the double bond at C-9 (11) was undesirable. As introduction of oxygen function into the double bond at C-9 (11) was unsuccessful, reduction of the double bond was examined. Reduction of the double bond at C-9 (11) of the tetrahydropyranyl (THP) ether **38** derived from the α,β-unsaturated ketone **37** was tried by three methods. The saturated ketone **39** was given in 48%, 77%, and 99% yield on catalytic hydrogenation using 10% palladium on carbon, Birch reduction using lithium, and reduction with sodium hydrogentelluride (NaHTe),[12] respectively. The stereochemistry of the newly generated chiral center (C-9) of **39** was suggested to be α-H, because hydrogen attacks from less hindered α-side on catalytic hydrogenation. Although the protecting group of the hydroxyl group at C-20 was necessary to be removed without significant effect on the acetal at C-3, the selective removal of the THP group of **39** was hard. After several trials, it was found that 1-ethoxyethyl (EE) group was a satisfactory protecting group which could be removed selectively in almost quantitative yield. The EE ether **40** obtained by the treatment of **37** with ethyl vinyl ether and pyridinium *p*-toluenesulfonate (PPTS) was reduced with NaHTe to give ketone **41** in 98% yield.

Introduction of a double bond at C-13 was necessary prior to addition of two carbon unit to C-14. Regioselectivity of phenylselenylation of the EE ether **41** was poor, but a methoxycarbonyl group was regioselectively introduced into C-13 of **41** giving **42** (83% yield) by treatment with dimethyl carbonate and sodium hydride containing catalytic amount of potassium hydride.[13] When the reaction was carried out without potassium hydride, the yield of **42** was very low. The ratio of keto and enol forms of β-keto ester **42** produced is variable. Phenylselenylation of **42** and successive oxidative elimination of the phenylseleno group

afforded α,β-unsaturated ester **43**.[14] Heathcock et al.[15] reported that addition of ketene acetal **44** to the "very reactive" Michael acceptor **45**, whose structure is very close to **43**, required 15 kbar for 24 h to do drive the reaction to completion. But a vinyl group was successfully introduced into the C-14 position of **43** to give **46** by conjugate addition of vinylmagnesium bromide catalyzed with a complex of copper(I) iodide and tributylphosphine[16] at −45 °C in 80% yield along with 1,2-addition product **47** (12% yield). The stereochemistry of the vinyl group of **46** was assumed to be α-axial, because the attack of the Grignard reagent was considered to occur from less hindered side. After our preliminary report it has been reported by Grieco et al.[17] that conjugate addition of C_2-unit to octalone **48** proceeded smoothly in ether at −78 °C, giving rise to **49** in 95% yield using an organocopper reagent derived from equimolar amounts of copper(I) iodide and vinyllithium and 2.6 equivalent of tributylphosphine. The compound **46** has all carbons contained in the skeletal structure **A** with desired stereochemistry.

Construction of ring E by attack of hydroxyl group at C-20 to C-13 was our selected strategy to be tried at first and introduction of a double bond at C-12 was necessary prior to the trial. Conversion of **46** into the α,β-unsaturated ester **51** via a mixture of stereoisomers of the alcohol **50** was carried out by the successive treatments with sodium borohydride in ethanol, methanesulfonyl chloride and triethylamine in dichloromethane, and then 1,8-diazabicyclo[5.4.0]undec-7-ene (DBU) in refluxing benzene. The overall yield of **51** from **46** was 73%. The EE group of **51** was removed by treatment in ethanol containing catalytic amount of PPTS to give alcohol **52** in 81% yield. The tricyclic compound **52** is ready to form bruceantin skeleton **A**.

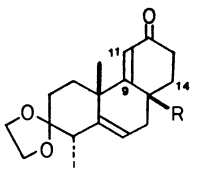

37: R=CH_2OH
38: R=CH_2OTHP
40: R=CH_2OEE
(EE: 1-ethoxyethyl)

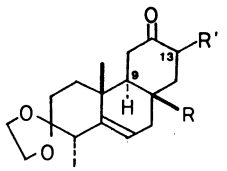

39: R=CH_2OTHP, R'=H
41: R=CH_2OEE, R'=H
42: R=CH_2OEE, R'=CO_2Me
(THP: tetrahydropyranyl)

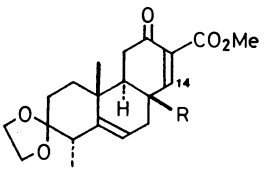

43: R=CH_2OEE
45: R=Me

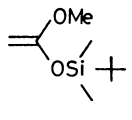

44

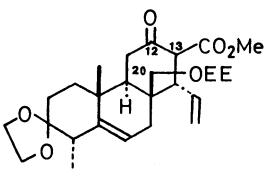

46

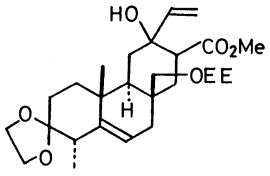

47

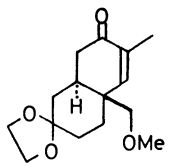

48

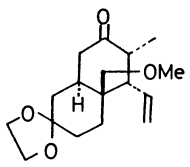

49

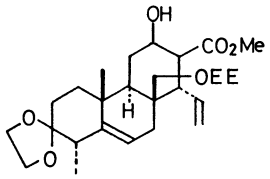

50

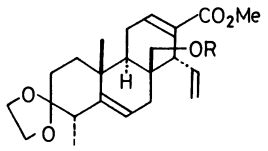

51: R=EE
52: R=H

The modest yield we encountered when scaling up the synthesis of the diacetal **33** led us to search for another route for the synthesis of **51**. If the double bond at C-9(11) is reduced prior to the introduction of an oxygen function into C-3, the use of the unstable acetals such as **33** can be avoided. It was eventually found that the double bond of the α,β-unsaturated ketone of **15** could be reduced selectively to give ketone **53** in a quantitative yield with NaHTe in ethanol at room temperature (the conjugated diene system of **15** was reduced on Birch reduction and catalytic hydrogenation). The keto alcohol **55** was obtained by LAH reduction of acetal **54** and following acid treatment of the product. The yield of **55** from **53** was almost quantitative. The hydroxyl group of **55** was protected with EE to give **56** in 94% yield. The α,β-unsaturated ester **60** was synthesized from **56** via **57**, **58**, and **59** by the same methods used to obtain **51** from **41**, namely methoxycarbonylation to give **57**, phenylselenylation followed by oxidative elimination to afford **58**, conjugate addition reaction of vinylmagnesium bromide to yield **59**, reduction with sodium borohydride, mesylation, and treatment with DBU to give **60**. The overall yield of **60** from **56** was 58%.

Before introduction of an oxygen function into C-3, the EE group of **60** was replaced with an acetyl group to give **61** in 90% yield, because the EE group was affected with MCPBA giving a complex mixture. On oxidation with MCPBA the acetate **61** afforded epoxide **62**. No other product was detected in the ^1H NMR spectrum of the crude **62**. The signal of the proton at C-3 in the ^1H NMR was observed as a singlet ($W_{1/2}$= 4.5 Hz) suggesting the configuration of the epoxide to be α which is preferable stereochemistry for introduc-

tion of an acetal group into C-3 as shown in the case of **28**. The epoxide **62** yielded the acetal **63** on treatment with 2-ethyl-2-methyl-1,3-dioxolane and $BF_3 \cdot Et_2O$ in dichloromethane. The yield of **63** from **61** was 87%. The replacement of the acetyl group of **63** with EE group was accomplished in 93% yield to afford **51**. Thus the preparation of enough amount of the tricyclic compound **51** for further syntheses toward antitumor quassinoids has become possible.

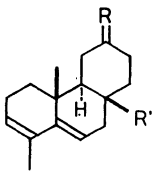

53: R=O, R'=CO_2Me
54: R=-O(CH_2)$_2$O-, R'=CO_2Me
55: R=O, R'=CH_2OH
56: R=O, R'=CH_2OEE

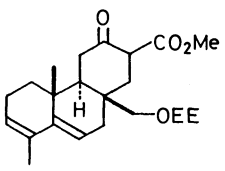

57

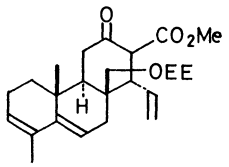

59

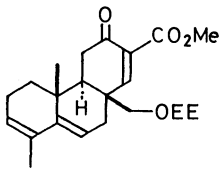

58

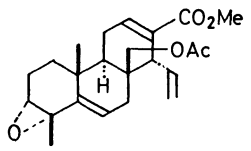

62

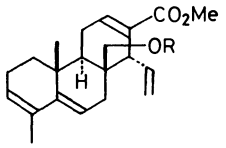

60: R=EE
61: R=Ac

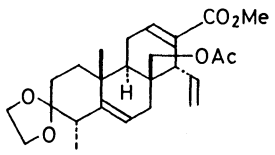

63

The next step in our strategy toward bruceantin skeleton was the construction of the epoxide ring E. The direct formation of tetracyclic triol **65** on MCPBA oxidation of triol **64** has been reported by Ziegler et al.[18] Therefore it was considered that the acid-catalyzed opening of 12,13-epoxide ring would provide a convenient access to ring E. For the regio- and stereospecific introduction of the epoxide into the C-12 double bond utilizing a hydroxyl group at C-21, the ester **51** was reduced to allylic alcohol **66** with DIBAL. The allylic alcohol **66** was oxidized with *t*-butyl hydroperoxide using titanium(IV) isopropoxide as a catalyst[19] to give epoxide **67** as a sole product in almost quantitative yield. The stereochemistry of the epoxide ring of **67** was hard to be determined by its NMR spectrum. On treatment with catalytic amount of PPTS in ethanol **67** afforded the diol **68** as nice crystalline compound in a quantitative yield. The similarity of the NMR spectra of **68** [^{1}H NMR signals for C-20H_2 (AB quartet at δ 3.33 and 4.36 with J=8 Hz) and C-12H (broad doublet at δ 4.05 with J=4 Hz) and ^{13}C NMR signals for C-12, C-13, C-20, and C-21] to those of the known compound **69**[20] suggested that the stereochemistry of the hydroxyl group at C-12 is α-axial. Therefore, the configuration of the epoxide ring of **67** was suggested to be α.

Even though the stereochemistry of the hydroxyl group at C-12 is axial, **68** gave diacetate **70** very easily. This facile acetylation of the axial hydroxyl group is compatible with acetylation of the primary hydroxyl group at C-21 followed by the migration of the acetyl group to the hydroxyl group at C-12 and successive acetylation of the regenerated primary hydroxyl group.

Migration of the protecting group of the hydroxyl group at C-21 to the hydroxyl group at C-12 was observed also for the *t*-butyldimethylsilyl (tBDMS) ether **71**. The acetate **72** derived from **71** showed the ^{1}H NMR signal of C-12H at δ ca. 5.0 suggesting the presence of the acetoxyl group at C-12. Although the silyl ether **71** was not affected by the treatment with chrolomethyl methyl ether (MOMCl) and *N,N*-diisopropylethylamine in refluxing dichloromethane, on treatment with MOMCl and potassium hydride in a mixed solvent of THF and *N,N*-dimethylformamide (DMF) **71** afforded methoxymethyl (MOM) ether **73**. On selective removal of the silyl protecting group with tetrabutylammonium fluoride followed by acetylation, **73** afforded the acetate **74** whose ^{1}H NMR spectrum suggested the presence of the acetoxyl group at C-12

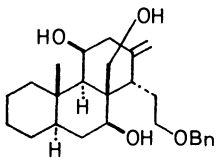

64

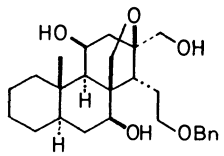

65

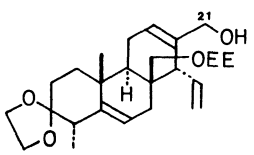

66

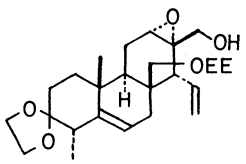

67

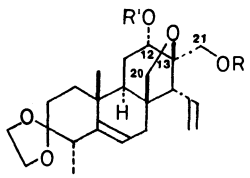

68: R=R'=H
70: R=R'=Ac
71: R=tBDMS, R'=H
72: R=tBDMS, R'=Ac
73: R=MOM, R'=tBDMS
74: R=MOM, R'=Ac
(tBDMS: t-butyldimethylsilyl)
(MOM: methoxymethyl)

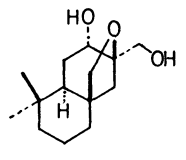

69

(C-12H: δ ca. 5.0). These observations indicate that the migration of the silyl group[21] from the hydroxyl group at C-21 to that of at C-12 occurred during the reaction of **71** to **73**.

The final step for the synthesis of the bruceantin skeleton was the construction of ring D (lactone or hemiacetal ring). Oxidation at C-7 and C-16 and reduction of the double bond at C-5 were inevitable in order to construct the ring D. Protection of the hydroxyl groups at C-12 and C-21 was necessary prior to these reactions. Silyl groups were considered to be desirable for the protection. The monosilyl derivative **71** was treated with potassium hydride in the mixed solvent of THF and DMF and then the solution of tBDMSCl in THF was added to the reaction mixture to give the disilyl derivative **75** in 96% yield.

Selective introduction of a hydroxyl group into C-16 of **75** was carried out by hydroboration-oxidation using thexylborane to yield alcohol **76**. Simultaneous oxidation of the hydroxyl group and the allylic position (C-7) of **76** was hard, and so **76** was converted into aldehyde **77** by Collins' oxidation. Although protection of the formyl group of **77** using trimethyl orthoformate in methanol containing PPTS was inefficient because of concurring hydrolysis of the acetal group at C-3, dimethyl acetal **78** was obtained in 94% yield by the use of dichloromethane instead of methanol as the solvent in the above reaction conditions.

Allylic oxidation of the acetal **78** with the complexes of chromium trioxide and 3,5-dimethylpyrazole[22] gave the α,β-unsaturated ketone **79** in 68% yield. The enhanced yield of allylic oxidation at C-7 of **78** compared with those of **29** and **33** is probably due to decrease of strain energy around the carbonyl at C-7 caused by saturation of the ring C and not due to simple change of steric hindrance around C-7. Birch reduction of **79** gave saturated ketone **80**. The stereo-

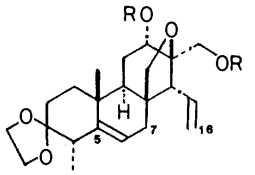

75: R=tBDMS

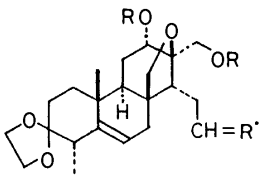

76: R=tBDMS, R'=H,OH
77: R=tBDMS, R'=O
78: R=tBDMS, R'=(OMe)$_2$

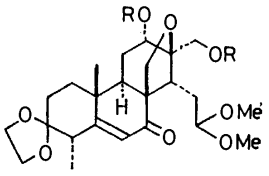

79: R=tBDMS

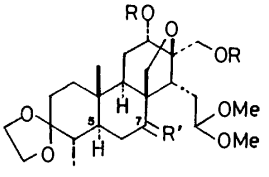

80: R=tBDMS, R'=O
81: R=tBDMS, R'=α-OH, β-H

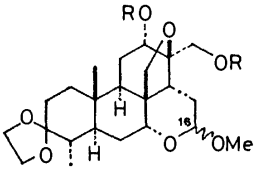

82: R=tBDMS

Table 1. Isolated Isomer of **3**: Assignments, Chemical Shifts, and Coupling Constants from 270 MHz ^{1}H NMR in $CDCl_3$

Proton	Chemical shift (δ)	Signal type	J/Hz
$C_{(1)}$-αH	ca. 1.3[a]		
$C_{(1)}$-βH	b)		
$C_{(2)}$-αH	b)		
$C_{(2)}$-βH	ca. 1.6[a]		
$C_{(4)}$-H	1.72	m	$J_{4,5}$=12, $J_{4,Me}$=6
$C_{(4)}$-Me	0.82	d	$J_{Me,4}$=6
$C_{(5)}$-H	1.92	dt	$J_{4,5}$=12, $J_{5,6\alpha}$=3, $J_{5,6\beta}$=12
$C_{(6)}$-αH	ca. 1.7[a]	ddd	$J_{6\alpha,6\beta}$=14, $J_{6\alpha,5}$=3, $J_{6\alpha,7}$=2
$C_{(6)}$-βH	1.20	ddd	$J_{6\beta,6\alpha}$=14, $J_{6\beta,5}$=12, $J_{6\beta,7}$=2
$C_{(7)}$-H	3.73	t	$J_{7,6\alpha}$=2, $J_{7,6\beta}$=2
$C_{(9)}$-H	2.06	dd	$J_{9,11\alpha}$=4, $J_{9,11\beta}$=14
$C_{(10)}$-Me	0.93	s	
$C_{(11)}$-αH	ca. 1.6[a]	dd	$J_{11\alpha,11\beta}$=14, $J_{11\alpha,9}$=4, $J_{11\alpha,12}$=ca. 0
$C_{(11)}$-βH	1.85	dt	$J_{11\beta,11\alpha}$=14, $J_{11\beta,9}$=14, $J_{11\beta,12}$=4
$C_{(12)}$-H	4.00	d	$J_{12,11\alpha}$=0, $J_{12,11\beta}$=4
$C_{(14)}$-H	2.02	dd	$J_{14,15\alpha}$=14, $J_{14,15\beta}$=4
$C_{(15)}$-αH	2.43	dt	$J_{15\alpha,14}$=14, $J_{15\alpha,15\beta}$=14, $J_{15\alpha,16}$=3
$C_{(15)}$-βH	1.71	dd	$J_{15\beta,14}$=4, $J_{15\beta,15\alpha}$=14, $J_{15\beta,16}$=ca. 0
$C_{(16)}$-H	4.80	d	$J_{16,15\alpha}$=3, $J_{16,15\beta}$=0
$C_{(20)}$-αH	3,31	d	$J_{20\alpha,20\beta}$=8
$C_{(20)}$-βH	4,23	d	$J_{20\beta,20\alpha}$=8
$C_{(21)}$-H_2	3.77	ABq	J=11, $\Delta\nu_{AB}$=15
Ethylenedioxy-H_4	3.93	m	

a) Determined by difference NOE. b) Undetermined because of overlapping with other signals.

chemistry at C-5 of **80** was supposed to be 5α-H, because the 5α-H compound is more stable than the 5β-H isomer.

For the completion of ring D, stereoselective reduction of the carbonyl group at C-7 into α hydroxyl group was necessary. Although bulky hydride reagents such as diisobutylaluminium hydride (DIBAL) were considered to give 7α-OH derivative selectively, 7β-OH derivative was obtained as the sole product on reduction of the ketone **80** with DIBAL and sodium borohydride. Chelation between the dimethyl acetal group and the hydride reagent may have controlled the stereochemistry of the reaction. On reduction with lithium triethylhydroborate the ketone **80** gave 7α-OH derivative **81** stereoselectively. The anomeric mixture at C-16 of the hemiacetal **82** was obtained smoothly by the treatment of **81** with catalytic amount of PPTS in MeOH at room temperature. The mixture could not be separated into each isomer, but an isomer of the anomeric mixture of the diol **3** obtained by the treatment of **82** with tetrabutylammonium fluoride could be separated.

Precise decoupling (Table 1) and difference NOE (Fig. 1) experiments using 270 MHz ^{1}H NMR confirmed the structure of the isolated isomer of **3** bearing 16β-methoxyl group to be that shown in Fig. 2. The stereochemistries of the epoxymethano bridge and the methyl group at C-4 are shown to be β-axial and α-equatorial, respectively, by the NOEs among $C_{(10)}$-Me, $C_{(20)}$-βH, and $C_{(4)}$-H (Fig. 1 A and B). The NOEs among $C_{(10)}$-Me, $C_{(20)}$-βH, and $C_{(11)}$-βH (Fig. 1 A and B) indicate that $C_{(11)}$-βH has axial conformation and the large coupling constant (14 Hz) between $C_{(9)}$-H and the $C_{(11)}$-βH suggests that the stereochemistry of the $C_{(9)}$-H is α-axial. The coupling constant (12 Hz) between $C_{(4)}$-H and $C_{(5)}$-H shows the α-axial nature of the $C_{(5)}$-H. The NOEs among $C_{(20)}$-αH, $C_{(14)}$-H, and $C_{(7)}$-H (Fig. 2 C, D, and E) indicate that these protons are located near place each other, therefore both of the protons at C-7 and C-14 have β-equatorial stereochemistry. This is also supported with the small coupling constants between the proton at C-7 and the protons at C-6. All of the NMR data of the isolated isomer of **3** are best compatible with the molecular structure (Fig. 3) having minimized steric energy (348.695 kJ mol^{-1}) given by MM2 force field calculation[23] for the 16β-methoxy isomer of **3** and unequivocally confirmed the stereochemical assignment.

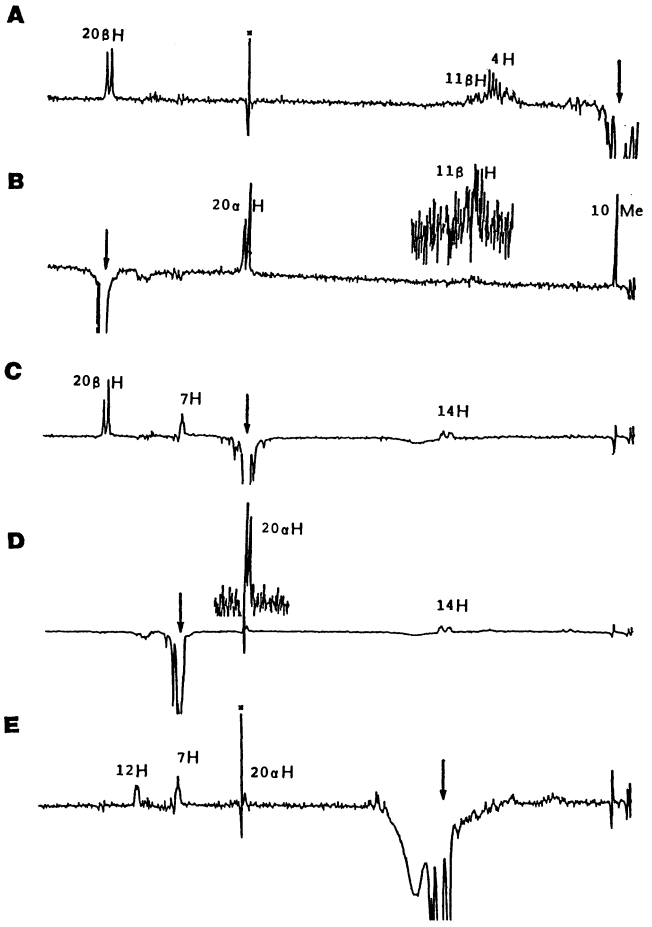

Fig. 1. Difference NOE spectra (270 MHz in $CDCl_3$) of 16β-methoxy isomer of **3**. ↓: Irradiated frequency. The NOE of 12H in E was induced by simultaneous irradiation on overlapping signal of 12-OH.

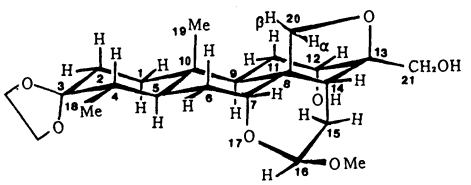

Fig. 2. Perspective drawing of the isolated isomer of **3**.

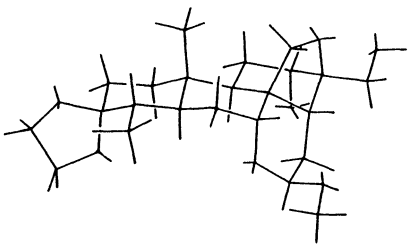

Fig. 3. Wire model generated by computer based on MM2 force field calculation for the 16β-methoxy isomer of **3** bearing minimum steric energy. Short lines from ether oxygen indicate lone pairs.

Experimental

General. All reactions were run under a nitrogen atmosphere with magnetic stirring unless otherwise noted. Unless otherwise noted, materials were obtained from commercial suppliers and used without further purification. Ether and tetrahydrofuran were distilled from lithium aluminium hydride immediately prior to use. Dichloromethane was distilled from P_2O_5. Absolute ethanol (EtOH) and methanol (MeOH) were distilled from magnesium. Hexane, benzene, toluene, pyridine, 1,2-dimethoxyethane (DME), acetonitrile, *N*,*N*-dimethylformamide (DMF), triethylamine, *N*,*N*-di-

isopropylethylamine, and dimethyl carbonate were distilled from calcium hydride. Chromium trioxide was dried overnight at reduced pressure and stored over P_2O_5. Liquid ammonia was distilled from sodium. Preparative chromatography was carried out on open column of silica gel (Wako, C-200). Thin-layer chromatography (TLC) was performed on E. Merck Kieselgel GF_{254} Art 7730.

Melting points were measured on Laboratory Devices Meltemp and are uncorrected.

^1H NMR spectra were determined with Varian EM 390 (90 MHz), JEOL FX 90Q (90 MHz), or Brucker WH 270 (270 MHz) spectrometers in $CDCl_3$ solutions with tetramethylsilane as internal standard. ^{13}C NMR spectra were recorded on JEOL FX 90Q spectrometer. ^1H NMR data are tabulated in order number of protons, multiplicity (s, singlet; brs, broad singlet; d, doublet; t, triplet; brt, broad triplet; q, quartet; m, multiplet), coupling constants in hertz. IR spectra were recorded on a Hitachi Model 260-30 grating infrared spectrometer. UV spectra were obtained on a Hitachi Model 340 instrument. Low- and high-resolution mass spectra were measured using JEOL JMS-D300 mass spectrometer equipped with JMA-2000 data analysis system.

3,7,8,8a-Tetrahydro-5,8a-dimethyl-1(2*H*)-naphthalenone (9): To a solution of monoacetal **8** (11.0 g, 46 mmol) in methanol (200 ml) was added sodium borohydride (3 g, 79 mmol) in portions under drying tube. The mixture was stirred at room temperature for 3 h. Acetic acid (200 ml) and 1 mol dm^{-3} HCl (100 ml) were added. After being set aside overnight, the solution was neutralized with 30% aqueous NaOH, extracted with ether, washed with water (×3) and then dried over $MgSO_4$. Removal of the solvent under reduced pressure and subsequent distillation afforded the diene **9** (6.1 g, 74%) as an oil: bp 83—94 °C (80.0 Pa); IR (oil) 1715 cm^{-1}; UV (EtOH) 237 nm (ε 16000); ^1H NMR δ=1.18 (3H, s, 10-CH_3), 1.81 (3H, brs, 4-CH_3), 5.50 (1H, m), and 5.75 (1H, brt, J=4 Hz); MS (70 eV) m/z (rel intensity) 176 (M^+, 36.5), 161 (13), and 118 (100); Found m/z 176.1217. Calcd for $C_{12}H_{16}O$: M, 176.1201.

3,7,8,8a-Tetrahydro-2α,5,8aβ-trimethyl-1(2*H*)-naphthalenone (10): To a solution of LDA (6.8 mmol) in THF (20 ml) was added a solution of **9** (1.11 g, 6.29 mmol) in THF (20 ml) dropwise with stirring at −78 °C. The mixture was stirred at room temperature for 30 min and to the solution was added MeI (0.8 ml, 13 mmol) which was passed through a neutral alumina column prior to use. After stirring at room temperature for 30 min the reaction was quenched by the addition of brine. The reaction mixture was acidified with dil HCl and extracted with ether. The ether solution was washed with brine and then dried (Na_2SO_4). Concentration in vacuo gave a residue that was chromatographed on silica gel (eluent: benzene) to give methylated compound **10** (1.02 g, 85%) which afforded colorless needles on crystallization from aqueous methanol: mp 47.0—48.8 °C; IR (oil) 1712 cm^{-1}; ^1H NMR δ=1.02 (3H, d, J=6 Hz, 8-CH_3), 1.16 (3H, s, 10-CH_3), 1.74 (3H, brs, 4-CH_3), 5.34 (1H, m), and 5.38 (1H, brt, J=4 Hz); MS (70 eV) m/z (rel intensity) 190 (M^+, 30), 175 (11), 134 (41), and 119 (100): Found: m/z 190.1357. Calcd for $C_{13}H_{18}O$: M, 190.1357.

1,4b,5,6,10,10a-Hexahydro-4bβ,8,10aβ-trimethyl-3(2*H*)-phenanthrenone (12): To a solution of 0.5 mol dm^{-3} NaOMe in MeOH (2.5 ml) was added **10** (0.70 g, 3.7 mmol) and then methyl vinyl ketone (0.65 ml). The mixture was stirred at room temperature for 20 h. (Michael adduct **11** could be obtained from the reaction mixture by usual work up.) To the reaction mixture was added 1 mol dm^{-3} NaOMe (2.5 ml) and the mixture was heated at reflux for 4 d. Brine was added into the mixture, which was extracted with ether and dried over Na_2SO_4. Evaporation of the solvent gave a residue which was purified by silica-gel column chromatography (50 g; eluent: 2% acetone in benzene) to give tricyclic compound **12** as a colorless oil (0.79g, 89%): IR (oil) 1672 and 1603 cm^{-1}; ^1H NMR δ=1.23 (3H, s), 1.42 (3H, s), 1.83 (3H, brs, 4-CH_3), 5.51 (1H, m), 5.66 (1H, brt, J=4 Hz), and 6.01 (1H, s, 11-CH); MS (70 eV) m/z (rel intensity) 242 (M^+, 100), and 227 (59); Found m/z 242.1689. Calcd for $C_{17}H_{22}O$: M, 242.1670.

3,7,8,8a-Tetrahydro-2-methoxycarbonyl-5,8a-dimethyl-1(2*H*)-naphthalenone (13): To a suspension of NaH (60 g, 1.5 mol 60% oil dispersion) and KH (1 g, 12 mmol, 50% oil dispersion) and dimethyl carbonate (110 ml) in DME was added **9** (200 g, 1.1 mol) in DME (250 ml) with stirring in an ice bath and releasing the hydrogen evolved by the reaction through mercury valve. The mixture was stirred in an ice bath until practical finish of evolution of hydrogen and then heated at reflux for 1 h. The reaction mixture was poured into saturated aqueous NH_4Cl and extracted with ether (11×1, 0.5 1×2). The ether solution was washed with saturated aqueous NH_4Cl (100 ml) and then brine (100 ml×2). Drying over Na_2SO_4 and evaporation of the solvent gave an orange oil, which crystallized upon standing. An analytical sample of **13**, mp 51.8—53 °C, was obtained as colorless plates (colored slightly yellow on exposure to air) by crystallization from methanol: IR (KBr) 1663, 1640, and 1618 cm^{-1}; UV (EtOH) 232 (ε 30000) and 238 nm (sh 25000); ^1H NMR δ=1.17 (3H, s, 10-CH_3), 1.76 (3H, brs, 4-CH_3), 2.92 (2H, brd 7-CH_2), 3.70 (3H, s, CO_2CH_3), and 5.30—5.65 (2H, m); MS (70 eV) m/z (rel intensity) 234 (M^+, 32), 219 (69), and 187 (100); Found m/z 234.1268. Calcd for $C_{14}H_{18}O_3$: M, 234.1256.

3,7,8,8a-Tetrahydro-2β-methoxycarbonyl-5,8aβ-dimethyl-2α-(3-oxobutyl)-1(2*H*)-naphthalenone (14): To a solution of **13** (4.24 g, 18 mmol) in MeOH (50 ml) was added 0.5 mol dm^{-3} NaOMe in MeOH (3.0 ml) and methyl vinyl ketone (4.0 ml). The mixture was stirred at 40 °C for 3 h. The solvent was distilled off under reduced pressure. The residue was dissolved in ether and brine. The ether solution was washed with brine and dried (Na_2SO_4). Evaporation of the solvent gave 5.50 g (100%) of crude **14** pure enough for further use. An analytical sample of **14**, mp 78.5—80 °C, was obtained by crystallization from hexane as colorless needles: IR (KBr) 1742, 1715, and 1708 cm^{-1}; UV (EtOH) 240 nm (ε 19000); ^1H NMR δ=1.17 (3H, s, 10-CH_3), 1.83 (3H, brs, 4-CH_3), 2.09 (3H, s, $COCH_3$), 3.70 (3H, s, CO_2CH_3), 5.60 (1H, m), and 5.72 (1H, dd, J=7 and 3 Hz); MS (70 eV) m/z (rel intensity) 304 (M^+, 5.8), 286 (5), 257 (9.2), 233 (94), and 201 (100); Found: C, 70.87; H, 7.82%. Calcd for $C_{18}H_{24}O_4$: C, 71.03; H, 7.95%.

1,4b,5,6,10,10a-Hexahydro-10aβ-methoxycarbonyl-4bβ,8-dimethyl-3(2*H*)-phenanthrenone (15): To a solution of diketone **14** (30.4 g, 0.1 mol) and *m*-toluic acid (16.3 g, 0.12 mol) in benzene (750 ml) was added pyrrolidine (1.7 ml, 0.02 mol) and the mixture was refluxed for 14 h passing through Molecular Sieves 4A. The cooled mixture was washed with 5% aqueous potassium hydroxide (100 ml×3) and the combined aqueous layers were extracted with ether (100 ml×3). The combined organic extracts were washed with 2 mol dm^{-3} HCl (100 ml×3) and the combined aqueous layers

were extracted with ether (100 ml×2). The combined organic extracts were washed with brine (100 ml), dried (Na_2SO_4-$MgSO_4$), filtered through a silica-gel column (70 g in benzene) and evaporated. The brown residue was chromatographed on silica-gel column (150 g in hexane, eluent: 2% AcOEt in hexane) to afford enone **15** (22.86 g, 80%) as a pale yellow solid. An analytical sample was obtained as colorless plates by recrystallization from ether-hexane: mp 80—82 °C; IR (Nujol) 1731, 1675, and 1608 cm^{-1}; UV (EtOH) 236.5 nm (ε 26000); ^1H NMR δ=1.05 (3H, s, 10-CH_3), 1.79 (3H, s, 4-CH_3), 3.72 (3H, s, CO_2CH_3), 5.53 (1H, m), 5.61 (1H, dd, J=7 and 3 Hz), and 6.18 (1H, s, 11-CH); ^{13}C NMR δ=198.67, 173.62, 166.44, 138.92, 130.30, 124.69, 123.75, 117.06, 51.88, 44.94, 38.82, 36.46, 35.59, 33.48, 31.45, 23.84, 22.13, and 19.56; MS (70 eV) m/z (rel intensity) 286 (M^+, 58) and 227 (100); Found: C, 75.46; H, 7.61%. Calcd for $C_{18}H_{22}O_3$: C, 75.49; H, 7.74%.

1,2,3,4b,5,6,10,10a-Octahydro-4bβ,8,10aβ-trimethyl-1-phenanthrenol (17): To a solution of **16** (6.0 g) in MeOH (180 ml) was added $NaBH_4$ (1.2 g) in portions with stirring in ice bath. After stirring at room temperature for 1 h, to the reaction mixture was added acetic acid (10 ml) and then 2 mol dm^{-3} hydrochloric acid (60 ml). After stirring for 1 h at room temperature, the reaction mixture was cooled in ice bath and was added 10% aqueous NaOH (120 ml). The reaction mixture was concentrated to ca. 150 ml with rotary evaporator and extracted with ether (100 ml×3). The combined ether extracts were washed with brine (100 ml×1) and dried over $MgSO_4$. Evaporation of the solvent afforded the alcohol **17** (5.88 g): IR (Nujol) 3400 and 1642 cm^{-1}; UV (MeOH) 239 nm (ε 10510) and 232 nm (ε 9716); ^1H NMR δ= 1.17 (3H, s), 1.20 (3H, s), 1.78 (3H, m, 4-CH_3), 3.50 (1H, dd, J=7 and 9 Hz, 14-CH), and 5.31—5.71 (3H, m); MS (70 eV) m/z (rel intensity) 244 (M^+, 89), 229 (69), 226 (26), and 211 (100); Found: m/z 244.1824. Calcd for $C_{17}H_{24}O$: M, 244.1825.

3,4b,5,6,10,10a-Hexahydro-4bβ,8,10aβ-trimethyl-1(2*H*)-phenanthrenone (18): To a solution of the alcohol **17** in CH_2Cl_2 (175 ml) was added pyridinium chlorochromate (13.0 g) and the mixture was stirred at room temperature for 1 h. The reaction mixture was decanted and the residue was washed with ether. The combined solution was passed through a florisil column and the solvent was evaporated to give a residue, which was chromatographed on a silica-gel column (50 g, eluent: benzene) to give the ketone **18** (3.4 g): IR (Nujol) 1720 cm^{-1}; UV (MeOH) 238 nm (ε 18660) and 232 nm (ε 17270); ^1H NMR δ=1.21 (3H, s), 1.43 (3H, s), 1.78 (3H, m, 4-CH_3), and 5.32—5.88 (3H, m); MS (70 eV) m/z (rel intensity) 242 (M^+, 64), 227 (20), 209 (77), and 184 (100); Found: m/z 242.1671. Calcd for $C_{17}H_{22}O$: M, 242.1671.

3,4b,5,6,10,10a-Hexahydro-4bβ,8,10aβ-trimethyl-1(2*H*)-phenanthrenone Tosylhydrazone (19): To a solution of the ketone **18** (3.4 g) in hot 95% EtOH (10 ml) was added a solution of tosylhydrazine (3.0 g) in hot 95% EtOH (6 ml) and the mixture was stirred for 10 min and then stood at room temperature for 12 h. Washing with 50% aqueous EtOH and crystallization from ether afforded the tosylhydrazone **19** as colorless crystals: mp 173—175 °C; IR (Nujol) 3215, 1602, and 1176 cm^{-1}; ^1H NMR δ=1.15 (3H, s), 1.30 (3H, s), 1.75 (3H, m, 4-CH_3), 2.37 (3H, s), 5.37—5.85 (3H, m), 7.28 (2H, d, J=8 Hz), and 7.86 (2H, d, J=8 Hz); MS (70 eV) m/z (rel intensity) 410 (M^+, 15), 395 (13), and 225 (100); Found: m/z 410.2071. Calcd for $C_{24}H_{30}N_2O_2S$: M, 410.2029.

1,4b,5,6,10,10a-Hexahydro-4bβ,8,10aβ-trimethyl-2-methylthiophenanthrene (20): To a solution of the tosylhydrazone **19** (869 mg) in THF (10 ml) and TMEDA (10 ml) was added 2 equiv of butyllithium in hexane dropwise with stirring at −78 °C and the mixture was stirred for 30 min at the temperature. After addition of dimethyl disulfide (0.22 ml, 1.1 equiv) dropwise at −78 °C, the reaction mixture was stirred at −30 °C for 1 h. *n*-Butyllithium (1.3 equiv) in hexane was added into the reaction mixture with stirring at −50 °C. The mixture was warmed to room temperature over 1 h and stirred at the temperature for 6 h. The reaction mixture was poured into saturated aqueous NH_4Cl (50 ml) and extracted with ether (50 ml×3). The combined extracts were washed with brine (20 ml×2) and dried over Na_2SO_4. The residue obtained by evaporation of the solvent was chromatographed on a silica-gel column (eluent: hexane) to give the enol thioether **20** (pale yellow viscous oil): IR (oil) 1620 and 1565 cm^{-1}; UV (MeOH) 302 nm (ε 8440), 238 nm (ε 16990), and 232 nm (ε 16780); ^1H NMR δ=1.13 (3H, s), 1.19 (3H, s), 1.77 (3H, m, 4-CH_3), 2.28 (3H, s, S-CH_3), 5.32—5.70 (3H, m), and 5.78 (1H, a part of ABq, J=6 Hz); MS (70 eV) m/z (rel intensity) 272 (M^+, 100) and 257 (74); Found: m/z 272.1594. Calcd for $C_{18}H_{24}S$: M, 272.1597.

4a,4b,5,6,10,10a-Hexahydro-4bβ,8,10aβ-trimethyl-2(1*H*)-phenanthrenone (21): To a solution of the enol thioether **20** (690 mg) in THF (6 ml) was added $TiCl_4$ (600 mg) in THF (20 ml) and the mixture was stirred at room temperature for 1 h. To the reaction mixture was added 80% aqueous acetic acid, stirred at room temperature for 4 d, poured into brine (20 ml), and then extracted with ether (40 ml×3). The combined ether layer was washed with brine (20 ml), saturated aqueous $NaHCO_3$ (50 ml×2), and then brine (20 ml) and dried over Na_2SO_4. The residue obtained by evaporation of the solvent was chromatographed on a silica-gel column (eluent: benzene) to give the α,β-unsaturated ketone **21** (410 mg) as colorless prisms (ether-hexane): mp 98—99.5 °C; IR (Nujol) 1680 cm^{-1}; UV (MeOH) 232 nm (ε 19000); ^1H NMR δ=0.99 (3H, s), 1.07 (3H, s), 1.80 (3H, m, 4-CH_3), 5.35—5.70 (2H, m), 6.11 (1H, dd, J=10 and 3.5 Hz, 12-CH), and 6.92 (1H, dd, J=10 and 2 Hz, 11-CH); MS (70 eV) m/z (rel intensity) 242 (M^+, 100) and 227 (50); Found: m/z 242.1665. Calcd for $C_{17}H_{22}O$: M, 242.1670.

1,4b,5,6,10,10a-Hexahydro-10aβ-methoxycarbonyl-4bβ,8-dimethyl-3(2*H*)-phenanthrenone 3-(Ethylene Acetal) (22): A mixture of enone **15** (2.162 g, 7.56 mmol), ethylene glycol (11.55 ml), and *p*-toluenesulfonic acid monohydrate (222 mg) in benzene (85 ml) was refluxed under Dean-Stark water separator for 9.5 h. The mixture was cooled to room temperature and the benzene layer was separated, and passed through an alumina column (eluent: benzene) to give monoacetal **22** (2.3661 g, 95%) as pale yellow crystals. An analytical sample was prepared by recrystallization from hexane to give colorless prisms: mp 121—122 °C; IR (Nujol) 1787 cm^{-1}; ^1H NMR δ=0.96 (3H, s, 10-CH_3), 1.78 (3H, brs, 4-CH_3), 3.66 (3H, s, CO_2CH_3), 3.96 (4H, m, acetal), 5.43 (1H, m), 5.57 (1H, dd, J=3 and 7 Hz), and 5.66 (1H, s, 11-CH); MS (70 eV) m/z (rel intensity) 330 (M^+, 35) and 271 (100); Found: C, 72.46; H, 7.74%. Calcd for $C_{20}H_{26}O_4$: C, 72.70; H, 7.93%.

Conversion of 15 into 12: A solution of the acetal **22** (2.88 g) in DME (5 ml) was added into a refluxing solution of LAH (230 mg) in ether (5 ml) dropwise. After refluxing for 10 min ethyl acetate (1 ml) was added into the reaction mixture. Ether and water were added into the mixture and then the mixture was filtered through a celite column. The filtrate was extracted with ether and the extract was dried over

Na_2SO_4. The residue obtained by evaporation of the solvent was purified by florisil column chromatography (eluent: benzene-acetone) to give 2.1 g of the alcohol **23**: ^{1}H NMR δ=1.10 (3H, s, 10-CH_3), 1.77 (3H, brs, 4-CH_3), 3.62 (2H, s, 20-CH_2), 3.92 (4H, s, acetal), 5.26—5.60 (2H, m), and 5.62 (1H, s, 11-CH).

The alcohol **23** (122 mg) in CH_2Cl_2 (0.5 ml) was added into the Collins' reagent prepared from CrO_3 (244 mg) and pyridine (0.39 ml) in CH_2Cl_2 (5 ml). After stirring for 15 min at room temperature the reaction mixture was decanted and the residue was washed with ether. The CH_2Cl_2 solution was combined with ether washes and the combined solution was washed with 5% aqueous NaOH (15 ml×3) and then water (10 ml×4) and dried over Na_2SO_4. Removal of the solvent gave a residue (84.5 mg) which was chromatographed on florisil (eluent: benzene-acetone) to give the aldehyde **24** (57.8 mg): IR (Nujol) 1718 cm^{-1}.

A mixture of **24** (50 mg), diethylene glycol (2 ml), 80% hydrazine hydrate (0.4 ml), and KOH (0.1 g) was heated under reflux at 160—180 °C for 3 h. After heating at 85—90 °C for 1 h under reduced pressure using rotary evaporator, the residual mixture was heated at 170 °C for 6 h. Water was added into cooled reaction mixture and the mixture was extracted with ether. The ether layer was washed three times with dil HCl and dried over Na_2SO_4. The residue (32 mg) given by evaporation of the solvent was chromatographed on preparative TLC to afford the major product which was identified with **12**.

Conversion of 12 into 21: A mixture of **12** (0.94 g) and tosylhydrazine (1.0 g) in EtOH (4.5 ml) was stirred for 10 min and set aside overnight. Evaporation of the solvent, silica-gel column chromatography of the residue and crystallization from ether gave tosylhydrazone **25** as colorless crystals (0.75 g): mp 160—165 °C; IR (Nujol) 3210 and 1170 cm^{-1}; ^{1}H NMR δ=1.14 (3H, s), 1.23 (3H, s), 1.79 (3H, brs, 4-CH_3), 2.43 (3H, s, -$SO_2C_6H_4$-$\underline{CH_3}$), 5.50 (1H, m), 5.60 (1H, m), 6.08 (1H, s, 11-CH), 7.29 (2H, d), and 7.88 (2H, d).

To a solution of the tosylhydrazone **25** (250 mg, 0.61 mmol) in a mixed solvent of THF (2.1 ml) and *N,N,N',N'*-tetramethylethylenediamine (TMEDA) (2.1 ml) was added 2.5 equiv of butyllithium in hexane and then dimethyl disulfide (0.1 ml, 1.5 equiv) with stirring at −78 °C. The mixture was stirred at −30 °C for 30 min. Hexane solution of butyllithium (1.7 equiv) was added to the reaction mixture at −78 °C to give deep red solution and the solution was warmed to room temperature over one hour and stirred at the temperature overnight. To the reaction mixture was added 15% aqueous ammonium chloride (50 ml) and extracted with hexane twice and with ether twice. The combined extracts were dried over $MgSO_4$ and the residue given on evaporation of the solvent was chromatographed on a silica-gel column (eluent: hexane-ether) to give a enol thioether (30 mg) whose spectra were identical with those of the enol thioether **20** derived from **16**.

To the enol thioether (30 mg) in THF (0.4 ml) was added a solution of $TiCl_4$ (30 mg) in THF (1 ml) and the mixture was stirred at room temperature for 90 min. Acetic acid (0.4 ml) and water (0.14 ml) were added into the reaction mixture and the mixture was stirred at room temperature for 4 d. The reaction mixture was cooled in ice bath and added NaOH (0.3 g) in water (2 ml). Extraction with ether, drying with Na_2SO_4, evaporation of the solvent and purification of the residue with preparative TLC gave an α,β-unsaturated ketone (13 mg), whose spectra were identical with those of the conjugated ketone **21** derived from **16**.

1,4b,5,6,10,10a-Hexahydro-10aβ-hydroxymethyl-4bβ,8-dimethyl-3(2*H*)-phenanthrenone (26): To a solution of LAH (230 mg, 6.06 mmol) in ether (5 ml) was added **22** (2.88 g, 8.73 mmol) in DME (5 ml) dropwise. The mixture was heated at reflux for 10 min and then AcOEt (1 ml) was added. Ether (50 ml) and water (20 ml) were added into the reaction mixture and the mixture was filtered through a column of celite. Aqueous 1 mol dm^{-3} HCl (30 ml) was added into the filtrate and stirred vigorously at room temperature for 30 min. The aqueous layer was extracted with ether, and combined organic layer was washed with brine and dried (Na_2SO_4). Removal of the solvent afforded keto alcohol **26** (2.25 g, 100%): IR (Nujol) 1655 and 1600 cm^{-1}; UV (EtOH) 237.5 nm (ε 24000); ^{1}H NMR δ=1.14 (3H, s, 10-CH_3), 1.80 (3H, brs, 4-CH_3), 3.74 (2H, ABq, J=13.5 Hz, $\Delta\nu_{AB}$=8.5 Hz, 20-CH_2), 5.48 (1H, m), 5.63 (1H, t, J=4 Hz), and 6.12 (1H, s, 11-CH); MS (70 eV) m/z (rel intensity) 258 (M^+, 69) and 227 (100); Found: m/z 258.1612. Calcd for $C_{17}H_{22}O_2$: M, 258.1620.

1,4b,5,6,10,10a-Hexahydro-10aβ-acetoxymethyl-4bβ,8-dimethyl-3(2*H*)-phenanthrenone (27): A solution of 209 mg (0.81 mmol) of alcohol **26** in 1 ml of pyridine and 0.5 ml of acetic anhydride was stirred at room temperature overnight. The reaction mixture was quenched by the addition of methanol. The solvent was evaporated in vacuo and the residue was chromatographed on a silica-gel column (10 g in hexane, eluent: ethyl acetate-hexane (1 : 2)) to afford 184 mg (76%) of acetate **27** as a colorless oil. An analytical sample was obtained by crystallization from ether-hexane as colorless prisms: mp 81—82.5 °C; IR (oil) 1740 and 1670 cm^{-1}; ^{1}H NMR δ=1.18 (3H, s, 10-CH_3), 1.82 (3H, brs, 4-CH_3), 2.10 (3H, s, $OCOCH_3$), 4.23 (2H, s, 20-CH_2), 5.50 (1H, m), 5.62 (1H, m), and 6.15 (1H, s, 11-CH); MS (70 eV) m/z (rel intensity) 300 (M^+, 23), 240 (43), and 227 (100); Found: C, 75.87; H, 7.93%. Calcd for $C_{19}H_{24}O_3$: C, 75.97; H, 8.05%.

1,4b,5,6,7,8,10,10a-Octahydro-10aβ-acetoxmethyl-7,8-epoxy-4bβ,8-dimethyl-3(2*H*)-phenanthrenone (28): To a cold (−15 °C) solution of **27** (208 mg, 0.69 mmol) in CH_2Cl_2 (4 ml) was added 80% MCPBA (165 mg, 0.76 mmol) in portions under drying tube. The mixture was stirred at −15 °C for 30 min and then at room temperature for 1 h. The reaction was quenched by the addition of saturated aqueous $NaHCO_3$ (2 ml) containing KI (ca. 20 mg). The mixture was taken up in ether, washed with aqueous Na_2SO_3, saturated aqueous $NaHCO_3$, and brine. Drying ($MgSO_4$) and evaporation of the solvent gave a mixture of α- and β-epoxide **28** (220 mg) in a 3 : 1 ratio (the ratio being determined by the ^{1}H NMR), which were separated by silica-gel column chromatography (5g in hexane, 20% to 50% ether-hexane) to afford α-epoxide **28α** (80 mg, more polar) and β-epoxide **28β** (48 mg, less polar) as colorless oil, respectively. **28α**: IR (oil) 1735 and 1665 cm^{-1}; ^{1}H NMR δ=1.13 (3H, s, 10-CH_3), 1.50 (3H, s, 4-CH_3), 2.28 (3H, s, $OCOCH_3$), 3.10 (1H, brs, $W_{1/2}$=4.5 Hz, 3-CH), 4.37 (2H, s, 20-CH_2), 6.05 (1H, m, 6-CH), and 6.32 (1H, s, 11-CH); MS (70 eV) m/z (rel intensity) 316 (M^+, 100), 256 (26), and 91 (86); Found: m/z 316.1705. Calcd for $C_{19}H_{24}O_4$: M, 316.1664. **28β**: IR (oil) 1740 and 1665 cm^{-1}; ^{1}H NMR δ=1.26 (3H, s, 10-CH_3), 1.52 (3H, m, 4-CH_3), 2.10 (3H, s, $OCOCH_3$), 3.60 (1H, d, J=3.6 Hz, 3-CH), 4.10 (2H, ABq, J=11 Hz, $\Delta\nu_{AB}$=7 Hz, 20-CH_2), 5.80 (1H, m, 6-CH), and 5.90 (1H, s, 11-CH); MS (70 eV) m/z (rel intensity) 316 (M^+, 56) and 91 (100); Found: m/z 316.1663. Calcd for $C_{19}H_{24}O_4$: M, 316.1664.

1,3,4,4a,7,8,8a,9-Octahydro-8aβ-acetoxymethyl-1α,4aβ-dimethyl-2,6-phenanthrenedione 2-(Ethylene Acetal) (29): To a solution of α-epoxide **28** (80 mg, 0.25 mmol) and ethylene glycol (0.5 ml) in benzene (2 ml) was added 2 drops of boron trifluoride etherate. The mixture was stirred at room temperature overnight and poured into saturated aqueous $NaHCO_3$ (5 ml), extracted with ether (10 ml), washed with saturated aqueous $NaHCO_3$ (5 ml) and brine (5 ml). The aqueous layer was reextracted twice with ether and washed as above. The combined ether layers were dried ($MgSO_4$) and concentrated in vacuo to afford 85.7 mg (94%) of **29** pure enough for further use: IR (oil) 1745 and 1675 cm^{-1}; ^1H NMR δ=1.00 (3H, d, J=6.6 Hz, 4-CH_3), 1.28 (3H, s, 10-CH_3), 2.06 (3H, s, $OCOCH_3$), 3.90 (4H, m, acetal), 4.34 (2H, brs, 20-CH_2), 5.40 (1H, m, 6-CH), and 6.34 (1H, s, 11-CH); MS (70 eV) m/z (rel intensity) 360 (M^+, 0.7) and 99 (100); Found: m/z 360.1931. Calcd for $C_{21}H_{28}O_5$: M, 360.1936.

1,3,4,4a,7,8,8a,9-Octahydro-8aβ-methoxycarbonyl-1α,4aβ-dimethyl-2,6-phenanthrenedione 2,6-Bis(ethylene acetal) (33): To a cold solution (−10 °C) of acetal **22** (135 mg, 0.409 mmol) in 1 ml of CH_2Cl_2 was added 97.1 mg (0.45 mmol) of 80% MCPBA in 1 ml of CH_2Cl_2 under drying tube. After being stirred at the same temperature for 30 min, the mixture was poured into saturated aqueous $NaHCO_3$ containing KI and extracted with ether. The organic layer was washed with saturated aqueous $NaHCO_3$ containing a small amount of sodium hydrogensulfide and then with brine, dried (Na_2SO_4) and concentrated in vacuo to afford a mixture of α-epoxide and β-epoxide (**30α** and **30β**) in a 5 : 1 ratio (the ratio being determined by the ^1H NMR) as colorless solids (150.9 mg), which were used directly in the next step. For analytical purposes, the pure α-epoxide **30α** was separated by crystallization from ether-hexane: mp 116.2—118.0 °C; IR (Nujol) 1620, 1246, 1102, 1020, 1010, and 922 cm^{-1}; ^1H NMR δ=0.98 (3H, s, 4-CH_3), 1.41 (3H, s, 10-CH_3), 1.95 (1H, dd, J=3 and 18 Hz, 7-CH), 2.99 (1H, dd, J=6 and 18 Hz, 7-CH), 3.04 (1H, brs, 3-CH), 3.66 (3H, s, CO_2CH_3), 4.00 (4H, m, acetal), 5.63 (1H, s, 11-CH), and 6.04 (1H, dd, J=3 and 6 Hz); MS (70 eV) m/z (rel intensity) 346 (M^+, 58), 287 (100), 269 (28), 243 (32), and 231 (16).

To a solution of the above mixture of epoxides **30** (150.9 mg) in benzene (8 ml) was added six drops of boron trifluoride etherate with vigorous stirring. After being stirred at room temperature for 15 min, the reaction was quenched with saturated aqueous $NaHCO_3$. The benzene layer was separated and washed with saturated aqueous $NaHCO_3$ and then brine. The combined aqueous layers were extracted with ether and the ether solution was washed with saturated aqueous $NaHCO_3$ and then brine. The combined organic extracts were dried (Na_2SO_4) and concentrated in vacuo to give a pale yellow solid which contained monoacetal **31** as a major component along with a small amount of diketone **32**.

A mixture of the above crude residue, ethylene glycol (1.5 ml), and a catalytic amount of p-toluenesulfonic acid monohydrate in benzene (15 ml) was refluxed under Dean-Stark water separator for 4.5 h. To the cooled mixture was added saturated aqueous $NaHCO_3$ and the aqueous layer was extracted with ether. Combined organic layer was washed with brine, dried (Na_2SO_4) and concentrated in vacuo. The residue was chromatographed on a silica-gel column (5 g in benzene, eluent: 10% to 30% ether-benzene) to afford diacetal **33** (94.8 mg, 64% overall from **22** in 3 steps) as a colorless oil: IR (KBr) 1736 and 1652 cm^{-1}; ^1H NMR δ=0.98 (3H, d, J=7 Hz, 4-CH_3), 1.20 (3H, s, 10-CH_3), 2.6 (1H, m, 4-CH), 2.82 (1H, dd, J=6 and 18 Hz, 7-CH), 3.63 (3H, s, CO_2CH_3), 3.9 (8H, m, acetal), 5.46 (1H, ddd, J=6, 1.5, and 1.5 Hz, 6-CH), and 5.63 (1H, s, 11-CH); MS (70 eV) m/z (rel intensity) 390 (M^+, 2), 346 (2.4), 331 (1), 302 (3.2), and 99 (100); Found: m/z 390.2096. Calcd for $C_{22}H_{30}O_6$: M, 390.2041.

3,4,4a,7,8,8a-Hexahydro-8aβ-methoxycarbonyl-1α,4aβ-dimethyl-2,6,9(1*H*)-phenanthrenetrione 2-(Ethylene Acetal) (35): To a solution of diacetal **33** (422 mg, 1.08 mmol) in CH_2Cl_2 (8 ml) was added a solution of $CrO_3 \cdot 2Pyr$ complex in CH_2Cl_2 (0.4 mol dm^{-3}, 40 ml) with vigorous stirring. The mixture was stirred at room temperature for 40 h and then quenched with $NaHSO_3$. The supernatant was filtered through a short column of florisil and the tarry solid in the flask was rinsed thoroughly with ether and the washings were filtered through a florisil column. The combined organic solutions were evaporated to give a residue, which was chromatographed on a silica-gel column (20 g in benzene, eluent: 10% to 40% ether-benzene) to afford 102.1 mg (27%) of **35** as a pale yellow oil and 170.5 mg (45%) of **31**. **35**: IR (oil) 1732, 1680, and 1668 cm^{-1}; ^1H NMR δ=1.12 (3H, d, J=7 Hz, 4-CH_3), 1.43 (3H, s, 10-CH_3), 3.73 (3H, s, CO_2CH_3), 3.95 (4H, m, acetal), 6.07 (1H, brs, 6-CH), and 6.23 (1H, s, 11-CH); MS (70 eV) m/z (rel intensity) 360 (M^+, 1.4), 301 (0.8), 99 (94), and 57 (100); Found: m/z 360.1567. Calcd for $C_{20}H_{24}O_6$: M, 360.1572.

1,3,4,4a,7,8,8a,9-Octahydro-8aβ-hydroxymethyl-1α,4aβ-dimethyl-2,6-phenanthrenedione 2-(Ethylene Acetal) (37): To a solution of diacetal **33** (10.1 g, 25.6 mmol) in THF (200 ml) was added LAH (1 g, 26.3 mmol). The mixture was stirred at room temperature for 1 h. To the reaction mixture was added AcOEt (5 ml) and then saturated aqueous NH_4Cl (20 ml). The mixture was filtered and the solid was washed with THF. The filtrate and washings were combined and washed with brine and then dried (Na_2SO_4). Removal of the solvent afforded a residue which was dissolved in acetone (50 ml). Pyridinium p-toluenesulfonate (PPTS, 0.1 g) was added to the solution and stirred at room temperature for 1 h. To the reaction mixture were added $NaHCO_3$ (1 g) and benzene (100 ml). The mixture was condensed to ca. 70 ml under reduced pressure. Ether (100 ml) was added to the condensed mixture and the organic layer was washed with half-saturated aqueous NaCl (100 ml×2) and dried (Na_2SO_4). Evaporation of the solvent gave a residue which was purified with silica-gel chromatography (100 g, eluent: 2% acetone in benzene) to give **37**. An analytical sample of **37** was obtained by recrystallization from acetone-hexane as colorless prisms: mp 184—184.5 °C; IR (Nujol) 3420 and 1650 cm^{-1}; ^1H NMR δ=1.02 (3H, d, J=7 Hz, 4-CH_3), 1.30 (3H, s, 10-CH_3), 3.68 (2H, brs, 20-CH_2), 3.90 (4H, m, acetal), 5.45 (1H, m, 6-CH), and 6.13 (1H, s, 11-CH); MS (70 eV) m/z (rel intensity) 318 (M^+, 4) and 99 (100); Found: m/z 318.1982. Calcd for $C_{23}H_{26}O_4$: M, 318.1982.

1,3,4,4a,7,8,8a,9-Octahydro-1α,4aβ-dimethyl-8aβ-[(tetrahydro-2-pyranyloxy)methyl]-2,6-phenanthrenedione 2-(Ethylene Acetal) (38): To a solution of **37** (706.9 mg, 2.22 mmol) in CH_2Cl_2 (30 ml) was added 55 mg of PPTS and 0.5 ml of dihydropyran. The mixture was stirred at room temperature for 5 h. The mixture was diluted with ether, washed with brine, dried over $MgSO_4$, and concentrated in vacuo. The residue was chromatographed on a silica-gel column (15 g in benzene, eluent: ether-benzene) to afford 904.5 mg (100%) of **38** as a pale yellow oil: IR (oil) 1672 cm^{-1}; ^1H NMR δ=1.02

(3H, d, J=7 Hz, 4-CH_3), 1.26 and 1.36 (1.5H each, s, 10-CH_3), 3.2—4.3 (8H, m), 4.53 (1H, m), 5.45 (1H, ddd, J=6, 2, and 2 Hz, 6-CH), and 6.13 (1H, s, 11-CH); MS (70 eV) m/z (rel intensity) 402 (M^+, 16), 318 (12), 99 (over), and 85 (100); Found: m/z 402.2423. Calcd for $C_{24}H_{14}O_5$: M, 402.2406.

1,3,4,4a,4b,5,7,8,8a,9-Decahydro-1α,4aβ-dimethyl-8aβ-[(tetrahydro-2-pyranyloxy)methyl]-2,6-phenanthrenedione 2-(Ethylene Acetal) (39): (a) Hydrogenation: A mixture of **38** (408 mg, 1.02 mmol) and palladium on carbon (10%, 45 mg) in 20 ml of ethanol was stirred at room temperature under an atmosphere of hydrogen for 45 h. The catalyst was removed by filtration and washed with ethanol, and the filtrate was evaporated. The residue was chromatographed on a silica-gel column (5 g in benzene, eluent: ether-benzene) to afford 195 mg (48%) of **39** as colorless oil: IR (oil) 1706 cm^{-1}; ^1H NMR δ=0.98 (3H, d, J=7 Hz, 4-CH_3), 1.04 (3H, s, 10-CH_3), 4.54 (1H, m), and 5.37 (1H, ddd, J=6, 2, and 2 Hz, 6-CH); MS (70 eV) m/z (rel intensity) 404 (M^+, 2.3), 320 (2.3), and 99 (100); Found: m/z 404.2569. Calcd for $C_{24}H_{36}O_5$: M, 404.2536. (b) Birch reduction: Lithium metal (150 mg, 21 mmol) was dissolved in 40 ml of liquid ammonia. To this solution was added **38** (905 mg, 2.25 mmol) in THF (10 ml). The mixture was stirred at −33 °C for 30 min and then quenched by the addition of NH_4Cl (5 g). The ammonia was allowed to evaporate to afford a residue, which was extracted with CH_2Cl_2 and washed with brine. Drying ($MgSO_4$) and evaporation of the solvent gave a residue, which was chromatographed on a silica-gel column to afford 705 mg (77.5%) of **39**. (c) Reduction with NaHTe: A mixture of tellurium powder (3.49 g, 27 mmol) and $NaBH_4$ (2.44 g, 64 mmol) in EtOH (80 ml, deoxygenated with argon) was heated to reflux under argon. After refluxing for 15 min, the resulting dark purple solution was cooled to −20 °C and a deoxygenated solution of acetic acid (1.4 ml) in EtOH (5.6 ml) was added to the mixture. After 5 min, to the above mixture was added **38** (4.31 g, 10 mmol) in EtOH (55 ml) and the resulting solution was stirred at 70 °C for 4.5 h followed by reflux for 3.5 h. The cooled mixture was filtered through a column of Celite with CH_2Cl_2. The solvent was evaporated to give a residue, which was extracted with ether, washed with brine, and dried ($MgSO_4$). Removal of the solvent gave 4.29 g (99%) of crude **39** pure enough for further use.

1,3,4,4a,7,8,8a,9-Octahydro-8aβ-[(1-ethoxyethoxy)methyl]-1α,4aβ-dimethyl-2,6-phenanthrenedione 2-(Ethylene Acetal) (40): A solution of **37** (132 mg, 0.41 mmol) and ethyl vinyl ether (0.3 ml, 3.14 mmol) in CH_2Cl_2 (5 ml) containing PPTS (13 mg) was stirred at room temperature for 1 h. The solution was diluted with CH_2Cl_2 (30 ml) and washed with brine (10 ml). The aqueous layer was extracted with CH_2Cl_2 (20 ml) and the combined organic extracts were dried ($MgSO_4$). Removal of the solvent in vacuo gave pure **40** (173 mg, 100%) as a pale yellow oil: IR (oil) 1670 cm^{-1}; ^1H NMR δ=1.02 (3H, d, J=7 Hz, 4-CH_3), 1.08—1.40 (9H, 3×CH_3), 3.2—3.8 (4H, m), 3.8—4.1 (4H, m, acetal), 4.65 (1H, m), 5.5 (1H, m, 6-CH), and 6.12 (1H, s, 11-CH); MS (70 eV) m/z (rel intensity) 390 (M^+, 5.7), 345 (3.6), 318 (2.7), 288 (6), 99 (over), and 73 (100); Found: m/z 390.2395. Calcd for $C_{23}H_{34}O_5$: M, 390.2404.

1,3,4,4a,4b,5,7,8,8a,9-Decahydro-8aβ-[(1-ethoxyethoxy)-methyl]-1α,4aβ-dimethyl-2,6-phenanthrenedione 2-(Ethylene Acetal) (41): A mixture of tellurium powder (16.58 g, 0.13 mol) and sodium borohydride (10.78 g, 0.29 mol) in EtOH (200 ml, deoxygenated with argon) was cautiously heated to reflux under argon. After refluxing for several min, the resulting dark brown solution was cooled to −20 °C and acetic acid (6.7 ml) in EtOH (28.3 ml) was added. The mixture was warmed to room temperature. To the mixture was added **40** (18.81 g, 0.048 mol) in EtOH (220 ml) and the reaction mixture was heated to reflux for 17 h. The cooled mixture was filtered through a pad of Celite using CH_2Cl_2, AcOEt, and acetone. The solvent was evaporated to give a residue, which was partitioned between CH_2Cl_2 (500 ml) and brine (300 ml). The aqueous layer was extracted with CH_2Cl_2 (200 ml×2). The combined organic extracts were dried ($MgSO_4$), filtered and concentrated in vacuo. The residue was chromatographed on a silica-gel column (200 g in benzene, eluent: 10% to 40% ether-benzene) to give 18.39 g (98%) of **41** as a pale yellow oil: IR (oil) 1705 cm^{-1}; ^1H NMR δ=0.9—1.4 (12H, 4×CH_3), 3.92 (4H, m, acetal), 4.67 (1H, m), and 5.39 (1H, m, 6-CH); MS (70 eV) m/z (rel intensity) 392 (M^+, 1.2), 346 (12), 320 (8), 302 (8), 99 (over), and 73 (100).

1,3,4,4a,4b,5,7,8,8a,9-Decahydro-8aβ-[(1-ethoxyethoxy)-methyl]-7-methoxycarbonyl-1α,4aβ-dimethyl-2,6-phenanthrenedione 2-(Ethylene Acetal) (42): To a suspension of sodium hydride (5.03 g, 12.5 mmol, 60% oil dispersion), potassium hydride (1 g, 8.7 mmol, 35% oil dispersion), and dimethyl carbonate (10 ml) in DME (150 ml) was added dropwise a solution of ketone **41** (18.39 g) in DME (270 ml) over 15 min. The mixture was refluxed for 2 h and then cooled to room temperature, poured into saturated aqueous NH_4Cl (200 ml), extracted with ether (500 ml, 300 ml×3) and dried ($MgSO_4$). Removal of the solvent gave an oily residue, which was chromatographed on a silica-gel column (200 g in benzene, eluent: 5% to 10% ether-benzene) to afford keto ester **42** (17.61 g, 83%) as a pale yellow oil: IR (oil) 1745, 1710, 1660, and 1620 cm^{-1}, ^1H NMR δ=0.9—1.3 (12H, 4×CH_3), 3.74 (3H, s, CO_2CH_3), 3.8—4.0 (4H, m, acetal), 4.65 (1H, m), 5.37 (1H, m, 6-CH), and 12.05 (0.5H, s, enol-OH); MS (70 eV) m/z (rel intensity) 450 (M^+, 3), 404 (22), 377 (20), 360 (14), 99 (over), and 73 (100); Found: m/z 450.2612. Calcd for $C_{25}H_{38}O_7$: M, 450.2615.

1,3,4,4a,4b,5,8a,9-Octahydro-8aβ-[(1-ethoxyethoxy)-methyl]-7-methoxycarbonyl-1α,4aβ-dimethyl-2,6-phenanthrenedione 2-(Ethylene Acetal) (43): To a cold (0 °C) suspension of sodium hydride (1.95 g, 48.75 mmol, 60% oil dispersion) in THF was added a solution of keto ester **42** (10.87 g, 24.15 mmol) in THF (70 ml) over 15 min. The mixture was stirred at room temperature for 15 min and then cooled to 0 °C. A solution of benzeneselenenyl chloride (6.97 g, 35.3 mmol) in THF was added rapidly, and the reaction mixture was quenched with saturated aqueous $NaHCO_3$ (50 ml), extracted with ether (500 ml) and washed with brine. The aqueous layer was saturated with NaCl and extracted with ether (200 ml). The combined organic extracts were dried over $MgSO_4$, filtered and concentrated in vacuo. To the crude product in 120 ml of CH_2Cl_2 was added 30% hydrogen peroxide (10 ml, 88 mmol) in 10 ml of water over 5 min at 0 °C. After being stirred at 0 °C for 30 min, the reaction mixture was diluted with CH_2Cl_2 (400 ml) and washed with saturated aqueous $NaHCO_3$ (200 ml). The aqueous layer was extracted with CH_2Cl_2 (200 ml) and the combined organic extracts were dried ($MgSO_4$) and concentrated in vacuo. The residue was chromatographed on a silica-gel column (100 g in benzene, eluent: 5% to 50% ether-benzene) to afford **43** (7.37 g, 67%) as a pale yellow oil: IR (oil) 1740, 1710, 1680, and 1620 cm^{-1}; ^1H NMR δ=0.9—1.3 (12H, 4×CH_3), 3.82 (3H, s, CO_2CH_3), 3.83—4.03 (4H, m, acetal),

4.58 (1H, m), 5.36 (1H, m, 6-CH), and 7.35 and 7.37 (1H, each s, 14-CH); MS (70 eV) *m/z* (rel intensity) 448 (M^+, 0.4), 404 (0.5), 403 (0.8), 377 (0.4), 347 (2), 314 (0.8), and 99 (100); Found: *m/z* 448.2460. Calcd for $C_{25}H_{46}O_7$: M, 448.2459.

1,3,4,4a,4b,5,7,8,8a,9-Decahydro-8aβ-[(1-ethoxyethoxy)-methyl]-7-methoxycarbonyl-1α,4aβ-dimethyl-8α-vinyl-2,6-phenanthrenedione 2-(Ethylene Acetal) (46) and 3,4,4a,4b,5,6,8a,9-Octahydro-8aβ-[(1-ethoxyethoxy)methyl]-6-hydroxy-7-methoxycarbonyl-1α,4aβ-dimethyl-6-vinyl-2(1*H*)-phenanthrenone 2-(Ethylene Acetal) (47): To a solution of $(Bu_3P \cdot CuI)_4$ complex (2.03 g) in THF (30 ml) was added vinylmagnesium bromide (from magnesium (700 mg, 29 mmol) and vinyl bromide (3 ml, 42 mmol)) in THF (50 ml) at −45 °C dropwise over a period of 15 min. The resulting solution was stirred at −45 °C for 15 min, and then keto ester **43** (6.54 g, 14.6 mmol) in THF (70 ml) was added over a period of 15 min. The solution was stirred for 2 h, during which time the temperature of the bath came to −20 °C. Saturated aqueous NH_4Cl (50 ml) was added and the mixture was extracted with ether (400 ml) and washed with brine. The aqueous layer was extracted with ether (100 ml×3) and the combined organic layers were dried ($MgSO_4$). Evaporation of the solvent gave a residue which was chromatographed on a silica-gel column (100 g in benzene, eluent: 5% to 50% ether-benzene) to afford 1,4-adduct **46** (5.81 g, 80%) and 1,2-adduct **47** (0.87 g, 12%). **46**: IR (oil) 1650 and 1615 cm^{-1}; ^1H NMR δ=0.93—1.30 (12H, 4×CH_3), 3.71 (3H, s, CO_2CH_3), 3.8—4.1 (4H, m, acetal), 4.54 (1H, m), 4.8—5.1 (2H, m, 16-CH_2), 5.2—5.9 (2H, m, 6-CH and 15-CH), and 12.28 and 12.30 (1H, each s, enol-OH); MS (70 eV) *m/z* (rel intensity) 476 (M^+, 0.6), 430 (22), 403 (4), 371 (6), 99 (over), and 73 (100); Found: *m/z* 430.2361. Calcd for $C_{25}H_{34}O_6$: M−EtOH, 430.2356. **47**: IR (oil) 3500, 1740, 1700, and 1650 cm^{-1}; ^1H NMR δ=0.9—1.3 (12H, 4×CH_3), 3.77 (3H, s, CO_2CH_3), 3.92 (4H, m, acetal), 4.61 (1H, m), 4.89 (1H, d, *J*=17 Hz), 5.02 (1H, d, *J*=11 Hz), 5.35 (1H, m, 6-CH), 5.96 (1H, dd, *J*=17 and 11 Hz), and 7.06 (1H, s, 14-CH); MS (70 eV) *m/z* (rel intensity) 476 (M^+, 1), 450 (1.3), 430 (10), 404 (6), 386 (7), 356 (42), 99 (over), and 73 (100).

3,4,4a,4b,5,8,8a,9-Octahydro-8aβ-[(1-ethoxyethoxy)methyl]-7-methoxycarbonyl-1α,4aβ-dimethyl-8α-vinyl-2(1*H*)-phenanthrenone 2-(Ethylene Acetal) (51): To a solution of keto ester **46** (9.48 g, 19.9 mmol) in EtOH (300 ml) was added sodium borohydride (0.91 g, 24 mmol) at 0 °C. The mixture was stirred at 0 °C overnight. Acetone (50 ml) was added to the reaction mixture and the solvent was evaporated to afford a residue, which was partitioned between ether (500 ml) and saturated aqueous NH_4Cl (100 ml). The aqueous layer was extracted with $CHCl_3$ (200 ml×2) and the combined organic extracts were dried ($MgSO_4$). Evaporation of the solvent gave a mixture of stereoisomers of the alcohol **50** which was used for further reaction without any purification. To a stirred solution of the above mixture of alcohols and triethylamine (20 ml, 0.14 mol) in CH_2Cl_2 (200 ml) was added methanesulfonyl chloride (6.5 ml, 84 mmol) over a period of 15 min at 0 °C. After being stirred at 0 °C for 1 h and at room temperature for 3 h, the mixture was diluted with water (100 ml) and extracted with $CHCl_3$, and the extract was dried ($MgSO_4$). Removal of the solvent gave a crude mesylate, which was dissolved in benzene (400 ml) and DBU (40 ml). The mixture was heated to reflux for 5 h. The cooled mixture was diluted with saturated aqueous NH_4Cl and extracted with ether (300 ml×3). The combined organic extracts were dried ($MgSO_4$) and evaporated to afford a residue which was chromatographed on silica-gel column (300 g dry, eluent: 5% to 20% ether-benzene) to give conjugated ester **51** (6.71 g, 73% yield from **46**). Recrystallization from ether-hexane gave colorless prisms: mp 116—118 °C; IR (Nujol) 1720 and 1660 cm^{-1}; ^1H NMR δ=0.9—1.3 (12H, 4×CH_3), 3.69 (3H, s, CO_2CH_3), 3.91 (4H, m, acetal), 4.56 (1H, m), 4.86—5.20 (2H, m, 16-CH_2), 5.26—6.00 (2H, m, 6-CH and 15-CH), and 7.04 (1H, t, *J*=3.6 Hz, 12-CH); MS (70 eV) *m/z* (rel intensity) 460 (M^+, 0.6), 429 (1.1), 414 (21), 370 (40), 99 (over), and 73 (100); Found: *m/z* 460.2841. Calcd for $C_{27}H_{40}O_6$: M, 460.2826; Found: C, 70.67; H, 8.77%. Calcd for $C_{27}H_{40}O_6$: C, 70.41; H, 8.75%.

1,4,4a,4b,5,6,10,10a-Octahydro-10aβ-methoxycarbonyl-4bβ,8-dimethyl-3(2*H*)-phenanthrenone (53): Reactions were carried out under argon atmosphere and the solvent was deoxygenated with argon prior to use. A mixture of tellurium powder (20.58 g, 0.16 mol) and sodium borohydride (12.17 g, 0.32 mol) in EtOH (500 ml) was stirred at room temperature. After the finish of evolution of hydrogen, the mixture was heated to reflux for 30 min. The resulting solution was cooled to 0 °C and acetic acid (10 ml) was added to the mixture. To the above solution of NaHTe was added **15** (22.86 g, 80 mmol) in EtOH (600 ml) and the reaction mixture was stirred at room temperature for 48 h. As TLC monitoring showed that the conversion was not complete, additional NaHTe solution (2.5 g (20 mmol) of tellurium, 1.5 g (40 mmol) of $NaBH_4$, and 1.2 ml of acetic acid in 80 ml of EtOH) was added to the reaction mixture. The starting material was consumed on stirring at room temperature for 18 h. Then the reaction mixture was stirred for 3 h under open air. The resulting black precipitate was filtered and the filtrate was evaporated to give a residue, which was taken up in ether (300 ml) and water (300 ml). The aqueous layer was extracted with ether (200 ml×2), and the combined organic extracts were washed with brine (100 ml). After drying (Na_2SO_4), the solvent was evaporated to give 22.81 g (99%) of **53** as colorless crystals pure enough for further use. An analytical sample was obtained by recrystallization from ether-hexane as colorless needles: mp 107—109 °C; IR (KBr) 1720 and 1215 cm^{-1}; ^1H NMR δ=0.78 (3H, s, 10-CH_3), 1.80 (3H, brs, 4-CH_3), 3.72 (3H, s, CO_2CH_3), 5.43 (1H, m), and 5.61 (1H, m); MS (70 eV) *m/z* (rel intensity) 288 (M^+, 14), 228 (40), and 161 (100); Found: *m/z* 288.1713. Calcd for $C_{18}H_{24}O_3$: M, 288.1725; Found: C, 74.68; H, 8.33%. Calcd for $C_{18}H_{24}O_3$: C, 74.97; H, 8.39%.

1,4,4a,4b,5,6,10,10a-Octahydro-10aβ-methoxycarbonyl-4bβ,8-dimethyl-3(2*H*)-phenanthrenone 3-(Ethylene Acetal) (54): A solution of **53** (22.81 g, 79.2 mmol), *p*-toluenesulfonic acid (1.3 g), and ethylene glycol (80 ml) in benzene (500 ml) was refluxed under Dean-Stark water separator for 1.5 h. The mixture was cooled to room temperature, quenched by the addition of $NaHCO_3$ (3 g), and the ethylene glycol layer was separated and extracted with benzene (200 ml×2). The combined benzene layers were washed with saturated aqueous $NaHCO_3$ (100 ml) and brine (100 ml), dried (Na_2SO_4), and evaporated to give a residue (27.82 g), which afforded crystalline **54** on standing. The crystals were pure enough for further use. An analytical sample was obtained by recrystallization from ether-hexane as colorless needles: mp 101.5—102.5 °C; IR (KBr) 1730 cm^{-1}; ^1H NMR δ=0.72 (3H, s, 10-CH_3), 1.78 (3H, brs, 4-CH_3), 3.66 (3H, s, CO_2CH_3), 3.96 (4H, brs, acetal), 5.39 (1H, m), and 5.58 (1H, m); MS (70 eV)

m/z (rel intensity) 332 (M^+, 100), 272 (66), and 99 (53); Found: C, 72.22; H, 8.28%. Calcd for $C_{20}H_{28}O_4$: C, 72.26; H, 8.49%.

1,4,4a,4b,5,6,10,10a-Octahydro-10aβ-hydroxymethyl-4bβ,8-dimethyl-3(2*H*)-phenanthrenone (55): To a solution of **54** (27.82 g) in THF (300 ml) was added $LiAlH_4$ (3 g) in portions. After being stirred at room temperature for 1 h, to the reaction mixture was added ethyl acetate (15 ml) and then saturated aqueous NH_4Cl (25 ml). The mixture was stirred for 30 min. The resulting precipitate was filtered, dissolved in 4 mol dm^{-3} HCl (200 ml), and extracted with ether (100 ml×2). The above filtrate, the washings, and the ether extracts were combined and evaporated. The residue was dissolved in 600 ml of 10% aqueous acetone containing *p*-toluenesulfonic acid (3 g). The mixture was stirred at room temperature for 20 h and then $NaHCO_3$ (3 g) was added. Removal of the solvent gave a yellow residue, which was taken up in 200 ml of water, filtered and washed with water (100 ml). The filtrate and the washings were combined, extracted with ether (200 ml×2). The above solid was dissolved in ether (500 ml) and combined with the ether extract and dried (Na_2SO_4). Evaporation of the solvent gave a crude residue, which was crystallized from ether-hexane to afford **55** (15.31 g). Chromatography on a silica-gel column (eluent: 5% acetone in benzene) followed by crystallization afforded 3.45 g of **55** from the mother liquor. The yield of the crystals of **55** was 90% overall from **15**. An analytical sample was obtained by recrystallization from ether as colorless prisms: mp 124—126 °C; IR (KBr) 3450 and 1715 cm^{-1}; ^1H NMR δ=0.93 (3H, s, 10-CH_3), 1.82 (3H, brs, 4-CH_3), 3.93 (2H, brs, 20-CH_2), and 5.50 (2H, m, 3-CH and 6-CH); MS (70 eV) *m/z* (rel intensity) 260 (M^+, 100) and 242 (27); Found: C, 78.43; H, 9.02%. Calcd for $C_{17}H_{24}O_2$: C, 78.42; H, 9.29%.

1,4,4a,4b,5,6,10,10a-Octahydro-10aβ-[(1-ethoxyethoxy)-methyl]-4bβ,8-dimethyl-3(2*H*)-phenanthrenone (56): To a solution of **55** (13.21 g, 50.8 mmol) in CH_2Cl_2 (250 ml) was added PPTS (3.4 g) and ethyl vinyl ether (10 ml). After being stirred at room temperature for 1 h, the mixture was washed with saturated aqueous $NaHCO_3$ (50 ml), dried ($MgSO_4$), and concentrated in vacuo. The residue was chromatographed on a silica-gel column (eluent: 20% ether in hexane) to afford 15.83 g (94%) of **56** as a pale yellow oil: IR (oil) 1710 cm^{-1}; ^1H NMR δ=0.95 (3H, s, 10-CH_3), 1.1—1.4 (6H, 2×CH_3), 1.74 (3H, brs, 4-CH_3), 4.70 (1H, q, *J*=5 Hz), and 5.4—5.6 (2H, m, 3-CH and 6-CH); MS (70 eV) *m/z* (rel intensity) 332 (M^+, 1.6), 286 (76), 260 (26), and 73 (100); Found: *m/z* 286.1932. Calcd for $C_{19}H_{26}O_2$: M−EtOH, 286.1932.

1,4,4a,4b,5,6,10,10a-Octahydro-10aβ-[(1-ethoxyethoxy)-methyl]-2-methoxycarbonyl-4bβ,8-dimethyl-3(2*H*)-phenanthrenone (57): To a suspension of NaH (5.85 g, 0.146 mol, 60% oil dispersion), KH (550 mg, 4.8 mmol, 35% oil dispersion), and dimethyl carbonate (15 ml) in DME (300 ml) was added **56** (15.83 g, 47.7 mmol) in DME (180 ml). The mixture was refluxed for 1 h, cooled to 0 °C, and quenched with the addition of saturated aqueous NH_4Cl (100 ml). The organic layer was separated, washed with brine, and dried (Na_2SO_4). Removal of the solvent gave a residue, which was chromatographed on a silica-gel column (150 g in hexane, eluent: 10% ether in hexane) to afford 17.84 g (96%) of **57** as a pale yellow oil: IR (oil) 1750, 1720, 1665, and 1625 cm^{-1}; ^1H NMR δ=0.94 (3H, s, 10-CH_3), 1.05—1.40 (6H, 2×CH_3), 1.77 (3H, brs, 4-CH_3), 3.73 (3H, s, CO_2CH_3), 4.58 (1H, m), and 5.3—5.6 (2H, m, 3-CH and 6-CH); MS (70 eV) *m/z* (rel intensity) 344 (M^+−EtOH, 2.6), 300 (14.6), and 73 (100); Found: *m/z* 344.2005. Calcd for $C_{21}H_{28}O_4$: M−EtOH, 344.1987.

4a,4b,5,6,10,10a-Hexahydro-10aβ-[(1-ethoxyethoxy)methyl]-2-methoxycarbonyl-4bβ,8-dimethyl-3(4*H*)-phenanthrenone (58): To a cold (0 °C) suspension of NaH (3.96 g, 99 mmol, 60% oil dispersion) in THF (200 ml) was added **57** (17.84 g, 46 mmol) in THF (170 ml) dropwise with stirring. The mixture was stirred at room temperature for 1 h and cooled to 0 °C. A solution of benzeneselenenyl chloride (10.80 g, 56 mmol) in THF (70 ml) was added rapidly to the mixture. After 5 min, saturated aqueous NH_4Cl (100 ml) was added to the reaction mixture and the mixture was extracted with ether. The extract was washed with brine, dried ($MgSO_4$), and concentrated in vacuo. The residue was dissolved in CH_2Cl_2 (200 ml) and cooled to 0 °C. Hydrogen peroxide (30%, 5.5 ml) was added and the mixture was stirred at 0 °C for 1.5 h. The mixture was washed with brine (100 ml), dried over $MgSO_4$, and concentrated in vacuo to give a residue, which was chromatographed on a silica-gel column (150 g in hexane, eluent: 30% ether in hexane) to afford 12.98 g (73%) of **58** as a yellow oil. IR (oil) 1745, 1720, and 1685 cm^{-1}; ^1H NMR δ=0.9—1.3 (9H, 3×CH_3), 1.80 (3H, brs, 4-CH_3), 3.83 (3H, s, CO_2CH_3), 4.60 (1H, q, *J*=5.4 Hz), 5.50 (2H, m, 3-CH and 6-CH), and 7.38 and 7.39 (1H, each s, 14-CH); MS (70 eV) *m/z* (rel intensity) 388 (M^+, 2), 342 (9), 316 (13), 298 (14), 285 (28), 254 (23), 253 (22), and 73 (100); Found: *m/z* 388.2246. Calcd for $C_{23}H_{32}O_5$: M, 388.2249.

1,4,4a,4b,5,6,10,10a-Octahydro-10aβ-[(1-ethoxyethoxy)-methyl]-2-methoxycarbonyl-4bβ,8-dimethyl-1α-vinyl-3(2*H*)-phenanthrenone (59): To a cold (−45 °C) solution of $(Bu_3P \cdot CuI)_4$ complex (3.2 g) in THF (50 ml) under nitrogen was added vinylmagnesium bromide (from 190 mg (32.5 mmol) of magnesium and 4.3 ml (61 mmol) of vinyl bromide) in THF (50 ml) dropwise. The resulting mixture was stirred at −45 °C for 20 min, and **58** (10.48 g, 27.01 mmol) in dry THF (100 ml) was added over a period of 30 min. After being stirred at −45 °C for 1.5 h, the mixture was washed with saturated aqueous NH_4Cl (100 ml) and then with brine (100 ml). Drying ($MgSO_4$) followed by evaporation of the solvent gave a residue, which was chromatographed on a silica-gel column (150 g in hexane, eluent: 5% to 10% ether-hexane) to afford 9.78 g (87%) of **59** as a colorless oil: IR (oil) 1655 and 1620 cm^{-1}; ^1H NMR δ=0.9—1.3 (3×CH_3), 1.78 (3H, brs, 4-CH_3), 3.73 (3H, s, CO_2CH_3), 4.57 (1H, m), 4.85—5.15 (2H, m, 16-CH_2), 5.3—5.9 (3H, m, 3-CH, 6-CH, and 15-CH), and 12.30 and 12.32 (0.8H, each s, enol-OH); MS (70 eV) *m/z* (rel intensity) 370 (M^+−EtOH, 16), 326 (19), 294 (10), 171 (48), and 73 (100); Found: *m/z* 370.2145. Calcd for $C_{23}H_{30}O_4$: M−EtOH, 370.2140.

1,4,4a,4b,5,6,10,10a-Octahydro-10aβ-[(1-ethoxyethoxy)-methyl]-2-methoxycarbonyl-4bβ,8-dimethyl-1α-vinylphenanthrene (60): To a cold (0 °C) solution of **59** (6.55 g, 15.7 mmol) in EtOH (150 ml) was added $NaBH_4$ (0.71 g, 18.7 mmol) in portions. The mixture was stirred at 0 °C overnight. Acetone was added to the mixture and the solvent was evaporated to afford a residue, which was partitioned between CH_2Cl_2 (200 ml) and saturated aqueous NH_4Cl (50 ml). The aqueous layer was extracted with CH_2Cl_2 (200 ml×2) and the combined organic extracts were dried ($MgSO_4$). Removal of the solvent gave a residue, which was dissolved in CH_2Cl_2 (100 ml) containing triethylamine (10 ml, 71 mmol). To the above cold (0 °C) mixture was added

methanesulfonyl chloride (3 ml, 39 mmol) dropwise over 10 min. After being stirred at 0 °C for 3.5 h, additional triethylamine (5 ml, 36 mmol) and methanesulfonyl chloride (2 ml, 26 mmol) was added to the mixture. The mixture was diluted with ether (300 ml) and washed with saturated aqueous NH_4Cl and then with brine. The aqueous layer was extracted with ether (100 ml×2) and the combined organic extracts were dried over $MgSO_4$. Removal of the solvent gave a residue, which was dissolved in benzene (100 ml) and DBU (20 ml). The mixture was refluxed until the mesylate was consumed. The cooling mixture was diluted with ether (300 ml) and washed with saturated aqueous NH_4Cl (100 ml). The aqueous layer was extracted with ether (100 ml×2) and the combined organic extracts were washed with water (100 ml) and brine (100 ml) and dried ($MgSO_4$). Removal of the solvent gave a residue which was chromatographed on a silica-gel column (60 g in hexane, eluent: 20% ether-hexane) to afford 4.82 g (76.5%) of **60** as a colorless oil: IR (oil) 1725 cm^{-1}; ^1H NMR δ=0.98 (3H, s, 10-CH_3), 1.09—1.39 (6H, 2×CH_3), 1.80 (3H, brs, 4-CH_3), 3.72 (3H, s, CO_2CH_3), 4.61 (1H, m), 4.89—5.24 (2H, m, 16-CH_2), 5.3—6.0 (1H, m, 15-CH), and 7.07 (1H, m, 12-CH); MS (70 eV) *m/z* (rel intensity) 368 (M^+—MeOH, 10), 354 (36), 310 (51), 295 (68), and 73 (100); Found: *m/z* 368.2359. Calcd for $C_{24}H_{32}O_3$: M—MeOH, 368.2351.

1,4,4a,4b,5,6,10,10a-Octahydro-10aβ-acetoxymethyl-2-methoxycarbonyl-4bβ,8-dimethyl-1α-vinylphenanthrene (61): A mixture of **60** (5.40 g, 13.5 mmol) and *p*-toluenesulfonic acid (0.5 g) in EtOH (100 ml) was stirred at room temperature for 30 min. The solvent was evaporated and the residue was diluted with ether (200 ml), washed with saturated aqueous $NaHCO_3$ (50 ml), and dried ($MgSO_4$). Removal of the solvent gave a residue, which was dissolved in pyridine (50 ml) and acetic anhydride (5 ml). The mixture was stirred at room temperature overnight. Excess acetic anhydride was decomposed by the addition of MeOH (10 ml) at 0 °C and the solvent was evaporated under reduced pressure. The residue was chromatographed on a silica-gel column (100 g in hexane, eluent: 20% to 40% ether-hexane) to afford 4.50 g (90%) of **61** as colorless crystals. An analytical sample of **61**, mp 108—108.5 °C, was obtained as colorless prisms by crystallization from ether-hexane: IR (KBr) 1740, 1715, and 1660 cm^{-1}; ^1H NMR δ=0.99 (3H, s, 10-CH_3), 1.78 (3H, brs, 4-CH_3), 2.06 (3H, s, $OCOCH_3$), 3.71(3H, s, CO_2CH_3), 3.96 and 4.17 (2H, ABq, *J*=10 Hz, 20-CH_2), 4.9—5.2 (2H, m, 16-CH_2), 5.3—5.9 (3H, m, 3-CH, 6-CH, and 15-CH), and 7.03 (1H, t, *J*=4 Hz, 12-CH); MS (70 eV) *m/z* (rel intensity) 370 (M^+, 1.6), 310 (100), and 171 (96); Found: *m/z* 370.2158. Calcd for $C_{23}H_{30}O_4$: M, 370.2144. Found: C, 74.35; H, 8.22%. Calcd for $C_{23}H_{30}O_4$: C, 74.56; H, 8.16%.

3,4,4a,4b,5,8,8a,9-Octahydro-8aβ-acetoxymethyl-7-methoxycarbonyl-1α,4aβ-dimethyl-8α-vinyl-2(1*H*)-phenanthrenone 2-(Ethylene Acetal) (63): To a cold (0 °C) solution of **61** (5.34 g, 14.4 mmol) in CH_2Cl_2 (100 ml) was added MCPBA (80%, 3.27 g, 15.1 mmol). After being stirred at 0 °C for 30 min under drying tube, the reaction mixture was poured into aqueous saturated Na_2SO_3 and extracted with ether (500 ml). The organic layer was washed with aqueous saturated $NaHCO_3$ (100 ml×2) and brine (60 ml), dried ($MgSO_4$) and concentrated in vacuo to afford the crude epoxide **62** (^1H NMR δ=0.97 (3H, s, 10-CH_3), 1.47 (3H, s, 4-CH_3), 2.09 (3H, s, $OCOCH_3$), 3.08 (1H, brs, $W_{1/2}$=4.5 Hz, 3-CH), 3.72 (3H, s, CO_2CH_3), 4.00 (2H, ABq, *J*=10 Hz, $\Delta\nu_{AB}$=5 Hz, 20-CH_2), 4.9—5.2 (2H, m, 16-CH_2), 5.4—5.9 (1H, m, 15-CH), 5.97 (1H, dd, *J*=5 and 3.5 Hz, 6-CH), and 7.00 (1H, *t*-like, 12-CH)), which was dried over P_2O_5 under reduced pressure for several hours. To a cold (0 °C) solution of the above epoxide and 2-ethyl-2-methyl-1,3-dioxolane (10 ml) in CH_2Cl_2 (100 ml) under argon was added boron trifluoride etherate (0.09 ml, 0.6 mmol) dropwise. The mixture was stirred at 0 °C for 1 h and additional $BF_3 \cdot Et_2O$ (0.04 ml, 0.3 mmol) was added. After being stirred at 0 °C for 30 min, the mixture was poured into saturated aqueous $NaHCO_3$ (100 ml), extracted with CH_2Cl_2 (200 ml×3), dried ($MgSO_4$), and concentrated in vacuo. The residue was chromatographed on a silica-gel column (eluent: ether-hexane) to afford **63** (5.39 g, 87% from **61**) as colorless crystals. An analytical sample was recrystallized from ether-hexane: mp 173—174 °C; IR (KBr) 1735, 1715, and 1655 cm^{-1}; ^1H NMR δ=1.00 (3H, d, *J*=7 Hz, 4-CH_3), 1.13 (3H, s, 10-CH_3), 2.06 (3H, s, $OCOCH_3$), 3.72 (3H, s, CO_2CH_3), 3.93 (4H, m, acetal), 4.9—5.2 (2H, m, 16-CH_2), 5.3—5.9 (2H, m, 6-CH and 15-CH), and 7.01 (1H, m, 12-CH); MS (70 eV) *m/z* (rel intensity) 430 (M^+, 0.8), 386 (0.8), 370 (3.2), and 99 (100); Found: *m/z* 430.2335. Calcd for $C_{25}H_{34}O_6$: M, 430.2355. Found: C, 69.60; H, 8.02%. Calcd for $C_{25}H_{34}O_6$: C, 69.74; H, 7.96%.

Conversion of Acetate 63 into 1-Ethoxyethyl Ether 51: A solution of **63** (2.22 g, 5.16 mmol) in MeOH (50 ml) was mixed with a solution of K_2CO_3 (0.5 g, 3.6 mmol) in water (10 ml). The mixture was stirred at room temperature overnight. The solvent was evaporated and the residue was taken up in saturated aqueous NH_4Cl (50 ml) and extracted with ether (100 ml×4). The combined organic layers were dried ($MgSO_4$) and concentrated in vacuo to afford crude alcohol **52**, which was dissolved in 50 ml of CH_2Cl_2. To this solution was added PPTS (350 mg) and ethyl vinyl ether (2 ml). The mixture was stirred at room temperature for 1 h. The solution was washed with saturated aqueous $NaHCO_3$ (30 ml), dried ($MgSO_4$) and evaporated. The residue was chromatographed on a silica-gel column (20 g in hexane, eluent: 30% ether-hexane) to afford 2.20 g (93%) of **51**.

3,4,4a,4b,5,8,8a,9-Octahydro-8aβ-[(1-ethoxyethoxy)methyl]-7-hydroxymethyl-1α,4aβ-dimethyl-8α-vinyl-2(1*H*)-phenanthrenone 2-(Ethylene Acetal) (66): To a cold (−78 °C) solution of conjugated ester **51** (2.35 g, 5.11 mmol) in toluene (50 ml) was added dropwise 16 ml of a ca. 1 mol dm^{-3} solution of diisobutylaluminium hydride (DIBAL) in hexane. After 1.5 h at this temperature, the mixture was quenched by the addition of methanol (25 ml) and stirred at room temperature for 30 min. The resulting precipitate was filtered and washed thoroughly with methanol. The combined filtrates were evaporated to give a residue, which was chromatographed on a silica-gel column (50 g in $CHCl_3$, eluent: 1% to 3% MeOH-$CHCl_3$) to afford allylic alcohol **66** (2.23 g, quant.) as a colorless oil: IR (oil) 3470 cm^{-1}; ^1H NMR δ=0.9—1.3 (12H, 4×CH_3), 3.8—4.0 (6H), 4.53 (1H, m), 4.85—5.20 (2H, m, 16-CH_2), 5.37 (1H, m, 6-CH), 5.74 (1H, m, 12-CH), and 5.3—5.9 (1H, m, 15-CH); MS (70 eV) *m/z* (rel intensity) 432 (M^+, 0.1), 414 (0.4), 386 (7), 342 (19), 99 (over), and 73 (100); Found: *m/z* 386.2426. Calcd for $C_{24}H_{34}O_4$: M—EtOH, 386.2458.

1,2,3,4,4a,4b,5,6,8,10-Decahydro-3α-hydroxy-2α-hydroxymethyl-4bβ,8α-dimethyl-1α-vinyl-7*H*-2β,10aβ-(epoxymethano)-phenanthren-7-one 7-(Ethylene Acetal) (68): To a cold (−20 °C) solution of allylic alcohol **66** (1.19 g, 2.75 mmol) in CH_2Cl_2 (30 ml) was added dropwise titanium(IV) isopropoxide (4 ml, 13.44 mmol). After 15 min, an anhydrous solution

of *t*-butyl hydroperoxide (5.9 M in 1,2-dichloroethane, 3.5 ml, 20.65 mmol) was added and the mixture was stirred at −20 °C for 3.5 h. Dimethyl sulfide (3 ml) and aqueous saturated sodium fluoride (5 ml) was added to the mixture at −20 °C and the mixture was stirred at room temperature for 1 h to result in white emulsion, which was filtered through a pad of Celite. The filtrate was extracted with $CHCl_3$ (100 ml×3), dried over $MgSO_4$, and concentrated in vacuo. The crude epoxy alcohol **67** without purification was dissolved in ethanol (100 ml) and treated with PPTS (70 mg, 0.28 mmol). The mixture was stirred at 40—50 °C for 30 min. Removal of the solvent gave a residue, which was chromatographed on a silica-gel column (40 g in $CHCl_3$, eluent: 1% to 3% MeOH-$CHCl_3$) to provide diol **68** (1.10 g, quant.) as colorless crystals. An analytical sample was obtained by recrystallization from acetone as colorless needles: mp 213—214 °C; IR (KBr) 3430, 1645, 1090, and 1045 cm^{-1}; ^1H NMR δ=0.99 (3H, d, J=6 Hz, 4-CH_3), 1.19 (3H, s, 10-CH_3), 3.33 (1H, d, J=8 Hz, 20-CH), 3.74 (2H, brs, 21-CH_2), 3.93 (4H, m, acetal), 4.05 (1H, brd, J=4 Hz, 12-CH), 4.36 (1H, d, J=8 Hz, 20-CH), 4.96—5.25 (2H, m, 16-CH_2), 5.36 (1H, m, 6-CH), and 6.1—6.6 (1H, m, 15-CH); ^{13}C NMR δ=9.89 (q), 19.72 (q), 29.88 (t), 30.82 (t), 31.07 (t), 36.81 (s), 37.08 (t), 40.47 (d), 40.90 (d), 44.04 (s), 58.29 (d), 64.79 (t), 64.95 (t), 65.22 (t), 70.64 (d), 76.38 (t), 84.51 (s), 111.14 (s), 117.99 (d), 118.86 (t), 134.99 (d), and 142.67 (s); MS (70 eV) m/z (rel intensity) 376 (M^+, 16), 358 (3), 292 (4), 100 (100), and 99 (over); Found: m/z 376.2226. Calcd for $C_{22}H_{32}O_5$: M, 376.2251.

1,2,3,4,4a,4b,5,6,8,10-Decahydro-3α-acetoxy-2α-acetoxymethyl-4bβ,8α-dimethyl-1α-vinyl-7*H*-2β,10aβ-(epoxymethano)phenanthren-7-one 7-(Ethylene Acetal) (70): A mixture of diol **68** (8.5 mg, 0.022 mmol), a catalytic amount of 4-dimethylaminopyridine (DMAP), acetic anhydride (0.3 ml), and pyridine (0.5 ml) was stirred at room temperature overnight. An excess acetic anhydride was decomposed by the addition of methanol and the volatiles were removed in vacuo. The residue was chromatographed on a silica-gel column (3 g in $CHCl_3$, eluent: 1% to 3% MeOH-$CHCl_3$) to afford diacetate **70** (7.9 mg, 76%): IR (oil) 1745 cm^{-1}; ^1H NMR δ=1.00 (3H, d, J=6 Hz, 4-CH_3), 1.16 (3H, s, 10-CH_3), 2.01 (3H, s, $OCOCH_3$), 2.08 (3H, s, $OCOCH_3$), 3.43 (1H, d, J=8 Hz, 20-CH), 3.83 (1H, d, J=12 Hz, 21-CH), 3.93 (4H, m, acetal), 4.38 (1H, d, J=12 Hz, 21-CH), 4.44 (1H, d, J=8 Hz, 20-CH), 4.83—5.35 (3H, m, 12-CH and 16-CH_2), 5.36 (1H, m, 6-CH), and 5.8—6.5 (1H, m, 15-CH); MS (70 eV) m/z (rel intensity) 460 (M^+, 1.6) and 99 (100); Found: m/z 460.2476. Calcd for $C_{26}H_{36}O_7$: M, 460.2462.

1,2,3,4,4a,4b,5,6,8,10-Decahydro-2α-(*t*-butyldimethylsiloxymethyl)-3α-hydroxy-4bβ,8α-dimethyl-1α-vinyl-7*H*-2β,10aβ-(epoxymethano)phenanthren-7-one 7-(Ethylene Acetal) (71): To a cold (0 °C) solution of diol **68** (1.4321 g, 3.81 mmol) and imidazole (0.549 g, 8.06 mmol) in DMF (15ml) was added *t*-buthyldimethylchlorosilane (tBDMSCl, 0.8625 g, 5.72 mmol). After being stirred at room temperature for 2 h, additional imidazole (0.39 g, 5.73 mmol) and tBDMSCl (0.57 g, 3.78 mmol) was added. After another 1 h, the mixture was poured into water (100 ml) and extracted with ether (100 ml×4). Drying ($MgSO_4$) and evaporation of the solvent gave a residue, which was chromatographed on a silica-gel column (40 g in hexane) with ether-hexane (1 : 2 to 1 : 1) to afford monosilyl ether **71** (1.8298 g, 98 %) as a colorless oil, which crystallized upon standing. An analytical sample was obtained by recrystallization from hexane as colorless prisms: mp 98—99 °C; IR (oil) 3500 cm^{-1}; ^1H NMR δ=0.90 (9H, s, *t*-Bu), 0.97 (3H, d, J=7 Hz, 4-CH_3), 1.15 (3H, s, 10-CH_3), 3.29 (1H, d, J=8 Hz, 20-CH), 3.77 (2H, ABq, J=10 Hz, $\Delta\nu_{AB}$=10 Hz, 21-CH_2), 3.91 (4H, m, acetal), 4.08 (1H, m, 12-CH), 4.32 (1H, d, J=8 Hz, 20-CH), 4.9—5.2 (2H, m, 16-CH_2), 5.33 (1H, m, 6-CH), and 6.2—6.7 (1H, m, 15-CH); MS (70 eV) m/z (rel intensity) 490 (M^+, 3), 433 (50), 415 (8), 99 (over), and 75 (100); Found: m/z 490.3107. Calcd for $C_{28}H_{46}O_5Si$: M, 490.3148. Found: C, 68.76; H, 9.68%. Calcd for $C_{28}H_{46}O_5Si$: C, 68.53, H, 9.45%.

1,2,3,4,4a,4b,5,6,8,10-Decahydro-3α-acetoxy-2α-(*t*-butyldimethylsiloxymethyl)-4bβ,8α-dimethyl-1α-vinyl-7*H*-2β,10aβ-(epoxymethano)phenanthren-7-one 7-(Ethylene Acetal) (72): A mixture of monosilyl ether **71** (12 mg), a catalytic amount of DMAP, acetic anhydride (0.5 ml), and pyridine (1 ml) was stirred at room temperature for 2.5 h. After the addition of methanol, the volatiles were removed in vacuo to give a residue. Chromatography on a silica-gel column (3 g in hexane) with ethyl acetate-hexane (1 : 5) afforded acetate **72** (11 mg, 84 %): IR (oil) 1745 cm^{-1}; ^1H NMR δ=0.90 (9H, s, *t*-Bu), 0.99 (3H, d, J=6 Hz, 4-CH_3), 1.15 (3H, s, 10-CH_3), 1.99 (3H, s, $OCOCH_3$), 3.33 (1H, d, J=8 Hz, 20-CH), 3.48 and 3.68 (2H, ABq, J=11 Hz, 21-CH_2), 3.92 (4H, m, acetal), 4.37 (1H, d, J=8 Hz, 20-CH), 4.95—5.25 (3H, m, 12-CH and 16-CH_2), 5.35 (1H, m, 6-CH), and 5.8—6.4 (1H, m, 15-CH); MS (70 eV) m/z (rel intensity) 532 (M^+, 0.1), 475 (3), 415 (8), and 99 (100); Found: m/z 475.2513. Calcd for $C_{26}H_{39}O_6Si$: M, 475.2517.

1,2,3,4,4a,4b,5,6,8,10-Decahydro-3α-(*t*-butyldimethylsiloxy)-2α-(methoxymethoxymethyl)-4bβ,8α-dimethyl-1α-vinyl-7*H*-2β,10aβ-(epoxymethano)phenanthren-7-one 7-(Ethylene Acetal) (73): Potassium hydride (1 g, 8.75 mmol, 35% oil dispersion) was washed with hexane (6 ml). To a suspension of the potassium hydride in a mixture of THF (20 ml) and DMF (10 ml) was added dropwise a solution of monosilyl ether **71** (1.00 g, 2.04 mmol) in THF (20 ml) at 0 °C. After 15 min, chloromethyl methyl ether (0.7 ml, 9.22 mmol) was added dropwise and the resulting mixture was stirred at room temperature for 80 min. The mixture was poured into saturated aqueous $NaHCO_3$ (60 ml), extracted with $CHCl_3$ (100 ml×1, 70 ml×2), and dried over $MgSO_4$. Removal of the solvent gave a residue, which was chromatographed on a silica-gel column (30 g in $CHCl_3$, eluent: 1% to 3% MeOH-$CHCl_3$) to afford methoxymethyl ether **73** (0.96 g, 88%) as a colorless viscous oil: IR (oil) no absorption due to hydroxyl group; ^1H NMR δ=0.90 (9H, s, *t*-Bu), 0.97 (3H, d, J=7 Hz, 4-CH_3), 1.15 (3H, s, 10-CH_3), 3.36 (3H, s, OCH_3), 3.37 (1H, 20-CH: broad signal due to overlapping with other signal), 3.57 (2H, brs, 21-CH_2), 3.92 (4H, m, acetal), 4.02 (1H, m, 12-CH), 4.34 (1H, d, J=8 Hz, 20-CH), 4.64 (2H, s, OCH_2O), 4.85—5.15 (2H, m, 16-CH_2), 5.34 (1H, m, 6-CH), and 6.1—6.6 (1H, m, 15-CH); MS (70 eV) m/z (rel intensity) 534 (M^+, 2), 503 (5), 477 (95), 445 (29), 415 (29), 99 (over), and 73 (100); Found: m/z 477.2673. Calcd for $C_{26}H_{41}O_6Si$: M, 477.2674.

1,2,3,4,4a,4b,5,6,8,10-Decahydro-3α-acetoxy-2α-(methoxymethoxymethyl)-4bβ,8α-dimethyl-1α-vinyl-7*H*-2β,10aβ-(epoxymethano)phenanthren-7-one 7-(Ethylene Acetal) (74): To a solution of **73** (25.8 mg, 0.048 mmol) in THF (1 ml) was added tetrabutylammonium fluoride (65 mg, 0.25 mmol) in THF (2 ml). The mixture was stirred at 50 °C for 23 h. The solvent was evaporated in vacuo to give a brown residue, which was filtered through florisil short column with ethyl acetate. The resulting crude alcohol was dissolved in pyri-

dine (1 ml) and acetic anhydride (0.3 ml) containing a catalytic amount of DMAP, and the mixture was stirred at room temperature for 95 min. After the addition of methanol, the volatiles were evaporated in vacuo to give a residue, which was chromatographed on a silica-gel column (5 g in hexane) with ether-hexane (1 : 1) to afford acetate **74** (21.1 mg, 94%) as colorless crystals. An analytical sample was obtained by recrystallization from ether-hexane as colorless prisms: mp 158—159 °C; IR (KBr) 1745, 1380, and 1250 cm^{-1}; ^1H NMR δ=0.99 (3H, d, J=6 Hz, 4-CH_3), 1.17 (3H, s, 10-CH_3), 2.03 (3H, s, $OCOCH_3$), 3.35 (3H, s, OCH_3), 3.36 (1H, d, J=8 Hz, 20-CH), 3.41 and 3.63 (2H, ABq, J=10 Hz, 21-CH_2), 3.92 (4H, m, acetal), 4.39 (1H, d, J=8 Hz, 20-CH), 4.60 (2H, brs, OCH_2O), 4.9—5.3 (3H, m, 12-CH and 16-CH_2), 5.35 (1H, m, 6-CH), and 5.9—6.4 (1H, m, 15-CH); MS (70 eV) m/z (rel intensity) 462 (M^+, 1), 431 (0.4), 402 (1.1), and 99 (100); Found: m/z 462.2622. Calcd for $C_{26}H_{38}O_7$: M, 462.2617.

1,2,3,4,4a,4b,5,6,8,10-Decahydro-3α-(*t*-butyldimethylsiloxy)-2α-(*t*-butyldimethylsiloxymethyl)-4bβ,8α-dimethyl-1α-vinyl-7*H*-2β,10aβ-(epoxymethano)phenanthren-7-one 7-(Ethylene Acetal) (75): To a cold (0 °C) suspension of potassium hydride (3.13 g, 27.4 mmol, 35% oil dispersion) in a mixture of THF (40 ml) and DMF (20 ml) was added dropwise a solution of **71** (2.76 g, 5.63 mmol) in THF (40 ml) over the period of 15 min. After 15 min, a solution of tBDMSCl (2.6 g, 17.2 mmol) in THF (5 ml) was added to the solution. The mixture was stirred at room temperature for 1 h, poured into brine (100 ml), and extracted with ether (150 ml×4). Drying ($MgSO_4$) and evaporation of the solvent gave a residue, which was chromatographed on a silica-gel column (60 g in hexane) with ether-hexane (1 : 4) to afford disilyl ether **75** (3.26 g, 96%) as a colorless viscous oil: IR (oil) no absorption due to hydroxyl group; ^1H NMR δ=0.04 (12H, s, 2×$Si(CH_3)_2$), 0.86 (9H, s, *t*-Bu), 0.90 (9H, s, *t*-Bu), 0.91 (3H, d, J=7 Hz, 4-CH_3), 1.12 (3H, s, 10-CH_3), 3.25 (1H, d, J=8 Hz, 20-CH), 3.60 (2H, s, 21-CH_2), 3.90 (4H, m, acetal), 4.29 (1H, d, J=8 Hz, 20-CH), 4.8—5.2 (2H, m, 16-CH_2), 5.33 (1H, m, 6-CH), and 6.0—6.6 (1H, m, 15-CH); MS (70 eV) m/z (rel intensity) 604 (M^+, 0.2), 547 (28), 503 (6), 415 (7), and 99 (100); Found: m/z 604.3997. Calcd for $C_{34}H_{60}O_5Si_2$: M, 604.3981.

1,2,3,4,4a,4b,5,6,8,10-Decahydro-3α-(*t*-butyldimethylsiloxy)-2α-(*t*-butyldimethylsiloxymethyl)-1α-(2-hydroxyethyl)-4bβ,8α-dimethyl-7*H*-2β,10aβ-(epoxymethano)phenanthren-7-one 7-(Ethylene Acetal) (76): In a 200 ml three-necked flask was placed ca. 2 mol dm^{-3} borane-THF solution (9.5 ml) and THF (50 ml) under argon atmosphere. To the solution was added dropwise 2,3-dimethyl-2-butene (6.5 ml, 54 mmol) at 0 °C and this solution was stirred at 0 °C for 2h. To this solution was added disilyl ether **75** (3.26 g, 5.40 mmol) in THF (40 ml) and the mixture was stirred at 0 °C for 3 h, then at room temperature for 1 h. The solution was cooled to 0 °C, quenched by the careful addition of water (6 ml), followed by 3 M NaOH solution (17 ml) and 30% H_2O_2 (17 ml). After being stirred at ca. 50 °C for 1.5 h, the mixture was cooled to room temperature and the aqueous layer was saturated with NaCl, extracted with ether (150 ml×3), and dried over $MgSO_4$. Evaporation of the solvent gave a residue, which was chromatographed on a silica-gel column (60 g in hexane) with ether-hexane (1 : 4 to 1 : 1) to afford alcohol **76** (2.71 g, 81%) as a colorless oil. An analytical sample was obtained by crystallization from ether-hexane as colorless prisms: mp 145—146 °C; IR (oil) 3500cm^{-1}; ^1H NMR δ=0.02 and 0.04 (12H, each s, 2×$Si(CH_3)_2$), 0.87 (9H, s, *t*-Bu), 0.93 (9H, s, *t*-Bu), 0.99 (3H, d, J=6 Hz, 4-CH_3), 1.12 (3H, s, 10-CH_3), 3.26 (1H, d, J=8 Hz, 20-CH), 3.95 (4H, m, acetal), 4.24 (1H, d, J=8 Hz, 20-CH), and 5.40 (1H, m, 6-CH); MS (70 eV) m/z (rel intensity) 622 (M^+, 1.8), 565 (6), 490 (15), 433 (26), and 99 (100); Found: m/z 622.4077. Calcd for $C_{34}H_{62}O_6Si_2$: M, 622.4087.

1,2,3,4,4a,4b,5,6,8,10-Decahydro-3α-(*t*-butyldimethylsiloxy)-2α-(*t*-butyldimethylsiloxymethyl)-1α-(2-oxoethyl)-4bβ,8α-dimethyl-7*H*-2β,10aβ-(epoxymethano)phenanthren-7-one 7-(Ethylene Acetal) (77): To a Collins' reagent, prepared from chromium trioxide (2 g, 20 mmol) and pyridine (5 ml, 62 mmol) in CH_2Cl_2 (50 ml), was added alcohol **76** (1.95 g, 3.10 mmol) in CH_2Cl_2 (35 ml). The mixture was stirred at room temperature for 1 h, then diluted with ether. The supernatant was filtered through florisil column and washed thoroughly with ether and ethyl acetate. The dark brown residue was dissolved in saturated $NaHCO_3$ solution (70 ml) and extracted with ether (150 ml), washed with aqueous $NaHSO_3$, saturated aqueous $NaHCO_3$, and brine, dried over $MgSO_4$. The combined filtrate and organic extract were concentrated in vacuo to give a residue, which was chromatographed on a silica-gel column (40 g in hexane) with ether-hexane (1 : 2) to afford aldehyde **77** (1.81 g, 93%) as a colorless amorphous solid: IR (oil) 2720 and 1725 cm^{-1}; ^1H NMR δ=0.90 (18H, s, 2×*t*-Bu), 0.98 (3H, d, J=6 Hz, 4-CH_3), 1.13 (3H, s, 10-CH_3), 3.33 (1H, d, J=8 Hz, 20-CH), 3.64 (2H, s, 21-CH_2), 3.7—4.0 (5H, m, 12-CH and acetal), 4.35 (1H, d, J=8 Hz, 20-CH), 5.34 (1H, m, 6-CH), and 9.73 (1H, *t*-like, 16-CH); MS (70 eV) m/z (rel intensity) 620 (M^+, 2), 563 (7), 519 (2), 431 (14), and 99 (100); Found: m/z 620.3906. Calcd for $C_{34}H_{60}O_6Si_2$: M, 620.3930.

1,2,3,4,4a,4b,5,6,8,10-Decahydro-3α-(*t*-butyldimethylsiloxy)-2α-(*t*-butyldimethylsiloxymethyl)-1α-(2,2-dimethoxyethyl)-4bβ,8α-dimethyl-7*H*-2β,10aβ-(epoxymethano)phenanthren-7-one 7-(Ethylene Acetal) (78): A mixture of aldehyde **77** (1.2125 g, 1.95 mmol), PPTS (60 mg, 0.24 mmol), and trimethyl orthoformate (5 ml) in CH_2Cl_2 (35 ml) was stirred at room temperature for 2 days. The reaction mixture was poured into saturated $NaHCO_3$ solution (30 ml), and extracted with $CHCl_3$ (100 ml×3), dried over $MgSO_4$, and concentrated in vacuo. The residue was chromatographed on a silica-gel column (25 g in hexane) with ether-hexane (1 : 3) to afford dimethyl acetal **78** (1.2196 g, 94%) as a pale yellow viscous oil: IR (oil) no absorption due to carbonyl group; ^1H NMR δ=0.06 and 0.08 (12H, each s, 2×$Si(CH_3)_2$), 0.91 (9H, s, *t*-Bu), 0.93 (9H, s, *t*-Bu), 0.99 (3H, d, J=6 Hz, 4-CH_3), 1.08 (3H, s, 10-CH_3), 3.26 (3H, s, OCH_3), 3.27 (1H, d, J=8 Hz, 20-CH), 3.28 (3H, s, OCH_3), 3.72 (2H, s, 21-CH_2), 3.8—4.1 (5H, m, 12-CH and acetal), 4.21 (1H, d, J=8 Hz, 20-CH), 4.4 (1H, m, 16-CH), and 5.38 (1H, m, 6-CH); MS (70 eV) m/z (rel intensity) 666 (M^+, 0.1), 651 (0.25), 634 (2), 609 (5), 577 (80), 499 (36), 445 (30), 99 (over), and 73 (100); Found: m/z 577.3390. Calcd for $C_{31}H_{53}O_6Si_2$: M−*t*-Bu−MeOH, 577.3382.

1,2,3,4,4a,4b,5,6-Octahydro-3α-(*t*-butyldimethylsiloxy)-2α-(*t*-butyldimethylsiloxymethyl)-1α-(2,2-dimethoxyethyl)-4bβ,8α-dimethyl-7*H*-2β,10aβ-(epoxymethano)phenanthrene-7,10(8*H*)-dione 7-(Ethylene Acetal) (79): To a cold (−20 °C) suspension of chromium trioxide (409 mg, 4.09 mmol) in CH_2Cl_2 (5 ml) was added 3,5-dimethylpyrazole (390 mg, 4.06 mmol) in one portion. The mixture was stirred at −20 °C for 20 min, and a solution of acetal **78** (135 mg, 0.20 mmol) in CH_2Cl_2 (10 ml) was added dropwise. After stirring at −20 °C

for 4 h, 3M NaOH solution (3 ml) was added and the mixture was stirred at 0 °C for 30 min. The solution was diluted with brine (20 ml), extracted with ether (50 ml×3), dried over $MgSO_4$, and concentrated in vacuo. The residue was chromatographed on a silica-gel column (10 g in benzene, eluent: 10% to 20% ether-benzene) to afford enone **79** (93.8 mg, 68%) as a pale yellow viscous oil: IR (oil) 1660 cm^{-1}; ^1H NMR δ=0.09 (12H, s, 2×Si(CH_3)$_2$), 0.91 (9H, s, *t*-Bu), 0.93 (9H, s, *t*-Bu), 1.08 (3H, d, J=7 Hz, 4-CH_3), 1.23 (3H, s, 10-CH_3), 3.13 (3H, s, OCH_3) 3.26 (3H, s, OCH_3), 3.95 (4H, m, acetal), and 5.95 (1H, d, J=2 Hz, 6-CH); MS (70 eV) m/z (rel intensity) 680 (M^+, 0.8), 649 (2), 623 (35), 591 (28), 459 (35), 99 (over), 75 (95), and 73 (100); Found: m/z 623.3412. Calcd for $C_{33}H_{55}O_8Si_2$: M−*t*-Bu, 623.3437.

1,2,3,4,4a,4b,5,6,8,8a-Decahydro-3α-(*t*-butyldimethylsiloxy)-2α-(*t*-butyldimethylsiloxymethyl)-1α-(2,2-dimethoxyethyl)-4bβ,8α-dimethyl-7*H*-2β,10aβ-(epoxymethano)phenanthrene-7,10(9*H*)-dione 7-(Ethylene Acetal) (80): To a solution of lithium (ca. 20 mg, 2.9 mmol) in 30 ml of liquid ammonia at −78 °C was added a solution of enone **79** (93.8 mg, 0.14 mmol) in THF (5 ml) containing *t*-butyl alcohol (0.01 ml). The mixture was stirred at −78 °C for 20 min, warmed to −33 °C, and stirred for 20 min, then quenched by the addition of methanol (2 ml). After the ammonia was allowed to evaporate, saturated aqueous NH_4Cl was added and the mixture was extracted with $CHCl_3$ (30 ml×3). Drying ($MgSO_4$) and evaporation of the solvent gave a residue, which was chromatographed on a silica-gel column (5 g in hexane, eluent: 25% to 50% ether-hexane) to afford ketone **80** (66.5 mg, 70%) as colorless crystals. An analytical sample was obtained by recrystallization from hexane as colorless needles: mp 154.5—155.5 °C; IR (oil) 1700 cm^{-1}; ^1H NMR δ=0.8—1.0 (24H, 8×CH_3), 3.12 (3H, s, OCH_3), 3.24 (3H, s, OCH_3), 3.48 (1H, d, J=7.5 Hz, 20-CH), 3.58 (2H, s, 21-CH_2), 3.80 (1H, m, 12-CH), 3.95 (4H, m, acetal), 4.10 (1H, dd, J=8, 2 Hz, 16-CH), and 4.14 (1H, d, J=7.5 Hz, 20-CH); MS (70 eV) m/z (rel intensity) 682 (M^+, 0.4), 667 (1.2), 651 (3.6), 625 (80), 593 (34), 461 (72), and 99 (100); Found: m/z 625.3572. Calcd for $C_{32}H_{57}O_8Si_2$: M−*t*-Bu, 625.3594.

12α,21-Bis(*t*-butyldimethylsiloxy)-13,20-epoxy-16-methoxy-3-picrasanone 3-(Ethylene Acetal) (82): To a cold (−78 °C) solution of ketone **80** (195.5 mg, 0.287 mmol) in THF (6 ml) was added lithium triethylhydroborate (1 mol dm^{-3} solution in THF, 2.5 ml) and the mixture was stirred at −78 °C, then allowed to warm to room temperature overnight. The mixture was quenched by the addition of water, followed by 3 mol dm^{-3} aqueous NaOH (2 ml) and 30% H_2O_2 solution (2 ml), and stirred at room temperature for 2 h. The solution was poured into brine and extracted with $CHCl_3$ (70 ml×3), dried over $MgSO_4$, and concentrated in vacuo to give a crude alcohol **81**, which without purification was dissolved in methanol (10 ml) and treated with a catalytic amount of PPTS. The reaction mixture was stirred at room temperature for 1 h and the solvent was evaporated in vacuo. The residue was chromatographed on a silica-gel column (15 g in hexane, eluent: 50% ether-hexane) to afford methylated hemiacetal **82** (168.3 mg, 90%) as an inseparable 1 : 1 (by NMR) mixture of diastereomers at C-16: IR (oil) no absorption due to hydroxyl and carbonyl group: ^1H NMR δ=−0.1—0.1 (12H, 2×Si(CH_3)$_2$), 0.8—1.0 (24H, 4-CH_3, 10-CH_3, and 2×*t*-Bu), 3.26 and 3.42 (3H, each s, OCH_3), and 3.93 (4H, m, acetal); MS (70 eV) m/z (rel intensity) 652 (M^+, 0.1), 637 (1), 595 (79), 563 (35), and 99 (100).

13,20-Epoxy-12α,21-dihydroxy-16-methoxy-3-picrasanone 3-(Ethylene Acetal) (3): To a cold (0 °C) solution of methylated hemiacetal **82** (187.5 mg, 0.287 mmol) in THF (6 ml) was added tetrabutylammonium fluoride (380 mg, 1.45 mmol) in THF (3 ml). After being stirred at room temperature for 18 h, the mixture was poured into saturated $NaHCO_3$ solution and extracted with $CHCl_3$ (50 ml×3). Drying ($MgSO_4$) and evaporation of the solvent gave a residue, which was chromatographed on a silica-gel column (15 g dry, eluent: 0% to 6% MeOH-$CHCl_3$) to afford 85.6 mg (70%) of a mixture of diastereomers **3** and 36.1 mg (30%) of a pure diastereomer (more polar, $C_{(16)}$ β-OMe isomer of **3**). An analytical sample of the more polar isomer of **3** was obtained by recrystallization from acetone-hexane as colorless needles: mp 213—216 °C; IR (KBr) 3420 cm^{-1}: ^1H NMR Table 1; MS (70 eV) m/z (rel intensity) 424 (M^+, 3), 374 (20), 361 (8), 100 (100), and 99 (over); Found: m/z 424.2446. Calcd for $C_{23}H_{36}O_7$, 424.2462.

References

1) J. Polonsky, "Progress in The Chemistry of Organic Natural Products," ed by W. Herz, H. Grisbach, G. W. Kirby, and Ch. Tamm, Springer-Verlag, Berlin, **47**, 220 (1985).

2) J. D. Connolly and R. A. Hill, *Natural Product Report*, **3**, 421 (1986) and references cited therein.

3) S. M. Kupchan, R. W. Britton, J. A. Lacadie, M. F. Ziegler, and C. W. Sigel, *J. Org. Chem.*, **40**, 648 (1975).

4) See references contained in the following recent papers: M. Kim, R. S. Gross, H. Sevestre, N. K. Dunlap, and D. S. Watt, *J. Org. Chem.*, **53**, 93 (1988); K. Shishido, K. Takahashi, K. Fukumoto, T. Kametani, and T. Honda, *ibid.*, **52**, 5704 (1987); P. A. Grieco, J. Inanaga, H. L. Sham, S. Sasaki, and H. Kim, *J. Chem. Soc., Chem. Commun.*, **1987**, 1044; D. M. Hedstrand, S. R. Byrn, A. T. Mckenzie, and P. L. Fuchs, *J. Org. Chem.*, **52**, 592 (1987); R. F. Spohn, P. A. Grieco, and R. P. Nargund, *Tetrahedron Lett.*, **28**, 2491 (1987); S. M. Kerwin, A. G. Paul, and C. H. Heathcock, *J. Org. Chem.*, **52**, 1686 (1987); F. Kuo and P. L. Fuchs, *J. Am. Chem. Soc.*, **109**, 1122 (1987); M. Yoshida and K. Kanematsu, *Heterocycles*, **26**, 3093 (1987); R. S. Gross and D. S. Watt, *Synth. Commun.*, **17**, 1749 (1987); K. Shishido, K. Takahashi, Y. Oshio, K. Fukumoto, T. Kametani, and T. Honda, *Tetrahedron Lett.*, **27**, 1339 (1986); T. Murae, M. Sasaki, T. Konosu, H. Matsuo, and T. Takahashi, *ibid.*, **27**, 3411 (1986); S. N. Suryawanshi and P. L. Fuchs, *J. Org. Chem.* **51**, 902 (1986); G. A. Kraus and M. E. Krolski, *ibid.*, **51**, 3347 (1986); F. E. Ziegler, S. I. Klein, U. K. Pati, and T.-F. Wang, *J. Am. Chem. Soc.*, **107**, 2730 (1985); J. Inanaga, S. Sasaki, P. A. Grieco, and H. Kim, *ibid.*, **107**, 4800 (1985); R. V. Stevens and A. P. Vinogradoff, *J. Org. Chem.*, **50**, 4056 (1985); B. A. McKittrick and B. Ganem, *ibid.*, **50**, 5898 (1985).

5) D. L. Snitman, M.-Y. Tsai, and D. S. Watt, *Synthetic Commun.*, **8**, 195 (1978).

6) The numbering was accorded with that for bruceantin.

7) J. S. Dutcher, J. G. Macmillan, and C. H. Heathcock, *J. Org. Chem.*, **41**, 2663 (1976).

8) H. O. House "The Michael Reaction" in "Modern Synthetic Reactions," 2nd ed, W. A. Benjamin, Inc, California (1972), pp. 595—623.

9) T. Honda, T. Murae, S. Ohta, Y. Kurata, H. Kawai, T. Takahashi, A. Itai, and Y. Iitaka, *Chem. Lett.*, **1981**, 299.

10) T. Nakai and T. Mimura, *Tetrahedron Lett.*, **1979**, 531.
11) T. Mukaiyama, K. Kamio, and S. Kobayashi, *Chem. Lett.*, **1973**, 261.
12) M. Yamashita, Y. Kato, and R. Suemitsu, *Chem. Lett.*, **1980**, 847; D. H. R. Barton and W. McCombie, *J. Chem. Soc., Perkin Trans. 1*, **1975**, 1574.
13) L. Ruest, G. Blouin, and P. Deslongchamps, *Synthetic Commun.*, **6**, 169 (1976).
14) H. J. Reich, J. M. Reuga, and I. L. Reich, *J. Am. Chem. Soc.*, **97**, 5434 (1975).
15) C. H. Heathcock, C. Mahaim, M. F. Schlecht, and T. Utawanit, *J. Org. Chem.*, **49**, 3264 (1984).
16) S. Danishefsky, K. Vaughan, R. Gadwood, and K. Tsuzuki, *J. Am. Chem. Soc.*, **103**, 4136 (1981).
17) T. Kawabata, P. A. Grieco, H.-L. Sham, H. Kim, J. Y. Jaw, and S. Tu, *J. Org. Chem.*, **52**, 3346 (1987).
18) F. E. Ziegler, S. I. Klein, U. K. Pati, and T.-F. Wang, *J. Am. Chem. Soc.*, **107**, 2730 (1985).
19) M. Isobe, M. Kitamura, S. Mio, and T. Goto, *Tetrahedron Lett.*, **23**, 221 (1982), M. Kitamura, M. Isobe, Y. Ichikawa, and T. Goto, *J. Org. Chem.*, **49**, 3517 (1984).
20) O. D. Dailey and P. L. Fuchs, *J. Org. Chem.*, **45**, 216 (1980).
21) Y. Torisawa, M. Sibasaki, and S. Ikegami, *Tetrahedron Lett.*, **1979**, 1865.
22) W. G. Salomond, M. A. Barta, and J. L. Havens, *J. Org. Chem.*, **43**, 2057 (1978).
23) N. L. Allinger and Y. H. Yuh, QCPE No. 395. Modified by E. Osawa, *Bull. Chem. Soc. Jpn.*, **58**, 1690 (1985).

 © 1988 The Chemical Society of Japan Bull. Chem. Soc. Jpn., 61, 3607—3612 (1988)

Chromium(VI) or Ruthenium(II) Complex Catalysis in Oxidation of Alcohols to Aldehydes and Ketones by Means of Bis(trimethylsilyl) Peroxide

Shigekazu KANEMOTO,† Seijiro MATSUBARA, Kazuhiko TAKAI, Koichiro OSHIMA,*
Kiitiro UTIMOTO, and Hitosi NOZAKI††
Department of Industrial Chemistry, Faculty of Engineering, Kyoto University, Yoshida, Kyoto 606
(Received April 28, 1988)

Bis(trimethylsilyl) peroxide (BTSP) serves as an effective oxidant of alcohols in the presence of chromium(VI) or ruthenium(II) complexes as catalysts in dichloromethane. Selective oxidation of primary alcohols in preference to secondary ones using $RuCl_2(PPh_3)_3$ as a catalyst is also described.

Dehydrogenative oxidation of alcohols to the corresponding carbonyl compounds is one of the most important reactions in organic synthesis. Many transition metal reagents have been widely employed[1] as stoichiometric oxidants or catalysts. Here we wish to report catalysis of pyridinium dichromate(VI) and dichlorotris(triphenylphosphine)ruthenium(II) for oxidation of alcohols by means of $Me_3SiOOSiMe_3$ as an oxidant.[2]

(1) Oxidation of Alcohols with $Me_3SiOOSiMe_3$ Catalyzed by Pyridinium Dichromate(VI). Hexavalent chromium reagents are commonly utilized in the oxidation of primary and/or secondary alcohols. Pyridinium chlorochromate (PCC),[3] pyridinium dichromate (PDC),[4] chromyl chloride,[5] the Collins reagent,[6] as well as the Jones reagent[7] are well-known ones used in the laboratories.[8] However, there are some significant difficulties associated with each oxidant. Particularly, the Collins reagent became popular because of the excellent yields of products, however, a large excess of the chromium complex was required due to the precipitating gummy product which occluded the oxidant and often provided troubles in carrying out the oxidation manipulation as well as workup. Moreover, toxicity of excess chromium trioxide is also a serious problem. A solution to these problems is to find out a suitable co-oxidant which can convert alcohols to the corresponding carbonyl compounds in the presence of a catalytic amount of chromium(VI) species.

The failure in the attempted oxidation of alcohols with a catalytic amount of chromium(VI) complex has been ascribed to the fact that the popular organic or inorganic oxidants can not reoxidize the resulting trivalent chromium into hexavalent because of its high oxidation potential (E^0=1.33 V in acid solutions).[9] Thus, we have turned our attention to utilize the peroxochromium-chromium(VI) trioxide cycle in which an oxodiperoxochromium complex (**1**) is a key reactant for the oxidation of alcohols.

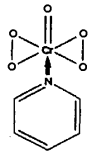

1

Wiede reported the generation of oxodiperoxochromium-pyridine complex (**1**) in 1897.[10] Treatment of chromium trioxide with hydrogen peroxide in the presence of pyridine gave the peroxo reagent as a deep blue solid. This was used only as a damp complex[11] because of the danger of explosion upon drying. It is desirable to generate the oxodiperoxochromium complex in highly diluted conditions and to utilize it in situ for the oxidation from the viewpoint of safety. We have examined suitable co-oxidants, which will oxidize chromium trioxide or its equivalent to the desired oxodiperoxychromium complex. Formation of the "peroxo complex" was checked by a visible absorption arround 580 nm.[12] Among such peroxides as *t*-BuOOH, *t*-BuOOBu-*t*, PhC(O)OOC(O)Ph, and aqueous hydrogen peroxide examined, only hydrogen peroxide produced desired oxodiperoxochromium species. In the case of hydrogen peroxide (30% in water), however, the transformation of primary alcohols to aldehydes accompanied overoxidation into carboxylic acid. Finally, the $Me_3SiOOSiMe_3$-pyridinium dichromate system has proved to be effective for the generation of the oxodiperoxochromium complex in dichloromethane solutions. As the peroxo complex decomposed easily, the oxidant $Me_3SiOOSiMe_3$ was added dropwise using a syringe drive to the reaction mixture. Bis(trimethylsilyl) peroxide was stable enough even upon contact with metallic surface of the syringe needle when it was diluted with dichloromethane (0.5 mol dm^{-3}). The typical results for the conversion of alcohols into carbonyl compounds are summarized in Table 1.

Each substrate was oxidized to the corresponding carbonyl compound in good yields. Moreover, the coexisting olefinic linkage remained intact upon treatment with the oxodiperoxochromium complex and no epoxy compounds were observed among the reaction mixture. Other hexavalent chromium reagents such as anhydrous chromium trioxide and pyri-

† Present address: The Institute of Physical and Chemical Research (RIKEN), 2-1 Hirosawa, Wako-shi, Saitama 351-01.
†† Present address: Dept. Applied Chemistry, Okayama University of Science, Ridai-cho, Okayama 700.

Table 1. Oxidation of Alcohols with Pyridinium Dichromate/$Me_3SiOOSiMe_3$ System[a]

Run	Substrate	Product	Yield/%[b]
1	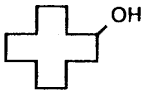	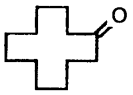	100
2	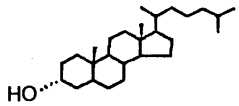	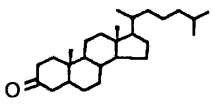	71
3	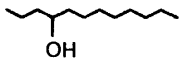	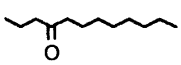	83
4		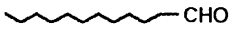	74
5		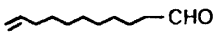	76
6	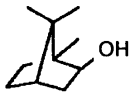	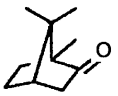	98
7	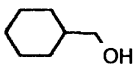	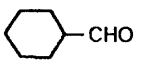	71[c]
8	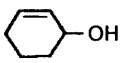	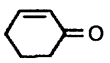	90[c]
9	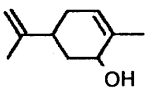	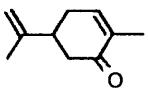	81[c]
10	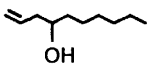	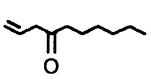	87[c]
11	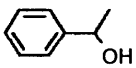	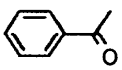	97
12	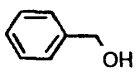	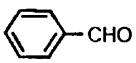	91

a) $Me_3SiOOSiMe_3$ (3.0 mmol) and pyridinium dichromate (0.1 mmol) were employed per one mol of alcohol. b) Isolated and purified yield. c) GLPC yields using decane, tridecane, or tetradecane as an internal standard.

dinium chlorochromate were examined as catalysts, and found to be less effective than pyridinium dichromate. For instance, oxidation of 4-*t*-butylcyclohexanol with CrO_3-$Me_3SiOOSiMe_3$ or PCC-$Me_3SiOOSiMe_3$ gave 4-*t*-butylcyclohexanone in 30% or 55% yield, respectively under the same reaction conditions as pyridinium dichromate-$Me_3SiOOSiMe_3$ system. These results show that oxodiperoxochromium complex is rather unstable either under acidic conditions or in the absence of pyridine.[13]

(2) Selective Oxidation of Primary Alcohols with Ruthenium Catalyst. Ruthenium complex is also a popular catalyst for the oxidation of alcohols. Many organic and inorganic co-oxidants such as amine oxide,[14] *t*-BuOOH,[15] hypervalent iodine compound,[16] molecular oxygen,[17] as well as inorganic $NaBrO_3$,[18] and periodate[19] were widely examined for the oxidation of alcohols. Dehydrogenative oxidation with hydrogen acceptor such as α,β-unsaturated carbonyl compounds has also been studied.[20] Being encouraged with the results obtained with chromium(VI)-catalyzed oxidation, we examined the combination of

$Me_3SiOOSiMe_3$ with a ruthenium complex, $RuCl_2(PPh_3)_3$ to find that simple mixing of the substrate, the catalyst, and the oxidant in one portion gave results as summarized in Table 2.[21] Olefinic double bonds in the substrate were completely inert under the reaction conditions. This observation shows that ruthenium is not oxidized to octavalent oxidation state with $Me_3SiOOSiMe_3$, in sharp contrast with the ruthenium catalysis reaction using periodate as oxidant.[19]

It is worth noting that the allylic alcohols are oxidized with retained configuration of the olefinic bond. Geraniol and nerol were oxidized to the corresponding (*E*)- and (*Z*)-α-enals, respectively. The ruthenium complex, when used stoichiometrically, has proved to be an efficient reagent for the selective oxidation of primary alcohols in the presence of secondary ones.[22] For instance, treatment of 1,10-undecanediol with $RuCl_2(PPh_3)_3$ in benzene gave 10-hydroxyundecanal in 89% yield. The oxidation presumably involves formation of a ruthenium alkoxide which undergoes β-elimination to produce the carbonyl compound and hydridochlorotris(triphenylphosphine)ruthenium. The oxidation of alcohols was completed with half mol of $RuCl_2(PPh_3)_3$, so that this hydridochloro complex is supposedly capable to oxidize another mol of the alcohol to the carbonyl compound. In fact, treatment of a mixture of 1-dodecanol and 4-dodecanol (1.0 mmol each) with $HRuCl(PPh_3)_3$ (1.0 mmol)[23] in benzene provided dodecanal in 75% yield along with a trace of 4-dodecanone (<2%). Possibly, the formation of a ruthenium alkoxide is a rate-determining step and bulkiness of triphenylphosphine ligand plays an important role for this selectivity.

$$RCH_2OH + RuCl_2(PPh_3)_3 \longrightarrow RCH_2O\text{-}RuCl(PPh_3)_3 + HCl$$
$$RCH_2O\text{-}RuCl(PPh_3)_3 \longrightarrow RCHO + HRuCl(PPh_3)_3$$
$$RCH_2OH + HRuCl(PPh_3)_3 \longrightarrow RCH_2O\text{-}RuH(PPh_3)_3 + HCl$$
$$RCH_2O\text{-}RuH(PPh_3)_3 \longrightarrow RCHO + H_2Ru(PPh_3)_3$$

Some attempted selective oxidations of primary alcohols with a catalytic amount of $RuCl_2(PPh_3)_3$ resulted in failure. Such usual co-oxidants as *t*-BuOOH, *N*-methylmorpholine *N*-oxide were effective not only for reoxidation of reduced ruthenium complex to higher oxidation state, but also for oxidation of triphenylphosphine to phosphine oxide which was no more a ligand of ruthenium metal. With *N*-methylmorphorine *N*-oxide-$RuCl_2(PPh_3)_3$ system, 1-dodecanol reacted at only three times the rate of

Table 2. Oxidation of Alcohols with $RuCl_2(PPh_3)_3/Me_3SiOOSiMe_3$ System[a]

Run	Substrate	Product	Yield/%[b]
1	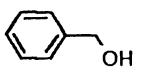	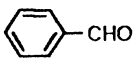	97
2	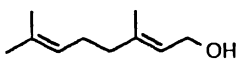	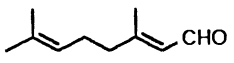	85
3	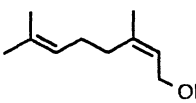	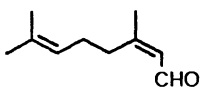	96
4	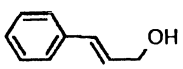	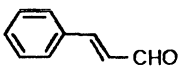	80
5	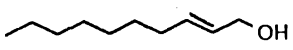	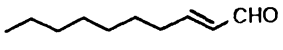	72
6	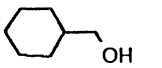	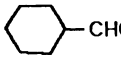	83[c]
7	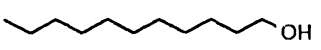	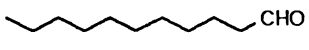	56
8	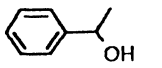	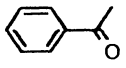	30[d]

a) $Me_3SiOOSiMe_3$ (2.0 mmol) and $RuCl_2(PPh_3)_3$ (0.05 mmol) were employed per one mmol of alcohol. b) Isolated and purified yield. c) GLPC yield using decane as an internal standard. b) Reaction mixture was stirred for 20 h. Starting material (60%) was recovered.

4-dodecanol. Meanwhile, in our new system, $Me_3SiOOSiMe_3$ was not too much strong to oxidize triphenylphosphine into triphenylphosphine oxide, so that the expected catalytic oxidation proceeded selectively. As expected, primary alcohols were oxidized faster than secondary ones with $RuCl_2(PPh_3)_3$-$Me_3SiOOSiMe_3$ system.[24] The relative rate of oxidation between 1-dodecanol and 4-dodecanol was 20 : 1 at the stage of 5% completion of the reaction.[25,26] Benzylic and allylic alcohols were more reactive than its saturated counterparts, and the ratio of reaction rate was more than 2/1. As a result, primary benzylic or allylic alcohols were oxidized more than 40 times as fast as saturated secondary alcohols. Table 3 shows the results of selective oxidation of benzylic and allylic primary alcohols to α-enals. Coexisting secondary alcohols were recovered unchanged nearly quantitatively.

The following Scheme 1 shows that the new system was applicable for the primary-secondary diols. Only hydroxy aldehyde was obtained in good yield.

Experimental

Infrared spectra of neat liquid film samples were determined on a Hitachi grating infrared spectrometer 215, or JASCO IR-810, mass spectra and exact masses on a Hitachi M-80. NMR spectra were recorded on a Varian EM-390, or Varian XL-200 spectrometer using TMS as an internal

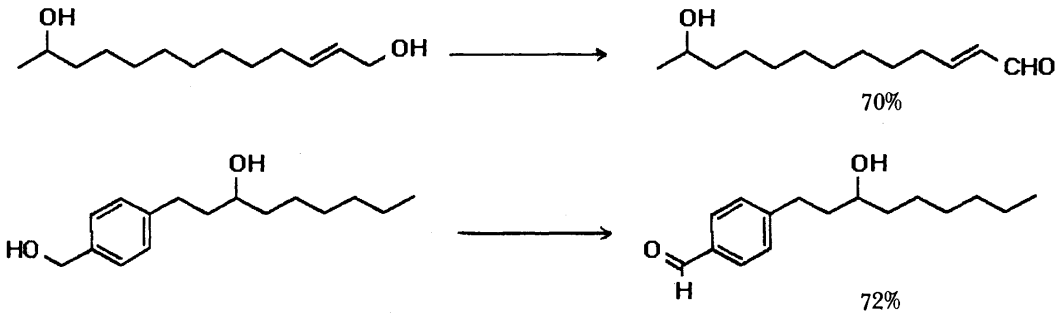

Scheme 1.

Diol (1.0 mmol), $RuCl_2(PPh_3)_3$ (0.1 mmol), and $Me_3SiOOSiMe_3$ (2.0 mmol) were combined in dichloromethane (10 ml) and the reaction mixture was stirred for 2 h at 25 °C.

Table 3. Selective Oxidation of Allyic Primary Alcohols in the Presence of Secondary Ones[a]

Run	Starting mixture of alcohols		Yields(%) of aldehyde and ketone[b]			
1	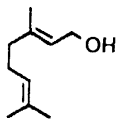	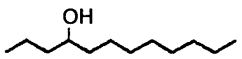	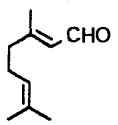	99	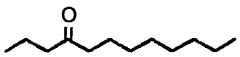	3(92)
2	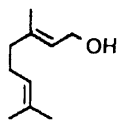	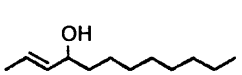	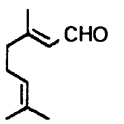	95	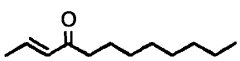	6(90)
3	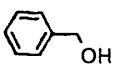	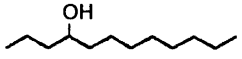	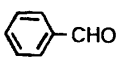	98	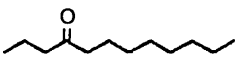	8(85)
4	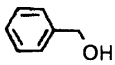	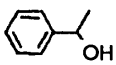	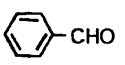	85	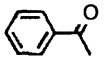	6(92)
5	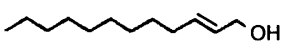	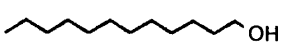	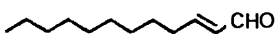	63	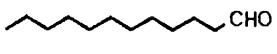	40

a) The hydroxy compounds (1.0 mmol each), $RuCl_2(PPh_3)_3$ (48 mg, 0.05 mmol), and $Me_3SiOOMe_3$ (0.45 g, 2.5 mmol) were combined in dichloromethane (15 ml) and the mixture was stirred for 3 h at 25 °C. b) Yields were calculated on the basis of GLPC (PEG 20 M, 20% on Celite 545, 1.5 m) using dodecane or tetradecane as an internal standard. Figures in parentheses vere recovery of starting secondary alcohols.

standard unless otherwise noted. Multiplicity is designated as s, singlet; d, doublet; t, triplet; q, quartet; m, multiplet. Preparative TLC plates were prepared with Merck Kiesel gel PF_{254}. Column chromatography was carried out with silica gel (Wakogel C-200) at atmospheric pressure.

Preparation of Bis(trimethylsilyl) Peroxide. The peroxide was prepared from hydrogen peroxide according to the reported procedure.[27] Bp 42—44 °C/30 Torr (1 Torr=133.322 Pa): IR (neat) 2960 (s), 1250 (s), 920 (w), 840 (s), 730 (s) cm^{-1}.

General Procedure for the Oxidation of Primary and Secondary Alcohols with Pyridinium Dichromate/Bis(trimethylsilyl) Peroxide. A solution of $Me_3SiOOSiMe_3$ (79 mg, 0.5 mmol) in dichloromethane (2.0 ml) was added to a solution of pyridinium dichromate (37 mg, 0.1 mmol) in the same solvent (5.0 ml). The color changed immediately from dark orange to deep blue, which indicated the formation of oxoperoxochromium complex. Substrate alcohol (1.0 mmol) in dichloromethane (1.0 ml) was added to the solution and the rest of $Me_3SiOOSiMe_3$ (0.45 g, 2.5 mmol) in dichloromethane (5.0 ml) was added dropwise over 1 h by syringe pump at 25°C. The resulting brown reaction mixture was stirred more than 30 min after the completion of the addition of peroxide. The mixture was poured into ice-cooled saturated aqueous sodium hydrogensulfite and extracted with ether (3×20 ml). The combined organic layers were washed with brine, dried over Na_2SO_4, and concentrated. Purification of crude product by silica-gel column chromatography gave a corresponding carbonyl compound in excellent yield (Table 1).

General Procedure for the Oxidation of Primary Alcohols to Aldehyde with $RuCl_2(PPh_3)_3/Me_3SiOOSiMe_3$ System. Oxidation of benzyl alcohol to benzaldehyde is representative. Benzyl alcohol (0.22 g, 2.0 mmol) and $Me_3SiOOSiMe_3$ (0.71 g, 4.0 mmol) were added to a solution of $RuCl_2(PPh_3)_3$ (96 mg, 0.1 mmol) in dichloromethane (15 ml) and the whole was stirred for 2 h at 25 °C. The resulting mixture was diluted with dichloromethane (20 ml) and poured into ice-cooled water. The organic layer was separated and water layer was extracted with dichloromethane and the combined organic layers were washed with saturated aqueous sodium hydrogensulfite and brine successively. Concentration followed by purification on preparative thin-layer chromatography gave benzaldehyde (0.19 g) in 91% yield (Table 2).

General Procedure for the Selective Oxidation of Allylic Primary Alcohols in the Presence of Secondary Ones. Selective oxidation of geraniol to (*E*)-citral in the presence of 4-dodecanol is representative. A solution of $Me_3SiOOSiMe_3$ (0.45 g, 2.5 mmol) in dichloromethane (5 ml) was added to a solution of geraniol (0.15 g, 1.0 mmol), 4-dodecanol (0.18 g, 1.0 mmol), and $RuCl_2(PPh_3)_3$ (0.05 g, 0.05 mmol) in dichloromethane (10 ml). The whole mixture was stirred for 3 h at 25 °C, and the resulting mixture was poured into ice water. The organic layer was separated and dried over Na_2SO_4. The yield of aldehyde and recovered secondary alcohol were checked by GLPC using tridecane as an internal standard (Table 3).

12-Hydroxy-2-tridecenal: To a solution of $RuCl_2(PPh_3)_3$ (96 mg, 0.1 mmol) in dichloromethane was added a mixture of $Me_3SiOOSiMe_3$ (0.37 g, 2.0 mmol) and 2-tridecene-1,12-diol (0.21 g, 1.0 mmol) in dichloromethane at 25 °C. The oxidation completed within 1.5 h and the reaction mixture was poured into ice water. Workup followed by purification gave 12-hydroxy-2-tridecenal in 70% yield: Bp 112—114 °C (0.05 Torr, bath temp); IR (neat) 3370, 2940, 2740, 1697, 975 cm^{-1}; ^1H NMR (CCl_4) δ=1.11 (d, 3H, J=6.0 Hz), 1.1—1.8 (m, 14H), 2.2—2.6, (m, 3H), 3.5—3.9 (m, 1H), 6.01 (dd, 1H, J=15.0 and 7.5 Hz), 6.68 (dt, 1H, J=15.0 and 7.0 Hz), 9.39 (d, 1H, J=7.5 Hz); exact mass spectrum m/z 211.1608. Calcd for $C_{13}H_{23}O_2$: M−1, 211.1698.

4-(3-Hydroxynonyl)benzaldehyde: Bp 116—118 °C (0.06 Torr, bath temp); IR (neat) 3380, 2933, 2740, 1700, 1608, 1218, 1167, cm^{-1}; ^1H NMR ($CDCl_3$) δ=0.85 (t, 3H, J=7.5 Hz), 1.05—1.85 (m, 11H), 2.43—3.0 (m, 2H), 3.75—3.95 (m, 1H), 7.05—7.50 (m, 2H), 7.7—7.95 (m, 2H), 10.0 (s. 1H); exact mass spectrum m/z 248.1720. Calcd for $C_{16}H_{24}O_2$: M, 248.1777.

References

1) R. A. Sheldon and J. K. Kochi "Metal-Catalyzed Oxidations of Organic Compounds," Academic Press, New York (1981).

2) A part of this work was published in a communication form: S. Kanemoto, K. Oshima, S. Matsubara, K. Takai, and H. Nozaki. *Tetrahedron Lett.*, **24**, 2185 (1983).

3) E. J. Corey and J. W. Suggs, *Tetrahedron Lett.*, **1975**, 2647; G. Piancatelli, A. Scettri, and M. D'Auria, *Synthesis*, **1982**, 245.

4) E. J. Corey and G. Schmidt, *Tetrahedron Lett.*, **1979**, 399.

5) K. B. Sharpless and K. Akashi, *J. Am. Chem. Soc.*, **97**, 5927 (1975).

6) J. C. Collins, W. W., Hess, and F. J. Frank, *Tetrahedron Lett.* **1968**, 3363; R. Ratcliffe and R. Rodehorst, *J. Org. Chem.*, **35**, 4000 (1970).

7) K. Bowden, I. M, Heilbron, E. R. H. Jones, and B. C. L. Weedon, *J. Chem. Soc.*, **1946**, 39.

8) For other reagents using hexavalent chromium as a key atom, see; E. Caradello, M. Orena, and S. Sandri, *Synthesis*, **6**, 396 (1976); W. G. Dauben and D. M. Michno. *J. Org. Chem.*, **42**, 682 (1977); G. Cainelli and F. Manescalchi, *J. Am. Chem. Soc.*, **98**, 6737 (1976).

9) G. Charlot, "Selected Constants of Oxydo-Reduction Potentials," Pergamon Press, New York (1958).

10) O. F. Wiede, *Ber.*, **30**, 2178 (1897).

11) G. W. Fleet and W. Little, *Tetrahedron Lett.*, **1977**, 3749.

12) D. M. Adams and J. B. Raynor, *J. Chem. Educ.*, **43**, 94 (1966), D. M. Adams and J. B. Raynor. "Advanced Practical Inorganic Chemistry," John Wiley, Cambridge, (1965), p. 50.; D. F. Evans, *J. Chem. Soc.*, **1957**, 4013.

13) Oxodiperoxochromium species was formed even in the absence of pyridine (checked by visible spectra), which decomposed easily within 5 min at room temp.

14) K. B. Sharpless, K. Akashi, and K. Oshima, *Tetrahedron Lett.*, **1976**, 2503.

15) Y. Tsuji, T. Ohta, T. Ido, H. Minbu, and Y. Watanabe, *J. Organomet. Chem.*, **270**, 333 (1984).

16) P. Müller and J. Godoy, *Tetrahedron Lett.*, **22**, 2361 (1981).

17) R. Tang, S. E. Diamond, N. Meary, and F. Mares, *J. Chem. Soc., Chem. Commun.*, **1978**, 562; M. Matsumoto and S. Ito, *ibid.*, **1981**, 907.

18) Y. Yamamoto, H. Suzuki, and Y. Moro-oka, *Tetrahedron Lett.*, **26**, 2107 (1985).

19) P. H. J. Carlsen, T. Katsuki, V. S. Martin, and K. B. Sharpless, *J. Org. Chem.*, **46**, 3936 (1981); V. M. Parikh and

J. K. N. Jones, *Can. J. Chem.*, **43**, 3452 (1965); P. Eaton and R. H. Mueller, *J. Am. Chem. Soc.*, **94**, 1014 (1972); "Oxidation in Organic Chemistry," Part B, ed by W. S. Trahanovsky, Academic Press, New York (1973).

20) Y. Sasson and J. Blum, *Tetrahedron Lett*, **1971**, 2167; Y. Sasson and G. L. Rempel, *ibid.*, **1974**, 4133; *idem*, *Can. J. Chem.*, **52**, 3825 (1974); S. L. Regan and G. M. Whitesides, *J. Org. Chem.*, **37**, 1832 (1972); S. Murahashi, K. Ito, T. Naota, and Y. Maeda, *Tetrahedron Lett.*, **22**, 5327 (1981).

21) Tishchenko type product, RCO_2CH_2R was not detected in the reaction mixture.

22) H. Tomioka, K. Takai, K. Oshima, and H. Nozaki, *Tetrahedron Lett.*, **22**, 1605 (1981).

23) P. S. Hallman, B. R. McGarvey, and G. Wilkinson, *J. Chem. Soc. A*, **1968**, 3143.

24) Oxidation of secondary alcohols were very slow even in the case of benzylic alcohol, and sometimes the reaction stops in less than 50% conversion.

25) The ratios were determined by monitoring the appearance of dodecanal and 4-dodecanone by GLPC (PEG 20M 5% on Celite 545, 1.5 m, 120 °C).

26) From the synthetical point of view, the ratio of >95:5 is necessary for "selective" reaction. In order to achieve this ratio, the relative rate should be more than 50/1, which was obtained in the case of oxidation using stoichiometrical amount of ruthenium complex as oxidant.[22]

27) S. Matsubara, K. Takai, and H. Nozaki, *Bull. Chem. Soc. Jpn.*, **56**, 2029 (1983).

 © 1988 The Chemical Society of Japan Bull. Chem. Soc. Jpn., 61, 3613—3618 (1988)

Efficient Electron Flux Conversion from Strongly Hydrophilic NADH Model in the Transmembrane Electron Transfer by Flavolipid

Itaru HAMACHI, Yoshiaki KOBUKE,* and (the late) Iwao TABUSHI
Department of Synthetic Chemistry, Faculty of Engineering, Kyoto University, Yoshida, Kyoto 606
(Received April 30, 1988)

By using a strongly hydrophilic NADH model, BzNAHCOOK in the external electron donor, a transmembrane electron transport to the internal acceptor, $K_3[Fe(CN)_6]$ through the flavolipid (**1**) was observed. BzNAHCOOK was proved to be an appropriate NADH model in the transmembrane electron transport study because of (i) the very low permeability through the bilayer membrane (k=1.0×10^{-3} s^{-1}) and (ii) the slow hydration rate (k=1.1×10^{-5} s^{-1}). The artificial liposome modified with the flavolipid showed a 6—7 times more efficient electron flux conversion from BzNAHCOOK to $K_3[Fe(CN)_6]$ than the liposome modified with the ubiquinone 10, a biologically important electron carrier. In association with the electron transport, electrochemical oxidation and reduction peaks of the flavolipid incorporated into the liposomal membrane were observed clearly by using Hg-electrode.

In the previous communications, we have reported a successful electron transport across the bilayer membrane of liposome functionalized with the flavolipid (**1**) from the external electron source to the internal acceptor.[1] This represents an artificial flavoprotein

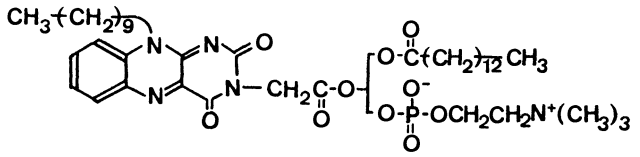

1

model which accepts electrons from $Na_2S_2O_4$ and donates them to $K_3[Fe(CN)_6]$. In an energetic view point, this means a large transmembrane driving force since $Na_2S_2O_4$ ($E_{1/2}$=−1.13 V vs. NHE) is a powerful reducing agent toward the flavin ($E_{1/2}$=−0.12 V and −0.37 V vs. NHE) and $K_3[Fe(CN)_6]$ ($E_{1/2}$=+0.36 vs. NHE). In native systems, the use of such an excess driving force is carefully avoided by choosing electron donors having appropriate reduction potentials. Dihydronicotinamide ($E_{1/2}$=−0.32 V vs. NHE) is the most important electron donor as seen in various NAD(P)H (hereafter abbreviated generally as RNAH) linked reductases, e.g. the NADH branch of the respiratory chain.[2] Here, RNAH interacts first with the membrane bound flavoprotein to initiate the transmembrane electron transport. RNAH molecular "flux" from the bulk aqueous to the membrane phase is converted to the electron "flux". This process is the first event of the respiratory chain and of primary importance even in the viewpoint of whole bioenergetics.[3]

According to the above considerations, it seems interesting and significant to construct an artificial Complex I of the respiratory chain.[4] The authors wish to report here a successful transmembrane electron transport through the flavoliposome system by using a RNAH model.

Results and Discussion

On the basis of the discussions described in the introductory section, the external electron donor

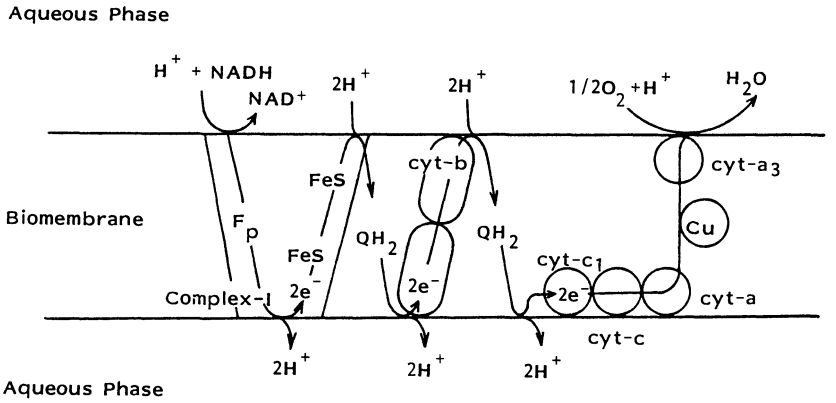

F_p: flavoprotein
FeS: iron-sulfur cluster
cyt: cytochrome
QH_2: ubiquinone 10

should be changed from a strong reducing agent such as $Na_2S_2O_4$ to RNAH derivatives. NADH itself is not a suitable reducing agent since it gives a too slow electron transport rate in the present flavoliposome system. This is not unusual and it is generally accepted that various NADH models give about 10^2 times faster rates toward flavin reduction than NADH itself in homogeneous solution.[5] This significant decrease of the reactivity of NADH is ascribed to the nature that a bulky and too hydrophilic NAD(P)H cannot get a molecular configuration appropriate for the electron transfer to flavin moiety without an assistance of the enzymatic binding. Therefore, a simple NADH model, 1-methyl-1,4-dihydronicotinamide (MeNAH) was considered as a candidate for the reductant. However the leakage rate of MeNAH through the lecithin bilayer membrane was too large (Table 1) to make practically difficult to estimate the net electron transport rate mediated by flavolipid because the material (MeNAH) transport overshadows the electron transport via flavolipid. MeNAH can not therefore be an appropriate NADH model. Introduction of stronger hydrophilicity is certainly required for the reductant to be used in the present membrane process. Therefore, we tested the potassium salt of *N*-(carboxymethyl)-1-benzyl-1,4-dihydronicotinamide (BzNAHCOOK)[6] as a reductant in the transmembrane electron transport study. The leakage rate of BzNAHCOOK was suppressed by a factor of 60 compared to that of MeNAH.

One of the disadvantages of the use of NADH model in the aqueous system arises often from its hydration.[7] BzNAHCOOK exhibited a superior characteristic in this point of view. The hydration rate of BzNAHCOOK in 5 mmol dm^{-3} Tris·HCl (pH=7.0) (k=1.1×10^{-5} s^{-1}) was 10^2 times slower than that of MeNAH in 5 mmol dm^{-3} Tris·HCl (pH=7.0) (k=1×10^{-3} s^{-1}). As will be illustrated later, this hydration

Table 1. Reduction Rate Constants of the Internal $K_3[Fe(CN)_6]$ in the Egg Lecithin Liposome by NADH-Models without the Flavolipid[a)]

NADH-model	k_{obs}/s^{-1} [b)]
MeNAH	60×10^{-3}
BzNAHCOOK	1×10^{-3}
NADH	0.03×10^{-3}

a) ($^{(o)}$NADH-models|lecithin|$^{(i)}$[Fe(CN)$_6$]$^{3-}$).
b) $-d[[Fe(CN)_6]^{3-}]/dt=k_{obs}[[Fe(CN)_6]^{3-}]$.

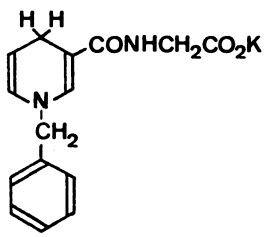

BzNAHCOOK

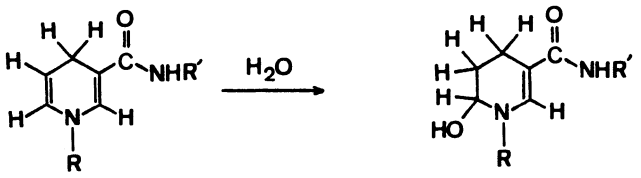

(RNAH)

Hydration of NADH and NADH-model compound.

rate of BzNAHCOOK is slow compared with rates of the facilitated electron transport across the membrane modified with flavolipid, the latter being 10^{-2}—10^{-1} s^{-1}. In the following, the electron transport through the artificial membrane functionalized with an efficient electron transport catalyst was investigated by using BzNAHCOOK as the external reductant. This electron transport system containing $K_3[Fe(CN)_6]$ in its internal aqueous phase ($^{(o)}$BzNAHCOOK|fl-Lip|$^{(i)}$ $K_3[Fe(CN)_6]$) is expected to give a simplified, isotopochemical model of the NADH dehydrogenase in the Complex I of the respiratory chain in the mitochondrial inner membrane.

Effective Flux Conversion of NADH Model by Flavolipid. Electron influx ($J_{o\to m}$) from the external BzNAHCOOK to the flavolipid (fl^{ox}: the oxidized form of the flavin moiety) locating in the membrane phase, was monitored by the reduction of flavolipid, which was incorporated into the liposome without $K_3[Fe(CN)_6]$ in its interior ($^{(o)}$|fl^{ox}-Lip|$^{(i)}$), by the external BzNAHCOOK. In the same way, the electron efflux ($J_{m\to i}$) from the reduced flavolipid (fl^{red}) locating in the bilayer membrane phase to the internal $K_3[Fe(CN)_6]$ was obtained by monitoring the oxidation of fl^{red} in the membrane by $K_3[Fe(CN)_6]$ in the external aqueous phase. The apparent flux constants of $k_{o\to m}$ and $k_{m\to i}$ were obtained from the following equation:

$$J_{o\to m} = -k_{o\to m}\, S(o)[fl^{ox}]$$
$$J_{m\to i} = -k_{m\to i}\, S(i)[fl^{red}]$$

where the inner and the outer surface areas, S(i) and S(o) were estimated from the observation that the mean radius and the thickness of the liposome used were 35

Table 2. Oxidation of fl^{red} and Reduction of fl^{ox} in the Membrane

Reductant	Oxidant	$k_{o\to m}$[a,b)]	$k_{m\to i}$[a,b)]
mmol dm^{-3}	mmol dm^{-3}	cm^{-2} s^{-1}	cm^{-2} s^{-1}
BzNAHCOOK	—		—
0.8		0.04×10^{-7}	
1.6		1.0 ×10^{-7}	
4.3		2.7 ×10^{-7}	
8.8		5.6 ×10^{-7}	
$Na_2S_2O_4$	—		
1.0		6.9 ×10^{-5}	
—	$K_3[Fe(CN)_6]$	—	
	0.9		1.2×10^{-5}

a) [liposome]=1.0×10^{-6} mol dm^{-3}, outer surface area=9×10^4 cm^2. b) $J_{o\to m}=-k_{o\to m}\cdot S(o)\,[fl^{ox}]$, $J_{m\to i}=-k_{m\to i}\cdot S(i)[fl^{red}]$.

and 4 nm, respectively. Since the apparent electron efflux constant ($k_{m\to i}$) can not be determined directly, it was estimated from the following:

$$k_{m\to i}=k_{m\to o}\cdot S(i)/S(o)=2/3\cdot k_{m\to o}$$

where $k_{m\to o}$ is a value determined by the oxidation of the reduced flavolipid by the externally added $K_3[Fe(CN)_6]$ (see Scheme 1). It should be mentioned that the local concentration of $K_3[Fe(CN)_6]$ in the internal aqueous phase was in the order of 10^{-1} mol dm^{-3} in the oxidation of fl^{red} by the internal $K_3[Fe(CN)_6]$ ($J_{m\to i}$), while the concentration of $K_3[Fe(CN)_6]$ in the external aqueous phase was in the order of 10^{-3} mol dm^{-3} in the oxidation of fl^{red} by the external $K_3[Fe(CN)_6]$ ($J_{m\to o}$). It is practically impossible to determine the value of $k_{m\to o}$ at the concentration range of 10^{-1} mol dm^{-3} $K_3[Fe(CN)_6]$. Therefore, $k_{m\to i}$ determined by this way may give an underestimated value. Even so, it is safely concluded that the apparent $J_{m\to i}$ from fl^{red} to Fe^{III} was much larger than the apparent $J_{o\to m}$ from BzNAHCOOK to fl^{ox}.

The apparent electron influx constant ($k_{o\to m}$) from BzNAHCOOK to fl^{ox} was 10^3—10^4 times slower than that from $Na_2S_2O_4$ to fl^{ox}, when compared at a similar reductant concentration (ca. 1.0×10^{-3} mol dm^{-3}). The much slower reduction rate of flavolipid by BzNAHCOOK than by $Na_2S_2O_4$ (−1.13 V vs. NHE)[8c] may reflect the nature of a much weaker electron donor

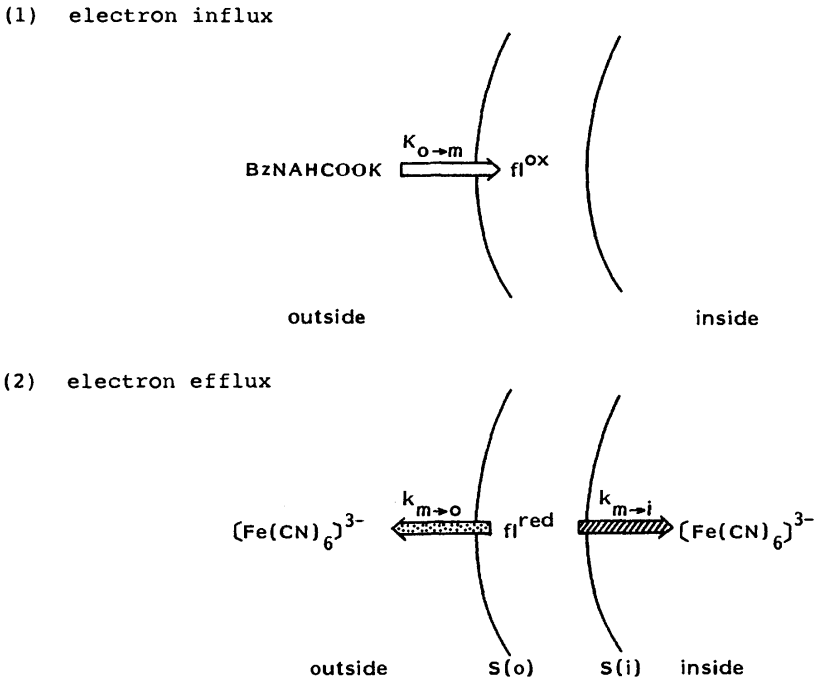

S(o) : outer surface area of the liposome

S(i) : inner surface area of the liposome

Scheme 1. Measurement of electron influx and electron efflux.

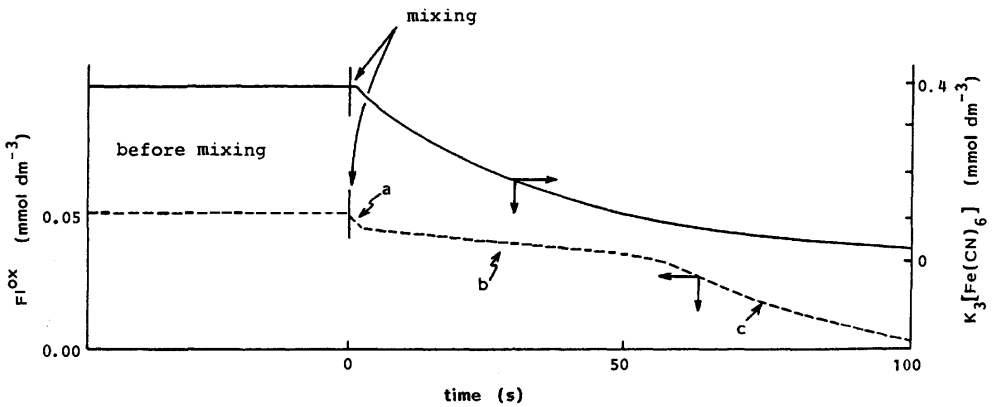

Fig. 1. Change of the concentration of the fl^{ox}-lip in the bilayer membrane (----) and the internal $K_3[Fe(CN)_6]$ (——) during the electron transport reaction by BzNAHCOOK. For a,b, and c, refer the text.

to the flavolipid than the latter.

In the reduction of internal $K_3[Fe(CN)_6]$ by the external BzNAHCOOK across the flavomembrane, a fast reduction of the flavin moiety to the corresponding dihydroflavin was observed at the very initial stage of the reaction (region "a" in Fig. 1). This process was followed by an apparent steady state, where the ratio fl^{red} to fl^{ox} was kept practically constant (region "b", fl^{red}/fl^{ox}=1/9—3/7), while most of the $K_3[Fe(CN)_6]$ was consumed during the period. This fl^{red}/fl^{ox} ratio was much smaller than that in the reduction of internal $K_3[Fe(CN)_6]$ by the external $Na_2S_2O_4$ (6/4=fl^{red}/fl^{ox}) under the same reductant concentration. This reflects the slower electron influx from the outside BzNAHCOOK to the fl^{ox} in the membrane than that from $Na_2S_2O_4$. When most of the $K_3[Fe(CN)_6]$ was reduced, the steady state disappeared and a first order decrease of the flavin (fl^{ox}) was followed (region "c"). In the above steady state, the rate-determining step of the total electron-transport reaction must be the electron influx step from the external BzNAHCOOK to the flavolipid in the membrane because the rate was first order with respect to the concentration of the external BzNAHCOOK as seen from Table 3 and Fig. 2. Even at the highest concentration of BzNAHCOOK, the rate was not saturated as observed. As reported previously for the case of $Na_2S_2O_4$, the saturation of the reduction rate of the internal $K_3[Fe(CN)_6]$ indicated that the rate determining step of the overall reaction was shifted from the electron influx process ($J_{o\to m}$) to the flavin-flavin electron transfer one (see Fig. 3).[1] Furthermore the rate observed here (k) was far slower than the $k_{m\to i}\cdot S(i)$. These observations are compatible with the idea of rate-determining influx. The rate constants of the overall electron transport are summarized in Table

Table 3. Reduction Rate Constants of Internal $K_3[Fe(CN)_6]$ by BzNAHCOOK in the Functionalized Liposomes

BzNAHCOOK	Mediator		k
mmol dm^{-3}	mmol dm^{-3}		s^{-1}
2.6	—		0.1×10^{-2}
0.9	Flavolipid	(0.05)	1.2×10^{-2}
2.6	Flavolipid	(0.05)	6.3×10^{-2}
4.2	Flavolipid	(0.05)	7.1×10^{-2}
9.2	Flavolipid	(0.05)	13×10^{-2}
0.9	UQ 10	(0.05)	0.2×10^{-2}
2.6	UQ 10	(0.05)	0.9×10^{-2}
9.2	UQ 10	(0.05)	2×10^{-2}
2.6	C_4-V^{2+}	(0.05)	0.1×10^{-2}
$Na_2S_2O_4$ (4.0)	Flavolipid	(0.07)	0.04
$Na_2S_2O_4$ (4.0)	UQ 10	(0.07)	1.70
DTT (2.6)	Flavolipid	(0.05)	0.6×10^{-2}
H_2/colloidal Pt	Flavolipid	(0.05)	0.6×10^{-2}

a) $-d[K_3[Fe(CN)_6]]/dt=k[K_3[Fe(CN)_6]]$, at 30 °C, pH 7.0. b) Flavolipid/Lecithin=UQ 10/Lecithin=2.5/97.5 (mol/mol), $[K_3[Fe(CN)_6]]$=0.39 mmol dm^{-3}. Local concentration of $K_3[Fe(CN)_6]$ was 0.75 mmol dm^{-3}. c) DTT: Dithiothreitol.

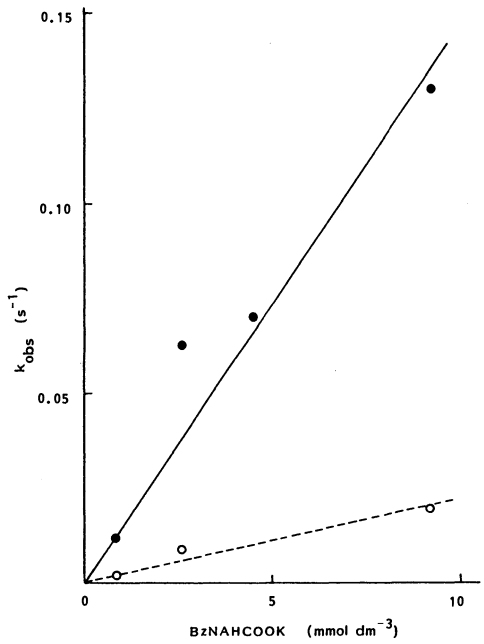

Fig. 2. $K_3[Fe(CN)_6]$ reduction by external BzNAHCOOK across the membrane modified with flavolipid or ubiquinone 10: fl-Lip (—●—), UQ 10 (--○--).

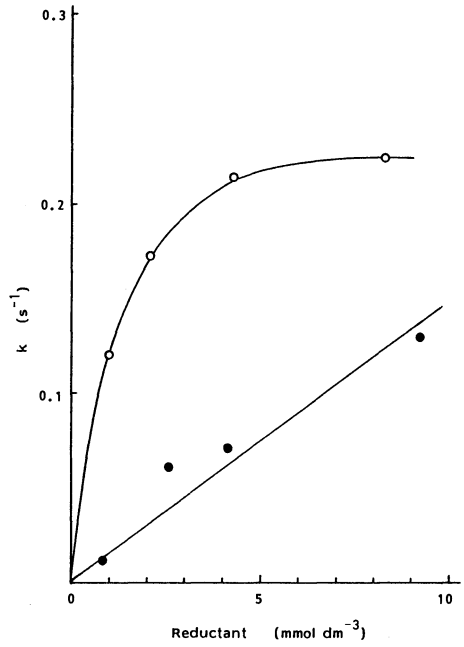

Fig. 3. Dependence of k on the concentration of the external reductant: $Na_2S_2O_4$ (—○—), BzNAHCOOK (—●—).

3 together with those of liposomes modified with ubiquinone 10 (UQ 10) and dibutylviologen (C_4V^{2+}). The flavolipid is a better catalyst for the electron transport from the external BzNAHCOOK to the internal $K_3[Fe(CN)_6]$ than ubiquinone 10. It is interesting to recall that in the case of $Na_2S_2O_4$, the liposome modified with ubiquinone 10 showed more than four time faster rate for the transmembrane electron

transport than the present flavoliposome. This rate order is reversed when the NADH model is employed as the reducing agent. In the electron transfer through the flavoliposome, it was demonstrated that the rate determining step was an influx, from the external reductant to the outer fl^{ox} (out) in the membrane in the case of BzNAHCOOK, while it was an efflux, from the inner fl^{red} to the $K_3[Fe(CN)_6]$ in the case of $Na_2S_2O_4$. Although the rate-determining step was determined to be the influx when BzNAHCOOK was employed, there is no information on it for the case of ubiquinone 10 modified liposome by the reductant of $Na_2S_2O_4$.[9] Therefore it is difficult to make a direct comparison of the overall electron-transfer rates for the flavoliposome and the ubiquinone 10 modified liposome in the case of $Na_2S_2O_4$. It is interesting that the flavoliposomes gave faster electron-transfer rates by the combination with a biologically important reducing agent such as NADH model than the ubiquinone 10 modified liposome system did. One of the important roles of the flavoprotein in the Complex I in the respiratory chain is the more efficient flux conversion from NADH in the bulk aqueous phase to the flavin moiety locating in the membrane phase than the direct flux conversion from NADH to ubiquinone 10. The result presented here may suggest a possible operation of such an electron relay system.

Dibutylviologen which is a moderately efficient electron-transport catalyst in the case of $Na_2S_2O_4$, showed only a poor catalytic activity in this case. This may reasonably be accounted for by considering the potential differences. The redox potential of C_4V^{2+} is -0.44 V vs. NHE,[8b] which means the reduction by BzNAHCOOK ($E_{1/2}=-0.36$ V vs. NHE at pH 7, two electron reduction-oxidation potential)[8a] is a thermally unfavorable reaction. Thus, the very slow electron-transport rate of C_4V^{2+} using BzNAHCOOK can be ascribed to the slow reduction rate of C_4V^{2+} by BzNAHCOOK.

The present flavoliposome can be reduced also by other weak electron donors. As a hydrogen-metabolizing system, hydrogen/colloidal platinum was used as a reducing agent in this system.[10] Dithiothreitol (DTT) also reduced this system, suggesting the possibility that the flavoliposome could work as a lipoyl dehydrogenase model.[11] From these various electron transport systems, the artificial liposome modified with the flavolipid was demonstrated to work as an effective model system for the study of biological electron transport.

Electrochemistry of Flavolipid Incorporated into the Bilayer Membrane. In order to know the oxidation states of the flavolipid in the electron transport process across the lipid membrane, electrochemical redox reactions of the flavolipid were examined. The cyclic voltammogram (CV) of the flavolipid incorporated into the lecithin bilayer membrane in water ($^{(o)}|$fl-Lip$|^{(i)}$) (pH 7.0) showed two clear pairs of cathodic and anodic

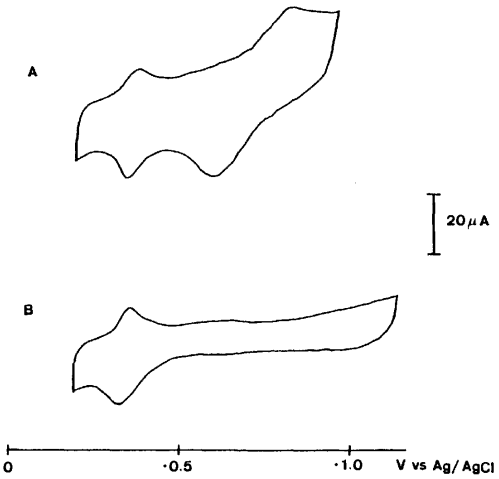

Fig. 4. Cyclic voltammograms on Hg-pool of the flavoliposome in 5 mmol dm^{-3} Tris HCl (pH=7.0). A: ($^{(o)}|$fl-Lip$|^{(i)}$), B: ($^{(o)}|$fl-Lip$|^{(i)}$ $K_3[Fe(CN)_6]$).

waves at -0.35 and -0.70 V vs. Ag/AgCl using a Hg-pool as a working electrode (Fig. 4). It is reported previously[12] that lecithin and other surfactants in water are adsorbed on a Hg electrode surface to inhibit the normal redox reactions of Cd^{2+} on the electrode.[13] In spite of such an inhibitory effect of lecithin, the present flavoliposome (0.025 mmol dm^{-3} flavolipid) afforded clear oxidation-reduction peaks. This may be explained by the idea that the flavin unit (redox site of the liposome) locates in the vicinity of the Hg-lecithin membrane interphase to favor the electron uptake and release from Hg to flavin and vice versa, respectively. In a contrast to the above case, the flavoliposome containing $K_3[Fe(CN)_6]$ in its internal aqueous phase ($^{(o)}|$fl-Lip$|^{(i)}$ $K_3[Fe(CN)_6]$) afforded only one redox couple of cathodic and anodic waves at -0.35 V vs. Ag/AgCl. Assignment of clearly separated two-step redox conversion is now under investigation in relation to the electron transfer reaction from BzNAHCOOK and/or $Na_2S_2O_4$ to $K_3[Fe(CN)_6]$ across the flavomembrane.

Experimental

Instruments. ^{1}H NMR spectra were obtained with a JEOL JNM PMX 60 SI NMR spectrometer, a JEOL JNM FX90Q FT NMR spectrometer or a JEOL JNM GX400 spectrometer. Mass spectra were obtained with a JEOL JMS-DX300 mass spectrometer. IR spectra were recorded on a Hitachi model 260-50 spectrophotometer. Fluorescence spectra were measured with a Shimadzu difference spectrofluorophotometer RF-503A. Electronic spectra were measured with either a Union SM-401 high sensitivity spectrometer or a Hitachi U-3400 spectrophotometer. Sonication was performed with an ultrasonic disruptor, Model UR-200P (Tomy Seiko). Centrifugation was carried out with a refrigerated centrifuge, Tomy Seiko Model RS-20III. Measurement of pH was performed on a Toa pH meter, Model HM 5-ES instrument.

Materials. Unless otherwise noted, all reagents and chemicals were obtained commercially and used without further purification. Egg yolk lecithin was carefully purified according to the literature method[14] and stored at −75 °C under Ar in the dark until its use. BzNAHCOOK was prepared according to the literature method[6] and identified by ^{1}H NMR, IR, electronic spectra and mass spectra.

Preparation of Artificial Single-Wall Bilayer Liposome. The artificial egg lecithin liposome containing $K_3[Fe(CN)_6]$ in its internal aq. phase ($^{(o)}$|lecithin|$^{(i)}$ $K_3[Fe(CN)_6]$), the artificial liposome modified with the flavolipid ($^{(o)}$|fl-Lip|$^{(i)}$) and the liposome modified with the flavolipid containing $K_3[Fe(CN)_6]$ in its internal aqueous phase ($^{(o)}$|fl-Lip|$^{(i)}$ $K_3[Fe(CN)_6]$) were prepared according to the sonication method reported previously by us.[16]

Measurement of Leakage Rate of NADH and its Models through the Bilayer Membrane. Leakage rates of NADH and its model compounds through the lecithin bilayer membrane were measured by observing the reduction of internal $K_3[Fe(CN)_6]$ in the lecithin liposome without the flavolipid ($^{(o)}$|lecithin|$^{(i)}$ $K_3[Fe(CN)_6]$). Into the 2.0 mL of the deaerated liposome solution (5 mmol dm^{-3}. Tris HCl, pH=7.0) was added 0.2 mL of the deaerated NADH model solution freshly prepared using a syringe stopped flow apparatus.[15] Reduction of the internal $K_3[Fe(CN)_6]$ was followed by monitoring the change in the absorbance at 425 nm.

Reduction of Flavolipid (fl^{ox}) Incorporated into the Bilayer Membrane by External BzNAHCOOK. Reduction of the flavolipid incorporated into the bilayer membrane by BzNAHCOOK was performed using the freshly prepared flavoliposome ($^{(o)}$|fl-Lip|$^{(i)}$) in a way similar to the reduction by $Na_2S_2O_4$ described previously.[15]

Oxidation of Flavolipid (fl^{red}) Incorporated into the Bilayer Membrane by External $K_3[Fe(CN)_6]$. A freshly prepared flavoliposome solution ($^{(o)}$|fl-Lip|$^{(i)}$), 2.0 mL) was placed in a 10 mm quartz cell equipped with a three-way stopcock. After the solution was deaerated by the usual method, 0.2 mL of a freshly prepared $Na_2S_2O_4$ (2.0 mmol dm^{-3}) solution was added. The reduction of fl^{ox} was ascertained to be complete within one minute by monitoring the change of absorbance at 444 nm. Then, into the reduced flavoliposome solution ($^{(o)}$ $Na_2S_2O_4$|fl^{red}-Lip|$^{(i)}$) at 25 °C, 0.2 mL of a deaerated $K_3[Fe(CN)_6]$ solution (11.0 mmol dm^{-3}) was added by using a specially designed syringe.[15] The reoxidation of fl^{red} in the bilayer membrane was followed by monitoring the change of the fluorescence intensity at 510 nm excited at 340 nm.

Reduction of $K_3[Fe(CN)_6]$ in the Internal Aqueous Phase of the Flavoliposome by External BzNAHCOOK. Reduction of the internal $K_3[Fe(CN)_6]$ by the external BzNAHCOOK was carried out by using the method similar to the reduction by $Na_2S_2O_4$, except that the ratio of fl^{red} to fl^{ox} was 1/9—3/7 in the steady state reduction.

Cyclic Voltammetry of the Flavoliposome. A Bioanalytical system CV-1B cyclic voltammograph was employed for the cyclic voltammetric determination of the flavolipid incorporated into the bilayer membrane. A freshly prepared flavoliposome solution (5 mL) was degassed by nitrogen bubbling for 0.5 h. As a supporting electrolyte, a KCl solution (0.1 mol dm^{-3}) was used and a Hg-pool electrode was used as a working electrode. Potentials were determined at 25 °C vs. an Ag/AgCl electrode as a reference.

Measurement of Hydration Rate of NADH Models in Tris Buffer Solution. Hydration rate of NADH models was monitored by the first order decrease of the intensity of the absorbance at 360 nm, characteristic of the reduced form of NADH models by using a freshly prepared solution of NADH model compound in 5 mmol dm^{-3} Tris·HCl (pH 7.0).

References

1) a) I. Tabushi and I. Hamachi, *Tetrahedron Lett.*, **28**, 3363 (1987). b) I. Tabushi, I. Hamachi, and Y. Kobuke, *ibid.*, **28**, 5899 (1987).

2) a) C. I. Ragan, *Biochim. Biophys. Acta*, **456**, 249 (1976). b) P. Mitchell, *Eur. J. Biochem.*, **95**, 1 (1979).

3) C. I. Ragan, *Biochem. J.*, **154**, 295 (1975).

4) Y. Hatefi and K. E. Stempel, *J. Biol. Chem.*, **244**, 2350 (1969).

5) T. C, Bruice, L. Main, S. Smith, and P. Y, Bruice, *J. Am. Chem. Soc.*, **93**, 7327 (1971).

6) S. Shinkai, Y. Ishikawa, H. Shinkai, T. Tsuno, H. Makishima, K. Ueda, and O. Manabe, *J. Am. Chem. Soc.*, **106**, 1801 (1984).

7) C. S. Y. Kim and S. Chaykin, *Biochemistry*, **7**, 2339 (1968).

8) a) G. Dryhurst, "Electrochemistry of Biological Molecules," Academic Press, New York (1977). b) "Hankbook of Biochemistry," 2nd ed., ed by H. A. Sober, The Chemical Rubber Co., Ohio (1970). c) M. W. Clark, "Oxidation-Reduction Potentials of Organic Systems," Williams and Wilkins, Baltimore, Md., (1960).

9) a) G. Hauska, *FEBS Lett.*, **79**, 345 (1977). b) A. Futami, E. Hurt, and G. Hauska, *Biochim. Biophys. Acta*, **547**, 583 (1979).

10) I. Tabushi and A. Yazaki, *J. Am. Chem. Soc.*, **103**, 7371 (1981).

11) "Flavins and Flavoproteins," ed by T. P. Singer, Elsevier, Amsterdam (1976).

12) a) B. Cosovic, N. Batina, and Z. Kozarac, *J. Electroanal. Chem.*, **113**, 239 (1980). b) L. Pospisil, J. Kuta, E. E. Mueller, and H. D. Doerfler, *ibid.*, **106**, 359 (1980).

13) Z. Kozarac and B. Cosovic, *Bioelectrochem. Bioenerg.*, **12**, 353 (1984).

14) W. S. Singleton, M. S. Gray, M. L. Brown, and J. L. White, *J. Am. Oil. Chem. Soc.*, **42**, 53 (1965).

15) a) I. Tabushi, T. Nishiya, T. Yagi, and H. Inokuchi, *J. Am. Chem. Soc.*, **103**, 6963 (1981). b) I. Tabushi, T. Nishiya, M. Shimomura, T. Kunitake, H. Inokuchi, and T. Yagi, *J. Am. Chem. Soc.*, **106**, 219 (1984). c) I. Tabushi and I. Hamachi, *Tetrahedron Lett.*, **27**, 5401 (1986).

 © 1988 The Chemical Society of Japan Bull. Chem. Soc. Jpn., 61, 3619—3627 (1988)

Synthesis, Structure, and Hypochromism of Pyrimidinopurinophanes[1)]

Kazuo Doyama, Takayuki Higashii, Fumio Seyama, Yoshiteru Sakata,* and Soichi Misumi
The Institute of Scientific and Industrial Research, Osaka University, Ibaraki, Osaka 567
(Received May 12, 1988)

Seventeen pyrimidinopurinophanes in which a pyrimidine and a purine ring are fixed with different mode of stacking were prepared. The synthesis was carried out by stepwise introduction of two bridging chains. In the final ring closure reaction, two isomers, i.e., isomers bridged at 9-position of a purine ring and those having the bridge at 7-position of a purine ring were obtained. The structures of the isomers were determined on the basis of ^{1}H NMR, IR, and UV spectra and X-ray analysis. In ^{1}H NMR spectra the bridge protons of the pyrimidinopurinophanes show complex multiplets, in contrast to the first order splittings in singly bridged reference compounds. This shows clearly the fixation of the conformations of the present cyclic compounds at room temperature. All of the pyrimidinopurinophanes show relatively large hypochromism (H) values. Even the compounds **2a—2d**, **4**, and **6** where the two base rings are not stacked in parallel, but inclined with the dihedral angle of around 50°, show H values of 10—20%. The H values did not change among the compounds **1c**, **1e—1g**, and **3** which have similar parallel-stacking structures of the two base rings. The results are well explained by the simplified equation of Ts'o et al.

Hypochromism — a decrease in the absorption intensity per unit chromophore — is observed frequently in various π-systems and biologically important substances such as proteins and DNA, where chromophores involved are stacked in a parallel fashion.[2)] The relationship between the stacking orientation and hypochromism values, however, has not been well-understood so far. Recently, we prepared a series of purinophanes where two purine rings are fixed with different mode of stacking.[3)] By analyzing the relationship between their hypochromism values and geometrical parameters from the X-ray results, we presented empirical formulas to estimate the hypochromism values for a given geometry of two stacked purine rings.

We set forward our study for the general understanding of the interaction between two nucleic acid bases other than two purine rings. Since purine-pyrimidine interaction is the greatest after purine-purine interaction,[4)] we planned to synthesize various pyrimidinopurinophanes, in which a purine and a pyrimidine ring is fixed with different modes of relative orientation. Related compounds, prepared so far, are singly bridged compounds, i.e., (pyrimidine)-$(CH_2)_n$-(purine)[4)] with changing the length of the chain and connecting positions at the base rings. They are, however, conformationally not frozen in solution and therefore, not well-suited for the quantitative treatment of hypochromism values in relation to the precise stacking orientation. The present rigid systems are expected to serve useful information about the structural dependence of hypochromism values.

Synthesis

All the pyrimidinopurinophanes **1—6** were prepared by step-wise introduction of the bridging chains. Thus, the singly bridged compounds **7—13** were first prepared starting from the corresponding pyrimidine and purine derivatives as shown in Chart 1. The second chain was introduced by ring closure with α,ω-

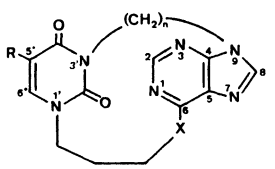

1

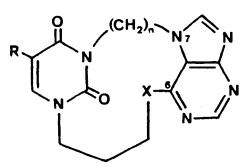

2

a X=NH, R=H, n=3
b X=NH, R=H, n=4
c X=S, R=H, n=3
d X=S, R=H, n=4
e X=S, R=CH_3, n=3
f X=S, R=OCH_3, n=3
g X=S, R=NO_2, n=3

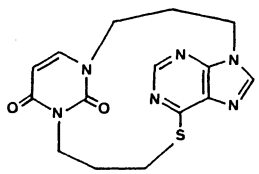

3

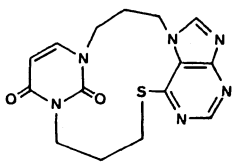

4

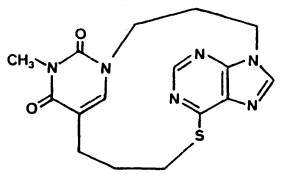

5

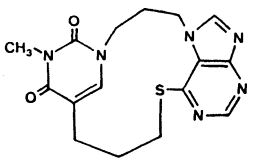

6

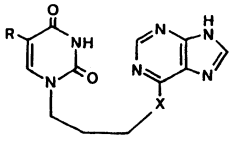

7 X=NH, R=H
8 X=S, R=H
9 X=S, R=CH_3
10 X=S, R=OCH_3
11 X=S, R=NO_2

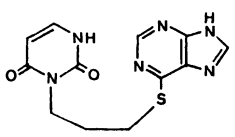

12

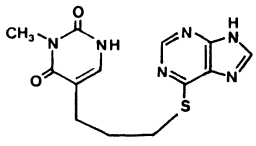

13

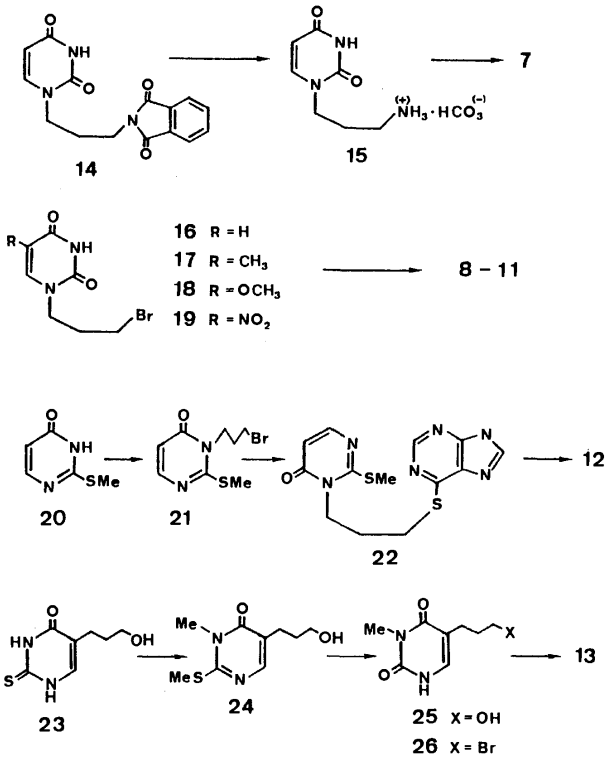

Chart 1.

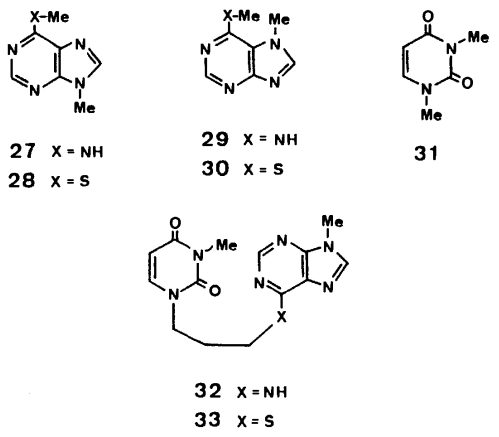

dibromoalkanes in the presence of sodium hydride in DMF (method A) and/or potassium carbonate in DMSO (method B). The coupling reaction gave two isomeric products, i.e., (1′,3′)pyrimidino(6,9)purinophanes **1** and (1′,3′)pyrimidino(6,7)purinophanes **2**. These structures were determined on the basis of spectral data and X-ray analysis as described later. The ratios of the two isomers are different in A and B methods as shown in Table 1. In all runs except for the ratio of **1b**/**2b** by the method B, the isomers **2** (bridged at 7-position of the purine ring) are the major or sole product. The other pyrimidino-purinophanes **1e**—**1g**, **2e**—**2g**, and **3**—**6** were prepared by the method A and the yields are summarized in Table 1.

Monomeric and dimeric references **27**,[3] **28**,[3] **29**,[5] **30**,[6] **31**,[7] **32**, and **33** were also prepared.

Structure

NMR Spectra. ^{1}H NMR spectra of the present molecules were measured in deuteriochloroform. The bridge protons of all the pyrimidinopurinophanes **1**—**6** show complex multiplets in contrast to the first order splitting patterns of acyclic reference compounds **32** and **33**. These results clearly indicate that the conformations of **1**—**6** are almost frozen at room temperature. The chemical shifts of the ring protons (H2, H8, H5′, and H6′) of the pyrimidinopurinophanes and reference compounds are summarized in Table 2. Since H2 and H8 protons of **27** or **28** resonate at higher field than the corresponding protons of **29** or **30**, the isomers which show the similar tendency in the chemical shifts of H2 and H8 to those of **27** or **28** were assigned to the structure having a linkage at 9-position of the purine ring, i.e., **1b**—**1g**, **3**, and **5** and the others were assigned to **2a**—**2g**, **4**, and **6**. The assignments were supported by IR and UV spectra and finally confirmed by X-ray analysis for **1d** and **2c**, described later. In Table 2, the protons H8 and H6′ of **1**, **3**, and **5** show high field shift, except for H8 of **5**, compared with the monomeric references, suggesting that the purine and the pyrimidine rings are stacked in face-to-face. On the other hand, **2**, **4**, and **6** might have the non-stacked orientation of the two base rings, because of the small $\Delta\delta$ values of the ring protons. The magnitude of $\Delta\delta$ values for all the ring protons of **1b**—**1g** in Table 3 are close with each other, indicating that the orientation of the purine and the pyrimidine ring in a molecule is not so different from that of **1d**, whose structure was determined by X-ray analysis. Similarly, the orientation of the two base rings in **2a**, **2b**, **2d**—**2g** might have close resemblance to that of **2c**, the structure of which was also determined by X-ray analysis.

Marked high field shift ($\Delta\delta$=−2.25 ppm) was observed for H6′ of **5**. One possible structure of **5** is that the two rings are hold in a orientation similar to that of [2.2]metaparacyclophane-1,9-diene, where the two aromatic rings are inclined to each other by 41°.[8] If **5** takes such conformation, H6′ locates closely above the center of the purine ring and hence, the large negative value of $\Delta\delta$ for H6′ and small positive one for H8 are reasonably accepted. In order to examine the rigidity of the conformation, temperature dependence of

Table 1. Yields(%) of **1**—**6** by A and B Methods

	1a/2a	**1b/2b**	**1c/2c**	**1d/2d**	**1e/2e**	**1f/2f**	**1g/2g**	**3/4**	**5/6**
Method A	—	—	6/14	19/21	10/28	12/34	11/11	13/25	16/40
Method B	0/44	17/15	0/40	0/28	—	—	—	—	—

Table 2. ^{1}H NMR Chemical Shifts (ppm) of H2, H8, H5′, and H6′ of Pyrimidinopurinophanes in $CDCl_3$ and Their Differences from Monomeric References (+ and − denote down- and up-field shifts, respectively)

Compd	H2		H8		H5′		H6′	
	δ	Δδ	δ	Δδ	δ	Δδ	δ	Δδ
27	8.43		7.71					
28	8.74		7.93					
31					5.73		7.18	
1b	8.29	−0.14	7.62	−0.09	5.70	−0.03	7.11	−0.07
1c	8.78	+0.04	7.81	−0.12	5.76	+0.03	6.98	−0.20
1d	8.73	−0.01	7.86	−0.07	5.78	+0.05	7.12	−0.06
1e	8.77	+0.03	7.71	−0.22			6.83	−0.16
1f	8.77	+0.03	7.78	−0.15			6.55	−0.16
1g	8.78	+0.04	7.83	−0.10			8.53	−0.20
3	8.79	+0.05	7.82	−0.11	5.83	(+0.10)	7.12	−0.06
5	8.83	+0.09	7.94	+0.01			4.74	−2.25
29	8.55		7.81					
30	8.84		8.06					
31					5.73		7.18	
2a	8.47	−0.08	7.87	+0.06	5.64	−0.09	7.11	−0.07
2b	8.49	−0.06	7.85	+0.04	5.81	+0.08	7.21	+0.03
2c	8.84	0.00	8.06	+0.07	5.89	+0.16	7.17	−0.01
2d	8.81	−0.03	8.00	+0.01	5.67	−0.06	7.12	−0.06
2e	8.83	−0.01	8.06	+0.07			7.02	+0.03
2f	8.85	+0.01	8.08	+0.09			6.74	+0.03
2g	8.86	+0.02	8.08	+0.09			8.74	+0.01
4	8.85	+0.01	8.05	+0.06	5.83	+0.10	7.17	−0.01
6	8.87	+0.03	8.13	+0.14			7.07	+0.08

the protons of **5** was measured in the range of −80—+150 °C. The signals of aromatic protons remain almost unchanged both in chemical shifts (less than 0.2 ppm) and in their shapes. Furthermore, the patterns of the complex multiplets due to the bridge protons of **5** did not change in the same temperature range. These results suggest that the conformation of **5** is much stable than that of [2.2]metaparacyclophane, where the coalescence temperature is 146 °C.[9]

IR Spectra. We found the easiest way to distinguish the isomers **1** (X=S) from **2** (X=S) by IR spectra. According to our empirical rule, there is only one absorption band in the region of 1500—1600 cm^{-1} for 9-substituted thiopurines **1** (X=S), **3**, **5**, and **28**, while two peaks are present for 7-substituted thiopurines **2** (X=S), **4**, **6**, and **30**. The results are summarized in Table 3. From the table the exceptions of the rule are only for **1g** and **2g**, where the nitro group is responsible for the additional peak.

Table 3. IR Peaks (cm^{-1}) in the Range of 1500—1600 cm^{-1} for **1c—1g**, **2c—2g**, **3—6**, and Reference Compounds

6-Alkylthio-9-alkylpurines		6-Alkylthio-7-alkylpurines	
28	1575	**30**	1585, 1545
1c	1560	**2c**	1570, 1540
1d	1560	**2d**	1575, 1545
1e	1560	**2e**	1570, 1540
1f	1560	**2f**	1575, 1545
1g	1555, 1510	**2g**	1575, 1540, 1510
3	1555	**4**	1575, 1545
5	1560	**6**	1570, 1540

Table 4. Absorption Maxima (λ_{max}, nm) and Extinction Coefficients (ε) of **1b**, **2a**, **2b**, and Related Compounds

6-Alkylamino-9-alkylpurine		6-Alkylamino-7-alkylpurine	
27+31	267(24600)	**29+31**	269(21600)
		2a	269(15700)
1b	265(19100)	**2b**	268(15800)

UV Spectra. Based on the difference (2 nm) of the longest-wavelength absorption band between 9-methyl- and 7-methyl-6-(methylamino)purines (**27** and **29**), the structures of the isomers **1b** and **2a**, **b** are assigned as shown in Table 4.[10]

X-Ray Analysis. In order to confirm the assignments of the structures of **1** and **2** in Tables 3 and 4, X-ray analysis was carried out for **1d** and **2c**. The crystal structures were solved[11] by a program MULTAN-78[12] and refined by least-squares method. The final R values are 0.038 for **1d** and 0.047 for **2c**. The resulting ORTEP drawings are shown in Figs. 1 and 2. The two base planes are almost parallel in **1d** (dihedral angle: 12.5°) with the interplanar distance of about 3.8 Å, while in **2c** they incline with each other with the dihedral angle of 50.4°. The bond angles and bond lengths of the two rings in **1d** and **2c** are almost the same values as those of 6-(methylthio)purine[13] and 1,3-dimethyluracil,[14] indicating that there is no special ring strain in the composite rings of **1d** and **2c**.

Hypochromism

Electronic spectra of the pyrimidinopurinophanes described above and reference compounds are mea-

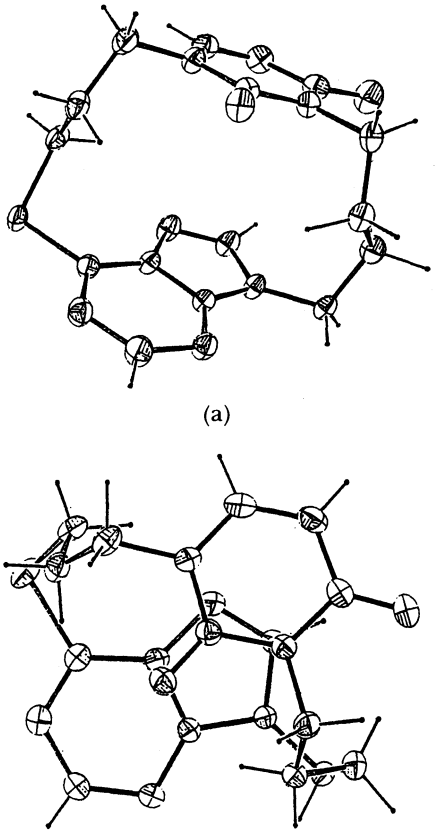

Fig. 1. Molecular structure (a) and views on the least-squars plane defined with a purine ring (b) in **1d**.

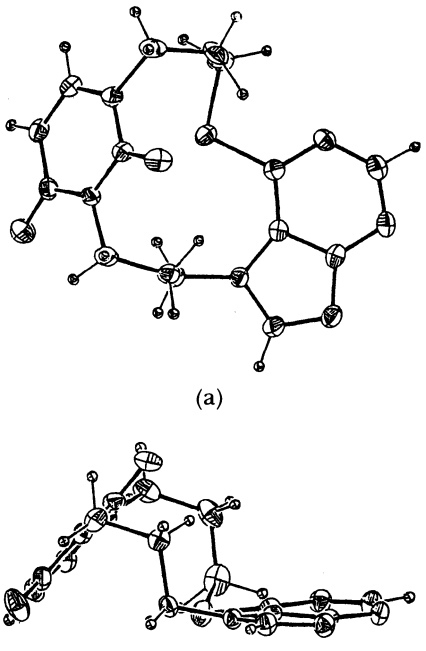

Fig. 2. Molecular structure (a) and side view (b) of **2c**.

sured in ethanol and in water. Typical examples are shown in Figs. 3—6. In the figures difference spectra, which were obtained by subtracting the intensities of a given pyrimidinopurinophane from the sum of the values of the two consisting monomeric references. Hypochromism values were calculated according to the following equations:

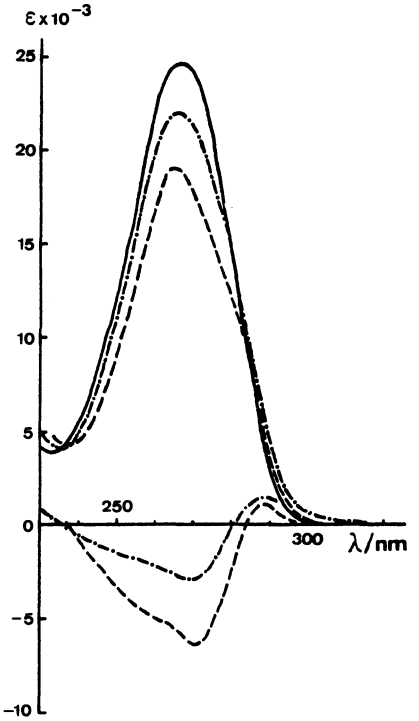

Fig. 3. Electronic spectra of **1b** (----), **32** (-·-·-), and (**27**+**31**) (——) in water and difference spetra of **1b** and **32** vs. (**27**+**31**).

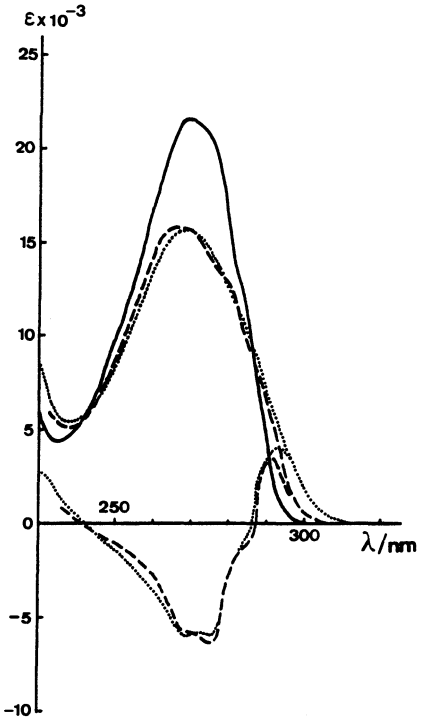

Fig. 4. Electronic spectra of **2a** (------), **2b** (----), and (**29**+**31**) (——) in water and difference spectra of **2a** and **2b** vs. (**29**+**31**).

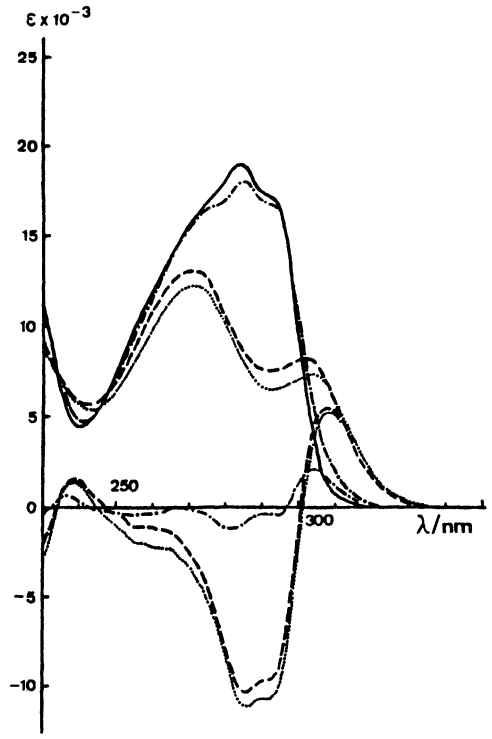

Fig. 5. Electronic spectra of **1c** (------), **1d** (----), **33** (-·-·-), and (**28**+**31**) (——) in water and difference spectra of **1c**, **1d**, and **33** vs. (**28**+**31**).

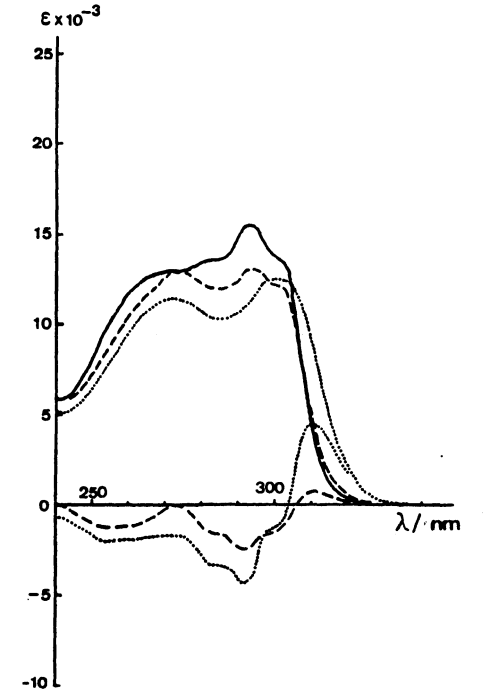

Fig. 6. Electronic spectra of **2c** (------), **2d** (----), and (**30**+**31**) (——) in water and difference spectra of **2c** and **2d** vs. (**30**+**31**).

$$\%H = (1 - (f_D/2f_M)) \times 100$$

$$f = 4.32 \times 10^{-9} \int (\varepsilon(\lambda)/\lambda^2) d\lambda, \quad (1)$$

where f_M and f_D are oscillator strength of monomer and dimer, respectively and these values were obtained by dividing the absorption curves into rectangles at intervals of 2 nm. The results are summarized in Table 5. In marked contrast to the small values for the linear dimers **32** and **33**, the hypochromism values of all the pyrimidinopurinophanes are relatively large and remain almost unchanged in ethanol and in water. This indicates that the structures of the present doubly bridged compounds in solution are almost the same as in the crystalline state. It is worthy of emphasis that **2a—2d** show relatively large hypochromism values in spite of the nonparallel orientation of the two base rings.

The almost parallel stacking of the two chromophores in **1a—1g** brings about larger hypochromism values than those of the corresponding isomers **2** having nonparallel orientation. However, the values of **1a—1g** are still smaller than those of purinophanes where two purine rings are held in face-to-face, due to the smaller interaction in pyrimidine-purine than in purine-purine.

The origin of hypochromism is the interaction between the lowest excited electronic state of a given chromophore and different electronic states of the neighboring chromophores. The theoretical calculation is very difficult since a number of configurational interactions must be taken into account. Ts'o et al.,[15] presented a simplified equation of evaluating hypochromism values (H%) for homodimers with parallel stacking:

$$H = A(1 - 3\cos^2\theta)/R_{ij}^3 \quad (2)$$

where R_{ij} is the distance between the center of i and j rings, θ is the angle between R_{ij} and the transition moment, and A is a constant. From the Eq. 2, H value is independent on the magnitude of the transition moments and if the two base rings of the pyrimidinopurinophanes are fixed with the same orientation, they should have the same H value. This is valid when the hypochromism values of **1c** and **1e—1g** in Table 5 are compared. Thus, the values of these compounds are almost identical with each other. The compounds should have very similar structure because of the same carbon framework, although the transition moments of the pyrimidine rings are different in magnitude owing to the introduction of the substituents. On the basis of molecular model considerations the stacking

Table 5. Hypochromism Values H(%) of Pyrimidinopurinophanes and Related Compounds in Two Solvents

	1b	**1c**	**1d**	**1e**	**1f**	**1g**	**2a**	**2b**	**2c**	**2d**	**3**	**5**	**32**	**33**
H_2O	24	28	20	27	30	26	15	17	11	8	29	27	9	2
EtOH	27	35	31	23	25	23	21	14	20	11	27	23	0	5

orientation of **3** is presumed that the two rings are kept in parallel with the same interplanar distance as that of **1c**, but one chromophore is rotated in its plane by 120° for **3**. In spite of the stacking geometry different from **1c**, *H* values of **3** are very similar to those of **1c**, supporting the validity of Eq. 2. These facts clearly show that the simplified Eq. 2 for homodimers is also applicable to the evaluation of H values for the parallel stacking of a pyrimidine and a purine ring without tedious molecular orbital calculations including a number of configurational interactions.

It is somewhat strange that the *H* values of **5**, where the two base rings seem to be not in parallel as discussed in NMR spectra, are identical with those of **1c**. Presumably, this is derived incidentally and the quantitative treatment of the H value in relation to the structure must wait for the structural determination of **5** by X-ray analysis.

The value of A in Eq. 2 is estimated to be around 1.2×10^3 by assuming that $\theta=90°$ and $R=3.5$ (from molecular model considerations) and 4.0 Å (from X-ray results) for **1c** and **1d**, respectively. The values are in good agreement with those estimated for the homodimers of 6-thiopurine ($A=1.30\times10^3$).[3]

The present and previous[3] results demonstrate that we can use Eq. 2 for the evaluation of *H* values of parallel-stacked nucleic acid base pairs, i.e., purine-purine and purine-pyrimidine rings.

Experimental

All melting points were uncorrected. NMR spectra were measured on a Hitachi R-24A (60 MHz), a JNM FX-100 (100 MHz), and a Bruker WH-360 (360 MHz). IR and mass spectra were recorded on a Hitachi EPI-G2 and a Hitachi RMU-7, respectively. Electronic spectra were taken on a Hitachi EPS-3T and a Hitachi 330. Liquid chromatography was performed on Nihon Bunsekikogyo LC-08 and LC-09.

1-(3-Aminopropyl)uracil, Formate Salt (15). To a stirred mixture of **14**[16] (3.0 g, 10 mmol) in ethanol (150 ml) heated to reflex was added hydrazine monohydrate (1.1 g, 22 mmol). The mixture was stirred at reflux for 8 h and ethanol was removed. To the residue was added 2 M HCl (30 ml; 1M=1 mol dm^{-3}) and the suspension was stirred at room temperature for 30 min. Insoluble solid was filtered off and the filtrate was concentrated. The solid was dissolved in a minimum amount of distilled water and the solution was passed through a column of Dowex 1-X8, formate form. Water was removed and the residue was recrystallized from absolute ethanol to give 1.66 g (77% yield) of **15**. **15**: Colorless solid; mp 152—155 °C; MS *m/z* 169 (M^+); ^{1}H NMR (DMSO-d_6, 60 MHz) δ=1.8 (q, *J*=7.0 Hz, 2, $NCH_2\underline{CH_2}$), 2.7 (t, *J*=7.0 Hz, 2, $\underline{CH_2}$-NH_3^+), 3.7 (t, *J*=7.0 Hz, 2, NCH_2), 5.6 (d, *J*=8.0 Hz, 1, ArH(5)), 7.7 (d, *J*=8.0 Hz, 1, ArH(6)), 8.4 (s, 1, CHO).

N^6-[3-(Uracil-1-yl)propyl]adenine (7). 6-Chloropurine (0.72 g, 4.6 mmol) and **15** (1.0 g, 4.6 mmol) was dissolved into ethanol (30 ml) containing triethylamine (1.4 ml, 10 mmol) and the solution was refluxed for 40 h under nitrogen atmosphere. After the reaction was over, the mixture was cooled at 0 °C for 2 h and yielded solid was filtered and washed well with cold water. This was dissolved into dil acetic acid (90 ml) with heating. After treatment with active carbon, the solution was neutralized with concd NH_3. Precipitates were filtered, washed with water and then, with acetone, and dried to give crude **7** (1.1 g, 80% as half hydrate). **7**: white solid from methanol-acetic acid, decomp>291 °C; MS *m/z* 287 (M^+); ^{1}H NMR (DMSO-d_6, 100 MHz) δ=1.91 (q, *J*=6.8 Hz, 2, $NCH_2\underline{CH_2}$), 3.54 (br.s, 2, $NH\underline{CH_2}$), 3.75 (t, *J*=6.8 Hz, 2, NCH_2), 5.53 (d, *J*=7.8 Hz, 1, ArH(5′)), 7.61 (br.t, 1, NH(6)), 7.70 (d, *J*=7.8 Hz, 1, ArH(6′)), 8.07 (s, 1, ArH(8)), 8.17 (s, 1, ArH(2)), 11.3 (br.s, 1, NH(3′)), 12.7 (br.s, 1, NH(9)); UV (EtOH) λ_{max} 268 nm ($\varepsilon=26.7\times10^3$). Found: C, 48.68; H, 4.61; N, 32.83%. Calcd for $C_{12}H_{13}N_7O_2\cdot1/2H_2O$: C, 48.64; H, 4.76; N, 33.09%. After heating of the above compound at 180 °C for 30 min, **7** without water of crystallization was obtained. Found: C, 50.22; H, 4.59; N, 33.91%. Calcd for $C_{12}H_{13}N_7O_2$: C, 50.17; H, 4.56; N, 34.13%.

6-[3-(Uracil-1-yl)propylthio]purine (8). A solution of **16**[4] (500 mg, 2.15 mmol) and thiourea (170 mg, 2.23 mmol) in ethanol (20 ml) was refluxed for 8 h. After reaction was over, ethanol was removed under reduced pressure. To the resulted semisolid was added water (15 ml) and nitrogen gas was passed through the apparatus to displace the air. To the heated mixture at 90 °C was added sodium hydroxide (170 mg, 4.3 mmol) and after ten minutes followed by the addition of 6-chloropurine (660 mg, 4.3 mmol) and the mixture was heated for 1 h. After cooling, yielded solid was filtered, washed with water and dried to give 540 mg (84% yield) of **8**. **8**: White powder from methanol-acetic acid; decomp >260 °C. MS *m/z* 304 (M^+). ^{1}H NMR (DMSO-d_6, 100 MHz) δ=2.04 (q, *J*=6.9 Hz, 2, $SCH_2\underline{CH_2}$), 3.35 (t, *J*=6.9 Hz, 2, SCH_2), 3.81 (t, *J*=6.9 Hz, 2, NCH_2), 5.56 (d, *J*=7.8 Hz,1, H5′), 7.67 (d, *J*=7.8 Hz, 1, H6′), 8.42 (s, 1, H8), 8.64 (s, 1, H2), 11.2 (br. s, 1, U-NH), 12.4 (br.s, 1, Pu-NH).

Found: C, 47.47; H, 4.05; N, 27.53; S, 10.42%. Calcd for $C_{12}H_{12}N_6SO_2$: C, 47.36; H, 3.98; N, 27.61; S, 10.53%.

6-[3-(Thymin-1-yl)propylthio]purine (9). Compound **9** was prepared starting from 1-(3-bromopropyl) thymine[3] by the similar procedure described for **8**. **9**: 89% yield; colorless fine needles from DMF-water; mp 279.0—282.5 °C with decomp. MS *m/z* 318 (M^+). ^{1}H NMR (DMSO-d_6, 360 MHz) δ=1.74 (d, *J*=1.0 Hz, 3, CH_3), 2.04 (q, *J*=7.0 Hz, 2, $SCH_2\underline{CH_2}$), 3.35 (t, *J*=6.8 Hz, 2, SCH_2), 3.78 (t, *J*=6.8 Hz, 2, Th-NCH_2), 7.53 (s, 1, H6′), 8.41 (s, 1, H8), 8.64 (s, 1, H2), 11.19 (br. s, 1, Th-NH).

Found: C, 49.09; H, 4.50; N, 26.18; S, 10.31%. Calcd for $C_{13}H_{14}N_6SO_2$: C, 49.05; H, 4.43; N, 26.40; S, 10.07%.

1-(3-Bromopropyl)-5-methoxyuracil (18). To a solution of 5-methoxyuracil[17] (7.1 g, 50 mmol) and trimethylsilyl chloride (10.9 g, 100 mmol) in dry benzene (150 ml) was added dropwise triethylamine (10.1 g, 100 mmol) and white suspension was stirred for 18 h. After filtration under atmosphere of dry nitrogen, the filtrate was concentrated under reduced pressure. To the resulted oil was added 1,3-dibromopropane (70 ml) and it was stand for a week at room temperature under nitrogen atmosphere. Water (200 ml) was added to the solution and it was extracted with chloroform. Organic phase was washed with water and dried over anhydrous sodiumsulfate. Evaporation of the solvent under reduced pressure gave yellow solid. Recrystallization from ethanol yielded **18** (3.5 g, 27% yield) as colorless columns; mp 130—131 °C. MS *m/z* 262 (M^+ for ^{79}Br). ^{1}H NMR ($CDCl_3$, 360 MHz) δ=2.34 (m, 2, $NCH_2\underline{CH_2}$), 3.47 (t, *J*=6.1 Hz, 2, CH_2Br), 3.76 (s, 3, OCH_3), 3.90 (t, *J*=6.6 Hz, 2, N-CH_2), 6.82

(s, 1, ArH), 9.61 (br, s, 1, NH).

Found: C, 36.52; H, 4.37; Br, 29.51; N, 9.95%. Calcd for $C_8H_{11}BrN_2O_3$: C, 36.52; H, 4.22; Br, 30.37; N, 10.65%.

6-[3-(5-Methoxyuracil-1-yl)propylthio]purine (10). Compound **11** was prepared in a yield of 75% by the similar procedure described for **8**. **10**: Colorless fine needles from water; decomp>190°C. MS *m/z* 334 (M^+). ^{1}H NMR (DMSO-d_6, 360 MHz) δ=2.06 (q, J=7.0 Hz, 2, $SCH_2\underline{CH_2}$), 3.36 (t, J=7.0 Hz, 2, SCH_2), 3.60 (s, 3, CH_3), 3.78 (t, J=6.9 Hz, 2, NCH_2), 7.36 (s, 1, H6'), 8.41 (br.s, 1, H8), 8.63 (s, 1, H2), 11.36 (br. s, 1, NH).

Found: C, 45.24; H, 4.21; N, 24.23; S, 9.57%. Calcd for $C_{13}H_{14}N_6O_3S \cdot 1/2\ H_2O$: C, 45.48; H, 4.40; N, 24.48; S, 9.34%.

1-(3-Bromopropyl)-5-nitrouracil (19). A mixture of 5-nitrouracil[18] (4.71 g, 30 mmol), 1,3-dibromopropane (60.0 g, 100 mmol), and anhydrous potassium carbonate (2.07 g, 15 mmol) in dry DMSO (70 ml) was stirred at room temperature for 1.5 d. The solvent was distilled off under reduced pressure. Water (200 ml) was added to the residue and it was extracted with chloroform and the extracts were dried over anhydrous sodium sulfate. The solution was concentrated under reduced pressure until about 100 ml of the solvent was left. Yielded precipitates of **19** was collected (2.67 g, 32% yield). Recrystallization from 2-propanol gave pure **19** as colorless prisms; mp 172—174 °C. MS *m/z* 277 (M^+ for ^{79}Br). ^{1}H NMR ($CDCl_3$, 360 MHz) δ=2.37 (m, 2, $NCH_2\underline{CH_2}$), 3.47 (t, J=6.0 Hz, 2, CH_2Br), 4.11 (t, J=6.8 Hz, 2, NCH_2), 8.79 (s, 1, ArH).

Found: C, 30.82; H, 3.16; N, 15.48%. Calcd for $C_7H_8BrN_3O_4$: C, 30.23; H, 2.90; N, 15.11%.

6-[3-(5-Nitrouracil-1-yl)propylthio]purine (11). A solution of **19** (1.39 g, 5 mmol), 6-mercaptopurine (0.84 g, 4.9 mmol), and sodium hydroxide (0.6 g, 15 mmol) in water (20 ml) was stirred for 3.5 h at room temperature. The solution was neutralized by dil HCl and then, few drops of ethanol were added. Yielded pale yellow solid was filtered, washed with water, and dried to give 1.51 g (87% yield) of **11**. **11**: Pale yellow powder from water; mp 270—271 °C with decomp. ^{1}H NMR (DMSO-d_6, 360 MHz) δ=2.13 (q, J=7.1 Hz, 2, $NCH_2\underline{CH_2}$), 3.37 (t, J=6.7 Hz, 2, SCH_2), 4.01 (t, J=6.7 Hz, 2, NCH_2), 8.41 (s, 1, H8), 8.63 (s, 1, H2), 9.31 (s, 1, H6'), 11.99 (br. s, 1, NH).

Found: C, 41.40; H, 3.36%. Calcd for $C_{12}H_{11}N_7O_4S$: C, 41.26; H, 3.17%.

3-(3-Bromopropyl)-*S*-methyl-2-thiouracil (21). To a stirred solution of **20**[19] (5.68 g, 40 mmol) in dry DMF (100 ml) was added 60% sodium hydride (1.68 g, 42 mmol). After stirring for 1 h, 1,3-dibromopropane (40 ml, 400 mmol) was added to the mixture and it was stirred for 1 h at room temperature and then, at 60 °C for 24 h. The solvent was removed under reduced pressure. The residue was purified by column chromatography on silica gel with chloroform to give **21** (8.67 g, 82% yield). **21**: Colorless prisms from methanol; mp 50.0—50.5 °C. MS *m/z* 263 (M^+ for ^{79}Br). ^{1}H NMR ($CDCl_3$, 100 MHz) δ=2.30 (m, 2, $NCH_2\underline{CH_2}$), 2.58 (s, 3, CH_3), 3.48 (t, J=6.6 Hz, 2, CH_2Br), 4.19 (m, 2, NCH_2), 6.18 (d, J=6.5 Hz, 1, ArH(5)), 7.75 (d, J=6.5 Hz, 1, ArH(6)).

Found: C, 36.57; H, 3.95; N, 10.75; S, 12.32%. Calcd for $C_8H_{11}N_2OSBr$: C, 36.51; H, 4.22; N, 10.65; S, 12.18%.

6-[3-(*S*-Methyl-2-thiouracil-3-yl)propylthio]purine (22). A solution of **21** (4.18 g, 15.9 mmol), 6-mercaptopurine monohydrate (2.70 g, 15.9 mmol), and sodium hydroxide (0.83 g, 20.8 mmol) in water (40 ml)-ethanol (10 ml) was stirred for 3 h at room temperature. The solution was neutralized by dil HCl and it was extracted by chloroform. The organic layer was dried over anhydrous sodium sulfate and concentrated. Crude product was purified by column chromatography on silica gel with chloroform-methanol (19:1) to give white solid (3.9 g, 73% yield). **22**: Colorless needles from methanol; mp 182.0—183.5 °C. MS *m/z* 334 (M^+). ^{1}H NMR ($CDCl_3$, 100 MHz) δ=2.29 (m, 2, $NCH_2\underline{CH_2}$), 2.54 (s, 3, CH_3), 3.50 (t, J=7.2 Hz, 2, SCH_2), 4.27 (m, 2, NCH_2), 6.23 (d, J=6.3 Hz, 1, H5'), 7.76 (d, J=6.6 Hz, 1, H6'), 8.21 (s, 1, H8), 8.71 (s, 1, H2).

Found: C, 46.83; H, 4.27; N, 25.31; S, 18.88%. Calcd for $C_{13}H_{14}N_6OS_2$: C, 46.69; H, 4.22; N, 25.13; S, 19.17%.

6-[3-(Uracil-3-yl)propylthio]purine (12). A solution of **22** (1.67 g, 5 mmol) in ethanol (20 ml)-2 M HCl (10 ml) was stirred for 2 d at room temperature. Yielded precipitates were filtered, washed with water, and dried to give 1.36 g (89% yield) of crude **12**. **12**: Colorless fine needles from water; mp 293—298 °C with decomp. MS *m/z* 304 (M^+). ^{1}H NMR (DMSO-d_6, 360 MHz) δ=1.97 (q, J=7.0 Hz, 2, $NCH_2\underline{CH_2}$), 3.34 (t, J=7.0 Hz, 2, SCH_2), 3.91 (t, J=7.0 Hz, 2, NCH_2), 5.58 (dd, J=1.4 Hz, 7.6 Hz, 1, H5'), 7.42 (m, 1, H6'), 8.39 (s, 1, H8), 8.63 (s, 1, H2), 10.21 (br. s, 1, NH(9)), 11.07 (br. d, 1, NH(1')).

Found: C, 47.39; H, 4.23; N, 27.90; S, 10.74%. Calcd for $C_{12}H_{12}N_6O_2S$: C, 47.36; H, 3.98; N, 27.61; S, 10.53%.

5-(3-Hydroxypropyl)-3-methyluracil (25). A mixture of 5-(3-hydroxypropyl)-2-thiouracil **23**[20] (14.88 g, 80 mmol), methyl iodide (25 ml, 400 mmol), and anhydrous potassium carbonate (24.29 g, 176 mmol) in dry DMF (50 ml) was stirred for 20 h at room temperature. Salts were filtered off and the filtrate was concentrated to dryness under reduced pressure. Water (100 ml) was added to the residue and it was extracted with chloroform. The organic phase was washed well with water and dried over anhydrous sodium sulfate. Evaporation of the solvent gave pale yellow solid of **24**. To the solid was added 20 ml of 1 M HCl and the mixture was refluxed for 1 h. After cooling, the solution was neutralized by sodium hydrogencarbonate and was concentrated to dryness. Yielded solid was extracted with chloroform. The extracts were dried and evaporated. The crude product was purified by column chromatography on silica gel with chloroform-methanol (19:1) to yield 9.3 g (63% yield) of **25**. Recrystallization from ethanol gave pure **25** as colorless prisms; mp 124—126 °C. MS *m/z* 184 (M^+). ^{1}H NMR ($CDCl_3$, 100 MHz) δ=1.76 (m, 2, $ArCH_2\underline{CH_2}$), 2.28 (t, J=6.0 Hz, 1, OH), 2.48 (t, J=7.1 Hz, 2, $ArCH_2$), 3.35 (s, 3, CH_2), 3.36 (q, J=5.9 Hz, 6.0 Hz, 2, $\underline{CH_2}OH$), 7.07 (d, J=5.6 Hz, 1, ArH), 9.22 (br. s, 1, NH).

Found: C, 51.95; H, 6.49; N, 15.23%. Calcd for $C_8H_{12}N_2O_3$: C, 52.16; H, 6.57; N, 15.21%.

5-(3-Bromopropyl)-3-methyluracil (26). A solution of **24** (1.84 g, 10 mmol) in concd hydrobromic acid (15 ml) and concd sulfuric acid (2 ml) was heated at 110 °C for 3 h with stirring. After cooling, the mixture was poured into cold water and it was extracted with chloroform. The organic layer was washed well with aqueous solution of sodium hydrogencarbonate and dried over anhydrous sodium sulfate. Evaporation of the solvent gave 1.54 g (62% yield) of **26**. **26**: Colorless columns from ethanol; mp 152.5—153.5°C. MS *m/z* 246 (M^+ for ^{79}Br). ^{1}H NMR ($CDCl_3$, 360 MHz) δ=2.12 (m, 2, $ArCH_2\underline{CH_2}$), 2.50 (t, J=7.1 Hz, 2, $ArCH_2$), 3.34 (s, 3, CH_3), 3.34 (t, J=6.3 Hz, 2, CH_2Br), 7.14 (d, J=5.7 Hz, 1, ArH), 9.64 (br, s, 1, NH).

Found: C, 38.74; H, 4.50; N, 11.25; Br, 32.07%. Calcd for

$C_8H_{11}N_2O_2Br$: C, 38.88; H, 4.49; N, 11.34; Br, 32.34%.

6-[3-(3-Methyluracil-5-yl)propylthio]purine(13). A solution of **26** (0.99 g, 4 mmol), thiourea (0.32 g, 4.2 mmol) in ethanol (10 ml) was refluxed for 8 h. After removal of ethanol, water (20 ml) was added to the residue. To the stirred mixture was added, at 90 °C under nitrogen atmosphere, sodium hydroxide (40 g, 10 mmol) and then (after 10 min), 6-chloropurine (1.24 g, 8 mmol). Heating and stirring were continued for 1 h. After cooling, yielded precipitates were collected to give 0.95 g (75% yield) of **13**. **13**: Colorless powder from water; mp 283—286 °C. MS m/z 318 (M^+). ^{1}H NMR (DMSO-d_6, 360 MHz) δ=1.89 (q, J=7.1 Hz, 2, $NCH_2\underline{CH_2}$), 2.39 (t, J=6.3 Hz, 2, $ArCH_2$), 3.33 (t, J=6.3 Hz, 2, SCH_2), 7.33 (d, J=5.8 Hz, 1, ArH(6')), 8.40 (s, 1, ArH(8)), 8.66 (s, 1, ArH(2)), 10.93 (d, J=5.8 Hz, 1, NH).

Found: C, 48.78; H, 4.61; N, 26.40; S, 10.32%. Calcd for $C_{13}H_{14}N_6O_2S$: C, 49.05; H, 4.43; N, 26.40; S, 10.07%.

General Procedure of Method A for the Synthesis of 1—6. To a suspension of **8—13** (3 mmol) in dry DMF (100 ml) was added 60% sodium hydride (259 mg, 6.25 mmol). After continuous stirring for 1 h at room temperature, the mixture became transparent solution. The solution was diluted with dry DMF until the total volume became 150 ml. The solution and a solution of 1,3-dibromopropane (0.305 ml, 3 mmol) in dry DMF (150 ml) were added simultaneously to dry DMF (300 ml) at room temperature in a period of 36—48 h (see Table 6) under nitrogen atmosphere. After addition was over, stirring was continued for 25—60 h (see Table 6). DMF was removed under reduced pressure and the residue was extracted with chloroform. The isomers having the bridge at 9-position of a purine ring (**1**, **3**, **5**) could be separated from the other isomers (**2**, **4**, **6**) by column chromatography on silica gel with chloroform-methanol (ratio: see Table 6).

General Procedure of Method B. To a stirred mixture of dry DMSO (400 ml) and potassium carbonate (0.9 g, 6.6 mmol) was added a solution of **7** or **8** (1 mmol) and 1,3-dibromopropane (1 mmol) in a period of 15 h at room temperature under nitrogen atmosphere. After addition was over, stirring was continued for 3 d. Salts were filtered off and the solvent was removed under reduced pressure. Crude product was separated into two isomers by column chromatography on silica gel with methanol-chloroform. Spectral and analytical data of **1c**, **1d**, **2c**, and **2d** are shown in Table 6.

2a: Colorless needles from water; decomp>300 °C. MS m/z 327 (M^+). ^{1}H NMR ($CDCl_3$, 100 MHz) δ=5.64 (d, J=8 Hz, 1, H5'), 7.11 (d,J=8 Hz, 1, H6'), 7.87 (s, 1, H8), 8.47 (s, 1, H2).

Found: C, 53.90; H, 5.46; N, 28.97%. Calcd for $C_{15}H_{17}N_7O_2 \cdot 1/2H_2O$: C, 53.57; H, 5.39; N, 29.15%.

1b: White powder from ethanol; decomp>320 °C. MS m/z 341 (M^+). ^{1}H NMR ($CDCl_3$, 100 MHz) δ=5.70 (d, J=7.8 Hz, 1, H5'), 7.11 (d, J=7.8 Hz, 1, H6'), 7.62 (s, 1, H8), 8.29 (s, 1, H2).

Found: C, 56.33; H, 5.60; N, 28.55%. Calcd for $C_{16}H_{19}N_7O_2$: C, 56.30; H, 5.61; N, 28.72%.

2b: Colorless crystals from methanol-ether; mp 207—209 °C. MS m/z 341 (M^+). ^{1}H NMR ($CDCl_3$, 100 MHz) δ=5.81 (d, J=7.8 Hz, 1, H5'), 7.21 (d, J=7.8 Hz, 1, H6'), 7.85 (s, 1, H8), 8.48 (s, 1, H2).

Found: C, 55.52; H, 5.80; N, 27.42%. Calcd for $C_{16}H_{19}N_7O_2 \cdot 1/2CH_3OH$: C, 55.45; H, 5.92; N, 27.43%.

9-Methyl-N^6[3-(3-methyluracil-1-yl)propyl]adenine (32). A mixture of **7** · $1/2H_2O$ (200 mg, 0.68 mmol), methyl iodide (0.21 g, 1.5 mmol) and potassium carbonate (0.28 g, 2.0 mmol) in dry DMSO (30 ml) was stirred for 24 h at room temperature under nitrogen atmosphere. After reaction was over, salts were filtered off and the filtrate was concentrated

Table 6. Reaction Conditions, Elution Solvents, Yields, Crystal Forms, Melting Points and Analytical Data of Pyrimidinopurinophanes

	Reaction condition	Elution solvent	Yield/%	Crystal		Analysis or MS Found/% (Calcd)			
	Dropping time(h)/ Reaction time(h)	$CHCl_3$: CH_3OH		Form	Mp θ_m/°C	C	H	N	S
1c	30/48	25 : 1	6	Needle	278—280	52.41	4.56	24.60	9.26
2c			14	Column	Decomp>322	52.04	4.75	24.54	9.16
						(52.31)	(4.68)	(24.40)	(9.31)
1d	30/48	25 : 1	19	Column	Decomp>275	53.64	5.02	23.16	9.16
2d			21	Column	281—283	53.88	5.10	23.15	8.90
						(53.62)	(5.06)	(23.45)	(8.94)
1e	36/60	99 : 1	9.6	Prism	Decomp>270	53.51	5.12	23.44	8.94
2e			28	Prism	>320	53.41	4.79	23.17	9.13
						(53.62)	(5.06)	(23.45)	(8.94)
1f	48/48	33 : 1	12	Needle	227—229	51.01	4.67	21.98	8.64
						(51.33)	(4.84)	(22.45)	(8.56)
2f			34	Plate	293—294	50.18	5.42	20.62	7.94
						(50.23)[a]	(5.46)[a]	(20.68)[a]	(7.89)[a]
1g	44/25	19 : 1	11	Powder	>300	46.21	3.92	24.96	8.09
2g			11	Powder	>300	46.01	4.02	25.28	8.44
						(46.27)	(3.88)	(25.18)	(8.23)
3	38/58	19 : 1	13	Powder	295—298	52.16	4.59	24.19	9.20
4			25	Prism	296—298		344 (M^+)		
						(52.31)	(4.68)	(24.40)	(9.31)
5	36/60	33 : 1	16	Prism	237—238	53.48	5.22	23.27	8.84
6			40	Powder	300—305	53.39	5.14	23.49	8.75
						(53.62)	(5.06)	(23.45)	(8.94)

a) For $C_{16}H_{18}O_3N_6S \cdot CH_3OH$.

to dryness under reduced pressure. Water (50 ml) was added to the residue and it was extracted with chloroform. The extracts were washed with water, dried over anhydrous sodium sulfate, and concentrated. The crude product was chromatographed on silica gel with methanol-chloroform and then, recrystallized from benzene-hexane to give pure **32** (88 mg, 41% yield). **32:** Colorless fine needles, mp 187.5—189.0 °C; MS *m/z* 315 (M^+). ^{1}H NMR ($CDCl_3$, 100 MHz) δ=2.10 (q, *J*=6.6 Hz, 2, $NCH_2\underline{CH_2}$), 3.35 (s, 3, N(3′)-CH_3), 3.76 (m, 2, N(6)-CH_2), 3.83 (s, 3, N(9)-CH_3), 3.91 (t, *J*=6.6 Hz, 2, N(1′)-CH_2), 5.71 (d, *J*=7.9 Hz, 1, ArH(5′)), 6.27 (br s, 1, NH), 7.20 (d, *J*=7.9 Hz, 1, ArH(6′)), 7.73 (s, 1, ArH(8)), 8.38 (s, 1, ArH(2)); UV (EtOH) λ_{max} 268 nm (ε=24.3×10^3); IR (Nujol mull) 3270 cm^{-1} (NH). Found: C, 53.06; H, 5.37; N, 31.02%. Calcd for $C_{14}H_{17}N_7O_2$: C, 53.32; H, 5.44; N, 31.09%.

9-Methyl-6-[3-(3-methyluracil-1-yl)propylthio]purine (33). The synthesis of **33** was carried out by the similar method described for **32**. Recrystallization of the crude product from benzene-hexane gave pure **33** in a yield of 34%. **33:** Colorless needles, mp 144—146 °C; MS *m/z* 332 (M^+); ^{1}H NMR ($CDCl_3$, 100 MHz) δ=2.24 (q, *J*=6.8 Hz, 2, $NCH_2\underline{CH_2}$), 3.34 (s, 3, N(9)-CH_3), 3.45 (t, *J*=6.8 Hz, 2, SCH_2), 3.89 (s, 3, N(3′)-CH_3), 3.94 (t, *J*=6.8 Hz, 2, NCH_2), 5.72 (d, *J*=7.8 Hz, 1, ArH(5′)), 7.19 (d, *J*=7.8 Hz, 1, ArH(6′)), 7.95 (s, 1, ArH(8)), 8.70 (s, 1, ArH(2)); UV (EtOH) λ_{max} 276 nm (ε=19.1×10^3), 282 (21.5×10^3), 290 (17.8×10^5). Found: C, 50.64: H, 4.81; N, 25.25; S, 9.64%. Calcd for $C_{14}H_{16}N_6SO_2$: C, 50.59; H, 4.85; N, 25.28; S, 9.65%.

This work was supported by Grants-in-Aid (Nos. 56470018 and 59470018) from the Ministry of Education, Science and Culture, to Yoshiteru Sakata.

References

1) Preliminary reports: K. Doyama, F. Hama, Y. Sakata, and S. Misumi, *Tetrahedron Lett.*, **22**, 4101 (1981); K. Doyama, F. Hama, Y. Sakata, and S. Misumi, *Tetrahedron Lett.*, **24**, 5253 (1983); T. Higashii, Y. Sakata, and S. Misumi, *Nucleic Acids Res. Symp. Ser.*, **16**, 125 (1985).

2) A general reference for hypochromism: C. R. Cantor and P. R. Schimmel, "Biophysical Chemistry," Part II "Techniques for the Study of Biological Structure and Function," W. H. Freeman and Co., San Francisco (1980), p. 399.

3) F. Seyama, K. Akahori, Y. Sakata, S. Misumi, M. Aida, and C. Nagata, *J. Am. Chem. Soc.*, **110**, 2192 (1988).

4) D. T. Browne, J. Eisinger, and N. J. Leonard, *J. Am. Chem. Soc.*, **90**, 7302 (1968).

5) R. N. Prasad and R. K. Robins, *J. Am. Chem. Soc.*, **79**, 6401 (1957).

6) E. Fischer, *Chem. Ber.*, **31**, 431 (1898).

7) D. Davidson and O. Baudisch, *J. Am. Chem. Soc.*, **48**, 2379 (1926).

8) A. W. Hanson, *Acta Crystallogr., Sect. B*, **27**, 197 (1971).

9) D. T. Hefelfinger and D. J. Cram, *J. Am. Chem. Soc.*, **93**, 4767 (1971).

10) The difference in absorption maxima in 6-dimethylamino-7- and -9-alkylpurines was originally observed by Baker et al.: B. R. Baker, R. E. Schaub, and J. P. Joseph, *J. Org. Chem.*, **19**, 638 (1954).

11) F. Seyama, Y. Sakata, N. Kasai, and S. Misumi, to be published.

12) P. Main, S. E. Hull, L. Lessinjer, G. Germained, J. P. Declercq, and M. M. Woolfson, MULTAN-78, University of York (1975).

13) W. J. Cook and C. E. Bugg, *J. Pharm. Sci.*, **64**, 221 (1975).

14) A. Banerjee, J. K. Dattagupta, W. Saenger, and A. Rabczenko, *Acta Crystallogr., Sect. B*, **33**, 90 (1977).

15) N. S. Kondo, H. M. Holmes, L. M. Stempel, and P. O. P. Ts'o, *Biochemistry*, **9**, 3479 (1970).

16) W. A. Summers, J. Y. Lee, and J. G. Burr, *J. Org. Chem.*, **40**, 1559 (1975).

17) J. H. Chesterfield, J. F. W. McOmie, and M. S. Tute, *J. Chem. Soc.*, **1960**, 4590.

18) T. B. Johnson and I. Matsuo, *J. Am. Chem. Soc.*, **41**, 782 (1919).

19) T. Matsukawa and B. Ohta, *J. Pharm. Soc. Jpn.*, **69**, 491 (1949).

20) N. J. Leonard and R. L. Cundall, *J. Am. Chem. Soc.*, **96**, 5904 (1974).

 © 1988 The Chemical Society of Japan Bull. Chem. Soc. Jpn., 61, 3629—3635 (1988)

On the Mechanism of Reductive Cleavage of the Carbon-Nitrogen Bond of Aliphatic Nitro Compounds with Tributyltin Hydride[1)]

Akio KAMIMURA* and Noboru ONO*,†

Department of Chemistry, Faculty of Liberal Arts, Yamaguchi University, Yamaguchi 753
†Department of Chemistry, Faculty of Science, Kyoto University, Kyoto 606

(Received June 1, 1988)

Denitrohydrogenation reaction of aliphatic nitro compounds with tributyltin hydride (Bu_3SnH) is accelerated in the presence of radical initiators. ESR and electrochemical measurements reveal that the reductive cleavage of the carbon-nitrogen bond proceeds not via anion radicals of nitro compounds such as $S_{RN}1$ reaction but via β-scission of (tributylstannyloxy)nitroxyl radicals. The relative reactivities of tin radicals toward substituted α-nitrocumenes, α-nitroethylbenzenes, and α-nitropropiophenones exhibits excellent Hammett correlations with positive ρ values. This tendency has also been found in the reaction of benzyl halides with tin radical. These results suggest that the carbon-nitrogen bond breaking from nitroxyl radical intermediates should take place in rate-determining step for the reaction.

Recently we and Tanner have reported that aliphatic nitro groups are readily replaced by hydrogen in good yield on treatment with tributyltin hydride (Bu_3SnH) in the presence of radical initiators.[2,3)] As Bu_3SnH can replace the nitro group by hydrogen without affecting other reducible groups such as carbonyl, alkoxycarbonyl, formyl, cyano, sulfinyl, or sulfonyl groups, this reaction has been widely used in organic synthesis.[4)] Mechanism of the reductive cleavage of the carbon-nitrogen bond with tin radicals has been of interest for recent years because of high chemoselectivity of the reaction. An electron-transfer mechanism is postulated from the analogy to $S_{RN}1$ reaction of nitro compounds.[2,3)] Namely, Tanner and co-workers have proposed that the reaction proceeds via mechanism A (see below) without concrete evidences, where anion radicals of nitro compounds are assumed as intermediates of the reaction.[5)] We have proposed two possible mechanism, mechanism A and B as shown in Scheme 1.[2)] The difference between mechanism A and B is that alkyl radicals are formed from anion radicals of nitro compounds in mechanism A, whereas alkyl radicals are formed from (tributylstannyloxy)nitroxyl radicals in mechanism B.

Mechanism A

$$\mathrm{R\text{-}NO_2 + Bu_3Sn\cdot \longrightarrow R\text{-}NO_2^{\cdot-} + Bu_3Sn^+}$$
$$\mathrm{R\text{-}NO_2^{\cdot-} \longrightarrow R\cdot + NO_2^-}$$
$$\mathrm{R\cdot + Bu_3SnH \longrightarrow R\text{-}H + Bu_3Sn\cdot}$$

Mechanism B

$$\mathrm{R\text{-}NO_2 + Bu_3Sn\cdot \longrightarrow R\text{-}N(O\cdot)O\text{-}SnBu_3}$$
$$\mathrm{R\text{-}N(O\cdot)O\text{-}SnBu_3 \longrightarrow R\cdot + Bu_3SnONO}$$
$$\mathrm{R\cdot + Bu_3SnH \longrightarrow R\text{-}H + Bu_3Sn\cdot}$$

Scheme 1.

The mechanism A is proposed based on following two facts.[3)] The reaction is catalyzed by radical initiators such as azobisisobutyronitrile (AIBN) and inhibited by the presence of a catalytic amount of *m*-dinitrobenzene (*m*-DNB). However, these evidences cannot exclude the mechanism B, for all radical reactions induced by tin radicals are catalyzed by AIBN and inhibited by *m*-DNB. For example, the reduction of alkyl bromides with tributyltin hydride, the typical radical reaction induced by tin radicals is inhibited by the presence of *m*-DNB. This reaction proceeds via S_H process and it is not certain whether electron-transfer mechanism is operated or not in the reduction of alkyl bromides with tributyltin radicals. Thus, there have been no concrete evidences for the reaction mechanism of denitration with tributyltin hydride.

Recently, Giese and co-workers also have shown that this reaction undergoes via mechanism B through their ESR and kinetic studies.[6)] Independently, we have reached the same conclusion and found that the (tributylstannyloxy)nitroxyl radicals undergo the different reaction from that of the anion radicals of nitro compounds. In this paper, we report that this reaction proceeds via nitroxyl radical intermediates and that kinetic studies support the carbon-nitrogen bond breaking from nitroxyl radical intermediates takes place in the transition state for the reaction.

Results and Discussion

The replacement of tertiary nitro groups by hydrogen with CH_3SNa[7)] or 1-benzyl-1,4-dihydronicotinamide (BNAH)[8)] involves anion radical intermediates. This mechanism has been well-established (Scheme 2). Collapse of anion radical of nitro compounds into a alkyl radical and nitrite ion is fundamental process of $S_{RN}1$ reaction of nitro compounds.[9)]

$$\mathrm{R\text{-}NO_2 + BNAH \longrightarrow R\text{-}NO_2^{\cdot-} + BNAH^{\ddagger}}$$
$$\mathrm{R\text{-}NO_2^{\cdot-} \longrightarrow R\cdot + NO_2^-}$$
$$\mathrm{R\cdot + BNAH \longrightarrow R\text{-}H + BNA\cdot}$$
$$\mathrm{BNA\cdot + R\text{-}NO_2 \longrightarrow R\text{-}NO_2^{\cdot-} + BNA^+}$$

Scheme 2.

On the other hand, the reaction of α-nitro sulfone **1** with BNAH gives 2-nitropropane, where the carbon-sulfur bond was cleaved in preference to the carbon-nitrogen bond (Eq. 1).[10)]

$$\underset{\mathbf{1}}{Me_2C(NO_2)SO_2Ph} + BNAH \longrightarrow Me_2CHNO_2 \quad (1)$$

Thus, the anion radicals of α-nitro sulfones collapsed to the α-nitroalkyl radicals and sulfinate ions (Eq. 2).

$$\mathbf{1}^{\cdot-} \longrightarrow Me_2\dot{C}NO_2 + PhSO_2^- \quad (2)$$

However, α-nitro sulfones do not react with tributyltin hydride under the conditions that the nitro groups of other nitro compounds are replaced by hydrogen. Namely, heating a mixture of **1**, Bu_3SnH (2 equiv), and AIBN (0.3 equiv) in toluene at 110 °C for 3 h resulted in clean recovery of **1** (Eq. 3).[11]

$$\mathbf{1} + Bu_3SnH \longrightarrow \text{No reaction} \quad (3)$$

In general, Bu_3SnH is much more reactive to nitro compounds for denitration than BNAH.[4] The low reactivity of **1** toward tin radicals suggest that the anion radicals are not intermediates for the reaction of nitro compounds with tin radicals. If the nitroxyl radicals **X** are intermediates, the above results are explained. The cleavage of carbon-sulfur bond is impossible from **X**, being easy from the corresponding anion radicals. And also the cleavage of carbon-sulfur bond is inhibited due to destabilization of radicals by the adjacent sulfonyl groups (Eq. 4).[12]

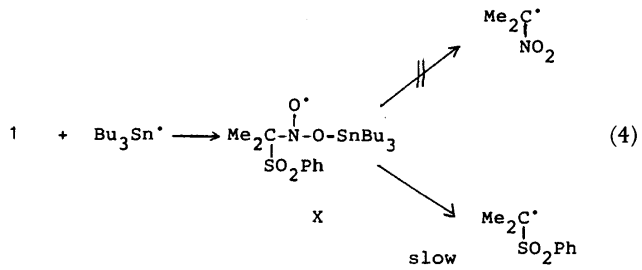

(4)

The reaction of α,*p*-dinitrocumene **2a** is also a good diagnosis for an electron-transfer process. This compounds react with various nucleophiles via electron-transfer processes and it is generally more reactive than other nitro compounds for $S_{RN}1$ reaction.[9] For example, **2a** react with various nucleophiles quite rapidly to give the substitution products in good yield, but α-nitrocumene **2b** does not undergo the $S_{RN}1$ reaction with most nucleophiles. *p*-Nitro group is essential for a smooth $S_{RN}1$ reaction.[9] However, **2a** was inert to Bu_3SnH for denitration, and the nitro group of **2b** is readily replaced by hydrogen on treatment with Bu_3SnH. Thus, these results show that the reaction of nitro compounds with Bu_3SnH proceeds via the completely different pathway from that of $S_{RN}1$ reaction. It is well-established that the $S_{RN}1$ reaction of nitro compounds proceeds via an electron-transfer process as shown in Scheme 3. Intramolecular electron transfer takes place in $S_{RN}1$ reaction.[13] The reaction of **2a** with tin radicals does not give $\mathbf{2a}^{\cdot-}$, for if anion radical is formed alkyl radical should be formed in the similar pathway as in Scheme 3. Tin radicals may attack the aromatic nitro group to give the nitroxyl radical, which is stable and does not collapse to alkyl radical. In fact, ESR measurements of the reaction mixture of **2a**, Bu_3SnH, and AIBN gave the spectra of the nitroxyl radical as shown in Fig. 1. It was reported that the similar ESR spectra was obtained by photolysis of hexamethyldistannane in the presence of aromatic nitro compounds (Eq. 5).[14] As the nitroxyl radicals

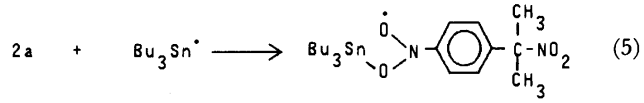

(5)

derived from aromatic nitro compounds are more stable than those derived from aliphatic ones, denitration does not proceeds from this intermediate. If observed spectra is from an anion radical, the α-nitro group should be eliminated very quickly. Consequently, aromatic nitro compounds act as excellent inhibitors for radical reduction with tin radicals. Although inhibition by *m*-DNB has been used as the diagnosis of an electron-transfer process from tin radicals in several cases,[3] it cannot be used as the diagnosis of an electron-transfer process as discussed here.

ESR measurements of the reaction mixture of various nitro compounds **3**—**7** and Bu_3SnH in benzene were carried out under the same reaction conditions as in denitration of nitro compounds in preparative works. When nitro compounds were mixed with

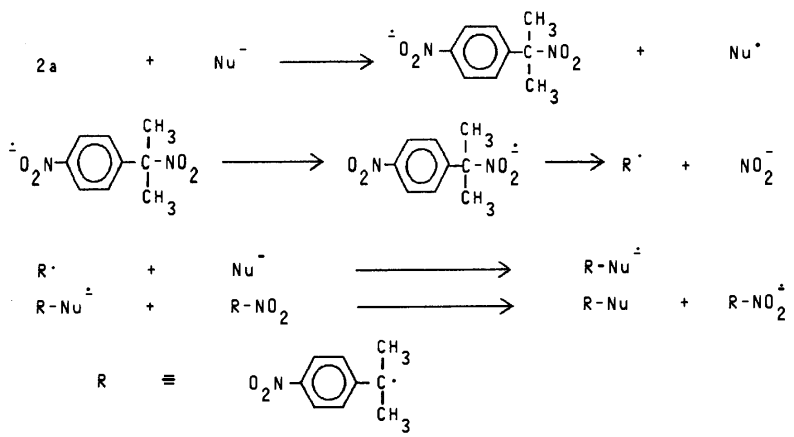

Scheme 3.

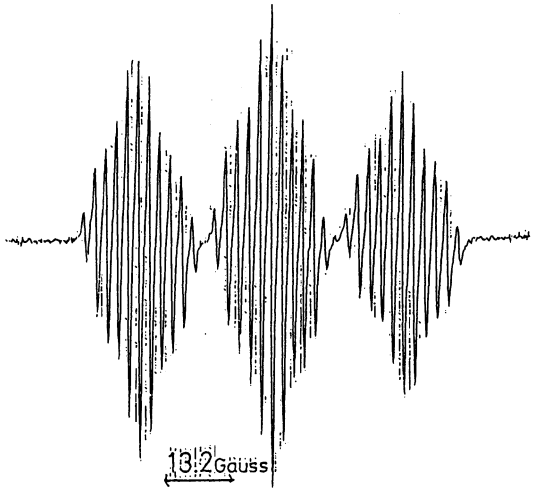

Fig. 1. ESR spectra of a solution of **2a**, Bu_3SnH, and AIBN in benzene at 65 °C.

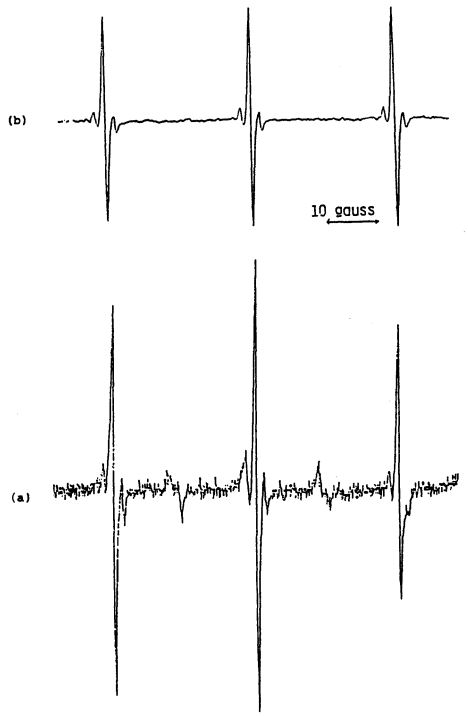

Fig. 2. ESR spectra (a): Solution of **7** and Bu_3SnH in benzene under irradiation with high pressure mercury lamp. (b): Solution of **3**, Bu_3SnH, and AIBN in benzene at 65 °C.

Bu_3SnH and AIBN in benzene and they were irradiated with UV light or heated at 65 °C, strong triplet or sextet [a(N)=27—28 G, a(H)=4—5 G (1G=10^{-4}T)] was detected. Typical spectra are shown in Fig. 2 and the ESR parameters are summarized in Table 1.

Me_3CNO_2 **3** Me_2CHNO_2 **4** $PhCH(Me)NO_2$ **5**

$Ph(C{=}O)CH(Me)NO_2$ **6** $Ph(C{=}O)CMe_2NO_2$ **7**

The ESR spectra also can be interpreted in terms of the formation of (tributylstannyloxy)nitroxyl radical as well as nitro anion radicals. Recently, Giese and his co-workers reported the similar ESR spectra by the reaction of several nitro compounds with Bu_3SnH.[6] They concluded that they were (tributylstannyloxy)-nitroxyl radicals. A weak coupling of tin isotope (^{119}Sn and ^{117}Sn) was detected in ESR spectra as shown in Fig. 2, where a triplet was surrounded by a weak doublet. This suggests that the tin radical adds to the nitro group to form tin-oxygen covalent bond. The ESR parameters obtained here are very close to those of anion radicals of nitro compounds. Considering these facts and low reactivity of **1** and **2a** for denitration, the observed spectra should be (tributylstannyloxy)-nitroxyl radicals. The detected radicals are real intermediates for denitration of nitro compounds, for they are not detected by ESR in the absence of AIBN. Further, Giese has reported that observed radicals decay by first order process.[6] In the photolytic experiment, the ESR signal disappears immediately, if the light is switched off, but comes back on further irradiation. Thus, the observed radicals are short-lived intermediates which decompose to give alkyl radicals.

Table 1. ESR Parameters in the Reaction of Nitro Compounds with Tin Radicals

Nitro compd	Initiator	g Factor	hfs/G	
			a_N	a_H
3	AIBN	2.0050	27.9	—
4	AIBN	2.0049	27.8	5.83
5	AIBN	2.0049	27.8	4.44
6	AIBN	2.0050	27.1	5.56
7	UV	2.0049	27.5	—

Electrochemical measurements were carried out for various kinds of nitro compounds. It is well-known that single electron reduction of aliphatic nitro compounds forms corresponding anion radicals of nitro compounds, which decompose readily to give alkyl radicals and nitrite ion.[15] As expected, cyclic voltammetry of α-nitroethylbenzene shows irreversible wave as shown in Fig. 3. The half wave reduction potentials ($E_{1/2}$) of various nitro compounds were measured by polarography. The results are summarized in Tables 2—4. Relative low reduction potentials were observed:

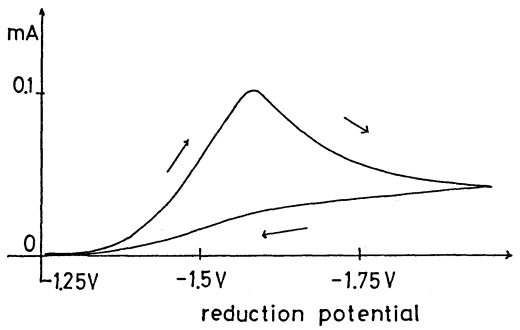

Fig. 3. Cyclic voltammetry of α-nitroethylbenzene, 0.10 M Bu_4NClO_4 in acetonitrile, at Hg.

Table 2. Relative Rate in the Reduction of Compounds **2** and $E_{1/2}$

Compound	X	σ	k_{rel}	$E_{1/2}$/V[a)]
2c	*p*-MeO	−0.27	0.68±0.01	−1.70
2d	*m*-Me	−0.07	0.93±0.03	
2b	H	0	1	−1.70
2e	*p*-F	+0.06	1.15±0.01	
2f	*m*-MeO	+0.12	1.11±0.04	
2g	*p*-Cl	+0.23	1.52±0.01	−1.60
2h	*m*-Cl	+0.37	1.49±0.05	
2i	*m*-CF_3	+0.43	1.66±0.03	
2j	*p*-CO_2Me	+0.45	1.71±0.07	−-1.60
2k	*p*-COMe	+0.50	1.57±0.07	
2l	*p*-CF_3	+0.54	1.74±0.01	
2m	*p*-CN	+0.66	1.62±0.04	−1.61
2a	*p*-NO_2	+0.78	0	

a) vs. Ag/Ag^+.

Table 3. Relative Rate in the Reaction of Compounds **9** and $E_{1/2}$

Compound	X	k_{rel}	$E_{1/2}$/V[a)]
9a	*p*-MeO	0.87±0.04	−1.55
9b	*p*-Me	0.92±0.01	−1.56
9c	*m*-Me	0.91±0.01	−1.62
9d	H	1	−1.68
9e	*m*-MeO	1.19±0.01	−1.57
9f	*p*-Cl	1.19±0.01	−1.66
9g	*m*-Cl	1.22±0.05	−1.51
9h	*p*-CO_2Me	1.59±0.01	−1.47
9i	*p*-CN	1.44±0.01	−1.49

a) vs. Ag/Ag^+.

Table 4. Relative Rate in the Reduction of Compounds **11** and $E_{1/2}$

Compound	X	k_{rel}	$E_{1/2}$/V[a)]
11a	*p*-MeO	0.76±0.01	−1.36
11b	*p*-Me	0.96±0.01	−1.36
11c	H	1	−1.37
11d	*p*-Cl	1.24±0.01	
11e	*p*-CO_2Me	1.36±0.14	−1.39
11f	*p*-CN	1.17±0.01	−1.32

a) vs. Ag/Ag^+.

compared to trifluoroacetophenone ($E_{1/2}$=−2.00 V) and acetophenone ($E_{1/2}$=−2.61 V):[16] α-nitropropiophenones, $E_{1/2}$=ca.−1.37 V; α-nitrocumenes $E_{1/2}$=ca. −1.58 V. These results are reasonable because the nitro group is strong electron acceptor. The positive ρ value was observed in Hammett plots of $E_{1/2}$. However, the value is very small (ρ=ca. 0.1—0.2), compared to that of the corresponding bromides (ρ=ca. 0.40).[17] This means that substituents have few effects on easiness of the electron transfer to the nitro groups.

Relationship between the relative reactivity of nitro compounds with Bu_3SnH and substituent constants σ was examined. The relative reactivities of substituted α-nitrocumenes **2** with Bu_3SnH in benzene at 80 °C were obtained by competitive reactions of **2** vs. **2b** on

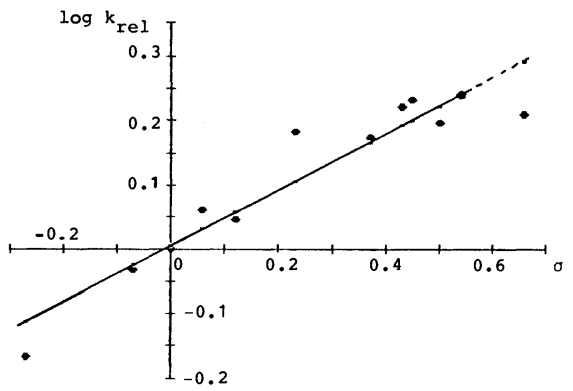

Fig. 4. Hammett plots of log k_{rel} vs. substituent constants σ for the reaction of **2** with Bu_3SnH.

the basis of measurement of appearance of products cumenes **8** and **8b**. The results are summarized in Table 2, and their Hammett plots are shown in Fig. 4. Hammett plots of log k_{rel} vs. substituent constants σ exhibits quite good correlation except for *p*-cyano-α-nitrocumene **2m**. ρ Value of **2** can be calculated by the least squares method (ρ=0.54, r=0.98). Similarly, the relative reactivities of substituted α-nitroethylbenzenes **9** and α-nitropropiophenones **11** with Bu_3SnH were obtained in the same way as above mentioned. The results are summarized in Tables 3 and 4. Good Hammett correlations between log k_{rel} and σ are obtained except *p*-cyano derivatives, which are less reactive than expected from the correlations. Obtained ρ values are as following; ρ=0.25 (r=0.97) for **9**, ρ=0.33 (r=0.96) for **11**. A positive Hammett correlations are

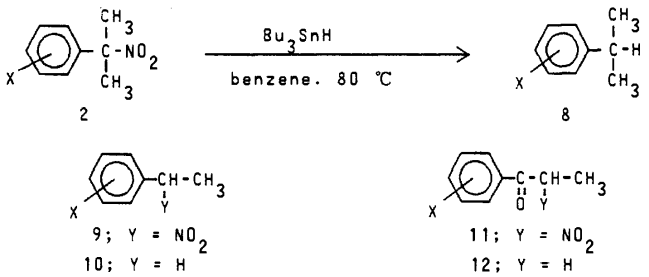

obtained both in any denitration reaction with Bu_3SnH and reduction potentials of nitro compounds. However, ρ values for the reaction with tin radicals are larger than those for electrochemical reduction. This result suggests that the formation of the anion radicals is not so much affected by variation of substituents. Thus, the larger ρ values for denitration with tin radical also support that this denitration reaction with tin radical proceeds not via the electron-transfer pathway but via the nitroxyl radical intermediates.

As related reactions, reductive cleavage of alkyl halides, sulfides, selenides, and xanthates with Bu_3SnH is well-known. The formation of alkyl radicals by tin radicals may be considered as shown in Scheme 4, where abstraction of X by tin radicals takes place via S_H process.[18,19]

$$R\text{-}X + Bu_3Sn^{\cdot} \underset{k_{-1}}{\overset{k_1}{\rightleftharpoons}} R\text{-}X\text{-}SnBu_3 \xrightarrow{k_2} R^{\cdot} + Bu_3SnX$$

X=Cl, Br, I

Scheme 4.

Hammett correlation for halogen abstraction with tin radical[19] and germyl radical[20] has been studied by Tanner and Sakurai, where positive ρ values are also obtained. They have concluded that these positive ρ values are attributed to following two reaction mechanism; an electron-transfer mechanism (Scheme 5) or polar effects on the halogen abstraction step (Scheme 6). In particular, carbon-halogen bond breaking step is considered as the rate-determining step of the reaction in the latter case.

$$R\text{-}X + Bu_3Sn^{\cdot} \overset{\text{single electron transfer}}{\rightleftharpoons} R\text{-}X^{\cdot-} + Bu_3Sn^{+}$$

anion radical

$$\longrightarrow R^{\cdot} + X^{-} + Bu_3Sn^{+}$$

X=Cl, Br, I

Scheme 5.

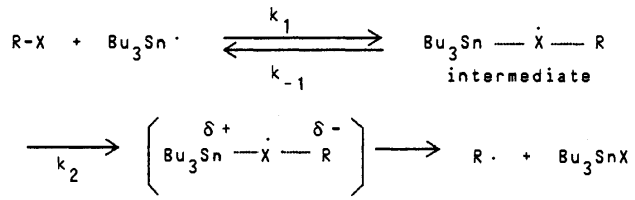

Scheme 6.

The denitration with tin radicals are quite similar to these results. As the electron-transfer mechanism is excluded as discussed above, the positive ρ values are attributed to the polar effects on the carbon-nitrogen bond scission. Although carbon-halogen bonds are so weak as to give alkyl radicals very quickly, carbon-nitrogen bond cleavage is so difficult that nitroxyl radical intermediates are readily observed by ESR spectroscopy. Thus, the carbon-nitrogen bond scission may be the rate-determining step of the denitration reaction. Considerable reaction process is depicted in Scheme 7.

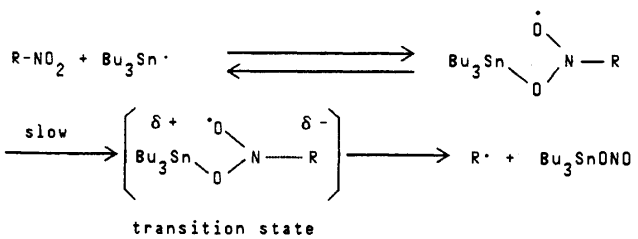

Scheme 7.

Experimental

Measurement. All melting points were uncorrected. ^{1}H NMR spectra were measured at 100 MHz with JEOL JNM-PS-100 spectrometer. IR spectra were recorded on Hitachi 215 spectrometer. GLC analyses were carried out with Shimadzu GC-8A gas chromatograph. Elemental analyses were performed by Kyoto University microanalyses center.

ESR Studies. ESR spectra were recorded using JEOL PX-3E spectrometer after mixing R-NO_2 (0.25 mmol), Bu_3SnH (0.25 mmol) and AIBN (0.05 mmol) in 0.5 ml of benzene under argon atmosphere, degassed and heating at 65 °C. ESR spectra were also recorded under irradiation of a solution of R-NO_2 (0.25 mmol) and Bu_3SnH (0.25 mmol) in 0.5 ml of benzene with high-pressure mercury lamp.

Polarography. PAR model 174 polarograph analyzer was used. The capillary constant for the dropping mercury electrode was 1.41 mg at −0.5 V vs. Ag/$AgClO_4$ in acetonitrile containing 2×10^{-2} M (1 M=1 mol dm^{-3}) Bu_4NClO_4. The anode was a 10 cm length of 1 mm diameter silver wire. All polarograms were determined at 25 °C with thoroughly deaerated solutions which was between 4×10^{-4} and 5×10^{-4} M in substrate and 2×10^{-2} M in Bu_4NClO_4.

Preparation of Nitro Compounds. α-Nitro sulfone **1** was prepared by the reaction of corresponding iodide with sodium benzenesulfinate.[21] α-Nitrocumene derivatives **2** substituted by electron-withdrawing groups were prepared by the reaction of the corresponding substituted nitrobenzenes with the lithium salt of 2-nitropropane in dimethyl sulfoxide (DMSO).[22] Other substituted nitrocumenes were prepared by the reaction of corresponding aryl lead(IV) compounds or diaryliodonium salts with the lithium salt of 2-nitropropane.[23] Physical properties of new compounds are summarized.

2c: ^{1}H NMR ($CDCl_3$) δ=1.91 (s, 6H), 3.72 (s, 3H), 6.83 (d, 2 H), 7.32 (d, 2H). IR (neat): 1250, 1350, 1530 cm^{-1}. Found: C, 61.38; H, 6.65; N, 7.13%. Calcd for $C_{10}H_{13}NO_3$: C, 61.53; H, 6.71; N, 7.18%.

2d: ^{1}H NMR ($CDCl_3$) δ=1.92 (s, 6H), 2.36 (s, 3H), 7.1—7.3 (m, 4H). IR (neat): 1350 and 1540 cm^{-1}. Found: C, 67.14; H, 7.39; N, 7.93%. Calcd for $C_{10}H_{13}NO_2$: C, 67.02; H, 7.31; N, 7.82%.

2e: ^{1}H NMR ($CDCl_3$) δ=1.98 (s, 6H), 7.1—7.6 (m, 4H). IR (neat): 1230, 1350, 1540 cm^{-1}. Found: C, 59.17; H, 5.45; N, 7.78%. Calcd for $C_9H_{10}NO_2F$: C, 59.01; H, 5.50; N, 7.65%.

2f: ^{1}H NMR ($CDCl_3$) δ=1.96 (s, 6H), 3.80 (s, 3H), 7.00 (m, 3 H), 7.36 (s, 1 H). IR (neat) 1220, 1350, 1530 cm^{-1}. Found: C, 61.47; H, 6.89; N, 7.13%. Calcd for $C_{10}H_{13}NO_3$: C, 61.53; H, 6.71; N, 7.18%.

2g: ^{1}H NMR ($CDCl_3$) δ=1.98 (s, 6H), 7.40 (s, 4H). IR (neat): 1100, 1350, 1540 cm^{-1}. Found: C, 54.16; H, 5.08; N, 7.16%. Calcd for $C_9H_{10}NO_2Cl$: C, 54.15; H, 5.05; N, 7.02%.

2h: ^{1}H NMR ($CDCl_3$) δ=1.92 (s, 6H), 7.3—7.4 (m, 4 H). IR (neat): 1080, 1350, 1540 cm^{-1}. Found: C, 54.29; H, 5.08; N, 7.08%. Calcd for $C_9H_{10}NO_2Cl$: C, 54.15; H, 5.05; N, 7.02%.

2i: ^{1}H NMR ($CDCl_3$) δ=2.00 (s, 6H), 7.64—7.72 (m, 4H). IR (neat): 1120, 1350, 1540 cm^{-1}. Found: C, 51.38; H, 4.28; N, 6.17%. Calcd for $C_{10}H_{10}NO_2F_3$: C, 51.51; H, 4.32; N, 6.01%.

2l: Mp 41.5—42 °C. ^{1}H NMR ($CDCl_3$) δ=2.04 (s, 6 H), 7.56—7.80 (m, 4 H). IR (Nujol): 1140, 1350, 1540 cm^{-1}. α-Nitroethylbenzenes **9** except **9i** were prepared by the reaction of the corresponding bromides with IRA-900 (NO_2^-)

in 60—70% yield.[24] Compound **9i** was prepared by the reaction of *p*-nitrobenzonitrile with lithium salt of nitroethane in hexamethylphosphoric triamide (HMPA). Physical properties of new compounds are shown here.

9a: ^{1}H NMR ($CDCl_3$) δ=1.83 (d, 3 H, J=7 Hz), 3.80 (s, 3 H), 5.56 (q, 1 H, J=7 Hz), 6.80—7.00 (m, 2H), 7.28—7.68 (m, 2H). IR (neat): 1250, 1350, 1540 cm^{-1}. Found: C, 59.62; H, 6.08; N, 7.89%. Calcd for $C_9H_{11}NO_2$: C, 59.66; H, 6.12; N, 7.73%.

9b: ^{1}H NMR ($CDCl_3$) δ=1.84 (d, 3H, J=7 Hz), 2.34 (s, 3H), 5.55 (q, 1H, J=7 Hz), 7.30 (m, 4 H). IR (neat): 1350 and 1540 cm^{-1}. Found: C, 65.58; H, 6.68; N, 8.25%. Calcd for $C_9H_{11}NO_2$: C, 65.43; H, 6.71; N, 8.48%.

9c: ^{1}H NMR ($CDCl_3$) δ=1.80 (d, 3H, J=7 Hz), 2.21 (s, 3H), 5.51 (q, 1H, J=7 Hz), 7.16—7.38 (m, 4H). IR (neat): 1350 and 1540 cm^{-1}. Found: C, 65.26; H, 6.64; N, 8.67%. Calcd for $C_9H_{11}NO_2$: C, 65.43; H, 6.71; N, 8.48%.

9e: ^{1}H NMR ($CDCl_3$) δ=1.84 (d, 3H, J=7 Hz), 3.78 (s, 3H), 5.53 (q, 1H, J=7 Hz), 6.84—7.40 (m, 4H). IR (neat): 1250, 1350, 1540 cm^{-1}. Found: C, 59.79; H, 6.19; N, 7.90%. Calcd for $C_9H_{11}NO_3$: C, 59.66; H, 6.12; N, 7.73%.

9f: ^{1}H NMR ($CDCl_3$) δ=1.84 (d, 3H, J=7 Hz), 5.56 (q, 1H, J=7 Hz), 7.40 (m, 4 H). IR (neat): 1090, 1350, 1540 cm^{-1}. Found: C, 51.97; H, 4.54; N, 7.51%. Calcd for $C_8H_8NO_2Cl$: C, 51.77; H, 4.34; N, 7.55%.

9g: ^{1}H NMR ($CDCl_3$) δ=1.87 (d, 3 H, J=7 Hz), 5.56 (q, 1H, J=7 Hz), 7.36—7.48 (m, 4H). IR (neat): 1080, 1350, 1540 cm^{-1}. Found: C, 51.85; H, 4.38; N, 7.67%. Calcd for $C_8H_8NO_2Cl$: C, 51.77; H, 4.34; N, 7.55%.

9h: ^{1}H NMR ($CDCl_3$) δ=1.94 (d, 3H, J=8 Hz), 3.96 (s, 3H), 5.69 (q, 1 H, J=7 Hz), 7.58 (d, 2H, J=8 Hz), 8.12 (d, 2H, J=8 Hz). IR (neat): 1350, 1540, 1705 cm^{-1}. Found: C, 57.28; H, 5.53; N, 6.93%. Calcd for $C_{10}H_{11}NO_4$: C, 57.41; H, 5.30; N, 6.70%.

9i: ^{1}H NMR ($CDCl_3$) δ=1.93 (d, 3H, J=8 Hz), 5.69 (q, 1 H, J=8 Hz), 7.70 (d,d, 4H). IR (neat): 1350, 1540, 2200 cm^{-1}. Found: C, 61.16; H, 4.68; N, 16.00%. Calcd for $C_9H_8N_2O_2$: C, 61.36; H, 4.58; N, 15.90%.

Preparation of α-nitro ketones **11** was carried out by oxidation of the corresponding nitro alcohols, which were prepared by the reaction of aldehydes with nitroethane.[25] Physical properties of new compounds are shown here.

11e: mp 86—86.5 °C. ^{1}H NMR ($CDCl_3$) δ=1.81 (d, 3H, J=7 Hz), 3.92 (s, 3H), 6.13 (q, 1H, J=7 Hz), 8.08 (q, 4H). IR (Nujol): 1350, 1560, 1700, 1720 cm^{-1}. Found: C, 55.56; H, 4.72; N, 5.90%. Calcd for $C_{11}H_{11}NO_5$: C, 55.70; H, 4.67; N, 5.90%.

11f: mp 119—120 °C. ^{1}H NMR ($CDCl_3$) δ=1.86 (d, 3H, J=7 Hz), 6.16 (q, 1H, J=7 Hz), 7.86 (d, 2H, J=8 Hz), 8.08 (d, 2H, J=8 Hz). IR (Nujor): 1350, 1540, 1700, 2250 cm^{-1}. Found: C, 58.78; H, 3.92; N, 13.86%. Calcd for $C_{10}H_8N_2O_3$: C, 58.83; H, 3.95; N, 13.72%.

Denitration of Compounds 2, 9, and 11. Denitration of these compounds with Bu_3SnH was described in a previous paper.[26] Denitrated products were obtained in 80—90% yield in most cases.

Competitive Reactions of 2. The substituted α-nitrocumene (0.25 mmol), α-nitrocumene (0.25 mmol), AIBN (0.01 mmol), and Bu_3SnH (0.02 mmol) were dissolved in 0.2 ml of benzene. The solution was degassed and sealed in a Pyrex tube. The tube was heated at 80 °C for 30 min, then opened and the products **8** were analyzed by GLC. Other compounds **9** and **11** were treated in the same way. The results are summarized in Tables 2, 3, and 4, respectively.

The authors wish to thank Professor Kazuhiro Maruyama for his helpful discussion concerning the ESR study. The authors also wish to thank Dr. Satoshi Okazaki, Dr. Kiminori Ushida, and Mr. Hideto Kato for measuring polarography and ESR. The present work was supported by a Grant-in-Aid for Scientific Research (No. 57540281) from the Ministry of Education, Science and Culture.

References

1) Preliminary accounts of this work were presented at the 47th National Meeting of the Chemical Society of Japan, Kyoto, April, 1983; abstract 2C14, and the 34th Organic Reaction Mechanism Symposium, Sapporo, August, 1983; abstract 2G11.

2) N. Ono, H. Miyake, R. Tamura, and A. Kaji, *Tetrahedron Lett.*, **22**, 1705 (1981).

3) D. D. Tanner, E. V. Blackburn, and D. D. Diaz, *J. Am. Chem. Soc.*, **103**, 1557 (1981).

4) For recent reviews, see: N. Ono and A. Kaji, *Synthesis*, **1986**, 693; N. Ono, H. Miyake, and A. Kaji, *Yuki Gosei Kagaku Kyoukai Shi*, **43**, 121 (1985); N. Ono, A. Kamimura, H. Miyake, I. Hamamoto, and A. Kaji, *J. Org. Chem.*, **50**, 3692 (1985); N. Ono, H. Miyake, A. Kamimura, and A. Kaji, *J. Chem. Soc., Perkin Trans. 1*, **1987**, 1929; N. Ono, M. Fujii, and A. Kaji, *Synthesis*, **1987**, 532; N. Ono, X. J. Tuo, and A. Kaji, *ibid.*, **1987**, 821; F. Baumberger and A. Vesella, *Helv. Chim. Acta*, **66**, 2210 (1983); G. Rossini, R. Ballini, M. Petrini, and P. Sorrenti, *Tetrahedron*, **40**, 3809 (1984).

5) Some papers cite Ref. 3 as typical example of electron transfer of tin radicals, G. A. Russell and D. F. Dedolph, *J. Org. Chem.*, **50**, 2598 (1985); D. D. Tanner, G. E. Diaz, and A. Potter, *ibid.*, **50**, 2149 (1985). However, there are no evidences to support complete one electron transfer from tin radicals to nitro compounds as discussed in this paper.

6) J. Dupuis, B. Giese, J. Hartung, M. Leising, H.-G. Korth, and R. Sustmann, *J. Am. Chem. Soc.*, **107**, 4332 (1985); H.-G. Korth, R. Sustmann, J. Dupuis, and B. Giese, *Chem. Ber.*, **120**, 1197 (1987).

7) N. Kornblum, S. C. Carlson, and R. G. Smith, *J. Am. Chem. Soc.*, **101**, 647 (1979).

8) N. Ono, R. Tamura, and A. Kaji, *J. Am. Chem. Soc.*, **105**, 4017 (1983).

9) N. Kornblum, T. M. Davis, G. W. Earl, G. S. Greene, N. L. Holy, R. C. Kerber, J. W. Manthey, M. T. Musser, and D. W. Show, *J. Am. Chem. Soc.*, **89**, 5714 (1967); N. Kornblum and J. Widmer, *ibid.*, **100**, 7086 (1978). Review: N. Kornblum, *Angew. Chem., Int. Ed. Engl.*, **14**, 734 (1975).

10) N. Ono, R, Tamura, R. Tanikaga, and A. Kaji, *J. Chem. Soc., Chem. Commun.*, **1981**, 71.

11) Bu_3SnH can replace the nitro group in the compounds, $R_2C(NO_2)X$ X=alkyl, aryl, H, CN, CO_2R, CH_2OH, $P(=O)(OR)_2$ by hydrogen. When X is SR, Cl, or Br, X is replaced by hygrogen on treatment with Bu_3SnH.

12) E. Block, "Reaction of Organosulfur Compounds," Academic Press, N. Y. (1978), p. 189.

13) J. P. Bay, S. T. Blumer, S. B. Tosh, D. Behar, and P. Neta, *J. Am. Chem. Soc.*, **105**, 320 (1985); M. C. R. Symons and W. P. Bowman, *J. Chem. Soc., Chem. Commun.*, **1984**,

1445; G. A. Russell and D. F. Dedolph, *J. Org. Chem.*, **50**, 2378 (1985).
14) K. Reuter and W. P. Neumann, *Tetrahedron Lett.*, **1978**, 5235.
15) A. K. Hoffmann, W. G. Hodgson, and W. H. Jura, *J. Am. Chem. Soc.*, **83**, 4675 (1961); A. K. Hoffmann, W. G. Hodgson, D. L. Maricle, and W. H. Jura, *ibid.*, **86**, 631, 639 (1964); H. Sayo and M. Masui, *Tetrahedron*, **24**, 1717 (1968).
16) D. D. Tanner, G. E. Diaz, and A. Potter, *J. Org. Chem.*, **50**, 2149 (1985).
17) J. W. Sease, G. G. Burton, and S. L. Nickol, *J. Am. Chem. Soc.*, **90**, 2595 (1968).
18) H. G. Kuivila, L. W. Menapace, and C. R. Warner, *J. Am. Chem. Soc.*, **84**, 3584 (1962); D. L. J. Clive, G. J. Chittattu, V. Farina, W. A. Kiel, S. Menchen, C. G. Russell, A. Singh, C. K. Wong, and N. J. Curtio, *ibid.*, **102**, 4438 (1980); P. J. Barker and A. L. J. Beckwith, *J. Chem. Soc., Chem. Commun.*, **1984**, 683; Review of Barton's deoxygenation: D. H. R. Barton and W. B. Motherwell, *Pure Appl. Chem.*, **53**, 15 (1981).
19) E. V. Blackburn and D. D. Tanner, *J. Am. Chem. Soc.*, **102**, 692 (1980).
20) H. Sakurai and K. Mochida, *J. Organomet. Chem.*, **42**, 339 (1972).
21) N. Kornblum, M. M. Kestner, S. D. Boyd, and L. C. Cattran, *J. Am. Chem. Soc.*, **95**, 3356 (1973).
22) N. Kornblum, L. Cheng, R. C. Kerber, M. M. Kestner, B. N. Newton, H. W. Pinnick, R. G. Smith, and P. A. Wade, *J. Org. Chem.*, **44**, 659 (1979).
23) P. P. Kozyrod and J. T. Pinhey, *Tetrahedron Lett.*, **22**, 789 (1981); **24**, 1301 (1983).
24) R. L. Crumbie, J. S. Nimitz, and H. S. Mosher, *J. Org. Chem.*, **47**, 4040 (1982).
25) G. Rosini and B. Ballini, *Synthesis*, **1983**, 547; N. Ono, M. Fujii, and A. Kaji, *ibid.*, **1987**, 532.
26) N. Ono, H. Miyake, A. Kamimura, I. Hamamoto, R. Tamura, and A. Kaji, *Tetrahedron*, **41**, 4013 (1985).

 © 1988 The Chemical Society of Japan Bull. Chem. Soc. Jpn., 61, 3637—3648 (1988)

General Reactivity of 2-Lithiobenzothiazole to Various Electrophiles and the Use as a Formyl Anion Equivalent in the Synthesis of α-Hydroxy Carbonyl Compounds

Hidenori CHIKASHITA,* Megumi ISHIBABA, Keiji ORI, and Kazuyoshi ITOH
Department of Applied Chemistry, Faculty of Engineering, Kansai University, Suita, Osaka 564
(Received June 7, 1988)

The reaction of 2-lithiobenzothiazole with a variety of electrophiles such as aldehydes, ketones, carboxylic esters, lactones, nitriles, and amides afforded the expected addition and substitution products. Trimethylsilyl chloride readily reacted with the benzothiazolyl anion to give 2-trimethylsilylbenzothiazole, while common alkyl halides including primary iodide and benzyl halides, as well as epoxides, did not react with the anion. This characteristic nucleophilicity of the anion was also demonstrated by its reaction with phenacyl halides and 5-chloro-2-pentanone leading to the formation of benzothiazolyl-substituted small-ring ethers. In order to demonstrate the value of 2-lithiobenzothiazole as a masked formyl anion, 2-(α-hydroxyalkyl)benzothiazoles were transformed into α-hydroxy carbonyl compounds in three reaction steps without masking the α-hydroxy groups. Quaternization of various 2-(α-hydroxyalkyl)benzothiazoles with methyl iodide in DMF afforded the corresponding 2-(α-hydroxyalkyl)-3-methylbenzothiazolium iodides in high yields and the subsequent alkylation or reduction of the C=N$^+$ link was readily accomplished with organolithium and Grignard reagents or sodium borohydride leading to the corresponding 2-(α-hydroxyalkyl)-3-methylbenzothiazolines with or without another 2-substituents. Hydrolysis of former compounds performed in aqueous acetonitrile, buffered to pH 7 and containing $AgNO_3$, gave the desired α-hydroxy ketones.

Umpolung[1] of the normal reactivity by modifying structural units has become one of the prevailing methods of choice in synthetic organic chemistry. Particularly, carbanions stabilized by adjacent sulfur atoms have been well-documented,[2] since Corey and Seebach[3] first utilized 2-lithio-1,3-dithiane as a formyl anion equivalent. Carbanions of cyclic imines stabilized by an adjacent heteroatom can also be regarded as an important formyl anion equivalent candidate due to the convertibility of the imine function with an adjacent heteroatom into a carbonyl group. However, notable differences in chemical stability between the cyclic imine adjacent oxygen atom and one adjacent sulfur atom have appeared. That is, the metalated oxazoline was reported to be unstable even at −78 °C,[4] while the corresponding benzothiazolyl anion seems to be stable as a masked formyl anion.[5] Despite much work in the benzothiazole field, however, only one example[6] of the use of 2-lithiobenzothiazole as a formyl anion equivalent has been described and there has been no study regarding its general reactivity to various electrophiles in spite of its importance and necessity. It is a purpose of the present paper to describe the fundamental and detailed studies of the general reactivity of 2-lithiobenzothiazole (**2**) toward different electrophiles (Scheme 1) and show the interesting differences in chemical reactivity between 2-lithio-1,3-dithiane or related reagents and **2**. We will also examine the utility of the lithium reagent **2** as a formyl anion equivalent with respect to the synthesis of α-hydroxy carbonyl compounds.

Preparation and Properties of 2-Lithiobenzothiazole (2). The conversion of benzothiazole (**1**) into the anion **2** was most conveniently achieved by adding 1.1 equiv of *n*-BuLi to a solution of **1** in THF at −78 °C which gave rise to a clear orange-colored solution. The progress of the lithiation was followed by deuteration of the reaction mixture with D_2O. When the solution was quickly quenched with D_2O after the addition of *n*-BuLi, the ^1H NMR spectrum of the product **3** (E=D), which had been isolated in 95% yield, showed 98% deuterium incorporation. This indicates that

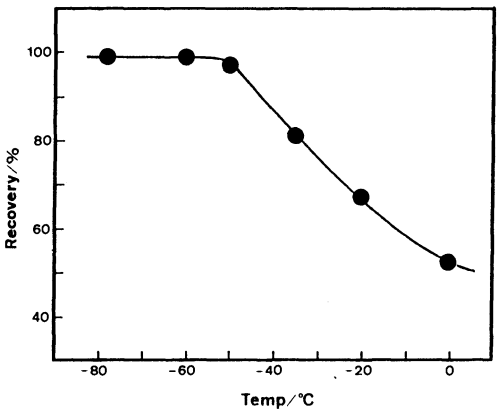

Fig. 1. Stability of 2-lithiobenzothiazole (**2**) in THF. Recovery percentages of benzothiazole (**1**) after quenching the anion solution with water at various temperatures.

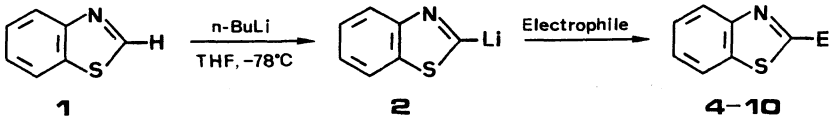

Scheme 1.

nearly quantitative metalation of **1** in THF at −78 °C occurs instantaneously. It is important and necessary for the reaction of **2** with a variety of electrophiles together with its operation to examine the stability of the anion **2** in THF at various temperatures. Thus, the yield of recovered **1** was monitored by quenching the THF solution containing the anion **2** with water after warming from −78 °C to several different temperatures (Fig. 1). As clearly indicated in Fig. 1, the anion **2** in THF is very stable below −50 °C, while it decomposes

Table 1. Reaction of 2-Lithiobenzothiazole (**2**) with Aldehydes and Ketones[a)]

Entry	Electrophile	Product	E	Yield/%[b)]
1	C_2H_5CHO	**4a**	$C_2H_5CH(OH)-$	70
2	n-C_3H_7CHO	**4b**	n-$C_3H_7CH(OH)-$	78
3	n-$C_5H_{11}CHO$	**4c**	n-$C_5H_{11}CH(OH)-$	89
4	i-C_3H_7CHO	**4d**	i-$C_3H_7CH(OH)-$	c)
5	t-C_4H_9CHO	**4e**	t-$C_4H_9CH(OH)-$	85
6	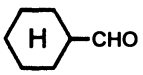	**4f**	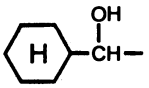	72
7	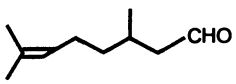	**4g**[d)]	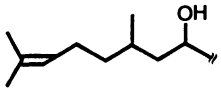	77[e)]
8	C_6H_5CHO	**4h**	$C_6H_5CH(OH)-$	77
9	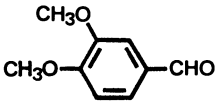	**4i**	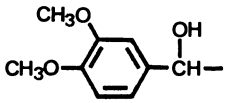	85[e)]
10	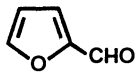	**4j**	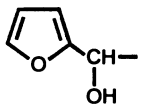	73
11	n-$C_6H_{13}COCH_3$	**5a**	n-$C_6H_{13}C(OH)(CH_3)-$	c)
12	$(n$-$C_4H_9)_2CO$	**5b**	$(n$-$C_4H_9)_2C(OH)-$	88[e)]
13	$(CH_3)_2CO$	**5c**	$(CH_3)_2C(OH)-$	77
14	$(C_6H_5)_2CO$	**5d**	$(C_6H_5)_2C(OH)-$	88
15	$C_6H_5COCH_3$	**5e**	$C_6H_5C(OH)(CH_3)-$	88
16	n-$C_3H_7COC_6H_5$	**5f**	n-$C_3H_7C(OH)(C_6H_5)-$	c)

Table 1. (Continued)

Entry	Electrophile	Product	E	Yield/%[b]
17	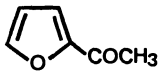	**5g**	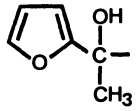	85
18	(*E*)-C_6H_5CH=$CHCOC_6H_5$	**5h**	(*E*)-C_6H_5CH=$CHC(OH)(C_6H_5)$-	83[f]
19	$C_6H_5C{\equiv}CCOCH_3$	**5i**	$C_6H_5C{\equiv}CC(OH)(CH_3)$-	78[f]
20	$(CH_3)_2C$=$CHCOCH_3$	**5j**	$(CH_3)_2C$=$CHC(OH)(CH_3)$-	71[f]
21	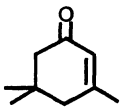	**5k**	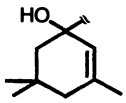	50[e,f]
22	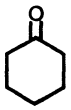	**5l**	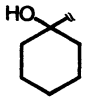	78
23	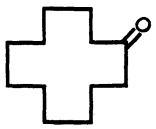	**5m**	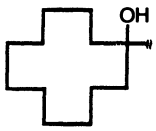	86

a) In all cases, 2-lithiobenzothiazole (**2**) was reacted with 1.1 equiv of the carbonyl compounds in THF at −78 °C for 1 h. b) Yields of pure products after recrystallization unless otherwise noted. c) The crude oily product was quantitatively obtained. d) A mixture of diastereomers. e) Yield of pure product after short-column chromatography on silica gel. f) Conjugate-addition product was not obtained.

Table 2. Reaction of 2-Lithiobenzothiazole (**2**) with Esters and Lactones[a]

Entry	Electrophile	Product	E	Yield/%[b]
1	$C_6H_5COOC_2H_5$	**6a**	C_6H_5CO-	76
2	$C_2H_5COOC_2H_5$	**6b**	C_2H_5CO-	68
3	n-$C_5H_{11}COOC_2H_5$	**6c**	n-$C_5H_{11}CO$-	63
4	i-$C_3H_7COOC_2H_5$	**6d**	i-C_3H_7CO-	64[c]
5	t-$C_4H_9COOCH_3$	**6e**	t-C_4H_9CO-	69[c]
6	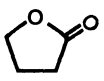	**7a**	$HO(CH_2)_3CO$-	79
7	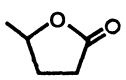	**7b**	$CH_3CH(OH)(CH_2)_2CO$-	80
8	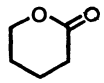	**7c**	$HO(CH_2)_4CO$-	99
9	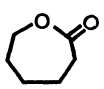	**7d**	$HO(CH_2)_5CO$-	96

a) In all cases, 2-lithiobenzothiazle (**2**) was reacted with 1.1 equiv of esters or lactones in THF at −78 °C to room temperature. b) Yields of pure products after recrystallization unless otherwise noted. c) Yield of pure product after short-column chromatography on silica gel.

considerably above −50 °C and the degree of this decomposition increased in proportion to the temperature of the solution. Accordingly, in the following experiments, electrophiles were added immediately to the anion solution after the addition of *n*-BuLi and the temperature of the reaction mixture was kept below −50 °C until the reaction was almost completed.

Hydroxyalkylation of 2 with Aldehydes and Ketones. Aldehydes and ketones reacted readily with the anion **2** to give the corresponding 2-(α-hydroxyalkyl)benzothiazoles in high yields. Table 1 lists a number of reaction products **4a—j** and **5a—m** together with their yields. The reactions were almost completed within 1 h at −78 °C and the reaction time did not vary with the steric and electronic character of the carbonyl compounds. Under the present conditions, a readily enolized ketone, such as cyclohexanone, produced the product **51** in high yield by carbonyl addition (Entry 22). This demonstrates the very effective nucleophilicity of the lithium reagent **2**. When α,β-unsaturated ketones were employed as carbonyl substrates (Entries 18—21), the α-hydroxy products **5h—k** were selectively obtained in good yields showing a high preference of the anion **2** for nonconjugate 1,2-addition to α,β-unsaturated carbonyl compounds.

Acylations of 2 with Esters and Lactones. The reactions of the anion **2** with esters effectively lead to the formation of 2-acylbenzothiazole derivatives **6a—e**. Lactones constituted with a variety of ring sizes can also be employed as an acylating reagent of the anion **2** producing the corresponding 2-(hydroxyacyl)benzothiazoles (**7a—d**) in excellent yields. These results are summarized in Table 2. In contrast to acylations of 2-lithio-1,3-dithianes in which a large excess of acylating reagents is required in order to avoid the proton abstraction of the primary product by the unreacted lithium reagent or the formation of diadduct, 1.1 equiv of esters or lactones were effectively used in the present reactions with no limitations on the acylations of **2**. Therefore, in the present acylations, the acylating reagents could be added to the anion solution at −78 °C. The reason for the efficient acylations in the present cases should ascribe to the high stability of the initial adducts **11** derived from the chelating effect peculiar to the benzothiazole ring shown in Scheme 2. In fact, in some cases, the adducts **11** separated from the reaction mixture and even an acidic hydrolysis of them was needed for effectively obtaining the acylated product.

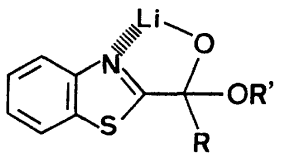

11

Scheme 2.

Reaction of 2 with Other Electrophiles. As well as esters and lactones, *N,N*-disubstituted amides and nitriles could also be used as acylating reagents as shown in Table 3. It is noteworthy that the reaction of the anion **2** with enolizable *N,N*-disubstituted amide, *N,N*-dimethylacetamide, proceeded effectively without enolization of the acylating reagent to afford 2-acetylbenzothiazole (**6f**) in excellent yield (Entry 2). This is in contrast to the similar acylation of 2-lithio-1,3-dithianes in which *N,N*-disubstituted amide as an acylating reagent is limited to a nonenolizable compound such as *N,N*-dimethylformamide. Alkylation of a formyl anion equivalent by using alkyl halides is one of useful and frequently encountered reactions. Many carbanions stabilized by adjacent heteroatoms have been known to be well-alkylated with common alkyl halides. However, we have found that alkylation of the anion **2** at −78—−50 °C could not proceed even with primary alkyl iodides or benzyl halides and in these reaction benzothiazole (**1**) was almost always rec-

Table 3. Reaction of 2-Lithiobenzothiazole (**2**) with Various Electrophiles[a]

Entry	Electrophile	Product	E	Yield/%[b]
1	C_6H_5CN	**6a**	C_6H_5CO-	82[c]
2	$(CH_3)_2NCOCH_3$	**6f**	CH_3CO-	77[c]
3	$(CH_3)_3SiCl$	**8**	$(CH_3)_3Si$-	96[d]
4	$C_6H_5COCH_2Br$	**9**	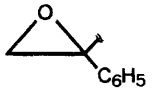	67
5	$C_6H_5COCH_2Cl$	**9**		92
6	$CH_3CO(CH_2)_3Cl$	**10**	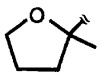	90

a) In all cases, 2-lithiobenzothiazole (**2**) was reacted with 1.1 equiv of electrophiles in THF at −78 °C to room temperature. b) Yields of pure products after short-column chromatography on silica gel unless otherwise noted. c) Yield of pure product after recrystallization. d) Yield of crude, nearly pure product.

overed after quenching with water. On the other hand, trimethylsilylation of **2** proceeded rapidly at −78 °C with trimethylsilyl chloride (Entry 3). Accordingly, common alkyl halides can not be used successfully in alkylations of the anion **2**. In order to assess the nucleophilic nature of **2**, the reactions with phenacyl bromide, phenacyl chloride, or 5-chloro-2-pentanone were carried out (Entries 4—6). Interestingly, the cyclic ether derivatives **9** and **10** were selectively obtained in excellent yields. These results show that the products are formed by the nucleophilic attack of **2** at the carbonyl carbon followed by intramolecular cyclization. This emphatically suggests that nucleophilicity of **2** towards the halogenated carbon is very low. The reaction of epoxides with **2** was also examined but this did not lead to the formation of the expected 2-(β-hydroxyalkyl)benzothiazole derivatives. In this case, **1** was recovered after quenching with

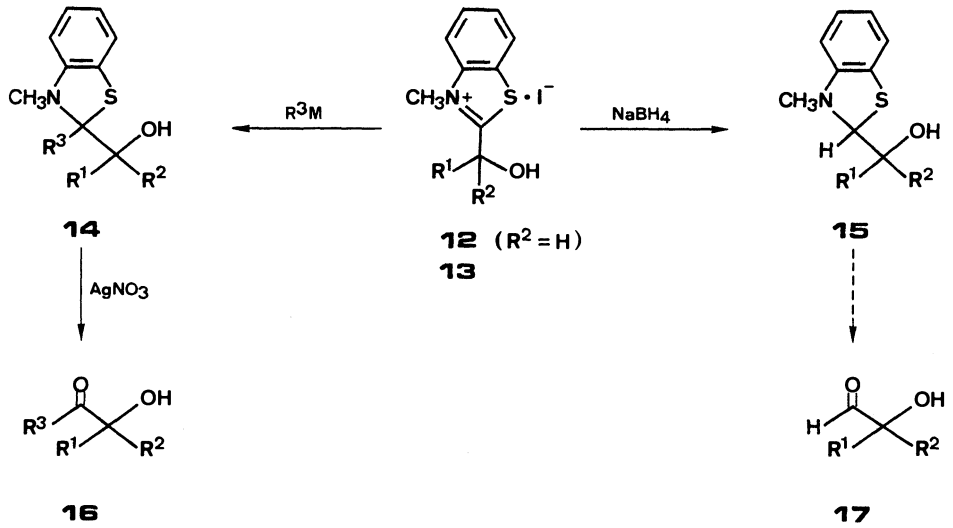

Scheme 3.

Table 4. Preparation of 2-(α-Hydroxyalkyl)-3-methylbenzothiazolium Iodides (**12** and **13**)[a)]

Entry	2-(α-Hydroxyalkyl)-benzothiazole	Product	R^1	R^2	Reaction time/h	Isolated yield/%
1	**4a**	**12a**	C_2H_5-	H	9.5	90
2	**4c**	**12b**	n-C_5H_{11}-	H	90	92
3	**4d**	**12c**	i-C_3H_7-	H	19.5	99[b,c)]
4	**4e**	**12d**	t-C_4H_9-	H	19.5	97
5	**4f**	**12e**		H	48	95
6	**4g**	**12f**	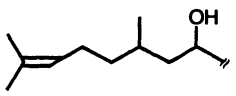	H	90	83
7	**4h**	**12g**	C_6H_5-	H	48	99
8	**4i**	**12h**	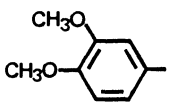	H	72	75
9	**5a**	**13a**	n-C_6H_{13}-	CH_3-	99	51[b,c)]
10	**5c**	**13b**	CH_3-	CH_3-	24	79
11	**5d**	**13c**	C_6H_5-	C_6H_5-	99	62
12	**5e**	**13d**	C_6H_5-	CH_3-	98	85
13	**5f**	**13e**	n-C_3H_7-	C_6H_5-	96	72[b,c)]
14	**5g**	**13f**	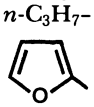	CH_3-	98	97
15	**5l**	**13g**		-$(CH_2)_5$-	96	84
16	**5m**	**13h**		-$(CH_2)_{11}$-	98	78

a) All the reactions were carried out with 6 equiv of iodomethane in DMF under refluxing.
b) Reaction was carried out with the corresponding crude oily 2-(α-hydroxyalkyl)benzothiazole.
c) Yield from benzothiazole (**1**).

water. Therefore, the reaction of 2-(lithiomethyl)-benzothiazole with carbonyl compounds is much more available rather than this reaction for obtaining 2-(β-hydroxyalkyl)benzothiazole derivatives.[7] It should be noted that the reaction of the anion **2** with alkyl halides or small-ring ethers at higher temperature (>−50 °C) was generally unavailable and unsatisfactory because the nucleophilicity of **2** towards the alkyl halides or the small-ring ethers did not depend on temperature and the reaction was not exempted from the decomposition of the anion itself as previously shown.

Table 5. Alkylation[a] of 2-(α-Hydroxyalkyl)-3-methylbenzothiazolium Salts (**12** and **13**) to 2-Substituted 2-(α-Hydroxyalkyl)-3-methylbenzothiazolines (**14**) and Hydrolysis[b] to α-Hydroxy Ketones (**16**)

Salt	R^3M	Alkylation product	Yield/%[c]	Hydrolysis product	Yield/%[d]
12a	*n*-C_4H_9Li	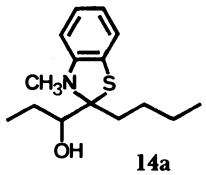 **14a**	Quant.	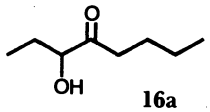 **16a**	49
12a	*n*-C_4H_9MgBr	**14a**	Quant.		
12a	*n*-$C_7H_{15}C{\equiv}CLi$	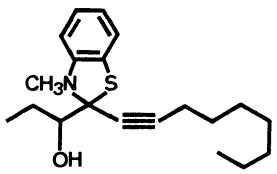 **14b**	98[c]	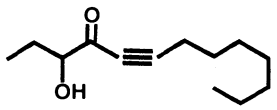 **16b**	64[e]
12b	*n*-C_4H_9Li	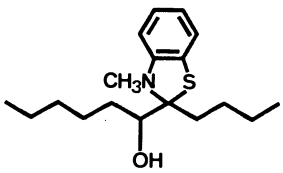 **14c**	93	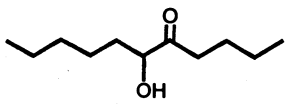 **16c**	47
12d	*n*-C_4H_9Li	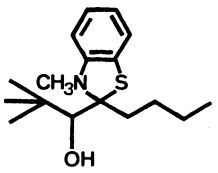 **14d**	Quant.	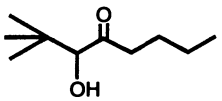 **16d**	41
12e	*n*-C_4H_9Li	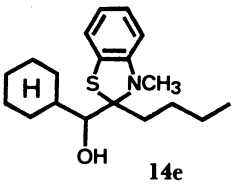 **14e**	Quant.	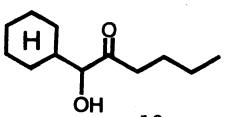 **16e**	45
13b	*n*-C_4H_9Li	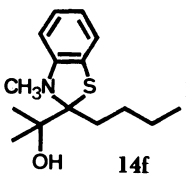 **14f**	49	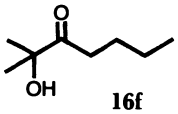 **16f**	44

a) All the reactions were carried out with 2.2 equiv of organometalic reagents in THF at −78 °C (30 min) to room temperature (1 h). b) All the reactions were carried out with 3 equiv of $AgNO_3$ in aqueous acetonitrile buffered to pH 7 at room temperature to 45°C. c) Yields of isolated nearly pure products unless otherwise noted. d) Isolated yields from the corresponding benzothiazolium salts unless otherwise noted. e) Yield from **14b** after purification by short-colum chromatography on silica gel.

An Application to the Synthesis of α-Hydroxy Carbonyl Compounds. We have further investigated the synthetic utility of the lithium reagent **2** as a formyl anion equivalent in the synthesis of α-hydroxy carbonyl compounds. As outlined in Scheme 3, the methodology comprises the quaternization of 2-(α-hydroxyalkyl)benzothiazoles (**4** and **5**) and the subsequent alkylation or reduction of the resulting salts **12** and **13** with organolithium and Grignard reagents or $NaBH_4$ leading to the corresponding 2,2-disubstituted benzothiazolines (**14**) or 2-substituted benzothiazolines (**15**), followed by their hydrolysis under mildly neutral conditions.

Methylation of **4** and **5** is very important not only for the present methodology but for our different methodology reported previously.[8] Therefore, we have examined this reaction with a variety of selected 2-(α-hydroxyalkyl)benzothiazoles (Table 4). It was found that these quaternizations could be conveniently and efficiently performed by the treatment with 6 equiv of methyl iodide in DMF at reflux temperature affording the desired iodides **12** and **13** in high yields, although the reaction of **5** derived from ketones (Entries 9—16) was generally more sluggish than that of **4** derived from aldehydes (Entries 1—8) and required a longer reaction time.

In order to obtain the 2-substituted 2-(α-hydroxyalkyl)benzothiazolines (**14**), we have studied the direct alkylation at the C-2 position of the thiazolium ring of **12** and **13** and discovered that 2 equiv of alkyl or alkynyllithium and Grignard reagents reacted cleanly with the several test α-hydroxy salts **12a**, **b**, **d**, **e**, and **13b** to give, after aqueous workup, the expected products **14a—f** in excellent yields (Table 5). Moreover, when the 2-(2-furyl)benzothiazolium iodide (**18**), which resulted from the aforementioned methylation of **10** (90% yield), was used in the reaction with *n*-BuMgBr (1.1 equiv), the benzothiazoline **19** was obtained in nearly quantitative yield (Scheme 4). However, we observed that the reaction of 2-(α-hydroxybenzyl)-3-methylbenzothiazolium iodide (**12g**) with *n*-BuLi or *n*-BuMgBr in THF gave considerable amounts of benzaldehyde together with the expected alkylation prod-

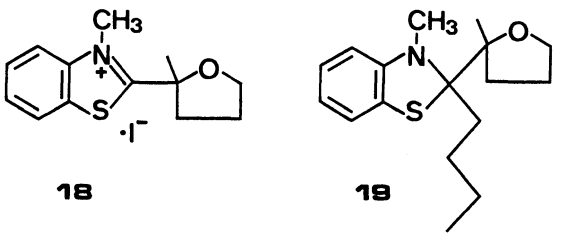

Scheme 4.

Table 6. $NaBH_4$ Reduction of 2-(α-Hydroxyalkyl)-3-methylbenzothiazolium Salts (**12** and **13**) to 2-(α-Hydroxyalkyl)-3-methylbenzothiazolines (**15**)[a]

Salt	Product		Yield/%[b]
12a	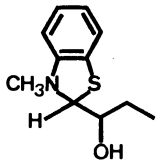	**15a**	88
12c	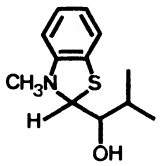	**15b**	Quant.
12d	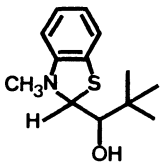	**15c**	Quant.
12e	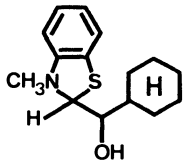	**15d**	Quant.
12f	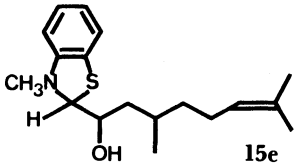	**15e**	Quant.
12h	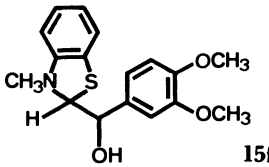	**15f**	71
13b	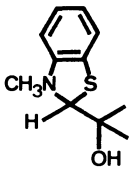	**15g**	82

a) All the reactions were carried out with 5 equiv of $NaBH_4$ in ethanol at 0 °C (30 min) to room temperature (1 h). b) Yields of isolated, nearly pure products.

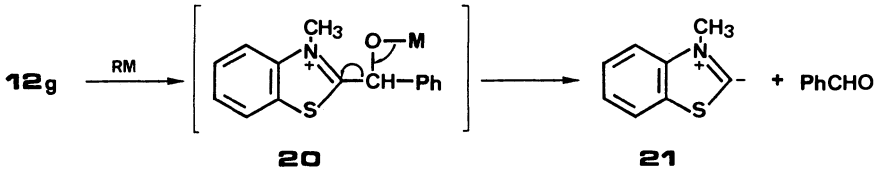

Scheme 5.

uct. This reaction most likely involves the elimination of the ylide **21** from the alkoxy intermediate **20** (Scheme 5).[9] Hydrolysis of crude 2-(α-hydroxyalkyl)-benzothiazolines (**14**) obtained here to the α-hydroxy ketones **16** was examined at the same time (Table 5). This could be effectively accomplished under mildly neutral conditions using $AgNO_3$ in an aqueous acetonitrile-phosphate buffer (0.05 M,† pH 7) solvent system,[10] affording the corresponding α-hydroxy ketones **16a—f** in good yields without any evidence of dehydration.

On the other hand, for obtaining the 2-substituted benzothiazolines (**15**), the reduction of the salts **12** and **13** with $NaBH_4$ was found to be very easy. Thus, the several test substances **12a**, **c**, **d**, **e**, **f**, h, and **13b** were cleanly reduced with no limitations by using 5 equiv of $NaBH_4$ in ethanol at 0 °C to room temperature to give **15a—g** in excellent yields (Table 6). In the present study, we did not examine the direct hydrolysis of **15** to α-hydroxy aldehydes **17**, since the latter compounds were well known to be generally unstable. However, it should be expected that these thiazolines **15** could be useful as a protected form of α-hydroxy aldehydes **17** because of easy convertibility of 2-substituted 3-methylbenzothiazoline function into a formyl group.[10]

Experimental

Melting points were recorded on a Yanagimoto micro melting-point apparatus and are uncorrected. ^1H NMR spectra were measured with a JEOL PMX-60 spectrometer at 60 MHz using tetramethylsilane as an internal reference. IR spectra were recorded on a JASCO A-202 spectrophotometer. GLC analyses were carried out on a Shimadzu Gas Chromatograph GC-6AM equipped with a hydrogen flame ionization detector using glass columns (1.5 m) packed with 2% Silicone OV-7 on Uniport HP (60—80 mesh). Silica gel (Wakogel C-300) was used for short-column chromatography. TLC was carried out on Merck precoated silica gel plates (Merck silica gel 60 F_{254}).

Materials. Tetrahydrofuran (THF) was freshly distilled over $LiAlH_4$ before use. Commercially available benzothiazole was purified by distillation. Butyllithium was obtained commercially as a 1.6 M solution in hexane. 0.05 M Phosphate buffer was prepared by dilution of the 0.1 M solution (pH 7, 0.4 M Na_2HPO_4+0.4 M KH_2PO_4) which was commercially available. The other reagents and solvents were obtained as high-grade commercial products and purified by the usual methods.

General Procedure for the Preparation of 2-Lithiobenzothiazole (2) Solution in THF. A stirred solution (0.5 M) of benzothiazole (**1**) in dry THF under nitrogen was cooled to −78 °C (Dry Ice/methanol bath) and 10% excess of butyllithium in hexane (1.6 M) was added dropwise (ca. 5 ml min^{-1}). Just before the addition had been completed, the anion solution gave rise to a clear and orange-colored solution. At the completion of the butyllithium addition, benzothiazole (**1**) was metalated quantitatively (>98% by ^1H NMR) as determined by deuteration of the solution with D_2O. The reaction vessel was continuously purged with nitrogen until the workup after the reaction with electrophiles.

The stability of the anion solution was determined by quenching the solutions (5 mmol scales) with a large excess of water after warming (ca. 5 °C min^{-1}) to several different temperatures. The aqueous mixtures were extracted with dichloromethane and the organic layers were dried with $MgSO_4$. Recovered yields of benzothiazole (**1**) were determined by GLC using pentylbenzene as an internal standard (Fig. 1).

General Procedure for the Reaction of the Anion 2 with Aldehydes and Ketones. A solution (0.55 M) of carbonyl compound (1.1 equiv to **1**) in dry THF was slowly added to the stirred solution of the anion **2** at −78 °C and the stirring was continued at the same temperature for 1 h. After removing the cold bath, the mixture was stirred for an additional 10 min and then quenched with a large excess of water. The aqueous mixture was extracted with benzene and the organic layer was washed thoroughly with water and then dried with $MgSO_4$. The mixture was evaporated under reduced pressure and the residue was completely dried in vacuo to give crude 2-(α-hydroxyalkyl)benzothiazoles (**4** and **5**). Purification of the products were performed by recrystallization for compounds **4a—c**, **4e**, **4h**, **4j**, **5c—e**, **5g—j**, **5l**, and **5m** or short-column chromatography for compounds **4d**, **4g**, **4i**, **5a**, **5b**, and **5k**. The results are summarized in Table 1. The ^1H NMR and physical data of the products are as follows (compounds **4f** and **5f** were characterized after conversion into the corresponding 3-methylbenzothiazolium iodides **12e** and **13e**).

4a: Colorless needles (acetone); mp 102—102.5 °C; ^1H NMR ($CDCl_3$) δ=1.00 (t, 3H, CH_3, J=7 Hz), 1.93 (m, 2H, CH_2), 4.50 (brs, 1H, OH), 4.90 (t, 1H, CH, J=6 Hz), 7.17 (m, 2H, Arom), and 7.68 (m, 2H, Arom). Found: C, 62.02; H, 5.80; N, 7.21%. Calcd for $C_{10}H_{11}NOS$: C, 62.15; H, 5.74; N, 7.25%.

4b: Colorless needles (acetone/hexane); mp 89—90 °C; ^1H NMR ($CDCl_3$) δ=0.92 (t, 3H, CH_3, J=7 Hz), 1.17—2.13 (m, 4H, $2CH_2$), 3.93 (d, 1H, OH, J=5 Hz), 4.95 (q, 1H, CH), 7.17 (m, 2H, Arom), and 7.67 (m, 2H, Arom). Found: C, 63.81; H, 6.30; N, 6.56%. Calcd for $C_{11}H_{13}NOS$: C, 63.73; H, 6.32; N, 6.76%.

4c: Colorless needles (acetone/hexane); mp 62.5—63 °C; ^1H NMR ($CDCl_3$) δ=0.67—2.17 (brm, 11H, n-C_5H_{11}), 3.27 (d, 1H, OH, J=5 Hz), 4.97 (q, 1H, CH), 7.27 (m, 2H, Arom), and 7.77 (m, 2H, Arom). Found: C, 66.37; H, 7.27; N, 5.86%. Calcd for $C_{13}H_{17}NOS$: C, 66.35; H, 7.28; N, 5.95%.

4d: Colorless oil; ^1H NMR ($CDCl_3$) δ=0.97 (d, 6H, $2CH_3$, J=7 Hz), 2.15 (m, 1H, CH), 4.77 (d, 1H, CHOH, J=5 Hz), 5.05 (brs, 1H, OH), 7.25 (m, 2H, Arom), and 7.80 (m, 2H, Arom). Found: C, 63.69; H, 6.21; N, 6.75%. Calcd for $C_{11}H_{13}NOS$: C, 63.73; H, 6.32; N, 6.76%.

4e: Colorless needles (acetone); mp 110—111 °C; ^1H NMR ($CDCl_3$) δ=1.00 (s, 9H, $3CH_3$), 4.35 (brs, 1H, OH), 4.60 (brs, 1H, CH), 7.26 (m, 2H, Arom), and 7.75 (m, 2H, Arom). Found: C, 65.05; H, 6.87; N, 6.34%. Calcd for $C_{12}H_{15}NOS$: C, 65.12; H, 6.83; N, 6.33%.

4g: Colorless oil; ^1H NMR ($CDCl_3$) δ=0.67—2.17 (brm, 16H), 3.73 (d, 1H, OH, J=5 Hz), 4.67, (brm, 1H, CHOH), 5.00 (brm, 1H, HC≡C), 7.23 (m, 2H, Arom), and 7.73 (m, 2H, Arom). Found: C, 70.52; H, 7.98; N, 4.65%. Calcd for $C_{17}H_{23}NOS$: C, 70.55; H, 8.01; N, 4.84%.

† 1M=1 mol dm^{-3}.

4h: Colorless needles (acetone/hexane); mp 124.5—125 °C; ^{1}H NMR ($CDCl_3$) δ=4.56 (brs, 1H, OH), 5.96 (s, 1H, CH), 7.19 (m, 7H, C_6H_5 and Arom), and 7.64 (m, 2H, Arom). Found: C, 69.73; H, 4.71; N, 5.69%. Calcd for $C_{14}H_{11}NOS$: C, 69.68; H, 4.60; N, 5.80%.

4i: Colorless needles; mp 78—79 °C; ^{1}H NMR ($CDCl_3$) δ=3.73 (s, 6H, $2CH_3O$), 4.67 (brs, 1H, OH), 5.93 (brs, 1H, CH), 6.70 (s, 1H, Arom), 6.87 (m, 2H, Arom), 7.20 (m, 2H, Arom), and 7.67 (m, 2H, Arom). Found: C, 63.55; H, 4.96; N, 4.51%. Calcd for $C_{16}H_{15}NO_3S$: C, 63.77; H, 5.02; N, 4.65%.

4j: Colorless needles (acetone/hexane); mp 155—155.5 °C; ^{1}H NMR ($CDCl_3$) δ=4.07 (br, 1H, OH), 6.02 (br, 1H, CH), 6.50 (q, 1H, Furan-H), 7.35 (m, 2H, Arom), 7.62 (d, 1H, Furan-H, J=2 Hz), 7.68 (m, 2H, Arom), and 8.13 (d, 1H, Furan-H, J=4 Hz). Found: C, 62.55; H, 3.76; N, 5.96%. Calcd for $C_{12}H_9NO_2S$: C, 62.32; H, 3.92; N, 6.06%.

5a: Colorless oil; ^{1}H NMR ($CDCl_3$) δ=0.60—2.17 (m, 16H, n-C_6H_{13} and CH_3), 3.90 (brs, 1H, OH), 7.20 (m, 2H, Arom), and 7.76 (m, 2H, Arom). Found: C, 68.59; H, 8.31; N, 5.39%. Calcd for $C_{15}H_{21}NOS$: C, 68.40; H, 8.04; N, 5.32%.

5b: Colorless oil; ^{1}H NMR ($CDCl_3$) δ=0.60—2.17 (m, 18H, 2n-C_4H_9), 3.50 (s, 1H, OH), 7.21 (m, 2H, Arom), and 7.75 (m, 2H, Arom). Found: C, 68.51; H, 8.26; N, 4.52%. Calcd for $C_{16}H_{23}NOS$: C, 69.27; H, 8.36; N, 5.05%.

5c: Colorless needles (hexane/acetone); mp 93—93.5 °C; ^{1}H NMR ($CDCl_3$) δ=1.70 (s, 6H, $2CH_3$), 3.60 (s, 1H, OH), 7.20 (m, 2H, Arom), and 7.72 (m, 2H, Arom). Found: C, 62.28; H, 5.73; N, 7.32%. Calcd for $C_{10}H_{11}NOS$: C, 62.15; H, 5.74; N, 7.25%.

5d: Colorless needles (acetone/hexane); mp 149.5—150 °C; ^{1}H NMR ($CDCl_3$) δ=4.47 (s, 1H, OH), 7.17 (m, 12H, $2C_6H_5$ and Arom), and 7.70 (m, 2H, Arom). Found: C, 75.63; H, 4.72; N, 4.46%. Calcd for $C_{20}H_{15}NOS$: C, 75.68; H, 4.76; N, 4.41%.

5e: Colorless needles (benzene/hexane); mp 80.5—81 °C; ^{1}H NMR ($CDCl_3$) δ=2.04 (s, 3H, CH_3), 4.07 (s, 1H, OH), and 6.93—7.90 (m, 9H, C_6H_5 and Arom). Found: C, 70.37; H, 5.21; N, 5.45%. Calcd for $C_{15}H_{13}NOS$: C, 70.56; H, 5.13; N, 5.49%.

5g: Colorless needles (acetone/hexane); mp 115.5—116 °C; ^{1}H NMR ($CDCl_3$) δ=2.03 (s, 3H, CH_3), 4.23 (s, 1H, OH), 6.23 (m, 2H, Furan-H), 7.23 (m, 3H, Furan-H and Arom), and 7.77 (m, 2H, Arom). Found: C, 63.69; H, 4.48; N, 5.85%. Calcd for $C_{13}H_{11}NO_2S$: C, 63.65; H, 4.52; N, 5.71%.

5h: Colorless needles (acetone/hexane); mp 169.5—170 °C; ^{1}H NMR ($CDCl_3$) δ=3.93 (s, 1H, OH), 6.78 (m, 2H, CH=CH), 7.20 (m, 12H, $2C_6H_5$ and Arom), and 7.77 (m, 2H, Arom). Found: C, 76.76; H, 4.95; N, 3.99%. Calcd for $C_{22}H_{17}NOS$: C, 76.94; H, 4.99; N, 4.08%.

5i: Colorless needles (acetone/pentane); mp 134.5—135 °C; ^{1}H NMR ($CDCl_3$) δ=2.07 (s, 3H, CH_3), 4.20 (brs, 1H, OH), 7.17 (m, 7H, C_6H_5 and Arom), and 7.79 (m, 2H, Arom). Found: C, 73.01; H, 4.77; N, 4.71%. Calcd for $C_{17}H_{13}NOS$: C, 73.09; H, 4.69; N, 5.01%.

5j: Colorless needles (acetone); mp 144—144.5 °C; ^{1}H NMR ($CDCl_3$) δ=1.57—1.87 (m, 9H, $3CH_3$), 3.38 (s, 1H, OH), 5.62 (m, 1H, HC=C), 7.20 (m, 2H, Arom), and 7.73 (m, 2H, Arom). Found: C, 66.87; H, 6.57; N, 5.82%. Calcd for $C_{13}H_{15}NOS$: C, 66.92; H, 6.48; N, 6.00%.

5k: Colorless needles; mp 105—106 °C; ^{1}H NMR ($CDCl_3$) δ=0.97 (s, 3H, CH_3), 1.13 (s, 3H, CH_3), 1.73 (s, 3H, CH_3), 1.88 (brd, 2H, CH_2, J=4 Hz), 2.00 (s, 1H, C<u>H</u>H), 2.01 (s, 1H, CH<u>H</u>), 3.47 (brs, 1H, OH), 5.52 (m, 1H, H-C=C-), 7.17 (m, 2H, Arom), and 7.72 (m, 2H, Arom). Found: C, 70.03; H, 7.12; N, 4.93%. Calcd for $C_{16}H_{19}NOS$: C, 70.29; H, 7.00; N, 5.12%.

5l: Colorless needles (acetone/hexane); mp 106.5—107 °C; ^{1}H NMR ($CDCl_3$) δ=1.10—2.43 (m, 10H, $5CH_2$), 3.27 (s, 1H, OH), 7.19 (m, 2H, Arom), and 7.73 (m, 2H, Arom). Found: C, 66.83; H, 6.56; N, 5.84%. Calcd for $C_{13}H_{15}NOS$: C, 66.92; H, 6.48; N, 6.00%.

5m: Colorless needles (acetone/hexane); mp 148—148.5 °C; ^{1}H NMR ($CDCl_3$) δ=1.40 (br, 18H, $9CH_2$), 2.00 (br, 4H, $2CH_2$), 2.97 (s, 1H, OH), 7.23 (m, 2H, Arom), and 7.77 (m, 2H, Arom). Found: C, 71.73; H, 8.65; N, 4.23%. Calcd for $C_{19}H_{27}NOS$: C, 71.88; H, 8.57; N, 4.41%.

General Procedure for the Reaction of the Anion 2 with Esters and Lactones. A solution (0.55 M) of ester or lactone (1.1 equiv to **1**) in dry THF was slowly added to the stirred solution of the anion **2** in THF at −78 °C and the mixture was stirred for 1 h. After removal of the cold bath, the mixture was continuously stirred for 30 min and then quenched with a large excess of water (in experiments with lactones, 0.1 M hydrochloric acid was used in place of water for the quenching). The aqueous mixture was extracted with benzene and the extract was washed thoroughly with water. The organic layer was dried with $MgSO_4$ and concentrated under reduced pressure to give crude 2-acylbenzothiazoles (**6** and **7**). Purification of the products was performed by recrystallization for compounds **6a—c** and **7a—d** or short-column chromatography for compounds **6d** and **6e**. The results are summarized in Table 2. The ^{1}H NMR and physical data of the products are as follows.

6a: Pale yellow needles (ethanol); mp 103.5—104.5 °C (lit,[5] mp 102.5 °C); ^{1}H NMR ($CDCl_3$) δ=7.30 (m, 5H, C_6H_5), 7.63 (m, 2H, Arom), and 8.10 (m, 2H, Arom).

6b: Colorless needles (ethanol); mp 76—77 °C; ^{1}H NMR ($CDCl_3$) δ=1.27 (t, 3H, CH_3, J=7 Hz), 3.25 (q, 2H, CH_2), 7.33 (m, 2H, Arom), and 7.85 (m, 2H, Arom). Found: C, 62.73; H, 4.65; N, 7.39%. Calcd for $C_{10}H_9NOS$: C, 62.80; H, 4.74; N, 7.32%.

6c: Colorless needles (ethanol); mp 61—62 °C; ^{1}H NMR ($CDCl_3$) δ=1.00 (t, 3H, CH_3, J=7 Hz), 1.12—1.73 (m, 6H, $3CH_2$), 3.20 (t, 2H, CH_2CO, J=6 Hz), 7.30 (m, 2H, Arom), and 7.82 (m, 2H, Arom). Found: C, 66.93; H, 6.45; N, 5.90%. Calcd for $C_{13}H_{15}NOS$: C, 66.92; H, 6.48; N, 6.00%.

6d: Colorless oil; ^{1}H NMR ($CDCl_3$) δ=1.30 (d, 6H, $2CH_3$, J=7 Hz), 3.92 (m, 1H, CH), 7.30 (m, 2H, Arom), and 7.83 (m, 2H, Arom). Found: C, 64.37; H, 5.38; N, 6.70%. Calcd for $C_{11}H_{11}NOS$: C, 64.36; H, 5.40; N, 6.82%.

6e: Colorless needles; mp 54.5—55.5 °C; ^{1}H NMR ($CDCl_3$) δ=1.53 (s, 9H, $3CH_3$), 7.33 (m, 2H, Arom), and 7.87 (m, 2H, Arom). Found: C, 65.75; H, 5.94; N, 6.29%. Calcd for $C_{12}H_{13}NOS$: C, 65.72; H, 5.97; N, 6.39%.

7a: Colorless needles (hexane/acetone); mp 93—93.5 °C; ^{1}H NMR ($CDCl_3$) δ=2.02 (m, 2H, CH_2), 3.30 (t, 2H, CH_2CO, J=7 Hz), 3.67 (t, 2H, C<u>H</u>$_2$OH, J=6 Hz), 3.67 (br, 1H, OH), 7.33 (m, 2H, Arom), and 7.85 (m, 2H, Arom). Found: C, 59.82; H, 5.06; 6.15%. Calcd for $C_{11}H_{11}NO_2S$: C, 59.71; H, 5.01; N, 6.33%.

7b: Colorless needles (acetone/hexane); mp 81—82 °C; ^{1}H NMR ($CDCl_3$) δ=1.23 (d, 3H, CH_3, J=6 Hz), 1.97 (q, 2H, CH_2), 3.32 (t, 2H, CH_2CO, J=7 Hz), 3.83 (m, 1H, CH), 4.35 (d, 1H, OH, J=8 Hz), 7.27 (m, 2H, Arom), and 7.83 (m, 2H, Arom). Found: C, 61.26; H, 5.50; N, 5.84%. Calcd for $C_{12}H_{13}NO_2S$: C, 61.25; H, 5.57; N, 5.95%.

7c: Colorless needles (acetone/hexane); mp 89.5—90.5 °C; ^{1}H NMR ($CDCl_3$) δ=1.33—2.50 (m, 4H, $2CH_2$), 3.22 (t, 2H, CH_2CO, J=7 Hz), 3.62 (t, 2H, $C\underline{H}_2OH$, J=6 Hz), 3.62 (br, 1H, OH), 7.27 (m, 2H, Arom), and 7.87 (m, 2H, Arom). Found: C, 61.24; H, 5.51; N, 5.89%. Calcd for $C_{12}H_{13}NO_2S$: C, 61.25; H, 5.57; N, 5.95%.

7d: Colorless needles (acetone/hexane); mp 81.5—82.5 °C; ^{1}H NMR ($CDCl_3$) δ=1.17—2.17 (m, 6H, $3CH_2$), 3.20 (t, 2H, CH_2CO, J=7 Hz), 3.50 (br, 1H, OH), 3.57 (t, 2H, $C\underline{H}_2OH$, J=6 Hz), 7.33 (m, 2H, Arom), and 7.85 (m, 2H, Arom). Found: C, 62.64; H, 6.18; N, 5.54%. Calcd for $C_{13}H_{15}NO_2S$: C, 62.63; H, 6.06; N, 5.62%.

Reaction of the Anion 2 with Benzonitrile. A solution of benzonitrile (2.84 g, 27.5 mmol) in dry THF (5 ml) was added to the stirred solution of the anion **2** (prepared from 25 mmol of **1**) at −78 °C and the mixture was continuously stirred for 1 h. After removing the cold bath, the mixture was stirred for an additional 10 min and then hydrolyzed with concd hydrochloric acid (5 ml). The acidic solution was continuously stirred until the temperature reached room temperature. The mixture was poured into same amount of water and the aqueous mixture was extracted with benzene. The benzene extract was washed thoroughly with water and the organic layer was dried with $MgSO_4$. The crystals obtained by evaporation of the organic layer under reduced pressure were triturated in pentane and filtered to give the crude 2-benzoylbenzothiazole (**6a**). Recrystallization from ethanol afforded pure **6a** as pale yellow needles (5.33 g, 82%); mp 103.5—104.5 °C (lit,[5] mp 102.5 °C).

Reaction of the Anion 2 with *N,N*-Dimethylacetamide. A solution of *N,N*-dimethylacetamide (2.40 g, 27.5 mmol) in dry THF (50 ml) was added to the stirred solution of the anion **2** (prepared from 25 mmol of **1**) at −78 °C and the mixture was continuously stirred for 1 h. The mixture was allowed to warm to room temperature and continuously stirred for an additional 30 min. The mixture was quenched with a large excess of water and extracted with benzene. The organic layer was washed thoroughly with water and dried with $MgSO_4$ and then evaporated under reduced pressure to give the crude crystalline 2-acetylbenzothiazole (**6f**). Recrystallization from acetone afforded pure **6f** as colorless needles (3.22 g, 73%); mp 108.5—109.5 °C; ^{1}H NMR ($CDCl_3$) δ=2.72 (s, 3H, CH_3), 7.30 (m, 2H, Arom), and 7.83 (m, 2H, Arom). Found: C, 60.83; H, 3.80; N, 7.78%. Calcd for C_9H_7NOS: C, 60.99; H, 3.98; N, 7.90%.

Reaction of the Anion 2 with Trimethylsilyl Chloride. Trimethylsilyl chloride (3.26 g, 30 mmol) was added to the stirred solution of the anion **2** (prepared from 25 mmol of **1**) at −78 °C and the mixture was continuously stirred for 1 h. The mixture was allowed to warm to room temperature and continuously stirred for 1 h. The mixture was concentrated under reduced pressure and the residue was extracted with hexane. The hexane extract was washed thoroughly with water and the organic layer was dried with $MgSO_4$. After evaporation of the solvent under reduced pressure gave the nearly pure (monitored by GLC) 2-trimethylsilylbenzothiazole (**8**) as a pale yellow oil (4.98 g, 96%). Purification by distillation afforded pure **8** as a colorless oil; bp 121—122 °C/ 5 mmHg†† (lit,[11] bp 139 °C/15 mmHg).

Reaction of the Anion 2 with Phenacyl Halides. A solution of phenacyl bromide or chloride (27.5 mmol) in dry THF (5 ml) was added to the stirred solution of the anion **2** (prepared from 25 mmol of **1**) at −78 °C and the mixture was then stirred for 1 h. The mixture was allowed to warm to room temperature and continuously stirred for 1 h. The mixture was concentrated under reduced pressure and the residue was diluted with benzene and then washed thoroughly with water. The organic layer was dried with $MgSO_4$ and evaporated under reduced pressure to give the crude oily 2-(2-phenyl-2-oxiranyl)benzothiazole (**9**). Purification by short-column chromatography afforded pure **9** as a colorless oil; ^{1}H NMR ($CDCl_3$) δ=3.15 (d, 1H, C$\underline{H}$H, J=6 Hz), 3.43 (d, 1H, CH$\underline{H}$, J=6 Hz), 7.17 (m, 7H, C_6H_5 and Arom), and 7.50 (m, 2H, Arom). Found: C, 70.83; H, 4.69; N, 5.48%. Calcd for $C_{15}H_{12}NOS$: C, 70.84; H, 4.76; N, 5.51%.

Reaction of the Anion 2 with 5-Chloro-2-pentanone. A solution of 5-chloro-2-pentanone (3.32 g, 27.5 mmol) in dry THF (5 ml) was added to the stirred solution of the anion **2** (prepared from 25 mmol of **1**) at −78 °C and the mixture was stirred for an additional 50 min at the same temperature. The mixture was allowed to warm to room temperature and continuously stirred for 2 h. The mixture was concentrated under reduced pressure and the residue was extracted with benzene. The benzene extract was washed thoroughly with water and the organic layer was dried with $MgSO_4$. Evaporation of the solvent under reduced pressure gave the crude oily 2-(2-methyltetrahydro-2-furanyl)benzothiazole (**10**). Purification by distillation afforded pure **10** as a colorless oil (4.94 g, 90%); bp 138.2 °C/2.5 mmHg; ^{1}H NMR ($CDCl_3$) δ=1.32 (s, 3H, CH_3), 1.84 (m, 4H, $2CH_2$), 3.83 (t, 2H, CH_2O), 7.16 (m, 2H, Arom), and 7.72 (m, 2H, Arom). Found: C, 65.72; H, 5.97; N, 6.39%. Calcd for $C_{12}H_{13}NOS$: C, 65.76; H, 6.18; N, 6.41%.

General Procedure for the Preparation of 2-(α-Hydroxyalkyl)-3-methylbenzothiazolium Iodides (12 and 13). The solution of 2-(α-hydroxyalkyl)benzothiazole (**4** or **5**) (48 mmol) in dimethylformamide (18 ml) and methyl iodide (18 ml) was refluxed with stirring for the appropriate times (see Table 4). After cooling to room temperature, the mixture was diluted with diethyl ether (50 ml) and cooled in an ice bath to completely precipitate the salt. The separated needles were collected by filtration, washed thoroughly with diethyl ether, and then dried in vacuo to afford the crude 2-(α-hydroxyalkyl)-3-methylbenzothiazolium salt (**12** or **13**). Recrystallization was performed from methanol to afford pure **12** and **13**. The results are summarized in Table 4. ^{1}H NMR and physical data of the products are as follows.

12a: Colorless needles (methanol); mp 206—209 °C (decomp); ^{1}H NMR (DMSO-d_6) δ=1.03 (t, 3H, CH_3, J=7 Hz), 1.85 (m, 2H, CH_2), 4.27 (s, 3H, CH_3N), 5.42 (q, 1H, CH), 7.31 (br, 1H, OH), 7.67 (m, 2H, Arom), and 8.23 (m, 2H, Arom). Found: C, 39.47; H, 4.21; N, 4.06%. Calcd for $C_{11}H_{14}NOSI$: C, 39.42; H, 4.21; N, 4.18%.

12b: Colorless needles (methanol/acetone); mp 126.5—127 °C (decomp); ^{1}H NMR (DMSO-d_6) δ=0.67—2.00 (br, 11H, n-C_5H_{11}), 4.22 (s, 3H, CH_3N), 5.42 (br, 1H, CH), 7.34 (br, 1H, OH), 7.72 (m, 2H, Arom), and 8.23 (m, 2H, Arom). Found: C, 44.33; H, 5.31; N, 3.62%. Calcd for $C_{14}H_{20}NOSI$: C, 44.57; H, 5.34; N, 3.71%.

12c: Colorless needles (methanol/acetone); mp 188.5—189 °C (decomp); ^{1}H NMR (DMSO-d_6) δ=1.12 (d, 3H, CH_3, J=7 Hz), 1.42 (d, 3H, CH_3, J=7 Hz), 2.53 (m, 1H, CH), 4.58 (s, 3H, CH_3N), 5.67 (br, 1H, C$\underline{H}$OH), 7.27 (br, 1H, OH), 8.02 (m, 2H, Arom), and 8.57 (m, 2H, Arom). Found: C, 41.33; H,

†† 1 mmHg≈133.322 Pa.

4.62; N, 3.84%. Calcd for $C_{12}H_{16}NOSI$: C, 41.27; H, 4.62; N, 4.01%.

12d: Colorless needles (methanol); mp 212—212.5 °C (decomp); ^{1}H NMR (DMSO-d_6) δ=1.33 (s, 9H, $3CH_3$), 4.67 (s, 3H, CH_3N), 5.63 (d, 1H, CH, J=4 Hz), 7.17 (d, 1H, OH, J=4 Hz), 8.03 (m, 2H, Arom), and 8.53 (m, 2H, Arom). Found: C, 43.02; H, 4.96; N, 3.65%. Calcd for $C_{13}H_{18}NOSI$: C, 42.98; H, 4.99; N, 3.86%.

12e: Colorless needles (methanol/acetone); mp 196.5—197 °C (decomp); ^{1}H NMR (DMSO-d_6) δ=1.17—2.50 (br, 11H, cyclohexyl), 4.53 (s, 3H, CH_3N), 5.60 (br, 1H, CH), 7.28 (br, 1H, OH), 8.00 (m, 2H, Arom), and 8.17 (m, 2H, Arom). Found: C, 46.04; H, 5.47; N, 3.53%. Calcd for $C_{15}H_{20}NOSI$: C, 46.28; H, 5.18; N, 3.60%.

12f: Colorless needles (methanol/acetone); mp 161.5—162 °C (decomp); ^{1}H NMR (DMSO-d_6) δ=1.17—2.67 (m, 16H), 4.63 (s, 3H, CH_3N), 5.33 (m, 1H, HC=C), 5.67 (br, 1H, CHOH), 7.33 (br, 1H, OH), 8.00 (m, 2H, Arom), and 8.52 (m, 2H, Arom). Found: C, 49.63; H, 6.19; N, 3.11%. Calcd for $C_{18}H_{26}NOSI$: C, 50.12; H, 6.07; N, 3.25%.

12g: Colorless needles (acetone/methanol); mp 122—123 °C (decomp); ^{1}H NMR (DMSO-d_6) δ=4.10 (s, 3H, CH_3N), 6.65 (s, 1H, CH), 7.38 (m, 6H, OH and C_6H_5), 7.70 (m, 2H, Arom), and 8.30 (m, 2H, Arom). Found: C, 47.08; H, 3.62; N, 3.61%. Calcd for $C_{15}H_{14}NOSI$: C, 47.01; H, 3.68; N, 3.66%.

12h: Colorless needles (methanol/acetone); mp 184.5—185.5 °C (decomp); ^{1}H NMR (DMSO-d_6) δ=4.03 (s, 6H, $2CH_3O$), 4.40 (s, 3H, CH_3N), 6.80 (s, 1H, CH), 7.27 (s, 2H, OH and Arom), 7.40 (m, 2H, Arom), 8.03 (m, 2H, Arom), and 8.53 (m, 2H, Arom). Found: C, 45.82; H, 3.99; N, 3.07%. Calcd for $C_{17}H_{18}NO_3SI$: C, 46.06; H, 4.09; N, 3.16%.

13a: Colorless needles (methanol/ether); mp 161.5—162 °C (decomp); ^{1}H NMR (DMSO-d_6) δ=0.60—1.67 (brm, 13H, n-C_6H_{13}), 1.82 (s, 3H, CH_3), 3.28 (br, 1H, OH), 4.35 (s, 3H, CH_3N), 7.73 (m, 2H, Arom), and 8.28 (m, 2H, Arom). Found: C, 47.40; H, 5.99; N, 3.58%. Calcd for $C_{16}H_{24}NOSI$: C, 47.41; H, 5.97; N, 3.46%.

13b: Colorless needles (methanol/acetone); mp 178.5—179 °C (decomp); ^{1}H NMR (DMSO-d_6) δ=2.08 (s, 6H, $2CH_3$), 4.60 (s, 3H, CH_3N), 7.33 (s, 1H, OH), 7.97 (m, 2H, Arom), and 8.50 (m, 2H, Arom). Found: C, 39.56; H, 4.17; N, 4.00%. Calcd for $C_{11}H_{14}NOSI$: C, 39.42; H, 4.21; N, 4.18%.

13c: Colorless needles (methanol/acetone); mp 203—204 °C (decomp); ^{1}H NMR (DMSO-d_6) δ=3.53 (br, 1H, OH), 4.05 (s, 3H, CH_3N), 7.32 (s, 10H, $2C_6H_5$), 7.73 (m, 2H, Arom), and 8.17 (m, 2H, Arom). Found: C, 54.89; H, 3.96; N, 3.17%. Calcd for $C_{21}H_{18}NOSI$: C, 54.91; H, 3.95; N, 3.05%.

13d: Colorless needles (methanol/acetone); mp 169.5—170 °C (decomp); ^{1}H NMR (DMSO-d_6) δ=2.02 (s, 3H, CH_3), 3.27 (br, 1H, OH), 3.93 (s, 3H, CH_3N), 7.40 (s, 5H, C_6H_5), 7.75 (m, 2H, Arom), and 8.30 (m, 2H, Arom). Found: C, 48.31; H, 3.99; N, 3.60%. Calcd for $C_{16}H_{16}NOSI$: C, 48.37; H, 4.06; N, 3.53%.

13e: Colorless needles (methanol/ether); mp 170.5—171 °C (decomp); ^{1}H NMR (DMSO-d_6) δ=0.67—1.67 (brm, 7H, n-C_3H_7), 3.67 (br, 1H, OH), 3.90 (s, 3H, CH_3N), 7.33 (s, 5H, C_6H_5), 7.73 (m, 2H, Arom), and 8.22 (m, 2H, Arom). Found: C, 50.86; H, 4.70; N, 3.38%. Calcd for $C_{18}H_{20}NOSI$: C, 50.83; H, 4.74; N, 3.29%.

13f: Colorless needles (methanol/acetone); mp 139—140 °C (decomp); ^{1}H NMR (DMSO-d_6) δ=2.10 (s, 3H, CH_3), 3.57 (brs, 1H, OH), 3.92 (s, 3H, CH_3N), 6.47 (q, 1H, Furan-H), 6.77 (d, 1H, Furan-H, J=3 Hz), 7.50—8.00 (m, 3H, Furan-H and Arom), and 8.23 (m, 2H, Arom). Found: C, 43.44; H, 3.65; N, 3.67%. Calcd for $C_{14}H_{14}NO_2SI$: C, 43.42; H, 3.64; N, 3.62%.

13g: Colorless needles (methanol/acetone); mp 179.5—180 °C (decomp); ^{1}H NMR (DMSO-d_6) δ=2.07 (s, 10H, $5CH_2$), 3.27 (br, 1H, OH), 4.43 (s, 3H, CH_3N), 7.77 (m, 2H, Arom), and 8.28 (m, 2H, Arom). Found: C, 44.82; H, 4.81; N, 3.69%. Calcd for $C_{14}H_{18}NOSI$: C, 44.81; H, 4.83; N, 3.73%.

13h: Colorless needles (methanol); mp 221—221.5 °C (decomp); ^{1}H NMR (DMSO-d_6) δ=1.33 (brs, 18H, $9CH_2$), 2.03 (br, 4H, $2CH_2$), 3.57 (br, 1H, OH), 4.67 (s, 3H, CH_3N), 7.80 (m, 2H, Arom), and 8.27 (m, 2H, Arom). Found: C, 51.96; H, 6.51; N, 2.83%. Calcd for $C_{20}H_{30}NOSI$: C, 52.29; H, 6.58; N, 3.05%.

18: Colorless needles (methanol/acetone); mp 195—195.5 °C (decomp); ^{1}H NMR (DMSO-d_6) δ=1.50 (s, 3H, CH_3), 2.00 (m, 4H, $2CH_2$), 3.99 (m, 2H, CH_2O), 4.25 (s, 3H, CH_3N), 7.69 (m, 2H, Arom), and 8.20 (m, 2H, Arom). Found: C, 43.33; H, 4.45; N, 3.94%. Calcd for $C_{13}H_{16}NOSI$: C, 43.22; H, 4.46; N, 3.88%.

General Procedure for the Alkylation of 2-(α-Hydroxyalkyl)-3-methylbenzothiazolium Iodides (12 and 13). A solution (1.6 M) of butyllithium (4.4 mmol) in hexane or a solution (0.8 M) of Grignard reagents (4.4 mmol; prepared from the corresponding bromide or chloride in THF) was added dropwise to a stirred and cooled suspension of 2-(α-hydroxyalkyl)benzothiazolium salt (**12** or **13**) (2 mmol) at −78 °C in the same solvent (10 ml). The mixture was stirred for 30 min at −78 °C and then allowed to warm to room temperature. After being stirred for 1 h, the mixture was quenched with large excess of water. After separation of the organic layer, the aqueous layer was extracted with dichloromethane. The combined organic layer was dried with $MgSO_4$ and filtered through silica gel (Wakogel C-300). Concentration of the solvent under reduced pressure afforded the nearly pure (monitored by TLC) 2-substituted 2-(α-hydroxyalkyl)-3-methylbenzothiazoline (**14**) as a viscous oil. A THF solution of 1-nonynyllithium (prepared by lithiation of 1,1-dibromo-1-nonene with butyllithium) was similarly used, giving the corresponding 2-(α-hydroxyalkyl)benzothiazolines (**14b**) which was isolated by short-column chromatography. These results are summarized in Table 5.

These compounds were used in the next hydrolysis step without further purification and identified at the same time by means of this hydrolysis transformation to the corresponding α-hydroxy ketones.

General Procedure for the Reduction of 2-(α-Hydroxyalkyl)-3-methylbenzothiazolium Iodides (12 and 13) with $NaBH_4$. The benzothiazolium salt **12** or **13** (2.0 mmol), dissolved in ethanol (8 ml), was treated with sodium borohydride (0.38 g, 10 mmol) at 0 °C. After stirring for 30 min at 0 °C and then 1 h at room temperature, the reaction mixture was diluted with water (30 ml) and the aqueous mixture was extracted with dichloromethane. The dichloromethane extract was dried with $MgSO_4$ and filtered through silica gel (Wakogel C-300). Concentration of the filtrate under reduced pressure afforded the nearly pure (monitored by TLC) 2-(α-hydroxyalkyl)-3-methylbenzothiazolines (**15**). The results are summarized in Table 6. ^{1}H NMR data of the products are as follows: **15a**: Viscous oil; ^{1}H NMR ($CDCl_3$) δ=1.05 (t, 3H, CH_3), 1.57 (m, 2H, CH_2), 2.62 (br, 1H, OH), 3.00 (s, 3H, CH_3N), 3.57 (m, 1H, CHOH), 4.81 (d, 1H, NCHS),

and 6.91 (m, 4H, Arom). **15b**: Viscous oil; ^{1}H NMR ($CDCl_3$) δ=0.87 (d, 3H, CH_3), 0.98 (d, 3H, CH_3), 1.93 (m, 1H, CH), 2.70 (s, 1H, OH), 2.87 (s, 3H, CH_3N), 3.30 (dd, 1H, CHOH), 4.60 (d, 1H, NCHS), and 6.67 (m, 4H, Arom). **15c**: Viscous oil; ^{1}H NMR ($CDCl_3$) δ=0.97 (s, 9H, $3CH_3$), 2.80 (s, 3H, CH_3N), 3.28 (dd, 1H, CHOH), 3.33 (s, 1H, OH), 4.54 (d, 1H, NCHS), and 6.73 (m, 4H, Arom). **15d**: Viscous oil; ^{1}H NMR ($CDCl_3$) δ=0.71—2.38 (br, 11H, cyclohexyl), 2.86 (s, 3H, CH_3N), 3.00 (br, 1H, OH), 3.33 (dd, 1H, CHOH), 4.71 (d, 1H, NCHS), and 6.79 (m, 4H, Arom). **15e**: Viscous oil; ^{1}H NMR ($CDCl_3$) δ=0.71—2.29 (m, 16H), 2.90 (s, 3H, CH_3N), 3.00 (br, 1H, OH), 3.81 (m, 1H, CHOH), 4.67 (d, 1H, NCHS), 5.00 (m, 1H, CH=C), and 6.72 (m, 4H, Arom). **15f**: Viscous oil; ^{1}H NMR ($CDCl_3$) δ=2.57 and 2.83 (s, 3H, CH_3N), 3.29 (br, 1H, OH), 3.76 (s, 6H, $2CH_3O$), 4.43 and 4.69 (d, 1H, CHOH), 4.86 and 5.04 (d, 1H, NCHS), and 6.10—7.00 (m, 7H, Arom). **15g**: Viscous oil; ^{1}H NMR ($CDCl_3$) δ=0.95 (s, 6H, $2CH_3$), 2.90 (s, 3H, CH_3N), 3.33 (dd, 1H, OH), 4.67 (d, 1H, NCHS), and 6.79 (m, 4H, Arom).

General Procedure for the Hydrolysis of 2-Substituted 2-(α-Hydroxyalkyl)-3-methylbenzothiazolines (14) to α-Hydroxy Ketones (16) with $AgNO_3$. Silver nitrate (0.51 g, 3.0 mmol), dissolved in water (5 ml), was added to the stirred solution of 2-substituted 2-(α-hydroxyalkyl)benzothiazoline (**14**) (prepared from 2.0 mmol of **12** or **13**) in acetonitrile (30 ml) and 0.05 M-pH 7-phosphate buffer (6.0 ml). After 15 min at room temperature, additional silver nitrate (0.51 g, 3.0 mmol), dissolved in water (5 ml), was added to the solution (in some cases, a yellow precipitate began to form during this second addition). After another 20 min at room temperature, triethylamine (0.20 g, 2.0 mmol) was added in order to neutralized the released acid (HNO_3) and stirring was continued for further 1 h at 45 °C. Saturated aqueous NaCl solution was added to the reaction mixture and the mixture was filtered through Celite. The filtrate was extracted with diethyl ether and ether extract was filtered through silica gel (Wakogel C-300). Evaporation of the solvent under reduced pressure gave the almost pure α-hydroxy ketones (**16**) that was free of 2-(methylamino)benzenethiol. The results are summarized in Table 5. Spectral data of the products are as follows: **16a**: Viscous oil; IR (neat) 3450 (OH) and 1700 cm^{-1} (C=O); ^{1}H NMR ($CDCl_3$) δ=1.00 (t, 6H, $2CH_3$), 1.13—2.10 (m, 6H, $3CH_2$), 2.40 (t, 2H, CH_2C=O), 3.50 (d, 1H, OH), and 4.12 (q, 1H, CHOH). **16b**: Viscous oil; IR (neat) 3450 (OH), 1695 (C=O), and 1590 cm^{-1} (C≡C); ^{1}H NMR ($CDCl_3$) δ=1.00 (t, 6H, $2CH_3$), 1.12—2.12 (m, 12H, $6CH_2$), 2.48 (t, 2H, CH_2C≡C), 4.33 (t, 1H, CHOH), and 5.33 (s, 1H, OH). **16c**: Viscous oil; IR (neat) 3450 (OH) and 1700 cm^{-1} (C=O); ^{1}H NMR ($CDCl_3$) δ=0.90 (m, 6H, $2CH_3$), 1.14—2.00 (m, 12H, $6CH_2$), 2.50 (t, 2H, CH_2C=O), 3.62 (d, 1H, OH), and 4.14 (q, 1H, CHOH). **16d**: Viscous oil; IR (neat) 3450 (OH) and 1670 cm^{-1} (C=O); ^{1}H NMR ($CDCl_3$) δ=1.06 (s, 9H, $3CH_3$), 1.06 (t, 3H, CH_3), 1.10—1.86 (m, 4H, $2CH_2$), 2.52 (t, 2H, CH_2C=O), 3.40 (d, 1H, OH), and 3.81 (d, 1H, CHOH). **16e**: Viscous oil; IR (neat) 3480 (OH) and 1710 cm^{-1} (C=O); ^{1}H NMR ($CDCl_3$) δ=0.71—2.10 (m, 18H, cyclohexyl and *n*-C_3H_7), 2.48 (t, 2H, CH_2C=O), 3.52 (d, 1H, OH), and 4.00 (dd, 1H, CHOH). **16f**: Viscous oil; IR (neat) 3450 (OH) and 1700 cm^{-1} (C=O); ^{1}H NMR ($CDCl_3$) δ=0.79 (t, 3H, CH_3), 1.14 (s, 6H, $2CH_3$), 1.20—1.90 (m, 4H, $2CH_2$), 2.48 (t, 2H, CH_2C=O), and 3.48 (d, 1H, OH).

References

1) D. Seebach and M. Kolb, *Chem. Ind. (London)*, **1974**, 687; D. Seebach, *Angew. Chem., Int. Ed. Engl.*, **18**, 239 (1979).

2) B. T. Grobel and D. Seebach, *Synthesis*, **1977**, 357; L. Field, *Synthesis*, **1978**, 713; T. A. Hase and J. K. Koskimies, *Aldrichimica Acta*, **14**, 73 (1981).

3) E. J. Corey and D. Seebach, *Angew. Chem., Int. Ed. Engl.*, **4**, 1075 (1965).

4) A. I. Meyers and E. W. Collington, *J. Am. Chem. Soc.*, **92**, 6676 (1970).

5) H. Gilman and J. A. Beel, *J. Am. Chem. Soc.*, **71**, 2328 (1949).

6) E. J. Corey and D. L. Boger, *Tetrahedron Lett.*, **1978**, 5.

7) H. Chikashita, S. Ikegami, T. Okumura, and K. Itoh, *Synthesis*, **1986**, 375.

8) H. Chikashita, M. Ishihara, and K. Itoh, *Heterocycles*, **23**, 2467 (1985).

9) A similar elimination of 2-(1-substituted 1-hydroxyalkyl)-3-methylbenzothiazolium iodides under basic conditions (aqueous K_2CO_3) has already been applied to a synthesis of ketones: see Ref. 8.

10) This method has been reported to be very effective for the hydrolysis of a variety of 3-methylbenzothiazoline derivatives to the corresponding parent carbonyl compounds: H. Chikashita, N. Ishimoto, S. Komazawa, and K. Itoh, *Heterocycles*, **23**, 2509 (1985); see also Refs. 6 and 7.

11) P. Jutzi and H. J. Hoffmann, *Chem. Ber.*, **106**, 594 (1973).

 © 1988 The Chemical Society of Japan Bull. Chem. Soc. Jpn., 61, 3649—3652 (1988)

Reactions of (Triphenylphosphine)gold(I) Enolates and Homoenolates

Masahiro MURAKAMI, Masahiko INOUYE, Michinori SUGINOME, and Yoshihiko ITO*
Department of Synthetic Chemistry, Faculty of Engineering, Kyoto University, Yoshida, Kyoto 606
(Received June 8, 1988)

Some reactions of (triphenylphosphine)gold(I) enolates and homoenolates, which are respectively prepared by the reaction of trimethylsilyl ethers of enols and cyclopropanols with (triphenylphosphine)gold(I) chloride in the presence of cesium fluoride, are described. The aldol reaction of (triphenylphosphine)gold(I) enolates with carbonyl compounds is efficiently promoted by Lewis acids such as titanium tetrachloride and diethylaluminum chloride to produce β-hydroxy carbonyl compounds. (Triphenylphosphine)gold(I) enolate reacts with phenyl acetylene to afford (triphenylphosphine)gold(I) phenylacetylide in good yield. Reaction of (benzoylmethyl)(triphenylphosphine)gold(I) (**3a**) with chlorotrimethylsilane produces α-(trimethylsilyloxy)styrene and (triphenylphosphine)gold(I) chloride, which is the reverse of the formation of **3a**. Gold(I) enolate undergoes an isocyanide insertion reaction into the linkage of carbon and gold. (2-Benzoylethyl)(triphenylphosphine)gold(I) reacts with 2-methyl-2-propanethiol to afford (triphenylphosphine)gold(I) *t*-butyl sulfide together with propiophenone.

Some gold(I) enolate complexes have been hitherto reported.[1] Carbon-bound gold(I) enolates of so-called active methylene compounds were prepared with thallium salts of active methylene compounds.[2] Carbon-bound gold(I) enolates of methyl ketones such as acetone and acetophenone were prepared by the reaction of methyl ketones with (triphenylphosphine)gold(I) bromide and silver oxide or with $(Ph_3PAu)_3O^+BF_4^-$.[3] Recently we reported a new preparative method for regioselectively forming carbon-bound (triphenylphosphine)gold(I) enolates (**3**) and homoenolates (**5**), in which trimethylsilyl ethers of enols **2** and cyclopropanols (**4**) are respectively treated with (triphenylphosphine)gold(I) chloride (**1**) in the presence of cesium fluoride (Eqs. 1, 2).[4] No reaction of **2** or **4** with **1** occurred in the absence of cesium fluoride.

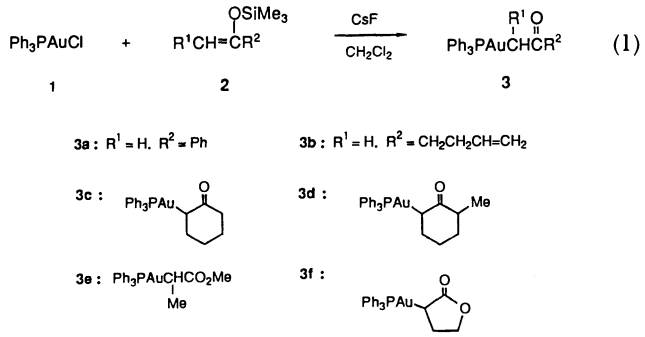

Unlike the previous method, our method features a regioselective formation of carbon-bound gold(I) enolates via trimethylsilyl ethers of enols from unsymmetrical ketones. X-Ray analyses of (benzoylmethyl)(triphenylphosphine)gold(I) (**3a**) and (2-benzoylethyl)(triphenylphosphine)gold(I) (**5a**) thus prepared unambiguously disclosed the carbon-bound gold(I) enolate and homoenolate structures with almost linear C-Au-P.[4]

Herein, we wish to report some reactions of gold(I) enolates and homoenolates.

Results and Discussion

Reactions of (Triphenylphosphine)gold(I) Enolates. [a] Lewis Acid Promoted Aldol Reactions: (Triphenylphosphine)gold(I) enolates (**3**) did not react with aldehydes. However, addition of Lewis acids efficiently promoted the aldol reaction of (triphenylphosphine)gold(I) enolates with carbonyl compounds to produce β-hydroxy carbonyl compounds (Table 1). Among a variety of Lewis acids, titanium tetrachloride and diethylaluminum chloride gave good results. It is noteworthy that gold(I) enolates readily reacted at −78 °C even with ketones, which are generally unreactive in aldol reaction, in the presence of titanium tetrachloride. Stereoselectivities of the Lewis acid promoted aldol reaction of gold(I) enolates were generally disappointing except for the high diastereoselectivity (91 : 9) observed in the titanium tetrachloride mediated reaction of gold(I) enolate of cyclohexanone with benzaldehyde. Intermediacy of titanium enolate generated by transmetallation of gold(I) enolate with titanium tetrachloride may be suggested in the present reaction, because the very similar diastereoselectivity was found in the reaction of titanium enolate of cyclohexanone with benzaldehyde.[5]

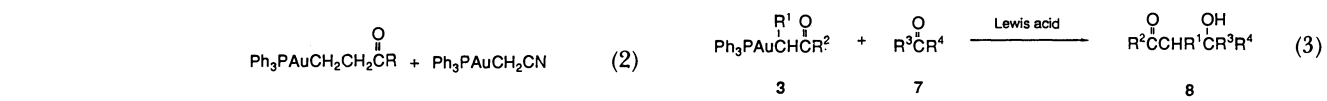

[b] Miscellaneous Reactions: (Triphenylphosphine)gold(I) enolates were relatively stable to oxygen and moisture and could be handled quickly in the open air, but gradually decomposed in solution. Some reactions with (benzoylmethyl)(triphenylphosphine)-gold(I) (**3a**) are shown in Eq. 4. Gold(I) enolate **3a** was inert to alcohol. But 2-methyl-2-propanethiol reacted

Table 1. Lewis Acid Promoted Aldol Reaction

Run	3	7	Lewis acid	Conditions	Yield/%	Syn : Anti[a] (erythro) (threo)
1	$PhCCH_2Au(PPh_3)$	PhCHO	$BF_3 \cdot OEt_2$	−78 °C, 8 h	33[b]	—
2			Et_2AlCl	−78 °C, 5.5 h	66[b]	—
3			$TiCl_4$	−78 °C, 2 h	88[b]	—
4		$PhCCH_3$	Et_2AlCl	−78 °C, 9.5 h	38[c]	—
5			$TiCl_4$	−78 °C, 5 h	64[c]	—
6		$PhCH_2CH_2CHO$	Et_2AlCl	−78 °C, 4.5 h	63[d]	—
7	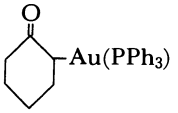	PhCHO	$TiCl_4$	−78 °C, 4 h	54[e]	91 : 9
8	$MeOCCHAu(PPh_3)$, Me	PhCHO	Et_2AlCl	−78 °C, 4.5 h	37[f]	61 : 39
9			$TiCl_4$	−78 °C, 3.5 h	81[f]	55 : 45
10			$Ti(OPr^i)_3Cl$	0 °C, 5 h	23[f]	50 : 50
11			$SnCl_4$	0 °C, 4 h	31[f]	50 : 50

a) Determined by ^1H NMR. b) Ref 6. c) Ref 7. d) Ref 8. e) Ref 9. f) Ref 10.

with **3a** at room temperature to give (triphenylphosphine)gold(I) *t*-butyl sulfide (**9**) together with acetophenone. Similarly, reaction of **3a** with phenylacetylene afforded (triphenylphosphine)gold(I) phenylacetylide (**10**) with acetophenone. Gold(I) enolate **3a** did not react with diphenyl disulfide but reacted with diphenyl diselenide to give (triphenylphosphine)-gold(I) phenyl selenide (**11**) with (phenylseleno)acetophenone (**12**).

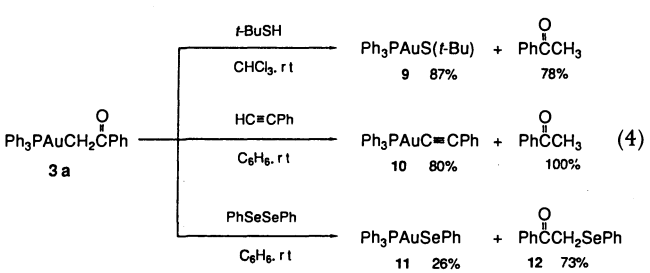

(4)

Reaction of **3a** with chlorotrimethylsilane produced α-(trimethylsilyloxy)styrene (**2a**) and (triphenylphosphine)gold(I) chloride (**1**). The reaction is the reverse of the formation of (triphenylphosphine)gold(I) enolate (**3a**). A similar reaction was observed with acetyl chloride.[3a] The gold(I) enolate (**3a**) was treated with acetyl chloride to give 1-phenylvinyl acetate (**13**) with (triphenylphosphine)gold(I) chloride (**1**).

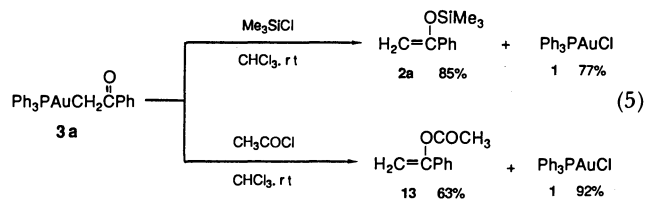

(5)

Reaction of **3a** with methyllithium in tetrahydrofuran (THF) at 0 °C gave rise to the formation of methyl-(triphenylphosphine)gold(I) (**14**) after workup with H_2O. Lithium enolate (**15**) of acetophenone, which may be concomitantly generated in the reaction, was indeed trapped. When **3a** was treated with methyllithium in THF at −78 °C and subsequently with benzaldehyde, chalcone (**16**) was isolated in 82% yield.

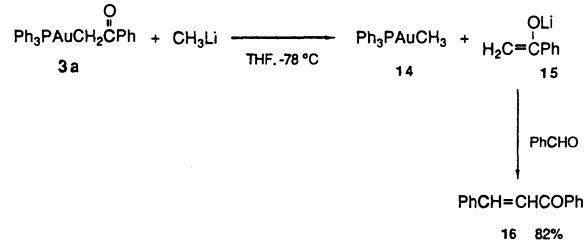

(6)

Gold(I) enolate **3a** underwent an isocyanide insertion reaction into the linkage of carbon and gold according to Eq. 7. NMR spectra revealed that the insertion product **17** exists in an enolized form.

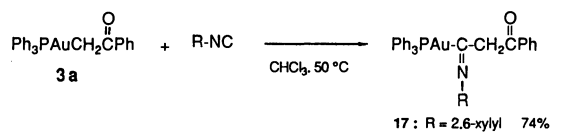

(7)

Reaction of (Triphenylphosphine)gold(I) Homoenolates. In contrast to gold(I) enolates, gold(I) homoenolates were rather unreactive and attempted reactions with gold(I) homoenolates were unsuccessful except for the reaction with 2-methyl-2-propanethiol shown in Eq. 8.

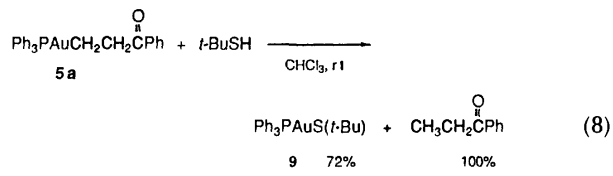

(8)

Experimental

General. Melting points were determined on a Yanaco MP-S3 apparatus and are uncorrected. ^{1}H NMR spectra were recorded on a JEOL JNM-MH 100 spectrometer (100 MHz) with Me_4Si as an internal standard. ^{13}C NMR spectra were obtained on a JNM-GX 400 spectrometer (100 MHz). Infrared spectra were obtained on a Hitachi 270-30 spectrophotometer. Cesium fluoride (Aldrich) was used after drying at ca. 200 °C in vacuo.

Preparation of Gold(I) Enolates 3a—e. Gold(I) enolates **3a—e** were prepared according to the procedure described.[4]

(2-Oxo-5-hexenyl)(triphenylphosphine)gold(I) (3b): 99%; ^{1}H NMR ($CDCl_3$) δ=2.00—2.61 (m, 4H), 2.61—2.87 (br. s, 2H), 4.73—5.12 (m, 2H), 5.61—6.10 (m, 1H), 7.03—7.80 (m, 15H); IR (neat) 1642, 1482, 1102, 910 cm^{-1}.

(2-Oxocyclohexyl)(triphenylphosphine)gold(I) (3c): 81%; ^{1}H NMR ($CDCl_3$) δ=0.86—2.84 (m, 8H), 3.13—3.26 (m, 1H), 7.06—7.85 (m, 15H); IR (neat) 1620, 1440, 1102, 910 cm^{-1}.

(3-Methyl-2-oxocyclohexyl)(triphenylphosphine)gold(I) (3d): 67%; ^{1}H NMR ($CDCl_3$) δ=0.75—2.96 (m, 7H), 1.07 (d, 3H, J=7 Hz), 3.08—3.35 (m, 1H), 7.04—7.86 (m, 15H); IR (neat) 1636, 1482, 1440, 1102 cm^{-1}.

[1-(Methoxycarbonyl)ethyl](triphenylphosphine)gold(I) (3e): 99%; ^{1}H NMR ($CDCl_3$) δ=1.16 (dd, 3H, J_{H-H}=6 Hz and J_{H-P}=6 Hz), 2.65 (dq, 1H, J_{H-H}=6 Hz and J_{H-P}=12 Hz), 3.66 (s, 3H), 7.16—7.69 (m, 15h); IR (neat) 1682, 1438, 1156, 1102 cm^{-1}.

(2-Oxotetrahydro-3-furyl)(triphenylphosphine)gold(I) (3f). To a suspension of anhydrous cesium fluoride (76 mg, 0.5 mmol) and (triphenylphosphine)gold(I) chloride (50 mg, 0.1 mmol) in acetonitrile (1.5 mL), 2-trimethylsilyloxy-4,5-dihydrofuran (**2f**, 32 mg, 0.2 mmol) was added. The mixture was stirred overnight at room temperature and filtered to remove insoluble inorganic salts. The filtrate was evaporated, washed with CH_2Cl_2, and subjected to column chromatography on silica gel pretreated with triethylamine to give **3f**; 28 mg, 51%; mp 149 °C (decomp); ^{1}H NMR ($CDCl_3$) δ=2.42—3.09 (m, 3H), 4.29—4.56 (m, 2H), 7.32—7.74 (m, 15H); ^{13}C NMR ($CDCl_3$) δ=31.1 (J_{C-P}=5 Hz), 42.2 (J_{C-P}=76 Hz), 68.5, 185.4; IR (KBr) 1692 cm^{-1}. Found: C, 48.28; H, 3.61; P, 5.43%. Calcd for $C_{22}H_{20}AuO_2P$: C, 48.54; H, 3.70; P, 5.69%.

(2-Benzoylethyl)(triphenylphosphine)gold(I) (5a). To a suspension of anhydrous cesium fluoride (286 mg, 1.95 mmol) and (triphenylphosphine)gold(I) chloride (193 mg, 0.390 mmol) in acetonitrile (6 mL), 1-phenyl-1-(trimethylsilyloxy)cyclopropane (111 mg, 0.539 mmol) was added and the mixture was stirred for 4 h at 50 °C. The resulting orange suspension was filtered and the filtrate was evaporated to leave brown oil, which was subjected to column chromatography on silica gel pretreated with triethylamine to give (2-benzoylethyl)(triphenylphosphine)gold(I) (**5a**, 176 mg, 76%) and (cyanomethyl)(triphenylphosphine)gold(I) (**6**, 34 mg, 17%). **5a**: mp 121—122 °C (decomp); ^{1}H NMR ($CDCl_3$) δ=1.48—1.79 (m, 2H), 3.28—3.58 (m, 2H), 7.22—7.74 (m, 18H), 7.99—8.15 (m, 2H); ^{13}C NMR ($CDCl_3$) δ=25.7 (d, J_{C-P}=95.5 Hz), 40.6 (d, J_{C-P}=4 Hz), 204.9 (d, J_{C-P}=5 Hz); IR (KBr) 1670 cm^{-1}. Found: C, 54.47; H, 3.98; P, 5.41%. Calcd for $C_{27}H_{24}OPAu$: C, 54.74; H, 4.08; P, 5.23%. **6**: mp 131—133 °C (decomp); ^{1}H NMR ($CDCl_3$) δ=1.66 (d, 2H, J=10.0 Hz), 7.31—7.76 (m, 15H); IR (KBr) 2200 cm^{-1}. Found: C, 48.00; H, 3.36; N, 2.65; P, 6.07%. Calcd for $C_{20}H_{17}AuNP$: C, 48.11; H, 3.43; N, 2.81; P, 6.20%.

[2-(Ethoxycarbonyl)ethyl](triphenylphosphine)gold(I) (5b): 78%; ^{1}H NMR ($CDCl_3$) δ=1.18 (t, 3H, J=7 Hz), 1.54 (m, 2H), 2.73 (m, 2H), 4.07 (q, 2H, J=7 Hz), 7.40—7.61 (m, 15H); IR (neat) 1728, 1484, 1440, 1100 cm^{-1}.

Lewis Acid Promoted Aldol Reaction. Representative procedure of Lewis acid promoted aldol reaction is given by the preparation of methyl 3-hydroxy-2-methyl-3-phenylpropanoate: To a dichloromethane solution (1 mL) of [1-(methoxycarbonyl)ethyl](triphenylphosphine)gold(I) (48 mg, 0.087 mmol) and benzaldehyde (11 mg, 0.10 mmol), a dichloromethane solution (0.13 mL) of titanium tetrachloride (0.13 mmol) was added at −78 °C, and the reaction mixture was stirred for 5 h at that temperature. Saturated aq. $NaHCO_3$ solution (5 mL) was added and, after usual extractive workup, methyl 3-hydroxy-2-methyl-3-phenylpropanoate (14 mg, 81%) was isolated by preparative TLC on silica gel.

(Triphenylphosphine)gold(I) *t*-Butyl Sulfide (9). A chloroform solution (0.3 mL) of (benzoylmethyl)(triphenylphosphine)gold(I) (**3a**, 24 mg, 0.041 mmol) and 2-methyl-2-propanethiol (5 mg, 0.05 mmol) was sonicated in a sealed tube at room temperature. After 1 h, hexane (0.9 mL) was added to give **9** as colorless crystals: 20 mg, 87%; mp 166—168 °C; ^{1}H NMR ($CDCl_3$) δ=1.60 (s, 9H), 7.27—7.71 (m, 15H). Found: C, 48.08; H, 4.35; P, 5.66%. Calcd for $C_{22}H_{24}AuPS$: C, 48.18; H, 4.41; P, 5.65%.

(Triphenylphosphine)gold(I) Phenylacetylide (10). A chloroform solution (0.3 mL) of **3a** (23 mg, 0.040 mmol) and phenylacetylene (7 mg, 0.07 mmol) was sonicated in a sealed tube at room temperature for 4 h. Then the reaction mixture was subjected to column chromatography on silica gel to give **10**: 18 mg, 80%; mp 165—166 °C (lit, 163—164 °C).[11]

Formation of (Triphenylphosphine)gold(I) Phenyl Selenide (11) and (Phenylseleno)acetophenone (12). In a sealed tube, a benzene solution (0.3 mL) of (benzoylmethyl)(triphenylphosphine)gold(I) (**3**, 23 mg, 0.040 mmol) and diphenyl diselenide (13 mg, 0.04 mmol) was sonicated at room temperature. After 12 h, the mixture was subjected to preparative TLC on silica gel to give **11** (6.3 mg, 26%) and **12** (8.0 mg, 73%). **11**: mp 146—149 °C (decomp); ^{1}H NMR ($CDCl_3$) δ=6.70—7.90 (m, 20H). Found: C, 46.81; H, 3.21; P, 5.03%. Calcd for $C_{24}H_{20}AuPSe$: C, 46.85; H, 3.28; P, 5.03%.

Formation of α-Trimethylsilyloxystyrene (2a). In a sealed tube, a $CDCl_3$ solution (0.3 mL) of (benzoylmethyl)-(triphenylphosphine)gold(I) (**3**, 23 mg, 0.040 mmol) and chlorotrimethylsilane (9 mg, 0.08 mmol) was sonicated at room temperature for 2.5 h. The formation of **2a** was observed by ^{1}H NMR [δ=0.25 (s), 4.47 (d, J=2 Hz), 4.95 (d, J=2 Hz)] and the yield was determined using an internal standard. (Triphenylphosphine)gold(I) chloride (**1**, 15 mg, 77%) was isolated by column chromatography on silica gel pretreated with triethylamine.

Formation of 1-Phenylvinyl Acetate (13). In a sealed tube, a chloroform solution (0.3 mL) of (benzoylmethyl)(triphen-

ylphosphine)gold(I) (**3**, 23 mg, 0.040 mmol) and acetyl chloride (5 mg, 0.06 mmol) was sonicated at room temperature. After 1 h, the mixture was subjected to column chromatography on silica gel pretreated with triethylamine to give **1** (18 mg, 92%) and **13** (4 mg, 63%).

Formation of Chalcone (16). To a solution of (benzoylmethyl)(triphenylphosphine)gold(I) (25 mg, 0.043 mmol) in THF (1 mL), an ether solution (0.14 mL) of methyllithium (0.055 mmol) was added at −78 °C under a nitrogen atmosphere. After stirring for 30 min, benzaldehyde was added (6.4 mg, 0.06 mmol) and the reaction mixture was allowed to warm gradually to room temperature and quenched with methanol (10 mL). The mixture was subjected to preparative TLC on silica gel to give chalcone (7.3 mg, 82%).

[2-Benzoyl-1-(2,6-xylylimino)ethyl](triphenylphosphine)-gold(I) (17). Under a nitrogen atmosphere, chloroform solution (2 mL) of **3a** (35 mg, 0.060 mmol) and 2,6-xylyl isocyanide (12 mg, 0.090 mmol) was heated at 50 °C for 6 h. Resulting yellow mixture was subjected to column chromatography on silica gel pretreated with triethylamine to give **17**: 32 mg, 74%; mp 160 °C (decomp); ^{1}H NMR ($CDCl_3$) δ= 2.37 (s, 6H), 6.08 (s, 1H), 6.95—8.12 (m, 23H); ^{13}C NMR ($CDCl_3$) δ=19.09, 101.22, 185.2, 209.1; IR (KBr) 1506, 1438 cm^{-1}. Found: C, 59.07; H, 4.58; N, 1.74: P, 4.62%. Calcd for $C_{35}H_{31}AuNOP$: C, 59.24; H, 4.40; N, 1.97, P, 4.37%.

References

1) R. J. Puddephatt, "Comprehensive Organometallic Chemistry," ed by G. Wilkinson, F. G. A. Stone, and E. W. Abel, Pergamon Press, Oxford, Vol. 2 (1982), p. 765.

2) a) B. J. Gregory and C. K. Ingold, *J. Chem. Soc. B*, **1969**, 276. b) D. Gibson, B. F. G. Johnson, and J. Lewis, *J. Chem. Soc. A*, **1970**, 367.

3) a) A. N. Nesmeyanov, E. G. Perevalova, K. I. Grandberg, and D. A. Lemenovskii, *Izv. Akad. Nauk SSSR, Ser. Khim.*, **1974**, 1124. b) A. N. Nesmeyanov, E. G. Perevalova, and D. A. Lemonovskii, *ibid.*, **1974**, 1661.

4) Y. Ito, M. Inouye, M. Suginome, and M. Murakami, *J. Organomet. Chem.*, **342**, C41 (1988).

5) E. Nakamura, J. Shimada, Y. Horiguchi, and I. Kuwajima, *Tetrahedron Lett.*, **24**, 3341 (1983).

6) K. Maruoka, S. Hashimoto, Y. Kitagawa, H. Yamamoto, and H. Nozaki, *J. Am. Chem. Soc.*, **99**, 7705 (1977).

7) J. Colonge, *Compt. Rend.*, **196**, 1414 (1933).

8) T. Mukaiyama and T. Inoue, *Chem. Lett.*, **1976**, 559.

9) T. Mukaiyama, K. Banno, and K. Narasaka, *J. Am. Chem. Soc.*, **96**, 7503 (1974).

10) J. Canceill, J. J. Basselier, and J. Jacques, *Bull. Soc. Chim. Fr.*, **1967**, 1024.

11) G. E. Coates and C. Parkin, *J. Chem. Soc.*, **1962**, 3220.

 © 1988 The Chemical Society of Japan Bull. Chem. Soc. Jpn., 61, 3653—3657 (1988)

Peptide Synthesis in Alcohol Solvents by the Mixed Anhydride Method Using Dimethylphosphinothioyl Chloride

Masaaki UEKI,* Takashi SAITO, Jun SASAYA, Shigeru IKEDA,† and Hidekazu OYAMADA
Department of Applied Chemistry, Science University of Tokyo, 1-3 Kagurazaka, Shinjuku-ku, Tokyo 162
(Received July 1, 1988)

The formation and coupling of the dimethylphosphinothioic mixed anhydrides of protected amino acids can be performed in alcohol solvents. Sparingly soluble protected C-terminal segments of vasoactive intestinal peptide (VIP) up to the heptapeptide stage were synthesized by this technique and fully characterized.

In peptide synthesis low solubility of even small peptides can result in incomplete reaction giving unpurifiable materials with lack of purification method. Thus, solubility problems may prevent further elongation of the peptide chain. The solid phase method[1] is one solution to this problem. For solution syntheses various kinds of organic solvents having high solubilizing power such as *N,N*-dimethylformamide, dimethyl sulfoxide, and hexamethylphosphoric triamide, all of which are classified as dipolar aprotic solvents, have been utilized. Among polar protic solvents alcohols, especially methanol, have high solubilizing ability for peptides, although their use as solvents in peptide bond formation is not normally possible because of their high reactivity toward the activated amino acid derivatives.

Recently we reported that dimethylphosphinothioic mixed anhydrides (Mpt-MAs), formed from protected amino acids by reaction with dimethylphosphinothioyl chloride (Mpt-Cl)[2] in the presence of a base, were stable toward isolation and reacted very selectively toward amino functions.[3]

Mpt-MAs react with alcohols only in presence of basic catalysts such as 4-dimethylaminopyridine and imidazole.[4] Such high stability toward alcohols and selectivity toward the amino group can be attributed to the presence of the P=S bond. In this study we applied the Mpt-MA method to peptide synthesis in alcohol solvents in order to determine whether the selectivity was high enough for use in practical peptide syntheses. If this were the case it would represent an efficient solution to the often serious solubility problem.

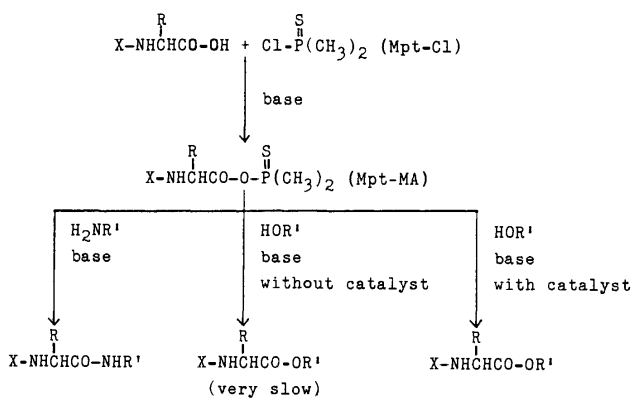

† Present address: Kokusan Chemical Works, Ltd., Gunma Factory, 2566 Oowa, Meiwa-mura, Oora-gun, Gunma 370-07.

Results and Discussion

The possibility of using alcohol solvents in peptide synthesis was first investigated by examination of the synthesis of model peptides. The results are summarized in Table 1.

In these experiments the Mpt-MAs were generated in situ. Generally the formation of Mpt-MAs can be easily followed by thin layer chromatography (TLC) since these compounds can be visualized, without removing the amino protecting group, simply by spraying with ninhydrin reagent followed by warming. For reasons not yet clear a color reaction toward ninhydrin arises from the Mpt mixed anhydride group itself.

Methanol (Entries 3 and 6) and ethanol (Entry 7) could be used as well as chloroform (Entries 1, 2, 4, and 5) in the mixed anhydride formation. However, when 2,2,2-trifluoroethanol was used (Entry 8) formation of ester was observed even during the activation step. Methanol (Entries 3 and 6) and ethanol (Entry 7) could be used in both activation and coupling steps and yields of peptides obtained in this way were high. Since methanol is a more effective solvent than ethanol for the peptide segments, the former was used in the following experiments.

Vasoactive intestinal peptide (VIP), isolated in 1970 by Said and Mutt from the small intestine of the hog,[5] is a linear octacosapeptide amide.[6] Total synthesis of VIP has been achieved by many groups by solution[7,8] and solid phase[9-11] methods. In all previous solution syntheses much effort was required to overcome the solubility problem.[12] In a recent synthesis Schaaper and Beyerman temporarily substituted Asn[28] by the corresponding β-*t*-butyl aspartate ester which was subsequently converted to Asn.[13] Clearly for such sparingly soluble peptides the development of a generally applicable solvent would offer significant improvements over current techniques. As an example to demonstrate the efficiency of methanol as a solvent for peptide bond formation, stepwise synthesis of the relatively insoluble C-terminal segments of VIP up to the heptapeptide stage was investigated. Results obtained in the case of di-, tri-, and tetrapeptide amides are

Table 1. Peptide Synthesis in Alcohol Solvents[a)]

$$\text{Prot-AA}^1\text{-OH} + \text{Cl-Mpt} \xrightarrow[\text{Solvent}^1]{\text{TEA}} [\text{Prot-AA}^1\text{-OMpt}] \xrightarrow[\text{Solvent}^2(\text{R}^2\text{-OH})]{\text{H-AA}^2\text{-OR}^1 + \text{TEA}} \text{Prot-AA}^1\text{-AA}^2\text{-OR}^1 + \text{Prot-AA}^1\text{-OR}^2$$

Entry	Peptide	Solvent[1]	Solvent[2]	Yield/%	Mp θ_m/°C	Yield (%) of Prot-AA[1]-OR[2]
1	Boc-Pro-Phe-OBzl	$CHCl_3$	$CHCl_3$	86	(oil)	—
2		$CHCl_3$	CH_3OH	93	(oil)	0
3		CH_3OH	CH_3OH	95	(oil)	0
4	Boc-Val-Val-OMe	$CHCl_3$	$CHCl_3$	96	165.0—166.5	—
5		$CHCl_3$	CH_3OH	93	163.0—165.0	0
6		CH_3OH	CH_3OH	82	163.0—165.0	0
7		C_2H_5OH	C_2H_5OH	93	162.0—163.5	0
8		CF_3CH_2OH	CF_3CH_2OH	14	160.5—161.5	37

a) Unless otherwise noted the MA was generated at 0 °C for 1 h and coupled with an amino component at 0 °C overnight.

Table 2. Synthesis of VIP C-terminal Di-, Tri-, and Tetrapeptide Amide

Entry	Peptide	Method	Solvent		Yield/%
			Activation	Coupling	
1	Z-Leu-Asn-NH_2	Mpt-MA(direct)	$CHCl_3$	CH_3OH	88
2		Mpt-MA(isolated)		CH_3OH	95
3		Mpt-MA(isolated)		CH_3OH-H_2O	98
4		NP active ester		DMF	93[a)]
5	Z-Ile-Leu-Asn-NH_2	Mpt-MA(direct)	$CHCl_3$	CH_3OH	52
6		Mpt-MA(isolated)		CH_3OH	95
7		NP active ester		DMF	87[a)]
8	Z-Ser-Ile-Leu-Asn-NH_2	Mpt-MA(direct)	$CHCl_3$	CH_3OH	94
9		Mpt-MA(isolated)		CH_3OH	94

a) Ref. 12.

summarized in Table 2.

In these reactions the desired products precipitated during the reaction. Z-Leu-Asn-NH_2 was obtained in 88% yield when Z-Leu-OMpt, generated in situ in chloroform, was added to a solution of H-Asn-NH_2·HBr in methanol containing triethylamine (Entry 1). However, when synthesis of the related tripeptide was carried out by the same method (Entry 5) the yield of Z-Ile-Leu-Asn-NH_2 was only 52%. In this case precipitation of the product began too early thus causing coprecipitation of the free amino component which was difficult to remove from the tripeptide. In order to avoid this problem Z-Ile-OMpt was first freed from triethylamine hydrochloride by washing the solution with water and then coupled with free H-Leu-Asn-NH_2 in methanol (Entry 6). This technique gave Z-Ile-Leu-Asn-NH_2 in a yield of 95%. Similar result was also obtained in the case of dipeptide synthesis (Entry 2). These results compare favorably with those obtained by Bodanszky, et al., which involved coupling of the *p*-nitrophenyl active ester in *N*,*N*-dimethylformamide.[12)]

At the tetrapeptide stage a somewhat different situation emerged. Serine is found as the fourth amino acid from the C-terminal position. As previously reported[3)] incorporation of serine into a peptide chain is possible without protecting the side-chain hydroxyl group when using the Mpt-MA method. However the isolated yield of Z-Ser-OMpt is exceptionally low because of the lactone formation. Since yields using isolated and in-situ-generated Z-Ser-OMpt are nearly the same, the method involving in situ activation is more convenient.

At the pentapeptide stage another difficulty was encountered. Solubility of the free tetrapeptide amide, H-Ser-Ile-Leu-Asn-NH_2, in methanol is much lower than the free C-terminal mono-, di-, and tripeptide amides. This may limit the use of methanol as a sole solvent in the synthesis of peptide segments containing asparagine and glutamine. However, it is known that peptides containing these amino acids, although not soluble in a single organic solvent, often dissolve in aqueous organic solvents. Synthesis was therefore examined in aqueous methanol.

When a methanolic solution of Z-Leu-OMpt was added, in 2 portions with a 20 min interval between additions, to a methanol-water (2 : 3) solution of asparaginamide, the dipeptide Z-Leu-Asn-NH_2 was obtained in 98% yield. This result shows that aqueous methanol can be more effective solvent than methanol itself for the synthesis of longer peptides containing asparagine and glutamine.

At the 24-position of VIP is found asparagine whose activation via the Mpt technique required some caution. Mpt-MA formation is usually performed at room temperature except in the case of serine which requires cooling to 0 °C in order to avoid lactone formation. In the case of asparagine, complex reactions, possibly including nitrile formation, were observed even at 0 °C. Fortunately this side-reaction could be suppressed by carrying out the reaction at −20 °C in either methanol or chloroform. These conditions were applied to the synthesis of Z-VIP(24—28)-NH_2.

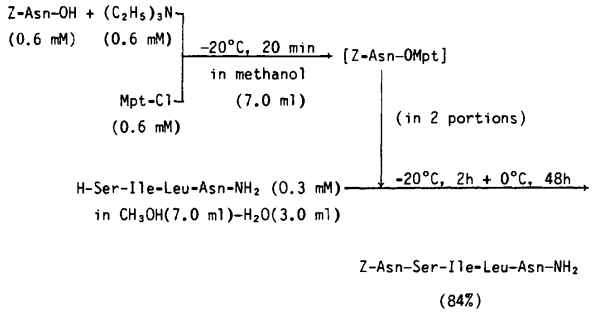

When a methanolic solution of Mpt-MA prepared from Z-Asn and Mpt-Cl at −20 °C for 20 min in the presence of triethylamine was added to a solution of H-Ser-Ile-Leu-Asn-NH_2 in methanol-water and the mixture stirred at the same temperature for 2 h and then at 0 °C for 48 h the pentapeptide Z-Asn-Ser-Ile-Leu-Asn-NH_2 was obtained in 84% yield in an analytically pure form.

The sixth amino acid, Leu, could be introduced without any problem using the salt-free, washed Mpt-MA along with free H-Asn-Ser-Ile-Leu-Asn-NH_2 dissolved in a methanol-water mixture. However, when Z-Tyr was coupled to H-Leu-Asn-Ser-Ile-Leu-Asn-NH_2 in a similar manner the crude product was contaminated with the free amino component and obtained in only 48% yield. Reprecipitation of the crude product from DMSO-H_2O or DMSO-methanol did not give pure material. Except for special amino acids such as Ser and Asn Mpt-MAs are sufficiently stable to be used for coupling reactions above room temperature thus avoiding premature precipitation. For example, when Z-Tyr-OMpt in methanol was added to a solution of H-Leu-Asn-Ser-Ile-Leu-Asn-NH_2 in a methanol-water mixture followed by stirring at 38—40 °C for 2 h and at room temperature for 46 h the desired product was obtained in 74% yield without contamination by the free amino component. In this case the unprotected tyrosine side-chain hydroxyl group caused no difficulty.

In the report of Bodanszky, et al.,[12] intermediates involved in the VIP synthesis could not be characterized except for the trifluoroacetates of *N*-deprotected peptide amides and for protected peptide amides longer than tripeptide only melting points and amino acid analyses were recorded. In the present study it was possible to characterize all of the protected and free peptide amides by amino acid analysis, elemental analysis and TLC. In addition melting points and optical rotation values could be recorded for the first time as shown in Tables 3 and 4.

In conclusion, peptide synthesis by the Mpt-MA method using methanol or methanol-water mixtures as solvents provides a convenient and efficient solution to the solubility problem in peptide synthesis.

Experimental

Amino acids and their derivatives used here are all of the L configuration. Abbreviations given by the IUPAC-IUB Commission (*J. Biol. Chem.*, **247**, 977 (1972)) are used throughout. Additional abbreviations: Z, benzyloxycarbonyl; Boc, *t*-butyloxycarbonyl; DCHA, dicyclohexylamine; TEA, triethylamine; AcOH, acetic acid; DMF, *N,N*-dimethylformamide; DMSO, dimethyl sulfoxide. DMF (Kokusan Chemical Works, special grade) was distilled at reduced pressure and stored over molecular sieves. Amino acid analyses were performed on the Atto Model MLC 203 Amino Acid Analyzer. Peptides were hydrolyzed in 6 mol dm^{-3} HCl in sealed, evacuated tubes at 110 °C for 24 h. TLC was carried out on precoated silica gel 60 (F-254) plates (Merck) in the following solvent systems: (A) 1-butanol-acetic acid-water (4:1:1); (B) chloroform-methanol-water (8:3:1).

Salt-Free, Washed Z-Amino Acid-Dimethylphosphinothioic Mixed Anhydrides (General Procedure): To a solution of Z-amino acid (2.0 mmol) and triethylamine (2.0 mmol) in chloroform (3.0 ml) was added Mpt-Cl[2] (2.2 mmol) in chloroform (1.0 ml) and the mixture stirred at room temperature for 20 min. Chloroform was removed under reduced pressure and the residue divided between ethyl acetate and water. The organic layer was successively washed with 5% aqueous citric acid solution (3 times), water (3 times), saturated NaCl solution, 5% aqueous sodium hydrogencarbonate solution (3 times), water (3 times), and saturated NaCl solution, and dried over anhydrous sodium sulfate. Removal of the solvent gave the Mpt-MAs as oils.

In the case of tyrosine 1.0 equiv of the Mpt-Cl was used in the presence of DCHA in order to avoid undesirable formation of *O*-dimethylphosphinothioylated product. The washing procedures were carried out without changing the solvent. After removal of the solvent Z-Tyr-OMpt was obtained as amorphous solid.

Thus obtained Mpt-MAs were used in the following experiments without further purification.

Preparation of Z-Ser-OMpt was already described in the previous communication.[3]

Preparation of Z-Leu-Asn-NH_2 (1): (A) To a suspension of Z-Asn-NH_2[12] (530.4 mg, 2.0 mmol) in AcOH (2.0 ml) was added 25% HBr/AcOH (8.3 ml). After 1 h the solution was diluted with ether to give a precipitate, which was dissolved in water and dehydrobrominated by stirring for 5 min with Dowex 1 resin. The resin was filtered and washed with water. The filtrate and washings were collected and evaporated under reduced pressure. The residue was dissolved in methanol and purified by gel filtration on Sephadex LH-20 to give the free asparaginamide as a white powder; 229.1 mg (87%), mp 138—139 °C, $[\alpha]_D^{27}$ +4.7° (*c* 2.0, H_2O), R_f(A) 0.12, R_f(B) 0.01.

To an ice-cooled solution of H-Asn-NH_2 (131.1 mg, 1.0 mmol) in methanol (6.5 ml) and TEA (209 μl, 1.5 mmol) was added Z-Leu-OMpt (536.1 mg, 1.5 mmol) in methanol (1.2 ml) and the mixture stirred at 0 °C for 24 h. The precipitate was collected by filtration and washed with chloroform, water and ether, and dried to give **1** as a white powder. After concentration of the filtrate and washings a second crop was obtained giving a total yield of 359.4 mg (95%). Physical properties and analytical data are given in Tables 3 and 4.

(B) H-Asn-NH_2 (19.7 mg, 0.15 mmol) and TEA (21 μl, 0.15 mmol) were dissolved in methanol (0.2 ml) and water (0.3 ml). To this solution was added at 0 °C a solution of Z-Leu-OMpt (53.6 mg, 0.15 mmol) in methanol (0.7 ml). After stirring for 20 min the same amounts of TEA and Z-Leu-OMpt were again added. After the mixture was stirred at 0 °C for 24 h the precipitate was collected as described above. Yield 55.5 mg (98%), mp 235—236 °C (decomp), $[\alpha]_D^{23}$ −7.6° (*c* 1, DMF).

(C) To a solution of Z-Leu-OH·DCHA (147.4 mg, 0.33 mmol) in chloroform (1.0 ml) was added Mpt-Cl (42.4 mg, 0.33 mmol) in chloroform (1.0 ml) and the mixture stirred at room temperature for 45 min. The solution was cooled to 0 °C and treated with a solution of asparaginamide hydrobromide (71.1 mg, 0.33 mmol) in methanol (2.5 ml) containing TEA (92.0 μl, 0.66 mmol) and the mixture stirred at the same temperature for 24 h. The precipitate was collected as described above to give 109.2 mg (88%) of the amide, mp 234—235 °C (decomp), $[\alpha]_D^{22}$ −7.6° (*c* 1.0, DMF).

Preparation of H-Leu-Asn-NH_2 (2): To a suspension of **1** (473.5 mg, 1.25 mmol) in AcOH (2.5 ml) was added 25% HBr/AcOH (5.2 ml) and the mixture kept standing at room temperature for 1 h and diluted with ether. The precipitate was collected, dehydrobrominated and purified as described for H-Asn-NH_2. Yield 257.0 mg (84%). Physical properties and analytical data are given in Tables 3 and 4.

Preparation of Z-Ile-Leu-Asn-NH_2 (3): (A) To an ice-cooled solution of **2** (244.3 mg, 1.0 mmol) and TEA (209 μl, 1.5 mmol) in methanol (6.7 ml) was added a solution of Z-Ile-OMpt (536.1 mg, 1.5 mmol) in methanol (1.1 ml), and the mixture stirred at 0 °C for 24 h. The precipitate was collected by filtration, washed as described for compound **1** and dried. Yield 468.3 mg (95%). Physical properties and analytical data are given in Tables 3 and 4.

(B) To a solution of Z-Ile-OH·DCHA (223.3 mg, 0.5 mmol) in chloroform (1.0 ml) was added a solution of Mpt-Cl (64.3 mg, 0.5 mmol) in chloroform (0.5 ml) and the mixture stirred for 1 h. The solution was cooled to 0 °C and treated with a solution of **2** hydrobromide (162.5 mg, 0.5 mmol) and TEA (140 μl, 1.0 mmol) in methanol (2.0 ml). The mixture was stirred at 0 °C for 24 h and worked up as described in (A). Yield 128.3 mg (52%), mp 262—263 °C (decomp).

Preparation of H-Ile-Leu-Asn-NH_2 (4): To a suspension of **3** (453.6mg, 0.92 mmol) in AcOH (5.0 ml) was added 25% HBr/AcOH (5.0 ml) and the mixture kept standing at room temperature for 1 h and diluted with ether. The precipitate was collected, dehydrobrominated and purified as described for H-Asn-NH_2. Yield 270.7 mg (82%). Physical properties and analytical data are given in Tables 3 and 4.

Preparation of Z-Ser-Ile-Leu-Asn-NH_2 (5): (A) To an ice-cooled solution of Z-Ser-OH (71.8 mg, 0.3 mmol) and TEA (41.8 μl, 0.3 mmol) in chloroform (1.0 ml) was added a solution of Mpt-Cl (38.5 mg, 0.3 mmol) in chloroform (0.5 ml). After stirring for 20 min the resulting solution was added to an ice-cooled solution of **4** (71.5 mg, 0.2 mmol) and TEA (41.8 μl, 0.3 mmol) in methanol (4.4 ml) and the mixture stirred at 0 °C for 24 h. The precipitate was collected by filtration and washed with chloroform, water and ether, and dried to give **5** as a white powder. After concentration of the filtrate and washings a second crop was obtained giving a total amount of 112.2 mg (94%). Physical properties and analytical data are given in Tables 3 and 4.

(B) To an ice-cooled solution of **4** (89.4 mg, 0.25 mmol) and TEA (52.2 μl, 0.375 mmol) in methanol (4.8 ml) was added a solution of Z-Ser-OMpt (124.3 mg, 0.375 mmol) in methanol (1.2 ml) and the mixture stirred at 0 °C for 24 h. Work up as described above gave **5**; 136.3 mg (94%), mp 257—258 °C (decomp).

Preparation of H-Ser-Ile-Leu-Asn-NH_2 (6): Compound **5** (597.2 mg, 1.03 mmol) was hydrogenolyzed for 4 h in the presence of 10% Pd-C in 80% AcOH (45 ml). The catalyst was filtered and washed with the same solvent. The filtrate and washings were combined and evaporated under reduced pressure. The residue was dissolved in water by addition of the minimum amount of methanol and the solution treated for 5 min with Dowex 1 resin. The resin was removed and washed with water, and the combined filtrate and washings were evaporated under reduced pressure. The residual mass was washed with ether to give **6**; 424.9 mg (93%). Physical properties and analytical data are given in Tables 3 and 4.

Preparation of Z-Asn-Ser-Ile-Leu-Asn-NH_2 (7): A solution of Z-Asn-OH (79.8 mg, 0.3 mmol) and TEA (41.8 μl, 0.3 mmol) in methanol (2.6 ml) was cooled to −20 °C, and treated with a solution of Mpt-Cl (38.5 mg, 0.3 mmol) in methanol (0.9 ml), and the mixture stirred for 20 min. The solution was added to a solution of **6** (133.3 mg, 0.3 mmol) and TEA (41.8 μl, 0.3 mmol) in methanol (7.0 ml) and water (3.0 ml) at −20 °C. After the mixture had been stirred for 40 min the Z-Asn-OMpt solution and TEA (0.3 mmol each) were added and the stirring continued at −20 °C for 2 h and at 0 °C for 48 h. The precipitate was filtered and washed with chloroform, ethanol, water, and ether, and dried to give **7**; 173.7 mg (84%). Physical properties and analytical data are given in Tables 3 and 4.

Preparation of H-Asn-Ser-Ile-Leu-Asn-NH_2 (8): Compound **7** (291.0 mg, 0.42 mmol) was hydrogenolyzed for 24 h in the presence of 10% Pd-C in 80% AcOH (45 ml). The same work up described for compound **6** gave **8**; 197.5 mg (82%). Physical properties and analytical data are given in Tables 3 and 4.

Preparation of Z-Leu-Asn-Ser-Ile-Leu-Asn-NH_2 (9): Compound **8** (55.9 mg, 0.1 mmol) and TEA (14.0 μl, 0.1 mmol) were dissolved in methanol (3.0 ml) and water (1.0 ml) and the solution cooled to 0 °C. To the solution was added Z-Leu-OMpt (35.8 mg, 0.1 mmol) in methanol (0.9 ml) and the mixture stirred at 0 °C for 20 min. After the same amounts of the Z-Leu-OMpt solution and TEA were again added the mixture was stirred at 0 °C for 48 h. Filtration, washing and drying as described for the compound **7** gave **9**; 64.5 mg (80%). Physical properties and analytical data are given in Tables 3 and 4.

Preparation of H-Leu-Asn-Ser-Ile-Leu-Asn-NH_2 (10): Compound **9** (133.5 mg, 0.165 mmol) was hydrogenolyzed for 8 h in the presence of 10% Pd-C in 80% AcOH (17 ml). The same work up described for compound **6** gave **10**; 97.0 mg (83%). Physical properties and analytical data are given

Table 3. Physical Properties of Synthetic Intermediates of VIP

Compound	Yield/%[a]	Mp (θ_m/°C)	$[\alpha]_D$ (solv., temp)	R_f(A)	R_f(B)
Z-VIP (27—28)-NH_2 (**1**)	95	235—236(decomp)	−7.5°(*c* 1 DMF, 22 °C)[b]	0.70	0.40
H-VIP(27—28)-NH_2 (**2**)	84	188—190(decomp)	−5.5°(*c* 1 H_2O, 26.5 °C)	0.33	0.06
Z-VIP (26—28)-NH_2 (**3**)	95	268—270(decomp)	−24.8°(*c* 0.5 DMSO, 24 °C)	0.78	0.64
H-VIP(26—28)-NH_2 (**4**)	82	218—220(decomp)	−20.3°(*c* 1 DMF, 19 °C)	0.51	0.21
Z-VIP (25—28)-NH_2 (**5**)	94[c]	261—262(decomp)	+6.0°(*c* 0.5 DMF, 25 °C)	0.73	0.43
H-VIP(25—28)-NH_2 (**6**)	93	216—220(decomp)	−29.1°(*c* 1 AcOH, 20.5 °C)	0.54	0.03
Z-VIP (24—28)-NH_2 (**7**)	84[c]	270—271(decomp)	−15.1°(*c* 0.5 DMSO, 20.5 °C)	0.72	0.11
H-VIP(24—28)-NH_2 (**8**)	82	230—233(decomp)	−33.5°(*c* 1 AcOH, 20.5 °C)	0.45	0.02
Z-VIP (23—28)-NH_2 (**9**)	80	259—261(decomp)	−20.7°(*c* 0.5 DMSO, 20.5 °C)	0.73	0.16
H-VIP(23—28)-NH_2 (**10**)	83	215—218(decomp)	−18.5°(*c* 1 AcOH, 27.5 °C)	0.35	0.04
Z-VIP (22—28)-NH_2 (**11**)	74	261—265(decomp)	−14.6°(*c* 0.5 DMSO, 27.0 °C)	0.66	0.30

a) Unless otherwise noted yields are given for reactions involving isolated Mpt-MAs. b) Lit,[12] −7.5°(*c* 1 DMF, 25 °C). c) In-situ-generated Mpt-MA was used.

Table 4. Analytical Data for Isolated Intermediates in the Synthesis of VIP

Compound	Amino Acid Ratios (6 mol dm^{-3}, 110 °C, 24 h)						Elemental Analysis
	Tyr	Ser	Ile	Leu	Asp	NH_3	
1				1.00(1)	1.00(1)	1.80(2)	
2				1.00(1)	1.00(1)	1.85(2)	($C_{10}H_{20}N_4O_3$)C,H,N
3			0.96(1)	1.00(1)	1.03(1)	1.85(2)	($C_{24}H_{37}N_5O_6$)C,H,N
4			0.94(1)	1.00(1)	1.00(1)	1.85(2)	($C_{16}H_{31}H_5O_4$)C,H,N
5		0.86(1)	0.96(1)	1.00(1)	1.00(1)	1.86(2)	($C_{27}H_{42}N_6O_8 \cdot H_2O$)C,H,N
6		0.88(1)	0.96(1)	1.02(1)	1.00(1)	1.80(2)	($C_{19}H_{36}N_6O_6$)C,H,N
7		0.92(1)	1.01(1)	1.05(1)	2.00(2)	2.91(3)	($C_{31}H_{48}N_8O_{10}$)C,H,N
8		0.97(1)	0.98(1)	1.03(1)	2.00(2)	2.69(3)	($C_{23}H_{42}N_8O_8$)C,H,N
9		0.87(1)	0.96(1)	2.00(2)	2.00(2)	2.88(3)	($C_{37}H_{59}N_9O_{11}$)C,H,N
10		0.93(1)	1.00(1)	2.05(2)	2.00(2)	3.12(3)	($C_{29}H_{53}N_9O_9 \cdot 2H_2O$)C,H,N
11	0.94(1)	0.97(1)	1.05(1)	2.17(2)	2.00(2)	3.22(3)	($C_{46}H_{68}N_{10}O_{13} \cdot 2.5H_2O$)C,H,N

in Tables 3 and 4.

Preparation of Z-Tyr-Leu-Asn-Ser-Ile-Leu-Asn-NH_2 (11): To a solution of **10** (26.9 mg, 0.04 mmol) and TEA (5.6 μl, 0.04 mmol) in methanol (1.5 ml) and water (0.5 ml) was added a solution of Z-Tyr-OMpt (16.3 mg, 0.04 mmol) in methanol (0.9 ml) and the mixture stirred at 38—40 °C for 20 min. After the same amounts of the Z-Tyr-OMpt solution and TEA were again added the mixture was stirred at 38—40 °C for 2 h and at room temperature for 46 h. The precipitate was filtered, washed successively with chloroform, ethanol, water and ether, and dried to give **11**. 30.0 mg (74%). Physical properties and analytical data are given in Tables 3 and 4.

The authers wish to express their thanks to Professor Louis A. Carpino, University of Massachusetts at Amherst, for stylistic revision of the manuscript.

References

1) R. B. Merrifield, *J. Am. Chem. Soc.*, **85**, 2149 (1963).
2) M. Ueki, T. Inazu, and S. Ikeda, *Bull. Chem. Soc. Jpn.*, **52**, 2424 (1979).
3) M. Ueki and T. Inazu, *Chem. Lett.*, **1982**, 45.
4) S. Ikeda and M. Ueki, 47th National Meeting of the Chemical Society of Japan, Kyoto, April 1983, Abstr., No. 4H09.
5) S. I. Said and V. Mutt, *Science*, **169**, 1217 (1970).
6) S. I. Said and V. Mutt, *Eur. J. Biochem.*, **28**, 199 (1972).
7) M. Bodanszky, Y. S. Klausner, and S. I. Said, *Proc. Natl. Acad. Sci. U. S. A.*, **70**, 382 (1973).
8) M. Takeyama, K. Koyama, K. Inoue, T. Kawano, H. Adachi, T. Tobe, and H. Yajima, *Chem. Pharm. Bull.*, **28**, 1873 (1980).
9) D. H. Coy and J. Gardner, *Int. J. Pept. Prot. Res.*, **15**, 73 (1980).
10) R. Colombo, *Experientia*, **38**, 773 (1982).
11) A. Fournier, J. K. Saunders, and S. St-Pierre, *Peptides*, **5**, 169 (1984).
12) M. Bodanszky, Y. S. Klausner, and V. Mutt, *Bioorg. Chem.*, **2**, 30 (1972).
13) W. M. M. Schaaper and H. C. Beyerman, *Peptides*, **5**, 167(1984).

 © 1988 The Chemical Society of Japan Bull. Chem. Soc. Jpn., 61, 3659—3665 (1988)

Preparation and Characterization of Large Surface Area $BaO \cdot 6Al_2O_3$

Masato MACHIDA, Koichi EGUCHI, and Hiromichi ARAI*
Department of Materials Science and Technology, Graduate School of Engineering Sciences, Kyushu University, 39, Kasuga, Fukuoka 816
(Received April 4, 1988)

Barium hexaaluminate, $BaO \cdot 6Al_2O_3$, exhibited excellent heat resistance in maintaining a large surface area. Preparation from hydrolysis of metal alkoxides was a superior process in deriving the large surface area of $BaO \cdot 6Al_2O_3$, to that from mixtures of $BaCO_3/\gamma$-Al_2O_3. Direct formation of $BaO \cdot 6Al_2O_3$ phase at low temperature plays the key role in retaining the fine particle size. The amount of water added for hydrolysis and the aging period of hydrolyzed precursors strongly influenced the surface area of alkoxide-derived $BaO \cdot 6Al_2O_3$. These effects of the preparation conditions originated from the difference in microstructure and chemical structure of the hydrolyzed precursors. Monodispersed fine precursor particles with high oxide content generated large surface area $BaO \cdot 6Al_2O_3$.

Catalytic combustion has many advantages over conventional flame combustion in suppressing NO_x emission and in improving combustion efficiency. Recently, much interest has arisen in new application of this technology in gas turbines, jet engines, and boilers above 1000 °C.[1,2] In maintaining catalytic activity under such a severe condition, high heat resistance is necessary in the catalytic materials. But this is not satisfied by the catalysts at present in use for low temperature combustion. One of the crucial problems is how to suppress sintering of the oxide support in a high temperature combustion catalyst. Our research has been focused on developing a support material endowed with high heat and thermal shock resistance which also maintains a large surface area even above 1400 °C.

Alumina is one of the most common support materials used around 1000 °C. Additive oxides, such as La_2O_3, BaO, CaO, MgO, SiO_2 etc., have been reported to aid in maintaining the large surface area at elevated temperatures.[3-6] We have previously reported[7,8] that the addition of BaO greatly increases the surface area of alumina above 1000 °C. The effect of BaO depends strongly on the oxide composition. The optimum composition agrees with the stoichiometric one for the formation of $BaO \cdot 6Al_2O_3$, at which the surface area reached more than 6 $m^2 g^{-1}$ even after calcination at 1450 °C. But the improvement is still unsatisfactory in practical use for high-temperature combustion. In this paper, we report the marked elevation of high-temperature surface area retention of $BaO \cdot 6Al_2O_3$ by employing the preparation from metal alkoxides. The powder characteristics of sol-gel prepared $BaO \cdot 6Al_2O_3$ were compared with the sample from the conventional technique. It has become evident that the formation process of $BaO \cdot 6Al_2O_3$ plays a key role in the retention of large surface area.

Experimental

Sample Preparation. Barium hexaaluminate ($BaO \cdot 6Al_2O_3$) was prepared from mixtures of $BaCO_3$ (99%, Kishida Chemical) and γ-Al_2O_3 (99.9%, Catalysis Soc. Jpn., JRC-ALO4). The average crystallite size of $BaCO_3$ and γ-Al_2O_3 were 0.8 μm and 5 nm, respectively. They were mixed with an automatic mortar grinder for 2 h before firing. The mixture was heated in air at a constant rate of 5 deg min^{-1} and kept at a desired temperature for 5 h in a high-density alumina crucible.

A sample with the same composition was prepared by hydrolysis of the corresponding metal alkoxides. Barium isopropoxide, $Ba(OC_3H_7)_2$, was prepared by the reaction between Ba metal (99%, Kishida Chemical) and 2-propanol (99.5%, Kishida Chemical) in N_2 stream at 80 °C.[9]

$$Ba + 2\,C_3H_7OH \rightarrow Ba(OC_3H_7)_2 + H_2$$

Calculated amounts of $Ba(OC_3H_7)_2$ and $Al(OC_3H_7)_3$ (99%, Kishida Chemical) were dissolved together in 2-propanol and refluxed at 80 °C for 5 h with vigorous stirring. All the procedure before the hydrolysis has been carried out in a dried N_2 atmosphere. As distilled water was slowly added to the resulting solution, gelation was observed immediately accompanied by a rise in temperature from 80 to 90 °C. After several hours of aging under stirring at 80 °C, the hydrolyzed alkoxides were evaporated to dryness in vacuo and the powders thus obtained were calcined in the above mentioned manner. In this study, the surface areas of alkoxide-derived $BaO \cdot 6Al_2O_3$ were investigated as a function of the amount of water for hydrolysis and the aging period of hydrolyzed alkoxides. Thus, a series of hydrolysis reactions were performed to demonstrate these optimum conditions.

Sample Characterization. The surface areas of oxide powders were determined by the BET method using nitrogen adsorption. The surface area thus obtained was reproducible within a 10% relative error on the average. The pore size distributions were also obtained from the nitrogen adsorption isotherms at 77 K. The crystal structures of the calcined samples were determined by X-ray diffraction (Rigaku Denki, 4011). The microstructures of the powder samples were measured by a scanning electron microscope (JEOL, JSM-50).

Thermal decomposition of the hydrolyzed precursors to the corresponding oxides was observed by differential thermal analysis and thermal gravimetry (ULVAC, TGD 5000RH) in air. The samples were heated at a constant rate of 10 deg min^{-1} up to 600 °C. The infrared spectra were taken on a JASCO IR 810 spectrometer before and after the thermal decomposition. Mixtures of the hydrolyzed precursors (30 mg) and KBr powder (300 mg) were pressed into

disks of 20 mm diameter and placed in the temperature-controlled in situ cell. The infrared spectra were recorded after evacuation at elevated temperatures and subsequent cooling to room temperature.

Results

The Surface Area of $BaO \cdot 6Al_2O_3$. γ-Alumina and the two BaO-Al_2O_3 precursors, which were prepared from powder mixtures and metal alkoxides, were heated at elevated temperatures for 5 h. The decrease in surface area during the heat treatment was measured as a function of the calcination temperature (Fig. 1). The present investigation was performed only on the samples with a composition of $(BaO)_{0.14}(Al_2O_3)_{0.86}$ at which the effect of BaO on the surface area is most prominent, as has been reported previously.[7,8] The three samples in Fig. 1 had similar surface areas after calcination at 1100 °C, but the surface area significantly decreased with a rise in calcination temperature. The decrease was most significant in pure alumina. The addition of BaO was obviously effective in maintaining the surface area at higher temperatures. The effect of BaO is related to the formation of a hexagonal layered aluminate ($BaO \cdot 6Al_2O_3$).[7,8] The surface area of barium hexaaluminate prepared from $BaCO_3/\gamma$-Al_2O_3 was 4 times larger than that of pure alumina above 1300 °C.

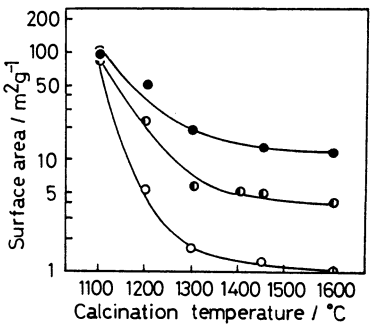

Fig. 1. Temperature dependence of surface areas of $(BaO)_{0.14}(Al_2O_3)_{0.86}$ and Al_2O_3. ● $(BaO)_{0.14}(Al_2O_3)_{0.86}$ (alkoxide), ◐ $(BaO)_{0.14}(Al_2O_3)_{0.86}$ ($BaCO_3/\gamma$-Al_2O_3), ○ Al_2O_3.

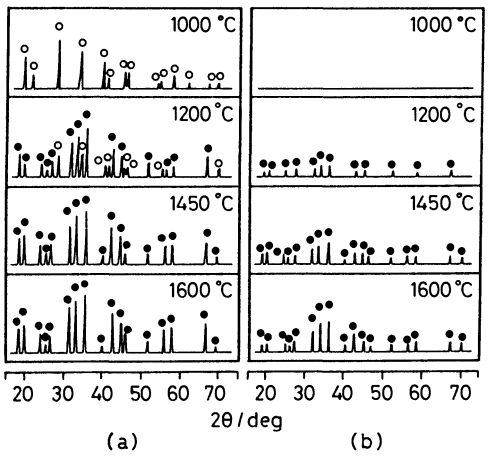

Fig. 2. X-Ray diffraction patterns of $(BaO)_{0.14}$-$(Al_2O_3)_{0.86}$ after calcination at various temperatures. (a) Powder mixture of $BaCO_3$ and γ-Al_2O_3. (b) Hydrolyzed alkoxides. ● $BaO \cdot 6Al_2O_3$, ○ $BaO \cdot Al_2O_3$.

Preparation from alkoxide precursors, which sometimes gives rise to the formation of ultrafine particles and/or low temperature processing of mixed oxides, was applied to the present system. The data for a typical alkoxide-derived sample are shown in Fig. 1. The loss of surface area upon heating was more gradual than that of the powder mixtures. The surface area was 3 times larger than that from $BaCO_3/\gamma$-Al_2O_3 mixtures above 1300 °C.[10] The value of 11 m^2g^{-1} after heating at 1600 °C has not been achieved by any oxide supports so far reported.

The Crystal Structure of BaO-Al_2O_3. The phase diagram of the system BaO-Al_2O_3 indicates that the $(BaO)_{0.14}(Al_2O_3)_{0.86}$ sample consists of a single phase of $BaO \cdot 6Al_2O_3$ in the equilibrium state.[11] However, the $BaCO_3/\gamma$-Al_2O_3 precursor underwent a complicated formation process to evolve this phase during the heating process, as shown in Fig. 2(a). After calcination at 1000 °C, the phase observed in $BaCO_3/\gamma$-Al_2O_3 was the equimolar compound ($BaO \cdot Al_2O_3$) and a trace amount of $BaCO_3$, instead of the equilibrium phase ($BaO \cdot 6Al_2O_3$). The sample at this calcination condition is almost completely composed of a mixture of $BaO \cdot Al_2O_3$ and Al_2O_3, though the diffraction lines from the latter phase are too weak to be observed by X-ray diffraction due to its poor crystallinity. With a rise in calcination temperature, the diffraction lines from $BaO \cdot 6Al_2O_3$ appeared and became intense. The formation of the equilibrium $BaO \cdot 6Al_2O_3$ phase was completed after heating at 1450 °C.

The samples from alkoxides, on the other hand, showed no diffraction lines after heating at 1000 °C. At 1200 °C, the diffraction lines which appeared in this case were only from the $BaO \cdot 6Al_2O_3$ phase (Fig. 2(b)). They became sharp and intense at elevated calcination temperatures, but the $BaO \cdot Al_2O_3$ phase was not observed at any temperature.

Microstructures and Pore Size Distributions. After calcination at 1450 °C, the particle morphology of alumina and $BaO \cdot 6Al_2O_3$ was observed by a scanning electron microscope (SEM), as shown in Fig. 3. The particle size of alumina (ca. 2 μm) was considerably larger than that of the $BaO \cdot 6Al_2O_3$ samples. Significant grain growth of alumina is evident from the large particle size and the smooth powder surface. In contrast, the $BaO \cdot 6Al_2O_3$ powder was clearly fine and possessed a rough surface. It is noted that the two $BaO \cdot 6Al_2O_3$ samples are obviously different in their particle sizes and microstructures. When the mixture of $BaCO_3$ and γ-Al_2O_3 was calcined at 1450 °C, the resultant particles (0.5—1.0 μm) were strongly agglomerated (Fig.3(b)). Such large agglomerates were absent in the sample obtained from hydrolyzed alkoxides. The particles were in a granular shape with uni-

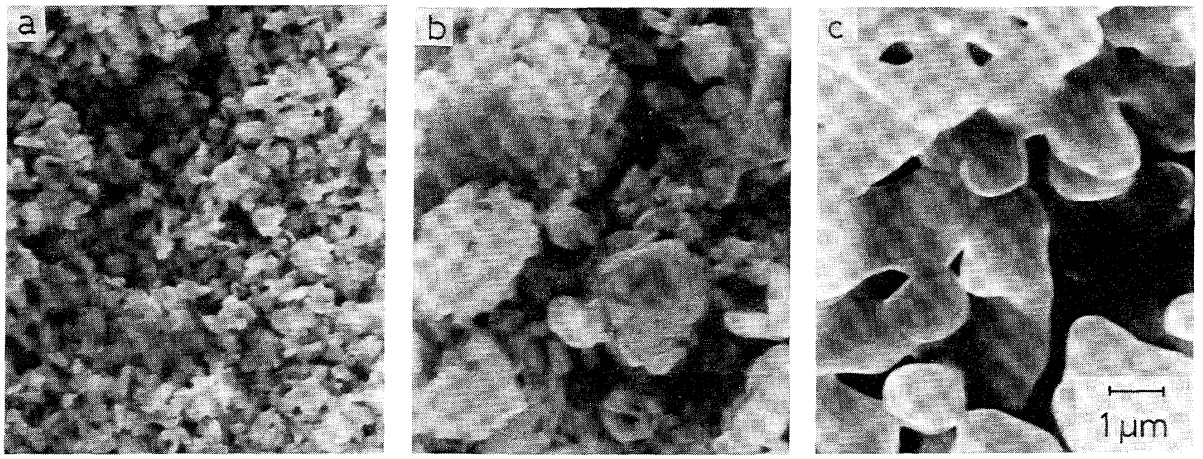

Fig. 3. SEM photographs of $BaO \cdot 6Al_2O_3$ and Al_2O_3 after calcination at 1450°C. a) $BaO \cdot 6Al_2O_3$ from alkoxides, b) $BaO \cdot 6Al_2O_3$ from $BaCO_3/\gamma\text{-}Al_2O_3$, c) Al_2O_3.

form (0.3 μm) size (Fig. 3(a)).

Pore size distributions of alumina and the $BaO \cdot 6Al_2O_3$ samples were measured after calcination at 1450 °C. The distribution was maximum at the pore size smaller than 10 nm (Fig. 4). The relative pore volume gradually decreased with increasing pore size. The barium hexaaluminate sample, in particular, that was prepared from alkoxides possessed obviously larger total pore volume than alumina. The sequence of total pore volume of three samples agreed with that of the surface area. The difference in surface area among the three alumina-based samples largely resulted from the population of pores with radius of ca. 10 nm or less.

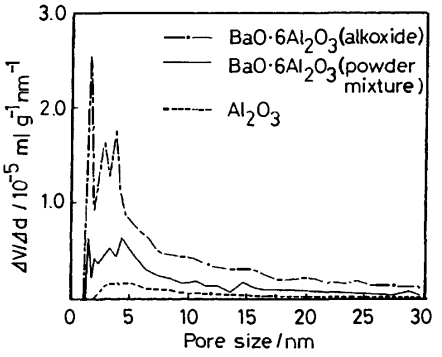

Fig. 4. Pore size distributions of $BaO \cdot 6Al_2O_3$ and Al_2O_3 after calcination at 1450°C.

Effect of Hydrolysis Conditions on Surface Area. The surface area of $BaO \cdot 6Al_2O_3$ is also sensitive to some preparation conditions during the alkoxide process such as the aging period of the hydrolyzed products and the amount of water. The surface area of alkoxide-derived $BaO \cdot 6Al_2O_3$ increased at the initial stage of aging and became almost constant after 12 h as shown in Fig. 5 ($R(H_2O/MOC_3H_7)$=10.0). After 12 h of aging and subsequent calcination at 1300 °C, the sample retained the surface area of 18.5 m^2g^{-1} which is about double that of the sample with 30 min of aging.

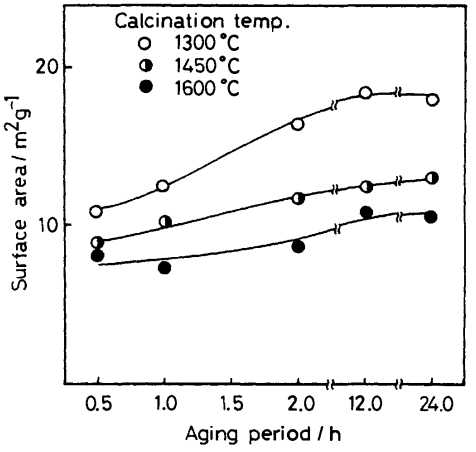

Fig. 5. Effect of the aging period of hydrolyzed precursors on the surface area of $BaO \cdot 6Al_2O_3$. ($R(H_2O/MOC_3H_7)$=10.0)

The amount of water added for hydrolysis is expressed as a molar ratio per metal isopropoxyl group ($R(H_2O/MOC_3H_7)$). The number of metal isopropoxyl groups, $-MOC_3H_7$, is the sum of $-AlOC_3H_7$ and $-BaOC_3H_7$. Figure 6 shows the effect of $R(H_2O/MOC_3H_7)$ on the surface area of $BaO \cdot 6Al_2O_3$. The surface area was maximum (20.2 m^2g^{-1}) at $R(H_2O/MOC_3H_7)$= 0.5, but it decreased either by an increase or by a decrease in the amount of water. The optimum condition, $R(H_2O/MOC_3H_7)$=0.5, agrees with the stoichiometric ratio for the hydrolysis of alkoxides. The effect of the amount of water is obvious especially when calcination was performed at lower temperatures such as 1300 °C.

The effect of the aging period was investigated by microscopic observation of the hydrolysis precursors (Fig. 7). In the initial stage, the sample contained large agglomerates (larger than 10 μm) which consisted of submicron primary particles. With the aging progress, the size of the agglomerate was significantly reduced. After aging for 24 h, the sample consisted

almost entirely of equal sized particles and agglomerates were rarely observed.

Figure 8 shows SEM photographs of precursors after a given amount of water was added to the alkoxide solution for hydrolysis. Corresponding to the two regions observed in the surface area changes (Fig. 6), the particle morphology was different between the sample with $R(H_2O/MOC_3H_7)<0.5$ and $R(H_2O/MOC_3H_7)>0.5$. The hydrolyzed sample at $R(H_2O/MOC_3H_7)>0.5$ consisted of submicron particles, but the particle morphology and size were almost unchanged with the amount of water so far as should be observed by SEM. In contrast, the particle size was obviously larger when less water ($R(H_2O/MOC_3H_7)<0.5$) was used for hydrolysis. In this region, the amount of water is not enough for complete hydrolysis of the alkoxides. Thus, the microstructures of the hydrolysis products well reflect the surface area of the $BaO \cdot 6Al_2O_3$. Large agglomerates and large precursor particles appear to result in low surface areas after calcination.

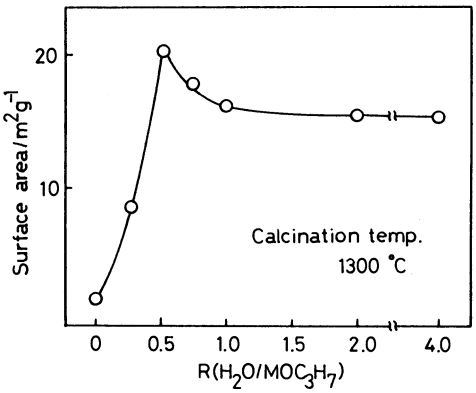

Fig. 6. Effect of the amount of water added to alkoxides on the surface area of $BaO \cdot 6Al_2O_3$. (12 h aging)

Thermal Behavior of Hydrolyzed Alkoxides. The decomposition of the hydrolyzed products was examined by in situ IR measurements. The IR spectra obtained after heating in vacuo at various temperatures are shown in Fig. 9. At room temperature, the hydrolyzed product showed the absorption band of the

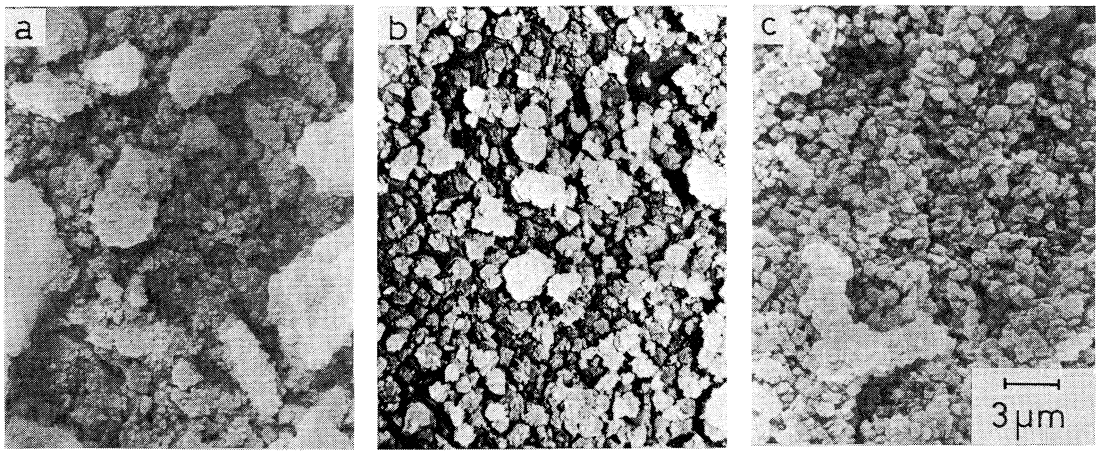

Fig. 7. Microstructures of hydrolyzed precursors with various aging period. a) 0.5 h, b) 2.0 h, c) 24.0 h. ($R(H_2O/MOC_3H_7=10.0$)

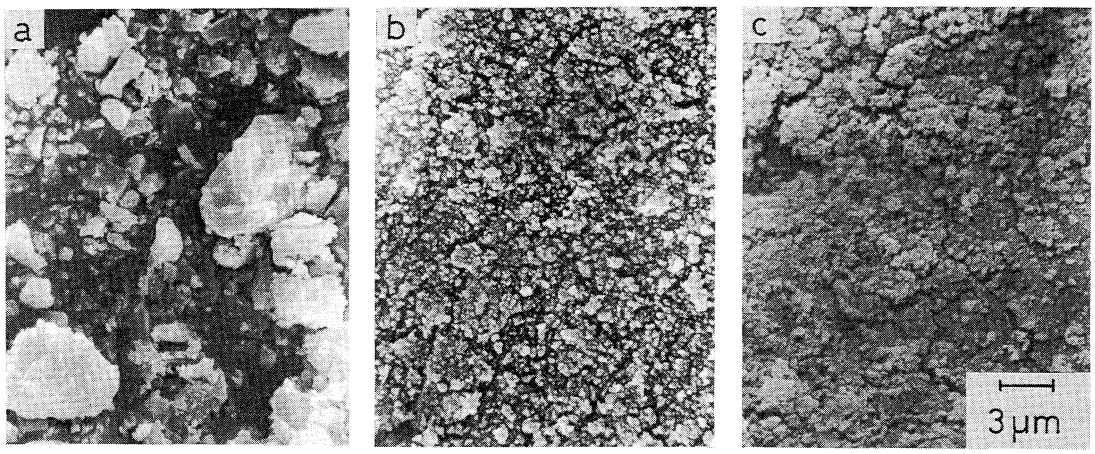

Fig. 8. Microstructures of hydrolyzed precursors with various $R(H_2O/MOC_3H_7)$. a) $R(H_2O/MOC_3H_7)=0.3$, b) 0.5, c) 1.0. (12 h aging)

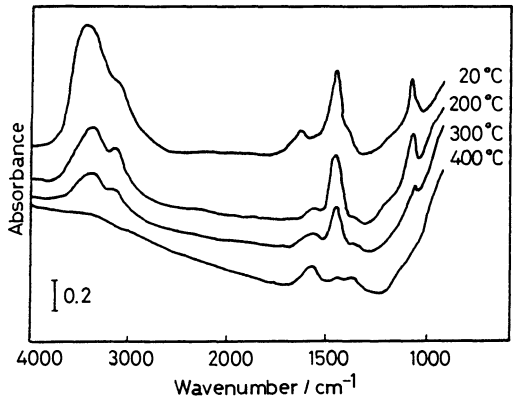

Fig. 9. Change of infrared spectrum of hydrolyzed alkoxides during the course of heating. Preparation condition of samples: $R(H_2O/MOC_3H_7)=1.0$, 12 h aging.

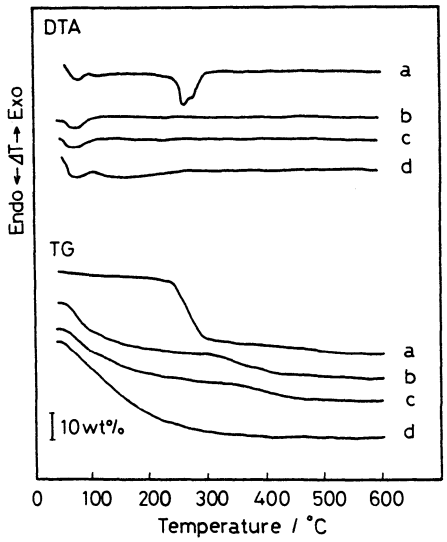

Fig. 10. DTA/TG analyses of the hydrolyzed precursors prepared under various $R(H_2O/MOC_3H_7)$ conditions. a) $R(H_2O/MOC_3H_7)=10.0$, b) 2.0, c) 1.0, d) 0.5.

H-O-H bending vibration around 1640 cm^{-1}. This band, being attributed to the physisorbed water, completely disappeared after evacuation at 200 °C. The bands at 3000—3500 cm^{-1} probably correspond to the O-H stretching mode of the metal hydroxides in the hydrolyzed precursors. These peaks were weakened at elevated temperatures due to the thermal decomposition of metal hydroxides to mixed oxides. The O-H bands disappeared at 400 °C after complete decomposition.

Figure 10 shows the DTA/TG curves of hydrolyzed precursors prepared under various $R(H_2O/MOC_3H_7)$ conditions. A broad endothermic peak below 100 °C, which was observed in every alkoxide-derived sample, is attributed to elimination of physisorbed water. A large and sharp endothermic peak with a 25% weight loss appeared for the sample with $R(H_2O/MOC_3H_7)=10$ around 250 °C. From the IR result, this weight loss can be attributed to dehydration accompanied by thermal decomposition of the metal hydroxides. Similar weight loss was observed in the samples with $R(H_2O/MOC_3H_7)<2.0$ at 250—400 °C, but they were small, corresponding to the small content of metal hydroxides.

Discussion

Effect of $BaO \cdot 6Al_2O_3$ Formation on Surface Area. Although a large surface area is one of the most important properties for combustion catalysts, only little is known about the support material for high-temperature combustion. Most support materials, which have been used so far below 1000 °C, sinter into particles with only a small surface area. γ-Alumina, which is most commonly used as a catalyst support below 1000 °C, is not adequate because of its significant decrease in surface area, as shown in Fig. 1. The decrease in the surface area around 1200 °C is accompanied by a phase transition from metastable states into the equilibrium phase (α-phase). In contrast, BaO added alumina is effective in maintaining the large surface area by forming the $BaO \cdot 6Al_2O_3$ phase.

The structure of $BaO \cdot 6Al_2O_3$ has been described as the intermediate of magnetoplumbite and β-alumina structures (Fig. 11).[12,13] But the detailed refinement of the crystal structure with this composition reported by Kimura et al.[14,15] revealed the existence of two compounds near the stoichiometric $BaO \cdot 6Al_2O_3$ composition. It was suggested that they are essentially β-alumina structures on the basis of the electron diffraction and crystallographic data. Both the magnetoplumbite and β-alumina structures are grouped into a layered aluminate type, but they differ from each other in the atomic arrangement in the mirror plane. In our previous reference on a series of alkaline earth oxide-alumina systems,[8] the aluminate samples which crystallize in the layered aluminate structures generally possessed the large surface area. It was also reported[16] that some rare earth metal aluminates with these layered structures exhibited large surface areas after heating at high temperatures. However, the $BaO \cdot 6Al_2O_3$ system is the most prominent in main-

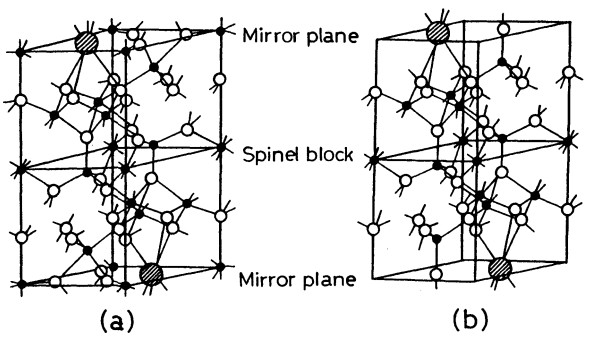

Fig. 11. Crystal structure of (a) magnetoplumbite and (b) β-alumina. ● Al^{3+}, ○ O^{2-}, ◉ Ba^{2+}.

taining the large surface area among the series of layered aluminates with large di- or trivalent cations. The real reason for such high thermal resistance against sintering is not sufficiently understood at present, but it is probably related to the crystal structure. In the layered aluminate structure, each layer is separated by the mirror plane (Fig. 11). The structure may suppress interlayer diffusion of atoms and crystal growth along the *c* direction (perpendicular to the mirror plane). In fact, polycrystalline sodium β-alumina, which is used as a solid electrolyte, grows as plate-shaped particles with their flat sides perpendicular to the *c* axis. Powers et al.[17] suggested that the stacking of layers in sodium β-alumina is very slow in comparison to the Al-O spinel formation. It was deduced that the mirror planes, which separate each spinel block, seem to play a key role in the large surface area of the layered aluminate family.

Effect of Preparation Procedure of $BaO \cdot 6Al_2O_3$. There are some superior points of an alkoxide process as compared with a conventional method, i.e., 1. high purity, 2. very fine primary particle, and 3. uniform mixing of components.[18,19] The first factor seems not to be so important for the high surface area of the system, because small amount of additives, such as Cr, Mn, and Co did not promote sintering.[20] Particles are desired to be fine to obtain a large surface area, but ultrafine particles are apt to sinter due to their large surface energy. At present, the third point is expected to be the most important in achieving the large surface area of $BaO \cdot 6Al_2O_3$. As mentioned above, the formation of barium hexaaluminate is essential for the large surface area of the present system. The alkoxide process permits direct formation of this phase by uniform mixing of the components at a molecular level (Fig. 2). To make a comparison with hydrolysis of the alkoxide mixture, barium isopropoxide and aluminium isopropoxide were separately hydrolyzed in 2-propanol solutions and the resulting hydroxide suspensions were mixed and evaporated to dryness. The phases appearing after calcination at 1300 °C were not only $BaO \cdot 6Al_2O_3$ but also $BaO \cdot Al_2O_3$. This indicates that high chemical homogeneity is attained only when a mixture of the two alkoxides is hydrolyzed simultaneously. In other words, the mixing at a particle level does not reduce the formation temperature of $BaO \cdot 6Al_2O_3$. It is likely that the mixing of the two alkoxides in 2-propanol leads to formation of mixed alkoxides;[21] but direct evidence for the formation of mixed alkoxides has not been obtained. The high chemical homogeneity in the alcoholic solution should be retained in alkoxide-derived precursors as a consequence of solution gelation.

On the other hand, in the case of powder mixtures, barium hexaaluminate is formed through the solid state reaction between $BaO \cdot Al_2O_3$ and alumina by diffusion. Since the excellent heat resistance is not achieved by the $BaO \cdot Al_2O_3$ phase, the $BaO \cdot Al_2O_3$ particles grow in size during the solid state reaction until they are converted to $BaO \cdot 6Al_2O_3$. Thus, it is concluded that the high surface area of the alkoxide-derived sample is a result of the low temperature formation of $BaO \cdot 6Al_2O_3$.

The difference in the reaction history is well reflected in the microstructures of the powders. The SEM photographs demonstrated a marked contrast in microstructure of the two barium hexaaluminate samples (Fig. 3). Although large agglomerates and unequal particle size are observed commonly in the powder mixtures, the alkoxide-derived samples consist of submicron particles with a uniform size. The difference in microstructure is reflected by the pore size distribution. Large primary particles in the powder mixture result in small overall pore volume as shown in Fig. 4. The pores smaller than 10 nm in diameter largely contribute to the difference in the total pore volume of the three samples. Pores of this size are in fact seen in the SEM photograph of the alkoxide-derived $BaO \cdot 6Al_2O_3$ sample as interparticle voids.

Effect of Preparation Condition in Alkoxide Process. The surface areas of samples from the alkoxide process were affected by the amount of water and the aging period after hydrolysis. The change in surface area with the amount of water is apparently divided into two regions as shown in Fig. 6. The stoichiometric amount of water for the decomposition of alkoxides is $R(H_2O/MOC_3H_7) = 0.5$.

$$2\text{-M-}(OC_3H_7) + H_2O \rightarrow \text{-M-O-M-} + 2\,C_3H_7OH \quad (1)$$

At $R(H_2O/MOC_3H_7) < 0.5$, the oxide is produced partly by hydrolysis (Reaction(1)) and partly by pyrolysis of the alkoxides. The increase in surface area in this region indicates that pyrolysis of the alkoxides does not contribute to the large surface area. Namely, a substantial amount of hydrolysis is required to produce a large surface area. The particle size of the incompletely hydrolyzed product is two orders of magnitude larger than that of the sample at $R(H_2O/MOC_3H_7) > 0.5$ (Fig. 8).

At the second region ($R(H_2O/MOC_3H_7) > 0.5$), the surface area decreases with an increase in $R(H_2O/MOC_3H_7)$ (Fig. 6). The partial formation of hydroxides (Reaction(2)) is included, due to the presence of excessive water in this region.[22]

$$M(OC_3H_7)_n + nH_2O \rightarrow M(OH)_n + nC_3H_7OH \quad (2)$$

As the amount of water increases, the reaction (2) becomes dominant, resulting in a high content of hydroxide groups in the product. The hydroxides thus formed are thermally decomposed into oxides accompanying elimination of water in the temperature range 250—400 °C as was observed by TG. The weight loss in this temperature range increased with $R(H_2O/MOC_3H_7)$, corresponding to the increase in the hydroxide content in the precursors. The formation temperature of $BaO \cdot 6Al_2O_3$ for the sample with a low

extent of hydrolysis ($R(H_2O/MOC_3H_7)<1.0$) was near 1100 °C, while it is above 1200 °C for the hydroxide-rich sample ($R(H_2O/MOC_3H_7)=10.0$). The decrease in surface area in the second region resulted from the hydroxide formation in precursors. This also elevates the temperature for the formation of $BaO \cdot 6Al_2O_3$

The effect of the aging period in Fig. 5 is somewhat smaller than that of the amount of water. The increase in surface area with aging is related to the extent of agglomeration of hydrolyzed products as was revealed by SEM observation in Fig. 7. The aging of hydrolyzed products in the presence of excessive water likely reduces the agglomeration of particles and brings about a high dispersion state. Large agglomerates, which are observed at a short aging period, grow into large particles in the course of heating. This only leads to the decrease in the surface area of the resultant $BaO \cdot 6Al_2O_3$

The authors are greatly indebted to the Center of Advanced Instrumental Analysis of Kyushu University for support in SEM measurements. This research was partially supported by a Grant-in-Aid for Scientific Research No. 61550598 from the Ministry of Education.

References

1) D. L. Trimm, *Appl. Catal.*, **7**, 249 (1983).
2) R. Prasad, L. A. Kennedy, and E. Ruckenstein, *Catal. Rev.*, **26**, 1 (1984).
3) I. Amato, D. Martorama, and B. Silengo, "Sintering and Catalysis," ed by G. C. Kuczynski, Plenum Press, New York and London (1975), p. 187.
4) H. Schaper, E. B. M. Doesburg, and L. L. Van Reijen, *Appl. Catal.*, **7**, 211 (1983).
5) H. Schaper, E. B. M. Doesburg, P. H. M. De Korte, and L. L. Van Reijen, *Solid State Ionics*, **16**, 261 (1985).
6) R. M. Levy and D. J. Bauer, *J. Catal.*, **9**, 76 (1967).
7) M. Machida, K. Eguchi, and H. Arai, *Chem. Lett.*, **1986**, 151.
8) M. Machida, K. Eguchi, and H. Arai, *J. Catal.*, **103**, 385 (1987).
9) K. S. Mazdiyansni, R. Dolloff, and J. S. Smith II, *J. Am. Ceram. Soc.*, **52**, 523 (1969).
10) M. Machida, K. Eguchi, and H. Arai, *Chem. Lett.*, **1986**, 1993.
11) E. M. Levin, C. R. Robbines, and H. F. McMurdie, "Phase Diagrams for Ceramists," Fig. 206. Am. Ceram. Soc. Columbus, (1964).
12) J. M. P. J. Verstegen and A. L. N. Stevels, *J. Lumin.*, **9**, 406 (1974).
13) A. L. N. Stevels and A. D. M. Schrama-de Pauw, *J. Electrochem.*, **123**, 691 (1976).
14) S. Kimura, E. Bannai, and I. Shindo, *Mat. Res. Bull.*, **17**, 209 (1982).
15) N. Iyi, S. Takekawa, Y. Bando, and S. Kimura, *J. Solid State Chem.*, **47**, 34 (1983).
16) H. Yamashita, A. Kato, N. Watanabe, and S. Matsuda, *Nippon Kagaku Kaishi*, **1986**, 1169.
17) R. W. Powers and S. P. Mitoff, "Solid Electrolytes," ed by P. Hagenmuller and W. Van Gool, Academic Press, New York (1978), pp. 123—144.
18) B. Yoldas, *Am. Ceram. Soc. Bull.*, **54**, 289 (1975).
19) D. W. Johnson, Jr., *Am. Ceram. Soc. Bull.*, **64**, 1597 (1985).
20) M. Machida, K. Eguchi, and H. Arai, *Chem. Lett.*, **1987**, 767.
21) D. C. Bradly, R. C. Mehrotra, and D. P. Gaur, "Metal Alkoxides," Academic Press, New York (1978), p. 199.
22) B. E. Yoldas, *J. Am. Ceram. Soc.*, **65**, 387 (1982).

 © 1988 The Chemical Society of Japan Bull. Chem. Soc. Jpn., 61, 3667—3672 (1988)

State of Polarization of Light Scattered by Anisotropic Spherical Particles

Yoh SANO
National Institute of Agrobiological Resources, Tsukuba Science City, Ibaraki 305
(Received March 25, 1988)

Using the light-scattering theory of Rayleigh-Gans, theoretical expressions were derived for the state of the polarization of light scattered by anisotropic spherical particles in the case of linearly polarized incident light with its electric vector inclined by an angle ψ to the scattering plane. The azimuth angle of the ellipse of the light scattered is a function of only the scattering angles, θ and ψ; the ellipticity of the ellipse of the scattered light is always equal to zero, meaning that the scattered light is linearly polarized for linearly polarized incident light. The degree of polarization of the scattered light, P, defined as the ratio of the polarized component to the total intensity of the scattered light, depends on the intrinsic anisotropy, p_m, the relative refractive index of the sphere to the solvent, m, and θ together with the angle ψ. Although P for isotropic spherical particles is always equal to 1 at any θ, P for anisotropic spherical particles is smaller than 1.0, but close to 1.0 if the incident light is unpolarized or linearly polarized with ψ=30°. If ψ is smaller than 30°, P varies from 1.0 to 0, depending strongly on the p_m and m of the anisotropic sphere. It has been suggested that the determination of P as a function of ψ and θ would provide good information about the optical intrinsic anisotropy of anisotropic spherical particles.

A particle may have two kinds of optical anisotropy: one is an "intrinsic" anisotropy and the other is a "form" anisotropy.[1] The form anisotropy is an optical anisotropy due to an anisometry. In other words, it is due to the anisotropic shape of a particle made of the isotropic phase. If the shape of the particle is non-spherical and is assumed to be a spheroid, the anisometry can be expressed by the ratio of the length of semiaxis of symmetry to the length of semitransverse axis of the spheroid. For an anisometric particle, the refractive index of the dispersed phase may be independent of the vibration direction of the electric vector. On the other hand, an intrinsic anisotropy occurs when the dispersed phase (the material composing the particle), itself, has an optical anisotropy because of, e.g., the orientation of valence bonds in the phase. For an intrinsic anisotropic particle, the refractive index of the dispersed phase depends on the vibration direction of the electric vector, and, even if the particle is spherical, the effect of the intrinsic anisotropy must be taken into consideration.

The light scattered by optically anisotropic scatterers will generally be partially polarized and contain some unpolarized component. To give a complete description of a partially elliptically polarized state of scattered light, we should analyze the intensities associated with both polarized and unpolarized components, and also give full specifications of the polarization ellipse.

In the case of randomly oriented, optically isotropic and anisometric particles, the state of the polarization of scattered light had already been calculated[2,3] on the basis of the Rayleigh[4]-Gans[5] theory (referred to as the Rayleigh-Gans theory of spheroids (RGS theory)). The RGS theory is used to avoid any confusion with the well-known Rayleigh-Gans (RG) theory of scattering, which involves a restrictive assumption that the refractive index of the particles is close to that of the surrounding medium.[6]

In the present paper, the effect of the intrinsic optical anisotropy to the state of polarization of light scattered by optically anisotropic spherical particles, such as spherical plant viruses, is discussed on the basis of the RGS theory and a set of parameters: i.e., the degree of polarization, ellipticity, azimuth, and handedness of the ellipse of the polarized component of scattered light is examined.

Theory

General Consideration. Let's consider light scattering by an optically anisotropic spherical particle. If a dispersed sphere is optically uniaxial, the excess polarizability can be expressed by a spheroid.[7] If the principal axes of the spheroid are α_a, α_b, α_b, the optical anisotropy is given by the ratio p_g,

$$p_g = \alpha_a/\alpha_b = g_a/g_b, \tag{1}$$

where

$$g_i = (3/4\pi)\,(m_i^2-1)/(m_i^2+2) \quad (i = a \text{ or } b), \tag{2}$$

and m_i is the relative refractive index of the i-direction.

When linearly polarized incident light with an electric vector oriented obliquely to the scattering plane (observation plane) reaches the scattering-volume element, the light scattered will be, in general, elliptically polarized and contain some unpolarized component as well.

All possible states of the scattered light are most easily analyzed by making use of the Stokes parameters as well as the Mueller or scattering matrix, which depends only on the characteristics of the scattering medium. The Stokes parameters(I, Q, U, and V) which completely characterize the intensity and polarization properties of a beam of light, including partially polarized and unpolarized light, are defined in terms of time averages of the electric field components of an electromagnetic wave.[8]

$$\begin{aligned} I &= \langle E_\pi E_\pi^* + E_\sigma E_\sigma^* \rangle, \\ Q &= \langle E_\pi E_\pi^* - E_\sigma E_\sigma^* \rangle, \\ U &= \langle E_\pi E_\sigma^* + E_\sigma E_\pi^* \rangle, \\ V &= \mathrm{i}\langle E_\pi E_\sigma^* - E_\sigma E_\pi^* \rangle. \end{aligned} \tag{3}$$

The subscripts π and σ refer to components of the electric field parallel and perpendicular, respectively, to the scattering plane, the brackets denote time averages, and the asterisks denote conjugate complex values. The four elements of the Stokes vector can be thought of as describing the total intensity (I), the excess of π-polarized over σ-polarized intensity (Q), the excess intensity of +45° linearly polarized over −45° linearly polarized light (U), and the excess of right (as opposed to left) circularly polarized intensity (V).

The Stokes vectors describing the incident and scattered light, $\boldsymbol{S}_0$ and $\boldsymbol{S}$, respectively, are connected by a 4×4 matrix called a Mueller's matrix or a scattering matrix, $\boldsymbol{M}$,

$$\boldsymbol{S} = \boldsymbol{M}\boldsymbol{S}_0, \tag{4}$$

where $\boldsymbol{S}=[I, Q, U, V]$ and $\boldsymbol{S}_0=[I_0, Q_0, U_0, V_0]$

Scattering Matrix. If the particle is sufficiently small compared to the wavelength of light, the scattering matrix $\boldsymbol{M}$ for a randomly oriented spheroid is given by RGS theory:[9]

$$\boldsymbol{M} = \begin{pmatrix} S_{11} & S_{12} & 0 & 0 \\ S_{12} & S_{22} & 0 & 0 \\ 0 & 0 & S_{33} & 0 \\ 0 & 0 & 0 & S_{44} \end{pmatrix}, \tag{5}$$

where the matrix elements S_{11}, S_{12}, S_{22}, S_{33}, S_{44} are given by

$$\begin{aligned} S_{11} &= F_1(1+\cos^2\theta) + 2F_2, \\ S_{12} &= F_1(\cos^2\theta - 1), \\ S_{22} &= F_1(\cos^2\theta + 1), \\ S_{33} &= 2F_1\cos\theta, \text{ and} \\ S_{44} &= 2(F_1 - F_2)\cos\theta, \end{aligned} \tag{6}$$

with

$$\begin{aligned} F_1 &= (\alpha^6/15)(p_g^2 + 3p_g + 7/2)F_0, \\ F_2 &= (\alpha^6/15)(p_g - 1)^2 F_0, \text{ and} \\ F_0 &= [(1+2p_m)(m^2-1)]^2/[(m^2-1) + p_m(2m^2+7)]^2. \end{aligned} \tag{7}$$

The α is the size parameter defined by

$$\alpha = 2\pi a/\lambda, \tag{8}$$

where a is the radius of the sphere and λ is the wavelength of light in the medium.

If the principal refractive indices in the a- or b-directions of the excess polarizabilities n_a and n_b are divided by the refractive index of the solvent n_0 and are represented by (m_a, m_b, m_b), the intrinsic (structural) anisotropy p_m is defined by

$$p_m = (m_a^2 - 1)/(m_b^2 - 1), \tag{9}$$

and the mean relative refractive index m of the spherical particle is defined by[1]

$$1/(m^2-1) = [1/(m_a^2-1) + 2/(m_b^2-1)]/3; \tag{10}$$

therefore, the optical anisotropy p_g defined by Eq. 1 for spherical anisotropic particles is given by

$$p_g = [p_m(2m^2+7) + (m^2-1)]/[2p_m(m^2-1) + (m^2+8)]. \tag{11}$$

State of Polarization of the Scattered Light. The scattered light is, in general, partially polarized and is an incoherent sum of the polarized, I_p (subscript "p" signifies the polarized component), and the unpolarized, I_u (subscript "u" signifies unpolarized), components. Both components are related to the Stokes parameters of scattered light by

$$I_p = (Q^2 + U^2 + V^2)^{1/2}, \tag{12}$$

and

$$I_u = I - I_p.$$

If we consider linearly polarized incident light with an electric vector which makes an angle ψ with the scattering plane, the Stokes vector can be expressed by the normalized Stokes parameters of the incident light beam as

$$\boldsymbol{S}_0 = [1, \cos 2\psi, \sin 2\psi, 0]. \tag{13}$$

By substituting the value of $\boldsymbol{S}_0$ in Eq.4, we obtain the values for each of the Stokes parameters of partially polarized scattered light as follows:

$$\begin{aligned} I_p &= I_p^\circ(1 - \cos^2\psi \sin^2\theta), \\ I &= I_p^\circ(1 - \cos^2\psi \sin^2\theta) + I_u, \\ I_p^\circ &= 2F_1, \; I_u = 2F_2, \text{ and} \\ \eta &= 0. \end{aligned} \tag{14}$$

The ellipticity, η, defined by the ratio of the semiminor to the semimajor axis of the ellipse of the polarized component of scattered light is always equal to 0, which means that the polarized component is linearly polarized in the case of linearly polarized incident light.

The azimuth angle, ζ, of the linearly polarized component of the scattered light, is given by

$$\tan\zeta = \tan\psi/\cos\theta, \tag{15}$$

and is only a function of ψ and θ.

The degree of polarization, P, is defined as the ratio of the intensity of the polarized portion to the total intensity,

$$P_\psi(\theta) = I_p/I. \tag{16}$$

Therefore, we obtain with Eq. 14

$$P_\psi(\theta) = (1 - \sin^2\theta\cos^2\psi)/[(1 - \sin^2\theta\cos^2\psi) + (F_2/F_1)]. \tag{17}$$

Since

$$F_2/F_1 = (p_g - 1)^2/(p_g^2 + 3p_g + 7/2), \tag{18}$$

and p_g is given by Eq. 11, the $P_\psi(\theta)$ depends on p_m, m, θ, and ψ. For anisotropic spherical particles ($p_m \neq 1$),

the $P_\psi(\theta)$ is smaller than 1.0 and is independent of α, as far as RGS theory holds.

A particle composed of isotropic material has a relative refractive index m equal in all directions of the electric vector of light, independently of the particle form. Therefore, in this case, p_m=1 (and p_g=1) and

$$F_1 = (\alpha^6/2)\, F_0,$$
$$F_2 = 0, \text{ and} \qquad (19)$$
$$F_0 = [(m^2-1)/(m^2+2)]^2.$$

The $P_\psi(\theta)$ is always equal to 1 over the entire range of θ in this case.

Numerical Results and Discussion

Variation of the Intensity of the Scattered Light. Numerical calculations were made with an ACOS 850/20 computer at the Computer Center of the Ministry of Agriculture and Forestry. Figure 1 shows the variation in the intensities of the scattered light for the unpolarized component I_u and the maximum of the polarized component $I_p{}^\circ$ as a function of the intrinsic anisotropy p_m for m=1.20. Here, the quantity I (and I_p and I_u as well) is called the "intensity" of the scattered light; however, it is a dimensionless quantity which is equal to the Rayleigh ratio per particle multiplied by k^2 (where $k=2\pi/\lambda$), and is usually expressed by i.

Bovine serum albumin is known to be somewhat asymmetrical and to possess an intrinsic (structural) anisotropy. The intrinsic anisotropy parameter of bovine serum albumin in the native state was calculated to be p_m=1.46.[10] Spherical plant viruses such as tomato bushy stunt virus, southern bean mosaic virus, satellite tobacco necrosis virus et al. contain different amounts of nucleic acids and proteins, although some of these viruses produce nucleic acid-free isometric particles. In some of the viruses the particles consist of various kinds of amino acid residues and in others the particles consist of a long backbone of alternating sugar and phosphate residues with one of five different purine or pyrimidine bases attached to each sugar residue. These residues have an anisotropic structure. Therefore, spherical plant viruses possess an intrinsic anisotropy due to the orientation of valence bonds of the amino acid and/or nucleic acid residues. Taking into account the experimental results of these spherical plant viruses, it is satisfactory to think about the values of p_m<1.9 and also to think the case of m_a>m_b, that is, the values of p_m>1.

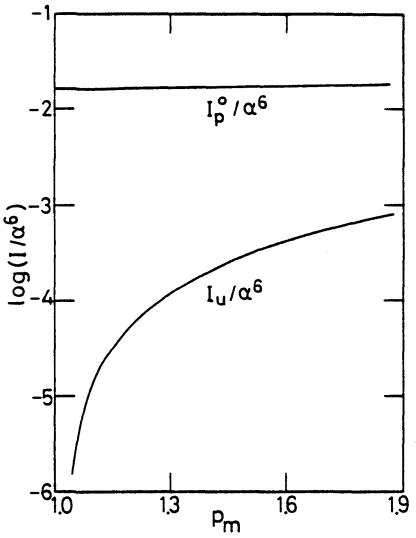

Fig. 1. Variation of $\log(I_u/\alpha^6)$ and $\log(I_p{}^\circ/\alpha^6)$ with the intrinsic anisotropy p_m>1 for m=1.20.

Variation of the Azimuth Angle ζ. Figure 2 shows the variation of the azimuth angle, ζ, with ψ for various θ. As is shown in Eq. 15, the value of ζ is independent of m, α and p_m. The ζ has the same sign as ψ for forward scattering ($0<\theta<90°$) and has the opposite sign for the backward scattering ($90°<\theta<180°$). ζ becomes greater as θ approaches 90°, and at θ=90° the value of ζ is equal to 90° for any value of ψ.

Variation of the Degree of Polarization. The degree of polarization at θ=90° given by Eq. 17 is

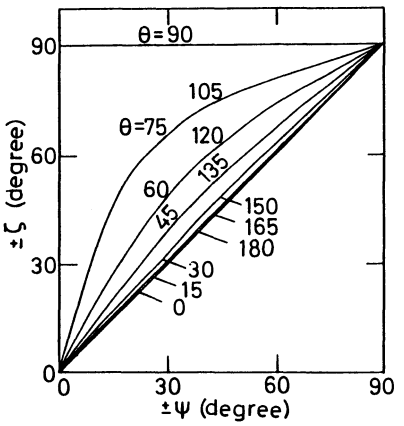

Fig. 2. Variation of the azimuth angle, ζ(degree), with ψ(degree) at various scattering angles θ(degree). For $\theta<90°$, ζ and ψ have the same sign, and for $\theta>90°$, ζ and ψ have the opposite sign.

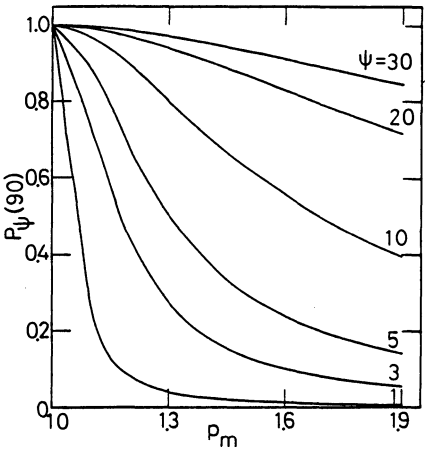

Fig. 3. Variation of the degree of polarization at θ=90°, $P_\psi(90)$, with the intrinsic anisotropy p_m>1 and m=1.20 for various values of ψ(degree).

$$P_\psi(90)=\sin^2\psi/(\sin^2\psi+F_2/F_1). \quad (20)$$

Figure 3 shows the variation of $P_\psi(90)$ with the intrinsic anisotropy p_m and ψ, at $m=1.20$. $P_\psi(90)$ depends strongly on p_m and ψ, especially in cases in which the ψ is smaller than 10°. When ψ is larger than 30°, the change of the $P_\psi(90)$ is relatively small. The $P_\psi(90)$ for isotropic spherical particles ($p_m=1$) is equal to 1.0 irrespective of the value of ψ.

Figure 4 shows the variation of $P_\psi(90)$ with $\pm\psi$. The $P_\psi(90)$ increases monotonously from 0 to almost 1 with the increase of $\pm\psi$, and its value becomes smaller as the p_m deviates from the isotropic materials ($p_m=1$).

Figure 5 shows the variation of $P_\psi(\theta)$ with $\pm\psi$ at various scattering angle θ for $p_m=1.4$. The $P_\psi(\theta)$ is symmetric around $\theta=90°$ since the intensities, I and I_p, are functions of $\sin^2\theta$, as is shown in Eq. 17. The dependence of $P_\psi(\theta)$ on $\pm\psi$ becomes smaller as the deviation of θ from 90° becomes larger. In the case of $\theta=0°$ or 180° the $P_\psi(\theta)$ is constant independent of $\pm\psi$.

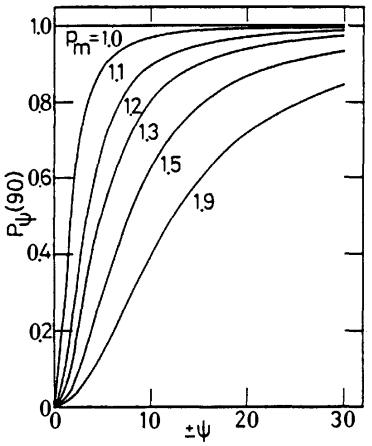

Fig. 4. Variation of the degree of polarization at $\theta=90°$, $P_\psi(90)$, with ψ(degree) and $m=1.20$ for various values of $p_m\geq 1$.

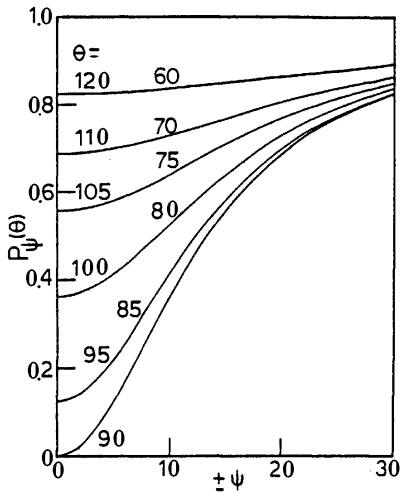

Fig. 5. Variation of the degree of polarization, $P_\psi(\theta)$, with ψ(degree) for $p_m=1.4$ and $m=1.20$. Parameters are scattering angle θ(degree).

Variation of the Degree of Depolarization. The intensity of the scattered light is measured practically by the irradiance transmitted through the analyzer with a transmission axis inclined by χ to the scattering plane. The degree of depolarization is defined by the ratio of the intensity of the parallel (i.e., $\chi=0°$) to the perpendicular (i.e., $\chi=90°$) component of the scattered light.

For unpolarized incident light, the degree of depolarization is given by

$$\rho_u(\theta)=[\cos^2\theta+F_2/F_1]/[1+F_2/F_1], \quad (21)$$

which is equal to $\cos^2\theta$ and is not equal to zero when the scattering angle θ is other than 90°, even if the unpolarized component I_u is zero for the optically isotropic particles ($p_m=1$). At $\theta=90°$, it becomes

$$\rho_u(90)=F_2/(F_1+F_2)=1-P_{90}(90), \quad (22)$$

where $P_{90}(90)$ is the degree of polarization for $\psi=90°$ and $\theta=90°$.

Instead of unpolarized light, if linearly polarized light with an azimuth angle of ψ is used as incident light, the degree of depolarization for $\theta=90°$ is

$$\rho_\psi(90)=F_2/[2F_1\sin^2\psi+F_2]. \quad (23)$$

The variation of $\rho_\psi(90)$ with p_m is shown in Fig. 6, which seems to be very similar to Fig. 3 if the direction of the ordinate is inverted. The value of $\rho_\psi(90)$ is very small if ψ is 30° or larger. The value, however, could become larger, if ψ is decreased.

For the Determination of Parameter Values. As is shown in Figs. 3—6, the degree of polarization, or degree of depolarization, depends strongly on the intrinsic anisotropy p_m, and is independent of α. If we measure a $P_\psi(\theta)$ or $P_\psi(90)$ value, and/or $\rho_\psi(\theta)$ or $\rho_\psi(90)$ value, the intrinsic anisotropy can be determined directly if the value of m is known. If we measure $P_\psi(\theta)$ or $\rho_\psi(\theta)$ values at several values of ψ and θ, it is possible to determine both m and p_m by fitting these values to the theoretical curves.

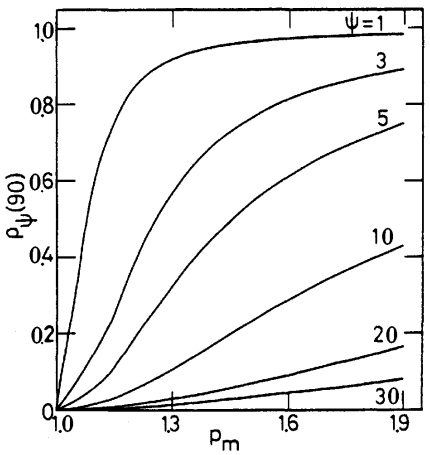

Fig. 6. Variation of the degree of depolarization at $\theta=90°$, $\rho_\psi(90)$, with the intrinsic anisotropy $p_m>1$ and $m=1.20$.

Knowledge about p_m and m immediately gives information regarding the refractive index of both the a- and b-axis of the intrinsic (structural) anisotropic spherical particle, n_a and n_b (according to Eqs. 9 and 10) if the refractive index of the solvent n_0 is known.

In conjunction with knowledge concerning the intrinsic anisotropy, p_m, the value of α is also obtained from the intensities (I, I_p, and I_u) according to Fig. 1. Also, knowledge concerning α immediately gives information on the molecular weight, M, if the partial specific volume is known.

The theory presented in this paper can be efficiently applied to small spherical plant viruses. However, plant virus particles sometimes form by a process, analogous to crystallization, by an orderly aggregation of similarly sized units into three-dimensional arrays. The nucleic acid of viruses also has a definite structure and is not simply a randomly coiled thread, stimulating the crystallization structure. In these cases the effect of the intrinsic anisotropy is large, and a slight modification is necessary for any determination of the intrinsic anisotropy, due to the nonrandom orientation of the segments.

Measurement of Degree of Polarization with the Analyzer. When the transmission axis of the analyzer χ is changed, the intensity of the scattered light $I_{\psi\chi}(\theta)$ is given by[8,11]

$$I_{\psi\chi}(\theta)=(I_u/2)+(I_p/2)[1+\cos^2(\chi-\zeta)],$$
$$=(I/2)[1+P_\psi(\theta)\cos^2(\chi-\zeta)], \quad (24)$$

where ζ is the azimuth angle of the linearly polarized, scattered component. The $I_{\psi\chi}(\theta)$ has a maximum, $I_{max}(\theta)$, and a minimum, $I_{min}(\theta)$, values at $\chi=\zeta$ and $\chi=\zeta+\pi/2$, respectively. The degree of polarization can, therefore, be experimentally measured using the equation

$$P_\psi(\theta)=[I_{max}(\theta)-I_{min}(\theta)]/[I_{max}(\theta)+I_{min}(\theta)]. \quad (25)$$

This is equivalent to thinking of the beam as being made up of two linearly polarized orthogonal incoherent beams of intensities $I_{max}(\theta)$ and $I_{min}(\theta)$.

If another kind of the degree of linear polarization is considered, which is defined directly by the experimentally measurable intensities of the irradiance through the transmission axis of the analyzer at χ and at $(\chi+\pi/2)$, respectively,

$$P_{\psi\chi}(\theta)=[I_{\psi\chi}(\theta)-I_{\psi(\chi+\pi/2)}(\theta)]/[I_{\psi\chi}(\theta)+I_{\psi(\chi+\pi/2)}(\theta)], \quad (26)$$

the deviation of $P_{\psi\chi}(\theta)$ from $P_\psi(\theta)$ is given by

$$P_{\psi\chi}(\theta)=P_\psi(\theta)\cos2(\chi-\zeta). \quad (27)$$

The maximum and minimum values of $P_{\psi\chi}(\theta)$ occur when χ is equal to the azimuth angle ζ and is equal to the orthogonal direction to the azimuth angle, respectively. The $P_{\psi\chi}(\theta)$ is equal to zero at $\chi=(\zeta+\pi/4)$.

Radiation Diagram of Intensity of the Transmitted Light through the Analyzer. The intensity of the irradiance transmitted through the analyzer can also be rewritten as

$$I_{\psi\chi}(\theta)=F_2+F_1\cdot F_{\psi\chi}(\theta), \quad (28)$$

and

$$F_{\psi\chi}(\theta)=(1-\sin^2\theta\cos^2\psi)+(\cos^2\theta\cos^2\psi-\sin^2\psi)\cos2\chi,$$

where both F_2 and F_1 are functions of p_m, m, and α (as explained before), while $F_{\psi\chi}(\theta)$ is a function which depends only on angles θ, ψ, and χ. Figures 7 and 8 are radiation diagrams of the function, $F_{\psi\chi}(\theta)$, which shows a maximum and a minimum, depending on ψ, χ, and θ.

For $\theta=0°$, the $F_{\psi\chi}(0)$ can be simplified as

$$F_{\psi\chi}(0)=2\cos^2(\psi-\chi). \quad (29)$$

If the angle between the transmission direction of the

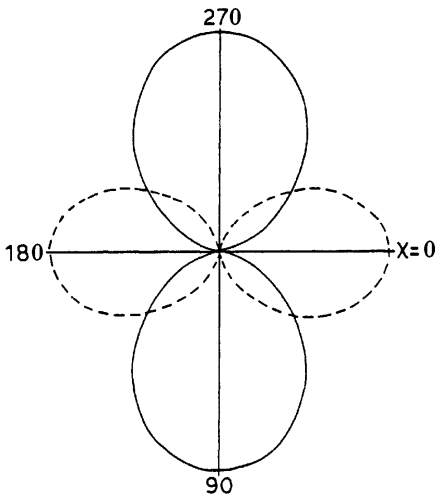

Fig. 7. Radiation diagram of the function of $F_{\psi\chi}(\theta)$. Parameters in the figure are transmission angles of analyzer χ(degree) to the scattering plane. Solid line represents the case for $\psi=90°$ without depending on θ. Broken line represents the case for $\psi=0°$ and $\theta=30°$ or 150°. The $F_{\psi\chi}(\theta)$ at $\theta=0°$ and $\theta=90°$ is situated on an origin.

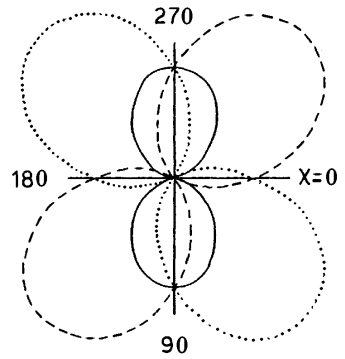

Fig. 8. Radiation diagram of the function of $F_{\psi\chi}(\theta)$ for $\psi=45°$ or $\psi=-45°$. Parameters in the figure are transmission angles of analyzer χ(degree). Solid line represents the value at $\theta=90°$ for $\psi=\pm45°$. Broken line indicates the value at $\theta=150°$ for $\psi=+45°$, and at $\theta=30°$ for $\psi=-45°$. Dotted line represents the value at $\theta=30°$ for $\psi=+45°$, and at $\theta=150°$ for $\psi=-45°$.

polarizer and the analyzer is $\pm\delta$,

$$I_{\psi\chi}(0) = (I_u/2) + I_p^\circ \cos^2\delta. \quad (30)$$

The second term in Eq. 30 is called Malus' law, which was discovered experimentally by Etienne Louis Malus in 1808.[8] Only the polarized component of the forward scattered light (θ=0°) follows Malus' law; half of the intensity of the unpolarized component of the scattered light must, furthermore, be introduced to the total intensity of the forward scattered light.

References

1) Y. Sano and M. Nakagaki, *J. Phy. Chem.*, **88**, 95 (1984).
2) Y. Sano and M. Nakagaki, *J. Colloid Interface Sci.*, **105**, 348 (1985).
3) Y. Sano and M. Nakagaki, *Bull. Chem. Soc. Jpn.*, **59**, 3023 (1986).
4) L. Rayleigh, *Philos. Mag.*, **44**, 28 (1897).
5) R. Gans, *Ann. Phys. (Leipzig)*, **37**, 881 (1912); **62**, 331 (1920).
6) For light scattering by polymer chains in solution Rayleigh-Gans-Debye theory is usually used. The intensity of light scattered by the optically anisotropic units (segments) has already examined. For example, H. Utiyama and M. Kurata, *Bull. Inst. Chem. Res. Kyoto Univ.*, **42**, 128 (1964), K. Nagai, *Polym. J.*, **3**, 67 and 563 (1972). However, state of polarization of scattered light is not examined.
7) M. Kerker, "The Scattering of Light and Other Electromagnetic Radiation," Academic Press, New York (1969).
8) W. A. Shurcliff, "Polarized Light," Harvard University Press, Massachusetts (1962).
9) H. C. Van de Hulst, "Light Scattering by Small Particles," Wiley, New York (1957).
10) Y. Sano, *J. Colloid Interface Sci.*, **124**, 403 (1988).
11) C. F. Bohren and D. R. Huffman, "Absorption and Scattering of Light by Small Particles," Wiley, New York (1983).

 © 1988 The Chemical Society of Japan Bull. Chem. Soc. Jpn., 61, 3673—3680 (1988)

Quenching of Excited Singlet and Triplet States of Some Polyfused Arenes by Dihalobenzenes

G. K. MALLIK, T. K. PAL, T. GANGULY, and S. B. BANERJEE*
Department of Spectroscopy, Indian Association for the Cultivation of Science, Jadavpur, Calcutta 700 032, India
(Received July 27, 1987)

External heavy atom effect on the emission spectra of naphthalene, phenanthrene, and chrysene by perturbers dihalobenzenes are investigated to estimate different nonradiative rate constants associated with the depletion of the singlet and the triplet states of the fluorescers. The bimolecular fluorescence quenching rate constant k_q has been evaluated at 300 K by applying Stern-Volmer relation. The dihalobenzene quenchers have triplet states lying below the singlet states of the fluorescers and the overall quenching rate k_q is composed of two rate constants, namely, the intramolecular intersystem crossing rate k_q^{ISC} and the singlet-triplet energy transfer rate constant k_q^{ST}. The relative magnitudes of the two rate constants k_q^{ISC} and k_q^{ST} have been examined in the light of the energy conditions controlling the associated processes. At 77 K, the phosphorescence decay curve of the fluorescers in the presence of dihalobenzenes is biexponential and the triplet decay of the perturbed fraction of the fluorescers is exponential. It is concluded that at the low temperature, heavy atom interaction in the systems studied mainly proceeds through CT mechanism. Speculative suggestion has been made to account for enhancement of phosphorescence emission of polyfused arenes in EtOH solution.

It is generally believed that the quenching of the excited singlet states of aromatic molecules (AM) in presence of another molecular species containing heavy atom like Cl, Br, and I proceeds via intermediate contact exciplex of charge transfer (CT) nature.[1-15] This CT exciplex is formed in a singlet state which may be higher than the singlet S_1 of the fluorescer AM. The reported observations were made mainly in dilute solutions and in a few cases in vapour phase[10,11] also. This intermediate contact CT exciplex increases the spin-orbit coupling as a result of which the spin forbiddeness of the intercombinational process decreases and consequently intramolecular intersystem crossing (ISC) rate increases. This intramolecular ISC $T_1 \leftrightsquigarrow S_1$ rate depends upon the energy gap between the singlet S_1 and triplet T_1 of the fluorescer AMs, the closer the gap, the greater will be the nonradiative transition probability from singlet to triplet.[16,17] In the presence of external heavy atom perturber another mechanism may be operative in causing depletion of singlet state. This is intermolecular singlet-triplet energy transfer depicted by the scheme[18]

$$S_d^1 + S_q^0 \rightarrow\rightarrow S_d^0 + T_q^1 \qquad (1)$$

where the subscripts d and q stand for donor and quencher molecules respectively. This transfer occurs by means of an exchange mechanism and is of short range nature. A required condition is that the triplet T_1 of the quencher should lie well-below the singlet S_1 of the fluorescer.

Heavy atom perturbation also modifies phosphorescence spectra of AMs[19-30] through the second order interactions which proceed via (1) electron exchange and (2) CT mechanism. There is still some controversy whether CT or electron exchange mechanism would be dominant in spin orbit interaction. Castino et al.[31] proposed exchange mechanism for pyrene-iodine system in cyclohexane solution. Lessard and Durocher[32] studied phosphorescence decay of indole and concluded that when halocarbons were used as quenchers heavy atom interaction proceeded through CT exciplex formation whereas in the case of the quencher propyl bromide the electron-exchange mechanism prevailed. Najbar et al.[28] stressed on second order electron exchange mechanism for the external heavy atom interaction between several AMs and KI.

The present paper reports the emission spectra of naphthalene, phenanthrene, and chrysene in ethanol (EtOH) at 300 and 77 K in presence of different concentrations of *p*-dichlorobenzene (DCB), *p*-dibromobenzene (DBB), and *p*-diiodobenzene (DIB). One of the objectives was to estimate the rates of the bimolecular fluorescence quenching proceeding via intramolecular ISC and intermolecular singlet-triplet energy transfer processes. It was also intended to determine the various photophysical parameters involved in the heavy atom interaction and to examine the role of CT or electron exchange in inducing depletion of singlet and triplet states of the fluorescer molecules.

Experimental

Source and method of purification of naphthalene, phenanthrene, and chrysene (used as fluorescer) were the same as described in our previous paper.[14] Both *p*-dichlorobenzene (DCB) and *p*-dibromobenzene (DBB) obtained from BDH were used after vacuum sublimation. *p*-Diiodobenzene (DIB) from Aldrich Chemical Ltd. was used without further purification. Solvent EtOH (E. Merck) of spectroscopic grade was used as such. 1,2-Dichloroethane (1,2-DCE) obtained from B D H London (LR Grade) was treated with calcium chloride for two days and then distilled over P_2O_5. 1,3-Dibromopropane (1,3-DBP) purchased from the same source was fractionally distilled at atmospheric pressure before use. The samples, quenchers, and solvents were tested for any possible interfering emission.

The concentrations of naphthalene, phenanthrene, and chrysene were chosen approximately at 10^{-4} mol dm^{-3} for all emission experiments at 300 and 77 K. The concentrations of the perturbers DCB, DBB, and DIB were varied between

0.32—2.30, 10^{-2}—0.25, and 10^{-4}—10^{-2} mol dm^{-3} respectively and those of 1,2-DCE and 1,3-DBP varied between 10^{-2}—10^{-1} and 0.41—4.00 mol dm^{-3} respectively.

The fluorescence and phosphorescence spectra were recorded with a Perkin Elmer model MPF 44 A fluorescence spectrophotometer provided with corrected spectra unit and the absorption spectra with a Shimadzu UV-VIS spectrophotometer model 210 A.

Naphthalene, phenanthrene, and chrysene were excited at 300, 295, and 320 nm, respectively when fluorescence and phosphorescence spectra were recorded both at 300 and 77 K. For phosphorescence decay study the emission wavelengths of naphthalene, phenanthrene, and chrysene were chosen at 469, 497, and 540 nm, respectively. After the phosphorescence intensity achieved a steady state, the exciting radiation was cut off to obtain the dark decay on the recorder.

Results and Discussion

The intensity of fluorescence emission of naphthalene, phenanthrene, and chrysene in EtOH falls off in a regular way when DCB, DBB, and DIB are added gradually (Fig. 1) to the binary mixtures. But the same dihalogen molecules do not produce any change in the absorption spectra of the polyfused arenes in EtOH. So, for these systems the static quenching may be ignored and the dynamic fluorescence quenching rate constant can be determined from the well-known relation (2)

$$f_o/f = 1 + K_{SV}[Q] = 1 + k_q\tau_o[Q]. \quad (2)$$

Here f_o and f refer to relative fluorescence intensities of fluorescer in EtOH without quencher [Q] and with quencher of concentration [Q] respectively, and K_{SV} is the Stern-Volmer (S-V) constant. Figure 2 gives the S-V plots and in Table 1 are given the k_q values measured in ternary solutions containing the dihalogens and also in solutions containing monohalogen quenchers chlorobenzene (ClB), bromobenzene (BrB), and iodobenzene (IB). The dihalogen perturbers are seen to be more efficient than the monohalogens in quenching fluorescence. The dependence of quenching efficiency on the number of chlorine, bromine, or iodine atoms in the quencher molecules or in other words on the electron affinities of the quencher molecules indicates that a possible route of depletion of the excited states of the fluorescer polyfused arenes is through contact exciplex of CT nature formed between fluorescer and quencher molecules. In the systems under study, the transfer of charge necessary for CT exciplex formation would be from the electron donor naphthalene, phenanthrene, or chrysene to the electron acceptor DCB, DBB, or DIB molecules. The CT interaction would induce large ISC with rate constant k_q^{ISC} in the chromophore. Another possible mechanism for nonradiative deactivation capable of significant con-

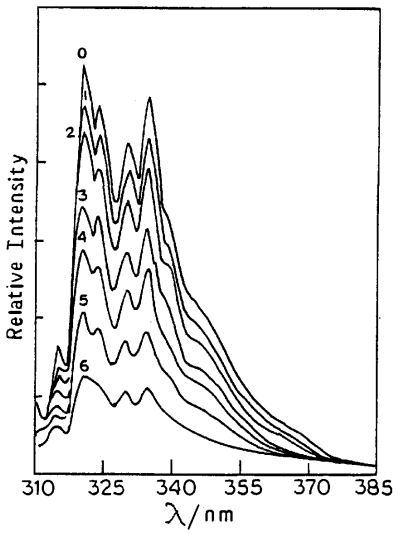

Fig. 1. Fluorescence spectra of naphthalene in EtOH (9.75×10^{-4} mol dm^{-3}) at 300 K (excitation wavelength: 300 nm). Concentration (mol dm^{-3}) of DBB in O,O; 1, 1.18×10^{-2}; 2, 1.96×10^{-2}; 3, 3.93×10^{-2}; 4, 6.56×10^{-2}; 5, 0.11; 6, 0.18.

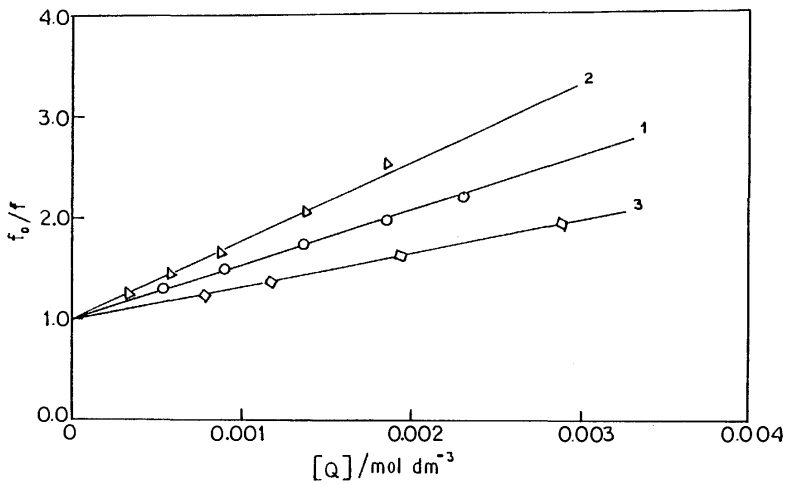

Fig. 2. f_o/f vs. [Q] relations for (1) naphthalene-DIB, (2) phenanthrene-DIB, and (3) chrysene-DIB.

Table 1. Values of Stern-Volmer Constant K_{SV} and Bimolecular Fluorescence Quenching Rate Constant k_q for the Systems of the Electron Donors Naphthalene, Phenanthrene, and Chrysene and Some Halobenzene Acceptors (Quenchers) in EtOH Solution at 300 K

Molecule	τ_0[a]/ns	Quencher	K_{SV}/ $dm^3 mol^{-1}$	k_q/ $dm^3 mol^{-1} s^{-1}$	k_q'/ $dm^3 mol^{-1} s^{-1}$	k_q^{ISC}/ $dm^3 mol^{-1} s^{-1}$	k_q^{ST}/ $dm^3 mol^{-1} s^{-1}$
Naphthalene	96.0	1) ClB[a]		No quenching			
		2) DCB	0.70	7.29×10^6	—	1.67×10^6	5.62×10^6
		3) 1,2-DCE	0.16	—	1.67×10^6	1.67×10^6	—
		1) BrB[a]	7.0	7.30×10^7	—	—	—
		2) DBB	24.8	2.58×10^8	—	1.25×10^8	1.33×10^8
		3) 1,3-DBP	12.0	—	1.25×10^8	1.25×10^8	—
		1) IB[a]	155.0	1.60×10^9	—	—	—
		2) DIB	543.7	5.66×10^9	—	—	—
Phenanthrene	57.5	1) ClB[a]		No quenching			
		2) DCB	0.35	6.09×10^6	—	2.61×10^6	3.48×10^6
		3) 1,2-DCE	0.15	—	2.61×10^6	2.61×10^6	—
		1) BrB	1.8	3.20×10^7	—	—	—
		2) DBB	7.0	1.22×10^8	—	6.09×10^7	6.11×10^7
		3) 1,3-DBP	3.5	—	6.09×10^7	6.09×10^7	—
		1) IB[a]	55.5	9.70×10^8	—	—	—
		2) DIB	772.3	1.34×10^{10}	—	—	—
Chrysene	42.6	1) ClB[a]		No quenching			
		2) DCB	0.14	3.28×10^6	—	2.35×10^6	0.93×10^6
		3) 1,2-DCB	0.10	—	2.35×10^6	2.35×10^6	—
		1) BrB[a]	2.4	5.60×10^7	—	—	—
		2) DBB	5.0	1.17×10^8	—	9.39×10^7	2.31×10^7
		3) 1,3-DBP	4.0	—	9.39×10^7	9.39×10^7	—
		1) IB	61.5	1.40×10^9	—	—	—
		2) DIB	106.90	2.52×10^9	—	—	—

a) Ref. 14.

tribution is singlet-triplet energy transfer, with rate constant k_q^{ST}, from the chromophore to the quencher. This energy transfer occurs through exchange mechanism and is of short range nature.[18] The dynamic rate constant may be assumed to be composed of mainly two independent rate constants k_q^{ISC} and k_q^{ST} and one may write

$$k_q = k_q^{ISC} + k_q^{ST}. \quad (3)$$

For the polyfused arene-dihalobenzene systems studied, it is not possible to estimate individual contribution of k_q^{ISC} and k_q^{ST} to k_q. Therefore, the fluorescence spectra of naphthalene, phenanthrene, and chrysene in EtOH have been measured with 1,2-DCE and 1,3-DBP as quenchers. In these aliphatic molecules the halogen atoms are well separated from each other by CH_2 group and, what is more important, these two molecules do not have any singlet or triplet state lying near the fluorescent state of naphthalene, phenanthrene, or chrysene. Therefore, energy transfer between the fluorescers and 1,2-DCE or 1,3-DBP should have no role in the deactivation process and only ISC would be operative through CT mechanism. The measured dynamic quenching rate constants, k_q', of the fluorescer in these aliphatic solvents (Table 1) would be composed of only k_q^{ISC}. If the k_q^{ISC} values of the aromatic fluorescers in dihalobenzene solvents are assumed to have the same values as k_q' then an estimate of k_q^{ST} for these systems may be made from the relation (3). The k_q^{ST} values thus determined are included in Table 1. The analysis of the rates k_q^{ST} and k_q^{ISC} so made, can only be very approximate and admittedly the procedure is open to criticism because it involves the tacit assumption that the external heavy atom effects induced by the aliphatic dihalogens and the aromatic dihalogens are the same. At the same time all other possible deactivation processes are disregarded. Nevertheless, such analysis may give a qualitative idea about the relative importance of the two processes in these systems and the relative magnitudes of the rate constants k_q^{ST} and k_q^{ISC} determined by the above procedure may be examined in the light of the energy condition controlling the associated processes. The triplet state T_1 of DCB and of DBB lies well below the singlet state S_1 of naphthalene and phenanthrene (Table 2) and the rate constant k_q^{ST} is large for two fluorophores in DCB and DBB, whereas T_1 states of DCB and DBB have energies higher than S_1 of chrysene and the singlet-triplet energy transfer process is less probable. Expectedly, for chrysene-DCB and chrysene-DBB systems the estimated k_q^{ST} is smaller than k_q^{ISC}. The intramolecular ISC rate k_{ISC} is, in general, large or small depending on whether the singlet-triplet energy interval ($\nu_f - \nu_p$) in a fluorescer is small or large. The k_q^{ISC} values of naphthalene, phenanthrene, and chrysene perturbed by DCB are in the expected order (Table 3), but in DBB the

Table 2. Difference in Energy ($\Delta\nu$) between the Singlet (S_1) of the Fluorescer and the Triplet (T_1) of the Quencher and k_{ST} values

Quencher	ν_p[a]/cm^{-1}	Molecule	ν_f[b]/ cm^{-1}	$d\nu(=\nu_f-\nu_p)$/ cm^{-1}	k_q^{ST}/ dm^3 mol^{-1} s^{-1}
DCB	27890[d]	Naphthalene	32249[c]	4359	5.62×10^6
		Phenanthrene	28893[c]	1003	3.48×10^6
		Chrysene	27692[c]	−198*	0.93×10^6
DBB	27910[e]	Naphthalene	32249	4339	1.33×10^8
		Phenanthrene	28893	983	6.11×10^7
		Chrysene	27692	−218*	2.31×10^7

* −Ve sign indicates that the triplet level of the quencher lies above the singlet level of the fluorescer.
a) ν_p denotes the phosphorescence 0-0 band (T_1) of quenchers. b) ν_f denotes the fluorescence 0-0 band (S_1) of fluorescers. c) Ref. 33. d) Ref. 34. e) Ref. 35.

Table 3. Difference between Singlet (ν_f) and Triplet (ν_p) Energy Levels of the Naphthalene, Phenanthrene, and Chrysene and k_q^{ISC} Values with Dihalobenzene Quenchers at 300 K in EtOH Solution

Molecule	ν_f^*/cm^{-1}	ν_p^*/cm^{-1}	$(\nu_f-\nu_p)$/cm^{-1}	k_q^{ISC}/dm^3 mol^{-1} s^{-1}	
				DCB	DBB
Naphthalene	32249	21274[a]	10975	1.67×10^6	1.25×10^8
Chrysene	27692	19800[a]	7892	2.35×10^6	9.39×10^7
Phenanthrene	28893	21730[a]	7163	2.61×10^6	6.09×10^7

* ν_f and ν_p denote the 0-0 bands of S_1 and T_1 levels of the polyfused arenes, respectively.
a) Ref. 36.

values calculated for naphthalene, phenanthrene, and chrysene are not so. Perhaps in the case of the aliphatic and aromatic quenchers containing bromine, the objections noted above are more valid. So far as relative magnitudes of k_q^{ST} and k_q^{ISC} for the individual polyfused arene fluorophores in DCB and DBB are concerned the following facts may be noted. For naphthalene in DCB as heavy atom perturber with large $(\nu_f-\nu_p)$ and $\Delta\nu$ (Tables 2 and 3), the k_q^{ST} rate process is more important than k_q^{ISC} (Table 1) while in the case of phenanthrene, the k_q^{ISC} is only marginally smaller than k_q^{ST}. In DBB, on the other hand, k_q^{ST} and k_q^{ISC} are of nearly the same magnitude for both naphthalene and phenanthrene. In the case of chrysene, where the energy condition for energy transfer from the singlet of the fluorescer to the triplet states of the heavy atom perturbers DCB and DBB is unfavourable, k_q^{ST} is smaller than k_q^{ISC} in both DCB and DBB. It is seen from Table 3 that k_q^{ST} is small when $\Delta\nu$ is small. This dependence of k_q^{ST} on $\Delta\nu$ is consistent with the expectation that small energy gap between the singlet of the fluorescer and the triplet of the quencher facilitates back transfer from the latter to the former. It is to be pointed out here that 1,2-diiodoethane or any other suitable aliphatic iodo compound of desired purity and stability, which does not have singlet or triplet level below S_1 state of the polyfused arenes, was not available. So individual contribution of k_q^{ST} and k_q^{ISC} with DIB as quencher could not be determined seperately. But it may be speculated that because of favorable energy condition, the S-T energy transfer (k_q^{ST}) in the case of chrysene in DIB will be larger than in DCB or DBB. The proposed quenching process may be represented by,

$$^1A^* + Q \underset{k_{-1}}{\overset{k_1}{\rightleftharpoons}} {}^1(A^{\delta+} \cdots\cdots Q^{\delta-})^* \xrightarrow{k_{ISC}} {}^3A^* + Q \rightarrow {}^1A + Q \qquad (3a)$$

The dihalobenzenes have favorable π-electronic structure efficiently forming CT complex and indicating quenching via process (3a). The low temperature measurements at 77 K discussed below favor this reaction.

Another process that might have some role is

$$^1A^* + Q \rightarrow\rightarrow {}^1A + {}^3Q^* \qquad (3b)$$

because the fluorescers and the quenchers have singlet and triplet states with favorable condition for energy transfer. But no direct evidence of ^3Q could be found. It may be pointed out that careful examination showed that the halobenzenes in EtOH did not phosphoresce at 300 K and even at 77 K, emission from these molecules was very weak.

The two second order mechanisms, charge transfer and electron exchange, through which external heavy atom perturbation by the dihalobenzenes on emission of the polyfused arenes proceeds, are known to affect the lowest triplet state of the aromatic polyfused arene fluorescers. Generally, these processes enhance the radiative character of $S_0 \leftarrow T$ transition of aromatic molecules (AM).[28,37] Study of decay of emissions from

the molecules and kinetic analysis of photophysical parameters of the singlet and triplet states of the molecules would therefore be expected to yield interesting information. With this idea in mind, the luminescence emissions of naphthalene, phenanthrene, and chrysene in EtOH rigid glass matrix at 77 K have been measured with and without addition of dihalobenzenes. When DCB is added to the binary mixture of phenanthrene or chrysene in EtOH at 77 K, both the fluorescence and phosphorescence emissions are reduced (Fig. 3). Only in the case of naphthalene, fluorescence is quenched and the phosphorescence is enhanced (Fig. 4). With DBB as quencher, fluorescence emission of all three polyfused arene fluorescers is quenched but their phosphorescence emission is enhanced (Fig. 5) while DIB quenches both the fluorescence and phosphorescence of the polyfused arenes (Fig. 6). In all the systems studied no change occurs in the shape and position of emission bands. The phosphorescence decay curves of polyfused arene-dihalobenzene systems are of biexponential nature. In the decay curve given in Fig. 7, $I_p(t)$ and $I_p(0)$ refer to time-dependent and stationary state phosphorescence intensity respectively. After a considerable time the decay curves become linear and identical with the unperturbed decay. The perturbed decay function which is obtained by subtracting the exponential decay component from the observed phosphorescence decay function is of exponential nature (Fig. 7). This lends support to the conclusion that the dominant process in external heavy atom perturbation in the systems investigated is charge transfer, because a nonexponential perturbed decay function would mean that major contribution comes through electron exchange mecha-

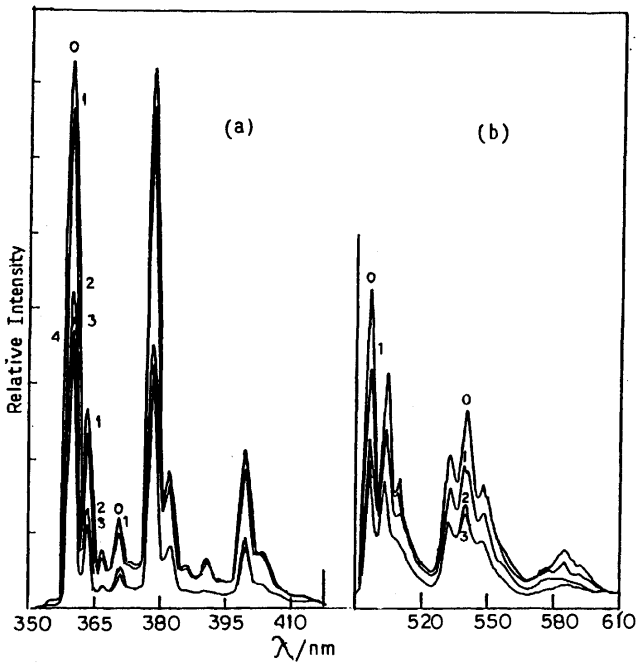

Fig. 3. Fluorescence (a) and phosphorescence (b) spectra of chrysene in EtOH (1.80×10^{-4} mol dm^{-3}) at 77 K (excitation wavelength: 320 nm). Concentration (mol dm^{-3}) of DCB in 0,0; 1, 0.34; 2, 0.67; 3, 0.81.

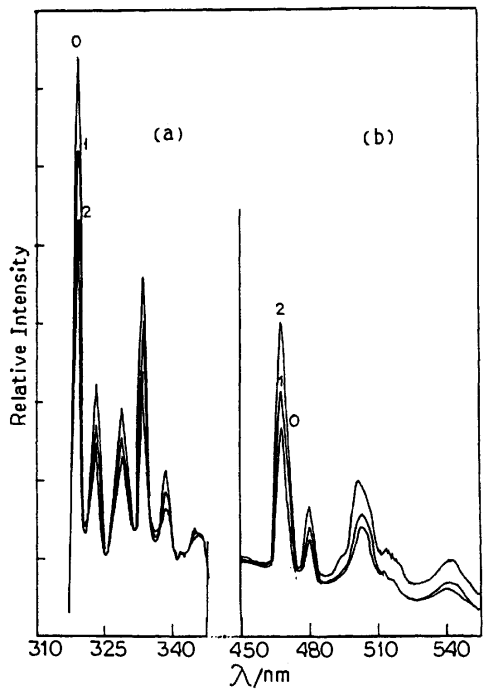

Fig. 4. Fluorescence (a) and phosphorescence (b) spectra of naphthalene in EtOH (5.20×10^{-4} mol dm^{-3}) at 77 K (excitation wavelength: 300 nm). Concentration (mol dm^{-3}) of DCB in 0,0; 1, 0.57, 2, 1.13.

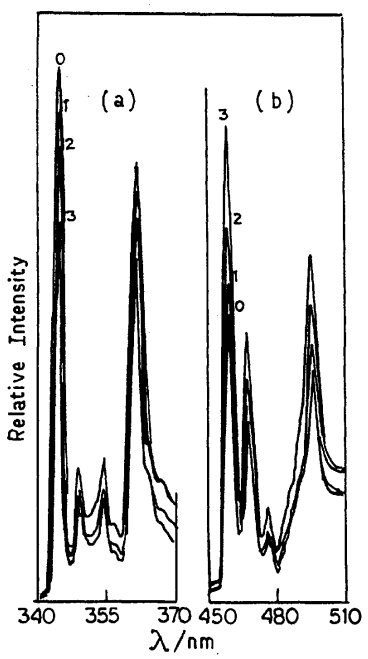

Fig. 5. Fluorescence (a) and phosphorescence (b) spectra of phenanthrene in EtOH (3.50×10^{-4} mol dm^{-3}) at 77 K (excitation wavelength: 295 nm). Concentration (mol dm^{-3}) of DBB in 0,0; 1, 0.11; 2, 0.18; 3, 0.25.

nism.[28,32] Referring to the decay curves, the phosphorescence intensity can be expressed as[13,22]

$$I_p(t)/I_p(0) = \beta e^{-t/\tau_p} + (1-\beta)e^{-t/\tau_p'}. \quad (4)$$

From the biexponential nature of the phosphorescence decay curve it is evident that the CT complex which may be formed in excited singlet state is also formed in the triplet state. But absence of any change in shape and position of phosphorescence bands of the polyfused arenes after addition of *p*-dihalobenzenes may mean that the triplet complex quickly dissociates into free molecules. With regard to possible phosphorescence emission from perturbed complex which has its own decay rate it may be that the peak positions and structure of phosphorescence spectra of the complex molecules are similar to those of the electron donor polyfused arenes. Cases of complexes showing donor type phosphorescence have been discussed and reviewed by previous authors.[32,38]

The values of β and other photophysical parameters are obtained by usual methods described earlier[13] are given in Tables 4—6. The photophysical parameters are all found to depend on concentration of the quenchers. The phosphorescence decay time τ_p' of a perturbed fluorescer molecule decreases regularly with increase of quencher concentration (Tables 4—6). Concomitantly relative intramolecular ISC rate k_i'/k_i (Prime sign denoting perturbed species) and the triplet

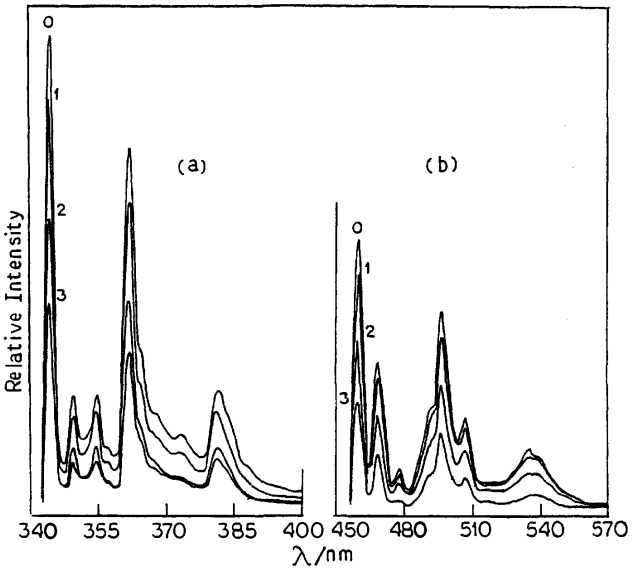

Fig. 6. Fluorescence (a) and phosphorescence (b) spectra of phenanthrene in EtOH (3.37×10^{-4} mol dm^{-3}) at 77 K (excitation wavelength: 295 nm). Concentration (mol dm^{-3}) of DIB in 0,0; 1, 1.88×10^{-2}; 2, 2.63×10^{-2}; 3, 2.78×10^{-2}.

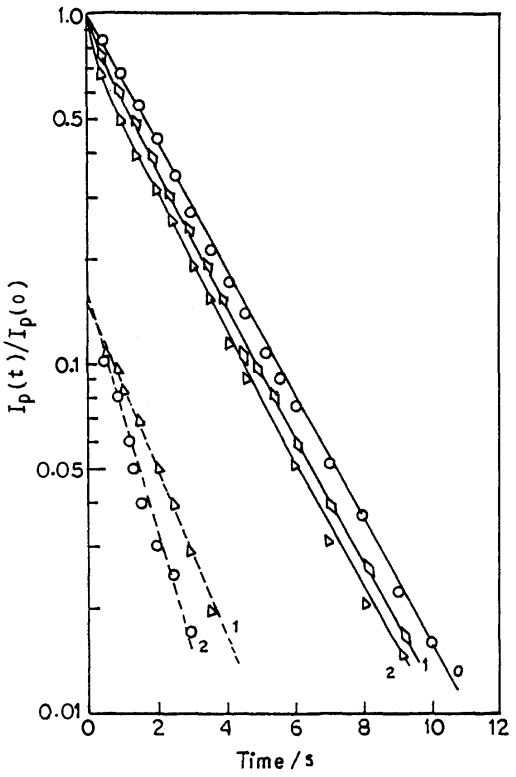

Fig. 7. Phosphorescence decay function of chrysene in EtOH (1.80×10^{-4} mol dm^{-3}) at 77 K without the perturber DIB (O); with the perturber DIB molecules of concentration (mol dm^{-3}) in (1) 1.73×10^{-2}; (2) 2.71×10^{-2}. Dotted curves 1 and 2 represent phosphorescence decay functions of the perturbed chrysene molecule by DIB.

Table 4. Influence of DCB on Fluorescence and Phosphorescence Photophysical Parameters of Chrysene, Naphthalene, and Phenanthrene in EtOH at 77 K

Compound	C_{DCB} / mol dm^{-3}	I_f/I_f°	I_p/I_p°	β	τ_p / s	τ_p' / s	α[a]	k_i'/k_i	k_p'/k_p	k_{ip}'/k_{ip}	Φ_t'/Φ_t	Φ_t'
Chrysene	0.34	0.93	0.73	0.78	2.38	1.73	0.57	1.25	0.49	1.46	1.05	0.81
	0.67	0.48	0.53	0.73	2.38	1.52	0.39	8.50	0.30	1.69	1.26	0.97
	0.81	0.41	0.45	0.71	2.38	1.44	0.32	9.51	0.25	1.79	1.26	0.97
Naphthalene	0.57	0.88	1.23	0.70	2.38	1.23	0.86	10.52	3.08	1.86	1.50	0.95
	1.13	0.78	1.50	0.50	2.38	1.15	0.75	12.64	4.08	1.93	1.52	0.96
	1.58	0.75	1.80	0.40	2.38	1.01	0.72	14.22	5.98	2.11	1.52	0.96
Phenanthrene	0.34	0.95	0.87	0.85	3.61	1.88	0.74	1.27	0.95	2.05	1.03	0.90
	1.13	0.77	0.77	0.80	3.61	1.80	0.62	2.76	0.75	2.17	1.09	0.95
	1.58	0.63	0.67	0.75	3.61	1.73	0.50	4.27	0.62	2.28	1.11	0.97

a) $\alpha=(I_p/I_p^\circ)\,\beta$.

Table 5. Influence of DBB on Fluorescence and Phosphorescence Photophysical Parameters of Chrysene, Naphthalene, and Phenanthrene in EtOH at 77 K

Compound	C_{DBB} / mol dm^{-3}	I_f/I_f°	I_p/I_p°	β	τ_p / s	τ_p' / s	α	k_i'/k_i	k_p'/k_p	k_{ip}'/k_{ip}	Φ_t'/Φ_t	Φ_t'
Chrysene	0.10	0.96	1.15	0.82	2.38	1.73	0.94	3.60	3.94	1.12	1.20	0.92
	0.14	0.93	1.25	0.72	2.38	1.58	0.90	4.03	4.32	1.21	1.21	0.93
	0.17	0.89	1.33	0.65	2.38	1.30	0.86	5.76	4.92	1.52	1.23	0.95
Naphthalene	0.04	0.85	1.20	0.68	2.38	1.23	0.82	8.94	2.78	1.88	1.49	0.94
	0.11	0.75	1.50	0.48	2.38	1.15	0.72	14.23	3.79	1.95	1.52	0.96
	0.18	0.66	1.57	0.40	2.38	1.01	0.63	18.99	3.91	2.25	1.54	0.97
Phenanthrene	0.11	0.96	1.09	0.87	3.30	1.59	0.95	5.60	5.26	1.66	1.12	0.97
	0.18	0.90	1.25	0.70	3.30	1.51	0.88	6.75	6.08	1.68	1.13	0.98
	0.25	0.80	1.48	0.52	3.30	1.44	0.77	8.28	6.27	1.77	1.13	0.98

Table 6. Influence of DIB on Fluorescence and Phosphorescence Photophysical Parameters of Chrysene, Naphthalene, and Phenanthrene in EtOH at 77 K

Compound	C_{DIB} / mol dm^{-3}	I_f/I_f°	I_p/I_p°	β	τ_p / s	τ_p' / s	α	k_i'/k_i	k_p'/k_p	k_{ip}'/k_{ip}	Φ_t'/Φ_t	Φ_t'
Chrysene	1.16×10^{-2}	0.77	0.89	0.73	2.38	1.88	0.65	3.49	0.73	1.32	1.20	0.92
	1.73×10^{-2}	0.66	0.87	0.70	2.38	1.73	0.61	9.83	0.73	1.44	1.26	0.97
	2.71×10^{-2}	0.50	0.73	0.67	2.38	1.23	0.49	32.80	0.71	2.06	1.29	0.99
Naphthalene	1.85×10^{-3}	0.88	0.93	0.75	2.38	1.59	0.70	2.06	0.93	1.54	1.24	0.78
	2.31×10^{-3}	0.81	0.73	0.80	2.38	1.44	0.58	2.31	0.45	1.74	1.27	0.80
	2.89×10^{-3}	0.68	0.44	0.86	2.38	1.30	0.38	2.69	0.14	1.95	1.30	0.82
Phenanthrene	1.88×10^{-2}	0.85	0.87	0.90	3.30	2.02	0.78	3.46	0.58	1.77	1.10	0.96
	2.63×10^{-2}	0.65	0.65	0.86	3.30	1.87	0.59	7.70	0.37	1.95	1.13	0.98
	2.78×10^{-2}	0.43	0.41	0.83	3.30	1.80	0.34	8.28	0.17	2.05	1.13	0.98

yield Φ_t' increase. The k_{ISC} rate is highly sensitive to concentration of the quencher (Tables 4—6). It has been noted above, that DBB enhances the intensity of phosphorescence bands of all three polyfused arenes whereas DCB enhances the phosphorescence of naphthalene only. On the other hand, DIB quenches phosphorescence of all three compounds. According to Eisenthal[39] electronic mixing of the donor triplet with the CT singlet may lead to an enhancement of the 0-0 band as well as all successive totally symmetric vibrational bands of the donor fluorescer molecule through borrowing of intensity from CT interaction by $S_0 \leftarrow T$ transition of the fluorescer. The mixing of the donor triplet with the CT singlet of the complex occurs via the CT triplet of the complex provided the mixing of the donor and CT triplets is permitted. A necessary condition is that the phosphorescence of the fluorescer is polarized parallel to the CT absorption.[39] It is tempting to speculate that these conditions are satisfied in the cases of those polyfused arene-dihalogen systems in which enhancement of intensity of phosphorescence emissions of polyfused arenes due to external heavy atom effect has been observed. These conditions might not be satisfied in the other systems such as phenanthrene and chrysene in DCB and the three polyfused arenes in DIB. In the case of these systems, addition of heavy atom quencher DCB or DIB to arenes concerned reduces phosphorescence radiative rates k_p'/k_p and simultaneously increases the non-radiative rates k_{ip}'/k_{ip} (Tables 4 and 6). The net result is quenching of phosphorescence on complexation in the triplet state.

References

1) S. Lipsky, W. P. Helman, and J. F. Merklin, "Luminescence of Organic and Inorganic Materials," ed by H. P. Kallmann and G. M. Spruch, Wiley, New York (1962), p. 83.

2) S. P. McGlynn, T. Azumi, and M. Kasha, *J. Chem. Phys.*, **40**, 507 (1964).

3) T. Medinger and F. Wilkinson, *Trans. Farad. Soc.*, **61**, 620 (1965).

4) J. Klein, V. Pinaud-Plazanet, and G. Laustrait, *J. Chem. Phys.*, **67**, 302 (1970).

5) W. R. Ware and C. Lewis, *J. Chem. Phys.*, **57**, 3546 (1972).

6) G. DasGupta and D. Phillips, *J. Chem. Soc., Faraday Trans. 2*, **68**, 2003 (1972).

7) D. Saperstein and E. Levin, *J. Chem. Phys.*, **62**, 3560. (1975).

8) J. Bending, M. Siegmund, and S. Helm, *Adv. Mol. Relax. Inter. Processes*, **14**, 121 (1979).

9) M. E. R. Marcondes, V. G. Toscano, and R. G. Weiss, *J. Photochem.*, **10**, 315 (1979).

10) H. A. Khawaja, G. P. Semeluk, and I. Unger, *Can. J. Chem.*, **60**, 1767 (1982).

11) H. A. Khwaja, G. P. Semeluk, and I. Unger, *Can. J. Chem.*, **61**, 1952 (1983).

12) F. Castano, S. Lombrana, E. Martinez, and M. T. Martinez, *Spectrosc. Lett.*, **16**, 805 (1983).
13) G. K. Mallik, T. K. Pal, S. Laha, T. Ganguly, and S. B. Banerjee, *J. Lumin.*, **33**, 377 (1985).
14) T. K. Pal, G. K. Mallik, T. Ganguly, and S. B. Banerjee, *Indian J. Phys.*, **60B**, 108 (1986).
15) K. Chatterjee, S. Chakravorti, T. Ganguly, and S. B. Banerjee, *IL NUOVO CIMENTO*, **8D**, 541 (1986).
16) M. Kasha, *J. Chem. Phys.*, **20**, 71 (1952).
17) K. K. Rohatgi-Mukherjee, "Fundamentals of Photochemistry," Wiley Eastern Ltd., New Delhi, Bangalore, Bombay, Calcutta, Madras, Hyderabad (1986), p. 136.
18) I. B. Berlmann, *J. Phys. Chem.*, **77**, 562 (1973).
19) K. B. Eisenthal and M. A. El-Sayed, *J. Chem. Phys.*, **42**, 794 (1965).
20) R. H. Hofeldt, R. Sehai, and S. H. Lin, *J. Chem. Phys.*, **52**, 4512 (1970).
21) G. G. Giachino and D. R. Kearns, *J. Chem. Phys.*, **52**, 2964 (1970).
22) G. G. Giachino and D. R. Kearns, *J. Chem. Phys.*, **52**, 3886 (1970).
23) G. J. Hoijtink, *Mol. Phys.*, **3**, 67 (1960).
24) G. W. Robinson, *J. Chem. Phys.*, **46**, 572 (1967).
25) H. Tsubomura and R. S. Mulliken, *J. Am. Chem. Soc.*, **82**, 5966 (1960).
26) J. N. Murrell, *Mol. Phys.*, **3**, 319 (1960).
27) S. E. Webber, *Chem. Phys. Lett.*, **5**, 466 (1970).
28) J. Najbar, J. B. Barks, and T. D. S. Hamilton, *Chem. Phys.*, **23**, 281 (1977).
29) J. C. Miller, J. S. Meek, and S. J. Strickler, *J. Am. Chem. Soc.*, **99**, 8175 (1977).
30) J. Najbar, J. Rodaliewicz-Nowak, and A. Chodkowska, *J. Lumin.*, **17**, 449 (1978).
31) F. Castano, A. Lazaro, S. Lombrana, and E. Martinez, *Spectrochim. Acta*, **39A**, 33 (1983).
32) G. Lessard and G. Durocher, *J. Phys. Chem.*, **82**, 2812 (1978).
33) J. B. Birks, "Organic Molecular Photophysics," Vol. 1, John Wiley and Sons, London, New York, Toronto, Sydney (1973), p. 10.
34) A. P. Marchetti and D. R. Kearns, *J. Am. Chem. Soc.*, **89**, 768 (1967).
35) G. Castro and R. M. Hochstrasser, *J. Chem. Phys.*, **46**, 3617 (1967).
36) S. P. McGlynn, T. Azumi, and M. Kinoshita, "Molecular Spectroscopy of the Triplet state," Prentice Hall Inc., New Jersey (1969), p. 159.
37) S. Yamauchi, Y. Komada, and N. Hirota, *Chem. Phys. Lett.*, **93**, 133 (1982).
38) S. Nagakura, "Excited states", ed by E. C. Lim, Vol. 2 (1975), p. 321.
39) K. B. Eisenthal, *J. Chem. Phys.*, **45**, 1850 (1966).

 © 1988 The Chemical Society of Japan Bull. Chem. Soc. Jpn., 61, 3681—3687 (1988)

Studies on Dielectric Permittivities, Refractive Indices for 1,1′-Bicyclohexyl Liquid Crystals in the Nematic and Isotropic Phases

Sushmita SEN, Krishnakoli KALI, and Subir K. ROY*
Department of Spectroscopy, Indian Association for the Cultivation of Science, Calcutta 700032, India
(Received September 7, 1987)

The dielectric permittivities $\varepsilon_{\parallel}$ and $\varepsilon_{\perp}$ and the refractive indices n_e, n_o of five 4-cyano-4′-alkyl-1,1′-bicyclohexyls (CCH 2, CCH 3, CCH 4, CCH 5, CCH 7 where 2, 3, 4, 5, 7 means ethyl, propyl, butyl, pentyl, heptyl respectively) have been measured at different temperatures in the nematic and isotropic phases. The orientational order parameter from the refractive indices data, calculated from (1) Vuks' method and (2) Neugebauer's method were in good agreement. At any reduced temperature, the order parameter for CCH 2 is largest and that of CCH 7 is smallest and those for the others are in between them. Unlike for cyanobiphenyls or cyclohexylbenzenes, the dielectric permittivity $\varepsilon_{\parallel}$ is obtained for $\vec{E} \perp \vec{H}$ and $\varepsilon_{\perp}$ for $E \parallel H$, where $\vec{E}$ is the electric and $\vec{H}$ is the magnetic field, and has been explained as due to these molecules having negative diamagnetic anisotropy. The dielectric anisotropy, $\Delta\varepsilon$ and optical anisotropy Δn for all the CCH's is much less than that of the corresponding CB or PCH molecules. All the CCH's show pretransitional permittivity just above the transition temperature T_{NI}.

Dielectric permittivities and refractive indices of liquid crystals are required for their selection for practical uses. The data for dielectric permittivities and refractive indices for alkylcyanobiphenyls,[1-3] cyclohexylbenzenes,[4] phenylcyclohexanecarboxylates[5] have been reported earlier. Such data for CCH's are rather scanty. The object of the present investigations were to study how the dielectric properties and refractive indices change when both the phenyl rings are replaced by cyclohexyl rings.

Studies on the temperature dependence of dielectric permittivities in the isotropic phase for nematics with strong dipole moments show pretransitional effects while in nonpolar nematics pretransitional effect is absent.[5,6] It was thought worthwhile to study the pretransitional effects in dielectric permittivity in the isotropic phase of 1,1′-bicyclohexyl liquid crystals. The results are discussed in this paper.

Experimental

Five CCH liquid crystals (CCH 2, CCH 3, CCH 4, CCH 5, CCH 7) procured from E. Merck, Germany were used in the investigations without further purification. Mesomorphic range of the samples,

Sample	Nematic range/°C
CCH 2 (4-cyano-4′-ethyl-1,1′-bicyclohexyl)	46—49
CCH 3 (4-cyano-4′-propyl-1,1′-bicyclohexyl)	50—80
CCH 4 (4-cyano-4′-butyl-1,1′-bicyclohexyl)	54—79
CCH 5 (4-cyano-4′-pentyl-1,1′-bicyclohexyl)	62—85
CCH 7 (4-cyano-4′-heptyl-1,1′-bicyclohexyl)	71—83

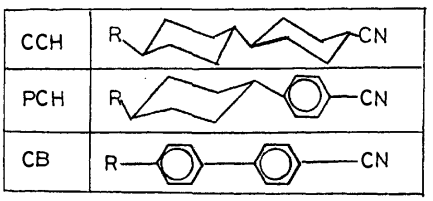

R=alkyl group

Measurement of Refractive Indices. The method of measurement of the refractive indices n_e, n_o for the extraordinary and ordinary rays with the help of ABBE refractometer and density measurements by means of capillary tube were de-

Table 1. Refractive Indices, Density, Polarizabilities and Order Parameter for CCH

T/°C	ρ/ g ml^{-1}	n_o	n_e	$\bar{\alpha}$	Vuks' method			Neugebauer's method		
				Å^3	α_o/Å^3	α_e/Å^3	S	α_o/Å^3	α_e/Å^3	S
(a) CCH 2										
46	0.925	1.4661	1.4959	26.486	25.822	27.806	0.62	25.903	27.652	0.65
46.5	0.924	1.4661	1.4953	26.498	25.846	27.791	0.60	25.922	27.648	0.64
47	0.923	1.4662	1.4942	26.503	25.878	27.744	0.58	25.950	27.607	0.62
47.5	0.923	1.4663	1.4934	26.507	25.903	27.709	0.56	25.968	27.586	0.60
48	0.922	1.4668	1.4919	26.518	25.959	27.605	0.52	26.025	27.503	0.55
49	0.919	1.4748								
49.5	0.918	1.4746								
50	0.918	1.4742								
50.5	0.917	1.4741								
51	0.917	1.4740								
53.5	0.915	1.4729			$\alpha_{\perp}$=	$\alpha_{\parallel}$=		$\alpha_{\perp}$=	$\alpha_{\parallel}$=	
55.5	0.913	1.4720			25.532	28.726		25.703	28.384	

Table 1. (Continued)

T/°C	ρ/ g ml^{-1}	n_o	n_e	$\bar{\alpha}$	Vuks' method			Neugebauer's method		
				Å^3	α_o/Å^3	α_e/Å^3	S	α_o/Å^3	α_e/Å^3	S
(b) CCH 3										
58.5	0.915	1.4590	1.5056	28.416	27.303	30.644	0.65	27.479	30.291	0.66
62	0.912	1.4578	1.5029	28.407	27.326	30.569	0.63	27.492	30.238	0.64
64	0.910	1.4575	1.5014	28.431	27.375	30.537	0.61	27.528	30.239	0.63
66.5	0.908	1.4567	1.4991	28.422	27.401	30.461	0.59	27.556	30.154	0.61
68.5	0.906	1.4564	1.4968	28.428	27.453	30.375	0.56	27.597	30.090	0.58
70.5	0.905	1.4560	1.4949	28.442	27.499	30.317	0.54	27.622	30.081	0.57
73	0.902	1.4553	1.4930	28.452	27.538	30.275	0.53	27.669	30.020	0.55
76	0.900	1.4546	1.4900	28.452	27.594	30.171	0.50	27.731	29.895	0.51
78	0.898	1.4545	1.4878	28.469	27.658	30.084	0.47	27.776	29.854	0.49
80.5	0.896	1.4548	1.4834	28.464	27.764	29.855	0.40	27.865	29.662	0.42
82.5	0.889	1.4635								
85	0.887	1.4625								
87	0.885	1.4615			$\alpha_\perp$=	$\alpha_\parallel$=		$\alpha_\perp$=	$\alpha_\parallel$=	
89	0.884	1.4605			26.910	32.093		27.212	31.490	
(c) CCH 4										
56	0.9109	1.4650	1.5081	30.503	29.407	32.695	0.64	29.601	32.305	0.61
58	0.9092	1.4642	1.5070	30.517	29.418	32.692	0.64	29.572	32.409	0.64
60	0.9066	1.4635	1.5048	30.540	29.481	32.645	0.62	29.607	32.404	0.63
64	0.9041	1.4616	1.5026	30.516	29.466	32.606	0.61	29.576	32.394	0.63
68	0.9005	1.4600	1.4998	30.518	29.496	32.583	0.60	29.678	32.199	0.63
76	0.8928	1.4554	1.4973	30.573	29.477	32.744	0.61	29.605	32.507	0.57
78	0.8909	1.4558	1.4939	30.582	29.593	32.560	0.58	29.742	32.267	0.57
79	0.8858	1.4680								
80	0.8850	1.4676								
82	0.8836	1.4663								
83	0.8826	1.4650								
85	0.8812	1.4644								
87	0.8799	1.4640								
90	0.8783	1.4620			$\alpha_\perp$=	$\alpha_\parallel$=		$\alpha_\perp$=	$\alpha_\parallel$=	
92	0.8762	1.4616			29.013	34.152		29.255	33.666	
(d) CCH 5										
68	0.906	1.4580	1.5093	32.516	30.796	34.960	0.64	31.018	35.514	0.64
72	0.902	1.4568	1.5061	32.198	30.861	34.876	0.62	31.076	34.440	0.61
76	0.898	1.4560	1.5020	32.218	30.963	34.726	0.58	31.151	34.353	0.58
78	0.897	1.4560	1.4991	32.226	31.048	34.580	0.54	31.223	34.231	0.55
81	0.894	1.4568	1.4931	32.238	31.231	34.259	0.46	31.396	33.923	0.46
83	0.892	1.4575	1.4823	32.252	31.378	33.999	0.40	31.511	33.733	0.41
85	0.884	1.4675								
86	0.883	1.4665								
87	0.883	1.4660								
88	0.882	1.4655								
89	0.881	1.4650			$\alpha_\perp$=	$\alpha_\parallel$=		$\alpha_\perp$=	$\alpha_\parallel$=	
92	0.880	1.4640			30.327	36.850		30.672	36.161	
(e) CCH 7										
71	0.893	1.4558	1.5009	35.858	34.487	38.600	0.52	34.713	38.157	0.54
72	0.892	1.4554	1.4997	35.843	34.500	38.539	0.51	34.716	38.103	0.53
73	0.891	1.4552	1.4980	35.843	34.542	38.449	0.49	34.751	38.026	0.52
74	0.890	1.4550	1.4966	35.842	34.573	38.374	0.48	34.758	38.009	0.51
75	0.889	1.4548	1.4952	35.840	34.607	38.302	0.47	34.786	37.948	0.50
76	0.888	1.4546	1.4936	35.838	34.652	38.220	0.45	34.849	37.816	0.47
77	0.887	1.4544	1.4919	35.822	34.678	38.114	0.43	34.859	37.748	0.45
78	0.886	1.4542	1.4905	35.826	34.717	38.102	0.43	34.894	37.689	0.44
79	0.885	1.4540	1.4891	35.840	34.764	37.987	0.40	34.915	37.689	0.44
80	0.884	1.4538	1.4874	35.841	34.810	37.902	0.39	34.959	37.605	0.42
81	0.883	1.4537	1.4859	35.851	34.862	37.828	0.37	35.004	37.547	0.40
82	0.880	1.4536								
84	0.877	1.4625								
87	0.875	1.4604			$\alpha_\perp$=	$\alpha_\parallel$=		$\alpha_\perp$=	$\alpha_\parallel$=	
89	0.873	1.4592			33.311	41.229		33.833	40.184	

Table 2. Dielectric Permittivities of CCH

T/°C	$\varepsilon_{\parallel}$	ε_{iso}	$\varepsilon_{\perp}$	$\bar{\varepsilon}$
(a) CCH 2				
46.5	9.85		5.696	7.081
47	9.782		5.757	7.099
47.5	9.760		5.869	7.166
48	9.684		5.892	7.156
48.5	9.440		5.939	7.106
50		7.503		
51		7.562		
52		7.603		
53		7.624		
54		7.607		
55		7.532		
56		7.503		
60		7.382		
(b) CCH 3				
58	9.419		4.673	6.255
60	9.598		4.732	6.354
62	9.725		4.863	6.484
64	10.015		4.905	6.608
66.5	10.184		5.099	6.794
68.5	10.112		5.185	6.827
70.5	10.094		5.385	6.955
73	9.998		5.459	6.972
76	9.968		5.593	7.051
78	9.953		5.702	7.119
79	9.490		5.722	6.978
80.5		7.855		
82.5		7.916		
83		8.207		
84		8.024		
85		7.959		
86		7.554		
88		7.463		
90		7.340		
(c) CCH 4				
56	8.871		4.361	5.864
58	8.876		4.404	5.895
60	9.119		4.386	5.964
64	9.119		4.592	6.101
68	9.120		4.635	6.130
72	9.117		4.893	6.301
76	9.037		5.049	6.378
78	8.934		5.467	6.623
79	8.869		5.472	6.604
80	8.741		5.474	6.563
82		7.072		
83		7.108		
85		7.159		
87		7.152		
90		7.146		
92		7.110		
(d) CCH 5				
51	8.586		4.365	5.772
56	8.910		4.371	5.884
60	8.992		4.479	5.983
65	9.146		4.631	6.136
69	9.214		4.723	6.220
73	9.251		4.753	6.252
77	9.279		4.832	6.314
81	9.333		4.951	6.412
84	8.752		5.412	6.525
85		6.596		
87		6.779		
88		7.173		
89		7.341		
90		7.337		
91		7.328		
93		7.319		
96		7.298		
(e) CCH 7				
74	7.169		3.888	4.982
75	7.181		3.963	5.036
76	7.175		4.020	5.072
77	7.182		4.045	5.091
78	7.155		4.067	5.096
79	7.132		4.050	5.077
80	6.939		4.037	5.004
82	6.919		4.022	4.988
83	6.490		4.036	4.854
84	6.444		3.985	4.805
86	5.895		4.246	4.796
87		4.891		
88		4.919		
89		4.925		
90		4.873		
91		4.849		
93		4.821		
94		4.806		
96		4.799		
98		4.796		

scribed elaborately in an earlier publication.[7]

Measurement of Dielectric Permittivities. The dielectric permittivities $\varepsilon_{\parallel}$ and $\varepsilon_{\perp}$ polarized parallel and perpendicular to the long molecular axes of the liquid crystals were measured at 1 kHz with a GR-1620 capacitance bridge using a capacitor of stainless steel electrodes of radius 1 cm separated by a 1 mm thick Teflon spacer. A magnetic field of 1.0 T was used to allign the molecules of the liquid crystals parallel and perpendicular to the electrode surfaces. The temperature of the sample was measured with a thermocouple mounted directly on one of the electrodes. The temperature of the cell was maintained constant within ±0.02 °C by means of a thermostat. The cell was calibrated with freshly distilled toluene and chlorobenzene and the values agree to 0.1% of the standard value.

Results

The experimental values of refractive indices n_e, n_o and the densities of the liquid crystals at different temperatures are given in Table 1. The effective polarizabilities α_e and α_o in the nematic phase calculated by using two methods Vuks[8] and Neugebauer[9] are included in Table 1. The principal polarizabilities $\alpha_{\parallel}$ and $\alpha_{\perp}$ parallel and perpendicular to the long axis of the molecules in the crystalline state were obtained from Hallers' et al.[10] graphical method. The orientational order parameters S were calculated from the relation $S=(\alpha_e-\alpha_o)/(\alpha_{\parallel}-\alpha_{\perp})$ and are included in Table 1.

Table 3a. Values of the Dielectric Anisotropy of CCH Compounds at Different Reduced Temperature

CCH 2		CCH 4		CCH 7	
T/T_{NI}	$\Delta\varepsilon$	T/T_{NI}	$\Delta\varepsilon$	T/T_{TN}	$\Delta\varepsilon$
0.989	4.154	0.927	4.510	0.964	3.281
0.991	4.025	0.932	4.472	0.967	3.218
0.992	3.891	0.949	4.527	0.972	3.137
0.994	3.792	0.961	4.485	0.975	3.088
0.995	3.501	0.972	4.224	0.981	2.902
		0.989	3.467	0.989	2.454
		0.992	3.397	0.997	1.649
		0.994	3.267		

Table 3b. Values of the Dielectric Ansotropy of CB 7, PCH 7, and CCH 7 at Different Reduced Temperature

CB 7		PCH 7		CCH 7	
T/T_{NI}	$\Delta\varepsilon$	T/T_{NI}	$\Delta\varepsilon$	T/T_{NI}	$\Delta\varepsilon$
0.930	12.1	0.930	8.12	0.964	3.28
0.955	11.7	0.954	7.84	0.972	3.14
0.970	11.1	0.967	7.41	0.975	3.09
0.980	10.3	0.980	6.92	0.980	2.90
0.995	8.6	0.990	6.03	0.992	2.46

Table 4a. Values of the Order Parameter of CCH Compounds at Different Reduced Temperature

CCH 2		CCH 4		CCH 7	
T/T_{NI}	S	T/T_{NI}	S	T/T_{NI}	S
0.991	0.65	0.935	0.61	0.969	0.54
0.992	0.64	0.940	0.64	0.971	0.53
0.994	0.62	0.957	0.63	0.977	0.51
0.995	0.60	0.969	0.63	0.980	0.50
0.997	0.55	0.991	0.57	0.983	0.47
				0.989	0.45
				0.994	0.42

Table 4b. Values of the Order Parameter of CB 7, PCH 7, and CCH 7 at Different Reduced Temperature

CB 7		PCH 7		CCH 7	
T/T_{NI}	S	T/T_{NI}	S	T/T_{NI}	S
0.950	0.62	0.948	0.50	0.969	0.54
0.959	0.58	0.954	0.49	0.971	0.53
0.968	0.56	0.967	0.46	0.977	0.51
0.978	0.52	0.979	0.41	0.980	0.50
		0.985	0.39	0.983	0.47
				0.989	0.44
				0.994	0.42

Discussion

The values of the dielectric anisotropy, $\Delta\varepsilon$, Table 3b, Fig. 4b for CB,[11] PCH,[4] and CCH compounds in the present paper shows that $\Delta\varepsilon$ gradually decreases from CB to PCH to CCH by the progressive replacement of one phenyl ring in PCH and both the phenyl rings in the CCH compounds by cyclohexyl groups. This may be attributed to the decrease in the degree of conjuga-

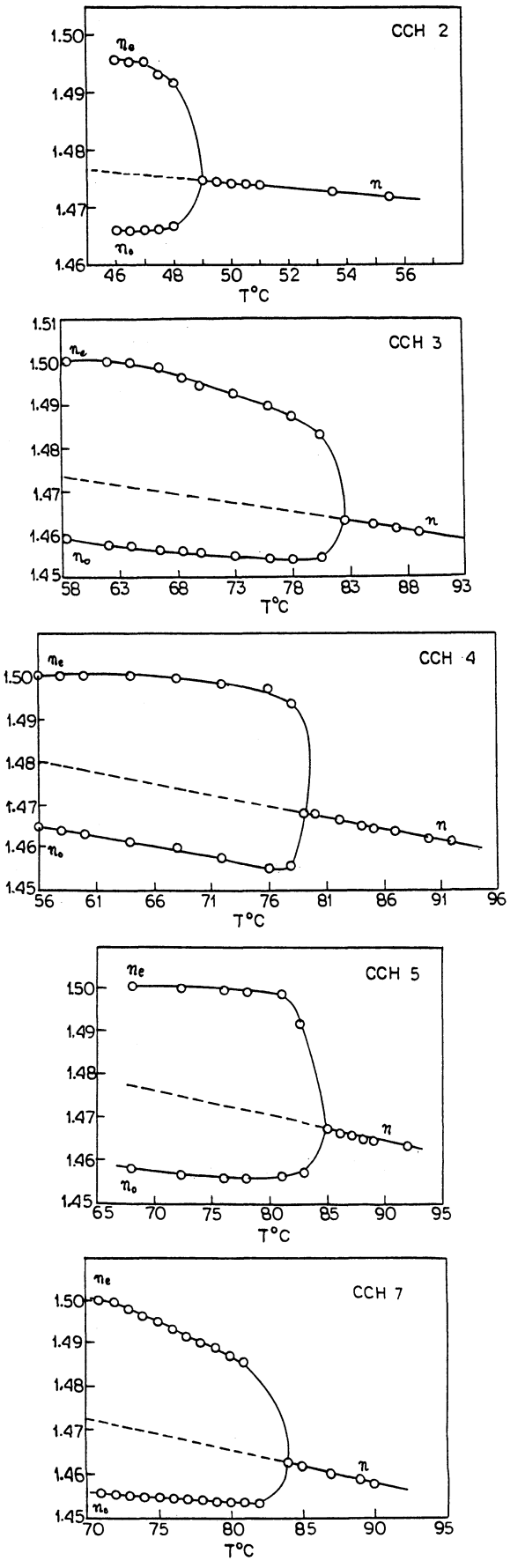

Fig. 1. Refractive index anisotropy plots for CCH 2, CCH 3, CCH 4, CCH 5, CCH 7 respectively.

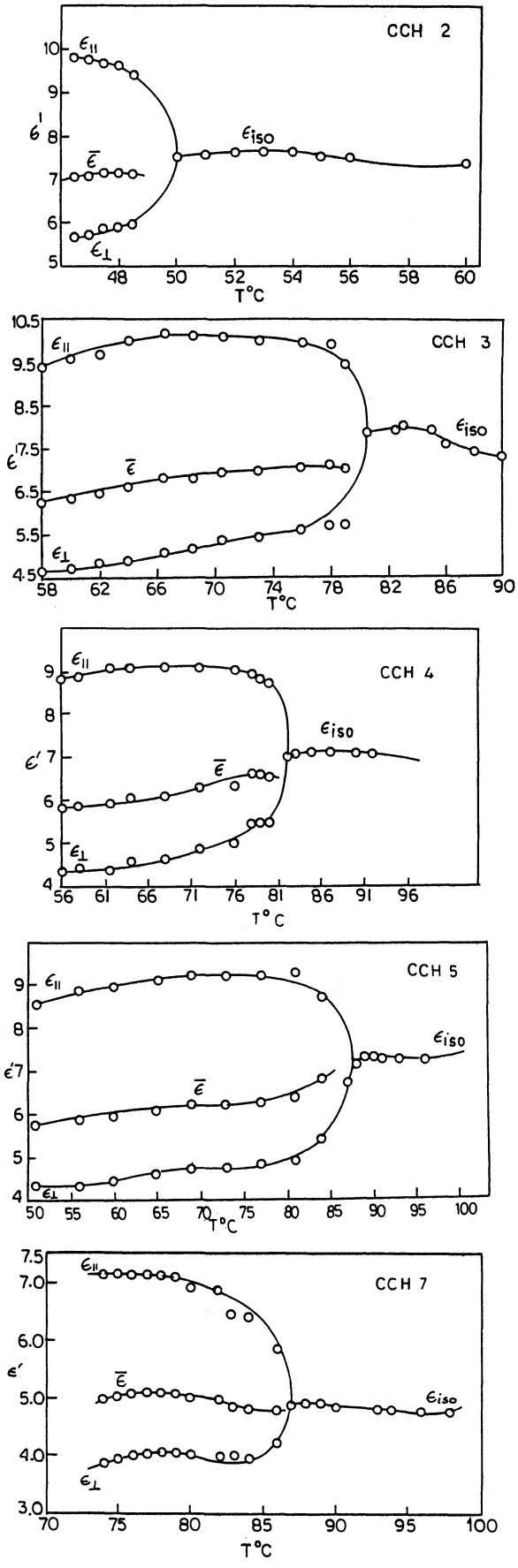

Fig. 2. Dielectric anisotropy plots for CCH 2, CCH 3, CCH 4, CCH 5, CCH 7 respectively.

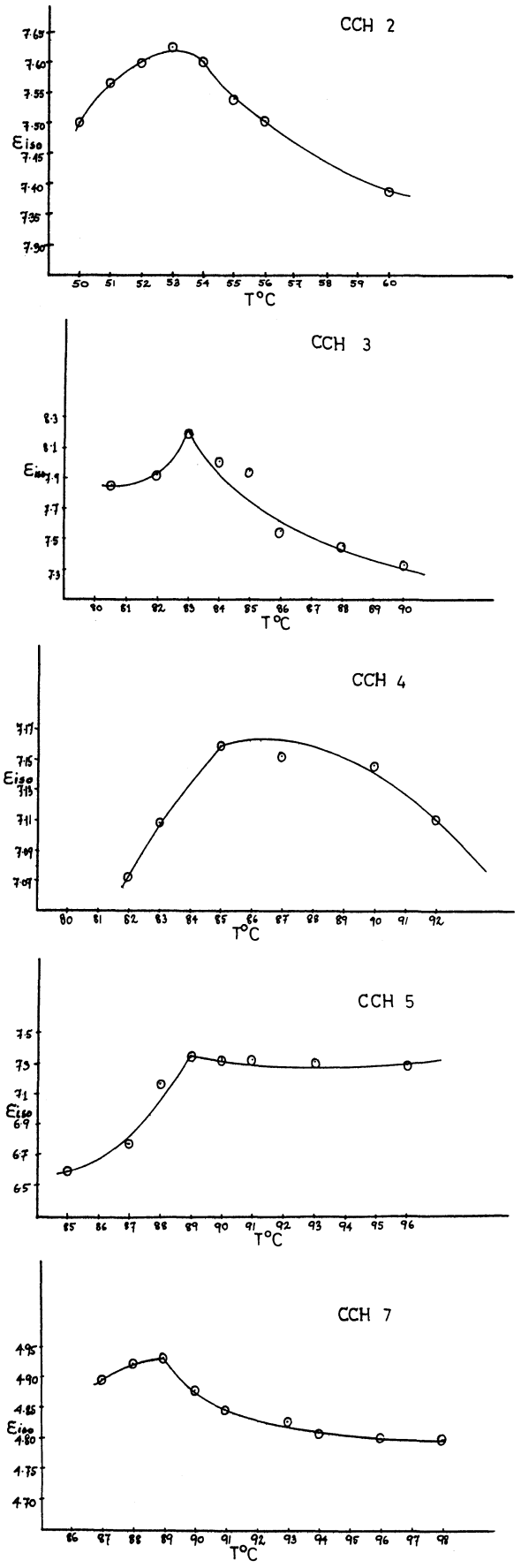

Fig. 3. Pretransition effect plots for CCH 2, CCH 3, CCH 4, CCH 5, CCH 7 respectively.

tion by progressive replacement of phenyl rings. This decrease of conjugation is more pronounced in the CCH compounds which are completely lacking in free π electrons.

The values of $\Delta\varepsilon$ within the CCH compounds, Table 3a, Fig. 4a, decreases with the increase of chain length which is also found in the case of PCH compounds by Schad et al.[11]

Schad[11] found that the experimental data for the PCH compounds hold the relation $\Delta\varepsilon(t_r) \alpha S(t_r)$, considering only the contribution of the predominant dipolar part of the dielectric polarization to $\Delta\varepsilon$, though one would expect that $S(t_r)/T$ should depend on $\Delta\varepsilon$. A possible explanation of the result was given[1] by a model of antiparallel dipole correlation.

In the case of the CCH compounds (Fig. 5a) the decrease of order parameter at any reduced temperature, with the increase of alkyl chain length may also be explained from the above relation.

From Table 1a—e, it can be seen that the order parameter S for each of the CCH liquid crystals evaluated from refractive indices and density data using Vuks' and Neugebauer's methods are in good agreement. Figure 5a, a comparison of the order parameter of the CCH liquid crystals at any common reduced temperature, $t_r=T/T_{NI}$, shows that the order parameter of CCH 2 is the largest and that for CCH 7 is the smallest and those for others are in between them. It appears that the larger the alkyl chain length the smaller is the order parameter.

The values of the order parameters at any reduced temperature t_r in CB, is the largest and in PCH is the smallest, Fig. 5b. But in the case of CCH compounds it is nearer to that of the CB compounds but greater than that for PCH. This cannot be explained from the above relation.[11]

The antiparallel local ordering in CCH compounds found by X-ray measurement[12] corresponds to the overlap of cyano group, which is quite different from

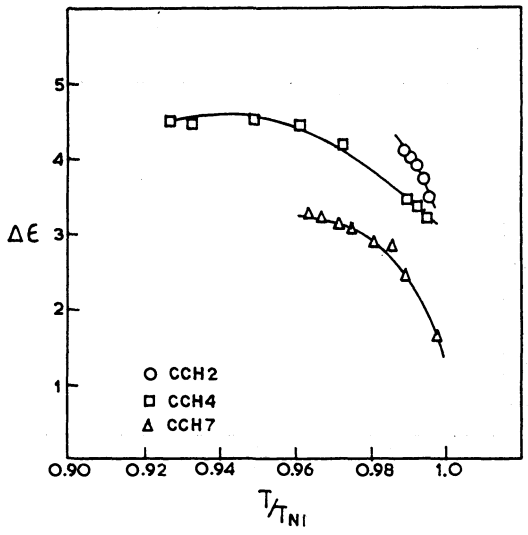

Fig. 4(a). Plots of $\Delta\varepsilon$ vs. T/T_{NI} for CCH 2, CCH 4. CCH 7.

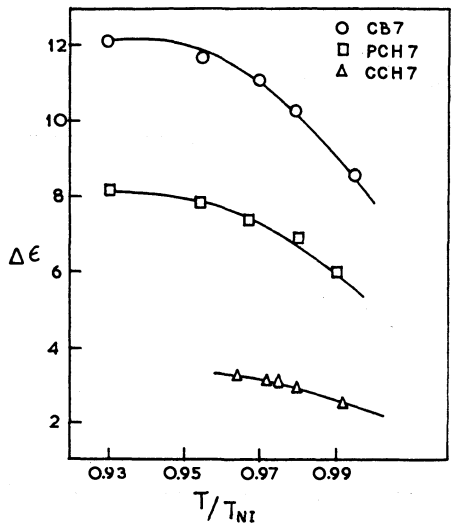

Fig. 4(b). Plots of $\Delta\varepsilon$ vs. T/T_{NI} for CB 7, PCH 7, CCH 7.

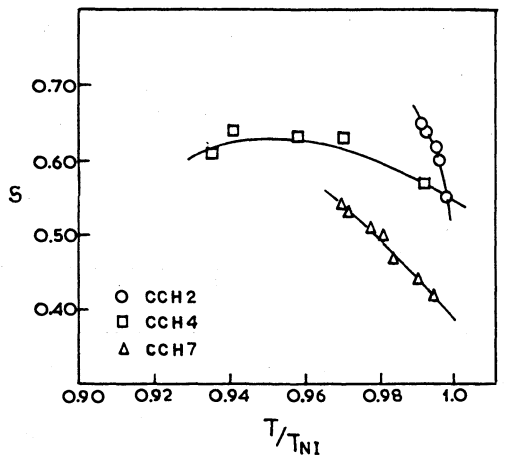

Fig. 5(a). Plots of S vs. T/T_{NI} for CCH 2, CCH 4, CCH 7.

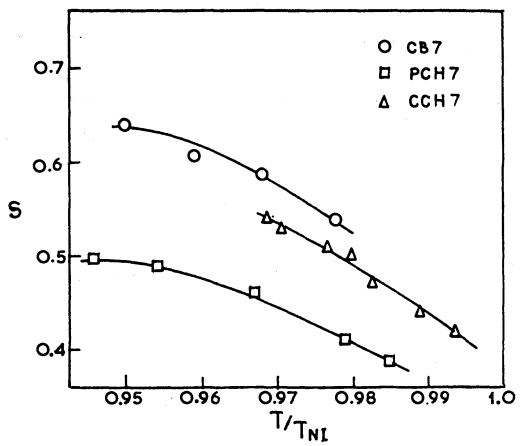

Fig. 5(b). Plots of S vs. T/T_{NI} for CB 7, PCH 7, CCH 7.

the core overlap in the case of CB and PCH compounds. This type of different local ordering in CCH compounds must affect the value of the order parameter and this may be the cause of the unexpected value of the order parameter in the CCH compound.

This type of unexpected observation of the ratio of Bend/splay (k_{33}/k_{11}) value of the elastic constant of the CCH compounds was found by Bradshaw et al.[5]

It is to be noted that for all the CCH liquid crystals, the dielectric permittivity $\varepsilon_{\parallel}$ is obtained for $\vec{E} \perp \vec{H}$ and $\varepsilon_{\perp}$ is obtained when $\vec{E} \parallel \vec{H}$ unlike the cyanobiphenyls, cyclohexylbenzenes, and other thermotropic liquid crystals, all of which have positive diamagnetic anisotropy. 1,1′-Bicyclohexyls have got negative diamagnetic anisotropy as was shown by Schad[11] in CCH 7 ($\Delta\chi=-2\times10^{-8}$ cm^3 g^{-1}). The negative diamagnetic anisotropy in CCH 5 was also confirmed by Pohl et al.[12] from the studies of the dependence of electric threshold voltage and switching time of a twisted layer of CCH 5, with the strength of the magnetic fleld.

Because of the negative anisotropy of the susceptibility, the CCH molecules orient themselves with the long molecular axis perpendicular to the magnetic field and this is why dielectric permittivity $\varepsilon_{\parallel}$ is obtained when $\vec{E} \perp \vec{H}$.

The anisotropy of the dielectric permittivity of the CCH's are shown in Fig. 2a—e. The average value of the dielectric permittivities $\bar{\varepsilon}$; shown in Table 2a—e in each case is found to increase with increase in temperature and is discontinuous with the isotropic value ε_{iso} at T_{NI}, Fig. 2a—e. This indicates the presence of strong antiparallel local ordering of the CCH molecules in the nematic phase in strongly polar molecules as reported earlier.[13]

Temperature dependence of dielectric permittivity ε_{iso} for the CCH liquid crystals in the isotropic phase is shown in Fig. 3a—e. It can be clearly seen that there is a peak in ε_{iso}, a little above the transition temperature T_{NI}. Such pretransition effects in dielectric permittivity in nematics with cyano end groups were reported by Bradshaw and Raynes,[5] Theon and Menu,[6] and recently by Krishnakoli et al.[14] The reduced contribution to dielectric permittivity ε_{iso} from dipole moment μ was attributed to apparent reduction in μ-values due to formation of dimers in antiparallel local ordering.[15] The pretransition in ε_{iso} near T_{NI} showing a maximum was explained as due to appreciable concentration of dimers in a dynamic dimer-monomer equilibrium.

References

1) S. Sen, P. Brahma, S. K. Roy, D. K. Mukherjee, and S. B. Roy, *Mol. Cryst. Liq. Cryst.*, **100**, 327 (1983).
2) S. Sen, P. Brahma, S. K. Roy, and S. B. Roy, *Acta Physica Polonica*, **A65**, 47 (1984).
3) B. R. Ratna and R. Sashidhar, *Pramana*, **6**, 278 (1976).
4) S. Sen, K. Kali, S. K. Roy, and S. B. Roy, *Mol. Cryst. Liq. Cryst.*, **126**, 269 (1985).
5) M. J. Bradshaw and E. P. Raynes, *Mol. Cryst. Liq. Cryst.*, **L72**, 73 (1981).
6) J. Theon and G. Menu, *Mol. Cryst. Liq. Cryst.*, **97**, 163 (1983).
7) K. Kali, S. Sen, and S. K. Roy, *Bull. Chem. Soc. Jpn.*, **58**, 3576 (1985).
8) M. F. Vuks, *Opt. Spectrosk*, **20**, 361 (1966).
9) H. E. J. Neugebauer, *Can. J. Phys.*, **32**, 1 (1954).
10) I. Haller, H. A. Huggins, H. R. Lilienthal, and T. R. McGuire, *J. Phys. Chem.*, **77**, 950 (1973).
11) Hp. Schad, G. Baur, and G. Meier, *J. Chem. Phys.*, **71**, 3174 (1979).
12) L. Pohl, R. Eidenchink, J. Krause, and G. Weber, *Phys. Lett.*, **65A**, 169 (1978).
13) N. V. Madhusudan and S. Chandrasekhar, Proc. International Conf. Liq. Cryst, Bangalore (1973), p. 427.
14) K. Kali, S. Sen, and S. K. Roy, *Acta Physica Polonica*, in press (1987).
15) L. Longa and W. H. de Jeu, *Phys. Rev. A*, **26**, 1632 (1982).

 © 1988 The Chemical Society of Japan Bull. Chem. Soc. Jpn., 61, 3689—3692 (1988)

Spectrophotometric Determination of Bismuth(III) and Indium(III) with 2,4,6-Tris(2-hydroxy-4-sulfo-1-naphthylazo)-1,3,5-triazine Trisodium Salt (THT)

Ishwar SINGH* and Pratap Singh KADYAN
Department of Chemistry, M. D. University, Rohtak-124001, India
(Received July 30, 1987)

Reaction behavior of bismuth(III) and indium(III) with 2,4,6-tris(2-hydroxy-4-sulfo-1-naphthylazo)-1,3,5-triazine trisodium salt (THT) is established under various conditions. Bismuth(III) forms a 2:3 dark red complex (absorption maximum at 530 nm) with the reagent at pH 4—6.5. Indium(III) reacts with THT to form a 1:2 dark red complex at pH 3—4.7 (λ_{max} 530 nm) and a 1:3 purple blue complex at pH ca. 10.5 (λ_{max} 620 nm). The molar absorptivities for the color reactions are 5.5×10^4 for bismuth(III), 8.4×10^4 for indium(III) at pH 3.5 and 7.9×10^4 L·mol^{-1}·cm^{-1} for indium(III) at pH ca. 10.5 (in sodium carbonate medium). Other physicochemical characteristics of the complexes are established. A number of foreign ions are tested for their interference and the use of masking agents wherever necessary is tabulated.

Recently, we proposed a water-soluble azo dye 2,4,6-tris(2-hydroxy-4-sulfo-1-naphthylazo)-1,3,5-triazine trisodium salt (THT) as chromogenic reagent for antimony and sulfide[1] and thorium and phosphate.[2] This reagent forms dark red color with bismuth(III) in weakly acidic medium and dark red and purple blue with indium(III) in weakly acidic and alkaline media, respectively. We propose spectrophotometric determination for these two elements in this communication.

Less attention has been given for microdetermination of bismuth and indium. Conventional iodide and thiourea methods[3,4] for bismuth are simple but lack sensitivity. Dithiocarbamate[5] is specific but is rather insensitive. Dithizone[3,4,6,7] has high sensitivity but the method is tedious and suffers lot of interferences. For indium, most of the methods are unselective and require separation of metals. Oxine[8,9] and bromo-substituted oxine[10-12] have been used as extractive reagents. However, PAR[13] is a better sensitive reagent for indium(III) at pH 6, but not selective. At pH 3, the selectivity increases, but sensitivity decreases.[14,15] The present reagent has been found to be highly sensitive, as well as selective for the determination of the two elements.

Experimental

Apparatus: A Bausch and Lomb Spectronic 2000 spectrophotometer with 10 mm matched glass cells was used for recording spectra and a Beckman Φ 60 pH meter was used for pH measurements.

Reagents: THT Solution: THT was synthesized as described earlier[1] and its 1×10^{-3} M solution (1M=1 mol dm^{-3}) was prepared by dissolving 0.900 g of THT in 1L of double-distilled water.

Bismuth(III) and Indium(III) Solution (1000 μg mL^{-1}): Standard solutions of bismuth(III) and indium(III) were prepared by dissolving an appropriate amount of bismuth nitrate pentahydrate $Bi(NO_3)_3\cdot5H_2O$ and indium sulfate monohydrate $In_2(SO_4)_3\cdot H_2O$ in double-distilled water and standardized by conventional methods.[16]

Acetate Buffer Solutions: Acetate buffer solution of pH 3.5 was prepared by diluting 940 mL 0.2 M acetic acid to 1L with 0.2 M sodium acetate and for pH 5.5, diluting 120 mL 0.2 M acetic acid to 1L with 0.2 M sodium acetate.

Sodium Carbonate Solution (0.02 M): Anhydrous sodium carbonate (2.12 g) was dissolved in 1L doubly distilled water for this concentration.

All the reagents used were of analytical grade during the experimental studies.

Procedures and Calibration Curves. Determination of Bismuth(III): To a suitable volume of sample containing 14—75 μg of bismuth(III) and 2 mL 1×10^{-3}M THT followed by 2 mL buffer solution of pH 5.5. Dilute to 25 mL with water and measure the absorbance at 530 nm against a corresponding reagent blank (2 mL 1×10^{-3}M THT+2 mL buffer diluted to 25 mL).

Determination of Indium(III): To a suitable volume of sample containing 6—35 μg of indium(III) add 2 mL 1×10^{-3}M THT followed by 2 mL of buffer solution of pH 3.5 or to an aliquot containing 6—27.5 μg of indium(III) and 2 mL 1×10^{-3}M THT followed by 2 mL 0.02 M carbonate solution. Make up the volume to 25 mL with water and measure the absorbance at 530 nm in the former case or at 620 nm for the latter against a corresponding reagent blank.

Deduce the amount of the metal ion from the standard calibration curve drawn under similar conditions.

Results and Discussion

Color Formation and Absorption Spectra. Bismuth(III) formed a dark red complex (absorption maximum at 530 nm) with an aqueous solution of THT at pH 4—6.5, while indium(III) formed two water soluble complexes, a dark red at pH 3—4.7 which absorbed maximally at 530 nm and a purple blue with a λ_{max} 620 nm. Color formation was instant and stable for several hours in each case. Acetate buffers were found siutable for maintaining weakly acidic pH's and thus 2 mL buffer of pH 5.5 for bismuth(III) and 2 mL buffer of pH 3.5 for indium(III) determinations were used. For determination of indium(III) at high pH, 2—8 mL 0.02 M sodium carbonate was found suitable and thus 2 mL of it was used in subsequent studies.

Table 1. Comparison of Sensitivities of Various Spectrophotometric Reagents for Bismuth(III) and Indium(III)

Reagent or reaction	Molar absorptivity (λ/nm)	Ref.	Molar absorptivity (λ/nm)	Ref.
	$L \cdot mol^{-1} \cdot cm^{-1}$ (for Bi)		$L \cdot mol^{-1} \cdot cm^{-1}$ (for In)	
Thiourea	3.6×10^4(322) 9.3×10^3(470)	3,4	—	
Iodide	9.1×10^3(645)	3,4	—	
Dithizone	7.92×10^4(490)	3,4	—	
Xylenol Orange	2.4×10^4(540)	17	—	
2,2′-(Ethylenediimino)bis[3-hydroxypropionic acid]	6.96×10^3(245)	18	—	
Propyldithiopyrylmethane	1.28×10^4(525)	19	—	
2-Thiobarbituric acid	2.4×10^4(416)	20	—	
Pyrogallol Red	2.0×10^4(615)	21	—	
Morpholine-4-dithioformate	4.01×10^4(615)	21	—	
8-Quinolinol (Oxine)	—		6.7×10^3(395)	8,9
5,7-Dibromo-8-quinolinol	—		8.8×10^3(415)	10
Pyrocatechol Violet	—		1.9×10^4(560)	27
Gallion	—		2.2×10^4(610)	28
Thoron I	—		6.1×10^3(520)	29
2-(3,5-Dibromo-2-pyridylazo)-5-dimethylaminophenol	9.9×10^4(600)	24	—	
2-(3,5-Dibromo-2-pyridylazo)-5-diethylaminophenol	8.0×10^4(600)	25	—	
N-Methylanabasine-α-azo-*p*-cresol	7.63×10^3 (550—600)	26	1.28×10^4(565)	30
4-(2-Pyridylazo)resorcinol (PAR)	1.07×10^4 (515, 530)	23	4.3×10^4(510) 1.8×10^4(510)	13—15
1-(2-Pyridylazo)-2-napthol (PAN)	—		1.9×10^4(560)	31
4-(2-Quinolylazo)resorcinol.	—		5.95×10^4	32
5-(2-Pyridylazo)-2-ethylamino-*p*-cresol	—		3.1×10^4(535)	33
2,4,6-Tris(2-hydroxy-4-sulfo-1-naphthylazo)-1,3,5-triazine trisodium salt (THT)	5.5×10^4(530)	Present method	8.4×10^4(530) 7.9×10^4(620)	Present method

The effect of THT concentration was investigated in each case at their respective λ_{max}'s containing a constant amount of bismuth(III) or indium(III) and varying amounts of the reagent. It was found that 2 times molar excess of THT was required for bismuth(III), while 3—4 times molar excess of THT was necessary for complete complexation for indium(III) at both pH levels. All further experiments were carried out with at least 5-fold molar excess of the reagent solution.

Other Characteristics of the Complexes. The complexes obeyed Beer's law over the range 0—3.8 ppm of bismuth(III) and 0—1.8 ppm at pH 3.5 and 0—1.3 ppm at pH ca. 10.5 of indium(III). The optimum concentration ranges as evaluated by Ringbom's plot are 0.56—3.0 ppm of bismuth(III) and 0.24—1.4 or 0.24—1.1 ppm of indium(III), at low and high pH, respectively. These are the optimum ranges in which the metal ions could be accurately determined. The respective Sandell's sensitivities of the bismuth(III) complex and indium(III) complexes at low and high pH are 0.0038, 0.0013, and 0.0014 $\mu g\,cm^{-2}$ with their respective molar absorptivities (ε), 5.5×10^4, 8.4×10^4, and 7.9×10^4 $L \cdot mol^{-1} \cdot cm^{-1}$. Table 1 gives a comparison of the sensitivities of some methods used for the determination of bismuth(III) and indium(III).

The stoichiometric ratios of metal to ligand in the complexes under the conditions mentioned above, were determined by Job's method of continuous variations. In case of indium(III) complexes, it was confirmed that the metal to ligand ratio was 1:2 for the dark red and 1:3 for the purple blue complexes. However, bismuth(III) unusually formed 2:3 com-

Table 2. Effect of Diverse Ions on the Determination of 1.7 $\mu g\,mL^{-1}$ of Bismuth(III)

Foreign ions	Tolerance limits in ppm	Masking agent
Fluoride	100	—
Chloride	100	—
Bromide	150	—
Iodide	200	—
Cyanide	400	—
Thiocyanate	500	—
Cadmium(II)	10	Masked by I^-
Mercury(II)	12	Masked by $S_2O_3^{2-}$
Iron(II)	20	Masked by CN^-
Cobalt(II)	10	Masked by CN^-
Nickel(II)	10	Masked by CN^-
Copper(II)	25	Masked by $S_2O_3^{2-}$
Lead(II)	20	Masked by $S_2O_3^{2-}$
Silver(I)	20	Masked by $S_2O_3^{2-}$
Antimony(III)	15	Masked by CNS^-
Thorium(IV)	25	Masked by PO_4^{3-}

Table 3. Effect of Diverse Ions on the Determination of 0.86 $\mu g\,mL^{-1}$ of Indium(III)

Foreign ion	Red complex (pH 3.5)		Purple-blue complex (pH ca. 10.5)	
	Tolerance limits in ppm	Masking agent	Tolerance limits in ppm	Masking agent
Citrate	250	—	180	—
Oxalate	160	—	150	—
Tartrate	220	—	150	—
Zinc(II)	4	Masked by CN^-	20	Masked by CN^-
Cadmium(II)	25	Masked by CN^- or I^-	28	Masked by CN^-
Mercury(II)	15	Masked by $S_2O_3^{2-}$ or I^-	25	Masked by $S_2O_3^{2-}$ or I^-
Iron(II)	20	Masked by F^- or CN^-	40	—
Manganese(II)	Interfere	—	10	—
Nickel(II)	20	Masked by CN^-	40	—
Cobalt(II)	20	Masked by CN^-	28	—
Copper(II)	40	Masked by $S_2O_3^{2-}$	64	—
Silver(I)	25	Masked by $S_2O_3^{2-}$	53	—
Lead(II)	20	Masked by $S_2O_3^{2-}$	15	Masked by $S_2O_3^{2-}$
Bismuth(III)	Interfere	—	7	—
Antimony(III)	10	Masked by CNS^-	10	—
Thorium(IV)	15	Masked by PO_4^{3-}	20	—
UO_2(VI)	Interfere	—	24	—

plex. THT(**1**) is a multidentate ligand[1] and a tentative structure for bismuth(III)-THT complex could be given as **2**. The complexes are not extractable in organic solvents and thus show the ionic character.

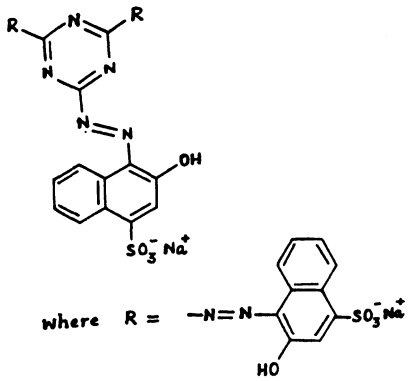

1

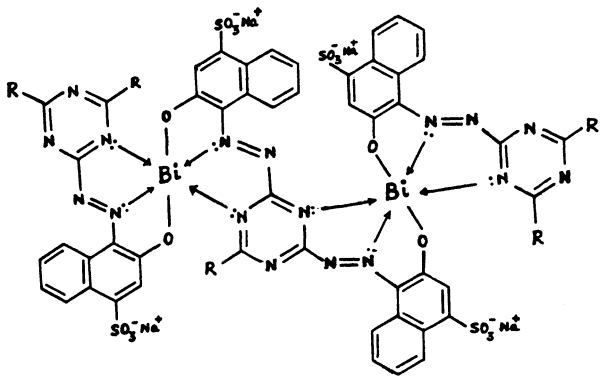

2

Effect of Diverse Ions on the Determination of Bismuth(III) and Indium(III). In the determination of bismuth(III) at the 1.7 $\mu g\,mL^{-1}$ level, nitrite, nitrate, sulfite, sulfate, thiosulfate, phosphate, citrate, tartrate, oxalate, thiourea, thiosemicarbazide up to 1000-fold excess, alkaline earths, lanthanoids, aluminium(III), chromium(III), and platinum metals up to 50-fold excess did not interfere. However, sulfide, EDTA, zinc(II), manganese(II), uranyl(VI), and indium(III) were found to interfere.

In the determination of indium(III) at the 0.86 $\mu g\,mL^{-1}$ level, fluoride, chloride, bromide, iodide, nitrite, nitrate, sulfite, thiosulfate, borate, phosphate, thiourea, thiosemicarbazide, cyanide, thiocyanate up to 1000-fold excess and alkaline earths, lanthanoids, aluminium(III), chromium(III), platinum metals up to 50-fold excess did not interfere. However, sulfide, EDTA, manganese(II), uranyl(VI), and bismuth(III) interfered at pH 3.5, while only sulfide and EDTA were found to interfere at high pH (ca. 10.5).

Tables 2 and 3 represent the tolerance limits in ppm of various ions in solution that caused a deviation smaller than ±2% in absorbance for the determination of bismuth(III) and indium(III) respectively.

One of the authors (PSK) is thankful to the Council of Scientific and Industrial Research, New Delhi, India for financial assistance.

References

1) I. Singh and P. S. Kadyan, *Analyst*, **110**, 309 (1985).
2) I. Singh and P. S. Kadyan, *Analyst*, **112**, 891 (1987).
3) Z. Marczenko, "Spectrophotometric Determination of Elements," Wiley, New York (1976).
4) F. D. Snell, "Photometric and Fluorometric Methods of Analysis, Metals, Part I," Wiley, New York (1978).
5) H. Bode, *Z. Anal. Chem.*, **144**, 165 (1955).
6) L. Barcza, *Acta Chem. Acad. Sci. Hung.*, **28**, 143 (1981).
7) T. F. Bidleman, *Anal. Chim. Acta*, **56**, 221 (1971).
8) C. L. Luke and M. E. Campbell, *Anal. Chem.*, **28**, 1340 (1956).

9) H. M. Irving, J. R. Smit, and L. Salmon, *Analyst*, **82**, 549 (1957).
10) J. E. Johnson, M. C. Lavine, and A. J. Rosenberg, *Anal. Chem.*, **30**, 2055 (1958).
11) J. Minczewski, U. Stolarczyk, and Z. Marczenko, *Chem. Anal. (Warsaw)*, **6**, 51 (1961).
12) N. S. Zuong and F. G. Zharovskii, *Ukr. Khim. Zh.*, **36**. 1159, 1273 (1970).
13) C. D. Dwivedi, K. N. Munshi, and A. K. Dey, *Chemist-Analyst*, **55**, 13 (1966); cf., A. I. Busev and V. M. Ivanov, *Izv. Vyssh. Uchebn. Zaved., Khim. Khim. Tekhnol.*, **5**, 202 (1962).
14) P. P. Kish and S. T. Orlovskii, *Zh. Analit. Khim.*, **17**, 1057 (1962).
15) M. Hniličkovă, *Collection Czech. Chem. Commun.* **29**, 1424 (1964).
16) A. I. Vogel, "A Text Book of Quantitative Inorganic Analysis," Fourth Edition, Longmans, London (1978).
17) K. L. Cheng, *Talanta*, **8**, 753 (1961).
18) B. Kopecka, V. Springer, and J. Majer, *Acta, Fac. Pharm. Univ. Commenianal*, **32**, 149 (1978); *Chem. Abstr.*, **92**, 208400n (1980).
19) A. V. Dolgorev and Ya. U. Lysak, *Zavod. Lab.*, **45**, 984 (1979); *Chem. Abstr.*, **92**, 51383j (1980).
20) B. Morelli, *Analyst*, **107**, 282 (1982).
21) Q. Xu and Xi. Xu, *Huaxue Xuebao*, **40**, 419 (1982); *Chem. Abstr.*, **97**, 119691u (1982).
22) B. K. Puri and M. Gautam, *Zh. Anal. Khim.*, **35**, 1024 (1980).
23) H. Tomioka and K. Terajima, *Bunseki Kagaku*, **16**, 698 (1967).
24) H. Sun and C. Li, *Fenxi Huaxue*, **11**, 767 (1983); *Chem. Abstr.*, **100**, 29023d (1984).
25) H. Sun and A. Liu, *Lanzhou Daxue Xuebao, Ziran Kexueban*, **19** (Huaxue Jikan), 124—30 (1983); *Chem. Abstr.*, **100**, 61075h (1984).
26) E. L. Krukorskaya and D. K. Ishanberlina, (USSR), *Sb. Nauchu. Tr-Tashk. Gos. Univ. Im. V. I. Lenina*, **622**, 43 (1980); *Chem. Abstr.*, **95**, 107996t (1981).
27) S. Rudolf and T. Janusz, *Chem. Anal. (Warsaw)*, **7**, 803 (1962).
28) A. P. Joshi and K. N. Munshi, *Mikrochim. Acta*, **1971**, 526.
29) H. A. Mottola, *Talanta*, **11**, 715 (1964).
30) E. L. Krukovskaya, Sh. T. Talipov, and N. T. Ponomareva, (USSR) Deposited DOC (1981) SPSTL 287 Khp-D p. 819; *Chem. Abstr.*, **97**, 229283 V (1982).
31) S. Shibata, *Anal. Chim. Acta*, **23**, 434 (1960).
32) Ch. Ibraimov, Sh. T. Talipov, N. B. Baber, and I. M. Nurmator, *Izv. Vyssh. Uchebn. Zaved., Khim. Khim. Tekhnol.*, **24**, 669 (1981); *Chem. Abstr.*, **95**, 161301a (1981).
33) K. Rakhmatullaev and B. G. Zakirov, *Uzb. Khim. Zh.*, **3**, 26 (1982); *Chem. Abstr.*, **97**, 207315e (1982).

 © 1988 The Chemical Society of Japan Bull. Chem. Soc. Jpn., 61, 3693—3697 (1988)

Antimony(V) Arsenatophosphate as a Thermally Stable Cation Exchanger: Selective Adsorption of Alkaline Earth and Transition Metal Ions on Its Column

K. G. VARSHNEY,* A. A. KHAN, and A. R. KHAN
Chemistry Section, Faculty of Engineering & Technology, Aligarh Muslim University, Aligarh-202001, India
(Received October 12, 1987)

A new inorganic ion exchanger based on antimony has been prepared viz. antimony(V) arsenatophosphate, which has shown a peculiarly high thermal stability and selectivity for alkaline earth and transition metal ions. As a result, its column use has been demonstrated for the separation of mercury from magnesium and zinc and of iron from other transition metals. A tentative formula has also been proposed for the material, on the basis of its chemical analysis and other characterization studies.

Antimony(V) salts have received attention because of their exceedingly good reproducible characteristics[1-4] and analytical potential[5,6] as inorganic ion exchangers. Antimony(V) silicate, synthesized in these laboratories,[7] has shown excellent stability and ion-exchange behavior. Since the mixed salts are found to show enhanced ion exchange properties over the single salts[8-10] it is important to study the properties of double salts based on antimony. In continuation of our such an effort the present paper deals with the synthesis, characterization and column applications of a thermally stable phase of the new inorganic ion exchanger viz. antimony(V) arsenatophosphate, exceptionally selective for some alkaline earths and transition metals.

Experimental

Reagents. Antimony pentachloride used in this study was of the 95% purity obtained from Fluka Switzerland. Trisodium orthophosphate and disodium hydrogenarsenate were of AnalaR grade (98.5—99%) obtained from B. D. H. Poole (England) and E. Merck (Darmstadt) respectively. All other reagents and chemicals were also of AnalaR grade.

Instruments Used. The following instruments were used for the various studies: A Philips X-ray diffraction unit with Cu$K\alpha$ target, an Elico (India) pH-meter Model LI-10, a Bausch and Lomb Spectronic-20 spectrophotometer, a Beckman IR-20 spectrophotometer, a Pye Unicam Model Sp-2900 atomic absorption spectrophotometer, a Systronics (India) flame photometer and a water bath incubator shaker with a temperature variation of ±0.5 °C.

Preparation of the Reagent Solutions. A stock solution (1M†) of antimony pentachloride ($SbCl_5$) was prepared in 4 M HCl. Further dilutions to the desired concentration were also made by 4 M HCl. Disodium hydrogenarsenate and trisodium phosphate were dissolved directly in demineralized water (DMW).

Synthesis of the Ion Exchange Material. Various samples of antimony(V) arsenatophosphate were prepared by mixing 0.05 M solutions of $SbCl_5$, disodium hydrogenarsenate and trisodium orthophosphate in different volume ratios and adjusting the pH of the mother liquor at 0 to 1 by adding aqueous ammonia with constant stirring. The gels thus obtained were conditioned for 24 h at room temperature before being separated with suction. The excess acid was washed off with DMW and the material was dried in an air oven at 40 °C before cracking in DMW to obtain granules of uniform size suitable for column operation. They were converted into the H^+-form by putting in 1M HNO_3 at least for 24 h with intermittently replacing the supernatant liquid. After washing off the excess acid the material was dried at 40 °C and passed through different sieves to obtain the various mesh sized particles. On the basis of the appearance and Na^+-ion exchange capacity (i.e.c.) determined by the column process, a sample obtained by mixing the Sb, arsenate and phosphate solutions in the volume ratio 3 : 1 : 1 was selected for all the studies. Its i.e.c. was found to be 2.2 meq (g dry)$^{-1}$.

Chemical Stability. The solubility of antimony(V) arsenatophosphate in various solvents was determined as given below:

250 mg portions of the material were kept with 25 ml of the solvent for 24 h at room temperature with intermittent shaking. 5 ml of the supernatant liquid was evaporated to dryness and the residue was dissolved in 10 ml DMW. Antimony, arsenic and phosphorus were then determined separately using the standard methods given below.

(1) Determination of Antimony. To the 2 ml portion of the above solution were added 1.6 ml of 18 M H_2SO_4 and 5 ml of KI reagent (11.2 g of KI+2 g of ascorbic acid in 100 ml water). The colored solution thus obtained was diluted to 10 ml with water in a standard volumetric flask and the absorbance was measured after 2—3 minutes at 420 nm against a reagent blank.[11]

(2) Determination of Arsenic. It was done by the molybdenum blue method.[12] The reagent solution was prepared by mixing 10 ml of solution A (1 g ammonium molybdate in 100 ml of 2.5M H_2SO_4) with 1 ml of solution B (0.15 g of hydrazine sulfate in 100 ml DMW) and diluting the mixture to 100 ml. Fresh reagent solution was prepared every time. 10 ml of this reagent solution was added to the sample solution (2 ml) and the mixture was heated on a steam bath for 15 min. After cooling to the room temperature, it was transferred to a 25 ml volumetric flask and diluted to the mark with DMW. The absorbance was taken at 840 nm.

Determination of Phosphorus. A teaspoonful carbon black was added to the sample solution (10 ml) followed by 100 ml of 0.5 M $NaHCO_3$. The contents of the flask were shaken for 30 min on a mechanical shaker and filtered through a Whatman No.42 filter paper. 15 ml of the filtrate

† 1M=1 mol dm^{-3}.

Table 1. Chemical Stability of Antimony(V) Arsenatophosphate in Various Solvents

Solvent (25ml)	Amount dissolved in mg		
	Antimony (Sb)	Arsenic (As)	Phosphorus (P)
1M HNO_3	0.58	0.79	0.03
2M HNO_3	0.85	1.7	0.05
4M HNO_3	1.2	1.7	0.06
1M HCl	0.83	1.6	0.05
2M HCl	1.0	1.8	0.01
4M HCl	2.3	1.9	0.06
1M H_2SO_4	1.2	1.6	0.03
2M H_2SO_4	1.3	1.7	0.04
1M $HClO_4$	0.58	1.9	0.02
1M $NaNO_3$	0.00	0.21	0.00
2M $NaNO_3$	0.23	0.24	0.00
0.05M NaOH	0.69	0.23	0.01
0.1M NaOH	1.1	1.7	0.04
0.1M aq. NH_3	1.4	1.5	0.02
0.5M aq. NH_3	1.5	2.2	0.03
1M CH_3COOH	1.5	1.5	0.02
0.1M KOH	1.4	0.30	0.59

Amount of the material taken=250 mg.

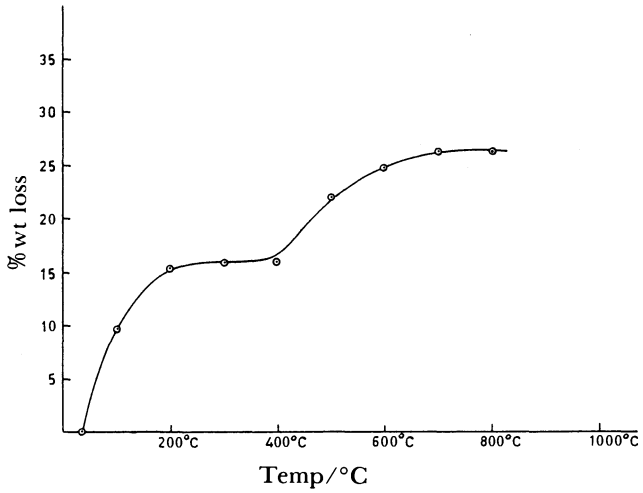

Fig. 1. % wt loss of the exchanger on heating to various temperatures.

Table 2. Effect of Heating on the Ion Exchange Capacity, Weight and Appearance of Antimony(V) Arsenatophosphate

Heating temperature °C	Appearance	Percent retention in i.e.c.	Percent weight loss
45	White	100	0.0
100	White	100	9.9
200	Light brown	100	15.5
400	Light brown	60	16.0
600	Pale yellow	18.2	25.0
800	Pale yellow	0.0	25.0

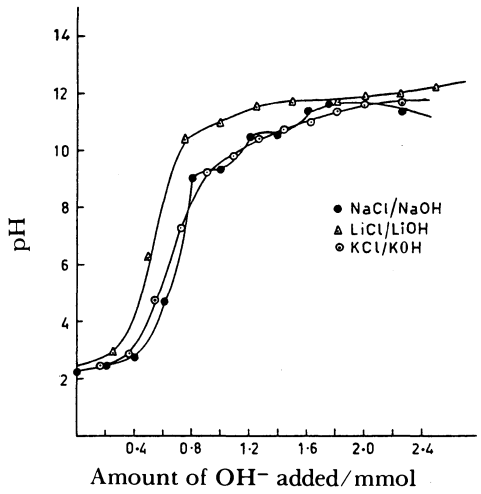

Fig. 2. pH titration curve for antimony(V) arsenatophosphate.

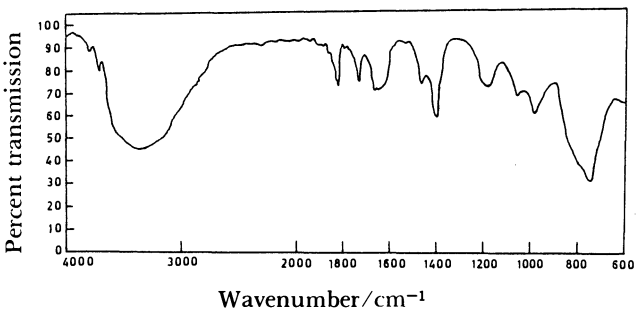

Fig. 3. Infrared spectra of antimony(V) arsenatophosphate in H^+ form.

was taken in a 25 ml volumetric flask followed by 5 ml of ammonium molybdate solution (1.5 g ammonium molybdate+100 ml of 3.2 M HCl+5 ml concd HCl). The sides of the flask were washed with distilled water and the solution was shaken thoroughly. 1 ml of $SnCl_2$ solution (10 g $SnCl_2 \cdot 2H_2O$ dissolved in 25 ml concd HCl diluted to 1320 ml with DMW) was then added to it and the volume was made up to the mark. The absorbance was taken at 660 nm, against a blank prepared in the similar manner.[13] Table 1 summarized the results.

Thermal Stability. Several 1 g portions of the exchanger were heated at various temperatures in a muffle furnace for 1 h each, and the i.e.c. was determined by the column process as usual after cooling them to room temperature. Percent weight loss was also recorded, the results of which are shown in Table 2 and Fig. 1.

Characterization of the Material. (A) Chemical Composition: 500 mg of the exchanger was dissolved in 20 ml concd HCl in a beaker by heating. The solution was further diluted to 50 ml by adding 4 M HCl. The amounts of antimony, arsenic and phosphorus were determined by the methods described above. The determinations were further confirmed by atomic absorption spectrophotometry. The mole ratio was found to be 6 : 1 : 5 for Sb, As, and P.

(B) pH Titrations: 500 mg of the exchanger in H^+-form was placed in each of the several 250 ml conical flasks, followed by the equimolar solutions of alkali metal chlorides and their hydroxides in different volume ratios, the final volume being 50 ml to maintain the ionic strength constant. The pH of the solution was recorded after equilibrium

(attained on keeping them for overnight) and plotted against the milliequivalents of the OH^- ions added as shown in Fig. 2.

(C) IR and X-Ray Studies: The IR spectrum of the exchanger in H^+-form was taken by the KBr disc method and is shown in Fig. 3. The X-ray diffraction patterns show the amorphous nature of the material.

Distribution Studies. 250 mg of the exchanger in H^+-form was shaken in an electric shaker at 30±2 °C for 4 h with 25 ml of the metal solution, adjusting the initial metal ion concentration less than 3% of the total ion-exchange capacity of the material. The metal ion concentrations in the solution before and after the equilibrium were determined by the standard volumetric methods using EDTA as the titrant.[14] The distribution coefficient (K_d) for alkaline earth and transition metal ions in DMW, $HClO_4$, and HNO_3 systems are summarized in Table 3.

The following formula was used for the calculation of the K_d values:

$$K_d = \frac{I-F}{F} \times \frac{V}{M} \text{ ml g}^{-1}$$

where

I = initial volume of the EDTA used,
F = final volume of the EDTA used,
V = total volume of the solution (ml),
M = mass of the exchanger (g).

Elution Behavior. 250 ml of the various $NaNO_3$ solutions (0.2, 0.4, 0.5, 0.8, 1.0, 1.2 M) were passed through the several columns (i.d. ca. 1 cm), each containing one gram of the exchanger in H^+-form with a flow rate ca. 0.5 ml min^{-1}. The H^+-ion thus eluted out was titrated against a standard (0.1M) NaOH solution. Maximum elution was observed with a 1M NaOH solution. Then, a similar column in H^+-form was eluted with a 1M $NaNO_3$ solution and the effluent collected in several 10 ml fractions, the total volume being again 250 ml. It was observed that the majority of the H^+-ion was released in the first 60 ml of the effluent.

Column Applications. Since the material appears to be highly selective for some transition metals such as Cu, Cd, Mn, and Zn, adsorption of these metal ions can be achieved on columns from a solution containing several other metal ions. Iron and mercury are not adsorbed appreciably and are excluded from the column of antimony(V) arsenatophosphate. Thus, the material can be used for exclusion of mercury, a chief pollutant, from an aqueous system by a simple column chromatographic method. Similarly, the method is applicable for some separations of analytical importance such as Fe(III) from Mn(II), Zn(II), Cu(II), Mg(II), Co(II), and Ba(II). Table 4 summarized the results of such separations on a column of i.d. ca. 0.6 cm containing 2 g of the 50—70 mesh size exchanger beads in H^+-form.

Results and Discussion

The main feature of this study has been to synthesize a chemically and thermally stable cation exchanger selective for certain heavy metals. As the results point out antimony(V) arsenatophosphate appears to have a high chemical stability in acids and alkalies (Table 1) and ion-exchange behavior. The most striking feature is, however, its extraordinary thermal stability (Table 2). It shows its original i.e.c. (2.20 meq (g dry)$^{-1}$) up to 200 °C and then loses slowly retaining 60% on heating upto 400 °C and 18% up to 600 °C. It is a peculiar behavior of this exchanger when compared with other materials of this class (Fig. 4).

Chemical analysis of the material points to the following emperical formula:

$$(Sb_2O_5)_3 \cdot H_3AsO_4 \cdot (H_3PO_4)_5 \cdot nH_2O$$

If it is assumed that whole of the external water is lost at 200 °C, then on the basis of the thermal studies (Table 2) we have the following expression for the number of external water molecules per molecule of the material, n

$$\frac{1800n}{M + 18n} = x$$

where x is the percent weight loss at 200 °C and M is the molecular weight of the exchanger excluding the

Table 3. K_d Values of Some Metal Ions on Antimony(V) Arsenatophosphate in DMW, $HClO_4$, and HNO_3 Systems

Sl. No.	Metal ion	K_d values				
		DMW	0.01M $HClO_4$	0.1M $HClO_4$	0.01M HNO_3	0.1M HNO_3
1	Na(I)	150	55	15	80	34
2	K(I)	935	225	43	225	62
3	Mg(II)	3880	3800	469	T.A.[a]	342
4	Ca(II)	1980	1286	940	494	420
5	Ba(II)	2900	1400	650	500	400
6	Sr(II)	3700	3700	1800	1800	1166
7	Cu(II)	T.A.[a]	T.A.[a]	1540	3180	720
8	Fe(II)	202	113	90	126	101
9	Cd(II)	T.A.[a]	3640	523	1770	434
10	Pb(II)	1860	684	460	790	684
11	Mn(II)	T.A.[a]	T.A.[a]	672	T.A.[a]	451
12	Zn(II)	T.A.[a]	3600	1750	1133	825
13	Hg(II)	400	178	108	78	56
14	Ni(II)	1166	442	375	322	192

a) T.A.=Total adsorption.

Table 4. Some Binary Separations of Metal Ions Achieved on Antimony(V) Arsenatophosphate Columns

Sl No.	Separation achieved	Amount loaded μg	Amount found μg	% Error	Eluent used	Volume of the eluent used/ml
1	Hg(II)-Mg(II)	1404 Hg(II)	1383 Hg(II)	−1.4%	0.01M HNO_3	100
		268 Mg(II)	266 Mg(II)	−0.6%	1M NH_4NO_3	50
2	Hg(II)-Zn(II)	1404 Hg(II)	1393 Hg(II)	−0.8%	0.01M HNO_3	100
		670 Zn(II)	654 Zn(II)	−2.4%	1M NH_4NO_3	80
3	Fe(III)-Mn(II)	408 Fe(III)	402 Fe(III)	−1.4%	0.01M $HClO_4$	100
		538 Mn(II)	541 Mn(II)	+0.5%	1M NH_4NO_3	80
4	Fe(III)-Zn(II)	407 Fe(III)	388 Fe(III)	−4.8%	0.01M $HClO_4$	100
		654 Zn(II)	644 Zn(II)	−1.5%	1M NH_4NO_3	100
5	Fe(III)-Cu(II)	396 Fe(III)	388 Fe(III)	−2.1%	0.01M $HClO_4$	100
		540 Cu(II)	543 Cu(II)	+0.6%	1M NH_4NO_3	50
6	Fe(III)-Mg(II)	408 Fe(III)	399 Fe(III)	−2.0%	0.01M HNO_3	100
		249 Mg(II)	251 Mg(II)	+1.0%	1M NH_4NO_3	80
7	Fe(III)-Ca(II)	382 Fe(III)	371 Fe(III)	−2.9%	0.01M $HClO_4$	100
		309 Ca(II)	309 Ca(II)	0%	1M NH_4NO_3	80
8	Fe(III)-Ba(II)	413 Fe(III)	408 Fe(III)	−1.4%	0.01M $HClO_4$	100
		1071 Ba(II)	1078 Ba(II)	+0.6%	1M NH_4NO_3	90

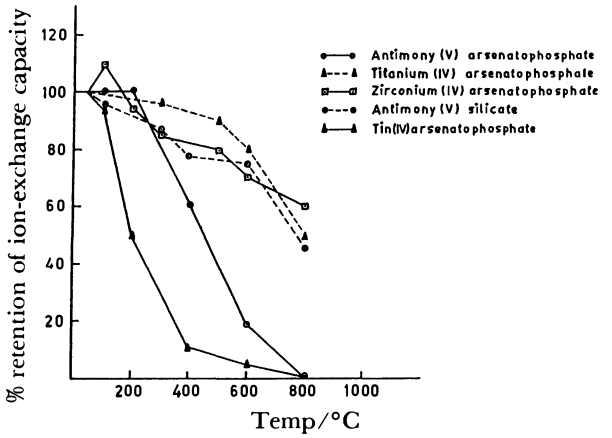

Fig. 4. Percent retention in the i.e.c. of antimony(V) arsenatophosphate and some other ion-exchangers on heating.

external water molecules. It gives the value of n as 16.

The pH-titration curves for alkali metals (Fig. 2) illustrate the maximum adsorption for Li^+ ions, which is obvious because of its highest hydrated radii ($Li^+_{(aq)}$=3.4 Å, $Na^+_{(aq)}$=2.76 Å, $K^+_{(aq)}$=2.32 Å). However, there is no appreciable difference in the adsorption behavior for Na^+ and K^+. It is also clear from the figure that the adsorption is a single step process. It is possible because the two acids, H_3AsO_4 and H_3PO_4 which provide the protogenic sites to the material, ionize almost to the same extent (pK_a for H_3PO_4=2.15 and pK_a for H_3AsO_4=2.3) thus releasing the H^+ ions simultaneously.

Infrared spectrum (Fig. 3) shows the peaks at wavenumbers 750, 950, 1100, 1200, 1400, 1700, 1750, 1800, and 3300 cm^{-1} representing the Sb-O stretchings (750), arsenate group (950), phosphate group (1100 and 1200) and the external water molecules (rest peaks) respectively.[15]

The most important aspect of an ion-exchange material is its analytical applications. Antimony(V) arsenatophosphate prepared in these studies has shown a maximum selectivity for Cu(II), Cd(II), Mg(II), Mn(II), and Zn(II) and a minimum selectivity for Hg(II), Ni(II), Fe(III). On the basis of these observations the following separations have been successfully achieved.

Hg(II)-Mg(II), Hg(II)-Zn(II), Fe(III)-Mg(II), Fe(III)-Ba(II), Fe(III)-Cu(II), Fe(III)-Zn(II), Fe(III)-Mn(II), Fe(III)-Ca(II).

Table 4 gives the salient features of these separations. Thus the material is useful for the separation of mercury from magnesium and zinc and of iron from magnesium, barium, copper, zinc manganese, and calcium.

The authors thank Prof. A. U. Malik for research facilities. The University Grants Commission and the Council of Scientific and Industrial Research (India) are thanked for the financial assistance to A.A.K. and A.R.K.

References

1) M. Abe and T. Ito, *Bull. Chem. Soc. Jpn.*, **41**, 333 (1968).

2) A. N. Lapitskii and V. F. Takavyi, *Zh. Khim.*, **2**, 19 (1969).

3) M. Qureshi and V. Kumar, *J. Chromatogr.*, **62**, 431 (1971).

4) B. G. Novikov, F. A. Belinskaya, and E. A. Materova, *Fiz. Khim.*, **1**, 29 (1971).

5) K. G. Varshney, S. Rani, U. Sharma, and S. Anwar, *Anal. Lett.*, **18**, 2033 (1985).

6) K. G. Varshney, S. Rani, and R. P. Singh, *Ecotoxicol. Environ. Safety*, **10**, 309 (1985).

7) K. G. Varshney, U. Sharma, S. Rani, and A. Premadas, *Sep. Sci. Tech.*, **17**, 1527 (1981—82).

8) K. G. Varshney and A. A. Khan, *Talanta*, **25**, 528 (1978).
9) K. G. Varshney and A. A. Khan, *J. Inorg. Nucl. Chem.*, **41**, 241 (1979).
10) K. G. Varshney and A. Premadas, *Sep. Sci. Tech.*, **16**, 793 (1981).
11) E. B. Sandell, "Colorimetric Determination of Traces of Metals," Vol. III, p. 266, Interscience Publishers, Inc., New York (1959).
12) Ref. 11, p. 282.
13) S. R. Olsen, C. V. Cole, F. S. Watanabe, and L. A. Dean, U. S. Dep. Agric., Circ. No. 939, 99 (1954).
14) C. N. Reilley, R. W. Schmidt, and Fawzes, *J. Chem. Educ.*, **36**, 555 (1959).
15) C. N. R. Rao, "Chemical Applications of Infrared Spectroscopy," Academic Press, New York (1963).

 © 1988 The Chemical Society of Japan Bull. Chem. Soc. Jpn., 61, 3699—3704 (1988)

Organophosphorus Analogues and Derivatives of the Natural L-Amino Carboxylic Acids and Peptides. I. Enzymatic Synthesis of D-, DL-, and L-Phosphinothricin and Their Cyclic Analogues

Ivan A. NATCHEV
Research Centre "Konstrukcionni Polymeri", 5-003 Gara Iskar, 1528 Sofia, Bulgaria
(Received April 28, 1987)

Acetylation of D-, DL-, and L-3-amino-2-pyrrolidinone (**1**) to the 3-acetamido derivative **2** and treatment with ethyl methylphosphinate afforded the addition product **3**. Strict selectivity was observed in the enzyme-catalyzed hydrolysis with the enzyme phosphodiesterase I, acylase, glutaminase, and α-chymotrypsin. The ester **7** and 1,2-azaphospholidine (**8**) were isolated by esterification of L-phosphinothricin (**6**).

The tripeptide γ-(hydroxymethylphosphinyl)-L-α-aminobutyryl-L-alanyl-L-alanine,[1] usually called Bialaphos (SF-1293), belongs to the small group of known natural phosphino analogues of the amino carboxylic acids. The antibiotic is produced from *Streptomices viridochromogenes strains* and has been found to possess herbicidal and fungicidal activity.[2,3] Upon enzyme decomposition with *E. coli* protease with a view to its structure elucidation, the unusual amino carboxylic acid 4-(hydroxymethylphosphinyl)-L-2-aminobutanoic acid (**6**), known as L-phosphinothricin, has been isolated.[4] It is produced[5] from *Streptomices hydroscopicus strains.*

The tripeptide Bialaphos has been synthesized[6] as a phosphonoethyl ester by the participation of the DL-forms of phosphinothricin and alanine, following a multistep procedure. In this case the yields were rather low. L-Phosphinothricin (**6**) has been synthesized[7] by Michael addition of chiral glycine Schiff base to a vinylphosphorus compound, $CH_2{=}CH{-}P(CH_3)(=O)OH$ The racemic phosphinothricin, widely used as herbicide and fungicide,[8] is produced synthetically. The introduction of the ethoxymethylphosphinyl, $EtO{-}P(CH_3){=}O$ group is achieved by the Arbuzov reaction. Thus, Wasielewski and Antczak[9] treated 4-bromobutanoic acid with diethyl methylphosphonite $CH_3P(OEt)_2$ and obtained the product after α-amination. Recently, Logusch[10] suggested that methyl DL-4-bromo-2-phtalimidobutanoate, could be used in a similar interaction, so that phosphinothricin is finally obtained by hydrolysis.

It is interesting to note that the biological activity of the natural L-phosphinothricin is twice as strong as that of the racemic mixture.[8]

The key approach in the pathway we chose to the synthesis of phosphinothricin (**6**) is a variant of the reaction of Michaelis-Becker,[11] usually applied to the alkylation hydrophosphoryl compounds, $>P(=O)H$ Despite the abundant data that have been published about this reaction, many of its aspects are still inadequately studied. Surprisingly, no one has as yet taken up McConnel and Coover[12] on their suggestion that lactams could be used in interactions of this type.

In view of the synthetic purposes in hand, the γ-lactam **1** of the D-, DL-, and L-2,4-diaminobutanoic acid was chosen as the starting material. It is very easily obtained[13] by dehydration.

In his work,[13] Adamson reports the acetylation of **1** with acetic anhydride, but his yields were very low and therefore unsatisfactory. It was found that, in the subsequent stages, any protective group, other that an acetyl group, caused considerable complications. The best acetylating agent proved to be acetic phosphoric anhydride, $AcOPO_3H_2$,[14] obtained immediately before use. The reaction proceeds at 60—70 °C for 15—20 min in the reagent medium the acetylated product **2** is isolated in a very high yield (95—98%).

The interaction of the lactam **2** with ethyl methylphosphinate takes 2.0—2.5 h of heating of the components at 120—130 °C in a closed steel cylinder and in an ambience of dry argon or nitrogen. Here, the presence of a catalyst is essential. Boron trifluoride etherate proved to be the most suitable catalyst in this case. Without it, the result is a resinous mass, from which the organophosphorus product is isolated in a very low yield (6—10%). To enhance the reaction, it is important that the temperature should be increased gradually, starting from ambient and going up to 120 °C for the duration of 1.0—1.5 h. When the process is completed, the volatile components are distilled off (100 °C/6×10^{-2} Torr (1 Torr=133.322 Pa)). The reaction product is then purified by column chromatography (silica gel and eluent chloroform : methanol=9 : 1). The product 2-acetamido-4-(ethoxymethylphosphinyl)butanamide (**3**) is obtained in a yield of 50—55%.

When the optically active D- and L-lactams **2** were used under the above conditions, no racemization was observed.

In our laboratory, we carried out analogous interactions, not only with the lactam of 2,4-diaminobutanoic acid, but also with the lactams of L-ornithine and L-lysine, where a cobalt-complex of 5-amino-1,10-

phenanthroline was used as catalyst. The results will be published separately.

The mineral hydrolysis of **3** is extremely difficult, due to the presence of an ethoxyphosphoryl group. Complete hydrolysis would require at least 8 h of boiling in 20—22% hydrochloric acid. Unfortunately, when the optically active starting esters **3** (D- or L-forms) were used, complete racemization of the product phosphinothricin (**6**) (approx. 90% yield) was observed.

We concentrated our efforts on such approaches as would help us to avoid the complications accompanying the hydrolysis of the esters of organophosphinic acids, at the same time preserving their optical activity.

The phosphoesterase enzymes, exo- and endonuclease, are widely employed in biochemical routine investigations of nucleic acids. To this moment, however, they have never been used to catalyzed the hydrolysis of the esters of organophosphinic acids. This approach was developed in our laboratory and will be discussed in a number of consecutive papers.

It was empirically established that the most favorable conditions for enzyme-catalyzed hydrolysis processes are as follows: 20 g substrate and 5 mg enzyme

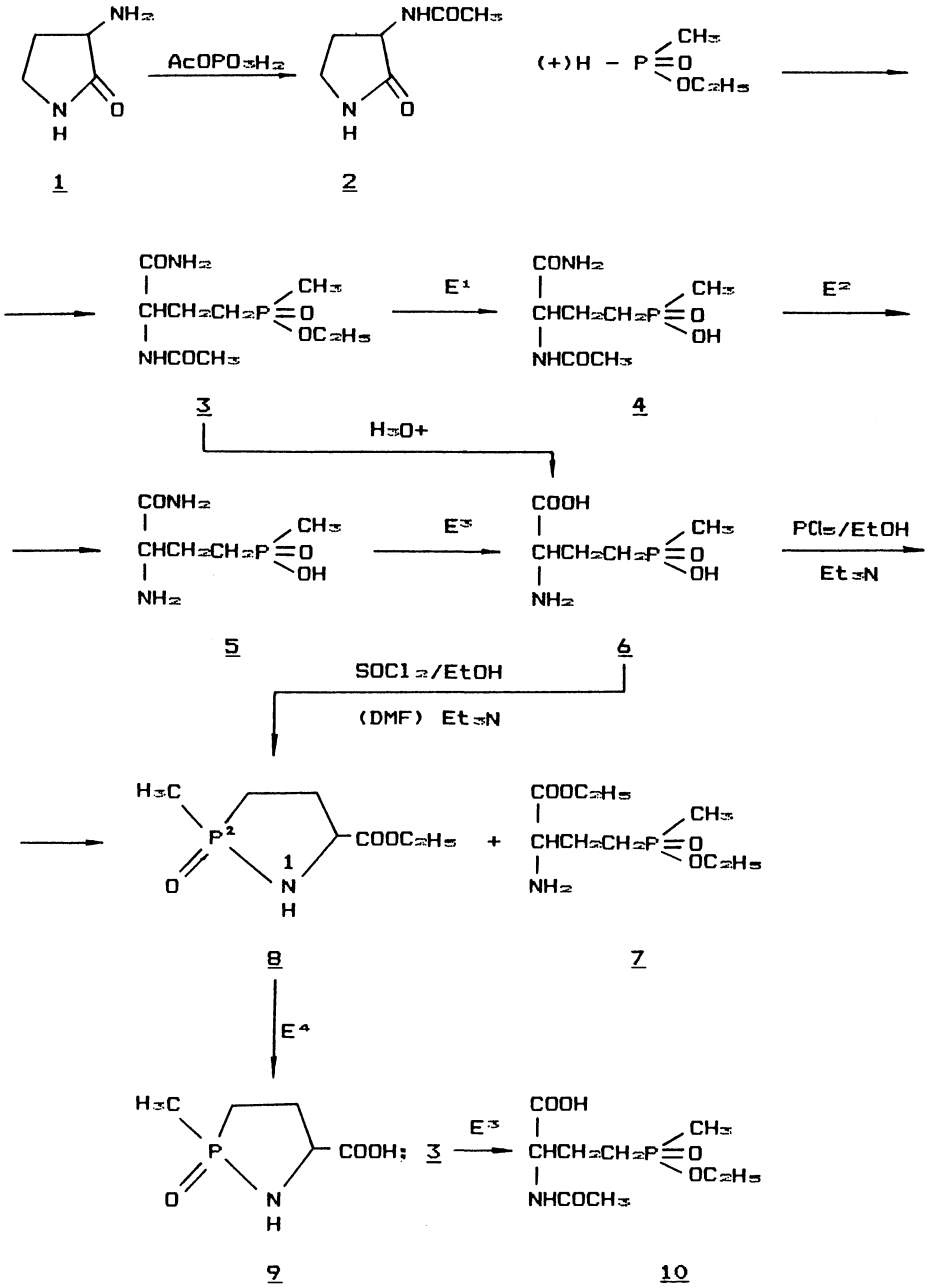

E^1 - Phosphodiesterase I; E^2 - Acylase I;
E^3 - Glutaminase; E^4 - α-Chymotrypsin.

Scheme 1.

are stirred for 6 h in an aqueous buffer solution, or emulsion, at the pH and temperature optimum of the enzyme. Naturally, larger of smaller quantities of the substrate can be used, provided that the ratio of substrate/enzyme remains the same. To ensure the easier manipulation and subsequent regeneration of the enzyme, especially if it is not easily available, a polymer carrier should be used, on which to spread the enzyme. In this case, 20 g substrate would require 10—15 mg enzyme. With very few exceptions, the enzyme-catalyzed hydrolysis affords practically quantitative yields and is strictly selective. If not inhibited, one and the same enzyme can be used in at least ten reactions. It is characteristic for the enzyme approach that no racemization occurs with optically active substrates, while the traditional hydrolysis methods usually lead to a complete loss of the optical activity. Of course, the different enzymes could be kinetically studied and the above conditions additionally refined to accomodate each separate type of enzyme. Where the synthesis of organophosphorus compounds is comcerned, however, this method is quite applicable. In our laboratory, we conducted experiments, using substrates that contain esters of the types R-P(=O)(H)OR^1, R-P(=O)(CH$_3$)OR^1, R-P(=O)(OR^1)OR^1, and R-P(=O)(OR^1)NHR^2 and other hydrolyzable groups (R, R^1, and R^2), with not only the enzymes phosphodiesterase I and alkaline phosphatase, but also with α-chymotrypsin, protease, mesintericopeptidase, acylase, urease, crude bee venom, and glutaminase. The concrete applications of these will be discussed separately.

With the phosphinic ester **3** we used the enzyme phosphodiesterase I in its free state and spread over polyacrylamide. As **3** is water-insoluble, a good initial homogenization of the substrate was achieved with 2—3 ml Tween-80^R per 20 g substrate the aqueous buffer (pH 8.8, 800 ml) was gradually added to the obtained jelly mass by continuous stirring. The homogeneous mixture was then tempered at 37 °C, and 5 mg (or 10—15 mg, if spread on polyacrylamide) phosphodiesterase I were added. After stirring for 6 h at the same temperature, the enzyme was removed by dialysis (ultrafiltration), or centrifugation, and was ready to use in next experiment. The buffer was acidified to pH 5.0 and extracted with diisopropyl ether. The acid **4** was isolated in a practically quantitative yield after drying with anhydrous magnesium sulfate and distillation of the extraction agent. Surprisingly, it was found that the catalytic action of the enzyme was not affected by the type of the optically active form: both the D- and L-forms of the D-, DL- and L-substrates **3** were hydrolyzed. It is interesting to note that alkaline phosphatase, which has a very similar activity, does not catalyze the hydrolysis of the substrate in question.

Acylase I was the next enzyme we applied to a rather unusual substrate, containing a phosphinic-acidic function. Under the above-mentioned conditions, at pH 7.0 and 25 °C, the enzyme catalyzed the hydrolysis of the *N*-acetyl group of the substrate L-**4** to the free amino phosphinic acid L-**5**, which was isolated in an approx. 80% yield after acidification, concentration and cooling. As a raw enzyme ("Sigma") was used, 25 mg of it were necessary for 25 g substrate **4**.

When trifluoroacetyl was used to protect the amino group in the starting lactam **1**, and when methyl methylphosphinate was employed in the reaction described above, the resultant trifluoroacetyl derivative (not given in the Scheme 1) was easily hydrolyzed in a practically quantitative yield after treatment with aqueous ammonia at pH 10.0. This is one of the rare cases (cf. also the case with acylase I above) when the classical methods for liberating the protective groups are to be preferred to the enzyme approach. However, when optically inactive (racemic) mixtures are used, the enzyme acylase I is quite suitable for the separation of optically active antipodes. The substrate DL-**4** leads to the isolation of the unchanged D-form D-**4**, and the hydrolysis product L-**5**.

The third enzyme investigated was glutaminase. Apart from the fact that this enzyme hydrolyzes the γ-amide function of glutamine to glutamic acid, it was found that using the α-amide of the modified glutamic acid, i.e. the substrate L-**5**, afforded the phosphinothricin L-**6** in a 95% yield. This is not very surprising, as in a separate experiment we used the diamide of the L-glutamic acid and obtained L-glutamic acid under the same conditions as for the enzyme-catalyzed hydrolysis of L-**5**. We discovered still another possible application of glutaminase, when a number of mono- and diamides of saturated and unsaturated dicarbonylic acids (malonoamide, succinamide, adipamide, pimelamide, fumaramide, citric 1,5-diamide, mesaconamide, ect.) were subjected to the catalytic action of glutaminase and gave the corresponding carboxylic acids. Sulfonamides R-SO_2NH_2 and amides of the type R-P(=O)(OR)NHR^2, as also aromatic mono- and diamides and cyclic imides, are not affected by the enzyme glutaminase.

In contrast to phosphodiesterase I, glutaminase is inactive towards the D-form of phosphinothricinamide **5**. It is interesting to note that, when the methylphosphinyl group of the substrate **5** is replaced with a dihydroxyphosphinyl group, the substrate 2-amino-4-phosphono-L-butanamide inhibits the enzyme completely. We have come to the conclusion that all experiments, involving glutaminase-catalyzed hydrolysis of carboxamides containing PO_3H_2 or P(O)(OH)H groups, should be approached with caution. Protection of the phosphono and phosphino groups as esters, however, does not result in the enzyme inhibition and a subsequent separation of the ester functions

with phosphonodiesterase I is easily possible.

In our case, the inevitable contamination of the enzyme does not seriously affect the enzyme-catalyzed hydrolysis process and glutaminase from *E. coli* can therefore be used, with an enzyme-content of about 50%.

In our laboratory, we developed a variant of the above method, where D-, DL-, and L-phosphinothricin are obtained by enzyme-catalyzed hydrolysis of the phosphinic ester **3** and a subsequent alkaline hydrolysis of the amide **4**. In this case, unlike the mineral hydrolysis of the ester **3**, no racemization of the optically active forms was observed. This method for production of phosphinothricin will be discussed separately.

Esterification was carried out with a view to obtaining derivatives of L-phosphinothricin, suitable for peptide synthesis. Treatment of the acid **6** with phosphorus pentachloride afforded a chloro-containing compound, which proved extremely unstable upon air-exposure and decomposed quickly releasing hydrogen chloride. For that reason, chlorination and esterification were conducted simultaneously in the presence of triethylamine as acceptor for the released hydrogen chloride. After the usual work-up for separation of the reaction products, we isolated the main product L-phosphinothricin *O,P*-diethyl ester (**7**) (yield approx. 65%) and 1,2-azaphospholidine (**8**) (yield approx. 20%). When a 1 equivalent phosphorus pentachloride was used, the yield of the 1,2-azaphospholidine (**8**) went up to 50%, whereas the diester of L-phosphinothricin (**7**) was found only in traces. Most probably, the improved experimental conditions have caused the initial chlorination, after which the carboxyl group is esterified and the phosphinyl and amino groups of phosphinothricin form an azaphospholidine cycle. If the *P*-ester of phosphinothricin is placed under the same conditions, no such cyclization occurs. An indirect was to proving the possible mechanism of this ring-formation is the isolation of 1,2-azaphospholidine (**8**) by treatment of L-phosphinothricin (**6**) with thionyl chloride and a catalytic quantity of *N,N*-dimethylformamide, followed by treatment with absolute ethanol. The product is obtained in a yield of about 60%.

When the fourth enzyme α-chymotrypsin, was used in an enzyme-catalyzed hydrolysis, the free acid **9** was isolated in a practically quantitative yield. The same product (cf. our subsequent publications) has been obtained by a variant of the reaction of Ugi: from 3-(hydroxymethylphosphinyl)propanal, ammonium, and cyclohexyl isocyanide, followed by enzyme hydrolysis. That enzyme-catalyzed hydrolysis should be preferred to mineral hydrolysis was due to the fact that the cyclic PONH-bond of 1,2-azaphospholidine (**8**) turned out to be highly sensitive to all interactions with acids or salts under the conditions accompanying the hydrolysis of the ethoxycarbonyl group. The enzyme-catalyzed hydrolysis is conducted by the method described above: 20 g substrate **8**, 15 mg raw α-chymotrypsin, stirring for 6 h at 25 °C in 500 ml buffer (pH 7.8). The enzyme could, of course, be spread over a polymer carrier, but as it is readily available, this was not actually necessary. An analogous deesterification occurred also when the enzyme alkaline mesintericopeptidase and protease were used.

The enzyme approach was again employed to obtain L-phosphonothricin with a free carboxyl function and protected $-P\lesssim^{CH_3}_{OEt}$ and amino groups. When the amide **3** was used as substrate of the enzyme glutaminase under the above conditions, the free carboxylic acid **10** was isolated in a practically quantitative yield.

Thus, by the slightly modified reaction of Michaelis-Becker and the new enzyme approach to the hydrolysis of alkoxymethylphosphinyl groups, carboxylic esters and amides, we succeeded in isolating L-phosphinothricin (**6**) in satisfactory yields. This product is rather valuable for its biological activity.

Experimental

General Notes: IR spectra, elemental analysis, HPLC, and determination of optical activity—on a Perkin-Elmer instrument; ^{1}H NMR spectra—on Jouel-100 MHz; mass-spectra—on LKB-900; melting point—measured on a Köfler apparatus; TLC—silica-gel film "Merck"; reagents and solvents— "Aldrich", "Merck"; enzymes and buffers—"Sigma"; α-chymotrypsin— "Pharmachim", Bulgaria. Special credit goes to Dr. N. Stambolieva, who kindly supplied the author with alkaline mesintericopeptidase.

Analytical data of all compounds, with their names, numbers in the text, schemes, and formulae, are given in the following order: yield; IR spectrum (*a.* KBr tablet, *b.* film, cm^{-1}); ^{1}H NMR spectrum taken in *c.* DMSO-d_6, *d.* $CDCl_3$, *e.* D_2O+NaOD, TMS standard, δ-scale, ppm (number of protons, calculated by the integral curve, multiplicity, position of proton in the molecule); mass-spectrum—*m/z*, Calcd/Found, %; elemental analysis for % C, H, N-Calcd/Found; mp; $[\alpha]_D^{20}$; R_f—phosphomolybdic acid ($12MoO_3 \cdot H_3PO_4 x H_2O$)—"Aldrich" or ninhydrin detection (for compounds containing an amino group), developed in systems:

A : *n*-BuOH: AcOH: H_2O=9 : 1 : 1;
B : *n*-BuOH: 25% aq. NH_3=4 : 1;
C : DMF: $CHCl_3$: MeOH=5 : 1 : 2;
D : $CHCl_3$: MeOH=9 : 1

The IR-spectra of the known natural compounds were compared with those of the compounds, obtained by the original methods described in the text, and elemental analysis was carried out. Full coincidence was observed in the range 4000—400 cm^{-1} and elemental analysis was satisfactory. For the optically active forms, which lack descriptions in the literature, mp's and $[\alpha]_D^{20}$ are also given.

Preparation of D-, DL-, and L-3-Acetamido-2-pyrrolidinone (2). Phosphorus pentaoxide (113 g) is dissolved at 60—70 °C in orthophosphoric acid (150 g). The obtained phosphoric acid (H_3PO_4) is stored in a refrigerator at −10 °C and is quickly melted in a hot oil bath immediately before use.

Phosphoric acid (8 ml) is dissolved in acetic anhydride (32 ml) (mole ratio 1.0:1.7) and D-, DL-, or L-3-amino-2-pyrrolidinone (10.01 g, 0.1 mol), is added. The mixture is stirred for 15—20 min at 80—85 °C and is then poured over crushed ice (approx. 50 g). Rapid cooling of the liquid phase occurs and the product 3-acetamido-2-pyrrolidinone (**2**) crystallizes: $C_6H_{10}N_2O_2$; 13.96 g (98.2%); D-form, 182—184 °C, L-form, 176—178 °C, DL-form, 175—177 °C (lit,[11] 176 °C); D-: =49.2°, L-: +43.5°, (*c* 0.1, MeOH).

Synthesis of Butanamide 3. A mixture of the lactam **2** (14.22 g, 0.1 mol), ethyl methylphosphinate (12.97 g, 0.12 mol), and boron trifluoride etherate (1 ml) is gradually heated for 1—1.5 h to 120 °C in a closed steel cylindrical container in an ambience of dry argon or nitrogen. Heating is kept up for another 2—2.5 h at 125—130 °C. After cooling, the reaction mixture is extracted with boiling benzene and the undissolved portion is decanted off. Cooling affords an oil, which crystallizes after being kept for a prolonged period at 0 °C over ethyl acetate/cyclohexane. L-3-Acetamido-4-(ethoxymethylphosphinyl)butanamide (**3**): $C_9H_{19}N_2O_4P$; 14.26 g (56.3%); *a*: 3350—3300, 3170—3010, 1650, 1640, 1320 (P-CH_3), 1280 (P=O), 1110—980 (P-O-C); *c*: 1.28 (3H, s, $COCH_3$), 1.38 (3H, t, *J*=7 Hz, $OC\underline{H}_2CH_3$), 2.03 (3H, d, *J*=17 Hz, PCH_3), 2.1—2.7 (4H, m, $PC\underline{H}_2C\underline{H}_2$), 4.12 (2H, q, $OC\underline{H}_2CH_3$), 4.52 (1H, t, *J*=8 Hz, $C\underline{H}CH_2$), 6.28 (1H, s, NH), 6.46 (2H, s, NH_2); after D_2O-exchange the protons N$\underline{H}$ and NH_2 do not appear; 250.23/250 (19%); 43.20/43.26, 7.65/7.39, 11.19/10.99; +43.9°, (*c* 0.1, MeOH); 162—164 °C (decomp); 0.43-A.

D-**3**: 11.96 g (50.8%); −40.2°, (*c* 0.1, MeOH); 162—164 °C (decomp).

DL-**3**: 12.54 g (53.3%); 149—152 °C (decomp).

Preparation of Phosphinothricin (6). Method A: The phosphinyl ester DL-**3** (25.02 g, 0.1 mol) is boiled for 8 hours in hydrochloric acid (150 ml, 22%). It is then evaporated in vacuum (80 °C/6×10^{-2} Torr) to dryness and placed in a column Dowex 50W-X8 H^+ resin. The column is washed with water, the first strongly acidic eluate is thrown away and washing continues with 0.5 M HCl (1 M=1 mol dm^{-3}). The ninhydrin-positive fraction is evaporated in vacuum to dryness and the residue is crystallized from ethanol/diethyl ether; DL-2-amino-4-(hydroxymethylphosphinyl)butanoic acid hydrochloride (**6**): $C_5H_{12}NO_4P \cdot HCl$; 20.02 g (92.1%); mp 203—205 °C (lit,[9] 202—204 °C).

Method B: Enzyme-Catalyzed Hydrolysis of D-, DL-, and L-3. 800 ml buffer (pH 8.8) are added to a well-homogenized mixture of D-, DL-, or L-**3** (20 g), and "Tween-80" (2 ml). After tempering at 37 °C, about 5 mg (or 10—15 mg, of spread on polyacrylamide) of the enzyme phosphodiesterase I are added. The mixture is stirred at the same temperature for 6 hours and the enzyme is then removed. Concentration and extraction with diisopropyl ether result in the isolation of: L-2-acetamido-4-(hydroxymethylphosphinyl)butanamide (L-**4**): $C_7H_{15}N_2O_4P$; 17.29 g (97.4%); *a*: 3350—3300, 3180—3025, 2845—2435, 1655, 1640, 1300, 1250, 765, 635; *c*: 1.21 (3H, s, $COCH_3$), 1.96 (3H, d, *J*=18 Hz, PCH_3), 2.2—2.7 (4H, m, PCH_2CH_2), 4.50 (1H, t, *J*=8 HZ, $CHCH_2$), 6.06 (1H, s, NH), 6.52 (2H, s, NH_2), 10.2—10.6 (1H, br., POOH); after D_2O-exchange no signals for the N$\underline{H}$, NH_2, and POOH protons appear; 222.18/222 (36%); 37.84/37.55, 6.80/7.01, 12.61/12.55; +64.8°, (*c* 0.1, MeOH); 185—189 °C (decomp).

D-**4**: 17.07 g (96.3%); −63.7 °, (*c* 0.1, MeOH); 192—194 °C (decomp).

DL-**4**: 17.39g (98.1%); 180—183 °C (decomp).

Enzyme-Catalyzed Hydrolysis of L-4. A mixture of the substrate L-**4** (20 g), "Tween-80" (2 ml) and raw acylase (25 mg, 50% enzyme content) is stirred for 6 h at 25 °C in 500 ml buffer (pH 70). After acidification, passing through an ion-exchange resin (eluent 0.5 M HCl) and evaporation in vacuum to dryness, the reaction residue is crystallized with ethanol/diethylether: L-2-amino-4-(hydroxymethylphosphinyl)butanamide hydrochloride (L-phosphinothricinamide hydrochloride) (L-**5**: $C_5H_{12}N_2O_3P \cdot HCl$: 15.52 g, (79.6%); *a*: 1550 (NH_3^+); *e*: 1.95 (3H, d, *J*=18Hz, PCH_3), 2.2—2.7 (4H, m, PCH_2CH_2), 4.33 (1H, t, $C\underline{H}CH_2$); 180.14/180 (25%); as hydrochloride — 27.73/27.65, 6.51/6.48, 12.93/13.11; +52.3°, (*c* 0.1, H_2O); 250 °C (decomp); 0.43-B.

Enzyme-Catalyzed Hydrolysis of 5. A mixture of the substrate L-**5** (21.65 g, 0.1 mol) and the enzyme glutaminase (5 mg) is stirred for 6 h at 25 °C in 500 ml buffer (pH 4.9). The enzyme is then removed and the reaction mixture is worked up as per Item 4, Method A. Yield of L-phosphinothricin hydrochloride: 21.24 g (97.6%).

Synthesis of Phosphinothricin *O,P*-Diethyl Ester- (7) and 1,2-Azaphospholidine (8). A suspension of D-, DL-, or L-phosphinothricin hydrochloride (**6**) (21.76 g, 0.1 mol), in 200 ml dry dioxane is continuously stirred in a humidity proof vessel, while phosphorus pentachloride (45.81 g, 0.22 mol) in dry dioxane and triethylamine (33.38 g, 0.33 mol) in 200 ml absolute ethanol are simultaneously and gradually added for 120 min at 40—45 °C. The mixture is boiled for 1 h and filtered. The filtrate is evaporated in vacuum to dryness. The reaction residue is dissolved in chloroform and a hydrogenchloride current is passed through it until no more oil is released from the D-, DL-, or L-phosphinothricin *O,P*-diethyl ester (**7**), which is then decanted out and, with some difficulty, crystallized. Yield 62—65%.

The mother layers, obtained after the isolation of the diester **7**, are evaporated in vacuum to dryness and the residue is placed in a silica-gel column and eluted with chloroform: methanol 9:1. The eluent is removed by evaporation and the product is crystallized, with some difficulty, from ethyl acetate/hexane. Ethyl (5*S*)-2-methyl-1,2-azaphospholidine-5-carboxylate 2-oxide (L-**8**): $C_7H_{14}NO_3P$; 3.69 g (19.3%); *a*: 1730, 1385 (P-N), 1320 (P-CH_3), 1270—1100 (P=O, C-O-C); *c*: 1.18 (3H, t, $OOH_2C\underline{H}_3$), 1.73 (3H, d, *J*=17 Hz, PCH_3), 2.2—2.7 (4H, m, PCH_2CH_2), 4.1—4.5 (3H, m, $CHCH_2OCH_2CH_3$), 7.03 (1H, s, NH); 191.17/191 (33%); 43.28/43.18, 7.38/7.03; 7.33/7.69; +74.3°; (*c* 0.1, MeOH); 93—95 °C; 0.72-D.

D-**8**: 3.85 g (21.5%); −70.2°; 90—92 °C.

DL-**8**: 3.65 g (20.4%); 89—91 °C.

Enzyme-Catalyzed Hydrolysis of the Ester 8. A well-homogenized mixture of the substrate L-**8** (19.71 g, 0.1 mol) and 2 ml "Tween-80" is added to a solution (thermostabilized at 25 °C) of the enzyme α-chymotrypsin (10 mg, raw, pancreatic), or 10 mg alkaline mesintericopeptidase, in 500 ml buffer (pH 7.8 and 8.2). The mixture is stirred for 6 h at the same temperature until pH 6.0 is reached and is then condensed. The product is filtered out after prolonged strage in a refrigirator: (5*S*)-2-methyl-1,2-azaphospholidine-5-carboxylic acid 2-oxide-(L-pyrophosphinothricin)-(L-**9**): $C_5H_{10}NO_3P$; 15.19 g (94.2%); *a*: 3320—2800, 1385, 1320, 1255; *e*: 1.71 (3H, d, *J*=17Hz. PCH_3), 2.2—2.7 (4H, m, PCH_2CH_2), 4.48 (1H, t, *J*=6 Hz,$CHCH_3$); 163.1/163 (26%); 36.82/37.05,

6.18/6.01, 859/8.63; +69.7°, (*c* 0.1, H_2O); 186—190 °C (decomp); 0.63-C.

Enzyme-Substrate Interaction of the Amide L-3 with Glutaminase. The method in Item 4.3 is employed. The following product is isolated: L-2-acetamido-4-(ethoxymethyl)-butanoic acid (**10**): $C_9H_{18}NO_5P$; 96.4%; *a*: 3510—3050, 1745, 1645, 1305, 1255, 1110—980; *c*: 1.18 (3H, t, *J*=7 Hz, OCH_2CH_3), 1.38 (3H, s, $COCH_3$), 2.18 (3H, d, *J*=18 Hz, PCH_3), 2.2—2.7 (4H, m, PCH_2CH_2), 4.18 (2H, q, OCH_2CH_3), 4.55 (1H, t, *J*=6 Hz, $CHCH_2$), 6.33 (1H, s, NH), 10.9—11.3 (1H, br., COOH); 251.22/251 (18%); 43.03/42.78, 7.22/7.36, 5.58/5.71; 46.7°, (*c* 0.1, MeOH); 132—135 °C; 0.33-A.

Synthesis of 1,2-Azaphospholidine L-8. Method-A: The method in Item 5 is employed, only now phosphorus pentachloride (22.91 g, 0.11 mol) and triethylamine (22.25 g, 0.22 mol) are used. L-**8** is obtained with a 50.6% (9.67 g) yield and its spectral data are identical with those of the same product obtained earlier.

Method B: A mixture of L-phosphinothricin hydrochloride (L-**6**) (21.76 g, 0.1 mol) and 2 ml *N,N*-dimethylformamide is stirred in dry benzene (200 ml) at room temperature. Thionyl chloride (13.09 g, 0.11 mol) is added in portions for the duration of 1 h, accompanied by a continuous current of dry nitrgen through the reaction mixture. The temperature is then increased to 40—45 °C and, while stirring is kept up, triethylamine (15.15 g, 0.15 mol) in 150 ml absolute ethanol is gradually added. The mixture is boiled for 1 h, filtered and worked up as above. Yield of L-**8**; 11.71 g (61.2%).

References

1) E. Bayer, K. Gugel, K. Högels, H. Hagenmeier, S Jessipow, W. König, and H. Zähner, *Helv. Chem. Acta*, **55**, 224 (1972).

2) K. Tacibana, T. Watanabe, Y. Suzuki, and Y. Sekizawa, *Sci. Reports Meiji Seika Kaisha*, **1980**, 27.

3) K. Weissermel, H. Kleiner, M. Finke, and U. Felcht, *Angew. Chem., Int. Ed. Engl.*, **20**, 223 (1981).

4) N. Ezaki, S. Amano, K. Fukushima, S. Inoue, and T. Niida, *Meiji Seika Kenkyu Nempo*, **1973**, 42.

5) Y. Kondo, T. Shomura, Y. Ogawa, T. Tutioka, H. Watanabe, K. Totsukawa, T. Suzuki, C. Moriyama, D. Yoshida, S Inoue, and T. Niida, *Sci. Reports Meiji Seika Kaisha*, **1973**, 34.

6) Y. Ogawa, H. Yoshida, S. Inoue, and T. Niida, *Meiji Seika Kenkyu Nempo*, **1973**, 60.

7) N. Minowa, M. Hirayama, and S. Fukatsu, *Tetrahedron Lett.*, **25**, 1147 (1984).

8) C. Fest and K. Schmidt, "The Chemistry of Organophosphorus Pesticides," Springer-Verlag (1982), p. 175.

9) C. Wasielewski and K. Antczak, *Synthesis*, **1981**, 540.

10) E. Logusch, *Tetrahedron Lett.*, **27**, 5935 (1986).

11) A. Michaelis and T. Becker, *Ber.*, **30**, 1003 (1897).

12) R. McConnel and H. Coover, *J. Am. Chem. Soc.*, **78**, 4453 (1956).

13) D. Adamson, *J. Chem. Soc.*, **1943**, 39.

14) A. Fatiadi, *Carbohydr. Res.*, **6**, 237 (1968).

 © 1988 The Chemical Society of Japan Bull. Chem. Soc. Jpn., 61, 3705—3709 (1988)

Organophosphorus Analogues and Derivatives of the Natural L-Amino Carboxylic Acids and Peptides. II. Synthesis, Enzyme-Substrate Interactions of "Bialaphos" (SF-1293) and Its Cyclic and Phosphinic Amide Type Analogues

Ivan. A. NATCHEV
Research Centre "Konstrukcionni Polymeri", 5-003 Gara Iskar, 1528 Sofia, Bulgaria
(Received April 28, 1987)

The natural tripeptide antibiotic "Bialaphos" (**5**) has been synthesized by condensation of the protected L-phosphinothricin (**1**) with the dipeptide alanylalanine ethyl ester. The dicyclohexylcarbodiimide method has been used, followed by enzyme-catalyzed hydrolysis. Analogously, a cyclic analogue and the phospha^{C}-peptide (phosphinic amide type) analogue (**14**) of the antibiotic (**5**) have been found to possess antitumour activity.

The tripeptide antibiotic γ-(hydroxymethylphosphinyl)-L-α-aminobutyryl-L-alanyl-L-alanine ("Bialaphos") (**5**) was isolated for the first time[1] from *Streptomices viridochromogenes strains* and it is known to possess herbicidal and fungicidal activity. The phosphinic acid analogue of glutamic acid: 2-amino-4-(hydroxymethylphosphinyl)butanoic acid (phosphinothricin), has a very wide application in agriculture. It should be noted that, while scientific literature abounds in methods for the synthesis of this compound, very limited information about the synthesis pathways of the tripeptide "Bialaphos" can be found. This is due to the complications that arise when attempts are made to release the blocking groups of the phosphinic function. Thus, researchers from Japan[2] synthesized the *P*-ester of "Bialaphos" (with the participation of the DL-forms of phosphinothricin and alanine), but when they tried to hydrolyze the ethoxymethylphosphinyl group to a free phosphinic acid, the "hard" hydrolysis conditions led to the hydrolysis of the peptide bonds. To solve this problem, we devised a method for enzyme-catalyzed hydrolysis[3] of esters of the type:

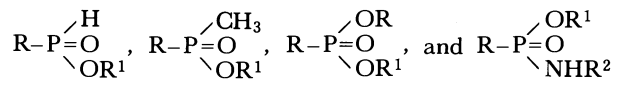

As starting compounds in the synthesis of "Bialaphos" we used protected phosphinothricin (**1**), prepared in our laboratory,[3] and the commercially available dipeptide L-alanyl-L-alanine ethyl ester. Condensation was carried out without complications by the dicyclohexylcarbodiimide method and the completely protected tripeptide **3** was isolated in an approx. 80% yield. Hydrolysis of the blocking *N*-acetyl and ethoxycarbonyl groups was also carried out by a standard method for peptide synthesis, i.e. mineral hydrolysis to the tripeptide **4**, obtained in an approx. 85% yield.

In our previous paper,[3] the enzyme phosphodiesterase I was successfully used in the enzyme-catalyzed hydrolysis of the *P*-ester of L-phosphinothricin. It could therefore be assumed that this enzyme would retain its catalytic activity in the case of the tripeptide **4**

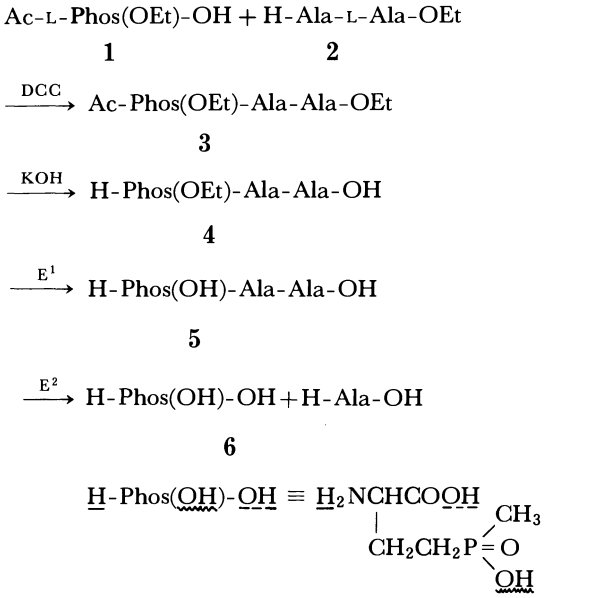

Scheme 1.

as well. Under the empirically confirmed most favorable hydrolysis conditions, i.e. 20 g substrate, 5 mg enzyme (of 15 mg enzyme, if spread on a polymer carrier), stirring for 6 h at 37 °C in 500 ml buffer (pH 8.8), the free tipeptide **5** was isolated in a yield of over 90%. Its spectral data were found to be identical with those of its natural counterpart. No additional purification of the phosphodiesterase I, supplied by "Sigma," was necessary. Its inevitable contamination did not noticeably affect the enzyme-catalyzed hydrolysis, despite the fact that, after the termination of the process, 6—8% phosphinothricin was isolated as a result of the hydrolysis of the phosphinothricin-alanyl peptide bond. It is interesting to note that when D-phosphinothricin (D-**1**) was used in an analogous synthesis, no presence of phosphinothricin was observed during the last phase of the enzyme hydrolysis. The occurence of the side hydrolysis process could be caused by some impurities of the commercial product, because phos-

phodiesterase I has never been found to possess any proteolytic activity. All our attempts to purify the phosphodiesterase I led to a marked decrease of its hydrolytic activity. When, under the same conditions, crude dried venom from *Crotalusatrox* was used, which hydrolyzes minimum 0.1 mmol bis(*p*-nitrophenyl)hydrogenphosphate per mg solid per minute at pH 8.8 and 37 °C, complete decomposition of the tripeptide **5** was observed and the only products that were isolated phosphinothricin and alanine.

The tripeptide "Bialaphos" **5** and its cyclic analogue "Pyrobialaphos" **9** (cf. below) have also been synthesized in our laboratory by the method of the activated esters and an *N*-protective group, *t*-butoxycarbonyl (*t*-BOC). This approach, though it is by no means better than the one described here, will be discussed separately.

With a view to elucidating the relationship of chemical structure-physiological activity, the cyclic analogue of phosphinothricin-2-amino-1,2-azaphospholidine-5-carboxylic acid **7**, recently synthesized by us,[3] was chosen as the N-terminal component of the tripeptide "Bialaphos". Condensation of **7** with the dipeptide alanylalanine ethyl ester was carried out by the dicyclohexylcarbodiimide method. The modified dipeptide **8** was isolated in an approx. 85% yield. When mineral hydrolysis was attempted of the ethoxycarbonyl group, the cyclic phosphinic amide group 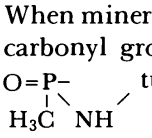 turned out to be highly unstable and the tripeptide "Bialaphos" **5** was isolated in a very good yield. This made it clear that the enzyme approach should in this case be used. Alkaline mesintericopeptidase was chosen as the esterase enzyme, as it is known to hydrolyze the peptide C-terminal pro-group rather faster, than the peptide bonds. Nevertheless, strict control of the hydrolysis process is essential until alanine is detected chromatographically. When 20 g substrate and 15—20 mg enzyme were used in a buffer medium

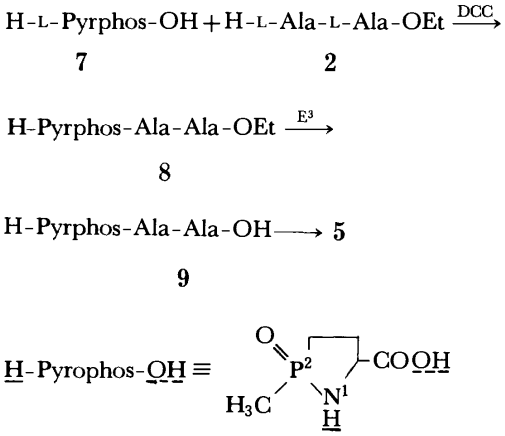

E^3 = Mesintericopeptidase.

Scheme 2.

(pH 7.8), the tripeptide 9 was isolated in about 70% yield. It differs from its natural counterpart in the presence in it of an N-terminal cyclic bond between the nitrogen and the phosphorus.

This modification leads to considerable changes in the physiological activity. Laboratory tests showed a marked decrease of the herbicidal activity. Surprisingly, the modified tripeptide **9** does not appear to have any bactericidal activity, which is characteristic for "Bialaphos". This fact can probably be accounted for by the absence of a free phosphinic acid group 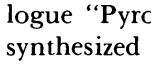 . The *P*-esterified tripeptide **4** shows a certain decrease of its bactericidal activity.

It would be interesting to try still another approach to bonding the unusual amino acid L-phosphino thricin with alanylalanine by creating a PONH bond.

Such di- and tripeptide were synthesized for the first time and quite independently from Imoto et al.[4] and Martell et al.[5] Unfortunately, no peptides with free terminal or side functional groups can be obtained, as "they are very sensitive to any mild alkaline or acidic treatment, aimed at the removal of the blocking groups".[5] Some Soviet researchers[6] were confronted with the same problem. They used the DCC-method to condense the phosphone analogue of phenylalanine, (1-acetamido-2-phenylethyl)phosphonic acid, 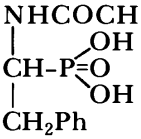 , with the methyl ester of phenylalanine.

Recently, it was reported in the patent literature that Issleib et al.[7] have succeeded in obtaining free phospha^C-peptides by condensation of the mono (trimethylsilyl) ester of 2-(benzyloxycarbonylamino)-ethylphosphonic acid, 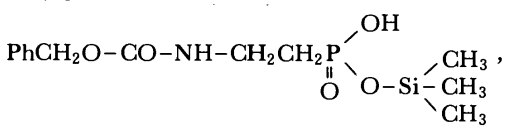 , with ethyl isocyanoacetoacetate $C^{\leftarrow}\equiv N\text{-}CH_2COCH_2COOEt$, and subsequent hydrogenation and hydrolysis of the trimethylsilyl protective group.

To this moment, no information is available in the literature about phospha^C-peptides with phosphinic acids.

The major problem in the synthesis of a phospha^C-peptide analogue of "Bialaphos" is finding a suitable protective group, which can be removed under such conditions, as do not noticably affect the PONH bond. Urethane-type protective groups provided to be unsuitable, because these derivatives of phosphinothricin are difficult to obtain and, besides, they lead to some side reactions upon treatment with hydrogen bromide-iced acetic acid. The use of an *N*-acetyl protective group is also undesirable, due to the instability

of the phosphinic amide group under conditions of mineral hydrolysis. Enzyme-catalyzed hydrolysis with α-chymotrypsin, protease, peptidase, etc., is also to be avoided, as in this case nonselective hydrolysis of the peptide alanylalanin bond occurs. Protective groups, released by hydrogenolysis, are ineligible as well, because they cause side reactions. The only group found suitable for the protection of the amino group of phosphinothricin, and with some reservations at that, is the trifluoroacetyl group.

The synthesis of the starting material **11**, having a free phosphinic acid function, $-P\begin{matrix}=O\\ \diagdown OH\end{matrix}$, and protected amino and carboxyl groups, was carried out by the method given in Ref. 8, where *N*-trifluoroacetyl protection has been applied to amino carboxylic acids.

Treatment of L-phosphinothricin ethyl ester, synthesized by us earlier, with *N*-ethyl trifluorothioacetate was carried out at room temperature in a borate buffer. The ester amide **11** was isolated in a yield of approx. 90%.

The dicyclohexylcarbodiimide method was used to condense the protected L-phosphinothricin **11** with the dipeptide L-alanyl-L-alanine ethyl ester. Conditions were analogous to those for the conventional peptide synthesis. The phospha^C-tripeptide **12** was isolated in an yield of about 75%. One equiv phosphinothricin **11**, 1 equiv dipeptide, and 1.1 equiv dicyclohexylcarbodiimide were kept for 12 h in an ambience of dry ethyl acetate and then the separated *N,N'*-dicyclohexylurea was filtered off. The filtrate was consecutively washed with 5% aqueous solution of sodium carbonate-water-1M HCl-water (1M=1 mol dm^{-3}), dried over anhydrous magnesium sulfate, evaporated to dryness in vacuum, and purified by column chromatography on silica gel.

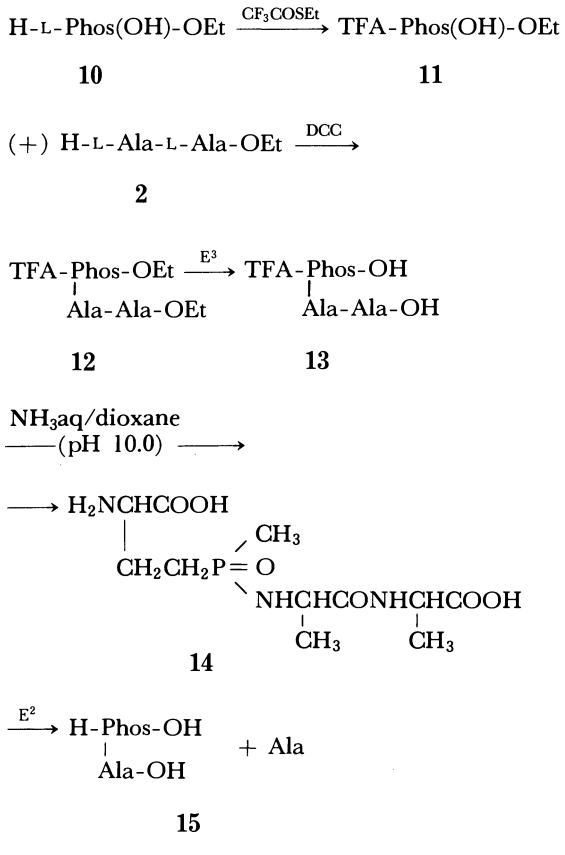

Scheme 3.

The carboxyl groups were released by the above-described method of enzyme-catalyzed hydrolysis with mesintericopeptidase to the protected phospha^C-peptide **13**, isolated in an approx. 80% yield. This yield, which is somewhat low for an enzyme-catalyzed process, is due to the fact that certain hydrolysis of the peptide bonds is observed as well.

The *N*-trifluoroacetyl protective group is removed by treatment with aqueous ammonia at pH 10.0. At lower pH values no hydrolysis occurs, whereas higher pH values lead to hydrolysis of the phosphinic amide bond. Despite the numerous experiments performed, the free phospha^C-peptide **14** was never isolated in a yield of over 40%.

In spite of the fact that the tripeptide **14** readily undergoes mineral hydrolysis, we failed in our attempts to find an enzyme that catalyzes the hydrolysis of the PO-NH bond. When alkaline phosphatase was used, the presence of about 10% phosphinothricin was established in the hydrolysate, but this was probably due to the alkalinity of the medium (pH 10.4), and not to the action of the enzyme.

The proteolytic enzymes α-chymotrypsin and protease catalyze the hydrolysis of the alanylalanine bond and as a result the phospha^C-dipeptide **15** is isolated in approx. 90% yield.

The tripeptide **14** has been statistically proved to possess antitumour activity. When applied to an experimental tumour L1210 in mice in doses of 20 (mg/kg) d^{-1} for the duration of 5 d, T/C of 168% was established (T/C%=ratio of median survival time, expressed as percent of untreated controls). The T/C ratio of the dipeptide **15** is 172%. When the tripeptide "Bialaphos" and phosphinothricin were subjected to parallel tests, no antitumour activity was registered. The relatively low toxicity of **14** (LD_{50}=428 mg/kg) and **15** (LD_{50}=523 mg/kg) promises very good results, should further studies in this direction be undertaken.

Experimental

General Notes: IR spectra, elemental analysis, and HPLC—on a Perkin-Elmer instruments; mp's—on a Kofler apparatus; TLC—silica-gel film "Merck". Solvents and reagents—"Aldrich", "Merck"; enzymes and buffers—"Sigma". The compounds obtained have been also proved by measuring the total and enzyme hydrolysate content. The IR-spectra and mp's of the known natural products have been compared with those of authentic samples.

Synthesis of Bialaphos *O,P*-Diethyl Ester (3). 2-Acet-

amido-4-(ethoxymethylphosphinyl)-L-butanoic acid (**1**) (23.52 g, 0.1 mol), L-alanyl-L-alanine ethyl ester (**2**) (19.02 g, 0.1 mol), and dicyclohexylcarbodiimide (22.69 g, 0.11 mol) are mixed in dry ethyl acetate (250 ml). The mixture is then stirred on a magnetic stirrer for 24 h in a closed Erlenmeier flask at room temperature. The *N,N'*-dicyclohexylurea is filtered out, 5—6 drops of 50% aqueous acetic acid are added and the filtrate is kept for 6 h at room temperature. After another filtration, the filtrate is washed with 5% aqueous solution of sodium carbonate-water-5% hydrochloric acid-water. It is then dried over anhydrous magnesium sulfate and distilled in vacuum to dryness. The obtained oil is dissolved in dry ethyl acetate and hexane is added until the solution becomes dull. After a prolonged storage in a refrigerator, the product is filtered out: γ-(Ethoxymethylphosphinyl)-L-α-acetamidobutyryl-L-alanyl-L-alanine ethyl ester (**3**): $C_{17}H_{32}N_3O_6P$; 33.69 g (83.1%); IR (KBr): 1745, 1650, 1520, 1305, 1200, 1110—970 cm^{-1}. Elemental analysis, % C, H, N, Calcd/Found: 50.36/50.48, 7.96/7.77, 10.36/10.77; mp 96—98 °C; total hydrolysate (after 12 hours' heating at 110 °C in 6 M HCl in a sealed ampule): phosphinothricin and alanine; enzyme hydrolysate (after 6 hours' stirring of 2 g substrate and 1 mg protease at pH 7.5 and 37 °C: phosphinothricin *P*-ethyl ester and alanine.

Isolation of Bialaphos *P*-Ethyl Ester 4.[2] The tripeptide **3** (20.54 g, 0.05 mol) is suspended in 200 ml 5% aqueous potassium hydroxide and the mixture is heated for 1 h at 40—50 °C. After cooling, acidification and extraction with diisopropyl ether, the organic extract is distilled in vacuum and the amorphous mass crystallized from dioxane/ethanol. The tripeptide **4** is obtained in an 84.6% yield (14.86 g).

Total hydrolysate-phosphinothricin, alanine; enzyme hydrolysate (protease)-phosphinothricin *P*-ethyl ester and alanine; satisfactory elemental analysis.

Isolation of Bialaphos (5).[1] The enzyme phosphodiesterase I (5 mg) is added to a buffer medium (500 ml, pH 8.8), containing the tripeptide **4** (20 g), at 37 °C. The mixture is stirred for 6 h at the same temperature. After dialysis, acidification and evaporation in vacuum (40—50 °C) to dryness, the solid mass is extracted with hot ethanol. The tripeptide **5** is isolated after cooling in a 90.6% yield. Its spectral data are identical with those of an authentic sample. Enzyme hydrolysis of Bialaphos with α-chymotrypsin: phosphinothricin (**6**) and alanine.

Synthesis of Pyrrobialaphos (9). The method described in Item 2 is employed, only now L-2-methyl-1,2-azaphospholidine-5-carboxylic acid 2-oxide (**7**) is used. The following product is isolated: *N*-/L-(2-methyl-1,2-azaphospholidine-5-carbonyl 2-oxide)/-L-alanyl-L-alanine ethyl ester (**8**): $C_{13}H_{24}N_3O_5P$; 29.10 g (87.3%); IR 1320 cm^{-1} (P-N); Calcd/Found (%): 46.84/46.59, 7.26/7.40, 12.61/12.55; mp 173—176 °C; total hydrolysate—phosphinothricin; enzyme hydrolysate (protease and α-chymotrypsin)-1,2-azaphospholidine analogue (pyrrophosphoshricin) (**7**) 20 g of the substrate, i.e. the protected tripeptide **8**, are well homogenized with 4—5 drops of "Tween-80" and added to a water-buffer medium (500 ml, pH 7.8), containing alkaline mesintericopeptidase (20 mg). Stirring is kept up for 3 h. The mixture is extracted with diisopropyl ether and the water layer is acidified and evaporated in vacuum to dryness. The residue is extracted with hot methanol to the product: *N*-/L-(2-methyl-1,2-azaphospholidine-5-carboxyl 2-oxide)/-L-alanyl-L-alanine (**9**): $C_{11}H_{20}N_3O_5P$; 21.16 g (69.3%); IR 3580—2920 cm^{-1} (COOH); Calcd/Found (%): 43.28/43.44, 6.60/6.51, 13.76/13.39; total hydrolysate—phosphinothricin, alanine; "mild" mineral hydrolysis (1 M HCl, 30 min., 50 °C)—Bialaphos (**5**); enzyme hydrolysis (α-chymotrypsin)-1,2-azaphospholidine (**7**), alanine; the product melts with decomposition at about 220 °C.

Synthesis of the Ester Amide 11. A mixture of L-phosphinothricin ethyl ester (**10**) (20.92 g, 0.1 mol) and *S*-ethyl trifluorothioacetate (24.71 g, 0.15 mol) in 100 ml 1 M NaOH and 400 ml borate buffer solution is shaken for 8 h on a mechanical shaker at room temperature. It is then acidified with 1M HCl, extracted with diisopropyl ether, dried over anhydrous magnesium sulfate, and distilled in vacuum to dryness. The following product is recrystallized from ethanol: L-2-trifluoroacetamido-4-(hydroxymethyl)butanoic acid ethyl ester **11**: $C_9H_{15}F_3NO_5P$; 27.56 g (90.3%); IR (KBr): 2860—2540, 2340—2100, 1740, 1650, 1520, 1310, 1170, 930, 840 cm^{-1}; Calcd/Found (%): 35.42/35.27, 4.95/5.01, 4.59/4.67; mp 163—165 °C; $[\alpha]_D^{22}$ +43.7°, (*c* 0.1, MeOH), R_f 0.43 (DMF: dioxane: MeOH=9:2:1).

Synthesis of the Phospha^C-peptide 14. A mixture of L-phosphinothricin (**11**) (30.52g, 0.1 mol), L-alanyl-L-alanine ethyl ester (**2**) (19.02 g, 0.1 mol) and dicyclohexylcarbodiimide (22.69 g, 0.11 mol) is stirred for 12 h in dry ethyl acetate (250 ml) at room temperature. This mixture is then filtered and the filtrate is washed with 5% aqueous solution of sodium carbonate, then with water, 0.5% aqueous solution of oxalic acid, again with water, and followed by drying over anhydrous magnesium sulfate and distillation in vacuum to dryness. The residue is dissolved in dry ethyl acetate and cooled. Hexane is added until the solution becomes dull. Crystallization is initiated by rubbing the flask walls with a glass stick and then leaving the solution in a refrigerator at −5 °C for prolonged period the following product is then filtered out: *N*-/L-3-ethoxycarbonyl-3-(trifluoroacetamido)-propyl/methylphosphinyl/-L-alanyl-L-alanine ethyl ester (**12**): $C_{17}H_{29}F_3N_3O_7P$; 35.56 g (74.8%); IR 1750, 1640, 1520, 1320—1270, 1189—940, 810, 720, 640, 560 cm^{-1}; Calcd/Found (%): 42.95/43.18, 6.18/6.01, 8.84/8.20; total hydrolysate—phosphinothricin, alanine; mp 93—95 °C.

A well homogenized mixture of the tripeptide **12** (47.54 g, 0.1 mol) and 5—6 drops of "Tween-80" is added to an aqueous buffer medium (800 ml, pH 7.8), which has been previously tempered at 30 °C and which contains 20 mg alkaline mesintericopeptidase. Stirring is kept up for 3 h at the same temperature (until a ninhydrin-positive detection occurs), the mixture is extracted with diisopropyl ether, acidified to pH 6.0, and evaporated in vacuum to dryness. The solid residue is extracted with boiling ethanol to the product: *N*-/L-3-carboxy-3-(trifluoroacetamido)propyl/methylphosphinyl/-L-alanyl-L-alanine (**13**): $C_{13}H_{21}F_3N_3O_7P$; 34.09 g (81.3%); IR 3200—2600 cm^{-1}; Calcd/Found (%): 34.24/37.56, 5.05/4.88, 10.02/10.13; total hydrolysate—phosphinothricin, alanine; mp 188—191 °C.

The tripeptide **13** (18.63 g, 0.05 mol) is stirred for 12 h at room temperature in a mixture of dioxane (200 ml) and aqueous ammonia, pH 9.6. After evaporation in vacuum to dryness (50 °C/18 mmHg) the reaction residue is passed through a silica-gel column, which results in the separation of phosphinothricin, the dipeptide alanylalanine and the tripeptide: *N*-/(L-3-carboxy-3-aminopropyl)methylphosphinyl/-L-alanyl-L-alanine (**14**): $C_{11}H_{22}N_3O_6P$; 6.24 g (38.6%); IR 3400—2860, 2340—2100, 1750, 1650, 1520, 1340, 1305, 1170, 930, 845, 620, 510 cm^{-1}; Calcd/Found (%): 40.87/40.90

6.86/6.49, 13.00/13.11; total hydrolysate—phosphinothricin, alanine; mp 216—219 °C (decomp).

Synthesis of the Phospha^{C}-dipeptide 15. The tripeptide **14** (3233 g, 0.1 mol) is stirred for 6 h at 25 °C in 800 ml aqueous buffer medium (pH 7.8), containing α-chymotrypsin (10 mg). After acidification (pH 6.0), the reaction mixture is evaporated in vacuum to dryness and the resultant organic mass is treated with hot dioxane to give: *N*-/(L-3-carboxy-3-aminopropyl)methylphosphinyl/-L-alanine (**15**): $C_8H_{17}N_2O_5P$; 24.01 g (95.2%); IR 3360—2840, 2320—2100, 1750, 1650, 1525, 1340, 11300,1170, 920, 840, 620, 515 cm^{-1}; Calcd/Found (%): 38.10/38.43, 6.79/6.62, 11.11/11.17; mp approx. 200 °C (decomp).

References

1) E. Bayer, K. Gugel, K. Högele, H. Hagenmeier, S. Jessipow, W. König, and H. Zähner, *Helv. Chem. Acta*, **55**, 224 (1972).

2) Y. Ogawa, H. Yoshida, S. Inoue, and T. Niida, *Meiji Seika Kenkyu Nempo*, **1973**, 60.

3) I. Natchev, *Bull. Chem. Soc. Jpn.*, **61**, 3699 (1988).

4) K. Yamauchi, M. Kinoshita, and M. Imoto, *Bull. Chem. Soc. Jpn.*, **45**, 2528 (1972).

5) M. Hariharan, S. Chaverek, and A. Martell, *Synth. Commun.*, **3**, 375 (1973).

6) N. Tarusova, I. Gandurina, Yu. Zhukov, G. Yakovleva, and R. Khomutov, *Izv. Akad. Nauk USSR, Ser. Khim.*, **1979**, 1596.

7) K. Issleib, A. Balszuweit, and K. Dopfer, DDR Patent 212739; *Chem. Abstr.*, **102**, 167168x (1985).

8) E. Schallenberg and M. Calvin, *J. Am. Chem. Soc.*, **77**, 2779 (1955).

 © 1988 The Chemical Society of Japan Bull. Chem. Soc. Jpn., 61, 3711—3715 (1988)

Organophosphorus Analogues and Derivatives of the Natural L-Amino Carboxylic Acids and Peptides. III. Synthesis and Enzyme-Substrate Interactions of D-, DL-, and L-5-Dihydroxyphosphinyl-3,4-didehydronorvaline and Their Cyclic Analogues and Derivatives

Ivan A. NATCHEV
Research Centre "Konstrukcionni Polymeri", 5-003 Gara Iskar, 1528 Sofia, Bulgaria
(Received April 28, 1987)

The unusual natural amino acid phosphorus containing didehydronorvaline (**5**) has been synthesized by consecutive treatment of the 4-bromo-2-butenal (**1**) with potassium cyanide and ammonium carbonate to the hydantoin (**2**), converted into the organophosphorus derivative **3**, followed by enzyme-catalyzed hydrolysis of the diethoxyphosphinyl group to the phosphonic acid **4**, and hydrolysis. The tetrahydro-1,2-azaphosphorine (**8**) and the protected didehydronorvaline derivatives **6**, **7**, **9**, and **10**, have been synthesized.

The tripeptide antibiotics Plumbemicin A: *N*-(*N*-L-alanyl-L-α-aspartyl)-3,4-didehydro-5-phosphono-D-norvaline, and Plumbemicin B: *N*-(N^2-L-alanyl-L-asparaginyl)-3,4-didehydro-5-phosphono-D-norvaline, have been isolated from *Streptomices plumbens strains* by Japanese researchers[1,2] and their biological activity has been studied.[3] To this moment, no information is available in the scientific and patent literature about the synthesis of the two tripeptides and of the unusual allylphosphonic acid **5**. The latter has been isolated and identified[2] by hydrolysis of the tripeptides. It is our intention, in two consecutive papers, to demonstrate the possibilities for their synthesis.

4-Bromo-2-butenal (**1**)[4] was chosen as the starting material for the synthesis of norvaline (**5**). Upon condensation with potassium cyanide/ammonium carbonate under the conditions of the Bucherer-Bergs reaction, the hydantoin (**2**) was obtained in a satisfactory yield (85%).

The next step was the Arbuzov reaction with the bromo-derivative **2** and triethyl phosphite. Despite the fact that a number of variations were introduced into the working conditions, the yield of the organophosphorus product never exceeded 50—55%. This could be explained with the rather "hard" conditions (3 h in boiling xylene) and with the sensitivity of the double bond. Varlet et al.[5] have synthesized the very similar structural analogue of the hydantoin (**3**), which has a saturated side chain, by using the Bucherer-Bergs 4-(diethoxyphosphinyl) butanal in their reaction. We employed an alternative approach, i.e. treatment of the acetal of 4-bromo-2-butenal, $BrCH_2CH{=}CHCH(OR)_2$ with triethyl phosphite, releasing the aldehyde and a subsequent treatment with potassium cyanide/ammonium carbonate. The yields were satisfactory and the approach will be discussed separately, accompanied with a demonstration of the catalytic activity of the enzyme α-chymotrypsin and urease towards the hydantoin (**3**) and its hydrolysis product.

We failed to achieve selective mineral hydrolysis of the diethoxyphosphinyl groups and the hydantoin ring. Under the markedly "hard" hydrolysis conditions, no individual products were obtained.

When the phosphonic diester **3** was treated with the enzyme phosphodiesterase I under conditions, described in our previous papers,[6] the free phosphonic acid **4** was isolated in a practically quantitative yield.

Patent data[7] report that 5-substituted hydantoins can be hydrolyzed by enzyme-catalyzed hydrolysis with dihydropyrimidinase to the corresponding carbamoyl derivatives. When the same enzyme was applied to the hydantoin (**3**), no enzyme-substrate interaction was observed. Furthermore, when the free phosphonic acid **4** was used as substrate, complete inhibition of the enzyme occurred.

To hydrolyze the hydantoin (**4**), we employed the method of Hiroi et al.[8] for preliminary N^3-tosylation, followed by mild mineral hydrolysis. It was found that isolation of the tosyl derivatives was unnecessary (cf. Experimental). Hydrolysis afforded the norvaline (**5**) as a racemic mixture in a yield of approx. 60%. Its spectral data were identical with those of an authentic sample.

It our laboratory, we succeeded in obtaining the same product **5**, as well as the tetrahydro-1,2-azaphosphorine analogue discussed below, by a four-component isonitrile condensation after the reaction of Ugi and a modified three-component condensation after the same reaction. This approach will be discussed separately.

With a view to obtaining optically active antipodes of 3,4-didehydronorvaline (**5**) and such derivatives as would be suitable for peptide synthesis, treatment was carried out with 1 equiv thionyl chloride in a medium of ethanol and in the presence of *N*,*N*-dimethylformamide in catalytic quantities. Thionyl chloride was gradually added to a cooled suspension of didehydronorvaline (**5**) in ethanol, which was continuously stirred. An argon, or nitrogen, current was passed through the reaction mixture, in order to carry off the released gases (sulfur dioxide and hydrogen chloride). The reaction mixture was then quickly brought to the boil,

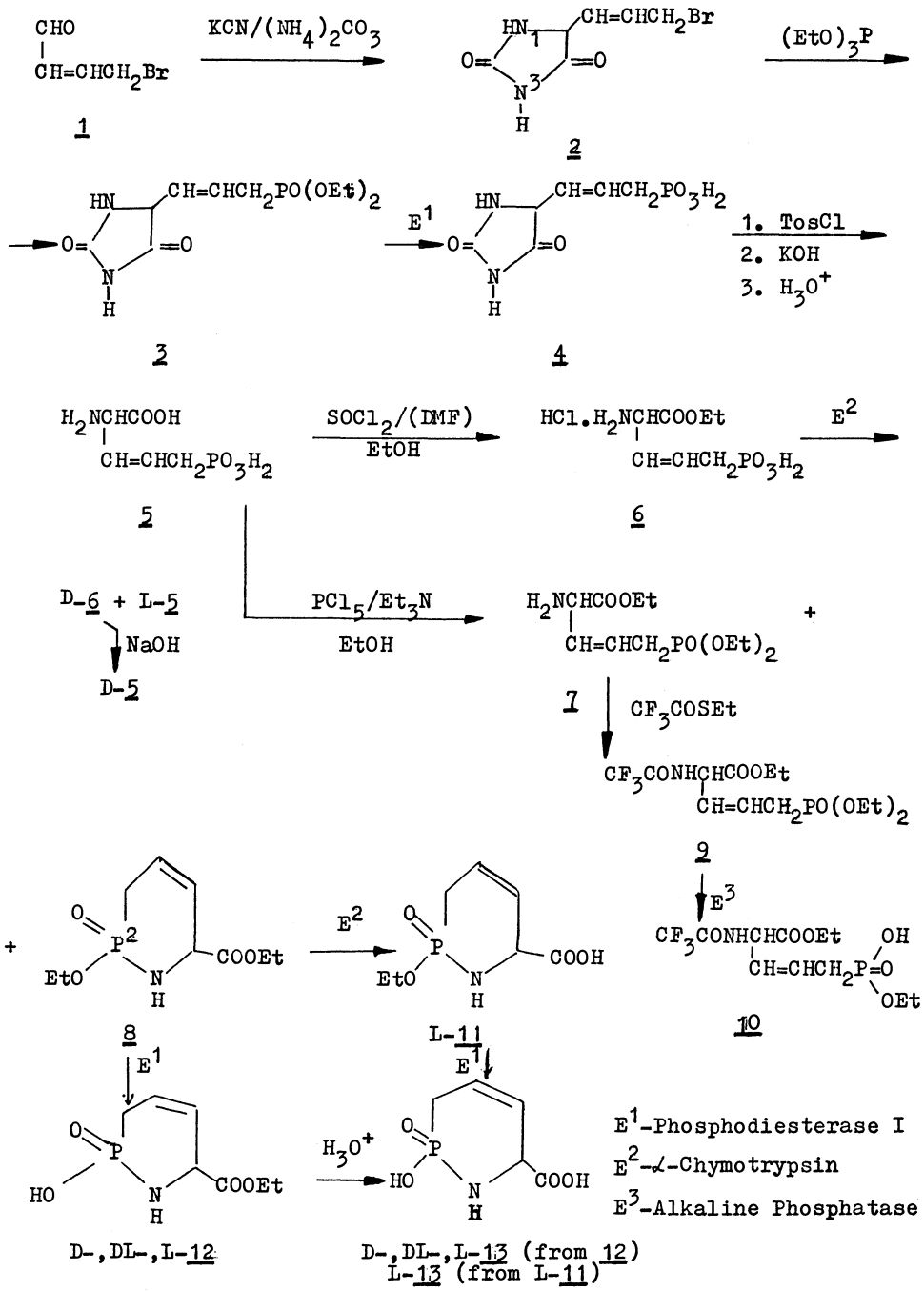

Scheme 1.

which was accompanied by dissolution and an intense release of gases, carried out of the reaction mixture by the argon (nitrogen). When a slight vacuum was applied to the reaction vessel and the released gases were collected in absorbers, it was found that sulfur dioxide and hydrogen chloride had been removed almost quantitatively, which clearly indicated that they could not have reacted with the starting material, or with the reaction product. Cooling resulted in spontaneously precipitation of the ethyl ester hydrochloride of the 3,4-didehydro-DL-norvaline (**6**), which was isolated in a yield of about 90%.

The separation of optically active antipodes was achieved by enzyme-catalyzed hydrolysis with α-chymotrypsin. When the method in reference[6] was used, the enzyme catalyzed hydrolysis of only the L-form of the racemic mixture DL-**6** to the 3,4-didehydro-L-norvaline L-**5**, while the D-form D-**6** remained unchanged. The D-form-**5**, free from its ester protection, was easily obtained by mineral hydrolysis of the ester D-**6**.

Norvaline with protected phosphono and carboxyl functions was obtained by treatment of D-, DL- and L-didehydronorvaline (**5**) with phosphorus pentachloride. Without isolating the rather unstable chlorinated products, we subjected them to treatment with

ethanol, with triethylamine as the condensation agent. As it was the case with our previous studies of phosphinothricin,[6] here, analogously, the interaction led to two products: triethyl ester **7** as the major one (yield of about 60%), and the ethyl ester of tetrahydro-1,2-azaphosphorinecarboxylic acid (**8**) (yield approx. 10%). All our attempts to increase the yield of **8** by using alternative synthetic methods were unsuccessful and even protection of the reactive double bond brought no results.

We succeeded in obtaining a completely protected norvaline by treating the triester **7** with *S*-ethyl trifluorothioacetate by the method in reference.[6] Thus, the *N*-trifluoroacetylated triester of the didehydronorvaline (**9**) was isolated in a yield of about 80%.

The enzyme alkaline phosphatase is very suitable when strict selectivity is needed in the enzyme-catalyzed hydrolysis of the diethoxyphosphinyl groups. When taken at its pH optimum (10.4) and at 37 °C, the enzyme enhances the hydrolysis of only one of the two ethoxyl groups to the phosphonic monoester **10**. The enzyme-substrate interaction was carried out under conditions which have been empirically proved effective in our laboratory: 20 g substrate, about 5 mg enzyme, 6 h. Of course, larger or smaller amounts of substrate can be used, provided that the quantitative ratio substrate/enzyme is kept within the prescribed limits. When one and the same enzyme is used repeatedly, or when larger amounts of substrate are involved, it is better to spread the enzyme on a polymer carrier, as for instance the polyacrylamide gel "Sigma", which is very good for the purpose. In this case, the quantity of the enzyme should be twice as much (10—15 mg per 20 g substrate) and it can be regenerated simply by centrifugation.

We already observed that the optical form of the substrate is quite independent of the catalytic action of phosphodiesterase I. The same was found to be also true about alkaline phosphatase. This enzyme, however, catalyzes both the D- and the L-forms of 5-(diethoxyphosphinyl)-3,4-didehydronorvaline.

When we tried to hydrolyze the ethoxy carbonyl and ethoxyphosphinyl groups of tetrahydro-1,2-azaphosphorine (**8**) by treatment with mineral acids and bases, it turned out that the cyclic phosphinic amide group was the most easily hydrolyzable. To overcome this problem, which occurred also with the cyclic analogue of phosphinothricin,[6] again we used the enzyme approach. The ethoxycarbonyl derivative **8**, as substrate of the enzyme α-chymotrypsin, affords the free acid L-**11** in a practically quantitative yield. As expected, the D-form-D-**8** does not participate in the interaction.

We already discussed some particular characteristics of the enzyme phosphodiesterase I. It is capable of catalyzing the substartes, irrespective of the type (D- or L-) of their optical activity. Thus, with the phosphonamidic ester (**8**) as substrate, the free acids D-, DL-, and L-**12** were isolated in practically quantitative yields. The free carbonyl group of the substrate L-**11** with the enzyme phosphodiesterase I afforded the free tetrahydro-1,2-azaphosphorine L-**13**, again with a quantitative yield.

Alkaline phosphatase does not have any catalytic action on the substrates **8**, **11**, **12**, and **13**.

It seems that the presence of a free hydroxyphosphinyl group, $O=P(HO)<$, increases, to a certain extent, the stability of the cyclic PO-NH bond. Thus, mineral hydrolysis of the esters D-, DL-, and L-**13**, although in yields of about 40%.

Studies on the physiological activity of the newly-synthesized products, as well as of the natural didehydro-D-norvaline (**5**), are under way and will be published soon.

Experimental

General Notes: IR-spectra, elemental analysis, optical activity and HPLC—on a Perkin-Elmer instrument; ^{1}H NMR-spectra—on Jouel-100 MHz; mass-spectra—on LKB-900; TLC—silica-gel film "Merck"; reagents and solvents—from "Aldrich" and "Merck"; enzymes and buffers—from "Sigma"; α-chymotrypsin—from "Pharmachim", Bulgaria. Special credit goes to Dr. N. Stambolieva of the Institute of Organic Chemistry, Bulgarian Academy of Sciences, for kindly supplying the mesintericopeptidase. The IR-spectra and mixed mp's of known compounds have been compared with those of authentic samples.

Synthesis of the Hydantoin (2). A mixture of 4-bromo-2-butenal (**1**) (14.90 g, 0.1 mol, potassium cyanide (7.81 g, 0.12 mol) and ammonium carbonate (14.41 g, 0.15 mol) is heated for 6 h at 55—60 °C in 150 ml 50% aqueous ethanol. A crystalline product is gradually released. After filtration, the filtrate is placed in a ventilation cupboard and strong draught is applied. The filtrate is then carefully acidified (the unreacted potassium cyanide releases hydrogen cyanide). After cooling, an additional quantity of the product is filtered out: 5-(3-bromo-1-propenyl)-2,4-imidazolidinedione (**2**): $C_6H_7BrN_2O_2$; 18.71 g (85.4%); IR (KBr, cm^{-1}): 3320—2860, 1750—1680, 860, 620; ^{1}H NMR ($CDCl_3$, TMS): δ=4.20 (3H, m, CHCO and CH_2Br), 6.20 and 6.76 (2H, m, C<u>H</u>=C<u>H</u>), 7.52 and 9.61 (2H, br.,NHX2); MS, *m/z* Calcd/Found: 219.04/219; elemental analysis, % C, H, N-Calcd/Found: 32.90/33.11, 3.22/3.46, 12.79/13.02; mp 183—186 °C (EtOH). (All analytical data to follow are given in the same order.)

Synthesis of the Diester 3. A mixture of the hydantoin (**2**) (21.90 g, 0.1 mol) and triethyl phosphite (19.94 g, 0.12 mol) is boiled for 3 h in 500 ml dry xylene in an ambience of dry argon, or nitrogen. The volatile components are evaporated in vacuum and the oily residue is passed first through florisil and then through a silica-gel column: 3-(2,5-dioxo-4-imidazolidinyl)-2-propenylphosphonic acid diethyl ester (**3**): $C_{10}H_{17}N_2O_5P$; 14.84 g (53.7%); IR (cm^{-1}) 3350—3200, 3030, 1750—1690, 1300, 1255, 1110—980, 865, 630; ^{1}H NMR (DMSO-d_6): δ=1.18 and 1.36 (6H, t, J=7 Hz, $OCH_2C\underline{H}_3$X2), 2.80 (2H, m, PCH_2), 3.50 and 3.62 (4H, q, $OC\underline{H}_2CH_3$X2), 4.18 (1H, d, J=8Hz, CHN), 5.62 and 6.12 (2H, m, C<u>H</u>=C<u>H</u>), 7.52 and 9.60 (2H, br., NHX2); MS, *m/z* Calcd/Found: 276.31/276; % C, H, N Calcd/Found: 43.48/43.56, 6.70/6.93,

10.14/10.16; mp 183—186 °C; R_f: 0.33 ($CHCl_3$: MeOH=9 : 1) and 0.83 (*n*-BuOH : AcOH : H_2O=9 : 1 : 1).

Enzyme Hydrolysis of the Phosphonic Diester 3. A homogeneous mixture of the substrate **3** (27.63 g, 0.1 mol) and the emulgator "Tween-80" is added to an aqueous buffer solution (500 ml, pH 8.8) of phosphodiesterase I (7 mg), tempered at 37 °C. Stirring is kept up for 6 h at the same temperature. After acidification, condensation and cooling, the following product is filtered out: 3-(2,5-dioxo-4-imidazolidinyl)-2-propenylphosphonic acid (**4**): $C_6H_7N_2O_2P$; 21.24 g (97.4%); IR (cm^{-1}) 2860—2430 (PO_3H_2); ^1H NMR (D_2O-NaOD): δ=2.98 (2H, m, PCH_2), 5.70 and 6.21 (2H, m, CH=CH-); MS *m/z* Calcd/Found: 218.11/218; % C, H, N Calcd/Found: 33.04/32.84, 3.24/3.56, 12.84/12.96; mp about 250 °C (decomp); R_f: 0.42 (*n*-BuOH : AcOH : H_2O=9 : 1 : 1).

Synthesis of Didehydronorvaline (5).[2] *p*-Toluenesulfonyl chloride (20.98 g, 0.11 mol) is gradually added for 1 h to 300 ml 80% aqueous ethanol, containing sodium hydroxide (10 mg) and the hydantoin (**4**) (21.81 g, 0.1 mol). After 30 min the reaction mixture is evaporated in vacuum to dryness, 20 g potassium hydroxide in 110 ml water are added and the mixture is heated for 30 min in a water bath. After acidification, heating for 30 min and elution through Amberlite IR-120 resin with 0.1 M (1 M=1 mol dm^{-3}) HCl, the following product is isolated: 3,4-didehydro-5-phosphono-DL-norvaline (**5**): $C_5H_{10}NO_5P$; 11.45 g (58.7%); spectral data coincided with those of an authentic sample; MS *m/z* Calcd/Found: 195.11/195; % C, H, N Calcd/Found: 30.78/31.01, 5.17/5.02, 41.00/39.78.

Synthesis of the Ethyl Ester 6. Thionyl chloride (13.09 g, 0.11 mol) is added dropwise to a continuously stirred suspension, cooled to 5 °C, of didehydronorvaline (**5**) (19.81 g, 0.1 mol) in 200 ml ethanol, containing 5 ml *N,N*-dimethylformamide. A swift current of dry argon, or nitrogen, is simultaneously passed through the reaction mixture. The cooling bath is replaced with a warmed-up heater. Gasses are removed from the system by a continuous flow of inert gas. After 5 min of boiling (highly-effective condenser), complete dissolution is observed. The product crystallizes after cooling: 3,4-didehydro-5-phosphono-DL-norvaline ethyl ester hydrochloride (**6**): $C_7H_{14}NO_5P \cdot HCl$; 20.31 g (91.0%); IR (cm^{-1}) 1750 (CO), 1550 (NH_3^+);% C, H, N Calcd/Found: 36.67/36.99, 6.32/6.11, 6.28/6.35; mp 210 °C (decomp).

Enzyme Hydrolysis and Separation of Optical Antipodes of the Ester 6. A mixture of the ester **6** (22.31 g, 0.1 mol) and α-chymotrypsin (6 mg) is stirred for 6 h at 25 °C in an aqueous buffer medium (pH 7.8, 500 ml). After acidification, evaporation to dryness and extraction with boiling ethanol, the following products are fractionally isolated: 3,4-didehydro-5-phoshono-D-norvaline ethyl ester hydrochloride D-**6**: $C_7H_{14}NO_5P \cdot HCl$; 9.00 g (96.4%); spectral data coicide with those of DL-**6**; mp: approx. 220 °C (decomposition); $[\alpha]_D^{20}$ +55.3°, (*c* 0.1, MeOH): 3,4-didehydro-5-phosphono-L-norvaline (L-**5**): $C_5H_{10}NO_5P$; 9.47 g (97.1%); spectral data identical with those of DL-**5**; mp 188—190 °C; $[\alpha]_D^{20}$ −53.3 (*c* 1, H_2O).

Hydrolysis of the Ester D-6. The ester D-**6** (22.32 g, 0.1 mol) is heated for 30 min at 40—45 °C in aqueous NaOH (2 M, 200 ml). After acidification, evaporation in vacuum to dryness and crystallization from ethanol, the following product is isolated: 3,4-didehydro-5-phosphono-D-norvaline (D-**5**): $C_5H_{10}NO_5P$; 17.57 g (90.1%); spectral data identical with those of D- and DL-**5**; $[\alpha]_D^{20}$ −53.3° (lit,[2] +51.4°), (*c* 1, H_2O).

Synthesis of the Triester 7 and Tetrahydro-1,2-azaphosphorine (8). Portions of phosphorus pentachloride (68.72 g, 0.33 mol) in 200 ml dry tetrachloromethane are added for 1 h at 80 °C to 300 ml dry tetrachloromethane, containing D-, DL-, or L-didehydronorvaline (**5**) (19.51 g, 0.1 mol). A current of dry argon, or nitrogen, is simultaneously passed through the suspension. After 30 min, the reaction mixture is evaporated in vacuum to dryness and mixed, first with 500 ml absolute ethanol, and then with 50 ml triethylamine. It is then boiled for 30 min, filtered and evaporated in vacuum to dryness. The residue is dissolved in dry chloroform and saturated with dry hydrogen chloride. The resultant residue is filtered and recrystallized from ethanol: 3,4-didehydro-5-diethoxyphosphinyl-(D-, DL-, L-)norvaline ethyl ester hydrochloride (**7**): $C_{11}H_{22}NO_5P \cdot HCl$; 18.72 g (59.3%); IR ($cm^{-1}$) 3020, 1740, 1525, 1255, 1110—975; ^1H NMR ($CDCl_3$, free base) δ=1.2—1.9 (9H, m, CH_3×2), 2.22 (2H, s, NH_2), 2.80 (2H, m, PCH_2), 3.20—3.60 (6H, m, OCH_2×3), 4.82 (1H, d, *J*=7 Hz, CHN), 578 and 6.20 (2H, m, CH=CH); MS *m/z* Calcd/Found 279.30/279; % C, H, N Calcd/Found: 41.85/42.01, 7.34/7.12, 4.44/4.69; R_f 0.55 (DMF: $CHCl_3$: MeOH=5 : 1 : 2); mp D-, DL-, D-: 140—146 °C (decomp); $[\alpha]_D^{20}$ +59.3°, (*c* 0.1, MeOH).

The filtrate, left after the filtration of the triester **7**, is evaporated in vacuum and eluted in a silica-gel column (eluent chloroform:hexane=5:2). Fractions of 50 ml each are collected. The fourth, fifth, and sixth fractions are combined, evaporated and passed through the columun: D-, DL-, L-2-ethoxy-6-ethoxycarbonyl-1,2,3,6-tetrahydro-1,2-azaphosphorine-2-oxide (**8**): $C_9H_{16}NO_4P$; 2.61 g (11.2%); IR (cm^{-1}) 1760, 1390, 1250, 920, 840; ^1H NMR ($CDCl_3$): δ=1.18 and 1.32 (6H, t, OCH_2CH_3×2), 2.46 (2H, m, PCH_2), 3.4—3.9 (4H, m, OCH_2CH_3×2), 4.62 (1H, d, *J*=8 Hz, CHCO), 5.82 and 6.35 (2H, m, CH=CH); MS *m/z* Calcd/Found: 233.20/233; % C, H, N Calcd/Found: 46.35/46.28, 6.91/7.07, 6.01/5.79; R_f: 0.72 ($CHCl_3$: *n*-C_6H_{14}=5 : 2); mp D-, DL-, L-: 86—90 °C; $[\alpha]_D^{20}$ +78.2° and −77.6°, (*c* 0.1, MeOH).

Synthesis of *N*-Trifluoroacetyl-(D-, DL-, L-)didehydronorvaline (9). The triester **5** (D-, DL-, or L-) (19.51 g, 0.1 mol) and *S*-ethyl trifluorothioacetate (24.72 g, 0.16 mol) are shaken for 8 h at room temperature in 100 ml 2 M NaOH, 600 ml borate buffer and 500 ml chloroform. The layers are separated and the aqueous layer acidified and extracted with chloroform (3×20 ml) and the combined organic extracts are dried over anhydrous magnesium sulfate and distilled in vacuum to dryness. The product is isolated as a noncrystallizing oil. For analytical purposes, purification is carried out by passing through a silica-gel column (eluent dioxane: chloroform=5 : 3): *N*-trifluoroacetyl-3,4-didehydro-5-diethoxyphosphinyl-(D-, DL-, L-)norvaline ethyl ester (**9**): $C_{13}H_{21}F_3NO_6P$; 28.87 g (average for the three forms, 79.6%); IR (film, cm^{-1}) 1760, 1520, 1210, 1110—860; % C, H, N Calcd/Found: 41.61/41.33, 5.64/5.81, 3.73/4.12; R_f: 0.65 (dioxane : chloroform=6 : 1); mp decomposes upon attempts at distillation; $[\alpha]_D^{20}$ +72.3° and −70.6°, (*c* 0.1, MeOH).

Enzyme Hydrolysis of the Didehydronorvaline (9). A homogeneous mixture of the ester **9** (18.77 g, 0.05 mol) and emulgator "Tween-80" is added to a buffer medium (pH 10.4, 800 ml), containing alkaline phosphatase (10 mg on agarose) and tempered at 37 °C. The mixture is stirred for 6 h and the enzyme is removed. The mixture is acidified, evaporated in vacuum to dryness and extracted with chloroform. The organic extract is dried over anhydrous magne-

sium sulfate and distilled in vacuum to dryness. The oily residue slowly crystallizes after a prolonged period in a refrigerator on hexane: *N*-trifluoroacetyl-3,4-didehydro-5-ethoxyhydroxyphosphinyl-(D-, DL-, L-)norvaline ethyl ester (**10**): $C_{11}H_{17}F_3NO_6P$; 16.86 g, (97.1%); IR (cm^{-1}) 2860—2420, 1760, 1540, 1260, 1110—840; ^1H NMR ($CDCl_3$): δ=1.13 and 1.30 (6H, t, $OCH_2C\underline{H}_3\times2$), 2.95 (2H, m, PCH_2), 4.1—4.4 (5H, m, $OC\underline{H}_2CH_3\times2$, C<u>H</u>NH), 5.38 (1H, m, CH=CHCH$_2$), 6.30 (2H, m, CH=C<u>H</u>CH$_2$, N<u>H</u>), 10.2—10.6 (1H, br., POOH); MS *m/z* Calcd/Found: 247.23/247; % C, H, N Calcd/Found: 38.05/34.44, 4.93/4.88, 4.03/3.96; R_f: 0.46 (dioxane : chloroform=6 : 1); $[\alpha]_D^{20}$ +76.2° and −73.1°, (*c* 0.1, MeOH); mp D-, DL-, L-: 95—96 °C (decomp).

Enzyme-Substrate Hydrolysis of the Ester 8: Each of the D-, DL-, and L-**8** substrates (23.32 g, 0.1 mol) is subjected to hydrolysis by the above method and using the enzymes α-chymotrypsin and phosphodiesterase I. The substrate L-**8** and α-chymotrypsin (6 mg) afford the product L-**1**, whereas D-, DL-, and L-**8** plus phosphodiesterase I (5 mg) afford the products D-, DL-, and L-**12**: L-2-ethoxy-1,2,3,6-tetrahydro-1,2-azaphosphorine-6-carboxylic acid 2-oxide L-**11**: $C_7H_{12}NO_4P$; 18.94 g (92.3%); IR (cm^{-1}) 3480—3200, 3025, 1760, 1390, 1250, 1110—960, 870, 640; ^1H NMR (DMSO-d_6) δ=1.21 (3H, t, *J*=7 Hz, $OCH_2C\underline{H}_3$), 2.36 (2H, m, PCH_2), 3.43 (2H, q, $OC\underline{H}_2CH_3$), 4.51 (1H, d, *J*=8 Hz, CHCO), 5.68 and 6.33 (2H, m, CH=CH), 10.4—11.0 (1H, br., COOH); MS *m/z* Calcd/Found: 205.15/205; % C, H, N Calcd/Found: 40.98/41.16, 5.90/5.71, 6.83/6.92; R_f: 0.72 (*n*-BuOH : 25%NH_3aq=8 : 1); mp 183—185 °C (decomp); $[\alpha]_D^{20}$ −82.6°, (*c* 0.1, MeOH), D-, DL-, L-6-ethoxycarbonyl-hydroxy-1,2,3,6-tetrahydro-1,2-azaphosphorine 2-oxide-D-, DL-, L-**12**: $C_7H_{12}NO_4P$; 19.92 g (97.1%); 2840—2420 (P-OH); MS *m/z* Calcd/Found: 205.15/205; % C, H, N Calcd/Found: 40.98/40.73, 5.90/6.11, 6.83/6.66; R_f: 0.52 (dioxane : chloroform=5 : 2); mp D-, DL-, L-: 118—121 °C (decomp); $[\alpha]_D^{20}$ +80.3° and −81.6°, (*c* 0.1, MeOH).

Enzyme-Substrate Hydrolysis of the Ester L-11. The above method for enzyme-catalyzed hydrolysis is used with phosphodiesterase I and the ester L-**11** (20.52 g, 0.1 mol) as substrate. The following product is isolated: L-2-hydroxy-1,2,3,6-tetrahydro-1,2-azaphosphorine-6-carboxylic acid 2-oxide L-**13**: $C_5H_8NO_4P$; 17.39 g (98.2%); IR (cm^{-1}) 3530—3200, 2840—2470, 1760, 1400, 1255, 870, 630; ^1H NMR (D_2O-NaOD): δ=2.31 (2H, m, PCH_2), 4.52 (1H, d, *J*=8 Hz, CHCO), 5.76 and 6.38 (2H, m, C<u>H</u>=C<u>H</u>), and three exchangeable protons — N<u>H</u>, PO<u>H</u>, and COOH; MS *m/z* Calcd/Found: 171.11/171; % C, H, N Calcd/Found: 33.91/34.11, 4.56/4.38, 7.91/8.06; R_f: 0.75 (*n*-BuOH : AcOH : H_2O= 9 : 1 : 1); mp approx. 230 °C (decomp); $[\alpha]_D^{20}$ −61.2° (*c* 0.1, 1 M NaOH).

Alkaline Hydrolysis of the Ester D-, DL-, and L-12. Each of the esters D-, DL-, and L-**12** (20.51 g, 0.1 mol) is stirred for 30 min at 40—45 °C in 2 M MaOH (150 ml). The reaction mixture is acidified, evaporated in vaccum to dryness and extracted with boiling ethanol. The esters D-, DL-, and L-**6** and D-, DL-, and L-**13**, respectively, are fractionally isolated in an average yield of 6.60 g (38.6%). Their spectral data are identical with those of the product L-**13**: mp D-, DL-, and L-: approx. 230 °C (decomp) $[\alpha]_D^{20}$ +59.8°, (*c* 0.1, 1 M NaOH).

References

1) T. Boku, A. Hirota, and H. Sakai, Japan Kokai 77-108904.

2) B. Park, A. Hirota, and H. Sakai, *Agr. Biol. Chem.*, **40**, 1905 (1976).

3) H. Diddens, M. Dorgerleh, and H. Zocher, *J. Antibiot.* **32**, 87 (1979).

4) M. Berenguer, J. Castella, J. Fernandez, and R. Galard, *Tetrahedron Lett.*, **1971**, 493.

5) J. Varlet, G. Fabre, F. Sanveur, N. Collignon, and Ph. Savignac, *Tetrahedron*, **37**, 1377 (1981).

6) I. Natchev, *Bull. Chem. Soc. Jpn.*, **61**, 3705 (1988).

7) Ger. Offen 2422737; *Chem. Abstr.*, **82**, P: 73473.

8) K. Hiroi, K. Achiwa, and S. Yamada, *Chem Pharm. Bull.*, **16**, 444 (1968).

 © 1988 The Chemical Society of Japan Bull. Chem. Soc. Jpn., 61, 3717—3722 (1988)

Mechanistic Study of the Oxidation of Substituted Benzylamines by *N*-Bromoacetamide

Kalyan K. BANERJI
Department of Chemistry, University of Jodhpur, Jodhpur 342 001, India
(Received October 22, 1987)

The oxidation of ortho-, meta-, and para-substituted benzylamines by *N*-bromoacetamide (NBA), to the corresponding benzaldehydes, is first order with respect to NBA and the amine. The pH dependence of the reaction rate suggests that the unprotonated benzylamine is the reductant. There is no effect of added acetamide. NBA itself has been postulated as the reactive oxidizing species. The oxidation of benzylamine-α,α-d_2 exhibited a substantial primary kinetic isotope effect (k_H/k_D=5.81). The rates of the oxidation of the meta- and para-substituted benzylamines were separately correlated in Taft's and Swain's dual substituent parameter equations. For the para-substituted compounds, the best correlation is obtained with σ_I and σ_R^+ values, while meta-substituted compounds correlated best with σ_I and σ_R° values. The reaction constants have negative values. The oxidation rates of the ortho-substituted compounds yield excellent correlation in a triparametric equation involving Taft's σ_I and σ_R^+ values and Charton's steric parameter, V. A mechanism involving transfer of a hydride ion from the amine to NBA, in the rate-determining step has been proposed.

We have been interested in the mechanisms of the oxidation of organic compounds by *N*-haloamides.[1-3] The oxidation of benzylamine also presents interesting possibilities. It is known to yield a large number of products including those resulting from condensation of intermediate products of the oxidation with the parent amine.[4] In addition benzamide, benzaldehyde, and benzoic acid are also formed.[4] Wei and Stewart have studied the oxidation of some substituted benzylamines with permanganate ion.[5] We now report the oxidation of a series of ortho-, meta-, and para-substituted benzylamines by *N*-bromoacetamide (NBA) in buffered alkaline solutions. Attempts have been made to correlate structure and reactivity in this reaction.

Experimental

General. Benzylamine-α,α-d_2 ($PhCD_2NH_2$) was prepared by the reduction of benzonitrile by lithium aluminium deuteride.[6] *m*-Amino- and *o*-nitrobenzylamines were prepared by the reported methods.[7,8] The other amines were commercially available. Borate buffers were used to keep the pH constant. NBA and its aqueous solutions were stored in dark brown bottles. The aqueous solutions of the amines were prepared from the freshly distilled amines and doubly distilled water. The concentrations of the amines were determined by titration with standard hydrochloric acid, using Methyl Red as an indicator.

Product Analysis. Ammonia was obtained in 93% yield by the oxidation of benzylamine at pH 10.6 as shown by partial distillation of the aqueous reaction mixture and titration of the distillate with standard acid. Benzaldehyde was isolated as the 2,4-dinitrophenylhydrazone (DNP).

Freshly distilled benzylamine (5.35 g, 0.05 mol) and NBA (1.4 g, 0.01 mol) were made up to 100 ml in water at pH 10.6. The reaction mixture was allowed to stand for ca. 8 h to ensure completion of the reaction. It was treated with an excess (250 ml) of a saturated solution of 2,4-dinitrophenylhydrazine in 2 M HCl (1 M=1 mol dm^{-3}) and kept overnight in a refrigerator. The precipitated DNP was filtered off, dried, weighed, recrystallized, and weighed again. The DNP was identical (mp and mixture mp) with an authentic sample of DNP of benzaldehyde. The yield of the DNP before and after recrystallization were 2.70 g (94%) and 2.52% (88%) respectively. In similar experiments with the other amines, the yields of DNP, after recrystallization, were 84—95%.

Kinetic Measurements. The reactions were studied under pseudo-first-order conditions by keeping a large excess of the amine over NBA. The reaction were carried out in flasks blackened from the outside to prevent any photochemical reaction. Preliminary experiments showed that the reaction is not sensitive to ionic strength (0.05—1.0 M) and hence no attempt was made to keep the ionic strength constant. The reactions were followed at pH 10.6, were the amines are almost completely unprotonated. Corrections were applied to the rate constants for the partial ionization of the amines. The reactions were followed iodometrically for up to 70% of the extent of the reactions. The psudo-first-order rate constant, k_1, was determined from the linear plots of log[NBA] vs. time. The second order rate constant, k_2, was obtained from the relation $k_2=k_1/$[benzylamine]. Duplicate kinetic runs showed that the rates were reproducible to within ±3%.

Results

The rate laws and other data were obtained for all the compounds investigated. Since results are similar only representative data are reproduced here.

The oxidation of the amines by NBA results in the formation of corresponding benzaldehydes and ammonia (Eq. 1).

$$PhCH_2NH_2 + MeCONHBr + H_2O \rightarrow PhCHO + NH_3 + HBr + MeCONH_2 \quad (1)$$

Rate Laws. The reactions are found to be of first order with respect to NBA and the amine (Table 1). The rate of oxidation of benzylamine increases with increasing pH but the dependence is not linear and the rate reaches a limiting value of $k_2=3.40\times10^{-2}\ M^{-1}\ s^{-1}$ at pH 11.3. The limiting rate is represented by k'. A plot of the rate constant vs. pH produces a typical ionization curve (Fig. 1).

Table 1. Rate Constants of the Oxidation of Benzylamine by NBA at 298 K, pH 10.6

$[PhCH_2NH_2]$	10^3[NBA]	10^4k_1
M	M	s^{-1}
0.05	5.0	2.00
0.10	5.0	4.21
0.20	5.0	8.52
0.30	5.0	13.0
0.40	5.0	16.4
0.50	5.0	21.0
0.20	2.0	8.72
0.20	3.5	8.63
0.20	7.5	8.25
0.20	10.0	8.60
0.20	15.0	8.52

Table 2. Kinetic Isotope Effect in the Oxidation of Benzylamine by NBA([NBA] 0.005 M, pH 10.6, Temp 298 K)

[amine]	Type	10^5k_1
M		s^{-1}
0.05	$^1H_2$	20.0
0.10	$^1H_2$	42.1
0.20	$^1H_2$	85.2
0.05	$^2H_2$	3.65
0.10	$^2H_2$	7.22
0.20	$^2H_2$	14.1

10^4k_H=41.6±0.1 M^{-1} s^{-1}
10^4k_D=7.14±0.09 M^{-1} s^{-1}
k_H/k_D=5.81±0.06
k_H and $k_D=k_1$/[amine]

Table 3. Effect of Acetamide on the Oxidation of Benzylamine by NBA, ([NBA]=0.005 M, [amine]=0.10 M, pH=10.6, Temp 298 K)

10^2[acetamide]/M	0	2.5	4.0	5.0	7.5	10.0
$10^4k_1/s^{-1}$	4.21	4.12	4.30	4.40	4.30	4.12

The curve in Fig. 1 indicates that neutral benzylamine is the reactive reducing species. In that case, it has been shown[5] that a plot of $\log[k_2/(k'-k_2)]$ vs. pH, where k' is the rate maxima, should be linear with a unit slope, whose intercept is the pK_{BH^+} of the benzylammonium ion. Figure 2 presents the plot (r=0.9981, slope=1.02±0.02), the pK_{BH^+} of benzylamine is 9.45±0.02, close to the literature value of 9.34.[9]

Kinetic Isotope Effect. To ascertain the importance of the cleavage of α-C-H bond in the rate-determining step, the oxidation of $PhCD_2NH_2$, was studied. The results showed the presence of a substantial primary kinetic isotope effect (Table 2).

Effect of Acetamide. The rate of the reaction is not affected by the addition of acetamide (Table 3).

Effect of Substituents. The rates of the oxidation of benzylamine, nine para-substituted, ten meta-substituted, and ten ortho-substituted benzylamines were

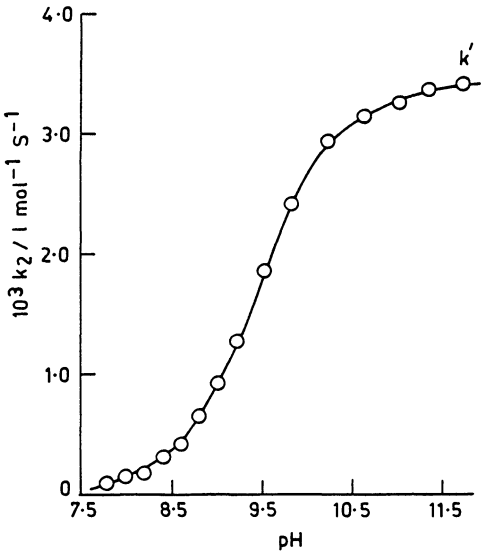

Fig. 1. Dependence of the rate of the oxidation of benzylamine on pH; temp 293 K.

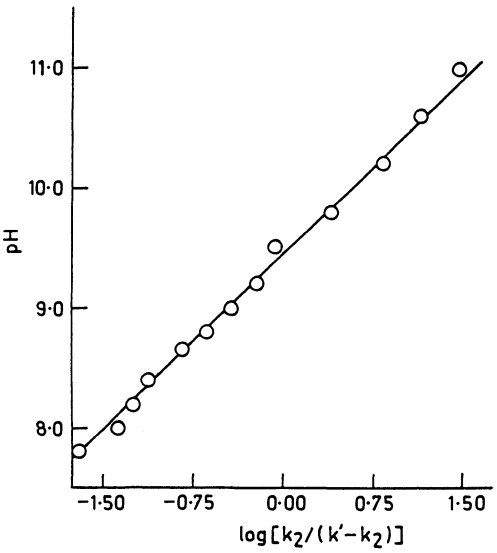

Fig. 2. Plot of pH against the function log $[k_2/(k'-k_2)]$ for the oxidation of benzylamine by NBA.

determined at different temperatures and the activation parameters were evaluated (Table 4).

Discussion

The linear correlation between log k_2 at 288 K and 308 K (r=0.9977, slope=0.8574) for the oxidation of the 30 amines shows that all the amines are oxidized by the same mechanism.[10] The value of isokinetic temperature is 529 K.

N-Haloamides are known to hydrolyzed and/or disproportionate in aqueous solutions to give hypohalous acids,[1-3] and hypohalous acids have been proposed as the reactive species in many reactions [1-3,11] of *N*-haloamides. However, no effect of the parent

amide on the reaction rate rules out the involvement of such preequilibria in the oxidation process and NBA itself seems to be the oxidizing species in the oxidation of benzylamines.

Correlation Analysis of the Reactivity. (i) Para- and Meta-Substituted Benzylamines: Since the rates of oxidation of the mono-substituted benzylamines failed to show satisfactory correlation with any single substituent parameter equation, the rates were subjected to analysis by Taft's[12] and Swain's[13] dual substituent parameter (DSP) equations. The rates of oxidation of the meta- and para-substituted benzylamines were separately correlated with σ_I and the four different σ_R substituent constants in Taft's equation[12] and with the field and resonance substituent constants of Swain et.al.[13] The results are summarized in Table 5. Both the meta- and para-series of substituted benzylamines meet the minimal basic requirements of substituents for the analysis by DSP equations.[14]

The results show that the rates of para-substituted amines show excellent correlation with σ_I and σ_R^+ values. The correlations with the other three σ_R values and in Swain's equation are relative poor. We have used the standard deviation (SD), coefficient of multiple correlation (R), and f as the measure of the goodness of fit. f has been defined by Dayal et al.[12] as

Table 4. Rate Constants and the Activation Parameters of the Oxidation of Substituted Benzylamines by NBA

Subs.	$10^5\ k_2/M^{-1}s^{-1}$					ΔH^*	ΔS^*
	288 K	293 K	298 K	303 K	308 K	kJ mol^{-1}	J mol^{-1} k^{-1}
H	200	316	421	688	950	54.9±1.6	−105±5.4
p-Me	660	976	1370	2200	2830	52.4±1.5	−104±5.2
p-OMe	5630	8330	11000	17100	21800	48.2±1.5	−101±5.0
p-F	350	548	712	1150	1670	54.5±1.8	−102±6.0
p-Cl	170	271	365	621	875	58.0±1.8	−96±6.1
p-Br	146	230	311	527	744	57.7±1.8	−98±5.9
p-NO_2	13.2	22.5	33.3	58.0	85.4	66.5±1.4	−87±4.6
p-CF_3	35.5	59.0	77.6	133	192	59.2±2.1	−105±7.0
p-COOMe	40.1	66.2	95.7	155	220	60.3±1.1	−100±3.8
p-NHCOMe	3540	5270	6690	10900	14600	50.1±1.9	−98±6.5
m-Me	304	480	635	1070	1490	56.2±1.9	−97±6.3
m-OMe	194	300	392	663	936	55.6±2.0	−103±6.8
m-F	55.0	83.4	105	171	233	50.6±2.0	−131±6.7
m-Cl	56.7	85.5	110	179	242	51.2±1.8	−129±6.1
m-I	69.3	107	139	222	305	52.0±1.5	−124±5.1
m-NO_2	11.5	16.8	21.6	32.0	42.8	45.8±1.1	−161±3.8
m-CF_3	26.5	41.3	60.6	81.2	113	50.3±1.3	−138±4.3
m-COOMe	41.2	61.0	80.3	132	183	52.8±1.8	−126±6.1
m-NH_2	319	496	683	1100	1580	56.4±1.3	−96±4.2
m-NHCOMe	142	222	298	474	664	54.2±1.4	−111±4.5
o-Me	1610	2430	3050	4900	6340	48.3±1.9	−111±6.5
o-OMe	2610	3850	4950	7610	9840	46.7±1.5	−112±4.9
o-F	231	351	462	782	1070	54.5±2.0	−106±6.7
o-Cl	262	413	555	920	1240	55.2±1.7	−102±5.8
o-Br	329	520	668	1080	1450	52.1±1.2	−111±4.1
o-I	534	786	1010	1650	2300	51.5±0.8	−109±2.8
o-NO_2	281	432	582	940	1260	53.2±1.5	−108±5.0
o-CF_3	240	368	495	798	1100	53.8±1.4	−108±4.8
o-COOMe	1600	2270	2910	4530	5950	46.4±1.6	−118±5.3
o-NHCOMe	4240	6100	7470	11500	15300	44.7±1.7	−116±5.9

Table 5. Correlation of the Rates of Oxidation of Substituted Benzylamines by NBA with Dual Substituent Parameters[a]

Substituent constant	Para-substituted						Meta-substituted					
	ρ_I	ρ_R	R	SD	f	n	ρ_I	ρ_R	R	SD	f	n
σ_I, σ_R°	−1.57	−3.16	0.9364	0.323	0.42	10	−1.76	−1.02	0.9951	0.053	0.09	11
σ_I, σ_R^{BA}	−1.62	−2.62	0.9617	0.252	0.33	10	−1.76	−0.70	0.9849	0.093	0.15	11
σ_I, σ_R^-	−1.17	−1.81	0.9136	0.351	0.72	9[b]	−1.67	−0.70	0.9890	0.084	0.13	10[b]
σ_I, σ_R^+	−1.43	−1.73	0.9984	0.053	0.07	10	−1.71	−0.38	0.9746	0.121	0.20	11
Swain et al.[c]	−0.36	−0.89	0.9914	0.120	0.16	10	−0.93	−0.30	0.9784	0.112	0.18	11

a) Temp 298 K, R=coefficient of multiple correlation; SD=standard deviation; f=SD/root mean squares of log k/k_0; n=No. of data points; σ_I and σ_R values are from Ref. 12. b) Data of NHCOMe substituted compounds not considered, no σ_R^- value is available. c) Field and resonance constants are from Ref. 13.

f=SD/RMS, where RMS is the root mean square of the data points (here log k/k_0). The comparison of f values shows that f is smaller for σ_R^+ scale than those for other scales by factors of ca. 3 to ca. 10. Therefore, it is apparent that the rates of the oxidation para-substituted benzylamines by NBA correlate best with σ_I and σ_R^+.

The rates of meta-substituted benzylamines show excellent correlation with σ_I and σ_R°, though the discriminating factor for the precision of fit with the other σ_R scales or with Swain's equation is not as sharp as in the case of para-substituted compounds. The comparison of f values shows that f is smaller for σ_R° scale than those for other scales by factors of ca. 1.5 to ca. 2.5. This agrees with the observation of Ehrenson, et al.[15] that the correlation of meta-substituted compounds is generally best with s_R° scale and meta-substituted compounds are less discriminating.

The reaction constants and the statistical data at different temperature are given in Table 6. The values of λ^p (ca. 1.24) showed that the oxidation of para-substituted benzylamines is more susceptible to the resonance effect than to the field effect. The selectivity of the reaction is decreased at higher temperature, but this decreases is of similar order for both the field and resonance effects resulting in the almost constant value of λ^p at different temperature.

In the oxidation of the meta-substituted compounds, the value of λ^m is ca. 0.56 indicating greater importance of the field effect. In the case meta-substituted compounds there is a small increase in the magnitude of the reaction constants with an increase in the temperature but this increase is of similar order for both the effects, reflected in the almost constant value of λ^m at different temperatures, the ratio of λ^m/λ^p is ca. 0.45.

(ii) Ortho-Substituted Benzylamines. It was found that the rates of oxidation of ortho-substituted benzylamines failed to yield any significant correlation with either Taft's polar or steric substituent constants.[16] The rates were, therefore, analyzed using Charton's method.[17] The rates were correlated using Eqs. 2 and 3, where σ_I, σ_R, and V are field, resonance and steric substituent constants and the values used were those compiled by Aslam et al.[18] h is the intercept term. α, β, and ϕ represent the susceptibility of the reaction to field, resonance, and steric effects respectively.

The results of correlation analysis in the terms of Eq. 2 are given in Eq. 4.

$$\log k_{ortho} = \alpha\,\sigma_I + \beta\,\sigma_R + h \quad (2)$$

$$\log k_{ortho} = \alpha\,\sigma_I + \beta\,\sigma_R + \phi V + h \quad (3)$$

$$\log k_2 = -0.85\,\sigma_I - 0.66\,\sigma_R - 1.74 \quad (4)$$

$$R = 0.5001;\ \mathrm{SD} = 0.48;\ n = 11.$$

where n is number of data points.

In the multiple linear regression using Eq. 2, the coefficient of correlation is poor and the standard deviation is high. The lack of a significant correlation with Eq. 2 leads to the conclusion that electric effects alone are not sufficient to account for the ortho-substituent effect in this reaction.

The correlation in the terms of Eq. 3 was performed assuming both orthogonal and planar conformations for NO_2 and COOMe groups. It was observed that the correlation was better with planar conformation of both the groups. The results Eq. 5 showed that the correlation with Eq. 3 is also not good.

$$\log k_2 = -2.19\sigma_I - 2.15\sigma_R + 1.29\,V - 2.43 \quad (5)$$

$$R = 0.9599;\ \mathrm{SD} = 0.17;\ n = 11.$$

It may be recalled that the rates of oxidation of para- and meta-substituted benzylamines showed excellent correlation in Taft's[12] DSP equation with σ_R^+ and σ_R° constants respectively. Therefore, the rates of the oxidation of ortho-substituted benzylamines were correlated in triparametric equations using Taft's σ_I, $\sigma_R^+/\sigma_R^\circ$ and Charton's steric parameters. The results showed that excellent correlations were obtained with Taft's σ_I, σ_R^+, and Charton's V values. The reaction constants and the statistical data are recorded in Table 7. The series of ortho-substituted benzylamines also meet the basic minimal requirements for the analysis by Taft's equation.[12]

The behavior of o-NO_2 and o-COOMe is consistent

Table 6. Temperature Dependence of the Reaction Constants

Temp / K	ρ_I	ρ_R[a]	λ[b]	R	SD	f
		Para-substituted				
288	−1.49	−1.80	1.21	0.9987	0.050	0.06
293	−1.43	−1.76	1.23	0.9984	0.052	0.07
298	−1.43	−1.73	1.21	0.9984	0.053	0.07
303	−1.39	−1.71	1.23	0.9983	0.053	0.07
308	−1.32	−1.68	1.27	0.9985	0.048	0.06
		Meta-substituted				
288	−1.69	−1.97	0.57	0.9968	0.041	0.07
293	−1.74	−0.99	0.57	0.9965	0.044	0.07
298	−1.76	−1.02	0.58	0.9951	0.058	0.09
303	−1.82	−1.01	0.55	0.9970	0.043	0.07
308	−1.84	−1.03	0.56	0.9975	0.040	0.06

a) ρ_R is ρ_R^+ and ρ_R° for the para- and meta-substituted compounds respectively. b) $\lambda = \rho_R/\rho_I$.

Table 7. Temperature Dependence of the Reaction Constants of the Oxidation of Ortho-Substituted Benzylamines by NBA

Temp / K	ρ_I	ρ_R^+	ϕ	R	SD	p_S	p_R
288	−1.81	−1.18	1.08	0.9988	0.028	39.5	26.5
293	−1.77	−1.15	1.04	0.9990	0.025	39.4	26.3
298	−1.72	−1.12	1.02	0.9987	0.030	39.4	26.4
303	−1.69	−1.09	0.99	0.9989	0.025	39.2	26.3
308	−1.64	−1.07	0.96	0.9988	0.026	39.5	26.2

with their planar conformation.

The significance of the correlation, tested by the F-test,[19] is >99.9%. Similarly the confidence level for the significance of σ_I, σ_R^+, and V terms, obtained by the Student's t-test,[19] is > 99.9%. This indicates the operation of significant field, resonance, and steric effects in the reaction.

To test the significance of the three substituent constants, multiple linear regression analyses were carried out with Taft's σ_I and σ_R^+, Taft's σ_I and V, and with σ_R^+ and V. The absence of significant correlations (Eqs. 6—8) showed that all the three σ_I, σ_R^+, and V substituent constants are significant.

$$\log k_2 = -0.79\sigma_I - 0.60\sigma_R^+ - 1.84 \quad (6)$$
$$R = 0.6518;\ \mathrm{SD} = 0.42;\ n = 11$$
$$\log k_2 = -1.39\sigma_I + 0.46V - 1.78 \quad (7)$$
$$R = 0.5731;\ \mathrm{SD} = 0.45;\ n = 11$$
$$\log k_2 = -0.97\sigma_R^+ + 0.58V - 2.61 \quad (8)$$
$$R = 0.7366;\ \mathrm{SD} = 0.37;\ n = 11$$

There is no significant colinearity between Taft's σ_I and V, σ_R^+ and V, and between Taft's σ_I and σ_R^+ (r= 0.4694, 0.3029, and 0.1076) for the eleven substituents.

The regression coefficients of σ_I and σ_R^+ terms are negative indicating that electron-releasing groups accelerate the reaction. The positive regression coefficient for the steric term indicates that the reaction is subject to steric acceleration by the ortho-substituents. The contribution of the resonance effect[17] to the total polar effect of the ortho-substituents was calculated using Eq. 9.

$$p_R = \frac{100 \times |\rho_R^+|}{|\rho_I| + |\rho_R^+|} \quad (9)$$

The contribution of steric parameter[17] to the total effect of the substituents, p_S, was determined using Eq. 10.

$$p_S = \frac{|\phi| \times 100}{|\rho_I| + |\rho_R^+| + |\phi|} \quad (10)$$

The values of p_R and p_S are also listed in Table 7. The values of p_R is ca. 39%. The value of p_R for the para-substituted compounds in ca. 55%. This shows that the balance of field and resonance effect is different for ortho- and para-positions, resonance effects being less pronounced in the former case. This may be due to the twisting away of the aminomethyl group from the plane of the benzene ring. The value of p_S shows that there is considerable steric effect in this reaction.

Mechanism. The kinetics are consistent with a mechanism in which as molecule each of the amine and NBA participate in the rate-determining step. The observed kinetic isotope effect confirms the rupture of the α-C-H bond in the rate-determining step. The large negative polar reaction constants and the correlation of the rates of para- and ortho-substituted benzylamines with σ_R^+ point to a transition state in which there is a strong resonance interaction between the substituent and a developing positive charge. This suggests the transfer of a hydride ion from the methylene group to the oxidant. There is no doubt that the amino group strongly activates the adjacent methylene and this supports the idea of hydride transfer. Thus the following mechanism may be proposed Eqs. 11—13.

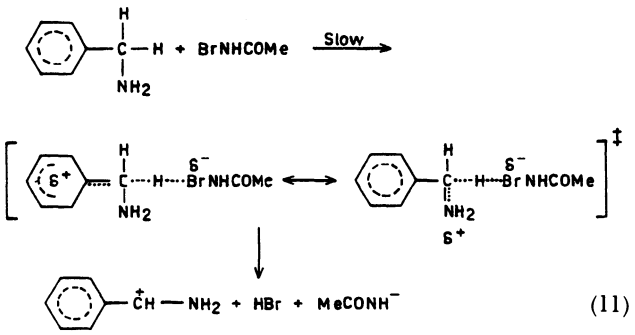

$$PhCHNH_2 + H_2O \xrightarrow{\text{Fast}} PhCHO + NH_4^+ \quad (12)$$

$$MeCONH^- + H^+ \xrightarrow{\text{Fast}} MeCONH_2 \quad (13)$$

The steric acceleration of the reaction may be explained on the basis of high ground state energy of the sterically crowded amines. Since the crowding is relieved in the product aldehyde as well as the transition state leading to it, the transition state energy of the crowded and uncrowded amines do not differ much and steric acceleration, therefore, result.

It is of interest the compare the oxidations of benzylamine by permanganate ion[5] and NBA. The rates of oxidation of 8 (out of 11 studied) meta- and para-substituted benzylamines by permanganate[5] correlate with σ^+ values, the reaction constant, ρ, being −0.28. The small value of ρ suggested the possibility of a one-electron oxidation. In the oxidation by NBA, the rates of 30 substituted benzylamine exhibited large negative polar reaction constants. A strong resonance interaction between the substituent and a developing positive charge, in the transition state, is also indicated. Hence a one-electron oxidation can be excluded.

Thanks are due to the University Grants Commission (India) and Council of Scientific and Industrial Research, India, for the financial support.

References

1) J. Mukherjee and K. K. Banerji, *J. Org. Chem.*, **46**, 2323 (1981).

2) V. Sharma and K. K. Banerji, *J. Chem. Res. (S)*, **1985**, 340; *idem*, *J. Chem. Res. (M)*, **1985**, 3551.

3) K. K. Banerji, *J. Org. Chem.*, **51**, 4764 (1986).

4) H. Shechter, S. S. Rawaley, and M. Tubis, *J. Am. Chem. Soc.*, **86**, 1701 (1964); H. Shechter and S. S. Rawaley, *J. Am. Chem. Soc.*, **86**, 1706 (1964).
5) M. M. Wei and R. Stewart, *J. Am. Chem. Soc.*, **88**, 1974 (1966).
6) E. A. Halevi, M. Nussim, and A. Ron, *J. Chem. Soc.*, **1963**, 866.
7) N. Kornblum and D. C. Iffland, *J. Am. Chem. Soc.*, **71**, 2137 (1949).
8) H. R. Ing and R. H. F. Manske, *J. Chem. Soc.*, **1926**, 2348.
9) F. Kieffer, *Compt. Rend.*, **238**, 1043 (1954).
10) O. Exner, *Prog. Phys. Org. Chem.*, **10**, 411 (1973).
11) E. H. Berlinger, *J. Chem. Educ.*, **43**, 124 (1966).
12) S. K. Dayal, S. Ehrenson, and R. W. Taft, *J. Am. Chem. Soc.*, **94**, 9113 (1972).
13) C. S. Swain, S. H. Unger, N. R. Rosenquest, and M. S. Swain, *J. Am. Chem. Soc.*, **105**, 492 (1983).
14) J. Shorter, "Correlation Analysis of Organic Reactivity," Research Studies Press, Chichester (1982), p. 50.
15) S. Ehrenson, R.T.C. Brownlee, and R. W. Taft, *Prog. Phys. Org. Chem.*, **10**, 1 (1973).
16) R.A.Y. Jones, "Physical and Mechanistic Organic Chemistry," Cambridge University Press, Cambridge (1979).
17) M. Charton, *J. Org. Chem.*, **40**, 407 (1975).
18) M. H. Aslem, A. G. Burden, N. B. Chapman, J. Shorter, and M. Charton, *J. Chem. Soc., Perkin Trans. 2*, **1981**, 500.
19) R. L. Wine, "Statistics for Scientists and Engineers," Prentice-Hall, New Delhi (1966).

Conductivity of Iron(II) Sulfate in Aqueous Solution at Various Temperatures

Eiji KUBOTA,* Yoshiaki MOCHIZUKI, and Masatoki YOKOI
Department of Chemistry, Faculty of Science, Shinshu University, Asahi, Matsumoto 390
(Received March 24, 1988)

Synopsis. The molar conductivity of iron(II) sulfate, $FeSO_4$, in water was measured in the temperature range 10—35 °C. Data were analyzed by the Quint-Viallard equation, and the resulting ion association constant, K_A, was applied to the Bjerrum equation to determine the contact ion size, R_B. The limiting ionic molar conductivity of iron(II) at 25 °C is $\lambda_0(1/2Fe^{2+})=53.8$ S cm^2 mol^{-1}. Thermodynamic properties of ion association reactions are $\Delta G^\circ_{298}=-13.7$ kJ mol^{-1}, $\Delta H^\circ=9.7$ kJ mol^{-1}, and $\Delta S^\circ_{298}=78.0$ J K^{-1} mol^{-1}.

Divalent metal sulfates have long been utilized as the most typical 2 : 2 type of electrolytes for the study of aqueous electrolyte solutions.[1-6] Regarding iron(II) sulfate, however, precise conductivity data of its aqueous solution are not available, except the work of Demassieux and Fedroff[3] at 25 °C. Conductivity data for the other iron(II) salts are not available either in the literature. This is probably because the salts undergo oxidation markedly on exposure to atmospheric oxygen. Thus we attempted to redetermine molar conductivities of iron(II) sulfate in aqueous solution at several temperatures by avoiding oxidation as carefully as possible.

Experimental

The preparation and purification of $FeSO_4$ were conducted in nitrogen atmosphere. A reagent grade $FeSO_4$ was recrystallized from water by adding a small amount of ethanol. The purified salt was dried at room temperature to obtain crystals of heptahydrate. The crystals were pulverized before use. Conductivity water was prepared by distilling water three times, and the distilled water was allowed to pass through a mixed bed ion-exchange resin shortly before use.

Measurements were made at a frequency of 1 kHz with a linear type bridge,[7] temperature variation being ±0.003 °C. The conductivity cell was equipped with a platinized electrode, and the cell constant was 0.99074±0.00001 cm^{-1} at 25 °C. No detectable change in the cell constant was observed in the temperature range 10—35 °C.

On starting each run, a nitrogen gas stream was bubbled gently through the conductivity water in the cell for about 30 to 40 min, and the conductivity of the water was measured after it reached an equilibrium value, which was less than 1.0×10^{-7} S cm^{-1}. The concentration (10^{-4} to 10^{-3} mol dm^{-3}) of $FeSO_4$ was adjusted by direct dissolution of pulverized specimen into the cell by utilizing Hawes-Kay's cup-dropping device[8] in an atmosphere of nitrogen. The variation in conductivity of the solution with time was 0.02% or less in 5 h after the preparation of the solution.

Results and Discussion

Conductivity data of aqueous solutions in the temperature range 10—35 °C are given in Table 1.

The conductivity data were analyzed by the Quint-Viallard conductivity theory in the form of Eq. 1:[9]

$$\Lambda=\gamma[\Lambda_0-Sc^{1/2}\gamma^{1/2}+Ec\gamma\log c\gamma+J_1c\gamma-J_2c^{3/2}\gamma^{3/2}], \quad (1)$$

$$K_A=(1-\gamma)/c\gamma^2f_\pm^2, \quad (2)$$

$$-\log f_\pm=Ac^{1/2}\gamma^{1/2}/(1+B\mathring{a}c^{1/2}\gamma^{1/2}), \quad (3)$$

where c is the concentration, γ is the degree of dissociation, K_A is the ion association constant, and $f_\pm$ is the mean ionic activity coefficient given by the extended Debye-Hückel theory of Eq. 3.[10] In Eq. 3, A and B depend upon solvent properties, and $\mathring{a}$ is the ion size

Table 1. Conductivity Data in Aqueous Solutions at Various Temperatures[a)]

10 °C		15 °C		20 °C	
10^4c	Λ	10^4c	Λ	10^4c	Λ
5.0500	81.447	3.5268	93.939	4.7768	104.15
9.5538	76.985	8.8480	87.161	8.5492	98.752
14.698	73.280	13.435	83.170	13.372	93.882
22.439	69.175	19.425	79.411	18.778	89.898
31.680	65.496	28.362	75.186	28.739	84.400
43.811	61.890	38.008	71.836	39.230	80.262
25 °C		**30 °C**		**35 °C**	
10^4c	Λ	10^4c	Λ	10^4c	Λ
5.5040	114.81	3.8277	132.38	4.0641	145.82
9.9449	108.22	8.3249	123.31	9.6007	133.80
14.446	103.40	13.478	116.32	15.528	125.76
21.856	97.592	20.955	109.43	22.871	118.71
29.661	92.999	32.964	101.69	33.314	111.56
45.036	86.622	49.691	94.615	45.505	105.43

a) c/mol dm^{-3}; $\Lambda(1/2FeSO_4)$/S cm^2 mol^{-1}, molar conductivity.

Table 2. Conductivity Parameters of $FeSO_4$ in Aqueous Solutions at Various Temperatures[a)]

T/°C	Λ_0	$\mathring{a}_{J2}$	K_A	$\sigma\Lambda$	R_B
10	93.1±0.3	12.6±0.2	201±4	0.06	4.3
15	105.0±0.1	11.4±0.1	215±3	0.06	4.3
20	119.4±0.1	11.4±0.2	231±3	0.05	4.2
25	133.8±0.1	11.5±0.1	247±2	0.05	4.1
30	150.4±0.2	11.3±0.1	264±3	0.08	4.1
35	167.1±0.1	11.4±0.1	281±3	0.07	4.0

a) $\Lambda_0(1/2\ FeSO_4)$/S cm^2 mol^{-1}, limiting molar conductivity. $\mathring{a}_{J2}$/Å, ion size parameter for the J_2 term. K_A/dm^3 mol^{-1}, ion association constant. $\sigma\Lambda$/%, relative standard deviation in Λ. R_B/Å, contact ion size for Bjerrum's equation.

Table 3. Limiting Molar Conductivity of Ions in Aqueous Solutions at 25 °C[a)]

Ion(M^{2+})	Mn^{2+}	Fe^{2+}	Co^{2+}	Ni^{2+}	Cu^{2+}	Zn^{2+}
$\lambda_0(1/2M^{2+})$	53.1[c)]	53.8[b)]	52.8[d)]	53.5[d)]	53.9[e)]	54.3[d)]

a) $\lambda_0(1/2M^{2+})$/S cm^2 mol^{-1}, limiting ionic molar conductivity. b) This work. c) Ref. 14. d) Ref. 4. e) Ref. 5.

Table 4. Thermodynamic Properties for Ion Association Reaction in Aqueous Solutions

Reaction	$K_{A\,298}$	ΔG°_{298}	ΔH°	ΔS°_{298}
	$dm^3\,mol^{-1}$	$kJ\,mol^{-1}$	$kJ\,mol^{-1}$	$J\,K^{-1}\,mol^{-1}$
$Fe^{2+}\cdot SO_4^{2-}$ a)	247	−13.7 ±0.1	9.72±0.05	78.5±0.4
$Co^{2+}\cdot SO_4^{2-}$ b)	178	−12.80±0.04	5.00±0.30	59.8±1.2
$Ni^{2+}\cdot SO_4^{2-}$ b)	187	−12.97±0.04	5.18±0.16	60.9±0.6
$Zn^{2+}\cdot SO_4^{2-}$ b)	165	−12.65±0.04	8.65±0.34	71.4±1.3

a) This work. b) Ref. 4.

parameter. The coefficients J_1 and J_2 are functions of ion size parameter δ_{J2}, and S, E, and J contain solvent properties.[10] The ion size parameters appearing in the J_1 and $f_\pm$ terms were fixed as equal to Bjerrum's q values, and the best fit δ_{J2} values for J_2 were calculated.[11] Table 2 shows the best fit parameters at the minimum value of $\sigma\Lambda$. $\sigma\Lambda(\%)$ is defined as

$$\sigma\Lambda=[\sum(\Lambda_{obsd}-\Lambda_{calcd})^2/(N-3)]^{1/2}, \quad (4)$$

where N is the number of experimental points.

When a conductivity equation containing a $c^{3/2}$ term is applied, the fitting of the data is generally better, but the ion size parameter δ_{J2} for the 2:2 type electrolyte is usually as large as 10—20 Å. In the present work δ_{J2} of 11—13 Å was obtained.[11] If one assumes the validity of Bjerrum's Eq. 5, the contact ion size R_B can be calculated from the resulting K_A:[12,13]

$$K_A(\text{calcd})=\frac{4\pi N}{1000}\int_{R_B}^{q} r^2\exp(e^2/rDkT)\mathrm{d}r. \quad (5)$$

The results are also given in Table 2. The parameters, Λ_0 and K_A increase with increasing temperature. The limiting molar conductivity of Fe^{2+} ion at 25 °C is obtained as λ_0 ($1/2\ Fe^{2+}$)=53.8 S $cm^2\,mol^{-1}$ by subtracting the value λ_0 ($1/2SO_4^{2-}$)=80.0 of SO_4^{2-} ion from the Λ_0 value.[10] Demassieux and Fedroff's data[3] give λ_0 ($1/2Fe^{2+}$)=49.8. Table 3 shows a comparison with other divalent transition metal ions. The ion size parameter δ_{J2} has a relatively large value, more than 10 Å, whereas R_B has a substantially reasonable value (the sum of the ionic crystal radii is ≈3.3 Å).[15] The log K_A-$1/T$ plot gives a good linearity. The resulting thermodynamic properties of ion association reaction are shown in Table 4 with data of other sulfate solutions. It can be seen that the properties of $Fe^{2+}\cdot SO_4^{2-}$ are in parallel with those of the other sulfates, though the absolute values are a little larger than the others. The positive ΔS° has been considered as due to the decreased orientation of water molecules when the ion-pair forms.[16]

The authors wish to thank the staffs of the Shinshuu University, Nagoya University, and Tokyo University Computation Centers for the use of the computers. The present work was partially supported by a Grant-in-Aid for Science Research No. 62540459 from the Ministry of Education, Science and Culture.

References

1) G. J. Janz and R. P. T. Tomkins, "Nonaqueous Electrolytes Handbook," Vol. 1, Academic Press, New York-London (1972), pp. 145, 1063; Vol. 2 (1973), p. 800.

2) V. M. M. Lobo, "Electrolyte Solutions: Literature Data on Thermodynamic and Transport Properties," Vol. I, Coimbra, Poltugal (1984); V. M. M. Lobo and J. L. Quaresma, Vol. II (1981).

3) N. Demassieux and B. Fedroff, *Ann. Chim.*, **16**, 215 (1941).

4) S. Katayama, *Bull. Chem. Soc. Jpn.*, **46**, 109 (1973); S. Katayama, *J. Solution Chem.*, **5**, 241 (1976).

5) B. B. Owen and R. W. Gurry, *J. Am. Chem. Soc.*, **60**, 3074 (1938).

6) A. D. Pethybridge and S. S. Taba, *Faraday Discuss. Chem. Soc.*, **64**, 274 (1977).

7) Conductivity bridge: Model 360-S by Fuso Seisakusho, Ltd. Standard resistor: esi, Ltd., within ±0.01 °C.

8) J. L. Hawes and R. L. Kay, *J. Phys. Chem.*, **69**, 2420 (1965).

9) J. Quint and A. Viallard, *J. Solution Chem.*, **7**, 135, 525, 533 (1978).

10) R. A. Robinson and R. H. Stokes, "Electrolyte Solutions," Butterworths, London (1965), pp. 229, 457, 463.

11) E. Kubota and M. Yokoi, *Bull. Chem. Soc. Jpn.*, **49**, 2674 (1976); E. Kubota and M. Yokoi, *ibid.*, **50**, 1422 (1977).

12) N. Bjerrum, *Kgl. Dan. Vidensk.*, **7**, No. 9 (1926).

13) J. C. Justice, *J. Chem. Phys. Physicochem. Biol.*, **65**, 353 (1968); J. C. Justice, *Electrochim. Acta*, **16**, 701 (1968); E. Renard and J. C. Justice, *J. Solution Chem.*, **3**, 633 (1974).

14) T. R. Broadwater and D. F. Evans, *J. Solution Chem.*, **3**, 757 (1974).

15) R. D. Shannon, *Acta Crystallogr., Sect. A*, **32**, 751 (1976); H. D. B. Jenkins and K. P. Thakur, *J. Chem. Educ.*, **56**, 576 (1979).

16) G. H. Nancollas, *Discussions Faraday Soc.*, **24**, 108 (1957); "Interactions in Electrolyte Solutions," Elsevier Publishing Company, Amsterdam-London-New York (1966), p. 133.

The Photochemical Debromination of Bromocyclopropane in the Presence of Amine

Hideo TOMIOKA* and Osamu INOUE
Department of Industrial Chemistry, Faculty of Engineering, Mie University, Tsu, Mie 514
(Received March 2, 1988)

Synopsis. The irradiation of bromoarylcyclopropanes (**1**) in the presence of tertiary amine resulted in the formation of the debrominated cyclopropanes as a mixture of geometrical isomers, whose ratios were essentially similar regardless of the stereochemistry of the bromide. The reactions were not, however, observed in the absence of amine. The results are interpreted as indicating that the reactions proceed through an initial single-electron transfer to the excited **1**, followed by debromination and hydrogen-abstraction.

Since the early 1980s, the scope of cyclopropane photochemistry has been greatly broadened by electron-transfer-sensitized reactions.[1] However, in most of these reactions cyclopropanes have been used as electron donors, which transfer single electrons to the excited-state acceptors (e.g., cyanoaromatics) to generate cyclopropane cation radicals. Recently we found, however, that some cyclopropanes can act as electron acceptors as well in the excited state when irradiated with an appropriate electron donor (e.g., amines). Thus, the irradiation of an arylcyclopropane bearing electron-withdrawing group in the presence of tertiary amine resulted in the regioselective addition of the amine, which can be explained as proceeding through a single-electron transfer mechanism.[2] As an extension of such works, we studied the photochemistry of halocyclopropanes in the presence of amine and found that bromocyclopropanes underwent efficient photodebromination,[3] most probably via single-electron transfer.

The irradiation of *r*-1-bromo-1,*t*-2-diphenylcyclopropane (**1a**) in acetonitrile or cyclohexane with a 300 W Hg lamp through a Pyrex filter did not result in the formation of any appreciable products, more than 95% of the starting compound being recovered unchanged even after a 16 h irradiation. In marked contrast, a similar irradiation of **1a** in the presence of a 5 molar excess of triethylamine led to the rapid disappearance of **1a** and the concurrent formation of the debrominated cyclopropanes (**2** and **3**) as a 6.1 : 1 mixture of geometrical isomers, predominantly **2**. Similarly, the irradiation of *r*-1-bromo-1,*c*-2-diphenylcyclopropane with the amine also afforded the debrominated cyclopropanes (**2** and **3**) in an isomer ratio almost identical with that observed in the irradiation of the trans isomer. 1-Bromo-3-methyl-1,2-diphenylcyclopropanes (**1b**) also underwent smooth photo-debromination in the presence of amine, although the yield and stereoselectivity of the reduction decreased considerably.[4] Control experiments showed that the reduction did not occur in the absence of light and that the product cyclopropanes did not isomerize under these conditions.

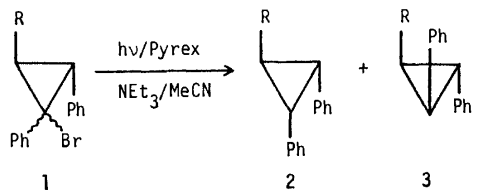

1 2 3

a: R=H

b: R=Me

In order to get insight into the mechanism of the present photoreduction, we carried out some additional experiments. First, the reactions were found to be somewhat sensitive to the solvent employed, as is summarized in Table 2. Thus, the photodebromination proceeded quite smoothly in acetonitrile, while the reduction was relatively inefficient in cyclohexane. This is, however, in marked contrast with the situation observed[2] in the photochemical addition of amines to electrophilic cyclopropanes, where the reactions did not proceed in any of those solvents listed in Table 2 except acetonitrile. Second, the bromocyclopropane fluorescence was quenched by the amine, indicating that the excited singlet state is involved in the present photoreduction.

The above findings can be better explained in terms of a mechanism involving electron transfer, as is

Table 1. Photodebromination of Bromocyclopropane (**1**) in the Presence of Amine[a]

1	R	1-Br/ 2-Ph	Conv/%[b]	Yield/%[b]		2/3
				2	3	
a	H	trans	94.6	46.5	7.6	6.1
	H	cis	85.3	53.1	7.7	6.9
b	Me	trans	100	12.4	5.2	2.4
	Me	cis	97.5	15.2	6.5	2.3

a) Irradiations were carried out on 10-mM degassed solution of **1** in MeCN in the presence of a 5-molar excess of NEt_3 for 2 h through a Pyrex filter with a 300 W high pressure Hg lamp. b) Determined by GC.

Table 2. Effect of Solvent on the Photodebromination of **1a**[a]

Solvent	Conv/%[b]	Yield/%[b]	
		2a	3a
MeCN	67.4	44.1	7.8
EtOH	41.9	40.8	14.0
CH_2Cl_2	42.0	36.9	9.7
THF	66.8	53.1	14.1
AcOEt	46.1	51.9	11.5
PhH	46.4	44.6	10.5
c-C_6H_{12}	23.0	32.0	13.5

a) See footnote a) in Table 1. The irradiation time was 1 h. b) See footnote b) in Table 1.

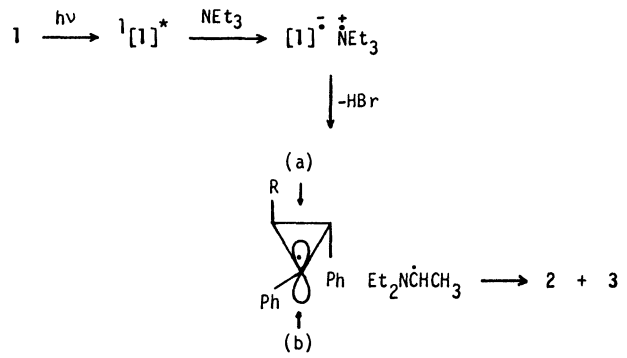

Scheme 1.

summarized in Scheme 1, rather than in terms of simple free-radical mechanism. Thus, **1** is first excited to its singlet state, which accepts an electron from the ground state amine to generate a cyclopropane-anion radical and an amine-cation radical. The cyclopropane anion radical, which had no bromine substituent, underwent efficient protonation by the amine cation radical, resulting in the ring cleavage.[2] The absence of any appreciable formation of such ring-opened products in the present photoreaction implies that the bromocyclopropane anion radical releases bromide, leaving the cyclopropyl radical, before it undergoes protonation. The solvent effects are worthy of comment in this connection. The effects of solvents in the electron-transfer reactions are usually explained in terms of the dissociation of the primary geminate-ion-radical pair, leading to a separated radical ion.[1a] Thus, a high polarity of the medium is usually required to solvate the separated radical ions. The moderate effect of solvents on the present photoreduction is in marked contrast with the fatal effects of solvent on the photoaddition[2] of amine to cyclopropane: this would indicate that the elimination of bromide ion is so efficient as to occur within the primary geminate pair. The abstraction of hydrogen from the resulting α-aminoalkyl radical by the cyclopropyl radical then affords the final products.

The fact that essentially similar isomer ratios are observed, regardless of the stereochemistry of the starting bromide, indicates that the geometry of the radical is planar rather than pyramidal. Apparently the attack of the hydrogen atom from a side (a) opposite to the 2-phenyl group leading to **2** is favored over that from the other side (b) giving **3**, since there is interference between the attacking hydrogen and the 2-phenyl group in the latter case. Obviously, the preference for the formation of **2** will be decreased by the introduction of the 3-methyl group since side (a)-attack is also subjected to steric hindrance by the methyl group, as was observed.

Experimental

Instrumentation. The UV and fluorescence spectra were recorded on a Hitachi 220-S spectrophotometer and a Hitachi MPF-2A spectrofluorometer respectively. The IR spectra were determined with a JASCO A-100 spectrometer, while the ^{1}H NMR spectra were measured on a JEOL JNM-MH-100 NMR spectrometer in CCl_4 with Me_4Si, as the internal reference. The mass spectra were recorded on a Shimadzu QP-1000 mass spectrometer (70 eV). The GC analyses were performed on a Yanagimoto instrument, Model G-80. The GC column A was prepared from 10% SE-30 on Diasolid L (5.0 mm×2.0 m); column B consisted of 5% PEG-20M on Diasolid L (5.0 mm×1.0 m).

Materials. The bromocyclopropanes (**1a** and **b**) were prepared by refluxing phenylbromodiazirine with alkenes (styrene and *trans*-β-methylstyrene respectively) in benzene according to the method of Padwa.[5] Geometrical isomers were separated by column chromatography (silica gel) eluted with ether. The data are show below.

trans-**1a:** Yield, 37%; yellow oil; ^{1}H NMR δ=7.5—6.6 (10H, m), 2.78 (1H, dd), 1.90 (1H, dd), 1.23 (1H, dd).

cis-**1a:** Yield, 42%; yellow oil; ^{1}H NMR δ=7.6—6.9 (10H, m), 2.42 (1H, dd), 1.93 (1H, dd), 1.83 (1H, dd).

trans-**1b:** Yield, 35%; yellowish semisolid; ^{1}H NMR δ=7.1—6.9 (10H, m), 2.46 (1H, bd), 1.69 (1H, d), 1.66 (3H, bs).

cis-**1b:** Yield, 27%; yellow oil; ^{1}H NMR δ=7.5—7.0 (10H, m), 2.11 (1H, d), 2.08 (1H, dq), 1.07 (3H, d).

The debrominated cyclopropanes **2a**[6] and **2b**[7] were prepared according to the reported procedures.

Irradiation for Product Identification. In a typical run, a solution of **1** (1 mmol) and triethylamine (5 mmol) in MeCN (50 cm^3) was placed in a quartz tube and irradiated using a high pressure, 300 W, Hg lamp with a water-cooled quartz jacket. The progress of the reaction was monitored by means of TLC. After irradiation for 5 h, the irradiation mixtures were concentrated on a rotary evaporator, chromatographed on preparative TLC (silica gel), and eluted with chloroform-hexane. The fast-moving fraction was found to contain the debrominated cyclopropanes as a mixture of geometrical isomers.

Irradiation for Analysis Purposes. All the irradiations outlined in the tables were carried out on 10 mM (1 M= 1 mol dm^{-3}) solutions of **1** in a quartz tube with a capacity of 5 cm^3 at 15 °C. The yields were conveniently determined by standard GC techniques, and the identity of the products was confirmed by GC using both A and B columns as well as GC-MS comparison with authentic samples prepared as above.

References

1) For reviews, see a) S. L. Mattes and S. Farid, "Organic Photochemistry," ed by A. Padwa, Marcel Dekker, New York (1983), Vol. 6; b) Y. Otsuji and K. Mizuno, *Rep. Asahi Glass Found. Ind. Technol.*, **49**, 215 (1986); c) K. Mizuno, *J. Syn. Org. Chem., Jpn.*, **44**, 1010 (1986).

2) H. Tomioka and H. Miyagawa, *J. Chem. Soc., Chem. Commun.*, in press.

3) The direct irradiation of *gem*-dibromocyclopropanes in ether has been reported to yield the corresponding monobromocyclopropanes. The photoreduction has, however, been explained in terms of the initial homolytic cleavage of the C-Br bond in the excited cyclopropanes to give the α-bromocyclopropyl radical, followed by hydrogen abstraction; N. Shimidzu and S. Nishida, *Chem. Lett.*, **1979**, 839.

4) GC analysis of the photo-mixtures showed the presence of many small peaks of higher-boiling products, which were not investigated further.

5) A. Padwa, M. J. Pulwer, and T. J. Blacklock, *Org. Synth.*, **60**, 53 (1981).

6) S. G. Beech, J. H. Turnbull, and W. Wilson, *J. Chem. Soc.*, **1952**, 4686; R. M. Dodson and G. Klose, *Chem. Ind. (London)*, **1963**, 450.

7) M. A. Fox and C. C. Chen, *J. Org. Chem.*, **48**, 321 (1983).

Stereochemistry of the Reactions of Trimethylgermyl Anions with 4-*t*-Butylcyclohexyl Derivatives

Kunio MOCHIDA* and Tsuyoshi KUGITA
Department of Chemistry, Faculty of Science, Gakushuin University, 1-5-1 Mejiro, Tokyo 171
(Received March 28, 1988)

Synopsis. The stereochemistry of trimethylgermyllithium, -sodium, and -potassium with *cis*- and *trans*-4-*t*-butylcyclohexyl bromides and trimethylstannanes was investigated by ^{1}H NMR spectroscopy. With the 4-*t*-butylcyclohexyl derivatives trimethylgermyl anions gave mixtures of *cis*- and *trans*-4-*t*-butylcyclohexyltrimethylgermanes. These results confirmed that free-radical pathways are important in such reactions.

In earlier reports we described the reactions of trialkylgermyl anions with aryl halides[1] and aryltrialkylstannanes.[2] These results revealed that free-radical pathways are important on the basis of the formation of products and radical trapping experiments.

Stereochemical studies also provide valuable mechanistic information concerning substitution reactions of trialkylgermyl anion with cyclohexyl derivatives. Recently, Kitching et al. reported that the reactions of trimethylgermyllithium with 4-methylcyclohexyl bromides gave mixtures of *cis*- and *trans*-4-methylcyclohexyltrimethylgermanes.[3,4] Since 4-methylcyclohexyl bromides exist as an equilibrium mixture of conformations, two steric courses of the reaction, i.e. axial and equatorial approaches of trimethylgermyl groups to cyclohexyl derivatives, cannot be distinguished. The introduction of a *t*-butyl group on the ring prevents a ring inversion. Then, a distinction of such two steric courses of the reaction may be possible.

In this paper, the stereochemical courses of the substitution reactions of trimethylgermyl anions with conformationally stable 4-*t*-butylcyclohexyl derivatives are described.

Results and Discussion

The stereochemistry of the substitution reactions of trimethylgermyllithium, -sodium, and -potassium with *cis*- and *trans*-4-*t*-butylcyclohexyl bromides and trimethylstannanes was examined by ^{1}H NMR spectroscopy.

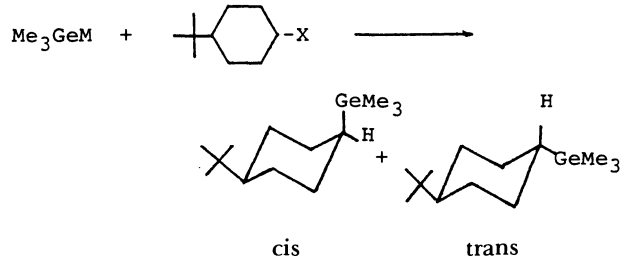

M=Li, Na, K; X=Br, $SnMe_3$

^{1}H NMR spectroscopy has been widely employed to determine the stereochemistry of 4-*t*-butylcyclohexyl derivatives, particularly, when electronegative groups, such as bromine atom, significantly deshield the methine proton (>C(H)X; X=Br) from the general cyclohexyl absorption and axial protons give rise to a resonance upfield from their counter parts.[5] In germanium and tin compounds, the methine proton (>C(H)Ge≤ and >C(H)Sn≤) would be of rather limited use. However, studies of the ^{13}C and ^{1}H NMR spectra of cyclohexyl and related organogermanes and -stannanes have shown that equatorial trimethylgermyl and trimethylstannyl groups give rise to a resonance upfield from their counterparts.[6]

trans-4-*t*-Butylcyclohexyl bromide (100%), prepared by the triphenylphosphine-bromine procedure for transforming an alcohol, reacted with trimethylgermyllithium to give *cis*- and *trans*-4-*t*-butylcyclohexyltrimethylgermanes in the ratio of 86 : 14. With *cis*-4-*t*-butylcyclohexyl bromide (100%), trimethylgermyllithium gave the corresponding trimethylgermanes (cis/trans=76 : 24).

trans-4-*t*-Butylcyclohexyltrimethylstannane (100%), prepared by a reaction of *cis*-4-*t*-butylcyclohexylmagnesium bromide with trimethylchlorostannane, reacted with trimethylgermyllithium to give *cis*- and *trans*-4-*t*-butylcyclohexyltrimethylgermanes in the ratio of 80 : 20. With *cis*-4-*t*-butylcyclohexyltrimethylstannane (100%), prepared by a treatment of *trans*-4-*t*-butylcyclohexyl tosylate with lithium trimethylstannate, reacted with trimethylgermyllithium to give the corresponding trimethylgermanes (cis/trans=81 : 19).

Reactions of trimethylgermylsodium and -potassium with *cis*- and *trans*-4-*t*-butylcyclohexyl bromides and trimethylstannanes were also examined. These results

Table 1. Reactions of Trimethylgermyl Anions with 4-*t*-Butylcyclohexyl Derivatives

No.	Reactants: Me_3GeM	Reactants:	Product: (isomeric purity/%) cis : trans
	M=	X=	
1	Li	*cis*-Br (100)	76 : 24
2		*trans*-Br (100)	86 : 14
3		*cis*-$SnMe_3$ (100)	81 : 19
4		*trans*-$SnMe_3$ (100)	80 : 20
5	Na	*cis*-Br	75 : 25
6		*trans*-Br	85 : 15
7		*cis*-$SnMe_3$	81 : 19
8		*trans*-$SnMe_3$	82 : 18
9	K	*cis*-Br	77 : 23
10		*trans*-Br	82 : 18
11		*cis*-$SnMe_3$	81 : 19
12		*trans*-$SnMe_3$	81 : 19

are summarized in Table 1.

The *cis*- and *trans*-4-*t*-butylcyclohexyltrimethylgermanes were conformationally stable with trimethylgermyl anions under these reaction conditions.

The counterions and leaving groups have little influence on the ratio of cis and trans products shown in Table 1.

Either cyclohexyl derivatives provided a mixture of the germanes, with the cis isomer being predominant. The present results are consistent with the electron-transfer and free-radical processes previously proposed by Kitching and co-workers, as well as us. Thus, an electron-transfer from trimethylgermyl anions to 4-*t*-butylcyclohexyl derivatives leads to a trimethylgermyl radical and anion radicals of 4-*t*-butylcyclohexyl derivatives. A subsequent dissociation of the 4-*t*-butylcyclohexyl radical from unstable radical anions of 4-*t*-butylcyclohexyl derivatives was followed by a combination with the trimethylgermyl radical. The trimethylgermyl radical approaches the 4-*t*-butylcyclohexyl radical from an axial direction.

Steric effects clearly do not explain the product distributions shown in Table 1. These reaction preferences may be explained by torsional effects.[7,8] A 4-*t*-butylcyclohexyl radical has a chair conformation with a dihedral angle between C-H_{2ax} and the axis of the p orbital of about 20°. For an axial attack of the trimethylgermyl radical (the cis germane), no torsional interactions occur since the hydrogen on the C_1 atom does not eclipse the equatorial hydrogens on the C_2 and C_6 atoms, On the other hand, the reaction of the 4-*t*-butylcyclohexyl radical from an equatorial attack of the germyl radical (the trans germane) results in the development of torsional interactions. Therefore, the cis germane is formed predominantly.

However, S_N2 displacement and four-center processes are not always excluded.

Experimental

NMR Spectra. ^1H NMR spectra were recorded on a JEOL GX-270 at 270 MHz for $CDCl_3$ solutions, and chemical shifts are with reference to internal Me_4Si.

Materials. Me_3GeCl[9] and Me_3SnCl[10] were prepared by established methods. *cis*-[11] and *trans*-4-*t*-Butylcyclohexyl bromides,[7] *cis*- and *trans*-4-*t*-butylcyclohexyltrimethylstannanes,[6] and *cis*- and *trans*-4-*t*-butylcyclohexyltrimethylgermanes[6] were prepared according to methods cited in the literature.

Preparation of Trimethylgermyl Anions. Trimethylgermyllithium, -sodium, and -potassium were prepared from reactions of trimethylchlorogermane with alkali metals in HMPA-ether in the manner described by Bulten and Noltes.[12]

Reactions of 4-*t*-Butylcyclohexyl Derivatives with Trimethylgermyl Anions. In a typical reaction, 10 cm^3 (ca. 0.4 mmol) of trimethylgermyllithium, prepared from a reaction of trimethylchlorogermane and lithium metal in HMPA-ether, was added by syringe to 100 mg (0.4 mmol) of 4-*t*-butylcyclohexyl bromide. Reactions were carried out under an atmosphere of argon at 15 °C for 30 min; then, the system was quenched with water. The ethereal layer was separated and the aqueous layer was extracted with ether. The combined organic layers were dried over sodium sulfate. The germane was obtained by a Varian 920 preparative GLC (6 mm×2 m column, 20% SE30 on celite 545).

Stability of 4-*t*-Butylcyclohexyltrimethylgermane. 4 cm^3 (ca. 1.6 mmol) of trimethylgermyllithium was added by syringe to 50 mg (0.20 mmol) of *trans*-4-*t*-butylcyclohexyltrimethylgermane (98% pure). Reactions were carried out under an atmosphere of argon at 15 °C for 1 h. After hydrolysis of the reaction mixture with water, the ethereal layers were dried over sodium sulfate. The germane product was recovered by a preparative GLC, which was unchanged to have a trans/cis ratio of 98:2.

The authors thank Professor Yasuhiro Nakadaira of the University of Electro-Communications for the JEOL GX-270 MHz NMR spectra.

References

1) K. Mochida and N. Matsushige, *J. Organomet. Chem.*, **229**, 11 (1982).
2) K. Mochida and T. Kugita, *Nippon Kagaku Kaishi*, **1985**, 334.
3) W. Kitching, H. Olszowy, and J. Waugh, *J. Org. Chem.*, **46**, 2423 (1981).
4) W. Kitching, H. Olszowy, and K. Harvey, *J. Org. Chem.*, **47**, 1893 (1982).
5) L. M. Jackman and S. Sternhell, "Nuclear Magnetic Resonance Spectroscopy in Organic Chemistry," 2nd ed., Pergamon, New York (1969).
6) W. Kitching, H. Olszowy, and K. Harvey, *J. Org. Chem.*, **43**, 898 (1978).
7) F. R. Jensen, L. H. Gale, and J. E. Rodgers, *J. Am. Chem. Soc.*, **90**, 5793 (1968).
8) P. von R. Schleyer, *J. Am. Chem. Soc.*, **89**, 699 (1967); **89**, 701 (1967).
9) A. E. Finholt, *Nucl. Sci. Abstr.*, **6**, 617 (1957).
10) D. Gant and J. R. van Wazer, *J. Organomet. Chem.*, **4**, 229 (1965).
11) E. L. Elies and R. G. Haber, *J. Org. Chem.*, **24**, 143 (1959).
12) E. J. Bulten and J. G. Noltes, *Tetrahedron Lett.*, **1966**, 4389.

Chemistry of Germanium Atoms. V. Deoxygenation of Carbonyl Compounds by Germanium Vapor (Atom)

Kunio MOCHIDA* and Yasuhiro MIZUNO
Department of Chemistry, Faculty of Science, Gakushuin University, 1-5-1 Mejiro, Tokyo 171
(Received April 8, 1988)

Synopsis. The co-condensation of thermally evaporated germanium vapor with carbonyl compounds was found to yield olefins and germanium monoxide.

Studies of metal-vapor reactions have been of considerable interest in organometallic chemistry and organic synthesis during the last few decades.[1] With this type method, it is proving to be feasible to synthesize organometallic compounds which would be difficult, if not impossible, to prepare by other methods and to study their reactive intermediates.

The study of a carbon atom as the homologue of a germanium atom has been well investigated, while the chemical properties of a germanium atom have been little studied.[2-7] In studying the reaction of germanium atoms in the condensed phase, we have found that germanium vapor (atom) abstracts oxygen atom from carbonyl compounds.

In this paper, we first describe the deoxygenation of carbonyl compounds by germanium vapor (atom).

Results and Discussion

The reaction of thermally vaporized germanium atoms with carbonyl compounds was examined. The results are summarized in Table 1.

The reaction of germanium atoms with acetone produced propylene (1.0%) and germanium monoxide.[8] Other aliphatic ketones showed a similar behavior; the reactions of germanium atoms with 3-pentanone, 2-pentanone, and 4-heptanone gave 2-pentene (3.6%), 1-pentene (3.6%) and 2-pentene (5.0%), and 3-heptene (2.6%), respectively, shown in Table 1. With cyclohexanone and methylcyclohexanones, germanium atoms gave cyclohexene and methylcyclohexenes (0.4—2.0%) as expected, and germanium monoxide. Other products, in addition to olefins and germanium monoxide, were negligible (>0.1%) in the reactions of germanium atoms with carbonyl compounds.

Table 1. The Reaction of Germanium Atoms with Carbonyl Compounds

Substrate	Product (Yield/%)[a]
CH_3COCH_3	$CH_3CH{=}CH_2$ (1.0)
$C_2H_5COC_2H_5$	$C_2H_5CH{=}CHCH_3$ (3.6)
$CH_3COC_3H_7$	$CH_2{=}CHC_3H_7$(3.6), $CH_3CH{=}CHC_2H_5$ (5.0)
$C_3H_7COC_3H_7$	$C_2H_5CH{=}CHC_3H_7$ (2.6)
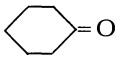	(0.5)
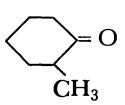	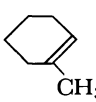 (0.4), 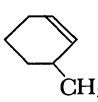 (1.2)
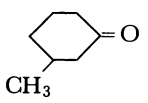	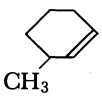 (0.8), 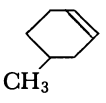 (0.4)
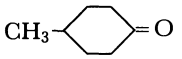	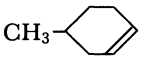 (2.0)

a) GLC yields. Yields of products were determined on the basis of the amount of the germanium metal consumed on the assumption that all of the germanium metal completely reacted with carbonyl compounds.

Blank experiments were carried out under identical conditions. As a result, the products shown in Table 1 were attributable to the interaction of germanium atoms with the starting carbonyl compounds.

The products, olefins shown in Table 1 are strong evidence for the intermediacy of carbenes in the deoxygenation of carbonyl compounds by germanium vapor (atoms). The carbenes are known to rearrange to isomeric olefins.[9,10]

When a mixture of carbonyl compounds and a large excess of cyclohexene as a carbene trapping reagent was used as a matrix for germanium vapor (atoms), no peak of 7,7-dialkylnorcaranes was detected by GC-MS. The yields of the olefins produced were almost

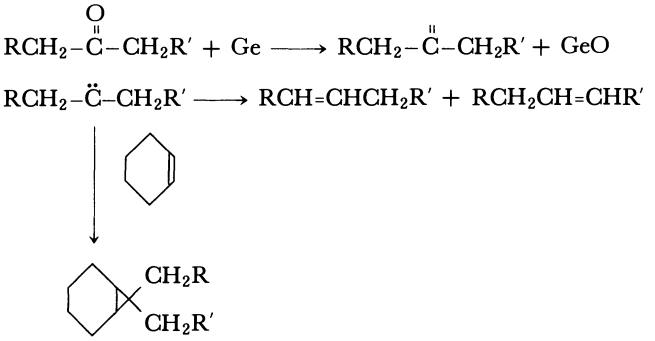

Scheme 1.

constant, despite the presence of cyclohexene. These results indicate that a ketone may complete for germanium atoms in the presence of an olefin and that intramolecular stabilization of alkylcarbenes by product formation is more rapid than an olefin addition, even at −196 °C.

The deoxygenation of oxygen-containing compounds by germanium vapor (atoms) can be rationalized in terms of the large value of the heat of combination of a germanium atom with an oxygen atom (155 kcal mol^{-1}, 1 cal=4.184 J).[11]

Similar results have been reported for the co-condensation of carbon atoms with carbonyl compounds.[12-14]

It is interesting that our results indicate no distinction between thermally generated germanium atoms

and nucleogenetic carbon atoms based on the reaction with carbonyl compounds.

Experimental

The reaction apparatus and conditions employed in this study have been described previously (ca. 1200—1300 °C, 5×10^{-3} Torr, 1 Torr=133.322 Pa).[5] In a typical experiment 0.5 g (6.9 mmol) of germanium metal was evaporated at a rate of ca. 10 mg·min^{-1} while an excess of acetone (ca. 15 cm^3) was co-condensed on the walls of a reaction flask containing an alumina-coated tungsten crucible and a perforated inlet tube through which acetone was introduced as vapor. The reaction flask was immersed in liquid nitrogen during the germanium evaporation. After germanium evaporation and the introduction of acetone were completed, the flask was warmed to room temperature and allowed to stand for 1.5 h.

The reaction mixture was fractionated by low-pressure trap-to-trap distillation on a vacuum line. The products were identified by comparing their GC-MS and retention times on GLC with those of authentic samples. The amounts of products were calculated by GLC with an internal-standard method.

GLC analyses were performed on a Shimadzu GC-4A and 8A gas chromatograph equipped with a 2-m column packed with 20% SE-30 or 20% squalane. GC-MS were obtained with a JEOL JMS-DX 303 mass spectrometer and data analyses were performed on a JMN-DA 5000 mass data system.

The authors thank Mitsubishi Metal Corporation for a gift of germanium metal. This work was supported in part by Grant-in-Aid for Specially Project Research (Nos. 61125004 and 62115003) provided by the Ministry of Education, Science and Culture.

References

1) For example: a) J. R. Blackborow, "Metal Vapor Synthesis in Organometallic Chemistry," Springer-Verlag, New York (1979); b) K. J. Klabunde, "Chemistry of Free Atoms and Particles," Academic Press, New York (1980); c) K. J. Klabunde, "Reactive Intermediates," ed by R. A. Abramovitch, Plenum, New York (1980), Vol. 1.

2) M. J. McGlinchey and T. -S. Tan, *Inorg. Chem.*, **14**, 1209 (1975).

3) R. T. Conlin, S. H. Lockhart, and P. P. Gasper, *Chem. Commun.*, **1975**, 825.

4) A. Bos, *Chem. Commun.*, **1972**, 26.

5) K. Mochida and K. Tashiro, *Nippon Kagaku Kaishi*, **1987**, 1168.

6) K. Mochida and K. Tashiro, *Chem. Lett.*, **1987**, 1105; K. Mochida, K. Tashiro, Y. Yoshida, and Y. Mizuno, *Bull. Chem. Soc. Jpn.*, **61**, 1247 (1988).

7) K. Mochida and Y. Yoshida, *Bull. Chem. Soc. Jpn.*, **61**, 1789 (1988).

8) IR (in KBr) of germanium monoxide containing unreacted germanium powder: 820 cm^{-1}.

9) L. Frieman and H. Schechter, *J. Am. Chem. Soc.*, **81**, 5512 (1951).

10) W. Kirme and B. V. Bülow, *Chem. Ber.*, **96**, 3316 (1963).

11) L. Brewer, *Chem. Ber.*, **52**, 2 (1953).

12) P. S. Skell, J. H. Plonka, and R. R. Engel, *J. Am. Chem. Soc.*, **89**, 1748 (1967).

13) P. S. Skell and J. H. Plonka, *J. Am. Chem. Soc.*, **92**, 836 (1970).

14) P. S. Skell and J. H. Plonka, *J. Am. Chem. Soc.*, **92**, 2160 (1970).

A Michael Reaction Product of Cyclohexylidenemalononitrile

Yoshiharu NAKANO,* Hiroaki YOKOTA, Minoru IGARASHI, and Shoichi SATO†
Depertment of Chemistry, Faculty of Science, Ibaraki University, Mito 310
†The Institute for Solid State Physics, The University of Tokyo, Roppongi 7-22-1, Tokyo 106
(Received March 31, 1988)

Synopsis. Cyclohexylidenemalononitriles dimerize and cyclize to give 3-amino-2,4-dicyano-2-[imino(methoxy)-methyl]spiro[bicyclo[4,4,0]deca-3,5-diene-1,1′-cyclohexane] (**3**). The crystal structure of **3** was determined by an X-ray diffraction method.

Alkylidenecyanoacetates and cyclohexanone undergo a Michael reaction to give cyclization products.[1] We investigated similar Michael-type cycloaddition reactions of alkylidenemalononitriles using sodium methoxide, and found that acyclic alkylidenemalononitriles dimerized and cyclized to give 2-azabicyclo[2.2.2]-octadiene derivatives (**1**)[2] whose crystal structure could be determined by an X-ray diffraction method, as shown in Fig. 1.[3] The bridged compounds release

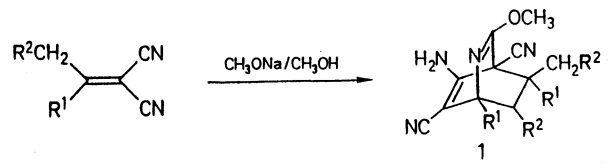

Fig. 1. Reactions of acyclic alkylidenemalononitliles.

alkene to give pyridine derivertives. Contrary to acyclic compounds, cyclohexylidenemalononitrile was found to give an imidate derivertive **3** which was different from expected bridged compounds (Fig. 2). We

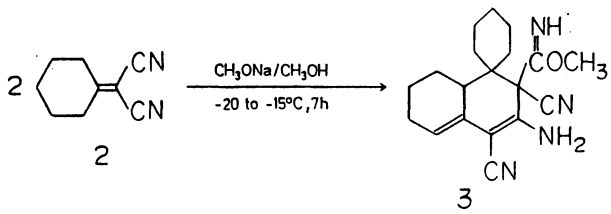

Fig. 2. Reaction of cyclohexylidenemalononitrile.

report here the results of an X-ray crystal diffraction of 3.

Experimental

Cyclohexylidene malononitriles were obtained according to usual Knoevenagel reaction procedure. Sodium methoxide was purchased from Kanto Chemical, and methanol was dried with magnesium methoxide.

Preparation of 3. To a solution of cyclohexylidenemalononitrile (2.92 g, 0.02 mol) in methanol (20 ml) was added sodium methoxide (0.54 g, 0.01 mol) at 5—7 °C with stirring. Stirring was continued for 6 h and then the reaction mixture was left for 6 h at 5—7 °C. The precipitate formed was filtered, washed with cold methanol, dried in vacuo, and recrystallized from acetone to give 0.9 g (yield 30%) of **3** (mp 227—230 °C. Found: C, 69.99; H, 7.35; N, 16.97%. Calcd for $C_{19}H_{24}N_4O$: C, 70.34; H, 7.46; N, 17.27%).

X-Ray Crystallography. A single crystal obtained from ethanol with approximate dimensions of 0.30×0.25×0.43 mm was used for data collection. The crystal data are as follows; $C_{19}H_{24}N_4O$, M_w=324.2, monoclinic, $P2_1/c$, a=16.141 (2), b=9.078(1), c=11.942(2) Å, β=100.45(2)°, U=1720.8(5) Å^3, Z=4, D_x=1.252 g cm^{-3}, D_m=1.258 g cm^{-3}, μ(Mo $K\alpha$)=0.867 cm^{-1}. The crystal was mounted on a Rigaku AFC 5R diffractometer at Institute for Molecular Science and intensity data were collected up to 2θ=60° with graphite monochromated Mo $K\alpha$ radiation. Unit cell parameters were determined by a least-squares refinement from setting angles of 42 accurately adjusted reflections ($27 \leq 2\theta \leq 41°$). In total, 2670 reflections ($|F_o| > 2.5\sigma(F_o)$) out of 5480 independent reflections ($0 \leq h \leq 22$, $0 \leq k \leq 12$, $-16 \leq l \leq 16$) were used for the refinement. Three standard reflections were measured at every 100 reflections, and no significant deterioration was observed. Lorentz and polarization corrections were applied. Subsequent calculations were carried out using a universal program (UNICS III)[4] at Institute for Molecular Science and at the University of Tokyo. The structure was solved by a direct method. All the non-hydrogen atoms appeared and almost all the interpeak distances were reasonable. The refinements were carried out by a block-diagonal least-squares method with anisotropic thermal parameters for non-hydrogen atoms. All the hydrogen atoms were located on the difference Fourier Maps and were refined isotropically to final R values

Table 1. Final Atomic Parameters with Estimated Stadard Deviations

Atom	X	Y	Z	B_{eq}
O	5651(1)	402(3)	2257(2)	3.3
N(1)	5386(2)	1753(3)	−247(3)	3.9
N(2)	6613(2)	−1447(3)	2563(2)	3.4
N(3)	6444(2)	−1470(3)	−402(2)	3.1
N(4)	8384(2)	−2724(4)	−924(3)	4.7
C(1)	8497(2)	−70(3)	1242(3)	2.5
C(2)	9324(2)	−160(4)	1207(4)	4.1
C(3)	9987(2)	565(5)	2065(5)	5.4
C(4)	9654(2)	917(5)	3140(4)	4.9
C(5)	8837(2)	1788(4)	2825(3)	3.3
C(6)	8150(2)	847(3)	2103(2)	2.3
C(7)	7358(2)	1708(3)	1498(2)	1.9
C(8)	6671(2)	465(3)	1049(2)	1.9
C(9)	7020(2)	−700(3)	329(2)	2.0
C(10)	7866(2)	−883(3)	436(2)	2.3
C(11)	7523(2)	2585(3)	444(2)	2.3
C(12)	7899(3)	4116(4)	648(3)	4.3
C(13)	7420(3)	5047(4)	1375(4)	4.9
C(14)	7368(2)	4277(4)	2485(3)	3.6
C(15)	6979(2)	2739(3)	2300(2)	2.7
C(16)	5941(2)	1186(3)	318(2)	2.4
C(17)	6328(2)	−317(3)	2033(2)	2.3
C(18)	5253(3)	−223(5)	3140(4)	5.0
C(19)	8160(2)	−1924(3)	−315(3)	3.0

Positional parameters are multiplied by 10**4. Thermal parameters are given by the equivalent temperature factors (A**2).

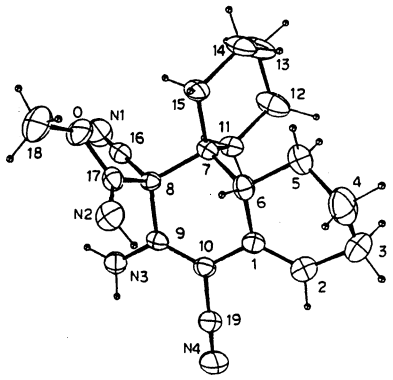

Fig. 3. Perspective view of **3** and the numbering of the atoms.

$0.060[R_w=0.088$, $w=1/(3.0+0.01|F_o|^2)$ for $|F_o|<15$ and $w=1/(\sigma^2(F_o)+0.0013|F_o|^2)$ for $|F_o|\geq 15]$. There was no residual peak greater than 0.7 e Å^{-3}.

Table 1 lists the non-hydrogen atomic coordinates with equivalent isotropic temperature factors.[5]

Results and Discussion

Molecular Structure. A perspective view of **3** is shown in Fig. 3. Table 2 lists selected bond distances and angles. We expected that **3** is a bridged compound, as described earlier,[2] on the basis of ^{1}H NMR spectra. Contrary to our expectation, it had a free imidate and a double bond instead of a bridged structure. We could not find any remarkable structural characteristics that favor a bicyclo compound instead of a bridged structure and stabilize the imidate group. The bond distances, C(17)-N(2) and O-C(17), are rather shorter than usual C-N double bond and C-O single bond, respectively. Thus, electrophilicity of C(17) should be rather small. A cyclohexane ring attaches perpendiculary to an almost planar hexalin system. The bond distances, C(7)-C(8) and C(8)-C(9), are elongated, probably due to a steric interaction among the substitutents. Other bond distances and angles are all normal. We are investigating similar reactions for other cycloalkylidenemalononitriles; their results will be reported elsewhere.

Table 2. Bond Distances and Angles with Estimated Standard Deviations

Atom	Distance/Å	Atom	Distance/Å
O-C(17)	1.341(4)	N(2)-C(17)	1.249(4)
N(3)-C(9)	1.348(4)	C(1)-C(2)	1.345(5)
C(1)-C(10)	1.467(4)	C(7)-C(8)	1.605(4)
C(8)-C(9)	1.533(4)	C(9)-C(10)	1.358(4)
	Angle/degree		Angle/degree
O-C(17)-N(2)	122.5(3)	C(7)-C(8)-C(9)	111.7(2)
O-C(17)-C(8)	110.0(2)	C(7)-C(8)-C(17)	112.7(2)
N(2)-C(17)-C(8)	127.3(3)	C(16)-C(8)-C(17)	106.9(2)

References

1) M. Igarashi, Y. Nakano, and M. Yatsu, *Synthesis*, **1984**, 1075.

2) M. Igarashi, Y. Nakano, M. Yatsu, T. Watanabe, and S. Sato, *Synthesis*, **1987**, 68.

3) Y. Nakano, M. Igarashi, and S. Sato, *Acta Crystallogr., Sect. C*, **43**, 738 (1987).

4) T. Sakurai and K. Kobayashi, *Rep. Inst. Phys. Chem. Res.*, **55**, 69 (1979).

5) The F_o-F_c table, anisotropic temperature facters, hydrogen positional parameters, isotropic thermal parameters, data of possible hydrogen bonds, and non-essential bond distances and angle are kept as Document No. 8840 at the Chemical Society of Japan.

Fries Rearrangement in Calixarene Esters: A New Entry for the Synthesis of *p*-Substituted Calixarenes

Takashi ARIMURA, Seiji SHINKAI,* Tsutomu MATSUDA, Yoshimi HIRATA,†
Hiroshi SATOH,† and Osamu MANABE†
Department of Organic Synthesis, Faculty of Engineering, Kyushu University, Fukuoka 812
†Department of Industrial Chemistry, Faculty of Engineering, Nagasaki University, Nagasaki 852
(Received June 23, 1988)

Synopsis. The Fries rearrangement was found to be a convenient method to synthesize *p*-acylcalixarenes from *O*-acylcalixarenes, the yields being relatively good (29—34%) as a synthetic method for *p*-substituted calixarenes.

Calixarenes are cyclic oligomers made up of benzene units as cyclodextrins are made up of glucose units. Since calixarenes possess a novel cylindrical architecture, they are expected to be useful for designing cavity-shaped host molecules.[1,2] In order to obtain functionalized calixarenes for host molecules, it is indispensable to find new synthetic methods to introduce various substituents into calixarenes. The first method is the direct substitution of the *p*-position (sulfonation, nitration, etc.).[1-5] However, this method is hampered by a fact that it is fairly difficult to isolate a fully-substituted product from lower-substituted by-products. Thus, the application of this method is limited to the very clean reactions. The second method is the rearrangement of the substituents on the OH groups to the *p*-position. Gutsche and Levine[6] introduced the Claisen rearrangement of the allyl ether of calixarenes to *p*-allylcalixarenes, but the allyl group is rather useless as an intermediate for functionalized calixarenes. We here address a new method to synthesize *p*-acylcalixarenes by the Fries rearrangement from esters of calix[6]arenes. The acyl group is a more versatile functional group to derive alcohols, imines, oximes, etc.

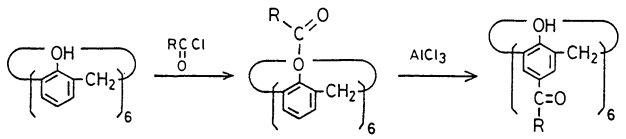

a: R = $CH_3(CH_2)_4$- b: R = $CH_3CH_2CH(CH_3)$-

Experimental

Acylation of calix[6]arene (**1**) was carried out according to the method of Gutsche and Lin for 25,26,27,28-tetraacetoxycalix[4]arene.[7] 37,38,39,40,41,42-Hexakis(hexanoyloxy)calix[6]arene (**2a**); recrystallized from hexane, mp 198—200 °C, yield 50%. IR (KBr): $\nu_{C=O}$ 1755 cm^{-1}, no ν_{OH} ^1H MNR (Me_2SO-d_6, 100 °C): CH_3, δ=0.84, 3H; $(CH_2)_3$, 1.24—1.49, 6H; $COCH_2$, 2.98, 2H; $ArCH_2Ar$, 3.66, 2H; aromatic protons, 6.80, 3H. Found: C, 76.42; H, 7.84%. Calcd for $(C_{13}H_{16}O_2)_6$: C, 76.44; H, 7.89%.

37,38,39,40,41,42-Hexakis[(2-methylbutanoyl)oxy]calix[6]arene (**2b**); recrystallized from *N*,*N*-dimethylformamide (DMF), mp 332—335 °C, yield 51%. IR(KBr): $\nu_{C=O}$ 1750 cm^{-1}, no ν_{OH}. ^1H NMR (Me_2SO-d_6, 160 °C): CH_3, δ=0.83 and 1.02, 3H each; CH_2, 1.42 and 1.63, 1H each; CH, 2.68, 1H; $ArCH_2Ar$, 3.62, 2H; aromatic protons, 6.84, 3H. Found: C, 75.17; H, 7.44; N, 0.41%. Calcd for $(C_{12}H_{14}O_2)_6 \cdot 0.35$DMF: C, 75.18; H,7.47; N, 0.42%. It was difficult to remove a trace amount of DMF which is possibly included in **2b** as a clathrate complex.

A typical experimental run for the Fries rearrangement of **2** to **3** is as follows: a mixture of **2** (0.88 mmol) and $AlCl_3$ (2.3 g, 15.8 mmol) was stirred in 40 ml of chlorobenzene at 45—50 °C for 17 h under a nitrogen atmosphere. After cooling water was added to the reaction mixture and the organic phase was diluted with 100 ml of chloroform, washed with 1 mol dm^{-3} HCl and water, and then dried over $MgSO_4$. The solution was concentrated in vacuo, and the oily residue was recrystallized from acetone. The crystals **3** were collected by centrifugation and then recrystallized from tetrahydrofuran for **3a** and chloroform-methanol for **3b**. The products gave satisfactory elemental analyses and spectral properties (IR, NMR) consistent with **3**.

5,11,17,23,29,35-Hexahexanoylcalix[6]arene (**3a**); mp 227—230 °C, yield 29%. IR (KBr): ν_{OH} 3375 cm^{-1}, $\nu_{C=O}$ 1670 cm^{-1}. ^1H NMR ($CDCl_3$, 25 °C): CH_3, δ= 0.91, 3H; $(CH_2)_3$, 1.38—1.72, 6H; $COCH_2$, 2.91, 2H; $ArCH_2Ar$, 4.00, 2H; aromatic protons, 7.87, 2H; OH, 10.42, 1H. Found:C, 76.41; H, 7.84%. Calcd for $(C_{13}H_{16}O_2)_6$:C, 76.44; H,7.89%.

5,11,17,23,35-Hexakis(2-methylbutanoyl)calix[6]arene (**3b**); >mp 360 °C, yield 34%. IR (KBr): ν_{OH} 3370 cm^{-1}, $\nu_{C=O}$1665 cm^{-1}. ^1H NMR ($CDCl_3$, 25 °C): CH_3, 0.89 and 1.13, 3H each; CH_2, 1.50 and 1.79, 1H each; CH, 3.36, 1H; $ArCH_2Ar$, 4.01, 2H; aromatic protons, 7.88, 2H; OH, 10.47, 1H. Found: C, 75.15; H, 7,14%. Calcd for $(C_{12}H_{14}O_2)_6 \cdot 0.09CHCl_3$: C, 75.15; H, 7.36%. A weak peak of included $CHCl_3$ was observed in the NMR spectrum when ^1H NMR was taken in Me_2SO-d_6.

All the ^1H NMR spectra were measured with JEOL GX-400.

Results and Discussion

We first tried the Fries rearrangement of 37,38,39,40,41,42-hexaacetoxycalix[6]arene. However, the rearrangement did not take place under the reaction conditions described in Experimental. When the more drastic reaction conditions (high temperature, increase in $AlCl_3$, etc.) were employed, the product was black resin insoluble in any solvents.** We thus used **2a** and **2b** as starting esters and found that the Fries rearangement really takes place.

It is not easy to enhance the yield for the synthesis of *p*-substituted calixarene derivatives. If the rearrange-

** It is not clear why the Fries rearrangement of the acetyl derivative does not take place. It is known that Friedel-Crafts acylation of benzocrown ethers catalyzed by aluminium chloride is impractical: W. W. Parish, P. E. Scott, and C. W. McCausland, *J. Org. Chem.*, **43**, 4597 (1978) and F. Wada and T. Matsuda, *Bull. Chem. Soc. Jpn.*, **53**, 421 (1980). The peculiar behavior may be attributable to an interaction between the smaller $AlCl_3$-CH_3COCl complex with the ionophoric calixarene ester.

Table 1. Melting Points, Yields, and Coalescence Temperatures of **2** and **3**

Calix[6]arene	Appearance	Mp θ_m/°C	Yield/%	T_c/°C[a]
2a	Colorless prisms	198—200	50	5
2b	Colorless prisms	332—335	51	50
3a	Colorless powder	227—230	29	−3
3b	Colorless powder	>360	34	0
p-Hexylcalix[6]arene[b]	Colorless powder	305—307	22[b]	−70

a) Pyridine-d_5. The methylene protons in these compounds (except **2a**) gave a singlet above T_c, whereas those in **2a** gave the two peaks in 2 : 1 ratio. b) This compound was synthesized from *p*-hexylphenol and formaldehyd[9].

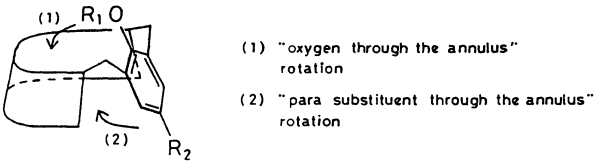

Fig. 1. Two possible rotation mechanisms in calixarenes.

ment is assumed to occur successively, the total yield for fully-substituted calix[6]arene becomes only 26.2% (=0.80^6) even though the yield for each benzene unit is 80%. This is a special situation in the modification of cyclic compounds. The yields obtained in the Fries rearrangement (29—34%) are apparently low. But, they are classified as good yields for the synthesis of *p*-substituted calix[6]arenes since these values imply that the rearrangement in each benzene unit occurs in 81—85% yields (i.e., 0.81^6=29%, 0.85^6=34%). The yields are higher than that for the Claisen rearrangement in calix[6]arene (21%).[7] This suggests that the Fries rearrangement well competes with or is superior to the Claisen rearrangement as a synthetic method for *p*-substituted calixarenes. Since the yield for **3b** is comparable with that for **3a**, this reaction is not so subject to the steric effect.

It is known that the temperature-dependent ^{1}H NMR spectrum of calix[6]arenes displays a few sets of overlapping pairs of doublets for the $ArCH_2Ar$ methylene hydrogens at low temperature and a singlet resonance at high temperature.[8] This behavior is interpreted in terms of conformational change form "cone" (or "hinged cone") to "alternate",[1,2] resulting in a coalescence temperature (T_c) at the intermediate. Determination of the T_c of **2** and **3** in pyridine-d_6 (−70—90 °C) (Table 1) showed that compounds **2** have the T_c higher than **3**, indicating that increased freezing of the partial conformations can be observed for the ester derivatives. In particular, **2b** has the very high T_c (50 °C) probably due to the bulky *s*-butyl group. Two possible mechanisms have been proposed for the rotation of the benzene unit, (1) oxygen through the annulus rotation and (2) para substituent through the annulus rotation (Fig. 1).[8] The fact that the T_c becomes higher only when the substituent is introduced into the OH group supports that the conformational change occurs according to the "oxygen through the annulus" rotation mechanism: that is, the T_c is sensitive to steric bulkiness of the substituent (R_1) on the oxygen but not so much to that of the para substituent (R_2).

Interestingly, the T_c values for **3a** and **3b** are surprisingly higher than those for calix[6]arene (−70 °C),[8] *p-t*-butylcalix[6]arene (−54 °C),[8] and *p*-hexylcalix[6]arene (−70 °C)[9] in pyridine-d_5. The origin of the remarkable T_c difference between *p*-acylcalix[6]arenes and *p*-alkylcalix[6]arenes is still a matter of controversy. We believe that the most probable rationale is the lower shift of the pK_a of the OH groups due to the electron-withdrawing *p*-acyl groups, which would strengthen the hydrogen-bonding interaction among the OH groups and stabilize accordingly the "cone" conformation in solution.

In conclusion, the present paper indicated that the Fries rearrangement is very useful for the synthesis of *p*-acylcalixarene derivatives. Further functionalization of *p*-acylcalixarenes is now under investigation in these laboratories.

References

1) C. D. Gutsche, *Acc. Chem. Res.*, **16**, 161 (1983).
2) C. D. Gutsche, "Host Guest Complex Chemistry/Macrocycles," Springer-Verlag, Berlin (1985), p. 375.
3) S. Shinkai, S. Mori, H. Koreishi, T. Tsubaki, and O. Manabe, *J. Am. Chem. Soc.*, **108**, 2409 (1986).
4) S. Shinkai, T. Tsubaki, T. Sone, and O. Manabe, *Tetrahedron Lett.*, **26**, 3343 (1985).
5) S. Shinkai, *Pure Appl. Chem.*, **58**, 1523 (1986).
6) C. D. Gutsche and J. A. Levine, *J. Am. Chem. Soc.*, **104**, 2652 (1982).
7) C. D. Gutsche and L.-G. Lin, *Tetrahedron*, **42**, 1633 (1986).
8) C. D. Gutsche and L. J. Bauer, *J. Am. Chem. Soc.*, **107**, 6052, 6059 (1985).
9) T. Arimura, H. Satoh, and S. Shinkai, unpublished.

Facile Reaction of *Te*-Aryl Benzenecarbotelluroates, ArCOTeAr', with Methyl Iodide and Halogens

Harkesh B. SINGH* and Narasimhan SUDHA
Department of Chemistry, Indian Institute of Technology, Powai, Bombay 400076, India
(Received November 26, 1987)

Synopsis. Reaction of *Te*-aryl benzenecarbotelluroates of the type ArCOTeAr' (Ar=phenyl *p*-tolyl, *p*-bromophenyl; Ar'=phenyl, *p*-methoxyphenyl) with methyl iodide was found to give symmetrical telluronium salts, $[Ar'Te(CH_3)_2]^+I^-$ in good yields. The reactivity of one of these benzene carbotelluroates towards halogens was also examined.

Although diaryl and dialkyl tellurides are known to react with methyl iodide to form the corresponding telluronium salts (Scheme 1),[1] it has been newly found that reaction of *Te*-aryl benzenecarbotelluroates with methyl iodide results in cleavage of the Te-CO bond.

$$R_2Te + CH_3I \rightarrow [R_2(CH_3)Te]^+I^-$$

Scheme 1.

When benzenecarbotelluroates (**1a—d**) were treated with excess of methyl at room temperature for 48 h, colorless $[Ar'Te(CH_3)_2]^+I^-$ (**2a—b**) were formed in yields of 70—90% based on the used tellurides **1**, together with trace amounts of as yet uncharacterized dark-violet compounds (Scheme 2) which contain carbonyl function. In no reaction was obtained the expected product **3**.

$$ArCTeAr' + CH_3I \longrightarrow \begin{cases} [Ar'Te(CH_3)_2]^+I^- & \mathbf{2} \\ [ArCTeAr'(CH_3)]^+I^- & \mathbf{3} \end{cases}$$

1a: Ar'=C_6H_5, Ar=C_6H_5 **2a**: Ar'=C_6H_5
1b: Ar'=C_6H_5, Ar=*p*-BrC_6H_4 **2b**: Ar'=*p*-$CH_3OC_6H_4$
1c: Ar'=C_6H_5, Ar=*p*-$CH_3C_6H_4$
1d: Ar'=*p*-$CH_3OC_6H_4$, Ar=*p*-$CH_3C_6H_4$

Scheme 2.

Whereas the halogenolysis reactions of similar compounds, tellurophthalide and tellurophthalic anhydride have been reported earlier,[2] to the best of our knowledge no reaction of benzenecarbotelluroates with methyl iodide has been previously described.

The scheme which most reasonably accounts for the results can be written as follows:

$$ArCTeAr' \xrightarrow[\text{Slow}]{CH_3I} [ArCTe^+CH_3Ar'\cdot I^-] \quad \mathbf{3}$$

$$\xrightarrow[\text{Fast}]{-ArCOI} [CH_3TeAr'] \xrightarrow[\text{Fast}]{CH_3I} (CH_3)_2Te^+Ar'\cdot I^- \quad \mathbf{2}$$

In order to learn more about the behavior of the Te-CO bond, we have investigated the halogenolysis reactions of **1d**. It was found that the benzenecarbotelluroate reacted with excess of SO_2Cl_2, Br_2, or I_2 at room temperature to afford the corresponding $Ar'TeX_3$ (X=Cl, Br, I) via cleavage of the Te-CO bond.

Experimental

Materials and Instruments. The *Te*-aryl benzenecarbotelluroates were prepared by the reaction of a benzoyl chloride with NaTeAr'.[3] All compounds had melting points and ν_{CO}'s in good agreement with those reported in the literature. IR spectra (4000—600 cm^{-1}) were obtained in KBr discs with Perkin Elmer 681. ^1H NMR (100 MHz) were obtained with a JEOL FX 100 instrument. Elemental analysis was by the Analytical Services Section, Regional Sophisticated Instrumentation Centre, Lucknow.

Reaction of $C_6H_5TeCOC_6H_5$ with CH_3I. To the benzenecarbotelluroate (0.25 g, 0.8 mmol) was added methyl iodide (2—3 ml) in a 50 ml flask and then capped. The resulting solution was allowed to stand for 48 h at ambient temperature during which time yellowish crystals separated out and the color of the solution turned dark-red. After 48 h absolute ether (10 ml) was added to the reaction mixture and allowed to stand for additional 12 h. The crystals were filtered, washed with ether, recrystallized from ethanol/water (1:1) to yield white crystals of $[C_6H_5Te(CH_3)_2]^+I^-$; yield 0.2 g (70% based on **1a** used), mp 168 °C.[4] Calcd (Found): C, 26.5 (25.9%); H, 3.06 (3.51%). ^1H NMR (DMSO-d_6) δ=2.38 (s, 6H), 7.5—7.9 (m, 5H). The red mother liquor was evaporated to dryness and the residue was washed with petroleum ether (40—60 °C) to give a dark violet solid of indefinite composition. IR (KBr) 1685 cm^{-1} (ν_{CO}). Reactions of $C_6H_5TeCOC_6H_4Br$-*p* and $C_6H_5TeCOC_6H_4CH_3$-*p* with CH_3I also gave $[C_6H_5Te(CH_3)_2]^+I^-$ in excellent yields (ca. 90%) and trace quantities of the brownish red solids. Reaction of *p*-$CH_3OC_6H_4TeCOC_6H_4CH_3$-*p* with CH_3I yielded [*p*-$CH_3OC_6H_4Te(CH_3)_2]^+I^-$ in excellent yield (ca. 86%), mp 172 °C (lit,[5] 170—172 °C). Calcd (Found): C, 27.5 (26.9%); H, 3.34 (3.57%). ^1H NMR (DMSO-d_6) δ=2.3 (s, 6H), 3.8 (s, 3H), 7.0—7.8 (m, 4H). A brownish red solid of indefinite composition was also obtained.

Halogenolysis Reactions. In a typical reaction, to a solution of *p*-$CH_3OC_6H_4TeCOC_6H_4$-*p* (0.4 g, 1.13 mmol) in chloroform (25 mL) was added dropwise iodine (0.28 g, 1.13 mmol) dissolved in chloroform at room temperature during 30 min. *p*-$CH_3OC_6H_4TeI_3$ is continuously precipitated as a dark violet solid, mp 130 °C (d), yield 0.35 g (91%) (based on **1d** used). Analogous reactions of Br_2 and SO_2Cl_2 with **1d** afforded *p*-$CH_3OC_6H_4TeBr_3$ and *p*-$CH_3OC_6H_4TeCl_3$ which were characterized by comparison with authentic samples (mp, IR, ^1H NMR).[1]

The authors would like to thank one of the referee(s) for his valuable suggestions.

References

1) K. J. Irgolic, "The Organic Chemistry of Tellurium," Gordon and Breach, New York (1974), p. 208.

2) L. Engman and M. P. Cava, *J. Org. Chem.*, **46**, 4194 (1981).
3) S. A. Gardner and H. J. Gysling, *J. Organomet. Chem.*, **197**, 111 (1980).
4) J. L. Piette and M. Renson, *Bull. Soc. Chim. Belges.*, **79**, 353 (1970).
5) G. T. Morgan and H. D. K. Drew, *J. Chem. Soc.*, **1925**, 2307.

The Vapor-Phase Preparation of V-P-O Catalysts Effective for Butane Oxidation to Maleic Anhydride

Yusaku TAKITA,* Takao HASHIGUCHI, and Hitoshi MATSUNOSAKO
Department of Environmental Chemistry and Engineering, Faculty of Engineering, Oita University, Oita 870-11
(Received February 29, 1988)

Synopsis. Almost pure α-$VOPO_4 \cdot 2H_2O$ powder was obtained by a vapor-phase reaction between $POCl_3$, $VOCl_3$, and water at about 763K in the presence of oxygen. Although α-$VOPO_4 \cdot 2H_2O$ changed into α- and β-$VOPO_4$ in the calcination in N_2, it was transformed into $(VO)_2P_2O_7$ and a small amount of β-$VOPO_4$ by in situ activation at 733 K at the heating rate of 10 K min^{-1} in a C_4H_{10}-O_2-N_2 stream, the resulting catalysts effected the selective oxidation of butane to maleic anhydride comparable to pure $(VO)_2P_2O_7$.

The production of maleic anhydride (MA) has been achieved practically by the oxidation of benzene and butenes (1-butene, *cis*-2-butene, *trans*-2-butene), MA production by the oxidation of butane has, however, been magnified since it has distinct economical merit.

V-P-O catalysts have been claimed to be effective for the oxidation of butane[1] and there are many studies on the catalysis of the V-P-O system from the viewpoint of the active phases for the reaction,[2] the role of a small excess of phosphorus in catalysts,[3,4] the differences in composition between bulk and surface,[5] the reaction path[6] and so on.

There also are much patent literature concerning the preparation method of the selective catalysts.[7] The preparation methods published so far can be classified into two large categories. One is the method using V_2O_5 as a starting material and the other is the method using organic or inorganic vanadium compounds. Each category can be further subdivided into many groups in terms of the reducing agents. Common to all is the use of a liquid reaction medium.

In this paper, the authors deal with a new vapor-phase preparation of V-P-O catalysts effective for MA synthesis from butane using vanadium chloride oxide and phosphoryl chloride as the starting materials.

First, the reaction conditions suitable for the preparation of powders containing V and P were explored extensively. The following conclusions were abstracted from the experiments.

(1) N_2 is suitable for the carrier gas of both $VOCl_3$ and $POCl_3$ vapor.

(2) $VOCl_3$ and $POCl_3$ should be mixed in a vapor phase at the place just before the entrance of a reactor.

(3) O_2 is favorable for the carrier gas of water vapor.

(4) The collector of the powders formed should be kept at about 420 K to prevent the condensation of the hydrochloric and phosphorus containing acids formed.

An improved apparatus for the catalyst preparation is shown in Fig. 1. The length of the reactor used here was about 15 cm which was sufficient to form oxide powders. The optimum flow rates of the introducing gases were dependent on the length and diameter of the reactor. The adoption of 1 ± 0.2 as the flow rate ratio, $F_{(O_2+H_2O)}/F_{(N_2)}$, and 9—10 as the linear velocity ratio, $L_{(O_2+H_2O)}/L_{(N_2)}$, maintained the powder formation for at least 17 h.

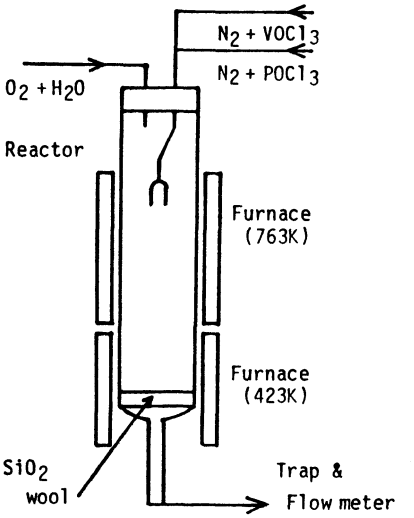

Fig. 1. Schematic diagram of the apparatus for powder preparation.

All of the vanadium atoms fed is seemed to be incorporated into the powders since no vanadium oxide was recovered from the effluent gas, however, phosphorus compounds were partly passed through the reactor and were recovered in a trap with a NaOH aqueous solution in most of the experiments. 0.06—0.15 g of the powders were formed per hour in each experiment.

The powders formed in this manner were subjected to XRD measurement and the results are summarized in Table 1. The mixture of α-$VOPO_4$ and V_2O_5 was obtained when the $POCl_3/VOCl_3$ ratio of the reactant gas was lower than unity (Run 1), on the contrary, a large $POCl_3/VOCl_3$ ratio gave the peaks assigned to $(VO)_2P_2O_7$, though the intensities were small. It is of interest that $(VO)_2P_2O_7$ with V(IV) ions was formed when an excess amount of $POCl_3$ was supplied.

The adoption of an intermediate $POCl_3/VOCl_3$ ratio brought about the formation of almost pure α-$VOPO_4 \cdot 2H_2O$ (ASTM Card 27-949) and the reproducibility of the experiments was fairly good (Runs 10—15). The P/V ratios of some of the powders obtained were examined by EPMA and these results are also shown in Table 1. The P/V ratio of the powder formed in Run 1 was 0.34 which is very close to the 0.33 of the $POCl_3/VOCl_3$ ratio of the feed gas. This suggests that all the $POCl_3$ in the feed gas was incorporated into the powder formed.

The ratios of the powders formed in Runs 13 and 15,

however, were 1.09 and 1.02 which were coincided the chemical formula of α-$VOPO_4 \cdot 2H_2O$ and the ratio of the former powder was unaltered after having been used for the oxidation of butane for 27 h. It can be inferred from these results that the 2.0—2.5 fold excess of $POCl_3$ to $VOCl_3$ is sufficient to form vanadium phosphate powder with a P/V ratio just exceeding unity. The powders formed in Runs 2, 3, and 6 contained a $(VO)_2P_2O_7$ phase in which vanadium atoms were reduced to V(IV) from the original V(V) of $VOCl_3$. According to Bordes and Courtine,[8] the reduction of α- and β-$VOPO_4$ begins at 920 K even in a N_2 stream. So that it is believed to be difficult for the reduction of V(V) of the powders to take place in the furnace kept at 763K. The Cl/V ratio of some catalysts were also determined by EPMA and were listed in Table 1. The powders formed in Runs 1 and 13 contained a small amount of chlorine, which was the extent of ca. 0.2% of the vanadium atoms but no chlorine was detected from the powder formed in Run 15. Although the chlorine content of the powders of Runs 2, 3, and 6 are not known, it can be inferred that the HCl formed by the hydrolysis of chloride oxides may play a role in the reduction.

The effects of the temperature and the surrounding gas in calcination on the phase of the α-$VOPO_4 \cdot 2H_2O$ were studied in order to obtain the optimum conditions of pretreatment suitable for the preparation of selective butane oxidation catalysts.

The portions of the powder formed in Run 13 were heated to 773 K at the different heating rates such as 2 K min^{-1} and 10 K min^{-1} in a N_2 or C_4H_{10}-O_2-N_2 (1.5, 9.0, and 89.5 vol% respectively) stream, and kept at 773 K for 2 h, and then steeply cooled down to the ambient temperature. The samples calcined in the N_2 stream were changed into α-$VOPO_4$ and β-$VOPO_4$ despite the heating rates in agreement with the results reported by Bordes and Courtine.[8]

The samples calcined in the C_4H_{10}-O_2-N_2 stream gave features different from those in N_2 stream. The XRD spectrum of the sample heated by 10 K min^{-1} consisted of sharp peaks of $(VO)_2P_2O_7$ in addition to weak peaks of β-$VOPO_4$, on the other hand the spectrum obtained at 2 K min^{-1} was mainly composed of β-$VOPO_4$ and α-$VOPO_4$. It can be concluded from these results that in situ pretreatment in the reactant gas mixture of butane oxidation and higher heating rates are favorable to obtain $(VO)_2P_2O_7$ which has been claimed to be the active phase for MA formation.

The results of the butane oxidation over several catalysts prepared by the method mentioned above are shown in Table 2 together with the results over $(VO)_2P_2O_7$ which was prepared from V_2O_5, $NH_2OH \cdot HCl$, and H_3PO_4 by the method described in the literature[2] and over pure V_2O_5 prepared by the thermal decomposition of ammonium metavanadate at 823 K.

Butane was mainly oxidized to carbon oxides over the pure V_2O_5 catalyst and MA was formed with only 13.5% selectivity under the reaction conditions. The MA selectivity reached 58.3% over the $(VO)_2P_2O_7$ catalyst. Although Catalyst 3 showed a considerably high activity, the distribution of products was much similar to that of pure V_2O_5. As shown in Table 1, Catalyst 3 was composed of an amorphous phase and a small amount of $(VO)_2P_2O_7$. The XRD spectrum from Catalyst 3 after the reaction was almost the same as that before pretreatment.

Catalysts 10 and 13, both derived from α-

Table 1. Preeparation of V-P-O Powders

Run	Reation time/h	Feed rate				$POCl_3/VOCl_3$	Prowders		
		$POCl_3$[a]	N_2[b]	$VOCl_3$[a]	N_2[b]		P/V	Cl/V	Phase[c]
1	50	0.6	29.7	1.83	27.8	0.33	0.34	0.0019	V_2O_5+[α-$VOPO_4$]
2	8	—	36.7	—	17.6	—	—		Amorphous+[$(VO)_2P_2O_7$]
3	8	—	56.0	—	23.8	—	2.32[d]		Amorphous+[$(VO)_2P_2O_7$]
6	17	3.10	35.3	1.96	30.3	1.58	0.50[d]		$(VO)_2P_2O_7$+β-$VOPO_4$
10	17	3.61	39.3	1.38	30.9	2.62	1.18	0	α-$VOPO_4 \cdot 2H_2O$
11	17	3.13	36.6	1.28	32.8	2.45	0.82[d]		α-$VOPO_4 \cdot 2H_2O$
13	17	3.35	37.7	1.42	33.2	2.36	1.09	0.0018	α-$VOPO_4 \cdot 2H_2O$
14	17	—	39.9	—	34.9	—	—		α-$VOPO_4 \cdot 2H_2O$
15	17	5.83	36.9	2.98	33.1	1.96	1.02	0	α-$VOPO_4 \cdot 2H_2O$

a) mmol $\cdot h^{-1}$. b) $cm^3 \cdot min^{-1}$. c) [ ] means minority. d) Chemical analysis.

Table 2. Oxidation of n-C_4H_{10} over P-V-O Catalysts

Catalyst	$(VO)_2P_2O_7$		V_2O_5	Cat. 3	Cat. 6	Cat. 10		Cat. 13	
Reaction time/h	3	76	27	27	27	27	3	6	27
Conv/%	16.0	15.6	39.8	54.0	18.3	20.6	13.3	13.4	15.3
MA[a]	60.9	58.3	13.5	12.4	52.5	50.0	47.2	47.6	52.9
CH_3COOH	—	—	0.14	0.27	0.94	0.75	—	—	—
$CH_2CHCOOH$	—	—	0.04	0.90	0.38	0.21	—	—	—
CO	33.1	32.9	59.6	54.2	8.82	32.8	36.8	36.5	33.5
CO_2	5.9	8.9	26.3	32.1	36.6	16.3	16.0	15.9	13.6
Others[b]	—	—	0.44	0.06	0.76	—	—	—	—

a) Maleic anhydride. b) C_1—C_3 Alkane, reaction temperature: 733 K, W/F: 0.46 g $\cdot$ s $\cdot$ cm^{-3}, feed gas composition: 1.5 vol% n-C_4H_{10}, 9.0 vol% O_2, 89.5 vol% N_2.

$VOPO_4 \cdot 2H_2O$ showed selectivities as high as that of the $(VO)_2P_2O_7$ catalyst. It can be seen from Table 2 that the activity and selectivity of Catalyst 13 improved with the reaction time. The XRD spectra from Catalysts 10 and 13 after the reaction were composed of many small broad peaks and a half of these peaks could be assigned to those of $(VO)_2P_2O_7$ and α-$VOPO_4$ but the rest could not be assigned. Observations of high base line position and the small broad peaks in all spectra suggested that the catalysts obtained by the gas phase reaction have an abundance of an amorphous solid or a very small crystalline. Since Catalyst 10 overcame the $(VO)_2P_2O_7$ catalyst in the conversion of butane, Catalyst 10 was superior to the $(VO)_2P_2O_7$ catalyst in MA yield.

It is concluded from these results that the vapor phase preparation of α-$VOPO_4 \cdot 2H_2O$ powder is one of the better methods of obtaining precursor of the selective catalysts.

Experimental

The $VOCl_3$ (Wako Pure Chem. 99+%) and $POCl_3$ (Wako Pure Chem., Special Grade) were used for powder preparation without further purification. The determination of the composition of the samples was carried out by means of either of a TN 5500 EPMA system or chemical analysis in conformity with a reference.[9] Reference files of the EPMA system were prepared using K lines from V, GaP, and KCl standards at 25 kV and were checked by analyzing mixtures of V_2O_5 and ammonium dihydrogen phosphate. Catalytic oxidation of butane was carried out using an ordinary flow type reaction system with fixed catalyst bed. The catalysts were in situ pretreated in the stream of a reaction gas mixture at a temperature which was regulated to raise to 773 K at the rate of 10 $K\,min^{-1}$ and then hold at 773 K for 2 h. The MA formed was collected for ca. 1 h after which the concentration of its aqueous solution was analyzed by means of GC (Thermon 1000 column, 423 K) or by titration with a NaOH aqueous solution.

References

1) US Patent 330354 (1973), US Patent 4043943 (1977).
2) T. Shimoda, T. Okuhara, and M. Misono, *Bull. Chem. Soc. Jpn.*, **58**, 2163 (1985).
3) B. K. Hodnett, Ph. Permanne, and B. Delmon, *Appl. Catal.*, **6**, 231 (1983).
4) I. Matsuura, K. Yoshida, and A. Mori, *Chem. Lett.*, **1987**, 585.
5) F. Grbassi, J. C. J. Bart, R. Tassinari, G. Vlaic, and P. Lagarde, *J. Catal.*, **98**, 317 (1986).
6) G. Centi, G. Fornasari, and F. Trifiro, *J. Catal.*, **89**, 44 (1984).
7) US Patent 3864280, 4013586, 4016105, 4209423, 4219484, 4244879, 4283288, 4315864, 4317778.
8) E. Bordes and P. Courtine, *J. Catal.*, **57**, 236 (1979).
9) "Shin Jikken Kagaku Koza," ed by Chem. Soc. Jpn., Maruzen, Tokyo (1976), Vol. 9, pp. 179, 275.

Electronic and ESR Spectral Studies of a Series of Phosphine and Phosphite Adducts with Cobaloxime Analog

Keisuke MITA,* Kazuhiko HOTTA, and Takeji TAKUI†
Osaka Municipal Technical Research Institute, Morinomiya, Joto-ku, Osaka 536
†Faculty of Science, Osaka City University, Sugimoto, Sumiyoshi-ku, Osaka 558
(Received November 30, 1987)

Synopsis. Electronic and ESR spectra were measured for solutions of $Co(dmgBF_2)_2$ in the presence of PX_3, where $Co(dmgBF_2)_2$ is a BF_2 capped species of bis(dimethylglyoximato)cobalt(II) ($Co(Hdmg)_2$) and PX_3 is PBu_3, PPh_3, $P(OEt)_3$, or $P(OPh_3)_3$. ^{31}P hyperfine splittings of their ESR spectra demonstrated that $Co(dmgBF_2)_2$ forms only 1:1 adducts with PX_3. The visible absorption spectrum of the dichloromethane solution of $Co(dmgBF_2)_2$ showed an absorption band at 444 nm at 20 °C. Upon PX_3 being added to the solution, the band shifted to a longer wavelength; the band shift increased with increasing the electron-donating ability of PX_3.

Bis(dimethylglyoximato)cobalt(II) complex ($Co(Hdmg)_2$) and its related compounds have been known as model compounds for vitamin B_{12}[1] or as hydrogenation catalysts.[2] Recently, during our investigation of the catalytic properties of those complexes, the methanol solution of $Co(dmgBF_2)_2$ (the BF_2 capped species of $Co(Hdmg)_2$, Fig. 1) was found to be thermochromic in the presence of tributylphosphine (PBu_3).[3] It was also found that the thermochromism is due to a shift of equilibrium between the Co^{II} and Co^{I} species.[3,4] On the other hand, no thermochromic behavior was observed for the methanol solution of $Co(dmgBF_2)_2$ in the presence of triphenylphosphine (PPh_3), triethylphosphite ($P(OEt)_3$), or triphenylphosphite ($P(OPh)_3$). In the present study, the electronic and ESR spectra of $Co(dmgBF_2)_2$ were measured in a methanol or dichloromethane solution in the presence of the above-mentioned four trivalent phosphorus ligands (PX_3); the influence of these phosphorus ligands is discussed in terms of the bonding properties between $Co(dmgBF_2)_2$ and PX_3.

Experimental

The ESR spectra were observed at 77 K with a Bruker ESP-300 and a JES ME-1X type spectrometer in the X band with a field modulation of 100 kHz. $Co(dmgBF_2)_2(2H_2O)$ was prepared according to the method of Bakac and Espenson.[5] The preparation of ESR samples was carried out under a dry atmosphere of argon. $Co(dmgBF_2)_2(2H_2O)$ was dissolved in methanol, and an amount of phosphorus ligand was added. A 1 ml solution was transferred to a quartz ESR tube, and the tube was then sealed. The visible absorption spectra were measured at 20 °C by a method described in a previous paper.[4]

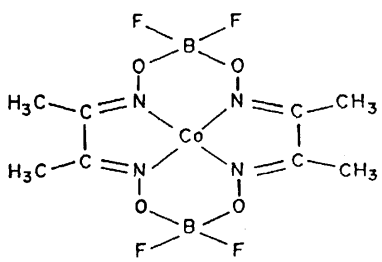

Fig. 1. The structure of $Co(dmgBF_2)_2$.

Results and Discussion

Figure 2a shows the ESR spectrum of $Co(dmgBF_2)_2$ observed in a frozen methanol solution at 77 K. The spectrum is characterized by the lineshape for a random orientation of paramagnetic species with anisotropic g values ($S=1/2$) and the hyperfine structure due to the magnetic interaction between an unpaired electron and a nucleus of $I=7/2$, where S and I denote an electron and a nuclear spin quantum number, respectively. No superhyperfine structure was resolved.

Figure 2b shows the ESR spectra of $Co(dmgBF_2)_2$ observed at 77 K in a frozen methanol solution in the presence of $P(OEt)_3$. The spectrum is distinctly different from that of the parent $Co(dmgBF_2)_2$ and is diagnostic for adduct formation. The additional doublet splitting of the hyperfine structure can be attributed to the superhyperfine structure due to the magnetic interaction of an unpaired electron with a ^{31}P nucleus ($I=1/2$). Assuming a tetragonal symmetry, $Co(Hdmg)_2$ is in the low-spin $^2A_1$ state and the unpaired electron is

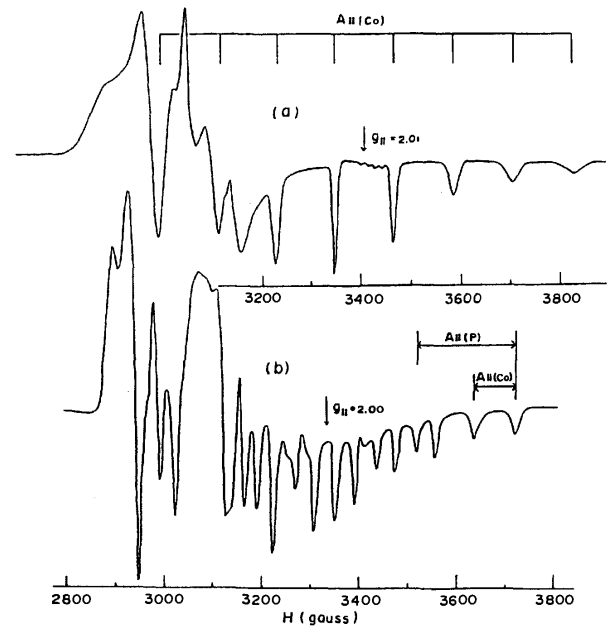

Fig. 2. ESR spectra of $Co(dmgBF_2)_2$ in a frozen methanol solution at 77 K.
(a) $[Co(dmgBF_2)_2]$: 0.89 mmol l^{-1}, microwave frequency: 9.570 GHz. (b) $[Co(dmgBF_2)_2]$: 0.48 mmol l^{-1}, $[P(OEt)_3]$: 5.7 mmol l^{-1}, microwave frequency: 9.32 GHz.

Table 1. ESR Parameters for $Co(dmgBF_2)(PX_3)$ Complexes

PX_3	$g_{\parallel}$	$A_{\parallel}(Co)$ G[a]	$A_{\parallel}(P)$ G[a]
None	2.01	120	—
PBu_3	2.00	82	125
PPh_3	2.00	92	127
$P(OEt)_3$	2.00	83	208
$P(OPh)_3$	2.00	89	230

a) 1 G=10^{-4} T.

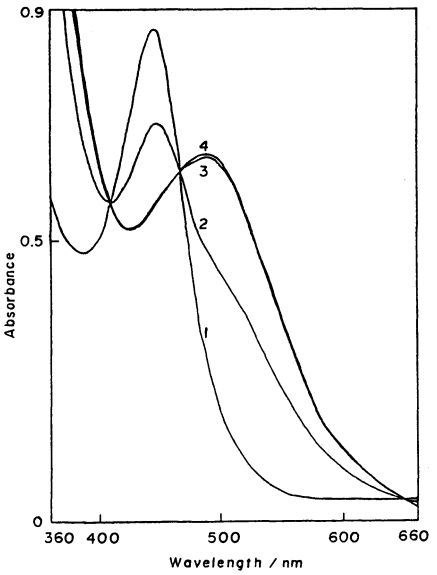

Fig. 3. Visible absorption spectra, 1, 2, 3, and 4 of 0.33 mM $Co(dmgBF_2)_2$ (1M=1 mol dm^{-3}) in the dichloromethane solution containing $P(OEt)_3$ with the concentration of 0, 0.22, 0.49, and 3.2 mM, respectively.

localized mainly in the d_{z^2} orbital.[6,7] Thus, the superhyperfine structure arises from the axial coordination of the phosphorus ligand, $P(OEt)_3$. The superhyperfine structure was not affected by the addition of excess of $P(OEt)_3$ to the solution, suggesting that $Co(dmgBF_2)_2$ forms only 1 : 1 adducts with $P(OEt)_3$ in the methanol solution. This finding parallels observations with $Co(Hdmg)_2(PX_3)$,[6,8] $Co(tpp)(PX_3)$,[9] and $Co(salen)(PX_3)$,[10-13] where Co(tpp) and Co(salen) are tetraphenylporphinatocobalt(II) and (*N,N'*-disalicylideneethylenediaminato)cobalt(II), respectively. A similar superhyperfine structure due to a ^{31}P nucleus was observed at 77 K for $Co(dmgBF_2)_2$ in a frozen methanol solution in the presence of the other phosphorus ligands, viz., PBu_3, PPh_3, or $P(OPh)_3$, conforming the 1 : 1 adducts formation of $Co(dmgBF_2)_2$ with these phosphorus ligands. (In the presence of excess PBu_3, however, the ESR signal could not be observed, because under that condition $Co^{II}(dmgBF_2)_2(PBu_3)$ is reduced to Co^{I} species.) The ESR parameters are shown in Table 1. A similar superhyperfine structure was observed for the 1 : 1 adducts in dichloromethane solution. The ESR parameters are quite the same as those listed in Table 1.

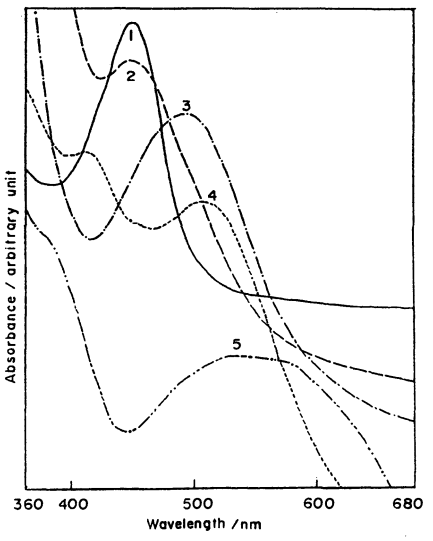

Fig. 4. Visible absorption spectra, 1, 2, 3, 4, and 5 of 0.30 mM $Co(dmgBF_2)_2$ in the dichloromethane solution containing none, 6.0 mM of $P(OPh)_3$, 6.0 mM of $P(OEt)_3$, 6.0 mM of PPh_3 and 1.1 mM of PBu_3, respectively.

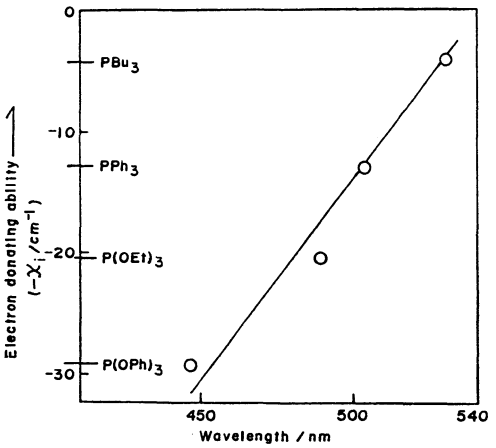

Fig. 5. Relationship between the electron-donating ability ($-X_i$) of PX_3 and the wavelength of the absorption band of $Co(dmgBF_2)_2(PX_3)$.

The visible absorption spectra of the methanol solution of $Co(dmgBF_2)_2$ showed an absorption band at 462 nm. When PBu_3 was added to the parent solution, the band shifted to 530 nm.[3] On the other hand, when PPh_3, $P(OEt)_3$, or $P(OPh)_3$ were added to the parent solution, no appreciable amount of the band shift was observed, suggesting that the interaction between these phosphorus ligands and $Co(dmgBF_2)_2$ is weak compared with that between PBu_3 and $Co(dmgBF_2)_2$ in the methanol solution.

The visible absorption spectra of the dichloromethane solution of $Co(dmgBF_2)_2$ showed an absorption band at 444 nm. Upon adding the trivalent phosphorus ligands to the parent solution, the band shifted to a longer wavelength while exhibiting isosbestic points. Figure 3 examplifies the spectral change observed upon increasing the amount of $P(OEt)_3$ from zero to 32×10^{-4} mol l^{-1} in a 3.3×10^{-4} mol l^{-1} of $Co(dmgBF_2)_2$

solution (the band at 444 nm shifted to 489 nm while exhibiting three isosbestic points at 408, 467, and 650 nm).

Figure 4 shows the visible absorption spectra (1, 2, 3, 4, and 5) of $Co(dmgBF_2)_2$ in the presence of none, $P(OPh)_3$, $P(OEt)_3$, PPh_3, and PBu_3, respectively, with the concentration; no more spectral change was observed upon a futher addition of each phosphorus ligand. Sice $Co(dmgBF_2)_2$ forms only 1 : 1 adducts with the phosphorus ligand, it is concluded from Fig. 4 that $Co(dmgBF_2)_2(PBu_3)$, $Co(dmgBF_2)_2(PPh_3)$, $Co(dmgBF_2)_2(P(OEt)_3)$, and $Co(dmgBF_2)_2(P(OPh)_3)$ have an absorption band at 530 nm (18900 cm^{-1}), 503 nm (19900 cm^{-1}), 489 nm (20400 cm^{-1}) and 446 nm (22400 cm^{-1}), respectively.

Figure 5 shows a relationship between the wavelength of the absorption band of $Co(dmgBF_2)_2(PX_3)$ and the electron-donating ability of PX_3 (the electron-donating ability is represented in units of Tolman X_i parameter).[14] This relationship shows that the absorption band of $Co(dmgBF_2)_2(PX_3)$ shifts to a longer wavelength upon increasing the electron-donating ability of PX_3 (namely with decreasing the Tolman X_i parameter of PX_3). The electronic configuration of square-pyramidal d^7 complexes is $(d_{xz})^2(d_{yz})^2(d_{xy})^2(d_{z^2})^1(d_{x^2-y^2})^0$ in the ground state. If the electron-donating ability of PX_3 (as an axial ligand) increases, the energy level of the d_{z^2} orbital would be increased. Thus, from the fact that the absorption bands of $Co(dmgBF_2)_2(PX_3)$ shift to a much longer wavelength upon increasing the electron donating ability of PX_3 (Fig. 5), the absorption band in Fig. 4 was assigned to the $d_{z^2} \rightarrow d_{x^2-y^2}$ transition. It was consequently concluded that the order of d_{z^2} σ-donor orbital mixing is $PBu_3 > PPh_3 > P(OEt)_3 > P(OPh)_3$.

References

1) G. N. Schrauzer, *Angew. Chem.*, **88**, 465 (1976).
2) Y. Ohgo, S. Takeuchi, and J. Yoshimura, *Bull. Chem. Soc. Jpn.*, **44**, 283, 583 (1971).
3) K. Mita, *Nippon Kagaku Kaishi*, **1986**, 771.
4) K. Mita, *Nippon Kagaku Kaishi*, **1987**, 823.
5) A. Bakac and J. H. Espenson, *J. Am. Chem. Soc.*, **106**, 5197 (1984).
6) G. N. Schrauzer and Lian-Pin Lee, *J. Am. Chem. Soc.*, **90**, 6541 (1968).
7) A. Rockenbauer, E. Budo-Zahonyi, and L. I. Simandi, *J. Chem. Soc., Dalton Trans.*, **1975**, 1729.
8) G. Labauze and J. B. Raynor, *J. Chem. Soc., Dalton Trans.* **1981**, 590.
9) B. B. Wayland and M. E. Abd-Elmageed, *J. Am. Chem. Soc.*, **96**, 4809 (1974).
10) B. B. Wayland and M. E. Abd-Elmageed, *Inorg. Chem.*, **14**, 1456 (1975).
11) G. Labauze and J. B. Raynor, *J. Chem. Soc., Dalton Trans.*, **1980**, 2388.
12) A. Pezeshk, F. T. Greenaway, J. C. Dabrowiak, and G. Vincow, *Inorg. Chem.*, **17**, 1717 (1978).
13) A. Pezeshk, F. T. Greenaway, and G. Vincow, *Inorg. Cnem.*, **17**, 3421 (1978).
14) C. A. Tolman, *J. Am. Chem. Soc.*, **92**, 2953 (1970).

Organic Derivatives of Layered Polysilicates. II.[1] Reaction of Magadiite and Kenyaite with Diphenylmethylchlorosilane

Tsuneo YANAGISAWA, Kazuyuki KURODA, and Chuzo KATO*
Department of Applied Chemistry, Waseda University, Ohkubo-3, Shinjuku-ku, Tokyo 160
(Received February 19, 1988)

Synopsis. Silanol groups on the interlayer surface of layered polysilicic acids (H-magadiite and H-kenyaite) were silylated by reaction with diphenylmethylchlorosilane. Dodecyltrimethylammonium magadiite and kenyaite intercalation compounds were used as the intermediates for the conversion. The interlayer modification was confirmed by XRD, IR, ^{29}Si-MAS NMR and elemental analysis.

Interlayer modification of layered materials by organic groups has attracted much attention from the viewpoint of the design of advanced materials with regulated structures. Layered polysilicates such as magadiite ($Na_2Si_{14}O_{29}\cdot xH_2O$) and kenyaite ($Na_2Si_{20}O_{41}\cdot xH_2O$) have exchangeable interlayer cations and acid treatment yields the corresponding layered polysilicic acids (H-magadiite ($H_2Si_{14}O_{29}\cdot xH_2O$) and H-kenyaite ($H_2Si_{20}O_{41}\cdot xH_2O$)). Since the layered polysilicic acids as well as the original layered polysilicates have interlamellar silanol groups,[2] they are expected to be one of the host materials for interlayer modification. In order to design the interlayer space freely, it is necessary to investigate the possibility of various types of interlayer modification. However, in the previous studies,[3,4] only trimethylsilylation was reported as the organic derivatizing method for polysilicic acids.

$$(\equiv Si\text{-}OH + ClSi(CH_3)_3 \rightarrow \equiv Si\text{-}O\text{-}Si(CH_3)_3)$$

These reports also showed that a bulky silylating agent such as diphenylmethylchlorosilane ($(C_6H_5)_2CH_3SiCl$, abbreviated as DPMCS) could not be intercalated.[4] These previous studies used only DMSO (or NMF) intercalated polysilicic acids as intermediates for the derivatization. In our previous study,[1] dodecyltrimethylammonium ($C_{12}H_{25}(CH_3)_3N^+$, abbreviated as DTMA) magadiite and kenyaite were preferable for the trimethylsilylation of the layered polysilicic acids. The advantage of the tetraalkylammonium intercalated polysilicic acids as intermediates for the organic derivatization was their relative stabilities and the variable enlargement of the interlayer space by variation in the number of carbon atoms in the organoammonium ions employed. Therefore, in this study, DPMCS was allowed to react with DTMA-magadiite and -kenyaite intercalation compounds and the silylated products were analyzed.

Experimental

Materials. The starting materials, Na-magadiite and K-kenyaite ($K_2Si_{20}O_{41}\cdot xH_2O$), were synthesized by the method described by Lagaly et al.[5,6] The exchange reaction of interlayer Na and K ions for DTMA ions to form the organoammonium intercalation compounds was also followed by the procedure by Lagaly et al.[5,7] The formation of the organoammonium intercalated compounds was checked by elemental analysis, X-ray, and IR data. Commercially available DPMCS was used in this study.

Silylation Reaction. The DTMA-magadiite and -kenyaite were mixed with DPMCS and the reaction mixtures were refluxed for 72 h. After the mixtures were filtered with suction, they were washed thoroughly with acetone and air-dried.

Analyses. X-Ray powder diffraction patterns were obtained by using Rigaku Rad IB (Cu $K\alpha$ radiation, Ni filtered). IR spectra were recorded on a Shimadzu IR-435 infrared spectrometer. ^{29}Si-MAS NMR spectra were obtained with a JEOL GSX-270 spectrometer at 53.67 MHz. The external standard was tetramethylsilane. Gated high power proton decoupling technique was employed with a 45° pulse, and the pulse repetition time was 7 s. Cross polarization (CP) technique with matched rf field amplitudes of 45 kHz was also employed. CP contact times were 5 and 8 ms, depending upon the sample, and the pulse repetition time was 5 s.

Results and Discussion

Table 1 shows the basal spacings of Na-magadiite, K-kenyaite, their DTMA complexes, and their silylated products. The spacing of DTMA-magadiite (29.4 Å) was larger than that of Na-magadiite (15.6 Å) by 13.8 Å. After the reaction with DPMCS, the spacing of the derivative decreased to 24.6 Å from 29.4 Å. However, the value was still larger than that of H-magadiite (11.2 Å) by 13.4 Å. The expansion of the layer spacing was retained after the heat treatment of the silylated products at 300—400 °C, suggesting the formation of $\equiv Si\text{-}O\text{-}SiCH_3(C_6H_5)_2$. The diphenylmethylsilylation of DTMA-kenyaite also gave similar results, although the d_{001} values were different because of the different layer thickness of kenyaite.

After the diphenylmethylsilylation, the IR absorption bands due to DTMA ions disappeared and new bands due to diphenylmethylsilyl (abbreviated as DPMS) groups appeared at 1430, 1270, 740, and 700 cm^{-1}. After the heat treatment up to 400 °C with a DTA instrument, the absorption peaks due to DPMS groups remained. Thus, these IR absorption peaks were not ascribed to by-products (ex. $(C_6H_5)_2CH_3SiOSiCH_3(C_6H_5)_2$) or the unreacted species, because

Table 1. Basal Spacings of Layered Polysilicates and Their Derivatives

	Na-magadiite(Å)	K-kenyaite(Å)
Original form	15.6	20.0
Dodecyltrimethylammonium exchanged form	29.4	35.6
Diphenylmethylsilylated form	24.6	31.4

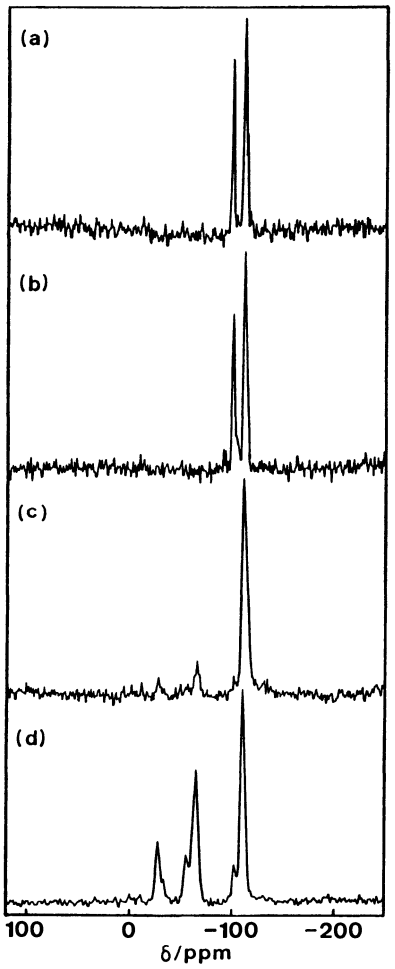

Fig. 1. ^{29}Si-MAS NMR spectra of (a) Na-magadiite, (b) dodecyltrimethylammonium magadiite, (c) and (d) diphenylmethylsilylated magadiite ((d): CP technique was used).

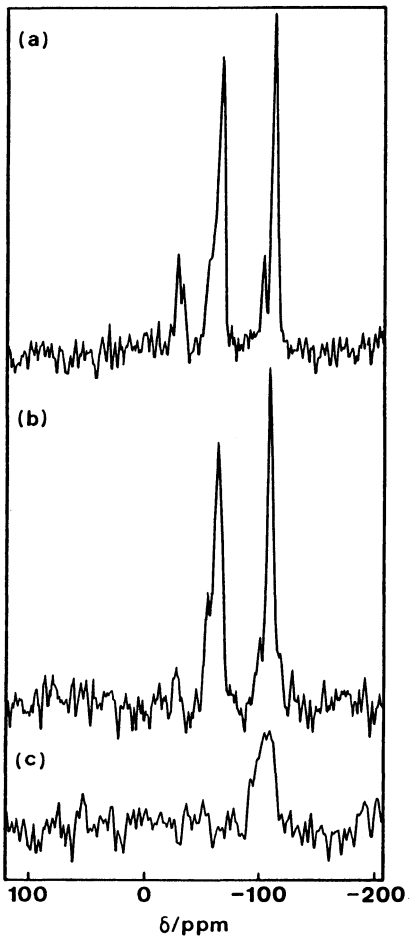

Fig. 2. ^{29}Si-CPMAS NMR spectra of heat treated diphenylmethylsilylated magadiite. (a) 300 °C, (b) 500 °C, and (c) 700 °C.

their boiling points were lower than 350 °C. The IR results of the silylated kenyaite also showed similar evidence of the linkage of the DPMS groups and the interlayer silanol groups.

Figure 1 shows the ^{29}Si-MAS NMR spectra of Na-magadiite, DTMA-magadiite, and the diphenylmethylsilylated magadiite. The NMR spectrum of Na-magadiite indicated the presence of two different SiO_4 units normally designated as Q^3 and Q^4 at −99.0 and −110.7 ppm, respectively. (Q^n means the SiO_4 having n siloxane bonds.) The spectrum was similar to the previous data reported by Pinnavaia et al.[8] The spectrum of the DTMA-magadiite did not show any significant changes in the chemical shifts and the intensities. However, in the spectrum of the diphenylmethylsilylated product, a remarkable change was observed. At first, the width of the peak due to Q^4 was broadened, indicating the presence of the newly formed Q^4 by silylation, (O_3SiOH (Q^3) → O_3SiO-SiR_3 (Q^4)). Secondly, the new peaks at −28 and −65 ppm appeared. With a further measurement using the cross polarization (CP) technique, these peaks were split, as shown in Fig. 1(d), although the reason for the splittings can not be explained definitely at present because the precise structure has not yet been clarified. The intensities of these peaks decreased with the combustion of the organic groups and finally unified into a single but relatively broad peak at −107 ppm (Fig. 2). Therefore, the peaks at −28 ppm were ascribed to the silicon atoms (Q^1) in the bonded DPMS groups. The latter signals at −65 ppm were thought to be assigned tentatively as the unsilylated Q^3 units strongly affected by the interlayer aromatic groups which usually caused an anisotropic magnetic effect. Possible bond distortion in the interlayer space may also influence the chemical shift.

Figure 3 shows the ^{29}Si-CP MAS NMR spectra of K-kenyaite, DTMA-kenyaite, and the silylated product. In the spectrum of the K-kenyaite, the Q^3 peak appeared at −98.5 ppm and the peak due to Q^4 at −109.7 ppm. In the spectrum of the DTMA-kenyaite, the peak due to Q^3 appeared at a similar position to that of K-kenyaite. However, the peak due to Q^4 was split into two peaks at −110.5 and −112.5 ppm. This difference between magadiite and kenyaite is probably ascribable to the difference in the layer structures. The spectrum of the silylated kenyaite indicated the presence of the Q^1 peak due to DPMS groups at −32.9 ppm. The signal at −64.9 ppm was tentatively assigned to Q^3. The peak due to Q^4 appeared at −110.2

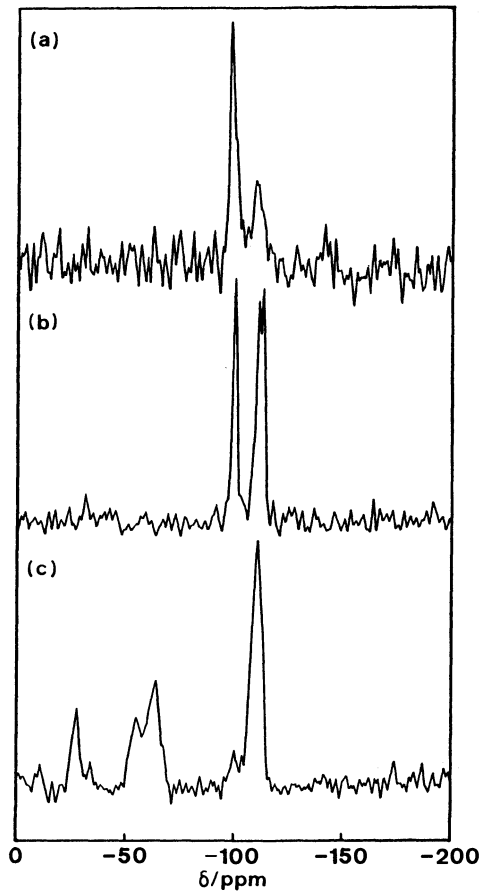

Fig. 3. ^{29}Si-CPMAS NMR spectra of (a) K-kenyaite, (b) dodecyltrimethylammonium kenyaite, and (c) diphenylmethylsilylated kenyaite.

ppm with a little broad peak width. These variations in the spectra corresponded to the partial diphenylmethylsilylation of interlamellar silanol groups.

The elemental analysis of the silylated magadiite and kenyaite also supported the silylation, though very small amounts of nitrogen due to remaining DTMA were detected. The H, C, and N contents (H, 2.01; C, 13.81; N, 0.15%) of the silylated magadiite indicated the ratio of DPMS group/$Si_{14}O_{29}$ was 0.79. The data of the silylated kenyaite (H, 1.39; C, 11.34; N, 0.10%) showed the ratio of DPMS group/$Si_{20}O_{41}$ was 0.92. As compared with the data on the trimethylsilylation of magadiite and kenyaite,[1] the values were lower because of the bulky nature of the DPMS groups.

The process of the diphenylmethylsilylation of DTMA-magadiite and -kenyaite can be expressed as a consecutive reaction. Since the silanol groups are present in the interlayer space of DTMA-magadiite and - kenyaite,[5,7] the silylating reagent can react with these silanol groups to form siloxane bonds;

$$\equiv Si\text{-}OH + (C_6H_5)_2CH_3SiCl \rightarrow \equiv Si\text{-}O\text{-}SiCH_3(C_6H_5)_2 + HCl.$$

The HCl produced can attack the DTMA silicate sites to form silanol groups. Then, the newly formed silanol groups can be silylated further.

In conclusion, the interlayer surface of magadiite and kenyaite was silylated with DPMCS using DTMA-magadiite and -kenyaite as intermediates, providing the possibility of various modifications of interlayer silanol groups.

We are indebted to Dr. Kenzo Deguchi and Mr. Katuya Hioka (JEOL) for their measurement and interpretation of ^{29}Si-MAS NMR spectra. One of the authors (K.K.) was supported financially by Nippon Sheet Glass Foundation for Materials Research. Waseda University also supported us financially as a Special Project Research.

References

1) T. Yanagisawa, K. Kuroda, and C. Kato, *Reactivity of Solids*, **5**, 167 (1988).
2) G. Lagaly, *Adv. Colloid Interface Sci.*, **11**, 105 (1979).
3) E. Ruiz-Hitzky and J. M. Rojo, *Nature (London)*, **287**, 28 (1980).
4) E. Ruiz-Hitzky, J. M. Rojo, and G. Lagaly, *Colloid Polym. Sci.*, **263**, 1025 (1985).
5) G. Lagaly, K. Beneke, and A. Weiss, *Am. Mineral.*, **60**, 642 (1975).
6) K. Beneke, H. H. Kruse, and G. Lagaly, *Z. Anorg. Allg. Chem.*, **518**, 65 (1984).
7) K. Beneke and G. Lagaly, *Am. Mineral.*, **68**, 818 (1983).
8) T. J. Pinnavaia, I. D. Johnson, and M. Lipsicas, *J. Solid State Chem.*, **63**, 118 (1986).

An ^{27}Al NMR Study on the Complexes Present in the Solutions of Potassium Hexathiocyanatoaluminate(III)

Noriyuki KOMATSU, Masatoki YOKOI,* and Eiji KUBOTA
Department of Chemistry, Faculty of Science, Shinshu University, Asahi, Matsumoto 390
(Received May 9, 1988)

Synopsis. The species present in the solutions of potassium hexathiocyanatoaluminate(III) in various solvents were identified by ^{27}Al NMR spectra of the solutions. In dimethyl sulfoxide solution containing excess KSCN, the spectrum consists of 7 resonances due to $[Al(NCS)_n(DMSO)_{6-n}]^{(3-n)+}$ (n=0—6), whereas a single resonance arising from $[Al(NCS)_6]^{3-}$ was observed in propylene carbonate or acetone.

The ^{27}Al NMR spectrum of an aqueous solution containing aluminum chloride and potassium thiocyanate shows a resonance at about 6 ppm upfield from the line due to $[Al(H_2O)_6]^{3+}$. The spectrum is similar to that of aqueous aluminum sulfate solution in which a separate resonance is located at 3 ppm upfield from the main one.[1] The upfield resonance of the former solution may be assigned to a species like $[Al(SCN)(H_2O)_5]^{2+}$.

Wehrli and Wehrli[2] studied species present in $AlCl_3$ solution of acetonitrile (AN) by ^{27}Al NMR. They showed that $AlCl_4^-$ and various hexacoordinated solvation complexes exist in the solutions and the relative amount of the species depends on the concentration of the solute. ^{27}Al NMR spectra of AN solution containing $KAlCl_x(SCN)_{4-x}$ have been reported.[3] It was shown that Cl^- and SCN^- mixed ligand tetracoordinated Al(III) species are in these solutions.

Since potassium hexathiocyanatoaluminate(III), is soluble in a variety of solvents, it seems interesting to identify the complexes present in aqueous and nonaqueous solutions. We have attempted to study the ^{27}Al NMR spectra of the solutions of the complex salt in various solvents.

Experimental

The preparation of potassium hexathiocyanatoaluminate(III) was almost similar to that described in the literature.[4] Anhydrous $AlCl_3$ was added to a solution of six equivalent KSCN in AN and the precipitated KCl was filtered off. The solvent was then removed with distillation under reduced pressure. The residue was recrystallized from acetone. ^{27}Al NMR spectra were recorded on a JEOL FT-90Q at 23.3 MHz or on a Bruker AC-250 at 65.18 MHz. The temperature of the sample was 28 °C. The Al NMR shift was measured with an external standard of aqueous $NaAlO_2$ solution. The shift data were then converted to the values with reference to the usual standard of $[Al(H_2O)_6]^{3+}$ line. The error in the shift was estimated as ±1 ppm.

Results and Discussion

Figure 1 reproduces ^{27}Al NMR spectra of the solutions of potassium hexathiocyanatoaluminate(III) and of the solutions containing the salt and excess KSCN in dimethyl sulfoxide (DMSO), *N,N*-dimethylacetamide (DMA), and AN. In these solutions, ^{27}Al NMR

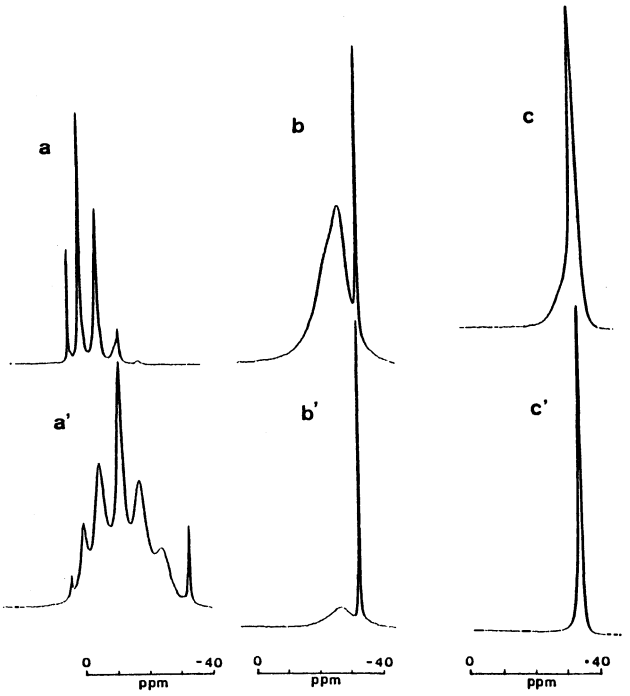

Fig. 1. ^{27}Al NMR spectra at 65.18 MHz of potassium hexathiocyanatoaluminate(III) in a) DMSO, a') DMSO containing KSCN, b) DMA, b') DMA containing KSCN, c) AN, c') AN containing KSCN. The concentration of the solutions are indicated in Tables 1 and 2.

resonances were observed only in the region of hexacoordinated Al(III) species.[5] In DMSO with excess KSCN the spectrum consists of 7 resonances, which can be assigned to the hexacoordinated SCN^- and DMSO mixed ligand complexes. Since two upfield lines newly appear by adding excess KSCN, the most upfield narrow line at −34.0 ppm should be the resonance caused by hexathiocyanatoaluminate(III) ion. In DMA a broad resonance was located at downfield of the narrow resonance at −34.2 ppm, the relative intensity of which was increased by adding excess KSCN. A shoulder was observed at downfield side of the resonance of −33.0 ppm in AN solution. It disappeared in the solution containing excess KSCN. As is shown in Fig. 2, in propylene carbonate (PC), the spectrum consists of only one narrow resonance at −33.9 ppm which was unchanged by addition of excess KSCN. Addition of DMSO to the PC solution produces lines of SCN^--DMSO mixed ligand complex that are seen in the DMSO solution. The intensity of the lines increased with the increase of DMSO content in the solution. This will be the evidence for the fact that hexathiocyanatoaluminate(III) ion is the only Al spe-

cies present in the solvent of low coordinating ability. In acetone (AC) the situation was similar to that in PC. The solution and that containing excess KSCN gave a single resonance at −33.9 ppm. In this way the shift of Al species containing six SCN^- in its coordination sphere was determined as −34 ppm.

The shift of $[Al(AN)_6]^{3+}$, in which AN coordinates to Al through N atom is reported as −32.7 ppm.[2] Since the shifts of hexaethylisocyanatoaluminum ion, $[Al(SCNEt)_6]^{3+}$, and tris(dimethyldithiocarbamato)-aluminum, $[Al(S_2CNMe_2)_3]$, are reported as 20[8] and 22 ppm,[9] respectively, the shift of $[Al(SCN)_6]^{3-}$ would be around 20 ppm, if SCN^- coordinates to Al through S atom. Thus it can be concluded that SCN^- coordinates to Al^{3+} through N atom in these solutions and we will write the formula of the complex as $[Al(NCS)_6]^{3-}$.

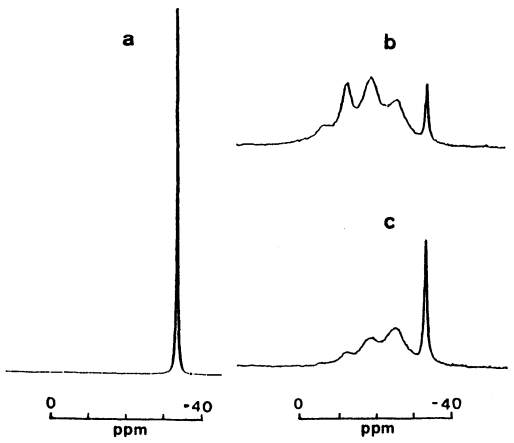

Fig. 2. ^{27}Al NMR spectra at 23.3 MHz of potassium hexathiocyanatoaluminate(III) in a) PC, b) PC-DMSO, Al:PC:DMSO mole ratio=1:122:10, and c) PC-DMSO, Al:PC:DMSO mole ratio=1:126:4.4.

All of the Al NMR shift of species coordinated octahedrally to ligands through O atom such as $[Al(DMF)_6]^{3+}$ (−2.6 ppm)[5] and $[Al(H_2O)_6]^{3+}$ (0 ppm) are around 0 ppm. Thus the most downfield resonance at 3.1 ppm in the DMSO solution can be assigned to $[Al(DMSO)_6]^{3+}$. Other 5 lines located between 3.1 and −34 ppm due to $[Al(NCS)_6]^{3-}$ may be assigned to $[Al(NCS)_n(DMSO)_{6-n}]^{(3-n)+}$, where n=1 to 5. Table 1 compares the observed shifts with those calculated by applying the pairwise additivity model.[6] In the present octahedral complex with two kinds of ligand, NCS^- and DMSO, the pairwise additivity parameters to be evaluated are $\eta_{O\text{-}O}$, $\eta_{N\text{-}N}$, and $\eta_{O\text{-}N}$, and the chemical shift of Al was calculated by summing the appropriate combination of twelve parameters corresponding to twelve edges of the octahedral complex in question. Although our spectra could not resolve lines from cis and trans isomers with n of 2, 3, and 4, the observed shifts are consistent with those calculated for cis isomers which were predicted[7] as giving narrower lines than those of trans isomers.

Table 1. Comparison between Observed and Calculated ^{27}Al Chemical Shifts of Al^{3+}- SCN^-- DMSO Mixed Ligand Complexes

Species	Obsd. shift/ppm (half width/Hz)		Calcd. shifts/ppm applying pair additive approximation[a]
	$K_3[Al(NCS)_6]$[b]	$K_3[Al(NCS)_6]$ +KSCN[c]	
$[Al(DMSO)_6]^{3+}$	3.1(25)	3.1(65)	3.10
$[Al(DMSO)_5(NCS)]^{2+}$	−0.7(52)	−0.7(80)	−0.70
$[Al(DMSO)_4(NCS)_2]$	−5.8(70)	−5.3(108)	cis −5.7 trans −4.5
$[Al(DMSO)_3(NCS)_3]$	−12.2(100)	−12.3(75)	cis −11.9 trans −10.7
$[Al(DMSO)_2(NCS)_4]^-$	−18.4(100)	−18.3(—)	cis −18.1 trans −16.9
$[Al(DMSO)(NCS)_5]^{2-}$	—	−25.3(—)	−25.4
$[Al(NCS)_6]^{3-}$	—	−34.0(52)	−34.00

a) Additivity parameter values(ppm): $\eta_{O\text{-}O}$=0.258; $\eta_{N\text{-}N}$=−2.833; $\eta_{O\text{-}N}$=−0.691. These values are estimated from the observed shifts of $[Al(DMSO)_6]^{3+}$, $[Al(NCS)_6]^{3-}$, and $[Al(DMSO)_5(NCS)]^{2+}$. b) 0.1 M. c) 0.3 M $K_3[Al(NCS)_6]$ and 3 M KSCN (1 M= 1 mol dm^{-3}).

Table 2. Chemical Shifts and Linewidths of Resonances in the Solutions of $K_3[Al(NCS)_6]$ and Those Containing Excess KSCN

Solvent	Solute	Shift/ppm (linewidth/Hz)	
AN	0.3 M $K_3[Al(NCS)_6]$		−33.0(140)
	0.4 M $K_3[Al(NCS)_6]$, 3 M KSCN		−33.3(65)
DMA	0.07 M $K_3[Al(NCS)_6]$	−28.5(610)	−34.2(35)
	0.05 M $K_3[Al(NCS)_6]$, 2 M KSCN	−28.5(580)	−34.2(20)
PC	0.2 M $K_3[Al(NCS)_6]$		−33.9(15)
	0.2 M $K_3[Al(NCS)_6]$, 2 M KSCN		−33.9(15)
AC	0.2 M $K_3[Al(NCS)_6]$		−33.9(65)
	0.2 M $K_3[Al(NCS)_6]$, 2 M KSCN		−33.9(41)

In DMA, the main species present in the solution of $K_3[Al(NCS)_6]$ appear to be $[Al(NCS)_n(DMA)_{6-n}]^{(3-n)+}$ of n of 5 or 4. Since the shift of $[Al(AN)_6]^{3+}$ is very close to that of $[Al(NCS)_6]^{3+}$, no definite conclusion could be drawn for the species present in the AN solution. It seems interesting that while a solvent of high coordinating ability like DMSO competes with SCN^- in coordinating Al^{3+}, a solvent of relatively low coordinating ability like AN competes with Cl^- in occupying the octahedral sites of Al^{3+}.[2] Table 2 gives the shifts of the complexes.

The authors wish to express their thanks to Prof. Ryozo Irie of Faculty of Agriculture, Shinshu University for obtaining NMR spectra at 65.18 MHz. The present work was partially supported by a Grant-in-Aid for Science Research No. 62540459 from the Ministry of Education, Science and Culture.

References

1) J. W. Akitt, J. A. Farnsworth, and P. Letellier, *J. Chem. Soc., Faraday Trans. 1*, **81**, 193 (1985).
2) F. W. Wehrli and S. Wehrli, *J. Magn. Reson.*, **44**, 197 (1981).
3) V. P. Tarasov, S. P. Petrosyants, G. A. Kirakosyan, and Yu. A. Buslaev, *Dokl. Akad. Nauk. SSSR*, **242**, 156 (1978).
4) O. Schmidtz-DuMont and B. Ross, *Angew. Chem.*, **76**, 647 (1964).
5) J. W. Akitt, "Multinuclear NMR," ed by J. Mason Plenum, New York (1987), Chap. 9.
6) T. Vladimiroff and E. R. Malinowski, *J. Chem. Phys.*, **46**, 1830 (1967).
7) K. A. Valiev and M. M. Zaripov, *Zh. Strukt. Khim.*, **7**, 494 (1966).
8) H. Haraguchi and S. Fujiwara, *J. Phys. Chem.*, **73**, 3467 (1969).
9) H. Nöth and P. Konrad, *Chem. Ber.*, **116**, 3552 (1983).

Oxidation of Benzylic and Allylic Alcohols with Cobalt(III) Acetate in Acetic Acid in the Presence and Absence of Sodium Bromide

Masao HIRANO, Takashi MORIMOTO,* and Keiko ITOH
Department of Industrial Chemistry, Faculty of Technology, Tokyo University of Agriculture and Technology, Koganei, Tokyo 184
(Received December 19, 1987)

Synopsis. Benzyl alcohol and its *o*-, *m*-, and *p*-substituted derivatives afforded fairly good yields of the corresponding benzaldehydes through a reaction with a Co(III)-NaBr system. With allylic alcohols, this system failed in a selective formation of unsaturated carbonyl compounds. In the latter cases, the products were effectively obtained by using a higher concentration of cobalt(III) acetate in the absence of NaBr.

Cobalt(III) acetate is a potent oxidant; on kinetic grounds,[1,2] the oxidation of organic compounds with it has been considered via an electron-transfer mechanism. Compared with other metal oxidants such as Pb(IV), Tl(III), Hg(II), Cr(VI), Se(IV) salts etc., some advantages in terms of relatively low cost, simple manipulation and, especially lower toxicity of cobalt(III) acetate make it considerably attractive in the oxidation of various olefins.[3-5] The present paper describes the oxidation of benzylic and allylic alcohols with cobalt(III) acetate in acetic acid since, hitherto, there has only been little data on this subject. In addition, the effect of added sodium bromide on the reaction rate as well as on the product yield is reported.

Results and Discussion

The oxidation of benzyl alcohol (**1**) in acetic acid with a stoichiometric amount (2 equiv. per mole of **1**) of cobalt(III) acetate was conducted under an inert atmosphere (argon) since the main product, benzaldehyde (**2**), is highly susceptible to autoxidation. After heating the reaction mixture at 60 °C for 2 h, it was observed that cobalt(III) acetate was not completely consumed, as judged from the dark-green color of the solution. A GLC analysis revealed that **1**, **2**, and a minor amount (GLC selectivity; 4.2%) of benzyl acetate (**3**) was involved in the product mixture. Then, the reaction was carried out in the presence of NaBr, known as a promoter in cobalt-catalyzed autoxidation of alkylbenzenes.[6,7] In this case, the initially dark-green solution became blue-black as the NaBr gradually disappeared. When the reaction mixture was poured into brine, the aqueous layer became cobaltous pink, suggesting that almost all the cobalt(III) acetate had been consumed. Indeed, the conversion of **1** was considerably increased upon the addition of a small amount of NaBr (Table 1), whereas **3** decreased to a trace amount. These observations imply that NaBr contributes not only to accelerate the reaction, but to inhibit any side-reaction. The yield of **2** gradually increased upon increasing the amount of NaBr and reached a maximum at NaBr/**1**=0.5. However, a further addition of NaBr no longer contributed to the formation of **2**.

The oxidation of substituted benzyl alcohols was performed in a manner similar to that of **1**, resulting in a predominant formation of the corresponding benzaldehydes. Compared with the other substrates, the oxidation of nitrobenzyl alcohols did not proceed so readily in the absence of NaBr, viz. the conversion of *p*-nitrobenzyl alcohol (**4**) was 65% at 60 °C for 2 h. On the other hand, *p*-methoxybenzyl alcohol (**5**) showed a higher reactivity. Thus, 77% of **5** was converted under comparable conditions.

As with the case of **1**, an addition of NaBr usually accelerated the oxidation of substituted benzyl alcohols, leading to a selective formation of the corresponding benzaldehydes. Indeed, the conversion of **4** increased to 97% upon the addition of NaBr(NaBr/**4**=

Table 1. Oxidation of Benzyl Alcohol in the Presence and Absence of Sodium Bromide[a]

NaBr/Sub. mole ratio	Recovered alcohol[b]	Yield of benzaldehyde[b]
0	21	75
0.1	7.3	81
0.3	4.4	83
0.5	4.2	89
0.7	4.9	83
1.0	4.2	76

a) Under argon, 60 °C, 2 h; ca. 0.5 g of substrate and a stoichiometric cobalt(III) acetate were used in every run. b) GLC yield in mol%.

Table 2. Oxidation of Benzyl Alcohols[a]

		Time	Temp	NaBr/Sub	Benzaldehyde[b]
		h	°C	mole ratio	%
H		2	60	0.5	86
Me	*o*-	2	50	0.5	75
	m-	2	50	0.5	91
	p-	2	60	0.5	81
OMe	*o*-	2.5	50	0.1	87
	m-	2	50	0.5	87
	p-	4	60	0.5	88
Br	*o*-	2	70	0.5	87
	m-	2	70	0.5	88
	p-	2	60	0.5	92
Cl	*o*-	2	70	0.5	91
	m-	2	70	0.5	91
	p-	4	60	0.1	85
NO_2	*o*-	2	70	0.5	72
	m-	2	70	0.5	83
	p-	2	60	0.5	82

a) Under argon; ca. 0.5 g of substrates and a stoichiometric cobalt(III) acetate were used in every run. b) Isolated yield.

Table 3. Oxidation of Allylic Alcohols[a)]

	Time	Temp	Co(III)/Sub.	Product[b)]
	h	°C	mole ratio	Yield/%
Cinnamyl alcohol	4	60	2.5	Cinnamaldehyde 62
Geraniol	24	40	2.5	Citral 63
1-Octen-3-ol	6	60	3.0	1-Octen-3-on 72
trans-2-Hexen-1-ol	6	60	5.0	*trans*-2-Hexenal 71

a) Under argon; ca. 0.5 g of substrates were used in every run. b) Isolated yield.

0.5) under the same conditions as mentioned above. The results of various substituted benzyl alcohols are summarized in Table 2. The reaction conditions (temperature, time, and concentration of NaBr) were determined on the basis of the reactivity of the substrates as well as the yield of the aldehydes. In all cases, GLC analyses showed that no neutral product, other than the aldehydes, was formed in a significant amount under the conditions employed. As shown in Table 2, substituted benzaldehydes were obtained in excellent yields, irrespective of the nature of the substituents or of the position of those on the benzene-ring. Consequently, the present procedure was proved to be applicable to a wide variety of substituted benzyl alcohols.

The reaction of allylic alcohol was also promoted upon the addition of NaBr. For example, conversions of 1-octen-3-ol in reactions with a stoichiometric amount of cobalt(III) acetate at 60 °C for 2 h were 26, 63, 70, and 77% when the mole ratios of NaBr/substrate were 0, 0.1, 0.5, and 1.0, respectively; at this time the GLC selectivities of the main product, 1-octen-3-on (**6**), were 24, 49, 52, and 50%, respectively. However, the unknown products increased and, thus, the selectivity of **6** decreased in proportion to the amount of NaBr added. The failure of a selective formation of **6** in the presence of NaBr might be explained by the facts that an olefinic double bond has been suggested to be as susceptible to cobalt(III) acetate as hydroxyl group[2)] and that cobalt(III)-NaBr system is an effective reagent for allylic oxidation.[8)] A close inspection of the reaction conditions revealed that a reaction with an excess amount of cobalt(III) acetate in the absence of NaBr for a relatively long time is appropriate for an effective formation of unsaturated carbonyl compounds from allylic alcohols (Table 3).

In connection with the initial stage of the reaction, cobalt monobromide has been suggested as being an active species in the autoxidation of hydrocarbons catalyzed by cobalt(II) acetate in the presence of NaBr.[6)] However, an intervention of the bromine radical cannot be ruled out, since any product study regarding the oxidation of alicyclic olefins with a cobalt(III)-NaBr system can be rationally interpreted in terms of a participation of the bromine radical.[8)] The specification of an active species is now under way in our laboratory.

The present reaction requires stoichiometric or higher amounts of cobalt(III) acetate and is of limited utility for large-scale oxidation. However, the oxidation of benzylic alcohols with a cobalt(III) acetate-NaBr system offers a conventional method for synthesizing benzaldehydes, since products can be selectively obtained within a reasonable period of time, regardless of nature or the position of the substituents on the benzene-ring.

Experimental

^{1}H NMR spectra were obtained with a JEOL model PMX-60 spectrometer for solutions in carbon tetrachloride. IR spectra were recorded for thin films or KBr disks on a JASCO DS-403G spectrophotometer. GLC was carried out on a Shimadzu GC-6A or GC-4CM instrument with a 2 m column packed with 5% PEG-20M or 1.5% OV-17, respectively, on Chromosorb WAW-DMCS.

Materials. All alcohols were commercially available and were purified by conventional procedures just before use. Cobalt(III) acetate in acetic acid was prepared according to method described in the literature;[9)] the concentration was determined by Fe(II) and back titration with Ce(IV).

Oxidation Procedures. The following procedures are representative. To a mixture of benzyl alcohol (ca. 0.5 g) and NaBr (0.5 mol equiv) in a round-bottomed flask was added cobalt(III) acetate in acetic acid (2 mol equiv); the flask was then flushed with argon. The reaction was carried out at a controlled temperature in a thermostat with magnetic agitation. After a given period, the reaction mixture was poured into brine and extracted three times with ether. The combined extract was successively washed with brine, 10% aqueous sodium carbonate, and brine and then dried (Na_2SO_4). Removing the ether on a rotary evaporator yielded a light-yellow oil, which was chromatographed on silica gel (hexane-AcOEt).

All products, so obtained, were known compounds and were identified by comparisons of their NMR and IR spectra with those of authentic samples.

References

1) Y. Kamiya and M. Kashima, *J. Catal.* **25**, 326 (1972).

2) R .Kawai and Y. Kamiya, *Nippon Kagaku Kaishi*, **1973**, 1533.

3) M. Hirano, K. Nakamura, and T. Morimoto, *J. Chem. Soc., Perkin Trans. 2*, **1981**, 817.

4) M. Hirano and T. Morimoto, *J. Chem. Soc., Perkin Trans. 2*, **1984**, 1033.

5) M. Hirano and T. Morimoto, *J. Chem. Soc., Perkin Trans. 2*, **1985**, 1105.

6) Y. Kamiya, T. Nakajima, and K. Sakota, *Bull. Chem. Soc. Jpn.*, **39**, 2211 (1966).
7) Y. Kamiya, "Oxidation of Organic Compounds," Am. Chem. Soc., (1968), p. 193.
8) T. Morimoto, M. Hirano, and T. Machida, *J. Chem. Soc., Perkin Trans. 2*, to be published.
9) S. S. Lande, C. D. Falk, and J. K. Kochi, *J. Inorg. Nucl. Chem.*, **33**, 4101 (1971).

Free Radical Addition of Thiophenol to 3-Substituted 1-Alkyne with or without Migration of the Substituents

Hideyoshi MIYAKE* and Kimiaki YAMAMURA
Department of Chemistry, College of General Education, Kobe University, Nada, Kobe 657
(Received February 9, 1988)

Synopsis. Thiophenol reacts with 3-phenylthio- and 3-bromo-1-alkyne in the presence of radical initiator to give 1,2-bis(phenylthio)-1-alkene and 2-bromo-1-phenylthio-1-alkene.

The free radical addition of a thiol to carbon-carbon double or triple bond is a well-established reaction.[1] It is one of the most useful methods to synthesize sulfides, under mild conditions. We studied further application of this reaction. We wish to report that the radical addition of thiophenol to 3-substituted 1-alkyne proceeds with or without migration of the substituents.

By heating thiophenol and 3-substituted 1-propyne such as **1** (X=SPh and Br; R=H), in benzene in the presence of azobis-isobutyronitrile (AIBN), we obtained neither 1-(phenylthio)allene (**2**) nor 3-substituted 1-phenylthio-1-alkene (**3**), but rearranged products **4** (Eq. 1). When the substituent (X) was PhS, 1,2-bis(phenylthio)-1-propene (**4a**) was obtained in an almost quantitative yield. However, when X was Br, 2-bromo-1-phenylthio-1-propene was obtained only in 45% yield with evolving HBr gas.

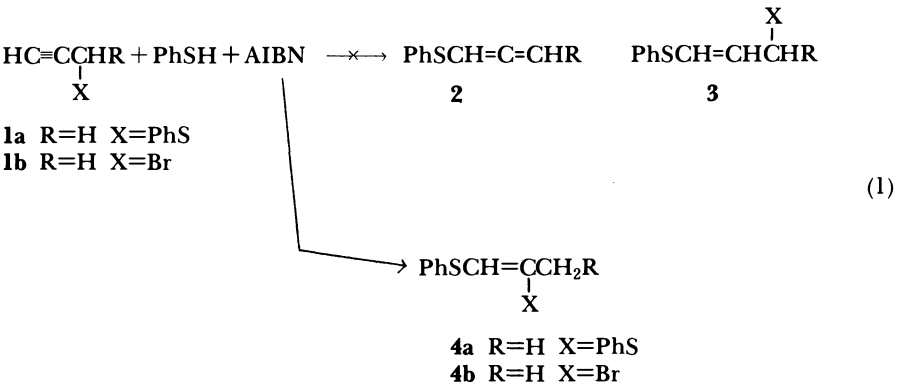

(1)

At first glance, this reaction seems to proceed with migration of the substituent (X) with a bridged radical intermediate (Eq. 2).[2] However, a more plausible mechanism is suggested as Scheme 1. It involves an initial attack of PhS· to triple bond followed by elimination of Br· or PhS·, because β-bromo or β-phenylthio radical easily eliminates Br· or PhS· to form double bond,[3] and the formation of 1-(phenylthio)allenes is quite reasonable. 1-(Phenylthio)-allenes are more reactive than **1**, and addition of HBr or PhSH occurs smoothly to give the adducts (**4a**, **b**).

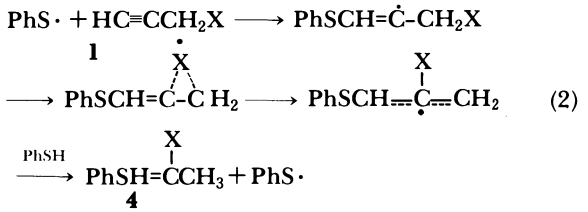

(2)

Regioselectivity and the mechanism of the addition of PhSH to allenes have been discussed by Heiba.[4] According to his discussion, the reaction involves (a) an initial attack of PhS· to allene and (b) hydrogen transfer to transient radical. The free radical intermediate formed by route 2 should undergo the reverse reaction.[5] However, the initial radical intermediate formed via route 1, although it may be initially non-allylic, undergoes rapid rotation of 90° around the C-C axis to form the conformation of the stable allylic radical. Such a rotation must have a very low activation energy and the resonance energy of allylic radical will make the reaction via route 1 faster than that via route 2.

This mechanism was supported by the following results. In the case of propargyl bromide, a small amount (<5%) of 1,2-bis(phenylthio)-1-propene (**4a**) was obtained as a by-product, and generation of HBr gas was observed. When two phase system of benzene-H_2O was used as solvent to remove HBr from the organic layer, the yield of **4b** decreased to 34%, and that of **4a** increased to 61% (Eq. 3).

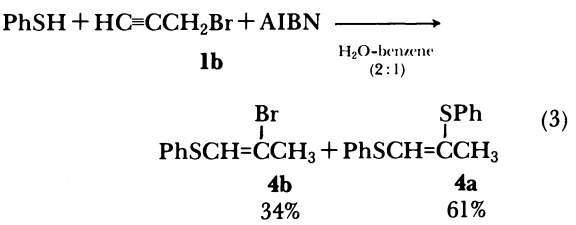

(3)

When 3-(4-methylphenylthio)-1-propyne (**1g**) was

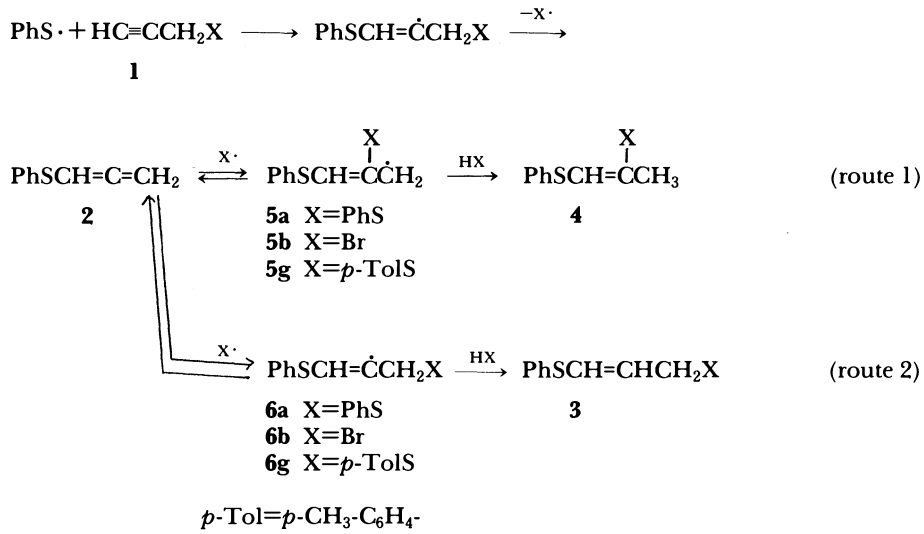

Scheme 1.

treated with 2 equivalent amount of thiophenol and 0.3 equivalent of AIBN, **4a** was obtained in 15% yield (Eq. 4). Although 1-(phenylthio)allene was not isolated, these results indicated the formation of 1-(phenylthio)allene intermediate. However, to our surprise, 2-(4-methylphenylthio)-1-phenylthio-1-propene (**4g**) was not obtained, but 3-(4-methylphenylthio)-1-phenylthio-1-propene (**3g**) was obtained in 66% yield.

$$p\text{-TolSCH}_2\text{C}{\equiv}\text{CH} + \text{PhSH} \xrightarrow{\text{AIBN}} \underset{\textbf{1g}}{} \quad \underset{(2\ \text{equiv})}{} \tag{4}$$

$$\textbf{4a} + p\text{-TolSCH}_2\text{CH=CHSPh}\ (\textbf{3g})$$

15% 66%

These results were explained as follows. Allylic radical **5g** was more stable than **5a**, and the activation energy of **5g** for hydrogen abstraction must be higher than that of **5a**. It suggests that the reaction of **1g** via route 1 is slower than that of **1a**. However, the stability of allylic radical **6** was not so influenced by aryl groups of the sulfides as that of **5**. And when **1g** was used, the relative reaction rate via route 2 became faster than that via route 1.

Although R in **1** is H, no simple adduct of thiophenol was obtained, when R is an alkyl group such as CH_3, n-C_3H_7, or n-C_5H_{11}, and X is SPh, a simple adduct like **3** was also obtained. The formation of such by-products as **3c**, **3d**, and **3f**, was similarly explained: Allylic radical **7** was more stable than **5a**, and the relative reaction rate to give **4** became slower. Results were summarized in Table 1.

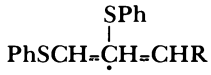

7

R=CH_3, n-C_3H_7, n-C_5H_{11}

When the substituents (X) is OH, OAc, and OCH_2Ph, which are not good leaving groups for the

Table 1. Free Radical Addition of PhSH to **1**

1	R	X	Products (yield/%,[a] E/Z[b])	
1a	H	PhS	PhSCH=CCH$_2$ (97, 69/31) SPh **4a**	
1b	H	Br	PhSCH=CCH$_3$ (45, 70/30) Br **4b**	
1c	CH_3	PhS	PhSCH=CC$_2$H$_5$ (53, 64/36) SPh **4c**	PhSCH=CHCHCH$_3$ (40, —[c]) SPh **3c**
1b	n-C_3H_7	PhS	PhSCH=CC$_4$H$_9^n$ (57, 68/32) SPh **4b**	PhSCH=CHCHC$_3$H$_7^n$ (27, —[c]) SPh **3d**
1e	n-C_3H_7	Br	PhSCH=CC$_4$H$_9^n$ (42, 71/29) Br **4e**	
1f	n-C_5H_{11}	PhS	PhSCH=CC$_6$H$_{13}^n$ (61, 66/34) SPh **4f**	PhSCH=CHCHC$_5$H$_{11}^n$ (22, —[c]) SPh **3f**

a) Isolated yield. b) Determined with isolation of each isomers. c) Not determined.

radical reaction, the migration of the substituents did not occur, and simple adducts of thiophenol were obtained. Results were shown below.

$$HC{\equiv}CCH_2X + PhSH \xrightarrow{AIBN} PhSCH{=}CHCH_2X$$

		isolated yield (%), (*E*/*Z*)	
X=OH	**3h**	83	(7/3)
X=OAc	**3i**	84	(7/3)
X=OCH_2Ph	**3j**	82	(7/3)

The *E*/*Z* ratio was determined by ^1H NMR.

This method is useful for synthesizing vinylic sulfides. Further application of this type of reaction is now under investigation.

Experimental

Reaction Procedure. As a typical experiment, the reaction of 3-phenylthio-1-propyne (**1a**) with thiophenol is as follows: 3-Phenylthio-1-propyne (**1a**) (1.48 g, 10 mmol), thiophenol (1.20 g, 10 mmol), and AIBN (0.49 g, 3 mmol) in benzene (10 ml) were stirred at 80 °C for 1 h. After removing the solvent under a reduced pressure, the product was purified by column chromatography on silica gel to give (*E*)-1,2-bis(phenylthio)-1-propene (1.74 g, 6.7 mmol) and (*Z*)-1,2-bis(phenylthio)-1-propene (0.80 g, 3.1 mmol) (**4a**).

(*E*)-1,2-Bis(phenylthio)-1-propene ((*E*)-4a): IR(neat): 800, 1435, 1472, and 1580 cm^{-1}; ^1H NMR($CDCl_3$) δ=2.05 (s, 3H), 6.30 (s, 1H), 7.0—7.4 (m, 10H); Anal. ($C_{15}H_{14}S_2$) C, H.

(*Z*)-1,2-Bis(phenylthio)-1-propene ((*Z*)-4a): IR(neat): 830, 1440, 1475, and 1582 cm^{-1}; ^1H NMR($CDCl_3$) δ=1.95 (s, 3H), 6.35 (s, 1H), 7.0—7.4 (m, 10H); Anal. ($C_{15}H_{14}S_2$) C, H.

(*E*)-2-Bromo-1-phenylthio-1-propene ((*E*)-4b): IR(neat): 823, 1438, 1478, and 1582 cm^{-1}; ^1H NMR($CDCl_3$) δ=2.30 (s, 3H), 6.30 (s, 1H), 7.0—7.4 (m, 5H); Anal. (C_9H_9SBr) C, H.

(*Z*)-2-Bromo-1-phenylthio-1-propene ((*Z*)-4b): IR(neat): 810, 1438, 1478, and 1582 cm^{-1}; ^1H NMR($CDCl_3$) δ=2.40 (s, 3H), 6.43 (s, 1H), 7.0—7.4 (m, 5H); Anal. (C_9H_9SBr) C, H.

(*E*)-1,2-Bis(phenylthio)-1-butene ((*E*)-4c): IR(neat): 1040, 1440, 1477, and 1582 cm^{-1}; ^1H NMR($CDCl_3$) δ=1.05 (t, 3H), 2.35 (q, 2H), 6.20 (s, 1H), 7.0—7.4 (m, 10H); Anal. ($C_{16}H_{16}S_2$) C, H.

(*Z*)-1,2-Bis(phenylthio)-1-butene ((*Z*)-4c): IR(neat): 1440, 1478, and 1580 cm^{-1}; ^1H NMR($CDCl_3$) δ=1.05 (t, 3H), 2.35 (q, 2H), 6.45 (s, 1H), 7.0—7.4 (m, 10H); Anal. ($C_{16}H_{16}S_2$) C, H.

1,3-Bis(phenylthio)-1-butene (3c): IR(neat): 942, 1022, 1438, 1478, and 1583 cm^{-1}; ^1H NMR($CDCl_3$) δ=1.35 (t, 3H), 3.5—4.0 (m, 1H), 5.7—5.9 (m, 2H), 6.8—7.4 (m, 10H); Anal. ($C_{16}H_{16}S_2$) C, H.

(*E*)-1,2-Bis(phenylthio)-1-hexene ((*E*)-4d): IR(neat): 1040, 1437, 1478, and 1580 cm^{-1}; ^1H NMR($CDCl_3$) δ=0.90 (t, 3H), 1.0—1.8 (m, 4H), 2.40 (t, 2H), 6.25 (s, 1H), 7.1—7.4 (m, 10H): Anal. ($C_{18}H_{20}S_2$) C, H.

(*Z*)-1,2-Bis(phenylthio)-1-hexene ((*Z*)-4d): IR(neat): 1040, 1437, 1476, and 1580 cm^{-1}; ^1H NMR($CDCl_3$) δ=0.90 (t, 3H), 1.0—1.8 (m, 4H), 2.25 (t, 2H), 6.50 (s, 1H), 7.1—7.4 (m, 10H); Anal. ($C_{18}H_{20}S_2$) C, H.

1,3-Bis(phenylthio)-1-hexene (3d): IR(neat): 1020, 1437, 1480, and 1580 cm^{-1}; ^1H NMR($CDCl_3$) δ=0.90 (t, 3H), 1.1—1.8 (m, 4H), 3.5—3.8 (m, 1H), 5.7—5.9 (m, 2H), 7.0—7.5 (m, 10H); Anal. ($C_{18}H_{20}S_2$) C, H.

(*E*)-2-Bromo-1-phenylthio-1-hexene ((*E*)-4e): IR(neat): 820, 1438, 1478, and 1580 cm^{-1}; ^1H NMR($CDCl_3$) δ=0.90 (t, 3H), 1.1—1.7 (m, 4H), 2.45 (t, 2H), 6.43 (s, 1H), 7.1—7.4 (m, 5H); Anal. ($C_{12}H_{15}BrS$) C, H.

(*Z*)-2-Bromo-1-phenylthio-1-hexene ((*Z*)-4e): IR(neat): 810, 1438, 1478, and 1580 cm^{-1}; ^1H NMR($CDCl_3$) δ=0.90 (t, 3H), 1.1—1.7 (m, 4H), 2.4—2.7 (m, 2H), 6.45 (s, 1H), 7.0—7.4 (m, 5H); Found: C, 53.49; H, 5.78%. Calcd for $C_{12}H_{15}BrS$: C, 53.14; H, 5.58%.

(*E*)-1,2-Bis(phenylthio)-1-octene ((*E*)-4f): IR(neat): 815, 1438, 1478, and 1580 cm^{-1}; ^1H NMR($CDCl_3$) δ=0.90 (t, 3H), 1.1—1.8 (m, 6H), 2.40 (t, 2H), 6.30 (s, 1H), 7.1—7.4 (m, 10H); Found: C, 72.78; H, 7.40%. Calcd for $C_{20}H_{24}S_2$: C, 73.11; H, 7.36%.

(*Z*)-1,2-Bis(phenylthio)-1-octene ((*Z*)-4f): IR(neat): 820, 1438, 1478, and 1580 cm^{-1}; ^1H NMR($CDCl_3$) δ=0.90 (t, 3H), 1.1—1.8 (m, 6H), 2.25 (t, 2H), 6.50 (s, 1H), 7.0—7.4 (m, 10H); Anal. ($C_{20}H_{24}S_2$) C, H.

1,3-Bis(phenylthio)-1-octene (3f): IR(neat): 1020, 1437, 1478, and 1578 cm^{-1}; ^1H NMR($CDCl_3$) δ=0.90 (t, 3H), 1.1—1.8 (m, 8H), 3.5—3.6 (m, 1H), 5.7—5.9 (m, 2H), 7.0—7.5 (m, 10H); Anal. ($C_{20}H_{24}S_2$) C, H.

3-(4-Methylphenylthio)-1-phenylthio-1-propene (3g): IR (neat): 1015, 1025, 1440, 1480, 1492, and 1583 cm^{-1}; ^1H NMR($CDCl_3$) δ=2.30 (s, 3H), 3.50 (d, 2H), 5.8—6.1 (m, 2H), 6.9—7.4 (m, 9H), Anal. ($C_{16}H_{16}S_2$) C, H.

3-Phenylthio-2-propen-1-ol (3h): IR(neat): 850, 1305, 1437, 1475, 1580, and 3400 cm^{-1}; ^1H NMR($CDCl_3$) δ=2.3—2.8 (m, 1H), 4.10 (d, 1.4H, *E*-isomer), 4.30 (d, 0.6H, *Z*-isomer), 5.8—6.4 (m, 2H), 7.0—7.4 (m, 5H); Found: C, 64.69; H, 6.20%. Calcd for $C_9H_{10}OS$: C, 65.02; H, 6.06%.

3-Phenylthio-2-propenyl Acetate (3i): IR(neat): 1437, 1477, 1580, and 1740 cm^{-1}; ^1H NMR($CDCl_3$) δ=2.00, 2.10 (two singlets, total 3H), 4.50 (d, 1.4H, *E*-isomer), 4.70 (d, 0.6H, *Z*-isomer), 5.5—6.0 (m, 1H), 6.3—6.6 (m, 1H), 7.0—7.4 (m, 5H): Anal. ($C_{11}H_{12}SO_2$) C, H.

3-Benzyloxy-1-phenylthio-1-propene (3j): IR(neat): 1308, 1440, 1480, and 1582 cm^{-1}; ^1H NMR($CDCl_3$) δ=3.95 (d, 1.4H, *E*-isomer), 4.15 (d, 0.6H, *Z*-isomer), 4.3—4.45 (m, 2H), 5.5—6.0 (m, 1H), 6.2—6.6 (m, 2H), 7.0—7.4 (m, 10H); Anal. ($C_{16}H_{16}OS$) C, H.

The present work was partly supported by a Grant-in-Aid for Encouragement of Young Scientists, No. 62740296 from the Ministry of Education, Science and Culture.

References

1) F. W. Stacy and J. F. Harris, Jr., *Org. React.*, **13**, 150 (1963).

2) P. S. Skell, D. L. Tuleen, and P. D. Readio, *J. Am. Chem. Soc.*, **85**, 2849, 2850 (1963); E. S. Huyser and R. H. C. Feng, *J. Org. Chem.*, **36**, 731 (1971).

3) J. A. Kampmeier, R. P. Geer, A. J. Meskin, and R. M. D'Silva, *J. Am. Chem. Soc.*, **88**, 1257 (1966).

4) E-A. I. Heiba, *J. Org. Chem.*, **31**, 776 (1966).

5) C. Walling and W. Helmreich, *J. Am. Chem. Soc.*, **81**, 1141 (1959); N. P. Neiureiter and F. G. Bordwell. *ibid.*, **82**, 5354 (1960).

Addition of *N*-(Hydroxymethyl)phthalimide to Methacrylates by Carbon-Carbon Bond Formation

Keisuke KURITA,* Hiroshi ITOH, Shunji CHIKAMORI, and Tomoyuki MABUCHI
Department of Industrial Chemistry, Faculty of Engineering, Seikei University, Musashino-shi, Tokyo 180
(Received February 26, 1988)

Synopsis. *N*-(Hydroxymethyl)phthalimide undergoes addition to the carbon-carbon bond of methacrylates effectively in sulfuric acid, resulting in the formation of a new carbon-carbon bond.

The hydroxymethyl group attached to the nitrogen of imides exhibits an interesting reactivity owing to a distinct cationic nature of the methylene group in an acidic medium such as sulfuric acid. Compounds having such a group are thus interesting intermediates in organic synthesis as electrophiles. *N*-(Hydroxymethyl)phthalimide is, for example, capable of electrophilic addition to cyano groups to form amide-imide compounds.[1] It also undergoes dehydration reaction with amines, while affording amine-imide derivatives.[2] These characteristic reactions have proved useful in providing convenient methods for synthesizing various types of polyamide-imides[3] and polyamine-imides.[4] This peculiar electrophilicity of hydroxymethylimides suggests the possibility of additions to carbon-carbon double bonds, if adequately polarized to permit the electrophilic attack, leading to new addition products by carbon-carbon bond formation.

N-(Hydroxymethyl)phthalimide (**1**) was subjected to the reactions with various kinds of compounds having a carbon-carbon double bond in concentrated sulfuric acid at 18 °C. The reaction with methyl methacrylate (**2a**) resulted in the formation of two products. Structural analysis revealed the major product to be a 1 : 1 adduct **3a** (78.5% yield) formed as a result of the electrophilic attack of **1** to the β-position of **2a**.

The minor product, on the other hand, was characterized by the presence of a carbon-carbon double bond and no hydroxyl group. Moreover, the ^{1}H NMR spectrum unambiguously indicated the double bond to be an exo methylene type. All these data supported the structure of **4a** (3.4% yield), which is formally a dehydrated form of **3a**. However, **3a** was not converted to **4a** when treated with sulfuric acid under the same conditions, suggesting **4a** to be formed by deprotonation from the intermediate species which results from the cationic attack of **1**, not by dehydration of **3a**. There is another possibility of deprotonation to give an alternate product having an endo double bond; however, **4a** was the only by-product we could isolate.

Since **1** seems to undergo decomposition in concentrated sulfuric acid in various fashions, the addition reaction would probably be dependent on the reaction temperature. When the temperature was lowered to 5 °C, the yield of **3a** increased to 82.0% as a result of suppression of side reactions at lower temperatures. Higher temperatures caused a marked reduction in the yield as shown in Table 1. In contrast, the formation of **4a** was not appreciably influenced by the reaction temperature. The reactions were also attempted in organic acidic solvents to prevent the possible degradation of **1** in sulfuric acid. No addition was, however, observed and only the starting materials were recovered in formic and dichloroacetic acids.

Ethyl methacrylate (**2b**) behaved quite similarly to **2a** in the reaction with **1** in sulfuric acid, giving the same kinds of addition products, **3b** and **4b**, in similar yields. Again, the minor product, **4b**, has an exo double bond.

Table 1. Reaction of *N*-(Hydroxymethyl)-phthalimide **1** with Methacrylates **2**

Methacrylate	Condition		Yield	
	Temp/°C	Time/h	%	
2a	5	20	**3a**, 82.0	**4a**, 3.2
2a	5	40	**3a**, 80.0	**4a**, 3.0
2a	18	20	**3a**, 78.6	**4a**, 3.4
2a	30	20	**3a**, 60.0	**4a**, 2.5
2a	43	20	**3a**, 23.6	**4a**, 2.5
2b	18	20	**3b**, 82.0	**4b**, 5.0

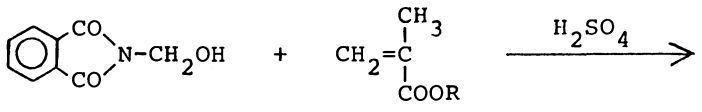

1 + **2a**, R=CH_3; **2b**, R=C_2H_5 $\xrightarrow{H_2SO_4}$

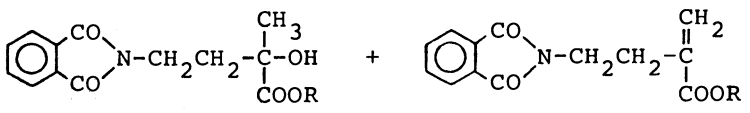

3a, R=CH_3; **3b**, R=C_2H_5 + **4a**, R=CH_3; **4b**, R=C_2H_5

If the addition of **1** also takes place to the carbon-carbon double bond as well as to the cyano group of acrylonitrile (**5a**) and methacrylonitrile (**5b**), these nitriles will afford 2 : 1 adducts. The addition reaction, however, turned out to proceed only at the cyano group even with two-fold excess **1**, and 1 : 1 adducts, **6a** and **6b**, were obtained in high yields along with three kinds of by-products formed from excess **1** by the elimination of formaldehyde and intermolecular dehydration. This indicates that the cyano group is more susceptible to electrophilic attack than the vinyl or vinylidene group on account of high electron density at the nitrogen atom and also that the resulting acrylamide and methacrylamide derivatives are resistive to the addition reaction.

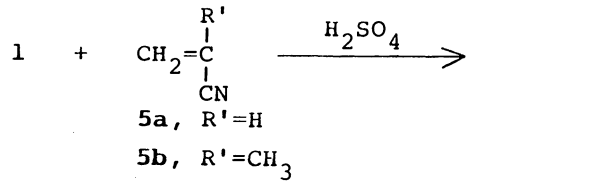

5a, R'=H

5b, R'=CH_3

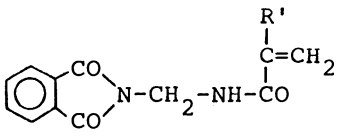

6a, R'=H

6b, R'=CH_3

Other vinyl compounds including methyl acrylate (**7**), ethyl acrylate (**8**), acrylic acid (**9**), methacrylic acid (**10**), methyl vinyl ketone (**11**), methyl isopropenyl ketone (**12**), acrylamide (**13**), vinyl acetate (**14**), butyl vinyl ether (**15**), styrene (**16**), fumaric acid (**17**), and cyclohexene (**18**) were also subjected to the reaction to understand the general scope of the reaction. No addition products were, however, detected in the reaction mixtures in all the cases, and only the by-products from **1** were isolated by column chromatography. It is noteworthy that while methacrylates **2a** and **2b** gave adducts in high yields, structurally similar vinyl compounds such as acrylates (**7** and **8**) and vinyl ketones (**11** and **12**) afforded no addition products, and only **1** and its degradation products were recovered. In the reaction with **11**, for example, most of the starting **1** was converted to the three kinds of by-products which were obtained in a total yield of 71%. This is probably ascribable to the higher electron availability at the α-position than β-position, as opposed to methacrylates,[8] which would make the reaction reluctant because of steric hindrance. Some reaction mixtures assumed dark colors and only small amounts of the by-products were recovered, indicating considerable extents of decomposition. The feasibility of the addition reaction thus appeared to be interpreted in terms of the electron availability at the β-position and the stability of the adducts; it is interesting to note that only the methacrylates meet these requirements among the vinyl compounds we examined.

Consequently, a new type of cationic addition of the hydroxymethyl group to C-C double bonds was effected, being quite sensitive to the substituents on the double bonds, and methacrylates were quite suitable for achieving a highly selective reaction.

Experimental

N-(Hydroxymethyl)phthalimide was prepared from phthalimide and formalin according to the procedure reported by Buc.[1]

^{1}H NMR spectra were recorded on a JEOL JNM-PMX60 (60 MHz) or JEOL JNM-GX270 (270 MHz) spectrometer, and ^{13}C NMR spectra on a JEOL PFT100 (25 MHz) or JEOL JNM-GX270 (68 MHz) spectrometer. Chemical shifts are relative to tetramethylsilane. IR spectra were taken with a JASCO IRA-1 spectrophotometer. Mass spectra were obtained with a Finnigan-MAT 4530 GC/MS spectrometer. Melting points were uncorrected.

Reaction of *N*-(Hydroxymethyl)phthalimide (1) with Methyl Methacrylate (2a). To 30 cm^3 of concentrated sulfuric acid kept at 0 °C was added 3.19 g (18 mmol) of pulverized **1**, which went into solution in 20 min with stirring. **2a** (1.80 g, 18 mmol) was added at 0 °C, and the solution was stirred at 18°C for 20 h. It was poured into ice-water, and the mixture was extracted with chloroform. The extract was washed with aqueous sodium hydrogencarbonate and then with water to neutral, dried over sodium sulfate, and evaporated to give 4.14 g of a white solid (mp 95—97 °C), whose TLC showed two spots. From the faster-moving band in column chromatography of the crude product on silicic acid in chloroform, an oily product was obtained and crystallized from acetone/petroleum ether to give 0.16 g (3.4% yield) of **4a** as colorless granules: mp 84—86 °C; IR (KBr) 1770, 1720 (shoulder), and 1700 cm^{-1} (C=O); ^{1}H NMR ($CDCl_3$) δ=2.72 (t, 2H, J=6 Hz, CH_2), 3.78 (s, 3H, OCH_3), 3.91 (t, 2H, J=6 Hz, CH_2), 5.53 (d, 1 H, J=1 Hz, =CH_2), 6.15 (d, 1H, J=1 Hz, =CH_2), and 7.76 (m, 4H, Ar H). Found: C, 64.67; H, 4.96; N, 5.38%. Calcd for $C_{14}H_{13}NO_4$: C, 64.86; H, 5.05; N, 5.40%.

The slower-moving band gave 3.92 g of adduct **3a** (78.6% yield): mp 102—104 °C. Recrystallization from cyclohexane afforded colorless needles: mp 105—106 °C; IR (KBr) 3470 (OH), 1770, 1730 (shoulder), and 1710 cm^{-1} (C=O); ^{1}H NMR ($CDCl_3$) δ=1.47 (s, 3H, CH_3), 2.13 (m, 2H, CH_2), 3.48 (br s, 1H, OH, exchangeable with D_2O), 3.69 (s, 3H, OCH_3), 3.80 (t, 2H, J=7 Hz, CH_2), and 7.78 (m, 4H, Ar H); ^{13}C NMR (DMSO-d_6) δ=25.97 (q, CH_3), 33.25 (t, CH_2), 37.67 (t, CH_2), 51.91 (q, OCH_3), 72.76 (s, -C-), 122.86 (d, Ar C), 131.74 (s, Ar C), 134.23 (d, Ar C), 167.61 (s, imide C=O), and 175.66 (s, C=O); MS m/z 277 (M^+). Found: C, 60.95; H, 5.37; N, 5.26%. Calcd for $C_{14}H_{15}NO_5$: C, 60.64; H, 5.45; N, 5.05%.

Reaction of *N*-(Hydroxymethyl)phthalimide (1) with Ethyl Methacrylate (2b). The reaction was carried out in the same way at 18°C for 20 h, and on chromatography, two products were isolated. One from the faster-moving band was an oil (adduct **4b**) which did not solidify (5.0% yield): IR (neat) 1770, 1730 (shoulder), and 1710 cm^{-1} (C=O); ^{1}H NMR ($CDCl_3$) δ=1.31 (t, 3H, J=7 Hz, CH_3), 2.70 (t, 2H, J=7 Hz, CH_2), 3.88 (t, 2H, J=7 Hz, CH_2), 4.22 (q, 2H, J=7 Hz, OCH_2), 5.51 (d, 1H, J=1 Hz, =CH_2), 6.12 (d, 1H, J=1 Hz, =CH_2), and 7.72 (m, 4H, Ar H).

The other from the slower-moving band was a white solid (adduct **3b**, 82.0% yield): mp 90—92 °C. Recrystallization from cyclohexane gave colorless needles: mp 93—95 °C; IR (KBr) 3500 (OH), 1770, 1725 (shoulder), and 1705 cm^{-1} (C=O); ^{1}H NMR ($CDCl_3$) δ=1.26 (t, 3H, J=7 Hz, CH_3), 1.45 (s, 3H, CH_3), 2.12 (m, 2H, CH_2), 3.41 (s, 1H, OH, exchangeable with D_2O), 3.78 (t, 2H, J=7 Hz, CH_2), 4.11 (q, 2H, J=7 Hz, OCH_2), and 7.73 (m, 4H, Ar H). Found: C, 62.01; H, 5.89; N, 5.24%. Calcd for $C_{15}H_{17}NO_5$: C, 61.85; H, 5.88; N, 4.81%.

Reaction of *N*-(Hydroxymethyl)phthalimide (1) with Acrylonitrile (5a) or Methacrylonitrile (5b). After the reaction of **5a** with two equivalents of **1** under the same reaction conditions, products were separated by column chromatography. The major product was **6a** (89.7% yield based on **5a**): mp 195—196 °C (lit,[5] 193 °C). Others are by-products formed from excess **1**: phthalimide (23% yield), bis(phthalimide)methane (1% yield); mp 227—229 °C (lit,[6] 226 °C), and bis(phthalimidemethyl) ether (2% yield); mp 205—207 °C (lit,[7] 207—209 °C).

With **5b** and two equivalents of **1**, the reaction proceeded in a similar manner giving rise to the formation of **6b** along with the by-products from **1** as in the case of **5a**. The yield of **6b** was 83.6% on the basis of **5b**: mp 159—161 °C; IR (KBr) 3390 (NH), 1775, 1720 (shoulder), and 1710 cm^{-1} (C=O); ^1H NMR ($CDCl_3$) δ=1.95 (s, 3H, CH_3), 5.27 (d, 2H, J=6 Hz, CH_2), 5.38 (s, 1H, =CH_2), 5.74 (s, 1H, =CH_2), 6.85 (br s, 1H, NH), and 7.72—7.87 (m, 4H, Ar H); ^{13}C NMR ($CDCl_3$) δ=18.4 (CH_3), 42.8 (CH_2), 120.7 (=CH_2), 123.5 (Ar C), 131.8 (Ar C), 134.2 (Ar C), 139.2 (=C), 167.4 (imide C=O), and 167.6 (C=O). Found: C, 64.06; H, 4.78; N, 11.65%. Calcd for $C_{13}H_{12}N_2O_3$: C, 63.92; H, 4.95; N, 11.47%.

References

1) S. R. Buc, *J. Am. Chem. Soc.*, **69**, 254 (1947).
2) M. B. Winstead and H. W. Heine, *J. Am. Chem. Soc.*, **77**, 1913 (1955).
3) K. Kurita, H. Itoh, and Y. Iwakura, *J. Polym. Sci., Polym. Chem. Ed.*, **16**, 779 (1978).
4) K. Kurita, H. Itoh, and Y. Iwakura, *J. Polym. Sci., Polym. Chem. Ed.*, **17**, 1187 (1979).
5) D. T. Mowry, U. S. Patent, 2529455 (1950); *Chem. Abstr.*, **45**, 2980 (1951).
6) R. O. Atkinson, *J. Chem. Soc.*, **1954**, 1329.
7) H. E. Zaugg, A. M. Kotre, and J. E. Fraser, *J. Org. Chem.*, **34**, 11 (1969).
8) M. Imoto, "Woodward Hoffmann Sokuo Tsukautameni," Kagakudoujin, Kyoto (1978), pp. 257—273.

Excimer Formation and Intramolecular Self-Complexation of Double-Armed γ-Cyclodextrin

Fumio HAMADA,† Koichi MURAI,† Akihiko UENO,* Iwao SUZUKI, and Tetsuo OSA*
Pharmaceutical Institute, Tohoku University, Aobayama, Sendai 980
†Department of Fuel Chemistry, Mining College, Akita University, Gakuen-cho, Tegata, Akita 010
(Received March 5, 1988)

Synopsis. Circular dichroism and fluorescence studies of γ-cyclodextrin bearing two naphthyl moieties (**1**) suggest that **1** exists as two intramolecular self-complexation forms in water-rich solutions with one or two of the naphthyl moieties included in its cavity. Upon addition of (−)-borneol as a guest, **1** forms a 1 : 1 host-guest complex, exhibiting slightly diminished excimer and circular dichroism bands. Ethylene glycol converts the intramolecular complexes into a relaxed form, in which two naphthyl moieties dangle outside the cavity.

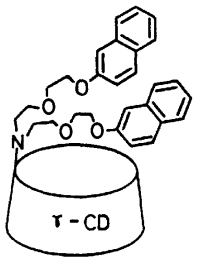

1

Many spectroscopic studies have shown that γ-cyclodextrin (γ-CD, cyclooctaamylose) can include two guest molecules in its large cavity.[1] When an aromatic moiety is covalently linked to γ-CD, it was suggested to enable γ-CD to form 1 : 1 host-guest complexes by narrowing the large cavity as a spacer.[2] When γ-CD has two naphthyl moieties located apart on its rim, the host accommodates one guest molecule in its cavity by moving the two naphthyl moieties outward from the interior of the cavity.[3] We describe here fluorescence and circular dichroism properties of another type of bi-chromophoric γ-CD (**1**), in which two naphthyl moieties are branched out from the nitrogen atom of amino-γ-CD.

The double armed γ-CD **1** was prepared as shown in Scheme 1. Since the reaction of γ-CD with 2-naphthalenesulfonyl chloride in pyridine is known to give a γ-CD derivative sulfonated regiospecifically at a primary hydroxyl, the amino moiety bearing two naphthalene rings is located at the narrower mouth of the primary hydroxyls of γ-CD.

Figure 1 shows the circular dichroism spectra of **1** in an aqueous 10% ethylene glycol solution. The spectrum of **1** at 8.42×10^{-5} mol dm^{-3} exhibits peaks around 220 nm and 280 nm and a trough around 240 nm. The dichroism intensities of the peak and the trough below 250 nm were reduced with decreasing concentration of **1**, and the spectrum, which has no trough around 240 nm, is eventually obtained. This concentration-dependency suggests that **1** associates with each other at its high concentrations. The change in the dichroism sign from negative to positive from the longer wavelength side below 250 nm may be related to the exciton coupling of S-helicity[4] arising from the electronic interaction between two naphthalene rings involved in the associated forms of **1**. Since no concentration-dependency was observed at lower concentrations than 2×10^{-5} mol dm^{-3} (Fig. 1 (B)), **1** is likely to exist as a monomer species in the concentration range. Upon addition of (−)-borneol to a dilute solution of **1**, the intensity of the positive peak around 218 nm was found to diminish, but the spectrum obtained in the presence of excess (−)-borneol still has the peak with a considerable intensity (Fig. 1). The analysis of the (−)-borneol-induced circular dichroism variations gave 720 mol^{-1} dm^3 as the binding constant.[3]

Figure 2 shows the fluorescence spectra of **1** in an aqueous 10% ethylene glycol solution, alone or in the presence of (−)-borneol. It is noted that the fluorescence pattern is hardly dependent on the concentration of **1**. The spectra exhibit a broad band around 410 nm in addition to the normal fluorescence around 358 nm. Since the broad band was observed even in acidic solu-

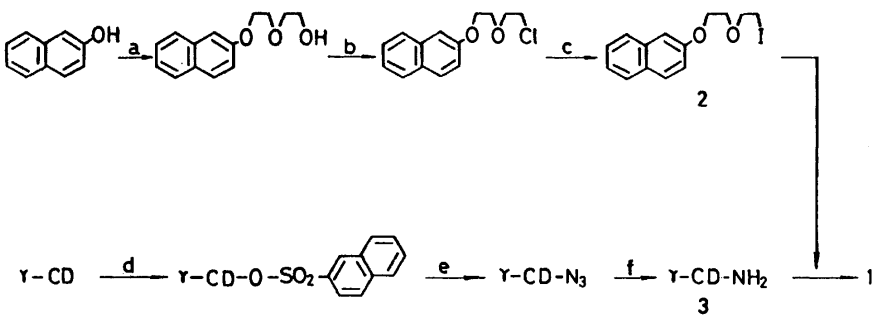

a, $ClCH_2CH_2OCH_2CH_2OH$, NaOH, 1-BuOH; b, $SOCl_2$; c, NaI, DMF; d, 2-$C_{10}H_7SO_2Cl$, pyridine; e, NaN_3; f, H_2/Pd-C

Scheme 1.

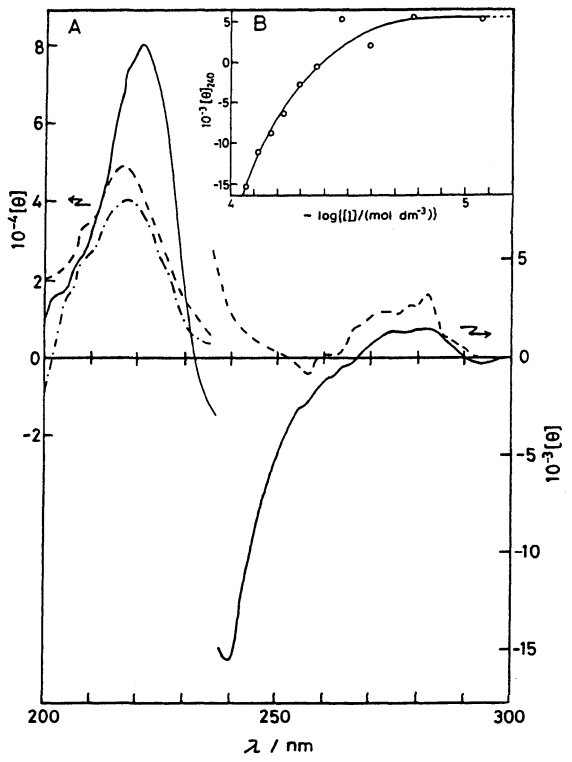

Fig. 1. Circular dichroism spectra of **1**, alone (——, 8.42×10^{-5} mol dm^{-3}; ----, 1.68×10^{-5} mol dm^{-3}) or in the presence of (−)-borneol (–·–: **1**, 1.68×10^{-5} mol dm^{-3}; (−)-borneol, 2.17×10^{-4} mol dm^{-3}) in an aqueous 10% ethylene glycol solution. The concentration-dependency of 240-nm dichroism intensity is shown in B.

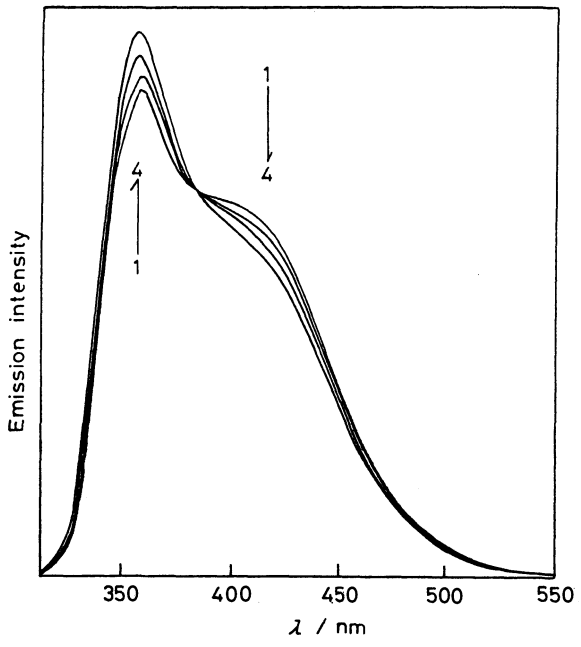

Fig. 2. Fluorescence spectra of **1** (7.68×10^{-6} mol dm^{-3}) in an aqueous 10% ethylene glycol solution at various (−)-borneol concentrations (1, 0; 2, 5.0×10^{-4}; 3, 2.0×10^{-3}; 4, 4.0×10^{-3} mol dm^{-3}).

tions, it was assigned to excimer emission, in other words, the band cannot be assigned to exciplex emission, which might have been caused by excited-state electronic interaction between the naphthyl chromophore and the nitrogen atom.[5] With increasing (−)-borneol concentration, the excimer intensity decreases while the monomer intensity increases. These (−)-borneol-induced variations are slight and suggest that excimer formation is possible even in the complexes.

When fluorescence spectra of **1** were measured at various ethylene glycol contents, the relative intensity of the excimer emission diminished with increasing ethylene glycol, and almost pure monomer fluorescence band was obtained in ethylene glycol. The absence of the excimer emission in ethylene glycol indicates that the two naphthyl moieties of **1** are separated from each other outside the cavity in the organic solvent.

Compound **1** may take three equilibrium forms **A**, **B**, and **C** in its dilute solutions as shown in Scheme 2. In **B** and **C**, **1** accommodates one or two of the pendant naphthyl moieties in its own cavity (intramolecular self-complexation). Since **1** exhibits induced circular dichroism in the naphthalene absorption regions, the naphthyl moiety is likely to be involved in the chiral CD cavity, and **B** and **C** forms are candidates for predominant species in water-rich solutions. In **B**, one of two naphthyl moieties acts as a cap[6] for another naphthyl moiety, which is included in the cavity, stabilizing the intramolecular complex. In **C**, the two naphthyl

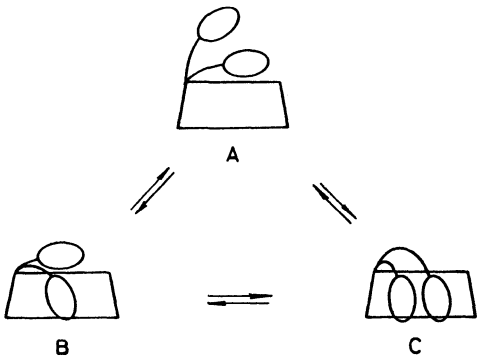

Scheme 2.

moieties are involved into the cavity together. The excimer emission observed in water-rich solutions confirms that **1** can take **C** form with two naphthyl moieties included in the cavity. On the other hand, the considerable intensity of the monomer emission suggests that **1** can also take **B** form, in which excimer is hardly formed because of the difficulty in face-to-face interactions between the two naphthyl moieties.[7] In ethylene glycol, **1** exhibits no excimer emission and may take **A** form due to weak hydrophobic interactions. The complex formation with (−)-borneol may convert **1** from intramolecular self-complexation forms **B** and **C** to an intermolecular complexation form **D** as shown in Scheme 3. Since excimer emission of **1** was still observed in the presence of (−)-borneol, the two naphthyl moieties are likely to be closely located in complex **D**. Examination of molecular

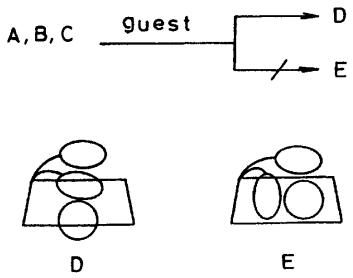

Scheme 3.

models indicates that complex form **E**, in which one of the two naphthyl moieties acts as a typical spacer for (−)-borneol, cannot be formed due to bulky size of (−)-borneol. The fact that the circular dichroism intensity of **1** is still large in the presence of excess (−)-borneol, suggests that one or two of the naphthyl moieties are likely to be involved partly in the γ-CD cavity in complex **D**, acting as flexible caps for the included guest.

Experimental

The circular dichroism and fluorescence spectra were measured at 25 °C using a JASCO J-400X spectrodichrometer and a Shimadzu RF-500 spectrofluorophotometer, respectively. The circular dichroism intensities were expressed as molar ellipticity (in degree cm^2dmol^{-1}) on the basis of the total concentration of **1**. Due to the poor solubility of **1** in pure water, an aqueous 10% ethylene glycol solution was used as the solvent. 2-Naphthylsulfonyl-γ-CD was prepared according to the reported method.[2b] Azido and amino derivatives of γ-CD were prepared by the methods similar to those reported by Melton et al.[8] for preparation of the corresponding α-CD derivatives.

Synthesis of 1. A mixture of the iodide **2** (2.7 g, 7.5 mmol), amino-γ-CD **3** (1.2 g, 0.93 mmol), K_2CO_3 (0.98 g), and *N*,*N*-dimethylformamide (40 ml) was heated at 80 °C for 40 h under nitrogen. After cooling, the reaction mixture was filtered and the filtrate was poured into 500 ml of acetone. The precipitates were collected by filtration, dissolved in water, and subjected to CM-Sephadex C-50 column chromatography with water as the eluting solvent. Recrystallization from methanol gave the desired product (0.202 g, 12%): R_f=0.46 (*n*-BuOH, EtOH, H_2O 5 : 4 : 3); ^1H NMR (DMSO-d_6) δ=2.6—3.8 (m, 64H), 4.50 (m, 7H, O_6H), 4.88 (m, 8H, C_1H), 5.63—5.96 (br. s, 16H, O_2H, O_3H), 7.13—7.88 (m, 14H, Ar); IR (KBr): 1628, 1600 cm^{-1}. Found: C, 50.76; H, 6.25; N, 0.76%. Calcd for $C_{76}H_{109}NO_{43}\cdot 4H_2O$: C, 50.80; H, 6.56; N, 0.78%.

This work was partly supported by Grant-in-Aid, Nos. 61470152 and 61550585 from the Ministry of Education, Science and Culture.

References

1) A. Ueno, F. Moriwaki, T. Osa, F. Hamada, and K. Murai, *Tetrahedron*, **43**, 1571 (1987) and references therein.

2) a) A. Ueno, Y. Tomita, and T. Osa, *J. Chem. Soc., Chem. Commun.*, **1983**, 976; b) A. Ueno, F. Moriwaki, Y. Hino, and T. Osa, *J. Chem. Soc., Perkin Trans. 2*, **1985**, 921 and references therein.

3) A. Ueno, F. Moriwaki, T. Osa, F. Hamada, and K. Murai, *Bull. Chem. Soc. Jpn.*, **59**, 465 (1986).

4) N. Harada and K. Nakanishi, "Circular Dichroic Spectroscopy, Exciton Coupling in Organic Stereochemistry," Tokyo-Kagaku-Dojin, Tokyo (1982).

5) G. S. Cox and N. J. Turro, *J. Am. Chem. Soc.*, **106**, 422 (1984).

6) J. Emert and R. Breslow, *J. Am. Chem. Soc.*, **97**, 670 (1975); I. Tabushi, K. Shimokawa, N. Shimizu, H. Shirakata, and K. Fujita, *J. Am. Chem. Soc.*, **98**, 7855 (1976).

7) J. B. Birks, "Organic Molecular Photophysics," John Wiley & Sons (1975).

8) L. D. Melton and K. N. Slesser, *Carbohydr. Res.*, **19**, 29 (1971).

Configurational Stability of Optically Active Selenoxides; Racemization via Achiral Hydrate

Toshio SHIMIZU,[1] Michio KOBAYASHI, and Nobumasa KAMIGATA*
Department of Chemistry, Faculty of Science, Tokyo Metropolitan University, Fukazawa, Setagaya-ku, Tokyo 158
(Received March 10, 1988)

Synopsis. Configurational stabilities of optically active diaryl selenoxides are examined under several conditions such as acidic, basic, or in the presence of water. It is found that the diaryl selenoxide which has two hindered *t*-butyl groups on the ortho positions is relatively stable toward racemization even under acidic conditions. Mechanism of racemization is ascertained to be via formation of the achiral hydrate ($R\text{-}Se(OH)_2\text{-}R'$) by the observation of oxygen exchange on the selenium atom.

Although optically active sulfoxides have been known for a long time, there has been no example of the isolation of an optically active selenoxide until recently. Davis et al. first reported the preparation of enantiomerically active selenoxides several years ago, although the enantiomeric excesses of the selenoxides were low.[2] Since then several optically active selenoxides were synthesized.[3-7] We reported the synthesis of optically active selenoxides by fractional recrystallization of diastereomeric mixture[4] or chromatographic separation using optically active column.[6] In addition, we obtained optically pure selenoxide as a stable solid by transesterification of the diastereomerically pure selenoxide.[7] The difficulty of the optical resolution of selenoxide has been attributed to its facile racemization.[8] Two mechanisms for the racemization of selenoxide are considered. One is the mechanism by the pyramidal inversion and the other is the mechanism via formation of its achiral hydrate ($R\text{-}Se(OH)_2\text{-}R'$). We previously estimated the stability of asymmetric selenoxides toward the pyramidal inversion. Optically active diaryl selenoxides were found to become more stable toward the pyramidal inversion by substitutions of bulky groups on the ortho positions.[9] However, the second mechanism of racemization involving the achiral hydrate is anticipated to be also important. We report here the configurational stability of optically active diaryl selenoxides which possess ortho substituents of various sizes under several conditions such as acidic, basic, or in the presence of water.

Results and Discussion

The optically active selenoxides were prepared by chromatographic resolution (optically active column) of the racemic samples.[6] Racemizations of selenoxides were measured at 26 °C in chloroform or methanol. Progress of the racemization was monitored by means of the circular dichroism spectrum. The racemizations in chloroform were examined, to begin with. However, no racemization was observed and the optical activities of selenoxides **1**—**4** were unchanged even after 5 days. When the racemizations were measured in

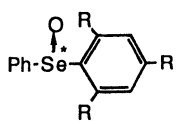

1 : R = Me
2 : R = Et
3 : R = i-Pr
4 : R = t-Bu

methanol, selenoxide **1**—**3** were found to racemize. The rate constants of the racemizations of **1**—**3** were 6.00×10^{-6}, 1.85×10^{-6}, 1.33×10^{-6} s^{-1} and the half-lives of the optical activities were 32.1, 104, 145 h, respectively. Larger ortho substituents were found to be more effective for retardation of the racemization. The selenoxide **4** which possessed the most bulky ortho substituents in this series was quite stable in methanol. The rate constants and half-lives of the racemizations are summarized in Table 1.

Influences of water, acid, and base were also examined. In the presence of water, racemizations were accelerated in the cases of selenoxides **1**—**3**, however selenoxide **4** was still stable even in the presence of water (Entries 3 and 4). The racemizations of selenox-

Table 1. Rate Constants and Half-Lives of Optical Activities[a]

Entry	Condition	k/s^{-1} ($t_{1/2}$/h)			
		1	**2**	**3**	**4**
1	$CHCl_3$	A[c]	A	A	A
2	MeOH	6.00×10^{-6} (32.1)	1.85×10^{-6} (104)	1.33×10^{-6} (145)	A
3	$MeOH+H_2O$[b]	6.31×10^{-6} (30.5)	2.18×10^{-6} (88.3)	1.40×10^{-6} (138)	A
4	$MeOH/H_2O(4/1)$	3.34×10^{-5} (5.76)	8.59×10^{-6} (22.4)	5.40×10^{-6} (35.6)	A
5	$MeOH/H_2O(4/1)+HCl$[b]	B[d]	B	B	1.85×10^{-5} (10.4)
6	$MeOH/H_2O(4/1)+NaOH$[b]	3.10×10^{-5} (6.21)			

a) Concentrations of selenoxides: 1 mmol l^{-1}. Temp: 26 °C. b) H_2O, HCl, NaOH: 30 mmol l^{-1}.
c) A: No racemization was observed after 5 days. d) B: Racemization was completed within 1 min.

ides **1**—**3** in dry methanol (distilled after drying with CaH_2) are suspected to be due to the presence of small traces of water in the methanol, because the racemizations were accelerated in aqueous methanol and no racemization occurred in chloroform which was a hydrophobic solvent. Remarkable acceleration of the racemization was observed in all selenoxides under acidic conditions (Entry 5). In the cases of selenoxides **1**—**3**, the racemizations were fast and completed within 1 min. The selenoxide **4** also racemized under these conditions, however, the half-life was long (10.4 h). Therefore, bulky ortho substituents of diaryl selenoxide particularly *t*-butyl groups were found to be effective to retard or prevent the racemization catalyzed by the acid and water. The racemization of selenoxide **1** was also examined in basic media. The racemization of the selenoxide was not accelerated by the addition of sodium hydroxide into aqueous methanol solution (Entry 6).

Since all the racemizations were examined at room temperature and no racemization occurred in chloroform and the racemizations were observed in aqueous conditions, the racemizations of selenoxides under these conditions are considered to proceed via its achiral hydrate. To clarify the mechanism via the hydrate, the racemization of selenoxide **2** with ^{18}O-labeled water was studied. A methanol solution of selenoxide **2** in the presence of $H_2{}^{18}O$ (97 atom%) was stirred at room temperature. The mass spectrum of selenoxide **2** after 10 days indicated the formation of ^{18}O-labeled selenoxide (M^+ 336(^{80}Se), 334(^{78}Se)) (Fig. 1). The high-resolution mass spectrum also supported the formation of the selenoxide-^{18}O. This result indicates the formation of the achiral hydrate. Though the achiral hydrate itself expected to be formed by hydration of the selenoxide **2** could not be detected by mass spectroscopy, it is attributed to the lability of the hydrate.

The results that the racemization was accelerated under acidic conditions and not accelerated in basic

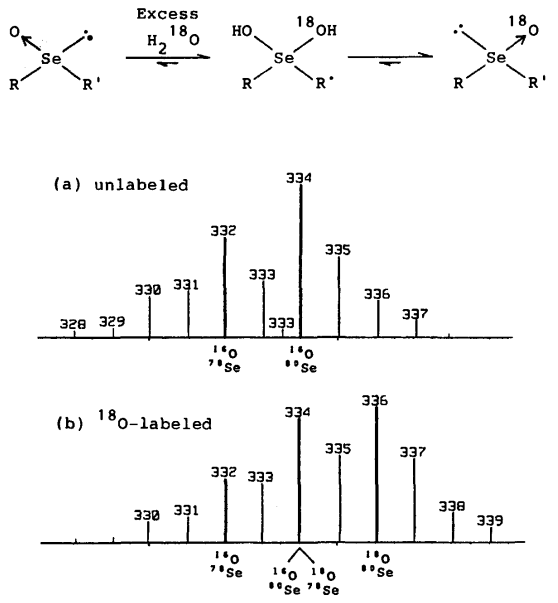

Fig. 1. Mass spectrum analysis of heavy oxygen exchange on selenium atom of selenoxide 2.

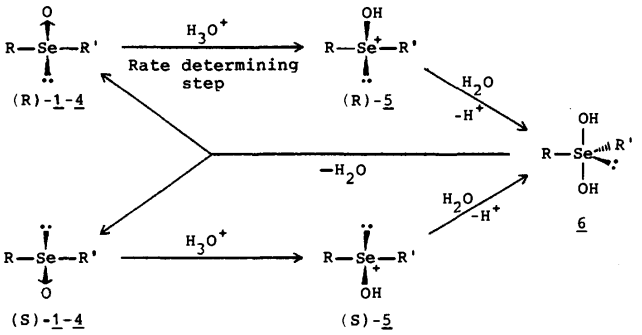

Scheme 1. Mechanism of racemization via achiral hydrate.

media suggest that the protonation on the oxygen atom of the selenoxide is the rate-determining step as shown in Scheme 1. This protonation on the selenoxide corresponds to the protonation of sulfoxide in strong acidic media.[10] The second step of the racemi-

$$Ph_2S{\rightarrow}O + H_2SO_4 \rightleftharpoons Ph_2S^+{-}OH + HSO_4^-$$

zation is fast addition of water to the hydroxy selenonium cation (*R*)-**5** or (*S*)-**5**. The addition of water to the hydroxy selenonium ion (*R*)-**5** or (*S*)-**5** followed by elimination of proton to give the achiral hydrate **6**. Finally, dehydration of the achiral hydrate **6** give the racemic mixture of selenoxide (*R*)-**1**—**4** and (*S*)-**1**—**4** resulting the exchange of the oxygen atom.

In conclusion, it was ascertained that the racemization of optically active selenoxides occurred through the achiral hydrate in aqueous media. Configurational stabilities of the optically active diaryl selenoxides toward the racemization via its achiral hydrate were found to be dependent on the ortho substituents.

Experimental

Materials. The optically active selenoxides **1**—**4** were prepared by optical resolution of racemic samples[3,11] using an optically active column.[6] Enantiomeric excesses (e.e.) of optically active selenoxides **1** and **2** were determined by ^1H NMR using Eu(hfc)$_3$ as an optically active shift reagent.[6] In the cases of optically active selenoxides **3** and **4**, e.e. were determined by HPLC using an optically active column.[11] The optical rotations and enantiomeric excesses (e.e.) of selenoxides used in the measurements of racemizations are shown below.

Phenyl Mesityl Selenoxide (1): $[\alpha]_D$ +40.2° (*c* 0.95, chloroform). E.e.=16%.

Phenyl 2,4,6-Triethylphenyl Selenoxide (2): $[\alpha]_D$ −29.0° (*c* 0.90, chloroform). E.e.=12%.

Phenyl 2,4,6-Triisopropylphenyl Selenoxide (3): $[\alpha]_D$ +58.4° (*c* 1.35, chloroform). E.e.=66%.

Phenyl 2,4,6-Tri-*t*-butylphenyl Selenoxide (4): $[\alpha]_D$ +96.5° (*c* 1.30, chloroform). E.e.=49%.

Measurement of Racemization. All racemizations of the selenoxides were carried out in 1 mmol l^{-1} concentration at 26 °C. Progress of the racemization was monitored by means of the circular dichroism spectrum (JASCO J-40A) at ca. 290 nm. The measurements of the racemizations were continued until about one half-life time.

Heavy Oxygen Exchange of Selenoxide. Heavy oxygen exchange of selenoxide **2** was carried out in methanol in the presence of ^{18}O-labeled water (Merck, 97 atom%). Concentra-

tions of selenoxide and the labeled water were 5 mmol l^{-1} and 0.5 mol l^{-1}, respectively. Formation of the ^{18}O-labeled selenoxide **2**-^{18}O was confirmed by the mass spectrum (JEOL JMS-DX300) after 10 days. M^+ 336(^{80}Se), 334(^{78}Se). Exact MS, Found: m/z 336.0867 (^{80}Se), Calcd for $C_{18}H_{22}{}^{18}O^{80}Se$: 336.0878. The relative intensities of the mass spectra shown in Fig. 1 are summarized below. Enriched oxygen-18 contained in the selenoxide **2**-^{18}O was estimated by measurements of both its low and high mass spectroscopy. The enriched oxygen-18 was calculated to be 38% by low mass spectroscopy based on intensities of the mass spectrum, m/z 328 ($C_{18}H_{22}{}^{16}O^{74}Se$, relative intensity: 3.5) and 338 ($C_{18}H_{22}{}^{18}O^{82}Se$, relative intensity: 22.3), since these mass numbers do not contain other isotope of oxygen and selenium. The oxygen-18 contained was also estimated to be 46% by high mass spectroscopy based on m/z 332 ($C_{18}H_{22}{}^{16}O^{78}Se$), 334 ($C_{18}H_{22}{}^{18}O^{78}Se$ and $C_{18}H_{22}{}^{16}O^{80}Se$), and 336 ($C_{18}H_{22}{}^{18}O^{80}Se$).

m/z	Relative Intensity	
	(a)unlabeled	(b)^{18}O-labeled
328	4.5	3.5
329	6.0	4.1
330	27.1	15.3
331	30.7	19.2
332	65.0	47.2
333	37.5	43.7
334	100	91.5
335	52.7	64.0
336	24.6	100
337	11.1	61.5
338	2.4	22.3
339	—	11.3
340	—	2.2

This work was supported by Grant-in-Aid for Scientific Research No. 62790152 from the Ministry of Education, Science and Culture.

References

1) Fellowship of the Japan Society for the Promotion of Science for Japanese Junior Scientists, 1987—.
2) F. A. Davis, J. M. Billmers, and O. D. Stringer, *Tetrahedron Lett.*, **24**, 3191 (1983).
3) M. Kobayashi, H. Ohkubo, and T. Shimizu, *Bull. Chem. Soc. Jpn.*, **59**, 503 (1986).
4) T. Shimizu and M. Kobayashi, *Chem. Lett.*, **1986**, 161.
5) F. Toda and K. Mori, *J. Chem. Soc., Chem. Commun.*, **1986**, 1357.
6) T. Shimizu and M. Kobayashi, *J. Org. Chem.*, **52**, 3399 (1987).
7) M. Kobayashi and T. Shimizu, *Nippon Kagaku Kaishi*, **1987**, 1437; T. Shimizu and M. Kobayashi, First International Conference on Heteroatom Chemistry, Kobe, July, 1987, Abstract p. 219.
8) M. Ōki and H. Iwamura, *Tetrahedron Lett.*, **1966**, 2917; K. B. Sharpless, M. W. Young, and R. F. Laure, *ibid.*, **1973**, 1979.
9) T. Shimizu, M. Yoshida, and M. Kobayashi, *Bull. Chem. Soc. Jpn.*, **60**, 1555 (1987).
10) S. Oae, *Quart. Rev. Sulfur Chem.*, **5**, 53 (1970).
11) T. Shimizu and M. Kobayashi, *Bull. Chem. Soc. Jpn.*, **59**, 2654 (1986).

The Synthesis of *Se*-Alkyl Alkaneselenoates via (1-Iodo-1-alkenyl)dialkylboranes

Masayuki HOSHI, Yuzuru MASUDA, and Akira ARASE*
Department of Industrial Chemistry, Kitami Institute of Technology, Kitami 090
(Received April 4, 1988)

Synopsis. *Se*-Alkyl alkaneselenoates were formed in moderate to good yields by successive reactions of (1-iodo-1-alkenyl)bis(1,2-dimethylpropyl)boranes with alkylselenomagnesium bromides and alkaline hydrogen peroxide.

Se-Alkyl alkaneselenoates (**5**) are receiving considerable attentions in organic syntheses.[1] A synthetic method for **5** has been developed employing carboxylic acid derivatives or selenocarboxylic acid derivatives as the substrates in most cases.[2] In our previous work, the reaction of (1-iodo-1-alkenyl)dialkylboranes (**1**) with alkylthiomagnesium bromides proceeded with inversion of configuration to give (*E*)-(1-alkylthio-1-alkenyl)dialkylboranes, which provided *S*-alkyl alkanethioates on alkaline hydrogen peroxide oxidation.[3] The above results led us to examine the synthesis of (*E*)-(1-alkylseleno-1-alkenyl)dialkylboranes (**4**) and, further, a new synthesis of **5** via **4**.

Preliminarily, (1-iodo-1-hexenyl)bis(1,2-dimethylpropyl)borane (**1a**), prepared by the hydroboration of 1-iodo-1-hexyne with bis(1,2-dimethylpropyl)borane in THF, was treated with an equimolar amount of butylselenomagnesium bromide (**2a**),[4] and the reaction mixture was then oxidized by alkaline hydrogen peroxide in the presence of *N,N,N′,N′*-tetramethylethylenediamine (TMEDA). As expected, *Se*-butyl hexaneselenoate (**5a**) was obtained in 58% yield. It was isolated from the oxidized mixture by column chromatography using silica gel (eluted by a mixture of benzene and hexane, 1 : 4). It was then identified by a comparison of its ^{1}H NMR, ^{13}C NMR, IR, and MS spectra with those of an authentic sample prepared by another method.[2a] The yield increased to 95% by employing a two-fold amount of **2a** under the same reaction conditions, though dibutyl selenide and dibutyl diselenide were competitively formed. These contaminants were easily separated from **5a** during the above-mentioned column chromatography. An addition of TMEDA was necessary; otherwise, the yield became nearly zero. A migration of 1,2-dimethylpropyl group from the boron atom to the α-alkenyl carbon atom,[5] a possible side reaction, did not occur under any cases. As shown in Table 1, several types of alkylselenomagnesium bromides may be employed in the present reaction. Thus, in the cases of primary and secondary alkylselenomagnesium bromides, the selenoates **5** were produced in 50—90% yields. The unsatisfactory results, which appeared in the case of 1,1-dimethylethyl-

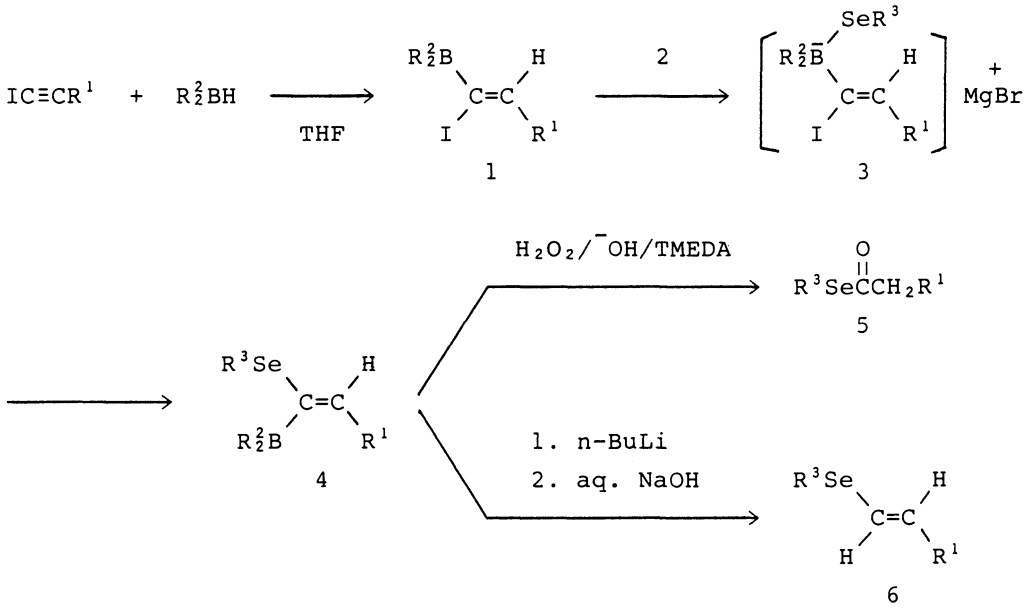

Scheme 1.

Table 1. Yields of *Se*-Alkyl Alkaneselenoates (**5**) and (*E*)-1-Alkylseleno-1-alkenes (**6**)

R^1 of $IC{\equiv}CR^1$	R^3 of $R^3SeMgBr$	Product and yield/%[a] $R^3SeCOCH_2R^1$[b] (**5**)	(*E*)-$R^3SeCH{=}CHR^1$[c] (**6**)
n-C_4H_9	C_2H_5[d]	80	67
n-C_4H_9	i-C_3H_7	73	80
n-C_4H_9	n-C_4H_9	90	70
n-C_4H_9	s-C_4H_9	75	65
n-C_4H_9	t-C_4H_9	0	—
n-C_4H_9	c-C_6H_{11}	52	42
n-C_4H_9	C_6H_5	33	64
n-C_4H_9	$C_6H_5CH_2$[e]	50	40
n-C_6H_{13}	n-C_4H_9	75	51

a) Based on starting 1-iodo-1-alkyne. b) Isolated. c) Determined by GLC. d) The preparation was carried out at −40 °C. e) The preparation was carried out in diethyl ether at −20 °C.

magnesium bromide, may be attributed to a difficulty regarding the presence of this reagent under the reaction conditions employed.

In a similar manner to the reaction of **1** with alkylthiomagnesium bromides,[3] **4** were suggested to be formed as precursors of **5**. Therefore, the boranes **4** would be expected to provide the corresponding (*E*)-1-alkylseleno-1-alkenes (**6**) on protonolysis of carbon-boron bond. Thus, an attempt to provide (*E*)-1-butylseleno-1-hexene (**6a**) was made by a protonolysis of **4a** with various carboxylic acids. A GLC examination of the protonolyzed mixture failed to show any detectable **6a**. However, a treatment of the same mixture successively with butyllithium and aqueous sodium hydroxide, a method reported by Negishi et al. for the conversion of the carbon-boron bond of alkenylboranes into a carbon-hydrogen bond with retention of configuration,[6] afforded highly pure **6a** in 67% yield, estimated by GLC. Compound **6a**, thus obtained, isomerized very easily to (*Z*)-isomer during the isolation procedure using column chromatography to give a mixture of *E*- and *Z*-isomer (*E*/*Z*=74/26). The *E*-isomer was assigned by an absorption band at 945 cm^{-1} in the IR spectrum and a coupling constant of 15 Hz between olefinic protons in the ^1H NMR spectrum. The *Z*-isomer was assigned by a coupling constant of 10 Hz between olefinic protons in the ^1H NMR spectrum. In similar reactions, several types of **6** were produced stereoselectively (Table 1); however, they also gave mixtures of *E*- and *Z*-isomer respectively in the isolation process. Thus, the above results strongly suggest an intermediary formation of **4**, though they have not yet been isolated and, thus, have not been directly analyzed. Accordingly, the reaction was speculated to proceed in the following way. Thus, with the alkylseleno anion, the boranes **1** form borate-complexes (**3**) which are transformed to **4** with an inversion of configuration; then, the boranes **4** are converted to **5** and **6**, respectively.

The present reaction not only offers a new synthetic method for *Se*-alkyl alkaneselenoates but also suggests the formation of alkenylboranes having the alkylseleno group on the α-alkenyl carbon atom. These alkenylboranes are expected to be versatile intermediates for various organoselenium compounds.

Experimental

Instruments. ^1H and ^{13}C NMR spectra were recorded on a Jeol FX-200 (200 MHz) spectrometer and obtained from a $CDCl_3$ solution containing TMS as the internal standard. IR spectra (film) were recorded with a Hitachi 285 spectrometer. Mass spectra were recorded with a Hitachi M-52 mass spectrometer.

Materials. Commercial 2-methyl-2-butene was purified by distillation over lithium aluminium hydride under an argon stream, and stored under an argon atmosphere. 1-Iodo-1-alkynes were prepared as described in the literature,[7] and used after drying over Molecular Sieves-4A. Commercial alkyl, phenyl, and benzyl bromides were dried with calcium chloride, purified by distillation, and stored over Molecular Sieves-4A under an argon atmosphere. Commercial selenium powder was used after drying in a vacuum desiccator containing phosphorus pentoxide. THF and diethyl ether were distilled over lithium aluminium hydride under argon stream, and stored under an argon atmosphere. TMEDA was purified by vacuum distillation over calcium hydride, and stored under an argon atmosphere. A THF solution of BH_3 was prepared by a method described in the literature.[8] Hexane and benzene, used as eluent for column chromatography, were distilled over sodium.

Representative Procedure. A solution of bis(1,2-dimethylpropyl)borane (10 mmol) in THF was prepared in a 50-ml argon-flushed round-bottom flask, and to the stirred solution was added 2.08 g of 1-iodo-1-hexyne (10 mmol) at −15 °C. The reaction mixture was stirred for 1 h at 0 °C and for additional 1 h at room temperature to complete the reaction. On the other hand, 0.48 g of magnesium turnings (20 mmol) was placed in a 100-ml round-bottom flask; the flask was then flushed with argon. The flask was charged with 20 ml of dry THF, and 2.74 g of butyl bromide (20 mmol) was slowly added to the vigorously stirred solution at room temperature giving a solution of butylmagnesium bromide in THF. After an addition of 40 ml of dry THF, the solution was cooled to −30 °C. Then, 1.58 g of selenium powder (20 mmol) was added through a sample inlet under argon flow to the vigorously stirred suspended solution of butylmagnesium bromide. After stirring for 1 h at −30 °C, the color of the suspension changed from black to cream. The resulting suspension of butylselenomagnesium bromide was further cooled to −50 °C.

The THF solution of (1-iodo-1-hexenyl)bis(1,2-dimethylpropyl)borane in the 50-ml round-bottom flask was then transferred to the suspended solution with a double-ended needle. The reaction mixture was stirred for 1 h at −50 °C and allowed to warm to room temperature. The reaction mixture was then oxidized by a successive addition of 5 ml of TMEDA, 5 ml of 3 mol dm^{-3} aqueous sodium hydroxide and 5 ml of 30% hydrogen peroxide for 1 h at 0 °C. The resulting mixture was extracted with diethyl ether; extract was then washed with brine, and dried over anhydrous magnesium sulfate. The solvent was removed on a rotary evaporator under reduced pressure, and the residue was put on a silica-gel column. The *Se*-butyl hexaneselenoate (2.12 g) was isolated by elution with a mixture of hexane and benzene (4 : 1) (90% yield).

The spectral data of the products are as follows:

***Se*-Ethyl Hexaneselenoate:** ^1H NMR ($CDCl_3$) δ=0.80—0.98 (m, 6H), 1.05—1.80 (m, 6H), 2.60 (t, *J*=7 Hz, 2H), and 2.89 (q, *J*=7 Hz, 2H); ^{13}C NMR ($CDCl_3$) δ=13.84, 15.97, 22.30, 25.17, 29.69, 30.98, 48.26, and 202.17 (>C=O); IR (film) 1715 (C=O) cm^{-1}; MS *m*/*z* 206 and 208 (M^+).

***Se*-(1-Methylethyl) Hexaneselenoate:** ^{1}H NMR δ=0.83—0.96 (m, 3H), 1.20—1.80 (m, 6H), 1.46 (d, J=7 Hz, 6H), 2.57 (t, J=7 Hz, 2H), and 3.50—3.75 (m, 1H); ^{13}C NMR δ=13.86, 22.33, 24.32 (CH_3-, 2C), 25.17, 31.00, 33.22 (>CH-), 48.44, and 202.99 (>C=O); IR 1710 (C=O) cm^{-1}; MS m/z 220 and 222 (M^+).

***Se*-Butyl Hexaneselenoate:** ^{1}H NMR δ=0.82—0.98 (m, 6H), 1.14—1.85 (m, 10H), 2.60 (t, J=7 Hz, 2H), and 2.90 (t, J=7 Hz, 2H); ^{13}C NMR δ=13.57, 13.86, 22.33, 23.09, 25.22 (-CH_2-, 2C), 31.00, 32.64, 48.26, and 202.29 (>C=O); IR 1715 (C=O) cm^{-1}; MS m/z 234 and 236 (M^+).

***Se*-(1-Methylpropyl) Hexaneselenoate:** ^{1}H NMR δ=0.80—1.03(m, 6H), 1.15—1.83 (m, 8H), 1.46 (d, J=7 Hz, 3H), 2.58 (t, J=7 Hz, 2H), and 3.37—3.63 (m, 1H); ^{13}C NMR δ=12.35, 13.86, 22.01, 22.33, 25.22, 30.60, 31.00, 40.58 (>CH-), 48.50, and 202.87 (>C=O); IR 1710 (C=O) cm^{-1} ; MS m/z 234 and 236 (M^+).

***Se*-Cyclohexyl Hexaneselenoate:** ^{1}H NMR δ=0.80—1.00 (m, 3H), 1.10—2.10 (m, 16H), 2.57 (t, J=7 Hz, 2H), and 3.43—3.72 (m, 1H); ^{13}C NMR δ=13.86, 22.33, 25.19, 25.69, 26.77 (-CH_2-, 2C), 31.00, 34.19 (-CH_2-, 2C), 42.16 (>CH-), 48.47, and 202.64 (>C=O); IR 1710 (C=O) cm^{-1} ; MS m/z 260 and 262 (M^+).

***Se*-Phenyl Hexaneselenoate:** ^{1}H NMR δ=0.78—0.98 (m, 3H), 1.10—1.85 (m, 6H), 2.69 (t, J=7 Hz, 2H), and 7.27—7.60 (m, 5H); ^{13}C NMR δ=13.86, 22.30, 25.08, 30.98, 47.50, 126.52 (>C=), 128.79 (-CH=), 129.29 (-CH=, 2C), 135.77 (-CH=, 2C), and 200.39 (>C=O); IR 1730 (C=O), 735, and 690 cm^{-1}; MS m/z 254 and 256 (M^+).

***Se*-Benzyl Hexaneselenoate:** ^{1}H NMR δ=0.80—0.96 (m, 3H), 1.10—1.43 (m, 4H), 1.50—1.70 (m, 2H), 2.62 (t, J=7 Hz, 2H), 4.14 (s, 2H), and 7.25 (s, 5H); ^{13}C NMR δ=13.84, 22.27, 25.11, 28.76, 30.98, 47.85, 126.84 (-CH=), 128.53 (-CH=, 2C), 128.82 (-CH=, 2C), 128.94 (>C=), and 201.56 (>C=O); IR 1710 (C=O), 755, and 695 cm^{-1}; MS m/z 268 and 270 (M^+).

***Se*-Butyl Octaneselenoate:** ^{1}H NMR δ=0.80—1.00 (m, 6H), 1.16—1.88 (m, 14H), 2.60 (t, J=7 Hz, 2H), and 2.89 (t, J=7 Hz, 2H); ^{13}C NMR δ=13.57, 14.07, 22.60, 23.09, 25.22, 25.54, 28.84, 28.93, 31.61, 32.67, 48.32, and 202.20 (>C=O); IR 1710 (C=O) cm^{-1}; MS m/z 262 and 264 (M^+).

References

1) a) G. Heppke, J. Martens, K. Praefcke, and H. Simon, *Angew. Chem.*, **89**, 328 (1977); b) G. Heppke, J. Martens, K. Praefcke, and H. Simon, *Angew. Chem., Int. Ed. Engl.*, **16**, 318 (1977); c) H. Ishihara and Y. Hirabayashi, *Chem. Lett.*, **1978**, 1007; d) A. P. Kozikowski and A. Ames, *J. Org. Chem.*, **43**, 2737 (1978); e) J. Pfeninger, C. Heuberger, and W. Graf, *Helv. Chim. Acta*, **63**, 2308 (1980); f) A. P. Kozikowski and A. Ames, *J. Am. Chem. Soc.*, **102**, 861 (1980); g) A. F. Sviridov, M. S. Ermolenko, D. V. Yashunsky, and N. K. Kochetkov, *Tetrahedron Lett.*, **24**, 4355 (1983); h) A. F. Sviridov, M. S. Ermolenko, D. V. Yashunsky, and N. K. Kochetkov, *Tetrahedron Lett.*, **24**, 4359 (1983).

2) a) H. Ishihara and Y. Hirabayashi, *Chem. Lett.*, **1976**, 203; b) H. J. Gais, *Angew. Chem.*, **89**, 251 (1977); c) P. A. Grieco, Y. Yokoyama, and E. Williams, *J. Org. Chem.*, **43**, 1283 (1978); d) H. Ishihara and Y. Hirabayashi, *Chem. Lett.*, **1978**, 1007; e) J. Pfeninger, C. Heuberger, and W. Graf, *Helv. Chim. Acta*, **63**, 2308 (1980); f) P. A. Grieco, J. Y. Jaw, D. A. Claremon, and K. C. Nicolaou, *J. Org. Chem.*, **46**, 1215 (1981); g) T. G. Back, S. Collins, and R. G. Kerr, *J. Org. Chem.*, **46**, 1564 (1981); h) T. G. Back and R. G. Kerr, *Tetrahedron Lett.*, **23**, 3241 (1982); i) A. F. Sviridov, M. S. Ermolenko, D. V. Yashunsky, and N. K. Kochetkov, *Tetrahedron Lett.*, **24**, 4355 (1983); j) S. Tomoda, Y. Takeuchi, and Y. Nomura, *Synthesis*, **1985**, 212; k) S. Kato, H. Kabuto, H. Hirabayashi, and T. Murai, *Synthesis*, **1985**, 520.

3) M. Hoshi, Y. Masuda, and A. Arase, *J. Chem. Soc., Chem. Commun.*, **1985**, 714.

4) The preparation of alkylseleno(or arylseleno)magnesium bromides was carried out by reference to the following literature; D. G. Foster and S. F. Brown, *J. Am. Chem. Soc.*, **50**, 1184, (1928).

5) A. Arase, M. Hoshi, and Y. Masuda, *Bull. Chem. Soc. Jpn.*, **57**, 209 (1984); M. Hoshi, Y. Masuda, and A. Arase, *Bull. Chem. Soc. Jpn.*, **58**, 1683 (1985).

6) E. Negishi and K. W. Chiu, *J. Org. Chem.*, **41**, 3484 (1976).

7) P. L. Southwick and J. R. Kirchner, *J. Org. Chem.*, **27**, 3305 (1962).

8) G. Zweifel and H. C. Brown, *Org. React.*, **13**, 1 (1963).

A Convenient Synthesis of 1,3-Pyrenedicarbaldehyde

Michael GOLTZ† and Ichiro MURATA*
Department of Chemistry, Faculty of Science, Osaka University, Toyonaka, Osaka 560
(Received April 14, 1988)

Synopsis. A convenient and preparatively useful access to the unknown 1,3-pyrenedicarbaldehyde is presented. When treated with an excess amount of *N,N*-dimethylformamide and phosphoryl chloride, 3,4-dihydro-2a*H*-cyclopenta[*cd*]phenalene was smoothly converted into dialdehyde in 57% yield. A plausible mechanism for this transformation was suggested from a labeling experiment using *N,N*-dimethylformamide-d_7.

Although pyrene is a reactive aromatic hydrocarbon and readily gives mono-, di-, tri-, and tetra-substitution in positions 1-, 1,6-, (and 1,8-), 1,3,6-, and 1,3,6,8-, respectively, by various electrophilic substitution reactions,[1] 1,3-disubstituted derivatives are hardly accessible. Quite recently, Harvey et al. reported that the acetylation of pyrene produced a mixture of 1,6- and 1,8-diacetylpyrene together with the 1,3-derivative, which was difficult to separate.[2] However, a selective introduction of carbon functionalities in these positions has not been reported so far. The only known 1,3-dialkyl derivatives are the 1,3-dimethylpyrene, which has been isolated together with its 1,8-isomer from a Vilsmeier formylation and reduction sequence of 1-methylpyrene,[3] and the 1,3-dipropylpyrene derived from 1-(2-chloro-1,3-dipropyl-2-cyclopropenyl)-1*H*-phenalene in poor yield.[4] During the course of our studies on nonalternant polycyclic hydrocarbons, we have found a convenient access to 1,3-pyrenedicarbaldehyde (**3**).

In order to synthesize the tetracyclic aldehyde **2** as a potential building block for the construction of various nonalternant hydrocarbons including a phenalene ring system,[5] the Vilsmeier reaction of 3,4-dihydro-2a*H*-cyclopenta[*cd*]phenalene (**1**)[6] was carried out. When treated with a large excess of *N,N*-dimethylformamide and phosphoryl chloride at room temperature for 14 h, compound **1** was smoothly converted into a stable crystalline product, yellow needles, mp 245—246 °C as the sole product in 57% yield. In contrast to our expectation, the structure of the obtained product was unambiguously established not as **2** but as 1,3-pyrenedicarbaldehyde (**3**), as shown in Scheme 1, from an elemental analysis and the following spectroscopic data. The electronic spectrum of **3** exhibits absorption bands similar to those of 1-pyrenecarbaldehyde.[7] Its IR spectrum shows the characteristic absorptions of aromatic aldehydes at 2700 and 1650 cm^{-1}. The presence of two formyl groups was established by its mass spectral fragmentation of *m/z* 258 (M^+, 33%), 229 (M^+ −CHO, 25%), and 200 (M^+ −2CHO, 100%). The NMR spectra reflect the C_{2v} symmetry. Thus, in $CDCl_3$ at 500 MHz, the two aldehyde protons appear as one singlet at δ 10.78 and the

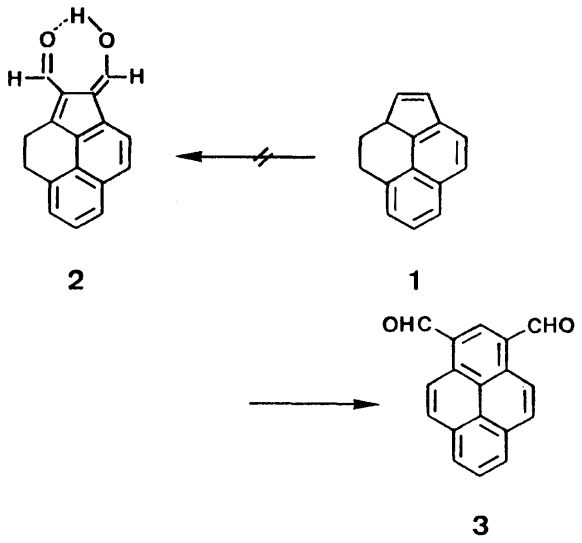

Scheme 1.

aromatic protons show an AB-quartet (4H) at δ 8.46 (H-5 and 9) and 9.49 (H-4 and 10) with *J*= 9.15 Hz, AX_2 pattern (3H) at δ 8.19 (H-7) and 8.43 (H-6 and 8) with *J*= 7.63 Hz, and 1H singlet at δ 8.83 (H-2). Its eleven carbon types was also revealed by the ^{13}C NMR spectrum (see Experimental).

The mechanism for the transformation of **1** to **3** is of particular interest. It should be noted that one CH-unit was incorporated into the ring skeleton of **1** and that the dehydrogenation took place during a reaction at room temperature under nitrogen.

The origin of the additional carbon atom was confirmed by a Vilsmeier reaction of **1** using *N,N*-dimethylformamide-d_7. Thus, the ^1H NMR spectrum of product **3**-d_3 from this reaction clearly reveals the deuterium incorporation at the 2-position of the pyrene skeleton in addition to the two formyl groups. Hence, the CH-unit at the 2-position must have arisen from the Vilsmeier reagent.

From a labeling experiment, together with the well-documented Vilsmeier reaction of cyclopentadiene derivatives,[8] we propose a plausible mechanism that might account for the transformation of **1** to **3** involving multi-step reactions, as shown in Scheme 2. As for the first and second steps, several precedents for the formation of 6-dimethylamino-1-[dimethyliminiomethyl]fulvenes appear in the literature.[8] Regarding the third step, we postulate that the Vilsmeier reagent attacks at the 6-position of the ring system to produce the tri-substituted intermediate **C**, which readily expels a proton owing to the generation of a naphthalene conjugation (**C**→**D**). The second deprotonation can occur with an expansion of the five-membered ring, followed by an elimination of dimethylamine to form a pyrene skeleton **F** which leads to the observed

† JSPS postdoctral fellow. M.G. expresses gratefully his thanks for a grant to the Japan Society for the Promotion of Science.

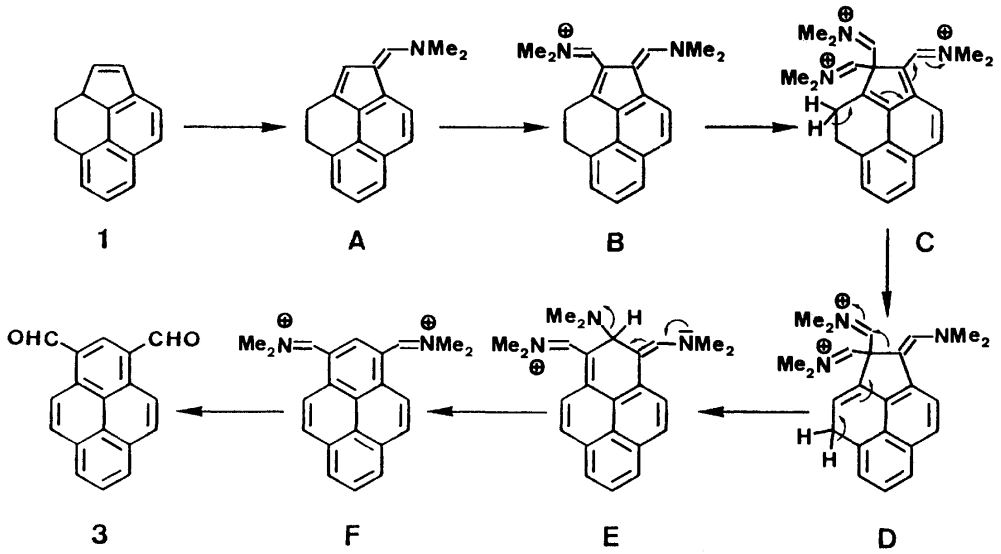

Scheme 2.

product **3** after a workup.

In summary, we have demonstrated that the Vilsmeier reaction of readily available hydrocarbon **1** provides a convenient, preparatively useful approach to **3** which might be used for the synthesis of hardly accessible [2.2]metapyrenophanes,[9] triangulenequinone,[10] and various carcinogenic polycyclic aromatic compounds.[11] We hope to report on additional experiments along this line in the near future.

Experimental

All melting points are uncorrected. IR spectra were measured in KBr with a JASCO A-100 spectrophotometer. The UV spectrum was measured with a Hitachi 340 recording spectrophotometer. Mass spectra were determined on a JEOL JMS-01SG-2 spectrometer. ^{1}H NMR spectra were recorded in $CDCl_3$ on JEOL JNM-GX 500 spectrometer (500 MHz). ^{13}C NMR spectra were taken on JEOL FX-90Q spectrometer (22.5 MHz). All chemical shifts are reported in δ units downfield from internal Me_4Si, and the J values are given in hertz. All reactions were carried out under a nitrogen atmosphere.

1,3-Pyrenedicarbaldehyde (3). To a stirred solution of 3,4-dihydro-2a*H*-cyclopenta[*cd*]phenalene (3.00 g, 15.6 mmol) (**1**) in tetrahydrofuran (20 cm^3, distilled from benzophenone ketyl) is added under nitrogen at room temperature a mixture of *N*,*N*-dimethylformamide (18.8 g, 0.25 mol, distilled from CaH_2) and phosphoryl chloride (19.8 g, 0.13 mol). The solution warms and iminium salt precipitates. After 14 h the solvent was removed under reduced pressure, 2 mol dm^{-3} sodium hydroxide (500 cm^3) was added and the mixture was extracted with dichloromethane (3×500 cm^3). The combined organic layers were dried with $MgSO_4$ and evaporated. Chromatography of the residue on silica gel (6% water) with dichloromethane gave a large yellow band which was collected. Removal of the solvent and recrystallization from dichloromethane afforded yellow crystals of 1,3-pyrenedicarbaldehyde (**3**) (2.3 g, 57% yield): yellow needles from dichloromethane, mp 245—246 °C (sealed capillary tube, sublimes at around 200 °C); IR (KBr) 1650, 2700 cm^{-1}; UV/VIS (in CH_2Cl_2) λ_{max} (ε) 244 (17200), 285 (25200), 292 (28000), 396 (29900), 400 (sh, 31500), 403 (32000), 407 (sh, 29900) nm; MS, (70 eV) *m*/*z* (rel intensity) 258 (M^+, 33%), 229 (M^+—CHO, 25%), 202 (30%), 201 (65%), 200 (M^+—2CHO, 100%), 199 (34%), 198 (30%); ^{1}H NMR ($CDCl_3$), δ= 10.78 (s, 2H, 1-CHO, 3-CHO), 9.49 (d, 2H, J= 9.15 Hz, H-4 and -10), 8.83 (s, 1H, H-2), 8.46 (d, 2H, J= 9.15 Hz, H-5 and -9), 8.43 (d, 2H, J= 7.63 Hz, H-6 and -8), 8.19 (t, 1H J= 7.63 Hz, H-7); ^{13}C NMR ($CDCl_3$), δ= 192.06, 137.34, 134.63, 133.98, 130.51, 129.04, 127.37, 127.14, 125.24, 123.81, 123.17. Found: C, 83.69; H, 3.90%. Calcd for $C_{18}H_{10}O_2$: C, 83.71; H, 3.90%.

A Vilsmeier reaction of the isomeric 3,4-dihydro-1*H*-cyclopenta[*cd*]phenalene gave comparable results. The treatment of **1** with two equivalents of *N*,*N*-dimethylformamide/phosphoryl chloride likewise leads to **3** and a recovery of the starting hydrocarbon **1**, while hydroxyfulvene **2** was not observed.

1,3-Pyrenedicarbaldehyde-d_3 (3-d_3). This compound was obtained from the Vilsmeier reaction of **1** with *N*,*N*-dimethylformamide-d_7 and phosphoryl chloride.

Exact mass, Found: *m*/*z* 261.0850; Calcd for $C_{18}H_7O_2D_3$; M, 261.0869. ^{1}H NMR signals at δ= 10.78 and 8.83 in **3** were completely disappeared.

The present study was partially supported by a Grant-in-Aid for Special Project Research No. 60129030 from the Ministry of Education, Science and Culture.

References

1) E. Clar "Polycyclic Hydrocarbons," Vol. II, Academic Press, New York (1964).

2) R.G. Harvey, J. Pataki, and H. Lee, *Org. Prep. Proced. Int.*, **16**, 144 (1984).

3) M. de Clercq and R.H. Martin, *Bull. Soc. Chim. Belg.*, **64**, 367 (1955).

4) I. Murata, T. Nakazawa, and K. Shima, *Chem. Lett.*, **1972**, 669.

5) For example, K. Nakasuji, K. Yoshida, and I. Murata, *J. Am. Chem. Soc.*, **105**, 5136 (1983).

6) I. Murata, K. Nakasuji, K. Yamamoto, T. Nakazawa, Y. Kayane, A. Kimura, and O. Hara, *Angew. Chem.*, **87**, 170 (1975); *Angew. Chem., Int. Ed. Engl.*, **14**, 170 (1975).

7) R.N. Jones, *J. Am. Chem. Soc.*, **67**, 2127 (1945).

8) K. Hafner, K.H. Vopel, G. Ploss, and C. Konig, *Justus Liebigs Ann. Chem.*, **661**, 52 (1963); see also: Houben-Weyl, Methoden der Organischen Chemie, Vol. 5/2c, Carbocyclische π-Elektronen-Systeme, Georg Thieme Verlag, Stut-

tgart, New York, 1985, pp. 553—557.
9) T. Umemoto, T. Kawashima, Y. Sakata, and S. Misumi, *Chem. Lett.*, **1975**, 837.
10) O. Hara, K. Tanaka, K. Yamamoto, T. Nakazawa, and I. Murata, *Tetrahedron Lett.*, **1977**, 2435.
11) R.G. Harvey and P.P. Fu, "Polycyclic Hydrocarbons and Cancer," Vol. 1, ed by H.V. Gelboin and P.O.P. Ts'o by Academic Press, New York (1978), Chap. 6.

A Short-Step Synthetic Approach to Eudesmane Skeleton. A Synthesis of (±)-β-Eudesmol and Related Eudesmane Sesquiterpenes

Takeshi KAWAMATA,* Kenzo HARIMAYA, and Seiichi INAYAMA
Pharmaceutical Institute, School of Medicine, Keio University, 35 Shinanomachi, Shinjuku-ku, Tokyo 160
(Received April 18, 1988)

Synopsis. The formal total syntheses of (±)-β-eudesmol and its related sesquiterpenes such as cryptomeridiol and neointermediol were accomplished by an efficient method using aldol cyclization as the key step starting from the known 3-vinyl-2-cyclohexen-1-one.

Although several different syntheses of eudesmane sesquiterpenes including (±)-β-eudesmol (**1**), one of the representatives of this class[1-3] have been reported, most of these approaches involved construction of the decalin ring system via the conventional Robinson annelation reaction. In the synthetic trial of **1**, approaches without recourse to this reaction have been reported recently.[4-7]

In connection with our interest in the development of an efficient general method for the synthesis of the eudesmane class of sesquiterpenoids, we have developed a short step approach to construct the eudesmane skeleton. This has enabled us to synthesize formally the well-known β-eudesmol (**1**) as well as cryptomeridiol (**4**)[8] and neointermediol (**5**).[9]

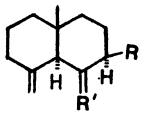

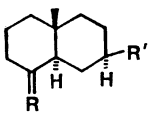

1 R: -C(OH)(CH$_3$)$_2$, R′: =H$_2$

2 R: -CH(CH$_3$)$_2$, R′:

3 R: -CH(CH$_3$)$_2$, R′: =O

4 R: , R′: -C(OH)(CH$_3$)$_2$

5 R: , R′: -CH$_2$=CHCH$_3$

Our synthetic strategy (Scheme 1) is based on the device of synthon like A or B as a common key intermediate and its intramolecular cyclization by aldol condensation (A) or Michael reaction (B) for the general construction of the eudesmane type of sesquiterpenes. These are represented by the above-mentioned β-eudesmol (**1**) and its close relatives, **4**, **5** and selinene[10] and C(6) oxygenated compounds, juneol (**2**)[11] and acolamone (**3**).[12] In this note the study of the synthon A is described.

Treatment of 3-vinyl-2-cyclohexen-1-one (**6**), readily available from 1,3-cyclohexanedione, with dimethyl malonate in methanol (MeOH) in the presence of sodium methoxide (NaOCH$_3$) gave mainly the 1,6-Michael adduct (**7**) (50%) along with a small amount of a dialkylation product. Conjugate addition of lithium dimethylcuprate (I) [(CH$_3$)$_2$CuLi] in dry ether at 0 °C provided methylated cyclohexanone (**8**) in good yield (88.4%). Acetalization of **8** with ethylene glycol [*p*-toluenesulfonic acid monohydrate (TsOH)/benzene] gave acetal diester (**9**) in almost quantitative yield. This was in turn subjected to reduction with lithium aluminum hydride (LiAlH$_4$) in ether to afford the corresponding dihydroxy acetal (**10**) (78%). Selective benzylation of **10** with benzyl bromide in tetrahydrofuran (THF) in the presence of tetrabutylammonium iodide (*n*-Bu$_4$NI) furnished almost exclusively the desired monobenzyl ether (**11a**) along with the dibenzyl ether (**11b**) [**11a** : **11b**=98 : 2]. Oxidation of **11a** with pyridinium dichromate (PDC) in dichloromethane (CH$_2$Cl$_2$) at room temperature afforded acetal aldehyde (**12**) in almost quantitative yield.

With the key intermediate **12** in hand, attention was turned to the crucial intramolecular aldol condensation. When **12** was exposed to the action of a 1 M (1 M=1 mol dm^{-3}) HCl in THF (1 : 2) at room temperature overnight, the desired α,β-unsaturated ketone **13** was constructed in a single step as a result of the simultaneous aldolization and dehydration (37%) along with the intermediary keto aldehyde (20%), which upon treatment of TsOH in benzene afforded additional **13** (ca. 7.5%). **13**: C$_{19}$H$_{24}$O$_2$ (MW 284). MS *m*/*z*: 284 (M$^+$). IR (KBr): 1687, 1620 (enone), 1068 cm^{-1}. Catalytic hydrogenation of **13** in the presence of 10% Pd-C in ethanol (EtOH)/ethyl acetate (AcOEt)(1 : 1) at room temperature proceeded smoothly with the concomitant cleavage of the benzyl group to furnish the keto alcohol (**14**)(66%). Oxidation of **14** with PDC in CH$_2$Cl$_2$ at room temperature followed by immediate treatment of the resulting unstable aldehyde **15** with Jones reagent in acetone afforded the keto carboxylic acid (**16**). This was, in turn, esterified with diazomethane (CH$_2$N$_2$) in ether to give the corresponding keto carboxylic acid methyl ester (**17**), IR (KBr): 1739, 1715 cm^{-1}. The ester

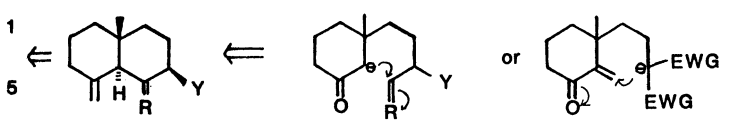

R: =H$_2$ or A R: =O or B

Scheme 1. Retrosynthetic analysis for the eudesmane skeleton.

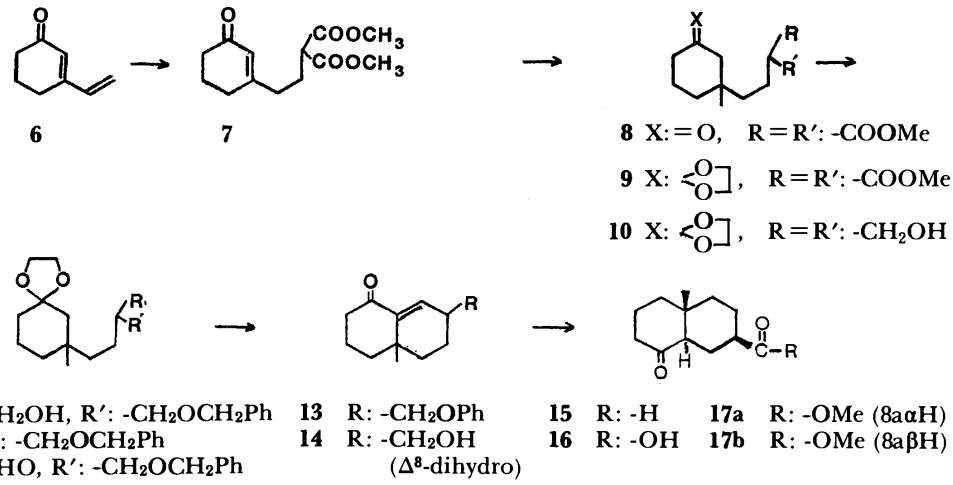

Scheme 2. Synthetic approach to (±)-β-eudesmol and its close relatives.

17 was found to be a 76 : 24 mixture of two components by the examination of its gas chromatographic data [Rt: 11.3 and 12.2]. On the other hand, ^{1}H NMR showed methyl signals at δ 1.17 and 0.82, methoxyl methyl signals at δ 3.67 and 3.68, and other signals between δ 1.1 and 2.4. The comparison of this data with that of the diastereomers[6] of **17** suggested that **17** was a mixture of **17a** and **17b** in an approximately 3 : 1 ratio. This was determined by evaluating the integration trace of the methyl and methoxyl methyl peaks described above. The ratio was in good agreement with that obtained from the GC-MS data; the presence of the C(2)-epimer of **17b** was easily ruled out since the ^{1}H NMR of **17** exhibited no signals below δ 2.4 .[6]

Since, not only the 4a-methyl-8-oxo-2-decalin carboxylic acid (**16**) and its ester **17a, b** but also the abovementioned mixture of four diastereomers of **17** have already been converted to β-eudesmol (**1**), which, in turn, has been converted to cryptomeridiol (**4**)[8] and neointermediol (**5**).[9] The synthesis of the former compounds (**16** and/or **17a, b**) constitute a formal total synthesis of (±)-β-eudesmol as well as (±)-**4** and (±)-**5**. Furthermore, since **17a** and **17b** could essentially be convertible to other isomeric eudesmols (α-, γ-eudesmol)[13] and its close relatives such as costal[14] and costic acid etc.,[14] this sequence should provide a general method of constructing the eudesmane sesquiterpenes exemplified by eudesmols.

Experimental

IR spectra were recorded on a Hitachi EPI-G3 spectrophotometer. Mass spectra were taken on a JEOL JMS-D300 instrument (JMA-2000 data analysis system). ^{1}H NMR spectra were recorded with JMN-GX-400 with TMS as an internal standard. TLC was performed on a Kieselgel 60 F_{254} plate (Merck) using ether-hexane (gradient).

Preparation of 7: To a cold (0 °C) stirred solution of $NaOCH_3$ (220 mg) in dry MeOH (15 ml) was added dropwise a solution of dimethyl malonate (2.4 g) in dry MeOH (15 ml) and then a solution of 3-vinyl-2-cyclohexen-1-one (**6**) (1.83 g) in dry MeOH (15 ml). The mixture was stirred at 0 °C for 2 h and then at room temperature overnight. The mixture was quenched with 2 M HCl, evaporated, and extracted with ether. The ether extract was washed with sat. NaCl and dried ($MgSO_4$). Removal of the solvent in vacuo left a crude oil, which was purified by chromatography on silica gel to give **7** as an oil, 1.90 g (ca. 50%), MS *m/z*: 254 (M^+). IR (KBr): 1749, 1733, 1644, 1620 cm^{-1}. From the polar fraction the dialkylation product, 371 mg (6.6%). MS *m/z*: 376 (M^+) ($C_{21}H_{28}O_6$) was obtained.

Conjugate Addition of $(CH_3)_2CuLi$ to 7 (8): To a cold (0 °C) stirred suspension of CuI (2.53 g) in dry ether (100 ml) was added dropwise CH_3Li (1.6 M hexane, 16.2 ml) under N_2 atmosphere and then **7** (1.5 g) in dry ether (120 ml). The mixture was stirred at 0 °C for 2 h and then at room temperature overnight. The mixture was quenched with sat. NH_4Cl, extracted with ether, washed with H_2O and dried over $CaCl_2$. Removal of the solvent at diminished pressure afforded 1.47 g of viscous oil, which was purified by chromatography on silica gel (ether : hexane=4 : 6) to give 1.26 g (88.4%) of an essentially pure oil, **8** (TLC homogeneous; ether : hexane=1 : 1). CI-MS *m/z*: 271 (M^++1) ($C_{14}H_{22}O_5$, MW 270). IR (KBr): 1751, 1733, 1710 cm^{-1}. ^{1}H NMR ($CDCl_3$) δ=0.98 (3H, s), 1.1—2.43 (12H, m), 3.3 (1H, d, 7), 3.75 (6H, s).

$LiAlH_4$ Reduction of 9: To a stirred suspension of $LiAlH_4$ (450 mg) in dry ether (80 ml) was added dropwise a solution of **9** (982 mg) in dry ether (60 ml) under ice-cooling. The mixture was refluxed for 2 h. The mixture was quenched carefully with sat. NH_4Cl, filtered and the filtered cake thoroughly washed with CH_2Cl_2. The filtrate was partitioned between the organic phase and the aqueous phase. The latter phase was extracted with CH_2Cl_2. The combined CH_2Cl_2 was washed with sat. NaCl and dried ($MgSO_4$). Removal of the solvent at reduced pressure left a viscous oil, which was purified by chromatography on silica gel eluting with ether to afford 630 mg (78%) of **10** as an oil. IR (KBr): 3387 (OH) cm^{-1}, which was used directly in the next step, and the recovered product, 79 mg (11.8%).

Preparation of Monobenzyl Ether (11a): To a stirred solution of **10** (600 mg) in dry THF (28 ml) was added NaH (104 mg) under N_2. After adding a catalytic amount of Bu_4NI, a solution of benzyl bromide (426 mg) in dry THF (12 ml) was added. The mixture was diluted with ether, washed with 2 M HCl and sat. NaCl and dried over $MgSO_4$. Evaporation of the solvent left a crude oil, which was purified by chromatography on silica gel. 10% ether-hexane fraction furnished 47 mg (4.6%) of dibenzyl ether (**11b**). MS *m/z*: 438 (M^+) ($C_{28}H_{38}O_4$, MW 438). IR (KBr): 1092, 1070 (sh), 1048, 944, 734, 697 cm^{-1}, and the ether eluant gave 710 mg (87.9%) of monobenzyl ether (**11a**) as an oil. MS *m/z*: 348 (M^+) ($C_{21}H_{32}O_4$, MW 348). IR (KBr): 3422, 1092, 1070 (sh), 1048,

944, 734, 697 cm^{-1}.

Cyclization of 11a (13): To a stirred solution of **11a** (100 mg) in CH_2Cl_2 (4 ml) was added PCC (80 mg) and the mixture was stirred at room temperature for 5 h. The reaction mixture was filtered through a pad of silica gel. The filtrate was evaporated to give a viscous oil **12**, IR (KBr): 1727 (-CHO), 1096 cm^{-1}, This was dissolved in 2 M HCl : THF (1 : 2) (1 ml) and stirred at room temperature overnight under an argon atmosphere. To the mixture sat. NaCl was added and it was extracted with ether, washed with sat. NaCl and dried ($MgSO_4$). Evaporation of the solvent followed by purification by chromatography on silica gel afforded 20 mg (ca. 30%) of **13** (oil), IR (KBr): 1687, 1620, 1086 cm^{-1}, MS *m/z*: 284 (M^+) ($C_{19}H_{24}O_2$, MW 284) and the intermediary keto aldehyde, 21 mg (20%), IR (KBr): 1728, 1287, 1129 (sh), 1115, 1068 cm^{-1}, which gave the additional enone **13** (5 mg, 7.5%) upon treatment with TsOH in refluxing benzene.

17a and 17b: 15 mg of **13** was dissolved in EtOH-AcOEt (1 : 1) (2 ml) and 10%-Pd/C (catalytic) was added. The mixture was stirred at room temperature under H_2 atmosphere for 4 days. After filtration of the mixture, the solvent was evaporated and the residue was purified by chromatography on silica gel to give 8 mg (66%) of **14**, which was dissolved in CH_2Cl_2 (1.5 ml), and PCC (12 mg) was added. The mixture was stirred for 3 h at room temperature. After filtration, the solvent was evaporated and the residue was purified by chromatography on silica gel to give 6 mg (79.9%) of the corresponding keto aldehyde (**15**). This was immediately dissolved in acetone (1 ml) and several drops of Jones reagent was added. After a few minutes a small amount of isopropyl alcohol was added. Filtration of the mixture followed by evaporation of the solvent left 5 mg (77.0%) of keto carboxylic acid (**16**), IR (KBr): 3500—2400, 1712 cm^{-1}. The above acid (**16**)(5 mg) was dissolved in ether (0.5 ml) and excess CH_2N_2 in ether was added. Evaporation of the solvent furnished 5 mg (ca. 100%) of the corresponding methyl ester (**17a** and **17b**). IR (KBr): 1739, 1715 cm^{-1}. GC-MS (2% OV-1, 200 °C), **17b**; R_t 11.3 min, *m/z*: 224 (M^+), 209 (M^+--15). **17a**; R_t 12 min, *m/z*: 224 (M^+), 209 (M^+—15). $C_{13}H_{20}O_3$ (MW 224). ^1H NMR (400 MHz) δ=0.82 (s), 3.67 (OCH_3) and 1.17 (s), 3.68 (OCH_3) [76 : 24]. High-resolution MS: *m/z* 224.1408 for **17a**, 224.1384 for **17b** [Theor. 224.1384 for $C_{13}H_{20}O_3$].

The authors are grateful to Hajime Yamanaka and Setuko Takei of the Joint Laboratory, School of Medicine, Keio University, for MS and IR measurements, respectively.

References

1) J. A. Marshall, M. T. Pike, and R. D. Carrol, *J. Org. Chem.*, **31**, 2933 (1966).
2) D. C. Humber, A. R. Pinder, and R. A. Williams, *J. Org. Chem.*, **32**, 2335 (1967).
3) C. H. Heathcock and T. R. Kelly, *Tetrahedron*, **24**, 1801 (1968).
4) J. B. A. Wijnberg, J. Vader, and A. de Groot, *J. Org. Chem.*, **48**, 4380 (1983).
5) J. W. Huffman and M. L. Mole, *J. Org. Chem.*,**37**, 13 (1972).
6) R. G. Carson and E. G. Zey, *J. Org. Chem.*, **37**, 2468 (1972).
7) R. B. Miller and R. D. Nash, *J. Org. Chem.*, **38**, 4424 (1973).
8) M. Sumimoto, H. Ito, H. Hirai, and K. Wada, *Chem. Ind., (London)*, **1963**, 780.
9) V. B. Zalkow, A. M. Shaligram and L. H. Zalkow, *Chem, Ind., (London)*, **1964**, 194.
10) L. Ruzicka and M. Stoll, *Helv. Chim, Acta*, **6**, 846 (1923).
11) S. C. Bhattacharyya, A. S. Rao and A. M. Shaligram, *Chem. Ind., (London)*, **1960**, 469.
12) M. Niwa, A. Nishiyama, M. Iguchi and S. Yamamura, *Bull. Chem. Soc. Jpn.*, **48**, 2930 (1975).
13) See Ref. 2 and references cited therein.
14) See Ref. 1 and references cited therein.

Study on Electroreduction Mechanism of Aromatic Dicarboxylic Acids. Electrosynthesis of 1,4-Benzenedimethanol[1)]

Ryu Oi, Kunio San-Nohe,† and Shinji Takenaka*
Omuta Research Institute, Mitsui Toatsu Chemicals, Inc., Omuta, Fukuoka 836
†Pharmaceutical Department, Central Research Institute, Mitsui Toatsu Chemicals Inc., Kasama-cho, Sakae-ku, Yokohama 247
(Received April 20, 1988)

Synopsis. The electroreduction mechanisms of terephthalic acid and isophthalic acid in acidic solution were studied by molecular orbital (MO) calculations. Further, a practical stepwise route to 1,4-benzenedimethanol has been developed by the electroreduction of *p*-(hydroxymethyl)-benzoic acid.

1,4-Benzenedimethanol (**4**) is of importance as a component of useful polymers,[2)] though a practical synthetic method has not yet been established. Namely, as a hitherto disclosed procedure for the synthesis of **4**, the chlorination of *p*-xylene followed by hydrolysis[3)] has been reported. However, the selectivity of the chlorination of each benzylic position is not necessarily satisfactory. The hydrogenation of terephthalic acid diester[4)] has also been reported, in which there still remains serious problems regarding the practical preparation of **4**, due to the vigorous reaction conditions and low yield of the product.

Incidentally, the electroreduction of aromatic carboxylic acids is both useful and a practical technique for the preparation of benzyl alcohols. We have therefore studied the synthesis of **4** starting from easily available terephthalic acid (**1**) by electrolysis. So far, it has been reported that the electroreduction of **1** in acidic aqueous media results in a nuclear reduction which affords 2,5-cyclohexadiene-1,4-dicarboxylic acid (**3**),[5)] while the electroreduction of **1** in aqueous ammoniacal media gives *p*-(hydroxymethyl) benzoic acid (**9**).[6)] However, no successful conversion of **1** to **4** has been mentioned in the literature.

In general, the mechanism of side chain reduction of aromatic carboxylic acid seems best accommodated[7)] by protonated carboxylic acid; the reduction is known to be promoted in a more acidic solution.[8)] Therefore, in order to investigate the possibility of a side-chain reduction of dicarboxylic acid **1** under the acidic conditions, we considered the reaction pathway of the electroreduction of **1**, compared with that of isophthalic acid (**5**), in terms of molecular orbital (MO) calculations; electroreduction of **5** in an aqueous acidic solution[9)] is reported to give 1,3-benzenedimethanol (**8**). According to our calculations, a direct reduction of **1** to **4** is unlikely to occur in acidic solution. We, therefore, investigated a combination of the electroreduction of **1** to **9** and that of **9** to **4** (two step conversion through **9**). In this paper, we discuss the mechanism and practical electroreduction of **9** for **4**.

Electroreduction Mechanism of 1 and 5 in Acidic Aqueous Media. Though no mechanistic study has so far been available concerning the exceptionally specific formation of nuclear reduced product **3** from **1** in an acidic media, it might be explained by assuming two different pathways (illustrated in Scheme 1): one involves a direct electroreduction of **1** followed by protonation (Route A), the other involves the protonation of **1** prior to electroreduction (Route B). A two-electron transfer should occur rather rapidly in an equilibrium state after the diprotonation of **1**, leading to the formation of **2**. The most important key step of each pathway (Route A and B) related to the product selectivity and rate determination may be the electron-uptake process of **1** and **2**, respectively. According to a MO calculation, the LUMO electron density of **1** is highly localized in the aromatic ring. Therefore, an electron uptake would take place, preferably, at the aromatic nuclear, affording **3** (Route A). On the other hand, an electron transfer on **2** would occur at the side chain to produce **4** (Route B), owing to the higher value of the LUMO electron density observed in the side chain of **2**.

Next, in order to assess the preferable route in Scheme 1, we compared the LUMO energy level of the key intermediate in the electron transfer. An intermediate having a lower LUMO energy would undergo an electron uptake, preferentially.[10)] The estimated value of the LUMO energy of **1** and **2** are shown in Scheme 1. The LUMO energy of **1** is lower than that of **2**, indicating that the electron uptake of **1** proceeds more smoothly than that of **2**. Thus, in turn, this fact suggests that Route A is preferable to Route B.

A MO calculation of meta derivative **5** was accomplished in a similar manner as that mentioned above, and opposite results were obtained. Thus, a reduction of **5** seems to occur, preferentially, according to Route B to give **8**, since the LUMO energy of **6** in Route B is lower than that of **5** in Route A.

Now, our calculations show a different reactivity of **1**, compared with that of **5**, suggesting the difficulty of a side-chain reduction of **1** in an acidic aqueous media;

Table 1. Electroreduction of Aromatic Carboxylic Acids[a)]

Entry	Substrate	Solvent electrolyte	Electricity passed / F mol^{-1}	Product (Yield/%)[b)]
1	**9**	12% aq. NH_4OH	10	—
2	**9**	10% aq. Et_4NOTs	10	**4** (3)
3	**9**	10% aq. H_2SO_4	10	**4** (68)
4	**1**	10% aq. H_2SO_4	43	**3** (3)[c)]
5	**5**	10% aq. H_2SO_4	90	**8** (6)[c)]

a) The electroreduction was carried out under constant current of 5 A dm^{-2} with an H-shaped divided cell fitted with two lead electrodes at 40 °C. b) Isolated yield based on substrate. c) Detected as a single product.

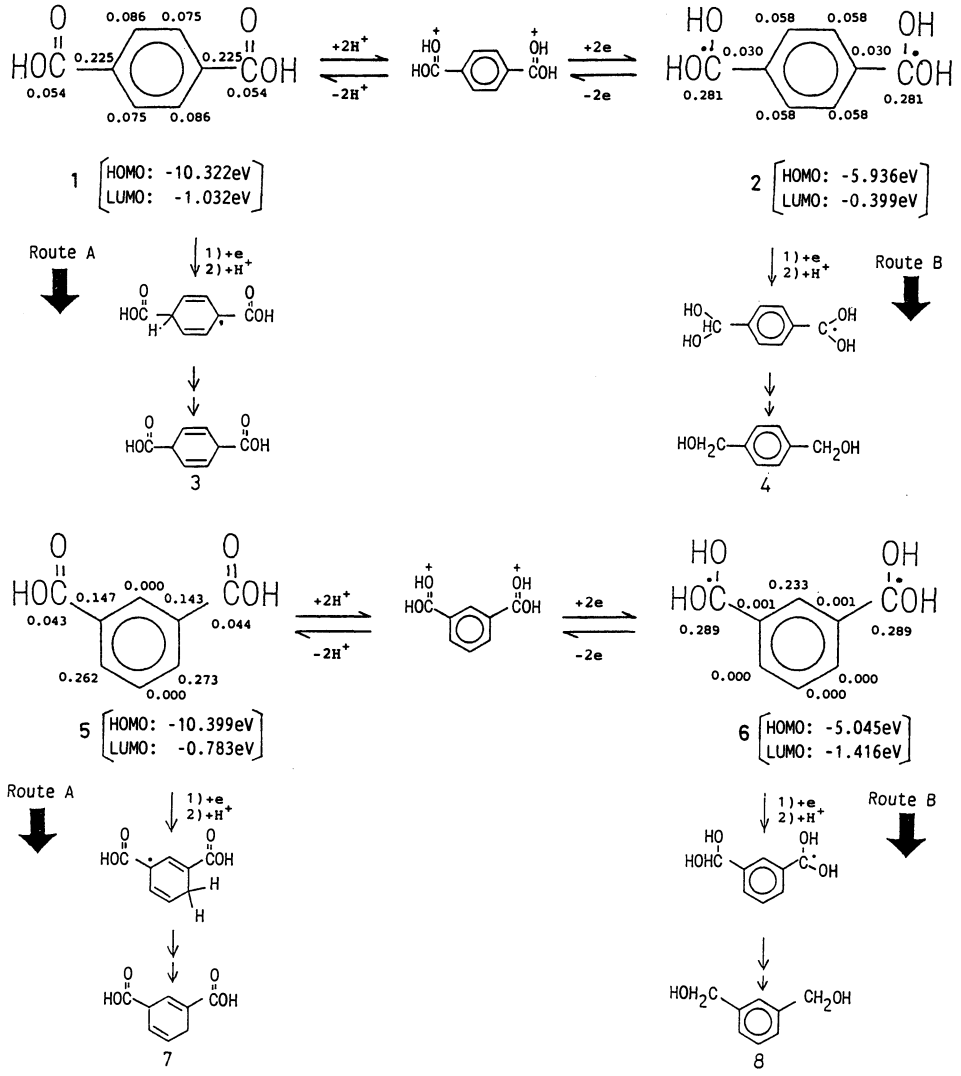

Scheme 1. LUMO electron densities are shown, and the values in parentheses represent HOMO and LUMO energy level. Molecular structures were designed by using STERIC1[14] program; equations used for calculations are as follows, 1: 1*BENZ (.1.-COOH)(.4.-COOH)**, charge of the molecule=0, 2: 1*BENZ-(.1.-C(-OH)2.+.)(.4.-C(-OH)2.+.)**, charge of the molecule=0, 5: 1*BENZ-(.1.-COOH)(.3.-COOH)**, charge of the molecule=0, 6: 1*BENZ-(.1.-C(-OH)2.+.)(.3.-C(-OH)2.+.)**, charge of the molecule=0, and RHF-AM1[15] calculations have been curried out.

the higher reactivity of **1**, in comparison with that of **2**, would displace the equilibrium to Route A. We changed the synthetic strategy in order to study the electroreduction of monocarboxylic acid (**9**) in an aqueous acidic media, which is easily synthesized by the electrolysis of **1** in an aqueous ammoniacal media.

Electroreduction of Aromatic Carboxylic Acids. Electroreduction was carried out with two lead electrodes using an H-shaped two-compartment cell divided by an ion-exchange membrane. The results under various electrolysis conditions are summarized in Table 1.

In the electroreduction of **9**, a satisfactory current efficiency was attained in an aqueous acidic media (Entry 3), while under neutral conditions (Entry 2), the reduction was very slow and no appreciable amount of **4** could be detected under ammoniacal basic conditions (Entry 1).

Incidentally, the electroreduction of **1** under the same reaction conditions as Entry 3 gave a nuclear reduced product **3** without the detection of a side chain reduction (Entry 4), whereas that of **5** afforded a single product **8** (Entry 5).

Experimental

Melting points are uncorrected and were determined in open-ended capillaries. IR spectra were recorded on a Hitachi 285 grating spectrometer.

Calculations. The calculations were performed on a Fujitsu FACOM M360R using MOPAC.[11]

Apparatus. An H-shaped cell divided by an ion-exchange membrane (Asahi Glass Co., Ltd. Selemion CMV) was used; it was equipped with two lead plate electrodes (50 cm^2, 12 cm apart), stirring bars, and a thermometer. A vessel was

immersed in a hot water bath at 40 °C and regulated dc power was supplied by Kikusui Electronics Co. Model PAD 35-60L.LP.

General Procedure. Electrochemical Reduction of *p*-(Hydroxymethyl)benzoic Acid (9). Into both the anode and cathode compartments was placed a 10% aqueous H_2SO_4 solution (200 g each). After regulated dc power (5 A dm^{-2}) was supplied at 40 °C, to the catholytes was portionwise added *p*-(hydroxymethyl)benzoic acid (**9**; 2.37 g h^{-1}, total 20.0 g, 0.131 mol) during the first 6 F mol^{-1} (8.4 h). After electrolysis (10 F mol^{-1}, 14.0 h) at 40 °C, the catholyte was extracted with diethyl ether. The extract was washed with brine, dried (Na_2SO_4), and concentrated in vacuo. The residue was purified by column chromatography (SiO_2, hexane/AcOEt, 3:1) to give **4** (13.0 g, 68.0%) as white crystal with an IR spectrums identical with that reported for the authentic material;[12] mp 113—116 °C (lit,[13] mp 118—119.4 °C).

We gratefully acknowledge Prof. Sigeru Torii, Dr. Hideo Tanaka (Okayama University), Dr. Tsuneo Hirano (The University of Tokyo), Dr. Kengo Oda (Central Research Institute), Mr. Kiyohisa Okano (Systems and Computing Department), and Dr. Akihiro Tamaki (Director of Omuta Research Institute) for support during this work. We also appreciate Mr. Masanao Esaki (Director of Omuta Factory, Mitsui Toatsu Chemicals, Inc.) for giving us an opportunity to present this work.

References

1) R. Oi and S. Takenaka, 9th Electroorganic Chemistry Symposium, Sendai, Jpn., June 1987, Abstr., No 31.
2) For example, J. C. Kilber, *Polym. Sci.*, **1964**, 2115.
3) For example, M. Furuya and K. Nakaoka, Jpn. Patent Kokai 85-32737(1985); *Chem. Abstr.*,**103**, 53800n (1985); C. Y. Huang and T. Maeno, U.S. Patent 3546301 (1970); *Chem. Abstr.*, **74**, 141241u (1971).
4) S. Watanabe, H. Namikawa, and Y. Shite, Jpn. Patent Kokai 74-31435 (1974); *Chem. Abstr.*, **82**, 125057y (1975).
5) Badische Anilin and Soda-Fabrik. Fr. Patent 1516599 (1968); *Chem. Abstr.*, **70**, 92677x (1969).
6) For example , BASF Ger. Patent 2642496 (1978); *Chem. Abstr.*, **89**, 6119e (1978); Standard Oil, U.S. Patent 4381229 (1983); *Chem. Abstr.*, **98**, 224292h (1983); Amuco, Aust. Patent 548059 (1985); *Chem. Abstr.*, **104**, 232965n (1986).
7) See the review by L. Eberson and J. H. P. Utley, "Organic Electrochemistry," ed by M. M. Baizer and H. Lund, Mercel Dekker, Inc., New York (1983), p. 375.
8) R. Oi, C. Shimakawa, Y. Shimokawa, and S. Takenaka, *Bull. Chem. Soc. Jpn.*, **60**, 4193 (1987).
9) C. Mettler, *Ber.*, **39**, 2933 (1906).
10) "Santei Ryoshikagaku Nyumon," ed by T. Yonezawa, C. Nagata, A. Imamura, H. Kato, and K. Morokuma, Kagaku Dojin, Kyoto (1983), p. 153 (jyo).
11) A Hitac version converted from MOPAC 3.1 version supplied from T. Hirano, Department of Synthetic Chemistry, Faculty of Engineering, The University of Tokyo, Jpn.
12) "Documentation of Molecular Spectroscopy," Verlag Chemie (1967), IR: No. 4829.
13) I. Wender, H. Greenfield, S. Metlin, and M. Orchin, *J. Am. Chem. Soc.*, **74**, 4079 (1952).
14) "Chemogram Steric/Chemo Input, Users Manual Ver 4.1," ed by S. Yoneda, Kagaku Jyoho Kyokai, Tokyo (1985)
15) M. J. S. Dewer, E. G. Zoeblisch, E. F. Healy, and J. J. P. Stewart, *J. Am. Chem. Soc.*, **107**, 3902 (1985).

Synthesis and Chemiluminescence of 5-[(2-Pyridyl)-, (2-Pyrazinyl)-, and (Substituted 2-pyrazinyl)amino]-1,2,4-trioxanes

Hideshi NAKAMURA† and Toshio GOTO*
Laboratory of Organic Chemistry, Faculty of Agriculture, Nagoya University, Chikusa, Nagoya 464
(Received May 6, 1988)

Synopsis. From pyridyl- and pyradinylamines and isobutylaldehyde were prepared the corresponding 5-arylamino-1,2,4-trioxanes, whose chemiluminescence was studied by comparing with those of *Cypridina* luciferin analogs.

Cypridina luciferin (**1a**) is one of the most efficient chemiluminescent substances in addition to its bioluminescent activity.[1] Accumulated results of studies on both of the bio- and chemiluminescence suggest the light-producing mechanism (Scheme 1) involving an intermediate, 1,2-dioxetane **2a**, which decomposes rapidly to yield predominantly a singlet excited state molecule. The efficient chemiluminescence and instability of the dioxetane **2a** would be explained in terms of conjugation of the electron-donating and highly fluorescent chromophore with the dioxetane ring. Akutagawa et al. treated 9-aminoanthracene **4a** with isobutyraldehyde in the presence of atmospheric oxygen and obtained a stable peroxide,[2] the 5-(9-anthrylamino)-1,2,4-trioxane **6a**[2-8] that caused efficient chemiluminescence when it was treated with a base in a polar aprotic solvent. Aminodioxetane **7a** is assumed to be an intermediate in the light producing process.[4,8] If the anthracene moiety is replaced with a pyrazine derivative, the expected aminodioxetane intermediate would have the structural similarity to the aminodioxetane **2a** in the *Cypridina* bioluminescence. In this paper, we describe the synthesis and chemiluminescence of the trioxanes (**6b—i**) which have the chromophore similar to *Cypridina* luciferin and *Watasenia* preluciferin (coelenterazine).[1]

Arylamines (**4b—i**) were oxidized with atmospheric oxygen in the presence of a large excess of isobutyraldehyde to afford the corresponding trioxanes (**6a—i**) in 6.5—50% yields (Table 1). The trioxanes may be formed via a Shiff-base as shown in Scheme 2. These compounds were fairly stable and showed a molecular ion peak in the EI mass spectra except **6b** and **6c**. The

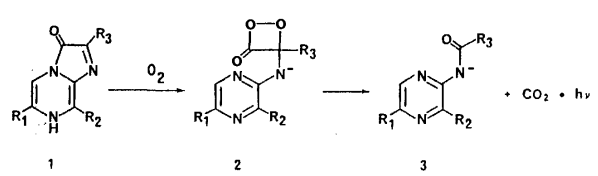

a: R_1= 3-indolyl, R_2= $CH_2CH_2CH_2$·NHC(=NH)NH_2, R_3= $CH(CH_3)CH_2CH_3$
b: R_1= phenyl, R_2=H, R_3= CH_3
c: R_1= 3-indolyl, R_2= H, R_3= CH_3

Scheme 1.

† Present address: The Research Institute for Life Sciences, Mitsubishi Kasei Co., Ltd., Minamiohtani, Machida, Tokyo 194.

^{1}H NMR spectrum of **6b** showed signals assignable to an isobutyl group at δ 0.98 (6H), 1.84 (1H), and 4.80(1H), and to a methine proton at δ 5.28 (1H), which was coupled with an NH proton signal at δ 4.82. In the ^{13}C NMR spectrum of **6b**, signals for an acetal methine carbon, a methine carbon bearing oxygen and nitrogen atoms, and a quaternary carbon attached to an oxygen atom were observed at δ 107.1, 84.0, and 79.9, respectively. The ^{1}H and ^{13}C NMR spectra of the trioxanes (**6c—g** and **6i**) resemble very closely those of **6b**. In the ^{1}H NMR spectra of **6a** and **6h**

Table 1. Synthetic Yield and Chemiluminescence Properties of the Trioxanes and Luciferin Analogs in Dimethyl Sulfoxide Containing *t*-BuOK

Compound	Yield/%	Φ_{CL}[a]×10^2	Φ_F[b]×10^2	Φ_S[c]×10^2
6a	12	4.6	37	12
6b	18	0.0086	2.7	0.32
6c	29	—	—	—
6d	19	0.045	8.4	0.54
6e	6.5	0.10	15	0.67
6f	26	0.049	8.1	0.60
6g	50	0.14	21	0.67
6h	45	0.13	20	0.65
6i	47	0.22	52	0.42
1b	—	0.12	11	1.1
1c	—	0.024	43	0.056

a) Quantum efficiency of chemiluminescence. b) Quantum efficiency of fluorescence of the corresponding amide (**8**). c) Quantum efficiency of excited singlet state formation.

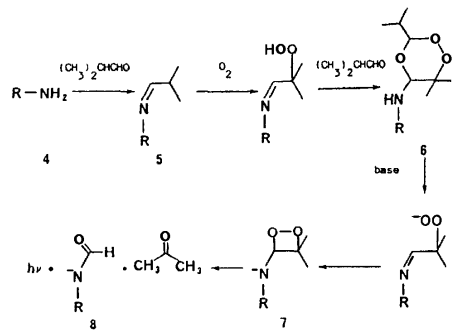

a: R = 9-anthryl
b: R = 2-pyridyl
c: R = 2-pyrazinyl
d: R = 5-methyl-2-pyrazinyl
e: R = 5-phenyl-2-pyrazinyl
f: R = 5-(p-bromophenyl)-2-pyrazinyl
g: R = 5-(p-methoxyphenyl)-2-pyrazinyl
h: R = 3-benzyl-5-(p-methoxyphenyl)-2-pyrazinyl
i: R = 5-(3-indolyl)-2-pyrazinyl

Scheme 2.

having substituents at ortho position to the amino group, an anisotropic effect on a methyl signal was observed.[4]

The trioxanes (**6b**, **d**—**i**) emitted light under basic conditions in dimethyl sulfoxide as well as **6a** (Table 1), but efficiencies of chemiluminescence and singlet excited state formation were much lower than those of **6a**. The luciferin analog **lb** also produced light under the same conditions and the efficiency of singlet excited state formation was about two times larger than those of the analogous trioxane **6e**, suggesting a slight difference between the dioxetanone and the dioxetane moiety for light production. On the other hand, the luciferin analog **lc** having an indole side chain showed only very weak chemiluminescence under the condition while it gave light efficiently in diethylene glycol dimethyl ether (diglyme) containing a trace of acetate buffer (pH 5.6);[1] the efficiency of singlet excited state formation being 0.16. Efficiency of singlet excited state formation of the analogous trioxane **6i** was about 8 times larger than that of **lc** under the basic condition, indicating the presence of some side reactions or quenching processes in the chemiluminescent reaction of **lc**.

Experimental

All melting points were uncorrected. ^{1}H and ^{13}C NMR spectra were recorded on a JEOL JNM-MH100 (100 MHz) and a JNM-FX100 (25 MHz) spectrometer, respectively. Chemical shifts (δ) are given in ppm from internal TMS and coupling constants (J) in Hz. IR spectra were taken on a JASCO IR-G spectrometer. UV spectra were obtained on a HITACHI EPS-3T spectrometer. Mass spectra were measured on a JEOL JMS-D100 and a JMS-0lSG-2 instrument. Fluorescence spectra were recorded on a Hitachi MPF-3 spectrofluorometer. Dimethyl sulfoxide and diglyme were distilled from KOH and sodium metal, respectively, under reduced pressure. The other solvents were of reagent grade (Wako Chemical Co., Ltd.). 2-Aminopyrazines (**4d**—**i**) were prepared by the methods described in our previous reports.[9]

Preparation of 5-(9-Anthrylamino)-3-isopropyl-6,6-dimethyl-1,2,4-trioxane (6a). This compound was prepared according to the method of Akutagawa et al.[2] Pale yellow prisms from CH_2Cl_2-hexane, mp 122—124 °C (lit,[2] 113 °C).

Preparation of the Trioxanes (6b—h). A solution of arylamine (**4b**—**h**) (2 mmol) and isobutyraldehyde (60 mmol) in diethyl ether (20 ml) was kept in a dark with stirring under atmospheric oxygen at room temperature. After about 10 days, the solution was diluted with diethyl ether, washed with aq. $NaHCO_3$ and saturated aq. NaCl, and dried over anhydrous Na_2SO_4. The solvent was removed under reduced pressure and the residue was chromatographed on TLC plates to give the corresponding trioxane (**6**).

6b: Needles (from hexane), mp 85—86 °C; ^{1}H NMR ($CDCl_3$) δ=0.98 (6H, d, J=6.5, 10 and 11-Me), 1.20 and 1.52 (each 3H, s, 7 and 8-Me), 1.84 (1H, m, 9-H), 4.82 (1H, d, J=11, NH), 5.16 (1H, d, J=5.2, 3-H), 5.28 (1H, d, J=11, 5-H), 6.60 (1H, d, J=8, 3-H), 6.72 (1H, dd, J=8 and 4), 7.48 (1H, td, J=8 and 1), 8.18 (1H, br d, J=4); ^{13}C NMR ($CDCl_3$) δ= 16.6 and 16.8 (each q, 10 and 11-Me); 17.5 and 21.7 (each q, 7 and 8-Me); 31.0 (d, C-9), 79.9 (s, C-6), 84.0 (d, C-5), 107.1 (d, C-3), 107.9 (d), 115.2 (d), 137.8 (d), 148.0 (d), 156.8 (s). Found: C, 61.65; H, 7.86; N, 10.96%. Calcd for $C_{13}H_{20}N_2O_3$: C, 61.88: H, 7.86; N, 10.96%.

6c: Colorless oil; ^{1}H NMR ($CDCl_3$) δ= 0.99 (6H, d, J=6.9), 1.20 (3H, s), 1.52 (3H, s), 1.83 (1H, m), 5.10 (1H, d, J=5.5), 5.17 (1H, d, J=10, NH), 5.42 (1H, d, J=10), 7.8—8.4 (3H, m); ^{13}C NMR ($CDCl_3$) δ=16.6 (q), 16.8 (q), 17.4 (q), 21.6 (q), 31.0 (d), 79.8 (s), 83.0 (d), 107.2 (d), 132.5 (d), 135.2 (d), 141.8 (d), 153.1 (s).

6d: Needles (from hexane), mp 104—105 °C; ^{1}H NMR ($CDCl_3$) δ= 0.95 (6H, d, J=6.8), 1.19 (3H, s), 1.52 (3H, s), 1.85 (1H, m), 2.43 (3H, s), 4.88 (1H, d, J=10, NH), 5.17 (1H, d, J=4.9), 5.38 (1H, d, J=10), 7.98 (2H, s); ^{13}C NMR ($CDCl_3$) δ=16.7 (q), 16.8 (q), 17.5 (q), 21.7 (q), 20.2 (q, ArMe), 31.0 (d), 79.9 (s), 83.4 (d), 107.3 (d), 131.2 (d), 141.0 (d), 143.8 (s), 151.0 (s). Found: C, 58.20; H, 7.81; N, 16.00%. Calcd for $C_{13}H_{21}N_3O_3$: C, 58.41; H, 7.92; N, 15.72%.

6e: Amorphous solid (from hexane), mp 100—110 °C; MS m/z 329 (M^+); ^{1}H NMR ($CDCl_3$) δ=0.98 (6H, d, J=6.4), 1.22 (3H, s), 1.56 (3H, s), 1.85 (1H, m), 4.90 (1H, d, J=10, NH), 5.18 (1H, d, J= 4.5), 5.42 (1H, d, J=12), 7.3—8.5 (7H, m); ^{13}C NMR ($CDCl_3$) δ= 16.7 (q), 16.8 (q), 17.5 (q), 21.7 (q), 31.0 (d), 79.8 (s), 83.2 (d), 107.3 (d), 125.8 (d), 128.4 (d), 128.8 (d), 131.4 (d), 136.7 (s), 139.1 (d), 144.2 (s), 151.6 (s). Found: C, 65.33; H, 7.03; N, 12.57%. Calcd for $C_{18}H_{23}N_3O_3$: C, 65.63; H, 7.04; N, 12.76%.

6f: Pale yellow amorphous solid (from hexane), mp 157—159 °C; MS m/z 407, 409 (M^+); ^{1}H NMR ($CDCl_3$) δ= 0.98 (6H, d, J=6.8), 1.23 (s), 1.56 (s), 1.88 (1H, m), 5.14 (1H, d, J=11, NH), 5.20 (1H, d, J=5.0), 5.48 (1H, d, J=11), 7.66 (4H, AB q), 8.12 (1H, d, J=1), 8.50 (1H, d, J=1); ^{13}C NMR ($CDCl_3$) δ=16.7 (q), 16.8 (q), 17.5 (q), 21.7 (q), 31.1 (d), 79.7 (s), 83.2 (d), 107.4 (d), 122.7 (s), 127.2 (d), 131.6 (d), 132.0 (d), 135.7 (s), 138.7 (d), 142.9 (s), 151.9 (s). Found: C, 51.87; H, 5.31; N, 10.04%. Calcd for $C_{18}H_{22}N_3O_3Br \cdot 1/2H_2O$: C, 51.81; H, 5.55; N, 10.06%.

6g: Amorphous solid (from hexane), mp 129.5—130.5 °C; MS m/z 359 (M^+); ^{1}H NMR ($CDCl_3$) δ= 0.96 (6H, d, J=6.8), 1.19 (3H, s), 1.53 (3H, s), 1.85 (1H, m), 3.80 (3H, s, OMe), 5.19 (1H, d, J=11, NH), 5.21 (1H, d, J=5.0), 5.47 (1H, d, J=11), 6.99 (2H, d, J=9), 7.87 (2H, d, J=9), 8.13 (1H, d, J=1), 8.51 (1H, d, J=1); ^{13}C NMR ($CDCl_3$) δ= 16.7 (q), 16.9 (q), 17.5 (s), 21.7 (s), 31.0 (d), 55.2 (q, OMe), 79.9 (s), 83.4 (d), 107.3 (d), 114.3 (d), 127.0 (d), 129.5 (s), 131.3 (d), 138.3 (d), 144.0 (s), 151.3 (s), 160.0 (s). Found: C, 63.44; H, 6.90; N, 11.76%. Calcd for $C_{19}H_{25}N_3O_4$: C, 63.49; H, 7.01; N, 11.69%.

6h: Plates (from hexane), mp 75.5—82 °C; MS m/z 449 (M^+); ^{1}H NMR ($CDCl_3$) δ=0.84 (6H, d, J=5.6), 1.13 (3H, s), 1.79 (3H, s), 1.79 (1H, m), 3.86 (3H, s, OMe), 4.24 (2H, AB q), 4.49 (1H, d, J=11, NH), 5.12 (1H, d, J=5.5), 5.59 (1H, d, J=11), 7.00 (2H, d, J=9), 7.2—7.4 (5H, m), 7.92 (2H, d, J=9), 8.42 (1H, br s); ^{13}C NMR ($CDCl_3$) δ=16.4 (q), 16.9 (q), 17.3 (q), 21.7 (q), 31.1 (d), 41.5 (t), 55.3 (q, OMe), 79.9 (s), 82.0 (d), 107.1 (d), 114.2, 127.1, 127.3, 128.4, 129.1, 129.4, 136.5, 136.6, 140.8, 142.6, 149.3, 159.8. Found: C, 69.23; H, 6.87; N, 9.24%. Calcd for $C_{26}H_{31}N_3O_4$: C, 69.46; H, 6.95; N, 9.35%.

Preparation of Trioxane 6i. A solution of aminopyrazine **4i** (200 mg, 0.91 mmol) and isobutyraldehyde (10.4 ml, 114 mmol) in diethyl ether (21 ml) was treated as described for the preparation of **6b**. After 5 days, pale yellow precipitates of **6i** were collected by filtration. The filtrate was treated as described in the case of **6b** to give additional amount of **6i**. **6i**: pale yellow amorphous solid, mp 204.5—205.5 °C; MS m/z 368 (M^+); ^{1}H NMR ($CDCl_3$) δ=0.98 (6H, d, J=6.8), 1.24 (3H, s), 1.57 (3H, s), 1.94 (1H, m), 4.91 (1H, d, J=12, NH), 5.20 (1H, d, J=5.0), 5.40 (1H, d, J=12), 7.71 (1H, d, J=2.5), 8.16 (1H, d, J=1), 8.40 (1H, br s, NH), 8.55 (1H, d, J=1), 7.1—8.2 (4H, m); ^{13}C NMR (DMSO-d_6) δ=16.5 (q), 16.6 (q), 17.7 (q), 21.4 (q), 30.5 (d), 80.1 (s), 82.8 (d), 106.5 (d), 111.6 (d), 112.8 (s), 119.5 (d), 120.9 (d), 121.4 (d), 123.5 (d), 124.9 (s), 131.9 (d), 136.7 (s), 137.5 (d), 141.3 (s), 150.6 (s). Found: C, 65.13; H, 6.54; N, 15.21%. Calcd for $C_{20}H_{24}N_4O_3$: C, 65.20; H, 6.57; N, 15.21%.

Preparation of the Formamides (8a, b, d—i). To a solution of each of the arylamines (**4**) (0.4 mmol) in pyridine (1 ml) was added acetic anhydride (0.1 ml) under cooling in an ice-water bath. The solution was warmed to room temperature and stirred for 2 h. The solvent was evaporated under reduced pressure to give the corresponding crude formamide (**8**), which was recrystallized from the solvent given.

8a: Pale yellow needles (from MeOH), mp 189—191 °C; MS *m/z* 221 (M^+). Found: C, 81.18; H, 5.21; N, 6.39%. Calcd for $C_{15}H_{11}NO$: C, 81.43; H, 5.01; N, 6.33%.

8b: Rods (from MeOH), mp 75—76 °C; MS *m/z* 122 (M^+). Found: C, 59.17; H, 4.95; N, 22.94%. Calcd for $C_6H_6N_2O$: C, 59.01; H, 4.95; N, 22.94%.

8d: Slightly yellowish plates (from benzene), mp 121—124 °C; MS *m/z* 137 (M^+). Found: C, 52.55; H, 5.17; N, 30.84%. Calcd for $C_6H_7N_3O$: C, 52.54; H, 5.15; N, 30.64%.

8e: Leaflets (from MeOH), mp 162—164 °C; MS *m/z* 199 (M^+). Found: C, 66.27; H, 4.70; N, 20.96%. Calcd for $C_{11}H_9N_3O$: C, 66.32; H, 4.55; N, 21.10%.

8f: Plates (from MeOH), mp 212—214 °C; MS *m/z* 277, 279 (M^+). Found: C, 47.49; H, 2.75; N, 15.11%. Calcd for $C_{11}H_8N_3OBr$: C, 47.50; H, 2.90; N, 15.11%.

8g: Plates (from MeOH), mp 205—206 °C; MS *m/z* 229 (M^+). Found: C, 62.60; H, 4.70; N, 18.43%. Calcd for $C_{12}H_{11}N_3O_2$: C, 62.87; H, 4.84; N, 18.33%.

8h: Pale yellow needles (from MeOH), mp 190.5—191 °C; MS *m/z* 319 (M^+). Found: C, 71.39; H, 5.30; N, 13.07%. Calcd for $C_{19}H_{17}N_3O_2$: C, 71.45; H, 5.37; N, 13.16%.

8i: Slightly yellowish amorphous solid (from MeOH), mp 262—263 °C; MS *m/z* 238 (M^+). Found: C, 65.53; H, 4.04; N, 23.75%. Calcd for $C_{13}H_{10}N_4O$: C, 65.53; H, 4.23; N, 23.52%.

Chemiluminescence and Fluorescence Measurements. A solution of dimethyl sulfoxide or diglyme (1 ml) containing 0.85 mol l^{-1} *t*-BuOK (*t*-BuOH solution, 5 μl) or acetate buffer pH 5.6 (50 μl) was added to a solution of a trioxane or a luciferin analog in dimethyl sulfoxide or diglyme (1 ml). The resulting light emission was recorded with a luminometer. Quantum yields of chemiluminescence and fluorescence were determined as previously described.[10]

References

1) T. Goto, *Pure Appl. Chem.*, **17**, 421 (1968); T. Goto, M. Isobe, D. A. Coviello, and Y. Kishi, *Tetrahedron*, **29**, 2035 (1973); T. Goto, "Bioluminescence of Marine Organisms," in "Marine Natural Products," ed by P. J. Scheuer, Academic Press, New York (1980), Vol. 3, pp. 179—222.

2) M. Akutagawa, H. Aoyama, Y. Omote, and H. Yamamoto, *J. Chem. Soc., Chem. Commun.*, **1976**, 180.

3) F. McCapra, Y. C. Chang, and A. Burford, *J. Chem. Soc., Chem. Commun.*, **1976**, 608.

4) T. Goto and H. Nakamura, *Tetrahedron Lett.*, **1976**, 4627.

5) H. Yamamoto, H. Aoyama, Y. Omote, M. Akutagawa, A. Takenaka, and Y. Sasada, *J. Chem. Soc., Chem. Commun.*, **1973**, 63.

6) A. Takenaka, Y. Sasada, and H. Yamamoto, *Acta Crystallogr., Sect. B*, **33**, 3564 (1977).

7) H. Yamamoto, M. Akutagawa, H. Aoyama, and Y. Omote, *J. Chem. Soc., Perkin Trans 1*, **1980**, 2300.

8) F. McCapra and A. Burford, *J. Chem. Soc., Chem. Commun.*, **1977**, 874.

9) S. Sugiura, S. Inoue, Y. Kishi, and T. Goto, *Yakugaku Zasshi*, **89**, 1646 (1969); Y. Kishi, H. Tanino, and T. Goto, *Tetrahedron Lett.*, **1972**, 2747.

10) H. Nakamura and T. Goto, *Photochem. Photobiol.*, **30**, 27 (1979).

A New and Simple Route to 3-Arylthiophenes[1)]

Tyo SONE,* Manabu INOUE, and Kazuaki SATO
Department of Applied Chemistry, Faculty of Engineering, Yamagata University, Yonezawa 992
(Received May 11, 1988)

Synopsis. 3-Arylthiophenes were prepared from 2,5-dichlorothiophene in two steps. 2,5-Dichlorothiophene reacted regioselectively with various aromatic compounds in the presence of $AlCl_3$ under mild conditions to give 4-aryl-2-chlorothiophenes. The latter compounds were easily converted to the corresponding 3-arylthiophenes by catalytic dechlorination in good yields.

Electrophilic substitutions of thiophene occur predominantly at the 2-position, making access to 3-substituted thiophenes rather troublesome.[2)] This is also the case with 3-arylthiophenes (**1**), one of the thiophene analogues of biphenyls; thus, it has been desired to find a general method for the preparation of **1**.[3)] Certain 3-substituted thiophenes,[3,4)] including **1** as well as the parent thiophene, have recently attracted attention in connection with the potential electric conductivity and their electrochromic property of their electrochemically prepared polymers. We wish to report here on a new and simple route to **1**.

It has been assumed that the chlorine atom(s) of chlorothiophenes is generally unreactive under Friedel-Crafts conditions, as is true for those of aryl chlorides. However, Ramsey et al. have reported that chlorothiophenes undergo polymerization by $AlCl_3$-$CuCl_2$ through a nuclear coupling with the elimination of HCl.[5)] Recently, we have also reported that, in the presence of $AlCl_3$, 2-chlorothiophene reacts with active aromatic compounds, giving the corresponding 2-arylthiophenes.[6)] Furthermore, we have observed an unusual $AlCl_3$-catalyzed Friedel-Crafts reaction of 2,5-dichloro-3-chloromethylthiophene with benzene and its simple alkyl derivatives, which yield 4-aryl-3-arylmethyl-2-chlorothiophenes, exclusively.[7)] In an extension of our studies, we found that under similar conditions 2,5-dichlorothiophene (**2**) reacted regioselectively with various aromatic compounds (**3**) to afford the unusual products, 4-aryl-2-chlorothiophenes (**4**). Early studies suggest that chlorine atom(s) in chlorothiophenes can be removed only with difficulty.[8,9)] However, contrary to expectation, **4** were found to be successfully dechlorinated by catalytic hydrogenation. Thus, the $AlCl_3$-catalyzed reaction provides a two-step synthesis (three-step from thiophene) of **1** from readily available **2** (Scheme 1).

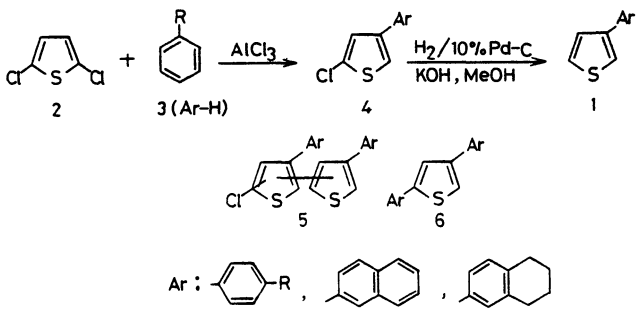

Scheme 1.

The procedure of the $AlCl_3$-catalyzed reaction is simple: one mole equiv of $AlCl_3$ was added to an equimolar mixture of **2** and **3** in CH_2Cl_2 under ice-cooling, and the mixture stirred below 40 °C for a total of 2 h. The results are summarized in Table 1. As shown in the Table, the reaction yielded the corresponding **4** as the major products in good yield, except for a reaction with chlorobenzene (**3f**), which yielded an inseparable mixture of 2,5-dichlorothiophene oligomers. In many cases, the presence of isomers due to the position of the substituent(s) on the aromatic ring, diarylthiophenes (**6**), and self-condensation products (**5**) which were derived from two moles of **4** with the elimination of HCl, were also suggested in the products (MS, UV, NMR). The corresponding 2-

Table 1. $AlCl_3$-Catalyzed Reaction of 2,5-Dichlorothiophene (**2**) with Aromatic Compounds (**3**)

Ar-H **3**	**4**	
	% Yield[a)]	Mp(θ_m/°C)
a R=H	62	74—75
b R=Me	54 (72)	117—118
c R=Et	66 (71)	97—98
d R=1,3-Me_2	63[b)]	bp 95—97/2 mmHg
e R=OMe	34[c)] (40)	126—127
f R=Cl	(5)	
g tetralin	63[d)]	49—50
h naphthalene	52[e)] (60)	114—15

a) Yields of the purified products based on **2** used; figures in parentheses are those of the crude products which contain the positional isomers. b) 2-Chloro-4-(2,4-dimethylphenyl)thiophene. c) Chlorobis(*p*-methoxyphenyl)bithienyl (**5e**; mp 103—104 °C, 17%) and 2,4-bis(*p*-methoxyphenyl)thiophene (**6e**; 4%) were also isolated. d) 2-Chloro-4-(5,6,7,8-tetrahydro-2-naphthyl)thiophene. e) 2-Chloro-4-(2-naphthyl)-thiophene.

Table 2. Catalytic Dechlorination of 4-Aryl-2-chlorothiophenes (**4**)

4 Ar	**1**	
	% Yield[a)]	Mp(θ_m/°C) (lit)
a R=H	85	93—94 (91—92,[17)] 89—91[15)])
b R=Me	83	112—113 (111—112,[17)] 113—113.5[15)])
c R=Et	80	96—97
d R=2,4-Me_2	68	bp 78—80/2 mmHg
e R=OMe	86	126—127 (129,[17)] 127[3)])
h 2-Naph[b)]	70	145—146 (145.5—146.5[15)])

a) Yields of the purified products based on **4** used. b) Naph: naphthyl.

arylthiophene derivatives, such as 2-aryl-5-chlorothiophenes, which might be expected, were not detected in the products. Interestingly, while naphthalene (**3h**) produced a mixture of the 1- and 2-naphthyl derivatives (**4h**; main product), tetralin (**3g**) yielded 2-chloro-4-(5,6,7,8-tetrahydro-2-naphthyl)thiophene (**4g**).

The structures of **4** were assigned on the basis of their elemental analyses and spectral data. The UV spectra excluded the presence of the 2-arylthiophene unit in the structures; instead, it suggested the presence of the 3-arylthiophene unit.[10] The NMR spectra showed, in addition to the absorption due to the aromatic ring protons, an AB quartet with a coupling of 1.25—1.70 Hz, characteristic for 2,4-disubstituted thiophenes[11] in the ring proton region. Further, the structure assignment of **4** was confirmed by chemical evidence. The reductive desulfurization of **4e** by Raney nickel, for example, gave *p-s*-butylanisole. Treatment of **4g** with 2,3-dichloro-5,6-dicyano-1,4-benzoquinone (DDQ) gave **4h**, which afforded 3-(2-naphthyl)-thiophene (**1h**) by dechlorination; this indicates that 2-naphthyl and the tetrahydro-2-naphthyl moieties are included in the molecules of **4h** and **4g**, respectively. When the reaction was conducted at −50 °C between **3** and the protonated **2**[12] which was prepared at the same temperature in advance, **4** were produced in somewhat higher yield. The reaction using $SnCl_4$ instead of $AlCl_3$ gave no products under the conditions studied.

The catalytic hydrogenation of **4** under atmospheric pressure using 10% Pd-C as a catalyst gave the corresponding **1** in satisfactory yield, as shown in Table 2.

The obtained results indicate that protonated **2** serves as electrophilic species in the $AlCl_3$-catalyzed reaction. An NMR spectroscopic method revealed that, in an $AlCl_3$-HCl-CH_2Cl_2 system at low temperature, **2** produced 2*H*-2,5-dichlorothiophenium ion.[12] However, the entire reaction pathway still remains unclear.

Finally, considering that the electrophilic substitutions of **1** occur in the 5-position as well as in the 2-position,[13] **4** could also be versatile intermediates for the selective syntheses of certain isomer-free 2-substituted 3-arylthiophenes. Namely, the introduction of an appropriate group into the vacant α-position of **4**, followed by a subsequent dechlorination would yield 2-substituted 3-arylthiophenes, the chlorine atom of **4** serving as a blocking group.

Experimental

All the melting and boiling points are uncorrected. The ^1H NMR (90 MHz, TMS as an internal reference), UV (in MeOH, unless otherwise noted), IR, and MS (70 eV) spectra were obtained on Hitachi R-22, Hitachi EPU-2A, Hitachi EPI-S2, and Hitachi RMU spectrometers, respectively.

2,5-Dichlorothiophene (**2**) was prepared by a method described in the literature.[14] Commercial $AlCl_3$ was used without special precautions against moisture.

$AlCl_3$-Catalyzed Reaction of 2,5-Dichlorothiophene (2) with Aromatic Compounds (3) (General Procedure). Pulverized $AlCl_3$ (20 mmol) was added in portions over ca. 5-min period to a mixture of **2** (20 mmol) and the substrate (**3**, 60 mmol) in CH_2Cl_2 (10 ml; 20 ml in the case of naphthalene) under ice-cooling. Exothermic reactions occurred with the appearance of a coloration and the rise of the temperature of the reaction mixture. The mixture was stirred at ca. 5 °C for 30 min, then at ambient temperature for 1 h, and at the reflux temperature of the solvent for an additional 30 min. The reaction mixture was poured into ice-water (ca. 70 ml) and extracted with $CHCl_3$ (10 ml×3). The extracts were combined, washed successively with water, 5% $NaHCO_3$ solution, and water, and dried. After removal of the solvent and the starting substances by distillation, the residue was sublimed under reduced pressure (2—3 mmHg (1 mmHg= 133.322 Pa)) yielding crude 4-aryl-2-chlorothiophene (**4**) which was contaminated with a small amount of the positional isomer. Chromatography (silica gel/hexane) of the residue of the sublimation gave another crop of **4**. The crude **4** was purified by recrystallization (hexane) or distillation. In the case of naphthalene (**3h**), the reaction mixture, after removal of the solvent, was sublimed under reduced pressure (7 mmHg) to recover **3h**, and the residue was directly chromatographed.

The minor products were not investigated further, except for those produced in the reaction of **2** with anisole (**3e**).

4a: MS *m/z* 194 (M^+, 100). UV λ_{max} 232 (4.25), 261 (3.95). ^1H NMR ($CDCl_3$) δ=7.1—7.6 (m, Ph+Th (thiophene; 3-H, 5-H)). Anal. ($C_{10}H_7ClS$) C, H.

4b: MS *m/z* 208 (M^+, 100). UV λ_{max} 235 (4.27), 267 (3.90). ^1H NMR (acetone-d_6) δ=2.29 (3H, s, CH_3), 7.17 and 7.26 (2H, AA'BB'm, *p*-Ph (*p*-substituted phenyl)), 7.41 and 7.51 (1H, d, $J_{3,5}$=1.6 Hz each, Th (3-H, 5-H)), 7.50 and 7.59 (2H, AA'BB'm, *p*-Ph). Anal. ($C_{11}H_9ClS$) C, H.

4c: MS *m/z* 222 (M^+, 100). UV λ_{max} 235 (4.36), 265 (4.06). ^1H NMR (acetone-d_6) δ=1.16 (3H, t, $J_{CH_2\text{-}CH_3}$=7.1 Hz, $CH_2\underline{CH_3}$), 2.62 (2H, q, $J_{CH_2\text{-}CH_3}$=7.1 Hz, $C\underline{H_2}CH_3$), 7.18 and 7.27 (2H, AA'BB'm, *p*-Ph), 7.39 and 7.49 (1H, d, $J_{3,5}$=1.6 Hz each, Th (3-H, 5-H)), 7.50 and 7.59 (2H, AA'BB'm, *p*-Ph). Anal. ($C_{12}H_{11}ClS$) C, H.

4d: MS *m/z* 222 (M^+, 100). UV λ_{max} 233 (4.28), 256sh (3.91). ^1H NMR (CCl_4) δ=2.22 and 2.25 (3H, s each, Me), 6.78 and 6.85 (d, $J_{3,5}$=1.3 Hz each, Th (3-H, 5-H)), 6.7—7.4 (5H, m, Ph+Th (3-H, 5-H)). Anal. ($C_{12}H_{11}ClS$) C, H.

4f: MS *m/z* 232 (M^++4, 14), 230 (M^++2, 69), 228 (M^+, 100).

4g: MS *m/z* 248 (M^+, 100). UV λ_{max} 236 (4.37), 267 (4.04). ^1H NMR ($CDCl_3$) δ=1.6—1.9 (4H, m, $PhCH_2\text{-}C\underline{H_2}\text{-}$), 2.78 (4H, br s, $Ph\text{-}C\underline{H_2}\text{-}CH_2\text{-}$), 6.9—7.3 (5H, m, Ph+Th (3-H, 5-H)). Anal. ($C_{14}H_{13}ClS$) C, H.

4h: MS *m/z* 244 (M^+, 100). UV λ_{max} 230 sh (4.63), 238 (4.75), 247 sh (4.66), 257sh (4.43), 265 sh (4.30), 281 (4.06), 290 (4.14), 302 (4.08). ^1H NMR ($CDCl_3$) δ= 7.1—8.0 (m, Naph+Th (3-H, 5-H; two doublets at 7.27 and 7.33 ($J_{3,5}$=1.7 Hz each)). Anal. ($C_{14}H_9ClS$) C, H.

Reaction with Anisole (3e). Chromatography (silica gel/hexane-benzene (1 : 1)) of the residue of the sublimation afforded the second crop of **4e** and the self-condensation product (**5e**; 0.7 g, mp 103—104 °C after crystallization from MeOH-acetone). The combined **4e** was recrystallized from EtOH. When the reaction mixture was poured into ice-water, a small amount of precipitate was separated out, which was recrystallized from *N,N*-dimethylformamide to give 2,4-bis(*p*-methoxyphenyl)thiophene (**6e**; 0.2 g, mp 220—221 °C (lit,[6] 219—221 °C).

4e: MS *m/z* 224 (M^+, 100). UV λ_{max} 242 (4.31), 273 (4.15). ^1H NMR ($CDCl_3$) δ= 3.81 (3H, s, OMe), 6.85 and 6.95 (2H, AA'BB'm, *p*-Ph), 7.05 and 7.15 (1H, d, $J_{3,5}$=1.6 Hz each, Th (3-H, 5-H)), 7.38 and 7.47 (2H, AA'BB'm, *p*-Ph). Anal. ($C_{11}H_9ClOS$) C, H.

5e: MS *m/z* 412 (M^+, 100). UV λ_{max} 245sh (4.40), 254 (4.43), 273 (4.42), 318—331 (3.89). ^1H NMR (acetone-d_6) δ= 3.79 (6H, s, OMe), 6.89 and 6.98 (4H, AA'BB'm, *p*-Ph), 7.05 (1H, s, Th), 7.2—7.7 (6H, m, *p*-Ph+Th). Anal. ($C_{22}H_{17}ClO_2S_2$) C, H.

Catalytic Dechlorination of 4-Aryl-2-chlorothiophenes (4). The procedure is a modification of the one used by Zwanenberg et al.[9] Hydrogenation was conducted by stirring a mixture of **4** (5 mmol), KOH (1.5 g), 10% Pd-C (0.7 g), and MeOH (100 ml) at room temperature in an atmospheric pressure hydrogenation apparatus filled with H_2. Within 1 h one equivalent of H_2 was consumed. After removal of the catalyst the solution was concentrated to ca. 30 ml. Water was added to the residue and the resulting crystalline mass was purified by sublimation under reduce pressure and/or recrystallization.

1a: MS *m/z* 160 (M^+, 100). UV λ_{max} 227 (4.15), 258 (4.14) (lit,[15] (96% EtOH) 227 (4.11), 259 (4.08)). ^{1}H NMR ($CDCl_3$) δ=7.1—7.8 (m, Ph+Th).

1b: MS *m/z* 174 (M^+, 100). UV λ_{max} 227 (4.27), 260 (4.23) (lit,[15] (96% EtOH) 228 (4.17), 261 (4.17)). ^{1}H NMR ($CDCl_3$) δ=2.35 (3H, s, Me), 7.13 and 7.22 (2H, AA'BB'm, *p*-Ph), 7.35 (3H, s, Th), 7.43—7.52 (2H, AA'BB'm, *p*-Ph).

1c: MS *m/z* 188 (M^+, 100). UV λ_{max} 228 (4.20), 262 (4.21). ^{1}H NMR ($CDCl_3$) δ=1.24 (3H, t, $J_{CH_2\text{-}CH_3}$=7.6 Hz, CH_2-$C\underline{H}_3$), 2.66 (2H, q, $J_{CH_2\text{-}CH_3}$=7.6 Hz, $C\underline{H}_2$-CH_3), 7.16 and 7.24 (2H, AA'BB'm, *p*-Ph), 7.35 (3H, s, Th), 7.45 and 7.54 (2H, AA'BB'm, *p*-Ph). Anal. ($C_{12}H_{12}S$) C, H.

1d: MS *m/z* 188 (M^+, 100). UV λ_{max} 227 sh (4.17), 248 (4.01). ^{1}H NMR ($CDCl_3$) δ=2.29 and 2.33 (3H, s each, Me), 6.9—7.4 (6H, m, Ph+Th). Anal. ($C_{12}H_{12}S$) C, H.

1e: MS *m/z* 190 (M^+, 100). UV λ_{max} 230 (4.11), 269 (4.21). ^{1}H NMR ($CDCl_3$) δ=3.81 (3H, s, -OMe), 6.85 and 6.95 (2H, AA'BB'm, *p*-Ph), 7.2—7.35 (3H, m, Th), 7.45 and 7.54 (2H, AA'BB'm, *p*-Ph).

1h: MS *m/z* 210 (M^+, 100). UV λ_{max} 226 (4.58), 244 (4.51), 252 (4.53), 280 (4.05), 290 (4.13), 301 (4.05) (lit,[15] (96% EtOH) 228 (4.59), 254 (4.57), 279 (4.11), 290 (4.16), 301 (4.08)). ^{1}H NMR ($CDCl_3$) δ=7.15—8.1 (m, Naph+Th).

Dehydrogenation of 4g. A mixture of **4g** (1.24 g, 5 mmol) and DDQ (2.27 g, 10 mmol) in benzene (30 ml) was stirred for 8 h at the reflux temperature of the solvent. After removal of the solvent by distillation, the residue was chromatographed (silica gel/hexane) to afford **4h** (mp 114—115 °C, 1.1 g, 90%).

Reductive Desulfurization of 4e with Raney Nickel. A mixture of 2-chloro-4-(*p*-methoxyphenyl)thiophene (**4e**; 1 g, 4.5 mmol) and W-7 Raney nickel (prepared from 10 g of the alloy) in benzene (100 ml) was stirred at the reflux temperature of the solvent for 20 h. The reaction mixture was filtered and the nickel was extracted with hot benzene for several hours in a Soxhlet extractor. The filtrate and the extract were combined and evaporated. The residue (0.6 g) were chromatographed (silica gel/hexane-chloroform (4:1) to give *p-s*-butylanisole (oil; 0.12 g, 17%) and 3-(*p*-methoxyphenyl)thiophene (**1e**; mp 123—125 °C; 0.09 g, 10%). The IR and NMR spectra of the oily product was identical with those of the authentic sample (bp 109—112 °C (16 mmHg); lit,[16] 106—108 °C (16 mmHg)) which was obtained by the methylation of *p-s*-butylphenol with dimethyl sulfate in basic solution.

This work was supported in part by a grant from The Japan Association of Chemistry, to which the authors' thanks are due. The authors also wish to thank Professor Kensuke Takahashi of Nagoya Institute of Technology for the NMR spectral measurements of the protonated 2,5-dichlorothiophene and helpful suggestions on the spectra.

References

1) Acid-catalyzed Reactions of Thiophene Nuclei. VI. Presented in part at the 8th International Congress of Heterocyclic Chemistry, Graz, August 1981, Abstr. 352. Part V: Ref. 6.

2) For example, E. Campaigne, "Comprehensive Heterocyclic Chemistry," ed by A. Katritzky and C. W. Rees, Pergamon Press (1984), Vol. 4, pp. 914—934.

3) J-P. Montheard, J-F. Delzant, and M. Gazard, *Synth. Commun.*, **14**, 289 (1984) and references cited therein.

4) For example, M. R. Bryce, A. Chissel, P. Kathirgamanathan, D. Parker, and N. R. M. Smith, *J. Chem. Soc., Chem. Commun.*, **1987**, 466; M. Sato, S. Tanaka, and K. Kaeriyama, *J. Chem. Soc., Chem. Commun.*, **1985**, 713; J. M. Bureau, M. Gazard, M. Champagne, J. C. Dubois, G. Tourillon, and F. Garnier, *Mol. Cryst. Liq. Cryst.*, **118**, 235 (1985); *Chem. Abstr.*, **102**, 158731y (1985), and references cited therein.

5) J. S. Ramsey and P. Kovacic, *J. Polym. Sci.*, **A-1**, **7**, 127 (1969).

6) T. Sone, R. Yokoyama, Y. Okuyama, and K. Sato, *Bull. Chem. Soc. Jpn.*, **59**, 83 (1986).

7) T. Sone, H. Kawasaki, S. Nagasawa, N. Takahashi, K. Tate, and K. Sato, *Chem. Lett.*, **1981**, 399.

8) For example, M. G. Reinecke and P. Pedaja, "Thiophene and Its Derivatives," ed by S. Gronowitz, John Wiley & Sons (1986), Part 2, pp. 351—420.

9) D. J. Zwanenburg and H. Wynberg, *J. Org. Chem.*, **34**, 340 (1969).

10) 2-Phenylthiophene, λ_{max}(MeOH) 220sh (3.82), 282 (4.17); 3-phenylthiophene, 226 (4.07), 258 (4.13).

11) S. Gronowitz, "Advances in Heterocyclic Chemistry," ed by A. R. Katritzky, Academic Press, New York (1963), Vol. 1, p. 7.

12) Y. Yokoyama, Y. Yamashita, K. Takahashi, and T. Sone, *Bull. Chem. Soc. Jpn.*, **56**, 2208 (1983).

13) N. Gjøs and S. Gronowitz, *Acta Chem. Scand.*, **24**, 99 (1970).

14) E. Campaigne and M. LeSuer, *J. Am. Chem. Soc.*, **70**, 415 (1948).

15) H. Wynberg, H. van Driel, R. M. Kellogg, and J. Buter, *J. Am. Chem. Soc.*, **89**, 3487 (1967).

16) A. Klages, *Chem. Ber.*, **37**, 3987 (1904).

17) A. Chrzaszczewska, *Roczniki Chem.*, **5**, 33 (1925); *Chem. Abstr.*, **20**, 1078 (1926).

A Reinvestigation of a Sensitized Photochemical Cycloaddition of Coumarin with Cyclopentene[1)]

Hiroshi SUGINOME* and Kazuhiro KOBAYASHI
Organic Synthesis Division, Faculty of Engineering, Hokkaido University, Sapporo 060
(Received May 18, 1988)

Synopsis. A reinvestigation of a sensitized photochemical cycloaddition of coumarin with cyclopentene reported by Hanifin and Cohen indicated that the cycloaddition gives a sterically disfavored cis-cisoid-cis adduct (18%) together with a cis-transoid-cis adduct (25%) and a head-to-head coumarin dimer with a cis-transoid-cis disposition. The two adducts behaved differently in hydrolysis and recyclization.

In connection with the program we have designed to explore the potential of the β-scission of the alkoxyl radicals generated from the cyclobutanols obtained by a [2+2]photocycloaddition of 4-hydroxycoumarin and olefins,[2,4)] we have been interested in the distinctly different behavior of coumarin reported by Hanifin and Cohen in 1966[3)] and 4-hydroxycoumarin in their photochemical cycloaddition.[5)]

Thus, while both Reid and his colleagues and we ourselves have found that the [2+2]photoaddition of 4-hydroxycoumarin (**1**) and cyclopentene (**2**) on direct irradiation gives a single [2+2]photocycloadduct **3** having a sterically disfavored cis-cisoid-cis configuration in a good yield (Scheme 1),[2,6)] Hanifin and Cohen[3)] have reported that the photoaddition of coumarin itself and cyclopentene does not give any cycloadducts on direct irradiation but gives single [2+2]photocycloadduct, mp 139 °C, on a sensitized irradiation. According to Hanifin and Cohen,[3)] the cyclopentane ring and the six-membered ring of the photoadduct are probably transoid oriented.

We have therefore reinvestigated the direct and sensitized photocycloadditions of coumarin and cyclopentene. Our results which differ from the previous report[3)] are described in this paper.

Results

A sensitized irradiation of coumarin and cyclopentene carried out according to the procedure of Hanifin and Cohen [**4** (5.6 mmol), **2** (5 ml), benzophenone (1 mmol), and dioxane (1 ml)] through a Pyrex filter with a 500-W high-pressure mercury arc for 5 days gave a mixture of three products, **5** (mp 82—84 °C, 25%), **6** (mp 138—139 °C, 18%), and **7** (mp 175—176 °C, 21%), which were separable by means of preparative TLC.

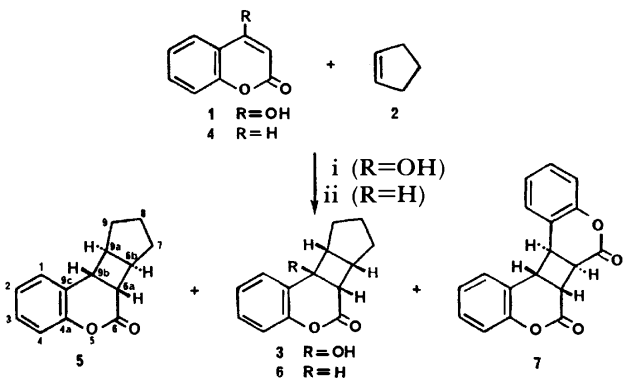

i) *t*-butyl alcohol-$h\nu$
ii) $C_6H_5COC_6H_5$-dioxan-$h\nu$

Scheme 1.

^{1}H NMR spectroscopy and their behaviors in hydrolysis and regeneration of the coumarin ring indicated that the stereochemistries of adducts **5** and **6** have cis-transoid-cis for **5** and cis-cisoid-cis for **6**.

A 500 MHz ^{1}H NMR spectrum of adduct **5** exhibited four signals (each 1H) at δ 2.70, 3.05, 3.14, and 3.19. The signal at δ 3.05 assignable to 6a-H split into a doublet of a doublet with $J_{6a,9b}$=9.28 Hz, $J_{6a,6b}$=4.88 Hz, and $J_{6a,9b}$=0.98 Hz. The signal at δ 3.19 assignable to 9b-H split into a doublet of a doublet with $J_{6a,9b}$=9.28 Hz and $J_{9a,9b}$=3.91 Hz. The signals at δ 3.41 (br. td, J=6.8 and 5.9 Hz) are assigned to the 9a-H and 6b-H. These coupling constants indicated that the cyclobutane-coumarin ring fusion as well as the cyclobutane-cyclopentane ring are cis and that the coumarin and cyclopentane ring are transoid oriented. The structure of the photoadducts **5** was thus established to be 6aα,6bβ,9aβ,9bα-($\pm$)-6b,7,8,9,9a,9b-hexahydrobenzo[*b*]cyclopenta[3,4]cyclobuta[1,2-*d*]pyran-6-(6a*H*)-one (**5**).

On the other hand, the results on the ^{1}H NMR spectrum of adduct **6**, the melting point of which is nearly in agreement with that of the adduct reported by Hanifin and Cohen, indicated that the cyclobutane-coumarin ring fusion as well as the cyclobutane-cyclopentane ring fusion are cis while the coumarin and cyclopentane ring are cisoid oriented in the adduct.

Thus, 500 MHz ^{1}H NMR spectrum of adduct **6** exhibited four signals each corresponding to ^{1}H at δ 3.23, 3.41, 3.73, and 3.97. The signal at δ 3.73 assignable to 5a-H split into a doublet of a doublet with $J_{6a,6b}$=11.23 Hz, and $J_{6a,9b}$=10.74 Hz. The signal at δ 3.97 assignable to 9b-H similarly split into a doublet of a doublet with $J_{6a,9b}$=11.23 Hz, and $J_{6b,9a}$=10.74 Hz. The signal at δ 3.97 assiganble to 9b-H similarly split into a doublet of a doublet with $J_{6a,9b}$=10.74 Hz and $J_{9b,9a}$=10.25 Hz. The rest of the signals at 3.23 (dq, J=7.81 and 8.3 Hz) and at δ 3.41 (dt, J=10.25 and 7.81 Hz) can be assigned to the 6b-H and 9a-H.

The spectroscopic analysis of the third photoadduct **7** indicated that it is a head-to-head and cis-transoid-cis dimer of coumarin obtained by Schenck and his colleagues by means of a sensitized irradiation of coumarin in ethanol or in benzene.[7)]

Thus, we conclude that the cycloadduct **6** previously reported by Hanifin and Cohen[3)] has cis-cisoid-cis structure and the cycloadduct **5**, newly isolated in the

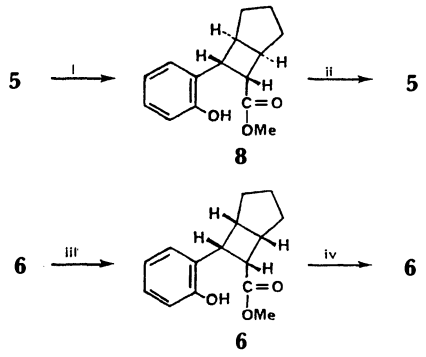

i) CH_3COONa-MeOH, r.t.
ii) *p*-toluenesulfonic acid-benzene-r.t. 10 min
iii) CH_3ONa-MeOH, r.t.
iv) concd HCl, r.t. 2 h

Scheme 2.

present work, has cis-transoid-cis structure (Scheme 1).

Irradiation of a solution of coumarin in cyclopentene and dioxane in the absence of a sensitizer for 5 days gave no [2+2]photocycloadducts: this agrees with the observation by Hanifin and Cohen.[3]

We found a clear difference between **5** and **6** in a base-catalyzed hydrolysis. Thus, while the cis-transoid-cis adducts **5** was readily hydrolyzed with sodium acetate in methanol at room temperature no hydrolysis took place when cis-cisoid-cis adduct **6** was exposed to the same conditions of hydrolysis. Hydrolysis of adduct **6** was, however, achieved with sodium methoxide in methanol for 2 h at room temperature (Scheme 2).

The molecular geometry of cis-cisoid-cis adduct **6** can be assumed to be similar to cis-cisoid-cis adduct **3**, whose molecular structure we determined by means of an X-ray crystallographic analysis.[2,3]

The difference in the behavior under hydrolysis of adducts **5** and **6** can be understood by comparing the geometries of these molecules since an inspection of the molecular models of adducts **5** and **6** indicated that the carbonyl carbon of adducts **6** is more shielded from an attacking nucleophile.

We also found a clear difference in the rates of the recyclizations of the hydrolyzed products **7** and **8**; the hydrolyzed product **8** gave the parent adduct **5** after treatment with *p*-toluenesulfonic acid in benzene at room temperature nearly spontaneously while no cyclization of **9** took place under these conditions. The ester **9** gave a more strained parent adduct **6** after treatment with concd HCl at pH 3 in ethanol at room temperature for 2 h (Scheme 2).

In has been reported as generally true that in an adduct of cycloalkenes and monocyclic enones where the cyclobutane ring fusion to the enones and alkene derived ring are cis, the rings are preferentially disposed transoid to each other.[5b]

It is worth noting that the present triplet sensitized photoaddition led to the production of a substantial proportion of the sterically disfavoured cis-cisoid-cis adduct in addition to an expected cis-transoid-cis adduct. The reason for this is not clear but the attractive interaction of an aromatic portion of coumarin and cycloalkene in the triplet exciplex or the biradical intermediate might be partly responsible for the formation of cis-cisoid-cis product.

Experimental

For the instruments and the experimental procedures see Ref. 2.

Photochemical Cycloaddition of Coumarin with Cyclopentene in the Presence of Benzophenone. Coumarin (820 mg, 6.5 mmol), cyclopentene (5 ml), benzophenone (180 mg, 1 mmol), and dioxane (1 ml) were irradiated through a Pyrex filter with a 500-W high-pressure Hg arc at room temperature for 5 days. After the removal of an excess of cyclopentene and dioxane under a reduced pressure, the product was subjected to preparative TLC with a 1:3 ethyl acetate and hexane to give three cycloadducts **5**, **6**, and **7** in the order of their mobility on the TLC plate. The most mobile adduct **5** (300 mg, 25%) was recrystallized from hexane to yield a specimen for analysis. Mp 82—84 °C. (Found: *m/z* 214.0989. Calcd for $C_{14}H_{14}O_2$: M, 214.0992). IR (Nujol) 1752 cm^{-1} (C=O); ^1H NMR (500 MHz) δ=1.57—1.67 (2H, m, 8-H), 1.86—2.02 (4H, m, 7-H and 9-H), 2.70 (1H, br. td, *J*=7.3 and 3.91 Hz, 9a-H), 3.50 (1H, ddd, *J*=9.28, 4.88, and 0.98 Hz, 6a-H), 3.14 (1H, br. td, *J*=6.8 and 5.9 Hz, 6b-H), 3.19 (1H, dd, *J*=9.28 and 3.91 Hz, 9b-H), and 7.00—7.31 (4H, m, 1,2,3,4-H); MS *m/z* (rel intensity), 214 (M^+, 4.6%), and 146 (100).

The second mobile adduct **6** (219 mg, 18%) was recrystallized from hexane. Mp 138—139 °C (lit,[3] mp 139 °C): (Found: *m/z* 214.0983. Calcd for $C_{14}H_{14}O_2$: M, 214.0992); IR (Nujol) 1746 cm^{-1} (C=O), 1172, amd 772; ^1H NMR (500 MHz), δ= 1.71—1.27 (1H, m), 1.34—1.62 (4H, m), 1.88 (1H, dd, *J*=13.67 and 6.35 Hz), 3.23 (1H, br. dq, *J*=7.81 and 8.3 Hz, 6b-H), 3.42 (1H, dt, *J*=10.25 and 7.81 Hz, 9a-H), 3.73 (1H, dd, *J*= 11.23 and 10.74 Hz, 6a-H), 3.97 (1H, dd, *J*=10.74 and 10.25 Hz, 9b-H), and 6.96—7.31 (4H, m, 1,2,3,4-H); MS *m/z* (rel intensity) 214 (M^+, 3.3%) and 146 (100).

The most polar adduct **7** (173 mg, 21%) was recrystallized from hexane. Mp 175—176 °C (lit,[6] mp 176.5 °C).

A Base-Catalyzed Hydrolysis of the Adduct 5. Adduct **5** (52 mg, 0.24 mmol) in methanol (1 ml) containing sodium acetate (20 mg, 0.24 mmol) was stirred overnight at room temperature. Examination of the solution by TLC (1:3 ethyl acetate-hexane) indicated the disappearance of the starting material. To this solution, dichloromethane (10 ml) was added and the solution was washed first with aq. saturated ammonium chloride and then with brine and dried over anhydrous magnesium sulfate. After the usual work-up, the product was dissolved in benzene (2 ml) containing *p*-toluenesulfonic acid (10 mg, 0.05 mmol). The solution was stirred for 10 min. at room temperature, washed with aq. sodium hydrogencarbonate and dried over anhydrous magnesium sulfate. The usual work-up of the solution gave the residue which was subjected to preparative TLC with a 1:3 ethyl acetate and hexane to yield the starting adduct **5** (31 mg, 60%).

A Base-Catalyzed Hydrolysis of Adduct 6. (a) Adduct **6** (26 mg, 0.12 mmol) in methanol (1 ml) containing sodium acetate (10 mg, 0.12 mmol) was stirred overnight at room temperature. The usual work-up of the solution gave the starting adduct **6** nearly quantitatively.

(b) To adduct **6** (54 mg, 0.25 mmol) in methanol (5 ml), a small amount of sodium metal was added. The solution was then stirred for 2 h at room temperature. Examination of the solution by means of TLC (a 1:3 ethyl acetate-hexane) indicated the disappearance of the starting adduct **6**. The solution was neutralized with concd hydrochloric acid (pH 3) and was stirred for another 2 h. After the removal of methanol under reduced pressure the residue was extracted with diethyl ether. The ethereal extract was washed first with aq.

sodium sulfate. The product was subjected to preparative TLC with a 1:3 ethyl acetate-hexane to yield the starting adduct **6** (41 mg, 76%).

References

1) Photoinduced Molecular Transformations. Part 97. Part 96. H. Suginome and T. Ohki, *J. Chem. Soc., Chem. Commun.*, in press.

2) H. Suginome, C. F. Liu, S. Seko, K. Kobayashi, and A. Furusaki, *J. Org. Chem.*, in press.

3) J. W. Hanifin and E. Cohen, *Tetrahedron Lett.*, **1966**, 1419.

4) H. Suginome, C. F. Liu, and A. Furusaki, *Chem. Lett.*, **1984**, 911.

5) For reviews on enone photochemical cycloaddition see a) S. W. Baldwin, "Organic Photochemistry," Vol. 5, ed by A. Padwa, Marcel Dekker, New York (1981), p. 123; b) A. C. Weedon, "Synthetic Organic Photochemistry," ed by W. M. Horspool, Plenum Press, New York (1984), p. 91.

6) D. J. Haywood, R. G. Hunt, C. J. Potter, and S. T. Reid, *J. Chem. Soc., Perkin Trans. 1*, **1977**, 2458.

7) G. O. Schenck, I. von Wilucki, and C. H. Krauch, *Chem. Ber.*, **95**, 1409 (1962).

New Applications of Crown Ethers. IX.[1] Crystal Structure of KSCN Complex of *N*-Heptylmonoaza-18-crown-6, and Conformational Features of the Pivot Nitrogen

Gong-Xin He, Kiyoshi Kikukawa,# Nobuaki Nishiyama,† Hiroshi Ohe,†† and Tsutomu Matsuda*
Department of Organic Synthesis, Faculty of Engineering, Kyushu University, Hakozaki, Higashi-ku, Fukuoka 812
†Center of Advanced Instrument Analysis, Kyushu University, Kasuga-kouen, Kasuga-shi 816
††Department of Physics, Faculty of Science, Kyushu University, Hakozaki, Higashi-ku, Fukuoka 812
(Received May 20, 1988)

Synopsis. Vertical arrangement of the alkyl side arm in the crystal structure of KSCN complex of *N*-heptylmonoaza-18-crown-6 is well-consonant with the effective side-arm participation in N-pivot lariat ether complexes and supports the lack of 'biscrown effect' for bis(monoaza-18-crown-6)s.

The lariat ethers are a family of the macrocyclic polyethers which bear one or more donor atoms in the side arm through a nitrogen or carbon pivot atom.[2,3] Complexation behavior of the N-pivot lariat ethers has been extensively studied in solutions by comparison with that of the *N*-alkylmonoazacrown ether, an analogue without donor atom in the side arm.[4,5] Gokel et al. have shown the unequivocal evidence for the side-arm participation in the crystal structures of N-pivot lariat ether complexes.[6,7] A similar X-ray analysis was also done for $NaClO_4$ complex of *N*-phenylmonoaza-15-crown-5[8] and KI complex of *N*-allylmonoaza-18-crown-6.[9] However, these studies could not give the arrangement of a flexible non-coordinating side arm and the conformational feature around the pivot nitrogen was also not emphasized in these complexes, while such structural information is very important for considering the interaction with a donating group in the side arm, such as a lariat group in lariat ethers or a second crown ring in bis(crown ether)s. The present paper shows a clear picture about KSCN complex of *N*-alkylmonoaza-18-crown-6, in which the non-coordinating side arm is arranged vertically to the ring plane, and the K^+ ion is located in the center of the ring. The fact in turn may give an answer for the question why a large enhanced binding can be obtained in the complexation of N-pivot lariat ethers, and why the two crown rings of bis(monoaza-18-crown-6)s could not cooperate in the complexation with larger cations.

Experimental

$C_{19}H_{39}NO_5 \cdot KSCN$. A white plate crystal was obtained from a methanol solution containing the ligand and excess KSCN by evaporating the solvent slowly at room temperature. Mp 78—80 °C; IR(Nujol): 2040, 1120, 960, 840 cm^{-1}; Calcd for $C_{20}H_{39}N_2O_5KS$: C, 52.37; H, 8.57; N, 6.11%. Found: C, 51.99; H, 8.49; N, 6.18%. The crystal used for X-ray analysis had approximate dimensions of 0.3×0.3×0.3 mm^3.

X-Ray Analysis. Crystal Data. monoclinic, $P2_1/c$, a=21.910(4), b=14.573(5), c=7.936(5) Å, β=94.36°, V=2527 $Å^3$, Z=4, D_m=1.21, D_c=1.21 g cm^{-3}. Intensity data were collected by ω-2θ scans of variable rate designed to yield measurements of equal relative precision for all significant reflections, using an Enraf-Nonius CAD4 diffractometer equipped with Mo $K\alpha$ radiation (λ=0.71073 Å) and a graphite monochromator. Data reduction included corrections for background, Lorentz, polarization, absorption. Independent 2702 reflections having $I>3\sigma(I)$ were used in the refinements. All structure were solved by MULTAN 82 and refined by full-matrix least square based on F with weights $w=\sigma^{-2}(F_o)$. Non-hydrogen atoms were refined anisotropically, and hydrogen atoms were located in calculated positions. The final residual values were R=0.052, R_w=0.077. The final atomic parameters for non-hydrogen atoms are listed in Table 1, and the selected bond distances and bond angles are shown in Fig 2. The complete tables of atomic coordinates, thermal parameters, bond distances and angles are kept as Document

Table 1. Final Atomic Parameters and Thermal Parameters, with Their Estimated Standard Deviations in Parentheses

Atom	X	Y	Z	B_{eq}/Å^2
K1	0.82150(4)	0.00067(5)	0.0242(1)	4.29(2)
N1	0.6965(1)	0.0516(2)	−0.0858(4)	4.10(6)
O1	0.7957(1)	0.1814(2)	−0.0686(3)	4.53(6)
O2	0.9041(1)	0.1444(2)	0.1263(3)	4.26(5)
O3	0.9358(1)	−0.0453(2)	0.1777(3)	4.61(6)
O4	0.8425(1)	−0.1778(2)	0.1398(3)	4.41(5)
O5	0.7339(1)	−0.1399(2)	−0.0593(3)	4.59(6)
S1	0.22658(8)	0.00009(9)	0.5711(2)	7.69(4)
C20	0.1697(2)	0.0041(3)	0.4198(6)	6.9(1)
N2	0.1299(1)	0.0049(2)	0.3235(4)	4.70(7)
C1	0.6987(2)	0.1338(3)	−0.1911(5)	4.65(9)
C2	0.7352(2)	0.2116(3)	−0.1101(5)	4.38(8)
C3	0.8355(2)	0.2526(2)	−0.0084(5)	4.72(9)
C4	0.8990(2)	0.2166(3)	0.0047(5)	5.27(9)
C5	0.9644(2)	0.1108(3)	0.1557(6)	5.9(1)
C6	0.9650(2)	0.0285(3)	0.2708(6)	5.7(1)
C7	0.9363(2)	−0.1271(3)	0.2745(5)	5.4(1)
C8	0.9045(2)	−0.2007(3)	0.1696(5)	5.23(9)
C9	0.8063(2)	−0.2483(2)	0.0576(5)	5.11(9)
C10	0.7414(2)	−0.2194(3)	0.0442(5)	5.11(9)
C11	0.6731(2)	−0.1157(3)	−0.0936(6)	5.30(9)
C12	0.6681(2)	−0.0240(3)	−0.1835(5)	5.04(9)
C13	0.6722(2)	0.0662(3)	0.0798(5)	5.2(1)
C14	0.6067(2)	0.0935(4)	0.0855(6)	7.4(1)
C15	0.5931(2)	0.1124(4)	0.2755(6)	7.3(1)
C16	0.5256(3)	0.1195(4)	0.2995(7)	9.1(2)
C17	0.5138(2)	0.1374(4)	0.4879(7)	8.3(1)
C18	0.4455(3)	0.1374(4)	0.5130(7)	10.2(2)
C19	0.4342(3)	0.1513(4)	0.6963(8)	10.4(2)

Anisotropically refined atoms given in the form of the isotropic equivalent thermal parameter defined as: $(4/3)\cdot[a2\cdot B(1,1)+b2\cdot B(2,2)+c2\cdot B(3,3)+ab(\cos \text{gamma})\cdot B(1,2)+ac(\cos \text{beta})\cdot B(1,3)+bc(\cos \text{alpha})\cdot B(2,3)]$.

Present address: Department of Industrial Chemistry, Faculty of Engineering (Kyushu Campus), Kinki University, Iizuka 820.

No. 8837 at the Editor of the Bulletin of the Chemical Society of Japan. All the measurements and calculations were performed at the Center of Advanced Instrument Analysis, Kyushu University.

Results and Discussion

The structure of the KSCN complex of *N*-heptylmonoaza-18-crown-6 is shown in Fig 1. Figure 2 gives its skeletal drawing along with the selected bond distances and bond angles. The skeletal drawing shows the arrangement of donor atoms around the cation. The macroring donor atoms are located in a chair-like arrangement to give the D_{3d} conformation of the ring, which is very close to those in the K^+ complexes of *N*-(2-methoxyethyl)monoaza-18-crown-6[6] and *N*-allylmonoaza-18-crown-6.[9] Interestingly, C13–N1–K1 bond angle of the complex is 99.5°, i.e. the non-coordinating alkyl side arm is directed almost upright to the ring plane. Although some effects might come from the crystal lattice packing the direction of C13–N1 bond is considered to be determined by the preferred conformation of the ring and coordination state of the pivot nitrogen. A further examination of CPK model shows that through simple rotations around the C13–N1 and C13–C14 bonds by 180° (two anti conformations to two eclipsed conformations) C15 can be put at such the position just above the K^+ ion without any deformation of the D_{3d} conformation, and this is just the position for the lariat oxygen atom in the N-pivot lariat ether complexes. Combined with the present result and the crystal structures of lariat ether complexes, we can conclude that the pyramidal structure of the pivot nitrogen and the conformation around the pivot nitrogen atom may account for the large enhanced binding observed in N-pivot lariat ether complexes. Very recently it was reported that the binding ability of C-pivot lariat ethers can be improved by introduction of an additional substituent (ex. methyl) on the pivot carbon, suggesting that the first side arm is arranged in an equatorial position in the C-pivot lariat ether complexes in the absence of the second substituent.[10,11]

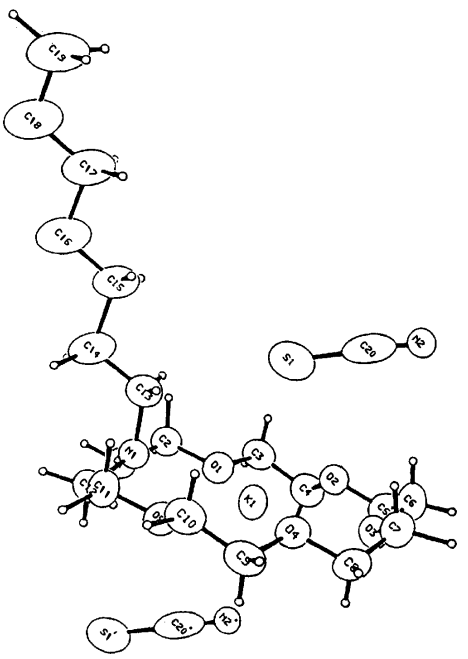

Fig. 1. Perspective drawing of the structure of KSCN complex of *N*-heptylmonoaza-18-crown-6.

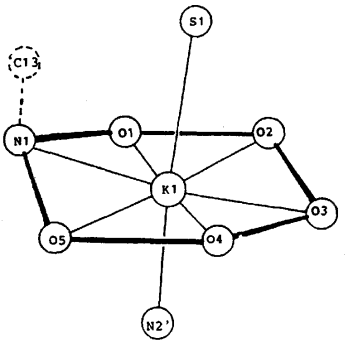

K1–N1	2.908(3)	K1–O3	2.783(2)
K1–O1	2.781(3)	K1–O4	2.785(2)
K1–O2	2.845(3)	K1–O5	2.851(2)
K1–S1	3.455	K1–N2′	3.043

C13–N1–K1	99.5(2)	N1–K1–O3	171.54(8)
C1–N1–K1	108.0(2)	O1–K1–O4	175.51(8)
C12–N1–K1	108.7(2)	O2–K1–O5	176.06(8)
S1–K1–N2′	176.7		

Fig. 2. Skeletal drawing of KSCN complex of *N*-heptylmonoaza-18-crown-6, along with the selected bond distances (Å) and bond angles (°).

For monoaza-18-crown-6 the presence of the pivot nitrogen differentiates each side of the macroring in D_{3d} conformation, which is so stable as to be maintained in the complexation with larger cations,[12] i.e., one side (the side below in Fig. 1) with three axial nonbonding lone pairs (n_{ax}) of oxygen, and the other side(up side in Fig. 1) with only two n_{ax}.[1,13] The vertical arrangement of the *N*-alkyl side arm makes the environment of the two sides more different, and a larger cation would be favorably located the side having three n_{ax} (below the ring in Fig. 1). So that the formation of an intramolecular sandwich complex with a larger cation is very difficult for the bis(monoaza-18-crown-6)s linked by a short bridging chain because two unfavorable sides with two n_{ax} have to be used, although there is no hindrance to form an intermolecular sandwich complex with two monoaza-18-crown-6 rings. This reasoning is consistent with the results that the bis(monoaza-18-crown-6)s behave very similarly with the corresponding monocyclic analogues in the solvent extraction, homogeneous binding constants and cation transport experiment.[1,14,15]

The position of K^+ ion in the present complex, in the center of the macroring, is also noticeable, since the cation is known to be located above the ring plane in the complexes containing a monoaza-18-crown-6 ring reported before.[6,9] It seems that the relative position of the cation to the macroring is determined not only by the ring size but also by the coordination balance of the axial ligands. In the present complex a good balance between the two axial anionic ligands makes the cation reside within the macroring.

This work was partly supported by a Grant-in-Aid for Scientific Research(No. 61470088) from the Ministry of Education, Science and Culture.

Reference

1) Part IIX. in this series: G.-X. He, K. Kikukawa, T. Ikeda, F. Wada, and T. Matsuda, *J. Chem. Soc., Perkin Trans. 2*, **1988**, 719.

2) G. W. Gokel, D. M. Dishong, and C. J. Diamond, *J. Chem. Soc., Chem. Commun.*, **1980**, 1053.

3) A. Masuyama, Y.Nakatsuji, I. Ikeda, and M. Okahara, *Tetrahedron Lett.*, **22**, 4665 (1981).

4) R. A. Schultz, D. M. Dishong, and G. W. Gokel, *Tetrahedron Lett.*, **22**, 2623 (1981).

5) R. A. Schultz, B. D. White, D. M. Dishong, K. A. Arnold, and G. W. Gokel, *J. Am. Chem. Soc.*, **107**, 6659 (1985).

6) F. R. Fronczek, V. J. Gatto, R. A. Schultz, S. J. Jungk, W. J. Colucci, R. D. Gandour, and G. W. Gokel, *J. Am. Chem. Soc.*, **105**, 6717 (1983).

7) F. R. Fronczek, V. J. Gatto, C. Minganti, R. A. Schultz, R. D. Gandour, and G. W. Gokel, *J. Am. Chem. Soc.*, **106**, 7244 (1984).

8) G. Weber, G. M. Sheldrick, J. P. Dix, and F. Vögtle, *Cryst. Struct. Commun.*, **9**, 1157 (1980).

9) R. D. Gandour, F. R. Fronczek, V. J. Gatto, C. Minganti, R. A. Schultz, B. D. White, K. A. Arnold, D. Mazzocchi, S. R. Miller, and G. W. Gokel, *J. Am. Chem. Soc.*, **108**, 4078 (1986).

10) M. Ouchi, Y. Inoue, K. Wada, S. Iketani, T. Hakushi, and E. Weber, *J. Org. Chem.*, **52**, 2420 (1987).

11) Y. Nakatsuji, T. Nakamura, M. Yonetani, H. Yuya, and M. Okahara, *J. Am. Chem. Soc.*, **110**, 531 (1988).

12) M. Dobler and R. P. Phizackerley, *Acta Crystallogr., Sect. B,: Crystallogr. Cryst. Chem.*, **B30**, 2748 (1974).

13) T. Yamabe, K. Hori, K. Akagi, and K. Fukui, *Tetrahedron*, **35**, 1065 (1979).

14) H. Sakamoto, K. Kimura, Y. Koseki, M. Matsuo, and T. Shono, *J. Org. Chem.*, **51**, 4974 (1986).

15) H. Sakamoto, K. Kimura, Y. Koseki, and T. Shono, *J. Chem. Soc., Perkin Trans. 2*, **1987**, 1181.

Catalytic Upgrading of SRC from Pyrolytic Coal Liquefaction and Hydrocracking of Polycyclic Aromatic Hydrocarbons

Chunshan SONG, Kouji HANAOKA, Tomohiro ONO, and Masakatsu NOMURA*
Department of Applied Chemistry, Faculty of Engineering, Osaka University, Yamadaoka 2-1, Suita, Osaka 565
(Received April 21, 1988)

Synopsis. Catalytic upgrading of SRC (solvent refined coal) derived from short contact time pyrolytic liquefaction of Wandoan subbituminous coal was carried out. The upgrading with unsulfided and sulfided nickel-molybdenum catalysts produced about 77 wt% and 85 wt% of oil plus light distillates from the SRC, respectively. The reactions occurring during the upgrading process were assessed by referring to the hydrocraking of related polycyclic aromatic hydrocarbons.

The upgrading of various coal-derived products has been the subject of much research work concerning the second stage of two- or multi-stage coal conversions.[1-3] Recently, we have found that when relatively low heating rates are used, subbituminous coal can be efficiently converted into THF-soluble products in high conversions (85—88 wt%, daf) by pyrolytic procedures in an N_2-tetralin system under high temperature and short contact time conditions.[4] The present work was conducted in order to evaluate the extent of convertibility of the pyrolytically derived SRC by upgrading over supported nickel-molybdenum catalysts. Hydrocracking of some related polycyclic aromatic hydrocarbons over the same catalysts was also carried out for assessing reactions occurring during the upgrading process.

Experimental

The SRC (Table 1) used in this work was prepared by short contact time pyrolytic liquefaction of Wandoan subbituminous coal.[4] The polycyclic aromatics used in hydrocracking reactions were reagent-grade anthracene, phenanthrene, and bibenzyl. The catalysts examined were NiO-MoO_3/Al_2O_3 (NiMo) catalyst (Ketjenfine 153S: NiO, 2.9 wt%; MoO_3, 15.8 wt%; surface area, 255 $m^2 g^{-1}$; pore volume, 0.56 ml g^{-1}) and the corresponding sulfided catalyst (S-NiMo). The upgrading was carried out at 425 °C for 1 h with 4.9 MPa H_2 in a 70-ml SUS-316 rocking autoclave with SRC (2.5 g, −32 mesh), tetralin (5 g) and a catalyst (1 g, −100 mesh) together with a small stainless-steel ball. The products were separated into gas, light distillates (LD, C_5-250 °C), oil (hexane-soluble), asphaltene (benzene-soluble), and preasphaltene (benzene insoluble). Hydrocracking of polycyclic aromatic hydrocarbons was carried out at 400 °C for 1 h with 9.8 MPa H_2 in the autoclave with a given reactant (3 g) and a catalyst (0.3 g, −100 mesh). The products were analyzed by GC and GC-MS. Experimental details concerning this work are similar to those described elsewhere.[4-6]

Results and Discussion

The results of catalytic upgrading of the SRC are shown in Fig. 1. The short-contact-time pyrolytically derived SRC showed a relatively high reactivity toward upgrading, and about 10 wt% of LD and 59 wt% of oil was obtained in the noncatalytic run (Run 1), without any consumption of gas-phase H_2. The use of a NiMo catalyst and the corresponding S-NiMo catalyst improved the conversion of preasphaltene and asphaltene to oil and LD, increased the consumption of H_2 and decreased the net hydrogen transfer from tetralin, as can be seen from Fig. 1. Relative to a noncatalytic run, the yield of LD rose from about 10 wt% to 18 wt% with a NiMo catalyst (Run 2), and to 23 wt% with a S-NiMo catalyst (Run 3). The total yields of light product, oil+LD+gas, were 87.8 wt% with S-NiMo, 80.0 wt% with NiMo and 70.9 wt% without catalyst. These results indicate the high extent of convertibility of the SRC. S-NiMo showed a higher catalytic activity than NiMo for the upgrading; such a trend was also observed in runs with asphaltene.[7]

Table 2 gives elemental analysis and structural parameters of oil products, and Fig. 2 shows the gel permeation chromatograms of oil products. As compared to a noncatalytic run, the use of NiMo and

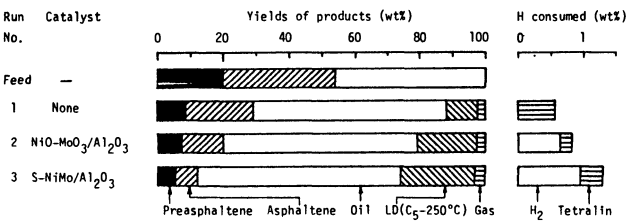

Fig. 1. Catalytic upgrading of SRC from short contact time pyrolytic liquefaction of Wandoan coal.

Table 1. Representative Analyses of SRC from Wandoan Coal

	Content (wt%, daf)			Elemental (wt%, daf)					Atomic ratio	
	Oil	Asp.	Preasp.	C	H	N	S	O[a]	H/C	O/C
SRC	31.3	23.3	13.5	86.3	6.7	1.2	—	5.8	0.93	0.05
Oil[b]	31.3	—	—	85.9	8.3	0.7	—	5.1	1.15	0.04
Asphaltene[c]	—	23.3	—	85.5	6.4	1.4	—	6.7	0.89	0.06
Preasphaltene[d]	—	—	13.5	85.6	4.9	1.6	—	7.9	0.68	0.07
Wandoan coal	0.9	4.7	1.7	78.3	5.9	1.0	0.1	14.7	0.90	0.14

a) By difference; b—d) Hexane-soluble (b), hexane-insoluble but benzene-soluble (c), and benzene-insoluble but THF-soluble (d) portions of the SRC.

Table 2. Elemental Analysis and Structural Parameters of Oil Products

Run No.	Catalyst	Elemental (wt%)				Atomic H/C	Parameters[a]		
		C	H	N	O[b]		f_a	σ	H_{aru}/C_{ar}
1	None	85.7	7.7	0.9	5.7	1.07	0.64	0.34	0.67
2	$NiO-MoO_3/Al_2O_3$	88.6	8.1	0.8	2.5	1.10	0.61	0.37	0.68
3	$S-NiMo/Al_2O_3$	88.8	8.3	0.7	2.2	1.12	0.59	0.39	0.67

a) Calculated from ^1H NMR and elemental analytical data using Brown-Ladner equations. f_a: ratio of number of aromatic carbons to total carbons (aromaticity); σ: degree of substitution in aromatic systems; H_{aru}/C_{ar}: ratio of number of aromatic hydrogens to number of aromatic carbons for a hypothetical unsubstituted aromatic system. b) By difference.

Table 3. Hydrocraking of Phenanthrene

Run No. / Catalyst	4 None	5 NiMo[a]	6 S-NiMo[b]
Products[c] (wt%)			
C_1—C_4	—	—	0.3
C_5—C_9	0.2	0.3	0.4
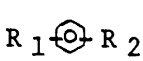	0.1	1.0	2.0
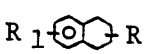	0.4	2.5	4.6
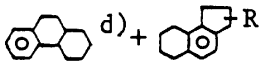	—	13.5	15.6
	—	38.9	37.6
	0.8	11.0	8.4
	1.3	10.9	8.4
	96.3	19.8	18.3
Others	0.9	2.1	4.4
Conversion	3.7	80.2	81.7

a) $NiO-MoO_3/Al_2O_3$. b) $S-NiMo/Al_2O_3$. c) R, R_1, and R_2 mean alkyl groups or hydrogen. d) *unsym*-Octahydrophenanthrene. e) *sym*-Octahydrophenanthene.

Table 4. Hydrocracking of Anthracene

Run No. / Catalyst	7 None	8 NiMo[a]	9 S-NiMo[b]
Products[c] (wt%)			
C_1—C_4	0.1	0.2	0.6
C_5—C_9	—	0.5	0.1
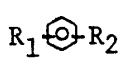	—	—	0.4
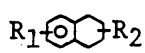	0.1	14.0	18.1
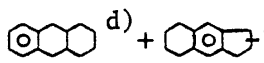	0.3	17.4	21.5
	—	64.5	56.4
	14.9	2.9	2.3
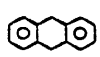	69.3	—	—
	14.4	—	—
Others	0.9	0.5	0.6
Conversion	85.6	100.0	100.0

a) $NiO-MoO_3/Al_2O_3$. b) $S-NiMo/Al_2O_3$. c) R, R_1, and R_2 mean alkyl groups or hydrogen. d) *unsym*-Octahydroanthracene. e) *sym*-Octahydroanthracene.

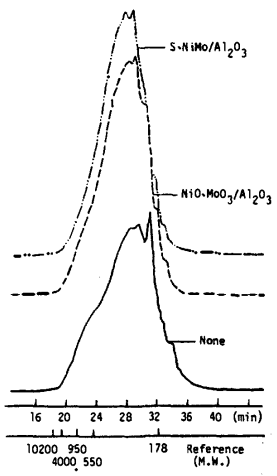

Fig. 2. Gel permeation chromatograms of oil products from catalytic upgrading (column, Shodex AC-801+AC-802; mobile phase, $CHCl_3$, 1 ml min^{-1}; UV detector, set at 254 nm).

S-NiMo facilitated a decreasing heteroatom content and aromaticity (f_a), and an increased atomic H/C ratio and the substitution extent of aromatics (σ) of oil products (Table 2), which correspond to the shift of the molecular size distribution of oil products of catalytic runs relative to a noncatalytic run toward the higher molecular size side (Fig. 2).

In order to assess the reactions occurring during the upgrading process, the hydrocracking of polyaromatics was carried out. The results in Tables 3 and 4 show that NiMo and S-NiMo significantly promoted hydrocracking reactions of phenanthrene and anthracene, whereas in the absence of catalyst a very limited amount of phenanthrene was converted (Table 3, Run 4) and anthracene was mainly converted into dihydroanthracene (Table 4, Run 7). Phenanthrene is known to have a low reactivity toward hydrogenation, and the major hydrogenated products of the catalytic runs are dihydro-, tetrahydro-, octahydrophenanthrene (Table 3). Anthracene showed much a higher reactivity, and in the catalytic runs, most of the intermediate

hydrogenation products, such as dihydro- and tetrahydroanthracene, were converted into octahydroanthracene and hydrocracked products (Table 4). The major hydrocracked products are monocyclic and bicyclic hydrocarbons. Both in runs involving phenanthrene and anthracene, S-NiMo afforded higher yields of hydrocracked products than NiMo, indicating a higher activity of the sulfided catalyst than the unsulfided one (Tables 3 and 4). In the reaction of bibenzyl, S-NiMo and NiMo also promoted conversion of the reactant to 1-cyclohexyl-2-phenylethane and 1,2-dicyclohexylethane, but the yields of hydrocracked products, such as benzene, toluene, and ethylbenzene, were only slightly higher than those of a noncatalytic run.

The above results provided a basis for assessing the hydrocracking reactions of aromatic compounds present in SRC during the upgrading process. Most of the hydrocracked products shown in Tables 3 and 4, if formed from catalytic upgrading of the SRC, would fall into the category of light distillates. On the other hand, fairly larger amounts of the products from catalytic runs (Tables 3 and 4) are hydrogenation products, which did not undergo hydrocracking (ring-opening) reactions. Therefore, apart from hydrocracking reactions, it is possible that some of the polyaromatic substances present in heavy portions of the SRC were converted into oil products by hydrogenation reactions, since an increase in naphthenic rings in asphaltene and preasphaltene can also increase their solubility in hexane.[8] This would rationalize the shift of the molecular size distribution of oil products from catalytic runs toward the higher molecular size side (Fig. 2). The SRC, of course, contains a significant percentage of heteroatom-containing compounds (heteroatom content, Table 1); their adsorption and reactions on the catalyst surface would also take place and they may partly interfere with those of aromatic compounds.[9] As can be seen from Table 2, the most considerable decrease of oxygen content of oil from catalytic runs relative to that of noncatalytic run suggests that the major reactions of heteroatom-containing compounds that occurred during the upgrading process were hydrodeoxygenation reactions. It seems that hydrodeoxygenation is easier than hydrodenitrogenation.[10]

The combination of results regarding upgrading of the SRC (Fig. 1), the hydrocracking of pure hydrocarbons (Tables 3 and 4) and the analytical results of oil products from upgrading (Table 2, Fig. 2) strongly suggest that NiMo and S-NiMo catalysts promoted hydrogenation and cracking of polyaromatic substances present in heavy portions of the SRC and, thus, enhanced their conversion to oil and light distillates. Hydrogenation reactions, such as those shown in Tables 3 and 4, decreased the aromaticity (f_a, Table 2), and hydrocracking-derived alkyl aromatics contributed to the increase of substitution extent (σ) of oil products. These reactions were simultaneously accompanied by heteroatom removal, mainly hydrodeoxygenation reactions. However, as estimated from the H_{aru}/C_{ar} values shown in Table 2, the remaining aromatic compounds in oil products after the catalytic upgrading, have (on the average) similar ring sizes as those contained in oil from a noncatalytic run.

References

1) "Upgrading Coal Liquids," ed by R. F. Sullivan, *Am. Chem. Soc. Sym. Ser.*, **139**, 39—251 (1981).

2) I. Mochida, K. Sakanishi, Y. Korai, and H. Fujitsu, *Fuel*, **65**, 1090 (1986).

3) A. Nishijima, *J. Fuel Soc. Jpn.*, **67**, 210 (1988).

4) C. Song, M. Nomura, and K. Hanaoka, *Coal Sci. Technol.*, **11**, 239 (1987).

5) C. Song and M. Nomura, *Fuel*, **66**, 1225 (1987).

6) S. Kikkawa, M. Nomura, and K. Murase, *J. Jpn. Petrol. Inst.*, **19**, 863 (1976).

7) P. A. Hertan, W. R. Jackson, and W. R. Larkins, *Fuel*, **64**, 1251 (1985).

8) H. Itoh and K. Ouchi, *Shokubai(Catalyst)*, **22**, 71 (1980); K. Ouchi, T. Chikada, and H. Itoh, *Fuel*, **58**, 37 (1979).

9) A. Nishijima, "Shokubai Koza," ed by Shokubai Gakkai, Kodansha, Tokyo (1986), Vol. 10, p. 47; I. Mochida, "Shokubai Koza," ed by Shokubai Gakkai, Kodansha, Tokyo (1985), Vol. 9, p. 162.

10) C. Li, Z. Xu, B. C. Gates, and L. Petrakis, *Ind. Eng. Chem. Process Des. Dev.*, **24**, 92 (1985).

Synthesis of 2-Aryl[1,2,4]triazolo[1,5-*a*]pyrimidines

K. KAMALA, P. JAYAPRASAD RAO, and K. KONDAL REDDY*
Department of Chemistry, Osmania University, Hyderabad 500007, India
(Received November 13, 1987)

Synopsis. 2-(Aroylamino)pyrimidines (**4**) have been converted into 1-(2-pyrimidyl)-5-aryl-1*H*-tetrazoles (**6**) by treatment with PCl_5 followed by azidolysis in aqueous acetone solution. Pyrolysis of **6** in decalin gave 2-aryl[1,2,4]triazolo-[1,5-*a*]pyrimidines (**8**). A reasonable pathway for the formation of **8** from **6** is suggested. Structures of all the compounds have been established by elemental analysis and spectral data.

1-Aminopyrimidinium salt (**1**), obtained from 2-aminopyrimidine and *O*-(mesitylsulfonyl)hydroxylamine, on reaction with benzoyl chloride is known to give 2-phenyl[1,2,4]triazolo[1,5-*a*]pyrimidine[1] (**2**, mp 185—0.5 °C) in a very low yield (8%). In view of the synthetic utility of 1,5-disubstituted tetrazoles[2] and in continuation of our studies on thermal decomposition of 1-heteroaryl-5-aryl-1*H*-tetrazoles,[3-6] we report a convenient synthesis of 2-aryl[1,2,4]triazolo[1,5-*a*]-pyrimidines by the pyrolysis of 1-(2-pyrimidyl)-5-aryl-1*H*-tetrazoles.

Results and Discussion

Benzoylation of 2-aminopyrimidine (**3**, X=H) in the presence of pyridine gave 2-benzamidopyrimidine[7] (**4a**). Treatment of **4a** with PCl_5, followed by reaction with NaN_3 of the resulting *N*-(2-pyrimidyl)arenecarboximidoyl chloride (**5a**) without isolation, led to the formation of a colorless compound, **6a**, mp 95 °C. The compound was analyzed for $C_{11}H_8N_6$. In its mass spectrum the molecular ion was observed at *m/z* 224. Its IR spectrum revealed the absence of amide and azide functions. The presence of >C=N- in the compound was indicated by the appearance of a band at 1600 cm^{-1}. Its ^1H NMR spectrum ($CDCl_3$) revealed two peaks—a multiplet at δ 7.1—7.5 and a doublet at δ 8.6 in 3 : 1 ratio. The doublet is assignable to protons in 4 and 6 positions of the pyrimidine ring. On the basis of these data the compound **6a** has been assigned as 1-(2-pyrimidyl)-5-phenyl-1*H*-tetrazole (**6a**) structure.

A number of 2-(aroylamino)pyrimidines (**4b—l**, Table 1) obtained by the reaction of 2-amino-, 2-amino-5-chloro-, and 2-amino-5-bromopyrimidines[8] with benzoyl, *p*-toluoyl, *p*-anisoyl, *p*-chlorobenzoyl chlorides in the presence of pyridine were converted into 1-(2-pyrimidyl)-5-aryl-1*H*-tetrazoles (**6b—l**) on treatment with PCl_5 followed by azidolysis.

Heating a mixture of **6a** and finely ground pure sand at 180—190 °C and column chromatography of the reaction mixture gave a colorless crystalline compound, **8a**, mp 186 °C. On the basis of the elemental analysis and spectral data [IR(KBr): 1600 cm^{-1} (>C=N), no absorptions due to >C=O, >NH, and N_3 functions. ^1H NMR ($CDCl_3$) δ 7.3—7.75 (m, phenyl protons), δ 8.2—9.0 (m, pyrimidine protons) in 5 : 3 ratio and MS: M^+ at *m/z* 196], the compound **8a** has been assigned as 2-phenyl[1,2,4]triazolo[1,5-*a*]pyrimidine

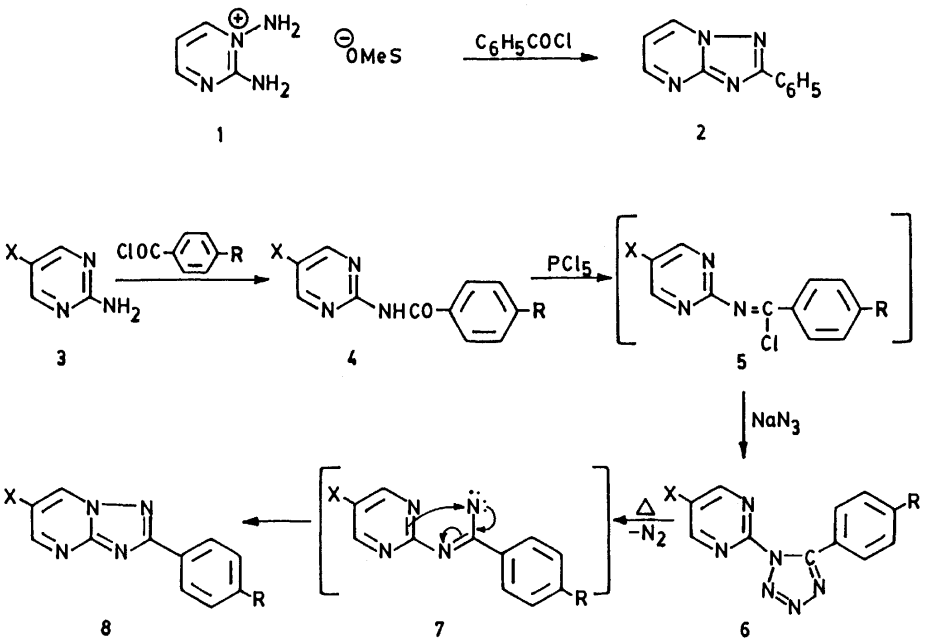

a: X = R = H; b: X = H, R = Me; c: X = H, R = OMe; d: X = H, R = Cl; e: X = Cl, R = H;
f: X = Cl, R = Me; g: X = Cl, R = OMe; h: X = R = Cl; i: X = Br, R = H; j: X = Br, R = Me;
k: X = Br, R = OMe; l: X = Br, R = Cl.

Table 1. Characterization Data of 2-(Aroylamino)pyrimidines (**4**), 1-(2-Pyrimidyl)-5-aryl-1*H*-tetrazoles (**6**) and 2-Aryl[1,2,4]triazolo[1,5-*a*]pyrimidines (**8**)

Compd.	Mp θ_m/°C	Yield %	IR cm^{-1} NH	IR cm^{-1} C=O	IR cm^{-1} C=N	Mol. formula	Calcd (%) C	Calcd (%) H	Calcd (%) N	Found (%) C	Found (%) H	Found (%) N
4a	142—143[7]	90	3300	1650	—	—	—	—	—	—	—	—
4b	148—149	85	3250	1660	—	$C_{12}H_{11}N_3O$	67.60	5.16	19.72	67.57	5.12	19.65
4c	181—182	78	3200	1650	—	$C_{12}H_{11}N_3O_2$	62.88	4.80	18.34	62.85	4.62	18.28
4d	109—111	95	3320	1670	—	$C_{11}H_8N_3OCl$	56.53	3.43	17.99	56.52	3.40	17.82
4e	139—140	85	3310	1650	—	$C_{11}H_8N_3OCl$	56.53	3.43	17.99	56.51	3.41	17.85
4f	129—130	82	3200	1665	—	$C_{12}H_{10}N_3OCl$	58.18	4.04	16.97	58.08	4.01	16.93
4g	184—185	87	3280	1660	—	$C_{12}H_{10}N_3O_2Cl$	54.65	3.79	15.94	54.62	3.75	15.88
4h	165—166	84	3310	1680	—	$C_{11}H_7N_3OCl_2$	49.25	2.61	15.67	49.20	2.58	15.62
4i	178—179	78	3320	1670	—	$C_{11}H_8N_3OBr$	47.48	2.88	15.11	47.38	2.65	15.08
4j	129—130	80	3250	1665	—	$C_{12}H_{10}N_3OBr$	49.32	3.42	14.38	49.29	3.31	14.28
4k	169—170	74	3330	1660	—	$C_{12}H_{10}N_3O_2Br$	46.75	3.25	13.64	46.72	3.18	13.60
4l	154—155	84	3300	1685	—	$C_{11}H_7N_3OBrCl$	42.24	2.24	13.44	42.22	2.20	13.42
6a	94—95	65	—	—	1600	$C_{11}H_8N_6$	58.93	3.57	37.50	58.91	3.52	37.42
6b	138—139	58	—	—	1600	$C_{12}H_{10}N_6$	60.50	4.20	35.29	60.40	4.16	35.22
6c	191—192	49	—	—	1600	$C_{12}H_{10}N_6O$	56.69	3.94	33.07	56.58	3.88	33.00
6d	185—186	68	—	—	1600	$C_{11}H_7N_6Cl$	51.06	2.71	32.50	51.00	2.60	32.39
6e	194—195	64	—	—	1600	$C_{11}H_7N_6Cl$	51.06	2.71	32.50	51.02	2.73	32.52
6f	146—147	55	—	—	1610	$C_{12}H_9N_6Cl$	52.84	3.30	30.83	52.86	3.33	30.80
6g	169—170	52	—	—	1600	$C_{12}H_9N_6OCl$	49.91	3.12	29.12	49.85	3.14	29.10
6h	151—152	60	—	—	1610	$C_{11}H_6N_6Cl_2$	45.05	2.05	28.67	45.00	2.00	28.62
6i	205—206	55	—	—	1605	$C_{11}H_7N_6Br$	43.56	2.31	27.73	43.50	2.30	27.78
6j	140—141	60	—	—	1590	$C_{12}H_9N_6Br$	45.43	2.84	26.50	45.60	2.71	26.45
6k	161—162	65	—	—	1610	$C_{12}H_9N_6OBr$	43.24	2.70	25.23	43.47	2.65	24.98
6l	148—149	62	—	—	1620	$C_{11}H_6N_6BrCl$	39.11	1.78	24.89	39.20	1.75	24.82
8a	186[1]	50	—	—	1600	$C_{11}H_8N_4$	67.35	4.08	28.57	67.30	4.01	28.50
8b**	200—201	42	—	—	1610	$C_{12}H_{10}N_4$	68.57	4.76	26.67	68.52	4.70	26.65
8c	280—281	40	—	—	1600	$C_{12}H_{10}N_4O$	63.72	4.42	24.78	63.69	4.38	24.70
8d	142—143	52	—	—	1580	$C_{11}H_7N_4Cl$	57.27	3.04	24.30	57.36	3.00	24.28
8e	230—231	55	—	—	1590	$C_{11}H_7N_4Cl$	57.27	3.04	24.30	57.30	3.02	24.20
8f	115—116	53	—	—	1605	$C_{12}H_9N_4Cl$	58.89	3.68	22.90	58.90	3.60	22.85
8g	218—219	45	—	—	1610	$C_{12}H_9N_4OCl$	55.28	3.45	21.50	55.26	3.40	21.38
8h	160—161	58	—	—	1605	$C_{11}H_6N_4Cl_2$	49.81	2.26	21.13	49.80	2.20	20.92
8i	144—145	50	—	—	1580	$C_{11}H_7N_4Br$	48.00	2.55	20.36	48.32	2.50	20.28
8j	203—204	52	—	—	1600	$C_{12}H_9N_4Br$	49.83	3.11	19.38	49.80	3.00	19.46
8k	165—166	53	—	—	1610	$C_{12}H_9N_4OBr$	47.21	2.95	18.36	47.19	2.86	18.38
8l	150—151	62	—	—	1610	$C_{11}H_6N_4BrCl$	42.65	1.94	18.09	42.60	1.90	18.06

6b* ^1H NMR ($CDCl_3$): δ 2.48 (s, 3H), 7.2—7.75 (m, 5H), 8.1 (d, 2H), M^+ at *m/z* 238.
8b** ^1H NMR ($CDCl_3$): δ 2.42 (s, 3H), 7.25—7.6 (m, 5H), 8.2 (d, 2H), M^+ at *m/z* 210.

(**8a**) structure. The yield of **8a** in this reaction was 25%. Pyrolysis of 1-(2-pyrimidyl)-5-phenyl-1*H*-tetrazole was also carried out in toluene, xylene, tetralin, and decalin. The tetrazole was recovered unchanged even after prolonged refluxing in toluene (bp 110 °C) or xylene (bp 140 °C). Refluxing the tetrazole in tetralin (bp 210 °C) for 3 h yielded **8a** in 35% yield. Decomposition of the tetrazole was complete by refluxing in decalin (bp 180 °C) for 3 h to give **8a** in 50% yield. Decomposition of other 1-(2-pyrimidyl)-5-aryl-1*H*-tetrazoles (**6b—l**) in decalin resulted in the formation of the corresponding **8b—l** (Table 1). The formation of **8**, in the pyrolysis of **6**, can be reasonably explained through stepwise elimination of a molecule of nitrogen from **6** and the cyclization of the resulting nitrene intermediate **7** in singlet state.[9]

Experimental

2-(Aroylamino)pyrimidines (4). General Procedure: To a solution of 2-aminopyrimidine in pyridine was added an equimolar amount of aroyl chloride with shaking. After the addition was complete, the reaction mixture was allowed to stand at room temperature for 2 h. The crude product that separated on dilution was filtered, washed with 10% sodium hydrogencarbonate solution, then several times with water. The dry solid was recrystallized from benzene-methanol to give pure **4** as summarized in Table 1.

1-(2-Pyrimidyl)-5-aryl-1*H*-tetrazoles (6). General Procedure: A mixture of **4** (5.00 mmol) and PCl_5 (1.3 g, 5.00 mmol) was heated at 100 °C for 1 h, when the evolution of fumes of HCl ceased. Excess of $POCl_3$ was removed under reduced pressure and the residual imidoyl chloride was treated with ice-cold sodium azide (0.37 g, 5.00 mmol) and excess of sodium acetate trihydrate in water (25 cm^3) and acetone (30 cm^3) with stirring. The stirring was continued overnight, acetone was removed under reduced pressure, and the remaining aqueous portion was extracted with chloroform. The dried chloroform extract was chromatographed over a column of neutral alumina, eluting with benzene to give pure **6** (Table 1).

Thermal Decomposition of 6. General Procedure: A solution of 1-(2-pyrimidyl)-5-aryl-1*H*-tetrazole (**6**, 2.50 mmol) in decalin (25 cm^3) was refluxed for 3 h. The decalin

was removed by distillation under reduced pressure. The residue was extracted with chloroform, the extract was concentrated and the residue was subjected to chromatography over a neutral alumina column, eluting with benzene-ethyl acetate (10:1) mixture to give pure **8** (Table 1).

One of the authors, K. Kamala, is thankful to CSIR, New Delhi, India for the award of SRF.

References

1) S. W. Schneller, "Comprehensive Heterocyclic Chemistry," ed by K. T. Potts, Pergamon Press, Oxford (1984), Vol. 5, Part 4A, p. 890, and also part therein Y. Tamura, K. Joong-Hyup, and M. Ikeda, *J. Heterocycl. Chem.*, **12**, 107 (1975).

2) R. N. Butler, "Advances in Heterocyclic Chemistry," ed by A. R. Katritzky and A. J. Boulton, Academic Press, New York (1977), Vol. 21, p. 324.

3) K. Kamala, P. Jayaprasad Rao, and K. Kondal Reddy, *Indian J. Chem.*, **22B**, 1194 (1983).

4) P. Jayaprasad Rao and K. Kondal Reddy, *Indian J. Chem.*, **22b**, 117 (1983).

5) G. Ramachandraiah and K. Kondal Reddy, *Indian J. Chem.*, **24B**, 808 (1985).

6) G. Ramachandraiah and K. Kondal Reddy, *Indian J. Chem.*, **24B**, 908 (1985).

7) T. Uro, K. Machida, and K. Hanai, *Chem. Pharm. Bull. Tokyo*, **14(7)**, 756 (1966).

8) Z. Carl, U.S. Patent 2609372; *Chem. Abstr.*, **48**, 746 (1954).

9) R. A. Abramovitch and E. P. Kyba, in the Chemistry of azido group, ed by Saul Patai, Interscience, London (1971), Chap. 5.

New Thiazolo[5,4-*d*]pyrimidines with Molluscicidal Properties

Khairy A. M. EL-BAYOUKI* and W. M. BASYOUNI
National Research Center, Dokki, Cairo, Egypt
(Received October 19, 1987)

Synopsis. Ethyl chloroformate/DMF mixture is used as a reagent for the facile ring closure of 5-amino-2-(ethylthio)-thiazole-4-carboxamide (**1a**) to afford an excellent yield of 2-ethylthiothiazolo[5,4-*d*]pyrimidin-7(6*H*)-one (**3**). The action of phosphoryl chloride on the latter product gave its 7-chloro derivative (**4**). The corresponding 7-(dicyanomethyl) (**5a**), 7-[cyano(ethoxycarbonyl)methyl] (**5b**), and 7-(substituted amino)derivatives (**6a—j**) are synthesized from reactions of malononitrile, ethyl cyanoacetate, and primary amines, respectively, with compound **4**. Most of the obtained products have been screened for activity against the intermediate host of schistosomiasis, *B. alexandrina* snails.

In connection with a program for preparing new purine and purine analogue derivatives with potentially useful biological properties,[1-3] the present paper reports the synthesis of some new thiazolo[5,4-*d*]pyrimidines and their molluscicidal effect.

Thus, when 5-amino-2-(ethylthio)thiazole-4-carboxamide (**1a**) was allowed to react with ethyl chloroformate/*N*,*N*-dimethylformamide (2 : 1), 2-(ethylthio)thiazolo[5,4-*d*]pyrimidin-7(6*H*)-one (**3**) was obtained in an excellent yield instead of the expected dione **2**. Compound **3** was found to be identical (mp and mixed mp) with the product obtained from the reaction of **1a** with triethyl orthoformate or from either **1a** or **1b** with formamide (2 h, 190 °C). Moreover, the ^{1}H NMR spectrum of **3** included a sharp signal at δ=8.24 representing H-5 of the thiazolopyrimidine nucleus,[4] and the mass spectrum of it observed M^+ 213 (100%). Such observations accord with structure **3** and exclude structure **2**.

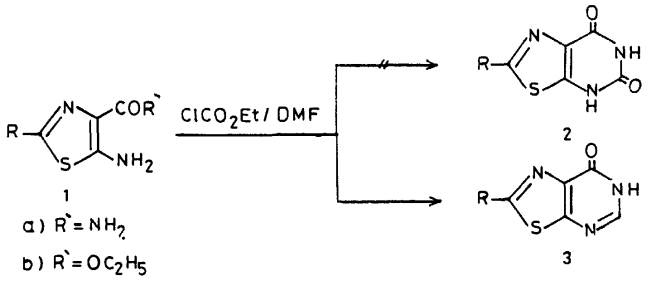

A possible mechanism consistent with this result is shown in Scheme 1. It involves the formation of intermediate **A** or **B** in the reaction medium, either of which can attack (or be attacked by) the 5-amino nitrogen of the thiazole system **1a** to give the intermediate **C** which in turn can eliminate dimethylamine leaving a formate residue for incorporating as C5 of the thiazolo[5,4-*d*]pyrimidin-7(6*H*)-one (**3**). The reaction under investigation, presumably, proceeds via intermediate formation of a Vilsmeier-Haack reagent.[5]

The present work employs product of type **3** for the synthesis of new 7-substituted 2-(ethylthio)thiazolo[5,4-*d*]pyrimidines required for biological screening as antischistosomal agents. Accordingly, 7-chloro-2-

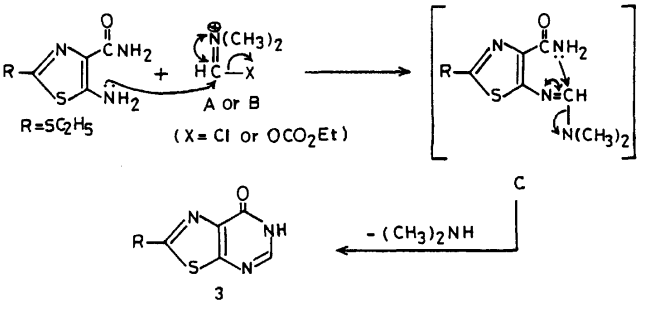

Scheme 1.

(ethylthio)thiazolo[5,4-*d*]pyrimidine (**4**) was prepared by the action of phosphoryl chloride on **3**. The chloro substituent of product **4** was easily replaced by the dicyanomethanide or the cyano(ethoxycarbonyl)methanide anion: reaction with malononitrile or ethyl cyanoacetate in DMSO and in presence of alkali gave the dinitrile **5a** and the nitrile ester **5b**,respectively. Treatment of **4** with primary amines in the presence of triethylamine likewise gave the corresponding 7-(substituted amino)-2-(ethylthio)thiazolo[5,4-*d*]pyrimidines (**6a—j**) in good yield.

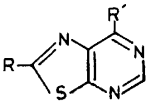

4, **5**, and **6**

R=SC_2H_5 for all cases.
4; R′=Cl.
5; R′=a) $CH(CN)_2$, and b) $CH(CN)CO_2Et$.
6; R′=a) $NHCH_3$, b) NHC_2H_5, c) $NHCH(CH_3)_2$,
d) $NHCH_2C_6H_5$,
e) NHC_6H_5, f) $NHC_6H_4CH_3$-*p*,
g) $NHC_6H_4OCH_3$-*p*,
h) NHC_6H_4Cl-*p*, i) NH-thiazolyl,
j) NH-CH_2-furyl.

Molluscicidal Activity. Snails: *Biomphalaria alexandrina*, the snail intermediate host of schistosomiasis, are used in this study. They are collected from

Table 1. Molluscicidal Activity of the Synthesized Products

Compound	% of mortality of adult snails/ppm			
	12.5	25	50	100 ppm
4	100	100	100	100
5a	0	50	100	100
5b	0	40	100	100
6a	15	25	100	100
6c	0	0	40	100
6e	30	70	100	100
6g	20	60	100	100
6i	0	25	100	100
6j	50	100	100	100

Table 2. Characterization of 7-(Substituted amino)-2-(ethylthio)thiazolo[5,4-*d*]pyrimidines (**6a—j**)

Compound	Mp/°C (solvent)	Yield %	Formula (Mol. wt.)	Analysis (%) Calcd (Found) C	H	N
6a	147—148 (ethanol)	79	$C_8H_{10}N_4S_2$ (226)	42.50 (42.50)	4.40 (4.10)	24.80 (24.40)
6b	79—81 (methanol)	67	$C_9H_{12}N_4S_2$ (240)	45.00 (44.60)	5.00 (5.20)	23.30 (23.30)
6c	89—91 (aqueous ethanol)	83	$C_{10}H_{14}N_4S_2$ (254)	47.20 (47.40)	5.50 (6.00)	22.00 (21.90)
6d	90—92 (methanol)	64	$C_{14}H_{14}N_4S_2$ (302)	55.60 (55.70)	4.60 (4.80)	18.50 (18.20)
6e	80—82 (aqueous ethanol)	72	$C_{13}H_{12}N_4S_2$ (288)	54.20 (54.50)	4.20 (4.40)	19.40 (19.60)
6f	103—105 (ethanol)	87	$C_{14}H_{14}N_4S_2$ (302)	55.60 (55.30)	4.60 (4.90)	18.50 (18.30)
6g	73—75 (ethanol)	76	$C_{14}H_{14}N_4OS_2$ (318)	52.80 (52.50)	4.40 (4.40)	17.60 (17.30)
6h	112—114 (ethanol)	75	$C_{13}H_{11}N_4ClS_2$ (322.5)	48.40 (48.40)	3.40 (3.70)	17.40 (17.60)
6i	89—90 (methanol)	82	$C_{10}H_9N_5S_3$ (295)	40.70 (40.50)	3.00 (3.10)	23.70 (23.80)
6j	85—87 (ethanol)	69	$C_{12}H_{12}N_4OS_2$ (292)	49.30 (49.60)	4.10 (4.10)	19.20 (19.30)

irrigation canals that were not already treated with molluscicides.

Exposure and recovery periods are 24 h each. Standard procedures are followed throughout this study.[6,7] Control experiments for each case are carried out. These experiments showed mortality of 0%. The results are recorded in Table 1.

From Table 1 the following comments are pointed out:

1. Most of the tested compounds showed a 100% snails mortality at 100 as well as at 50 ppm dilution.

2. For compounds **4**, **5a**, **6e**, and **6j** a 50—100% snails mortality is attained at 25 ppm dilution.

3. Compounds **4** and **6j** reached, comparatively to the others, the highly active status at 12.5 ppm.

Moreover, the activity showed by products **4** and **6j** is found to be stable >12.5 ppm to pH changes "4—10", temperature changes "10—30 °C", sun radiations, and high mud concentration media (up to 10000 ppm mud).

So, incorporating a chloro or furfurylamino residue on C7 of the thiazolo[5,4-*d*]pyrimidine ring system bearing ethylthio moiety on position 2 is recommended for obtaining antischistosomal agents with a stable activity against *B. alexandrina* snails.

Experimental

Melting points are uncorrected.

2-(Ethylthio)thiazolo[5,4-*d*]pyrimidin-7(6*H*)-one (3). A) A mixture of **1a** (2 g) (prepared from 5-amino-2-mercaptothiazole-4-carboxamide[8] and ethyl iodide) and ethyl chloroformate (5 ml) in *N,N*-dimethylformamide (7 ml) was left overnight at 25 °C. The reaction mixture was then diluted with water and the obtained solid was filtered off, washed with water, dried and crystallized from ethanol to give **3** (2 g, 95%), mp 184—6 °C.

B) When the same reaction was repeated under reflux for 5—10 min, **3** (77%) was obtained.

C) A solution of **1a** (2 g) in formamide (15 ml) was heated in an oil bath (180—190 °C) for 1 h. The solid which separated on cooling, was filtered off, washed with water, dried and crystallized from ethanol to give **3** (68%), undepressed on admixture with the product above.

D) When **1b** (2 g) was allowed to react in formamide as described above, **3** (65%) was obtained. (Found: C, 39.8; H, 2.9; N, 19.7%. Calcd for $C_7H_7N_3OS_2$: C, 39.4 ; H, 3.3; N, 19.7%. IR (KBr), ν/cm^{-1}; 3300—2600 (NH and SC_2H_5), 1715 (CO-NH). UV (ethanol) λ_{max}/nm ($\varepsilon\times10^{-3}$); 325 (7.55), 311 (10.90), 270 (7.07), 223 (14.15), 214 (15.33). ^{1}H NMR (DMSO-d_6), δ=1.4 (s, t, 3H, CH_3), 3.38 (s, q, 2H, CH_2), 8.25 (s, s, 1H, C-5), 12.4 (b, s, 1H, NH). MS: *m/z* 213 (100%).

7-Chloro-2-(ethylthio)thiazolo[5,4-*d*]pyrimidine (4). A mixture of **3** (5 g) and phosphoryl chloride (30 ml) was heated in an oil bath at 120—25 °C for 1.5 h. After cooling, the reaction mixture was poured onto crushed ice. The solid was filtered off, washed with water several times, dried, then crystallized from ethanol to give **4** (4 g, 73.6%) mp 73—5 °C. Found: C, 36.1; H, 2.9; N, 17.8%. Calcd for $C_7H_6N_3S_2Cl$: C, 36.3; H, 2.6; N, 18.1%. UV (ethanol) λ_{max}/nm ($\varepsilon\times10^{-3}$); 300 (18.10), 295(18.63), 241(9.76), 229(13.54), 208—202(10.35). ^{1}H NMR ($CDCl_3$) δ=1.5 (s, t, CH_3), 3.4 (s, q, 2H, CH_2), 8.63 (s, s, 1H, C-5).

α-[2-(Ethylthio)thiazolo[5,4-*d*]pyrimidin-2-yl]malononitrile (5a). A mixture of **4** (2.3 g), malononitrile (0.73 g), and potassium hydroxide (0.5 g in 2 ml water) in dimethyl sulfoxide (15 ml) is heated on a steam-bath for 1 h. After cooling, the reaction mixture was diluted with water and then treated with cold dilute acetic acid solution. The solid was filtered off, washed with water, dried, then crystallized from ethanol to give **5a** (1.9 g, 73%) mp 258—60 °C. Found: C, 46.1; H, 2.8; N,26.4%. Calcd for $C_{10}H_7N_5S_2$: C, 46.0; H, 2.7; N, 26.8%. IR (KBr) ν/cm^{-1}, 2220, 2200 (CN). UV (ethanol) λ_{max}/nm ($\varepsilon\times10^{-3}$), 343 (24.34), 261(17.11), 231(14.54), 201 (13.72). ^{1}H NMR (DMSO-d_6) δ=1.45 (s, t, 3H, CH_3), 3.17 (s, q, 2H, CH_2), 8.3 (s, s, 1H, C-5). MS *m/z* 261(100%).

Ethyl α-Cyano-α-[2-(ethylthio)thiazolo[5,4-*d*]pyrimidin-2-yl]acetate (5b). To a solution of **4** (2.34 g) in dimethyl sulfoxide (15 ml) it was added ethyl cyanoacetate (1.24 g) and potassium hydroxide (0.5 g in 2 ml water) and the solution was heated on a steam-bath for 1 h. After cooling, the reaction mixture was treated with cold dilute acetic acid to give a solid which was filtered off, washed with water, dried, then crystallized from 1-butanol to give **5b** (2.1 g, 67.5%), mp

Table 3. Spectral Properties of 7-(Substituted amino)-2-(ethylthio)thiazolo-[5,4-*d*]pyrimidines (**6a—j**)

Compound	IR (KBr) ν/cm^{-1} NH	UV (ethanol) (λ_{max}/nm ($\varepsilon\times10^{-3}$))	^{1}H NMR ($CDCl_3$) (δ values from TMS)	MS *m/z* (% intensity)
6a	3350	312 (10.66); 287 (13.18); 282 (12.30); 246 (16.97); 213 (14.71) and 207 (13.84)	1.5 (s, t, 3H, CH_3); 3—3.4 (s, m, 5H, CH_2, NCH_3); 6.1 (b, 1H, NH) and 8.43 (s, s, 1H, C-5).	226 (100)
6b	3460—3100	307 (10.04); 287 (15.82); 279 (15.82); 247 (17.84); 213 (13.72); 205(13.55).	1.15—1.17(s, m, 6H, $2CH_3$); 3.8—3.9 (s, m, 4H, $2CH_2$); 5.9(b, 1H, NH); 8.33 (s, s, 1H, C-5).	
6c	3400—3100	312.5 (11.10); 288 (14.80); 285 (14.09); 247 (18.13); 213 (14.57), 206 (14.24).	1.2—1.7 (s, m, 9H, $3CH_3$); 3.35 (s, q, 2H, CH_2; 4.6 (s, m, 1H, CH); 5.8 (b, 1H, NH); 8.46 (s, s, 1H, C-5).	
6d	3440—3130	311 (11.34); 289 (15.98); 284 (15.29); 248 (14.39); 205 (22.04).	1.4 (s, t, 3H, CH_3); 3.25 (s, q, 2H, CH_2); 4.8 (s, d, 2H, CH_2 of benzyl); 6.3 (b, 1H, NH); 7.4—8.0 (s, m, 5H, C_6H_5); 8.5(s, s, 1H, C-5).	
6e	3420—3100	310 (25.01); 265 (16.55); 214 (21.23); 204 (24.44).	1.45 (s, t, 3H, CH_3); 3.30 (s, q, 2H, CH_2); 7.30—8.0 (s, m, 6H, NH, C_6H_5); 85 (s, s, 1H, C-5).	
6f	3420—3240	309 (25.00); 263 (16.44); 214 (21.06); 204 (24.44).	1.45 (s, t, 3H, CH_3); 2.3 (s, s, 3H, CH_3); 3.3 (s, q, 2H, CH_2); 7.30—8.0(s, m, 5H, NH, C_6H_4); 8.5 (s, s, 1H, C-5).	
6g	3500—3050	309 (22.13); 267 (16.53); 214 (19.71); 204 (23.83).	1.45 (s, t, 3H, CH_3); 3.35 (s, q, 2H, CH_2); 3.80 (s, s, 3H, OCH_3); 7.30—7.90 (s, 5H, NH, C_6H_5); 8.47 (s, s, 1H, C-5).	318 (100)
6h	3400—3220	311 (22.02); 270 (16.34); 213 (19.60); 204 (23.55).	1.51 (s, t, 3H, CH_3); 3.40 (s, q, 2H, OH_2); 7.2—8.0 (s, m, 5H, NH, C_6H_4); 8.6 (s, s, 1H, C-5).	
6i	3440—3220	293 (23.02); 241 (11.86); 229 (17.06); 207 (12.68); 201 (12.98).	1.53 (s, t, 3H, CH_3); 3.50 (s, q, 2H, CH_2); 5.25 (b, 1H, NH); 6.45—7.02 (s, 2d, 2H, CH=CH); 8.8 (s, s, 1H, C-5).	
6j	3440—3140	308 (11.48); 287 (15.43); 280 (14.33); 246 (19.20); 214 (21.14).	143 (s, t, 3H, CH_3); 3.30 (s, q, 2H, CH_2); 4.90 (s, d, N, CH_2); 6.3—7.4 (s, m, 4H, NH, furyl); 8.45 (s, s, 1H, C-5).	

189—91 °C. Found: C, 46.6; H, 3.8; N, 17.9%. Calcd for $C_{12}H_{12}N_4O_2S_2$: C, 46.7; H, 3.9; N, 18.2%. IR(KBr) ν/cm^{-1}: 2210 (CN), 1650 (CO). UV (ethanol) λ_{max}/nm ($\varepsilon\times10^{-3}$), 348 (31.08), 263 (17.61), 229 (21.04), 202 (15.65). ^{1}H NMR (DMSO-d_6) δ=1.4 (s, m, 6H, $2CH_3$), 3.5 (s, q, 2H, CH_2), 4.3 (s, q, 2H, CH_2), 8.47 (s, s, 1H, C-5). MS *m/z* 308(100%).

7-(Substituted amino)-2-(ethylthio)thiazolo[5,4-*d*]pyrimidines (6). General Method: To a mixture of **4** (0.01 mol) and the desired primary amine (0.01 mol) in absolute ethanol (20 ml) it was added triethylamine (few drops), and the mixture was heated under reflux for 1 h. The solution was then concentrated and left to cool. The solid obtained was identified and characterized (cf. Tables 2 and 3).

References

1) Kh. A. M. El-Bayouki, E. N. Flemming, and B. P. Erik, *Synthesis*, **1985**, 104.

2) J. Frank, J. Anker, Kh. A. M. El-Bayouki, and B. P. Erik, *Chem. Scri.*, **26**, 337 (1986).

3) B. P. Erik, K. E. Andersen, Kh. A. El-Bayouki, and E. N. Flemming, Eur. Patent. Appl., EP 155,911; *Chem. Abstr.*, **104**, 186245c (1986).

4) M. Benedek-Vamos and R. Promei, *Tetrahedron Lett.*, **1969**, 1011; K. E. Andersen, M. Hammad, B. P. Erik, *Liebigs Ann. Chem.*, **1986**, 1255.

5) K. Ikawa, F. Takami, Y. Fukui, and K. Tokuyama, *Tetrahedron Lett.*, **1969**, 3279.

6) World Health Organization. Expert Committee on Bilharziasis. Control methods of molluscicides and other means of snails distruction. *Wld. Hlth. Org.*, **65**, 33—38 (1953).

7) World Health Org. Molluscicides Screening and evaluation, *Bull. Wld. Hlth. Org.*, **33**, 567—81 (1956).

8) A. H. Cook, I. Heilbron, and E. Smith, *J. Chem. Soc.*, **1949**, 1440.

 © 1988 The Chemical Society of Japan Bull. Chem. Soc. Jpn., 61, 3797—3800 (1988)

Theoretical Treatment of Solvent Effects on the Frequency Shifts of Fluorescence Spectra

Takehiro ABE
College of General Education, Tohoku University, Kawauchi, Sendai 980
(Received April 14, 1988)

A theoretical expression for the solvent fluorescence spectral shifts of a neutral solute molecule has been developed by following the same treatment as in Abe's expression for solvent absorption spectral shifts (*Bull. Chem. Soc. Jpn.*, **54**, 327 (1981); **58**, 3415 (1985)). Compared with all previous applicable expressions being applied to only polar solute molecules, the present expression has the advantage that it can be applied to not only the polar solute molecules but also nonpolar solute molecules. The polarizabilities of the ground and excited states concerning fluorescence are treated as being different from the corresponding values concerning absorption. Applications to nonpolar solute molecules are successfully presented.

Many theories have hitherto been proposed for solvent effects on the frequency shifts of fluorescence spectra.[1-10] All presented theoretical expressions are easily applicable except Liptay's.[4] Liptay's expression is so complicated that it is practically difficult to apply. Among the theoretical expressions, the first-appearing expression presented independently by Mataga et al.[1] and by Lippert[2] has been famous and frequently used. However, all these applicable expressions give no frequency shifts for nonpolar solute molecules having no dipole moments in both the ground and excited states, though some frequency shifts are, in fact, observed even for the nonpolar solute molecules in nonpolar solvents. In this case, the frequency shifts are obviously due to dispersion effects. Accordingly, the dispersion effects should be considered in the applicable theoretical expression for the solvent fluorescence frequency shift.

In this paper, therefore, an attempt has been made to present an expression for the solvent fluorescence spectral shift of a neutral solute molecule by explicitly considering the dispersion forces between the solute and solvent molecules on the basis of a previous theory[11] for the solvent absorption spectral frequency shift.

Theory

Fluorescence spectra of solutions are generally measured at very low concentrations of solutes. Let us, therefore, consider a system consisting of a spherical neutral solute molecule and N identical spherical neutral solvent molecules. The solvent molecules are assumed to form no hydrogen bonds or complexes with the solute and to have sufficiently small dipole moments so that they are not tightly oriented with respect to each other. In the fluorescence spectral measurements of solutes in solution, one usually chooses solvents that absorb light at much shorter wavelengths than the solutes do. One, therefore, assumes that the solvent molecules remain in their ground states when a transition from the ground state to the i-th excited state occurs in a solute molecule.

Then, one can write the ith electronic state of the system in the zeroth-order as

$$\Phi_i^\circ = \phi_i^A \prod_{s=1}^{N} \phi_0^s. \tag{1}$$

Here, the zeroth-order wave functions of ϕ_i^A and ϕ_0^s denote the i-th state of the solute and the ground state of the s-th solvent molecule, respectively. In the present paper, the suffices and shoulders of A and s denote the solute and the s-th solvent molecule, respectively. The energy of the i-th state of the system in which all the molecules interact with one another can be written by the second-order perturbation theory as

$$E_i = E_i^\circ + (\Phi_i^\circ|\boldsymbol{H}'|\Phi_i^\circ) + \sum_{m\neq i} \frac{(\Phi_m^\circ|\boldsymbol{H}'|\Phi_i^\circ)(\Phi_i^\circ|\boldsymbol{H}'|\Phi_m^\circ)}{E_i^\circ - E_m^\circ}, \tag{2}$$

where E_i° and E_m° are the unperturbed energies corresponding to Φ_i° and the m-th excited state, respectively, of the system, and $\boldsymbol{H}'$ is the perturbation due to interactions among the molecules in the system. The wave function and energy of the ground state of the system are obtained by replacing i by 0 in Eqs. 1 and 2, respectively.

From Ref. 11, one can write $\boldsymbol{H}'$ as

$$\boldsymbol{H}' = \boldsymbol{H}'_{As} + \boldsymbol{H}'_{st}, \tag{3}$$

where

$$\boldsymbol{H}'_{As} = \frac{1}{4\pi\varepsilon_0} \sum_{s=1}^{N} \boldsymbol{p}_A \cdot \boldsymbol{T}_{As} \cdot \boldsymbol{p}_s \tag{4}$$

and

$$\boldsymbol{H}'_{st} = \frac{1}{8\pi\varepsilon_0} \sum_{s=1}^{N} \sum_{t=1}^{N} \boldsymbol{p}_s \cdot \boldsymbol{T}_{st} \cdot \boldsymbol{p}_t. \tag{5}$$

Here, ε_0 is the permittivity of vacuum, $\boldsymbol{p}$ the operator of dipole moment, $\boldsymbol{T}_{As}$ the dipole-dipole interaction tensor of $R_{As}^{-3}(\boldsymbol{I}-3R_{As}^{-2}\boldsymbol{R}_{As}\boldsymbol{R}_{As})$, where $\boldsymbol{I}$ is a unit tensor, $\boldsymbol{R}_{As}$ the position vector from A to s, and t denotes the t-th solvent molecule.

When the wavenumbers of the fluorescence frequencies (cm^{-1}) of the solute molecule in vapor and in a solution are denoted by σ_{i0}° and σ_{i0}, respectively,

one obtains the following expression for the solvent fluorescence spectral frequency shift:

$$\sigma_{i0} - \sigma_{i0}^{\circ} = \frac{1}{hc}\{<E_i - E_i^{\circ}>_{av} - <E_0 - E_0^{\circ}>_{av}\}, \quad (6)$$

where c is the speed of light in vacuum, h Plank's constant, and $< >_{av}$ denotes the average over-all orientations of all the solvent molecules. In the calculation of $<E_i - E_i^{\circ}>_{av}$, terms containing powers higher than the sixth power of $1/R$ may always be neglected. Moreover, for convenience, common terms appearing in both $<E_i - E_i^{\circ}>_{av}$ and $<E_0 - E_0^{\circ}>_{av}$ may be omitted in a calculation of $<E_i - E_i^{\circ}>_{av}$.

Calculations of the terms of Eq. 6 will briefly be shown below. Using Eqs. 3—5, one can write:

$$(\Phi_i^{\circ}|\boldsymbol{H}'|\Phi_i^{\circ}) = \frac{1}{4\pi\varepsilon_0}\sum_{s=1}^{N}\boldsymbol{p}_{ii}^{A}\cdot\boldsymbol{T}_{As}\cdot\boldsymbol{p}_{00}^{s} + \frac{1}{8\pi\varepsilon_0}\sum_{s=1}^{N}\sum_{t=1}^{N}\boldsymbol{p}_{00}^{s}\cdot\boldsymbol{T}_{st}\cdot\boldsymbol{p}_{00}^{t}, \quad (7)$$

where $\boldsymbol{p}_{00}$ and $\boldsymbol{p}_{ii}$ are the ground and ith-excited state dipole moments, respectively. Accordingly, considering the Franck–Condon principle, one obtains:

$$\begin{aligned}
&<(\Phi_i^{\circ}|\boldsymbol{H}'|\Phi_i^{\circ})>_{av}\\
&=<(\Phi_i^{\circ}|\boldsymbol{H}'_{As}|\Phi_i^{\circ})\ \exp\{-(\Phi_i^{\circ}|\boldsymbol{H}'|\Phi_i^{\circ})/kT\}>_{av}\\
&+<(\Phi_i^{\circ}|\boldsymbol{H}'_{st}|\Phi_i^{\circ})\ \exp\{-(\Phi_i^{\circ}|\boldsymbol{H}'|\Phi_i^{\circ})/kT\}>_{av}\\
&\approx -\frac{1}{(4\pi\varepsilon_0)^2kT}\sum_{s=1}^{N}<(\boldsymbol{p}_{ii}^{A}\cdot\boldsymbol{T}_{As}\cdot\boldsymbol{p}_{00}^{s})(\boldsymbol{p}_{ii}^{A}\cdot\boldsymbol{T}_{As}\cdot\boldsymbol{p}_{00}^{s})>_{av}\\
&=-\frac{2(p_{00}^{s})^2(p_{ii}^{A})^2}{3(4\pi\varepsilon_0)^2kT}\sum_{s=1}^{N}\frac{1}{R_{As}^6}, \quad (8)
\end{aligned}$$

where k is Boltzmann's constant and T the thermodynamic temperature. In the same way, one obtains

$$\begin{aligned}
&<(\Phi_0^{\circ}|\boldsymbol{H}'|\Phi_0^{\circ})>_{av}\\
&=<(\Phi_0^{\circ}|\boldsymbol{H}'|\Phi_0^{\circ})\ \exp\{-(\Phi_i^{\circ}|\boldsymbol{H}'|\Phi_i^{\circ})/kT\}>_{av}\\
&\approx -\frac{2(p_{00}^{s})^2(\boldsymbol{p}_{00}^{A}\cdot\boldsymbol{p}_{ii}^{A})^2}{3(4\pi\varepsilon_0)^2kT}\sum_{s=1}^{N}\frac{1}{R_{As}^6}. \quad (9)
\end{aligned}$$

On the other hand, the calculation of the average value of the second term of Eq. 2 is quite the same as in the case of the absorption.[11] Thus, following the procedure given in Refs. 11 and 12, one finally obtains the following expression for the fluorescence frequency in solution:

$$\begin{aligned}
\sigma_{i0} = \sigma_{i0}^{\circ} &+ \frac{\pi}{hc}\left(\frac{4\pi L}{3}\right)^{2/3}\times\frac{(d^s/M_r^s)^{2/3}(p_{00}^{s})^2}{(r_A+r_s)^4}\\
&\times\left[\frac{2\{(\boldsymbol{p}_{00}^{A}\cdot\boldsymbol{p}_{ii}^{A})-(p_{ii}^{A})^2\}}{3(4\pi\varepsilon_0)^2kT}+\frac{(\alpha_{00,F}^{A}-\alpha_{ii,F}^{A})}{4\pi\varepsilon_0}\right]\\
&+\frac{\pi}{hc(4\pi\varepsilon_0)}\left(\frac{4\pi L}{3}\right)^{2/3}\times\frac{(d^s/M_r^s)^{2/3}\alpha_{00}^{s}}{(r_A+r_s)^4}\\
&\times[\{(p_{00}^{A})^2-(p_{ii}^{A})^2\}+\frac{3}{2}\\
&\times\frac{I_0^s\cdot I_0^A}{I_0^s+I_0^A}(\alpha_{00,F}^{A}-\alpha_{ii,F}^{A})], \quad (10)
\end{aligned}$$

where L is Avogadro's constant, M_r the relative molecular mass, d the density, α_{00} and α_{ii} are the electric isotropic polarizabilities of the ground and excited states, respectively, and r is the radius of a spherical molecule. The suffix F for $\alpha_{00,F}^{A}$ and $\alpha_{ii,F}^{A}$ means that these polarizabilities are not those concerning the absorption, but those concerning the fluorescence (for the reason mentioned below). In Eq. 10, the average transition energy for all transitions from the ground state or the i-th excited state to all other excited states is assumed to be equal to the ionization potential of the ground state (I_0), as shown in Ref. 12.

According to only Eq. 10, it is practically impossible to evaluate three values for p_{00}^{A}, p_{ii}^{A} and $(\alpha_{00,F}^{A}-\alpha_{ii,F}^{A})$ from data for the solvent fluorescence spectral shifts. In order to apply Eq. 10 for the fluorescence, therefore, the dipole moments of the ground and i-th excited states appearing in Eq. 10 must be assumed to be equal to the corresponding dipole moments concerning the absorption, as is usually assumed in all previous theories for fluorescence. This assumption will be approximately fulfilled, if the nuclear equilibrium configuration of the i-th excited state does not significantly differ from that of the ground state. Then, the dipole moments appearing in Eq. 10 must be estimated in advance from data for the solvent absorption spectral shifts according to an expression for the solvent absorption spectral shift. Of course, in the case of a nonpolar solute molecule, values for σ_{i0}° and $(\alpha_{00,F}^{A}-\alpha_{ii,F}^{A})$ can be estimated according to Eq. 10.

The isotropic polarizability of the i-th excited state of the solute molecule is written as $\alpha_{ii}^{A}=\{2/3(4\pi\varepsilon_0)\}\times\sum_{j\neq i}|\boldsymbol{\mu}_{ij}^{A}|^2/(E_j^{A}-E_i^{A})$, where $\boldsymbol{\mu}_{ij}^{A}$ is the transition dipole moment from the i-th state to the j-th excited state. Here, we will discuss whether or not the ground- and excited-state polarizabilities concerning the fluorescence are equal to the corresponding values concerning the absorption.

First, for the present purpose we consider the value of $\boldsymbol{\mu}_{ij}^{A}$ according to the conventional treatment of Orlandi and Siebrand[13] for the Herzberg-Teller coupling mechanism as follows. Here, the vibronic state involved in the transition of the solute molecule is written as

$$\psi_{iv}(q,Q) = \phi_i(q,Q)\chi_v^{(i)}(Q), \quad (11)$$

where q and Q denote the sets of electronic and nuclear coordinates, respectively, so that i is an electronic quantum number and v a vibrational one. Then, according to Orlandi and Siebrand,[13] the transition dipole moment from $\psi_{iv}(q,Q)$ to $\psi_{jw}(q,Q)$ (where j and w are the electronic and vibrational

quantum numbers, respectively) is approximately given by

$$\begin{aligned}\mu_{ij,vw} &= \langle \chi_v^{(i)} | P_{ij}(Q) | \chi_w^{(j)} \rangle \\ &\approx P_{ij}(Q_0) \langle \chi_v^{(i)} | \chi_w^{(j)} \rangle \\ &+ \sum_k [\sum_l (\langle \phi_j | P | \phi_l \rangle \langle \phi_l | \partial / \partial Q_k | \phi_i \rangle)_{Q_0} \\ &\times (\hbar / 2\mu_k \omega_k)^{1/2}] \times \langle \chi_{w'}^{(j)} | \chi_v^{(i)} \rangle, \end{aligned} \quad (12)$$

where

$$P_{ij}(Q) = \langle \phi_i | P | \phi_j \rangle; \; P = \sum_\mu e r_\mu, \quad (13)$$

r_μ being the position vector of the μ-th electron in the solute molecule, μ_k and ω_k denoting the reduced mass and angular frequency of induced mode k, respectively, and w' denoting the ω value in which mode k is excluded. Moreover, Q_0 is a nuclear equilibrium configuration, about which $P_{ij}(Q)$ is expanded. In the case of the absorption, Q_0 should be a nuclear equilibrium configuration of the ground state and in the case of fluorescence, Q_0 should be an equilibrium configuration of the i-th excited state.

Equation 12 shows that the value of μ_{ij} varies with both the nuclear equilibrium configuration and the vibrational quantum number v in the i-th state, even if $P_{ij}(Q_0)=0$ for forbidden electronic transitions. Accordingly, the value of $|\mu_{ij}^A|^2$ involved in the expression for the polarizability will vary with the equilibrium configuration and the vibrational quantum number v. Moreover, the polarizability of the i-th state will vary with the vibrational quantum number v through the change of the value of $1/(E_j^A - E_i^A)$ with v, because the E_i^A value varies with v. After all, the polarizability of the i-th state will vary with its equilibrium configuration and vibrational quantum number. In the same i-th electronic state, both the vibrational quantum number and equilibrium configuration of the vibronic state concerning the fluorescence may differ from the corresponding values of the vibronic state concerning absorption. These differences between the two vibronic states will cause differences between the polarizabilities of the vibronic states. Thus, the polarizabilities of the ground and i-th excited states concerning fluorescence will differ from the corresponding values concerning absorption. For this reason, the polarizabilities concerning fluorescence are clearly denoted by the subscript F in Eq. 10.

The transition energies (in cm^{-1}) of the solute molecule from the ground state to the i-th excited state in vapor and in a solution are denoted by σ_{0i}° and σ_{0i}, respectively. The polarizabilities of the ground and i-th excited states concerning absorption are denoted by $\alpha_{00,A}^A$ and $\alpha_{ii,A}^A$, respectively. For a nonpolar solute molecule having no dipole moments in both the ground and excited states, values for σ_{0i}° and $\alpha_{ii,A}^A$ can be obtained from data for the solvent absorption spectral shifts according to Ref. 12. By applying Eq. 10 to data for the solvent fluorescence spectral shifts of a nonpolar molecule, values for σ_{i0}° and $(\alpha_{00,F}^A - \alpha_{ii,F}^A)$ can be obtained by the least-squares method. On the other hand, for a polar solute molecule, values for p_{ii}^A and $\alpha_{ii,A}^A$ ought to be obtained in advance (according to Ref. 12) on the condition that the σ_{0i}° value is known. Then, by using the p_{ii}^A value, values for σ_{i0}° and $(\alpha_{00,F}^A - \alpha_{ii,F}^A)$ can be obtained by means of a least-squares analysis of data for the solvent fluorescence spectral shifts, according to Eq. 10.

Applications

Equation 10 improves on a weak point of all the previous expressions which can not be applied to nonpolar solute molecules. In this paper, therefore, examples of the applications of Eq. 10 to only nonpolar solute molecules of anthracene, *all-trans*-1,3,5,7-octatetraene and pyrazine will been shown below, although Eq. 10 was also successfully applied to some polar solute molecules.

In applying Eq. 10, as well as the expression for the absorption in Ref. 12, to nonpolar solute molecules, the temperature was always assumed to be 20 °C. All values used for $\alpha_{00,A}^A$ and α_{00}^s were calculated from values for molar refraction, which were obtained by summing up bond refractions. The calculations of r_A and r_s were made in the same way as in Ref. 12. The gas-phase dipole moments of solvent molecules and the ionization potentials of all the solute and solvent molecules, except octatetraene, were taken from the usual chemical handbooks. Only the ionization potential of the ground state of an octatetraene molecule having four conjugated double bonds was estimated to be 8.22 eV (1 eV=1.602×10^{-19} J) in the same way as in the case of a lycopene molecule,[12] since no observed ionization potential value for the molecule was found. The author excluded data for solvents lacking information regarding their ground-state dipole moments and ionization potentials and for solvents which are capable of forming hydrogen bonds and complexes with solutes.

According to the procedure described above, the expression for the absorption in Ref. 12 and Eq. 10 were applied to data for the solvent absorption- and fluorescence-spectral shifts, respectively, of anthracene,[14] *all-trans*-1,3,5,7-octatetraene[15] and pyrazine.[6] Values estimated for σ_{0i}°, σ_{i0}°, $(\alpha_{ii,A}^A - \alpha_{00,A}^A)$ and $(\alpha_{ii,F}^A - \alpha_{00,F}^A)$ are listed in Table 1. By using these values, values for σ_{0i} and σ_{i0} were calculated and compared with the corresponding observed values, as shown in Fig. 1. This figure shows that the correlation between the observed and calculated values of σ_{0i} and σ_{i0} is good.

Table 1 shows that the present values for σ_{0i}° and σ_{i0}° roughly approach the corresponding observed values. As shown in Table 1, the estimated value of $(\alpha_{ii,A}^A - \alpha_{00,A}^A)$ for anthracene agrees well with the observed values measured by electric field tech-

Table 1. Differences in Polarizabilities between the Ground- and Excited-States of Nonpolar Molecules

	Anthracene	*trans*-1,3,5,7-Octatetraene	Pyrazine
$\sigma^{\circ}_{0i}/cm^{-1}$	27470	34785	31460
(Obsd)	(27560)[a]	(35523)[b]	(30870)[c]
$(\alpha^{A}_{ii,A}-\alpha^{A}_{00,A})/10^{-24}$ cm^3	18.5	36.71	−2.35
(Obsd)	(16.7±2.3)[d]		
$\sigma^{\circ}_{i0}/cm^{-1}$	27580	25666	29280
(Obsd)	(27380)[a]		
$(\alpha^{A}_{ii,F}-\alpha^{A}_{00,F})/10^{-24}$ cm^3	25.1	6.90	2.76

a) Ref. 14. b) Ref. 15. c) Ref. 16. d) Refs. 17 and 18.

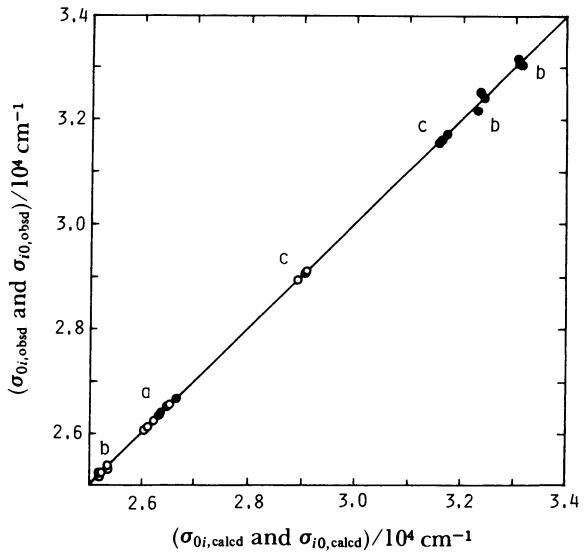

Fig. 1. Correlation between the observed and calculated values of σ_{0i} (●) and σ_{i0} (○), for anthracene (a), *all-trans*-1,3,5,7-octatetraene (b) and pyrazine (c).

niques.[17,18] The present result of $\alpha^{A}_{00,A}>\alpha^{A}_{ii,A}$ for pyrazine is probably due to the great contribution of the $|\mu_{i0}|^2/(E^{A}_{0}-E^{A}_{i})$ term to the $\alpha^{A}_{ii,A}$ value, since $(E^{A}_{0}-E^{A}_{i})<0$ in this case. Table 1 shows that the values for $(\alpha^{A}_{ii,F}-\alpha^{A}_{00,F})$ are considerably different from the corresponding values for $(\alpha^{A}_{ii,A}-\alpha^{A}_{00,A})$. This means that the ground- and excited-state polarizabilities concerning fluorescence are considerably different from the corresponding values concerning absorption. In the case of octatetraene, the absorption band is the 0–0 band. Therefore, the estimated value (51.51×10^{-24} cm^3) for $\alpha^{A}_{ii,A}$ is equal to $\alpha^{A}_{ii,F}$. In this case, therefore, the value for $\alpha^{A}_{00,F}$ can be estimated to be 44.61×10^{-24} cm^3, which is much greater than the $\alpha^{A}_{00,A}$ value (14.80×10^{-24} cm^3).

References

1) N. Mataga, Y. Kaifu, and M. Koizumi, *Bull. Chem. Soc. Jpn.*, **28**, 690 (1955); **29**, 465 (1956).
2) E. Lippert, *Z. Naturforsch.*, **10a**, 541 (1955); *Z. Elektrochem.*, **61**, 962 (1957).
3) N. G. Bakhshiev, *Opt. Spektrosk.*, **10**, 717 (1961); **16**, 821 (1964).
4) V. L. Bilot and A. Kawski, *Z. Naturforsch.*, **17a**, 621 (1962).
5) W. Liptay, *Z. Naturforsch.*, **20a**, 1441 (1965).
6) H. Baba, L. Goodman, and P. C. Valenti, *J. Am. Chem. Soc.*, **88**, 5410 (1966).
7) A. Chamma and P. Viallet, *C. R. Acad. Sci. Paris, Sec. C*, **270**, 1901 (1970).
8) Yu. T. Mazurenko and N. G. Bakhshiev, *Opt. Spektrosk.*, **28**, 905 (1970); Yu. T. Mazurenko, *Opt. Spectrosk.*, **55**, 277 (1983).
9) P. Suppan, *Chem. Phys. Lett.*, **94**, 272 (1983); P. Suppan and E. Guerry-Butty, *J. Lumin.*, **33**, 335 (1985).
10) B. S. Brunschwig, S. Ehrenson, and N. Sutin, *J. Phys. Chem.*, **91**, 4714 (1987).
11) T. Abe, *Bull. Chem. Soc. Jpn.*, **54**, 327 (1981).
12) T. Abe and I. Iweibo, *Bull. Chem. Soc. Jpn.*, **58**, 3415 (1985).
13) G. Orlandi and W. Siebrand, *J. Chem. Phys.*, **58**, 4513 (1973).
14) M. Koizumi, "Koukagaku Gairon (Introduction of Photochemistry)," Asakura Shoten, Tokyo (1963), p. 163.
15) R. W. Gavin, Jr., C. Weisman, J. K. MoVey, and S. A. Rice, *J. Chem. Phys.*, **68**, 522 (1978).
16) S. F. Mason, *J. Chem. Soc.*, **1959**, 1240.
17) W. Liptay, G. Walz, W. Bauman, H.-J. Schlosser, H. Deckers, and N. Detzer, *Z. Naturforsch.*, **26a**, 2020 (1971).
18) R. Mathies and A. C. Albrecht, *J. Chem. Phys.*, **60**, 2500 (1974).

 © 1988 The Chemical Society of Japan Bull. Chem. Soc. Jpn., 61, 3801—3805 (1988)

Classification of DNA Sequences by Hayashi's Quantification (III) Method. Sequences Involving 5′-Splice Signals in Pre-mRNA of Higher Eukaryotes' Genes

Yôichi IIDA
Department of Chemistry, Faculty of Science, Hokkaido University, Sapporo 060
(Received April 15, 1988)

Concerning the signals which direct the excision of introns from mRNA precursors in higher eukaryotes' genes, a consensus sequence, $\overset{C}{\underset{A}{}}AG/GT\overset{}{\underset{}{G}}$AGT, has been proposed with a 5′-splice site, but actual 5′-splice site sequences differ from it to a greater or lesser degree. In the present paper, we took a set of 1751 sequences, which are composed of 9-nucleotide sequences including 5′-splice signals and of other sequences including no such signals. Hayashi's quantification analysis (Class III) was applied to such a system. Assuming no external criterion for 5′-splice signals, we examined how the 1751 sequences show responses to the positions and species of nucleotides. The optimum classification led to a fair separation of the 5′-splice signal sequences from sequences including no such signals. The results were compared with those derived previously by the use of the quantification (Class II) method.

Many eukaryotic genes are interrupted by introns, which have been removed from the mRNA precursors (pre-mRNAs) by the use of the RNA splicing mechanism. It became clear that the splicing pathway could be divided into two stages. In the first stage, the pre-mRNA is cleaved at the 5′-splice site of the intron, generating the first exon and a species composed of the intron and the following exon. The latter intermediate is present in a lariat form, where the 5′-end of the intron is joind by a 2′–5′ phosphodiester linkage to an A residue upstream of the 3′-splice junction. The sequence encompassing the A residue is called "the branch-point sequence". The second stage involves cleavage at the 3′-splice site and ligation of the exons, with a concomitant release of the intron lariat. Both stages are related to several reactions which occur in a large multicomponent complex termed a "spliceosome". Small nuclear ribonucleoprotein particles (snRNPs) including U1, U2, U4—6 are important components of the spliceosome (for reviews, see Refs. 1—3).

Nucleotide sequences defining 5′- and 3′-splice junctions in pre-mRNAs have been found to share considerable homology in higher eukaryotes.[4] In the case of 5′-splice sites, a consensus sequence, 5′-(exon)-$\overset{C}{\underset{A}{}}AG/GT\overset{}{\underset{}{G}}$AGT-(intron)-3′, has been known, where the stroke (/) indicates the boundary between exon and intron. However, this is only a qualitative description of the splice signal. The consensus sequence cannot tell what degree of matching between the observed sequence and the consensus sequence is necessary to specify the exact splice site. Another major problem involves the relative importance of each of the nucleotides in the sequence. That is, mutational studies have demonstrated that the importance of nucleotide matching to the consensus sequence differs from position to position. For example, a few positions, such as the G at the 5′- end of intron, are absolutely necessary, while mutations in the other positions, though they reduce the efficiency of correct splicing, sometimes do not affect correct splicing seriously.[5,6] In order to study such splice signals more quantitatively and to ascertain the relative importance of each of the nucleotides, we previously studied multivariate statistical analysis and then performed Hayashi's quantification analysis (Class II).[7,8] For this purpose, we took 1751 samples of the 9-nucleotide sequences belonging to either of two groups. Group 1 is composed of sequences including 5′-splice signals, while sequences of Group 2 include no such signals. In the Class II analysis, using external criterion for the 5′-splice signals, we searched for the optimum condition under which sequences of the two groups could be discriminated most distinctly; we also determined the optimum weights for the position and species of nucleotides.

In the present paper, we utilizes another approach of Hayashi's quantification analysis (Class III)[9,10] to the same set of 1751 sequences. In contrast to the Class II method, the Class III method distributes the total of 1751 sequences most distinctly and determines the optimum weights for the position and species of nucleotides, assuming an absence of external criterion as to whether a sequence may belong to the 5′-splice sequence or not. It was found that the classification by this technique could well separate the sequences of Group 1 from those of Group 2. This approach enables us, to a considerable extent, to characterize 5′-splice site sequences in terms of position and species of nucleotides, even if there is no external criterion for 5′-splice signals.

Analysis by Quantification (III) Method

The nucleotide sequence data used in the present paper are the same as those used by quantification (Class II) in a previous paper.[7] In Table 1, some of the 9-nucleotide sequences are reproduced. Here, sequences belonging to Group 1 include 5′-splice signals, where nine nucleotides (composed of three at the 3′-end of the exon and six at the 5′-end of the intron) are

truncated in each sequence. In the group, we summarized 155 sequences (i_1=1, 2, ···, 155), which were taken from authentic 5′-splice site sequences in various mammalian genes containing introns: globin genes, insulin genes, etc.[11] On the other hand, Group 2 is composed of sequences other than the 5′-splice site. Those sequences were taken from the human β-globin gene, as was described in the previous paper.[7] Excluding the two sequences of the authentic 5′-splice sites in the β-globin, we gave 1596 sequences (i_1=156, 157, ···, 1751) composed of 9-nucleotides in Group 2. Therefore, a total of N_1=1751 sample sequences (i_1=1, 2, ···, N_1) are summarized in Table 1.

In constrast to the Class II analysis, the Class III method does not use the criterion of Groups 1 and 2, but examines how uniquely the 1751 sequences respond to items and categories.[9,10] This method is similar to the dual scaling approach of Maung and Guttman.[12,13] In our case, there are nine items, identified k=1, 2, ···, 9. They correspond to the positions of nucleotides in the 9-nucleotide sequence, being defined in terms of their order from the 5′ to 3′ ends of the sequence. On the other hand, the category denotes the kind of nucleotide, where A, G, C, or T is specified by α=1, 2, 3, or 4 respectively at every item.

Table 1. Some of the 9-Nucleotide Sequences Belonging to Group 1 and Group 2[a]

No.	Group	Sequence	Gene
1	1	GAGGTGAGG	Human alpha-Globin
2	1	AAGGTGAGC	
3	1	CAGGTTGGT	Human beta-Globin
4	1	AGGGTGAGT	
:	:	:	
155	1	AGGGTGAGC	Dog Insulin
156	2	ACATTTGCT	Human beta-Globin
157	2	CATTTGCTT	
:	:	:	
1751	2	TTTCATTGC	

a) Group 1 is composed of 5′-splice site sequences, while Group 2 is composed of sequences other than 5′-splice sites. For further details, see text.

We introduce a running suffix $i_2=4(k-1)+\alpha$, (i_2=1, 2, ···, N_2; N_2=36), and transform the sequence data of Table 1 into the item-category data by using a dummy variable, $n(i_1, i_2)$. It takes a value of 1 if the sample sequence (i_1) has a nucleotide (α) at the position (k), but otherwise it takes 0. Such item-category data are shown in Table 2.

The Class III method rearranges sample sequences and item-categories in such a way that sample sequences showing similar responses to items and categories are gathered together. If we obtain the optimum condition for this, we can find what responses to items and categories are similar to each other. Moreover, we can classify not only items and categories, but also sample sequences in the most characteristic way. For this purpose, let us give the quantity $x(i_1)$ to the i_1-th sample sequence (i_1=1, 2, ···, N_1) and a quantity $y(i_2)$ to the i_2-th item-category ($i_2=4(k-1)+\alpha$; i_2=1, 2, ···, N_2). Then we introduce the correlation coefficient, $r(X, Y)$, by the use of

$$r(X,Y) = V(X,Y)/\{S(X)S(Y)\}, \tag{1}$$

$$V(X,Y) = (1/N)\sum_{i_1=1}^{N_1}\sum_{i_2=1}^{N_2} x(i_1)y(i_2)n(i_1,i_2) - \bar{x}\bar{y}, \tag{2}$$

$$S(X) = \{(1/N)\sum_{i_1=1}^{N_1} x(i_1)^2 n_1(i_1) - (\bar{x})^2\}^{1/2}, \tag{3}$$

$$S(Y) = \{(1/N)\sum_{i_2=1}^{N_2} y(i_2)^2 n_2(i_2) - (\bar{y})^2\}^{1/2}, \tag{4}$$

where;

$$N = \sum_{i_1=1}^{N_1}\sum_{i_2=1}^{N_2} n(i_1,i_2), \tag{5}$$

$$\bar{x} = (1/N)\sum_{i_1=1}^{N_1} x(i_1)n_1(i_1), \tag{6}$$

$$\bar{y} = (1/N)\sum_{i_2=1}^{N_2} y(i_2)n_2(i_2), \tag{7}$$

$$n_1(i_1) = \sum_{i_2=1}^{N_2} n(i_1,i_2), \tag{8}$$

$$n_2(i_2) = \sum_{i_1=1}^{N_1} n(i_1,i_2). \tag{9}$$

In order to classify sample sequences together with items and categories most distinctly, we maximize $|r(X, Y)|$. That is, if the correlation coefficient

Table 2. Categorical Data to be Used in Hayashi's Quantification Analysis (Class III)[a]

No.	Group	Item 1				Item 2				···	Item 9			
		Category				Category					Category			
		1	2	3	4	1	2	3	4		1	2	3	4
1	1	0	1	0	0	1	0	0	0	···	0	1	0	0
2	1	1	0	0	0	1	0	0	0	···	0	0	1	0
:	:			:				:					:	
155	1	1	0	0	0	0	1	0	0	···	0	0	1	0
156	2	1	0	0	0	0	0	1	0	···	0	0	0	1
:	:			:				:					:	
1751	2	0	0	0	1	0	0	0	1	···	0	0	1	0

a) For the 9-nucleotide sequences given in Table 1, the position of nucleotide (item) and the kind of nucleotide (category) are specified with a dummy variable (0 or 1). In the Class III analysis, the item number (k) and the category number (α), where k=1, 2, ···, 9 and α=1, 2, 3, 4, are further combined into a parameter: $i_2=4(k-1)+\alpha$, where i_2=1, 2, ···, 36. For further details, see text.

approaches 1, the arrangements of $n(i_1, i_2)=1$ versus i_1 and i_2 become linear. In this case, the (i_1) sequence may be well characterized by the item-category (i_2). The maximization of $|r(X, Y)|$ can be done by differentiating:

$$\partial r(X, Y)^2/\partial x(i_1) = 0, \quad (i_1 = 1, 2, \cdots, N_1), \tag{10}$$
$$\partial r(X, Y)^2/\partial y(i_2) = 0, \quad (i_2 = 1, 2, \cdots, N_2), \tag{11}$$

where we can put $\bar{x}=0$ and $\bar{y}=0$ without loss of generality. These equations lead to:

$$\sum_{i_2'=1}^{N_2}\sum_{i=1}^{N_1} n(i, i_2)n(i, i_2')y(i_2')/n_1(i) = r(X, Y)^2 n_2(i_2)y(i_2), \quad (i_2 = 1, 2, \cdots, N_2), \tag{12}$$

$$x(i_1) = \{1/r(X, Y)\}\sum_{j=1}^{N_2} n(i_1, j)y(j)/n_2(j), \quad (i_1 = 1, 2, \cdots, N_1). \tag{13}$$

Eq. 12 can be solved by eigen value problem with the aid of computer calculation. It has the maximum eigen value of 1. However, this value is a trivial solution and is excluded, because it gives an inadequate value of $\bar{y}=(1/N)\sum_{i_2=1}^{N_2} y(i_2)n_2(i_2)\neq 0$. Therefore, we take the second largest eigen value of $r(X, Y)^2$. This value, together with Eq. 12, leads to the eigen vector of $\boldsymbol{y}_2=\{y(12), \cdots, y(i_2 2), \cdots, y(N_2 2)\}^t$, where the suffix 2 corresponds to the second largest eigen value and where the superscript t indicates the transposition of the vector. From $\boldsymbol{y}_2$ together with Eq. 13, we can obtain the eigen vector of $\boldsymbol{x}_2=\{x(12), \cdots, x(i_1 2), \cdots, x(N_1 2)\}^t$. If we arrange the components of $\boldsymbol{x}_2$ and $\boldsymbol{y}_2$ in the order of their magnitudes, we can classify not only items and categories, but also sample sequences most distinctly.

In a similar way, if we obtain the third and fourth largest eigen values of Eq. 12, we can calculate the corresponding eigen vectors: $\boldsymbol{y}_3$, $\boldsymbol{y}_4$, and $\boldsymbol{x}_3$, $\boldsymbol{x}_4$. If a sample sequence i_1, $(i_1=1, 2, \cdots, N_1)$, is plotted by the use of the coordinate of $\{x(i_1 2), x(i_1 3)\}$, we can map sample sequences on a two-dimensional graph most distinctly. It is also possible to distribute the items and categories i_2, $(i_2=1, 2, \cdots, N_2)$, in the most characteristic way by plotting $\{y(i_2 2), y(i_2 3)\}$.

Results and Discussion

For the item-category data of Table 2, the second, third, and fourth largest eigen values of $r(X, Y)^2$ were calculated as 0.2155, 0.1571, and 0.1511 respectively. From Eq. 12, we estimated the components of $\boldsymbol{y}_2$, $\boldsymbol{y}_3$ and $\boldsymbol{y}_4$ (normalized item-category scores), where the variance of the components was normalized to unity. In view of the magnitudes of $r(X, Y)^2$, the vector of $\boldsymbol{y}_2$ distinguishes item-categories and sample sequences most strongly, while the vectors of $\boldsymbol{y}_3$ and $\boldsymbol{y}_4$ have less distinguishing power. The degree of distinction by $\boldsymbol{y}_3$ is almost the same as that by $\boldsymbol{y}_4$. Such normalized scores are summarized for item (k) and category (α), where $i_2=4(k-1)+\alpha$, $(i_2=1, 2, \cdots, 36)$. For example, we give in Fig. 1 a graph of normalized item-category scores obtained by plotting $\{y(i_2 2), y(i_2 3)\}$ with $i_2=1, 2, \cdots, 36$. This graph corresponds to the second and third largest eight values and shows the most distinct distribution among item-categories, where some form a cluster. For item-categories $(k-\alpha)$, (4–2), (3–2), (8–2), (7–1), (2–1), (6–2), (5–4), (6–1), (1–1), and (1–3) form a cluster and show relatively high scores in the direction of the second largest eigen value. These item-categories come from G at the fourth position, G at the third position, G at the eighth position, A at the seventh position, A at the second position, G at the sixth position, T at the fifth position, A at the sixth position, A at the first position, and C at the first position respectively in the 9-nucleotide sequence of Table 1. These nucleotides and positions coincide well with the consensus sequence $\overset{C}{A}AG/GT\overset{A}{G}AGT$ proposed by Mount,[4] possessing a strong power to distinguish the 5′-splice site sequence. From the magnitudes of the $y(i_2 2)$ values, G at the fourth position seems to be most effective. This result may correspond to the invariant G nucleotide at the 5′-end of every intron. As is shown in Fig. 1, the item-categories other than those due to the consensus

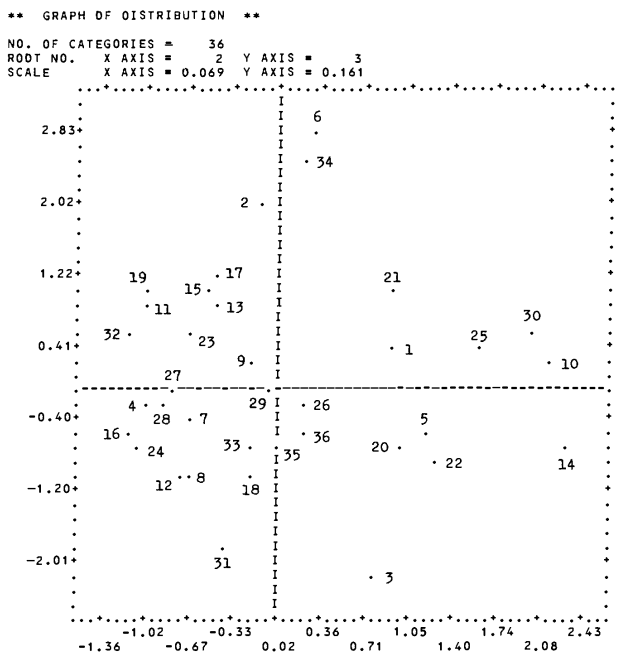

Fig. 1. Two-dimensional mapping of item-categories in Hayashi's quantification analysis (Class III) of 1751 members of 9-nucleotide sequences given in Tables 1 and 2. Abscissa shows normalized score of $y(i_2 2)$, which is calculated from the second largest eigen value of Eq. 12. Ordinate shows normalized score of $y(i_2 3)$ calculated from the third largest eigen value. Parameter i_2, $(i_2=1, 2, \cdots, 36)$, is related to item (k) and category (α) by $i_2=4(k-1)+\alpha$. Note that points of $i_2=1, 3, 5, 10, 14, 20, 21, 22, 25$, and 30 form a cluster. For further details, see text.

sequence form another cluster. Althogh some of them are located around the positive region of $y(i_2 2)$, most of the item-categories other than the consensus sequence lie in the negative region of $y(i_2 2)$. It appears that they make negative contribution to 5′-splice site signals.

Next let us examine how uniquely the 1751 sequences respond to the positions and species of nucleotides. For this purpose, we will calculate the sample scores of $x(i_1 2)$, $x(i_1 3)$ and $x(i_1 4)$, (i_1=1, 2, ···, N_1). As was mentioned above, the sample score of $x(i_1 2)$ can classify the 1751 sequences most distinctly. Therefore, we first arranged their $x(i_1 2)$ values in the order of their magnitudes, as is shown in Fig. 2. Here, we categorized the sample scores at appropriate equal intervals, and constructed a graph of the distribution and the frequency percentage versus the categorized sample score ($z=x(i_1 2)$) for the 1751 members of the 9-nucleotide sequences shown in Table 1. For the sake of comparison, the lower half of the graph illustrates a histogram of the sequences belonging to Group 1 (155 members of the 5′-splice site sequences), while the upper half illustrates those belonging to Group 2 (1596 members of sequences other than the 5′-splice sites). As has already been mentioned, the present Class III approach assumes no external criterion as to whether or not a sequence may belong to the 5′-splice site sequence. However, Fig. 2 clearly shows that the Class III approach can discriminate, to considerable extent, sequences of Group 1 from those of Group 2. In order to estimate the rate of discrimination in terms of the sample score z, we note the overlapping of the distribution curve of Group 1, $f_1(z)$, and that of Group 2, $f_2(z)$, around z=0.55. The optimum discrimination rate, P, at the critical sample score, z^*, may be determined by using this relation:

$$P=\int_{-\infty}^{z^*} f_2(z)dz=\int_{z^*}^{\infty} f_1(z)dz=1-\int_{-\infty}^{z^*} f_1(z)dz. \quad (14)$$

Here, the values for $\int_{-\infty}^{z^*} f_1(z)dz$ and $\int_{-\infty}^{z^*} f_2(z)dz$ can be obtained by estimating the cumulative frequency percentage curves for the distributions of sample scores in Groups 1 and 2 respectively. If we then plot $\int_{-\infty}^{z} f_2(z)dz$ and $1-\int_{-\infty}^{z} f_1(z)dz$ versus z, the intersect of their curves will give the values for z^* and P. In this way, z^*=0.572 and P=96.8% were estimated from the cases given in Fig. 2. This result implies that any sequence with a sample score of $z>0.572$ may be classified into Group 1 with a 96.8% probability, while a sequence with a sample score of $z<0.572$ may be placed in Group 2 with a 96.8% probability.

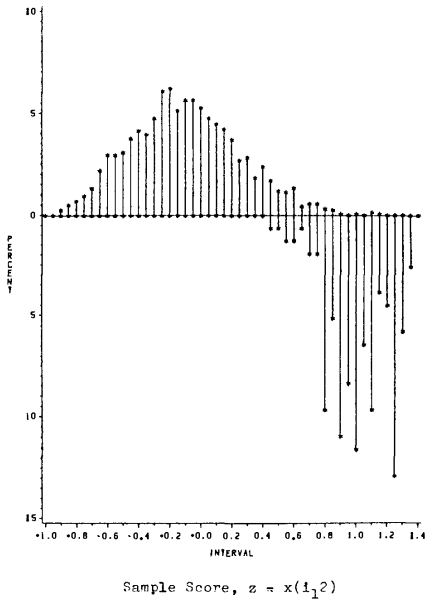

Fig. 2. Graph of distribution and frequency percentage versus categorized sample score ($z=x(i_1 2)$) for 1751 members of 9-nucleotide sequences shown in Table 1. Values of $x(i_1 2)$, (i_1=1, 2, ···, 1751), are calculated from the second largest eigen value of Eqs. 12 and 13. For purposes of comparison, the lower half of the graph shows a histogram of the sequences belonging to Group 1 (155 members of 5′-splice site sequences in Table 1), while the upper half, those belonging to Group 2 (1596 members of sequences other than 5′-splice sites). For further details, see text.

Let us compare the discrimination rate of the present Class III analysis with that of the Class II analysis reported previously.[7] The Class II analysis used an external criterion for Group 1 (5′-splice site sequences) and Group 2 (sequences other than 5′-splice sites), and discriminated the two groups most distinctly by maximizing the σ_B^2/σ^2 value, where σ^2 is the variance of the total samples and σ_B^2, the variance between Groups 1 and 2. Then, the optimum discrimination rate, P, was estimated to be as high as 98.2%. It is reasonable that this value is larger than the 96.8% value of the present Class III analysis. However, it is important to note that, even without any external criterion, Groups 1 and 2 can be discriminated as much as 96.8%. This implies that the sequences belonging to Group 1 show unique responses to the positions and species of nucleotides and that the 5′-splice signal may be composed of a particular pattern of nucleotide sequences.

In order to examine this situation more extensively, we map 1751 sequences on a two-dimensional graph by plotting the coordinates of $\{x(i_1 2), x(i_1 3)\}$, (i_1=1, 2, ···, N_1); as is shown in Fig. 3. Here, any sequence is represented by a dot (·), but multiple overlapping of dots is given by signs (*, +, etc.) (see the captions of Fig. 3). It is found that the 1751 sequences may be roughly classified into two clusters on the two-dimensional map. The first cluster lies around the origin of the coordinate: most of the members of this cluster belong to Group 2 (sequences other than 5′-splice sites). Those members are distributed almost symmetrically around the point of origin, indicating that their sequences exhibit no particular (random)

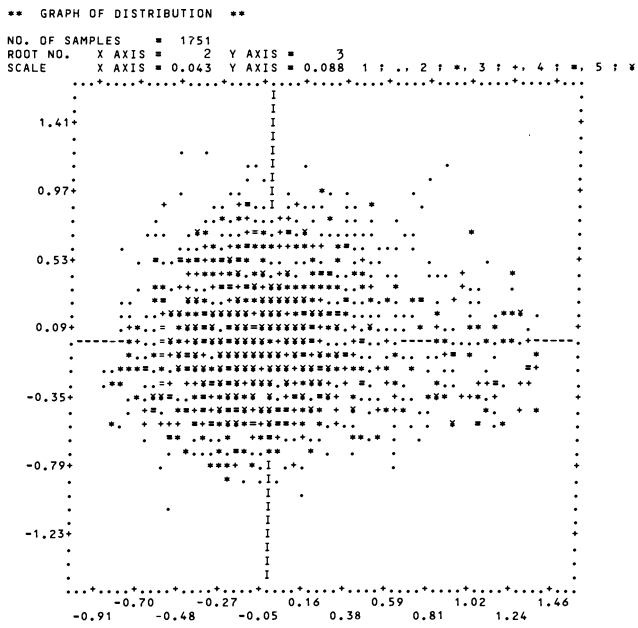

Fig. 3. Two-dimensional mapping of 1751 members of 9-nucleotide sequences (i_1=1, 2, ···, 1751) in Hayashi's quantification analysis (class III). Abscissa shows value of $x(i_12)$, which is calculated from the second largest eigen value of Eqs. 12 and 13. Ordinate shows value of $x(i_13)$ calculated from the third largest eigen value. Each sample sequence is given by a dot (·), but multiple overlapping of dots is indicated by signs (*, +, etc.). For example, the sign (*) shows double overlapping of dots. For further details, see text.

responses to the positions and species of nucleotides. On the other hand, the second cluster is out of the first cluster, deviating remarkably from the point of origin and lying around the positive region of $x(i_12)$=0.55—1.50. Most of the members of the second cluster belong to Group 1, as has been described previously. The distribution of those members versus the $x(i_13)$ axis is almost symmetrical, suggesting that the $x(i_13)$ value has no appreciable power to separate Group 1 (5′-splice site sequences) from Group 2. These observations are in good accordance with our previous calculation, where $x(i_13)$ comes from the third largest eigen value of Eq. 12 and has a lesser correlation coefficient than has $x(i_12)$. Even in the two-dimensional mapping of the 1751 sequences, the two clusters can be mostly separated by the use of the $x(i_12)$ parameter.

We further carried out two-dimensional mapping of the 1751 sequences (i_1=1, 2, ···, N_1) by plotting $\{x(i_12), x(i_14)\}$ or $\{x(i_13), x(i_14)\}$ (data not shown). In these cases also, the parameters of $x(i_13)$ and $x(i_14)$ are found to have no practical ability to discriminate: only the parameter of $x(i_12)$ is very effective.

Concluding Remarks

Hayashi's quantification analysis (Class III) is similar to the principal-component analysis for data of samples composed of continuous variables. However, the Class III analysis differs from the principal-component analysis in several points:

(1) The Class III analysis deals with samples composed of categorical data or item-category data.

(2) In the Class III analysis, we give appropriate quantities to both samples and item-categories in such a way that the correlation coefficient between samples and item-categories may be maximized (see Eq. 12).

(3) In this process, using the second largest eigen value, we can simultaneously classify not only item-categories, but also samples, in the most characteristic way. We can map them in two- or three-dimensional coordinates, using the third and fourth largest eigen values.

The Class III approach is applicable when samples have no external criterion. In the present investigation, the 1751 sample sequences composed of 5′-splice site sequences and sequences other than 5′-splice sites were analyzed with the Class III method, and a discrimination rate of up to 96.8% was attained. If there is an external criterion, the Class II method gives a higher rate of discrimination. However, if sample sequences exhibit unique responses to the positions and species of nucleotides, the Class III approach may give a satisfactory rate of discrimination even without any external criterion. In this respect, the Class III method is "an automatic classification technique" of unknown nucleotide sequences, and it may become generally useful in the analysis of nucleotide sequences other than those of splicing.

References

1) B. Ruskin and M. R. Green, *Science*, **229**, 135 (1985).
2) T. Maniatis and R. Reed, *Nature (London)*, **325** 673 (1987).
3) M. M. Konarska and P. A. Sharp, *Cell*, **49**, 763 (1987).
4) S. M. Mount, *Nucleic Acids Res.*, **10**, 459 (1982).
5) R. Treisman, S. H. Orkin, and T. Maniatis, *Nature (London)*, **302**, 591 (1983).
6) M. Aebi, H. Hornig, R. H. Padgett, J. Reiser, and C. Weissmann, *Cell*, **47**, 555 (1986).
7) Y. Iida, *Comput. Appl. Biosci.*, **3**, 93 (1987).
8) Y. Iida, *Bull. Chem. Soc. Jpn.*, **60**, 2977 (1987).
9) C. Hayashi, *Ann. Inst. Statist. Math.*, **3**, 69 (1952).
10) C. Hayashi, *Bull. Inst. Statist. Math.*, **4**, 19 (1956).
11) GenBank, Genetic Sequence Data Bank, Release 55.0, USA (1988).
12) L. Guttman, The Prediction of Personal Adjustment, ed by The Committee on Social Adjustment, New York: Social Science Research Council, 319 (1941).
13) K. Maung, *Ann. Eugenics*, **11**, 189 (1941).

 © 1988 The Chemical Society of Japan Bull. Chem. Soc. Jpn., 61, 3807—3812 (1988)

Surface Activity of Complexes Formed with *N*-Dodecyl-β-alanine and Copper(II) Ion in Aqueous Solution

Akio NAKAMURA* and Kazuo TAJIMA†
Nagoya Municipal Women's Junior College, Kitachikusa, Chikusa-ku, Nagoya 464
†Department of Chemistry, Faculty of Engineering, Kanagawa University, Rokkakubashi, Kanagawa-ku, Yokohama 221

(Received April 21, 1988)

The surface activity of the equimolar mixed solutions of *N*-dodecyl-β-alanine (NDA) and inorganic salts was studied at 30 °C. The surface tension of the NDA-$CuCl_2$ solution decreased more than that of the single NDA solution, whereas the surface tensions of the NDA-NaCl, NDA-$CaCl_2$, and NDA-$MgCl_2$ solutions were almost the same as that of the single NDA solution in the concentration region studied. The experiments with the bulk solution have shown that the 1:1-complex ion formed with NDA and the copper(II) ion is soluble and more surface-active than NDA alone, but the 1:2-complex is not effective in the surface activity because of its extremely low solubility. The formation constant of the 1:1-complex ion was determined, by potentiometry with both copper(II) and hydrogen ion-selective electrodes, to be 5.5×10^{-5}, while the standard free energy of the complex formation was found to be 24.7 kJ mol^{-1}. The composition and structure of the 1:2-complex were studied by means of X-ray diffractometry, IR spectroscopy, and elemental analyses for the precipitate. The total amounts of NDA adsorbed at the air/aqueous solution interface were determined by radiometry using tritium-labeled NDA, and the amount of the 1:1-complex adsorbed was calculated by the Gibbs adsorption isotherm. Thus, the compositions were determined in both the adsorbed and bulk phases. It was seen that the relative adsorbability of the 1:1-complex was larger than that of NDA by a factor of about 1.5×10^2 and, further, was larger than that of a 1:1-complex formed with NDA and sodium dodecylsulfate by a factor of about 3.7.

Ampholytic surfactants of the amino-acid type have been used in various fields because of their excellent characteristics (e.g., high detergency, bactericidal effect, low irritating to the skin, definite effect of pH on the solution properties, high biodegradability, and wide compatibility with other types of surfactants).[1] In spite of such characteristics of ampholytic surfactants, however, reports of their basic surface-chemical properties seem to be rather rare compared to the cases of anionic, cationic, and nonionic surfactants.

We have investigated some of the properties of *N*-dodecyl-β-alanine (NDA), which is one of most simple surfactants of the amino-acid type (e.g., the adsorption isotherms and the interfacial tensions at the air/aqueous solution[2] and oil/aqueous solution[3] interfaces, the pH effects on the surface activity,[4] and the interactions with anionic surfactants[5,6] and with insoluble monolayers).[7]

On the other hand, it is well-known that amino acids and the transition metal ions form a number of stable complexes in their aqueous solutions, and some of their structural properties have been investigated as models of metal complexes in biological systems.[8] Therefore, a similar interaction can be expected to occur between the transition metal ions and the ampholytic surfactants of the amino-acid type. However, little has been reported concerning the surface activity of such a complex in its aqueous solution.[9]

The purpose of the present study is to elucidate the surface activity of the complex formed in the mixed solution of the copper(II) ion and NDA.

Experimental

Materials. *N*-Dodecyl-β-alanine (NDA) (i.e., 3-(dodecylammonio)propionate) was synthesized from dodecylamine and β-propiolactone in acetonitrile; also, tritiated NDA was synthesized by the same procedure except that tritiated dodecylamine was used instead of dodecylamine. The details of the synthesis and purification of the materials have been reported elsewhere.[2] The salts of NaCl, $CaCl_2$, $MgCl_2$, and $CuCl_2$ were purified by recrystallization, repeated three times, from distilled water. Water was purified by distillation after it had been refluxed overnight with acidic permanganate and subsequently with alkaline permanganate.

Methods. The adsorption of NDA was measured by the same radiometry as that reported previously.[2,10] The surface tension was measured by the Wilhelmy plate method. The time dependence of the surface tension was self-recorded to obtain an equilibrium value.[11] The activities of the copper(II) and hydrogen ions in the solutions were measured with the ion-selective electrodes connected to the ion meter (Orion Research, U.S.A., model 920). To minimize the effect of the photo-sensitivity of the copper(II) ion-selective electrode on the output current, the apparatus was set up and operated in as dark a room as possible. All the measurements were made at 30±0.2 °C in the pH region of about 4.3—5.5, where the NDA molecules are mostly zwitterionic[4] and where copper(II) hydroxide is essentially absent.

Results and Discussion

Surface Activity of the Solution. Figure 1 shows the surface tension (γ) vs. concentration curves of the NDA solution (C) with and without an equimolar amount of $CuCl_2$. The abscissa of Fig. 1 shows the

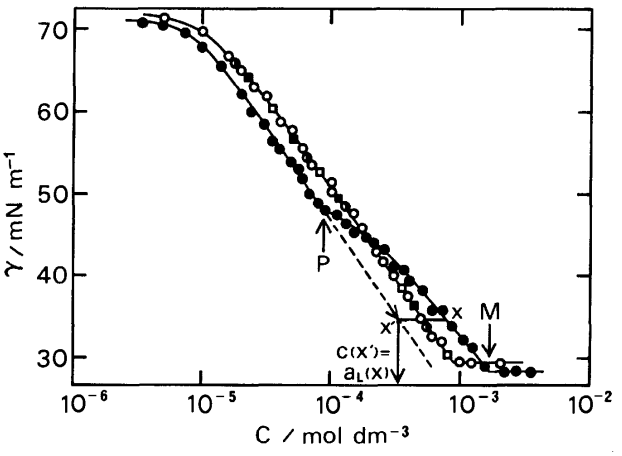

Fig. 1. Surface tension vs. concentration curves for NDA solutions alone (O), and with equimolar amount of $CuCl_2$ (●), $MgCl_2$ (□), $CaCl_2$ (■), and $NaCl_2$ (◑). Dashed line shows the extrapolation of the curve for NDA-$CuCl_2$ system above P point (see text).

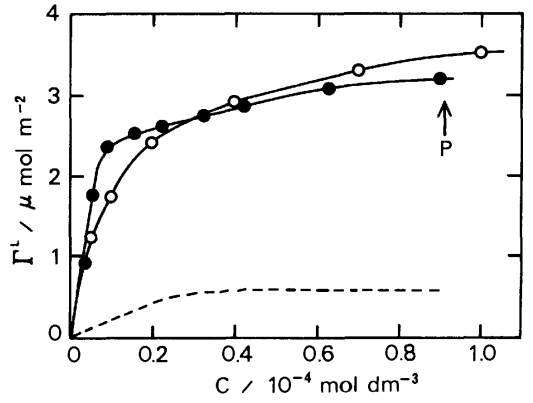

Fig. 2. Adsorption isotherms of NDA measured by a radiometry for NDA solution (O) and equimolar mixed solution of NDA-$CuCl_2$ (●). Dashed line shows the calculated adsorbed amount of the 1:1-complex ion (ML^+).

concentration of each component in the equimolar mixed solution. It is worthy of notice that the lowering of surface tension of NDA-$CuCl_2$ is larger than that of a single NDA solution and has a kink point at the concentration of 9.0×10^{-5} mol dm^{-3}. Here, we call this point P. Above the concentration of the P point, a flickering light was visible upon the irradiation of the He-Ne laser beam to the solution. This means that very fine crystalline particles would be generated, whereas a further lowering of the surface tension is observed until the micelle formation at 1.65×10^{-3} mol dm^{-3}. Here, we call this point M. On the other hand, the surface tensions of the other solutions, which had been prepared by an equimolar mixing of NDA-NaCl, NDA-$CaCl_2$, and NDA-$MgCl_2$, were almost the same as that of the single NDA solution in the corresponding concentration region. This finding indicates that the addition of such amounts of these salts caused no enhancement of the surface activity of the NDA solution. In other words, the salting-out effects were not observed in these systems. Therefore, the results obviously suggest the occurrence of a favorable and specific interaction of NDA with the copper(II) ion in the solution.

Figure 2 shows the adsorbed amounts of NDA (Γ^L) observed by radiometry at the air/solution interface with and without an equimolar amount of $CuCl_2$ in the concentration region below the P point in Fig. 1. The presence of $CuCl_2$ obviously enhanced the adsorption in the lower concentration region, but depressed it in the higher one, compared with that of the single NDA solution. This may be due to the formation of a surface-active complex, as may be expected from the results in Fig. 1. The depression of the adsorption isotherm in the higher concentration region is probably caused by both the ionic repulsion between the net charges of the adsorbed complexes and its geometrically large cross-section area due to the formation of a six-membered ring with NDA and the copper(II) ion, as will be shown later.

In general, it is well-known that the complexes of copper(II) ions and amino acids have the 1:2-composition and a planar structure, with the coordination number being 4.[8] Thus, in a dilute aqueous solution the complex-formation equilibria of NDA with the copper(II) ion are assumed to be described by the following two-step reactions:

$$M^{2+} + L^{\pm} \rightleftarrows ML^+ + H^+ \quad (1)$$

$$ML^+ + L^{\pm} \rightleftarrows ML_2 + H^+, \quad (2)$$

where M^{2+}, ML^+, ML_2, $L^{\pm}$, and H^+ denote the copper(II) ion, the 1(copper(II)):1(NDA)-complex ion, the 1:2-complex, the zwitterionic NDA, and the hydrogen ion respectively. Thus, we have presumed that the enhanced surface activity of the solution at the concentrations below the P point, as seen in Fig. 1, is due mainly to the presence of the 1:1-complex ion (ML^+), while the depression above the P point is mainly attributable to the formation of the 1:2-complex (ML_2), which is essentially insoluble because of having two long chains in a molecule. In order to confirm this reasoning, the solution properties were studied precisely, as will be described in the following sections.

1:1-Complex (ML^+) Formation. In Fig. 3 the surface tension of the mixed solution of NDA with $CuCl_2$ is plotted against the concentration of NDA (C). The total concentrations of the mixed solutions were kept at 1.0×10^{-4} mol dm^{-3}. The maximum deviation of the surface tension of the mixed solution from that of the single NDA solution is found at the equimolar ratio of NDA/$CuCl_2$; this suggests the formation of the surface-active 1:1-complex ion (ML^+) in the solution.

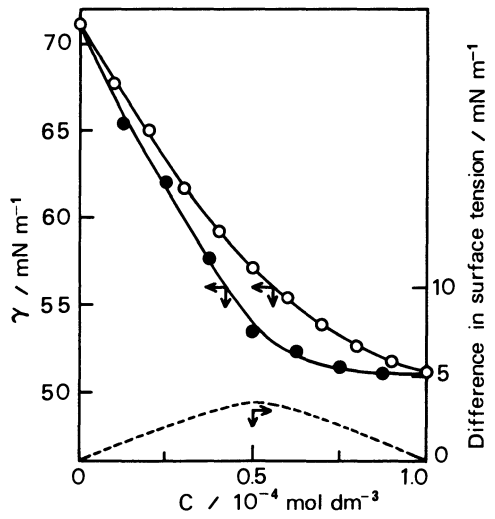

Fig. 3. Surface tensions of NDA (O) solution and NDA-$CuCl_2$ (●) solution (total concentration kept at 1.0×10^{-4} mol dm^{-3}) vs. NDA concentration curves. Dashed line shows the difference in surface tensions of NDA and NDA-$CuCl_2$ solutions.

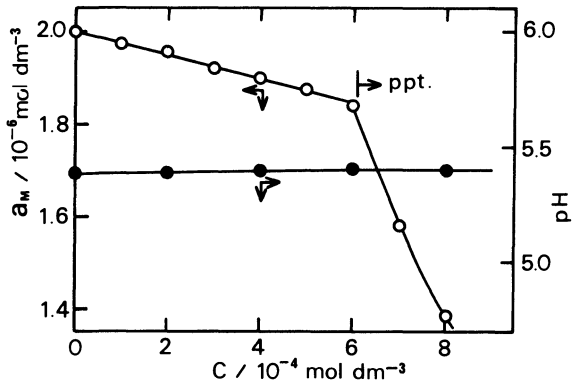

Fig. 4. Activities of copper(II) ion (a_M) (O) and hydrogen ion (pH) (●) vs. the concentration of NDA.

In order to determine the formation constant of the 1:1-complex ion, the activity measurements of the copper(II) ion (a_M) and the hydrogen ion (a_H) in the mixed solution of NDA-$CuCl_2$ were made by means of potentiometry, but the results were not so reliable as to enable us to determine accurately the trace quantities of complexes formed in a dilute concentration region, as is shown in Fig. 2. Therefore, an alternative system was introduced. Pure NDA powder in a given amount was stirred into the $CuCl_2$ solution (2.0×10^{-6} mol dm^{-3}) in a thermostat. The values of a_M and a_H were measured as a function of the C value. The results are shown in Fig. 4. The a_M value gradually decreased with the increase in the C value and steeply decreased at about 5.8×10^{-4} mol dm^{-3} above which point the precipitate was observed in the solution as has been described in the surface tension measurements. On

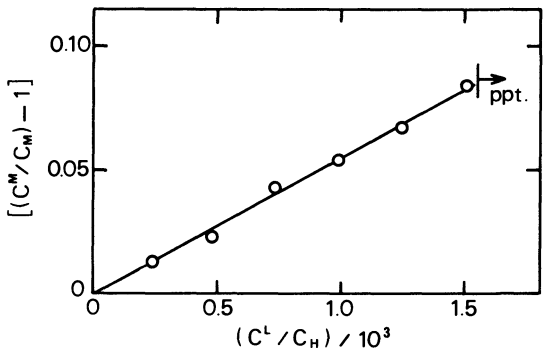

Fig. 5. $[(C^M/C_M)-1]$ vs. (C^L/C_H) plot according to Eq. 5.

the other hand, the a_H value was almost invariable at pH 5.4, in spite of the increase in the C value due to the buffer action of the solution for a small amount of the released H^+ ion. Here, we obtain from Eqs. 1 and 2:

$$a_{ML}\,a_H/a_M\,a_L = K_1 \quad (3)$$

$$a_{ML2}\,a_H/a_{ML}\,a_L = K_2, \quad (4)$$

where K_1 and K_2 denote the successive formation constants of ML^+ and ML_2 and where a_M, a_L, a_{ML}, a_{ML2}, and a_H denote the activities of M^{2+}, $L^{\pm}$, ML^+, ML_2, and H^+ respectively. Further, since the concentration of each species is of the order of magnitude of 10^{-4}—10^{-6} mol dm^{-3}, the activities in Eqs. 3 and 4 can reasonably be replaced by these concentrations:

$$C_{ML}\,C_H/C_M\,C_L = K_1 \quad (3')$$

$$C_{ML2}\,C_H/C_{ML}\,C_L = K_2 \quad (4')$$

where C_i denotes the concentration of species i. Then, under the condition of $C^L \gg C^M$, as in the case of Fig. 4, the combination of Eqs. 3′ and 4′ gives:

$$(C^M/C_M) - 1 = K_1(C^L/C_H) + K_1K_2(C^L/C_H)^2, \quad (5)$$

where C^M and C^L are the total concentrations defined as:

$$C^M = C_M + C_{ML} + C_{ML2} \quad (6)$$

$$C^L = C_L + C_{ML} + 2C_{ML2}. \quad (7)$$

If the ratio of K_2 to K_1 is assumed to be far less than unity, by analogy with the case of the β-alanine solution ($K_1 = 1.5\times10^{-3}$ and $K_2=5.9\times10^{-5}$),[12] the second term of R.H.S. in Eq. 5 is negligible. Therefore, the plot of $[(C^M/C_M)-1]$ against (C^L/C_H) should be linear, and its slope should give us the K_1 value. Here, for the actual plot, the values of a_M and a_H were used as the values of C_M and C_H respectively. The results are shown in Fig. 5; the K_1 value was found to be 5.5×10^{-5}.

Then, the standard free energy change ($\Delta G°$) in the 1:1-complex ion formation was calculated to be

24.7 kJ mol^{-1} according to this relation:

$$\Delta G^\circ = -RT \ln K_1. \quad (8)$$

This value is slightly larger than that of β-alanine (16.4 kJ mol^{-1}) calculated using the K_1 value obtained above, and fairly larger than those of some α-amino acids, for instance, glycine (7.1 kJ mol^{-1}) and α-alanine (7.7 kJ mol^{-1}).[13] This means that NDA is less reactive with the copper(II) ion than these amino acids. This result may reflect primarily the differences in the basicities of the nitrogen donors in these amino acids, and secondarily the differences in the structures of the chelate-rings of the 1:1-complexes.

Adsorbed Amount of the 1:1-Complex. In order to correlate the composition of the solution interior with that of the surface phase, the Gibbs adsorption isotherm was applied. The Gibbs adsorption isotherm is written generally[14] at a constant temperature and pressure as follows:

$$-d\gamma/RT = \sum_i \Gamma_i \, d(\ln a_i), \quad (9)$$

where γ denotes the surface tension, and Γ_i and a_i, the surface excess and the activity of the i-th species of solutes in the solution interior respectively. Here, since the formulation is limited to the concentration region below the P point in Fig. 1, the adsorbed species of solutes are assumed to be $L^\pm$, ML^+, and Cl^-; these species are related by Eq. 1, and the activity of each species can be replaced by the concentration for the reason described above. Thus, Eq. 9 can be rewritten as:

$$-d\gamma/RT = \Gamma_L \, d(\ln C_L) + \Gamma_{ML} \, d(\ln C_{ML}) + \Gamma_{Cl} \, d(\ln C_{Cl}), \quad (10)$$

where the subscript Cl denotes Cl^-.

The following relations are introduced to the total quantity (superscripts) of surface-active species in the surface phase and to the conditions of electrical neutrality in the surface and bulk phases:

$$\Gamma^L = \Gamma_L + \Gamma_{ML} \quad (11)$$

$$\Gamma_{ML} = \Gamma_{Cl} \quad (12)$$

$$C^M = (1/2)C_{Cl}. \quad (13)$$

Under the condition of equimolar mixing, from Eqs. 6 and 7, and neglecting the third terms of R.H.S. for the reason described above, we obtain:

$$C^M = C^L = C \quad (14)$$

$$C_M = C_L = C_S, \quad (15)$$

where C denotes the total concentrations of the respective solutes in the mixture (corresponding to the abscissa in Figs. 1 and 2) and where C_S denotes the single-ion concentrations of copper(II) and NDA. From Eqs. 10 and 12—15, we obtain:

$$-(d\gamma/RT)_{1:1} = \Gamma_L \, d(\ln C_S) + \Gamma_{ML} \, d(\ln C_{ML}) + \Gamma_{ML} \, d(\ln C), \quad (16)$$

where the subscript 1:1 indicates the value for the equimolar mixed solution of NDA-$CuCl_2$. Since, under the present experimental conditions, the solution pH actually remains constant, as has been described previously and as shown in the case of Fig. 4, we obtain from Eq. 3′:

$$d(\ln C_{ML}) = 2 \, d(\ln C_S). \quad (17)$$

By substituting Eqs. 11 and 17 into Eq. 16 we obtain:

$$-(d\gamma/RT)_{1:1} = (\Gamma^L + \Gamma_{ML}) \, d(\ln C_S) + \Gamma_{ML} \, d(\ln C). \quad (18)$$

By differentiating Eq. 18 with respect to $(\ln C)$, we obtain:

$$-(1/RT)[\partial\gamma/\partial(\ln C)]_{1:1} \equiv I_{1:1} = (\Gamma^L + \Gamma_{ML})[\partial(\ln C_S)/\partial(\ln C)]_{1:1} + \Gamma_{ML}, \quad (19)$$

Moreover, from Eq. 3′ we obtain:

$$[\partial(\ln C_S)/\partial(\ln C)]_{1:1} \equiv r = (q + q^{1/2})/2q, \quad (20)$$

where $q = [1 + 4K_1(C/C_H)]$.

By substituting Eq. 20 into Eq. 19, we obtain:

$$\Gamma_{ML} = (I_{1:1} - r\Gamma^L)/(r + 1). \quad (21)$$

Thus, we may calculate the adsorbed amount of the 1:1-complex ion (ML^+) from Eq. 21 by using the K_1 and Γ^L values determined by the potentiometry and radiometry respectively, and also the $I_{1:1}$ value given as the inclination of the surface tension vs. the equimolar concentration curve in Fig. 1. The amount of copper(II) in the adsorbed phase, estimated as ML^+, is shown with a dashed line in Fig. 2. While the molar ratio of ML^+ to the total NDA in the adsorbed phase, Γ_{ML}/Γ^L, is about 0.16 in the higher concentration region in Fig. 2, that in the solution interior, C_{ML}/C^L, as calculated using the K_1 value, is about 1.3×10^{-3} in the same concentration region. Consequently, it turns out that the surface activity of ML^+ is fairly larger than that of NDA alone.

Surface Activity of the 1:1-Complex. The surface activity of the 1:1-complex ion in this co-adsorption system was compared to that of NDA in terms of the relative adsorbability (α), which was defined as follows:[6]

Table 1. Relative Adsorbability of 1:1-Complexes and SDS to NDA

Adsorbate	$\lim_{C\to0}(\Gamma/C)$/m	α
NDA	3.1×10^{-4}	1
SDS	4.1×10^{-5}	0.13
NDA-SDS	1.0×10^{-2}	33[6]
NDA-Cu	3.7×10^{-2}	150

$$\alpha = \lim_{C \to 0} (\Gamma_{ML}/C_{ML})/(\Gamma_L/C_L). \quad (22)$$

The results are shown in Table 1, together with the values of the 1:1-complex ion formed between NDA and sodium dodecylsulfate (SDS).[6] It is worthy of notice that the surface activity of the 1:1-complex ion of copper(II) and NDA is larger than that of NDA by a factor of 1.5×10^2 and larger than that of the 1:1-complex of NDA and SDS by a factor of 3.6.

1:2-Complex Formation. In order to elucidate the effect of the precipitation on the surface tension of the solutions above the P point in Fig. 1, analyses of the precipitate were carried out. The precipitate which was generated in the equimolar mixed solution at 8.0×10^{-4} mol dm^{-3} was collected on a membrane filter (pore size, 3 μm) and dried in a desiccator for a week. The precipitate consisted of bluish and flaky microcrystals, and it was so hydrophobic as to repel its mother solution. The results of the elemental analyses of the precipitate are shown in Table 2.

In Table 3 the IR spectra of pure NDA and the precipitate obtained by the KBr disk method are compared. The precipitate lacks the absorption bands at 1650 cm^{-1} and 2330 cm^{-1} due to $=NH_2^+$. The absorption bands at 860 cm^{-1} due to $-(CH_2)_2-$ in the polar group of NDA, and also the absorption bands at 1400 cm^{-1} and 1570 cm^{-1} due to $-COO^-$ shift to higher frequencies. These results confirm that the precipitate is the hydrated 1:2-complex, $[Cu(NDA)_2]\cdot2H_2O$, with a ring structure formed between the hydrophilic group of NDA and the copper(II) ion.

Further, in order to obtain information on the crystal structure of the 1:2-complex, the X-ray (Cu $K\alpha$ 0.154 nm) diffraction pattern was measured for the powdery precipitate. The main peaks, at the angles of 2θ=3.93° (1.00), 7.86° (0.24), 11.82° (0.16), and 15.44° (0.05), can all be assigned to a lattice space of 2.24 nm on the basis of the Bragg condition; here, the figures in parentheses indicate the relative intensity of each peak. This long lattice spacing may correspond to the distance between copper(II) ions aligned in a adjacent layers of the 1:2-complex with a multilayer structure. Since the total length of the single ML_2 molecule with the trans-form on a plane is about 3.35 nm, as estimated from the STS molecular model, the packing of ML_2 molecules in the crystal state represented schematically in Fig. 6 may explain the X-ray data. The crystallographic structure will be described more precisely elsewhere.

Solubility Product of the 1:2-Complex. The solubility product (K_{SP}) of the 1:2-complex described above is defined from Eqs. 3 and 4 as follows:

$$K_{SP} = a_M a_L^2 / a_H^2, \quad (23)$$

As the observed values of a_M and a_H, and the calculated value of a_L from Eq. 3 have been given at the P point in Fig. 1, the value of K_{SP} is calculated to be 3.9×10^{-2} mol dm^{-3}. Figure 7 shows the activities of copper(II) and hydrogen ions in $CuCl_2$ solutions with and without equimolar NDA, whose concentration region corresponds to that below the M point in Fig. 1. When we put the data of a_M and a_H in Fig. 7 into Eq. 23, it turns out that the calculated values of a_L still increased until the M point. Consequently, the a_L value calculated at a given surface tension (e.g., X point) between P and M points in Fig. 1 nearly coincides with the C value obtained by the extrapolation of the γ vs. log C curve smoothly over the P point to the given surface tension (X′ point). The extrapolated curve is shown by a dashed line in Fig. 1. Thus, this finding explains why the surface tension lowers continuously above the P point, even after forming the precipitate of the 1:2-complex, until the

Table 2. Elemental Analyses of Precipitate

	Found (%)	Calcd (%)[a]
C	57.8	58.7
H	11.4	11.1
N	4.50	4.56
Cu	10.3	10.3
Cl	—	—
Molar ratio of N/Cu	1.98	2.00

a) For $Cu(NDA)_2\cdot2H_2O$.

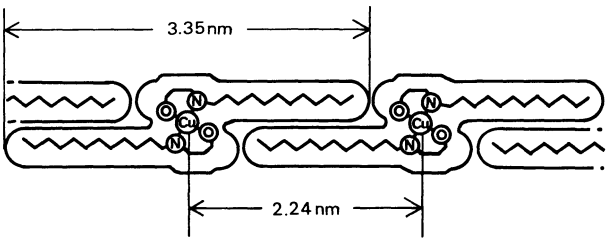

Fig. 6. A model for the molecular arrangement of the 1:2-complex in the precipitate.

Table 3. IR Spectra of the 1:2-Complex

Group	NDA (cm^{-1})	$Cu(NDA)_2\cdot2H_2O$ (cm^{-1})	Assignment
$-(CH_2)_2-$[a]	860	890	gauche
$-COO^-$	1410	1430	sym. str.
	1560	1580	asym. str.
$-NH_2^+$	1650	—	asym. deg. def.
	2330	—	asym. deg. def. +twisting

a) In the ammonio-propionate group.

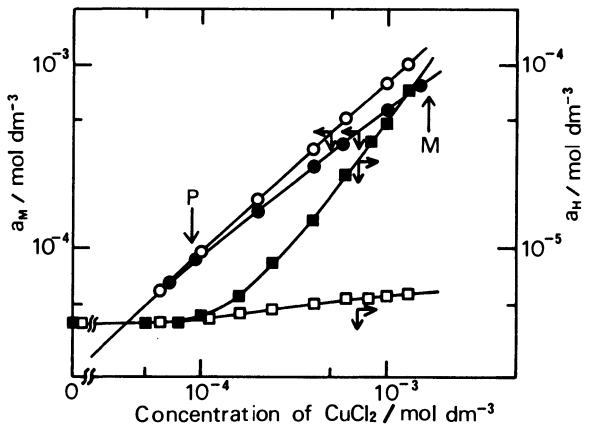

Fig. 7. Activities of copper(II) ion (a_M) and hydrogen ion (a_H) vs. the concentration of $CuCl_2$ with and without of equimolar amount of NDA: Copper(II) ion; (●) with and (○) without NDA. Hydrogen ion; (■) with and (□) without NDA.

micelle is formed at the M point.

Though, the 1:2-complex can be expected to be essentially highly surface-active, the complex has been considered in the present study as if it were surface-inactive. This was because the complex is not soluble at all as a result of its large hydrophobic moiety, as is shown in Fig. 6. However, it is conceivable that apparently the same composition may be observed at the co-adsorbing surface or in the mixed micelle formed with NDA and the 1:1-complex. The discrimination of such an ambiguous effect should be made in mixed solutions of the copper(II) ion and the short-chain compounds of *N*-alkyl-β-alanine, where the 1:2-complex may become soluble as one of the surface-active species. The study performed for this purpose will be presented elsewhere.

References

1) M. J. Rosen, "Surfactants and Interfacial Phenomena," Wiley-Interscience, New York (1978), p. 22.

2) T. Okumura, A. Nakamura, K. Tajima, and T. Sasaki, *Bull. Chem. Soc. Jpn.*, **47**, 2986 (1974).

3) K. Tajima, T. Tsutsui, and H. Murata, *Bull. Chem. Soc. Jpn.*, **53**, 1165 (1980).

4) A. Nakamura, K. Tajima, and T. Sasaki, *Bull. Chem. Soc. Jpn.*, **48**, 214 (1975).

5) A. Nakamura, *Bull. Chem. Soc. Jpn.*, **48**, 1720 (1975); A. Nakamura and M. Muramatsu, *J. Colloid Interface Sci.*, **62**, 165 (1977).

6) K. Tajima, A. Nakamura, and T. Tsutsui, *Bull. Chem. Soc. Jpn.*, **52**, 2060 (1979).

7) K. Tajima and T. Tsutsui, *Bull. Chem. Soc. Jpn.*, **54**, 109 (1981); **54**, 114 (1981).

8) T. Ono, H. Shimanouchi, Y. Sasada, T. Sakurai, O. Yamauchi, and A. Nakahara, *Bull. Chem. Soc. Jpn.*, **52**, 2229 (1979); T. Ono and Y. Sasada, *ibid.*, **54**, 90 (1981); Y. Sasada, A. Takenaka, and T. Furuya, *ibid.*, **56**, 1745 (1983); Y. Inomata, T. Takeuchi, and T. Moriwaki, *Spectrochim. Acta*, **40A**, No. 2, 179 (1984); M. A. Hitchman and L. Kwan, *J. Chem. Soc., Dalton Trans.*, **1987**, 457.

9) H. A. Eliott and C. P. Huang, *J. Colloid Interface Sci.*, **70**, 29 (1979).

10) K. Tajima, M. Muramatsu, and T. Sasaki, *Bull. Chem. Soc. Jpn.*, **43**, 1991 (1970).

11) M. Koshinuma, A. Nakamura, T. Seimiya, and T. Sasaki, *Bull. Chem. Soc. Jpn.*, **45**, 344 (1972).

12) These values could be determined for β-alanine using Eq. 5 by means of a procedure similar to that described in the text, since the values of a_M and a_H could be measured in a sufficiently high concentration region without precipitation.

13) The K_1 values used in the calculation of $\Delta G°$ for these amino acids were obtained according to this relation: $K_1 = K_1^* K_A$, where K_1^* denotes the formation constant of the 1:1-complex between the copper(II) ion and anionic amino acid ($M^{2+} + L^- \rightleftarrows ML^+$) and where K_A denotes the second dissociation constant of amino acid ($L^\pm \rightleftarrows L^- + H^+$). The K_1^* and K_A values are cited from: A. E. Martell and R. M. Smith, "Critical Stability Constants," Plenum Press, New York (1974), Vol. 1.

14) E. A. Guggenheim, "Thermodynamics," North Holland Publishing Co., Amsterdam (1957), p. 50.

 © 1988 The Chemical Society of Japan Bull. Chem. Soc. Jpn., 61, 3813—3817 (1988)

Environmental Intensity Increments of the $S_1(n\pi^*)\leftarrow S_0$ Absorption Spectra of Benzil in Fluid Solutions[1)]

Kaori MIYATA and Motohiko KOYANAGI*
Department of Chemistry, Faculty of Science, Kyushu University,
Hakozaki, Higashi-ku, Fukuoka 812
(Received April 22, 1988)

A remarkable solvent effect on intensity of molecular electronic transitions has been found in near UV absorption spectra of benzil. Great intensity enhancement is observed in alcohols and in chloromethanes as well as in nitriles. Parameters which are required to explain the origin of those environmental intensity enhancement are neither solvent refractive indexes nor polarities. A some rotationally flexible freedom around the -OC-CO- axis of benzil in the solvent seems important. Week complex formation between the solute and the solvent molecule is likely to play an important role. Similar solvent effects are found for absorption spectra of benzophenone and dicyclohexyl ketone, but with more complexity regarding their spectral shifts in contrast to the case of benzil.

There have been reported a lot of experimental data on the originally weak electronic transitions which become substantially enhanced through interactions with environmental solvent molecules. Roughly, two types of environmental intensification in the transitions have been reported. One is associated largely with solvent polarities (and partly to dielectric constants): e.g., $^1L_b\leftrightarrow S_0$ transition spectra of pyrene[2-4)] and coronene.[3)] The other is closely related to solvent dispersion forces or refractive indexes: e.g., $^1L_b\leftrightarrow S_0$ transition spectra of benzene[5-8)] and naphthalene[5,9)] and $^1U\leftarrow S_0$ absorption spectra of *p*-benzoquinone,[5)] aliphatic monoketones[10)] and benzaldehyde.[11)] Recently, Abe has proposed experimental and theoretical expressions for the molecular electronic oscillator strength of the latter type of molecules and successfully applied those equations to several ketones and benzenes.[12,13)]

In the present work we studied the $S_1(n\pi^*)\leftarrow S_0$ absorption spectra of benzil in various solvents and found that there was a remarkable solvent intensification on the electronic transition.

Experimental

Benzil (a Tokyo Kasei Co. zone-melting reagent) was used as received. Dicyclohexyl ketone, benzophenone, cyclobutanone, and cyclopentanone (all commercially pure grade reagents) were purified through repeated vacuum distillations. These ketones were stored in sealed-off glass tubings in vacuo. Almost all of the solvents employed (Dotite spectroscopically pure grade reagents) were deoxygenated by nitrogen gas bubbling before the measurements and used without further purification. Benzonitrile was purified by vacuum distillation. Carbon disulfide was purified in the same way as reported previously.[14)]

The oscillator strength of the $S_1(n\pi^*)\leftarrow S_0$ transition for each of the aromatic ketones in fluid solutions is difficult to estimate accurately from the observed spectrum because there is almost always its overlap with the $S_2(\pi\,\pi^*)\leftarrow S_0$ transition absorption. Integration over a certain part of the absorption system may in principle give relative oscillator strengths correctly as long as there are little changes in the Franck-Condon factors and as long as there is no strong intermolecular interaction. For benzil, in almost all cases we employed a band maximum around 27—28000 cm^{-1} as the upper wavenumber limit of the integration although small spectral pattern changes are found in benzene solution and the two nitriles (especially in benzonitrile solution) probably because of band overlappings (see Fig. 1). The exception is for CS_2 which has a substantial absorption originating from the onset around 430 nm; for this case the integration was taken up to the first band maximum and then the integration value was compared to another intensity integration value over the corresponding band region in a standard solution, hexane. For benzophenone, a treatment similar to that for benzaldehyde[10)] was employed. The other experimental details are similar to those described previously.[11)]

Results and Discussion

Benzil. Although the molecular structure of benzil in fluid solutions has been reported nowhere, we may suppose that it is close to the crystal[15-18)] or the vapor[19)] structure which has proven to belong to the C_2 point group with a CO/CO torsional angle of ca. 110° (for crystal)[15,16)] or 117°±3° (for vapor)[19)] and with the phenyl rings nearly coplanar with the carbonyl groups. Under this assumed molecular symmetry, the $S_1(n\pi^*)\leftarrow S_0$ absorption transition may formally be allowed. Further, if benzil is simply assumed to be an electronically composite compound of two equivalent aromatic monocarbonyls (e.g., benzaldehyde or acetophenone), the relevant $\pi^*\leftarrow n$ transitions involve both allowed and forbidden characters. Despite this drastic assumption and the formal geometrical discussion, however, the $S_1(n\pi^*)\leftarrow S_0$ transition of benzil still retains substantial forbidden character originating from $\pi^*\leftarrow n$ transition properties; the very small oscillator strength observed confirms that this is the case.

Near UV absorption spectra of benzil were studied in various solvents at room temperature. Several spectra were picked up and shown in Fig. 1. The spectra show a few broad vibronic bands irrespective of

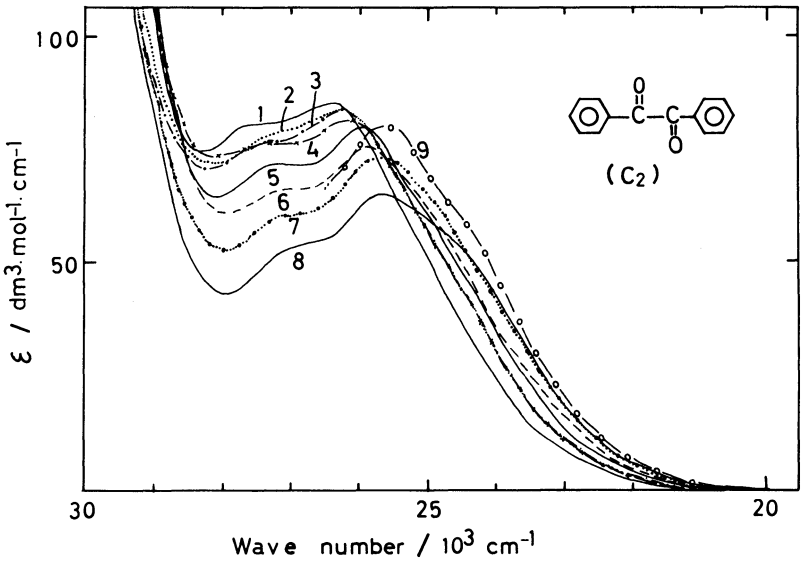

Fig. 1. $S_1(n\pi^*)\leftarrow S_0$ absorption spectra of benzil in various solvents at 20 °C. The solvents are: 1, acetonitrile; 2, 2-propanol; 3, chloroform; 4, benzonitrile; 5, benzene; 6, *p*-xylene; 7, carbon tetrachloride; 8, methylcyclohexane; and 9, carbon disulfide.

solvent polarity. Except for the spectrum in CS_2, it is generally found that toward the shorter the absorption wavelength of the peak maximum shifts, the greater the environmental intensity enhancement is. Solvents which effect such great intensity enhancement are alcohols, CH_2Cl_2, $CHCl_3$, and nitriles. With respect to the spectral increment in nonpolar and in several nearly nonpolar solvents such as hexane, methylcyclohexane, CCl_4, benzene, toluene, *p*-xylene, and CS_2, the usual refractive index or the dispersion force dependence[10–13] seems to hold qualitatively. The great intensity enhancement of the spectra in alcohols and chloromethanes differs from the case of pyrene.[2–4]

Cyclobutanone. Generally, cycloalkanones are chemically reactive and photochemically unstable.[20,21] Especially it has been known from the observation of the fluorescence excitation spectrum that cyclobutanone undergoes predissociation from its $S_1(n\pi^*)$ state.[22] As such, we were interested in observing near UV absorption spectra of cyclobutanone in fluid solutions. Similarly to the cases of acetone and cyclopentanone,[11] however, its $S_1(n\pi^*)\leftarrow S_0$ spectrum shows that the absorption transition is almost isolated from other absorption transitions lying at higher energies and gives a good example for a study on solvent intensification. The observed spectra are in part shown in Fig. 2. The deduced conclusion is in line with that reported previously for acetone and cyclopentanone[11]: The intensity enhancement observed is ascribed to the perturbation of dispersion forces between the solute and solvent molecules.

Benzophenone and Dicyclohexyl Ketone. Near UV absorption bands of benzophenone and dicyclohexyl

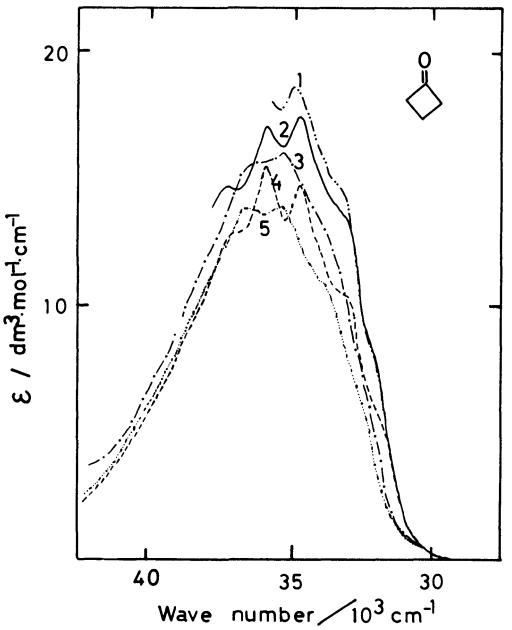

Fig. 2. $S_1(n\pi^*)\leftarrow S_0$ absorption spectra of cyclobutanone in some solvents at 20 °C. The solvents are: 1, benzene; 2, carbon tetrachloride; 3, chloroform; 4, cyclohexane; and 5, acetonitrile.

ketone in polar solvents such as dichloromethane, chloroform, and acetonitrile become much broad and undergo intensity enhancement (see Fig. 3). This is a contrast to the results obtained for cyclobutanone, loc. cit. (cf. Fig. 2), for the other aliphatic monoketones,[11] and for benzaldehyde.[10] It has been known that these polar solvents form stoichiometric complexes with several aromatic carbonyl compounds such as benzo-

phenone[23] and benzaldehyde[10] and with several aliphatic ketones.[24] Despite these facts of complex formation, however, it should be noted that the intensity enhancement of benzaldehyde (and also acetophenone) in dichloromethane and nitriles is not substantial; these solvents never belong to the most effective intensity perturbers, but are nearly in the dispersion force correlation line (for such a correlation diagram, see Fig. 3 of Ref. 10). For benzophenone, however, the great intensity enhancement in chloromethanes is quite remarkable.

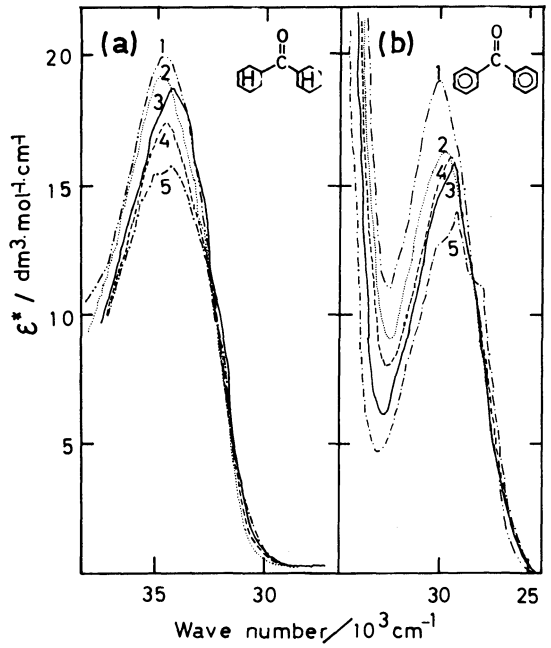

Fig. 3. $S_1(n\pi^*)\leftarrow S_0$ absorption spectra of (a) dicyclohexyl ketone and (b) benzophenone in some solvents at 20°C. Note that the ordinate axis denotes ε^*, but not ε; where ε^* is a constricted molar extinction coefficient, i.e., $\varepsilon^*=c\cdot\varepsilon$ (c: constant). For case (a), $c=1/2$; and for case (b), $c=1/9$. The solvents are: 1, chloroform; 2, acetonitrile; 3, carbon tetrachloride; 4, benzene; and 5, cyclohexane.

Although no data on the ground state geometry of dicyclohexyl ketone has been reported, the molecule is thought to be considerably skewed as is supposed from photoselection experiments by Chandler and Goodman.[25] With the help of their experimental results, we investigated the near UV spectra of the molecule. The observed spectra are partially shown in Fig. 3a. Since this absorption system is almost isolated from other higher energy transitions like the other aliphatic monoketones, it is more clearly demonstrated that the absorption spectral intensity is certainly enhanced in acetonitrile and especially chloroform (and also in dichloromethane).

Complex Formation between Ketones and Polar Solvents. By measuring near UV and IR spectra in various fluid solutions, Becker has concluded that benzophenone forms 1:1 weak complexes with certain polar solvents such as nitriles, alcohols, and halomethanes.[23] We also confirmed that benzaldehyde belongs to the case.[10] These facts necessitated a simlar investigation for benzil, acetone, dicyclohexyl ketone, and the cyclic ketones. In almost all of the cases, we measured several isosbestic points which are manifestations of such 1:1 complex formation. As an

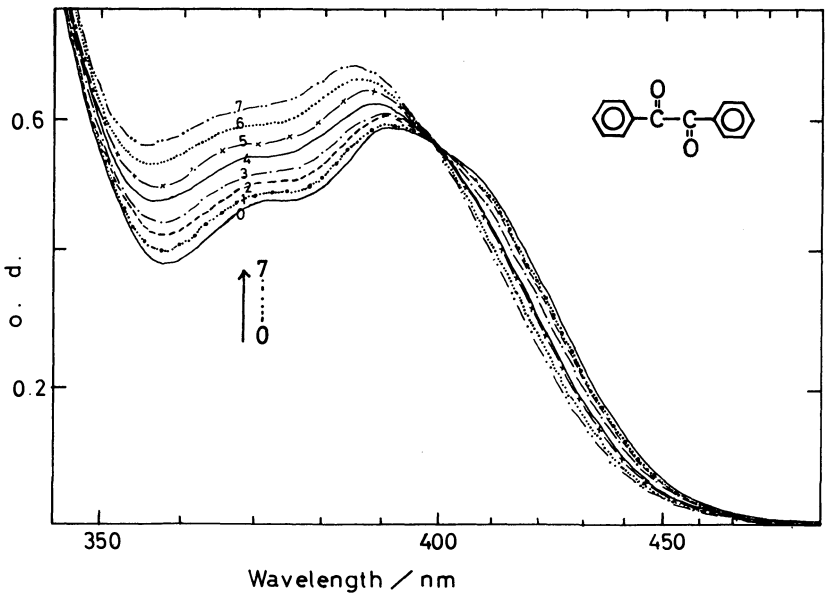

Fig. 4. Absorption spectral change of benzil with an increase in propionitrile concentraton. [Benzil]= 9×10^{-3} M in propionitrile-methylcyclohexane mixed solvents at 20°C. Propionitrile concentrations in 10^{-1} M units are: (0), 0; (1), 1.41; (2), 2.83; (3), 5.66; (4), 11.3; (5), 14.2; (6), 28.3; and (7), 42.5.

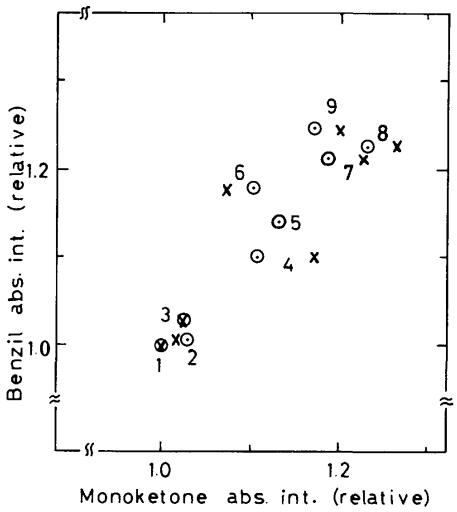

Fig. 5. Correlation between the environmental absorption intensity increment of benzil and that of each flexible monoketone: ×, for benzophenone; and ○, for dicyclohexyl ketone. The solvents are: 1, hexane; 2, cyclohexane; 3, methylcyclohexane; 4, carbon tetrachloride 5, *p*-xylene; 6, benzene; 7, dichloromethane; 8, chloroform; and 9, acetonitrile.

example, the absorption spectra of benzil in propionitrile-methylcyclohexane binary solvent solutions are shown in Fig. 4 although those are not so stoichiometric as the other monoketones' spectra (vide infra).

The absorption spectra of the ketones investigated are characterized and classified as follows:

(1) Almost all the spectra give several isosbestic (or nearly isosbestic) points when changing concentration of an active solvent in binary mixed solvent solutions. Such active solvents are: CH_3CN, C_2H_5CN, CH_2Cl_2, $CHCl_3$, ethanol, and 2-propanol. Appearance of these isosbestic points is a manifestation of 1:1 complex formation between the ketone and the solvent molecule. The equilibrium constants obtained are lying in the range of 10^0—10^{-2} M^{-1} (mostly at ca. 10^{-1} M^{-1}; 1 M=1 mol dm^{-3}).

(2) From their environmental intensity enhancement behaviors, the ketones observed are classified into two groups: (i) acetone and the cyclic ketones[26] and (ii) benzophenone, dicyclohexyl ketone, and benzil (see also Fig. 5).

(3) Despite of the existence of two carbonyl groups in benzil, nearly isosbestic points in binary mixed solvent solutions are observed even at a high concentration of such a polar solvent. This suggests that the kinetic reaction of 1:1 complex formation occurs dominantly. (An example for the benzil in propionitrile-methylcyclohexane mixed solvent system is shown in Fig. 4.)

(4) Among the group (ii) molecules, benzil seems to show a nearly linear relation between intensity enhancements and spectral shifts. This means that

Table 1. Intensities of $S_1(n\pi^*) \leftarrow S_0$ Absorptions for Some Ketones[a]

Ketone	f[b]$/10^{-4}$	$\varepsilon_{max}/M^{-1}\cdot cm^{-1}$
Group(i)		
Cyclobutanone	4.7	18
Cyclopentanone	4.8	18
Acetone	4.1	14
Benzaldehyde	(5.6)	24
Group(ii)		
Benzophenone	(22)	115
Dicyclohexyl ketone	7.8	33
Benzil	(12)	54

a) In cyclohexane solution at 20°C. b) Evaluated oscillator strengths within ±5% errors. However, parentheses indicate some roughly evaluated values with larger errors (±15%) because of band overlaps.

predominant environmental perturbing forces are, to a certain extent, restricted in the case of benzil. As such, benzil may be considered as a representative of the group (ii) molecules.

The environmental intensity enhancement for the group (i) ketones is interpreted in terms of the dispersion force (or the solvent refractive index) scheme[10,11] while that for the group (ii) is neither in terms of the solvent polarity nor in terms of the refractive index.

Although we can not proceed further without speculations, a comparison among the absorption oscillator strengths (or absorption molar extinction coefficients) of those ketones is very interesting (see Table 1). The intensity of dicyclohexyl ketone in a hydrocarbon is about 1.6 times as great as that of cyclobutanone or cyclopentanone (or acetone) in the same solvent while the intensity of benzophenone is about four times greater than that of benzaldehyde (or acetophenone). Similarly, the intensity of benzil is about twice as great as that of benzaldehyde (or acetophenone) and also that of 2,3-butanedione (i. e., biacetyl).[27,28] A common factor in the group (ii) ketones is a rotationally flexible freedom about the adjacent bond(s) to the carbonyl group(s). A hydrogen bond[29] or a charge transfer type complex formation may deform the ground state geometry a little bit along the relevant torsional coordinate(s). This may bring forth further intensity increment by borrowing from $^1n\sigma^* \leftarrow S_0$ (and also $^1\pi\pi^* \leftarrow S_0$ for the aromatic ketones) transitions. In order to discuss further on benzil somewhat quantitatively, we feel a need to seek a much more suitable complex system in which the spectral intensity change may surpass ordinary solvent effects.

Concluding Remarks

In this paper we used the term "solvent effects" in a broad sense. On the occasion of comparison between the theoretical and the experimental data many authors have rather kept away from solvents with a

special local interaction with guests as best as possible. As for clear-cut complex forming systems, there is no problem in selecting out such solvents. However, a problem arises when the solvent forms a very weak complex with a certain solute with its low stabilization energy which is comparable to or somewhat higher than the usual Boltzmann energy, i.e.,~kT: Even an "inert" solvent may generally form complexes (or clusters) at low temperature. Pyrene is one typical example of such cases.[30] The present case for benzil may be another one: Intensity increment observed in the present work seems to occur in most all hydrogen donating solvents.[29] This is in part supported by a preliminary work, that is in progress, on benzil in many binary solvent solutions into which 10^{-2}—10^{-3} mol dm^{-3} of trifluoroacetic acid or trichloroacetic acid added.

We are now being inclined to accept an assumption that a big deviation of an experimental data from the theory, if it is not easily explainable, is due to these weak local interactions.

We are thankful to Professor Kenichi Nakashima, University of Saga, for his helpful discussion and to the referee for his letting us know Ref. 29. This work was in part supported by a Grant-in-Aid for Scientific Research from the Ministry of Education, Science and Culture (No. 62540358).

References

1) A preliminary report of this work was presented at the Annual Meeting of the Chemical Society of Japan, Fukuoka, Oct. 1987.

2) A. Nakajima, *Bull. Chem. Soc. Jpn.*, **44**, 3272 (1971).

3) A. Nakajima, *Kagaku no Ryoiki*, **33**, 394 (1979) and references cited therein.

4) K. Kalyanasundaram and J. K. Thomas, *J. Am. Chem. Soc.*, **99**, 2039 (1977).

5) M. Koyanagi, *J. Mol. Spectrosc.*, **25**, 273 (1968).

6) N. S. Bayliss, *J. Mol. Spectrosc.*, **31**, 406 (1969).

7) G. W. Robinson, *J. Chem. Phys.*, **46**, 572 (1967).

8) J. W. Eastmann and S. J. Rehfeld, *J. Phys. Chem.*, **74**, 1438 (1970).

9) G. Durocher and C. Sandorfy, *J. Mol. Spectrosc.*, **20**, 410 (1966).

10) K. Nakashima and M. Koyanagi, *Bull. Chem. Soc. Jpn.*, **55**, 3923 (1982).

11) K. Nakashima, K. Uchida-Kai, M. Koyanagi, and Y. Kanda, *Bull. Chem. Soc. Jpn.*, **55**, 415 (1982).

12) T. Abe and I. Iweibo, *J. Chem. Phys.*, **83**, 1546 (1985).

13) T. Abe and I. Iweibo, *Bull. Chem. Soc. Jpn.*, **59**, 2381 (1986).

14) M. Koyanagi and Y. Kanda, *Spectrochim. Acta*, **20**, 973 (1964).

15) G. J. Brown and R. Sadanaga, *Acta Crystallogr.*, **18**, 158 (1965).

16) I. Y. Chan and B. N. Nelson, *J. Chem. Phys.*, **62**, 4080 (1975).

17) E. J. Gabe, Y. LePage, F. L. Lee, and L. R. C. Barclay, *Acta Crystallogr., Sect. B*, **37**, 197 (1981).

18) H. Terauchi, T. Kojima, K. Sakaue, F. Tajiri, and Y. Maeda. *J. Phys. Chem.*, **76**, 612 (1982).

19) Q. Shen and K. Hagen, *J. Phys. Chem.*, **91**, 1357 (1987).

20) K. Y. Tang and E. K. C. Lee, *J. Phys. Chem.*, **80**, 1833 (1976) and references cited therein.

21) E. Hamer and J. R. Huber, *Chem. Phys.*, **35**, 387 (1978).

22) J. C. Hemminger and E. C. K. Lee, *J. Chem. Phys.*, **55**, 1405 (1971).

23) R. S. Becker, *J. Mol. Spectrosc.*, **3**, 1 (1959).

24) L. J. Bellamy and R. L. Williams, *Proc. R. Soc., London, Ser. A*, **25**, 22 (1960).

25) W. D. Chandler and L. Goodman, *J. Mol. Spectrosc.*, **36**, 141 (1970).

26) Benzaldehyde, acetophenone, and *p*-benzoquinone seem to belong to this group. As for *p*-benzoquinone, the solvent effects on the $S_{1,2}$←S_0 absorption spectra in several nonpolar solvents have been reported in Ref. 5. In acetonitrile and chloroform, the spectra become very broad, but no anomaly in the intensity enhancement has been found (M. Koyanagi, Doctoral Thesis, Kyushu University, 1966).

27) L. S. Forster, *J. Am. Chem. Soc.*, **77**, 1417 (1955).

28) M. Koyanagi, K. Miyata, and K. Nakashima, *J. Photochem. Photobiol.*, submitted for publication.

29) Almost all solvents which showed great intensification in this paper have been reported to have hydrogen-bond donating natures: M. J. Kamlet, J-L. Abboud, M. H. Abraham, and R. W. Taft, *J. Org. Chem.*, **48**, 2877 (1983).

30) K. Nakashima and M. Koyanagi, *Photochem. Photobiol.*, **44**, 169 (1986) and references cited therein.

 © 1988 The Chemical Society of Japan Bull. Chem. Soc. Jpn., 61, 3819—3823 (1988)

Vibrational Analysis of Tangled Spectra. II. Role of Phonon Side Band Structure in the T←S Spectra of Acetophenones

Kenichi NAKASHIMA,† Hiroshi FUTAMI, and Motohiko KOYANAGI*
Department of Chemistry, Faculty of Science, Kyushu University,
Hakozaki, Higashi-ku, Fukuoka 812
(Received May 13, 1988)

$T_{1,2}$←S_0 phosphorescence excitation spectra of acetophenone, acetophenone-*methyl-d*$_3$, and acetophenone-*phenyl-d*$_5$ have been observed in the crystals at 4.2 K. Vibration analysis for the observed tangled spectra becomes possible only by the help of calculations which allow untangling of the tangled spectra. The calculations involve interstate mixings, by vibronic and environmental interactions, among 36 crude adiabatic Born-Oppenheimer vibronic functions of $^3\pi\pi^*$ and $^3n\pi^*$ states. A new aspect of the present work is introduction of a role of intermolecular phonon side bands into the calculations; this clearly showing that the observed spectra are reproduced much better than unless otherwise.

In the preceding paper,[1] we analyzed the tangled $T_{1,2}$←S_0 spectrum of acetophenone in the crystal and showed how conventional analysis was of no use for such a tangled system. Qualitatively, the band structure was explained in terms of canonical mixture of 36 BO vibronic functions of the T_1 and T_2 states. However, several disparities remained unsettled between the observed and the calculated spectrum. These are: (i) an abrupt decrease in calculated intensity in the zeroth order 0–0 band region of the $T_2(n\pi^*)$←S_0 transition, (ii) a discrepancy in the overall spectral intensity distributions, (iii) the lack of several structured bands in the calculation, etc.

In the present paper we report on three items. The first is to give the experimental $T_{1,2}$←S_0 absorption spectra of acetophenone-*methyl-d*$_3$ (hereafter abbreviated as $\mathbf{d_3}$) and acetophenone-*phenyl-d*$_5$ ($\mathbf{d_5}$). To our knowledge, no experimental data thereof have been reported. The second is to simulate these spectra by means of a similar method as given previously for $\mathbf{d_0}$.[1] The third is to take fully into account intermolecular phonon side bands. The simulation with such a phonon correction leads to a great improvement over the earlier one. At least, the extent of the disparities (i) and (ii), loc. cit., seems to be greatly diminished.

Experimental

The guest molecules, nonlabeled acetophenone ($\mathbf{d_0}$, a GR grade reagent from Tokyo Kasei Co.) and $\mathbf{d_3}$ and $\mathbf{d_5}$ (both reagents from Merck, Sharp and Dohme of Canada), were purified by distillation in vacuo. All T←S phosphorescence excitation and absorption spectra were observed at 4.2 K in the crystals. For the measurements of the excitation spectra, ca. 10^{-3} M§ benzaldehyde was doped as an effective phosphorescence emitter while for the absorption measurements, pure crystals with ca. 5 mm thickness were used. All spectra were recorded on a 3/4 m Nalumi Spectrometer with an HTV R375 photomultiplier tube. Other experimental details were similar to those described elsewhere.[1,2]

Theoretical

First, $T_{1,2}$←S_0 spectra of the two deuterated acetophenones were simulated in almost all the same way as reported for $\mathbf{d_0}$.[1] Some suitable frequency changes for many fundamental vibrations were made according to the same procedure as given for benzaldehydes.[2] The exceptions are in the determination of three out-of-plane vibrational frequencies of T_1: ν'_{43}, ν'_{42}, and ν'_{41}. The modes, especially ν''_{43} and ν''_{41}, have been well known to be delocalized over the ring and C–$COCH_3$ framework.[1,3–6] Furthermore, it is expected that a large increase in the C–(CXO) bond order consequent to π^*←π promotion leads to an increase in the CXO-wagging vibrational frequency on going from the ground to the $\pi\pi^*$ excited state. For these reasons, the three diagonal matrix elements were treated as independent parameters. Crystal field and vibronic interaction matrix elements were determined on the basis of the phosphorescence intensity data for mixed isotopic crystal systems.[2] The final data employed for $\mathbf{d_3}$ are partially given in Tables 1 and 2. For $\mathbf{d_5}$, a part of only the diagonal elements are given in Table 1.

Secondly, intermolecular phonon bands were taken into account for the explanation of a broad, but some structured, background absorption which is presumed to dominate a large part of the total absorption intensity. It is found that a similar sub-structure always attends both on almost all prominent phosphorescence bands and on several absorption bands. On the assumption that this was due to a pile of Franck–Condon (FC) type phonon bands, we synthesized a model function for such a feature on a computer by using ten independent gaussians. The three parameters of each gaussian (i.e., location of the frequency center, weight, and bandwidth) were chosen so that the origin band structure of each T←S spectrum was reproduced as best as possible. A final model structure for $\mathbf{d_0}$ is shown in Fig. 1.

The first few bands in the T←S spectra of $\mathbf{d_3}$ and $\mathbf{d_5}$ were sharper than those in $\mathbf{d_0}$ (as demonstrated in Fig.

† Present address: Laboratory of Chemistry, College of Liberal Arts, University of Saga, Honjo, Saga 840.

§ 1 M=1 mol·dm^{-3}.

Table 1. Zeroth Order Diagonal Matrix Elements Employed for Acetophenone, Acetophenone-*methyl-d*$_3$, and Acetophenone-*phenyl-d*$_5$[a]

Band	$\Delta\tilde{\nu}$/cm^{-1}[b]			Band	$\Delta\tilde{\nu}$/cm^{-1}[b]			Band	$\Delta\tilde{\nu}$/cm^{-1}[b]		
	d_0	d_3	d_5		d_0	d_3	d_5		d_0	d_3	d_5
|0>	0	0	0	|27>	590	535	570	|45*>	*50*	*45*	*50*
|45>	70	70	65	|40>	600	590	465	|44*>	*125*	*110*	*125*
|44>	90	85	90	|39>	700	685	565	|30*>	*170*	*160*	*170*
|30>	190	185	185	|38>	735	715	620	|43*>	*195*	*180*	*195*
|43>	245	270	225	|37>	835	800	675	|29*>	*360*	*305*	*360*
|41>	325	340	290	|36>	930	880	800	|42*>	*380*	*360*	*340*
|29>	360	355	370	|35>	970	965	980	|41*>	*430*	*390*	*375*
|42>	445	445	425	|0*>	*0*	*0*	*0*	|27*>	*550*	*495*	*550*

a) Only the representative vibronic levels are shown here. Asterisked states denote the BO vibronic levels of $T_2^0(n\pi^*)$ and the others $T_1^0(\pi\pi^*)$. b) Diagonal matrix elements are calculable on the basis: for d_0, $|0> \leftrightarrow 26150$ cm^{-1} and $|0^*> \leftrightarrow 26555$ cm^{-1}; for d_3, $|0> \leftrightarrow 26145$ cm^{-1} and $|0^*> \leftrightarrow 26560$ cm^{-1}; and for d_5, $|0> \leftrightarrow 26225$ cm^{-1} and $|0^*> \leftrightarrow 26575$ cm^{-1}. Underlined values give energy separation from the $|0^*>$ level.

Table 2. Off-Diagonal Matrix Elements Employed for Acetophenone-*methyl-d*$_3$[a]

T_1	T_2								
	|0*>	|30*>	|29*>	|27*>	|45*>	|44*>	|43*>	|42*>	|41*>
|0>	70.00	17.15	7.00	33.60	25.67	43.18	23.38	85.00	36.21
|30>	17.15	4.20	1.71	8.23	6.29	10.58	5.73	20.82	8.87
|27>	33.60	8.23	3.36	16.13	12.32	20.73	11.22	40.80	17.38
|45>	25.67	6.29	2.57	12.32	0	0	0	0	0
|44>	43.18	10.58	4.32	20.73	0	0	0	0	0
|43>	26.08	6.39	2.61	12.52	0	0	0	0	0
|42>	85.00	20.82	8.50	40.80	0	0	0	0	0
|41>	36.21	8.87	3.62	17.38	0	0	0	0	0
|40>	8.50	2.08	0.85	4.08	0	0	0	0	0
|39>	8.50	2.08	0.85	4.08	0	0	0	0	0
|38>	36.21	8.87	3.62	17.38	0	0	0	0	0
|45+30>	6.29	1.54	0.63	3.02	0	0	0	0	0
|44+30>	10.54	2.58	1.05	5.06	0	0	0	0	0
|43+30>	5.69	1.40	0.57	2.73	0	0	0	0	0
|42+30>	20.82	5.10	2.08	10.00	0	0	0	0	0

a) Only the representative elements are given here although 99×99 values are employed for the calculations. In cm^{-1} units.

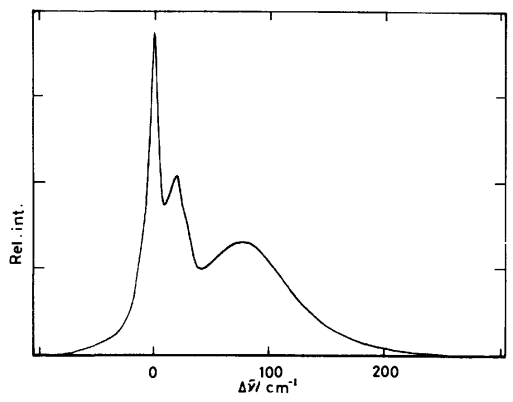

Fig. 1. A model shape function for the background FC type phonons. The fundamental zero-phonon line at $\Delta\nu$=0 cm^{-1} is lorentzian with Γ_{fwhm}=10 cm^{-1} while the other part is synthesized using ten different gaussian functions with various values of Γ_{fwhm}.

2). We thus assumed that each fundamental band of the former had a lorentzian shape with a 7 cm^{-1} fwhm while that of the latter a 10 cm^{-1} fwhm.

Results and Discussion

T←S Phosphorescence Excitation Spectra of the Deuterated Acetophenones. The observed T←S phosphorescence excitation spectra of d_3 and d_5 in the crystals[7] are shown in Fig. 2. For comparison, the spectrum of d_0 is added. At glance, most intensive bands of each spectrum appear to display one-to-one correspondence. However, the correspondence is in appearance only (vide infra).

The prominent band at the longest wavelength (26112 cm^{-1} for d_3 and 26177 cm^{-1} for d_5) is assigned to the T_1 origin band of the $T_1(\pi\pi^*) \leftarrow S_0$ transition. Energy closeness between the phosphorescence origin band of d_3 in d_5 (at 26099 cm^{-1})[3] and the crystal absorption origin band (at 26112 cm^{-1}) seems to support this assignment. The large (ca. 70 cm^{-1})

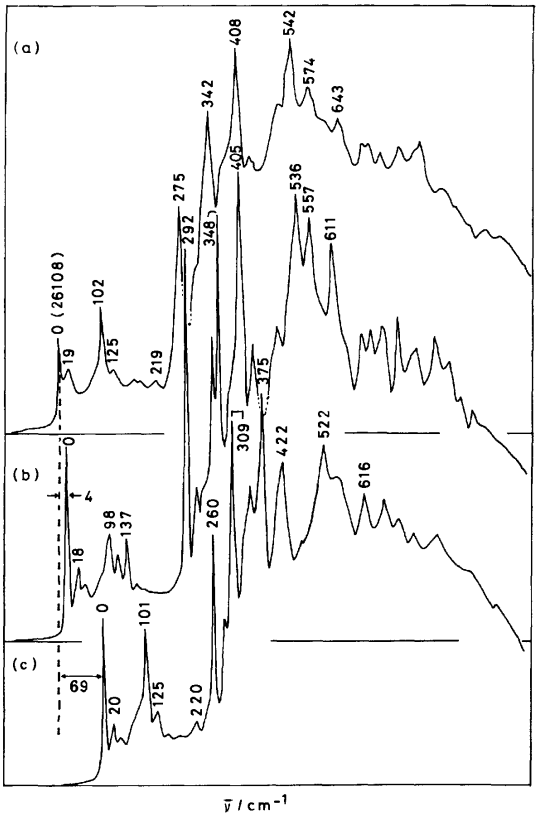

Fig. 2. Observed T←S phosphorescence excitation spectra of (a) ($\mathbf{d_0}$), (b) $\mathbf{d_3}$, and (c) $\mathbf{d_5}$ in the crystals at 4.2 K.

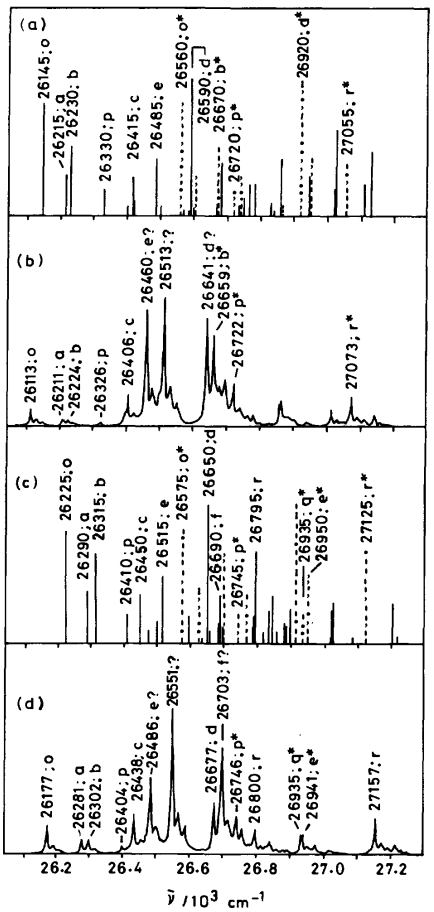

Fig. 3. (a,c) Zeroth order levels employed and (b,d) simulated T←S spectra at 0 K. (a, b) For $\mathbf{d_3}$; and (c, d) for $\mathbf{d_5}$. For band designations, see Ref. 1.

origin band deuteration shift on going from $\mathbf{d_0}$ to $\mathbf{d_5}$ allows assignment of the lowest excited triplet state to $\pi\pi^*$ since a similar deuteration shift has been established for the $\pi\pi^*$ transition of benzaldehyde-*phenyl*-d_5.[8] The very small (4 cm^{-1}) deuteration shift in $\mathbf{d_3}$ gives another piece of evidence for the validity of the $\pi\pi^*$ assignment.

Satellite bands were observed for all T←S spectra at ca. 20, ca. 40, and ca. 90 cm^{-1} from each origin band (and also first several strong false origins) to the higher wavenumber side. Similar sub-structured bands to the lower wavenumber side have also been observed in T→S spectra.[3] These are assigned to lattice vibrations in a similar way to the cases of T←S and T→S electronic spectra of *p*-dihalobenzenes[9] and *p*-benzoquinone[10] in the pure and isotopic mixed crystals. No evidence is obtained for alternative assignments: e.g., either trap bands or Davydov splitting components. The observed band broadness never contradicts our interpretation.

The bands in the 90—140 cm^{-1} region are quite interesting, but complicated (especially for $\mathbf{d_3}$). Such small frequencies may generally be ascribed to two torsional vibration modes, i.e., τ (-$COCH_3$) and τ (-CH_3). Although no information has been presented about these potential surfaces of the crystal phase acetophenones both for the ground and for the excited state, the reasonably sharp origin bands observed both in the phosphorescence and in the excitation spectrum suggest that the rotational potential barriers thereof are high relative to those for the $S_1(n\pi^*)$ state: The $S_1(n\pi^*)$←S_0 phosphorescence excitation spectra in the pure crystal and mixed crystals showed all poorly resolved features.[11,12] Recent jet works[13-15] may be helpful for obtaining information on those potentials.[16]

Simulated T←S Spectra of $\mathbf{d_3}$ and $\mathbf{d_5}$ in the Crystal. The zeroth order levels of $\mathbf{d_3}$ and $\mathbf{d_5}$ are shown in Figs. 3a and 3c, respectively. The height of the solid lines represents the relative value of the interaction between two levels of $T_1(0,0+\nu_i)$ and $T_2(0-0)$; and that of the dashed lines the interaction between the levels of $T_1(0-0)$ and $T_2(0,0+\nu_i)$. Refined calculation spectra of the two deuterated compounds are shown in Figs. 3b and 3d, respectively (for the observed spectra, see Figs. 2b and 2c). The eigenfunction corresponding to each calculated origin band (at 26113 cm^{-1} for $\mathbf{d_3}$ and 26177 cm^{-1} for $\mathbf{d_5}$) is approximately described by

$$|26113> = 0.18|0^*> - 0.96|0> + 0.10|42^*> + \cdots \quad (1)$$

and

$$|26177> = 0.23|0^*> - 0.93|0> + 0.12|42^*> + \cdots \quad (2)$$

A significant mixing of $|0^*>$ with $|0>$ is clear for each case. This explains why the origin band appears with remarkable intensity despite its substantial $\pi\pi^*$ character.

In contrast to the above, there is no convincing band which is assignable to the origin band of the $T_2(n\pi^*)\leftarrow S_0$ transition. Here we give only three eigenfunctions. These may be combined with three of the most intensive observed bands (see also Figs. 2b, 2c, 3b, and 3d):

for $\mathbf{d_3}$,

$$|26460> = 0.75|41> + 0.32|42> - 0.45|0^*> + \cdots \quad (3)$$

$$|26513> = 0.61|41> - 0.55|42> + 0.47|0^*> + \cdots \quad (4)$$

$$|26641> = 0.62|42> - 0.52|27> + 0.44|0^*> + \cdots, \quad (5)$$

and for $\mathbf{d_5}$,

$$|26486> = 0.62|41> + 0.45|44 + 30> - 0.36|0^*> + \cdots \quad (6)$$

$$|26551> = 0.59|41> - 0.46|42> + 0.51|0^*> + \cdots \quad (7)$$

$$|26703> = 0.46|40> + 0.57|41 + 31> + 0.39|0^*> + \cdots, \quad (8)$$

Despite superficial one-to-one band correspondence between the observed prominent bands of $\mathbf{d_3}$ and those of $\mathbf{d_5}$, there are considerable differences between the relevant calculated eigenvector-components of the two compounds as well as between the expansion coefficients of the corresponding components (e.g., compare Eq. 3 with Eq. 6 and Eq. 5 with Eq. 8). A similarity of these results for acetophenones to other results for aromatic aldehydes[2,17,18] leads us to a deduction that this kind of mixing is general for a molecule with a lower excited state of a strongly forbidden character. This deduction is important.

Role of Background Phonon Bands. If discussion is restricted to the spectral intensity distribution, the mimicking is poor. Here let us put aside an obvious experimental fact that spectral bands become broader on going toward shorter wavelengths. To be noted is a big difference between the observed and the calculated spectral intensity distributions: e.g., an abrupt decrease in intensity of the calculated spectra in the zeroth order 0–0 band region of the $T_2(n\pi^*)\leftarrow S_0$ transition and another decrease in intensity of 26.7—26.8×10³ cm⁻¹ region bands. In order to find a solution to the disparity, we introduced an intermolecular phonon ensemble to the calculations. The ensemble is presumed to closely concern a pile of FC type phonon vibrations.

The model structure employed is shown in Fig. 1. The revised calculation is then straightforward. The resultant spectrum for $\mathbf{d_0}$ is shown in Fig. 4 together with the uncorrected spectrum. Clearly, the revised spectrum is much close to the observed one. However, a question might be raised: Is such a band feature as shown in Fig. 1 due to another FC structure? Instead of the assumed intermolecular lattice vibrations, there are two intramolecular vibrations with small frequency as what comes under this category: the ϕ-$COCH_3$ tortional (i.e., ν_{45}) and the CH_3-rotational vibration (ν_{44}). As regards this, we have no unambiguous evidence which discriminates between them. However, we know that similar broad features also do appear for several other aromatic aldehydes with high τ (ϕ-CHO) potential barriers[2,4,17] and, further, almost all of these are explainable by FC-type phonon bands.[18] We are thus inclined to conclude that the substructure in the acetophenone crystal is also mostly explained by FC type intermolecular phonons.

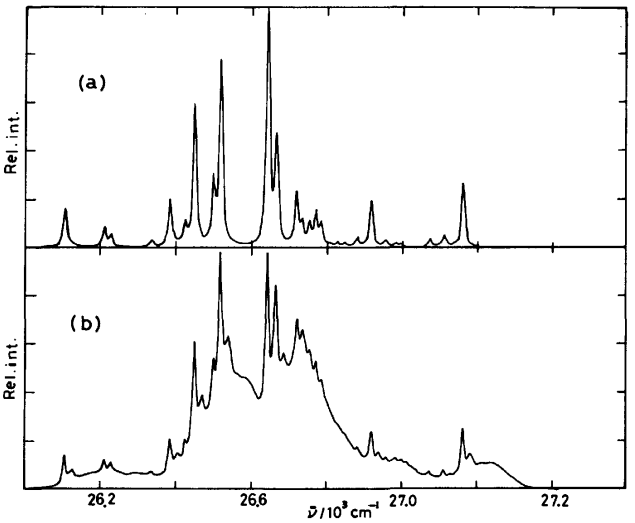

Fig. 4. Simulated T←S spectra of $\mathbf{d_0}$ at 0 K. (a) Without and (b) with the background phonon structure introduced (see the text and Fig. 1). Figure 4a is the same one as reported previously (cf. Fig. 4b of Ref. 1).

The calculations reported in this paper were carried out at the Computation Center of Kyushu University. This work was in part supported by a Grant-in-Aid from the Ministry of Education, Science and Culture (No. 62540358).

References

1) K. Nakashima and M. Koyanagi, *Bull. Chem. Soc. Jpn.*, **58**, 2000 (1985). Paper I of this series.

2) M. Koyanagi, K. Nakashima, and L. Goodman, *Chem. Phys.*, **92**, 435 (1985).

3) M. Koyanagi, R. J. Zwarich, and L. Goodman, *J. Chem. Phys.*, **56**, 3044 (1972).

4) L. Goodman and M. Koyanagi, *Mol. Photochem.*, **4**, 369 (1972).

5) A. Gambi, S. Giorgianni, A. Passerini, R. Visinoni, and S. Ghersetti, *Spectrochim. Acta*, **36A**, 871 (1980).

6) A. J. Duben, L. Goodman, and M. Koyanagi, "Excited States," ed. by E. C. Lim, Academic Press, New York and London (1974), Vol. 1, p. 295.

7) Each phosphorescence excitation spectrum at 4.2 K was confirmed to be very close to the corresponding direct T←S absorption spectrum at the same temperature.

8) M. Koyanagi and L. Goodman, *Chem. Phys.*, **39**, 237 (1979).

9) G. Castro and R. M. Hochstrasser, *J. Chem. Phys.*, **46**, 3617 (1967).

10) M. Koyanagi, Y. Kogo, and Y. Kanda, *J. Mol. Spectrosc.*, **34**, 450 (1970).

11) W. A. Case and D. R. Kearns, *J. Chem. Phys.*, **52**, 2175 (1970).

12) Despite many trials, only considerably broad bands were observed for the $S_1(n\pi^*)$←S_0 spectra of acetophenone in the crystal and in mixed crystals at 1.8 and 4.2 K. This is in big contrast to the T→S phosphorescence and T←S excitation spectra of acetophenone itself [and the $S_1(n\pi^*)$←S_0 spectra of benzaldehyde (see Ref. 4)]. The hosts employed were deuterated acetophenones, methylbenzoate, benzoic acid, pentane, hexane, methylcyclohexane, and benzene. See also Ref. 16 for a similar problem.

13) N. Omori, T. Suzuki, and M. Ito, *J. Phys. Chem.*, **92**, 1086 (1988).

14) J. L. Tomer, J. H. Spangler, and D. W. Pratt, *J. Am. Chem. Soc.*, **110**, 1615 (1988).

15) E. Villa, A. Amirav, W. Chen, and E. C. Lim, *Chem. Phys. Lett.*, **147**, 43 (1988).

16) Aside from several minor points, recently reported supersonic jet T_1←S_0 spectra of acetophenone (Refs. 13 and 14) are in good accord with the predicted spectra (Ref. 19), one of which (the case of $\Delta E \approx -405\ cm^{-1}$ in the crystal where the minus means $T_1={}^3n\pi^*$) was demonstrated previously (see Fig. 5 in Ref. 1). Our preliminary calculation for the same system, but with $F_c=0$ (gas model), also shows that an almost similar band pattern is realized when $\Delta E[({}^3n\pi^*)-({}^3\pi\pi^*)]$ is small (say, less than $200\ cm^{-1}$). However, a problem is that there never appear remarkably intense two bands in the 70—90 cm^{-1} region in contrast to the observed jet spectra. According to our rough estimation, smallness in ν''_{45} frequency (e.g., $44\ cm^{-1}$ according to Ref. 3) requires that any jet experiments for a molecule with such a small fundamental frequency must be done at very low vibrational temperature [say, less than 20 K, at least, to attain a relation of I(hot-band system)<0.1×I(cold-band system)]. Because we believe that the S←S and a large part of the T←S jet spectrum of benzaldehyde (Ref. 13 and private communications from Prof. D. W. Pratt) quite resemble the corresponding spectra in methylcyclohexane matrices at 4.2 K (see Refs. 4, 6, 17 for the assignments and discussion), we wonder if an analogous discussion might be possible also for the acetophenone cases. For making the points clear, an investigation on the simulation T←S spectra of the vapor phase acetophenone is in progress.

17) M. Koyanagi, H. Futami, and K. Nakashima, *J. Chem. Phys.*, **89**, 2662 (1988).

18) H. Futami, Master Thesis, Kyushu University, 1988; H. Futami and M. Koyanagi, *Mem. Fac. Sci. Kyushu Univ., Ser. C*, **16**, 101 (1988).

19) K. Nakashima, Doctoral Disertation, Kyushu University, 1985, Chap. 5.

 © 1988 The Chemical Society of Japan Bull. Chem. Soc. Jpn., 61, 3825—3830 (1988)

Crystal and Molecular Structure of Double Macrocyclic Inclusion Complexes, γ-Cyclodextrin·12-Crown-4·NaCl, a Model for the Transport of Ions through Membranes

Shigehiro KAMITORI, Ken HIROTSU,* and Taiichi HIGUCHI
Department of Chemistry, Faculty of Science, Osaka City University, Sumiyoshi-ku, Osaka 558
(Received April 28, 1988)

The crystal structure of a γ-cyclodextrin·12-crown-4·NaCl (3:3:1) inclusion complex was determined by an X-ray method to be space group $P42_12$, $a=b=23.816(3)$ Å, $c=23.072(3)$ Å. The inclusion complex has a C_4 symmetry, and the cation, Na^+, is coordinated by two 12-crown-4 molecules in a hydrophobic channel formed by tail-to-tail oriented two γ-cyclodextrin molecules.

γ-Cyclodextrin (CD) is a truncated cone-shaped cyclic oligosaccharide composed of eight D-glucoses. It has a hydrophobic cavity with a diameter of 8.5 Å, and eight hydroxyl groups (primary hydroxyl group) at the narrow side and sixteen hydroxyl groups (secondary hydroxyl group) at the wide side of the molecule. γ-CD has an ability to form inclusion complexes with various organic compounds, as well as α-CD and β-CD. It was therefore expected to mimic a biological function, such as enzyme catalysis.[1,2]

There have been many structural investigations of the inclusion compounds of α-CD and β-CD by X-ray crystal analyses, whose guest molecules are relatively rigid, e.g. benzene, adamantane, and their derivatives.[3,13] However X-ray structural studies of the CD's inclusion complexes which have flexible or functional molecules as guests have been very few. We expected that the structures of flexible guest molecules in the inclusion complexes are affected by the interior shape of the host molecules, and reported on an X-ray structural study of the γ-CD·12-crown-4 (1:1) inclusion complex.[14] The 12-crown-4 molecule is flexible and can have various conformations to form complexes with cations; also, its affinities to various cations are different, depending on cation diameters.[15] As expected, the 12-crown-4 molecule in a γ-CD cavity of approximate C_8 symmetry has a C_4 ring conformation, which was found in its complexes with cations, e.g. 12-crown-4·LiSCN,[16] $(12\text{-crown-4})_2NaClO_4$,[17] while free 12-crown-4 molecule has a C_i symmetry.[18] This result suggested that the 12-crown-4 molecules included in γ-CD cavities have an ability to coordinate cations.

Next, we prepared the crystals of two inclusion complexes composed of γ-CD, 12-crown-4, and Li^+ or K^+ cation,[19] and determined their crystal structures in order to reveal the cations' positions in the inclusion complexes. According to our work, a cation coordinates eight oxygen atoms of two 12-crown-4 molecules; this sandwich-type complex of $(12\text{-crown-4})_2\cdot Li^+$ or $(12\text{-crown-4})_2\cdot K^+$ was completely encapsulated in the hydrophobic channel formed by two tail-to-tail oriented γ-CD molecules. These double macrocyclic inclusion complexes showed some interesting characteristics, as follows: 1) Cations exist in a hydrophobic environment by means of 12-crown-4 molecules. 2) Because the $(12\text{-crown-4})_2$·cation complexes suffer from particular constraints of γ-CD cavities, abnormal structural changes in 12-crown-4·cation complexes occur, e.g. the cation-oxygen distances and the chirality of the 12-crown-4 ring conformation. 3) These double macrocyclic inclusion complexes may be models of the transport of ions through membranes; γ-CDs act as lipid bilayer membranes forming hydrophobic region in their interior,[3] and 12-crown-4 molecules act as ionophores.

Here, we report on the crystal structure of an inclusion complex composed of γ-CD, 12-crown-4 and Na^+, with an intermediate cation diameter between Li^+ and K^+. Na^+ forms a double macrocyclic inclusion complex as well as Li^+, K^+. We then tried to make a double macrocyclic inclusion complex with Rb^+; it was in vain because of the large cation diameter of Rb^+.

For a clear discussion, the inclusion complexes were numbered as follows:

γ-CD·12-crown-4 (1:1)	**(1)**
γ-CD·12-crown-4·LiSCN (3:3:1)	**(2)**
γ-CD·12-crown-4·NaCl (3:3:1)	**(3)**
γ-CD·12-crown-4·KCl (3:3:1)	**(4)**

Experimental

Preparation of the Crystalline Complex of γ-CD·12-Crown-4·NaCl (3:3:1) (3). Equimolar quantities of dry NaCl, 12-crown-4, and γ-CD were dissolved in a hot, aqueous solution, and left in an open test tube at 50 °C. Beautiful crystals of γ-CD·12-crown-4·NaCl appeared within 2 weeks.

X-Ray Structure Determination. A crystal for data collection, a rectangular block of 0.4×0.4×0.6 mm, was sealed in a glass capillary with a drop of mother liquor in order to avoid any crystal degradation. Diffraction intensities were measured on a Rigaku AFC-6A automatic diffractometer using Cu $K\alpha$ radiation ($\lambda=1.5418$ Å). Lattice constants were determined by least-squares methods with 20 reflections in $38°<2\theta<48°$. 3844 independent reflections (2833 with $I>3\sigma(I_0)$) were collected up to $2\theta=100°$, using a $\omega/2\theta$-scan mode at room temperature. No correction was

made for an absorption effect. Crystal data of **3** are as follows.

$C_{48}H_{80}O_{40} \cdot C_8H_{16}O_4 \cdot 1/3(NaCl) \cdot 7.7H_2O$, tetragonal, space group $P4_12_12$, $a=b=23.816$ (4)Å, $c=23.0.72(3)$Å, $Z=6$

This complex is isomorphous with the γ-CD·12-crown-4 inclusion complex **1** which we reported previously.[14] The phase problem was solved by using atomic coordinates of γ-CDs of **1**; guest molecules and water molecules were located on a difference Fourier synthesis.[20] One of the primary oxygen atoms O(6)1 is disordered at two positions (O(6)A1 and O(6)B1). The structures were refined to $R=0.168$ by full-matrix least-squares methods,[21] using isotropic temperature factors for all atoms. The R value is pretty high because of insufficient data at high angles in 2θ and the highly disordered water molecules. The quantity minimized was $\sum w(|F_o|-|F_c|)^2$ with $w=1.0$. Final atomic coordinates and temperature factors are given in Table 1. Tables of the complete bond distances and bond angles, and observed and calculated structure factor amplitudes, are deposited to the Chemical Society of Japan (Document No. 8831).

Results and Discussion

1. The Crystal Structure of γ-CD·12-Crown-4·NaCl Inclusion Complex (3). Three γ-CD molecules are stacked along the c-axis, forming a channel-type structure, and 12-crown-4 molecules are included in 1:1 stoichiometry in γ-CDs at the secondary sides of γ-CDs. Also, Na^+ is located between two γ-CD·12-crown-4 inclusion complexes, as shown in Fig. 1.[22] Host and guest molecules are centered on the four-fold crystallographic rotation axis so that three quarters of the γ-CD molecules are in an asymmetric unit. γ-CD **A** (the γ-CD molecule in the complex **A**) and γ-CD **B**, **B** and **C** and **C** and **A'** are in tail-to-tail, head-to-head, and tail-to-head orientations, respectively. Intermolec-

Table 1. Fractional Coordinates and Temperature Factors with Estimated Standard Deviations

Atom	X	Y	Z	B	Atom	X	Y	Z	B
Na(1)	0.5	0.0	0.792(1)	3.4(7)	O(3)4	0.721(1)	0.188(1)	0.734(1)	2.6(5)
C(1)1	0.666(2)	0.241(2)	0.951(2)	2.6(8)	O(4)4	0.646(1)	0.198(1)	0.644(1)	2.2(5)
C(2)1	0.705(2)	0.228(2)	0.899(1)	2.4(8)	O(5)4	0.755(1)	0.109(1)	0.578(1)	3.1(6)
C(3)1	0.712(2)	0.161(2)	0.893(2)	2.6(8)	O(6)4	0.717(1)	0.195(1)	0.508(1)	6.2(8)
C(4)1	0.733(2)	0.136(2)	0.944(2)	2.8(8)	C(1)5	0.740(2)	0.161(2)	0.281(2)	2.9(9)
C(5)1	0.688(2)	0.148(2)	0.995(2)	3.2(9)	C(2)5	0.774(2)	0.136(2)	0.234(2)	3.7(9)
C(6)1	0.707(2)	0.122(2)	1.054(2)	4.(1)	C(3)5	0.757(2)	0.076(2)	0.223(2)	3.3(9)
O(2)1	0.681(1)	0.252(1)	0.851(1)	3.3(6)	C(4)5	0.767(2)	0.045(2)	0.277(2)	3.0(9)
O(3)1	0.752(1)	0.154(1)	0.845(1)	2.5(5)	C(5)5	0.730(2)	0.069(2)	0.323(2)	3.2(9)
O(4)1	0.734(1)	0.078(1)	0.937(1)	2.4(5)	C(6)5	0.730(2)	0.043(2)	0.385(2)	6.(1)
O(5)1	0.687(1)	0.210(1)	1.001(1)	2.8(5)	O(2)5	0.765(1)	0.168(1)	0.180(1)	3.8(6)
O(6)A1	0.662(3)	0.134(3)	1.093(2)	5.(1)	O(3)5	0.794(1)	0.053(1)	0.178(2)	5.6(8)
O(6)B1	0.769(2)	0.142(2)	1.061(2)	3.(1)	O(4)5	0.748(1)	−0.015(1)	0.2668(9)	2.4(5)
C(1)2	0.450(2)	0.286(2)	0.948(2)	3.5(9)	O(5)5	0.748(1)	0.127(1)	0.329(1)	3.6(6)
C(2)2	0.484(2)	0.304(2)	0.899(2)	3.5(9)	O(6)5	0.788(2)	0.048(2)	0.403(2)	8.(1)
C(3)2	0.533(2)	0.263(2)	0.892(2)	2.9(8)	C(1)6	0.559(1)	0.286(1)	0.282(2)	1.9(7)
C(4)2	0.568(2)	0.262(2)	0.946(2)	4.(1)	C(2)6	0.597(2)	0.292(2)	0.235(2)	3.1(9)
C(5)2	0.529(2)	0.240(2)	0.996(2)	3.4(9)	C(3)6	0.628(2)	0.236(2)	0.221(2)	3.5(9)
C(6)2	0.558(2)	0.234(2)	1.055(2)	4.(1)	C(4)6	0.657(2)	0.218(2)	0.277(2)	2.3(8)
O(2)2	0.451(1)	0.306(1)	0.847(1)	3.6(6)	C(5)6	0.611(2)	0.212(2)	0.325(2)	3.8(9)
O(3)2	0.569(1)	0.287(1)	0.845(1)	3.7(6)	C(6)6	0.636(2)	0.193(2)	0.384(2)	4.(1)
O(4)2	0.612(1)	0.221(1)	0.938(1)	1.9(5)	O(2)6	0.567(1)	0.308(1)	0.181(1)	3.3(6)
O(5)2	0.483(1)	0.280(1)	1.000(1)	3.5(6)	O(3)6	0.667(1)	0.241(1)	0.173(1)	2.8(5)
O(6)2	0.588(2)	0.285(2)	1.063(2)	9.(1)	O(4)6	0.684(1)	0.164(1)	0.266(1)	2.5(5)
C(1)3	0.640(2)	0.257(2)	0.628(2)	3.2(8)	O(5)6	0.585(1)	0.265(1)	0.331(1)	3.8(6)
C(2)3	0.611(2)	0.285(2)	0.680(2)	2.8(9)	O(6)6	0.679(1)	0.236(1)	0.403(1)	4.4(7)
C(3)3	0.553(2)	0.263(2)	0.692(2)	2.9(9)	O(1)A	0.512(2)	0.086(2)	0.859(2)	9.(1)
C(4)3	0.519(2)	0.270(2)	0.631(2)	2.8(8)	C(1)A	0.558(4)	0.076(4)	0.889(3)	11.(2)
C(5)3	0.548(2)	0.234(2)	0.583(2)	2.7(8)	C(2)A	0.595(3)	0.035(3)	0.893(3)	9.(2)
C(6)3	0.520(2)	0.237(2)	0.526(2)	3.7(9)	O(1)B	0.573(1)	0.048(1)	0.725(1)	5.4(8)
O(2)3	0.645(1)	0.281(1)	0.730(1)	3.5(6)	C(1)B	0.549(3)	0.082(3)	0.685(2)	7.(1)
O(3)3	0.523(1)	0.295(1)	0.731(1)	3.6(6)	C(2)B	0.487(3)	0.095(3)	0.700(3)	8.(2)
O(4)3	0.4642(9)	0.244(1)	0.643(1)	2.0(5)	O(1)C	0.531(3)	0.085(3)	0.189(3)	14.(2)
O(5)3	0.604(1)	0.259(1)	0.577(1)	2.7(5)	C(1)C	0.579(3)	0.064(3)	0.213(3)	10.(2)
O(6)3	0.519(1)	0.294(1)	0.508(2)	6.2(9)	C(2)C	0.589(3)	0.010(4)	0.235(3)	12.(2)
C(1)4	0.777(2)	0.085(2)	0.626(2)	3.2(9)	Cl(1)	0.121(2)	0.175(2)	0.543(2)	4.(1)
C(2)4	0.778(2)	0.123(2)	0.679(2)	3.3(9)	Ow1	0.811(3)	0.150(3)	0.468(3)	18.(3)
C(3)4	0.720(2)	0.146(2)	0.691(2)	2.4(8)	Ow2	0.417(2)	0.426(2)	0.166(2)	11.(1)
C(4)4	0.700(2)	0.174(2)	0.632(2)	3.1(9)	Ow3	0.084(2)	0.088(2)	0.153(2)	13.(2)
C(5)4	0.699(2)	0.131(2)	0.586(2)	3.0(9)	Ow4	0.561(2)	0.416(2)	0.386(2)	12.(2)
C(6)4	0.683(2)	0.153(2)	0.525(2)	4.(1)	Ow5	0.548(3)	0.410(3)	0.047(3)	15.(2)
O(2)4	0.801(1)	0.097(1)	0.729(1)	3.2(6)	Ow6	0.100(3)	0.156(3)	0.557(3)	13.(3)

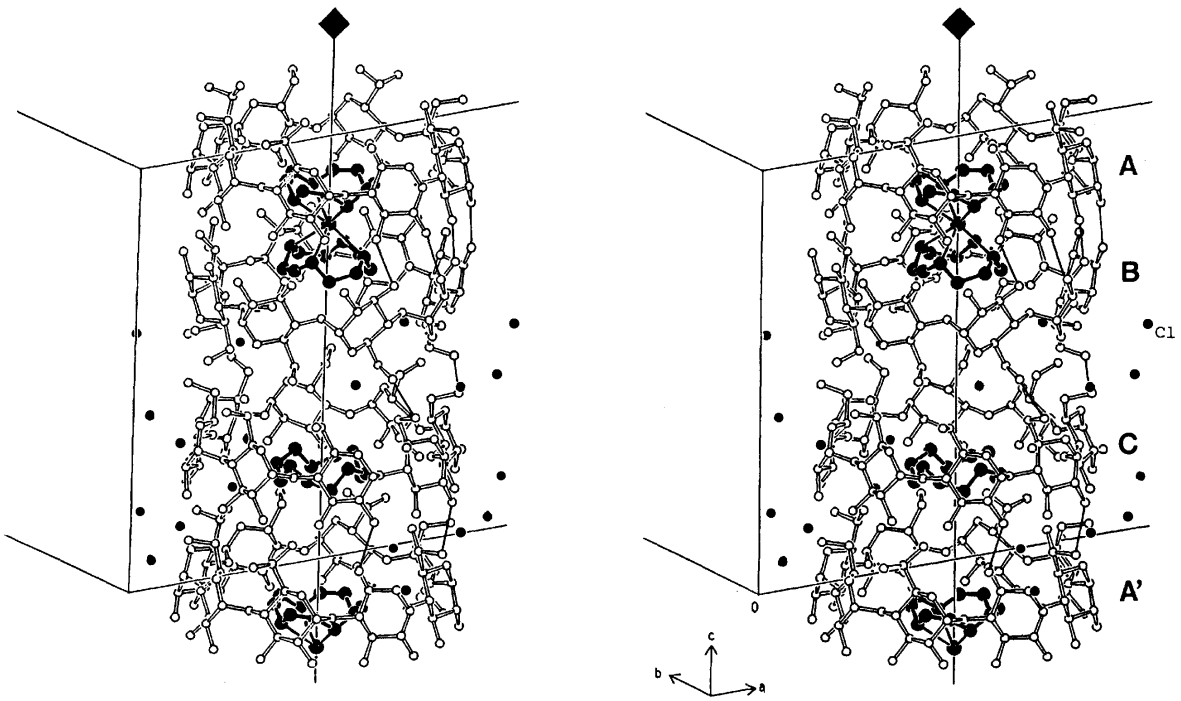

Fig. 1. The stereo view of the channel-type structure of γ-CD·12-crown-4·NaCl (3:3:1) inclusion complex. Na^+, 12-crown-4 molecules, Cl^- labeled by "Cl" and water molecules are shown by full circles. Only symmetry independent intermolecular hydrogen bonds are indicated by straight lines.

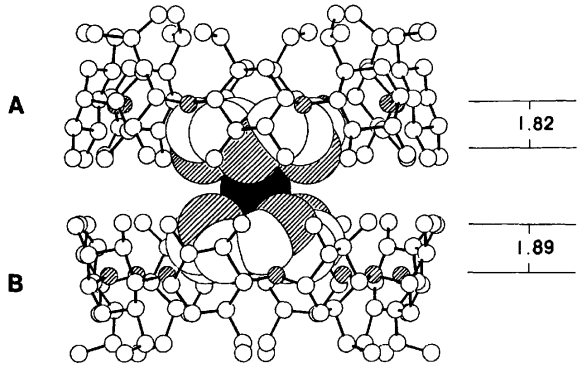

Fig. 2. The structures of γ-CD·12-crown-4·Na^+ inclusion complexes. Cations and 12-crown-4 molecules are plotted in space filling mode, indicated by full and hatched circles, respectively. O(4) atoms are also indicated by hatching. Interplanar distances(Å) between O(4) atoms plane and oxygen atoms of 12-crown-4 molecules are given.

ular hydrogen bonds are formed between O(2,3) (secondary hydroxyl groups (see Fig. 3.)) of the γ-CD **A** and O(2,3) of the γ-CD **B**, O(6) (primary hydroxyl groups) of **B** and O(6) of **C**, O(2,3) of **C** and O(6) of **A'**; the hydrogen bond distance of O(2)1···O(2)3 is 3.00, O(3)1···O(3)4 2.79, O(2)2···O(2)4 2.95, O(3)2···O(3)3 2.85, O(6)3···O(6)5 2.90, O(6)4···O(6)6 2.80, O(2)5···O(6)B1 2.82, O(2)6···O(6)2 2.85 Å.

The Na^+ coordinates to eight oxygen atoms of two

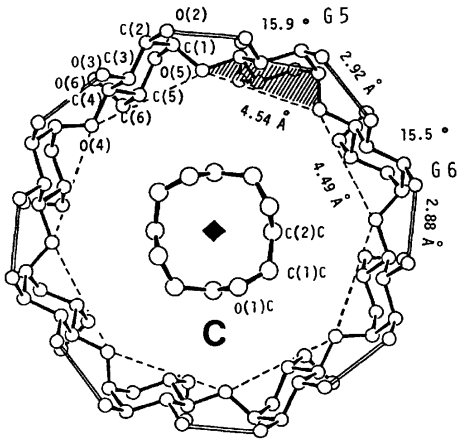

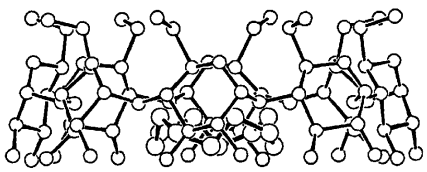

Fig. 3. The structure of the complex C with C_4 symmetry. One of O(4)'-C(1)-C(4)-O(4) atoms planes is indicated by hatching, and geometrical values are shown.

Table 2. Geometrical Data

Complex		H-Bond distance (Å)	Distance (Å)	Tilt-angle (°)
A	G1	2.81	4.45	11.9
	G2	2.80	4.55	11.3
B	G3	2.89	4.48	15.9
	G4	2.86	4.50	17.6
C	G5	2.92	4.54	15.9
	G6	2.89	4.49	15.5

a) The H-bond distance is defined as the O(3)n-O(2)n+1 distance. b) The distance is defined as the O(4)n-O(4)n+1 distance. c) The tilt-angle is defined as the angle made by (O)4 atoms plane and the plane formed by O(4)n+1, C(1)n, C(4)n, O(4)n of each glucose residue.

12-crown-4 molecules to form a 1:2 sandwich-structure complex, which is included by two tail-to-tail oriented γ-CDs **A** and **B**. Therefore, as shown in Fig. 2,[23] 12-crown-4 and γ-CD molecules could form complexs with Na^+ in a 2:2:1 ratio, as well as Li^+ and K^+. The distance between a Na^+ and Cl^- is 11.5 Å, showing a very weak electrostatic interaction between them.

The conformation of complex **B** is shown in Fig. 3, and the geometrical data of γ-CDs are given in Table 2, indicating very normal and more symmetrical structures compared with γ-CD hydrates.[24,25] As is well known, the secondary hydroxyl groups between neighboring glucose residues form intramolecular hydrogen bonds to maintain the round shape of the γ-CD ring; O(2)n···O(3)n+1 hydrogen bond distances are in the range 2.80—2.92 Å. The eight glycosidic O(4) oxygen atoms are coplanar within 0.01, 0.01, and 0.02 Å for γ-CDs **A**, **B**, and **C**, and the average distances of O(4)n···O(4)n+1 in each complex are 4.50, 4.49, and 4.51 Å. The glucose residues are inclined to the four-fold rotation axis so as to make the primary hydroxyl side narrow, and the secondary hydroxyl side wide. The tilt angles of glucose residues are defined as the angles made by the plane through O(4) atoms and the plane formed by O(4)n+1, C(1)n, C(4)n, O(4)n of each glucose.[24] The average tilt angles are 11.6, 16.8, and 15.7° for **A**, **B**, and **C**, respectively.

As pointed out in previous X-ray studies, the differences of the tilt angles among three γ-CDs are derived from the intermolecular hydrogen bonds between γ-CDs; the intermolecular hydrogen bonds between γ-CD **A** and **C** make the ring of γ-CD **A** wide at the primary site, so γ-CD **A** has more cylindrical geometry than **B** and **C**. This difference of γ-CD's geometries directly affects the locatins of 12-crown-4 molecules in **1**; the 12-crown-4 molecule is included more deeply in γ-CD **A** than in **B** and **C**, which have inclined cone structures. However, in **2**, **3**, and **4**, the existence of cations make this situation more complicated.

The interplanar distance between the four O(1) atoms plane of a 12-crown-4 molecule and the eight O(4) atoms plane of γ-CD could be adopted as an indicator of the inclusion depth. These distances in complexes **A** and **B** are given in Table 3 for **1**, **2**, **3**, and **4**. The distances of complexes **A** and **B** in **1** are 1.25 and 1.64 Å, respectively, and each value is the smallest among the corresponding complexes in Table 3, showing that each 12-crown-4 molecule of complexes **A** and **B** in **1** are deeply included in the γ-CD cavity. In the cases of **2**, **3**, and **4**, the locations of 12-crown-4 molecules depend not only on the shape of γ-CDs but also on the cation diameters. In **2** where the small cation, Li^+, exists, 12-crown-4 molecules are shallowly included in γ-CDs; on the other hand, in **4** 12-crown-4 molecules enter the γ-CD's cavities deeply due to the large cation diameter of K^+. In **3**, the distance at complex **A** is an intermediate value between the values of **2** (Li^+) and **4** (K^+), but the distance at complex **B** is almost same as in **2**. This result is due to the difference in the geometries of γ-CDs **A** and **B** mentioned above. Since γ-CD **A** is in a cylindrical structure and γ-CD **B** is in a cone-like structure, a 12-crown-4 molecule could more easily enter the cavity of γ-CD **A** than that of γ-CD **B**, as in **1**.

Table 3. Interplanar Distances

Complex	1	2	3	4
A	1.25	2.09	1.82	1.50
B	1.64	1.86	1.89	1.69

The conformation of the (12-crown-4)$_2$·Na^+ complex and the main short contacts between the γ-CD molecules and the (12-crown-4)$_2$·Na^+ complex are shown in Fig. 4. The structure of the (12-crown-4)$_2$·Na^+ complex in the hydrophobic channel of γ-CD molecules is quite normal. This complex has an approximate S_8 symmetry and the Na^+–O bond distances at the sites of complexes **A** and **B** are 2.58(5) and 2.58(4) Å, respectively. These values are normal compared with the Na^+–O distances of 2.474(8)—2.543(8) Å of (12-crown-4)$_2$·$NaClO_4$.[17] However, the Li^+–O distances of **2** are unusually long; 2.45(8) and 2.54(8) Å at complexes **A** and **B**. The Li^+–O average distance of the 12-crown-4·LiSCN 1:1 complex[26] is 2.08 Å, and that of [Li(12-crown-4)$_2$][$AsPh_2$] and

$[Li(12\text{-crown-}4)_2][PPh_2]$,[27] where Li^+ has a coordination number of 8, as in **2** is 2.35 Å. The attractive forces by the van der Waals interaction between 12-crown-4 molecules and γ-CD molecules make the Li^+–O bond distances long. The K^+–O bond distances of **3** are 2.80(8) and 2.99(9) Å at complexes **A** and **B**, respectively. Although in terms of the large esd's, these values are almost normal compared with the K^+–O distances of 2.77—2.83 Å in the 18-crown-6·KSCN complex,[28] the 12-crown-4 molecule can not form a complex with K^+ by itself.

2. Attempt to Form the Double Macrocyclic Inclusion Complex by 12-Crown-4, γ-CD and Rb^+. Comparing the interplanar distances at complexes **A** and **B** in **1** with the values in **4**, it was expected that 12-crown-4 molecules and γ-CDs might form a double macrocyclic inclusion complex with a larger cation than K^+, i.e. Rb^+. The crystal was prepared by the same procedure as in **3**, using RbCl instead of NaCl.

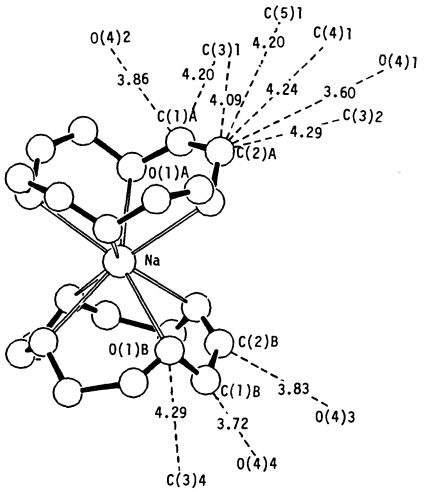

Fig. 4. The structures of $(12\text{-crown-}4)_2Na^+$ complexes. Intermolecular contacts with γ-CDs (less than 4.3 Å) are shown by dotted lines.

3845 independent reflections (2663 with $I > 3\sigma(I_0)$) were collected up to 100° in 2θ. A diffference Fourier synthesis was calculated using the atomic coordinates of the γ-CDs of **3**. Atoms of 12-crown-4 molecules were found, but the peak of cation did not appear, as is shown in Fig. 5. There was a very low peak (0.50, 0.0, 0.79) compared with the peak of Na^+. However, the peak of Rb^+ does not appear with a low ocupancy, but may be that of contaminated cation, probably Na^+ with a low occupancy, since, in **2**, a contaminated Na^+ of 1.9% was detected by atomic absorption analysis.[19] Therefore, this system composed of γ-CDs and 12-crown-4 molecules can not catch Rb^+ cations.

Conclusion

The Na^+ cation can exist in a hydrophobic circumstance of γ-CD cavities by forming a sandwich structure complex with two 12-crown-4 molecules, as well as Li^+ and K^+. The $(12\text{-crown-}4)_2\cdot Na^+$ sandwich structure complex in the γ-CDs **A** and **B** has normal Na^+–O bond distances, while unusually long Li^+–O bond distances of 2.45 and 2.54 Å were found in **2**.[19] The cation–oxygen bond distances are mainly determined by two interactions, i.e., electrostatic interaction between the cation and oxygen atoms of 12-crown-4 molecules, and van der Waals interaction between 12-crown-4 molecules and γ-CDs. The latter strongly affects the Li^+–O bond distances in **2**. The Na^+ may be more fit to enter the space between complexes **A** and **B** than Li^+, since these two interactions are reasonably balanced in **3**.

These double macrocyclic inclusion complexes catching cations may be models of the transport of ions through lipid bilayer membranes by an ionophore, such as Valinomycin. Although CD molecules are not as flexible as lipid bilayer membranes, the channel of two tail-to-tail oriented CDs, γ-CDs **A** and **B** in this paper, is analogous to lipid bilayer membranes at several points, such as the existence in

Z= 79/100

X	Y= 0	1	2	3	4	5	6
50	1134	948	524	141			
51	947	785	421	99			
52	524	420	193	10			
53	140	94	3				
54							
55							
56							

Z= 79/100

X	Y= 0	1	2	3	4	5	6
50	89	82	66	45	20		
51	82	74	61	49	31		
52	65	51	35	26	17		
53	45	23	3				
54	20						
55							
56							

Fig. 5. Difference Fourier map of the Na^+ position (left) and corresponding map of the complex with Rb^+(right). These two difference Fourier syntheses were calculated by the same scale.

an aqueous solution and the exchange of their guest molecules, as described by Stezowski et al.[3] The presented system, that γ-CDs include cations through the intermediary of the hydrophobic methylene rings of 12-crown-4 molecules, is similar to the situation that lipid bilayer membranes permit cations caught by ionophores to diffuse in them by an interaction between the hydrophobic interior of membranes and the hydrophobic exterior of ionophore·cation complexes.

This system could also have ion selectivity by the above-mentioned interactions among γ-CDs, 12-crown-4 molecules and cations. From only the presented work about this system, it is difficult to elucidate the difference of affinities of the double macrocyclic inclusion complex to three cations (Li^+, Na^+, and K^+) in detail. However, at least, the affinity of this system to Rb^+ is very small.

We are indebted to the Crystallographic Research Center, Institute for Protein Research, Osaka University, for computer calculations. We thank Nihon Shokuhin Kako Co., Ltd., Tokyo, Japan for a supply of γ-CD. This work was supported by a Grant-in-Aid for Special Project Reseach (No. 62216018) from the Ministry of Education, Science and Culture.

References

1) M. L. Bender and M. Komiyama, "Cyclodextrin Chemistry," Springer-Verlag, Berlin (1978).
2) W. Saenger, *Angew. Chem., Int. Ed. Engl.*, **19**, 344 (1980).
3) J. J. Stezowski, K. H. Jogun, E. Eckel, and K. Bartels, *Nature (London)*, **274**, 621 (1978).
4) M. M. Hording, J. M. Maclennen, and R. M. Parton, *Nature (London)*, **274**, 617 (1978).
5) K. Harata, *Bull. Chem. Soc. Jpn.*, **53**, 2782 (1980).
6) K. Harata, K. Uekama, M. Otagiri, F. Hirayama, and H. Ogino, *Bull. Chem. Soc. Jpn.*, **54**, 1954 (1981).
7) K. Harata, *Bull. Chem. Soc. Jpn.*, **55**, 2315 (1982).
8) K. Harata, K. Uekama, M. Otagiri, F. Hirayama, and Y. Ohtani, *Bull. Chem. Soc. Jpn.*, **58**, 1234 (1985).
9) R. Tokuoka, T. Fujiwara, and K. Tomita, *Acta Crystallogr., Sect. B*, **37**, 1158 (1981).
10) J. A. Hamilton and M. N. Sabesan, *Acta Crystallogr., Sect. B*, **38**, 3063 (1982).
11) M. Czubler, E. Eckle, and J. J. Stezowski, *J. Chem. Soc., Chem. Commun.*, **1981**, 1291.
12) J. J. Stezowski, *'Trans. A. C. A.'*, **20**, 73 (1985).
13) G. Le Bas, C. De Rango, N. Rysanek, and G. Tsoucaris, *J. Inclusion Phenomena*, **2**, 861 (1984).
14) S. Kamitori, K. Hirotsu, and T. Higuchi, *J. Chem. Soc., Chem. Commun.*, **1986**, 690.
15) F. Vögtel, "Host Guest Complex Chemistry," Springer-verlag: Berlin, Heidelberg, New York (1982).
16) P. Groth, *Acta Chem. Scand.*, **35**, 463 (1981).
17) E. Mason and H. A. Eick, *Acta Crystallogr., Sect. B*, **38**, 1821 (1976).
18) P. Groth, *Acta Chem. Scand.*, **32**, 279 (1978).
19) S. Kamitori, K. Hirotsu, and T. Higuchi, *J. Am. Chem. Soc.*, **109**, 2409 (1987).
20) T. Sakurai, "The Universal Crystallographic Computing System," The Crystallographic Society of Japan, (1967).
21) W. R. Busing, K. O. Martin, and H. A. Levy, ORFLS, Report ORNL-TM-305, Oak Ridge National Laboratory, Oak Ridge, (1965).
22) C. K. Johnson, ORTEP 2, Report ORNL-5138, Oak Ridge National Laboratory, Tenessee, (1976).
23) W. D. S. Motherwell, PLUTO78, A Program for plotting Molecular and Crystal Structures., University Chemical Laboratory, Cambridge.
24) K. Harata, *Bull. Chem. Soc. Jpn.*, **60**, 2763 (1987).
25) J. M. Maclennan and J. J. Stezowski, *Biochem. Biophys. Res. Commun.*, **92**, 933 (1980).
26) P. Groth, *Acta Crystallogr., Sect. B*, **38**, 1821 (1982).
27) H. Hope, M. M. Olmstead, P. P. Power, and X. Xu, *J. Am. Chem. Soc.*, **106**, 819 (1984).
28) M. Dobler and R. P. Phizackerley, *Acta Crystallogr., Sect. B*, **30**, 2748 (1974).

 © 1988 The Chemical Society of Japan Bull. Chem. Soc. Jpn., 61, 3831—3837 (1988)

The Valence Control and Catalytic Properties of $La_{2-x}Sr_xNiO_4$

Taihei NITADORI,* Motohiko MURAMATSU, and Makoto MISONO†
Tabacco Science Research Laboratory, Japan Tobacco, Inc.,
Umegaoka, Midori-ku, Yokohama, Kanagawa 227
†Department of Synthetic Chemistry, Faculty of Engineering, The University
of Tokyo, Hongo, Bunkyo-ku, Tokyo 113
(Received April 30, 1988)

A series of $La_{2-x}Sr_xNiO_4$ catalysts (x=0—1.0) with a K_2NiF_4-type structure were prepared, and the average oxidation number of the Ni ion and the stoichiometry of the oxygen in the catalysts were measured. We also investigated the relationships between the reactivity of the catalysts and their catalytic activity for oxidation. The average oxidation number of the Ni ion increased monotonously from 2.32 (x=0) to 2.90 (x=1.0) upon the Sr substitution, and the composition changed with the x value from oxygen-excess (x=0—0.2) to oxygen-deficient (x=0.6—1.0), via a stoichiometric composition at x=0.4. In the range of x=0—0.2 (oxygen excess), the desorption peaks of oxygen in TPD (temperature-programmed desorption) were observed at about 300 °C; these results were ascribable to the excess oxygen. In this range, the oxidizing power of the surface, which was measured by the reduction of the catalysts by CO, was comparatively high. For x=0.4—1.0 (stoichiometric to oxygen-deficient), the oxygen desorbed at a higher temperature, and the amounts increased in accordance with the increase in the oxygen deficiency. The oxidizing power of the surface similarly increased with x values up to x=0.8. The composition of metal on the surface generally reflected that in the bulk, as judged from XPS. The catalytic activity for the oxidation was in parallel with the oxidizing power of the surface in x=0.4—1.0.

K_2NiF_4-type mixed oxide (A_2BO_4) consists of alternating layers of ABO_3 perovskite and AO rock salt, being a kind of two-dimensional analogue of perovskite.[1] K_2NiF_4-type oxides with various A- and B-site metal ions are known,[2] as in the case of perovskite-type mixed oxides.[3] It is also possible to control the valence and stoichiometry by the appropriate substitution of constituent metal elements. Hence, a series of catalysts with a K_2NiF_4-type structure are suitable materials for research into the relationships between the reactivity of the oxygen on the surface and in the bulk and the catalytic activity, as in the case of such perovskites as $LnBO_3$ (Ln: rare earth, B: Mn, Fe, Co).[4-8]

Recently we reported the catalytic activity of $La_{2-x}Sr_xCoO_4$, a K_2NiF_4-type mixed oxide, and compared the results with those for $La_{1-x}Sr_xCoO_3$, perovskite.[9] In the case of simple 3d-transition metal oxides, nickel oxide shows a relatively high oxidation activity, coming next to cobalt and manganese oxides,[10] while $LaNiO_3$ perovskite shows an activity in the same level.[4,11] However, $LaNiO_3$ is not stable on a usual atmosphere, and the preparation of Sr-substituted $LaNiO_3$ is very difficult under ordinary conditions. Therefore, in the present study, we prepared a series of Sr-substituted La_2NiO_4 catalysts and determined the valence of the nickel ion at the B-site and the change in the nonstoichiometry of oxygen upon the Sr substitution. We also measured the catalytic activities for oxidation as well as the reactivity of the oxygen on the surface and in the bulk of the catalysts, and discussed the relationships between them.

Experimental

Preparation of $La_{2-x}Sr_xNiO_4$. The $La_{2-x}Sr_xNiO_4$ (x=0—1.5) catalysts (the actual compositions of these mixed oxides were, in general, nonstoichiometric, $La_{2-x}Sr_xNiO_{4+\delta}$, but the stoichiometric formulae will be used in this paper unless explicit presentation is necessary) were prepared from mixtures of acetates of the metal components. First, the mixed acetate solution was evaporated to dryness in a rotary evaporator (70 °C), and then the residual solid was decomposed in air at 300 °C for 3 h and finally calcined in a quartz crucible in air at 1000 °C for 10 h.

Powder X-ray diffraction patterns were recorded on a powder X-ray diffractometer (Rigaku Denki, Geigerflex, RAD-IIA) using Cu $K\alpha$ radiation. The surface area of the samples was measured by the BET method (static N_2 adsorption; Micromeritics; AccuSorb 2100).

The oxidation number of the nickel ion in the catalysts was measured by means of iodometry. This method has usually been used as a direct method for the measurement of the excess oxygen in nickel oxide[12] and for the measurement of the average oxidation number of a Co or Ni ion in mixed oxides.[13] A sample (ca. 100 mg) which was dried at 100 °C for 3 h was dissolved in 25 ml of 0.4 mol l^{-1} HCl plus 25 ml of 0.16 mol l^{-1} KI aqueous solution. The solution was then titrated with a standard thiosulfate solution.

The composition of metal ions was determined with the aid of inductively coupled plasma spectrometry (ICP) (Nippon Jarrell-Ash, ICAP-575-II). The X-ray photoelectron spectra (XPS) were obtained with a Shimadzu ESCA-750 apparatus employing Mg $K\alpha$ radiation (1253.6 eV) under a high vacuum of 10^{-6} Pa. The binding energy was calibrated by using a Cls electron line (285.0 eV) coming from the background.

Apparatus. Conventional flow and pulse systems described previously were used.[4-6]

Procedure. Temperature Programmed Desorption (TPD) of Oxygen: The TPD of oxygen was carried out with a flow system using helium as the carrier gas. Prior to each run, the sample (1.0 g) was pretreated in an O_2 stream for 1 h at 800 °C and then cooled to room temperature. Then, O_2 was replaced by He at room temperature. Any oxygen impurity in He was removed by the use of a Molecular Sieve (MS) 5A

trap kept at the temperature of liquid nitrogen. The temperature of the sample was raised at a constant rate of 20 deg min^{-1} in the He stream (25 cm^3 min^{-1}), and the oxygen desorbed was detected with a thermal conductivity detector. It was confirmed by a gas chromatograph that only oxygen existed in the effluent He gas. The TPD curves were reproduced in repeated runs (3 times) after the pretreatments above.

Reduction of Catalysts by CO: The reduction of the catalysts by CO was conducted in the pulse reactor. Prior to the reaction, the catalysts (50 mg) were treated in an O_2 stream (20 cm^3 min^{-1}) for 1 h at 300 °C, and then the O_2 stream was replaced by a He stream purified by the use of a MS-5A trap kept at the temperature of liquid N_2. The flow rate of the carrier gas (He) was 25 cm^3 min^{-1}, and the size of each pulse was 0.1 cm^3. The products were analyzed by means of a gas chromatograph.

Oxidation of Propane: The catalytic oxidation of propane was carried out with a flow system. Prior to each reaction, the catalysts (300 mg) were treated in an O_2 stream for 1 h at 300 °C. A gas mixture of propane (0.83%), O_2 (33.3%), and N_2 (balance) was fed into the reactor. The flow rate of the mixed gas was 60 cm^3 min^{-1}. The products were analyzed by means of a gas chromatograph.

Results

Catalysts and Their Physical Properties. The surface area, the crystal structure, and the compositions of the prepared catalysts, $La_{2-x}Sr_xNiO_4$, are summarized in Table 1. In the range of x=0—1.0, samples with a tetragonal K_2NiF_4-type structure were obtained, judging from the XRD patterns. At x=1.5, the sample was a mixture of K_2NiF_4-type oxide, SrO, and NiO, the content of the latter two both being about 10—20%. No XRD peaks of La_2O_3 were observed. The surface areas of the samples were all less than 3 m^2 g^{-1} because of the high calcination temperature, and they tended to increase with the x value. The bulk compositions of the metal ions measured by ICP are shown in Fig. 1. The bulk composition agreed well with the nominal composition expected from the quantities of starting materials, within the limits of experimental error. Hence, there was no substantial loss of any specific components during the preparation of the catalysts (for example, evaporation during the calcination).

Figure 2 shows the average oxidation number of the nickel ion at the B-site, as measured by iodometry. The average oxidation number of the nickel ion increased monotonously from 2.32 (x=0) to 2.90 (x=1.0) with the increase in x, as has been expected. It should further be noted that the nonstoichiometry varied from an oxygen-excess composition for x=0—0.2, through almost a stoichiometric one for x=0.4, to an oxygen-deficient one (x=0.6—1.0).

TPD of Oxygen. Figure 3 shows the TPD profiles of oxygen from the catalysts, where the rate of desorption, as calculated from the oxygen concentration in the effluent gas, is plotted against the catalyst temperature. As is shown in this figure, the amount of the oxygen desorbed below 800 °C decreased with the

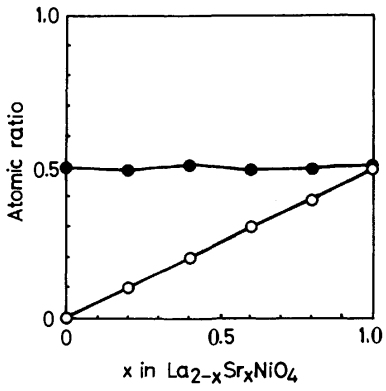

Fig. 1. The metal ion composition in the bulk.
○: Sr/La+Sr, ●: Ni/La+Sr.

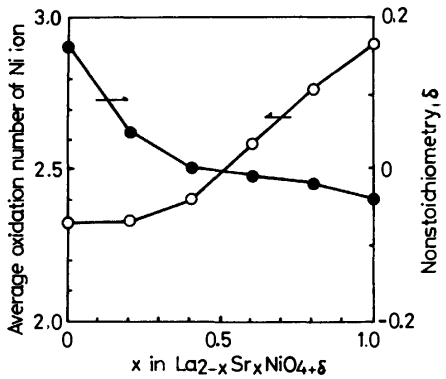

Fig. 2. The average oxidation number of Ni ion and the nonstoichiometry (δ) of $La_{2-x}Sr_xNiO_4$.

Table 1. The Surface Areas, Structures, and Compositions of Catalysts

x	Surface area/m^2 g^{-1}	Structure	Composition[a]
0	1.6	K_2NiF_4-type	$La_{2.0}$ $Ni^{2+}_{0.68}Ni^{3+}_{0.32}O_{4.16}$
0.2	2.0	K_2NiF_4-type	$La_{1.8}Sr_{0.2}Ni^{2+}_{0.67}Ni^{3+}_{0.33}O_{4.07}$
0.4	1.9	K_2NiF_4-type	$La_{1.6}Sr_{0.4}Ni^{2+}_{0.60}Ni^{3+}_{0.40}O_{4.00}$
0.6	2.5	K_2NiF_4-type	$La_{1.4}Sr_{0.6}Ni^{2+}_{0.42}Ni^{3+}_{0.58}O_{3.99}$
0.8	2.9	K_2NiF_4-type	$La_{1.2}Sr_{0.8}Ni^{2+}_{0.24}Ni^{3+}_{0.76}O_{3.98}$
1.0	2.5	K_2NiF_4-type	$La_{1.0}Sr_{1.0}Ni^{2+}_{0.09}Ni^{3+}_{0.91}O_{3.96}$
1.5	2.5	K_2NiF_4-type, NiO, SrO	—

a) The metal ions were measured by ICP. The contents of oxygen were calculated from the oxidation number of the Ni ion, as measured by iodometry.

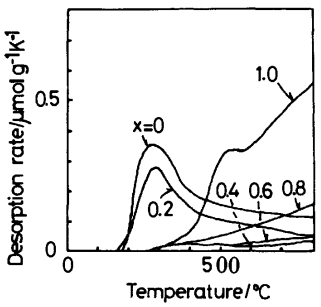

Fig. 3. TPD profiles of oxygen from $La_{2-x}Sr_xNiO_4$.

Table 2. The Amount of Oxygen Desorption, the Corresponding Layers, and the Change in the Nonstoichiometry (see text)

x	Amount of oxygen desorbed/cm³ g⁻¹	Corresponding layer	$\Delta\delta$
0	2.48	8.6	0.09
0.2	1.77	5.0	0.06
0.4	0.26	0.8	0.01
0.6	0.30	0.7	0.01
0.8	0.78	1.5	0.03
1.0	3.25	6.3	0.10

a) The amount of oxygen in TPD desorbed up to 800 °C. The surface layers corresponding to the amounts of desorbed oxygen (assuming that the amount of oxygen in the surface monolayer was 0.96×10^{19} atom m^{-2}). The change in the nonstoichiometry attributed to the oxygen desorption ($\Delta\delta$: $La_{2-x}Sr_xNiO_{4+\delta-\Delta\delta}$).

increase in the Sr content in the range of x=0—0.4, showed a minimum at x=0.4, and then increased with x (x=0.4—1.0). The TPD profiles for x=0 and 0.2 were similar to each other, both having a peak at around 300 °C, but were quite different from those for x=0.4—1.0. This difference in the TPD profiles seems to correspond to the transition of the nonstoichiometry of the catalysts from an oxygen-excess (x=0—0.2) to a stoichiometric and an oxygen-deficient composition (x=0.4—1.0).

The amounts of oxygen desorbed below 800 °C, as well as the number of surface layers and the change in the nonstoichiometry (δ) corresponding to the amounts of oxygen, are shown in Table 2, where the surface layers were calculated by assuming that the density of the oxygen in the monolayer is 0.96×10^{19} atom m^{-2} and where the change of the nonstoichiometry, $\Delta\delta$, caused by desorption was expressed by; $La_{2-x}Sr_xNiO_{4+\delta-\Delta\delta}$. All of these values varied in a similar way, showing a minimum at x=0.4—0.6. The amounts of oxygen desorbed were always more than one surface monolayer except for the values of x=0.4 and 0.6. This indicates that the desorption of the lattice oxygen in the bulk took place in addition to the adsorbed oxygen. In the range of x=0.4—0.6, the nonstoichiometry and the average oxidation number

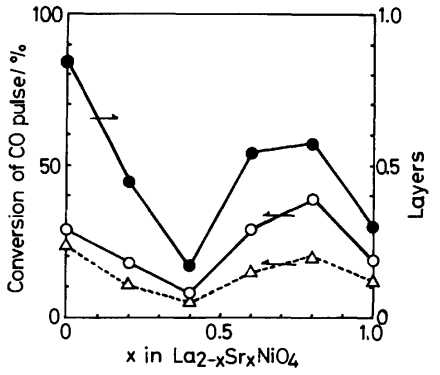

Fig. 4. The % conversion of CO to CO_2 in the first and in the fifth pulse and the amount of oxygen consumed by the first CO pulse in the unit of surface layers.
O: the first pulse, △: the fifth pulse, ●: layers.

of the Ni ion in catalysts, being nearly stoichiometric, are less influenced by the change in the atmosphere (partial oxygen pressure) or the temperature.

Reduction of the Catalyst by CO (Oxidizing Power of the Surface). The % conversions of CO to CO_2 decreased gradually upon repeated pulses (at 10 min intervals). The decrease was smaller for x=0—0.2 (oxygen-excess) than for x=0.6—1.0 (oxygen-deficient). The values in the first and fifth pulses are shown in Fig. 4, where the amount of oxygen consumed by the first CO pulse is also given in the unit of surface layers. The conversion may be regarded as a measure of the oxidizing power per unit of catalyst weight. The oxidizing power expressed by the % conversion in the first pulse decreased first with the increase in x, showing its lowest value at x=0.4. It then increased with x up to x=0.8 and decreased at x=1.0. The amount of oxygen consumed by the first CO pulse for x=0 corresponded to about 6% of the excess oxygen. As this amount was less than the monolayer, this value may express the oxidizing power of the catalyst surface (the reducibility of the surface).

Surface Composition of the Catalyst. The surface compositions of the catalysts were measured by XPS; the results are shown in Fig. 5, where Eq. 1[14] was used for the calculation.

$$(N_a/N_b) = (n_a/n_b)(\lambda_a/\lambda_b)(\sigma_a/\sigma_b)(S_a/S_b) \quad (1)$$

where N: peak intensity, n: atoms per unit volume, λ: mean free path of the electron, σ: ionization cross section, and S: instrumental factor. The peak areas of La4d, Sr3d, and Ni3p, including the satellite peak, were used for N, while the values of σ were taken from the literature.[15] "$\lambda\cdot S$" was assumed to be constant, as in a previous work.[16] The surface compositions of the catalysts, as determined by Eq. 1, are not very accurate, but they may be sufficient to compare the relative change in the surface composition for a series of catalysts. As may be seen from this figure, though the

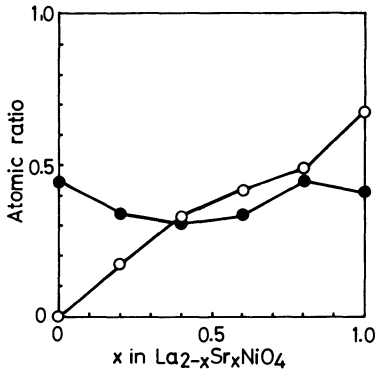

Fig. 5. The surface composition of metal ion determined by XPS.
O: Sr/La+Sr, ●: Ni/La+Sr.

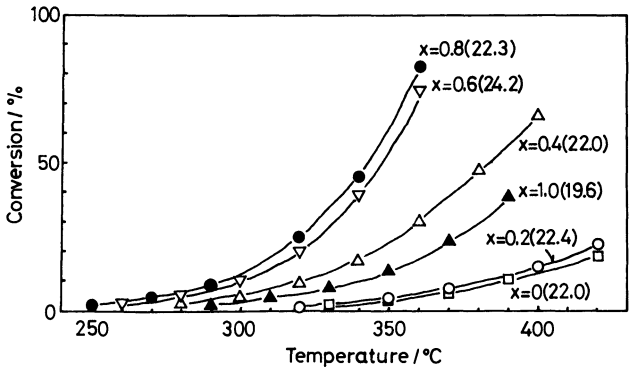

Fig. 6. The catalytic activity for propane oxidation over $La_{2-x}Sr_xNiO_4$. The activation energy in parenthesis: kcal mol^{-1}.

atomic ratio at Sr in the A-site (O) increased monotonously with x, this value was generally higher than that in the bulk composition. On the other hand, the atomic ratio of the Ni ion was considerably lower than that in the bulk, except for the values of x=0 and 0.8. The ratio of La:Sr:Ni, as calculated from Eq. 1, was 51:25:24 (54:13:33 in the bulk) at x=0.4 and 33:34:31 (bulk, 40:27:33) at x=0.8. The binding energies of La4d, Sr3d, and Ni3p in XPS changed little from one catalyst to another.

Catalytic Activity for the Complete Oxidation of Propane. The activity for the propane oxidation is shown in Fig. 6. The only reaction products were CO_2 and H_2O for all the catalysts. As is shown in this figure, the oxidation activities per unit of weight of the catalysts were very low at x=0—0.2; they then became higher with x up to x=0.8 and then decreased at x=1.0, showing a maximum at x=0.8. The activation energy obtained from the data at a low conversion level (below 10%) was 19.6—24.1 kcal mol^{-1}, as is shown in parentheses in Fig. 6.

Discussion

Structure and Composition of $La_{2-x}Sr_xNiO_4$. As K_2NiF_4-type mixed oxides often show interesting electrical properties, quite a few studies have been reported about this type of mixed oxides, formed by various A- and B-site ions.[2] The structure and the electrical properties of $La_{2-x}Sr_xNiO_4$ have also been studied.[17-19] All of these reports show that $La_{2-x}Sr_xNiO_4$ has a K_2NiF_4-type structure in the range of x=0—1.0, in agreement with the results of the present study. However, the formation of a K_2NiF_4 structure with x=1.5 has not been reported. The reason may be the necessity of an extremely high and unstable oxidation state of tetravalent Ni. This corresponds to the difficulty of Sr substitution in $LaNiO_3$ perovskite.

In the case of La_2NiO_4, a part of the Ni ion is oxidized to make it trivalent, since its tolerance factor is close to the lower limit of the tetragonal K_2NiF_4-type structure.[2] Hence, the composition becomes oxygen-excess. The average oxidation number of the Ni ion (2.32) and the oxygen-excess composition observed for x=0 in the present work are consistent with those data. It is probable that cation deficiencies at both A- and B-sites were formed in La_2NiO_4, as in the case of $LaMnO_3$.[20] The oxidation number of the Ni ion increased monotonously from 2.32 (x=0) to 2.90 (x=1.0) with the increase in the extent of the Sr substitution for the A-site (Table 1). Gopalakrishnan et al. also reported a monotonous increase in the number from 2.15 (x=0) to 3.00 (x=1.0)[17] with a change in the stoichiometry with x from an oxygen-excess to a stoichiometric composition. This trend is consistent with that found in the present work, except that the composition in the present work became oxygen-deficient at a higher x value.. This difference may be due to the different calcination conditions. In this work, the oxides were calcined in air at 1000 °C, while in the oxygen these were caclined at 1200 °C for more than 72 h for x=0.4—1.0 in their case.

The valence control of the B-site ion as well as the variation in the nonstoichiometry upon the Sr substitution obtained in this work may be compared with those results previously obtained for perovskites and $La_{2-x}Sr_xCoO_4$. In the case of $La_{2-x}Sr_xCoO_4$, the average oxidation number of the Co ion increased monotonously from 2.28 (x=0) to 3.34 (x=1.5) with the increase in x, and its composition varied from $La_2CoO_{4.14}$ to $La_{0.5}Sr_{1.5}CoO_{3.92}$.[9] This variation is very similar to that found in this study for $La_{2-x}Sr_xNiO_4$. The change in nonstoichiometry was also similar for $La_{1-x}Sr_xMnO_3$.[8] On the other hand, in the case of the $La_{1-x}Sr_xCoO_3$ or $La_{1-x}Sr_xFeO_3$ system,[6,7] although the averag oxidation number of the B-site ion increased monotonously with the x value, the composition varied from stoichiometric to oxygen-deficient. This variation corresponds to that found in the present study for $La_{2-x}Sr_xNiO_4$ above x=0.4.

Thus, it may be stated that the $La_{2-x}Sr_xNiO_4$

catalysts prepared in the present study have well-controlled oxidation numbers of the Ni ion and nonstoichiometry, in general agreement with those of the previous studies of related mixed oxides.

The Effect of Sr Substitution on the Oxidizing Power of the Surface, the Surface Composition, and the TPD. The oxidizing power of the surface, as measured by the CO pulse, varied as is shown in Fig. 4. This trend appears to correspond closely to the changes in the nonstoichiometry and the TPD profiles. The initial decrease in the oxidizing power (x=0—0.4) apparently parallels the desorption peak at about 300 °C in the TPD.[21] On the other hand, the variation in the oxidizing power of the surface in the range of x=0.4—0.8 corresponds to the variation in the oxygen desorption in TPD in the high-temperature region. The low oxidizing power of the surface at x=1.0 may be due to the stability of the oxygen-deficient composition or to the formation of a Sr^- rich phase on the surface, as will be described below.

The reactivity of the oxide ion in the bulk may be seen in the TPD profiles (Fig. 3). In x=0—0.2, the large peaks in the TPD profiles at about 300 °C are ascribed to the desorption of the excess oxygen (the amount of oxygen desorbed was about 4 times the monolayer).

For x=0.4—1.0, the TPD profiles were similar, with no peak at about 300 °C, and the amount of the desorbed oxygen increased with the x. The oxygen desorbed at a higher temperature may be assigned to the formation of the oxygen deficiency if one considers the relationship between the amounts of desorbed oxygen, the valence change in the B-site ion, and the change in the nonstoichiometry (Table 2). Consequently, the valence control by the following scheme, as in the $La_{1-x}Sr_xCoO_3$ system,[4-6] is probable for x=0.4—1.0.

$$La_2^{3+}Ni^{2+}O_4 \xrightarrow{Sr^{2+}} La_{2-x}^{3+}Sr_x^{2+}Ni_{1-x}^{2+}Ni_x^{3+}O_4 \quad (2)$$

$$La_{2-x}Sr_xNi_{1-x}^{2+}Ni_x^{3+}O_4 \longrightarrow La_{2-x}Sr_xNi_{1-x+2\delta}^{2+}Ni_{x-2\delta}^{3+}O_{4-\delta} + \delta/2O_2 \quad (3)$$

First, a some of the divalent Ni ions are oxidized to the trivalent state upon the Sr substitution (Eq. 2). With further Sr substitution, the oxygen desorbs, forming a lattice oxygen deficiency, therefore, a some of the trivalent Ni ions are reduced to the divalent state (Eq. 3). The lattice oxygen deficiency should tend to increase with the increase in x and the rise in the temperature, as reflected in the TPD profiles at x=0.4—1.0.

The concentration of Sr on the surface was higher than that in the bulk in the whole range of x values studies. Especially at x=1.0, Sr occupied about half of the metal ions on the surface layer (about 33%, in bulk). Accordingly, a Sr-rich phase on the surface, which may be formed in this catalyst, is a possible reason for the lower oxidizing power of the surface at x=1.0. The Ni concentration on the surface varied with the x value, but it accounted for 24—33% of the total metal ions; this value did not change much among the catalysts, though it was always lower than the concentration in the bulk. On the whole, though the bulk composition was generally reflected in the surface composition, caution must be exercised when the property in the bulk is used for the discussion of the surface properties.

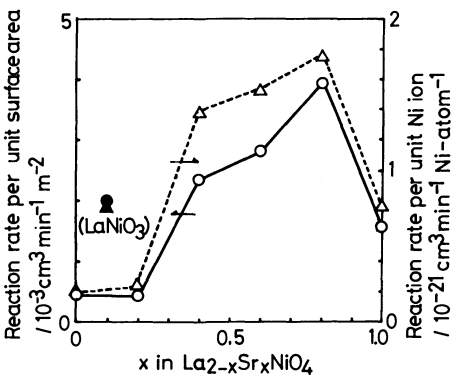

Fig. 7. The reaction rate for propane oxidation at 227 °C per unit surface area and unit Ni ion on the surface.

The Effect of Sr Substitution on the Catalytic Activity for Oxidation. Though the catalytic properties of $LaNiO_3$ perovskite have been reported in several papers,[22] there have been only a few studies of the catalysis of La_2NiO_4,[23-25] and no studies on the effect of the valence control have been reported. When the catalytic activity for oxidation is compared per unit of surface area of the catalysts, the catalytic activities of x=0.4—0.8 in this work were comparable with or higher than that of $LaNiO_3$[4] (Fig. 7). The reaction rate of the propane oxidation, normalized to the Ni atom on the surface, is also shown in Fig. 7; it was calculated from the surface composition (Fig. 5).[26] The activity per surface Ni ion thus calculated was higher for $La_{2-x}Sr_xNiO_4$ (x=0.4—0.8) than for $LaNiO_3$.

The catalytic activity for oxidation increased steeply from x=0.2 to 0.4 (Fig. 7). If one considers this result together with the changes in the composition, the TPD profiles, and the oxidizing power of the surface described above, the catalysts may be divided again into two groups, x=0—0.2 and 0.4—1.0.

First we will discuss the latter group. In this range (x=0.4—1.0), the oxygen deficiency and the reactivity of the lattice oxygen increased with the x value up to x=0.8. A similar increase in the catalytic activity has already been reported for $La_{1-x}Sr_xCoO_3$ perovskite.[4-6] Further, the oxidizing power of the surface and the oxidation activity showed parallel variations in this range of x, as in the cases of $La_{1-x}Sr_xMnO_3$ and $La_{2-x}Sr_xCoO_4$.[8,9] It is noteworthy that the oxidizing power of the surface showed a maximum where the

composition of the catalysts was slightly shifted from stoichiometric to oxygen-deficient. It is probable that, in this state, the redox cycles of the desorption and adsorption of oxygen on the surface and/or in the vicinity of the surface occurred smoothly; therefore, the catalytic activity increased. Hence, the catalytic activity in the present Ni system is closely related to the reactivity of the oxygen on the surface, as in $La_{1-x}Sr_xMnO_3$,[8] but the contribution of the oxygen in the bulk may not be neglected, especially in x=0.4—1.0, as in $La_{1-x}Sr_xCoO_3$.[4-6]

On the other hand, in the range of x=0—0.2, the oxidation activity was low, although large peaks were observed around 300 °C (due to the excess oxygen) in TPD and the oxidizing power of the surface was comparatively high. It may be suggested as the reason for this discrepancy that the excess oxygen is inactive for the catalytic oxidation reaction, although it is responsible for the TPD peaks at about 300 °C and the reducibility of the surface. In the cases of $La_{1-x}Sr_xMnO_3$ and $La_{2-x}Sr_xCoO_4$, the composition for low x values was oxygen-excess[8,9] and the catalytic activities were lower than for those with higher x values. This result also indicates that the low catalytic activity is correlated to the oxygen-excess composition. The reason for this is not clear at present, but it is possible that the ability of the dissociation or the activation of the oxygen is low because of the very small oxygen deficiency on the surface, as in the case of $La_{1-x}Sr_xMnO_3$.[8]

Conclusion

A series of $La_{2-x}Sr_xNiO_4$ (x=0—1.0) catalysts with a K_2NiF_4-type structure were prepared. With the increase in the x value, the average oxidation number of the Ni ion increased monotonously from 2.32 (x=0) to 2.90 (x=1.0) and the nonstoichiometry changed from an oxygen-excess to an oxygen-deficient composition via a stoichiometric one.

Based on the variation in the TPD of oxygen and the oxidizing power of the catalyst surface (as measured by the CO pulse), the catalysts were divided into two groups; (1) x=0—0.2 (oxygen-excess composition) and (2) x=0.4—1.0 (stoichiometric and oxygen-deficient). In Group (1), the desorption peak of oxygen ascribable to the excess oxygen was observed at about 300 °C, and the oxidizing power of the surface was comparatively high. On the other hand, in Group (2) oxygen desorbed at a relatively high temperature, with the formation of a lattice oxygen deficiency. The amount of oxygen desorbed and the oxidizing power of the surface increased from x=0.4 to x=0.8, much as with other perovskites and K_2NiF_4-type oxides.

The catalytic activity for the oxidation was in parallel with the oxidizing power of the surface in Group (2). However, the catalytic activity of Group (1) was low in spite of the considerable oxidizing power of the surface. Though the reason for this is not clear at present, it appears that the excess oxygen was inactive for the catalytical oxidation and/or that the ability of dissociation and activation of the oxygen on the surface was low.

References

1) D. Balz and K. Plieth, *Z. Elektrochem.*, **59**, 545 (1955); F. Galasso and W. Darby, *J. Phy. Chem.*, **66**, 1318 (1962).

2) P. Ganguly and C. N. R. Rao, *J. Solid State Chem.*, **53**, 193 (1984).

3) R. J. H. Voorhoeve, "Advanced Materials in Catalysis," ed. by J. J. Burton and R. L. Garton, Academic Press, New York (1977), p. 129.

4) T. Nakamura, M. Misono, T. Uchijima, and Y. Yoneda, *Nippon Kagaku Kaishi*, **1980**, 1679.

5) T. Nakamura, M. Misono, and Y. Yoneda, *Bull. Chem. Soc. Jpn.*, **55**, 394 (1982).

6) T. Nakamura, M. Misono, and Y. Yoneda, *J. Catal.*, **83**, 151 (1983); *Chem. Lett.*, **1981**, 1589.

7) T. Nitadori and M. Misono, *J. Catal.*, **93**, 459 (1985).

8) T. Nitadori, S. Kurihara, and M. Misono, *J. Catal.*, **98**, 221 (1986).

9) T. Nitadori and M. Misono, *Chem. Lett.*, **1986**, 1255.

10) G. E. Boreskov, *Kinet. Katal.*, **14**, 2 (1973).

11) N. Yamazoe and Y. Teraoka, *Shokubai*, **25**, 196 (1983).

12) S. W. Weller and S. E. Voltz, *J. Am. Chem. Soc.*, **76**, 4695 (1954).

13) B. E. Gushee, L. Kaz, and R. Ward, *J. Am. Chem. Soc.*, **79**, 5601 (1957).

14) Y. Hirooka, *Hyomen Kagaku*, **7**, 231 (1986).

15) J. H. Scofield, *J. Electr. Spectr. Relat. Phenom.*, **8**, 129 (1976).

16) T. Nitadori, T. Ichiki, and M. Misono, *Bull. Chem. Soc. Jpn.*, **61**, 621 (1988).

17) J. Goparakrishnan, G. Colsmann, and B. Reuter, *J. Solid State Chem.*, **22**, 145 (1977).

18) L. F. Kononynk, N. G. Surmach, and L. V. Makhnack, *Izv. Adad. Nauk, SSSR, Neorg, Mater.*, **18**, 1222 (1982); *Inorg. Mater.*, **18** 1029 (1982).

19) K. Ishikawa, S. Kondo, Y. Suzuki, S. Takayama, K. Shimada, and Y. Suzuki, *Bull. Chem. Soc. Jpn.*, **59**, 703 (1986).

20) B. C. Tofield and W. R. Scott, *J. Solid State Chem.*, **10**, 183 (1974).

21) Here, it must be considered that, in the CO pulse experiments, the catalysts were pretreated in a He stream at 300 °C, so the oxidation state may be different between the CO pulse and TPD experiments. In the TPD profile of x=0 after the pretreatment in the CO pulse, the peak about 300 °C did not appear, while oxygen desorption started at 320 °C. However, the composition of this sample was $La_2NiO_{4.11}$, still an oxygen-excess composition; therefore, the oxidizing power of the surface measured as in the CO pulse experiment must be related to this excess oxygen.

22) For example, 2, 4, 10 in these references.

23) N. Gunasekaran and A. Meenashisundaram, *Indian J. Chem.*, **21A**, 346 (1982).

24) N. Gunasekaran, A. Meenashisundaram, and V. Srinivasan, *React. Kinet. Catal. Lett.*, **21**, 243 (1982); *Surface Technology*, **22**, 89 (1984).

25) K. V. Ramanujachary and C. S. Swamy, *J. Catal.*, **93**, 279 (1985).

26) The calculation was carried out by assuming that the amounts of the surface oxygen of a perovskite and a K_2NiF_4-type oxide are the same and that the total numbers of metal ions on the surface are 2/3 (perovskite) and 3/4 (K_2NiF_4-type oxide) the number of oxygen atoms. The La:Ni ratio was used as the surface composition of $LaNiO_3$ (unpublished data by T. Nitadori and M. Misono).

Catalytic Activity of Nb-Si Mixed Oxides Induced by Reduction with Hydrogen

Yuji WADA,* Masakatsu INAIDA, Yasushi MURAKAMI, and Akira MORIKAWA
Department of Chemical Engineering, Tokyo Institute of Technology, O-okayama, Meguro-ku, Tokyo 152
(Received May 9, 1988)

Mixed oxides of niobium and silicon became catalytically active for butene isomerization by a reduction with hydrogen, and their catalytic activities depended on the duration of the reduction. The activity was irreversibly poisoned by oxygen. The formation of Nb^{4+} by the hydrogen reduction was revealed by ESR technique. Nb^{4+} was oxidized to Nb^{5+} by the admission of oxygen gas, and at the same time O_2^- was formed. It was concluded that the catalytically active site on the mixed oxide surface was Nb^{4+} ion formed by the reduction. The importance of isolation of Nb^{4+} ion in silica network was suggested for the retention of the catalytic activity.

It has been pointed out that the geometry of a surface in the molecular dimension, such as a step or kink, is an important factor for metal crystalline catalysts resulting in structure sensitive and insensitive reactions.[1] For metal oxide catalysts, however, it is still not clear whether this type of concept can be a leading principle for interpreting their catalytic activity, since most of metal oxide catalysts are amorphous in their structure in the working state. Even for some oxides of tungsten,[2] vanadium,[3] and rhenium,[4] whose catalytic activities depend on their type of crystal phase, a relation between their catalysis and the microscopic geometry of their surface has not yet been well understood.

The authors have observed that niobium oxide, which was catalytically inactive for butene isomerization, became active for a reaction through only a slight reduction in the mixture of hydrogen gas and water vapor.[5] The catalytic activity induced by the reduction depended on the extent of the reduction; it increased with the extent of the reduction up to a composition of $NbO_{2.494}$, and then decreased by a further reduction, though the niobium oxide of the compositions between $NbO_{2.500}$ and $NbO_{2.488}$ maintains a T-type crystal structure. These facts have led us to the idea that the high dispersion of niobium(IV) ions, which is achieved by a slight reduction, is important for maintaining the catalytic activity of the reduced niobium oxide.[5] In other words, the geometric environment around Nb^{4+}, which depends on its dispersion, may determine whether Nb^{4+} becomes catalytically active or not.

To elucidate the roll of the dispersion for catalysis on reduced niobium oxide, the authors have examined the catalytic properties of mixed oxides of niobium and silicon, since niobium ions are probably dispersed in an inactive matrix of silica. The amount of Nb contained in the oxide can be changed to a wide extent so that the dispersion can be controlled over a wide range.

Experimental

Preparation of Catalysts. Niobium chloride with a purity of 99.97% (kindly supplied by Prof. Nangyo at Tohoku Univ.) was dissolved into ethanol at a concentration of 0.1 mol-Nb/l under a dry nitrogen atmospher. This solution was mixed with ethyl orthosilicate(Wako Chemical Co., Research Grade) and stirred for 0.5 h. A coprecipitate obtained by adding agueous ammonia to the above-mentioned mixture was aged for 14 h at room temperature. The coprecipitate was heated at 373 K to remove ethanol and was washed with deionized water until chloride ion was undetectable by a test with an aqueous silver nitrate solution. It was then dried on a hot-water bath and calcined at 873 K for 2 h in air. The catalyst is denoted as Nb-Si(number), where the number in the parentheses indicates 100 Nb/(Nb+Si). The X-ray diffraction spectra of the catalysts showed that they maintained an amorphous structure, even after being calcined at 873 K, though pure niobium oxide was crystallized by calcination at the same temperature, indicating that niobium atoms were well dispersed in the oxides so as to be unable to form an ordered structure.

Procedures. The reaction was carried out with a conventional gas-circulation system of 320 ml. A catalyst of 50 mg was heated at 823 K in oxygen gas for 1 h and then degassed for 0.5 h. The catalyst was reduced with hydrogen gas at 823 K. Water formed by the reduction of the catalyst was collected with a trap cooled with liquid nitrogen. After cooling the catalyst to 298 K, the reaction was started by introducing *cis*-2-butene to the reaction system. The composition of the reaction mixture was determined by gas chromatography.

ESR Measurement. The ESR spectra were recorded with a JEOL-PE-1X at 77 K. The catalyst was pretreated in the same manner as described in the above section. A tube made of quartz for ESR measurements was connected to the upper part of the reaction cell. The catalyst preliminarily pretreated in the cell was transferred to the tube for ESR measurements. A small space was provided at the top of the tube to admit oxygen gas onto the catalyst. For the observation of a tetracyanoethylene (TCNE) radical, a benzene solution of TCNE (1 ml, 8×10^{-2} mol l^{-1}) was brought into contact with the pretreated catalyst in the ESR tube. The spin density was determined by a comparison of

the ESR signal of the samples with that of Mn^{2+} inserted in the ESR cavity. The latter has been frequently titrated by a standard benzene solution of DPPH in the same condition of ESR measurements applied to the samples.

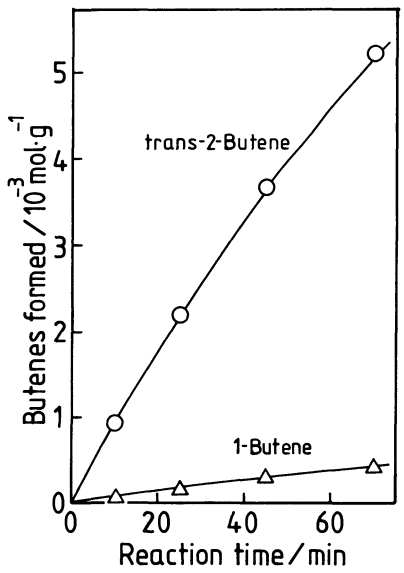

Fig. 1. Isomerization of *cis*-2-butene on the reduced Nb-Si(10). The catalyst was reduced with hydrogen gas at 823 K for 2.5 h. The reaction was carried out at 298 K with a pressure of *cis*-2-butene, 1.33×10^5 Pa.

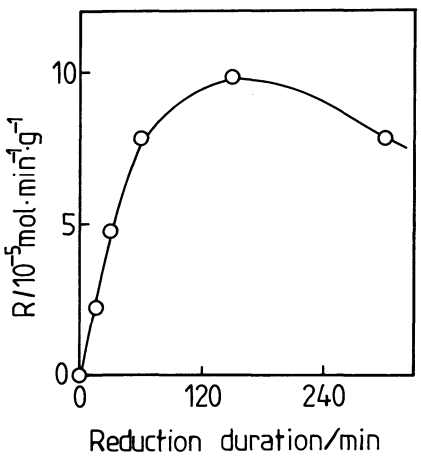

Fig. 2. Dependence of the catalytic activity of the Nb-Si(10) mixed oxide on the reduction duration at 823 K. The reaction conditions were the same as in Fig. 1.

Table 1. Poisoning of the Reduced Nb-Si(10) Mixed Oxide Catalyst

Additive	Non	O_2	NO	N_2O	CO	NH_3
Amount[a)]	—	0.8	6.0	6.0	6.0	6.0
Activity[b)]	2.3	0.2	0.0	1.2	1.8	0.7

a) The amount of the additives admitted/10^{-5} mol g^{-1}.
b) The catalytic activity/10^{-5} mol min^{-1} g^{-1}. The catalyst was reduced at 823 K for 0.25 h before the experiment.

Results and Discussion

Isomerization of *cis*-2-Butene. The Nb–Si mixed oxide, itself, was catalytically inactive for the isomerization of *cis*- 2-butene. It became catalytically active for the reaction by its reduction with hydrogen gas at 823 K. Figure 1 shows the progress of a reaction on Nb–Si(10) reduced for 2.5 h. Products were only 1-butene and *trans*-2-butene. The rate of the formation of *trans*-2-butene was 10-times faster than that of 1-butene. The average rate of the reaction calculated from the amount of *cis*-2-butene converted to 1-butene and *trans*-2-butene during the initial 10 min was taken as a measure of the catalytic activity.

Figure 2 shows the dependence of the catalytic activity on the reduction duration of the oxide (Nb–Si(10)). The catalytic activity could be increased by increasing the reduction duration (by up to 2.5 h) and slightly decreased upon further reduction. The induction of catalytic activity by reduction with hydrogen gas suggests that the catalytically active site for butene isomerization is a Nb cation with a lower oxidation state formed by reduction.

The catalytic activities observed for the reduced catalyst, which was preliminarily exposed to various compounds, are listed in Table 1. All the tested compounds (O_2, NO, NH_3, CO, and N_2O) retarded the catalytic activity. NO and O_2 were the most poisonous to the catalyst among them. Figure 3 shows the relation between the catalytic activity on Nb–Si poisoned by oxygen and the amount of oxygen admitted. The admission of oxygen of 5×10^{-6} mol g^{-1} reduced the catalytic activity to 1/10 of that of non-poisoned catalyst.

Oxidants, such as O_2 and NO, were the most effective poisons. However, NH_3 was less poisonous than these two compounds. Therefore, it is stressed

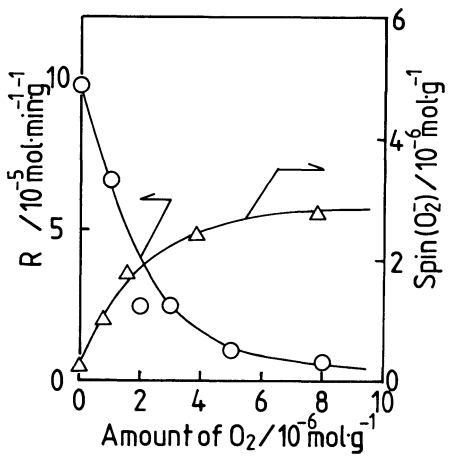

Fig. 3. Poisoning of the catalytic activity and the formation of O_2^- radical on the surface by admission of oxygen gas. The reaction conditions were the same as in Fig. 1.

that the observed activity is not attributed to the catalysis by the acidic property of the Nb–Si oxide, although Iizuka et al. have reported on the acid catalysis by hydrated niobium oxide.[6] The strong poisoning effect of the two oxidants suggests that the active site loses its catalytic activity by oxidation. Therefore, it is reasonable to assume that the active site is a Nb^{4+} ion formed by reduction with H_2. This assumption is supported by the experimental result that the formation of Nb^{4+} by reduction was assured by ESR spectroscopy for niobium oxide, which became catalytically active by reduction.[1]

ESR Investigation. While the catalysts showed no ESR absorption after a pretreatment, their reduction induced the spectrum shown in Fig. 4-a. An apparent g value of 1.91±0.02 was obtained, independent of the content of niobium, except for pure niobium oxide. Since the g value is similar to those reported for a Nb^{4+} ion in silicate glass,[7] the ESR absorption observed for the reduced Nb–Si oxide is attributed to the Nb^{4+} ion. The poor resolution of the spectrum might be due to a low symmetry and irregularity of the environment around the ions.

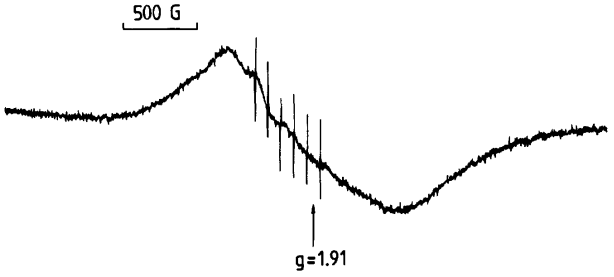

Fig. 4-a. ESR spectrum measured at 77 K of the reduced Nb-Si(50). The catalyst was reduced with hydrogen gas at 823 K for 0.25 h. The six sharp signals overlapping that of Nb^{4+} are due to Mn^{2+} as the standard.

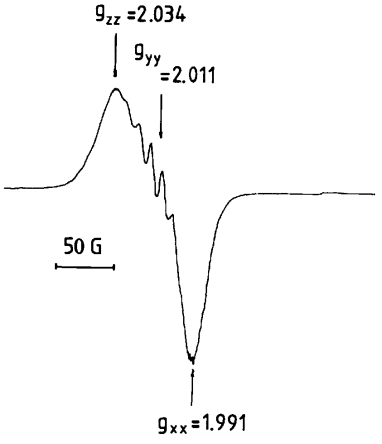

Fig. 4-b. ESR spectrum of O_2^- formed by admission of oxygen gas onto the reduced Nb-Si(10). The catalyst was reduced at 823 K for 2.5 h before the admission of oxygen gas.

When oxygen gas was admitted onto the reduced catalyst, a new signal (Fig. 4-b) appeared. The g values (g_{xx}=1.991±0.001, g_{yy}=2.011±0.001, and g_{zz}= 2.034±0.005) were obtained. The shape of the spectrum is similar to that of the O_2^- formed on La_2O_3 (reported by Wang et at.[8]) and on other materials.[9,10] When ethene or propene was brought into contact with a catalyst showing the ESR spectrum of Fig. 4-b at room temperature, no change in the spectrum occurred, that is, the species formed on the catalysts by the admission of oxygen gas did not react with the olefins. From the g values, the shape of the spectrum, and the poor reactivity with olefins, the species giving the ESR absorption spectrum of Fig. 4-b could be identified as being an O_2^- ion. Since the ESR absorption due to Nb^{4+} was decreased, in contrast with the formation of O_2^-, this O_2^- ion must be formed by electron transfer from Nb^{4+} ion as shown in Reaction 1:

$$Nb^{4+} + O_2 \rightarrow Nb^{5+} \cdots O_2^-. \quad (1)$$

That the hyperfine structure in the spectrum resulted from an interaction of O_2^- with the niobium nucleus (I=9/2) indicates that O_2^- is located at a Nb atom. It is plausible that the hyperfine structure observed in the spectrum resulted from an interaction of O_2^- with a niobium nucleus (I=9/2), although the series of hyperfine signals can not be completely identified in the spectrum because of the low resolution of the ESR spectrum. The relation between the amount of O_2 admitted and that of O_2^- formed is shown in Fig. 3. The spin density of O_2^- formed was increased linearly up to the amount of admitted O_2 (2×10^{-6} mol g^{-1}) at a slope of unity, suggesting that O_2 was stoichiometrically converted to O_2^- on the reduced catalyst.

The inverse changes of the catalytic activity and the amount of O_2^- formed by the admission of O_2 shown in Fig. 3, strongly support the idea that the

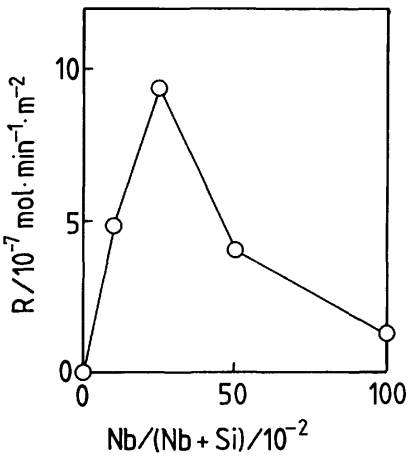

Fig. 5. Dependence of the catalytic activity on the content of Nb in the catalysts.

catalytically active site is a Nb^{4+} ion. Poisoning of the catalytic activity for butene isomerization by O_2 must be caused by the oxidation of Nb^{4+}, as indicated in Reaction 1. The number of the active sites was estimated to be 4×10^{-6} mol g^{-1} from an extrapolation of the linear part obtained at small amounts of the admitted O_2 (Fig. 3).

Catalysis and Content of Nb. Figure 5 shows the catalytic activity for *cis*-2-butene isomerization obtained on reduced Nb–Si catalysts containing various amounts of niobium. The catalytic activity showed a maximum at a content of 25%-Nb and decreased above this value. Figure 6 shows the amount of O_2^- formed on the reduced catalysts after the admission of a sufficient amount of oxygen gas to convert all Nb^{4+} to Nb^{5+} on the surface. The amount of O_2^- formed passed through a maximum at 10% of Nb and was decreased for the Nb content more than the value. Though the color change of the catalysts after a treatment with hydrogen at 823 K confirmed the occurrence of the reduction of the catalysts, almost no formation of O_2^- was observed for Nb–Si(50) and Nb–Si(100), or Nb_2O_5.

When TCNE was brought into contact with a reduced catalyst, a new ESR absorption spectrum of a single peak (g=2.011) appeared. It has been reported that TCNE is converted to its anion radical when the species with electron-donating character is present on the solid surfaces.[11,12] It is reasonable to say that a TCNE molecule, whose electron affinity is larger than that of oxygen molecule, can be converted to its anion radical on reduced Nb–Si where Nb^{4+} acts as an electron donor. Figure 7 shows the relation between the Nb content in the catalysts and the amount of TCNE radical formed on catalysts pretreated in the same manner as mentioned in Fig. 6. The TCNE radical increased linearly with an increase in the Nb content. The monotonous increase in the TCNE radical with an increase in the Nb content simply results from the increase in the amount of Nb^{4+} on the surface of the reduced catalysts. On the other hand, the O_2^- formation showed an optimum for change of the Nb atom content in the oxide. These contrasted results for the two electron acceptors, TCNE and O_2, may be explained as described below; an O_2^- radical is stable only on the isolated Nb atom on the surface, since this radical is further reduced to be an ESR inactive oxygen species, such as O_2^{2-} or O^{2-}, by a neighboring Nb^{4+}. On catalysts containing a small amount of Nb, the number of isolated Nb atoms is increased with an increase in the Nb content, since the atoms are highly dispersed. At a high content, however, the local aggregation of niobium ions occurs so as to result in a decrease in the number of isolated Nb^{4+} ions.

The resemblance in the dependences of the catalytic activity and the formation of O_2^- suggests that highly dispersed Nb^{4+} ions are catalytically more active than

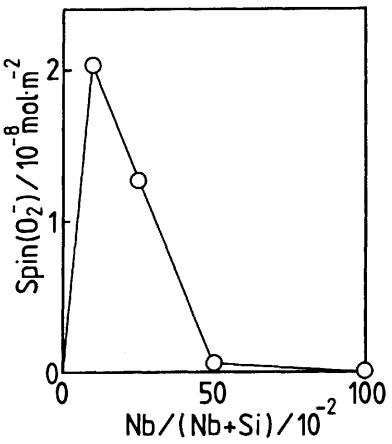

Fig. 6. Dependence of the amount of O_2^- on the content of Nb. The catalysts were reduced at 823 K for 2.5 h before the admission of oxygen gas.

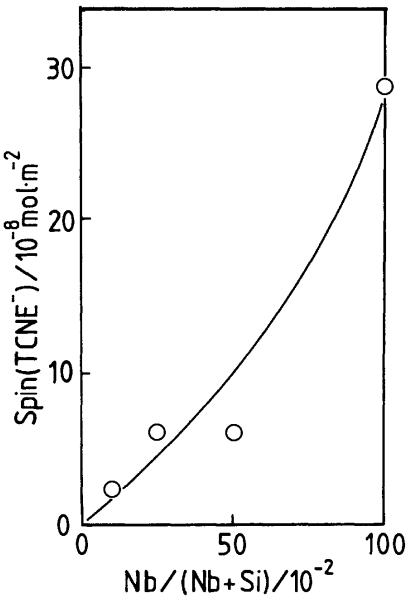

Fig. 7. Dependence of the amount of TCNE anion radical on the content of Nb in the catalysts. The catalysts were reduced at the same conditions as in Fig. 6.

aggregated ions.

The dependence of the catalytic activity observed over slightly reduced niobium oxide on the Nb/O ratio in the oxide has been explained by a change in the dispersion of Nb^{4+} formed on the surface.[5] It has been concluded that an isolated Nb^{4+} ion with coordinative unsaturation, which is formed predominantly on a highly dispersed surface, is the catalytically active site. Coordinative unsaturation is lost by coupling of two Nb^{4+} ions on a catalyst with low dispersion. It is, therefore, stressed that similarly to a reduced Nb_2O_5 catalyst[5] the catalytic activity for a Nb–Si system originates from a coordinative unsaturation of the Nb^{4+} ion.

The importance of the dispersion of active species on the surface has been reported for Nb_2O_5/SiO_2,[13] MoO_3/SiO_2,[14] MoO_3/porous Vycor glass,[15] TiO_2/porous Vycor glass,[16] Ti–Si mixed oxide,[17] and MoO_3/Al_2O_3.[18,19] Nishimura et al. have demonstrated that well-defined Nb monomers attached on SiO_2 exhibited high activity and selectivity for the dehydrogenation of ethanol.[13] Ono et al. have attributed the catalytic activity of MoO_3/SiO_2 for dehydrogenation of ethanol to tetrahedrally coordinated Mo ion formed predominantly at high dispersion.[14]

The coordination environment of metal ions in metal oxides, such as the coordination number and symmetry, which are important for the induction of catalytic activity, should depend on the dispersion for both supported oxide and mixed oxide systems. Especially for Nb–Si mixed oxide system, an isolated Nb^{4+} ion is more stable than that formed in Nb_2O_5, since a Nb atom is isolated in a matrix of silica at a low content of Nb during the preparation process.

The present research was supported by a Grant from CBMM INTERNACIONAL LTDA.

References

1) M. Boudart, *Adv. Catal.*, **20**, 153 (1969).
2) S. De. Rossi, E. Iguchi, M. Schiavello, and R. J. D. Tilley, *Z. Phys. Chem., N. F.*, **103**, 193 (1976).
3) A. Anderson and S. T. Lundin, *J. Catal.*, **58**, 383 (1979).
4) N. Tsuda and A. Fujimori, *J. Catal.*, **69**, 410 (1981).
5) Y. Murakami, Y. Wada, and A. Morikawa, *Bull. Chem. Soc. Jpn.*, **61**, 2747 (1988).
6) T. Iizuka, K. Ogasawara, and K. Tanabe, *Bull. Chem. Soc. Jpn.*, **56**, 2927 (1983).
7) N. R. Yafaev and N. S. Garif'yanov, *Soviet Physics Solid State*, **5**, 2213 (1964).
8) J.-X. Wang and J. Lunsford, *J. Phys. Chem.*, **90**, 3890 (1986).
9) J. H. Lunsford, *Catal. Rev.*, **8**, 135 (1973).
10) M. Che and A. J. Tench, *Adv. Catal.*, **32**, 1 (1983).
11) M. Che, C. Naccache, and B. Imelik, *J. Catal.*, **24**, 328 (1972).
12) R. S. Davidson and R. M. Slater, *J. Chem. Soc., Faraday Trans. 1*, **72**, 2416 (1976).
13) M. Nishimura, K. Asakura, and Y. Iwasawa, "Proceedings of the 9th International Congress on Catalysis," ed by M. J. Phillips and M. Ternan, The Chemical Institute of Canada, Ottawa, Canada (1988), Vol. 4, p. 1842.
14) T. Ono, M. Anpo, and Y. Kubokawa, *J. Phys. Chem.*, **90**, 4780 (1986).
15) M. Anpo, T. Suzuki. T. Tanaka, S. Yamashita, and Y. Kubokawa, *J. Phys. Chem.*, **88**, 5778 (1984).
16) M. Anpo, N. Aizawa, Y. Kubokawa, M. Che, C. Louis, and E. Giamello, *J. Phys. Chem.*, **89**, 5689 (1985).
17) M. Anpo, H. Nakaya, S. Kodama, Y. Kubokawa, K. Domen, and T. Onishi, *J. Phys. Chem.*, **90**, 1633 (1986).
18) D. S. Zingg, L. E. Makovsky, R. E. Tischer, F. R. Brown, and D. M. Hercules, *J. Phys. Chem.*, **84**, 2898 (1980).
19) H. Weigold, *J. Catal.*, **83**, 85 (1983).

 © 1988 The Chemical Society of Japan Bull. Chem. Soc. Jpn., 61, 3845—3852 (1988)

Liquid Structure of *N,N*-Dimethylformamide, Acetonitrile, and Their 1:1 Molar Mixture

Tamas RADNAI,†† Sumiko ITOH, and Hitoshi OHTAKI*,†
Department of Electronic Chemistry, Tokyo Institute of Technology at Nagatsuta, 4259 Nagatsuta, Midori-ku, Yokohama 227
(Received May 12, 1988)

Liquid structures of pure *N,N*-dimethylformamide (DMF) and acetonitrile (AN) as well as of their 1:1 molar mixture were investigated by X-ray diffraction at 25 °C. The careful reinvestigation of pure DMF led to a good reproducibility of the previous result. Slight deviations in the structural parameters are discussed and a detailed parameter table is reported. A simple model in which each AN molecule has 2 neighbors at an average distance of 330 pm describes the more ordered first neighbor structure of pure AN. The main interaction forming the structure is of dipole-dipole type, in agreement with previous findings. In the 1:1 molar mixture a dipole–dipole model also leads to a satisfactory description of the first neighbor structure. The preferred orientation is that with dipoles in the antiparallel position. A central DMF molecule has 1.75 neighboring AN molecules in average at a distance of 316 pm. The same stands for DMF around AN. No evidence for other kinds of interaction, e.g., weak H-bond type intermolecular interactions could be found in the mixture.

Both *N,N*-dimethylformamide (DMF) and acetonitrile (AN) are typical aprotic, dipolar, simple organic solvents. They are widely used in the chemical practice due to their advantageous physicochemical properties like the broad temperature range in which they are liquid; relatively high dielectric constants as well as good donor and acceptor properties which enable them to be excellent solvents for a great number of compounds. Their basic physical and chemical properties are often subjects of studies.

Recently, their liquid structure was also a matter of investigations.[1-4] An X-ray diffraction study of liquid DMF revealed the intramolecular structure,[1] while no direct evidence could be found for ordering effects between the molecules. The joined MO calculations suggested a slight tendency for dimer formation, but the interactions between the molecules were found to be weak. Generally acetonitrile is also considered as a structureless liquid, because of the lack of H-bonds, in spite of the appearance of the definite short range ordering between the molecules. The ordering is mainly due to the dipole–dipole interactions, as derived from diffraction and theoretical studies.[2-4]

Surprisingly enough, the properties of the binary mixtures of DMF and AN have not been studied extensively. They are miscible at any concentration, forming non-azeotropic mixtures, but no detailed data of the physicochemical properties as well as their structures are available up to now. It is generally assumed that the solvent structural effects are very weak and can be neglected when compared with solute-solvent interactions in their binary solutions.

Some indications, however, point to the existence of molecular associations between DMF and AN in mixtures. Comparing Gutmann's donor and acceptor numbers of the two solvents, one can conclude that a remarkable difference is in the donicity (D_N(AN)=14.1, D_N(DMF)=26.6), while the acceptor numbers are similar (A_N(AN)=19.3, A_N(DMF)=16.0). These differences lead to variations in the metal–ligand complex formation as well as to differences in the solvation of the metal ions in the pure solvents. Moreover, the solvation and complex formation phenomena can also be affected in the mixtures. Indeed, it was proved that a preferential solvation of copper(II) ions by DMF occurs in the mixtures of DMF and AN when studying the $[CuCl_n]^{(2-n)+}$ complex formation.[5] It is obvious to think that the differences in their donor and acceptor properties can also lead to a measurable degree of DMF–AN complex formation, even if the governing interaction is weak.

Literature data also support the hypothesis. Evidence of attractive interactions between DMF and AN is reported on the basis of light scattering studies.[6] These interactions are in competition with the ones between the like molecules and a great number of single molecules have also to be present in the liquid, according to the measured excess free energy data. More direct evidence for solute–solute type interactions between DMF and AN as solutes even at low concentrations in benzene solutions was found by the dielectric relaxation method[7] practically at every stoichiometric ratio of the solutes. In a previous work, however, from electro-osmotic measurements the weakness of such interactions, if any, was emphasized.[8] Indeed, guesswork on possible type of interactions suggests weak H-bond-like interactions between CH group of DMF and N atom of AN, and electric multipole–multipole interactions between the two kinds of molecules.

In order to determine the structural consequences of such presumed interactions, an X-ray diffraction measurement was performed on the 1:1 molar mixture of DMF and AN. For the sake of comparison, X-ray

† Present address: Coordination Chemistry Laboratories, Institute for Molecular Science, Myodaiji-cho, Okazaki 444.

†† On leave from: Central Research Institute for Chemistry of the Hungarian Academy of Sciences, Budapest, P.O.B.17, H-1525, Hungary.

measurements on pure DMF and AN were also carried out, and their structural data were compared with those reported in the literature.

Experimental

Sample Solutions. Both DMF and AN of reagent grade were distilled twice before use. A mixture of 1:1 molar ratio, corresponding to 1:1.781 mass ratio, was prepared by measuring the weights of the components. Densities of the samples were checked pycnometrically.

X-Ray Scattering Measurements. The scattering experiments were carried out with a JEOL θ-θ diffractometer by using Mo $K\alpha$ radiation (λ=71.07 pm) and a bent LiF monochromator in a room thermostated at (25±1) °C. The accessible range of scattering angle (2θ) was 2—140°, corresponding to the s-range from 0.006 pm^{-1} to 0.168 pm^{-1}, s being the scattering variable ($s=4\pi\lambda^{-1}\sin\theta$). Times requiring to accumulate 80000 counts were recorded at each angle of the measurements. Special care was taken of the low X-ray absorption as well as the high evaporation rates of the samples. The levels of the horizontal surface of the liquids were checked every 2—3 hours. Additionally, the low-angle region for the mixture and the whole experiment for the AN were measured repeatedly in order to obtain better results for data reduction. A typical result for the agreement between the data from two consecutive experiments was within 2—3%, and the deviation never exceeded 5%.

Beyond the above specialities, the method of measurements and data treatments were the same as those described in previous papers.[9]

Analysis of the Scattering Data. Experimental intensities were corrected for background, absorption, double scattering, polarization and incoherent scattering by the standard methods. The reduced intensities $i(s)$ were calculated as:

$$i(s) = KI(s) - \sum n_j\{[f_j(s) + \Delta f_j']^2 + (\Delta f_j'')^2\}, \quad (1)$$

where $I(s)$ is the experimental intensity and is normalized to the absolute scale with respect to a stoichiometric volume V containing one DMF and AN molecule in the pure liquids, and one molecule of both kinds in the mixture, K is the normalizing factor, n_j is the number of atom j in the stoichiometric volume, $f_j(s)$ is the scattering factor of atom j at s, $\Delta f_j'$, and $\Delta f_j''$ are the real and imaginary parts of anomalous dispersion of atom j. The experimental radial distribution functions $D(r)$ and pair-correlation functions $G(r)$ were calculated by the Fourier transform of the $i(s)$ functions according to

$$D(r) = 4\pi r^2\rho_0 + (2r/\pi)\int_0^{s_{max}} si(s)M(s)\sin(sr)ds, \quad (2)$$

and

$$G(r) = D(r) / (4\pi r^2\rho_0), \quad (3)$$

where ρ_0 denotes the average electron density in the sample defined as

$$\rho_0 = \sum\sum n_i n_j f_i(0) f_j(0) / V. \quad (4)$$

$M(s)$ is the modification function of the form

$$M(s) = \sum\{[f_i(0) + \Delta f_i']^2 + (\Delta f_i'')^2\} / \{[f_N(s) + \Delta f_N']^2 + (\Delta f_N'')^2\}\exp(-ks^2). \quad (5)$$

All calculations were performed by using appropriate versions of programs KURVLR[10] and NLPLSQ.[11]

Results and Discussion

Method of Structural Analysis. At first, a semi-quantitative analysis was done for each sample at the radial distribution level. $D(r)$ and $G(r)$ functions for DMF and AN were compared with those available from the literature, and the differences in the $D(r)$ functions of the three samples were discussed. As a second step, the intramolecular structural parameters for both DMF and AN were calculated by the least squares method (LSQ) at the reduced intensity level. Then models for intermolecular interactions were tested, trying to find the average configuration of the nearest neighbors by LSQ. When building up the model for the mixture, the parameters fixed previously in the LSQ analysis for the pure liquids were used for describing the intramolecular structure without changing them. Finally, the structural parameters for the random distribution of the atoms around the central ones were determined.

For the LSQ, theoretical reduced intensities $i_{th}(s)$ were calculated as

$$i_{th}(s) = \sum\sum n_{pq}c_{pq}j_0(sr_{pq})\exp(-b_{pq}s^2) - 4\pi\rho_0 / s\sum\sum n_p n_q c_{pq}R_{pq}^2 j_1(sR_{pq})\exp(-B_{pq}s^2). \quad (6)$$

where

$$c_{pq}(s) = \{[f_p(s) + \Delta f_p'][f_q(s) + \Delta f_q'] + \Delta f_p''\Delta f_q''\}M(s), \quad (7)$$

and r_{pq}, b_{pq}, and n_{pq} denote the distance, temperature factor, and frequency factor (coordination number) of the p-q atom-pair, respectively. R_{pq} is the distance beyond which a continuous distribution of atoms of type q around the p type atom in the center is assumed, while B_{pq} is the parameter describing the sharpness of the boundary at R_{pq}. For brevity, $j_m(x)$ stands for the spherical Bessel function of the mth order.

$$U = \sum_{s_{min}}^{s_{max}} \omega(s)[i(s) - i_{th}(s)]^2, \quad (8)$$

The LSQ procedure was applied in order to find the minimum of the error-square sum using the weighting functions $w(s)=s^2$. During the fitting procedure several s ranges were tried. Finally an extended range from s_{min}=0.005 pm^{-1} to s_{max}=0.16 pm^{-1} could be applied. The quality of the fit was checked through the value of U and the usually defined Hamilton R-factor.

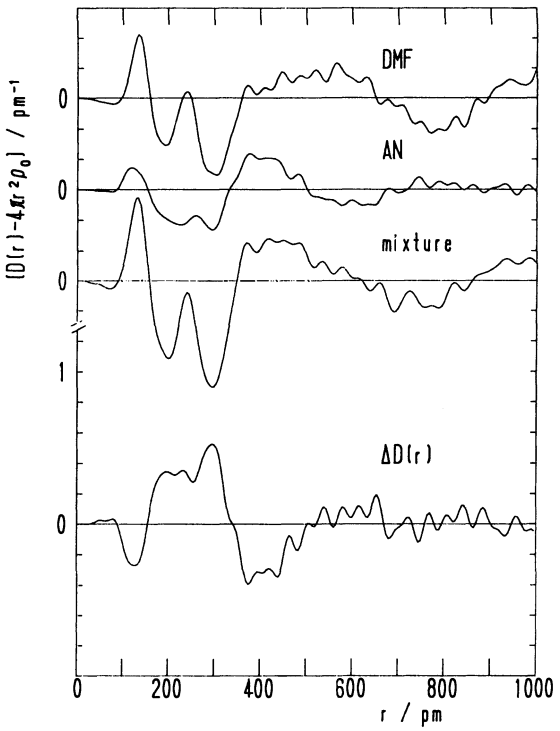

Fig. 1. Experimental RDF's for pure DMF, AN, their 1:1 molar mixture, and the weighted difference of the three curves. The RDF's are given in form of $D(r)-4\pi r^2\rho_0$, the difference curve as defined in Eq. 9.

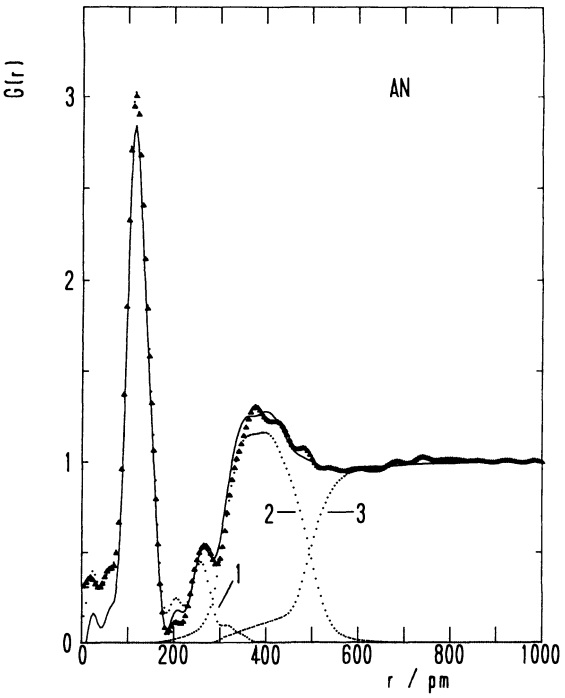

Fig. 3. Experimental $G(r)$ (triangles) is compared with the theoretical one from the best fit of the models (solid line) for pure AN. The dotted curves are: intramolecular contribution (1), intermolecular part from dipole-dipole model (2), and the continuum (3).

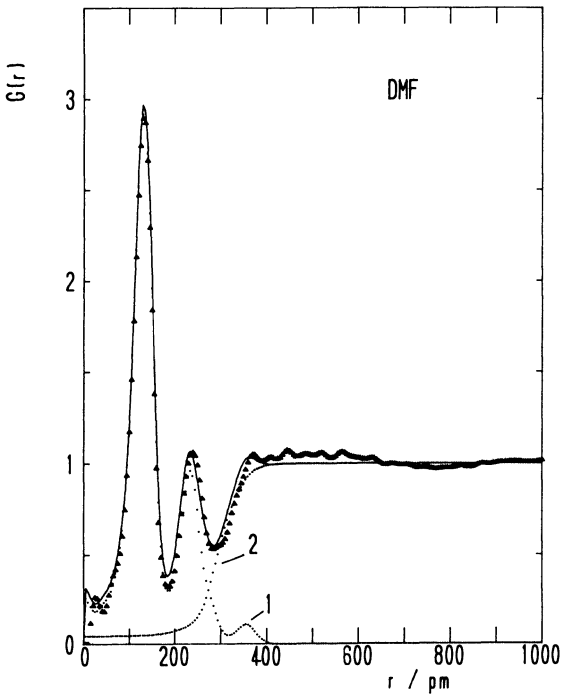

Fig. 2. Experimental $G(r)$ (triangles) is compared with the theoretical one from the best fit of the models (solid line) for pure DMF. The dots represent the intramolecular (1) and the continuum (2) contributions.

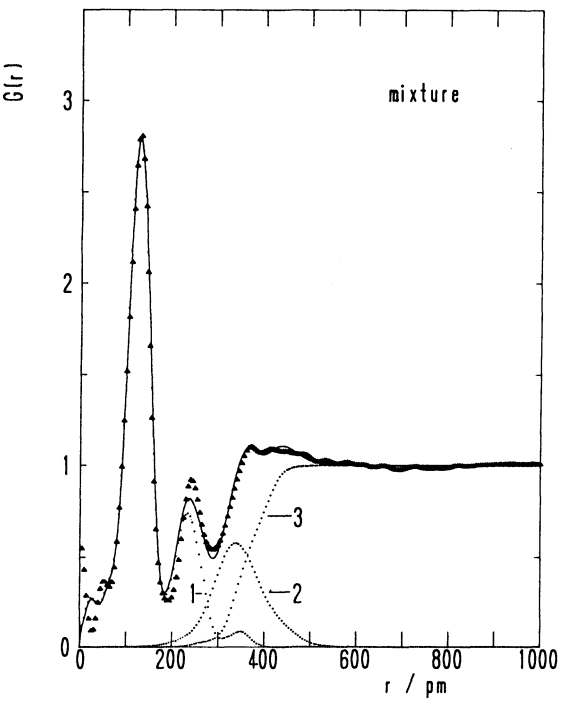

Fig. 4. Experimental $G(r)$ (triangles) is compared with the theoretical one from the best fit of the models (solid line) for 1:1 molar mixture of DMF and AN. The dotted curves are: intramolecular contribution (1), intermolecular part from the complete dipole-dipole model (2), and the continuum (3).

X-Ray Radial Distribution Functions (RDF's). The total experimental X-ray radial distribution curves of the three samples are shown in Fig. 1 in the form of $D(r)-4\pi r^2\rho_0$. The corresponding $G(r)$ functions are also shown in Figs. 2—4.

The two distinct peaks at about 130 and 230 pm for pure DMF were ascribed to the intramolecular interactions in a previous paper.[1] The peak positions are very well reproduced in the present work (the resolution of the RDF was 5 pm, the agreement is within this limit). The peak shapes also agree well, except the small ripples which still remained after that a correction had been applied to remove them as far as possible. Since only a small modulation appears from 350 to 650 pm, it witnesses about the absence of any significant interaction between the molecules.

There are also two distinct peaks at about 120 and 270 pm on the RDF of pure AN, with a small peak at about 200 pm (see Fig. 1). The last one emerges as a hump at the corresponding $G(r)$ in Fig. 3. The peak positions and their relative heights are in good agreement with those reported earlier.[2] It is obvious to ascribe these three peaks to the intramolecular distances, similar to the DMF case. The peak appearing between 300 and 500 pm is less broad and significantly higher than that of DMF. It also has a shoulder at about 320 pm, and its shape is rather complex, reflecting stronger intermolecular interactions and as a consequence, more definite short-range ordering in the liquid.

The two main peaks in the RDF of the 1:1 molar mixture obviously include the intramolecular distances both from DMF and AN. Consequently, they become broader and the peak positions are shifted from those of pure liquids. As for the peak beyond to 300 pm, it is more definite than that for pure DMF, but less pronounced than for pure AN. It seems to be rather complex, and a more quantitative analysis is needed in order to decide if it reflects only the concentration effect, i.e., the simple mixing of the AN-like and DMF-like structures (which is physically not relevant) or is a sign of a specific interaction between the two kinds of molecules.

The first step towards the solution of this problem was the construction of the weighted difference of the experimental RDF's according to

$$\Delta D(r) = [D_M(r)-4\pi r^2\rho_{0,M}] - K_1[D_{DMF}(r)-4\pi r^2\rho_{0,DMF}] - K_2[D_{AN}(r) - 4\pi r^2\rho_{0,AN}], \quad (9)$$

where $K_1=\rho_{0,M}/\rho_{0,DMF}$, $K_2=\rho_{0,M}/\rho_{0,AN}$ are two weights which account for the differences in the average atom densities between the samples (M stands for the mixture). The $\Delta D(r)$ curve is shown in Fig. 1. It is easy to prove that the function defined by Eq. 9 tends to zero when r is beyond the boundaries of the continuum. Accordingly, the ripples beyond 600 pm are clearly spurious, summing up the experimental errors after the double subtractions and determine the accuracy of the peak resolution. On the other hand, the minimum and the maximum found in the intramolecular range up to 250 pm are also physically irrelevant, and are due to the enlarged errors from the inaccuracy of the ripple correction in the low-r range. The interesting feature of this difference curve is the sharp peak near 300 pm followed by a deep minimum around 380 pm. Both are larger than those found to be irrelevant, and give a clear indication not only for the presence of the intermolecular interaction between the molecules but also a detectable shift in the average interatomic distances between adjacent molecules towards the lower-r region.

Structure of Pure DMF. In spite of the visibly good agreement between the new and the previously reported experimental results, a detailed LSQ analysis of the $i(s)$ curve was carried out in order to see the influence of minor experimental deviations on the structural parameters. The planar structure for the DMF molecule was retained. In the structural model examined in the present study only two slight modifications were applied. The non-bonding C···H distances were not neglected in the fitting procedure although they give only small contributions to the X-ray scattering, and the treatment of the continuum (the second term in Eq. 6) was employed by separated atom–atom contributions of each kind of atoms (this latter change does not influence the intramolecular parameters).

The experimental and theoretical $si(s)$ functions of

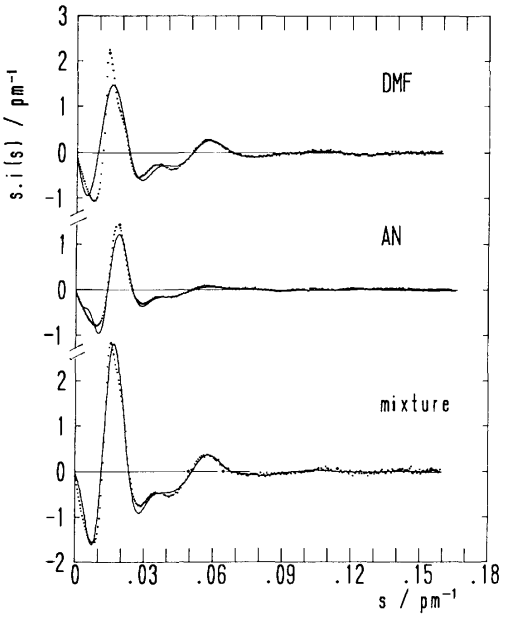

Fig. 5. Experimental structure functions $si(s)$ (dots) are compared with the theoretical ones from the best fit of the models (solid lines) for pure DMF, AN, and their 1:1 molar mixture.

Table 1. Intramolecular Parameters for Liquid DMF

Interaction	This work		Ref. 1		Ref. 12	
	r	$b/10$	r	$b/10$	r	$b/10$
C-H	109(1)	1(1)	109(1)	1(1)	—	—
C_1=O	124(2)	3(1)	124(2)	3(1)	120(1)	3(1)
C_1-N	135(2)	5(1)	135(2)	5(1)	140(1)	4(1)
C_2-N	145(2)	5(1)	145(2)	5(1)	143(1)	4(1)
N···H	202(2)	5(1)	202(2)	5(1)	—	—
O···H	202(2)	5(1)	203(2)	5(1)	—	—
N···H	207(3)	5(1)	208(2)	5(1)	—	—
O···N	235(5)	2(1)	225(3)	2(1)	231(2)	3(2)
C_1···C_2	238(5)	2(1)	239(5)	2(1)	247(3)	1(1)
C_2···C_3	261(5)	2(1)	257(5)	2(1)	244(2)	1(1)
C_2···O	281(5)	5(2)	270(5)	5(2)	285(2)	1(1)
C_3···O	358(5)	10(3)	354(5)	10(3)	359(5)	7(2)
C_3···H	238(5)	2(2)	—	—	—	—
C_2···H	331(5)	6(5)	—	—	—	—
<NC$_1$O	130		121		127	
<C$_1$NC$_2$	116		116		121	
<C$_2$NC$_3$	129		128		121	

a) Distances (r) in pm, and temperature factor (b) in pm^2. The calculated bond angles are also given (in degrees). The numbering of the atoms is the same as in Ref. 1 and is shown in Fig. 6.

Table 2. Parameters Describing the Continuum Parts of the Structure in Liquid DMF, AN, and Their 1:1 Molar Mixture

Atom pair	DMF		AN		Mixture	
	R_{pq}	$B_{pq}/10$	R_{pq}	$B_{pq}/10$	R_{pq}	$B_{pq}/10$
C-C	290(9)	18(2)	285(4)	109(44)	337(2)	40(5)
C-N	269(9)	37(3)	505(15)	18(5)	378(3)	37(3)
C-O	311(9)	36(4)	—	—	395(36)	36(9)
N-N	—	—	479(29)	6(2)	396(75)	38(19)
N-O	—	—	—	—	419(100)	4(4)

a) The contributions were calculated in an atom-atom distribution form. The boundaries of the continuum parts (R_{pq}) are given in pm, the corresponding B_{pq} values in pm^2.

the best fit are shown in Fig. 5. The intramolecular structural parameters for DMF are given in Table 1. As it is seen from the comparison with those parameters reported earlier,[1] no change occurred in the bonding distances, and only minor changes resulted in the nonbonding distances, leading to slight variation in the bond angles. For a further comparison, structural parameters derived from an independent X-ray study on pure DMF,[12] applying transmission geometry, are also given in Table 1. Although these structural parameters are somewhat different, but not contradictory to the results reported here.

The intermolecular part of the liquid structure of DMF is completely described by assuming random distribution of atoms around the central ones beyond to the boundaries given by the set of R_{pq} and B_{pq} parameters listed in Table 2. Only the C–C, C–N, and C–O contributions were fitted because of their major weights. The parameters obtained support the internal consistency of the model.

Structure of Pure AN. Intramolecular structural parameters for liquid AN were determined earlier from X-ray diffraction experiments.[2,3] Since there are slight differences between them, these parameters were also recalculated during the structural analysis. The values finally accepted are compared with the literature data in Table 3. No significant change in the intramolecular parameters was observed.

As for the intermolecular structure, the previous works employed two completely different approaches. The first one[2] interpreted the liquid structure in crystallographic terms, computing all possible interactions between eight molecules within an orthorhombic unit cell, and determining a "correlation-cluster" size resulting in a diameter of about 1300 pm. The molecules are arranged in the clusters with the parallel or antiparallel position of their dipoles. Although a decrease in the positional and orientational correlations was considered in the model, the ordering seems still to be exaggerated.

The other approach[3,4] had the aim at determining the molecular pair-correlation function of liquid AN from combined neutron and X-ray diffraction exper-

Table 3. Intramolecular Parameters for Liquid AN

Interaction	This work		Ref. 2		Ref. 3	
	r	$b/10$	r	$b/10$	r	$b/10$
C′-H′	109(1)	1(1)	109	—	—	—
C′-C″	147(2)	1.7(3)	146.5(1)	2.7(3)	148(3)	3(1)
C′-N′	115(1)	1.6(3)	115.3(1)	1.4(1)	114(3)	4(1)
C″···N′	262(2)	5(1)	261.8(2)	4.1(2)	—	5(1)
C′···H′	208(3)	5(1)	—	—	212(3)	4(2)
N′···H′	314(3)	10(5)	—	—	—	8(1)

a) Distances (r) in pm, and temperature factor (b) in pm². The numbering of the atoms is given in Fig. 6.

iments. From the total experimental pair-correlation function and calculations by the perturbation theory combined with it, the leading terms of the invariant series expansion could be derived, characteristic to the positional and also the orientational correlations between the molecules. This information is much more beyond to that which is accessible only by one diffraction experiment. The results showed that the dipole-dipole and quadrupole-quadrupole interactions were essential at small intermolecular distances and that the antiparallel orientation of the dipoles was preferred. The average configuration of the first neighbors, however, was not given in terms of structural parameters.

In order to derive the simplest possible model for the first-neighbor structure of AN, an LSQ analysis was carried out. In the applied model two neighbors were assumed around a central molecule, with their dipoles in the antiparallel position. The separation distance l between the centers of the molecules was a fitted parameter, together with the b values rendered to the interatomic distances. Beyond the first neighbors, a random distribution of atoms was assumed. The agreement between the experimental and theoretical $si(s)$ functions is shown in Fig. 5, and the corresponding $G(r)$ curves in Fig. 3.

As a result of the fit, a separation distance between the neighboring molecules l=330 pm was obtained. This value agreed well with that of 335 pm which can be calculated from the coordinates of atoms in the unit cell given in Ref. 2. Beyond the two nearest neighbors no more molecules were needed to obtain a good fit, and random distribution of atoms was enough to describe the remaining structure.

Intermolecular Structure of the Mixture. Since the analysis of the RDF's suggested that structural effect may occur when mixing the two pure solvents, a detailed LSQ analysis of the $i(s)$ for 1:1 molar mixture was also carried out. Various model combinations were tested. At first, a rough estimate gave the average number of 5.5 for N or C atoms at about 330 pm distant from a central one. Similarly, 8.7 N or C atoms were found around a central O atom at a distance of about 380 pm. This result would correspond to 2.7—2.9 AN molecules around a central DMF molecule. Of course, this picture is very rough, since it does not distinguish between the types of atoms and does not specify any geometry for the structure. Correspondingly, the fit was not satisfactory enough.

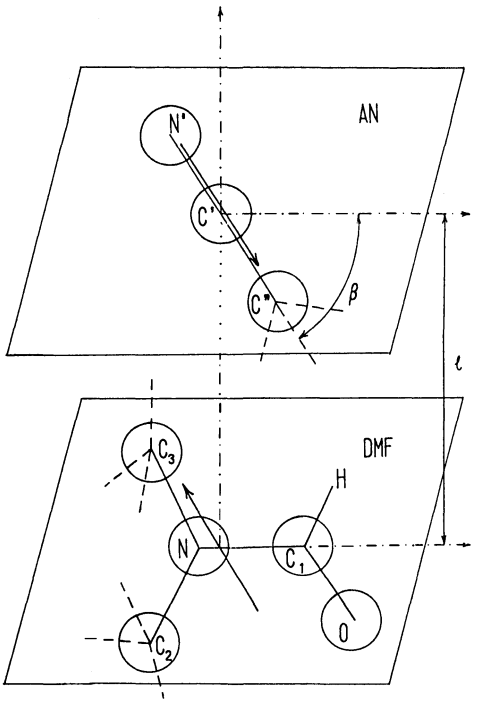

Fig. 6. Schematic drawing of the structural model for DMF-AN complexes. For the sake of simplicity, only one DMF and one AN molecules are shown, the unlike molecules above and below should be arranged accordingly. The direction of the dipoles of the molecules are indicated by arrows. The numbering of the atoms is also shown (primes always refer to atoms belonging to AN). The H atoms of the methyl groups are indicated by dashed lines.

As a second step, a complete model was constructed. From the results of pure AN it was supposed that the dominant interaction between DMF and AN molecule is via their dipoles. The idea for formulating the model was that while retaining the nearest neighbor model for pure AN, the central molecule should be changed to a DMF one in the mixture. The DMF molecule was allowed then to change its orientation to construct various types of the DMF-AN complex. Figure 6 shows the schematic drawing of the model and defines the structural parameters included. It was

Table 4. Calculated Intermolecular Distances (in pm) and b Values (in pm^2) between the Neighboring DMF and AN Molecules from the Best Fit for the 1:1 Molar Mixture

Interaction	r	$b/10$
C′···N	317	51(7)
N′···C_3	319	167(20)
C″···O	329	40(10)
N′···N	332	167(20)
C′···C_1	332	51(7)
C″···C_1	341	40(10)
C′···C_2	355	51(7)
C′···C_3	355	51(7)
C″...N	356	40(10)
C″···C_2	361	40(10)
N′···C_1	369	167(20)
C′···O	373	51(7)
N′···C_2	391	167(20)
N′···O	439	167(20)
C″···C_3	441	40(10)

supposed that the axis of the two molecules lay in parallel planes, and their centers lay on a line perpendicular to the planes. Independent parameters for the fit were: the number n of AN molecules around the central DMF, which corresponds to a set of equal atomic coordination numbers by definition, the separation distance l between the centers of the molecules, corresponding also to a set of atom–atom distances; the rotation angle β around the l-axis, and three b_{ij} values where i and j indicate different molecules. Continuum parameters for each kind of atom-pairs were also included in the fit, but later the terms of less importance (those containing H atoms) were excluded. The interactions of the central DMF molecules with those molecules which are at a distance larger than l, e.g., being within the same plane, were considered in the continuum part. This model obviously has some-rather arbitrary-restrictions, but the requirement of using the least number of structural parameters was always kept in mind during the calculations.

The corresponding pair-correlation functions $G(r)$ and the structure functions $si(s)$ after reaching the best fit are shown in Figs. 4 and 5, respectively. Table 4 shows the (dependent) interatomic distances between DMF and AN molecules calculated from the best fitted independent parameters. Parameters for describing the continuum are given in Table 2.

The final values of n=1.75±0.08, l=316±20 pm, and β=59±10 degree were obtained. The number of AN molecules around a central DMF molecule being somewhat less than 2 seems to be reasonable, because the structure of the DMF–AN mixture, in which a half of AN molecules in the pure state are replaced to DMF molecules, may have a similar, but slightly disordered molecular arrangement, to the pure liquid of AN. For a further consideration, the whole procedure was repeated when an AN molecule was placed in the middle. Similarly, a number of n=1.86±0.1 DMF molecules were determined to be around the AN.

The obtained value for the rotation angle β corresponds to the antiparallel orientation of the dipoles. The least squares sum, in fact, was not very sensitive to the variation of β alone. The R-factor change only about 10% when β varied from 0 to 60 degrees. The only sharp increase in R-factor occurred, amounting up to 300% of the minimum value obtained when the unfavorable parallel orientation was tested.

It is very interesting to note that the separation distance l proved to be less than between two neighboring molecules in pure AN. Its shift from 330 pm to 316 pm going from the pure liquid to the mixture is meaningful, without doubt. It is also noteworthy that when letting to vary l and β together, the favorable antiparallel orientation occurred by accompanying a decrease in the separation distance. It can not be concluded from this fact directly, however, that the interaction between the DMF and AN is stronger than between two AN molecules, but only that the yielded configuration is sterically the most favorable. This may be due to the fortunate coincidence of a more bulky, basically planar DMF molecule with a smaller, and essentially linear AN molecule. For determining the strength of interactions more extended, energetic studies are needed with more appropriate methods.

Several additional tries for finding evidence for other kinds of possible first neighbor configurations were also carried out, but all they failed. Especially when searching for contributions due to weak H-bond type interactions between CH groups of DMF and N atoms of AN at about their characteristic distance of 290—310 pm, no noticeable finding was obtained. The LSQ fit could not be improved, and no remaining peak in the radial distribution function could be observed in the given range neither before constructing the H-bond type model, nor looking for some minor contribution still to be considered after the complete model had been applied.

The work has been supported, in part, by the Ministry of Education, Science and Culture (Grant-in-Aid for Scientific Research on Priority Area of Macromolecular Complexes, No. 62612005). One of us (T.R.) is greatly indebted to the Tokyo Institute of Technology and the Hungarian Academy of Sciences to allow for being engaged into the present study. Computers at the Tokyo Institute of Technology were used for the calculations.

References

1) H. Ohtaki, S. Itoh, T. Yamaguchi, S. Ishiguro, and B. M. Rode, *Bull. Chem. Soc. Jpn.*, **56**, 3406 (1983).

2) A. Kratochwill, J. U. Weidner, and H. Zimmermann, *Ber. Buns. Ges.*, **77**, 408 (1973).
3) H. Bertagnolli and M. Zeidler, *Mol. Phys.*, **36**, 177 (1978).
4) O. Steinhauser and H. Bertagnolli, *Chem. Phys. Lett.*, **78**, 555 (1981).
5) S. Ishiguro and H. Ohtaki, *J. Coord. Chem.*, **15**, 237 (1987).
6) I. Katime and L. C. Cesteros, *J. Chem. Soc., Faraday Trans. 2*, **80**, 1215 (1984).
7) A. K. Sharma, D. R. Sharma, and D. S. Gill, *J. Phys., D*, **18**, 1199 (1985).
8) R. L. Blokhra, M. L. Parmar, and S. K. Agarval, *J. Electroanal. Chem.*, **89**, 417 (1978).
9) See e.g., H. Ohtaki, M. Maeda, and S. Ito, *Bull. Chem. Soc. Jpn.*, **47**, 2217 (1974) or H. Ohtaki, T. Yamaguchi, and M. Maeda, *Bull. Chem. Soc. Jpn.*, **49**, 701 (1976).
10) G. Johansson and M. Sandström, *Chem. Scr.*, **4**, 195 (1973).
11) T. Yamaguchi, Doctor Thesis, Tokyo Inst. of Technol., March (1983).
12) I. Serke, Doctor Thesis, Central Res. Inst. of Hung. Acad. Sci., (1983).

 © 1988 The Chemical Society of Japan Bull. Chem. Soc. Jpn., 61, 3853—3857 (1988)

Study of the Effect of Structural Factors on Magnetism of Di-μ-alkoxodicopper(II) Complexes by Ab Initio MO Calculations[1)]

Makoto HANDA,† Nobuaki KOGA,† and Sigeo KIDA*
Department of Chemistry, Faculty of Science, Kyushu University 33, Hakozaki, Higashi-ku, Fukuoka 812
†Institute for Molecular Science, Myodaiji, Okazaki 444[2)]
(Received June 3, 1988)

The effect of variation of structural factors on the spin-exchange interaction between copper(II) centers in dialkoxo-bridged dinuclear copper complexes were studied by the ab initio MO method with UHF formalism. The calculations were performed on di-μ-methoxotetraamminedicopper(II). The *J*-values were obtained as functions of Cu-O-Cu angle, dihedral angle between two coordination planes, planarity of bonds on the bridging oxygens, tetrahedral distortion of coordination planes, and the tilt of O-C bond from the O-O axis. The results demonstrated that the Cu-O-Cu angle most effectively affect the *J*-value but the other factors are less effective.

A great number of dinuclear copper complexes have been synthesized in the recent two decades, and their structures and magnetisms have been extensively studied.

Hodgson, Hatfield, and the co-workers first showed the relation between a structural factor and magnetic coupling of dinuclear copper(II) complexes. Based on experimental data of several dihydroxo-bridged copper complexes, they showed that there is a linear relationship between the Cu-O-Cu bond angle and the *J*-value, where $-2J$ represents the energy separation between the lowest spin-triplet and singlet states.[3)] Merz and Haase,[4)] and Nieminen[5)] pointed out that a similar relation also exists for dialkoxo-bridged copper(II) complexes based on numerous experimental results. These relations were theoretically interpreted in terms of extended Hückel MO by Hoffmann et al.,[6)] and later by Kahn.[7)] Bencini and Gatteschi[8)] applied the angular overlap approach to a two-atom-bridged dinuclear copper(II) system, and obtained a result similar to that of Hoffmann et al.[6)] However, some other structural factors such as the planarity of Cu_2O_2 entity, the dihedral angle formed by two coordination planes, and the planarity of bonds about bridging oxygen, have been claimed by several workers to be important factors to determine the spin coupling as well as or rather than the Cu-O-Cu angle.[5,7-11)] Indeed, such factors seem to have a good correlation with experimentally obtained *J*-values of dialkoxo-bridged copper(II) complexes. However, in practice, such factors are not independent of other structural factors, but are linked to each other in more or less degree. Hence, it is difficult to determine which factor is the most important one for the spin-exchange interaction from the experimental data.

Thus, theoretical approaches were attempted to see the correlation between each of structural factors and *J*-value. Bencini and Gatteschi also examined effects of various structural factors on the spin coupling by the angular overlap approach.[8)] However, there is limitation in their results, since the angular overlap approach cannot expect quantitative results. De Loth et al. calculated *J*-values by an ab initio SCF MO method on copper(II) acetate monohydrate[12)] and a μ-oxalato-dicopper(II) complex.[13)] Haase et al. applied a similar approach to di-μ-hydroxo and di-μ-methoxo-dicopper(II) complexes shown below.[14)]

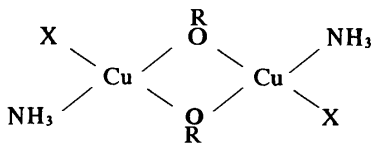

R = H or CH_3

X = F, Cl, or Br

They calculated *J*-values on the model complexes using ps HONDO program with pseudo potential for core electrons of copper, varying the Cu-O-Cu angle, the Cu-O distance, coordination geometry, and the planarity of bonds about the bridging oxygens, and they concluded that the magnitude of exchange coupling strongly depends on these factors. However, they did not investigate the effect of variation of the dihedral angle formed by the two coordination planes, in spite of that the importance of this factor has been pointed out by some workers.[7,11)] Furthermore, they did not discuss on which structural factor the *J* value most deeply depends.

As we have been much interested to clarify which structural factor is the major factor to determine the magnetic interaction in dialkoxo-bridged copper(II) complexes, in this study, we have calculated *J*-values

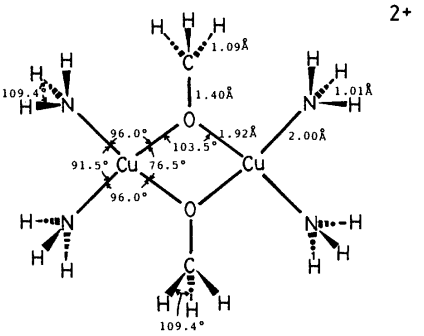

Fig. 1. Structure of the basic model.

on the model compound cited in Fig. 1 by an ab initio MO method, employing the unrestricted Hartree-Fock operator. In this calculation, in order to elucidate the effect of each structural factor on the spin coupling, we systematically varied each of various structural factors such as 1) the Cu–O–Cu angle (ϕ), 2) the dihedral angle formed by the two coordination planes (α), 3) the angle formed by the O–C vector and the Cu_2O_2 plane (θ), 4) the dihedral angle between the Cu_2O_2 plane and the plane formed by the four ammonia nitrogens (τ), and 5) the angle between the O–C and O–O vectors (δ), keeping the other factors constant as far as possible.

Calculation

The calculations were carried out by the GAUSSIAN82[15] program implemented with effective core potential code,[16a,b] the unrestricted Hartree-Fock(UHF) method being employed to estimate J value. The energies of two magnetic orbitals were calculated by the restricted Hartree-Fock (RHF) method.

The copper core electrons were described in terms of effective core potential,[16c] and the valence electrons in terms of basis function [1s1p2d] contracted from (5s2p5d).[16c] The 4-31G[16d] basis set was used for CH_3O and the STO-3G[16e] for NH_3. J values were calculated with the equation,

$$J = -(E_{TUHF} - E_{SUHF})/(\langle S^2\rangle_T - \langle S^2\rangle_S)$$

following Yamaguchi's treatment,[17] where $\langle S^2\rangle_T$ and $\langle S^2\rangle_S$ represent the spin eigenvalues of $\hat{S}^2$ for triplet and singlet states, respectively, and E_{TUHF} and E_{SUHF} are energies for the triplet and singlet states, respectively. The E_{SUHF} value was approximately represented with E_{SPUHF} which was obtained by projecting out the triplet component and using the following equation.

$$E_{SPUHF} = E_{SUHF} + \langle S^2\rangle_{SUHF}(E_{SUHF} - E_{TUHF})/(\langle S^2\rangle_{TUHF} - \langle S^2\rangle_{SUHF})$$

Results and Discussion

Throughout the calculations all bond lengths were fixed. During calculations with varying a structural parameter, all other bond angles were also fixed at the values cited in the basic model, unless there is a geometrical necessity. The results are shown diagramatically in Figs. 2—6. In each diagram the calculated J values and the energy gaps (ΔE) between the two magnetic orbitals (HOMO and LUMO) are plotted versus structural parameter. Each diagram shows that the variation of J is parallel to that of ΔE, implying that the results of the calculations by UHF and RHF are consistent with each other. The experimental data for J, ϕ, α, θ, and τ so far available are summarized in Table 1.

Effect of the Cu–O–Cu angle, ϕ. Since all the atoms

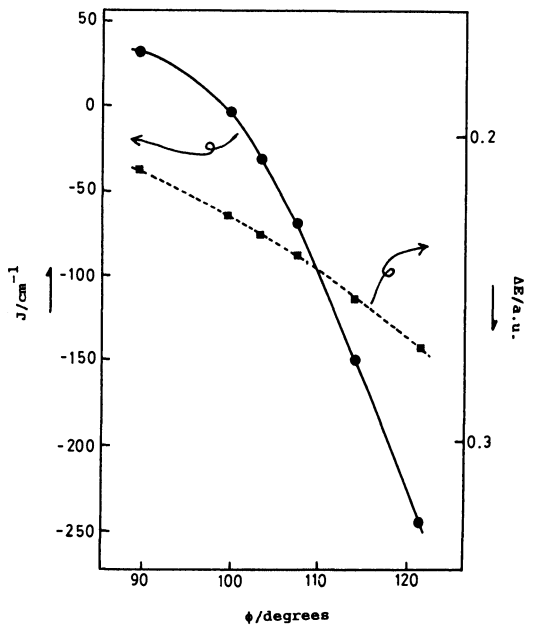

Fig. 2. Variation of the calculated J(——) and ΔE(---) with Cu-O-Cu angle ϕ. (1 a.u.= 2.62550×10^{-6} J mol^{-1}).

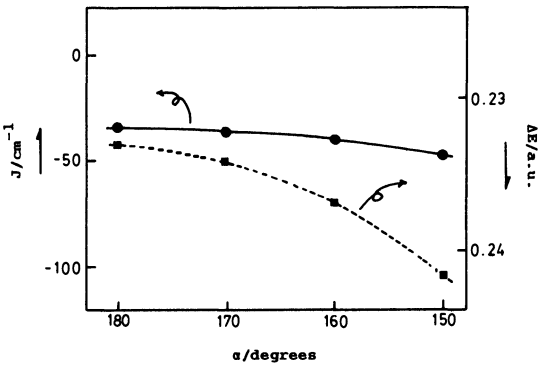

Fig. 3. Variation of the calculated J(——) and ΔE(---) with the dihedral angle formed by the two coordination planes α.

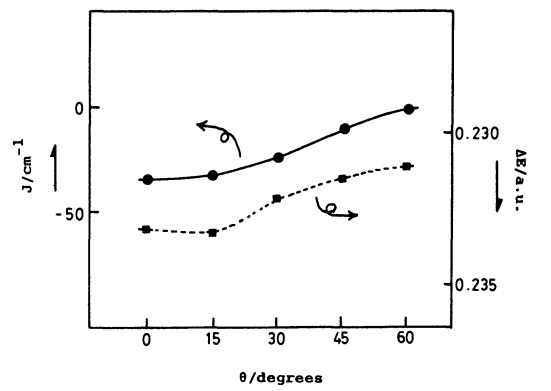

Fig. 4. Variation of the calculated J(——) and ΔE(---) with the angle formed by the O-C vector and the Cu_2O_2 planes θ.

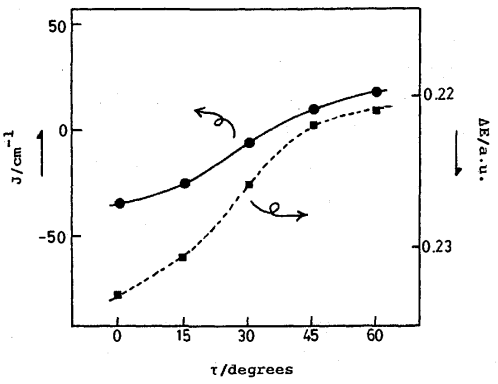

Fig. 5. Variation of the calculated J(——) and ΔE(---) with the dihedral angle between the Cu_2O_2 plane and the plane formed by the four ammonia nitrogen τ.

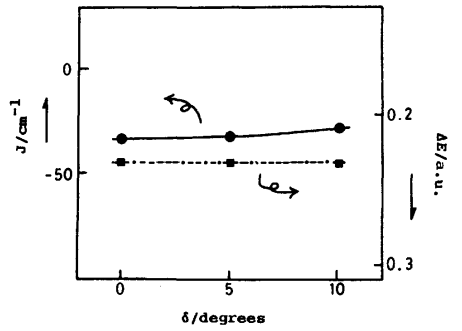

Fig. 6. Variation of the calculated J(——) and ΔE(---) with the angle between the O-C and O-O vectors δ.

are kept in a plane, the variation of ϕ is necessarily required to vary the angles about the copper atoms to keep the summation of angles around the copper atom at 360°. In order to fulfil the requirement, the necessary angle variation was equivalently portioned out on ∠OCuN, ∠NCuN, and ∠NCuO, so that the strain due to the angle variation is made minimum.

As seen in Fig. 2, $-J$ value increases with increasing

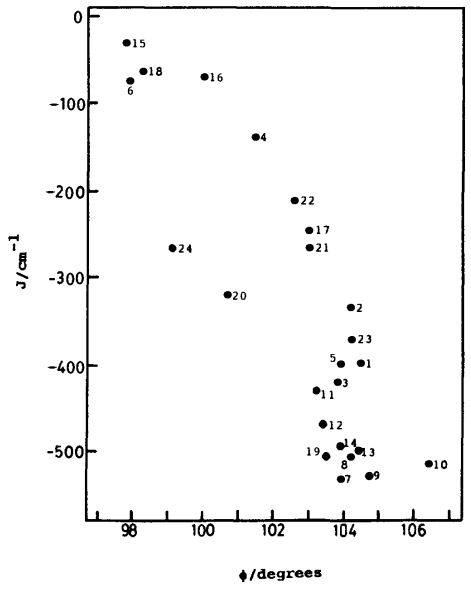

Fig. 7. A plot of experimental J versus Cu–O–Cu angle ϕ. Numbers refer to the complexes listed in Table 1.

Table 1. Experimental Data of $-2J, \phi, \alpha, \theta$, and τ

Compd.	$-2J$/cm^{-1}	ϕ/°	α/°	θ/°[a]	τ/°[a]	Ref.
1	799	104.5	180	4.5	5.2	18
2	670	104.2	180	4.5	8.5	19
3	845	103.8[b]	176.5	1.3[b,c]	—	20,21
4	279	101.5	180	26.1	20.5	22,23
5	800	103.9	180	4.5	16.7	24,25
6	149	97.9[b]	148.5	27.9[b,c]	—	26
7	1065	103.9	180	23.1	12.2	27
8	1020	104.2	180	22.8	15.0	27
9	1056	104.7	180	1.5	12.6	27
10	1030	106.4	180	0.7	0.5	28
11	863	103.2	180	23.5	5.5	29
12	940	103.4	180	12.5	6.8	29
13	1001	103.9	180	7.3	13.9	29
14	988	103.9	180	14.2	16.3	29
15	65	97.8[b]	180	40.8[b]	20.4	30
16	141	100.0	180	31.9	15.8	31
17	495	103.1	180	7.9	30.2	32
18	128	98.3	164.1	36.5[c]	—	33
19	1015	103.5	180	3.5	4.8	34
20	640	100.7[b]	167.9	27.4[b,c]	—	35
21	535	103.0	180	7.2	13.2	36
22	425	102.6	180	13.4	18.0	7
23	745	104.2	180	5.4	12.6	37
24	530	99.4[b]	164.7	23.0[b,c]	—	38,39

a) Calculated from atomic coordinates in the references except for 3 and 5 which were taken from the literature values. b) Mean value of two angles. c) Angle formed by the O-C vector and the Cu_2 O plane.

ϕ as has been pointed out by many workers on the bases of either experimental results[3-5] or quantum mechanical approaches.[6-8,14] The experimentally obtained J values so far available were plotted versus ϕ, and shown in Fig. 7. A good agreement was obtained between our results (Fig. 2) and experimental ones (Fig. 7) in general trend with some exceptions, though the agreement in numerical values is poor. As for the exceptions, we will discuss in the later part of this paper.

Ferromagnetic interactions were observed for some hydroxo-bridged dicopper(II) complexes with small Cu–O–Cu angles,[3] and were reasonably explained in terms of Hückel MO by Hoffmann et al.[6] The present result also predicts the possibility of ferromagnetism in alkoxo-bridged copper(II) complexes with small ϕ. In fact,the complex with ϕ=97.8° bears $-2J$=65 cm^{-1} (cf. compound 15 in Table 1), suggesting that ferromagnetism may be observed for alkoxo-bridged complexes with ϕ<97°.

Angle Formed by Two Coordination Planes, α. The variation of α necessitates to vary the O–O distance in order to keep the Cu–O–Cu angle at the value of the basic structure (Fig. 1).

As seen in Fig. 3, the variation of J per degree is very small compared with that in the case of ϕ, especially, J is practically constant in the range 180—170°, inspite of that some workers[11] regarded this angle as an important factor to determine the spin coupling. According to Bencini and Gatteschi's calculations by angular overlap approach[8] $-J$ increases when α decreases from 180°. On the other hand, Kahn[7] reported the opposite trend based on the Hückel MO calculations. Kahn's result may be due to that the O–O distance was kept constant in his calculations so that the Cu–O–Cu angle also decreases with decreasing α. Such feature has been often observed in practical examples, hence in such cases the decrease in antiferromagnetic interaction should be attributed not to the change in α but to the change in ϕ which is usually linked to α.

Angle between the Cu_2O_2 Plane and O–C Vector, θ. This angle can be varied without any change of the other factors.

As seen in Fig. 4, $-J$ gradually decreases with increasing θ. Figure 4 implies that there is the transition point from antiferro- to ferromagnetic interaction at about θ=60°. However, the extent of the effect of θ on J is much small compared with that of ϕ.

Dihedral Angle between the Cu_2O_2 Plane and the Plane Formed by the Four Ammonia Nitrogens, τ. This parameter was first proposed by Sinn to represent the extent of terahedral distorsion of the coordination plane.[9] He considered this angle an important factor to determine the spin coupling.

As seen in Fig. 5, $-J$ decreases with increasing τ, and there is the antiferro—ferro transition point at about τ=35°. According to Bencini and Gatteschi's calculations the transition point exsists at about 60°.[8] However, in practical examples the variations of τ all fall in the range of 0—20°(cf. Table 1), and Fig. 5 shows that the variation of J/degree is relatively small in this range. Accordingly, the effect of τ on J value would be minor compared with that of ϕ.

Angle between O–O and O–C Vectors, δ. This angle represents the deviation of the O–C bond from the O–O axis due to the strain of chelate ring formation.

Figure 6 shows that the effect of δ on J is very small at least in the range of δ=0—10° which covers whole range of δ for practical compounds.

Concluding Remarks

J-values of dialkoxo-bridged dinuclear copper(II) complexes were obtained as functions of each of five structural parameters by ab initio MO calculations using the unrestricted Hartree-Fock method. Each parameter was varied in keeping the other ones unchanged unless there is any geometrical requirement. The results revealed that the Cu–O–Cu angle is the major factor to determine J value, and the other factors bring only minor effects on J value. This is readily seen in Table 2, in which $|\Delta J|$/degree for each parameter is summarized in the third column. Further, taking into consideration the practical range of the parameters, we have compared effects of variation of these parameters in the last column of Table 2, which shows that the Cu–O–Cu angle is still the major factor to determine J value. However, it should be noted that these structural parameters are not independent, but linked to each other. Therefore, one must be careful to discuss the variation of J as a function of a single parameter. Thus, the existence of exceptions observed in Fig. 7 may be ascribed to the above mentioned reason, i.e., J varies linking to other

Table 2. $|\Delta J|$/degree and $|\Delta J|$/(the pratically variable range of each parameter)

Structural parameter	Practically[a] variable range/°	$\|\Delta J\|$/degree[b]/cm^{-1}	$\|\Delta J\|$/range/cm^{-1}
ϕ	97—107	7.4	74
α	180—150	0.41	12
θ	0—40	0.48	19
τ	0—30	0.96	29
δ	0—10	0.12	1.2

a) Estimated from the data in Table 1. b) Averaged value of $|\Delta J|$/degree in the variable range.

structural parameters in practical compounds, though it is difficult to assign which factor plays the major role to cause deviation from the general rule at present.

References

1) This work was partly presented at 37th Symposium on Coordination Chemistry, Tokyo (1987).

2) This work was mainly carried out at the Institute for Molecular Science and partly at Kyushu University.

3) D. J. Hodgson, *Prog. Inorg. Chem.*, **19**, 173 (1975); V. H. Crawford, H. W. Richardson, J. R. Wasson, D. J. Hodgson, and W. E. Hatfield, *Inorg. Chem.*, **15**, 2107 (1976).

4) L. Merz and W. Haase, *J. Chem. Soc., Dalton Trans.*, **1980**, 875.

5) K. Nieminen, *Ann. Acad. Sci. Fenn., Ser. A, 2*, **197**, 8 (1983).

6) P. J. Hay, J. C. Thibeault, and R. Hoffmann, *J. Am. Chem. Soc.*, **97**, 4884 (1975).

7) O. Kahn, *Inorg. Chim. Acta*, **62**, 3 (1982).

8) A. Bencini and D. Gatteschi, *Inorg. Chim. Acta*, **31**, 11 (1978).

9) R. M. Countryman, W. T. Robinson, and E. Sinn, *Inorg. Chem.*, **13**, 2013 (1974); E. Sinn, *ibid.*, **15**, 358 (1976).

10) M. Mikuriya, K. Toriumi, T. Ito, and S. Kida, *Inorg. Chem.*, **24**, 629 (1985).

11) G. D. Fallon, K. S. Murray, W. Mazurek, and M. J. O'connor, *Inorg. Chim. Acta*, **96**, L53 (1985); W. Mazurek, B. J. Kennedy, K. S. Murray, M. J. O'connor, J. R. Rodgers, M. R. Snow, A. G. Wedd, and P. R. Zwack, *Inorg. Chem.*, **24**, 3258 (1985).

12) P. de Loth, P. Cassoux, J. P. Daudey, and J. P. Malrieu, *J. Am. Chem. Soc.*, **103**, 4007 (1981).

13) M. F. Charlot, M. Verdaguer, Y. Journaux, P. de Loth, and J. P. Daudey, *Inorg. Chem.*, **23**, 3802 (1984).

14) H. Astheimer and W. Haase, *J. Chem. Phys.*, **85**, 1427 (1986).

15) J. S. Binkley, M. J. Frisch, D. J. DeFrees, K. Raghavachari, R. A. Whiteside, H. B. Schlegel, and J. A. Pople, Carnegie-Mellon Chemistry Publishing Unit, Pittsburgh, PA, (1984).

16) a) L. E. McMurchie and E. R. Davidson, *J. Comput. Phys.*, **44**, 289 (1981); b) R. L. Martin , unpublished; c) P. J. Hay and W. R. Wadt, *J. Chem. Phys.*, **82**, 270, (1985); d) R. Ditchfield, W. J. Hehre, and J. A. Pople, *J. Chem. Phys.*, **54**, 724 (1971); e) W. J. Hehre, R. F. Stewart, and J. A. Pople, *J. Chem. Phys.*, **51**, 2657 (1969).

17) K. Yamaguchi, H. Fukui, and T. Fueno, *Chem. Lett.*, **1986**, 625; K. Yamaguchi, Y. Takahara, and T. Fueno, "Applied Quantum Chemistry," ed by V. H. Smith, H. F. Schaefer, and K. Morokuma, Reidel, Dordrecht (1986), p. 155.

18) A. Pajunen and M. Lehtonen, *Soum. Kemistil., B*, **44**, 200 (1971); M. Lehtonen, E. Luukkonen, and R. Uggla, *ibid., B*, **44**, 399 (1971).

19) L. Merz and W. Haase, *Acta Crystallogr., Sect. B*, **34**, 2128 (1978).

20) Y. Nishida and S. Kida, *J. Inorg. Nucl. Chem.*, **38**, 451 (1976).

21) R. Mergehenn and W. Haase, *Z. Naturforsch., Teil B*, **30**, 155 (1975).

22) A. Pajunen and K. Smolander, *Finn. Chem. Lett.*, **1974**, 99.

23) R. Uggla, M. Melnik, O. Orama, M. Kilinga, and C. Harjulin, *Soum. Kemistil., B*, **45**, 323 (1972).

24) E. Uhlig and K. Steiger, *Z. Anorg. All. Chem.*, **360**, 39 (1968).

25) R. Mergehenn, L. Merz, and W. Haase, *Z. Naturforsch., Teil B*, **30**, 14 (1975).

26) M. Nasakkala, *Ann. Acad. Sci. Fenn., Ser. A, 2*, **181**, 6 (1977).

27) L. Walz, H. Paulus, and W. Haase, *J. Chem. Soc., Dalton Trans.*, **1985**, 913.

28) J. A. Bertrand and J. A. Kelley, *Inorg. Chim. Acta*, **4**, 203 (1970).

29) L. Walz and W. Haase, *J. Chem. Soc., Dalton Trans.*, **1985**, 1243.

30) K. Nieminen and M. Nasakkala, *Acta Chem. Scand., A*, **34**, 375 (1980).

31) K. Nieminen, *Acta Chem. Scand., A*, **35**, 753 (1981).

32) L. Banci, A. Bencini, P. Dapporto, A. Dei, and D. Gatteschi, *Inorg. Chem.*, **19**, 3395 (1980).

33) J. A. Bertrand, E. Fujita, and P. G. Eller, *Inorg. Chem.*, **13**, 2067 (1974).

34) M. Mikuriya, T. Harada, H. Okawa, and S. Kida, *Inorg. Chim. Acta*, **75**, 1 (1983).

35) Y. Nishida and S. Kida, *Mem. Fac. Sci. Kyushu Univ., Ser. C*, **13**, 35 (1981).

36) M. Mikuriya, H. Okawa, and S. Kida, *Bull. Chem. Soc. Jpn.*, **54**, 2979 (1981).

37) M. Mikuriya, H. Okawa, and S. Kida, *Bull. Chem. Soc. Jpn.*, **55**, 1086 (1982).

38) A. C. Villa, L. Coghi, A. G. Manfredotti, and C. Guastini, *Cryst. Struct. Commun.*, **3**, 543 (1974).

39) Y. Nishida, F. Numata, and S. Kida, *Inorg. Chim. Acta*, **11**, 189 (1974).

 © 1988 The Chemical Society of Japan Bull. Chem. Soc. Jpn., 61, 3859—3867 (1988)

Crystal Structures of Chiral Smectogenic 4-Pentyloxyphenyl and 4-Heptyloxyphenyl 4′-[(*S*)-2-Methylbutyl]biphenyl-4-carboxylates

Kayako HORI* and Yuji OHASHI
Department of Chemistry, Ochanomizu University, Otsuka, Bunkyo-ku, Tokyo 112
(Received June 15, 1988)

Crystal structures of the title compounds, which have a Sm* C phase adjacent to a cholesteric, have been determined by single crystal X-ray analysis. 4-Pentyloxyphenyl 4′-[(*S*)-2-methylbutyl]biphenyl-4-carboxylate: monoclinic, $P2_1$, a=25.085(2), b=5.7522(3), c=18.668(1) Å, β=110.275(9)°, Z=4. 4-Heptyloxyphenyl 4′-[(*S*)-2-methylbutyl]biphenyl-4-carboxylate: triclinic, $P\bar{1}$, a=14.607(1), b=17.212(2), c=5.7322(8) Å, α=94.84(1), β=84.03(1), γ=108.607(9)°, Z=2. Final R-values were 0.113 and 0.083, respectively. Both crystals have layer structures similar to those of Sm* C phase. Two crystallographically independent molecules in each crystal are related by a pseudo-inversion. Paraffin chains with extended conformations have close contacts between layers.

The Sm* C phase of liquid crystals has become of interest because of its unique ferroelectricity. Precise structures and molecular interaction in the phase, however, are not sufficiently clear, because it is very difficult to obtain microscopic structural information due to rapid molecular motions. So, we intended to find a relationship between the mesophase characteristics (phase sequences, structures and properties) and molecular interaction revealed in the crystal structures, by X-ray crystal structure analysis for a series of compounds with various mesophase characteristics.

For this purpose, three types of compounds containing biphenyl esters were chosen, since their mesophase characteristics have already been examined.[1] The first type, 4-alkoxyphenyl 4′-[(*S*)-2-methylbutyl]biphenyl-4-carboxylates, has a Sm* C phase with iridescent color caused by a short-pitched helical structure, between crystalline and cholesteric phases.[2] Powder X-ray diffraction patterns showed that I-5 and I-7 are isomorphous with I-6 and I-8, respectively.[3] This paper describes the crystal structures of I-5 and I-7 in detail.

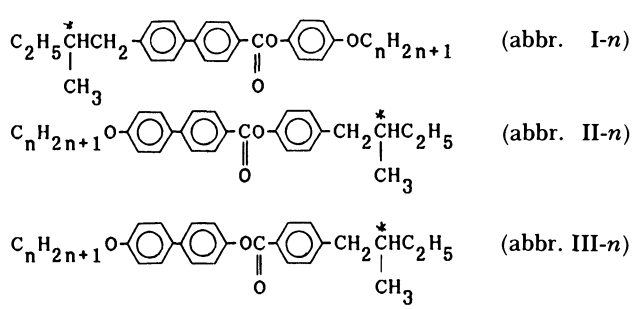

Experimental

The compounds were obtained in the same way as described previously.[4] Transparent long parallelepiped crystals were grown from a methanol–chloroform solution. Crystals of dimensions, 0.4×0.3×0.1 mm (I-5) and 0.5×0.4×0.1 mm (I-7) were used. The unit cell dimensions and space groups were determined from oscillation and Weissenberg photographs. Accurate cell parameters were determined by a least-squares fit for 16 reflections within the range $39°<2\theta<52°$ (I-5) and 20 reflections within the range $33°<2\theta<52°$ (I-7), measured on a Rigaku AFC-4 diffractometer with Cu $K\alpha$ radiation (λ=1.54184 Å) monochromatised by graphite. Crystal data. I-5, M_r=430.56, $C_{29}H_{34}O_3$, monoclinic, $P2_1$, T=298 K, a=25.085(2), b=5.7522(3), c=18.668(1) Å, β=110.275(9)°, V=2526.8(4) Å^3, Z=4, d_x=1.131 g cm^{-3}, μ=4.90 cm^{-1}, $F(000)$=928; I-7, M_r=458.61, $C_{31}H_{38}O_3$, triclinic, $P\bar{1}$, T=298 K, a=14.607(1), b=17.212(2), c=5.7322(8) Å, α=94.84(1), β=84.03(1), γ=108.607(9)°, V=1356.4(3) Å^3, Z=2, d_x=1.123 g cm^{-3}, μ=4.79 cm^{-1}, $F(000)$=496. Intensity data were collected by 2θ–ω scan mode, up to 2θ=125°. Scan width was $\Delta\omega=(1.0+0.15\tan\theta)°$. Backgrounds were counted for 5 s at both ends of a scan. Three standard reflections were recorded after every 50 reflections. No significant intensity variations were observed. For I-5, a total of 4497 reflections were collected at a rate of $4°(2\theta)$ min^{-1}, of which 3345 were treated as significant ($|F_o|>3\sigma(|F_o|)$). For I-7, 4345 reflections were collected at a rate of $8°(2\theta)$ min^{-1}, of which 3692 were used in the calculation. The data were corrected for Lorentz and polarization factors but not for absorption.

The structures were determined by applying the program MULTAN78[5] and refined by constrained block-matrix least-squares using SHELX76.[6] The quantity minimized was $\Sigma w(|F_o|-|F_c|)^2$, where $w=(\sigma(F_o)^2+0.004|F_o|)^{-1}$. In the course of the refinement of both structures, additional peaks of 0.5—1.0 e Å^{-3} were found around the chiral groups, whose atoms revealed considerably large temperature factors. These peaks were included as disordered atoms in further refinement. For I-5, C(22) to C(25) of the molecule A and C(23) to C(25) of B were disordered, whereas only the terminal C(24) atoms of A and B were disordered for I-7. All the non-hydrogen atoms except for the disordered ones of I-7 were refined anisotropically with loosely constrained condition to have normal geometries. Some hydrogen atoms were found in the difference Fourier maps and others were derived geometrically except for the chiral parts and the terminal atoms of the alkyl chains of I-5. Final refinement including the hydrogen atoms were performed with the program HBLS,[7] since the numbers of the parameters became too large for SHELX76. Max. Δ/σ and max. $\Delta\rho$ in the final difference map were 0.52 and 0.25 e Å^{-3} for I-5, and 0.54 and 0.30 e Å^{-3} for I-7. Final R (and R_w) were 0.113 (0.139) and 0.083 (0.098) for I-5 and I-7, respectively. Rather large R-value of I-5 is due to the disordered structures of the chiral parts. Atomic scattering factors were taken from the International Tables for X-ray Crystallography.[8] The final

Table 1. Final Atomic Coordinates with Their Estimated Standard Deviations of 4-Pentyloxyphenyl 4′-[(S)-2-Methylbutyl]biphenyl-4-carboxylate (I-5)

Atom	x	y	z	B_{eq}/Å$^{2a)}$
O(1A)	0.1630(2)	1.1093(15)	0.8335(3)	10.7
O(2A)	0.2156(2)	0.8131(11)	0.8180(3)	7.0
O(3A)	0.3178(2)	0.6911(14)	1.1284(3)	8.8
C(1A)	0.0019(4)	0.9993(17)	0.3075(4)	8.1
C(2A)	0.0400(4)	0.8260(19)	0.3413(5)	9.7
C(3A)	0.0702(4)	0.8224(17)	0.4176(5)	8.4
C(4A)	0.0654(3)	1.0052(16)	0.4644(4)	6.9
C(5A)	0.0270(3)	1.1835(17)	0.4305(4)	7.6
C(6A)	−0.0050(4)	1.174(2)	0.3547(5)	8.7
C(7A)	0.0950(3)	0.9984(13)	0.5489(4)	5.8
C(8A)	0.1316(3)	0.818(2)	0.5824(4)	7.8
C(9A)	0.1593(3)	0.8067(15)	0.6603(4)	6.4
C(10A)	0.1507(3)	0.9816(19)	0.7072(5)	8.0
C(11A)	0.1151(4)	1.1695(16)	0.6743(5)	8.0
C(12A)	0.0893(4)	1.1783(18)	0.5943(4)	8.3
C(13A)	0.1759(3)	0.9872(18)	0.7909(4)	7.3
C(14A)	0.2396(3)	0.7904(19)	0.8956(5)	7.5
C(15A)	0.2260(4)	0.5884(19)	0.9269(4)	8.3
C(16A)	0.2527(3)	0.5507(17)	1.0045(5)	8.0
C(17A)	0.2920(3)	0.7064(18)	1.0496(4)	7.3
C(18A)	0.3038(3)	0.9022(17)	1.0173(4)	7.4
C(19A)	0.2790(3)	0.9481(18)	0.9405(4)	7.2
C(21A)	−0.0369(4)	1.001(3)	0.2225(5)	10.5
C(22A)$^{b)}$	−0.0059(11)	1.068(4)	0.1677(12)	14.0
C(23A)$^{b)}$	−0.0003(8)	1.323(4)	0.1687(9)	11.3
C(24A)$^{b)}$	0.0261(11)	1.380(6)	0.1124(14)	17.0
C(25A)$^{b)}$	−0.0409(13)	1.005(6)	0.0851(14)	20.6
C(22A′)$^{b)}$	−0.0162(11)	1.175(10)	0.1767(11)	23.7
C(23A′)$^{b)}$	−0.0581(12)	1.213(7)	0.0960(14)	16.0
C(24A′)$^{b)}$	−0.0570(10)	0.989(7)	0.0681(10)	15.6
C(25A′)$^{b)}$	0.0454(9)	1.271(7)	0.1978(14)	13.8
C(31A)	0.3075(3)	0.492(2)	1.1657(4)	8.9
C(32A)	0.3334(3)	0.531(2)	1.2536(5)	9.2
C(33A)	0.3248(4)	0.328(3)	1.2994(5)	11.4
C(34A)	0.3494(4)	0.3777(19)	1.3845(5)	10.6
C(35A)	0.3342(4)	0.187(2)	1.4334(6)	10.4
O(1B)	0.3353(2)	0.1458(12)	0.6592(3)	8.5
O(2B)	0.2846(2)	0.4424(10)	0.6757(3)	6.8
O(3B)	0.1813(2)	0.5549(11)	0.3638(3)	7.6
C(1B)	0.4969(3)	0.2217(18)	1.1872(4)	7.3
C(2B)	0.4588(3)	0.401(2)	1.1561(4)	7.8
C(3B)	0.4283(3)	0.4047(18)	1.0785(4)	7.1
C(4B)	0.4358(3)	0.2350(14)	1.0298(4)	5.5
C(5B)	0.4730(4)	0.060(2)	1.0615(5)	8.5
C(6B)	0.5020(4)	0.0443(19)	1.1398(4)	8.2
C(7B)	0.4032(3)	0.2471(16)	0.9455(4)	6.2
C(8B)	0.3675(3)	0.4299(14)	0.9110(4)	5.8
C(9B)	0.3388(3)	0.4366(16)	0.8318(4)	7.0
C(10B)	0.3472(2)	0.2618(12)	0.7872(3)	4.6
C(11B)	0.3820(3)	0.0752(16)	0.8203(4)	6.7
C(12B)	0.4100(3)	0.0686(16)	0.8979(4)	6.4
C(13B)	0.3225(3)	0.2741(14)	0.7016(4)	6.8
C(14B)	0.2602(3)	0.4676(12)	0.5955(4)	5.1
C(15B)	0.2721(3)	0.6659(14)	0.5625(4)	6.0
C(16B)	0.2473(3)	0.6988(16)	0.4842(4)	6.4
C(17B)	0.2096(3)	0.5341(15)	0.4404(4)	5.9
C(18B)	0.1953(3)	0.3408(16)	0.4741(4)	7.2
C(19B)	0.2202(3)	0.3107(16)	0.5528(4)	6.4
C(21B)	0.5329(4)	0.229(3)	1.2725(4)	9.4
C(22B)	0.5002(4)	0.164(3)	1.3246(4)	12.2
C(23B)$^{b)}$	0.5383(7)	0.127(4)	1.4079(7)	13.0
C(24B)$^{b)}$	0.5650(8)	0.345(7)	1.4361(8)	17.7
C(25B)$^{b)}$	0.4627(6)	−0.040(4)	1.3023(7)	9.9
C(23B′)$^{b)}$	0.5443(17)	0.230(11)	1.401(3)	26.3
C(24B′)$^{b)}$	0.5286(13)	0.222(10)	1.4653(14)	13.6

Table 1. (Continued)

Atom	x	y	z	B_{eq}/Å$^{2a)}$
C(25B')[b]	0.4831(16)	−0.075(10)	1.2994(18)	15.4
C(31B)	0.1963(4)	0.7440(16)	0.3259(4)	7.7
C(32B)	0.1632(4)	0.709(2)	0.2400(4)	9.2
C(33B)	0.1810(3)	0.9026(19)	0.1964(4)	7.5
C(34B)	0.1510(3)	0.873(3)	0.1095(4)	10.3
C(35B)	0.1682(5)	1.066(3)	0.0662(6)	13.0

a) $B_{eq}=(4/3)\sum_{ij}\beta_{ij}(a_i\cdot a_j)$. b) Occupation factors are fixed as 0.55, 0.45, 0.66, and 0.34 for C(22A)–C(25A), C(22A')–C(25A'), C(23B)–C(25B), and C(23B')–C(25B'), respectively.

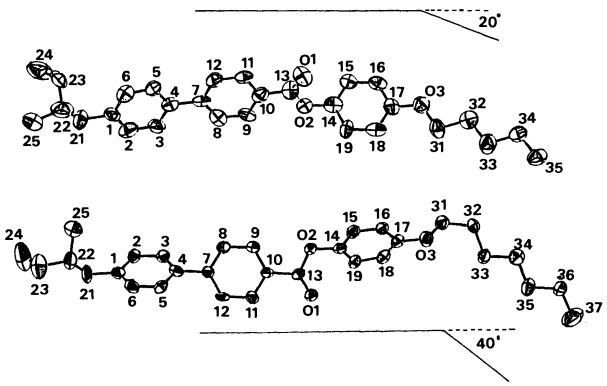

Fig. 1. ORTEP views of the molecules A of 4-pentyloxyphenyl 4'-[(*S*)-2-methylbutyl]biphenyl-4-carboxylate (I-5, upper) and 4-heptyloxyphenyl 4'-[(*S*)-2-methylbutyl]biphenyl-4-carboxylate (I-7, lower) with 50% probability thermal ellipsoids. Only one of the two conformers of the disordered part is shown for simplicity.

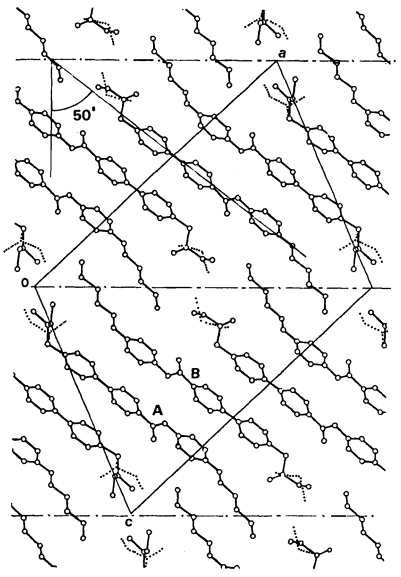

Fig. 2. Crystal structure of I-5 viewed along the b axis. The dot-and-dash lines denote interfaces of the layer. The dotted lines denote disordered conformers.

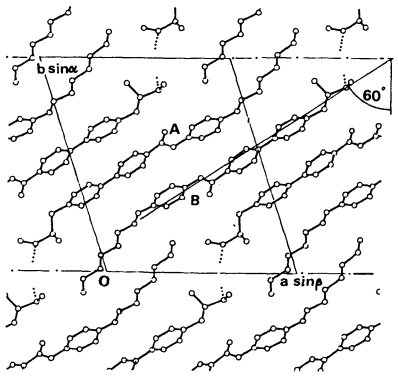

Fig. 3. Crystal structure of I-7 viewed along the c axis. The dot-and-dash lines denote interfaces of the layer. The dotted lines denote disordered conformers.

coordinates of non-hydrogen atoms are given in Tables 1 (I-5) and 2 (I-7).[9] Computations were done on a HITAC M-280H at the Computer Center of the University of Tokyo.

Results and Discussion

Molecular Conformations. There are two crystallographically independent molecules with approximately the same conformation in an asymmetric unit for both crystals. The ORTEP drawings of the molecular structures with numbering schemes are shown in Fig. 1.[10] Chiral parts are highly disordered even in the crystalline state for I-5, while they are only slightly disordered for I-7. All the bond lengths and bond angles, as given in Tables 3 and 4, are compatible with those found in other mesogens.[11] All the phenyl rings are planar within the experimental error.

Table 5 shows torsion angles characteristic to the molecular conformations. Each molecule in the I-5 crystal has an approximately coplanar biphenyl moiety and an all-trans zigzag paraffin chain, while a largely twisted biphenyl moiety and an extended paraffin chain with a twisted O–C–C–C part are found in the I-7 crystal. In each crystal, an extended alkyl chain results in a bent shape of a molecule as a whole, as shown in Fig. 1. The angles between the chains and the other part of the molecules are approximately 20° (I-5) and 40° (I-7).

Crystal Packing. Figures 2 and 3 show the crystal

Table 2. Final Atomic Coordinates with Their Estimated Standard Deviations of 4-Heptyloxyphenyl 4′-[(*S*)-2-Methylbutyl]biphenyl-4-carboxylate (I-7)

Atom	*x*	*y*	*z*	B_{eq}/Å$^{2a)}$
O(1A)	0.5409(3)	0.6614(3)	0.4871(10)	8.1
O(2A)	0.5624(3)	0.5910(2)	0.7792(7)	5.4
O(3A)	0.9550(3)	0.7584(3)	0.7960(8)	6.5
C(1A)	−0.0876(5)	0.3158(4)	0.6937(12)	5.8
C(2A)	−0.0458(4)	0.3625(4)	0.8884(11)	5.3
C(3A)	0.0513(4)	0.4097(4)	0.8781(11)	5.5
C(4A)	0.1104(5)	0.4036(3)	0.6759(10)	5.0
C(5A)	0.0717(5)	0.3561(4)	0.4795(11)	5.8
C(6A)	−0.0261(6)	0.3098(4)	0.4955(13)	6.7
C(7A)	0.2150(4)	0.4544(3)	0.6554(9)	4.5
C(8A)	0.2724(4)	0.4566(4)	0.8358(10)	4.9
C(9A)	0.3702(4)	0.5029(3)	0.8238(9)	4.5
C(10A)	0.4071(4)	0.5554(3)	0.6412(9)	4.4
C(11A)	0.3492(4)	0.5584(4)	0.4661(10)	5.2
C(12A)	0.2536(4)	0.5072(4)	0.4747(8)	4.2
C(13A)	0.5090(4)	0.6095(3)	0.6267(9)	4.6
C(14A)	0.6606(4)	0.6377(4)	0.7734(10)	5.2
C(15A)	0.6923(5)	0.6835(4)	0.9767(11)	5.8
C(16A)	0.7902(5)	0.7255(4)	0.9897(11)	5.6
C(17A)	0.8560(4)	0.7205(3)	0.8013(11)	5.2
C(18A)	0.8243(4)	0.6707(3)	0.6024(11)	5.3
C(19A)	0.7258(4)	0.6333(4)	0.5830(10)	5.1
C(21A)	−0.1963(5)	0.2705(6)	0.705(2)	9.4
C(22A)	−0.2246(6)	0.1784(6)	0.702(2)	10.6
C(23A)	−0.3300(8)	0.1327(9)	0.665(3)	14.2
C(24A)$^{c)}$	−0.4035(14)	0.1466(19)	0.848(6)	24.0
C(24A′)$^{c)}$	−0.377(5)	0.045(4)	0.624(13)	13.6$^{b)}$
C(25A)	−0.2021(10)	0.1475(12)	0.918(3)	18.2
C(31A)	0.9944(5)	0.8083(4)	0.9954(12)	6.6
C(32A)	1.1016(5)	0.8473(4)	0.9336(12)	6.1
C(33A)	1.1223(5)	0.9038(4)	0.7312(14)	6.7
C(34A)	1.2282(6)	0.9579(5)	0.7175(15)	7.3
C(35A)	1.2522(5)	1.0167(5)	0.5165(18)	8.3
C(36A)	1.3572(5)	1.0740(5)	0.5039(14)	7.3
C(37A)	1.3874(11)	1.1303(8)	0.298(3)	14.2
O(1B)	0.6751(3)	0.3699(3)	1.3815(8)	6.6
O(2B)	0.6558(3)	0.4456(3)	1.1017(7)	6.0
O(3B)	0.2640(3)	0.2769(2)	1.0858(7)	4.8
C(1B)	1.3041(4)	0.7262(4)	1.1888(14)	6.6
C(2B)	1.2670(5)	0.6770(5)	0.9950(14)	6.7
C(3B)	1.1681(4)	0.6356(3)	0.9974(10)	4.8
C(4B)	1.1073(4)	0.6345(4)	1.2028(9)	4.5
C(5B)	1.1447(5)	0.6859(4)	1.3936(11)	6.4
C(6B)	1.2432(5)	0.7298(5)	1.3905(12)	7.0
C(7B)	1.0029(4)	0.5811(3)	1.2090(8)	4.4
C(8B)	0.9425(4)	0.5841(3)	1.0401(9)	4.4
C(9B)	0.8464(4)	0.5337(4)	1.0465(10)	4.9
C(10B)	0.8099(4)	0.4817(3)	1.2312(9)	4.5
C(11B)	0.8690(4)	0.4799(3)	1.4052(9)	4.9
C(12B)	0.9648(4)	0.5296(4)	1.3919(12)	5.6
C(13B)	0.7087(4)	0.4264(4)	1.2565(11)	5.4
C(14B)	0.5561(4)	0.4003(4)	1.0975(10)	4.8
C(15B)	0.5245(4)	0.3529(4)	0.8954(10)	5.4
C(16B)	0.4265(5)	0.3107(4)	0.8871(10)	5.4
C(17B)	0.3611(4)	0.3148(3)	1.0777(9)	4.4
C(18B)	0.3952(4)	0.3605(3)	1.2803(9)	4.5
C(19B)	0.4919(4)	0.4071(4)	1.2869(10)	4.9
C(21B)	1.4135(6)	0.7675(5)	1.1815(16)	8.2
C(22B)	1.4536(7)	0.8318(8)	1.006(3)	15.9
C(23B)	1.5638(9)	0.8652(9)	0.971(4)	18.2
C(24B)$^{c)}$	1.5997(16)	0.8910(16)	1.209(8)	27.2
C(24B′)$^{c)}$	1.576(5)	0.931(4)	1.153(12)	18.1$^{b)}$
C(25B)	1.4050(9)	0.8958(6)	1.037(3)	15.2
C(31B)	0.2278(5)	0.2276(4)	0.8827(12)	6.3
C(32B)	0.1202(6)	0.1843(5)	0.9355(15)	7.7

Table 2. (Continued)

Atom	x	y	z	B_{eq}/Å[2a)]
C(33B)	0.0991(5)	0.1236(4)	1.1306(14)	7.0
C(34B)	−0.0091(5)	0.0788(4)	1.1801(14)	7.1
C(35B)	−0.0324(6)	0.0154(4)	1.3635(12)	7.0
C(36B)	−0.1397(7)	−0.0322(5)	1.387(2)	9.8
C(37B)	−0.1582(7)	−0.0970(6)	1.5671(17)	9.5

a) $B_{eq}=(4/3)\sum_{ij}\beta_{ij}(a_i\cdot a_j)$. b) Isotropic temperature factors. c) Occupation factors are fixed as 0.8, 0.2, 0.7, and 0.3 for C(24A), C(24A'),C(24B), and C(24B'), respectively.

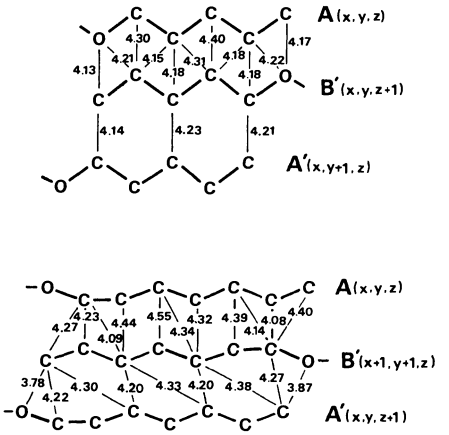

Fig. 4. Inter-chain distances (Å) of I-5 (upper) and I-7 (lower). Symmetry codes are shown in parentheses.

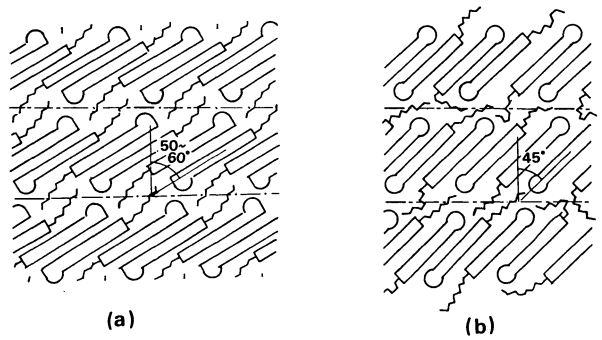

Fig. 5. Schematic diagrams of the structures of the crystal (a) and Sm* C (b). In the latter, the tilt direction forms a slightly helical distribution on moving from layer to layer. A half-rounded head in (a) denotes a static bulky 2-methylbutyl group, while a round head in (b) denotes a rotating one.

structures of I-5 and I-7, respectively. They have a similar packing mode. Layer structures similar to those of smectics are composed of two crystallographically independent molecules A and B, which are related by a pseudo-inversion except for the chiral parts. In a crystal of an achiral compound, 4,4'-bis(pentyloxy)azoxybenzene had a layer structure composed of equivalent molecules, in which a layer plane was very clear, corresponding to the existence of an "intermediately highly ordered smectics".[12] In the present case, layer planes, although less clear, are parallel to the (10$\bar{1}$) plane (I-5) and the (010) plane (I-7). The molecular long axis is largely tilted in the layer. The tilt angles are estimated to be 50° (I-5) and 60° (I-7).

Paraffin chains of adjacent molecules are in contact with each other between layers. The inter-chain distances are shown in Fig. 4. The molecules A and B' are contact in the range of 4.13—4.40 Å for I-5 and 4.08—4.55 Å for I-7. The wider range of I-7 is caused by the twisted O–C–C–C parts. Neverthless, the inter-chain distances in the two crystals are very close to the values found in the crystalline long-chain compounds; 4.14 and 4.20 Å for hexatriacontane[13] or 4.13 and 4.20 Å for normal-chain fatty acids.[14] Furthermore, the chains of the molecules B' and A' are also relatively close, though the zigzag chains are out of phase each other. Therefore, the inter-chain association between layers plays an important role in molecular aggregation in these crystals. The bent shape of each molecule mentioned above is resulted from this inter-chain contact. This bending also favors the packing of bulky 2-methylbutyl groups.

Concerning a packing mode within a layer, there are two kinds of intermolecular overlapping. Each molecule overlaps largely, i.e., from head to tail, with one of the nearest neighbor molecules. On the contrary, the overlaps with the other molecule is small and alkyl chains are related to the interlayer aggregation. So, the two molecules displace largely each other along their long axes, and the large displacement leads to a large tilt angle of the molecule in a layer. Nearest phenyl rings between adjacent molecules make angles of 60° (I-5) and 54° (I-7) in average. This fact also suggests that lateral intermolecular forces are not so strong as in the case of 4,4'-bis(pentyloxy)azoxybenzene with a more ordered smectic than Sm* C, since nearest phenyl rings of the latter crystal are parallel between adjacent molecules.

Relationship between the Crystal and Sm* C Structures. Characteristic features of the two crystal structures are summarized schematically in Fig. 5(a). This is compared with a Sm* C structure shown in Fig. 5(b), which was estimated in the previous study[4] by measuring temperature dependence of the interlayer distances in the Sm* C phase in the series I (n=6, 7, 8, 9, 10, 12, 14, and 16) by X-ray diffraction. Linear

Table 3. Bond Lengths (l/Å) and Bond Angles (ϕ/°) of I-5

Bond	l/Å or ϕ/°	Bond	l/Å or ϕ/°
O(1A)-C(13A)	1.187(14)	O(1B)-C(13B)	1.205(11)
O(2A)-C(13A)	1.379(13)	O(2B)-C(13B)	1.326(10)
O(2A)-C(14A)	1.369(13)	O(2B)-C(14B)	1.415(9)
O(3A)-C(17A)	1.389(13)	O(3B)-C(17B)	1.364(11)
O(3A)-C(31A)	1.412(16)	O(3B)-C(31B)	1.417(12)
C(1A)-C(2A)	1.374(16)	C(1B)-C(2B)	1.391(16)
C(1A)-C(6A)	1.387(16)	C(1B)-C(6B)	1.386(16)
C(2A)-C(3A)	1.362(15)	C(2B)-C(3B)	1.385(16)
C(3A)-C(4A)	1.398(14)	C(3B)-C(4B)	1.391(13)
C(4A)-C(5A)	1.399(14)	C(4B)-C(5B)	1.362(14)
C(5A)-C(6A)	1.364(16)	C(5B)-C(6B)	1.392(17)
C(7A)-C(8A)	1.382(15)	C(7B)-C(8B)	1.387(13)
C(7A)-C(12A)	1.376(13)	C(7B)-C(12B)	1.407(13)
C(8A)-C(9A)	1.378(15)	C(8B)-C(9B)	1.403(12)
C(9A)-C(10A)	1.400(14)	C(9B)-C(10B)	1.367(12)
C(10A)-C(11A)	1.401(15)	C(10B)-C(11B)	1.386(12)
C(11A)-C(12A)	1.408(14)	C(11B)-C(12B)	1.373(13)
C(14A)-C(15A)	1.396(16)	C(14B)-C(15B)	1.377(11)
C(14A)-C(19A)	1.389(15)	C(14B)-C(19B)	1.379(12)
C(15A)-C(16A)	1.386(15)	C(15B)-C(16B)	1.390(13)
C(16A)-C(17A)	1.381(15)	C(16B)-C(17B)	1.387(13)
C(17A)-C(18A)	1.358(15)	C(17B)-C(18B)	1.385(13)
C(18A)-C(19A)	1.376(15)	C(18B)-C(19B)	1.393(13)
C(1A)-C(21A)	1.547(18)	C(1B)-C(21B)	1.535(18)
C(4A)-C(7A)	1.492(13)	C(4B)-C(7B)	1.503(13)
C(10A)-C(13A)	1.468(16)	C(10B)-C(13B)	1.503(11)
C(21A)-C(22A)	1.53(3)	C(21B)-C(22B)	1.52(2)
C(21A)-C(22A′)	1.52(6)	C(22B)-C(23B)	1.53(3)
C(22A)-C(23A)	1.48(4)	C(22B)-C(25B)	1.47(3)
C(22A)-C(25A)	1.53(4)	C(22B)-C(23B′)	1.51(7)
C(23A)-C(24A)	1.46(4)	C(22B)-C(25B′)	1.47(6)
C(22A′)-C(23A′)	1.52(7)	C(23B)-C(24B)	1.44(5)
C(22A′)-C(25A′)	1.56(7)	C(23B′)-C(24B′)	1.40(9)
C(23A′)-C(24A′)	1.39(6)	C(31B)-C(32B)	1.543(16)
C(31A)-C(32A)	1.558(19)	C(32B)-C(33B)	1.534(17)
C(32A)-C(33A)	1.51(2)	C(33B)-C(34B)	1.544(19)
C(33A)-C(34A)	1.52(2)	C(34B)-C(35B)	1.52(2)
C(34A)-C(35A)	1.555(18)		
C(13A)-O(2A)-C(14A)	117.0(8)	C(13B)-O(2B)-C(14B)	117.0(6)
C(17A)-O(3A)-C(31A)	118.4(9)	O(1B)-C(13B)-O(2B)	121.9(8)
O(1A)-C(13A)-O(2A)	120.9(10)	O(1B)-C(13B)-C(10B)	124.4(8)
O(1A)-C(13A)-C(10A)	127.5(11)	O(2B)-C(13B)-C(10B)	113.7(7)
O(2A)-C(13A)-C(10A)	111.3(9)	O(2B)-C(14B)-C(15B)	118.4(7)
O(2A)-C(14A)-C(15A)	116.2(10)	O(2B)-C(14B)-C(19B)	120.4(7)
O(2A)-C(14A)-C(19A)	122.5(10)	O(3B)-C(17B)-C(16B)	124.0(8)
O(3A)-C(17A)-C(16A)	125.2(9)	O(3B)-C(17B)-C(18B)	115.1(8)
O(3A)-C(17A)-C(18A)	115.4(9)	C(17B)-O(3B)-C(31B)	117.3(7)
C(2A)-C(1A)-C(6A)	117.0(10)	C(2B)-C(1B)-C(6B)	118.8(10)
C(1A)-C(2A)-C(3A)	122.5(10)	C(1B)-C(2B)-C(3B)	119.9(10)
C(2A)-C(3A)-C(4A)	120.4(10)	C(2B)-C(3B)-C(4B)	121.5(9)
C(3A)-C(4A)-C(5A)	117.5(9)	C(3B)-C(4B)-C(5B)	117.7(9)
C(4A)-C(5A)-C(6A)	120.4(10)	C(4B)-C(5B)-C(6B)	122.2(11)
C(1A)-C(6A)-C(5A)	122.0(11)	C(1B)-C(6B)-C(5B)	119.6(11)
C(8A)-C(7A)-C(12A)	118.6(9)	C(8B)-C(7B)-C(12B)	117.4(8)
C(7A)-C(8A)-C(9A)	121.8(10)	C(7B)-C(8B)-C(9B)	121.6(8)
C(8A)-C(9A)-C(10A)	119.7(9)	C(8B)-C(9B)-C(10B)	119.3(8)
C(9A)-C(10A)-C(11A)	119.5(10)	C(9B)-C(10B)-C(11B)	120.3(8)
C(10A)-C(11A)-C(12A)	118.8(9)	C(10B)-C(11B)-C(12B)	120.3(8)
C(7A)-C(12A)-C(11A)	121.2(9)	C(7B)-C(12B)-C(11B)	121.1(9)
C(15A)-C(14A)-C(19A)	121.1(10)	C(15B)-C(14B)-C(19B)	120.7(7)
C(14A)-C(15A)-C(16A)	118.0(10)	C(14B)-C(15B)-C(16B)	119.7(8)
C(15A)-C(16A)-C(17A)	121.3(10)	C(15B)-C(16B)-C(17B)	119.5(9)
C(16A)-C(17A)-C(18A)	119.1(10)	C(16B)-C(17B)-C(18B)	120.7(9)
C(17A)-C(18A)-C(19A)	122.1(10)	C(17B)-C(18B)-C(19B)	119.2(9)
C(14A)-C(19A)-C(18A)	118.4(10)	C(14B)-C(19B)-C(18B)	119.9(8)
C(2A)-C(1A)-C(21A)	124.4(10)	C(2B)-C(1B)-C(21B)	119.0(10)
C(6A)-C(1A)-C(21A)	118.4(10)	C(6B)-C(1B)-C(21B)	122.2(10)

Table 3. (Continued)

Bond	ϕ/°	Bond	ϕ/°
C(3A)-C(4A)-C(7A)	121.5(8)	C(3B)-C(4B)-C(7B)	120.2(8)
C(5A)-C(4A)-C(7A)	120.7(8)	C(5B)-C(4B)-C(7B)	122.1(8)
C(4A)-C(7A)-C(8A)	120.5(8)	C(4B)-C(7B)-C(8B)	123.5(8)
C(4A)-C(7A)-C(12A)	120.8(8)	C(4B)-C(7B)-C(12B)	119.1(8)
C(9A)-C(10A)-C(13A)	125.4(10)	C(9B)-C(10B)-C(13B)	121.2(7)
C(11A)-C(10A)-C(13A)	115.1(10)	C(11B)-C(10B)-C(13B)	118.3(7)
C(1A)-C(21A)-C(22A)	113.8(14)	C(1B)-C(21B)-C(22B)	113.7(12)
C(1A)-C(21A)-C(22A′)	111(2)	C(21B)-C(22B)-C(23B)	113.5(16)
C(21A)-C(22A)-C(23A)	108(2)	C(21B)-C(22B)-C(25B)	116.7(15)
C(21A)-C(22A)-C(25A)	112(2)	C(21B)-C(22B)-C(23B′)	99(3)
C(23A)-C(22A)-C(25A)	106(2)	C(21B)-C(22B)-C(25B′)	101(3)
C(22A)-C(23A)-C(24A)	106(2)	C(23B)-C(22B)-C(25B)	107(2)
C(21A)-C(22A′)-C(23A′)	113(4)	C(23B′)-C(22B)-C(25B′)	125(4)
C(21A)-C(22A′)-C(25A′)	126(4)	C(22B)-C(23B)-C(24B)	107(2)
C(23A′)-C(22A′)-C(25A′)	119(4)	C(22B)-C(23B′)-C(24B′)	118(5)
C(22A′)-C(23A′)-C(24A′)	98(4)	O(3B)-C(31B)-C(32B)	106.2(8)
O(3A)-C(31A)-C(32A)	108.6(10)	C(31B)-C(32B)-C(33B)	107.8(10)
C(31A)-C(32A)-C(33A)	113.2(11)	C(32B)-C(33B)-C(34B)	110.7(10)
C(32A)-C(33A)-C(34A)	111.2(12)	C(33B)-C(34B)-C(35B)	110.9(12)
C(33A)-C(34A)-C(35A)	112.9(11)		

Table 4. Bond Lengths (l/Å) and Bond Angles (ϕ/°) of I-7

Bond	l/Å	Bond	l/Å
O(1A)-C(13A)	1.197(9)	O(1B)-C(13B)	1.200(9)
O(2A)-C(13A)	1.349(8)	O(2B)-C(13B)	1.361(9)
O(2A)-C(14A)	1.402(8)	O(2B)-C(14B)	1.418(8)
O(3A)-C(17A)	1.382(8)	O(3B)-C(17B)	1.356(7)
O(3A)-C(31A)	1.425(11)	O(3B)-C(31B)	1.425(9)
C(1A)-C(2A)	1.393(10)	C(1B)-C(2B)	1.385(11)
C(1A)-C(6A)	1.391(10)	C(1B)-C(6B)	1.394(11)
C(1A)-C(21A)	1.526(14)	C(1B)-C(21B)	1.525(13)
C(2A)-C(3A)	1.390(10)	C(2B)-C(3B)	1.391(10)
C(3A)-C(4A)	1.389(9)	C(3B)-C(4B)	1.396(9)
C(4A)-C(5A)	1.392(9)	C(4B)-C(5B)	1.390(10)
C(4A)-C(7A)	1.497(8)	C(4B)-C(7B)	1.507(8)
C(5A)-C(6A)	1.393(11)	C(5B)-C(6B)	1.393(11)
C(7A)-C(8A)	1.389(9)	C(7B)-C(8B)	1.390(8)
C(7A)-C(12A)	1.388(8)	C(7B)-C(12B)	1.384(9)
C(8A)-C(9A)	1.394(9)	C(8B)-C(9B)	1.393(8)
C(9A)-C(10A)	1.390(8)	C(9B)-C(10B)	1.394(9)
C(10A)-C(11A)	1.393(9)	C(10B)-C(11B)	1.393(9)
C(10A)-C(13A)	1.480(9)	C(10B)-C(13B)	1.481(9)
C(11A)-C(12A)	1.392(9)	C(11B)-C(12B)	1.386(9)
C(14A)-C(15A)	1.385(9)	C(14B)-C(15B)	1.389(10)
C(14A)-C(19A)	1.386(9)	C(14B)-C(19B)	1.381(9)
C(15A)-C(16A)	1.388(10)	C(15B)-C(16B)	1.388(10)
C(16A)-C(17A)	1.385(9)	C(16B)-C(17B)	1.386(9)
C(17A)-C(18A)	1.393(9)	C(17B)-C(18B)	1.390(8)
C(18A)-C(19A)	1.387(9)	C(18A)-C(19B)	1.387(9)
C(21A)-C(22A)	1.504(18)	C(21B)-C(22B)	1.50(2)
C(22A)-C(23A)	1.52(2)	C(22B)-C(23B)	1.53(3)
C(22A)-C(25A)	1.50(3)	C(22B)-C(25B)	1.48(3)
C(23A)-C(24A)	1.48(4)	C(23B)-C(24B)	1.50(6)
C(23A)-C(24A′)	1.45(7)	C(23B)-C(24B′)	1.45(6)
C(31A)-C(32A)	1.511(13)	C(31B)-C(32B)	1.519(13)
C(32A)-C(33A)	1.520(13)	C(32B)-C(33B)	1.535(14)
C(33A)-C(34A)	1.528(14)	C(33B)-C(34B)	1.530(13)
C(34A)-C(35A)	1.537(15)	C(34B)-C(35B)	1.515(13)
C(35A)-C(36A)	1.534(14)	C(35B)-C(36B)	1.518(17)
C(36A)-C(37A)	1.53(2)	C(36B)-C(37B)	1.523(19)

Table 4. (Continued)

Bond	ϕ/°	Bond	ϕ/°
C(13A)-O(2A)-C(14A)	116.6(5)	C(13B)-O(2B)-C(14B)	118.8(5)
C(17A)-O(3A)-C(31A)	118.9(6)	C(17B)-O(3B)-C(31B)	116.6(5)
C(2A)-C(1A)-C(6A)	117.5(6)	C(2B)-C(1B)-C(6B)	119.7(7)
C(2A)-C(1A)-C(21A)	120.4(7)	C(2B)-C(1B)-C(21B)	117.8(7)
C(6A)-C(1A)-C(21A)	122.1(7)	C(6B)-C(1B)-C(21B)	122.1(7)
C(1A)-C(2A)-C(3A)	121.8(6)	C(1B)-C(2B)-C(3B)	119.8(7)
C(2A)-C(3A)-C(4A)	118.9(6)	C(2B)-C(3B)-C(4B)	120.8(6)
C(3A)-C(4A)-C(5A)	120.7(6)	C(3B)-C(4B)-C(5B)	118.3(6)
C(3A)-C(4A)-C(7A)	120.7(6)	C(3B)-C(4B)-C(7B)	119.8(5)
C(5A)-C(4A)-C(7A)	118.3(6)	C(5B)-C(4B)-C(7B)	121.9(6)
C(4A)-C(5A)-C(6A)	118.7(6)	C(4B)-C(5B)-C(6B)	120.8(7)
C(1A)-C(6A)-C(5A)	121.8(7)	C(1B)-C(6B)-C(5B)	119.9(8)
C(4A)-C(7A)-C(8A)	119.3(5)	C(4B)-C(7B)-C(8B)	121.8(5)
C(4A)-C(7A)-C(12A)	121.8(5)	C(4B)-C(7B)-C(12B)	119.3(5)
C(8A)-C(7A)-C(12A)	118.5(6)	C(8B)-C(7B)-C(12B)	118.8(5)
C(7A)-C(8A)-C(9A)	121.2(6)	C(7B)-C(8B)-C(9B)	121.2(5)
C(8A)-C(9A)-C(10A)	118.7(6)	C(8B)-C(9B)-C(10B)	118.8(5)
C(9A)-C(10A)-C(11A)	120.9(5)	C(9B)-C(10B)-C(11B)	120.4(6)
C(9A)-C(10A)-C(13A)	121.1(5)	C(9B)-C(10B)-C(13B)	123.3(6)
C(11A)-C(10A)-C(13A)	118.0(5)	C(11B)-C(10B)-C(13B)	116.3(6)
C(10A)-C(11A)-C(12A)	118.9(6)	C(10B)-C(11B)-C(12B)	119.4(6)
C(7A)-C(12A)-C(11A)	121.4(6)	C(7B)-C(12B)-C(11B)	121.2(6)
O(1A)-C(13A)-O(2A)	124.0(6)	O(1B)-C(13B)-O(2B)	122.2(7)
O(1A)-C(13A)-C(10A)	123.2(6)	O(1B)-C(13B)-C(10B)	128.2(7)
O(2A)-C(13A)-C(10A)	112.7(5)	O(2B)-C(13B)-C(10B)	109.4(6)
O(2A)-C(14A)-C(15A)	116.8(6)	O(2B)-C(14B)-C(15B)	118.5(6)
O(2A)-C(14A)-C(19A)	122.4(6)	O(2B)-C(14B)-C(19B)	119.9(6)
C(15A)-C(14A)-C(19A)	120.6(6)	C(15B)-C(14B)-C(19B)	121.5(6)
C(14A)-C(15A)-C(16A)	119.7(6)	C(14B)-C(15B)-C(16B)	118.8(7)
C(15A)-C(16A)-C(17A)	120.1(6)	C(15B)-C(16B)-C(17B)	120.8(7)
O(3A)-C(17A)-C(16A)	125.1(6)	O(3B)-C(17B)-C(16B)	125.3(6)
O(3A)-C(17A)-C(18A)	115.0(6)	O(3B)-C(17B)-C(18B)	115.5(5)
C(16A)-C(17A)-C(18A)	119.9(6)	C(16B)-C(17B)-C(18B)	119.2(6)
C(17A)-C(18A)-C(19A)	119.8(6)	C(17B)-C(18B)-C(19B)	120.8(5)
C(14A)-C(19A)-C(18A)	119.5(6)	C(14B)-C(19B)-C(18B)	118.7(6)
C(1A)-C(21A)-C(22A)	115.6(10)	C(1B)-C(21B)-C(22B)	114.9(10)
C(21A)-C(22A)-C(23A)	115.7(12)	C(21B)-C(22B)-C(23B)	115.8(15)
C(21A)-C(22A)-C(25A)	113.4(13)	C(21B)-C(22B)-C(25B)	112.1(14)
C(23A)-C(22A)-C(25A)	107.0(14)	C(23B)-C(22B)-C(25B)	114.2(16)
C(22A)-C(23A)-C(24A)	116.9(18)	C(22B)-C(23B)-C(24B)	107(3)
C(22A)-C(23A)-C(24A′)	129(3)	C(22B)-C(23B)-C(24B′)	97(3)
O(3A)-C(31A)-C(32A)	107.5(7)	O(3B)-C(31B)-C(32B)	108.4(7)
C(31A)-C(32A)-C(33A)	112.6(7)	C(31B)-C(32B)-C(33B)	112.9(8)
C(32A)-C(33A)-C(34A)	110.2(8)	C(32B)-C(33B)-C(34B)	112.8(8)
C(33A)-C(34A)-C(35A)	112.0(8)	C(33B)-C(34B)-C(35B)	114.3(8)
C(34A)-C(35A)-C(36A)	113.2(9)	C(34B)-C(35B)-C(36B)	111.5(9)
C(35A)-C(36A)-C(37A)	115.7(11)	C(35B)-C(36B)-C(37B)	109.2(11)

Table 5. Torsion Angles (ϕ/°)

	I-5		I-7	
	A	B	A	B
Phenyl groups				
ring(C1-C6)-ring(C7-C12)	5.5	2.9	51.5	−52.5
ring(C7-C12)-ring(C14-C19)	59.2	−59.6	54.2	−54.4
Alkyl chains				
O(3)-C(31)-C(32)-C(33)	180.0	183.5	62.7	−64.6
C(31)-C(32)-C(33)-C(34)	181.5	178.0	165.4	181.1
C(32)-C(33)-C(34)-C(35)	172.0	179.5	180.7	177.2
C(33)-C(34)-C(35)-C(36)	—	—	177.9	185.4
C(34)-C(35)-C(36)-C(37)	—	—	176.2	182.0

increase in the interlayer distances with increase in temperature was attributed mainly to the large change of paraffin chain organization. However, the tilt angle of the core part is kept constant (45°), until the transition to a cholesteric phase occurs. This behavior is well interpreted by the crystal structures, as follows. The tilt angles in the crystal structures (50° and 60°) are close to that in the Sm* C phase. This fact suggests that molecular arrangements as a whole do not change largely at the transition, though the transition is of first-order with a large enthalpy change (6—7 kcal mol^{-1}).[2] Transition from crystals to Sm* C is caused by melting of the paraffin chains, which are regularly organized in the crystalline states. Each molecule begins to rotate around its long molecular axis, because the packing between adjacent phenyl rings is not so close, as is suggested by their nonparallel contact. In Sm* C phase, the chains would change their conformations largely, while the inclination angle of molecular axis should be kept relatively constant, owing to the interaction between the alkyl chains. When the chains are sufficiently disordered, molecules no longer have smectic layers because of relatively small molecular interaction of the core part. Then the transition to a cholesteric phase should occur. In the case of I-5, the chains are so short that Sm* C phase appears only monotropically; with increase in temperature the I-5 crystal transforms directly to a cholesteric phase.

It is concluded that the Sm* C phase behavior observed in a series of biphenyl esters is well interpreted by the molecular packing modes in the crystals. This fact suggests that single crystal X-ray analyses give powerful and useful information to elucidate precise mesophase structures.

The present work was partially supported by a Grant-in-Aid for Scientific Research No. 60540280 from the Ministry of Education, Science and Culture.

References

1) J. W. Goodby and T. M. Leslie, *Mol. Cryst. Liq. Cryst.*, **110**, 175 (1984).

2) G. W. Gray and D. G. McDonnell, *Mol. Cryst. Liq. Cryst.*, **37**, 189 (1976).

3) K. Hori, M. Takamatsu, and Y. Ohashi, *Ferroelectrics*, in press.

4) K. Hori, *Mol. Cryst. Liq. Cryst.*, **123**, 321 (1985).

5) P. Main, S. E. Hull, L. Lessinger, G. Germain, J.-P. Declercq, and M. M. Woolfson, MULTAN78. A System of Computor Programs for the Automatic Solution of X-ray Diffraction Data. Univs. of York, England and Loivain, Belgium (1978).

6) G. M. Sheldrick, SHELX76. A Program for Crystal Structure Determination. Univ. of Cambridge (1976).

7) Y. Ohashi, Unpublished version of an original program by T. Ashida.

8) "International Tables for X-ray Crystallography," Birmingham, Kynoch Press (1974), Vol. IV.

9) The tables for the anisotropic temperature factors for non-hydrogen atoms, the tables for the atomic parameters for the hydrogen atoms and the F_o-F_c list are deposited as Document No. 8844 at the Office of the Editor of the Bulletin of the Chemical Society of Japan.

10) C. Johnson, ORTEP. Report ORNL-3794, Oak Ridge National Laboratory, Tennessee (1965).

11) P. Mandal, S. Paul, H. Shenk, and K. Goubitz, *Mol. Cryst. Liq. Cryst.*, **135**, 35 (1986).

12) N. C. Shivaprakash, M. M. M. Abdoh, and J. Shashidhara Prasad, *Z. Kristallogr.*, **172**, 79 (1985).

13) H. M. M. Shearer and V. Vand, *Acta Crystallogr.*, **9**, 379 (1956).

14) E. von Sydow, *Ark. Kemi*, **9**, 231 (1955).

 © 1988 The Chemical Society of Japan Bull. Chem. Soc. Jpn., 61, 3869—3875 (1988)

Structure of Mixed Ligand Complex [Cu(pan)(phen)]BF_4 with Special Reference to the Acceleration of the Ligand Substitution Reaction

Hiroko WADA,* Motoo SHIRO,† Akio YUCHI, and Genkichi NAKAGAWA
Department of Applied Chemistry, Nagoya Institute of Technology, Gokiso-cho, Showa-ku, Nagoya 466
†Shionogi Research Laboratories, Shionogi & Co., Ltd., Fukushima-ku, Osaka 553
(Received March 22, 1988)

The crystal structures of [1-(2-pyridylazo)-2-naphtholato]copper(II) complexes, [Cu(pan)(phen)]BF_4 as well as [Cu(pan)(H_2O)]ClO_4 and [Cu_2(pan)$_2$(H_2O)$_3$](BF_4)$_2$ have been determined. In these complexes pan^- anion coordinates with copper(II) as a tridentate ligand and all complexes have square pyramidal geometry. In the mixed ligand complex [(Cu(pan)(phen)]BF_4, 1,10-phenanthroline occupies the forth position in the basal plane and the apical site, thus the structure is fairly distorted. This distorted structure is responsible for the fast substitution of [Cu(pan)(phen)]$^+$ complex with $edta^{4-}$.

In the series of studies on the ligand substitution reaction, Tanaka and his coworkers found that the reactivity of the complexes can be quantitatively accounted for by the electron donation from the ligand already bound to the metal ion.[1]

In our previous works,[2–4] it was found that the color change of 1-(2-pyridylazo)-2-naphthol (PAN, Hpan) or Xylenol Orange indicator in chelatometric titration of copper(II) with ethylenediamine-*N*,*N*,*N*′,*N*′-tetraacetic acid (EDTA, H_4edta) is accelerated by the addition of a small amount of bidentate ligand such as 1,10-phenanthroline (phen), 2,2′-bipyridine, 8-quinolinol, sodium diethyldithiocarbamate. The rate and mechanism of substitution reaction of [Cu(pan)]$^+$ complex with EDTA had been studied in detail.[3] In the absence of phen, the ligand substitution reaction with EDTA proceeds as

$$\mathrm{Cu(pan)^+ + edta' \rightleftharpoons Cu(pan)(edta) \longrightarrow Cu(edta)^{2-} + Hpan} \quad (1)$$

The rate depends on the total concentration of EDTA not combined with copper(II), [edta′], and the rate constant is; $k=1.7\times10^3$ dm^3 mol^{-1} s^{-1}, whereas in the presence of phen, the rate does not depend on the concentration of edta′, but depends mainly on the concentration of hydrogen ion. The mechanism of the substitution reaction is expressed as

$$\mathrm{[Cu(pan)(phen)]^+ + H^+ \longrightarrow Cu(phen)^{2+} + Hpan} \quad (2)$$
$$\mathrm{Cu(phen)^{2+} + edta' \rightleftharpoons Cu(edta)^{2-} + phen}$$

The rate constant is; $k=1.6\times10^6$ dm^3 mol^{-1} s^{-1}. The faster substitution Reaction (2) compared with Reaction (1) is attributed to the distorted structure of the mixed ligand complex [Cu(pan)(phen)]$^+$. Also the formation of the mixed ligand complex of [Cu(pan)]$^+$ with some other bidentate ligands such as 2,2′-bipyridine, bathophenanthroline, 8-quinolinol, diethyldithiocarbamate, etc. was found, and the stability constants of these mixed ligand complexes were determined spectrophotometrically.[5]

In this work the crystal structure of [Cu(pan)(phen)]BF_4 (**1**) was determined as well as [Cu(pan)(H_2O)]ClO_4 (**2**), [Cu_2(pan)$_2$(H_2O)$_3$](BF_4)$_2$ (**3**) for comparison. Although crystal structure of complex **2** had been determined previously by Ooi et al.,[6] the refined geometry as well as the other complexes was determined. The influence of phen on the acceleration of the substitution reaction is discussed by comparing the bond lengths of Cu–pan in the complex **1** with those in the complexes **2**, **3**, and [Cu(pan)Cl] (**4**).[7]

Experimental

Preparation of the Complexes. [Cu(pan)(phen)]BF_4(**1**) was prepared by adding an ethanol solution of equal concentration of Hpan and phen to an aqueous solution of $Cu(BF_4)_2$ in the molar ratio of 1:1. After slow evaporation of the solvent at room temperature, dark green crystals with metallic luster were obtained together with orange ones of Hpan. The results of elemental analysis of the dark green crystal: C, 55.9%; H, 2.9%; N, 12.1%, Calcd for [Cu(pan)(phen)]BF_4: C, 56.0%; H, 3.1%; N, 12.1%. [Cu(pan)(H_2O)]ClO_4 (**2**) was prepared from Hpan and $Cu(ClO_4)_2$ and [Cu_2(pan)$_2$(H_2O)$_3$](BF_4)$_2$ (**3**) from Hpan and $Cu(BF_4)_2$ in the similar way. All crystals have similar color as [Cu(pan)(phen)]BF_4.

X-Ray Analysis. Crystallographic details for **1**, **2**, and **3** are listed in Table 1. The unit cell parameters were determined by least-squares fitting of 2θ values of 20 reflections ($0.20<\sin\theta/\lambda<0.24$ Å^{-1}) measured on a Rigaku AFC-5 diffractometer equipped with a graphite monochromator.

Three-dimensional intensity data were collected by ω–2θ scan technique using Cu $K\alpha$ radiation (λ=1.54178 Å) for **1** and using Mo $K\alpha$ radiation (λ=0.71069 Å) for **2** and **3**. Three standard reflections monitored every 100 reflections showed no significant change during the data collection. All intensities were corrected for Lorentz and polarization factors, but not for absorption effects.

The structures were solved by the conventional heavy atom method, and improved by block-diagonal least-squares refinement of the positional and the thermal parameters of the non-H atoms and the positional ones of the H atoms

Table 1. Crystallographic Details for **1**, **2**, and **3**

Complex	**1**	**2**	**3**
Formula	[Cu(pan)(phen)]BF_4	[Cu(pan)(H_2O)]ClO_4	[Cu(pan)(H_2O)](BF_4) ·[Cu(pan)(H_2O)$_2$]BF_4
Formula weight	578.8	429.3	851.3
Crystal system	Triclinic	Triclinic	Triclinic
Space group	$P\bar{1}$	$P\bar{1}$	$P\bar{1}$
a/Å	11.945(1)	9.342(7)[a]	11.095(5)
b/Å	13.630(3)	10.356(5)	20.367(5)
c/Å	7.651(2)	8.208(5)	7.539(2)
α/°	103.63(3)	93.31(5)	96.13(2)
β/°	92.09(3)	95.01(6)	102.14(2)
γ/°	84.43(2)	83.33(5)	80.98(3)
V/Å^3	1204.7(6)	784.8(8)	1640(1)
Z	2	2	2
D_c/g cm^{-3}	1.596	1.817	1.724
μ/cm^{-1}	18.9 (Cu $K\alpha$)	16.6 (Mo $K\alpha$)	14.5 (Mo $K\alpha$)
Crystal size/mm	0.3×0.1×0.1	0.3×0.15×0.1	0.4×0.15×0.05
$\sin\theta_{max}\cdot\lambda^{-1}$/Å^{-1}	0.588	0.595	0.595
Number of unique reflections	4092	2761	5761
Number of observed reflections [$\|F_o\|>2\sigma(F_o)$]	3708	2424	4652
Number of reflections used for least-squares refinement	3586	2417	4625
R	0.054	0.040	0.045
R_w	0.079	0.053	0.060
S	1.164	0.938	1.170

a) The unit cell parameters described in Ref. 6 are as follows: a=10.38, b=8.22, c=9.35 Å, α=85°20′, β=96°48′, γ=93°19′.

which were located on difference electron density maps. The temperature factor of each H atom was assumed to be isotropic and equal to the equivalent isotropic temperature factor of the attached atom. The function minimized in the refinement was $\Sigma(w|\Delta F|^2)$. The weighting scheme was $w=[\sigma^2(F_o)+c^2|F_o|^2]^{-1}$ for observed reflections with $w^{1/2}|\Delta F|<4$ and $w=0$ otherwise. The values of c^2 were 0.00381, 0.00231, and 0.00144 for **1**, **2**, and **3**, respectively. The parameter shifts in the final cycle were less than half the corresponding σ values. The atomic scattering factors were calculated using the analytical expression $f=\Sigma[a_i\exp(-b_i\sin^2\theta/\lambda^2)]+c$ (i=1—4).[8] Computations using the programs of MULTAN84, PLUTO, and XPACK86 SHIONOGI were performed by a FACOM M-340R computer at Shionogi Research Laboratories.

Structural Description

Perspective views of **1** and **2** are shown in Figs. 1 and 2, respectively. In the crystal of **3**, the two complexes which should be differently described as [Cu(pan)-(H_2O)]BF_4 (**3A**) and [Cu(pan)(H_2O)$_2$]BF_4 (**3B**) are included (Figs. 3 and 4). All the complexes have the same type of coordination geometry around Cu(II): square pyramidal geometry or square planar one with weak interaction between Cu and the atom at the position corresponding to the apex. Three corners of the basal plane are occupied by the atoms of pyridyl N, azo N adjacent to the naphthol group and naphthol O of the pan$^-$ ligand. The atoms at the fourth corner of the plane (X) and the apical position (Y) are shown in Fig. 5 along with the atom-numbering systems of the

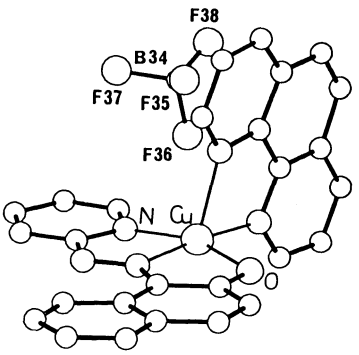

Fig. 1. Perspective drawing of **1** with atomic numbering system for BF_4^-.

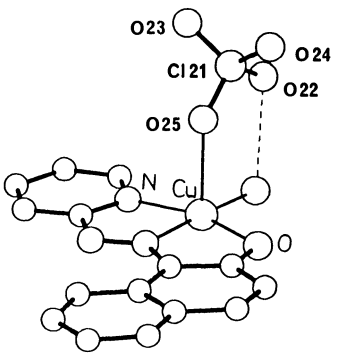

Fig. 2. Perspective drawing of **2** with atomic numbering system for ClO_4^-. Broken line represents the intramolecular hydrogen bond of O(20)···O(22).

phen and pan$^-$ ligands. The square pyramid of **1**, in which the axial Cu–N bond is considerably tilted to the basal plane [$\angle$N(20)–Cu–N(29)=79.4(1)°], is the most distorted in those of the complexes.

Atomic coordinates and equivalent isotropic temperature factors are listed in Table 2. The bond lengths and angles involving Cu, and the deviations of Cu from the basal plane are given in Table 3, where those of [Cu(pan)Cl] (**4**)[7] are listed together for comparison. The less planarity of the basal plane in **3A** and **3B**, judged based on the rms deviation of the constituent atoms from the plane, may be mainly caused by that of the pan$^-$ ligand as described later.

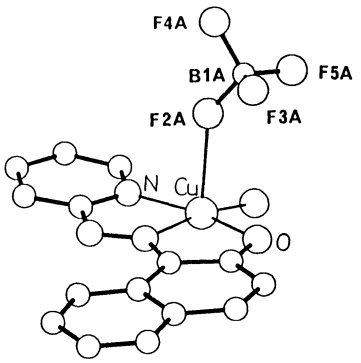

Fig. 3. Perspective drawing of **3A** with atomic numbering system for BF_4^-.

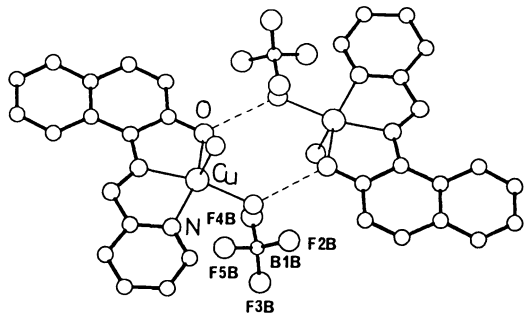

Fig. 4. Perspective drawing of **3B** with atomic numbering system for BF_4^-. Broken lines represent the intermolecular hydrogen bonds of O(19)···O(20).

The bond length of Cu–N(20) in **1** is compatible with the equatorial Cu–N bonds in [Cu(gg)(phen)]-$3H_2O$,[9] 2.009(5) Å, and in [Cu(phen)$_3$]$(ClO_4)_2$,[10] 2.00(1) and 2.02(1) Å (gg=glycylglycine dianion). However, the bond of Cu–N(29) in **1** is shorter than the axial Cu–N bonds, 2.275(5) Å in [Cu(gg)(phen)]-$3H_2O$ and 2.34(1) and 2.32(1) Å in [Cu(phen)$_3$]$(ClO_4)_2$, indicating the N(29) atom to be tightly bound to Cu.

For **2**, **3A**, and **3B** (X=H_2O), the deviation of Cu from the basal plane increases as the distance between Cu and the apical atom decreases. The bonds of Cu–N(1), Cu–N(8), Cu–O(19), and Cu–O(20), according to usual statistical tests, are respectively lengthened in the order of [**2**, **3A**]<**3B**, **2**<[**3A**, **3B**], **3A**<[**2**, **3B**], and [**2**, **3A**]<**3B**, though differences among those in [ ] are not significant. This suggests that the equatorial bonds tend to be weakened with shortening the interatomic distance between Cu and Y. The bonds in **1**, except Cu–N(8), are significantly longer than the corresponding ones in **3B**, a similar tendency having been pointed out on comparison between [Cu(gg)(phen)]$3H_2O$ and [Cu(gg)$(H_2O)_2$]-H_2O.[9]

In the crystal of **4**, the centrosymmetric binuclear complex molecule, [Cu(pan)Cl]$_2$, bridged through two Cl atoms is formed: each Cl atom lies at the basal plane of one square pyramid and at the apex of another one. The bond lengths of Cu–pan$^-$ are very similar to the corresponding one in **1**.

The bond lengths and angles of the phen and pan$^-$ ligands are normal and agree well within experimental errors with those in the respective free ligands. The phen ligand in **1** is bowed along its longest molecular axis, the dihedral angle between the two C_5N rings being 4.3°. For pan$^-$ ligand, the rms deviations of the constituent atoms from the mean plane are 0.016, 0.030, 0.055, 0.040, and 0.016 Å for **1**, **2**, **3A**, **3B**, and **4**, respectively. The less planarity of the ligand observed in **3A** and **3B** is mainly caused by the twist between the pyridine and naphthol rings: the

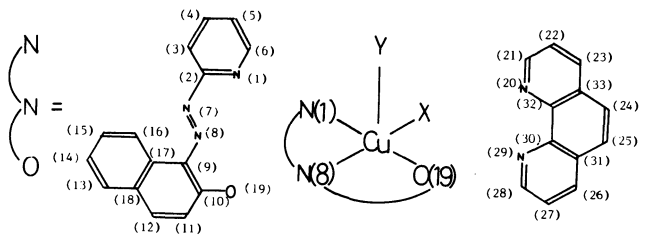

	1	2	3A	3B	4
X	phen[N(20)]	H_2O[O(20)]	H_2O[O(20A)]	H_2O[O(20B)]	Cl
Y	phen[N(29)]	ClO_4[O(25)]	BF_4[F(2A)]	H_2O[O(21B)]	Cl

Fig. 5. Coordination geometry of the compexes and atomic numbering systems of pan$^-$ and phen ligands.

Table 2. Atomic Coordinates ($\times 10^4$) and Equivalent Isotropic Temperature Factors ($Å^2 \times 10^2$) with Estimated Standard Deviations in Parentheses for **1**, **2**, and **3**

1	x	y	z	B_{eq}
Cu	7761.6(3)	3557.3(3)	1282.6(5)	408(1)
N(1)	9030(2)	2601(2)	1846(3)	327(6)
C(2)	9955(2)	3089(2)	2419(4)	316(7)
C(3)	10923(3)	2601(2)	3003(5)	409(9)
C(4)	10938(3)	1589(3)	2983(5)	480(11)
C(5)	9996(3)	1095(3)	2406(6)	508(12)
C(6)	9063(3)	1616(2)	1836(5)	441(10)
N(7)	9941(2)	4117(2)	2426(3)	312(6)
N(8)	8980(2)	4444(2)	1834(3)	297(6)
C(9)	8717(2)	5403(2)	1651(3)	306(7)
C(10)	7599(2)	5504(2)	908(4)	358(8)
C(11)	7157(3)	6470(2)	648(5)	419(9)
C(12)	7791(3)	7271(2)	1055(4)	385(9)
C(13)	9522(3)	8043(2)	2211(4)	382(9)
C(14)	10581(3)	7993(2)	2941(5)	407(9)
C(15)	11070(2)	7069(2)	3226(4)	388(9)
C(16)	10491(2)	6215(2)	2800(4)	328(7)
C(17)	9394(2)	6251(2)	2081(3)	289(7)
C(18)	8910(2)	7183(2)	1784(4)	315(7)
O(19)	6994(2)	4743(2)	501(3)	446(7)
N(20)	6586(2)	2583(2)	407(3)	305(6)
C(21)	6505(3)	1989(2)	−1230(4)	388(9)
C(22)	5685(3)	1309(3)	−1715(5)	454(10)
C(23)	4933(3)	1245(2)	−462(5)	455(10)
C(24)	4226(3)	1828(4)	2678(7)	669(16)
C(25)	4285(4)	2459(5)	4298(7)	731(18)
C(26)	5193(5)	3901(5)	6367(5)	935(23)
C(27)	6003(5)	4547(4)	6631(5)	885(20)
C(28)	6764(4)	4511(3)	5268(5)	670(14)
N(29)	6714(2)	3842(2)	3686(3)	431(8)
C(30)	5894(3)	3207(2)	3407(4)	408(9)
C(31)	5102(4)	3177(4)	4703(5)	622(14)
C(32)	5827(2)	2531(2)	1659(4)	320(7)
C(33)	4995(2)	1860(2)	1278(5)	412(9)
B(34)	7185(3)	231(3)	3858(5)	430(11)
F(35)	6989(3)	1277(2)	4436(4)	728(10)
F(36)	7380(2)	−47(2)	2025(3)	567(8)
F(37)	8201(3)	13(2)	4707(5)	921(13)
F(38)	6372(4)	−275(4)	4223(5)	1514(25)
2	x	y	z	B_{eq}
Cu	2904.4(3)	1764.3(3)	4929.2(4)	235(1)
N(1)	1943(3)	3233(2)	6212(3)	250(6)
C(2)	484(3)	3316(3)	5933(3)	238(9)
C(3)	−426(3)	4259(3)	6698(4)	300(10)
C(4)	191(4)	5154(3)	7783(4)	354(11)
C(5)	1680(4)	5066(3)	8086(4)	391(12)
C(6)	2524(4)	4098(3)	7273(4)	331(11)
N(7)	−110(2)	2383(2)	4828(3)	237(7)
N(8)	896(2)	1566(2)	4273(3)	206(7)
C(9)	677(3)	538(3)	3208(3)	218(8)
C(10)	2027(3)	−202(3)	2884(3)	236(9)
C(11)	2028(3)	−1309(3)	1779(4)	286(10)
C(12)	765(3)	−1662(3)	1074(4)	278(9)
C(13)	−1892(4)	−1410(3)	653(4)	314(10)
C(14)	−3226(4)	−762(4)	997(4)	344(11)
C(15)	−3293(3)	339(4)	2049(4)	340(11)
C(16)	−2050(3)	812(3)	2772(4)	271(9)
C(17)	−682(3)	148(3)	2473(3)	232(9)
C(18)	−615(3)	−966(3)	1393(3)	255(9)
O(19)	3234(2)	139(2)	3606(3)	275(7)
O(20)	4882(2)	1939(2)	5772(3)	317(7)
Cl(21)	4322(1)	3845(1)	2329(1)	341(3)
O(22)	5519(3)	3622(3)	3551(4)	528(11)

Table 2. (Continued)

2	*x*	*y*	*z*	B_{eq}
O(23)	3837(3)	5189(3)	2304(5)	620(12)
O(24)	4789(4)	3379(4)	777(4)	704(15)
O(25)	3163(3)	3133(3)	2717(3)	475(10)
3	*x*	*y*	*z*	B_{eq}
Cu(1A)	5775.2(4)	3747.3(2)	5096.7(6)	278(1)
N(1A)	5520(3)	2850(1)	5563(4)	290(9)
C(2A)	6479(3)	2384(2)	5216(4)	277(11)
C(3A)	6498(4)	1715(2)	5417(5)	333(12)
C(4A)	5489(4)	1518(2)	5916(5)	390(13)
C(5A)	4499(4)	1993(2)	6260(5)	386(13)
C(6A)	4558(4)	2655(2)	6075(5)	345(12)
N(7A)	7479(3)	2591(1)	4656(4)	283(9)
N(8A)	7288(3)	3228(1)	4508(4)	256(9)
C(9A)	8074(3)	3591(2)	4041(4)	268(10)
C(10A)	7556(3)	4278(2)	4018(5)	288(11)
C(11A)	8252(4)	4739(2)	3547(5)	354(12)
C(12A)	9394(4)	4527(2)	3182(6)	371(13)
C(13A)	11184(4)	3663(2)	2955(5)	397(14)
C(14A)	11734(4)	3016(2)	3032(6)	420(14)
C(15A)	11095(4)	2529(2)	3432(6)	420(14)
C(16A)	9899(4)	2703(2)	3759(5)	344(12)
C(17A)	9311(3)	3358(2)	3685(4)	267(10)
C(18A)	9973(3)	3848(2)	3276(5)	325(12)
O(19A)	6475(2)	4479(1)	4431(4)	333(8)
O(20A)	4474(3)	4263(1)	6205(4)	386(9)
B(1A)	3876(5)	3941(3)	622(7)	419(16)
F(2A)	4475(3)	3616(2)	2122(4)	744(13)
F(3A)	4728(3)	4130(2)	−210(5)	924(17)
F(4A)	3214(4)	3490(2)	−527(5)	925(17)
F(5A)	3115(5)	4442(2)	1112(8)	1420(26)
Cu(1B)	8213.9(4)	897.2(2)	10255.6(7)	337(1)
N(1B)	6504(3)	1058(1)	10774(4)	316(10)
C(2B)	6013(3)	1706(2)	10651(5)	292(11)
C(3B)	4820(3)	1939(2)	10926(5)	342(12)
C(4B)	4134(4)	1492(2)	11399(5)	385(13)
C(5B)	4665(4)	836(2)	11597(6)	410(14)
C(6B)	5842(4)	638(2)	11254(6)	382(13)
N(7B)	6721(3)	2151(1)	10173(4)	299(9)
N(8B)	7776(3)	1844(2)	9897(4)	294(9)
C(9B)	8653(3)	2135(2)	9369(5)	283(11)
C(10B)	9691(3)	1639(2)	9107(5)	332(12)
C(11B)	10727(4)	1849(2)	8578(6)	407(14)
C(12B)	10729(4)	2497(2)	8381(6)	407(14)
C(13B)	9752(4)	3674(2)	8388(5)	397(14)
C(14B)	8764(4)	4153(2)	8600(5)	417(14)
C(15B)	7703(4)	3977(2)	9069(5)	363(13)
C(16B)	7633(3)	3329(2)	9316(5)	316(12)
C(17B)	8639(3)	2824(2)	9120(4)	290(11)
C(18B)	9704(4)	3003(2)	8614(5)	346(13)
O(19B)	9682(3)	1017(1)	9344(4)	438(10)
O(20B)	8324(3)	−89(1)	9807(5)	484(10)
O(21B)	9163(3)	838(2)	13103(5)	612(13)
B(1B)	7569(5)	−438(3)	5010(9)	514(19)
F(2B)	8093(4)	−872(2)	6290(6)	962(17)
F(3B)	6759(4)	−676(2)	3622(6)	1175(22)
F(4B)	8424(5)	−210(3)	4366(7)	1497(30)
F(5B)	7046(6)	75(3)	5903(8)	1608(33)

dihedral angles between the two rings are 1.4, 1.9, 4.5, 3.9, and 1.2° in the above order.

The atom-numbering systems of the BF_4^- and ClO_4^- anions are presented in Figs. 1—4. The bond lengths of B–F average 1.37 Å for **1**, 1.35 Å for **3A** and 1.33 Å for **3B**, and those of Cl–O average 1.43 Å for **2**. The mean bond angles of F–B–F are all 109° for **1**, **3A**, and **3B**, and that of O–Cl–O is 110° for **2**. The temperature

Table 3. Geometries of the Complexes of **1**, **2**, **3A**, **3B**, and **4** (Standard Deviations in Parentheses)

Complex	**1**	**2**	**3A**	**3B**	**4**
(a) Bond length/Å					
Cu-N(1)	2.003(3)	1.973(3)	1.971(3)	1.987(3)	1.991(2)
Cu-N(8)	1.953(3)	1.937(2)	1.947(3)	1.947(4)	1.964(2)
Cu-O(19)	1.985(3)	1.958(2)	1.940(3)	1.954(3)	1.984(2)
Cu-X	2.015(3)	1.940(2)	1.931(3)	1.990(4)	2.263(1)
Cu-Y	2.199(3)	2.412(2)	2.411(4)	2.190(4)	2.647(1)
(b) Bond angles/°					
N(1)-Cu-N(8)	78.7(1)	79.7(1)	79.9(1)	79.4(2)	78.53(9)
N(1)-Cu-O(19)	158.5(1)	161.6(1)	162.7(1)	160.6(1)	159.3
N(1)-Cu-X	100.2(1)	98.0(1)	98.6(1)	96.8(1)	97.36(7)
N(1)-Cu-Y	102.5(1)	92.0(1)	89.0(1)	95.4(1)	91.26(7)
N(8)-Cu-O(19)	81.9(1)	82.7(1)	82.7(1)	82.3(2)	81.50(9)
N(8)-Cu-Y	172.9(1)	175.2(1)	167.8(1)	161.2(2)	170.0
N(8)-Cu-Y	107.8(1)	94.2(1)	97.1(1)	105.8(2)	96.90(7)
O(19)-Cu-X	97.8(1)	99.2(1)	98.4(1)	98.5(1)	101.50(7)
O(19)-Cu-Y	92.2(1)	94.3(1)	92.5(1)	95.7(1)	96.34(7)
X-Cu-Y	79.4(1)	90.0(1)	94.9(1)	92.8(2)	92.21(3)
Cu-N(1)-C(2)	111.2(2)	111.6(2)	111.2(3)	111.1(3)	112.2
Cu-N(1)-C(6)	130.4(2)	129.5(2)	129.6(3)	129.9(3)	129.5
Cu-N(8)-N(7)	120.1(2)	120.0(2)	119.3(3)	119.9(3)	120.1
Cu-N(8)-C(9)	115.4(2)	115.0(2)	114.5(3)	115.5(3)	115.3
Cu-O(19)-C(10)	110.6(2)	111.3(2)	111.3(3)	111.5(3)	111.4
Cu-N(20)-C(21)	126.4(2)				
Cu-N(20)-C(32)	115.2(2)				
Cu-N(29)-C(28)	131.4(3)				
Cu-N(29)-C(30)	110.1(2)				
(c) Deviations of Cu from the basal plane towards the apex/Å					
	0.152(1)	0.084(1)	0.109(1)	0.228(1)	0.145
(d) Deviations of the equatorial donor atoms from the basal plane and their rms values in parentheses/Å					
	−0.029	−0.015	−0.109	−0.113	−0.036
	ca. 0.034	ca. 0.013	ca. 0.096	ca. 0.066	ca. 0.030
	(0.029)	(0.012)	(0.092)	(0.081)	(0.026)

factors of the atoms of the anions are larger than those of the constituent atoms of the pan⁻ and phen ligands, some of which exhibit a large anisotropy. The H atoms of all the complexes lie at the positions not far from those expected on chemical grounds.

In **2** and **3**, the two complexes related by an inversion center are linked to form a binuclear unit by the hydrogen bonds between O(19) and O(20) individually lying on different basal planes of the two square pyramids: the interatomic distances are 2.661(3), 2.666(4), and 2.688(5) Å for **2**, **3A**, and **3B**, respectively. This is represented for **3B** in Fig. 4. The basal planes of the two complexes, parallel to each other, are differently separated in each binuclear unit probably subjected to different packing effects: the distances are respectively 1.40, 0.61, and 1.14 Å for **2**, **3A**, and **3B**. The above-mentioned dihedral angle between the pyridine and naphthol rings in the pan⁻ ligand increases with decreasing distance in the order of **2**>**3B**>**3A**. Smaller angles are observed for **1** and **4** in which such hydrogen bonds are not formed. Therefore, we assumed that the distortion in the pan⁻ ligand may be caused by the formation of the intermolecular hydrogen bonds in the binuclear unit. The O(20) atom forms a hydrogen bonds with O(22) [2.741(4) Å] in **2** and a bifurcated one with F(2B) and F(5B) [2.929(4) and 3.015(4) Å] in **3B**.

Discussion

The bond lengths of Cu-pan in the mixed complex **1** were similar to those in complex **4**. However, the mixed ligand phen complex **1** is expected to have the same structure in aqueous solution, whereas in the mixed ligand chloro complex **4** Cl^- at apical position should be replaced with water molecule. The resulted complex may have the structure close to complex **3B**, because the interaction with inert anions at apical site is weak even in solid as shown in complexes **2** and **3A**.

In the ligand substitution reaction of the mixed ligand complex $[Cu(pan)(phen)]^+$ with multidentate ligand such as $edta^{4-}$, the reaction mechanism is different from that of the unidentate mixed ligand complex. The mixed ligand complex with the

unidentate ligand has at least one water molecule in X or Y position. The water molecule is labile and easily displaced by a moiety of the entering ligand before or in the rate-determining step. Thus the rate is propotional to the concentration of the entering ligand. The reaction is accelerated by the presence of unidentate ligand (L), because the bonds between Cu(II) and pan^- are weakened depending on the electron donation from L to Cu(II).

On the other hand, a bidentate ligand such as phen occupies not only the basal site but also the apical one, then there left no site for the entering ligand to attack, but Cu-pan bonds are weakened by the coordination of phen as seen from the results of the X-ray analysis. This is also found from the decreased stability constant of $[Cu(pan)(phen)]^+$ compared with that of $[Cu(pan)]^+$: $\log K^{pan}_{Cu(pan)(phen)}=12.20$ and $\log K^{pan}_{Cu(pan)}=15.58$ (5%dioxane, 0.1 mol dm^{-3} KNO_3 at 25 °C). Therefore, the Cu-pan bond in the mixed ligand complex **1** is easily broken by the attack of proton (rate-determining step). The rate of the reaction does not depend on the concentration of the entering ligand but depends on the concentration of hydrogen ion. The resulted $[Cu(phen)]^{2+}$ complex is rapidly replaced with $edta^{4-}$. As the rate constant of Reaction (2) is much larger than that of Reaction (1), the rate of the color change of PAN indicator is accelerated by the addition of phen in the chelatometric titration of copper(II).

References

1) M. Tabata and M. Tanaka, *Inorg. Chem.*, **17**, 2779 (1978) and the references cited therein.
2) G. Nakagawa and H. Wada, *Talanta*, **20**, 829 (1973).
3) G. Nakagawa and H. Wada, *Talanta*, **22**, 563 (1975).
4) H. Wada, T. Ishizuki, and G. Nakagawa, *Bull. Chem. Soc. Jpn.*, **50**, 2104 (1977).
5) H. Wada, K. Ikuta, and G. Nakagawa, *Bull. Chem. Soc. Jpn.*, **51**, 2916 (1978).
6) S. Ooi, D. Carter, and Q. Fernando, *J. Chem. Soc., Chem. Commun.*, **1967**, 1301.
7) G. R. Desiraju, H. R. Luss, and D. L. Smith, *J. Am. Chem. Soc.*, **100**, 6375 (1978).
8) International Tables for X-ray Crystallography, (1974) Vol. IV, Birmingham, Kynoch Press.
9) M. C. Lim, E. Sinn, and R. B. Martin, *Inorg. Chem.*, **15**, 807 (1976).
10) O. P. Anderson, *J. Chem. Soc., Dalton Trans.*, **1973**, 1237.

The Synthesis and Thermal Behavior of Lithium *cyclo*-Hexaphosphate

Makoto WATANABE,* Khoichi MURATA, and Mioko MAEDA
Department of Industrial Chemistry, Chubu University,
Matsumoto-cho, Kasugai, Aichi 487
(Received April 9, 1988)

Lithium *cyclo*-hexaphosphate hexahydrate was made by heating a mixture of 85%-phosphoric acid and dilithium carbonate at an Li/P molar ratio of 1.4 at 200 (1 h), 275 (5 h), and then 420 °C (3 h). The thermal product was handled with a wet chemical method developed in this study. The *cyclo*-hexaphosphate was stable at room temperature (20—30 °C), while a small part of it decomposed to phosphates with shorter chain lengths above about 60 °C in air. The *cyclo*-hexaphosphate was transformed thermally to crystalline long-chain polyphosphates upon heating above 530 °C.

Some oligophosphates and long-chain polyphosphates have been made by the thermal condensation of orthophosphates. These polyphosphates have been used for water treatment, food additives, detergents, and so forth.[1] Griffith and Buxton have reported on the synthesis of lithium *cyclo*-hexaphosphate hexahydrate by heating a mixture of phosphoric acid and dilithium carbonate and then recrystallizing the *cyclo*-phosphate from the thermal product. They also indicated that the hydrated *cyclo*-phosphate could be dehydrated by heating at about 120 °C without decomposition.[2] The present authors followed up the method and found that there are several problems regarding the preparation of the hydrated and unhydrated *cyclo*-hexaphosphates. This paper describes the problems and an improvement in the preparation method for the *cyclo*-phosphate. The thermal property of the *cyclo*-phosphate was also studied.

Experimental

Preparation of Lithium *cyclo*-Hexaphosphate. According to Griffith and Buxton, a mixture of dilithium carbonate and 85%-phosphoric acid with an Li/P molar ratio of 1.4 was heated at 200 °C for 1 h and at 275 °C for 5—7 h; then, the resulting thermal product was dissolved in water and lithium *cyclo*-hexaphosphate hexahydrate was crystallized by adding methanol to the solution. The present authors found that it was difficult to prepare the *cyclo*-phosphate by this method and that it was necessary to study the effect of the mixing ratio of dilithium carbnate and 85%-phosphoric acid, the heating temperature, and the heating time for the distribution of phosphate species in the thermal product. It was also necessary to improve the wet process in order to purify the *cyclo*-phosphate from the thermal product.

Chemical Analysis. An atomic absorption analysis was used for a determination of any lithium ions in the sample solution by using a Shimadzu atomic absorption spectrophotometer (AA-646). Phosphorus was determined according to the Molybdenum Blue method.[3]

Paper Chromatography. A one-dimensional paper-chromatographic separation was employed by using acidic (for the separation of chain phosphates) and basic (for the separation of ring phosphates) solvents.[4] A sample (0.1 g) was dissolved in 10 cm^3 of a 6% aqueous disodium dihydrogen ethylenediaminetetraacetate dihydrate (Na_2H_2-edta·$2H_2O$) solution. The solution (8 mm^3) was spotted on Toyo No. 51A filter paper (2 by 50 cm). The development was run at 3 °C for 2 d.

Colorimetric Measurement of Phosphates. Every individual spot on the chromatogram was cut at its demarcation line and put into a 100-cm^3 beaker containing 10 cm^3 of 0.1 mol dm^{-3} aqueous ammonia. The phosphate extracted in aqueous ammonia was determined colorimetrically by a method described in our previous paper.[5]

HPLC Analysis. An HPLC technique (developed by Yoza) was also used for a separation and determination of any phosphate species in a sample solution.[6] Aqueous 0.26- and 0.40-mol dm^{-3} solutions of potassium chloride were run at a flow rate of 1 cm^3 s^{-1}.

^{31}P NMR Measurement. The ^{31}P NMR spectrum of an aqueous phosphate solution was taken by a JNM-GX270 instrument. Phosphoric acid (85%) was employed as a reference with the positive chemical shifts being downfield.

X-Ray Diffractometry. An X-ray diffraction diagram of a powder sample was taken with nickel filtered Cu $K\alpha$ radiation by using a Rigaku X-ray diffractometer, RAD-1B.

TG-DTA Measurement. The TG-DTA measurement was used to study the thermal behavior of the product by using a Cho Balance TRDA-H apparatus with the heating rate of 5 °C min^{-1} in air.

Results and Discussion

Li/P Molar Ratio and Reaction Temperature. The process of the synthesis of *cyclo*-hexaphosphate developed by Griffith and Buxton is shown in Fig. 1. Mixtures of 85%-orthophosphoric acid and dilithium carbonate with Li/P ratios of 1.0—1.5 were heated in the same manner as that of Griffith and Buxton. The compositions of the phosphate species of these thermal products are shown in Table 1. (The values listed in Tables 1—4 are average values for, at least, three times.) The main product was high polyphosphate or diphosphate. The content of *cyclo*-hexaphosphate was at most 19.0% at an Li/P ratio of 1.4. The resulting thermal products were again heated at 350 or 420 °C for 3 h. The compositions of the phosphate species of the thermal products are listed in Tables 2 and 3, respectively. The content of *cyclo*-hexaphosphate increased when the thermal products were reheated at 350 and 420 °C. The *cyclo*-phosphate content at 420 °C was higher than that at 350 °C. The best Li/P ratio was 1.4, in agreement with the result of Griffith

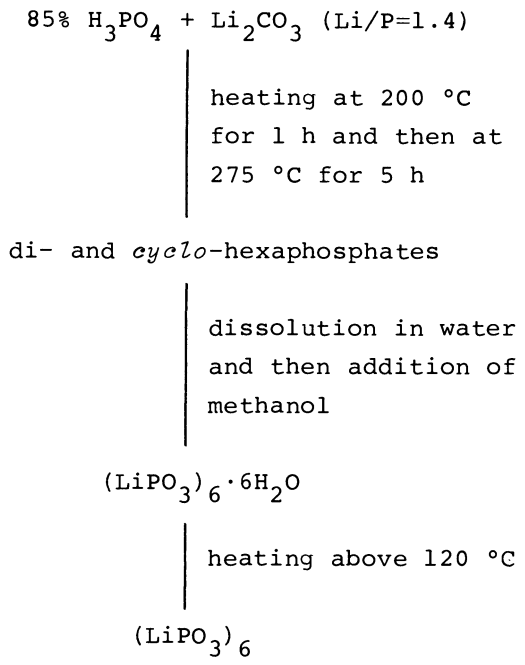

Fig. 1. Synthetic process of *cyclo*-hexaphosphate by Griffith and Buxton.

Table 1. Compositions of the Thermal Products Heated at 200 °C for 1 h and at 275 °C for 5 h

Li/P	Phosphates/P%				
	Ortho	Di	Tri	*cyclo*-Hexa	Higher
1.0	3.9	4.8	—	—	91.3
1.1	3.4	29.6	2.8	—	64.2
1.2	—	45.0	—	11.6	43.4
1.3	—	68.0	—	13.5	18.5
1.4	—	74.7	—	19.0	6.3
1.5	—	81.4	—	11.5	7.1

Table 2. Compositions of the Thermal Products Heated at 200 °C for 1 h, at 275 °C for 5 h, and then at 350 °C for 3 h

Li/P	Phosphates/P%				
	Ortho	Di	Tri	*cyclo*-Hexa	Higher
1.0	—	—	—	—	100
1.1	—	11.8	—	2.9	85.3
1.2	—	18.6	—	16.1	65.3
1.3	—	36.2	—	36.4	27.4
1.4	—	31.0	—	35.2	33.8
1.5	—	33.9	—	31.3	34.8

and Buxton. The effect of the reaction temperature on the content of the *cyclo*-phosphate was studied for the thermal product with an Li/P ratio of 1.4 (prepared by Griffith and Buxton's method). The results are shown in Table 4. The best reaction temperature seemed to be 420 °C. The either product at a temperature higher or lower than 420 °C showed a decrease in the *cyclo*-phosphate content.

Table 3. Compositions of the Thermal Products Heated at 200 °C for 1 h, at 275 °C for 5 h, and then at 420 °C for 3 h

Li/P	Phosphates/P%				
	Ortho	Di	Tri	*cyclo*-Hexa	Higher
1.0	—	—	—	—	100
1.1	—	13.8	—	—	86.2
1.2	—	22.6	—	15.3	62.1
1.3	—	28.1	—	39.5	32.4
1.4	—	29.6	—	44.4	26.0
1.5	—	37.2	—	25.1	37.7

Table 4. The Effect of Heating Temperature on the Composition of the Thermal Product with Li/P Ratio of 1.4[a)]

t/°C	Phosphates/P%				
	Ortho	Di	Tri	*cyclo*-Hexa	Higher
300	—	63.7	—	26.1	10.7
320	—	37.1	—	35.5	27.4
350	—	31.0	—	35.2	33.8
370	—	27.7	—	43.7	28.6
400	—	29.9	—	40.0	30.1
420	—	29.6		44.4	26.0
450	—	28.1	—	33.3	38.6

a) The thermal product was preheated at 200 °C for 1 h and at 275 °C for 5 h.

Purification of the *cyclo*-Hexaphosphate. The highest content of the *cyclo*-phosphate in the thermal products was about 45% and a purification of the *cyclo*-phosphate was required. Griffith and Buxton described how *cyclo*-phosphate was purified by dissolving the thermal product in water and then adding methanol to the solution. The thermal product obtained by heating at 420 °C for 3 h did not dissolve in water, but dissolved in a 1% ethylenediaminetetraacetic acid (H_4edta) solution of pH 9. The pH of the solution was controlled with a 1-mol dm^{-3} aqueous lithium hydroxide solution. The thermal product (7.3 g) was dissolved in 100 cm^3 of a H_4edta solution and the residue (di- and highpolyphosphates) was filtered off. Methanol (110 cm^3) was added to the filtrate and a white precipitate was removed by filtration. Lithium chloride (8 g) was added to the filtrate. A small amount of white precipitate (*cyclo*-hexa- and highpolyphosphates) was filtered off; then, lithium chloride (18.5 g) was added to the filtrate. A white precipitate was obtained by filtration, washed with 75 vol% aqueous acetone, and dried in air. The process is shown in Fig. 2. Found: P, 29.5; Li, 6.8;

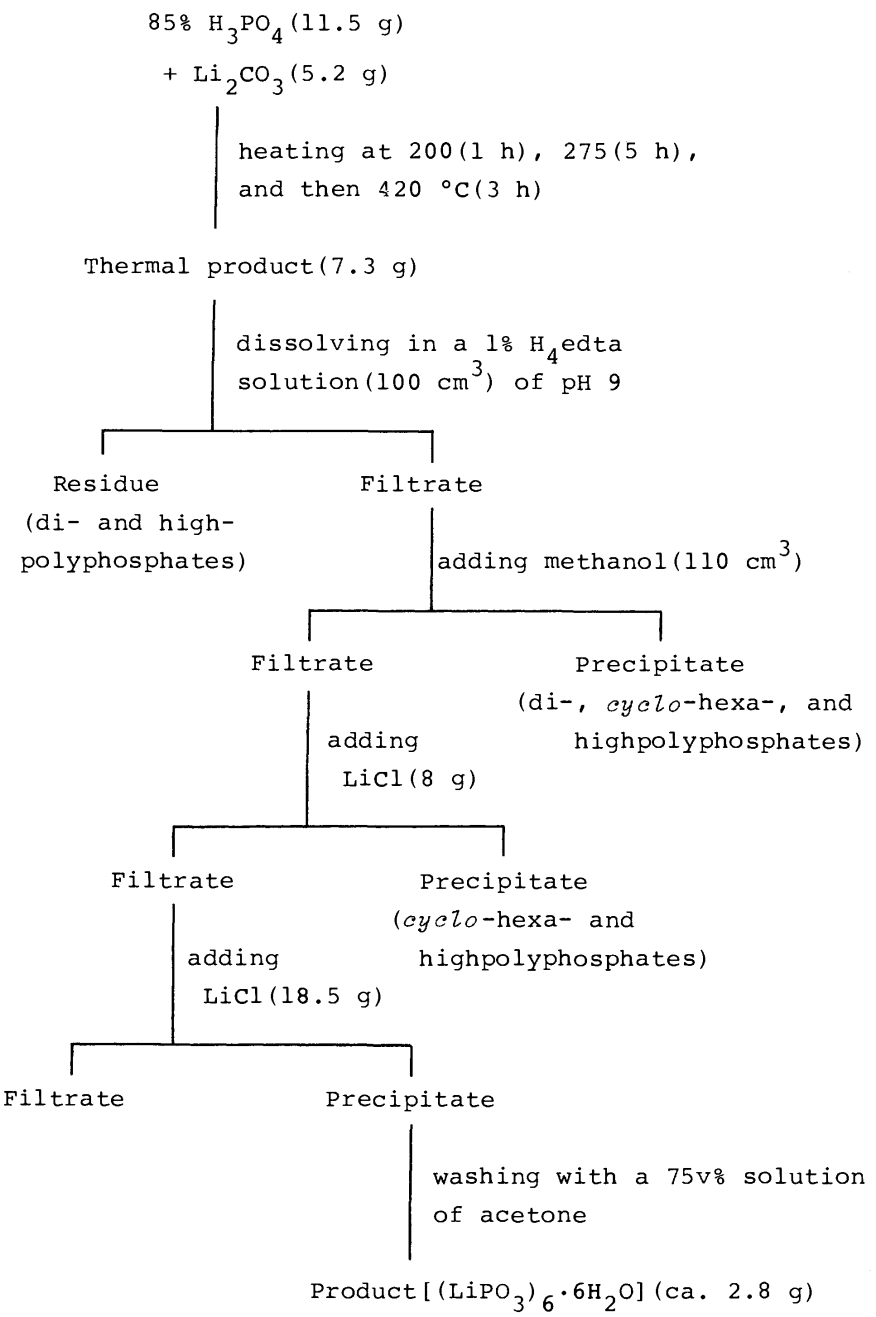

Fig. 2. Synthetic process of *cyclo*-hexaphosphate hexahydrate.

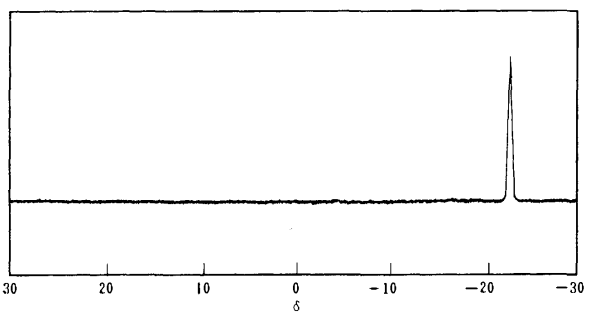

Fig. 3. ^{31}P NMR spectrum of $(LiPO_3)_6 \cdot 6H_2O$.

H_2O, 17.5%. Calcd for $(LiPO_3)_6 \cdot 6H_2O$: P, 29.8; Li, 6.7; H_2O, 17.3%. The ^{31}P NMR spectrum of the product shown in Fig. 3 exhibited only one singlet at −22.6 ppm and the peak is due to a middle-PO_4 group. The product also gave only one HPLC peak in the profile. Accordingly, the product is lithium *cyclo*-hexaphosphate hexahydrate, $(LiPO_3)_6 \cdot 6H_2O$. The X-ray diffraction data of *cyclo*-phosphate are presented in Table 5, together with the data of Griffith and Buxton. They gave a rough order of intensity of the peak without the I/I_0 value. The yield of the product was about 30%. The *cyclo*-phosphate was stable at room

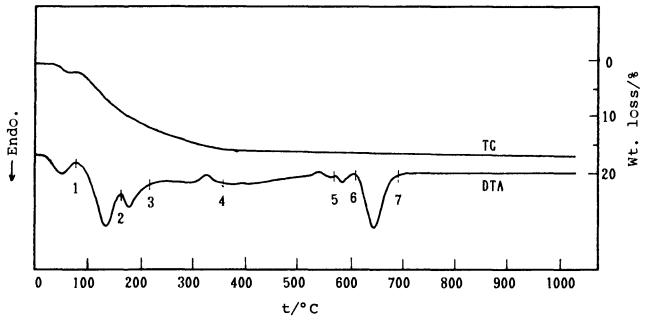

Fig. 4. TG and DTA curves of $(LiPO_3)_6 \cdot 6H_2O$.

Table 5. X-Ray Diffraction Data of $(LiPO_3)_6 \cdot 6H_2O$

(This study)		(Griffith and Buxton)	
d/Å	I/I_0	d/Å	I/I_0
7.22	28	6.91	—
6.67	5	5.53	—
6.28	100	4.39	—
5.47	45	3.40	—
4.68	40	2.96	—
4.23	60		
4.18	7		
4.09	45		
3.92	60		
3.83	4		
3.74	4		
3.71	6		
3.62	11		
3.53	35		
3.13	30		
2.94	80		
2.90	13		
2.88	16		
2.72	30		
2.63	4		
2.58	7		
2.41	6		
2.39	4		
2.35	6		
2.33	20		
2.26	5		

temperature (20—30 °C), with a solubility of 3.03 at 20 °C.

TG-DTA Measurement. TG and DTA curves of lithium *cyclo*-hexaphosphate hexahydrate are shown in Fig. 4. The thermal products (as numbered in Fig. 4) were taken out of a furnace and subjected to further analysis in order to study the thermal reactions of the *cyclo*-phosphate. The first endothermic peak accompanying a small amount of weight loss seemed to be due to the removal of the adsorbed water, since the product showed an X-ray diffraction pattern of $(LiPO_3)_6 \cdot 6H_2O$. However, the results listed in Table 6 indicate that a small part of the *cyclo*-phosphate decomposed to diphosphate:

$$(LiPO_3)_6 + 3H_2O \longrightarrow 3Li_2H_2P_2O_7. \quad (1)$$

The water in the above equation might have come from the water of crystallization of the *cyclo*-phosphate. The next big endothermic reaction accompanying the weight loss was considered to be due to an elimination of the water of crystallization along with a simultaneous decomposition of the *cyclo*-phosphate. The third small endothermic peak accompanying the weight loss may have been caused by an elimination of the rest water of crystallization, and a condensation of the phosphates to phosphates with longer chain lengths, since the content of ortho-, di-, and triphosphate in the thermal product decreased and that of *cyclo*-hexaphosphate increased after the endothermic reaction. A small exothermic peak was observed at about 330 °C. As Table 6 shows, most parts of the thermal products of Nos. 2—4 were *cyclo*-hexaphosphate; the weight loss of thermal product No. 4 agrees well with the following dehydration:

$$(LiPO_3)_6 \cdot 6H_2O \longrightarrow (LiPO_3)_6 + 6H_2O. \quad (2)$$

Thermal product No. 4 gave a different X-ray diffraction diagram than those of Nos. 2 and 3. Therefore, the exothermic reaction can be attributed to a transition of *cyclo*-hexaphosphate. The X-ray diffraction pattern of No. 4 agreed with that of anhydrous lithium *cyclo*-hexaphosphate by Griffith and Buxton. After the next exothermic reaction at about 530 °C, the

Table 6. Composition and Weight Loss of the Thermal Products of $(LiPO_3)_6 \cdot 6H_2O$

Sample No.	Wt. loss	X-Ray dif.	Phosphates/P%				
			Ortho	Di	Tri	*cyclo*-Hexa	Higher
1	2.8	SM	—	1.0		99.0	—
2	10.9	UK	1.1	1.9	3.4	93.6	—
3	13.4	UK	1.0	1.4	2.2	95.4	—
4	17.2	$(LiPO_3)_6$	—	2.0	—	98.0	—
5	17.3	$LiPO_3$ JCPDS 26-1177	—	6.6	—	7.1	86.3
6	17.3	JCPDS 26-1177	—	14.2	—	—	85.8
7	17.3	AM	—	—	—	—	100

SM, UK, and AM stand for the starting material, an unknown substance, and an amorphous species respectively.

crystalline *cyclo*-hexaphosphate transformed to crystalline lithium methaphosphate (highpolyphosphate). The thermal product was sintered through the next small endothermic reaction at about 590 °C. The metaphosphate melted at about 650 °C. Griffith and Buxton reported that the *cyclo*-hexaphosphate hexahydrate can be dehydrated by heating above 120 °C and pure anhydrous *cyclo*-hexaphosphate can be prepared. According to the above results, a samll part of the *cyclo*-hexaphosphate hexahydrate is decomposed to phosphates with shorter chain lengths by heating above about 60 °C and pure anhydrous *cyclo*-hexaphosphate can not be prepared by heating the hexahydrate.

References

1) J. R. Van Wazer, "Phosphorus and its compounds," Interscience Publishers Inc., New York (1961), Vol. II.

2) E. J. Griffith and R. L. Buxton, *Inorg. Chem.*, **4**, 549 (1965).

3) Y. Hirai, N. Yoza, and S. Ohashi, *Anal. Chim. Acta*, **115**, 269 (1980).

4) S. Ohashi, *Kagaku To Kogyo*, **21**, 878 (1968). The A_2 and B_2 solvents in Table 3 were used.

5) M. Watanabe, H. Suzumori, M. Maeda, and T. Yamada, *Bull. Chem. Soc. Jpn.*, **53**, 2663 (1980).

6) Presented at the 4th symposium of Inorganic Phosphorus Chemistry, Nagoya, November 1983.

 © 1988 The Chemical Society of Japan Bull. Chem. Soc. Jpn., 61, 3883—3887 (1988)

Synthesis, Properties, and Crystal Structure of Binuclear Nickel(II) and Palladium(II) Complexes of Tridentate Thiolic Ligands with NNS-Donor Set

Makoto HANDA,† Masahiro MIKURIYA,††,* Zhuang Jin ZHONG, Hisashi ŌKAWA, and Sigeo KIDA
Department of Chemistry, Faculty of Science, Kyushu University 33,
Hakozaki, Higashi-ku, Fukuoka 812
††Department of Chemistry, School of Science, Kwansei Gakuin University,
Uegahara, Nishinomiya 662
(Received April 21, 1988)

Nickel(II) and palladium(II) complexes with tridentate thiolic ligands of the NNS-donor set have been prepared and characterized on the basis of elemental analyses, IR and electronic spectra, molar conductances, and magnetic susceptibilities. The crystal structure of the nickel(II) perchlorate of 3-[2-(2-pyridyl)ethylamino]-1-propanethiol was determined by single-crystal X-ray diffraction method. The structure consists of thiolate-bridged binuclear units. Each metal ion is coordinated by the amino nitrogen, pyridine nitrogen, and two bridging sulfur atoms, forming an essentially planar coordination unit, and the two N_2S_2 planes are connected at the S1-S2 edge with a dihedral angle of 136.1°.

Tridentate alcoholic ligands have been extensively utilized for synthesizing binuclear metal complexes bridged by their deprotonated alcoholic oxygens. As reported in the previous papers, we carried out systematic investigations on binuclear copper(II) complexes of tridentate alcoholic ligands of NSO-,[1-6] SNO-,[4,6,7] or SSO-donor set,[4,8] and revealed that the substitution of thioether sulfur for nitrogen donor atom substantially affects the formation, structure, magnetism, and electrochemical and spectral properties of the complexes. In this study the interest is focused on the effect of the change of the bridging atom from alcoholic oxygen to thiolic sulfur on the structure and physicochemical properties of binuclear complexes. All attempts to synthesize binuclear copper(II) complexes with thiolate-bridge have been unsuccessful, because thiols in general reduce copper(II) to copper(I) ($2R\text{-}S^- + 2Cu^{2+} \rightarrow R\text{-}SS\text{-}R + 2Cu^+$). However, formation of thiolate-bridged metal complexes is feasible by the use of other transition metal ions. In spite of great interests in structure and properties of such thiolate-bridged complexes, investigation on binuclear metal complexes with tridentate thiolic ligands is very limited.[9-12] Thus, we have initiated a systematic investigation on thiolate-bridged binuclear complexes using tridentate thiolic ligands.

In this study we have examined binuclear nickel(II) and palladium(II) complexes of thiolic ligands of NNS-donor set. The ligands utilized in this study are 2-(2-aminoethylamino)ethanethiol (HL^1), 2-(3-aminopropylamino)ethanethiol (HL^2), 2-(2-pyridylmethylamino)ethanethiol (HL^3), 2-[2-(2-pyridyl)ethylamino]ethanethiol (HL^4), and 3-[2-(2-pyridyl)ethylamino]-1-propanethiol (HL^5). Of these ligands, HL^1 and HL^2

HL^1: $NH_2CH_2CH_2NHCH_2CH_2SH$

HL^2: $NH_2CH_2CH_2CH_2NHCH_2CH_2SH$

HL^3: 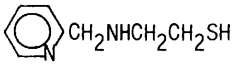

HL^4: 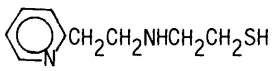

HL^5: 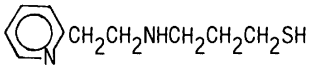

were used for the preparation of chloride and tetraphenylborate complexes of nickel(II) by Rose et al.[9] The chloride complexes were practically diamagnetic, whereas the tetraphenylborate complexes showed a subnormal magnetic moment in solid state (1.07 B.M. for $Ni(L^1)B(C_6H_5)_4$ and 1.29 B.M. for $Ni(L^2)B(C_6H_5)_4$). They presumed that the tetraphenylborate complexes were polymeric and contained both diamagnetic nickel(II) of square plane and paramagnetic nickel(II) of a coordination number larger than four. However, the structures of the tetraphenylborate and chloride complexes have not been confirmed yet. Thus, we have reinvestigated the nickel(II) complexes (perchlorate and tetrafluoroborate) of HL^1 and HL^2 together with the new complexes of HL^3, HL^4, and HL^5. During the course of this study, we found the X-ray structural data of $Ni(L^4)ClO_4$ had been already reported by Seff et al.[10] In this complex, a five-membered chelate ring is formed by the mercapto group with Ni(II), whereas $Ni(L^5)ClO_4$ has a six-membered chelate ring. The difference in the chelate ring size may affect the thiolate-bridged binuclear structure. Therefore we have determined the X-ray crystal structure of $Ni(L^5)ClO_4$ in order to compare the structure with that of $Ni(L^4)ClO_4$.

Experimental

Preparations. The ligands except HL^5 were prepared by the literature methods.[9,13] HL^1, HL^3, and HL^4 were

† Present address: Department of Chemistry, Faculty of Science, Shimane University, Matsue 690.

purified by distillation under reduced pressure and HL^2 was purified by sublimation. HL^5 was prepared by the application of the method of Murase et al.[14] 3-[2-(2-pyridyl)ethylamino]-1-propanol[3] was converted to *N*-[2-(2-pyridyl)ethyl]-3-bromopropylamine (**1**) according to the standard method.[15] Conversion of **1** to the corresponding thiol ($HL^5 \cdot 2HBr$) was proceeded via the phosphorothioate, which was obtained by the reaction of **1** with trisodium phosphorothioate.[14] $HL^5 \cdot 2HBr$ was used for the preparation of the complex without purification.

$Ni(L)ClO_4$ ($L=L^1, L^2, L^3, L^4$). To a solution of nickel(II) perchlorate hexahydrate (1 mmol) in methanol (10 cm^3) was added a methanolic solution of the ligand (1 mmol), and the mixture was stirred for 30 min to give violet microcrystals. They were collected, washed with methanol, and dried over P_2O_5 in a vacuum desiccator.

$Ni(L^5)ClO_4$. Crude ligand ($HL^5 \cdot 2HBr$, 1.4 g, ca. 4 mmol) and nickel(II) perchlorate hexahydrate (3.0 g, 8 mmol) were dissolved in 30 cm^3 of water and the pH of the solution was adjusted to ca. 9 by the addition of triethylamine. The resulting deep brown solution was heated on a water bath for ten minutes and undissolved material was filtered off. Addition of excess sodium perchlorate to the filtrate resulted in the precipitation of reddish brown crystals, which were recrystallized from an acetonitrile-ethanol mixture and dried over P_2O_5 under vacuum.

$Ni(L)BF_4$ ($L=L^2, L^4$). To an aqueous solution (10 cm^3) of nickel(II) acetate tetrahydrate (1 mmol) was added a solution of the ligand (1 mmol) in water (10 cm^3) to form a red solution. A saturated aqueous solution of $NaBF_4$ (2 mmol) was added to this solution to give violet microcrystals, which were collected, washed with methanol, and dried over P_2O_5 in a vacuum desiccator.

$Pd(L^2)ClO_4$. An aqueous solution of $[PdCl_4]^{2-}$ was prepared by dissolving $PdCl_2$ (2 mmol) in water containing NaCl (4.4 mmol). To this were added HL^2 (2 mmol) and NaOH pellets (2.2 mmol), and the mixture was stirred for a half hour. Then, an aqueous solution of $NaClO_4 \cdot H_2O$ (large excess) was added to give a yellow precipitate. It was recrystallized from water as yellow microcrystals.

Elemental analyses of the complexes are given in Table 1.

Measurements. Infrared spectra were measured on a Hitachi 215 infrared spectrometer, and electronic spectra were recorded on a Shimadzu UV-VISIBLE recording spectrometer Model UV-240 in acetone or water. Reflectance

Table 1. Elemental Analyses of Complexes

	Found(%)			Calcd(%)		
	C	H	N	C	H	N
$Ni(L^1)ClO_4 \cdot 1/2H_2O$	16.72	4.18	9.77	16.78	4.22	9.78
$Ni(L^2)ClO_4$	20.65	4.49	9.59	20.61	4.50	9.61
$Ni(L^2)BF_4$	21.34	4.57	9.90	21.55	4.70	10.05
$Ni(L^3)ClO_4 \cdot 1/2H_2O$	28.63	3.51	8.10	28.73	3.62	8.38
$Ni(L^4)ClO_4$	31.66	3.96	7.92	31.85	3.86	8.25
$Ni(L^4)BF_4$	32.87	3.95	8.62	33.08	4.01	8.57
$Ni(L^5)ClO_4$	34.05	4.31	7.94	33.98	4.28	7.93
$Pd(L^2)ClO_4$	17.49	3.79	8.12	17.71	3.86	8.26

Table 2. Atomic Coordinates ($\times 10^4$) and Thermal Parameters

Atom	*x*	*y*	*z*	B_{eq}/Å$^{2b)}$	Atom	*x*	*y*	*z*	B_{eq}/Å$^{2b)}$
Ni1	4088(1)	3530(1)	−1217(1)	3.0	N4	486(5)	4046(2)	−162(7)	3.4
Ni2	1430(1)	3599(1)	−964(1)	3.2	C1	3256(9)	4300(4)	989(20)	10.1
Cl1	−2009(2)	3186(1)	704(3)	5.4	C2	4442(9)	4480(3)	1121(14)	6.5
Cl2	2708(2)	4940(1)	5396(3)	6.5	C3	5512(8)	4169(3)	1020(12)	5.8
S1	3063(2)	3715(1)	734(2)	4.0	C4	5660(8)	4230(3)	−2011(11)	5.0
S2	2550(2)	3107(1)	−1834(3)	3.5	C5	5160(8)	4045(3)	−3726(11)	4.8
O1	−2066(6)	3524(2)	−452(9)	7.1	C6	5479(7)	3567(3)	−3877(10)	3.9
O2	−3203(8)	3090(3)	955(11)	10.1	C7	6235(7)	3412(3)	−4962(10)	4.6
O3	−1694(12)	2822(4)	−115(18)	18.4	C8	6455(8)	2984(3)	−5034(11)	5.1
O4	−1295(12)	3252(4)	2050(16)	20.8	C9	5941(7)	2703(3)	−4020(10)	4.7
O5[a)]	2553(11)	5454(4)	5508(16)	7.6	C10	5184(7)	2874(3)	−2964(10)	3.9
O5'[a)]	1862(17)	4746(6)	4375(24)	8.2	C11	2099(8)	3160(3)	−4122(10)	5.1
O6[a)]	2977(9)	4772(3)	7008(14)	6.1	C12	880(8)	2969(3)	−4654(12)	6.0
O6'[a)]	3387(14)	4929(5)	6925(20)	6.1	C13	−14(8)	3015(3)	−3370(13)	5.7
O7[a)]	3298(11)	4968(4)	4091(16)	8.1	C14	−431(8)	3791(3)	−3744(10)	5.2
O7'[a)]	3940(15)	4951(6)	4787(21)	6.7	C15	40(8)	4230(3)	−3089(10)	4.6
O8[a)]	1482(10)	4969(4)	5231(15)	7.3	C16	−179(7)	4293(2)	−1310(9)	3.4
O8'[a)]	2485(17)	4404(7)	4887(24)	8.3	C17	−1008(7)	4592(3)	−875(10)	4.0
N1	5427(5)	3925(2)	−598(8)	4.1	C18	−1130(7)	4631(3)	826(11)	4.5
N2	4975(5)	3295(2)	−2871(7)	3.1	C19	−428(8)	4383(3)	1986(11)	4.6
N3	8(5)	3439(2)	−2550(8)	4.1	C20	358(7)	4086(3)	1464(10)	4.2

a) Atoms refined with occupancy factors of 0.5. b) $B_{eq}=4/3[a^2B(1,1)+b^2B(2,2)+c^2B(3,3)+ab(\cos\gamma)B(1,2)+ac(\cos\beta)B(1,3)+bc(\cos\alpha)B(2,3)]$.

spectra were recorded on Shimadzu multipurpose spectrophotometer Model MPS-5000. Conductance measurements were carried out with a Yanagimoto Conductivity Outfit Model MY-8 in acetone or in water. Magnetic susceptibilities were measured by the Faraday method. The apparatus was calibrated by the use of $[Ni(en)_3]S_2O_3$.[16] The diamagnetic corrections were made with Pascal's constants[17] and magnetic moments were calculated by the equation, $\mu_{eff}=(8\chi_A T)^{1/2}$.

X-Ray Crystal Structure Analysis of Ni(L^5)ClO$_4$. A crystal with dimensions 0.12×0.30×0.31 mm^3 was used for the X-ray analysis. The unit-cell parameters and intensities were measured on a Rigaku AFC-5R automated four-circle diffractometer with graphite-monochromated Mo $K\alpha$ radiation (λ=0.71073 Å). The intensity data were collected by the ω scan technique with a scan rate of 4° min^{-1}.

Crystal Data: $C_{20}H_{28}Cl_2N_4Ni_2O_8S_2$, F.W.=704.9; monoclinic, $P2_1/n$; a=11.303(2), b=31.142(5), c=8.104(1) Å, β=98.17(1)°; D_c=1.66 g cm^{-3}; Z=4; μ(Mo $K\alpha$)=17.2 cm^{-1}.

A total of 4254 reflections with $2\theta<46°$ were collected. The intensity data were corrected for Lorentz-polarization effects and for absorption. Independent 3125 reflections with $|F_o|>3\sigma(F_o)$ were considered as "observed" and were used for structure analysis. The structure was solved by the direct method. Refinements were carried out by the block-diagonal least-squares method. The weighting scheme $w=[\sigma_{count}^2+(0.015|F_o|)^2]^{-1}$ was employed. Hydrogen atoms were inserted in their calculated positions and fixed at their positions. The final discrepancy factors are $R=\Sigma||F_o|-|F_c||/\Sigma|F_o|=0.059$ and $R_w=[\Sigma w(|F_o|-|F_c|)^2/\Sigma w|F_o|^2]^{1/2}=0.076$.

All the calculations were carried out on the HITAC M-680H computer at the Computer Center of the Institute for Molecular Science using a local version of the MULTAN 78, UNICS-III, and ORTEP programs.[18] Atomic coordinates and thermal parameters of nonhydrogen atoms are listed in Table 2. The anisotropic thermal parameters of nonhydrogen atoms, the atomic coordinates and thermal parameters of hydrogen atoms, and the F_o-F_c tables have been deposited as a Document No. 8841 at the Office of the Editor.

Results and Discussion

Nickel(II) complexes with the general formula NiLX (X=ClO$_4^-$, L=L^1, L^2, L^3, L^4, L^5; and X=BF$_4^-$, L=L^2, L^4) were obtained. As for the palladium(II) complex, only Pd(L^2)ClO$_4$ could be isolated as crystals. Magnetic moments at room temperature and molar conductance data are given in Table 3.

The magnetic moments of the complexes are not zero. These residual paramagnetism can be ascribed to the temperature independent paramagnetism of nickel atom. Thus, we can conclude that all these complexes are diamagnetic. The S–H vibration near 2500 cm^{-1} of the free ligands was absent in the IR spectra of the complexes. This suggests that the thiol is deprotonated and coordinated to the metal. IR spectra also suggested no coodination of the perchlorate and tetrafluoroborate ions to the metal; ClO$_4^-$ and BF$_4^-$ vibrations appeared as a broad band at ca. 1100 and ca. 1050 cm^{-1}, respectively. Molar conductance data indicated that all the complexes are 2:1 electrolyte in acetone or water. Based on these facts, the complexes are presumed to be binuclear bridged by the mercaptide sulfur atoms.

The crystal structure of Ni(L^5)ClO$_4$ consists of binuclear complex cations and perchlorate ions. Perchlorate ions do not participate in any coordination as suggested from IR spectra. A perspective drawing of the binuclear cation is illustrated in Fig. 1. Selected bond distances and angles are given in Table 4. Both the nickel ions adopt an essentially planar configuration with aliphatic amino nitrogen, pyridine nitrogen, and bridging sulfur atoms. The deviations of atoms from the least-squares planes of N$_2$S$_2$ are less than 0.11 Å and the deviations of Ni1 and Ni2 from the planes are only 0.05 and 0.01 Å, respectively. The Ni–S

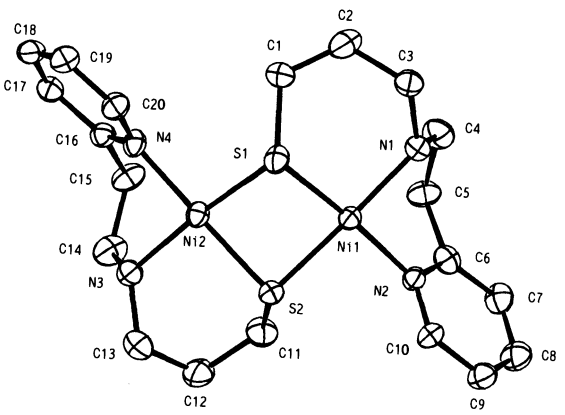

Fig. 1. A perspective view of $[Ni_2(L^5)_2]^{2+}$ ion.

Table 3. Magnetic Moments and Molar Conductances of Complexes

	μ_{eff}/B.M.[a]	λ_M/Ω^{-1} cm^{-2} mol^{-1}
Ni(L^1)ClO$_4$·1/2H$_2$O	0.28	204[b]
Ni(L^2)ClO$_4$	0.21	183[b]
Ni(L^2)BF$_4$	0.28	198[b]
Ni(L^3)ClO$_4$·1/2H$_2$O	0.67	154[b]
Ni(L^4)ClO$_4$	0.40	214[b]
Ni(L^4)BF$_4$	0.26	231[b]
Ni(L^5)ClO$_4$	0.28	223[b]
Pd(L^2)ClO$_4$	0.23	214[c]

a) Magnetic moment at room temperature. Temperature-independent paramagnetism is not included for the calculation of μ_{eff}. b) In acetone. c) In water.

distances are 2.166(2)—2.180(2) Å, which are common for other thiolate-bridged bi- and oligonuclear nickel(II) complexes.[19-24] The Ni1–Ni2 distance is 3.047(1) Å, making a contrast with that of $Ni(L^4)ClO_4$ (2.739(1) Å)[10] and other thiolate-bridged binuclear nickel(II) complexes,[19-21] whose structurtes are characterized by the small dihedral angle (82.3—114.3°) between the two NiN_2S_2 planes sharing the S–S′ edge and by the small Ni–S–Ni angle (76.7—79.5°). As the result, the Ni–Ni′ distances are very short (2.733—2.795 Å).[25] In $Ni(L^5)ClO_4$, the two N_2S_2 planes are bent at the S1–S2 edge with a dihedral angle of 136.1° and the Ni–S–Ni angles are 89.02(8) and 89.27(8)°. This may be ascribed to the steric requirement of the six-membered chelate ring which favors the coplanar structure. A similar structural feature was observed in $[Ni_2\{SCH(CH_2CH_2NH_2)_2\}_2]Br_2$ which contains two adjacent six-membered chelate rings.[24]

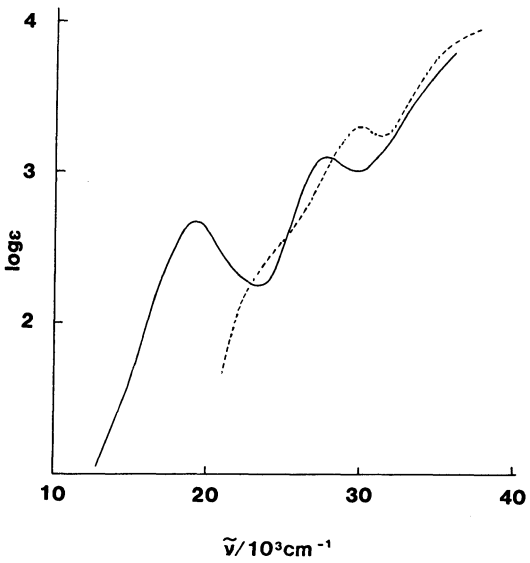

Fig. 2. Electronic spectra of (——) $Ni(L^2)ClO_4$ and (-----) $Pd(L^2)ClO_4$.

Table 4. Selected Interatomic Distances (l/Å) and Bond Angles (ϕ/°)

Ni1–Ni2	3.047(1)	Ni1–N1	1.960(6)
Ni1–S1	2.167(2)	Ni1–N2	1.928(6)
Ni1–S2	2.180(2)	Ni2–N3	1.974(6)
Ni2–S1	2.170(2)	Ni2–N4	1.923(6)
Ni2–S2	2.166(2)		
Ni1–S1–Ni2	89.27(8)	N1–Ni1–N2	87.5(3)
Ni1–S2–Ni2	89.02(8)	S1–Ni2–S2	80.9(1)
S1–Ni1–S2	80.6(1)	S1–Ni2–N4	97.3(2)
S1–Ni1–N1	96.9(2)	S2–Ni2–N3	94.0(2)
S2–Ni1–N2	95.1(2)	N3–Ni2–N4	87.9(3)

Electronic spectra of the nickel(II) complexes in acetone exhibit a d–d band near 19×10^3 cm^{-1} (ε: 400—500 dm^3 mol^{-1} cm^{-1}) (Fig. 2 and Table 5), characteristic of planar nickel(II). The spectra were also characterized by an absorption in a near-ultraviolet region (27—28×10^3 cm^{-1}), whose extinction coefficient is more than 10^3 dm^3 mol^{-1} cm^{-1}. Judging from its frequency and intensity it can not be a d–d transition band, but should be assigned to a charge-transfer transition. Such a near-ultraviolet band was also observed for other thiolate-bridged binuclear nickel(II) complex.[14]

The electronic spectrum of $Pd(L^2)ClO_4$ in water shows absorption bands at ca. 24×10^3 and 30×10^3cm^{-1}, which can be assigned to a d–d and a charge-transfer transitions, respectively.

Electronic spectra of the nickel(II) complexes in water (immediately after the dissolution) were essentially the same as the spectra in acetone. However, the purple color of the aqueous solutions faded gradually and the solutions became pale green in a day or two, suggesting the decomposition of the complexes in water. The tendency to decompose in water was prominent in $Ni(L^1)ClO_4$ and $Ni(L^3)ClO_4$, whereas the complexes with $(L^2)^-$, $(L^4)^-$, and $(L^5)^-$ were fairly stable in water. The low stability of the former complexes seems to be due to the strain in the 5–5 fused-ring system.

Each powder spectrum of the nickel(II) complexes resembles that in acetone solution in the region 14—30×10^3 cm^{-1} (Table 5). Thus, the magnetic, electronic spectral, and X-ray structural results indicate that the coordination geometries are invariably planar in solution as well as in solid state for all the present nickel complexes.

References

1) M. Mikuriya, H. Okawa, and S. Kida, *Bull. Chem. Soc. Jpn.*, **53**, 2871 (1980); **54**, 2979 (1981); **55**, 1086 (1982).

Table 5. Electronic Spectral Data ($\tilde{\nu}/10^3$ cm^{-1} (ε))

	Absorption		Reflectance	
$Ni(L^1)ClO_4\cdot1/2H_2O$	19.6(420)	27.7(1100)[a]	19.4	26.7
$Ni(L^2)ClO_4$	19.3(470)	27.6(1230)[a]	19.0	27.2
$Ni(L^2)BF_4$	19.3(480)	27.7(1230)[a]	18.9	27.0
$Ni(L^3)ClO_4\cdot1/2H_2O$	19.3(460)	ca. 28(1800)[a]	19.0	ca. 27
$Ni(L^4)ClO_4$	19.3(500)	ca. 27(1480)[a]	19.0	ca. 27
$Ni(L^4)BF_4$	19.4(490)	ca. 27(1390)[a]	19.1	ca. 27
$Ni(L^5)ClO_4$	20.1(450)	26.8(2030)[a]	20.2	26.7
$Pd(L^2)ClO_4$	ca. 24(200)	30.0(2000)[b]		

a) In acetone. b) In water.

2) M. Mikuriya, H. Okawa, and S. Kida, *Bull. Chem. Soc. Jpn.*, **53**, 3717 (1980).
3) M. Nakamura, M. Mikuriya, H. Okawa, and S. Kida, *Bull. Chem. Soc. Jpn.*, **54**, 1825 (1981).
4) M. Mikuriya, M. Nakamura, H. Okawa, and S. Kida, *Chem. Lett.*, **1982**, 839.
5) M. Mikuriya, M. Nakamura, H. Okawa, and S. Kida, *Inorg. Chim. Acta*, **68**, 111 (1983).
6) M. Mikuriya, M. Aihara, Y. Nishi, H. Okawa, and S. Kida, *Chem. Lett.*, **1980**, 795.
7) M. Mikuriya, H. Okawa, and S. Kida, *Inorg. Chim. Acta*, **34**, 13 (1979); **42**, 233 (1980).
8) M. Mikuriya, M. Nakamura, H. Okawa, and S. Kida, *Inorg. Chim. Acta*, **70**, 223 (1983).
9) S. L. Rose, R. E. Hoskin, J. E. Cavanaugh, C. J. Smith, and E. L. Blinn, *Inorg. Chim. Acta*, **40**, 7 (1980).
10) T. B. Vance, L. G. Warner, and K. Seff, *Inorg. Chem.*, **16**, 2106 (1977).
11) D. H. Busch, D. C. Jicha, M. C. Thompson, J. W. Wrathall, and E. Blinn, *J. Am. Chem. Soc.*, **86**, 3642 (1964).
12) J. Harley-Mason, *J. Chem. Soc.*, **1952**, 146.
13) H. R. Snyder, J. M. Stewart, and J. B. Ziegler, *J. Am. Chem. Soc.*, **69**, 2672 (1947).
14) I. Murase, S. Ueno, and S. Kida, *Bull. Chem. Soc. Jpn.*, **56**, 2748 (1983).
15) F. Cortese, *Org. Synth.*, Coll. Vol. II, 91 (1948).
16) N. F. Curtis, *J. Chem. Soc.*, **1961**, 3147.
17) F. E. Mabbs and D. J. Machin, "Magnetism and Transition Metal Complexes," Chapman and Hall, London (1973).
18) T. Sakurai and K. Kobayashi, *Rikagaku Kenkyusho Hokoku*, **55**, 69 (1979); P. Main, S. E. Hull, L. Lessinger, G. Germain, J-P. Declercq, and M. M. Woolfson, MULTAN 78 (1978). A System of Computer Programs for the Automatic Solution of Crystal Structure from X-Ray Diffraction Data. Univ. of York, England and Louvain, Belgium; C. K. Johnson, Report No. 3794, Oak Ridge National Laboratory, Oak Ridge, Tennessee (1965).
19) G. A. Barclay, E. M. McPartlin, and N. C. Stephenson, *Inorg. Nucl. Chem. Lett.*, **3**, 397 (1967); *Acta Crystallogr., Sect. B*, **25**, 1262 (1969); D. J. Baker, D. C. Doodall, and D. S. Moss, *Chem. Commun.*, **1969**, 325.
20) J. P. Fackler, Jr., and W. J. Zegarski, *J. Am. Chem. Soc.*, **95**, 8566 (1973).
21) A. C. Villa, A. G. Manfredotti, M. Nardell, and C. Pelizzi, *Chem. Commun.*, **1970**, 1322.
22) C. H. Wei and L. F. Dahl, *Inorg. Chem.*, **9**, 1878 (1970).
23) P. Woodward, L. F. Dahl, E. W. Abel, and B. C. Crosse, *J. Am. Chem. Soc.*, **87**, 5251 (1965).
24) M. Mikuriya, S. Kida, and I. Murase, *Bull. Chem. Soc. Jpn.*, **60**, 1180 (1987).
25) J. P. Fackler, Jr., *Prog. Inorg. Chem.*, **21**, 55 (1976).

 © 1988 The Chemical Society of Japan Bull. Chem. Soc. Jpn., 61, 3889—3893 (1988)

Equilibrium Study on the Characteristic Color-Changing Reaction of Lanthanum Complex of 3-[[Bis(carboxymethyl)amino]-methyl]-1,2-dihydroxyanthraquinone (Alizarin Complexon) with Fluoride Ion

Akio YUCHI,* Hiroki MORI, Hitoshi HOTTA, Hiroko WADA, and Genkichi NAKAGAWA
Department of Applied Chemistry, Nagoya Institute of Technology,
Gokiso-cho, Showa-ku, Nagoya 466
(Received April 25, 1988)

Complexation equilibria between lanthanum (M), 3-[[bis(carboxymethyl)amino]methyl]-1,2-dihydroxyanthraquinone (Alizarin Complexon, H_4L) and fluoride were studied by potentiometry with fluoride ion selective electrodes and by spectrophotometry. M_2HL_2 and a further protonated species react with fluoride to form M_2HL_2F and $M_2H_2L_2F$, whereas M_2L_2 does not. The unexpectedly large stability constant of $10^{4.12}$ for the reaction, $M_2HL_2+F^- \rightleftharpoons M_2HL_2F$, may be ascribed to the incorporation of fluoride ion in a specially organized core of M_2HL_2.

Rare earth metal (M) complexes of alizarin complexon(3-[[bis(carboxymethyl)amino]methyl]-1,2-dihydroxyanthraquinone; ALC or H_4L; Fig. 1) react with fluoride ion to show a characteristic color change from red to blue.[1] This reaction provides the selective and sensitive photometric method for fluoride.[2] Various modifications of this reaction have been proposed to overcome the disadvantages of large reagent blank, slow attainment of equilibria and insufficient affinities toward fluoride.[3] In contrast to abundance of conventional bleaching methods which utilize the dissociation of a color-forming reagent from the metal complex by the reaction with fluoride ion, no other reaction systems involving the formation of the mixed ligand complex have been found except those with the derivatives.[4-6]

Although several attempts have been made to elucidate the mechanism of this color development, they are not sufficient.[10-13] From the similarity of the absorption spectrum of the blue species to that of completely deprotonated ALC, the following equation was first proposed by Leonard and West.[10]

$$MHL + F^- \rightleftharpoons MLF + H^+$$
(Charges of the complexes are omitted)

Formation of the mixed ligand complex, MLF, by displacement of one of the water molecules with fluoride was supposed to promote the dissociation of the last proton on ALC, causing the color change. Later on, rather complicated formulas such as $M_5L_4F_4$,[11] $M_2H_2L_2F_2$,[12] and $M_5L_4F_2$[13] have been proposed as the composition of the mixed ligand complexes. Various molar ratio methods used in these studies were not suited for the system, because ALC has so many functional groups that various species can be formed in a successive manner as in the case of Xylenol Orange,[14] and because affinity to fluoride is too low to give a well-defined break point on the plots.

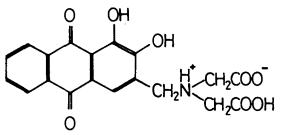

Fig. 1. Structure of ALC.

We have made systematic studies on the formation of mixed ligand complexes with fluoride and simpler ligands,[15-17] using fluoride ion-selective electrodes. The same approach is applied to this system.

Experimental

Reagents. Lanthanum solution was prepared from the nitrate hexahydrate and was standardized against Na_2H_2edta. Potassium fluoride was dried in a platinum crucible for 24 hours at 110 °C. Fluoride solutions were stored in polyethylene containers. Potassium nitrate was recrystallized twice. Carbonate-free potassium hydroxide solution was prepared as described elsewhere.[18]

ALC ($H_4L \cdot 2H_2O$) was prepared and purified as described in literature.[19,20] Purity of the reagent was confirmed by elemental analysis and potentiometric titration. It was dissolved in known amounts of carbonate-free potassium hydroxide solution. Acetate buffer has been used for the earlier equilibrium studies of this system by photometry.[10-12] As the buffer proved to alter the equilibria,[21] no buffer was used in this study except 2-morpholino-1-propanesulfonic acid.

Measurement. Details of the potentiometry were the same as described previously.[14-16] Visible absorption spectra were recorded with a UNION high-sens spectrophotometer SM-401 and a Shimadzu UV-250.

Results

Protonation Equilibria of ALC. Solutions containing 3 to 9×10^{-3} mol dm^{-3} ALC were potentiometrically titrated with a nitric acid or a potassium hydroxide solution between $-\log[H^+]$ 3 and 8. At lower $-\log[H^+]$ the reagent precipitated as H_4L, the solubility of which has been reported to be 5×10^{-4} mol dm^{-3}.[20] The average number of protons bound to the ligand, $\bar{n}_H$ was calculated by

$$\bar{n}_{H,o} = \frac{4C_L + C_H - C_{OH} - [H^+] + [OH^-]}{C_L}, \quad (1)$$

where C_L, C_H, and C_{OH} are the analytical concentrations of the ligand, hydrogen, and hydroxide ions added, respectively (Fig. 2). The third and fourth protonation constants were determined by the conventional method.

Visible absorption spectra were recorded for the solutions containing 1×10^{-4} mol dm^{-3} ALC at various $-\log[H^+]$ values between 2.0 and 7.1. A distinct isosbestic point was observed at 455 nm. The third protonation constant was determined by fitting a set of normalized curves to the plot of the absorbance change at 540 nm (squares in Fig. 3).

The constants obtained are as follows: $\log K_3=5.58$ by potentiometry, and 5.52 by spectrophotometry; $\log K_4=2.48$ by potentiometry. These are in good agreement with those in literature: $\log K_3=5.47$[13] and 5.54[22]; $\log K_4=2.54$[13] and 2.40.[22]

Complexation Equilibria of Lanthanum Ion with ALC. Complexation equilibria between lanthanum ion and ALC were potentiometrically studied. Preliminary experiments showed that addition of excess lanthanum ion over ALC causes precipitation of complexes at any $-\log[H^+]$ and that even in the presence of excess ALC precipitation occurs at lower $-\log[H^+]$. Thus, 0.2 to 1×10^{-3} mol dm^{-3} solutions containing lanthanum ion and a slight excess of ALC were subjected to potentiometry. The $\bar{n}_H$ value was likewise calculated by Eq. 1 and is shown as a function of $-\log[H^+]$ in Fig. 2. The plateau at $\bar{n}_H$ equal to 0.5 suggests the presence of polynuclear species.

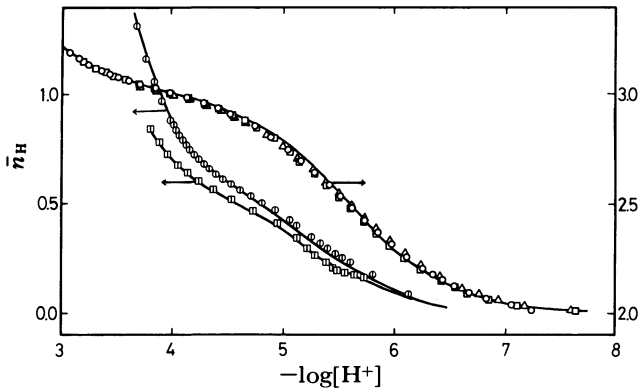

Fig. 2. Plots of $\bar{n}_H$ vs. $-\log[H^+]$ for the La^{3+}-ALC system (25 °C, 0.1 mol dm^{-3} KNO_3). $C_M/10^{-3}$ mol dm^{-3}: (○,□,△) 0; (Ⓓ) 0.19; (▣) 0.51. $C_L/10^{-3}$ mol dm^{-3}: (○) 4.8; (□) 6.7; (△) 8.6; (Ⓓ) 0.20; (▣) 0.52. The solid lines are calculated with the constants obtained.

Table 1. Average Deviation of $\bar{n}_H$ for Various Combination of Species in La-ALC System

No.	Species considered					$\Delta\bar{n}_H$[a]
	MHL	$M_2H_2L_2$	M_2HL_2	ML	M_2L_2	
1	○	×	×	○	×	0.090
2	○	×	×	×	○	0.153
3	○	×	○	○	×	0.021
④	○	×	○	×	○	0.010
5	×	×	○	○	×	0.045
6	×	×	○	×	○	0.023
7	×	○	○	○	×	0.031
⑧	×	○	○	×	○	0.015
9	×	○	×	○	×	0.162
10	×	○	×	×	○	0.225

a) $\Delta\bar{n}_H=(\Sigma(\bar{n}_{H,c}-\bar{n}_{H,o})^2/N)^{1/2}$; N: number of data.

The complexation equilibria are generally expressed by

$$pM^{3+} + rH_2L \rightleftharpoons M_pH_qL_r + (2r-q)H^+ : K_{pqr}. \quad (2)$$

Then $\bar{n}_H$ is given by

$$\bar{n}_{H,c} = \frac{\Sigma\Sigma\Sigma q[M_pH_qL_r]}{C_L}. \quad (3)$$

Various combinations of the possible complexes were assumed and K_{pqr} values in each set were refined to give a minimum error square sum about $\bar{n}_H$'s expressed by Eqs. 1 and 3 (Table 1). Both the combinations of species, Nos. 4 and 8 gave satisfactory agreement. Formation of M_2L_2 and M_2HL_2 is definite, whereas the composition of the other species present at lower $-\log[H^+]$ region could not be determined whether MHL or $M_2H_2L_2$, since $\Delta\bar{n}_H$ did not differ so much between Nos. 4 and 8. The constants obtained are summarized in Table 2.

These equilibria were also studied spectrophotometrically with the solutions containing 0.1×10^{-3} mol dm^{-3} La^{3+} and a small excess of ALC at $-\log[H^+]$ between 2 and 8 (Fig. 4). Spectral change between $-\log[H^+]$ 2—4 with an isosbestic point at 453 nm corresponds to the formation of M_2HL_2, whereas that between $-\log[H^+]$ 6—8 with an isosbestic point at

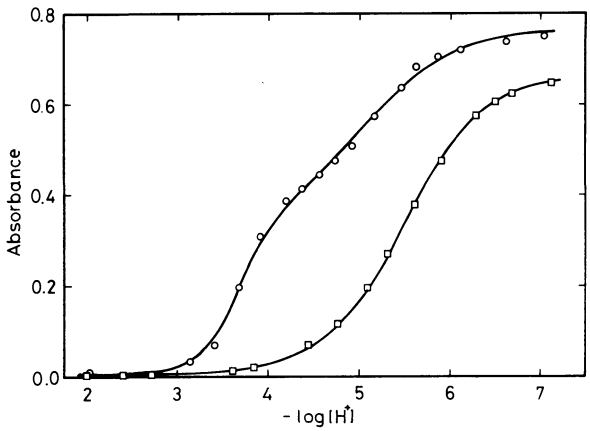

Fig. 3. Absorbance change of ALC as a function of $-\log[H^+]$ in the presence and absence of La^{3+} (25 °C, 0.1 mol dm^{-3} KNO_3). Wavelength, 540 nm. C_M: (□) 0; (○) 9.4×10^{-5} mol dm^{-3}. C_L: (□,○) 9.5×10^{-5} mol dm^{-3}. The solid lines are calculated with the constants obtained.

Table 2. Stability Constants for the Species Found in La-ALC and La-ALC-F Systems at 25 °C and at 0.1 mol dm^{-3} KNO_3

Equilibrium	Equilibrium constant
A. La-ALC system[a]	
$2M + 2H_2L \rightleftharpoons M_2L_2 + 4H^+$	$\log K_{202} = 0.28$
$2M + 2H_2L \rightleftharpoons M_2HL_2 + 3H^+$	$\log K_{212} = 5.58$
B. La-ALC-F system	
$2M + 2H_2L + F^- \rightleftharpoons M_2HL_2F + 3H^+$	$\log K_{2121} = 9.70$
$2M + 2H_2L + F^- \rightleftharpoons M_2H_2L_2F + 2H^+$	$\log K_{2221} = 14.17$

a) In more acidic medium, the third species was found (see text for details).

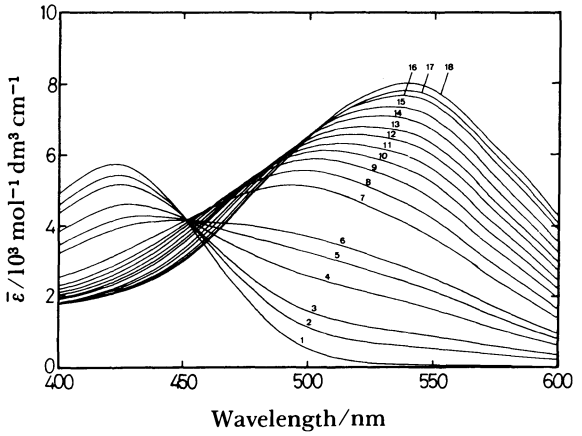

Fig. 4. Absorption spectra of La-ALC system at various −log[H$^+$] (25 °C, 0.1 mol dm^{-3} KNO_3). C_M=9.4×10^{-5} mol dm^{-3}; C_L=9.5×10^{-5} mol dm^{-3}. −log[H$^+$]: (1) 2.014; (2) 3.359; (3) 3.495; (4) 3.651; (5) 3.760; (6) 3.846; (7) 4.196 (8) 4.392; (9) 4.457; (10) 4.740; (11) 4.920; (12) 5.116; (13) 5.275; (14) 5.481; (15) 5.638; (16) 5.838; (17) 6.046; (18) 7.075.

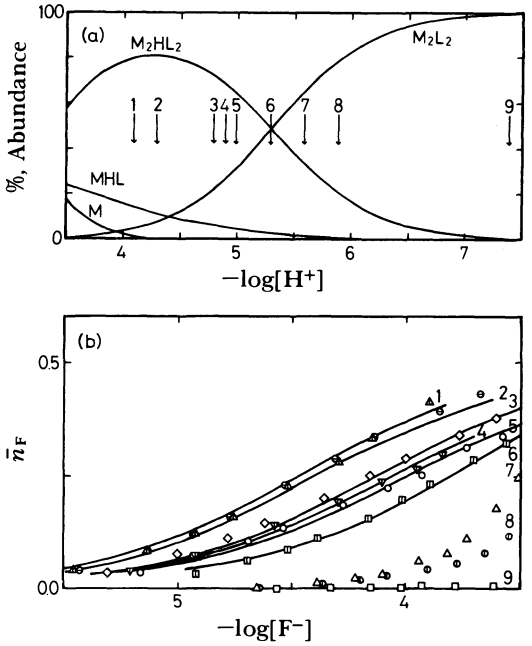

Fig. 5. (a) Distribution of species for the La-ALC system. C_M=0.5×10^{-3} mol dm^{-3}; C_L=0.55×10^{-3} mol dm^{-3}. MHL is arbitrarily taken as a minor species formed in acidic media (see text for details). The numbers in (a) correspond to the experimental conditions in (b). (b) $\bar{n}_F$ vs. −log[F$^-$] for the La-ALC-F system. The solid lines are calculated with the constants obtained.

505 nm to the deprotonation of M_2HL_2 to form M_2L_2. At intermediate −log[H$^+$], both reactions are concerned in the spectral change. The change in absorbance at 540 nm is shown as a function of −log[H$^+$] in Fig. 3. By using the constants potentiometrically obtained and refining the molar absorptivities for M_2HL_2 and MHL or $M_2H_2L_2$, this curve could be reproduced as shown by the solid curve in Fig. 3.

Mixed Ligand Complexes of La-ALC with Fluoride. The distribution of each species in the solution of C_M=0.5×10^{-3} and C_L=0.55×10^{-3} mol dm^{-3} was calculated with the constants obtained above, and was shown as a function of −log[H$^+$] in Fig. 5(a). A minor species formed in acidic media was assumed to be MHL. Even if $M_2H_2L_2$ was assumed instead of MHL, distribution of other species was practically the same. The reaction of these species with fluoride was examined at various −log[H$^+$] values indicated by arrows in Fig. 5(a). It took 30 min for equilibration at −log[H$^+$] 4, whereas 2 h at 5.5. Thus all the solutions were subjected to measurements after 3 h.

With the −log[H$^+$] and −log[F$^-$] values for each experimental point, the average number of fluoride ions bound to lanthanum complexes, $\bar{n}_F$ was calculated by

$$\bar{n}_{F,o} = \frac{C_F - [F^-] - [HF] - 2[HF_2^-]}{C_M} \quad (4)$$

and is shown as a function of −log[F$^-$] in Fig. 5(b). No increase in $\bar{n}_F$ at higher −log[H$^+$] indicates that M_2L_2 does not react with fluoride ion. At lower −log[H$^+$], on the other hand, the curves well fit a normalized curve, $X=\log x$; $Y=0.5x/(1+x)$. This suggests the formation of polynuclear species.

Formation of a mixed ligand complex is expressed by

$$pM + rH_2L + sF^- \rightleftharpoons M_pH_qL_rF_s + (2r - q)H^+ : K_{pqrs}. \quad (5)$$

Then $\bar{n}_F$ is given by

Table 3. Average Deviation of $\bar{n}_F$ for Various Combination of Species in La-ALC-F System

No.	Species considered				$\Delta\bar{n}_F$[a]
	MHLF	M_2HL_2F	$M_2H_2L_2F$	$M_4H_3L_4F_2$	
1	○	×	×	×	0.069
2	×	○	×	×	0.039
3	×	×	○	×	0.057
4	×	×	×	○	0.039
5	○	○	×	×	0.033
⑥	×	○	○	×	0.015

a) $\Delta\bar{n}_F=(\Sigma(\bar{n}_{F,o}-\bar{n}_{F,c})^2/N)^{1/2}$; N: number of data.

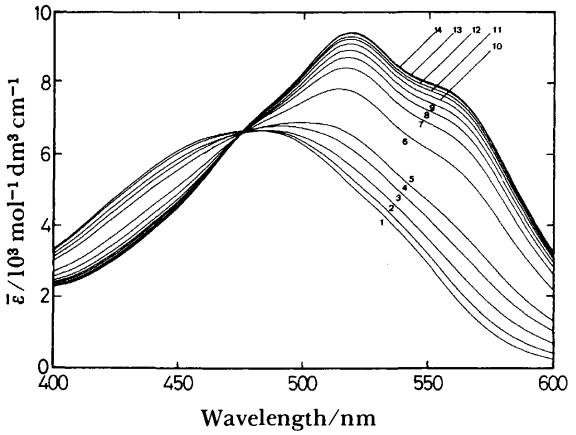

Fig. 6. Absorption spectra of La-ALC-F system at various fluoride concentrations (25°C, 0.1 mol dm^{-3} KNO_3). C_M=9.3×10^{-5} mol dm^{-3}; C_L=9.5×10^{-5} mol dm^{-3}; −log[H$^+$]=5.10. C_F/10^{-5} mol dm^{-3}: (1) 0; (2) 1.05; (3) 2.09; (4) 3.14; (5) 4.19; (6) 8.38; (7) 12.6; (8) 16.8; (9) 21.0; (10) 26.2; (11) 31.4; (12) 41.9; (13) 52.4; (14) 105.

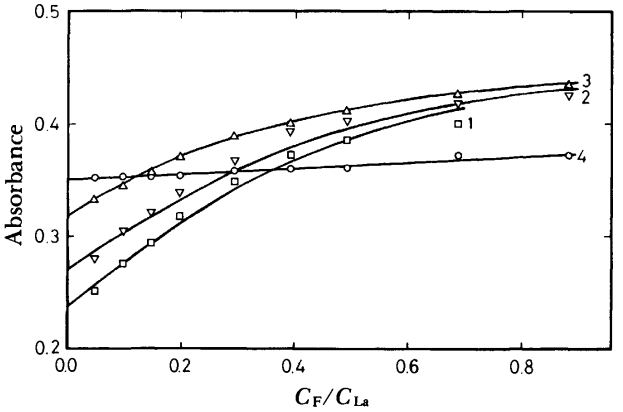

Fig. 7. Absorbance change by the addition of fluoride to La-ALC. C_M=0.5×10^{-3} mol dm^{-3}; C_L=0.55×10^{-3} mol dm^{-3}. Wavelength, 620 nm; pathlength, 1 mm. −log[H$^+$]: (1) 4.3; (2) 4.8; (3) 5.3; (4) 5.9.

$$\bar{n}_{F,c}=\frac{\Sigma\Sigma\Sigma\Sigma_s[M_pH_qL_rF_s]}{C_M} \quad (6)$$

Various combinations of the possible mixed ligand complexes were assumed and K_{pqrs} values in each set were refined to give a minimum error square sum about $\bar{n}_F$'s expressed by Eqs. 4 and 6 (Table 3). Only the combination of species, No. 6 gave satisfactory agreement. Stability constants of $M_2H_2L_2F$ and M_2HL_2F were summarized in Table 2. The constant for the latter species can be recalculated as

$$M_2HL_2 + F^- \rightleftharpoons M_2HL_2F: K^F_{M_2HL_2F} = 10^{4.12}. \quad (7)$$

Visible absorption spectra of La-ALC solutions were recorded in the presence of various amounts of fluoride. Figure 6 shows the results at −log[H$^+$] 5.10. The spectra of the mixed ligand complexes measured in the presence of appropriate amounts of fluoride varied with −log[H$^+$]. This agrees with the presence of two mixed ligand complexes deduced above. Absorbance at 620 nm was plotted against molar ratio of fluoride to lanthanum, C_F/C_M(Fig. 7). By using the constants obtained and refining the molar absorptivities, the change could be reproduced as shown by the solid curves.

Discussion

La-ALC Complexes. The La-ALC species formed at pH 4.6 was first considered to be MHL from the similarity of the absorption spectrum to that of H_2L.[10] Langmyhr et. at. later pointed out the presence of another minor species at higher pH (5.5 or 6.5) from the results of continuous variation method.[12] Anfält and Jagner obtained the $\bar{n}_H$ value of 0.56 in their potentiometric titration of ALC with La^{3+} at constant pH of 4.5, and deduced that MHL and another species coexisted.[13]

In this study, similar values for $\bar{n}_H$ were obtained under the same conditions, but are ascribed to only one species, M_2HL_2 from the detailed analysis of the equilibria. In alkaline media, this species releases the proton to form M_2L_2($\log K^H_{M_2HL_2}$=5.30). ALC has several donor atoms which cannot coordinate to one metal ion at the same time. The ligand in a 1:1 complex still keeps the coordination ability. On the other hand, La in a 1:1 complex is coordination-unsaturated and can interact with other donor atoms. Thus polynuclear species such as M_2HL_2 and M_2L_2 are formed.

Mixed Ligand Complexes. Anfält and Jagner

concluded, from their potentiometric data, that no protons were left on the mixed ligand complex.[13] If it were the case, the reactivity of La-ALC complex to fluoride would increase with pH. As shown in Figs. 5 and 7, however, the reverse trend is observed. This is just explained by that protonated species such as M_2HL_2 and MHL or $M_2H_2L_2$ do have affinities for fluoride to form M_2HL_2F and $M_2H_2L_2F$, whereas completely deprotonated species does not.

In a previous paper, we made a systematic study on the formation of the mixed ligand complexes with fluoride.[16] Reactivity of a metal ion with fluoride generally decreases by the coordination of another ligand: for example, K^F_{LaF} is $10^{2.69}$, whereas K^F_{LaLF} is $10^{2.0}$ for nta^{3-} as L, $10^{1.7}$ for $hedta^{3-}$, $10^{1.4}$ for $edta^{4-}$, and $10^{1.8}$ for $cdta^{4-}$. Compared to these values, La-ALC complexes have unexpectedly high affinities (Eq. 7), which can be ascribed to the incorporation of fluoride ion in a specially organized core of M_2HL_2. The structure is not certain at this stage.

Analytical Implication. The optimum pH for the determination of fluoride has empirically been determined to be around 4.3. This agrees with that of maximum proportion of M_2HL_2 as shown in Fig. 5(a). At lower pH the complex dissociates, whereas at higher pH it becomes M_2L_2 unreactive to fluoride ion.

Even at the optimum pH, calibration curve is straight only in lower fluoride concentration range (Fig. 7), because the conditional stability constant is not high enough. Thus large excess of the La-ALC reagent is essential.

The authors wish to thank the Grant-in-Aid for Scientific Research No. 61127007 from the Ministry of Education, Science and Culture.

References

1) R. Belcher, M. A. Leonard, and T. S. West, *Talanta*, **2**, 92 (1959).

2) R. Belcher, M. A. Leonard, and T. S. West, *J. Chem. Soc.*, **1959**, 3577.

3) H. Wada, H. Mori, and G. Nakagawa, *Anal. Chim. Acta*, **172**, 297 (1985) and references therein.

4) M. A. Leonard and G. T. Murray, *Analyst (London)*, **99**, 645 (1974); M. A. Leonard, *ibid.* **100**, 275 (1975); S. F. Deane and M. A. Leonard, *ibid.* **102**, 340 (1977); S. F. Deane, M. A. Leonard, V. McKee, and G. Svehla, *ibid.*, **103**, 1134 (1978).

5) A. A. Minin, G. A. Barmina, and I. G. Khakhalkina, *J. Anal. Chem. USSR.*, **1975**, 1845.

6) Recently several papers have been published on the positive photometric method for fluoride in the presence of surfactants.[7-9]

7) L. Lenarczyk, Z. Marczenko, and M. Jarosz, *Mikrochim. Acta*, **1984III**, 485 (1985).

8) M. Yamazaki, I. Mori, Y. Fujita, S. Kitano, and Y. Kamada, *Bunseki Kagaku*, **33**, 170 (1984).

9) I. Mori, Y. Fujita, K. Fujita, S. Kitano, and T. Kotake, *Bunseki Kagaku*, **35**, 136 (1986).

10) M. A. Leonard and T. S. West, *J. Chem. Soc.*, **1960**, 4477.

11) P. G. Jeffery and D. Williams, *Analyst (London)*, **86**, 590 (1961).

12) F. J. Langmyhr, K. S. Klausen, and M. H. Nouri-Nekoui, *Anal. Chim. Acta*, **57**, 341 (1971).

13) T. Anfält and D. Jagner, *Anal. Chim. Acta*, **70**, 365 (1974).

14) A. Yuchi, T. Okubo, H. Wada, and G. Nakagawa, *Anal. Sci.*, **3**, 151 (1987).

15) A. Yuchi, K. Ueda, H. Wada, and G. Nakagawa, *Anal. Chim. Acta*, **186**, 313 (1986).

16) A. Yuchi, H. Hotta, H. Wada, and G. Nakagawa, *Bull. Chem. Soc. Jpn.*, **60**, 1379 (1987).

17) A. Yuchi, N. Yanai, H. Wada, and G. Nakagawa, *Analyst (London)*, **113**, 1405 (1988).

18) J. E. Powell and M. A. Hiller, *J. Chem. Educ.*, **34**, 330 (1957).

19) K. Al-ani and M. A. Leonard, *Analyst (London)*, **95**, 1039 (1970).

20) C. K. Laird and M. A. Leonard, *Talanta*, **17**, 173 (1970).

21) Analytical Methods Committee, *Analyst (London)*, **96**, 384 (1971).

22) F. Ingman, *Talanta*, **20**, 135 (1973).

 © 1988 The Chemical Society of Japan Bull. Chem. Soc. Jpn., 61, 3895—3900 (1988)

Oxygen-17 NMR Study of the Uranyl Ion. V.[1] Kinetics and Mechanisms of Formation and Decomposition Reactions of Di-μ-hydroxo-bis-[uranyl(VI)] Ion in Aqueous Nitrate Solutions

Woo-Sik JUNG,† Masayuki HARADA, Hiroshi TOMIYASU,* and Hiroshi FUKUTOMI††
Research Laboratory for Nuclear Reactors, Tokyo Institute of Technology,
O-okayama, Meguro-ku, Tokyo 152
(Received May 11, 1988)

The rates of formation and decomposition reactions of di-μ-hydroxo-bis[uranyl(VI)] ion, $(UO_2)_2(OH)_2^{2+}$, have been measured in aqueous nitrate solutions (ionic strength=0.5 M; M=mol dm^{-3}) by ^{17}O NMR spectroscopy. In weakly acidic solutions the reactions obey the rate law:

$$d[(UO_2)_2(OH)_2^{2+}]/dt = k_2[UO_2^{2+}][UO_2OH^+] - k_{-2}K_a[H^+][(UO_2)_2(OH)_2^{2+}]/2,$$

where $K_a=[(UO_2)_2OH^{3+}]/[H^+][(UO_2)_2(OH)_2^{2+}]$. A mechanism involving a single-bridged binuclear intermediate, $(UO_2)_2OH^{3+}$, is proposed. Rate constants (M^{-1} s^{-1}) at 25 °C and activation parameters ΔH^* (kJ mol^{-1}) and ΔS^* (J K^{-1} mol^{-1}) for the formation and decomposition are as follows: 1.52×10^5, 18.9±1.5, and −82.4±5.0 for k_2 and 2.10×10^5, 23.6±1.3, and −64.0±4.2 for $k_{-2}K_a$. The rate of the decomposition reaction is compared with that in several related systems.

Thermodynamic studies of the hydrolysis reaction of uranyl ions have been carried out extensively.[2-5] Although the equilibrium quotients (Q_{11}, Q_{22}, and Q_{35}) of the reactions differ depending on the ionic medium, the following reactions have been established as main ones:[2]

$$UO_2^{2+} + H_2O = UO_2OH^+ + H^+ \qquad Q_{11} \qquad (1)$$

$$2UO_2^{2+} + 2H_2O = (UO_2)_2(OH)_2^{2+} + 2H^+ \qquad Q_{22} \qquad (2)$$

$$3UO_2^{2+} + 5H_2O = (UO_2)_3(OH)_5^+ + 5H^+ \qquad Q_{35} \qquad (3)$$

where hereafter $(UO_2)_p(OH)_q^{(2p-q)+}$ ion will be abbreviated as (p, q) and their concentrations as $[p, q]$ for brevity. There seems to be little doubt about the existence of (2,2) and (3,5) species as major ones, the former of which has been confirmed by X-ray investigations.[6] This binuclear complex has a dihydroxo-bridged and not an oxo-bridged structure. Recently the two major species have been identified by Raman spectroscopy.[7] Our recent study[8] showed that ^{17}O NMR signals of the major hydrolysis species are resolved from the signal of the uranyl ion below room temperature and the rate of the equilibrium reaction (Eq. 2) between (1,0) and (2,2) species is within the range of ^{17}O NMR measurements. Kinetic studies of the reaction have been undertaken by several workers,[9-12] but the mechanism remains unclear. We studied the kinetics of formation and decomposition reactions of (2,2) species by the ^{17}O NMR spectroscopic method and the kinetic results are reported in this paper.

Experimental

Preparation of Sample Solutions. Uranyl complex used is uranyl(VI) nitrate hexahydrate $UO_2(NO_3)_2\cdot6H_2O$, which was prepared by the same method as described in a previous paper[1] by using ^{17}O enriched water (^{17}O=42.1% atom%). ^{17}O enrichment of uranyl oxygen atoms (henceforth called uranyl oxygens) of the stock solution was so performed that oxygen isotope effects may not occur in ^{17}O NMR spectra of uranyl oxygens.[13] Therefore, the ^{17}O signal of uranyl oxygens of the stock solution consisted of a single line of Lorentzian shape, which corresponds to $[^{16}O=U=^{17}O]^{2+}$. The sample solutions for NMR measurements were prepared by diluting the stock solution with doubly distilled deionized water and adjusting the hydrogen ion concentration with either NaOH or HNO_3 solutions. The hydrogen ion concentrations of the solutions were measured with a Toa IM-20E pH meter. The pH meter readings at each temperature were calibrated to give $-\log[H^+]$ by using standard HNO_3 solutions at 0.5 M ionic strength (1 M= 1 mol dm^{-3}), which was adjusted with KNO_3. The hydrogen ion concentrations of the sample solutions increased with increasing temperature in weakly acidic solutions, while remained almost constant irrespective of temperature in strongly acidic solutions. The total uranyl ion concentration ($[UO_2^{2+}]_t$) of all sample solutions was 0.17 M. The hydrogen ion concentrations of the solutions were calculated on the assumption that the activity coefficient of the hydrogen ion in the self media is the same as that in KNO_3 media. The rates were measured at 0.5 M ionic strength because, to our knowledge, the thermodynamic parameters of equilibrium constants for hydrolysis reactions (Eqs. 1—3) of uranyl ions are available only for this ionic strength.[3]

Measurements of NMR Spectra and Kinetic Analysis. The measurements of the ^{17}O NMR spectra were carried out by JEOL JNM-GX 500 and JEOL JNM-GX 400 FT-NMR spectrometers operating at 67.83 and 54.26 MHz, respectively equipped with a GVT-3 temperature controller which was calibrated directly by use of a digital resistance thermometer (Tsuruga Electric Work, Ltd.). The measurements were performed with a 5-mm-o.d. NMR sample tube, which was

† Present address: Korea Advanced Energy Research Institure, Chung-Nam, Korea.

†† Present address: Department of Chemistry, Okayama University, Tsushima-naka, Okayama 700.

immersed in a 10-mm-o.d. concentric NMR tube containing D_2O as a lock solvent. Conditions for NMR measurement were: pulse width, 22 μs (corresponding to 45°); spectral width, 30 kHz; number of scans, 2000—30000. The kinetic analysis was carried out by using a computer program of two-site exchange model as described previously.[14] The ^{17}O transverse relaxation time of (2,2) species in the absence of chemical exchange was not measured directly in the temperature range studied, but was estimated to be 4.08×10^{-2} s at 5 °C by the computer simulation. This value was relatively smaller than the relaxation time (6.68×10^{-2} s) of (1,0) in the absence of chemical exchange. Owing to the quadrupole relaxation, the transverse relaxation time T_2 of ^{17}O changes with temperature. The relation between T_2 and temperature is usually reported by an Arrhenius-type function

$$1/T_2 = A\exp(-E_Q/RT)$$

where E_Q is an activation energy. In the earlier paper,[1] the activation energies for T_2 of free water and water coordinated to uranyl ion were determined to be 22.4±0.1 and 24.8±0.8 kJ mol^{-1}, respectively, and the activation energy for T_2 of uranyl oxygens was 24.2±0.3 kJ mol^{-1} in the temperature range from 7 to 35 °C. Based on these results, it is reasonable to assume that the activation energies for T_2 of both (1,0) and (2,2) are close to 24 kJ mol^{-1}. Therefore, the correction was made for T_2 based on the above assumption.

Results and Discussion

^{17}O resonances of uranyl oxygens in strongly acidic solutions are always observed as a single Lorentzian resonance (Fig. 1A), the chemical shift of which is ca. 1118 ppm relative to pure water at room temperature. In weakly acidic solutions the line shapes of the resonances are sensitive to [H$^+$], i.e. to the degree of hydrolysis, as shown in Fig. 1. At 25 °C two resonances were observed (Fig. 1B-D) in the range of −log[H$^+$] from 3.15 to 3.38, while three resonances (Fig. 1E) at −log[H$^+$]=3.71. The ratios of intensities of three resonances from the high field agree with [1,0]:2[2,2]:3[3,5] at 5 °C, which can be estimated on the basis of thermodynamic parameters reported by Baes and Meyer.[3] For example, the estimated ratio at −log[H$^+$] of 3.71 is 40.9:52.5:6.5, which agree well with the ratio of intensities in Fig. 1E. This fact supports our previous assignment[8] that the resonances at 2.0 and 6.7 ppm downfield relative to the uranyl ion correspond to (2,2) and (3,5) species, respectively.

Figure 2 shows that the resonances of (1,0) and (2,2) species tend to coalesce with increasing temperature. This indicates that there occurs a chemical exchange reaction between the two species. The τ values at each temperature were obtained from the best fit of the line shapes. The calculated lines are shown at the right-hand side in Fig. 2. In the calculations of τ we

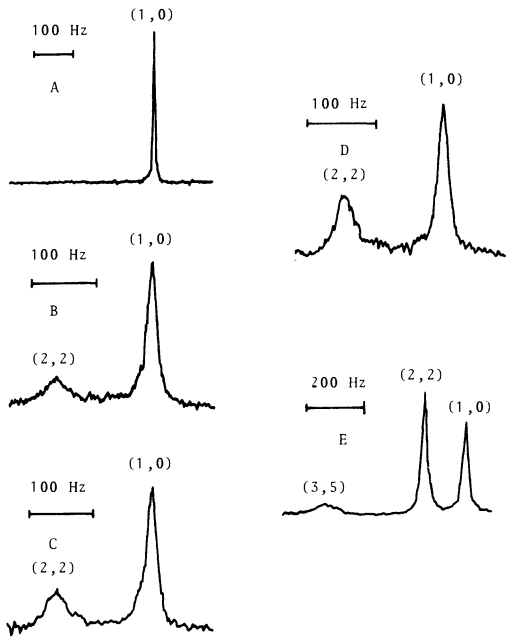

Fig. 1. ^{17}O spectra of uranyl solutions at −log[H$^+$] of 1.17 (A), 3.15 (B), 3.28 (C), 3.38 (D), 3.71 (E); $[UO_2^{2+}]_t$=0.17 M. The NMR spectra were recorded on a JEOL GX-500 at 25 °C except for (E), which was measured with a JEOL GX-400 at 5 °C.

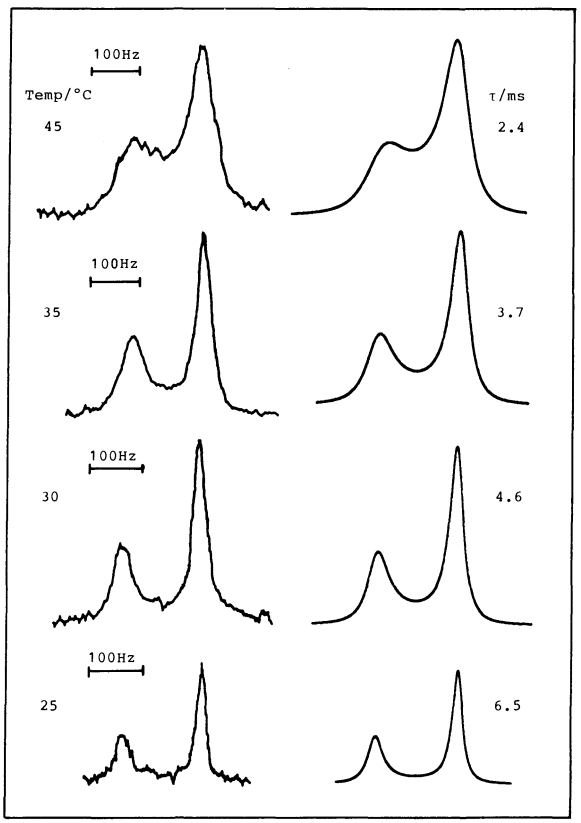

Fig. 2. Experimental (left side) and best-fit calculated ^{17}O NMR lineshapes of uranyl solutions which were recorded on a JEOL GX-500; $[UO_2^{2+}]_t$=0.17 M and −log[H$^+$]=3.38 at 20 °C. Temperatures and best-fit τ values are shown at left and right sides in the figure, respectively.

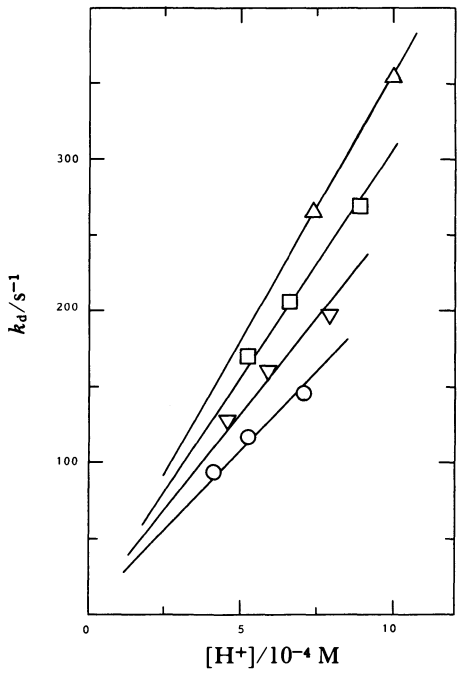

Fig. 3. Plots of k_d against $[H^+]$ for the decomposition of $(UO_2)_2(OH)_2^{2+}$ complex: (○) 25 °C; (▽) 30 °C; (□) 35 °C; (△) 40 °C. The measurements were made by a JEOL GX-500.

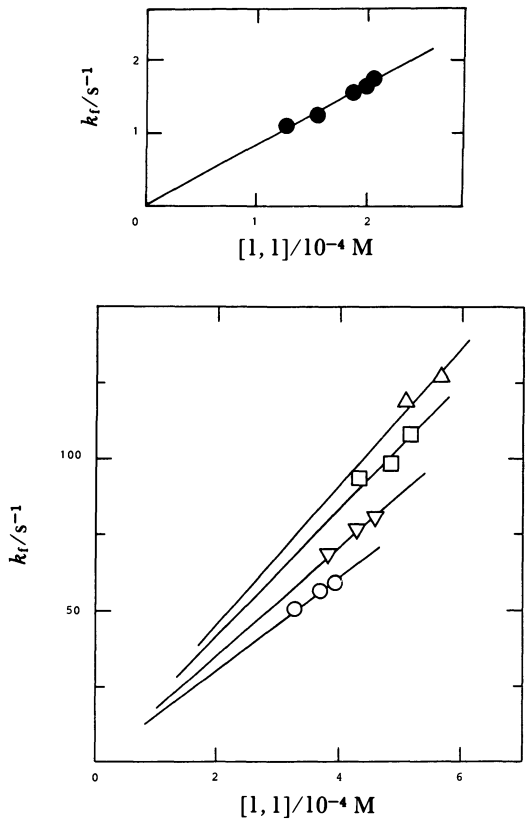

Fig. 4. a) A plot of k_f against $[UO_2OH^+]$ at 5 °C. b) Plots of k_f against $[UO_2OH^+]$ at various temperatures: (○) 25 °C; (▽) 30 °C; (□) 35 °C; (△) 40 °C. The NMR measurements were carried out by using a JEOL GX-400 (a) and a JEOL GX-500 (b).

neglected the effect of the existence of (3,5) species on τ, because the ^{17}O line-broadening of (3,5) species with increasing temperature is smaller than those of (1,0) and (2,2) species and [3,5] is much lower tha [1,1] and [2,2] in the sample solutions studied. The mean lifetimes of (1,0) and (2,2) species, $\tau_{1,0}$ and $\tau_{2,2}$, were evaluated from Eq. 4.

$$\tau = \tau_{1,0} P_{2,2} = \tau_{2,2} P_{1,0} \quad (4)$$

where the $P_{1,0}$ ($=1-P_{2,2}$) value is defined as [1,0]/([1,0]+2[2,2]). The values of P were calculated on the basis of thermodynamic parameters. The pseudo-first-order rate constants for formation and decomposition reactions, k_f and k_d, are expressed as

$$k_f = 1/\tau_{1,0} = -\mathrm{d}[1,0]/[1,0]\mathrm{d}t, \quad (5a)$$

$$k_d = 1/\tau_{2,2} = -\mathrm{d}[2,2]/2[2,2]\mathrm{d}t. \quad (5b)$$

The pseudo-first-order rate constants calculated are listed in Table 1. The rate constants for the formation of (2,2) species decrease with increasing $[H^+]$, while the rate constants for the decomposition increase linearly with $[H^+]$ (Fig. 4).

Eyring and co-workers[9] and Hurwitz and Atkinson[10] studied the kinetics of the formation reaction of (2,2) species by temperature- and pressure-jump relaxation methods and interpreted the relaxation times on the basis of the mechanism that the formation is initiated by the direct interaction of two uranyl ions, followed by fast subsequent abstraction of two hydrogen ions. This formation mechanism can be ruled out by the above results that the rate of the formation has an inverse relationship to $[H^+]$. However, it seems likely that the formation mechanism involves (1,1) species, because its concentration changes proportionally to $1/[H^+]$ as described by Eq. 1. As a result, the rate determining step in the formation of (2,2) species is postulated to be the bimolecular reaction (k_2, second-order rate constant) between (1,0) and (1,1) ions, followed by the fast abstraction of a hydrogen ion. Then k_f should be equal to $k_2(1,1)$. This is demonstrated in Fig. 4-a. A plot of k_f determined at 5 °C by use of the GX-400 NMR spectrometer vs. [1,1] gives a straight line passing through the origin and the slope corresponds to the k_2 value. In Fig. 4-b, similar plots of k_f determined at various temperatures by the GX-500 NMR spectrometer vs. [1,1] are illustrated.

Table 1. Rate Constants for the Formation and Decomposition of $(UO_2)_2(OH)_2^{2+}$ Complex at 25 °C

Solution	i	ii	iii
$-\log[H^+]$	3.15	3.28	3.38
k_f/s^{-1}	59.3	56.0	50.8
k_d/s^{-1}	93.8	117	146

A JEOL GX-500 NMR spectrometer was used for the NMR measurements.

Table 2. The Second-Order Rate Constants for the Formation and Decomposition of $(UO_2)_2(OH)_2^{2+}$ Complex

	25 °C	30 °C	35 °C	40 °C
$k_2/10^5$ M^{-1} s^{-1} [a]	1.52±0.02	1.77±0.01	2.08±0.06	2.28±0.06
$k_{-2}K_a/10^5$ M^{-1} s^{-1} [b]	2.10±0.09	2.54±0.13	3.04±0.08	3.46±0.11

a) ΔH^*=18.9±1.5 kJ mol^{-1} and ΔS^*=−82.4±5.0 J K^{-1} mol^{-1}.
b) ΔH^*=23.6±1.3 kJ mol^{-1} and ΔS^*=−64.0±4.2 J K^{-1} mol^{-1}.

A JEOL GX-500 NMR spectrometer was used for the NMR measurements.

The GX-500 spectrometer gives better resolution for the signals of (1,0) and (2,2) than the GX-400 particularly at temperatures above 25 °C. The k_2 values are calculated from Fig. 4-b on the assumption that all the plots pass through the origin. The results are listed in Table 2 together with activation parameters for k_2 path. The k_2 value in the present study is about two times larger than the value (6.4×10^4 M^{-1} s^{-1} in 0.5 M KNO_3 media at 25 °C) reported by Eyring et al.[11] using the temperature-jump relaxation method. Wendt[15,16] explained the formation reaction of dimer from $2MOH^{(z-1)+}$ (M^{z+}= Fe^{3+} and VO^{2+}) in terms of the Eigen-Wilkins mechanism[17] that the rate-determining step in the reaction is the loss of a water molecule from the inner hydration sphere of one $MOH^{(z-1)+}$ cation. The formation of (2,2) species from UO_2^{2+} and UO_2OH^+ may also be represented by

$$UO_2^{2+} + UO_2OH^+ \overset{K_E}{\rightleftharpoons} (UO_2^{2+} \cdots UO_2OH^+) \xrightarrow{k_{ex}}$$
$$[UO_2\text{-}OH\text{-}UO_2]^{3+} \xrightarrow[\text{fast}]{} (UO_2)_2(OH)_2^{2+} + H^+$$

where k_{ex} is the rate constant of water exchange in UO_2^{2+} ion, not in UO_2OH^+ ion because loss of a hydrogen ion from coordinated water is known to labilize metal ions for substitution reaction at another position,[18,19] i.e. the rate for water exchange is expected to be faster in UO_2OH^+ than in UO_2^{2+}. The mechanism of water exchange in the uranyl ion was proposed to be dissociative interchange (I_d).[20] The rate constant k_2 is given by

$$k_2 = K_E k_{ex} \tag{6}$$

The equilibrium constant, K_E, for the contact pair association between UO_2^{2+} and UO_2OH^+ ions can be estimated from the Eigen-Fuoss equation:[21]

$$K_E = \frac{4\pi Na^3}{3000} \exp\left[-\left\{\frac{z_1z_2e^2}{aD} - \frac{z_1z_2e^2\kappa}{D(1+\kappa a)}\right\}/k_BT\right] \tag{7}$$

where

$$\kappa^2 = \frac{8\pi Ne^2\mu}{1000Dk_BT} \tag{8}$$

In these equations, N is Avogadro's number, a is the distance of closest approach between the two ions, e the electronic charge, D the dielectric constant, k_B the Boltzmann constant, T the absolute temperature, z_1 and z_2 the signed numbers of electronic charges on ions 1 and 2, and μ the ionic strength. In cases in which D=78.5, T=298 K, μ=0.5 M, and $a=6\times10^{-8}$ cm, Eq. 7 yields K_E=0.20 M^{-1}. Rate constant k_{ex} is thus estimated to be 7.6×10^5 s^{-1} at 25 °C from Eq. 6. This estimated value is close to the rate constant for water exchange (9.8×10^5 s^{-1} at 25 °C),[20] which was determined in water–acetone mixture by the ^1H NMR line-broadening method on the assumption that the hydration number of the uranyl ion is four. This leads to the conclusion that the rate-determining step in the k_2 path is the loss of a water molecule in the equatorial plane of the uranyl ion.

The pseudo-first-order rate constants for the decomposition reaction of (2,2) species increase linearly with $[H^+]$ in such low acid region as in this study. Frei and Wendt[12] studied the decomposition reaction by $HClO_4$ ($[H^+]<0.05$ M) with the stopped-flow method and showed that the rate constant for the reaction approaches a limiting value at $[H^+]$ in its high region. These results can be explained by the following two mechanisms: mechanism 1, the A–B–D–E pathway with B–D as the rate-determining step and mechanism 2, the A–C–D–E or A–C–D–E pathways with D–E as the rate-determining step. The basic

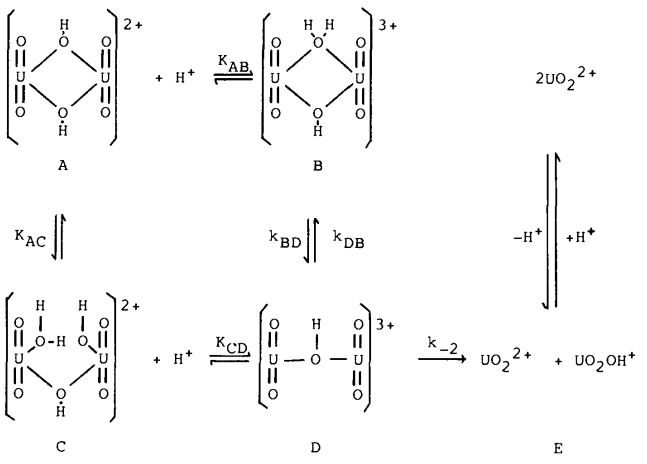

distinction between the two mechanisms is that the rate-determining steps in mechanisms 1 and 2 are assumed to be the cleavage of the first and second

Table 3. The Second-Order Rate Constants for the Acid Decomposition Reaction of Di-μ-hydroxo Binuclear Complexes and Rate Constants for Water Exchange of the Composite Metal Ions at 25°C

Binuclear complex	Rate const $M^{-1}s^{-1}$	Ref.	Metal ion	k_{ex} s^{-1}	Ref.
$[Cr(phen)_2OH]_2^{4+}$	2.3×10^{-6}	24	$Cr(NH_3)_5OH_2^{3+}$	5.5×10^{-5}	a)
$[Co(en)_2OH]_2^{4+}$	5×10^{-4}	28	$Co(en)_2(OH_2)_2^{3+}$	5.2×10^{-6}	b)
$[Co(NH_3)_4OH]_2^{4+}$	1.2×10^{-3}	c)	$Co(NH_3)_5OH_2^{3+}$	6.1×10^{-6}	19
$(VOH)_2^{4+}$	1.54	27	$V(OH_2)_6^{3+}$	5×10^{2}	d)
$(FeOH)_2^{4+}$	3.33	26	$Fe(OH_2)_6^{3+}$	1.6×10^{2}	18
$(VOOH)_2^{2+}$	2.6×10^{2}	16	$VO(OH_2)_5^{2+}$	5×10^{2}	e)
$(UO_2OH)_2^{2+}$	2.14×10^{5}	f)	$UO_2(OH_2)_5^{2+}$	7.6×10^{5}	f)

a) H. R. Hunt and H. Taube, *J. Am. Chem. Soc.*, **80**, 2642 (1958). b) S. Aygen, H. Hanssum, and R. van Eldik, *Inorg. Chem.*, **24**, 2853 (1985). c) A. B. Hoffmann and H. Taube, *Inorg. Chem.*, **7**, 903 (1968). d) A. D. Hugi, L. Helm, and A. E. Merbach, *Helv. Chim. Acta*, **68**, 508 (1985). e) K. Wüthrich and R. E. Connick, *Inorg. Chem.*, **6**, 583 (1967). f) This work.

hydroxo bridges, respectively. Based on these mechanisms, k_d are given by

$$k_d = \frac{1}{2}\frac{K_{AB}[H^+]}{1+K_{AB}[H^+]}k_{BD} \quad (9a)$$

or

$$k_d = \frac{1}{2}\frac{K_a[H^+]}{1+K_a[H^+]}k_{-2} \quad (9b)$$

where K_a is defined as $[(UO_2)_2OH^{3+}]/[H^+][(UO_2)_2(OH)_2^{2+}]$. In the limiting case of $K_{AB}[H^+]\ll1$ or $K_a[H^+]\ll1$, k_d becomes $k_{BD}K_{AB}[H^+]/2$ or $k_{-2}K_a[H^+]/2$, either being the same form as the observed rate law. However, it appears unlikely that the rate for B–D step is slow to determine the whole, rate, because the dissociation of water in complex B will be labilized by the coordinated hydroxyl group and the rate is expected to be much faster than that of water exchange in the uranyl ion. Consequently we propose that the acid decomposition of (2,2) species proceeds through mechanism 2 rather than mechanism 1. According to mechanism 2 the slopes in Fig. 3 correspond to $k_{-2}K_a/2$, and the $k_{-2}K_a$ values at each temperature are listed in Table 2 along with activation parameters.

The existence of complex D, $(UO_2)_2OH^{3+}$, proposed in this study has been postulated in investigations of equilibrium reactions by several groups.[5,22,23] The approximate value of the equilibrium constant K_a can be obtained from the relationship $K_a=K_{21}/K_{22}$, where K_{21} is the equilibrium constant for the reaction $2UO_2^{2+}+H_2O=(UO_2)_2OH^{3+}+H^+$. With the use of the earlier data on K_{21} and K_{22},[5,22] K_a values at 25 °C are determined to be 63 and 28 M^{-1} in 3 and 0.1 M KNO_3 solutions, respectively. The limiting condition $K_a[H^+]\ll1$ is therefore satisfied in the range of the acid concentrations in this study. The mechanism with the breakage of the second bridge as the rate-determining step, in which a single-bridged binuclear intermediate is formed, was also proposed in the decomposition reaction of di-μ-hydroxo-tetrakis(1,10-phenanthroline)-dichromium(III) ion.[24]

The rate law for the decomposition of $(UO_2)_2(OH)_2^{2+}$ ion is different from those of $(FeOH)_2^{4+}$,[16,25,26] $(VOOH)_2^{2+}$,[16] $(VOH)_2^{4+}$,[27] and [Co(ethylenediamine)$_2$-OH]$_2^{4+}$,[28] which have both acid-independent and -dependent terms. The second-order rate constants for the acid-dependent path in the decomposition of related di-μ-hydroxo binuclear complexes are summarized in Table 3, which also contains the rate constants for water-exchange reaction in the composite metal ions. There appears to be some correlation between two rate constants, i.e. the more labile the substitution reactions, the faster the decomposition reactions.

The existence of $(UO_2)_2OH^{3+}$, which is one of the minor hydrolysis species of uranyl ions, has not been justified hitherto but is confirmed by this kinetic measurement.

The authors wish to express their thanks to Mr. Yoshiyuki Nakamura of Natural Products Laboratory Chemistry, Tokyo Institute of Technology and Mr. Naoyuki Fujii of JEOL, Ltd. for measuring NMR spectra and helpful advice. This paper is partly supported by a Grant-in-Aid for Scientific Research No. 62470039 from the Ministry of Education, Science and Culture.

References

1) Part IV: W.-S. Jung, H. Tomiyasu, and H. Fukutomi, *Bull. Chem. Soc. Jpn.*, **60**, 489 (1987).

2) C. F. Jr. Baes and R. E. Mesmer, "The Hydrolysis of Cations"; Wiley-Interscience, New York, 1976. Chap. 9.

3) C. F. Baes Jr. and N. J. Meyer, *Inorg. Chem.*, **1**, 780 (1962).

4) R. M. Rush and J. S. Johnson, *J. Phys. Chem.*, **67**, 821 (1963).

5) H. S. Dunsmore, S. Hietanen, and L. G. Sillen, *Acta Chem. Scand.*, **17**, 2644 (1963); S. Hietanen, B. R. L. Row, and L. G. Sillen, *Acta Chem. Scand.*, **17**, 2735 (1963).

6) M. Åberg, *Acta Chem. Scand.*, **23**, 791 (1969); A. Perrin,

Acta Crystallogr., Sect. B, **32**, 1658 (1976); A. Navaza, F. Villain, and P. Charpin, *Polyhedron*, **3**, 143 (1984).

7) L. M. Toth, and G. M. Begun, *J. Phys. Chem.*, **85**, 547 (1981); M. Asano and J. A. Koningstein, *Can. J. Chem.*, **60**, 2207 (1982).

8) W.-S. Jung, H. Tomiyasu, and H. Fukutomi, *J. Chem. Soc., Chem. Commun.*, **1987**, 372.

9) M. P. Whittaker, E. M. Eyring, and E. J. Dibble, *J. Phys. Chem.*, **69**, 2319 (1965); hereafter they reinterpreted the relaxation times as bimolecular reaction between (1,0) and (1,1) ions in Ref. 11.

10) P. A. Hurwitz and G. Atkinson, *J. Phys. Chem.*, **71**, 4142 (1967).

11) M. P. Whittaker, J. Assay, and E. M. Eyring, *J. Phys. Chem.*, **70**, 1005 (1966).

12) V. Frei and H. Wendt, *Ber. Bunsenges. Phys. Chem.*, **74**, 593 (1970).

13) W.-S. Jung, Y. Ikeda, H. Tomiyasu, and H. Fukutomi, *Bull. Chem. Soc. Jpn.*, **57**, 2317 (1984).

14) Y. Ikeda, H. Tomiyasu, and H. Fukutomi, *Inorg. Chem.*, **23**, 1356 (1984).

15) H. Wendt, *Inorg. Chem.*, **8**, 1527 (1969).

16) B. Lutz, and H. Wendt, *Ber. Bunsenges. Phys. Chem.*, **74**, 372 (1970).

17) M. Eigen, *Pure Appl. Chem.*, **6**, 97 (1963); R. G. Wilkins, *Acc. Chem. Res.*, **3**, 408 (1970).

18) M. W. Grant and R. B. Jordan, *Inorg. Chem.*, **20**, 55 (1981).

19) F.-C. Xu, H. R. Krouse, and T. W. Swaddle, *Inorg. Chem.*, **24**, 267 (1985).

20) Y. Ikeda, S. Soya, H. Fukutomi, and H. Tomiyasu, *J. Inorg. Nucl. Chem.*, **41**, 1333 (1979).

21) M. Eigen, *Z. Phys. Chem. (Frankfurt)*, **1**, 176 (1954); R. M. Fuoss, *J. Am. Chem. Soc.*, **80**, 5059 (1958).

22) P. A. Overvoll and W. Lund, *Anal. Chim. Acta*, **143**, 153 (1982).

23) L. H. J. Lajunen and S. Parhi, *Finn. Chem. Lett.*, **1979**, 143.

24) D. Wolcott and J. B. Hunt, *Inorg. Chem.*, **7**, 755 (1968).

25) B. A. Sommer and D. W. Margerum, *Inorg. Chem.*, **9**, 2517 (1970).

26) H. N. Po and N. Sutin, *Inorg. Chem.*, **10**, 428 (1971).

27) T. W. Newton and F. B. Baker, *Inorg. Chem.*, **4**, 1533 (1965).

28) S. E. Rasmussen and J. Bjerrum, *Acta Chem. Scand.*, **9**, 735 (1955).

 © 1988 The Chemical Society of Japan Bull. Chem. Soc. Jpn., 61, 3901—3906 (1988)

Calorimetric and Raman Spectroscopic Studies of Cadmium(II) Thiocyanato Complexes in *N,N*-Dimethylformamide

Shin-ichi ISHIGURO,* Toshiyuki TAKAMUKU, and Hitoshi OHTAKI†
Department of Electronic Chemistry, Tokyo Institute of Technology at Nagatsuta, Midori-ku, Yokohama 227
†Coordination Chemistry Laboratories, Institute for Molecular Science, Myodaiji, Okazaki 444
(Received June 17, 1988)

Formation of thiocyanato complexes of cadmium(II) ion has been calorimetrically studied in *N,N*-dimethylformamide (DMF) at 25 °C. Calorimetric data obtained were well explained in terms of the formation of a series of four mononuclear $[CdX_n]^{(2-n)+}$ (n=1—4, X=SCN) complexes, and their formation constants, enthalpies, and entropies were determined. Raman band shifts for the C-S stretching vibration of SCN^- ion indicated that SCN^- ion binds to cadmium(II) ion only with the N end within the mono- or dithiocyanato complex, $[Cd(NCS)]^+$ or $[Cd(NCS)_2]$. Within the tri- and tetrathiocyanato complexes, thiocyanate ions binds with both the N and S ends, and the coordination modes, $[Cd(NCS)_2(SCN)]^-$ and $[Cd(NCS)_3(SCN)]^{2-}$, were suggested. The coordination modes for the di- and tetrathiocyanato complexes in DMF, $[Cd(NCS)_2]$ and $[Cd(NCS)_3(SCN)]^{2-}$, are different from those in water, $[Cd(NCS)(SCN)]$ and $[Cd(NCS)_2(SCN)_2]^{2-}$.[1] It is thus shown that the N-bonding becomes more favorable in DMF than in water. Such a result may mainly be ascribed to relatively weakened solvation of the SCN^- ion in DMF, especially at the N atom site which is hydrogen-bonded with water molecules but not with DMF.

Thiocyanate ion is capable of bonding through either the hard nitrogen or soft sulfur end with Lewis acids depending on hardness and softness of the Lewis acids. Among thiocyanato complexes of d^{10} metal(II) ions, N-bonding was found in the $[Zn(NCS)_4]^{2-}$ complex that contains a relatively hard zinc(II) ion, while S-bonding was observed in the $[Hg(SCN)_4]^{2-}$ complex of soft mercury(II) ion.[2-4] For cadmium(II) ion, its hardness is weaker than that of zinc(II) ion and its softness is also less than that of mercury(II) ion, thiocyanate ions bind through two N and two S ends to form $[Cd(NCS)_2(SCN)_2]^{2-}$ in water.[2] Furthermore, the coordination of thiocyanate ions in lower complexes has been suggested to be $[Cd(NCS)]^+$ (N-bonding), $[Cd(NCS)(SCN)]$ (N- and S-bondings), and $[Cd(NCS)_2(SCN)]^-$ (two N- and one S-bondings) in water.[1] The result implies that the apparent hard and soft characters of cadmium(II) ion changes in the course of the stepwise complexation with thiocyanate ions. It is thus expected that the binding energies to cadmium(II) ion of the hard N and soft S ends of the SCN^- ion are very close to each other in water. In such a case, solvation of thiocyanate ion might also play an essential role for determining the N- or S-bonding of the ion to cadmium(II) ion.

We therefore aimed at investigating the formation and structure of cadmium(II) thiocyanato complexes in aprotic solvents with different solvating abilities. In this work we report the complexation between cadmium(II) and thiocyanate ions in *N,N*-dimethylformamide (DMF) studied by calorimetry. Raman spectra of cadmium(II) thiocyanate solutions were measured to elucidate the bonding types of SCN^- ion to cadmium(II) ion within the thiocyanato complexes.

Experimental

Reagents. All chemicals used were of reagent grade. Cadmium(II) perchlorate DMF solvate was prepared by dissolving $Cd(ClO_4)_2 \cdot 6H_2O$ crystals in DMF and then by recrystallizing it three times from DMF. The DMF solvate thus obtained is finally recrystallized from acetone and washed with ether. The cadmium(II) perchlorate DMF solvate thus obtained was dried at about 40 °C in a vacuum oven for several days and kept in a desiccator over P_2O_5. The value of x in the $Cd(ClO_4)_2 \cdot x$dmf was found to be 6 from the analysis of the metal concentration by EDTA titration. Tetraethylammonium perchlorate was recrystallized once from water and dried in a vacuum oven at 100 °C. Ammonium perchlorate of reagent grade was dried at 100 °C. Tetraethylammonium thiocyanate and ammonium thiocyanate of reagent grade were used without further purification and dried in vacuum in a desiccator over P_2O_5. *N,N*-Dimethylformamide was dried for several weeks over Molecular Sieve 4A 1/16 and then distilled at 25 °C under reduced pressure and stored over molecular sieve in a dark bottle with a P_2O_5 drying-tube.

Measurements. Calorimetric measurements were carried out in a room thermostated at (25±0.2) °C.[1] Test solutions contained either 0.4 mol dm^{-3} $(C_2H_5)_4NClO_4$ or 1 mol dm^{-3} NH_4ClO_4 as a constant ionic medium. A cadmium(II) perchlorate solution (50 cm^3) was placed in a stainless steel vessel, the inside wall of which was coated with Teflon. The vessel was inserted into an aluminium block thermostated at (25.0±0.0001) °C in an air-bath. The vessel was filled with dry nitrogen gas and isolated from moisture with a P_2O_5 drying-tube. A $Cd(ClO_4)_2$ solution in the vessel was then titrated with a 0.4 mol dm^{-3} $(C_2H_5)_4NSCN$ or a 1 mol dm^{-3} NH_4SCN DMF solution by using an autoburet (APB-118, Kyoto Electronics). Heats of complexation at each titration point were measured with a certainty of ±0.02 J and were corrected for heat of dilution of the titrant. The heat of dilution had been determined by separate experiments by titrating a 0.4 mol dm^{-3} $(C_2H_5)_4NClO_4$ (or 1 mol dm^{-3} NH_4ClO_4) DMF solution with a 0.4 mol dm^{-3} $(C_2H_5)_4NSCN$ (or 1 mol dm^{-3} NH_4SCN) DMF solution. The heat of dilution observed in this measurement was found to be very small. Calorimetric measurements were carried out by using a fully automatic on-line system developed in our

Table 1. The Total Concentrations (mol dm^{-3}) of Cd^{2+} and SCN^- Ions in the Various Cadmium(II) Thiocyanate Solutions Used for Raman Spectroscopic Measurements

	Cd^{2+}	SCN^-	$\bar{n}$[a]
A	0.4006	0.4065	1.0
B	0.3997	0.8321	2.0
C	0.3998	1.321	3.0
D	0.3992	4.171	3.9

a) The average number of SCN^- ions bound per cadmium(II) ion calculated by using the formation constants in Table 2 obtained in the 1 mol dm^{-3} NH_4ClO_4 ionic medium at 25 °C.

laboratory.

Raman spectra of cadmium(II) thiocyanate solutions were measured with a JRS-400T Raman spectrometer (JEOL) using 514.5 nm line of an NEC GLG argon ion laser in a room at 25 °C. The composition of solutions for the Raman spectroscopic measurements is listed in Table 1.

Data Analysis. A heat q_i measured at the ith titration point is represented by Eq. 1 using overall formation constants β_n and overall enthalpies $\Delta H^\circ_{\beta n}$ of formation of the $[CdX_n]^{(2-n)+}$ complexes.

$$q_i = -(V_i \sum \beta_n \Delta H^\circ_{\beta n} m_i x_i^n - V_{i-1} \sum \beta_n \Delta H^\circ_{\beta n} m_{i-1} x_{i-1}^n), \quad (1)$$

where V denotes the volume of a test solution, and m and x stand for the concentrations of free cadmium(II) and thiocyanate ions, respectively, which are related to their total concentrations C_M and C_X according to the mass-balance equations:

$$C_{M,i} = \sum \beta_n m_i x_i^n + m_i, \quad (2)$$

$$C_{X,i} = \sum n\beta_n m_i x_i^n + x_i. \quad (3)$$

The formation constants and enthalpies were simultaneously determined by minimizing the error-square sum, $U=\sum(q_{i,obsd}-q_{i,calcd})^2$ by using a non-linear least-squares program.

Results and Discussion

Calorimetric titration curves for the complexation of cadmium(II) with thiocyanate ions obtained in the $(C_2H_5)_4NClO_4$ DMF solution are depicted in Fig. 1, in which the values $-q/(\delta v C_{X,tit})$ are plotted against C_X/C_M, where q, δv, $C_{X,tit}$, C_X, and C_M denote the heat evolved and the volume of an aliquot of the titrant added at each titration point, the concentration of $(C_2H_5)_4NSCN$ in the titrant solution, and the total concentrations of SCN^- and Cd^{2+} ions in the test solution, respectively. The calorimetric data were analyzed by assuming the formation of various sets of mononuclear cadmium(II) thiocyanato complexes. Among various sets examined, the set (1—4) assuming the formation of $[CdX]^+$, $[CdX_2]$, $[CdX_3]^-$, and $[CdX_4]^{2-}$ (X=SCN), and the set (1,2,4) eliminating

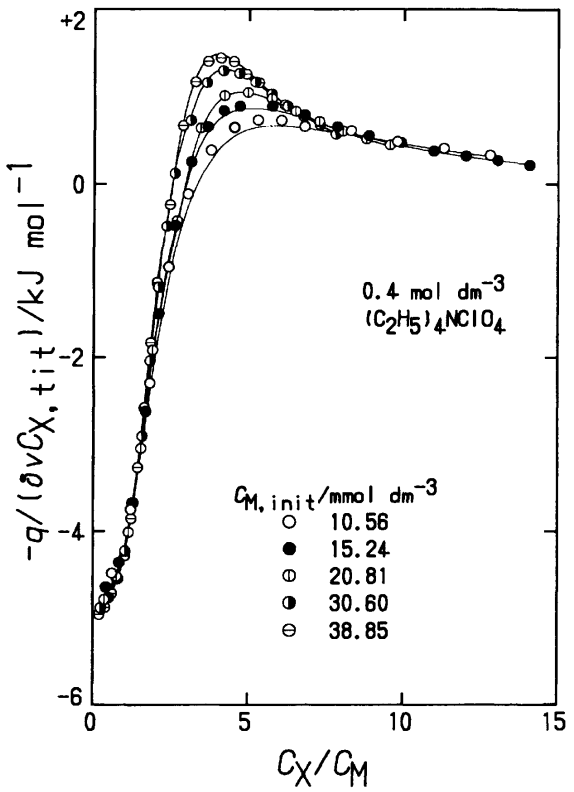

Fig. 1. Calorimetric titration curves of cadmium(II) thiocyanate DMF solutions containing 0.4 mol dm^{-3} $(C_2H_5)_4NClO_4$ at 25 °C. Concentrations of cadmium(II) ions, $C_{M,init}$/mmol dm^{-3}, in initial test solutions are given. The solid lines show the curves calculated by using the constants of the set (1—4) in the $(C_2H_5)_4NClO_4$ ionic medium in Table 2.

$[CdX_3]^-$ from the set (1—4) gave relatively small Hamilton R factors. The results for these sets are listed in Table 2. Other sets gave significantly large R values. Since both $\log \beta_3$ and $\Delta H^\circ_{\beta 3}$ values were obtained with small standard deviations and they laid within the reasonable range, we concluded that the $[CdX_3]^-$ can not be eliminated, and thus the set (1—4) is the best choice for describing the complexation of cadmium(II) with thiocyanate ions in DMF. In fact, as seen in Fig. 1, the solid lines calculated by using the constants for the set (1—4) in Table 2 well reproduce the experimental points over the whole range of C_X/C_M.

The titration curves obtained in the NH_4ClO_4 DMF solution are shown in Figs. 2 and 3. The data were analyzed by a similar way to that employed for data in the $(C_2H_5)_4NClO_4$ solution. In the NH_4ClO_4 solution, among various sets examined, the sets (1—4) and (1,2,3) gave relatively small R factors as shown in Table 2. Since the R value of the set (1—4) is appreciably smaller than that of the set (1,2,3), we adopted the parameters of the set (1—4) as the final choice.

Distribution of the cadmium(II) thiocyanato com-

Table 2. Least-Squares Refinement of Overall Formation Constants, $\log(\beta_n/\text{mol}^{-n}\,\text{dm}^{3n})$, and Enthalpies, $\Delta H^{\circ}_{\beta n}/\text{kJ mol}^{-1}$, of the Thiocyanato Complexes of Cadmium(II) Ion in *N,N*-Dimethylformamide at 25 °C[a]

	$(C_2H_5)_4NClO_4$[b]		NH_4ClO_4[c]	
	(1—4)	(1,2,4)	(1—4)	(1,2,3)
$\log\beta_1$	3.57(0.11)	3.47(0.14)	2.77(0.08)	2.40(0.07)
$\log\beta_2$	5.98(0.15)	5.73(0.17)	4.61(0.11)	3.86(0.07)
$\log\beta_3$	7.59(0.14)	—	5.69(0.12)	4.65(0.07)
$\log\beta_4$	8.81(0.16)	8.39(0.15)	6.55(0.13)	—
$\Delta H^{\circ}_{\beta 1}$	−4.9(0.04)	−5.0(0.07)	−5.8(0.1)	−6.1(0.2)
$\Delta H^{\circ}_{\beta 2}$	−9.2(0.2)	−9.1(0.2)	−11.7(0.3)	−15.7(0.8)
$\Delta H^{\circ}_{\beta 3}$	−7.3(0.2)	—	−11.2(0.4)	−0.4(0.6)
$\Delta H^{\circ}_{\beta 4}$	2.6(0.4)	−0.2(0.1)	−2.3(0.1)	—
U[d]	0.045	0.161	0.695	1.49
R[e]	0.023	0.044	0.034	0.050
N[f]	88	88	156	156

a) Values in parentheses refer to three standard deviations. b) 0.4 mol dm^{-3}. c) 1 mol dm^{-3}. d) Error-square sum. e) The Hamilton R factor. f) The number of calorimetric data points.

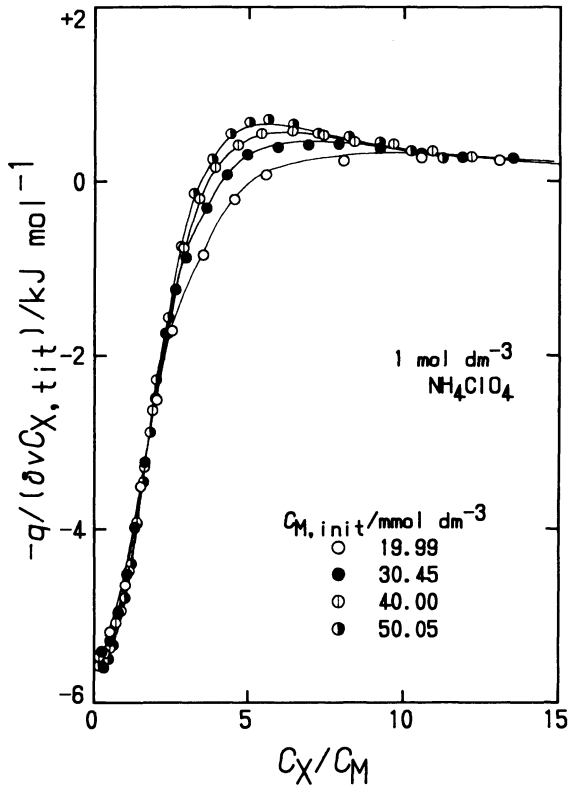

Fig. 2. Calorimetric titration curves of cadmium(II) thiocyanate DMF solutions containing 1 mol dm^{-3} NH_4ClO_4 at 25 °C. Concentrations of cadmium(II) ions, $C_{M,init}$/mmol dm^{-3}, in initial test solutions are given. The solid lines show the curves calculated by using the constants of the set (1—4) in the NH_4ClO_4 ionic medium in Table 2.

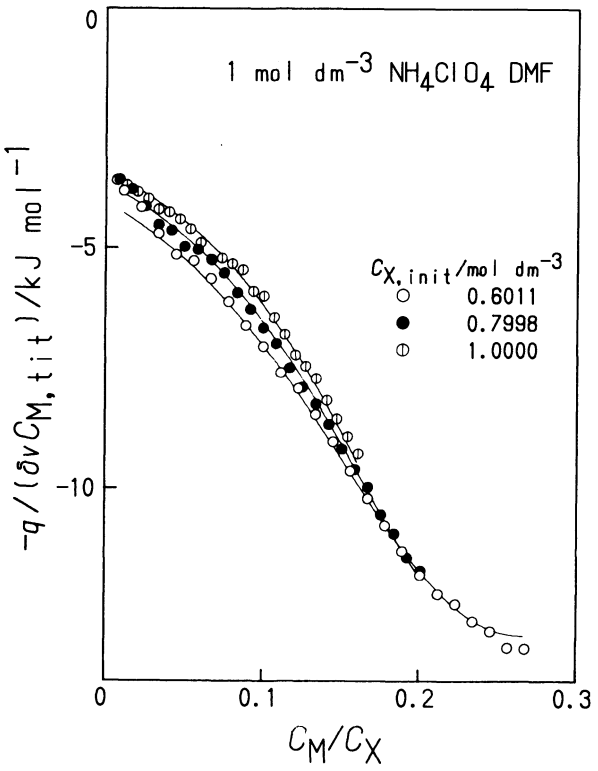

Fig. 3. Calorimetric back titration curves of cadmium(II) thiocyanate DMF solutions containing 1 mol dm^{-3} NH_4ClO_4 at 25 °C. Concentrations of cobalt(II) ions, $C_{X,init}$/mmol dm^{-3}, in initial test solutions are given. The solid lines show the curves calculated by using the constants of the set (1—4) in the NH_4ClO_4 ionic medium in Table 2.

plexes in these $(C_2H_5)_4NClO_4$ and NH_4ClO_4 DMF solutions in shown in Fig. 4, which is calculated by using the formation constants for the sets (1—4) in Table 2. It is demonstrated that the complexation is more favorable in 0.4 mol dm^{-3} $(C_2H_5)_4NClO_4$ than in 1 mol dm^{-3} NH_4ClO_4 ionic medium. A similar result has been obtained also in the copper(II) bromide system in DMF,[5] where it is suggested that bromide ion forms appreciably ion pairs with NH_4^+ ion, while the ion pair formation of bromide ion with $(C_5H_5)_4N^+$ ions is practically negligible.

Raman Spectra of the Cadmium(II) Thiocyanate Solutions. Raman spectra for the C-S stretching vibrations are shown in Fig. 5. The observed Raman bands were assigned to each complex by taking into

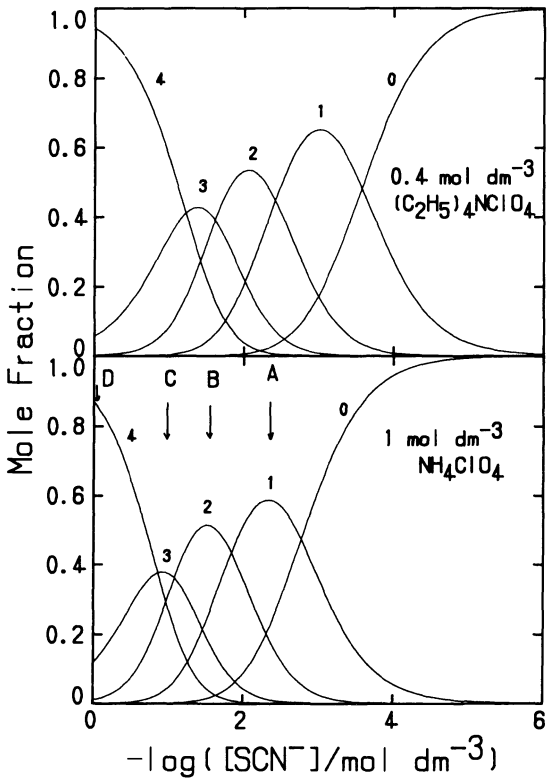

Fig. 4. Distribution of the cadmium(II) thiocyanato complexes in 0.4 mol dm^{-3} $(C_2H_5)_4NClO_4$ and 1 mol dm^{-3} NH_4ClO_4 DMF solutions. The numbers represent n within the $[CdX_n]^{(2-n)+}$ (X=SCN) complex. Distribution of species in solutions A, B, C, and D used for the Raman spectral measurements is indicated.

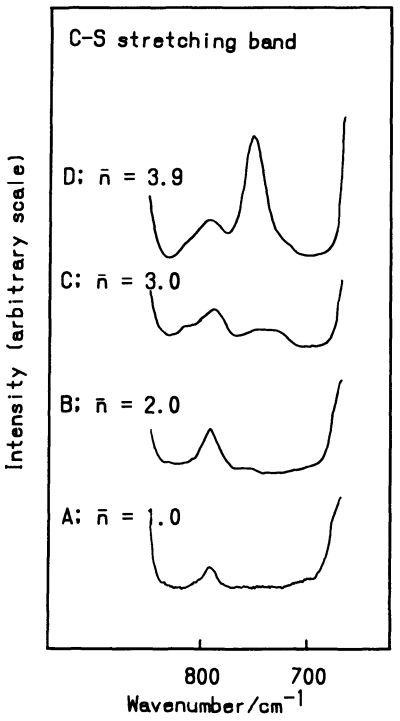

Fig. 5. Raman spectra for the C-S stretching vibration of SCN^- ion in various cadmium(II) thiocyanate DMF solutions.

account the distribution of the cadmium(II) thiocyanato complexes in the NH_4ClO_4 solution in Fig. 4.

The C-S stretching vibrational band of free SCN^- ion appears at ca. 755 cm^{-1} in DMF. It is known that the band shifts toward higher and lower frequencies when SCN^- ion binds to a metal ion with the N and S ends, respectively.[6-11] Solutions A and B show a sole band at 795 cm^{-1}, which involve the mono- and di(thiocyanato)cadmium(II) complexes, respectively, as the main species. This shift for the C-S stretching band toward a higher frequency from 755 to 795 cm^{-1} evidently indicates that the SCN^- ions bind with the N end to cadmium(II) ion to yield the $[Cd(NCS)]^+$ and $[Cd(NCS)_2]$ complexes. For solution C are observed a band at 795 cm^{-1}, indicative of the Cd-NCS linkage, and a broad one ranging 730—760 cm^{-1}, showing the alternative Cd-SCN bonding, i.e., the tri(thiocyanato)-cadmate(II) complex may involve the Cd-SCN linkage suggesting the $[Cd(NCS)_2(SCN)]^-$ coordination. Solution D containing predominantly the tetra-(thiocyanato)cadmate(II) complex shows the 795 cm^{-1} band and a weak shoulder at 735 cm^{-1}, indicating that the complex involves both Cd-NCS and Cd-SCN linkages. According to the X-ray diffraction measurement,[12] the four-coordinate tetrahedral $[Cd(NCS)_3(SCN)]^{2-}$ complex with three Cd-N and one Cd-S arrangements is elucidated.

On the other hand, Raman spectra for the C-N stretching vibration of SCN^- ion show a sole band for all the cadmium(II) thiocyanate solutions examined. No significant shift of the band is observed with the successive complexation. Therefore, it was hard to conclude the binding mode of SCN^- ion to cadmium(II) ion from the C-N stretching vibrational band.

The Coordination Structure Change. In DMF cadmium(II) ion is present as the hexa-solvate $[Cd(dmf)_6]^{2+}$ complex according to the X-ray diffraction measurement.[12] The formation of the four-coordinate $[Cd(NCS)_3(SCN)]^{2-}$ complex thus indicates that the coordination structure changes from octahedral to tetrahedral at a certain step of the complexation between cadmium(II) and thiocyanate ions.

Stepwise thermodynamic quantities of formation of the cadmium(II) thiocyanato complexes in DMF are summarized in Table 3. In any solution examined, the ΔS_4° value is large and positive, even larger than the ΔS_n° (n=1,2,3) values. This result is in contrast to that obtained in the cadmium(II)-halide systems,[13] in which the tri(halogeno)cadmate(II) complexes have a tetrahedral coordination. Such a relatively large and positive ΔS_4° value, together with a relatively large and positive ΔH_4° value for breaking metal-solvent bonds, observed in the cadmium(II) thiocyanate system

Table 3. The Stepwise Formation Constants, $\log(K_n/\text{mol}^{-1}\,\text{dm}^3)$, Enthalpies, $\Delta H_n^\circ/\text{kJ mol}^{-1}$, and Entropies, $\Delta S_n^\circ/\text{J K}^{-1}\,\text{mol}^{-1}$, for the Cadmium(II)-$SCN^-$ System in *N,N*-Dimethylformamide at 25 °C

	Water $NaClO_4$[a]	*N,N*-Dimethylformamide $(C_2H_5)_4NClO_4$[b]	NH_4ClO_4[c]
$\log K_1$	1.378	3.57	2.77
$\log K_2$	0.396	2.41	1.84
$\log K_3$	0.052	1.61	1.08
$\log K_4$	0.180	1.23	0.86
ΔH_1°	−10.2	−4.9	−5.8
ΔH_2°	−20.1	−4.3	−5.9
ΔH_3°	22.6	1.9	0.5
ΔH_4°	−22.8	9.9	8.9
ΔS_1°	−8	52	33
ΔS_2°	−60	32	16
ΔS_3°	77	37	22
ΔS_4°	−73	56	46
$\Delta G_{\beta_4}^\circ$[d]	−11.4	−50.3	−37.4
$\Delta H_{\beta_4}^\circ$[d]	−30.5	2.6	−2.3
$\Delta S_{\beta_4}^\circ$[d]	−64	178	118

a) Ref. 1, the concentration of ionic medium is 3 mol dm^{-3}. b) 0.4 mol dm^{-3}. c) 1 mol dm^{-3}. d) For the overall reaction, $Cd^{2+}+4X^-=[CdX_4]^{2-}$ (X=SCN).

suggests that an extensive liberation of DMF molecules occurs at the fourth step, i.e., the tri(thiocyanato)cadmate(II) complex is octahedral, and the coordination structure changes from octahedral to tetrahedral at the formation of the tetra(thiocyanato)-cadmate(II) one.[14]

In water it was indicated that the corresponding coordination structure change occurs at the formation of the tri(thiocyanato)cadmate(II) complex.[1] Consequently, we note that the change in coordination about cadmium(II) ion from octahedral to tetrahedral takes place at the latter step of the complexation in DMF than that in water in the cadmium(II) thiocyanate system. A similar result has been found for the cadmium(II) halide systems in water and in DMSO,[15] in which the coordination changes from octahedral to tetrahedral at the second step in water, while at the third one in DMSO.

The Binding Mode Difference of Thiocyanate Ion in Water and in DMF. It is suggested in a previous section that a six-coordination for $[Cd(NCS)]^+$, $[Cd(NCS)_2]$, and $[Cd(NCS)_2(SCN)]^-$, and a four-coordination for $[Cd(NCS)_3(SCN)]^{2-}$ occur in DMF. It is noted that a six-coordination for $[Cd(NCS)]^+$ and $[Cd(NCS)(SCN)]$, and a four-coordination for $[Cd(NCS)_2(SCN)]^-$ and $[Cd(NCS)_2(SCN)_2]^{2-}$ are concluded in water.[1,2] These results imply that the apparent hard and soft characters of cadmium(II) ion changes with the stepwise complexation of thiocyanate ions. Furthermore, it is indicated that solvent properties are also responsible for determining the N- or S-bonding of an SCN^- ion to cadmium(II) ion.

Thiocyanate ion binds to cadmium(II) ion through the N end at the first step in both water and DMF, giving a slightly more negative ΔH_1° value in water than that in DMF. At the second step thiocyanate ion ligates to the metal(II) ion through the S end in water, while through the N end in DMF. The difference in the N- or S-bonding of SCN^- ion reflects on the ΔH_2° values. As seen in Table 3 the ΔH_2° value is less negative than the ΔH_1° value in DMF, while the reverse in the case in water. The binding of a soft S atom of SCN^- ion to cadmium(II) ion leads to remarkable exothermicity in water as compared with that of a hard N atom in DMF.

Solvation of SCN^- ion in aprotic DMF solvent may be very different from that in protic water, especially at the hydrogen-bonding N atom site. When the enthalpies are compared, despite the fact that cadmium(II) ion is more strongly solvated by ca. −63 kJ mol^{-1} in a strong donor solvent DMF than in water,[16] the ΔH_1° value for the formation of $[Cd(NCS)]^+$ in the former solvent is only slightly less negative than that in the latter. For the corresponding ΔH_1° values for the halogeno complexes,[13] even more negative value in DMF than that in water is in fact observed for chloride ion that is strongly hydrogen-bonded, i.e., strongly solvated in water. The ΔH_1° value is slightly less negative for bromide ion like thiocyanate ion, and much less negative for iodide ion in DMF than in water.[17,18] It is thus shown that thiocyanate ion is also hydrogen-bonded at the N atom site in water, although the interaction with water molecules is not so strong as in the case of chloride ion.

Cadmium(II) ion may behave as a harder ion in aprotic DMF solvent than in protic water.[15] In fact, the stability of $[CdX]^+$ increases in the sequence Cl<Br<I in water,[17,18] i.e. the decreasing order of the hydrogen-bonding abilities of halide ions, while the sequence is reversed in DMF[12] and also in DMSO.[19] Thiocyanate ion forms hydrogen bonds, especially at

the N atom site, with water molecules but not with DMF. On the other hand, solvation of SCN^- ion at the soft and large S atom site may be weak in both solvents, or even weaker in water than in DMF.[20] Therefore, the reactivity at the N atom site of SCN^- ion may be enhanced in DMF over water. Consequently, thiocyanate ion may favorably bind with cadmium(II) ion through the N end in DMF, while through the S end in water. It is thus reasonably expected that the $[Cd(NCS)_2]$ and $[Cd(NCS)_3(SCN)]^{2-}$ complexes are formed in DMF, while the [Cd(NCS)-(SCN)] and $[Cd(NCS)_2(SCN)_2]^{2-}$ ones in water.[1]

The present work has been financially supported by Grant-in-Aid for Scientific Research on Priority Area of "Dynamic Interactions and Electronic Processes of Macromolecular Complexes" No. 62612005 from the Ministry of Education, Science and Culture.

References

1) S. Ishiguro, K. Yamamoto, and H. Ohtaki, *Bull. Chem. Soc. Jpn.*, **59**, 531 (1986).
2) T. Yamaguchi, K. Yamamoto, and H. Ohtaki, *Bull. Chem. Soc. Jpn.*, **58**, 3235 (1985).
3) S. Ahrland and L. Kullberg, *Acta Chem. Scand.*, **25**, 3692 (1971).
4) I. Persson, Å. Iverfeldt, and S. Ahrland, *Acta Chem. Scand.*, **A35**, 295 (1981).
5) S. Ishiguro, K. Ozutsumi, L. Nagy, and H. Ohtaki, *Bull. Chem. Soc. Jpn.*, **60**, 1691 (1987).
6) A. Tramer, *J. Chim. Phys.*, **59**, 232 (1962).
7) S. Froaeous and R. Larsson, *Acta Chem. Scand.*, **16**, 1447 (1962).
8) K. A. Taylor, T. V. Long II, and R. A. Plane, *J. Chem. Phys.*, **47**, 138 (1967).
9) R. E. Hester and K. Krishnan, *J. Chem. Phys.*, **48**, 825 (1968).
10) D. P. Strommen and R. A. Plane, *J. Chem. Phys.*, **60**, 2643 (1974).
11) A. Antić-Jovanović, M. Jemeric, and D. A. Long, *J. Raman Spectrosc.*, **12**, 91 (1982).
12) K. Ozutsumi, T. Takamuku, S. Ishiguro, and H. Ohtaki, to be published.
13) S. Ishiguro, K. Ozutsumi, S. Miyauchi, and H. Ohtaki, to be published.
14) S. Ishiguro, K. Ozutsumi, and H. Ohtaki, *Bull. Chem. Soc. Jpn.*, **60**, 531 (1987); *J. Chem. Soc., Faraday Trans. 1*, **84**, 2409 (1988).
15) S. Ahrland, *Pure Appl. Chem.*, **51**, 2019 (1979).
16) G. R. Hedwing, D. A. Owensby, and A. J. Parker, *J. Am. Chem. Soc.*, **96**, 6589 (1974).
17) P. Gerding, *Acta Chem. Scand.*, **20**, 79 (1966).
18) P. Gerding and B. Johannson, *Acta Chem. Scand.*, **22**, 2255 (1968).
19) S. Ahrland and N.-O. Björk, *Acta Chem. Scand.*, **A30**, 257 (1976).
20) P. Bacelon, J. Corset, and C. de Loze, *J. Solution Chem.*, **12**, 1 (1983); **12**, 13 (1983); **12**, 23 (1983).

Syntheses and Characterization of Dinuclear High-Spin Iron(II,III) and (III,III) Complexes with 2,6-Bis[bis(2-benzimidazolylmethyl)-aminomethyl]-4-methylphenolate(1−)

Masatatsu SUZUKI, Hiroki OSHIO,† Akira UEHARA,* Kazutoyo ENDO,††
Makoto YANAGA,†† Sigeo KIDA,† and Kazuo SAITO†††
Department of Chemistry, Faculty of Science, Kanazawa University, Kanazawa 920
†Coordination Chemistry Laboratories, Institute for Molecular Science, Okazaki 444
††Department of Chemistry, Faculty of Science, Tokyo Metropolitan University, Fukazawa, Setagaya, Tokyo 158
†††International Christian University, Osawa, Mitaka, Tokyo 181
(Received July 2, 1988)

Two types of dinuclear high-spin mixed valence iron(II,III) complexes, $[Fe_2(L\text{-}Bzim)(RCOO)_2](BF_4)_2\cdot nH_2O$ (RCOO=CH_3COO (**1**) or C_6H_5COO (**2**)), and $[Fe_2(L\text{-}Bzim)(C_6H_5COO)_2(OH)]BF_4\cdot H_2O$ (**3**), and dinuclear high-spin iron(III,III) complexes, $[Fe_2(L\text{-}Bzim)(CH_3COO)_2](ClO_4)_3\cdot 3.5H_2O$ (**4**) and $[Fe_2(L\text{-}py)(C_6H_5COO)_2](ClO_4)_3\cdot CH_3CN\cdot H_2O$ (**5**) were prepared, where L-Bzim is 2,6-bis[bis(2-benzimidazolylmethyl)aminomethyl]-4-methylphenolate(1−) and L-py is 2,6-bis[bis(2-pyridylmethyl)aminomethyl]-4-methylphenolate(1−). Mössbauer spectra of the mixed valence complexes revealed that they involve high-spin iron(II) and (III) ions in equimolar amount. Their ESR spectra exhibited a signal at g_{av}=1.7 near liquid helium temperature characteristic of an antiferromagnetically spin coupled high-spin iron(II,III) dimer. Magnetic susceptibility measurements over the temperature range 80—300 K revealed that weak antiferromagnetic spin-exchange interactions are present between iron(II) and iron(III) ions ($J\approx-5$ cm^{-1}). The complexes showed an intervalence absorption band in the near infrared region, indicating that they belong to class II mixed valence type on the classification of Robin and Day. Cyclic voltammogram of **3** in acetonitrile showed two sets of reversible redox couples at 0.00 and 0.66 V vs. SCE, which are assigned to the redox reactions of Fe(II,III)/Fe(II,II) and Fe(III,III)/Fe(II,III), respectively. The complexes **4** and **5** exhibited weak antiferromagnetic interaction (J=−9—−12 cm^{-1}). ESR spectra of **4** and **5** showed a significant temperature dependence.

Dinuclear mixed valence iron(II,III) centers have been found to exist in some iron proteins such as pink uteroferrin,[1-5] the reduced form of bovine spleen acid phosphatase,[1,2,6] and semi-methemerythrin.[7-9] Those iron proteins were characterized mainly by ESR spectroscopy. They exhibit an ESR signal at $g<2.0$, which was interpreted in terms of antiferromagnetic exchange interaction between high-spin iron(II) and high-spin iron(III) ions.

In the previous studies,[10,11] we reported preparation of the first examples of dinuclear high-spin iron(II, III) complexes with the dinucleating ligand 2,6-bis-[bis(2-benzimidazolylmethyl)aminomethyl]-4-methylphenolate(1−)=L-Bzim or 2,6-bis[bis(2-pyridylmethyl)-aminomethyl]-4-methylphenolate(1−)=L-py (Fig. 1). The L-py complexes were characterized by various spectroscopies such as ESR and Mössbauer. Recently Brovik and Que determined the crystal structure of $[Fe_2(L\text{-}py)(C_2H_5COO)_2](BPh_4)_2\cdot CH_3COCH_3$, where two irons are triply bridged by phenolato and two carboxylato groups.[12] It is interesting to investigate how the ligand environment influences physicochemical properties of mixed valence iron(II,III) complexes. As an extension of our current work on the mixed valence iron(II,III) complexes with various dinucleating ligands, we report here details of physicochemical properties of the iron(II,III) and (III,III) complexes with L-Bzim in comparison with those of the L-py complexes. Recently such dinuclear mixed valence complexes with three bridging ligands (two carboxylate ions and oxide or phenolate ion) have been reported by two groups.[13,14]

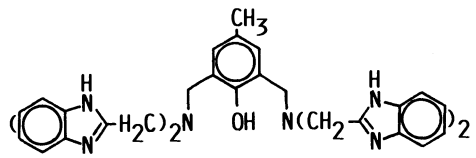

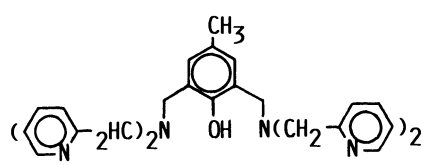

Fig. 1. Dinucleating ligands (HL-Bzim): 2,6-bis[bis(2-benzimidazolylmethyl)aminomethyl]-4-methylphenol and (HL-py): 2,6-bis[bis(2-pyridylmethyl)aminomethyl]-4-methylphenol.

Experimental

Materials. HL-Bzim and HL-py were prepared as previously described.[15,16] $Fe(BF_4)_2\cdot 6H_2O$ was prepared by the know method.[17] The other chemicals were of reagent grade.

Preparation of Iron(II,III) Complexes. $[Fe_2(L\text{-}Bzim)(RCOO)_2](BF_4)_2\cdot nH_2O$ (RCOO=CH_3COO (**1**) or C_6H_5COO (**2**)): A solution of $Fe(BF_4)_2\cdot 6H_2O$ (2 mmol) in 20 cm^3 of ethanol was added with stirring to a solution of HL-Bzim (1 mmol), RCOOH (2 mmol), and triethylamine (1 mmol) in 20 cm^3 of ethanol under N_2. The resulting pale brown solution was exposed to air to form dark brown solution,

which was allowed to stand for a few hours at room temperature to give greenish brown crystals. They were filtered off, washed with ethanol and ether, and dried in vacuo. The complexes were recrystallized from acetonitrile-diethyl ether.

$[Fe_2(L\text{-}Bzim)(C_6H_5COO)_2(OH)]BF_4\cdot H_2O$ (3): A solution of $Fe(BF_4)_2\cdot 6H_2O$ (2 mmol) in 20 cm^3 of ethanol was added to an ethanol solution (20 cm^3) of HL-Bzim (1 mmol), C_6H_5COOH (1 mmol), and triethylamine (3 mmol) with stirring. The solution was exposed to air at 10 °C. The color changed to violet instantaneously. The violet solution was allowed to stand for several hours to give violet crystals, which were filtered off, washed with ethanol and ether, and dried in vacuo.

Preparation of Iron(III,III) Complexes. $[Fe_2(L\text{-}Bzim)(CH_3COO)_2](ClO_4)_3\cdot 3.5H_2O$ (4): A solution of $Fe(ClO_4)_3\cdot 9H_2O$ (2 mmol) in 30 cm^3 of ethanol was mixed with a solution of HL-Bzim (1 mmol) and CH_3COONH_4 (2 mmol) in 20 cm^3 of ethanol with stirring. The resulting reddish brown solution was allowed to stand for several hours to give reddish brown crystals, which were collected by filtration, washed with ethanol and ether, and dried in vacuo.

$[Fe_2(L\text{-}py)(C_6H_5COO)_2](ClO_4)_3\cdot CH_3CN\cdot H_2O$ (5): A solution of $Fe(ClO_4)_3\cdot 9H_2O$ (2 mmol) in 20 cm^3 of acetonitrile was added to a solution of HL-Bzim (1 mmol), C_6H_5COOH (2 mmol), and triethylamine (2 mmol) in 30 cm^3 of ethanol. The resulting dark green solution was allowed to stand overnight to give dark green crystals, which were collected by filtration, washed with ethanol and ether, and dried in vacuo.

Analyses of iron(II) and iron(III) ions in the mixed valence complexes were carried out by the same method as that described in the literature.[11] The results are given in Table 1.

Measurements. The electronic spectra were measured on a Jasco UVIDEC 505 UV/VIS recording digital spectrophotometer and a Hitachi U-3400 spectrophotometer. Infrared spectra were obtained by the KBr-disk and Nujol mull methods with a Jasco A-3 infrared spectrophotometer. Magnetic susceptibilities were measured with a Shimadzu torsion magnetometer MB-2 which was calibrated with $Hg[Co(NCS)_4]$. Diamagnetic correction was made by using Pascal's constants.[18] Cyclic voltammograms were obtained with a Hokuto Denko HA-301 Potentiostat/Galvanostat and a Hokuto Denko HB-104 Function Generator in a cell containing a glassy carbon working electrode, a platinum-coil auxiliary electrode, and a saturated calomel electrode as reference electrode. Acetonitrile was used as the solvent and tetrabutylammonium perchlorate as the supporting electrolyte. Ferrocene was added for an internal check of redox potential and reversibility. $E_{1/2}$ of ferrocene was 0.39 V (vs. SCE) with a peak-to-peak separation (ΔE=70 mV). Mössbauer spectra were measured at 77 K against a $^{57}Co(Pt)$ source moving in a mode of constant acceleration. Velocity calibration was carried out by the resonance lines of metallic iron, and isomer shifts were given relative to iron metal at room temperature. The spectra of the mixed valence complexes were analyzed with a least square fitting program of Lorenztian functions into two sets of quadrupole doublets, each of which was fitted with an equal line width and intensity. ESR spectra were measured on a JEOL JES-FE2XG ESR spectrometer (X-band microwave unit, 100 KHz field modulation) equipped with an Air Product LTD-3-110 liquid helium transfer system. The microwave frequency was monitored with a Takeda Riken TR5212 microwave counter, and the resonance magnetic field values of the signals were measured with an NMR field meter (ECHO Electronics Co., Ltd.).

Results and Discussion

Characterization of Complexes. Chemical analyses of iron(II) and iron(III) ions in the complexes **1**, **2**, and **3** revealed that the complexes contain iron(II) and iron(III) ions in equimolar ratio. Mössbauer spectra also support the chemical analyses (vide infra). The molar conductivity of **1** in acetonitrile is 227 Ω^{-1} cm^2 mol^{-1}, characteristic of an 1:2 electrolyte. From the dinucleating nature of L-Bzim and the elemental analyses as well as the molar conductivities, the complexes **1** and **2** are formulated as $[Fe_2(L\text{-}Bzim)(RCOO)_2](BF_4)_2\cdot nH_2O$ (RCOO=CH_3COO or C_6H_5COO). Recently Jameson et al. determined the crystal structure of $[Fe_2(L\text{-}Bzim)(C_6H_5COO)_2](BF_4)_2\cdot 2[CF_3SO_3HN(C_2H_5)_3]$ where two iron ions are triply bridged by phenolato and two benzoato bridges in syn-syn configuration.[19] Such triply bridging structure has been found for similar mixed valence iron(II, III) and manganese(II, III) complexes.[12,20,21]

The complex **3** was also isolated by treating the complex **2** with one equivalent of triethylamine; the addition of base to the acetonitrile–ethanol (1:1) solution of **2** resulted in an instantaneous color change from brown to reddish violet. When diethyl ether was

Table 1. Analytical Data of the Complexes

No.	Complex	Found (Calcd) (%)				
		C	H	N	Fe(II)	Fe(III)
1	$[Fe_2(L\text{-}Bzim)(CH_3COO)_2](BF_4)_2\cdot 2H_2O$	47.67 (48.03)	3.96 (4.21)	12.44 (12.45)	4.9 (4.97)	5.1 (4.97)
2	$[Fe_2(L\text{-}Bzim)(C_6H_5COO)_2](BF_4)_2\cdot 3H_2O$	51.87 (52.12)	4.12 (4.21)	11.12 (11.05)	4.2 (4.41)	4.4 (4.41)
3	$[Fe_2(L\text{-}Bzim)(C_6H_5COO)_2(OH)]BF_4\cdot H_2O$	56.52 (56.87)	4.20 (4.34)	11.93 (12.06)	4.7 (4.81)	5.0 (4.81)
4	$[Fe_2(L\text{-}Bzim)(CH_3COO)_2](ClO_4)_3\cdot 3.5H_2O$	42.23 (42.33)	3.74 (3.95)	11.17 (11.09)		9.0 (8.87)
5	$[Fe_2(L\text{-}py)(C_6H_5COO)_2](ClO_4)_3\cdot CH_3CN\cdot H_2O$	47.48 (47.42)	4.14 (3.90)	7.76 (7.90)		8.9 (9.00)

added to this solution under an inert atmosphere, violet crystals were obtained. Thus basic conditions are necessary for the formation of **3**. The conductivity measurement in DMF (66 Ω^{-1} cm^2 mol^{-1}) revealed that the complex is an 1:1 electrolyte. From the above results, it seems reasonable that the complex contains hydroxide ion and is formulated as $[Fe_2(Bzim)(C_6H_5COO)_2(OH)]BF_4 \cdot H_2O$. At the present stage, however, the structure of **3** is not clear. The iron(III,III) complexes **4** and **5** also seem to have a triply bridging unit consisting of phenolato and two carboxylato bridges.

Magnetism. The effective magnetic moments of the mixed valence complexes **1**, **2**, and **3** at room temerature are all 7.7 B.M./Fe_2 and those of the iron(III,III) complexes **4** and **5** are 5.1 and 4.8 B.M./Fe, respectively. These values indicate that all the iron(II) and (III) ions are in high-spin state. Magnetic susceptivilities of the complexes were analyzed by the usual spin-spin interaction model based on exchange Hamiltonian $\mathscr{H}=-2JS_1 \cdot S_2$. The molar susceptibilities (χ_A) of spin coupling dimers, (S_1=2, S_2=5/2), and (S_1=5/2, S_2=5/2) are given in Eqs. 1 and 2, respectively.

$$\chi_A = \frac{N\beta^2 g^2}{4kT} \cdot \frac{x^{24} + 10x^{21} + 35x^{16} + 84x^9 + 165}{x^{24} + 2x^{21} + 3x^{16} + 4x^9 + 5} \quad (1)$$

$$\chi_A = \frac{2N\beta^2 g^2(1-P)}{kT} \cdot \frac{x^{28} + 5x^{24} + 14x^{18} + 30x^{10} + 55}{x^{30} + 3x^{28} + 5x^{24} + 7x^{18} + 9x^{10} + 11} + \frac{4.34P}{T} \quad (2)$$

where $x=\exp(-J/kT)$, the symbols have usual meanings, and temperature independent paramagnetisms ($N\alpha$) are assumed to be zero. The magnetic susceptibilities of the iron(II,III) and iron(III,III) complexes were interpreted in terms of the above equations with the parameters listed in Table 2 (Fig. 2). These results indicate that high-spin iron(II) and iron(III) ions in the iron(II, III) complexes are weakly antiferromagnetically coupled to yield an S=1/2 spin ground state. The iron (III, III) complexes also exhibit weak antiferromagnetic exchange interacrion to yield an S=0 spin ground state. Analogous mixed valence dinuclear iron(II,III) and manganese(II,III) complexes with phenolato and two carboxylato bridges show comparable magnitude of antiferromagnetic interaction (J=−3——8 cm^{-1}).[11,20,21] Thus phenolato and carboxylato bridges seem to provide weak antiferromagnetic interaction for all the iron and manganese dinuclear systems, regardless of homoval-ent or mixed valent system.

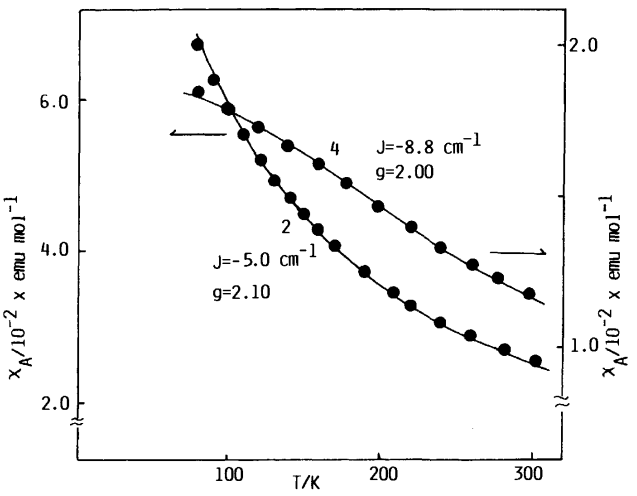

Fig. 2. Temperature dependence of magnetic susceptibilities of $[Fe_2(L\text{-}Bzim)(C_6H_5COO)_2](BF_4)_2 \cdot 3H_2O$ (**2**) and $[Fe_2(L\text{-}Bzim)(CH_3COO)_2](ClO_4)_3 \cdot 3.5H_2O$ (**4**).

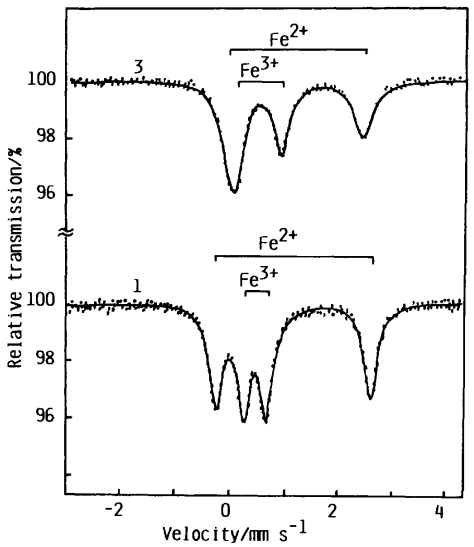

Fig. 3. Mössbauer spectra of $[Fe_2(L\text{-}Bzim)(CH_3COO)_2](BF_4)_2 \cdot 2H_2O$ (**1**), and $[Fe_2(L\text{-}Bzim)(C_6H_5COO)_2(OH)]BF_4 \cdot H_2O$ (**3**) at 77 K.

Table 2. Magnetic Parameters of the Complexes[a]

No.	Complex	J/cm^{-1}	g
1	$[Fe_2(L\text{-}Bzim)(CH_3COO)_2](BF_4)_2 \cdot 2H_2O$	−5.0	2.10
2	$[Fe_2(L\text{-}Bzim)(C_6H_5COO)_2](BF_4)_2 \cdot 3H_2O$	−5.0	2.10
3	$[Fe_2(L\text{-}Bzim)(C_6H_5COO)_2(OH)]BF_4 \cdot H_2O$	−4.0	2.10
4	$[Fe_2(L\text{-}Bzim)(CH_3COO)_2](ClO_4)_3 \cdot 3.5H_2O$	−8.8	2.00
5	$[Fe_2(L\text{-}py)(C_6H_5COO)_2](ClO_4)_3 \cdot CH_3CN \cdot H_2O$[b]	−12.0	2.00

a) $N\alpha$ is assumed to be zero. b) Fitted with contamination of 2% of monomeric high-spin iron(III) impurity.

Table 3. Mössbauer Parameters of the Complexes at 77 K[a]

No.	Complex	Fe(II)			Fe(III)			A(Fe(III)/Fe(II))[c]
		δ[b]	ΔE	Γ	δ[b]	ΔE	Γ	
1	$[Fe_2(L\text{-}Bzim)(CH_3COO)_2](BF_4)_2\cdot 2H_2O$[d]	1.29	2.81	0.28	0.58	0.40	0.30	1.11
2	$[Fe_2(L\text{-}Bzim)(C_6H_5COO)_2](BF_4)_2\cdot 3H_2O$[d]	1.18	2.15	0.37	0.56	0.96	0.40	1.10
3	$[Fe_2(L\text{-}Bzim)(C_6H_5COO)_2(OH)]BF_4\cdot H_2O$[d]	1.29	2.45	0.37	0.61	0.81	0.32	1.06
4	$[Fe_2(L\text{-}Bzim)(CH_3COO)_2](ClO_4)_3\cdot 3.5H_2O$[d]				0.27	0.71	0.59	
	$[Fe_2(L\text{-}py)(CH_3COO)_2](BF_4)_2\cdot 2H_2O$[e]	1.16	2.42	0.41	0.47	0.51	0.33	
	$[Fe_2(L\text{-}py)(C_6H_5COO)_2](BF_4)_2\cdot 2H_2O$[e]	1.15	2.06	0.56	0.56	0.47	0.27	

a) All data in mm s^{-1} except for A(Fe(III)/Fe(II)). b) Isomer shift, δ, relative to iron metal. c) Ratios of areas of Fe(III) to Fe(II). d) This work. e) Ref. 11.

Mössbauer Spectra. Mössbauer spectra of **2** and **3** are given in Fig. 3 and their parameters are listed in Table 3. The presence of iron(II) and iron(III) ions in equimolar ratio in mixed valence complexes is evidenced by the fact that the ratios of area of two sets of quadrupole doublets are nearly unity (Table 3). This fact agrees with the results of the chemical analyses. The quadrupole splitting ΔE and isomer shift δ in mm s^{-1} of the mixed valence complexes are 2.15—2.81 and 1.18—1.29 for iron(II) moieties, and 0.40—0.96 and 0.56—0.61 for iron(III) moieties, respectively. The former quadrupole splitting and isomer shift fall in the range of those of the high spin iron(II) complexes and the latters in the range of iron(III) complexes, respectively.[22] Although the structure of **1** and **2** seem to be almost identical, the quadrupole splittings of the iron(II) and iron(III) moieties in **1** and **2** significantly differ from each other. The iron(II) moiety of **1** exhibits a larger ΔE (2.81) than that of **2** (2.15), whereas the iron(III) moiety of **2** exhibits a larger ΔE (0.96) than that of **1** (0.40). A larger quadrupole splitting reflects a larger electric field gradient at the nucleus, suggesting a lower symmetry of ligand field; i.e., the distortion from octahedron in iron(II) moiety of **1** is larger than that of **2**, but this relation is reversed for iron(III) moieties. The quadrupole splittings of iron(II) and iron(III) moieties in the acetato and benzoato complexes with L-py are 2.42 and 2.06, and 0.51 and 0.47 mm s^{-1}, respectively, suggesting that structural difference between acetato and benzoato complexes with L-py is smaller than that between the L-Bzim complexes and a distortion from octahedron in the L-Bzim complexes is larger than that in L-py complexes. For further discussion, structural details are necessary.

ESR Spectra. All the ESR spectra of the mixed valence complexes in frozen glass of acetonitrile solution as well as in the polycrystalline phase (Fig. 4) show a broad signal at $g\approx 1.7$ at 12 K, indicative of the existence of dinuclear high-spin iron(II,III) mixed valence center where iron(II) and (III) ions are antiferromagnetically coupled to yield a spin ground state of $S=1/2$. The $g\approx 1.7$ signals are observable only near liguid helium temperature and almost disappear above 30 K. Such a spectral behavior is very similar to those of the mixed valence iron proteins such as semimethemerythrin[8] and the L-py complexes,[11] although the signal of the present complexes is very broad as compared with those of the iron proteins. All the frozen solution spectra exhibit a sharp signal at $g\approx 4.3$ attributable to a mononuclear rhombic high-spin iron(III) complex present as impurity formed by slight decomposition in solution. In fact, the spectrum of **3** in polycrystalline phase has no such signal at $g\approx 4.3$. It should be noted that in all the present mixed valence complexes there is a broad signal at $g\approx 5$—6 which is absent in the iron proteins and the L-py complexes.[11] As illustrated in Fig. 4a, b, and c, the $g\approx 5$—6 signals also show a temperature dependence which is similar to that at $g\approx 1.7$. The signals at $g\approx 5$—6 may be ascribed to the complex in $S=3/2$ spin state. The mixed valence manganese(II, III) complexes also have such a broad signal at $g\approx 4$.[20,21]

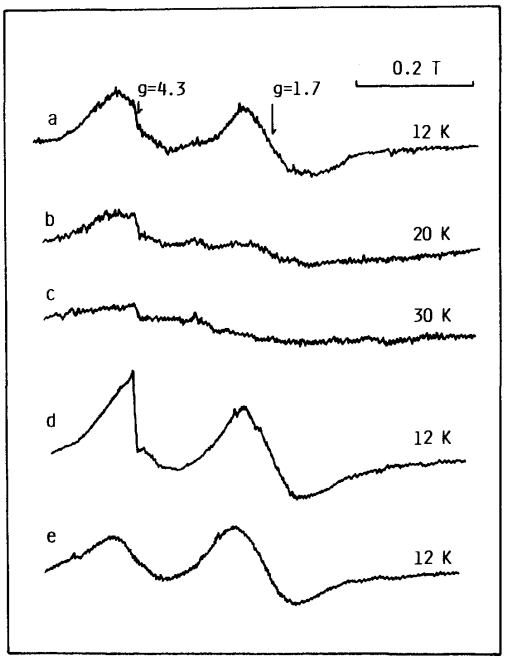

Fig. 4. ESR spectra of $[Fe_2(L\text{-}Bzim)(C_6H_5COO)_2](BF_4)_2\cdot 3H_2O$ (**2**) at 12 K (a), 20 K (b), and 30 K (c) in acetonitrile, and $[Fe_2(L\text{-}Bzim)(C_6H_5COO)_2(OH)]BF_4\cdot H_2O$ (**3**) at 12 K (d) in acetonitrile and at 12 K (e) in polycrystalline phase.

Table 4. Electronic Spectral Data of the Complexes[a)]

No.	Complex	ν_{max}/cm^{-1}, (ε/mol^{-1} dm^3 cm^{-1}) CT band	IT band	
1	$[Fe_2(L\text{-}Bzim)(CH_3COO)_2](BF_4)_2\cdot 2H_2O$[d)]	19200(940)[s]	7400(230)	10300[s]
2	$[Fe_2(L\text{-}Bzim)(C_6H_5COO)_2](BF_4)_2\cdot 3H_2O$[d)]	18500(880)[s]	7040(220)	10200[s]
3	$[Fe_2(L\text{-}Bzim)(C_6H_5COO)_2(OH)]BF_4\cdot H_2O$[d)]	18520(3200)	8000(200)[b)]	
4	$[Fe_2(L\text{-}Bzim)(CH_3COO)_2](ClO_4)_3\cdot 3.5H_2O$[d)]	21740(4120) 19800(2060)[c)]		
5	$[Fe_2(L\text{-}py)(C_6H_5COO)_2](ClO_4)_3\cdot CH_3CN\cdot H_2O$[d)]	16950(920)		
	$[Fe_2(L\text{-}py)(CH_3COO)_2](BF_4)_2\cdot H_2O$[e)]	18000(900)	7700(290)	
	$[Fe_2(L\text{-}py)(C_6H_5COO)_2](BF_4)_2\cdot 2H_2O$[e)]	17400(970)	7400(290)	

a) In acetontrile under N_2. b) Broad band. c) In DMF. d) This work. e) Ref. 11. s: Shoulder.

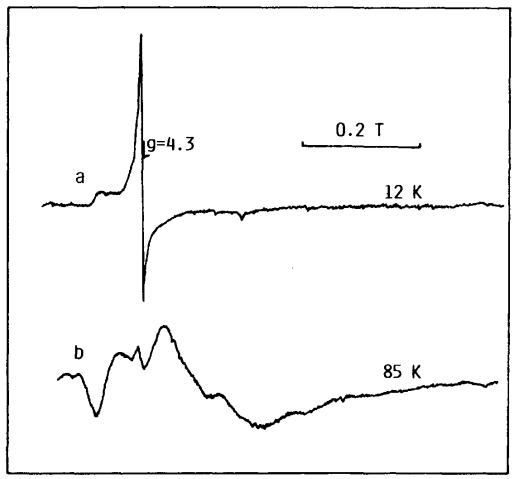

Fig. 5. ESR spectra of $[Fe_2(L\text{-}py)(C_6H_5COO)_2](ClO_4)_3\cdot CH_3CN\cdot H_2O$ (**5**) at 12 K (a) and at 85 K (b) in acetonitrile.

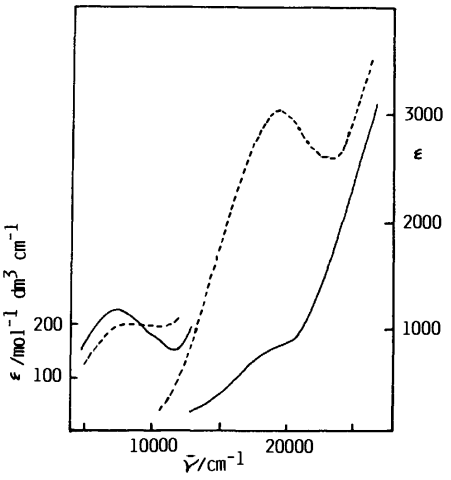

Fig. 6. Electronic spectra of $[Fe_2(L\text{-}Bzim)(C_6H_5COO)_2](BF_4)_2\cdot 3H_2O$ (**2**) (——) and $[Fe_2(L\text{-}Bzim)(C_6H_5COO)_2(OH)]BF_4\cdot H_2O$ (**3**) (------) in acetonitrile under nitrogen atmosphere.

The ESR spectrum of **5** is illustrated in Fig. 5. A significant temperature dependence is observed in the spectra. The spectral behavior of **4** is very similar to that of **5**. They have six spin states of S=0, 1, 2, 3, 4, and 5, in which an S=0 state is the lowest. The spectrum at 12 K exhibits an intense signal at $g\approx 4.3$ and weaker one at higher g values which are attributable to mononuclear iron(III) impurity. Since at 12 K, the population in the ESR active states (S=1, 2, 3, 4, and 5) is about 14%, which was estimated on the basis of Boltzmann distribution by using $J=-12$ cm^{-1}, the signals would be expected to be very weak. On the other hand, at 85 K the population of those states becomes larger (S=0: 19%, S=1: 38%, S=2: 28%, S=3: 11%, S=4: 3%, S=5: 1%) and signals would be expected. In fact, several broad and complicated signals are observed at 85 K (Fig. 5). Such complex spectra were also reported for dinuclear complexes.[23,24)]

Electronic Spectra. The electronic spectra of the mixed valence complexes exhibit an absorption band in the near infrared region (ε=200 mol^{-1} dm^3 cm^{-1}/Fe_2) in acetonitrile (Fig. 6 and Table 4), whereas no such band is observed in this region for the iron(III, III) complexes. The analogous iron(II, III) complexes with L-py also have a near infrared band. Such bands can be assigned to the intervalence transition (IT) of the type $[Fe^{2+}\text{-}Fe^{3+}]\xrightarrow{h\nu}[Fe^{3+}\text{-}Fe^{2+}]^*$. All the complexes have an IT band with a shoulder at higher energy side, while the L-py complexes exhibit only a single IT band. The presence of shoulder may reflect a splitting of t_{2g} orbitals of iron(III) moiety resulting from a lower ligand field symmerty.

All the mixed valence complexes have a charge-transfer transition (CT) from bridging phenolato group to iron(III) moiety in the visible region. The molar extinction coefficients of the CT bands in **1** and **2** are ca. 900 mol^{-1} dm^3 cm^{-1}, whereas that of **3** is 3200 mol^{-1} dm^3 cm^{-1}. The CT band of the iron(III, III) complex **4** showed a remarkable solvent effect (Table 4); the CT band appeared at 21740 cm^{-1} (ε=4120 mol^{-1} dm^3 cm^{-1}) in acetonitrile, and at 19800 cm^{-1} (ε=2060 mol^{-1} dm^3 cm^{-1}) in DMF. Thus such significant energy and intensity variations of the CT band may reflect some structural change in the phenolato bridge.

Ainscough et al.[25)] and Pyrz et al.[26)] pointed out that for mononuclear iron(III)-phenolate complexes the energy of CT band of phenolate moiety to iron(III) ion is sensitive to the donor strength of the other ligands

Table 5. Cyclic Voltammetric Data of the Mixed Valence Complexes

No.	Complex	$E_{1/2}$[a] (E/V vs. SCE)	$E_{1/2}$[b]	$(i_{pa}/i_{pc})^{a}$	$(i_{pa}/i_{pc})^{b}$	K_c
1	$[Fe_2(L\text{-}Bzim)(CH_3COO)_2](BF_4)_2\cdot 2H_2O$[e]	−0.12	+0.56	1.2	1.1	5.0×10^{11}
2	$[Fe_2(L\text{-}Bzim)(C_6H_5COO)_2](BF_4)_2\cdot 3H_2O$[e]	0.00	+0.66	1.1	0.9	2.2×10^{11}
3	$[Fe_2(L\text{-}Bzim)(C_6H_5COO)_2(OH)]BF_4\cdot H_2O$[e]	−0.16	+0.28			
	$[Fe_2(L\text{-}py)(CH_3COO)_2](BF_4)_2\cdot H_2O$[f]	−0.03	+0.68			1.6×10^{12}
	$[Fe_2(L\text{-}py)(C_6H_5COO)_2](BF_4)_2\cdot 2H_2O$[f]	+0.05	+0.73			5.0×10^{11}

a) For Fe(II,III)/Fe(II,II) redox couple. b) Fe(III,III)/Fe(II,III) redox couple. c) Comproportionation constant at 20 °C. d) Irreversible. e) This work. f) Ref. 11.

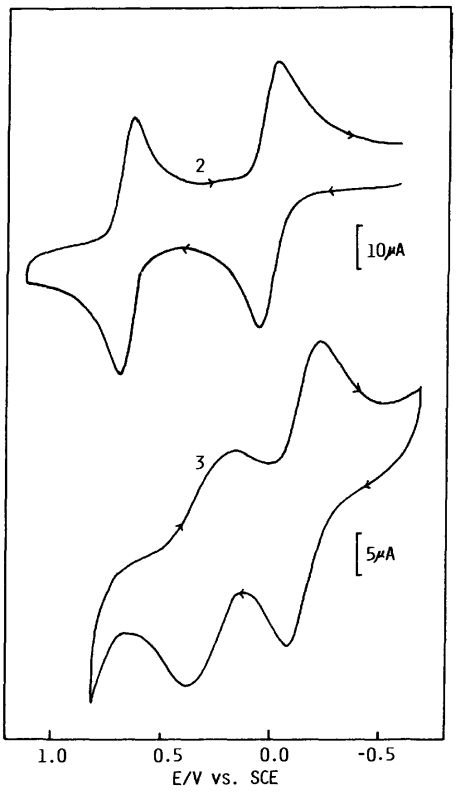

Fig. 7. Cyclic voltammograms of $[Fe_2(L\text{-}Bzim)(C_6H_5COO)_2](BF_4)_2\cdot 3H_2O$ (**2**) and $[Fe_2(L\text{-}Bzim)(C_6H_5COO)_2(OH)]BF_4\cdot H_2O$ (**3**) in 0.1 mol dm^3 tetrabutylammonium perchlorate in acetonitrile at a glassy carbon electrode at a scan rate of 100 mV s^{-1}.

coordinated and the redox potential of the complex; i.e., the donor strength of the other ligands becomes stronger, the more negative the redox potential and the higher the energy of the charge-transfer transition. The present iron(II, III) and (III, III) complexes have a charge-transfer band at higher energy region than the corresponding L-py complexes and the redox potentials of the L-Bzim complexes are more negative than those of the L-py complexes (vide infra). This observation implies that the benzimidazolyl group of L-Bzim is a stronger donor than the pyridyl group of L-py.

Cyclic Voltammogram. Figure 7 illustrates the cyclic voltammograms of **2** and **3** in acetonitrile (Table 5). The complex **2** shows two reversible redox couples at +0.00 and +0.66 V vs. SCE, which correspond to the redox reactions of Fe(II,III)/Fe(II,II) and Fe(III, III)/Fe(II,III). A similar CV was observed for **1**. The redox potentials of **1** and **2** are more negative by 50—120 mV than those of the corresponding L-py complexes. Such negative shifts are consistent with the shift of the CT band energies of the L-Bzim and L-py complexes. The CV of **3** also exhibits two redox couples at ca. −0.16 and +0.28 V vs. SCE, although the reversibility is poor as compared with those of **1** and **2**. Introduction of hydroxide ion seems to cause a poor reversibility and negative shift. A similar situation was obseved for the L-py complexes.[11]

Comproportionation constants of **1** and **2** in the following equilibrium are 5—2×10^{11}, indicating that the mixed valence

$$Fe(II, II) + Fe(III, III) \rightleftharpoons 2Fe(II, III)$$

complexes are significantly stabilized. Thus, the present ligand system (L-Bzim and two carboxylato) also provides favorable coordination sites toward M^{2+} and M^{3+} ions to form a mixed valence complex as the L-py ligand system (L-py and two carboxylate ions) does.

References

1) L. Que, Jr., *Coord. Chem. Rev.*, **50**, 73 (1983).
2) B. C. Antanaitis and P. Aisen, *Adv. Inorg. Biochem.*, **5**, 111 (1983).
3) B. C. Antanaitis, P. Aisen, and H. E. Lilienthal, *J. Biol. Chem.*, **258**, 3166 (1983).
4) R. B. Lauffer, B. C. Antanaitis, P. Aisen, and L. Que, Jr., *J, Biol. Chem.*, **258**, 14212 (1983).
5) P. G. Debrunner, M. P. Hendrich, J. D. Jersey, D. T. Keough, J. T. Sage, and B. Zerner, *Biochim. Biophys. Acta*, **745**, 103 (1983).
6) J. C. Davis and B. A. Averill, *Proc. Natl. Acad. Sci. U.S.A.*, **79**, 4623 (1982).
7) R. G. Wilkins and P. C. Harrington, *Adv. Inorg. Biochem.*, **5**, 51 (1983).
8) B. B. Muhoberac, D. C. Wharton, L. M. Babcock, P. C. Harrington, and R. G. Wilkins, *Biochim. Biophys. Acta*, **626**, 337 (1980).
9) D. M. Kurtz, Jr., J. T. Sage, M. Hendrich, P. G. Debrunner, and G. S. Lukat, *J. Biol. Chem.*, **258**, 2115 (1983).

10) M. Suzuki, A. Uehara, and K. Endo, *Inorg. Chim. Acta*, **123**, L9 (1986).
11) M. Suzuki, A. Uehara, H. Oshio, K. Endo, M. Yanaga, S. Kida, and K. Saito, *Bull. Chem. Soc. Jpn.*, **60**, 3547 (1987).
12) A. S. Brovik and L. Que, Jr., *J. Am. Chem. Soc.*, **110**, 2345 (1988).
13) A. S. Borovik, B. P. Murch, and L. Que, Jr., *J. Am. Chem. Soc.*, **109**, 7190 (1987).
14) J. R. Hartman, R. L. Rardin, P. Chaudhuri, K. Pohl, K. Wieghardt, B. Nuber, J. Weiss, G. C. Papaefthymiou, R. B. Frankel, and S. J. Lippard, *J. Am. Chem. Soc.*, **109**, 7387 (1987).
15) M. Suzuki, H. Kanatomi, and I. Murase, *Chem. Lett.*, **1981**, 1745.
16) M. Suzuki, H. Kanatomi, and I. Murase, *Bull. Chem. Soc. Jpn.*, **57**, 36 (1984).
17) C. L. Spiro, S. L. Lambert, T. J. Smith, E. N. Duesler, R. R. Gagné, and D. N. Hendrickson, *Inorg. Chem.*, **20**, 1229 (1981).
18) F. E. Mabbs and D. J. Marchin "Magnetisms and Transition Metal Complexes," Chapman and Hall, London (1975), p. 5.
19) A. B. Hussein, N. L. Morris, P. G. Romero, and G. B. Jameson, private communication.
20) a) M. Suziki, S. Murata, A. Uehara, and S. Kida, *Chem Lett.*, **1987**, 281; b) M. Suzuki, M. Mikuriya, S. Murata, A. Uehara, H. Oshio, S. Kida, and K. Saito, *Bull. Chem. Soc. Jpn.*, **60**, 4305 (1987).
21) H. Diril, H. R. Chang, X. Zhang, S. K. Larsen, J. A. Potenza, C. G. Pierpont, H. J. Schugar, S. S. Isied, and D. N. Hendrickson, *J. Am. Chem. Soc.*, **109**, 6207 (1987).
22) N. N. Greenwood and G. T. Gibbs, "Mössbauer Spectroscopy," Chapman and Hall, London (1971), p. 148.
23) R. G. Wollmann and D. N. Hendrickson, *Inorg. Chem.*, **17**, 926 (1978).
24) E. W. Aniscough, A. M. Brodie, and S. J. McLachlan, *J. Chem. Soc., Dalton Trans.*, **1983**, 1385.
25) E. W. Aniscough, A. M. Brodie, J. E. Plowman, K. L. Brown, A. W. Addison, and A. R. Gainsford, *Inorg. Chem.*, **19**, 3655 (1980).
26) J. W. Pyrz, A. L. Roe, L. J. Stern, and L. Que, Jr., *J. Am. Chem. Soc.*, **107**, 614 (1985).

 © 1988 The Chemical Society of Japan Bull. Chem. Soc. Jpn., 61, 3915—3918 (1988)

A Convenient Synthesis of 1α-Hydroxyvitamin D_2

Yoji TACHIBANA
Central Research Laboratory, Nisshin Flour Milling, Co., Ltd.,
Tsurugaoka, Ooimachi, Iruma-gun, Saitama 354
(Received February 20, 1988)

The enol acetylation of ergosta-1,4,6,22-tetraen-3-one (**4**) by treatment with isopropenyl acetate under acidic condition gave 3-acetoxy-1,3,5,7,22-ergostapentaene (**5**). The reduction of **5** with calcium borohydride afforded ergosta-1,5,7,22-tetraen-3β-ol (**6**). The *t*-butyldimethylsilyl ether derivatives (**8**) of the Diels–Alder cyclo adduct (**7**) derived from **6** and 4-phenyl-3*H*-1,2,4-triazole-3,5-dione was oxidized with *m*-CPBA to the diepoxide adduct (**9**). The 1α,2α-epoxide of the diepoxy alcohol (**10**) obtained after the removal of the silyl group of **9** was selectively reduced with $LiAlH_4$ to yield the 22,23-epoxy-1α,3β-diol (**11**) and **11** was subsequently converted to the corresponding diacetate (**12**). The deoxygenation of the 22,23-epoxide of **12** with a combination of sodium iodide and trifluoroacetic anhydride gave the 1α-acetoxyergosteryl acetate (**13**). Irradiation of **13** with a high-pressure mercury lamp followed by thermal isomerization, saponification, purification on silica gel and crystallization gave 1α-hydroxyvitamin D_2 (**1**) as colorless crystals.

It is reported that 1α-hydroxyvitamin D_2 (**1**)[1] is about ten times less toxic than 1α-hydroxyvitamin D_3 (**2**),[2] and yet appears to be almost equally potent in vitamin D activity.[3] This suggests that **1** might represent a therapeutically superior compound. DeLuca et al. reported the synthesis of **1** by the irradiation of 1α-acetoxyergosteryl acetate (**13**) followed by the thermal isomerization and saponification. However, concerning the synthesis of **13**, their preparative process utilizing ergost-5-en-3β-ol as a key intermediate generally gave a poor yield of **13** due to the side reactions involving the formation of a considerable amount of the 4,6-diene isomer.[4]

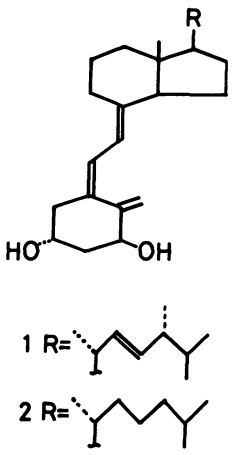

Thus, it is desirable to obtain **13** in higher yiled for the preparation of **1**. We have reported the conversion of cholesta-1,4,6-trien-3-one to cholesta-5,7-diene-1α,3β-diol via 3-acetoxy-1,3,5,7-cholestatetraene as a key intermediate.[5] This procedure seemed to be applicable to the synthesis of **13**. In the present paper, an alternative convenient method for the preparation of 1α-acetoxyergosteryl acetate (**13**) and its conversion to 1α-hydroxyvitamin D_2 (**1**) are described.

Ergosta-4,6,22-trien-3-one (**3**)[6] was dehydrogenated to ergosta-1,4,6,22-tetraen-3-one (**4**) by the modified method of Pelć et al.[7] Treatment of the 4,6,22-trienone (**3**) with 2,3-dichloro-5,6-dicyano-*p*-benzoquinone (DDQ) in the presence of a catalytic amount of 5-sulfosalicylic acid gave the tetraenone (**4**) in a fairly good yield. The tetraenone (**4**) was converted to 3-acetoxy-1,3,5,7,22-ergostapentaene (**5**) by the enol acetylation in the presence of a combination of isopropenyl acetate and *p*-toluenesulfonic acid. Longer time is required to complete this enol acetylation compared with that of cholesta-1,4,6-trien-3-one.[5] The pentaenyl acetate (**5**) was subsequently reduced with calcium borohydride[8] to yield ergosta-1,5,7,22-tetraen-3β-ol (**6**) in good yield.

After the 5,7-diene of **6** was protected with 4-phenyl-3*H*-1,2,4-triazole-3,5-dione[9] as a Diels–Alder adduct (**7**), the hydroxyl group was protected by conversion to *t*-butyldimethylsilyl derivative (**8**) for performing the selective α-epoxidation of the double bond (C-1).[10] In the next stage, the reactivity of the oxidizing reagent to the two different double bond (C-1 and C-22) was examined. When an equimolar amount of *m*-chloroperbenzoic acid (*m*-CPBA) was allowed to react with **8**, the ^1H NMR spectrum of the product showed that the signals due to the double bond at C-22 disappeared completely, indicating the double bond at C-22 was epoxidized selectively. Therefore, we planned to regenerate the double bond by removal of the epoxide after the hydroxyl group was introduced at the α position of C-1.

Theatment of **8** with excess *m*-CPBA afforded the diepoxide derivative (**9**) as diastereomeric mixtures with respect to the 22,23-epoxide, showing two spots on thin-layer chromatography.[11] On the other hand, the orientation of the 1,2-epoxide was confirmed as α-configuration by comparison of the ^1H NMR spectra of the compounds **9** and **10** (described later) with those of corresponding established 1α,2α-epoxide derivatives obtained from cholesterol.[8,10] Removal of the silyl group of **9** by treatment with tetrabutylammonium fluoride tetrahydrofuran solution gave the diepoxy

alcohol (**10**). The resulting **10** was reduced with excess $LiAlH_4$ to yield 22,23-epoxy diol (**11**). Crump et al. reported the reduction of the 22,23-epoxide of ergostery acetate protected with 4-phenyl-3*H*-1,2,4-triazole-3,5-dione ($LiAlH_4$ in tetrahydrofuran-ether, reflux for 3 days).[12] However, the 22,23-epoxide of **11** was not reduced under the conditions employed here (in tetrahydrofuran, reflux for 1 h).[13] The epoxy diol (**11**) was treated with pyridine–acetyl chloride to afford the corresponding diacetate (**12**). After trying several deoxygenating reagents,[14] we found that a combination of sodium iodide and trifluoroacetic anhydride[15] successfully deoxygenated the 22,23-epoxide of **12** to yield the desired 1α-acetoxyergosteryl acetate (**13**). The deoxygenation should be carried out at relatively low temperature (0—5 °C) to avoid side reactions involving the formation of the cis isomer. The *E* stereochemistry of the regenerated double bond (C-22) in **13** was supported by the ^1H NMR spectrum, where the coupling pattern of the olefinic protons at the side chain was in quite agreement with that of 1α-acetoxyergosteryl acetate obtained by the method described in the literature.[1] The diacetate (**13**) was hydrolyzed upon treatment with ethanolic potassium hydroxide to give the corresponding diol (**14**).

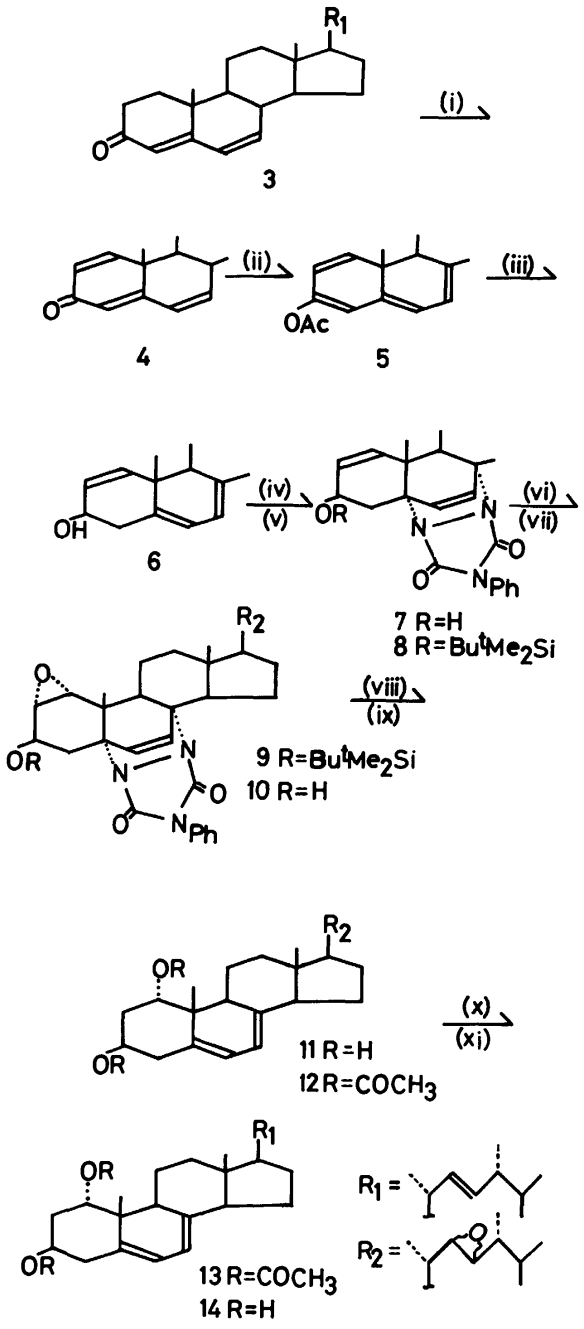

Scheme 1. (i) DDQ-5-sulfosalicylic acid. (ii) Isopropenyl acetate-*p*-TsOH. (iii) $Ca(BH_4)_2$, 0 °C in MeOH-EtOH. (iv) 4-Phenyl-3*H*-1,2,4-triazole-3,5-dione. (v) Bu^tMe_2SiCl-imidazole, 35 °C in DMF. (vi) *m*-CPBA. (vii) Bu_4NF, 5 °C in THF. (viii) $LiAlH_4$-THF. (ix) CH_3COCl-pyridine. (x) NaI-$(CF_3CO)_2O$, 5 °C in THF-acetonitrile. (xi) KOH-EtOH.

The irradiation of the diacetate (**13**) with high-pressure mercury lamp using aq. 1.2% KNO_3 solution as a filter followed by the thermal isomerization of precalciferol to calciferol and the subsequent saponification afforded the crude 1α-hydroxyvitamin D_2 (**1**). Purification by column chromatography on silica gel and crystallization gave **1** as colorless crystals.

Since 1α-acetoxyergosteryl acetate (**13**) is obtainable readily from ergosterol as described above, the present study provides an efficient method for the preparation of 1α-hydroxyvitamin D_2 (**1**).

Experimental

Melting points are uncorrected. UV spectra were taken on a Hitachi 320 spectrometer. ^1H NMR spectra were recorded in $CDCl_3$ on a JEOL JNF-FX200 spectrometer with TMS as an internal standard. Mass spectra were measured on a Hitachi M-80 mass spectrometer. Optical rotations were determined with a JASCO DIP-4 polarimeter. Solvents were removed under reduced pressure.

Ergosta-1,4,6,22-tetraen-3-one (4). A mixture of ergosta-4,6,22-trien-3-one (**3**) (65 g, 165.0 mmol), DDQ (65 g, 286.3 mmol) and 5-sulfosalicylic acid (12 g, 47.2 mmol) in dioxane (500 ml) was heated under reflux for 3 h. The solution was filtered to remove the hydroquinone formed and the filtrate was concentrated to dryness. The mixture was extracted with ethyl acetate. The extract was washed with aq. 10% KOH solution and brine, dried over sodium sulfate and evaporated. The residue was chromatographed on silica gel. Elution with ethyl acetate-hexane (1/9, v/v) gave crude tetraenone (**4**) (45 g), which was crystallized from acetone to afford pale yellow needles. 35 g (54%): mp 112—114 °C (lit,[6] 104—106 °C).

3-Acetoxy-1,3,5,7,22-ergostapentaene (5). A mixture of **4** (10 g, 25.5 mmol), *p*-toluenesulfonic acid (10 g, 52.6 mmol), and isopropenyl acetate (100 ml, 900.0 mmol) in butyl acetate (100 ml) was allowed to reflux for 16 h. The mixture solution was washed with water, aq. $NaHCO_3$ solution and brine, dried over sodium sulfate and evaporated. The residue was crystallized from acetone to give the pentaene (**5**) as yellow needles. 7.6 g (69%): mp 154—156 °C; λ_{max} 252 nm

(ε=9200, EtOH); *m/z* 434 (M^+); ^1H NMR δ 5.64—5.98 (m, 5H, H-1, H-2, H-4, H-6, H-7), 5.21 (m, 2H, H-22, H-23), 2.20 (s, 3H, $COCH_3$). Found: C, 82.53; H, 9.87%. Calcd for $C_{30}H_{42}O_2$: C, 82.88; H, 9.76%; $[\alpha]_D^{25}$ −508° (*c* 0.2, $CHCl_3$).

Ergosta-1,5,7,22-tetraen-3β-ol (6). The ether solution (100 ml) of the pentaene (**5**) (10 g, 23.0 mmol) was added dropwise at −10 °C to a stirred solution of calcium borohydride in ethanol-methanol (calcium chloride (30 g, 333.3 mmol) in methanol (300 ml) and sodium borohydride (15 g, 405.4 mmol) in ethanol (150 ml)). The mixture was stirred at 0 °C for 3 h and at room temperature overnight. After addition of 50% acetic acid to dissolve the resulted precipitates, the product was extracted with ethyl acetate. The extract was washed with water, aq. $NaHCO_3$ solution, brine and dried over sodium sulfate. The ethyl acetate was evaporated to dryness and the residue was chromatographed on silica gel. The product, which was eluted with hexane-ethyl acetate (4/1, v/v) was crystallized from acetone to give the tetraene (**6**). 7.7 g (85%): mp 156—157 °C; λ_{max} 282 nm (ε=11000, EtOH); *m/z* 394 (M^+); ^1H NMR δ=5.47—5.78 (m, 4H, H-1, H-2, H-6, H-7), 5.21 (m, 2H, H-22, H-23), 4.31 (1H, m, H-3). Found: C, 85.06; H, 10.71%. Calcd for $C_{28}H_{42}O$: C, 85.19; H, 10.75%.

The Diels-Alder Adduct of Ergosta-1,5,7,22-tetraen-3β-ol (7). The tetraenol (**6**) (9.6 g, 24.4 mmol) was dissolved in ethyl acetate (100 ml). To the solution, 4-phenyl-3*H*-1,2,4-triazole-3,5-dione (4.8 g, 27.4 mmol) was added by portion until a faint pink color persisted. The solvent was removed and the residue was purified by silica-gel column chromatography (eluted with chloroform) to give the adduct (**7**). 12.5 g (90%): mp 170—171 °C (crystallized from methanol); *m/z* 394 (M^+−175); ^1H NMR δ=7.40 (5H, m, C_6H_5), 6.44, 6.26 (2H, AB q, *J*=8 Hz, H-6, H-7), 6.04 (2H, m, H-1, H-2), 5.20 (2H, m, H-22, H-23), 5.06 (1H, m, H-3). Found: C, 75.74; H, 8.34; N, 7.29%. Calcd for $C_{36}H_{47}N_3O_3$: C, 75.87; H, 8.33; N, 7.37%.

The 3β-*O*-(*t*-Butyldimethylsilyl) Derivative (8) of the Diels-Alder Adduct (7). To the solution of the Diels-Alder adduct (**7**) (8.4 g, 14.8 mmol) in *N,N*-dimethylformamide (20 ml), *t*-butyldimethylsilyl chloride (3.6 g, 23.8 mmol) and imidazole (3.6 g, 52.9 mmol) was added. The mixture solution was warmed at 35° for 1 h and extracted with ether. The ether solution was washed with brine, dried over sodium sulfate and evaporated. The residue was crystallized from methanol-ether to give the silyl derivative (**8**). 9.1 g (90%): mp 186—188 °C; ^1H NMR δ=7.40 (5H, m, C_6H_5), 6.44, 6.26 (2H, AB q, *J*=8 Hz, H-6, H-7), 5.69 (2H, m, H-1, H-2), 5.18 (2H, m, H-22, H-23), 4.99 (1H, m, H-3). Found: C, 73.71; H, 9.07; N, 6.15%. Calcd for $C_{42}H_{61}N_3O_3Si$: C, 73.73; H, 9.01; N, 6.14%.

1α,2α:22,23-Diepoxide Derivative (9). The silyl derivative of the Diels-Alder adduct (**8**) (7.5 g, 10.7 mmol) was dissolved in chloroform (100 ml) and *m*-chloroperbenzoic acid (*m*-CPBA) (7.5 g, 43.5 mmol) was added. After the mixture was stirred at room temperature for 24 h, the solution was washed with sodium carbonate and brine, dried over sodium sulfate and evaporated to give the diepoxide (**9**). 7.1 g (90%): mp 194—195 °C (crystallized from methanol); *m/z* 541 (M^+−175); ^1H NMR δ=7.45 (5H, m, C_6H_5), 6.42, 6.20 (2H, AB q, *J*=8 Hz, H-6, H-7), 4.94 (1H, m, H-3), 3.17—3.34 (2H, m, H-1, H-2). Found: C, 70.34; H, 8.61; N, 5.85%. Calcd for $C_{42}H_{61}N_3O_5Si$: C, 70.43; H, 8.60; N, 5.87%.

22,23-Epoxy-ergosta-5,7-diene-1α,3β-diol (11). A tetrahydrofuran solution (50 ml) of the crude **9** (5.6 g, 7.8 mmol) and 1 M (1 M=1 mol dm^{-3}) tetrabutylammonium fluoride tetrahydrofuran solution (12 ml) was allowed to react at 5 °C for 16 h. The mixture was extracted with ethyl acetate, washed with brine and dried over sodium sulfate. Evaporation to dryness left a residue, which was chromatographed on silica gel with chloroform as eluent to afford the diepoxy alcohol **10** as oil. 3.7 g (79%): *m/z* 427 (M^+−175); ^1H NMR δ=7.45 (5H, m, C_6H_5), 6.43, 6.21 (2H, AB q, *J*=8 Hz, H-6, H-7), 5.04 (1H, m, H-3), 3.27 (2H, m, H-1, H-2).

To the tetrahydrofuran solution (400 ml) of $LiAlH_4$ (8.1 g, 213.7 mmol), **10** (2.7 g, 4.5 mmol) in tetrahydrofuran (150 ml) was added dropwise. The mixture was heated under reflux for 1 h. After decomposition of the excess $LiAlH_4$ by addition of water, dil. hydrochloric acid was added to give a clear solution. The solution was extracted with ethyl acetate, washed with aq. $NaHCO_3$ solution and brine, and dried over sodium sulfate. Chromatography on silica gel of the crude oil obtained after evaporation of ethyl acetate (eluted with chloroform-ethyl acetate) (4/1, v/v) yielded the epoxy diol (**11**). 1.2 g (63%): mp 155—157 °C (crystallized from acetone); *m/z* 428 (M^+); λ_{max} 282 nm (ε=10900, EtOH); ^1H NMR δ=5.70, 5.38 (2H, m, H-6, H-7), 4.05 (1H, m, H-3), 3.73 (1H, bs, H-1). Found: C, 78.11; H, 10.31%. Calcd for $C_{28}H_{44}O_3$: C, 78.44; H, 10.37%.

1α-Acetoxyergosteryl Acetate (13). The epoxy diol (**11**) (2.0 g, 4.7 mmol) was treated with pyridine (5 ml)-acetyl chloride (1 ml, 14.0 mmol) at room temperature for 2 h. The mixture was extracted with hexane, washed with dil. hydrochloric acid and brine, and dried over sodium sulfate. Chromatography on silica gel (eluted with hexane) gave the epoxy diacetate (**12**) as oil. 1.9 g (81%): *m/z* 512 (M^+); ^1H NMR δ=5.67, 5.39 (2H, m, H-6, H-7), 4.99 (2H, m, H-1, H-3), 2.09, 2.03 (6H, s, $COCH_3$).

Trifluoroacetic anhydride (1.5 ml, 10.6 mmol) was added to the solution of sodium iodide (6.0 g, 40.0 mmol) in 30 ml of acetonitrile-tetrahydrofuran (1/1, v/v). The mixture was stirred at room temperature for 30 min. After the solution was cooled to 0 °C, the epoxy diacetate (**12**) (900 mg, 1.8 mmol) in 10 ml of acetonitrile-tetrahydrofuran (1/1, v/v) was added dropwise. The mixture solution was kept at 5 °C for 48 h. The reaction mixture was extracted with hexane, washed with 5% sodium hydrogensulfite and brine, and dried over sodium sulfate. The residue after evaporation of the solvent was purified by column chromatography on silica gel (eluted with hexane-ethyl acetate, 95/5, v/v) to afford the crude **13**, which was crystallized from ethanol to yield the diacetate as colorless crystals. 350 mg (40%): mp 129—130 °C; *m/z* 496 (M^+); λ_{max} 282 nm (ε=10800, EtOH); ^1H NMR δ=5.68, 5.40 (2H, m, H-6, H-7), 5.19 (2H, m, H-22, H-23), 5.01 (2H, m, H-1, H-3), 2.08, 2.03 (6H, s, $COCH_3$). Found: C, 77.14; H, 9.78%. Calcd for $C_{32}H_{48}O_4$: C, 77.36; H, 9.76%.

The diacetate (**13**) (300 mg, 0.6 mmol) was treated with ethanolic potassium hydroxide (KOH 150 mg, EtOH 10 ml) under reflux for 10 min. The mixture was extracted with ether and washed with brine. Evaporation of the solvent followed by the crystallization from ethanol yielded the diol (**14**) as colorless crystals. 210 mg (84%): mp 197—198 °C; λ_{max} 282 nm (ε=11000, EtOH); *m/z* 412 (M^+); ^1H NMR δ=5.74,

5.37 (2H, m, H-6, H-7), 5.19 (2H, m, H-22, H-23), 4.07 (1H, m, H-3), 3.78 (1H, bs, H-1). Found: C, 80.92; H, 10.72%. Calcd for $C_{28}H_{44}O_2$: C, 81.48; H, 10.77%.

1α-Hydroxyvitamin D_2 (1). The ether solution of the diacetate (**13**) (200 mg, 0.4 mmol) was irradiated at room temperature for 2 min (high pressure mercury lamp, Ushio UM-452; aq. 1.2% KNO_3 solution as filter). After the ether was removed, the resulted residue was dissolved in ethanol (10 ml) and the solution heated under reflux for 1 h. To the solution, 1 M ethanolic potassium hydroxide solution (2 ml) was added and the mixture refluxed for a further 10 min. The solution was extracted with ether, washed with brine, and dried over sodium sulfate. Column chromatography on silica gel after evaporation of ether (eluted with chloroform–ethyl acetate, 9/1, v/v) afforded the crude hydroxyvitamin D_2 (**1**). Crystallization from hexane–ethyl acetate gave **1** as colorless crystals. 28 mg (17%): mp 136—138 °C (lit,[16] 138—140 °C); λ_{max} 265 nm (ε=18500, EtOH); $[\alpha]_D^{25}$ +47.5° (*c* 0.5, EtOH).

References

1) H.-Y. Lam, H. K. Schnoes, and H. F. DeLuca, *Science*, **186**, 1038 (1974); H.-Y. Lam, H. K. Schnoes, and H. F. DeLuca, *Steroids*, **30**, 2181 (1977).

2) M. F. Holich, E. J. Semmler, H. K. Schnoes, and H. F. DeLuea, *Science*, **180**, 190 (1973); D. H. R. Barton, R. H. Hesse, M. M. Pechet, and E. Rizzardo, *J. Am. Chem. Soc.*, **95**, 2748 (1973).

3) G. Sjödén, C. Smith, U. Lindgren, and H. F. DeLuca, *Proc. Soc. Exp. Biol. Med.*, **178**, 432 (1985).

4) O. Nishikawa, J. Oshido, and H. Tsuruta, *Chem. Pharm. Bull.*, **32**, 3244 (1984).

5) Y. Tachibana, *Bull. Chem. Soc. Jpn.*, **59**, 3702 (1986).

6) D. A. Schepherd, R. A. Donia, J. A. Campbell, B. A. Johnson, R. P. Holysz, G. Slomp, Jr., J. E. Stafford, R. L. Pederson, and A. C. Ott, *J. Am. Chem. Soc.*, **77**, 1212 (1955).

7) B. Pelć and Kodicek, *J. Chem. Soc. C*, **1971**, 860.

8) C. Kaneko, A. Sugimoto, Y. Eguchi, S. Yamada, and M. Ishikawa, *Tetrahedron*, **30**, 2701 (1974).

9) D. H. R. Barton, T. Shioiri, and D. A. Widdowson, *J. Chem. Soc. C*, **1971**, 1968; M. Anastasia and M. Derossi, *J. Chem. Soc., Chem. Commun.*, **1979**, 164.

10) A. Emke, D. Hands, J. M. Midgley, W. B. Whalley, and R. Ahmad, *J. Chem. Soc., Perkin Trans. 1*, **1977**, 820; D. W. Guest and D. H. Williams, *J. Chem. Soc., Perkin Trans. 1*, **1979**, 1695.

11) It was reported that the epoxidation of a 22,23-double bond of the ergosterol type gave β isomer as the major product. D. H. R. Barton, J. P. Poyster, P. G. Sammes, M. B. Hursthouse, and S. Neidle, *J. Chem. Soc., Chem. Commun.*, **1971**, 715.

12) D. R. Crump, D. H. Williams, and B. Pelć, *J. Chem. Soc., Perkin Trans. 1*, **1973**, 2731; J. C. Bontekoe, A. Wignall, M. R. Rappoldt, and J. R. Roborgh, *Int. Z. Vitaminforsch*, **40**, 589 (1970).

13) M. Morisaki, J. R. Lightbourn, and N. Ikekawa, *Chem. Pharm. Bull.*, **21**, 457 (1973); K. Ochi, I. Matsunaga, and M. Shindo, *J. Chem. Soc., Perkin Trans. 1*, **1979**, 161; S. Fung and J. B. Siddall, *J. Am. Chem. Soc.*, **102**, 6580 (1980); S. Takatsuto, N. Yazawa, M. Ishiguro, M. Morisaki, and N. Ikekawa, *J. Chem. Soc., Perkin Trans. 1*, **1984**, 139.

14) J. W. Cornforth and D. T. Green, *J. Chem. Soc. C*, **1970**, 846; T. Fujisawa, K. Sugimoto, and H. Ohta, *Chem. Lett.*, **1974**, 883; J. E. McMurry, M. G. Sievestri, M. P. Fleming, T. Hoz, and M. W. Grayston, *J. Org. Chem.*, **43**, 3249 (1978); S. Matsubara, T. Nonaka, Y. Okuda, S. Kanemoto, K. Oshima, and H. Nozaki, *Bull. Chem. Soc. Jpn.*, **58**, 1480 (1985); M. Mori, Y. Uozumi, M. Kimura, and Y. Ban, *Tetrahedron*, **42**, 3793 (1986).

15) P. E. Sonnet, *J. Org. Chem.*, **43**, 1841 (1978).

16) H. E. Paaren, H. F. DeLuca, and H. K. Schnoes, *J. Org. Chem.*, **45**, 3253 (1980).

Rotational Isomerism in Fluorene Derivatives. XIII.[1] Conformational Equilibria of 9-(2-Methylaminophenyl)-fluorene and the Effect of Acid on It

Akiko NISHIDA, Makoto TAKESHITA, Shizuo FUJISAKI, and Shoji KAJIGAESHI*
Department of Industrial Chemistry, Faculty of Engineering,
Yamaguchi University, Tokiwadai, Ube 755
(Received March 18, 1988)

The compound 9-(2-methylaminophenyl)fluorene (**2**) was obtained by treatment of 9-(2-dimethylaminophenyl)-9-fluorenol (**1b**) with dry hydrogen bromide in acetic acid. The conformational equilibrium (*ap*⇄*sp*) of **2** was investigated on the basis of dynamic ^{1}H NMR spectra in $CDCl_3$. The stabilization of the *ap*-form could be ascribed to an N–H···π interaction between the methylamino group and the fluorene ring. The effect of trifluoroacetic acid on the equilibrium of **2** is also discussed.

Recently, we have investigated the conformational equilibria of 9-substituted 9-(2-dimethylaminophenyl)-fluorenes (**1**) on the basis of D NMR spectra. We also discussed the effect of trifluoroacetic acid on 9-(2-dimethylaminophenyl)fluorene (**1a**). In that case, we recognized the presence of N–H···π interaction in the *ap*-trifluoroacetate.[2] In the present paper, we wish to report on the preparation of 9-(2-methylaminophenyl)-fluorene (**2**) and on the conformational equilibrium of **2**, which essentially has an N–H group in the molecule. We also discuss the effect of trifluoroacetic acid on the equilibrium of **2**.

Results and Discussion

Preparation of 9-(2-Methylaminophenyl)fluorene (2). The reaction of 9-fluorenone with 2-dimethylaminophenylmagnesium bromide in dry ether-benzene gave 9-(2-dimethylaminophenyl)-9-fluorenol[2] (**1b**). Bubbling hydrogen bromide into a solution of **1b** in acetic acid unexpectedly afforded **2** in satisfactory yield (75%). In this case, the expected product, 9-bromo-9-(2-dimethylaminophenyl)fluorene (**1c**), was not obtained at all. The structure of **2** could be confirmed by elementary analysis and from its ^{1}H NMR and IR spectra. Furthermore, **2** could be converted into **1a** by treatment with methyl iodide in acetone at room temperature for a week, followed by treatment with aqueous sodium hydroxide.

It is interesting to form **2** by the reaction of **1b** with hydrogen bromide. The following mechanism has been suggested to account for the formation of **2** from **1b** with the aid of hydrogen bromide (Scheme 2). Actually, we confirmed the production of bromine by the usual test using iodo-starch paper. Elimination of methyl bromide from the four membered ring ammonium salt (**3**) to give four membered ring amine (**4**) is inferred from analogy with the von Braun

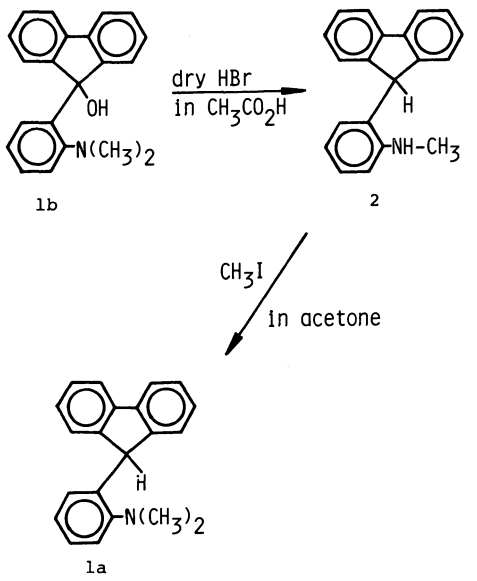

Scheme 1.

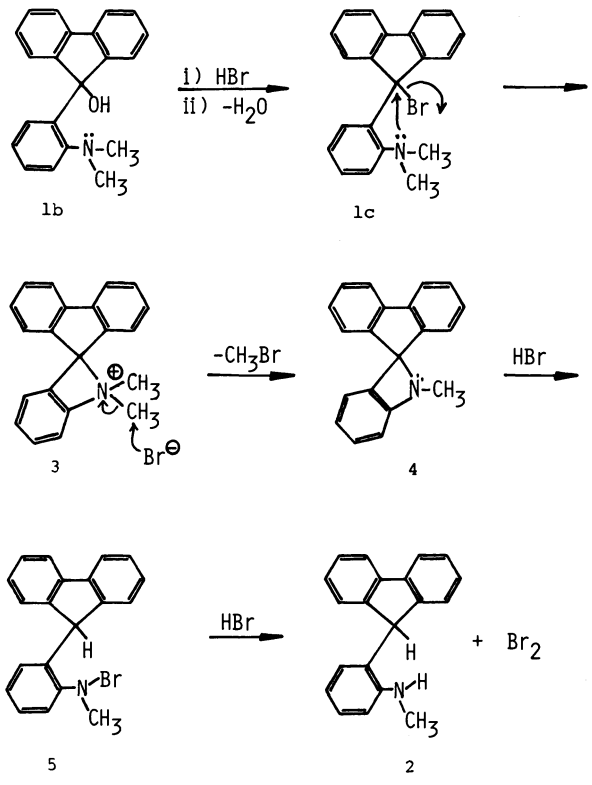

Scheme 2.

reaction,[3] in which a tertiary amine eliminates alkyl bromide to give a disubstituted cyanamide by means of cyanogen bromide. An *N*-bromoamine derivative (**5**) should be derived from **4** with hydrogen bromide owing to the release of the unstable four membered ring system.

On the other hand, the reaction of 9-(4-dimethylaminophenyl)-9-fluorenol (**6**) with hydrogen bromide in acetic acid and subsequent treatment of sodium hydroxide produced **6** instead of 9-(4-methylaminophenyl)fluorene (**7**). The result supported the above reaction mechanism which includes the four membered ring system.

Conformational Equilibria of 2 in Chloroform. Usually, in 9-(2-substituted phenyl)fluorene derivatives, two rotamers (*ap* and *sp*) were identified by their NMR spectra because of their high barriers to rotation about the C(9)–C(Ar) bond. The conformational equilibria *ap*⇄*sp* of these compounds are mainly controlled by intramolecular steric effects, nonbonding intramolecular interaction (attraction or repulsion), and solvent effects. The isomerization of **2** by rotation about the C(9)–C(Ar) bond is shown in Fig. 1.

As shown in Table 1, the two CH_3 signals were observed at δ 2.22 and 2.98 as broad singlets at room temperature, respectively. The dynamic NMR spectra of the methyl protons at various temperatures from 60 to −30 °C are shown in Fig. 2. The signal for the methyl group appeared as a sharp singlet at 60 °C, and this signal gradually split into two broad singlets with lowering of the temperature. Finally, the methyl signal showed one singlet (δ 3.00) and one doublet (δ 2.20, J=5 Hz) (1:2.1) at −30 °C. The former corresponded to the methyl proton of the *sp*-form; the latter corresponded to that of the *ap*-form. Two amino protons (N–H) were observed as a broad singlet at δ 4.36 (*sp*-form) and a broad quartet at δ 2.42 (*ap*-form) at −30 °C.

Since the amino protons easily exchange with one another, if the rate of the exchange is faster than the time scale of NMR, no coupling of the amino proton with the vicinal proton should occur. Therefore, in the case of the *sp*-form of **2**, both the methyl and amino protons are observed as singlets. For the other *ap*-form, the methyl and amino protons couple with one another; that is, the rate of the exchange of the amino proton is found to be slower than the NMR time scale.

Iwamura et al.[4] already proposed the presence of the N–H···π internal hydrogen bonding in the *ap*-form of 9-(2-aminophenyl)fluorene (**8**) to stabilize this form (the ratio; *ap*/*sp*=4/1 at −51 °C). Similarly,for compound **2**, we can show that N–H···π interaction exists between the methylamino group and the fluorene ring. This stabilizes the *ap*-form (*ap*/*sp*=2.1/1 at −30 °C) (Fig. 3). Thus, the methyl signal of **2**-*ap*

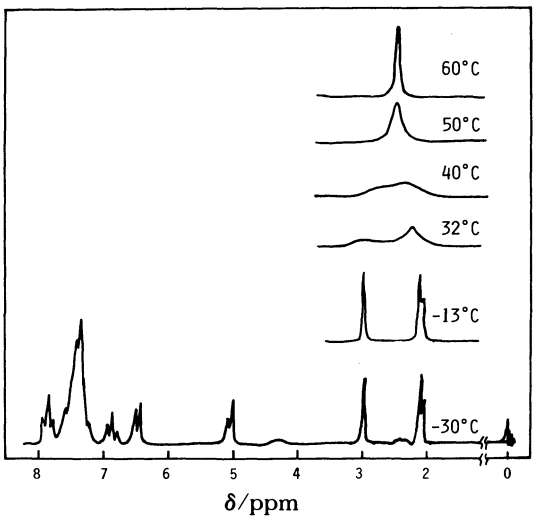

Fig. 2. Temperature-dependent spectra of **2** in $CDCl_3$.

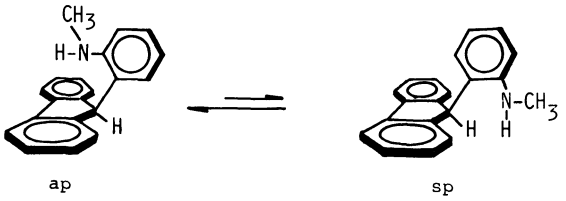

Fig. 1. Isomerization process between *ap* and *sp* form of 9-(2-methylaminophenyl)fluorene **2**.

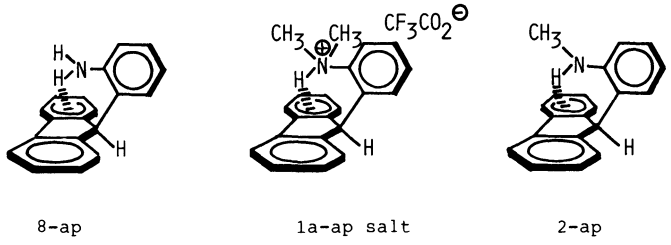

Fig. 3. N–H···π interaction in **8**-*ap*, **1a**-*ap* salt, and **2**-*ap*.

Table 1. ^{1}H NMR Data of **2** in $CDCl_3$

Temp/°C	δ/ppm				
	$NHCH_3$	$NHCH_3$	9-H	6′-H	Aromatics
25	2.22br.s 2.98br.s	—	5.02br.s	—	6.02—7.70m
−30	2.20d[a] 3.00s	2.42br.q 4.36br.s	4.98s 5.02s	— 6.48d[b]	6.08—7.90m

a) J=5 Hz. b) J=7 Hz.

should be observed as a doublet.

The IR spectrum of **2** in 0.1 mol l^{-1} solution of carbon tetrachloride exhibited an N–H streching frequency at 3435 cm^{-1}. This value did not alter on dilution with the solvent down to 0.02 mol l^{-1} concentration. According to this phenomenon, we can not detect the presence of the N–H···π hydrogen bonding in **2**, because intermolecular hydrogen bonding due to an N–H group is usually not influenced with respect to variation of its concentration.[5] The reference compound **7**, which was obtained from the reaction of 9-(4-dimethylaminophenyl)-fluorene (**9**) with cyanogen bromide, showed corresponding absorption at the same 3435 cm^{-1} in 0.05 mol l^{-1} solution of carbon tetrachloride.

Iwamura et al. observed the frequencies of the N–H stretching in **8** and 9-(4-aminophenyl)fluorene (**10**), and proposed that the low frequency shift of the symmetric NH vibration in **8** relative to the para isomer **10** indicates the presence of N–H···π hydrogen bonding in **8**.[4] However, Ōki et al. have recently examined the N–H streching frequencies of 9-(2-amino-1-naphthyl)fluorene (*ap*- and *sp*-) (**11**) and 9-(2-methylamino-1-naphthyl)fluorene (*ap*- and *sp*-) (**12**). They have confirmed that the N–H···π interactions in **11**-*ap* and **12**-*ap* have little affected on the N–H stretching frequencies because the frequencies are almost the same in both the *ap*- and *sp*-rotamers.[6] Thus, unfortunately, the N–H···π interaction in **2**-*ap* had not been confirmed from its IR spectral behavior because **2** and **7** give the same N–H stretching frequencies.

DNMR spectra of **2** were measured in $CDCl_3$ containing D_2O. The *ap*-methyl signal was observed as a singlet peak because the vicinal N–H proton exchanges rapidly with D^+ (Fig. 4). By line-shape analyses of the methyl signal in the DNMR spectra,[7] the activation free energies ($\Delta G^{\ddagger}$) of internal rotation (*ap*⇄*sp*) of **2** in $CDCl_3$–D_2O were obtained as 15.5 and 15.9 kcal mol^{-1} for the *sp*→*ap* and *ap*→*sp* processes, respectively. As compared with the $\Delta G^{\ddagger}$ values in **1a** ($\Delta G^{\ddagger}_{sp\to ap}$=15.5, $\Delta G^{\ddagger}_{ap\to sp}$=13.8 kcal mol^{-1}; 1 cal=4.184 J), it turned out that the ground state of **2**-*d*-*ap* is considerably stabilized.

Variation of Conformational Equilibria of 2 by Adding Trifluoroacetic Acid in the Chloroform Solution. As shown above, it is recognized that compound **2** maintains an equilibrium *ap*/*sp*=2.1/1 in chloroform at −10 °C. When trifluoroacetic acid was added dropwise to the solution of **2** in chlorofrm, the ^1H NMR signal of the methylamino group gradually changed in an interesting manner as shown in Fig. 5.

Compound **2** reacts with trifluoroacetic acid and gives a salt ammonium trifluoroacetate. In the process shown in Fig. 5, we can explain the variation of the methyl signal on adding trifluoroacetic acid as follows. (1) In the case of [CF_3COOH]≦[**2**]: By protonation of the methylamino group, the *sp*-methyl signal (singlet) gradually develops with shift to lower field, while the *ap*-methyl signal (doublet) changes into a singlet and gradually sinks with shift to higher

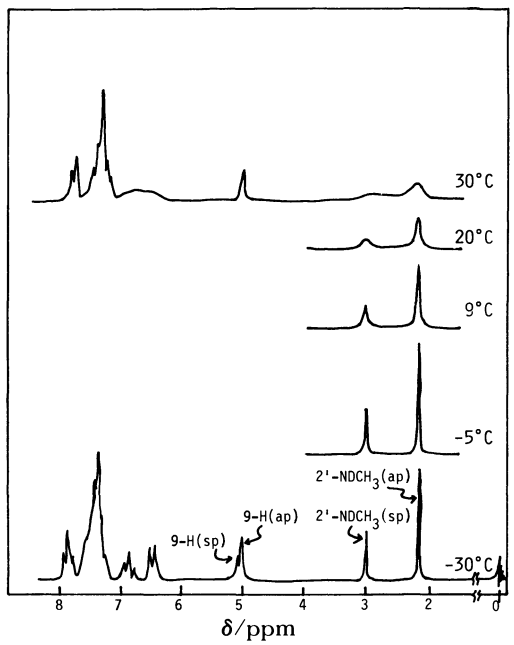

Fig. 4. Temperature-dependent spectra of **2** in $CDCl_3$–D_2O.

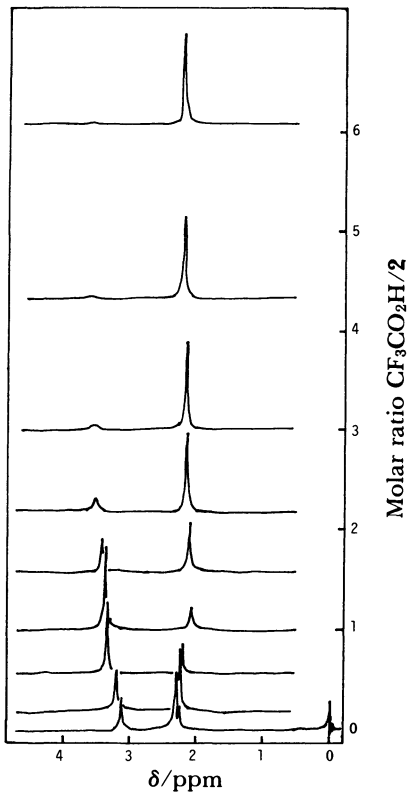

Fig. 5. ^1H NMR spectra of **2** and **2**–CF_3CO_2H salt at −10 °C.

field. That is, in the resulting ammonium trifluoroacetate the *sp*-form is more stable than the *ap*-form, contrary to the case of the free amine **2**. It is presumed that the trifluoroacetate ion acts as a medium to reduce the distance between the methylammonium group and the 9-proton (Fig. 6). This suggested bridging effect of the trifluoroacetate ion will make the *ap*⇄*sp* equilibrium incline predominantly to the *sp*-form. (2) In the case of [CF_3COOH]> [**2**]: The *sp* signal gradually shrinks with convergence to about δ 3.6, and the *ap* signal gradually enhances with convergence to about δ 2.2. That is, when excess equivalent of the acid is added, the trifluoroacetate ion associates with excess trifluoroacetic acid and loses its bridging effect between the methylammonium group and the 9-proton. In fact, with addition of methanol (or dimethylsulfoxide) to the solution of **2** in excess amount of acid, the *ap* signal, which had considerably developed, almost disappeared. In this case, the acid is associated with added methanol and its concentration is essentially diluted. Thus, it can be postulated that by increasing the concentration of the acid, the N–H···π interaction between the methylammonium group and the fluorene ring in the *ap*-salt predominates over the bridging effect of the trifluoroacetate ion in the *sp*-salt. In this way the *ap*-salt may be stabilized. Furthermore, in the case of [CF_3COOH]⩾[**2**], the *sp* signal almost disappears and the sharp *ap* signal (about δ 2.2) is observed. Accordingly, the N–H···π interaction makes the equilibria *ap*⇄*sp* incline to the *ap*-form, exclusively. However in any case, both the *ap*- and *sp*-methyl signals are probably observed together as weighted average of those of **2** and **2**-salt.

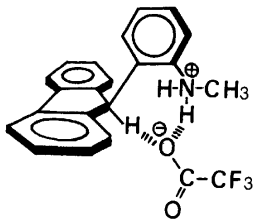

Fig. 6. A bridging effect of trifluoroacetate ion in **2**-*sp*-salt.

In this system, we can recognize a conformational equilibrium of **2** owing to the restricted rotation about the C(9)–C(Ar) bond, and both acid-base equilibria owing to the protonation of each conformer of **2** with trifluoroacetic acid, and additionally a conformational equilibrium exists between the two **2**-salts. Thus, at least the four equilibria described above participate in this system. The first and last equilibria can be determined by the relative stability of the two rotamers (*ap*- and *sp*-) in **2** and **2**-salt, respectively. Also the acid-base equilibria are governed by the concentration

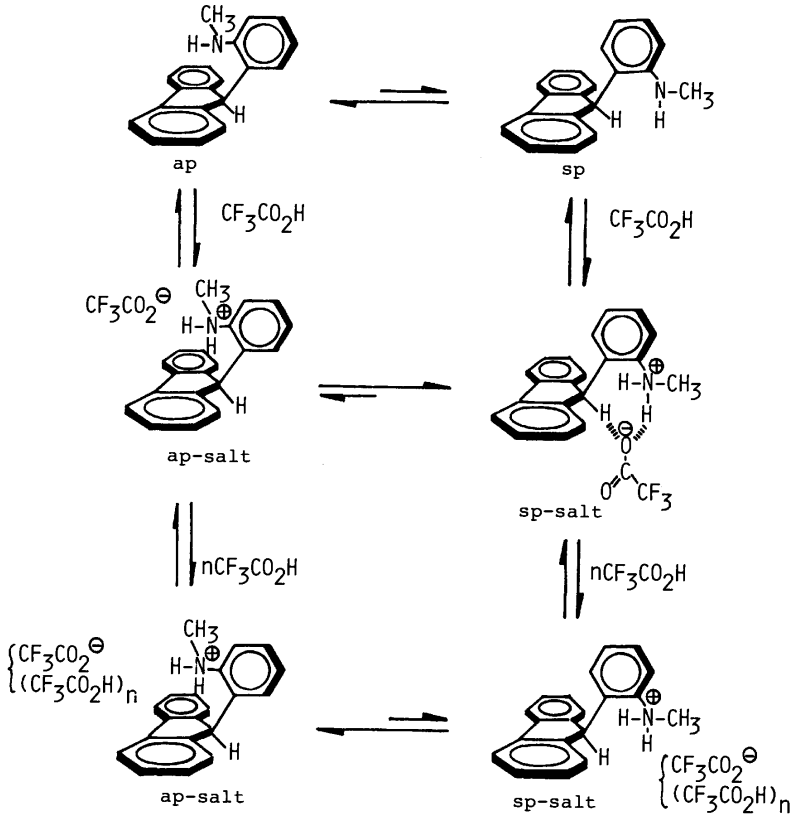

Fig. 7. Isomerization processes for **2** (*ap* and *sp*) and their trifluoroacetate salts.

of trifluoroacetic acid because the quantity of **2** is held constant. However, we consider that the stability of the rotamer may be independent of the rate of proton exchange between the acid and base.

We now show the above-mentioned interconversion for the conformers of the free amine **2** and its salt in Fig. 7.

Experimental

^{1}H NMR spectra were recorded on a JEOL-MH-100 spectrometer with a JEOL model JES-VT-3 variable temperature controller. The chemical shifts are expressed in ppm, with tetramethylsilane as an internal standard. Dynamic NMR spectra were analized by using a modified version of the computer program DNMR 3. The IR spectra were measured on a JASCO IRA-1 spectrometer solutions in carbon tetrachloride. Melting points are uncorrected.

9-(2-Methylaminophenyl)fluorene (2). To a solution of 9-(2-dimethylaminophenyl)-9-fluorenol (**1b**) (0.2 g, 0.7 mmol) in acetic acid (5 ml) was bubbled hydrogen bromide gas generated for 1 h. The mixture was concentrated, alkalized by sodium hydroxide solution, and extracted with benzene. The benzene solution was dried with magnesium sulfate, and concentrated in vacuo to obtain the residue which was recrystallized from acetone to give **2** as colorless needles; yield: 0.14 g (75%); mp 121—122 °C. IR (CCl_4): 3420 cm^{-1} (NH). Found: C, 88.38; H, 6.13; N, 5.05%. Calcd for $C_{20}H_{17}N$: C, 88.52; H, 6.32; N, 5.16%.

^{1}H NMR data of **2** in $CDCl_3$ at 25 and −30 °C were shown in Table 1.

9-(4-Dimethylaminophenyl)-9-fluorenol (6). A solution of fluorenone (1.8 g, 0.01 mol) in dry THF was added to the Grignard reagent prepared from magnesium turnings (0.4 g, 0.017 mol) and *p*-bromo-*N*,*N*-dimethylaniline (3 g, 0.015 mol). The mixture was refluxed for 1 h. After cooling, the solution was poured into dil. hydrochloric acid, alkalized by sodium hydroxide solution and extracted with benzene. The benzene solution was dried with magnesium sulfate, distilled off in vacuo, leaving a residue which was recrystallized from benzene to give **6** as colorless prisms; yield 2.0 g (66%); mp 157—158 °C. ^{1}H NMR ($CDCl_3$) δ=2.52 (1H, s, OH), 2.89 (6H, s, $2CH_3$), 6.68 (2H, d, J=8 Hz, 3′,5′-H), 7.16—7.73 (11H, m, 2′,6′-H and fluorenyl protons). Found: C, 83.99; H, 6.18; N, 4.41%. Calcd for $C_{21}H_{19}NO$: C, 83.69; H, 6.36; N, 4.65%.

9-(4-Dimethylaminophenyl)fluorene (9). Hydriodic acid (57%, 6.0 g, 50 mmol) was added to a solution of **6** (1.2 g, 4 mmol) in acetic acid (30 ml), and refluxed for 1.5 h. The reaction mixture was concentrated in vacuo to obtain a residue which was treated by sodium bisulfite, alkalized by sodium hydroxide solution, and extracted with benzene. The benzene solution was dried with magnesium sulfate and evaporated in vacuo to give **9** yield: 0.8 g (70%); colorless needles; mp 155—156 °C (from benzene-hexane (1:2)). ^{1}H NMR ($CDCl_3$) δ=2.92 (6H, s, $2CH_3$), 5.02 (1H, s, 9-H), 6.72 (2H, d, J=8 Hz, 3′, 5′-H), 7.06 (2H, d, J=8 Hz, 2′, 6′-H), 7.28—7.96 (8H, m, fluorenyl protons). Found: C, 88.72; H, 6.56; N, 4.68%. Calcd for $C_{21}H_{19}N$: C, 88.38; H, 6.71; N, 4.91%.

9-(4-Methylaminophenyl)fluorene (7). A solution of **9** (0.3 g, 1.05 mmol) and cyanogen bromide (0.3 g, 3.2 mmol) in acetone(5 ml) was refluxed for 16 h, and concentrated at atmospheric pressure to obtain a residue, which was extracted with dry ether. The ether filtrate was extracted with 15% hydrochloric acid solution and washed with water. The ether solution was dried with magnesium sulfate and concentrated in vacuo. The crude product (9[4-(*N*-cyano-*N*-methylamino)phenyl]fluorene (0.2 g)) was refluxed continuously in 20% hydrochloric acid solution for 6 h. The reaction mixture was alkalized by sodium hydroxide solution, extracted with benzene, dried with magnesium sulfate. The solution was evaporated in vacuo, leaving a residue which was column-chromatographed on alumina using benzene as an eluent to give **7**; yield: 0.06 g (22%); colorless needles; mp 126—127 °C. IR (CCl_4): 3420 cm^{-1} (NH). ^{1}H NMR ($CDCl_3$) δ=2.83 (3H, s, CH_3), 3.52 (1H, br. s, NH), 5.06 (1H, s, 9-H), 6.60 (2H, d, J=8 Hz, 3′,5′-H), 7.02 (2H, d, J=8 Hz, 2′,6′-H), 7.20—8.0 (8H, m, fluorenyl protons). Found: C, 88.40; H, 6.29; N, 5.07%. Calcd for $C_{20}H_{17}N$: C, 88.52; H, 6.32; N, 5.16%.

***N*-Methylation of 2.** To a solution of **2** (0.22 g, 0.8 mmol) was added methyl iodide (0.22 g, 1.6 mmol) and the mixture was allowed to stand for a week at room temperature. The reaction mixture was concentrated, alkalized by sodium hydroxide solution, and extracted with benzene. The benzene solution was dried with magnesium sulfate and the solvent distilled off in vacuo to give **1a**; yield: 0.14 g (60%); colorless crystals; mp 121—122 °C (from methanol–benzene). ^{1}H NMR ($CDCl_3$) δ=2.86 (6H, br.s, $2CH_3$), 5.86 (1H, br. s, 9-H), 6.34 (1H, d, 6′-H), 6.92—7.70 (11H, m, aromatic protons).

The authors wish to thank Professor Masashi Tashiro, Institute of Advanced Material Study, Kyushu University, for the elemental analyses, and are grateful for the financial support of this work by Research Grant-in-Aid from the Ministry of Education, Science and Culture (No. 60470023).

References

1) Part XII of this series: A. Nishida, S. Shirakawa, S. Fujisaki, and S. Kajigaeshi, *Mem. Fac. of Eng. Yamaguchi Univ.*, **38**, 269 (1988).

2) A. Nishida, M. Takeshita, S. Fujisaki, and S. Kajigaeshi, *Nippon Kagaku Kaishi*, **1987**, 1791.

3) H. Hageman, *Org. Reac.*, **7**, 198 (1953).

4) H. Tukada, M. Iwamura, T. Sugawara, and H. Iwamura, *Org. Mag. Reson.*, **19**, 78 (1982).

5) K. Nakanishi and P. H. Solomon, "Infrared Absorption Spectroscopy-Practical," 2nd ed., Holden-Day, San Francisco (1977).

6) K. Moriyama, N. Nakamura, M. Nakamura, and M. Oki, *Gazz. Chim. Ital.*, **117**, 655 (1987).

7) G. Binsch, *J. Am. Chem. Soc.*, **91**, 1304 (1969); H. Kihara, *JAPC*, **4**, 9 (1983).

Synthesis of Gramicidin S Analogues Consisting of Fourteen Amino Acid Residues

Makoto TAMAKI,* Michiaki TAKIMOTO, and Ichiro MURAMATSU†
Department of Chemistry, Faculty of Science, Toho University, Miyama, Funabashi-shi, Chiba 274
†Department of Chemistry, College of Science, Rikkyo University, Nishi-ikebukuro, Tokyo 171
(Received March 22, 1988)

Four cyclotetradecapeptides related to gramicidin S, *cyclo*(-Val-Orn-Leu-Leu-D-Phe-Pro-Leu-)$_2$ (14-peptide-**1**), *cyclo*(-Val-Orn-Leu-D-Leu-D-Phe-Pro-Leu-)$_2$ (14-peptide-**2**), *cyclo*(-Val-Orn-Leu-Leu-D-Phe-Pro-D-Leu-)$_2$ (14-peptide-**3**), *cyclo*(-Val-Orn-Leu-D-Leu-D-Phe-Pro-D-Leu-)$_2$ (14-peptide-**4**), were prepared in order to investigate the contribution of the ring size and the amino acid sequences around the Pro residue to the antibiotic activity and conformation. The CD spectra of these synthetic peptides in ethanol solutions were different from each other, indicating that they possess various conformations in ethanol solutions. 14-Peptides-**1**, -**2**, and -**3** showed 1/4—1/8 of the antibiotic activity of gramicidin S against the gram-positive microorganisms tested, whereas 14-peptide-**4** showed no activity. A clear relationship between CD spectra and the antibiotic activity of these synthetic peptides could not be found.

Gramicidin S-1 (GS)[1] is an antibiotic cyclodecapeptide, *cyclo*(-Val-Orn-Leu-D-Phe-Pro-)$_2$,[2] with a rigid β-pleated sheet conformation.[3] From numerous investigations of the relationship between the structure and the antibiotic activity of this antibiotic, it has been proposed that the D-Phe-Pro-Val sequence in the β-turn part is essential for its antibiotic activity.[4,5] On the other hand, we found during studies of an antibiotic cyclododecapeptide, gratisin (GR),[6] that *cyclo*(-Val-Orn-Leu-D-Phe-Pro-D-Tyr-)$_2$, *cyclo*(-Val-Orn-Leu-D-Phe-D-Tyr-Pro-)$_2$, and *cyclo*(-Val-Orn-Leu-Pro-D-Phe-D-Phe-)$_2$ possess a strong activity, although their sequences in the β-turn part are different from each other.[7] These results suggest that the presence of an amino acid residue, D-Tyr or D-Phe,

	1 2 3 4 5 6 7
14-peptide-1	cyclo(-Val-Orn-Leu-Leu-D-Phe-Pro-Leu-)$_2$
14-peptide-2	cyclo(-Val-Orn-Leu-D-Leu-D-Phe-Pro-Leu-)$_2$
14-peptide-3	cyclo(-Val-Orn-Leu-Leu-D-Phe-Pro-D-Leu-)$_2$
14-peptide-4	cyclo(-Val-Orn-Leu-D-Leu-D-Phe-Pro-D-Leu-)$_2$

Fig. 1. Primary structures of synthetic cyclotetradecapeptides.

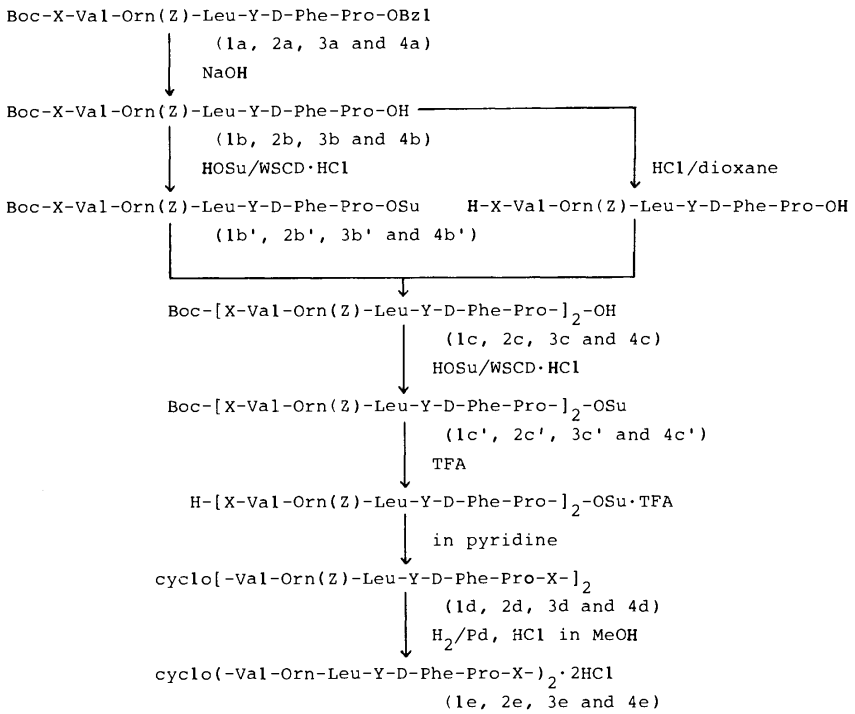

Fig. 2. Synthesis of cyclotetradecapeptides.
[X=Leu, Y=Leu (14-peptide-**1**), X=Leu, Y=D-Leu (14-peptide-**2**), X=D-Leu, Y=Leu (14-peptide-**3**), X=D-Leu Y=D-Leu (14-peptide-**4**)].

in gratisin peptides makes it possible for them to adopt a suitable conformation for antibiotic activity, regardless of the position of the Pro residue. Thus, it is of interest to study the structure–activity relationship of a cyclic peptide with a larger ring size than those of GS and GR. The configuration and the hydrophobic side chain of the amino acid residues around the D-Phe–Pro sequence are known to play an important role in stabilizing the β-turn formed by the D-Phe–Pro sequence.[4,7] In order to further investigate the contribution of the ring size and the amino acid sequence around the β-turn to the secondary structure and the antibiotic activity, we synthesized four cyclotetradecapeptides (Fig. 1) containing, respectively, partial sequences: Leu–D-Phe–Pro–Leu, D-Leu–D-Phe–Pro–Leu, Leu–D-Phe–Pro–D-Leu, and D-

Table 1. Yields, Physical Properties, and Analytical Data of Intermediary Products of 14-Peptide-**1**—**4**

		Yield/%	Mp θ_m/°C
1a	Boc-Leu-Val-Orn(Z)-Leu-Leu-D-Phe-Pro-OBzl	47	213—217
1b	Boc-Leu-Val-Orn(Z)-Leu-Leu-D-Phe-Pro-OH	88	196—198
1c	Boc-[Leu-Val-Orn(Z)-Leu-Leu-D-Phe-Pro-]$_2$-OH	83	255—260
1d	*cyclo*[-Val-Orn(Z)-Leu-Leu-D-Phe-Pro-Leu-]$_2$	55	>340
2a	Boc-Leu-Val-Orn(Z)-Leu-D-Leu-D-Phe-Pro-OBzl	68	210—215
2b	Boc-Leu-Val-Orn(Z)-Leu-D-Leu-D-Phe-Pro-OH	82	206—207
2c	Boc-[Leu-Val-Orn(Z)-Leu-D-Leu-D-Phe-Pro-]$_2$-OH	87	223—225
2d	*cyclo*[-Val-Orn(Z)-Leu-D-Leu-D-Phe-Pro-Leu-]$_2$	60	323—325 (decomp)
3a	Boc-D-Leu-Val-Orn(Z)-Leu-Leu-D-Phe-Pro-OBzl	71	204—207
3b	Boc-D-Leu-Val-Orn(Z)-Leu-Leu-D-Phe-Pro-OH	90	199—202
3c	Boc-[D-Leu-Val-Orn(Z)-Leu-Leu-D-Phe-Pro-]$_2$-OH	30	209—210
3d	*cyclo*[-Val-Orn(Z)-Leu-Leu-D-Phe-Pro-D-Leu-]$_2$	69	235—239
4a	Boc-D-Leu-Val-Orn(Z)-Leu-D-Leu-D-Phe-Pro-OBzl	44	190—194
4b	Boc-D-Leu-Val-Orn(Z)-Leu-D-Leu-D-Phe-Pro-OH	92	159—164
4c	Boc-[D-Leu-Val-Orn(Z)-Leu-D-Leu-D-Phe-Pro-]$_2$-OH	67	197—201
4d	*cyclo*[-Val-Orn(Z)-Leu-D-Leu-D-Phe-Pro-D-Leu-]$_2$	67	303—304

	$[\alpha]_D^{20}$/° (DMF)			Elemental analysis (%) C	H	N	R_f^1	R_f^2
1a	−39.09	$C_{62}H_{90}O_{12}N_8 \cdot 0.5H_2O$	C:	64.84	7.99	9.76	0.69	0.56
	(*c* 1.1)		F:	64.86	8.05	9.76		
1b	−42.25	$C_{55}H_{84}O_{12}N_8 \cdot 0.5H_2O$	C:	62.42	8.10	10.59	0.36	0.42
	(*c* 1.1)		F:	62.32	8.18	10.52		
1c	−32.72	$C_{105}H_{158}O_{21}N_{16} \cdot 2.5H_2O$	C:	62.26	8.11	11.06	0.29	0.31
	(*c* 1.1)		F:	62.18	8.10	11.21		
1d	−137.12	$C_{100}H_{148}O_{18}N_{16} \cdot 2H_2O$	C:	63.27	8.07	11.81	0.55	0.57
	(*c* 0.7)		F:	63.47	8.00	11.93		
2a	−23.73	$C_{62}H_{90}O_{12}N_8$	C:	65.36	7.96	9.83	0.63	0.51
	(*c* 1.2)		F:	65.12	8.14	9.51		
2b	−20.89	$C_{55}H_{84}O_{12}N_8 \cdot 0.5H_2O$	C:	62.42	8.10	10.59	0.36	0.43
	(*c* 1.5)		F:	62.32	7.93	10.56		
2c	−18.38	$C_{105}H_{158}O_{21}N_{16} \cdot 2.5H_2O$	C:	62.26	8.11	11.06	0.34	0.32
	(*c* 1.2)		F:	62.48	8.18	10.80		
2d	−37.10	$C_{100}H_{148}O_{18}N_{16} \cdot H_2O$	C:	62.88	8.04	11.92	0.55	0.42
	(*c* 0.6)		F:	63.90	7.89	11.93		
3a	−22.58	$C_{62}H_{90}O_{12}N_8$	C:	65.36	7.96	9.83	0.60	0.48
	(*c* 1.2)		F:	65.11	7.97	9.66		
3b	−23.62	$C_{55}H_{84}O_{12}N_8 \cdot H_2O$	C:	61.89	8.12	10.50	0.28	0.34
	(*c* 1.0)		F:	61.92	8.07	10.09		
3c	−18.72	$C_{105}H_{158}O_{21}N_{16} \cdot 2.5H_2O$	C:	62.26	8.11	11.06	0.20	0.24
	(*c* 0.9)		F:	62.59	8.03	10.78		
3d	−38.60	$C_{100}H_{148}O_{18}N_{16} \cdot 2.5H_2O$	C:	62.97	8.08	11.75	0.55	0.48
	(*c* 0.9)		F:	62.71	7.95	11.88		
4a	−2.57	$C_{62}H_{90}O_{12}N_8$	C:	65.36	7.96	9.83	0.71	0.61
	(*c* 1.2)		F:	65.10	8.02	9.90		
4b	+1.17	$C_{55}H_{84}O_{12}N_8 \cdot 0.5H_2O$	C:	62.42	8.10	10.59	0.40	0.50
	(*c* 1.0)		F:	62.36	8.00	10.91		
4c	−2.74	$C_{105}H_{158}O_{21}N_{16} \cdot 1.5H_2O$	C:	62.82	8.08	11.16	0.40	0.52
	(*c* 1.0)		F:	62.88	8.00	11.14		
4d	+28.88	$C_{100}H_{148}O_{18}N_{16} \cdot 2H_2O$	C:	63.27	8.07	11.81	0.68	0.61
	(*c* 0.7)		F:	63.36	7.99	11.90		

Table 2. Yields, Physical Properties, and Analytical Data of 14-Peptide-**1**—**4**

1e *cyclo*(-Val-Orn-Leu-Leu-D-Phe-Pro-Leu-)$_2$·2HCl
Yield, 85%; mp 291—294 °C (decomp); $[\alpha]_D^{20}$ −95.28° (*c* 0.45, EtOH); R_f^3 0.76, R_f^4 0.68.
Amino acid ratios: Val, 1.01; Orn, 0.88; Leu, 3.04; Phe, 1.09; Pro, 0.97.
MS (FAB), *m/z* 1594 ($C_{84}H_{136}O_{14}N_{16}$, MH^+). Found: C, 57.01; H, 8.20; N, 12.12%.
Calcd for $C_{84}H_{136}O_{14}N_{16}$·2HCl·6$H_2O$: C, 56.84; H, 8.52; N, 12.62%.

2e *cyclo*(-Val-Orn-Leu-D-Leu-D-Phe-Pro-Leu-)$_2$·2HCl
Yield, 83%; mp 281—283 °C (decomp); $[\alpha]_D^{20}$ −76.72° (*c* 0.37, EtOH); R_f^3 0.76, R_f^4 0.65.
Amino acid ratios: Val, 1.03; Orn, 0.88; Leu, 3.00; Phe, 1.20; Pro, 0.90.
MS (FAB), *m/z* 1594 ($C_{84}H_{136}O_{14}N_{16}$, MH^+). Found: C, 57.41; H, 8.21; N, 12.33%.
Calcd for $C_{84}H_{136}O_{14}N_{16}$·2HCl·5$H_2O$: C, 57.42; H, 8.49; N, 12.75%.

3e *cyclo*(-Val-Orn-Leu-Leu-D-Phe-Pro-D-Leu-)$_2$·2HCl
Yield, 88%; mp 234—238 °C; $[\alpha]_D^{20}$ −52.0° (*c* 0.3, DMF); R_f^3 0.77, R_f^4 0.66.
Amino acid ratios: Val, 1.03; Orn, 0.93; Leu, 3.02; Phe, 1.05; Pro, 0.97.
MS (SIMS), *m/z* 1594 ($C_{84}H_{136}O_{14}N_{16}$, MH^+). Found: C, 57.77; H, 8.04; N, 12.91%.
Calcd for $C_{84}H_{136}O_{14}N_{16}$·2HCl·5$H_2O$: C, 57.42; H, 8.49; N, 12.75%.

4e *cyclo*(-Val-Orn-Leu-D-Leu-D-Phe-Pro-D-Leu-)$_2$·2HCl
Yield, 76%; mp 280—282 °C (decomp); $[\alpha]_D^{20}$ −9.15° (*c* 0.27, EtOH); R_f^3 0.79, R_f^4 0.67.
Amino acid ratios: Val, 1.06; Orn, 0.91; Leu, 3.00; Phe, 1.22; Pro, 0.90.
MS (SIMS), *m/z* 1594 ($C_{84}H_{136}O_{14}N_{16}$, MH^+). Found: C, 58.89; H, 8.42; N, 13.29%.
Calcd for $C_{84}H_{136}O_{14}N_{16}$·2HCl·2.5$H_2O$: C, 58.93; H, 8.42; N, 13.09%.

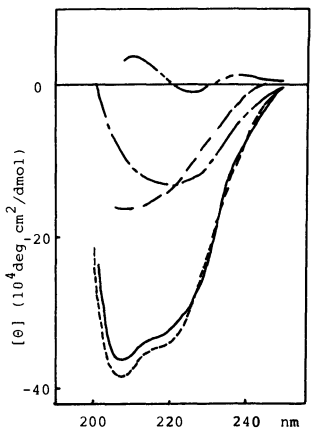

Fig. 3. CD spectra of synthetic cyclotetradecapeptides and GS in ethanol.
14-Peptide-**1** ——, 14-peptide-**2** — —, 14-peptide-**3** —·—, 14-peptide-**4** —···—, and GS ------.

Leu-D-Phe-Pro-D-Leu. The Leu residue was chosen as an amino acid residue having a hydrophobic side chain for an enlargement of the ring size.

These peptides were synthesized by conventional methods, as shown in Fig. 2. The yields, physical properties and analytical data regarding intermediary products are summarized in Table 1. The homogeneity of 14-peptide **1**—**4** was confirmed by means of thin-layer chromatography (TLC), amino acid analysis, high-performance liquid chromatography (HPLC), elemental analysis, and fast atom bombardment (FAB) or secondary ion (SI) mass spectrometry (Table 2).

The CD spectra of these synthetic peptides and GS in ethanol solutions are shown in Fig. 3. The spectral shapes of 14-peptide-**1**, -**2**, -**3**, and -**4** differ from each other, indicating that their peptides have different conformations in ethanol solutions. Recently, in CD spectroscopic studies of GS and GR, we reported that the CD spectra of their synthetic isomers could be classified into four groups, and that the isomers belonging to each group possess analogous partial sequences around the Pro residues.[5,7] 14-Peptide-**1**, having a D-Phe-Pro-Leu sequence, showed a similar CD curve to that of GS and GR-peptides having a D-Phe-Pro-X (X=Val or Tyr) sequence at the β-turn part, although the number of ring members of this peptide is different from that of GS or GR, and its ellipticity is almost the same as that of GS. This result indicates that 14-peptide-**1** possesses a conformation similar to that of GS in an ethanol solution, and that the amino acid sequence at the β-turn part makes a large contribution to the conformation. On the other hand, 14-peptides-**2**, -**3**, and -**4** showed CD spectra different from GS analogs and GR-peptides possessing Phe-Pro-D-X or D-Phe-Pro-D-X (X=Val or Tyr). These results suggest that it might be impossible to evaluate the contribution of the conformation around the Pro residue to the CD spectra of these 14-peptides by comparing their CD curves.

The antibiotic activity of these synthetic peptides against several microorganisms is summarized in Table 3. 14-Peptide-**1**, having a D-Phe-Pro-Leu sequence, showed 1/4—1/8 of the activity of GS against the gram-positive microorganisms tested. Recently, we reported that a GR-peptide having a D-Phe-Pro-Tyr sequence at the β-turn part possessed 1/4—1/16 of the activity of GS, and that its CD spectrum is similar to that of GS.[7] Supposing that the mode of action of these peptides having a -D-Phe-Pro- sequence at the β-turn part is the same as that of GS, the present results indicate that the ring size of a molecule is important in order to exhibit a strong and characteristic antibiotic activity, though it is not essential to exhibit activity. 14-Peptide-**2** and -**3** showed almost the same activity as that of 14-peptide-**1** toward gram-postive microorganisms, although their

Table 3. Antibiotic Activity of 14-Peptides-**1**—**4** and GS[a)]

Test organisms	GS	**1**	**2**	**3**	**4**
Staph. aureus MS353 C36 C	3.13	25	25	12.5	>50
Strept. pyogenes N.Y. 5	3.13	12.5	12.5	12.5	>50
Corynebact. diphtheriae P.W. 8	1.56	12.5	12.5	25	>50
Bac. subtilis ATCC 6633	3.13	12.5	25	25	>50
E. coli NIHJ-JC2	>100	>50	>100	>50	>50

a) Minimum inhibitory concentration ($\mu g\,ml^{-1}$) was determined by an agar dilution method with 10^6 organisms per milliliter.

sequences at the β-turn part are different from each other. Similar results were obtained in studies of peptides related to GR.[7] These results indicate that, for exhibiting activity, the amino acid sequence at the β-turn part is not limited to a D-Phe-Pro-Val sequence, which is of GS. On the other hand, 14-peptide-**4** showed no activity. This result indicates that Leu residues at positions 7 and 7′ in 14-peptide-**2**, or at positions 4 and 4′ in 14-peptide-**3**, could not be substituted by D-Leu residues without affecting the activities.

Experimental

All melting points are uncorrected. The CD spectra were obtained by use of a JASCO spectropolarimeter, model J-500, using a 0.5-mm quartz cell at room temperature. The CD spectroscopy of GS and four cyclotetradecapeptides were carried out with ethanol solutions of their dihydrochlorides at a concentration of 1.5—2.0×10^{-4} M (1 M=1 mol dm^{-3}). The molecular weights of these synthetic peptides were determined by FAB mass spectrometry using a JEOL JMS-D-300 mass spectrometer and SI mass spectrometry using a HITACHI M-80. Amino acid analyses were carried out by a Hitachi 835 amino acid analyzer, after hydrolysis of the peptides in 6 M HCl at 110 °C for 24 h. HPLC was performed by an ODS column (ϕ 4.6×250 mm) using MeOH-5% aq $NaClO_4$(5:1) as an elution solvent. TLC was performed on Merck silica-gel F_{254} plates with the following solvent systems (v/v): R_f^1, $CHCl_3$-MeOH (9:1); R_f^2, $CHCl_3$-MeOH-AcOH (95:5:3); R_f^3, *n*-BuOH-AcOH-H_2O (4:1:1); R_f^4, *n*-BuOH-pyridine-AcOH-H_2O (4:1:1:2). The yields of **1a**, **2a**, **3a**, and **4a** were calculated on the basis of the amount of Pro-OBzl as a starting material.

Boc-Leu-Val-Orn(Z)-Leu-Leu-D-Phe-Pro-OBzl (1a). HCl·Pro-OBzl (1.70 g, 7 mmol) was dissolved in $CHCl_3$ (30 ml); the solution was then washed with 5% Na_2CO_3 and water under cooling in an ice bath. To this solution were added Boc-D-Phe (1.85 g, 7 mmol), HOBt (1.08 g, 8 mmol) and WSCD·HCl (1.33 g, 7 mmol) at 0 °C. This solution was stirred for 1 h at 0 °C and 2 h at room temperature. The reaction mixture was washed successively with 5% citric acid, water, and 5% Na_2CO_3 and water; the solvent was then evaporated in vacuo. The residue was dissolved in 4 M HCl/dioxane (20 ml) at 0 °C. After stirring for 30 min at room temperature, the solution was concentrated in vacuo. The residue was dissolved in $CHCl_3$ (30 ml); the solution was then washed with 5% Na_2CO_3 and water under cooling in an ice bath. To this solution were added Boc-Leu(1.68 g, 7 mmol), HOBt (1.08 g, 8 mmol) and WSCD·HCl (1.33 g, 7 mmol) at 0 °C. The same procedure as described above was repeated for this reaction mixture. Further, Boc-Leu, Boc-Orn(Z), Boc-Val, Boc-Leu were successively coupled by the same method. All reactions were followed by TLC on a silica-gel plate. The crude protected heptapeptide obtained from the final reaction mixture was purified by reprecipitation from AcOEt-ether; overall yield, 3.73 g (47% from Pro-OBzl).

Compounds **2a**, **3a**, and **4a** were prepared in a similar manner. Compounds **2a** and **4a** were purified by chromatography on a silica-gel column (ϕ 1.2×40 cm) using a solvent system of $CHCl_3$-MeOH (50:1) and reprecipitation from AcOEt-ether.

Boc-Leu-Val-Orn(Z)-Leu-Leu-D-Phe-Pro-OH (1b). To a solution of **1a** (3.00 g, 2.63 mmol) in MeOH (20 ml) and dioxane (10 ml), 1 M NaOH (5.3 ml) was added. The solution was stirred for 10 h at room temperature. 5% citric acid (100 ml) was added to the reaction mixture. The resulting solid was collected by filtration, washed with water and dried. The product was recrystallized from MeOH-ether-hexane; yield 2.42 g (88%).

Compounds **2b**, **3b**, and **4b** were prepared in a similar manner.

Boc-[Leu-Val-Orn(Z)-Leu-Leu-D-Phe-Pro-]$_2$-OH (1c). To a solution of **1b** (1.05 g, 1.0 mmol) in DMF (10 ml) were added HOSu (0.23 g, 2.0 mmol) and WSCD·HCl (0.38 g, 2.0 mmol) at 0 °C, and then the mixture was stirred for 5 h at room temperature. After the solution was evaporated, water was added to the residue. The resulting solid, Boc-Leu-Val-Orn(Z)-Leu-Leu-D-Phe-Pro-OSu (**1b′**), was collected by filtration, washed with water and then dried. Another crop of **1b** (1.05 g, 1.0 mmol) was dissolved in 4 M HCl/dioxane (10 ml) at 0 °C. After stirring a room temperature for 30 min, the solution was concentrated in vacuo. To a solution of H-Leu-Val-Orn(Z)-Leu-Leu-D-Phe-Pro-OH (prepared as mentioned above) and TEA (0.28 ml, 2.00 mmol) in DMF (15 ml) at 0 °C was added **1b′** derived from **1b**. The mixture was left to stand for 2 h at 0 °C and overnight at room temperature. The solution was evaporated; then 5% citric acid was added to the residue. The resulting solid was collected by filtration, washed with water and then dried. The product was recrystallized from MeOH-ether-hexane; yield, 1.64 g (83%).

Compounds **2c**, **3c**, and **4c** were prepared in a similar manner.

***cyclo*[-Val-Orn(Z)-Leu-Leu-D-Phe-Pro-Leu-]$_2$ (1d).** Compound **1c** (0.80 g, 0.40 mmol) was converted into the *N*-hydroxysuccinimide ester (**1c′**) by the method described for **1c**. It was then dissolved in TFA (10 ml) at 0 °C. The mixture was stirred for 40 min at room temperature and then concentrated in vacuo. The residue, the trifluoroacetate of

the tetradecapeptide active ester, was triturated with ether and collected by filtration and dissolved in DMF (10 ml). The solution was poured, dropwise, into pyridine (350 ml) at 45 °C. After stirring for 3 h at 45 °C, the solution was concentrated. The addition of water to the residue afforded precipitates, which were filtered and washed with water. The purification of this compound was performed by chromatography on a silica-gel column (ϕ 1×20 cm) using a solvent system of $CHCl_3$–MeOH (50:1), followed by reprecipitation from MeOH–ether; yield, 0.41 g (55%).

Compounds **2d**, **3d**, and **4d** were prepared in a similar manner.

***cyclo*(-Val-Orn-Leu-Leu-D-Phe-Pro-Leu-)$_2$·2 HCl (1e).** Compound **1d** (121 mg, 0.065 mmol) was dissolved in 90% aq MeOH (15 ml) and dioxane (10 ml); then, 1 M HCl (0.15 ml) was added to the solution. This mixture was hydrogenolyzed in the presence of palladium black for 15 h. After removing the catalyst, the filtrate was concentrated in vacuo. The product was purified by gel filtration on a Sephadex LH-20 column (ϕ 1.2×120 cm) using MeOH as a solvent, and by reprecipitation from MeOH–ether; yield, 92 mg (85%).

Compounds **2e**, **3e**, and **4e** were prepared in a similar manner. However, in **2e**, the gel-filtration procedure was not required.

We are grateful to the staff of the Research Laboratories of Toyo Jozo Co. for elemental analyses, microbiological assays and the measurement of FAB mass spectra, and also to Professor Makoto Suzuki, Meijo University for the SIMS measurements.

References

1) Recently, it was reported that natural GS is a mixture of several homologs. The GS signified in the present paper corresponds to gramicidin S-1 in the report: S. Nozaki and I. Muramatsu, *J. Antibiot.*, **37**, 689 (1983).

2) Amino acid residues with no prefix are of L-configuration unless otherwise noted. The abbreviations for amino acids and peptides are in accordance with the rules of IUPAC-IBU Commission of Biological Nomenclature. Abbreviations used are as follows: Boc, *t*-butoxycarbonyl; Z, benzyloxycarbonyl; OBzl, benzyloxy; HOBt, 1-hydroxybenzotriazole; HOSu, *N*-hydroxysuccinimide; WSCD·HCl, 1-ethyl-3-(3-dimethylaminopropyl)carbodiimidehydrochloride; DMF, *N*,*N*-dimethylformamide; AcOEt, ethyl acetate; TEA, triethylamine; TFA, trifluoroacetic acid.

3) D. C. Hodgkin and B. M. Oughton, *Biochem. J.*, **65**, 752 (1957).

4) N. Izumiya, T. Kato, H. Aoyagi, M. Waki, and M. Kondo, "Synthetic Aspects of Biologically Active Cyclic-peptide-Gramicidin S and Tyrocidines," Kodansha, Tokyo, and Halsted Press, New York (1979), pp. 49—97.

5) M. Tamaki, T. Okitsu, M. Araki, H. Sakamoto, M. Takimoto, and I. Muramatsu, *Bull. Chem. Soc. Jpn.*, **58**, 531 (1985).

6) An antibiotic peptide, gratisin, showing activity toward Bacillus subtilis 720 was isolated from *Bacillus brevis* Y-33 by Silaev et al. The primary structure of gratisin was proposed to be a cyclic dodecapeptide, *cyclo*(-Val-Orn-Leu-Phe-Pro-Tyr-)$_2$. However, the configuration of each amino acid residue has not yet been established. G. G. Zharikova, S. P. Myaskovskaya, and A. B. Silaev, *Vestn. Mosk. Univ., Biol. Pochovoved.*, **27**, 110 (1972); *Chem. Abstr.*, **77**, 162982p (1972); S. P. Myaskovskaya, G. G. Zharikova, and A. B. Silaev, *Vestn. Mosk. Univ. Biol. Pochovoved.*, **28**, 123 (1973); *Chem. Abstr.*, **80**, 37446c (1974).

7) M. Tamaki, *Bull. Chem. Soc. Jpn.*, **57**, 3210 (1984).

 © 1988 The Chemical Society of Japan Bull. Chem. Soc. Jpn., 61, 3931—3942 (1988)

Se-Aryl Alkane- or Arenecarboselenothioates: Synthesis and Some Reactions[1)]

Shinzi KATO,* Eiji YASUI, Kiyomitsu TERASHIMA, Hideharu ISHIHARA, and Toshiaki MURAI

Department of Chemistry, Faculty of Engineering, Gifu University, 1-1 Yanagido, Gifu 501-11

(Received March 30, 1988)

A series of *Se*-aryl carboselenothioates **3** (RCSSeAr, R=alkyl, aryl) were synthesized and characterized from the reaction of bis(thioacyl) sulfides **1** with sodium areneselenolates. The thionselenolesters **3** are stable (liquid or crystals) both thermally and to moisture. Reactions of **3** with aliphatic primary and secondary amines gave the corresponding ammonium carbodithioates **8** together with diphenyl diselenide **7**. In contrast, treatment with aromatic amines or sodium alcoholates afforded the corresponding thioamides or *O*-alkyl or *O*-aryl thionesters in good yields. The oxidation of **3** with *m*-chloroperbenzoic acid gave the corresponding sulfides **12** [RCS(O)SeAr] and acyl arylseleno sulfides **13** [RCOSSeAr] which are formed by a rearrangement of the ArSe group to the thiocarbonyl sulfur atom.

In the past decades, a number of esters of carboselenoic and carbotelluroic acids (RCOER', E=Se, Te) have been prepared and their physical and chemical properties have been revealed.[2)] In contrast, the chemistry of carboselenothioic acid esters **3** (RCSSeR')[3)] (hereafter cited as thionselenolesters) have virtually not been studied, because of their synthetic difficulty, though they are interesting compounds synthetically and spectroscopically. In earlier studies, we succeeded in isolating bis(thioacyl) sulfides **1**[4)] and demonstrated that they are very useful for the thioacylation of amines, alcoholates, and thiolates.[5)] We now wish to report on the synthesis of a series of thionselenolesters **3** from the reaction of bis(thioacyl) sulfides **1** with sodium areneselenolates and their various reactions.

Results and Discussion

For the synthesis of thionselenolesters **3**, the reaction conditions (using bis[4-methyl(thiobenzoyl)] sulfide **1i** and sodium benzeneselenolate) have been preliminary investigated in detail. As a result, the reaction conditions of bis(thioacyl) sulfides with a large excess of sodium areneselenolate at 0 °C for 1 h seemed to be preferable. For example, when a dichloromethane solution of the sulfide **1i** was added to three equivalents of sodium benzeneselenolate in ethanol at 0 °C, the color of the mixture quickly changed from dark green to reddish pink. After the usual work-up of the reaction mixture, a chromatographic separation on silica gel afforded 73% of *Se*-

Table 1. Yields and Bp or Mp of *Se*-Aryl Alkane- and Arenecarboselenothioates **3**

No.	RCSSeAr R	Ar	Method[a)]	Yield[b)] %	Bp (°C/Torr)[c)] or Mp (°C)
3a	CH_3	C_6H_5	A	26	85 / 1.5
3b	C_2H_5	C_6H_5	A	51	114 / 3.5
3c	n-C_3H_7	C_6H_5	A	68	127 / 3.5
3d	i-C_3H_7	C_6H_5	A	77	111 / 3.0
3e	n-C_4H_9	C_6H_5	A	60	132 / 3.5
3f	n-C_5H_{11}	C_6H_5	A	69	152 / 3.5
3g	*cyclo*-C_6H_{11}	C_6H_5	A	83	119 / 1.0
3h	C_6H_5	C_6H_5	A	44	44—46
			B	60	
			C	12	
3i	4-$CH_3C_6H_4$	C_6H_5	A	73	83—84
			B	77	
			C	12	
3j	4-$CH_3C_6H_4$	4-$CH_3C_6H_4$	A	81	118—120
3k	4-$CH_3C_6H_4$	4-ClC_6H_4	A	70	96—97
3l	2,4,6-$(CH_3)_3C_6H_2$	C_6H_5	A	0	
3m	4-$CH_3OC_6H_4$	C_6H_5	A	68	63—65
			B	31	
			C	0	
3n	4-ClC_6H_4	C_6H_5	A	78	87—88
			B	80	
			C	37	

a) Method A: $(RCS)_2S$+ArSeNa; Method B: RCSCl+ArSeNa; Method C: RCSCl+$ArSeSi(CH_3)_3$. b) Isolated yield. c) Kugelrohr oven temp, 1 Torr≈133.322 Pa.

phenyl 4-methylbenzenecarboselenothioate **3i** as reddish-pink crystals. Through an analogous treatment of other bis(thioacyl) sulfides **1a—h, j—n** with sodium areneselenolates, the corresponding aliphatic and aromatic thionselenolesters **3a—h, j—n** were isolated in good yields[6] (Eq. 1, Table 1). However, a number

$$\underset{\mathbf{1}}{RC(=S)-S-C(=S)R} + \underset{\mathbf{2}}{ArSeNa} \xrightarrow[CH_2Cl_2/CH_3OH]{0\,^\circ C,\ 30\ min} \underset{\mathbf{3}}{R-C(=S)-SeAr} \quad (1)$$

(Method A)

No.	R	Ar
3a	CH_3	C_6H_5
3b	C_2H_5	C_6H_5
3c	n-C_3H_7	C_6H_5
3d	i-C_3H_7	C_6H_5
3e	n-C_4H_9	C_6H_5
3f	n-C_5H_{11}	C_6H_5
3g	*cyclo*-C_6H_{11}	C_6H_5
3h	C_6H_5	C_6H_5
3i	4-$CH_3C_6H_4$	C_6H_5
3j	4-$CH_3C_6H_4$	4-$CH_3C_6H_4$
3k	4-$CH_3C_6H_4$	4-ClC_6H_4
3l	2,4,6-$(CH_3)_3C_6H_2$	C_6H_5
3m	4-$CH_3OC_6H_4$	C_6H_5
3n	4-ClC_6H_4	C_6H_5

of attempts to prepare a sterically hindered 2,4,6-trimethylphenyl derivative **3l** failed. In order to make a comparison with the above mentioned method, the following two synthetic methods were also examined: a) Reaction of thioacyl chloride with sodium benzeneselenolate (Method B) and b) with (phenylseleno)-trimethylsilane (Method C) (Eq. 2). As shown in

$$\underset{\mathbf{4}}{RC(=S)Cl} + \underset{\mathbf{2}}{C_6H_5SeNa} \xrightarrow[\text{Method B}]{0\,^\circ C,\ 30\ min,\ CH_2Cl_2} \underset{\mathbf{3}}{}$$

$$\underset{\mathbf{4}}{} + \underset{\mathbf{5}}{C_6H_5SeSi(CH_3)_3} \xrightarrow[\text{Method C}]{40\,^\circ C,\ 30\ min,\ CH_2Cl_2} \underset{\mathbf{3}}{} \quad (2)$$

Table 1, the former method led to analogous yields of **3**, while the later to low yields, because of the unexpected low reactivity of (phenylseleno)trimethylsilane.[7] It is noted that both methods are limited to the synthesis of aromatic derivatives (**3**, R=aromatic), because of a synthetic difficulty involving aliphatic thioacyl chlorides.[8]

The structures of the obtained thionselenolesters **3** were determined on the basis of mass, IR, UV/Vis, and ^1H and ^{13}C NMR spectroscopic data, and the results of microanalysis. The stretching frequencies, n–π^* transitions, and ^{13}C NMR spectra of the thiocarbonyl group of **3** are summarized in Table 2.

The thionselenolesters **3** are colored compounds: aliphatic derivatives (R=aliphatic) are yellow to orange and aromatic ones (R=aromatic) are red to reddish pink. They are stable both thermally and to moisture. They did not change at room temperaure for one week and can be storred in the refrigerator (0 °C) for over 3 years.

Spectra. It is known that νC=S bands of dithiocarboxylic acid esters appear in the region 1100—1200 cm^{-1} for the aliphatic derivatives and 1200—1250 cm^{-1} for the aromatic ones. As listed in Table 2, the characteristic thiocarbonyl stretching frequencies of **3** were observed in the 1220—1250 cm^{-1} region for the aliphatic derivatives and the 1000—1200 and/or 840—900 cm^{-1} regions for the aromatic derivatives. In the electron spectra of **3**, two characteristic absorption maxima were observed at 300—320 nm (π–π^*) and 480—495 nm (n–π^*,[10] C=S group) for the aliphatic derivatives and 530—540 nm (n–π^*,[10] C=S group) for the aromatic ones. The π–π^* and n–π^* transitions of the C=S group of *O*-phenyl 4-methylbenzenecarbothioate **11c**, phenyl 4-methylbenzenecarbodithioate **18**, and *Se*-phenyl 4-methylbenzenecarboselenothioate **3i** in both cyclohexane and ethanol are collected in Table 3. In going from E=*O*, to *S*, and *Se*, both absorption maxima shift to a longer-wavelength region. This is the first example of a bathochromic effect regarding the π–π^* and n–π^* transitions by an

Table 2. The IR, Visible, and ^{13}C NMR Spectra of the C=S Group of **3**

No.	RCSSeAr R	Ar	IR (neat) νC=S/cm^{-1}	Vis (hexane) λ_{max}/nm (log ε)	^{13}C NMR[c] [δ] (C=S)
3a	CH_3	C_6H_5	1195, 831	492	240.1
3b	C_2H_5	C_6H_5	1191, 860	486	246.4
3c	n-C_3H_7	C_6H_5	1184, 832	486	244.4
3d	i-C_3H_7	C_6H_5	1210	493	242.2
3e	n-C_4H_9	C_6H_5	1180, 867	486	244.3
3f	n-C_5clH_{11}	C_6H_5	1170, 878	486	245.4
3g	*cyclo*-C_6H_{11}	C_6H_5	1190, 860	488	250.2
3h	C_6H_5	C_6H_5	1245[a]	542 (1.92)	232.2
3i	4-$CH_3C_6H_4$	C_6H_5	1250[a]	541 (1.97)[b]	231.8
3j	4-$CH_3C_6H_4$	4-$CH_3C_6H_4$	1250[a]	528 (2.05)	232.4
3k	4-$CH_3C_6H_4$	4-ClC_6H_4	1223[a]	540 (1.99)	230.7
3m	4-$CH_3OC_6H_4$	C_6H_5	1240[a]	538 (2.09)	229.5
3n	4-ClC_6H_4	C_6H_5	1238[a]	542 (1.92)	230.5

a) KBr. b) CH_2Cl_2. c) $CDCl_3$.

Table 3. The π-π^* and n-π^* Transitions of *O*-Phenyl 4-Methylbenzenecarbothioate (**11c**), Phenyl 4-Methylbenzenecarbodithioate (**18**), and *Se*-Phenyl 4-Methylbenzenecarboselenothioate (**3i**) and ^{13}C NMR Spectra of the Thiocarbonyl Groups

No.	R-C(=S)-E-C$_6$H$_5$ R	E	λ_{max}/nm π-π^* *cyclo*-C$_6$H$_{12}$	π-π^* C$_2$H$_5$OH	n-π^* *cyclo*-C$_6$H$_{12}$	n-π^* C$_2$H$_5$OH	^{13}C=S (CDCl$_3$) [δ]
11c	4-CH$_3$C$_6$H$_4$	O	297	301	438	431	210.9
18	4-CH$_3$C$_6$H$_4$	S	310	314	528	518	227.6
3i	4-CH$_3$C$_6$H$_4$	Se	314	319	540	533	231.8
	4-CH$_3$C$_6$H$_4$	Te	318 (?)		550 (?)		236 (?)

Table 4. Selected Ions from Mass Spectra (70 eV) of *Se*-Phenyl 4-Methylbenzenecarbothioselenoate (**3i**), and *O*-Phenyl 4-Methylbenzenecarbothioate (**11c**), and Phenyl 4-Methylbenzenecarbodithioate (**18**)

4-CH$_3$C$_6$H$_4$C(S)SeC$_6$H$_5$	*m/z*	RI	4-CH$_3$C$_6$H$_4$C(S)OC$_6$H$_5$	*m/z*	RI	4-CH$_3$C$_6$H$_4$CS$_2$C$_6$H$_5$	*m/z*	RI
[C$_3$H$_3$]$^+$	39	9	[C$_3$H$_3$]$^+$	39	31	[C$_3$H$_3$]$^+$	39	14
[C$_4$H$_3$]$^+$	51	12	[C$_4$H$_3$]$^+$	51	17	[C$_4$H$_3$]$^+$	51	9.5
[C$_5$H$_5$]$^+$	65	14	[C$_5$H$_5$]$^+$	65	35	[C$_5$H$_5$]$^+$	65	25
[C$_6$H$_5$]$^+$	77	13	[C$_6$H$_5$]$^+$	77	10.5	[C$_6$H$_5$]$^+$	77	4.5
[CH$_3$C$_6$H$_4$]$^+$	91	30	[CH$_3$C$_6$H$_4$]$^+$	91	61.5	[CH$_3$C$_6$H$_4$]$^+$	91	39.5
[C$_6$H$_5$S]$^+$	109	2.5	[C$_6$H$_5$O]$^+$	93	5.5	[C$_6$H$_5$S]$^+$	109	13.5
[CH$_3$C$_6$H$_4$C≡S]$^+$	135	100	[C$_6$H$_5$S]$^+$	109	7	[CH$_3$C$_6$H$_4$C≡S]$^+$	135	100
[C$_6$H$_5$Se]$^+$	157	7	[CH$_3$C$_6$H$_4$C≡O]$^+$	119	53	[M]$^+$	244	
[CH$_3$C$_6$H$_4$C≡Se]$^+$	183	2.5	[CH$_3$C$_6$H$_4$C≡S]$^+$	135	100			
[M]$^+$	292		[M]$^+$	228				

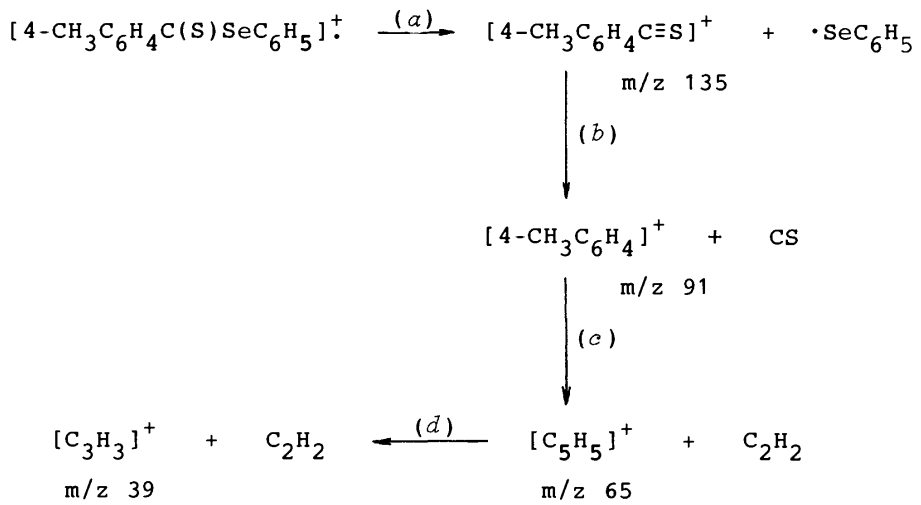

Scheme 1.

adjacent chalcogen element. In ^{13}C NMR spectra, ^{13}C=S values appear at δ 240—246 for the aliphatic derivatives and at 229—233 for the aromatic derivatives, respectively. As shown in Table 3, lower-field shifts of the thiocarbonyl carbon of the thion- **11c**, dithio- **18**, and thionselenolesters **3i** were observed in going from E=*O*, to *S*, and *Se*. Analogous lower shifts of the carbonyl carbon were observed for chalcogeno esters (RCOER′, E=*O*, *S*, *Se*, *Te*).[2]

It is well-known that *S*-alkyl benzenecarbothioates undergo a rearrangement of the alkyl group to the carbonyl oxygen atom, while the alkyl group of *O*-alkyl benzenecarbothioates migrates to the thiocarbonyl sulfur atom.[11-14] The obtained thionselenolesters **3** all afforded molecular ions. The fragment ions and the relative intensity of the 4-methyl derivative **3i** together with those of the corresponding thion- **11c** and dithioester **18** are shown in Table 4. As shown in the table, the cleavage pattern of the thionselenolester is substantially similar to those of the corresponding thion- and dithioesters.[15] Thus, the base peak is [4-CH$_3$C$_6$H$_4$C≡S]$^+$ peak at *m/z* 135 and the second highest one is the [C$_7$H$_7$]$^+$ peak at *m/z* 91; other significant peaks are those of the [C$_5$H$_5$]$^+$, [C$_6$H$_5$]$^+$, [C$_4$H$_3$]$^+$, [C$_3$H$_3$]$^+$, and [C$_6$H$_5$Se]$^+$, ions at *m/z* 65, 77, 51, 39, and 157, respectively. The most important successive frag-

mentations are (*a*)→(*b*)→(*c*), and→(*d*) (Scheme 1). In addition to these peaks, two characteristic peaks at *m/z* 183 and 109 can be observed corresponding to $[CH_3C_6H_4C{\equiv}Se]^+$ and $[C_6H_5S]^+$, respectively. This fact suggests a possible rearrangement of the phenyl group to the thiocarbonyl sulfur atom, followed by a fragmentation ion (**I**), though no metastable peaks corresponding to the fragmentation from the ion (**I**) could be observed (Scheme 2). Such a migration of the phenyl group bonded to a Se atom to the thiocarbonyl sulfur atom is the first example.

Reactions: In general, thion-[16] and dithioesters[17,18] react with primary and secondary amines to give the corresponding thioamides. In order to clarify the reactivity of the thionselenolester **3i**, several reactions with nucleophiles, such as amines and alcoholates, and oxidation by *m*-chloroperbenzoic acid were carried out using the 4-methyl derivative **3i** as the model thionselenolester. In Table 5, the reaction conditions of **3i** with primary and secondary amines and the products are summarized. At room temperature, **3i** does not react with an aromatic amine, such as aniline, though the reaction does occur under reflux in hexane to afford the corresponding thioanilide **6a** and diphenyl diselenide **7** in 68 and 99%, respectively. In contrast, the reaction with aliphatic amines, such as cyclohexylamine, diethylamine, and piperidine, occurrs at room temperature to give the corresponding ammonium salts **8** in 30—40% yields together with diselenide **7** and a dark-brown oil. No formation of the expected thioamides was observed.[18] In these reactions, the yields of diphenyl diselenide were quantitative. Over 60% the sulfur in the used **3i** was recovered as a dithio salt **8**, while the recovery of the $CH_3C_6H_4$ moiety was less than 45%. In order to elucidate the formation mechanism of **8**, a number of attempts to analyze the dark-brown oily substances have been undertaken. However, at the present stage, no appropriate explanation has been found regarding the formation of the ammonium dithiocarboxyates **8**.

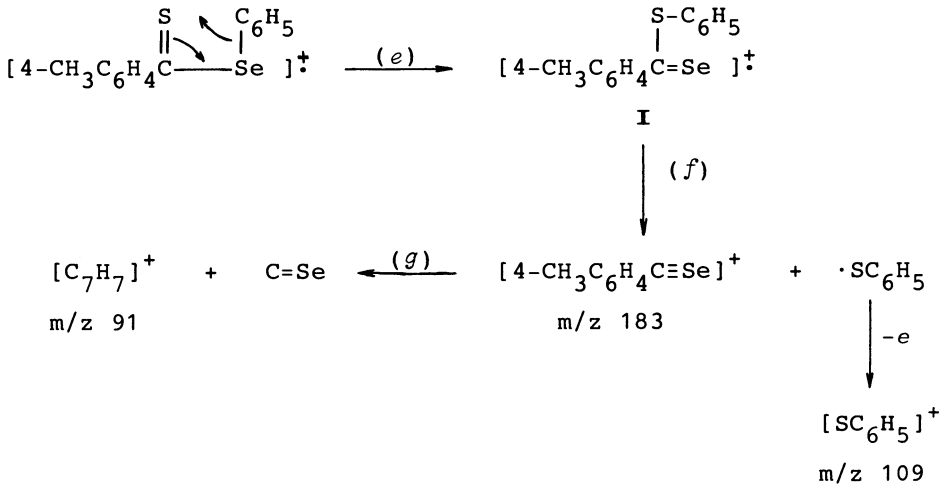

Scheme 2.

Table 5. Reaction of Thionselenolesters **3i** with Amines[a]

$ArCSSeC_6H_5$ Ar	Ar′ or R_2NH	Solvent	Temp °C	Time h	Product/% $ArCSNHAr'$ (**6**)	$ArCS_2^-NH_2R_2$ (**8**)	$C_6H_5SeSeC_6H_5$ (**7**)
4-$CH_3C_6H_4$	$C_6H_5NH_2$	*n*-C_6H_{14}	69	24	68 (**6a**)		99
3i	*cyclo*-$C_6H_{11}NH_2$	*n*-C_6H_{14}	20	5		40 (**8a**)	90
	$(C_2H_5)_2NH$	*n*-C_6H_{14}	25	24		44 (**8b**)	94
		n-C_6H_{14}	20	0.5		31 (**8c**)	97
	NH_2NH_2	*n*-C_6H_{14}	18	1	29 (**6b**)		
		C_2H_5OH	20	1	78 (**6b**)		98
		C_2H_5OH	78	24	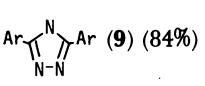 (**9**) (84%)		
	$NH_2CSNHNH_2$	C_2H_5OH	78	6	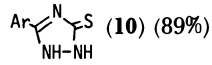 (**10**) (89%)		

a) Mole ratio: **3i**/NH_2NH_2=1:2.

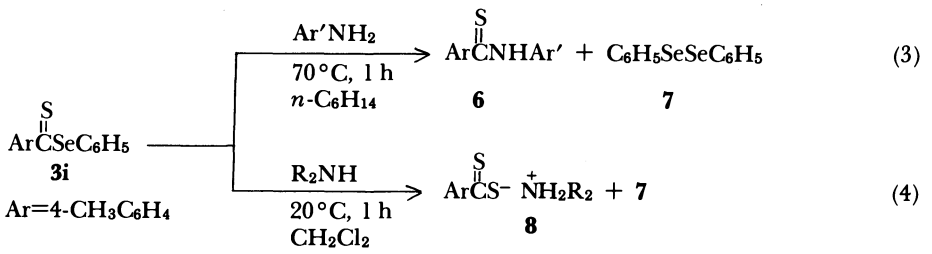

No.	Ar'
6a	C_6H_5
6b	NH_2
6c	NH_2CSNH

No.	R_2NH
8a	*cyclo*-$C_6H_{11}NH_2$
8b	$(C_2H_5)_2NH$
8c	

The reaction with hydrazine at room temperature readily proceeded to give the corresponding thiohydrazide **6b**. When the reaction was carried out under reflux in ethanol, however, 1,3,4-thiadiazole **9** was obtained in a good yield. In addition, a reaction with thiosemicarbazide under the same conditions yielded 3,4-dihydro-2*H*-1,3,4-triazole-2-thione (**10**) in an almost quantitative yield. Presumably, **9** and **10** would be formed via the corresponding thioamide **6b** or **6c**, respectively. The same products **9** and **10** were obtained in reactions using the corresponding dithioesters **18**.

The thionselenolesters **3** do not react with methanol and ethanol at room temperature and even under refluxing conditions. However **3i** readily reacted with alkali metal alcoholates at room temperature to give the corresponding thionesters **11** in good yields (Eq. 5, Table 6). The formation of those thionesters seemed to proceed more smoothly than in cases using the corresponding phenyl arenecarbodithioates.[19]

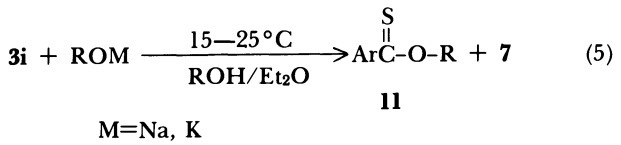

(5)

No.	R
11a	CH_3
11b	C_2H_5
11c	C_6H_5

The oxidation of dithioesters with peroxy acid provides a route to (alkyl- or arylthio)-, (alkyl- or arylsulfinyl)-, and (alkyl- or arylsulfonyl)sulfines.[20] The thionselenolesters **3i** upon treatment with peroxy acids are expected to produce the corresponding sulfines. In fact, the treatment of *Se*-phenyl 4-methylbenzenecarboselenothioate **3i** with one equivalent of *m*-chloroperbenzoic acid (mCPBA) in ether at 0 °C gave a 34% yield of a mixture of two isomeric phenylseleno(4-methylphenyl)sulfines (**12i** and **12'i**). No formation of the expected phenyl selenenyl (PhSeO–CSO–$C_6H_4CH_3$-4) and phenylselenonylsulfines (PhSeO$_2$–CSO–$C_6H_4CH_3$-4) were observed. Instead, phenylseleno 4-methylbenzoyl sulfides (**13i**), bis(4-methylbenzoyl) disulfide (**14**, R=4-$CH_3C_6H_4$), and diphenyl diselenide (**7**) were obtained in 11, 3, and 14% yields, respectively. Similarly, the oxidation of the aliphatic thionselenolesters, **3d** and **3e** afforded the corresponding sulfines as a mixture of the trans- (**12d**, **12e**) and cis-isomer (**12'd**, **12'e**), phenylseleno acyl sulfides **13d**, **13e**,[1] and diphenyl diselenide **7** in analogous yields.[21] The trans- **12** and cis-isomer **12'** were separated by thin-layer chromatography. The structures of the products, **12**, **13**, **14**, were established on the basis of the IR, ^1H and ^{13}C NMR, and mass spectra, and/or by comparisons of the spectra with those of authentic samples. In addition, the conformation of the trans- **12e** and cis-isomer **12'e** were deduced by the ^1H NMR spectra. For example, the methine and methylene protons of the trans- **12e** were shifted down field, compared with those of the cis-isomers **12'd** and **12'e**, respectively. In addition, the ortho-protons on the 4-methylbenzene ring of the trans-isomer **12i** showed a broad multiplet without

Table 6. Reaction of Thionselenolesters **3i** with Sodium Alcoholates

$ArCSSeC_6H_5$ Ar	ROM[a]	Solvent	Temp °C	Time h	Product/% ArCSOR (**11**)	Product/% $C_6H_5SeSeC_6H_5$ (**7**)
4-$CH_3C_6H_4$ **3i**	CH_3ONa	$(C_2H_5)_2O/CH_3OH$	20	2	86 (**11a**)	90
	C_2H_5ONa	$(C_2H_5)_2O/C_2H_5OH$	22	2	91 (**11b**)	95
	C_6H_5ONa	$(C_2H_5)_2O$	18	24	79 (**11c**)	90

a) Mole ratio: **3i**/ROM=1:1.

Table 7. Reaction of Thionselenolesters **3** with *m*-Chloroperbenzoic Acid[a)]

$RCSSeC_6H_5$ (**3**) R	Product/% Diselenide (**7**)	*trans*-Sulfine (**12**)	*cis*-Sulfine (**12′**)	$RCOSSeC_6H_5$	Disulfide (**14**)
i-C_3H_7 (**3d**)	35	13 (**12d**)	13 (**12′d**)	19 (**13d**)	—
n-C_4H_9 (**3e**)	Trace	32 (**12e**)	21 (**12′e**)	38 (**13e**)	—
4-$CH_3C_6H_4$ (**3i**)	14	26 (**12i**)	8 (**12′i**)	11 (**13i**)	3

a) Reaction conditions: 0 °C, 90 min in ether; mole ratio **3**/*m*-CPBA=1:1.

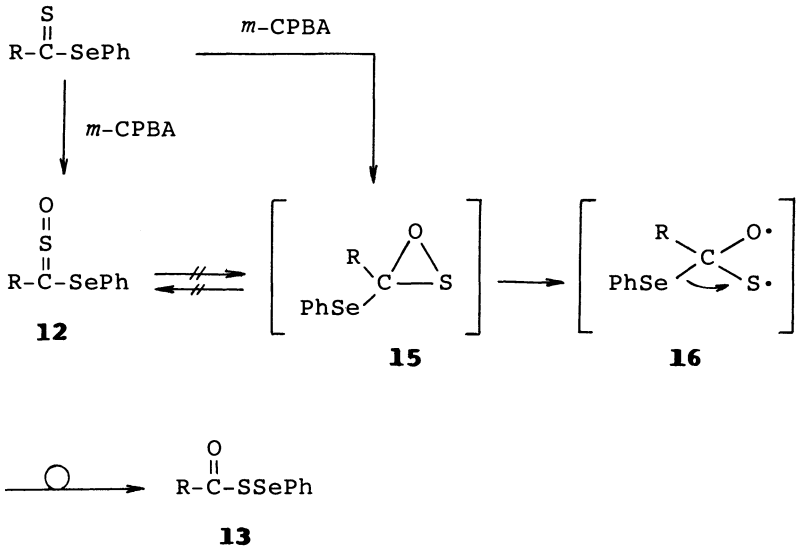

Scheme 3.

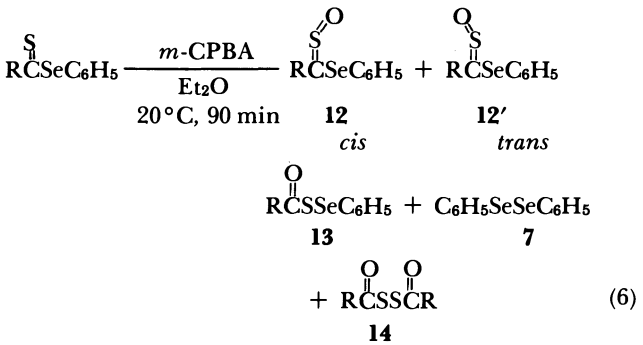

(6)

No.	R
12d, 12′d, 13d	*i*-C_3H_7
12e, 12′e, 13e	*n*-C_4H_9
12i, 12′i, 13i, 14	4-$CH_3C_6H_4$

any downfield shift, while those of the cis-isomer **12′i** showed a singlet.[22)] Presumably, one of the reasons for such downfield shifts of the methine and methylene protons seems to be due to a deshielding action of the sulfinyl group.[23)] It is noted that the methine, methyl, and sulfine carbons of the *trans*-isopropyl(phenylseleno)sulfine **12d** were shifted upfield compared with those of the cis-isomer **12′i**. Similar upfield shifts of trans-isomer were observed for the ^{13}C NMR spectra of butyl(phenylseleno)sulfine, **12e** and **12′e**.

For the formation of phenylseleno acyl sulfides **13**, the possibility via the sulfine **12** and then 2-

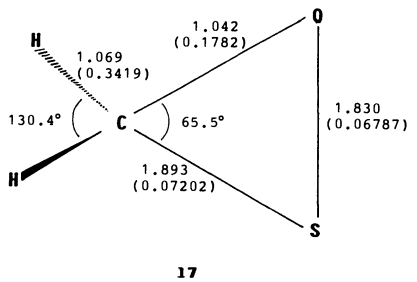

Fig. 1. Optimized geometry, bond lengths in Å, angles in deg. and bond populations in parentheses from 3-21G level MO calculations.

phenylseleno-3-alkyl (or aryl) oxathiirane **15** as intermediates can be considered (Scheme 3). However, after stirring trans- **12** or cis-isomer **12″** in dichloromethane at 20 °C for 2 h, no conversion between the trans- **12** and cis-isomers **12′** was observed. This result suggests that the possibility of a formation roue of **13** via the sulfine **12**, can be ruled out. In order to obtain additional information regarding the formation of the sulfine **12** via the oxathiirane **15**, an ab initio molecular orbital study was carried out by employing oxathiirane **17** as a model. The optimized molecular geometries[24)] of **17** were calculated by ab initio MO calculations at the 3-21G level using on energy-gradient method. As illustrated in Fig. 1, the bond population between sulfur and oxygen was smaller

than those of the carbon–oxygen and carbon–sulfur bonds. Thus, the S–O bond of the oxathiirane ring is weaker than the C–O and C–S bonds. Most probably, phenylseleno acyl sulfide **13** is formed by a migration of the phenylseleno group of the opening intermediate **16**.

Experimental

The melting points were obtained by using a Yanagimoto micromelting point apparatus and are uncorrected. The IR spectra were measured on a JASCO grating IR spectrophotometer (IR-G and A-302). The UV/Vis spectra were taken from a Hitachi 124 and 330 spectrometer. The ^{1}H and ^{13}C NMR spectra were recorded on Hitachi R-24 (60 MHz), R-22 (90 MHz), and JEOL JNM GX-270 (270 MHz) with tetramethylsilane as an internal standard.

The mass spectra were taken from a Hitachi RMU-6M mass spectrometer (70 eV, 180—190 °C). High-resolution mass spectroscopy was taken by a Shimazu high-resolution mass spectrometer (GCMS 9020-DF/PAC-1100). Elemental analyses were carried out by Elemental Analyses Center of Kyoto University and Alfred Bernhardt Analytical Laboratory, Engelskirhen (Germany).

Materials: Bis(thioacyl) sulfides,[4] piperidinium carbodithioates,[25] thioacyl chlorides,[26] phenylselenotrimethylsilanes,[27] diphenyl-,[27] bis(4-methylphenyl)-,[28] and bis(4-chlorophenyl) diselenides,[29] were prepared according to methods described in the literature. Sodium areneselenolates were prepared by a treatment of the corresponding diaryl diselenides with sodium borohydride, respectively.[30] Aniline, cyclohexylamine, diethylamine, and piperidine were dried by refluxing with potassium hydroxide, and distilled before use. Hydrazine hydrate, thiosemicarbazide, and *m*-chloroperbenzoic acid (80%) were of commercial grade and were used without further purification. The solvents were dried by the use of sodium metal or calcium chloride. Column chromatography was performed on Wako Gel 200.

The preparation methods of *Se*-phenyl 2-propane- (**3d**) and 4-methylbenzenecarboselenothioate (**3i**) (as typical procedures) are described in detail. All manipulations are carried out under nitrogen.

***Se*-Phenyl Methanecarboselenothioate (3a):** In a manner similar to the synthesis of **3d**, the reaction of bis[methyl(thiocarbonyl)] sulfide (**1a**, 3 mmol) in hexane (20 ml), freshly prepared from ethanedithioic acid (533 mg, 6 mmol) and dicyclohexylcarbodiimide (619 mg, 3 mmol), with a solution of sodium benzeneselenolate (3 mmol) in dichloromethane/methanol (3:1, 20 ml) at −60 °C for 30 min, followed by silica-gel column chromatography (hexane) and then bulb-to-bulb distillation yielded 170 mg (26%) of **3a** as orange liquid: bp 85 °C/1.5 Torr. IR (neat), 3047, 1582, 1480, 1442, 1359, 1208, 1195 (C=S), 1092, 1070, 1021, 1001, 831 (C=S) 737, 688, 494, and 468 cm^{-1}. UV/Vis (hexane) 258, 328, and 492 nm. ^{1}H NMR ($CDCl_3$) δ=2.84 (3H, s, CH_3), and 7.4—7.6 (5H, m, Ar). ^{13}C NMR ($CDCl_3$) δ=42.3 (CH_3), and 240.1 (C=S). MS (70 eV) *m/z* (rel intensity), 216 (M^+; 12), 157 ($C_6H_5Se^+$, 24), and 59 (CH_3CS^+, 100). Found: *m/z* 215.9503. Calcd for C_8H_8SSe: M, 215.9512.

***Se*-Phenyl Ethanecarboselenothioate (3b):** In a manner similar to the synthesis of **3d**, the reaction of bis[ethyl(thiocarbonyl)] sulfide (**1b**) (3 mmol) in hexane (20 ml), freshly prepared from propane dithioic acid (637 mg, 6 mmol) and dicyclohexylcarbodiimide (619 mg, 3 mmol), with a solution of sodium benzeneselenolate (3 mmol) in a mixed solvent of dichloromethane/methanol (3:1, 20 ml) at −10 °C for 30 min, followed by silica-gel column chromatography (hexane) and then bulb-to-bulb distillation yielded 353 mg (51%) of **3b** as orange liquid: bp 114 °C/3.5 Torr. IR (neat), 3025, 2950, 2290, 1577, 1480, 1441, 1280, 1191 (C=S), 1067, 1022, 1002, 968, 860 (C=S), 744, 691, and 471 cm^{-1}. UV/Vis (hexane) 258, 328, and 486 nm. ^{1}H NMR ($CDCl_3$) δ=1.35 (3H, t, CH_3), 3.04 (2H, q, CH_2), and 7.3—7.6 (5H, m, Ar). ^{13}C NMR ($CDCl_3$) δ=15.0 (CH_3), 47.1 (CH_2), and 246.4 (C=S). MS (70 eV) *m/z* (rel intensity), 230 (M^+; 5), 157 ($C_6H_5Se^+$, 5), and 73 ($C_2H_5CS^+$, 100). Found: *m/z* 229.9661. Calcd for $C_9H_{10}SSe$: M, 229.9668.

***Se*-Phenyl 1-Propanecarboselenothioate (3c):** In a manner similar to the synthesis of **3d**, bis[propyl(thiocarbonyl)] sulfide (**1c**) (3 mmol) in hexane (20 ml), freshly prepared from butanedithioic acid (721 mg, 6 mmol) and dicyclohexylcarbodiimide (619 mg, 3 mmol), was added to a solution of sodium benzeneselenolate (3 mmol) in a mixed solvent of dichloromethane/methanol (3:1, 20 ml) at 0 °C for 30 min, followed by silica-gel column chromatography and then bulb-to-bulb distillation yielded 496 mg (68%) of **3c** as orange liquid: bp 127 °C/3.5 Torr. IR (neat) 3025, 2980, 2950, 2880, 1580, 1478, 1460, 1440, 1380, 1240, 1184 (C=S), 1063, 1020, 1000, 922, 832 (C=S), 737, 687, and 468 cm^{-1}; UV/Vis (hexane) 258, 330, and 486 nm. ^{1}H NMR ($CDCl_3$) δ=0.99 (3H, t, CH_3), 1.88 (2H, m, CH_2), 3.04 (2H, t, CH_2), and 7.34—7.57 (5H, m, Ar). ^{13}C NMR ($CDCl_3$) δ=13.0 (CH_3), 23.7 (CH_2), 55.6 (CH_2), and 244.4 (C=S). MS (70 eV) *m/z* (rel intensity), 244 (M^+; 12), 157 ($C_6H_5Se^+$, 12), and 87 ($C_3H_7CS^+$, 100). Found: *m/z* 243.9836. Calcd for $C_{10}H_{12}SSe$: M, 243.9825.

***Se*-Phenyl 2-Propanecarboselenothioate (3d):** A solution of bis[isopropyl(thiocarbonyl)] sulfide (**1d**, 3 mmol) in hexane (20 ml), freshly prepared by a reaction of 2-methylpropanedithioic acid (721 mg, 6 mmol) with dicyclohexylcarbodiimide (619 mg, 3 mmol) in hexane (20 ml) at −70 °C for 30 min, was added to a solution of freshly prepared sodium benzeneselenolate (3 mmol) in a mixed solvent of dichloromethane/methanol (3:1, 20 ml) at 0 °C. The reaction mixture was then stirred at this temperature for 30 min. The color of the solution quickly changed from violet to orange. Hexane (15 ml) was added; the mixture was then washed with water (3×50 ml), followed by drying with anhydrous sodium sulfate. The solvent was evaporated in vacuo. The residue was chromatographed on silica gel [hexane/dichloromethane (9:1)]; then, a bulb-to-bulb distillation of the resulting orange eluent yielded 560 mg (77%) of **3d** as orange liquid: bp 111 °C/3.0 Torr. IR (neat) 3045, 3000, 2950, 2900, 1581, 1480, 1441, 1384, 1210 (C=S), 1160, 1067, 1031, 1021, 1001, 905, 815, 738, 688, and 470 cm^{-1}. UV/Vis (hexane) 258, 328, and 493 nm. ^{1}H NMR ($CDCl_3$) δ=1.36 (6H, d, CH_3), 3.59 (1H, m, CH), and 7.41—7.53 (5H, m, Ar). ^{13}C NMR ($CDCl_3$) δ=23.9, 50.8, and 242.2 (C=S). MS (70 eV) *m/z* (rel intensity), 244 (M^+; 12), 157 ($C_6H_5Se^+$, 42), and 87 (i-$C_3H_7CS^+$, 100). Found: *m/z* 243.9825. Calcd for $C_{10}H_{12}SSe$: M, 243.9825.

***Se*-Phenyl 1-Butanecarbothioselenoate (3e):** In a manner similar to the synthesis of **3d**, bis[butyl(thiocarbonyl)] sulfide (**1e**, 3 mmol) in hexane (20 ml), freshly prepared from pentanedithioic acid (806 mg, 6 mmol) and dicyclohexylcarbodiimide (619 mg, 3 mmol), was added to a solution of

sodium benzeneselenolate (3 mmol) in a mixed solvent of dichloromethane/methanol (3:1, 20 ml) at 0 °C for 30 min, followed by silica-gel column chromatography (hexane) and then bulb-to-bulb distillation of the resulting orange eluent yielded 460 mg (60%) of **3e** as orange liquid: bp 132 °C/3.5 Torr. IR (neat) 3050, 2970, 2950, 2580, 1580, 1478, 1440, 1380, 1300, 1220, 1180 (C=S), 1091, 1064, 1021, 1000, 867, 732, 688, and 468 cm^{-1}. UV/Vis (hexane) 258, 330, and 486 nm. ^1H NMR ($CDCl_3$) δ=0.91 (3H, t, CH_3), 1.39 (2H, m, CH_2), 1.82 (2H, m, CH_2), 3.06 (2H, t, CH_2), and 7.34—7.54 (5H, m, Ar). ^{13}C NMR ($CDCl_3$) δ=13.6, 21.6, 32.7, 53.5, and 244.3 (C=S). MS (70 eV) *m/z* (rel intensity), 258 (M^+; 10), 156 ($C_6H_5Se^+$, 50), and 101 (n-$C_4H_9CS^+$, 100). Found: *m/z* 257.9987. Calcd for $C_{11}H_{14}SSe$: M, 257.9987.

***Se*-Phenyl 1-Pentanecarboselenothioate (3f):** In a manner similar to the synthesis of **3d**, bis[1-pentyl(thiocarbonyl)] sulfide (**1f**, 3 mmol) in hexane (20 ml), freshly prepared from 1-hexanedithioic acid (890 mg, 6 mmol) and dicyclohexylcarbodiimide (619 mg, 3 mmol), was added to a solution of sodium benzeneselenolate (3 mmol) in dichloromethane/methanol (3:1, 20 ml) at 0 °C for 30 min, followed by silica-gel column chromatography [hexane/carbon tetrachloride (2:1)] and then bulb-to-bulb distillation yielded 560 mg (69%) of **3f** as orange liquid: bp 152 °C/3.5 Torr. IR (neat) 3027, 2990, 2950, 2880, 1578, 1475, 1460, 1448, 1376, 1210 (C=S), 1070, 1061, 1019, 999, 878, 821, 730, 681, and 464 cm^{-1}. UV/Vis (hexane) 258, 332, and 486 nm. ^1H NMR ($CDCl_3$) δ=0.90 (3H, t, CH_3), 1.33 (4H, m, CH_2), 1.84 (2H, m, CH_2), 3.06 (2H, t, CH_2), and 7.33—7.57 (5H, m, Ar). ^{13}C NMR ($CDCl_3$) δ=13.9 (CH_3), 22.3 (CH_2), 30.7 (CH_2), 30.9 (CH_2), 54.1 (CH_2), and 245.4 (C=S). MS (70 eV) *m/z* (rel intensity), 272 (M^+; trace), 157 ($C_6H_5Se^+$, 32), and 115 (n-$C_5H_{11}CS^+$, 100). Found: *m/z* 272.0147. Calcd for $C_{12}H_{16}SSe$: M, 272.0138.

***Se*-Phenyl Cyclohexanecarbothioselenoate (3g):** In a manner similar to the synthesis of **3d**, bis[cyclohexyl(thiocarbonyl)] sulfide (**1g**) (3 mmol) in hexane (20 ml), freshly prepared from cyclohexanecarbodithioic acid (962 mg, 6 mmol) and dicyclohexylcarbodiimide (619 mg, 3 mmol), was added to a solution of sodium benzeneselenolate (3 mmol) in dichloromethane/methanol (3:1, 20 ml) at 0 °C for 30 min. Silica-gel column chromatography [hexane/dichloromethane (3:1)] and then bulb-to-bulb distillation of the resulting orange eluent yielded 705 mg (83%) of **3g** as orange liquid: bp 119 °C/1.0 Torr. IR (neat) 3030, 2950, 2880, 1583, 1478, 1450, 1440, 1241, 1190 (C=S), 1131, 1066, 1020, 1001, 990, 919, 888, 860, 845, 780, 736, 687, and 470 cm^{-1}. UV/Vis (hexane) 261, 331, and 488 nm. ^1H NMR ($CDCl_3$) δ=1.15—2.03 (10H, m, CH_2), 3.25 (1H, tt, CH), and 7.4—7.6 (5H, m, Ar). ^{13}C NMR ($CDCl_3$) δ=25.5, 26.0, 34.6, 61.9, and 250.2 (C=S). MS (70 eV) *m/z* (rel intensity), 284 (M^+; 9), 157 ($C_6H_5Se^+$, 5) 127 (*cyclo*-$C_6H_{11}CS^+$, 100), and 83 (*cyclo*-$C_6H_{11}^+$, 51). Found: *m/z* 284.0133. Calcd for $C_{13}H_{16}SSe$: M, 284.0138.

***Se*-Phenyl Benzenecarboselenothioate (3h) (Method A):** In a manner similar to synthesis Method A of **3i**, the reaction of bis(thiobenzoyl) sulfide (**1h**, 3 mmol) in hexane (50 ml) with sodium benzeneselenolate (3 mmol), followed by silica-gel column chromatography [hexane/dichloromethane (5:1)], yielded 122 mg (44%) of chemically pure **3h** as violet crystals: mp 44—46 °C. IR (neat) 3120, 3100, 1595, 1582, 1578, 1480, 1444, 1318, 1245 (C=S), 1186, 1160, 1109, 1086, 1045, 1022, 1003, 836, 759, 738, 685, 622, 611, 560, and 471 cm^{-1}. UV/Vis (hexane) 302 (4.18), and 542 (1.92) nm. ^1H NMR ($CDCl_3$) δ=7.0—8.0 (10H, m, Ar). ^{13}C NMR ($CDCl_3$) δ=126.3—146.6 (Ar), and 232.2 (C=S). MS (70 eV) *m/z* (rel intensity), 278 (M^+; 3), 121 ($C_6H_5CS^+$, 100), and 77 ($C_6H_5^+$, 5). Found: *m/z* 277.9668. Calcd for $C_{13}H_{10}SSe$: M, 277.9668.

Method B: In a manner similar to synthesis Method B of **3i**, the reaction of thiobenzoyl chloride (**4a**, 386 mg, 2 mmol) with sodium benzeneselenolate (2 mmol), followed by silica-gel column chromatography [hexane/dichloromethane (5:1)], yielded 330 mg (60%) of **3h**.

Method C: In a manner similar to synthesis Method C of **3i**, the treatment of thiobenzoyl chloride (**4a**, 156 mg, 1 mmol) with (phenylseleno) trimethylsilane (229 mg, 1 mmol) in hexane (15 ml) at 20 °C for 1 h, followed by silica-gel column chromatography [hexane/dichloromethane (5:1)], yielded 33 mg (12%) of **3h** and 119 mg (76%) of diphenyl diselenide.

***Se*-Phenyl 4-Methylbenzenecarboselenothioate (3i) (Method A):** A solution of bis[4-methyl(thiobenzoyl)] sulfide (**1i**, 302 mg, 1 mmol) in dichloromethane (3 ml) was added to sodium benzeneselenolate (1 mmol) in a mixed solvent of dichloromethane and methanol (2:1, 15 ml) at 0 °C; the reaction mixture was then stirred at this temperature for 30 min. The color of the reaction mixture quickly changed from dark green to red. Dichloromethane (20 ml) was added; the mixture was then washed with water (3×30 ml), followed by drying with anhydrous sodium sulfate. After the solvent had been evaporated in vacuo, the residue was chromatographed on silica-gel column [hexane/dichloromethane (5:1)] to yield 213 mg (73%) of **3i** as reddish-pink crystals: mp 83—84 °C. IR (KBr) 1600, 1475, 1440, 1309, 1250 (C=S), 1181, 1045, 1020, 1010, 848, 817, 767, 732, 684, 630, 554, 471, and 458 cm^{-1}. UV/Vis (hexane) 265 (3.83), 315 (4.23), and 541 (1.97) nm. ^1H NMR ($CDCl_3$) δ=2.30 (3H, s, CH_3) and 7.22—7.93 (9H, m, Ar). ^{13}C NMR ($CDCl_3$) δ=21.6 (CH_3), 126.7—144.5 (Ar), and 231.8 (C=S). MS (70 eV) *m/z* (rel intensity), 292 (M^+; 12), 135 (4-$CH_3C_6H_4CS^+$, 100), and 91 (4-$CH_3C_6H_4^+$, 64). Found: C, 57.82; H, 4.49; S, 11.13; Se, 27.26%. Calcd for $C_{14}H_{12}SSe$: C, 57.57; H, 4.42; S, 10.99; Se, 27.03%.

Method B: A solution of 4-methyl(thiobenzoyl) chloride (**4b**, 341 mg, 2 mmol) in benzene (3 ml) was added to sodium benzeneselenolate (2 mmol) in a mixed solvent of benzene/methanol (1:1, 10 ml) at 0 °C; the mixture was stirred at this temperature for 30 min. Dichloromethane (50 ml) was added; the mixture was then washed with water (3×30 ml), followed by drying over anhydrous sodium sulfate. The solvent was evaporated using a rotary evaporator. The residue was chromatographed on a silica-gel column [hexane/dichloromethane (5:1)] to yield 330 mg (60%) of **3i**.

Method C: A solution of 4-methyl(thiobenzoyl) chloride (**4b**, 171 mg, 1 mmol) in hexane (3 ml) was added to (phenylseleno)trimethylsilane (229 mg, 1 mmol) in hexane (15 ml); the mixture was then stirred at 20 °C for 1 h. The solvent was evaporated in vacuo and the residue chromatographed on silica gel [hexane/dichloromethane (5:1)] the second red eluent)] to yield 34 mg (12%) of **3i** and 127 mg (81%) of diphenyl diselenide.

***Se*-(4-Methylphenyl) 4-Methylbenzenecarboselenothioate (3j) (Method A):** In a manner similar to synthesis Method A of **3i**, the reaction of sodium 4-methylbenzeneselenolate (1 mmol) in 15 ml of dichloromethane/methanol (2:1) with bis[4-methyl(thiobenzoyl)] sulfide (**1i**, 302 mg, 1 mmol) in

dichloromethane (5 ml) yielded 247 mg (81%) of **3j** as reddish-pink crystals: mp 118—120 °C. IR (KBr) 2920, 1595, 1485, 1305, 1250 (C=S), 1235, 1208, 1176, 1040, 1036, 1008, 890, 811, 800, 757, 629, 552, 485, and 467 cm^{-1}. UV/Vis (CH_2Cl_2) 226 (4.45), 258 (4.02), 323 (4.34), and 528 (2.05) nm. ^1H NMR ($CDCl_3$) δ=2.17 (3H, s, CH_3ArSe), 2.38 (3H, s, CH_3ArCS), and 7.2—8.0 (8H, m, Ar). ^{13}C NMR ($CDCl_3$) δ=21.5 (CH_3), 21.6 (CH_3), 126.6—144.5 (Ar), and 232.4 (C=S). MS (70 eV) *m/z* (rel intensity), 306 (M^+; 3), 171 ($CH_3C_6H_4Se^+$, <1), 135 ($CH_3C_6H_4CS^+$, 100), and 91 ($CH_3C_6H_4^+$, 3). Found: C, 59.11; H, 4.49%. Calcd for $C_{15}H_{14}SSe$: C, 59.01; H, 4.62%.

***Se*-(4-Chlorophenyl) 4-Methylbenzenecarboselenothioate (3k) (Method A):** In a manner similar to synthesis Method A of **3i**, the reaction of 4-chlorobenzeneselenolate (1 mmol) in 15 ml of dichloromethane/methanol (2:1) with bis[4-methyl(thiobenzoyl)] sulfide (**1i**, 302 mg, 1 mmol) in dichloromethane (5 ml) yielded 229 mg (70%) of **3k** as reddish pink needles: mp 96—97 °C. IR (KBr) 2980, 1594, 1468, 1384, 1306, 1253, 1223, 1177, 1086, 1036, 1005, 850, 839, 812, 760, 721, 621, 550, 490, 478, and 448 cm^{-1}. UV/Vis (hexane) 227 (4.61), 269 (4.11), 316 (4.48), and 540 (1.99) nm. ^1H NMR ($CDCl_3$) δ=2.38 (3H, s, CH_3), and 7.2—8.0 (8H, m, Ar). ^{13}C NMR ($CDCl_3$) δ=21.6 (CH_3), 126.7—144.2 (Ar), and 230.7 (C=S). MS (70 eV) *m/z* (rel intensity), 326 (M^+; 2), 191 ($ClC_6H_4Se^+$, <1), 135 ($CH_3C_6H_4CS^+$, 100), and 91 ($CH_3C_6H_4^+$, 5). Found: C, 51.63; H, 3.32%. Calcd for $C_{14}H_{11}SSeCl$: C, 51.62; H, 3.40%.

Attempt to Synthesize *Se*-Phenyl 2,4,6-Trimethylbenzenecarboselenothioate (3l) (Method A): A dichloromethane solution (5 ml) of bis[2,4,6-trimethyl(thiobenzoyl) sulfide (**1l**, 359 mg, 1 mmol) was added to a solution of freshly prepared sodium benzeneselenolate (1 mmol) in dichloromethane/methanol (1:1); the reaction mixture was then stirred at 0 °C for 30 min. After the usual work-up of the reaction mixture, the resulting residue was chromatographed on a silica-gel column [hexane/dichloromethane (10:1)] to give 150 mg (96%) of diphenyl diselenide **7** and 183 mg (51%) of the starting sulfide **1l**.

***Se*-Phenyl 4-Methoxybenzenecarboselenothioate (3m) (Method A):** In a manner similar to synthesis Method A of **3i**, the reaction of sodium benzeneselenolate (1 mmol) in dichloromethane/methanol(1:1) with bis[4-methoxy(thiobenzoyl)] sulfide (**1j** 334 mg, 1 mmol) in dichloromethane (3 ml) yielded 155 mg (51%) of **3m** as reddish-pink crystals: mp 63—65 °C. IR (KBr) 1595, 1568, 1501, 1440, 1310, 1259, 1240 (C=S), 1186, 1174, 1034, 1020, 845, 830, 737, 688, 627, 570, and 553 cm^{-1}. UV/Vis (hexane) 240 (4.05), 264 (3.77), 339 (4.38), and 538 (2.09) nm. ^1H NMR ($CDCl_3$) δ=3.85 (3H, s, CH_3O), and 6.9—8.1 (9H, m, Ar). ^{13}C NMR ($CDCl_3$) δ=55.6 (CH_3O), 113.7—163.9 (Ar), and 229.5 (C=S). MS (70 eV) *m/z* (rel intensity), 308 (M^+; 2), 151 ($4\text{-}CH_3OC_6H_4\text{-}CS^+$, 100), and 107 ($4\text{-}CH_3OC_6H_4^+$, 5). Found: C, 54.40; H, 4.33%. Calcd for $C_{14}H_{12}OSSe$: C, 54.58; H, 4.19%.

Method B: In a manner similar to synthesis Method B of **3i**, treatment of 4-methoxy(thiobenzoyl) chloride (**4c**, 374 mg, 2 mmol) in benzene (3 ml) with sodium benzeneselenolate (2 mmol) in a mixed solvent (1:1, 10 ml) at 0 °C for 30 min, followed by silica-gel column chromatography [hexane/dichloromethane (10:1)] yielded 188 mg (31%) of **3m**.

Method C: In a manner similar to synthesis Method C of **3i**, the reaction of 4-methoxy(thiobenzoyl) chloride (**4c**, 187 mg, 1 mmol) with phenylselenotrimethylsilane (229 mg, 1 mmol) in hexane (18 ml) at 0 °C for 1 h, followed by silica-gel column chromatograpy [hexane/dichloromethane (10:1)], gave 129 mg (82%) of diphenyl diselenide (**7**).

***Se*-Phenyl 4-Chlorobenzenecarboselenothioate (3n) (Method A):** In a manner similar to synthesis Method A of **3i**, the reaction of sodium benzeneselenolate (1 mmol) in a mixed solvent of dichloromethane/methanol (3:1, 20 ml) with bis[4-chloro(thiobenzoyl)] sulfide (**1i**, 1.1 mmol) in hexane (50 ml) at 0 °C for 30 min, followed by column chromatography on silica gel [hexane/dichloromethane (10:1)] yielded 244 mg (78%) of **3n** as reddish-pink crystals: mp 87—88 °C. IR (KBr) 1580, 1479, 1448, 1396, 1298, 1238 (C=S), 1173, 1090, 1041, 1018, 1009, 891, 822, 731, 691, 681, 621, 550, 490, 420, and 400 cm^{-1}. UV/Vis (hexane) 230sh (4.12), 312 (4.17), and 542 (1.92) nm. ^1H NMR ($CDCl_3$) δ=7.0—7.8 (9H, m, Ar). ^{13}C NMR ($CDCl_3$) δ=127.8—145.1 (Ar) and 230.5 (C=S). MS (70 eV) *m/z* (rel intensity), 312 (M^+; 8), 155 ($4\text{-}ClC_6H_4CS^+$, 100), and 111 ($4\text{-}ClC_6H_4^+$, 5). Found: C, 50.37; H, 3.09%. Calcd for $C_{13}H_9SSeCl$: C, 50.10; H, 2.96%.

Method B: In a manner similar to synthesis Method B of **3i**, treatment of 4-chloro(thiobenzoyl) chloride (**4d**, 382 mg, 2 mmol) in benzene (3 ml) with sodium benzeneselenolate (2 mmol) in a mixed solvent of benzene/methanol (1:1, 10 ml) at 0 °C for 30 min, followed by silica-gel column chromatography [hexane/dichloromethane (5:2)] yielded 500 mg (80%) of **3n**.

Method C: In a manner similar to synthesis Method C of **3g**, the reaction of 4-chloro(thiobenzoyl) chloride (**4d**, 191 mg, 1 mmol) with phenylselenotrimethylsilane (229 mg, 1 mmol) in 20 °C for 1 h, followed by silica-gel column chromatography [hexane/dichloromethane (10:1)] yielded 115 mg (37%) of **3n** and 62 mg (32%) of diphenyl diselenide (**7**).

For the reaction of thionselenolester **3** with amine, sodium alcoholates, typical procedures are described. The products were confirmed by comparisons of the melting point and IR or NMR spectra with those of authentic sample.

Reaction with Aniline: Aniline (93 mg, 1 mmol) was added to a solution of *Se*-phenyl 4-methylbenzenecarboselenothioate (**3i**, 291 mg, 1 mmol) in hexane (30 ml); the reaction mixture was then refluxed for 24 h. Filtration of the resulting precipitates gave 154 mg (68%) of 4-methylthiobenzanilide **6a**. The solvent was evaporated by a rotary evaporator then the residue was chromatographed on a silica-gel column (hexane), giving 152 mg (98%) of diphenyl diselenide (**7**).

Reaction with Cyclohexylamine: To a suspension of **3i** (291 mg, 1 mmol) in hexane (30 ml) was added cyclohexylamine (97 mg, 1 mmol). The reaction mixture was then stirred at 20 °C for 5 h. Filtration of the resulting red precipitates gave 96 mg (41%) of cyclohexylammonium 4-methylbenzenecarbodithioate (**8a**) as red crystals. Evaporation of the filtrate by a rotary evaporator, followed by a chromatographic separation of the resulting residue on silica gel (hexane), gave 140 mg (90%) of diphenyl diselenide (**7**).

Reaction with Diethylamine: The reaction of **3i** (291 mg, 1 mmol) with diethylamine (73 mg, 1 mmol) in hexane (30 ml) at 18 °C for 2 h, followed by silica-gel column chromatography (hexane), yielded 107 mg (44%) of diethylammonium 4-methylbenzenecarbodithioate (**8b**) as red crystals and 147 mg (94%) of **7**.

Reaction with Piperidine: The reaction of **3i** (291 mg, 1 mmol) with piperidine (85 mg, 1 mmol) in hexane (30 ml) at 20 °C for 30 min, followed by silica-gel column chroma-

tograph (hexane), yielded 78 mg (31%) of piperidinium 4-methylbenzenecarbodithioate (**8c**) as red crystals and 151 mg (97%) of **7**.

Reaction with Hydrazine: (Conditions A): A solution of hydrazine hydrate (80%, 63 mg, 1 mmol) in hexane (5 ml) was added dropwise to *Se*-phenyl 4-methylbenzenecarboselenothioate (**3i**, 291 mg, 1 mmol) in hexane (40 ml); the mixture was then stirred at 18 °C for 1 h. Filtration of the resulting precipitates gave 48 mg (29%) of 4-methylbenzenecarbothionohydrazide (**6b**) as slightly yellow crystals. After evaporating the filtrate, the residue was chromatographed on silica-gel column [hexane/dichloromethane (5:1)] to give 151 mg (96%) of **7**.

6b: Mp 115—125 °C. IR (KBr) 3200, 1590, 1519, 1492, 1410, 1365, 1312, 1287, 1240, 1220, 1180, 1021, 1001, 937, 821, 719, 671, 629, and 612 cm^{-1}. ^1H NMR ($CDCl_3$) δ=2.38 (3H, s, CH_3), 4.99 (2H, br, NH_2), 7.1—7.7 (4H, m, Ar), and 8.74 (1H, br, NH). MS (70 eV) *m/z* (rel intensity), 166 (M^+; 26), 135 (4-$CH_3C_6H_4CS^+$, 96), 91 (4-$CH_3C_6H_4^+$, 100), and 65 ($C_5H_5^+$, 45).

(Conditions B): Hydrazine hydrate (80%, 63 mg, 1 mmol) and **3i** (291 mg, 1 mmol) was stirred in ethanol (40 ml) at 18 °C for 1 h. The solvent was removed by a rotary evaporator; then, hexane (30 ml) was added. Filtration of the precipitates yielded 130 mg (78%) of 4-methylbenzenecarboselenohydrazide (**6b**). Evaporation of the filtrate, followed by silica-gel column chromatography [hexane/dichloromethane (5:1)], gave 150 mg (96%) of **7**.

Reaction with Sodium Methanolate: A solution of sodium methanolate (27 mg, 0.5 mmol) in methanol (10 ml) was added dropwise to a solution of *Se*-phenyl 4-methylbenzenecarboselenothioate (**3i**, 146 mg, 0.5 mmol) in ether (10 ml). The reaction mixture was stirred at ca. 20 °C for 2 h. The solvent was evaporated and ether (20 ml) was added. The resulting precipitates (C_6H_5SeNa) was filtered, followed by acidlysis with 1 mol dm^{-3} HCl (5 ml) and by extraction with hexane (50 ml). Evaporation of the extract under reduced pressure gave 70 mg (90%) of diphenyl diselenide. The filtrate (ether soluble part) was concentrated to ca. 1 ml, followed by silica-gel column chromatography [hexane/dichloromethane (5:1)],to give 71 mg (86%) of *O*-methyl 4-methylbenzenecarbothioate (**11a**).

Reaction with Sodium Ethanolate: Similarly, the reaction of **3i** (146 mg, 0.5 mmol) with sodium ethanolate (34 mg, 0.5 mmol) in ethanol (10 ml) yielded 82 mg (91%) of *O*-ethyl 4-methylbenzenecarbothioate (**11b**) and 72 mg (95%) of **7**.

Reaction with Sodium Phenolate: The reaction of **3i** (146 mg, 0.5 mmol) with sodium phenolate (146 mg, 0.5 mmol) in ether at 20 °C for 24 h yielded 91 mg (79%) of *O*-phenyl 4-methylbenzenecarbothioate (**11c**) and 68 mg (90%) of **7**.

Reaction of *Se*-Phenyl 2-Propanecarboselenothioate (3d) with *m*-Chloroperbenzoic acid: A solution of *m*-chloroperbenzoic acid (217 mg, 1 mmol) in ether (10 ml) was added to *Se*-phenyl 2-propanecarboselenothioate (**3d**, 243 mg, 1 mmol) in the same solvent (30 ml); the mixture was then stirred at 0 °C for 90 min. The reaction mixture was washed with saturated aqueous sodium hydrogen carbonate (50 ml) and then water (3×50 ml), followed by drying using anhydrous sodium sulfate. After evaporating the solvent by a rotary evaporator, the residue was separated by thin-layer chromatography [hexane/dichloromethane (5:1)] to yield 50 mg (35%) of diphenyl diselenide (**7**, R_f=0.76), 52 mg (19%) of 2-methylpropionyl phenylseleno sulfide (**13d**, R_f=0.51) as slightly yellow oil, 34 mg (13%) of *trans*-isopropyl(phenylseleno)sulfine(**12d**, R_f=0.22) as yellow oil, and 33 mg (13%) of *cis*-isopropyl(phenylseleno)sulfine (**12'd**, R_f=0.11) as slightly yellow oil.

12'd: IR (neat) 3080, 3000, 2950, 1573, 1471, 1460, 1452, 1437, 1380, 1358, 1190, 1140, 1050, 1019, 998, 930, 738, and 687 cm^{-1}. ^1H NMR ($CDCl_3$) δ=1.08 (6H, d, CH_3), 4.07 (1H, m, CH), and 7.3—7.7 (5H, m, Ar). ^{13}C NMR ($CDCl_3$) δ=20.9 (CH_3), 32.5 (CH), 128.8—132.9 (Ar), and 197.9 (C=S=O). MS (70 eV) *m/z* (rel intensity), 260 (M^+; <1), 87 ($C_3H_7CS^+$, 62), 71 (*i*-$C_3H_7CO^+$, 100), and 43 (*i*-$C_3H_7^+$, 46).

12'd: IR (neat) 3080, 3000, 2950, 1573, 1471, 1460, 1452, 1437, 1205, 1190, 1140, 1070, 1050, 1019, 998, 930, 738, and 687 cm^{-1}. ^1H NMR ($CDCl_3$) δ=1.18 (6H, d, CH_3), 2.77 (1H, m, CH), and 7.3—7.8 (5H, m, Ar). ^{13}C NMR ($CDCl_3$) δ=23.3 (CH_3), 33.7 (CH), 125.2 (Ar), and 205.8 (C=S=O). MS (70 eV) *m/z* (rel intensity), 260 (M^+; 5), 87 (*i*-$C_3H_7CS^+$, 100), 71 (*i*-$C_3H_7CO^+$, 22), and 43 (*i*-$C_3H_7^+$, 18).

13d: IR (Neat) 2980, 2940, 1710 (C=O), 1570, 1470, 1451, 1433, 1087, 1015, 947, 845, 730, and 681 cm^{-1}. ^1H NMR ($CDCl_3$) δ=1.24 (6H, d, CH_3), 3.02 (1H, sept, CH), and 7.2—7.8 (5H, m, Ar). MS (70 eV) *m/z* (rel intensity), 260 (M^+; <1), 157 ($C_6H_5Se^+$, 21), 87 (*i*-$C_3H_7CS^+$, 5), 71 (*i*-$C_3H_7CO^+$, 100), and 43 (*i*-$C_3H_7^+$, 43).

Reaction of *Se*-Phenyl 1-Butanecarboselenothioate (3e) with *m*-Chloroperbenzoic Acid: In a manner similar to the reaction of **3d**, the reaction of *Se*-phenyl 1-butanecarboselenothioate (**3e**, 257 mg, 1 mmol) with *m*-chloroperbenzoic acid (217 mg, 1 mmol) at 0 °C for 90 min, followed by dry silica-gel column chromatography [hexane/dichloromethane (5:1)], yielded 20 mg (28%) of pentanoyl phenylseleno sulfide† (**13e**, the first eluent), as slightly yellow oil 89 mg (32%) of *trans*-1-butyl(phenylseleno)sulfine (**12e** the second eluent) as yellow oil, and 58 mg (21%) of *cis*-butyl(phenylseleno)sulfine (**12'e** the third eluent) as yellow oil.

12e: IR (neat) 3060, 2950, 2870, 1573, 1470, 1460, 1455, 1434, 1420, 1180, 1076, 1017, 998, 970, 733, and 684 cm^{-1}. ^1H NMR ($CDCl_3$) δ=0.87 (3H, t, CH_3), 1.28—1.81 (4H, m, CH_2), 2.94 (2H, t, CH_2), and 7.2—7.6 (5H, m, Ar). ^{13}C NMR ($CDCl_3$) δ=13.6 (CH_3), 21.9 (CH_2), 29.9 (CH_2), 32.1 (CH_2CSO), 128.8—136.9 (Ar), and 191.8 (C=S=O). MS (70 eV) *m/z* (rel intensity), 274 (M^+; 15), 181 ($C_4H_9CSSe^+$, 11), 117 ($C_4H_9CSO^+$, 9), 101 ($C_4H_9CS^+$, 100), 85 ($C_4H_9CO^+$, 28), and 57 ($C_4H_9^+$, 36).

12'e: IR (neat) 3060, 2950, 2870, 1573, 1479, 1460, 1455, 1434, 1420, 1375, 1300, 1228, 1160, 1138, 1070, 1017, 998, 970, 733, and 684 cm^{-1}. ^1H NMR ($CDCl_3$) δ=0.69 (3H, t, CH_3), 1.1—1.6 (4H, m, CH_2), 2.47 (2H, t, CH_2), and 7.3—7.7 (5H, m, Ar). ^{13}C NMR ($CDCl_3$) δ=13.2 (CH_3), 21.6 (CH_2), 29.9 (CH_2), 31.7 (CH_2CSO), 124.1—136.9 (Ar), and 197.2 (C=S=O). MS (70 eV) *m/z* (rel intensity), 274 (M^+; 10), 181 ($C_4H_9CSSe^+$, 10), 101 ($C_4H_9CS^+$, 100), 85 ($C_4H_9CO^+$, 28), and 57 ($C_4H_9^+$, 33).

13e: IR (neat) 3050, 2950, 2900, 2850, 1710, 1572, 1467, 1450, 1430, 1110, 1011, 990, 785, and 730 cm^{-1}. ^1H NMR ($CDCl_3$) δ=0.93 (3H, t, CH_3), 1.3—1.7 (4H, m, CH_2), 2.74 (2H, t, CH_2), and 7.1—7.8 (5H, m, Ar). MS (70 eV) *m/z* (rel intensity), 274 (M^+; 10), 157 ($C_6H_5Se^+$, 11), 101 ($C_4H_9CS^+$, 6), 85 ($C_4H_9CO^+$, 13), and 57 ($C_4H_9^+$, 100).

† Containing below 2% of diphenyl diselenide.

Reaction of *Se*-Phenyl 4-Methylbenzenecarboselenothioate (3i) with *m*-Chloroperbenzoic Acid: A solution of *m*-chloroperbenzoic acid (216 mg, 1 mmol) in ether (20 ml) was added to a solution of *Se*-phenyl 4-methylbenzenecarboselenothioate (**3i**, 291 mg, 1 mmol) in the same solvent (30 ml); the mixture was then stirred at 0 °C for 90 min. The reaction mixture was washed with saturated aqueous sodium hydrogen carbonate (50 ml) and then with water (3×50 ml), followed by drying with anhydrous sodium sulfate. The solvent was evaporated by a rotary evaporator. The residue was chromatographed on silica gel [hexane/dichloromethane (2:1)] to give a first eluent (orange), a second (pink), and third eluent (yellow). The repeated chromatographic separation of the first eluent [hexane/dichloromethane (20:1)] gave 22 mg (14%) of diphenyl diselenide (**7**). Similarly, a chromatographic separation of the second eluent [hexane/dichloromethane (5:1)] gave 34 mg (11%) of phenylseleno 4-methyl(thiobenzoyl) sulfide (**13i**) as slightly yellow crystals 9 mg (3%) of bis[4-methyl(thiobenzoyl)] disulfide (**14**). Thin-layer chromatography [20 cm×20 cm, hexane/dichloromethane (2:1)] of the third eluent gave 81 mg (26%) of *trans*-4-methylphenyl(phenylseleno) sulfine (**12i**, R_f=0.39) as yellow oil and 25 mg (8%) of *cis*-4-methylphenyl(phenylseleno) sulfine (**12'i**, R_f=0.07) as yellow oil.

12i: IR (neat) 3050, 1601, 1571, 1480, 1438, 1276, 1183, 1100, 1017, 995, 810, 740, 690, 618, 542, 471, 438, and 410 cm^{-1}. ^1H NMR ($CDCl_3$) δ=2.25 (3H, s, CH_3) and 6.9—7.5 (9H, m, Ar). ^{13}C NMR ($CDCl_3$) δ=21.7 (CH_3), 128.8—142.9 (Ar), and 178.5 (C=S=O). MS (70 eV) *m/z* (rel intensity), 308 (M^+; 7), 215 (4-$CH_3C_6H_4CSSe^+$, 79), 135 (4-$CH_3C_6H_4CS^+$, 100), 119 (4-$CH_3C_6H_4CO^+$, 28), and 91 (4-$CH_3C_6H_4^+$, 9).

12'i: IR (neat) 3050, 1601, 1571, 1480, 1438, 1276, 1201, 1183, 1170, 1100, 1017, 995, 810, 740, 690, 618, 542, 471, 438, and 410 cm^{-1}. ^1H NMR ($CDCl_3$) δ=2.35 (3H, s, CH_3), and 7.0—8.3 (9H, m, Ar). ^{13}C NMR ($CDCl_3$) δ=21.3 (CH_3), 126.1—141.1 (Ar), and 194.1 (C=S=O). MS (70 eV) *m/z* (rel intensity), 308 (M^+; 8), 215 (4-$CH_3C_6H_4CSSe^+$, 83), 135 (4-CH_3CS^+, 100), 119 (4-$CH_3C_6H_4CO^+$, 29), and 91 ($CH_3C_6H_4^+$, 23).

13i: Mp 86—88 °C (lit,[3] 86—88 °C). ^1H NMR ($CDCl_3$) δ=2.38 (3H, s, CH_3) and 6.9—8.1 (9H, m, Ar). IR (KBr) 1660 cm^{-1}.

14: Mp 117—119 °C. IR (KBr) 1693 cm^{-1}. UV/Vis (*cyclo*-C_6H_{12}) 250sh, 265 (4.55), and 267sh nm

We wish to thank Professor Satoshi Inagaki of Gifu University for his helpful suggestions to regarding the ab initio molecular orbital calculation.

References

1) The oral presentation of this work: K. Terashima, T. Katada, S. Kato, and M. Mizuta, The Central District Chemical Joint Meeting of The Japan Chemical Society, Nagoya, October, 1979, Abstr. No. 3F-08. It was taken for 9 years in order to confirm the curious experimental results, where the thionselenol esters react with primary and secondary amines to give the corresponding ammonium dithiocarboxylates; The formation of the sulfines **12** and sulfides **13** was presented at the First International Conference of Heteroatom Chemistry, Kobe, Japan, July 1987, Abstr. No. PS1026.

2) S. Kato, T. Murai, and M. Ishida, *Org. Prep. Proc. Int.*, **18**, 369 (1986).

3) Only three compounds have been described in literature—Selenothiophthalide from the reaction of iminoselenophthalide with hydrogen sulfide: a) M. Renson and R. Collinene, *Bull. Soc. Chim. Belg.*, **73**, 491 (1964). $C_6H_5CSSeCH_2CH_2\overset{+}{N}(CH_3)_2Cl^-$ from the reaction of thiobenzoyl chloride with 2-aminoethylselenomagnesium chloride, followed by treatment with hydrogen chloride: b) S. H. Chu and H. G. Mautner, *J. Med. Chem.*, **13**, 214 (1970). $(CF_3)_2CHCSSeC_6H_5$ from the reaction of bis(trifluoromethyl)thioketene with benzeneselenol: M. A. Raash, *J. Org. Chem.*, **37**, 1347 (1972).

4) a) S. Kato, T. Katada, and M. Mizuta, *Angew. Chem.*, **88**, 844 (1976); *Angew. Chem., Int. Ed. Engl.*, **15**, 766 (1976); b) S. Kato, K. Sugino, M. Yamada, T. Katada, and M. Mizuta, *Angew. Chem.*, **89**, 917 (1977); *Angew. Chem., Int. Ed. Engl.*, **16**, 788 (1977).

5) S. Kato, H. Shibahashi, T. Katada, T. Takagi, I. Noda, M. Mizuta, and M. Goto, *Liebigs Ann. Chem.*, **1982**, 1229.

6) The low yield of the methyl derivative **3a** seems to be due to decomposition of the starting sulfide **1a**, which is very unstable thermally.

7) The elevation of the reaction temperature over 40 °C leads to decomposition of (phenylseleno)trimethylsilane.

8) The synthesis of thioacyl chlorides are limited to the aromatic ones. The reaction of aliphatic dithiocarboxyl acid with sulfuryl chloride or phosphorus pentachloride to afford the sulfenyl chloride of structure $RCCl(SCl)_2$.

9) a) A. Bak, L. Hanzen-Nygarred, and C. Pedersen, *Acta Chem. Scand.*, **12**, 1451 (1958); b) L. T. Bellamy and P. F. Rogasch, *J. Chem. Soc.*, **1960**, 2218; c) S. Kato, M. Mizuta, and Y. Ishii, *J. Organometal. Chem.*, **55**, 121 (1973).

10) The hypsochromic shifts of these absorption maxima are observed by changing of the solvent from cyclohexane to ethanol, indicating the n-π^* transitions of the thioacyl group.

11) W. H. McFadden, R. M. Siefert, and J. Wasserman, *Anal. Chem.*, **32**, 1495 (1960).

12) A. Ohno, Y. Ohnishi, R. Koizumi, and G. Tsuchihashi *Tetrahedron Lett.*, **1968**, 4032.

13) A. Ohno, T. Koizumi, Y. Ohnishi, and G. Tsuchihashi, *Org. Mass Spec.*, **3**, 261 (1970).

14) S. Scheithauer and R. Mayer, "Thio- and Dithiocarboxylic Acids and Their Derivatives" in Topics in Sulfur Chemistry, ed by A. Senning, George Thieme, Stuttgartt (1979), p. 200.

15) It was reported that *O*-alkyl and *S*-alkyl thiobenzoates undergo the similar type of rearrangement thermally and under the conditions of electron impact: Y. Araki and A. Kaji, *Bull. Chem. Soc. Jpn.*, **43**, 3214 (1970).

16) P. Reynaud, R. C. Moreau, and J. P. Samana, *Bull. Soc. Chim. Fr.*, **1965**, 3628.

17) a) B. Holmberg, *Arkiv Kemi. Mineral. Geol. A*, **17** (No. 23), 1 (1944); b) A. Kjaer, *Acta Chem. Scand.*, **4**, 1437 (1950).

18) The reactions of *O*-phenyl 4-methylbenzenecarbothioate or *S*-phenyl 4-methylbenzenecarbodithioate with excess of piperidine gradually proceed at room temperature to give the corresponding thioamide in almost quantitative yields.

19) The reaction of phenyl benzenecarbodithioate with sodium ethanolate in ether does not occur at 10—25 °C.

20) a) B. Zwanenburg, L. Thijs, and J. Strating, *Tetrahedron Lett.*, **1967**, 3453; b) B. Zwanenburg, L. Thijs, and J. Strating, *Rec. Trav. Chim. Pays-Bas*, **90**, 614 (1971).

21) The low yields of the aliphatic esters are considered to be due to decomposition of the starting bis(thioacyl) sulfides **1**.

22) The ortho proton of the phenyl ring of *trans*-phenylthio(phenyl)sulfine (**12'**) shifted downfield compared with those of the corresponding cis-isomer **12**.

23) The similar downfield shifts were observed for the methyl protons of phenyl(methylthio)sulfine [$C_6H_5C(S{=}O)$-SCH_3].[19]

24) Karlström et al. obtained the similar result for decomposition of the oxathiirane **15** using the ab initio CASSCF method: G. Karlström, B. O. Roos, and L. Carlsen, *J. Am. Chem. Soc.*, **106**, 1557 (1984).

25) a) S. Kato and M. Mizuta, *Bull. Chem. Soc. Jpn.*, **45**, 3492 (1972); b) S. Kato, T. Mitani, and M. Mizuta, *Int. J. Sulfur Chem.*, **8**, 359 (1973).

26) a) R. Mayer and S. Scheithauer, *J. Prakt. Chem.*, **21**, 214 (1963); b) R. Mayer and S. Scheithauer, *Chem. Ber.*, **98**, 829 (1965).

27) J. E. Drake and R. T. Hemmings, *J. Chem. Soc., Dalton Trans.*, **1979**, 1730.

28) N. Marziano and R. Passerrini, *Gazz. Chim. Ital.*, **94**, 1137 (1964).

29) H. G. Mautner, *J. Am. Chem. Soc.*, **78**, 5292 (1956).

30) J. L. Piette and M. Renson, *Bull. Soc. Chim. Belg.*, **79** 360 (1970).

Synthesis of Branched-Chain Oligosaccharides in Sarsasaponins by Dehydrative Glycosylation

Shinkiti KOTO,* Naohiko MORISHIMA,[1] Masaharu UCHINO, Misa FUKUDA, Masayo YAMAZAKI, and Shonosuke ZEN
School of Pharmaceutical Sciences, Kitasato University, Shirokane, Minato-ku, Tokyo 108
(Received April 12, 1988)

The branched-chain oligosaccharides, 6-*O*-(β-D-glucopyranosyl)-4-*O*-(α-L-rhamnopyranosyl)-D-glucopyranose, and 2,6-di-*O*-(β-D-glucopyranosyl)-4-*O*-(α-L-rhamnopyranosyl)-D-glucopyranose, which compose sarsasaponins, as well as the structurally related 2-*O*-(β-D-glucopyranosyl)-4-*O*-(α-L-rhamnopyranosyl)-D-glucopyranose were synthesized stepwise via dehydrative glycosylation by a ternary mixture of *p*-nitrobenzenesulfonyl chloride, silver triflate, and triethylamine.

The dehydrative condensation of a protected monosaccharide, in which a reducing hydroxyl group and one of the nonreducing hydroxyl groups are unprotected, proceeds slowly, even under forced conditions, and its selectivity is generally poor.[2] The starting material used in such glycosylation is an anomeric mixture which may undergo self-condensation to give a nonreducing disaccharide. Because of these deficiencies, oligosaccharides with a fine structure have never been attempted using dehydrative glycosylation. Glycosylation of this kind, however, has an attractive feature in that it uses glycosyl donors with much longer shelf-lives compared to those of such hydrolyzable donors[3] as glycosyl halides and their equivalents. Studies of dehydrative glycosylation[4] have indicated that a ternary mixture of *p*-nitrobenzenesulfonyl chloride (NsCl), silver triflate (AgOTf), and triethylamine (Et_3N) (NST mixture) performs cross-condensation between 2,3,4,6-tetra-*O*-benzyl-D-glucopyranose (**1**) and various alcohols.[5] The reaction proceeds with moderate efficiencies and its selectivity depends on the type of donors,[6–9] reactivity of acceptors,[5,10] as well as the nature of any additives.[11] This report deals with the synthesis of bifurcated *O*-β-D-glucopyranosyl-(1→2)-*O*-[α-L-rhamnopyranosyl-(1→4)]-D-glucopyranose (**2**) and *O*-β-D-glucopyranosyl-(1→6)-*O*-[α-L-rhamnopyranosyl-(1→4)]-D-glucopyranose (**3**) as well as of trifurcated *O*-β-D-glucopyranosyl-(1→2)-*O*-[β-D-glucopyranosyl-(1→6)]-O-[α-L-rhamnopyranosyl-(1→4)]-D-glucopyranose (**4**),[12] while showing a practical limitation of glycosylation with an NST mixture.[5] The tetrasaccharide **4** composes the antibiotic saponins, parillin and sarsaparilloside from *Radix sarsaparillae*,[13] whereas the trisaccharide **2** might possibly constitute avenacoside A from the leaves and seeds of *Avena sativa*,[14] and another trisaccharide **3** is contained in a harb saponin, saikosaponin-*c* from the root of *Bupleurum falcatum* L.[15]

α-L-Rhap-(1→4)-D-Glcp
2
↑
↓
β-D-Glcp

2

β-D-Glcp
1
↓
6
α-L-Rhap-(1→4)-D-Glcp

3

β-D-Glcp
1
↓
6
α-L-Rhap-(1→4)-D-Glcp
2
↑
↓
β-D-Glcp

4

Synthesis of the Trisaccharide 2. The acceptor **5** for the synthesis of **2** was prepared from a known acetal **6**.[16] A controlled allylation of **6** with allyl bromide and sodium hydride gave 2-*O*-allyl ether **7** (54%) and an isomer **8** (11%). The structure of **7** was confirmed by measuring the ^1H NMR of its 3-acetate. Benzylation of **7** and a subsequent hydrolysis gave the diol **9**, which was subjected to controlled benzylation with benzyl chloride and sodium hydride to afford the desired **5** (55%) and the isomer **10** (11%).

Condensation of 2,3,4-tri-*O*-benzyl-L-rhamnopyranose[17] (**11**) and methyl 2,3,6-tri-*O*-benzyl-β-D-glucopyranoside[11] (**12**) using the NST mixture was first examined. The use of a 1.5 molar amount of the donor **11** produced a cross-condensate **13** (72% from **12**) and a self-condensate **14** (36% from **11**). The configuration of the interglycoside linkage was confirmed by measuring a $^1J_{CH}$[18] (170 Hz) for the signal (δ 98.4) of the anomeric carbon of the rhamnosyl residue in **13** and that in the corresponding debenzylated compound **15** (δ 102.3, 170 Hz). Rhamnosylation of **16**[16] with **11** was similarly carried out in order to furnish the disaccharide derivative **17** (68% from **16**) and **14** (36% from **11**). The anomeric carbon of the α-rhamnosyl residue of **17** appeared at δ 98.2 again with a $^1J_{CH}$ of 170 Hz (Table 1), whereas the corresponding proton gave a characteristic doublet (δ 5.07) with a small splitting (1.8 Hz). Thus, rhamnosylation with **11** of the 4-OH group was stereoselective but was apt to let the self-condensation of the donor undergo, differing from the case of glucosylation with **1**.[11] The acceptor **5** was then similarly condensed with **11** to give the

condensate **18** (81%). The anomeric carbon of the α-rhamnosyl moiety resonated at δ 98.2 with a $^1J_{CH}$ of 169 Hz. Deallylation of **18** with a rhodium complex and a subsequent hydrolysis[9] afforded the disaccharide acceptor **19**.

The 2-OH group of the simple acceptor **20**, which was readily prepared from **9**, was glucosylated with a 1.3 molar amount of **1** and the NST mixture to give the sophorose derivative **22** (38%) and a kojibiose derivative **21** (29%). The chemical shift of the anomeric proton (δ 5.20) and the anomeric carbon (δ 98.9) of the reducing end of **22** showed characteristic downfield shifts caused by a substitution by the tetra-*O*-benzylglucosyl residue at the 2-OH group in **20** (Table 1). Thus, glucosylation with **1** of the 2-OH group was marginally selective for the β-anomer.[10] Then, a similar glucosylation was applied to **19** to afford the desired trisaccharide derivative **24** (41%) and

Table 1. ^1H[a] and ^{13}C[b] NMR Data (δ) for the Anomeric Centers of the Fully Benzylated Glycosides

Compd. confgn.	H-1 α-D-Glc	H-1′→2 β-D-Glc	H-1″→4 α-L-Rha	H-1‴→6 β-D-Glc	C-1 α-D-Glc	C-1′→2 β-D-Glc	C-1″→4 α-L-Rha	C-1‴→6 β-D-Glc
22	5.20(3.5)	4.83(7.8)			98.9	103.4		
17	4.85(3.5)		5.07(1.8)		95.1(167)		98.2(170)	
30	4.88(4.0)			4.42(8.0)	95.2			103.8
24	5.11(3.0)	4.76(7.6)	5.08(2.0)		98.6(168)	103.2(162)	98.8(171)	
32	4.80(4.0)		5.10(2.0)	4.38(8.0)	95.0(168)		97.8(168)	104.0(159)
45	5.12(3.5)	4.72(7.5)	5.11(2>)	4.41(8.0)	97.7(167)	103.2(159)	98.5(173)	103.8(157)

a) The values in parentheses are those for $^3J_{HH}$(Hz) of the anomeric protons. b) The values in parentheses are those for $^1J_{CH}$(Hz) of the anomeric carbons.

Table 2. ^{13}C NMR Data (δ)[a] for the Glycosides in D_2O

	C-atom	MR[b]	S[c]	MS[d]	**15**	G[e]	**2**	**3**	**4**
	1α		92.4			92.5	92.5(172)	93.3(172)	93.1(173)
	1β		95.1	102.4	104.5(161)	96.4	95.5(164)	97.4(164)	96.2(162)
	2α		81.4			72.1	81.7	72.9	82.1
	2β		82.1	82.1	74.8	74.7	82.3	75.2	81.8
	3α		72.5			73.7	72.8	73.1	73.3
	3β		76.5	77.0	76.4	76.3	75.4	75.8	75.9
D-Glc	4α		70.4			70.3	78.2	78.7	78.5
	4β		70.4	70.1	78.8	70.3	78.2	78.7	78.5
	5α		71.8			71.0	71.3	70.6	70.4
	5β		76.5	77.0	75.9	75.3	75.9	75.8	75.2
	6α		61.7			69.4	61.0	69.3	69.3
	6β		61.7	61.4	61.6	69.4	61.0	69.3	69.3
	1′α		104.4				104.8(159)		105.4(162)
	1′β		103.2	104.6			103.5(159)		103.8(160)
	2′		74.2	75.0			74.2		74.7
β-D-Glc-(1′→2)	3′		76.5	77.0			76.6		77.1
	4′		70.4	70.4			70.3		71.0
	5′		76.5	77.3			76.4		77.1
	6′		61.7	61.4			61.5		62.1
	1″	101.9			102.3(170)		101.8(169)	102.2(171)	102.2(168)
	2″	71.0			71.5		71.0	71.6	71.6
	3″	71.3			71.7		71.3	71.8	71.8
α-L-Rha-(1″→4)	4″	73.1			73.3		72.8	73.3	73.3
	5″	69.4			70.5		69.9	70.5	70.4
	6″	17.7			17.8		17.8	17.8	17.8
	1‴					103.0		103.8(159)	103.8(160)
	2‴					73.3		74.3	74.3
β-D-Glc-(1‴→6)	3‴					76.3		77.3	77.1
	4‴					70.3		71.0	71.0
	5‴					76.3		77.1	77.1
	6‴					61.7		62.1	62.1

a) The values in parentheses are those for $^1J_{CH}$(Hz). b) MR=methyl α-L-rhamunopyranoside (Ref. 22). c) S=sophorose (Ref. 20). d) MS=methyl β-sophoroside: the values are those in C_5D_5N (Ref. 21) subtracted by 1.0 arbitrarily. e) G=gentiobiose (Ref. 20).

the α-isomer **23** (29%). The new anomeric carbon resonated at δ 103.2 with a $^1J_{CH}$ of 162 Hz, indicating the β-configuration. The chemical shifts of the anomeric protons and carbons of **24** correspond well with those of the relevant disaccharide derivatives, **17** and **22** (Table 1).

A hydrogenolytic debenzylation of **24** furnished the trisaccharide **2**, the ^{13}C NMR spectrum of which was consistent with the proposed structure (Table 2); the assignment was tentatively carried out based on the spectra of sophorose,[20] methyl sophoroside,[21] methyl α-L-rhamnopyranoside,[22] and **15**.

Synthesis of the Trisaccharide 3. The synthesis was started from the known acceptor **25**.[16] The first glycosylation of **25** with **1** in the presence of the NST mixture afforded the gentiobiose derivative **27** (64%) and the isomaltose derivative **26** (21%). The new anomeric carbon of **27** appeared at δ 103.8, indicating the β-configuration. The glucosylation of the acceptor **28**[23] with **1** also gave the gentiobiose derivative **30**[24,25] (75%) and the α-isomer **29** (22%). Deallylation of **27** gave **31**, which was then subjected to the α-rhamnosylation with **11**. In this case, however, the 4-OH group of **31** was so unreactive to the activated **11**, due to the presence of the tetra-*O*-benzylglucosyloxyl group at the C-6 position, that a significant amount (18%) of the *p*-nitrobenzenesulfonate of **31** was formed expectedly,[26] indicating a practical limitation of the rhamnosylation with **11** and the NST mixture. Nevertheless, the desired trisaccharide derivative **32** was produced in a 36% yield with complete selectivity. The anomeric carbon of the α-rhamnosyl moiety in **32** appeared at δ 97.8 with a $^1J_{CH}$ of 168 Hz; the chemical shifts of the anomeric protons and carbons nicely correspond with those of the relevant disaccharide derivatives, **17** and **30** (Table 1).

Hydrogenolysis of **32** afforded the trisaccharide **3**, the ^{13}C NMR spectrum of which was tentatively assigned based on the spectra of gentiobiose[20] and **15** and was consistent with the proposed structure (Table 2).

Synthesis of the Tetrasaccharide 4. The key

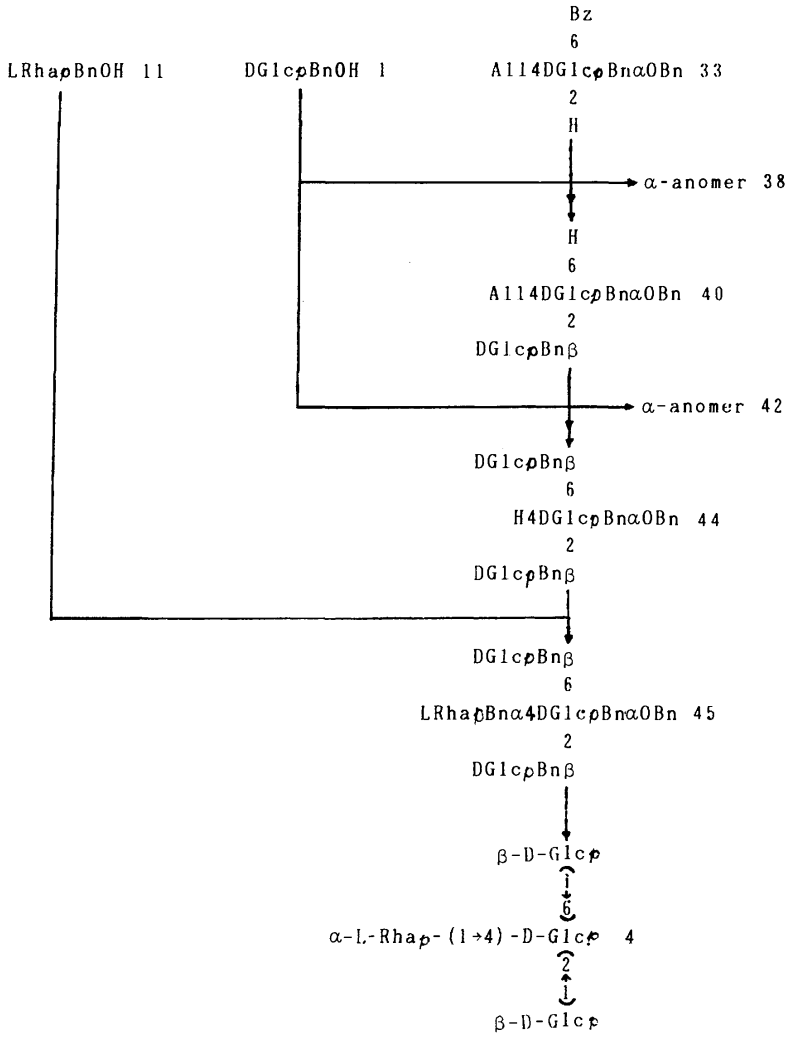

Fig. 1. Synthetic diagram[24] for the tetrasaccharide **4** (All=-$CH_2CH{=}CH_2$, Bn=CH_2Ph, Bz=-COPh).

acceptor **33** was prepared from the dityrityl ether **34**.[27] Brief heating of **34** in allyl bromide in the presence of a limited amount of sodium hydride, followed by forced benzylation by hot benzyl chloride and excess potassium hydroxide, and a subsequent detritylation with trifluoroacetic acid in methanolic chloroform gave the 4-*O*-allyl derivative **35** (79%) and the isomer **36** (9%). A bulky trityloxyl group at the C-2 position in **34** well diminished the reactivity of the neighboring 3-OH group. The structure of **35** was confirmed by converting it into the known **16**.[16] A mild benzoylation of **35** with benzoyl chloride in pyridine gave the desired acceptor **33** (52%) and the isomer **37** (12%). The H-2 of the 6-benzoate **33** resonates at δ 3.53, whereas that of the 2-benzoate **37** was so deshielded that it gave a signal at δ 4.90.

The first glucosylation of **33** with **1** and the NST mixture gave the desired product **39** (45%) and the α-isomer **38** (39%). As described above, a significant formation of the α-glucosides was also observed in glucosylation with **1** for the 2-OH group of **19** and **20**. The anomeric carbon of the nonreducing β-glucosyl residue of **39** appeared at δ 103.6. Debenzoylation of **39** gave the acceptor **40**. This was successively benzylated and deallylated to give another acceptor **41**. Rhamnosylation of **41** with **11** and the NST mixture provided the trisaccharide derivative **24** described above. Thus, the structure of **33** was strictly confirmed.

The second glucosylation of the 6-OH group of **40**

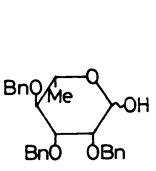

11

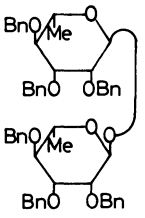

14

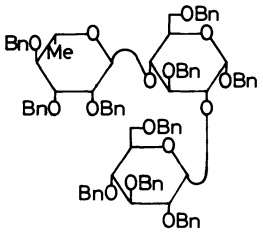

23

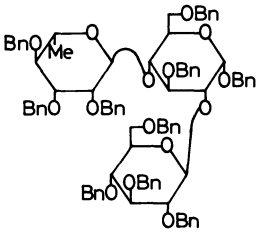

24

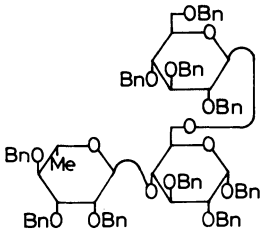

32

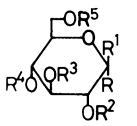

	R	R¹	R²	R³	R⁴	R⁵
1	OH, H		Bn	Bn	Bn	Bn
5	OBn	H	All	Bn	H	Bn
6	OBn	H	H	H	Bd	
7	OBn	H	All	H	Bd	
8	OBn	H	H	All	Bd	
9	OBn	H	All	Bn	H	H
10	OBn	H	All	Bn	Bn	H
12	H	OMe	Bn	Bn	H	Bn
16	OBn	H	Bn	Bn	H	Bn
20	OBn	H	H	Bn	Bn	Bn
25	OBn	H	Bn	Bn	All	H
28	OBn	H	Bn	Bn	Bn	H
33	OBn	H	H	Bn	All	Bz
34	OBn	H	Tr	H	H	Tr
35	OBn	H	H	Bn	All	H
36	OBn	H	H	All	Bn	H
37	OBn	H	Bz	Bn	All	H

All = $-CH_2-CH=CH_2$
Bd = $>CH(Ph)$
Bn = $-CH_2Ph$
Bz = $-COPh$
Tr = $-CPh_3$

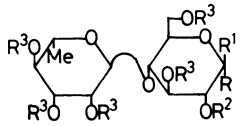

	R	R¹	R²	R³
13	H	OMe	Bn	Bn
15	H	OMe	H	H
17	OBn	H	Bn	Bn
18	OBn	H	All	Bn
19	OBn	H	H	Bn

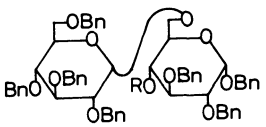

26 R = All
29 R = Bn

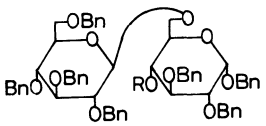

27 R = All
30 R = Bn
31 R = H

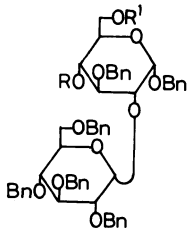

21 R = R' = Bn
38 R = All, R' = Bz

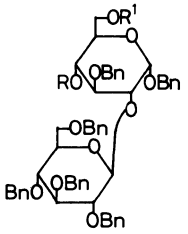

22 R = R' = Bn
39 R = All, R' = Bz
40 R = All, R' = H
41 R = H , R' = Bn

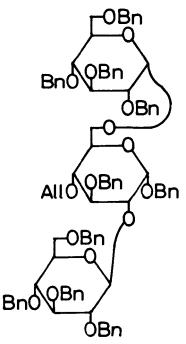

42

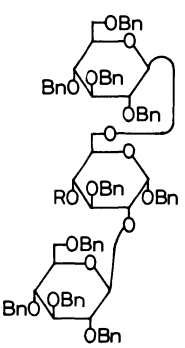

43 R = All
44 R = H

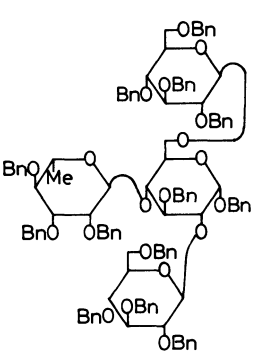

45

with **1** and the NST mixture furnished the desired **43** (68%) and the α-anomer **42** (31%). The anomeric carbon of the newly introduced β-glucosyl moiety of **43** appeared at δ 104.0. Deallylation of **43** smoothly gave the trisaccharide acceptor **44**.

The final rhamnosylation of **44** with **11** and the NST mixture afforded the fully benzylated tetrasaccharide **45** in a 37% yield, as the sole cross-condensate. The anomeric carbon of the α-rhamnosyl moiety appeared at δ 98.5 with a $^1J_{CH}$ of 173 Hz. All the anomeric carbons and protons of **45** are well correlated with those of the component trisaccharide derivative **24** and **32** (Table 1).

A catalytic hydrogenolysis of **45** gave the trifurcated tetrasaccharide **4**, the ^{13}C NMR spectrum of which was consistent with the proposed structure (Table 2). The assignment was tentatively carried out based on the spectra of sophorose,[20] gentiobiose,[20] **15**, **2**, and **3**.

Thus, the work described may illustrate the scope and limitations for the synthesis of complex oligosaccharides using the dehydrative glycosylation with an NST mixture.[5]

Experimental

The solvent systems for chromatography on a silica-gel column (gradient elution) and TLC were toluene-2-butanone (TB), hexane-ethyl acetate (HE), hexane-acetone (HA), IPE†-ethyl acetate (IE), and chloroform-methanol (CM) systems. The glycosylation with the NST mixture and the accompanying processing were performed as described earlier.[5,6,10] Sodium hydride in an oil suspension (60% of NaH by wt) was used without pre-washing. Hydrogenolytic debenzylation was carried out using a Parr-3911 hydrogenation apparatus under 340 kPa of H_2 at room temp. A concentration of the solution was carried out under reduced pressure. The NMR spectra were recorded with a Varian XL-400 spectrometer at 400 MHz for ^1H and at 100.6 MHz for ^{13}C or with a Varian VXR-300 spectrometer at 300 MHz for ^1H and at 75.5 MHz for ^{13}C; the chemical shifts of ^1H NMR are relative to the satelite peak of $CDCl_3$ at δ 7.26 in $CDCl_3$ and the peak of DOH at δ 4.70 in D_2O and those for ^{13}C NMR are to the central peak of $CDCl_3$ at δ 77.0 in $CDCl_3$ and the peak of 1,4-dioxane at δ 67.4 in D_2O. A routine measurement of the NMR spectra was carried out with a Varian EM-390 spectrometer at 90 MHz for ^1H and with a JEOL-PS-100 spectrometer linked to a JEOL-EC-100 computer at 25.2 MHz for ^{13}C; the chemical shifts are relative to the peak of internal TMS at δ 0.0 in $CDCl_3$ and that of external TMS at δ 0.0 in D_2O. For other items, refer to previous reports,[5,10,11] unless otherwise described.

Benzyl 2-*O*- and 3-*O*-Allyl-4,6-*O*-benzylidene-α-D-glucopyranosides (7 and 8). A mixture of **6**[16] (1.00 g), NaH in an oil suspension (144 mg) and allyl bromide (12 ml) was stirred for 3 h at 80 °C. The mixture was diluted with toluene and washed with cold H_2O. The organic layer was concentrated and chromatographed (IE system) to give the diallyl ether (0.11 g, 9%), **7** (0.60 g, 54%), mp 153—154 °C (from IPE), $[\alpha]_D^{20}$ +138° (*c* 0.7, $CHCl_3$), ^1H NMR ($CDCl_3$, 90 MHz) δ=3.42 (1H, dd, $J_{1,2}$=3.6 Hz, $J_{2,3}$=9.3 Hz, H-2), 5.01 (1H, d, H-1), 5.53 (1H, s, benzylidene), 5.7—6.2 (1H, m, allyl), ^{13}C NMR ($CDCl_3$, 75 MHz) δ=62.4 (C-5), 69.0 (C-6), 79.4 (C-2), 81.3 (C-4), 95.8 (C-1), 102.0 (benzylidene), 118.0, 134.4 (allyl), and **8** (0.12 g, 11%), mp 95—97 °C (from hexane), $[\alpha]_D^{20}$ +83° (*c* 2.8, $CHCl_3$), ^1H NMR ($CDCl_3$, 90 MHz) δ=5.01 (1H, d, $J_{1,2}$=3.0 Hz, H-1), 5.51 (1H, s, benzylidene), 5.7—6.2 (1H, m, allyl), ^{13}C NMR ($CDCl_3$, 75 MHz) δ=62.9 (C-5), 68.9 (C-6), 78.6 (C-4), 81.9 (C-3), 98.3 (C-1), 101.2 (benzylidene), 117.2, 135.0 (allyl).

Found: **7**, C, 68.91; H, 6.55%. **8**, C, 68.89; H, 6.51%. Calcd for $C_{23}H_{26}O_6$: C, 69.33; H, 6.58%.

A sample of **7** was acetylated with acetic anhydride and pyridine, followed by chromatography (HA system) to give the homogeneous acetate, ^1H NMR (CCl_4, 90 MHz) δ=2.02 (3H, s, Ac), 3.42 (1H, dd, $J_{1,2}$=3.6 Hz, $J_{2,3}$=9.6 Hz, H-2), 3.43 (1H, dd, $J_{3,4}$=9.6 Hz, $J_{4,5}$=9.0 Hz, H-4), 4.88 (1H, d, H-1), 5.36 (1H, s, benzylidene), 5.47 (1H, t, H-3) indicating that Ac is at the O-3 of **7**.

Benzyl 2-*O*-Allyl-3-*O*-benzyl-α-D-glucopyranoside (9). A mixture of **7** (0.55 g), crushed KOH (0.3 g), and $PhCH_2Cl$ (2.8 ml) was stirred for 1 h at 125 °C. The mixture was diluted with toluene and washed with cold H_2O. The organic layer was concentrated at 95 °C and then heated in aq AcOH (80%, 16 ml) for 1 h at 95 °C. The mixture was concentrated and chromatographed (TB system) to give **9** (0.52 g, 94%), mp 78—80 °C (from IPE), $[\alpha]_D^{20}$ +94° (*c* 2.1, $CHCl_3$), ^{13}C NMR ($CDCl_3$, 75 MHz) δ=62.3 (C-6), 79.7 (C-2), 81.2 (C-3), 95.5 (C-1), 117.5, 134.6 (allyl).

Found: C, 68.71; H, 6.93%. Calcd for $C_{23}H_{28}O_6$: C, 68.98; H, 7.05%.

Benzyl 2-*O*-Allyl-3,6- and -3,4-di-*O*-benzyl-α-D-glucopyranosides (5 and 10). A mixture of **9** (294 mg), NaH in an oil suspension (40 mg) and $PhCH_2Cl$ (2.9 ml) was stirred for 2 h at 110 °C. The mixture was processed and chromatographed (TB system) to give a fully benzylated product (49 mg, 11%), **5** (198 mg, 55%), $[\alpha]_D^{20}$ +79° (*c* 2.7, $CHCl_3$), ^{13}C NMR ($CDCl_3$, 75 MHz) δ=79.5 (C-2), 81.4 (C-3), 95.4 (C-1), 117.4, 134.6 (allyl), and **10** (38 mg, 11%), mp 55—56 °C, $[\alpha]_D^{20}$ +86° (*c* 5.8, $CHCl_3$), ^{13}C NMR ($CDCl_3$, 75 MHz) δ=61.7 (C-6), 77.4 (C-4), 79.9 (C-2), 81.8 (C-3), 95.5 (C-1), 117.4, 134.7 (allyl).

Found: **5**, C, 73.07; H, 6.93%. **10**, C, 73.77; H, 6.92%. Calcd for $C_{30}H_{34}O_6$: C, 73.45; H, 6.99%.

A sample of **5** was acetylated with acetic anhydride and pyridine, followed by chromatography (HA system) to afford the homogeneous acetate, ^1H NMR (CCl_4, 90 MHz) δ=1.71 (3H, s, Ac), 3.38 (1H, dd, $J_{1,2}$=3.6 Hz, $J_{2,3}$=9.3 Hz, H-2), 3.83 (1H, t, $J_{3,4}$=9.3 Hz), 4.83 (1H, d, H-1), 4.87 (1H, dd, $J_{4,5}$=9.6 Hz) indicating the presence of Ac at the O-4 or **5**.

Methyl *O*-(2,3,4-Tri-*O*-benzyl-α-L-rhamnopyranosyl)-(1→4)-2,3,6-tri-*O*-benzyl-β-D-glucopyranoside (13) and *O*-(2,3,4-Tri-*O*-benzyl-α-L-rhamnopyranosyl)-(1→1)-2,3,4-tri-*O*-benzyl-α-L-rhamnopyranoside (14). The acceptor **12**[11] (30.0 mg) was condensed with **11**[17] (42.1 mg) in the presence of NsCl (43.0 mg), AgOTf (Aldrich, 49.8 mg), and Et_3N (27.1 μl) in CH_2Cl_2 (0.4 ml), followed by chromatography (TB system) to give **14** (15.2 mg, 36% from **11**), $[\alpha]_D^{20}$ −74° (*c* 0.9, $CHCl_3$), ^{13}C NMR ($CDCl_3$, 25 MHz) δ=18.0 (C-6), 68.8 (C-5), 93.7 (C-1), and **13** (41.2 mg, 72% from **12**), $[\alpha]_D^{20}$ −23° (*c* 2, $CHCl_3$), ^{13}C NMR ($CDCl_3$, 25 MHz) δ=17.8 (C-6′), 56.8 (MeO), 98.4 ($^1J_{CH}$=170 Hz, C-1′), 104.9 ($^1J_{CH}$=156 Hz, C-1).

13, Found: C, 74.94; H, 6.73%. Calcd for $C_{55}H_{60}O_{10}$: C, 74.98; H, 6.86%.

† IPE=diisopropyl ether.

14, Found: C, 76.00; H, 6.88%. Calcd for $C_{54}H_{58}O_9$: C, 76.21; H, 6.87%.

Methyl *O*-α-L-Rhamnopyranosyl-(1→4)-β-D-glucopyranoside (15). Hydrogenolysis of **13** (76.5 mg) over Pd on C (10%, 50 mg) in AcOH (6 ml) containing H_2O (50 μl) overnight, followed by chromatography (CM system), gave a hygroscopic foam of **15** (17.3 mg, 59%), $[\alpha]_D^{20}$ −58° (*c* 1.2, H_2O), ^1H NMR (D_2O, 90 MHz) δ=1.28 (3H, d, $J_{5',6'}$=6.0 Hz, H-6'), 3.57 (3H, s, MeO), 4.39 (1H, d, $J_{1,2}$=7.8 Hz, H-1), 4.87 (1H, d, $J_{1',2'}$=1.8 Hz, H-1').

Found: C, 45.64; H, 7.16%. Calcd for $C_{13}H_{24}O_{10}$: C, 45.88; H, 7.11%.

Benzyl *O*-(2,3,4-Tri-*O*-benzyl-α-L-rhamnopyranosyl)-(1→4)-2,3,6-tri-*O*-benzyl-α-D-glucopyranoside (17). Rhamnosylation of **16**[16] (45.8 mg) with **11** (55.2 mg), NsCl (54.6 mg), AgOTf (65.4 mg), and Et_3N (35.5 μl) in CH_2Cl_2 (0.3 ml), followed by chromatography (TB system), furnished **14** (19.7 mg, 36% from **11**) and then **17** (55.4 mg, 68% from **16**), $[\alpha]_D^{20}$ +16° (*c* 1.9, $CHCl_3$).

Found: C, 76.28; H, 6.55%. Calcd for $C_{61}H_{64}O_{10}$: C, 76.54; H, 6.74%.

Benzyl *O*-(2,3,4-Tri-*O*-benzyl-α-L-rhamnopyranosyl)-(1→4)-2-*O*-allyl-3,6-di-*O*-benzyl-α-D-glucopyranoside (18). The acceptor **5** (260.7 mg) was treated with **11** (346.4 mg) in the presence of NsCl (353.5 mg), AgOTf (410.2 mg), and Et_3N (224.0 μl) in CH_2Cl_2 (2 ml). Chromatography (TB system) gave **14** (55.7 mg, 16% from **11**) and then **18** (388.8 mg, 81% from **5**), $[\alpha]_D^{20}$ +32° (*c* 1.3, $CHCl_3$), ^{13}C NMR ($CDCl_3$, 100 MHz) δ=18.0 (C-6'), 95.1 ($^1J_{CH}$=168 Hz, C-1), 98.2 ($^1J_{CH}$=169 Hz, C-1'), 117.6, 134.7 (allyl).

Found: C, 75.29; H, 6.93%. Calcd for $C_{57}H_{64}O_{11}$: C, 75.47; H, 6.89%.

Benzyl *O*-(2,3,4-Tri-*O*-benzyl-α-L-rhamnopyranosyl)-(1→4)-3,6-di-*O*-benzyl-α-D-glucopyranoside (19). A mixture of **18** (346.1 mg), TRC†† (Aldrich, 30 mg) and EBW†† (7.7 ml) was refluxed overnight. The mixture was concentrated and then heated in acetone (6 ml) containing aq HCl (3.5%, 60 μl) for 1 h at 45 °C. Chromatography (HE system) gave **19** (277.9 mg, 85%), $[\alpha]_D^{20}$ +32° (*c* 1.7, $CHCl_3$), ^{13}C NMR ($CDCl_3$, 100 MHz) δ=17.8 (C-6'), 97.6 ($^1J_{CH}$=168 Hz, C-1), 98.2 ($^1J_{CH}$=170 Hz, C-1').

Found: C, 74.85; H, 6.63%. Calcd for $C_{54}H_{58}O_{10}$: C, 74.80; H, 6.74%.

Benzyl 3,4,6-Tri-*O*-benzyl-α-D-glucopyranoside (20). A mixture of **9** (0.44 g), crushed KOH (0.74 g), and $PhCH_2Cl$ (5.3 ml) was stirred for 2 h at 125 °C. After processing, chromatography (HE system) gave the product, which was then refluxed in EBW (4 ml) in the presence of TRC (20 mg) overnight. After concentration, the residue was heated in acetone (4 ml) containing aq HCl (3.5%, 40 μl) for 1 h at 45 °C. Chromatography (HE system) furnished **20** (0.27 g, 45%), $[\alpha]_D^{20}$ +105° (*c* 1.8, $CHCl_3$) ^{13}C NMR ($CDCl_3$, 75 MHz) δ=68.4 (C-6). 69.8 (C-5), 70.7 (C-2), 73.1, 73.5, 75.0, 75.4 (benzyl), 77.4 (C-4), 83.5 (C-3), 97.9 (C-1).

Found: C, 75.60; H, 6.66%. Calcd for $C_{34}H_{36}O_6$: C, 75.53; H, 6.71%.

Benzyl *O*-(2,3,4,6-Tetra-*O*-benzyl-α- and β-D-glucopyranosyl)-(1→2)-3,4,6-tri-*O*-benzyl-α-D-glucopyranosides (21 and 22). The acceptor **20** (53.5 mg) was glucosylated with **1** (Pfânstiehl, 69.5 mg), NsCl (37.3 mg), AgOTf (43.3 mg), and Et_3N (23.5 μl) in CH_2Cl_2 (0.5 ml), followed by chromatography (TB system), gave **22** (40.1 mg, 38%), $[\alpha]_D^{20}$ +48° (*c* 0.9, $CHCl_3$), and then **21** (30.5 mg, 29%), $[\alpha]_D^{20}$ +79° (*c* 1.9, $CHCl_3$), ^1H NMR ($CDCl_3$, 400 MHz) δ=5.09 (1H, d, $J_{1',2'}$=3.6 Hz, H-1'), 5.24 (1H, d, $J_{1,2}$=3.5 Hz, H-1), ^{13}C NMR ($CDCl_3$, 100 MHz) δ=94.0 (C-1'), 95.0 (C-1).

Found: **21**, C, 76.76; H, 6.73%. **22**, C, 76.53; H, 6.62%. Calcd for $C_{68}H_{70}O_{11}$: C, 76.81; H, 6.64%.

Benzyl *O*-(2,3,4,6-Tetra-*O*-benzyl-α- and β-D-glucopyranosyl)-(1→2)-*O*-[(2,3,4-tri-*O*-benzyl-α-L-rhamnopyranosyl)-(1→4)]-3,6-di-*O*-benzyl-α-D-glucopyranosides (23 and 24). (i) The acceptor **19** (48.4 mg) was glucosylated with **1** (39.2 mg) in the presence of NsCl (24.8 mg), AgOTf (28.8 mg), and Et_3N (15.6 mg) in CH_2Cl_2 (0.4 ml), followed by chromatography (TB system), gave **24** (32.1 mg, 41%), $[\alpha]_D^{20}$ +20° (*c* 1.2, $CHCl_3$), and **23** (22.6 mg, 29%), $[\alpha]_D^{20}$ +48° (*c* 0.7, $CHCl_3$), ^{13}C NMR ($CDCl_3$, 100 MHz) δ=94.1 (C-1'), 94.9 (C-1), 98.3 (C-1'').

Found: **23**, C, 76.19; H, 6.64%. **24**, C, 76.27; H, 6.82%. Calcd for $C_{88}H_{92}O_{15}$: C, 76.06; H, 6.67%.

(ii) Rhamnosylation of **41** (see below, 38.9 mg) with **11** (26.0 mg), NsCl (26.6 mg), AgOTf (30.9 mg), and Et_3N (14.7 μl) in CH_2Cl_2 (0.4 ml), followed by chromatography (TB system), gave **14** (5.8 mg, 15%) and **24** (21.1 mg, 38%), the ^{13}C NMR spectrum of which was identical with that of **24** described above.

***O*-β-D-Glucopyranosyl-(1→2)-*O*-[α-L-rhamnopyranosyl-(1→4)]-D-glucopyranose (2).** Hydrogenolysis of **24** (58.8 mg) over Pd on C (10%, 36 mg) in AcOH (6 ml) containing H_2O (50 μl) overnight, followed by chromatography (CM system), afforded a hygroscopic foam of **2** (17.0 mg, 82%), $[\alpha]_D^{20}$ +1.4° (*c* 1.2, H_2O), ^1H NMR (D_2O, 300 MHz) δ=4.53 (0.7H, d, $J_{1',2'}$=7.5 Hz, H-1'α), 4.60 (0.3H, d, $J_{1,2}$=7.6 Hz, H-1β), 4.75 (1H, d, $J_{1'',2''}$=1.5 Hz, H-1''), 5.32 (0.7H, d, $J_{1,2}$=4.0 Hz, H-1α).

Found: C, 44.54; H, 6.98%. Calcd for $C_{18}H_{32}O_{15}$: C, 44.26; H, 6.60%.

Benzyl *O*-(2,3,4,6-Tetra-*O*-benzyl-α- and β-D-glucopyranosyl)-(1→6)-4-*O*-allyl-2,3-di-*O*-benzyl-α-D-glucopyranosides (26 and 27). The acceptor **25**[16] (50.0 mg) was condensed with **1** (60.0 mg) in the presence of NsCl (34.0 mg), AgOTf (39.5 mg), and Et_3N (21.4 μl) in CH_2Cl_2 (0.6 ml), followed by chromatography (TB system), gave **26** (22.2 mg, 21%), $[\alpha]_D^{20}$ +76° (*c* 1.3, $CHCl_3$), ^{13}C NMR ($CDCl_3$, 75 MHz) δ=94.5 (C-1), 97.3 (C-1'), 116.8, 135.0 (allyl), and **27** (65.8 mg, 64%), $[\alpha]_D^{20}$ +51° (*c* 1.1, $CHCl_3$), ^{13}C NMR ($CDCl_3$, 75 MHz) δ=95.2 (C-1), 103.8 (C-1'), 116.6, 134.8 (allyl).

Found: **26**, C, 76.12; H, 6.89%. **27**, C, 75.97; H, 6.83%. Calcd for $C_{64}H_{68}O_{11}$: C, 75.87; H, 6.76%.

Benzyl *O*-(2,3,4,6-Tetra-*O*-benzyl-α- and β-D-glucopyranosyl)-(1→6)-2,3,4-tri-*O*-benzyl-α-D-glucopyranosides (29 and 30). Condensation of **28**[23] (54.0 mg) with **1** (70.2 mg) in the presence of NsCl (37.7 mg), AgOTf (43.7 mg), and Et_3N (23.7 μl) in CH_2Cl_2 (0.54 ml), followed by chromatography (TB system), gave **29** (23.3 mg, 22%), mp 106—107 °C, $[\alpha]_D^{20}$ +79° (*c* 1.7, $CHCl_3$) [lit,[24] mp 102—105 °C, $[\alpha]_D^{20}$ +64° (*c* 0.6, $CHCl_3$)], ^{13}C NMR ($CDCl_3$, 75 MHz) δ=94.6 (C-1), 97.3 (C-1'), and **30** (79.2 mg, 75%), mp 132—134 °C, $[\alpha]_D^{20}$ +41° (*c* 0.7, $CHCl_3$) [lit, mp 128—130 °C,[24] 133—134 °C,[25] $[\alpha]_D^{20}$ +39° (*c* 0.4, $CHCl_3$),[24] +17.1° (*c* 1, $CHCl_3$)[25]].

Found: **29**, C, 76.53; H, 6.63%. **30**, C, 76.53; H, 6.54%.

†† TRC=tris(triphenylphosphine)rhodium(I) chloride and EBW is the mixture of EtOH, benzene, and H_2O (7:3:1, v/v) (Ref. 19).

Calcd for $C_{68}H_{70}O_{11}$: C, 76.81; H, 6.64%.

Benzyl *O*-(2,3,4,6-Tetra-*O*-benzyl-β-D-glucopyranosyl)-(1→6)-2,3-di-*O*-benzyl-α-D-glucopyranoside (31). A mixture of **27** (73.5 mg), TRC (20 mg), and EBW (4 ml) was refluxed overnight. After concentration, the residue was heated in acetone (2 ml) containing aq HCl (3.5%, 50 μl) for 1 h at 45 °C. Chromatography (HE system) gave **31** (43.6 mg, 62%), mp 128—129 °C, $[\alpha]_D^{20}$ +35° (*c* 0.7, $CHCl_3$), ^{13}C NMR ($CDCl_3$, 25 MHz) δ=95.6 (C-1), 103.9 (C-1′).

Found: C, 75.18; H, 6.67%. Calcd for $C_{61}H_{64}O_{11}$: C, 75.29; H, 6.63%.

Benzyl *O*-(2,3,4,6-Tetra-*O*-benzyl-β-D-glucopyranosyl)-(1→6)-*O*-[(2,3,4-tri-*O*-benzyl-α-L-rhamnopyranosyl)-(1→4)]-2,3-di-*O*-benzyl-α-D-glucopyranoside (32). Rhamnosylation of **31** (54.4 mg) with **11** (36.5 mg) in the presence of NsCl (27.3 mg), AgOTf (43.2 mg), and Et_3N (23.5 μl) in CH_2Cl_2 (0.4 ml), followed by chromatography (TB system), gave **14** (16.0 mg, 45% from **11**), the *p*-nitrobenzenesulfonate of **31** (12.0 mg, 18% from **31**), $[\alpha]_D^{20}$ +31° (*c* 1.3, $CHCl_3$), ^{13}C NMR ($CDCl_3$, 75 MHz) δ=94.5 (C-1), 103.7 (C-1′), 123.8, 125.8, 142.3, 149.9 (*p*-nitrobenzenesulfonyl) [Found: C, 69.64; H, 5.81; N, 1.28%. Calcd for $C_{67}H_{67}NO_{15}S$: C, 69.47; H, 5.83; N, 1.21%], and then **32** (27.7 mg, 36% from **31**), $[\alpha]_D^{20}$ +17 (*c* 1.7, $CHCl_3$).

Found: C, 75.64; H, 6.54%. Calcd for $C_{88}H_{92}O_{15}$: C, 76.06; H, 6.67%.

***O*-β-D-Glucopyranosyl-(1→6)-*O*-[α-L-rhamnopyranosyl-(1→4)]-D-glucopyranose (3).** Hydrogenolysis of **32** (77.6 mg) over Pd on C (10%, 50 mg) in AcOH (6 ml) containing H_2O (50 μl) for 2 d, followed by chromatography (CM system), gave a hygroscopic glass of **3** (15.4 mg, 56%), $[\alpha]_D^{20}$ −5.1° (*c* 1.1, H_2O), ^1H NMR (D_2O, 300 MHz) δ=4.35 (0.4H, d, $J_{1'',2''}$=8.0 Hz, H-1″α), 4.37 (0.6H, $J_{1'',2''}$=8.0 Hz, H-1″β), 4.54 (0.6H, $J_{1,2}$=8.0 Hz, H-1β), 4.80 (1H, s, H-1′), 5.11 (0.4H, $J_{1,2}$=4.0 Hz, H-1α).

Found: C, 43.98; H, 6.98%. Calcd for $C_{18}H_{32}O_{15}$: C, 44.26; H, 6.60%.

Benzyl 4-*O*-Allyl-3-*O*-benzyl- and 3-*O*-Allyl-4-*O*-benzyl-α-D-glucopyranosides (35 and 36). A mixture of **34**[27] (6.09 g), NaH in an oil suspension (0.49 g) and allyl bromide (30.7 ml) was stirred for 4 h at 60 °C. After removing some insoluble matter by filtration, the solution was evaporated to dryness. The residue was vigorously stirred in $PhCH_2Cl$ (160 ml) containing crushed KOH (60 g) for 6 h at 120 °C. After filtration and evaporation at 95 °C, the residue was refluxed in a mixture of MeOH (20 ml), $CHCl_3$ (30 ml), and trifluoroacetic acid (Tokyo Kasei, 5 ml) for 1.5 h. After Et_3N (11 ml) being added, evaporation and chromatography (TB system) gave **35** (2.56 g, 79%), mp 81—82 °C (from hexane containing IPE), $[\alpha]_D^{20}$ +131° (*c* 1.0, $CHCl_3$), ^{13}C NMR ($CDCl_3$, 75 MHz) δ=61.7 (C-6), 69.9 (C-5), 71.3 (C-2), 77.2 (C-4), 83.0 (C-3), 97.8 (C-1), 117.3, 134.5 (allyl), 136.8, 138.6 (benzyl), and **36** (0.28 g, 9%), mp 94.5—95.5 °C (from IPE), $[\alpha]_D^{20}$ +105° (*c* 0.3, $CHCl_3$), ^{13}C NMR ($CDCl_3$, 75 MHz) 61.7 (C-6), 69.9 (C-5), 71.3 (C-2), 77.2 (C-4), 82.8 (C-3), 97.8 (C-1), 116.8, 135.1 (allyl), 136.8, 137.8 (benzyl).

Found: **35**, C, 68.84; H, 7.01%. **36**, C, 68.75; H, 7.03%. Calcd for $C_{23}H_{28}O_6$: C; 68.98, H; 7.05%.

A sample (28.2 mg) of **35** was treated in DMF (0.6 ml) with NaH in an oil suspension (17 mg) and $PhCH_2Br$ (52 μl) at room temp for 1 h. Processing followed by chromatography (HE system) gave a product which was refluxed overnight in EBW (4 ml) containing TRC (8 ml). After concentration, the residue was heated in acetone (4 ml) containing aq HCl (3.5%, 40 μl) for 1 h at 45 °C. Chromatography (HE system) gave **16** (19.4 mg, 51%), which was identified with a sample prepared following the known method.[16]

Benzyl 4-*O*-Allyl-6- and -2-*O*-benzoyl-3-*O*-benzyl-α-D-glucopyranosides (33 and 37). To a solution of **35** (2.71 g) in pyridine (13.5 ml) was added PhCOCl (0.79 ml) portionwise at −10 °C. The mixture was then stirred overnight at 0 °C. Processing and chromatography (TB system) gave the dibenzoate (0.77 g, 19%), **33** (1.79 g, 52%), $[\alpha]_D^{20}$ +105° (*c* 1.0, $CHCl_3$), ^1H NMR (CCl_4, 90 MHz) δ=3.53 (1H, dd, $J_{1,2}$=4 Hz, $J_{2,3}$=10 Hz, H-2), 4.82 (1H, d, H-1), and **37** (0.40 g, 12%), $[\alpha]_D^{20}$ +174° (*c* 3.1, $CHCl_3$) ^1H NMR (CCl_4, 90 MHz) 4.06 (1H, dd, $J_{2,3}$=10 Hz, $J_{3,4}$=9 Hz, H-3), 4.90 (1H, dd, $J_{1,2}$=4 Hz, H-2), 5.12 (1H, d, H-1).

Found: **33**, C, 71.11; H, 6.32%. **37**, C, 71.01; H, 6.32%. Calcd for $C_{30}H_{32}O_7$: C, 71.41; H, 6.39%.

Benzyl *O*-(2,3,4,6-Tetra-*O*-benzyl-α- and β-D-glucopyranosyl)-(1→2)-4-*O*-allyl-6-*O*-benzoyl-3-*O*-benzyl-α-D-glucopyranosides (38 and 39). The acceptor **33** (1.749 g) was glucosylated with **1** (2.44 g) in the presence of NsCl (1.31 g), AgOTf (1.52 g), and Et_3N (0.82 ml) in CH_2Cl_2 (18 ml), followed by chromatography (TB system), gave **39** (1.6 g, 45%), $[\alpha]_D^{20}$ +56° (*c* 5.4, $CHCl_3$), ^{13}C NMR ($CDCl_3$, 25 MHz) δ=98.9 (C-1), 103.6 (C-1′), 117.6, 134.6 (allyl), 166.0 (C=O), and **38** (1.37 g, 39%), $[\alpha]_D^{20}$ +93° (*c* 2.3, $CHCl_3$), ^{13}C NMR ($CDCl_3$, 25 MHz) δ=94.5 (C-1′), 95.2 (C-1), 117.6, 133.3 (allyl), 166.6 (C=O).

Found: **38**, C, 74.79; H, 6.67%. **39**, C, 74.57; H, 6.54%. Calcd for $C_{64}H_{66}O_{12}$: C, 74.83; H, 6.48%.

Benzyl *O*-(2,3,4,6-Tetra-*O*-benzyl-β-D-glucopyranosyl)-(1→2)-4-*O*-allyl-3-*O*-benzyl-α-D-glucopyranoside (40). A mixture of **39** (1.53 g), MeOH (20 ml), and 1,4-dioxane (7.5 ml) was treated with dil methanolic NaOMe (7.5%, 7.5 ml) for 6.5 h at room temp. After AcOH was added, evaporation and chromatography (TB system) gave **40** (1.19 g, 87%), $[\alpha]_D^{20}$ +67° (*c* 0.6, $CHCl_3$), ^{13}C NMR ($CDCl_3$, 25 MHz) δ=99.1 (C-1), 103.6 (C-1′), 117.3, 134.9 (allyl).

Found: C, 74.13; H, 6.91%. Calcd for $C_{57}H_{62}O_{11}$: C, 74.17; H, 6.77%.

Benzyl *O*-(2,3,4,6-Tetra-*O*-benzyl-β-D-glucopyranosyl)-(1→2)-3,6-di-*O*-benzyl-α-D-glucopyranoside (41). A mixture of **40** (199.5 mg), NaH in oil suspension (41 mg), and DMF (1.5 ml) was stirred for 0.5 h at −5 °C. After $PhCH_2Br$ (0.13 ml) was added, the mixture was stirred for 1 h at room temp. Quenching with MeOH, processing, and subsequent chromatography (HE system) gave the product, which was then refluxed in EBW (4 ml) containing TRC (30 mg). After evaporation, the residue was heated in acetone (2 ml) containing aq HCl (3.5%, 30 μl) for 1 h at 45 °C. Chromatography (HE system) afforded **41** (80.1 mg, 40%), $[\alpha]_D^{20}$ +45° (*c* 1.3, $CHCl_3$), ^{13}C NMR ($CDCl_3$, 100 MHz) δ=99.0 (C-1), 103.5 (C-1′).

Found: C, 75.02; H, 6.72%. Calcd for $C_{61}H_{64}O_{11}$: C, 75.29; H, 6.63%.

Benzyl *O*-(2,3,4,6-Tetra-*O*-benzyl-β-D-glucopyranosyl)-(1→2)-*O*-[(2,3,4,6-tetra-*O*-benzyl-α- and -β-D-glucopyranosyl)-(1→6)]-4-*O*-allyl-3-*O*-benzyl-α-D-glucopyranosides (42 and 43). The acceptor **40** (1.19 g) was glucosylated with **1** (0.91 g), NsCl (0.49 g), AgOTf (0.57 g), and Et_3N (0.31 ml) in CH_2Cl_2 (7.0 ml), followed by chromatography (TB system) to afford

42 (0.58 g, 31%), $[\alpha]_D^{20}$ +69° (*c* 1.7, $CHCl_3$), ^{13}C NMR ($CDCl_3$, 25 MHz) δ=97.5 (C-1″), 98.6 (C-1), 103.6 (C-1′), 117.0, 135.2 (allyl), and **43** (1.26 g, 68%), $[\alpha]_D^{20}$ +43° (*c* 2.6, $CHCl_3$), ^{13}C NMR ($CDCl_3$, 25 MHz) δ=98.9 (C-1), 103.6 (C-1′), 104.0 (C-1″), 116.7, 135.0 (allyl).

Found: **42**, C, 75.34; H, 6.50%. **43**, C, 75.52; H, 6.52%. Calcd for $C_{91}H_{96}O_{16}$: C, 75.60; H, 6.69%.

Benzyl *O*-(2,3,4,6-Tetra-*O*-benzyl-β-D-glucopyranosyl)-(1→2)-*O*-[(2,3,4,6-tetra-*O*-benzyl-β-D-glucopyranosyl)-(1→6)]-3-*O*-benzyl-α-D-glucopyranoside (44). A mixture of **43** (1.04 g), TRC (0.20 g), and EBW (33 ml) was refluxed for 3 h. After evaporation, the residue was refluxed in acetone (50 ml) containing aq HCl (3.5%, 2 ml) for 0.5 h. Chromatography (TB system) furnished **44** (0.82 g, 81%), $[\alpha]_D^{20}$ +34° (*c* 1.1, $CHCl_3$), ^{13}C NMR ($CDCl_3$, 25 MHz) δ=99.2 (C-1), 103.8 (2C, C-1′ and C-1″).

Found: C, 75.28; H, 6.55%. Calcd for $C_{88}H_{92}O_{16}$: C, 75.19; H, 6.60%.

Benzyl *O*-(2,3,4,6-Tetra-*O*-benzyl-β-D-glucopyranosyl)-(1→2)-*O*-[(2,3,4,6-tetra-*O*-benzyl-β-D-glucopyranosyl)-(1→6)]-*O*-[(2,3,4-tri-*O*-benzyl-α-L-rhamnopyranosyl)-(1→4)]-3-*O*-benzyl-α-D-glucopyranoside (45). Rhamnosylation of **44** (735 mg) with **11** (431 mg) in the presence of NsCl (348 mg), AgOTf (404 mg), and Et_3N (219 μl) in CH_2Cl_2 (2.8 ml) and subsequent chromatography (TB system) gave, after the elution of **14** and the *p*-nitrobenzenesulfonate of **44**, ^{13}C NMR ($CDCl_3$, 25 MHz) δ=98.4 (C-1), 103.3 (C-1′), 104.0 (C-1″), 124.2, 126.3, 142.6, 150.2 (*p*-nitrobenzenesulfonyl), the sole cross-condensate **45** (352 mg, 37%), $[\alpha]_D^{20}$ +19° (*c* 1.3, $CHCl_3$).

Found: C, 75.63; H, 6.68%. Calcd for $C_{115}H_{120}O_{20}$: C, 75.80; H, 6.64%.

***O*-β-D-Glucopyranosyl-(1→2)-*O*-[β-D-glucopyranosyl-(1→6)]-*O*-[α-L-rhamnopyranosyl-(1→4)]-D-glucopyranose (4).** Hydrogenolysis of **45** (75 mg) over Pd on C (10%, 75 mg) in AcOH (6 ml) containing H_2O (50 μl) for 3 d, followed by chromatography (CM system), afforded **4** (11.5 mg, 43%), mp 179—180 °C (decomp), $[\alpha]_D^{20}$ −16° (*c* 0.3, H_2O), ^1H NMR (D_2O, 300 MHz) δ=4.35 (0.7H, d, $J_{1''',2'''}$=8.0 Hz, H-1‴α), 4.37 (0.3H, d, $J_{1''',2'''}$=8.0 Hz, H-1‴β), 4.52 (0.7H, d, $J_{1',2'}$=8.0 Hz, H-1′α), 4.60 (0.3H, d, $J_{1,2}$=8.0 Hz, H-1β), 4.80 (1H, d, $J_{1'',2''}$= 1.5 Hz, H-1″), 5.31 (0.7H, d, $J_{1,2}$=4.0 Hz, H-1α).

Found: C, 44.04; H, 6.65%. Calcd for $C_{24}H_{42}O_{20}$: C, 44.31; H, 6.51%.

References

1) Present address: School of Nursing, Kitasato University, Kitasato, Sagamihara 228.

2) K. Matsuzaki and T. Uryu, *Seibutsu Butsuri*, **20**, 1 (1980).

3) H. Paulsen, *Chem. Soc. Rev.*, **13**, 15 (1984); R. R. Schmidt, *Angew. Chem., Int. Ed. Engl.*, **25**, 212 (1986); H. Kunz, *ibid.*, **26**, 294 (1987).

4) S. Koto, N. Morishima, T. Irisawa, Y. Hashimoto, M. Yamazaki, and S. Zen, *Nippon Kagaku Kaishi*, **1982**, 1651.

5) S. Koto, T. Sato, N. Morishima, and S. Zen, *Bull. Chem. Soc. Jpn.*, **53**, 1761 (1980).

6) S. Koto, N. Morishima, Y. Kihara, H. Suzuki, S. Kosugi, and S. Zen, *Bull. Chem. Soc. Jpn.*, **56**, 188 (1983).

7) S. Koto, N. Morishima, H. Sato, Y. Sato, and S. Zen, *Bull. Chem. Soc. Jpn.*, **58**, 120 (1985).

8) N. Morishima, S. Koto, T. Irisawa, Y. Hashimoto, M. Yamazaki, T. Higuchi, and S. Zen, *Chem. Lett.*, **1982**, 1383.

9) S. Koto, N. Morishima, K. Takenaka, C. Uchida, and S. Zen, *Bull. Chem. Soc. Jpn.*, **58**, 1464 (1985).

10) S. Koto, S. Inada, T. Yoshida, M. Toyama, and S. Zen, *Can. J. Chem.*, **59**, 255 (1981).

11) S. Koto, N. Morishima, M. Owa, and S. Zen, *Carbohydr. Res.*, **130**, 73 (1984).

12) N. Morishima, S. Koto, M. Uchino, and S. Zen, *Chem. Lett.*, **1982**, 1183.

13) R. Tschesche, R. Kottler, and G. Wulff, *Justus Liebigs Ann. Chem.*, **699**, 212 (1966); R. Tschesche, G. Luedke, and G. Wulff, *Chem. Ber.*, **102**, 1253 (1969).

14) R. Tschesche, M. Tauscher, H.-W. Fehlhaber, and G. Wulff, *Chem. Ber.*, **102**, 2072 (1969).

15) T. Kubota and H. Hinoh, *Tetrahedron Lett.*, **1968**, 303.

16) A. Lubineau, A. Thieffry, and A. Veyrières, *Carbohydr. Res.*, **46**, 143 (1976).

17) J. M. J. Fréchet and H. H. Baer, *Carbohydr. Res.*, **42**, 369 (1975).

18) K. Bock and C. Pedersen, *J. Chem. Soc., Perkin Trans. 2*, **1974**, 293.

19) P. A. Gent and R. Gigg, *Carbohydr. Res.*, **49**, 325 (1976).

20) T. Usui, N. Yamaoka, K. Matsuda, K. Tuzimura, H. Sugiyama, and S. Seto, *J. Chem. Soc., Perkin Trans. 1*, **1973**, 2425.

21) K. Mizutani, H. Kajita, K. Tashima, and O. Tanaka, *Nippon Kagaku Kaishi*, **1982**, 1595.

22) K. Bock and C. Pedersen, *Adv. Carbohydr. Chem. Biochem.*, **41**, 27 (1983).

23) S. David, A. Lubineau, and A. Thieffry, *Tetrahedron*, **34**, 299 (1978).

24) S. Koto, N. Morishima, C. Kusuhara, S. Sekido, T. Yoshida, and S. Zen, *Bull. Chem. Soc. Jpn.*, **55**, 2995 (1982).

25) R. R. Schmidt, M. Reichrath, and U. Moering, *J. Carbohydr. Chem.*, **3**, 67 (1984).

26) S. Koto, Y. Hamada, and S. Zen, *Chem. Lett.*, **1975**, 587.

27) S. Koto, N. Morishima, T. Yoshida, M. Uchino, and S. Zen, *Bull. Chem. Soc. Jpn.*, **56**, 1171 (1983).

 © 1988 The Chemical Society of Japan Bull. Chem. Soc. Jpn., 61, 3951—3955 (1988)

Reduction of Sulfur Dioxide and Carbon Dioxide with Benzoin Carbanion. Oxygen Transfer from Products Formed by the Reduction of Sulfur Dioxide to 7,7,8,8-Tetracyanoquinodimethane

Fuminori Akiyama
Chemical Research Institute of Nonaqueous Solutions, Tohoku University, Sendai 980
(Received April 28, 1988)

A reaction of sulfur dioxide (SO_2) with benzoin carbanion (the lithium salt of benzoin dianion, **1**) in tetrahydrofuran (THF) gave a mixture of benzil (**2**) and benzoin (**3**) in yields of 83 and 17%, respectively, irrespective of the reaction temperature between −78 and 25 °C. The reaction of carbon dioxide (CO_2) with **1** in THF gave a mixture of **2** and **3** accompanied by the formation of a small amount of lithium benzoate (**4**). The proportion of **2** in a mixture of **2** and **3** formed in the reaction of CO_2 with **1** were 49, 30, and 20% at −78, −22, and 25 °C, respectively. The reaction of SO_2 with **1** in the presence of 7,7,8,8-tetracyanoquinodimethane (TCNQ) gave oligomers of TCNQ with a yield of 60%, in which some parts of the cyano groups were transformed to carboxylato groups.

From the view point of the use of resources it is important to investigate the reaction of sulfur dioxide (SO_2) or carbon dioxide (CO_2) with organic compounds. Especially, reductions of CO_2 or SO_2 have been extensively investigated for many years. It has been reported that a reduction of SO_2 with hydrogen sulfide,[1] methane,[2] carbon,[3] carbon monoxide[4] gave elemental sulfur. A reduction of CO_2 in the presence of various catalysts have been reported to give formic acid,[5] methanol,[6] or methane.[7] Electrochemical or photoelectrochemical reduction of CO_2 has also been investigated.[8] In these reactions SO_2 or CO_2 is converted to compounds having relatively low reactivity, such as carbon monoxide, formic acid, methanol, or elemental sulfur. If a reduction of SO_2 or CO_2 is conducted using mild reducing reagents, there is a possibility that unstable oxides, which are very reactive, may be formed. If we can use the high reactivity of these unstable oxides effectively, there is a possibility that we can fruitfully utilize SO_2 or CO_2. An outline of this concept for the reduction of SO_2 was shown in a previous paper.[9] That for the reduction of CO_2 is shown in Scheme 1.

Various types of sulfur oxides are known.[10] Unstable sulfur monoxide has been known.[11] There might be other unstable sulfur oxides which have not been reported. Recently, unstable carbon oxides such as $C_2O_2^+$,[12] $C_2O_2^-$,[13] C_2O,[14] and C_3O[15] have been reported. In a previous paper the reduction of SO_2 with a mild reducing reagent, benzoin carbanion (the lithium salt of benzoin dianion, **1**), was reported to give unstable sulfur oxides which gave sulfur atoms to cyclopentadiene to form oligomers having sulfide linkages.[9] Although **1** has not been used as a reducing reagent in synthetic organic chemistry, it was found in a previous paper[9] that **1** reduced SO_2. In the present report it will be described that CO_2 is also reduced with **1**. The reaction scheme of a reduction of SO_2 with **1** was shown in the previous paper.[9] That for the reduction of CO_2 with **1** is shown as follows:

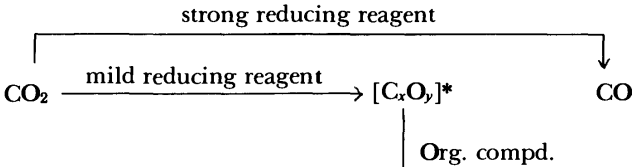

Scheme 1.

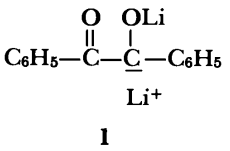

1

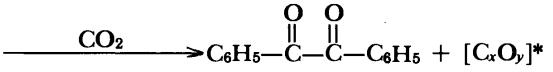

In addition to this result it will be described that the reduction products of SO_2 with **1** have sufficient reactivity to give an oxygen atom to 7,7,8,8-tetracyanoquinodimethane (TCNQ) and that the reduction products of CO_2 with **1** do not have sufficient reactivity to react with TCNQ.

Results and Discussion

Reaction of Benzoin Carbanion 1 with SO_2 (System A) or CO_2 (System B). Reactions of **1** with SO_2 or CO_2 were carried out in tetrahydrofuran (THF) at three reaction temperatures −78, −22, and 25 °C. The products were divided into water-soluble and -insoluble portions. Proportions of benzil (**2**) and benzoin (**3**) (the ratio of **2** to **3**) were measured from the NMR spectra of the water-insoluble portion and the yield of lithium benzoate (**4**) was measured from the NMR spectra of materials in the water-soluble portion (see Experimental).

In system A there was no **4** in the water-soluble portion and there were no organic compounds other than **2**, **3**, trace amounts of benzoic acid, and a small

Table 1. Products and Yields in the Reaction of Benzoin Carbanion 1 with SO_2 or CO_2 in THF

Reaction	Temp °C	Proportion (%)[a] of benzil and benzoin Benzil (2) / Benzoin (3)	Yield (%)[b] Lithium benzoate (4)	Benzoic acid
SO_2[c]	25 −22 −78	83 / 17	0	Trace
CO_2[d]	25	20 / 80[e]	4[f]	0
	−22	30 / 70[e]	10[f]	0
	−78	49 / 51[e]	18[f]	0

a) Proportions mean the ratio of **2** to **3**. b) 0.5 mol of product ×100/mol of **3** used. c) Proportion in the system A means actual yield.[16] Since several runs at three reaction temperature gave products having almost same proportions of **2** and **3**, the average value of the proportions was calculated. Although the yield of **2** in system A was reported to be 85% in the previous paper,[9] several times of reinvestigation showed that 83% was correct value. d) Actual yield of **2** or **3** can be calculated by multiplying proportion of them with (100−yield of **4**)/100.[17] e) Average values of three runs at each temperature are shown. f) Average values of two runs at each temperature are shown.

amount of the reaction products of SO_2 with diisopropylamine in the water-insoluble portion,[16] proportion of **2** and **3** being shown in Table 1.

Since in system B a small amount of **4** was formed and was found in the water-soluble portion, its yields were measured at three reaction temperature (Table 1). The proportions of **2** and **3** in the water-insoluble portion were measured (Table 1).[17]

Since one might suppose that a small amount of the oxygen contained in CO_2 or SO_2 or in the reaction vessel as an impurity plays an important role in the production of benzil, a reaction of **1** with air was undertaken at −22 °C in order to show that the reaction product of **1** with air was mainly **4**. Therefore, such a possibility can be excluded.

The possibility that oxygen of **4** comes from the oxygen contained as an impurity in the reaction vessel can be excluded for the following reasons. The facts that system A does not give **4** and scarcely gives benzoic acid and that the purity of CO_2 is more than 99 vol% exclude the existence of oxygen in system B. The fact that the yields of **2** and **4** increase as the reaction temperature decreases suggests that these two compounds are oxidation products of **1** with CO_2.

In system B, the lower was the reaction temperature, the higher was the yield of **2**. An increase in the yield of the oxidation product of **1** with a decreasing reaction temperature is, presumably, concerned with a change in the solvation of reaction intermediate (adduct of **1** with SO_2 or CO_2). Szwarc et al. have suggested that a decrease in the temperature facilitates the formation of a solvent-separated ion pair by the solvation of an ion pair.[18] If in system A the intermediate is well solvated and a change in temperature does not have any effect on the solvation, the yield of **2** is expected not to be affected by a change in the reaction temperature. If in system B the intermediate is poorly solvated at room temperature and the solvation of the intermediate is facilitated as the temperature decreases, the yield of **2** is expected to be affected by a change in the reaction temperature. The well-solvated structure of the intermediate presumably has a higher probability of an oxidation-reduction reaction than a poorly solvated one.

It was confirmed by means of TLC and gel-permeation chromatography of the products that elemental sulfur was not formed in system A. It was also confirmed by means of GLC or NMR analyses that carbon monoxide or formic acid was not formed in system B. These facts indicate the possibility that unstable oxides are formed in system A or B. Several attempts for their isolation were unsuccessful, presumably because of their instabilities.

In order to check the reactivities of the unstable oxides or intermediate formed in a reaction of SO_2 or CO_2 with **1**, the reaction of **1** with a mixture of TCNQ with an excess amount of SO_2 or CO_2 was carried out.

Reaction of Benzoin Carbanion 1 with a Mixture of TCNQ and SO_2 (System C) or CO_2 (System D). An experiment in which air or nitrogen was used in place of SO_2 or CO_2 was also carried out. The reaction products were mainly salt (LiTCNQ) and oligomers of TCNQ. The IR spectrum of the salt (KTCNQ, see Experimental) is well coincident with that of the authentic sample prepared by the method of Melby[19] and other workers.[20] Yields of the salt are shown in Table 2. Low yields of KTCNQ in the reaction in the presence of air or nitrogen are presumably attributed to hydrolysis of LiTCNQ or KTCNQ during the separation procedure (contact with saturated aqueous KCl solution) because of the strong basicity of the products.[21] The highest yield of KTCNQ was obtained in system D, as is shown in Table 2.

Oligomers of TCNQ formed in the reactions were separated; their yields are shown in Table 2. The yield of the oligomer of TCNQ was obtained in system C. The IR spectra of these oligomers obtained by four sorts of reactions were similar. The IR absorptions at 1587 and 1360 cm^{-1} for the oligomers indicate the presence of carboxylato groups.[22] The IR absorption

Table 2. Yields of the Oligomers of TCNQ and KTCNQ Obtained by the Reaction of Benzoin Carbanion **1** with a Mixture of TCNQ and SO_2, CO_2, Air, or Nitrogen at −22°C in THF

Reaction	Yield (%) of the oligomer of TCNQ[a)]	Yield (%) of KTCNQ[b)]
SO_2	60	31
CO_2	7	74
Air	13	7
Nitrogen	7	5

a) Yields were calculated as 100×wt of oligomer/wt of TCNQ used.[30] b) LiTCNQ formed was converted to KTCNQ (see work-up procedure in Experimental). Yields were calculated as 100×mol of KTCNQ/mol of TCNQ used.

of a COO^- symmetric stretching vibration at a relatively low frequency, such as 1360 cm^{-1}, has been reported for formates[23] or metal salts of amino acids.[24] The absence of IR absorption of 1540 and 860 cm^{-1}, which are seen in a spectrum of TCNQ, indicates that all of the TCNQ used were consumed. Two ^{13}C NMR signals at δ 160 and 170 in ^{13}C NMR of the oligomers indicate the presence of carboxylato groups. Steric crowding of the groups in the oligomers presumably brings about a slight upfield shift of the carboxylato group compared to the value reported in the literature (δ 170—185).[25] The difference in the chemical shift of these two signals is presumably attributed to different structures to which the carboxylato groups are attached. Elemental analyses of the oligomer obtained in system C indicated that N/C (ratio of N and C content) was 0.29, which was less than 0.39 (the calculated value for TCNQ). This fact indicates that the formation of the carboxylato group brought about the removal of a nitrogen atom from the oligomer of TCNQ. The molecular weight of these oligomers (calibrated to the molecular weight of standard polystyrene) was between 800—200 judged from the analyses by means of gel-permeation chromatography.

These above-stated facts show that in system C TCNQ was converted to low molecular weight oligomers of TCNQ in which some of the CN groups are transformed to a carboxylato group in considerable yield. One might suppose that the oxygen of the carboxylato group in this oligomer of TCNQ comes about from the moisture or oxygen contained in the reaction vessel as an impurity. However, the fact that only system C gave an oligomer having a carboxylato group in high yield and that other reactions carried out using CO_2, air or nitrogen by almost the same procedure as system C, did not give the oligomer so much supports the conclusion that the oxygen of the carboxylato group of the oligomer obtained in the former reaction comes about from the reduction products of SO_2. The formation of the oligomer of TCNQ in a yield of around 10% (see Table 2) is presumably concerned with the hydrolyses of TCNQ by the moisture contained in the reaction vessel as an impurity or hydrolysis during the work-up procedure by moisture in the atmosphere. Therefore, it can be concluded that the oxygen of the carboxylato group in a small amount of the oligomer obtained in system D does not come from the reduction products of CO_2.

The fact that the oligomer of TCNQ, having a carboxylato group, is formed in system C presumably indicates that an oxygen atom transfers from the formed unstable sulfur oxides to TCNQ. Previously, unstable sulfur oxides were trapped (see previous paper) and IR spectra were shown (see Fig. 4 in that paper).[9] Although one might suppose that water is possibly formed by a reduction of SO_2 with **1** and it hydrolyzes the CN groups of TCNQ to form a carboxylato group, the fact that system D, in which the reduction of CO_2 with **1** also possibly gives water, slightly gives a carboxylato group suggests the possibility that a carboxylato group is formed by an oxygen transfer from the formed unstable oxides. In order to show that the formation of oligomer in 60% yield in system C can not be attributed to a hydrolysis of the CN group by the formed water, a control experiment was carried out.[26] Since water formed, even if the reduction gives water in system C, is far less than the water added in the control experiment, it can be considered that 60% yield of the oligomer is too high to be attributed to hydrolyses by a small amount of the formed water.

The sulfur-transfer reaction in the previous paper gave an oligomer of cyclopentadiene which contained almost 20 wt% of sulfur.[9] On the other hand, the oligomer of TCNQ obtained in system C was found to have only less than 1 wt% of sulfur. It is not yet clear why TCNQ does not accept sulfur so much but accept oxygen atoms from the formed unstable sulfur oxides.

The reaction of unstable sulfur oxides or carbon oxides formed in system A or B with various reagents are now being investigated.

Experimental

General Procedures. The IR spectra were measured using a JEOL Fourier transform IR spectrophotometer. The ^1H NMR spectra were recorded on a JEOL Fourier transform NMR spectrometer operating at 89.55 MHz and a JNM-PMX 60SI NMR spectrometer operating at 60 MHz. The ^{13}C NMR spectra were recorded on a JEOL Fourier transform NMR spectrometer operating at 22.50 MHz. Thin-layer chromatography separations were carried out on silica

gel (Merk Art. 5717). Sulfur dioxide was distilled over phosphorous pentaoxide prior to use. Tetrahydrofuran was distilled over $LiAlH_4$ under a nitrogen atmosphere immediately prior to use. Diisopropylamine was distilled and dried over molecular sieves. Reagent-grade TCNQ was recrystalized from ethyl acetate prior to use. All other chemicals were of reagent grade and were obtained from commercial sources. In all reactions in the present report two-necked round-bottomed flask, one neck of which was capped with a serum cap and the other neck of which was installed with a delivery tube for SO_2, CO_2, air, or nitrogen, was used.

Reaction of Benzoin Carbanion 1 with SO_2 (System A) or CO_2 (System B). Since it has been reported that two sites of benzoin are converted to anion,[27] slight excess amount of lithium diisopropylamide (LDA) compared to 2 equivalent of benzoin was used to form **1**. To a THF solution of **1**, formed using 3 mmol of benzoin with the same procedure as that described in a previous paper,[9] 9 mmol of SO_2 or a large excess amount of CO_2 was bubbled as gas through a delivery tube. During the introduction of SO_2 or CO_2 into the reaction solution, the solution changed in color from orange-red to dark red (almost black), and then to yellow. In the case of the reaction of CO_2, the introduction of CO_2 was continued for at least 30 minutes after the reaction mixture changed in color to yellow. After the completion of the introduction of SO_2 or CO_2, THF was evaporated to give a yellow residue. The residue was washed with water several times in order to separate the products into a water-soluble portion and a water-insoluble organic portion. From the water-insoluble organic portion **2** and **3** were separated by means of preparative TLC using chloroform as an eluent; their structures were confirmed by comparisons of their IR and NMR spectra with those of authentic samples. For quantitative analyses the water-insoluble organic products were dissolved in $CDCl_3$ and their ^1H NMR were taken to give a ratio of **2** to **3** from signals of methine (δ 6.06) and aromatic protons (δ 7.17—8.17). Since benzoic acid was not formed in system B and was formed in only trace amount in system A, **2** and **3** are the only components derived from **1** in the water-insoluble portion (the proportions are shown in Table 1). The water-soluble portion was evaporated to give a white residue. This residue was treated several times with silica-gel column chromatography using water as an eluent to give pure **4**, the structure of which was confirmed by a comparison of their IR and NMR spectra with authentic samples. For quantitative analyses hexamethyldisiloxane was added to the white residue and its ^1H NMR spectra were taken in CD_3OD in order to measure the ratio of CH_3 protons of hexamethyldisiloxane (δ 0.07) and aromatic protons (δ 7.2—7.4 and 7.8—8.0) of **4**.

Reaction of Benzoin Carbanion 1 with a Mixture of TCNQ and SO_2 (System C). To 3 mmol of TCNQ in a nitrogen-containing two-necked 200 ml round-bottomed flask, 120 ml of absolute THF was added using a syringe and stirred for 30 minutes at room temperature under nitrogen atmosphere to obtain a homogeneous solution. This mixture was cooled to −22°C and 20 mmol of SO_2 was intriduced through delivery tube to this mixture. To this mixture THF solution of 3 mmol of **1**, which was prepared in other 100 ml two necked round-bottomed flask, was added dropewise through a serum cap using a syringe at −22 °C.

Work-up Procedure for the Reactions of the Systems C, D, E, and F. THF was evaporated from the reaction solutions to give residues. Each residue was treated with two different separation procedures in order to isolate metal-TCNQ salt and the oligomer of TCNQ.

One separation procedure is that for the separation of the metal-TCNQ salt. Since LiTCNQ has been known to be a little soluble in water and organic solvents (about 1%[19]), LiTCNQ was converted to KTCNQ, which was reported to be practically insoluble in water or organic solvents, in order to separate the metal-TCNQ salt from the reaction mixture. In this separation procedure 50 ml of saturated aqueous potassium chloride and 100 ml of ethyl acetate was added to the residue. The resulting mixture was shaken and filtered to give a purple powder, followed by washing it with water several times and then with ethyl acetate several times. The obtained powder was dried and elemental analyses were undertaken to show it to be KTCNQ (Found: C, 59.25; H, 1.66; N, 22.33; K, 16.25%. Calcd for $C_{12}H_4N_4K$: C, 59.24, H, 1.66; N, 23.02, K, 16.07%). Since there is no method for the purification of this salt (other than washing), a little discrepancy between the observed and calculated N contents is unavoidable. Analyses of potassium were undertaken using sodium tetraphenylborate.

In another separation procedure the residue was extracted with ethyl acetate several times and the extracts were treated with preparative TLC using ethyl acetate as an eluent to give oligomers of TCNQ. **2** and **3** were located in the range of a larger R_f value than 0.75. The oligomer of TCNQ obtained in system C or D were located in a TLC plate in the range of R_f=0.05—0.60 or R_f=0.03—0.08, respectively. The oligomers obtained in systems E and F were located in the range R_f=0.03—0.27. The obtained oligomers of TCNQ were colored dark brown. In the latter cases there was a trace amount of blue powder, which were located in the TLC plate in the range R_f=0.35—0.68, which showed an IR spectra different from those of the oligomer shown in Table 2. Since the amount of this blue powder was less than those located in R_f=0.03—0.27, this powder was not characterized and was not included in the oligomer shown in Table 2.

Reaction of Benzoin Carbanion 1 with a Mixture of TCNQ and CO_2 (System D). To a homogeneous mixture of 3 mmol of TCNQ and 120 ml of absolute THF in a nitrogen-containing two-necked 200 ml round-bottomed flask, CO_2, which was passed through an drying reagent, was introduced through a delivery tube for 30 minutes at −22 °C (during the introduction of CO_2 a part of CO_2 escapes from a needle which is attached to a serum cap). A 3-mmol THF solution of **1**, which was prepared in other 100 ml two-necked round-bottomed flask, was added dropwise to the THF solution of TCNQ, which was saturated with CO_2. During the addition of **1** CO_2 was continued to be introduced through a delivery tube. To our knowledge the solubility of CO_2 in THF has not been reported. However, the solubility of CO_2 in dichloromethane,[28] cyclohexane,[29] or dimethyl sulfoxide[29] at above room temperature has been reported. Since the solubilities in these solvents are not so much different form each other, the solubility of CO_2 in THF can be assumed to be not so much different from the solublities in these three solvents. Since we can assume that a decrease in the temperature from room temperature to −22°C brings about at least a two-fold increase in the solubility of CO_2 (on

the basis of the data in those literatures),[28,29] we can assume that the contained CO_2 is at least 9 times greater than TCNQ in the reaction mixture.

Reaction of Benzoin Carbanion 1 with TCNQ in the Presence of Air (System E). Almost the same reaction procedure that for system D was adopted, except for the use of air, which was passed through a 10% KOH aqueous solution in order to remove the CO_2 contained in air and drying reagent, in place of CO_2.

Reaction of Benzoin Carbanion 1 with TCNQ in the presence of Nitrogen Atmosphere (System F). Almost the same reaction procedure as that used in system D was adopted, except for the use of nitrogen, which was passed through a drying reagent, in place of CO_2.

References

1) S. Peter and H. Woy, *Chem. Ing. Techn.*, **41**, 1 (1969).

2) J. J. Helstrom and G. A. Atwood, *Ind. Eng. Chem. Process Des. Dev.*, **17**, 114 (1978).

3) K. Blomster, P. Taskinen, and J. Myyri, *Inst. Min. Metall., Sect C.*, **86**, 147 (1977).

4) W. A. Blanton, U. S. Patent 4066573 (1978).

5) Y. Inoue, H. Izumida, Y. Sakai, and H. Hashimoto, *Chem. Lett.*, **1976**, 863.

6) T. Tatsumi, A. Muramatsu, and H. Tominaga, *Chem. Lett.*, **1985**, 593; H. Baussart, R. Delobel, M. L. Bras, D. L. Maquer, and J. M. Leroy, *Appl. Catal.*, **14**, 381 (1985); S. Gusi, F. Trifiro, A. Vaccari, and G. D. Piero, *J. Catal.*, **94**, 120 (1985); G. C. Chinchen, K. C. Wauch, and D. A. Whan, *Appl. Catal.*, **25**, 101 (1986).

7) H. Inoue, and M. Funakoshi, *J. Chem. Eng. Jpn.*, **17**, 602 (1984); D. J. Darensbourg and C. Ovalles, *Inorg. Chem.*, **25**, 1603 (1986).

8) M. Ulman, B. Aurian-Blajeni, and M. Halman, *CHEMTECH.*, **1984**, 235; M, G. Bradley, T. Tysak, D. J. Graves, and N. A. Vlachopoulos, *J. Chem. Soc., Chem. Commun.*, **1983**, 349; J. Hawecker, J. M. Lehn, and R. J. Zissel, *J. Chem. Soc., Chem. Commun.*, **1985**, 56; R. Maidan and I. Willner, *J. Am. Chem. Soc.*, **108**, 8100, (1986).

9) F. Akiyama, *J. Polym. Sci., Polym. Lett. Ed.*, **24**, 631 (1986).

10) M. Schmidt and W. Siebert, "Comprehensive Inorganic Chemistry," ed by J. C. Bailer, Jr., H. J. Emeleus, R. Nyholm, and A. F. Trotman-Dickenson, Pargamon Press, New York (1973), Vol. 2, p. 859.

11) N. Basco and R. D. Morse, *Chem. Phys. Lett.*, **20**, 557 (1973); A. Grillo, R. Reed, and M. W. Slack, *J. Chem. Phys.*, **70**, 1634 (1979).

12) L. B. Knight, Jr., J. Steadman, P. K. Miller, and D. E. Bowman, *J. Chem. Phys.*, **80**, 4593 (1984), references are cited therein.

13) D. Cordishi, V. Indovina, and M. Occhiuzzi, *J. Chem. Soc., Faraday Trans. 1*, **76**, 1147 (1980); S. Olivella, M. P. Pericas, and F. Seratosa, *THEOCHEM*, **14**, 91 (1983).

14) C. Devillers, *Compt. Rend. Acad. Sci. (Paris)*, **262**C, 1485 (1966); W. Bauen, R. Meuser, and K. H. Becker, *J. Photochem.*, **24**, 99 (1984); G. Parker, D. Wiseman, C. Winter, and C. Mackey, *J. Org. Chem.*, **49**, 4494 (1984); C. Yamada, H. Kanamori, H. Horiguchi, S. Tsuchiya, and E. Hirota, *J. Chem. Phys.*, **84**, 2573 (1986); W. Bauer, K. H. Becker, and R. Meuser, *Ber. Bunsen-Ges. Phys. Chem.*, **89**, 340 (1985).

15) R. D. Brown, F. W. Eastwood, P. S. Elmes, and P. D. Godfrey, *J. Am. Chem. Soc.*, **105**, 6496 (1983); T. B. Tang, H. Inokuchi, S. Saito, C. Yamada, and E. Hirota, *Chem. Phys. Lett.*, **116**, 83 (1985).

16) In the system A the weight of the water-insoluble portion, which contained the reaction products of diisopropylamine with SO_2 in the amount of 6 mol% of the sum of **2** and **3**, was 2—3 wt% more than the weight of **3** used.

17) In the system B the weight of the water-insoluble portion, which contained the reaction products of diisopropylamine with CO_2 in the amount of 3 mol% of the sum of **2** and **3**, was less than the weight of **3** used by the weight correspondent to a decrease owing to the formation of **4**.

18) J. Smid, "Ion and Ion Pair in Organic Reactions," ed by M. Szwarc, Wiley-Intersience, New York (1972), Vol. 1, p. 85.

19) L. R. Melby, R. J. Harder, W. R. Hertler, W. Mahler, R. E. Benson, and W. E. Mochel, *J. Am. Chem. Soc.*, **84**, 3374 (1962).

20) D. S. Acker and D. C. Blomster, U. S. Patent 3162641 (1963).

21) In the system E or F ethyl acetate solution obtained from work-up procedure for separation of KTCNQ (contact with aqueous KCl solution) contained larger amount of oligomer of TCNQ (30% yield, compare with the yields in Table 2) than those obtained by the separation procedure of oligomer (TLC procedure without contact with water).

22) Oligomer contained in the ethyl acetate solution obtained from the separation procedure of KTCNQ in the systems E and F (see Ref. 21) also showed IR spectra having absorptions at 1587 and 1360 cm^{-1}. The fact that contact of the products with aqueous KCl solution gave oligomer having IR absorptions at 1587 and 1360 cm^{-1} supports conclusion that these absorptions can be attributed to carboxylato group.

23) K. Itoh and H. J. Bernstein, *Can. J. Chem.*, **170**, 34 (1956).

24) K. Nakamoto, Y. Morimoto, and A. E. Martell, *J. Am. Chem. Soc.*, **83**, 4528 (1961).

25) F. W. Wehrli and T. Wirthlin, "Interpretation of Carbon-13 NMR Spectra," HEYDEN and SON Ltd., London (1976), inside back cover.

26) After 13 ml of 1 mol dm^{-3} aqueous hydrochloric acid solution, amount of which was enough to neutralize the basic material, was added to the reaction solution of the system F carried out using 3 mmol of benzoin, the whole solution was evaporated and extracted with ethyl acetate. The oligomer of TCNQ was separated from this extract by means of TLC to show that the yield of oligomer was 30%.

27) H. G. Heine, *Liebigs Ann. Chem.*, **735**, 56 (1970).

28) F. H. Vonderheiden and J. W. Eldrige, *J. Chem. Eng. Data*, **8**, 20 (1963).

29) J. H. Dymond, *J. Phys. Chem.*, **71**, 1829 (1967).

30) IR spectra of the oligomers obtained in the system D, E, and F showed contamination of small amount of LiTCNQ in the oligomer separated with TLC. Therefore, actual yields of the oligomers in these three cases are a little lower than those shown in Table 2. Since solubility of LiTCNQ in ethyl acetate is relatively small and Rf of LiTCNQ is very low, contamination of LiTCNQ in the oligomer obtained in the system C can be neglected.

 © 1988 The Chemical Society of Japan Bull. Chem. Soc. Jpn., 61, 3957—3964 (1988)

A Michael Addition and Peterson Olefination Sequence Using 1-Silylethenyl Sulfides and Sulfoxide

Shuji KANEMASA,* Hiroshi KOBAYASHI, Junji TANAKA, and Otohiko TSUGE*
Institute of Advanced Material Study, and Department of Molecular Science and Technology,
Interdisciplinary Graduate School of Engineering Sciences,
Kyushu University, Kasugakoen, Kasuga 816
(Received April 30, 1988)

Reaction of organolithiums with a 1-(trimethylsilyl)ethenyl sulfide produces 1,2-bis(trimethylsilyl)-cyclopropanes, while use of 1-silylethenyl sulfides bearing a bulkier silyl moiety results in exclusive formation of the corresponding Michael adduct anions which are then quenched with aldehydes to give vinyl sulfides. On the contrary, a 1-(trimethylsilyl)ethenyl sulfoxide undergoes smooth Michael addition with a variety of organometallics and the resulting carbanion intermediates can be quenched with aldehydes to produce vinyl sulfoxides. Scope and limitations of these sequential reactions are discussed.

Development of a step-saving procedure for the sequence including several reaction steps is important from a standpoint of efficiency and simplification of synthetic route. Especially attractive is a one-flask procedure in which more than two steps of carbon–carbon bond forming processes are involved.

In a previous communication,[1] we reported the Michael addition–Peterson olefination sequence of methyl 2-(trimethylsilyl)acrylate (Eq. 1, EWG=COOMe). Thereafter we have been continuing our research program aiming at a wide extension of this consecutive reaction to other systems using electrophilic olefins such as 1-silylethenyl sulfides,[2] sulfoxides,[2] and ketones.

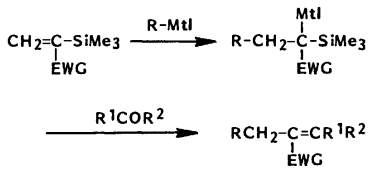

(1)

Meantime Ager reported Michael additions of phenyl 1-silylethenyl sulfide with organolithiums followed by alkylations or Peterson olefinations.[3,4] His two reports stimulated us to present our own results obtained in a similar research using the same 1-silylethenyl sulfide, its derivatives, and a silylethenyl sulfoxide. As discussed below, our results differ from the Ager's ones in some points.

The Michael addition of 1-silyl-1-alkenyl sulfides was first reported by Seebach who briefly investigated the Michael addition–Peterson olefination sequence of a 1-silylethenyl sulfide.[5] Later this reaction was applied to a synthetic approach of sulfines[6] and 1-silylalkyl sulfides.[7] Although yields of the Michael addition step were unsatisfactory at the early stage of these investigations, they were improved by slow addition of a diluted solution of the Michael acceptors to excess nucleophiles.[7]

Compared with the relatively many reaction examples on 1-silyl-1-alkenyl sulfides, the corresponding sulfoxides and sulfones[6] with higher oxidation levels have been rarely utilized in the related reaction sequence. As 1-silylalkyl sulfoxides are labile compounds[6] so as to undergo sila-Pummerer rearrangement under mild conditions, the Michael addition to 1-silyl-1-alkenyl sulfoxides must be useful as a new method of generating 1-silyl-1-sulfinyl carbanions.[8]

The present article describes the scope and limitation of the Michael addition–Peterson olefination sequence of 1-silylethenyl sulfides and sulfoxide.

Results and Discussion

Michael Reactions of 1-Silylethenyl Sulfides. In the first place, the reactivity of phenyl 1-(trimethylsilyl)ethenyl sulfide (**1**) in Michael additions was examined by use of nucleophiles such as phenyllithium and phenylmagnesium bromide; the resulting anionic adduct was quenched with water. Although silane **1** was recovered quantitatively in the reaction with the Grignard reagent, phenyllithium underwent a smooth addition in diethyl ether or tetrahydrofuran (THF) in the presence of *N,N,N′,N′*-tetramethyl-1,2-ethanediamine (TMEDA) to afford **4a** as a single product (Scheme 1). The product **4a** which consisted of two stereoisomers in a 4.3:1 ratio was assigned not to be the expected 1-silylalkyl sulfide **5a** but 1-benzyl-2-phenylthio-1,2-bis(trimethylsilyl)cyclopropane (**4a**) on

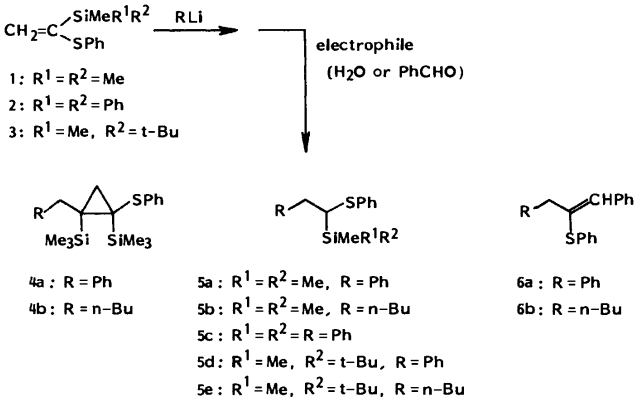

Scheme 1.

the basis of spectral data. The maximum yield of **4a** reached 88% when the reaction was carried out in THF (Table 1, Entry 2). Nevertheless the formation of neither **4a** nor related compounds was reported in the previous works accomplished by Ager[3,4,7] and others.[5,6]

As shown in Scheme 2, phenyllithium adds to the β-carbon of vinylsilane **1** to provide carbanion intermediate **A** (R=Ph, R^1=R^2=Me, Mtl=Li). Exclusive formation of cyclopropane **4a** indicates that the resulting carbanion **A**, stabilized by both silyl and phenylthio moieties, is much more nucleophilic than the starting phenyllithium. Thus relatively rapid addition of **A** to **1** leads to bisadduct **B** (R=Ph) followed by internal nucleophilic substitution into **4a**. A related cyclopropanation has been recently demonstrated by Cohen who carried out the reactions of vinylsilane **1** with 1-(phenylthio)allyllithiums.[9] Use of two equivalents of phenyllithium also gave cyclopropane **4a** as a sole product (Table 1, Entry 3). Even when **1** was slowly added to excess phenyllithium (2 equiv) in a period of 1 h, **4a** was the major

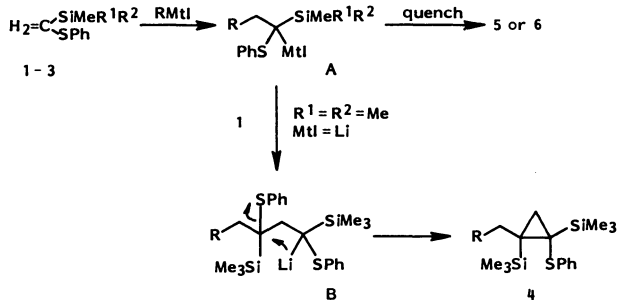

Scheme 2.

product (62%); the 1:1 adduct **5a** was obtained only in 17% yield (Entry 4).

Use of butyllithium instead of phenyllithium in the Michael addition of **1** in diethyl ether and subsequent hydrolytic quench furnished a 1:1 mixture of cyclopropane **4b** and the expected Michael adduct **5b** (Scheme 1 and Table 1, Entry 6). They can be separated from each other by column chromatography. On the other hand, both the same reaction in THF (Entry 7) and the reaction using a catalytic amount of copper(I) chloride (Entry 8) in diethyl ether produced only cyclopropane **4b**.

Though quench of the carbanion intermediates **A** (R^1=R^2=Me, Mtl=Li) with benzaldehyde gave the expected phenyl vinyl sulfides **6a, b** as a 1:1 mixture of *E*- and *Z*-isomers, their yields remained unsatisfactory because of the competitive formation of undesired cyclopropanes **4a, b** (Entries 5 and 10). According to the reaction pathway shown in Scheme 2, Michael acceptors bearing a bulkier silyl moiety, e.g. *t*-butyldimethylsilyl or methyldiphenylsilyl, would effectively suppress the cyclopropanation.

1-(Methyldiphenylsilyl)ethenyl phenyl sulfide (**2**) and 1-(*t*-butyldimethylsilyl)ethenyl phenyl sulfide (**3**), prepared by treating 1-(phenylthio)ethenyllithium with the corresponding silyl chlorides, reacted with phenyl- or butyllithium under similar reaction conditions to afford the Michael adducts **5a—c** after hydrolytic quench, or vinyl phenyl sulfides **6a,b** after treatment with benzaldehyde (Scheme 1 and Table 1, Entries 11—15). No cyclopropanes were even detected as expected, but water-quenched adducts **5c** and **5e** were accompanied instead (Entries 12 and 15).

Structures of phenyl vinyl sulfides **6a,b** were based on the ^{1}H and ^{13}C chemical shifts (**6a**: CH_2C=: 3.46 (*Z*), 3.79 (*E*) and 44.29 (*Z*), 37.23 (*E*); =CHPh: 6.75 (*Z*), 6.81

Table 1. Reactions of 1-Silylethenyl Sulfides **1—3** with Organolithium Compounds and Subsequent Quench with Electrophiles

Entry	Silane	RLi (equiv)	Solvent[a]	Additive (equiv)[b]	Time/h[c]	Electrophile[d]	Product (yield/%)[e]
1	**1**	PhLi (1)	DEE	TMEDA (1)	1	H_2O	**4a** (65)
2	**1**	PhLi (1)	THF	TMEDA (1)	1	H_2O	**4a** (88)
3	**1**	PhLi (2)	DEE	TMEDA (2)	1	H_2O	**4a** (69)
4	**1**	PhLi (2)	DEE	TMEDA (2)	1[f]	H_2O	**4a** (62)+**5a** (17)
5	**1**	PhLi (2)	DEE	TMEDA (2)	1[f]	PhCHO	**4a** (73)+**6a** (21, 1:1)[g]
6	**1**	*n*-BuLi (1)	DEE	TMEDA (1)	1.5	H_2O	**4b** (48)+**5b** (49)
7	**1**	*n*-BuLi (1)	THF	TMEDA (1)	1	H_2O	**4b** (88)
8	**1**	*n*-BuLi (1)	DEE	CuCl (0.03)	1	H_2O	**4b** (88)
9	**1**	*n*-BuLi (2)	DEE	TMEDA (2)	1	H_2O	**4b+5b** (45, 92:8)[h]
10	**1**	*n*-BuLi (1)	DEE	TMEDA (1)	1	PhCHO	**4b** (30)+**6b** (56, 1:1)[g]
11	**2**	PhLi (1)	DEE	TMEDA (1)	1	H_2O	**5c** (65)
12	**2**	PhLi (1)	DEE	TMEDA (1)	1	PhCHO	**5c+6a** (53, 1:3)[g]
13	**3**	PhLi (1)	DEE	TMEDA (1)	1	H_2O	**5d** (54)
14	**3**	*n*-BuLi (1)	DEE	TMEDA (1)	1	H_2O	**5e** (71)
15	**3**	*n*-BuLi (1)	DEE	TMEDA (1)	1	PhCHO	**5e+6b** (100, 3:7)[g]

a) DEE: diethyl ether; THF: tetrahydrofuran. b) TMEDA: *N,N,N′,N′*-tetramethyl-1,2-ethanediamine. c) All the reactions were carried out at 0 °C. d) After the addition of PhCHO, the reaction was continued for 1 h at 0 °C. e) Yield of isolated products. f) Silane **1** was added dropwise in a period of 1 h. g) Not separated. The ratio of two isomers of **6** was determined by ^{1}H NMR. h) Not separated. The ratio was determined by GLC.

(*E*). **6b**: CH_2C=: 38.26 (*Z*), 31.06 (*E*); =CHPh: 6.60 (*Z*), 6.76 (*E*)).

Donor molecules effectively employable in the Michael reactions of 1-silylethenyl sulfide **1** are quite limited to some organolithiums. Thus Grignard reagents and lithium enolates of esters, amides, and ketones are all ineffective.[10]

A Michael Addition-Peterson Olefination Sequence of a 1-Silylethenyl Sulfoxide. 1-Silylethenyl sulfoxides must be better Michael acceptors than 1-silylethenyl sulfides because of their higher capability of stabilizing the α-anionic center by a sulfinyl moiety. Accordingly were investigated Michael additions of phenyl 1-(trimethylsilyl)ethenyl sulfoxide (**7**) which was prepared by oxidation of **1** with *m*-chloroperbenzoic acid (MCPBA).

Treatment of **7** with TMEDA and phenyllithium (both 1 equiv) in THF at −78 °C for 1 h followed by hydrolytic quench gave a mixture of 2-phenyl-1-phenylsulfinyl-1-(trimethylsilyl)ethane (**9**) and phenylacetaldehyde (**10**) whose separation from each other was unsuccessful because of their lability (Scheme 3). No formation of cyclopropane derivatives was observed. As the relative ratio of **10** was gradually increased with liberation of benzenethiol when this mixture was allowed to stand at room temperature, aldehyde **10** was presumably formed from **9** via sila-Pummerer rearrangement,[11] not from the Michael adduct anion **C** (R=Ph).

Under similar reaction conditions, the anion **C** (R=Ph) was generated and then quenched with benzaldehyde to give the expected 1-alkenyl sulfoxide **8a** as a single stereoisomer in 71% yield based on **7** (Scheme 3, Table 2, Entry 1). Although the stereostructure of **8a** could not be determined only on the basis of spectral data, its assignment as *E*-isomer was accomplished by a chemical conversion. Thus **8a** was quantitatively deoxygenated into *E*-isomer of **6a** on treatment with trifluoroacetic anhydride, sodium iodide, and triethylamine.[12]

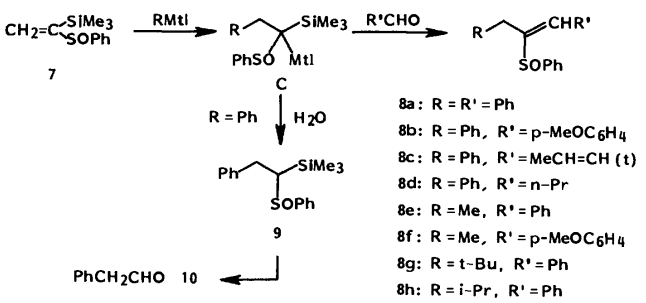

Scheme 3.

Methyllithium as a Michael donor (Entries 8 and 9) and aromatic, α,β-unsaturated, and aliphatic aldehydes as carbonyl quenchers (Entries 6 and 7) can be employed effectively. Grignard reagents (Entries 2 and 10), a lithium cuprate (Entry 3), and magnesium cuprates (Entries 4 and 11) are also reactive albeit yields of the Michael addition steps are relatively low.

As shown in Table 2 Peterson olefinations of the silyl- and sulfinyl-stabilized intermediates **C** (Mtl=Li) derived from **7** were highly *E*-selective (Entries 1—7, 10, and 11) except for the cases where a sterically small Michael donor such as methyllithium was employed in the initial Michael additions (Entries 8 and 9). This high *E*-selectivity makes a striking contrast to the aforementioned nonstereoselective Peterson condensations of the intermediates **A** (R^1=R^2=Me, Mtl=Li) derived from **1** and also contrast to the poor

Table 2. A Michael Addition and Peterson Olefination Sequence of 1-Silylvinyl Sulfoxide **7**[a]

Entry	R-Mtl (equiv)	Michael reaction	R'CHO[b]	Peterson reaction	Product yield (%)[c]	*E*/*Z*
1	PhLi (1.5)	−78 °C, 1 h[d]	PhCHO	−78 °C, 1 h	**8a** (71)	*E*
2	PhMgBr (1.2)	−15 °C, 1 h	PhCHO	−15—0 °C, 1 h	**8a** (50)	*E*
3	Ph_2CuLi (1.2)	0 °C, 1 h	PhCHO	0 °C, 1 h	**8a** (56)	*E*
4	$Ph_2CuMgBr$ (1)	−15 °C, 1 h	PhCHO	−15—0 °C, 1 h	**8a** (68)	*E*
5	PhLi (1.5)	−78 °C, 1 h[d]	*p*-$MeOC_6H_4CHO$	−78 °C, 1 h	**8b** (92)	*E*
6	PhLi (1.5)	−78 °C, 1 h[d]	MeCH=CHCHO(*t*)	−78 °C, 1 h	**8c** (87)	*E*
7	PhLi (1.5)	−78 °C, 1 h[d]	*n*-PrCHO	−78 °C, 1 h	**8d** (86)	*E*
8	MeLi (1.5)	−78 °C, 1 h[d]	PhCHO	−78 °C, 1 h	**8e** (76)	1.7[e]
9	MeLi (1.5)	−78 °C, 1 h[d]	*p*-$MeOC_6H_4CHO$	−78 °C, 1 h	**8f** (73)	2.3[e]
10	*t*-BuMgBr (1.2)	−15 °C, 1 h	PhCHO	−15 °C, 1 h	**8g** (26)	*E*
11	*i*-$Pr_2CuMgBr$ (1.1)	−15 °C, 1 h	PhCHO	−15—0 °C, 1 h	**8h** (44)	*E*
12	CH_2=C(OLi)OEt (1)	−78 °C, 20 min	PhCHO	−78 °C, 1 h	**11a** (66)	1.8[f]
13	CH_2=C(OLi)OEt (1)	−78 °C, 20 min	*p*-$MeOC_6H_4CHO$	−78 °C, 1 h	**11b** (73)	2[e]
14	CH_2=C(OLi)OEt (1)	−78 °C, 20 min	2-furylCHO	−78 °C, 1 h	**11c** (75)	2[e]
15	CH_2=C(OLi)OEt (1)	−78 °C, 20 min	*n*-PrCHO	−78 °C, 1 h	**11d** (60)	*E*
16	CH_2=C(OLi)OEt (1)	−78 °C, 20 min	MeCH=CHCHO(*t*)	−78 °C, 1 h	**11e** (73)	*E*
17	MeCH=C(OLi)OEt (1)	−78 °C, 1 h	PhCHO	−78 °C, 1 h	**12** (33)	g)

a) All reactions were carried out in dry THF under nitrogen. b) One equimolar amount of an aldehyde was used. c) Yield of isolated products. d) In the presence of TMEDA (1.5 equiv). e) Determined by ^{13}C NMR. f) Determined by ^1H NMR. g) Three diastereomers are involved (^{13}C NMR).

stereoselectivity observed in the Peterson reactions of the lithium anions derived from phenyl trimethylsilylmethyl sulfoxide.[8] Such high stereoselectivity will be discussed below.

1-Silylethenyl sulfoxide **7** also showed a high reactivity toward lithium enolates of esters. For example, the lithium enolate of ethyl acetate underwent a smooth Michael addition to **7** at −78 °C in 20 min and the resulting adduct anion was quenched with a variety of aldehydes to give vinyl sulfoxides **11a—e**, *E*-isomers as major products (Scheme 4 and Table 2, Entries 12—16). The *E*-selectivity is absolutely exclusive unless the Michael additions with a lithium enolate are followed by the Peterson olefinations with aromatic aldehydes (Entries 12—14).

Though in a low yield, a similar product **12** was obtained in the reaction of the lithium enolate of ethyl propanoate with **7** and benzaldehyde (Entry 17).

The stereoselectivity observed above is interpreted in Fig. 1. The sterically more favored intermediate adduct **D**[13] would be predominantly formed in the Michael addition step. Two chair transition states **E** and **F** are possible[14] where the bulky phenyl and silyl moieties always occupy equatorial positions. As Peterson olefination of the resulting adducts must occur, under the employed conditions, through cis-elimination of a silanol,[15] the carbonyl adducts formed via **E** and **F** should selectively lead to *E*- and *Z*-isomers, respectively, of **8**, **11**, and **12**. In the approach **F** there are two gausche interactions between R′–RCH_2 and R′–Me_3Si, whereas axial R′ in the approach **E** causes a less critical 1,3-diaxial interaction. This is the major reason for the selective or exclusive formation of *E*-olefins.

When R is small in size (R=Me), the gauche interaction between RCH_2 and R′ is relatively reduced. On the other hand the gauche repulsion is partly cancelled by an attractive interaction between the aromatic plane and the ester moiety when R is CH_2COOEt and R′ is aryl or hetero aryl (approach **G**). In these cases, relative stability of approach **F** is increased to lead to the decrease of *E*-selectivity.

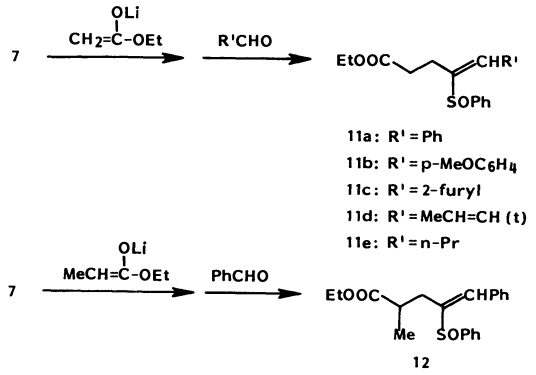

Scheme 4.

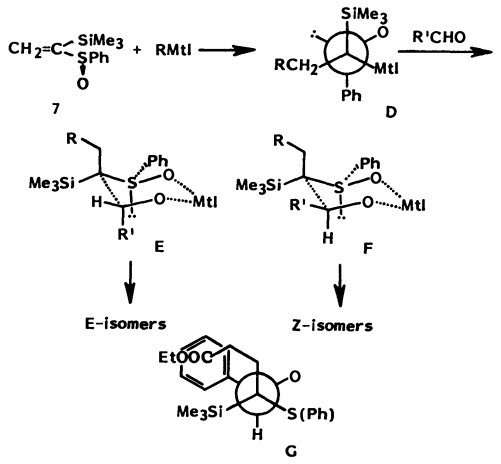

Fig. 1. Stereoselectivity in the Michael/Peterson sequences of 1-silylethenyl sulfoxide **7**.

Experimental

General. Melting points were determined on a Yanagimoto melting point apparatus and are uncorrected. IR spectra were taken with a JASCO IRA-1 or a JASCO A-702 spectrometer. ^1H NMR spectra were recorded on a Hitachi R-40 (90 MHz), a JEOL FX-100 (100 MHz), or a JEOL GSX-270 instrument (270 MHz), and ^{13}C NMR on a JEOL FX-100 (25.05 MHz) or a JEOL GSX-270 spectrometer (67.94 MHz). Chemical shifts are expressed in parts per million downfield from tetramethylsilane as an internal standard. Mass spectra were measured with a JEOL-O1SG-2 spectrometer at 70 eV of ionization energy. GC-mass spectra as well as high-resolution mass spectra were obtained on the same instrument. Elemental analyses were performed on a Hitachi 026 CHN analyzer. Thin-layer chromatography (TLC) was accomplished on 0.2 mm precoated plates of silica gel 60 F-254 (Merck) or of aluminum oxide 60 F-254 type-E (Merck). Visualization was made with ultraviolet light (254 and 365 nm), iodine, molybdophosphoric acid (5% in ethanol), or *p*-anisaldehyde (5% in ethanol containing 5% of sulfuric acid). For preparative column chromatography, Wakogel C-200, C-300 (Wako), and Silicagel 60 (Merck) were employed. Flash chromatography was carried out on an EYELA EF-10 apparatus using a column (20×180 mm) packed with Silicagel 60 (Merck, size: 0.04—0.063 mm). preparative high performance liquid chromatography (HPLC) was performed on a Kusano KHLC-201 apparatus with a UV-detector Uvilog-III using a column (22×300 mm) packed with silica gel (Wakogel LC-50H). Gas liquid chromatography (GLC) was accomplished on a Yanaco G-2800 gas chromatograph (Yanagimoto) with an ionization flame detector using a glass column (SE-30, 3×2000 mm) or a glass capillary column (Silicone GE, SE-30, 0.25×50000 mm). Micro vacuum distillation was carried out on a Sibata GTO-250R Kugelrohr distilling apparatus. Solvents were evaporated with a Tokyo Rikakikai rotary evaporator type-V at about 50 °C unless otherwise stated.

Materials. Phenyl 1-(trimethylsilyl)ethenyl sulfide (**1**) was prepared by reaction of 1-lithioethenyl phenyl sulfide with chlorotrimethylsilane.[7] Lithium diphenylcuprate,

magnesium bromide diphenylcuprate, and magnesium bromide diisopropylcuprate were in situ prepared from two equivalents of the corresponding organometallics and copper(I) iodide. The lithium enolates of ethyl acetate and propanoate were in situ prepared from equimolar amounts of lithium diisopropylamide (LDA) and the corresponding esters. Tetrahydrofuran (THF) or diethyl ether was distilled from lithium aluminum hydride or sodium metal, respectively, immediately before use. Diisopropylamine was distilled from sodium hydride.

Phenyl 1-(Methyldiphenylsilyl)ethenyl Sulfide (2): To a freshly prepared solution of LDA (66 mmol) in hexane was added dropwise, at −78 °C under nitrogen, phenyl vinyl sulfide (9 g, 66 mmol) in dry THF (40 ml) in a period of 15 min. After stirring for 1 h, chloro(methyl)diphenylsilane (15.5 g, 66 mmol) was slowly added. The resulting mixture was stirred at −78 °C for 30 min and then at 0 °C for additional 30 min, poured into saturated aqueous sodium chloride (30 ml), and extracted with dichloromethane (35 ml×2). The combined extracts were dried over magnesium sulfate and evaporated in vacuo. The residue was chromatographed over silica gel with hexane-ethyl acetate (20:1 v/v) to give **2** (16.8 g, 77%): Colorless liquid; bp 215—220 °C/27 Pa; IR (neat) 1420, 1240, 1100, 875, and 695 cm^{-1}; ^1H NMR ($CDCl_3$) δ=0.73 (3H, s, SiMe), 5.40, 5.47 (each 1H, s, $=CH_2$), and 7.1—7.7 (15H, m, Ph); ^{13}C NMR ($CDCl_3$) δ=−3.88 (q, SiMe), 124.01 (t, $=CH_2$), 127.95, 128.42, 129.30, 129.77, 132.07, 134.89, 135.24, and 144.72; MS *m/z* (rel intensity, %) 332 (M^+, 22), 241 (13), 213 (10), 198 (20), 197 (base peak), 195 (17), 181 (17), 165 (13), 151 (13), 145 (16), 119 (14), 109 (12), 105 (43), 93 (11), 91 (38), and 77 (28). Found: C, 75.95; H, 6.13%. Calcd for $C_{21}H_{20}SSi$: C, 75.85; H, 6.06%.

1-(*t*-Butyldimethylsilyl)ethenyl Phenyl Sulfide (3). A similar procedure using LDA (66 mmol), phenyl vinyl sulfide (9 g, 66mmol) in THF (40 ml), and *t*-butylchlorodimethylsilane (9.9 g, 66 mmol) gave **3** (7.2 g, 61%) after vacuum distillation of the crude product: Colorless liquid; bp 73—76 °C/19 Pa; IR (neat) 1250 and 825 cm^{-1}; ^1H NMR ($CDCl_3$) δ=0.18 (6H, s, $SiMe_2$), 0.98 (9H, s, *t*-Bu), 5.17, 5.41 (each 1H, s, $=CH_2$), and 7.2—7.5 (5H, m, Ph); ^{13}C NMR ($CDCl_3$) δ=−5.88 (q, $SiMe_2$), 17.00 (s, *t*-Bu), 26.83 (q, *t*-Bu), 120.30 (t, $=CH_2$), 128.41, 129.36 (each d), 132.18, 135.13 (each s), and 145.83 (s); MS *m/z* (rel intensity, %) 250 (M^+, 10), 193 (43), 177 (12), 168 (14), 167 (base peak),151 (48), 91 (24), 82 (16), 76 (23), and 75 (17).

General Procedure for the Michael Addition/Water Quench Sequence of Vinyl Sulfides 1—3 Leading to 4a,b and 5a—e. As a typical procedure, the reaction of phenyllithium with **1** is described (Entry 1 in Table 1): To a solution of *N,N,N′,N′*-tetramethyl-1,2-ethanediamine (TMEDA, 0.116 g, 1 mmol) in dry diethyl ether (3 ml) was added phenyllithium (or butyllithium) at 0 °C under nitrogen. After vinylsilane **1** (0.208 g, 1 mmol) in diethyl ether (10 ml) was added in a period of 1 h, the mixture was stirred for additional 1 h. It was poured into saturated aqueous ammonium chloride and extracted with diethyl ether (30 ml×2). The combined extracts were dried over magnesium sulfate and evaporated in vacuo. The residue was subjected to column chromatography over silica gel by using hexane to give **4a** (0.125 g, 65%). Other reactions were carried out under the reaction conditions listed in Table 1 and the results are summarized in the same table.

4a (a 4.3:1 mixture of two stereoisomers (^1H NMR)): Colorless liquid; IR (neat) 1250 and 839 cm^{-1}; ^1H NMR ($CDCl_3$) δ=0.02, 0.09, 0.14, 0.21 (18H, each s, 4.3:1:4.3:1, $SiMe_3$), 1.4—1.6 (2H, m, ring CH_2), 2.98, 3.29 (2H, each s, $PhCH_2$), and 7.0—7.3 (10H, m, Ph); ^{13}C NMR ($CDCl_3$) δ=0.54, 1.22 (each q, $SiMe_3$), 21.97, 24.46 (each s, ring C), 25.39 (t, ring CH_2), 39.55, 39.99 (each t, 4.3:1, $PhCH_2$), 124.32, 124.61, 125.59, 125.88, 126.66, 127.34, 127.93, 128.32, 128.80 (each d, Ph), 139.65, 140.77, and 141.89 (each s, 4.4:4.2:1, Ph); MS *m/z* (rel intensity, %) 384 (M^+, 32), 218 (21), 167 (12), 135 (15), 129 (19), 128 (15), 110 (17), 109 (17), 91 (11), and 73 (base peak). Found; C, 68.68; H, 8.45%. Calcd for $C_{22}H_{32}SSi_2$: C, 68.68; H, 8.38%.

4b (a 2.2:1 mixture of two stereoisomers (^1H NMR)): Colorless liquid; IR (neat) 1250 and 839 cm^{-1}; ^1H NMR ($CDCl_3$) δ=0.08, 0.11, 0.18 (18H, each s, 2.2:3.2:1, $SiMe_3$), 0.89 (3H, t, J=6.0 Hz, n-C_5H_{11}), 1.0—1.8 (10H, m, n-C_5H_{11}), and 6.9—7.3 (10H, m, Ph); ^{13}C NMR ($CDCl_3$) δ=1.00, 1.12, 1.29, 1.88 (each q, 2.6:1.2:2.0:1, $SiMe_3$), 14.35 (q, n-C_5H_{11}), 21.83, 22.83 (1:2.6), 23.41, 26.88 (1:3.1), 23.71, 24.47 (1:2.6), 29.36, 29.88 (2.5:1), 32.41, 32.65 (1:2.1) 34.13, 35.35 (1:2.6), 124.36, 124.65, 126.72, 127.36, 128.48 (each d, Ph), 140.30, and 140.66 (each s, 2.5:1, Ph); MS *m/z* (rel intensity, %), 364 (M^+, 11), 73 (base peak), 44 (16), and 42 (12). Found: C, 65.67; H, 9.95%. Calcd for $C_{20}H_{30}SSi_2$: C, 65.87; H, 9.93%.

5a: Colorless liquid; IR (neat) 1250 and 841 cm^{-1}; ^1H NMR ($CDCl_3$) δ=0.16 (9H, s, $SiMe_3$), 2.7—3.1 (3H, CH_2 and CH), and 7.0—7.4 (10H, m, Ph); ^{13}C NMR ($CDCl_3$) δ=−2.22 (q, $SiMe_3$), 36.76 (d, CH), 38.14 (t, CH_2), 125.84, 126.17, 128.13, 128.62, 129.23, 129.97 (each d, Ph), 137.62, and 140.76 (each s, Ph); MS *m/z* (rel intensity, %) 286 (M^+, 17), 195 (20), 167 (45), 135 (44), 109 (21), 91 (40), 77 (21) 73 (base peak), and 65 (22). HRMS Found: *m/z* 286.1199. Calcd for $C_{17}H_{22}SiS$: M, 286.1210.

5b: Colorless liquid; IR (neat) 1250, 858, and 837 cm^{-1}; ^1H NMR ($CDCl_3$) δ=0.12 (9H, s, $SiMe_3$), 0.83 (3H, t, J=5.0 Hz, n-C_5H_{11}), 1.0—1.9 (8H, m, n-C_5H_{11}), 2.45 (1H, dd, J=5.0 and 6.0 Hz, CH), and 7.0—7.5 (5H, m, Ph); ^{13}C NMR ($CDCl_3$) δ=−1.88(q, $SiMe_3$), 14.18 (q, n-C_5H_{11}), 22.65, 28.18, 31.94, 32.12 (each t, n-C_5H_{11}), 34.65 (d, CH), 125.89, 129.01, 129.77 (each d, Ph), and 138.89 (s, Ph); MS *m/z* (rel intensity, %) 266 (M^+, 23), 183 (10), 182 (66), 167 (28), 151 (12), 135 (11), 123 (13), 109 (12), 91 (14), and 73 (base peak). Found: C, 67.39; H, 9.83%. Calcd for $C_{15}H_{26}SSi$: C, 67.60; H, 9.83%.

5c: Yellow liquid; IR (neat) 1425, 1250, and 1110 cm^{-1}; ^1H NMR ($CDCl_3$) δ=0.00 (3H, s, SiMe), 2.0—2.7 (3H, m, CH_2 and CH), and 6.0—7.2 (20H, m, Ph); ^{13}C NMR δ=−5.03 (q, SiMe), 36.67 (d, CH), 38.48 (t, CH_2), 126.12, 126.22, 128.02, 128.12, 128.56, 129.54, 129.69, 130.56, 135.20, 137.79, and 140.57; MS *m/z* (rel intensity, %) 410 (M^+, 36), 241 (22), 197 (base peak), and 91 (22). Found: C, 79.03; H, 6.45%. Calcd for $C_{27}H_{26}SiS$: C, 78.97; H, 6.38%.

5d: Colorless liquid; IR (neat) 1250 and 820 cm^{-1}; ^1H NMR ($CDCl_3$) δ=0.04, 0.08 (each 3H, $SiMe_2$), 1.00 (9H, *t*-Bu), 2.7—3.3 (3H, m, CH_2 and CH), and 7.0—7.1 (10H, m, Ph); ^{13}C NMR ($CDCl_3$) δ=−6.41, −5.76 (each q, $SiMe_2$), 17.88 (s, *t*-Bu), 27.59 (q, *t*-Bu), 35.18 (d, CH), 39.36 (t, CH_2), 125.71, 126.18, 128.18, 128.60, 129.36, 129.71 (each d, Ph), 138.30, and 141.13 (each s, Ph); MS *m/z* (rel intensity, %) 328 (M^+, 2), 167 (46), 151 (24),135 (51), 109 (31), 91 (56), 73 (base peak), 65 (33), 57 (58), and 41 (34). Found: C, 73.29; H, 8.68%. Calcd for $C_{20}H_{28}SiS$: C, 73.11; H 8.59%.

5e: Pale yellow liquid; IR (neat) 1250 and 830 cm^{-1}; ^1H NMR ($CDCl_3$) δ=−0.04, 0.00 (each 3H, s, $SiMe_2$), 0.7—1.6 (11H, m, n-C_5H_{11}), 0.86 (9H, s, t-Bu), 2.52 (1H, dd, J=6.6 and 4.4 Hz, CH), and 6.9—7.3 (5H, m, Ph); ^{13}C NMR ($CDCl_3$) δ=−6.00 ($SiMe_2$), 14.01 (n-C_5H_{11}), 17.68, 27.93 (t-Bu), 22.49, 27.93, 31.89, 31.92, 32.68 (n-C_5H_{11} and CH), 125.53, 128.68 129.20, and 138.73 (Ph); MS m/z (rel intensity, %) 308 (M^+, 5), 251 (20), 167 (base peak), and 73 (43). HRMS Found: m/z 308.2006. Calcd for $C_{18}H_{32}SiS$: M, 308.2018.

General Procedure for the Michael Addition/Peterson Olefination Sequence of Vinyl Sulfides 1—3 Leading to 6. The reaction of **1** with phenyllithium and benzaldehyde is described as a typical example (Entry 5 in Table 1): To a solution of TMEDA (0.232 g, 2 mmol) in dry diethyl ether (10 ml) was added phenyllithium (2 mmole) at 0 °C under nitrogen. After vinylsilane **1** (0.208 g, 1 mmol) in diethyl ether (10 ml) was added in a period of 1 h, the mixture was stirred for additional 1 h. Benzaldehyde (0.212 g, 2 mmol) in diethyl ether (2 ml) was added and stirring was continued for 1 h. The mixture was poured into saturated aqueous ammonium chloride and extracted with diethyl ether (30 ml×2). The combined extracts were dried over magnesium sulfate and evaporated in vacuo. The residue was chromatographed over silica gel with hexane-ethyl acetate (50:1 v/v) to give **6a** (0.064 g, 21% $E:Z$=1:1) and then **4a** (0.141 g, 73%). Other reactions were carried out under the reaction conditions listed in Table 1 and the results are shown in the same table.

6a (a 1:1 mixture of E- and Z-isomers (^1H NMR)): Pale yellow liquid; IR (neat) 2854 cm^{-1}; ^1H NMR ($CDCl_3$) δ=3.46, 3.79 (2H, each s, CH_2), 6.75, 6.81 (1H, each s, =CH), and 7.0—7.9 (15H, m, Ph); ^{13}C NMR ($CDCl_3$) δ=37.23, 44.29 (each t, CH_2), 126.37, 126.46, 127.02, 127.15, 127.35, 127.68, 127.89, 128.02, 128.25, 128.29, 128.46, 128.56, 128.91, 129.05, 129.12, 129.24, 129.28, 129.69, 131.59, 132.29, 132.75, 133.50, 133.85, 134.80, 135.07, 135.16, 136.48, 136.77, 137.14, 138.50, and 138.89; MS m/z (rel intensity, %) 302 (M^+, 21), 192 (36), 191 (27), 178 (32), 165 (38), 115 (94), 109 (65), 91 (base peak), 89 (24), 78(34), 77 (38), and 65 (79). HRMS Found: m/z 302.1123. Calcd for $C_{21}H_{18}S$: M, 302.1128.

Pure (E)-**6a** was obtained by deoxygenation of (E)-**8a** with trifluoroacetic anhydride-sodium iodide-triethylamine: Pale yellow plates (hexane); mp 80—81 °C; IR (KBr) 1630, 1628, 1600, 800, 790, 780 748 and 731 cm^{-1}; ^1H NMR ($CDCl_3$) δ=3.82 (2H, s, CH_2C=), 6.85 (2H, s, =CH), and 7.1—7.6 (15H, m, Ph).

6b (a 1:1 mixture of E- and Z-isomers (^1H NMR)): Pale yellow liquid; IR (neat) 2858 cm^{-1}; ^1H NMR ($CDCl_3$) δ=0.83 (3H, t, J=6.0 Hz, n-C_5H_{11}), 1.1—1.9 (6H, m, n-C_5H_{11}), 2.1—2.5 (2H, m, n-C_5H_{11}), 6.60, 6.76 (1H, s, =CH), and 7.1—7.6 (10H, m, Ph); ^{13}C NMR ($CDCl_3$) δ=13.95, 13.99, 22.35, 22.42, 28.49, 28.57, 31.06, 31.49, 31.60, 38.26 (n-C_5H_{11}), 126.62, 126.75, 127.11, 127.30, 127.56, 127.96, 128.30, 128.39, 128.82, 129.07, 129.21, 130.95, 132.11, 134.26, 134.42, 136.05, 136.77, 137.17, and 139.82 (Ph); MS m/z (rel intensity, %) 282 (M^+, 44), 226 (27), 135 (43), 117 (37), 116 (47), 115 (base peak), 91 (66), and 42 (35). HRMS Found: m/z 282.1435. Calcd for $C_{19}H_{22}S$: M, 282.1430.

Phenyl 1-(Trimethylsilyl)ethenyl Sulfoxide (7):[16] To a solution of sulfide **1** (6 g, 29 mmol) in dichloromethane (60 ml) was added dropwise 3-chloroperbenzoic acid (MCPBA, 6.7 g, 29.1 mmol in dichloromethane (100 ml)) in a period of 30 min. The mixture was stirred at room temperature for 30 min, poured into saturated aqueous sodium hydrogensulfite (100 ml) and extracted with dichloromethane (60 ml×3). The combined extracts were washed with saturated sodium hydrogencarbonate, dried over magnesium sulfate, and evaporated in vacuo. The residue was chromatographed over silica gel by using hexane-ethyl acetate (10:1 v/v) to give **7** (6.16 g, 95%): Colorless liquid; IR (neat) 1240, 1040, and 840 cm^{-1}; ^1H NMR ($CDCl_3$) δ=0.05 (9H, s, $SiMe_3$), 6.19, 6.77 (each 1H, s, =CH_2), and 7.5—7.6 (5H, m, Ph);^{13}C NMR ($CDCl_3$) δ=−1.21 (q, $SiMe_3$), 126.63, 129.15, 129.24 (each d, Ph), 131.53 (t, =CH_2), 143.67 (s, Ph), and 157.22 (s, =C); MS m/z (rel intensity, %) 224 (M^+, 27), 167 (89), 126 (89), 77 (19), 75 (11), 73 (base peak), and 45 (12). HRMS Found: m/z 224.0683. Calcd for $C_{11}H_{16}OSiS$: M, 224.0690.

General Procedure for the Michael Addition/Peterson Olefination Sequence of Vinyl Sulfoxide 7 Leading to 8a—h, 11a—e, and 12. As a typical procedure, the reaction of **2** with phenyllithium and benzaldehyde is described (Entry 1 in Table 2): To a solution of TMEDA (0.174 g, 1.5 mmol) in dry THF (3 ml) was added phenyllithium (1.5 mmol) at −78 °C under nitrogen. After 30 min, vinyl sulfoxide **7** (0.224 g, 1 mmol) in THF (1 ml) was added in a period of 5 min and the mixture was stirred for 1 h. Benzaldehyde (0.16 g, 1.5 mmol) in THF (1 ml) was added and stirring was continued at the same temperature for 1 h. The mixture was poured into saturated aqueous ammonium chloride and extracted with diethyl ether (30 ml×2). The combined extracts were dried over magnesium sulfate and evaporated in vacuo. The residue was chromatographed over silica gel by using hexane-diethyl ether (20:1 v/v) to give **8a** (0.216 g, 71%) as a single isomer. Other reactions were carried out under the reaction conditions listed in Table 2. The results are also summarized in the same table.

8a: Colorless needles (hexane); mp 98—99 °C; IR (KBr) 1050 cm^{-1}; ^1H NMR ($CDCl_3$) δ=3.46, 3.82 (each 1H, d, J_{gem}=16.5 Hz, CH_2C=), and 6.9—7.7 (16H, Ph and =CH); ^{13}C NMR ($CDCl_3$) δ=31.40 (t, CH_2C=), 125.78 (d, =CH), 129.24, 131.49, 132.81 (each d, Ph), 134.27, 136.62, 142.58 (each s, Ph), and 143.84 (s, =C); MS m/z (rel intensity, %) 318 (M^+, 2), 184 (43), 183 (78), 105 (base peak), 79 (24), 78 (31), and 77 (56). Found: C, 79.40; H, 5.94%. Calcd for $C_{21}H_{18}OS$: C, 79.21; H, 5.70%.

The sulfoxide **8a** was converted into (E)-**6a** by the following procedure: To a solution of **8a** (0.244 g, 0.76 mmol) in acetone (5 ml) were added sodium iodide (0.3 g, 2 mmol) and triethylamine (0.25 ml, 2 mmol). After cooled to 0 °C, trifluoroacetic anhydride (0.3 ml, 2 mmol) was slowly added. The mixture was stirred at the same temperature for 10 min and evaporated in vacuo. The residue was treated with water and extracted with diethyl ether (30 ml×3). The combined extracts were washed with diluted aqueous sodium thiosulfate and dried over magnesium sulfate. Evaporation of the ether in vacuo provided (E)-**6** (0.227 g, 98%).

8b: Colorless prisms (hexane); mp 91—93 °C; IR (KBr) 1040 cm^{-1}; ^1H NMR ($CDCl_3$) δ=3.51, 3.98 (each 1H, d, J_{gem}=17.3 Hz,CH_2C=), 3.75 (3H, s, p-OMe), 6.8—6.9 (2H, m, Ar), and 6.9—7.7 (13H, m, Ar and =CH); ^{13}C NMR ($CDCl_3$) δ=31.30 (t, CH_2C=), 55.42 (q, OMe), 114.36 (d, Ar), 125.77 (d, =CH), 126.54, 127.07, 128.35, 128.36, 129.24, 131.13, 131.36 (each d, Ar), 133.13, 136.95, 141.48 (each s, Ar), 143.31 (s, =C), and 160.36 (s, Ar); MS m/z (rel intensity, %), 348 (M^+, 5), 223

(61), 222 (base peak), 207 (31), 178 (24), 116 (32), and 91 (47). Found: C, 76.01; H, 5.71%. Calcd for $C_{22}H_{20}O_2S$: C, 75.83; H, 5.78%.

8c: Pale yellow liquid; IR (neat) 1040 cm^{-1}; ^1H NMR ($CDCl_3$) δ=1.82 (3H, d, J=5.1 Hz, Me), 3.33, 3.67 (each 1H, d, J_{gem}=15.3 Hz, CH_2C=), 6.14 (1H, dq, J=15.0 and 5.1 Hz, MeCH=), 6.24 (1H, dd, J=15.0 and 10.6 Hz, =CH), and 6.9—7.7 (11H, m, Ar and =CH); ^{13}C NMR ($CDCl_3$) δ=18.36 (q, Me), 29.88 (t, CH_2C=), 124.95 (d, =CH), 125.34, 125.93, 127.98, 128.07, 128.71, 130.61 (each d, Ph), 133.40, 137.84 (each d, =CH), 137.59, 140.87 (each s, Ph), and 142.83 (s, =C); MS m/z (rel intensity, %) 282 (M^+, 16), 157 (29), 142 (25), 141 (43), 129 (43), 128 (37), 126 (19), 125 (19), 116 (61), 97 (27), 91 (base peak), 78 (80), 77 (80), and 65 (44). Found: C, 76.40; H, 6.57%. Calcd for $C_{18}H_{18}OS$: C, 76.56; H, 6.42%.

8d: Colorless liquid; IR (neat) 1040 cm^{-1}; ^1H NMR ($CDCl_3$) δ=0.80 (3H, t, J=7.0 Hz, n-Pr), 1.2—1.8, 1.9—2.4 (each 2H, m, n-Pr), 3.15, 3.52 (each 1H, d, J_{gem}=15.6 Hz, CH_2C=), 6.57 (1H, t, J=6.0 Hz, =CH), and 6.8—7.6 (10H, m, Ph); ^{13}C NMR ($CDCl_3$) δ=13.38 (q, n-Pr), 21.53, 29.78 (each t, n-Pr), 30.18 (t, CH_2C=), 124.95, 125.98, 128.17, 128.80, 130.66, 137.20 (each d, Ph and =CH), 137.59, 142.77 (each s, Ph), and 143.55 (s, =C); MS m/z (rel intensity, %) 284 (M^+, 23), 159 (base peak), 130 (28), 126 (86), 117 (89), 115 (32), 91 (98), 89 (72), 78 (23), 77 (21), 71 (67), and 56 (41). HRMS Found: m/z 284.1231. Calcd for $C_{18}H_{20}OS$: M, 284.1234.

8e (a 1.7:1 mixture of E- and Z-isomers (^{13}C NMR)): Pale yellow liquid; IR (neat) 1040 cm^{-1}; ^1H NMR ($CDCl_3$) δ=0.90 (1/2.7×3H, t, J=7.6 Hz, Et (Z)), 1.05 (1.7/2.7×3H, t, J=7.6 Hz, Et (E)), 1.8—2.8 (2H, m, Et), 7.00 (1/2.7H, br s, =CH (Z)), and 7.2—7.8 (10H+1.7/2.7H, m, Ph and =CH (E)); ^{13}C NMR ($CDCl_3$) δ=12.87, 13.10 (each q, Et), 18.84, 19.01 (each t, Et),124.26, 125.43, 126.72, 126.90, 128.18, 128.30, 128.41, 128.65, 128.99, 129.12, 129.47, 130.17, 131.10, 134.56, 135.08, 142.98 (s, Ph), 143.98 (s, Ph), 147.60, and 148.25 (each s, =C); MS m/z (rel intensity, %) 256 (M^+, 5), 131 (42), 116 (32), 115 (56), 91 (base peak) 79 (62), 78 (34), 77 (90), and 52 (61). Found: C, 74.75; H, 6.37%. Calcd for $C_{16}H_{16}OS$: C, 74.96; H, 6.29%.

8f (a 2.3:1 mixture of E- and Z-isomers (^{13}C NMR)): Pale yellow liquid; IR (neat) 1040 cm^{-1}; ^1H NMR ($CDCl_3$) δ=0.89 (1/3.3×3H, t, J=7.0 Hz, Et (Z)), 0.97 (2.3/3.3×3H, t, J=7.0 Hz, Et (E)), 2.38 (1/3.3×2H, q, J=7.0 Hz, Et (Z)), 2.40 (2.3/3.3×2H, t, J=7.0 Hz, Et (E)), 3.80 (3H, s, p-OMe), 6.7—7.0 (2H, m, Ar), 7.24 (1/3.3H, s, =CH (Z)), and 7.3—7.8 (8H+2.3/3.3H, m, Ar and =CH (E)); ^{13}C NMR ($CDCl_3$) δ=13.09 (q, Et), 18.65 (t, Et), 55.37 (q, OMe), 114.16, 114.40 (each d, Ar), 124.61, 125.63 (each d, =CH), 127.25, 128.71, 129.30, 130.37, 131.00, 131.15, 131.34, 131.69, 135.20, 143.75, 145.36, and 160.16 (s, Ar); MS m/z (rel intensity, %) 286 (M^+, 9), 161 (77), 145 (44), 125 (47), 121 (43), 117 (32), 103 (37), 97 (33), 91(58), 78 (44), and 77 (base peak). Found: C, 71.03; H, 6.16%. Calcd for $C_{17}H_{18}O_2S$: C, 71.30; H, 6.33%.

8g: Colorless prisms (hexane); mp 115—116 °C; IR (KBr) 1040 cm^{-1}; ^1H NMR ($CDCl_3$) δ=0.86 (9H, s, t-Bu), 1.58, 2.85 (each 1H, d, J_{gem}=14.7 Hz, CH_2C=), 7.3—7.4 (5H, m, Ph), 7.4—7.5 (3H, m, Ph), and 7.7—7.8 (3H, m, Ph and =CH); ^{13}C NMR ($CDCl_3$) δ=30.40 (t-Bu), 33.51 (t-Bu), 39.18 (CH_2C=), 126.63, 127.82, 128.51, 128.97, 129.36, 129.87, 131.64, 135.88, 143.74, and 144.32 (=C); MS m/z (rel intensity, %) 298 (M^+, 1), 131 (22), 126 (23), 125 (27), 117 (21), 116 (51), 115 (base peak), 91 (31), 78 (33), and 77 (29). Found: C, 76.30; H, 7.46%. Calcd for $C_{19}H_{22}OS$: C, 76.47; H, 7.43%.

8h: Colorless liquid; IR (neat) 1050 cm^{-1}; ^1H NMR ($CDCl_3$) δ=0.82, 0.85 (each 3H, d, J=6.6Hz, i-Pr), 1.8—2.0 (2H, m, i-Pr and one of CH_2C=) 2.48 (1H, dd, J=14.3 and 6.6 Hz, the other of CH_2C=), 7.3—7.4 (5H, m, Ph), 7.4—7.5 (4H, m, Ph and =CH), and 7.6—7.7 (2H, m, Ph); ^{13}C NMR ($CDCl_3$) δ=22.15, 22.69 (each i-Pr), 27.07 (i-Pr), 35.12 (CH_2C=), 125.99, 128.16, 128.59, 129.05, 129.27, 130.28, 131.37, 135.06, 143.34 (Ph and =CH), and 145.39 (=C); MS m/z (rel intensity, %) 284 (M^+, 8), 117 (25), 115 (29), 108 (78), 107 (59), 103 (21), 91 (61), 79 (base peak), 78 (22), 77 (65), and 51 (37). Found: C, 75.92; H, 7.30%. Calcd for $C_{18}H_{20}OS$: C, 76.02; H, 7.09%.

11a (a 1.8:1 mixture of E- and Z-isomers (^1H NMR)): Pale yellow liquid; IR (neat) 1730 and 1040 cm^{-1}; ^1H NMR ($CDCl_3$) δ=1.16 (1/2.8×3H, t, J=7.2 Hz, OEt (E)), 1.17 (1.8/2.8×3H, t, J=7.2 Hz, OEt (Z)), 2.0—2.8 (4H, m, CH_2CH_2), 4.19 (1/2.8×2H, q, J=7.2 Hz, OEt (Z)), 4.25 (1.8/2.8×2H, q, J=7.2 Hz, OEt (E)), 7.02 (1/2.8H, br s, =CH (Z)), and 7.2—7.8 (10H+1.8/2.8H, m, Ph and =CH (E)); ^{13}C NMR ($CDCl_3$) δ=14.06 (q, OEt), 20.88, 32.65 (each t, CH_2CH_2 (E)), 22.65, 33.83 (each t, CH_2CH_2 (Z)), 60.48, 60.59 (each t, OEt), 124.42, 125.54 (each d, =CH), 128.72, 129.01, 129.13, 129.42, 129.71, 130.60, 131.42, 132.89, 134.30, 137.19, 143.07 (s), 144.95, 145.42 (each s, =C), 172.07, and 172.42 (each s, COOEt); MS m/z (rel intensity, %) 312 (M^+ −16, 4), 283 (2), 223 (37), 203 (38), 149 (base peak), 110 (50), 109 (42), 84 (30), 76 (38), 73 (31), and 43 (43). Found: C, 69.45; H, 6.16%. Calcd for $C_{19}H_{20}O_3S$: C, 69.49; H, 6.14%.

11b (a 2:1 mixture of E- and Z-isomers (^{13}C NMR)): Pale yellow liquid; IR (neat) 1730 and 1040 cm^{-1}; ^1H NMR ($CDCl_3$) δ=1.20 (3H, t, J=7.0 Hz, OEt), 2.0—2.8 (4H, m, CH_2CH_2), 3.80 (3H, s, p-OMe), 4.06 (2H, q, J=7.0 Hz, OEt), 6.7—7.0 (2H, m, Ar), 7.00 (1/3H, s, =CH (Z)), and 7.2—7.8 (7H+2/3H, m, Ar and =CH (E)); ^{13}C NMR ($CDCl_3$) δ=14.18 (q, OEt), 20.88, 32.71 (each t, CH_2CH_2, (E)), 23.00, 34.12 (each t, CH_2CH_2 (Z)), 55.42 (q, OMe), 60.71 (t, OEt), 114.24, 114.60 (each d, Ar), 124.60, 125.54, 126.89, 129.42, 130.60, 131.07, 131.30, 142.36, 143.42 (s, =C), 160.25 (s, Ar), 172.42, and 174.66 (each s, COOEt); MS m/z (rel intensity, %) 342 (M^+ −16, 5), 313 (12), 233 (base peak), 204 (28), 203 (42), 191 (38), 163 (61), 161 (23), 159 (22), 145 (52), 116 (25), and 77 (22). Found: C, 66.91; H, 6.27%. Calcd for $C_{20}H_{22}O_4S$: C, 67.02; H, 6.19%.

11c (a 2:1 mixture of E- and Z-isomers (^{13}C NMR)): Yellow liquid; IR (neat) 1730 and 1040 cm^{-1}; ^1H NMR ($CDCl_3$) δ=1.18 (2/3×3H, t, J=7.0 Hz, OEt (E)), 1.20 (1/3×3H, t, J=7.0 Hz, OEt (Z)), 2.0—3.0 (4H, m, CH_2CH_2), 4.04 (2/3×2H, q, J=7.0 Hz, OEt (E)), 4.08 (1/3×2H, q, J=7.0 Hz, OEt (Z)), 6.0—6.7 (2H, m, Ar), 7.16 (1/3H, br s, =CH), and 7.3—7.8 (6H, m, Ar); ^{13}C NMR ($CDCl_3$) δ=14.24 (q, OEt), 21.77, 33.41 (each t, CH_2CH_2 (E)), 22.12, 34.06 (each t, CH_2CH_2 (Z)) 60.65 (t, OEt), 114.36, 119.54 (each d), 124.24, 125.83 (each d), 141.60, 142.50 (s, =C), 144.48 (d), and 172.60 (s, COOEt); MS m/z (rel intensity, %) 273 (M^+ −45, 4), 193 (42), 164 (30), 125 (19), 123 (70), 109 (20), 107 (67), 91 (base peak), 78 (56), 77 (63), and 65 (49). Found: C, 63.90; H, 5.70%. Calcd for $C_{17}H_{18}O_4S$: C, 64.13; H, 5.70%.

11d: Pale yellow liquid; IR (neat) 1725 and 1040 cm^{-1}; ^1H NMR ($CDCl_3$) δ=1.22 (3H, t, J=7.0 Hz, OEt), 1.88 (3H, dd, J=6.6 and 1.1 Hz, Me), 2.0—2.6 (4H, m, CH_2CH_2), 4.07 (2H, q, J=7.0 Hz, OEt), 6.15 (1H, dq, J=15.0 and 6.6 Hz,

MeCH=), 6.29 (1H, ddd, J=15.0, 6.6, and 1.1 Hz, =CH), and 7.1—7.7 (6H, m, Ph and =CH); ^{13}C NMR ($CDCl_3$) δ=14.80 (q, OEt), 18.77 (q, Me), 29.36, 34.00 (each t, CH_2CH_2), 60.59 (t, OEt), 125.24, 129.36 (each d, =CH), 131.19, 134.13, 138.54 (each d), 141.24 (s), 143.48 (s, =C), and 172.31 (s, COOEt); MS m/z (rel intensity, %) 247 (M^+ −45, 17), 167 (57), 97 (base peak), 95 (50), 93 (42), 91 (35), 78 (58), and 77 (37). Found: C, 65.72; H, 6.99%. Calcd for $C_{16}H_{20}O_3S$: C, 65.73; H, 6.89%.

11e: Colorless liquid; IR (neat) 1720 and 1040 cm^{-1}; ^{1}H NMR ($CDCl_3$) δ=0.95 (3H, t, J=7.0 Hz, n-Pr), 1.09 (3H, t, J=7.0 Hz, OEt), 1.4—1.7 (2H, m, n-Pr), 1.7—2.6 (6H, m, CH_2CH_2 and n-Pr), 4.04 (2H, q, J=7.0 Hz, OEt), 6.46 (1H, t, J=7.5 Hz, =CH), and 7.3—7.7(5H, m, Ph); ^{13}C NMR ($CDCl_3$) δ=13.82 (q, n-Pr), 14.18 (q, OEt), 19.94, 22.18, 30.30, 33.77 (each t, n-Pr and CH_2CH_2), 60.59 (t, OEt), 125.19, 129.36, 131.13 (each d), 137.17(d), 143.42 (s), 143.83 (s, =Ct), and 172.42 (s, COOEt); MS m/z (rel intensity, %), 294 (M^+, 3), 249 (25), 169 (base peak), 141 (29), 123 (27), 95 (37), and 81 (56). Found: C, 65.09; H, 7.60%. Calcd for $C_{16}H_{22}O_3S$: C, 65.28; H, 7.53%.

12 (a mixture of three isomers including E- and Z-isomers (^{1}H and ^{13}C NMR)): Pale yellow liquid; bp 250 °C/80 Pa (bulb-to-bulb); IR (neat) 1730 and 1050 cm^{-1}; ^{1}H NMR ($CDCl_3$) δ=1.04, 1.16 (3H, each d, J=6.6 Hz, Me), 1.18, 1.19 (3H, each t, J=7.0 Hz, OEt), 1.9—3.1 (3H, m, $CHCH_2$), 3.97, 4.04 (2H, each q, J=7.0 Hz, OEt), 7.00 (0.5H, br s, =CH (Z)), and 7.0—7.8 (10H+0.5H, m, Ph and =CH (E)); ^{13}C NMR ($CDCl_3$) δ=14.12, 16.71, 16.82, 17.59 (each q), 29.47, 29.83, 31.28 (each t, CH_2), 37.77, 38.06, 39.53 (each d, CH), 60.42, 60.59, 60.71 (each t, OEt), 124.48, 125.89, 126.01 (each d), 128.72, 128.89, 129.13, 129.24, 129.48, 129.71, 130.60, 131.66, 132.30 (each d), 134.42, 134.60, 134.72, 137.48 (each s), 143.36, 143.42, 143.78 (each s), 175.24, 175.54, and 176.01 (each s, COOEt); MS m/z (rel intensity, %) 326 (M^+ −16, 10), 297 (16), 217 (base peak), 143 (34), 133 (55), 129 (28), 128 (47), 116 (42), and 91 (35). Found: C, 70.23; H, 6.55%. Calcd for $C_{20}H_{22}O_3S$: C, 70.15; H, 6.48%.

References

1) O. Tsuge, S. Kanemasa, and Y. Ninomiya, *Chem. Lett.*, **1984**, 1993.

2) O. Tsuge, S. Kanemasa, H. Kobayashi, and J. Tanaka, 54th Annual Meeting of Chemical Society of Japan, Tokyo, April 1987, Abstr., No. 1-III M-32.

3) D. J. Ager, *J. Chem. Soc., Perkin Trans. 1*, **1986**, 183.

4) D. J. Ager, *J. Chem. Soc., Perkin Trans. 1*, **1986**, 195.

5) D. Seebach, R. Burstinghaus, B. T. Grobel, and M. Kolb, *Justus Liebigs Ann. Chem.*, **1977**, 830.

6) M. van der Leji and B. Zwanenburg, *Tetrahedron Lett.*, **1978**, 3383.

7) D. J. Ager, *Tetrahedron Lett.*, **22**, 587 (1981); D. J. Ager, *ibid.*, **24**, 95 (1983); D. J. Ager, *J. Chem. Soc., Perkin Trans. 1*, **1983**, 1131.

8) An example is known for the Peterson olefination using 1-silyl-1-sulfinyl carbanions (F. A. Carey and O. Fernandez, *J. Org. Chem.*, **38**, 2670 (1973)).

9) T. Cohen, J. P. Sherbine, S. A. Mendelson, and M. Myers, *Tetrahedron Lett.*, **26**, 2965 (1985).

10) The reactions of **1** with butyllithium or the lithium enolates generated from methyl 2-(trimethylsilyl)acetate, *N,N*-dimethylacetamide, acetone, and methyl methylsulfinylmethyl sulfide led to complex mixture. The monolithium enolates of dimethyl succinate and glutarate as well as the lithium enolate of methyl cyanoacetate were inactive to **1**.

11) A. G. Brook and D. G. Anderson, *Can. J. Chem.*, **46**, 2115 (1968); D. J. Hart and Y.-M. Tsai, *Tetrahedron Lett.*, **24**, 4387 (1983).

12) J. Drabowicz and S. Oae, *Synthesis*, **1977**, 404; J. D. Buynak, M. N. Rao, R. Y. Chandrasekaran, E. Haley, P. de Meester, and S. C. Chu, *Tetrahedron Lett.*, **26**, 5001 (1985).

13) J. F. Biellman and J. J. Vicens, *Tetrahedron Lett.*, **1974**, 2915; G. Chassaing, R. Lett, and A. Marquet, *ibid.*, **1978**, 471.

14) C. A. Kingsbury, *J. Org. Chem.*, **37**, 102 (1972).

15) D. J. Ager, *Synthesis*, **1984**, 384.

16) B. Harirchian and P. Magnus, *J. Chem. Soc., Chem. Commun.*, **1977**, 522.

Facile Formations of *o*- and *p*-Tropoquinone Mono- and Bisacetals by Anodic Oxidations of 2,3-, 2,5-, 2,7-, and 4,5-Dimethoxytropones[1)]

Akira MORI, Tadahiko KUBOTA,† and Hitoshi TAKESHITA*
Institute of Advanced Material Study, 86, Kyushu University,
Kasuga-koen, Kasuga, Fukuoka 816
†Graduate School of Engineering Sciences, 39, Kyushu University,
Kasuga-koen, Kasuga, Fukuoka 816
(Received May 9, 1988)

o- and *p*-Tropoquinone mono- and bisacetals (tetramethoxycycloheptadienones) were prepared from 2,3-, 2,5-, 2,7-, and 4,5-dimethoxytropones by means of anodic oxidations in practical yields. Cerium(IV) salt oxidations of dimethoxytropones afforded a mixture of products i.e., a hydrolysis product and/or a methanol adduct of tropoquinone bisacetals. By treating with sulfuric acid in a mixture of acetic acid and acetic anhydride, 4,4,7,7- and 2,2,7,7-tetramethoxycycloheptadienones gave the Thiele-type reaction products with a high positional selectivity. Similarly, 2-bromo-7-methoxytropone was anodically oxidized to 4,4,7,7-tetramethoxycycloheptadienone and its 2-bromo derivative. The mechanism of the reaction is also discussed in detail.

The facile acetal formation of *p*-tropoquinone (3,6-cycloheptadiene-1,2,5-trione) in methanol and the hydrate formation of *o*-tropoquinone (4,6-cycloheptadiene-1,2,3-trione) in water are well-known and repulsive dipole–dipole interactions of 1,2-dione and 1,2,3-trione moieties are attributable for the phenomena.[2,3)] Recently, we prepared tropoquinone acetals, which are useful for further transformations, toward functionalized troponoids: i.e., a) the 2,3-dichloro-5,6-dicyano-*p*-benzoquinone (DDQ) oxidation of the ketol, derived from tropone via a photosensitized oxidation, an acetalization, and a bond cleavage of the endoperoxide with triethylamine[4)] and b) DDQ,[5)] thallium(III) nitrate (TTN),[6)] and cerium(IV) ammonium nitrate (CAN)[7)] oxidations of 2-alkoxy-5-hydroxytropones. We have now developed an improved preparation of bisacetals by the anodic oxidation of 2,3-, 2,5-, 2,7-, and 4,5-dimethoxytropones. This anodic oxidation was also applicable to tropone, 2-methoxytropone, and 2-bromo-7-methoxytropone.

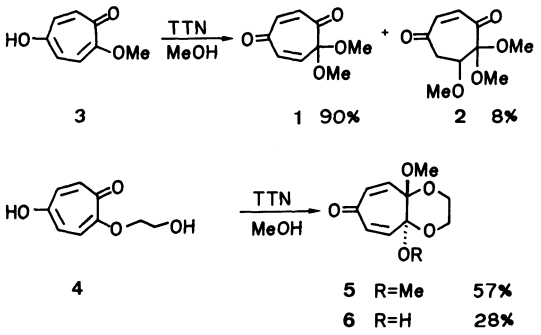

Scheme 1.

Results and Disccusion

2,5-Disubstituted Tropones. We have already shown that 7,7-dimethoxycyclohepta-2,5-diene-1,4-dione (**1**) can be prepared in good yield together with its methanol adduct (**2**) by the TTN-oxidation of 5-hydroxy-2-methoxytropone (**3**) in methanol.[6)] Similarly, 2-(2-hydroxyethoxy)-5-hydroxytropone (**4**) gave two bisacetals **5** and **6** in good combined yields.[6)] However, it is desirable to develop a selective formation of either of the two. Thus, when **3** was anodically oxidized in a singel-cell apparatus without accurate potential control in anhydrous methanol with lithium perchlorate, a single product **1** was obtained in 62% yield. In parallel, **4** gave **6** in 75% yield. Consequently, anodic oxidation is a practical method to obtain a single product selectively.

Table 1. Anodic and CAN Oxidations of Troponoids

Substrate	Anodic Oxidation	CAN Oxidation
3	1 62%	not tried
4	6 75%	not tried
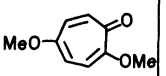 7	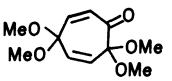 8 97%	1 15% 2 77%
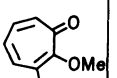 9	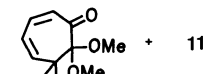 + 11* 10 57% 7%	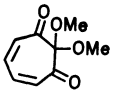 12 59%
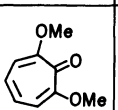 13	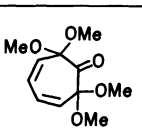 14 94%	14 6%
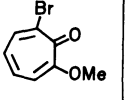 15	8 + 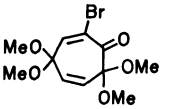 23% 16 67%	not reacted

*11 = 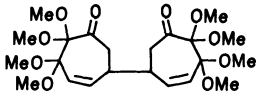

A similar electrolysis of 2,5-dimethoxytropone (**7**) also gave a single product (**8**) in quantitative yield. Its ^{1}H NMR spectrum showed two sets of an *AB*-quartet around δ 5.8—6.4, suggesting the structure to be 4,4,7,7-tetramethoxy-2,5-cycloheptadien-1-one. Again, the CAN-oxidation of **7** gave **1** and **2** in 15 and 77% yields. The difference in product distributions might depend on the reaction conditions, i.e., hydrolysis and Michael addition reactions must follow in an acidic medium under CAN-oxidation conditions, while the bisacetal **8** was stable under neutral electrolysis conditions.

2,3-Disubstituted Tropones. The electrode oxidation of 2,3-dimethoxytropone (**9**)[8] gave two products **10** and **11** in 57 and 7% yields: the major product **10** was deduced to be 6,6,7,7-tetramethoxy-2,4-cycloheptadien-1-one from its ^{1}H NMR spectrum, showing four methoxyl and four olefinic proton signals. The by-product **11**, four methoxyl signals and two olefinic and three aliphatic proton signals, was suggested to be 4,4,4′,4′,5,5,5′,5′-octamethoxy-[bi-2-cyclohepten-1-yl]-6,6′-dione. The CAN-oxidation of **9** gave the symmetrical monoacetal **12** in 59% yield. Its structure was determined by spectral data.

2,7-Disubstituted Tropones. The anodic oxidation of 2,7-dimethoxytropone (**13**)[8] gave a single product **14** in 94%, whose NMR spectrum suggested it to be 2,2,7,7-tetramethoxy-3,5-cycloheptadien-1-one. On the other hand, **13** was slightly reactive to the CAN-oxidation to give **14** in only 6% yield with 9% conversion.

In the case of 2-bromo-7-methoxytropone (**15**), the CAN-oxidation gave no identifiable product at all. However, electrolysis afforded two products: one was **8** in 23% and the other, its relatively unstable bromo derivative **16**, in 67%. The oxidation occurred selectively at C-4, the para position to the methoxyl group and the bromine atom was removed to give **8** during electrolysis.

4,5-Dimethoxytropones. The anodic oxidation of 4,5-dimethoxytropone (**17**)[9] gave 4,4,5,5-tetramethoxy-2,6-cycloheptadien-1-one (**18**) in 41% and its methanol adduct **19** in 10% yields. The structure of **19** was unambiguously ascertained from the spectral data. The position of the methoxyl group in **19** was elucidated to be at C-2 from a consideration of the ^{13}C chemical shifts[10] i.e., C-2 at δ 152.6 and C-3 at δ 109.3 together with an absence of a long-range coupling between a singlet at δ 5.37 and a doublet at δ 6.13.

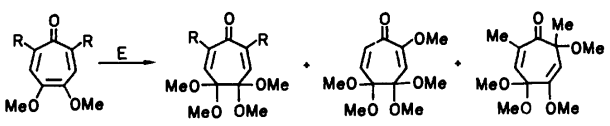

Scheme 2.

Therefore, the structure of **19** was determined to be 2,4,4,5,5-pentamethoxy-2,6-cycloheptadien-1-one.

Electrolysis of 4,5-dimethoxy-2,7-dimethyltropone (**20**)[5] gave 4,4,5,5-tetramethoxy-2,7-dimethyl-2,6-cycloheptadien-1-one (**21**) in 77% and its methanol adduct **22** in 8%. The structure of **22** was deduced from the ^{1}H chemical shifts of methyl signals at δ 1.37 and 1.92. No further transformation under anodic oxidation conditions occurred from **22** because of the presence of the methyl group, being different from the case of **19**.

Moreover, the oxidation of 4,5-dimethoxy-2,7-dipropyltropone (**23**) gave a single product **24** in 97%. The structure of **24** was determined to be 4,4,5,5-tetramethoxy-2,7-dipropyl-2,6-cycloheptadien-1-one from the same spectral criteria as **18** and **21**.

Other Troponoids. Since a further oxidation, **18** to **19**, took place in the anodic oxidation of **17**, other tropones, 2-methoxytropone (**25**) and tropone (**26**), should be examined: 2-Methoxytropone gave four products (**1**; 7%, **7**; 20%, **8**; 6%, and **27**; 6%) with a recovery of **25** in 56% after the consumption of 2 F mol^{-1} of electricity. By passing 4 F mol^{-1} of electricity, yields of **8** and **7** increased to 49 and 15%, respectively. Three (**1**, **7**, and **8**) of them were identical with authentic samples. The structure of a new product, **27**, was identified as 6,7,7-trimethoxy-2,4-cycloheptadien-1-one on the basis of the doublet methine proton at δ 4.09 and the carbonyl absorption at 1685 cm^{-1}. On the other hand, the CAN-oxidation of **25** afforded **2** in 7% and **27** in 1% yields. Tropone gave **7**, **8**, and **25** in 7, 7, and 5% yields, respectively.

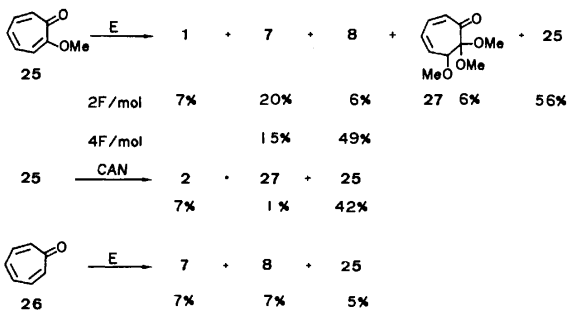

Scheme 3.

Thus, anodic oxidations of tropone and 2-methoxytropone were less satisfactory. Although the yields of products were not always high, a one-step formation of methoxylated troponoids is of practical value.

Thiele-Type Reactions of Bisacetals. As has been seen in CAN-oxidations of **7** and **25** and in anodic oxidations of **17** and **20**, methanol added to the C=O conjugated C=C double bond. It has been shown[6] that Thiele-type reactions of acetal **1** and bisacetals **5** and **6**, respectively, gave 4,5-diacetoxy-2-methoxytropone (**28**) and 6-acetoxy-2,3-(ethylenedioxy)tropone (**29**) with a high positional selectivity. The treatment of **8** with a 1 : 1-mixture of acetic acid and acetic anhydride with a catalytic amount of concd sulfuric acid gave three

products (**1**; 28%, **30**; 35%, **31**; 5%). The structures of **30** and **31** were determined by the spectral data. Since **31** showed a carbonyl carbon at δ 168.4 in the ^{13}C NMR spectrum, an acetotropy, which is common in 2-acetoxytropones,[11] is operative in **31**. Additionally, the decoupled ^1H NMR spectrum disclosed a long-range coupled ABX_3 system. Therefore, **31**, was 2-acetoxy-4,7-dimethoxytropone.

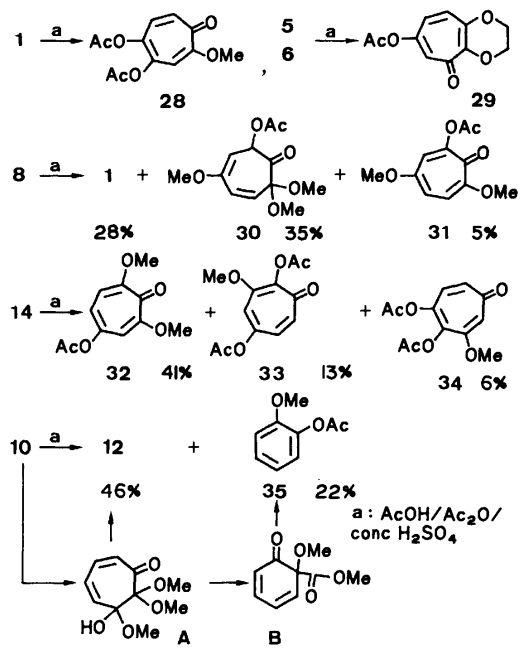

Scheme 4.

The ^1H NMR of the major product, **30**, showed an acetoxyl and three methoxyl signals together with three olefinic proton signals and a doublet methine proton signal at δ 5.65 (J=8.2 Hz). Taking the IR carbonyl absorption (1690 cm^{-1}) into account, the structure of **30** was assigned to be 2-acetoxy-4,7,7-trimethoxy-3,5-cycloheptadien-1-one.

Next, **14** furnished three troponoids (**32**; 41%, **33**; 13%, **34**; 6%) by a treatment under Thiele-type reaction conditions. All ^1H NMR spectral splittings of these compounds were suggested to be 5,7-disubstituted tropolone derivatives; i.e., two of three olefinic protons vicinally coupled (J=10.3—12.8 Hz) and the third proton appeared as a doublet with a small coupling constant (J≈2.5 Hz). From the presence of an acetoxyl and two methoxyl signals, the structure of **32** was deduced to be 4-acetoxy-2,7-dimethoxytropone. As **33** and **34** showed a methoxyl and two acetoxyl signals, the structures of **33** and **34** were 2,5-diacetoxy-3-methoxytropone[12] (J=10.3 Hz) and 4,5-diacetoxy-3-methoxytropone (J=12.8 Hz), respectively. On the contrary, **10** afforded only the hydrolysis product **12** in 46% and 2-acetoxyanisole (**35**) in 22% yields, but no Thiele-type product.

The formation of **35** from **10** could be explained in terms of a hydrolysis of one of the methoxyl groups at C-6 to give **A**, followed by a ring contraction and a decarbonylation via a six-membered dienone **B**.

Mechanistic Consideration of the Anodic Oxidation. According to mechanistic studies for anisoles[13] and 1,4-dimethoxybenzenes described in literature,[14] a sequence involving a methoxyl radical attack to the aryl radical cations (EECC sequence) in methanolic potassium hydroxide has been proposed. Under conditions without methoxide ion, the nucleophilic attack of methanol to anodically formed radical cations was predominant to give cations; further oxidation and methoxylation followed (ECEC sequence).

Since the present anodic oxidations of troponoids were performed in the presence of lithium perchlorate, methoxyl radicals would hardly exist under the reaction conditions. Therefore, the ECEC mechanism to **10** was assumed as shown in Scheme 5. An attack of a methoxide ion to the radical cation **C** occurred to give **D** at C-2 since the resultant radical could be more stabilized than the alternative from a C-3 attack of a methoxide ion in **C**. Further electrolysis and methoxylation should give **10**. The mechanism for the dimeric product **11** could be explained in terms of an intermediary formation of **E** from **D**. Successive oxidation, dimerization, and methoxylation gave product **11**. An attempted electrolysis of **10** gave no **11**. Additionally, the ECEC mechanism was also favored in the oxidation of **4**. If an EECC mechanism was operative, the attack of a methoxyl radical to **H** would be more preferable at C-a to give **J** than at C-b bacause of the steric hindrance. From **J**, a mixture of acetals **5** and **6** should be obtained via **K**. On the other hand, an internal attack of the hydroxyethoxy group in **H** led to radical **L**, which was further oxidized and a methoxylation followed to give **6**. Thus, an ECEC mechanism was favored.

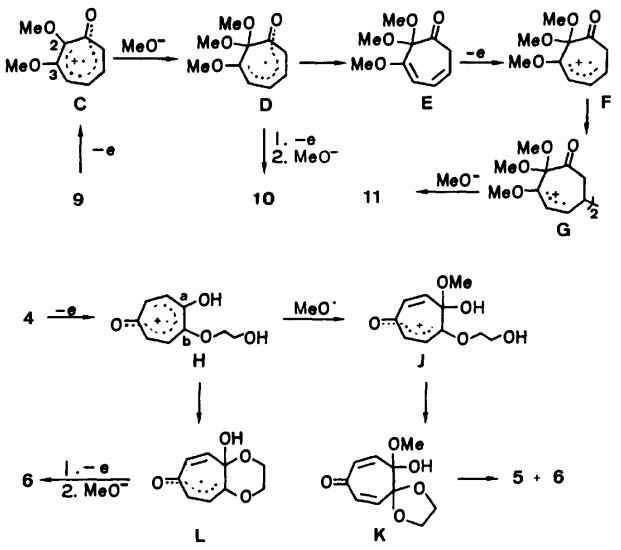

Scheme 5.

Next, for the formation of **8**, from **15**, a reduction process might be involved, since the reactions were

Table 2. Results of Controlled Anodic Oxidation of **15**

Electricity	Ratio of component				
F mol^{-1}	**15**	**36**	**16**	**8**	**37**
2.4	17	5	1	0	0
3.2	15	6	2	Trace	0
4.1	6	2	6	6	Trace
5.0	4	1	9	6	Trace
5.9	2	Trace	9	5	Trace
6.8	2	0	9	5	Trace
7.7	1.5	0	9	5.5	0.5
10.1	0	0	3	2.5	2.5
12.3	0	0	4	4	3
			(16)	(22)	(17)

Numbers in parentheses are yields isolated.

conducted in an undivided cell. In order to make the point clear, we investigated the reaction of **15** in some detail. When the reaction was traced by the ^{1}H NMR spectrum of the whole reaction mixture every hour, product distributions were obtained, as summarized in Table 2. After 3 h, a new product **36** was formed. After 5 h, the amount of **36** decreased with increasing amounts of **8** and **16**. Finally, another new product **37** was produced while **15** and **36** were consumed. Compound **36** was identical with the authentic 2-bromo-4,7-dimethoxytropone, which was prepared from the reaction of *N*-bromosuccinimide and **7** together with the dibromo derivative **38**.[15] Compound **37** was a methanol adduct of **16** from the spectral data.

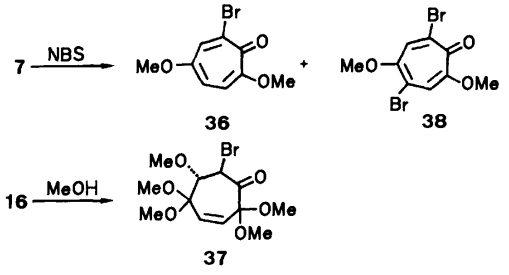

Scheme 6.

An attempted oxidation of **16** gave only **37** but no **8** at all. The formation of **37** required no electricity since **37** was formed simply by standing in a methanol solution of **16**. On the other hand, an anodic oxidation of **36** gave **16** in quantitative yield.

Taking these evidences into account, the mechanism shown in Scheme 7 can be proposed. Compound **15** was electrolyzed to the cation radical **M**, where the attack of methanol, further oxidation, and methoxylation occurred to give **Q**. A subsequent elimination of methanol from **Q** led to **36**, which was again oxidized and methoxylated to **16**. On the other hand, a prototropy occurred from **Q** to **R** and a subsequent addition-elimination process led to give **8**. An exclusive attack of a methoxide ion to C-4 of **P** could be explained by a steric hindrance from the bromine and dimethyl acetal groups.

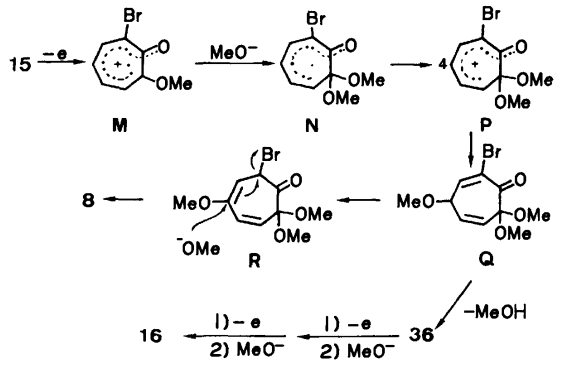

Scheme 7.

Conclusion

As has been described, the oxidation of twelve troponoids proceeded in practical yields. Interestingly, an electrode oxidation and a CAN-oxidation were complementary to some extent with each other. For instance, **13** having shown a better result regarding electrode oxidation, was inert to CAN-oxidation. Its conversion to **14** after 4.5 h was only 7%.

The reactivities of bisacetals to Thiele-type reactions were quite different and the site of the reaction with the acetate anion was selective in each case.

Experimental

The elemental analyses were performed by Miss S. Hirashima, of Institute of Advanced Material Study, Kyushu University. NMR spectra were measured by a JEOL 270H spectrometer in a $CDCl_3$ solution (unless otherwise specified); chemical shifts are expressed in the unit δ. Mass spectra were measured with a JEOL 01SG -2 spectrometer. IR spectra were taken as KBr disks or as a liquid film inserted between NaCl plates using a Jasco IR-A 102 spectrometer. UV spectra were measured by a Hitachi U-3200 spectrophotometer.

Anodic Oxidation of 5-Hydroxy-2-methoxytropone (3). An anhydrous MeOH solution (90 cm^3) of **3** (51.4 mg) and $LiClO_4$ (41 mg) was electrolyzed in an undivided cell fitted with a circular Pt-gauze (10 mm in diameter×20 mm in height) anode and a Pt cathode under a constant current (10 mA). After 2.2 F mol^{-1} of electricity were passed at room temperature under an N_2 atmosphere, the solvent was evaporated in vacuo. The residue was diluted with water and extracted with $CHCl_3$. The solvent was evaporated and the residue was chromatographed on a silica-gel column to give 37.9 mg (62%) of **1**: a pale-yellow oil, which was identical with the authentic sample.[6]

Anodic Oxidation of 5-Hydroxy-2-(2-hydroxyethoxy)-tropone (4). An anhydrous MeOH solution (90 cm^3) of **4** (100 mg) and $LiClO_4$ (40 mg) was oxidized anodically to give 87.7 mg (75%) of **6**: colorless crystals, mp 123—124 °C, which was identical with the authentic sample.[6]

Anodic Oxidation of 2,5-Dimethoxytropone (7). An anhydrous MeOH solution (80 cm^3) of **7** (101.6 mg) and $LiClO_4$ (44 mg) was electrolyzed (2 F mol^{-1}) to give 135 mg (97%) of **8**: a colorless oil; ^1H NMR δ=3.29 (6H, s), 3.30 (6H, s), 5.82 (1H, d, J=12.5 Hz), 6.01 (1H, d, J=12.5 Hz), 6.09 (1H, dd, J=12.5, 2.0 Hz), and 6.34 (1H, dd, J=12.5, 2.0 Hz); ^{13}C NMR δ=49.7 (2C), 50.4 (2C), 98.5, 101.9, 127.4, 131.2, 135.9, 139.8, and 193.0; IR 1705, 1460, 1440, 1390, 1300, and 1210 cm^{-1}; UV (MeOH) 202 (ε 6000), 229 (sh 2900), and 336 nm (140).

Found: C, 57.62; H, 7.12%. Calcd for $C_{11}H_{16}O_5$: C, 57.88; H, 7.07%.

CAN-Oxidation of 7. An anhydrous MeOH solution (1.5 cm^3) of **7** (60 mg) and CAN (396 mg) was stirred at 0 °C and the mixture was kept at room temperature for 4.5 h with stirring. Silica-gel chromatography of the mixture afforded 9.7 mg (15%) of **1** and 59.4 mg (77%) of **2**: a colorless oil. The latter was identical with the authentic sample.[6]

Anodic Oxidation of 2,3-Dimethoxytropone (9). An anhydrous MeOH solution (100 cm^3) of **9** (122 mg) and $LiClO_4$ (104 mg) was electrolyzed (2.8 F mol^{-1}) to give 95.4 mg (57%) of **10** and 11.6 mg (7%) of **11**.

10: Colorless crystals, mp 107—108 °C; ^1H NMR δ=3.36 (6H, br s), 3.42 (6H, s), 5.86 (1H, dd, J=12.0, 1.0 Hz), 6.06 (2H, m), and 6.40 (1H, ddd, J=12.0, 6.0, 2.0 Hz); ^{13}C NMR δ=51.3 (2C), 52.9 (2C), 101.2, 103.5, 126.2, 128.1, 133.4, 137.9, and 194.5; IR 1670, 1420, 1140, and 1120—980 cm^{-1}; UV (MeOH) 201 (ε 3800), 231 (2400), and 293 nm (4700).

Found: C, 57.99; H, 6.88%. Calcd for $C_{11}H_{16}O_5$: C, 57.88; H, 7.07%.

11: Colorless crystals, mp 150—152 °C; ^1H NMR δ=2.26 (2H, d, J=11.0 Hz), 2.62 (2H, m), 2.96 (2H, t, J=11.0 Hz), 3.17 (6H, s), 3.35 (6H, s), 3.38 (6H, s), 3.47 (6H, s), 5.73 (2H, dd, J=11.7, 2.2 Hz), and 5.93 (2H, dd, J=11.7, 3.7 Hz); ^{13}C NMR δ=39.1 (2C), 44.8 (2C), 50.6 (2C), 51.1 (2C), 51.2 (2C), 51.5 (2C), 101.6 (2C), 106.2 (2C), 132.1 (2C), 134.3 (2C), and 202.7 (2C); IR 1720, 1440, 1170, and 1100 cm^{-1}; UV (MeOH) 297 nm (ε 130).

Found: C, 56.49; H, 7.39%. Calcd for $C_{22}H_{34}O_{10}\cdot 1/2H_2O$: C, 56.53; H, 7.49%.

CAN-Oxidation of 9. An anhydrous MeOH solution (2 cm^3) of **9** (31.6 mg) was treated with CAN (115 mg) to give 20.3 mg (59%) of **12** and 11.3 mg of unreacted **9**.

12: Pale-yellow crystals, mp 69—70 °C; ^1H NMR δ=3.38 (6H, s), 6.0—6.1 (2H, m), and 6.5—6.6 (2H, m); ^{13}C NMR δ=52.7 (2C), 104.6, 129.5 (2C), 133.0 (2C), and 195.1 (2C); IR 1700, 1450, 1420, and 1220 cm^{-1}; UV (MeOH) 313 nm (ε 3500).

Found: C, 59.42; H, 5.61%. Calcd for $C_9H_{10}O_4$: C, 59.33; H, 5.53%.

Anodic Oxidation of 2,7-Dimethoxytropone (13). An anhydrous MeOH solution (50 cm^3) of **13** (48.2 mg) and $LiClO_4$ (54 mg) was electrolyzed (3.1 F mol^{-1}) to give 62.1 mg (94%) of **14**: a colorless oil; ^1H NMR δ=3.26 (12H, s), 5.5—5.7 (2H, m), and 6.1—6.3 (2H, m); ^{13}C NMR δ=50.5 (4C), 101.0 (2C), 127.4 (2C), 130.2 (2C), and 192.5; IR 1740, 1175, 1140, 1080, and 1050 cm^{-1}; UV (MeOH) 206 (ε 7600) and 259.6 nm (2900).

Found: C, 57.74; H, 7.07%. Calcd for $C_{11}H_{16}O_5$: C, 57.88; H, 7.07%.

CAN-Oxidation of 13. a) An anhydrous MeOH solution (2 cm^3) of **13** (43.4 mg) was oxidized with CAN (145 mg) to give 3.4 mg (6%) of **14** and 39.3 mg of unreacted **13**.

b) An anhydrous MeOH solution (4 cm^3) of **13** (12.1 mg) was oxidized with CAN (130 mg) to give a complex mixture.

Anodic Oxidation of 2-Bromo-7-methoxytropone (15). a) An anhydrous MeOH solution (50 cm^3) of **15** (98 mg) and $LiClO_4$ (57 mg) was electrolyzed (8.1 F mol^{-1}) to give 23.6 mg (23%) of **8** and 94.7 mg (67%) of **16**: a pale-yellow oil; ^1H NMR δ=3.24 (6H, s), 3.27 (6H, s), 5.82 (1H, d, J=12.0 Hz), 6.07 (1H, dd, J=12.0, 2.0 Hz), and 6.84 (1H, d, J=2.0 Hz); ^{13}C NMR δ=49.8 (2C), 50.6 (2C), 99.4, 101.0, 121.2, 131.0, 135.5, 140.1, and 188.3; IR 1720, 1620, 1460—1440, 1380, and 1100—1020 cm^{-1}.

Found: m/z 306.0074 and 308.0041. Calcd for $C_{11}H_{15}O_5Br$: M, 306.0101 and 308.0081.

b) An anhydrous MeOH solution (50 cm^3) of **15** (98 mg) and $LiClO_4$ (58 mg) was electrolyzed. Every 1 cm^3 of the mixture was taken out, evaporated, and filtered by a silica cartridge (Sep-pak) in order to monitor by ^1H NMR spectroscopy. After 3 h, the work-up gave the crude **36**, whose ^1H NMR spectrum was identical with that of an authentic sample. After 11 h, the whole mixture was evaporated and the residue was chromatographed to give 19.3 mg (16%) of **16**, 19.2 mg (22%) of **8**, and 22 mg (17%) of **37**: pale-yellow crystals, mp 76—78 °C; ^1H NMR δ=3.08 (3H, s), 3.13 (3H, s), 3.29 (3H, s), 3.38 (3H, s), 3.67 (3H, s), 3.95 (1H, d, J=6.2 Hz), 4.80 (1H, d, J=6.2 Hz), 5.86 (1H, d, J=11.8 Hz), and 6.01 (1H, d, J=11.8 Hz); ^{13}C NMR δ=48.9, 49.1, 49.6, 50.3, 54.8, 60.0, 87.5, 97.8, 101.0, 130.0, 133.5, and 188.3; IR 1750, 1460, and 1390 cm^{-1}; UV (MeOH) 201.8 (ε 2600) and 290 nm (170).

Found: C, 42.31; H, 5.57%. Calcd for $C_{12}H_{19}O_6Br$: C, 42.49; H, 5.65%.

NBS-Bromination of 2,5-Dimethoxytropone (7). Preparation of 2-Bromo-4,7-dimethoxytropone (36). A CCl_4 solution (4 cm^3) of **7** (222 mg) and NBS (248 mg) was refluxed for 2 h. After cooling the mixture to room temperature, the precipitate was filtered. The solvent was evaporated and the residue was chromatographed on a silica-gel column to give 38 mg (12%) of **36**, 28 mg (6%) of **38**, and 90 mg of recovered **7**.

36: Pale-yellow crystals, mp 146—147 °C; ^1H NMR δ=3.78 (3H, s), 3.88 (3H, s), 6.43 (1H, dd, J=11.0, 3.0 Hz), 6.79 (1H, d, J=11.0 Hz), and 8.07 (1H, d, J=3.0 Hz); ^{13}C NMR δ=55.9, 56.6, 108.3, 113.7, 135.9, 138.5, 156.6, 157.3, and 173.6; IR 1580, 1495, 1390, 1340, 1245, 1210, 1185, and 1120 cm^{-1}.

Found: C, 43.86; H, 3.76%. Calcd for $C_9H_9O_3Br$: C, 44.11; H, 3.70%.

38: Pale-yellow crystals, mp 139—142 °C (lit,[15] mp 140—142 °C).

Anodic Oxidation of 36. An anhydrous MeOH solution (50 cm^3) of **36** (30 mg) and $LiClO_4$ (51 mg) was electrolyzed (5.6 F mol^{-1}) to give 37 mg (99%) of **16**, which was identical with the authentic sample.

CAN-Oxidation of 15. An anhydrous MeOH solution (2 cm^3) of **15** (59 mg) was treated with CAN (301 mg). The starting material was completely recovered.

Anodic Oxidation of 4,5-Dimethoxytropone (17). An anhydrous MeOH solution (40 cm^3) of **17** (53 mg) and $LiClO_4$ (54 mg) was electrolyzed (5.2 F mol^{-1}) to give 29.6 mg (41%) of **18** and 8.5 mg (10%) of **19**.

18: A colorless oil; ^1H NMR δ=3.31 (6H, br s), 3.48 (6H, br s), 6.10 (2H, dm, J=12.5 Hz), and 6.42 (2H, dm, J=12.5 Hz); ^{13}C NMR δ=50.4 (2C, br), 51.7 (2C, br), 102.2 (2C), 131.0 (2C), 141.2 (2C), and 190.8; IR 1665, 1620, 1460,

and 1390 cm^{-1}; UV (MeOH) 209 nm (ε 9000).

Found: C, 57.83; H, 6.90%. Calcd for $C_{11}H_{16}O_5$: C, 57.88; H, 7.07%.

19: A colorless oil; ^1H NMR δ=3.30 (6H, br s), 3.51 (6H, br s), 3.67 (3H, s), 5.37 (1H, s), 6.13 (1H, d, J=12.6 Hz), and 6.41 (1H, d, J=12.6 Hz); ^{13}C NMR δ=50.4 (2C, br), 51.6 (2C, br), 55.4, 101.6, 103.3, 109.3, 130.0, 140.7, 152.6, and 186.4; IR 1720, 1670, 1640, and 1460 cm^{-1}.

Found: m/z 258.1103. Calcd for $C_{12}H_{18}O_5$: M, 258.1108.

Anodic Oxidation of 4,5-Dimethoxy-2,7-dimethyltropone (20). An anhydrous MeOH solution (120 cm^3) of **20** (186 mg) and $LiClO_4$ (116 mg) was electrolyzed (3.7 F mol^{-1}) to give 188 mg (77%) of **21** and 20.3 mg (8%) of **22**.

21: Colorless crystals, mp 98—100 °C; ^1H NMR δ=1.93 (6H, d, J=1.4 Hz), 3.27 (6H, br s), 3.45 (6H, br s), and 6.14 (2H, d, J=1.4 Hz); ^{13}C NMR δ=20.4 (2C), 50.2 (2C, br), 51.5 (2C, br), 102.0 (2C), 134.1 (2C), 138.1 (2C), and 194.9; IR 1635, 1440, and 1385 cm^{-1}; UV (MeOH) 240 nm (ε 6400).

Found: C, 60.80; H, 7.92%. Calcd for $C_{13}H_{20}O_5$: C, 60.92; H, 7.87%.

22: A colorless oil; ^1H NMR δ=1.37 (3H, s), 1.92 (3H, d, J=1.4 Hz), 3.15 (3H, s), 3.26 (3H, s), 3.28 (3H, s), 3.63 (3H, s), 4.46 (1H, s), and 6.06 (1H, d, J=1.4 Hz); ^{13}C NMR δ=19.3, 25.8, 49.6, 50.3, 52.4, 55.1, 81.9, 99.6, 101.3, 134.8, 139.2, 158.6, and 203.8; IR 1710, 1650, 1450, and 1350 cm^{-1}.

Found: m/z 256.1307. Calcd for $C_{13}H_{20}O_5$: M, 256.1308.

Anodic Oxidation of 4,5-Dimethoxy-2,7-dipropyltropone (23). An anhydrous MeOH solution (50 cm^3) of **23** (26 mg) and $LiClO_4$ (52 mg) was electrolyzed (6.7 F mol^{-1}) to give 31.6 mg (97%) of **24**: a colorless oil; ^1H NMR δ=0.90 (6H, t, J=7.3 Hz), 1.41 (4H, m), 2.29 (4H, m), 3.25 (6H, br s), 3.45 (6H, br s), and 6.01 (1H, t, J=1.1 Hz); ^{13}C NMR δ=13.6 (2C), 21.8 (2C), 36.0 (2C), 50.4 (2C, br), 51.4 (2C, br), 102.1 (2C), 133.1 (2C), 143.0 (2C), and 196.3; IR 1670, 1650, 1460, 1430, 1380, and 1360 cm^{-1}; UV (MeOH) 243 nm (ε 6300).

Found: C, 65.27; H, 8.91%. Calcd for $C_{17}H_{28}O_5$: C, 65.36; H, 9.03%.

Anodic Oxidation of 2-Methoxytropone (25). a) An anhydrous MeOH solution (50 cm^3) of **25** (427.4 mg) and $LiClO_4$ (53 mg) was electrolyzed (2.0 F mol^{-1}) to give 103.5 mg (20%) of **7**, 44.5 mg (6%) of **8**, 37.5 mg (7%) of **1**, 37 mg (6%) of **27**, and 237.8 mg of unreacted **25**.

27: A pale-yellow oil; ^1H NMR δ=3.28 (3H, s), 3.40 (3H, s), 3.41 (3H, s), 4.09 (1H, d, J=6.0 Hz), 5.90 (1H, d, J=12.0 Hz), 6.10 (1H, dd, J=11.5, 6.5 Hz), 6.33 (1H, ddd, J=11.5, 6.0, 1.0 Hz), and 6.48 (1H, ddd, J=12.0, 6.5, 1.0 Hz); ^{13}C NMR δ=51.2, 51.4, 58.7, 76.8, 102.0, 127.4, 127.5, 134.3, 135.0, and 195.0; IR 1685, 1595, 1450, and 1425 cm^{-1}.

Found: m/z 198.0890. Calcd for $C_{10}H_{14}O_4$: M, 198.0859.

b) An anhydrous MeOH solution (65 cm^3) of **25** (101 mg) and $LiClO_4$ (40 mg) was electrolyzed (4.0 F mol^{-1}) to give 18.4 mg (15%) of **7** and 82.5 mg (49%) of **8**.

CAN-Oxidation of 25. An anhydrous MeOH solution (2 cm^3) of **25** (48 mg) was treated with CAN (437 mg) to give 5.6 mg (7%) of **2**, 1 mg (1%) of **27**, and 20 mg of unreacted **25**.

Anodic Oxidation of Tropone (26). An anhydrous MeOH solution (50 cm^3) of **26** (84 mg) and $LiClO_4$ (58 mg) was electrolyzed (2.5 F mol^{-1}) to give 5.3 mg (5%) of **25**, 9.8 mg (7%) of **7**, 11.8 mg (7%) of **8**, and 40 mg of unreacted **26**.

Thiele-Type Reaction of 8. A 1:1-mixture (3 cm^3) of AcOH and Ac_2O, and **8** (177.5 mg) was stirred with a catalytic amount of concd H_2SO_4 at room temperature for 2 h. The mixture was diluted with water and extracted with $CHCl_3$. The solvent was evaporated in vacuo and the residue was chromatographed on a silica-gel column to give 39.5 mg (28%) of **1**, 67 mg (35%) of **30**, and 8.7 mg (5%) of **31**.

30: A pale-yellow oil; ^1H NMR δ=2.01 (3H, s), 3.25 (3H, s), 3.37 (3H, s), 3.60 (3H, s), 5.25 (1H, dd J=8.2, 2.2 Hz), 5.65 (1H, d, J=8.2 Hz), 5.98 (1H, d, J=13.2 Hz), and 6.41 (1H, dd, J=13.2, 2.2 Hz); ^{13}C NMR δ=21.0, 49.9, 52.0, 54.9, 69.4, 97.5, 100.4, 126.7, 136.4, 156.6, 169.9, and 193.2; IR 1750, 1690, 1650, 1405, 1370, and 1230 cm^{-1}.

Found: m/z 256.0945. Calcd for $C_{12}H_{16}O_6$: M, 256.0945.

31: Colorless crystals, mp 131—133 °C; ^1H NMR δ=2.37 (3H, s), 3.78 (3H, s), 3.89 (3H, s), 6.65 (1H, dd, J=12.1, 2.9 Hz), 6.84 (1H, d, J=2.9 Hz), and 6.90 (1H, d, J=12.1 Hz); ^{13}C NMR δ=20.7, 55.8, 57.4, 120.0, 120.4 (2C), 156.9, 160.6, and 168.4 (3C); IR 1770, 1590, 1510, 1460, 1250, and 1170 cm^{-1}.

Found: m/z 224.0684. Calcd for $C_{11}H_{12}O_5$: M, 224.0684.

Thiele-Type Reaction of 10. A 1:1-mixture of AcOH and Ac_2O (1 cm^3) of **10** (97 mg) was stirred in the presence with a catalytic amount of concd H_2SO_4 to give 35.9 mg (46%) of **12** and 15.5 mg (22%) of **35**. The latter was identical with an authentic sample.

Thiele-Type Reaction of 14. A 1:1-mixture of AcOH and Ac_2O (0.4 cm^3) and **14** (31.6 mg) was stirred with a catalytic amount of concd H_2SO_4 to give 12.6 mg (41%) of **32**, 4.5 mg (13%) of **33**, and 2.1 mg (6%) of **34**.

32: A pale-yellow oil; ^1H NMR δ=2.32 (3H, s), 3.93 (6H, s), 6.62 (1H, d, J=2.6 Hz), 6.65 (1H, dd, J=10.3, 2.6 Hz), and 6.80 (1H, d, J=10.3 Hz); ^{13}C NMR δ=21.1, 56.6 (2C), 111.6, 112.2, 117.3, 147.8, 160.6, 161.2, 169.5, and 173.1; IR 1760, 1595, 1500, 1450, 1380, and 1360 cm^{-1}.

Found: m/z 224.0685. Calcd for $C_{11}H_{12}O_5$: M, 224.0685.

33: A colorless oil; ^1H NMR δ=2.33 (3H, s), 2.36 (3H, s), 3.94 (3H, s), 6.59 (1H, d, J=2.2 Hz), 6.62 (1H, dd, J=10.3, 2.2 Hz), and 7.24 (1H, d, J=10.3 Hz); ^{13}C NMR δ=20.6, 21.1, 56.7, 111.3, 116.4, 127.1, 152.9, 163.9, 168.4 (2C), and 168.8 (2C); IR 1785, 1600, 1500, and 1370 cm^{-1}.

Found: m/z 252.0631. Calcd for $C_{12}H_{12}O_6$: M, 252.0631.

34: A colorless oil; ^1H NMR δ=2.29 (6H, s), 3.80 (3H, s), 6.51 (1H, d, J=2.2 Hz), 6.78 (1H, d, J=12.8 Hz), and 6.91 (1H, dd, J=12.8, 2.2 Hz).

Found: m/z 252.0633. Calcd for $C_{12}H_{12}O_6$: M, 252.0631.

The authors thank Mr. Seishi Kasai for his experimental assistance and the Ministry of Education, Science and Culture for financial support, a Grant-in-Aid for Scientific Research given to A. M. (No. 60470025).

References

1) One part of this work has been reported. See A. Mori, T. Kubota, S. Kasai, and H. Takeshita, *Chem. Lett.*, **1987**, 1931.

2) S. Itô, Y. Shoji, H. Takeshita, M. Hirama, and K. Takahashi, *Tetrahedron Lett.*, **1975**, 1075.

3) M. Hirama and S. Itô, *Tetrahedron Lett.*, **1975**, 1071.

4) A. Mori and H. Takeshita, *Kyushu Daigaku Sogo Rikogaku Kenkyuka Hokoku*, **3**, 125 (1982).

5) A. Mori, Y. Isayama, T. Kusaba, and H. Takeshita, *Kyushu Daigaku Sogo Rikogaku Kenkyuka Hokoku*, **6**, 185

(1985).

6) H. Takeshita, A. Mori, and Y. Isayama, *Bull. Chem. Soc. Jpn.*, **58**, 1678 (1985).

7) A. Mori, Y. Isayama, and H. Takeshita, *Bull. Chem. Soc. Jpn.*, **59**, 511 (1986).

8) J. F. Bagli, T. Bogri, B. Palameta, and M. St-Jacques, *Can. J. Chem.*, **57**, 1949 (1979).

9) H. Takeshita, A. Mori, Y. Goto, and T. Nagao, *Bull. Chem. Soc. Jpn.*, **60**, 1747 (1987).

10) In 3-ethoxycyclohexenone, the C-2 carbon appeared at δ 102.7 and the C-3 at δ 176.8. See G. R. Bedford and P. J. Taylor, *Org. Magn. Reson.*, **9**, 49 (1977).

11) S. Masamune, A. V. Kemp-Jones, J. Green, D. L. Rabenstein, M. Yasunami, K. Takase, and T. Nozoe, *J. Chem. Soc., Chem. Commun.*, **1973**, 283; H. Takeshita, A. Mori, H. Watanabe, T. Kusaba, S. Sugiyama, and M. Kodama, *Bull. Chem. Soc. Jpn.*, **60**, 4335 (1987).

12) Due to the 1,9-sigmatropy generally operative in 2-acetoxytropones,[11b] the first priority for the numberings of carbons should be given to the acetoxyl group adjacent to the C-1 carbonyl (like the hydroxyl in tropolones). Then, **33** should be designated as 2,5-diacetoxy-3-methoxytropone, regardless of its tautomeric contribution.

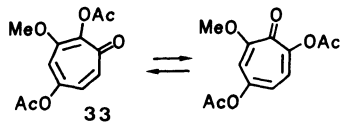

33

13) A. Nilsson, U. Palmquist, T. Pettersson, and A. Ronlan, *J. Chem. Soc., Perkin Trans. 1*, **1978**, 708.

14) M. G. Dolson and J. S. Swenton, *J. Am. Chem. Soc.*, **103**, 2361 (1981).

15) A. Mori, M. Kasuga, and H. Takeshita, *Kyushu Daigaku Sogo Rikogaku Kenkyuka Hokoku*, **8**, 195 (1987).

 © 1988 The Chemical Society of Japan Bull. Chem. Soc. Jpn., 61, 3973—3982 (1988)

Generation of Sulfur-Functionalized Nitrile Oxide, (Phenylthio)-acetonitrile Oxide, and Synthetic Applications

Shuji KANEMASA,* Yasumasa NORISUE, Hiroyuki SUGA, and Otohiko TSUGE*
Institute of Advanced Material Study, and Department of Molecular Science and Technology,
Interdisciplinary Graduate School of Engineering Sciences,
Kyushu University, Kasugakoen, Kasuga 816
(Received June 1, 1988)

The first generation of a new sulfur-functionalized nitrile oxide 1,3-dipole, (phenylthio)acetonitrile oxide, is presented. Its cycloadditions to a variety of olefins and acetylenes lead to 3-(phenylthiomethyl)-2-isoxazolines and -oxazoles, the formers being selectively deprotonated at the carbon substituted by the sulfur moiety. The resulting sulfur-stabilized carbanions react with aldehydes, esteric Michael acceptors, and alkyl halides to enable the introduction of a carbon substituent to the side chain on 3-position. Raney Ni reduction of these 2-isoxazolines gives β,β'-dihydroxy ketones and β-hydroxy ketones.

A phosphorus-functionalized nitrile oxide, (diethoxyphosphinyl)acetonitrile oxide, was first prepared in our laboratory[1] and its synthetic versatility is now gradually established.[2-4] Advantages of the phosphorus-functionalized nitrile oxide in organic synthesis are that 1) its cycloadditions to olefins or acetylenes regioselectively lead to 3-(phosphinylmethyl)-2-isoxazolines or -oxazoles bearing a variety of substituents at the 5-position, 2) these heterocycles can be converted into 3-[1-(diethoxyphosphinyl)alkyl], 3-(1-alkenyl), and 3-acyl derivatives via the phosphorus-stabilized carbanions, 3) the phosphorus moiety of the cycloadducts can survive intact on their reductive cleavage of the nitrogen–oxygen bond with Raney Ni to afford 4-hydroxy-2-oxoalkylphosphonates which undergo Horner–Emmons olefinations under mild conditions.

A sulfur-functionalized nitrile oxide, (phenylthio)-acetonitrile oxide, is an additional example for the family of α-functionalized nitrile oxides. Its synthetic applications would be characterized by its cycloadditions with olefins or acetylenes leading to 3-(phenylthio)-substituted 2-isoxazolines or isoxazoles and the generation of sulfur-stabilized carbanions followed by the subsequent reactions with electrophiles. The most characteristic advantage would be that reductive cleavage of the nitrogen–oxygen bond and elimination of the sulfur moiety can be carried out in one step.[5]

The present paper presents the first preparation of a sulfur-functionalized nitrile oxide, (phenylthio)acetonitrile oxide, and its synthetic application.

Results and Discussion

Generation of (Phenylthio)acetonitrile Oxide. Two routes were examined for the generation of (phenylthio)acetonitrile oxide (**3**). One consists of the direct oxidation of (phenylthio)acetaldehyde oxime (**2**) with sodium hypochlorite–triethylamine in dichloromethane (Scheme 1). As oxime **2** (syn:anti=4:5 by ^{1}H NNR; 91% from **1**) can be readily prepared in quantities and in a good yield from commercially available bromoacetaldehyde diethyl acetal via (phenylthio)acetaldehyde diethyl acetal (**1**, 95% based on the starting acetal), the rather low yield oxidation step of **2** into **3** is enough compensated. The nitrile oxide **3** is trapped, as soon as it is generated, in a 1,3-dipolar cycloaddition with an olefinic dipolarophile. This will be mentioned below.

The other route involves the Mukaiyama reaction[6] using 2-phenylthio-1-nitroethane (**5**). A mixture of the nitro compound **5** and phenyl isocyanate was heated in benzene in the presence of triethylamine and an olefin. The strating **5** is available from 2-nitroethanol via 1-bromo-2-nitroethane (**4**), however this preparation involves the use of rather expensive and difficult-to-handle 2-nitroethanol and the poor yield of **4**.[7]

The bromination of oxime **3** with *N*-bromosuccinimide (NBS)[8] or the chlorination with *N*-chlorosuccinimide (NCS) followed by the dehydrohalogenation with triethylamine failed to generate nitrile oxide **3**.

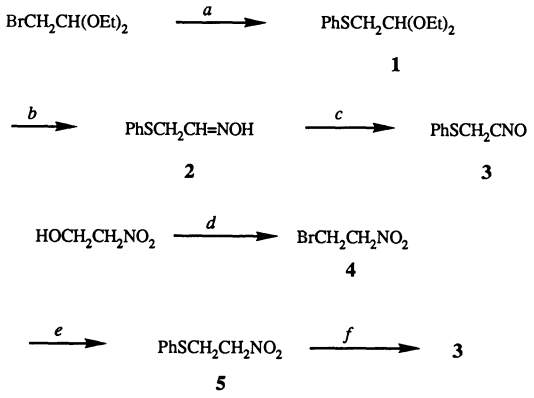

a: NaOEt in EtOH, *b*: NH_2OH HCl in EtOH, 50 °C, *c*: $NaOCl/NEt_3$ in dichloromethane, *d*: PBr_3 in diethyl ether, 0 °C, *e*: PhSH/Na in THF, *f*: $PhNCO/NEt_3$ in benzene

Scheme 1.

Cycloadditions of (Phenylthio)acetonitrile Oxide to Olefins and Acetylenes. Efficiency in the generation of (phenylthio)acetonitrile oxide (**3**) from the above two precursors, oxime **2** and nitro compound **5**, was evaluated in the trapping reactions of **3** with olefinic dipolarophiles. An equimolar mixture of oxime **2** and *N*-(*p*-tolyl)maleimide in dichloromethane was treated with 5% aqueous sodium hypochlorite (3 equiv) and a catalytic amount of triethylamine in benzene at room temperature for 4 h. After chromatographic purification, the expected 2-isoxazoline **6a** was obtained in 65% yield based on **2** (Scheme 2 and Table 1, Entry 1).

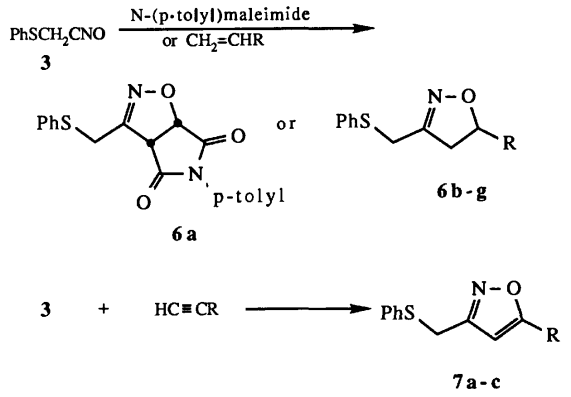

Scheme 2.

The generation step of nitrile oxide **3** from oxime **2** was, first of all, optimized in its cycloaddition reaction with *N*-(*p*-tolyl)maleimide as a highly reactive dipolarophile. Employment of a phase-transfer catalyst (Entry 6) did not improve the yield of **6a**; replacement of aqueous hypochlorite with the sodium hypochlorite supported on Celite 545[9] failed to generate nitrile oxide **3** (Entry 7). The use of 3 equivalents of aqueous sodium hypochlorite at room temperature (Entry 5) gave the best yield of **6a** (compare with Entries 1—3 and 8—10).

Trapping experiments of nitrile oxide **3** with other olefinic dipolarophiles were performed under the conditions which gave the best yield of **6a** (Table 1, Entry 5). Nitrile oxide **3** could be regioselectively trapped with electron-deficient olefins, 1-alkenes, and electron-rich olefins to produce 5-substituted 3-(phenylthiomethyl)-2-isoxazolines **6b—g** (Scheme 2 and Table 2, Entries 2, 4, 6—8, and 10). Similar

Table 1. Generation of (Phenylthio)acetonitrile Oxide **3** from Oxime **2** and Its Trapping with *N*-(*p*-Tolyl)maleimide Leading to **6a**

Entry	NaOCl (equiv)[a]	Condition[b]	Yield/%[c]
1	1	rt, 18 h	27
2	2	0°C, 1 h→rt, 1.5 h	33
3	3	0°C, 1 h→rt, 4 h	46
4	3	0°C, 5 min→rt, 17 h	51
5	3	rt, 4 h	65
6	3[d]	rt, 4 h	61
7	3[e]	rt, 4 h	0
8	5	rt, 5 h	48
9	5	reflux, 5 h	40
10	7	0°C, 5 min→rt, 5 h	47

a) Aqueous solution was used (5%). b) To an equimolar mixture of oxime **3**, and *N*-(*p*-tolyl)maleimide in dichloromethane were added NaOCl and a catalytic amount of triethylamine. The resulting mixture was allowed to react under the conditions listed above. c) Yield of isolated **6a** based on **2**. d) A catalytic amount of tetrabutylammonium hydrogensulfate was used as a phase transfer catalyst. e) NaOCl supported on Celite 545 was used in ethyl acetate.

Table 2. Generation and Cycloaddition of (Phenylthio)acetonitrile Oxide **3**

Entry	Precursor	Dipolarophile (equiv)	Condition[a]	Time/h	Product	R	Yield/%[b]
1	**2**	*N*-(*p*-Tolyl)maleimide (1)	A, rt	5	**6a**	—	65
2	**2**	Styrene (5)	A, rt	5	**6b**	Ph	52
3	**5**	Styrene (2.5)	B, rt→reflux	1→4	**6b**		90
4	**2**	Methyl acrylate (1.2)	A, rt	5	**6c**	COOMe	43
5	**5**	Methyl acrylate (2)	B, rt→reflux	1→4	**6c**		78
6	**2**	3-Buten-2-one (2)	A, rt	5	**6d**	COMe	46
7	**2**	3-Butenenitrile (1.5)	A, rt	4	**6e**	CH_2CN	22
8	**2**	1-Heptene (5)	A, rt	5	**6f**	*n*-C_5H_{11}	39
9	**5**	1-Heptene (2)	B, rt→reflux	1→4	**6f**		57
10	**2**	Vinyl acetate (5)	A, rt	5	**6g**	OCOMe	41
11	**2**	Methyl propiolate (2)	C, reflux	4	**7a**	COOMe	17
12	**2**	2-Propyn-1-ol (2)	C, reflux	4	**7b**	CH_2OH	21
13	**2**	3-Chloropropyne (2)	C, reflux	4	**7c**	CH_2Cl	15
14	**5**	3-Chloropropyne (2)	B, rt→reflux	1→4	**7c**		54

a) A: NaOCl (3 equiv)-NEt_3 (0.1 equiv) in dichloromethane; B: PhNCO (2 equiv)-NEt_3 (cat.) in benzene; C: NaOCl (2.5 equiv)-NEt_3 (0.25 equiv) in dichloromethane. b) Yield of isolated product based on **2** or **5**.

cycloadditions to electron-deficient acetylenes and 1-alkynes gave isoxazoles **7a—c** as single regioisomers, albeit in low yields (Scheme 2 and Table 2, Entries 11—13).

The relatively low yield formation of **6** and **7** mentioned above is apparently due to the poor efficiency in the generation step of **3** from **2** since the same nitrile oxide **3** undergoes a high-yield cycloaddition (90%) to styrene when generated by the dehydration of **5** with phenyl isocyanate (Table 2, Entry 3). In all the attempted cases the generation of **3** from **5** is much more effective than the generation from **2** (Entries 3, 5, 9, and 14).

Reactions of the Carbanions of 3-(Phenylthiomethyl)-2-isoxazolines with Electrophiles. The phenylthio functionality of 2-isoxazolines **6** would permit the selective deprotonation at the position adjacent to the sulfur moiety rather than 4-position.[10] Accordingly the styrene adduct **6b** as an example was deprotonated with lithium diisopropylamide (LDA) and the resulting anion was captured with aromatic and aliphatic aldehydes. Thus excellent yields of adducts **8a—d** were obtained as mixtures of diastereomers when the anions were treated with three equivalents of aldehydes (Scheme 3 and Table 3, Entries 1—4).

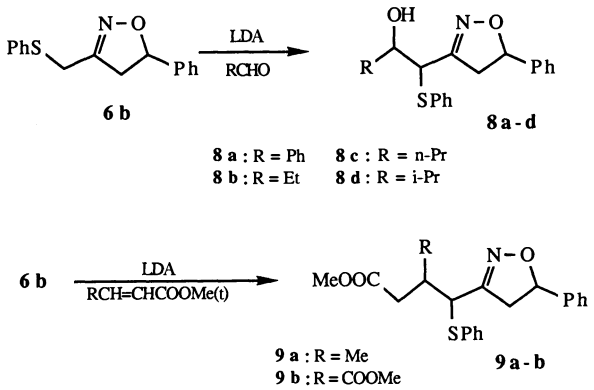

Scheme 3.

Although Michael additions of the carbanion derived from **6b** with methyl crotonate as an acceptor did not take place at −78 °C in THF, the presence of hexamethylphosphoric triamide (HMPA, 1.2 equiv) highly accelerated the addition reaction. Thus the Michael adducts **9a,b** were produced, as mixtures of diastereomers, in the reactions with methyl crotonate and dimethyl fumarate (Scheme 3 and Table 3, Entries 5,6). Use of 3-buten-2-one as a Michael acceptor led to a mixture of complex products with the 53% recovery of **6b**. Presumably the olefin acceptor underwent a base-catalyzed polymerization under the above basic conditions.

The carbanion of 2-isoxazoline **6b** was similarly alkylated at −78 °C in the presence of HMPA (Scheme 4 and Table 3). Not only alkyl iodides (Entries 7,8) but also alkyl bromides could be employed as well (Entries 9—11). Especially methylation, benzylation, and allylation were effective. On the other hand, the carbanion derived from methyl 2-isoxazoline-5-carboxylate **6c** could not be smoothly alkylated with methyl iodide, the starting **11** being partly recovered (44%). Accordingly the ester **6c** was first hydrolyzed quantitatively by aqueous lithium hydroxide in *t*-

Table 3. Reactions of the Carbanions of 2-Isoxazolines **6** and **11** with Electrophiles

Entry	2-Isoxazoline	Electrophile (equiv)	Condition[a]	Time/h	Product	Yield/%[b]
1	**6b**	PhCHO (3)	A	1	**8a**	85
2	**6b**	EtCHO (3)	A	1	**8b**	86
3	**6b**	*n*-PrCHO (3)	A	1	**8c**	99
4	**6b**	*i*-PrCHO (3)	A	1	**8d**	92
5	**6b**	Methyl crotonate (1.2)	B	2	**9a**	86
6	**6b**	Dimethyl fumarate (1.2)	B	2	**9b**	45
7	**6b**	MeI (2)	B	2	**10a**	91
8	**6b**	EtI (3)	B	2	**10b**	67[c]
9	**6b**	*i*-BuBr (1.2)	C	4	**10c**	47[d]
10	**6b**	$PhCH_2Br$ (1.2)	C	2	**10d**	92
11	**6b**	$CH_2=CHCH_2Br$ (1.2)	D	2	**10e**	77
12	**11**	MeI (2)	E	3	**12a**	82
13	**11**	EtI (1.2)	E	24	**12b**	32[e]
14	**11**	*n*-$C_5H_{11}Br$ (1.5)	E	8	**12c**	49[f]
15	**11**	7-Iodo-2-heptanone ethylene acetal (1.2)	E	48	**12d**	35[g]
16	**6b**	$Br(CH_2)_2Br$ (4)	E	2	**13a**	35[h]
17	**6b**	$Br(CH_2)_4Br$ (3)	E	2	**13b**	77
18	**6b**	$Br(CH_2)_5Br$ (2)	E	2	**13c**	74

a) A—D: The carbanion of **6b** was generated by treating with LDA (1.2 equiv) in THF at −78 °C. After an electrophile was added, the reaction was continued at −78 °C in the absence (Condition A) or presence of HMPA (B: 1.2 equiv; C: 5.7 equiv; D: 11.5 equiv). E: The carbanion of **6b** or **11** was generated by treating with LDA (2.2—2.4 equiv) in THF at −78 °C. After an electrophile and HMPA (11.5 equiv) were added, the reaction was continued at −78 °C. b) Yield of isolated products. c) Recovered **6b**: 27%. d) Recovered **6b**: 40%. e) Recovered **11**: 30%. f) Recovered **11**: 34%. g) Recovered **11**: 17%. h) Recovered **6b**: 41%.

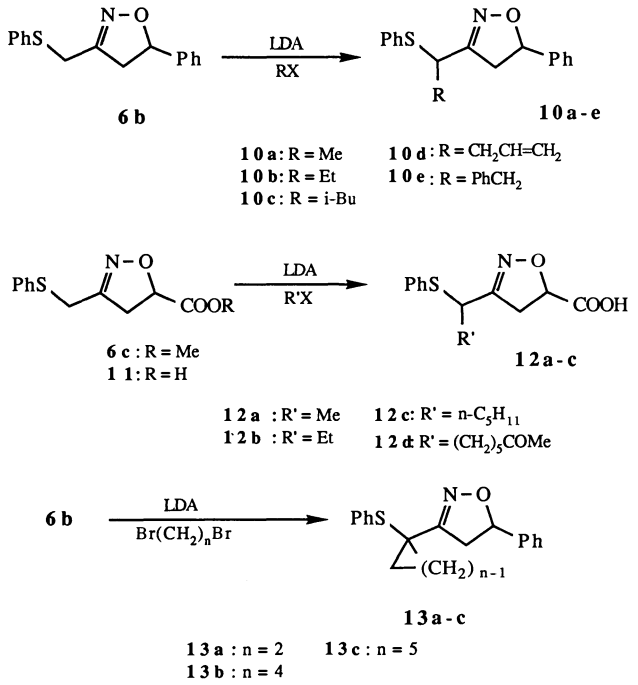

Scheme 4.

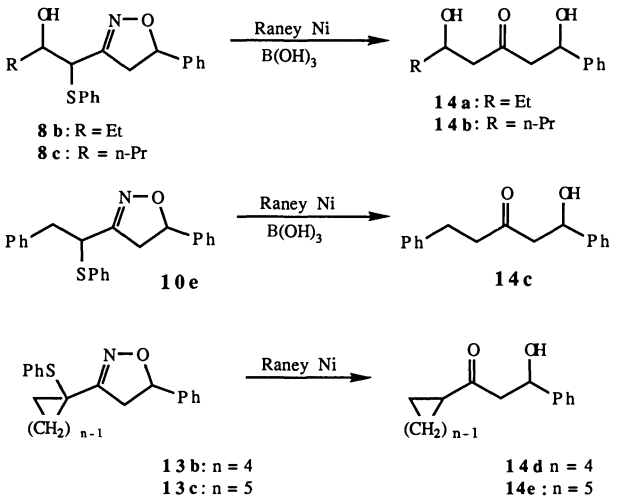

Scheme 5.

butyl alcohol and the resulting acid **11** was used for alkylation. The acid **11** was converted into the dianion with a little excess than two equivalents of LDA and then alkylations with several alkyl halides were performed to give moderate to good yields of alkylated acids **12a—d** (Entries 12—15). In the alkylation with 7-iodo-2-heptanone ethylene acetal, the dioxolane protecting group was cleaved on the usual acidic work up to give **12d**.

Alkylations of **6b** with 1,2-dibromoethane, 1,4-dibromobutane, and 1,5-dibromopentane in the presence of more than two equivalents of LDA produced 3-[1-(phenylthio)cycloalkyl]-2-isoxazolines **13a—c** (Entries 16—19).

Raney Ni Reduction of 2-Isoxazolines Leading to β-Hydroxy Ketones. It was anticipated that the sulfur moiety of 3-[1-(phenylthio)alkyl]-2-isoxazolines would be concurrently removed on the reductive cleavage of the nitrogen–oxygen bond with Raney Ni.[5] This desulfurization must be particularly important in the synthetic applications of sulfur-functionalized nitrile oxide **3** since the sulfur functionality can serve as a side chain-activating group through a sequence of deprotonation and reactions with nucleophiles.

Aldehyde adducts **8b,c** were treated with Raney Ni in aqueous ethanol in the presence of boric acid to give β,β′-dihydroxy ketones **14a,b** as mixtures of two diastereomers of desulfurized products, respectively (Scheme 5). Alkylated 2-isoxazolines **10e** and **13b,c** were similarly reduced to produce the corresponding β-hydroxy ketones **14c—e**.

Although sulfur-functionalized nitrile oxides are quite rare,[11] organic synthesis using 3-sulfinyl-2-isoxazolines has been recently reported.[5] These isoxazolines could be prepared in an optically pure form by treatment of 3-lithiomethyl-2-isoxazolines with a chiral sulfinate after separation of two diastereomers. Though the cycloadducts of our nitrile oxide **3** are synthetically equivalent to these precedents, one advantage is that a variety of functionalities can be introduced at the 5-position of 2-isoxazoline ring by use of **3**.[12]

Experimental

General. Melting points were determined on a Yanagimoto melting point apparatus and are uncorrected. IR spectra were taken with a JASCO IRA-1 or a JASCO A-702 spectrometer. ^{1}H NMR spectra were recorded on a Hitachi R-40 (90 MHz), a JEOL FX-100 (100 MHz), or a JEOL GSX-270 (270 MHz) instrument and ^{13}C NMR on a JEOL FX-100 (25.05 MHz) or a GSX-270 spectrometer (67.94 MH). Chemical shifts are expressed in parts per million downfield from tetramethylsilane as an internal standard. Mass spectra were measured with a JEOL-01SG-2 spectrometer at 70 eV of ionization energy. High-resolution mass spectra were obtained on the same instrument. Elemental analyses were performed on a Hitachi 026 CHN analyzer. Thin-layer chromatography (TLC) was accomplished on 0.2 mm precoated plates of silica gel 60 F-254 (Merck). Visualization was made with ultraviolet light (254 and 365 nm), iodine, molybdophosphoric acid (5% in ethanol), or *p*-anisaldehyde (5% in ethanol containing 5% of sulfuric acid). For preparative column chromatography, Wakogel C-200, C-300 (Wako), and Silicagel 60 (Merck) were employed.

(Phenylthio)acetaldehyde Diethyl Acetal (1). To a solution of sodium ethoxide (20.4 g, 0.30 mol) in dry ethanol (90 ml) was added thiophenol (33.0 g, 0.30 mol). After the mixture was stirred at room temperature for 0.5 h, bromoacetaldehyde diethyl acetal (68.43 g, 0.33 mol) was added in a period of 1.5 h. The mixture was stirred for 22 h, poured into water (80 ml), and extracted with diethyl ether (100 ml×2). The combined extracts were dried over magnesium sulfate and evaporated in vacuo. The residue

was subjected to vacuum distillation to give **1** (64.95 g, 95%): Colorless liquid; bp 103—104 °C/106 Pa; ^{1}H NMR ($CDCl_3$) δ=1.18 (6H, t, J=7.0 Hz, Me), 3.13 (2H, d, J=5.4 Hz, SCH_2), 3.32—3.81 (4H, m, OEt), 4.61 (1H, t, J=5.4 Hz, CH), and 7.06—7.42 (5H, m, Ph); ^{13}C NMR ($CDCl_3$) δ=15.24 (q, Me), 37.53 (t, SCH_2), 62.24 (t, OEt), 102.01 (d, CH), 126.24, 129.07, 129.54 (each d), and 136.72 (s); MS m/z (rel intensity, %) 226 (M^+, 5), 135 (47), 123 (58), 109 (35), 103 (59), 77 (Ph, 34), 75 (66), 65 (30), 51 (35), 47 (base peak), 45 (63), 43 (24), and 39 (21). Found: C, 63.63; H, 7.94%. Calcd for $C_{12}H_{18}O_2S$: C, 63.68, H, 8.02%.

(Phenylthio)acetaldehyde Oxime (2). To a solution of acetal **1** (10.0 g, 44.25 mmol) in ethanol (60 ml) was added aqueous hydroxylamine hydrochloride (3.38 g, 48.67 mmol in 30 ml of water). This mixture was stirred at 50 °C for 5 h and the ethanol was evaporated in vacuo. From the resulting aqueous solution products were extracted with dichloromethane (30 ml×2). The combined extracts were dried over magnesium sulfate and evaporated in vacuo. The residue was chromatographed over silica gel with hexane-ethyl acetate (5:1 v/v) to give oxime **2** (6.69 g, 91%) as a 4:5 mixture of syn and anti isomers: Pale yellow viscous oil; IR (neat) 3000 and 1570 cm^{-1}; ^{1}H NMR ($CDCl_3$) δ=3.53 (1H, d, J=6.5 Hz, one of SCH_2), 3.75 (1H, d, J=5.8 Hz, the other of SCH_2), 6.74 (4/9H, t, J=5.8 Hz, CH (syn)), 7.08—7.50 (6H, m, Ph and CH (anti)), and 8.90 (1H, br s, OH); ^{13}C NMR ($CDCl_3$) δ=26.95 (t, SCH_2 (syn)), 32.88 (t, SCH_2 (anti)), 126.72, 127.19, 129.18, 129.42, 130.77 (each d), 134.30, 135.01 (each s), 148.01, and 148.66 (each d); MS m/z (rel intensity, %) 167 (M^+, 21), 123 (49), 110 (71), 109 (base peak), 104 (21), 77 (54), 69 (50), 66 (24), 65 (86), 63 (22), 51 (91), 50 (41), 45 (85), and 39 (77). HRMS Found: m/z 167.0404. Calcd for C_8H_9NOS: M, 167.0399.

General Procedure for the Generation of Nitrile Oxide 3 from Oxime 2 and Its Cycloadditions with Olefins Leading to 6a—g. To a solution of oxime **2** (0.167 g, 1 mmol) and an olefin (1 to 5 mmol) in dichloromethane (20 ml) was added slowly an aqueous solution of soduim hypochlorite (5%, 4.47 g, 3 mmol) and triethylamine (0.01 g, 0.1 mmol). The mixture was stirred at room temperature for 4 to 5 h, poured into ice water (30 ml), and extracted with dichloromethane (20 ml×2). The combined extracts were dried over magnesium sulfate and evaporated in vacuo. The residue was chromatographed over silica gel by using hexane-ethyl acetate as an eluent to give cycloadduct **6**. The ratios of hexane-ethyl acetate employed are as follows: **6a**, **6c**, **6d**: 4:1 v/v; **6b**: 20:1 v/v; **6e**: 1:1 v/v; **6f**: 10:1 v/v; **6g**: 6:1 v/v. Yields of **6**, molar amounts of the olefin used, and reaction times are summarized in Table 2.

6a: Colorless needles (ethyl acetate-hexane); mp 129—130 °C; IR (KBr) 1700 and 1570 cm^{-1}; ^{1}H NMR ($CDCl_3$) δ=2.34 (3H, s, Me), 3.75 (1H, d, J=14.5 Hz, one of SCH_2), 4.63 (1H, d, J=14.5 Hz, the other of SCH_2), 5.29 (1H, d, J=9.5 Hz, 4-H), 5.29 (1H, d, J=9.5 H, 5-H), and 7.00—7.44 (9H, m, Ph); ^{13}C NMR ($CDCl_3$) δ=21.24 (q, Me), 29.30 (t, SCH_2), 54.89 (d, 4-C), 79.59 (d, 5-C), 126.07, 127.77, 128.30, 129.54, 130.13, 130.78 (each d), 133.66, 139.60 (each s), 152.01 (s, 3-C), 170.30, and 171.48 (each s, C=O); MS m/z (rel intensity, %) 352 (M^+, 81), 187 (26), 162 (22), 146 (24), 133 (56), 132 (45), 130 (24), 109 (base peak), 104 (39), 91 (51), 78 (33), 77 (58), 69 (20), 65 (68), 52 (50), 51 (50), 45 (47), and 39 (34). Found: C, 64.66; H, 4.67; N, 8.12%. Calcd for $C_{19}H_{16}N_2O_3S$: C, 64.76; H, 4.58; N, 7.95%.

6b: Yellow oil; IR (neat) 1580 cm^{-1}; ^{1}H NMR ($CDCl_3$) δ=2.94 (1H, dd, J=8.3 and 17.0 Hz, one of 4-H), 3.37 (1H, dd, J=11.0 and 17.0 Hz, the other of 4-H), 3.67 (1H, d, J=14.7 Hz, one of SCH_2), 3.87 (1H, d, J=14.7 Hz, the other of SCH_2), 5.45 (1H, dd, J=8.3 and 11.0 Hz, 5-H), and 7.02—7.38 (10H, m, Ph); ^{13}C NMR ($CDCl_3$) δ=30.76 (t, SCH_2), 43.55 (t, 4-C), 82.32 (d, 5-C), 125.88, 127.15, 128.17, 129.24, 130.33 (each d), 134.18, 141.02 (each s), and 155.83 (s, 3-C); MS m/z (rel intensity, %) 269 (M^+, 4), 125 (74), 109 (21), 97 (35), 76 (base peak), 51 (63), and 50 (25). HRMS Found: m/z 269.0875. Calcd for $C_{16}H_{15}NOS$: M, 269.0874.

6c: Yellow oil; IR (neat) 1740 and 1585 cm^{-1}; ^{1}H NMR ($CDCl_3$) δ=3.28 (2H, d, J=9.0 Hz, 4-H), 3.67 (3H, s, Me of COOMe), 3.77 (2H, s, SCH_2), 4.92 (1H, t, J=9.0 Hz, 5-H), and 7.13—7.40 (5H, m, Ph); ^{13}C NMR ($CDCl_3$) δ=30.47 (t, SCH_2), 39.53 (t, 4-C), 52.71 (q, COOMe), 77.77 (d, 5-C), 127.36, 129.30, 130.42 (each d), 134.13 (s), 155.71 (s, 3-C), and 170.66 (s, C=O); MS m/z (rel intensity, %) 251 (M^+, 20), 123 (46), 109 (68), 77 (34), 69 (23), 65 (50), 59 (base peak), 54 (23), 51 (47), 44 (57), and 38 (36). HRMS Found: m/z 251.0617. Calcd for $C_{12}H_{13}NO_3S$: M, 251.0615.

6d: Yellow oil; IR (neat) 1720 and 580 cm^{-1}; ^{1}H NMR ($CDCl_3$) δ=1.04 (3H, s, Me), 3.18 (1H, d, J=11.0 Hz, one of 4-H), 3.20 (1H, d, J=7.2 Hz, the other of 4-H), 3.66 (1H, d, J=16.0 Hz, one of SCH_2), 3.84 (1H, d, J=16.0 Hz, the other of SCH_2), 4.75 (1H, dd, J=11.0 and 7.2 Hz, 5-H), and 7.12—7.39 (5H, m, Ph); ^{13}C NMR ($CDCl_3$) δ=25.94 (q, Me), 30.47 (t, SCH_2), 37.94 (t, 4-C), 84.06 (d, 5-C), 127.42, 129.30, 130.60 (each d), 133.83 (s), 156.01 (s, 3-C), and 207.66 (s, C=O); MS m/z (rel intensity, %) 235 (M^+, 11), 123 (67), 109 (32), 77 (27), 65 (27), 51 (28), 45 (33), 43 (base peak), and 39 (20). HRMS Found: m/z 235.0665. Calcd for $C_{12}H_{13}NO_2S$: M, 235.0666.

6e: Yellow viscous oil; ^{1}H NMR ($CDCl_3$) δ=2.37 (1H, d, J=6.0 Hz, one of CH_2CN), 2.39 (1H, d, J=5.5 Hz, the other of CH_2CN), 2.84 (1H, dd, J=6.0 and 17.2 Hz, one of 4-H), 3.23 (1H, dd, J=10.0 and 17.4 Hz, the other of 4-H), 3.72 (1H, d, J=17.2 Hz, one of SCH_2), 3.86 (1H, ddd, J=6.0, 6.0, and 5.5 Hz, 5-H), and 7.14—7.43 (5H, m, Ph); ^{13}C NMR ($CDCl_3$) δ=23.18 (t, CH_2CN), 30.53 (t, SCH_2), 40.47 (t, 4-C), 75.54 (d, 5-C), 116.36 (s, CN), 127.54, 129.48, 130.54 (each d), 133.95 (s), and 156.12 (s, 3-C); MS m/z (rel intensity, %) 232 (M^+, base peak), 164 (21), 163 (35), 162 (25), 130 (40), 123 (44), 109 (78), 77 (30), 65 (46), 54 (38), 51 (29), 45 (37), and 39 (28). HRMS Found: m/z 232.0666. Calcd for $C_{12}H_{12}N_2OS$: M, 232.0669.

6f: Colorless needles (ethyl acetate-hexane); mp 32—33 °C; IR (KBr) 1575 cm^{-1}; ^{1}H NMR ($CDCl_3$) δ=0.85 (3H, t, J=6.0 Hz, Me), 1.02—1.68 (8H, m, CH_2 of n-C_5H_{11}), 2.61 (1H, dd, J=8.2 and 7.0 Hz, one of 4-H), 3.02 (1H, dd, J=10.1 and 17.0 Hz, the other of 4-H), 3.67 (1H, d, J=14.5 Hz, one of SCH_2), 3.85 (1H, d, J=14.5 Hz, the other of SCH_2), 4.28—4.65 (1H, m, 5-H), and 7.10—7.42 (5H, m, Ph); ^{13}C NMR ($CDCl_3$) δ=14.00 (q, Me), 22.47, 24.94, 31.00, 31.59, 35.00 (each t, CH_2 of n-C_5H_{11}), 40.41 (t, 4-C), 81.36 (d, 5-C), 127.01, 129.24, 130.07 (each d), 134.66 (s), and 155.71 (s, 3-C); MS m/z (rel intensity, %) 263 (M^+, 72), 192 (base peak), 130 (21), 123 (51), 110 (29), 109 (42), 77 (45), 64 (22), 56 (21), 55 (29), 44 (29), 40 (36), and 38 (20). Found: C, 68.35; H, 7.95; N, 5.24%. Calcd for $C_{15}H_{21}NOS$: C, 68.40; H, 8.04; N, 5.32%.

6g: Yellow oil; IR (neat) 1740 and 1580 cm^{-1}; ^{1}H NMR ($CDCl_3$) δ=1.96 (3H, s, Me), 2.96 (1H, dd, J=1.5 and 18.0 Hz, one of 4-H), 3.26 (1H, dd, J=6.2 and 18.0 Hz, the other of 4-H), 3.81 (2H, s, SCH_2), 6.55 (1H, dd, J=1.5 and 6.2 Hz, 5-H), and 7.14—7.43 (5H, m, Ph); ^{13}C NMR ($CDCl_3$) δ=20.94

(q, Me), 30.59 (t, SCH_2), 41.83 (t, 4-C), 95.83 (d, 5-C), 127.60, 129.36, 130.83 (each d), 133.83 (s), 156.89 (s, 3-C), and 169.72 (s, C=O); MS *m/z* (rel intensity, %) 251 (M^+, 43), 163 (28), 123 (29), 109 (25), 45 (22), and 43 (base peak). HRMS Found: *m/z* 251.0610. Calcd for $C_{12}H_{13}NO_3S$: M, 251.0615.

General Procedure for the Cycloadditions of Nitrile Oxide 3 Generated from Oxime 2 with Acetylenes Leading to 7a—c. To a solution of oxime **2** (0.334 g, 2 mmol) and acetylene (3 mmol to 4 mmol) in dichloromethane (15 ml) was added slowly an aqueous solution of sodium hypochlorite (5%, 7.45 g, 5 mmol) and triethylamine (0.051 g, 0.5 mmol). The mixture was stirred at 50 °C for 4 h, poured into water (15 ml), and extracted with dichloromethane (20 ml×2). The combined extracts were dried over magnesium sulfate and evaporated in vacuo. The residue was chromatographed over silica gel by using hexane–ethyl acetate to give cycloadduct **7**. The ratios of hexane–ethyl acetate employed as eluents are as follows: **7a**: 50:1 v/v; **7b**: 2:1 v/v **7c**: 100:1 v/v. Yields of **7**, molar amounts of the acetylene used, and reaction times are summarized in Table 2.

7a: Colorless needles (diethyl ether–hexane); mp 39—40 °C; ^{1}H NMR ($CDCl_3$) δ=3.87 (3H, s, Me), 4.10 (2H, s, SCH_2), 6.86 (1H, s, 4-H), and 7.12—7.40 (5H, m, Ph); ^{13}C NMR ($CDCl_3$) δ=29.00 (t, SCH_2), 52.89 (q, Me), 109.42 (d, 4-C), 127.48, 129.19, 130.48 (each d), 134.13 (s), 157.25 (s, C=O), 160.54 (s, 3-C), and 162.42 (s, 5-C); MS *m/z* (rel intensity, %) 249 (M^+, 60), 190 (base peak), 162 (22), 144 (34), 125 (26), 123 (52), 110 (22), 109 (80), 77 (69), 65 (38), 51 (50), 45 (59), and 39 (27). Found: C, 58.05; H, 4.76; N, 5.72%. Calcd for $C_{12}H_{11}NO_3S$: C, 57.82; H, 4.45; N, 5.62%.

7b: Yellow oil; ^{1}H NMR ($CDCl_3$) δ=3.58 (1H, br s, OH), 4.00 (2H, s, SCH_2), 4.56 (2H, s, CH_2OH), 6.14 (1H, s, 4-H), and 7.06—7.36 (5H, m, Ph) ^{13}C NMR ($CDCl_3$) δ=28.91 (t, SCH_2), 56.15 (t, CH_2OH), 101.76 (d, 4-C), 127.05, 129.24, 129.98 (each d), 134.77 (s), 161.57 (s, 3-C), and 172.41 (s, 5-C); MS *m/z* (rel intensity, %) 221 (M^+, 17), 190 (39), 162 (29), 144 (26), 130 (22), 123 (64), 109 (base peak), 77 (59), 69 (35), 65 (64), 53 (25), 52 (23), 51 (77), 50 (25), 45 (88), 39 (66), and 31 (69). HRMS Found: *m/z* 221.0508. Calcd for $C_{11}H_{11}NO_2S$: M, 221.0509.

7c: Pale yellow needles (diethyl ether–hexane); mp 47—48 °C; ^{1}H NMR ($CDCl_3$) δ=4.03 (2H, s, SCH_2), 4.47 (2H, s, CH_2Cl), 6.21 (1H, s, 4-H), and 7.10—7.39 (5H, m, Ph); ^{13}C NMR ($CDCl_3$) δ=29.10 (t, SCH_2), 34.47 (t, CH_2Cl), 103.71 (d, 4-C), 127.29, 129.34, 130.27 (each d), 134.66 (s), 161.96 (s, 3-C), and 168.06 (s, 5-C); MS *m/z* (rel intensity, %) 241 (M^+ +2, 16), 239 (M^+, 37), 206 (20), 198 (27), 190 (33), 162 (39), 149 (26), 145 (20), 142 (28), 123 (31), 110 (21), 109 (base peak), 76 (68), 65 (37), 45 (37), 43 (25), and 39 (27). Found: C, 55.21; H, 4.34; N, 5.74%. Calcd for $C_{11}H_{10}NOSCl$: C, 55.11; H, 4.20; N, 5.84%.

General Procedure for the Cycloadditions of Nitrile Oxide 3 Generated from 2-Phenylthio-1-nitroethane 5. To a solution of the nitro compound **5** (1.5 g, 8.2 mmol) and triethylamine (0.10 g, 1.0 mmol) in dry benzene (5 ml) was added the solution of an olefin (16.4 mmol) and phenyl isocyanate (1.95 g, 6.4 mmol). The mixture was stirred at room temperature for 1 h, and then refluxed for 4 h. The insoluble material (*N,N'*-diphenylurea) was filtered off, and the filtrate was evaporated in vacuo. The residue was chromatographed over silica gel with hexane–ethyl acetate to give cycloadduct **6** or **7**. The ratios of hexane–ethyl acetate employed are as follows: **6b**, **6f**, **7c**: 20:1 v/v; **6c**: 4:1 v/v. Yields of **6** or **7**, molar amounts of the olefin or acetylene used, and reaction times are summarized in Table 2.

General Procedure for the Addition Reactions of 2-Isoxazoline 6b with Aldehydes Leading to 8a—d. To a solution of diisopropylamine (0.242 g, 2.4 mmol) in dry THF (25 ml) was added butyllithium (15% in hexane, 1.5 ml, 2.4 mol) at −78 °C under nitrogen. After 5 min, a solution of 2- isoxazoline **6b** (0.538 g, 2 mmol) in dry THF (15 ml) was added. After 0.5 h at −78 °C, an aldehyde (6 mmol) was added. The mixture was stirred at the same temperature for 1 h, poured into saturated aqueous ammonium chloride (50 ml), and extracted with dichloromethane (40 ml×2). The combined extracts were dried over magnesium sulfate and evaporated in vacuo. The residue was chromatographed over silica gel by using hexane–ethyl acetate (10:1 v/v) as an eluent to give adduct **8**. All the adducts **8** were mixtures of more than three diastereomers (^{13}C NMR). The results are summarized in Table 3.

8a: Yellow viscous oil; IR (neat) 3400 and 1575 cm^{-1}; ^{1}H NMR ($CDCl_3$) δ=2.64—3.50 (2H, m, 4-H), 3.70 (1H, br s, OH), 4.20—4.44 (1H, m, SCH), 4.81—5.08 (1H, m, CHOH), 5.11—5.44 (1H, m, 5-H), and 6.82—7.42 (15H, m, Ph); ^{13}C NMR ($CDCl_3$) δ=43.30 (t, 4-C), 55.12, 55.36 (each d, SCH), 74.01, 74.42 (each d, CHOH), 81.89 (d, 5-C), 125.89, 126.54, 126.89, 127.07, 127.89, 128.13, 128.36, 128.54, 128.65, 129.24, 132.25, 132.54, (each d), 133.30, 133.48, 140.13, 140.60, 140.77 (each s), 157.01, 157.25, and 157.36 (each s, 3-C); MS *m/z* (rel intensity, %) 269 (M^+ −PhCHO), and 105 (22). Satisfactory elemental analysis was not available because of its instability.

8b: Yellow oil; IR (neat) 3400 and 1580 cm^{-1}; ^{1}H NMR ($CDCl_3$) δ=0.81—1.08 (3H, m, Me), 1.40—1.80 (2H, m, CH_2), 2.80—3.64 (3H, m, 4-H and OH), 3.64—3.96 (1H, m, CHOH), 3.96—4.26 (1H, m, SCH), 5.27—5.57 (1H, m, 5-H), and 6.94—7.47 (10H, m, Ph); ^{13}C NMR ($CDCl_3$) δ=9.94 (q, Me), 27.59, 27.88, 28.18 (each t, CH_2), 43.00, 43.36 (each t, 4-C), 51.42, 51.77, 53.24, 53.47 (each d, SCH_2), 72.95, 73.12, 73.53, 73.65 (each d, CHOH), 125.95, 126.13, 127.71, 127.83, 128.25, 129.30, 132.07, 132.25 (each d), 133.19, 133.42, 133.71, 140.95, 141.07 (each s), 157.77, 157.89, and 158.19 (each s, 3-C); MS *m/z* (rel intensity, %) 327 (M^+, 5), 269 (base peak), and 77 (22). HRMS Found: *m/z* 327.1288. Calcd for $C_{19}H_{21}N_2OS$: M, 327.1292.

8c: Yellow oil; IR (neat) 3400 and 1580 cm^{-1}; ^{1}H NMR ($CDCl_3$) δ=1.91 (3H, t, *J*=7.0 Hz, Me), 2.15—2.77 (4H, m, CH_2), 2.80—3.64 (3H, m, 4-H, CHOH), 3.76—4.22 (2H, m, SCH and OH), 5.30—5.58 (1H, m, 5-H), and 6.95—7.47 (10H, m, Ph); ^{13}C NMR ($CDCl_3$) δ=13.88 (q, Me), 18.88 (t, CH_2), 36.71, 37.00, 37.36, (each t, CH_2), 43.12, 43.24, 43.47 (each t, 4-C), 51.89, 52.18, 53.77, 54.00 (each d, SCH), 71.42, 71.59, 72.06 (each d, CHOH), 82.01 (d, 5-C), 125.95, 127.89, 128.25, 128.77, 129.36, 132.25 (each d), 133.13, 133.54, 133.71 (each s), 140.95, 141.07 (each s), 157.30, 157.72, 157.95, and 158.06 (each s, 3-C); MS *m/z* (rel intensity, %) 341 (M^+, 7), 269 (base peak), 126 (45), 111 (31), 110 (22), 78 (27), 77 (39), 51 (22), and 43 (30). HRMS Found: *m/z* 341.1447. Calcd for $C_{20}H_{23}NO_2S$: M, 341.1448.

8d: Yellow oil; IR (neat) 3400 and 1580 cm^{-1}; ^{1}H NMR ($CDCl_3$) δ=0.99 (6H, d, *J*=6.8 Hz, Me), 1.77—2.08 (1H, m, CH), 2.65 (1H, br s, OH), 2.90—3.77 (3H, m, 4-H, CHOH), 4.20—4.41 (1H, m, SCH), 5.47 (1H, dd, *J*=8.2 and 10.8 Hz, 5-H), and 6.97—7.44 (10H, m, Ph); ^{13}C NMR ($CDCl_3$)

δ=16.41, 17.24, 19.41, 19.94 (each q, Me), 31.36 (d, CH), 42.94, 43.30 (each t, 4-C), 49.94, 51.95 (each d, SCH), 76.48, 77.18 (each d, CHOH), 82.06 (d, 5-C), 126.01, 127.89, 128.18, 128.77, 129.36, 132.30 (each d), 133.07, 133.30, 141.13 (each s), 157.25, and 157.83 (each s, 3-C); MS *m/z* (rel intensity, %) 341 (M^+, 5), 269 (base peak), 126 (27), 111 (23), 77 (23), and 43 (23). HRMS Found: *m/z* 341.1444. Calcd for $C_{20}H_{23}NO_2S$: M, 341.1446.

General Procedure for the Michael Additions of 2-Isoxazoline 6b Leading to 9a,b. To a solution of diisopropylamine (0.121 g, 1.2 mmol) in dry THF (10 ml) was added butyllithium (15% in hexane, 0.75 ml, 1.20 mol) at −78 °C under nitrogen. After a solution of 2-isoxazoline **6b** (0.269 g, 1 mmol) in dry THF (10 ml) was added, stirring was continued at −78 °C for 0.5 h. An α,β-unsaturated ester (1.2 mmol) and HMPA (0.215 g, 1.2 mmol) were added. The mixture was stirred at the same temperature for 2 h, poured into saturated aqueous ammonium chloride (30 ml), and extracted with dichloromethane (40 ml×2). The combined extracts were dried over magnesium sulfate and evaporated in vacuo. The residue was chromatographed over silica gel by using the following eluent to give adduct **9**: **9a**: hexane-ethyl acetate (6:1 v/v); **9b**: chloroform. All the adducts **9** were mixtures of more than two diastereomers. The results are summarized in Table 3.

9a: Yellow oil; ^{1}H NMR ($CDCl_3$) δ=1.04—1.33 (3H, m, Me), 2.06—2.66 (3H, m, CH and CH_2), 2.72—3.81 (2H, m, 4-H), 3.51, 3.57 (3H, each s, CO_2Me), 3.94—4.18 (1H, m, SCH), 5.22—5.55 (1H, m, 5-H), and 6.80—7.46 (10H, m, Ph); ^{13}C NMR ($CDCl_3$) δ=18.12 (q, Me), 32.41 (t), 38.71, 39.24 (each d, SCH), 42.12 (t, 4-C), 51.36, 51.47 (each q, CO_2Me), 81.77 (d, 5-C), 125.71, 127.36, 127.89, 128.48, 129.07, 130.01, 131.71 (each d), 133.36, 133.77, 140.60, 140.95 (each s), 157.42, 157.95 (each s, 3-C), 172.25, and 172.36 (each s, C=O); MS *m/z* (rel intensity, %) 369 (M^+, base peak), 260 (67), 228 (73), 129 (23), 115 (27), 113 (30), 109 (45), 105 (25), 104 (33), 103 (30), 91 (39), 78 (20), 77 (50), 65 (29), 55 (22), 51 (22), 38 (20), and 25 (21). HRMS Found: *m/z* 369.1400. Calcd for $C_{21}H_{23}NO_3S$: M, 369.1399.

9b: Yellow oil; ^{1}H NMR ($CDCl_3$) δ=2.53—3.79 (11H, m, 4-H, CH_2, CH, and CO_2Me), 4.16—4.44 (1H, m, SCH), 5.32—5.62 (1H, m, 5-H), and 6.94—7.47 (10H, m, Ph); ^{13}C NMR ($CDCl_3$) δ=34.47 (t), 42.71, 43.30, 43.94, 47.94 (each d, SCH), 51.95, 52.36 (each q, CO_2Me), 82.30 (d, 5-C), 125.89, 128.30, 128.77, 129.42, 132.54, 132.83 (each d), 133.01, 140.77, 140.60 (each s), 156.18, 156.36 (each s, 3-C), 171.71, 171.89, 172.31, and 172.54 (each s, C=O); MS *m/z* (rel intensity, %) 413 (M^+, 37), 272 (29), 168 (22), 155 (21), 153 (20), 147 (28), 141 (29), 129 (23), 128 (43), 116 (20), 115 (42), 110 (21), 109 (base peak), 105 (36), 104 (49), 103 (33), 51 (43), and 40 (34). HRMS Found: *m/z* 413.1296. Calcd for $C_{22}H_{23}NO_5S$: M, 413.1296.

General Procedure for the Alkylations of 2-Isoxazoline 6b Leading to 10a—e. To a solution of diisopropylamine (0.121 g, 1.2 mmol) in dry THF (10 ml) was added butyllithium (15% in hexane, 0.75 ml, 1.2 mol) at −78 °C under nitrogen. A solution of 2-isoxazoline **6b** (0.269 g, 1 mmol) in dry THF (10 ml) was added. After stirring was continued for 0.5 h at −78 °C, an alkyl halide (1.2 to 3 mmol) and HMPA (1.2 mmol to 11.5 mmol) were added. The mixture was stirred at −78 °C for 2 h, poured into saturated aqueous ammonium chloride (30 ml), and extracted with dichloromethane (40 ml×2). The combined extracts were dried over magnesium sulfate and evaporated in vacuo. The residue was chromatographed over silica gel by using hexane-ethyl acetate as an eluent to give **10**. The ratios of hexane-ethyl acetate employed are as follows: **10a**: 6:1 v/v; **10b**, **10c**, and **10e**: 15:1 v/v; **10d**: 10:1 v/v. These adducts **10** were all mixtures of two diastereomers. The results are summarized in Table 3.

10a: Pale yellow oil; ^{1}H NMR ($CDCl_3$) δ=1.46, 1.47 (3H, each d, each J=7.0 Hz, Me), 2.95 (H, dd, J_{4-5}=8.5 and J=16.7 Hz, one of 4-H), 3.37 (1H, dd, J_{4-5}=11.0 and J=16.7 Hz, the other of 4-H), 4.14, 4.28 (1H, each q, J=7.0 Hz, SCH), 5.25—5.54 (1H, m, 5-H), and 6.87—7.40 (10H, m, Ph); ^{13}C NMR ($CDCl_3$) δ=18.12, 18.35 (each q, Me), 40.00, 40.41 (each d, SCH), 41.30, 41.94 (each t, 4-C), 81.89, 82.06 (each d, 5-C), 125.83, 127.66, 127.83, 128.01, 128.18, 128.65, 129.13, 132.07, 132.30 (each d), 133.42, 140.95, 141.24 (each s), 159.01, and 159.42 (each s, 3-C); MS *m/z* (rel intensity, %) 283 (M^+, 63), 174 (base peak), 156 (34), 131 (44), 129 (71), 128 (31), 126 (20), 115 (20), 110 (34), 109 (43), 104 (28), 103 (32), 91 (28), and 77 (27). HRMS Found: *m/z* 283.0980. Calcd for $C_{17}H_{17}NOS$: M, 283.1030.

10b: Pale yellow oil; ^{1}H NMR ($CDCl_3$) δ=0.95, 1.02 (3H, each t, J=7.5 Hz, Me), 1.53—1.89 (2H, m, CH_2), 2.48—3.56 (2H, m, 4-H), 3.98, 4.08 (1H, each t, J=7.0 Hz, SCH), 5.37 (1/2H, dd, J_{5-4}=8.2 and 11.0 Hz, 5-H), 5.41 (1/2H, dd, J_{5-4}=8.0 and 11.0 Hz, 5-H), and 6.83—7.44 (10H, m, Ph); ^{13}C NMR ($CDCl_3$) δ=11.82, 11.94 (each q, Me), 25.18, 25.35 (each t, CH_2), 41.06, 41.59 (each t, 4-C), 46.71, 47.12 (each d, SCH), 81.59 (d, 5-H), 125.60, 127.24, 127.42, 127.83, 127.95, 128.48, 128.60, 128.95, 131.66 (each d), 133.42, 133.60, 140.95, 141.13 (each s), 157.89, and 158.30 (each s,3-C); MS *m/z* (rel intensity, %) 297 (M^+, 4), 109 (base peak), and 77 (56). HRMS Found: *m/z* 297.1180. Calcd for $C_{18}H_{19}NOS$: M, 297.1186.

10c: Pale yellow oil; ^{1}H NMR ($CDCl_3$) δ=0.76—1.04 (6H, m, Me), 1.46—1.73 (3H, m, CH_2CH), 2.83 (1/2H, dd, J_{4-5}=8.5 and J=16.5 Hz, one of 4-H), 2.99 (1/2H, dd J_{4-5}=8.3 and J=16.5 Hz, one of 4-H), 3.29 (1/2H, dd, J_{4-5}=10.8 and J=16.5 Hz, the other of 4-H), 3.42 (1/2H, dd, J_{4-5}=10.8 and J=16.5 Hz, the other of 4-H), 4.20, 4.32 (1H, each t, each J=7.0 Hz, SCH_2), 5.35 (1/2H, dd, J_{5-4}=8.5 and 10.8 Hz, 5-H), 5.40 (1/2H, dd, J_{5-4}=8.3 and 10.8 Hz, 5-H), and 6.83—7.42 (10H, m, Ph); ^{13}C NMR ($CDCl_3$) δ=21.94, 22.41, 22.53 (each q, Me), 25.77, 25.94 (each d, *i*-Pr), 40.59, 40.77 (each t, CH_2), 41.06, 41.59 (each t, 4-C), 43.41, 43.89 (each d, SCH), 81.77, 81.89 (each d, 5-C), 125.83, 127.42, 127.60, 128.01, 128.13, 128.72, 129.13, 131.89 (each d), 133.54, 133.77, 141.01, 141.30 (each s), 158.13, and 158.71 (each s, 3-C). MS *m/z* (rel intensity, %) 325 (M^+, 22), 269 (38), 218 (27), 216 (base peak), 109 (32), 44 (43), 42 (35), and 40 (30). HRMS Found: *m/z* 325.1506. Calcd for $C_{20}H_{23}NOS$: M, 325.1499.

10d: Colorless prisms (diethyl ether); mp 110—111 °C; ^{1}H NMR ($CDCl_3$) δ=2.96 (1H, dd, J_{4-5}= 8.5 and J=17.0 Hz, one of 4-H), 3.34 (1H, dd, J_{4-5}= 10.8 and J=17.0 Hz, the other of 4-H), 3.10 (2H, d, J=8.0 Hz, CH_2), 4.41, 4.47 (1H, each t, J=8.0 Hz, SCH), 5.37 (1H, dd, J_{5-4}= 8.5 and 10.8 Hz, 5-H), and 6.84—7.38 (15H, m, Ph); ^{13}C NMR ($CDCl_3$) δ=38.43, 38.57 (each t, CH_2), 41.80, 42.09 (each t, 4-C), 46.73, 46.87 (each d, SCH), 81.98 (d, 5-C), 125.93, 127.20, 127.73, 128.12, 128.76, 129.20, 132.23 (each d), 133.30, 137.50, 141.02 (each s), and 157.66 (s, 3-C); MS *m/z* (rel intensity, %) 359 (M^+, 7), 109 (22), 91 (base peak), 77 (39), 65 (32), 51 (22), and 39 (21). Found: C, 76.70; H, 5.83; N, 4.05%. Calcd for $C_{23}H_{21}NOS$: C, 76.85, H, 5.89; N, 3.90%.

10e: Pale yellow oil; ^{1}H NMR ($CDCl_3$) δ=2.34—2.62 (2H,

m, CH_2), 2.72—3.56 (2H, m, 4-H), 4.17, 4.24 (1H, each t, J=8.0 Hz, SCH), 4.84—6.01 (4H, m, 5-H, CH_2=CH), and 6.83—7.20 (10H, m, Ph); ^{13}C NMR ($CDCl_3$) δ=36.24, 36.41 (each t), 41.41, 41.94 (each t, 4-C), 44.77, 45.12 (each d, SCH), 81.89, 82.01 (each d, 5-C), 118.18 (t,=CH_2), 125.83, 127.66, 127.83, 128.07, 128.65, 129.19, 132.13 (each d), 133.13 (s), 133.95 (d, =CH), 141.01, 141.13 (each s), 157.72, and 158.13 (each s, 3-C); MS m/z (rel intensity, %) 309 (M^+, 4), 129 (29), 128 (46), 115 (32), 109 (base peak), 105 (30), 104 (28), 103 (24), 91 (44), 77 (36), 76 (86), 69 (22), 65 (63), 53 (23), 51 (51), 41 (35), and 39 (49). HRMS Found: m/z 309.1179. Calcd for $C_{19}H_{19}NOS$: M, 309.1186.

Hydrolysis of 2-Isoxazoline-5-carboxylate 6c into 2-Isoxazoline-5-carboxylic Acid 11. To a solution of 2-isoxazoline **6a** (1 g, 4 mmol) in aqueous 2-methyl-2-propanol (50%, 20 ml) was added lithium hydroxide (monohydrate, 0.18 g, 4.2 mmol). The mixture was stirred at room temperature for 1 h, poured into water (20 ml), and washed with diethyl ether (20 ml). The pH of the aqueous layer was adjusted below 5 with 1 M hydrochloric acid, and the resulting water layer was extracted with dichloromethane (40 ml). The extract was dried over magnesium sulfate and evaporated in vacuo to give 2-isoxazoline-5-carboxylic acid **11** (0.92 g, 97%): Pale yellow solid; mp 72—73 °C; IR (KBr) 3000 and 1700 cm^{-1}; ^{1}H NMR ($CDCl_3$) δ=3.28 (1H, d, J_{4-5}=8.5 Hz, one of 4-H), 3.29 (1H, d, J_{4-5}=9.5 Hz, the other of 4-H), 3.73 (2H, s, SCH_2), 4.92 (1H, dd, J_{5-4}=8.5 and 9.5 Hz, 5-H), 7.01—7.38 (5H, m, Ph), and 9.19 (1H, s, CO_2H); ^{13}C NMR ($CDCl_3$) δ=30.47 (t, SCH_2), 39.83 (t, 4-C), 77.30 (d, 5-C), 127.66, 129.48, 130.83 (each d), 133.83 (s), 156.54 (s, 3-C), and 174.01 (s, C=O); MS m/z (rel intensity, %) 237 (M^+, 21), 192 (28), 164 (26), 130 (38), 123 (93), 109 (base peak), 76 (49), 69 (27), 65 (61), 54 (27), 51 (59), 50 (20), 45 (96), and 39 (46). Found: C, 55.46; H, 4.72; N, 5.86%. Calcd for $C_{11}H_{11}NO_3S$: C, 55.68; H, 4.67; N, 5.90%.

General Procedure for the Alkylations of 2-Isoxazoline-5-carboxylic Acid 11 Leading to 12a—c. To a solution of diisopropylamine (0.222 g, 2.2 mmol) in dry THF was added butyllithium (15% in hexane, 1.38 ml, 2.2 mmol) at −78°C under nitrogen. A solution of 2-isoxazoline **11** (0.237 g, 1 mmol) in dry THF (5 ml) was added. After 0.5 h at −78 °C, an alkyl iodide (1.2—2 mmol) and HMPA (2 ml, 11.5 mmol) were added, and the mixture was stirred for the time shown in Table 3. Saturated aqueous ammonium chloride (30 ml) was added, the mixture was acidified to pH 5 by adding 1 M hydrochloric acid, and extracted with dichloromethane (30 ml×2). The combined extracts were dried over magnesium sulfate and evaporated in vacuo. The residue was chromatographed over silica gel by using hexane–ethyl acetate containing acetic acid as an eluent to give **12**: The ratios of hexane–ethyl acetate–acetic acid employed are as follows: **12a**: 10:10:1 v/v **12b**: 50:10:3 v/v; **12c**: 15:5:1 v/v. All the alkylated 2-isoxazoline-5-carboxylic acids **12** were mixtures of two diastereomers. The results are summarized in Table 3.

12a: Yellow viscous oil; IR (neat) 2920, 1730, and 1580 cm^{-1}; ^{1}H NMR ($CDCl_3$) δ=1.48 (3H, d, J=7.0 Hz, Me), 3.35 (1H, d, J_{4-5}=8,6 Hz, one of 4-H), 3.37 (1H, d, J_{4-5}=9.0 Hz, the other of 4-H), 4.15 (1H, q, J=7.0 Hz, SCH), 4.91 (1/2H, t, J_{5-4}=8.6 Hz, 5-H), 4.96 (1/2H, J_{5-4}=9.0 Hz, 5-H), 7.12—7.44 (5H, m, Ph), and 8.32 (1H, br s, CO_2H); ^{13}C NMR ($CDCl_3$) δ=17.97, 18.36 (each q, Me), 38.04 (t, 4-C), 39.84, 40.48 (each d, SCH), 77.05 (d, 5-C), 128.22, 128.41, 129.34, (each d), 132.66 (s), 160.10 (s, 3-C), 173.83, and 173.97 (each s, C=O); MS m/z (rel intensity, %) 251 (M^+, 7), 177 (28), 150 (25), 111 (base peak), 110 (55), 66 (30), 43 (30), 41 (22), 39 (29), and 32 (21), HRMS Found: m/z 251.0605. Calcd for $C_{12}H_{13}NO_3S$: M, 251.0613.

12b: Pale yellow viscous oil; IR (neat) 3000, 1730, and 1580 cm^{-1}; ^{1}H NMR ($CDCl_3$) δ=1.02, 1.04 (3H, each t, J=7.2 Hz, Me), 1.61—1.99 (2H, m, CH_2), 3.21—3.45 (2H, m, 4-H), 3.99 (1/2H, dd, J_{5-4}=7.0 and 10.5 Hz, 5-H), 4.98 (1/2H, dd, J_{5-4}=6.6 and 10.8 Hz, 5-H), 7.09—7.43 (5H, m, Ph), and 9.81 (1H, br s, CO_2H); ^{13}C NMR ($CDCl_3$) δ=12.00 (q, Me), 25.24, 25.65 (each t, CH_2), 37.71, 37.83, (each t, 4-C), 46.65, 47.42 (each d, SCH), 76.83, 77.01 (d, 5-C), 127.89, 128.25, 129.30, 132.07, 132.95 (each d), 133.19 (s), 159.18, 159.36 (each s, 3-C), and 174.48 (s, C=O); MS m/z (rel intensity, %) 265 (M^+, 31), 156 (34), 110 (58), 109 (39), 65 (20), and 41 (base peak). HRMS Found: m/z 265.0782. Calcd for $C_{13}H_{15}NO_3S$: M, 265.0772.

12c: Pale yellow oil; IR (neat) 3000, 1730, and 1580 cm^{-1}; ^{1}H NMR ($CDCl_3$) δ=0.89 (3H, t, J=7.0 Hz, Me), 1.09—1.94 (8H, m, CH_2), 3.04—3.63 (2H, m, 4-H), 3.95—4.22 (1H, m, SCH), 4.77—5.09 (1H, m, 5-H), 7.08—7.44 (5H, m, Ph), and 10.24 (1H, br s, CO_2H); ^{13}C NMR ($CDCl_3$) δ=13.94 (q, Me), 22.35, 27.00, 31.24, 31.77, 32.12 (each t, CH_2), 37.71 (t, 4-C), 44.94, 45.71 (each d, SCH), 76.83, 77.01 (each d, 5-C), 127.89, 128.25, 129.30, 132.07, 132.95 (each d), 133.24 (s, 1-C of Ph), 159.48 (s, 3-C), and 174.60 (s, C=O); MS m/z (rel intensity, %) 307 (M^+, 17), 198 (45), 135 (24), 123 (30), 110 (59), 109 (86), 91 (21), 77 (27), 65 (43), 56 (95), 52 (22), 46 (24), 42 (31), 41 (base peak), and 39 (47). HRMS Found: m/z 307.1242. Calcd for $C_{16}H_{21}NO_3S$: M, 307.1241.

Alkylation of 2-Isoxazoline-5-carboxylic Acid 11 with 7-Iodo-2-heptanone Ethylene Acetal Leading to 12d. To a solution of LDA prepared from diisopropylamine (0.355 g, 3.51 mmol) and butyllithium (15% in hexane, 2.2 ml, 3.51 mmol) in dry THF (21 ml) was added 2-isoxazoline-5-carboxylic acid **11** (0.379 g, 1.67 mmol) in dry THF (12 ml) at −78 °C under nitrogen. After 0.5 h, 7-iodo-2-heptanone ethylene acetal (0.951 g, 3.35 mmol) and HMPA (3.3 ml, 19.0 mmol) were added. The mixture was stirred at −78 °C for 48 h and poured into saturated aqueous ammonium chloride (50 ml). After acidified to pH 1 by adding diluted sulfuric acid (10%), the mixture was extracted with dichloromethane (50 ml×3). The combined dichloromethane extracts were washed with water, dried over magnesium sulfate, and evaporated in vacuo. The residue was chromatographed over silica gel with hexane–ethyl acetate–acetic acid (10:10:1 v/v) to give isoxazoline **12d** (0.202 g, 35%) and **11** (0.067 g, 17%).

12d: Pale yellow viscous oil; ^{1}H NMR ($CDCl_3$) δ=1.19—2.00 (8H, m, CH_2), 2.12 (3H, s, Me), 2.44 (2H, t, J=6.8 Hz, CH_2CO), 3.10—3.64 (2H, m, 4-H), 4.06 (1H, t, J=7.5 Hz, SCH), 4.84—5.14 (1H, m, 5-H), 7.16—7.30 (5H, m, Ph), and 8.62 (1H, s, CO_2H); MS m/z (rel intensity, %) 349 (M^+, 19), 137 (21), 123 (23), 110 (46), 109 (36), and 52 (base peak). HRMS Found: m/z 349.1321. Calcd for $C_{18}H_{23}O_4NS$: M, 349.1346.

General Procedure for the Dialkylations of 2-Isoxazoline 6b Leading to 13a—c. To a solution of diisopropylamine (0.242 g, 2.4 mmol) in dry THF (10 ml) was added butyllithium (15% in hexane, 1.5 ml, 2.4 mol) at −78 °C under nitrogen. A solution of 2-isoxazoline **6b** (0.269 g, 1 mmol) in dry THF (10 ml) was added at −78 °C. After

0.5 h, an α,ω-dibromoalkane (2 to 4 mmol) and HMPA (2 ml, 11.5 mmol) were added. The mixture was stirred at −78 °C for 2 h, poured into saturated aqueous ammonium chloride (30 ml), and extracted with dichloromethane (40 ml×2). The combined extracts were dried over magnesium sulfate and evaporated in vacuo. The residue was subjected to column chromatography over silica gel by using hexane-ethyl acetate as an eluent to give **13**. The ratios of hexane-ethyl acetate employed are as follows: **13a** and **13c**: 10:1 v/v; **13b**: 15:1 v/v. The results are summarized in Table 3.

13a: Pale yellow oil; ^{1}H NMR ($CDCl_3$) δ=1.16—1.43, 1.45—1.69 (4H, m, CH_2CH_2), 3.06 (1H, dd, $J_{4\text{-}5}$=8.0 and J=17.5 Hz, one of 4-H), 3.49 (1H, dd, $J_{4\text{-}5}$=10.8 and J=17.5 Hz, the other of 4-H), 5.47 (1H, dd, $J_{5\text{-}4}$=8.0 and 10.8 Hz, 5-H), and 6.83—7.52 (10H, m, Ph); ^{13}C NMR ($CDCl_3$) δ=17.24, 17.63 (each t), 21.97 (s, q-C), 44.48 (t, 4-C), 82.86 (d, 5-C), 125.83, 125.98, 126.12, 127.68, 128.17, 128.76, 129.15, 129.34, 132.81 (each d), 136.18, 141.06 (each s), and 160.88 (s, 3-C); MS m/z (rel intensity, %) 295 (M^+, 89), 278 (49), 218 (47), 189 (28), 188 (72), 169 (29), 168 (64), 156 (37), 149 (22), 147 (23), 141 (27), 128 (37), 117 (24), 116 (22), 115 (60), 110 (45), 109 (base peak), 105 (39), 104 (41), 103 (29), 91 (58), 78 (31), 77 (90), 69 (23), 65 (54), 51 (50), 45 (21), 43 (39), and 39 (33). HRMS Found: m/z 295.1027. Calcd for $C_{18}H_{17}NOS$: M, 295.1030.

13b: Pale yellow oil; ^{1}H NMR ($CDCl_3$) δ=1.44—2.24 (8H, m, CH_2), 3.12 (1H, dd, $J_{4\text{-}5}$=8.5 and J=16.7 Hz, one of 4-H), 3.54 (1H, dd, $J_{4\text{-}5}$=10.8 and J=16.7 Hz, the other of 4-H), 5.51 (1H, dd, $J_{5\text{-}4}$=8.5 and 10.8 Hz, 5-H), and 6.94—7.38 (10H, m, Ph); ^{13}C NMR ($CDCl_3$) δ=23.41, 36.65, 36.88 (each t, CH_2), 43.41 (t, 4-C), 58.12 (s, q-C), 82.18 (d, 5-C), 125.77, 128.01, 128.72, 128.89, 134.60 (each d), 132.72, 141.24 (each s), and 161.25 (s, 3-C); MS m/z (rel intensity, %) 323 (M^+, 6), and 214 (base peak). HRMS Found: m/z 323.1345. Calcd for $C_{20}H_{21}NOS$: M, 323.1345.

13c: Pale yellow oil; ^{1}H NMR ($CDCl_3$) δ−1.17—2.12(10H, m, CH_2), 3.10 (1H, dd, $J_{4\text{-}5}$=8.5 and J=16.5 Hz, one of 4-H), 3.53 (1H, dd, $J_{4\text{-}5}$=11.0 and J=16.5 Hz, the other of 4-H), 5.51 (1H, dd, $J_{5\text{-}4}$=8.5 and 11.0 Hz, 5-H), and 7.21—7.27 (10H, m, Ph); ^{13}C NMR ($CDCl_3$) δ=22.65, 25.47, 35.00, (each t, CH_2), 42.47 (t, 4-C), 52.53 (s, q-C), 81.77 (d, 5-C), 125.89, 128.06, 128.77, 129.18, 136.54 (each d), 130.65, 141.30 (each s), and 160.54 (s, 3-C); MS m/z (rel intensity, %) 337 (M^+, 2), 228 (78), 115 (23), 110 (22), 109 (base peak), 104 (28), 91 (36), 81 (30), 79 (28), 78 (27), 77 (57), 65 (54), 53 (21), 51 (34), 41 (33), and 39 (44). HRMS Found: m/z 337.1512. Calcd for $C_{21}H_{23}NOS$: M, 337.1491.

General Procedure for the Raney Ni Hydrogenolysis of 2-Isoxazolines 8, 10, and 13 Leading to 14. To a solution of 2-isoxazoline **8**, **10**, or **13** (0.809 mmol) in aqueous ethanol (17%, 9.8 ml) were added boric acid (0.25 g, 4.045 mmol) and Raney Ni (W-2, 0.4 ml, 0.8 ml suspension in ethanol). Air in the reaction flask was replaced with hydrogen gas by repeated (5 times) evacuation and flushing with hydrogen. The mixture was stirred under hydrogen at room temperature. Insoluble materials were removed off by filtration through Celite 545. To the filtrate was added water (100 ml) and the organic layer was extracted with dichloromethane (100 ml×3). The combined extracts were dried over magnesium sulfate and evaporated in vacuo to give **14**. Reaction times, yields of **14**, and purification methods are as follows: **14a**: 16 h, 97%, silica-gel chromatography with hexane-diethyl ether (3:2 v/v) **14b**: 13 h, 76%, silica-gel chromatography with hexane-diethyl ether (2:1 v/v); **14c**: 18.5 h, 56%, silica-gel chromatography with dichloroethane; **14d**: 14.5 h, 91%, silica-gel chromatography with hexane-diethyl ether (3:1 v/v); **14e**: 16 h, 91%, silica-gel chromatography with hexane-diethyl ether (3:1 v/v).

14a: (a 1:1 mixture of two diastereomers (by ^{13}C NMR)): Colorless viscous oil; IR (neat) 3400 and 1700 cm^{-1}; ^{1}H NMR ($CDCl_3$) δ=0.95 (3H, t, J=7.0 Hz, Et), 1.27—1.68 (2H, m, Et), 2.50—3.10 (4H, m, $COCH_2$), 3.98 (2H, m, OH), 5.16 (2H, dd, J=4.0 and 9.0 Hz, CHOH), and 7.16—7.40 (5H, m, Ph); ^{13}C NMR ($CDCl_3$) δ=9.79 (Me), 29.52, 29.56 (Et), 49.93, 49.99, 52.11, 52.37, ($COCH_2$), 68.93, 69.16, 69.83, 69.99 (CHOH), 125.65, 127.67, 128.53, 143.02, 143.06, 211.27 (CO), and 211.44 (CO); MS m/z (rel intensity, %) 232 (M^+, 64), 149 (base peak), 107 (81), 104 (32), 83 (50), 79 (39), 77 (37), 55 (37), and 41 (25). HRMS Found: m/z 222.1255. Calcd for $C_{13}H_{18}O_3$: M, 222.1255.

14b: (a 1:1 mixture of two diastereomers (by ^{13}C NMR)): Pale yellow viscous oil; IR (neat) 3400 and 1700 cm^{-1}; ^{1}H NMR ($CDCl_3$) δ=0.76—1.02 (3H, m, n-Pr), 1.12—1.70 (4H, m, n-Pr), 2.31—3.07 (4H, m, $COCH_2$), 4.00 (2H, br s, OH), 5.02—5.22 (2H, m, CHOH), and 7.12—7.40 (5H, m, Ph); ^{13}C NMR ($CDCl_3$) δ=13.86 (Me), 18.48 (CH_2), 38.72 (CH_2), 50.12, 51.12, 52.06, 52.35 ($COCH_2$), 67.15, 67.33, 69.55, 69.72 (CHOH), 125.54, 127.35, 128.23, 143.21, 210.72 (CO), and 210.90 (CO); MS m/z (rel intensity, %) 236 (M^+, 16), 162 (23), 120 (64), 107 (base peak), 106 (25), 105 (85), 104 (35), 78 (45), 76 (38), 73 (20), 58 (33), 55 (34), and 42 (42). HRMS Found: m/z 236.1414. Calcd for $C_{14}H_{20}O_3$: M, 236.1411.

14c: Colorless viscous oil; IR (neat) 3440 and 1720 cm^{-1}; ^{1}H NMR ($CDCl_3$) δ=2.52—3.06 (6H, m, CH_2), 3.26 (1H, br s, OH), 5.14 (1H, dd, J=5.0 and 7.5 Hz, CHOH), and 7.04—7.40 (10H, m, Ph); MS m/z (rel intensity, %) 254 (M^+, 23), 236 (53), 229 (39), 149 (20), 145 (21), 135 (23), 131 (22), 121 (44), 107 (65), 105 (80), 104 (99), 91 (base peak), 79 (56), and 77 (53). Found: C, 80.07; H, 7.12%. Calcd for $C_{17}H_{18}O_2$: C, 80.28; H, 7.13%.

14d: Pale yellow viscous oil; IR (neat) 3440 and 1700 cm^{-1}; ^{1}H NMR ($CDCl_3$) δ=1.40—1.92 (8H, m, cyclopentyl), 2.65—3.03 (3H, m, $CHCOCH_2$), 3.56 (1H, br s, OH), 5.09 (1H, dd, J=5.0 and 7.0 Hz, CHOH), and 7.12—7.38 (5H, m, Ph); MS m/z (rel intensity, %) 218 (M^+, 13), 149 (33), 107 (65), 105 (23), 104 (40), 103 (22), 79 (base peak), 78 (29), 77 (98), 71 (22), 69 (69), 51 (33), 43 (25), 41 (87), and 39 (42). HRMS Found: m/z 218.1303. Calcd for $C_{14}H_{18}O_2$: M, 218.1306.

14e: Colorless viscous oil; IR (neat) 3440 and 1700 cm^{-1}; ^{1}H NMR ($CDCl_3$) δ=1.04—2.00 (10H, m, cyclohexyl) 2.12—2.50 (1H, m, cyclohexyl), 2.76 (1H, dd, J=17.0 and 5.5 Hz, one of $COCH_2$), 2.92 (1H, dd, J=17.0 and 7.0 Hz, the other of $COCH_2$), 3.60 (1H, br s, OH), 5.11 (1H, dd, J=7.0 and 5.5 Hz, CHOH), and 7.18—7.40 (5H, m, Ph); MS m/z (rel intensity, %) 222 (M^+, 20), 204 (30), 120 (58), 107 (base peak), 106 (26), 105 (70), 104 (25), 79 (58), 78 (26), 77 (51), 59 (32), 58 (38), and 43 (45). HRMS Found: m/z 232.1464. Calcd for $C_{15}H_{20}O_2$: M, 232.1462.

The present work was financially supported in part by a Grant-in-Aid for Scientific Research (No. 61470095) from the Ministry of Education, Science and Culture.

References

1) O. Tsuge, S. Kanemasa, and H. Suga, *Chem. Lett.*, **1986**, 183.

2) O. Tsuge, S. Kanemasa, H. Suga, and N. Nakagawa, *Bull. Chem. Soc. Jpn.*, **60**, 2463 (1987).

3) O. Tsuge, S. Kanemasa, and H. Suga, *Chem. Lett.*, **1987**, 323.

4) O. Tsuge, S. Kanemasa, N. Nakagawa, and H. Suga, *Bull. Chem. Soc. Jpn.*, **60**, 4091 (1987).

5) R. Annunziata, M. Cinquini, F. Cozzi, A. Gilardi, and A. Restelli, *J. Chem. Soc., Perkin Trans. 1*, **1985**, 2289 and 2293.

6) T. Mukaiyama and T. Hoshino, *J. Am. Chem. Soc.*, **82**, 5339 (1960).

7) D. Ranganathan, *J. Chem. Res. (S)*, **1983**, 78.

8) The bromination-dehydrobromination route of oximes leading to nitrile oxides have been well documented (Refs. 1, 2, and references cited therein).

9) O. Tsuge, H. Watanabe, and S. Kanemasa, *Chem. Lett.*, **1984**, 1415.

10) H. Grund and V. Jäger, *Liebigs Ann. Chem.*, **1980**, 80; S. Shatzmiller, E. Shalom, R. Lidor, and E. Tartkovski, *ibid.*, **1983**, 906; W. Schwab and V. Jäger, *Angew. Chem., Int. Ed. Engl.*, **20**, 603 (1981); A. P. Kozikowski and A. K. Ghosh, *J. Org. Chem.*, **49**, 2762 (1984).

11) An arylsulfonyl-substituted methanenitrile oxide is known: P. A. Wade and J. F. Bereznak, *J. Org. Chem.*, **52**, 2973 (1987); D. Sarlo, A. Guarna, A. Brandi, and A. Goti, *Tetrahedron*, **41**, 5181 (1985); P. A. Wade and H. R. Hinney, *J. Am. Chem. Soc.*, **101**, 1319 (1979).

12) So far neither successful lithiations at the side chain of the 2-isoxazolines bearing a carbonyl-type substituent at 5-position nor smooth reactions of the resulting anions with sulfinates are known.

 © 1988 The Chemical Society of Japan Bull. Chem. Soc. Jpn., 61, 3983—3989 (1988)

Interaction of Poly[*N*-(3-aminopropyl)glycine] and Its Derivatives with Lipid Membrane

Yoshiko YAGI, Shunsaku KIMURA, and Yukio IMANISHI*
Department of Polymer Chemistry, Kyoto University,
Yoshida Honmachi, Sakyo-ku, Kyoto 606
(Received November 14, 1987)

Poly[*N*-(3-aminopropyl)glycine] (PolyNAPGly, **5**) and its derivatives were synthesized as model peptides of the membrane-bound enzymes, and investigated on their interactions with lipid membrane. PolyNAPGly (**5**) was shown to be distributed to dipalmitoylphosphatidyl choline bilayer membrane without destruction of the vesicle structure. Dodecyl groups were introduced to the side chains of PolyNAPGly (**5**), and found to facilitate binding of the polymer to lipid membrane. However, the introduction of the excess amount of hydrophobic groups to PolyNAPGly (**5**) caused the formation of polymer micelles, and the addition of such polymers to lipid vesicles destroyed the membrane structure. The derivative of PolyNAPGly (**5**) (n=35) bearing one or two dodecyl groups and some N^{ε}-benzyloxycarbonylhistidyl groups was found to be bound tightly to lipid membrane without destruction of the membrane structure. The addition of these polypeptides to vesicles decreased the membrane fluidity.

The significance of the membrane-bound enzymes in cell physiology is well recognized. For example, in the case of signal transduction through cell membrane, binding of a hormone to its receptor on the cell membrane induces the activation of phospholipase C to break down phosphatidylinositol to yield diacylglyceride, which is known to trigger the activation of protein kinase C in the presence of Ca^{2+} ion. The well-known protein kinase C is a cytosolic enzyme, but associated with lipid membrane in cooperation with Ca^{2+} and diacylglycerol.[1] Under these conditions, it is activated for phosphorylation of proteins, which is the key step for the regulation of the protein function.[2] Another instance of membrane-bound enzyme in relation to the signal transduction is the hormone-sensitive adenylate cyclase, activated by binding of a hormone to the receptor through GTP-binding protein.[3] These functions of membrane-bound enzymes must be deeply dependent on the nature of membrane environments.[4]

Peptide hormones have also been shown to interact specifically with lipid membrane, and their physiological activities have been discussed in terms of their conformation and orientation in lipid membrane. For example, Kaiser and Kezdy have succeeded in synthesizing biologically active peptides which possess a sequence designed to take a specific secondary structure.[5] Furthermore, Schwyzer has shown that the mode of interaction of opioid peptides with lipid membrane can be correlated with the receptor subtype selection.[6] These reports emphasize the significance of amphiphilic structures of peptides in their interactions with lipid membrane. In the present investigation, we aimed at the elucidation of fundamental aspects of interactions between enzymes and lipid membrane using enzyme-model polypeptides.

Various kinds of polymer models of enzymes have been investigated in a homogeneous solution. Kiefer et al. synthesized branched poly(ethyleneimine)s containing nucleophilic catalytic and hydrophobic groups, and observed that they efficiently hydrolyzed hydrophobic esters.[7] The flexibility of polymer structures was suggested as one of the key factors of catalytic efficacy. Overberger and his coworkers have reported on efficient solvolytic activity of poly(*N*-vinylimidazole) and copolymers.[8] However, application of such polymers to a membrane system has not been reported, probably because they were not distributed well to lipid membrane or because they collapsed membrane structures.

The interactions of cationic polymers with lipid membrane has been studied on poly(lysine).[9,10] Poly(lysine) did not interact with a neutral lipid membrane, but was distributed into a negatively charged membrane due to electrostatic and hydrophobic interactions. The solution conformation and the chirality of the polypeptide affect the mechanism of the interactions.

We chose poly[*N*-(3-aminopropyl)glycine] (PolyNAPGly) as a starting polypeptide and its derivatives were prepared by the reaction of amino groups in side chains. These polymers are characterized by flexible chains for the *N*-substituted amide linkages: lack of amide protons to form a hydrogen bond and cis/trans isomerization around the amide bond.[11] This flexibility would be favorable for the polymers to be partitioned into lipid membrane and to function as a catalyst by a conformational adjustment at membrane surface.

N^{ε}-Benzyloxycarbonylhistidyl (ZHis) and dodecyl groups were introduced into the polymers as a nucleophilic catalytic moiety and as an anchor to lipid membrane, respectively, and the interactions of these polymers with lipid membrane were investigated. Perturbation of lipid membrane is represented by the change in membrane fluidity and by the leakage of carboxyfluorescein (CF) entrapped in the vesicle. Perturbation is discriminated from destruction of vesicle structure.

Experimental

Synthesis. Synthetic scheme of the polymer is shown in Fig. 1.

***N*-(3-Aminopropyl)glycine (1)**: Bromoacetic acid (3.5 g) in ethanol was added dropwise to 1,3-propanediamine (18.5 g) in ethanol. After refluxing for 72 h, ethanol was evaporated, and 5 M NaOH (25 ml; 1 M=1 mol dm^{-3}) was added and evaporated. The water addition/evaporation was repeated, and the residue was dissolved in ether/water, and evaporated. The obtained oil was used for the next step without further purifications.

***N*-Benzyloxycarbonyl-*N*-[3-(benzyloxycarbonylamino)-propyl]glycine (2)**: Benzyloxycarbonyl chloride (0.1 M) was added to 2.5 M NaOH aqueous solution (40 ml) of *N*-(3-aminopropyl)glycine at 0 °C under a vigorous stirring. After stirring for 24 h at room temperature, the aqueous phase was washed with ether and acidified with HCl, and extracted with ethyl acetate. The ethyl acetate solution was washed with water and dried over Na_2SO_4. After eluting on silica gel with chloroform/methanol/acetic acid (95/5/3 v/v) as an eluant, the oil was crystallized from ether/ethanol, yield 4.2 g (42%); mp 96—98 °C. Found: C, 62.88 ; H, 6.07; N, 7.09%. Calcd for $C_{21}H_{24}N_2O_6$: C, 62.99; H, 6.04; N, 6.96%.

Poly[*N*-[3-(benzyloxycarbonylamino)propyl]glycine] (4): Compound **2** (8.5 g) was reacted with thionyl chloride (10 ml) at 60 °C for 20 min. The solution was added into hexane (200 ml). The obtained white precipitate was recrystallized from benzene, yield 3.4 g (56%); mp 86—87 °C. The purified *N*-carboxy anhydride (NCA) (**3**) was polymerized in dichloromethane (40 ml) using hexylamine as an initiator (25.9 mg). After 70 h, the solution was added into ether (200 ml) to precipitate the product. The obtained polymer was reprecipitated from acetone. The degree of polymerization of the polymer was estimated to be 35 by vapor-pressure osmometry.

Poly[*N*-(3-aminopropyl)glycine] (PolyNAPGly) (5): Compound **4** (0.5 g) in acetic acid (20 ml) was treated with 3 M HBr/acetic acid (2 ml) at room temperature for 1 h. The solution was added into ether to precipitate the product. The white solid obtained was purified by dialysis (Spectrapore 1000, Ieda Inc.), yield 106 mg (30%).

Poly[*N*-[3-(dodecylamino)propyl]glycine] (Poly(C_{12})$_n$-NAPGly) (6,7): PolyNAPGly(**5**) (0.1 g) in dimethyl sulfoxide (2 ml) was reacted with dodecyl iodide (15.2 mg, in the case of n=1) in the presence of lutidine (1 ml) under a nitrogen atmosphere at 60 °C for 60 h. The solution was added to acetic acid/ether (1/4 v/v), and the obtained solid was purified by dialysis, yield 24 mg (25%). It was shown by NMR measurement that dodecyl groups were introduced on 2.8% of amino groups in the polymer.

Poly[*N*-[3-[[N^{α}-(benzyloxycarbonyl)histidyl]amino]propyl]-glycine] (PolyZHis$_n$NAPGly) (8,9): A solution of PolyNAPGly (50 mg) in dimethyl sulfoxide (2 ml) was reacted overnight with $N^{\alpha,im}$-bis(benzyloxycarbonyl)histidine *p*-nitrophenyl ester (15.8 mg, in the case of n=4) in the presence of triethylamine (100 ml) under a nitrogen atmosphere at 30 °C. Then the solution was added to ether (100 ml). The obtained oil was dissolved in *N*,*N*-dimethylformamide (2 ml), and pH was adjusted to 9 with 2 M NaOH. After standing for 30 min for deblocking the protected imidazolyl group, the solution was acidified by acetic acid, and added to ether. The obtained polymer was purified by dialysis, yield 12.5 mg (20%). Histidyl groups were introduced on 12.5% of total amino groups in the polymer.

Preparation of Small Unilamellar Vesicles (SUV). The lipid dispersion in a buffer (2-[4-(2-hydroxyethyl-1-piperazyl]ethanesulfonic acid (HEPES) (pH 7.2) or tris(hydroxymethyl)aminomethane (Tris) (pH 9.0) (10 mM), NaCl (0.1 M), and EDTA (0.1 mM)) was sonicated under a nitrogen atmosphere above the phase transition temperature for 20 min using a probe type of ultrasonic disruptor (TOMY SEIKO Co., Ltd., Japan) at the power of range 3, and ultracentrifuged at 100000 g to remove aggregates other than small unilamellar vesicles[12] and any titanium from the probe.[13] Vesicles, in which CF was trapped, were prepared according to the method reported by Barbet et al.[12]

Lipid concentration was determined by the method reported by Raheja et al.[14]

Measurements. Fluorescence measurements were carried out on a Hitachi MPF-4 fluorescence spectrophotometer. Fluorescence depolarization was measured by a modified MPF-4 apparatus installed with a fixed polarizer at the monitor side and a rotating polarizer at the excitation side which is driven by a stepping motor to 0° or 90° with respect to another polarizer. A depolarizer was set in front of the polarizer at the excitation side. At each position of the rotating polarizer, four data points were measured, processed by microcomputer, and averaged out. One polarization value was obtained at every 30 s. Excitation wavelengths of 8-anilino-1-naphthalenesulfonoic acid (ANS), 1,6-diphenyl-1,3,5-hexatriene (DPH), and CF were 380, 360, and 490 nm, respectively.

The concentration of polymer is represented in terms of the peptide residue unit.

Results

Derivatives of PolyNAPGly (5). PolyNAPGly (**5**) derivatives carrying one and two dodecyl groups in a polymer chain are represented as PolyC_{12}-NAPGly(**6**) and Poly(C_{12})$_2$-NAPGly (**7**), respectively. Other derivatives are PolyZHis$_4$-NAPGly (**8**), PolyZHis$_5$-NAPGly (**9**), and PolyC_{12}ZHis$_3$-NAPGly (**10**), which contain in a polymer chain four ZHis groups, five ZHis groups, and one dodecyl and three ZHis groups, respectively (Fig. 1). These derivatives were purified by dialysis to eliminate contamination by low molecular weight compounds.

CF Leakage from Vesicles by Polymer Addition. CF leakage from vesicles induced by the addition of the polymers represents perturbation to the membrane structure.[12] Figure 2 shows the time course of the CF leakage from dipalmitoylphosphatidyl choline (DPPC) vesicles induced by the addition of the polymers above the phase transition temperature of DPPC membranes. The addition of PolyNAPGly (**5**) and PolyZHis$_5$-NAPGly (**9**) did not increase the leakage so much, but the addition of Poly(C_{12})$_2$-NAPGly (**7**) and PolyC_{12}-ZHis$_3$-NAPGly (**10**) increased the CF leakage. Therefore, the polymers are tightly bound to the lipid

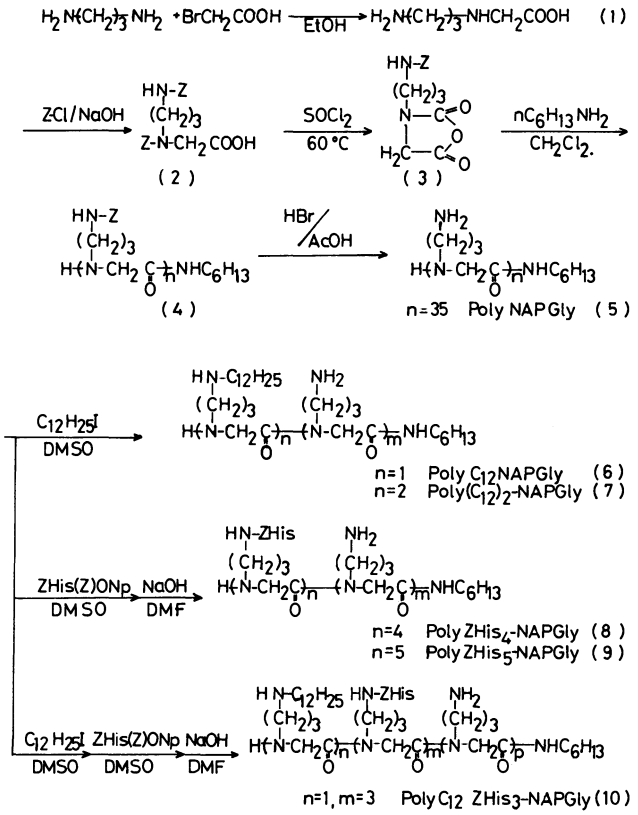

Fig. 1. Synthetic scheme of PolyNAPGly and its derivatives.

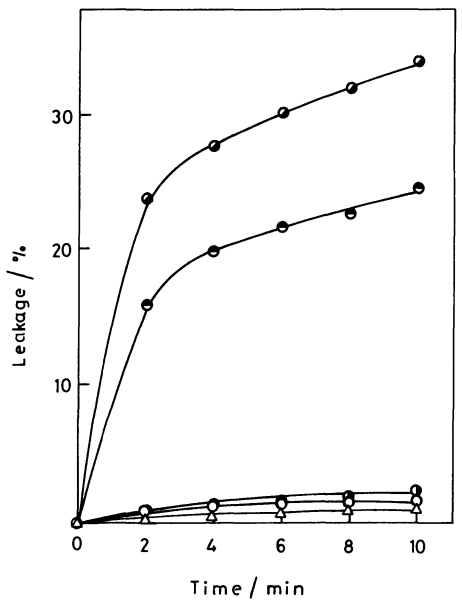

Fig. 2. Time course of CF leakage from DPPC vesicles by the addition of polymers at 46°C and at pH 9.0. DPPC lipid, 17 μM; polymer, 3.2 μM. △, Buffer; ○, PolyNAPGly (**5**); ◓, Poly(C_{12})$_2$-NAPGly (**7**); ◑, PolyZHis$_5$-NAPGly (**9**); ◕, Poly-C_{12}ZHis$_3$-NAPGly (**10**).

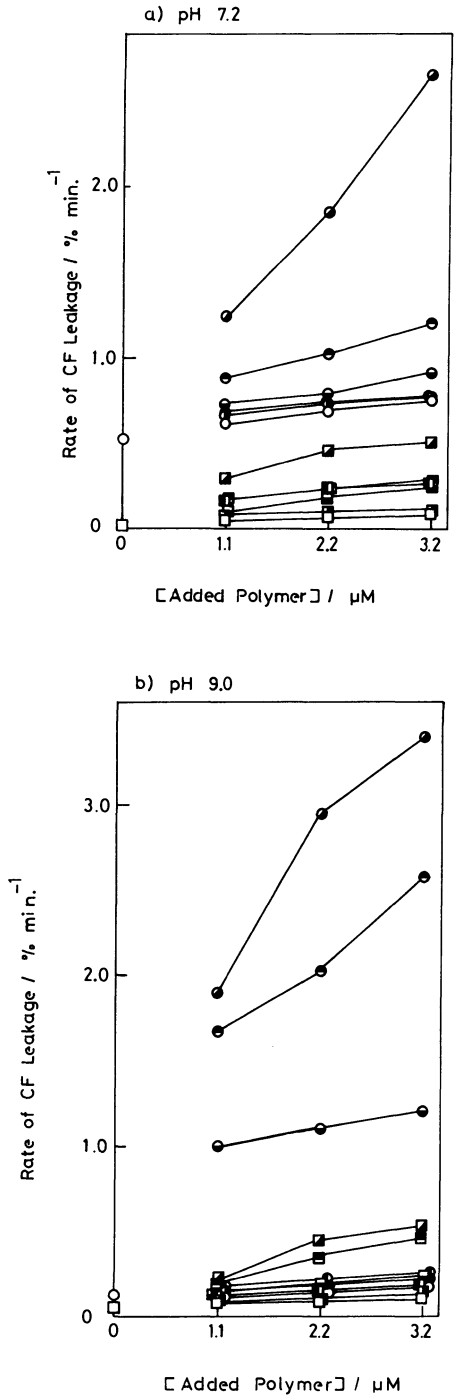

Fig. 3. The dependence of CF leakage from DPPC vesicles on the concentration of added polymers. The rate of CF leakage was determined at 10 min after the polymer addition. DPPC lipid, 17 μM. a) Experiment at pH 7.2, b) experiment at pH 9.0. □ and ○, PolyNAPGly (**5**); ◘ and ◒, PolyC_{12}-NAPGly (**6**); ◘ and ◒, Poly(C_{12})$_2$-NAPGly (**7**); ◧ and ◐, PolyZHis$_4$-NAPGly (**8**); ◧ and ◑, PolyZHis$_5$-NAPGly (**9**); ◪ and ◕, PolyC_{12}ZHis$_3$-NAPGly (**10**). Square and circle symbols represent the experiments carried out at 33°C and 46°C, respectively.

membrane by the action of the dodecyl groups as anchoring groups.

Dependence of CF Leakage on pH, Temperature, and Amount of Added Polymer. The rate of CF leakage from DPPC vesicles was determined at 10 min after the polymer addition. Figure 3 shows the rates of CF leakage at different pH values, temperatures, and concentrations of added polymers. The rate of CF leakage at pH 9.0 was larger than that at pH 7.2, while it is considered that distribution to and permeation across lipid membrane of CF are more difficult at pH 9.0 than at pH 7.2 because of its pK_a values of 4.5 and 6.3.[12] The rate of CF leakage was small at 33 °C, which is lower than the phase transition temperature. However, it was enhanced at 46 °C, which is higher than the phase transition temperature. The higher the hydrophobicity of the polymer is, the more the CF leakage was enhanced. In the case of less hydrophobic polymer, the CF leakage was not increased so much with increasing concentration of added polymers. This indicates weak interactions of these polymers with bilayer membranes and a small number of binding sites in the lipid membranes for these polymers. On the other hand, the CF leakage induced by the addition of Poly(C_{12})$_2$-NAPGly (**7**) and PolyC_{12}-ZHis$_3$-NAPGly (**10**) increased with an increase in the concentration of added polymers, indicating a strong binding of these polymers to the membrane.

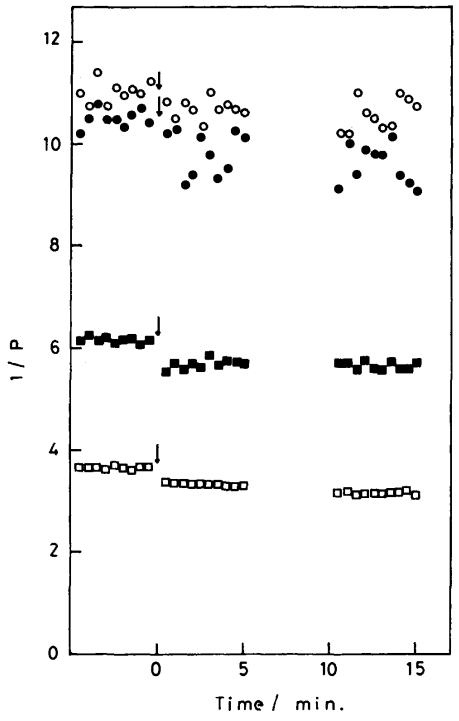

Fig. 4. Change in membrane fluidity of DPPC vesicles on the addition of Poly(C_{12})$_2$-NAPGly(7) at pH 9.0. DPPC lipid, 84 μM; Polymer, 20 μM.
□, DPH at 33 °C; ■, ANS at 33 °C; ○, DPH at 46 °C; ●, ANS at 46 °C.

The Change in Membrane Fluidity upon the Polymer Addition. The change in membrane fluidity induced by the addition of a polymer was investigated by measuring fluorescence depolarization of ANS and DPH in the membrane (Fig. 4). The fluorescent probes, ANS and DPH, reflect the fluidity of the surface region and the hydrophobic domain of lipid membrane, respectively. Figure 5 shows the relative change in fluorescent polarization induced by the polymer addition. It was found that the addition of every polymer increases the polarization, that is, it decreases the membrane fluidity. Poly(C_{12})$_2$-NAPGly (**7**) and PolyC_{12}ZHis$_3$-NAPGly (**10**) were shown to effectively decrease the membrane fluidity below the phase transition temperature.

Discussion

Dissolution of the polymers into lipid bilayer membrane without a serious destruction of the membrane structure is indispensable for polymers to be a model compound of membrane-bound enzymes. PolyNAPGly (**5**) was expected to satisfy the conditions as follows. i) A propyl group should act as an anchor group for the polypeptide to be bound to membrane. ii) The backbone of the polypeptide is flexible due to *N*-substituted amide bonds, hence the polypeptide easily fits to the membrane surface. iii) PolyNAPGly (**5**) is difficult to go deeply into the membrane, because it is positively charged at the neutral pH and the lack of amide protons makes carbonyl groups unshielded from solvents. Taking these points into consideration, it is suggested that the polypeptides tend to be incorporated into the membrane surface compartment.

The synthetic polymers are soluble in water. The molecular structures of these polymers are composed of hydrophilic and hydrophobic regions. However, they were designed not to form a polymer micelle by avoiding the introduction of hydrophobic substituents excessively to the polymer. The absence of micelle formation was confirmed by a hydrophobic fluorescent probe, ANS.[15,16] The derivatives neither enhanced nor shifted the emission from ANS in aqueous solution. This indicates the absence of hydrophobic environment imposed on ANS by micelle formation. An extensive introduction of hydrophobic groups to PolyNAPGly (**5**) makes it a polymer micelle, which is an unfavorable structure to collapse the vesicles. For instance, the polymer bearing nine ZHis groups in a chain enhanced the emission intensity of ANS in solution, indicating the formation of polymer micelle. The addition of this polymer to CF-trapped vesicles induced a complete leakage of CF immediately after polymer addition, indicating the destruction of vesicle structures. Such polymers were not used in the present investigation. After all, the amount of dodecyl and ZHis substituents in a polymer chain should be less than two and five, respectively, in order for the

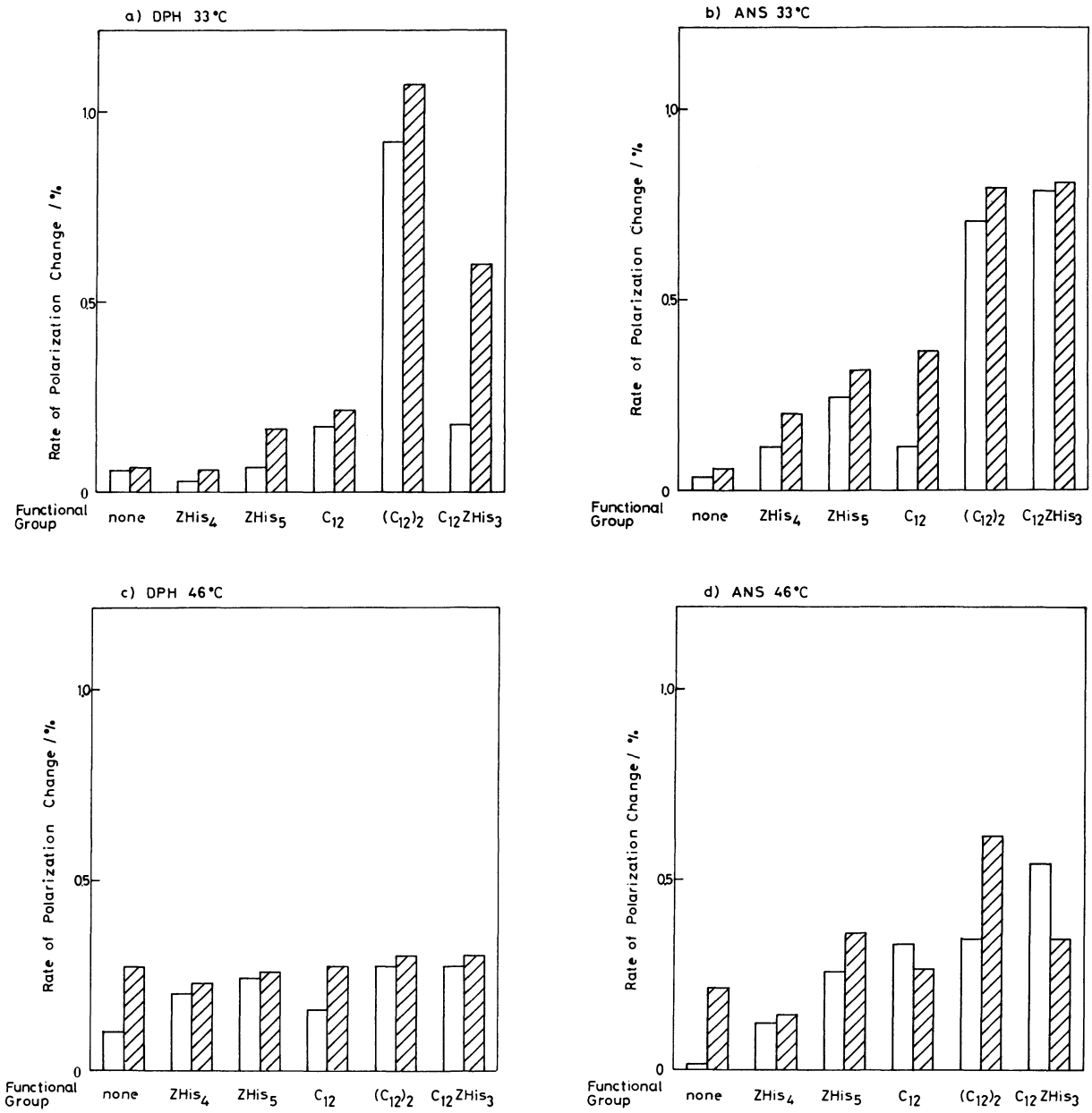

Fig. 5. The relative change in fluorescence polarization of DPH and ANS in DPPC vesicles induced by the addition of polymers. The relative change in fluoresence polarization is represented by $(P-P_0)/P_0$, where P designates the average polarization value at 5 min after the addition of polymer (20 μM), and P_0 means the polarization value in the absence of polymer. The temperature and used fluorescent probe are indicated at the top of each figure. The observed P_0 values are a) 0.285 (pH 7.2) and 0.275 (pH 9.0), b) 0.163 (pH 7.2 and 9.0), c) 0.096 (pH 7.2) and 0.091 (pH 9.0), and d) 0.098 (pH 7.2) and 0.095 (pH 9.0).
□, pH 7.2; ▨, pH 9.0.

derivatives of PolyNAPGly(**5**) to interact with lipid membrane without a serious damage of the membrane structure.

In the presence of DPPC vesicles, the addition of PolyNAPGly (**5**) changed the polarization of ANS in the lipid membrane. The varied polarizations of ANS should be attributed to the fluidity change of the membrane on interaction of PolyNAPGly (**5**) with the lipid membrane. While, CF leakage from DPPC vesicles was not influenced so much by the addition of PolyNAPGly (**5**), indicating the absence of the serious damage of the lipid membrane. These observations strongly support that PolyNAPGly (**5**) is a suitable polymer for the investigation of membrane-bound enzymes.

The effect of substituents of the polymer on binding to the membrane was investigated. The introduction of ZHis groups to PolyNAPGly (**5**) did not affect its

interaction with lipid membrane so much. However, the incorporation of dodecyl groups enhanced the binding to membrane (Fig. 2). Since PolyC$_{12}$ZHis$_3$-NAPGly (**10**) disturbed the membrane structure more extensively than PolyZHis$_4$-NAPGly (**8**), the dodecyl group of PolyC$_{12}$ZHis$_3$-NAPGly (**10**) should enhance the binding of the polymer to membrane (Fig. 3). Therefore, dodecyl group is effective in anchoring water-soluble compounds to lipid membrane. This result is consistent with that reported by Sunamoto, who succeeded in coating lipid vesicles with polysaccharide carrying a few hydrophobic alkyl chains.[17]

Cationic charges on the amino groups of the polymer also influence the affinity of the polymer with lipid membrane. Figure 3 shows that the effect of polymer addition on the CF leakage is larger at pH 9.0 than at pH 7.2. At pH 9.0 positive charges on the polymer are less than those at pH 7.2. Therefore, the polymer is bound to the neutral membrane at pH 9.0 more favorably than at pH 7.2. CF leakage did not reach 100% under the conditions in which several polymer molecules per one vesicle were added, indicating that the polymers do not completely destroy the vesicle structure. The time course of the CF leakage is biphasic (Fig. 2). One is just after the polymer addition, which is a transient state accompanied by the insertion of the polymer molecules into the membrane. The following slow leakage of CF should be attributed to a disordering of the membrane structure occurring after the complete incorporation of the polymers into the membrane.

The phase transition temperature of DPPC vesicles was raised by about 1 °C on addition of PolyNAPGly, PolyZHis$_4$-NAPGly (**8**), PolyC$_{12}$-NAPGly (**6**), or PolyC$_{12}$ZHis$_3$-NAPGly (**10**). This was detected by investigating the temperature dependence of fluorescence intensity of ANS according to the method by Mayer et al. (data not shown).[16] This observation also indicates that the polymers are absorbed on the membrane surface and slightly decreased the mobility of lipid molecules.

This effect of the polymers on the membrane fluidity was more prominent below the phase transition temperature. Based on the polarization of DPH, fluidity of the hydrophobic domain of a lipid membrane was almost independent of the nature of added polymers above the phase transition temperature, indicating that these polymers do not have serious effects on the structure of hydrophobic domain of a lipid membrane. However, below the phase transition temperature, effects of polymers on the fluidity of the hydrophobic domain of a lipid membrane were strongly dependent on the nature of polymers (Fig. 5). Especially, Poly(C$_{12}$)$_2$-NAPGly (**7**) and PolyC$_{12}$ZHis$_3$-NAPGly (**10**) perturbed markedly the structure of hydrophobic domain of lipid membrane. Dufourcq and his coworkers have reported that interactions of melittin, which is an amphiphilic polypeptide toxin, with phosphatidyl choline bilayers are stronger above the phase transition temperature than those below it.[18] However, it might be inferred that amphiphilic compounds tend to be bound more tightly to gel-state membrane than to liquid-crystalline membrane. Since the complex formed between amphiphilic compounds and lipid molecules should be highly ordered, the binding should accompany a large entropy loss. The entropy loss upon binding might be smaller for gel-state membrane than for liquid-crystalline membrane, leading to a larger loss of free energy upon binding to gel-state membrane than to liquid-crystalline membrane. For example, it has been reported that glucagon is bound tightly to gel-state membrane.[19,20] The present polymers behaved similarly to glucagon in the interaction with lipid membranes.

It should be noted that binding of polymer to lipid membrane decreased the membrane fluidity. Decrease in membrane fluidity by Ca^{2+} has been observed and attributed to the dehydration of head groups of lipid molecules by Ca^{2+} binding.[21] The decrease in membrane fluidity on the polymer addition might be explained by the same reason—that is, the ammonium and carbonyl groups of the polymer are bound to the polar groups of lipid molecules to dehydrate the membrane surface.[22]

To conclude, water-soluble polymers can be bound to lipid membrane by introducing hydrophobic groups as anchoring groups. The membrane affinity is adjustable by the number and the properties of the hydrophobic group. These points are very essential in the simulation of membrane-bound enzymes, since they affect sensitively physical properties of membrane, such as membrane fluidity and packing of lipid molecules.

References

1) M. D. Bazzi and G. L. Nelsestuen, *Biochemistry*, **26**, 115 (1987).
2) Y. Nishizuka, *TIBS*, **1983**, 13.
3) A. Levitzki and E. Helmreich, *FEBS Lett.*, **101**, 213 (1979).
4) E. Hauski, G. Rimon, and A. Levitzki, *Biochemistry*, **18**, 846 (1979).
5) E. T. Kaiser and F. J. Kezdy, *Science*, **223**, 249 (1984).
6) R. Schwyzer, *Biochemistry*, **25**, 6335 (1986).
7) H. C. Kiefer, W. I. Congdon, I. S. Scarpa, and I. M. Klotz, *Proc. Natl. Acad. Sci. U.S.A.*, **69**, 2155 (1972).
8) C. G. Overberger and J. C. Salamone, *Acc. Chem. Res.*, **2**, 217 (1969).
9) D. Carrier, J. Dufourcq, J. F. Faucon, and M. Pezolet, *Biochim. Biophys. Acta*, **820**, 131 (1985).
10) P. T. Shafer, *Biochim. Biophys. Acta*, **373**, 425 (1974).
11) Y. Imanishi, *Adv. Polym. Sci.*, **20**, 1 (1976).
12) J. Barbet, P. Machy, A. Truneh, and L. D. Leserman, *Biochim. Biophys. Acta*, **772**, 347 (1984).
13) J. Bramhall, J. Hofmann, R. DeGuzman, S.

Montestruque, and R. Schell, *Biochemistry*, **26**, 6330 (1987).
14) R. K. Raheja, C. Kaur, A. Singh, and I. S. Bhatia, *J. Lipid Res.*, **14**, 695 (1973).
15) A. Azzi, B. Chance, G. K. Radda, and C. P. Lee, *Proc. Natl. Acad. Sci. U.S.A.*, **62**, 612 (1969).
16) L. D. Mayer and G. L. Nelsestuen, *Biochemistry*, **20**, 2457 (1981).
17) J. Sunamoto, *Pharmacia*, **21**, 1229 (1985).
18) J. Dufourcq, J. F. Faucon, G. Fourche, J. L. Dasseux, M. L. Maire, and T. Gulik-Krzywicki, *Biochim. Biophys. Acta*, **859**, 33 (1986).
19) R. M. Epand, A. J. S. Jones, and B. Sayer, *Biochemistry*, **16**, 4360 (1977).
20) A. J. S. Lones, R. M. Epand, K. F. Lin, D. Walton, and W. J. Vail, *Biochemistry*, **17**, 2301 (1978).
21) H. Hauser, E. G. Finer, and A. Darke, *Biochem. Biophys. Res. Commun.*, **76**, 267 (1977).
22) T. Ohtoyo, M. Shimagaki, K. Otoda, S. Kimura, and Y. Imanishi, *Biochemistry*, **27**, 6458 (1988).

 © 1988 The Chemical Society of Japan Bull. Chem. Soc. Jpn., 61, 3991—3998 (1988)

Footprint Catalysis. I. A New Method for Designing "Tailor-Made" Catalysts with Substrate Specificity: Silica (Alumina) Catalysts for Butanolysis of Benzoic Anhydride

Kensaku MORIHARA,* Sachiyo KURIHARA, and Junko SUZUKI
Department of Chemistry, Faculty of Science, Nara Women's University, Kitauoyanishi-machi, Nara 630
(Received March 22, 1988)

The design of tailor-made specific catalysts for a given organic reaction was investigated. Dibenzamide or *N*-benzoylbenzenesulfonamide, transition state analogs of benzoic anhydride on transacylation, was found to act as a template upon aluminium ion-doped silica gel and to imprint specific adsorption sites, "footprints," on the surface. The footprints were particular Lewis acid sites with a complementary structure to the template. They demonstrated an enzyme-like specific catalytic function on the butanolysis of benzoic anhydride through their specific affinities for substrate molecules in the transition state.

Several kinds of enzyme-simulating catalysts consisting of a binding site and catalytic functional group(s) have been extensively investigated, and fair success has been reported.[1-4] However, there remain some problems,[5] and their catalytic features might seem, to date, somewhat unlike those of real enzymes. This is mainly because the present synthetic means encounters much difficulty in preparing so highly organized catalytic sites as those of natural enzymes and, consequently, the catalytic sites of such enzyme mimics cannot effectively used the non-covalent binding energy of E–S complexes to lower the activation energy barrier to a reaction as do the active sites of natural enzymes in their activities.[6-8]

Another approach to enzyme mimics, however, might be possible if the competitive inhibition mechanism for enzymes by transition state analogs, proposed by Wolfenden,[9] is applicable to designing enzyme-like catalytic sites. According to this mechanism, transition state analogs are specifically adsorbed on the active sites of enzymes much more tightly than the substrates themselves. Since these strong bonding in E–I complexes are similar in kind to those in E–S complexes, such a large bonding energy in E–I complexes can be applicable to the design of catalysts. If adsorption sites of any kind are available that possess complementary structures to the transition state analogs and, thereby, have a specific affinity for them, the sites might show a catalytic function when they bind the substrate molecules of the reaction. This is because the sites might misuse their specific affinity for the substrate molecules in a transition state to stabilize them and to lower the activation energy barrier of the reaction, which is, say, a reversed application of the inhibition mechanism by transition state analogs[9] to catalysis.

Such specific adsorption sites can be prepared on the surfaces of appropriate materials by rather easy imprinting procedures using chemically stable transition state analogs as template molecules. Thus, how to design a specific catalyst for a given reaction becomes directly how to design a specific adsorbent for a transition state analog of the substrate for the reaction. One of the present authors has found a method for imprinting specific adsorption sites for Methyl Red on the surface of silica(alumina) gels,[10,11] by a similar procedure as that described by Dickey.[12] These adsorption sites, regarded as "footprints" of Methyl Red, possess a Lewis acidic nature, keeping a complementary structure to the template molecules. This leads to a possibility of their use as an acid catalyst with substrate specificity.

The present paper reports that the "footprints" could be marked on the surface of commercially available silica gel by surface modification using aluminium ions and transition state analogs, e.g., dibenzamide or *N*-benzoylbenzenesulfonamide†, and that the "footprints" revealed unusual and specific catalytic behaviors on butanolysis of benzoic anhydride.

Experimental

Materials and Apparatus. All materials, if not specified, were of guaranteed grade of Nacalai Tesque Co. Ltd., and were used without further purification.

Silica gel; Merck Kieselgel 60, art. no. 7754, particle size 0.06—0.20 mm, mesh 70—230.

Dibenzamide (Bz-NH-Bz); prepared from benzonitrile.[13] Mp 145 °C (lit, 148 °); (Found: C, 74.81; H, 4.88; N, 6.18%).

N-Benzoylbenzenesulfonamide (Ph-SO_2-NH-Bz); prepared by usual pyridine-assisted benzoylation of benzenesulfonamide. Mp 148 °C (lit, 147 °C); (Found: C, 59.51; H, 4.26; N, 5.37%).

Dibenzoylmethane; recrystallized from petroleum benzine. Mp 74.5 °C (lit, 77.5—78 °C).

Benzoic anhydride; recrystallized from benzene-petroleum benzine. Mp 42 °C (lit, 42 °C).

Phthalic anhydride; recrystallized from benzene. Mp 130 °C (lit, 138.8 °C).

† In the strict sence, this compound is not a true transition state analog, but a tetrahedral intermediate analog as shown in Scheme 1. Its action on catalysis, however, nearly the same as a transition state analog according to Hammond rule.

Acetone; purified by distillation after refluxing with potassium permanganate.

1-Butanol; purified by distillation.

Benzene; purified by distillation over sodium metal.

Acetonitrile; purified by distillation after drying with calcium sulfate, and phosphorus pentoxide.

Anhydrous barium perchlorate; obtained by dehydration of barium perchlorate (3—4 H_2O) at 140 °C in vacuo.

pH-meter; Toa Electronics Ltd. HM-5B with a glass electrode GC-125.

Preparation of Catalysts. Kieselgel (100 g) was refluxed with concd hydrochloric acid for 4 h to release free surface silanol groups according to Fritz et al. and King et al.[14,15] The gel was throughly washed with water and, successively, with dil. aqueous ammonia till pH of supernatant reached 6.0—7.0. The gel was collected by filtration and pressed on filter papers. The "wet" gel, thus obtained, (equivalent to 10 g of dry weight), was added to 0.2 mol·l^{-1} aluminium chloride aqueous solution (50 cm^3) and the pH of the supernatant was adjusted to 7.0—8.0 with dil. aqueous ammonia. The mixture was then allowed to stand for one or two days. The precipitated aluminium hydroxide was removed off by decantation, and the silica(alumina) gel was washed three times with dil. hydrochloric acid (pH 4.0). To this gel, was added dibenzamide (450 mg) (or *N*-benzoylbenzenesulfonamide) in aqueous ammonia (40 cm^3) or in a minimum amount of acetone in order to dissolve the templates immediately. The supernatant was acidified to pH 4.0 quickly, and the mixture was allowed to stand for one or two days with an occasional pH adjustment. The gel was collected by filtration, and added to dil. hydrochloric acid (50 cm^3, pH 4.0) for washing, and collected by filtration and again washed on filter paper with the same hydrochloric acid. It was then air-dried at room temperature for 2—5 days to reach constant weight. The dried gel was subjected to methanol extraction by the use of a Soxhlet extractor untill no more absorbance at 243 nm could be observed. After extraction, the gel was quickly transfered into a desiccator over calcium chloride and dried under atmospheric pressure for one day and then under reduced pressure (25 mHg[††]) for a further one or two days. Finally, it was dried at 120—140 °C under reduced pressure (3 mHg) to give a sample ("imprinted") silica(alumina) gel catalyst preparation. A blank gel catalyst which omitted aluminium ions and templates, and a control gel catalyst which omitted only templates were prepared, respectively, by quite the same procedure as the sample gel catalyst preparation (always in parallel). All final gel preparations were carefully stored in tightly stoppered vinials for protection against moisture. The gel catalysts, inactivated by moisture, could be re-activated by repeated azeotropic dehydration with 2-propanol (20 cm^3) and benzene (80 cm^3) for 1 h.

Acidic Properties of Gel Catalysts. An acid strength determination was carried out by a method of Benesi with Hammett indicators,[16] and Lewis acid site detection was made with phenolphthalein according to a method of Pines and Haag.[17]

Kinetic Measurements. The reaction conditions for the butanolysis of benzoic anhydride was the same as that of phthalic anhydride described by Tarama et al.[18] To a mixture of benzene (70 cm^3) and 1-butanol (30 cm^3), was added a weighed amount of catalysts; the mixture was equilibrated at 55 °C for 1 h. In inhibition studies, an inhibitor was added 40 min later, and the mixture was kept at 55 °C for a further 20 min. Under vigorous stirring with a magnetic stirrer, an exactly weighed quantity of benzoic anhydride (2.262 g) was added to the mixture in order to initiate the reaction. Aliquots of 5 cm^3 were taken out at proper intervals in order to analyze the benzoic acid formed by the method of Greenhow,[19] as follows. To acetonitrile (10 cm^3) containing anhydrous barium perchlorate (0.225 g), was added an aliquot of the reaction mixture; the resulting solution was subjected to potentiometric titration with a 0.01 M[†††]-tripropylamine acetone solution using a glass electrode. Time courses of the butanolyses were practically linear up to 120 min and V_{obs}s were obtained from the slope. $V=V_{obs}-V_{uncat}$, where V_{uncat} was V_{obs} of catalyst amount extrapolated to zero. Kinetic parameters, K_ms and V_{max}s, were obtained from the usual Lineweaver-Burk plots, and activation parameters were calculated from the V_{max} values obtained at 50 °C, 55 °C, and 62 °C, respectively, where $\ln V_{max}$ vs. T^{-1} plots were finely linear (Fig. 3). Since the catalysts varied in activity by preparation lots and were very susceptible to moisture during storage, the kinetic parameters of catalysts of the same lots and of the same determination were always compared for a meaningful discussion of the catalytic behaviors of the gels.

Results

Table 1 demonstrates the acidic properties of gels, and the catalytic activities observed thereof. The purple coloration of sample (imprinted) gels by phenolphthalein for Lewis acid sites was immediately lost by an addition of the original template molecules. Table 2 shows that inactivated catalysts by moisture were regenerated by azeotropic dehydration. Figure 1 (A, B, C) displays typical Lineweaver-Burk plots for the catalytic butanolysis by the sample (imprinted) catalysts and the control catalyst, suggesting that the catalyzed reaction follows Michaelis-Menten kinetics with respect to the benzoic anhydride concentration in the range of 0.5—5.5 M of 1-butanol. Figure 2 shows that the initial velocity is nearly linear with respect to 1-butanol concentration below 0.8 M and, thereafter, leveled off. The rate of the catalyzed reaction can be expressed as follows:

$$\text{rate} = \frac{V_{max}[\text{benzoic anhydride}][\text{1-butanol}]}{K_m + [\text{benzoic anhydride}]} \quad (1)$$

In Table 3, are shown the kinetic parameters, and in Table 4, the activation parameters calculated from data shown in Table 3 and Fig. 3. In Figs. 4 and 5 are shown competitive inhibition plots by the original templates, and in Fig. 6, those plots by dibenzoylmethane, for sample (imprinted) gels-catalyzed butanolysis, respectively. The inhibition constants, K_is, are

†† 1 mmHg≈133.322 Pa.

††† 1 M=1 mol dm^{-3}.

Table 1. Acidic Properties and Catalytic Activity

Catalyst	Acid site above pK_a; +1.5[b]	+4.8[c]	+6.8[d]	Lewis acid site[e]	Activity[a] $10^4 \times V/M\ min^{-1}$
Sample (footprint) gel imprinted by dibenzamide					
not dried	+	+	+	−	0.00
dried[f]	+	+	+	+[g]	1.24
Control gel					
not dried	+	+	+	−	0.00
dried[f]	+	+	+	+	0.35
Blank gel					
dried[f]	−	−	−	−	0.00

a) Per 300 mg of catalysts. b) Determined with 4-(phenylazo)diphenylamine. c) With Methyl Red. d) With Neutral Red. e) Detected with phenolphthalein. f) Dried in vacuo at 120—140°C. g) Decolorized by dibenzamide addition.

Table 2. Regeneration of Catalytic Activity

Catalyst[a]	Activity: $10^4 \times V/M\ min^{-1}$ 300 mg	500 mg	700 mg
Original	1.2	2.2	3.0
Inactivated[b]	—	—	0.0
Regenerated[c]	—	1.1	1.9
Regenerated[d]	—	0.7	1.1

a) Imprinted by dibenzamide. b) Allowed to stand for one day toward room humidity. c) Azeotropically dehydrated with 2-propanol-benzene (20:80 v/v), 2 times. d) Another catalyst, dehydrated 4 times.

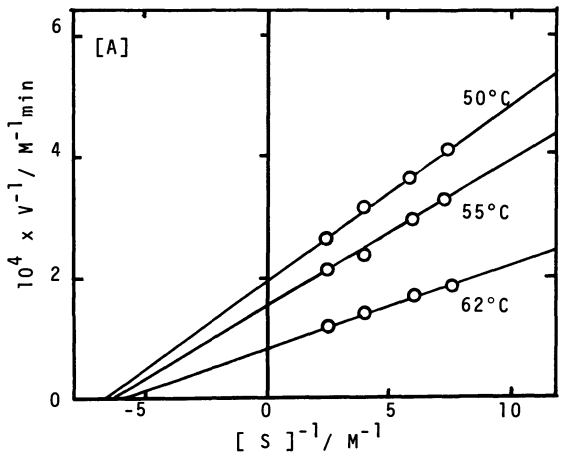

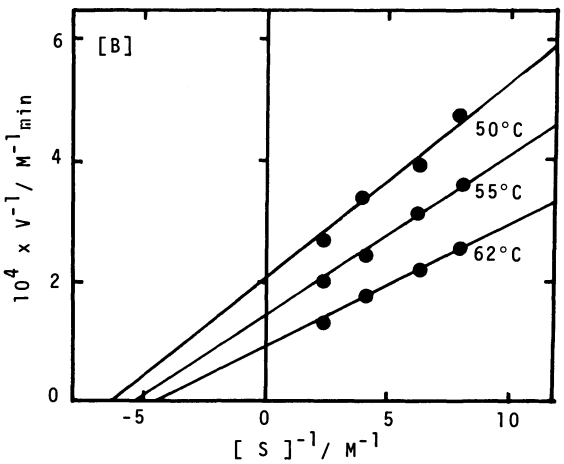

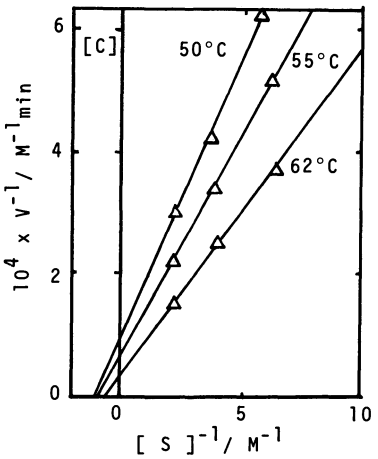

Fig. 1. Linewever-Burk plots for butanolysis of benzoic anhydride catalyzed by silica (alumina) gel catalysts.
(A): Catalyst imprinted by Bz-NH-Bz; 700 mg. (B): Catalyst imprinted by Ph-SO_2-NH-Bz; 700 mg. (C): Control catalyst; 700 mg. [S]: Benzoic anhydride concentration. $V = V_{observed} - V_{uncatalyzed}$.

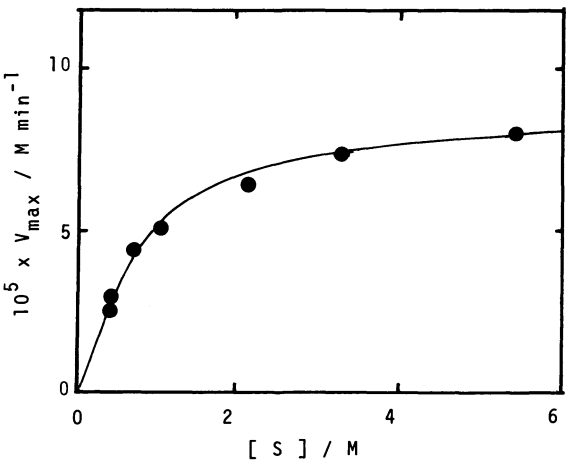

Fig. 2. Relationship between maximum velocity and 1-butanol concentration.
Catalyst imprinted by Ph-SO_2-NH-Bz; 700 mg: [S]: 1-Butanol concentration.

shown in Table 5. No competitive inhibition by the templates (Bz–NH–Bz, Ph–SO_2–NH–Bz, 2.24×10^{-3} M) was observed on Lineweaver-Burk plots (not shown) for the control gel-catalyzed butanolysis. Lineweaver-Burk plots (not shown) for the sample (imprinted) gels and the control gel-catalyzed butanolyses of phthalic anhydride are almost identical, and the kinetic parameters are shown in Table 6.

Discussion

The butanolysis of benzoic anhydride, a water-free esterification, was selected as a catalysis assay system because water was known to be poison for silica alumina catalysts, and benzoic anhydride was preferable to phthalic anhydride because its related derivatives for further studies were more easily available.

The linear relationship between the amounts of the sample (imprinted) and the control catalysts and the increase in reaction rates comfirms that the butanolyses are catalyzed reactions.

As shown in Table 1, the catalytic activities of the sample (imprinted) gel and the control gel are evidently caused by Lewis acid sites on the silica

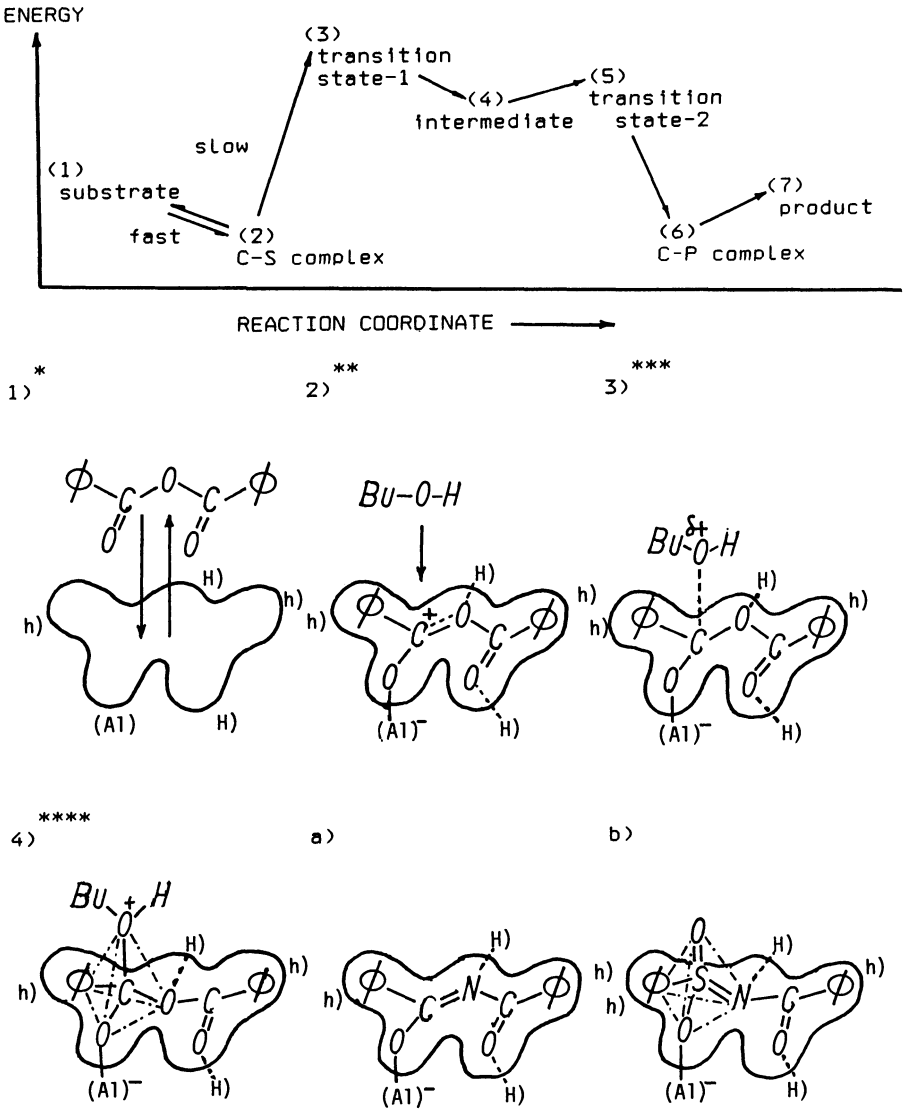

Scheme 1. Speculated catalytic mechanism for butanolysis of benzoic anhydride upon a footprint catalytic site.

* Substrate and footprint, a shallow hollow, imprinted by Bz–NH–Bz. (Al): Lewis acid site at bottom of the hollow. h): Hydrophobic subsite. H): Hydrogen bond donor.

** Adsorbed substrate on a catalytic site, carbocation.

*** Transition state. Bu–OH: 1-butanol as nucleophile.

**** Tetrahedral intermediate for transacylation.

a) Analog for the transition state (3), dibenzamide (Bz–NH–Bz), bound onto the footprint. b) Analog for the tetrahedral intermediate (4), *N*-benzolybenzenesulfonamide (Ph–SO_2–NH–Bz), bound onto the footprint.

(alumina) gels, since both the blank gel lacking all kinds of acid sites and the "not dried" gels possessing acid sits, but lacking Lewis acid sites, are fully inactive. Furthermore, Lewis acid sites, not Brønsted acid sites, are assured to participate in the catalysis on the "imprinted" catalytic sites for following reasons: 1) Only such catalyst preparation as are positive (purple) to phenolphthalein for Lewis acid sites and lose immediately the purple collor upon the addition of templates showed the characteristic catalytic behaviors of "imprinted" catalytic sites, as mentioned below. 2) The catalytic activities were strongly affected by a Lewis base, such as water. 3) Dibenzoylmethane showed a competitive inhibition effect (Fig. 6) which could bind only onto Lewis acid sites through its enol-form but not to Brønsted acid sites.

The rate law of Eq. 1 for the butanolysis suggests that the reaction proceeds through a Rideal-Eley mechanism in which benzoic anhydride molecules initially adsorb onto the catalytic sites to activate carbonyl groups for the rate-limitting nucleophilic attack of 1-butanol in solution, as shown in Scheme 1.

As shown in Table 3, the K_m values of "imprinted" catalytic sites of the sample gels are clearly smaller than those of the corresponding control catalysts. Repeated the preparation of catalysts demonstrated that these difference in K_ms were reproducible: The K_ms observed on several sample (imprinted) catalysts laid between 0.13—0.28 M, and those of control catalysts laid between 1.25—2.31 M. Such differences in the K_ms indicate that the "imprinted" catalytic sites of the sample gels always possess about a 10-times stronger affinity ($1/K_m$) for benzoic anhydride than those of the control gels. An exact comparison of the substrate specificity (V_{max}/K_m) of the catalytic sites between the two catalysts is impossible, since amounts of the catalytic sites are unkown here. However, the number of "imprinted" catalytic sites of a sample catalyst is assumed to be nearly same, or less than those of the corresponding control catalyst, since the two catalyst have been prepared in parallel from the same aluminium ion-doped silica gel preparation. Therefore, the "imprinted" catalytic sites of sample catalysts

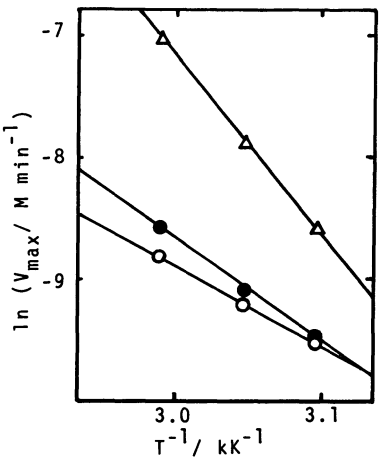

Fig. 3. Arrhenius plots for the catalyzed butanolyses. --○--: catalyst imprinted by Bz-NH-Bz, --●--: catalyst imprinted by Ph-SO_2-NH-Bz, --△--: control catalyst.

Table 3. Kinetic Parameters for Butanolysis of Benzoic Anhydride

Catalyst[a] imprinted by:	T	K_m	$10^5 \times V_{max}$	$10^5 \times V_{max}/K_m$
	°C	M	M min^{-1}	min^{-1}
Bz-NH-Bz[b]	50	0.14	4.8	34.3
	55	0.16	6.8	42.5
	62	0.18	11.2	62.2
Ph-SO_2-NH-Bz	50	0.16	5.1	31.2
	55	0.20	7.5	37.5
	62	0.33	12.5	37.9
Control	50	1.25	13.8	11.0
	55	1.67	22.7	13.6
	62	2.50	62.5	25.0
Bz-NH-Bz[c]	55	0.13	6.6	50.8
Control[f]	55	1.25	7.9	6.3

a) 700 mg. b) Bz: benzoyl. c) A set of another catalyst preparation.

Table 4. Activation Parameters for Butanolysis of Benzoic Anhydride

Catalyst imprinted by:	E_a	ΔH^*	ΔS^*
	kJ deg^{-1} M^{-1}	kJ M^{-1}	kJ deg^{-1} M^{-1}
Bz-NH-Bz[a]	63.2	60.7	−137.2
Ph-SO_2-NH-Bz	66.5	64.0	−126.4
Control	113.0	110.5	23.8

a) Bz-: benzoyl.

are assured to be more "specific" (with larger V_{max}/K_m) than the "native" catalytic sites of control catalysts.

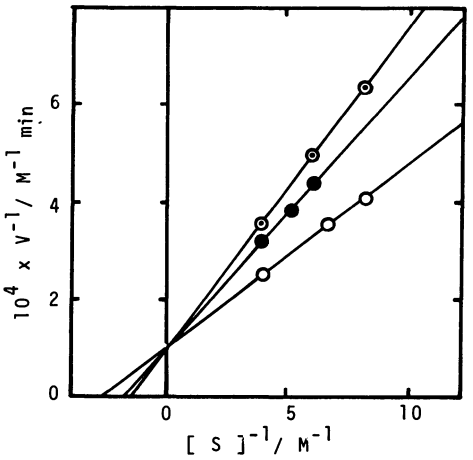

Fig. 4. Inhibitory effect of template molecules on footprint catalyst: Competitive inhibition.
Catalyst imprinted by Bz-NH-Bz; 700 mg: inhibitor; Bz-NH-Bz:
--○--: [I]=0, --●--: [I]=2×10^{-4} M, --⊙--: [I]=3×10^{-4} M.

The "imprinted" catalytic sites can also be characterized by the activation parameters, shown in Table 4. There is a distinct difference in the E_a values between the "imprinted" and the "native" catalytic sites, which confirms that the former are more effective catalytic sites, and supports the idea that an increase in the specificity of the former are caused by not only binding steps (K_m), but also by catalytic steps (V_{max}). The difference in ΔS^* values suggests that substrate molecules in transition states on the "imprinted" catalytic sites are assumed to be more firmly restricted than on the "native" catalytic sites of the control gel.

The other characteristic of the "imprinted" catalytic sites are their unusual behaviors toward the inhibitory effect by the template molecules. As shown in Figs. 4 and 5, markedly strong competitive inhibitions have been observed in catalysis on the "imprinted" catalytic sites by action of the templates used for imprinting, where the ratio of K_m/K_i is 2765 in one case. On the other hand, absolutely no inhibition by the templates has been found on Lineweaver-Burk plots (not shown) for a catalyzed reaction on "native" catalytic sites.

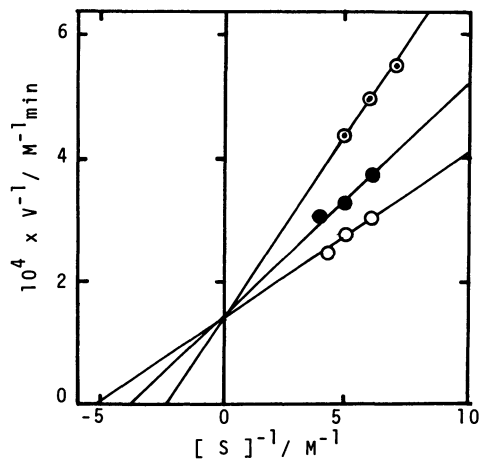

Fig. 5. Inhibitory effect of template molecules on footprint catalyst: Competitive inhibition.
Catalyst imprinted by Ph-SO_2-NH-Bz; 700 mg: inhibitor; Ph-SO_2-NH-Bz:
--○--: [I]=0, --●--: [I]=2×10^{-4} M, --⊙--: [I]=3×10^{-3} M.

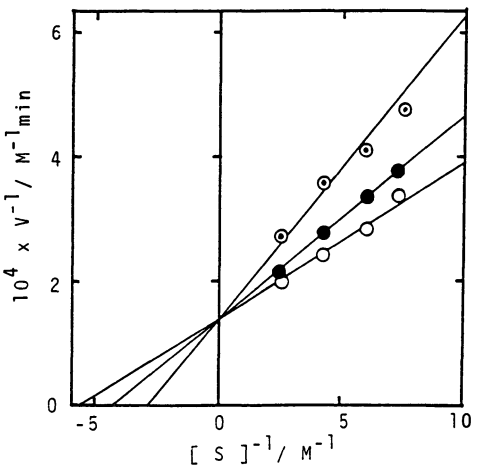

Fig. 6. Inhibitory effect of dibenzoylmethane on footprint catalyst: Competitive inhibition.
Catalyst imprinted by Bz-NH-Bz; 700 mg: inhibitor; dibenzoylmethane:
--○--: [I]=0, --●--: [I]=1.26×10^{-3} M, --⊙--: [I]=8.93×10^{-3} M.

Table 5. Inhibition Constants for Butanolysis of Benzoic Anhydride

Catalyst imprinted by:	Inhibitor:	$10^4 \times K_i$ / M	K_m / M	K_m/K_i
Bz-NH-Bz[a)]	Bz-NH-Bz	0.47	0.13	2765
Bz-NH-Bz[b)]	Bz-NH-Bz	2.50	0.50	520
Bz-NH-Bz	Dibenzoylmethane	33.70	0.16	48
Ph-SO_2-NH-Bz	Ph-SO_2-NH-Bz	1.95	0.19	974
Control	Bz-NH-Bz	No inhibition	1.54	—
Control	Ph-SO_2-NH-Bz	No inhibition	1.54	—

a) Bz-: benzoyl. b) Another catalyst preparation.

Table 6. Kinetic Parameters for Butanolysis of Phthalic Anhydride

Catalyst[a] imprinted by:	K_m(K_m[b])	$10^4 \times V_{max}$	$10^4 \times V_{max}/K_m$
	M	M min^{-1}	min^{-1}
Bz-NH-Bz	0.45 (0.16)	1.67	3.75
Ph-SO_2-NH-Bz	0.45 (0.20)	1.67	3.75
Control	0.45 (1.67)	1.67	3.75
Bz-NH-Bz[c]	0.40 (0.13)	1.79	4.48
Control[c]	0.40 (1.25)	1.79	4.48

a) 500 mg. b) K_m for benzoic anhydride. c) A set of another catalyst preparation.

Furthermore, butanolysis with another substrate, phthalic anhydride,[18] was examined in order to characterize the "imprinted" catalytic sites. No difference in Lineweaver-Burk plots (not shown) was observed between the "imprinted" and the "native" catalytic sites. As can be seen from the kinetic parameters in Table 6, the "imprinted" catalytic sites show no particular affinity for phthalic anhydride at all and simply serve as usual acidic catalytic sites.

These unusual behaviors of the "imprinted" catalytic sites cannot be attributed merely to their acidic nature, since no difference in the acidic character was detected between the two catalysts, as shown in Table 1. Therefore, it is necessary to assume the presence of particular adsorption sites of Lewis acidic nature like "footprints" of the templates used for imprinting, as illustrated in Scheme 1. The following speculation is probable regarding the formation and molecular recognition capability of the "footprints".

Isomorphic substitutions of surface silicate by aluminate can form potential Lewis acid sites which coordinate to the conjugate bases of template molecules to yield surface acid-base complexes. Among some models of Lewis acid sites of silica alumina gels reported thus far, the model proposed by Tamele[20] is the most favorable in this case, since the "imprinted" catalytic sites have been formed by surface modification in mild conditions.

The acid-base complexes must make maximal interaction, such as hydrogen bonding and hydrophobic bonding, etc., with surrounding silicates throughout a continual and reversible rearrangement being subjected to thermodynamic control, which gives rise to most energetically stable surface complexes. A subsequent repeated extraction with hot methanol forces the removal of template molecules from stable acid-base complexes; the resulting decomposition of the complexes leaves energetically unstable particular sites, "footprints", on the surface with "complementarity" toward the templates. The term "complementarity" has dual meaning, i.e., "geometric" and "electronic".[21] The latter affords the footprints "electronic strain", a situation of high energy, postulated by Blow and Steiz[21] for the active sites of enzymes. The "electronic strain" arises from an unpaired lone-pair acceptor (Lewis acid), unpaired hydrogen bond donor(s) and/or acceptor(s), and so on toward even weaker forces, as can be seen in Scheme 1. This may provide a driving force for the molecular recognition capability to the footprints. This must be an origin of the enzyme-like "specific" Lewis acid catalysis on "footprint" catalytic sites.

Since the net structure of bulk silica gel must remain unchanged and shrinking never occurs during drying, unlike Dickey's silica gel,[12] the destruction of a surface structure can be prevented and a reproducible preparation of catalytic sites can be possible.

The "footprint" catalysis reported here has unprecedented features, such as substrate specificities, turnover capability, and easy and "tailor-made" preparability, etc., which are of greater advantage than any other stoichiometric synthetic reactions using template effects on surfaces of synthetic polymers recently reported,[22] and further studies on the "footprint" catalysis are in progress.

The authors are indebted to Professor Yujiro Imanaga for his interest throughout this work and also to Ms. Naoko Matzumoto and Ms. Kazue Kobayashi for help in parts of the experiments.

References

1) D. J. Cram, P. Y. Lam, and S. P. Ho, *J. Am. Chem. Soc.*, **108**, 839 (1986).

2) V. T. D'Souza, K. Hanabusa, T. O'Leary, R. C. Gadwood, and M. L. Bender, *Biochem. Biophys. Res. Commun.*, **129**, 727 (1985).

3) R. Breslow, G. Trainor, and A Ueno, *J. Am. Chem. Soc.*, **105**, 2739 (1983).

4) J.-M. Lehn and C. Sirlin, *Chem. Commun.*, **1978**, 949.

5) F. M. Menger and M. Ladika, *J. Am. Chem. Soc.*, **109**, 3145 (1987).

6) W. P. Jencks, *Adv. Enzymol.*, **43**, 219 (1975); "Catalysis in Chemistry and Enzymology," McGraw-Hill, New York (1969).

7) M. I. Page, *Angew. Chem., Int. Ed. Engl.*, **16**, 449 (1977).

8) M. L. Sinnot, *Chem. Brit.*, **15**, 293 (1979).

9) R. Wolfenden, *Acc. Chem. Res.*, **5**, 10 (1972); *Ann. Rev. Biophys. Bioeng.*, **5**, 271 (1976).

10) K. Morihara, H. Manabe, and A. Ishino, unpublished data.

11) K. Morihara, M. Uei, and H. Namikoshi, unpublished

data.
12) F. H. Dickey, *J. Phys. Chem.*, **59**, 695 (1955).
13) "Beilstein Handbuch der Organischen Chemie," **IX**, 214.
14) J. F. Fritz and J. N. King, *Anal. Chem.*, **48**, 570 (1976).
15) P. Jundo and P. Venturello, *J. Am. Chem. Soc.*, **101**, 6606 (1979).
16) H. A. Benesi, *J. Phys. Chem.*, **61**, 970 (1957).
17) H. Pines and W. O. Haag, *J. Am. Chem. Soc.*, **82**, 2471 (1960).
18) K. Tarama, S. Teranishi, K. Hattori, and T. Ishibashi, *Shokubai (Tokyo)*, **4**, 69 (1962).
19) E. J. Greenhow, *Analyst*, **97**, 346 (1972).
20) M. W. Tamele, *Discuss. Faraday Soc.*, **8**, 270 (1950).
21) D. M. Blow and T. A. Steiz, *Ann. Rev. Biochem.*, **39**, 63 (1970).
22) G. Wulff, *Am. Chem. Soc., Symp. Ser.*, **308**, (Polym. Reagents Catal.) 186—230 (1986).

 © 1988 The Chemical Society of Japan Bull. Chem. Soc. Jpn., 61, 3999—4003 (1988)

Footprint Catalysis. II. Molecular Recognition of Footprint Catalytic Sites

Kensaku MORIHARA,* Emiko NISHIHATA, Mari KOJIMA, and Sayoko MIYAKE
Department of Chemistry, Faculty of Science, Nara Women's University,
Kitauoyanishi-machi, Nara 630
(Received March 22, 1988)

In order to investigate the molecular recognition capability of "footprint" catalytic sites, the affinities of nine "footprint" catalysts for eleven competitive inhibitors, closely related to template molecules, were estimated through the competitive inhibition constants, K_i. An examination of the affinity revealed that the recognition by "footprint" catalytic sites was so highly specific that it could recognize not only the whole, but also the partial, structures of the bound molecules.

Our preceding paper of this series[1] reported that a new imprinting procedure for aluminium ion-doped silica gel by the action of a transition state analog (i.e., dibenzamide or *N*-benzoylbenzenesulfonamide) as a template formed unprecedented "imprinted" Lewis acid sites ("footprints") with a structure complementary to the template used, and that the "footprints" showed enzyme-like specific catalytic behavior regarding the butanolysis of benzoic anhydride.

The unique specific catalysis by the footprints has been assumed to arise from the molecular recognition capability of the "imprinted" catalytic sites through their "complementarity"[1] (or "electronic strain"[2]) to the molecule of transition state analog used.

The present paper describes a further investigation regarding the molecular recognition capability of the "imprinted" catalytic sites in order to prove the assumptive "complementarity"[1] and to obtain fundamental data necessary for designing tailor-made catalysts with substrate specificity by this imprinting method.

Since both substrate specificity in catalysis and susceptibility to competitive inhibitors originate from the same "complementarity" of the footprints, an examination of the suceptibility ($=K_i$) was carried out, before any investigation of the substrate specificity.

Nine "imprinted" catalysts were prepared by the imprinting method using nine different templates which were closely related to dibenzamide or *N*-benzoylbenzenesulfonamide, respectively. They were subjected to a "cross" inhibition study, in which all catalytic sites were crosswise affected by several competitive inhibitors, including the original template, in order to estimate the binding affinity ($1/K_i$) between the catalytic sites and the inhibitors.

The magnitude of the recognition capability of the catalytic sites was defined as $-dG\{=RT\ln(1/K_i)\}$. An examination of the observed $-dG$ values proved that the recognition by the footprints were so highly specific and exact that the catalytic sites could recognize not only whole bound molecules but also even partial structures of the molecules.

Experimental

Materials. Template molecules and related compounds (**1**—**15**) were prepared by the usual pyridine-assisted acylation of benzamide, benzenesulfonamide, and their para-substituted derivatives with benzoyl chloride, *p*-toluoyl chloride, and acetic anhydride, and characterized by mp, IR (JASCO IRA-1), NMR (HITACHI R-600, 60 MHz), and elemental analysis, if necessary. Other materials were the commercial products of guaranteed grade from Nacalai Tesque Co. Ltd., which were used without further purification, if not specified.

N-Benzoylbenzenesulfonamide (**1**); mp 148 °C (lit, 147 °C).

Dibenzamide (**2**); mp 145.5—148 °C (lit, 148 °C); (Found; C, 74.81; H, 4.88; N, 6.14%).

N-Acetylbenzamide (**3**); mp 116—117 °C (lit, 115 °C); (Found; C, 66.25; H, 5.52; N, 8.58%).

N-Benzoyl-*p*-toluenensulfonamide (**4**); mp 145 °C (lit, 147—150 °C).

N-(*p*-Toluoyl)-*p*-toluenesulfonamide (**5**); mp 138—139 °C; IR(Nujol) 3300 (N–H), 1700 (C=O), 1345 and 1175 cm^{-1} (SO_2); ^1H NMR ($CDCl_3$) δ=8.18—6.87 (m, 8H, ArH), 2.36 (s, 3H, CH_3–), and 2.29 (s, 3H, CH_3–); (Found; C, 61.98; H, 5.20; N, 4.78%).

N-Acetylbenzenesulfonamide (**6**); mp 125—126 °C; IR (Nujol) 1690 (C=O), 1360 and 1165 cm^{-1} (SO_2); ^1H NMR ($CDCl_3$) δ=9.47 (s, 1H, NH), 8.40—7.35 (m, 5H, ArH), and 2.05 (s, 3H, CH_3–); (Found; C, 48.38; H, 4.57; N, 7.00%).

N-Benzoyl-4-(decanoylamino)benzenesulfonamide (**7**); mp 211 °C; IR (Nujol) 3285, 3200 (N–H), 1720, 1695 (C=O), 1340 and 1180 cm^{-1} (SO_2); ^1H NMR($CDCl_3$) δ=7.26 (m, 9H, ArH), 1.90 (s, 2H, $-CH_2-CO-$) and 0.98 (s, 3H, CH_3–); (Found; C, 63.89; H, 7.01; N, 6.66%).

N-Benzoyl-4-(acetamido)benzenesulfonamide (**8**); mp 257—260 °C; IR (Nujol) 3300 (N–H), 1655 (C=O), 1535 (amide II), 1320 and 1170 cm^{-1} (SO_2); ^1H NMR ($CDCl_3$) δ=7.22 (m, 9H, ArH) and 1.47 (s, 3H, CH_3–).

4-(Decanoylamino)benzenesulfonamide (**9**); prepared by chlorosulfonation and succesive amination of decananilide; mp 207—209 °C; IR (Nujol) 3265 (N–H), 1685 (C=O), 1535 (amide II), 1320 and 1155 cm^{-1} (SO_2); ^1H NMR($CDCl_3$) δ=7.24 (m, 4H, ArH), 1.95 (s, 2H, $-CH_2-CO-$), 1.51 (m, 14H, $-CH_2-$), and 0.96 (s, 3H, CH_3–); (Found; C, 59.11; H; 8.00; N, 8.62%).

4-(Acetamido)benzenesulfonamide (**10**); mp 219.5 °C (lit, 219 °C).

N-Acetyl-4-(decanoylamino)benzenesulfonamide (**11**); mp

165 °C; IR(Nujol) 3340, 3290 (N-H), 1730, 1690 (C=O), 1520 (amide II), 1320, 1160 cm^{-1} (SO_2); ^1H NMR ($CDCl_3$) δ=8.1—7.1 (m, 6H, ArH), 2.01 (s, 2H, $-CH_2-CO-$), 1.49 (s, 14H, $-CH_2-$) and 1.21 (S, 6H, CH_3-); (Found; C, 58.77; H, 7.72; N, 7.71%).

N-Acetyl-4-(acetamido)benzenesulfonamide (**12**); mp 251°C; IR(Nujol) 3330(N-H), 1705, 1680(C=O), 1550 (amide II), 1320 and 1170 cm^{-1} (SO_2); ^1H NMR ($CDCl_3$) δ=7.24 (m, 4H, ArH), and 1.52 (s, 6H, CH_3-); (Found; 46.79; H, 4.64; N, 11.00%).

N-Benzoyl-4-(methanesulfonamido)benzenesulfonamide (**13**); mp 264—267 °C; IR (Nujol) 3190 (N-H), 1690 (C=O), 1350, 1330, 1170, and 1140 cm^{-1} (SO_2); ^1H NMR (DMSO-d_6) δ=7.50 (m, 9H, ArH) and 3.22 (s, 3H, CH_3-SO_2-); (Found; C, 47.49; H, 3.83; N, 8.04%).

4-(Methanesulfonamido)benzenesulfonamide (**14**); prepared by methanesulfonylation of sulfanilamide; mp 184—187 °C; IR (Nujol) 3400, 3310, 3260 (N-H), 1625, 1350 and 1170 cm^{-1} (SO_2); ^1H NMR (DMSO-d_6) δ=7.6 (m, 4H, ArH) and 3.19 (s, 3H, CH_3-SO_2-); (Found; C, 33.73; H, 3.93; N, 11.10%).

Diacetamide **15**; prepared from acetamide according to a method described in the literature.[2] Mp 75—76 °C (lit, 77.5—78 °C).

Dibenzoylmethane **16**; recrystallized from ethanol. mp 74.5 °C (lit, 77.5—78 °C).

Catalysts. The preparation procedures and acid sites characterizations of catalysts were the same as those described in the preceding paper, except for the use of different compounds as templates.

Kinetic Measurement. The reaction conditions and procedures were the same as those reported in the preceding paper, i.e., 1-butanolysis of benzoic anhydride at 55 °C in 1-butanol–benzene mixture (30:70 v/v), and the kinetic parameters, V_{max}, K_m, and K_i were obtained as usual from Lineweaver–Burk plots.

Reslts and Discussion

All the butanolyses obeyed Michaelis–Menten kinetics with respect to the concentration of benzoic anhydride; the kinetic parameters for catalized reactions are shown in Table 1. Some typical competitive inhibition plots are shown in Figs. 1—5. A coincidence of the intercepts on the $1/V$ axis were observed in all Lineweaver–Burk plots in the presence of different inhibitors (Figs. 2—5), which confirmed that all the different inhibitors were bound onto the same catalytic sites. Therefore, the affinities of a catalytic site for different inhibitors can be estimated and significantly compared with each other. The affinity, molecular recognition, by the catalytic sites is

Table 1. Kinetic Parameters of Footprint Catalysts

Footprint catalyst {N}[a]	K_m	$10^5 \times V_{max}$[b]
	M[c]	M min^{-1}
{**1**}	0.54	40.9
{**1**}[d]	0.57	31.7
{**2**}	0.19	19.0
{**2**}[d]	0.50	35.7
{**3**}	0.54	3.6
{**3**}[d]	1.05	6.5
{**4**}	0.17	19.0
{**5**}	0.29	21.1
{**7**}	0.13	8.1
{**8**}	0.06	4.7
{**8**}	0.23	10.2
{**9**}	0.35	11.2
{**13**}	0.08	1.3

a) Footprint catalyst {**N**} represents the catalyst imprinted by template **N**. b) Per catalyst 1.0 g. c) 1 M=1 mol dm^{-3}. d) Other catalyst preparation used mainly in preliminary experiments.

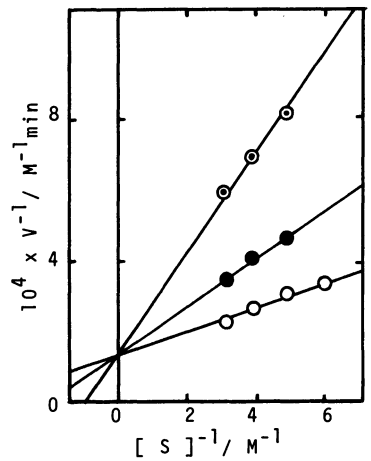

Fig. 1. A criterion for footprint catalytic sites; competitive inhibition of the catalyst {**8**} by the original template **8**. Catalyst {**8**} (K_m 0.23 M), 700 mg; $V=V_{obs}-V_{uncat}$; [S]=benzoic anhydride concentration; [I]=inhibitor (=template **8**) concentration. ○: [I]=0, ●: [I]=3.0×10^{-4} M, ⊙: [I]=5.0×10^{-4} M, $K_i=2.79\times10^{-4}$ M, $-dG=RT\ln(1/K_i)$=22.3 kJ.

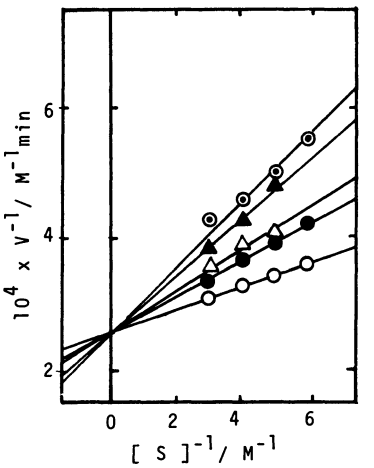

Fig. 2. Competitive inhibition of footprint catalyst {**8**} by **1**, **8**, **10**, and **12**.
Catalyst {**8**} (K_m 0.06 M), 700 mg; [I]=5.0×10^{-4} M; ⊙: by **8**, $K_i=2.62\times10^{-4}$ M ($-dG$=22.6 kJ), ▲: by **10**, $K_i=3.29\times10^{-4}$ M (21.8 kJ), △: by **12**, $K_i=5.46\times10^{-4}$ M (20.5 kJ), ●: by **1**, $K_i=8.22\times10^{-4}$ M (20.1 kJ), ○: no inhibitor.

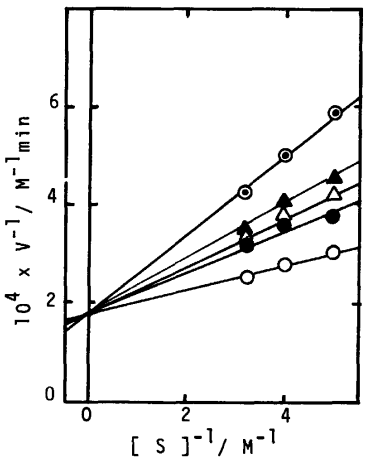

Fig. 3. Competitive inhibition of footprint catalyst {7} by **1**, **7**, **9**, and **11**.
Catalyst {7} (K_m 0.13 M), 700 mg; [I]=5.0×10^{-4} M; ⊙: by **7**, K_i=2.05×10^{-4} M (−dG=23.0 kJ), ▲: by **9**, K_i=3.56×10^{-4} M (21.8 kJ), △: by **11**, K_i=4.53×10^{-4} M (20.9 kJ), ●: by **1**, K_i=5.59×10^{-4} M (20.5 kJ), O: no inhibitor.

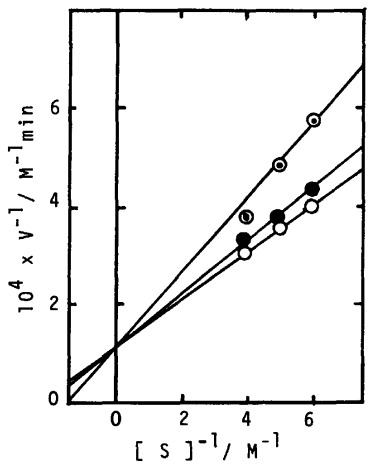

Fig. 4. Competitive inhibition of footprint catalyst {9} by **1** and **9**.
Catalyst {9} (K_m 0.35 M), 700 mg; [I]=3.0×10^{-4} M; ⊙: by **9**, K_i=4.32×10^{-4} M (−dG=21.3 kJ), ●: by **1**, K_i=2.77×10^{-3} M (15.9 kJ), O: no inhibitor.

expressed by the negative value of the free-energy change on binding; $-dG=RT\ln(1/K_i)$, where K_i is a competitive inhibition constant.

As can be seen in Table 2, each catalytic site reveals the maximum affinity(specified by *) for its original template (the template used in imprinting process.) as an inhibitor without exception. This fact strongly suggests that the molecular recognition capability of the footprints must be closely related to its formation process, and that the it must arise from a "complementarity" to its original template. Since molecular recognition is based on the "complementarity",[1] ("electronic strain"),[2] the magnitude of the affinity for a bound molecule greatly depends upon the resemblance in shapes and structures between the original template of the footprint and the inhibitors, e.g., footprint {1}* clearly differentiates **1** from **3**, **4**, **5**, **6**, and **15** by more than 14.7 kJ (=23.9−9.2 kJ; dG for **3**), whereas it hardly differentiates **1** from the structurally resembling **2** by only 1.3 kJ (=23.9−22.6 kJ), and similar feature is also seen on footprint {2} and {3}. Footprints show less affinity for molecules and/or groups that are too small to fit into the "complementary" structures, e.g., footprint {2} prefers **2** to **3** by 14 kJ, and exclude molecules and/or group that are too large to fit the structures, e.g., footprint {1} excludes **4** and **5** by about 20 kJ.

* Footprint{N} represents the footprint imprinted by template **N**.

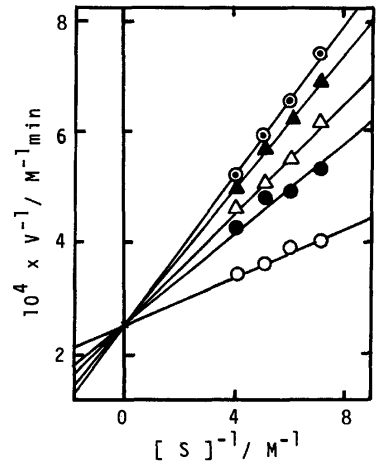

Fig. 5. Competitive inhibition of footprint catalyst {13} by **1**, **8**, **13**, and **14**.
Catalyst {13} (K_m 0.08 M), 300 mg; [I]=5.0×10^{-4} M; ⊙: by **13**, K_i=2.29×10^{-4}M (−dG=23.0 kJ), ▲: by **14**, K_i=2.68×10^{-4} M (22.6 kJ), △: by **8**, K_i=3.68×10^{-4} M (21.8 kJ), ●: by **1**, K_i=5.59×10^{-4} M (20.5 kJ), O: no inhibitor.

It should be noted that the magnitude of differentiation by the "imprinted" catalytic sites mentioned above is sufficiently large to be comparable to those by the "built-in" receptor sites of macrocycles, considering that 18-crown-6 differentiates K^+ from Na^+ by 10.15 kJ,† and dibenzo-18-crown-6 does so by 3.66 kJ† in methanol at 25 °C.

Furthermore, an examination of the data in Table 2 proves that the affinity for whole molecules(dG_w) can be expressed as the sum of those for partial structures(dG_p s) of the binders(inhibitors and templates); $dG_w=\sum dG_p$, as shown in Scheme 1. Assuming that the footprint {7} consists of three subsites (**X**, **Y**, **Z**) (**X** is situated for the *p*-substituent moiety, **Y** for the benzenesulfonamide moiety, and **Z** for the *N*-acyl

† Calculated from data in Ref. 4.

Table 2. Molecular Recognition by Footprints; Specific Affinities

Inhibitor	Molecular recognition by footprint {N}; $-dG\{=RT\ln(1/K_i)\}$/kJ								
	{1}	{2}	{3}	{4}	{5}	{7}	{8}	{9}	{13}
1: Ph-SO_2-NH-Bz	23.9*	20.5	8.0			20.5	20.1	15.9	20.5
2: Bz-NH-Bz	22.6	22.6*	8.4						
3: Ac-NH-Bz	9.2	8.4	13.0*						
4: Tosyl-NH-Bz	2.9	2.9		21.3*	4.6				
5: Tosyl-NH-Toluoyl	4.2	0.0	4.2		18.8*				
6: Ac-NH-Tosyl	5.0	0.8	2.9						
	7.1**	3.3**	10.9**						
7: *p*-(C_9H_{19}-CO-NH-)C_6H_4-SO_2-NH-Bz						23.0*			
8: *p*-(Ac-NH-)C_6H_4-SO_2-NH-Bz							22.6*		21.8
9: *p*-(C_9H_{19}-CO-NH-)C_6H_4-SO_2-NH_2						21.8		21.3*	
								21.8**	
10: *p*-(Ac-NH-)C_6H_4-SO_2-NH_2							21.8		
11: *p*-(C_9H_{19}-CO-NH-)C_6H_4-SO_2-NH-Ac						20.9			
12: *p*-(Ac-NH-)C_6H_4-SO_2-NH-Ac							20.5		
13: *p*-(Mesyl-NH-)C_6H_4-SO_2-NH-Bz									23.0*
14: *p*-(Mesyl-NH-)C_6H_4-SO_2-NH_2									22.6
15: Ac-NH-Ac	6.7	2.5	10.9						
	7.3**	6.3**	11.1**						
16: Bz-CH_2-Bz		15.5							

* Maximum values of molecular recognition of footprints to the original template molecules. ** Values calculated from partial affinities shown in Table 4.

Binding of inhibitor **7** onto footprint {7}[a)]
C_9H_{19}-CO-NH-/-C_6H_4-SO_2-NH-/-CO-C_6H_5 $dG=dG_x+dG_y+dG_z=23.0$ kJ
/----**X**-------//--------**Y**---------//------**Z**---/
subsite **X** subsite **Y** subsite **Z**
Binding of **9** onto fotprint {7}
C_9H_{19}-CO-NH-/-C_6H_4-SO_2-NH_2 $dG=dG_x+dG_y=21.8$ kJ
/---**X**------//-------**Y**------//---**Z**---/

Binding of **1** onto footprint {7}
C_6H_5-SO_2-NH-/-CO-C_6H_5 $dG=dG_y+dG_z=20.5$ kJ
/----**X**-----//------**Y**---------//------**Z**---/
Binding of **11** onto footprint {7}
C_9H_{19}-CO-NH-/-C_6H_4-SO_2-NH-/-CO-CH_3 $dG=dG_x+dG_y+dG_z=20.9$ kJ
/----**X**---------//------**Y**-------//---**Z**---/

a) Footprint {7} represents the footprint imprinted by template **7**.

Scheme 1. Estimation of partial affinities of footprints.

moiety), then the difference in affinity (1.2 kJ=dG_z) between dG_w (23.0 kJ) of the footprint {7} for inhibitor-(=template) **7** and dG_w (21.8 kJ) of the footprint {7} for inhibitor **9** can be attributable to the partial affinity of the subsite *Z* for the benzoyl moiety of the inhibitor **7**. Similarly, the difference (2.5 kJ=dG_x) between dG_w (20.5 kJ) of the footprint {7} for the inhibitor **1** and dG_w (23.0 kJ) of the footprint {7} for the inhibitor **7** can also be attributed to a partial affinity of subsite **X** for decanoylamino group of inhibitor **7**. The residual affinity (19.3 kJ) should be ascribed to the partial affinity of subsite **Y** for benzenesulfonamide moiety of the inhibitor **7**.

Table 3. Estimated Partial Footprint Affinities

Inhibitors bound	Footprint {N}*	dG (kJ)	$=dG_x+$	dG_y+	dG_z
7	{7}	23.0	= 2.5 +	19.3 +	1.2
8	{8}	22.6	= 2.5 +	19.3 +	0.8
				av.	1.0
13	{13}	23.0	= 2.5 +	20.1 +	0.4
11	{7}	20.9	= 2.5 +	19.3 −	0.9
12	{8}	20.5	= 2.5 +	19.3 −	1.3
				av.19.5	av. −1.1

* Footprint {N} represents the footprint imprinted by template **N**.

Similar substructive treatments are applicable to footprints {8} and {13}, as shown in Table 3. A closely similar feature is observed in the dG_y and dG_z values, which are identical within experimental errors. The

Table 4. Molecular Recognition of Subsites of Footprints toward Partial Structures of Bound Molecules

Partial structures (**A**-**H**) of bound molecules onto subsite **Y**;	Partial affinity ($-dG_p$/kJ) of subsite **Y**{N}* toward **A**-**E**; {N} = {A},	{B},	{C},	{D},	{E}
A; Ph-SO_2-NH-	22.9	19.5		19.5	7.0
B; Ph-CO-NH-	21.6	21.6			7.4
C; *p*-CH_3-C_6H_4-SO_2-NH-			21.3		
D; *p*-NH-C_6H_4-SO_2-NH-				19.3	
E; CH_3-CO-NH-	8.2	7.4			12.0

subsite **Z**;	$-dG_p$ of subsite **Z**{N}* toward **F**-**G**; {N} = {G}	{no footprint}
F; -SO_2-Ph	−1.1	
G; -CO-Ph	1.0	−12.1
H; -CO-CH_3	−1.1	

subsite **X**;	$-dG_p$ of subsite **X**{N}* toward **I**-**K**; {N} = {I}	{J}	{K}
I; *p*-(CH_3-CO-NH-)	2.5		1.2
J; *p*-(C_9H_{19}-CO-NH-)		2.5	
K; *p*-(CH_3-SO_2-NH-)			2.5

* Subsite **Y**{N} represents the subsite **Y** of the footprint imprinted by template **N**.

dG_y values (19.3—20.1 kJ) are much higher than the dG_z values (0.4–1.2 kJ) and the dG_x value (2.5 kJ), which indicates that only one Lewis acid site has been formed and located at subsite **Y** (in each case).

Footprints {**7**}, and {**8**} differentiate acetyl groups of inhibitors **11** and **12** from th benzoyl groups of inhibitors **7** and **8**, respectively, with a negative partial affinity (−0.9, −1.3 kJ). This reveals that an enforced binding occurs to give an intramolecular strain to the bound molecule since the catalytic sites are rigid.

The partial affinities of footprints can be estimated from the data given in Table 2 and shown in Table 4. In the estimation process, the average value of dG_z (1.0 kJ) of footprints {**7**} and {**8**} was used as a starting standard value under the assumption of a priority order for subsite **Y**, *N*-acetyl > -C_6H_4-SO_2-NH- > *N*-benzoyl, because all the inhibitors in Table 2 are ambiguous in action mode during the imprintig and the binding(inhibition) processes. Such a priority order is therefore necessary to define their action mode in the inhibition. Only the above order has offered reasonable estimates agreeable to the observed values shown in the Table 2. The true calculated values (** in Table 2) obtained from the partial footprint affinity (Table 4) agree reasonably well with the practically reliable observed values (> ca. 5 kJ). This finding confirms that the assumption that $dG_w = \sum dG_p$ is reasonable, i.e., the molecular recognition of the footprints can govern even the partial structures of the bound molecules. It also shows that the data given in Table 3 are reliable as a whole.

Though the values given in Tables 2 and 4 have been obtained only from the present catalyst preparations and the reaction system employed in the present work, the whole feature might not change so very much in other reaction systems.

Since the specific affinities and intramolecular strain effects would be essential in enzymatic catalysis,[5] the data for the partial affinities and strains shown in Tables 2 and 3 might be applicable to the design of tailor-made enzyme-simulated catalysts with any substrate specificities. Various attempts are now in progress.

References

1) K. Morihara, S. Kurihara, and J. Suzuki, *Bull. Chem. Soc. Jpn.*, **61**, 3991 (1988).

2) D. M. Blow and T. A. Steiz, *Ann. Rev. Biochem.*, **39**, 63 (1970).

3) "Beilstein Handbuch der Organischen Chemie" **II**, 181.

4) H. K. Frensdorff, *J. Am. Chem. Soc.*, **93**, 600, 606 (1971).

5) W. P. Jencks, *Adv. Enzymol.*, **43**, 219 (1975); "Catalysis in Chemistry and Enzymology," McGraw-Hill, New York (1969).

 © 1988 The Chemical Society of Japan Bull. Chem. Soc. Jpn., 61, 4005—4014 (1988)

The Photochemistry of Steroidal 6-Membered Cyclic α-Nitro Ketones[1)]

Hiroshi SUGINOME,* Yoshitaka KUROKAWA, and Kazuhiko ORITO
Organic Synthesis Division, Department of Chemical Process Engineering,
Faculty of Engineering, Hokkaido University, Sapporo 060
(Received April 25, 1988)

The results of the photolysis of five steroidal 6-membered cyclic α-nitro ketones in ethanol are described. Irradiation with a Pyrex-filtered light of 2-nitro-5α-cholestan-3-one in ethanol, which exists exclusively in the enol form in the solvent, resulted in a new photorearrangement and gave 5α-cholestane-2,3-dione 3-oxime with the accompanying formation of the corresponding α-diketone. We propose a path involving a nitro–nitrite rearrangement for this anomalous formation of 5α-cholestane-2,3-dione 3-oxime. However, similar irradiation of 4,4-dimethyl-2-nitro-5α-choloestan-3-one, which exists exclusively as the enol form in ethanol, and 3-nitro-5α-cholestan-2-one, which is in an 1:1 equilibrium mixture of keto and enol forms in ethanol, gave the corresponding α-hydroxyimino ketone and α-diketone respectively. Irradiation of 4β-nitro-5β-cholestan-3-one and 6α-nitro-5α-cholestan-7-one, both of which exist as the keto form in ethanol, gave similarly the corresponding α-hydroxyimino ketone respectively, but without the accompanying formation of α-diketone. The α-hydroxyimino ketones from the above four 6-membered cyclic α-nitro ketones arise through the hydrogen abstraction by the n,π* excited nitro group of the keto forms of the α-nitro ketones followed by the elimination of the element of water, while α-diketones are formed via the nitro–nitrite rearrangement of the excited nitro group of the enol forms.

In connection with our studies of nitrite photolysis[2)] and of photoinduced nitro–nitrite rearrangement,[3)] we have been interested, too, in the photochemistry of cyclic α-nitro ketones.

In this paper, we report the photochemistry of five steroidal 6-membered cyclic α-nitro ketones, three of which exist in solution predominantly in their enol form. The photochemistry of cyclic α-nitro ketones which in solution exist in their keto forms has been reported by Reid and Tucker, who found that 2-nitrocycloheptanone and α-nitro camphor rearrange to give cyclic *N*-hydroxy imides and α-hydroxyimino ketones on irradiation in solution.[4)]

Results

Preparations and Structures of the α-Nitro Ketones. Five steroidal 6-membered cyclic α-nitro ketones, 2-nitro-5α-cholestan-3-one (**3**)[5,6)] 4,4-dimethyl-2-nitro-5α-cholestan-3-one (**4**), 3-nitro-5α-cholestan-2-one (**11**), 4β-nitro-5β-cholestan-3-one (**13**), and 6α-nitro-5α-cholestan-7-one (**17**),[6)] chosen for the present study, were prepared by mononitration of the corresponding steroidal ketones with alkyl nitrate and bases.[7,8)]

We found that nitration of 5α-cholestan-3-one (**1**) under the conditions reported by previous investigators [butyl nitrate (3.35 mol) and potassium *t*-butoxide (5.78 mol) in *t*-butyl alcohol at 17—20 °C][5)] led to the substantial formation of α,ω-dinitro secosteroid; this arose from the hydrolytic cleavage of the dipotassium salt of α,α′-dinitro ketone.[9)] The formation of α,ω-dinitro secosteroid as a by-product in the nitration of ketone **1** with an excess of ethyl nitrate and potassium *t*-butoxide in THF at −40—0 °C has also been reported by Meakins and his colleagues.[6)] We found that the formation of the α,ω-dinitro secosteroid that is formed by the hydrolysis of the dipotassium salt of 2,4-dinitro-5α-cholestan-3-one can be avoided; no α,ω-dinitro secosteroids or ω-nitro carboxylic esters[7)] that arise from cleavage reactions were found in the products when a lesser amount of a base was used [propyl nitrate (2.9 mol) and potassium *t*-butoxide (2.6 mol)].

All five steroidal 2-nitro ketones are crystalline compounds. The IR spectra of 2-nitro-5α-cholestan-3-one (**3**) in Nujol exhibited strong bands at 1616 and 1513 cm^{-1} due to the carbon–carbon double bond and a conjugated nitro group. There were also very weak bands at 1746 and 1561 cm^{-1} owing to the carbonyl and a nonconjugated nitro group. 2-Nitro-5α-cholestan-3-one (**3**) seems therefore to exist almost exclusively as its enol form in the mulled state although a small portion exists as the keto form.[10)]

The absence of any bands due to the presence of non-conjugated 2-nitro ketone indicates that 4,4-dimethyl-2-nitro-5α-cholestane (**4**) in the mulled state exists exclusively in its enol form. The IR spectrum of 3-nitro-5α-cholestan-2-one (**11**) in Nujol exhibited two bands at 1619 and 1509 cm^{-1} due to the conjugated nitro group, and two bands at 1735 and 1562 cm^{-1} due to the carbonyl and nonconjugated nitro groups. It is clear that this nitro ketone in the mulled state exists as an equilibrium mixture of the keto and enol forms. On the other hand, the IR spectra of 4β-nitro-5β-cholestan-3-one (**13**) and 6α-nitro-5α-cholestan-7-one (**17**) indicated that these ketones in the mulled state exist almost exclusively in their keto form (Table 1).

The ^1H NMR spectra of 2-nitro-5α-cholestan-3-one (**3**) and its 4,4-dimethyl derivative (**4**) in $CDCl_3$ indicated that these 2-nitro ketones in the solution exist entirely as their enol form (see Experimental). It thus becomes apparent that these 2-nitro ketones in a more polar protic solvents such as the ethanol used in the present photolysis exist exclusively in their enol form.

In contrast to the behavior of these 2-nitro ketones,

Table 1. Infrared Absorptions of Cyclic α-Nitro Ketones[a]

α-Nitro ketone	Absorptions of functional groups (cm^{-1})	
	HO-C=C-NO_2	O=C-CH-NO_2
3	1513 and 1616	1561[b] and 1746[b]
4	1513 and 1605	—
11	1509 and 1619	1562 and 1735
13	—	1558 and 1714
17	—	1558 and 1728

a) In Nujol mull. b) A very weak band.

the ^{1}H NMR spectrum of 3-nitro-5α-cholestan-2-one (**11**) in $CDCl_3$ exhibited the presence of signals assignable to the 3α-H of its keto form (see Experimental) and indicated that it exists in an equilibrium with the enol form in $CDCl_3$. The ^{1}H NMR spectrum of **11** in methanol exhibited a singlet at δ 0.69 and a doublet of a doublet at δ 5.60 (J=7.2 and 11.9 Hz); these were assignable to the 18-H and the 3α-H of its keto form respectively; there was also a singlet at δ 0.71, assignable to the 18-H of its enol form. The ratio of the keto and enol forms in methanol estimated by their signal area was 45.5:54.5.

The ^{1}H NMR spectra of 4β-nitro-5β-cholestan-3-one (**13**) and 6α-nitro-5α-cholestan-7-one (**17**)[6] in $CDCl_3$ indicated that in solution they exist exclusively in their keto forms.

The aliphatic nitro group is known to exhibit two absorption bands, one in 210 nm and another in the 270—280 nm region.[11] The band at the lower wavelengths with a low intensity is due to the n→π* transition while the 210 nm band is due to the π→π* transition.[12-14] The α,β-unsaturated nitro compounds, on the other hand, are known to show absorption maxima with high intensity; these are assignable to the π→π* transitions, in the region 220—250 nm.[11-14]

The absorption maxima and the intensities of the UV spectra of the above five α-nitro ketones in three solvents are summarized in Table 2. The spectral data are in agreement with the conclusion on the keto-enol equilibria deduced by the ^{1}H NMR spectroscopy. 2-Nitro-5α-cholestan-3-one **3** and its 4,4-dimethyl derivative **4** in ethanol exhibited intense absorption maxima due to the π→π* transitions of a conjugated nitro group at 343 and 337 nm. The displacement of the absorption maxima to the longer wavelengths, when compared with the absorption maxima of the corresponding nitro olefins, is attributable to the effects of the additional hydroxyl group in the chromophore.

The nitro ketones **3** and **4** also exhibited intense absorption maxima at 310 and 315 nm in hexane respectively although their intensities were reduced in hexane in the case of **3** presumably owing to the presence of a greater amount of the keto form in the nonpolar solvent. 3-Nitro-5α-cholestan-2-one (**11**) exhibited weaker absorption maxima at 330 nm in ethanol and at 312 nm in hexane, assignable to the π→π* transitions. The decreased intensities are apparently due to the greater extent of the keto form. As expected, the intensities of absorptions due to the enol forms of the above three α-nitro ketones enhanced in ethanol containing sodium ethoxide where these α-nitro ketones exist exclusively in their enol forms.

Table 2. UV Spectra of 6-Membered Cyclic α-Nitro Ketones

	λ_{max}/nm (ε)		
	EtOH	Hexane	EtOH-NaOEt
3	343 (14800)	310 (8900)	338 (13800)
4	337 (12300)	315 (10400)	330 (18400)
11	330 (5100)	312 (7700)	338 (14900)
13	345 (60) 284 (110)	270—330 (ca. 400)	342 (450) 235 (9800)
17	239 (1550) 291 (220)	226 (1890) 274 (160)	235 (6500)

6α-Nitro-5α-cholestan-7-one (**17**), on the other hand, exhibited broad weak absorption at 274 nm in hexane. The absorption maximum is assignable to the n→π* transition of the nitro- and/or the carbonyl groups on the basis of a bathochromic shift of the band in ethanol as well as its intensity. This α-nitro ketone **17** was found to be hardly enolizable at room temperature since no appreciable change of the UV spectrum was observed when it was taken in ethanol containing sodium ethoxide.

4β-Nitro-5β-cholestan-3-one (**13**) in hexane exhibited broad and weak absorption maxima from 270 to 330 nm attributable to the n→π* transitions of the nitro and/or the carbonyl group of the keto form as well as the band attributable to the π→π* transition of the conjugated nitro group of the enol form which is present in a trace amount.

Photochemistry of Cyclic α-Nitro Ketones. (a) 2-Nitro-5α-cholestan-3-one (3) (Scheme 1). Photolysis of **3** in ethanol with a Hanovia 450-W high pressure Hg arc through Pyrex for 2.5 h in an atmosphere of nitrogen gave a product mixture from which a crystalline mixture of diosphenols, (22.5%) 2-hydroxy-5α-cholest-1-en-3-one (**5a**) and its isomer **5b**,[15-21] as well as a ketonic product **6** (11.6%) were isolated by means of preparative TLC (Scheme 1). No other pure

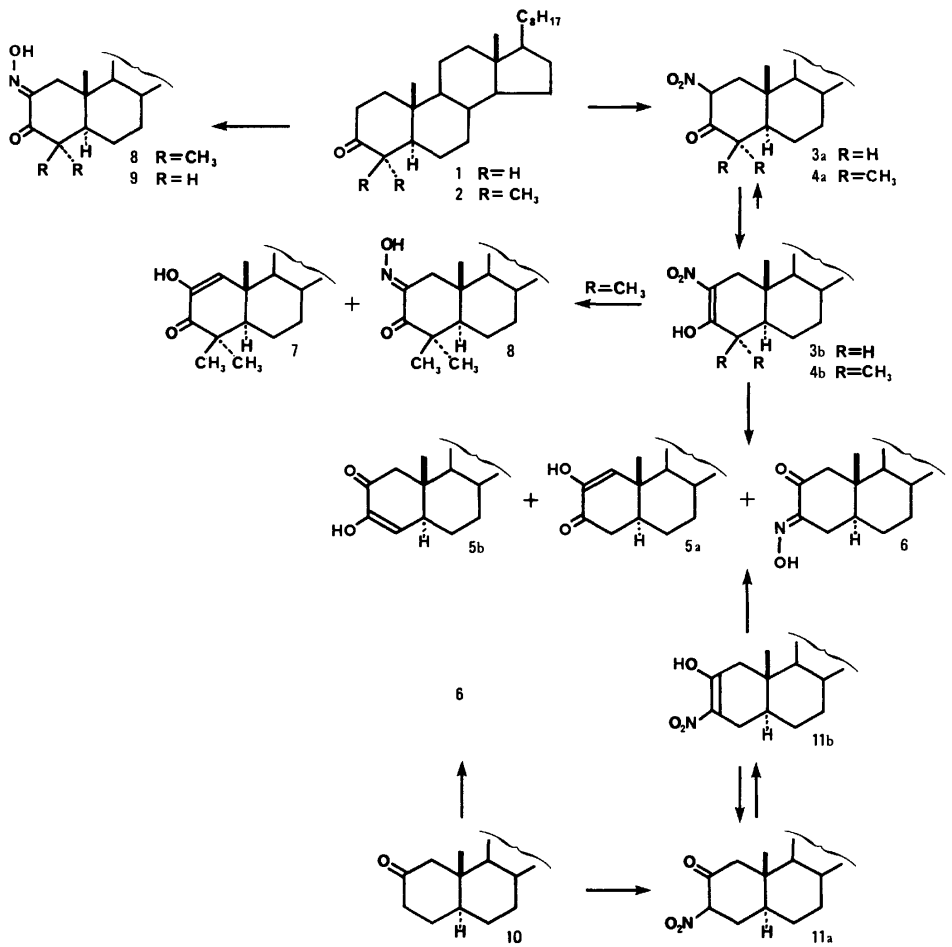

Scheme 1.

products were isolated. Recrystallization of the mixture of diosphenols from ethanol gave a mixture of **5a** and **5b**. The ratio of **5a** and **5b** determined before and after recrystallization by ^{1}H NMR spectroscopy was approximately 1:1.

High resolution mass spectrometry indicated that the ketonic product **6** has the molecular formula $C_{27}H_{45}NO_2$. The IR spectrum exhibited a series of bands assignable to a hydroxyimino and an unstrained carbonyl group. The ^{1}H NMR spectrum of **6** exhibited two one-proton doublets at δ 2.77 and 2.09 (J=17.58 Hz) and a doublet of a doublet centered at δ 2.99 (J=19.42 and 5.5 Hz). These spectral results suggested that the structure of **6** was either 5α-cholestane-2,3-dione 2-oxime (**8**)[6,16,22,23] or 5α-cholestane-2,3-dione 3-oxime (**6**). The structure of **6** was determined to be the latter by a direct comparison between oximes **6** and **8** prepared by means of nitrosation of 5α-cholestan-2-one and 5α-cholestan-3-one. The oxime **6** obtained by the photolysis was identical with the oxime prepared by the nitrosation of 5α-cholestan-2-one and differed from the oxime prepared by the nitrosation of 5α-cholestan-3-one. The signals at δ 2.77, 2.09, and 2.99 in the ^{1}H NMR of **6** were then assignable to the 1α-H, 1β-H, and 4α-H respectively. The considerable downfield shift of the signal due to the 4α-H is attributable to the deshielding by the hydroxyl group of the hydroxyimino function and indicates that the hydroxyl of the hydroxyimino group was oriented anti to the 2-carbonyl group.[24] The ^{1}H NMR spectrum of **8** exhibited two doublets at δ 1.93 and 3.22 assignable to the 1α-H and 1β-H. The considerable downfield shift of the signal due to the 1β-H is similarly attributable to the deshielding by the hydroxyimino group, which is oriented anti to the carbonyl group.

(b) Photolysis of 4,4-Dimethyl-2-nitro-5α-cholestan-3-one (4) (Scheme 1). Photolysis of 4,4-dimethyl derivative **4** was then undertaken. The photolysis of **4** in ethanol for 1 h under the same conditions as for the photolysis of **3b** led to a 76% conversion of the oxime and gave a mixture of the products. Preparative TLC of the products gave a diosphenol, 4,4-dimethyl-2-hydroxy-5α-cholest-1-en-3-one (**7**),[25,26] and ketonic product **8** in 22% and 11.6% yields. The structure of **8** was deduced by means of spectroscopy (see Experimental). High resolution mass spectrometry indicated that the ketonic product **8** had the molecular

formula $C_{29}H_{49}NO_2$. The IR spectrum exhibited bands assignable to a hydroxyimino and an unstrained carbonyl group. The ^1H NMR spectrum indicated two doublets at δ 2.17 and 3.03 (J=18.7 Hz). These spectral results suggested that the structure of the product was 4,4-dimethyl-5α-cholestane-2,3-dione 2-oxime (**8**).[27] This assumed structure was confirmed by a direct comparison with the specimen obtained by the synthesis. The signals at δ 2.81 and 3.02 in the ^1H NMR spectrum are assignable to the 1α-H and 1β-H respectively. Thanks to a considerable shift of the signal of the 1β-H to the low field in comparison with the signal of the 1α-H, it was confirmed that the hydroxyl group in the hydroxyimino group is again oriented anti to the carbonyl group.

(c) Photolysis of 3-Nitro-5α-cholestan-2-one (11). Photolysis of nitro ketone **11** in ethanol with a Eikosha 500-W high pressure Hg arc through a Pyrex for 3 h in an atmosphere of nitrogen resulted in a 93% conversion of the nitro ketone and gave a mixture of products from which we obtained a poor yield of the diosphenols, 5α-cholestane-2,3-dione (**5a** and **5b**)(4%) produced by the photolysis of nitro ketone **3** and a ketonic product **6** (18%). The product **6** had the molecular formula $C_{27}H_{45}NO_2$ and was identical in every respects with 5α-cholestane-2,3-dione 3-oxime (**6**) obtained by the photolysis of 2-nitro-5α-cholestan-3-one (**3**).

(d) Photolysis of 4β-Nitro-5β-cholestan-3-one (13) (Scheme 2). As we have said, nitro ketone **13** exists as its keto form in ethanol while nitro ketones, **3**, **4**, and **11** exist mostly as their enol froms **3b**, **4b**, and **11b** in the solvent. It is, therefore, of considerable interest to know how the difference in the tautomeric nature of the nitro ketones is reflected in the products of their photolysis.

The photolysis of nitro ketones **13** in ethanol for 3 h under the conditions described above resulted in a 51% conversion of the substrate and gave a mixture cf products which was subjected to column chromatography

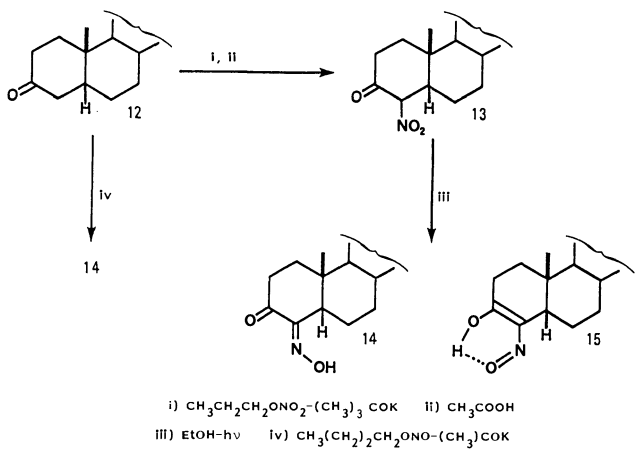

Scheme 2.

to give two crystalline products **14** and **15**. The compound **14** had the molecular formula $C_{27}H_{45}NO_2$ (high resolution mass spectrometry). The IR spectrum exhibited bands at 3340, 1693, and 1571 cm^{-1} assignable to a hydroxyimino group conjugated with a carbonyl group. This result, together with the ^1H NMR spectrum, indicated that it was 5β-cholestane-3,4-dione 4-oxime (**14**). The structure was confirmed by a direct comparison with oxime **14** which was prepared by nitrosation of 5β-cholestan-3-one **12**.

The ^1H NMR spectrum of **14** exhibited a doublet of a doublet at δ 2.93 (1H) with J=5.5 and 2.9 Hz assignable to the angular 5β-H. The observed displacement of this signal to the low field indicates that the 5β-H is deshielded by the hydroxyl of the hydroxyimino function which is oriented anti to the carbonyl group. High resolution mass spectrometry of compouhd **15** indicated that compound **15** is an isomer of α-hydroxyimino ketone **14**. The product had a double melting point and the higher melting point was nearly in agreement with that exhibited by α-hydroxyimino ketone **14**. IR spectrum exhibited a broad band at 3330 cm^{-1} due to a hydrogen-bonded hydroxyl group but no band due to a carbonyl group. Instead, there was a weak band at 1650 cm^{-1} due to a C=C bond in the IR spectrum. These results together with its ^1H NMR spectrum indicated that compound **15** was 4-nitroso-5β-cholest-3-en-3-ol. The assigned structure was then confirmed by isomerizing **15** to the oxime **14**. The nitroso steroid **15** was heated up to 140 °C and recrystallization of the melt gave a specimen which was identical with α-hydroxyimino ketone **14**. So far the nitroso-monomer has rarely been isolated. The nitroso-monomer **15** in this case may perhaps be isolated as a result of stabilization by an intramolecular hydrogen bond between the hydroxyl group and the nitroso oxygen. The mixture of the products of the photolysis was carefully examined by means of TLC but no cyclic α-diketones and cyclic imides were found.

(e) Photolysis of 6α-Nitro-5α-cholestan-7-one (17)[6] (Scheme 3). Nitro ketone **17** is again in a keto form in ethanol as in the case of nitro ketone **13**. Photolysis of nitro ketone **17** in ethanol for 7 h under the conditions as mentioned above, resulted in a 59% conversion and gave a complex mixture of the products. Two crystalline products **18** and **19** were isolated in 13 and 12% yields from the products by means of preparative TLC. The molecular formulae of **18** and **19** were determined to be $C_{27}H_{46}O_2$ and $C_{27}H_{45}NO_2$ by means of high-resolution mass spectrometry. The structure of product **18** was confirmed to be 6α-hydroxy-5α-cholestan-7-one on the basis of their IR and ^1H NMR spectra (see Experimental). The structure of product **19** was also deduced to be 5α-cholestane-6,7-dione 6-oxime on the basis of the IR, ^1H NMR, and mass

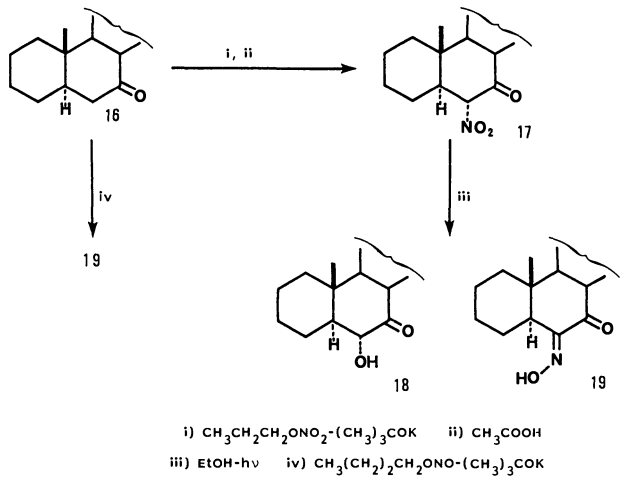

Scheme 3.

spectra (see Experimental) and this was finally confirmed by its preparation by nitrosation of 5α-cholestan-7-one (**16**). The ^1H NMR spectrum of **19** exhibited a doublet of a doublet at δ 2.17 (J=11.6 and 2.9 Hz) assignable to the 5α-H and a triplet at δ 2.48 (J=10.8 Hz) assignable to the 8β-H. It should be noted that although the hydroxyl group of the hydroxyimino function is almost certainly oriented anti to the carbonyl group, the 5α-proton is not deshielded to the same extent as 5β-proton of 5β-cholestane-3,4-dione 4-oxime. An inspection of the molecular model indicates that the orientation of the hydroxyl group is unable to deshield the axial 5α-proton. In the ^1H NMR spectrum of **19**, there was another one-proton multiplet centered at δ 2.28 assignable to the 4α-H which is likely to be deshielded by the hydroxyl group.

Discussion

A wide variety of photochemical transformations of aromatic, α,β-unsaturated, and aliphatic nitro compounds have been reported. The subject was first reviewed in 1969[14] and has recently been updated.[28]

Although the photochemistry of some cyclic α-nitro ketones which exist in their keto form in solution has been investigated by Reid and Tucker,[4] no investigation has been carried out on the photochemistry of cyclic α-nitro ketones which in solution exist predominantly as their enol forms. The cyclic α-nitro ketones which exist as their enol forms are regarded as substituted α,β-unsaturated nitro compounds.

Chapman and his colleagues were the first to report the photochemical transformation of 2-nitro-1-phenylpropane into 1-hydroxyimino-1-phenyl-2-propanone via nitro–nitrite rearrangement.[29] Analogous photorearrangements to hydroxyimino ketones via the Chapman rearrangement have since been reported of several acyclic nitroalkenes, β-bromo-β-nitrostyrene,[30] *cis*-α,4-dinitrostilbene,[31] 1-aryl-2-nitro-1-propenes,[32] 1-(2-pyridyl)- and 1-(3-pyridyl)-2-nitro-1-alkenes,[33] and simple aliphatic nitroalkenes.[34] Intramolecular cycloaddition followed by a carbon–carbon double bond cleavage has been reported[31,32] to compete with the nitro–nitrite rearrangements in some of the above nitroalkenes.

The analogous photochemical formation of α-hydroxyimino ketones with the accompanying formation of cyclic ketones and enones via nitro–nitrite rearrangements have been observed for 6-membered cyclic nitroalkenes.[34,35] Another variation of the reported photochemistry of nitroalkenes is a photoinduced deconjugation which takes place when intramolecular abstraction of γ-hydrogen is possible.[34]

Our experiments have shown that the common products of the photolysis of the 6-membered cyclic α-nitro ketones which exist as their enol forms in protic solvents are cyclic α-diketones and cyclic α-hydroxyimino ketones. It should be noted that no cyclic imides, which have been found in the products of the photolysis of 2-nitrocycloheptanones and α-nitrocamphor,[4] were found in the products of the present photolysis.

The formation of α-diketones **5** and **7** from **3b**, **4b**, and **11b** is analogous to the formation of cyclic ketones in the photolysis of cyclic nitroalkenes. The pathway to these α-diketones involving the nitro–nitrite rearrangement is outlined in Scheme 4. Thus, excited 6-membered cyclic α-nitro ketones (**A**) rearrange to the corresponding cyclic α-hydroxy ketone nitrites (**C**) through oxaziridine intermediate (**B**). Disproportionation or the scission of a hydrogen atom of the alkoxyl

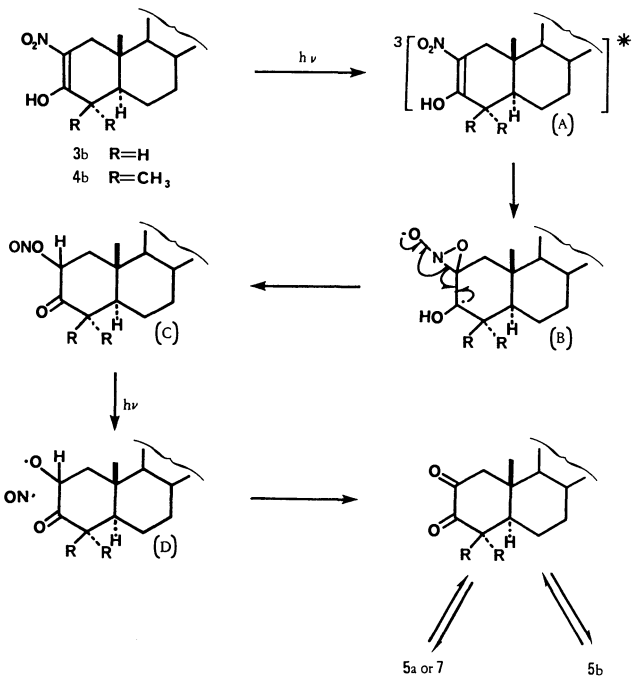

Scheme 4.

radical (**D**) generated from the nitrite (**C**) affords cyclic α-diketones such as **5a**, **5b**, or **7**.

On the other hand, the path of the formation of cyclic α-hydroxyimino ketones from the excited cyclic α-nitro ketones (**4a**→**8**, **11a**→**6**) is outlined in Scheme 5. As outlined, these cyclic α-hydroxyimino ketones are simply derived through the isomerization of α-nitroso ketone (**G**) which can be formed from the intermediate (**F**) generated by the hydrogen abstraction from the solvent by the n,π* triplet excited nitro group[36–39] of the keto form (e.g., **E**) or the enol forms (e.g., **A**).

It is very likely, however, that α-hydroxyimino ketone **6** or **8** from α-nitro ketone **4** or **11** is formed from their keto form since α-hydroxyimino ketone **14** is obtained in the photolysis of α-nitro ketone **13** which exists exclusively in the keto form in ethanol.

An anomalous result in the present experiments, however, is the formation of 5α-cholestane-2,3-dione 3-oxime (**6**) in the photolysis of 2-nitro-5α-cholestan-3-one (**3a**).

One of the probable geneses of the anomalous formation of α-hydroxyimino ketones **6** from 2-nitro-5α-cholestan-3-one **3** is outlined in Scheme 6. Thus, irradiation of 2-nitro-5α-cholestan-3-one (**3**) generates the n,π* triplet from which the nitrite (**I**) is formed by the Chapman rearrangement.[28–35] The combination of nitrogen monoxide with the C-3 of the enoloxyl radical (**J**) generated from the nitrite may give a nitroso ketone (**K**). The hydrogen abstraction by the excited nitroso ketone (**K**) then may give α-hydroxyimino ketone **6** through the removal of a hydroxyl radical from a ketyl radical (**L**). The competing process from the n,π* triplet, a hydrogen abstraction from the solvent, leading to the formation of α-hydroxyimino ketone **8** is unlikely to be as efficient as the Chapman rearrangement.

No α-hydroxyimino ketones based on the pathway involving the Chapman rearrangement outlined in Scheme 6 were formed in the photolysis of 3-nitro-5α-cholestan-2-one (**11**) and 4,4-dimethyl-2-nitro-5α-cholestan-3-one (**4**) even though photolysis resulted in the

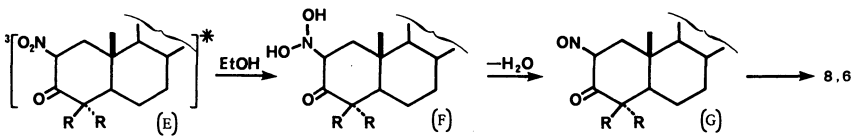

Scheme 5.

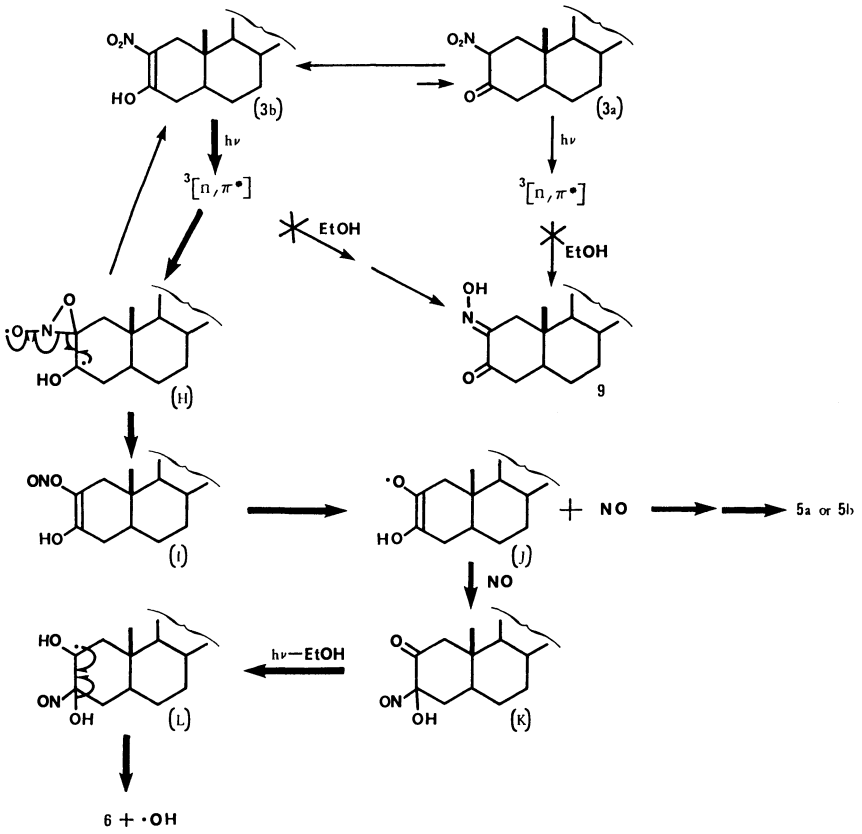

Scheme 6.

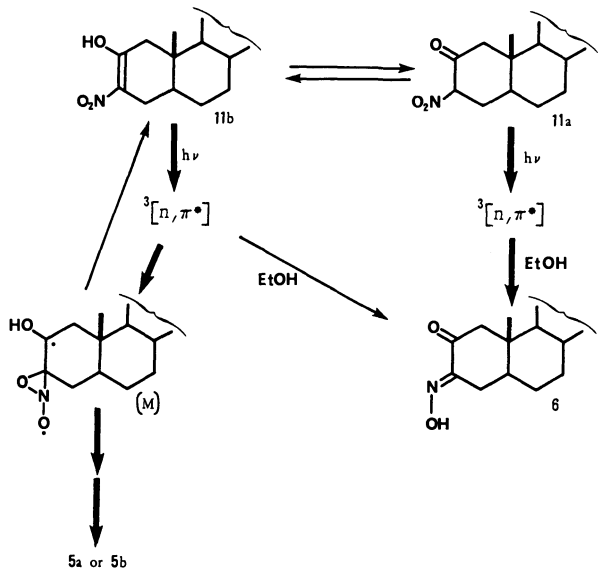

Scheme 7.

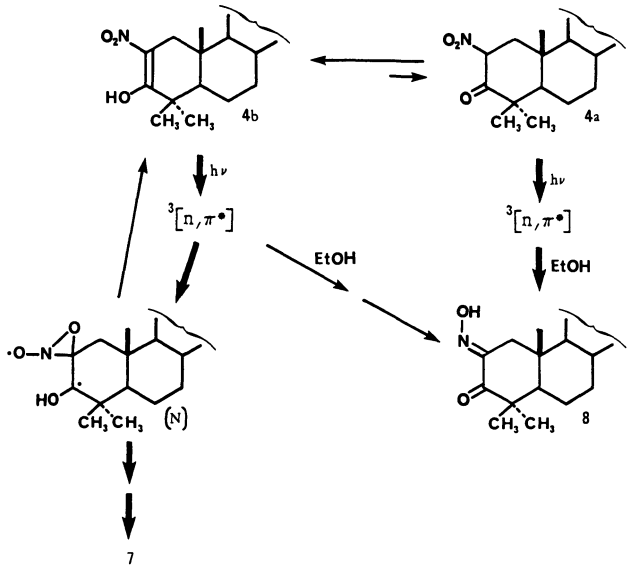

Scheme 8.

formation of diketones **5** or **7**, which involves the nitro–nitrite rearrangement as outlined in Schemes 7 and 8. The absence of α-hydroxyimino ketone **9** in the photolysis of nitro ketone **11** based on the mechanism outlined in Scheme 6 is attributable to steric inhibition of the combination of nitrogen monoxide with the C-2 of the intermediate by the 10β-methyl group. The absence of 4,4-dimethyl-5α-cholestane-2,3-dione 3-oxime in the photolysis of nitro ketone **4** is similarly attributable to the steric inhibition of the combination of nitrogen monoxide with the C-3 of the intermediate such as (**J**) (Scheme 6) by the C-4 *gem*-dimethyl group.

There are precedents for the formation of α-hydroxyimino ketones **14** and **19** in the photolysis of α-nitro ketones **13** and **17**, which exist in their keto forms.[4] These products are apparently formed by the elimination of the element of water from the intermediate formed from the hydrogen abstraction from the solvent by the n,π* excited nitro group. The unprecedented isolation of the unstable nitroso intermediate **15** in the photolysis of α-nitro ketone **13** is of interest in connection with this pathway.

The α-hydroxy ketone **18** is likely to be generated from the corresponding nitrite. The nitrite in this case may be formed either through the Chapman rearrangement of the enol form, which exists in a trace amount, or through the dissociation–recombination mechanism[3] of the nitro group of the keto form.[40]

Experimental

Mp's were recorded with a Yanagimoto micro mp apparatus. IR spectra were determined for Nujol mulls with a Hitachi Model 285 infrared spectrophotometer or a JASCO IR 810 infrared spectrophotometer unless otherwise indicated. ^{1}H NMR spectra were determined with a JEOL PS 200 high resolution FT-NMR spectrometer (200 MHz) or a JEOL JNM-FX 270 spectrometer (270 MHz) (solvent, $CDCl_3$; $SiMe_4$ as an internal standard) (Faculty of Pharmaceutical Sciences of this University). TLC was carried out on a Merck Kiesel gel 60-PF_{254}. The high and low resolution mass spectra were determined with a JEOL JMS-D-300 spectrometer (70 eV) (Faculty of Pharmaceutical Sciences of this University). Elemental analyses were performed by the staff of the analytical laboratory of Faculty of Pharmaceutical Sciences.

2-Nitro-5α-cholestan-3-one (2-Nitro-5α-cholest-2-en-3-ol) (3). 5α-Cholestan-3-one (**1**) (2 g 5.18 mmol) was dissolved in *t*-butyl alcohol (50 ml) containing potassium *t*-butoxide (1.5 g, 13.4 mmol). To this solution at 22 °C propyl nitrate (1.5 ml, 15 mmol) was added and the solution was stirred for 2 h at room temperature. The solution was then poured into iced water (200 ml). A yellow-colored potassium salt of α-nitro compound **3** (2.512 g) was collected by filtration. The potassium salt was dissolved in glacial acetic acid (100 ml) by heating. The solution was cooled to room temperature and water was added to the solution to yield colorless crystals of 2-nitro-5α-cholestan-3-one (**3**) (2.157 g, 96.6%), mp 117—125 °C. This nitro ketone was recrystallized from ethanol to yield analytical specimen (1.487 g, 66.6%), mp 132—135 °C (lit,[5] mp 135—136 °C). IR (Nujol) 1616 (C=C), 1513 (conjugated NO_2) 1746, (very weak band, C=O), and 1561 cm^{-1} (very weak bond non-conjugated NO_2); ^{1}H NMR (100 MHz) δ=0.67 (3H, s, 18-H), 0.83 (3H, s, 19-H), and 2.70 (1H, *J*=15.9 Hz, 1-H); MS, *m/z* (rel intensity) 431 (M^+, 83.8%), 227 (64.8, M^+—D-ring) 276 (89.7), 95 (64.0), 81 (65.4), 69 (61.8), 57 (67.4), 55 (94.4), and 43 (100).

4,4-Dimethyl-2-nitro-5α-cholestan-3-one (4). 4,4-Dimethyl-5α-cholestan-3-one (**2**) (5 g) was dissolved in *t*-butyl alcohol (185 ml) containing potassium *t*-butoxide (7.5 g). To this solution, propyl nitrate (5.15 ml) was added and the solution was stirred for 3 h 45 min at room temperature. The solution was then poured into iced water (700 ml). A yellow-colored potassium salt of α-nitro compound (7.4 g) was collected by filtration. The potassium salt was dissolved in glacial acetic acid (200 ml), and water was slowly added to

the solution to yield colorless crystals of 4,4-dimethyl-2-nitro-5α-cholestan-3-one (**4**) (4.2 g, 75.6%). This nitro ketone was recrystallized from hexane to yield an analytical specimen (3.0 g, 54%), mp 123—127 °C. Found: C, 75.74; H, 10.95; N, 2.95%. Calcd for $C_{29}H_{49}NO_3$; C, 75.77; H, 10.74; N, 3.05%. IR (Nujol) 1605 (C=C), 1513 (conjugated NO_2), and 1297 cm^{-1}; ^1H NMR (270 MHz) δ=0.66 (3H, s, 18-H), 0.88 (3H, s, 19-H), 1.30 and 1.32 (each 3H, each s, 4-Me), 2.05 and 2.80 (each 1H, each d, J=15.38 Hz, 1α-H and 1β-H). MS, m/z (rel intensity) 459 (M^+, 100%), 441 (15.3), 412 (M^+-HNO_2, 15.0), 403 (29.2), 315 (58.0), 304 (59.6), 95 (80.8), 81 (70.7), 69 (70.7), 55 (74.1), and 43 (79.1).

3-Nitro-5α-cholestan-2-one (11). 5α-Cholestan-2-one (**10**) (1.5 g) was dissolved in THF (50 ml) containing potassium t-butoxide (1.4 g). To this solution, isopentyl nitrate (2 g) in THF (3 ml) was added over the course of 20 min, while being cooled with Dry Ice–methanol. After the solution was stirred for 40 min at room temperature, the solution was neutralized by the addition of glacial acetic acid. The solution was then poured into water (250 ml) and the solution was extracted with dichloromethane. Combined organic layers were worked up by the usual method. The crude oily nitro ketone (1.786 g) was recrystallized from ethanol to yield crystals of nitro ketone **11** (1.372 g. 81.7%), mp 117—120 °C, ^1H NMR (270 MHz) δ=0.67 (3H, s, 18-H), 0.85 (3H, s, 19-H), 5.28 (0.37H, dd, J=12.9 and 6.9 Hz, 3β-H of the keto form **11b**) and 13.8 (0.63H, s, OH); IR (Nujol) 1735 (C=O), 1619 (C=C), 1562 (non-conjugated NO_2), 1509 cm^{-1} (conjugated NO_2); MS (70 eV), m/z (rel intensity) 431 (M^+, 91.4%), 416 (6.9), 291 (11.3), 276 (M^+—D-ring, 100), 262 (27.9), and 55 (43.3). Found: C, 74.99; H, 10.45; N, 3.09%. Calcd for $C_{27}H_{45}NO_3$: C, 75.13; H. 10.50; N, 3.25%.

4β-Nitro-5β-cholestan-3-one (13). 5β-Cholestan-3-one (**12**) (500 mg, 1.30 mmol) was dissolved in t-butyl alcohol (10 ml) containing potassium t-butoxide (200 mg, 1.79 mmol). To this solution at 22 °C, propyl nitrate (0.15 ml, 1.5 mmol) was added and the solution was stirred for 2.5 h at room temperature. The solution was then poured into iced water (70 ml). Glacial acetic acid was added to this aqueous pale yellow solution of the potassium salt of α-nitro ketone until pH 3. The solution was stirred for 30 min and extracted with dichloromethane. The organic layer was washed with water and dried over anhydrous Na_2SO_4. The workup in the usual way gave an oil (546 mg). This oily 4β-nitro-5β-cholestan-3-one (**13**) crystallized upon the addition of ethanol. (123 mg, 22%), mp 157—160 °C. The filtrate contained the starting 3-ketone and 2,4-dinitro ketone. Found: C, 75.02; H, 10.39; N, 3.27%. Calcd for $C_{27}H_{45}NO_3$: C, 75.13; H, 10.51; N, 3.25%. IR (Nujol) 1714 (C=O), 1558 cm^{-1} (NO_2); ^1H NMR (200 MHz) δ=0.69 (3H, s, 18-H), 1.13 (3H, s, 19-H), and 5.67 (1H, d, J=12.7 Hz, 4α-H); MS, m/z (rel intensity) 431 (M^+, 34.8%), 385 (M^+-NO_2, 30.7), 276 (22.3), 231 (30.7), 229 (37.2), 140 (38.8), 95 (72.4), 81 (75.1), 69 (69.7), 55 (100), and 43 (84.1).

6α-Nitro-5α-cholestan-7-one (17). The α-nitro ketone **17** was prepared according to the procedure reported by Meakins et al.[6] Yield was 34%. Mp 143—144 °C (lit,[6] mp 137—139 °C). IR (Nujol) 1728 (C=O) and 1558 cm^{-1} (non-conjugated NO_2).

Photolysis of 2-Nitro-5α-cholestan-3-one (3). 2-Nitro-5α-cholestan-3-one (**3**) (300 mg, 10.7 mmol) in absolute ethanol (450 ml) was irradiated with a Pyrex-filtered light (Hanovia 450-W high pressure Hg arc) for 1.5 h in an atmosphere of dry nitrogen. The removal of the solvent under a reduced pressure gave an oily residue (341 mg) which was subjected to preparative TLC with benzene to yield two fractions. The more mobile oily fraction (63 mg, 22.5%) was 5α-cholestane-2,3-dione (**5**). Its NMR spectrum indicated that it was a 1:1 mixture of two isomeric enols **5a** and **5b**. Recrystallization of the mixture with ethanol gave a crystalline mixture of 2-hydroxy-5α-cholest-1-en-3-one (**5a**) and its isomer **5b** in a 1 to 1 ratio. Mp 119—155 °C (lit,[21] mp of pure enol **5a**, 163—167 °C). ^1H NMR δ=0.56 (s, 18-H of **5b**), 0.68 (s, 18-H of **5a**), 5.70 (d, J=2.6Hz, 4-H of **5b**), 5.68 (s, OH of **5a** and **5b**), 6.38 (s, 1H of **5a**). The polar fraction (190 ml) was subjected to preparative TLC with a 3:1 benzene–ethyl acetate to yield 5α-cholestan-2,3-dione 3-oxime (**6**) (34 mg, 11.6%). An analytical specimen was obtained by recrystallization with ethanol. Mp 196—198 °C. IR (Nujol) 3628, 3445, and 3228 (OH), 1708, and 1687 (C=O), 1608 and 1585 (C=N), 1272, 1031, and 985 cm^{-1}; ^1H NMR (270 MHz), δ=0.66 (3H, s, 18-H), 0.85 (3H, s, 19-H), 2.77 (1H, d, J=17.6 Hz, 1β-H), 2.09 (1H, d, J=17.2 Hz, 1α-H), and 2.99 (1H, dd, J=19.4 and 5.5 Hz, 4α-H); EIMS (rel intensity) 415 (M^+, 100%), 400 (6.3), 399 (6.3), 398 (9.5), 261 (28.3), 260 (55.6), and 43 (95.8). Found: m/z 415.3480. Calcd for $C_{27}H_{45}NO_2$: M, 415.3450.

Synthesis of 5α-Cholestan-2,3-dione 3-Oxime (6). To a solution of the ketone (100 mg) in t-butyl alcohol (10 ml) containing potassium t-butoxide (35 ml), butyl nitrite (0.035 ml) was added and the solution was stirred for 30 min at room temperature. The solution was then poured into iced water. After aq. 2 M hydrochloric acid (1 M=1 mol dm^{-3}) had been added, the solution was extracted with diethyl ether. The combined organic layers were washed with water and dried over anhydrous sodium sulfate. The usual workup of the solution gave an oily product (193 mg) which was subjected to preparative TLC with a 2:1 benzene–ethyl acetate to give a crude oxime (83 mg, 77%). Recrystallizations from ethyl acetate–methanol gave pure oxime **6**, (54 mg), mp 196—198 °C. This oxime was identical with oxime **6** obtained from the photolysis of nitro ketone **3**.

Synthesis of 5α-Cholestane-2,3-dione 2-Oxime (9),[6,16,22,23] This hydroxyimino ketone **9** was prepared according to the procedure reported by Chadwick et al.[6] Butyl nitrite was used instead of pentyl nitrite. The oxime which was recrystallized from THF melted at 271—274 °C. (lit, mp 240—242 °C;[6] 203—205 °C;[16] 268—270 °C[22,23]). IR (Nujol) 3136 (OH), 1718 (C=O), 1619 (C=N), 1294, 975, and 817 cm^{-1}; MS, m/z (rel intensity) 415 (M^+, 79.8%), 398 [$(M-OH)^+$, 100], 384 (27.9), 314 (20.7), 260 (76.3), 244 (27.1), 216 (22.3), 136 (36.3), 121 (39.1), 107 (37.0), 95 (55.8), 81 (55.1), 69 (52.4), 55 (73.8), and 43 (66.7%); ^1H NMR (270 MHz) δ=0.67 (3H, s, 18-H), 0.85 (3H, s, 19-H), 1.93 (1H, d, J=18.0 Hz, 1α-H), 2.44 (1H, dd, J=5.5 and 18.9 Hz, 4-H), and 3.22 (1H, d, J=18.0 Hz, 1β-H).

Photolysis of 4,4-Dimethyl-2-nitro-5α-cholestan-3-one (4). 2-Nitro steroid (**4**) (350 mg, 0.76 mmol) in absolute ethanol (350 ml) was flashed with nitrogen and was irradiated with a Pyrex-filtered light (Eikosha 500-W high pressure Hg arc) for 1 h in an atmosphere of dry nitrogen. The removal of the solvent under a reduced pressure gave an oily residue (352 mg) which was subjected to preparative TLC with chloroform to yield three fractions. The most mobile fraction (83 mg, 24%) was the starting material (**4**). The second mobile fraction (54 mg, 21.6%) was 4,4-dimethyl-2-hydroxy-5α-cholest-1-en-3-one (**7**) which was recrystallized

from ethanol-water to yield crystals, mp 165—169 °C (lit, mp 165—167 °C,[25] 168 °C[26]). IR (Nujol) 3442, 3412 (OH), 1668, and 1652 cm^{-1} (C=C and C=O of diosphenol); EIMS, *m/z* (rel intensity) 428 (M^+, 67.2%), 425 [$(M-Me)^+$, 25.4]. 400 [$(M-CO)^+$, 16.3], 385 (14.9), 341 (13.1), 315 (37.1), 300 (37.5), 247 (22.8), 166 (28.8), 81 (54.6), 69 (55.1), 55 (64.5), and 43 (100); ^1H NMR (270 MHz) δ=0.68 (3H, s, 18-H), 1.11 (3H, s, 19-H), 1.13 (3H, s, 4β-Me), 1.91 (3H, s, 4α-Me), 5.99 (1H, s, OH), and 6.40 (1H, s, 1-H). The most polar fraction (33 mg, 12.7%) was 4,4-dimethyl-5α-cholestane-2,3-dione 2-oxime (**8**)[27] which was recrystallized from ethanol-water. Mp 202—205 °C (lit,[27] mp 197—198 °C). IR (Nujol), 3270 (OH), 1705 (C=O), 1612 (C=N), 962, and 759 cm^{-1}; ^1H NMR (270 MHz) δ=0.66 (3H, s, 18-Me), 0.85 (3H, s, 19-Me), 1.12 (3H, s, 4β-Me), 1.17 (3H, s, 4α-Me), 2.17 (1H, d, J=18.7 Hz, 1α-H), and 3.03 (1H, d J=18.7 Hz, 1β-H).

Synthesis of 4,4-Dimethyl-5α-cholestane-2,3-dione 2-Oxime (8). This oxime was prepared according to the procedure reported by French workers.[27] Mp 202—205 °C (lit,[27] mp 197—198 °C). This hydroxyimino ketone was identical with the specimen obtained by the photolysis of 4,4-dimethyl-2-nitro-5α-cholestan-3-one.

Photolysis of 3-Nitro-5α-cholestan-2-one (11). 3-Nitro-5α-cholestan-2-one (**11**) (300 mg, 0.7 mmol) in ethanol (300 ml) was irradiated with a Pyrex-filtered light (Eikosha 500-W high pressure Hg arc) for 3 h in an atmosphere of a nitrogen. A workup of the irradiated solution as in the case of 2-nitro steroid **3b** gave an oily residue (323 mg) which was subjected to preparative TLC with dichloromethane to yield three fractions. The most mobile fraction (22 mg, 7.5%) was the starting material **11b**. The second mobile fraction (11 mg, 4.2%) was a mixture of α-diketones **5a** and **5b** and it was recrystallized from methanol-water to yield a mixture of α-diketones **5a** and **5b** mp 116—158 °C. The most polar fraction (47 mg, 17.7%) was 5α-cholestane-2,3-dione 3-oxime (**6**) which was recrystallized from methanol-water. Mp 196—198 °C. This oxime was identical with the specimen obtained by the photolysis of 2-nitro-5α-cholestan-3-one (**3a**).

Photolysis of 4β-Nitro-5β-cholestan-3-one (13). Nitro steroid **13** (300 mg, 0.7 mmol) in absolute ethanol (400 ml) in a quartz vessel was irradiated with a low pressure Hg arc in a Rayonet chamber reactor for 3 h in an atmosphere of dry nitrogen. The removal of the solvent under reduced pressure gave an oily residue (330 mg) which was subjected to the separation by means of column chromatography (silica gel). Elution with benzene gave the starting nitro steroid (148 mg) and then nitroso steroid **15** (37 mg, 25.2%). The latter was recrystallized from ethanol to yield a specimen for analysis, mp 113—119 °C and 167—174 °C. IR (Nujol) 1650 (C=C), 1528 and 1000 cm^{-1}; ^1H NMR (200 MHz) δ=0.67 (3H, s, 18-H), 1.14 (3H, s, 19-H); EIMS *m/z* (rel intensity) 415 (M^+, 14.2%), 398 [$(M-OH)^+$, 43.1], 356 (21.9), 140 (39.7), and 124 (100). Found: *m/z* 415.3457. Calcd for $C_{27}H_{45}NO_2$: M, 415.3450. Elution with a 99:1 diethyl ether-methanol gave a crude α-keto oxime **14** (74 mg, 50.4%) which was subjected to preparative TLC with a 97:3 dichloromethane-methanol to yield 30 mg of α-keto oxime **14**. It was recrystallized from ethanol to yield an analytical specimen, mp 186—188 °C. IR (Nujol) 3340 (OH), 1693 (C=O), and 1571 cm^{-1} (C=N); ^1H NMR (270 MHz), δ=0.66 (3H, s, 18-H) and 1.09 (3H, s, 19-H), 2.93 (1H, dd, J=5.5 and 2.9 Hz, 5β-H), and 2.47 (2H, m, 2-H);MS, *m/z* (rel intensity) 415 (M^+, 9.4%), 398 [$(M-OH)^+$, 33.0], 356 (24.5), 276 (14.0), 260 (100), 160 (6.5), 128 (31.2), 124 (86.8), 109 (31.4), 95 (38.5), 81 (41.6), 69 (40.5), 55 (52.0), and 41 (44.7); Found: *m/z* 415.3440. Calcd for $C_{27}H_{45}NO_2$: M, 415.3448.

Synthesis of 5α-Cholestane-3,4-dione 4-Oxime (14). To 5β-cholestan-3-one (100 mg) in *t*-butyl alcohol (10 mg) containing potassium *t*-butoxide (35 ml), butyl nitrite (0.035 ml) was added. The solution was stirred for half an hour at room temperature and poured into iced water. After aq. 2 M hydrochloric acid had been added, the aq. solution was extracted with diethyl ether. The combined ethereal extracts were washed with water and dried over anhydrous sodium sulfate. The usual work-up of the solution gave an oily hydroxyimino ketone (141 mg). This crude product was subjected to preparative TLC with a 2:1 benzene-ethyl acetate to give a crude oxime (66 mg, 66%). The specimen for analysis (27 mg) was obtained by recrystallizing from methanol-water. It was identical with oxime **14** obtained by the photolysis of 4β-nitro-5β-cholestan-3-one (**13**). Mp 186—188 °C.

Photolysis of 6α-Nitro-5α-cholestan-7-one (17). 6α-Nitro-5α-cholestan-7-one (**17**)(300 mg, 0.7 mmol) in ethanol (300 ml) was irradiated with a Pyrex-filtered light (Eikosha 500-W high pressure Hg arc) for 7 h in an atmosphere of a nitrogen. Evaporation of the solvent under a reduced pressure gave an oily residue (315 mg) which was subjected to preparative TLC with dichloromethane to yield three fractions. The most mobile fraction (122 mg, 40.6%) was the starting material. The second mobile fraction (27 mg, 13.2%) was 6α-hydroxy-5α-cholestan-7-one (**18**). The ketone **18** was recrystallized from ethanol-water to yield the specimen for analysis. Mp 123—128 °C. IR (Nujol) 3468 (OH) and 1705 cm^{-1} (C=O); ^1H NMR (270 MHz) δ=0.67 (3H, s, 18-H) 1.11 (3H, s, 19-H), 2.44 (1H, br. t, J=11.7 Hz, 8β-H), 3.15 (1H, d, J=4.5 Hz, OH), and 3.86 (1H, ddd, J=11.82, 4.5 and 1.1 Hz, 6β-H); ($CDCl_3$-D_2O) δ=3.86 (1H, dd, J=11.72 and 1.1 Hz, 6β-H); MS *m/z* (rel intensity) 402 (M^+, 100%), 384 [$(M-H_2O)^+$, 23], 271 (13.4), 257 (13.5), 247 (16.3), 231 (15.7), 194 (24.9), 125 (45.9), 109 (37.8), 95 (47.3), 81 (52), 55 (60.6), and 43 (55.8); Found: *m/z* 402.3517. Calcd for $C_{27}H_{46}O_2$: M, 402.3498.

The most polar fraction (25 mg, 12.2%) was 5α-cholestane-6,7-dione 6-oxime (**19**) and this was recrystallized from methanol-water to give an analytical specimen. Mp 155—158 °C. IR (Nujol) 3292 cm^{-1} (OH), 1717 (C=O), and 1673 (w, C≡N): ^1H NMR (270 MHz) δ=0.67 (3H, s, 18-H), 0.98 (3H, s, 19-H), 2.17 (1H, dd, J=11.72 and 2.94 Hz, 5α-H), 2.49 (1H, t, J=11.0 Hz, 8β-H) and 8.76 (1H, s, NOH); MS *m/z* (rel intensity) 415 (M^+, 43.6%), 398 [$(OH)^+$, 43.0%)], 370 (73.0), 344 (100), 95 (90.4), 81 (68.3), 69 (84.5); Found: *m/z* 415.3443; Calcd for $C_{23}H_{45}NO_2$: M, 415.3449.

As in the case of the photoreaction of nitro ketone **13** the absence of cyclic α-diketone and cyclic imides in the products was confirmed by means of TLC and a color reaction ($FeCl_3$-water).

Synthesis of 5α-Cholestane-6,7-dione 6-Oxime (19). To 5α-cholestan-7-one (500 mg) in *t*-butyl alcohol (20 ml) containing potassium *t*-butoxide (500 mg), butyl nitrite (1.8 ml) was added. The solution was stirred for 12 h at room temperature and poured into iced water. After aq. 2 M-hydrochloric acid had been added the aq. solution was extracted with diethyl ether, washed with water and dried over anhydrous sodium sulfate. The usual workup gave an

oily oxime (647 mg) which was subjected to preparative TLC to give a crude keto oxime **19** (97 mg). The oxime was recrystallized from methanol to give the specimen for analysis (40 mg). Mp 155—158 °C. This oxime was identical in every respect with the specimen obtained by the photolysis of nitro ketone **17**.

References

1) Photoinduced Molecular Transformations. Part 98. Part 97. H. Suginome and K. Kobayashi, *Bull. Chem. Soc. Jpn.*, **61**, 3782 (1988).

2) H. Suginome, M. Murakami, and T. Masamune, *J. Chem. Soc., Chem. Commun.*, **1966**, 343; H. Suginome, N, Sato, and T. Masamune, *Tetrahedron Lett.*, **1967**, 1557; H. Suginome, M. Murakami, and T. Masamune, *Bull. Chem. Soc. Jpn.*, **41**, 468 (1968); H. Suginome, N. Sato, and T. Masamune, *ibid.*, **42**, 215 (1969); H. Suginome, I. Yamazaki, H. Ono, and T. Masamune, *Tetrahedron Lett.*, **1968**, 5259; H. Suginome, N. Sato, and T. Masamune, *ibid.*, **1969**, 3353; H. Suginome, T. Kojima, K. Orito, and T. Masamune, *Tetrahedron*, **27**, 291 (1971); H. Suginome, N. Sato, and T. Masamune, *ibid.*, **27**, 4863 (1971); H. Suginome, T. Mizuguchi, and T. Masamune, *J. Chem. Soc., Chem. Commun.*, **1972**, 276; H. Suginome, T. Mizuguchi, and T. Masamune, *Tetrahedron Lett.*, **1971**, 4723; H. Suginome, T. Tsuneno, N. Sato, T. Masamune, H. Shimanouchi, Y. Tsuchida, and Y. Sasada, *ibid.*, **1972**, 661; H. Suginome, N. Maeda, and T. Masamune, *J. Chem. Soc., Perkin Trans.1*, **1976**, 1312; H. Suginome, T. Mizuguchi, and T. Masamune, *ibid.*, **1976**, 2365; H. Suginome, T. Mizuguchi, S. Honda, and T. Masamune, *ibid.*, **1977**, 927; H. Takahashi, M. Ito, and H. Suginome, *Chem. Lett.*, **1977**, 241; H. Suginome, N. Yonekura, T. Mizuguchi, and T. Masamune, *Bull. Chem. Soc. Jpn.*, **50**, 3010 (1977); H. Suginome, S. Sugiura, N. Yonekura, T. Masamune, and E. Osawa, *J. Chem. Soc., Perkin Trans. 1*, **1978**, 613; H. Suginome and T. Uchida, *J. Chem. Soc., Chem. Commun.*, **1979**, 701; H. Suginome and A. Osada, *J. Chem. Soc., Perkin Trans. 1*, **1982**, 1963; H. Suginome, N. Maeda, and M. Kaji, *ibid.*, **1982**, 111.

3) H. Suginome, K. Takakuwa, and K. Orito, *Chem. Lett.*, **1982**, 1357.

4) S. T. Reid and J. N. Tucker, *J. Chem. Soc., Chem. Commun.*, **1971**, 1609.

5) A. Hassner, J. M. Larkin, and J. E. Dawd, *J. Org. Chem.*, **33**, 1733 (1968).

6) D. J. Chadwick, W. R. T. Cottrell, and G. D. Meakins, *J. Chem. Soc., Perkin Trans. 1*, **1972**, 655.

7) H. Feuer and P. M. Pivawer, *J. Org. Chem.*, **31**, 3152 (1966).

8) For a recent review on preparation of cyclic α-nitro ketones, see R. H. Fischer and H. M. Weitz, *Synthesis*, **1980**, 261.

9) H. Feuer, J. W. Shepherd, and C. Savides, *J. Am. Chem. Soc.*, **78**, 4364 (1956) and the papers cited therein.

10) The same results were reported by Hassner et al.[5] on the nitro ketone in KBr disk.

11) For a review of early literatures see A. E. Gillam, E. S. Stern, and E. R. H. Jones, "An Introduction to Electronic Absorption Spectroscopy in Organic Chemistry," 2nd ed., Edward Arnold Ltd., London (1958), pp. 65—66.

12) S. Nagakura, *Mol. Phys.*, **3**, 152 (1960).

13) H. H. Jaffe and M. Orchin, "Theory and Applications of Ultraviolet Spectroscopy," John Wiley, New York (1962), p. 182.

14) For reviews see a) C. N. R. Rao, "The Chemistry of the Nitro and Nitroso groups, Part 1," ed by H. Feuer, Interscience Publ., New York (1969), pp. 92—106; b) H. A. Morrison, *ibid.*, pp. 167—168.

15) E. T. Stiller and O. Rosenheim, *J. Chem. Soc.*, **1938**, 353.

16) J. C. Sheehan and W. F. Erman, *J. Am. Chem. Soc.*, **79**, 6050 (1957).

17) W. Reusch and R. Lemahieu, *J. Org. Chem.*, **28**, 2443 (1963).

18) L. Ruzicka, P. A. Plattner, and M. Furrer, *Helv. Chim. Acta*, **27**, 524 (1944).

19) C. Djerassi and T. Nakano, *Chem. Ind. (London)*, **1960**, 1385.

20) E. J. Bailey, D. H. R. Barton, J. Elks, and J. F. Templeton, *J. Chem. Soc.*, **1962**, 1578.

21) S. Nakajma, R. Konaka, and K. Takeda, *Yakugaku Zasshi*, **96**, 764 (1976).

22) M. P. Cava, P. M. Weintraub, and E. J. Glamkowski, *J. Org. Chem.*, **31**, 2015 (1966).

23) M. Avaro and J. Levisalles, *Bull. Soc. Chim. Fr.*, **1969**, 3166.

24) H. Suginome and F. Yagihashi, *J. Chem. Soc., Perkin Trans. 1*, **1977**, 2488.

25) R. Hanna and G. Ourisson, *Bull. Soc. Chim. Fr.*, **1961**, 1945.

26) G. R. Chaudhry, T. G. Halsall, and E. R. H. Jones, *J. Chem. Soc.*, **1961**, 2725.

27) M. Avaro and J. Levisalles, *Bull. Soc. Chim. Fr.*, **1967**, 3173.

28) Y. L. Chow, "The Chemistry of Amino, Nitroso, Nitro compounds and Their Derivatives," ed by S. Patai, Wiley, New York (1982), pp. 181—290.

29) O. L. Chapman, P. G. Cleveland, and E. D. Hoganson, *J. Chem. Soc., Chem. Commun.*, **1966**, 101.

30) G. W. Shaffer, *Can. J. Chem.*, **48**, 1948 (1970).

31) J. T. Pinhey and E. Rizzardo, *Tetrahedron Lett.*, **1973**, 4057.

32) I. Saito, M. Takami, and T. Matsuura, *Tetrahedron Lett.*, **1975**, 3155.

33) R. G. Hunt and S. T. Reid, *J. Chem. Soc., Perkin Trans. 1*, **1977**, 2462.

34) J. S. Cridland, P. J. Moles, S. T. Reid, and K. T. Taylor, *Tetrahedron Lett.*, **1976**, 4497.

35) H. E. Zimmerman, L. C. Roberts, and R. Arnold, *J. Org. Chem.*, **42**, 621 (1977).

36) J. K. Brown and W. G. Williams, *J. Chem. Soc., Chem. Commun.*, **1966**, 495.

37) R. Hurley and A. C. Testa, *J. Am. Chem. Soc.*, **88**, 4330 (1966).

38) J. A. Barltrop and N. J. Bunce, *J. Chem. Soc. C.*, **1986**, 1467.

39) Y. Kitaura and T. Matsuura, *Tetrahedron*, **27**, 1583 (1971).

40) The nitro-nitrite rearrangement of nitro ketone **13** through a homolytic dissociation-recombination of the nitro group may give rise to 6β-hydroxy-5α-cholestan-7-one nitrite[3] which leads to 6β-hydroxy-5α-cholestan-7-one. The 6β-hydroxy-7-one, however, may readily isomerize to the 6α-isomer **18** through its enol form.

^{1}H NMR Study of Intramolecular Hydrogen-Bonding Interaction in Cyclodextrins and Their Di-*O*-methylated Derivatives

Mitsuhiko ONDA, Yasuhiko YAMAMOTO, Yoshio INOUE,* and Riichirô CHÛJÔ
Department of Biomolecular Engineering, Tokyo Institute of Technology,
O-okayama 2-chome, Meguro-ku, Tokyo 152
(Received May 17, 1988)

Intramolecular hydrogen bonding of α-, β-, and γ-cyclodextrins, and α- and β-dimethyl cyclodextrins has been investigated in dimethyl sulfoxide-d_6 by ^{1}H NMR spectroscopy. The temperature dependence of ^{1}H chemical shifts of secondary hydroxyl protons of cyclodextrins and dimethyl cyclodextrins reveals the existence of the intramolecular hydrogen bond. The strength of hydrogen bond becomes stronger as the ring size becomes smaller and by methylation. The intramolecular hydrogen bond in which the OH(3) is proton donor is preferred in α-cyclodextrin as well as in α- and β-dimethyl cyclodextrins. The orientation of secondary hydroxyl groups was estimated with the Karplus-type equation and the orientation is found to be suitable for making intramolecular hydrogen bond.

Cyclodextrins (CDs) are cyclic oligosaccharides consisting of six or more D-glucose units, which are connected by α-1,4-glucosidic linkages.[1] α-, β-, and γ-CDs are typical CDs composed of 6, 7, and 8 glucose units, respectively. Since CDs can accommodate guest molecules of suitable size in their cavities in both solid and solution states,[1–5] they have been paid great attention in various fields. The CD molecules have been modified chemically in attempts to improve properties such as the solubility and the complexation ability.[2,4,6–9] 2,6-Di-*O*-methyl-α- and β-CDs (α- and β-DMCDs, respectively) are typical examples of such modified CDs and they not only have higher solubility to both water and organic solvents but also appear to have significantly enhanced abilities of complexation and improved chiral recognition upon the inclusion processes.[2,10,11]

Hydrogen bonding is one of important interactions involved in determining the three-dimensional structures of biopolymers such as proteins, nucleic acids, and carbohydrates. The hydrogen bonds in these systems can be located by crystal structure analysis, especially by the neutron diffraction study which can directly prove the location of hydrogen atoms in the crystal lattice.[12,13] In solution state, on the contrary, it is not always easy to detect directly hydrogen-bond formation. Nuclear magnetic resonance spectroscopy (NMR) is one of potential physicochemical techniques which can provide the information about the hydrogen bonding in solution. Chemical shift or coupling constant, and temperature dependence of chemical shift, deuterium exchange and/or isotope effect, have been effectively used to study the hydrogen bonds, and in some case, to distinguish between the inter- and the intramolecular hydrogen bonds.[15–19]

X-Ray[20–24] and neutron diffraction[12,13] studies have shown that in solid state round but slightly conical form of CD macrocyclic ring structure is stabilized by the intramolecular hydrogen bonds between OH(2) and OH(3) groups of the adjacent glucose units. The existence of intramolecular hydrogen bonds of both O(3)–H···O(2) and O(3)···H–O(2) types in solid state have been suggested for α- and β-CDs. In DMCDs the formation of O(3)–H···O(2) type hydrogen bonds has also been suggested.[23,25]

There have been many attempts to determine the driving forces for complexation processes of CD and to make use of CDs inclusion ability in various field. Since CD inclusion complexation usually occurs in solution, the determination of CD conformation in solution could give some information on the complexation mechanism of CD inclusion complexes. The intramolecular hydrogen bond might play an important role for stabilizing the structure of CD macrocycle in solution. In the present work, the hydrogen bonding properties of CDs and DMCDs in DMSO-d_6 solution and orientation of their hydroxyl group were studied by the temperature dependence of chemical shifts and coupling constants of hydroxyl protons.

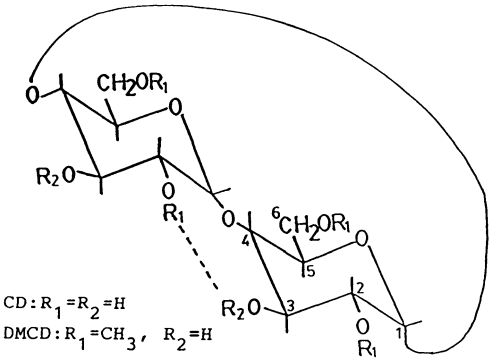

Experimental

α-, β-, and γ-CDs were generous gifts from Nihon Shokuhin Kako Co. Ltd. and methyl α-D-glucoside (MG) was purchased from Nakarai Chemicals and were dried in vacua at 120 °C before use to remove most of the hydrated water. α-DMCD was purchased from Toshin Chemical Co., and was used after recrystallization from water. β-DMCD

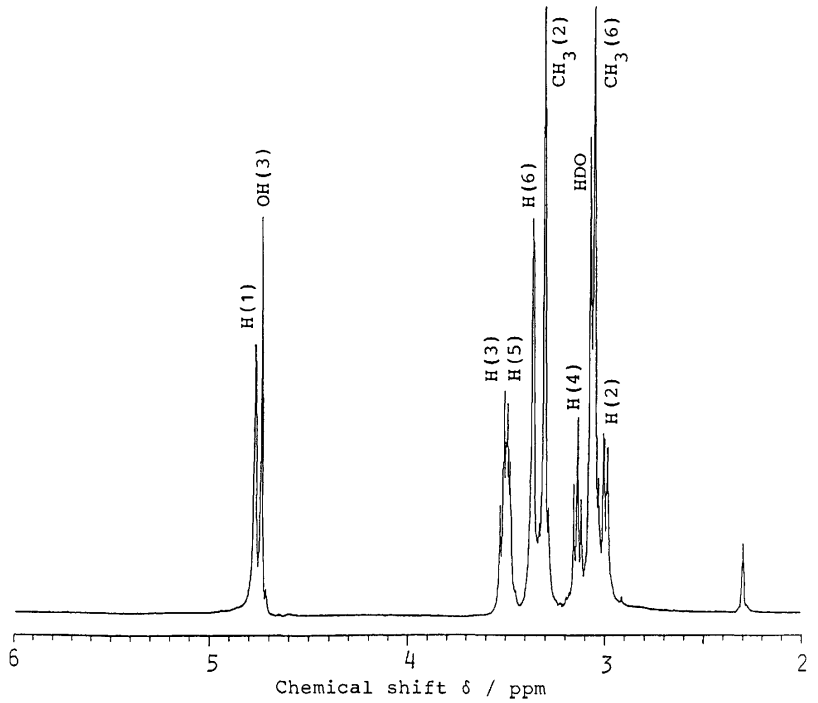

Fig. 1. The 500 MHz ^{1}H NMR spectrum of β-DMCD in DMSO-d_6 solution at 35 °C.

was obtained from Toshin Chemical Co., and was purified using the procedures reported by Koizumi et al.[26] The NMR solvent, deuterated dimethyl sulfoxide (DMSO-d_6), was purchased from Merck Co.

500 MHz ^{1}H NMR spectra were recorded on a JEOL GX-500 spectrometer in DMSO-d_6 at several temperatures from 25 to 75 °C. Concentration of all samples is 0.02 M (1 M= 1 mol dm^{-3}). Chemical shifts are given in parts per million (ppm) down field from tetramethylsilane (TMS). Digital resolution of the spectra is 0.0006 ppm (0.3 Hz).

Results and Discussion

Chemical Shift of Hydroxyl Proton Resonances in CDs. In Fig. 1 is shown the 500 MHz ^{1}H NMR spectrum of β-DMCD at 35 °C. In a previous paper,[27] we have assigned ^{1}H NMR spectra of some CDs and permethylated CDs by means of two-dimensional NMR techniques. ^{1}H NMR chemical shifts and coupling constants of hydroxyl groups and H(1) of α-, β-, and γ-CDs, and α- and β-DMCDs and MG in DMSO-d_6 at 35 °C are listed in Table 1. The resonances of the secondary hydroxyl protons of α-, β-, and γ-CDs (δ 5.2—5.6), and that of β-DMCD (δ 4.70) appear at lower field than those of the primary hydroxyl protons (δ 4.2—4.4) and the hydroxyl protons of MG (δ 4.1—4.6). These results suggest that the secondary hydroxyl groups form intramolecular hydrogen bond in α-, β-, and γ-CDs and β-DMCD. When the hydrogen bond is formed, polarization like $O^{\delta-}\cdots H^{\delta+}\text{-}O^{\delta-}$ along the hydrogen bond net work is enhanced and the proton participating in hydrogen bond becomes more positive in its electronic character. Therefore, such proton is deshielded compared to the proton that is not concerned with the hydrogen bond, i.e. its signal shifts to lower field. The resonance of secondary hydroxyl proton of α-DMCD appears at δ 4.45, which is clearly at higher field than the chemical shifts of other secondary proton resonances of CDs. But ^{1}H chemical shift data alone are not sufficient, and another supporting data are necessary to conclude that the intramolecular hydrogen bond is present in CDs and DMCDs (see below).

Table 1. Chemical Shifts[a] of H(1) and Hydroxyl Protons of Some CDs, DMCDs and MG in DMSO-d_6 at 35 °C

	H(1)	OH(2)	OH(3)	OH(6)	OH(4)
α-CD	4.60	5.32	5.26	4.28	
β-CD	4.68	5.52	5.48	4.26	
γ-CD	4.74	5.53	5.57	4.32	
α-DMCD	4.77		4.45		
β-DMCD	4.77		4.70		
MG	4.32	4.41	4.46	4.12	4.58

a) Chemical shifts are expressed in ppm from TMS.

Temperature Dependence of Hydroxyl Proton Chemical Shifts. Figure 2 shows the chemical shift changes of hydroxyl proton resonances of α-CD over the temperature range examined. Although the chemical shift of H(1) changes little with temperature, those of hydroxyl protons shift to higher field almost linearly with the increase of temperature (Fig. 3). Similar results are found for β- and γ-CDs, α- and

β-DMCDs, and MG.

For dilute solutions of CDs, DMCDs, and MG in DMSO-d_6, the following equilibrium of hydrogen bonding is present.

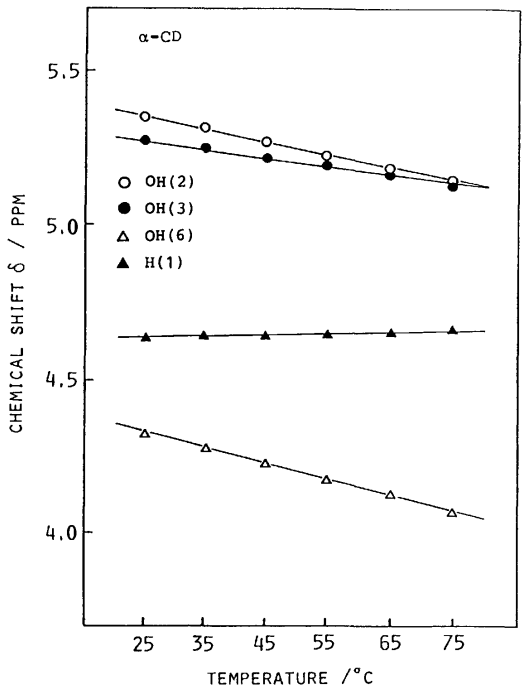

Fig. 2. Temperature dependence of the chemical shift of the hydroxyl and anomeric protons in α-CD.

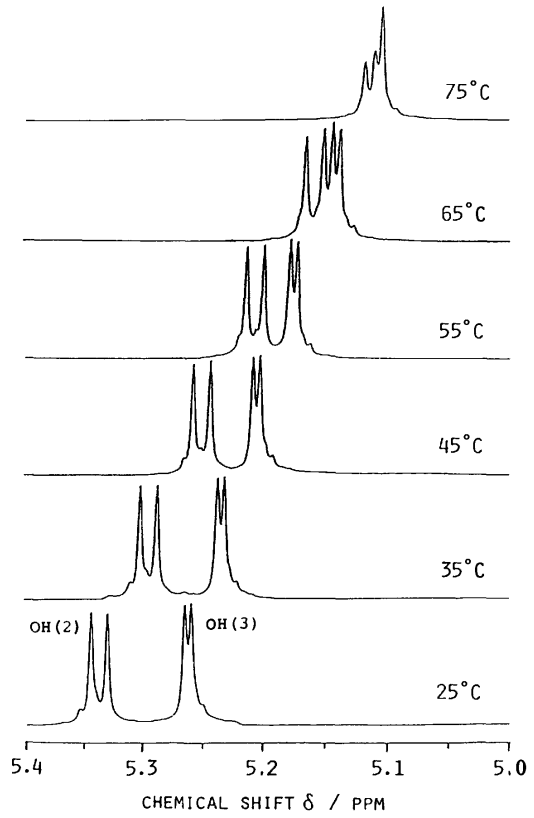

Fig. 3. The 500 MHz ^{1}H NMR spectrum of the secondary protons of α-CD at indicated temperature.

$$-OH\cdots HO- \rightleftarrows -OH\cdots O{=}S(CD_3)_2$$

The observed upfield shift of hydroxyl proton resonances with increase of temperature is attributed to decrease in the strength of the solvent-solute association. The smaller value of temperature coefficient of the chemical shift ($d\delta/dT$) means that the above equilibrium more prefers to lie to the left side i.e. hydroxyl groups preferentially form the intramolecular hydrogen bonds. The temperature dependent chemical shifts of hydroxyl protons of α-, β-, and γ-CDs and MG show that the $d\delta/dT$ values of all OH(6) proton signals are large and are nearly equal with each other (Fig. 4-A, Table 2). This observation suggests that all OH(6) protons are exposed to solvent DMSO-d_6 in a similar fashion. Since MG can't form intramolecular hydrogen bond, hydrogens of OH(6) of CDs do not participate in intramolecular hydrogen bonding. On the other hand, the $d\delta/dT$ values for OH(2) and OH(3) of CDs and DMCDs are significantly smaller than those of MG (Figs. 4-B and 4-C, respectively). This suggests that the secondary hydroxyl groups of α-, β-, and γ-CDs, and α- and β-DMCD prefer to form intramolecular hydrogen bond between OH(2) (in the case of DMCD, methoxy group) and OH(3) of the adjacent glucose units rather than to form a hydrogen bond with DMSO-d_6. The $d\delta/dT$ values for both OH(2) (α-, β-, and γ-CDs) and OH(3) increase in the following order: α-DMCD≒β-DMCD<α-CD<β-CD<γ-CD, indicating that the strength of the intramolecular hydrogen bond in DMSO-d_6 is in the following order: γ-CD<β-CD<α-CD<β-DMCD≒α-DMCD. The strength becomes weaker according to increase the ring size except α- and β-DMCDs. The macrocycle size of γ-CD might be

Table 2. Temperature Dependence ($d\delta/dT$) of the Hydroxyl Proton Resonances of Some CDs and MG in DMSO-d_6 at Concentration 0.02 M

	$(d\delta/dT)/10^{-3}$ ppm deg^{-1}		
	OH(2)	OH(3)	OH(6)
α-CD	4.36 (0.60)[a]	2.67 (0.41)[a]	5.21 (0.87)[a]
β-CD	5.42 (0.74)[a]	4.16 (0.56)[a]	5.66 (0.95)[a]
γ-CD	5.59 (0.77)[a]	4.64 (0.72)[a]	5.59 (0.94)[a]
α-DMCD		1.61 (0.25)[a]	
β-DMCD		1.67 (0.26)[a]	
MG	7.25	6.36	5.93

a) Data in parentheses represent the R valuse; where

$$R = \frac{d_j^i\delta/dT}{d_j^{MG}\delta/dT}$$

i = α-, β-, and γ-CDs, and α- and β-DMCDs
j = OH(2), OH(3), and OH(6).

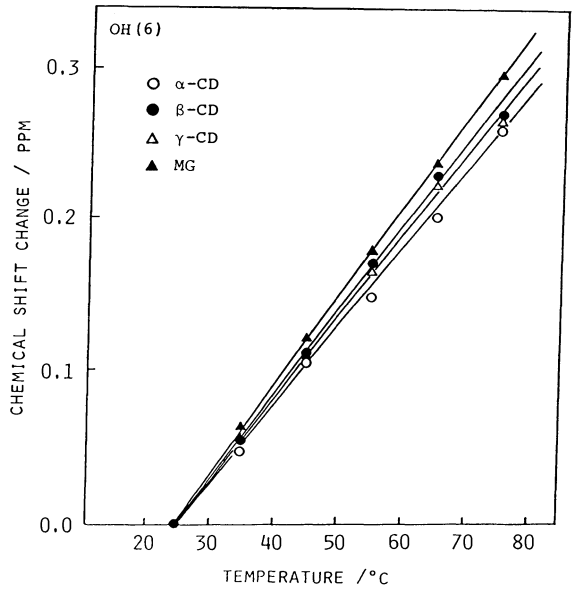

(A)

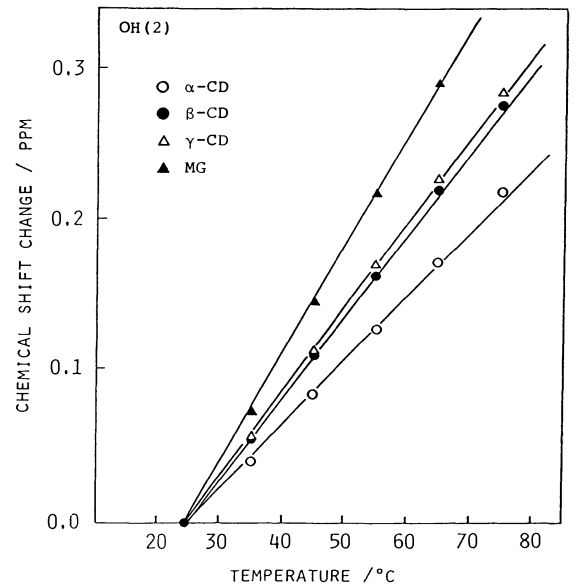

(B)

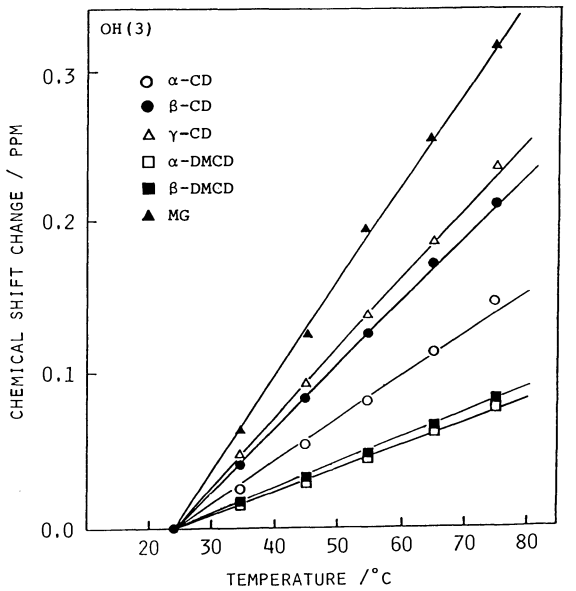

(C)

Fig. 4. Temperature dependence of the chemical shifts of the hydroxyl protons of α-, β-, and γ-CDs, and α- and β-DMCDs and MG; (A) OH(6), (B) OH(2), (C) OH(3). The ordinate refers to the magnitude of the upfield shift relative to the chemical shift observed at 25 °C.

too large to form the tight intramolecular hydrogen bond, and so its macrocyclic ring might be flexible. The ring size could be an important factor to form the strong intramolecular hydrogen bond.

Harata[22] has found from the X-ray study that in the hydrated crystal state the OH(2)···OH(3′) distance of adjacent glucose units is in order of α-CD>β-CD>γ-CD, indicating that the OH(2)···OH(3′) intramolecular hydrated crystal state the OH(2)···OH(3′) distance of adjacent glucose units is in order of α-CD>β-CD>γ-CD, indicating that the OH(2)···OH(3′) intramolecular remarkably distorted and two intramolecular hydrogen bonds are disrupted because of the sharp inclination of one glucose unit.[20,24] This can make weak the intramolecular hydrogen bond of α-CD. In solution, the flexibility of α-CD macrocyclic ring is sufficiently high to compensate for the disruption of intramolecular hydrogen bond. On occasion of crystallization, CDs may take energetically stable conformations, which are not necessarily suitable to form a strong hydrogen bond. Thus, it is concluded that not all of the results for the solids necessarily correspond with those for solution. For solutions, the role of solvent molecules must be considered also. The methylation of OH(2) groups are found to lead the formation of stronger intramolecular hydrogen bond. This point will be discussed in a following section.

Type of Intramolecular Hydrogen Bond. Three different modes (Fig. 5) are possible for the intramolecular hydrogen bonds of CD in DMSO-d_6, i.e. in types 1 and 2, OH(2) and OH(3) groups are main proton donors of the intramolecular hydrogen bond, respectively, and in type 3 (flip-flop type) the rapid exchange is assumed to occur between type 1 and type 2. St-Jacques et al.[17] have reported from the analysis of coupling constant $^3J_{HOCH}$ that α- and β-CDs form type 2 intramolecular hydrogen bond and Christofides et al.[18,19] have also reported from the studies of ^2H isotope effect on ^1H and ^{13}C chemical shifts that α- and β-CDs form type 2 hydrogen bond, but there is no description about the difference between α- and β-CDs. For DMCDs the type of intramolecular hydrogen bond to be considered is only type 4, because there is only one type of secondary hydroxyl group in each glucose constituent. To identify the type of

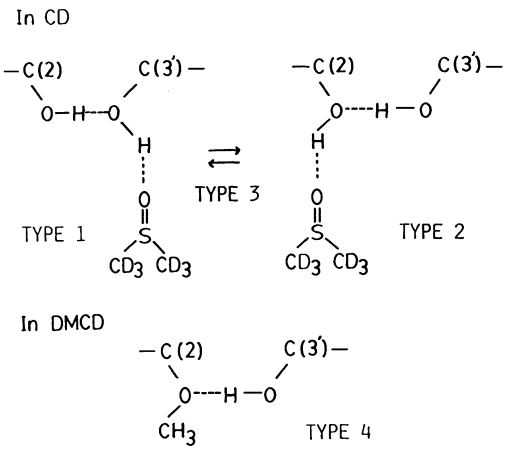

Fig. 5. The schematic representation of the intramolecular hydrogen bonds in CDs and DMCDs.

intramolecular hydrogen bond, we have tried to measure deuterium exchange rates of CD hydroxyl protons upon an addition of small amounts of deuterium oxide. If the hydrogen bond is type 1 or 2, ^1H–^2H exchange rate of hydrogen-donating hydroxyl group is slower than that of free hydroxyl group. But, ^1H–^2H exchange rate could not be estimated, since it was too rapid as compared to the NMR time scale. Then, the type of intramolecular hydrogen bond is identified based on R values (Table 2), defined as follows,

$$R = \frac{d_j^i \delta/dT}{d_j^{MG}\delta/dT}$$

where $d_j^i\delta/dT$ and $d_j^{MG}\delta/dT$ indicate the temperature coefficients of chemical shifts of j-th hydroxyl group of CD and MG, respectively, and superscript i and subscript j are,

i = α-, β-, and γ-CDs, and α- and β-DMCDs
j = OH(2), OH(3), and OH(6).

A hydroxyl group with R value of 1 is considered to be forming the intermolecular hydrogen bond with DMSO-d_6 in a similar way as that of MG. The R value smaller than 1 means that a hydroxyl group prefers to form the intramolecular hydrogen bond. The R values for the OH(6) groups of all CDs are nearly equal to 1, indicating they form the intermolecular hydrogen bond with DMSO-d_6. The OH(3) groups of α- and β-DMCDs have the smallest R values of 0.25 and 0.26, which are strongly supporting the conclusion obtained from the $d\delta/dT$ values that α- and β-DMCDs form the strongest intramolecular hydrogen bond. In α-CD the R value for the OH(3) groups (0.41) is much smaller than that for the OH(2) groups (0.60). So the OH(3) group is considered to be a dominant proton donor (type 2) for the intramolecular hydrogen bond between it and the OH(2) group of the adjacent glucose unit. Similar tendency is also observed for β-CD, though the absolute R values for OH(2) and OH(3) become larger. Thus in β-CD the type 2 intramolecular hydrogen bond is dominant, but the type 3 intramolecular hydrogen bond and the intermolecular hydrogen bond with solvent DMSO-d_6 are also formed more frequently than in α-CD. In γ-CD the R value for OH(2) is nearly equal to that for OH(3) and both are relatively large, although they are clearly less than 1. So the preferred intramolecular hydrogen bond in γ-CD is type 3, and the extent of hydrogen bond with DMSO-d_6 is not negligibly small. Therefore the character of intramolecular hydrogen bond is found to change from type 2 to type 3 with increasing the ring size of CD. The ring size of CD is considered to be an important factor determining not only the strength but also the type of the intramolecular hydrogen bond.

Orientation of Secondary Hydroxyl Groups. The values of vicinal coupling constants $^3J_{HOCH}$ for OH(2) and OH(3) groups of α-, β-, and γ-CDs didn't change within experimental error over the temperature ranged from 25 to 75 °C. This result indicates that the orientation of hydroxyl group is independent of the temperature range examined here, because the $^3J_{HOCH}$ value can be related to the dihedral angle Φ around the HO–CH bond through the Karplus type equation;[28]

$$^3J_{HOCH} = 10.4\cos^2\Phi - 1.5\cos\Phi + 0.2. \quad (1)$$

The values of coupling constants for the secondary hydroxyl groups and the estimated dihedral angles Φ are listed in Table 3. Some sets of values of dihedral angles Φ for α-, β-, and γ-CDs appear to be reasonable for making an intramolecular hydrogen bond. From the CPK molecular model study, in the case of combination of $\Phi_{OH(2)}$ and $\Phi_{OH(3)}$ values both of which are positive, formation of the intramolecular hydrogen bond between adjacent glucose units is impossible.

It is noteworthy that the $^3J_{HOCH}$ values for OH(2) of α-, β-, and γ-CDs are almost the same with that of MG, while those for OH(3) of all CDs are quite different from that of MG. This result implies that significant conformational change occurs not at OH(2) but at OH(3) group by cyclization. Needless to say that MG is monosaccharide, so it does not form the intramolecular hydrogen bond like CDs. Thus, such conformational change of the secondary hydroxyl groups of CDs might be attributed to the formation of the intramolecular hydrogen bond. The change of orientation of OH(3) group implies again that OH(3) is a major proton donor of the hydrogen bond, i.e., the predominant type of the hydrogen bond in all CDs is type 2. For these cases, the negative values of $\Phi_{OH(3)}$ are adequate for α- and β-CDs. The OH(3) group is directed to opposite direction of OH(2′) of the adjacent glucose unit, when $\Phi_{OH(3)}$ value is positive.

Table 3. The Observed Vicinal Coupling Constants $^3J_{HCOH}$ and the Calculated Dihedral Angles of Secondary Hydroxyl Groups of Some CDs in DMSO-d_6 at 35°C

	OH(2)			OH(3)		
	J/Hz	Φ/deg[a]		J/Hz	Φ/deg[a]	
α-CD	7.0	±27.9,	±137.7	2.8	±54.7,	±115.7
β-CD	6.7	±30.0,	±136.1	2.5	±56.8,	±113.8
γ-CD	7.0	±27.9,	±137.7	2.5	±56.8,	±113.8
α-DMCD				ca. 0.0	ca. ±85.9	
β-DMCD				ca. 0.0	ca. ±85.9	
MG	6.6	±30.7,	±135.7	5.1	±40.3,	±135.7

a) Φ's were computed based on the following Karplus type equation,
$^3J_{HCOH} = 10.4\cos^2\Phi - 1.5\cos\Phi + 0.2$.

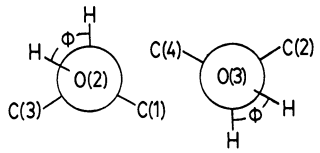

For β-DMCD we can not determine the exact value of coupling constant $^3J_{HOCH}$, since the splitting of the OH(3) resonance is too small even at 500 MHz. If $^3J_{HOCH}$ value for OH(3) of β-DMCD is assumed to be 0.0 Hz, the dihedral angles estimated from Eq. 1 are ±85°. When the type 4 hydrogen bond is formed, the value of +85° is ruled out. Making CPK model with the value of −85°, the distance between OH(3′) and O(2) is found to become the shortest. This results corresponds well with small temperature coefficient of OH(3) proton chemical shift, indicating the formation of very strong intramolecular hydrogen bond in β-DMCD. It is also found from the CPK model study that the rim of β-DMCD made by the secondary hydroxyl and the methoxyl groups is slightly wider than that of β-CD made by the secondary hydroxyl groups. For 2,3,6-tri-*O*-methyl-β-CD with no intramolecular hydrogen bond, some conformational changes around the glucosidic linkage have been detected from ^{13}C NMR study,[27] but for β-DMCD any obvious changes have not been detected. The secondary hydroxyl groups of β-DMCD form the intramolecular hydrogen-bond network which maintains the stable macrocyclic structure in DMSO-d_6. For α-DMCD we can not also determine the exact value of coupling constant $^3J_{HOCH}$, because the line width of the secondary hydroxyl proton is too large in this system. The value of the coupling constant of α-DMCD is expected to be the same order as that of β-DMCD. In such case, the distance between OH(3′) and O(2) of α-DMCD becomes nearly the same as that of β-DMCD. Hence it is reasonably expected that the strength of the intramolecular hydrogen bond of α-DMCD is about the same as that of β-DMCD. This expectation is also derived from the values of $d\delta/dT$ and R.

Conclusion

In α-, β-, and γ-CDs and α- and β-DMCDs the intramolecular hydrogen bond is formed between OH(2) and OH(3′) groups of adjacent glucose units in DMSO-d_6. The strength of the intramolecular hydrogen bond of CDs in DMSO-d_6 is in the following order: α-DMCD≒β-DMCD>α-CD>β-CD>γ-CD, and this order is opposite to that found in solid. For solutions, the role of solvent molecules must be considered. α- and β-CDs prefer to form the intramolecular hydrogen bond in which OH(3) is the donor of proton. The intramolecular hydrogen bond plays an important role to maintain the stable macrocyclic structure of CDs and DMCDs investigated here.

This work was supported by a Grant-in-Aid for Scientific Research (No. 62430019) from The Ministry of Education, Science and Culture.

References

1) M. L. Bender and M. Komiyama, "Cyclodextrin Chemistry," Springer-Verlag, New York (1978).
2) J. Szejtli, "Cyclodextrins and Their Inclusion Complexes," Akademiai Kiado, Budapest (1982).
3) W. Saenger, *Angew. Chem., Int. Ed. Engl.*, **19**, 344 (1980).
4) I. Tabushi, *Acc. Chem. Res.*, **15**, 62 (1982).
5) Y. Inoue, *Kagaku (Iwanami)*, **55**, 710 (1985).
6) Y. Inoue, *JEOL NEWS*, **23A**, 36 (1987).
7) Y. Inoue, F. Kuan, and R. Chûjô, *Bull. Chem. Soc. Jpn.*, **60**, 2539 (1987).
8) Y. Inoue, Y. Takahashi, and R. Chûjô, *Carbohydr. Res.*, **144**, C9 (1985).
9) Y. Inoue, Y. Takahashi, and R. Chûjô, *Carbohydr. Res.*, **148**, 109 (1986).
10) K. Uekama and T. Irie, *Seiyaku Kojo*, **5**, 20 (1985).
11) K. Uekama and F. Hirayama, *Kagaku to Kogyo*, **59**, 443 (1985).
12) C. Betzel, W. Saenger, B. E. Hingerty, and G. M. Brown, *J. Am. Chem. Soc.*, **106**, 7545 (1984).
13) V. Zabel, W. Saenger, and S. A. Mason, *J. Am. Chem. Soc.*, **108**, 3664 (1986).
14) T. D. Ditner and D. W. Urry, *J. Am. Chem. Soc.*, **94**,

1399 (1972).
15) K. D. Kopple, A. Go, I. J. Schamper, and C. S. Wilcox, *J. Am. Chem. Soc.*, **95**, 6090 (1973).
16) N. Niccolai, C. Rossi, V. Brizzi, and W. A. Gibbong, *J. Am. Chem. Soc.*, **106**, 5732 (1984).
17) M. St-Jacques, P. R. Sundararajan, K. J. Taylor, and R. H. Marchessault, *J. Am. Chem. Soc.*, **98**, 4386 (1976).
18) J. C. Christofides and D. B. Davies, *J. Chem. Soc., Chem. Commun.*, **1982**, 560.
19) J. C. Christofides, D. B. Davies, and E. B. Rathbone, *J. Am. Chem. Soc.*, **108**, 5738 (1986).
20) P. C. Manor and W. Saenger, *J. Am. Chem. Soc.*, **96**, 3630 (1974).
21) K. Linder and W. Saenger, *Carbohydr. Res.*, **99**, 103 (1982).
22) K. Harata, *Bull. Chem. Soc. Jpn.*, **60**, 2763 (1987).
23) K. Harata, *Chem. Lett.*, **1984**, 1641.
24) K. Harata, *Bull. Chem. Soc. Jpn.*, **51**, 1644 (1978).
25) B. Casu, M. Rebiani, G. G. Gallo, and A. Vigeani, *Tetrahedron*, **22**, 3061 (1966).
26) K. Koizumi, Y. Kubota, T. Utamura, and S. Horiyama, *J. Chromatogr.*, **368**, 329 (1986).
27) Y. Yamamoto, M. Onda, Y. Takahashi, Y. Inoue, and R. Chûjô, *Carbohydr. Res.*, **170**, 229 (1987).
28) R. R. Fraser, M. Kaufman, P. Morand, and G. Govil, *Can. J. Chem.*, **47**, 403 (1969).

 © 1988 The Chemical Society of Japan Bull. Chem. Soc. Jpn., 61, 4023—4028 (1988)

Stereoselective Total Synthesis of (±)-Labdane-8α,15-diol and (±)-Eperuane-8β,15-diol[1]

Hiroshi HIROTA,* Toshio NAKAMURA, Takahiko TSUYUKI, and Takeyoshi TAKAHASHI†
Department of Chemistry, Faculty of Science, The University of Tokyo,
Hongo, Bunkyo-ku, Tokyo 113
(Received May 17, 1988)

(±)-Labdane-8α,15-diol and (±)-eperuane-8β,15-diol, diastereomeric diterpenes to each other, were prepared separately and stereoselectively, via a common 7-membered lactone from the known tricyclic keto alcohol.

A large number of diterpenoids possessing a labdane skeleton (**1**) occur in nature[2] and labdanolic acid (**2**) and eperuic acid (**3**) are two of the representative labdane-type diterpenoids. These acids are antipodal except for the asymmetric center at C-13 position, which was assigned to be the same (*S*)-configuration. Stereochemical assignment at C-13 position has been difficult on most of labdane-type compounds,[3] and therefore X-ray structure analysis of a derivative of labdanolic acid has been applied to establish the C-13 configuration.[4]

Concerning the synthetic works, Barltrop et al. have reported the total synthesis of methyl labdanolate (**4**) and its 13-epimer corresponding to an enantiomer of methyl eperuate (**5**), but their synthesis included non-stereoselective formation of the C-13 methyl group by hydrogenation at the final stage.[5] In this paper, we wish to report the stereoselective total synthesis of (±)-labdane-8α,15-diol (**6**) and (±)-eperuane-8β,15-diol (**7**) from a common key intermediate ((±)-**8**).

Our fundamental synthetic strategies were based on the following considerations. i) Alkylation at the α-position of the lactone carbonyl group of **8** via an enolate ion would proceed stereoselectively from the sterically less-hindered α-side. ii) If a methyl group was introduced from the α-side at this position and then one carbon-unit was homologated at the lactone carbonyl carbon, (±)-labdane-8α,15-diol (**6**) would be afforded unambiguously. iii) On the other hand, if some C_2-unit equivalent was introduced from the α-side at this position and then the lactone carbonyl carbon was converted into a methyl group, (±)-eperuane-8β,15-diol (**7**) could be obtained stereoselectively.

Preparation of the Tricyclic Lactone ((±)-8). The racemic α,β-unsaturated ketone (**9**), which could be obtained easily via the known procedure,[6] was treated with 3.5 equivalent moles of lithium in liquid ammonia, and the resulting alkoxy enolate was trapped with methyl iodide[7] to afford a methylated keto alcohol (**10**) quantitatively. The carbonyl group of **10** was removed by Huang-Minlon reduction to give unsaturated alcohol (**11**) in 95% yield. Hydrogenation of **11** over platinum catalyst afforded a saturated alcohol (**12**) in 98% yield. Jones oxidation of the alcohol (**12**) gave the corresponding ketone (**13**) quantitatively. The ketone (**13**) was treated with perbenzoic acid[8] to afford a single lactone (**8**), the Baeyer-Villiger oxidation product, in 61% yield.

Thus, (±)-**8** was obtained from the known ketone (**9**) via a five-step reaction sequence in 57% overall yield.

Synthesis of (±)-Labdane-8α,15-diol (6). The lactone (**8**) was treated with lithium diisopropylamide (LDA) followed by methyl iodide to afford a 13α-methylated lactone (**14**) in 72% yield. Since no peak due to the stereoisomeric compound could be detected in the ^{13}C NMR spectrum of the reaction product, it was concluded that the stereoselective methylation had

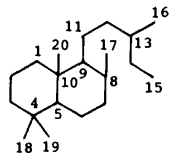

1

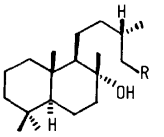

2 R = CO_2H
4 R = CO_2CH_3
6 R = CH_2OH

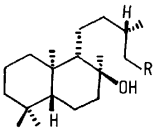

3 R = CO_2H
5 R = CO_2CH_3
7 R = CH_2OH

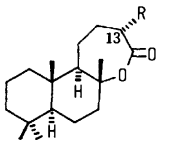

8 R = H
14 R = CH_3
19 R = $CH_2CH{=}CH_2$

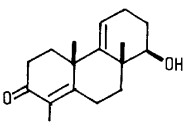

9

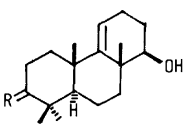

10 R = O
11 R = H_2

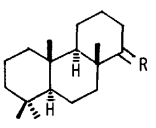

12 R = α-H, β-OH
13 R = O

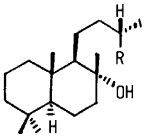

15 R = CH_2OH
16 R = CHO
17 R = CH_2OTs
18 R = CH_2CN

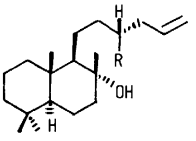

20 R = CH_2OH
21 R = CH_3

† Present address: Department of Applied Biological Science, College of Agriculture and Veterinary Medicine, Nihon University, Kameino, Fujisawa 252.

occurred from the sterically less-hindered α-side of the enolate. Lithium aluminium hydride reduction of this lactone (**14**) gave the corresponding diol (**15**) quantitatively.

The C_1-unit homologation at the hydroxymethyl group of **15** was attempted by Wittig reaction. Pyridinium chlorochromate oxidation of the diol (**15**) gave an aldehyde (**16**) in 46% yield, which was treated with methylenetriphenylphosphorane and hydroboration was followed. A mixture of (±)-labdane-8α,15-diol (**6**) and (±)-eperuane-8β,15-diol (**7**) was obtained in a ratio of ca. 2:1 in 65% yield. This means that the isomerization at C-13 position would take place under the Wittig reaction conditions. Hence, the transformation of hydroxyl group into cyano group was next examined to synthesize **6** without isomerization at the C-13 position.

The diol (**15**) was treated with *p*-toluenesulfonyl chloride at 0 °C to afford a monotosylate (**17**) in 87% yield. On treatment with sodium cyanide,[9] **17** afforded a cyanide (**18**) in 93% yield, which was hydrolyzed with sodium hydroxide in the presence of aqueous hydrogen peroxide[10] to give (±)-labdanolic acid (**2**) stereoselec-

Table 1. ^{13}C NMR Spectra of Methyl Labdanolate (**4**), Methyl Eperuate (**5**), Labdane-8α,15-diol (**6**), and Eperuane-8β,15-diol (**7**) in $CDCl_3$

No. of carbon	Methyl labdanolate (**4**)		Methyl eperuate (**5**)	
	Synthetic	Authentic[a]	Synthetic	Authentic[a]
1	39.82	39.86	39.90	39.86
2	18.53	18.56	18.61	18.56
3	41.47	41.45	41.37	41.34
4	33.27	33.25	33.35	33.31
5	56.21	56.25	56.29	56.31
6	20.59	20.61	20.70	20.61
7	44.43	44.35	44.67	44.64
8	74.20	73.90	74.20	74.13
9	62.31	62.17	62.15	62.12
10	39.20	39.17	39.25	39.23
11	22.86	22.83	22.57	22.49
12	40.69	40.65	40.39	40.37
13	31.32	31.26	31.21	31.14
14	42.10	42.13	42.15	42.13
15	173.78	173.77	173.92	174.00
16	19.94	19.93	20.07	20.04
17	24.08	24.03	24.08	24.03
18	33.46	33.48	33.54	33.48
19	21.54	21.58	21.62	21.58
20	15.50	15.49	15.55	15.49
MeO	51.31	51.24	51.34	51.30

No. of carbon	Labdane-8α,15-diol (**6**)		Eperuane-8β,15-diol (**7**)	
	Synthetic	Literature[17]	Synthetic	Authentic[a]
1	39.77	39.8	39.82	39.91
2	18.50	18.5	18.50	18.56
3	42.04	42.1	42.02	42.13
4	33.27	33.3	33.27	33.31
5	56.16	56.2	56.16	56.25
6	20.56	20.6	20.56	20.61
7	41.15	40.9	40.45	40.42
8	74.44	74.4	74.47	74.47
9	62.47	62.5	61.79	61.89
10	39.17	39.2	39.23	39.29
11	24.03	24.0	24.08	24.14
12	44.43	44.3	44.51	44.58
13	30.61	30.6	30.07	30.12
14	39.77	39.8	39.23	39.29
15	60.98	60.3	61.25	61.21
16	19.83	20.1	20.07	20.10
17	23.00	23.2	22.16	22.15
18	33.43	33.5	33.43	33.48
19	21.51	21.5	21.51	21.58
20	15.50	15.5	15.47	15.49

a) Shift values were obtained from the ^{13}C NMR charts of authentic samples which were sent from Profs. E. L. Ghisalberti and P. R. Jefferies. Eperuane-8β,15-diol (**7**) was a natural compound and other samples (**4** and **5**) were derived from natural ones.

tively in 75% yield. This acid (**2**) was converted into (±)-methyl labdanolate (**4**) and then into (±)-labdane-8α,15-diol (**6**) via known procedures.[11]

The ^{13}C and ^{1}H NMR spectral data of synthetic **4** and **6** were completely identical with those of natural methyl labdanolate[5,12-15] and labdane-8α,15-diol[12,14,16,17] (see Table 1 for the comparison of ^{13}C NMR spectral data). Thus (±)-labdane-8α,15-diol (**6**) was synthesized stereoselectively from the lactone (**8**) by a seven-step reaction sequence in 43% overall yield.

Synthesis of (±)-Eperuane-8β,15-diol (7). As mentioned before, it is necessary to introduce a C_2-unit equivalent at the α-position of lactone carbonyl group of **8** to build up the side chain of **7**. Ethylene oxide being turned out to be ineffective,[18] the introduction of C_2-unit equivalent was achieved by allylation followed by ozonolysis. The lactone (**8**) was treated with LDA followed by allyl bromide to afford the 13α-allylated lactone (**19**) in 62% yield. No stereoisomer could be detected by ^{13}C NMR spectrum examination of the reaction product. This result indicates that allylation exclusively occurred from the sterically less-hindered α-side of the enolate. On reduction with lithium aluminium hydride, this lactone (**19**) gave the corresponding diol (**20**) in 97% yield, which was monotosylated with *p*-toluenesulfonyl chloride. The reaction product was then reduced with lithium aluminium hydride to afford an alcohol (**21**) in 80% yield, which was treated with ozone. A reductive treatment with sodium borohydride[19] was followed to give (±)-eperuane-8β,15-diol (**7**) in 82% yield. This diol (**7**) was transformed into (±)-eperuic acid (**3**) and methyl eperuate (**5**) by known procedures.[20]

The ^{13}C and ^{1}H NMR spectral data of synthetic **5** and **7** were completely identical with those of natural methyl eperuate[5,12,13,20] and eperuane-8β,15-diol,[12,20] respectively (see Table 1 for ^{13}C NMR spectral data).

Thus, (±)-eperuane-8β,15-diol (**7**) was synthesized stereoselectively by five step reactions in 39% overall yield from the same intermediate (**8**) as that used for a preparation of **6**.

Experimental

General Procedures. All melting points were measured on a Mel-temp capillary melting point apparatus (Laboratory Devices) and uncorrected. Infrared (IR) spectra were measured on a Hitachi 260-30 spectrometer. Proton nuclear magnetic resonance (^{1}H NMR) spectra were taken using a Varian EM-390 and a JEOL FX-90Q (both 90 MHz) spectrometers at ambident temperature. ^{13}C NMR spectra were measured on a JEOL FX-90Q (22.5 MHz) spectrometer. Chloroform-*d* was used as the NMR solvent unless otherwise mentioned. Chemical shifts were expressed in δ (ppm) downfield from tetramethylsilane as an internal standard and coupling constants in Hz. Mass spectra (MS) were run on a JEOL JMS-D300 mass spectrometer operating at 70 eV. Thin-layer chromatography (TLC) was carried out on Kieselgel 60 GF_{254} coated in 0.25 mm thickness. Wakogel C-200 (Wako) was used for silica-gel column chromatography.

(±)-8β-Hydroxy-1,1,4aβ,8aβ-tetramethyl-3,4,4a,6,7,8,8a,9,10,10aα-decahydro-2(1*H*)-phenanthrenone (10). In a three-necked flask, lithium metal (570 mg) and liquid ammonia (150 ml) were placed at −78 °C and stirred for 10 min under a nitrogen atmosphere. A tetrahydrofuran (THF; 70 ml) solution of keto alcohol (**9**; 6.00 g) was added to the mixture and stirred at a refluxing temperature of ammonia for 1 h. At −78 °C methyl iodide (12 ml) was added to the mixture, and the whole was again stirred at a refluxing temperature of ammonia for 2 h. After removal of ammonia at room temperature, the reaction mixture was neutralized with about 2 M hydrochloric acid (1 M=1 mol dm^{-3}) and was extracted with chloroform four times. The combined chloroform extract was washed with saturated brine, and was dried over sodium sulfate. Removal of the solvent afforded keto alcohol (**10**; 6.37 g; quantitative yield) as white crystals (from acetone), mp 139.5—142.5 °C; IR (KBr) 3400 and 1710 cm^{-1}; ^{1}H NMR δ=1.08(6H, s), 1.17 (3H, s), 1.28 (3H, s), 3.41 (1H, dd, *J*=8.5 and 7 Hz), and 5.33 (1H, t, *J*=4 Hz); MS *m/z* (%) 276 (M^+, 37), 258 (100), and 232 (82); Found: *m/z* 276.2099. Calcd for $C_{18}H_{28}O_2$: M, 276.2090.

(±)-4bβ,8,8,10aβ-Tetramethyl-1,2,3,4b,5,6,7,8,8aα,9,10,10a-dodecahydro-1β-phenanthrenol (11). To a suspension of keto alcohol (**10**; 3.70 g) in diethylene glycol (64 ml) were added 80% hydrazine hydrate (7 ml) and potassium hydroxide (9.1 g). After the mixture was heated for 2 h at 170 °C (bath temperature) about 10 ml of the solvent was distilled off and the mixture was heated for 1 h at 230 °C. Water (70 ml) and 6 M hydrochloric acid (70 ml) were added, and the mixture was extracted with benzene. The usual work-up yielded the reduction product (**11**; 3.34 g) in 95% yield as white crystals (from benzene), mp 153.5—155 °C; IR (KBr) 3300 cm^{-1}; ^{1}H NMR δ=0.87 (6H, s), 1.13 (6H, s), 3.41 (1H, dd, *J*=8.5 and 7 Hz), and 5.27 (1H, t, *J*=4 Hz); MS *m/z* (%) 262 (M^+, 21), 244 (61), 203 (75), and 106 (100); Found: C, 82.57; H, 11.61%; and *m/z* 262.2291. Calcd for $C_{18}H_{30}O$: C, 82.38; H, 11.52%; and M, 262.2298.

(±)-4bβ,8,8,10aβ-Tetramethyl-4aα*H*,8aα*H*-tetradecahydro-1β-phenanthrenol (12). A catalytic amount of platinum oxide was added to a solution of **11** (1.91 g) in acetic acid (60 ml) and the mixture was stirred under a hydrogen atmosphere at room temperature for 2.5 d. The reaction was monitored as follows; a small portion of the reaction mixture was treated with *m*-chloroperbenzoic acid. Only starting material (**11**), if present, was transformed into an epoxide, which could be differentiated from **12** by TLC examination. Filtration and evaporation afforded an alcohol (**12**; 1.89 g) in 98% yield as white crystals (from benzene), mp 179—182 °C; IR (KBr) 3300 cm^{-1}; ^{1}H NMR δ=0.81(3H, s), 0.86 (6H, s), 0.88 (3H, s), and 3.12 (1H, dd, *J*=10 and 5 Hz); MS *m/z* (%) 264 (M^+, 41), 249 (26), and 191 (100); Found: *m/z* 264.2452. Calcd for $C_{18}H_{32}O$: M, 264.2455.

(±)-4bβ,8,8,10aβ-Tetramethyl-3,4,4aα,4b,5,6,7,8,8aα,9,10,10a-dodecahydro-1(2*H*)-phenanthrenone (13). Jones reagent (5 ml) was added to a solution of the saturated alcohol (**12**; 3.47 g) in acetone (450 ml) at 0 °C , and the mixture was stirred for 30 min at the same temperature. To the mixture, a saturated aqueous solution (ca. 100 ml) of sodium sulfite was added, and then acetone was removed under reduced pressure. The reaction product was extracted with benzene

three times and dried over sodium sulfate. The benzene solution was passed through a small amount of Florisil, and the solvent was evaporated to afford ketone (**13**; 3.44 g) quantitatively, as white crystals (from ether), mp 102.5—103 °C; IR (KBr) 1710 cm^{-1}. ^1H NMR δ=0.83 (3H, s), 0.87 (3H, s), 0.95 (3H, s), and 1.14 (3H, s); MS *m/z* (%) 262 (M^+, 78), 247 (43), and 191 (100); Found: C, 82.06; H, 11.82%; and *m/z* 262.2304. Calcd for $C_{18}H_{30}O$: C, 82.38; H, 11.52%; and M, 262.2298.

(±)-5aβ,8,8,11aβ-Tetramethyl-7aαH,11bαH-tetradecahydronaphth[2,1-*b*]oxepin-4-one (8). Perbenzoic acid (9.7 g) was added to a solution of the saturated ketone (**13**; 6.20 g) in chloroform (90 ml), and the mixture was stirred at room temperature for 2 d under dark. A saturated aqueous solution (20 ml) of sodium hydrogensulfite was added to the reaction mixture, and the chloroform layer was separated, washed three times with a saturated aqueous solution of sodium hydrogencarbonate, and dried over sodium sulfate. Purification by silica-gel column chromatography (0.6% acetone in benzene) afforded 7-membered lactone (**8**; 4.00 g) in 61% yield, as white crystals (from benzene), mp 100.5—102.5 °C; IR (KBr) 1705 cm^{-1}; ^1H NMR δ=0.83 (6H, s), 0.90 (3H, s), and 1.51 (3H, s); MS *m/z* (%) 278 (M^+, 42), 263 (72), and 137 (100); Found: C, 77.81; H, 11.18%; and *m/z* 278.2238. Calcd for $C_{18}H_{30}O_2$: C, 77.65; H, 10.86%; and M, 278.2247.

(±)-3α,5aβ,8,8,11aβ-Pentamethyl-7aαH,11bαH-tetradecahydronaphth[2,1-*b*]oxepin-4-one (14). Under an argon atmosphere, a hexane solution of butyllithium (1.6 M; 5.7 ml) and diisopropylamine (1.7 ml) were added successively to THF (80 ml) at −78 °C. The mixture was stirred for 20 min at room temperature and then kept to −78 °C, to which a THF (50 ml) solution of the lactone (**8**; 1.89 g) was added. After stirring for 30 min at −78 °C and addition of methyl iodide (0.90 ml), the whole mixture was stirred at room temperature for 2 h and then a mixture of 14% aqueous solution of ammonium chloride and a small amount of sodium sulfite was added. The reaction product was extracted with ether three times, worked up as the usual manner, and separated by silica-gel column chromatography (0.3% acetone in benzene) to afford methylated lactone (**14**; 1.42 g) in 72% yield as white crystals, mp 125.5—127 °C; IR (KBr) 1715 cm^{-1}; ^1H NMR δ=0.81 (6H, s), 0.90 (3H, s), 1.17 (3H, d, *J*=7 Hz), 1.15 (3H, s); ^{13}C NMR δ=15.1, 18.8, 18.8, 19.7, 21.8, 22.9, 24.4, 32.9, 33.4, 33.6, 38.8, 39.9, 40.3, 41.6, 43.7, 55.6, 57.9, 85.5, and 177.4; MS *m/z* (%) 292 (M^+, 34), 277 (56), and 137 (100); Found: *m/z* 292.2390. Calcd for $C_{19}H_{32}O_2$: M, 292.2404.

(±)-1β-[(3*S*)-4-Hydroxy-3-methylbutyl]-2β,5,5,8aβ-tetramethyl-4aαH-decahydro-2α-naphthalenol (15). Under an argon atmosphere, lithium aluminium hydride (140 ml) was added to a solution of the methylated lactone (**14**; 1.40 g) in ether (5 ml), and the mixture was stirred at 0 °C for 30 min. The reaction was stopped by addition of a small amount of water and the mixture was filtered. The filtrate, after addition of water (50 ml), was extracted with ether three times, and the ethereal layer was dried over magnesium sulfate and successively evaporated to give diol **15** (1.42 g) quantitatively as white crystals, mp 114—115 °C; IR (KBr) 3350 cm^{-1}; ^1H NMR δ=0.80 (6H, s), 0.88 (3H, s), 0.91 (3H, d, *J*=6 Hz), 1.15 (3H, s), and 3.46 (2H, br t, *J*=5 Hz); MS *m/z* (%) 296 (M^+, 8), 278 (21), 263 (25), and 69 (100); Found: *m/z* 296.2714. Calcd for $C_{19}H_{36}O_2$: M, 296.2717.

(±)-1β-[(3*S*)-3-Methyl-4-oxobutyl]-2β,5,5,8aβ-tetramethyl-4aαH-decahydro-2α-naphthalenol (16). A solution of diol **15** (300 mg) in dichloromethane (20 ml) was added to a solution of pyridinium chlorochromate (1.04 g) in dichloromethane (70 ml) and the mixture was stirred at room temperature for 40 min. A saturated aqueous solution (100 ml) of sodium hydrogencarbonate together with a small amount of sodium sulfite was added. After filtration with Celite under reduced pressure, the reaction mixture was extracted three times with chloroform, dried over magnesium sulfate, and separated by a silica-gel column chromatography (1% acetone in benzene). Pure hydroxy aldehyde **16** (140 mg) was obtained in 46% yield as a colorless oil; IR (neat) 3450 and 1720 cm^{-1}; ^1H NMR δ=0.78 (6H, s), 0.86 (3H, s), 1.08 (3H, d, *J*=9 Hz), 1.13 (3H, s), 2.33 (1H, br sextet, *J*=6 Hz), and 9.57 (1H, d, *J*=2 Hz); MS *m/z* (%) 294 (M^+, 7), 276 (28), and 109 (100); Found: *m/z* 294.2541. Calcd for $C_{19}H_{34}O_2$: M, 294.2560.

Preparation of a Mixture of (±)-Labdane-8α,15-diol (6) and (±)-Eperuane-8β,15-diol (7) from the Hydroxy Aldehyde (16). Under a nitrogen atmosphere, a solution of methyltriphenylphosphonium iodide (426 mg) in THF (25 ml) was added to a hexane solution of butyllithium (1.6 M; 0.7 ml) at 0 °C, and the mixture was stirred at room temperature for 1.5 h. A solution of the hydroxy aldehyde **16** (140 mg) in THF (10 ml) was added to the mixture, and was refluxed for 18 h. Addition of a saturated aqueous solution (30 ml) of ammonium chloride followed by evaporation of THF gave a residue, which was extracted with hexane three times and dried over magnesium sulfate. Separation by column chromatography on silica gel (0.5% acetone in benzene) afforded a diastereomeric mixture of the Wittig reaction product (60 mg) as an oil; IR (neat) 3450 and 1635 cm^{-1}; ^1H NMR δ=0.77 (6H, s), 0.85 (3H, s), 0.97 (3H, d, *J*=6 Hz), 1.11 (3H, s), 4.88 (1H, br d, *J*=11 Hz), 4.92 (1H, br d, *J*=17 Hz), and 5.63 (1H, ddd, *J*=17, 11, and 4 Hz); MS *m/z* (%) 292 (M^+, 19), 274 (10), and 69 (100); Found: *m/z* 292.2776. Calcd for $C_{20}H_{36}O$: M, 292.2768. To a solution of the diastereomeric mixture (60 mg) in THF (7 ml) was added a THF solution of diborane (0.4 M; 1 ml) at 0 °C under nitrogen atmosphere, and the mixture was stirred at room temperature for 1.5 h. Water (1 ml), 3 M aqueous solution of sodium hydroxide (1 ml), and 30% aqueous solution of hydrogen peroxide (1 ml) were successively added, and the mixture was stirred at 40 °C for 1.5 h, and then extracted with ether three times. The ethereal layer was dried over magnesium sulfate and purified by silica-gel column chromatography (5% acetone in benzene) to afford 27 mg of labdane-8α,15-diol (**6**; 42% yield) and 14.5 mg of eperuane-8β,15-diol (**7**; 23% yield), both as crystalline compounds. Physical and spectral data of these diols (**6** and **7**) were completely identical with those synthesized from separate routes mentioned below.

(±)-1β-[(3*S*)-3-Methyl-4-(*p*-tolylsulfonyl)butyl]-2β,5,5,8aβ-tetramethyl-4aαH-decahydro-2α-naphthalenol (17). The diol (**15**; 191 mg) and *p*-toluenesulfonyl chloride (300 mg) were dissolved into pyridine (6 ml), and the mixture was stirred at 0 °C for 12 h. After addition of water and 2 M hydrochloric acid, the reaction product was extracted. The ethereal extract was worked up as usual and subjected to separation by Florisil column chromatography to afford monotosylate (**17**; 254 mg; 87% yield) as white crystals (from ether), mp 97—98.5 °C; IR (KBr) 3600—3400, 1360, and 1180 cm^{-1}; ^1H NMR δ=0.75 (3H, s), 0.78 (3H, s), 0.86 (3H, s),

0.89 (3H, d, J=6 Hz), 1.06 (3H, s), 2.43 (3H, s), 3.80 (2H, d, J=6 Hz), 7.27 (2H, d, J=8 Hz), and 7.71 (2H, d, J=8 Hz); MS m/z (%) 450 (M^+, 6), 432 (59), 417 (42), and 191 (100); Found: m/z 450.2788. Calcd for $C_{26}H_{42}O_4S$: M, 450.2803.

(±)-1β-[(3*S*)-4-Cyano-3-methylbutyl]-2β,5,5,8aβ-tetramethyl-4aα*H*-decahydro-2α-naphthalenol (18). The monotosylate (**17**; 226 mg) and sodium cyanide (260 mg) were added to a mixture of tributylamine (0.2 ml) and water (1 ml), and the whole mixture was refluxed with vigorous stirring for 6 h. The reaction product was extracted with ether and worked up as usual. Column chromatography on Florisil afforded nitrile (**18**; 142 mg; 93% yield) as white crystals (from ether–hexane), mp 51—52 °C; IR (KBr) 3600—3400, 2250, and 940 cm^{-1}; ^1H NMR (CCl_4) δ=0.79 (6H, s), 0.85 (3H, s), 1.07 (3H, d, J=7 Hz), 1.09 (3H, s), and 2.26 (2H, m); MS m/z (%) 305 (M^+, 5), 290 (4), 287 (3), 272 (7), and 71 (100); Found: m/z 305.2689. Calcd for $C_{20}H_{35}NO$: M, 305.2717.

(±)-Labdanolic Acid (2). A mixture of the nitrile **18** (49 mg), sodium hydroxide (500 mg), ethanol (5 ml), and 30% aqueous hydrogen peroxide (5 ml) was stirred at ca. 70 °C for about 30 min until the evolution of oxygen ceased. Then the mixture was refluxed for 7.5 h. After addition of an aqueous solution of sodium sulfite, evaporation of ethanol, and then addition of 2 M hydrochloric acid, the reaction product was extracted with ether. The ethereal layer was washed with a saturated brine, dried over sodium sulfate and evaporated to give a crude reaction mixture, which was separated by silica-gel column chromatography. From the ether eluant, 39 mg (75% yield) of labdanolic acid (**2**) was obtained as white crystals (from hexane–ether), mp 150.5—152 °C; IR (KBr) 3400, 1705, and 1690 cm^{-1}; ^1H NMR δ=0.80 (6H, s), 0.87 (3H, s), 0.98 (3H, d, J=6.5 Hz), 1.15 (3H, s), and 2.27 (2H, m); MS m/z (%) 324 (M^+, 45), 306 (45), 291 (43), and 69 (100); Found: m/z 324.2671. Calcd for $C_{20}H_{36}O_3$: M, 324.2665.

(±)-Methyl Labdanolate (4). To an ethereal solution of labdanolic acid (**2**; 34 mg) was added an ethereal solution of diazomethane (about three equivalent moles), and the mixture was stood for 5 h at room temperature. Removal of ether afforded the corresponding methyl ester **4** quantitatively as an oil; IR (neat) 3500 and 1740 cm^{-1}; ^1H NMR δ=0.80 (6H, s), 0.86 (3H, s), 0.95 (3H, d, J=6.5 Hz), 1.15 (3H, s), 2.25 (2H, m), and 3.64 (3H, s); ^{13}C NMR (Table 1); MS m/z (%) 338 (M^+, 13), 320 (8), 305 (8), 144 (60), and 69 (100); Found: m/z 338.2802. Calcd for $C_{21}H_{38}O_3$: M, 338.2819.

(±)-Labdane-8α,15-diol (6). To a solution of methyl labdanolate (**4**; 31.5 mg) in THF (10 ml) was added lithium aluminium hydride (20 mg), and the mixture was stirred at room temperature for 1 h. After addition of 2 M hydrochloric acid, the reaction mixture was extracted with ether. The ethereal layer was worked up in the usual manner and separated by silica-gel column chromatography. Pure labdane-8α,15-diol (**6**; 28.5 mg) was obtained in 99% yield as white crystals (from chloroform–hexane), mp 111.5—112.5 °C; IR (KBr) 3350 cm^{-1}; ^1H NMR δ=0.79 (6H, s), 0.87 (3H, s), 0.90 (3H, d, J=6.5 Hz), 1.14 (3H, s), and 3.66 (2H, t, J=6 Hz); ^{13}C NMR (Table 1); MS m/z (%) 310 (M^+, 3), 292 (17), 277 (20), and 69 (100); Found: m/z 310.2856. Calcd for $C_{20}H_{38}O_2$: M, 310.2873.

(±)-5aβ,8,8,11aβ-Tetramethyl-3α-(2-propenyl)-7aα*H*, 11bα*H*-tetradecahydronaphth[2,1-*b*]oxepin-4-one (19). Under an argon atmosphere, a hexane solution of butyllithium (1.6 M; 6.3 ml) and diisopropylamine (1.75 ml) were added successively to THF (70 ml) at −78 °C. The mixture was stirred for 20 min at room temperature and then kept at −78 °C. A solution of the lactone (**8**; 2.10 g) in THF (60 ml) was added to the mixture and the stirring was continued for 30 min at −78 °C. Then a mixture of allyl bromide (1.7 g) and THF (5 ml) was added, and the whole mixture was stirred at room temperature for 2 h. The reaction mixture was subjected to the same work-up as that for **14** and separated on silica-gel column chromatography (0.3% acetone in benzene), and the allylated lactone **19** (1.49 g) was obtained in 62% yield as white crystals (from benzene), mp 78.5—79.5 °C; IR (KBr) 1720 and 1650 cm^{-1}; ^1H NMR δ=0.77 (6H, s), 0.85 (3H, s), 1.48 (3H, s), 5.00 (1H, br d, J=11 Hz), 5.03 (1H, br d, J=15 Hz), and 5.63 (1H, ddt, J=15, 11, and 5 Hz); ^{13}C NMR δ=15.0, 18.7, 19.6, 21.7, 22.9, 24.3, 29.6, 33.3, 33.5, 36.7, 38.7, 39.8, 41.5, 43.6, 45.1, 55.5, 57.9, 85.7, 116.8, 136.3, and 176.2; MS m/z (%) 318 (M^+, 18), 303 (39), and 191 (100); Found: m/z 318.2546. Calcd for $C_{21}H_{34}O_2$: M, 318.2560.

(±)-1β-[(3*R*)-3-Hydroxymethyl-5-hexenyl]-2β,5,5,8aβ-tetramethyl-4aα*H*-decahydro-2α-naphthalenol (20). Under an argon atmosphere, lithium aluminium hydride (160 mg) was added to a solution of the allylated lactone (**19**; 1.40 g) in ether (7 ml), and the mixture was stirred at 0 °C for 30 min. The same work-up as that for **15** was followed to afford diol **20** (1.38 g) in 97% yield as white crystals, mp 109—110 °C; IR (KBr) 3350 and 1640 cm^{-1}; ^1H NMR δ=0.79 (6H, s), 0.86 (3H, s), 1.14 (3H, s),2.09 (2H, br t, J=7 Hz), 3.47 (1H, dd, J=11 and 3 Hz), 3.65 (1H, dd, J=11 and 3 Hz), 4.96 (1H, br d, J=11 Hz), 5.02 (1H, br d, J=16 Hz), and 5.80 (1H, ddt, J=16, 11, and 7 Hz); MS m/z (%) 332 (M^+, 4), 304 (9), 289 (16), and 95 (100); Found: C, 78.10; H, 11.95%; m/z 322.2867. Calcd for $C_{21}H_{38}O_2$: C, 78.20; H, 11.87%; M, 322.2873.

(±)-1β-[(3*R*)-3-Methyl-5-hexenyl]-2β,5,5,8aβ-tetramethyl-4aα*H*-decahydro-2α-naphthalenol (21). Under an argon atmosphere, *p*-toluenesulfonyl chloride (1.60 g) was added to a solution of the diol **20** (1.30 g) in pyridine (50 ml) at 0 °C, and the mixture was stirred at room temperature for 10 h. The reaction mixture was subjected to the same work-up as that for **17**, and separated by silica-gel column chromatography (0.7% acetone in benzene) to afford monotosylate (1.80 g) as an oil. To a solution of this crude monotosylate, without further purification, in ether (60 ml) was added lithium aluminium hydride (1.20 g), and the mixture was refluxed for 7 h under an argon atmosphere. The reaction was completely stopped by addition of water, and the mixture was filtered under reduced pressure. The filtrate was extracted with ether three times, and the ethereal extract was worked up as usual to yield olefinic alcohol **21** (1.00 g) in 80% yield as white crystals, mp 47—47.5 °C; IR (KBr) 3350 and 1640 cm^{-1}; ^1H NMR δ=0.78 (6H, s), 0.86 (3H, s), 0.89 (3H, d, J=6.5 Hz), 1.15 (3H, s), 4.97 (1H, br d, J=10 Hz), 4.99 (1H, br d, J=17 Hz), and 5.78 (1H, ddt, J=17, 10, and 7 Hz); MS m/z (%) 306 (M^+, 15), 288 (12), 273 (16), and 69 (100); Found: C, 82.25; H, 12.78%; m/z 306.2927. Calcd for $C_{21}H_{38}O$: C, 82.29; H, 12.49%; M, 306.2924.

(±)-Eperuane-8β,15-diol (7). To a solution of the olefin alcohol **21** (935 mg) in chloroform (45 ml) was introduced ozone (8%; 0.015 mol h^{-1}) at −20 °C for 1.5 h with stirring. Sodium borohydride (935 mg) in a 50% ethanol aqueous solution (80 ml) was added at 0 °C, and the whole mixture was stirred at 50 °C for 1 h, and then at room temperature for 5 h. After neutralization with 10% sulfuric acid, the reaction product was extracted with chloroform three times and the

organic layer was worked up as usual. Evaporation followed by silica-gel column chromatography (5% acetone in benzene) afforded eperuane-8β,15-diol (**7**; 773 mg) in 82% yield as white crystals (from benzene), mp 126—128 °C; IR (KBr) 3300 cm^{-1}; ^1H NMR δ=0.79 (6H, s), 0.87 (3H, s), 0.91 (3H, d, J=7.5 Hz), 1.15 (3H, s), 3.68 (2H, td, J=6 and 1.5 Hz); ^{13}C NMR (Table 1); MS m/z (%) 310 (M^+, 11), 292 (8), 277 (9), and 69 (100); Found: C, 75.16; H, 12.44%. Calcd for $C_{20}H_{38}O_2 \cdot 1/2\,H_2O$: C, 75.18; H, 12.30%; Found: m/z 310.2893. Calcd for $C_{20}H_{38}O_2$: M, 310.2873.

The authors wish to thank Professors E. L. Ghisalberti and P. R. Jefferies, Department of Organic Chemistry, the University of Western Australia for the kind sending of the ^1H and ^{13}C NMR spectral charts of optically active methyl labdanolate (**4**), methyl eperuate (**5**), and eperuane-8β,15-diol (**7**).

References

1) A part of this work was reported as a preliminary form: T. Nakamura, H. Hirota, and T. Takahashi, *Chem. Pharm. Bull.*, **34**, 3518 (1986).

2) e.g., J. R. Hanson, *Natural Products Reports*, **4**, 399 (1987).

3) e.g., Chiral lanthanoides shift reagents have been used to differenciate manool from its 13-epimer by ^1H NMR: A. H. Conner and J. W. Rowe, *Phytochemistry*, **15**, 1949 (1976).

4) K. Bjåmer, G. Ferguson, and R. D. Melville, *Acta Crystallogr., Sect. B*, **24**, 855 (1968); and references cited therein.

5) D. B. Bigley, N. A. J. Rogers, and J. A. Barltrop, *J. Chem. Soc.*, **1960**, 4613.

6) T. Honda, T. Murae, S. Ohta, Y. Kurata, H. Kawai, T. Takahashi, A. Itai, and Y. Iitaka, *Chem. Lett.*, **1981**, 299; cf., K. Miyaji, T. Nakamura, H. Hirota, M. Igarashi, and T. Takahashi, *Tetrahedron Lett.*, **25**, 5299 (1984); H. Hirota, A. Yokoyama, K. Miyaji, T. Nakamura, and T. Takahashi, *ibid.*, **28**, 435 (1987); H. Hirota and T. Takahashi, *Yuki Gosei Kagaku Kyokai Shi*, **45**, 1199 (1987).

7) Methyl iodide should be added to the well-cooled (below −40 °C) enolate solution. Otherwise, multiply methylated compounds would be obtained. cf., G. Stork, P. Rosen, N. Goldman, R. V. Coombs, and J. Tsuji, *J. Am. Chem. Soc.*, **87**, 275 (1965).

8) Perbenzoic acid was prepared following the literature (G. Braun, *Org. Synth.*, Coll. Vol. 1, 431 (1941)). *m*-Chloroperbenzoic acid was ineffective to this system. When peracetic acid was used, decomposition reaction of the product (**8**) was taken place quickly.

9) cf., W. P. Reeves and M. R. White, *Synth. Commun.*, **6**, 193 (1976).

10) D. Hartley, *J. Chem. Soc.*, **1962**, 4722.

11) e.g., J. D. Cocker and T. G. Halsall, *J. Chem. Soc.*, **1956**, 4262; K. H. Overton and A. J. Renfrew, *J. Chem. Soc. C*, **1967**, 931.

12) C. A. Henrick, P. R. Jefferies, and R. S. Rosich, *Tetrahedron Lett.*, **1964**, 3475.

13) S. Bory and E. Lederer, *Croat. Chem. Acta*, **29**, 157 (1957).

14) J. De Pascual Teresa, J. G. Urones, and A. Montes Sanchez, *An. Quim.*, **74**, 959 (1978).

15) F. Bohlmann and C. Zdero, *Phytochemistry*, **16**, 1583 (1977).

16) A. J. Baker, G. Eglinton, A. G. Gonzalez, R. J. Hamilton, and P. A. Raphael, *J. Chem. Soc.*, **1962**, 4705.

17) A. G. Gonzalez, C. G. Francisco, R. Freire, R. Hernandez, J. A. Salazar, and E. Suarez, *Tetrahedron Lett.*, **1976**, 1897.

18) As a model experiment, methyl palmitate was treated with lithium diisopropylamide followed by addition of ethylene oxide at 0 °C; only starting material (methyl palmitate) was recovered.

19) J. A. Sousa and A. L. Bluhm, *J. Org. Chem.*, **25**, 108 (1960).

20) C. A. Henrick and P. R. Jefferies, *Tetrahedron*, **21**, 1175 (1965).

 © 1988 The Chemical Society of Japan Bull. Chem. Soc. Jpn., 61, 4029—4035 (1988)

A Highly Chemoselective Reduction of Conjugated Nitro Olefins with Hantzsch Ester in the Presence of Silica Gel

Masayuki FUJII
Department of Industrial Chemistry, Faculty of Engineering, Kinki University in Kyushu, 11-6 Kaya-no-mori, Iizuka, Fukuoka 820
(Received May 19, 1988)

An effective system to reduce conjugated nitro olefins into the corresponding nitroalkanes is described. The system composed of Hantzsch ester (HEH) and silica gel in benzene exerts high yield and excellent chemoselectivity under almost neutral conditions. Facile applications of the system to the syntheses of natural products are also described.

The importance of aliphatic nitro compounds has remarkably increased in synthetic organic chemistry.[1] They are very useful tools for carbon–carbon bond formation because the strongly electron-withdrawing property of nitro group makes it possible to generate an α-carbanion adjacent to the group and to react with various electrophiles under mild reaction conditions. Moreover, nitro group itself can be converted into other functions such as carbonyl,[2] amino,[3] oxime,[4] hydrogen,[5] and so on. Namely the preparation[6] and reaction[7] of conjugated nitro olefins have been studied extensively and the compounds of this class have been widely accepted as intermediates to nitroalkanes via reductive hydrogenation.[8–12] Although a number of reducing reagents to convert a nitro olefin into the corresponding nitroalkane have been reported, there still remain several problems to be improved. For example, catalytic hydrogenation also reduces non-conjugated carbon–carbon double bonds,[9] and sodium borohydride cannot be employed for the reduction of compounds with a carbonyl function.[10]

On the other hand, reduction with NAD(P)H or its analogs received a wide interest in the recent decade. Particularly, the discussion on the mechanism of reduction has involved a lot of researchers not only in organic chemistry but also physical, analytical, and biochemistries.[13] It is suspected that 1,4-dihydropyridine derivatives might be characterized as a remarkable reducing reagent because the compounds in this category have too low potentials to reduce most of various functional groups, which, in turn, may exert interesting selectivity (chemo-, regio-, stereo-, or some other), especially for substrates with a variety of functional groups, under certain reaction conditions. However, unfortunately, studies on 1,4-dihydropyridine derivatives as tools in synthetic chemistry have enjoyed little attention and only few reports have been published concerning to this subject.[14,15] Namely, we found that silica gel catalyzes the reduction of certain functional groups while others remain unaffected.[14,16,17]

As a part of our research to find a selective organic reaction, it was elucidated that 3,5-bis(ethoxycarbonyl)-2,6-dimethyl-1,4-dihydropyridine (Hantzsch ester, HEH) is indeed a useful reagent to reduce certain functional groups selectively. In this report, the author wishes to describe a convenient method for the reduction of nitro olefins with HEH, in the presence of silica gel, with high chemoselectivity and in high yield under mild reaction conditions.[18]

Experimental

Instruments. ^{1}H NMR spectra were measured at 100 MHz with a JOEL JUN-FX 100 Fourier transform NMR spectrometer and at 400 MHz with a JOEL GX400 Fourier transform NMR spectrometer. IR spectra were recorded on a Hitachi EPI-S2 infrared spectrometer. Elemental analyses were performed with a Yanaco MT-3 elemental analyzer. Gas chromatographic data were recorded on a Yanaco G-1800 gas chromatograph (OV 330). GC mass data were recorded on a Hitachi M-80A GC Mass analyzer.

Materials. Hantzsch ester (HEH) and its 4,4-dideuteriated analog (HEH-4,4-d_2) were prepared as reported in a previous paper.[19] The deuterium content in HEH-4,4-d_2 was confirmed to be 98% by 400 MHz ^{1}H NMR analysis. Solvents were freshly distilled before the use. Silica gel (Nakarai Silica Gel 60, 35—70 mesh) was dried in an oven at 80 °C for a few days.

Preparation of Nitro Olefins. 1-Nitro-4-methyl-1-pentene (1a): A mixture of 8.6 g of 3-methylbutanal, 9.2 g of nitromethane, and 2.0 g of triethylamine was stirred at room temperature for 17 h, then quenched by addition of 50 ml of 2 M (1 M=1 mol·dm^{-3}) hydrochloric acid. The resulting solution was washed with water (2×50 ml) and 50 ml of brine, and dried on anhydrous sodium sulfate. After removal of the solvent, the residue was purified by a column chromatography on silica gel with benzene eluent to give 11.4 g (78%) of 1-nitro-4-methyl-2-pentanol. The β-nitro alcohol was then added into a mixture of 16 g of acetic anhydride and 18.4 g of pyridine and the solution was stirred at room temperature for 2 h. The reaction mixture was poured into 50 ml of 2 M hydrochloric acid and extracted with ether (3×30 ml). The organic layer was washed with water (3×30 ml) and brine (1×30 ml) and then dried on anhydrous sodium sulfate. After removal of the solvent the residue was purified by column chromatography on silica gel with hexane–benzene (1:1) as an eluent to give 14.4 g (98%) of the acetate. 14.4 g of the acetate was dissolved in 100 ml of benzene and the resulting solution was refluxed with 32 g of sodium carbonate for 5 h. The reaction mixture was filtered and the filtrate was washed with water (2×50 ml)

and brine (1×50 ml). The organic layer was dried and the solvent was evaporated under reduced pressure. Distillation of the residue with a Kugelrohr distillator gave 5.7 g (58%) of **1a**: bp 100 °C (2.7×10^3 Pa). ^{1}H NMR ($CDCl_3$) δ=0.98 (d, 6H, J=6 Hz), 1.65—2.04 (m, 1H), 2.18 (t, 2H, J=6 Hz), 6.95 (d, 1H, J=14 Hz) and 7.25 (dt, 1H, J=14, 6 Hz). IR (neat) 3000 (m), 1655 (s), 1530, and 1383 cm^{-1} (s).

Other nitro olefins except **1i** were prepared with the same method as described for **1a**.

1-Nitro-1-nonene (1b): Yield 43%. ^{1}H NMR ($CDCl_3$) δ=0.88 (t, 3H, J=6 Hz), 1.20—1.63 (m, 10H), 2.26 (q, 2H, J=6 Hz), 6.94 (d, 1H, J=14 Hz), and 7.25 (dt, 1H, J=14, 6 Hz). IR (neat) 3000 (m), 1656 (m), 1532, and 1357 cm^{-1} (s).

Methyl 4-Nitro-4-heptenoate (1c): Yield 67%. ^{1}H NMR ($CDCl_3$) δ=1.14 (t, 3H, J=7 Hz), 2.16—2.48 (m, 2H), 2.78—3.01 (m, 4H), 3.68 (s, 3H), and 7.06 (t, 1H, J=7 Hz). IR (neat) 3000 (m), 1750 (s), 1644(m), 1530, and 1375 cm^{-1} (s).

5-Nitro-5-octen-2-one (1d): Yield 51%. ^{1}H NMR ($CDCl_3$) δ=1.13(t, 3H, J=7 Hz), 2.16—2.48 (m, 2H), 2.63—2.96 (m, 4H), and 7.11 (t, 1H, J=7 Hz). IR (neat) 3000 (m), 1725 (s), 1644 (m), 1530, and 1370 cm^{-1} (s).

3,6-Dimethyl-9-nitro-2,8-undecadiene (1e): Yield 60%. Bp 80—90 °C (9.3×10 Pa) (by Kugelrohr distillation). ^{1}H NMR ($CDCl_3$) δ=0.95 (d, 3H, J=6 Hz), 1.10 (t, 3H, J=7 Hz), 1.07—1.44 (m, 3H), 1.60 (s, 3H), 1.68 (s, 3H), 1.91—2.27 (m, 4H), 2.61 (q, 2H, J=7 Hz), 5.07 (m, 1H), and 7.06 (t, 1H, J=8 Hz). IR (neat) 3000 (m), 1670 (m), 1527, and 1380 cm^{-1} (s).

4,8-Dimethyl-1-nitro-1,7-nonadiene (1f): Yield 63%. Bp 100—120 °C (3.3×10 Pa) (by Kugelrohr distillation). ^{1}H NMR ($CDCl_3$) δ=0.95 (d, 3H, J=6 Hz), 1.10—1.44 (m, 3H), 1.60 (m, 3H), 1.68 (m, 3H), 1.93—2.44 (m, 4H), 5.07 (m, 1H), 6.95 (d, 1H, J=14 Hz), and 7.25 (dt, 1H, J=14, 8 Hz). IR (neat) 3000 (m), 1650 (m), 1530, and 1380 cm^{-1} (s).

β-Nitrostyrene (1j): Yield 60%. Mp 58 °C. ^{1}H NMR ($CDCl_3$) δ=7.36—7.50 (m, 5H), 7.53 (d, 1H, J=14 Hz), and 7.96 (d, 1H, J=14 Hz). IR (Nujol) 3000 (m), 1630 (m), 1515, and 1385 cm^{-1} (s).

***o*-Methoxy-β-nitrostyrene (1k):** Yield 78%. Mp 81.5—82 °C. ^{1}H NMR ($CDCl_3$) δ=3.91 (s, 3H), 6.90—7.05 (m, 2H), 7.35—7.52 (m, 2H), 7.80 (d, 2H, J=14 Hz), and 8.06 (d, 2H, J=14 Hz). IR (Nujol) 3000 (m), 1628 (m), 1538, and 1375 cm^{-1} (s).

***p*-Methoxy-β-nitrostyrene (1l):** Yield 74%. Mp 85.5—86.5 °C. ^{1}H NMR ($CDCl_3$) δ=3.85 (s, 3H), 6.85—7.00 (m, 2H), 7.41—7.56 (m, 2H), 7.48 (d, 1H, J=14 Hz), and 7.95 (d, 1H, J=14 Hz). IR (Nujol) 3000 (m), 1608 (m), 1608 (m), 1513, and 1375 cm^{-1} (s).

β-Methyl-β-nitrostyrene (1m): Yield 82%. Mp 64 °C. ^{1}H NMR ($CDCl_3$) δ=2.42 (s. 3H), 7.39 (m, 5H), and 8.02 (m, 1H). IR (Nujol) 3000 (m), 1650 (m), 1530, and 1378 cm^{-1} (s).

***p*-Methoxy-β-methyl-β-nitrostyrene (1n):** Yield 50%. Mp 46.5—47 °C. ^{1}H NMR ($CDCl_3$) δ=2.45 (s, 3H), 3.84 (s, 3H), 6.86—7.01 (m, 2H), 7.31—7.44 (m, 2H), and 8.02 (m, 1H). IR (Nujol) 3000 (m), 1605(m), 1515, and 1380 (s).

2-(2-Furyl)-1-nitroethene (1o): Yield 32%. Mp 72 °C. ^{1}H NMR ($CDCl_3$) δ=6.51—6.58 (m, 1H), 6.84—6.88 (m, 2H), 7.49 (d, 1H, 14 Hz), and 7.69 (d, 1H, J=14 Hz). IR (Nujol) 3000 (m), 1635 (m), 1500, and 1375 cm^{-1} (s).

2-(2-Thienyl)-1-nitroethene (1p): Yield 66%. Mp 79—80 °C. ^{1}H NMR ($CDCl_3$) δ=7.07—7.16 (m, 1H), 7.21—7.56 (m, 2H), 7.43 (d, 1H, J=13 Hz), and 8.12 (d, 1H, J=13 Hz). IR (Nujol) 3000 (m), 1622(m), 1525, and 1380 cm^{-1} (s).

Ethyl 3-Methyl-2-nitro-2-butenoate (1g): A mixture of 7.6 ml of 90% fuming nitric acid and 1.1 ml of water was cooled to 0 °C, and 2.56 g of ethyl 3-methyl-2-butenoate was added to this mixture over 1.25 h with vigorous stirring. The solution was stirred for 1.5 h at 0 °C and 1 h at room temperature, and then poured onto 50 ml of crushed ice and extracted three times with 30 ml of chloroform. The extracts were combined and washed three times with 50 ml of water, six times with 30 ml of saturated aqueous sodium hydrogencarbonate and twice with 30 ml of brine, dried over anhydrous sodium sulfate, and concentrated under reduced pressure. The residual oil was distilled to give 3.14 g (91%) of **1i** as colorless oil. Bp 87.5 °C (3.1×10^2 Pa). ^{1}H NMR ($CDCl_3$) δ=1.29 (t, 3H, J=7 Hz), 1.97 (s, 3H), 2.25 (s, 3H), and 4.27 (q, 2H, J=7 Hz). IR (neat) 3000 (m), 1725 (s), 1650 (m), 1540, and 1375 cm^{-1} (s).

2-Methyl-2-(2-nitroethenyl)cyclohexanone (**1h**) and 1-(2-nitroethenyl)cyclohexanecarbaldehyde (**1i**) were supplied by Prof. K. Fuji of Institute for Chemical Research, Kyoto University.

Reduction of Nitro Olefins. 1-Nitro-4-methylpentane (2a): In a 30 ml round-bottom flask equipped with a magnetic stirrer and a reflux condenser were placed 258 mg (2.0 mmol) of **1a**, 560 mg (2.2 mmol) of HEH, 2.0 g of silica gel (Nakarai Silica Gel 60, 35—70 mesh), and 10 ml of anhydrous benzene. The reaction mixture was heated to reflux for 30 minutes under an argon atmosphere. The reaction mixture was cooled to room temperature, filtered, and the precipitate was washed with 30 ml of benzene. The combined organic solution was concentrated under reduced pressure and the residue was subjected to column chromatography on silica gel with hexane–benzene (1 : 1) as an eluent. As a pure product, 202 mg (78%) of **2a** was obtained. ^{1}H NMR ($CDCl_3$) δ=0.91 (d, 6H, J=6 Hz), 1.14—1.36 (m, 2H), 1.42—1.74 (m, 1H), 1.86—2.08 (m, 2H), and 4.34 (t, 2H, J=7 Hz). IR (neat) 3000 (m), 1555, and 1390 cm^{-1} (s).

Reductions of the other nitro olefins were carrried out following the general procedure described above.

1-Nitrononane (2b): Yield 91%. ^{1}H NMR ($CDCl_3$) δ=0.88 (t, 3H, J=6 Hz), 1.20—1.40 (m, 12H), 2.00 (m, 2H), and 4.36 (t, 2H, J= 7 Hz). IR (neat) 3000 (m), 1558, and 1385 cm^{-1} (s).

Methyl 4-Nitroheptanoate (2c): Yield 87%. ^{1}H NMR ($CDCl_3$) δ=0.95 (t, 3H, J=6 Hz), 1.20—1.53 (m, 2H), 2.00—2.46 (m, 6H), 3.70(s, 3H), and 4.42—4.69 (m, 1H). IR (neat) 3000 (m), 1743 (s), 1550, and 1380 cm^{-1} (s).

5-Nitro-2-octanone (2d): Yield 86%. ^{1}H NMR ($CDCl_3$) δ=0.95 (t, 3H, J=6 Hz), 1.20—1.53 (m, 6H), 2.08 (s, 3H), and 4.44—4.71 (m, 1H). IR (neat) 3000 (m), 1715 (s), 1550, and 1370 cm^{-1} (s).

3,6-Dimethyl-9-nitro-2-undecene (2e): Yield 88%. ^{1}H NMR ($CDCl_3$) δ=0.87 (d, 3H, J=6 Hz), 0.95 (t, 3H, J=7 Hz), 1.08—1.48 (m, 6H), 1.59 (s, 3H), 1.75—2.08 (m, 5H), 4.21—4.48 (m, 1H), and 4.97—5.16 (m, 1H). IR (neat) 3000 (m), 1560, and 1380 cm^{-1} (s).

2,6-Dimethyl-9-nitro-2-nonene (2f): Yield 83%. ^{1}H NMR ($CDCl_3$) δ=0.91, (d, 3H, J=6 Hz), 1.12—1.44 (m, 5H), 1.60 (s, 3H), 1.68 (s, 3H), 1.97 (q, 2H, J=7 Hz), 2.03 (t, 2H, J=7 Hz), 4.35 (t, 2H, J=7 Hz), and 4.98—5.16 (m, 1H). IR (neat) 3000 (m), 1563, and 1390 cm^{-1} (s).

Ethyl 3-Methyl-2-nitrobutanoate (2g): Yield 71%. ^{1}H

NMR ($CDCl_3$) δ=1.13 (d, 6H, J=7 Hz), 1.35 (t, 3H, J=7 Hz), 2.47—2.96 (m, 1H, J=7 Hz), 4.34 (q, 2H, J=7 Hz), and 5.93 (d, 1H, J=8 Hz). IR (neat) 3000 (m), 1760 (s), 1570, and 1380 cm^{-1} (s).

2-Methyl-2-(2-nitroethyl)cyclohexan-1-one (2h): Yield 90%. ^1H NMR ($CDCl_3$) δ=1.20 (s, 3H), 1.68—1.90 (m, 6H), 2.04—2.46 (m, 4H), and 4.43 (t, 2H, J=7 Hz). IR (neat) 3000 (m), 1715 (s), 1560, and 1390 cm^{-1} (s).

1-(2-Nitroethyl)cyclohexanecarbaldehyde (2i): Yield 45%. ^1H NMR ($CDCl_3$) δ=1.27—1.98 (m, 10H), 2.22 (t, 2H, J=7 Hz), 4.32 (t, 2H, J=8 Hz), and 9.23 (s, 1H). IR (neat): 3000 (m), 1710 (s), 1561, and 1390 cm^{-1} (s).

(2-Nitroethyl)benzene (2j): Yield 84%. ^1H NMR ($CDCl_3$) δ=3.30 (t, 2H, J=7 Hz), 4.58 (t, 2H, J=7 Hz), and 7.11—7.33 (m, 5H). IR (neat) 3000 (m), 1530, and 1380 cm^{-1} (s).

1-Methoxy-2-(2-nitroethyl)benzene (2k): Yield 84%. ^1H NMR ($CDCl_3$) δ=3.31 (t, 2H, J=7 Hz), 3.81 (s, 3H), 4.59 (t, 2H, J=7 Hz), and 6.81—7.35 (m, 4H). IR (neat) 3000 (m), 1556, and 1383 cm^{-1} (s).

1-Methoxy-4-(2-nitroethyl)benzene (2l): Yield 65%. ^1H NMR ($CDCl_3$) δ=3.27 (t, 2H, J=7 Hz), 3.91 (s, 3H), 4.58 (t, 2H, J=7 Hz), and 6.80—7.17 (m, 4H). IR (neat) 3000 (m), 1550, and 1380 cm^{-1} (s).

2-Nitropropylbenzene (2m): Yield 87%. ^1H NMR ($CDCl_3$) δ=1.51 (d, 3H, J=6 Hz), 2.86—3.40 (m, 2H), 4.57—4.92 (m, 1H), and 7.07—7.30 (m, 5H). IR (neat) 3000 (m), 1550, and 1390 cm^{-1} (s).

1-Methoxy-4-(2-nitropropyl)benzene (2n): Yield 100%. ^1H NMR ($CDCl_3$) δ=1.50 (d, 3H, J=6 Hz), 2.80—3.32 (m, 2H), 3.74 (s, 3H), 4.52—4.87 (m, 1H), and 6.74—7.08 (m, 4H). IR (neat) 3000 (m), 1545, and 1385 cm^{-1} (s).

2-(2-Furyl)-1-nitroethane (2o): Yield 62%. ^1H NMR ($CDCl_3$) δ=3.34 (t, 2H, J=7 Hz), 4.62 (t, 2H, J=7 Hz), 6.08—6.14 (m, 1H), 6.26—6.32 (m, 1H), and 7.30—7.33 (m, 1H). IR (neat) 3000 (m), 1555, and 1380 cm^{-1} (s)

2-(2-Thienyl)-1-nitroethane (2p): Yield 83%. ^1H NMR ($CDCl_3$) δ=3.49 (t, 2H, J=7 Hz), 4.57 (t, 2H, J=7 Hz), 6.02—6.95 (m, 2H), and 7.03—7.18 (m, 1H). IR (neat) 3000 (m), 1550, and 1382 cm^{-1} (s).

Reduction of 1j with HEH-4,4-d_2: A mixture of 75 mg (0.5 mmol) of **1j**, 280 mg (1.1 mmol) of HEH-4,4-d_2 (98% purity in deuterium) and 500 mg of silica gel in 5 ml of anhydrous benzene was refluxed for 30 minutes under a nitrogen atmosphere. The reaction mixture was worked up as described above giving 71 mg (93%) of **2j**-d_1. The analysis of the 400 MHz ^1H NMR spectrum revealed that the deuterium was incorporated into the 2-position of **2j** quantitatively.

400 MHz ^1H NMR ($CDCl_3$) δ=3.24 (tt, 1H, J=2, 8 Hz), 4.53 (d, 2H, J=8 Hz), 7.19—7.35 (m, 5H). GC-MS: m/z 152 (M^+).

Synthesis of 3,7,11-Trimethyl-1-dodecanol (8). The nitro olefin, **4**, was prepared starting from 7.8 g of 3,7-dimethyloctanal (**3**) and 6.1 g of nitromethane in 81% yield following the procedure described above for **1a**.

^1H NMR ($CDCl_3$), δ=0.83 (d, 6H, J=7 Hz), 0.90 (d, 3H, J=7 Hz), 1.03—1.78 (m, 8H), 2.23 (t, 2H, J=6 Hz), 6.93 (d, 1H, J=14 Hz), and 7.22 (dt, 1H, J=14, 6 Hz). IR (neat) 3000 (m), 1663 (m), 1530, and 1350 cm^{-1} (s).

Reduction of 1.99 g of **4** with 2.80 g of HEH and 10 g of silica gel was carried out as described for **1a** to give 1.95 g (97%) of 4,8-dimethyl-1-nitrononane (**5**).

^1H NMR ($CDCl_3$) δ=0.86 (d, 6H, J=7 Hz), 0.88 (d, 3H, J=7 Hz), 1.03—1.56 (m, 10H), 1.83—2.12 (m, 2H), and 4.33 (t, 2H, J=6 Hz). IR (neat) 2950 (m), 1576, and 1380 cm^{-1} (s). Found: C, 65.89; H, 11.34; N, 6.88%. Calcd for $C_{11}H_{23}NO_2$: C, 65.61; H, 11.52; N, 6.96%.

A mixture of 1.0 g of **5**, 0.57 g of ethyl crotonate, 0.8 g of DBU and 5 ml of DMF was stirred at room temperature for 20 h. The reaction mixture was worked up as an usual way to give 0.87 g (55%) of ethyl 3,7,11-trimethyl-4-nitrododecanoate (**6**).

^1H NMR ($CDCl_3$) δ=0.82 (d, 9H, J=7 Hz), 0.95—2.51 (m, 21H), 4.05—4.18 (m, 2H), and 4.32—4.49 (m, 1H). IR (neat) 3000 (m), 1750 (s), 1575, and 1380 cm^{-1} (s). Found: C, 65.08; H, 10.53; N, 4.37%. Calcd for $C_{17}H_{33}NO_4$: C, 64.71; H, 10.55; N, 4.44%.

A mixture of 630 mg (2.0 mmol) of **6**, 700 mg (2.4 mmol) of tributyltin hydride, and 100 mg (0.6 mmol) of AIBN in 5 ml of benzene was heated to reflux for 5 h. The reaction mixture was chromatographed on silica gel using benzene/hexane (1/1) as an eluent to give 351 mg (65%) of ethyl 3,7,11-trimethyldodecanoate (**7**).

^1H NMR ($CDCl_3$) δ=0.82 (d, 6H, J=7 Hz), 0.86 (d, 6H, J=7 Hz), 0.95—1.61 (m, 11H), 2.24 (d, 2H, J=6 Hz), and 4.12 (q, 2H, J=6 Hz). IR (neat) 3000 (m) and 1745 cm^{-1} (s). Found: C, 75.86; H, 12.55%. Calcd for $C_{17}H_{34}O_2$: C, 75.48; H, 12.68%.

The ester **7** was reduced with $LiAlH_4$ in ether at 0 °C to give the aimed alcohol **8** in 90% yield.

^1H NMR ($CDCl_3$) δ=1.78—1.88 (m, 12H), 1.95—1.62 (m, 17H), 3.20 (bs, 1H), and 3.58 (t, 2H, J=6 Hz). IR (neat) 3580 (s), and 2975 cm^{-1}.

Synthesis of Dendrolasin: To a solution of 6.1 g of nitromethane and 9.6 g of 3-furancarbaldehyde (**9**) in 100 ml of ethanol was added 10 ml of 10 M KOH over 30 minutes at 0 °C with vigorous stirring. The reaction mixture was stirred for 30 minutes and poured onto 100 ml of ice water. The precipitate was filtered and recrystallized from hot ethanol to give 12.0 g (86%) of 1-(3-furyl)-2-nitroethene (**10**) as yellow needles. Mp 68—70 °C.

^1H NMR ($CDCl_3$) δ=6.60 (dd, 1H, J=6, 1 Hz), 6.93 (d, 1H, J=6 Hz), 7.54 (d, 1H, J=14 Hz), 7.60 (m, 1H), and 7.79 (d, 1H, J=14 Hz). IR (KBr) 3010 (m), 1640 (m), 1500, and 1375 cm^{-1} (s).

A mixture of 1.39 g of **10**, 3.08 g of HEH, 10.0 g of silica gel and 50 ml of benzene was heated to reflux under a nitrogen atmosphere for 30 minutes. Silica gel was filtered off and the filtrate was chromatographed on silica gel using benzene as an eluent to give 1.33 g (94%) of 1-(3-furyl)-2-nitroethane (**11**) as yellowish oil.

^1H NMR ($CDCl_3$) δ=3.34 (t, 2H, J=7 Hz), 4.62 (t, 2H, J=7 Hz), 6.13 (m, 1H), 6.31 (m, 1H), and 7.35 (m, 1H). IR (neat) 3000 (s), 1550, and 1375 cm^{-1} (s).

To a solution of 705 mg (5 mmol) of **11** and 700 mg of 2,6-dimethyl-5-heptenal in 10 ml of toluene was added 132 mg (1.5 mmol) of *N*,*N*-dimethylethylenediamine. The mixture was heated to reflux for 24 h. The reaction mixture was diluted with 20 ml of 2 M hydrochrolic acid and extracted with ethyl acetate. The extract was condensed and chromatographed on silica gel to give two isomeric products, 46% of **12** and 25% of **13**. The nitro olefin **13** was easily isomerized into allylic nitro compound **12** in quantitative yield by refluxing it in benzene in the presence of 0.1 equivalent amount of triethylamine for 5 h.

^{1}H NMR ($CDCl_3$) δ=1.61 (s, 6H), 1.86 (s, 3H), 2.20—2.61 (m, 5H), 5.08 (q, 1H, J=7 Hz), 5.23—5.64 (m, 2H), 6.31 (s, 1H), 7.21 (s, 1H), and 7.41 (t, 1H, J=2 Hz). IR (neat) 2950 (s), 1625 (m), 1560, and 1375 cm^{-1} (m).

A mixture of 526 mg (2.0 mmol) of **12**, 1.75 g (6.0 mmol) of tributyltin hydride 98 mg of AIBN, and 10 ml of benzene was refluxed for 5 h and then washed with water and brine. The solution was condensed under reduced pressure and chromatographed on silica gel using benzene as an eluent to give 187 mg (43%) of dendrolasin (**14**).

^{1}H NMR ($CDCl_3$) δ=1.59 (s, 6H), 1.85 (s, 3H), 2.23—2.58 (m, 8H), 5.18—5.43 (m, 2H), 6.30 (s, 1H), 7.22 (s, 1H), and 7.36 (t, 1H, J=2 Hz). IR (neat) 2950 (s), and 1620 cm^{-1} (m). GC-Ms m/z 218 (M^+).

Results and Discussion

Reduction of Nitro Olefins: It was reported that silica gel activates HEH in benzene effectively and α,β-unsaturated carbonyl compounds are reduced with this system in satisfactory yields and with high chemo- and regioselectivities.[20] The reduction of carbon-carbon double bonds in α,β-conjugated nitro olefins also proceeds with the same reducing system; as shown in Scheme 1, a mixture of a nitro olefin, 1.1 equivalent amount of HEH, and silica gel in refluxing benzene

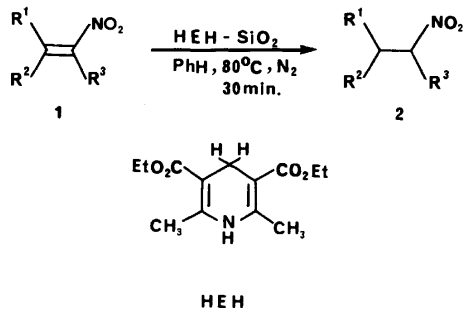

Scheme 1.

affords the corresponding nitroalkane quite smoothly. The results are summerized in Table 1. Both aromatic and aliphatic nitro olefins are reduced in excellent to good yields. It is worth while to note that the carbon-carbon double bonds in nitro olefins that bear carbonyl functional groups can be reduced with the present system without affecting any influence on the carbonyl functions.

The carbon-carbon double bond in an α,β-unsaturated ketone is a function which is reduced with the HEH–silica gel system. However, when an α,β-unsaturated carbonyl compound was subjected to the reduction competitively with an equivalent amount of nitro olefin, 95% of the latter was reduced after 5 h whereas 95% of the former was found unreacted (Scheme 2).

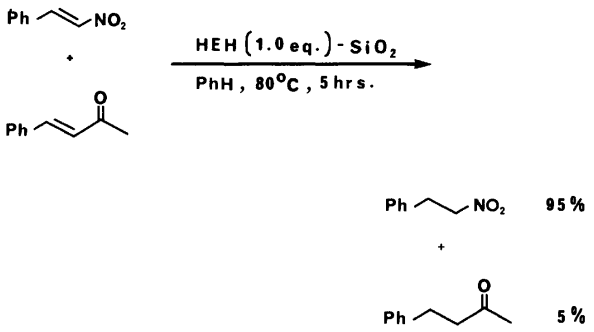

Scheme 2.

When 3,5-bis(ethoxycarbonyl)-2,6-dimethyl-1,4-dihydropyridine-4,4-d_2 (HEH-4,4-d_2) was subjected to the reduction of β-nitrostyrene and 1-nitro-2-phenylethane produced was analyzed on 400 MHz ^{1}H NMR spectrometer, it was found that more than 98% of the deuterium was incorporated into the 2-position, which indicates that the hydrogen on the 4-position of HEH migrates onto the substrate without exchanging with hydrogens in the solvent.

The reduction of nitro olefin is accompanied by the formation of dimeric products.[10] No dimer was detected, however, in the products from the present reduction system. In previous papers of the series, it was reported that silica gel plays not only a role of a Lewis acid catalyst to activate HEH but also a role of a proton donner with the silanol group on its surface.[17] Here again, it seems reasonable to expect that a carbanion formed from the substrate nitro olefin by accepting a (net) hydride from HEH is immediately protonated on the surface of silica gel to afford a stable product.

Although stereoselective reduction has not been examined yet, the author believes that the present reduction system can provide a versatile method in organic synthesis with its high yield, excellent chemoselectivity, and facility of the procedure, and the method has been applied to the syntheses of natural products as will be described in the following section.

Syntheses of Natural Product. Synthesis of 3,7,11-Trimethyl-1-dodecanol: A sesquiterpene alcohol, 3,7,11-trimethyl-1-dodecanol (**8**), has been widely accepted as a key intermediate in the synthesis of α-Tocopherol (Vitamin E).[21] The present reduction system can usefully be applied to the synthesis of this alcohol. The whole reaction scheme is shown in Scheme 3.

3,7-Dimethyloctanal (**3**) was condensed with nitromethane to give a β-nitro alcohol in the presence of triethylamine as a catalyst. The nitro alcohol was then converted into conjugated nitro olefin, **4**, via acetylation and elimination of acetic acid. The nitro olefin **4** was reduced with 1.1 equivalent amount of HEH into the corresponding nitroalkane **5** in 97% yield. Michael-type addition of **5** to ethyl crotonate in the presence of DBU[22] gave the γ-nitro ester **6**, which was subjected to the reaction with tributyltin hydride and AIBN as a free radical initiator, to substitute the

Table 1. Reduction of Conjugated Nitroolefins with HEH-SiO_2

	Substrate 1	Product 2	Yield[a]/%
a	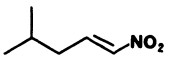	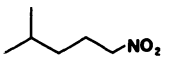	78
b	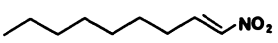	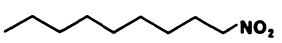	91
c	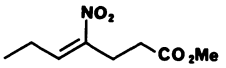	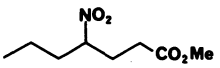	87
d	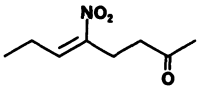	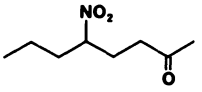	86
e	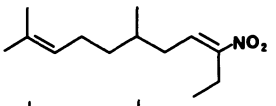	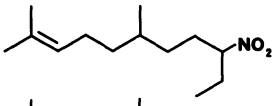	88
f	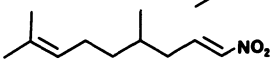	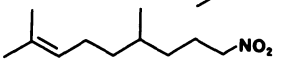	83
g	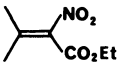	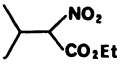	71
h	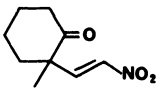	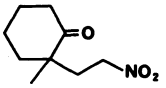	90
i	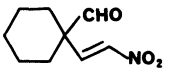	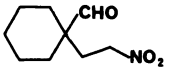	45
j	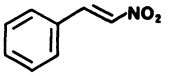	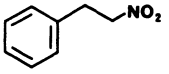	84
k	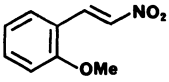	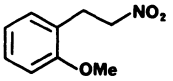	84
l	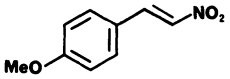	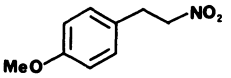	65
m	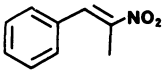	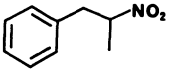	87
n	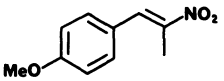	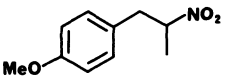	100
o	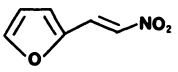	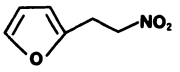	62
p	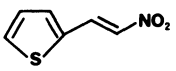	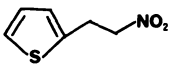	83

a) Isolated yield.

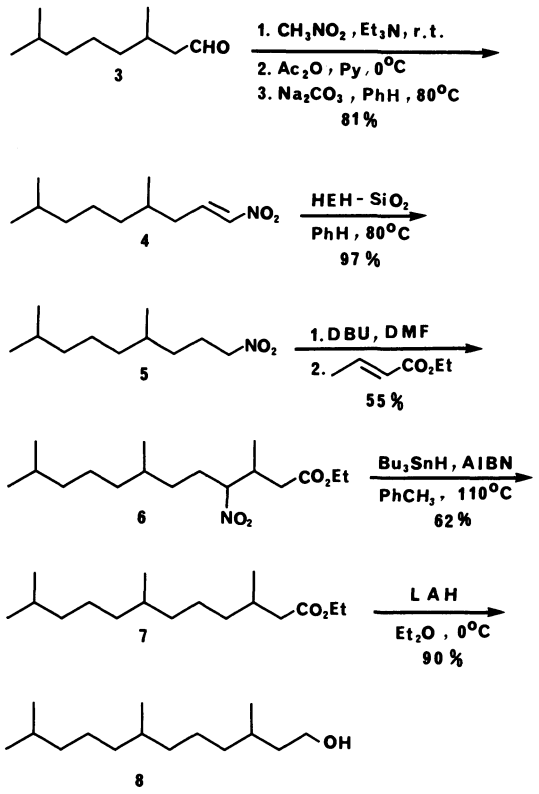

Scheme 3.

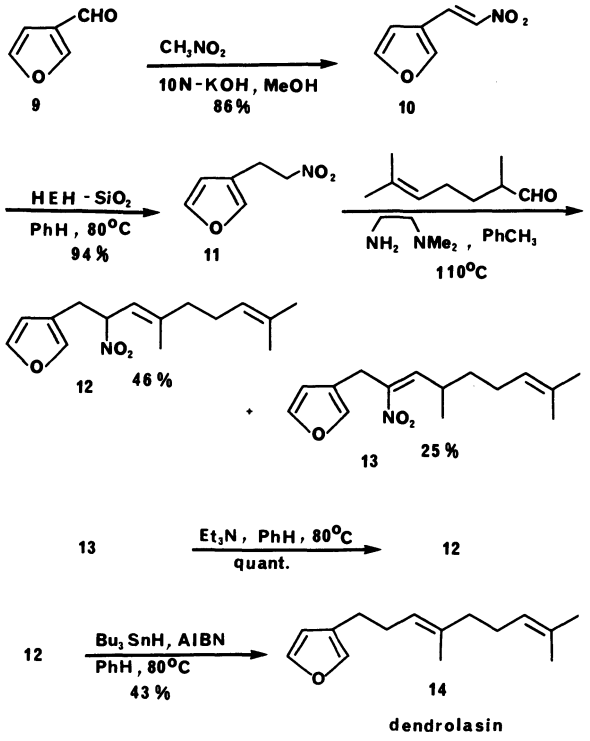

Scheme 4.

nitro group by a hydrogen.[5] The resulting ester **7** was converted into the alcohol **8** by the reduction with lithium aluminum hydride in 90% yield. The overall yield of **8** based on the aldehyde **3** was 24%.

Synthesis of Dendrolasin: A furanoterpenoid, dendrolasin (**14**) was isolated from *Lasius (Dendrolasius) fuliginosus*, an ant, as an alarm pheromone[23] and synthesized by several groups.[24] It is found that the application of the present reduction system provides a very short (4 steps, 25% overall yield) process for **14** as shown in Scheme 4.

Condensation of furan-3-carbaldehyde (**9**) with nitromethane in 10 M KOH–MeOH gave 1-(3-furyl)-2-nitroethene (**10**) in 86% yield. The nitro olefin **10** was reduced into the corresponding saturated nitro compound **11** in 94% yield, which was condensed with 2,6-dimethyl-5-heptenal in the presence of *N,N*-dimethylethylenediamine under reflux in toluene[25] to yield the allylic nitro compound **12** (46% yield) together with the conjugated nitro olefin **13** (25% yield). The latter can be isomerized into the former quantitatively under reflux in benzene with triethylamine. Substitution of the nitro group in **13** by a hydrogen can be achieved in 43% yield by treating **13** with tributyltin hydride in the presence of AIBN to give dendrolasin (**14**).

The author deeply thanks Prof. Atsuyoshi Ohno and Dr. Kaoru Nakamura of Institute for Chemical Reseach, Kyoto University, and Prof. Tetsuo Aida of Kinki University in Kyushu for their helpful discussion.

References

1) H. H. Baer and L. Urbas, "Activating and directing effects of the nitro group in aliphatic system," in "The Chemistry of the Nitro and Nitroso groups," Part 2, Chap. 3, ed by H. Feuer, Interscience Pub., New York, N. Y. (1970), pp. 75—200; N. Ono and A. Kaji, *Yuki Gosei Kagaku Kyokai Shi*, **38**, 115 (1980); N. Ono, H. Miyake, and A. Kaji, *ibid.*, **43**, 121 (1985).

2) I. E. McMurry and J. Melton, *J. Org. Chem.*, **38**, 4367 (1973).

3) E. W. Colvin and D. Seebach, *J. Chem. Soc., Chem. Commun.*, **1978**, 689.

4) J. R. Hadson and E. Premuzic, *J. Chem. Soc. C*, **1970**, 1182.

5) N. Ono, R. Tamura, and A. Kaji, *J. Am. Chem. Soc.*, **102**, 2581 (1980); N. Ono, H. Miyake, R. Tamura, and A. Kaji, *Tetrahedron Lett.*, **22**, 1705 (1981).

6) G. D. Backley and C. W. Scaife, *J. Chem. Soc.*, **1947**, 1471; J. Melton and I. E. McMurry, *J. Org. Chem.*, **40**, 2138 (1975).

7) D. Seebach and P. Knochel, *Helv. Chim. Acta*, **67**, 261, (1984).

8) a. Pd/C-H_2; J. C. Sowden and H. O. L. Fischer, *J. Am. Chem. Soc.*, **69**, 1048 (1947).

9) $RhCl(PPh_3)_3$-H_2; R. E. Harmon, J. L. Parsons, D. W.

Cooke, S. K. Gupta, and J. Schoolenberg, *J. Org. Chem.*, **34**, 3684 (1969).

10) $NaBH_4$; A. I. Meyers and J. C. Sircan, *J. Org. Chem.*, **32**, 4134 (1967); A. K. Sinhabobu and R. T. Borchardt, *Tetrahedron Lett.*, **24**, 227 (1983); A. Bhattacharjya, R. Mukhopahyay, and S. C. Pakrashi, *Synthesis*, **1985**, 886.

11) NAD(P)H-models; K. Wallenfels, W. Ertel, A. Hockendorf, J. Rieser, and K. H. Uberscher, *Naturwissenschaften*, **62**, 459 (1975): S. Shinkai, Y. Kusano, T. Ide, T. Sone, and O. Manabe, *Bull. Chem. Soc. Jpn.*, **51**, 3544 (1978); T. Trefouel, P. Tintillier, G. Dupas, J. Bourguignon, and G. Queguiner, *Bull. Chem. Soc. Jpn.*, **60**, 4492 (1987).

12) Microorganisms; H. Ohta, K. Ozaki, and G. Tsuchihashi, *Chem. Lett.*, **1987**, 191.

13) For a recent review, see S. Yasui and A. Ohno, *Bioorg. Chem.*, **14**, 70 (1986).

14) M. Fujii, K. Nakamura, S. Yasui, S. Oka, and A. Ohno, *Bull. Chem. Soc. Jpn.*, **60**, 2423 (1987).

15) M. Fujii, K. Nakamura, H. Mekata, S. Oka, and A. Ohno, *Bull. Chem. Soc. Jpn.*, **61**, 495 (1988).

16) S. Yasui, M. Fujii, K. Nakamura, and A. Ohno, *Bull. Chem. Soc. Jpn.*, **60**, 963 (1987).

17) S. Yasui, M. Fujii, and A. Ohno, *Bull. Chem. Soc. Jpn.*, **60**, 4019 (1987).

18) For a preliminary communication, see K. Nakamura, M. Fujii, S. Oka, and A. Ohno, *Chem. Lett.*, **1985**, 523.

19) A. Singer and S. M. McElvain, *Org. Synth.*, Coll. Vol. II, 214 (1966).

20) K. Nakamura, M. Fujii, S. Oka, and A. Ohno, *Chem. Lett.*, **1985**, 523; M. Fujii, K. Nakamura, S. Yasui, S. Oka, and A. Ohno, *Bull. Chem. Soc. Jpn.*, **60**, 2423 (1987).

21) K. K. Chan, N. Cohen, J. P. D. Noble, A. C. Specian, Jr., and G. Saucy, *J. Org. Chem.*, **41**, 3497 (1976): For a recent review, see S. Yamada, T. Takeshita, and J. Tanaka, *Yuki Gosei Kagaku Kyokai Shi*, **40**, 268 (1982).

22) N. Ono, H. Miyake, and A. Kaji, *Synthesis*, **1984**, 226.

23) R. Bernardi, C. Cardani, D. Ghiringhelli, A. Silva, A. Baggini, and M. Paran, *Tetrahedron Lett.*, **1967**, 3893.

24) M. Nishizawa, H. Yamada, and Y. Hayashi, *Tetrahedron Lett.*, **27**, 187 (1986); D. J. Fauokner, *Natural Product Reports*, **1**, 551, (1984); S. P. Tanis and P. M. Herrinton, *J. Org. Chem.*, **48**, 4572 (1983); D. Nasipuri and G. J. Das, *J. Chem. Soc., Perkin Trans. 1*, **1979**, 2776.

25) R. Tamura, M. Sato, and D. Oda, *J. Org. Chem.*, **51**, 4318 (1986).

 © 1988 The Chemical Society of Japan Bull. Chem. Soc. Jpn., 61, 4037—4042 (1988)

A Convenient Method for the Preparation of Secondary Propargylic Ethers. The Reactions of Acetals with 1-Trimethylsilyl-1-alkynes Promoted by the Combined Use of Catalytic Amounts of Tin(IV) Chloride and Zinc Chloride

Masaji HAYASHI,* Atsuro INUBUSHI, and Teruaki MUKAIYAMA
Department of Applied Chemistry, Faculty of Science, Science University of Tokyo, Kagurazaka, Shinjuku-ku, Tokyo 162
(Received May 20, 1988)

In the coexistence of catalytic amounts of $SnCl_4$ and $ZnCl_2$, acetals undergo a coupling with 1-trimethylsilylalkynes to give secondary propargylic ethers in good yields. Similarly, propargylic ethers are directly produced from aldehydes by the treatment with alkoxytrimethylsilanes and 1-trimethylsilylalkynes under the same conditions. This catalyst system also efficiently promotes aldol reaction of silyl enol ethers with acetals or aldehydes, and the Michael reaction of silyl enol ethers with α,β-unsaturated ketones.

Over the years there have been a large body of efforts directed to the construction of carbon skeleton by employment of various kinds of silyl carbon nucleophiles, and those to develop catalysts which efficiently promote the coupling with electrophiles have been extensively studied.[1] Recently, various carbon–carbon bond forming reactions[2] were shown to be achieved by the use of a catalytic amount of Lewis acids such as trityl salts developed by us[2b] for example, and it becomes apparent that a stoichiometric amount of Lewis acid, such as $TiCl_4$ or $SnCl_4$,[3] is not necessarily required in these types of acid-promoted reactions of carbonyl compounds with silyl nucleophiles. During our continuing work on the development of efficient promotors, a convenient carbon–carbon bond forming reaction was developed by the combined use of catalytic amounts of various neutral molecules and weakly acidic Lewis acids such as TrCl–$SnCl_2$, TMSCl–$SnCl_2$.[4] Thus divalent tin is able to accept halogen ion from the above mentioned active organic halide or silyl halide to generate cationic species (Tr^+, TMS^+-like cation etc.). In an extension of this concept, we considered that higher capability of $SnCl_2$ could accept halogen ion from the other Lewis acid such as $TiCl_4$ to generate $TiCl_3^+$–$SnCl_3^-$, or by the combination of Lewis acids such as $ZnCl_2$–$SnCl_4$ to generate $ZnCl^+$–$SnCl_5^-$, and that such species should be applicable for the activation of electrophiles, as promotors, in various reactions with moderately reactive silyl nucleophiles.

We screened further more effective combination of various Lewis acids and it was found that the combined use of $SnCl_4$ and $ZnCl_2$ is quite efficient for a coupling reaction of acetals with 1-trimethylsilyl-1-alkynes, as we have briefly reported in a preliminary communication.[5] We now describe in full the results of our investigation on the above coupling reaction using this new catalyst system and further the application to aldol and the Michael reactions.

Results and Discussion

Ethynylation (1). The reaction of 1-trimethylsilyl-1-alkynes with acetals generally requires an equimolar amount or a large exess of Lewis acids, such as $TiCl_4$,[6] and it was also shown that the above mentioned reaction was hardly promoted by a catalytic amount of Lewis acid. In the first place, we examined the reaction of 3-phenylpropanal dimethyl acetal (**2**) with (trimethylsilylethynyl)benzene (**1**) in the presence of 10 mol% each of two metal salts (A and B), as shown in Table 1. The reactions were carried out as follows: A suspension of 10 mol% each of catalysts A and B in CH_2Cl_2, was stirred for 30 min at room temperature. After cooling to 0 °C, **2** was added, followed by the addition of **1** at the same temperature, and the reaction mixture was stirred at 0 °C. Usual workup of the

Table 1. Ethynylation of 3-Phenylpropanol Dimethyl Acetal with (Trimethylsilylethynyl)benzene in the Presence of Various Combination of Metal Salts[a]

Entry No.	Catalyst[b] A	Catalyst[b] B	Time/h	Yield/%[c]
1	TrCl	$SnCl_2$	24	Trace
2	TMSCl	$SnCl_2$	3.5	Trace
3	SnF_2	$TiCl_4$	24	6
4	$SnCl_2$	$TiCl_4$	24	47
5	$SnCl_2$	$SnCl_4$	3.5	39
6	$SnCl_2$	$TiCl_2(OTf)_2$	24	50
7	$SnCl_2$	$ZnCl_2$	2.5	0
8	$SnBr_2$	$TiCl_4$	24	33
9	$ZnCl_2$	$TiCl_4$	3.5	49
10	$ZnCl_2$	$SnCl_4$	3.5	68
11	$ZnBr_2$	$SnCl_4$	3.5	53
12	$SnCl_2$	—	3.5	0
13	$ZnCl_2$	—	3.5	0
14	$TiCl_4$	—	24	7
15	$SnCl_4$	—	3.5	30

a) Reaction were carried out in CH_2Cl_2 with 1.0 equivalent of **1**. b) 10 mol% of catalysts were used except for Entry 15. c) Isolated yield.

reaction mixture afforded 1,5-diphenyl-3-methoxy-1-pentyne (**3**).

Conventionally employed promotors, such as TrCl-$SnCl_2$ or TMSCl-$SnCl_2$[4] were not effective in the above mentioned reaction (Entries 1 and 2). The results indicate that these catalysts are insufficient to activate the acetal to produce the coupling product with **1**. Now, from the point of view that $SnCl_2$ is a potential metal salt to accept halogen ion from organic halide or silyl halide, it was assumed that more active cationic species than Tr^+-$SnCl_3^-$ or TMS^+-$SnCl_3^-$ should be generated by the combined use of strong Lewis acids ($TiCl_4$, $SnCl_4$, etc.) and weak Lewis acids ($SnCl_2$, $ZnCl_2$, etc.). As the result, in almost cases the reactions proceeded effectively to afford the desired product (**3**) in high yields (Entries 3—11). The combination of $SnCl_4$ and $ZnCl_2$ gave the best result concerning the yield of **3**. The mechanism of the reformation of $SnCl_4$-$ZnCl_2$ catalyst system could be explained as follows; In $ZnCl^+$-$SnCl_5^-$-like species initially generated,[7] $ZnCl^+$ activates oxygen atom of the acetal and at the same time $SnCl_5^-$ attacks silicon atom of the 1-trimethylsilyl-1-alkyne to activate the acetylene by way of forming TMS^+-$SnCl_5^-$-like species, which is in turn transformed into TMS-OR^2 and the original catalytic species. In the case of the combined use of $TiCl_4$ and $SnCl_2$, initially $TiCl_3^+$-$SnCl_3^-$-like species will be generated.

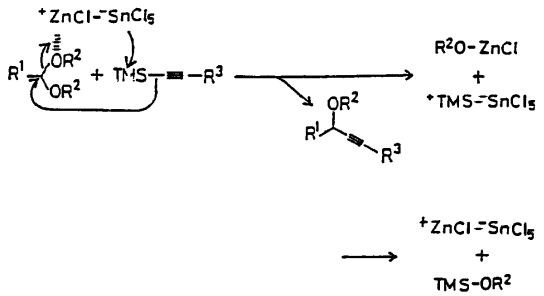

In the case of using $SnCl_2$, the yields of **3** were influenced by the co-catalyst, that is, the yields depended on the strength of Lewis acidity of co-catalyst (Entries 4—7). On the other hand, by the use of $ZnCl_2$ instead of $SnCl_2$, the yields of **3** did not consist with the Lewis acidity[7] of the co-catalyst (Entries 9 and 10). As shown in Entries 3,4,8 and 10,11, the substituents of tin(II) or zinc(II) salts remarkably influenced on the turn-over of the catalyst. It is assumed that Sn(II) with more electronegative atom can accept halogen ion from co-catalyst such as $TiCl_4$ to generate $TiCl_3^+$, and that Zn(II) with more electronegative atom as Cl can generate stronger cationic species as $ZnCl^+$, and consequently the oxygen atom of the acetal group would be activated more effectively. In the case of SnF_2, the yield was not so high because of its insolubility to the solvent.

The combination of Zn(II)-Sn(IV) proved better than those of Sn(II)-Sn(IV), Zn(II)-Ti(IV), Sn(II)-Ti(IV) in the present reaction. However, these tendencies can not be explained by considering solely the Lewis acid strength of $SnCl_4$ and $TiCl_4$,[7] and it may be pointed out that the difference of the affinities of central metal as Ti, Si, and Zn toward oxygen atom reflects on the regeneration step of the catalysts. By the use of 20 mol% of $SnCl_4$ as catalyst in the absence of other co-catalyst (Entyl 15), the same reaction resulted in the formation of **3** in a moderate yield.

Next, we examied the optimum reaction conditions by using the above reaction as a model, and the results are summarized in Table 2. As shown in the Table, the coupling reaction proceeded effectively in CH_2Cl_2 at 0 °C in the coexistence of 10 mol% each of $SnCl_4$ and $ZnCl_2$. It should be noted that the ratio of $SnCl_4/ZnCl_2$ influences the yield of **3**, assuming that the unbalance of the amounts of $SnCl_4$ and $ZnCl_2$ should give rise to decrease in the population of a key species $ZnCl^+$-$SnCl_5^-$.

Then we examined the coupling reaction of various 1-trimethylsilyl-1-alkynes (**5**) with dimethyl acetals (**4**) in the presence of catalytic amounts of $SnCl_4$-$ZnCl_2$ as shown in Table 3, and the corresponding secondary propargylic ethers (**6**) were obtained in good yields. In the case of the reaction of aromatic or conjugated aldehyde dimethyl acetal (Entries 1,10,11), the side reactions forming a dipropargyl derivative (for example, **7** or **8**) took place because of the high reactivities of benzyl or allyl cations. Concerning the effect of acetals, the yield of propargylic ethers indicates a

Table 2. Effect of Solvent, Ratio of $SnCl_4/ZnCl_2$ and Temperature

Entry No.	1/2	Solvent	$SnCl_4/ZnCl_2$	Temp/°C	Time/h	Yield/%[a]
1	1/1	CH_2Cl_2	10/10	0	3.5	68
2	1/1	CH_3CN	10/10	20	24	9
3	1/1	Et_2O	10/10	20	24	0
4	1/1	Toluene	10/10	20	24	0
5	1/1.5	CH_2Cl_2	10/10	20	3.5	85
6	1/1.5	CH_2Cl_2	20/10	20	3.5	71
7	1/1.5	CH_2Cl_2	10/20	20	3.5	58
8	1/1.5	CH_2Cl_2	10/10	−20	7	74

a) Isolated yield. Yields are based on **1**.

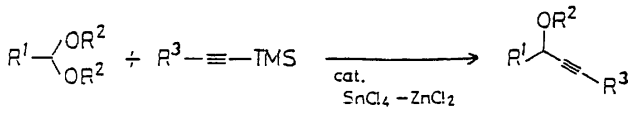

4 5 6

Table 3. Ethynylation of Acetals with 1-Trimethylsilyl-1-alkynes[a]

Entry No.	R^1	R^2	R^3	4/5	Time/h	Yield/%[b]
1	Ph	CH_3	Ph	1/1	3.5	33
2	$Ph(CH_2)_2$	CH_3	Ph	1.5/1	3.5	85
3[c]	$Ph(CH_2)_2$	CH_3	CH_3	2/1	3.5	82
4	$Ph(CH_2)_2$	CH_3	$CH_3(CH_2)_4$	1.4/1	3.5	78
5	$Ph(CH_2)_2$	$PhCH_2$	Ph	1.5/1	3.5	44
6	$PhCH(CH_3)$	CH_3	Ph	1.5/1	10.5	13
7	$CH_3(CH_2)_7$	CH_3	Ph	1.5/1	3.5	79
8	$CH_3(CH_2)_7$	CH_3	CH_3	2/1	3.5	74
9	$CH_3(CH_2)_7$	CH_3	$CH_3(CH_2)_4$	1.5/1	48	71
10	PhCH=CH	CH_3	Ph	1/1	3.5	29
11	CH_3CH=CH	CH_3	Ph	1/1	3.5	15
12	CH_3	CH_3CH_2	Ph	1.5/1	3.5	53

a) Reaction was carried out in CH_2Cl_2 at room temperature in the coexistence of 10 mol% each of $SnCl_4$ and $ZnCl_2$. b) Isolated yield. c) 20 mol% each of $SnCl_4$ and $ZnCl_2$ was used.

tendency to decrease as R^2 substituent becomes more bulky (Entry 12), and cyclic acetals such as 1,3-dioxolane did not react with 1-trimethylsilyl-1-alkynes under the above condition. When benzyl acetal was used as a substrate, unknown side reactions accompanied. The reaction of α-substituted aldehyde dimethyl acetal with **5** was very slow to afford **6** in poor yield (Entry 6). In addition, under the above conditions, silylalkynes having bulky substituents on the silicon atom, such as (triphenylsilylethynyl)benzene, did not react with acetals.

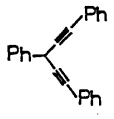

7

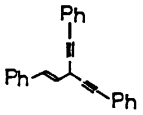

8

Ethynylation (2). From the synthetic point of view, it is more desirable to prepare the above-mentioned propargylic ethers directly from the corresponding aldehydes. On the basis of such consideration, the reaction of in situ formed hemiacetal-type compounds (**9**) with **5** was examined. As shown in Table 4, in the coexistence of 20 mol% each of $SnCl_4$ and $ZnCl_2$, adducts **9** were initially formed from alkoxytrimethylsilanes and aldehydes, and **9** in turn reacted with **5** to form the desired secondary propargylic ethers **6**. In the case of benzyloxytrimethylsilane, the yield was not so high (Entry 1) and unknown side reactions accompanied as same as the above mentioned reaction.

Allylation of Propargylic Ethers. It was reported that allyl ethers reacts with silyl nucleophiles, such as allylsilane[8] or silyl enol ethers,[9] in the presence of a catalytic amount of $TrClO_4$ to result in the formation

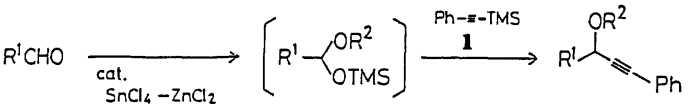

9 6

Table 4. Synthesis of Secondary Propargylic from Aldehydes[a]

Entry No.	R^1	R^2	Time/h	Yield/%[b]
1	$Ph(CH_2)_2$	$PhCH_2$	6	67
2	$Ph(CH_2)_2$	CH_3	6	78
3	$Ph(CH_2)_2$	CH_2CH_2	6	77
4	$CH_3(CH_2)_5$	CH_3	6	73
5	$Ph(CH_2)_2$	c)	21	37(20%d.e.)
6	$Ph(CH_2)_2$		22	0

a) Reaction was carried out in CH_2Cl_2 at −78 °C for 4 h, then at room temperature for 6 h in the coexistence of 20 mol% each of $SnCl_4$ and $ZnCl_2$. b) Isolated yield. Yields are based on aldehydes. c) *S*-configuration.

of a new carbon skeleton having tertiary carbon. These facts and the above-mentioned side reaction to form bis propargyl compounds **7** or **8** suggested us to develop a convenient method for the two carbon-carbon bond formations by one-pot procedure, that is, the secondary propargylic ethers thus obtained had a potentiality to couple with the second nucleophile such as allylsilane. Expectedly, **3** smoothly reacted with allyltrimethylsilane at 0 °C in the coexistance of 20 mol% each of $SnCl_4$ and $ZnCl_2$ to afford the 1,5-enyne compound (**10**) in 56% yield. And **10** was also

obtained according to the above-mentioned methods from acetal (**1**) (in 29% yield), from 3-phenylpropanal (in 60% yield) by one-pot procedure.

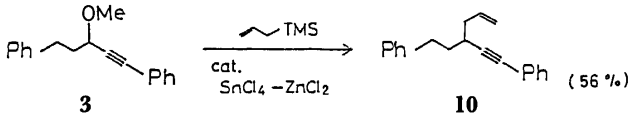

3 **10**

Aldol Reaction. This new catalyst system ($SnCl_4$-$ZnCl_2$) also promoted the aldol reaction of silyl enol ethers and aldehydes or acetals smoothly and some experimental results are shown in Table 5. The ratios of anti/syn (threo/erythro) adducts are slightly different from those in the cases of using other promotors, such as $TrClO_4$,[1] TrCl-$SnCl_2$, or TMSCl-$SnCl_2$.[4]

The Michael Reaction. Tin(IV) chloride and zinc chloride catalyst system also promoted the Michael reaction of silyl enol ethers with α,β-unsaturated ketones as shown in Table 6. The uk (anti) adducts[4] were obtained preferentially similar to the reactions using other promotors (Tr^+ or TMS^+-like cation). These diastereoselectivities are almost the same as consistent with those of Tr^+ or TMS^+-like cation-promoted Michael reactions.

Allylation of Aldehydes. Under the acidic condition, allyltrimethylsilane generally reacts with aldehyde to give a complicated product mixture by the occurrence of further reactions, which contains the reaction of hemiacetal (**11**) formed by the addition of initially formed silyl alkoxide to the starting aldehyde followed by the addition of the allyltrimethylsilane. In contrast, by using the present catalyst system, the desired homoallyl alcohols were obtained in good yields as shown below.

Table 5. Aldol Reaction of Aldehydes or Dimethyl Acetals with Trimethylsilyl Enol Ethers

Entry No.	Nucleophiles	Electrophiles	Time/h	Yield/%	Ratio of anti/syn[b]
1			2	65	—
2	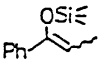	PhCHO	2	99	58:42
3		$PhCH(OMe)_2$	4	99	73:27
4		PhCHO	4	83	32:69
5		$PhCH(OMe)_2$	2	87	36:64
6			2	58	89:11
7		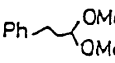	2	80	87:13

a) All products gave satisfactory NMR and IR spectra.[3] b) Determined by ^1H NMR.[4]

Table 6. Michael Reaction of α,β-Unsaturated Ketones with Trimethylsilyl Enol Ethers

Entry No.	Nuleophile	Electrophile	Products[a]	Time/h	Yielde/%	Ratio of anti/syn[b]
1	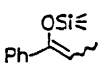		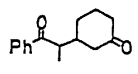	4	87	87:23
2			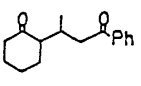	2	84	65:35
3		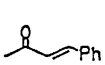	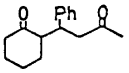	3	100	55:45

a) All products gave satisfactory NMR and IR spectra. b) Determined by ^1H NMR.

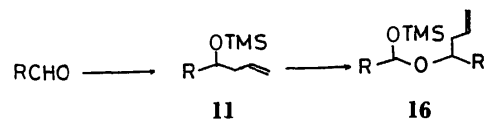

11 16

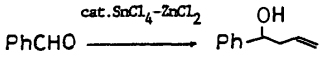

61%

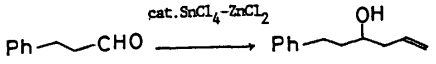

74%

It is concluded that the catalytic use of equimolar amounts of $SnCl_4$ and $ZnCl_2$ effectively promotes the reaction of 1-trimethylsilyl-1-alkynes with acetals, and also secondary propargylic ethers thus obtained are converted into 1,5-enyne compounds by the further reaction with allyltrimethylsilane in the same flask. The present cationic promotors based on the combination of two metal salts will open many synthetic and theoritical possibilities in carbon-carbon bond forming reactions.

Experimental

The IR spectra were determined on Hitachi Model 260-30 spectrometer. The ^1H NMR spectra were recorded with a Hitachi R-24B, a Varian EM-390, and a JEOL GX-400 spectrometers in $CDCl_3$ with trimethylsilane as an internal standard. The mass spectra were taken on a JEOL JMS-D300. Diethyl ether was freshly distilled from sodium benzophenone ketyl. Dichloromethane was distilled from CaH_2 and stored over Molecular Sieve. Purification of products was performed by column chromatography on silica gel (Wakogel C-200, C-300 or Merck, Art. 9385 Kieselgel 60, 230—400 mesh), preparative TLC on silica gel (Wakogel B-5F).

1-Trimethylsilyl-1-alkynes **1a—g** were prepared by trimethylsilylation of the corresponding lithium acetylide (butyllithium and alkynes), and purified by distillation or column chromatography on silica gel. Dimethyl acetals **2a—h** were prepared by transacetalization of the corresponding aldehydes with trimethyl orthoformate in the presence of *p*-TsOH·H_2O.

Preparation of Propargylic Ethers (6). (Table 3) A typical reaction procedure is described for 3-phenylpropanal dimethyl acetal with (trimethylsilylethynyl)benzene (Entry 2): a CH_2Cl_2 (4 ml) suspension of $SnCl_4$ (0.11 mmol) and $ZnCl_2$ (0.11 mmol) was stirred for 30 min at room temperature, to which were added succeccively (trimethylsilylethynyl)benzene (1.0 mmol) in CH_2Cl_2 (3 ml) and 3-phenylpropanal dimethyl acetal (1.5 mmol) in CH_2Cl_2. The reaction mixture was stirred for 3.5 h at the same temperature, then quenched with aqueous solution of sodium hydrogencarbonate. The organic materials were extracted with CH_2Cl_2, and the combined extracts were dried over $MgSO_4$. After evaporation of the solvent, the residue was purified by preparative TLC (silica gel) to afford 1,5-diphenyl-3-methoxy-1-pentyne (**1a**) (0.85 mmol, 85%). IR (neat) 2835, 2240, 1610, 1500 cm^{-1}; ^1H NMR ($CDCl_3$) δ=1.87—2.30 (m, 2H), 2.72—2.97 (m, 2H), 3.45 (s, 3H), 4.11 (t, J=6 Hz, 1H), 6.95—7.60 (m, 10H); MS m/z 250 (M^+). Found: C, 86.29; H, 7.26%. Calcd for $C_{18}H_{18}O$: C, 86.36; H, 7.25%.

Other analysis data are presented: 1,3-Diphenyl-3-methoxy-1-propyne (Entry 1). IR (neat) 2815, 2215, 1600, 1490 cm^{-1}; ^1H NMR ($CDCl_3$) δ=3.47 (s, 3H), 5.27 (s, 1H), 7.2—7.6 (9m, 10H); MS, m/z 222 (M^+).

6-Phenyl-4-methoxy-1-hexyne (Entry 3). IR (neat) 2825, 2235, 1610, 1500; ^1H NMR ($CDCl_3$) δ=1.84 (d, 3H, J=1.8 Hz), 1.75—2.20 (m, 2H), 2.53—2.97 (m, 2H), 3.53 (s, 3H), 3.63—4.08 (m, 1H), 7.17 (s, 5H); MS, m/z 188 (M^+).

3-Methoxy-1-phenyl-1-decyne (Entry 4). IR (neat) 2815, 2220, 1600, 1495 cm^{-1}; ^1H NMR ($CDCl_3$) δ=0.63—1.73 (m, 11H), 1.73—2.46 (m, 4H), 3.38 (s, 3H), 3.55—4.16 (m, 1H), 7.18 (s, 5H); MS, m/z 244 (M^+). Found: C, 83.61; H, 9.95%. Calcd for $C_{17}H_{24}O$: C, 83.55; H, 9.90%.

1,5-Diphenyl-3-benzyloxy-1-pentyne (Entry 5). IR (neat) 2225, 1610, 1495, 1270, 1040 cm^{-1}; ^1H NMR ($CDCl_3$) δ=1.93—2.40 (m, 2H), 2.58—3.06 (m, 2H), 4.28 (dd, 1H, J=6.5, 6.5 Hz), 4.28 (d, 2H, J=11 Hz), 6.85—7.27 (m, 15H); MS, m/z 326 (M^+). Found: C, 88.45; H, 6.78%. Calcd for $C_{24}H_{22}O$: C, 88.31; H, 6.79%.

1,4-Diphenyl-3-methoxy-1-pentyne (Entry 6). ^1H NMR ($CDCl_3$) δ=1.43 (d, 2H, J=7 Hz), 2.83—3.35 (m, 1H), 3.42 (s, 1H), 4.22 (dd, 1H, J=7 Hz, 6.7 Hz), 7.26 (s, 5H); MS, m/z 250 (M^+).

1-Phenyl-3-methoxy-1-undecyne (Entry 7). IR (neat) 1600, 1490 cm^{-1}; ^1H NMR ($CDCl_3$) δ=0.67—2.07 (m, 17H), 4.50 (s, 3), 4.15 (t, 1H), 7.1—7.6 (m, 5H); MS, m/z 258 (M^+).

4-Methoxy-1-hexadecyne (Entry 8). IR (neat) 2235 cm^{-1}; ^1H NMR ($CDCl_3$) δ=0.67—1.99 (m, 17H), 3.36 (s, 3H), 3.72—4.05 (m, 1H) MS, m/z 196 (M^+).

8-Methoxy-1-hexadecyne (Entry 9). ^1H NMR ($CDCl_3$) δ=1.56—1.93 (m, 26H), 1.97—2.38 (m, 2H), 3.35 (s, 3H), 3.68—4.03 (m, 1H); MS, m/z 252 (M^+).

1,5-Diphenyl-3-methoxy-1-penten-4-yne (Entry 10). IR (neat) 2815, 1675 (m), 1595, 1490, 960 cm^{-1}; ^1H NMR ($CDCl_3$) δ=3.32, 3.43 (s, 3H), 4.74 (d, 1.5H, J=5.5 Hz), 5.25 (d, 1.5 H, J=9.5 Hz), 5.72—6.27 (m, 2H), 7.1—7.25 (m, 10) (cis, trans mixture).

3-Methoxy-1-phenyl-4-hexen-1-yne (Entry 11). IR (neat) 2815, 2195, 1590, 1490, 960 cm^{-1}; ^1H NMR ($CDCl_3$) δ=1.26 (d, 3H, J=6.5 Hz), 3.28 (s, 3H), 4.78 (t, 1H, J=6.5 Hz), 5.65—6.32 (m, 2H), 7.17—7.56 (m, 5H); MS, m/z 186 (M^+).

3-Ethoxy-1-phenyl-1-butyne (Entry 12). IR (neat) 2210, 1600, 1490 cm^{-1}; ^1H NMR ($CDCl_3$) δ=1.15 (t, 3H, J=6.6 Hz), 1.35 (d, 3H, J=7.5 Hz), 3.23—4.10 (m, 2H), 4.34 (q, 1H, J=6.6 Hz), 7.09—7.58 (m, 5H); MS, m/z 174 (M^+). Found: C, 82.58; H, 8.08%. Calcd for $C_{12}H_{14}O$: C, 82.72; H, 8.10%.

Preparation of Propargylic Ether (6). (Table 4). A typical reaction procedure is described for 3-phenylpropanal with methoxytrimethylsilane and (trimethylsilylethynyl)-benzene (Entry 2): a CH_2Cl_2 (4 ml) suspension of $SnCl_4$ (0.2 mmol) and $ZnCl_2$ (0.2 mmol) was stirred for 30 min at room temperature, to which were added successively methoxytrimethylsilane (1.6 mmol) in CH_2Cl_2 (2 ml) and

3-phenylpropanal (1.0 mmol) in CH_2Cl_2 (2 ml) at −78 °C and stirred for 4 h, then warmed to room temperature, a solution of (trimethylsilylethynyl)benzene (1.5 mmol) in CH_2Cl_2 (2 ml) was added to the reaction mixture and stirred for 6 h at the same temperature. After quenching with aqueous solution of sodium hydrogencarbonate, the solution was extracted with CH_2Cl_2. The extracts were dried over $MgSO_4$ and condensed in vacuo. Purification by preparative TLC on silica gel (hexane:ether 1:1, v/v) afforded 1,5-diphenyl-3-methoxy-1-pentyne (0.78 mmol, 78%).

Other spectral data presented: 1,5-Diphenyl-3-ethoxy-1-pentyne (Entry 3), IR (neat) 2200, 1600, 1490 cm^{-1}; ^1H NMR ($CDCl_3$) δ=1.22 (t, 3H, J=7.5 Hz), 1.91—2.32 (m, 2H), 2.70—3.03 (m, 2H), 3.27—4.03 (m, 1H), 4.17 (q, 2H, J=7.5 Hz), 7.0—7.5 (m, 10H); MS, m/z 246 (M^+). Found: C, 86.50; H, 7.71%. Calcd for $C_{19}H_{20}O$: C, 86.32; H, 7.63%.

4-Methoxy-2-decyne (Entry 4). IR (neat) 2830, 2210, 1605, 1495 cm^{-1}; ^1H NMR ($CDCl_3$) δ=0.73—2.35 (m, 13H), 3.42 (s, 3H), 3.92—4.21 (m, 1H), 7.07—7.53 (m, 5H); MS, m/z 230 (M^+).

1,5-Diphenyl-3-(1-phenylethoxy)-1-pentyne (Entry 5). ^1H NMR ($CDCl_3$) δ=1.27, 1.43 (d, 3H, J=6.5 Hz), 1.80—2.28 (m, 2H), 2.57—3.03 (m, 2H), 4.03 (q, 1H, J=6.5 Hz), 4.1—5.0 (m, 1H), 6.90—7.47 (m, 10H); MS, m/z 340 (M^+).

Preparation of 1,5-Diphenyl-3-methoxy-1-pentene (Cis-Isomer): 1,5-Diphenyl-3-methoxy-1-pentyne (1 mmol) was dissolved in AcOEt (5 ml) and hydrogenated with Lindler catalyst (50 mg) and quinoline (30 mg) at 1 atm. The catalyst was removed by filtration and the solvent was condensed in vacuo. Then the residue was purified by preparative TLC on silica gel to afford 1,5-diphenyl-3-methoxy-1-pentene (0.89 mmol, 89%). IR (neat) 2810, 1600, 1490, 1405 cm^{-1}; ^1H NMR ($CDCl_3$) δ=1.63—2.07 (m, 2H), 2.55—2.90 (m, 2H), 3.11 (s, 3H), 3.82—4.27 (m, 1H), 5.50 (dd, 1H, J=12 Hz, 8.5 Hz), 6.52 (d, 1H, J=12 Hz), 6.77—7.40 (m, 10H); MS, m/z 252 (M^+). Found: C, 85.90; H, 7.97%. Calcd for $C_{18}H_{20}O$: C, 85.67; H, 7.99%.

Allylation of Propargylic Ethers: A CH_2Cl_2 suspension of $SnCl_4$ (0.4 mmol) and $ZnCl_2$ (0.4 mmol) was stirred for 30 min at room temperature, to which were added successively methoxytrimethylsilane (1.5 mmol) in CH_2Cl_2 (2 ml) and 3-phenylpropanal (1.0 mmol) in CH_2Cl_2 (2 ml) at 0 °C, and stirred for 4 h. Then to the reaction mixture was added (trimethylsilylethynyl)benzene (1.5 mmol) in CH_2Cl_2 (2 ml) at the same temperature and stirred for 6 h. After warming to room temperature allyltrimethylsilane (5 mmol) in CH_2Cl_2 (3 ml) was added and stirred for 15 h at the same temperature. Usual workup and purification by preparative TLC on silica gel afforded 1-phenyl-3-(2-phenylethyl)-5-hexen-1-yne (0.6 mmol, 60%). IR (neat) 1640, 1595, 1485, 910 cm^{-1}; ^1H NMR ($CDCl_3$) δ=1.58—3.03 (m, 3H), 4.90—5.29 (m, 2H), 5.57—6.34 (m, 1H), 7.05—7.66 (m, 10H); MS, m/z 260 (M^+).

Aldol Reaction and the Michael Reaction: Representative procedure is described for the reaction of silyl enol ether of propiophenone and benzaldehyde; a CH_2Cl_2 (4 ml) suspension of $SnCl_4$ (0.1 mmol) and $ZnCl_2$ (0.1 mmol) was stirred for 30 min at room temperature, to which was added a CH_2Cl_2 solution (2 ml) of silyl enol ether of propiophenone (1.1 mmol) and a CH_2Cl_2 (2 ml) solution of benzaldehyde (1.0 mmol) successively at −78 °C. The reaction mixture was further stirred for 2 h at this temperature, and the reaction quenched with satd. $NaHCO_3$ solution. The organic materials were extracted with CH_2Cl_2 twice, and the combined extracts were washed with brine and dried over Na_2SO_4. After evaporation of the solvent, the crude product was purified by silica gel thin layer chromatography to give the product in 99% yield.

Allylation of Aldehydes: A typical procedure is described for the reaction of 3-phenylpropnal with allyltrimethylsilane; a CH_2Cl_2 (4 ml) suspension of $SnCl_4$ (0.1 mmol) and $ZnCl_2$ (0.1 mmol) was stirred for 30 min at room temperature, to which was added allyltrimethylsilane (1.2 mmol) in CH_2Cl_2 (2 ml) and benzaldehyde (1.0 mmol) in CH_2Cl_2 (2 ml) successively at 0 °C. The reaction mixture was further stirred for 2 h at this temperature. Usual workup and purification by preparative TLC on silica gel afforded the product in 74% yield.

References

1) E. Colvin, "Silicon in Organic Synthesis," Butterworths (1981); W. P. Weber, "Silicon Reagentsfor Organic Synthesis," Springer-Verlag (1983).

2) a) R. Noyori, S. Murata, and M. Suzuki, *Tetrahedron*, **37**, 3899 (1981). b) T. Mukaiyama, S. Kobayashi, and M. Murakami, *Chem. Lett.*, **1984**, 1759; S. Kobayashi, M. Murakami, and T. Mukaiyama, *ibid.*, **1985**, 1535, and references cited therein.

3) T. Mukaiyama, K. Narasaka, and K. Banno, *Chem. Lett.*, **1973**, 1011; T. Mukaiyama, *Angew. Chem., Int. Ed. Engl.*, **16**, 817 (1977); K. Narasaka, K. Soai, Y. Aikawa, and T. Mukaiyama, *Bull. Chem. Soc. Jpn.*, **49**, 779 (1976).

4) N. Iwasawa and T. Mukaiyama, *Chem. Lett.*, **1987**, 463; T. Mukaiyama, S. Kobayashi, M. Tamura, and Y. Sagawa, *ibid.*, **1987**, 491.

5) M. Hayashi, A. Inubushi, and T. Mukaiyama, *Chem. Lett.*, **1987**, 1975.

6) W. S. Johnson, R. Elliott, and J. D. Elliott, *J. Am. Chem. Soc.*, **105**, 2904 (1983).

7) D. Cook, *Can. J. Chem.*, **41**, 522 (1963). Generally the strength of Lewis acidity is as follows. $TiCl_4$>$SnCl_4$>$ZnCl_2$>$SnCl_2$.

8) M. Murakami, T. Kato, and T. Mukaiyama, *Chem. Lett.*, **1987**, 1167.

9) T. Mukaiyama, H. Nagaoka, and M. Murakami, *Chem. Lett.*, **1986**, 1009.

Reaction of 1,4,2-Dithiazolium Salts with Amino Compounds

Katsumi YONEMOTO* and Isao SHIBUYA*
National Chemical Laboratory for Industry, Tsukuba, Ibaraki 305
(Received June 10, 1988)

Systematic studies on the behavior of 1,4,2-dithiazolium cations (**1**) toward various amino compounds (ammonia, aliphatic and aromatic amines, hydrazine, semicarbazide, thiosemicarbazide derivatives, etc.) were performed. The reaction pathway could be classified into three types depending on possible three fission modes of the initially-formed adduct. The main products were 5-imino-1,4,2-dithiazole, thiourea, and 1,3,4-thiadiazole derivatives, through the three different pathways, respectively. In order to clarify the factors controlling the reaction courses, the reactions of **1** with *p*-substituted aniline derivatives were carried out under systematically varying conditions. The strength of bases and the polarity of solvents had clear influence on the reactivity. The reaction mechanism is also discussed.

Chemistry of five-membered heteroaromatic cations, which are stabilized by 6 π-electron system satisfying Hückel's rule, has been extensively studied and reviewed. These cations have attracted much attention to their reactivity as potentially versatile intermediates for a wide range of heterocyclic compounds involving sulfur and/or nitrogen atoms. In particular, the reactivity of 1,3-dithiolium (**2**)[1] or 1,3-oxathiolium cations (**3**)[2] toward nucleophiles such as active methylene and amino compounds has been the subject of detailed investigations. Convenient synthetic methods for 1,2-dithiolium (**4**)[3] and 1,2,4-dithiazolium cations (**5**)[4] and their reactions with a number of active methylene compounds have been also reported. On the other hand, chemistry of 1,4,2-dithiazolium cations (**1**), aza-analogues of **2** as well as isomeric ring system of **5**, has not been fully explored. The synthesis of **1** was recently established by Paton,[5] Sammes,[6] and the authors.[7] Some reactions of **1** with nucleophiles were also attempted.[5,6b] However, no systematic study on the reactivity of **1** has been reported. In our continued investigation on the chemistry of 1,4,2-dithiazolium cations (**1**), we have examined systematically the behavior of **1** toward various amino compounds.

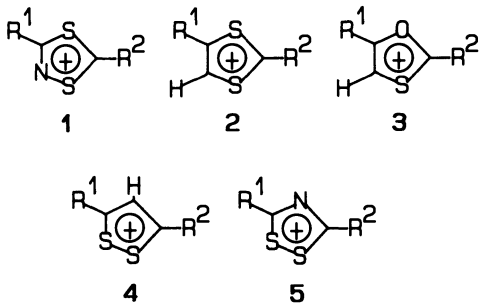

Results and Discussion

The reaction of **1** with amino compounds took place by initial attack of the terminal nitrogen of nucleophiles at the C-5 position of cations **1**, leading to the intermediate adducts (**6**) (Scheme 1), analogously to the case for **2** or **3**. However, the subsequent

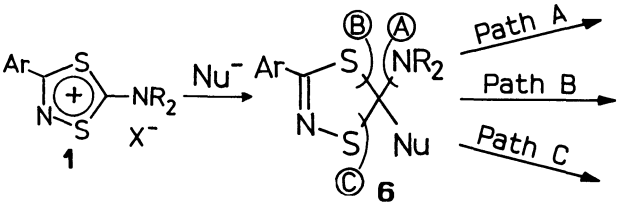

Scheme 1.

pathway from this stage was unique and can be classified into the following three types depending on possible three fission modes (A, B, and C in Scheme 1).

Path A: Proton abstraction by base followed by liberation of dialkylamino group to give 5-imino-1,4,2-dithiazole derivatives.

Path B: Loss of proton results in, in turn, the C–S bond cleavage to afford an open-chain intermediate, which then undergoes either recyclization or decomposition leading to final products.

Path C: Spontaneous fragmentation of dithiazole ring to form thiourea derivatives together with nitrile and sulfur.

The reaction conditions, products (classified according to these three pathways), and their yields are summarized in Table 1.

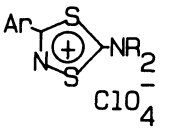

No.	Ar	NR_2
1a	Ph	NMe_2
1b	"	NEt_2
1c	"	molpholino
1d	"	NPhMe
1e	4-ClC_6H_4	NEt_2
1f	4-MeC_6H_4	"
1g	4-$MeOC_6H_4$	"

When 1,4,2-dithiazolium salt (**1a**) was allowed to react with aniline (Entry 1), hydrazine derivatives (Entries 2—4), and benzoylsulfenamide (Entry 5) in the absence of base, the sole formation of the correspond-

Table 1. The Reaction of 1,4,2-Dithiazolium Salts **1** with Various Amino Compounds

Entry	NR_2 of **1**	Amino compd	Solvent	Base	Time	Temp	Product (Yield/%)[a] path A	path B[b]	path C
1	NMe_2	$PhNH_2$	MeCN	—	6 h	refl.	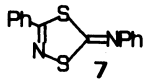 **7** (90)	—	—
2	NMe_2	$PhNHNH_2$	CH_2Cl_2	—	1 h	refl.	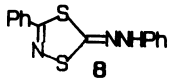 **8** (88)	—	—
3	NMe_2	$PhCONHNH_2$	CH_2Cl_2	—	0.5 h	refl.	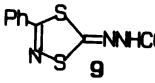 **9** (87)	—	—
4	NMe_2	$PhNHCONHNH_2$	CH_2Cl_2	—	0.5 h	refl.	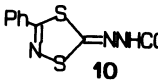 **10** (80)	—	—
5	NMe_2	$PhCOSNH_2$	MeCN	—	3 d	r.t.	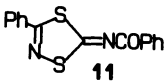 **11** (29)	—	—
6	NMe_2	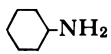	MeCN	—	2 h	r.t.	—	—	**12** (88)
7	NMe_2	$Ph_2S{\rightarrow}NH$	MeCN	—	2 h	r.t.	—	—	$Me_2NCSN{\leftarrow}SPh_2$ **13** (33)
8	NMe_2	NH_4OH	H_2O	—	0.5 d	r.t.	—	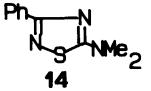 **14** (1)	Me_2NCSNH_2 **16** (62)
9	NMe_2	Me_2NNH_2	CH_2Cl_2	—	0.5 h	refl.	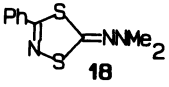 **18** (29)	—	$Me_2NCSNHNMe_2$ **19** (18)
10	NEt_2	$NH_2NH_2{\cdot}H_2O$	H_2O	—	2 h	r.t.	—	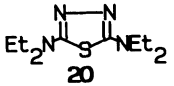 **20** (43)[b,c]	—
11	NEt_2	$Et_2NCSNHNH_2$	H_2O	Et_3N	0.5 h	r.t.	—	**20** (63)	—
12	NEt_2	$PhCSNHNH_2$	MeCN	Et_3N	1 h	r.t.	—	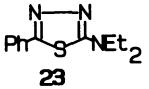 **23** (78)	—
13	NMe_2	$PhCONHNH_2$	MeCN	Et_3N	1 h	r.t.	—	—	$Me_2NCSNHNHCOPh$ **24** (49)

a) Isolated yield. b) Conversion yield based on **1b**. c) 3,6-Diphenyl-1,4-dihydro-1,2,4,5-tetrazine **22** was also obtained in 3% yield. d) Thiobenzamide **15** was formed via Path B (Entries 8—12): 27% (Entry 8), 18% (Entry 9), 30% (Entry 10), 55% (Entry 11), 84% (Entry 12).

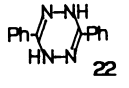
22

ing 3-phenyl-5-substituted imino-1,4,2-dithiazoles (**7**—**11**) (via Path A) was observed. In the case of Entry 5, extrusion of sulfur from sulfenamide moiety simultaneously proceeded. On the other hand, the reaction of **1** with *N*-unsubstituted sulfenamides such as *S*-dimethylthiocarbamoyl substituted sulfenamide did not give this type of compounds, but afforded 1,4,2,5-dithiadiazine derivatives, arising from ring expansion on nitrogen atom.[8]

The reaction of **1a** with cyclohexylamine (Entry 6) and *S,S*-diphenylsulfilimine (Entry 7) gave *N*-cyclohexyl-*N'*,*N'*-dimethylthiourea (**12**) and *N*-(dimethylthiocarbamoyl)-*S,S*-diphenylsulfilimine (**13**), respectively, together with benzonitrile and sulfur via Path C (Scheme 2).

On treatment with a large excess of aqueous ammonia (Entry 8), **1a** yielded not only *N,N*-dimethylthiourea (**16**) (via Path C) but 5-dimethylamino-3-phenyl-1,2,4-thiadiazole (**14**) and thiobenzamide (**15**) (both via Path B). The formation of **14** and **15** can be rationalized as follows. The initially-formed adduct **6a** (Scheme 3) opens the ring (via Path B) to form the second intermediate **17**, which then undergoes either ring closure reaction accomplished by elimination of H_2S or decomposition reaction, to give final products **14** and **15**, respectively. Furthermore, when treated with *N,N*-dimethylhydrazine (Entry 9), **1a** gave three types of products, i.e., dithiazole derivative (**18**) (via Path A), thiobenzamide (**15**) (via Path B), and thiourea derivative (**19**) (via Path C).

In the case of an excess of hydrazine hydrate (Entry 10), the reaction with **1b** gave an unexpected product 2,5-bis(diethylamino)-1,3,4-thiadiazole (**20**) togther with thiobenzamide (**15**). A mechanistic interpretation for the formation of **20** is shown in Scheme 4. The intermediate adduct by the reaction of **1b** with NH_2NH_2 undergoes ring scission to provide *N,N*-diethylthiosemicarbazide (**21**) (via Path C), which then reacts with another molecule of **1b** as a nucleophile to afford the alternative adduct **6b** followed by ring opening (via Path B) and ring closure reaction with liberation of **15** and sulfur to give the final product **20**. The reason why **1b** reacts exclusively with **21** even in the presence of an excess of hydrazine hydrate seems to be as follows. **1b** is almost insoluble in water and the reaction of **1b** with hydrazine proceeds slowly. Thus, the crystalline **1b** reacts preferentially with oily **21** free from water in contrast with NH_2NH_2 in aqueous solution. The concomitant formation of 3,6-diphenyl-1,4-dihydro-1,2,4,5-tetrazine (**22**) in 3% yield seems to result from a side reaction of PhCN with NH_2NH_2. In order to confirm this latter pathway, the reaction of **1b** with **21** (Entry 11) was carried out in the presence of triethylamine in aqueous solution. The reaction also gave **20** in a good yield.

A similar reaction was observed with thiobenzoylhydrazine (Entry 12) in the presence of Et_3N to give

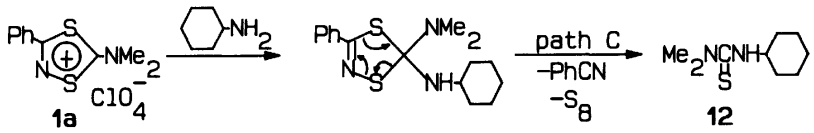

Scheme 2.

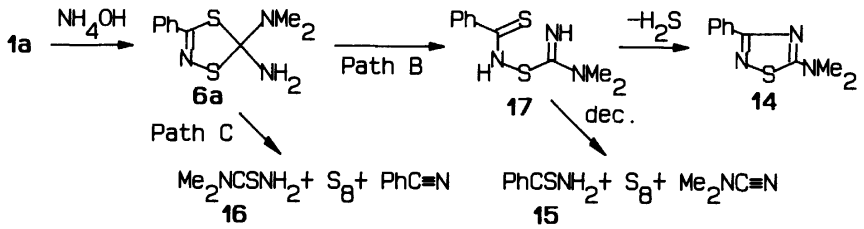

Scheme 3.

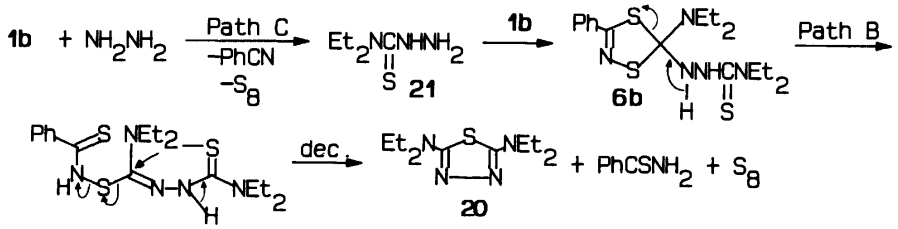

Scheme 4.

Table 2. ^{1}H NMR, IR, MS, Mp, and Elemental Analysis for the Products

Compd	^{1}H NMR ($CDCl_3$)[a]	IR (KBr) cm^{-1}
8	6.16 (1H, s), 6.8—7.6 (8H, m), 7.7—7.9 (2H, m)	1599, 1491, 1244, 928
9	7.3—7.6 (6H, m), 7.7—7.9 (2H, m), 7.9—8.1 (2H, m), 10.6 (1H, br. s)	1628, 1522, 1286, 926
10	6.6—6.8 (1H, m), 6.9—7.1 (2H, m), 7.2—7.4 (5H, m), 7.4—7.6[b] (2H, m), 8.5 (1H, br. s), 9.5 (1H, br. s)	3372, 1673, 1529, 1114
11	7.5—7.7 (6H, m), 7.9—8.1 (2H, m), 8.3—8.5 (2H, m)	1606, 1421, 1315, 1281
12	0.9—2.3 (10H, m), 3.26 (6H, s), 4.3 (1H, br. s)	1593, 1389, 1010, 603
18	2.60 (6H, s), 7.4—7.6 (3H, m), 7.7—7.9 (2H, m)	1556, 1653, 1232, 948
19	2.68 (6H, s), 3.23 (6H, s)	3184, 1543, 1004, 1115
20	1.20 (12H, t, J=7.2Hz), 3.39 (8H, q, J=7.2Hz)	1508, 1431, 1367, 736
22	5.70 (2H, s), 7.5—7.6 (6H, m), 8.0—8.2 (4H, m)	1473, 1444, 769, 699
23	1.27 (6H, t, J=7.0Hz), 3.56 (4H, q, J=7.0Hz), 7.3—7.5 (3H, m), 7.8—8.0 (2H, m)	1529, 1452, 1350, 1307
24	3.35 (6H, s), 7.4—7.6 (3H, m), 7.8—8.0 (2H, m), 8.8 (1H, br. d), 10.1 (1H, br. d)	3260, 3200, 1652, 1524

Compd	MS (rel. intensity) m/z	Mp θ_m (solv.) °C	Found (Calcd)/% C	H	N	S
8	285 (M^+, 16), 103 (100)	136.5—137.0 ($CHCl_3$-MeCN)	58.79 (58.92)	3.81 (3.89)	14.85 (14.72)	22.55 (22.47)
9	313 (M^+, 9), 105 (100)	134.0—135.0 ($CHCl_3$-MeCN)	57.45 (57.49)	3.50 (3.54)	13.62 (13.41)	20.40 (20.46)
10	328 (M^+, 9), 103 (77)	186.5—187.0 (DMSO)	54.65 (54.86)	3.68 (3.68)	17.15 (17.06)	19.37 (19.52)
11	298 (M^+, 4), 105 (100)	191.5—192.0 (CH_2Cl_2-MeCN)	60.18 (60.38)	3.32 (3.38)	9.37 (9.39)	21.49 (21.49)
12	186 (M^+, 100), 88 (88)	91.5—92.0 (CH_2Cl_2-pentane)	58.19 (58.02)	9.74 (9.74)	15.04 (15.04)	17.24 (17.21)
18	237 (M^+, 45), 135 (27)	78.5—79.0 (CH_2Cl_2-pentane)	50.63 (50.61)	4.67 (4.67)	17.72 (17.70)	27.05 (27.02)
19	147 (M^+, 59), 88 (100)	88.5—89.0 (CH_2Cl_2-pentane)	40.73 (40.79)	8.79 (8.90)	28.46 (28.54)	21.78 (21.77)
20	228 (M^+, 100), 116 (27)	52.5—53.0 (Pentane-Et_2O)	52.35 (52.60)	8.74 (8.83)	24.40 (24.53)	14.00 (14.04)
22	236 (M^+, 44), 104 (100)	263.5—264.5 (CH_2Cl_2-Et_2O)	70.92 (71.17)	5.11 (5.12)	23.66 (23.71)	
23	233 (M^+, 76), 190 (100)	43.0—44.0 (Pentane)	61.75 (61.77)	6.48 (6.48)	18.03 (18.01)	13.80 (13.74)
24	223 (M^+, 28), 88 (100)	164.5—165.0 (MeCN)	53.80 (53.79)	5.87 (5.87)	18.89 (18.82)	14.39 (14.36)

a) ppm from internal TMS. b) In DMSO-d_6.

2-diethylamino-5-phenyl-1,3,4-thiadiazole (**23**) in a good yield via the same pathway (Path B) mentioned above. On the other hand, on treatment with its oxa-analogue, benzoylhydrazine, **1a** gave only a product **9** in the absence of base (via Path A) (Entry 3), whereas, in the presence of Et_3N (Entry 13), **1a** afforded 4-benzoyl-1,1-dimethylthiosemicarbazide (**24**) (via Path C).

From the above results, the basicity of reaction solution as well as the nature of nucleophiles seem to be important factors determining the reaction modes. In order to get additional information on the factors controlling the three reaction courses, we selected the combination of **1a—g** with *p*-substituted anilines to examine the reaction under various conditions (Table 3).

First of all, to explore the effects of base strength, the reaction of **1a** with *p*-toluidine was examined in the presence of four different bases and in the absence of base. It was found that the formation of *N,N*-dimethyl-*N'*-(*p*-tolyl)thiourea (**26e**) (via Path C) predominates in comparison with that of 5-(*p*-tolyl)imino-3-phenyl-1,4,2-dithiazole (**25e**) (via Path A) with increasing value of pK_a (Entries 14—18); the ratio between the two products varies widely. Toluidine itself (pK_a 5.09) can act as a base, although its basicity is lower than that of pyridine. A similar trend was evident in the reaction of **1b** with *p*-toluidine (Entries 19—21). Furthermore, even when triphenylphosphine was used instead of amine base, **26** was produced selectively (Entries 22, 23).

These results can be interpreted as follows. Attack

Table 3. The Reaction of **1** with *p*-Substituted Aniline Derivatives

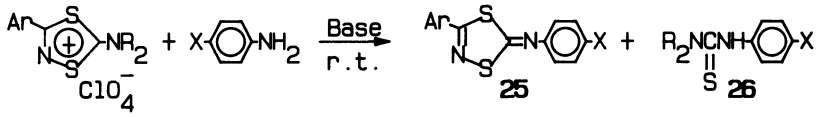

Entry	NR_2	Ar	X	Base (pK_a)	Solvent (ε_γ)	Yield/%	
						25	**26**
14	NMe_2	Ph	Me	—	MeCN	71	—
15	NMe_2	Ph	Me	Pyridine (5.19)	MeCN	73	18
16	NMe_2	Ph	Me	γ-Picoline (6.02)	MeCN	73	24
17	NMe_2	Ph	Me	2,6-Lutidine (6.72)	MeCN	42	44
18	NMe_2	Ph	Me	Triethylamine (10.9)	MeCN	—	64
19	NEt_2	Ph	Me	Pyridine	MeCN	53	Tr.
20	NEt_2	Ph	Me	γ-Picoline	MeCN	48	38
21	NEt_2	Ph	Me	2,6-Lutidine	MeCN	15	48
22	NMe_2	Ph	Me	Ph_3P	MeCN	Tr.	45
23	NMe_2	Ph	Me	Ph_3P	CH_2Cl_2	—	53
24	NEt_2	4-ClC_6H_4	Me	γ-Picoline	MeCN	42	50
25	NEt_2	Ph	Me	γ-Picoline	MeCN	48	38
26	NEt_2	4-MeC_6H_4	Me	γ-Picoline	MeCN	53	32
27	NEt_2	4-$MeOC_6H_4$	Me	γ-Picoline	MeCN	41	29
28	NMe_2	Ph	Me	γ-Picoline	MeCN	48	38
29	NEt_2	Ph	Me	γ-Picoline	MeCN	73	24
30	Morpholino	Ph	Me	γ-Picoline	MeCN	44	8
31	NPhMe	Ph	Me	γ-Picoline	MeCN	85	11
32	NMe_2	Ph	Me	γ-Picoline	CH_2Cl_2 (9.1)	93	7
33	NMe_2	Ph	Me	γ-Picoline	EtOH (27.0)	81	13
34	NMe_2	Ph	Me	γ-Picoline	MeCN (37.5)	73	24
35	NMe_2	Ph	Me	γ-Picoline	DMSO (46.7)	50	47
36	NMe_2	Ph	MeO	γ-Picoline	MeCN	72	20
37	NMe_2	Ph	Me	γ-Picoline	MeCN	73	24
38	NMe_2	Ph	Cl	γ-Picoline	MeCN	42	23

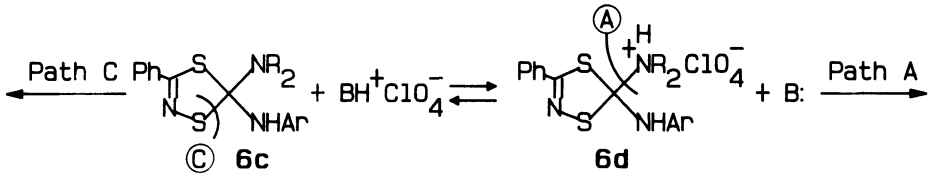

Scheme 5.

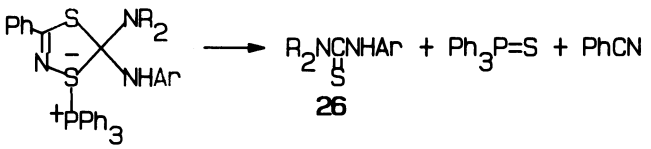

Scheme 6.

of *p*-toluidine on the C-5 position of **1** leads to intermediate **6c** which is in equilibrium with **6d** as shown in Scheme 5. The equilibrium is shifted toward **6c** in the presence of a stronger base by effective trapping of perchloric acid, and hence fragmentation of **6c** proceeds preferentially to afford **26** (via Path C). On the other hand, in the presence of a weaker base, considerable contribution of **6d** leads to the pre-

ferential liberation of dialkylamino group to give **25** (via Path A). In the case of phosphine, nucleophilic attack by Ph_3P on the sulfur atom (1- or 4-position) of adduct **6c** promotes the sulfur extrusion resulting in the preferential formation of **26**; triphenylphosphine sulfide was also formed as expected.

In order to examine the influence of substituents in 1,4,2-dithiazolium cations (**1**), the reactions of **1a—g**, bearing different aryl groups at the C-3 position (Entries 24—27) and different di-substituted amino groups at the C-5 position (Entries 28—31), with *p*-toluidine in the presence of γ-picoline were carried out. The yields and the ratio of products **25** and **26** depend mainly on the substituents at the C-5 position which is the reaction center, but almost negligible dependence upon those at C-3 was found. According to the rationalization mentioned above, the equilibrium should be shifted toward **6d** (Scheme 5) with high basicity of the di-substituted amino groups at C-5. Therefore, the formation of **25** should be favored. However, the fact obtained stands in contrast to this expected result. It may be attributable to an extra factor: a liberating secondary amine from **6d**, in turn, acts as a base. The increasing order of basicity of the corresponding secondary amines is known as follows: $Et_2NH \approx Me_2NH > O(C_2H_4)_2NH > PhMeNH$.[9] Thus, in the case where the liberating amine has relatively strong basicity (e.g. Me_2NH and Et_2NH), the yield of **26** somewhat increased.

When the reaction was carried out in four different solvents (Entries 32—35), the selectivity proved to be clearly solvent-dependent, where the ratio of **25** to **26** decreased linearly with increase in dielectric constant (ε_γ). It could be postulated that adduct **6** tends to cleave in polar solvents, probably because the transition state in the ring scission reaction has some

Table 4. Characterization Data of Compounds **25**

No.	Ar	X	^{1}H NMR ($CDCl_3$, ppm from TMS)	MS (rel. intensity) *m/z*	Mp θ_m/°C
25a	4-ClC_6H_4	Me	2.37 (3H, m), 6.98, 7.24 (2H, d, *J*=9Hz), 7.43, 7.72 (2H, d, *J*=9Hz)	320 (M^++2, 6.2), 318 (M^+, 14.7), 181 (100)	128.0—130.0
25b	4-MeC_6H_4	Me	2.37 (3H, s), 2.39 (3H, s), 6.99, 7.23 (2H, d, *J*=9Hz), 7.25, 7.66 (2H, d, *J*=9Hz)	298 (M^+, 12), 181 (61), 149 (100)	128.0—129.5
25c	4-$MeOC_6H_4$	Me	2.36 (3H, s), 3.84 (3H, s), 6.95, 7.24 (2H, d, *J*=9Hz), 6.9—7.1, 7.6—7.8 (2H, m)	314 (M^+, 12), 165 (100), 133 (48)	128.0—128.5
25d	Ph	Cl	7.04, 7.33 (2H, d, *J*=9Hz), 7.4—7.6 (3H, m), 7.7—7.9 (2H, m)	306 (M^++2, 3.5), 304 (M^+, 7.6), 135 (100)	129.0—129.5
25e	Ph	Me	2.36 (3H, s), 6.99, 7.24 (2H, d, *J*=9Hz), 7.4—7.6 (3H, m), 7.7—7.9 (2H, m)	284 (M^+, 19), 181 (100), 135 (95)	88.0—88.5
25f	Ph	MeO	3.83 (3H, s), 6.9—7.2 (4H, m), 7.4—7.6 (3H, m), 7.7—7.9 (2H, m)	300 (M^+, 18), 165 (77), 133 (100)	124.0—125.0

Table 5. Characterization Data of Compounds **26**

No.	R_2N	X	^{1}H NMR ($CDCl_3$, ppm from TMS)	MS (rel. intensity) *m/z*	Mp θ_m/°C
26a	Et_2N	Me	1.27 (6H, t, *J*=7.2Hz), 2.33 (3H, s), 3.75 (4H, q, *J*=7.2Hz), 7.17 (4H, s)	222 (M^+, 49), 189 (23), 116 (100)	Oil
26b	Morpholino	Me	2.32 (3H, s), 3.6—3.9 (8H, m), 7.0—7.2 (4H, m)	236 (M^+, 65), 130 (66), 86 (100)	141.5—143.0
26c	PhMeN	Me	2.30 (3H, s), 3.74 (3H, s), 7.16 (4H, s), 7.3—7.7 (5H, m)	256 (M^+, 65), 150 (100), 106 (100)	116.5—117.5
26d	Me_2N	Cl	3.06 (6H, s), 6.62, 7.12 (2H, d, *J*=9Hz)	216 (M^++2, 9), 214 (M^+, 24), 88 (100)	150.0—151.5
26e	Me_2N	Me	2.33 (3H, s), 3.33 (3H, s), 7.17 (4H, s)	194 (M^+, 42), 91 (33), 88 (100)	166.0—167.0
26f	Me_2N	MeO	3.29 (6H, s), 3.80 (3H, s), 6.88, 7.20 (2H, d, *J*=9Hz)	210 (M^+, 33), 121 (11), 88 (100)	121.5—122.0

polar character and scission energy is reduced in polar media.

Finally, the reactions of **1** with aniline derivatives bearing different substituents X (MeO, Me, and Cl) at the para-position were examined (Entries 36—38). However, the substituents X showed little effect on both the yields and the ratio of **25** to **26**. For definite interpretation on the factors which favor Path B, further detailed information will be needed.

In summary, the reactivity of 1,4,2-dithiazolium cations (**1**) proved to be partly similar to that of 1,3-dithiolium cations (**2**)[1] or 1,3-oxathiolium cations (**3**)[2] (Path A and a part of Path B), but partly different from that of all of other five-membered heteroaromatic cations[1-4] (Path C and a part of Path B). The reaction of **1** with various active methylene compounds has currently been studied; the results will be reported in a separate paper.

Experimental

All the melting points were uncorrected. The ^{1}H NMR spectra were recorded on a Hitachi R-40, in $CDCl_3$, using TMS as an internal standard. The IR spectra were measured on a JASCO A-302 spectrometer using KBr disks. The low-resolution mass spectra were taken on Hewlett Packard 5995A spectrometer by electron impact ionizing technique at 70 eV.

1,4,2-Dithiazolium salts (**1**),[7] *S*-benzoylsulfenamide,[10] *N,N*-diethylthiocarbazide (**21**),[11] and thiobenzoylhydrazine[12] were prepared according to the procedures in the literatures. Other reagents were commercially available and used without any purification.

Reaction of 1a, b with Amino Compounds; General Procedure. 1,4,2-Dithiazolium perchlorates **1a,b** (1 mmol) were added to stirred solutions (6 ml) of amino compounds (2 mmol), except for aqueous ammonia (28%) (4 ml) (Entry 8) and hydrazine monohydrate (80%) (0.2ml) (Entry 10). In the case of using base, the combination of **1** (1 mmol), amino compounds (1 mmol), and triethylamine (1 mmol) was adopted (Entries 11—13). Other reaction conditions were listed in Table 1. After the solvent was removed in vacuo, the residue was purified by column chromatography on silica gel and recrystallization from appropriate solvents listed in Table 3. The yields of products are presented in Table 1 and their characterization data are shown in Table 3. On the other hand, **7**,[5] **13**,[13] **14**,[14] and **16**[15] were identified by direct comparison with each authentic sample.

Reaction of 1a—g with *p*-Substituted Aniline Derivatives. 1,4,2-Dithiazolium perchlorates (**1a—g**) (1 mmol) were added to stirred solutions (4 ml) of the aniline derivatives (1.1 mmol) in the presence of base (1.1 mmol). The reaction mixture was stirred for 6 h at room temperature. The crude products were extracted with dichloromethane (20 ml×2) after addition of 2% hydrochloric acid. The two products **25** and **26** were isolated by preparative TLC. Their mps and spectral data are shown in Tables 4 and 5. The elemental analyses of **25e** and **26e** are shown below. Identification of other **25** and **26**'s was based only on spectral data.

25e: Found: C, 63.18; H, 4.21; N, 9.75%. Calcd for $C_{15}H_{12}N_2S_2$: C, 63.35; H, 4.25; N, 9.85%.

26e: Found: C, 61.71; H, 7.28; N, 14.37%. Calcd for $C_{10}H_{14}N_2S$: C, 61.82; H, 7.26; N, 14.42%.

References

1) K. Hirai, T. Ishiba, and H. Sugimoto, *Chem. Pharm. Bull.*, **20**, 1711 (1972); K. Hirai, *Tetrahedron Lett.*, **1971**, 1137.

2) K. Hirai and T. Ishiba, *Heterocycles*, **9**, 1223 (1978); *idem*, *Chem. Pharm. Bull.*, **26**, 3017 (1978); **20**, 2384 (1972). For a review: K. Hirai, H. Sugimoto, and T. Ishiba, *Yuki Gosei Kagaku Kyokai Shi*, **39**, 192 (1981).

3) I. Shibuya, *Bull. Chem. Soc. Jpn.*, **52**, 1235 (1979).

4) I. Shibuya, *Bull. Chem. Soc. Jpn.*, **57**, 605 (1984).

5) D. J. Greig, M. McPherson, R. M. Paton, and J. Crosby, *J. Chem. Soc., Chem. Commun.*, **1985**, 1641.

6) a) F. S. Y. Chan and M. P. Sammes, *J. Chem. Soc., Chem. Commun.*, **1985**, 1641. b) F. S. Y. Chan, M. P. Sammes, and R. L. Harlow, *J. Chem. Soc., Perkin Trans. 1*, **1988**, 899.

7) I. Shibuya and K. Yonemoto, *Bull. Chem. Soc. Jpn.*, **59**, 2017 (1986).

8) K. Yonemoto, I. Shibuya, and K. Honda, *Bull. Chem. Soc. Jpn.*, **61**, 2232 (1988).

9) "Dissociation Constants of Organic Bases in Aqueous Solution" in "CRC Handbook of Chemistry and Physics," 67th ed, ed by R. C. Weast, CRC Press, Inc., Florida (1986), P. D-159.

10) M. S. Raasch, *J. Org. Chem.*, **37**, 3820 (1972).

11) K. A. Jensen, *J. Prakt. Chem.*, **159**, 192 (1941).

12) K. A. Jensen and C. Pedersen, *Acta Chem. Scand.*, **15**, 1097 (1961).

13) H. Yoshida, H. Taketani, T. Ogata, and S. Inokawa, *Bull. Chem. Soc. Jpn.*, **49**, 3124 (1976).

14) J. Goerdeler, A. Hupperts, and K. Wember, *Chem. Ber.*, **87**, 68 (1954).

15) F. Kurzer and P. M. Sanderson, *J. Chem. Soc.*, **1957**, 4461.

 © 1988 The Chemical Society of Japan Bull. Chem. Soc. Jpn., 61, 4051—4055 (1988)

Highly Regio- and Stereoselective Ring-Opening Reaction of γ-Alkenyl-γ-butyrolactones with Allylsilanes in the Presence of Trimethyloxonium Salt Leading to Methyl 4,8-Alkadienoates

Masatoshi KAWASHIMA and Tamotsu FUJISAWA*
Chemistry Department of Resources, Mie University, Tsu, Mie 514
(Received June 29, 1988)

The reaction of γ-alkenyl-γ-butyrolactones with allylic trimethylsilanes in the presence of trimethyloxonium tetrafluoroborate proceeded regio- and stereoselectively with an allylic rearrangement of the substrate to afford methyl (*E*)-4,8-alkadienoates in high yields. On the other hand, the ring opening of 4-hexen-6-olide afforded exclusively methyl (*Z*)-4,8-alkadienoates in high yields. The synthetic utility of the reaction was demonstrated by the short step synthesis of β-sinensal and β-farnesene.

Alkadienoic acids possessing 1,5-diene structure such as 2,6-, 3,7-, and 4,8-alkadienoic acids are incorporated in terpenoid carboxylic acids and many synthetic methods have been developed. For example, the Claisen rearrangement of 2-alkenoic acid allylic esters via trimethylsilylketene acetals produces 3-carboxy-1,5-diene derivatives, which are subsequently converted into 2,6-alkadienoic acids by the Cope rearrangement.[1] Palladium-catalyzed carbonylation accompanying allylic rearrangement of 3-hydroxy-1,6-diene derivatives gives 3,7-alkadienoic acids.[2] The Claisen rearrangement of 3-acetoxy-1,6-heptadiene via *t*-butyldimethylsilylketene acetal gives 4,8-nonadienoic acid.[3] In these synthetic methods, there is no example which satisfies both convenience of the operative procedure and the stereoselectivity of the carbon–carbon double bond. In our laboratory, the ring opening of ω-alkenyllactones such as β-alkenyl-β-propiolactone, γ-vinyl-γ-butyrolactone, and δ-vinyl-δ-valero lactone with organocopper reagents were developed and utilized for the synthesis of the various kinds of alkenoic acids.[4] Alkadienoic acids such as 3,7- ,4,8-, and 5,9-alkadienoic acids were prepared by this method using diallylcuprate, however, the product yields are not so high and the predomination of *E*-configuration of the carbon-carbon double bond is not perfect. The reason may be due to the lack of thermal stability of the cuprate and formation of copper π-allyl complex.[5] The yield and the stereoselectivity of the carbon-carbon double bond of 4,8-nonadienoic acid obtained by the ring opening of γ-vinyl-γ-butyrolactone are the lowest among these alkadienoic acids and not adequate for the further utilization of the acid. Therefore to develop more stereoselective synthetic method of 4,8-alkadienoic acids or their esters, allylsilane, which is thermally stable compound, was noticed for the nucleophile as the source of allyl group toward the ring opening of γ-vinyl-γ-butyrolactone. The present paper describes details on the regio- and stereoselective reaction of γ-alkenyl-γ-butyrolactones and the analogous lactone, 4-hexen-6-olide, with allylsilanes in the presence of trimethyloxonium tetrafluoroborate to afford methyl (4*E*)- and (4*Z*)-4,8-alkadienoates in high yields, respectively.[6]

The reactions of allylsilane with acetal,[7] aldehyde,[8] enone,[9] and so on,[10] are achieved in the presence of the activator of the electrophile such as Lewis acids because of the low nucleophilicity of allylsilane. Therefore, the reactions of γ-vinyl-γ-butyrolactone (**1**) with allyltrimethylsilane were carried out in the presence of catalytic or equimolar amount of Lewis acid such as $TiCl_4$, $SnCl_4$, $AlCl_3$, $Me_3SiOSO_2CF_3$, and Me_3SiI, however, the desired allylation of the lactone did not proceed to result in a recovery of the starting material **1**. When the Meerwein reagent, triethyloxonium tetrafluoroborate, which was known as the ethylating agent of the oxygen atom of γ-butyrolactone,[11] was used as the activator of the lactone **1**, the reaction of **1** with allylsilane proceeded in CH_2Cl_2 at room temperature to afford ethyl 4,8-nonadienoate (**2**) in 49% yield accompanying with many complex products formed by the over alkylation of the initial product **2**. Since the side reaction seemed to be attributed to the high reactivity of triethyloxonium salt, trimethyloxonium tetrafluoroborate was used instead of triethyloxonium salt resulting in remarkable increase of the yield of the corresponding methyl ester, methyl 4,8-nonadienoate (**3a**) (100%) in spite of heterogeneous reaction. The product showed the regioselective attack of allylsilane to the terminal vinyl carbon of the lactone **1** without accompanying the attack to the γ-carbon. The present result of the allylic rearrangement of the electrophile in the reaction of allylic silanes has been rarely reported.[12] Moreover the exclusive *E*-configuration of the newly formed carbon-carbon double bond of the ester **3a** was confirmed by NMR, IR spectra, and GLPC analysis in

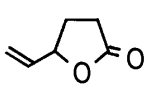

1

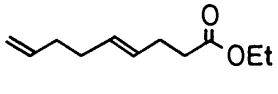

2

Table 1. Ring Opening of γ-Vinyl-γ-butyrolactone[a]

Oxonium salt	Solvent	Temp	Time/h	Yield of Ester/%
Et_3OBF_4	CH_2Cl_2	rt	13	49
Me_3OBF_4	CH_2Cl_2	rt	94	100
Me_3OBF_4	CH_2Cl_2	reflux	8	83
Me_3OBF_4	$CHCl_3$	reflux	10	72
Me_3OBF_4	Benzene	rt	94	—[b]
Me_3OBF_4	CH_2Cl_2–CH_3NO_2	rt	13	26

a) The molar ratio of lactone, oxonium salt, and allylsilane is 1:2:3. b) No reaction proceeded.

comparison with those of methyl ester of 4,8-nonadienoic acid obtained by the reaction of **1** with diallylcuprate.[4] The reaction did not proceed at all in nonpolar solvent such as benzene. When nitromethane was used as the co-solvent of dichloromethane to dissolve the oxonium salt, the yield of the methyl ester **3a** was remarkably decreased. The reactions in

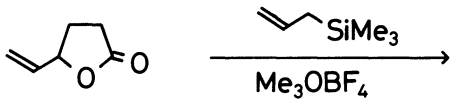

1

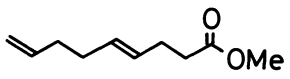

3a

refluxing CH_2Cl_2 and $CHCl_3$ decreased the yields to 83% and 72%, respectively, although the reaction time was markedly shortened to about a tenth. These representative results are summarized in Table 1.

Wide applicability of this ring opening of γ-vinyl-γ-butyrolactones was elucidated by the reaction of various γ-alkenyl-γ-butyrolactones with allylic silanes. In the reactions of allyltrimethylsilane with methyl substituted γ-vinyl-γ-butyrolactones such as

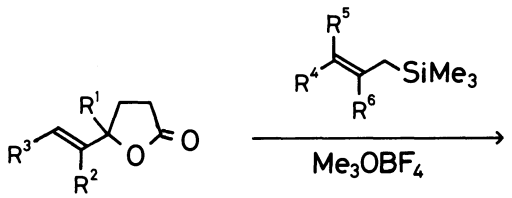

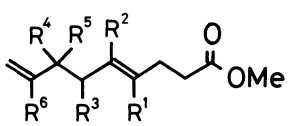

3

γ-isopropenyl- and γ-(1-propenyl)-γ-butyrolactones, the ring opening of both lactones afforded the corresponding methyl 4,8-alkadienoates **3b,c** with

Table 2. Ring Opening of γ-Alkenyl-γ-butyrolactones[a]

Lactone	Allylsilane	Product	Yield/%
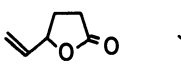	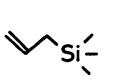	**3a** 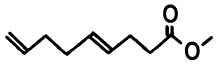	100
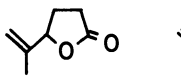	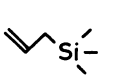	**3b** 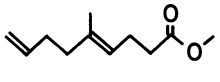	85
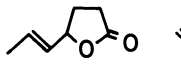	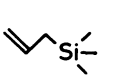	**3c** 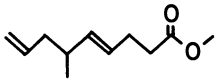	81
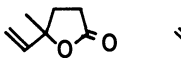	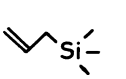	**3d** 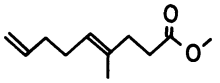	90
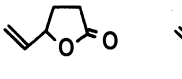	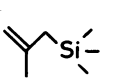	**3e**	93
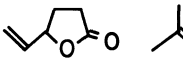	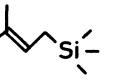	**3f** 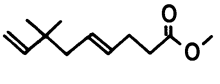	74
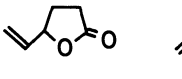	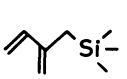	**3g**	74

a) All reactions were performed at room temperature for 94 h in CH_2Cl_2. The molar ratio of lactone, oxonium salt, and allylsilane is 1:2:3.

methyl group at 5- and 6-positions in high ylelds (81% and 85%, respectively). The reaction of γ-methyl-γ-vinyl-γ-butyrolactone gave the corresponding ester **3d** with methyl group at 4-position in 74% yield. The ring opening of γ-vinyl-γ-butyrolactone with substituted allylsilanes such as (2-methyl-2-propenyl)-trimethylsilane, (3-methyl-2-butenyl)trimethylsilane, and 2-(trimethylsilylmethyl)-1,3-butadiene also proceeded regio- and stereoselectively to afford the corresponding methyl 4,8-alkadienoates **3e—g** with substituent at 7- and 8-positions. In a recent report on the ring opening of 2-vinyltetrahydrofuran with allylsilanes, the regioselectivity is affected by the substituent on the allylsilane.[12a] In the present ring opening of γ-alkenyl-γ-butyrolactones, no formation of regioisomer produced by the attack of allylsilane to the γ-carbon of γ-alkenyl-γ-butyrolactones could be confirmed. Moreover, IR spectra and GLPC analyses of

Table 3. Ring Opening of 4-Hexen-6-olide[a)]

Allylsilane		Product	Yield/%
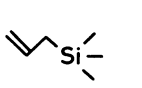	5a	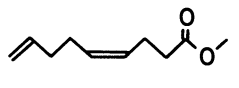	87
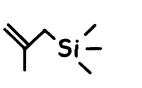	5b	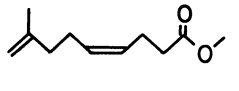	84
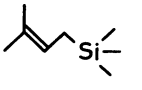	5c	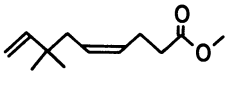	86
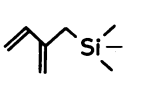	5d	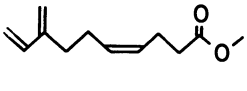	60

a) All reactions were performed at room temperature for 94 h in CH_2Cl_2. The molar ratio of lactone, oxonium salt, and allylsilane is 1:2:3.

the products showed exclusive *E*-configuration of the newly formed carbon–carbon double bond on 4-position of the esters. These results are summarized in Table 2.

4-Hexen-6-olide (**4**) is also a kind of allylic esters similar to γ-alkenyl-γ-butyrolactones. It is significant to investigate whether allylic rearrangement of the lactone **4** in reaction of **4** with allylic silane in the presence of trimethyloxonium tetrafluoroborate arises or not. Reaction with allyltrimethylsilane was carried out under the same conditions for the ring opening of **1**, in CH_2Cl_2 at room temperature to give a single product. Surprisingly, the product was methyl 4,8-nonadienoate, without accompanying a trace amount of methyl 4-vinyl-6-heptenoate. Moreover the carbon–carbon double bond at 4-position of the obtained ester retained completely the *Z*-configuration of 4-hexen-6-olide. This is noticeable result compared with the ring opening of 4-hexen-6-olide with organocuprate to give a mixture of (*E*)- and (*Z*)-4-alkenoic acids (S_N2 product) and 4-vinylalkanoic acid (S_N2' product).[13)] Oxonium salt-promoted reaction of **4** with other methyl-substituted allylsilanes proceeded with high regio- and stereoselectivity to afford methyl (4*Z*)-4,8-alkadienoate **5**. The results are summarized in Table 3. Thus perfect S_N2' reaction in the ring opening of γ-alkenyl-γ-butyrolactones and perfect S_N2 reaction in that of 4-hexen-6-olide provide both geometrically pure (4*E*)- and (4*Z*)-4,8-alkadienoates.

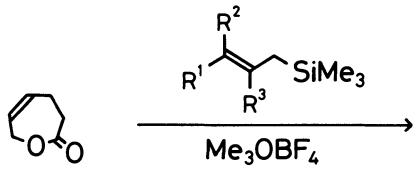

4

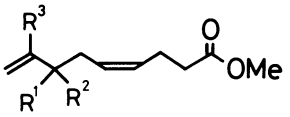

5

The applicability of the present stereoselective synthetic method of methyl 4,8-alkadienoate is demonstrated in a short step synthesis of β-sinensal **6**, an important constituent of the odor and taste of Chinese orange oil (*Citrus sinensus* L.)[14)] and β-farnesene **7**, natural aphid alarm pheromone. Methyl 4-methyl-8-methylene-4,9-decadienoate (**3h**), obtained in a yield of 65% by the reaction of γ-methyl-γ-vinyl-γ-butyrolactone with 2-(trimethylsilylmethyl)-

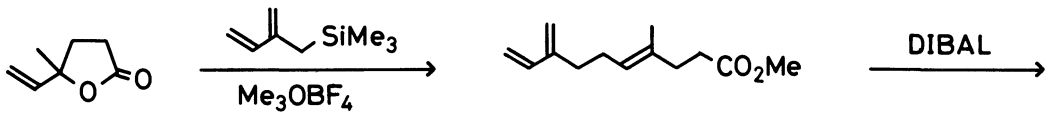

3h

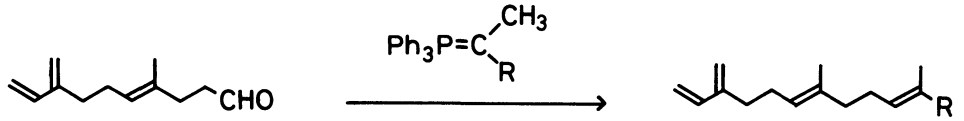

8

R = CHO 6

R = CH_3 7

1,3-butadiene, was reduced by diisobutylaluminum hydride in THF–toluene to give 4-methyl-8-methylene-4,9-decadienal (**8**) in 83% yield. The Wittig reaction of the aldehyde **8** with (α-formylethylidene)-triphenylphosphorane and with isopropylidenetriphenylphosphorane afforded the desired *trans,trans*-β-sinensal **6** and *trans*-β-farnesene **7** in 82% and 54% yields, respectively.

The present ring opening reaction of γ-alkenyl-γ-butyrolactone and 4-hexen-6-olide with allylsilanes in the presence of trimethyloxonium tetrafluoroborate involves several characteristic features as follows: (1) Both isomers of (*E*)- and (*Z*)-4,8-alkadienoic acid methyl esters are obtained in high yields, respectively, by selecting the starting lactone, either γ-alkenyl-γ-butyrolactone or 4-hexen-6-olide. (2) High regio- and stereoselectivity is easily achieved at room temperature. (3) The operative procedure is extremely simple.

Experimental

General. Boiling points were measured at the pressure indicated and are uncorrected. Infrared spectra were recorded on a Hitachi EPI-G2 spectrometer. ^{1}H NMR spectra were recorded on a Varian A-60 spectrometer and on a Jeol JNM-PMX60SI spectrometer and are reported in parts per million (δ) from TMS. Samples were dissolved in CCl_4 containing TMS as an internal standard. Preparative thin-layer chromatography (TLC) was performed on 20×20 cm glass plates coated with 1.5 mm of silica gel (Wakogel B-5F). All reactions were run under a positive pressure of dry argon. Reactions requiring anhydrous conditions were performed in a flame-dried glassware that was cooled under argon. Anhydrous solvents were transferred by an oven-dried syringe. Solvents were distilled before use: Dichloromethane was distilled from phosphorus pentaoxide.

Materials. γ-Vinyl-, γ-isopropenyl-, and γ-(1-propenyl)-γ-butyrolactones were prepared according to the published method.[16] γ-Methyl-γ-vinyl-γ-butyrolactone[17] and 4-hexen-6-olide[13] were prepared by the reported method. Trimethyl-[18] and triethyloxonium tetrafluoroborates[19] were prepared by the published method. Allyltrimethylsilane, (3-methyl-2-butenyl)trimethylsilane, and 2-(trimethylsilylmethyl)-1,3-butadiene were purchased from Petrarch Systems Inc. (2-Methyl-2-propenyl)trimethylsilane was prepared by the reported procedure.[20]

Procedure for the Reaction of γ-Alkenyl-γ-butyrolactones with Allylsilanes in the Presence of Trimethyloxonium Tetrafluoroborate. In a typical experiment, a flask equipped with a magnetic stirring bar and septum was charged 592 mg (4.00 mmol) of Me_3OBF_4. After flushing with dry argon, a solution of 686 mg (6.00 mmol) of allyltrimethylsilane in CH_2Cl_2 (6 ml) was added to the flask at room temperature. Then a solution of 224 mg (2.00mmol) of γ-vinyl-γ-butyrolactone in CH_2Cl_2 (6 ml) was added and the reaction mixture was stirred at the same temperature for 94 h. The reaction was quenched with 10 ml of saturated $NaHCO_3$. The organic layer was separated and aqueous layer was extracted with CH_2Cl_2. The combined organic layer was washed with brine, dried with anhydrous $MgSO_4$, and concentrated. The residue was purified by TLC (hexane:CH_2Cl_2=2:1) to afford 336 mg (2.00 mmol) (100%) of methyl 4,8-nonadienoate (**3a**). R_f=0.5; ^{1}H NMR δ=2.07 (br d, *J*=3 Hz, 4H), 2.27 (br s, 4H), 3.55 (s, 3H), 4.70—5.95 (m, 5H); IR (neat) 1740, 1000, 970, 910 cm^{-1}; Anal. ($C_{10}H_{16}O_2$) C, H.

In the same manner as above, all other ring opening reactions of γ-alkenyl-γ-butyrolactones and 4-hexen-6-olide were performed.

Methyl (*E*)-5-Methyl-4,8-nonadienoate (3b): R_f=0.5; ^{1}H NMR δ=1.60 (s, 3H), 2.08 (br s, 4H), 2.27 (br d, *J*=4 Hz, 4H), 3.57 (s, 3H), 4.73—5.97 (m, 4H); IR (neat) 1740, 990, 910, 840 cm^{-1}; Anal. ($C_{11}H_{18}O_2$) C, H.

Methyl (*E*)-6-Methyl-4,8-nonadienoate (3c): R_f=0.5; ^{1}H NMR δ=0.94 (d, *J*=7 Hz, 3H), 1.80—2.13 (m, 3H), 2.25 (br s, 4H), 3.57 (s, 3H), 4.67—5.97 (m, 5H); IR (neat) 1740, 990, 970, 910 cm^{-1}; Anal. ($C_{11}H_{18}O_2$) C, H.

Methyl (*E*)-4-Methyl-4,8-nonadienoate (3d): R_f=0.5; ^{1}H NMR δ=1.60 (s, 3H), 1.93—2.18 (m, 4H), 2.27 (br s, 4H), 3.57 (s, 3H), 4.73—5.98 (m, 4H); IR (neat) 1740, 990, 910, 840 cm^{-1}; Anal. ($C_{11}H_{18}O_2$) C, H.

Methyl (*E*)-8-Methyl-4,8-nonadienoate (3e): R_f=0.5; ^{1}H NMR δ=1.72 (s, 3H), 2.07 (br s, 4H), 2.29 (br s, 4H), 3.57 (s, 3H), 4.65 (br s, 2H), 5.27—5.59 (m, 2H); IR (neat) 1740, 970, 890 cm^{-1}; Anal. ($C_{11}H_{18}O_2$) C, H.

Methyl (*E*)-7,7-Dimethyl-4,8-nonadienoate (3f): R_f=0.5; ^{1}H NMR δ=0.92 (s, 6H), 1.82—2.08 (m, 2H), 2.25 (br s, 4H), 3.55 (s, 3H), 4.58—5.98 (m, 5H); IR (neat) 1740, 1000, 970, 910 cm^{-1}; Anal. ($C_{12}H_{20}O_2$) C, H.

Methyl (*E*)-8-Methylene-4,9-decadienoate (3g): R_f=0.5; ^{1}H NMR δ=2.17 (br s, 4H), 2.23 (br s, 4H), 3.55 (s, 3H), 4.80—5.50 (m, 6H), 6.28 (dd, *J*=18 Hz, 11 Hz, 1H); IR (neat) 1740, 990, 970, 890 cm^{-1}; Anal. ($C_{12}H_{18}O_2$) C, H.

Methyl (*Z*)-4,8-Nonadienoate (5a): R_f=0.5; ^{1}H NMR δ=2.05 (br d, *J*=3 Hz, 4H), 2.24 (br s, 4H), 3.55 (s, 3H), 4.60—5.97 (m, 5H); IR (neat) 1740, 990, 910 cm^{-1}; Anal. ($C_{10}H_{16}O_2$) C, H.

Methyl (*Z*)-8-Methyl-4,8-nonadienoate (5b): R_f=0.5; ^{1}H NMR δ=1.72 (s, 3H), 2.07 (br s, 4H), 2.27 (br s, 4H), 3.57 (s, 3H), 4.60 (br s, 2H), 5.20—5.50 (m, 2H); IR (neat) 1740, 890 cm^{-1}; Anal. ($C_{11}H_{18}O_2$) C, H.

Methyl (*Z*)-7,7-Dimethyl-4,8-nonadienoate (5c): R_f=0.5; ^{1}H NMR δ=0.95 (s, 6H), 1.83—2.17 (m, 2H), 2.28 (br s, 4H), 3.57 (s, 3H), 4.57—6.03 (m, 5H); IR (neat) 1740, 990, 910 cm^{-1}; Anal. ($C_{12}H_{20}O_2$) C, H.

Methyl (*Z*)-8-Methylene-4,9-decadienoate (5d): R_f=0.5; ^{1}H NMR δ=2.20 (br s, 4H), 2.27 (br s, 4H), 3.57 (s, 3H), 4.83—5.57 (m, 6H), 6.30 (dd, *J*=18 Hz, 11 Hz, 1H); IR (neat) 1740, 990, 890 cm^{-1}; Anal. ($C_{12}H_{18}O_2$) C, H.

Methyl (*E*)-4-Methyl-8-methylene-4,9-decadienoate (3h).[21] In the same manner as above, **3h** was prepared in a yield of 65% by the reaction of γ-methyl-γ-vinyl-γ-butyrolactone 131 mg (1.04 mmol) with (trimethylsilylmethyl)-1,3-butadiene 438 mg (3.12 mmol) in the presence of trimethyloxonium tetrafluoroborate 154 mg (1.04 mmol) in CH_2Cl_2 10 ml at room temperature for 71 h. R_f=0.5; IR (neat) 1740, 990, 890, 850 cm^{-1}.

(*E*)-4-Methyl-8-methylene-4,9-decadienal (8).[22] Under an argon atmosphere, to a solution of **3h** 140 mg (0.676 mmol) in THF 2 ml, was added dropwise a toluene solution of 1 M (1 M=1 mol dm^{-3}) diisobutylaluminum hydride 0.7 ml (0.7 mmol) at −78 °C. After the mixture was stirred at the same

temperature for 2.7 h, the reaction was quenched by the addition of 10 ml of saturated aqueous NH_4Cl solution. Organic layer was separated and aqueous layer was extracted with twice of 10 ml of ether. The combined organic layer was washed with brine, dried with anhydrous $MgSO_4$, and concentrated. The residual crude product was purified by preparative TLC (hexane:Et_2O=2:1, R_f=0.7) to afford 100 mg (0.561 mmol) of **8**.

β-Sinensal (6).[22] According to the published procedure,[22] **6** was prepared by the Wittig reaction of **8** with (α-formylethylidene)triphenylphosphoran in refluxing benzene.

β-Farnesene (7).[23] Under an argon atmosphere, to a solution of isopropylidenetriphenylphosphorane, prepared from isopropyltriphenylphosphonium bromide 1.40 g (3.64 mmol) and 1.59 M butyllithium 2.40 ml (3.82 mmol) in ether (10 ml) at room temperature for 3 h, a solution of **8** (324 mg, 1.82 mmol) in ether (2 ml) was added at the same temperature. After the mixture was stirred at room temperature for 3 h, precipitated phosphine oxide was removed by filtration. The filtrate was concentrated to give an oil. The crude product was purified by preparative TLC (Hexane, R_f=0.8) to afford 200 mg (0.979 mmol) of **7**.

We thank Mr. Shogo Ando for his invaluable assistance in the experimental work.

References

1) G. Fráter, *Helv. Chim. Acta*, **58**, 442 (1975).
2) W. Himmele, W. Hoffmann, and L. Janitschke, Ger. Offen. DE 3345375 Al, (1985); *Chem. Abstr.*, **104**, 33773y (1986).
3) R. Rossi, A. Carpita, and M. G. Quirici, *Gazz. Chim. Ital.*, **111**, 173 (1981).
4) T. Sato, M. Takeuchi, T. Itoh, M. Kawashima, and T. Fujisawa, *Tetrahedron Lett.*, **22**, 1817 (1981); T. Fujisawa, T. Sato, M. Kawashima, and M. Nakagawa, *Chem. Lett.*, **1981**, 1307; T. Fujisawa, T. Sato, M. Kawashima, K. Naruse, and K. Tamai, *Tetrahedron Lett.*, **23**, 3583 (1982); M. Kawashima and T. Fujisawa, *Chem. Lett.*, **1984**, 1851; T. Fujisawa, T. Sato, and M. Takeuchi, *ibid.*, **1982**, 71; M. Kawashima, T. Sato, and T. Fujisawa, *Bull. Chem. Soc. Jpn.*, **61**, 3255 (1988).
5) H. L. Goering and S. S. Kantner, *J. Org. Chem.*, **48**, 721 (1983).
6) For preliminary reports on aspects of the present study, see: T. Fujisawa, M. Kawashima, and S. Ando, *Tetrahedron Lett.*, **25**, 3213 (1984).
7) T. Mukaiyama, H. Nagaoka, M. Murakami, and M. Ohshima, *Chem. Lett.*, **1985**, 977; M. Kawai, M. Onaka, and Y. Izumi, *ibid.*, **1986**, 381; A. Hosomi, M. Ando, and H. Sakurai, *ibid.*, **1986**, 365, and references cited therein.
8) S. Danishefsky and M. DeNinno, *Tetrahedron Lett.*, **26**, 823 (1985), and references cited therein.
9) R. L. Danheiser and D. M. Fink, *Tetrahedron Lett.*, **26**, 2509 (1985); G. Majetich, J. Defauw, K. Hull, and T. Shawe, *ibid.*, **26**, 4711 (1985), and references cited therein.
10) M. Ohno, S. Matsuoka, and S. Eguchi, *J. Org. Chem.*, **51**, 4553 (1986); H. Hamana and T. Sugasawa, *Chem. Lett.*, **1985**, 921; S. L. Schreiber, T. Sammakia, and W. E. Crowe, *J. Am. Chem. Soc.*, **108**, 3128 (1986); S. A. Carr and W. P. Weber, *J. Org. Chem.*, **50**, 2782 (1985); T. S. Tan, A. N. Mather, G. Procter, and A. H. Davidson, *J. Chem. Soc., Chem. Commun.*, **1984**, 585, and references cited therein.
11) M. K. Kaloustian and F. Khouri, *Tetrahedron Lett.*, **22**, 413 (1981); H. Meerwein, *Angew. Chem.*, **67**, 374 (1955); H. Meerwein, P. Borner, O. Fuchs, H. J. Sasse, H. Schrodt, and J. Spille, *Chem. Ber.*, **89**, 2060 (1956); P. Deslongchamps, R. Chenevert, R. J. Taillefer, C. Moreau, and J. K. Saunders, *Can. J. Chem.*, **53**, 1601 (1975).
12) a) A. Oku, Y. Homoto, and T. Harada, *Chem. Lett.*, **1986**, 1495; b) S. Danishefsky and J. F. Kerwin, Jr., *J. Org. Chem.*, **47**, 3803 (1982).
13) T. Fujisawa, K. Umezu, and M. Kawashima, *Chem. Lett.*, **1984**, 1795.
14) T. Hiyama, A. Kanakura, H. Yamamoto, and H. Nozaki, *Tetrahedron Lett.*, **1978**, 3051.
15) W. S. Bowers, L. R. Nault, R. E. Webb, and S. R. Dutky, *Science* (Washington, D. C.), **1778**, 1121 (1972).
16) S. Danishefsky, R. L. Funk, and J. F. Kerwin, Jr., *J. Am. Chem Soc.*, **101**, 6756 (1979); M. Kawashima and T. Fujisawa, *Bull. Chem. Soc. Jpn.*, **61**, 3377 (1988).
17) B. M. Trost, D. E. Keeley, H. C. Arndt, and M. J. Bogdanowicz, *J. Am. Chem. Soc.*, **99**, 3088 (1977).
18) T. J. Curphey, *Org. Synth.*, **51**, 142 (1971).
19) H. Meerwein, *Org. Synth.*, Coll. Vol. V, 1080 (1973).
20) A. Hosomi and H. Sakurai, *Tetrahedron Lett.*, **1977**, 4041.
21) Y. Masaki, K. Sakuma, and K. Kaji, *Chem. Pharm. Bull.*, **33**, 1930 (1985).
22) E. Bertele and P. Schudel, *Helv. Chim. Acta*, **50**, 2445 (1967).
23) A. Yasuda, S. Tanaka, H. Yamamoto, and H. Nozaki, *Bull. Chem. Soc. Jpn.*, **52**, 1752 (1979).

 © 1988 The Chemical Society of Japan Bull. Chem. Soc. Jpn., 61, 4057—4065 (1988)

Multinuclear NMR and the Rotational Barriers about the C-N Bonds of Several, *N,N*-Disubstituted Arenecarboxamides

Hiroko SUEZAWA,* Kin-ya TSUCHIYA, Eiji TAHARA, and Minoru HIROTA
Department of Synthetic Chemistry, Division of Material Science and Engineering,
Faculty of Engineering, Yokohama National University,
Hodogaya-ku, Yokohama 240
(Received July 6, 1988)

The ^{15}N, ^{17}O, and ^{13}C NMR spectra of substituted *N,N*-dimethyl- and *N,N*-dibenzylbenzamides and *N,N*-dimethylnaphthamides were measured and correlated with the height of their rotational barriers. The ^{15}N and ^{17}O chemical shifts of the amides were shown to be controlled predominantly by the extent of the contribution of the polar mesomeric structure (**II**) and, especially in the case of ^{15}N, could be used to estimate the rotational barrier.

In recent decades, dynamic nuclear magnetic resonance spectroscopy has supplied much useful information on the exchange and the dynamic behaviors of molecules. Amides and related nitrogen compounds were investigated most extensively by this method partly because their NMR spectra show the coalescence phenomena at temperatures near ambient.[1-7]

Rotational barrier about the C–N bond of the amide is directly related to the partial double bond character of the bond and often used to examine the electronic properties of amides, such as the effect of conjugation, the effect of the electronegativity of the substituent on the acyl carbon, etc. For instance, the rotational barriers about the C–N bond of unsaturated and aromatic amides have been shown to be affected very sensitively by the conjugative properties of their hydrocarbon moieties with the carbonyl group. The fact is reflected in the rotational barriers of *N,N*-dimethylacrylamide (69.8 kJ mol^{-1})[1] and *N,N*-dimethylbenzamide (64.9 kJ mol^{-1})[2] which are considerably lower than that of *N,N*-dimethylformamide (87.4 kJ mol^{-1}).[3] The partial double bond character of the C–N bond is usually assumed to be originated from the polar mesomeric structure (**II**) bearing a positive charge on the nitrogen and a negative charge on the carbonyl oxygen; the higher C–N bond order should be expected when the contribution of the canonical structure **II** becomes more predominant. Hence, the pi-electron densities on the nitrogen and the oxygen atoms should be correlated with the height of the rotational barrier.

Very extensive studies on the ^{1}H and ^{13}C chemical shifts of aromatic compounds revealed the fact that the chemical shift could be correlated linearly with the electron density of the carbon atom derived from MO calculations for the series of aromatic compounds having closely related structures.[8-10] It has thus become a well-known fact that the electron density should be correlated linearly with the chemical shift of the respective nucleus in a manner to induce a shift towards a higher field by the increase in the electron density. As to ^{15}N chemical shifts, this fact was substantiated by Mason.[11] Carbonyl ^{17}O chemical shifts of many acyl derivatives were also measured and correlated with the electron densities by Delseth and coworkers.[12]

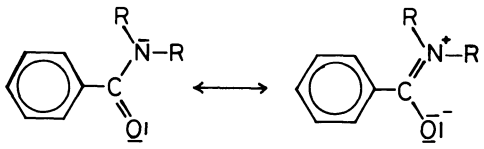

(I) (II)

For this reason, the increase in the rotational barrier should cause the down-field shift of ^{15}N signal and the up-field shift of ^{17}O signal. From this point of view, the ^{13}C, ^{15}N, and ^{17}O chemical shifts were measured with several arenecarboxamides and correlated with their rotational barriers, or their activation free energies of internal rotation, about the C–N bonds.

Results and Discussion

Carbonyl and *N*-methyl carbons, amide nitrogen, and carbonyl oxygen are expected to be affected most significantly by the change in the partial double bond character of the amide moiety. Hence, the NMR spectra were reported only with the nuclei concerned (viz., ^{13}C of carbonyl and *N*-methyl, ^{15}N of amide, and ^{17}O of carbonyl) in several solvents; the chemical shifts are given in Table 1. The table also includes the rotational barriers of the amides reported previously by the present authors.[13,14] In order to examine the correlation with the rotational barrier, the chemical shifts were plotted as ordinate and the rotational barriers as abscissa; the results are given in Figs. 1 and 2 for the ^{15}N chemical shift and in Fig. 3 for the ^{17}O chemical shift. Throughout this paper chemical shifts were expressed by the conventional δ-scale, which assigns a positive value to the region more deshielded than the standard. Here the chemical shifts (δ/ppm) were correlated linearly with the height of the rotational barrier ($\Delta G^{\ddagger}$/kJ mol^{-1}) by the following equation:

Table 1. ^{15}N, ^{17}O, and ^{13}C NMR Chemical Shifts of *N,N*-Dialkyl Aromatic Amides

No.	X	Solvent	$\delta_{^{15}N}$	$\delta_{^{17}O}$	$\delta_{^{13}C(CO)}$	$\delta_{^{13}C(Me)}$	$\Delta G^{\ddagger}$[13,14]
			ppm				kJ mol^{-1}
(a) *N,N*-Dimethylbenzamides $XC_6H_4CONMe_2$							
1	H	$CDCl_3$	101.4	341	171.0	39.0, 34.7	65.5
		C_5D_5N	101.6	342	171.4	39.6, 34.5	63.2
		CD_3SOCD_3	105.2	332	170.0	38.6, 34.5	—
		CD_3OD	108.3	326	173.2	39.9, 35.6	67.8
2	4-Cl	$CDCl_3$	101.3	—	170.0	39.1, 35.0	64.6
		C_5D_5N	99.0	—	169.9	39.1, 35.1	63.3
		CD_3SOCD_3	105.9	—	169.0	38.9, 34.3	65.1
		CD_3OD	108.8	—	171.1	39.8, 35.7	67.2
3	4-CH_3O	$CDCl_3$	100.0	368	170.4	38.5, 35.2	61.4
		C_5D_5N	99.5	370	171.2	37.7*	58.8
		CD_3SOCD_3	103.9	342	170.0	35.9*	—
		CD_3OD	107.4	—	172.5	38.2*	63.3
4	4-CH_3	$CDCl_3$	99.6	345	171.2	39.0, 35.1	64.0
		C_5D_5N	98.7	338	171.0	37.7*	62.0
		CD_3SOCD_3	104.8	320	170.3	38.6, 34.8	—
		CD_3OD	107.7	320	173.3	39.9, 35.7	66.5
5	2-Cl	$CDCl_3$	105.1	328	167.6	37.3, 33.9	—
		C_5D_5N	104.7	331	168.0	37.8, 34.5	78.5
		CD_3SOCD_3	108.8	—	166.9	37.3, 33.9	80.4
		CD_3OD	111.6	310	170.0	38.5, 34.9	—
6	2-CH_3O	$CDCl_3$	104.5	330	168.2	37.1, 33.5	—
		C_5D_5N	103.7	344	168.9	37.5, 34.2	75.7
		CD_3SOCD_3	108.0	315	170.9	37.3, 33.9	77.5
		CD_3OD	111.3	312	167.9	38.4, 34.8	—
7	2-CH_3	$CDCl_3$	104.3	335	170.6	37.6, 33.8	74.1
		C_5D_5N	102.9	339	171.0	38.0, 34.3	72.6
		CD_3SOCD_3	107.9	315	169.8	37.6, 33.7	74.6
		CD_3OD	111.5	311	172.6	38.7, 34.8	—
8	2-OH	$CDCl_3$	103.1	—	172.1	38.5*	51.1
		C_5D_5N	103.4	328	169.8	38.9, 34.8	57.1
		CD_3SOCD_3	108.6	342	168.8	35.3*	—
		CD_3OD	—	—	—	—	59.6
9	2-OH	$CDCl_3$	103.7	—	170.6	38.5*	51.3
	5-Cl	C_5D_5N	103.4	—	168.2	36.0*	59.2
		CD_3SOCD_3	108.2	—	167.1	35.4*	63.1
		CD_3OD	—	—	170.8	36.8*	61.1
10	2-OH	$CDCl_3$	—	—	—	—	51.6
	5-NO_2	C_5D_5N	104.3	—	167.5	36.4*	61.0
		CD_3SOCD_3	109.2	—	167.1	36.0*	64.1
		CD_3OD	—	—	—	—	61.6
11	2-OH	$CDCl_3$	106.7	284	170.5	37.0*	51.3
	5-CH_3O	C_5D_5N	103.4	358	169.6	36.1*	56.8
		CD_3SOCD_3	108.3	340	168.4	35.9*	—
		CD_3OD	112.6	348	172.0	36.9*	59.7
12	2-OH	$CDCl_3$	104.2	283	171.5	37.8*	50.9
	5-CH_3	C_5D_5N	103.0	369	170.1	36.2*	57.0
		CD_3SOCD_3	108.7	330	169.1	36.1*	—
		CD_3OD	111.4	345	172.5	37.4*	59.9
13	2-OH	$CDCl_3$	103.0	288	171.9	37.8*	50.9
	3,5-$(CH_3)_2$	C_5D_5N	103.6	—	171.9	37.4*	53.6
		CD_3SOCD_3	108.3	—	169.6	36.4*	—
		CD_3OD	112.2	—	172.7	37.5*	55.4

Table 1. (Continued)

No.	X	Solvent	$\delta^{15}N$	$\delta^{17}O$	$\delta^{13}C(CO)$	$\delta^{13}C(Me)$	$\Delta G^{\neq 13,14)}$
			ppm				kJ mol^{-1}
(b) *N,N*-Dibenzylbenzamides $XC_6H_4CON(CH_2Ph)_2$ (b benzyl CH_2)							
14	H	$CDCl_3$	125.7	360	171.8	51.2, 46.7[b)]	64.3
		C_5D_5N	124.6	—	172.0	51.8, 47.5[b)]	62.6
		CD_3SOCD_3	128.8	—	171.1	51.6, 46.7[b)]	63.5
		CD_3OD	—	—	—	—	65.0
15	4-Cl	$CDCl_3$	125.9	—	170.9	51.4, 47.1[b)]	63.1
		C_5D_5N	124.3	—	171.0	51.6, 47.8[b)]	62.8
		CD_3SOCD_3	129.0	—	170.2	—	63.6
		CD_3OD	—	—	—	—	63.3
16	4-CH_3O	$CDCl_3$	123.9	384	171.7	49.8*[b)]	60.3
		C_5D_5N	124.2	396	171.9	49.2*[b)]	59.0
		CD_3SOCD_3	127.5[a)]	354	170.9	49.3*[b)]	—
		CD_3OD	131.6[a)]	—	174.5	—	59.9
17	4-CH_3	$CDCl_3$	124.9	—	171.8	51.2, 46.9[b)]	63.3
		C_5D_5N	123.6	—	172.1	49.7*[b)]	62.0
		CD_3SOCD_3	127.9	—	171.3	51.0, 47.8[b)]	—
		CD_3OD	131.9[a)]	—	174.5	49.0*[b)]	63.8
18	2-OH	$CDCl_3$	126.6	305	172.3	50.1*[b)]	54.5
		C_5D_5N	123.8	—	172.0	51.8, 47.4[b)]	61.8
		CD_3SOCD_3	130.6	—	169.5	50.9, 46.1[b)]	65.9
		CD_3OD	—	—	—	—	62.1
19	2-Cl	$CDCl_3$	130.0	—	168.9	50.7, 46.5[b)]	68.3
		C_5D_5N	128.4	—	168.7	51.1, 46.8[b)]	67.0
		CD_3SOCD_3	132.5	—	167.9	50.7, 46.5[b)]	—
		CD_3OD	136.1[a)]	—	171.0	52.4, 48.2[b)]	—
20	2-OCH_3	$CDCl_3$	129.3	350	169.6	50.8, 46.0[b)]	67.0
		C_5D_5N	128.0	363	170.3	51.7, 47.0[b)]	67.7
		CD_3SOCD_3	131.3	327	168.9	50.8, 46.1[b)]	68.4
		CD_3OD	131.5	—	172.3	52.5, 47.8[b)]	68.2
(c) *N,N*-Dimethylnaphthamides $XC_{10}H_6CONMe_2$							
21	1-$CONMe_2$	$CDCl_3$	105.8	331	170.2	38.1, 34.4	—
		C_5D_5N	103.8	335	170.9	38.7, 35.0	74.6
		CD_3SOCD_3	109.8	304	169.3	38.0, 34.1	76.4
		CD_3OD	113.4	—	173.0	39.2, 35.1	—
		C_6D_6	102.7	—	169.9	37.9, 34.2	71.4
22	2-$CONMe_2$	$CDCl_3$	101.9	352	170.9	38.9, 34.7	65.9
		C_5D_5N	99.7	360	171.7	39.7, 35.5	64.2
		CD_3SOCD_3	105.6	315	170.1	38.8, 34.8	—
		CD_3OD	108.7	—	173.3	39.9, 35.6	68.6
		C_6D_6	97.9	—	170.7	36.4*	<64
23	1-$CONMe_2$	$CDCl_3$	107.5	290	170.8	37.3*	55.9
	2-OH	C_5D_5N	106.3	364	169.3	37.5, 34.5	65.4
		CD_3SOCD_3	111.6	—	167.7	37.1, 33.9	69.0
		CD_3OD	115.4	—	171.3	36.8*	66.9
24	2-$CONMe_2$	$CDCl_3$	101.9	296	172.7	38.1*	49.0
	1-OH	C_5D_5N	104.4	—	172.1	37.7*	—
		CD_3SOCD_3	109.2	—	169.9	36.7*	—
		CD_3OD	112.9[a)]	—	173.1	37.7*	52.0
25	2-$CONMe_2$	$CDCl_3$	103.6	292	171.1	38.0*	55.6
	3-OH	C_5D_5N	104.0	337	169.8	36.0*	63.6
		CD_3SOCD_3	109.2	345	168.6	36.7, 34.3	67.4
		CD_3OD	110.8[a)]	352	172.0	38.7, 35.3	66.3
26	1-$CONMe_2$	$CDCl_3$	107.7	309	168.7	37.7, 34.5,	—
	2-OCH_3	C_5D_5N	105.6	302	168.2	37.3, 34.3	90.5

Table 1. (Continued)

No.	X	Solvent	$\delta^{15}N$	$\delta^{17}O$	$\delta^{13}C(CO)$	$\delta^{13}C(Me)$	$\Delta G^{*13,14}$
			ppm				kJ mol^{-1}
26		CD_3SOCD_3	111.1	281	167.2	37.0, 33.8	91.9
		CD_3OD	115.4	—	170.6	38.1, 34.8	—
		C_6D_6	104.0	—	167.9	37.0, 34.1	—
27	2-$CONMe_2$	$CDCl_3$	105.7	340	169.0	37.8, 34.5	—
	1-OCH_3	C_5D_5N	103.8	336	169.2	38.0, 34.4	78.2
		CD_3SOCD_3	109.4	309	168.2	37.7, 34.1	79.8
		CD_3OD	113.4	—	171.9	39.0, 35.2	—
28	2-$CONMe_2$	$CDCl_3$	104.9	336	167.8	37.0, 33.5	—
	3-OCH_3	C_5D_5N	102.7	335	168.5	37.7, 34.4	78.9
		CD_3SOCD_3	108.6	329	167.6	37.5, 34.0	81.7
		CD_3OD	112.7	—	172.2	38.7, 35.0	—
		C_6D_6	101.4	—	168.2	37.5, 34.3	75.0

a) Measured at 55 °C. b) CH_2 signals of benzyl group. * denotes a coalesced peak.

Table 2. Chemical Shift vs. Rotational Barrier Correlations[a)]

(a) ^{15}N chemical shift vs. rotational barrier correlation with the amides lacking *o*-hydroxyl group.

Amide[c)]	Solvent[c)]	*n*	*k*	*m*	*r*
a,c	C	6	0.362	77.58	0.94
a,c	P	12	0.230	85.60	0.91
a,c	D	8	0.182	94.41	0.89
a,c	M	5	0.250	91.48	0.83
a,c	C,P	18	0.229	85.92	0.90
a	C,P	12	0.300	81.28	0.92
c	C,P	6	0.188	88.76	0.90
b	C,P	12	0.697	81.49	0.92

(b) ^{17}O chemical shift vs. rotational barrier correlation with the amides lacking *o*-hydroxyl group.

Amide[b)]	Solvent	*n*	*k*	*m*	*r*
a,c	C	5	−2.07	485.40	0.78
a,c	P	11	−1.47	447.60	0.80
a,c	C,P	16	−1.48	447.73	0.80
a,c	D,M	7	−1.62	433.57	0.93
a,b,c	C	8	−3.05	553.40	0.81
a,b,c	P	13	−1.92	483.01	0.82
a,b,c	C,P	21	−1.95	483.97	0.81

(c) ^{15}N chemical shift vs. rotational barrier correlation with the *o*-hydroxyl amides.

Amide[b)]	Solvent	*n*	*k*	*m*	*r*
a*,c*	C	8	0.447	80.95	0.57
a*,c*	P	8	0.204	91.83	0.77
a*,c*	D	4	0.446	80.13	0.86
a*,c*	M	6	0.116	105.90	0.51

a) *n*; number of plotted data, *k*; slope of the regression line, *m*; intercept of the regression line, *r*; correlation coefficient. b) The amides are classified as follows: a; **1—7**, b; **14—17**, **19**, and **20**, c; **21**, **22**, and **26—28**, a*; **8—13**, c*; **23—25**. a* and c* are *o*-hydroxylated amides. c) C; $CDCl_3$, P; C_5D_5N, D; CD_3SOCD_3, M; CD_3OD.

$$\delta = k\Delta G^* + m$$

The best fit slope (k) and the intercept (m) values for the plot were calculated by the least squares calculations and given in Table 2. In order to show the limit of reliability of the plot explicitly, the correlation coefficient (r) was given in the same table.

The plotted data of *o*-hydroxy derivatives constitute a group clearly distinguishable from those of other amides lacking *o*-hydroxyl group in the chemical shift vs. rotational barrier diagram of both ^{15}N and ^{17}O series. Besides the presence of the *o*-hydroxyl group, the important factors affecting the chemical shifts are (i) the polar and the conjugative properties of the substituents and (ii) the nature of the solvent. However, the influence induced by these factors were sometimes obscured because the rotational barriers are also perturbed by the similar factors in a manner proportional to the effect on the chemical shift.

In order to make the discussion more straightfor-

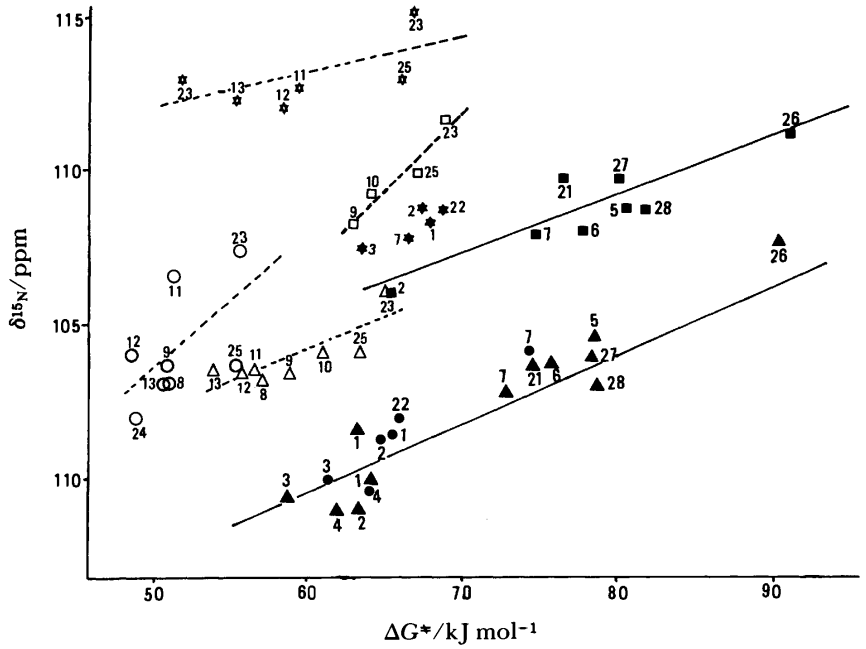

Fig. 1. The ^{15}N chemical shift (δ_{15N}) vs. the height of the rotational barrier[14] ($\Delta G^{\ddagger}$) plots of *N,N*-dimethylbenzamides (a) and *N,N*-dimethylnaphthamides (c) in various solvents [chloroform-*d* (●), pyridine-d_5 (▲), dimethyl-d_6 sulfoxide (■), and methanol-d_4 (★)]. The amides bearing *o*-hydroxyl group are shown by open marks; those without *o*-hydroxyl group shown by filled marks.

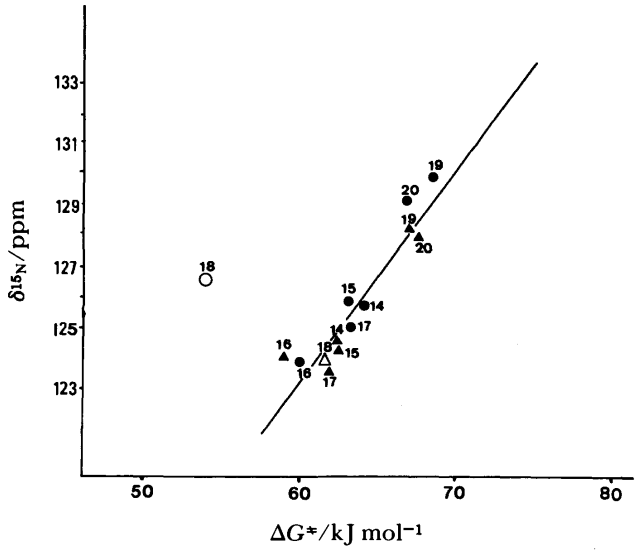

Fig. 2. The ^{15}N chemical shift (δ_{15N}) vs. the height of the rotational barrier[14] ($\Delta G^{\ddagger}$) plots of *N,N*-dibenzylbenzamides (b) in various solvents. The points have the same meaning as in Fig. 1.

ward, the amides employed in this work were classified on the basis of their structural feature into three groups; namely, (a) *N,N*-dimethylbenzamides **1—13**, (b) *N,N*-dibenzylbenzamides **14—20**, and (c) *N,N*-dimethylnaphthamides **21—28**. As the chemical shift was perturbed considerably by the solvent, the chemical shift data in each solvent were correlated individually with the rotational barriers in the same solvent; the difference in the solvent was also discussed. In several cases, the plots in several different solvents were combined in the statistical treatment. Except for the *o*-hydroxy derivatives, good to excellent correlations were obtained. Since these factors affect each nucleus of the atoms comprising the $CONR_2$ moiety in a different way, their chemical shift vs. rotational barrier correlations will be discussed individually.

The Correlation of ^{15}N Chemical Shifts with the Rotational Barriers. As expected, the ^{15}N chemical shift vs. rotational barrier plots in various solvents were shown to have positive slopes, which means that the chemical shift moves towards down-field as the height of the rotational barrier increases. The trend is in line with the rotational barrier vs. ^{15}N chemical shift plots for a series of *m*- and *p*-substituted benzamides reported by Randall and coworkers.[15] Since the ^{15}N chemical shifts were perturbed most predominantly by the nature of the substituent on the nitrogen atom, the *N,N*-dibenzyl derivatives (b) resonate at far lower fields than the *N,N*-dimethyl derivatives (a) and (c), constituting a group of plotted points in the upper half of Fig. 1. The down-field shift might be caused by either or both of the electronic and the magnetic anisotropy effects.

The effects on the ^{15}N chemical shift of the

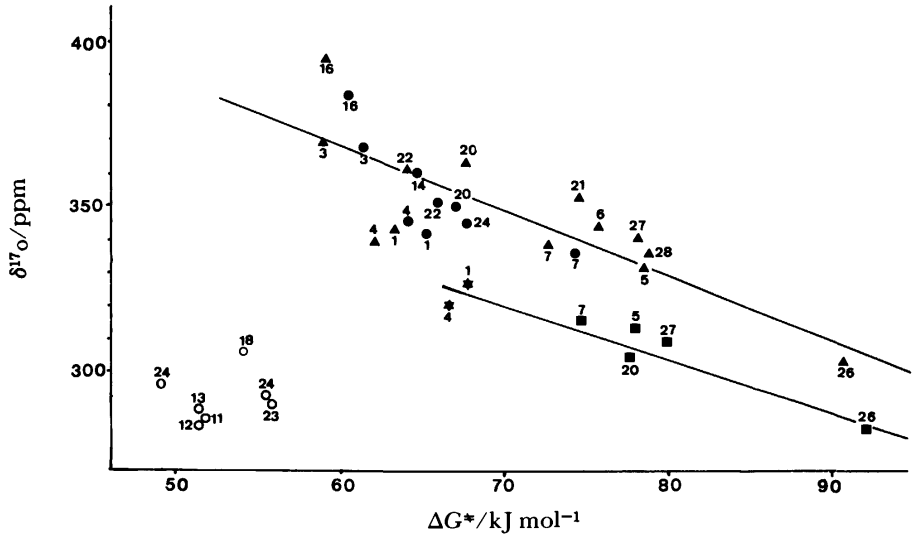

Fig. 3. The ^{17}O chemical shift (δ_{17O}) vs. the height of the rotational barrier[14] (ΔG^*) plots of the three series of the *N,N*-dialkylarenecarboxamides (a, b, and c) in various solvents. The points have the same meaning as in Fig. 1.

structural changes and of the substituent(s) in the aromatic part of the molecule do not seem to cause apparently observable deviation from the combined regression lines for the series of *N,N*-dimethylbenzamide (a) and -naphthamide (c) except for *o*-hydroxy derivatives (Fig. 1). This implies that the direct through-space effects, such as anisotropy and steric effects, due to the structural change far apart from the ^{15}N nucleus do not induce a serious deviation of the ^{15}N chemical shifts of these amides.

If we assume (i) that the chemical shift should be controlled exclusively by the electron density on the nitrogen atom throughout these two series of *N,N*-dimethyl derivatives [(a) and (c)], and (ii) that the solvent effect is merely electrostatic,[16] both the increase in the rotational barrier and the down-field shift should be originated by the increase in the contribution of the polar mesomeric structure (**II**), which causes the descreening of the nitrogen nucleus. Therefore, the chemical shift vs. rotational barrier plot should merge into a single regression line irrespective of the solvent used. This situation may be realized approximately when the solvent is less polar as in the cases of chloroform and pyridine solutions. Thus, the plots in these two solvents constitute a group, giving a regression line with r=0.90. However, the correlation is better with the regression lines drawn by use of the data in the two solvent independently (r=0.94 for the $CDCl_3$ solutions and r=0.914 for the C_5D_5N solutions). The solvent effect becomes more evident in dimethyl sulfoxide and methanol.

In cases of the *o*-hydroxy derivatives (**8—13**, **18**, and **23—25**), the plots deviate strikingly from those for the amides lacking *o*-hydroxyl group. However, the chemical shift vs. rotational barrier plots still hold positive slopes analogous to the other series of amides investigated; the plots showed clearly that the ^{15}N chemical shift is controlled by the contribution of polar mesomeric structure (**II**) even in this series of amides. The regression lines separately drawn for the plot of the *o*-hydroxy amides occupy considerably upward positions in Fig. 1 in comparison with the corresponding lines for the amides lacking *o*-hydroxyl group; which means that the nitrogen is more deshielded than estimated by the screening of the nucleus probably due to the strong neighbor anisotropy effect of the hydrogen-bonded chelate ring.

The Correlation of ^{17}O Chemical Shifts with the Rotational Barriers. The ^{17}O chemical shift vs. rotational barrier plots are given in Fig. 3. As rationalized by the increased contribution of the polar mesomeric structure **II** which increases the negative charge on the oxygen, the regression lines for the plots have negative slopes (negative k values). In sharp contrast to the large separation between the plots of ^{15}N chemical shifts, the plotted points of ^{17}O chemical shifts for the *N,N*-dimethyl amides [(a) and (c)] and those for the *N,N*-dibenzyl amides (b) constitute a rather scattered but single group in Fig. 3. The fact suggest that the effect of *N*-substituent is attenuated significantly on the carbonyl oxygen.

The direct through-space effect caused by the *o*-substituent (and peri-substituent) becomes more important in the ^{17}O chemical shift, which may cause irregular fluctuation of the chemical shift and decreased the reliability of the correlation (lowering of r value).

The chelate ring formation by intramolecular

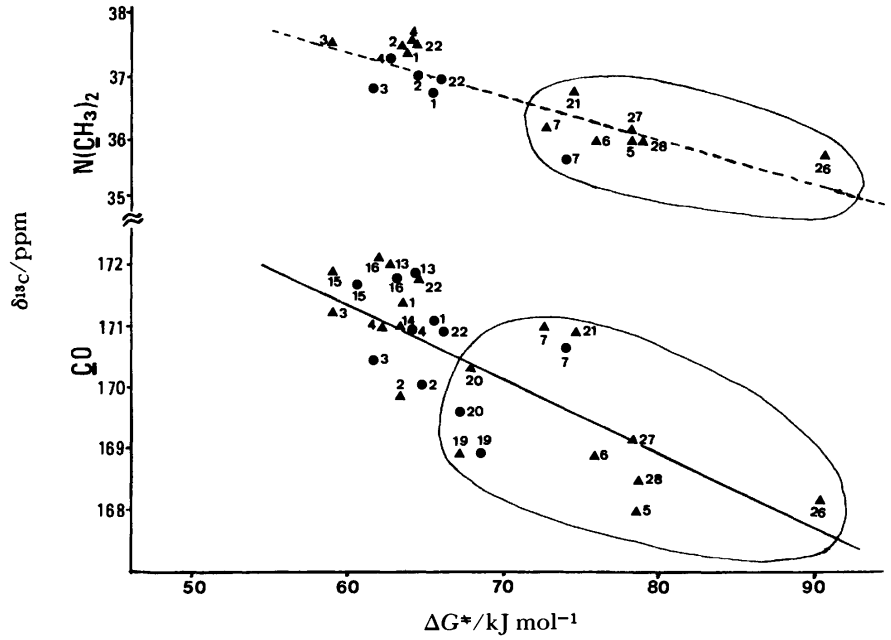

Fig. 4. The ^{13}C chemical shift (δ_{13C}) vs. the height of the rotational barrier[14] (ΔG^*) plots of the three series of the *N,N*-dialkylarenecarboxamides (a, b, and c) in chloroform-*d* and pyridine-d_5. The points have the same meaning as in Fig. 1.

hydrogen bonding with the *o*-hydroxyl group causes a considerable up-field shift of carbonyl ^{17}O chemical shift. This tendency is in accord with the reported chemical shifts of salicylaldehyde and methyl salicylate.[17]

The Correlation of ^{13}C Chemical Shifts with the Rotational Barrier. The ^{13}C chemical shifts of the *N*-methyl and the carbonyl carbons were also measured and given together in Table 1 and correlated with the rotational barriers in Fig. 4. It is remarkable that the ^{13}C chemical shift of the *N*-methyl carbon would move apparently towards high field as the rotational barrier increases, since this trend is just opposite to the direction of the shift observed with ^{15}N which moves down-field during the similar change. The methyl ^{13}C chemical shift can be expected to move in the same direction as the ^{15}N if the inductive effect which decreases the carbon electron density alone is assumed to operate. Thus we need an explanation for this apparently contradictory behavior of the carbon chemical shift.

The *N*-methyl ^{13}C chemical shift is generally rather insensitive to the structural modification of the aromatic part and also to the nature of the solvent; populating in a narrow range of the chemical shift. The range became far narrower when the amides were classified in reference to the presence of the ortho substituent. Thus, the *o*-unsubstituted amides resonate within the range 36.8—37.6 ppm and most of the *o*-substituted amides (but void of *o*-hydroxyl group) in the range 35.7—36.2 ppm.

If we adopt the geometries estimated by Baumstark and co-workers,[18] one of the *N*-methyl groups of *N,N*-dimethyl-1-naphthamide (**21**) should be subjected to the strong diamagnetic anisotropy effect from the aromatic ring. If we assume that the *o*-substituted amide takes a conformation similar to **21** due to the steric hindrance caused by the ortho-substituent, this conclusion is effective to all ortho-substituted amides. In contrast, the methyl group does not seem to be exposed to diamagnetic magnetic field induced by the aromatic ring in the cases of the *o*-unsubstituted amides. When we examined the ^{13}C chemical shift vs. rotational barrier plot closely, superficial negative slope is suspected to arise from the fact that the plotted points for the *o*-substituted amides (encircled points in Fig. 4) lie in the right bottom part of the diagram. This comes, of course, from the anisotropy effect just described. The explanation could be extended to the *o*-hydroxy amides whose methyl carbons resonate at lower fields and which are assumed to become more planar due to chelate ring formation.

The ^{13}C chemical shifts of *p*-substituted *N,N*-dimethylbenzamides were correlated with σ_p and also with Dewar's F constants by Jones and Wilkins.[19] Analogously, the carbonyl ^{13}C chemical shifts of **5—13** could be interpreted by the somewhat exaggerated electronic effect caused by the ortho-substituent, or by the combined substituent effect in the cases of polysubstituted derivatives, operating in a through-bond manner.

Solvent Effect on the ^{15}N and ^{17}O Chemical

Table 3. Solvent Effect on the ^{15}N and ^{17}O Chemical Shifts[a]

Compd No.	$\Delta\delta^{15}_{N}$ ($\Delta\delta^{17}_{O}$)/ppm			
	C_5D_5N	$(CD_3)_2SO$	CD_3OD	C_6D_6
(a) *N,N*-Dimethylbenzamides				
1	0.2 (1)	3.8 (−9)	6.9 (−15)	
2	−1.3 (2)	4.6 (−26)	7.5	
3	−0.5	3.9	7.4	
4	−0.9 (7)	5.2 (−25)	8.1 (−25)	
5	−0.4 (3)	3.7	6.5 (−18)	
6	−0.8 (14)	3.5 (−15)	6.8 (−18)	
7	−1.4 (4)	3.6 (−20)	7.2 (−24)	
8	0.3	7.5	—	
9	−0.4	4.5	—	
10	—	—	—	
11	−3.4 (74)	1.6 (56)	5.9 (64)	
12	−1.2 (86)	4.5 (47)	7.2 (62)	
13	0.6	2.3	9.2	
(b) *N,N*-Dibenzylbenzamides				
14	−1.1	3.1	—	
15	−1.6	3.1	—	
16	−0.3 (12)	3.6 (−30)	7.5	
17	−1.3	3.0	7.0	
18	−2.8	4.0	—	
19	−1.6	2.5	6.1	
20	−1.3 (13)	2.0 (−23)	2.2	
(c) *N,N*-Dimethylnaphthamides				
21	−2.0 (18)	4.0 (−27)	7.6	−3.1
22	−2.2 (8)	3.7 (−37)	6.8	−4.0
23	−1.2 (74)	4.1	7.9	—
24	2.3	7.3	11.0	—
25	0.4 (45)	5.6 (53)	7.2 (60)	—
26	−2.1 (−7)	3.4 (−28)	7.7	−3.7
27	−1.9 (−4)	3.7 (−31)	7.7	—
28	−2.1 (−1)	3.7 (−7)	7.8	−3.5

a) $\Delta\delta=\delta_{solv}-\delta_{CDCl_3}$.

Shifts. The solvent induced shifts with reference to the chemical shifts in chloroform-*d* solutions are given in Table 3. At a glance of the whole data, they seemed to be in line with a very simple and straightforward interpretation that the polarity of the solvent favors the contribution of the dipolar mesomeric structure **II**.

However, the whole of the solvent induced shift could not be attributed merely to the dielectric nature of the solvents, since the rotational barrier vs. chemical shift plots were solvent dependent giving a different regression line for each solvent. Moreover, the down-field shift of the ^{15}N chemical shift and the up-field shift of the ^{17}O chemical shift becomes more predominant in the following order of the solvent: benzene<pyridine<chloroform<DMSO<methanol. Pyridine is exceptional when the solvent effect is compared in reference to the dielectric nature of the solvent, inducing an up-field shift of ^{15}N signal and a down-field shift of ^{17}O signal. Similar irregularity was observed with the rotational barrier of the same amides reported in our previous paper.[14] This trend of the solvent effect is in accord with the order of the hydrogen-donating ability[20] (in forming hydrogen bonds) of the C–H or OH group in the solvent molecule. Association by forming hydrogen bonds is a specific solvent–solute interaction which requires the access of the solvent molecule with an appropriate orientation from a specified direction. In this situation, the solvent molecule, usually anisotropic, should induce an anisotropic field around the amide molecule. Thus the observed solvent dependency of the regression lines is explicable by the hydrogen-bond-like interaction between the solvent and the solute molecules.

In conclusion, both the rotational barrier and the ^{15}N and ^{17}O chemical shifts can be assumed to be controlled by the same origin, the extent of the mesomeric contribution of the canonical structure **II**, or the C–N bond order and the electron densities on the nitrogen and oxygen atoms, when their measurements were carried out in the same solvent. The correlation is excellent with the rotational barrier vs. ^{15}N chemical shift plot for the dimethylamides lacking *o*-hydroxyl group. Consequently, ^{15}N chemical shifts of the amides should be a probe of the heights of their rotational barriers.

Experimental

N,N-Dimethyl- and *N,N*-dibenzylarenecarboxamides were prepared as usual by the reaction of the corresponding aroyl chlorides with dimethyl- and dibenzylamines, respectively.

^{15}N, ^{17}O, and ^{13}C NMR spectra were recorded on a JEOL FX-90Q spectrometer using 10-mm probe. In order to obtain strong signals from ^{15}N and ^{17}O nuclei of natural abundance, the samples for the measurements were prepared by dissolving as concentrated as possible, ca. 500 mg of the amide in ca. 1.5 ml of the solvent. Chloroform-*d*, methanol-d_4, pyridine-d_5, dimethyl-d_6 sulfoxide (DMSO-d_6), and benzene-d_6 were used as solvents throughout this work. The multi-nuclear measurements were carried out under the following conditions:

Nucleus	^{15}N	^{17}O	^{13}C
Resonance frequency (MHz)	9.04	12.10	22.50
Pulse length (μs)	18(45°)	20(90°)	12(45°)
Delay	3 s	100 ms	2 s
Number of data points	8K	1K	8K
Spectral width (Hz)	3000	10000	5000
Accuracy (Hz)	0.7 (0.08 ppm)	10 (0.8 ppm)	1.2 (0.05 ppm)
Number of scans	ca. 10000	ca. 100000	ca. 500
Reference	liq. NH_3 external	H_2O external	TMS internal

The authors wish to express their hearty thanks to Professor Masatsune Kainosho, Tokyo Metropolitan University, for his valuable advice throughout this work. The ^{15}N experiments were set forth by his suggestion to which we are especially grateful. This research is partly supported by a Grant-in-Aid for Scientific Research from the Ministry of Education, Science and Culture.

References

1) R. F. Hobson and L. W. Reeves, *J. Magn. Reson.*, **10**, 243 (1974).

2) L. M. Jackman, T. E. Kavanagh, and R. C. Haddon, *Org. Magn. Reson.*, **1**, 109 (1969).

3) M. Ravinovitz and A. Pines, *J. Am. Chem. Soc.*, **91**, 1585 (1969).

4) M. T. Rogers and J. C. Woodbrey, *J. Phys. Chem.*, **66**, 540 (1962); R. H. Garner and T. H. Siddall, III, *Tetrahedron Lett.*, **1966**, 3513; R. C. Neuman, Jr. and V. Jonas, *J. Am. Chem. Soc.*, **90**, 1970 (1968); G. P. Schiemenz and G. Stein, *Tetrahedron*, **26**, 2007 (1970); L. W. Reeves, R. C. Shaddick, and K. N. Shaw, *Can. J. Chem.*, **49**, 3684 (1971); T. Drakenberg, *Tetrahedron Lett.*, **1972**, 1743; C. H. Yoder and R. D. Gardner, *J. Org. Chem.*, **46**, 64 (1981).

5) P. K. Korver, K. Spaargaren, P. J. van der Haak, and Th. J. de Boer, *Org. Magn. Reson.*, **2**, 295 (1970); **3**, 605 and 615 (1971).

6) K. Spaargaren, C. Kruk, T. A. Molenaar-Langeveld, P. K. Korver, P. J. van der Haak, and Th. J. de Boer, *Spectrochim. Acta, Part A*, **28**, 965 (1972).

7) L. M. Jackman, "Dynamic Nuclear Magnetic Resonance Spectroscopy," ed. by L. M. Jackman and F. A. Cotton, Academic Press, N. Y. (1975), p. 208.

8) P. C. lauterbur, *Tetrahedron Lett.*, **1961**, 274; J. E. Bloor and D. L. Green, *J. Phys. Chem.*, **72**, 716 (1968); P. Lazzeretti and F. Taddei, *Org. Magn. Reson.*, **3**, 283 (1971).

9) G. L. Nelson, G. C. Levy, and J. D. Cargioli, *J. Am. Chem. Soc.*, **94**, 3090 (1972).

10) M. Hirota, K. Abe, H. Endo, and H. Masuda, *Rep. Asahi Glass Found. Ind. Technol.*, **35**, 109 (1979).

11) J. Mason, *J. Chem. Soc., Faraday Trans. 2*, **73**, 1464 (1977).

12) C. Delseth, T. T. T. Nguyen, and J. P. Kintzger, *Helv. Chim. Acta*, **63**, 498 (1980).

13) M. Hirota and K. Todokoro, *Chem. Lett.*, **1974**, 777.

14) H. Suezawa, K. Tsuchiya, E. Tahara, and M. Hirota, *Bull. Chem. Soc. Jpn.*, **60**, 3973 (1987).

15) P. S. Pregosin, E. W. Randall, and A. I. White, *J. Chem. Soc., Perkin Trans. 2*, **1972**, 513.

16) General electrostatic interaction between the solvent and solute molecules, usually called general polarity effect, can be evaluated by the dielectric constant or by the Kirkwood-Bauer-Magat parameter of the solvent. Dielectric constants of the solvents employed are 4.80 for $CHCl_3$, 12.3 for C_5H_5N(pyridine), 32.6 for CH_3OH, and 40.0 for CH_3SOCH_3. Corresponding K-B-M parameters are 0.358, 0.441, 0.477, and 0.481, respectively. Neither dielectric constants nor K-B-M parameters could be correlated with the observed solvent shifts.

17) C. Delseth, T. Thanh-Tam Nguyen, and J.-P. Kintzinger, *Helv. Chim. Acta*, **63**, 498 (1980).

18) A. L. Baumstark, P. Balakrishnan, M. Dotrong, C. J. McCloskey, M. G. Oakey, and D. W. Boykin, *J. Am. Chem. Soc.*, **87**, 1059 (1987).

19) R. G. Jones and J. M. Wilkins, *Org. Magn. Reson.*, **11**, 20 (1978).

20) The substituent effect could not be rationalized by the hydrogen-bond donor acidity defined by Taft and coworkers (R. W. Taft and M. J. Kamlet, *J. Am. Chem. Soc.*, **98**, 2886 (1976)).

 © 1988 The Chemical Society of Japan Bull. Chem. Soc. Jpn., 61, 4067—4070 (1988)

ESR Studies of Copper(II) Ion Doped in Single Crystal of Benzo-15-crown-5 Complex

Yong Li, Kunihiko Tajima, Kazuhiko Ishizu,* and Nagao Azuma†
Department of Chemistry, Faculty of Science, Ehime University, Matsuyama 790
†Faculty of General Education, Ehime University, Matsuyama 790
(Received February 6, 1988)

Angular-dependent ESR measurements were carried out at 77 K for ^{65}Cu(II) ions doped in a single crystal of benzo-15-crown-5 (B15C5) magnesium complex. Not only the allowed resonance lines of copper(II) ions, but also the forbidden lines arising from a nuclear quadrupole interaction were observed. Based on an analysis of the single crystal ESR spectra, the spin Hamiltonian containing the quadrupole term was determined for a B15C5–^{65}Cu(II) complex having a $3d_{z^2}$ ground state in a B15C5–Mg(II) solid matrix.

Regarding previous work, we have reported ESR studies on copper(II) complexes with 15-crown-5 (15C5) derivatives in solution,[1] where the benzo-15-crown-5–copper(II) complexes (B15C5–Cu(II)) revealed the characteristic ESR g-anisotropies ($g_Z < g_X, g_Y$) which are typical of the copper(II) ion with a $3d_{z^2}$ ground-state doublet. In the ESR spectra measured in solution, however, the full Hamiltonian involving the nuclear quadrupole interaction could not be determined.

In the present paper, we report on the ESR spectra observed at 77 K for a B15C5–^{65}Cu(II) complex doped in a diamagnetic single crystal composed of a benzo-15-crown-5–Mg(II) complex. The copper(II) complex also exhibited the inverse g-values ($g_Z < g_X, g_Y$) featured by the $3d_{z^2}$ ground state. In addition, strong lines due to a forbidden transition of the copper(II), ascribed to a quadrupole interaction, were successfully observed for the $3d_{z^2}$ ground state. An analysis of the angular-dependent ESR spectra determined the magnitude of the nuclear quadrupole interaction, which would be affected by a strong axial perturbation in the present complex.

Experimental

B15C5 was prepared according to Pedersen's method.[2] $Mg(ClO_4)_2 \cdot 6H_2O$ and 60%-$HClO_4$ were purchased.

In order to obtain a B15C5–Mg(II) single crystal doped with copper(II), $^{65}CuSO_4 \cdot 5H_2O$ was added to a 0.5 mol dm^{-3} 60%-$HClO_4$ solution of B15C5 and $Mg(ClO_4)_2 \cdot 6H_2O$ mixed in an equivalent molar ratio, in which the ^{65}Cu(II) concentration was controlled to be 1% of the total Mg(II) concentration. The mixture was left standing for one week, after which yellow single crystals were obtained.

A doped single crystal was mounted on the plane of a goniometer rod with silicone grease. The single crystal ESR spectra were recorded at 77 K. Figure 1 (a) illustrates the relation between the magnetic field $\boldsymbol{H}$ and the coordinate systems used. The coordinate systems, (*0-xyz*) and (*0-123*), represent those fixed to the goniometer and to the single crystal, respectively. By appropriate intervals in the ϕ angle, the crystal was rotated around the z-axis (Fig. 1(a)) with α=2.8° and 18.2° being adopted. The direction of the magnetic field $\boldsymbol{H}$ is taken in the x-y plane. Figure 1 (b) shows the arrangement of the (*0-123*) coordinate system in the single crystal with its dimensions.

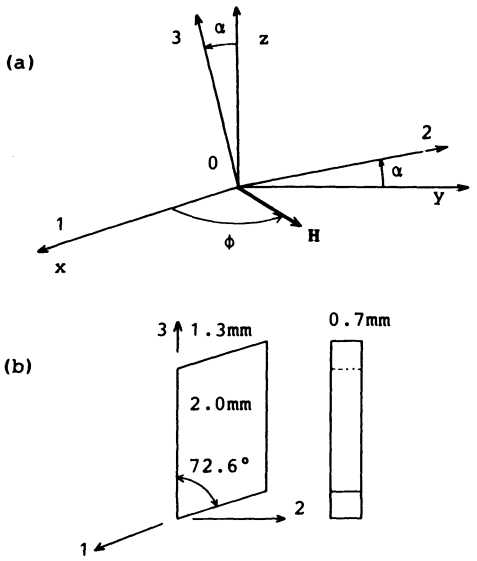

Fig. 1. (a) Coordinate systems adopted in the ESR measurement. The systems (*0-xyz*) and (*0-123*) were fixed to the goniometer and to the crystal, respectively. The crystal is mounted on the y-z plane, with keeping the axis *1* parallel to the x axis, and α is the angle between the axes *3* and z. The crystal is rotated around the z axis, so the magnetic field $\boldsymbol{H}$ is also rotated in the x-y plane by ϕ angle. (b) The arrangement of the (*0-123*) coordinate system in the single crystal with its dimension.

The ESR measurements were carried out on a JEOL-FX-2XG X-band ESR spectrometer operating with a 100-kHz magnetic-field modulation. The positions of the resonance lines were determined by taking Li-TCNQ (g=2.0025) as a standard. The magnetic fields were calibrated based on the hyperfine splitting of Mn(II) in powdered MgO (8.69 mT).

Results and Discussion

Figure 2 (a) shows the powder ESR spectrum observed at room temperature. The spectrum revealed a typical g-anisotropy, $g_Z < g_X, g_Y$, which was similar to that of a B15C5–copper(II) complex also having a $3d_{z^2}$

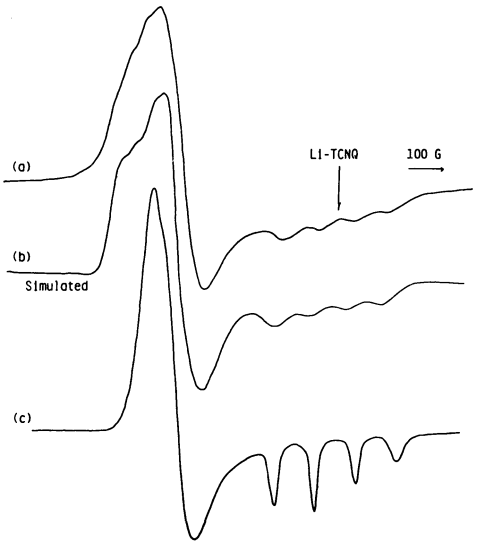

Fig. 2. Powder ESR spectrum of ^{65}Cu(II) doped in the crystal of B15C5-Mg(II) complex, measured at room temperature (a) and its simulation (b). Spectrum (c) was obtained from the B15C5-^{65}Cu(II) complex in 60%-$HClO_4$ aqueous solution at 77 K.

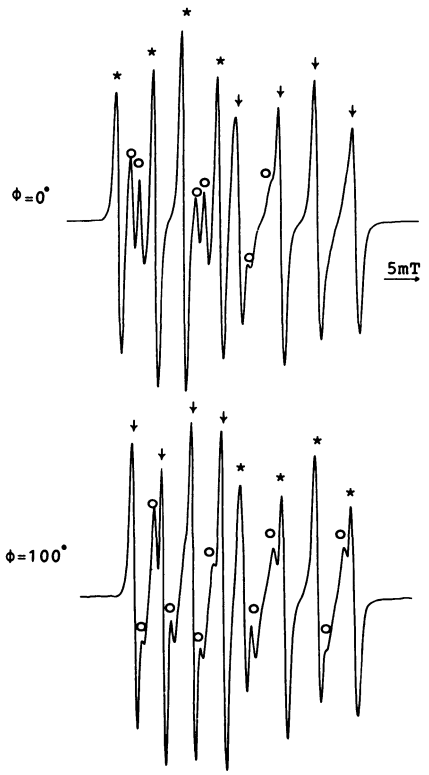

Fig. 3. ESR spectra of ^{65}Cu(II) doped in the single crystal of B15C5-Mg(II) complex. The temperature of the sample was 77 K and the α angle was 2.8°. The definition of the α and ϕ angles are given in Fig. 1. Asterisk and arrow indicate the allowed hyperfine splittings of the sites 1 and 2, respectively. The other spectral lines with open circle are due to the forbidden transitions.

ground state in solution (Fig. 2(c)).

Figures 3 and 4 show the angular-dependent ESR spectra of the ^{65}Cu(II) doped in a single crystal. The eight lines marked with asterisks and arrows have been assigned to the allowed transitions in two magnetically unequivalent copper sites. The other lines are ascribed to the forbidden transition ($\Delta M_I=\pm 1$). However, the range of the rotation angle (ϕ), in which one could observe each of those forbidden lines, has been very small. This is because the hindrance by the much stronger eight allowed lines and the overlapping between the forbidden transition lines themselves are inevitable. Therefore, an analysis of the angular variation of the forbidden lines has been almost impossible. We therefore confined our spectral analysis to only the allowed lines. In a usual case, the forbidden transition of copper(II) ion can not be detected in the X-band ESR spectra, because of its small transition probability. Thus, information concerning the quadrupole coupling is usually obtained from the Q-band ESR spectra for a single crystal.[3] Here, it is quite noteworthy that the forbidden lines were observed, even in the X-band spectra. This indicates that the probability of a forbidden transition is large enough to allow a clear detection in the observed ESR hyperfine structures.

In addition, it has been widely accepted that forbidden hyperfine lines are enhanced in intensity and that their resonant field positions are affected by a combination of the nuclear Zeeman interaction and nuclear quadrupole interaction.[3] If the magnitudes of the two terms are about the same and sufficiently enough for the detection of a forbidden transition, one can expect three pairs of forbidden transition lines to occur in middle of the respective allowed ^{65}Cu(II) hyperfine splittings; that is, the low-, medium-, and high-field pairs of forbidden transitions should be detected at a medium magnetic field, between those of four hyperfine lines of the copper(II) ion. The intensity of the medium-field pair is affected by the nuclear Zeeman term. On the other hand, the nuclear quadrupole term, as well as the nuclear Zeeman term, contribute to the intensity of the low- and high-field pairs, which results in the asymmetry of the observed forbidden hyperfine structure. In the present case, however, the line intensity for each of the low- and high-field pairs is nearly the same, while the intensity for the medium-field pair is greatly reduced in comparison with those of the low- and high-field pairs, as can be seen in Figs. 3 and 4. The contribution of the nuclear quadrupole term to the intensity of the low- and high-field pairs is calculated as to be the same. Therefore, it is suggested that the forbidden transitions mainly arise from a nuclear quadrupole interaction, and that the contribution to the line intensity from the nuclear quadrupole term is rather larger than that from the nuclear Zeeman term in this

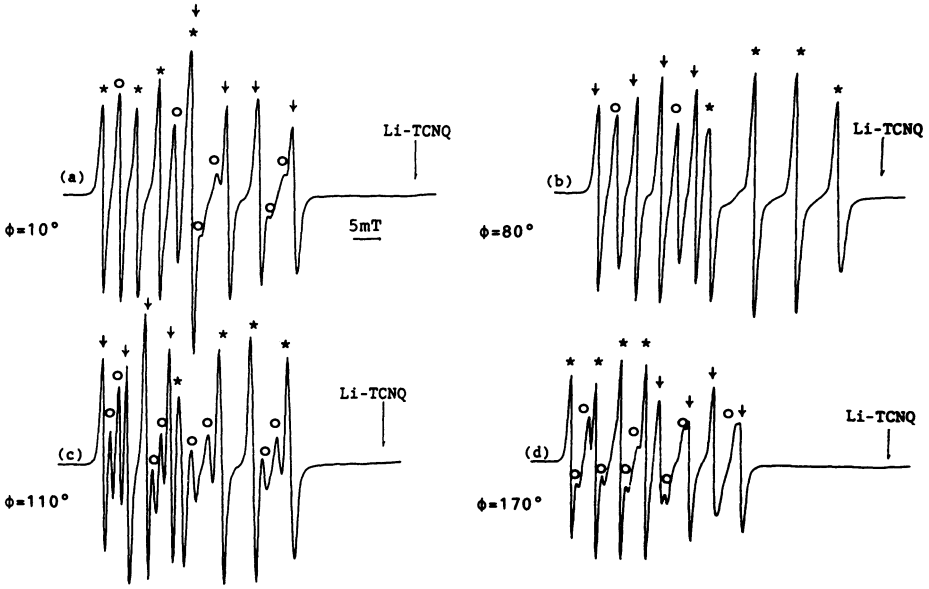

Fig. 4. The angular dependent forbidden ESR spectra of ^{65}Cu(II) doped in the single crystal of B15C5-Mg(II) complex, which are labeled with open circle. The symbols and the condition in the experiment are the same as those in Fig. 3, except for α=18.2°.

case.

By taking account of the view described above, an analysis of the single-crystal ESR spectra was performed based on the spin Hamiltonian given by

$$\mathscr{H} = \beta \boldsymbol{H}\boldsymbol{S}\cdot\boldsymbol{g}\cdot\boldsymbol{h} + \boldsymbol{I}\cdot\boldsymbol{A}\cdot\boldsymbol{S} + \boldsymbol{I}\cdot\boldsymbol{Q}\cdot\boldsymbol{I},$$

where $\boldsymbol{h}$ is a unit vector along the external magnetic field and the other symbols refer to the usual conventions. Within the limits of a high-field approximation, a general solution to the second order has been derived by Iwasaki[4] for the Hamiltonian in an arbitrary coordinate system without making any assumption that the $\boldsymbol{g}$, $\boldsymbol{A}$, and $\boldsymbol{Q}$ tensors are coaxial. According to the general solution, a computer analysis was carried out for the angular variation of the single crystal ESR spectra.

Figure 5 shows the angular variation of the allowed hyperfine lines of ^{65}Cu(II) doped in a single-crystal of B15C5-Mg(II). The open and solid circles indicate the observed line positions of the two copper sites. The spin Hamiltonian parameters estimated from the single-crystal ESR study are listed in Table 1. The solid lines in Fig. 5 represent the angular variations calculated based on the spin Hamiltonian parameters.

As shown in Fig. 5, the measured values agree well with the calculated values. At some ϕ angles, the high-field and low-field spacings of the ^{65}Cu(II) hyperfine splittings are not equal to the medium-field spacing. This has also been realized by means of the quadrupole interaction, since the second-order perturbation due to this interaction shifts the respective positions of the four lines.

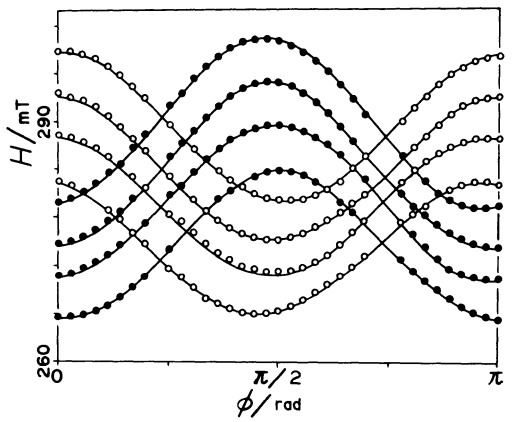

Fig. 5. The angular variation of the allowed hyperfine line positions of ^{65}Cu(II) doped in the single crystal of B15C5-Mg(II) complex at α=2.8°. The solid and open circles are of the sites 1 and 2, respectively. The solid lines are the reproduction calculated with the parameters in Table 1.

The simulated powder ESR spectrum based on the same parameters is close to the observed spectrum, as shown in Figs. 2 (a) and (b). This fact confirmed that the copper(II) ion was doped in the single crystal in the form of a B15C5-copper(II) complex. The spin Hamiltonian parameters of the two sites are in agreement within the error limit. Therefore, the two copper(II) sites are in the same ligand field environ-

Table 1. Estimated Principal Values and Axes of g, A, and Q tensors of B15C5-^{65}Cu(II) Complex

Principal value[a] and (estimated standard deviation)		Direction cosine[b]		Corresponding parameters in 60%-$HClO_4$ solution
Site 1 (with * mark in Figs. 3 and 4)				
g_X	2.408(0.002)	0.8333	−0.5034	−0.2282	2.330
g_Y	2.296(0.001)	0.2933	0.7527	−0.5894	
g_Z	2.030(0.003)	0.4685	0.4242	0.7750	1.990
A_X	5.00(0.03)	0.9462	−0.2420	−0.2147	3.2
A_Y	3.00(0.03)	0.0941	0.8409	−0.5330	
A_Z	10.39(0.04)	0.3095	0.4841	0.8184	11.5
Q_X	−0.51(0.03)	0.7665	−0.5823	−0.2709	
Q_Y	−0.24(0.03)	0.2573	0.6650	−0.7012	
Q_Z	0.71(0.03)	0.5884	0.4678	0.6595	
Site 2 (with arrow mark in Figs. 3 and 4)				
g_X	2.389(0.002)	−0.4595	0.8804	−0.1169	2.330
g_Y	2.287(0.003)	0.7458	0.3111	−0.5890	
g_Z	2.036(0.007)	0.4822	0.3579	0.7996	1.990
A_X	5.64(0.05)	−0.4301	0.9021	−0.0342	3.2
A_Y	2.72(0.06)	0.7632	0.3431	−0.5476	
A_Z	10.54(0.09)	0.4822	0.2616	0.8361	11.5
Q_X	−0.48(0.05)	−0.2131	0.9701	−0.1164	
Q_Y	−0.27(0.05)	0.7716	0.0940	−0.6291	
Q_Z	0.59(0.05)	0.5993	0.2239	0.7686	

a) Principal values of the A and Q tensors are in mT. b) Direction cosines of the principal axis are referred to the (*0-123*) coordinate system.

Table 2. Relation between Principal Axes of the g, A, and Q tensors of B15C5-^{65}Cu(II) Complex

Between	Angle/deg	
	Site 1	Site 2
g_X and A_X	16.4	5.2
g_Y and A_Y	12.9	3.2
g_Z and A_Z	10.1	5.9
<mean>	13.1	4.8
g_X and Q_X	6.4	15.1
g_Y and Q_Y	8.4	12.8
g_Z and Q_Z	9.9	10.4
<mean>	8.2	12.7
A_X and Q_X	22.4	13.9
A_Y and Q_Y	16.9	15.1
A_Z and Q_Z	18.5	8.1
<mean>	19.3	12.3

ment.

The angles between the estimated principal axes of the g and A tensors, and those of g and Q tensors, are listed in Table 2. Those values are varied from 3.2° to 16.4° and the simple mean value is 9.7°. In order to determine whether these values are significant or not, the error limit required in the direction cosines is less than 2%. However, the accuracy in the present meurements is not considered enough to do so.

The marked nuclear quadrupole interaction can be attributed to the considerable perturbing effect of the axial ligands on the copper(II) ion with a $3d_{z^2}$ ground state in a B15C5–Cu(II) complex,[1,5] since a strong axial ligation results in a large molecular electric field gradient which interacts with the nuclear electric quadrupole.

In the present paper, the relation between the principal axes of the g, A, and Q tensors and the crystallographic axes of the single crystal is not discussed, since X-ray structural analysis of the host crystal has not yet been performed.

ESR measurements were carried out at the Advanced Instrumentation Center for Chemical Analysis of this University. The calculations were performed at the Computer Center of this University.

References

1) K. Ishizu, T. Haruta, K. Nakai, K. Miyoshi, and Y. Sugiura, *Chem. Lett.*, **1978**, 579; K. Ishizu, T. Haruta, Y. Kohno, K. Mukai, and Y. Sugiura, *Bull. Chem. Soc. Jpn.*, **53**, 3513 (1980); Y. Li, K. Tajima, K. Ishizu, and N. Azuma, *Bull. Chem. Soc. Jpn.*, **60**, 557 (1987).

2) C. J. Pedersen, *J. Am. Chem. Soc.*, **89**, 7017 (1967).

3) H. So and R. L. Belford, *J. Am. Chem. Soc.*, **91**, 2392 (1969); L. K. White and R. L. Belford, *J. Am. Chem. Soc.*, **98**, 4428 (1976).

4) M. Iwasaki, *J. Magn. Reson.*, **16**, 417 (1974).

5) T. Sakurai, K. Kobayashi, S. Tsuboyama, Y. Kohno, N. Azuma, and K. Ishizu, *Acta Crystallogr., Sect. C*, **39**, 206 (1983).

 © 1988 The Chemical Society of Japan Bull. Chem. Soc. Jpn., 61, 4071—4075 (1988)

Bistability and Oscillations in the Bromate-Bromide-Cerium(III) System in Continuous-Flow Stirred Tank Reactor. A Simulation Using a New Set of Rate Constants of the FKN Scheme

Yoshihiro SASAKI
Institute for Chemical Research, Kyoto University, Uji, Kyoto 611
(Received June 7, 1988)

The bahavior of a bromate-bromide-cerium(III) system in a continuous-flow stirred tank reactor was simulated within the framework of the FKN reaction scheme and a new set of rate constants prepared by Field and Försterling. The characteristic properties such as bistability, hysteresis and minimal oscillations could be reproduced. In order to understand bistability in this system, the dynamic behavior of a four-variable model was examined by means of a two-variable approximation.

The bromate-bromide-cerium(III) system in a sulfuric acid medium in a continuous-flow stirred tank reactor (CSTR) can possess either one or two steady states or an oscillatory state.[1-4] The bistable system exists in either of the two steady states under the same set of constraints. When the system is perturbed, it relaxes to either of the two steady states, depending on the magnitude and direction of the perturbation. When the constraints are slowly changed, the system moves via a hysteresis loop between the two steady states. While the system does not contain organic substrates, it can exhibit minimal oscillations under certain conditions.

The reaction behavior of the system has been reproduced successfully through the FKN reaction scheme.[2,4-9] However, it was confirmed that several rate constants in the FKN scheme are inconsistent with some kinetic studies.[10-12] Therefore, Field and Försterling prepared a new set of rate constants (FF set of rate constants) on the basis of the recent results.[13] The FF values are similar to the Tyson's "Lo" values.[9,14] However, Bar-Eli and Ronkin found that the "Lo" values do not reproduce experiment very well, compared with the FKN values.[9] Therefore, we may become interested in a computation using the FF values. In this study, the bistability and oscillations of the bromate-bromide-cerium(III) system in a CSTR were re-investigated by means of a simulation method.

Calculations

The FKN reaction scheme can be described as follows:

$$Br^- + HOBr + H^+ \rightleftharpoons Br_2 + H_2O \quad (1)$$

$$Br^- + HBrO_2 + H^+ \rightleftharpoons 2HOBr \quad (2)$$

$$Br^- + BrO_3^- + 2H^+ \rightleftharpoons HOBr + HBrO_2 \quad (3)$$

$$2HBrO_2 \rightleftharpoons HOBr + BrO_3^- + H^+ \quad (4)$$

$$HBrO_2 + BrO_3^- + H^+ \rightleftharpoons 2BrO_2\cdot + H_2O \quad (5)$$

$$Ce(III) + BrO_2\cdot + H^+ \rightleftharpoons Ce(IV) + HBrO_2 \quad (6)$$

$$Ce(IV) + BrO_2\cdot + H_2O \rightleftharpoons Ce(III) + BrO_3^- + 2H^+ \quad (7)$$

Table 1. FF Sets of Rate Constants at 20 °C

Reaction	Forward	Backward
1	8×10^9 M^{-2} s^{-1}	110 s^{-1}
2	3×10^6 M^{-2} s^{-1}	2×10^{-5} M^{-1} s^{-1}
3	2 M^{-3} s^{-1}	3.2 M^{-1} s^{-1}
4	3000 M^{-1} s^{-1}	10^{-8} M^{-2} s^{-1}
5	42 M^{-2} s^{-1}	4.2×10^7 M^{-1} s^{-1}
6	8×10^4 M^{-2} s^{-1}	8.9×10^3 M^{-1} s^{-1}
7	0	0

1 M=1 mol dm^{-3}.

This scheme has been used in order to explain the oxidation of cerium(III) by bromate in a sulfuric acid solution.[13,15,16] The new set of rate constants at 20 °C prepared by Field and Försterling is shown in Table 1.[13] When the oxidation reaction is carried out in a CSTR, the term, $k_0(C_{0i}-C_i)$, is added to the rate equations generated from Reactions 1—6, where C_i and C_{0i} are the concentrations of species i in the solution and in the feed flow, respectively. k_0 is the ratio between the flow rate, dV/dt, and the volume of the reaction vessel. The external parameters, or constraints, for the reaction system are $[BrO_3^-]_0$, $[Br^-]_0$, $[Ce(III)]_0$, $[H^+]_0$, k_0, and the temperature.[2] Therefore, the states of the system are dependent on the constraints.

In this study, the seven-variable rate equations were employed because the value of $[H^+]_0$ was assumed to be large. The calculation of the steady states was performed by Newton's method. The temporal evolution of the system was obtained by using Gear's algorithm.[17] The stability of the steady states was surveyed by means of linearized stability analysis.[18]

Results and Discussion

Figure 1 shows the relationship between $[Br^-]_0$ and the concentration of bromide in the steady states, $[Br^-]_{ss}$, when $[H^+]_0=1.5$ mol dm^{-3}, $[Ce(III)]_0=1.5\times10^{-4}$ mol dm^{-3} and $k_0=0.004$ s^{-1}. The state of the reaction system depended on the concentration of bromate in the feed flow. That is, when $[BrO_3^-]_0\leq6\times10^{-5}$ mol dm^{-3}, the system existed in ssI, which was characterized by a relatively high $[Br^-]_{ss}$ and a low $[Ce(IV)]_{ss}$.

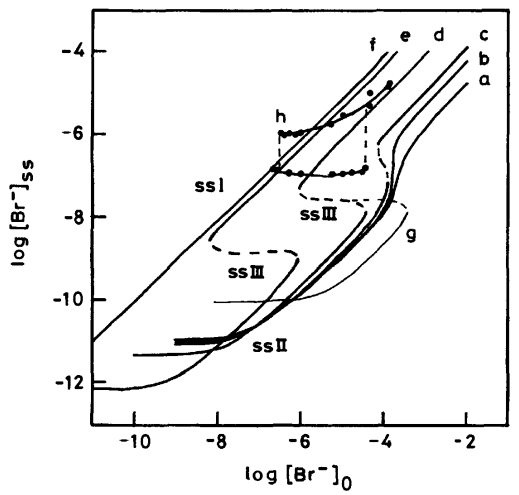

Fig. 1. Relationship between $[Br^-]_0$ and $[Br^-]_{ss}$. $[Ce(III)]_0=1.5\times10^{-4}$ M, $[H^+]_0=1.5$ M, and $k_0=0.004$ s^{-1}. $[BrO_3^-]_0$ (M) a: 0.1, b: 0.032, c: 0.016, d: 0.002, e: 2×10^{-4}, f: 5×10^{-5}. g: calculated according to the four-variable model under the same conditions in d. h: experimental results at 25°C under the same conditions in d.[2]

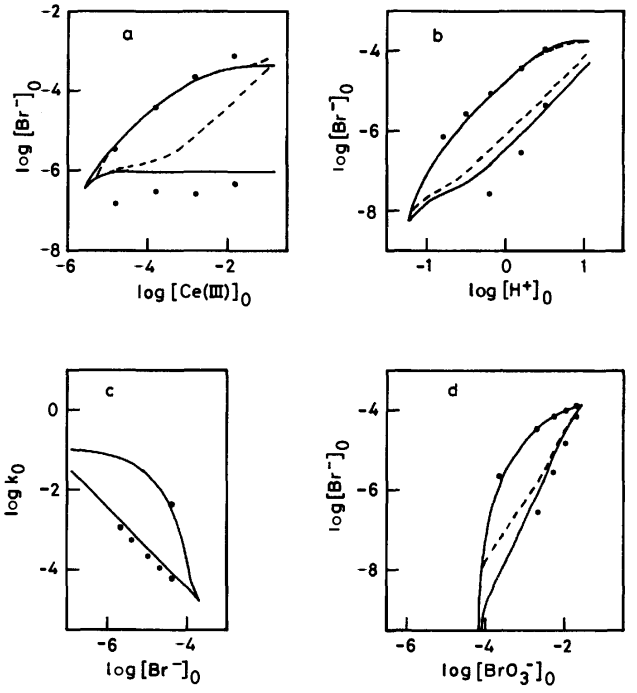

Fig. 2. Hysteresis limits. Solid lines: calculated, points: experimental (25°C),[2] dashed lines: calculated when $k_{-7}=0.001$ M^{-3} s^{-1}. Subspaces and fixed constraints a: $[Ce(III)]_0$-$[Br^-]_0$, $[BrO_3^-]_0=0.002$ M, $[H^+]_0=1.5$ M, $k_0=0.004$ s^{-1}; b: $[H^+]_0$-$[Br^-]_0$, $[BrO_3^-]_0=0.002$ M, $[Ce(III)]_0=1.5\times10^{-4}$ M, $k_0=0.004$ s^{-1}; c: $[Br^-]_0$-k_0, $[BrO_3^-]_0=0.002$ M, $[Ce(III)]_0=1.5\times10^{-4}$ M, $[H^+]_0=1.5$ M; d: $[BrO_3^-]_0$-$[Br^-]_0$, $[Ce(III)]_0=1.5\times10^{-4}$ M, $[H^+]_0=1.5$ M, $k_0=0.004$ s^{-1}.

When $[BrO_3^-]_0\geq0.032$ mol dm^{-3}, the steady state of the system varied smoothly from ssI to ssII (low concentration of bromide and high concentration of cerium(IV)) with a decrease of $[Br^-]_0$. On the other hand, when 7.5×10^{-5} mol $dm^{-3}\leq[BrO_3^-]_0\leq2.2\times10^{-2}$ mol dm^{-3}, the system could possess three steady states (ssI, ssII, and ssIII) under the same set of $[BrO_3^-]_0$ and $[Br^-]_0$. The steady states (ssI and ssII) were stable and had all the negative eigen-values (nodes). The steady state (ssIII) was unstable and had one positive and the other negative eigenvalues (saddle point). These results mean that we can not attain ssIII experimentally and that the system exists in either ssI or ssII. Also, if $[Br^-]_0$ is continually changed to a sligtly different value, the system in one steady state suddenly moves to the other steady state at a critical value of $[Br^-]_0$. Thus, we obtain a hysteresis loop. The calculated curve, d, was not consistent with the experimental results at 25 °C due to Geiseler and Bar-Eli[2] in the region of low bromide-concentration. The inconsistency may be attributed to a difficulty involving the determination of bromide in the region by means of a bromide-sensitive electrode.[19] However, the dynamical behavior, such as bistability and hysteresis, could be reproduced successfully.

Figure 2 shows the calculated hysteresis limits together with the experimental results due to Geiseler and Bal-Eli.[2] The bistable region of the system lays in a five-dimensional space of $[BrO_3^-]_0$, $[Ce(III)]_0$, $[H^+]_0$, $[Br^-]_0$, and k_0. Four of 10 two-dimensional subspaces were examined in this study. In the figure, the system existed in ssII below the lower lines and in ssI above the upper lines, respectively. In the intermediate region, the two steady states coexisted. All of the upper lines were consistent with the experimental data. However, the lower lines deviated slightly from the experimental data. The reason for the deviation is not apparent at present.

The bromate-bromide-cerium(III) system which we studied possessed a small oscillation region in the neighborhood of the bistable domain. Figure 3 shows the oscillation region projected on the $[BrO_3^-]_0$-$[Br^-]_0$ subspace, where a represents an oscillation domain having one unstable steady state ($Re(\lambda)>0$) and b denotes a bistable region. In regions c and d, there were three steady states (one saddle point, one stable node and one unstable steady state ($Re(\lambda)>0$)). The system then settled in a stable node after a long time. However, in the domain where c and d were piled up, three unstable states were obtained and the system exhibited one limit cycle. In the other region of Fig. 3, one stable steady state existed. The region, a, calculated here seems to reproduce the experimental oscillation region at 25 °C, e, due to Bar-Eli and Geiseler in location, size and shape.[4] The oscillation preiod and the ratio, $[Br^-]_{max}/[Br^-]_{min}$, calculated are shown in Table 2. At high $[BrO_3^-]_0$ and $[Br^-]_0$, the amplitude and the period were comparably small and at low $[BrO_3^-]_0$ and $[Br^-]_0$, comparably large. A similar trend was obtained experimentally.[4] The

Table 2. Period and Amplitude of the Oscillations

$[BrO_3^-]_0$/M	$[Br^-]_0$/M	Period/s	$[Br^-]_{max}/[Br^-]_{min}$
0.116	3.2×10^{-4}	307	2.5
0.11	3.1×10^{-4}	345	3.5
0.10	2.8×10^{-4}	370	6.4
0.09	2.65×10^{-4}	445	11.3
0.082	2.45×10^{-4}	643	17.3
0.078	2.37×10^{-4}	905	22.3

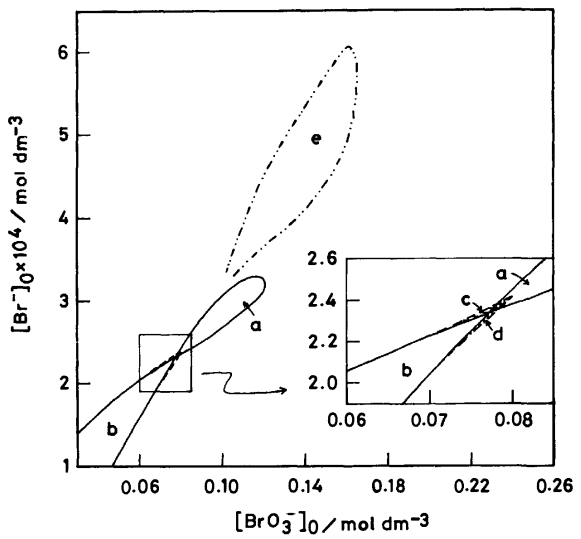

Fig. 3. Oscillation and bistability regions in the $[BrO_3^-]_0$-$[Br^-]_0$ subspace. $[H^+]_0$=0.75 M, $[Ce(III)]_0$= 3×10^{-4} M, and k_0=0.005 s^{-1}. a: oscillation, b: bistability, c and d: regions having one stable and two unstable steady states e: experimental oscillation region at 25 °C.[4] The domain where c and d intersect has three unstable steady states.

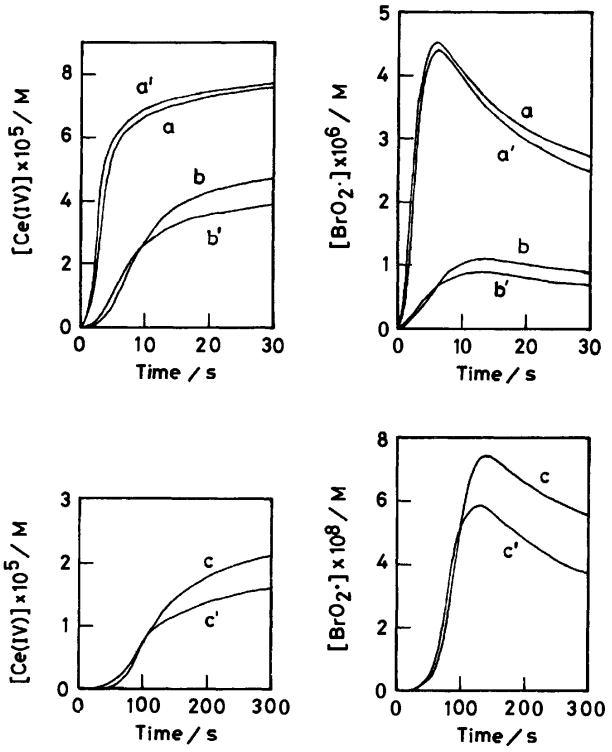

Fig. 4. Simulations of [Ce(IV)] and $[BrO_2\cdot]$ in the oxidation reaction of Ce(III) with bromate in 1 M sulfuric acid solution. $[H^+]_{initial}$=1 M, $[Ce(III)]_{initial}$= 10^{-4} M. $[BrO_3^-]_{initial}$ (M) a: 1, b: 0.1, c: 0.002. The prime represents the experiment due to Field and Försterling.[13]

magnitudes of the oscillation period and the amplitude were also consistent with the experiment (the oscillation period: 156—493 s and the amplitude: 1.6—15).

The FF set of rate constants, prepared on the basis of recent kinetic data, reproduces the reaction behavior of the bromate-bromide-cerium(III) system well, as is shown in Figs. 1—3. In the calculation, the contribution of Reaction 7 is not taken into account due to Field and Försterling, who assumed that a small quantity of bromide remaining as an impurity in bromate is a trigger for the oxidation of Ce(III) by bromate in a sulfuric acid medium. It is reported that the induced period varies in the oxidation of Ce(III) (3×10^{-4} mol dm^{-3}) by 0.001 mol dm^{-3} of bromate,[20] which may support the assumption by Field and Försterling.

However, Reaction 7 is a conceivable trigger for the oxidation of Ce(III) by bromate. Therefore, in order to examine the contribution of Reaction 7, we simulated the observed [Ce(IV)] and $[BrO_2\cdot]$ during the overall reaction of Ce(III) with bromate and the hysteresis limits by taking account of the reaction. The unknown value of k_{-7} was estimated by trial and k_7 was obtained according to the relationship, $k_5k_6k_{-7}=k_{-5}k_{-6}k_7$. Figure 4 shows the calculated concentrations of Ce(IV) and $BrO_2\cdot$ when k_{-7}=0.001 mol^{-3} dm^9 s^{-1}. The calculated curves in Fig. 4 were consistent with the experimental results due to Field and Försterling.[13] The hysteresis limits calculated when k_{-7}=0.001 mol^{-3} dm^9 s^{-1} are shown in Figs. 2a, b, and d. Reaction 7 influenced mainly the lower lines, especially in the regions of relatively large $[Ce(III)]_0$ and small $[BrO_3^-]_0$. Figures 2a, b, and d suggest that the contribution of Reaction 7 to the behavior of the bromate-bromide-cerium(III) system in a CSTR is not so large.

As is described above, a bromate-bromide-cerium-(III) system kept far from thermodynamic equilibrium can possess two steady states under the same set of

constraints. The behavior is based on the autocatalytic formation of $HBrO_2$ by Reactions 5 and 6, and based on competition between Reactions 2 and 5. However, because this explanation is not sufficient to understand the properties of the system, we examined the dynamical behavior of a four-variable model composed of Reactions 1—4 and 8.

$$BrO_3^- + HBrO_2 + 2Ce(III) + 3H^+ \longrightarrow$$

$$2HBrO_2 + 2Ce(IV) + H_2O \quad (8)$$

Reaction 8 is obtained when the backward reactions in Reactions 5 and 6 are neglected. In this model, Reaction 5 is assumed to be rate determining in the autocatalytic reaction. Such a condition can be realized when $[Ce(III)]_0$ is very large. Thus, the rate of Reaction 8 is yielded as follows:

$$v_8 = k_5[H^+]_0[BrO_3^-][HBrO_2] \quad (9)$$

Because the bromate–bromide–cerium(III) system studied here contains a large excess of bromate, $[BrO_3^-]$ is substantially equal to $[BrO_3^-]_0$ and the backward reactions in Reactions 2 and 4 can be neglected. The state of the model system depends on four constraints, $[H^+]_0$, $[BrO_3^-]_0$, $[Br^-]_0$, and k_0.

The rate equations generated from the four-variable model are written as follows:

$$d[Br_2]/dt = k_1[H^+]_0[Br^-][HOBr] - (k_0 + k_{-1})[Br_2] \quad (10)$$

$$d[HBrO_2]/dt = k_3[H^+]_0^2[BrO_3^-]_0[Br^-] - k_{-3}[HOBr][HBrO_2] - k_2[H^+]_0[Br^-][HBrO_2] + k_5[H^+]_0[BrO_3^-]_0[HBrO_2] - 2k_4[HBrO_2]^2 - k_0[HBrO_2] \quad (11)$$

$$d[HOBr]/dt = k_3[H^+]_0^2[BrO_3^-]_0[Br^-] - k_{-3}[HOBr][HBrO_2] + k_{-1}[Br_2] - k_1[H^+]_0[Br^-][HOBr] + 2k_2[H^+]_0[Br^-][HBrO_2] + k_4[HBrO_2]^2 - k_0[HOBr] \quad (12)$$

$$d[Br^-]/dt = k_{-3}[HOBr][HBrO_2] - k_3[H^+]_0^2[BrO_3^-]_0[Br^-] - k_1[H^+]_0[Br^-][HOBr] + k_{-1}[Br_2] - k_2[H^+]_0[Br^-][HBrO_2] + k_0([Br^-]_0 - [Br^-]) \quad (13)$$

The curve, g, in Fig. 1 shows the relationship between $[Br^-]_0$ and $[Br^-]_{ss}$ calculated by using Eqs. 10—13 when $[BrO_3^-]_0=0.002$ mol dm^{-3}, $[H^+]_0=1.5$ mol dm^{-3}, and $k_0=0.004$ s^{-1}. The curve suggests that the four-variable model is essentially equal to the FKN reaction scheme. In order to reduce the number of independent variables to two, we adopt the approximation that $d[Br_2]/dt=0$ and $d[HBrO_2]/dt=0$ at all times according to Bar-Eli and Noyes.[21] Thus, we can obtain the following equations:

$$[Br_2] = (k_1[H^+]_0/(k_0 + k_{-1}))[Br^-][HOBr] \quad (14)$$

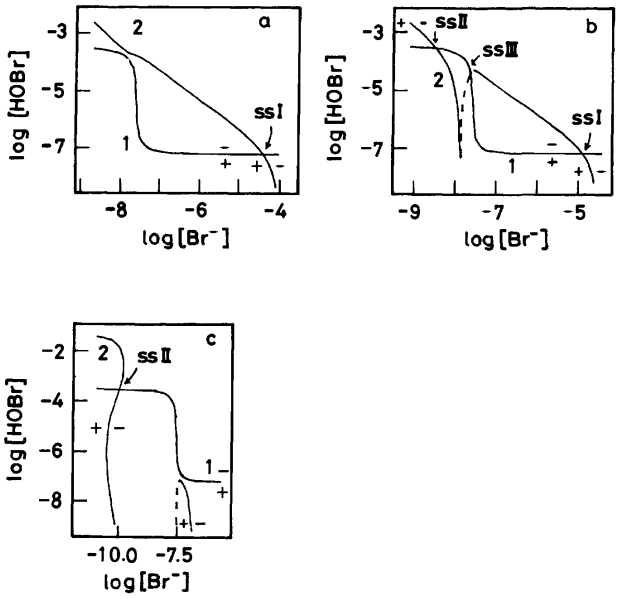

Fig. 5. Nullclines of the four-variable model. $[BrO_3^-]_0=0.002$ M, $[H^+]_0=1.5$ M, and $k_0=0.004$ s^{-1}. $[Br^-]_0$ a: 5×10^{-4} M, b: 1.55×10^{-4} M, c: 7×10^{-7} M. 1: $d[HOBr]/dt=0$, 2: $d[Br^-]/dt=0$. +: $d[HOBr]/dt>0$ or $d[Br^-]/dt>0$, −: $d[HOBr]/dt<0$ or $d[Br^-]/dt<0$.

$$[HOBr] = (k_3[H^+]_0^2[BrO_3^-]_0[Br^-] - k_2[H^+]_0[Br^-][HBrO_2] + k_5[H^+]_0[BrO_3^-]_0[HBrO_2] - k_0[HBrO_2] - 2k_4[HBrO_2]^2)/(k_{-3}[HBrO_2]) \quad (15)$$

A domain of $[HBrO_2]$ where $[HBrO_2]>0$ and $[HOBr]>0$, is defined from Eq. 15. We can depict the trajectory of the model system by using Eqs. 12—15.

Figure 5 shows the dependency of the HOBr and Br^- nullclines on $[Br^-]_0$ when $[BrO_3^-]_0=0.002$ mol dm^{-3}, $[H^+]_0=1.5$ mol dm^{-3} and $k_0=0.004$ s^{-1}. In Fig. 5b ($[Br^-]_0=1.55\times10^{-4}$ mol dm^{-3}), there are three intersections, i.e., three steady states (two stable nodes and one saddle point). Because the Br^- nullcline has an S-shape, interesting circumstances occur. In the left side of the Br^- nullcline, $d[Br^-]/dt>0$ and a state of the model system in the region varies temporally to the right. A state in the right side of the Br^- nullcline moves to the left for a similar reason. Therefore, the solid lines in the Br^- nullcline are stable because a state of the model system moves temporally toward the solid lines. On the other hand, the dashed line is unstable because a state of the model system temporally goes away from the dashed line. Thus, the middle intersection corresponds to an unstable steady state (saddle point) and the intersections of both sides to stable steady states (stable nodes). There is a separatrix through the saddle point, which separates the basins of attraction associated with the nodes. When the model system in a steady state is perturbed to pass the separatrix, the system relaxes to the other

steady state. On the other hand, Figs. 5a and c correspond to the case that the system has one stable steady state. Figures 5a—c suggest that at a critical value of $[Br^-]_0$, the nullclines yield one intersection and one point of contact and that at the $[Br^-]_0$, the model system jumps to the other steady state.

The four-variable model gives dynamical information on bistability in the bromate–bromide–cerium-(III) system, but the oscillatory state in the model system has not yet been found at present.

References

1) W. Geiseler and H. H. Föllner, *Biophys. Chem.*, **6**, 107 (1977).
2) W. Geiseler and K. Bar-Eli, *J. Phys. Chem.*, **85**, 908 (1981).
3) W. Geiseler, *Ber. Bunsenges. Phys. Chem.*, **86**, 721 (1982).
4) K. Bar-Eli and W. Geiseler, *J. Phys. Chem.*, **87**, 3769 (1983).
5) R. J. Field, E. Körös, and R. M. Noyes, *J. Am. Chem. Soc.*, **94**, 8649 (1972).
6) K. Bar-Eli and R. M. Noyes, *J. Phys. Chem.*, **81**, 1988 (1977).
7) K. Bar-Eli and R. M. Noyes, *J. Phys. Chem.*, **82**, 1352 (1978).
8) K. Bar-Eli, "Nonlinear Phenomena in Chemical Dynamics," ed by C. Vidal and A. Pacault, Springer-Verlag, West Berlin (1981), pp. 228—239.
9) K. Bar-Eli and J. Ronkin, *J. Phys. Chem.*, **88**, 2844 (1984).
10) Z. Noszticzius, E. Noszticzius, and Z. A. Schelly, *J. Phys. Chem.*, **87**, 510 (1983).
11) F. Ariese and Z. Ungvàrai-Nagy, *J. Phys. Chem.*, **90**, 1 (1986).
12) F. Ariese and Z. Ungvàrai-Nagy, *J. Phys. Chem.*, **90**, 1496 (1986).
13) R. J. Field and H. -D. Försterling, *J. Phys. Chem.*, **90**, 5400 (1986).
14) J. J. Tyson, "Oscillations and Traveling Waves in Chemical Systems," ed by R. J. Field and M. Burger, Wiley-Interscience, New York (1985), p. 95.
15) S. Barkin, M. Bixon, R. M. Noyes, and K. Bar-Eli, *Int. J. Chem. Kinet.*, **9**, 841 (1977).
16) R. J. Field and P. M. Boyd, *J. Phys. Chem.*, **89**, 3707 (1985).
17) C. W. Gear, "Numerical Initial Value Probrems in Ordinary Differential Equations," Prentice-Hall, Englewood Cliffs, N. J. (1971), Chap. 11.
18) P. Gransdorff and I. Prigogine, "Thermodynamic Theory of Structure, Stability, and Fluctuations," Wiley-Interscience, New York (1971).
19) J. H. Woodson and H. A. Liebhafsky, *Anal. Chem.*, **41**, 1894 (1969).
20) G. J. Kasparek and T. C. Bruice, *Inorg. Chem.*, **10**, 382 (1971).
21) K. Bar-Eli and R. M. Noyes, *J. Chem. Phys.*, **86**, 1927 (1987).

 © 1988 The Chemical Society of Japan Bull. Chem. Soc. Jpn., 61, 4077—4082 (1988)

Solvation and Ionic Association of Bis(β-diketonato)(diamine)-cobalt(III) Perchlorates in Alcohols and Ketones

Kazuaki Ito,* Hiroyuki Isono,† Etsuro Iwamoto,† and Yuroku Yamamoto††
Department of Environmental Science, Faculty of Engineering, Hiroshima University, Saijo, Higashi-Hiroshima 724
†Department of Chemistry, Faculty of Science, Hiroshima University, Naka-ku, Hiroshima 730
††Environmental and Safety Engineering Department, Fukui Institute of Technology, Gakuen, Fukui 910
(Received March 28, 1988)

The conductances of bis(2,4-pentanedionato)(diamine)cobalt(III) perchlorates, $[Co(acac)_2(diamine)]ClO_4$ (where acac: 2,4-pentanedionato; diamine: en (ethylenediamine) and *N,N,N',N'*-tmen (*N,N,N',N'*-tetramethylethylenediamine)) in methanol (MeOH), ethanol (EtOH), 2-propanol (*i*-PrOH), methyl ethyl ketone (MEK), and methyl isobutyl ketone (MIBK) and of bis(β-diketonato)(ethylenediamine)cobalt(III) perchlorates, $[Co(\beta\text{-dik})_2(en)]ClO_4$ (where β-dik: acacBr (3-bromo-2,4-pentanedionato) and $acacNO_2$ (3-nitro-2,4-pentanedionato)) in EtOH, acetone (Me_2CO), and MEK were measured at 25 °C. $[Co(acac)_2(en)]ClO_4$ in the alcohols was found to be more dissociated than $[Co(acac)_2(N,N,N'N'\text{-tmen})]ClO_4$. This behavior was explained as being due to the strong solvation of $[Co(acac)_2(en)]^+$ by the alcohols. $[Co(acac)_2(N,N,N',N'\text{-tmen})]^+$ seems to be solvated in ketones rather than alcohols. The sequence of the ionic association constant for $[Co(\beta\text{-dik})_2(en)]ClO_4$, acac<acacBr<$acacNO_2$, could be interpreted in terms of an enhanced polarity of the cations with the electron-withdrawing groups.

In order to understand the solute-solvent interactions characteristic of metal-chelate ions, we have measured the conductances of 17 metal-chelate electrolytes, bis(β-diketonato)(diamine)cobalt(III) complexes, $[Co(\beta\text{-dik})_2(diamine)]X$ (X^-=ClO_4^-, I^-, and Br^-) in organic solvents at 25 °C.[1-5] From the obtained conductance parameters (the limiting conductance, Λ_0, the Walden product of the cations, $\lambda_0^+ \cdot \eta$, and the ionic association constant, K_a), we have clarified the effects of the following factors on the mobility of the chelate cations and ionic association: (a) interactions between NH protons of diamine in the cations and solvent dipole;[1,2] (b) solvation of the ligands in the cations through hydrogen bonding;[3] (c) *N*-methylation of the ligand ethylenediamine in the cations[1-3] and the relative acidity of the residual NH protons;[4] and (d) polar substituents such as the nitro group in the ligand β-diketonato.[5]

However, factors (b) and (d) have been examined only in 1-propanol (*n*-PrOH) and acetone (Me_2CO), and nitrobenzene ($PhNO_2$), respectively. In this study, in order to obtain more information on their factors, the conductances of $[Co(\beta\text{-dik})_2(diamine)]ClO_4$ were measured in several alcohols and ketones. The obtained results are discussed in detail regarding the difference in solvation of the chelate cations by alcohols and ketones as well as the polarity of the chelate cations.

Experimental

(a) $[Co(\beta\text{-dik})_2(diamine)]ClO_4$ was prepared and purified as described previously.[1,5] Tetraethylammonium perchlorate (Et_4NClO_4, commercial product) was purified by two recrystallizations. The purity of all products was checked by chemical analyses of C, H, and N. Methanol (MeOH) and ethanol (EtOH) were refluxed for 3 days over magnesium methoxide and magnesium ethoxide, respectively, and fractionally distilled. 1-Propanol (*n*-PrOH) and 2-propanol (*i*-PrOH) were refluxed over calcium oxide for 2 days and fractionally distilled. Acetone (Me_2CO), methyl ethyl ketone (MEK), and methyl isobutyl ketone (MIBK) were refluxed over Drierite after dehydration and fractionally distilled. The distillation was performed under a flow of N_2 gas.

(b) The procedure for the conductance measurements and other measurements (viscosity and density) were described previously.[1] The dielectric constant (ε) and viscosity (η in mPa s) of the solvents for an analysis were as follows: for MeOH ε=32.62,[6] η=0.5460; for EtOH ε=24.33,[7] η=1.082; for *n*-PrOH ε=20.45,[7] η=1.948; for *i*-PrOH ε=19.41,[8] η=2.078; for Me_2CO ε=20.56,[9] η=0.3052; for MEK ε=18.01,[10] η=0.3803; for MIBK ε=12.8,[11] η=0.5478.

Results

The conductances Λ(S cm^2 mol^{-1}) at six to nine concentrations, C(mol dm^{-3}) of $[Co(\beta\text{-dik})_2(diamine)]ClO_4$ and Et_4NClO_4 covering the range from 4.2×10^{-3} to 10^{-5} mol dm^{-3} in the alcohols and the ketones were measured at 25 °C.[12] The data were analyzed by the Fuoss-Hsia equation with $E=E_1\Lambda_0-2E_2$ in the form,[13]

$$\Lambda = \Lambda_0 - SC^{1/2}\gamma^{1/2} + EC\gamma\log C\gamma + J_1(d)C\gamma - J_2(d)C^{3/2}\gamma^{3/2} - K_aC\gamma f_\pm^2\Lambda, \quad (1)$$

where Λ_0 and K_a refer to the limiting conductance and the ionic association constant, respectively, and the other symbols have their usual meanings. The procedure for fitting in terms of Λ_0, K_a, and the distance parameter d has been described previously.[1]

The obtained conductance parameters are given in Tables 1 and 2 for the alcohols and the ketones,

Table 1. Conductance Results in Alcohols at 25 °C

Electrolyte	Solvent	Λ_0 / S cm² mol⁻¹	K_a / dm³ mol⁻¹	d[a] / Å	σ_Λ[b]
$[Co(acac)_2(en)]ClO_4$	MeOH	106.08±0.06	37±12	8.5	0.020
Et_4NClO_4	MeOH	131.0 ±0.1	60±16	8.8	0.028
$[Co(acac)_2(en)]ClO_4$	EtOH	48.68±0.02	147± 8	13.7	0.012
$[Co(acac)_2(N,N,N',N'\text{-tmen})]ClO_4$	EtOH	53.36±0.01	180± 3	14.4	0.009
$[Co(acacBr)_2(en)]ClO_4$	EtOH	46.68±0.01	179± 2	14.6	0.003
$[Co(acacNO_2)_2(en)]ClO_4$	EtOH	46.06±0.05	297± 6	18.0	0.012
Et_4NClO_4	EtOH	61.31±0.16	295±30	11.4	0.008
$[Co(acac)_2(en)]ClO_4$[c]	*n*-PrOH	25.81±0.02	411±45	14.1	0.011
$[Co(acac)_2(N,N,N',N'\text{-tmen})]ClO_4$[c]	*n*-PrOH	28.57±0.02	480±15	16.4	0.015
Et_4NClO_4	*n*-PrOH	31.50±0.02	895±19	19.3	0.015
$[Co(acac)_2(en)]ClO_4$	*i*-PrOH	23.67±0.02	812±36	14.4	0.016
$[Co(acac)_2(N,N,N',N'\text{-tmen})]ClO_4$	*i*-PrOH	26.63±0.05	837± 9	22.9	0.026

a) Distance parameter with a minimum σ_Λ value in Eq. 1. b) Standard deviation of Λ ($\sigma_\Lambda = [\sum(\Lambda_{calcd} - \Lambda_{obsd})^2/(n-3)]^{1/2}$). c) Ref. 3.

Table 2. Conductance Results in Ketones at 25 °C

Electrolyte	Solvent	Λ_0 / S cm² mol⁻¹	K_a / dm³ mol⁻¹	d[a] / Å	σ_Λ[b]
$[Co(acac)_2(en)]ClO_4$[c]	Me_2CO	180.03±0.09	180± 4	14.0	0.06
$[Co(acac)_2(N,N,N',N'\text{-tmen})]ClO_4$[c]	Me_2CO	186.40±0.04	137± 2	13.1	0.03
$[Co(acacBr)_2(en)]ClO_4$	Me_2CO	175.84±0.07	231± 4	15.0	0.06
$[Co(acacNO_2)_2(en)]ClO_4$	Me_2CO	174.74±0.08	368± 4	15.6	0.06
Et_4NClO_4	Me_2CO	208.85±0.09	210± 5	13.6	0.08
$[Co(acac)_2(en)]ClO_4$	MEK	140.44±0.03	374± 4	16.6	0.02
$[Co(acac)_2(N,N,N',N'\text{-tmen})]ClO_4$	MEK	145.3 ±0.1	253± 9	16.2	0.15
$[Co(acacBr)_2(en)]ClO_4$	MEK	136.93±0.06	524± 7	17.2	0.04
$[Co(acacNO_2)_2(en)]ClO_4$	MEK	136.52±0.07	981± 14	18.2	0.05
Et_4NClO_4	MEK	164.40±0.04	455± 7	16.8	0.04
$[Co(acac)_2(en)]ClO_4$	MIBK	93.5 ±0.1	3120±150	22.6	0.09
$[Co(acac)_2(N,N,N',N'\text{-tmen})]ClO_4$	MIBK	97.71±0.08	1710± 40	22.2	0.10
Et_4NClO_4	MIBK	109.5 ±0.2	4190±130	20.8	0.20

a) and b) are the same as in Table 1. c) Ref. 3.

respectively, together with those in 1-propanol (*n*-PrOH) and acetone (Me_2CO). The limiting conductances (λ_0^+/S cm² mol⁻¹) and Walden products ($\lambda_0^+ \cdot \eta$/S cm² mol⁻¹ 10⁻¹ Pa s) of the chelate cations are given in Table 3, together with those in *n*-PrOH, Me_2CO, nitrobenzene ($PhNO_2$), and 1,2-dichloroethane (1,2-DCE) for comparison. The data were obtained from the limiting conductances of the perchlorate ion, λ_0^- (ClO_4^-): in MeOH, 70.94;[6] in EtOH, 32.04;[7] in *i*-PrOH, 15.24;[8] in Me_2CO, 118.35;[9] in MEK, 93.0;[10] in MIBK, $\lambda_0^- \cdot \eta = 0.34$.[14]

Discussion

(1) Solvation and Association of $[Co(acac)_2(diamine)]ClO_4$. (a) Ionic Mobility: Figure 1 shows the Walden products ($\lambda_0^+ \cdot \eta$) for $[Co(acac)_2(en)]^+$ and $[Co(acac)_2(N,N,N',N'\text{-tmen})]^+$ in each solvent. It is clear that $\lambda_0^+ \cdot \eta$ for $[Co(acac)_2(en)]^+$ is much smaller than that for $[Co(acac)_2(N,N,N',N'\text{-tmen})]^+$ except for the result in 1,2-DCE, although the size of $[Co(acac)_2(en)]^+$ is smaller than $[Co(acac)_2(N,N,N',N'\text{-tmen})]^+$

Table 3. Ionic Mobilities and Walden Products of [Co(β-dik)$_2$(diamine)]$^+$ in Organic Solvents at 25 °C

Chelate Cation	Solvent	λ_0^+ / S cm^2 mol^{-1}	$\lambda_0^+ \cdot \eta$ / S cm^2 mol^{-1} 10^{-1} Pa s
[Co(acac)$_2$(en)]$^+$	MeOH	35.14	0.192
[Co(acac)$_2$(en)]$^+$	EtOH	16.64	0.180
[Co(acac)$_2$(*N*,*N*,*N*′,*N*′-tmen)]$^+$	EtOH	21.32	0.231
[Co(acacBr)$_2$(en)]$^+$	EtOH	14.64	0.158
[Co(acacNO$_2$)$_2$(en)]$^+$	EtOH	14.02	0.152
[Co(acac)$_2$(en)]$^+$[a]	*n*-PrOH	9.39	0.183
[Co(acac)$_2$(*N*,*N*,*N*′,*N*′-tmen)]$^+$[a]	*n*-PrOH	12.15	0.237
[Co(acac)$_2$(en)]$^+$	*i*-PrOH	8.43	0.175
[Co(acac)$_2$(*N*,*N*,*N*′,*N*′-tmen)]$^+$	*i*-PrOH	11.39	0.237
[Co(acac)$_2$(en)]$^+$[a]	Me$_2$CO	61.63	0.188
[Co(acac)$_2$(*N*,*N*,*N*′,*N*′-tmen)]$^+$[a]	Me$_2$CO	68.0	0.208
[Co(acacBr)$_2$(en)]$^+$	Me$_2$CO	57.44	0.175
[Co(acacNO$_2$)$_2$(en)]$^+$	Me$_2$CO	56.34	0.172
[Co(acac)$_2$(en)]$^+$	MEK	47.44	0.180
[Co(acac)$_2$(*N*,*N*,*N*′,*N*′-tmen)]$^+$	MEK	52.3	0.199
[Co(acacBr)$_2$(en)]$^+$	MEK	43.93	0.167
[Co(acacNO$_2$)$_2$(en)]$^+$	MEK	43.52	0.166
[Co(acac)$_2$(en)]$^+$	MIBK	—	0.17
[C(acac)$_2$(*N*,*N*,*N*′,*N*′-tmen)]$^+$	MIBK	—	0.19
[Co(acac)$_2$(en)]$^+$[b]	PhNO$_2$	10.9	0.201
[Co(acac)$_2$(*N*,*N*,*N*′,*N*′-tmen)]$^+$[b]	PhNO$_2$	11.9	0.220
[Co(acacBr)$_2$(en)]$^+$[c]	PhNO$_2$	9.77	0.180
[Co(acacNO$_2$)$_2$(en)]$^+$[c]	PhNO$_2$	9.29	0.172
[Co(acac)$_2$(en)]$^+$[b]	1,2-DCE	25.7	0.201
[Co(acac)$_2$(*N*,*N*,*N*′,*N*′-tmen)]$^+$[b]	1,2-DCE	26.0	0.204

a) Ref. 3. b) Ref. 1. c) Ref. 5.

with four *N*-methyl groups.[15] The difference in $\lambda_0^+ \cdot \eta$ is larger in the alcohols than in the other solvents.

These are in opposition to the results for tetraalkylammonium ion (R_4N^+), for which $\lambda_0^+ \cdot \eta$ decreases with increasing the ionic size in the order $Et_4N^+ < Pr_4N^+ < Bu_4N^+ < (i\text{-Am})_3BuN^+$ in each solvent, as is hydrodynamically expected.[1,6–10,16]

It is considered that there exist three main factors for solute-solvent interactions of [Co(acac)$_2$(diamine)]$^+$: (1) Lewis acid-base interaction ; (2) an ion-dipole interaction; and (3) van der Waals interactions. Table 4 gives the solvent properties: (1-a) donor number (DN),[17] (1-b) acceptor number (AN);[17] (2) dipole moment (μ);[11] (3) solubility parameter (δ).[18] These parameters correspond to the above factors (1—3), respectively.

The alcohols have both basic (oxygen atom) and acidic (OH proton) parts for which the corresponding parameters are DN and AN, respectively (Table 4).

Table 4. Solvent Parameters

Solvent	DN[a]	AN[b]	μ[c]	δ[d]
MeOH	19	41.3	1.70	14.5
EtOH	20	37.9	1.69	12.7
n-PrOH	—	—	1.68	11.9
i-PrOH	—	33.5	1.66	11.5
Me$_2$CO	17	12.5	2.88	9.9
MEK	—	—	2.74	9.3
MIBK	—	—	2.79	8.4
PhNO$_2$	4.4	14.8	4.22	10.0
1,2-DCE	0	16.7	1.40	9.8

a) Donor number (DN), Ref. 17. b) Acceptor number (AN), Ref. 17. c) Dipole moment (μ), Ref. 11. d) Solubility parameter (δ), Ref. 18.

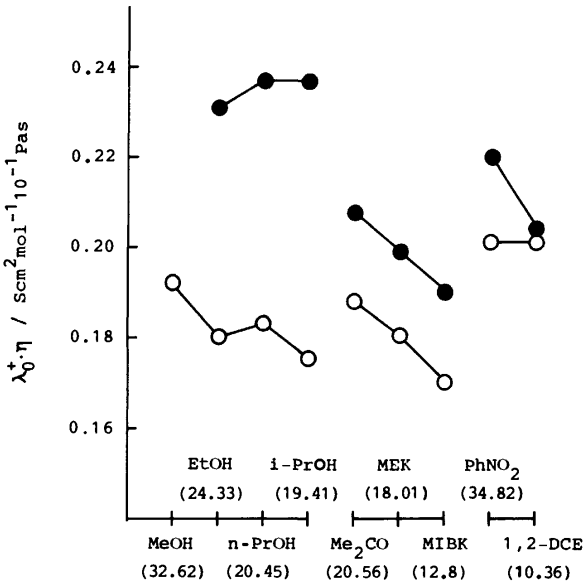

Fig. 1. Walden products for O, $[Co(acac)_2(en)]^+$ and ●, $[Co(acac)_2(N,N,N',N'\text{-tmen})]^+$. The values in parentheses are the dielectric constant (ε) of each solvent.

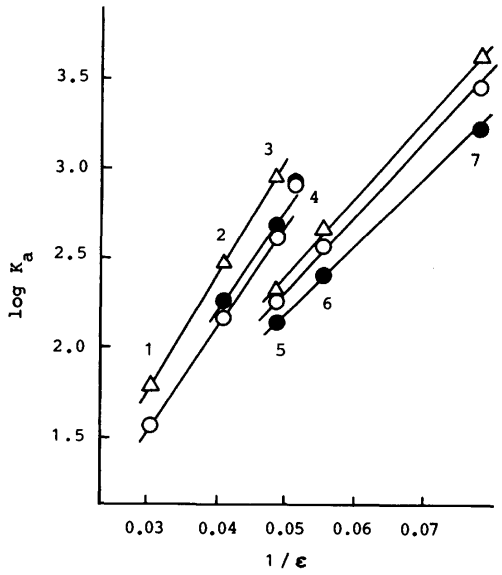

Fig. 2. Plots of log K_a with $1/\varepsilon$ for O, $[Co(acac)_2(en)]ClO_4$; ●, $[Co(acac)_2(N,N,N',N'\text{-tmen})]ClO_4$; and △, Et_4NClO_4.
Alcohols: 1, MeOH; 2, EtOH; 3, *n*-PrOH;[3] 4, *i*-PrOH. Ketones: 5, Me_2CO;[3] 6, MEK; 7, MIBK.

Thus, they can solvate the NH protons of the ligand en and the oxygen atoms of the ligand acac in $[Co(acac)_2(en)]^+$. A molecular model for the solvation of $[Co(acac)_2(en)]^+$ by one alcohol molecule is possible without crowding. This acid-base interaction contributes to a lower mobility in the alcohols than in the ketones. The effect of an ion-dipole interaction (factor 2) in the alcohols is small due to their lower dipole moments. This was confirmed from the result in 1,2-DCE with low polarity, in which the mobility of $[Co(acac)_2(en)]^+$ was comparable to that of $[Co(acac)_2(N,N,N',N'\text{-tmen})]^+$.[1]

The ketones have a basic (CO group) part and act as a hydrogen bonding donor for the NH protons in $[Co(acac)_2(en)]^+$ (factor 1-a). This solvation may result in a lower mobility. However, since the μ values of the ketones are smaller than that of $PhNO_2$ which strongly solvates the NH protons by an ion-dipole interaction,[1] factor 2 is not so effective.

Further, it is noteworthy that the Walden products for $[Co(acac)_2(N,N,N',N'\text{-tmen})]^+$ in the ketones are much smaller than in the alcohols, as is shown in Table 3. On the other hand, for Bu_4N^+ there is no appreciable change with solvents: $\lambda_0^+ \cdot \eta$ is 0.212,[6] 0.213,[7] 0.209,[7] and 0.211[8] for MeOH, EtOH, *n*-PrOH, and *i*-PrOH, and 0.201[9] and 0.199[10] for Me_2CO and MEK, respectively.

Since $[Co(acac)_2(N,N,N',N'\text{-tmen})]^+$ has no NH protons, another factor should be considered regarding the decreased mobility in the ketones. Van der Waals forces between $[Co(acac)_2(N,N,N',N'\text{-tmen})]^+$ and the ketones/alcohols may be operative compared to $[Co(acac)_2(en)]^+$, because the charge of Co(III) is shielded by the bulky ligands, *N,N,N',N'*-tmen and acac. The solubility parameter, δ is an indication for the van der Waals interactions. Although δ values of charged species are not available, δ values of $[Co(acac)_3]$ (9.72, 10.12, and 10.7)[19] are more close to those of the ketones than the alcohols (Table 4), suggesting that the ketone molecules solvate more strongly $[Co(acac)_2(N,N,N',N'\text{-tmen})]^+$. Furthermore, the fact that the chelate electrolyte is more soluble in the ketones than the alcohols supports the above view. Another factor may be dipole (ion)–dipole (solvent) interactions, because of the polarity of this cation, in addition to ion-dipole (solvent) interactions. These effects are also larger for ketones with high polarity.

(b) Ionic Association: Figure 2 shows that the variation of K_a with $1/\varepsilon$ for $[Co(acac)_2(diamine)]ClO_4$ and Et_4NClO_4. With good approximations, straight lines are obtained for all electrolytes, as is expected from the coulombic theory of ionic association,[20]

$$\log K_a = e^2 / akT \cdot 1/\varepsilon + \log K_a^\circ, \qquad (2)$$

where a is the contact distance between the cation and the anion, k is the Boltzman constant and T is the absolute temperature. K_a° contains the contribution to the association for all factors, except for the long-range coulombic interaction.

Two trends are shown: (i) Each electrolyte is more associated in the alcohols than the ketones at the same dielectric constant and (ii) the slope of log K_a vs. $1/\varepsilon$ is a little larger in the alcohols than the ketones. Trend (i) has been observed for tetraalkylammonium per-

chlorates:[7-9] The larger association constant in the alcohols could be explained in terms of (1) diminution in dielectric constant in the vicinity of an ion pair and (2) a multiple-step association process with solvation and desolvation of ClO_4^- by the alcohol molecules. The increasing effect of K_a due to this multiple-step association process[8,9] increases in the order MeOH< EtOH<*n*-PrOH<*i*-PrOH, which may be responsible for trend (ii).

The different pattern of K_a for [Co(acac)$_2$(diamine)]-ClO$_4$ was observed. In the ketones, K_a for [Co(acac)$_2$-(en)]ClO$_4$ is larger than that for [Co(acac)$_2$(*N*,*N*,*N'*,*N'*-tmen)]ClO$_4$. In the alcohols, on the other hand, the reverse trend is observed although the difference in K_a is small. Since [Co(acac)$_2$(*N*,*N*,*N'*,*N'*-tmen)]$^+$ has a large molal volume compared to [Co(acac)$_2$(en)]$^+$, its cation charge may be more shielded. Therefore, K_a for [Co(acac)$_2$(*N*,*N*,*N'*,*N'*-tmen)]ClO$_4$ should be smaller than that for [Co(acac)$_2$(en)]ClO$_4$, though this is not the case in alcohols.

An explanation is based on the strong solvation of [Co(acac)$_2$(en)]$^+$ by the alcohols: solvation of the NH protons (en) by the oxygen atom of alcohols and of the oxygen atoms (acac) by the OH proton of the alcohols through hydrogen bonding, as is discussed in the preceding section. This leads to the formation of strongly solvated cation and the cation may be behave as a distinct entity which has a larger molal volume compared to [Co(acac)$_2$(*N*,*N*,*N'*,*N'*-tmen)]$^+$. However, the steric structure of the chelate cation would not be affected, even if the alcohols solvate the cation firmly. This has been confirmed from a result which showed that the absorption spectra of $^1A_{1g}$–$^1T_{1g}$ have no appreciable change with solvents.[15] In the ketones, the NH protons in [Co(acac)$_2$(en)]$^+$ are solvated by the oxygen atom of the CO group. However, since they have no acidic part for solvation of the acac in [Co(acac)$_2$(en)]$^+$, the solvation may not be so effective compared to that by the alcohols.

The K_a values in *i*-PrOH are larger than those expected from the line of the plots of the primary alcohols, showing weaker solvation by *i*-PrOH, which may result from its lower acidity or steric hindrance.

(2) Solvation and Association of [Co(β-dik)$_2$(en)]-ClO$_4$: The coordinated acac in this type of metal-chelate cations is of pseudo aromatic character with a ring current[21] and has a electron-mediating ability. Therefore, it is expected that the introduction of the electron-withdrawing substituents, Br and NO_2 at the C-3 position of the acac in [Co(acac)$_2$(en)]$^+$ increases the relative acidity of the NH protons of the ligand en through the pseudo aromatic chelate ring, although these are far from the substituents. This is justified from the result that the rate of H-D exchange of the NH protons in a deuterium oxide/dimethyl-d_6-sulfoxide mixture (weight ratio 1:3.9) by ^{1}H NMR measurement increase in the sequence acac<acacBr<

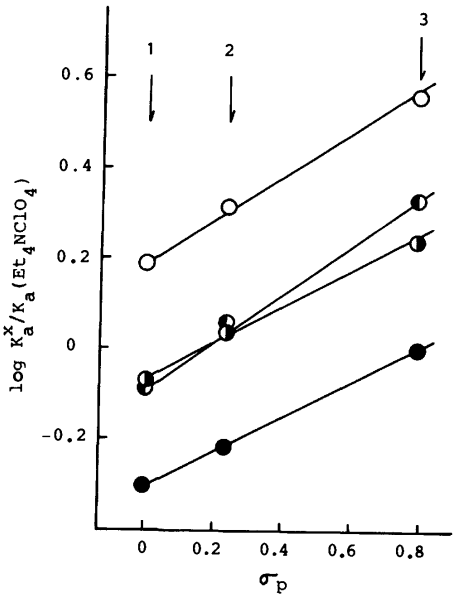

Fig. 3. Hammett's relationship for the ratio of K_a for [Co(β-dik)$_2$(en)]ClO$_4$ to Et$_4$NClO$_4$.
β-dik: 1, acac; 2, acacBr; 3, acacNO_2. Organic solvents: ●, EtOH; ◑, Me_2CO; ◐, MEK; ○, $PhNO_2$.[1,5]

acacNO_2,[5] in accordance with Hammett's σ_p values of electron-withdrawing tendency of the substituents.

Figure 3 shows a plot of the ratio of K_a for [Co(β-dik)$_2$(en)]ClO$_4$ to Et$_4$NClO$_4$ vs. Hammett's σ_p value. Since the Et$_4$N$^+$ ion has no specific site for solvation or ion pair formation in each solvent, the change in the ratio of K_a may suggest specific interactions of the chelate electrolytes. The trends indicated in Fig. 3 show two characteristics: (i) The ratio of K_a for [Co(acac)$_2$(en)]ClO$_4$ to Et$_4$NClO$_4$ increases in the order EtOH<MEK≈Me_2CO<$PhNO_2$, and (ii) the ratio increases in the same order [Co(acac)$_2$(en)]ClO$_4$< [Co(acacBr)$_2$(en)]ClO$_4$<[Co(acacNO_2)$_2$(en)]ClO$_4$ as the rate of H-D exchange. Furthermore, a linear relationship with a similar slope is obtained for all the solvent systems.

For [Co(acac)$_2$(en)]ClO$_4$, a solvent-separated ion pair is formed in the alcohols and ketones and the solvation of the cation by the alcohols is much stronger. On the other hand, a contact ion pair between the NH protons and ClO_4^- is formed in $PhNO_2$ by a partial exclusion of nitrobenzene molecules, leading to a larger K_a value.[1] These correspond to the order of the ratio of K_a for [Co(acac)$_2$(en)]ClO$_4$ to Et$_4$NClO$_4$, EtOH<MEK≈Me_2-CO<$PhNO_2$.

For the introduction of substituents, Br and NO_2, the two effects on the increase in K_a should be considered: (1) The increase in the relative acidity of the NH protons in the ligand en, leading to a stronger interaction between the NH protons and ClO_4^- and (2) the increase in the polarity of the chelate cations,

leading to a stronger cation–anion interaction. At the same time, the two effects also enhance the solvation of the cations, leading to a decrease in K_a. The increased solvation of the cations is supported by the fact that the introduction of Br and NO_2 largely decreases the mobility of the cations in the order acac>acacBr> acacNO_2 (Table 3). In practice, however, since K_a values are increased by the introduction of Br and NO_2, the decreasing effect of solvation on K_a is overcome by the increasing effects, (1) and (2). In EtOH, since the $[Co(acac)_2(en)]^+$ cation is strongly solvated, the increase in K_a by the introduction of Br and NO_2 is attributed to effect (2). In Me_2CO and MEK, a solvent-separated ion pair is similarly formed, although the solvation is not so effective compared to that in EtOH. Thus, it seems that the contribution of effect (1) is small and that of effect (2) is large. In $PhNO_2$, where a contact ion pair between the NH protons and ClO_4^- is formed, the contribution of both effects (1) and (2) is considered. However, in view of the fact that the slope for $PhNO_2$ is similar to that for EtOH (Fig. 3), it is likely that effect (2) is predominant.

References

1) K. Ito, *Inorg. Chem.*, **22**, 2872 (1983).

2) K. Ito, E. Iwamoto, and Y. Yamamoto, *Bull. Chem. Soc. Jpn.*, **55**, 3190 (1982).

3) K. Ito, E. Iwamoto, S. Suehisa, H. Isono, and Y. Yamamoto, *Bull. Chem. Soc. Jpn.*, **59**, 3841 (1986).

4) K. Ito, E. Iwamoto, K. Hasegawa, M. Yamamoto, and Y. Yamamoto, *Bull. Chem. Soc. Jpn.*, **58**, 1287 (1985).

5) K. Ito, H. Isono, E. Iwamoto, and Y. Yamamoto, *Inorg. Chem.*, **23**, 850 (1984).

6) R. L. Kay, C. Zawoyski, and D. F. Evans, *J. Phys. Chem.*, **69**, 4208 (1965); R. L. Kay, D. F. Evans, and G. P. Cunningham, *ibid.*, **73**, 3322 (1969).

7) D. F. Evans and P. Gardam, *J. Phys. Chem.*, **72**, 3281 (1968). $\lambda_0^-(ClO_4^-)$=32.04 was obtained from Λ_0 (Et_4NClO_4) and λ_0^+ (Et_4N^+).

8) S. M. A. Matesich, J. A. Nadas, and D. F. Evans, *J. Phys. Chem.*, **74**, 4568 (1970).

9) D. F. Evans, J. Thomas, J. A. Nadas, and S. M. A. Matesich, *J. Phys. Chem.*, **75**, 1714 (1971).

10) S. R. C. Hughes and D. H. Price, *J. Chem. Soc. A*, **1967**, 1093. λ_0^- (ClO_4^-)=93.0 was obtained from Λ_0 (Et_4NClO_4) and λ_0^+ (Et_4N^+).

11) "Handbook of Chemistry and Physics," 64th ed., ed. by R. C. West, CRC Press: Florida (1983). The dielectric constant (ε=12.8) for MIBK at 25 °C was estimated from 13.11 (ε) for MIBK at 20 °C and the temperature dependence of the dielectric constants for Me_2CO and MEK.

12) The equivalent conductance data at various concentrations of $[Co(\beta\text{-dik})_2(diamine)]ClO_4$ and Et_4NClO_4 in the alcohols and the ketones at 25 °C can be ordered directly to the author (K.I.).

13) R. M. Fuoss and K. L. Hsia, *Proc. Natl. Acad. Sci. U.S.A.*, **57**, 1550 (1967); R. Fernández-Prini, *Trans. Faraday Soc.*, **65**, 3311 (1969).

14) λ_0^- (ClO_4^-)$\cdot\eta$ (=0.34) in MIBK was estimated from (a) 0.36 for λ_0^- (ClO_4^-)$\cdot\eta$ in Me_2CO and 0.35 in MEK and (b) $\Lambda_0\cdot\eta$ for the chelate electrolytes in Me_2CO, MEK, and MIBK.

15) This is further confirmed from the result that the *N*-methylation lengthens the Co–N bond length, which is justified from the absorption peak in the visible region of $^1A_{1g}$–$^1T_{1g}$ red-shifted with *N*-methylation (541 and 542 nm for $[Co(acac)_2(en)]^+$ and 598 and 596 nm for $[Co(acac)_2(N,N,N',N'$-tmen)]$^+$ in *n*-PrOH and Me_2CO, respectively, in analogy with the results in $PhNO_2$ and 1,2-DCE (Ref. 1)).

16) R. Fernández-Prini, "Physical Chemistry of Organic Solvent Systems," ed. by A. K. Covington and T. Dickson, Plenum Press, London (1973), Chap. 5.

17) V. Gutmann, "The Donor-Acceptor Approach to Molecular Interactions," Plenum Press, New York (1978).

18) A. F. M. Barton, *Chem. Rev.*, **75**, 731 (1975).

19) M. Yamamoto and Y. Yamamoto, *Anal. Chim. Acta*, **87**, 375 (1976); J. F. Huber, F. C. Kraak, and H. Veening, *Anal. Chem.*, **44**, 1554 (1972).

20) W. R. Gilkerson, *J. Chem. Phys.*, **25**, 1199 (1956); R. M. Fuoss, *J. Am. Chem. Soc.*, **80**, 5059 (1958).

21) J. J. Bellary and R. F. Branch, *J. Chem. Soc.*, **1945**, 4491; J. P. Colemann, R. L. Marchall, and W. L. Young III, *Chem. Ind. (London)*, **1962**, 1380.

 © 1988 The Chemical Society of Japan Bull. Chem. Soc. Jpn., 61, 4083—4086 (1988)

The Potentiometric Detection of Complex Formation between IgG and anti-IgG Using a Chemically Modified Tantalum Electrode

Toshihiko TANAKA,† (the late) Naoto YAMAMOTO, and Hiroshi TSUBOMURA*
Faculty of Engineering Science, Osaka University,
1-1 Machikaneyama, Toyonaka, Osaka 560
†Takatsuki Research Laboratory, Sumitomo Chemical Co., Ltd.,
2-10-1 Tsukahara, Takatsuki, Osaka 569
(Received April 2, 1988)

Tantalum electrodes were chemically modified with anti-IgG to detect IgG (immunoglobulin G) or with IgG to detect anti-IgG by using cyanuric bromide. Changes in the potential as a result of the antigen-antibody reaction can be explained by a simple first-order kinetics equation, while the polarity of the changes at various pH's can be explained in terms of the charge transfer between anti-IgG and IgG in a way similar to that shown in previous reports for the case of Ti electrodes. The surface modification was confirmed by Auger Electron Spectroscopy (AES).

Many kinds of electrochemical methods have been investigated in order to detect biological substances.[1-7] Among them, the potentiometric detection method using chemically modified electrodes,[4-7] developed in our laboratory, is unique in that the responses depend directly on the complex formation on the electrode surface, and so quantitative detection can be achieved without using any enzymes which produce H_2O_2, NH_4^+ , or other electrochemically active species. For example, antigen (hCG) was detected[4-6] by the use of a titanium electrode chemically modified with antibody (anti-hCG) without being marked by any reactive chemicals like peroxidase. In a similar way, other immunological substances, enzymes (e.g., trypsin), or enzyme inhibitor (e.g., aprotinin) were detected by the use of modified titanium or tungsten electrodes.[6,7]

The stability in the potential of these chemically modified electrodes critically influences the detection limits, reliability, accuracy, and precision of the potentiometric determination. In a recent attempt, we coated a tungsten electrode with a plasma polymerized film prior to the chemical modification in order to improve its electrochemical stability.[7] Tantalum/tantalum oxide electrodes were foumd by Lerner et al.[8] to be stable as implanted stimulating electrodes.

In this paper, a tantalum electrode chemically modified with an antibody (anti-human IgG-Fc, momoclonal) and an antigen (human IgG) were investigated to determine their possible use as a potentiometric sensors for an antigen (human IgG) and an antibody (anti-human IgG) respectively. The kinetic properties and the pH effects on the response of the tantalum electrodes were also investigated for the further elucidation of the potential change.

Electron spectroscopic analysis techniques such as X-ray photoelectron spectroscopy (XPS), Auger electron spectroscopy (AES), and electron energy-loss spectroscopy (ELS) are efficient for analyzing the surfaces of chemically modified electrodes. The surfaces of graphite, tin oxide, and indium oxide electrodes chemically modified with hydroxymethylferrocene (HMF) or 1,1′-bis(hydroxymethyl)ferrocene (BHMF) by using cyanuric chloride were investigated by means of XPS by Yacynych and Lin.[9,10] In this report, the chemical modification of a tantalum surface by using cyanuric bromide was monitored by AES.

Experimental

Material. Lyophilized IgG from human serum (98% pure) was obtained from the Green Cross Co. The anti-human IgG-Fc, monoclonal antibody, and lyophilized bovine serum albumin (BSA) were obtained from Wako Pure Chemical Industries Ltd. Tantalum sheets, 0.1 mm thick and 99.9% pure, for the surface investigations, and a tantalum rod 4 mm in diameter (99.95% pure) for use as an electrode were obtained from the Japan Lamp Industrial Co., Ltd.

Preparation of Tantalum Electrodes. Figure 1 shows the structure of a typical tantalum electrode for the potentiometric measurement; it consists of a tantalum tip 4 mm in diameter, a tantalum rod 2 mm in diameter and 40 mm in length, a stainless steel nut, and a chlorotrifluroethylene (CTFE) pipe. The tantalum tip was washed by ultrasonifi-

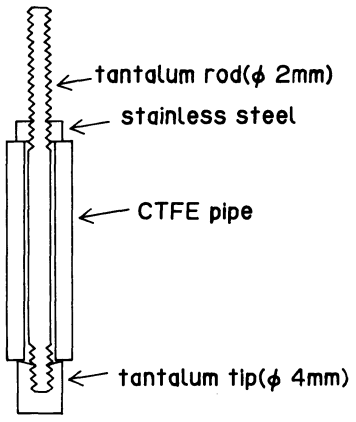

Fig. 1. The structure of a tantalum electrode.

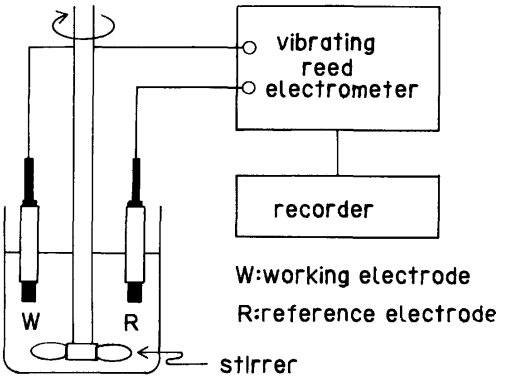

Fig. 2. A schematic illustration of the apparatus for the potentiometric measurement.

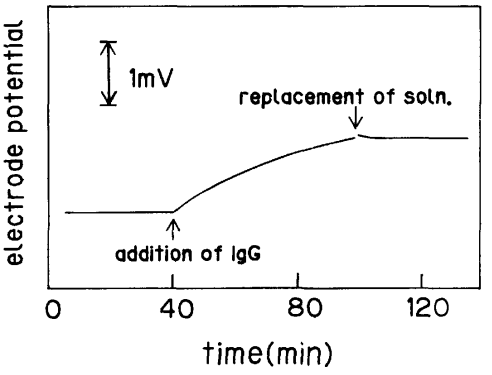

Fig. 3. The potential change of an anti-IgG-Fc electrode caused by addition of human IgG(2.5×10^{-8} M) in veronal buffer (pH 8.6).

cation in 2 M hydrochloric acid (1 M=1 mol dm^{-3}), a 2 M sodium hydroxide solution, acetone, and then in purified water, each for 10 min. Then the tip was treated with a ca. 500 V low-frequency plasma discharge in a vacuum chamber for 20 min under an oxygen atmosphere of 0.15 Torr (1 Torr≈133.322 Pa) before chemical modification.

Chemical Modification. The chemical modification of the tantalum electrode surface was performed by a method similar to that of March et al.[11] The tip was chemically activated in a stirred aqueous solution containing 1.2 M sodium carbonate, 0.5 M cyanogen bromide, and 1 M acetonitrile. Then, the tip was immersed in a borate buffer solution (pH 8.1) containing a 0.02 wt% anti-human IgG-Fc monoclonal antibody for 90 min to form an anti-IgG-Fc electrode. A human IgG electrode was made similarly in a buffer solution containing 0.02 wt% human IgG instead of anti-human IgG-Fc. A BSA electrode, used as the reference, was similarly made in a buffer containing 0.02 wt% BSA instead of human IgG. At the end of the chemical modification, all the electrodes were immersed in a borate buffer solution (pH 8.1) containing 0.7 M urea for 30 min in order to block the unreacted part of the electrode surface.

Potentiometric Measurement. The potential between the working and reference electrodes were measured by using a vibrating reed electrometer, TR8411, of the Takeda Riken Industry Co., Ltd. The experimental set-up is shown schematically in Fig. 2. The solution in the measuring vessel is a 15 ml veronal buffer solution (pH 8.6, 0.05 M) kept at 30°C and stirred constantly. The pH effect was measured in Britton Robinson buffers[12] whose ionic strength was adjusted to 0.1 by diluting with water,[13] although it is known from our previous work that the ionic strength of a solution scarcely affects the electrode response.

Surface Analysis. The structure of the tantalum surfaces at each step of the chemical modification were investigated by AES using a PhiModel 10-155 cyrindrical mirror analyzer (CMA) at an electron-beam voltage of 3.0 keV and with a current of 10^{-6} A. The differential spectra were obtained by a 6 V modulation. Tantalum sheets (13 mm×13 mm) were treated in the same manner as with the anti-human IgG-Fc electrodes and were then used as specimens for the surface analysis.

Results and Discussion

Potentiometric Measurement. Compared with the titanium electrode used in our previous work, the tantalum electrode is electrochemically more stable, and the time necessary for stabilizing the electrode potentioal for the tantalum electrode became about one tenth of that for the titanium electrodes.

As is shown in Fig. 3, the potential of an anti-human IgG-Fc electrode changes irreversibly to the positive upon the addition of human IgG to the veronal buffer solution at pH 8.6. The potential did not, however, change after the replacement of the sample solution with a fresh buffer solution. In an irreversible case, the complex-formation on the surface is expressed as follows:[4-6]

$$A_{fixed} + B \xrightarrow{k} C \qquad (1)$$

where A_{fixed} is an immobilized antibody on the surface; B, an antigen in solution; C, the complex formed on the surface, and k, the rate constant. On the assumption that the potentiometric response of the electrode, $U(t)$, is proportional to the surface concentration of C, [C], $U(t)$ is expressed as follows:

$$U(t) = U_m [1 - \exp(-k[B]_0 t)] \qquad (2)$$

where $[B]_0$ is the initial concentration of [B], t is the reaction time after the addition of B, and U_m is the response to be realized when all surface fixed anti-IgG molecules are complexed. In this equation, [B] is assumed to keep the initial value $[B]_0$, because the quantity of B in the solution is much larger than that of A_{fixed}. The obtained potential changes from Fig. 3 fit in well with Eq. 2, and by treating the data, $k=3.8\times10^4$ ($M^{-1}\,s^{-1}$) and $U_m=1.3$ mV (pH 8.6, 30°C) are derived. The k value is of the same order of magnitude as the $k=1.6\times10^4$ ($M^{-1}\,s^{-1}$) previously obtained for a titanium anti-hCG electrode to hCG.

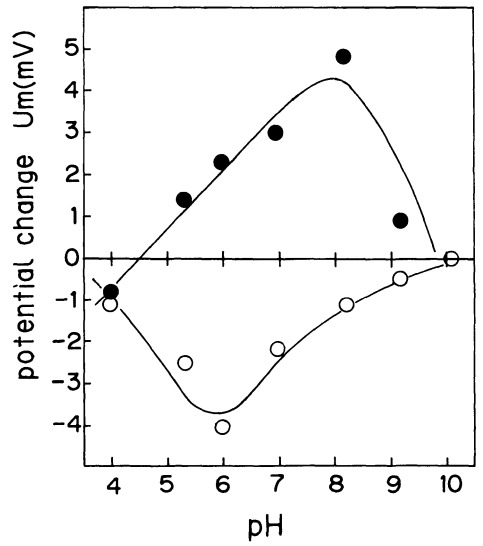

Fig. 4. The response of anti-IgG and IgG electrodes at various pH. ●: an anti-IgG electrode by an addition of IgG. ○: an IgG electrode by an addition of anti-IgG.

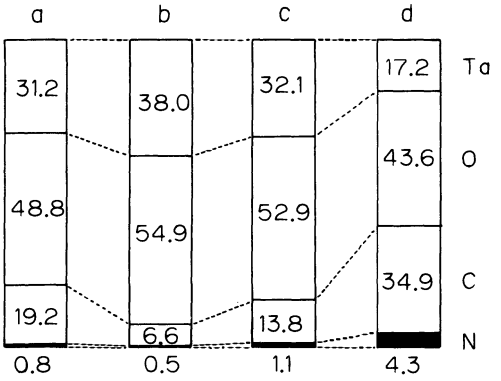

Fig. 5. The atomic concentration(%) of a tantalum surface measured by AES for each step of chemical modification. (a) After washing, (b) after O_2 plasma treatment, (c) after CNBr treatment, (d) after immersing in antibody soln.

The k values for reactions between various sets of antigens and antibodies, as determined by Karush, lie between 2×10^5 (M^{-1} s^{-1}) and 4.8×10^8 (M^{-1} s^{-1}).[14] Our present values are appreciably smaller than Karush's, like those obtained in our previous work.[4-6]

The antigen-antibody complex formed on the tantalum electrode can be dissociated by immersing it in a 2 M $MgCl_2$ stirred aqueous solution containing 1 M urea for 20—30 min. After this has been done, the anti-IgG electrode again shows a response to the antigen. Thus, the electrode could be used 7 to 8 times, although the response gradually became small; the potential could be restored by immersion in a fresh buffer. This degradation indicates a denaturation of the antibody by urea. In the case of IgG electrodes, the potential change upon the addition of anti-IgG-Fc is of almost the same order of magnitude as in the case of the anti-IgG-Fc electrode upon the addition of IgG except that the direction is negative.

pH Effect. The U_m values for the anti-IgG electrode in the reaction with IgG were determined from the data of the potential shift and Eq. 2 at various pH's. The U_m values thus obtained are always positive, from pH=5 to 9.2 (Fig. 4). The negative value at pH4 might have been caused by the partial denaturation of the protein, and so this value can be omitted. On the other hand, for the IgG electrode, the U_m value is always negative, from pH=4 to pH=9.2, with the minimum at pH=6. These results (shown in Fig. 4) indicate that the direction of the potential shift in the anti-IgG electrode is generally the opposite of that in the IgG electrode. As can be seen from Eq. 2, the U_m value is independent of the kinetics of the reaction or the binding energy between the proteins. It should be dependent on (1) the electrical dipole moment or the charge polarization between the antigen and antibody and (2) the coverage of the protein chemically attached to the electrode surface, because the change of the surface potential is linearly dependent on the electrical double layer at the interface, that is, the polarization per unit of surface area. Therefore, the results shown in Fig. 4 indicate that the direction of the electrical polarization between complexed protein molecules is independent of the pH. This implies that the polarization is mainly caused by a weak chemical bonding (a sort of charge transfer complexation or hydrogen bonding) between antigen and antibody. If, on the other hand, we assume that the potential shift is caused by the net charge of the protein molecule to be detected, its direction must be reversed at its isoelectric point (pH=5.8—7.3). The results in Fig. 4 clearly show this is not the case.

Surface Analysis. Figure 5 shows the relative atomic concentrations of the electrode surface at the successive steps of the chemical modification, calculated from the AES peak to peak heights for Ta(174 eV), C(273 eV), N(384 eV), and O(510 eV).[15] As the surface concentrations of N and C decrease from (a) to (b), one can see that organic contaminations are taken away by O_2 plasma treatment. The increase in the concentrations of N and C from (b) to (c) shows the attachment of an organic group such as imidocarbonate by BrCN. The incerase in the concentrations of N and C from (c) to (d) shows the attachment of a significant amount of anti-IgG to the surface. These results confirm each of the steps of the chemical treatment and support the idea that the result obtained from the potentiometric measurement is really caused by the specific complexing of immuno-proteins.

In conclusion, the specific detection of immunoactive proteins , IgG or anti-IgG, can be performed by the use of a tantalum electrode modified with the

antibody or antigen. The steps of the protein immobilization of the tantalum surface have been confirmed by AES.

References

1) R. M. Ianniello, T. J. Lindsay, and A. M. Yacynych, *Anal. Chim. Acta*, **141**, 23 (1982).
2) R. M. Ianniello, T. J. Lindsay, and A. M. Yacynych, *Anal. Chem.*, **54**, 1098 (1982).
3) R. M. Ianniello, T. J. Lindsay, and A. M. Yacynych, *Anal. Chem.*, **54**, 1980 (1982).
4) N. Yamamoto, Y. Nagasawa , M. Sawai, S. Sudo, and H. Tsubomura, *J. Immunol. Methods*, **22**, 309 (1978).
5) N. Yamamoto, Y. Nagasawa, S. Shuto, H. Tsubomura, M. Sawai, and H. Okumura, *Clin. Chem.*, **26**, 1569 (1980).
6) N. Yamamoto, S. Shuto, and H. Tsubomura, *Appl. Biochem. Biotech.*, **6**, 319 (1981).
7) N. Yamamoto, S. Nagaoka, T. Tanaka, T. Shiro, K. Honma, and H. Tsubomura, Proceedings of the International Meeting on Chemical Sensors, Fukuoka, Japan, Sept 19—22, Kodansha-Elsevier (1983).
8) H. Lerner, R. Z. Zahradnik, and M. Buchbinder, *IEEE Trans. Biomed. Eng.*, **BME-29** (4), 290 (1982).
9) A. W. C. Lin, P. Yeh, A. M. Yacynych, and T. Kuwana, *J. Electroanal. Chem.*, **84**, 411 (1977).
10) A. M. Yacynych and T. Kuwana, *Anal. Chem.*, **50**, 640 (1978).
11) S. C. March, I. Parich, and P. Cuatrecasas, *Anal. Biochem.*, **60**, 149 (1974).
12) H. T. S. Britton and R. A. Robinson, *J. Chem. Soc.*, **1931**, 458, 1456.
13) J. A. C. Frugoni, *Gass. Chim. Ital.*, **87**, 403 (1957).
14) F. Karush, *Compr. Immunol.*, **5** (immunoglobulins), 85 (1978).
15) L. E. Davis et al., "Handbook of Auger Electron Spectroscopy", second ed., Physical Electronics Division, Perkin Elmer Co., Minnesota, U.S.A. (1978).

 © 1988 The Chemical Society of Japan Bull. Chem. Soc. Jpn., 61, 4087—4092 (1988)

Transesterification Reaction of Tetraethoxysilane and Butyl Alcohols

Isao HASEGAWA and Sumio SAKKA*,†
Division of Molecular Engineering, Graduate School of Engineering, Kyoto University, Sakyo-Ku, Kyoto, Kyoto-Fu 606
†Institute for Chemical Research, Kyoto University, Uji, Kyoto-Fu 611
(Received June 14, 1988)

Tetraethoxysilane was treated with Amberlyst 15 cation-exchange resin in the presence of butyl alcohols. On treating the mixture of tetraethoxysilane and 1-butanol, the transesterification took place in which butoxyl groups were substituted for ethoxyl groups in tetraethoxysilane. The degree of the transesterification depended on the molar ratio of tetraethoxysilane to 1-butanol of the mixture. The distribution of alkoxysilane species present in the tetraethoxysilane–1-butanol solution was compared with the tetrabutoxysilane–ethanol solution, and it was found that the degree of the transesterification depended on the ratio of numbers of alkyl groups in tetraalkoxysilane and alcohol used. The time required for equilibrium in the distribution of alkoxysilane species in the solution was different with the variety of butyl alcohols used, suggesting the presence of steric effect of butyl alcohols on this reaction.

Tetraethoxysilane ($Si(OC_2H_5)_4$, abbreviated to TEOS) has been widely used for syntheses of silica-based materials as starting material for silica, especially for the synthesis of silica glass by the sol–gel method.[1] For the preparation of silica gels, the mixture of TEOS, alcohol as solvent, water for the hydrolysis and catalyst, such as hydrochloric acid, is usually used. In the course of hydrolysis and polymerization of TEOS, it is reported that transesterification, in which alcohols used displace ethoxyl groups in TEOS to produce ethanols, occurs.[2,3]

The purpose of this study is to investigate the transesterification reaction between TEOS and different isomers of butyl alcohols by using Amberlyst 15 cation-exchange resin. Since no water is used in this study, polymerization reaction caused by the hydrolysis of TEOS can be suppressed to a low percentage.

Amberlyst 15 is a powerful proton donor which acts for the cleavage of siloxane bond in the similar way to trichloroacetic acid and concentrated sulfuric acid.[4] This cation-exchange resin has been used for the post-treatment of trimethylsilylation of silicates, since incompletely trimethylsilylated derivatives with a silanol group or alkoxyl groups are formed in the crude products.[5–7] The trimethylsilylation reaction is completed by treating the crude products in the excess of hexamethyldisiloxane with Amberlyst 15. It is also reported that partially trimethylsilylated derivatives from tetraalkoxysilanes or alkyltriethoxysilanes are produced by treating them with Amberlyst 15 in the presence of hexamethyldisiloxane.[8,9]

Experimental

Materials. Tetraethoxysilane, tetrabutoxysilane ($Si(OC_4H_9)_4$, TBOS), 1-butanol (Bu^nOH), 2-butanol (Bu^sOH), 2-methyl-1-propanol (Bu^iOH), 2-methyl-2-propanol (Bu^tOH), and ethanol (EtOH) were of reagent grade. Amberlyst 15 cation-exchange resin was used after heating in an oven of 80 °C and cooling in a desiccator, as suggested by Garzó et al.[10]

Preparation of Solutions. TEOS was added to 1-butanol so that the mixed solutions might have various mixing molar ratio. The mixing molar ratio of alcohol (ROH) to tetraalkoxysilane (TAOS) is expressed as the ROH/TAOS ratio in this study. After stirring 20 cm^3 of the mixture for 5 min for homogenization of the solution, 0.5 g of Amberlyst 15 was added. After the vessel of the solution was sealed up, the solution was kept standing in an oven of 40 °C. In this way, the solutions with the Bu^nOH/TEOS ratios from 1.0 to 10.0 were prepared.

In order to estimate the degree of polymerization of TEOS which occurs as a side reaction, the TEOS–EtOH solutions whose EtOH/TEOS ratios ranged from 1.0 to 10.0 were prepared by mixing TEOS and ethanol. Quantity of the monomeric species after Amberlyst treatment can be estimated as the residual ratio of TEOS, since only the compounds with ethoxyl groups are present in this system even when the transesterification reaction occurs.

For comparison of the distribution of ester-exchanged derivatives in the TEOS–Bu^nOH solutions, the TBOS–EtOH solutions with the EtOH/TBOS ratios from 1.0 to 8.0 were prepared in the same way as described above by using TBOS and ethanol.

Moreover, for investigating the effect of the structure of butyl alcohols on the transesterification reaction, TEOS–Bu^iOH, TEOS–Bu^sOH, TEOS–Bu^tOH solutions at the BuOH/TEOS ratio of 4.0 were also prepared in the same way.

Analytical Procedure. All the solutions were analyzed with a Shimadzu GC-12A gas chromatograph equipped with a hydrogen flame ionization detector and a CLH-702 split sample injector for capillary gas chromatography. The analytical conditions were the same as those described in the previous paper.[8] Each peak on the gas chromatograms was identified with a JEOL JMS-DX 300 gas chromatograph-mass spectrometer in the same analytical conditions described previously.[9]

Quantitative analysis was performed on TEOS and TBOS by using tetradecane as an internal standard. Since standard samples of other compounds formed could not be obtained, however, the distribution of each alkoxysilane species in the solutions was expressed in terms of the peak area ratio.

Results and Discussion

Gas Chromatography. Figure 1 shows the gas chromatograms of (a) the TEOS-Bu^{n}OH solution without Amberlyst treatment, (b) the TEOS-EtOH solution with Amberlyst treatment and (c) the TEOS-Bu^{n}OH solution with Amberlyst treatment. These solutions were kept standing in an oven of 40 °C for 120 h and the ROH/TEOS ratios of the solutions are all 4.0. When Amberlyst 15 is not added, only the peak of TEOS, which is the starting material, is detected, indicating that no transesterification reaction occurs. When Amberlyst 15 is added, however, other peaks than TEOS appear, as seen in Fig. 1 (b) and (c). These peaks were identified by conducting combined gas chromatograph-mass spectrometry and the assignments of the peaks on Fig. 1 (a)—(c) are summarized in Table 1.

In this table, it is seen that polymerization of TEOS occurs by treating the TEOS-EtOH solution with Amberlyst 15, as hexaethoxydisiloxane ($Si_2O_7(C_2H_5)_6$) and octaethoxytrisiloxane ($Si_3O_{10}(C_2H_5)_8$) were detected. The peaks corresponding to other compounds than TEOS on the gas chromatogram shown in Fig. 1 (c) are assigned to partially or fully ester-exchanged products formed from TEOS and those from hexaethoxydisiloxane. This fact indicates that the transesterification reaction occurs by treating the mixture of TEOS and Bu^{n}OH with Amberlyst 15, although the polymerization occurs slightly at the same time.

Polymerization of TEOS by Amberlyst Treatment. Figure 2 shows the variation in the distribution of alkoxysilane species and the residual ratio of TEOS in the TEOS-EtOH solutions with the EtOH/TEOS ratio after treating with Amberlyst 15 at 40 °C for 120 h. With the increase of the EtOH/TEOS ratio, TEOS decreases, and the dimer ($Si_2O_7(C_2H_5)_6$) and trimer ($Si_3O_{10}(C_2H_5)_8$) increase, and the residual ratio of TEOS is only 66% at the EtOH/TEOS ratio of 10.0, suggesting that the polymerization as a side reaction

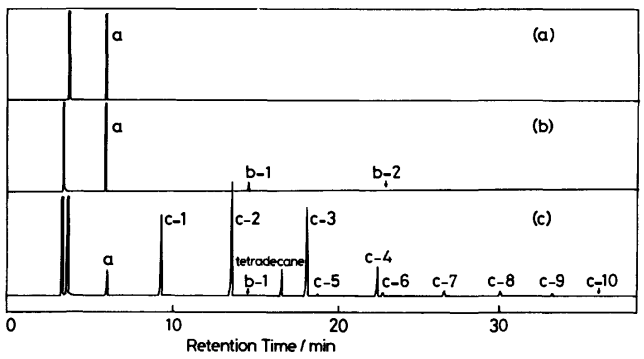

Fig. 1. Gas chromatograms of alkoxysilane species present in (a) the TEOS-Bu^{n}OH solution without Amberlyst treatment, (b) the TEOS-EtOH solution, and (c) the TEOS-Bu^{n}OH solution with Amberlyst treatment after keeping the solutions standing in an oven of 40 °C. The ROH/TEOS ratios of the solutions are all 4.0.

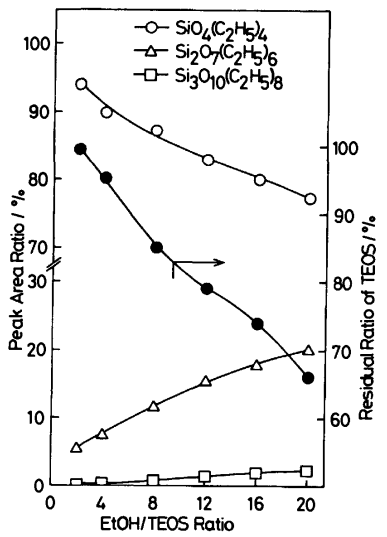

Fig. 2. Variation in the distribution of alkoxysilane species and the residual ratio of TEOS with the EtOH/TEOS ratio in the TEOS-EtOH solutions after treating with Amberlyst 15 at 40 °C for 120 h.

Table 1. Identification of Peaks on the Gas Chromatograms Shown in Fig. 1(a)—(c)

Peak	Retention time/min	Formula	Molecular weight
a	5.6	$SiO_4(C_2H_5)_4$	208
b-1	14.4	$Si_2O_7(C_2H_5)_6$	342
b-2	23.3	$Si_3O_{10}(C_2H_5)_8$	428
c-1	9.0	$SiO_4(C_2H_5)_3(C_4H_9)$	236
c-2	13.4	$SiO_4(C_2H_5)_2(C_4H_9)_2$	264
c-3	18.1	$SiO_4(C_2H_5)(C_4H_9)_3$	292
c-4	22.5	$SiO_4(C_4H_9)_4$	320
c-5	18.7	$Si_2O_7(C_2H_5)_5(C_4H_9)$	370
c-6	22.8	$Si_2O_7(C_2H_5)_4(C_4H_9)_2$	398
c-7	26.6	$Si_2O_7(C_2H_5)_3(C_4H_9)_3$	426
c-8	30.1	$Si_2O_7(C_2H_5)_2(C_4H_9)_4$	454
c-9	33.3	$Si_2O_7(C_2H_5)(C_4H_9)_5$	482
c-10	36.2	$Si_2O_7(C_4H_9)_6$	510

proceeds by this treatment.

It was reported that the recovery of the monomeric silicate species was only 0.3% after soaking the TEOS-EtOH-water-hydrochloric acid solution at the TEOS:EtOH:water:hydrochloric acid molar ratio of 1:7:2:0.01 in a water bath of 40 °C.[11] Although the residual ratio of TEOS is fairly low in the solutions at higher EtOH/TEOS ratios as is shown in Fig. 2, the value is much higher than the recovery of monomeric silicate species in the TEOS-EtOH-water-hydrochloric acid system, that is, water containing system after only 10 h of soaking at 40 °C. This fact suggests that polymerization of TEOS in the present study is fairly suppressed because of the absence of water. Therefore, it is thought that the ester-exchange reaction in TAOS-ROH solutions can be investigated with the Amberlyst treatment.

Transesterification of TEOS with 1-Butanol. Figure 3 shows the variation in the distribution of each alkoxysilane species present in the TEOS-Bu^{n}OH solutions with the Bu^{n}OH/TEOS ratio after Amberlyst treatment at 40 °C for 120 h and the recoveries of TEOS and TBOS at each Bu^{n}OH/TEOS ratio are shown in Fig. 4. The degree of transesterification varies with the Bu^{n}OH/TEOS ratio, increasing with increasing Bu^{n}OH/TEOS ratio. At the Bu^{n}OH/TEOS ratio of 20.0, 35.5% of TEOS added to the solution changes to TBOS after the treatment. It seems that there are optimum conditions for the formations of species with different ester-exchanged ratios. The optimum conditions for the formation of $Si(OEt)_3(OBu^n)$, $Si(OEt)_2(OBu^n)_2$, and $Si(OEt)(OBu^n)_3$ can be determined as the ratios of 2.0, 4.0, and 8.0, respectively, from Fig. 3.

Figure 3 also indicates that there may be no linear relationship on the optimum Bu^{n}OH/TEOS ratio for obtaining a species with a specific degree of transesterification as a main product. It appears, however, that larger amounts of Bu^{n}OH against TEOS are required to change $Si(OEt)_2(OBu^n)_2$ to $Si(OEt)(OBu^n)_3$ than to change $Si(OEt)_3(OBu^n)$ to $Si(OEt)_2(OBu^n)_2$. Actually, even when the solution with the Bu^{n}OH/TEOS ratio of 80.0 is treated in the same manner, the change of TEOS to TBOS is not complete. The peak area ratio of $Si(OBu^n)_4$ is 66.9 %, that of $Si(OEt)(OBu^n)_3$ is 9.5% and that of $Si(OEt)_2(OBu^n)_2$ is 2.2%, while $Si(OEt)_4$ and $Si(OEt)_3(OBu^n)$ are hardly confirmed on the chromatogram. This fact suggests that the transesterification reaction does not occur at a constant rate on relative steps and larger amounts of Bu^{n}OH to TEOS are required to form the species with higher degrees of transesterification.

Transesterification of TBOS with Ethanol. Figure 5 shows the variation in the distribution of each species present in the TBOS-EtOH solutions with the EtOH/TBOS ratio after Amberlyst treatment at 40 °C

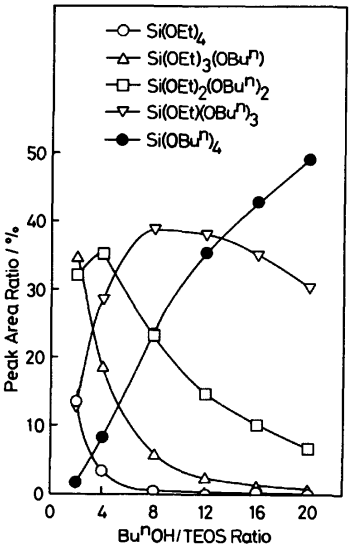

Fig. 3. Variation in the distribution of alkoxysilane species in the TEOS-Bu^{n}OH solutions with the Bu^{n}OH/TEOS ratio after Amberlyst treatment at 40 °C for 120 h.

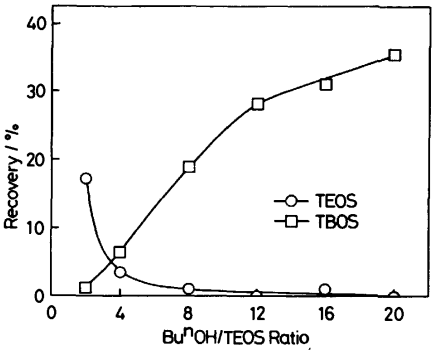

Fig. 4. Variation in the recoveries of TEOS and TBOS in the TEOS-Bu^{n}OH solutions with the Bu^{n}OH/TEOS ratio after Amberlyst treatment at 40 °C for 120 h.

for 120 h. With the increase of this ratio, the degree of substitution of ethoxyl group for butoxyl increases. Compared with the distribution in TEOS-Bu^{n}OH solutions shown in Fig. 3, peak area ratios of each alkoxysilane species at the EtOH/TBOS ratios of 1.0, 2.0, 4.0, and 8.0 show almost the same values as those at the Bu^{n}OH/TEOS ratios of 16.0, 8.0, 4.0, and 2.0, respectively. This fact means that the distribution of alkoxysilane species after Amberlyst treatment depends on the ratio of number of alkyl group in TAOS and that in ROH used, since the ratio of $-C_2H_5/-C_4H_9$ (the ratio of number of ethyl group to that of butyl group) both at the EtOH/TBOS ratio of 1.0 and the Bu^{n}OH/TEOS ratio of 16.0 is 0.25 and the ratio of $-C_2H_5/-C_4H_9$ both at the EtOH/TBOS ratio of 8.0 and the Bu^{n}OH/TEOS ratio of 2.0 is 2.0.

Effect of Treatment Time. Figure 6 shows the

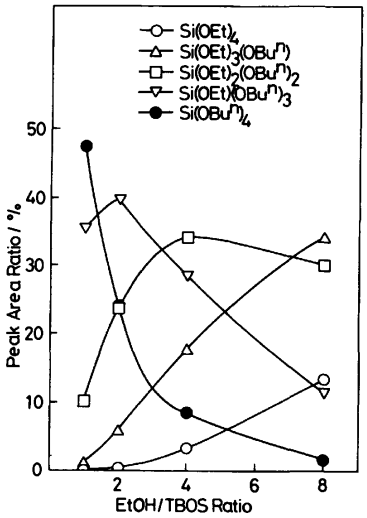

Fig. 5. Variation in the distribution of alkoxysilane species in the TBOS-EtOH solutions with the EtOH/TBOS ratio after Amberlyst treatment at 40 °C for 120 h.

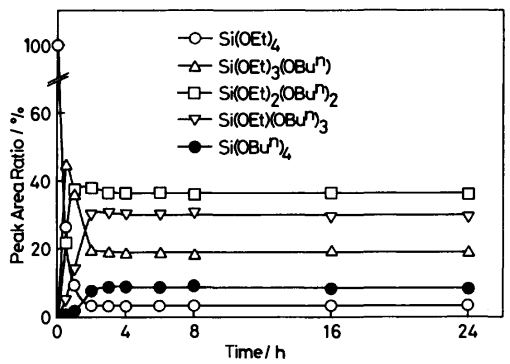

Fig. 6. Variation in the distribution of alkoxysilane species in the TEOS-Bu^{n}OH solution at the Bu^{n}OH/TEOS ratio of 4.0 with time of Amberlyst treatment at 40 °C.

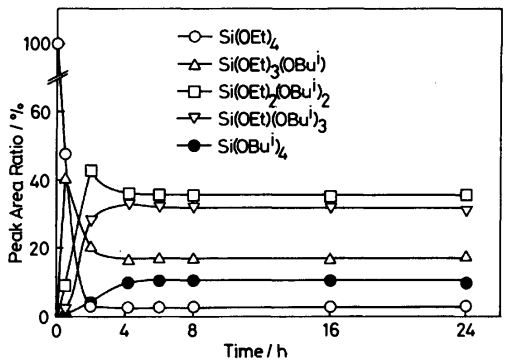

Fig. 7. Variation in the distribution of alkoxysilane species in the TEOS-Bu^{i}OH solution at the Bu^{i}OH/TEOS ratio of 4.0 with time of Amberlyst treatment at 40 °C.

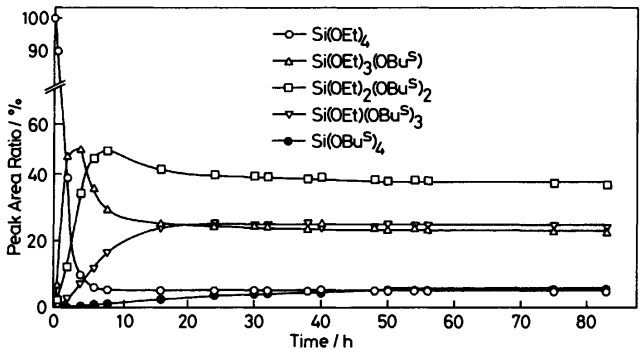

Fig. 8. Variation in the distribution of alkoxysilane species in the TEOS-Bu^{s}OH solution at the Bu^{s}OH/TEOS ratio of 4.0 with time of Amberlyst treatment at 40 °C.

variation in the distribution of alkoxysilane species in the TEOS-Bu^{n}OH solution at the Bu^{n}OH/TEOS ratio of 4.0 with time of Amberlyst treatment at 40 °C. In this figure, it is seen that the distribution of each alkoxysilane species does not vary and the equilibrium on the distribution is established on and after 2 h, indicating that the transesterification reaction between TEOS and Bu^{n}OH proceeds very rapidly.

Effect of the Structure of Butyl Alcohols. Variations in the distribution of alkoxysilane species with time of Amberlyst treatment at 40 °C in the TEOS-Bu^{i}OH and the TEOS-Bu^{s}OH solutions both at the BuOH/TEOS ratio of 4.0 are shown in Figs. 7 and 8, respectively. It is seen that the equilibrium on the transesterification is achieved in 6 h in the TEOS-Bu^{i}OH solution and in 50 h in the TEOS-Bu^{s}OH solution. The times for attaining the equilibrium in the TEOS-Bu^{i}OH and TEOS-Bu^{s}OH solutions are longer than that in the TEOS-Bu^{n}OH solution and the time is shorter in the TEOS-Bu^{i}OH system than in the TEOS-Bu^{s}OH system. It is considered that these differences are attributed to the steric effect of butyl alcohols on this transesterification reaction, and the time for the equilibrium seems to be shorter when the number of branching of alkyl group in a butyl alcohol is less and the number of C-C bond at the carbon atom to which a hydroxyl group attaches in a butyl alcohol is less.

When the TEOS-Bu^{t}OH solution at the Bu^{t}OH/TEOS ratio of 4.0 is treated with Amberlyst 15, however, the peak of TEOS become smaller with the treatment time and is hardly seen on the gas chromatogram after keeping the solution standing in an oven of 40 °C for 84 h. Then the solution gels after ca. 20 days. This suggests that the main reaction in this system is polymerization of TEOS. Typical gas chromatogram of the TEOS-Bu^{t}OH solution is shown in Fig. 9. By identifying the peaks on Fig. 9 with combined gas chromatograph-mass spectrometry, the peak a is assigned to $Si(OC_2H_5)_3(OH)$ (M, 180), which hardly appears in the other systems, and

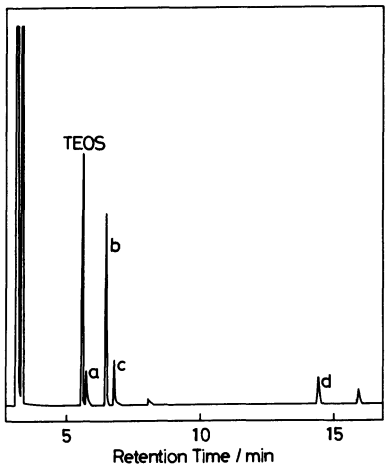

Fig. 9. Gas chromatogram of the TEOS-Bu^{t}OH solution at the Bu^{t}OH/TEOS ratio of 4.0 after Amberlyst treatment at 40 °C for 16 h.

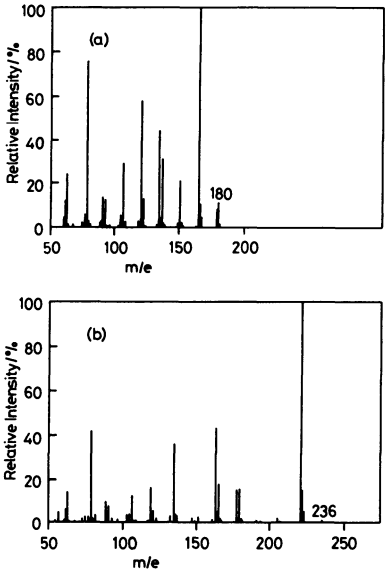

Fig. 10. 70-eV mass spectra of (a) Si(OEt)$_3$(OH) and (b) Si(OEt)$_3$(OBu^t) corresponding to peaks a and b in Fig. 9.

the peak b is assigned to Si(OC$_2$H$_5$)$_3$(OBu^t) (M, 236). The mass spectra of these compounds are shown in Fig. 10 (a) and (b), respectively. The peak c is assigned to Si(OC$_2$H$_5$)$_2$(OBu^t)(OH) and the peak d is assigned to Si$_2$O$_7$(C$_2$H$_5$)$_6$. It is considered that the polymerization rather than the transesterification occurs in this system because of the presence of the species with a reactive silanol group.

General Reaction Mechanism. The results described above suggest that the fundamental reaction of the transesterification in the present study may proceed as follows;

$$\text{A-H} + \text{Si(OR}^1\text{)}_4 \longrightarrow \text{A-Si(OR}^1\text{)}_3 + \text{R}^1\text{OH} \quad (1)$$

(A-H: Amberlyst-H)

$$\text{A-Si(OR}^1\text{)}_3 + \text{R}^2\text{OH} \longrightarrow \text{A-H} + \text{Si(OR}^1\text{)}_3\text{(OR}^2\text{)} \quad (2)$$

The ester-exchange reaction would proceed to the degree which is determined by the ROH/TAOS ratio.

The differences in the time for establishing the equilibrium in the TEOS-Bu^{n}OH, TEOS-Bu^{t}OH, and TEOS-Bu^{s}OH systems may be attributed to the steric effect of butyl alcohols. It is supposed that the differences arise in Reaction (2). In Reaction (2), butyl alcohol molecules present in the solution and EtOH formed by Reaction (1) would react with A-Si(OR)$_3$ competitively. In the final stage, however, the quantity of a butyl alcohol in the solution is expected to determine the degree of transesterification, since the main products in these three systems are Si(OEt)$_2$-(OBu)$_2$ in spite of the variety of butyl alcohols.

The presence of alkoxydisiloxane and alkoxytrisiloxane species, as is seen in Fig. 1 (b) and (c), and the occurrence of gelation in the TEOS-Bu^{t}OH solution indicate that polymerization of TEOS occurs together with the transesterification. The following polymerization reactions are assumed.

$$\text{A-H} + \text{Si(OR)}_4 \longrightarrow \text{A-R} + \text{Si(OR)}_3\text{(OH)} \quad (3)$$

$$\text{Si(OR)}_3\text{(OH)} + \text{Si(OR)}_4 \longrightarrow (\text{RO})_3\text{Si-O-Si(OR)}_3 + \text{ROH} \quad (4)$$

$$\text{Si(OR)}_3\text{(OH)} + \text{A-Si(OR)}_3 \longrightarrow (\text{RO})_3\text{Si-O-Si(OR)}_3 + \text{A-H} \quad (5)$$

$$\text{Si(OR)}_3\text{(OH)} + \text{Si(OR)}_3\text{(OH)} \longrightarrow (\text{RO})_3\text{Si-O-Si(OR)}_3 + \text{H}_2\text{O} \quad (6)$$

The occurrence of gelation in the TEOS-Bu^{t}OH solution may be explained by the presence of the species with a reactive silanol group formed by Reaction (3), which may lead to the polymerization.

Conclusion

Transesterification reaction took place when the mixture of TEOS and a butyl alcohol was treated with Amberlyst 15 cation-exchange resin except for Bu^{t}OH. A slight degree of polymerization of TEOS also took place as a side reaction. The degree of transesterification of TEOS depended mainly on the ratio of mixing of TEOS and a butyl alcohol, indicating that alkoxysilane species with a specific ester-exchanged ratio can be obtained as the main product in a solution by choosing the optimum ratio of mixing of TAOS and ROH. Additionally, the distribution of alkoxysilane species with different degrees of transesterification in a solution was governed by the ratio of numbers of alkyl groups in TAOS and ROH used, regardless of the kinds of TAOS and ROH used as starting materials. The kind of butyl alcohols also affected the time for attaining the equilibrium of transesterification reaction. When Bu^{t}OH was used as

a butyl alcohol, polymerization of TEOS was more dominant than the transesterification, which led to the gelation of the solution.

This work was supported by a Grant-in-Aid for Scientific Research on Priority Areas, New Functionality Materials—Design, Preparation and Control, The Ministry of Education, Science and Culture, No. 62604011.

References

1) S. Sakka, "Treatise on Material Science and Technology, Vol. 22," Academic Press, New York (1982), p. 129.
2) C. J. Brinker, K. D. Keefer, D. W. Schaefer, R. A. Assink, B. D. Kay, and C. S. Ashley, *J. Non-Cryst. Solids*, **63**, 45 (1984).
3) J. C. Pouxviel, J. P. Boilot, J. C. Beloeil, and J. Y. Lallemand, *J. Non-Cryst. Solids*, **89**, 345 (1987).
4) W. Noll, "Chemistry and Technology of Silicones," Academic Press, New York (1968), p. 230.
5) C. W. Lentz, *Inorg. Chem.*, **3**, 574 (1964).
6) G. Eglinton, J. N. M. Firth, and B. L. Welters, *Chem. Geol.*, **13**, 25 (1974).
7) J. Götz and C. R. Masson, *J. Chem. Soc. A*, **1970**, 2683.
8) I. Hasegawa and S. Sakka, *Bull. Chem. Soc. Jpn.*, **60**, 4313 (1987).
9) I. Hasegawa and S. Sakka, *J. Organomet. Chem.*, **340**, 31 (1988).
10) G. Garzó, A. Vargha, T. Székely, and D. Hoebbel, *J. Chem. Soc., Dalton Trans.*, **1980**, 2068.
11) I. Hasegawa and S. Sakka, *J. Non-Cryst. Solids*, **100**, 201 (1988).

 © 1988 The Chemical Society of Japan Bull. Chem. Soc. Jpn., 61, 4093—4097 (1988)

Structural Study of Na_2O-TeO_2 Glasses by Mössbauer Spectroscopy and Differential Thermal Analysis

Tetsuaki NISHIDA,* Setsuko SARUWATARI, and Yoshimasa TAKASHIMA
Department of Chemistry, Faculty of Science, Kyushu University 33,
Hakozaki, Higashiku, Fukuoka 812
(Received June 22, 1988)

A Mössbauer spectrum of $x$$Na_2O$·$(95-x)$$TeO_2$·$5Fe_2O_3$ glasses ($0 \leqq x \leqq 35$) consists of a paramagnetic quadrupole doublet peak with an isomer shift of 0.39 ± 0.01 mm s^{-1} with respect to metallic iron. Quadrupole splitting of the doublet peak changes gradually from 0.76 to 0.60 mm s^{-1} when Na_2O content is changed from 0 to 35 mol% at 5 mol% intervals. These results suggest that Fe^{3+} ions are present at substitutional sites of Te^{4+} ions constituting distorted TeO_4 trigonal bipyramids. Each of the distorted TeO_4 trigonal bipyramids has an oxygen vacancy and a lone electron pair at one of the equatorial sites. Decreased quadrupole splitting is ascribed to an increased symmetry of FeO_4 (and also TeO_4) trigonal bipyramids, due to a formation of nonbridging oxygen atoms followed by a gradual change of the glass matrix from a two-(β-TeO_2) or three-(α-TeO_2) dimensional network structure to a lower dimensional network structure. These structural changes are also deduced from a composition dependency of glass transition temperatures (T_g), which decrease continuously from 318 to 232 °C with increasing Na_2O content.

It is known that tellurite (TeO_2-based) glasses have some excellent physical properties such as low glass transition temperature (T_g), high refractive index, high dielectric constant, high thermal expansion coefficient, and high transmission in the IR region.[1-5] Structural study of tellurite glasses has been performed by several researchers by means of X-ray diffraction,[6-8] IR,[8-11] neutron diffraction,[12-16] and Mössbauer spectroscopy.[11,17-19] Local structure of TeO_2 glass was first studied by Brady,[6] who indicated that TeO_2 glass is composed of distorted TeO_6 octahedra. On the other hand, an X-ray diffraction study of V_2O_5-TeO_2 glasses performed by Dimitriev and Dimitrov[7] showed that coordination number of Te^{4+} ion changes from 4 to 3 when V_2O_5 is incorporated into TeO_2 matrix. An X-ray diffraction and IR absorption study of alkali tellurite glasses was performed by Dimitriev et al.,[8] who elucidated that alkali tellurite glasses are composed of TeO_4 groups. An IR study of binary alkali or alkaline earth tellurite glasses was performed by Mochida et al.,[9] who elucidated that these tellurite glasses have a layer structure composed of distorted TeO_4 trigonal bipyramids having a lone electron pair at one of the equatorial sites (in the xy plane). Each Te^{4+} ion has an oxygen vacancy at one of the equatorial sites.[9] The IR results obtained by Mochida et al.[9] were supported by Dimitriev et al.,[10] who showed that an introduction of MoO_3 into TeO_2 matrix results in a structural change from TeO_4 trigonal bipyramids to TeO_3 trigonal pyramids, similarly to the structural change of V_2O_5-TeO_2 glasses.[7] Neutron diffraction studies revealed that tellurite glasses are composed of distorted TeO_4 trigonal bipyramids.[12-16] Neov et al. proposed that tellurite glasses are composed of TeO_4 tetrahedra.[13] A neutron diffraction study performed by Neov et al.[14] revealed that TeO_4 trigonal bipyramids, constituting the glass matrix of tellurite glasses, gradually change into TeO_3 trigonal pyramids when P_2O_5 is incorporated into TeO_2 matrix. This structural change is similar to that of V_2O_5-TeO_2[7] and MoO_3-TeO_2[10] glasses described above. Structural change of V_2O_5-TeO_2 glasses was also observed by Johnson et al.[16] by using a neutron diffraction method. Mössbauer studies on the structure of tellurite glasses were performed by Binczycka et al.[17] and Bahgat et al.[11,18,19] Some of the Mössbauer studies[17,18] suggested that iron is present as octahedral Fe^{3+} ions in tellurite glasses, in spite that both the isomer shift (<0.40 mm s^{-1} with respect to metallic iron) and the quadrupole splitting (0.6—0.9 mm s^{-1}) indicated the coordination number smaller than 6. On the other hand, Mössbauer studies performed by Bahgat et al.[11,19] lead to a conclusion that Fe^{3+} ions are present at tetrahedral environments in strontium tellurite and several rare earth tellurite glasses. This conclusion[11,19] was drawn because the Mössbauer parameters of Fe^{3+} ions in these tellurite glasses were almost comparable to those of tetrahedral Fe^{3+} ions obtained for several oxide glasses. In Ref. 19, it was concluded that an increased SrO content results in an increased number of nonbridging oxygen atoms in FeO_4 and TeO_4 tetrahedra.

Present Mössbauer study of a series of Na_2O-TeO_2 glasses containing a small amount (5 mol%) of Fe_2O_3 was carried out in order to elucidate the short-range (local) and also middle- or long-range structures of tellurite glasses, e.g., a steric configuration around the iron (and also tellurium) atom and a structural change caused by alkali oxide (Na_2O) which was incorporated into TeO_2 matrix. DTA measurements of the Na_2O-TeO_2 glasses containing 5 mol% Fe_2O_3 were also performed in parallel, because glass transition temperature (T_g) is known to be sensitive to a change in the coordination number of network-forming atoms and to a formation of nonbridging oxygen,[20-24] chlorine,[25] and fluorine[26] atoms followed by a depolymerization of the network structure.

Experimental

A series of xNa$_2$O·(95−x)TeO$_2$·5Fe$_2$O$_3$ glasses were prepared by fusing individual mixtures (1 g) of commercially available Na$_2$CO$_3$, TeO$_2$, and Fe$_2$O$_3$, of guaranteed reagent grade. Each of the mixtures, in which x was changed at 5 intervals, was fused at 750 °C for 1 h in air by using an electric muffle furnace. After the fusion, each melt in a platinum crucible was immediately quenched with ice-cold water. Transparent and light brown glasses were obtained in a compositional region $0 \leqq x \leqq 35$. Mössbauer and DTA measurements were performed on pulverized tellurite glasses. Mössbauer measurements were performed by a constant acceleration method at room temperature, by using a proportional counter and a multichannel (1024-channel) analyzer. Cobalt-57 (10 mCi) diffused into a palladium foil was used as a Mössbauer source. As a standard material for the isomer shift, a piece of metallic iron foil enriched with iron-57 was used. The iron foil was also used for calibrating the velocity of Mössbauer spectrometer. Each Mössbauer spectrum was analyzed into a quadrupole doublet by a least-squares method. DTA measurements of tellurite glasses were performed in the temperature range between room temperature and 600 °C, with a heating rate of 5 °C min^{-1}. Powder of α-Al$_2$O$_3$ was used as a standard material in the DTA measurements.

Results and Discussion

A Mössbauer spectrum of 20Na$_2$O·75TeO$_2$·5Fe$_2$O$_3$ glass is shown in Fig. 1, which indicates a characteristic doublet peak due to paramagnetic Fe^{3+} ions of high spin state.[27,28] Since the absorption is symmetric, each Mössbauer spectrum is analyzed into a quadrupole doublet peak having equal linewidth and equal intensity. All the Mössbauer parameters of Na$_2$O–TeO$_2$–Fe$_2$O$_3$ glasses are shown in Figs. 2 and 3. Figure 2a indicates that isomer shift is independent of the composition, showing a constant value of 0.39±0.01 mm s^{-1}. Comparing the present results with recent Mössbauer results of alkali borate,[25,29–32] alkali borosilicate,[32–34] and other glasses cited in review articles,[35–37] we can deduce that Fe^{3+} ions are four-fold coordinated in Na$_2$O–TeO$_2$ glasses, and that they are not octahedrally coordinated as in several phosphate glasses.[38–41] In the Mössbauer spectra of tetrahedrally coordinated Fe^{3+} ions, isomer shifts were located in a range of 0.22—0.38 mm s^{-1} with respect to metallic iron.[25,29–37] These experimental results obtained so far indicate that isomer shift of Fe^{3+} ions is less than 0.40 mm s^{-1} when they are four-fold coordinated. The experimental error of isomer shift is estimated to be ±0.01 mm s^{-1}. On the other hand, Mössbauer spectra of Fe^{3+} ions in several phosphate glasses[38–41] indicate that isomer shift is more than 0.42 mm s^{-1} when they are octahedrally coordinated with oxygen atoms. These results suggest that a boundary of isomer shift lies at about 0.40 mm s^{-1} for four-fold and six-fold coordinated Fe^{3+} ions with oxygen atoms.[42] Therefore, the isomer shift of

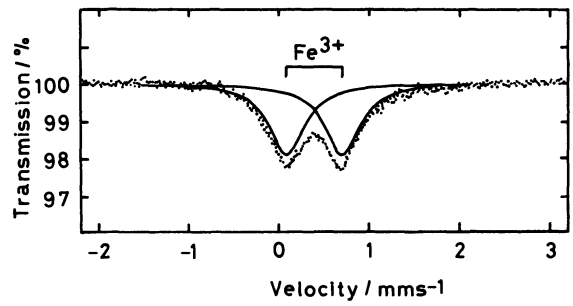

Fig. 1. Mössbauer spectrum of 20Na$_2$O·75TeO$_2$·5Fe$_2$O$_3$ glass measured at room temperature.

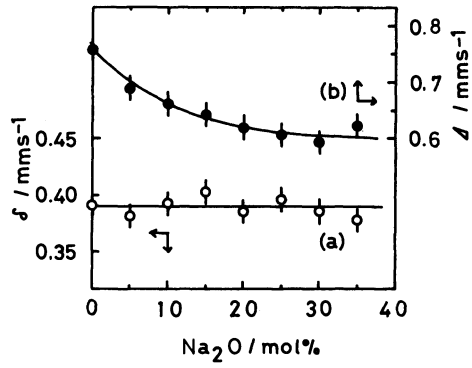

Fig. 2. Composition dependencies of (a) isomer shift (δ) and (b) quadrupole splitting (Δ) of Fe^{3+} ions in xNa$_2$O·(95−x)TeO$_2$·5Fe$_2$O$_3$ glasses.

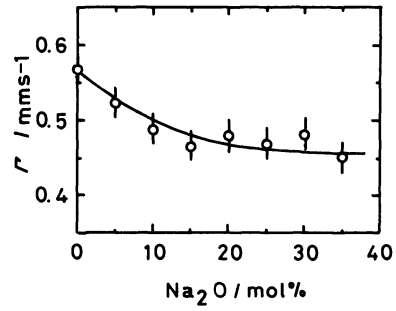

Fig. 3. Composition dependency of linewidth (Γ) of Fe^{3+} ions in xNa$_2$O·(95−x)TeO$_2$·5Fe$_2$O$_3$ glasses.

0.39±0.01 mm s^{-1} (Fig. 2a) will suggest four-fold coordinated Fe^{3+} ions (of high spin state). The relatively large isomer shift values (0.39±0.01 mm s^{-1}) suggest that s-electron density at iron nucleus is lower than that of tetrahedral Fe^{3+} ions observed in several oxide glasses.[25,29–37] Earlier Mössbauer results on tellurite glasses obtained by Binczycka et al.[17] and Bahgat et al.,[18] suggesting that Fe^{3+} ions are octahedrally present in tellurite glasses, are unlikely because the isomer shift values were less than 0.40 mm s^{-1} with respect to metallic iron. It should be noted that recent IR[9,10] and neutron diffraction[12–16] studies propose a presence of distorted

TeO_4 trigonal bipyramids having an oxygen vacancy and a lone electron pair at one of the equatorial sites. Taking into account these IR and neutron diffraction results,[9,10,12–16] we can tentatively conclude that the present Mössbauer results (isomer shift) suggest distorted FeO_4 trigonal bipyramids having an oxygen vacancy at one of the equatorial sites. Apart from Te^{4+} ions, Fe^{3+} ions will not have a lone electron pair at the equatorial sites. They will form sp^3d hybrid orbital, similarly to the Te^{4+} ions constituting TeO_4 trigonal bipyramids.

From the electronic point of view, the four-fold coordinated FeO_4 trigonal bipyramid having one oxygen vacancy is equivalent to an FeO_4 tetrahedron without oxygen vacancy. The almost constant and large isomer shift values located around 0.39 mm s^{-1} (Fig. 2a), irrespective of the composition, may be concerned with the oxygen vacancy at one of the equatorial sites in FeO_4 trigonal bipyramids. A part of negative charge on the Fe^{3+} ion will be attracted to the oxygen vacancy. As a result, 4s-electron density at the iron nucleus will be decreased. This will cause a relatively large isomer shift values. Also, the larger isomer shift values will be concerned with lower s-electron density in an sp^3d hybrid orbital, because a contribution of s-orbital to the sp^3d hybrid orbital is lower as compared with sp^3 hybrid orbital. The Fe^{3+} ions attached to oxygen vacancies will be less sensitive to a change of electron densities at iron nucleus. In several vanadate glasses,[20,21,42,43] a drastic change of glass matrix was observed from VO_5 tetragonal pyramids to VO_4 tetrahedra when alkali or alkaline earth oxide was incorporated into V_2O_5 matrix. This structural change corresponds to an orbital change in the V^{5+} or V^{4+} (and also Fe^{3+}) ions from sp^3d to sp^3 hybrid orbital. From the relatively large and constant isomer shift values (0.39 ± 0.01 mm s^{-1}) observed in tellurite glasses, we can deduce the presence of oxygen vacancies at neighboring sites of Fe^{3+} ions in FeO_4 trigonal bipyramids and also sp^3d hybrid orbital in the Fe^{3+} ions. This will be discussed later in connection with a formation of nonbridging oxygen atoms.

Continuous decrease in the quadrupole splitting shown in Fig. 2b suggests that a symmetry of FeO_4 (and also TeO_4) trigonal bipyramids increases with increasing Na_2O content. In the case of high-spin Fe^{3+} ions, an electric field gradient brought about by neighboring atoms (q_{lat}) primarily causes the quadrupole interaction. Similar decrease in the quadrupole splitting of Fe^{3+} ions was observed in several alkali borate[25,29–32] and alkali borosilicate[32–34] glasses, where the decrease was ascribed to a formation of nonbridging oxygen and chlorine atoms in BO_4, SiO_4, and BO_3Cl tetrahedra. Decrease in the quadrupole splitting of Fe^{3+} ions has also been observed in alkali vanadate[20,21,42] glasses, from which we could know a formation of nonbridging oxygen atoms in VO_4 tetrahedra and a depolymerization of the layer structure originally composed of VO_5 tetragonal pyramids. The experimental error of quadrupole splitting is estimated to be ±0.02 mm s^{-1}. Quadrupole splitting of Fe^{3+} ions octahedrally coordinated with oxygen atoms (e.g. 0.3—0.6 mm s^{-1}) is usually smaller than that of tetrahedrally coordinated Fe^{3+} ions (e.g. 0.6—0.9 mm s^{-1}), owing to a higher symmetry of the former. It should be noted that a change of middle- or long-range structure, as well as a change of short-range structure, is sometimes reflected in the quadrupole splitting of Fe^{3+} ions. Therefore, the continuous decrease in quadrupole splitting (Fig. 2b) is ascribed to a formation of nonbridging oxygen atoms in distorted FeO_4 (and also TeO_4) trigonal bipyramids having an oxygen vacancy at one of the equatorial sites. Furthermore, a lone electron pair will be present in the sp^3d hybrid orbital of Te^{4+} ion constituting a TeO_4 trigonal bipyramid. An introduction of alkali oxide (Na_2O) into TeO_2 matrix will result in a depolymerization of original α-TeO_2[10,13,14] or β-TeO_2[9,16] type structure, composed of distorted TeO_4 trigonal bipyramids having a lone electron pair at one of the equatorial sites. Comparing Fig. 2a with Fig. 2b, we can know that quadrupole splitting (Δ) is more sensitive to the structural change than isomer shift (δ). Similar phenomenon was observed in a crystallization study of several borate and borosilicate glasses.[32]

Figure 3 indicates that a formation of nonbridging oxygen atoms and a depolymerization of the glass matrix are reflected in the linewidth. It is generally known that linewidth of the absorption peak due to iron in glasses is greater than about 0.4 mm s^{-1}. This is a characteristic feature of the absorption for amorphous materials. Each linewidth shown in Fig. 3 is in a range of 0.46—0.57 mm s^{-1}. A continuous decrease in linewidth (Fig. 3) suggests that bond length and bond angle between Fe^{3+} (and also Te^{4+}) ions and neighboring oxygen atoms become more uniform when nonbridging oxygen atoms are formed in FeO_4 (and also TeO_4) trigonal bipyramids. Figure 3 demonstrates that linewidth decreases by adding Na_2O into TeO_2 matrix and becomes almost constant (about 0.46 mm s^{-1}) when Na_2O content is higher than about 20 mol%. This indicates that a distinct structural change occurs in tellurite glasses of low alkali oxide content. The composition dependency is in good agreement with that of quadrupole splitting described above.

Glass transition temperatures (T_g) of tellurite glasses obtained from DTA measurements are plotted in Fig. 4. Each DTA curve of Na_2O–TeO_2 glasses containing 5 mol% Fe_2O_3 shows a broad endothermic peak due to glass transition and exothermic peaks due to crystallization. Recent DTA studies on the structure of several glasses revealed that T_g is closely concerned with a change in the coordination number of network-

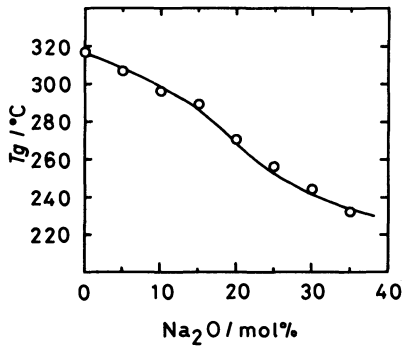

Fig. 4. Composition dependency of glass transition temperature (T_g) of xNaO·(95−x)TeO$_2$·5Fe$_2$O$_3$ glasses.

forming atoms and with a formation of nonbridging oxygen or halogen atoms.[20–26,42–44] The latter structural change causes a depolymerization of network structure. T_g shows a distinct increase/decrease with increasing/decreasing coordination number of network-forming atoms, because the coordination number is responsible for the degree of bridging in the glass matrix. Also, a formation of nonbridging oxygen atoms is deduced from a decrease in T_g.[20–24,42–44] Therefore, a continuous decrease in T_g ranging from 318 to 232 °C (Fig. 4) is ascribed to an increased fraction of less distorted TeO_4 and FeO_4 trigonal bipyramids having nonbridging oxygen atoms. At the same time, it is concluded that a middle- or long-range structural change occurs from the original three-dimensional network (α-TeO_2) structure or two-dimensional layer (β-TeO_2) structure to a lower dimensional network structure, i.e., one-dimensional chain structure. This structural change is similar to that of alkali vanadate (K_2O–V_2O_5,[20] Na_2O–V_2O_5,[21] and Li_2O–V_2O_5[42]) glasses. In alkali vanadate glasses,[20,21,42] a simultaneous decrease in T_g and quadrupole splitting (of the Fe^{3+} ions) was ascribed to a structural change from a two-dimensional layer structure composed of VO_5 tetragonal pyramids to a one-dimensional chain structure composed of VO_4 tetrahedra which have nonbridging oxygen atoms.

A simultaneous decrease in T_g and quadrupole splitting (of Fe^{3+} or Sn^{4+} ions) has been observed when nonbridging oxygen atoms are formed in GeO_4 and GaO_4 tetrahedra constituting alkali (K_2O-) germanate[24] and gallate[44] glasses, respectively. Concordant composition dependencies of T_g and quadrupole splitting, observed in several vanadate,[20,21,42,43] germanate,[24] gallate,[44] and tellurite glasses, suggest that a structural information obtained from Mössbauer measurements is representative of the whole glass matrix. Mössbauer atoms will be homogeneously distributed in the glass matrix either at the substitutional sites of the individual network-forming ions (e.g. V^{5+}, V^{4+}, Ga^{3+}, and Te^{4+}) or at the interstitial sites in the glass matrix (e.g. phosphate glasses), depending on the type of glass matrix. From the constant isomer shifts described above (Fig. 2a), it is speculated that nonbridging oxygen atoms will be preferentially formed at axial oxygen sites. The longer interatomic distance and resultant weaker covalent bond between Fe^{3+} (and also Te^{4+}) ions and oxygen atoms at axial sites will bring about little effect on the s-electron density and therefore on the isomer shift.

It is concluded that Fe^{3+} ions are present at substitutional sites of the Te^{4+} ions constituting TeO_4 trigonal bipyramids. Each of the TeO_4 trigonal bipyramids has an oxygen vacancy and a lone electron pair at one of the equatorial sites. An Fe^{3+} ion in the FeO_4 trigonal bipyramid does not have a lone electron pair. It is also concluded that an introduction of Na_2O into TeO_2 matrix results in a change of the glass matrix from an original three-dimensional network (α-TeO_2) or a two-dimensional layer (β-TeO_2) structure to a lower dimensional network structure, i.e., a chain structure composed of less distorted TeO_4 trigonal bipyramids which have nonbridging oxygen atoms.

The authors are grateful to Prof. Toshinobu Yoko of Kyoto University for his useful comments and discussion. One of the authors (TN) is indebted to Yoshida Science Foundation and Kazuchika Ohkura Memorial Foundation for a financial support.

References

1) J. E. Stanworth, *Nature (London)*, **169**, 581 (1952).
2) J. E. Stanworth, *J. Soc. Glass Tech.*, **36**, 217T (1952).
3) J. A. James and J. E. Stanworth, *J. Soc. Glass Tech.*, **38**, 421T (1954).
4) J. E. Stanworth, *J. Soc. Glass Tech.*, **38**, 425T (1954).
5) M. Imaoka and I. Satake, *Seisankenkyu*, **9**, 505 (1957).
6) G. W. Brady, *J. Chem. Phys.*, **27**, 300 (1957).
7) Y. Dimitriev and V. Dimitrov, *Mater. Res. Bull.*, **13**, 1071 (1978).
8) Y. Dimitriev, V. Dimitrov, and M. Arnaudov, *J. Mater. Sci.*, **14**, 723 (1979).
9) N. Mochida, K. Takahashi, K. Nakata, and S. Shibusawa, *Yogyo Kyokai Shi*, **86**, 26 (1978).
10) Y. Dimitriev, V. Dimitrov, and M. Arnaudov, *J. Mater. Sci.*, **18**, 1353 (1983).
11) A. A. Bahgat, E. E. Shaisha, and A. I. Sabry, *J. Mater. Sci.*, **22**, 1323 (1987).
12) S. Neov, I. Gerassimova, K. Krezhov, B. Sydzhimov, and V. Kozhukharov, *Phys. Status Solidi A*, **47**, 743 (1978).
13) S. Neov, V. Kozhukharov, I. Gerasimova, K. Krezhov, and B. Sydzhimov, *J. Phys. C*, **12**, 2475 (1979).
14) S. Neov, I. Gerasimova, V. Kozhukharov, and M. Marinov, *J. Mater. Sci.*, **15**, 1153 (1980).
15) V. Kozhukharov, S. Neov, I. Gerasimova, and P. Mikula, *J. Mater. Sci.*, **21**, 1707 (1986).
16) P. A. V. Johnson, A. C. Wright, C. A. Yarker, and R. N. Sinclair, *J. Non-Cryst. Solids*, **81**, 163 (1986).
17) H. Binczycka, O. Gzowski, L. Murawski, and J.

Sawicki, *Phys. Status Solidi A*, **70**, 51 (1982).
18) A. A. Bahgat, E. E. Shaisha, A. I. Sabry, and N. A. Eissa, *Phys. Status Solidi A*, **90**, K25 (1985).
19) E. E. Shaisha, A. A. Bahgat, A. I. Sabry, and N. A. Eissa, *Phys. Chem. Glasses*, **26**, 91 (1985).
20) T. Nishida and Y. Takashima, *Bull. Chem. Soc. Jpn.*, **60**, 941 (1987).
21) T. Nishida, M. Ogata, and Y. Takashima, *Bull. Chem. Soc. Jpn.*, **60**, 2887 (1987).
22) J. E. Shelby, *J. Am. Ceram. Soc.*, **57**, 436 (1974).
23) J. E. Shelby, *J. Appl. Phys.*, **46**, 193 (1975).
24) T. Nishida, M. Katada, and Y. Takashima, *Bull. Chem. Soc. Jpn.*, **57**, 3566 (1984).
25) T. Nishida, M. Ogata, and Y. Takashima, *Bull. Chem. Soc. Jpn.*, **59**, 2401 (1986).
26) T. Nishida, T. Nonaka, and Y. Takashima, *Bull. Chem. Soc. Jpn.*, **58**, 2255 (1985).
27) N. N. Greenwood and T. C. Gibb, "Mössbauer Spectroscopy," Chapman and Hall Ltd., London (1971), Chaps. 3 and 5.
28) R. Ingalls, F. Van der Woude, and G. A. Sawatzky, "Iron and Nickel," in "Mössbauer Isomer Shifts," ed by G. K. Shenoy and F. E. Wagner, North-Holland Pub Co., Amsterdam (1978), Chap. 7.
29) T. Nishida and Y. Takashima, *J. Non-Cryst. Solids*, **37**, 37 (1980).
30) T. Nishida, T. Shiotsuki, and Y. Takashima, *J. Non-Cryst. Solids*, **41**, 161 (1980).
31) T. Nishida, T. Hirai, and Y. Takashima, *J. Non-Cryst. Solids*, **43**, 221 (1981).
32) T. Nishida and Y. Takashima, "Application of Mössbauer Effect on the Crystallization of Several Glasses," in "Industrial Applications of the Mössbauer Effect," ed by G. J. Long and J. G. Stevens, Plenum Press, New York & London (1986), pp. 409—421.
33) T. Nishida, T. Hirai, and Y. Takashima, *Phys. Chem. Glasses*, **22**, 94 (1981).
34) T. Nishida, T. Hirai, and Y. Takashima, *Bull. Chem. Soc. Jpn.*, **54**, 3735 (1981).
35) C. R. Kurkjian, *J. Non-Cryst. Solids*, **3**, 157 (1970).
36) J. M. D. Coey, *J. Phys.*, **35**, C6-89 (1974).
37) W. Müller-Warmuth and H. Eckert, *Phys. Rep.*, **88**, 91 (1982).
38) M. F. Taragin, J. C. Eisenstein, and W. Haller, *Phys. Chem. Glasses*, **13**, 149 (1972).
39) T. Nishida, T. Shiotsuki, and Y. Takashima, *J. Non-Cryst. Solids*, **43**, 115 (1981).
40) T. Nishida, T. Shiotsuki, and Y. Takashima, *J. Non-Cryst. Solids*, **43**, 123 (1981).
41) T. Nishida, Y. Miyamoto, and Y. Takashima, *Bull. Chem. Soc. Jpn.*, **56**, 439 (1983).
42) T. Nishida, M. Ogata, and Y. Takashima, Proc. VI Int. Conf. Phys. Non-Cryst. Solids, 1987 (Kyoto); *J. Non-Cryst. Solids*, **95/96**, 241 (1987).
43) T. Nishida and Y. Takashima, *J. Non-Cryst. Solids*, **94**, 229 (1987).
44) T. Nishida, S. Saruwatari, and Y. Takashima, *Bull. Chem. Soc. Jpn.*, **61**, 2347 (1988).

 © 1988 The Chemical Society of Japan Bull. Chem. Soc. Jpn., 61, 4099—4105 (1988)

Redox-Linked Protonation of $[Fe_4X_4(YR)_4]^{2-}$ (X,Y=S and Se; R=*n*-$C_{12}H_{25}$ and C_6H_4-*p*-*t*-Bu) in Aqueous Solutions

Masami NAKAMOTO,† Koji TANAKA,* and Toshio TANAKA*
Department of Applied Chemistry, Faculty of Engineering, Osaka University, Yamada-oka, Suita, Osaka 565
†Osaka Municipal Technical Research Institute, Morinomiya, Joto-ku, Osaka 536
(Received June 25, 1988)

A series of $[Fe_4X_4(YR)_4]^{2-}$ (X,Y=S and Se; R=*n*-$C_{12}H_{25}$ and C_6H_4-*p*-*t*-Bu) were prepared as *n*-Bu_4N^+ salts. In aqueous Triton X-100 micellar solutions, only the reduced forms of $[Fe_4X_4(YR)_4]^{2-}$ (X,Y=S and Se; R=*n*-$C_{12}H_{25}$ and C_6H_4-*p*-*t*-Bu) undergo protonation reactions at the sulfur or selenium atom of the Fe_4X_4 (X=S and Se) core to exist as an equilibrium mixture of the protonated and unprotonated clusters. On the other hand, not only the oxidized but also the reduced forms of $[Fe_4X_4(YC_6H_4$-*p*-*t*-$Bu)_4]^{2-}$ (X,Y=S and Se) undergo protonation reactions in aqueous poly[2-(dimethylamino)hexanamide] (PDACA) solutions. The pK_{ox} values of $[Fe_4X_4(YC_6H_4$-*p*-*t*-$Bu)_4]^{2-}$ (X,Y=S and Se) vary depending on the terminal thiolate and selenolate ligands; 5.9 for Y=S and 6.8 for Y=Se, whereas the pK_{red} values of $[Fe_4X_4(YC_6H_4$-*p*-*t*-$Bu)_4]^{3-}$ are controlled by the core sulfur and selenium; 8.8 for X=S and 7.3 for X=Se. Such characteristic pK_{ox} and pK_{red} values suggest that the protonation takes place at the terminal sulfur or selenium atom of the oxidized clusters $[Fe_4X_4(YC_6H_4$-*p*-*t*-$Bu)_4]^{2-}$ (X,Y=S and Se), while it occurs at the sulfur or selenium atom of the Fe_4X_4 core of the reduced clusters $[Fe_4X_4(YC_6H_4$-*p*-*t*-$Bu)_4]^{3-}$ (X,Y=S and Se).

Iron-sulfur proteins containing Fe_4S_4 cores function as electron transfer catalysts in various biological redox reactions, such as photosynthesis,[1] nitrate reduction,[2] dinitrogen fixation,[3] and so on. As models of active sites of iron-sulfur proteins, the various iron-sulfur clusters with thiolate ligands have been synthesized.[4-9] The electrochemistry of those clusters[10-16] has elucidated that synthetic water soluble Fe_4S_4 clusters in aqueous solutions exhibit more positive redox potentials than water insoluble Fe_4S_4 clusters in organic solvents.[10,12,17] The redox potentials of the former, however, are still more negative than those of 4-Fe and 8-Fe ferredoxins (−0.52 to −0.73 V vs. SCE around pH 7.0) in water.[18] Such negative redox potentials of synthetic Fe_4S_4 clusters may be associated with the absence of hydrogen bondings formed between amide hydrogen of the peptide chain and sulfur of the Fe_4S_4 core and/or of the terminal cysteine residue ligated on the iron atoms in 4-Fe ferredoxins.[19-21] In accordance with this, the redox potential of $[Fe_4S_4(SCH_2CH_2CO_2)_4]^{6-}$ in water in the presence of bovine serum albumin or bovine insulin is 170—220 mV more positive than that of the cluster in water.[17] Recently, we have demonstrated that a Fe_4S_4 cluster $[Fe_4S_4(SC_6H_4$-*p*-*n*-$C_8H_{17})_4]^{2-}$ undergoes a redox-linked protonation in an aqueous micellar solution, and the protonated and unprotonated clusters exist as an equilibrium mixture below pH 10.[22] Such a redox-linked protonation of $[Fe_4X_4(Y$-*n*-$C_{12}H_{25})_4]^{2-}$ (X, Y=S and Se) has briefly been communicated to take place at the sulfur atom of the Fe_4S_4 core rather than the terminal thiolate sulfur on the basis of the electrochemical study in aqueous micellar solutions.[23] This paper describes the protonation behaviors of a series of $[Fe_4X_4(YC_6H_4$-*p*-*t*-$Bu)_4]^{2-}$ (**I**) as well as $[Fe_4X_4(Y$-*n*-$C_{12}H_{25})_4]^{2-}$ (**II**) (X, Y=S and Se) in aqueous micellar and poly[2-(dimethylamino)hexanamide] (PDACA) solutions in more detail.

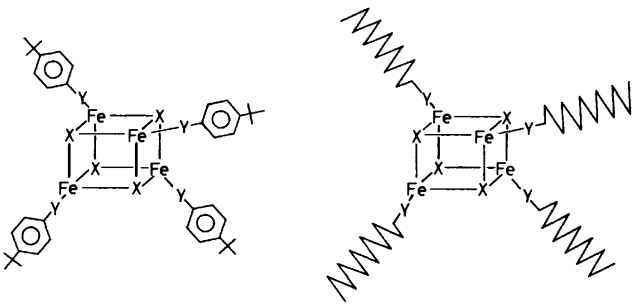

I **II**

(X, Y=S and Se)

Experimental

General Procedure and Materials. All manipulations were carried out under N_2 atmosphere. Solvents used for preparations and physical measurements were purified by distillations over dehydration chemicals; magnesium methoxide for MeOH, calcium hydride for MeCN, and calcium oxide for DMF. Commercially available guaranteed reagent grades of 1-dodecanethiol and *p*-*t*-butylbenzenethiol were used without purification. 1-Dodecaneselenol was obtained by the reaction of 1-bromododecane with selenourea supplied by Shinko Chemical Co., Ltd. in EtOH by the similar manner to the preparation of 1-dodecanethiol.[24] *p*-*t*-Butylbenzeneselenol,[25] $[n\text{-}Bu_4N]_2[Fe_4S_4(S\text{-}t\text{-}Bu)_4]$,[4] and $[n\text{-}Bu_4N]_2[Fe_4Se_4(S\text{-}t\text{-}Bu)_4]$[26] were prepared according to the literature. Poly[2-(dimethylamino)hexanamide] (PDACA) supplied by Toray Co., Ltd. was purified by dialysis.

Preparation of $[n\text{-}Bu_4N]_2[Fe_4S_4(SR)_4]$ (R=*n*-$C_{12}H_{25}$ and C_6H_4-*p*-*t*-Bu). To a MeOH (100 cm³) solution containing MeONa (2.43 g, 45 mmol) and 1-dodecanethiol or *p*-*t*-butylbenzenethiol (45 mmol) was added a filtered MeOH (50 cm³) solution of $FeCl_3$ (2.5 g, 15 mmol), and a MeOH (50 cm³) solution containing MeONa (0.81 g, 15 mmol) and

NaSH (0.84 g, 30 mmol) successively. After stirred for 24 h, the resulting black solution was filtered. To the filtrate was added slowly *n*-Bu_4NBr (4.0 g, 12 mmol) in MeOH (50 cm^3) to give a black precipitate of $[n\text{-}Bu_4N]_2[Fe_4S_4(SR)_4]$, which was collected by filtration and recrystallized from MeCN, 47% for R=*n*-$C_{12}H_{25}$ and 51% for R=C_6H_4-*p*-*t*-Bu. Found for $[n\text{-}Bu_4N]_2[Fe_4S_4(S\text{-}n\text{-}C_{12}H_{25})_4]$: C, 58.37; H, 10.37; N, 1.68%. Calcd for $C_{80}H_{172}Fe_4N_2S_8$: C, 58.51; H, 10.56; N, 1.71%. Found for $[n\text{-}Bu_4N]_2[Fe_4S_4(SC_6H_4\text{-}p\text{-}t\text{-}Bu)_4]$: C, 57.76; H, 8.28; N, 1.45%. Calcd for $C_{72}H_{124}Fe_4N_2S_8$: C, 57.74; H, 8.35; N, 1.87%.

Preparation of $[n\text{-}Bu_4N]_2[Fe_4S_4(SeR)_4]$ (R=*n*-$C_{12}H_{25}$ and C_6H_4-*p*-*t*-Bu). The selenolate ligated cluster $[n\text{-}Bu_4N]_2[Fe_4S_4(SeR)_4]$ (R=*n*-$C_{12}H_{25}$ and C_6H_4-*p*-*t*-Bu) was prepared by the ligand substitution reaction[27] of $[Fe_4S_4(S\text{-}t\text{-}Bu)_4]^{2-}$ with selenol as follows; a DMF (80 cm^3) solution containing $[n\text{-}Bu_4N]_2[Fe_4S_4(S\text{-}t\text{-}Bu)_4]$ (1.0 g, 0.84 mmol) and 1-dodecaneselenol (2.0 g, 8.0 mmol) or *p*-*t*-butylbenzeneselenol (1.8 g, 8.4 mmol) was stirred at 50 °C for 7 h, during which time N_2 gas was bubbled into the solution every 5 min to remove *t*-BuSH from the solution. The resulting solution was evaporated to dryness under reduced pressure. The residual solid was recrystallized from MeCN to give black crystals, 50% for R=*n*-$C_{12}H_{25}$ and 61% for R=C_6H_4-*p*-*t*-Bu. Found for $[n\text{-}Bu_4N]_2[Fe_4S_4(Se\text{-}n\text{-}C_{12}H_{25})_4]$: C, 52.07; H, 9.37; N, 1.62%. Calcd for $C_{80}H_{172}Fe_4N_2S_4Se_4$: C, 52.51; H, 9.48; N, 1.53%. Found for $[n\text{-}Bu_4N]_2[Fe_4S_4(SeC_6H_4\text{-}p\text{-}t\text{-}Bu)_4]$: C, 51.63; H, 7.44; N, 1.66%. Calcd for $C_{72}H_{124}Fe_4N_2S_4Se_4$: C, 51.31; H, 7.42; N, 1.66%.

Preparation of $[n\text{-}Bu_4N]_2[Fe_4Se_4(SR)_4]$ (R=*n*-$C_{12}H_{25}$ and C_6H_4-*p*-*t*-Bu). To a MeOH (20 cm^3) solution containing MeOLi (0.76 g, 20 mmol) and 1-dodecanethiol or *p*-*t*-butylbenzenethiol (20 mmol) was added a filtered MeOH (20 cm^3) solution of $FeCl_3$ (0.82 g, 5.0 mmol) in 10 min, followed by the addition of selenium powder (0.40 g, 5.0 mmol) rapidly. After stirred for 24 h, the resulting solution was filtered. To the filtrate was added slowly *n*-Bu_4NBr (1.2 g, 3.8 mmol) in MeOH (15 cm^3) to give a precipitate, which was collected by filtration, washed with MeOH, and dried in vacuo. The resulting powder was recrystallized from MeCN to give black crystals, 48% for R=*n*-$C_{12}H_{25}$ and 51% for R=C_6H_4-*p*-*t*-Bu. Found for $[n\text{-}Bu_4N]_2[Fe_4Se_4(S\text{-}n\text{-}C_{12}H_{25})_4]$: C, 52.14; H, 9.54; N, 1.50%. Calcd for $C_{80}H_{172}Fe_4N_2S_4Se_4$:C, 52.51; H, 9.48; N, 1.53%. Found for $[n\text{-}Bu_4N]_2[Fe_4Se_4(SC_6H_4\text{-}p\text{-}t\text{-}Bu)_4]$: C, 51.52; H, 7.43; N, 1.34%. Calcd for $C_{72}H_{124}Fe_4N_2S_4Se_4$: C, 51.31; H, 7.42; N, 1.66%.

Preparation of $[n\text{-}Bu_4N]_2[Fe_4Se_4(SeR)_4]$ (R=*n*-$C_{12}H_{25}$ and C_6H_4-*p*-*t*-Bu). A DMF (80 cm^3) solution containing $[n\text{-}Bu_4N]_2[Fe_4Se_4(S\text{-}t\text{-}Bu)_4]$ (1.16 g, 0.84 mmol) and 1-dodecaneselenol (2.1 g, 8.4 mmol) or *p*-*t*-butylbenzeneselenol (1.8 g, 8.4 mmol) was stirred at 50 °C for 7 h, during which time N_2 gas was bubbled into the solution. The resulting solution was evaporated to dryness under reduced pressure. The residual solid was recrystallized from MeCN to give black crystals, 45% for R=*n*-$C_{12}H_{25}$ and 67% for R=C_6H_4-*p*-*t*-Bu. Found for $[n\text{-}Bu_4N]_2[Fe_4Se_4(Se\text{-}n\text{-}C_{12}H_{25})_4]$: C, 47.39; H, 8.76; N, 1.18%. Calcd for $C_{80}H_{172}Fe_4N_2Se_8$: C, 47.63; H, 8.59; N, 1.39%. Found for $[n\text{-}Bu_4N]_2[Fe_4Se_4(SeC_6H_4\text{-}p\text{-}t\text{-}Bu)_4]$: C, 46.59; H, 6.69; N, 1.54%. Calcd for $C_{72}H_{124}Fe_4N_2Se_8$: C, 46.17; H, 6.67; N, 1.50%.

Preparation of Aqueous Micellar Solutions. A DMF (1.0 cm^3) solution of the cluster (12 μmol) was added to a stirred aqueous solution (25 cm^3, pH 5—10) containing NaOH-H_3PO_4 (0.1 mol dm^{-3}) and either Triton X-100 (0.025—0.5 mol dm^{-3}) or poly[2-(dimethylamino)hexanamide] (PDACA) (0.1 g). Dark brown aqueous Triton X-100 micellar or PDACA solutions thus prepared was used after filtration.

Physical Measurements. Cyclic voltammetry measurements were performed with a Hokuto Denko HA-501 potentiostat/galvanostat using a glassy carbon electrode in DMF or with a hanging mercury drop electrode (HMDE) in aqueous micellar solutions, respectively. As supporting electrolytes were used *n*-Bu_4NClO_4 in DMF and H_3PO_4-NaOH in aqueous solutions. A saturated calomel electrode (SCE) was used as a reference.

Results and Discussion

Redox Behaviors of $[Fe_4X_4(YR)_4]^{2-}$ (X, Y=S and Se; R=*n*-$C_{12}H_{25}$ and C_6H_4-*p*-*t*-Bu) in Aqueous Triton X-100 Micellar Solutions. Cyclic voltammograms of the present clusters show reversible $[Fe_4X_4(YR)_4]^{2-/3-}$ redox couples in the range $E_{1/2}$=−0.94 to −1.37 V vs. SCE in DMF (Table 1), where $E_{1/2}$ is approximated by the average of the cathodic and anodic peak potentials. As typical examples, the cyclic voltammograms of $[Fe_4S_4(S\text{-}n\text{-}C_{12}H_{25})_4]^{2-}$ and $[Fe_4S_4(SC_6H_4\text{-}p\text{-}t\text{-}Bu)_4]^{2-}$ are depicted in Fig. 1a and 1c. The redox potentials of synthetic Fe_4S_4 clusters as well as ferredoxins are affected significantly by the change of a medium.[10,18] The redox behaviors of synthetic Fe_4S_4 clusters in

Table 1. Electrochemical Parameters of the Clusters in DMF and in Aqueous Triton X-100 Micellar Solutions (pH 7.0)

Cluster	In DMF	In aq. micellar soln.		
	$E_{1/2}$[a]	$E_{1/2}$[a]	pK_a	$E_{1/2}$[a] at pH>pK_a
$[Fe_4S_4(S\text{-}n\text{-}C_{12}H_{25})_4]^{2-}$	−1.37	−0.59	9.1	−0.71
$[Fe_4S_4(Se\text{-}n\text{-}C_{12}H_{25})_4]^{2-}$	−1.35	−0.89	8.9	−1.04
$[Fe_4Se_4(S\text{-}n\text{-}C_{12}H_{25})_4]^{2-}$	−1.27	−0.85	7.7	−0.87
$[Fe_4Se_4(Se\text{-}n\text{-}C_{12}H_{25})_4]^{2-}$	−1.24	−0.91	7.7	−0.96
$[Fe_4S_4(SC_6H_4\text{-}p\text{-}t\text{-}Bu)_4]^{2-}$	−1.00	−0.55	8.5	−0.65
$[Fe_4S_4(SeC_6H_4\text{-}p\text{-}t\text{-}Bu)_4]^{2-}$	−0.99	−0.65	8.5	−0.67
$[Fe_4Se_4(SC_6H_4\text{-}p\text{-}t\text{-}Bu)_4]^{2-}$	−0.96	−0.78	7.5	−0.79
$[Fe_4Se_4(SeC_6H_4\text{-}p\text{-}t\text{-}Bu)_4]^{2-}$	−0.94	−0.79	7.3	−0.79

a) Values for the 2−/3− couple, V vs. SCE.

water, therefore, seem to be very important in connection with those of 4-Fe and 8-Fe ferredoxins. However, the fact that Fe_4S_4 clusters with alkanethiolate ligands such as $[Fe_4S_4(S\text{-}t\text{-}Bu)_4]^{2-}$ and $[Fe_4S_4(SCH_2CH_2CO_2)_4]^{6-}$ are subject to hydrolysis reactions in an aqueous medium[28] makes it difficult to study on the redox behaviors of synthetic Fe_4S_4 clusters in water. In order to protect the present clusters $[Fe_4X_4(YR)_4]^{2-}$ (X, Y=S and Se; R=n-$C_{12}H_{25}$ and C_6H_4-p-t-Bu) from such a hydrolysis reaction, those clusters are solubilized in an aqueous Triton X-100 micellar solution. The high stability of those clusters in this medium was confirmed by their electronic absorption spectra showing no appreciable change for 4 h under N_2. It has been reported that various surfactants strongly adsorb on solid electrodes such as glassy carbon and platinum plates and almost completely inhibit a direct electron transfer between those electrodes and the electrochemically active species in aqueous micellar solutions.[29] On the other hand, cyclic voltammograms of $[Fe_4S_4(SC_6H_4\text{-}p\text{-}n\text{-}C_8H_{17})_4]^{2-}$ solubilized in aqueous micellar and vesicle solutions have been obtained successfully[22,30] by taking advantage of a strong affinity of sulfur for an Hg electrode.[31] In accordance with this, the cyclic voltammograms of $[Fe_4S_4(S\text{-}n\text{-}C_{12}H_{25})_4]^{2-}$ and $[Fe_4S_4(SC_6H_4\text{-}p\text{-}t\text{-}Bu)_4]^{2-}$ by the use of a hanging mercury drop electrode (HMDE) clearly show the (2−/3−) redox couple at $E_{1/2}$=−0.59 and −0.55 V vs. SCE, respectively, in aqueous Triton X-100 micellar solution at pH 7.0 (Fig. 1b and 1d). A large cathodic peak current compared with anodic one

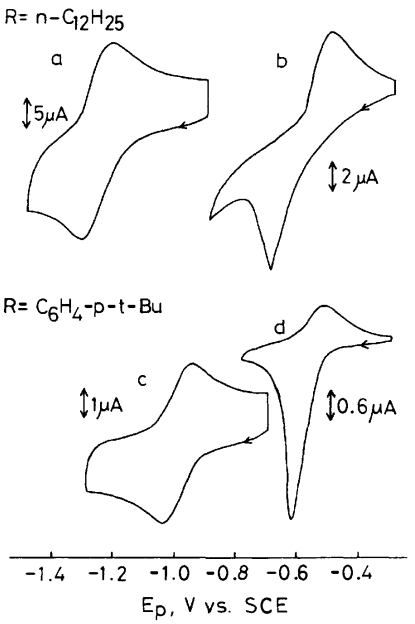

Fig. 1. Cyclic voltammograms of $[Fe_4S_4(SR)_4]^{2-}$ with a glassy carbon electrode in DMF (a, c) and with a hanging mercury drop electrode in aqueous Triton X-100 micellar solutions at pH 7.0 (b, d); scan rate 0.2 V s^{-1}.

of the $[Fe_4S_4(SR)_4]^{2-/3-}$ (R=n-$C_{12}H_{25}$ and C_6H_4-p-t-Bu) redox couple (Fig. 1b and 1d) suggests that adsorption of the oxidized cluster $[Fe_4S_4(SR)_4]^{2-}$ is stronger than that of the reduced species $[Fe_4S_4(SR)_4]^{3-}$ (R=n-$C_{12}H_{25}$ and C_6H_4-p-t-Bu) on the surface of an HMDE.[22,29,30] It has been shown that the adsorption of $[Fe_4S_4(SC_6H_4\text{-}p\text{-}n\text{-}C_8H_{17})_4]^{2-}$ on an Hg electrode causes the $E_{1/2}$ value of the cluster to shift cathodically by 80 mV compared with that of the free species in solutions.[30] Based on this fact, the $E_{1/2}$ values of $[Fe_4X_4(YR)_4]^{2-/3-}$ couple (X, Y=S and Se; R=n-$C_{12}H_{25}$ and C_6H_4-p-t-Bu) in aqueous Triton X-100 micellar solutions at pH 7.0 are considered to be shifted anodically by at least 150—780 mV compared with those in DMF and fall in the range −0.55 to −0.91 V vs. SCE at pH 7.0 (Table 1), which are compared to the redox potentials of 4-Fe (−0.52 to −0.67 V vs. SCE) and 8-Fe ferredoxins (−0.65 to −0.73 V vs. SCE) in water.[18] Thus, the redox potentials of Fe_4X_4 (X=S and Se) clusters are affected significantly by the extrinsic effect of the medium used.

Although the concentration of Triton X-100 (0.025—0.5 mol dm^{-3}) hardly influences the redox potentials of the present clusters, proton concentrations gave a significant effect on the redox potentials. Figure 2 shows the plots of the $E_{1/2}$ values of the present clusters vs. pH of aqueous Triton X-100 micellar solutions at 20 °C. The $E_{1/2}$ values of the $[Fe_4S_4(Y\text{-}n\text{-}C_{12}H_{25})_4]^{2-/3-}$ (Y=S (○) and Se (●) in Fig. 2a) and $[Fe_4Se_4(Y\text{-}n\text{-}C_{12}H_{25})_4]^{2-/3-}$ (Y=S (△) and Se (▲) in Fig. 2a) couples are shifted by about −55 mV/pH in the pH lower than ca. 9.0 and 7.7, respectively, while they remain constant in the pH higher than those values. Similarly, $[Fe_4S_4(YC_6H_4\text{-}p\text{-}t\text{-}Bu)_4]^{2-}$ (Y=S (○) and Se (●) in Fig. 2b) and $[Fe_4Se_4(YC_6H_4\text{-}p\text{-}t\text{-}Bu)_4]^{2-}$ (Y=S (△) and Se (▲) in Fig. 2b) display the same shifts of $E_{1/2}$ in the pH lower than ca. 8.5 and 7.3, respectively, and the $E_{1/2}$ values are constant in the pH higher than those values. The pH dependence of $E_{1/2}$ values (ca. −55.0 mV/pH) for the present clusters indicates that the redox-linked protonation of the clusters takes place and the resulting protonated cluster exists as an equilibrium mixture with unprotonated one. The electron density of $[Fe_4X_4(YR)_4]^{3-}$ (X, Y=S, Se; R=n-$C_{12}H_{25}$, C_6H_4-p-t-Bu) is apparently larger than that of $[Fe_4X_4(YR)_4]^{2-}$. The turning point of each plot in Fig. 2a and 2b, therefore, corresponds to the pK_a value of the reduced forms of the clusters, which is classified into four groups: ca. 9.0, 7.7, 8.5, and 7.3 for the $[Fe_4S_4(Y\text{-}n\text{-}C_{12}H_{25})_4]^{3-}$, $[Fe_4Se_4(Y\text{-}n\text{-}C_{12}H_{25})_4]^{3-}$, $[Fe_4S_4(YC_6H_4\text{-}p\text{-}t\text{-}Bu)_4]^{3-}$, and $[Fe_4Se_4(YC_6H_4\text{-}p\text{-}t\text{-}Bu)_4]^{3-}$ (Y=S and Se), respectively (Table 1). Thus, the pK_a values of the $[Fe_4X_4(YR)_4]^{3-}$ (X, Y=S and Se; R=n-$C_{12}H_{25}$ and C_6H_4-p-t-Bu) are controlled by the difference of the Fe_4S_4 and Fe_4Se_4 cores rather than that of the terminal sulfur and selenium atoms of the Y-n-$C_{12}H_{25}$ or YC_6H_4-p-t-Bu moiety. This result

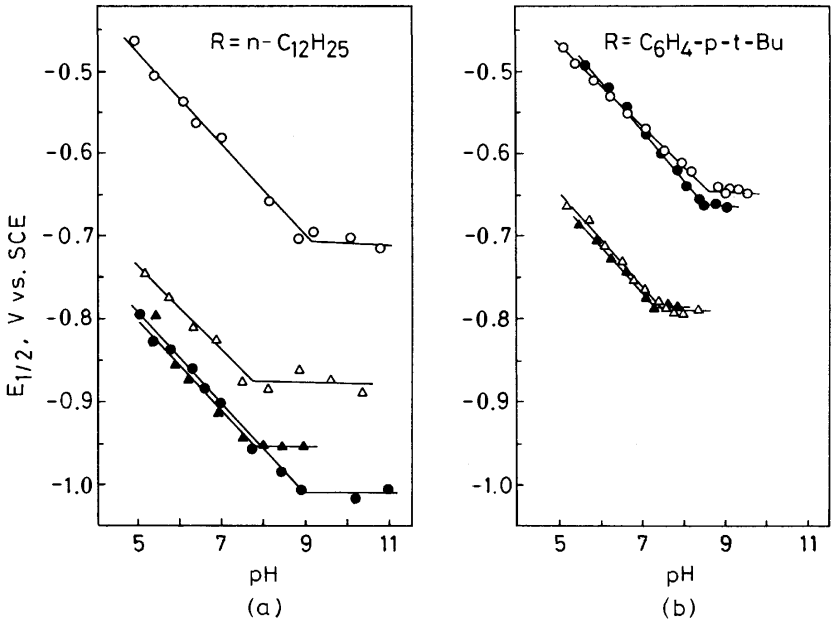

Fig. 2. Plots of the $E_{1/2}$ values of the $[Fe_4X_4(YR)_4]^{2-/3-}$ (R=n-$C_{12}H_{25}$ (a) and C_6H_4-p-t-Bu (b)) redox couples vs. pH in aqueous Triton X-100 micellar solutions at 20°C; X,Y=S,S (○); S,Se (●); Se,S (△); Se,Se (▲).

suggests that the present redox-linked protonation takes place at the sulfur or selenium atom of the Fe_4X_4 core (X=S and Se) of $[Fe_4X_4(YR)_4]^{3-}$ (X, Y=S and Se; R=n-$C_{12}H_{25}$ and C_6H_4-p-t-Bu).

Redox Behaviors of $[Fe_4X_3(YC_6H_4$-p-t-Bu$)_4]^{2-}$ (X, Y=S and Se) in an Aqueous Poly[2-(dimethylamino)-hexanamide] (PDACA) Solution. The preceding discussion reveals that the protonation of $[Fe_4X_4(YR)_4]^{3-}$ (X, Y=S and Se; R=n-$C_{12}H_{25}$ and C_6H_4-p-t-Bu) in aqueous Triton X-100 micellar solutions takes place at the sulfur or selenium atom of the Fe_4X_4 (X=S and Se) core. The hydrophobic sphere of a nonionic Triton X-100 micelle is, however, apparently different from the environments formed by polypeptide chains of 4-Fe ferredoxins, which may be stabilized by hydrogen bondings between amide protons of peptide chains and terminal and/or core sulfur atoms. In order to introduce amide groups around the Fe_4S_4 core in a model system, poly[2-(dimethylamino)hexanamide] (PDACA) involving both amide and amino groups in the polymer chains was employed for solubilizing the clusters in aqueous solutions. The

PDACA: $-(-NHCH_2CH_2CH_2CH_2CHCO-)_n$ with $N(CH_3)_2$ on the CH

electronic absorption spectrum of $[Fe_4S_4(S$-n-$C_{12}H_{25})_4]^{2-}$ in an aqueous PDACA solution (pH 7.0), however, showed a decrease of the absorption maximum at 420 nm with a half-life $t_{1/2}=1.3\times10^3$ s at 20 °C, suggesting that $[Fe_4S_4(S$-n-$C_{12}H_{25})_4]^{2-}$ slowly undergoes a hydrolysis reaction in this medium. On the other hand, the cluster in the Triton X-100 micellar solution exhibited no spectral change for 4 h under N_2. Such a difference may result from a strong hydrophobicity of Triton X-100 micelle compared with an aqueous PDACA solution. The hydrolysis of $[Fe_4S_4(S$-n-$C_{12}H_{25})_4]^{2-}$ in an aqueous PDACA solution may result in a dissociation of the terminal ligand, which is adsorbed strongly on an HMDE.[31] In fact, the cyclic voltammogram of $[Fe_4S_4(S$-n-$C_{12}H_{25})_4]^{2-}$ in an aqueous PDACA solution at pH 7.0 showed a pair of cathodic and anodic waves at $E_{pc}=-0.63$ V and $E_{pa}=-0.56$ V vs. SCE, respectively, which are consistent not only with the peak potentials but also with the appearance of those of S-n-$C_{12}H_{25}^-$ (n-Bu_4N^+ salt) in the same medium. Similarly, the redox waves due to S-n-$C_{12}H_{25}^-$ or Se-n-$C_{12}H_{25}^-$ were observed in the cyclic voltammograms of other three clusters in aqueous PDACA solutions. Thus, the 1-dodecanethiolate and -selenolate ligated clusters $[Fe_4X_4(Y$-n-$C_{12}H_{25})_4]^{2-}$ (X, Y=S and Se) undergo the ligand dissociation in aqueous PDACA solutions.

In contrast to the lability of $[Fe_4X_4(Y$-n-$C_{12}H_{25})_4]^{2-}$ in aqueous PDACA solution, $[Fe_4X_4(YC_6H_4$-p-t-Bu$)_4]^{2-}$ (X, Y=S and Se) is fairly stable in this medium, since the electronic absorption spectra of the latter except for $[Fe_4Se_4(SeC_6H_4$-p-t-Bu$)_4]^{2-}$ [32] in an aqueous PDACA solution (pH 7.0) were almost unchanged for 6 h. In fact, $[Fe_4X_4(YC_6H_4$-p-t-Bu$)_4]^{2-}$ (X, Y=S and Se) in aqueous PDACA solution at pH 7.0 exhibit each redox couple arising from the cluster ($E_{1/2}=-0.57$ for

X, Y=S, S; −0.56 for X, Y=S, Se; −0.79 for X, Y=Se, S; −0.77 V vs. SCE for X, Y=Se, Se), and the redox couple neither of SC_6H_4-*p*-*t*-Bu$^-$ (E_{pc}=−0.70 and E_{pa}=−0.60 V) nor of SeC_6H_4-*p*-*t*-Bu$^-$ (E_{pc}=−1.01 and E_{pa}=−0.89 V vs. SCE) was observed, indicating that $[Fe_4X_4(YC_6H_4\text{-}p\text{-}t\text{-}Bu)_4]^{2-}$ (X, Y=S and Se) undergoes one-electron redox reaction in aqueous PDACA solution without dissociation of the YC_6H_4-*p*-*t*-Bu$^-$ ligand at pH 7.0. Moreover, the cyclic voltammograms of those clusters obtained even after applying the electrode potential at −1.00 V vs. SCE for 5 min exhibited only the redox waves of those clusters. The electrochemical study on the clusters in aqueous PDACA solutions, therefore, is restricted to $[Fe_4X_4(YC_6H_4\text{-}p\text{-}t\text{-}Bu)_4]^{2-}$ (X, Y=S and Se) in the present study.

The $E_{1/2}$ values of the $[Fe_4X_4(YC_6H_4\text{-}p\text{-}t\text{-}Bu)_4]^{2-/3-}$ redox couples at various pH are depicted in Fig. 3, which reveals that all the $E_{1/2}$ values for X, Y=S and Se are shifted cathodically in linear fashion with increasing the pH value in the intermediate pH range,

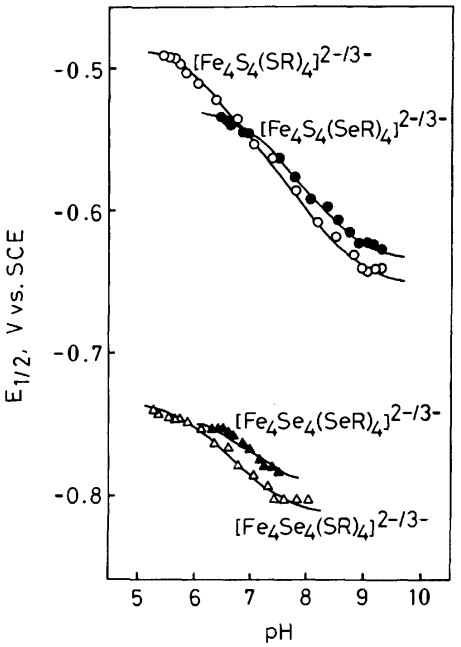

Fig. 3. Plots of the $E_{1/2}$ values of the $[Fe_4X_4(YR)_4]^{2-/3-}$ (R=C_6H_4-*p*-*t*-Bu) redox couples in aqueous PDACA solutions vs. pH at 10°C; X,Y=S,S (○); S,Se (●); Se,S (△); Se,Se (▲).

being similar to those in aqueous Triton X-100 micellar solutions, while the values are likely to show a tendency to level off from each linear relation not only in alkaline but also in acidic sides.[33] Such characteristic pH dependence of the $E_{1/2}$ value may be interpreted in terms of protonation/deprotonation equilibria of the oxidized clusters $[Fe_4X_4(YC_6H_4\text{-}p\text{-}t\text{-}Bu)_4]^{2-}$ as well as of the reduced species $[Fe_4X_4(YC_6H_4\text{-}p\text{-}t\text{-}Bu)_4]^{3-}$ (X, Y=S and Se) in aqueous PDACA solutions, as shown in Scheme 1, where K_{ox} and K_{red} are the acid dissociation constants of the protonated species $[Fe_4X_4(YR)_4H]^-$ and $[Fe_4X_4(YR)_4H]^{2-}$ (X, Y=S and Se; R=C_6H_4-*p*-*t*-Bu), respectively, as expressed by Eqs. 1 and 2, and

$$K_{ox} = \frac{[[Fe_4X_4(YR)_4]^{2-}][H^+]}{[[Fe_4X_4(YR)_4H]^-]} \quad (1)$$

$$K_{red} = \frac{[[Fe_4X_4(YR)_4]^{3-}][H^+]}{[[Fe_4X_4(YR)_4H]^{2-}]} \quad (2)$$

$E^1_{1/2}$ and $E^2_{1/2}$ are the half-wave potentials of the redox couples of unprotonated and protonated species, respectively. The half-wave potential $E_{1/2}$ for the overall electrode reaction, therefore, can be written as Eq. 3 or 4,[34,35] where R, T, and F are the gas constant,

$$E_{1/2} = E^1_{1/2} + \frac{RT}{F}\ln\frac{K_{ox}(K_{red} + [H^+])}{K_{red}(K_{ox} + [H^+])} \quad (3)$$

$$E_{1/2} = E^2_{1/2} + \frac{RT}{F}\ln\frac{K_{red} + [H^+]}{K_{ox} + [H^+]} \quad (4)$$

temperature, and the Faraday constant, respectively. An anodic shift of $E_{1/2}$ values with increasing the proton concentration (Fig. 3) suggests that the K_{ox} value is larger than the K_{red} value (Eq. 3). Therefore, $E_{1/2}$ approaches to $E^1_{1/2}$ (Eq. 3) and $E^2_{1/2}$ (Eq. 4) under the proton concentrations being $[H^+] \ll K_{red}$ (Eq. 3) and $[H^+] \gg K_{ox}$ (Eq. 4), respectively. Thus, the redox potential $E_{1/2}$ of $[Fe_4X_4(YC_6H_4\text{-}p\text{-}t\text{-}Bu)_4]^{2-/3-}$ (X, Y=S and Se) in aqueous PDACA solution may be leveled off both in acidic and in alkaline regions (Fig. 3). Computer simulation curves of the $E_{1/2}$ value using Eq. 3 or 4 with the pK_{red}, pK_{ox}, and $E^1_{1/2}$ or $E^2_{1/2}$ values listed in Table 2 give reasonable agreement with the observed $E_{1/2}$ values of those clusters,[36] as shown by solid lines in Fig. 3.

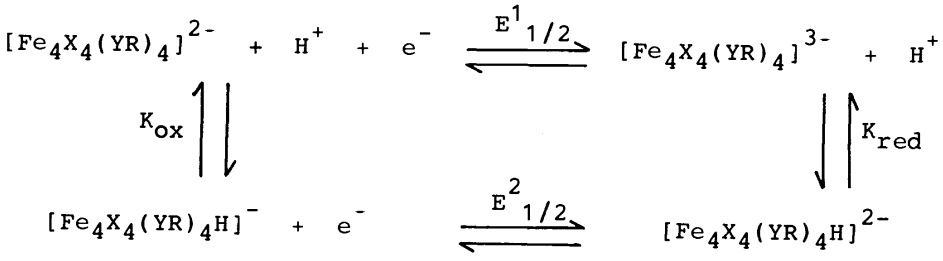

Scheme 1. R=C_6H_4-*p*-*t*-Bu.

Table 2. pK Values of the Oxidized and Reduced Clusters in Aqueous PDACA Solution

Cluster	pK_{ox}	pK_{red}[a]	$E^1_{1/2}$[b]	$E^2_{1/2}$[b]
$[Fe_4S_4(SC_6H_4$-p-t-$Bu)_4]^{2-}$	5.85	8.80	−0.650	−0.484
$[Fe_4S_4(SeC_6H_4$-p-t-$Bu)_4]^{2-}$	6.90	8.80	−0.632	−0.526
$[Fe_4Se_4(SC_6H_4$-p-t-$Bu)_4]^{2-}$	5.85	7.30	−0.811	−0.732
$[Fe_4Se_4(SeC_6H_4$-p-t-$Bu)_4]^{2-}$	6.70	7.30	−0.795	−0.744

a) Values for the 3− species. b) Values for the 2−/3− couple.

The pK_{red} values of $[Fe_4X_4(YC_6H_4$-p-t-$Bu)_4]^{3-}$ (Table 2) obtained from the simulation are devided into two groups; 8.8 for X=S and 7.3 for X=Se, where Y=S and Se. The close similarity of the pK_{red} values of the clusters with Fe_4S_4 and Fe_4Se_4 cores in an aqueous PDACA solution to the pK_a values of those in an aqueous Triton X-100 micellar solution also supports the view that the pK_a values in Triton X-100 micellar solutions are associated with the proton dissociation constants of the reduced species of the clusters. Thus, the protonation of the reduced clusters takes place at the sulfur or selenium of the Fe_4X_4 core (X=S and Se) both in aqueous Triton X-100 micellar and in aqueous PDACA solutions. On the other hand, the pK_{ox} values of $[Fe_4X_4(YC_6H_4$-p-t-$Bu)_4]^{2-}$ (Table 2) are devided into two group; 5.85 for $[Fe_4X_4(SC_6H_4$-p-t-$Bu)_4]^{2-}$ and 6.8±0.1 for $[Fe_4X_4(SeC_6H_4$-p-t-$Bu)_4]^{2-}$ (X=S and Se). This behavior indicates that pK_{ox} values are controlled by the terminal sulfur and selenium atoms in contrast to pK_{red} which depends on the core sulfur or selenium atom. Thus, the protonation of the oxidized clusters $[Fe_4X_4(YC_6H_4$-p-t-$Bu)_4]^{2-}$ (X, Y=S and Se) takes place at the terminal sulfur or selenium atoms in aqueous PDACA solutions. These results lead us to the conclusion that the basicities of the terminal sulfur and selenium in the oxidized clusters may be stronger than those of the core sulfur and selenium atoms, while in the reduced cluster, the basicities may be opposite; the core sulfur and selenium atoms stronger than the terminal those atoms.

References

1) D. C. Yoch, D. I. Arnon, and W. V. Sweeney, *J. Biol. Chem.*, **250**, 8330 (1975); H. Hiura, T. Kakuno, J. Yamashita, H. Matsubara, and T. Horio, *J. Biochem.*, **89**, 1787 (1981); K. T. S. Shanmugan, D. B. Buchanan, and D. E. Arnon, *Biochim. Biophys. Acta*, **256**, 477 (1972).

2) K. M. Werber and M. Mevarech, *Arch. Biochem. Biophys.*, **186**, 60 (1978); S. Seki, M. Hagiwara, K. Kudo, and M. Ishimoto, *J. Biochem.*, **85**, 833 (1979).

3) B. E. Smith, D. J. Lowe, and R. C. Bray, *Biochem. J.*, **137**, 169 (1974); M. Tanaka, M. Haniu, K. T. Yasunobu, and L. E. Mortenson, *J. Biol. Chem.*, **252**, 7093 (1977); V. Sunderson and F. M. Ausubel, *J. Biol. Chem.*, **256**, 2808 (1981).

4) B. A. Averill, T. Herskovitz, R. H. Holm, and J. A. Ibers, *J. Am. Chem. Soc.*, **95**, 3523 (1973).

5) R. H. Holm, W. D. Philips, B. A. Averill, J. J. Mayerle, and T. Herskovitz, *J. Am. Chem. Soc.*, **96**, 2109 (1974).

6) G. R. Dukes and R. H. Holm, *J. Am. Chem. Soc.*, **97**, 528 (1975).

7) R. W. Johnson and R. H. Holm, *J. Am. Chem. Soc.*, **100**, 5338 (1978).

8) G. B. Wong, D. M. Kurtz, Jr., R. H. Holm, L. E. Mortenson, and R. G. Upchurch, *J. Am. Chem. Soc.*, **101**, 3078 (1979).

9) M. A. Bobrik, E. J. Laskowski, R. W. Johnson, W. O. Gillum, J. M. Berg, K. O. Hodgson, and R. H. Holm, *Inorg. Chem.*, **17**, 1402 (1978).

10) B. V. DePamphilis, B. A. Averill, T. Herskovitz, L. Que, Jr., and R. H. Holm, *J. Am. Chem. Soc.*, **96**, 4159 (1974).

11) L. Que, Jr., J. R. Anglin, M. A. Bobrik, A. Davison, and R. H. Holm, *J. Am. Chem. Soc.*, **96**, 6042 (1974).

12) C. L. Hill, J. Renaud, R. H. Holm, and L. E. Mortenson, *J. Am. Chem. Soc.*, **99**, 2549 (1977).

13) G. Christou, P. M. Mascharak, W. H. Armstrong, G. C. Papaefthymiou, R. B. Frankel, and R. H. Holm, *J. Am. Chem. Soc.*, **104**, 2820 (1982).

14) W. H. Armstrong, P. K. Mascharak, and R. H. Holm, *J. Am. Chem. Soc.*, **104**, 4373 (1982).

15) R. E. Johnson, G. C. Papaefthymiou, R. B. Frankel, and R. H. Holm, *J. Am. Chem. Soc.*, **105**, 7280 (1983).

16) G. Christou, C. D. Garner, R. M. Miller, C. E. Johnson, and J. D. Rush, *J. Chem. Soc., Dalton Trans.*, **1983**, 2363.

17) T. C. Bruice and R. Maskiewicz, *J. Chem. Soc., Chem. Commun.*, **1978**, 703; B. Odell and P. J. Geary, *J. Chem. Soc., Dalton Trans.*, **1984**, 29.

18) C. L. Hill, J. Renaud, R. H. Holm, and L. E. Mortenson, *J. Am. Chem. Soc.*, **99**, 2549 (1977).

19) E. T. Lode, C. L. Murray, and J. C. Rabinowitz, *J. Biol. Chem.*, **251**, 1683 (1976).

20) J. C. Rabinovitz and W. V. Sweeney, *Annu. Rev. Biochem.*, **49**, 139 (1980).

21) E. Adman, K. D. Watenpaugh, and L. H. Jensen, *Proc. Natl. Acad. Sci. U.S.A.*, **72**, 4854 (1975).

22) K. Tanaka, T. Tanaka, and I. Kawafune, *Inorg. Chem.*, **23**, 517 (1984); K. Tanaka, M. Moriya, and T. Tanaka, *Inorg. Chem.*, **25**, 835 (1986).

23) M. Nakamoto, K. Tanaka, and T. Tanaka, *J. Chem. Soc., Chem. Commun.*, **1986**, 1669.

24) G. G. Urquhart, J. W. Gates, Jr., R. Connor, L. I. Smith, R. T. Arnold, and K. Stevenson, *Org. Synth.*, Coll. Vol. 3, 363 (1955).

25) T. H. Colle and E. S. Lewis, *J. Am. Chem. Soc.*, **101**, 1810 (1979).

26) G. Christou, B. Ridge, and H. N. Rydon, *J. Chem. Soc., Dalton Trans.*, **1978**, 1423.

27) L. Que, Jr., M. A. Bobrick, J. A. Ibers, and R. H.

Holm, *J. Am. Chem. Soc.*, **96**, 4168 (1974); K. Tanaka, M. Nakamoto, Y. Tashiro, and T. Tanaka, *Bull. Chem. Soc. Jpn.*, **58**, 316 (1985).

28) T. C. Bruice, R. Maskiewicz, and R. C. Job, *Proc. Natl. Sci. U.S.A.*, **72**, 231 (1975); R. C. Job and T. C. Bruice, *ibid.*, **72**, 2478 (1975).

29) Z. Kozarac and B. Cosovic, *Bioelectrochem. Bioenerg.*, **12**, 353 (1984); B. Cosovic, N. Matina, and Z. Kozarac, *J. Electroanal. Chem.*, **113**, 239 (1980); L. Pospisil, J. Kuta, E. Muller, and H.-D. Dorfler, *J. Electroanal. Chem.*, **106**, 359 (1980); F. Muller, H. Emons, and H.-D. Dorfler, *Bioelectrochem. Bioenerg.*, **10**, 279 (1983).

30) K. Tanaka, M. Masanaga, and T. Tanaka, *J. Am. Chem. Soc.*, **108**, 5448 (1986).

31) R. Parsons and P. C. Symons, *Trans. Faraday Soc.*, **64**, 1077 (1968); N. Kobayashi, A. Osawa, K. Shimizu, Y. Hayashi, H. Kimoto, and T. Fujisawa, *J. Polym. Sci., Polym. Lett. Ed.*, **15**, 137 (1977); P. J. Peerce and F. C. Anson, *J. Electroanal. Chem. Interfacial Electrochem.*, **105**, 317 (1979).

32) The electronic absorption spectrum of $[Fe_4Se_4(SeC_6H_4\text{-}p\text{-}t\text{-}Bu)_4]^{2-}$ in aqueous PDACA showed the 76% decrease of the absorptivity of the CT band at 490 nm for 6 h.

33) The cyclic voltammogram of $[Fe_4X_4(YC_6H_4\text{-}p\text{-}t\text{-}Bu)_4]^{2-}$ (X, Y=S and Se) exhibits only a (2−/3−) redox couple in the intermediate pH range (Fig. 3). When pH is higher than ca. 7.3 or 8.8 and lower than ca. 5.9 or 6.8, however, a new redox couple due to free $YC_6H_4\text{-}p\text{-}t\text{-}Bu^-$ (Y=S and Se) appeared besides a redox couple of the clusters, suggesting the partial dissociation of $YC_6H_4\text{-}p\text{-}t\text{-}Bu^-$ (Y=S and Se) in the pH range higher than ca. 7.3 or 8.8 and lower than ca. 5.9 or 6.8 in the PDACA solution.

34) M. Masanaga, S. Kuwabata, K. Tanaka, and T. Tanaka, *Chem. Lett.*, **1986**, 1531.

35) P. L. Dutton and D. F. Wilson, *Biochim. Biophys. Acta*, **346**, 165 (1974); R. S. Magliozzo, B. A. McIntosh, and W. V. Sweeny, *J. Biol. Chem.*, **257**, 3506 (1982).

36) The $E_{1/2}$ value of the $[Fe_4Se_4(SeC_6H_4\text{-}p\text{-}t\text{-}Bu)_4]^{2-/3-}$ couple observed in acid and alkaline regions is slightly deviated from computer simulation curves of the $E_{1/2}$ value, which may be due to the instability of the Fe_4Se_4 cluster with selenolate ligands, as described elsewhere.[9,32]

 © 1988 The Chemical Society of Japan Bull. Chem. Soc. Jpn., 61, 4107—4112 (1988)

Ion-Solvent Interaction of Amino Acids. The Role of the "Zwitterionic" and the "Ionic" Forms in the Modification of Water Structure over the Temperature Range 25—45 °C

Moni Mohan Bhattacharyya and Mihir Sengupta*
Department of Chemistry, University College of Science, Calcutta 700 009, India
(Received October 2, 1987)

Viscosities and densities of aqueous glycine, glycinium chloride, sodium glycinate, betaine, betainium chloride [$(CH_3)_3\overset{+}{N}CH_2COOH \cdot Cl^-$], and tetramethylammonium bromide solutions have been measured at 25, 30, and 40 °C over the concentration range 0.01 to 0.1 M. The sequence of the viscosity B-coefficient values obtained is in the order: $B_{anion} > B_{cation} > B_{zwitterion}$ for the glycine and betaine systems. The comparatively higher structure promoting behavior of the anion has been discussed in terms of the charge delocalization effect. Apparent molal volumes at infinite dilution have also been calculated, and the ratio B/ϕ_v° furnishes important information about the nature of solvation around the ion. The present study indicates that in the betaine molecule, the opposing nature of ion-water interaction at the two charge centers renders the system neither a "structure maker" nor a "breaker" in aqueous solution.

In an earlier communication[1] viscosity studies on amino acids at different pH's in presence of free acids and alkalis, and at different temperatures have been reported. It was found that the viscosity data of amino acids in the acidic and basic solutions used could not be processed properly using the Jones-Dole equation[2]

$$\eta/\eta_0 = 1 + A\sqrt{c} + Bc, \quad (1)$$

as unreasonable negative A coefficient values, together with B-values with large standard deviations, were obtained. Instead, the use of the following equation, generally obeyed by uncharged molecules and neutral (zwitterionic) amino acids,[3] viz.

$$\eta/\eta_0 = 1 + Bc \quad (2)$$

was found to be more satisfactory. The B-coefficient values obtained from the above two equations are of course not the same, and in fact significant differences were observed.[3]

For a dilute solution of spherical particles, the Einstein equation[4] $\eta/\eta_0 = 1 + 2.5\theta$, ($\theta$=solute volume fraction) when combined with Eq. 2 gives the hydrodynamic volume per mole (V_h) of the (solute) particles, which tend to rotate in the fluid streamlines:

$$B = 2.5\, V_h \times 10^{-3} \quad (3)$$

For ellipsoidal particles at low concentrations a more general expression for V_h may also be derived:[5]

$$B = k\, V_h \times 10^{-3} \quad (4)$$

where k is a shape factor, being equal to 2.5 for spherical molecules. Since the apparent molal volume at infinite dilution: ϕ_v° ($=\overline{V}^\circ$) and V_h are approximately equal, the magnitude of the ratio B/ϕ_v° is expected to offer valuable information about the nature of interaction of solute molecules with the solvent.

Both neutral glycine and tetramethylammonium ion are the lowest members in the respective series of compounds, and also are well-known structure breakers[3,6] in aqueous solutions due to the presence of peripheral charge. It is interesting to investigate how these moieties, when conjoined in the form of a single molecule (e.g., in betaine) interact with the solvent water. The study of betaine and its homologues is also important in view of the current interest[7] in the potential utilization of their surfactant properties for tertiary oil recovery. Further, the purpose of the present work is also to investigate the comparative applicability of the Jones-Dole equation (Eq. 1) or Eq. 2, using amino acid salts in water only, instead of in acids or alkalis as done earlier,[1] and also the effects of the "zwitterionic" and the "ionic" form surface charges on the solvent water while either keeping unaltered, or else altering suitably, the size of the solute molecule.

With these objects in view, we have measured the viscosities of solutions of glycine, glycinium chloride, sodium glycinate, tetramethylammonium bromide, betaine, and betainium chloride, at three different temperatures over the range 25—40 °C. For betaine solutions measurements were also made at two other temperatures (35 and 45 °C). The density measurements enable the calculation of the apparent molal volumes directly, which further enables us to study the ion-solvent interactions from the complementary view points of viscosity and apparent molal volume.

Experimental

Glycine used was medicinal grade (E. Merck) and was purified as described earlier.[1] Sodium glycinate and glycinium chloride were prepared by mixing equivalent amounts of glycine and the corresponding alkali or acid as required. Betaine was obtained from betaine monohydrate (Fluka, Purum) by dissolving in hot absolute ethanol and precipitating white anhydrous betaine by adding anhydrous ether;[5] it was dried in vacuo at 100 °C, and stored in a desiccator under a reduced pressure. Betainium chloride (B.D.H.) was purified by precipitating from a saturated aqueous solution with ethyl alcohol.[8] It was dried at 110 °C for a few hours and stored in a desiccator. Tetramethylam-

Table 1. Viscosity and Density data ($g\,cm^{-3}$) for the Glycine and Betaine Systems and Tetramethylammonium Bromide, in aqueous Solution at Different Temperatures

Glycine			Glycinium chloride		
Concn (C/M)	Density	(η/η_0-1)	Concn ($C^{1/2}$/M$^{1/2}$)	Density	$(\eta/\eta_0-1)/C^{1/2}$
	25°C			25°C	
0.13555	1.01806	0.01800	0.31904	1.00153	0.05650
0.06447	0.99914	0.00760	0.25203	0.99991	0.04570
0.02765	0.99795	0.00370	0.15201	0.99812	0.03060
0.01582	0.99760	0.00200			
0.00818	0.99734	0.00092			
				30°C	
			0.18260	0.99752	0.0296
			0.16940	0.99729	0.0279
			0.15480	0.99676	0.0255
			0.10970	0.99599	0.0184
				40°C	
			0.22516	0.99440	0.0396
			0.20856	0.99392	0.0358
			0.17204	0.99337	0.0290
			0.13531	0.99294	0.0241
			0.09434	0.99265	0.0188

Sodium glycinate			Betaine		
Concn ($C^{1/2}$/M$^{1/2}$)	Density	$(\eta/\eta_0-1)/C^{1/2}$	Concn (C/M)	Density	(η/η_0-1)
	25°C			25°C	
0.31555	1.00272	0.11120	0.08251	0.99880	0.0179
0.24747	1.00060	0.08850	0.06337	0.99857	0.0139
0.20005	0.99938	0.07190	0.03987	0.99783	0.0077
0.15669	0.99826	0.06010	0.02452	0.99752	0.0051
0.07959	0.99723	0.03350			
	30°C			30°C	
0.27510	0.99986	0.0953	0.08496	0.99739	0.0191
0.23619	0.99864	0.0829	0.06009	0.99667	0.0136
0.21220	0.99803	0.0769	0.04339	0.99650	0.0105
0.16120	0.99728	0.0601	0.02499	0.99613	0.0055
0.10469	0.99629	0.0431	0.02002	0.99602	0.0040
			0.01295	0.99596	0.0032
	40°C				
0.29799	0.99668	0.1008			
0.25104	0.99531	0.0831			
0.21045	0.99437	0.0747			
0.17510	0.99328	0.0639			
0.15530	0.99328	0.0549			
0.11920	0.99272	0.0417			

Betaine hydrochloride			Tetramethylammonium bromide		
Concn ($C^{1/2}$/M$^{1/2}$)	Density	$(\eta/\eta_0-1)/C^{1/2}$	Concn ($C^{1/2}$/M$^{1/2}$)	Density	$(\eta/\eta_0-1)/C^{1/2}$
	25°C			25°C	
0.38850	1.00205	0.0970	0.25069	0.99952	0.0257
0.31980	1.00018	0.0808	0.22578	0.99903	0.0247
0.17086	0.99776	0.0454	0.17640	0.99829	0.0199
0.11920	0.99751	0.0335			
	30°C			30°C	
0.38763	1.00027	0.0982	0.40899	1.00206	0.0477
0.34531	0.99924	0.0866	0.30587	0.99918	0.0375
0.32040	0.99876	0.0811			
0.27109	0.99788	0.0690	0.29189	0.99942	0.0358
0.24430	0.99736	0.0634	0.2300	0.99758	0.0291
0.19519	0.99683	0.0521			

Table 1. (Continued)

Betaine hydrochloride			Tetramethylammonium bromide		
Concn ($C^{1/2}/M^{1/2}$)	Density	$(\eta/\eta_0-1)/C^{1/2}$	Concn ($C^{1/2}/M^{1/2}$)	Density	$(\eta/\eta_0-1)/C^{1/2}$
	40 °C				
0.29375	0.99476	0.0747			
0.24361	0.99381	0.0635			
0.19219	0.99322	0.0518			
0.15931	0.99278	0.0433			

Betaine 35 °C			Betaine 45 °C		
Concn (C/M)	Density	(η/η_0-1)	Concn (C/M)	Density	(η/η_0-1)
0.18457	0.99738	0.0409	0.10806	0.99213	0.0233
0.09755	0.99582	0.0212	0.10552	0.99203	0.0228
0.06222	0.99519	0.0128	0.07349	0.99152	0.0153
0.04413	0.99485	0.0093	0.04640	0.99103	0.0096
0.03126	0.99459	0.0059	0.03473	0.99082	0.0072
0.02431	0.99447	0.0050	0.02645	0.99064	0.0047
0.01873	0.99436	0.0037			

Table 2. B-Coefficient $(kg\,mol^{-1})^{-1}$ and $A(kg\,mol^{-1})^{-1/2}$ Values of the Viscosity Plots

System		25 °C	30 °C
Betaine	B coeff.	0.227±0.009	0.226±0.015
Betaine hydrochloride	B coeff.	0.236±0.0007	0.237±0.002
	A coeff.	0.0052±0.0001	0.0052±0.0005
Glycine	B coeff.	0.132±0.008	0.137±0.009
Sodium glycinate	B coeff.	0.327±0.004	0.306±0.002
	A coeff.	0.0076±0.0007	0.011±0.0004
Glycinium chloride	B coeff.	0.155±0.0007	0.155±0.0007
	A coeff.	0.0069±0.0002	0.0014±0.0001
Tetramethylammonium bromide	B coeff.	0.081±0.002	0.107±0.001
	A coeff.	0.0058±0.0004	0.0043±0.0003

System	35 °C	40 °C	45 °C
Betaine	0.225±0.008		0.225±0.006
Betaine hydrochloride		0.232±0.002	
		0.0067±0.0003	
Glycine		0.145±0.004	
Sodium glycinate		0.319±0.009	
		0.0054±0.0018	
Glycinium chloride		0.156±0.003	
		0.0034±0.0006	
Tetramethylammonium bromide			

monium bromide was purified as described earlier.[9] All the amino acids and their salts were dried at 100 °C for about two hours before being dissolved in redistilled water (from an all Pyrex still), and the solutions were prepared and dilutions made on molal basis.

Details of the method of viscosity measurement have been described earlier.[1] The densities were measured in a 30 cm^3 Sprengel type bicapillary pycnometer, fitted with ground glass caps, and are precise to $\pm10^{-5}$ g cm^{-3} (bouyancy corrections not made). A constant temperature bath, controlled to within ±0.005 °C was used. The literature values[10] of the density of water used in the calculations were 0.99707, 0.99568, 0.99406, 0.99220, and 0.99024 g cm^{-3} at 25, 30, 35, 40, and 45 °C, respectively. The viscosity and density data at different concentrations and at different temperatures are recorded in Table 1.

Calculations and Results. For the computerised least squares analysis of the viscosity data of glycine and betaine Eq. 2 was used, whereas for the salt forms of the amino acids both Eqs. 1 and 2 were tried. In the case of the salts, the acceptable positive values of the intercepts as also B-values with comparatively smaller standard deviations obtained, showed the better applicability of the Jones-Dole equation (Eq. 1) rather than Eq. 2 in contrast to the earlier finding.[1] The B and A-values thus obtained, at different temperatures, are recorded in Table 2 (together with the s.d. of fit only).

The apparent molal volumes were calculated from the density data by the use of the usual equation $\phi_v=\frac{1}{m}[(1000+mM_2)/\rho_m-(1000/\rho_o)]$; the values at infinite dilution for the salts were obtained from a least-squares fit of the Redlich-Meyer equation[11]

$$\phi_v - S_v\sqrt{c} = \phi_v^\circ + hC \qquad (5)$$

where h is an empirical constant, and S_v the Debye-Hückel limiting slope, the different values of which at the different temperatures were taken from literature.[11] The "hydrolysis effect" corrections[12] for the ϕ_v values have been made, but

Table 3. ϕ_v° Values ($cm^3 mol^{-1}$) at Different Temperature

System	25 °C	30 °C	35 °C	40 °C	45 °C
Betaine	100	102	103		103
Betaine hydrochloride	123			123	
Glycinium chloride	66			66	
Sodium glycinate	40	43			
Tetramethylammonium bromide	114			116	
Glycine		39	42	43	

Table 4. Ionic values of B, ϕ_v°, and B/ϕ_v° at Different Temperatures

System	25 °C B_{ion} / kg mol^{-1}	25 °C $\phi_{v(ion)}^\circ$ / cm^3 mol^{-1}	B/ϕ_v°	30 °C B_{ion} / kg mol^{-1}	30 °C $\phi_{v(ion)}^\circ$ / cm^3 mol^{-1}	B/ϕ_v°
Glycinium chloride	0.162	44	3.8	0.156		
Sodium glycinate	0.241	46	5.3	0.221	49	4.6
Betaine hydrochloride	0.243	101	2.4	0.238		
Tetramethylammonium bromide	0.123	85	1.4	0.142		
Betaine			2.3			2.2
Glycine			3.5			

System	40 °C B_{ion} / kg mol^{-1}	40 °C $\phi_{v(ion)}^\circ$ / cm^3 mol^{-1}	B/ϕ_v°
Glycinium chloride	0.145	44	3.3
Sodium glycinate	0.235		
Betaine hydrochloride	0.221	101	2.2
Tetramethylammonium bromide		87	
Betaine			2.2
Glycine			3.4

the correction for the "dissociation effect" was found to be negligibly small (<1 $cm^3 mol^{-1}$).[12] The ϕ_v values for the neutral amino acids were analyzed according to the equation:

$$\phi_v = \phi_v^\circ + aC \quad (6)$$

where a is an empirical constant. The ϕ_v° values for all the systems mentioned are shown in Table 3. Both B and ϕ_v° values for the salts of amino acids have been further reduced to the corresponding ionic values, and then the ratio B/ϕ_v° for the ions calculated for different temperatures; these are incorporated in Table 4.

Discussion

A comparison of the B-value of glycine at 25 °C (0.132)† with literature data shows that our value is slightly lower than that reported by Devine and Lowe[3] (0.143) and Mason and Kampmeyer[13] (0.142), but is close to that reported by Tsangaris and Martin[8] and Tyrrell and Kennerly[5] when these values are extrapolated to 25 °C. Our earlier found value for glycine at 40 °C also agreed well with that reported by Tsangaris and Martin.[8] Both the latter two groups of workers reported B-values for betaine which are significantly different from each other, the present value at 25 °C (0.226) is close to the extrapolated value (0.224) for the same system reported by Tyrrell and Kennerley.[5] The B-value of tetramethylammonium bromide at 25 °C agrees with that reported by Kay et al.[14] Tsangaris and Martin's reported B-value for glycinium chloride at 40 °C (0.15)[8] agrees satisfactorily with ours (0.152), but their own calculated B-value for betainium chloride at 16 °C (−0.06) from the data procured from other sources seems to be in error, and thus largely disagrees with the present value (0.236 at 25 °C).

The ϕ_v° value for betaine at 25 °C (100) is consistent with the value reported by Tyrrell and Kennerley[5] at 20 °C (98.4 $cm^3 mol^{-1}$). Our ϕ_v° values for glycinium chloride and sodium glycinate at 25 °C (66 and 40 cm^3 respectively) are slightly lower than those reported by Shahidi[12] for the same systems (67.22 and 42.81 respectively).

The earlier found better suitability of Eq. 2 (valid for uncharged species in solution) for reproducing the concentration variation of the viscosity of amino acids in acidic or alkaline medium was suprising, because amino acids are known to be present in such solutions rather as salts. The said experimental observation was also apparently justified on the basis of theoretical calculations according to the Fuoss–Onsager theory[15] of mixed electrolyte solutions, which showed that the

† All B values expressed in kg mol^{-1} units.

net electrostatic contribution part: $(A_{mix}-A_{HCl\ or\ NaOH})\sqrt{I}$ out of the total relative viscosity value, was negligibly small, thereby apparently rendering redundant the applicability of the Jones–Dole equation (Eq. 1). In the present more comprehensive investigation where purely aqueous solutions of salts of different amino acids of varying cationic and anionic sizes were taken, the experimental results at all the temperatures have convincingly shown the better applicability of Eq. 1 rather.

The observed sequence of *B*-coefficient values for the present systems is: $B_{anion}>B_{cation}>B_{zwitterion}$, which was also obtained by Tsangaris and Martin[8] for the glycine system. However, for the betaine system, they reported a different sequence, i.e., $B_{zwitterion}>B_{cation}$, which is quite at variance with the observation in the present case. As mentioned, their reported negative value for betainium chloride at 16 °C appears unacceptable.

The ionisation of glycine is as follows:

$$^{+}NH_3CH_2COOH \underset{}{\overset{+H^+}{\rightleftharpoons}} {}^{+}NH_3CH_2COO^- \overset{+OH^-}{\rightleftharpoons} NH_2CH_2COO^- + H_2O$$

The different *B*-values obtained for the three different ionic species, having almost identical sizes and structures, indicate substantially different types of solvent–solute interactions, due entirely to the varying nature of charge on the three molecules. The high *B* value of the glycinate anion clearly points to extra structure promotion by this ion. This type of structure enhancement was also observed by Laurence and Wolfenden[16] for the acetate anion (B_{HAc}=0.117 and B_{Ac^-}=0.245). The glycinate ion being essentially the amino acetate ion, the exactly similar observation here is quite in order. The fact that the acetate anion is stabilized by the extremely effective delocalization of charge between the two canonical structures of identical energy involved, accounts for the extra order produced by this ion, compared to the zwitterion or acetic acid. By contrast, for the glycinium cation any such delocalization effect would be much less effective because it would first involve a separation of charge in the COOH group; this is seen reflected in the lower value of *B*-coefficient for this cation.††

The simultaneous presence of the two charge centers in the zwitterion makes it a unique system, as is seen from the abrupt reduction of *B*-coefficient value compared to either of the two ionic forms. An exactly similar situation arises also in the case of the $\overline{V}^\circ$ values of the dipolar ions. In the zwitterionic glycine system, the electron-withdrawing inductive effect[19] of the NH_3^+ from the acetate anion largely reduces the availability of the negative charge at the other end, thereby resulting in a net reduction of both the *B*-coefficient and $\overline{V}^\circ$ values.

The temperature coefficient of the *B*-value of glycine is positive, while that for both glycinate and glycinium ions are negative, thus indicating the latter two to be net structure makers in water, over the temperature range investigated. Both the ions are therefore solvated to some extent, and definitely have their primary solvation sheath.

In the context of the above discussion, the betaine system appears to be very interesting. The betaine molecule is obtained by substituting the three hydrogen atoms of the charged nitrogen atom by methyl groups, the result of which is faithfully reflected in the higher *B*-coefficient value (Einstein volume effect). The comparatively slightly higher value of *B*-coefficient of the betaine cation ($(CH_3)_3\overset{+}{N}CH_2COOH$) as compared to that for betaine itself, may be due to the same reason as mentioned earlier in the case of the glycinium cation.

The temperature coefficient of the *B*-value of betaine better reflects its structural interaction with the solvent than does the *B*-coefficient value itself. The *B* value remains almost unchanged over the temperature range (25—45 °C) investigated; this was also observed by Tyrrell and Kennerley over the range 5—20 °C (whose results are consistent with ours). By introducing three methyl groups at the charged nitrogen atom of the glycine molecule, this part of the betaine molecule virtually becomes a tetramethylammonium moiety. It therefore appears that in betaine, the extent of structure breaking by the "tetramethyl" moiety and structure making by the acetate moiety within the molecule are evenly balanced, therefore rendering the betaine molecule neither a "maker" nor a "breaker" in the solvent at all the temperatures.

The temperature coefficient of betaine cation is also negative, making it a structure maker like the glycinium cation. In both these molecular ions, the localized positive charge facilitates the separation of proton on the other end through the inductive effect, and therefore, not as much available at the periphery of the molecule as in the tetramethylammonium ion, thus causing it to behave like a structure maker.

The B/ϕ_v° values are important indicators[5] as to whether a particular solute is solvated or unsolvated, since a value between 0 and 2.5 points to unsolvated species, and any higher value to solvated ones. Based upon this criterion, the tetramethylammonium and betaine systems fall in the "unsolvated" category, whereas the glycinium, glycinate, and glycine are well

†† Nightingale[17] also explained the higher *B*-value of the iodate ion in comparison to that of the periodate ion, as due to the more effective delocalization of charge by the oxygen atoms in the former, thus permitting more extensive interaction with the solvent. Were localization of charge the more effective solvent puller (than the charge-delocalization effect) for such larger molecular ions, as observed by Gurney,[18] glycinium cation or periodate ion would give rise to higher *B*-values.

within the "solvated" class having definite primary solvation sheaths. Tyrrell and Kennerley[5] also observed similar interaction with the solvent for the glycine, tetramethylammonium, and betaine systems. The high value of B/ϕ_v°, together with the very low value of ϕ_v° for the glycinate anion, clearly indicates that this system interacts much more strongly with the solvent molecules, as compared to either the glycine or glycinium systems.

The betaine cation seems to have a primary solvation sheath, as is also evident from the negative temperature dependence of B/ϕ_v° value. The peculiar behavior of betaine is also reflected in the value of B/ϕ_v° and its temperature invariance. The fact that the ϕ_v values of betaine decrease with concentration at all temperatures is another point of departure from the common trend shown by amino acids. This type of concentration dependence was also noted by Tyrrell and Kennerley[5] for the same system, and by Wen and Saito[20] for the larger tetraalkylammonium bromide system. The explanation furnished for the latter was that when the cosphere of the bromide ion interacts with that of the tetraalkylammonium cation, there results a negative contribution to the partial molal volume. It is highly probable that in the betaine system a similar interaction between the hydration spheres of the tetramethylammonium and the "acetate" moieties takes place, resulting in a diminution of apparent molal volumes.

References

1) M. M. Bhattacharya and M. Sengupta, *Z. Phys. Chem. (N.F.)*, **79**, 133 (1982).

2) G. Jones and M. Dole, *J. Am. Chem. Soc.*, **51**, 2950 (1929).

3) W. Devine and B. M. Lowe, *J. Chem. Soc. A*, **1971**, 2113.

4) A. Einstein, *Ann. Phys.*, **19**, 289 (1906).

5) J. V. Tyrrell and M. Kennerley, *J. Chem. Soc. A*, **1968**, 2724.

6) E. R. Nightingale, Jr., *J. Phys. Chem.*, **66**, 895 (1962).

7) Tronel-Peyroz, Emmanuel, and D. Schumann, *J. Colloid Interface Sci.*, **92**, 136 (1983).

8) J. M. Tsangaris and R. B. Martin, *Arch. Biochem. Biophys.*, **112**, 267 (1965).

9) M. M. Bhattacharya and M. Sengupta, *Electrochim. Acta*, **30**, 857 (1985).

10) R. A. Robinson and R. H. Stokes, "Electrolyte solutions," Butterworth Scientific Publication (1959).

11) O. Redlich and D. M. Meyer, *Chem. Rev.*, **64**, 221 (1964).

12) F. Shahidi, *J. Chem. Soc., Faraday Trans. 1*, **76**, 101 (1980).

13) L. S. Mason, P. M. Kampmeyer, and A. L. Robinson, *J. Am. Chem. Soc.*, **74**, 1287 (1952).

14) R. L. Kay, T. Vituccio, C. Zawoski, and D. F. Evans, *J. Phys. Chem.*, **70**, 2336 (1966).

15) L. Onsager and R. M. Fuoss, *J. Phys. Chem.*, **36**, 2689 (1932).

16) V. D. Laurence and J. H. Wolfenden, *J. Chem. Soc. (London)*, **1934**, 1144.

17) E. R. Nightingale and R. F. Benck, *J. Phys. Chem.*, **63**, 1777 (1959).

18) R. W. Gurney, "Ionic Processes in Solution," McGraw-Hill Book Company, N.Y. (1953), p. 169.

19) F. J. Millero, A. L. Surdo, and C. Shin, *J. Phys. Chem.*, **82**, 784 (1978).

20) W. Y. Wen and S. Saito, *J. Phys. Chem.*, **68**, 2639 (1964).

 © 1988 The Chemical Society of Japan Bull. Chem. Soc. Jpn., 61, 4113—4119 (1988)

Extraction-Spectrophotometric Determination of Pd(II) with 4-(3,5-Dichloro-2-pyridylazo)-1,3-diaminobenzene and Trichloroacetate. I

C. A. Fontán,* (the late) C. B. Marone, and R. Olsina
Departamento de Química Analítica "Dr. Carlos B. Marone"
Universidad Nacional de San Luis, Argentina
(Received April 11, 1987)

In acid acqueous ethanol solutions Pd(II) reacts with 4-(3,5-dichloro-2-pyridylazo)-1,3-diaminobenzene (3,5-Cl2PADAB=L) making up three colored complex species. The three complexes have a 1:1 metal-ligand molar ratio and they differ from each other only in their protonation degree. In solutions with H_2SO_4 or $HClO_4$ concentrations higher than 10 or 8 M, respectively, the complex species is yellow, and in less acid solutions (pH 0.80 to 2 M H_2SO_4 or pH 0.8 to 3 M $HClO_4$ range) it changes in a reversible way to a violet color while its intensity increases (molar absorptivity 8.2×10^4 $dm^3\,mol^{-1}\,cm^{-1}$ at 588 nm and 5.2×10^4 $dm^3\,mol^{-1}\,cm^{-1}$ at 545 nm). The red purple complex formed in the pH range 3—4 are insoluble in 10% (v/v) ethanol-water solutions. The complex species were given the formulation $PdH_nL^{(n+2)+}$ ($n>1$) ($H_2SO_4>10$ M, or $HClO_4>8$ M), $PdHL^{3+}$ (pH 0.8 to 2 M H_2SO_4 or pH 0.8 to 3 M $HClO_4$ range) and PdL^{2+} (pH 3—4), and the existence of one or another depends exclusively upon the acidity of the reaction medium. In 10% (v/v) ethanol-water solutions acidified with H_2SO_4 or $HClO_4$, only the last two species are extracted into benzene as $PdL^{2+}\cdot(TCA^-)_2$ and $PdHL^{3+}(TCA^-)_3$ (TCA^-=trichloroacetate) ion-associations. The composition of the complexes formed in aqueous solutions was estimated by the composition of the ion-association complexes transferred to the organic phase.

4-2(-Pyridylazo)-1,3-diaminobenzene (PADAB), 5-(2-pyridylazo)-2,4-diaminotoluene (PADAT) and its halogen-substituted compounds constitute a relatively new type of *o*-amino azo analytical reagents. All of them react chromatically only with a few metallic ions (Co(II), Pd(II), Zn(II), Cu(II), Au(III), Fe(II), Fe(III), Ni(II), and Ag(I)). Several of them have been used for the spectrophotometric determination of Co(II)[1–6] and Pd(II).[7–13] Cobalt(II) reacts with these reagents to form CoL_2 complexes (pH range 3—11) which are changed into other deeply colored monoprotonated and diprotonated complexes by the addition of hydrochloric or other mineral acids. The CoL_2 complexes,[3] or their ion-association species formed with a suitable organic base, can be extracted into an organic solvent.[3,14]

In the course of a systematic investigation on the reaction between one of these pyridylazo reagents, 3,5-Cl2PADAB, and Pd(II),[12] and on the extraction of the complexes formed, we have found that the behavior of the Pd(II)–3,5-Cl2PADAB complexes resembles those of Co(II).

As we have not found detailed information about the reaction between Pd(II) and this type of reagents, this work is devoted to elucidate the mechanisms of formation of the Pd(II)–3,5-Cl2PADAB complexes and their extraction as ion-association species formed with trichloroacetate.

Bearing in mind that in the search of new sensitive and selective chromogenic reagents, a full knowledge of the reactions involved in the formation and extraction of metallic complexes yields important information, which can be used as the basis for the development of new spectrophotometric methods.

Experimental

Apparatus. pH was measured on a digital Orion Mod. 701-A pH-meter provided with a glass/Ag–AgCl combination electrode. Both absorbance measurements and spectral recordings were carried out on a Varian Mod. 634-UV spectrometer equipped with 10-mm glass cells.

For the extractions, 100×35 mm "Pyrex"-type glass tubes with polyethylene stoppers were used. Equilibrations were carried out by mechanical shaking of the tubes with longitudinal desplacements of 35—40 mm and a rate of 300 fluctuations per minute. Temperature was kept at 20±0.5 °C.

Reagents. 3,5-Cl2PADAB Solutions: The synthesis of the reagent was described earlier.[12] A 1×10^{-3} M solution (1 M=1 mol dm^{-3}) was prepared in 96% pure ethanol by using a purified and solid reagent. Other solutions having the concentration required for each particular test were prepared by means of dilutions, with the same solvent, of that solution.

Pd(II) Standard Solution (5×10^{-3} M). $Pd(NO_3)_2\cdot2H_2O$ (0.2665 g) was dissolved in 50 cm^3 of (4+6) H_2SO_4. The solution was heated to guarantee complete dissolution. Once cold, it was put in a volumetric flask and distilled water was added up to 200 cm^3. The effective concentration of the metal was complexometrically determined.[15] More diluted solutions were daily prepared from the previous one. Pd(II) solutions remain unaltered during 5 days if kept in glass vessels.

Trichloroacetic Acid (HTCA) Solution. The acid solution (500 cm^3, 5 M) was prepared from the solid drug. The exact content of the trichloroacetic acid was alkalimetrically determined on aliquot portions of the previous solution.[16]

General Procedures. Color Development. Aliquots of conveniently diluted Pd(II) solutions were diluted with distilled water up to about 15 cm^3. Acidity was adjusted to the value required for each test by adding concentrated

H_2SO_4 or $HClO_4$. When the medium acidity corresponded to the pH values higher than 0, the concentration of Na_2SO_4 or $NaClO_4$ was kept at 1 or 2 M, respectively. In these cases the pH of the solutions was adjusted at the required values by the addition of the diluted solution of H_2SO_4, $HClO_4$, or NaOH. The solutions were transferred to 25 cm^3 volumetric flasks, and 2.5 cm^3 of the ethanolic solution of the reagent were added. The absorbance of the solutions, as well as the absorption spectra of the solutes dissolved in them, were recorded when the color of each test reached its maximum insensity and remained, at least for ten minutes, unchanged.

Extractions. The complexation reactions were promoted on Pd(II) solutions (10—15 cm^3), put in extractions tubes and conditioned in the above-described way. The total initial HTCA concentration was kept constant at 1 M in all tests. Once the complexation was finished, a volume of pure benzene equal to that of the aqueous solution contained in the tubes was added, and the whole was mechanically shaken from 40min to 1 h. Then the organic phases were transferred to 25 cm^3 dried volumetric flask. The aqueous phases were washed twice, each time with 3 cm^3 portions of pure benzene, and the washing liquids were put together with the bulk of each benzenic extract, adding, in the end, benzene until completing 25 cm^3. After reaching the equilibrium, the pH of the aqueous phases was potentiometrically measured. The percentage of palladium extracted was spectrophotometrically determined by using 3,5-Cl2PADAB as chromogenic reagent.

Results and Discussion

In a previous paper,[12] we showed that in aqueous ethanol solutions Pd(II) reacts slowly with 3,5-Cl2PADAB in a wide range of concentrations of H_2SO_4 or $HClO_4$. The spectra of the palladium(II) chelates were measured for the 10% (v/v) ethanol-water solutions containing various concentrations of the components at different acidity conditions.

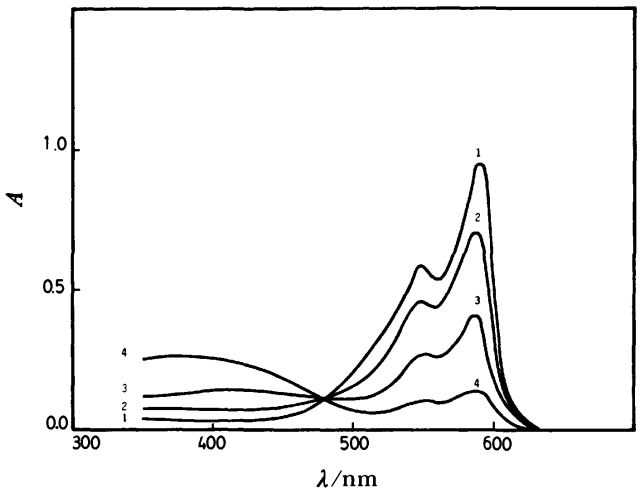

Fig. 1. Absorption spectra of Pd(II)-3,5-Cl2PADAB complexes in aqueous ethanol acid solution with 1.20×10^{-5} M reagent. Sulfuric acid concentration: (1) 2 M; (2) 7 M; (3) 8.30 M; (4) 9.80 M. Ethanol 10% (v/v).

Figures 1 and 2 show the absorption spectra of a mixture containing an excess of Pd(II) compared with 3,5-Cl2PADAB. The wavelength of maximum absorbance and intensities at the maxima (Table 1) remained without changes for mixtures containing a 10 mole

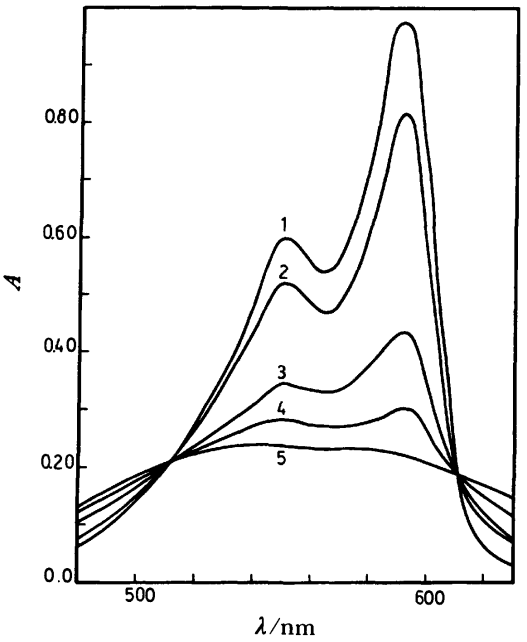

Fig. 2. Absorption spectra of Pd(II)-3,5-Cl2PADAB complexes in aqueous ethanol acid solution. Reagent, Pd(II) and ethanol concentrations as for Fig. 1. pH: (1) 1.00; (2) 1.70; (3) 2.30; (4) 2.80; (5) 3.20.

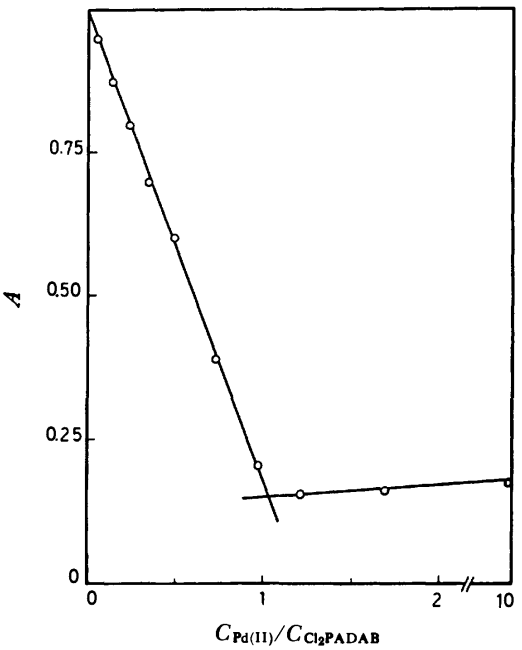

Fig. 3. Saturation curve of Pd(II)-3,5-Cl2PADAB complex in aqueous solution. 3,5-Cl2PADAB concentration was kept constant=3.50×10^{-5} M; Pd(II)= variable; 10% (v/v) ethanol; pH=3; λ=430 nm; water as blank.

excess of reagent. In these cases, the spectra were scanned with similar 3,5-Cl2PADAB solutions as reference because the mixtures showed a strong absorption due to of the great concentration of 3,5-Cl2PADAB.

As is evident from the comparison of the spectra in Figs. 1 and 2, two Pd(II)–3,5-Cl2PADAB complexes exist in aqueous ethanol, depending only on the acidity. The color of the complex formed in H_2SO_4>10 M solutions is yellow, similar to the reagent at this acidity, while the solutions containing the complex formed in the acidity range from pH 1 to 2 M H_2SO_4 or from pH 1 to 3 M $HClO_4$ showed a violet color. An insoluble red purple complex was precipitated in less acidic media (pH 3—4), starting from pH 1. Anyone of these comlexes was generated either by promoting the chelation reaction at the suitable acidity, or by conveniently adjusting the acidity of media of the solution containing any of them.

The Composition of the Complex and the Mechanism of Complex Formation. Earlier studies[12] have shown that the Pd(II): 3,5-Cl2PADAB ratio of the violet complex is 1:1. In spite of its low solubility in aqueous ethanol solutions, the composition of the complex prevailing in the pH range 3—4 was spectrophotometrically obtained by means of absorbance variations, measured at the reagent maximum absorption wavelength (420 nm), of the pH 3 solutions containing constant concentration of 3,5-Cl2PADAB and varied proportions of Pd(II) (Fig. 3). The molar ratio obtained was also 1:1. Because of its low molar absorptivity, no further studies were carried out on the yellow complex, but it is likely to have contain the same molar ratio as the others. Similar situations have been indicated by Shibata et al. with respect to the Co(II)–5-Cl2PADAB[3] and Co(II)–3,5-Cl2PADAT[6] complexes. In agreement with the above considerations, the spectral changes observed when the acidity of the Pd(II)–3,5-Cl2PADAB complex solutions was varied were due to protonation or acid dissociation of these complexes, rather than to a cange in the Pd(II):reagent molar ratio. Furthermore, knowing that the Pd(II) complex formed depends on the acidity of the reaction media and that in the pH 4 to 18 M H_2SO_4 or pH 4 to 10 M $HClO_4$ range three species of 3,5-Cl2PADAB,[12] H_3L^{3+}, H_2L^{2+}, and HL^+ are involved in its acid-base behavior, it can be assumed that the reaction between Pd(II) and 3,5-Cl2PADAB is described by the following equilibria:

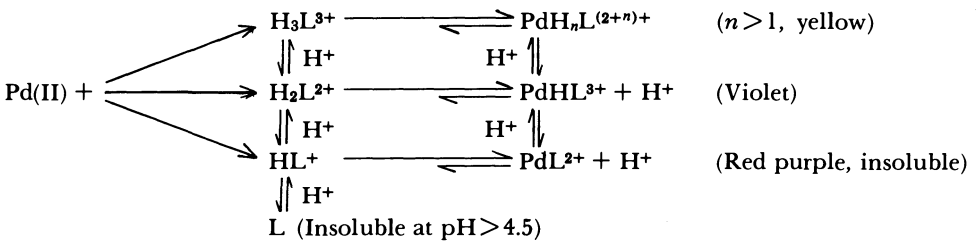

The above scheme is in good agreement with the experimental facts observed. In order to prove, at least partially, the validity of the above equilibria, the number of protons released in the reaction as

$$PdHL^{3+} \rightleftharpoons PdL^{2+} + H^+ \quad (1)$$

was spectrophotometrically examined for solutions containing excess of Pd(II). Studies in solutions showed that the $PdH_nL^{(2+n)+}$ and $PdHL^{3+}$ acid dissociation equilibria are sufficiently separated, so that they can be treated independently. If the acid dissociation constant for Eq. 1 is given by Eq. 2

$$K_a^{PdHL^{3+}} = [PdL^{2+}][H^+]/[PdHL^{3+}] \quad (2)$$

the dependence of $\log\{[PdL^{2+}]/[PdHL^{3+}]\}$ is written as

$$pK_a^{PdHL^{3+}} = \log\{(A - A_{PdHL^{3+}})/(A_{PdL^{2+}} - A)\} + pH \quad (3)$$

were A is the total absorbance of the solutions at a specified pH, and $A_{PdHL^{3+}}$ and $A_{PdL^{2+}}$ are the absorbance of solutions containing only the protonated complex and the soluble fraction of the non-protonated complex, respectively. The plot $\log\{(A-A_{PdHL^{3+}})/(A_{PdL^{2+}}-A)\}$ against pH gave a straight line with a slope of unity, value that is in good agreement with the supposition of Eq. 1. The $pK_a^{PdHL^{3+}}$=2 was calculated from the pH at which $\log\{(A-A_{PdHL^{3+}})/(A_{PdL^{2+}}-A)\}$ equals zero.

General Study of Extractable Pd(II)-3,5-Cl2PADAB-TCA^- Ion-Association Complexes. Considering that only positively charged Pd(II)–3,5-Cl2PADAB complexes can be formed, the extraction of such chelates can be carried out in the presence of suitable organic bases which form extractable ion-association complexes. In this sense, the best results were obtained for the trichloroacetate–benzene system. Pd(II) is quantitatively extracted into benzene in the presence of 3,5-Cl2PADAB, ethanol and high concentrations of trichloroacetate anion (TCA^-) within the acidity range from pH 4 to 2 M H_2SO_4 or from pH 4 to 1 M $HClO_4$ (Fig. 4). In strongly acidic solutions (pH 1 to 2 M H_2SO_4 or pH 1 to 1 M $HClO_4$ range), only a violet ion association complex is extracted into benzene.

Comparing the absorption spectra of this compound in benzene with those of the Pd(II)-3,5-Cl2PADAB complexes formed in aqueous solutions with the same mineral acid concentration, and in the presence or absence of trichloroacetate (Table 1) showed that the violet complex extracted was that stated as $PdHL^{3+}$. Although some Pd(II) complexes were formed in aqueous solutions of H_2SO_4 (C>10 M), they were not extracted into benzene, probably because under such conditions the HTCA dissociation is repressed to such

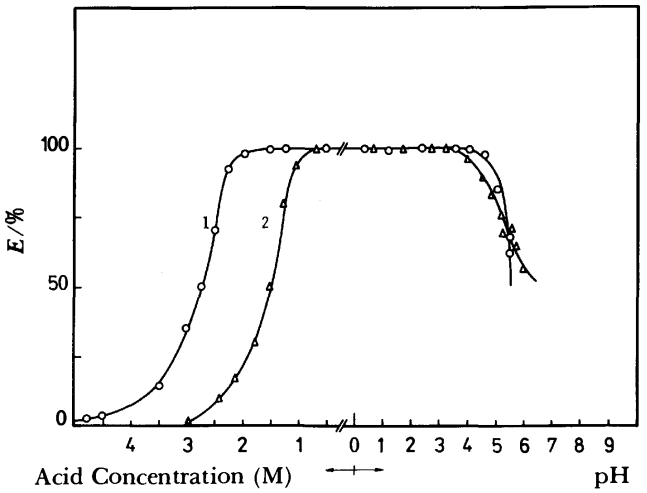

Fig. 4. Effect of pH or mineral acid concentration on extraction of the Pd(II)-3,5-Cl2PADAB-TCA^- system. Extractions from aqueous 10% (v/v) ethanol solutions with 1.80×10^{-5} M Pd(II), 1.20×10^{-4} M 3,5-Cl2PADAB and 1 M HTCA. Curves: (1) H_2SO_4; (2) $HClO_4$. $V_o=V_w$. Time of full color development of the Pd(II)-3,5-Cl2PADAB complexes=period of equilibration=40 min.

Table 1. Absorption Maxima and Molar Absorptivity of Pd(II) Complexes in 10% Ethanol-Water Solutions and of Ion-Association Extracted into Benzene

Complex	λ_{max}/nm	Molar absorptivity/ $dm^3\,mol^{-1}\,cm^{-1}$
PdL^{2+}	Insoluble	—
$PdHL^{3+}$ [a]	588	8.20×10^4
	548	5.20×10^4
$PdH_nL^{(2+n)+}$	380—400	2.00×10^4
$PdHL^{3+}$ [b]	594	8.40×10^4
	560	5.90×10^4
$PdL^{2+}\cdot(TCA^-)_2$	545	2.00×10^4
	515—530	1.80×10^4
$PdHL^{3+}\cdot(TCA^-)_3$ [c]	600	8.60×10^4
	555	5.50×10^4

L=3,5-Cl2PADAB. a) Complex formed in 1 M H_2SO_4 aqueous solution with 10% (v/v) ethanol. b) Complex formed in 1 M H_2SO_4 solution with 10% (v/v) ethanol and 1 M HTCA. c) Ion-association extracted into benzene from solution b).

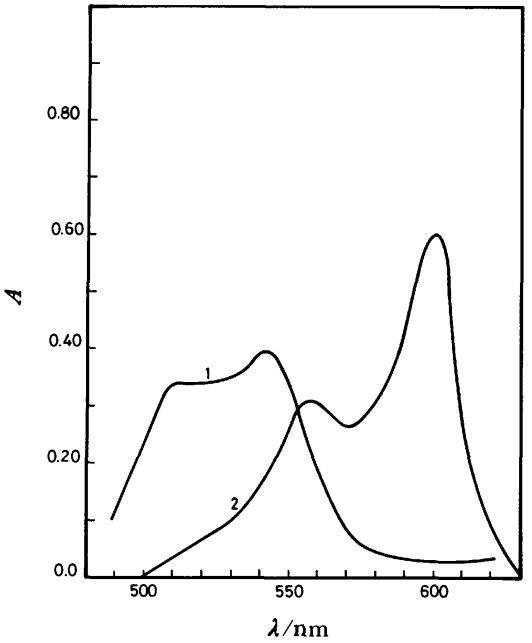

Fig. 5. Absorption spectra in benzene of the extracted ion-association compounds for the Pd(II)-3,5-Cl2PADAB-TCA^- system. Concentrations in the aqueous phases: Pd(II)=1.90×10^{-5} M; 3,5-Cl2PADAB=2.00×10^{-4} M; HTCA=1 M; ethanol 10%. Acidity: (1) pH=4.00; (2) 1—2 M H_2SO_4 with 7.00×10^{-6} M final concentration of Pd(II) in the organic extract. Measurements against corresponding reagents blanks in 10-nm cell. Time of full color development=period of equilibration=40 min. Organic extracts (10 cm^3) diluted to 25 cm^3 with pure benzene after extraction.

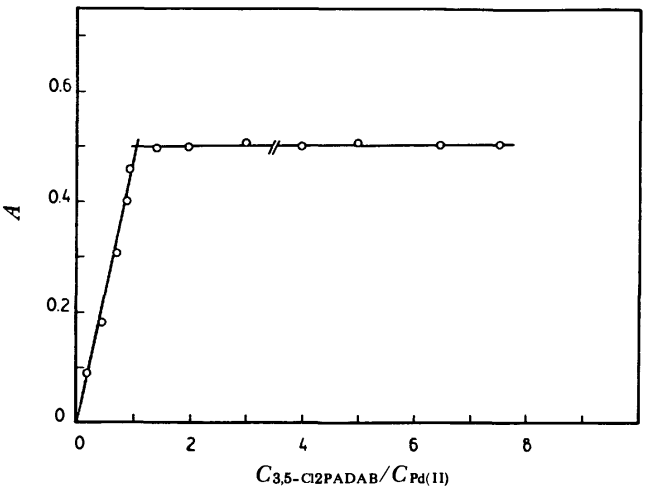

Fig. 6. Saturation curve of Pd(II)-3,5-Cl2PADAB complex extracted into benzene. Concentrations in the aqueous phase (10 cm^3): Pd(II) 6.00×10^{-5} M; HTCA 1 M; ethanol 10% (v/v); pH=3; λ=545 nm; Extracts (10 cm^3) dilute to 25 cm^3 with pure benzene after equilibrations.

an extent that practically no free anion occurs.

When the pH of the aqueous phases was increased from 1 to 4, the extraction was accompanied by a change in the absorption spectra of the extracts (Fig. 5), which is reversible with the acidity variations of the aqueous phases. In the pH range 3—4, only a red purple ion-association complex is extracted. This compound, and the reagent excess at pH 3—4, are not greatly soluble in benzene or in ethanol-benzene mixtures. In Table 1 are summarized the wavelength of maximum absorption and the molar absorptivities of the two ion-associations extracted.

The 1:1 Pd(II):3,5-Cl2PADAB molar ratio of the colored ion-association complexes in the organic phases were corroborated at 2 M H_2SO_4 by the molar ratio and slope-ratio methods, and at pH 3 by the molar ratio method (Fig. 6). The total Pd(II)-3,5-Cl2PADAB-TCA^- composition was also spectrophotometrically studied. The knowledge of the number of trichloroacetate anion molecules associated to each of the complexes extracted confirmed their charge and, consequently, the $PdHL^{3+}$ and PdL^{2+} composition postulated in aqueous solutions. The expression applied to establish the total (Pd(II)-3,5-Cl2PADAB)-TCA^- composition was derived as follows.

In some additional experiments on the extraction into organic solvents, it was established that Pd(II)-3,5-Cl2PADAB complexes are not extracted in the presence of the anions sulfate, perchlorate, nitrate, or chloride. They were extracted only in the presence of trichloroacetate anion. Therefore, it was concluded that this is the anion that takes part in the formulation of the extracted compound, and not any other. Bearing this in mind, as well as the 1:1 Pd(II):3,5-Cl2PADAB composition observed during complex formation and extraction, a general quantitative description of the complex extraction must consider the following ion-association reaction and distribution equilibria:

$$PdH_nL^{s+} + s\,TCA^- \rightleftharpoons PdH_nL^{s+}\cdot(TCA^-)_s \quad (4)$$

$$PdH_nL^{s+}\cdot(TCA^-)_s \rightleftharpoons (PdH_nL^{s+}\cdot(TCA^-)_s)_{org} \quad (5)$$

were the subscript org refers to the benzene phase, and the absence of a subscript indicates the aqueous phase. The ion-association formation constant and the distribution constant are given by:

$$K_{ass} = [PdH_nL^{s+}\cdot(TCA^-)_s]/\{[PdH_nL^{s+}][TCA^-]^s\}, \quad (6)$$

$$K_D^{ass} = [PdH_nL^{s+}\cdot(TCA^-)_s]_{org}/[PdH_nL^{s+}\cdot(TCA^-)_s]. \quad (7)$$

The extraction constant of ion-association is given by:

$$K_{ex} = K_D^{ass}\cdot K_{ass} = [PdH_nL^{s+}\cdot(TCA^-)_s]_{org}/\{[PdH_nL^{s+}][TCA^-]^s\} \quad (8)$$

Introducing the HTCA acid association constant (K_a^{HTCA}) and distribution constant (K_D^{HTCA}) in material balance for HTCA after extraction, and taking into account that $C_{Pd(II)} \ll\ll C_{HTCA}$, it can be shown that

$$[TCA^-] = C_{HTCA}/\{1 + [H^+]/(K_a^{HTCA} + K_D^{HTCA}\cdot[H^+]/K_a^{HTCA})\} \quad (9)$$

At constant proton concentration and salt content, Eq. 9 becomes:

$$[TCA^-] = C_{HTCA}/cte \quad (10)$$

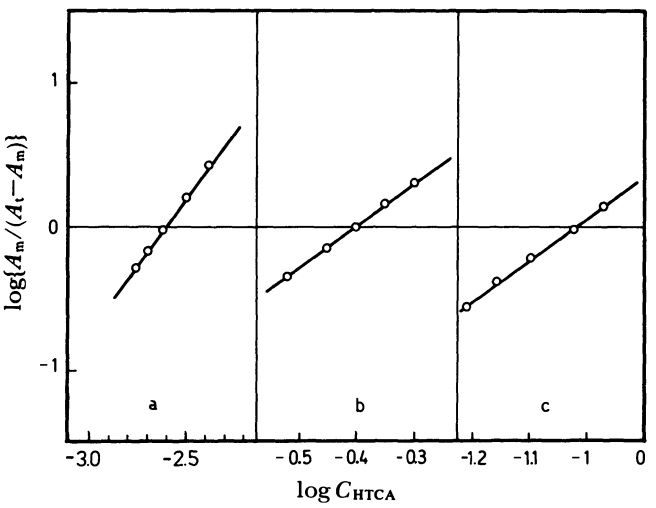

Fig. 7. $\log\{A_m/(A_t-A_m)\}$ vs. log C_{HTCA} curves for the Pd(II)-3,5-Cl2PADAB-TCA^- system. See text.

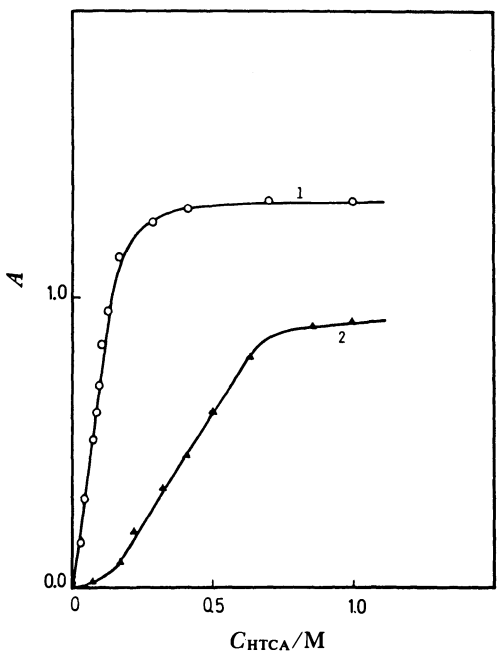

Fig. 8. Absorbance of Pd(II)-3,5-Cl2PADAB-TCA^- compounds in benzene vs. HTCA concentration in the aqueous phases. Concentrations present in the aqueous phases (10 cm^3): 3.90×10^{-5} M Pd(II), 10% ethanol, (1) 4.00×10^{-4} M 3,5-Cl2PADAB, 1 M H_2SO_4, λ_{max}=600 nm; (2) pH 1.50 (H_2SO_4), 5.90×10^{-5} M 3,5-Cl2PADAB, λ_{max}=600 nm. Benzene as blank. Organic extracts (10 cm^3) diluted to 25 cm^3 with pure benzene after equilibration.

Introducing Eq. 10 in Eq. 8, rearranging and taking logarithm, the Eq. 8 takes the form:

$$\log[\mathrm{PdH}_n\mathrm{L}^{s+}\cdot(\mathrm{TCA}^-)_s]_{org}/[\mathrm{PdH}_n\mathrm{L}^{s+}] = \log K^*_{ex} + s\log C_{HTCA} \quad (11)$$

where K^*_{ex} is the extraction constant based on total initial HTCA concentration in the aqueous phase:

$$K^*_{ex} = K_{ex}\cdot \mathrm{cte}^s \quad (12)$$

where cte is defined by Eqs. 9 and 10.

For any C_{HTCA}, the ratio $[\mathrm{PdH}_n\mathrm{L}^{s+}\cdot(\mathrm{TCA}^-)_s]_{org}/[\mathrm{PdH}_n\mathrm{L}^{2+}]$ could be calculated from absorbance of $\mathrm{PdH}_n\mathrm{L}^{s+}\cdot(\mathrm{TCA}^-)_s$ in benzene vs. C_{HTCA} curves. In this case, this ratio becomes equal to $A_m/(A_t-A_m)$, where A_t is the absorbance of extracts for the C_{HTCA} at which the extraction is quantitative, and A_m is the absorbance of extracts for any C_{HTCA} lower than the suitable for the quantitative extraction. Thus, the concentration of $\mathrm{PdH}_n\mathrm{L}^{s+}$ remaining in the aqueous phase will be A_t-A_m; Eq. 11, then, becomes,

$$\log\{A_m/(A_t - A_m)\} = \log K^*_{ex} + s\cdot\log C_{HTCA} \quad (13)$$

Eq. 13 indicates that the plot of $\log\{A_m/(A_t-A_m)\}$ against $\log C_{HTCA}$ should give a straight line with a slope of s, that is the number of trichloroacetate anion associated to the complex. Figure 7c shows this plot for A_t and A_m values taken from the absorbance (600 nm) vs. C_{HTCA} curve (Fig. 8 curve 1) obtained at 1 M H_2SO_4. The straight line has a slope of 3. Carrying out the extractions at pH 3—4, the value s calculated was not completely reliable owing to the very great absorbance even of a slight reagent excess, that disturbed seriously the absorbance measurements.

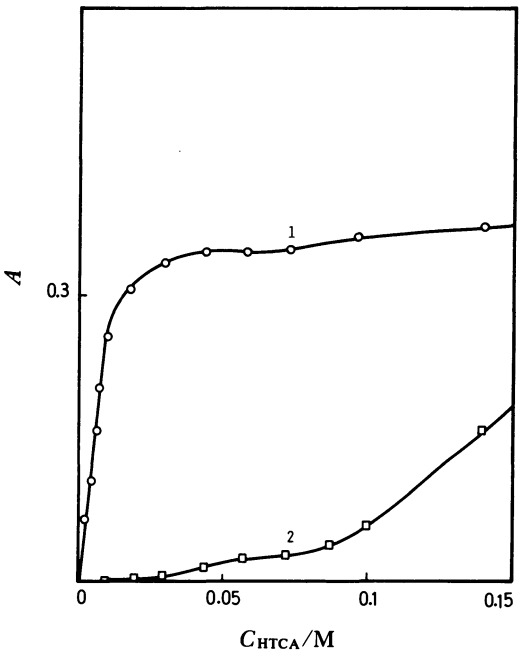

Fig. 9. Absorbance of Pd(II)-3,5-Cl2PADAB-TCA$^-$ ion-association compound in benzene vs. HTCA concentration in the aqueous phases. Amounts present in the aqueous phases (10 cm^3) 3.90×10^{-5} M Pd(II); 5.90×10^{-5} M 3,5-Cl2PADAB; 10% ethanol; pH 1.50. (1) λ_{max}=545 nm; (2) λ_{max}=600 nm. Benzene as blank. Organic extracts diluted to 25 cm^3 with pure benzene after equilibrations.

The complex-to-TCA$^-$ molar ratio of the red purple ion-association was established carrying out extractions at pH 1.5 in solutions containing a 1.5-fold molar excess of 3,5-Cl2PADAB with respect to Pd(II), and reading the absorbance against pure benzene. At pH 1.5 both complexes are formed and exracted. However, in the C_{HTCA} range from "0" to 0.07 M practically only the red purple ion-association complex is extracted (Fig. 9), while for C_{HTCA} higher than 0.07 M both ion-association complexes are simultaneous extracted. In the latter case, the absorbance measures at 600 nm were not disturbed by the presence of the red purple ion-association complex in the extracts (Fig. 8, curve 2).

According to what has been said above, it can be shown that, carrying out the extractions at pH 1.5 within the appropriate C_{HTCA} range and reading the absorbance of extracts at the suitable wavelength, Eq. 13 can be applied to establishing simultaneously the composition of the two ion-association complexes.

Figures 7a and 7b show the results obtained by applying Eq. 13 when the extractions were carried out in the C_{HTCA} ranges from "0" to 0.07 M and from 0.07 M to 1 M, respectively.

In the first case, the slope value of the straight line is 2, and in the second, such value is 3. This values agree with the essential electroneutrality of the extracted compound, assuming that the Pd(II) chelates have the composition PdL^{2+} and PdHL^{3+}, as suggested.

For the purpose of analytical applications, because of its very high molar absorptivity (600 nm) in benzene, the $\mathrm{PdHL}^{3+}\cdot(\mathrm{TCA}^-)_3$ ion-association complex is the most important.

References

1) S. Shibata, M. Furukawa, Y. Ishiguro, and S. Sasaki, *Anal. Chim. Acta*, **55**, 231 (1971).
2) S. Shibata, *Bunseki Kagaku*, **21**, 551 (1972).
3) S. Shibata, M. Furukawa, and K. Goto, *Anal. Chim. Acta*, **71**, 85 (1974).
4) E. Kiss, *Anal. Chim. Acta*, **66**, 385 (1973).
5) S. Shibata, M. Furukawa, and K. Goto, *Talanta*, **20**, 426 (1973).
6) S. Shibata, M. Furukawa, and E. Kamata, *Anal. Chim. Acta*, **73**, 107 (1974).
7) S. Shibata, Y. Ishiguro, and R. Nakashima, *Anal. Chim. Acta*, **64**, 305 (1973).
8) W. H. Po and T. T. Hu, *Fen Hsi Hua Hsueh*, **6**, Vol. 2, 94 (1978).
9) F. Kai, Y. Sakanashi, S. Satoh, and S. Uchikawa, *Anal. Lett.*, **16**, 1013 (1983).

10) M. Huang and T. Kang, *Fenxi Huaxue*, **11**, 600 (1983).
11) M. Xu, Z. Pan, N. Xie, and S. Yu, Wuhan Daxue Xuebao, *Ziran Kexueban*, **3**, 59 (1983).
12) C. A. Fontán and C. B. Marone, *Anales Asoc. Quím. Argentina*, **71**, 449 (1983).
13) Z. Ma, Q. Rong, and Q Pan, *Huaxue Shiji*, **7**, 17 (1985).
14) O. Baudino and C. B. Marone, *Anal. Chim. Acta*, **119**, 393 (1980).
15) G. Schwarzenbach and H. Flaschka, "Complexometric Titrations," ed by Methuen and Co., Ltd. 2nd ed., G. Britain (1969), p. 251.
16) American Chemical Specifications, "Reagents Chemicals," 4th ed., ACS. (1964).

 © 1988 The Chemical Society of Japan Bull. Chem. Soc. Jpn., 61, 4121—4125 (1988)

Extraction-Spectrophotometric Determination of Pd(II) with 4-(3,5-Dichloro-2-pyridylazo)-1,3-diaminobenzene and Trichloroacetate. II

C. A. Fontán,* (the late) C. B. Marone, and R. Olsina
Departamento de Química Analítica "Dr. Carlos B. Marone"
Universidad Nacional de San Luis, Argentina
(Received April 11, 1987)

The influence of different variables affecting the extraction of Pd(II) with 4-(3,5-dichloro-2-pyridylazo)-1,3-diaminobenzene (3,5-Cl2PADAB) and trichloroacetate are described. The complexation reaction between palladium(II) and 3,5-Cl2PADAB, in 1 M trichloroacetic acid aqueous solutions containing ethanol (10% v/v) and an acidity range from pH near 1 to 2 M H_2SO_4 is completed 10 min after having mixed the reagents. Under these experimental conditions, Pd(II) is extracted into benzene as an colored ion-association compound with trichloroacetate. At 600 nm, Beer's law is fulfilled up to a Pd(II) concentration of 2.16 ppm, being the most appropriate concentrations for the metal spectrometry those ranging from 0.24 to 2.12 ppm. The apparent molar absorptivity is 8.60×10^4 dm^3 mol^{-1} cm^{-1}, and the method's sensitivity (Sandell) of 0.00123 μg Pd(II)·cm^{-2}. The assayed procedures for suppressing the most serious interferences produced by Au(III) and Hg(II) are specified, and the procedure for increasing the tolerance as to Ag(I), Cu(II), Co(II), Cr(III)-(IV), Ir(III)-(IV), Os(VIII), and Ru(III)-(VIII) are described.

In previous papers[1,2] we showed that Pd(II) reacts with 4-(3,5-dichloro-2-pyridylazo)-1,3-diaminobenzene (3,5-Cl2PADAB=L) in an acidity range from pH 4 to 2 M† H_2SO_4 (or from pH 4 to 3 M $HClO_4$) to form three complexes having an equal metal-to-reagent molar ratio (1:1) though different Pd(II)-to-H^+ ratio.

These complexes were assigned as the formulas of $PdH_nL^{(2+n)+}$ ($n>1$), $PdHL^{3+}$, and PdL^{2+}. They are related to each other by means of reversible acid-base equilibria, and the formation of one species or another depends on the acidity of the reaction medium.

The complex species $PdHL^{3+}$ and PdL^{2+} are quantitatively extracted into benzene in the form of ion-association compounds formed with trichloroacetate (TCA^-) under different acidity conditions.[2] Pd(II) is extracted as $PdHL^{3+}\cdot(TCA^-)_3$ in the acidity range from pH near 1 to 2 M H_2SO_4, while in less acid aqueous ethanol phase (pH range 3—4) it is quantitatively extracted as $PdL^{2+}\cdot(TCA^-)_2$. The high molar absorptivity of the ion-association compound $PdHL^{3+}\cdot(TCA^-)_3$ dissolved in benzene, as well as its suitable solubility in this solvent, accounted for carrying-out a study focused on establishing the most appropriate experimental conditions for the separation and spectrophotometric determination of palladium(II).

This is the aim of this work, as well as to describe the procedures assayed in order to avoid the interference of some metallic ions, and eliminate or, at least, reduce to allowable values their concentrations in solutions containing together with Pd(II), in those particular cases in which they are found at higher proportions than the tolerated by the proposed procedure.

† 1 M=1 mol dm^{-3}.

Experimental

Apparatus. A Varian 634 UV model spectrophotometer was used for recording spectra and individual absorbance measurements, with 10-mm path-length glass or quartz cells. The pH was measured on an Orion pH-meter model 701 A, equipped with a glass/Ag-AgCl combination electrode.

Reagents. 3,5-Cl2PADAB Solutions: The reagent was synthesized as previously described.[1] Ethanol solution (0.025% (w/v) of the pure material was generally used. When necessary, other solutions with the required concentration were prepared either by diluting the previous solutions with the same solvent, or by direct weighing of the reagent.

5×10^{-3} M Pd(II) Solution: Distilled water (50 ml) and concentrated sulfuric acid (2 ml) were added to 0.2664 g of $Pd(NO_3)_2\cdot2H_2O$ contained in a 150 ml precipitation flask. The whole was softly heated until complete dissolution of the salt. Once cooled, the resulting solution was transferred to a 200 ml volumetric flask and then the volume made up to the mark with distilled water. The metal's actual concentration was complexometrically determined.[3] This solution, stored in a glass vessel, keeps its concentrations unchanged for 5 days. More diluted solutions of Pd(II) were daily prepared from the previous one.

Trichloroacetic Acid Standardized Solution: An approximately 5 M solution (500 cm^3) of the acid was prepared from the solid reagent. The exact content of trichloroacetic acid was alkalimetrically determined on portions of the previous solutions.[4] All other reagents used were of analytical grade.

General Procedures. The trichloroacetate anion was added in the aqueous phases as trichloroacetic acid standardized solution, and the 3,5-Cl2PADAB reagent as an ethanol solution. For the extraction, the solutions were mechanically shaken in 100 mm long.×35 mm diameter "Pyrex-type" glass tubes with polyethylene stoppers. The temperature was kept at 20±0.5 °C. The percentage of palladium(II) extracted was calculated by determining both the amount of metallic ion transferred to the organic phase and that remaining in the aqueous phase after the

equilibrium is reached, using a spectrophotometric procedure that employes 3,5-Cl2PADAB.[1] When dealing with the extraction of single ion-association compound, the %E was evaluated by means of the absorbance measurements of its organic extracts at the maximum absorption wavelength of the spectral curve of that compound. To do this, it was necessary to previously determine the value of its molar absorptivity under the experimental conditions of the quantitative extraction of Pd(II).

Recommended Procedure for the Extraction-Spectrophotometric Determination of Palladium(II). In an extraction tube, put 2 cm^3 of acid solution of the sample containing no more than 27 ppm of Pd(II), 5 cm^3 of 2 M HTCA solution, 0.5—1 cm^3 of 96% H_2SO_4, 1 cm^3 of 0.025% ethanol solution of the reagent, and make volume up to 10 cm^3 with distilled water. Let it stand for 15 minutes and then, add 10 cm^3 of pure benzene. Shake the whole mechanically during 15 minutes. Allow the phases to separe, and then decant the organic layer into a 25 cm^3 dry volumetric flask. Wash the aqueous phase twice with 3 cm^3 portion of pure benzene; mix the washing liquids together with the bulk of the organic extract and, afterwards dilute up to the mark with pure benzene. If the so-obtained solution shows any turbidity, centrifuge before carrying out the absorbance measurement at 600 nm against a reagent blank. Calculate the palladium concentration from a calibration curve obtained by operating in the same way.

Results and Discussion

Although 3,5-Cl2PADAB is soluble in benzene, no less than a 45 min agitation period was required for the quantitative extraction of Pd(II) when the reagent dissolved in benzene was used. This is because, on the one hand, the complexation reaction needs at least 10 min to become complete and, on the other, the reagent is only slightly transferred to the aqueous phase under the experimental conditions exacted for the quantitative extraction of the metallic ion. This latter fact contributes to reduce the rate of the complexation reaction in the aqueous phase. Thus, in order to reduce the time interval employed in the extraction, the reagent has to be added as the ethanol solution to the aqueous phase. Once the Pd(II)–3,5-Cl2PADAB complexation reaction is over, the complex formed can be extracted into benzene in a second stage.

For the extraction of Pd(II) with 3,5-Cl2PADAB and trichloroacetate other organic solvents immiscible with water, such as higher alcohols, esters, ethers, chloroform, carbon tetrachloride, etc., were tested, but benzene was selected due to the greater stability of the extracted solute dissolved in this solvent.

Influence of the Trichloroacetic Acid and Ethanol Concentrations. The extraction was studied up to 2 M HTCA concentration. Different minimum concentrations of the organic acid was required for extracting the PHL^{3+} mixed-complex and the excess of the reagent (Fig. 1). 1 M was the optimum concentration of HTCA which ensures complete extraction of both complex and reagent excess. With higher values the percentage extraction did not drop although strongly emulsified extracts were obtained. Ethanol was necessarily added in the aqueous phases together with the reagent. In 1 M HTCA with 1—2 M H_2SO_4 solutions, both the percentage extraction and color stability of the organic extracts do not change significantly up to 15% (v/v) ethanol concentration; whereas contents greather than the previous one disminish the extraction yield. Ethanol also stabilizes the extract color. The absorbance remains virtually unchanged for at least 10 h in its presence, but for only 20 min in its absence.

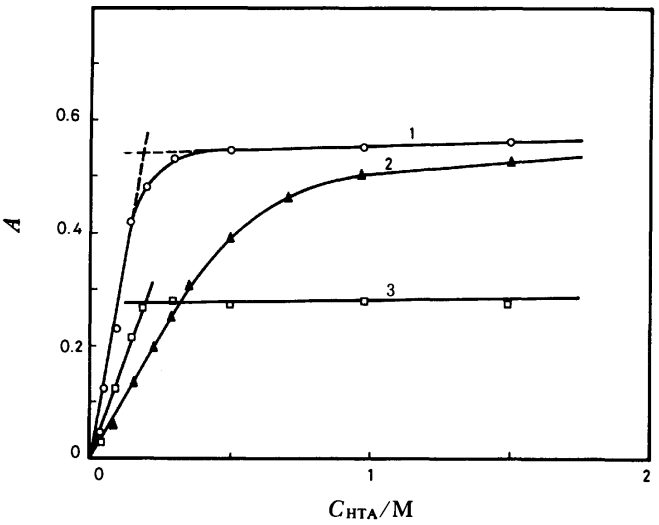

Fig. 1. Influence of total trichloroacetic acid concentration in the aqueous phase on benzene extraction of $PdHL^{3+}\cdot(TCA^-)_3$ ion-association compound. Concentrations in the aqueous phases: (1) and (2) 1.60×10^{-5} M Pd(II); 9.00×10^{-5} M 3,5-Cl2PADAB. (3) 4.60×10^{-5} M 3,5-Cl2PADAB. (1), (2), and (3) HTCA=variable; 1 M H_2SO_4; 10% ethanol. (1) λ_{max}= 600 nm, (2) λ_{max}=555 nm, (3) λ_{max}=440 nm. V_o= V_w=10 ml. Organic extracts diluted to 25 cm^3 with pure benzene after equilibrations. Time of full color development of $HLPd^{3+}$ complex=period of equilibration=45 min. Absorbance measures vs. (1) and (2) reagents, (3) water.

Still under the best experimental conditions, ethanol and HTCA were partially extracted by benzene, changing in this way the initial phase volumes. A strong scattering of absorbance measures was observed with phase volume changes. To increase reproducibility, a dilution step of the benzene extracts to a final fixed volume was included after extraction.

Periods of Color Development and Equilibration. In 1—2 M H_2SO_4 solutions with 1 M HTCA and 10% ethanol, Pd(II)–3,5-Cl2PADAB reaction was completed about 10 min after reagent addition. Being the complexation over, a few seconds' equilibration were required for the quantitative extraction. In practice, however, it was necessary to prolong both periods (color development and equilibration) to 15 min in

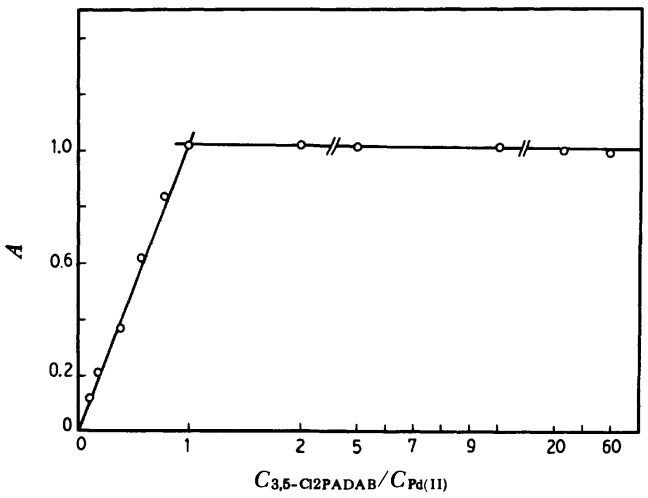

Fig. 2. Effect of 3,5-Cl2PADAB concentration on benzene extraction of $PdHL^{3+}\cdot(TCA^-)_3$ ion-association complex. Saturation curve. Concentrations in the aqueous phases: 3.00×10^{-5} M Pd(II); 3,5-Cl2PADAB=variable; HTCA 1 M; 1 M H_2SO_4; 10% ethanol. λ_{max}=600 nm. Reagent blank. Time of full color development=period of equilibration= 15 min. $V_o=V_w$=10 ml. Organic extracts diluted to 25 cm^3 with pure benzene after equilibrations.

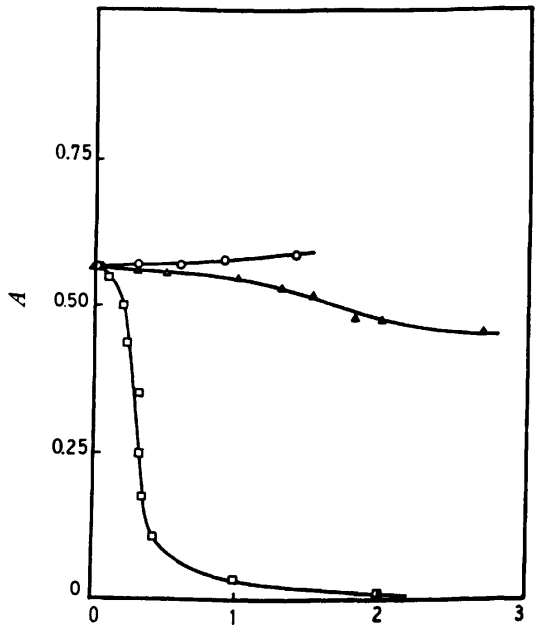

Fig. 3. Effect of aqueous salts on benzene extraction of the $PdHL^{3+}\cdot(TCA^-)_3$ association complex. Concentrations in the aqueous phases (10 cm^3): 1.60×10^{-5} M Pd(II); 1.60×10^{-4} M 3,5-Cl2PADAB; 1 M HTCA; 1 M H_2SO_4; 10% ethanol. (1) Na_2SO_4 (2) $NaClO_4$; (3) NaCl. λ_{max}=600 nm. Reagent blank. Organic extracts (10 cm^3) diluted to 25 cm^3 with pure benzene after equilibrations.

order not to obtain strongly emulsified benzene extracts.

Effect of Reagent Concentration. All other factors being kept constant, the reagent concentration was varied. It was found that a slight excess of reagent sufficed to extract completely the complex and to reach the maximum benzene extracts absorbance. Although this last magnitude remained unaltered for high 3,5-Cl2PADAB-to-Pd(II) ratios (Fig. 2), large amounts of reagent are not convenient because the absorption of reagent blanks becomes too high. Accordingly, 1 cm^3 of 0.025% (w/v) 3,5-Cl2PADAB solution every 10 cm^3 of aqueous phase is specified in the procedure. Figure 2 also shows that the extracted complex has high stability.

Influence of Foreign Salts. The influence of the salt content in the aqueous phases on the absorbance of the benzene extracts was studied by extracting Pd(II) in solutions where the H_2SO_4, 3,5-Cl2PADAB, HTCA, and ethanol concentrations were kept constant, and at the most convenient values. In separate test, different concentrations of sodium salts of sulfuric, perchloric, and hydrochloric acids were assayed. Figure 3 shows the results obtained. Chloride ions decrease the extraction yield and therefore, HCl cannot be recommended for dissolution of samples. Na_2SO_4 or $NaClO_4$ concentrations lower than 1 M influence significantly neither on the absorbance of benzene extracts of $PdHL^{3+}\cdot(TCA^-)_3$ nor on the yield of the extraction. For $NaClO_4$ concentrations higher than 1 M, the yield of the extraction diminishes due to the occlusion of Pd(II) and $PdHL^{3+}$ by the $NaClO_4$ crystals, precipited by the addition of the ethanolic solution of the reagent.

Beer's Law. Sensitivity. Under the experimental conditions described in the recommended procedure for the extraction-spectrophotometric determination of Pd(II), Beer's law is fulfilled up to a concentration of 2.16 ppm of Pd(II) in the organic extracts. The method's sensitivity, estimated according to Sandell's criterion, is 0.00123 μg of Pd(II) cm^{-2} for $\log(I_o/I_t)$= 0.001, and the apparent molar absorptivity of the ion-association compound extracted happened to be 8.6×10^4 $dm^3\,mol^{-1}\,cm^{-1}$ (s=900; $CL_{\alpha=0.05}^{85360-86640}$), at 600 nm. The reproducibility of the method, expressed by the percentual relative standard deviation, which was calculated on the basis of 20 determinations, is 0.59—0.39 depending on the metallic ion concentration.[5] The color of the diluted organic extracts is stable at least during 10 h.

Effect of Foreign Ions. The influence of foreign ions on the determination of Pd(II) by applying the proposed method, was studied for 18 cations that may generally appear with palladium in an analytical system, as well as for some common anions and masking agents. The criterion for interference was a change of ±3% in the absorbance for 2 ppm of palladium. Table 1 shows the results obtained. The greatest limitations are brought by Au(III). The interference of Au(III), when it is found in concen-

Table 1. Tolerances for Some Common Cations and Anions on Spectrophotometric Determination of Pd(II). Pd(II) taken=2 ppm

Ion	Ion-to-Pd(II) tolerated molar ratio[b]	Ion	Ion-to-Pd(II) tolerated molar ratio
Pt(IV)	1000	Mn(II)	3000
Ir(III)	10	Ag(I)	50
Ru(III)	2.5	Cd(II)	3000
Os(VIII)	5	Hg(II)	<1
Rh(III)	170	AsO_3^{3-}	6700
Au(III)	<1	Tartrate	4500
Cu(II)	300	Ascorbic acid	5000
Co(II)	500	SCN^-	1
Ni(II)	1000	Br^-	1
Fe(III)	1000	Co(II)[a]	5000
Fe(II)	2000	Ir(III)-(IV)[a]	400
Cr(III)	1000	Cu(II)[a]	5000
Zn(II)	1000	Ag(I)[a]	10000
Al(III)	3000		

a) Previous extraction with benzenic 0.02% (v/v) acetylacetone solution. b) Maximum tolerated values.

trations lower than 7 ppm, was avoided reducing it to metal by adding a few mg of solid $FeSO_4$, $NaNO_2$, Na_3AsO_3, or oxalic acid to its aqueous solutions and allowing the system to stand for 15 min before adding the reagent and HTCA. In higher concentrations, it was quantitatively extracted by means of Yoe and Overholser's technique[1,6] without change in the palladium concentration. Hg(II) interference could be controlled neither by masking nor by reducing it to metal; prior separation proved to be the only way of avoiding its interference. For that purpose, and in order to expand the method's applications to samples containing large amounts of Cr(III)-(VI), Os(IV)-(VIII), Ru(III)-(VIII), Cu(II), Co(II), Ir(III)-(IV), or Ag(I), several separative procedures were assayed. Volatilization[7,8] in hot concentrate H_2SO_4 or $HClO_4$ solutions proved to be the most efficient and practical method to separate mercury, chromium, osmium, and ruthenium. By combining the previous extraction of Pd(II) that uses acetylacetone dissolved in benzene[9] with the procedure suggested in this work, was the most convenient way for the Pd(II) determination in solutions containing high proportions of Cu(II), Co(II), Ir(III)-(IV), or Ag(I).

Volatilization Procedure. (i) Place 2—20 cm^3 of sample solution containing up to 50 μg of Pd(II) in an extraction tube. Add 10 cm^3 of 94—96% sulfuric acid and 10—15 drops of 72% $HClO_4$ and fume in hot plate until decoloration of the solution or reduction of the volume up to 5 cm^3. (ii) On reaching this stage, add carefully 20 cm^3 of a mixture solution of concentrate HCl and $HClO_4$ (1:8), drop by drop, and keep on heating. During the operation, stop adding the acid mixture whenever the sample color becomes greenish-grey, and keep on adding when it turns red-orange. (iii) Being the solution decolorized, go on heating until almost dried. Let it cool and then continue with the recommended procedure for Pd(II) determination.

If the sample had a great amount of chromium (up to 5.000 ppm) it was volatilized as chromyl chloride through the applications of steps (i) and (ii). But if only osmium and ruthenium occur (up to 6.000 ppm each), the steps to follow were just (i) and (iii). This procedure also enabled the removal of Hg(II) (as $HgCl_2$) up to 1.000 ppm by replacing in step (ii) the acid mixture by 30 cm^3 of 37% HCl.

Procedure Using Acetylacetone Dissolved in Benzene. Into an extraction tube place 20 cm^3 of solution containing between 10 and 100 μg of Pd(II). Adjust the pH to 0.5—0.8 with $HClO_4$ or NaOH solution. Next, add 20 cm^3 of benzenic 0.02% (v/v) acetylacetone solution and shake the tube for 30 min. Allow the phases to separate, and then shake 10 cm^3 of the benzene extract during 30 min with equal volume of an aqueous solution containing 1 M H_2SO_4, 1 M HTCA, 9×10^{-5} M 3,5-Cl2PADAB, and 10% ethanol. Afterwards, transfer the extract, by now colored, to a 25 cm^3 volumetric flask and dilute to the mark with pure benzene. Measure the absorbance of the benzene solution at 600 nm against a blank obtained in the same manner as described for the tests. Calculate the concentration of palladium from a calibration curve obtained under identical conditions.

Applications. The effectiveness of the one-step extraction procedure described in this paper, was evaluated by carrying out Pd(II) determinations on six synthetic solutions prepared from pure solutions of their components. Tables 2 and 3 outlines the compositions of the solutions and the results obtained. Sample No. 2 in Table 2 simulated, both in its compositions and in the component contents, the dissolution of a sample of a concentrate mineral of native platinum. A final stage of sample decomposition was simulated by repeated treatment (2—3 times) of the synthetic solution aliquots with portions of concentrate HCl-HNO_3 (3:1) mixture. Next, in order to eliminate completely osmium and virtual traces of chloride ions, these sample portions were heated until

Table 2. Results Obtained in the Benzene Extraction and Spectrophotometric Determination of Pd(II) with 3,5-Cl2PADAB and TCA^- in Synthetic Samples

Sample No.	Sample composition/% (w/w)	Solution/ppm	Pd(II) found[d]/ppm	E_r/%
1	Au (—)[a]	2000		
	Os (—)[b]	5000		
	Ru (—)[b]	2000		
	Pd (—)	1.50	1.49 ($s=1.4\times10^{-2}$ $Cl^{1.51-1.49}_{\alpha=0.05}$)	−0.66
2	Pt (87.47)	1081		
	Ir (1.24)	15.22		
	Os (0.48)[b]	6		
	Rh (0.25)	3		
	Au (0.02)[c]	0.5		
	Cu (0.71)	0.01		
	Fe (7.41)	91.6		
	Ni (0.10)	1.22		
	Pd (0.85)	9.95	9.86 ($s=1\times10^{-2}$ $Cl^{9.88-9.85}_{\alpha=0.05}$)	−1.00

a) Extracted into ethyl acetate in 3 M HCl solution. b) Volatilized as their respective tetroxides in hot 96% H_2SO_4 solution containing 10—15 drops of 72% $HClO_4$. c) Reduced to metal by adding solid FeSO. d) Mean of ten determinations ($n=10$) on five sample portions.

Table 3. Results Obtained in the Benzene Extraction and Spectrophotometric Determination of Pd(II) with 3,5-Cl2PADAB and TCA^- in Synthetic Samples. Previous Extraction of Pd(II) in pH 0.5—0.8 ($HClO_4$) Solutions with Acetylacetone Dissolved in Benzene

Sample No.	Sample composition/ppm		Pd(II) found[a]/ppm	E_r/%
1	Co(II)	2400		
	Pd(II)	0.80	0.79 ($s=6\times10^{-3}$ $Cl^{0.794-0.785}_{\alpha=0.05}$)	−1.80
2	Cu(II)	2500		
	Pd(II)	0.80	0.79 ($s=5\times10^{-3}$ $Cl^{0.794-0.786}_{\alpha=0.05}$)	−1.80
3	Ir(III)	580		
	Pd(II)	0.80	0.79 ($s=7\times10^{-3}$ $Cl^{0.795-0.785}_{\alpha=0.05}$)	−1.80
4	Ag(I)	17000		
	Pd(II)	1.61	1.62 ($s=3\times10^{-2}$ $Cl^{1.63-1.58}_{\alpha=0.05}$)	+0.62

a) Mean of ten determinations ($n=10$) on five sample portions.

dryness two times, upon adding 5 cm^3 of concentrate nitric acid containing 4—5 drops of 72% $HClO_4$. Before the color development stage, Au(III) and Ir(IV) were reduced to metal and Ir(III), respectively, by adding 20 mg of solid $FeSO_4$.

Sample No. 4 in Table 3 simulated, as far as its composition is concerned, the dissolution of a silver base alloy sample composed of 99.99% Ag and 0.01% Pd.

References

1) C. A. Fontán and C. B. Marone, *Anales Asoc. Quím. Argentina*, **71**, 449 (1983).

2) C. A. Fontán, C. B. Marone, and R. A. Olsina, Under consideration for publication.

3) G. Schwarzenbach and H. Flaschka, "Complexometric Titrations," ed by Methuen and Co., Ltd, London (1969).

4) American Chemical Specifications, "Reagents Chemicals," 4th ed., ACS (1964).

5) IUPAC, "Quantitative Characterization of Procedures Using Ultraviolet and Visible Molecular Absorption Spectrophotometry," *Pure Appl. Chem.*, **58**, 1015 (1986).

6) J. H. Yoe and L. G. Overholser, *J. Am. Chem. Soc.*, **61**, 2058 (1939).

7) F. E. Beamish, "The Analytical Chemistry of the Noble Metals," ed by Pergamon Press, 1st ed. (1966).

8) E. B. Sandell and H. Onishi, "Photometric Determination of Traces of Metals," Vol. III, part I, Jhon Wiley & Sons Inc., 4th. ed., U.S.A. (1978).

9) J. Stary, "The Solvent Extraction of Metal Chelates," ed by Pergamon Press, N.Y. (1964).

 © 1988 The Chemical Society of Japan Bull. Chem. Soc. Jpn., 61, 4127—4131 (1988)

Conformational Dependence of Mass Spectral Fragmentation of Pinane Derivatives

Tse-Lok Ho†
SCM Organic Chemicals Division, P.O.Box 389, Jacksonville, FL 32201, U.S.A.
(Received September 18, 1987)

The major fragmentation pathway for pinane derivatives on electron impact involves cleavage of the cyclobutane bond which is part of a boat-cyclohexane. This trend is followed by ketones, alcohols, and hydrocarbons of the same skeleton.

Stereochemical correlation of mass spectrometric fragmentations has been investigated by many chemists.[1] While the majority of the reported data is concerned with the differences arising from configuration variation of functional groups, the effects of molecular conformations on the fragmentation pathways remain a subject of great interest but insufficient inquiry. The reason for this apparent lack of activity in the area is two fold: general consensus indicates that highly energetic species are generated in the mass spectrometer and the decomposition of these species must be accompanied by the destruction of conformational integrity of the original molecules; more importantly, adequate conformational isomers are difficult to identify.

We are convinced that the electron impact-induced fragmentation of a molecule must be biased by conformational factors. For studying this possibility we chose the diastereoisomeric 3-pinanones, i.e., pinocamphone (*trans*-3-pinanone (**1**)) and isopinocamphone (*cis*-3-pinanone (**2**)). They are a pair of stable compounds which can be regarded as closest to being conformationally isomeric.[2] Thus, if we ignore the methylene bridge of the bicyclic structure, pinocamphone is reduced to 2,4,4-trimethylcyclohexanone in a flattened chair form, whereas isopinocamphone, that a flattened boat.

(1)

(2)

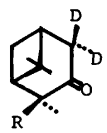

(1-d_3) R=D
(1-d_2) R=H

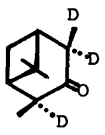

(2-d_3)

Since both ketones contain an equatorial α-methyl group, there is only a conformational difference between the two with respect to the cyclohexanone moiety. As ionization in the mass spectrometer of such ketones is commonly localized at the carbonyl group, factors affecting their fragmentation pathways other than the conformations must be the same. The pairwise comparison of the principal peaks in their mass spectra should then provide clues to the conformational influence on the fragmentation of the 3-pinanones.

In the electron impact mass spectra of the 3-pinanones the relative intensities of ions *m/z* 83 and 55 are reversed (see Figs. 1 and 2). The *m/z* 83 ion is stronger and *m/z* 55 ion is weaker in the spectrum of **1**, and the opposite is true for that of **2**. These results are clear-cut and reproducible under GC-MS conditions. With the help of high resolution mass analysis and by examination of the corresponding deuterated ketones, Schemes 1 and 2 can be postulated to account for the differences.

The rationale is supported by spectral analysis of pinocamphone-2,4,4-d_3 (**1**-d_3), pinocamphone-4,4-d_2 (**1**-d_2), and isopinocamphone-2,4,4-d_3 (**2**-d_3). The following mass shifts were observed: with the trideuterated ketones— *m/z* 83→84, 69→71, 55→56, and 41→43. Furthermore, the negligible 55→56 shift in the spectrum of **1**-d_2 and the much lower intensity of *m/z* 84 in the same spectrum confirm the assignment of the ion structure.

While these ions are actually doublets, invariably the hydrocarbon species are in much higher abundance, therefore there is no possibility of misinterpreting the trends. The ratios of the hydrocarbon ions to acylium ions for **1** are 10.63 for *m/z* 83, 8.28 for *m/z* 69, 64.91 for *m/z* 55, and those for **2** are 4.74 (*m/z* 83), 10.85 (*m/z* 69), 29.33 (*m/z* 55) as determined by high resolution scans.

It appears then the α-cleavage at the C(2)-C(3) bond of the ketones is rapidly followed by a rupture of the four-membered ring, with the latter fragmentation displaying a remarkable degree of selectivity. It may be concluded that the cyclobutane bond which also constitutes a part of the boat-shaped cyclohexanone, and the one subtended by it, break preferentially. This process, but not the alternative mode of cleavage,

† Present address: The NutraSweet Co., 601 Kensington Rd., Mt. Prospect, IL 60056, U.S.A.

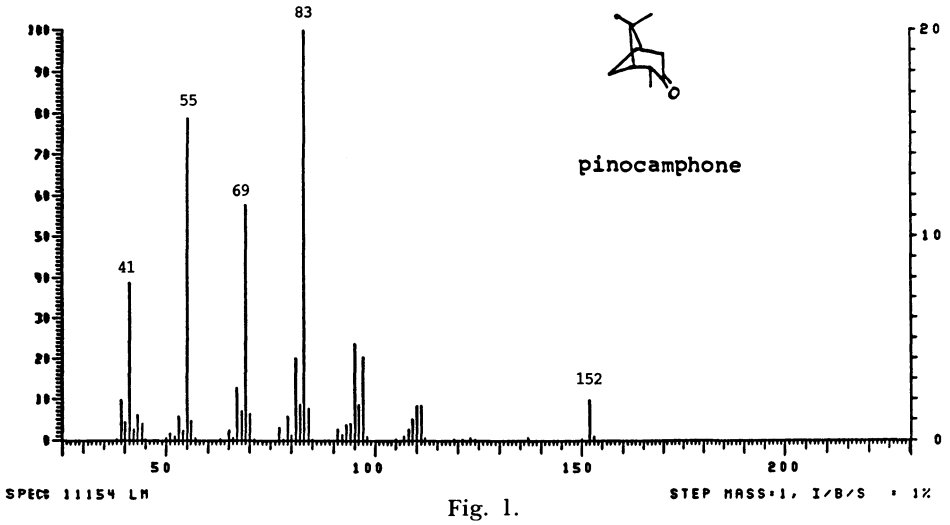

Fig. 1.

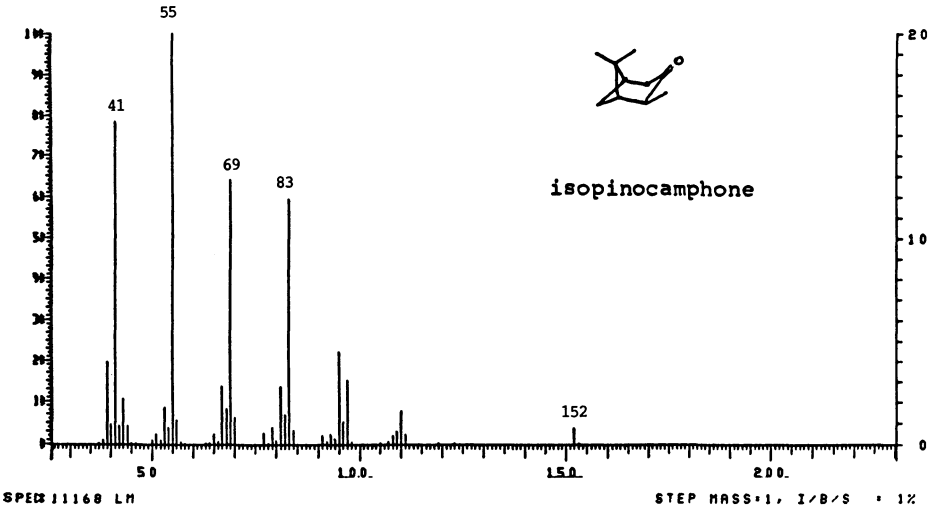

Fig. 2.

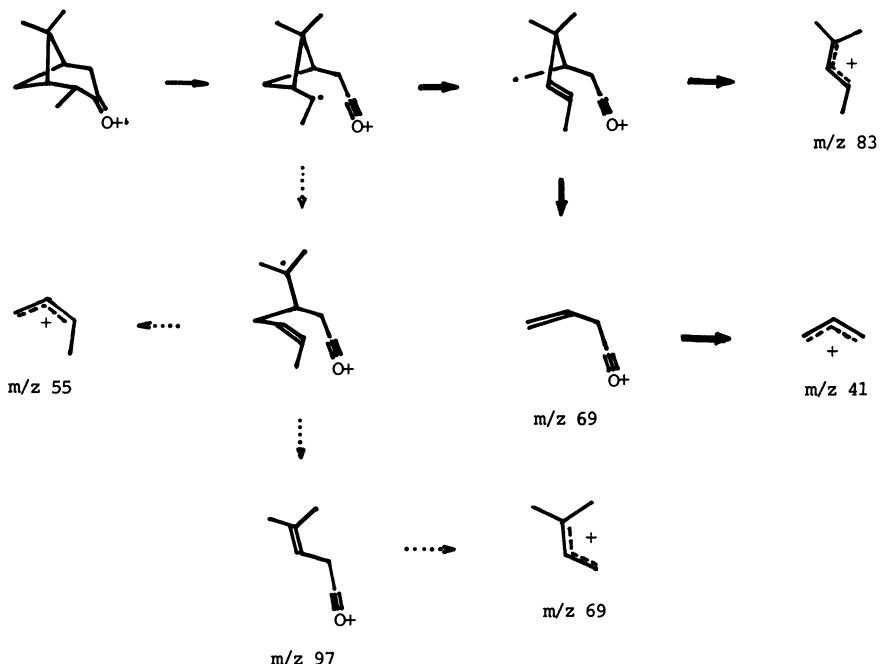

Scheme 1.

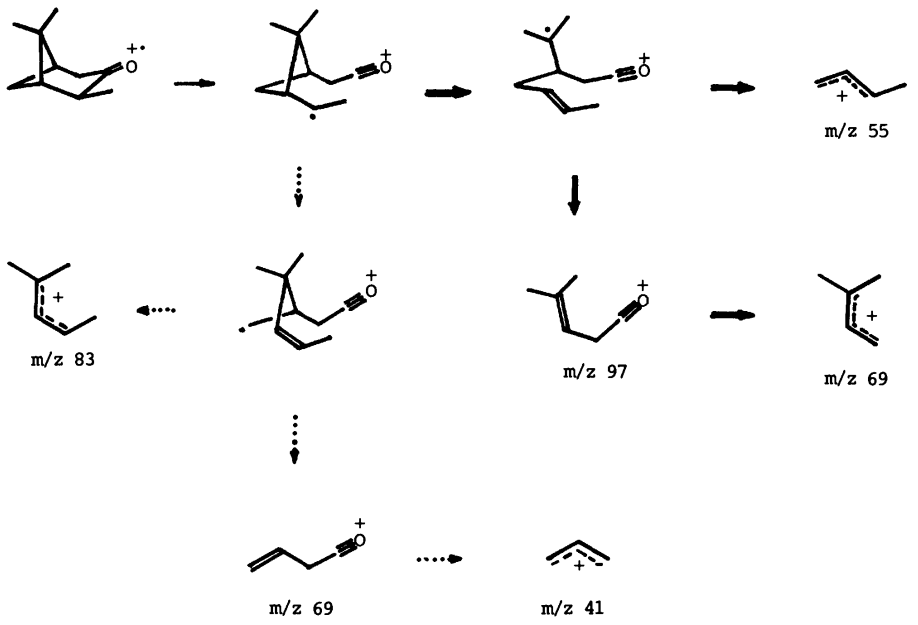

Scheme 2.

relieves a larger portion of the inherent strain of the molecule.

While the strain relief must play a contributory role in the selective fragmentation, the more important factor may be related to the Principle of Least Motion. Newman projections along the C(2)-C(1) bond of the ketones clearly show a smaller dihedral angle subtended by C(3) and C(7) than that subtended by C(3) and C(6) in pinocamphone (**1**) and a larger dihedral angle in isopinocamphone (**2**). Cyclobutane cleavage of the 2,3-seco radical ion is favored at the bond nearly parallel to the original C(2)-C(3) bond for easier development of a double bond involving the empty orbital $C(2)^+$ or radical $C(2)^{\cdot}$. This preference for bond cleavage finds analogy in the E2 elimination which is least favored when the departing groups are close to being orthogonal and becomes progressively more favorable as the dihedral angle narrowed or widened, maximizing at 0° or 180°.

Perhaps it should be emphasized that the fragmentation of the 2,3-seco radical ions is instantaneous such that their intermediacy is unnecessary. In other words, acyclic species could have been generated more or less directly. This transiency explains the maintenance of the original conformations and their influence on the fragmentation pathways.

It may be interesting to speculate also that molecular conformations have subtle effects on the initial cleavage sites. Undoubtedly the more highly substituted C(2)-C(3) bond is the preferred locale of fragmentation, but this mode is not to the exclusion of the C(3)-C(4) bond fission, as evinced by the appearance of $C_5H_7O^+$ and $C_3H_3O^+$ ions. An increased percentage of the C(3)-C(4) bond cleavage in **2** relative to that in **1** is apparent from examination of the $C_nH_{2n-1}^+/C_nH_mO^+$ ratio of the twin peaks at *m/z* 83 and 55.

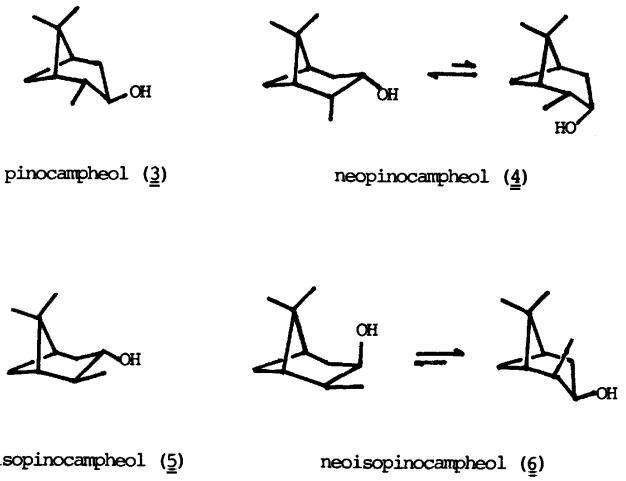

The four stereoisomeric 3-pinanols[3] also exhibit discernible intensity variations in a number of fragments. The members of the neo alcohols, each being capable of assuming a conformation in which the hydroxyl group is axially oriented and juxtaposed to a remote hydrogen atom, give rise to more abundant ($M-H_2O$) and ($M-H_2O-CH_3$) peaks— *m/z* 136: neopinocampheol (**4**) 6%, neoisopinocampheol (**6**) 5%, pinocampheol (**3**) 3%, isopinocampheol (**5**) 2%; *m/z* 121: **4** 9%, **6** 14%, **3** 0.5%, **5** 1%. On the other hand, the normal/iso compounds, having equatorial hydroxyl groups, display considerably stronger ions at *m/z* 43: **3** 85%, **5** 82%, **4** 40%, **6** 46%. Based on the conformations of the four alcohols (Fig. 3) the more

facile dehydration and the tandem demethylation of the neo alcohols becomes clear (Scheme 3).

The *m/z* 55 fragment is the base peak of pinocampheol **3**. In the spectra of the other isomers this fragment is approximately half as intense. The appearance of *m/z* 56 as the major peak in the cluster of the surrounding region in the mass spectrum of the 2,4,4-trideuterated alcohols suggests its main component as a crotyl cation composing of a carbon segment of C(7,1,2,10) (Scheme 4).

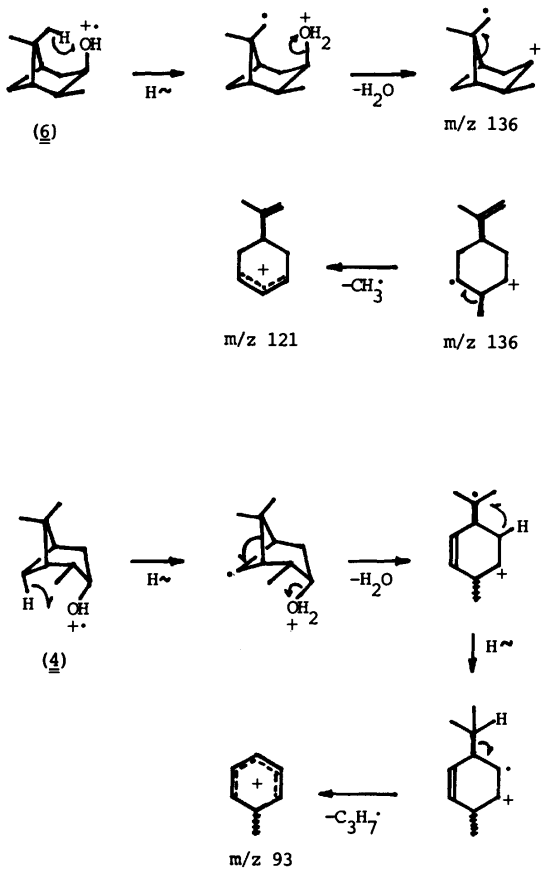

Scheme 3.

The most noticeable peak shift in the spectra of the 3-deuterio alcohols is *m/z* 81→82, in addition to the (M−H_2O) and (M−H_2O−CH_3) ions. Thus the *m/z* 81 ion could arise from the same seco species by losing a crotyl radical, and subsequent dehydration.

It is likely that *m/z* 84 and 70 are interrelated. Both peaks are derivable from the molecular ions via analogous processes albeit involving scission of different bonds. The relative intensities of *m/z* 84 are in the descending order of **4>3≈6>5**, whereas those of *m/z* 70 are **5≈6>3>4**. The trends are most satisfactorily explained by Scheme 5 in which a preferential ring fission involving C(1)-C(7) and C(5)-C(6) bonds when the compound contains a chair-like trimethylcyclohexane and cleavage at C(1)-C(6) and C(5)-C(7) bonds when the trimethylcyclohexane moiety is forced into a boat-like conformation is indicated. Assignment of the fragment is also consistent with the observed mass shifts of *m/z* 70→72 and 84→85 in the 2,4,4-trideuterio alcohols. Mass shift is absent with regard to these two ions in the 3-deuterio alcohols.

The major direction of cyclobutane ring cleavage for the alcohols follows the two ketones. Remarkably, even the parent hydrocarbons *cis*-pinane (**7**) and *trans*-pinane (**8**) manifest parallel intensity differences in the relevant peaks. While we observed approximately equal intensity of the *m/z* 83 and 69 ions for **7** at ca. 54%, the corresponding peaks registered at 63% and 48%, respectively, in **8**. The coincidental balance of the fragmentation pathways for *cis*-pinane may be actually due to further conformational modification or flattening of the boat-shaped trimethylcyclohexane ring as flagpole interaction between the axial hydrogen at C(3) and the syn-methyl group at C(6) is rather severe. Scheme 6 showing two extreme conformational isomers is only presented for the sake of clarity. It should also be stated that the seco ions indicated

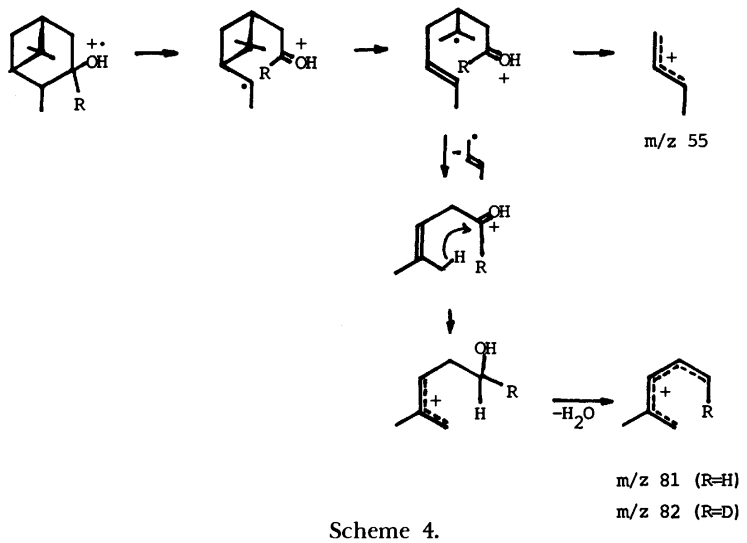

Scheme 4.

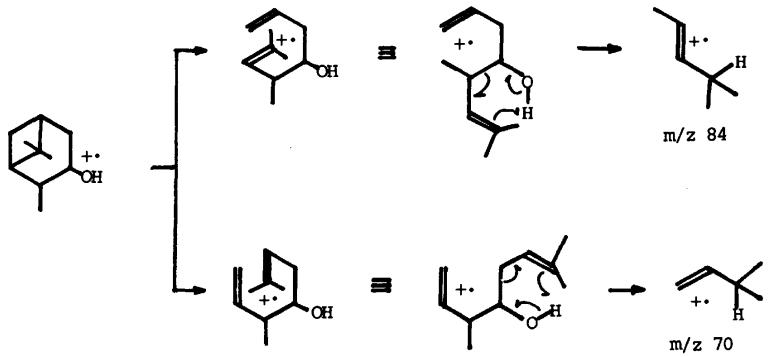

Scheme 5.

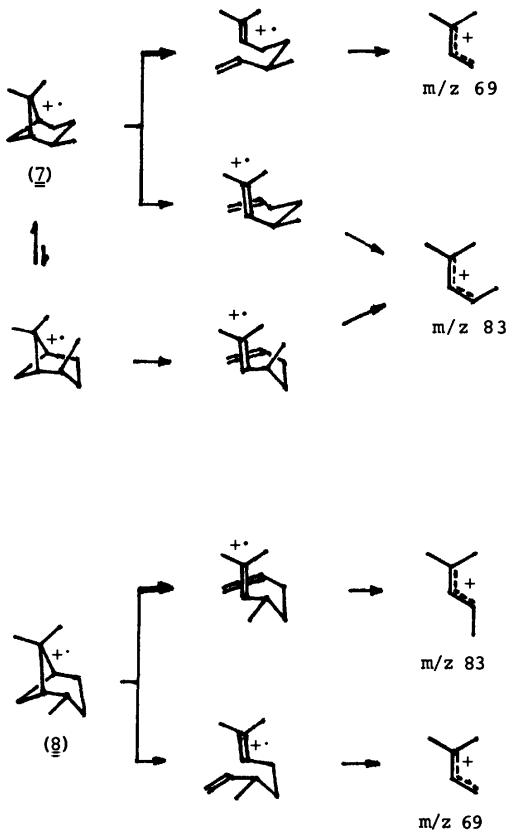

Scheme 6.

in Schemes 5 and 6 could be generated in a stepwise manner instead of a synchronous process.

The recognizable differences in the mass fragmentation of pinane derivatives are hardly fortuitous. As the only dissimilarity among members of the three series of compounds is in their conformations, it seems that the fragmentation pathways are indeed affected to a large extent by those factors.

The origin of the conformational preferences of the compounds discussed above can be traced to the secondary methyl group. It appears that this group has an additional effect in causing the cyclobutane bond nearest to dihedrally orthogonal to it to undergo rupture preferentially. The destabilization of that cyclobutane bond and/or slight stabilization of the antiperiplanar counterpart may be expected on the basis of an electronic transmission which is operated in the three-bond spin-spin coupling (Karplus relationship).

Experimental

All known compounds were prepared according to literature methods.[3] Deuteration of **1** and **2** were carried out in a mixture of dioxane and deuterium oxide in the presence of sodium methoxide at room temperature. The alcohols were obtained by reduction of the ketones with either sodium borohydride or lithium aluminum deuteride.

Mass spectra were measured in a Finnigan MAT 112 mass spectrometer connected to a Perkin Elmer Sigma gas chromatograph which was equipped with a DX-4 column (30 m×0.246 mm) and temperature-programmed at 4 °C min^{-1} from 60 to 250 °C using helium as carrier gas.

The author is greatly indebted to Dr. A. F. Thomas (Firmenich Cie.) for his criticisms and help, Sonya Sapp for her expert operation of the GC-MS system.

References

1) S. Meyerson and A. W. Weitkamp, *Org. Mass Spectrom.*, **1**, 659 (1968); M. M. Green, *Topics in Stereochem.*, **9**, 35 (1976); *Tetrahedron*, **36**, 2687 (1980); A. Mandelbaum, *Mass Spectrom. Rev.*, **2**, 223 (1983); A. F. Thomas and B. Wilhalm, *Helv. Chim. Acta*, **50**, 826 (1967).

2) M. V. Bhatt, *Chem. Ind.*, **1959**, 1452; Y. Bessiere-Chretien and C. Grison, *Bull. Soc. Chim. Fr.*, **1971**, 1454.

3) H. Schmidt, *Chem. Ber.*, **77**, 544 (1944).

 © 1988 The Chemical Society of Japan Bull. Chem. Soc. Jpn., 61, 4133—4136 (1988)

Kinetics of Reduction of Silver(II) by Sodium Tetrahydroborate

Manash DASGUPTA and Mahendra K. MAHANTI*
Department of Chemistry, North-Eastern Hill University, Shillong 793003, India
(Received September 28, 1987)

The kinetics of reduction of silver(II) by sodium tetrahydroborate in aqueous acidic solution has been investigated. The reaction was observed to proceed in two steps, namely, (a) the formation of the intermediate Ag^{I} and (b) the subsequent conversion of Ag^{I} to Ag^{0}. The activation parameters for the two steps have been separately calculated. The intermediate Ag^{I} species, and the final products, were characterized by chemical and spectral methods. A plausible mechanism for the reduction of Ag^{II} ions has been proposed.

The mechanism of oxidation by Ag^{II} has been the subject of several investigations in which organic[1] and inorganic[2] substrates have been used. The Ag^{II}/Ag^{I} couple has a high reduction potential of +2.00 V in 1.0 M $HClO_4$ (1 M=1 mol dm^{-3}).[3] Silver(II) reacts rapidly even with substrates that exhibit sluggish behavior towards other commonly employed reagents. The kinetics of oxidation of Fe^{2+}, Mn^{2+}, Co^{2+}, Ce^{3+}, and V^{4+} by Ag^{II} revealed a wide range of reduction potentials and self-exchange rates.[4] Many oxidation reactions such as the oxidation of Hg^{I} by Ce^{4+} ions,[5] the peroxydisulfate oxidations of Ce^{III}, Cr^{III}, V^{IV}, and N_2H_4,[6] and of oxalate,[7] are all catalyzed by Ag^{+} ions, and the kinetics have been visualized as proceeding via the initial oxidation of Ag^{I} to Ag^{II}, which then undergoes reduction by the substrate. The reactions of the tetrahydroborate ion with transition metal compounds usually result either in a reduction of metal to a lower oxidation state and possibly the formation of a hydride compound, or the formation of a tetrahydroborate or a diborane derivative.[8,9] Sodium tetrahydroborate in water or methanol solution was found to be an effective reducing agent for the conversion of aldehydes and ketones to the corresponding alcohols.[10,11] In an earlier paper, we had reported our results on the kinetics of reduction of hexacyanoferrate(III) by sodium tetrahydroborate.[12] In continuation of our work on the kinetics of reduction of transition metal ions by sodium tetrahydroborate, we report here the kinetic features of the reduction of silver(II) by sodium tetrahydroborate in aqueous acidic medium, at constant ionic strength, under a nitrogen atmosphere. A plausible mechanistic pathway for the reduction reaction has been suggested.

Experimental

Materials, Methods, and Stoichiometry. Sodium tetrahydroborate (Loba Chemical Co.) was kept under vacuum. Tetrakis(pyridine)silver(II) peroxodisulfate, $[Ag(py)_4]S_2O_8$, was prepared by the standard procedure,[13] and was used as the source of Ag(II). Perchloric acid and sodium perchlorate were of E. Merck products. All solutions were prepared in dark-colored flasks in order to prevent exposure of Ag^{II} solutions to light.

Solutions of sodium tetrahydroborate were prepared in water. Since sodium tetrahydroborate undergoes hydrolysis in aqueous medium,[12] all the solutions used for the kinetic runs were prepared by dissolving 2.5 times more of $NaBH_4$ than what was theoretically necessary. Solutions of Ag^{II} were prepared in $HClO_4$ and $NaClO_4$ to maintain a constant ionic strength. It has been shown that Ag(II) can undergo disproportionation according to:[14,15]

$$2\,Ag^{II} \rightleftharpoons Ag^{I} + Ag^{III}$$

Hence, an excess of Ag^{I} solution (0.10 M) was added to prevent disproportionation of Ag^{II}. The two solutions were separately thermostated at 15 °C for 1 h under nitrogen, and then mixed in equal volumes by syringing into the spectrophotometric cell (UV-26, Beckman). The progress of the reaction was monitored at 375 nm by observing:

(i) An increase in the optical density due to the reduction of the Ag^{II} to the Ag^{I} species. This solution does not contain any Ag^{II} ion at the end of this reaction.

(ii) The subsequent decrease in the optical density at 375 nm (due to the reduction of the Ag^{I} to the Ag^{0} species).

The pH of the reaction mixture was checked periodically during the course of the reaction (Control Dynamics, digital model), and found to remain constant. Since the grey-colored Ag^{0} species was formed as the final reaction product, care was taken to ensure that the reaction mixture remained homogeneous for the duration of the kinetic runs. It was observed that there was no precipitation during the course of the kinetic runs.

The stoichiometry of the reaction was determined in the following manner: reaction mixtures containing $NaBH_4$ and an excess of Ag^{II} were allowed to react at 15 °C for 24 h under nitrogen, and then analyzed, spectrophotometrically at 375 nm for the Ag^{II} which was left. The results gave a ratio of substrate to reductant according to the equation:

$$2\,BH_4^- + 8\,Ag^{2+} + 6\,H_2O \longrightarrow 8\,Ag^{0} + 2\,B(OH)_3 + 14\,H^+.$$

Analysis of the Ag(I) Intermediate. Two milliliters of the reaction mixture were withdrawn within 1 min of the initiation of the reaction, and spectrally analyzed over a range of wavelengths from 300 nm to 900 nm. The dark colored species[16] was found to absorb at 375 nm, which was due to the presence of the Ag^{I} intermediate species. In an earlier investigation, it was shown that Ag^{II} was reduced to an Ag^{I} species.[17]

Product Analysis. A solution of $NaBH_4$ (2×10^{-5} M) in 100 ml of water, was mixed with a solution containing the

Ag^{II} complex (2×10^{-5} M) in $HClO_4$, and excess of Ag^{I} solution (ionic strength adjusted to 0.05 M by the addition of $NaClO_4$), and the reaction mixture allowed to stand at 15 °C for 24 h under nitrogen. Greyish colored particles were precipitated along with a thin layer of shining silver mirror formed on the walls of the reaction vessel. The reaction mixture was filtered. The precipitate was washed with distilled water, tested for the complete removal of Ag^{+} ions, and then dried. The filtrate was analyzed for the presence of borate, as described earlier.[12]

The precipitate (0.5187 g) was taken, and converted to AgCl by the standard method,[18] and gravimetrically estimated as AgCl. The weight of AgCl was 0.6682 g, which corresponded to 0.5029 g of silver. This value compared favorably, within the limits of experimental error, with the theoretical percentage of silver present in the final product (theoretically, 100%; experimentally obtained by this method, 96.9%). This confirmed that the silver was present in the final product as Ag^{0}.

Results and Discussion

Kinetics Results. The rates of the reactions (the formation of Ag^{I} from Ag^{II} and the subsequent conversion of Ag^{I} to Ag^{0} species) were dependent on the first powers of the concentrations of each of the reactants (Table 1). The two rate constants have been separated, and individually calculated as k_1 (conversion of the Ag^{II} to the Ag^{I} species) and k_2 (conversion of the Ag^{I} to the Ag^{0} species). Plots of k_1 and k_2, respectively, versus a twenty-five fold range of concentration of BH_4^- ions, gave a straight line passing through the origin, indicating that the rate of the reaction was dependent on the first power of the concentration of BH_4^- ions. At constant BH_4^- concentration (large excess), the first-order rate constants (k_1 and k_2, respectively) did not change with changing Ag^{2+} ion concentrations (twenty-fold range), which indicated a first order dependence on the Ag^{2+} ion concentration (Table 1).

The reaction was studied at varying pH (Table 1). The logarithm of the rate of disappearance of Ag^{2+} ion divided by the tetrahydroborate ion concentration, was plotted against pH. The plot was linear, indicating a first order dependence of the rate of the reaction on the hydrogen ion concentration.

The reaction was influenced by changes in the temperature (Table 1), and the activation parameters have been evaluated and shown in Table 2. It has been suggested[14] that in the exchange of Ag^{I} with Ag^{II}, the

Table 1. Rate Data for the Reduction of Ag^{II} by $NaBH_4$ at 15°C (μ=0.05 M)

$[BH_4^-]$ / 10^3 M	$[Ag^{II}]$ / 10^4 M	pH	$10^3 k_1/s^{-1}$ $Ag^{II} \longrightarrow Ag^{I}$	$10^3 k_2/s^{-1}$ $Ag^{I} \longrightarrow Ag^{0}$
1.0	1.0	2.0	14.2	6.2
5.0	1.0	2.0	72.5	31.5
10.0	1.0	2.0	145.0	61.2
25.0	1.0	2.0	360.0	156.0
1.0	0.75	2.0	14.0	5.8
1.0	0.50	2.0	14.8	6.0
1.0	0.25	2.0	14.5	6.5
1.0	0.10	2.0	14.0	6.0
1.0	0.05	2.0	14.5	6.5
1.0	1.0	2.5	12.6	5.5
1.0	1.0	3.0	11.0	4.8
1.0	1.0	3.5	9.8	4.3
1.0	1.0	4.0	8.5	3.7
1.0	1.0	5.0	6.6	2.9
1.0	1.0	6.0	5.1	2.2
1.0	1.0	2.0	18.0[a]	7.4[a]
1.0	1.0	2.0	20.9[b]	10.5[b]
1.0	1.0	2.0	25.2[c]	13.5[c]
1.0	1.0	2.0	29.5[d]	17.6[b]

a) 20°C; b) 25°C; c) 30°C; d) 35°C (all temperature corrections were ±0.1°C). All values of rate constants were the average of three experiments, agreement being ±3%.

Table 2. Activation Parameters

Parameter	$Ag^{II} \longrightarrow Ag^{I}$	$Ag^{I} \longrightarrow Ag^{0}$
E	28±2 kJ mol^{-1}	43±2 kJ mol^{-1}
A	2×10^2 s^{-1}	5×10^4 s^{-1}
ΔH^{*}	25±2 kJ mol^{-1}	40±2 kJ mol^{-1}
ΔS^{*}	−208±4 J K^{-1} mol^{-1}	−166±4 J K^{-1} mol^{-1}

rate law was consistent with a disproportionation mechanism

$$2Ag^{II} \rightleftharpoons Ag^{I} + Ag^{III}$$

the rate of exchange being equal to the rate of the disproportionation reaction at equilibrium. This would necessarily imply that the rate constant for the reverse reaction (the reaction between the Ag^{I} and the Ag^{III} species) must be quite large. In the present investigation, since excess Ag^{I} has been added to the initial Ag^{II} solution, one might envisage the suppression of the disproportionation reaction involving the formation of the Ag^{III} species. This would enable the facile conversion of Ag^{II} to Ag^{I} which has been reflected in the activation parameters (Table 2) for the first step of the reaction. The conversion of Ag^{I} to Ag^{0} has been observed in this investigation.

Variations in the ionic strength of the medium using $NaClO_4$ (range of ionic strength 0.01 to 0.075 mol l^{-1}), did not affect the rate of the reaction.

Under the present experimental conditions, the rate law could be expressed as:

$$\text{Rate} = -\frac{d[\text{Ag(II)}]}{dt} = k_{obs}[\text{Ag(II)}][BH_4^-][H^+]$$

where k_{obs} corresponds to the composite rate constant for the reaction, which has been separated into the individual rate constants, k_1 and k_2 (Table 1).

Mechanism. Since the rate of the reaction was dependent on the concentrations of each of the reactants, the first step of the reaction could be represented as:

$$BH_4^- + H^+ \longrightarrow H^+BH_4^-. \quad (1)$$

The redox steps following Eq. 1 would involve the reaction of Ag^{II} with the tetrahydroborate species. There is evidence from the hydrolysis of diborane[19] that intermediates of partially hydrolyzed boron hydride compounds do exist, and that these intermediates differ in their reducing capacities. In the present investigation, the intermediate boron compounds could not be isolated, although the reactions of diborane with ice and with the "bound water" in silica gel do indeed suggest the existence of intermediate boron compounds.[19]

Molecular hydrogen reacts homogeneously with a number of metal ions in solution, reducing them to a lower oxidation state. For example, the mechanism of reduction of Cu^{2+} to Cu^{+} has been shown to be [20,21]

$$Cu^{2+} + H_2 \rightleftharpoons CuH^+ + H^+$$

$$CuH^+ + Cu^{2+} \longrightarrow 2Cu^+ + H^+,$$

the intermediate CuH^+ being stabilized by covalent bonding.

The reactions of Hg^{2+}, Hg_2^{2+}, and MnO_4^- with molecular hydrogen had indicated that hydrogen behaved as a two-equivalent reductant. Thus, the mechanism for the reduction of Hg^{2+} to Hg_2^{2+} was suggested to be:[22]

$$Hg^{2+} + H_2 \longrightarrow Hg^0 + 2H^+$$

$$Hg^0 + Hg^{2+} \xrightarrow{\text{fast}} Hg_2^{2+}.$$

In the reactions with Hg_2^{2+} and MnO_4^-, the rate-determining step appeared to be a two-equivalent reduction, leading to the formation of Hg_2^0 and Mn^{V}, respectively, as intermediates.

It has been earlier reported that acidic solutions of Ag^{2+} ions have been reduced to metallic silver by a variety of reducing agents.[23–28] Aqueous solutions of $AgClO_4$ were reduced by hydrogen to the metal,[29] a homolytic cleavage of hydrogen being suggested as follows:

$$2Ag^+ + H_2 \longrightarrow 2AgH^+$$

$$2AgH^+ + \text{Substrate} \longrightarrow \text{Products} + 2Ag^+.$$

At lower concentrations of Ag^+, a heterolytic splitting of H_2 was proposed:[30]

$$Ag^+ + H_2 \longrightarrow AgH + H^+$$

$$AgH + Ag^+ \longrightarrow \text{Intermediate} \xrightarrow{\text{Substrate}} \text{Products}.$$

The effect of complex formation with ligands other than water was studied by following the reduction of silver complexes by hydrogen to the metal,[31] and the rate data indicated a heterolytic cleavage of hydrogen. The reduction of silver–amine complexes to metallic silver by hydrogen was investigated in an attempt to correlate reactivity with ligand properties,[32] thus:

$$[Ag(NR_3)_2]^+ + H_2 \longrightarrow Ag + 2R_3NH^+.$$

The kinetic results of the present investigation would suggest a stepwise reduction of Ag^{2+} ions by sodium tetrahydroborate. In the first instance, the Ag^{2+} ion would be reduced to Ag^{I}, which in turn, is converted to Ag^{0}.

In the present investigation, the reaction sequence could be represented as follows:

$$H^+ + BH_4^- \longrightarrow H^+BH_4^-$$

$$H^+BH_4^- \longrightarrow \frac{1}{2}B_2H_6 + H_2$$

$$4H_2 + 8Ag^{2+} \longrightarrow 8Ag^+ + 8H^+$$

$$8Ag^+ + BH_4^- + 3H_2O \longrightarrow 8Ag^0 + B(OH)_3 + 7H^+$$

$$\frac{1}{2}B_2H_6 + 3H_2O \longrightarrow B(OH)_3 + 3H_2.$$

The overall stoichiometric reaction is:

$$2BH_4^- + 8Ag^{2+} + 6H_2O \longrightarrow 8Ag^0 + 2B(OH)_3 + 14H^+$$

The intermediate formation of the Ag(I) species, and also the formation of Ag^0 as the final product, have

been confirmed by spectral and chemical methods, in the present investigation.

References

1) C. Baiocchi, G. Bovio, and E. Mentasti, *Int. J. Chem. Kinet.*, **14**, 1017 (1982); E. Mentasti and E. Palizzetti, *J. Chem. Soc., Perkin Trans. 1*, **1978**, 77.

2) A. K. Indrayan, B. K. Mishra, and P. K. Gupta, *Inorg. Chem.*, **20**, 450 (1981); D. S. Honig, K. Kustin, and J. E. Martin, *Inorg. Chem.*, **11**, 1895 (1972).

3) G. Biederman, F. Maggio, V. Romano, and R. Zingales, *Acta Chem. Scand., Ser. A*, **35**, 287 (1981).

4) P. Arsalli, C. Baiocchi, E. Mentasti, and J. S. Coe, *J. Chem. Soc., Dalton Trans.*, **1984**, 475.

5) W. C. E. Higginson, D. R. Rosseinsky, B. Stead, and A. G. Sykes, *Disc. Faraday Soc.*, **29**, 49 (1960).

6) W. M. Cone, *J. Am. Chem. Soc.*, **67**, 78 (1945).

7) J. M. Anderson and J. K. Kochi, *J. Am. Chem. Soc.*, **92**, 1651 (1970); *J. Org. Chem.*, **35**, 986 (1970).

8) A. G. Ginsberg, *Adv. Trans. Metal Chem.*, **1**, 111 (1965).

9) M. L. H. Green and D. J. Jones, *Adv. Inorg. Radiochem.*, **7**, 215 (1965).

10) S. W. Chaikin and W. G. Brown, *J. Am. Chem. Soc.*, **71**, 122 (1949).

11) H. C. Brown, E. J. Mead, and B. C. Subba Rao, *J. Am. Chem. Soc.*, **77**, 6209 (1955).

12) M. Bhattacharjee, A. K. Bhattacharjee, and M. K. Mahanti, *Bull. Chem. Soc. Jpn.*, **54**, 3566 (1981).

13) G. Pass and H. Sutcliffe, "Practical Inorganic Chemistry," Chapman and Hall, London (1974), p. 79.

14) B. M. Gordon and A. C. Wahl, *J. Am. Chem. Soc.*, **80**, 273 (1958).

15) J. B. Kirwin, F. D. Peat, P. J. Proll, and L. H. Sutcliffe, *J. Phys. Chem.*, **67**, 1617 (1963).

16) E. T. Borish, L. J. Kirchenbaum, and E. Mentasti, *J. Chem. Soc., Dalton Trans.*, **1985**, 1789.

17) L. J. Kirschenbaum, E. T. Borish, and J. D. Rush, *Isr. J. Chem.*, **25**, 159 (1985).

18) A. I. Vogel, "A Text Book of Quantitative Analysis," ELBS (1985), p. 479.

19) I. Shapiro and H. G. Weiss, *J. Phys. Chem.*, **57**, 219 (1953).

20) E. Peters and J. Halpern, *J. Phys. Chem.*, **59**, 793 (1955).

21) J. Halpern, E. R. Macgregor, and E. Peters, *J. Phys. Chem.*, **60**, 1455 (1956).

22) G. J. Korinek and J. Halpern, *J. Phys. Chem.*, **60**, 285 (1956).

23) J. Kleinberg, *Chem. Rev.*, **40**, 381 (1947).

24) C. Wagner, *J. Metals*, **4**, 214 (1952).

25) L. Andrussow, *Z. Phys., Chem.*, **208**, 78 (1958).

26) M. A. Bernard and B. Nocher, *Compt. Rend.*, **258**, 3309 (1964).

27) G. A. Rechnitz and S. B. Zamochnick, *Talanta*, **11**, 713 (1964); **12**, 479 (1965).

28) R. J. Kline and C. J. Kershner, *Inorg. Chem.*, **5**, 932 (1966).

29) A. H. Webster and J. Halpern, *J. Phys. Chem.*, **60**, 280 (1956).

30) A. H. Webster and J. Halpern, *J. Phys. Chem.*, **61**, 1239 (1957).

31) A. H. Webster and J. Halpern, *J. Phys. Chem.*, **61**, 1245 (1957).

32) J. Halpern and J. B. Milne, Proc. 2nd Intl. Cong. Catal., Paris (1961), p. 445.

 © 1988 The Chemical Society of Japan Bull. Chem. Soc. Jpn., 61, 4137—4141 (1988)

Visible Light Assisted Heterogeneous Catalysis. Decomposition of Peroxomonosulfate over Doped and Undoped WO_3 Dispersions in Aqueous Medium

Pichai MARUTHAMUTHU,* Muthupandian ASHOKKUMAR, and Lakshmanan VENKATASUBRAMANIAN
Department of Energy, University of Madras, A.C. College Campus, Madras 600025, India
(Received December 7, 1987)

Aqueous suspension of RuO_2-loaded WO_3 powder on illumination with light of $\lambda \geqslant 410$ nm was found to decompose peroxomonosulfate (PMS, HSO_5^-) efficiently. The rate and other kinetic parameters indicated that the decomposition process followed Langmuir kinetics; at low concentrations of HSO_5^- ($0.54—2.06\times10^{-3}$ mol dm^{-3}) the reaction obeyed a first-order kinetics and at higher concentrations, ($[HSO_5^-]>3.00\times10^{-3}$ mol dm^{-3}) the rate became independent of $[HSO_5^-]$. The effects of pH and the molar percentage of the dopant on the rates were also investigated. Small amount of doping by RuO_2 (2.5 molar percentage) was found to increase the photocatalytic decomposition of HSO_5^- whereas the higher amount of doping decreased the rate. Added 2-propanol to the system was found to increase the rate of decomposition of peroxomonosulfate. The proposed mechanism of the decomposition of PMS involves the reactions of the photogenerated valence band holes and the conduction band electrons of WO_3, by radiation of wavelength $\geqslant 410$ nm, in presence and absence of 2-propanol. The rate constants and quantum yields have also been evaluated. The photocatalytic decomposition of peroxomonosulfate is one of the few examples of a unimolecular reaction catalyzed by both the photogenerated holes (h^+_{vb}) and electrons (e^-_{cb}).

The photocatalytic and photosynthetic reactions involving homogeneous and heterogeneous catalyses have recently attracted much attention because of their possible applications in solar energy conversion processes.[1] Particular interest has been focussed on the generation of hydrogen from water using semiconductors[2] and radiations of wavelength matching the sunlight. Recent works involve the simplified conventional photoelectrochemical cell with the use of semiconductor dispersions to carry out photocatalytic[3] and photosynthetic[4] reactions. These dispersed particles consist of single semiconductor alone or metallized semiconductor.[5,6] It has also been shown that a combination of redox systems with metal catalysts is indispensable for the efficient transfer of photon-induced conduction band electrons and valence band holes for redox reactions as well as protection of semiconductors against photocorrosion.[7,8] Since the photons absorbed in a thin layer close to the semiconductor–electrolyte interface alone are responsible for the chemical process, a large surface area of the active catalyst is desirable. This is best provided by catalysts in the form of powders and colloids. Although the area of illuminated surfaces is almost independent of the total surface area, as the size of the particle is decreased the density of the catalyst in the form of powder or colloid in the area of illumination gets increased and hence the catalytic efficiency will also be increased. Krasnovskii and Brin[9] have investigated the photocatalytic oxygen evolution reaction using WO_3 as a photocatalyst and Fe^{3+} as the electron acceptors. Darwent and Mills[10] have investigated the effect of RuO_2-loaded on WO_3 on oxygen evolution from water using Fe^{3+} as an electron acceptor. Recently Gratzel and coworkers[11] have reported the reactions of WO_3-coated electrodes and Nozik et al. have explored the electron-transfer reactions with WO_3 colloids.[12]

In this article we report the photocatalytic decomposition reactions of an inorganic peroxide namely peroxomonosulfate, $HOOSO_3^-$ (PMS) in aqueous suspension of WO_3 powder with radiation of wavelength $\geqslant 410$ nm. During the decomposition of PMS by the e^-_{cb} and h^+_{vb} of WO_3, oxidation of water to oxygen was also observed. Hence PMS may be considered as a sacrificial agent for the production of oxygen from water. PMS itself is an oxidizing agent ($E^\circ=1.82$ V) similar to peroxodisulfate and undergoes radiolytic and photolytic reactions.[13,14] It does not undergo photochemical decomposition unless the wavelength used is $\leqslant 260$ nm. However, in presence of WO_3 powder, with and without RuO_2 loading, efficient decomposition of PMS is observed on illumination with light of $\lambda \geqslant 410$ nm. The effects of (i) pH, (ii) catalyst amount, (iii) percentage doping of RuO_2, and (iv) 2-propanol on the heterogeneous photocatalytic decomposition of PMS are discussed. The significance of this investigation is that the substrate chosen (PMS) itself is an oxidant, but capable of simultaneously scavenging the e^-_{cb} and h^+_{vb} formed by band-gap irradiation of WO_3. The reaction is also a typical example for visible light induced catalytic decomposition of PMS which otherwise happens by UV irradiation.

Experimental

WO_3 used was from Fluka (>99.99%). RuO_2 loading was done using the technique described by Gratzel and coworkers[15] by dissolving calculated amount of $RuCl_3\cdot H_2O$ in water and mixing thoroughly with WO_3. The slurry was dried and heated in a muffle furnace in argon atmosphere at 800—900 °C for 4 h. Diffuse reflection measurements were

taken using Beckman Quartz Spectrophotometer (Model-DU: Serial 92906) at room temperature in the wavelength region 350—700 nm. Scanning Electron Microscope pictures (Fig. 1) were taken with JEOL JSM-35 CF Model. The particle sizes varied from 1—10 μm. An interesting observation in SEM pictures is that the doping increases the crystallinity of WO_3 semiconductor powders.

The surface areas of the catalysts were determined by BET method and found to be 1.0 to 1.5 m^2g^{-1}. PMS was from E.I. du Pont de Nemours & Co., USA, in the form of triple salt ($2KHSO_5 \cdot KHSO_4 \cdot K_2SO_4$) and was used as such. Other chemicals used were of the purest research grade available. Photocatalytic reactions were carried out in a rectangular all quartz reactor. Prior to irradiation, WO_3 dispersions were freed from dissolved oxygen by purging with purified Argon. A high pressure Mercury lamp (250 watt, Applied Photophysics, London) in combination with suitable cut-off filters emitting the light of $\lambda \geqslant 410$ nm was used as the light source. The intensity of the incident radiation, I_0, determined by trisoxalatoferrate(III) actinometry[16] was 6.91×10^{-8} Eins s^{-1}. The emission spectrum of the mercury lamp shows that the emitted light above 410 nm has the maximum intensity (ca. 99%) only at λ=436 nm. The IR radiations were removed using a water jacket. The change in the concentration of PMS with time was estimated iodometrically as reported in literature.[13] Unless otherwise mentioned, all the reactions were carried out with 25 mg of the 2.5% RuO_2/WO_3 photocatalyst in 35 ml of the reaction mixture.

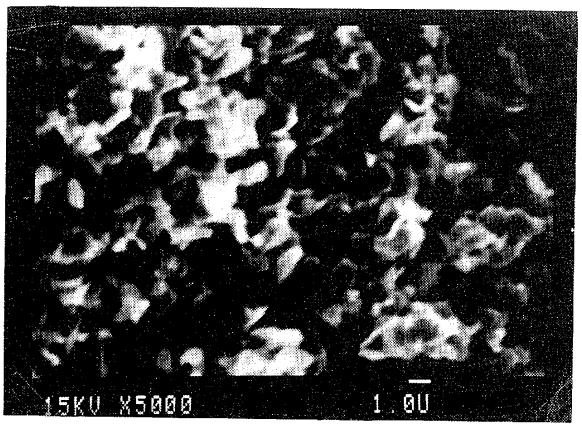

(A)

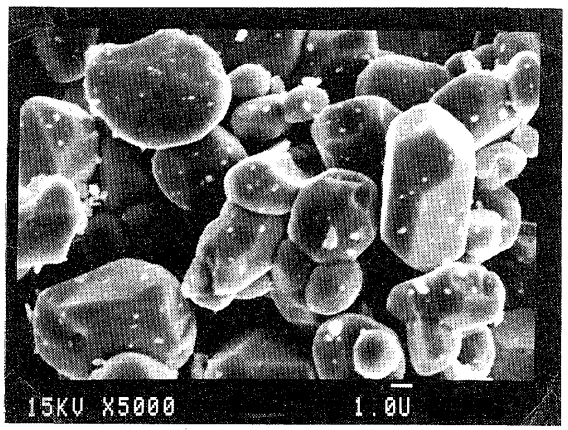

(B)

Fig. 1. SEM photographs of (A) unloaded WO_3 (sintered at 800—900 °C) and (B) 2.5% RuO_2/WO_3 (sintered at 800—900 °C).

Quantum yields (Φ) of the photocatalytic reactions were determined using the relation,

$$\Phi = \frac{\text{Rate of decomposition of PMS}}{[\,(I_0 \times \text{Absorbance of the catalyst at } \lambda = 436\,\text{nm})/100\,]} \qquad \text{(a)}$$

which has been derived from the basic definition,

$$\Phi = \frac{\text{Number of moles decomposed per unit time}}{\text{Number of Einsteins absorbed per unit time}}$$

In this study the number of moles decomposed per unit time is nothing but the rate of decomposition of PMS. From the diffuse reflection spectra it has been found that the catalyst powder absorbs only a fraction of the total incident radiation at λ=436 nm. Hence number of Einstein absorbed per unit time from the total incident radiation (I_0) has been calculated using the expression written in the denominator of the relation (a). Also the absorbances of undoped and 2.5% RuO_2 doped WO_3 are found to be 70% and 87% of the incident radiations respectively. Oxygen evolution was identified using TL's Digital Oxygen Analyser Model DP 2M.

Results and Discussion

About 90% of PMS was decomposed in about three hours of illumination of an aqueous slurry containing PMS ($0.54—2.06 \times 10^{-3}$ mol dm^{-3}) and RuO_2/WO_3 (25 mg). No dissolution of WO_3 was observed even after six hours of continuous irradiation. Blank experiments were also conducted under the similar conditions without the photocatalyst and there was no decomposition of PMS observed even after four hours of prolonged irradiation.

Effect of Initial Concentrations of PMS. At low concentrations of PMS, the initial rate (r_0) of decomposition of PMS, $-d[PMS]/dt$ was found to increase with increase in the initial concentrations but at higher concentrations, the rate became independent of $[PMS]_0$. The plots of r_0 vs. $[PMS]_0$ exhibited a curvature, characteristic of saturable surface and the rates are described by a simple Langmuir form,

$$r_0 = \frac{kK[PMS]_0}{1 + K[PMS]_0} \qquad (1)$$

where k is the proportionality constant and K is the equilibrium constant. The first order rate constant k_1 can be calculated from k using the relation, $k_1 = k/[PMS]_0$. These observations are conveniently demonstrated by the linearity of the plot of $1/r_0$ vs. $1/[PMS]_0$ (Fig. 2) as given by the relation,

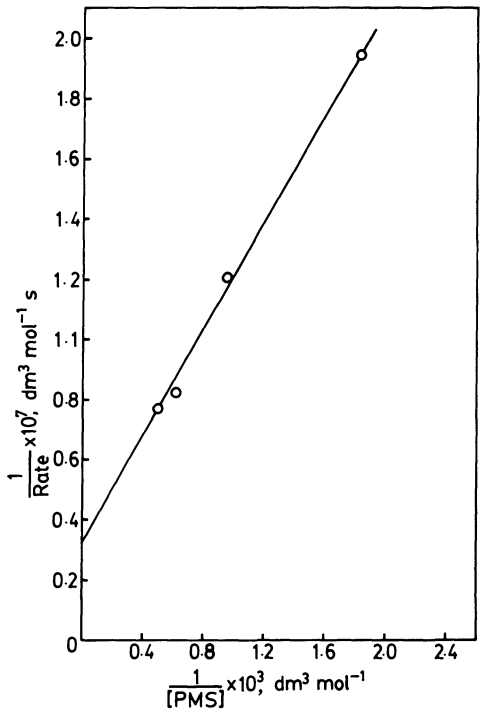

Fig. 2. Evaluation of k and K.

$$\frac{1}{\text{rate}_0} = \frac{1}{kK[\text{PMS}]_0} + \frac{1}{K} \quad . \tag{2}$$

From the slope and intercept of the above plot, the values of k and K were evaluated as 3.19×10^{-7} mol dm^{-3} s^{-1} and 3.52×10^2 dm^3 mol^{-1} respectively. At lower concentrations of PMS, Eq. 1 is reduced to

$$\text{rate}_0 = kK[\text{PMS}]_0 \tag{3}$$

and the overall reaction obeyed a first-order kinetics (assuming the surface to be truly Langmurian).

Effect of pH. The photocatalytic decomposition of PMS over RuO_2-doped WO_3 powders at different pH (1.0—5.0), at constant $[PMS]_0$ (1.00×10^{-3} mol dm^{-3}) as well as catalyst amount (25 mg) exhibited a maximum rate at pH=3.0 (Fig. 3) with a sharp decrease above and below this pH. Since the pK_a values of PMS ($pK_1<0$ and $pK_2=9.4$)[17] are not within the pH of the reaction slurry, the rate profile with pH may be due to the energetics of the conduction band and valence band edges with respect to the redox potential of PMS ($E^\circ=1.82$ V).[18] Photocatalysis implies an excess charge carrier transfer between the catalyst and reactant across the interface. The efficiency of the catalytic process is determined by the contribution of this transfer to the total excess charge carrier decay. This charge transfer between WO_3 and PMS is probably much favored at pH=3 as evidenced by the kinetic data.

Effect of Catalyst Amount. The photocatalytic effect of RuO_2/WO_3 powders is proved by its successful cleavage of PMS. The reactivity of the catalyst is maintained even after its successive participation in the photodecomposition reaction of PMS. The nonphotocorrosive nature of this catalyst is seen by the absence of tungsten ions in the reaction solution even after six hours of prolonged irradiation. Increase in the amount of catalyst is found to increase the rate of decomposition of PMS at constant $[PMS]_0$ (1.00×10^{-3} mol dm^{-3}). The calculated rates for different catalyst amounts at constant $[PMS]_0$ are given in Table 1.

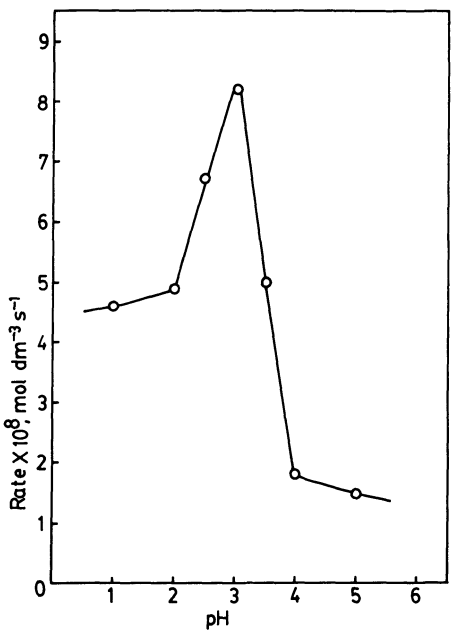

Fig. 3. Effect of pH.

Table 1. Effect of Catalyst Amount

Catalyst amount/mg	Rate$\times10^7$/mol dm^{-3} s^{-1}
15	0.44
25	0.82
35	1.20
45	1.29

Effect of RuO_2 Loading. Doping at different molar percentages (1.0%—12.5%) of RuO_2 shows that upto 2.5% loading of RuO_2 on WO_3 increases PMS decomposition beyond which there is a decrease. Although RuO_2 is a well-known catalyst for oxygen evolution[19] it has been widely employed as a good catalyst for hydrogen evolution.[20] Sakata and coworkers[19] have examined the catalytic properties of RuO_2 on n-type semiconductors under illumination for both oxygen and hydrogen evolution from water. In the present investigation, the rates of decomposition of PMS for 1.0 and 2.5% RuO_2/WO_3 photocatalysts are more than that for undoped WO_3 and the rates decrease beyond this percentage (Table 2). This might be due to the nature of deposition of RuO_2 on WO_3 surface. RuO_2 is deposited very finely (Fig. 1B)

Table 2. Effect of RuO_2-Loading

Molar percentage of RuO_2 loading	Rate$\times 10^8$/mol dm^{-3} s^{-1}
Undoped WO_3	3.00
1.0	5.95
2.5	8.23
5.0	3.26
7.5	2.50
10.0	1.82
12.5	1.56

on the WO_3 surface. With increasing amount of RuO_2, the density of deposition is increased. For this kind of deposition, RuO_2 particles on WO_3 surface would be expected to function as recombination centers since the distance between the particles becomes shorter than the distance at which the image force to both electron and hole is effective. The other reason would be that the photoejected electrons are also consumed for the reduction of RuO_2 prior to PMS reduction.

Reaction Pathway. It has been shown by Krasnovskii[9] that the aqueous dispersions of WO_3 illuminated by visible light produce oxygen as a result of the reaction of the valence band holes (h^+_{vb}) with water,

$$4h^+_{vb} + 2H_2O \longrightarrow O_2 + 4H^+. \quad (4)$$

It is also proved by Gratzel and co-workers[11a] that valence band hole of WO_3 is capable of oxidizing SO_4^{2-} to $SO_4^{\cdot-}$. Hence it is probable that PMS is also attacked by h^+_{vb} eventhough PMS is a powerful oxidizing agent ($E°$=1.82 V).[18] Moreover, it is well established that electrons (e^-_{aq}) react with PMS almost at a diffusion controlled rate.[14a] Hence, it is not surprising that both h^+_{vb} and e^-_{cb} react with PMS. This type of reactivity of PMS, as an electrophile as well as nucleophile, has already been observed by us[21] in visible light induced photochemical reactions of PMS with excited state $[Ru(bpy)_3]^{2+}$. While the conduction band electrons generate $SO_4^{\cdot-}$ and/or ·OH, the valence band holes are capable of removing the hydrogen atom from $HOOSO_3^-$ forming $SO_5^{\cdot-}$. These radicals and radical ions should favor the evolution of oxygen appreciably than the water oxidation by h^+_{vb} alone. Considering these reactions, we propose the following mechanism (Fig. 4):

$$WO_3 \xrightarrow[\lambda \geqslant 410\,nm]{h\nu} h^+_{vb} + e^-_{cb} \quad (5)$$

$$[HSO_5^-] + WO_3 \longrightarrow [HSO_5^-]_{ad.}\,WO_3 \quad (6)$$

$$[HSO_5^-]_{ad.} + e^-_{cb} \longrightarrow \begin{cases} SO_4^{\cdot-} + OH^- & (7a) \\ SO_4^{2-} + \dot{O}H & (7b) \end{cases}$$

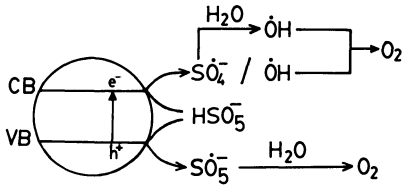

Fig. 4. Schematic representation of PMS decomposition by WO_3 particle.

$$HSO_5^- + SO_4^{\cdot-} \longrightarrow SO_5^{\cdot-} + HSO_4^- \quad (8)$$

$$SO_4^{\cdot-} + H_2O \longrightarrow SO_4^{2-} + H^+ + \dot{O}H \quad (9)$$

$$HSO_5^- + \dot{O}H \longrightarrow SO_5^{\cdot-} + H_2O \quad (10)$$

$$2\dot{O}H \longrightarrow 1/2O_2 + H_2O \quad (11)$$

$$[HSO_5^-]_{ad.} + h^+_{vb} \longrightarrow SO_5^{\cdot-} + H^+ \quad (12)$$

$$2SO_5^{\cdot-} \xrightarrow{H_2O} 2HSO_4^- + O_2 \quad (13)$$

The reaction of the electron with PMS occurs in two ways, Reactions 7a and 7b. The formation of $SO_5^{\cdot-}$, $SO_4^{\cdot-}$, and ·OH as radical products from PMS were identified by optical pulse radiolysis[14a] and in-situ-photolysis ESR investigation using spin-trapping agents[22] such as fumaric and maleic acids.

The overall reaction for the decomposition of PMS by illuminated WO_3 could be written as

$$HSO_5^- \xrightarrow[\lambda \geqslant 410\,nm]{WO_3,\ h\nu} 1/2\,O_2 + SO_4^{2-} + H^+.$$

The quantum yields (Φ) determined, as explained previously, for the undoped and 2.5% RuO_2 doped WO_3 were 0.62 and 1.36 respectively. Since both the photogenerated e^-_{cb} and h^+_{vb} are capable of decomposing PMS, the expected quantum yield is 2. The low value observed in our experiments might be due to (i) all the photons hitting the surface of the reaction vessel are not absorbed by the semiconductor slurry (ii) electron–hole recombination and (iii) recombination of $SO_4^{\cdot-}$ and ·OH to form PMS.

Effect of 2-Propanol. Addition of 2-propanol is found to increase the rate of decomposition of PMS. The reaction was investigated by photolysing aqueous slurry containing various concentrations of 2-propanol (0.25—1.00 mol dm^{-3}) with a constant $[PMS]_0$ (1.00×10^{-3} mol dm^{-3}) and catalyst amount (25 mg). The rate of decomposition of PMS increased with increase in [2-PrOH]. The enhanced decomposition of PMS in the presence of 2-propanol is due to the additional Reactions 14 and 15 along with Reactions 8—13.

$$(CH_3)_2CHOH + h^+_{vb}, SO_4^{\dot{-}}, \dot{O}H \longrightarrow (CH_3)_2\dot{C}OH \quad (14)$$

$$(CH_3)_2\dot{C}OH + HSO_5^- \longrightarrow (CH_3)_2C{=}O + SO_4^{\dot{-}} + H_2O \quad (15)$$

In the presence of 2-propanol (0.50 mol dm^{-3}) the Φ values are 2.21 and 2.71 for undoped and 2.5% RuO_2 doped WO_3 respectively. The comparatively high Φ values observed here could be due to the reaction of $SO_4^{\dot{-}}$ and $\dot{O}H$ with 2-propanol instead of recombination and also due to the reduction of PMS by the alcohol radical formed (Eqs. 14 and 15).

It may be concluded that peroxomonosulfate which is photochemically active at $\lambda \leqslant 260$ nm is found to be decomposed in the presence of WO_3, doped and undoped with RuO_2, by visible radiation. The presence of 2-propanol further enhanced the decomposition of PMS.

The authors are indebted to Dr. K. I. Vasu, Director and his fellow Scientists, of Central Electrochemical Research Institute, Karaikudi, India for their assistance in taking diffuse reflection spectra and SEM photographs. One of the authors (M. Ashokkumar) acknowledges the financial support (as fellowship) from the University Grants Commission, New Delhi, India.

References

1) "Energy Resources through Photochemistry and Photocatalysis", ed by M. Gratzel, Academic Press, New York (1983).

2) a) M.Gratzel, *Acc. Chem. Res.*, **14**, 376 (1981); b) A. J. Bard, *J. Phys. Chem.*, **86**, 2 (1982).

3) A. J. Bard, *J. Photochem.*, **10**, 59 (1979).

4) W. W. Dunn, Y. Aikawa, and A. J. Bard, *J. Am. Chem. Soc.*, **103**, 6893 (1981).

5) T. Watanabe, T. Takizawa, and K. Honda, *J. Phys. Chem.*, **81**, 1845 (1977).

6) M. B. St. John, A. J. Furgala, and A. F. Sammuells, *J. Phys. Chem.*, **87**, 801 (1983).

7) H. Metlee, J. W. Otovs, and M. Calvin, *Solar Energy Mat.*, **4**, 443 (1981).

8) T. Kawai and T. Sakata, *J. Chem. Soc., Chem. Commun.*, **1980**, 694.

9) a) A. A. Krasnovskii and G. P. Brin, *Dokl. Akad. Nauk, SSSR*, **147**, 656 (1962); b) *idem, Dokl. Akad. Nauk, SSSR*, **168**, 1100 (1966).

10) J. R. Darwent and A. Mills, *J. Chem. Soc., Faraday Trans. 2*, **78**, 359 (1982).

11) a) J. Desilvestro and M. Gratzel, *J. Chem. Soc., Chem. Commun.*, **1982**, 107; b) W. Erbs, J. Desilvestro, E. Borgarello, and M. Gratzel, *J. Phys. Chem.*, **88**, 4001 (1984).

12) M. T. Nenadovic, T. Rajh, O. I. Mićić, and A. J. Nozik, *J. Phys. Chem.*, **88**, 5827 (1984).

13) R. Renganathan, Ph. D. Thesis, Madras University (1984).

14) a) P. Maruthamuthu and P. Neta, *J. Phys. Chem.*, **81**, 937 (1977); b) P. Maruthamuthu and P. Kanakaraj, *Int. J. Chem. Kinet.*, **15**, 1301 (1983).

15) N. M. Li, S. Dimitriferic, and M. Gratzel, *J. Am. Chem. Soc.*, **106**, 6565 (1984).

16) J. M. Fitzgerald, "Analytical Photochemistry and Photochemical Analysis," Marcel Dekker, New York (1971), p.92.

17) D. L. Ball and J. O. Edwards, *J. Am. Chem. Soc.*, **78**, 1125 (1956).

18) M. Spiro, *Electrochim. Acta*, **24**, 313 (1979).

19) T. Sakata, K. Hashimoto, and T. Kawai, *J. Phys. Chem.*, **88**, 5214 (1984).

20) E. Amouyel, P. Keller, and A. Moradpur, *J. Chem. Soc., Chem. Commun.*, **1980**, 1019.

21) P. Maruthamuthu, L. Venkatasubramanian, and P. Dharmalingam (Communicated).

22) P. Maruthamuthu and H. Taniguchi (unpublished results).

 © 1988 The Chemical Society of Japan Bull. Chem. Soc. Jpn., 61, 4143—4146 (1988)

Studies on Metal Chelates of 8-Hydroxy-5-quinolyl Ketone Oxime, *O*-Carbamoyl and *O*-Thiocarbamoyl Derivatives as Bactericides

Z. H. KHALIL, A. A. ABDEL-HAFEZ, A. S. YANNI,* and A. M. MOHARAM
Chemistry and Botany Departments, Faculty of Science, Assiut University, Egypt
(Received February 29, 1988)

The reaction of 5-acetyl-8-quinolinol (**1**) and corresponding chalcone derivatives **2a—f** with hydroxylamine hydrochloride in boiling pyridine gave the corresponding oximes **3** and **4a—f** respectively in almost quantitative yields. Further interaction of **3** and **4a—e** with phenyl isocyanate and/or thiocyanate the corresponding carbamate and/or thiocarbamate (**5a,b**) and (**6a—e**, **7a—e**) were achieved. Metal chelates of **1**, **3**, and **4e,f** with bivalent metal cations like Fe(II), Cu(II), and Zn(II) have been synthesized and characterized by elemental and IR-spectral analysis. The synthesized compounds were biologically screened to study the structure activity relationship, (SAR) and the effect of complexation and type of metal cation on the potency of the more biologically active compounds.

The biological activity of oximes, carbamates, and thiocarbamates is of interest. Acetophenone *O*-methylcarbamoyl oxime and esters of dithiocarbamic acids, have clearly been established as insecticides,[1] leading anthelmintic[2-4] and herbicidal[5] agents. It has been observed recently that some drugs have increased activity when administered as metal complexes more so their metal chelates.[6,7]

In this work SAR has been done to evaluate the bactericidal activity of the oxime, carbamate, thiocarbamate derived from 5-acetyl-8-quinolinol and/or its chalcone derivatives. Effect of complexation and type of metal cation on the potency of the more effective compounds was considered.

Results and Discussion

Interaction of **1** and the chalones **2a—f** with hydroxylamine hydrochloride gave the corresponding oximes **3** and **4a—f** respectively.

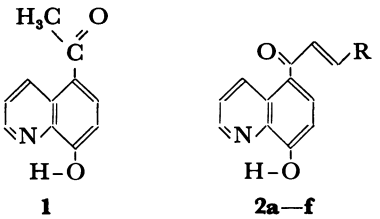

1

2a—f

a, R = C_6H_5
b, R = *p*-$CH_3OC_6H_4$
c, R = *p*-ClC_6H_4
d, R =
e, R = *n*-C_3H_7
f, R = *n*-C_6H_{13}

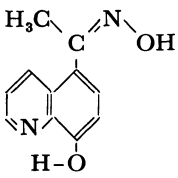

3

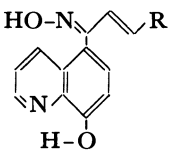

4a—f

The IR spectra of compound **3** and **4a—f** showed a broad band at 3200—2800 cm^{-1} characteristic to the oxime hydroxyl group in addition to ν C=N at 1600 cm^{-1} with the lack of ν C=O group. The NMR (DMSO) of compound **3** revealed signals at δ 2.3 (s, 1H, OH), 2.8—3.2 (s, 3H, CH_3), and 6.75—7.4 (m, 5H, aromatic), the proton of Q-OH was appeared at δ 7.2 confusing with the aromatic protons.

Phenyl isocyanate and phenyl isothiocyanate react readily with the oximes **3** and **4a—e** in boiling dry benzene in presence of triethylamine to afford the corresponding carbamates and thiocarbamates **5a,b**; **6a—e** and **7a—e** in good yields.

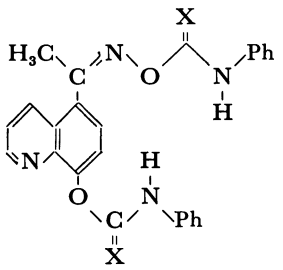

5a, X=O
b, X=S

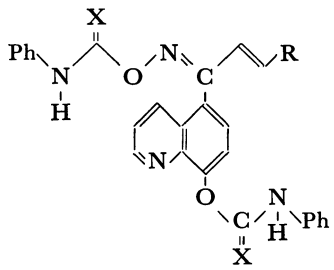

6a—e, X=O
7a—e, X=S

The structure of the carbamates **6a—e** and thiocarbamates **7a—e** was assigned on both analytical and spectral data. The IR spectra of carbamates showed the lack of (ν OH) and presence of (ν NH) as a single band in the 3200 cm^{-1} region and (ν C=O) in the region 1700 cm^{-1}. The NMR (DMSO) spectra of **5b** showed signals at δ 3.25 (s, 3H, CH_3), 7.5—8.5 (m, 10H, aromatics), and 8.7 (s, 1H, NH); **6b** δ 2.8 (s, 3H, CH_3), 6.5—7.0 (m, 15H, aromatics), and 8.2 (s, 1H, NH).

Interaction of compounds **1**, **3**, **4e,f** with the appropriate amounts of metal salt solution gave the corresponding complex. The IR spectra showed a broad distinct band at 3200—3100 cm^{-1} in the ligands were found due to hydrogen bonding.[8,9] On this basis the intramolecular hydrogen bonded chelate structures (-O-H-N-) have been proposed for the ligands. A critical examination of the spectra of metal chelates indicates that the bands at 3100 cm^{-1} present in the ligands is shifted to higher values (3600—3300 cm^{-1}) in the chelates. Thus on metal chelate formation, the bands between 3600—3300 cm^{-1} which appear in all chelates are not present in the original ligands.[10,11] The disappearance of hydrogen-bonded -OH in the

ligands and its reappearance in the metal chelates are suggestive of O–M–N bond formation, where M is a metal atom. The bands of medium intensity around 1600 cm^{-1} in the spectra of ligands due to (ν C=N–) is shifted to lower values with weak intensity in the spectra of chelates. It is due to M←N bond formation. The bands between 1600—1490 cm^{-1} are due to aromatic rings. The overall study and the analytical data show that the ligands form chelates of the type ML_2 where L=ligand. The reaction may be written as follows:

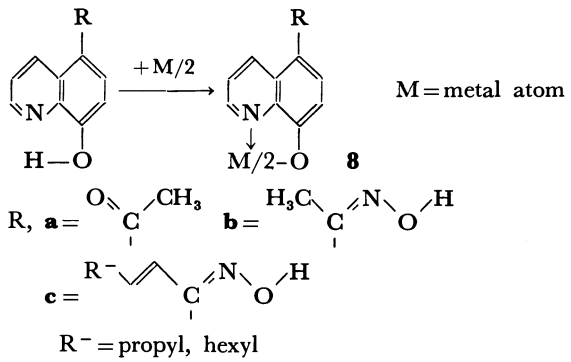

The structure of the metal chelate is in good agreement with previous work.[12,13]

Screening for Antimicrobial Activity: The bacteriostatic properties of the oxime, carbamates, and metal chelate complexes were studied by the usual cupplate agar diffusion technique[12] against some selected Gram positive: *Bacillus cereus, Staphylococcus aureus,* and *Micrococcus luteus*; and Gram negative bacteria: *Serratia* sp., *E. coli,* and *Pseudomonas aeruginosa.*

A final concentration of 100 ppm of the tested compounds in ethylene glycol was used.

5-[1-(Hydroxyimino)ethyl]-8-quinolinol (**3**) is effective only against the tested Gram positive bacteria. Substituting the methyl group by a styryl Ph–CH=CH (**4a**) abolishes its potency, while further substitution by an electron releasing or activating group at the phenyl neucleus (**4b,c**) restore this activity towards *Bacillus cereus* and *Staph. aureus.* The same observation was noticed also on using furfurylidene instead of benzylidene Ph–CH= derivative (**4d**). On the other hand, substitution by a 1-pentenyl or 1-octenyl group (**4e** and **f**) enhances similarly the bactericidal activity and is also extends towards other tested *Gram negative* bacteria.

Converting the oxime **3** to its carbamate **5a** or thiocarbamate derivative **5b** removes its activity while the carbamate or thiocarbamate **6** or **7** have no effect on *micrococcus luteus,* and their activity either abolishes or have no changes on the other *Gram positive* bacterial species. It is worthy to mention that the thiocarbamate is less effective than the carbamate derivative (cf. **6e**, **7e**).

Metal chelation of the more effective bactericidal compounds **3**, **4e,f** with bivalent metal cations e.g. Cu^{2+}, Zn^{2+}, Fe^{2+} has different effect depending on the type of substituent at the 5-position within 8-quinolinol nucleus and the type of metal cation. Complexing with zinc increases largely its potency towards both *Gram positive* and *Gram negative* bacteria and is not significantly affected by the type of substitution at the 5-position of 8-quinolinol while complexing with Cu has different effect depending on the type of 5-substituent. The larger effect was noticed on increasing the alkyl side chain length within the 5-substituent relative to unsubstituted 5-acetyloxime, cf. $[\mathbf{3}]_2Cu$, $[\mathbf{4e}]_2Cu$, and $[\mathbf{4f}]_2Cu$; and 5-[1-(hydroxyimino)ethyl] complex $[\mathbf{3}]_2Cu$ is less effective than its precursor 5-acetyl $[\mathbf{1}]_2Cu$. On the other hand complexing with Fe^{3+} has different effect. It decreases sharply or abolishes the potency after complexation especially on enlarging alkyl side chain with the 5-substituent, (cf. $[\mathbf{4e}]_2Fe$, $[\mathbf{4f}]_2Fe$).

Conclusion

5-Acetyl-8-quinolinol is more effective as bactericides than its oxime, while the chalcone oxime derivatives **4a—f** have variable effect depending on the type of the substituent R. Conversion of the oxime to carbamate or thiocarbamate decreases or abolishes this activity and the carbamates are more effective than corresponding thiocarbamates.

On complexation of the ligands it increases and extends the activity towards *Gram negative* bacteria depending on the type of metal cation used. The more effective complexes are those containing Zn metal independing on the 5-substituent which is not the case of Cu.

Experimental

All the melting points are uncorrected. IR spectra were recorded on a Perkin-Elemer infrared 137B spectrophotometer. NMR spectra in DMSO were measured on a Varian, 90 MHz. The time allowed for the completion of the reaction and the purity of the prepared compounds were monitored by TLC.

Reaction of 5-Acetyl-8-quinolinol (1) and Its Chalcone Derivatives 2a—f with Hydroxylamine Hydrochloride: A solution of 5-acetyl-8-quinolinol (**1**) and/or corresponding chalcones **2a—f** (0.01 mol) and hydroxylamine hydrochloride (0.015 mol) in dry pyridine[14] (20 ml) was heated under reflux for 3 h. The reaction mixture was poured onto crushed ice and the precipitated solid was filtered off and crystallized from the suitable solvent to give the corresponding oximes **3** and **4a—f** respectively. The results are given in Table 1.

Reaction of Oximes 3 and 4a—f with Phenyl Isocyanate and Phenyl Isothiocyanate: A solution of the oximes **3**, **4a—e** (0.01 mol), phenyl isocyanate or phenyl isothiocyanate (0.01 mol) in dry benzene 25 ml containing triethylamine (0.5 ml) was heated under reflux for 4 h. The

Table 1a. Physical and Analytical Data of Oximes **3**, **4a—p**, *O*-Phenylcarbamoyl Oximes **5a**, **6a—e**, and *O*-Phenylthiocarbamoyl Oximes **5b**, **7a—e**

Compd	Yield	Mp θ_m/°C	Molecular formula	Analysis (%)[a] Found			Calcd		
				N	Cl	S	N	Cl	S
3	96	193	$C_{11}H_{10}O_2N_2$	14.05			13.86		
4a	75	240	$C_{18}H_{14}O_2N_2$	9.99			9.65		
b	85	330	$C_{19}H_{16}O_3N_2$	8.90			8.75		
c	70	310	$C_{18}H_{13}O_2N_2Cl$	8.88	10.69		8.63	10.94	
d	72	340(decomp)	$C_{16}H_{12}O_3N_2$	10.29			10.00		
e	65	310—312	$C_{15}H_{16}O_2N_2$	11.20			10.94		
f	60	327—329	$C_{18}H_{22}O_2N_2$	9.72			9.40		
5a	75	225	$C_{25}H_{20}O_4N_4$	12.95			12.73		
b	71	235	$C_{25}H_{20}O_2N_4S_2$	12.00		13.35	11.86		13.56
6a	65	328—330	$C_{32}H_{24}O_4N_4$	10.88			10.61		
b	68	260—262	$C_{33}H_{26}O_5N_4$	10.30			10.03		
c	53	235—237	$C_{32}H_{23}O_4N_4Cl$	10.12	6.52		9.95	6.31	
d	60	288—290	$C_{30}H_{22}O_5N_4$	11.08			10.81		
e	46	250(decomp)	$C_{29}H_{26}O_4N_4$	11.65			11.34		
7a	62	293—295	$C_{32}H_{24}O_2N_4S_2$	10.18	11.68		10.00		11.43
b	64	>340	$C_{33}H_{26}O_3N_4S_2$	9.62	11.03		9.49		10.85
c	49	>340	$C_{32}H_{23}O_2N_4S_2Cl$	9.60	10.98		9.42		10.76
d	56	248—250	$C_{30}H_{22}O_3S_2$	10.50	11.83		10.18		11.64
e	43	340	$C_{32}N_{32}O_2N_4$	9.97	11.49		9.86		11.27

a) All C, H analysis gave satisfactory results.

Table 1b. Physical and Analytical Data of Metal Chelate Complexes of **1**, **3**, **4e**, and **6f**

Compd	Mp θ_m/°C	Molecular formula	Analysis (%)[a] Found/Calcd N	Metal	UV spectra[b] λ_{max}/nm
$\mathbf{1}_2Cu$	335—337 (decomp)	$[C_{11}H_8O_2N]_2Cu$	6.55 6.43	14.76 14.59	255, 283, 378
$\mathbf{1}_2Zn$	350	$[C_{11}H_8O_2N]_2Zn$	6.63 6.40	15.19 14.95	258, 288, 385
$\mathbf{1}_2Fe$	350	$[C_{11}H_8O_2N]_2Fe$	6.82 6.50	13.29 13.05	247, 278, 368, 430(sh)
$\mathbf{3}_2Cu$	350	$[C_{11}H_9O_2N_2]_2Cu$	12.28 12.03	13.90 13.65	250(sh), 310(sh), 358
$\mathbf{3}_2Zn$	296—298	$[C_{11}H_9O_2N_2]_2Zn$	12.10 11.98	14.15 13.99	260, 338, 383
$\mathbf{3}_2Fe$	>350	$[C_{11}H_9O_2N_2]_2Fe$	12.50 12.23	12.45 12.20	250, 290(sh), 350
$\mathbf{4e}_2Cu$	>350	$[C_{15}H_{15}O_2N_2]_2Cu$	9.99 9.76	11.25 11.08	240, 280(sh), 370(sh)
$\mathbf{4e}_2Zn$	>350	$[C_{15}H_{15}O_2N_2]_2Zn$	9.90 9.73	11.53 11.36	260, 284(sh), 350
$\mathbf{4e}_2Fe$	>350	$[C_{15}H_{15}O_2N_2]_2Fe$	10.05 9.89	10.10 9.87	
$\mathbf{6f}_2Cu$	>350	$[C_{18}H_{21}O_2N_2]_2Cu$	8.88 8.51	9.95 9.66	258 285, 330, 390
$\mathbf{4f}_2Zn$	>350	$[C_{18}H_{21}O_2N_2]_2Zn$	8.70 8.49	10.15 9.91	255, 283, 355, 400(sh)
$\mathbf{4f}_2Fe$	>350	$[C_{18}H_{21}O_2N_2]_2Fe$	8.85 8.62	8.80 8.59	

a) All C, H analysis gave satisfactory results. b) Saturated solution in methanol (1:5 dilution).

separated crystalline solid was filtered off, washed with ether and recrystallized from dioxane to give the corresponding carbamate or thiocarbamate derivatives **5a,b**; **6a—e** and **7a—e** respectively. The results are given in Table 1a.

Chelation of 1 and Oximes 3, 4e,f with Bivalent Metal Cation, e.g. Fe(II), Cu(II), and Zn(II): The complexes were prepared by dissolving the ligands **1**, **3**, and **4e,f** in warm aqueous ethanol and treated with an appropriate amount of

Table 2. Bactericidal Screening of Compounds **3**—**7** and Some of Their Complexes

Compd No.	Gram positive (inhibition zones in mm)			Gram negative (inhibition zones in mm)		
	Becillus cereus	*Staphylococcus aureus*	*Micrococcus luteus*	*Serratia* sp.	*E. coli*	*Pseudom. aeruginose*
3	10	10	10	—	—	—
4a	—	—	—	—	—	—
b	10	10	—	—	—	—
c	12	11	—	—	—	—
d	10	12	—	—	—	—
e	18	16	10	10	9	8
f	18	16	10	10	8	9
5a	—	—	—	—	—	—
b	—	—	—	—	—	—
6a	—	—	—	—	—	—
b	—	—	—	—	—	—
c	10	10	—	—	—	—
d	—	—	—	—	—	—
e	10	10	—	—	—	—
f	10	10	—	—	—	—
7a	—	—	—	—	—	—
b	—	—	—	—	—	—
c	10	10	—	—	—	—
d	10	12	—	—	—	—
e	—	—	—	—	—	—
f	—	—	—	—	—	—
[**1**]$_2$Cu	15	18	16	7	6	7
[**1**]$_2$Zn	25	25	18	20	25	10
[**1**]$_2$Fe	12	14	12	13	8	12
[**3**]$_2$Cu	7	—	—	—	—	—
[**3**]$_2$Zn	20	22	18	20	15	10
[**3**]$_2$Fe	10	8	—	8	—	—
[**4e**]$_2$Cu	12	15	14	10	8	7
[**4e**]$_2$Zn	22	22	20	20	22	10
[**4e**]$_2$Fe	8	10	—	10	—	—
[**4f**]$_2$Cu	37	38	22	10	11	—
[**4f**]$_2$Zn	22	22	18	15	20	10
[**4f**]$_2$Fe	8	7	—	7	—	—

metal salt solution in aqueous ethanol. The mixture was heated under reflux on a water bath for 1 h. The resulting precipitates of the complexes were filtered off, washed well with hot water and dried. The physical and analytical data are recorded in Table 1b.

References

1) T. R. Fukuto, R. L. Metkalf, R. L. Jones, and R. O. Meyers, *J. Agric. Food Chem.*, **17**, 923 (1969).

2) R. C. Twirt, R. D. Muir, and S. Mizuba, *J. Med. Chem.*, **12**, 349 (1969).

3) A. G. Farbwerks Hoechst, Fr. Demande, 2015026, 1970; Ger. Appl., 03, Agu., 1968; *Chem. Abstr.*, 5534 K (1971).

4) A. Roger Mathfs (to B .F. Goodrich Co.), U.S. Patent 2608575 (1952); *Chem. Abstr.*, 479352 F (1953).

5) T. B. Balph (to Universal Oil Products Co.), U.S. Patent 2710872 (1955); *Chem. Abstr.*, 505735 (1956).

6) D. R. Williams, *Chem. Rev.*, **72**, 203 (1972).

7) A. Furst and R. T. Haro, *Progr. Exp. Tumor Res.*, **12**, 102 (1969).

8) J. B. Hendrickson, D. J. Cram, and G. S. Hammond, "Organic Chemistry," McGraw Hill Kogakuaba Ltd., Tokyo, 3rd ed. (1970), p. 260.

9) C. N. R. Rao, "Chemical Application of Infrared Spectroscopy," Academic Press, Inc., New York (1968), p. 184.

10) L. J. Bellamy, "The IR Spectra of Complex Molecules," Methuen (1964), p. 105.

11) K. Ueno and A. E. Marthell, *J. Phys. Chem.*, **60**, 1270 (1956).

12) British Pharmacopacia, Pharmaceutical Press, London, 796 (1953).

13) G. V. Villeual'd, N. N. Anshets, and J. A. Osdchil, USSR, 579, 271 (OlC 070 215/24), 05 No (1977), Appl. 2, 362, 762, 19 May (1976).

14) N. Latif, N. Mishriky, and N. S. Girgis, *Ind. J. Chem.*, **15B**, 118 (1977).

Terpenoids. XI.[1] Mayurone Oxide

Shizuo NAGAHAMA,* Takafumi FUCHINOUE, and Masato TAZAKI
The Kumamoto Institute of Technology, Ikeda 4-22-1, Kumamoto 860
(Received April 30, 1988)

Synopsis. Epoxidation of mayurone **7** gave mayurone oxide **21** in good yield. Grignard methylation of **21** gave epoxy alcohols, **17** and **22**. Thujopsadiene monoepoxide **23** was synthesized from **21** by Wittig reaction. Oxide **21** and **23** were found in the autoxidation product of **1**. Oxide **21** was found in the autoxidation product of **2**, **3**, and **6**.

Oxidation of thujopsene **1** under various conditions[1-3] generally gave a complicated mixture including mayurone **7**.[4] Our current concern is the full characterization of the complicated mixture in order to determine the reaction mechanism and to control the reaction specific to a chiral thujopsane derivative bearing versatile functionalities. During the time consuming separation and isolation of the minor products from permanganate oxidation of **1**, some epoxy ring containing products are indicated as well as **5**[3] and **17**[1] isolated earlier.

Direct epoxidation of **1** failed under various conditions,[5] but an epoxidation of mayurone **7** gave a new oxide **21** in high yield. The compound **21** was a useful intermediate to synthesize some standard samples of epoxy-ring-containing thujopsanes for the characterization of minor products in the oxidation products of **1**.

Results and Discussion

Mayurone **7** gave only an epoxide in high yield upon treatment with alkaline hydrogen peroxide in aqueous methanol. The epoxidation is highly diastereoselective, i.e., no epimeric epoxide was found in the products by GLC and ^{1}H NMR analyses. The ^{1}H NMR of the epoxide showed two vicinal protons on an epoxy ring, one of which showed a long-range coupling constant of 1.6 Hz. The configuration of the epoxy ring was further established as the structure **21** by correlation to a known epoxide **17**[1] as described below. A Grignard methylation of **21** at low temperature occurred at the carbonyl group, giving a mixture of two epoxy alcohols. They were separated by silica-gel chromatography to about an 8:1 product ratio. Since the minor product was identical with **17**,[1] α-configuration of the epoxy ring in **21** was established. The major epoxy alcohol mp 80 °C was assigned as structure **22**. Interestingly, the stereoselectivity in the methylation is reversed on going from mayurone[3] **7** to its epoxide **21**, due to a subtle difference in steric hindrance around the carbonyl groups.

Reaction of **21** with triphenylphosphonium methylide gave a new thujopsane derivative **23**, assigned by IR and ^{1}H NMR spectra.

Since our major interest was the full characterization of the complicated mixture from **1** by permanganate oxidation in anhydrous acetone,[3] reanalysis by GLC of the mixture was attempted briefly. The result suggested the presence of the new compounds **21** and **23**, but their direct formation by permanganate oxidation is unlikely. Rather they were considered to have arisen from secondary autoxidation of the major components in the product, i.e., **1** (unreacted), **2**, **3**, and **6**,[3] during the time consuming separations. Therefore the autoxidation was examined on these components separately. Mayurone oxide **21** and thujopsadiene 8α,9-epoxide **23** were found in the products of the autoxidation of **1**. Mayurone oxide **21** was also found in the autoxidation products of thujopsadiene **6** and 9-thujopsen-8-ols **2** and **3** besides **7**. These results show that the complex mixture from permanganate oxidation of **1** is partly due to the autoxidation of the primary products.

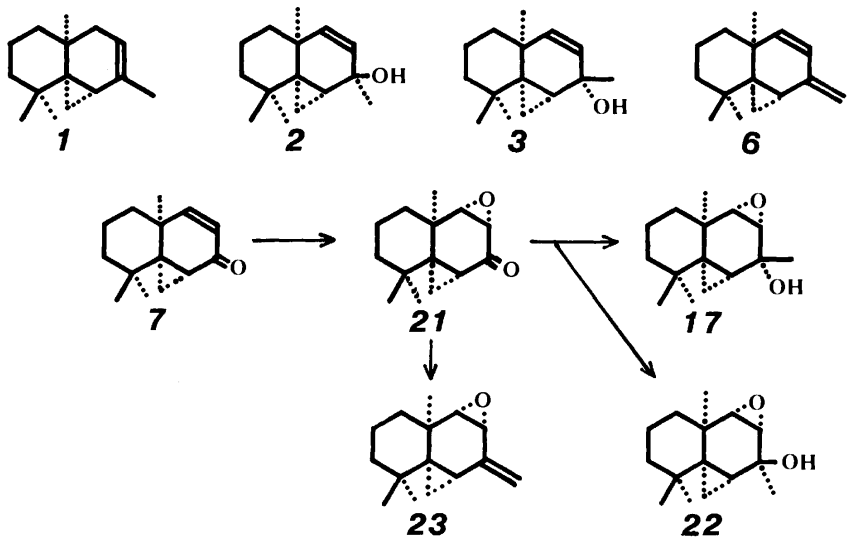

Experimental

Mayurone oxide 21 from Mayurone 7: Mayurone 74 mg was added to a mixture of 30% H_2O_2 (0.15 ml), 6 M-NaOH (0.024 ml; 1 M=1 mol dm^{-3}) and methanol (1.0 ml) and the mixture was stirred for 1 h at room temperature. After the addition of water (50 ml) and sat. NaCl (20 ml), the mixture was extracted with ether-hexane (2:1). Evaporation of the solvent gave **21** 79 mg as the sole product. **21**: mp 93.5—94.5 °C (from methanol). IR (KBr) 3020, 2950, 1680, 1488, 1465, 1446, 1390, 1380, 1366, 1290, 1247, 1172, 1040, 1018, 980, 965, 945, 912, 868, 840, 828, 780, 770, 650, and 446 cm^{-1}. ^1H NMR ($CDCl_3$) δ=0.57 (3H, s), 1.10 (3H, s), 1.53 (3H, s), 3.04 (1H, d, J=4.0 Hz), 3.25 (1H, dd, J=4.0 and 1.6 Hz), and 0.64—2.18 (9H, m).

Grignard Methylation of 21: Mayurone oxide **21** (0.50 g) in dry THF (10 ml) was cooled to −70 °C. Methylmagnesium iodide (1.37 M, 1.66 ml) was added under an argon atmosphere and stirred for 1 h at −70 °C. The reaction mixture was hydrolyzed with aqueous ammonium acetate solution at −50 °C, extracted with ether-hexane (1:1), and dried over sodium sulfate. The solvent was evaporated and the residue was chromatographed on a silica-gel column. Hexane-CH_2Cl_2 (8:2 to 7:3) eluted unchanged **21** (0.25 g). Hexane-CH_2Cl_2 (1:1) and CH_2Cl_2 eluted **22** (228 mg) and ether-CH_2Cl_2 (1:19) eluted **17** (27.5 mg) mp 106 °C, identified by IR and ^1H NMR.[1] **22**: mp 78—80 °C. IR (KBr) 3470, 3380 (OH), 3100, 2950, 2930, 1480, 1370, 1128, 1090, 1050, 965, 938, 908, 858, 822, 812, 801, 742, 606, and 503 cm^{-1}. ^1H NMR ($CDCl_3$) δ=0.26 (1H, dd, J=10.1 and 4.3 Hz), 0.55 (3H, s), 0.89 (1H, dd, J=5.6 and 4.3 Hz), 1.02 (3H, s), 1.33 (3H, s), 1.46 (3H, s), 2.66 (1H, d, J=3.8 Hz), and 2.93 (1H, dd, J=3.8 and 2.0 Hz).

Thujopsadiene Monoepoxide 23 from Mayurone Oxide 21: To a suspension of methyltriphenylphosphonium bromide, 200 mg (0.56 mmol) in 5 ml of tetrahydrofuran, 0.28 ml of 1.55 M butyl lithium in hexane was added at −40 °C. After stirring the mixture for 30 min, 100 mg of mayurone oxide **21**, 0.46 mmol was added at room temperature and the mixture was refluxed for 4 h. Four ml of aqueous sodium chloride solution was added and the organic layer was separated. GLC analysis of the layer showed **23**, 39%, **21**, 11%, triphenylphosphine oxide 39% and unidentifiable products 11%. The products were chromatographed on silica gel. Hexane-CH_2Cl_2 eluted 47 mg of **23**. Oil, IR (neat) 3080, 3050, 3000, 2850, 1633 (CH_2=C), 1460, 1385, 1370, 1253, 1170, 1043, 945, 903, 878, 863, 832, 805, 762, and 682 cm^{-1}. ^1H NMR ($CDCl_3$) δ=0.58 (3H, s), 1.04 (3H, s), 1.38 (3H, s), 2.77 (1H, d, J=4 Hz), 3.41 (1H, dd, J=4 and 1.5 Hz), and 5.16 (2H, broad s).

Compounds 21 and 23 in Autoxidation Products of 1: In the autoxidation products of thujopsene (23.8 g) reported previously,[1] a fraction (265 mg, 1.1%, 90% pure by GC) just after the elution of dimeric peroxide **16** was found to be **23** by comparison of the IR. The crude mayurone fraction was combined and rechromatographed on SiO_2 gel affording **21** (28 mg, 0.1%) preceeding the mayurone fraction, identified by IR.

Compound 21 from Allylic Alcohol 2: A sample of alcohol **2** (93% pure) was autoxidized on standing for 6 months. Gas chromatography showed **6**, 6%, **2**, 21%, **7**, 33%, and **21**, 14%.

Compound 21 from Allylic Alcohol 3: Alcohol **3** 0.50 g was autoxidized on standing for more than 6 months. Gas chromatography showed **6**, 52%, **3**, 2%, **7**, 23%, and **21**, 10%. Alumina and silica gel chromatography gave 0.02 g of **21**, identified by IR.

Compound 21 from Thujopsadiene 6: Thujopsadiene **6** was synthesized from mayurone and methylmagnesium iodide. The diene **6**, 2.88 g was autoxidized on standing for more than 6 months. Gas chromatography showed **6**, 53%, **7**, 32%, and **21**, 6%. Silica-gel chromatography gave 0.05 g of **21**, identified by IR.

References

1) Part X, S. Nagahama and M. Tazaki, *Bull. Chem. Soc. Jpn.*, **60**, 4453 (1987).

2) S. Akiyoshi and S. Nagahama, *Bull. Chem. Soc. Jpn.*, **30**, 886 (1957); T. Nozoe, H. Takeshita, S. Ito, T. Ozaki, and S. Seto, *Chem. Pharm. Bull.*, **8**, 936 (1960); S. Nagahama, H. Kobayashi, and S. Akiyoshi, *Bull. Chem. Soc. Jpn.*, **35**, 1410 (1962); H. Takeshita, T. Sato, T. Muroi, and S. Ito, *Tetrahedron Lett.*, **1969**, 3095; M. Ito, T. Nishimura, and K. Abe, *Bull. Chem. Soc. Jpn.*, **45**, 1914 (1972).

3) S. Nagahama and M. Tazaki, *Bull. Chem. Soc. Jpn.*, **60**, 4175 (1987).

4) G. L. Chetty and Sukh Dev, *Tetrahedron Lett.*, **1964**, 73; **1965**, 3773; S. Ito, K. Endo, H. Homma, and K. Oka, *Tetrahedron Lett.*, **1965**, 3777; B. Tomita, Y. Hirose, and T. Nakatsuka, *Tetrahedron Lett.*, **1968**, 843.

5) S. P. Acharrya and H. C. Brown, *J. Org. Chem.*, **35**, 3874 (1970); P. C. Traas, L. M. van der Linde, and H. J. Takken, *Rec. Trav. Chim. Pays-Bas*, **93**, 264 (1974).

Selective Nuclear Halogenation of Polymethylbenzenes with Alumina-Supported Copper(II) Halides

Mitsuo KODOMARI,* Hiroaki SATOH, and Suehiko YOSHITOMI
Department of Industrial Chemistry, Shibaura Institute of Technology, Shibaura, Minato-ku, Tokyo 108
(Received May 19, 1988)

Synopsis. The halogenation of polymethylbenzenes with alumina-supported copper(II) halides under heterogeneous conditions in nonpolar solvents gave nuclear-halogenated compounds selectively in high yields; no side-chain-halogenated compounds were formed.

Although copper(II) halides have been used to halogenate aromatic hydrocarbons under heterogenous conditions in nonpolar solvents,[1] aromatic hydrocarbons with ionization potential (IP) higher than approximately 7.55 eV are entirely unreactive toward chlorination with copper(II) chloride.[2] For example, chlorination of naphthalene (IP=8.10[3]) or phenanthrene (IP=8.03[3]) does not occur, even under reflux, with copper(II) chloride in high-boiling solvents, such as chlorobenzene and nitrobenzene.[1,4] Previously, we reported that copper(II) halides can be activated remarkably by supporting onto neutral alumina,[5] and polycyclic aromatic hydrocarbons or alkoxybenzenes are halogenated selectively to give corresponding halides by use of copper(II) halides supported onto neutral alumina.[6,7] In reactions of alkylbenzenes with metal halides, side-chain-halogenation and polymerization in addition to nuclear-halogenation occur.[8] In contrast, we found that similar reactions with alumina-supported copper(II) halides gave selectively nuclear-halogenated products in high yields. In this paper, we report on a convenient method of selective nuclear halogenation of polymethylbenzenes with alumina-supported copper(II) halides.

Results and Discussion

The halogenation of polymethylbenzenes with alumina-supported copper(II) halides in nonpolar solvents in which copper(II) halides were not soluble, occurred as a heterogeneous reaction on the surface and gave only nuclear-halogenated compounds in high yields; no side-chain-halogenated compounds were obtained. The reaction of copper(II) bromide with mesitylene in carbon tetrachloride at reflux yielded no detectable products after 5 h. In contrast, in a similar reaction using alumina-supported copper(II) bromide, bromomesitylene in 97% yield from a reaction run at 50 °C for 1 h and dibromomesitylene in 99% yield from the reaction run at 80 °C for 5 h were obtained. The results of chlorination and bromination of polymethylbenzenes are summarized in Tables 1 and 2. The reactivity of polymethylbenzenes toward copper(II) halides increased with increasing the number of methyl groups. For instance, bromination of toluene in carbon tetrachloride did not proceed at reflux, even though pentamethylbenzene was brominated at 30 °C to give bromopentamethylbenzene quantitatively. Toluene and copper(II) bromide reacted at reflux for 72 h to give benzyl bromide as the main product. In a similar reaction with alumina-supported copper(II) bromide, bromotoluene (*o*/*p*=1) was obtained in good yield and no side-chain-brominated compounds were detected.

The reaction of alkylbenzene with copper(II) bromide is critically influenced by the presence of water in small quantities.[9] With toluene, nuclear bromination predominates in a rigorously anhydrous system. When small amounts of water are added, phenyl(*p*-tolyl)methane is the main product, in addition to benzyl bromide. In contrast, in a reaction with alumina-supported copper(II) bromide in the presence of water in small quantities, only nuclear bromination occurred and no products resulting from side-chain-bromination were formed. It seems that alumina not only activates copper(II) halides but also acts as a dehydrating agent in this system. Copper(II) chloride was less reactive than copper(II) bromide toward the polymethylbenzenes. The chlorination of the polymethylbenzenes required more severe conditions than that of bromination. The chlorination of xylene did not occur under the same conditions, even though the bromination proceeded at 80 °C in carbon tetrachloride. With polymethylbenzenes containing more than three methyl groups. The corresponding nuclear-monochlorinated compounds were obtained selectively in high yield. A reaction of pentamethylbenzene, even at 80 °C for 5 h gave chloropentamethylbenzene in 98% yield (isolated).

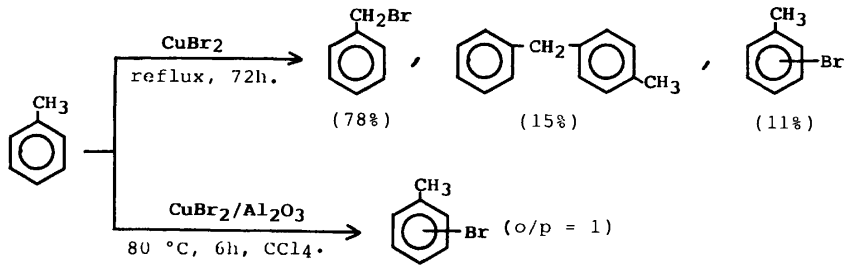

Scheme 1.

Table 1. Bromination of Polymethylbenzenes with $CuBr_2/Al_2O_3$[a]

Polymethylbenzene	Reaction temp/°C	Reaction time/h	Product	Yield/%[b]
a Methyl-	80	6	2- and 4-Br	85[c]
b 1,3-Dimethyl-	80	2	4-Br	98(85)
c 1,2,3-Trimethyl-	80	1	4-Br	97(87)
d 1,3,5-Trimethyl-	50	1	2-Br	97(86)
	80	5	2,4-Br	99(97)
e 1,2,3,5-Tetramethyl-	50	1	4-Br	92(90)
	80	5	4,6-Br	99(98)
f 1,2,3,4,5-Pentamethyl-	30	1	6-Br	(99)

a) All the reaction was carried out in carbon tetrachloride. The molar ratio of CuBr/polymethylbenzene was 5. b) Determined by GLC; figures in parentheses show the yield of isolated product. c) $o/p=1$.

Table 2. Chlorination of Polymethylbenzenes with $CuCl_2/Al_2O_3$[a]

Polymethylbenzene	Reaction temp/°C	Reaction time/h	Product	Yield/%[b]
c	110	4	4-Cl	95(80)
d	110	5	2-Cl	90(78)
e	130	3	4-Cl	91(82)
f	80[c]	5	6-Cl	(98)

a) Reactions were carried out in chlorobenzene. The molar ratio of $CuCl_2$/polymethylbenzene was 5. b) Determined by GLC; figures in parentheses show the yield of isolated product. c) The reaction was carried out in carbon tetrachloride.

The advantages of this procedure are simple workups, mild reaction conditions and higher selectivities. Products can be isolated by simple filtration and solvent evaporation, and no extraction steps are required.

Experimental

Preparation of Copper(II) Bromide Supported on Alumina: To a solution of copper(II) bromide (10 g) in distilled water (30 ml) was added neutral alumina (20 g, Woelm N-Super 1) at room temperature. The water was evaporated by using a rotary evaporator at 80 °C under reduced pressure. The resulting reagent was then dried under vacuum (4 Torr; 1 Torr≈133.322 Pa) at 100 °C for 15 h. The preparation of alumina-supported copper(II) chloride was similar to that described above.

4-Bromo-*m*-xylene: General Procedure for Bromination of Polymethylbenzenes. A mixture of *m*-xylene (2.4 g, 22.6 mmol), alumina-supported copper(II) bromide (50.5 g), and carbon tetrachloride (60 ml) was placed in a 100 ml round-bottom flask and stirred with a Teflon-coated magetic stirring bar at 80 °C for 1 h. The products mixture was filtered, and the spent and unused reagent were washed with carbon tetrachloride (30 ml). The solvent was evaporated from the combined filtrate under reduced pressure, and the residue was distilled under vacuum to give 3.6 g (86%) of 4-bromo-*m*-xylene. Bp 89—91 °C/14 Torr (lit,[10] 203 °C). The ^1H NMR and IR spectra was identical with those of an authentic sample.

6-Chloro-1,2,3,4,5-Pentamethylbenzene: General Procedure for Chlorination of Polymethylbenzenes. A mixture of pentamethylbenzene (2.0 g, 13.5 mmol), alumina-supported copper(II) chloride (28 g) and carbon tetrachloride (40 ml) was stirred at 80 °C for 5 h. The product mixture was filtered, and the spent and unused reagents were washed with carbon tetrachloride (30 ml). Evaporation of the solvent from the combined filtrate under reduced pressure yielded 2.42 g (98%) of 6-chloro-1,2,3,4,5-pentamethylbenzene as a white solid having mp 152—153 °C (lit,[11] mp 154.5—155 °C). The ^1H NMR and IR spectra was identical with those of an authentic sample.

References

1) D. C. Nonhebel, *J. Chem. Soc.*, **1963**, 1216.
2) I. Tanimoto, K. Kushioka, T. Kitagawa, and K. Maruyama, *Bull. Chem. Soc. Jpn.*, **52**, 3586 (1976).
3) J. B. Birks and M. A. Slifkin, *Nature (London)*, **191**, 762 (1961).
4) J. C. Ware and E. E. Brochert, *J. Org. Chem.*, **26**, 2267 (1961).
5) M. Kodomari, H. Satoh, and S. Yoshitomi, *Nippon Kagaku Kaishi*, **1986**, 1813.
6) M. Kodomari, H. Satoh, and S. Yoshitomi, *J. Org. Chem.*, **53**, 2093 (1988).
7) M. Kodomari, S. Takahashi, and S. Yoshitomi, *Chem. Lett.*, **1987**, 1901.
8) P. Kovacic and C. Wu, *J. Org. Chem.*, **26**, 759, 762 (1961).
9) P. Kovacic and K. E. Davis, *J. Am. Chem. Soc.*, **86**, 427 (1964).
10) *Beilstein*, **5**(2), p. 293.
11) *Beilstein*, **5**(3), p. 1011.

Normal Pressure Double Carbonylation of Aryl Halides Using Cobalt(II) Chloride in the Presence of either Sodium Sulfide or Sodium Borohydride

Kenji ITOH, Masahiro MIURA,* and Masakatsu NOMURA
Department of Applied Chemistry, Faculty of Engineering, Osaka University, Suita, Osaka 565
(Received May 27, 1988)

Synopsis. Tetracarbonylcobaltate ion generated by a treatment of cobalt(II) chloride with either sodium sulfide or sodium borohydride under a normal pressure of carbon monoxide was capable of catalyzing carbonylation of aryl halides in the presence of calcium hydroxide and methyl iodide to give arylglyoxylic acids in good selectivity.

Several effective methods for cobalt-catalyzed carbonylation of aryl halides to produce the corresponding carboxylic acids, α-keto carboxylic acids, and alkyl aryl ketones have recently been developed, using either tetracarbonylcobaltate ion $Co(CO)_4^-$ under photostimulation[1,2] or alkyltetracarbonylcobalt complexes $RCo(CO)_4$.[3,4] In the latter case, we reported that the product distribution is a marked function of the solvent system employed.[4] These reactions smoothly proceed in the presence of an appropriate base under extremely mild conditions. The catalytically active species are usually prepared in situ from somewhat air-sensitive octacarbonyldicobalt $Co_2(CO)_8$. Simple inorganic cobalt salts have also been successfully used as the catalyst precursors;[5-7] however only the monocarboxylic acids were isolated.

As part of our study, we have undertaken the synthesis of the α-keto carboxylic acids using cobalt salts in order to provide a convenient route to the acids.[8] We observed that the tetracarbonylcobaltate ion prepared by a treatment of cobalt chloride with either sodium sulfide in water[9] or sodium borohydride in dioxane[10] can catalyze the carbonylation of aryl halides (**1**) at room temperature under a normal pressure of carbon monoxide to give the corresponding α-keto acids (**2**) in good selectivity along with the glycolic acids (**3**) and the mono acids (**4**) (Eq. 1 and Table 1).[11]

$$\mathrm{ArX} \xrightarrow[\mathrm{Na_2S\ or\ NaBH_4\ /Ca(OH)_2}]{\mathrm{CO/CoCl_2/MeI}} \mathrm{ArCOCOOH} + \mathrm{ArCH(OH)COOH} + \mathrm{ArCOOH} \quad (1)$$

1 **2** **3** **4**

1a: 1-bromonaphthalene
1b: bromobenzene
1c: iodobenzene

Table 1. Carbonylation of Aryl Halides with Cobalt Chloride[a]

Run	**1** (mmol)	Co-catalyst	Solvent[b]	Conv./%	Product yield/%[c]		
					2	**3**	**4**
1	**1a** (5)	Na_2S	A	51	86	9	4
2	**1a** (10)[d]	Na_2S	A	41	87	5	4
3	**1a** (5)	$NaSCH_3$	A	20	75	5	17
4	**1a** (10)	$NaBH_4$	A	39	80	3	5
5	**1a** (5)	—[e]	A	55	85	4	5
6	**1a** (5)	Na_2S	B	90	89	3	6
7	**1a** (10)	Na_2S	B	53	89	4	7
8	**1a** (10)	Na_2S	B[f]	31	88	7	2
9	**1a** (10)	Na_2S	B[g]	31	82	3	10
10	**1a** (5)[h]	Na_2S	B	11	20	17	60
11	**1b** (5)	Na_2S	A	42	53[i]	4	5
12	**1b** (5)	$NaBH_4$	A	40	57[i]	2	8
13	**1b** (5)	Na_2S	B	74	48[i]	2	8
14	**1c** (5)	Na_2S	A	61	62[i]	3	5
15	**1c** (5)	$NaBH_4$	A	48	68[i]	3	5
16	**1c** (5)	Na_2S	B	78	64[i]	3	13

a) The reaction was carried out using $CoCl_2$ (0.5 mmol), Na_2S (0.25 mmol) or $NaBH_4$ (1 mmol), $Ca(OH)_2$ (35 mmol), and methyl iodide (25 mmol) at 20 °C for 20 h. b) A: Dioxane–H_2O (3:1, v/v). B: 2-Propanol–H_2O (1:1, v/v). c) Yield based on the halide consumed was determined by GLC after trimethylsilylation with *N,O*-bis(trimethylsilyl)acetamide or methylation with diazomethane. d) Reaction for 40 h. e) $Co_2(CO)_8$ (0.25 mmol). f) 2-Propanol–H_2O (3:1, v/v). g) 2-Propanol–H_2O (1:2, v/v). h) Reaction at 60 °C. i) The keto acid was obtained as a mixture of the acid and the condensated product with pyruvic acid. The value indicates that after hydrolysis of the product mixture with NaOH.[3,4]

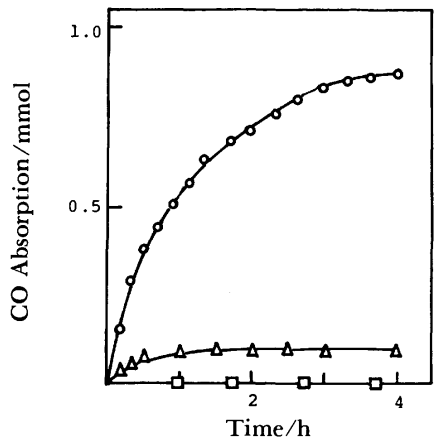

Fig. 1. CO Absorption in the treatment of $CoCl_2$ (0.5 mmol) with sulfur-containing compounds in the presence of $Ca(OH)_2$ (35 mmol): Na_2S (0.25 mmol) ○, $NaSCH_3$ (0.5 mmol) △, and $C_2H_5OCS_2K$ (0.5 mmol) □.

When cobalt chloride (0.5 mmol) was treated with sodium sulfide (0.25 mmol) in the presence of calcium hydroxide in water at 20 °C under carbon monoxide (1 atm) for 4 h, about 0.9 mmol of carbon monoxide was consumed (Fig. 1). The IR spectrum of the solution showed a single characteristic peak for $Co(CO)_4^-$ at 1913 cm^{-1} in the region 1700 to 2000 cm^{-1}. The addition of **1** (5 or 10 mmol) in dioxane, together with methyl iodide to the solution, gave **2** along with **3** and **4**. The formation of aryl methyl ketone was not detected in each reaction. The conversion of **1** and the selectivity of **2** were comparable with those using $Co_2(CO)_8$ (0.25 mmol) (Runs 1 and 5). Cobalt sulfide could not be used in place of $CoCl_2$–Na_2S, suggesting that the sulfide does not participate in the formation of the active species. While sodium methanethiolate, which is an efficient reagent for the preparation of nickel(0) carbonyl derivatives from nickel chloride,[12] could also be used in place of sodium sulfide, it was considerably less effective than the sulfide (Run 3 and Fig. 1). Potassium ethylxanthogenate and sodium diethyldithiocarbamate were ineffective.

As an alternative catalyst system for the carbonylation, $CoCl_2/NaBH_4/Ca(OH)_2$ could also be successfully used (Runs 4, 12, and 15). In this case, the cobaltate ion was prepared within 1.5 h (see Experimental).

It is noteworthy that, in the reaction in 2-propanol-water (1 : 1, v/v), a remarkably higher conversion of **1**, accompanied by a little decrease of the selectivity of **2**, was observed (Runs 6, 13, and 16). This is in contrast with the reactions in dioxane–water (1 : 1) and ethanol–water (1 : 1) in which the mono acids **4** were the major products.[4] The conversion of **1**, however, decreased as a result of changes in the 2-propanol–water ratio from 1 : 1 to both 3 : 1 and 1 : 2 (Runs 8 and 9).

In conclusion, the double carbonylation reaction of aryl halides to give arylglyoxylic acids was conveniently carried out using only simple reagents which are inexpensive and easily handled.

Experimental

Generation of Tetracarbonylcobaltate Ion. (a) To a flask containing cobalt chloride (0.5 mmol), sodium sulfide nonahydrate (0.25 mmol), and calcium hydroxide (35 mmol) was added water (10 cm^3). The mixture was stirred for 4 h at room temperature under carbon monoxide (1 atm). (b) A mixture of cobalt chloride (0.5 mmol) and sodium borohydride (1 mmol) in dioxane (10 cm^3) was stirred at 20 °C for 1 h, while bubbling carbon monoxide. Then, water (5 cm^3) and calcium hydroxide (35 mmol) were added and stirred for a further 20 min.

Carbonylation of Aryl Halides 1 and the Product Analysis. The methods were essentially the same as those described previously.[4]

The present work was partly supported by a Grant-in-Aid for Scientific Research No. 62750783 from the Ministry of Education, Science and Culture.

References

1) J. J. Brunet, C. Sidot, and P. Caubere, *Tetrahedron Lett.*, **22**, 1013 (1981); J. J. Brunet, C. Sidot, and P. Caubere, *J. Org. Chem.*, **48**, 1166 (1983).

2) T. Kashimura, K. Kudo, S. Mori, and N. Sugita, *Chem. Lett.*, **1986**, 299; 483; 851.

3) M. Foa, F. Francalanci, E. Bencini, and A. Gardano, *J. Organomet. Chem.*, **285**, 293 (1985); F. Francalanci, E. Bencini, A. Gardano, M. Vincenti, and M. Foa, *J. Organomet. Chem.*, **301**, C27 (1986); M. Foa and F. Francalanci, *J. Mol. Catal.*, **41**, 89 (1987).

4) M. Miura, F. Akase, and M. Nomura, *J. Chem. Soc., Chem. Commun.*, **1986**, 241; M. Miura, F. Akase, M. Shinohara, and M. Nomura, *J. Chem. Soc., Perkin Trans. 1*, **1987**, 1021; M. Miura, F. Akase, and M. Nomura, *J. Org. Chem.*, **52**, 2623 (1987).

5) J. J. Brunet, C. Sidot, B. Loubinuoux, and P. Caubere, *J. Org. Chem.*, **44**, 2199 (1979).

6) K. Kudo, T. Shibata, T. Kashimura, S. Mori, and N. Sugita, *Chem. Lett.*, **1987**, 577.

7) M. Miura, K. Itoh, and M. Nomura, *J. Mol. Catal.*, **48**, 11 (1988).

8) Palladium-catalyzed synthesis of arylglyoxylic acid derivatives: F. Ozawa, N. Kawasaki, H. Okamoto, T. Yamamoto, and A. Yamamoto, *Organometallics*, **6**, 1640 (1987); T. Sakakura, H. Yamashita, T. Kobayashi, T. Hayashi, and M. Tanaka, *J. Org. Chem.*, **52**, 5733 (1987) and references therein.

9) The method for the preparation of tetracarbonylcobaltate ion using cobalt salts in the presence of $Na_2S_2O_3$ and/or Na_2S under a medium pressure of carbon monoxide has been claimed, which was applied to the double carbonylation of relatively more reactive benzyl halides: J. Gauthier-Lafaye and R. Perron, *Jpn. Kokai Tokkyo Koho*, 59-102825 (1984); Eur. Patent 108698 (1984); *Chem. Abstr.*, **101**, 130413b (1984).

10) The $CoCl_2/NaBH_4/NaOH$ system has been used for the carbonylation of benzyl bromide: N. Satyanarayana and M. Periasamy, *Tetrahedron Lett.*, **28**, 2633 (1987).

11) While tetracarbonylcobaltate ion has also been hitherto prepared from simple cobalt salts by the other several means, they required to use unsuitable solvent and base for the double carbonylation: M. P. Schubert, *J. Am. Chem. Soc.*, **55**, 4563 (1933); P. Gilmont and A. A. Blanchard, *Inorg. Synth.*, **2**, 238 (1946); W. Hieber, E. O. Fischer, and E. Bockly, *Z. Anorg. Allg. Chem.*, **269**, 308 (1952); R. J. Clark, S. E. Whiddon, and R. E. Serfass, *J. Organomet. Chem.*, **11**, 637 (1968); L. Cassar, G. P. Chiusoli, and F. Guerrieri, *Synthesis*, **1973**, 509.

12) K. Tanaka, Y. Kawata, and T. Tanaka, *Chem. Lett.*, **1974**, 831.

The Hammett Relationship in the Reduction of Aldehydes with 2-Propanol by Catalysis with Hydrous Zirconium Oxide

Makoto SHIBAGAKI,* Hideyuki KUNO, Kyoko TAKAHASHI, and Hajime MATSUSHITA
Life Science Research Laboratory, Japan Tobacco INC.,
6-2 Umegaoka, Midori-ku, Yokohama, Kanagawa 227
(Received June 7, 1988)

Synopsis. A linear correlation of the Hammett relationship was obtained for a catalytic reduction of substituted benzaldehydes with 2-propanol with hydrous zirconium oxide. The reaction constant ρ was 1.35, indicating that the electronic effect on the reaction is larger than that on the standard one.

In a previous paper, we reported that the reduction of aldehydes and ketones with 2-propanol proceeds efficiently in the presence of hydrous zirconium oxide.[1,2] All the conjugated ketones, as well as sterically hindered ones, could be substantially reduced by this method. The reduction of conjugated, as well as sterically hindered ketones, took a long time. The reduction of ketones with chloride substituted at the α-position was faster. There results suggested that both steric and electronic factors affect the reaction. The Hammett relationship is a useful method for an interpretation of the reaction mechanism, since it indicates the relative electronic effect quantitatively.[3]

In this paper, we report on the relative electronic effect on the reduction by use of the reaction constant (ρ), which was obtained by the Hammett relationship.

Experimental

Catalyst and Materials. Hydrous zirconium oxide was prepared in the manner described in a previous paper.[2] The calcination of the catalyst was performed at 300 °C for 5 h. Commercial reagents were used for the reaction without further purification.

Reduction and Analysis. In a 10 cm^3 round-bottom flask equipped with a reflux condenser, 1 mmol of aldehyde, 0.1 mmol of a hydrocarbon as an internal standard, 2 cm^3 of 2-propanol, and 0.1 g of hydrous zirconium oxide were placed. The reaction mixture was immersed in an oil bath which was kept at 78±0.1 °C, and 0.1—0.2 μl samples were removed at appropriate time intervals and analyzed by gas chromatography (capilary column PEG 20M 30m).

Results and Discussion

The reduction of substituted benzaldehydes proceeded efficiently to give the corresponding alcohols. No by-products were detected. Exceptionally, *p*-hydroxybenzaldehyde and *p*-(dimethylamino)benzaldehyde were mainly converted to *p*-hydroxybenzyl isopropyl ether and *p*-(dimethylamino)benzyl isopropyl ether, respectively. In all cases, a linear correlation between the natural logarithm of the concentration of aldehyde and reaction time was obtained. It indicated that the reaction rate is of pseudo-first-order in the aldehyde concentration,[2] and the rate constants, k, were calculated from the slope of the line, and are listed in Table 1.

The Hammett relationship for the reduction is illustrated in Fig. 1, and shows ln k/k_0, where k_0 is the rate constant for the reduction of benzaldehyde, plotted against σ, where σ is the substituent constant.[4] A linear correlation was obtained, except for the cases of *p*-hydroxybenzaldehyde and *p*-(dimethylamino)-benzaldehyde. This result suggests that a linear free

Table 1. Substituent Effect on the Reduction of Substituted Benzaldehydes[a]

Entry	Substituent	Rate const.[b]
1	*m*-NO_2	3.25
2	*p*-CN	2.83
3	*m*-Br	2.68
4	*m*-Cl	2.60
5	*m*-F	2.41
6	*p*-Cl	2.03
7	H	1.41
8	*p*-C_2H_5	1.01
9	*p*-CH_3	1.22
10	*p*-OCH_3	1.02
11	*p*-OH	0.34[c]
12	*p*-$N(CH_3)_2$	0.30[c]

a) Aldehyde 1 mmol, 2-propanol 2 cm^3, Catalyst 0.2 g, 78.0±0.1 °C. b) $\times 10^{-4}$ s^{-1}. c) Only isopropyl ether was obtained.

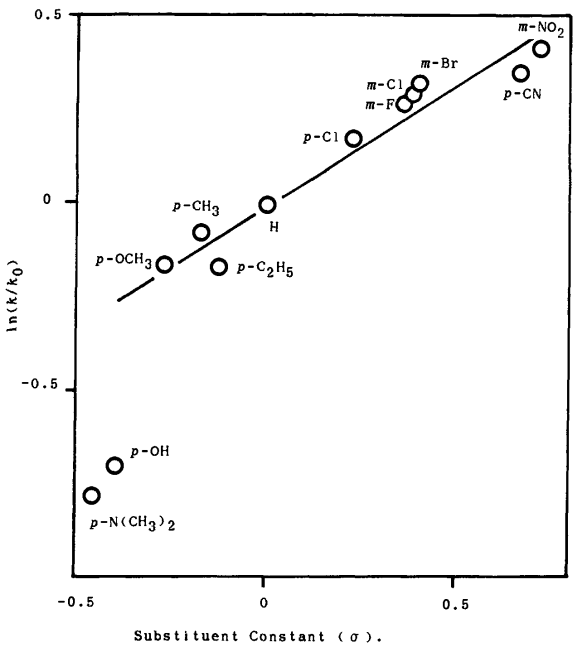

Fig. 1. Correlation between substituent constant, σ, and rate constant of the reduction.
k: Rate constant of substituted benzaldehyde.
k_0: Rate constant of benzaldehyde.

energy relationship exists in the reduction, and that the electronic effect can be directly evaluated.

The reaction constant, ρ, which was obtained from the slope of the line, reflects the sensitivity of the reaction rate to the electronic effect. The value of ρ was 1.35, which indicates that the electronic effect on the reduction was larger than that on the standard reaction (the esterification of substituted benzoic acids).[4]

The reduction of aldehyde with 2-propanol was believed to proceed via the attack on the carbonyl by the hydride from 2-propanol. From this it follows that the electronic deficient aldehyde was reduced faster. This interpretation is supported by the results for the Hammett relationship.

In the case of the reduction of *p*-hydroxybenzaldehyde and *p*-(dimethylamino)benzaldehyde, the rates were too slow and the products were mainly ethers. This is because the affinity of the hydroxyl or dimethylamino group to hydrous zirconium oxide is stronger than that of the carbonyl group.

References

1) H. Matsushita, S. Ishiguro, H. Ichinose, A. Izumi, and S. Mizusaki, *Chem. Lett.*, **1985**, 731.

2) M. Shibagaki, K. Takahashi, and H. Matsushita, *Bull. Chem . Soc. Jpn.*, **61**, 3283 (1988).

3) L. P. Hammett, *Chem. Rev.*, **17**, 125 (1935); L. P. Hammett, "Physical Organic Chemistry," McGraw-Hill Book Co., New York (1940), p. 184.

4) C. G. Swain and E. C. Lupton, Jr., *J. Am. Chem. Soc.*, **90**, 4328 (1968); P. R. Wells, "Linear Free Energy Relationships," Academic Press, New York (1968).

The Synthesis and Characterization of Manganese(III) Complexes with the General Formula of $[Mn(X)(L)]^{n+}$ (n=0, 1) (X=Cl^-, N_3^-, Pyridine, *N*-Methylimidazole, L=*N*,*N*′-[(Methylimino)bis(trimethylene)]-bis[salicylideneaminate]: The X-Ray Crystal Structure of $[Mn(N\text{-MeIm})(L)][BPh_4]$

Toshifumi AKUI, Akira OHYOSHI, Naohide MATSUMOTO,*,† and Hisashi ŌKAWA†
Department of Applied Chemistry, Faculty of Engineering, Kumamoto University, Kurokami 2-39-1, Kumamoto 860
†Department of Chemistry, Faculty of Science, Kyushu University, Hakozaki, Higashi-ku, Fukuoka 812
(Received March 18, 1988)

Synopsis. A series of manganese(III) complexes with the general formula of $[Mn(X)(L)]^{n+}$ (n=0, 1) have been prepared and characterized, where X=Cl^-, N_3^-, pyridine, *N*-methylimidazole, and L=quinquedentate Schiff base ligand *N*,*N*′-[(methylimino)bis(trimethylene)]bis[salicylideneaminate]. The X-ray analysis of $[Mn(N\text{-MeIm})(L)][BPh_4]$ confirmed that the coordination geometry of the manganese(III) ion is a tetragonal bipyramid in which two axial positions are occupied by a central amine nitrogen atom N(3) and an imidazole nitrogen atom N(4), with elongated bond distances of Mn–N(3)=2.388(6) Å and Mn–N(4)=2.251(6) Å.

Recently we have reported on imidazolate-bridged iron(III)–copper(II) and manganese(III)–copper(II) binuclear complexes.[1] As for the iron(III) and the manganese(III) component complexes of their binuclear complexes, complexes with a quinquedentate ligand *N*,*N*′-[methylimino)bis(trimethylene)]bis[salicylideneaminate], $[Fe(L)][BPh_4]$ and $[Mn(L)][BPh_4]$, were employed, because they can provide a coordination site by expanding coordination number. We have already reported on iron(III) complexes with the ligand and found that the iron(III) complexes with $[Fe(X)(L)]^{n+}$ (n=0, 1) constitute a family of spin-equilibrium complexes.[2,3] In this study, a series of manganese(III) complexes $[Mn(X)(L)]^{n+}$ (n=0, 1) (see the drawing) have been prepared and characterized.

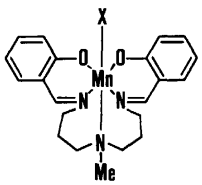

Experimental

Syntheses. Ligand $[H_2L]$. The quinquedentate ligand was prepared by mixing salicylaldehyde (40 mmol) and bis(3-aminopropyl)amine (20 mmol) in 100 cm^3 of methanol. This ligand solution was subsequently used for the preparation of the manganese(III) complexes.

$[Mn(Cl^-)(L)]\cdot 1.5CH_3OH$. To a solution of $[H_2L]$ (20 mmol) in 100 cm^3 of methanol was added a solution of manganese(III) acetate dihydrate (20 mmol) in 30 cm^3 of methanol. The mixture was then stirred at room temperature for 10 min. The resulting solution was gently warmed under stirring for 30 min. To the mixture was added LiCl (50 mmol). The dark green needle crystals thus precipitated were collected by suction filtration and dried.

$[Mn(L)][BPh_4]\cdot 2CH_3OH$. To a solution of $[H_2L]$ (10 mmol) in 50 cm^3 of methanol was added a solution of manganese(III) acetate dihydrate (10 mmol) in 30 cm^3 of methanol. The mixture was then stirred at room temperature for 30 min. To the mixture was added a solution of sodium tetraphenylborate (15 mmol) in 30 cm^3 of methanol. The resulting solution was gently warmed on a water bath for 20 min and then cooled to room temperature. After several hours, black needle crystals thus precipitated were collected by filtration and dried.

$[Mn(N_3^-)(L)]\cdot 0.5H_2O$. To a solution of $[Mn(Cl^-)(L)]$ $2CH_3OH$ (1 mmol) in 30 cm^3 of methanol was added sodium azide (1.5 mmol) in a minimum amount of water. The solution was then gently warmed on a water bath for 10 min and filtered. The filtrate was cooled to room temperature. After several hours, the black crystals thus precipitated were collected by filtration and dried.

$[Mn(X)(L)][BPh_4]$ (X=Py, *N*-MeIm). To a solution of $[Mn(L)][BPh_4]$ in 30 cm^3 of methanol was added pyridine or *N*-methylimidazole (ca. 1.5 times by mole ratio). The solution was then warmed on a water bath for 10 min and then filtered. The filtrate was cooled to room temperature. After several hours, the black crystals thus precipitated were collected and dried.

Physical Measurements. The elemental analyses were performed by Mr. Shinichi Miyazaki at the Technical Service Center of Kumamoto University. The melting points were measured on a Yanagimoto micro melting point apparatus and were uncorrected. The electrical conductivity measurements were carried out on a Denki Kagaku Keiki AOC-10 digital conductometer on ca. 10^{-3} mol dm^{-3} acetonitrile solutions. The infrared spectra were recorded on KBr discs with a JASCO A-702 spectrophotometer. The magnetic susceptibilities were obtained by the Faraday method at room temperature using a Cahn 2000 electric balance. The susceptibilities were corrected for the diamagnetism of component atoms by the use of Pascal's constants. The molar effective magnetic moment was calculated by means of this equation $\mu_{eff}=2.828\sqrt{\chi_A T}$.

X-Ray Diffraction Study of $[Mn(N\text{-MeIm})(L)][BPh_4]$. The diffraction data were obtained on a Rigaku AFC-5 four-circle diffractometer at the Faculty of Science, Kyushu University, using graphite-monochromatized Mo $K\alpha$ radiation at 20±1 °C. Data concerning the conditions for crystallographic data collection and structure refinement is as follows: Formula=$MnO_2N_5C_{49}BH_{51}$, F.W.=807.7, triclinic, space group=$P\bar{1}$, a=11.680(5) Å, b=16.617(4) Å, c=11.649(4) Å, α=104.30(4)°, β=99.81(2)°, γ=93.26(2)°, V=2147.2 $Å^3$, D_{calcd}=1.249 g cm^{-3} (Z=2), D_{measd}=1.22 g cm^{-3} (by the floatation method in an aqueous KI solution), crystal dimension 0.4×0.3×0.3 mm,

Table 1. Fractional Atomic Coordinates ($\times 10^4$) of [Mn(N-MeIm)(L)][BPh_4], with their Estimated Standard Deviations in Parentheses

Atom	X	Y	Z	B_{eqv}	Atom	X	Y	Z	B_{eqv}
Mn	943(1)	2497(1)	2863(1)	3.9	C22	2840(7)	3904(5)	2563(7)	6.8
O1	1361(3)	1490(2)	1965(3)	4.1	C23	3228(8)	4185(6)	1694(10)	9.2
O2	574(4)	3553(3)	3662(4)	4.6	C24	2160(7)	2970(5)	847(7)	6.4
N1	2207(4)	2465(3)	4261(4)	4.0	C25	2983(8)	3607(7)	−596(9)	9.0
N2	−500(4)	2419(3)	1601(4)	3.7	B	3998(6)	7621(4)	2099(6)	3.4
N3	−295(4)	1793(3)	3821(4)	3.8	C26	2750(5)	8022(4)	2105(5)	3.2
N4	2168(4)	3164(3)	2024(4)	4.4	C27	1704(5)	7489(4)	1838(5)	3.9
N5	2804(6)	3572(5)	572(6)	7.7	C28	622(5)	7778(4)	1790(6)	4.7
C1	2452(5)	1295(4)	1984(5)	3.8	C29	523(6)	8632(5)	2018(7)	5.5
C2	2707(6)	749(4)	948(6)	4.9	C30	1527(6)	9171(4)	2267(6)	5.3
C3	3812(7)	500(5)	958(7)	6.1	C31	2617(5)	8870(4)	2308(5)	4.1
C4	4690(6)	764(5)	1972(7)	5.8	C32	5118(5)	8336(4)	2647(6)	4.0
C5	4447(6)	1303(4)	2978(6)	5.0	C33	5203(6)	8870(4)	3808(6)	5.1
C6	3345(5)	1583(4)	3009(5)	3.8	C34	6157(7)	9453(5)	4368(7)	6.5
C7	3129(5)	2103(4)	4135(5)	4.3	C35	7054(7)	9537(5)	3776(9)	7.8
C8	2021(6)	2866(5)	5494(5)	5.1	C36	7016(7)	9041(5)	2634(9)	7.7
C9	1098(6)	2339(5)	5846(6)	6.1	C37	6053(6)	8450(4)	2072(7)	5.6
C10	−153(8)	2280(6)	5094(7)	8.2	C38	4129(5)	7003(3)	3018(5)	3.2
C11	−3(8)	955(6)	3805(9)	8.7	C39	4946(5)	6422(4)	2981(5)	3.9
C12	−1517(7)	1796(6)	3280(8)	7.6	C40	5149(6)	5953(4)	3827(6)	4.8
C13	−1865(6)	1315(4)	1906(6)	5.2	C41	4513(7)	6056(4)	4747(6)	5.3
C14	−1155(6)	1584(4)	1049(6)	4.5	C42	3712(6)	6624(4)	4820(6)	5.2
C15	−888(6)	3056(4)	1309(5)	4.2	C43	3515(5)	7089(4)	3970(5)	4.1
C16	−393(6)	3910(4)	1885(6)	4.5	C44	3963(5)	7112(4)	686(5)	3.4
C17	−629(6)	4530(4)	1281(7)	5.7	C45	4097(6)	7563(4)	−173(6)	4.7
C18	−185(7)	5345(5)	1801(8)	7.0	C46	4050(7)	7166(5)	−1381(6)	5.8
C19	469(8)	5564(4)	2955(8)	7.0	C47	3840(7)	6319(5)	−1804(6)	6.3
C20	702(7)	4971(4)	3611(7)	6.0	C48	3659(7)	5849(4)	−1008(6)	5.8
C21	296(6)	4124(4)	3059(6)	4.4	C49	3728(6)	6252(4)	214(6)	4.5

Table 2. Elemental Analytical Data, Melting Points, Molar Electrical Conductances Measured in Acetonitrile, and Effective Magnetic Moments at 293 K

Complex	C(%)	H(%)	N(%)
[Mn(Cl^-)(L)·1.5CH_3OH	55.25(55.16)	5.96(6.38)	8.97(8.58)
[Mn(N_3^-)(L)·0.5H_2O	55.16(55.14)	5.71(5.73)	18.11(18.37)
[Mn(L)][BPh_4]·2CH_3OH	71.71(71.48)	6.71(6.76)	5.40(5.32)
[Mn(Py)(L)][BPh_4]·0.5CH_3OH	74.00(73.90)	6.44(6.39)	6.58(6.83)
[Mn(N-MeIm)(L)][BPh_4]	72.76(72.86)	6.43(6.36)	8.24(8.67)

Complex	Mp θ_m/°C	Λ_M/S mol^{-1} cm^2	μ_{eff}/B.M.
[Mn(Cl^-)(L)]·1.5CH_3OH	210	35	4.9
[Mn(N_3^-)(L)]·0.5H_2O	205	10	4.6
[Mn(L)][BPh_4]·2CH_3OH	185	92	4.9
[Mn(Py)](L)][BPh_4]·0.5CH_3OH	166	92	4.7
[Mn(N-MeIm)(L)][BPh_4]	163	96	4.7

Calcd values are in parentheses.

μ(Mo $K\alpha$)10.2 cm^{-1}, scan mode θ-2θ, scan speed 6° min^{-1}, scan width (1.1+0.5 tanθ)°, 2θ range 2.5—48°, octant collected h, $\pm k$, $\pm l$, no. of unique reflections data used 3960, R=6.48%, R_w=6.60%.

The intensity data were corrected for the Lorentz-polarization effect but not for the absorption. The structure was solved by the heavy atom method and refined by the block-diagonal least-squares method, in which weight w=1 was adopted for all the reflections. The hydrogen atoms were included in the structure factor calculations, but not refined. The calculations were carried out by the use of UNICS III computer program system[4] on a FACOM M 780 computer at the Computer Center of Kyushu University. The final positional parameters are given in Table 1.

Results and Discussion

The elemental analytical data, melting points, molar electrical conductivities, and effective magnetic moments at room temperature are given in Table 2. Either complex, [Mn(Cl^-)(L)] or [Mn(L)][BPh_4]2CH_3-OH, can be used as the starting compound for the synthesis of other complexes by using a way similar to that used for iron(III) complexes.[2,3] The chloro ion of [Mn(Cl^-)(L)] is easily substituted by N_3^- ion to

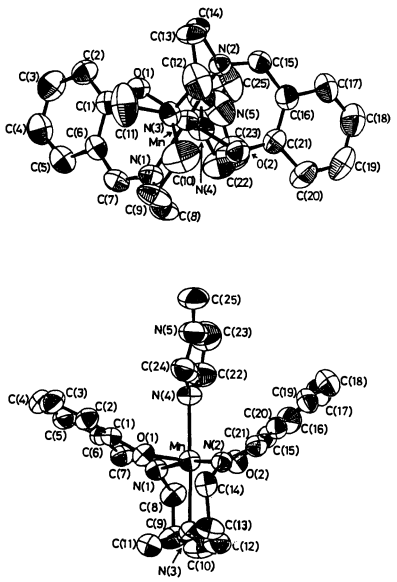

Fig. 1. Perspective drawing of the cation [Mn(*N*-MeIm)(L)]$^+$ with the atom numbering scheme.

produce the azide complex. The molar electrical conductances of the complexes [Mn(Cl^-)(L)] and [Mn(N_3^-)(L)] are not zero. This indicates that the unidentate ligands, such as Cl^- and N_3^-, are partially dissociated in the acetonitrile solutions. The electrical conductances of [Mn(L)][BPh_4], [Mn(*N*-MeIm)(L)]-[BPh_4], and [Mn(Py)(L)][BPh_4] are consistent with that of the 1:1 electrolyte. The effective magnetic moments of all the complexes indicate that the manganese(III) ions are in high-spin state (S=2).

Structural Description of [Mn(*N*-MeIm)(L)][BPh_4].[5] A perspective drawing of the [Mn(*N*-MeIm)(L)]$^+$ cation with the atom numbering scheme is shown in Fig. 1. The bond distances and angles are given in tables which are deposited as supplementary data.[5] The manganese(III) ion assumes a tetragonal bipyramidal coordination geometry, where the equatorial plane comprises N_2O_2 donors of two salicylideneamine moieties and where the two axial positions are occupied by the central amine nitrogen of L and a nitrogen of *N*-methylimidazole. The two salicylideneaminate moieties construct a shallow cave, in which the *N*-MeIm ligand is positioned. The geometry is similar to that of the analogous iron(III) complex [Fe(4-Mepy)(L)]$^+$.[2] A drastic difference between the iron(III) and manganese(III) complexes is found in the metal-axial ligand bond distances. The bond distances between the manganese(III) ion and the axial ligands are elongated, as in Mn–N(3)=2.388(6) Å and Mn–N(4)=2.251(6) Å, while the corresponding distances of the iron(III) analogue are 2.035(6) Å and 2.010(6) Å.[2]

This work was in part supported by a Grant-in-Aid from the Ministry of Education, Science and Culture.

References

1) N. Matsumoto, Y. Maeda, H. $\overline{O}$ kawa, T. Akui, T. Kawaji, A. Ohyoshi, M. Kodera, H. Ohshio, and S. Kida, *J. Chem. Soc., Dalton Trans.*, in press.

2) N. Matsumoto, S. Ohta, C. Yoshimura, A. Ohyoshi, S. Kohata, H. $\overline{O}$ kawa, and Y. Maeda, *J. Chem. Soc., Dalton Trans.*, **1985**, 2575.

3) A. Ohyoshi, J. Honbo, N. Matsumoto, S. Ohta, and S. Sakamoto, *Bull. Chem. Soc. Jpn.*, **59**, 1611 (1986).

4) T. Sakurai and K. Kobayashi, *Rikagaku Kenkyusho Houkoku*, **55**, 69 (1987); S. Kawano, *Rep. Comput. Cent. Kyushu Univ.*, **13**, 39 (1980).

5) The bond distances and angles, H-atom coordinates, and anisotropic thermal parameters are deposited as supplementary data as Document No. 8830 at the office of the Editor of the Bull. Chem. Soc. Jpn.

Racemization of Optically Active Cysteine via Formation of 2,2-Dimethyl-4-thiazolidinecarboxylic Acid

Tadashi SHIRAIWA,* Kazuo KATAOKA, Shinji SAKATA, and Hidemoto KUROKAWA
Faculty of Engineering, Kansai University,
Yamate-cho, Suita, Osaka 564
(Received April 9, 1988)

Synopsis. Optically active cysteine (Cys) was racemized via formation of (*RS*)-2,2-dimethyl-4-thiazolidinecarboxylic acid ((*RS*)-DMT) by refluxing in the presence of acetone in 10-fold molar amount in acetic acid. The formed (*RS*)-DMT was hydrolyzed by adding water to the reaction mixture to give (*RS*)-Cys in 95—97% yield.

(*R*)-Cysteine (abbreviated as (*R*)-Cys), a useful material for medicines, food additives, and cosmetics, has been obtained mainly from hair. Such acquisition of (*R*)-Cys from natural products is apt to be unstationary. (*S*)-Cys, a useful material for antibiotics, is difficult to obtain from natural products. An efficient synthesis of (*RS*)-Cys has been reported, [1,2] and (*R*)- and (*S*)-Cys can be obtained by an optical resolution using preferential crystallization.[3-5] (*R*)-Cys has been demanded in large amounts, but (*S*)-Cys is not in so large an amount. Therefore, a practical method for the racemization of optically active Cys must also be established to use the preferential crystallization procedure for industrial purposes.

Optically active amino acids are racemized in the presence of aldehydes in several organic acids, such as formic acid and acetic acid, and the racemization rate is largest in acetic acid.[6] However, Cys forms 4-thiazolidinecarboxylic acid derivatives by reacting with aldehydes or ketones.[7-9] Of these derivatives, 2,2-dimethyl-4-thiazolidinecarboxylic acid (DMT) is obtained by reacting Cys with acetone and easily hydrolyzed in water to regenerate Cys.[8,9] Threfore, the racemization of optically active Cys via formation of (*RS*)-DMT was tried in the presence of acetone in acetic acid.

Experimental

Materials (*R*)-Cysteine hydrochloride monohydrate was purchased from Wako Pure Chemicals Ind. and recrystallized from water. An aqueous solution of the hydrochloride was adjusted with concentrated aqueous ammonia to pH 6 to obtain (*R*)-Cys: $[\alpha]_D^{20}$ +6.49° (*c* 4.04, 5 mol dm^{-3} HCl) (lit,[10] $[\alpha]_D^{25}$ +6.5° (*c* 2, 5 mol dm^{-3} HCl)). (*S*)-Cys ($[\alpha]_D^{20}$ −6.52° (*c* 3.99, 5 mol dm^{-3} HCl)) was obtained by optical resolution using the preferential crystallization of (*RS*)-4-thiazolidinecarboxylic acid[4] or (*RS*)-cysteine salt of 4-ethylbenzenesulfonic acid.[5]

Racemization. A mixture of 0.0200 mol (2.42 g) of (*R*)- or (*S*)-Cys and 0.200 mol (11.6 g) of acetone in 30 cm^3 of acetic acid was refluxed (approximately 93 °C) for 1—2.5 h. After adding 10 cm^3 of water to the mixture, the solution was dried under reduced pressure at 45 °C and the residue was redissolved in 10 cm^3 of water. The solution was dried under reduced pressure at 45 °C. The suspension of the residue in 50 cm^3 of methanol was stirred for 30 min at room temperature. (*RS*)-Cys was collected by filtration, washed with methanol, and dried; the (*RS*)-Cys showed no optical rotation in water or 5 mol dm^{-3} hydrochloric acid having mp 222—225 °C (decomp). The ^{1}H NMR spectrum of the obtained (*RS*)-Cys in deuterium oxide was recorded on a JEOL JNM-PMX 60 NMR spectrometer, with no methyl protons indicated.

Synthesis of (*R*)-2,2-Dimethyl-4-thiazolidinecarboxylic Acid. A mixture of 0.0200 mol of (*R*)-Cys and 0.0400 mol of acetone in 30 cm^3 of acetic acid was stirred at 30 °C for 0.5 h. After evaporating the mixture to 5 cm^3 at 45 °C, 50 cm^3 of diethyl ether was added to the solution and the suspension was stirred for 4 h at room temperature. The formed (*R*)-DMT was collected by filtration and washed thoroughly with diethyl ether. Found: C, 44.53; H, 6.84; N, 8.55% (Calcd for $C_6H_{11}NO_2S$: C, 44.70; H, 6.88; N, 8.69%); yield 2.52 g (78.2%); mp 144—145 °C (lit,[8] 138—140 °C); $[\alpha]_D^{20}$ −188° (*c* 0.102, acetone) (lit,[8] $[\alpha]_D^{22}$ −183° (acetone)), $[\alpha]_D^{20}$ −144° (*c* 0.503, methanol).

Rate Constant of Racemization. A mixture of 0.0200 mol of (*R*)-Cys and 30 cm^3 of acetic acid was heated at 60, 70, 80, or 90 °C. After adding 0.100, 0.200, or 0.400 mol of acetone to the mixture, the resulting solution was stirred at each temperature; (*R*)-Cys was dissolved completely by stirring for several minutes. One cm^3 portions of the solution were pipetted out at appropriate time intervals and diluted rapidly to 10 cm^3 with acetic acid. The optical rotation at 589 nm was measured with a Union Giken PM-101 digital polarimeter equipped with a quartz cell of 0.50 dm path length. The rate constant of racemization (k_R/h) was calculated by the least-squares method from

$$\ln \alpha_0 / \alpha_t = k_R t, \quad (1)$$

where α_t is the optical rotation at time t h and α_0 that extrapolated to zero time. The half-life period ($t_{1/2}$/h) was calculated on the basis of k_R values obtained by Eq. 1.

The racemization rate for (*R*)-DMT was similarly measured at 90 °C by using 0.0200 mol of (*R*)-DMT and 0.180 mol of acetone.

Results and Discussion

Formation and Hydrolysis of (*R*)-2,2-Dimethyl-4-thiazolidinecarboxylic Acid. (*R*)-DMT was obtained in 78.2% yield by reacting 0.0200 mol of (*R*)-Cys with 0.0400 mol of acetone in acetic acid at 30 °C for 0.5 h, as described in the experimental section. In this reaction, (*R*)-Cys was completely dissolved by stirring for 20 min, and the resulting solution showed a negative optical rotation. If (*R*)-Cys is merely dissolved and (*R*)-DMT does not form, the solution should show a positive optical rotation since (*R*)-Cys has $[\alpha]_D$ +13.0° (acetic acid)[12] and (*R*)-DMT $[\alpha]_D^{20}$ −109° (*c* 0.103, acetic acid). This result indicates that (*R*)-DMT forms rapidly with dissolution of (*R*)-Cys. Optically active amino acids and their derivatives are racemized in the presence of aldehydes or ketones.[6,11]

The (*R*)-DMT obtained under the above conditions is optically pure because the specific rotation (−188 °) in acetone agrees closely with the reported value (−183 °).[8]

After stirring the above reaction mixture for 0.5 h at 30 °C followed by adding water, a drying of the solution gave (*R*)-Cys($[\alpha]_D^{20}$ +6.50 ° (*c* 3.97, 5 mol dm^{-3} HCl)) as the residue in 89.1% (2.16 g) recovery.

The above result indicates that (*R*)-DMT is formed rapidly by reacting (*R*)-Cys with acetone in acetic acid and is easily hydrolyzed by adding water to regenerate (*R*)-Cys.

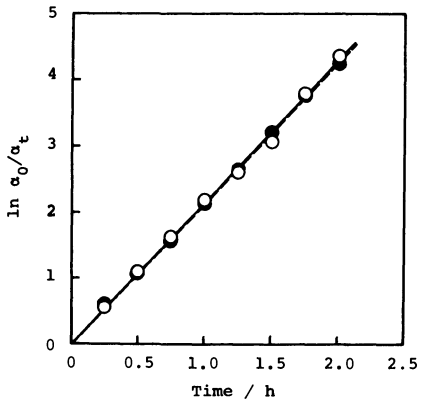

Fig. 1. First-order reaction for racemization.
Conditions: (*R*)-Cysteine ((*R*)-Cys) or (*R*)-2,2-dimethyl-4-thiazolidinecarboxylic acid ((*R*)-DMT) 0.0200 mol; acetic acid 30 cm^3; temperature 90 °C. —○—: (*R*)-Cys; acetone 0.200 mol. --●--: (*R*)-DMT; acetone 0.180 mol. α_0: Optical rotation extrapolated to zero time. α_t: Optical rotation at time *t* h.

Racemization of (*R*)-2,2-Dimethyl-4-thiazolidinecarboxylic Acid. (*R*)-Cys (0.0200 mol) was also reacted similarly with 0.200 mol of acetone at 50 °C for 1 h to give (*R*)-DMT in 85.9% (2.77 g) yield. The obtained (*R*)-DMT seemed to be partially racemized: $[\alpha]_D^{20}$ −139 ° (*c* 0.494, methanol); 96.5% optical purity. This result indicates that the formed (*R*)-DMT is racemized by increasing the amount of acetone and heating.

The optical rotation (α_t) of (*R*)-DMT or (*R*)-Cys was measured at 90 °C in the presence of acetone in 9- or 10-fold molar amount in acetic acid at 15 min intervals, as described in the experimental section. These racemizations can be regarded as first-order reactions because linear relationships are found between ln α_0/α_t and time *t*, as shown in Fig. 1. The rate constant (2.14 h^{-1}) for (*R*)-Cys agrees well with that (2.13 h^{-1}) for (*R*)-DMT. These results indicate that the rate-determining step is the racemization of (*R*)-DMT.

The rate constant for the racemization (k_R/h^{-1}) was measured at 60, 70, 80, or 90 °C. Acetone was used in 0.100, 0.200, and 0.400 mol for 0.0200 mol of (*R*)-Cys, the corresponding k_R's being represented as $k_{R(0.1)}$, $k_{R(0.2)}$, and $k_{R(0.4)}$, respectively. The k_R values and half-life periods ($t_{1/2}$/h) are listed in Table 1 for which the correlation coefficients between ln α_0/α_t and time *t* are over 0.99.

The $k_{R(0.2)}$ value (0.820 h^{-1}) at 80 °C is approximately equal to $k_{R(0.4)}$ (0.838 h^{-1}), though the $k_{R(0.1)}$ value (0.675 h^{-1}) is smaller than these values. Therefore, this racemization does not require acetone more than 10 times the molar amount of (*R*)-Cys. The dependence of $k_{R(0.2)}$ on temperature is given in the range 60—90 °C by

$$\ln k_{R(0.2)} = -12951 / T + 36.44, \quad (2)$$

Table 1. Rate Constant and Half-Life Period for Racemization[a]

Conditions		Rate constant	Half-life period
Temperature	Acetone	h^{-1}	h
°C	mol		
60	0.200	0.089	7.80
70	0.200	0.258	2.68
80	0.100	0.675	1.03
80	0.200	0.820	0.85
80	0.400	0.838	0.83
90	0.200	2.14	0.32

a) (*R*)-Cysteine (0.0200 mol) and acetone were stirred in 30 cm^3 of acetic acid.

Table 2. Racemization of Optically Active Cysteine[a]

Configuration of optically active Cys	Racemization period	Yield of (*RS*)-Cys
	h	g [%[b]]
(*R*)	1.0	2.32 [95.7]
(*R*)	1.5	2.33 [96.0]
(*R*)	2.0	2.34 [96.7]
(*S*)	2.0	2.35 [96.9]
(*S*)	2.5	2.35 [96.9]

a) Cys: Cysteine. Conditions: (*R*)- or (*S*)-Cys 0.0200 mol; acetone 0.200 mol; acetic acid 30 cm^3; temperature approximately 93 °C. b) The yield was calculated on the basis of the amount of (*R*)- or (S)-Cys used by reaction.

where T/K is temperature, and the correlation coefficient has been found to be 0.999. The $k_{R(0.2)}$ value at 50 °C was calculated to be 0.0262 h^{-1} from Eq. 2, which value suggests that the (*R*)-DMT obtained from the reaction at 50 °C for 1 h has 97.4% optical purity. The calculated optical purity agrees well with that (96.5%) of the obtained (*R*)-DMT.

Racemization of Optically Active Cysteine. Based on the above results, (*R*)- or (*S*)-Cys was racemized in the presence of acetone in 10-fold molar amount under reflux (approximately 93 °C). The results are listed in Table 2.

The k_R and $t_{1/2}$ values at 93 °C were calculated from Eq. 2 to be 2.90 h^{-1} and 0.24 h, respectively. These values suggest that 99.7% of optically active Cys is racemized by reacting for 2 h. As seen in Table 2, the racemization is almost complete in reaction for 2 h, and (*RS*)-Cys is obtained in high yield (97%).

References

1) J. Martens, H. Offermans, and P. Scherberich, *Angew. Chem., Int. Ed. Engl.*, **20**, 668 (1981).
2) Y. Irie, F. Kakizaki, and A. Ezaki, Jpn. Patent, 10577 (1983); *Chem. Abstr.*, **98**, 198746n (1983).
3) C. Inoue, Y. Kurima, and S. Moriguchi, Jpn. Patent, 70859 (1982); *Chem. Abstr.*, **97**, 163490b (1982).
4) T. Shiraiwa, Y. Sado, M. Komure, and H. Kurokawa, *Bull. Chem. Soc. Jpn.*, **60**, 3277 (1987).
5) T. Shiraiwa, H. Tazoh, M. Sunami, Y. Sado, and H. Kurokawa, *Bull. Chem. Soc. Jpn.*, **60**, 3985 (1987).
6) S. Yamada, C. Hongo, and I. Chibata, *J. Org. Chem.*, **48**, 843 (1983).
7) S. Ratner and H. T. Clarke, *J. Am. Chem. Soc.*, **59**, 200 (1937).
8) G. E. Woodward and E. F. Schroeder, *J. Am. Chem. Soc.*, **59**, 1690 (1937).
9) J. C. Sheehan and D. H. Yang, *J. Am. Chem. Soc.*, **80**, 1158 (1958).
10) J. S. Davis, "Amino Acids and Peptides," Chapman and Hall, London, New York (1985), p. 130.
11) J. C. Clark, G. H. Phillipps, and M. R. Steer, *J. Chem. Soc., Perkin Trans. 1*, **1976**, 475.
12) "The Merck Index," 10th ed, ed by M. Windholz, Merck and Co., Inc., New Jersey (1983), p. 400.

Asymmetric Induction during the Aminolysis of 5(4*H*)-Oxazolones from *N*-Benzoyl Amino Acids; Almost Specific Formation of One Epimer in the Reaction of the Oxazolone from *N*-Benzoyl-DL-*t*-leucine with Methyl L-Prolinate

Toshifumi MIYAZAWA,* Toshihiko OTOMATSU, Katsutoshi HIGASHI, Takashi YAMADA, and Shigeru KUWATA

Department of Chemistry, Faculty of Science, Konan University, Higashinada-ku, Kobe 658

(Received May 25, 1988)

Synopsis. Asymmetric induction during the aminolysis of 5(4*H*)-oxazolones from *N*-benzoyl amino acids was investigated using a series of amino acid esters as amine nucleophiles. The reaction of the oxazolone from *N*-benzoyl-DL-*t*-leucine with methyl L-prolinate was found to produce the diastereomeric D–L isomer, almost specifically, under appropriate conditions.

The formation of a chirally labile 5(4*H*)-oxazolone has been regarded as one of the main causes of racemization during segment coupling in peptide synthesis.[1] When a racemic oxazolone is allowed to react with an optically active amino acid ester, the peptide product is usually not a 1:1 mixture of diastereomers because of the occurrence of asymmetric induction. However, such asymmetric induction, reported first by Weygand et al.,[2] has not hitherto been explicitly taken into account in the problem of racemization during the segment coupling of two chiral residues.[3] Recently, Benoiton et al.[4] have studied the solvent and temperature effects on asymmetric induction during the aminolysis of the oxazolones from Bz-DL-Leu[5] and Z-Gly-DL-Leu with N^{ε}-Z-L-lysine esters, and have showed that the diastereomeric D–L isomer is formed in excess in a non-polar solvent (dichloromethane or THF) and the L–L isomer is formed in excess in a polar solvent (DMF), the proportion of the L–L isomer increasing with decreasing temperature. On the contrary, in the aminolysis of the pseudooxazolones from *N*-trifluoroacetyl amino acids in THF, it has been reported that the L–L isomer is formed in excess when the esters of amino acids (except proline, as mentioned below) are used as amine nucleophiles.[2b,6] These results indicate that the direction of asymmetric induction depends not only on the solvents but also on the nature of the reactants. It is difficult to draw general conclusions concerning the direction and the extent of asymmetric induction, because relevant experimental data have so far been very limited. This is partly due to the restriction of the methods for the analysis of peptide diastereomers.

We have recently found that diastereomeric pairs of a variety of *N*-acyl dipeptide esters can be separated well by reversed phase high performance liquid chromatography (RP-HPLC).[7] Taking advantage of this procedure we set about to conduct a further study on asymmetric induction in peptide synthesis from the viewpoint of the substituent, solvent, and temperature effects. During the course of this investigation we found a reaction system which generates the largest degree of induction reported to date.

We first investigated asymmetric induction during the aminolysis of the oxazolone from Bz-DL-Val with a series of L-amino acid esters both in a representative non-polar solvent, dichloromethane, and in a representative polar solvent, DMF. As shown in Table 1, even in DMF it is only when L-alanine methyl ester was used as an amine nucleophile that the L–L isomer

Table 1. Asymmetric Induction during the Aminolysis of the 5(4*H*)-Oxazolones from Bz-DL-Val and Bz-DL-Leu with a Series of L-AA-OMe[a,b]

AA	5(4*H*)-Oxazolone from Bz-DL-Val		5(4*H*)-Oxazolone from Bz-DL-Leu
	in CH_2Cl_2	in DMF	in DMF
Ala	62	46	47
Abu	65	60	56
Val	67	65	64
Leu	67	63	59
Nle	78	60	55
Ile	64	66	64
Hep	63	60	57
Pro[c]	84	72	72
Phe	73	58	56
Tyr	66	64	
Phg	57	53	51
Ser	—[d]	—[d]	51
Met	74	51	

a) Data given as % D-L peptide formed. Duration and temperature of the reaction: 24 h at 5 °C. b) The amino acid esters were used in the form of hydrochloride in the presence of an equimolar amount of TEA. c) *p*-Toluenesulfonate. d) The diastereomers of the resulting peptide were not separated.

was formed in excess, while the D-L isomer was the predominant one in other cases. This was also the case with the aminolysis of the oxazolone from Bz-DL-Leu. When the solvent was changed from DMF to dichloromethane, the proportion of the D-L isomer increased in most cases, though there was observed one exception where L-isoleucine methyl ester was used as an amine nucleophile.

Amine nucleophiles had a profound effect on asymmetric induction. The most prominent was the fact that the proportion of the D-L isomer was exceedingly large both in dichloromethane and in DMF when L-proline methyl ester was used as an amine nucleophile. In the aminolysis of 2-trifluoromethyl-5(2*H*)-oxazolones, it has been reported that when an L-proline ester is used as an amine nucleophile, the direction of asymmetric induction is reversed, that is, the D-L isomer is formed predominantly in this case, in contrast to the cases using other L-amino acid esters which generate the L-L isomer in excess.[6] The direction of asymmetric induction during the aminolysis of 2-phenyl-5(4*H*)-oxazolones with proline methyl ester, however, was the same as that caused by the other amino acid esters as amine nucleophiles.

Next, using the proline ester as an amine nucleophile, we examined the aminolysis of the oxazolone derived from *t*-leucine (2-amino-3,3-dimethylbutanoic acid, Tle),[8] an unusual amino acid with a bulkier side chain than valine, in expectation of the generation of a higher degree of asymmetric induction. Thus, the oxazolone from Bz-DL-Tle was allowed to react with L-proline methyl ester in a variety of solvents at different temperatures (50 to −20 °C). The results are summarized in Table 2. Under all the conditions examined the D-L isomer was formed in excess to a large extent (≥70% D-L isomer), as expected. The effect of the solvent was extremely significant. Thus, the proportion of the D-L isomer was smallest in DMF and became largest in aromatic hydrocarbons. A similar effect of aromatic hydrocarbons was observed in the aminolysis (24 h at 0 °C) of other oxazolones with L-proline methyl ester as follows: the percentage of D-Val-L-Pro formed in the aminolysis of the oxazolone from Bz-DL-Val, 66 (DMF), 87 (toluene), 88 (*m*-xylene), 89 (*o*-xylene); percentage of D-aIle-L-Pro formed in the aminolysis of the oxazolone from Bz-DL-Ile, 79 (DMF), 92 (toluene), 92 (*m*-xylene), 92 (*o*-xylene). The effect of the temperature was also profound, especially in less apolar solvents. A lower temperature favored the formation of the D-L isomer in the present case. As a result of both the solvent and the temperature effects, the D-L isomer was formed almost specifically (97% D-L isomer) in the aminolysis of the oxazolone from Bz-DL-Tle in toluene or xylenes at −20 °C. This is the largest degree of asymmetric induction during the aminolysis of the oxazolones reported to date,[9] and makes a unique example of nearly exclusive formation of one epimer via the kinetic resolution of stereochemically labile enantiomers by a chiral reagent.

Table 2. Solvent and Temperature Effects on the Asymmetric Induction during the Aminolysis of the 5(4*H*)-Oxazolone from Bz-DL-Tle with L-Pro-OMe[a,b]

Solvent	Temp/°C			
	50	30	0	−20
DMF	70	76	82	86
Pyridine		79	86	88
CH_2Cl_2		82	92	95
Acetonitrile		84	91	95
Benzene	75	86		
Dioxane	74	89		
THF	87	89	92	93
Ethyl acetate		90	93	95
Toluene		90	95	97
Mesitylene		92	95	96
m-Xylene		92	96	97
o-Xylene	78	93	96	97

a) Data given as % D-L peptide formed. Duration of the reaction: 24 h. b) The amino acid ester was used in the form of *p*-toluenesulfonate in the presence of an equimolar amount of TEA.

Experimental

Optical rotations were measured with a JASCO DIP-4 polarimeter. TLC and preparative TLC were performed on Merck Kieselgel $60F_{254}$ and Kieselgel GF_{254} (Type 60), respectively. The liquid chromatograph employed was a Shimadzu LC-3A instrument, equipped with a Shimadzu SPD-2A variable wavelength UV monitor and a Shimadzu Chromatopac C-R1A data processor. A prepacked ODS column (Cosmosil $5C_{18}$) consisted of a stainless-steel tube, 4.6 mm I.D. and 150 mm long. Bz-DL-Val-OH, Bz-DL-Leu-OH, Bz-DL-Ile-OH, and Bz-DL-Tle-OH[8b] were obtained as described by Greenstein and Winitz.[10] They were converted to 5(4*H*)-oxazolones using DCC or EDC·HCl according to methods described in the literature.[11,12]

HPLC Separation of the Diastereomers of *N*-Benzoyl Dipeptide Methyl Esters. Bz-DL-Val-OH (0.15 mmol) was coupled with H-L-AA-OMe·HCl (or TosOH) (where AA denotes the amino acid residues listed in Table 3) (0.15 mmol) in CH_2Cl_2 (2 ml) at 0 °C in the presence of TEA (0.14 mmol) by the DCC method. The neutral fraction was separated from the reaction mixture as usual. This fraction was submitted to a separation of the diastereomers by RP-HPLC under the conditions shown in Table 3. On the other hand, authentic samples to identify the L-L isomer on the chromatogram were prepared as follows: H-L-Val-L-AA-OMe·HCl (prepared via the coupling of Z-L-Val-OH (1 mmol) with H-L-AA-OMe·HCl (or TosOH) (1 mmol) in the presence of TEA (1 mmol) by means of EDC·HCl (1 mmol) and the subsequent debenzyloxycarbonylation by hydrogenation in the presence of 5% Pd-C and concd HCl) was dissolved in $CHCl_3$ (12 ml) and treated with benzoyl chloride (1.5 mmol) in the presence of TEA (2.2 mmol) for several hours. The neutral fraction was separated from the reaction mixture as usual. The capacity factors ($k'=(t_R-t_0)/t_0$, where t_R=retention time and t_0=void time) and the separation factors ($\alpha=k'_{D-L}/k'_{L-L}$) are listed in Table 3. The diastereomers of Bz-D/L-Val-L-AA-OMe for AA=Ser, Thr, Asp(OMe), Asn, Glu(OMe), Gln, Trp, and His could not be separated ($\alpha=1$) under any conditions examined.

Samples of a diastereomer mixture (L-L isomer + D-L isomer) and the corresponding L-L isomer for Bz-Leu-AA-OMe were prepared in the same manner as mentioned above.

Table 3. HPLC Separation[a] of the Diastereomers of Bz-Val-AA-OMe and Bz-Leu-AA-OMe

AA	Bz-Val-AA-OMe				Bz-Leu-AA-OMe			
	Conditions[b]	k'_{L-L}	k'_{D-L}	α	Conditions[b]	k'_{L-L}	k'_{D-L}	α
Ala	A	2.86	3.01	1.05	C	7.56	8.49	1.12
Abu	A	4.32	4.89	1.13	A	7.02	8.25	1.17
Val	B	3.42	4.05	1.18	B	5.41	6.45	1.19
Leu	B	5.76	6.70	1.16	B	8.46	10.23	1.21
Nle	B	6.37	7.36	1.16	B	9.41	11.37	1.21
Ile	B	5.61	6.68	1.19	B	8.52	10.42	1.22
Hep	B	11.63	13.69	1.18	B	16.94	20.85	1.23
Pro	A	4.45	3.86	1.15[c]	C	13.83	13.03	1.06[c]
Phe	B	5.86	6.77	1.16	B	8.75	9.98	1.14
Tyr	A	3.71	3.47	1.07[c]	A	6.06	5.43	1.12[c]
Phg	B	4.17	4.59	1.10	B	6.20	7.39	1.19
Ser	C	2.97	2.97	1.00	D	7.08	6.65	1.07
Met	A	5.76	6.24	1.08	A	9.60	10.19	1.10

a) Capacity factor, $k'=(t_R-t_0)/t_0$, where t_R=retention time and t_0=void time. Separation factor, $\alpha=k'_{D-L}/k'_{L-L}$. b) A: mobile phase, 50% MeOH aq; flow rate, 1.0 ml min^{-1}; column temp, 50°C. B: mobile phase, 60% MeOH aq; flow rate, 1.0 ml min^{-1}; column temp, 30°C. C: mobile phase, 45% MeOH aq; flow rate, 1.0 ml min^{-1}; column temp, 50°C. D: mobile phase, 45% MeOH aq; flow rate, 0.8 ml min^{-1}; column temp; 50°C. c) In this case, $\alpha=k'_{L-L}/k'_{D-L}$.

Their HPLC data are also listed in Table 3. The diastereomers of Bz-D/L-Leu-L-AA-OMe for AA=Thr, Asp(OMe), Asn, Glu(OMe), Gln, and Trp could not be separated under any of the conditions examined.

Samples of a diastereomer mixture, L-Ile-L-Pro + D-aIle-L-Pro, and the corresponding L-L isomer were prepared in the same manner as mentioned above: k' for D-aIle-L-Pro was 3.67 and k' for L-Ile-L-Pro 4.30, and α=1.17 under the conditions B in the footnote b of Table 3.

Bz-L-Tle-L-Pro-OMe and Bz-D-Tle-L-Pro-OMe. These were obtained through a treatment of H-L(or D)-Tle-L-Pro-OMe·HCl (prepared in the same manner as described above for the valyl peptide derivatives) with benzoyl chloride in the presence of *N,N*-diisopropylethylamine in $CHCl_3$. L-L Isomer: syrup, purified by preparative TLC on silica gel with $CHCl_3$-EtOAc (9:1); $[\alpha]_D^{25}$ −70.5° (*c* 1.5, MeOH); Anal. ($C_{19}H_{26}N_2O_4$) C, H, N. D-L Isomer: mp 123—124°C (uncorrected) (EtOAc-petroleum ether); $[\alpha]_D^{22}$ −26.1° (*c* 1.0, MeOH); Anal. ($C_{19}H_{26}N_2O_4$) C, H, N. HPLC k'_{L-L}=5.20, k'_{D-L}=4.58, and α=1.14 (t_0=ca. 3.3 min) under the following conditions: mobile phase, 50% MeOH aq; flow rate, 1.0 ml min^{-1}; column temperature, 30°C; detection, 254 nm; sensitivity range, 0.02 absorbance units full scale (a.u.f.s.).

Aminolysis of 5(4*H*)-Oxazolones with L-Amino Acid Methyl Esters. A 5(4*H*)-oxazolone (0.15 mmol) and H-L-AA-OMe·HCl (or TosOH) (where AA denotes the amino acid residues listed in Table 1) (0.15 mmol) were dissolved (or suspended) in 1.5 ml of solvent, and the mixture was placed into a thermostatted bath (−20°C, 0°C, 5°C, 30°C, or 50°C). After 15 min, a solution of TEA (0.15 mmol) in 0.5 ml of the solvent was added and the reaction mixture was stirred for 24 h at the set temperature. After an addition of EtOAc (20 ml), the organic layer was separated, washed with 5% HCl, water, sat. $NaHCO_3$, and water, and dried over Na_2SO_4. One part of the residue obtained by the evaporation of the solvent was dissolved in MeOH and submitted to HPLC analysis. The results are summarized in Tables 1 and 2.

References

1) D. S. Kemp, "The Peptides," ed by E. Gross and J. Meienhofer, Academic Press, New York (1979), Vol. 1, Chap. 7.

2) a) F. Weygand, W. Steglich, and X. Barocio de la Lama, *Tetrahedron, Suppl.*, **8**, Part 1, 9 (1966); b) W. Steglich, D. Mayer, X. Barocio de la Lama, H. Tanner, and F. Weygand, "Peptide 1966," ed by H. C. Beyerman, A. van de Linde, and W. Maassen van den Brink, North-Holland Publ., Amsterdam (1967), p. 67.

3) N. L. Benoiton, "The Peptides," ed by E. Gross and J. Meienhofer, Academic Press, New York (1983), Vol. 5, Chap. 4, p. 263.

4) N. L. Benoiton, K. Kuroda, and F. M. F. Chen, *Tetrahedron Lett.*, **22**, 3361 (1981).

5) Abbreviations given by the IUPAC-IUB Joint Commission (*Eur. J. Biochem.*, **138**, 9 (1984) are used throughout. Additional abbreviations: Bz, benzoyl; Z, benzyloxycarbonyl; THF, tetrahydrofuran; DMF, *N,N*-dimethylformamide; Abu, 2-aminobutanoic acid; Nle, norleucine; Hep, heptyline (2-aminoheptanoic acid); Phg, *C*-phenylglycine; aIle, alloisoleucine; DCC, dicyclohexylcarbodiimide; EDC, 1-ethyl-3-(3-dimethylaminopropyl)carbodiimide; TosOH, *p*-toluene-sulfonic acid; TEA, triethylamine.

6) I. Tomida, S. Senda, T. Kuwabara, and K. Katayama, *Agric. Biol. Chem.*, **40**, 2033 (1976), and references cited therein.

7) T. Miyazawa, T. Yamada, and S. Kuwata, "Peptide Chemistry 1982," ed by S. Sakakibara, Protein Research Foundation, Osaka (1983), p. 69.

8) For the synthesis of the racemic compound, see, a) T. Miyazawa, K. Takashima, Y. Mitsuda, T. Yamada, S. Kuwata, and H. Watanabe, *Bull. Chem. Soc. Jpn.*, **52**, 1593 (1979); b) T. Miyazawa, T. Nagai, T. Yamada, S. Kuwata, and H. Watanabe, *Mem. Konan Univ., Sci. Ser.*, **1979**, 51.

9) The proportion of the L-L isomer was reported to be 89% in the reaction of the 5(2*H*)-oxazolone from *N*-trifluoroacetyl-DL-*t*-leucine with *t*-butyl L-valinate in THF at ambient temperature for 90 h; E. Frauendorfer, W. Steglich, and F. Weygand, *Chem. Ber.*, **106**, 1019 (1973).

10) J. P. Greenstein and M. Winitz, "Chemistry of the Amino Acids," John Wiely & Sons, New York (1961), p. 1266.

11) F. M. F. Chen, K. Kuroda, and N. L. Benoiton, *Synthesis*, **1979**, 230, and references cited therein.

12) For the 5(4*H*)-oxazolone from Bz-DL-Tle-OH, see, A. Kjaer, *Acta Chem. Scand.*, **7**, 889 (1953).

Decalino-14-crown-4. New Type of Lithium Ion Selective Ionophore

Kazuya KOBIRO,* Toshitaka HIRO, Toshihiro MATSUOKA, Kiyomi KAKIUCHI, Yoshito TOBE, and Yoshinobu ODAIRA
Department of Applied Fine Chemistry, Faculty of Engineering, Osaka University, Suita, Osaka 565
(Received June 24, 1988)

Synopsis. A new type of crown ether, decalino-14-crown-4, has been synthesized and found to be a highly selective and effective ionophore for lithium ion.

Recently, lithium has become increasingly important not only in the wide area of the synthetic and industrial chemistry but also in the field of the atomic fusion as a vital raw material for tritium.[1] From the viewpoint of supplying for its great demand, much attention has been paid even to the concentration of lithium from the sea water. But the extration of lithium ion from the aqueous phase has been very difficult because of the strong hydration of water molecules around the cation. Only a few reports have been so far presented on the extraction or transport of lithium ion. Bartsch et al. reported that 14-crown-4 derivative bearing carboxyphenyl group as an additional binding site exhibited good lithium/sodium ion selectivity in competitive extraction.[2] Takagi,[3] Sasaki,[4] Shono,[5] and their co-workers independently reported that crown ethers with phenolic group as an additional binding site showed the excellent lithium/sodium ion selectivity in extraction of alkali metal ions.

On the other hand, as an extension of a decalin wall strategy for the design of new host molecules with high guest-selectivity,[6] we have previously reported that the cylindrical crown ether, didecalino-14-crown-4† (**1**), with no additional binding site exhibits highly effective extractabilty for lithium ion due to the embedding effect of decalin wall, by which the coordinated lithium ion was buried deep in lipophilic cylinder and was protected from the hydration of water molecules.[7] Althogh the crown ether **1** was an excellent **extractant** for lithium ion, it is not expected to be a selective and effective **ionophore** for lithium ion, because of the low efficiency of decomplexation process suppressed by the embedding effect of the decalin walls.

We now design a new type of lithium ion selective ionophore, decalino-14-crown-4 (**2**), containing one decalin subunit. This molecule is expected to satisfy the indispensable conditions as a selective ionophore: i) the appropriate balance between complexation and decomplexation abilities with the cation and ii) high lipophilicity required for efficient recycle of ionophore. In this paper, we wish to report on the synthesis of **2** and the effect of incorporated decalin subunits on lithium ion transport.

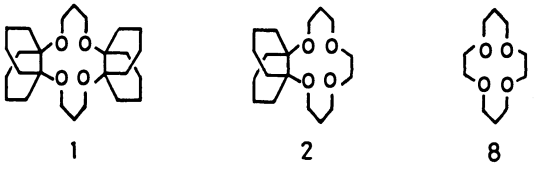

1 2 8

† Ortho-fused cyclic compound is tentatively named "decalino" for decahydronaphtho[4a, 8a].

Results and Discussion

The target ionophore **2** was synthesized by the similar procedure described by Liotta et al.[8] Reaction of 4a,8a-decalindiol (**3**) with 1,10-dichloro-4,7-dioxadecane (**4**) in dimethyl sulfoxide (DMSO) with NaOH as a base at 110 °C gave **2** as crystals (mp 69—70 °C), as shown in Scheme 1. As a reference compound, stilbene-incorporated decalino-18-crown-6, 7,8-dipheyl-2,6,9,13-tetraoxatricyclo[12.4.4.0^{1,14}]docos-7-ene (**7**), was designed. In this molecule, the stilbene unit is expected to have high lipophilicity as well as the decalin subunit. But, there is a marked difference in influence on the structure of crown ether ring between two subunits. Namely, two vinyl oxygen atoms bonding to the stilbene subunit must be fixed on the same plane, in contrast with gauche conformation of two oxygen atoms bonding to the decalin subunit or flexible conformation of them bonding to the ethane subunit. Crown ether **7** was synthesized by the method similar to that described by Merz[9a] and Inoue et al.[9b] Namely, reaction of 4a,8a,-bis[3-(tosyloxy)propoxy]-decalin (**5**) and benzoin with aqueous NaOH under phase-transfer conditions produced **7** in 22% yield as crystals (mp 154—155 °C).

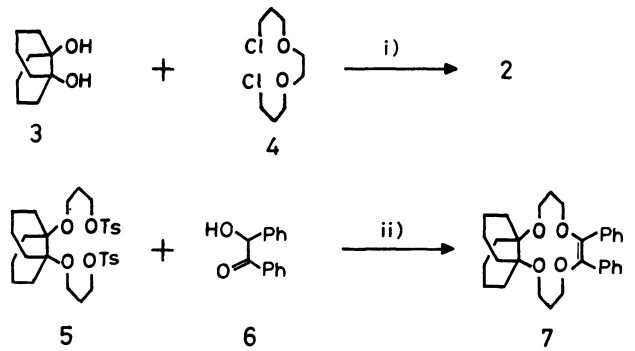

i) NaOH, $LiClO_4$ ii) NaOH, Bu_4NBr

Scheme 1.

Prior to the transport experiment of alkali metal ions, solvent extraction was carried out in water/dichloromethane system[7] in order to know the complexation ability of the ionophore **2** toward some alkali metal ions. The results are listed in Table 1. The data in Table 1 clearly show that ionophore **2** has both excellent extractability for lithium ion (81%) and prominent Li^+/Na^+ selectivity (Li^+/Na^+=16), as

compared with **1** ($Li^+/Na^+=5$) and the reference compounds, **7** ($Li^+/Na^+=4$) and 14-crown-4 (**8**) ($Li^+/Na^+=11$). In addition, ionophore **2** could hardly extract K^+, Rb^+, and Cs^+. The selectivity order of **2** is $Li^+ \gg Na^+ > K^+ \simeq Rb^+ \simeq Cs^+$, indicating that ionophore **2** would be an efficient and selective ionophore for lithium ion. These high extractability of **1** and **2** is ascribed to the embedding effect of decalin wall by which the coordinated lithium ion is buried deep in the lipophilic atmosphere and is protected from hydration by excluding water molecules out of its coordination sphere. The difference of Li^+ and Na^+ extractability by using **1** and **2** is explained as follows: In the case of **1** having two decalin subunits, the embedding effect is expected to be very strong. Accordingly, ionophore **1** extracts Na^+ which is somewhat larger than the cavity size of **1**, not to mention Li^+ being suitable for its cavity. In the case of **2** having one decalin subunit, the embedding effect is not so strong as compared with in the case of **1**. Therefore, ionophore **2** extracts only Li^+ effectively being suitable for its cavity, while does not Na^+ being somewhat larger than its cavity.

Next, the competitive alkali metal ion transport was executed at 25 °C in a double glass cell where two aqueous phases were separated by the chloroform membrane containing the ionophore. Figure 1a illustrates the plots for competitive transport of Li^+ by using **2**, **7**, or **8** and in which those for other alkali metal ions are omitted from a graph for clarification.[10] As expected, the target ionophore **2** turned out to be an effective ionophore for Li^+ as compared with the reference compounds **7** and **8** (Fig. 1a). The rate of Li^+ transport by using **2** is about ten-fold faster than those by using **7** and **8**. Figure 1b illustrates the results of competitive transport of alkali metal ions by using **2**. The ionophore **2** did not transport K^+, Rb^+, and Cs^+ at all. The most outstanding in Fig. 1b is the high Li^+/Na^+ selectivity of **2**. Significantly, the Li^+/Na^+ selectivity, although not very accurate because of the slow transport of Na^+, was determined to be 20 (calculated from the ratio of the average flux during 24 h). As a result, a new type of ionophore **2** having one decalin subunit without additional binding site is proved to be a highly lithium ion selective and effective ionophore.

Further studies on the separation of isotopes ($^6Li^+$ and $^7Li^+$) by the decalino-14-crown-4 derivatives are now in progress.

Table 1. Extraction of Alkali Metal Picrates in Water/Dichloromethane System by Ionophores, **2**, **7**, and **8**

Ionophore	Extractability/%				
	Li^+	Na^+	K^+	Rb^+	Cs^+
1	ca. 100	20			
2	81	5	1	1	ca. 0
7	13	3	3	3	3
8	11	1	ca. 0	ca. 0	ca. 0

[ionophore]=7.0×10^{-4} M, [picric acid]=7.0×10^{-5} M, and [alkali metal hydroxide]=0.1 M at 25.0±0.1 °C.

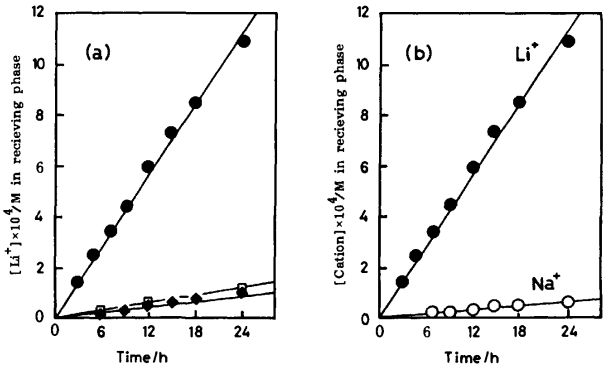

Fig. 1. Competitive transport of alkali metal ions through chloroform membrane containing ionophores.
(a): Plots for transport of Li^+ by using —●— **2**, —◆— **7**, or —□— **8**. Plots for Na^+, K^+, Rb^+, and Cs^+ were omitted from the graph for clarification.
(b): Plots for competitive transport of alkali metal ions by using **2**. K^+, Rb^+, and Cs^+ were not transported under these conditions.

Experimental

All melting points were uncorrected. IR spectra were recorded on a Hitachi 260-10 spectrometer. Mass spectra were recorded on a Hitachi RMU-6E spectrometer at 70 eV ionization energy. ^1H NMR spectra were measured on a JEOL JNM-PS 100 spectrometer in $CDCl_3$ solution using Me_4Si as an internal standard. ^{13}C NMR spectrum was measured on a JEOL JNM-FX-60 spectrometer in $CDCl_3$ solution. Electronic spectra were taken with a Hitachi 356 spectrophotometer. Flame photometric analyses were performed on a Nippon Jarrell Ash AA-8500 Mark II spectrophotometer.

Materials. Benzoin and dimethyl sulfoxide (DMSO) were purchased from Wako Pure Chemical Industries.

Synthesis. 1,10-Dichloro-4,7-dioxadecane (**4**) was prepared from 4,7-dioxadecane-1,10-diol[5] by chlorination as an oil: IR (neat) 1120 cm^{-1}; MS *m/z* (rel intensity) 214 (M^+), 151 (4), 122 (24), 108 (72), 41 (100); ^1H NMR (CCl_4) δ=1.95 (q, *J*=6 Hz, 4H), 3.4—3.7 (m, 12H). Found: C, 44.62; H, 7.55; Cl, 32.75%. Calcd for $C_8H_{16}Cl_2O_4$: C, 44.67; H, 7.50; Cl, 32.96%. 4a,8a-Bis[3-(tosyloxy)propoxy]decalin (**5**) was prepared from 4a,8a-bis(3-hydroxypropoxy)decalin by usual method and was used without further purification. 4a,8a-Bis(3-hydroxypropoxy)decalin was prepared from 4a,8a-decalindiol (**3**) by reaction with allyl bromide followed by hydroboration-oxidation: IR (neat) 3400, 1080 cm^{-1}; MS *m/z* (rel intensity) 286 (M^+), 211 (8), 136 (100); ^1H NMR (CCl_4) δ=1.0—2.1 (m, 20H), 3.3—4.2 (m, 10H). Found: C, 65.93; H, 10.55%. Calcd for $C_{16}H_{30}O_4 \cdot 0.3\ (H_2O)$; C, 65.86; H, 10.56%.

Decalino-14-crown-4 (2). A mixture of 4.5 g (0.11 mol) of NaOH and 12 g (0.11 mol) of $LiClO_4$ in 80 ml of DMSO was brought to 100 °C slowly and stirred for 20 min. After being cooled to room temperature, 8.2 g (48 mmol) of diol **3** was added. To this mixture was added dropwise a solution of 5.1 g (24 mmol) of dichloride **4** in 5 ml of DMSO over 2 h. The mixture was stirred at 110 °C for 24 h and then another 5.2 g (24 mmol) of **4** in 5 ml of DMSO was added dropwise over 2 h. The mixture was stirred for 12 h at 110 °C and cooled to room temperature. To this mixture was added 400 ml of water and the resulting solution was extracted with dichloromethane. The organic phase was dried over $MgSO_4$ and the solvent was evaporated in vacuo. The residure was

chromatographed on silica gel (ether/light petroleum=5/95) to afford 100 mg (1%) of **2**: mp 69—70 °C (recrystallized from light petroleum); IR (KBr) 1120 cm^{-1}; MS *m/z* (rel intensity) 312 (M^+), 178 (6), 136 (100); ^1H NMR δ=1.0—1.9 (m, 20H), 3.0—4.0 (m, 12H, s at 3.69); ^{13}C NMR δ=20.7 (t, 2C), 23.4 (t, 2C), 30.4 (t, 2C), 31.3 (t, 4C), 56.7 (t, 2C), 67.6 (t, 2C), 71.3 (t, 2C), 78.0 (s, 2C). Found: C, 69.01; H, 10.35%. Calcd for $C_{18}H_{32}O_4$: C, 69.20; H, 10.32%.

7,8-Diphenyl-2,6,9,13-tetraoxatricyclo[12.4.4.0^{1,14}]docos-7-ene (7). A mixture of 10.9 g (18 mmol) of ditosylate **5** and 3.9 g (18 mmol) of benzoin in 130 ml of benzene was stirred mechanically for 1 h at 40 °C. After being cooled, 98 mg (0.47 mmol) of tetrabutylammonium bromide was added. To this mixture was added 20 ml of 50% NaOH. After continuous stirring for 40 h at 70 °C, the mixture was cooled to room temperature, washed with 100 ml of water and the organic phase was separated. The aqueous phase was extracted with dichloromethane and the combined organic phase was dried over $MgSO_4$. The solvent was removed by evaporation and the residue was chromatographed on silica gel (ether/light petroleum=3/97) to give 1.89 g (22%) of **7**: mp 154—155 °C (recrystallized from light petroleum); IR (KBr) 3050, 1590, 1100 cm^{-1}; MS *m/z* (rel intensity) 462 (M^+), 252 (65), 147 (100); ^1H NMR δ=1.2—2.1 (m, 20H), 3.4—4.2 (m, 8H), 7.0—7.4 (m, 10H). Found: C, 77.84; H, 8.33%. Calcd for $C_{30}H_{38}O_4$:, C, 77.89; H, 8.28%.

Extraction. Extraction of alkali metal picrates by crown ethers into dichloromethane was preformed by the method described previously.[7]

Transport. Competitive transport of alkali metal ions through chloroform membrane containing ionophore was performed at 25.0±0.1°C using a double glass cell (diameters: inner 2.6 cm and outer 5.0 cm) where two aqueous phases were separated by chloroform membrane containing ionophore. Membrane: ionophore (1.5×10^{-4} M; 1 M=1 mol dm^{-3}) in 60.0 ml of chloroform; source phase: LiOH, NaOH, KOH, RbOH, and CsOH (each 1.0×10^{-2} M) and picric acid (6.0×10^{-3} M) in 15.0 ml of deionized water; recieving phase: 20.0 ml of deionized water. Metal ion concentrations were determined by flame photometry.

We are grateful to Professor Toshiyuki Shono and Dr. Keiichi Kimura for their helpful discussion and advice.

References

1) For example see: K. Nishizawa, H. Watanabe, S. Ishino, and M. Shinagawa, *J. Nucl. Sci. Technol.*, **21**, 133 (1984); K. Nishizawa, S. Ishino, H. Watanabe, and M. Shinagawa, *ibid.*, **21**, 694 (1984).

2) R. A. Bartsch, B. P. Czech, S. I. Kang, L. E. Stewart, W. Walkowiak, W. A. Charewicz, G. S. Heo, and B. Son, *J. Am. Chem. Soc.*, **107**, 4997 (1985).

3) Y. Katayama, K. Nita, M. Ueda, H. Nakamura, and M. Takagi, *Anal. Chim. Acta*, **173**, 193 (1985).

4) K. Sasaki and G. Pacey, *Anal. Chim. Acta*, **174**, 141 (1985).

5) K. Kimura, M. Tanaka, S. Iketani, and T. Shono, *J. Org. Chem.*, **52**, 836 (1987).

6) K. Kobiro, M. Takahashi, Y. Odaira, Y. Kawasaki, Y. Kai, and N. Kasai, *J. Chem. Soc., Dalton Trans.*, **1986**, 2613; K. Kobiro, M. Takahashi, S. Takada, K. Kakiuchi, Y. Tobe, and Y. Odaira, *Chem. Lett.*, **1986**, 455.

7) K. Kobiro, T. Matsuoka, S. Takada, K. Kakiuchi, Y. Tobe, and Y. Odaira, *Chem. Lett.*, **1986**, 713.

8) F. L. Cook, T. C. Caruso, M. P. Byrne, C. W. Bowers, D. H. Spech, and C. L. Liotta, *Tetrahedron Lett.*, **1974**, 4029.

9) a) A. Merz, *Angew. Chem.*, **89**, 484 (1977); *Angew. Chem., Int. Ed. Engl.*, **16**, 467 (1977). b) Y. Inoue, M. Ouchi, T. Nakazato, T. Matsuda, and T. Hakushi, *Chem. Lett.*, **1982**, 781.

10) Na^+, K^+, Rb^+, and Cs^+ concentration in recieving phase by using **2**, **7**, and **8** are as follows: **2**: Na^+, 0.55×10^{-4} M/24 h; K^+, Rb^+, and Cs^+ were not transported after 24h under there conditions. **7** and **8**: Na^+, K^+, Rb^+, and Cs^+ were not detected after 24 h under these conditions.

A Determination Method of Absolute Configuration

Fumio TODA,* Koji MORI, and Atsushi SATŌ
Department of Industrial Chemistry, Faculty of Engineering,
Ehime University, Matsuyama 790
(Received June 29, 1988)

Synopsis. A determination method of absolute configuration of sulfoxides, amines, and aminoalcohols by measuring their ^{1}H NMR spectra in the presence of optically active 2,2′-dihydroxy-1,1′-binaphthyl and 1,6-di(*o*-chlorophenyl)-1,6-diphenyl-2,4-hexadiyne-1,6-diol, was reported.

There are mainly three determination methods of absolute configuration of chiral compounds, CD- and X-ray analyses and chemical conversion to a configurationally known compound. However, each method has own problem. We report a simple method of determining the absolute configuration by a combination of host–guest complexation and ^{1}H NMR spectra measurement. Previously, it was reported that optically active 2,2′-dihydroxy-1,1′-binaphthyl (**1**) and 1,6-di(*o*-chlorophenyl)-1,6-diphenylhexa-2,4-diyne-1,6-diol (**2**) form complex with a wide variety of organic compounds not only in the solid state[1] but also in solution,[2] and these host compounds can be used as chiral shift reagents.[2]

We recently found that the direction and magnitude of shifts of the proton signals of the complex depend on the difference of absolute configuration of the host and guest compounds, and that the phenomena are applicable to determining the absolute configuration of the guest compounds. Although a similar determination method of the absolute configuration of sulfinate esters[3] and γ-lactones[4,5] by using optically active 1-phenyl- (**3a**), 1-(1-naphthyl)- (**3b**), and 1-(9-anthryl)-2,2,2-trifluoroethanol (**3c**) has been known, application of this method to sulfoxides, amines, and aminoalcohols has not been reported.

Experimental

General. All the ^{1}H NMR spectra were measured in $CDCl_3$ by JEOL-PMX 60 Spectrometer. All the host (**1** and **2**) and the guest compounds (**4**—**18**) were prepared according to the reported method in the literature cited.[1]

Results and Discussion

For example, the methyl signal (δ 2.717) of racemic methyl phenyl sulfoxide (**4**) is split into two signals at δ 2.654 and 2.667 in the presence of an equimolar amount of (*S*)-(−)-**1** (**1a**) (Table 1). The optically pure (*R*)-(+)- and (*S*)-(−)-**4**[6] show the former and the latter signals, respectively, under the same conditions. In the case of other alkyl aryl sulfoxides, **6**[7] and **7**,[8] the methyl signals of (*S*)-(−)-enantiomers are also in higher field than those of (*R*)-(+)-ones (Table 1). (*S*)-(+)-Enantiomer of butyl methyl sulfoxide (**7**)[9] showed its methyl signal at higher field than did (*R*)-(−)-one. Although the configuration of other dialkyl sulfoxides **8**—**10** has not been determined, their (+)-enantiomers which show the methyl signal at higher field probably have (*S*)-configuration. This assignment is probably correct because (+)-enantiomers of many alkyl methyl sulfoxides such as ethyl methyl,[9] methyl propyl, isopropyl methyl,[10,11] isobutyl methyl,[11] and *t*-butyl methyl sulfoxides[9] have been reported to have (*S*)-configuration. In the case of dialkyl sulfoxides, however, more than two molar amounts of **1a** are necessary for a splitting of the methyl signal (Table 1).

In the case of amines, **11**,[12] **12**,[13] **13**,[14] and **14**, the methyl signals of their (*R*)-enantiomers appeared at higher field than did those of (*S*)-ones in the presence of **1a** (Table 1). However, the methine signal of **15**[15] or **16** appeared at higher field when the configuration is (*S*). Although the methine signals of **12** (δ 4.117) and **13** (4.217) were not split by **1a**, these were split to δ 3.801 and 3.843, and 4.040 and 4.067, respectively, in the presence of (*R*,*R*)-(−)-**2** (**2a**), and the signal of (*S*)-enantiomers appeared at higher field. Methyl signals of aminoalcohols **17**[16] and **18**[17] were also split by **1a**, and those of (*S*)-enantiomers appeared at higher field (Table 1). These data clearly show again the presence of a correlation between the manner of shift in

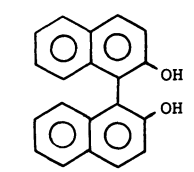

1
a: (*S*)-(−)-enantiomer
b: (*R*)-(+)-enantiomer

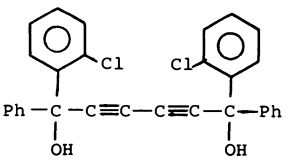

2
a: (*R*,*R*)-(−)-enantiomer
b: (*S*,*S*)-(+)-enantiomer

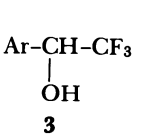

3
a: Ar=Ph
b: Ar=

c: Ar=

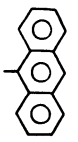

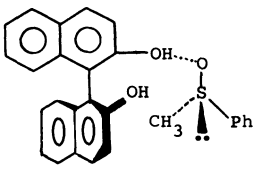

1a·(*S*)-(−)-**4**
19

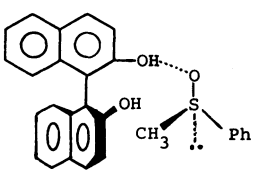

1a·(*R*)-(+)-**4**
20

Fig. 1. Shielding effect in the complex.

Table 1. Chemical Shift Values of the Italicized Protons of Guest Compounds in the Absence and Presence of **1a**, and Assignment of Absolute Configuration to the Shifted Signal to Relatively Higher Magnetic Field[a)]

Guest compound	Chemical shift δ/ppm			Absolute configuration
	Molar ratio of **1a** to the guest			
	0	0.5—3		
Ph-SO-C*H*$_3$ (**4**)	2.717	1	2.654 2.667	(*S*)-(−)
m-Tol-SO-C*H*$_3$ (**5**)	2.717	2	2.616 2.633	(*S*)-(−)
p-Tol-SO-C*H*$_3$ (**6**)	2.700	1	2.667 2.680	(*S*)-(−)
Bu^n-SO-C*H*$_3$ (**7**)	2.367	3	2.315 2.333	(*S*)-(+)
Am^n-SO-C*H*$_3$ (**8**)	2.517	2	2.413 2.433	(*S*)-(+)
Hex^n-SO-C*H*$_3$ (**9**)	2.517	2	2.417 2.433	(*S*)-(+)
Hep^n-SO-C*H*$_3$ (**10**)	2.583	2	2.453 2.470	(*S*)-(+)
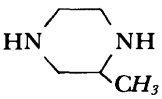 (**11**)	0.958	1	0.640 0.683	(*R*)-(−)
Ph-CH(NH$_2$)-C*H*$_3$ (**12**)	1.377	1	1.124 1.167	(*R*)-(+)
2-Naph-CH(NH$_2$)-C*H*$_3$ (**13**)	1.450	1	1.235 1.267	(*R*)-(+)
C*H*$_3$-CH(NH$_2$)-COOCH$_3$ (**14**)	1.333	0.5	1.170 1.200	(*R*)-(−)
CH$_3$CH$_2$-C*H*(NH$_2$)-CH$_3$ (**15**)	2.806	1	2.317 2.367	(*S*)-(+)
(CH$_3$)$_2$CHCH$_2$-C*H*(NH$_2$)-COOCH$_3$ (**16**)	3.500	0.5	3.250 3.317	(*S*)-(+)
C*H*$_3$-CH(OH)-CH$_2$-NH$_2$ (**17**)	1.150	0.5	0.900 0.917	(*S*)-(+)
HO-CH$_2$-CH(NH$_2$)-CH(C*H*$_3$)$_2$ (**18**)	0.917	0.5	0.583 0.665	(*S*)-(+)

a) All the spectra were measured at a concentration of guest compound 0.02 g in 1 ml $CDCl_3$. When the signal is multiplet, chemical shift value at a center of the signal is indicated.

^{1}H NMR spectra and absolute configuration. Using the relation, absolute configuration of amines and aminoalcohols can be determined.

Of course, the two signals at higher and lower fields take turn when **1b** and **2b** are used instead of **1a** and **2a**, respectively.

The regular correlation between the configuration and the manner of shift of signal is probably due to the shielding effect in the complex of the components (Fig. 1). For example, **1a** forms complexes with (*S*)-**4** (**19**) and with (*R*)-**4** (**20**). In **19**, the methyl is shielded by the naphthyl group of **1a** and its signal appears at higher field than that of **20** (Fig. 1).

In all complexes, hydrogen bond may play an important role as is shown in Fig. 1. Since amines and aminoalcohols form relatively stronger hydrogen bond with **1a** than do dialkyl sulfoxide, smaller amount of **1a** is probably enough for the splitting of the former's signal. Nevertheless, the complex formation in solution does not always support the formation of crystalline inclusion complex. For example, **4**, **5**, and **7** form crystalline complex with **1**, and these are effectively resolved.[1)] However, **6**, **8**, **9**, and **10** do not form complex with **1**. Contrarily, **7**—**10** form complex with **2** and these are resolved.[1)] Although **11** forms complex with **2** and is efficiently resolved,[18)] **12**—**18** do not from comlex with **2**. Nevertheless, **17** and **18** form complex with **1** and are resolved.[19)]

References

1) F. Toda, *Top. Curr. Chem.*, **140**, 43 (1987).
2) F. Toda, K. Mori, J. Okada, M. Node, A. Itoh, K. Oomine, and K. Fuji, *Chem. Lett.*, **1988**, 131.
3) W. H. Pirkle and M. S. Hoekstra, *J. Am. Chem. Soc.*, **98**, 1832 (1976).
4) W. H. Pirkle, D. L. Sikkenga, and M. S. Pavlin, *J. Org. Chem.*, **42**, 384 (1977).
5) W. H. Pirkle and D. L. Siggenga, *J. Org. Chem.*, **42**, 1370 (1977).
6) U. Folli, D. Iarassi, F. Montanari, and G. Torre, *J. Chem. Soc. C*, **1968**, 1317.
7) F. Toda, K. Tanaka, and T. C. W. Mak, *Chem. Lett.*, **1984**, 2085.
8) K. Mislow, M. M. Green, P. Laur, J. T. Melillo, T. Simmons, and A. L. Ternay, Jr., *J. Am. Chem. Soc.*, **87**, 1958 (1965).
9) M. Axelroad, P. Bickart, M. L. Goldstein, M. M.

Green, A, Kiaer, and K. Mislow, *Tetrahedron Lett.*, **1968**, 3249.
10) M. Mikolajczyk and J. Drabowicz, *Tetrahedron Lett.*, **1972**, 2379.
11) W. G. Gallet and W. Gaffield, *J. Chem. Soc. C*, **1969**, 2437.
12) W. L. F. Argarego, H. Sshou, and P. Waring, *J. Chem. Res. (S)*, **1980**, 133.
13) W. Leithe, *Chem. Ber.*, **64**, 2827 (1931).
14) H. Wolf, E. Bunnenberg, and C. Djerass, *Chem. Ber.*, **97**, 533 (1964).
15) J. A. Mills and W. Klyne, "Progress in Stereochemistry," Academic Press, Inc., New York, N. Y. (1954), Vol. 1, p. 195.
16) D. E. Wolf, W. H. Jones, J. Valiant, and K. Folkers, *J. Am. Chem. Soc.*, **72**, 2820 (1950).
17) F. Barrow and G. W. Ferguson, *J. Chem. Soc.*, **1935**, 410.
18) F. Toda, K. Tanaka, and M. Kido, *Chem. Lett.*, **1988**, 513.
19) F. Toda and K. Mori, unpublished data.

 © 1988 The Chemical Society of Japan Bull. Chem. Soc. Jpn., 61, 4171—4175 (1988)

Measurements of the Polarized ATR Spectra for Adsorbed Dye Layers by Using a Stack of Thin Glass Plates

Michio KOBAYASHI,* Hitoshi TOKUNAGA, Jun OKUBO,† Toshihiko HOSHI,† and Yoshie TANIZAKI
Department of Chemistry, Nagaoka University of Technology, Nagaoka-shi 940-21
†Department of Chemistry, College of Science and Engineering, Aoyama Gakuin University, Chitosedai, Setagaya-ku 157
(Received January 16, 1988)

Polarized ATR spectra have been measured for the dye layers adsorbed on stacked, thin glass plates. For the adsorbed Crystal Violet (CV) layer, the metachromasy band in the || polarized ATR spectrum is blue-shifted and intensified in comparison with that in the ⊥ polarized ATR spectrum. This is in marked contrast to the observation for the adsorbed Methylene Blue (MB) layer that the || polarized ATR spectrum is similar in shape and position to the ⊥ polarized ATR spectrum. The blue shift and the enhancement of the metachromasy band in the || polarized ATR spectrum for the adsorbed CV layer is ascribed to an optical property characteristic of the adsorbed CV layer; the adsorbed CV layer exhibits an extra electronic transition band located at the high-energy side of the metachromasy band and polarized normal to the glass plane. Two possible explanations for the occurrence of this extra band are presented.

A conventional measurement of the absorption spectrum of molecules adsorbed on a glass surface using a polarized light with normal incidence allows only a two-dimensional detection of the optical anisotropy in the glass plane. In contrast, the polarized ATR (attenuated total reflection) method enables observations of the three-dimensional optical anisotropy of the adsorbed layer, including the anisotropy in the direction of the thickness.[1] Wilks and Hirschfeld proposed a method for obtaining the ATR spectra by employing a stack of thin internal-reflection plates, the sample material being sandwiched between the plates.[2] This method is ideal for liquids contained between the plates by capillary action. In the present study we measured the polarized ATR spectra in the visible region for adsorbed dye layers using a stack of thin glass plates whose surfaces adsorbed dye molecules.

Experimental

Commercial Crystal Violet (CV) and Methylene Blue (MB) were used without further purification. A borosilicate glass plate (55×9.5×0.16 mm) was thoroughly washed by successive sonications in isopropyl alcohol, hot distilled water, concd nitric acid and hot distilled water and finally by steam washing with distilled water. Sixty sheets of the glass plates, thus cleaned, were placed in a holder appropriate for preventing stacking, and dipped in CV or MB aqueous solution for several hours. These glass plates which adsorbed CV or MB were, after rinsing several times with distilled water, placed in a plastic cell filled with distilled water, as illustrated in Fig. 1a. The polarized ATR spectrum for this sample cell was measured using a Shimadzu UV-360 spectrophotometer equipped with a Rochon-type polarizer made of synthetic quartz (Karl Lambrecht Corp.). The optical arrangement is shown in Fig. 1b. Ordinary rays from a Rochon-type polarizer are almost perfectly plane-polarized and the plane of their electric field vector can be rotated by rotating the polarizer. The || and ⊥ polarized light thus obtained, the vibrating electric field vectors of which are parallel and perpendicular, respectively, to the plane of incidence, as defined in Fig. 1a, are introduced into the side of the stack of thin glass plates with an angle of incidence of θ, defined in Fig.

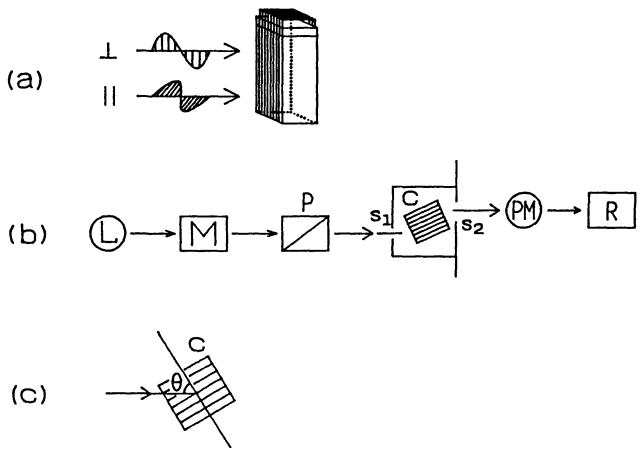

Fig. 1. Optical arrangement.
(a): definitions of the || and ⊥ polarized lights. (b): optical path for the measurement of the polarized ATR spectrum. L: tungsten lamp, M: monochromator(prism+grating), P: Rochon-type polarizer, S_1 and S_2: slit, C: cell containing a stack of thin glass plates, PM: photomultiplier, R: recorder. (c): definition of the angle of incidence (θ).

1c. Part of the incident light is scattered from the side surface of the glass plates, and a major part of the light entering the glass plates propagates within each plate, being totally reflected if θ is larger than the critical angle (θ_c=61° for the light passing from the glass layer to the water layer); the number of total reflections is about 20 for θ=70° and about 10 for θ=80°. In the case of these multiple total reflections, the || (⊥) polarized light remains || (⊥) polarized and the evanescent wave penetrates into the adsorbed dye layer; thus, the so-called || (⊥) polarized ATR spectrum for the adsorbed dye layer can be obtained. A correct, undistorted ATR spectrum can be obtained only when θ is well above θ_c.[3] To compensate for the effect of light scattering from the glass surface and so forth, we used a reference cell which was identical with the sample cell, except that glass plates with no adsorbed dye layer were employed. As shown in Fig. 1b, we cut extraordinary rays from the Rochon-type polarizer by entrance slit S_1 in order to avoid their disturbance on the ATR spectra, and admitted totally reflected ordinary rays

only to the detector by exit slit S_2, which was shifted in position from the entrance slit, S_1.

Results

Unpolarized and Polarized ATR Spectra of the Adsorbed CV Layer. It is well-known that an aqueous solution of CV shows a metachromasy band in the visible region, with a shape and location which depends on the CV concentration, as shown in Fig. 2.[4] With increasing CV concentration, the monomer band at 590 nm is weakened and a metachromasy band appears at 535 nm with an enhanced intensity.

We first confirmed that a reference cell containing 60 glass plates and filled with water gives no characteristic band and that the amount of the light loss is constant over the whole wavelength region examined, i.e., the absorbance of the reference cell was wavelength-independent, irrespective of the light polarization and θ. Figure 3 shows the unpolarized ATR spectra for the adsorbed CV layer with several values of θ. As θ decreased, the metachromasy band at 526 nm was intensified to a greater degree than the monomer band at 590 nm. A correct, undistorted ATR spectrum giving a spectral pattern similar to the ordinary transmission spectrum was obtained when $70° \leqq \theta \leqq 80°$ ($\theta_c < \theta$).

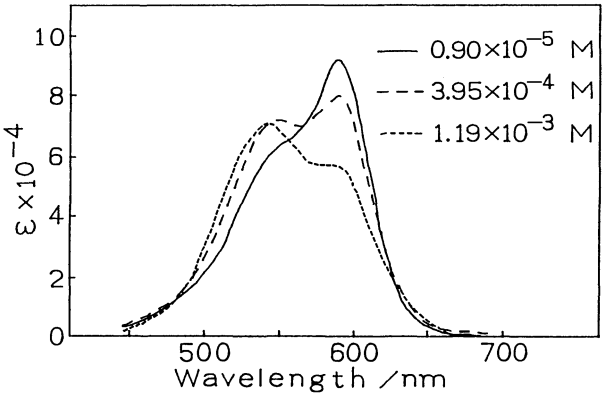

Fig. 2. Absorption spectra for the CV aqueous solutions of various concentrations.

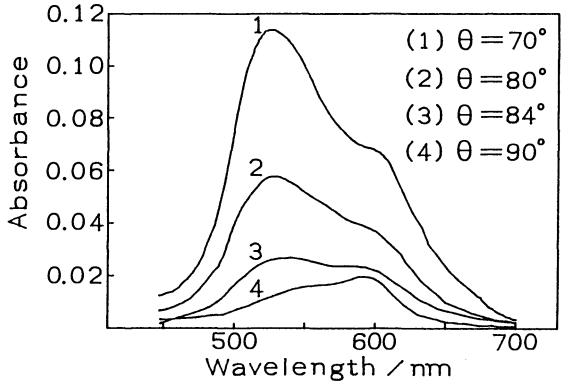

Fig. 3. Unpolarized ATR spectra for the adsorbed CV layer with several values of θ.

Figure 4 shows the changes in absorbance at the band peak of the CV layer with respect to the adsorption time. According to the curve for $\theta=0°$ (normal incidence), the absorbance increased with increasing adsorption time. This means that the adsorption of CV molecules on the glass surface is not completed, even after 300 hours. In contrast to the curve for $\theta=0°$, the absorbance is almost saturated in the curve for $\theta=70°$. This may reflect some aspects characteristic of the ATR spectrum, i.e., the inapplicability of Lambert's law due to the attenuation or the finite penetration depth of the evanescent wave.

In Fig. 5 the unpolarized ATR spectrum for $\theta=70°$ is compared with the unpolarized transmission spectrum measured with $\theta=0°$ (normal incidence). On going from $\theta=70°$ to $\theta=0°$, the absorbance increased as a whole; this seems to agree with the trend shown in Fig. 3. However, it should be emphasized that the peak position of the metachromasy band for $\theta=70°$, 526 nm, is different from that for $\theta=0°$, 535 nm. The spectrum for $\theta=0°$ in Fig. 5 agrees with that for a highly concentrated aqueous solution of CV regarding peak position

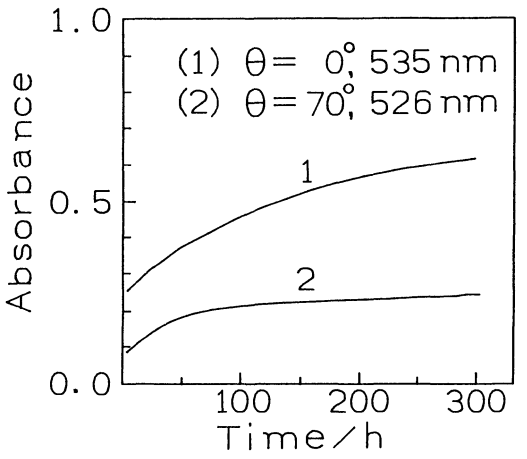

Fig. 4. Changes in the absorbance at the band peak of the adsorbed CV layer for $\theta=0°$ and 70° with respect to the adsorption time.

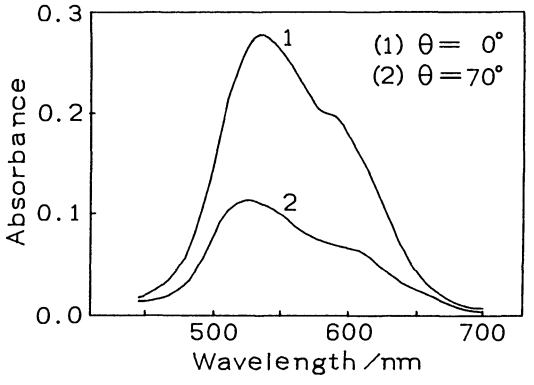

Fig. 5. Comparison of the unpolarized ATR spectrum of the adsorbed CV layer for $\theta=70°$ with the unpolarized transmission spectrum for $\theta=0°$.

and shape.

The polarized transmission and ATR spectra measured for the adsorbed CV layer are summarized in Fig. 6. The essential coincidence of the || and ⊥ polarized transmission spectra (θ=0°, Fig. 6a) implies that the adsorbed CV layer is optically isotropic within the surface plane of the glass plate. However, differences in the peak positions and absorbances are observed between the || and ⊥ spectra for θ=70° and 80° (Figs. 6b and 6c). The differences are especially pronounced for θ=70°. The ⊥ polarized ATR spectrum for θ=70° (Fig. 6b) is nearly identical to the transmission spectrum (θ=0°, Fig. 6a), except for the band intensity (about twice), whereas the metachromasy band of the || polarized ATR spectrum for θ=70° in Fig. 6b is largely blue-shifted in comparison with that of the ⊥ spectrum. This blue shift may be related to the origin of the difference in the peak positions observed in the unpolarized ATR and transmission spectra shown in Fig. 5. This blue shift is further enhanced with an increasing amount of adsorbed CV, as inferred from Fig. 6d.

Unpolalized and Polarized ATR Spectra of the Adsorbed MB Layer. Like CV, MB shows a metachromasy band at the high-energy side of the monomer band in higher MB concentrations.[5] In order to check whether the behavior of this ATR spectra is similar to that of the adsorbed CV layer, we measured the unpolarized and polarized ATR spectra of the adsorbed MB layer. The unpolarized ATR spectrum of the adsorbed MB layer measured with θ=70° is compared in Fig. 7 with the unpolarized transmission spectrum measured with θ=0° (normal incidence). In contrast to the unpolarized ATR and transmission spectra of the adsorved CV layer shown in Fig. 5, the two spectra are quite similar and there is no difference in the peak positions. Figure 8 shows the polarized ATR spectra of the adsorbed MB layer for θ=70°; the || and ⊥ polarized ATR spectra are similar in shape, and the peak positions are coincident. This is, again, in marked contrast to the case of the adsorbed CV layer given in Fig. 6b or 6d.

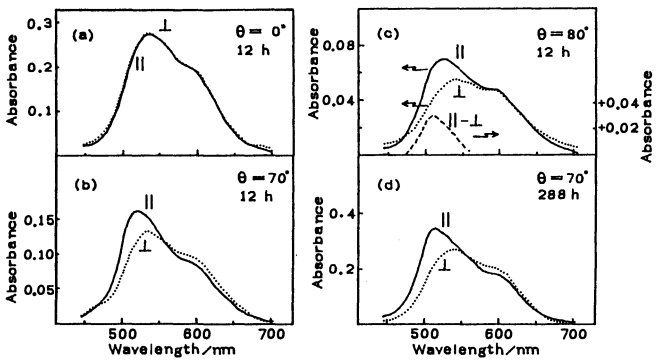

Fig. 6. Polarized transmission (θ=0°) and ATR (θ=70 and 80°) spectra of the adsorbed CV layer. The adsorption times are indicated.

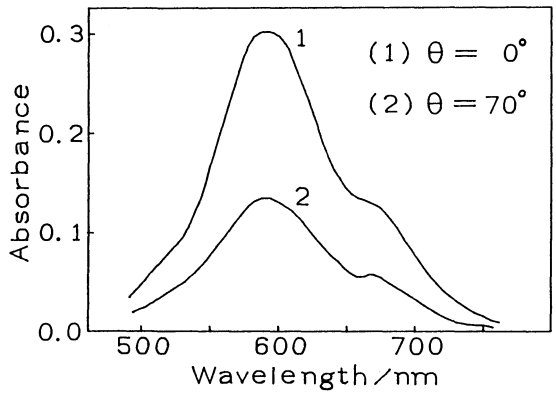

Fig. 7. Comparison of the unpolarized ATR spectrum of the adsorbed MB layer for θ=70° with the unpolarized transmission spectrum for θ=0°

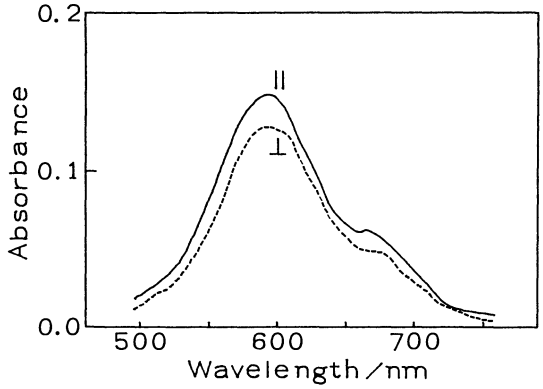

Fig. 8. Polarized ATR spectra of the adsorbed MB layer for θ=70°.

Discussion

For bulk materials or thick films, it is well-known that the || and ⊥ ATR spectra are both red-shifted and that the longer-wavelength bands are relatively more intense in comparison with the ordinary transmission spectrum measured with normal incidence (θ=0°)[6] by the following factors: (a) an anomalous dispersion in the refractive index, n,[7,8] and (b) a wavelength dependence of the penetration depth of the evanescent wave.[9]

From the viewpoint of the general trend of the || and ⊥ ATR spectra for bulk materials, the most remarkable features of the present observations are the differences in the polarized ATR spectra for the adsorbed CV (Fig. 6b) and the MB (Fig. 8) layers. As shown in Fig. 6b (CV), the metachromasy band of || (520 nm) is blue-shifted from that of ⊥ (535 nm) and the intensity ratio of the metachromasy band to the monomer band for || is larger than that for ⊥. In contrast, the main feature of Fig. 8 (MB) is that the peak position of || coincides with that of ⊥ and that the intensity ratio in question for || is essentially equal to that for ⊥. This feature of Fig. 8 excludes the possible influence of the

above-mentioned two factors that cause a deviation of the polarized ATR spectra from the transmission spectrum. This leads to the following conclusions: (1) The influence of non-total reflection[7] due to the anomalous dispersion in n of an adsorbed dye layer is negligible for $\theta=70°$ in the case of the adsorbed MB layer, i.e., the dispersion in n of the adsorbed MB layer is not sufficiently large, even in the wavelength region of the absorption band, to influence the band location and intensity. (2) The evanescent wave penetrates the adsorbed MB layer perfectly, invalidating the wavelength dependence of the penetration depth of the evanescent wave. The former is in accordance with the known fact that the polarized and unpolarized ATR spectra of a thin film resemble its transmission spectrum unless there is a very strong dispersion in n,[10] as is the case for the adsorbed MB layer, which is considered to be a very thin film. The latter is also in accordance with the observation that the thickness of the adsorbed MB layer is estimated to be at most two or three molecular layers, if we assume that the molecular planes of MB are parallel to the surface of the glass plate. On the other hand, the penetration depth of the evanescent wave for visible light is several hundred Å; that is, the evanescent wave can penetrate into about one hundred molecular layers of the adsorbed MB.

As pointed out in the Results section, the $\perp$ ATR spectrum for CV in Fig. 6b is considered to be equivalent to the transmission spectrum for CV in Fig. 6a measured with normal incidence. Therefore, the above-mentioned spectral features of the $\parallel$ ATR spectra for the adsorbed CV layer concerning the location and intensity, in comparison with that of the $\perp$ ATR spectra, are in marked contrast to those of the ATR spectra for bulk materials. This difference can be explained as follows: If there is a very strong dispersion in n of the thin film, the absorption maxima for the $\parallel$ and $\perp$ polarizations may not occur at the same wavelength; that is, the band for $\parallel$ polarization is displaced to a shorter wavelength relative to the band for $\perp$ polarization.[10] If this is the case, the results in Fig. 6b could be explained as being due to a strong dispersion in n of the adsorbed CV layer. However, the following reasons can be used to eliminate this possibility. First, the magnitude of the molecular extinction coefficient (ε) in the visible region for CV (ε=70000—92000) is comparable to that for MB (ε=60000—85000). Second, the actual absorbance, i.e., the thickness of the adsorbed dye layer is also similar for CV and MB. Third, the degree to which the two bands in the visible region are overlapped is essentially the same for CV and MB, implying that there is no significant difference between CV and MB in the overlapping effect[8] of the two anomalous dispersion curves in n. It must be recalled here that the peak for the $\parallel$ ATR spectrum of CV adsorbed on an absorbing gold film electrode was blue-shifted from that of CV adsorbed on a transparent glass.[11] That is, the presence of an extra absorption due to the gold film can cause a shift in the $\parallel$ ATR spectrum of the adsorbed dye layer to a shorter wavelength. In conformity with this observation, we may conclude that the blue shift and the enhancement of the metachromasy band of the $\parallel$ ATR spectra in Fig. 6b reflect an optical property characteristic of the adsorbed CV layer. We, thus, propose that the adsorbed CV layer exhibits an extra electronic transition band which is located at the high-energy side of the metachromasy band and is polarized normal to the glass plane. This extra electronic transition band can be detected only in the $\parallel$ ATR spectrum, not in the $\perp$ ATR spectrum nor in the transmission spectrum observed with $\theta=0°$. We obtained this extra electronic transition band as a difference spectrum between the $\parallel$ and $\perp$ ATR spectra, as shown in Fig. 6c by the ($\parallel-\perp$) curve.

There are two possible explanations for the occurrence of this extra electronic transition band under the assumption that CV molecules are adsorbed with their molecular planes parallel to the glass plane. First, CV has a nonplanar structure which gives rise to an out-of-plane polarized component of the electronic transition; it may, in turn, give rise to an extra electronic transition band polarized normal to the glass plane, under the present assumption. Second, the adsorption process gives an electronic perturbation to each CV molecule in the adsorbed CV layer to a different degree, being dependent on the distance from the glass plane, which may induce an intermolecular charge-transfer band with a nonvanishing intensity. In this charge-transfer band, the charge transfer occurs in the direction (z) perpendicular to the glass plane; the transition moment should also be in the same direction.

We now give an explanation for the spectra shown in Fig. 3. With a decrease in θ for $90°>\theta>\theta_c$, the electric field amplitude of the $\parallel$ polarized evanescent wave ($E_\parallel$) increases to a larger degree than that of the $\perp$ polarized evanescent wave ($E_\perp$), although both $E_\parallel$ and $E_\perp$ increase.[12] Among the electric field components of the evanescent wave that contribute to $E_\parallel$, especially the E_z component polarized perpendicularly to the glass surface increases in amplitude very sharply with a decrease in θ for $90°>\theta>70°$.[12] In conformity with this variation, the ATR spectrum for the extra electronic transition band, polarized perpendicularly to the glass surface and detected by the E_z component of unpolarized natural light, should increase in intensity with a decerase in θ for $90°>\theta>70°$. The above change yields, along with an enhancement of the entire ATR band, an increase in the intensity of the metachromasy ATR band to a greater degree than the monomer ATR band with a decrease in θ. There is, of course, the influence of an increasing number of total reflections with a decrease in θ for $90°>\theta>70°$, which should also cause an enhancement of the entire ATR band.

The authors wish to express their thanks to

Professor Kozo Kuchitsu, Nagaoka University of Technology, for his critical reading of the manuscript.

References

1) N. J. Harrick, "Internal Reflection Spectroscopy," John Wiley & Sons (1967), p. 30.

2) Ref. 1, p. 205; P. A. Wilks (Jr.) and T. Hirschfeld, Internal Reflection Spectroscopy, "Applied Spectroscopy Reviews," ed by E. G. Brame, Marcel Dekker, New York (1967).

3) Ref. 1, p. 73.

4) M. Schubert and A. Levine, *J. Am. Chem. Soc.*, **77**, 4197 (1955); L. V. Levshin and V. K. Gorshkov, *Opt. Spectrosc.*, **10**, 401 (1961); W. H. J. Stork, G. J. M. Lippits, and M. Mandel, *J. Phys. Chem.*, **76**, 1772 (1972).

5) E. Rabinowitch and L. F. Epstein, *J. Am. Chem. Soc.*, **63**, 69 (1941); L. Michaelis and S. Granick, *ibid.*, **67**, 1212 (1945); E. Braswell, *J. Phys. Chem.*, **72**, 2477 (1968).

6) Ref. 1, pp. 63—65 and 69—73.

7) T. Fujiyama, "Bunkokagaku '68-B," the supplement 85 of "Kagaku No Ryoiki," ed by Y. Morino, T. Shimanouchi, S. Fujiwara, and M. Oki, Nankodo, Tokyo (1968), pp. 69 and 70; Ref. 1, pp. 83—87.

8) T. Fujiyama, "Bunkokagaku '68-B," pp. 71 and 72.

9) Ref. 1, Eq. 22 on p. 30.

10) Ref. 1, pp. 68 and 69.

11) W. N. Hansen, Internal Reflection Spectroscopy in Electrochemistry, p. 41, "Advances in Electrochemistry and Electrochemical Engineering (Vol. 9)," ed by P. Delahey and C. W. Tobias, John Wiley & Sons, New York (1973).

12) Ref. 1, Fig. 10 on p. 29; Ref. 11, Fig. 3 on p. 16 and Fig. 4 on p. 17.

 © 1988 The Chemical Society of Japan Bull. Chem. Soc. Jpn., 61, 4177—4181 (1988)

The Charge Carried by a Layer Formed by an Aggregation of Polyelectrolytes in a Solution Containing a Salt

Tetsuo KANEKO
Kogane Kazusa-cho 16-1, Matsudo-shi, Chiba-ken 270
(Received February 22, 1988)

A layer formed by the aggregation of polyelectrolyte molecules is charged according to the ionic dissociation of the layer in a simple salt solution. The charge carried by the layer is estimated on a basis of solutions of the Poisson-Boltzmann equation. It has been found that this charge is independent of the concentration, n_s, of a salt, in spite of the permanence of the layer to counter ions when the density, n_g, of charged groups in the polyelectrolyte molecules is much higher than the concentration n_s. As the result, the charge may be given as a function of three parameters (temperature, density n_g, and thickness of the layer) except for n_s. Moreover, it has been found that the distribution of counter ions within the layer and their distribution in the vicinity of the layer may be independent of n_s and that these distributions of counter ions may agree with that in a salt-free solution.

An electric field is formed around a polyelectrolyte molecule in an aqueous solution because of the ionic dissociation of the polyelectrolyte molecule. This formed electric field restricts the diffusion of counter ions due to thermal motion and a repulsive force between the counter ions. In general, it is known that the charge density of a polyion in a solution may be independent of the concentration of a salt.[1]

Guéron and Weisbuch noted, on a basis of calculations using the Poisson-Boltzmann equation, that counter ions exist with quite high densities in the immediate vicinity of the surface of highly charged polyelectrolyte molecules.[2] Moreover, they found that the distribution of counter ions in the vicinity of these polyelectrolyte molecules is insensitive to the concentration, n_s, of a salt, as has been noted by Stigter,[3] and that this distribution is not strongly dependent on the shapes of the polyelectrolyte molecules.[2]

Plates, cylinders, and spheres, the surfaces of which hold constant surface-charge densities, were introduced as models of polyelctrolytes in order to ascertain these properties of counter-ion distributions.[2] In the layer-model system of a polyelectrolyte solution,[4] layers formed by the aggregations of polyelectrolyte molecules were immersed in a solvent instead of plates, which hold a constant surface-charge density. This layer model was capable of giving a quantitative estimation of the charged characteristics of a polyion in a salt-free solution. Counter ions in the layer-model system distribute continuously from the inside of the layers of polyelectrolytes to the outside of the layers, since the layers are permeable to counter ions. The purpose of this investigation was to show that the charge carried by such layers of polyelectrolytes may be independent of the salt concentration. If a salt is added to a layer-model system, it is doubtful whether the charge of the layers would be influenced by the salt, owing to an effect related to the permeance of the layers which may not occur on charged surfaces of constant surface-charge density. If the layer model is capable of having a nature found in the relation between the charge density of polyion and the concentration of a salt (as described above), the charge of the polyelectrolyte layers should not be affected by a salt added to a layer-model system.

Engström and Wennerström used the Gouy-Chapman solution in order to estimate the density of counter ions in the immediate vicinity of charged plates which maintain a constant surface-charge density and which immerse in a simple salt solution; they showed that this density of cunter ions is independent of the concentration of a salt, and that it agrees with the counter-ion density in a salt-free solution.[5] Similarly, by using the Gouy-Chapman solution in this study it has been shown that the distribution of counter ions in the vicinity of the surface of the layers may be independent of n_s under the condition that any effect dependent on the distance between the layers can be ignored. Also, this counter-ion distribution may agree with that in a salt-free solution. In accordance with the above condition, the layer-model system described in this paper is composed of one layer of polyelectrolytes immersed in a simple salt solution. It is shown here that any charge carried by the layer can be independent of n_s.

In addition, the charged circumstance of the layer can be represented as the total charge contained in an imaginary cylinder. This imaginary cylinder is perpendicular to the surface of the layer and has a unit cross section. Also, the both ends of the imaginary cylinder are at the center of the layer and on the surface of the layer, respectively. A system composed of a layer can be an electric equivalent to a system composed of a charged plate of a conductor substituted for the layer, if the charge per unit area on the surface of the plate is equal to the total charge in an imaginary cylinder as is described above. On the basis of this situation, the total charge in the imaginary cylinder was regarded as being the surface-charge density on a polyelectrolyte layer in a previous paper,[4] although this surface-charge density was imaginary. The charged circumstance of the layer differs, in fact, from the charged circumstance of the dielectric in an electric field in which the dielectric induces a charge on its surface and

from the charged circumstance of a charged conductor in which a charge accumulates on its surface. In this paper, the total charge in the imaginary cylinder will be called the layer-charge density (LCD), in order to avoid any confusion between these charged circumstances.

Model

Structure of a Layer Model. The layer-model system used in order to estimate the charged characteristics of polyions in a salt-free solution consisted of many layers formed by aggregations of polyelectrolyte molecules and arranged in a solvent.[4] When these layers are immersed in a simple salt solution, it is difficult to estimate the charge carried by the layers (i.e., LCD), the distribution of counter ions, etc., by considering any effect dependent on the distance between the layers and by solving the Poisson-Boltzmann equation. In this paper, a certain condition, which corresponds to the dilute concentration of polyelectrolytes, is assumed in order to avoide this difficulty, i.e., it is assumed that the electrostatic interaction between layers of polyelectrolytes is negligible. The estimations of the LCD, of the electric field, and of the counter-ion distribution under this condition are the objects of this investigation. Consequently, the layer-model system used in this paper consists of one layer of polyelectrolytes (Fig. 1); this layer is immersed in a simple salt solution. The thickness of the layer is Δx and the density of the charged groups packed in the layer is n_g. The concentration of a salt in the solution, in which the layer is immersed, is n_s. In addition, even in the layer-model system which is salt-free, though the distance between neighboring layers of polyelectrolytes is of the order 10^2 Å, the electrostatic interaction between the layers hardly affects the LCD in the system when this LCD is of the order 10^{-2} C·m^{-2}.[4]

Electrostatic Potential. Though it is assumed that the absolute value of the charge of a counter ion is the same as that of a co-ion, the electrostatic potential ψ in the layer-model system (as is shown in Fig. 1) can be described by the following Poisson-Boltzmann equation: within a layer of polyelectolytes ($-\Delta x/2 < x < \Delta x/2$) it is

$$\frac{d^2\psi_1}{dx^2} = -\frac{1}{\varepsilon}\{-z'en_g - zen_s \exp[ze\psi_1/kT] + zen_s \exp[-ze\psi_1/kT]\}, \quad (1)$$

while outside the layer ($\Delta x/2 \leqq x$) it is

$$\frac{d^2\psi_2}{dx^2} = \frac{2zen_s}{\varepsilon} \sinh[ze\psi_2/kT]. \quad (2)$$

In the above, ε is the dielectric constant of a solvent, $-z'e$ is the charge of a charged group, ze is the charge of a counter ion, $-ze$ is the charge of a co-ion, k is Boltzmann's constant, and T is the absolute temperature. In addition, it is assumed that the dielectric constant within the layer is the same as that of a solvent.

For boundary conditions

$$\psi_1\left(\frac{\Delta x}{2}\right) = \psi_2\left(\frac{\Delta x}{2}\right) \text{ and } -\varepsilon \frac{d\psi_1}{dx}\Big|_{x=\Delta x/2} = -\sigma,$$

the approximate solution of Eq. 1 can be obtained as follows:[4,6]

$$\begin{aligned}\psi_1(x) = &-\frac{kT}{ze} \cdot \operatorname{arcsinh} f \\ &+ \frac{kT}{2ze} \cdot \left\{\sqrt{2}\,\Lambda\sigma + \frac{ze\psi_2(\Delta x/2)}{kT} + \operatorname{arcsinh} f\right\} \cdot \exp\left[-\mu\left(\frac{\Delta x}{2} - x\right)\right] \\ &+ \frac{kT}{2ze} \cdot \left\{-\sqrt{2}\,\Lambda\sigma + \frac{ze\psi_2(\Delta x/2)}{kT} + \operatorname{arcsinh} f\right\} \cdot \exp\left[\mu\left(\frac{\Delta x}{2} - x\right)\right], \end{aligned} \quad (3)$$

where $\Lambda^2 \equiv z/(2z'kT\varepsilon n_g)$, $\mu^2 \equiv zz'e^2n_g/(\varepsilon kT)$, and $f \equiv z'n_g/(2zn_s)$. Also, $-\sigma$ is the layer-charge density (LCD). By considering the continuity of the electric field in the layer, it can be described as

$$-\sigma = \int_0^{\Delta x/2} \{-z'en_g - 2zen_s \sinh[ze\psi_1/kT]\}\, dx.$$

On the other hand, the Gouy-Chapman solution given for the following boundary conditions is used as a solution of Eq. 2:

$$\psi_2(\infty) = 0, \quad -\varepsilon \frac{d\psi_2}{dx}\Big|_{x=\infty} = 0, \quad -\varepsilon \frac{d\psi_2}{dx}\Big|_{x=\Delta x/2} = -\sigma.$$

The Formulation of the LCD. A formula which represents the LCD, $-\sigma$, in a simple salt solution can be formed by substituting the Gouy-Chapman solution into $\psi_2(\Delta x/2)$ in Eq. 3 and by considering the following condition in conectin with the continuity of the electric field $-\varepsilon\, d\psi_1/dx$ in the layer:

$$-\varepsilon \frac{d\psi_1}{dx}\Big|_{x=0} = 0. \quad (4)$$

As a result, the obtained formula is

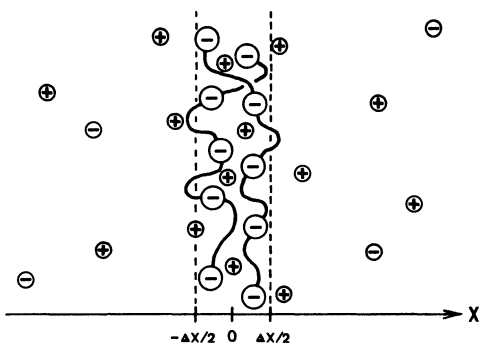

Fig. 1. A layer model. Charged groups, counter ions, and co-ions are represented by ~(−)~, (+), and (−), respectively.

$$\Delta\sigma\cdot\left[\ln\left\{\left(\sqrt{\frac{1}{4}+\left(\frac{zn_s}{z'n_g}\right)^2}+\frac{1}{2}\right)^{-1/2}\cdot\left(\sqrt{\frac{1}{4}\Delta^2\sigma^2+\frac{zn_s}{z'n_g}}+\frac{1}{2}\Delta\sigma\right)\right\}\right]^{-1}=-\sqrt{2}\tanh\left[\mu\frac{\Delta x}{2}\right]. \quad (5)$$

Thus, the LCD is given by Eq. 5 as a function of four parameters (T, n_g, n_s, Δx).

If the existance of co-ions in the layer can be ignored, the $-zen_s\cdot\exp[ze\psi_1/kT]$ term disappears in Eq. 1 and, as a result, the $(zn_s/z'n_g)^2$ term disappears in Eq. 5. Moreover, if the existance of co-ions on the surface of the layer can be ignored, the $zn_s/z'n_g$ term also disappears in Eq. 5. It has been suggested that, if co-ions can be sufficiently excluded in the vicinity of the layer, the LCD may be independent of n_s.

In addition, an approximation to Eq. 5 can be given when $zn_s/z'n_g$ is small. It is possible that the $zn_s/z'n_g$ ratio is sufficiently small, because the value of n_g is of the order of 10^{28} m^{-3},[4] if a polyacrylate molecule is considered as an example. For a small $zn_s/z'n_g$ ratio, the magnitude of $\Delta\sigma$, in accordance with the sign of the right-hand side of Eq. 5, must satisfy $\Delta\sigma<1$. In accordance with the magnitude of this right-hand side, $\Delta\sigma$ can be close to 1. By considering this magnitude of $\Delta\sigma$ and the sign of $\Delta\sigma$, the following approximation for $-\sigma$ is found when $zn_s/z'n_g$ is sufficiently small:

$$-\sigma=-\sigma_0+\Delta\sigma(n_s), \quad (6)$$

where $-\sigma_0$ is the LCD in a salt-free solution[4] and it is

$$-\sigma_0=-\frac{Y}{2\Delta}\{(2+Y)-\sqrt{Y(Y+4)}\},$$

In Eq. 6, $\Delta\sigma(n_s)$ is defined as

$$\Delta\sigma(n_s)\equiv\frac{2kT\varepsilon}{\sigma_0}\sqrt{\frac{Y}{Y+4}}\cdot n_s.$$

In the above formulae, Y is defined as

$$Y\equiv 2\sqrt{2}\tanh[\mu\Delta x/2].$$

Results and Discussion

Layer-Charge Density (LCD). LCD in a simple salt solution can be given as a function of four parameters (T, n_g, n_s, Δx). It can be shown, however, that this LCD becomes a function of three parameters (T, n_g, Δx) if the $zn_s/z'n_g$ ratio is sufficiently small.

When $zn_s/z'n_g$ is small, Eq. 6 becomes an approximation of Eq. 5, and the relationship between $-\sigma$ and n_s can be well understood in Eq. 6. For the conditions used in order to estimate the charge density of polyion in a salt-free, dilute solution of a polyelectrolyte (the T, n_g and Δx parameters are 298 K, 1.7×10^{28} m^{-3}, and 3 Å, respectively, and both z and z' are 1),[4] the $\Delta\sigma(n_s)/\sigma_0$ ratio is of the order of 10^{-2} if n_s is 10^{-1} mol·dm^{-3}. This ratio is much smaller than 1. Thus, the second term in the right-hand side of Eq. 6 reduces, when $zn_s/z'n_g$ is small. As is shown in Fig. 2, the LCD $-\sigma$ may become independent of n_s, even though the layer is permeable to counter ions. Moreover, this LCD, which is independent of n_s, may agree with that in a salt-free solution, as can be seen from Eq. 6. In addition, if n_g is small, $-\sigma$ is liable to be influenced by n_s, as can be seen in Fig. 2.

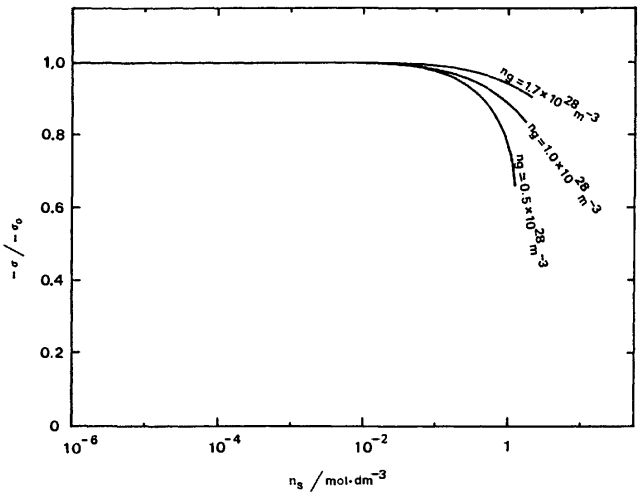

Fig. 2. The dependence of $-\sigma/\sigma_0$ on n_s at 298 K on the basis Eq. 6. The $-\sigma/\sigma_0$ ratio is values calculated for Δx=3 Å.

On the other hand, when the distribution of co-ions within the layer and in the vicinity of the layer can be ignored, the $zn_s/z'n_g$ and $(zn_s/z'n_g)^2$ terms disappear in Eq. 5; then, LCD agrees with that in a salt-free solution. This result shows that when $z'n_g$ is much larger than zn_s, co-ions are sufficiently excluded within the layer and in the vicinity of the layer.

Ultimately, it is inferred that the independence of the charge density of polyions from the concentration of a salt occurs owing to the quite high density of charged groups contained in the polyions (then, co-ions are sufficiently excluded in the vicinity of the polyions).

Electric Field. The electric field, $-\varepsilon d\psi/dx$, on the surface of the layer is proportional to $-\sigma$. Since $-\sigma$ for the small value of $zn_s/z'n_g$ is independent of n_s, for such a value of $zn_s/z'n_g$ the electric field on the surface is independent of n_s. Moreover, it can be shown that the electric field in the vicinity of the layer is insensitive to n_s if n_s is sufficiently small. The electric field in the vicinity of the layer is given by

$$-\varepsilon\frac{d\psi_2}{dx}=\varepsilon E_0+\varepsilon E(n_s), \quad (7)$$

where εE_0 is the electric field occurring in a salt-free solution[4] and it is

$$\varepsilon E_0=\frac{-\sigma_0}{1-\frac{\Delta\sigma_0}{\sqrt{2}}\cdot\mu\left(\frac{\Delta x}{2}-x\right)}$$

In Eq. 7, $\varepsilon E(n_s)$ is defined as

$$\varepsilon E(n_s) \equiv \varepsilon E_0 \cdot \left[- \frac{\Delta\sigma/\sigma_0}{1 - \frac{\Delta\sigma_0}{\sqrt{2}}\mu\left(\frac{\Delta x}{2} - x\right)} \right.$$

$$+ \frac{\sqrt{2}}{f\Delta\sigma_0} \cdot \frac{\mu\left(\frac{\Delta x}{2} - x\right)}{\left\{1 - \frac{\Delta\sigma_0}{\sqrt{2}}\mu\left(\frac{\Delta x}{2} - x\right)\right\}^2} \cdot \left\{1 - \sqrt{2}\Delta\sigma_0\mu\left(\frac{\Delta x}{2} - x\right)\right.$$

$$\left. \left. + \frac{1}{3}\left(\sqrt{2}\Delta\sigma_0\mu\left(\frac{\Delta x}{2} - x\right)\right)^2 - \frac{1}{24}\left(\sqrt{2}\Delta\sigma_0\mu\left(\frac{\Delta x}{2} - x\right)\right)^3 \right\} \right].$$

In the Guoy-Chapman solution, the coefficient κ defined as

$$\kappa^2 \equiv \frac{2z^2e^2n_s}{\varepsilon kT},$$

is contained. Equation 7 is obtained by considering n_s and $\kappa\cdot(\Delta x/2 - x)$ to be small and by approximating $-\varepsilon d\psi/dx$ given by the Gouy-Chapman solution. The ratio of the second term to the first term in the right-hand side of Eq. 7, $|E(n_s)/E_0|$, is much smaller than 1 in the vicinity of the layer, as is found from the dependence of $\{E_0+E(n_s)\}/E_0$ on x in Fig. 3. As a result, it is found that the electric field in the vicinity of the layer may be independent of n_s, and that it may agree with the electric field in a salt-free solution. Moreover, the dependence of $\{E_0+E(n_s)\}/E_0$ on x in Fig. 3 suggests that the extent of the electric field insensitive to n_s expands more if n_s decreases more.

In addition, the electric field within the layer is given by the following formula obtained by using Eq. 3 and by considering Eq. 4:

$$-\varepsilon\frac{d\psi_1}{dx} = -\frac{\sigma}{2}\left\{\left(1 + \frac{2\sqrt{2}}{Y}\right)\cdot\exp\left[-\mu\left(\frac{\Delta x}{2} - x\right)\right]\right.$$

$$\left. + \left(1 - \frac{2\sqrt{2}}{Y}\right)\cdot\exp\left[\mu\left(\frac{\Delta x}{2} - x\right)\right]\right\}.$$

As is noted by this formula, the dependence of this electric field on n_s is the same as the dependence of $-\sigma$ on n_s. If $zn_s/z'n_g$ is sufficiently small, $-\varepsilon d\psi_1/dx$ may be independent of n_s and may agree with the electric field in a salt-free solution (as can be noted according to Ref. 4).

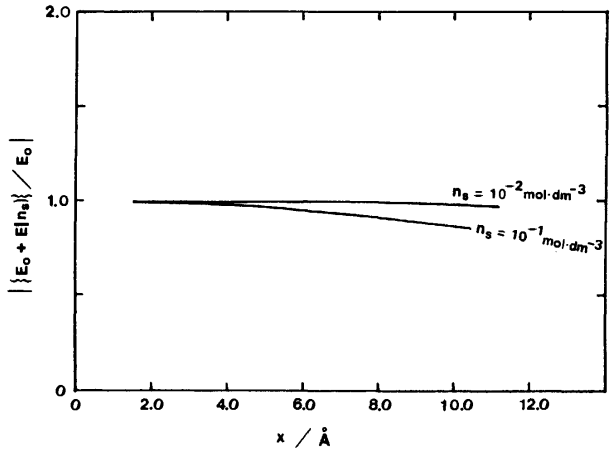

Fig. 3. The dependence of $\{E+E(n_s)\}/E_0$ on x at 298 K on the basis of Eq. 7. The $\{E+E(n_s)\}/E_0$ ratio is values calculated for n_g=1.7×10^{28} m^{-3} and Δx=3 Å.

The Distribution of Counter Ions. The property of the electric field in the vicinity of the layer suggests that the distribution of ions in the vicinity of the layer is insensitive to n_s and that the extent of the ion-distribution insensitive to n_s expands in accordance with a reduction in n_s. The relationship between the counter-ion distribution and n_s in the vicinity of the layer may be represented by

$$n_2(x) = n_0(x) + n_0(x)\cdot\left[- \frac{2\Delta\sigma/\sigma_0}{1 - \frac{\Delta\sigma_0}{\sqrt{2}}\mu\left(\frac{\Delta x}{2} - x\right)} \right.$$

$$+ \frac{2}{f\Delta^2\sigma_0^2}\cdot\frac{1}{\left\{1 - \frac{\Delta\sigma_0}{\sqrt{2}}\mu\left(\frac{\Delta x}{2} - x\right)\right\}^2}\cdot\left\{1 - \sqrt{2}\Delta\sigma_0\mu\left(\frac{\Delta x}{2} - x\right)\right.$$

$$+ \frac{1}{2}\left(\sqrt{2}\Delta\sigma_0\mu\left(\frac{\Delta x}{2} - x\right)\right)^2 - \frac{1}{6}\left(\sqrt{2}\Delta\sigma_0\mu\left(\frac{\Delta x}{2} - x\right)\right)^3$$

$$\left. \left. + \frac{1}{48}\left(\sqrt{2}\Delta\sigma_0\mu\left(\frac{\Delta x}{2} - x\right)\right)^4 \right\} \right], \quad (8)$$

where $n_2(x)$ is the density of counter ions, and $n_0(x)$ is the density of counter ions in a salt-free solution,[4] i.e.:

$$n_0(x) = \frac{{\sigma_0}^2}{2kT\varepsilon\left\{1 - \frac{\Delta\sigma_0}{\sqrt{2}}\cdot\mu\left(\frac{\Delta x}{2} - x\right)\right\}^2}.$$

In addition, Eq. 8 is obtained by considering n_s and $\kappa\cdot(\Delta x/2 - x)$ to be small and by approximating the counter-ion density given by the Gouy-Chapman solution. It is noted in Fig. 4 (depicted in accordance with Eq. 8) that the density of counter ions in the vicinity of the layer, $n_2(x)$, may be insensitive to n_s if n_s is less than 0.1 mol·dm^{-3} ($zn_s/z'n_g$ is less than 10^{-2}). The insensitivity of $n_2(x)$ to n_s is similar to the property of the counter-ion distribution in the vicinity of the charged surfaces of plates, cylinders, and spheres.[2,3] The behavior of $n_2(x)$ (Fig. 4) suggests that the extent of the distribution of counter ions insensitive to n_s expands in accordance with a reduction in n_s. Furthermore, when n_s is so small that the second term in the right-hand side of Eq. 8 can be ignored, the density $n_2(x)$ may agree with the counter-ion density in a salt-free solution. This result is similar to that regarding the charged-plates model of Engström and Wennerström.[5]

On the other hand, the density of co-ions in the vicinity of the layer is given by

$$n_s^2/n_2(x).$$

This formula does not include terms independent of n_s. The formula shows that the density of co-ions is quite small when $zn_s/z'n_g \ll 1$ is satisfied. As a result, the co-ion distribution in the vicinity of the layer may be ignored, although this distribution depends on n_s. Therefore, it is deduced that the insensitivity of the electric field to n_s is attributable to only the property of the counter-ion distribution in the vicinity of the layer.

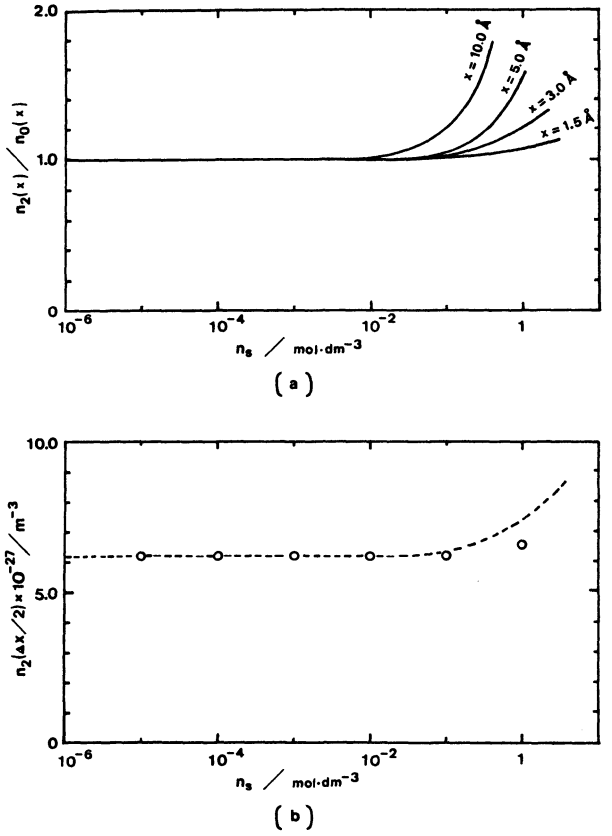

Fig. 4. The dependence of $n_2(x)$ on n_s at 298K on the basis of Eq. 8. The $n_2(x)/n_0(x)$ ratio is values calculated for n_g=1.7×1.0^{28} m^{-3} and Δx=3 Å. The circles represent the $n_2(\Delta x/2)$ counter-ion density on the surface of the layer. The broken line represents the counter-ion density in the immediate vicinity of a charged plate and its surfaces hold a constant surface-charge density 0.190 C·m^{-2} (which equals to a value given by the layer model under the above condition when n_s=0).

In addition, in Fig. 4 the behavior of counter-ion distribution in the immediate vicinity of a charged plate, which holds a constant surface-charge density (0.190 C·m^{-2}), agrees well with the behavior of n_2 $(\Delta x/2)$ (which is n_2 (x) on the surface of the layer) depicted by the circles. The insensitivity of the LCD to n_s is reconfirmed by means of an agreement between these circles and the broken line in Fig. 4.

The density of counter ions within the layer, n_1 (x), is given by using Eq. 3 and by considering Eq. 4; it is represented as

$$n_1(x)=\frac{z'n_g}{z}\cdot\left(\sqrt{\frac{1}{4}+\left(\frac{zn_s}{z'n_g}\right)^2}+\frac{1}{2}\right)\cdot\exp\left[-\frac{\Delta\sigma}{\sqrt{2}}\left\{\left(1+\frac{2\sqrt{2}}{Y}\right)\cdot\exp\left[-\mu\left(\frac{\Delta x}{2}-x\right)\right]-\left(1-\frac{2\sqrt{2}}{Y}\right)\cdot\exp\left[\mu\left(\frac{\Delta x}{2}-x\right)\right]\right\}\right].$$

The density n_1 (x) described by this formula may be as insensitive as n_2 (x), expressed by Eq. 8, if $zn_s/z'n_g$ is sufficiently small. Under the condition that satisfies $zn_s/z'n_g \ll 1$, the density n_1 (x) may agree with the counter-ion density in a salt-free solution (as can be noted according to Ref. 4). Ultimately, it is found that the counter-ion distribution within the layer and in the vicinity of the layer may agree with that in a salt-free solution not only when n_s is zero, but also when it is small.

Conclusion

The LCD in a layer model system containing a salt is given as a function of three parameters (T, n_g, Δx) when $zn_s/z'n_g$ is sufficiently small, even though a layer of polyelectrolytes is immersed in a simple salt solution. Thus, in spite of the permeance of the layer to counter ions, it has been determined that the LCD in this system may be quite insensitive to n_s, though the system satisfies $zn_s/z'n_g \ll 1$. It may be inferred that the independence of the polyion-charge density from the concentration of a salt is attributable to the much higher density of charged groups than the concentratin of the salt. In addition, under the condition that the existance of co-ions in the layer can not be ignored (i.e., $zn_s/z'n_g$ is not small) the LCD in the layer model system may depend on four parameters (T, n_g, n_s, Δx).

The independence of the LCD from n_s in the layer model system is attributable to the insensitivity of counter-ion distribution to n_s. When $zn_s/z'n_g$ is small, the counter-ion distribution in the vicinity of the layer may become quite insensitive to n_s. This result indicates an insensitivity similar to that found from the behavior of the counter-ion distribution in the vicinity of the charged surfaces of the plates, of the cylinders, and of the spheres which hold a constant surface-charge density. Moreover, it has been found that a counter-ion distribution which shows a behavior independent of n_s may agree with the counter-ion distribution in a salt-free solution. If a polyelectrolyte molecule satisfies $zn_s/z'n_g \ll 1$, it is inferred that the cunter-ion distribution in the vicinity of its polyion may be identified with that in a salt-free solution, although n_s is not zero.

The author wishes to express his thanks to Dr. Kazumi Kogure for her many helpful discussions. He also wishes to express his thanks to the members of Japan NUS Co., Ltd. for permission to use the electronic typewriter equiped in the office of Japan NUS Co., Ltd.

References

1) G. S. Manning, *Biophys. Chem.*, **7**, 95 (1977).
2) M. Guéron and G. Weisbuch, *Biopolymers*, **19**, 353 (1980).
3) D. Stigter, *Prog. Colloid Polym. Sci.*, **65**, 45 (1978).
4) T. Kaneko, *Bull. Chem. Soc. Jpn.*, **61**, 363 (1988).
5) S. Engström and H. Wennerström, *J. Phys. Chem.*, **82**, 2711 (1978).
6) S. Lifson, *J. Chem. Phys.*, **27**, 700 (1957).

Application of the SPE Method to Organic Electrochemistry. IX. Reaction Profiles of an Iron Redox Couple Incorporated into Pt-Nafion with Ascorbic Acid

Zempachi OGUMI,* Toshiyuki MIZOE, and Zen-ichiro TAKEHARA
Department of Industrial Chemistry, Faculty of Engineering, Kyoto University, Sakyo-ku, Kyoto 606
(Received March 16, 1988)

Fe^{3+} has been incorporated into Pt-Nafion. The behavior of Fe^{3+} as a mediator was examined in detail in a system comprising the oxidation of L-ascorbic acid (AA) to dehydroascorbic acid (AD). The diffusion of AA in Nafion is slower than that of Fe^{3+}. The concentration profiles of Fe^{3+} and AA in Pt-Nafion have been clarified and a reaction of the mediator with AA took place within a very narrow zone close to the surface. The averaged diffusion coefficients of Fe^{3+} and AA are 1.5×10^{-7} $cm^2 s^{-1}$ and 4.7×10^{-8} $cm^2 s^{-1}$, respectively.

The present authors have investigated the application of the SPE method to organic electrochemistry[1,2] using Nafion as an SPE material. The use of a mediator system in electroorganic syntheses gives some advantages, such as a higher reaction selectivity, easier separation, higher reactivity etc. It was clarified in a previous paper[3] by the present authors that an iron redox couple incorporated into Pt-Nafion acted as a mediator for the oxidation of L-ascorbic acid, AA, to dehydroascorbic acid, AD. In this work, the reaction of Fe^{3+} with AA and their concentration profiles in Pt-Nafion were both examined in detail.

Two configurations are possible in the use of SPE composite electrodes, as described in a previous paper.[3] In configuration a, in Fig. 3 in Ref. 3, substrates are introduced into the working electrode compartment. In configuration b of the same figure, substrates are introduced into the counter electrode compartment. The former configuration is more useful for enhancing the reaction rate. On the other hand, it is easier in the latter configuration to investigate concentration profiles in a composite electrode, since the contribution from any direct electrode reaction of the substrates is suppressed. The latter configuration (b) is focused upon here.

Pt-Nafion has, inherently, the structure of a Nafion-coated electrode. Many workers have investigated Nafion-coated electrodes prepared by the casting of a Nafion solution,[4-6] owing to their potential applications to such electrochemical devices as sensors and electrochromic displays. The concentration profiles on polymer-coated-electrodes have been extensively investigated by Saveant and co-workers[7,8] as well as others. Polymer-coated electrodes were mainly prepared by using a solution casting method including Nafion-coating. Solution-cast films are thin and it is not easy to characterize their structure well. In some cases, the structure of a solution-cast film is different from that of a thicker membrane prepared by a conventional method. For example, a Nafion film cast from its solution, without an adequate following curing treatment, is different from the characteristic ionomer structure of Nafion. In the case of Pt-Nafion, the coating layer is thick (100—300 μm) and its structure is well characterized.[9] Utilizing these advantages, concentration profiles and a reaction zone inside the Nafion which coated a porous Pt electrode were investigated. The obtained results present a clearer typical model of the concentration distribution on Nafion-coated electrodes. These are useful in giving higher functions to SPE composite electrodes regarding their applications to organic electrochemistry.

Experimental

Chemicals. Commercially available chemicals of reagent grade were used without further purification.

Pt-Nafion Composite Electrodes. Nafion 125 and Nafion 120 were used as SPE materials. These two Nafions are different only in their thickness, and are nominally 125 and 250 μm (5 and 10 mil) thick. After standard boiling water treatments, platinum was deposited on one side of the Nafion by a method previously described.[3] An iron redox couple was incorporated into Pt-Nafion by a previously described method.[3]

Electrolysis Cell. The electrolysis cell was composed of two compartments, a working electrode compartment (w.e.c. 15 cm^3) and a counter electrode compartment (c.e.c. 14.5 cm^3), which were divided by Pt-Nafion. Argon was filled in w.e.c. and an aqueous sulfuric acid solution (in most cases 0.025 mol dm^{-3}) without or with AA (in most cases 0.15 mol dm^{-3}) in c.e.c. The cell was thermostated at 25 °C.

Electrochemical Measurements. Chronopotentiometry, chronoamperometry, and steady state current measurements were adopted in order to obtain information on the concentration profiles of Fe^{3+} and AA. The apparent effective surface area of composite electrodes was 3.1 cm^2.

Results

The Concentration of Fe^{3+} inside Pt-Nafion. By a method similar to that used before,[3] the exchange selectivity of Nafion for Fe^{3+} was investigated. The concentration of Fe^{3+} in Pt-Nafion equilibrated with an Fe^{3+}solution of concentration higher than 0.3 mol dm^{-3} was 0.31 mol dm^{-3}-whole-wet-resin. Fe^{3+} is exchanged with other cations in the solution when it is soaked in an electrolyte solution free from Fe^{3+} until the concentration distribution reaches an equilibrium state between the contacting solution and Pt-Nafion. Therefore, after the electrolytic cell was set up and

filled with a sulfuric acid solution in c.e.c. (14.5 cm^3), the concentration of Fe^{3+} inside Pt-Nafion decreased to 0.29 and 0.12 mol dm^{-3}-whole-wet-resin (Nafion 125) for 0.050 and 0.10 mol dm^{-3} in c.e.c., respectively.

The Thickness of Pt-Nafion. Swelling changes the volume of Nafion, resulting in a change in its thickness. The degree of swelling is known to be dependent on its pretreatment conditions. After the standard boiling water treatment, the thickness of Nafion 125 and 120 was measured using a micrometer. The averaged values were 139 and 284 μm, respectively, which approximately agreed with values 143 and 289 μm calculated using an empirical equation[9] of swelling while assuming an isotropic expansion by swelling.

Diffusion of Fe^{3+}. Chronopotentiometry measurements gave $i\tau^{1/2}$ of 29.6 mA $s^{1/2}$ on Pt-Nafion containing Fe^{3+} and contacting with 0.05 mol dm^{-3} H_2SO_4. Substituting 0.29 mol dm^{-3} for the concentration of Fe^{3+}, the Sand equation,[10] Eq. 1, gave the diffusion coefficient of Fe^{3+} in Pt-Nafion, and $D_{Fe}=1.5\times10^{-7}$ $cm^2\,s^{-1}$ was obtained.

$$I\tau^{1/2}=nFAcD^{1/2}\pi^{1/2}/2 \quad (1)$$

This value is reasonable, compared with the value for Na^+, $D_{Na}=9.44\times10^{-7}$ $cm^2\,s^{-1}$, measured by a tracer method for Nafion 120.[11]

The constant current for a reduction of Fe^{3+} on Pt-Nafion contacting 0.5 mol dm^{-3} $Fe_2(SO_4)_3$ was measured under mass-transfer limiting conditions using Nafion 125 and Nafion 120 at 200 mV vs. Ag/AgCl. Assuming that the diffusion layer thickness is equal to the Nafion thickness (139 and 284 μm, respectively), a calculation using Eq. 2 and c=0.31 mol dm^{-3} gave $D_{Fe}=1.4\times10^{-7}$ $cm^3\,s^{-1}$.

$$I=nFADc/d \quad (2)$$

After equilibrating Fe-type Pt-Nafion with 0.05 mol dm^{-3} H_2SO_4, the electrode potential was stepped from 700 mV (vs. Ag/AgCl) to 200 mV, where Fe^{3+} was reduced to Fe^{2+} under mass-transfer limiting conditions. As plotted in Fig.1, in the range of small t the transient current decreased linearly with $t^{1/2}$, and in the range of larger t the current remained constant. Using the Cottrell Eq. 3,[12] and substituting c=0.29 mol dm^{-3}, $D_{Fe}=1.8\times10^{-7}$ $cm^2\,s^{-1}$ was obtained.

$$I=nFAcD^{1/2}/\pi^{1/2}t^{1/2} \quad (3)$$

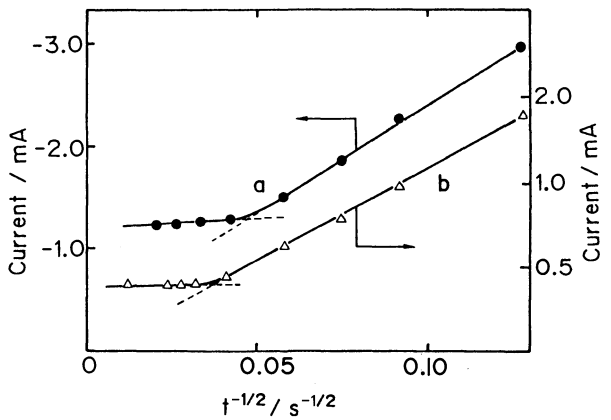

Fig. 1. Cottrell plots of the reduction of Fe^{3+} (a) and oxidation of L-ascorbic acid (b) on Pt-Nafion 125.
Fe^{3+}: 0.75—0.20V, 0.2 M Fe^{3+} and 25 mM H_2SO_4 in c.e.c.
AA: 0.25—0.75V, 0.15 M AA, 25 mM H_2SO_4 in c.e.c.

The diffusion layer thickness increased with the time after the potential stepping; a model involving semiinfinite diffusion was no longer valid after the time that the surface of Nafion began to significantly affect the diffusion of Fe^{3+}. On the other hand, at a longer time, the reduction was controlled by the mass transfer, which was limited by the linear diffusion through the Nafion layer of Pt-Nafion under steady state conditions. This situation leads to a constant current as shown in the figure. The intersecting point of two linear lines gives the time when the thickness of the diffusion layer becomes equal to the thickness of the Nafion. Using $d=(\pi Dt)^{1/2}$ and $t^{-1/2}=0.05$ $s^{-1/2}$ (at the intersecting point), a calculation gave the thickness of 143 μm, which agreed fairly well with the directly measured value, 139 μm.

Diffusion of AA. Since AA is known to be oxidized on a Pt electrode, the diffusion coefficient of AA in Pt-Nafion was measured by electrochemical methods. Chronoamperometry measurements were carried out by stepping a potential of Pt-Nafion without any incorporation of iron ions from 250 to 750 mV, at which all AA reaching the electrode surface on Pt-Nafion through the Nafion layer was sufficiently quickly oxidized to dehydroascorbic acid. As shown in Fig. 1, the transient current decreased proportionally to $t^{-1/2}$ for a shorter time. A slope of i-$t^{-1/2}$ gives the diffusion coefficient using the Cottrell equation, Eq. 3, if the concentration of AA inside the Pt-Nafion c_{At} is known. As discussed below, a concentration in a solution contacting Pt-Nafion can be adopted as the value in Pt-Nafion within an error of less than 10%. Under this situation, the Cottrell equation, Eq. 3, leads to the diffusion coefficient of AA in Pt-Nafion, $D_{AA}=4.4\times10^{-8}$ $cm^2\,s^{-1}$. By a treatment similar to that in the chronopotentiometry of Fe^{3+}, the intersecting point of a Cottrell plot with a steady state current (which corresponds to the diffusion limiting current through the Nafion 125 layer on Pt-Nafion) gave a thickness of 127 μm. The value is about 10% less than the measured value for Nafion 125 (139 μm). The diffusion current of AA through the Nafion layer on Pt-Nafion at 750 mV was proportional to the concentration of AA in the contacting solution. The diffusion current using Nafion 125 was two-times larger than that with Nafion 120, as expected from the difference in the diffusion flux through two membranes of different thickness.

Discussion

The concentration profiles of AA and Fe^{3+} inside Pt-Nafion is discussed. The reaction of AA, with Fe^{3+}, in an aqueous solution is described as follows.[13]

$$-dc_{At}/dt = kc_{At}[Fe^{3+}] \quad (4)$$

c_{At}; total concentration of ascorbic acid AA dissociates to AA^- and AA^{2-} in an aqueous solution. Neglecting the second dissociation, AA^{2-} since it makes a very small contribution,[13] Eq. 4 can be rewritten

$$-dc_{At}/dt = k_1[AA^0][Fe^{3+}] + k_2[AA^-][Fe^{3+}]. \quad (5)$$

Using the dissociation constant, K_1,

$$-dc_{At}/dt = (k_1 + k_2K_1/[H^+])[AA^0][Fe^{3+}]. \quad (6)$$

The rate constants, k_1 and k_2, and the dissociation constant, K_1, were obtained previously:[13]

$$k_1 = 1.6\times10^2\ mol^{-1}\,dm^3\,s^{-1},$$
$$k_2 = 6.4\times10^3\ mol^{-1}\,dm^3\,s^{-1},$$

and

$$K_1 = 9.2\times10^{-5}\ mol\,dm^{-3}.$$

Since Fe^{2+} is generated inside Pt-Nafion by a reaction of Fe^{3+} with AA, the cation is demanded in Nafion in order to satisfy the requirements of electroneutrality there. In this system, H^+ produced by the oxidation of AA satisfies this requirement. Further, as discussed previously, not all counter ions of Nafion are changed to Fe^{3+}, but some H^+ coexists in the Nafion as a counter ion. For these reasons, the concentration of H^+ at the reaction site in Pt-Nafion is higher than 0.29 mol dm^{-3} under the situation that the reaction between AA and Fe^{3+} takes place. This consideration allows one to neglect the second term in the parenthesis of Eq. 6, namely to neglect the contribution from the reaction of dissociated ascorbic acid. Equation 6 simplifies as follows:

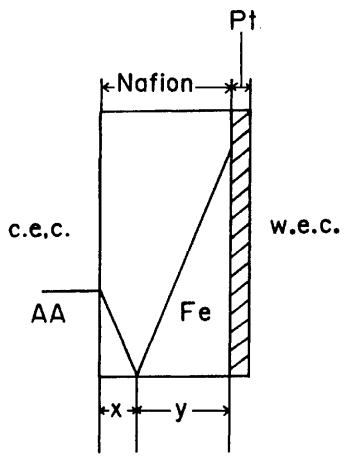

Fig. 2. A simplified model of the concentration profile of indirect oxidation of AA by Fe(3+/2+) redox couple inside the Pt-Nafion. x: diffusion layer thickness of AA, y: diffusion layer thickness of Fe^{3+}.

$$-dc_{At}/dt = k_1[AA^0][Fe^{3+}]. \quad (7)$$

Assuming the simple model shown in Fig. 2, the concentration profiles of AA and Fe^{3+} were calculated using this equation. In this model it was assumed that a reaction is completed at the surface where AA and Fe^{3+} meet. Saveant and co-workers have extensively investigated the concentration profiles on polymer-coated electrodes.[7,8] The rate constants and diffusion coefficients of electroactive species and substrates through both a coating layer and a solution should be taken into consideration as factors which affect the concentration profiles in the coating layer. In the present treatment, the diffusion through a solution contacting Pt-Nafion is neglected because a much slower diffusion through the coating layer is expected. Yeager et al. investigated the mass transport of Na^+ through Nafion and through a depletion layer formed on the surface of Nafion.[14] Their result that the thickness of the depletion layer was as thin as 15 μm, supports the expectation that the mass transfer is predominantly controlled by the diffusion through Nafion. The reaction rate is also considered to be very fast, compared with the rate of mass transfer.

Some specific partition has been observed for many species at the interface between an ion-exchange membrane and the solution.[15] Therefore, the concentration of AA inside Pt-Nafion might be different from that in the solution. As discussed above, all ascorbic acid exists in its neutral form in Pt-Nafion. At the intersecting point in Fig. 1, the current obtained by a chronoamperometry measurement must be equal to the steady state current, though the former value can be estimated by extrapolation. Using Eqs. 2 and 3,

$$I_s = nFAlc_{At}/\pi t_l. \quad (8)$$

Substituting the values into I_s, n, F, A, l, and t_l in Eq. 8, c_{At} becomes 0.16 mol dm^{-3}, which is close to 0.15 mol dm^{-3}, the concentration in the contacting solution. From the above discussion it is concluded that the above assumption, that c_{At} is equal to the concentration of the contacting solution within the experimental error in the concentration range examined here, is acceptable and that there exists neither a specific affinity nor a repulsion between Nafion and ascorbic acid in the present system, though a strong affinity was often reported between organic substances and ion exchange membranes.

In the model of Fig. 2, the followings are applicable:

$$x + y = 0.0139, \quad (9)$$

$$J_{Fe} = 2J_{AA}, \quad (10)$$

$$\text{The flux of AA, } J_{AA} = D_{AA}c_{At}/x, \quad (11)$$

and

$$\text{The flux of } Fe^{3+},\ J_{Fe} = D_{Fe}c_{Fe}/y, \quad (12)$$

From the above equations,

$$y = D_{Fe}c_{Fe}\times0.0139/(2D_{AA}c_{At} + D_{Fe}c_{Fe}). \quad (13)$$

The calculated values of y are plotted as a function of c_{At} in Fig. 3. Using the values for y and Eq. 2, the oxidation current of AA was calculated and is described in Fig. 4 (open circle, solid line) together with the experimental results (triangle and black circle). The experimental values are smaller than the calculated values. The difference can partly be ascribed to the exclusion of Fe^{3+} by H^+ formed by the oxidation of AA from the membrane.

In the above treatment, it was assumed that the reaction between AA and Fe^{3+} proceeded instantaneously at the surface where two species met. The concept of a reaction zone was introduced in order to examine whether the model of instantaneous reaction between Fe^{3+} and AA is valid or not. The model shown in Fig. 5 describes the reaction zone. The concentration of reactants is assumed to be uniform inside the zone (thickness; d) and equal to each other (c_{av}).

$$dc/dt = k_1 c_{av}^2 \qquad (14)$$

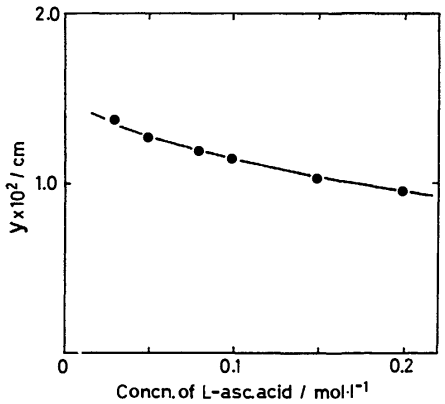

Fig. 3. The dependence of the thickness of diffusion layer for AA (y) on the concentration of AA in c.e.c. on Pt-Nafion 125 incorporated with Fe(3+/2+) redox couple (x+y=139 μm).

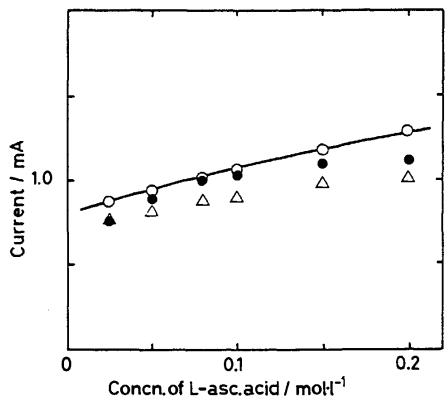

Fig. 4. Dependencies of oxidation current of AA on the concentration of AA in c.e.c. using Pt-Nafion 125 incorporated with Fe(3+/2+) redox couple. Solid line: values calculated using y in Fig. 3 and D_{Fe} and D_{AA}.
△: Run 1, ●:Run 2.

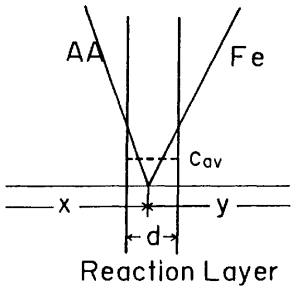

Fig. 5. A reaction layer model of indirect oxidation of AA on Pt-Nafion incorporated with Fe(3+/2+) redox couple.
d: reaction layer thickness, x: diffusion layer thickness of AA, y: diffusion layer thickness of Fe^{3+}, c_{av}: average concentration of AA and Fe^{3+}.

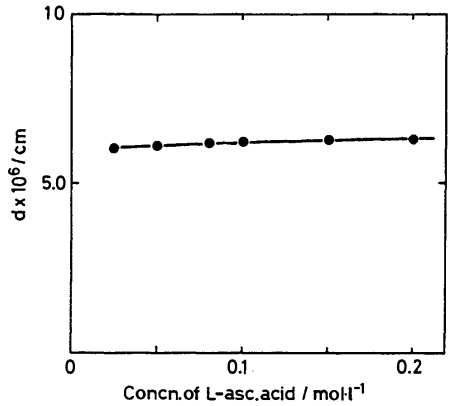

Fig. .6. The dependence of the reaction layer thickness (d in Fig. 5) on the concentration of AA in c.e.c. on Pt-Nafion 125 incorporated with Fe(3+/2+) redox couple.

Under a steady state,

$$k_1 c_{av}^2 \times d/1000 = D_{AA} c_{At}/x. \qquad (15)$$

A numerical calculation gave d, which is plotted in Fig. 6 as a function of c_{At}. As shown in the figure, the thickness is about 6 μm, about 4% of the Nafion thickness. This results reveals that the model of Fig. 2 is valid.

From the above discussion, it is shown that the rate of a mediated reaction is mainly controlled by the slow diffusion of AA and takes place within a narrow zone very close to the Nafion surface facing against c.e.c. Configuration a in Fig. 3 of Ref. 3, where substrates are contained in w.e.c., will make the diffusion pass of Fe^{3+} shorter and will remarkably enhance the reaction rate, though a direct reaction of substrates on the electrode bound on Nafion must proceed rapidly in this configuration.

Conclusion

Pt-Nafion incorporated with iron ions gave an example of a polymer coated electrodes containing redox mediators. Details of the concentration profiles

of the reactants in the coating polymer, Nafion, were examined. A Fe^{2+}/Fe^{3+} redox couple incorporated into Pt-Nafion worked as a mediator in the oxidation of ascorbic acid. The diffusion of Fe^{3+} and AA was rate-determining, and the diffusion of the latter was slower. The mediation reaction proceeded in the very narrow zone, quite close to the Nafion surface. The averaged diffusion coefficients in Nafion, D_{Fe} and D_{AA}, were 1.5×10^{-7} cm^2 s^{-1} and 4.7×10^{-8} $cm^2 s^{-1}$, respectively. Ascorbic acid did not show any specific affinity to Nafion.

SPE composite electrodes were functionalized by the incorporation of mediator systems into SPE materials. This modification is expected to enhance its activity and reaction selectivities in its application to organic electrochemistry, sensors, etc. Configurations in which substrates are contained in the w.e.c. will enhance the activity of SPE composites electrodes incorporated with mediators.

This work was partly supported by a Grant-in-Aid for Scientific Research (No. 61850147) from the Ministry of Education, Science and Culture.

References

1) Z. Ogumi, H. Yamashita, K. Nishio, Z. Takehara, and S. Yoshizawa, *Electrochim. Acta*, **28**, 1687 (1983).

2) Z. Ogumi, S. Ohashi, and Z. Takehara, *Nippon Kagaku Kaishi*, **1984**, 1788.

3) Z. Ogumi, T. Mizoe, N. Yoshida, and Z. Takehara, *Bull. Chem. Soc. Jpn.*, **60**, 4233 (1987).

4) I. Rubinstein and A. J. Bard, *J. Am. Chem. Soc.*, **102**, 6641 (1980).

5) D. A. Buttry and F. C. Anson, *J. Am. Chem. Soc.*, **104**, 4824 (1982).

6) E. W. Kristensen, W. G. Kuhn, and R. M. Wightman, *Anal. Chem.*, **59**, 1752 (1987).

7) C. P. Andrieux and J. M. Saveant, *J. Electroanal. Chem.*, **142**, 1 (1982).

8) C. P. Andrieux and J. M. Saveant, *J. Electroanal. Chem.*, **93**, 163 (1978).

9) W. G. Grot, G. E. Munn, and D. N. Walmsley, 141st National Meeting, The Electrochemical Society, Houston, Texas (1972).

10) A. J. Bard and L. R. Foulkner, "Electrochemical Methods," John Wiley & Sons, New York (1980), Chap. 7.

11) H. L. Yeager and A. Steck, *J. Electrochem. Soc.*, **128**, 1880 (1981).

12) A. J. Bard and L. R. Foalkner, "Electrochemical Methods," John Wiley & Sons, New York (1980), Chap. 5.

13) M. M. T-Khan and A. E. Martell, *J. Am. Chem. Soc.*, **86**, 4176 (1967).

14) H. L. Yeager and B. Kipling, *J. Phys. Chem.*, **83**, 1836 (1979).

15) C. R. Martin and H. Freiser, *Anal. Chem.*, **53**, 904 (1981).

A Novel Approach to the Enumeration of Reaction Types by Counting Reaction-Center Graphs Which Appear as the Substructures of Imaginary Transition Structures

Shinsaku FUJITA
Research Laboratories, Ashigara, Fuji Photo Film Co., Ltd., Minami-Ashigara, Kanagawa 250-01
(Received March 30, 1988)

A novel method of enumerating reaction types is presented. The reaction types are formulated as reaction-center graphs (RCGs) that are derived from a parent basic reaction graph (BRG) or from a parent reaction graph (RG) by the substitution of various atoms on the vertices and/or by the attachment of single, double, or triple par-bonds to the edges. The counting of the isomeric RCGs is solved by applying Pólya's theorem to the derivation of a cycle index, in which different variables are introduced to the different orbits of the permutation group of a parent BRG (or RG). Various atom-figure and bond-figure inventories are described in order to count the isomers of RCGs. The numbers of the RCGs are given in the form of the coefficients of a generating function called an RCG-counting polynomial series.

The collection of reaction types as a knowledge database is necessary for the construction of a computer system dealing with organic reactions.[1-12] The reaction data should be classified clearly and consistently in order to keep the database manageable. A well-defined classification of reaction types is also of fundamental importance for the purpose of retrieving organic reactions[13] as well as for the intention of providing organic chemistry with a more logical and systematic format.[14]

The classification of reaction types necessitates their enumeration, since the expanse of the information regarding them must be preestimated.[15] In addition, the enumeration implies the generation of new organic reactions that fundamentally supports a system of synthetic design.[2c]

The systematic enumeration of reaction types has been achieved only to a limited extent. This stems from the fact that an individual organic reaction is represented by a conventional reaction diagram which contains substrates and products combined with an arrow, as shown in Scheme 1.[16,17j] The conventional enumeration of reaction types thereby requires a multiple comparison among the molecules contained in both sides of the respective diagrams. The treatment of such dual representations is cumbersom and may lead to an overlooking of various possibilities and/or to duplicated counting.

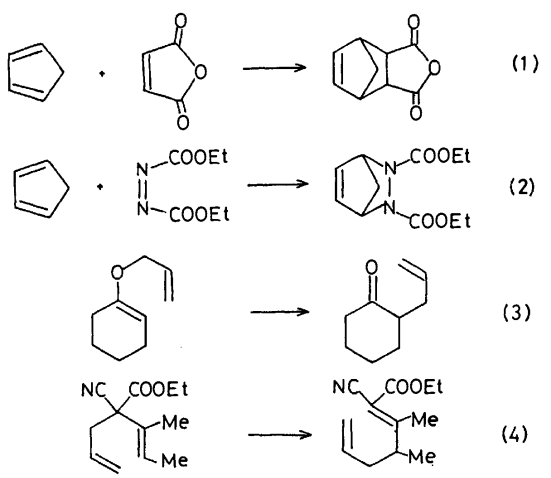

Scheme 1.

In previous papers,[17] we have proposed the concept of imaginary transition structures (ITS) which afford unitary representations of individual organic reactions. As a result, the manipulation of reaction data is transformed to that of ITSs as a kind of structural formulas. An abstraction of the reaction types is thereby accomplished by finding appropriate subgraphs or substructures of ITSs. Among the useful subgraphs, imaginary rings (ITS rings),[17a,i] reaction-center graphs (RCG),[17a] reaction graphs (RG),[17b,c,f,g] and three- or four-nodal subgraphs[17d,k] are especially effective for characterizing organic reactions.

By a formulation based on the ITSs, an enumeration of the reaction types is transformed into the counting of the subgraphs. In this connection, we have enumerated reaction graphs (RG) to afford a generic classification of reaction types.[17b,c,f,g] As a continuation of this work, the present report deals with a general method for counting reaction types and, especially, with an enumeration of the RC graphs (RCG) which provide us with more detailed information concerning reaction types than the reaction graphs do.

Formulation and Methods

Unique Representations of Reaction Types. Scheme 2 summarizes the formulation of the reaction types discussed in this paper. These ITSs and the related substructures correspond to the diagrams shown in Scheme 1. Although the respective concepts have been reported in the previous papers,[17a,b] they should be restated and extended with the purpose of being applied to the present problem of enumeration.

The *imaginary transition structure (ITS)* of a given reaction contains the participating atoms (C, H, N, O, etc.) and three kinds of bonds (in- (⊖), out- (⧺), and par-bonds (—)), which bonds correspond to the structural changes during the reaction.[17a]

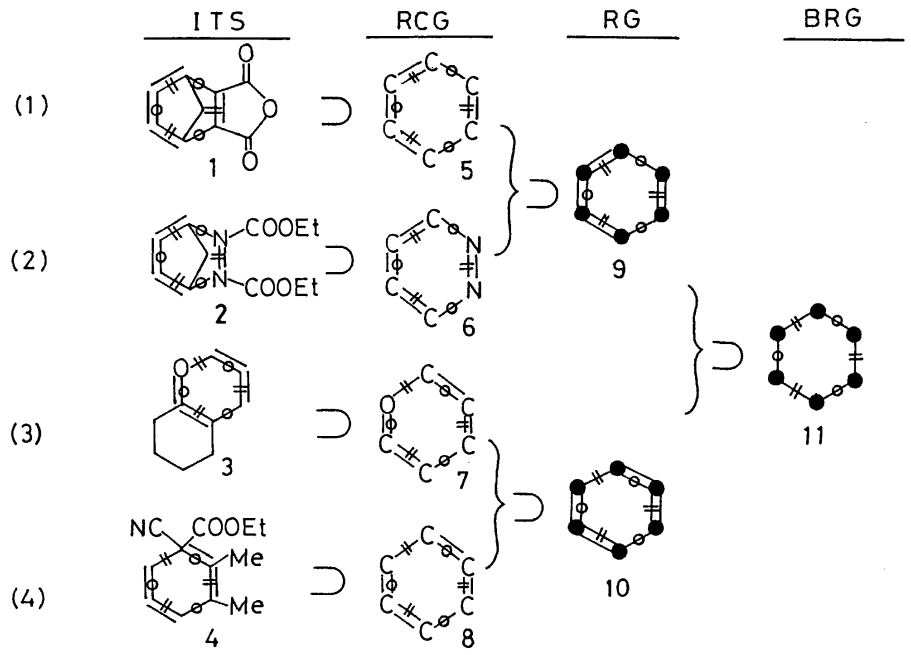

Scheme 2.

A *reaction-center graph (RCG)* is defined as a substructure or a subgraph of a given ITS, in which all reaction centers and imaginary bonds between them are collected.[17b] For example, the RCGs (**5**—**8**) are extracted from the corresponding ITSs (**1**—**4**), as shown in Scheme 2. The RCGs (**5** and **6**) represent generic reaction types, both of which are called *Diels-Alder reactions.* They are discriminated from each other in the light of node values (i.e., C_6 and C_4N_2). The Claisen and Cope rearrangements are represented by the RCGs (**7** and **8**), which are the substructures of the ITSs (**3** and **4**) respectively. The RCGs (**7** and **8**) differ from each other in their node values (i.e. C_5O vs. C_6).

A *reaction graph (RG)* is a more abstract substructure that disregards the node values of an RC graph.[17b] The RCGs (**5** and **6**) give the same RG (**9**), which coresponds to a generic class of the Diels-Alder reactions. The RCGs (**7** and **8**) afford another reaction graph (**10**) that represents a [3,3]sigmatropic rearrangement.

A *basic reaction graph (BRG)* is defined as a substructure that contains reaction centers without node values and has in- and out-bonds but no par-bonds on the edges.[17b] The BRG indicates an electron-shift pattern, which is a descriptor of a broad class of organic reactions. A common basic reaction graph (**11**) is obtained from the RGs (**9** and **10**) by deleting all of the par-bonds therefrom (Scheme 2).

A *reaction pair* consists of two graphs (ITSs, RCGs, RGs, or BRGs) interchangeable by an operation which exchanges all in-bonds and out-bonds with each other (*transformation to reverse reaction*: TRR). For example, the TRR operation on RG (**9**) affords the RG of the corresponding reverse reaction, i.e., retro-Diels-Alder reaction. We call a reaction pair of RG level *an RG pair,* and distinguish it from an RCG pair that is a reaction pair of the RCG level.

A *self reaction pair* is a special case of a reaction pair, the graph of which is invariant on the TRR operation. For example, RCG **8** and RG **10** are self-reaction pairs in the respective levels.

Scheme 2 indicates a hierarchical classification of organic reactions in terms of the ITS approach. It should be emphasized that the levels of the hierarchy, i.e., RCG, RG, and BRG, give explicit representations to the respective generic reaction types.

In order to avoid any unfamiliarity with the ITS approach, we introduce *projections to starting stage (PS)* and *to product stage (PP)* that derive conventional diagrams or general schemes from the corresponding ITS, RCG, RG, and BRG (Scheme 3). The PS operation involves a deletion of in-bonds (or taking up par- and out-bonds), and the PP operation involves a deletion of out-bonds (or the taking-up of par- and in-bonds).

Formulation of the Enumeration Problem of Reaction Types. In the light of the formulation described above, our subject to enumerate reaction types is now regarded as the counting of RCGs, RGs, and BRGs. In the present paper, we will discuss two approaches to the enumeration of RCGs (Scheme 4).

The first approach is a one-step method (Scheme 4(1)). An RC graph (RCG) is, thus, considered as being a derivative of a parent BRG that is attached by l_1 single par-bonds (—) and/or l_2 double par-bonds (=) on its edges and is substituted by an appropriate number of atoms on its vertices (nodes). The RCGs (**5**, **6**, **7**, and **8**) are derivatives based on BRG **11** in this sense.

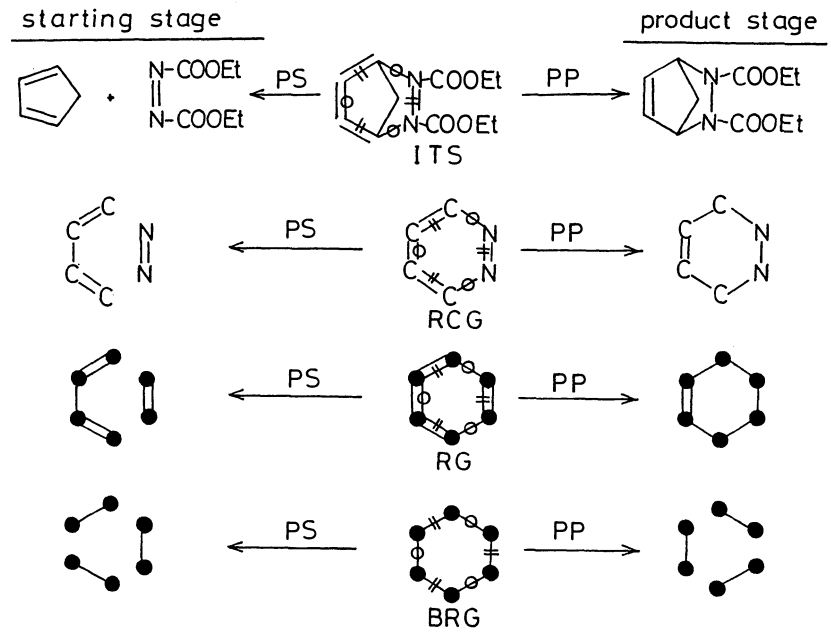

Scheme 3.

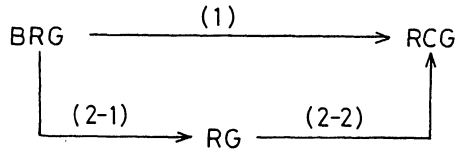

Scheme 4.

An alternative approach consists of two steps (2-1 and 2-2 of Scheme 4). In the first step (2-1), a reaction graph (RG) is considered to be a derivative of a basic reaction graph (BRG) that is substituted by l_1 single par-bonds and/or l_2 double par-bonds on its edges. For example, the RGs (**9** and **10**) are isomers that contain 4 single par-bonds but differ from one another in their manner of substitution (Scheme 2). Several RGs have been enumerated in this line and reported in previous papers.[17b,c,f,g] The present paper affords a more general treatment regarding this step than the previous reports. The 2nd step (2-2) concerns an RCG as the derivative of a parent RG that is substituted by an appropriate number of atoms on its vertices.[18] For example, the RCGs (**5** and **6**) are derivatives that have C_6 and C_4N_2, respectively, on the vertices of the RG (**9**). Similarly, the RCGs (**7** and **8**) are derivatives having C_5O and C_6, respectively, on the vertices of the RG (**10**).

One-Step Enumeration. In the one-step approach, an appropriate BRG is selected as a parent graph. Let **G** be the group of symmetry (order g) of the parent BRG, there being p vertices (nodes) at which atoms can be substituted and being q edges to which par-bonds can be attached. Let **H** (degree: $p+q$ and order: g) be a permutation group isomorphic to **G**. Let h_C be the number of the permutations in **H** which have a cycle structure of the type:

$$C=[i_1+j_1, i_2+j_2, \cdots, i_r+j_r, \cdots],$$

wherein i_r cycles of length r are concerned with a substitution to the vertices and j_r cycles or length r are with respect to the edges; they satisfy the following relationships:

$$1i_1+2j_2+\cdots+pi_p=p$$
$$1j_1+2j_2+\cdots+qi_q=q$$

Since the edges and vertices obviously are not interchangeable by **H** (in other words, the two construct different classes or orbits), the cycle index of **H** is obtained by restating Pólya's theorem[19] in an applicable form to our cases:

$$Z(\mathbf{H})=(1/g)\sum_C h_C(s_1^{i_1}s_2^{i_2}\cdots s_p^{i_p})(t_1^{j_1}t_2^{j_2}\cdots t_q^{j_q}), \quad (1)$$

where the summation is taken over all different types (C) of partitions (Appendix 1).

Then, let s_r be an atom-figure inventory that indicates the manner of atom constitution (an atom figure). Also let t_r be a bond-figure inventory that shows the mode of par-bond substitution (a bond-figure). They are defined as shown in the following equations:

$$s_r=1+u_1^r+u_2^r+u_3^r+\cdots \quad (2)$$
$$t_r=1+x_1^r+x_2^r. \quad (3)$$

By introducing s_r (Eq. 2) and t_r (Eq. 3) into the cycle index (Eq. 1), we obtain an RCG-counting polynomial series (Eq. 4) in the form of a generating function:

$$G(u_1, u_2, \cdots x_1, x_2)=Z(\mathbf{H}, 1+u_1+u_2+\cdots, 1+x_1+x_2)$$
$$=\sum A(k_1k_2\cdots l_1l_2)(u_1^{k_1}u_2^{k_2}\cdots)(x_1^{l_1}x_2^{l_2}). \quad (4)$$

The coefficient $A(k_1k_2\cdots l_1l_2)$ of $(u_1^{k_1}u_2^{k_2}\cdots)(x_1^{l_1}x_2^{l_2})$ gives the number of RC graphs when k_1 atoms of the first kind, k_2 of the second kind and so on are introduced to the vertices of the parent BRG, and l_1 of sin-

gle par-bonds and l_2 of double par-bonds are attached to the edges of the BRG. It should be noted that the two kinds of figure-counting series, which we call an *atom-figure inventory* and a *bond-figure one*, can take various forms according to the objects of enumeration. Although they are obviously equivalent from a mathematical point of view, the discrimination between them is convenient in chemical usage. This point will be exemplified in the following discussions.

The cycle index (Eq. 1) can be further generalized so as to be applicable to a case in which the vertices and/or edges subdivided to two or more intransitive orbits in a permutation group (Appendix 1).

An RCG pair-counting polynomial series $P(u_1, u_2, \cdots, x_1, x_2)$ can be obtained in a similar manner, except that the group of the parent BRG is replaced by that of a structure in which the difference between in- and out-bonds is disregarded.[20] The explicit forms for specific cases are listed in the discussions below.

Two-Step Enumeration. This approach contains two successive steps of enumeration (Scheme 4(2-1) and (2-2)). Suppose that a parent BRG has p edges belonging to one orbit and q edges to another different orbit of a permutation group **H** (degree: $p+q$ and order: g) and that the p edges can be attached by single par-bonds and that the q edges can be attached by single or double par-bonds. Variables t_{ar} and t_{br} are assigned to the respective orbits. The mathematical framework described above is thereby applicable to this case and, hence, the corresponding cycle index can be represented as

$$Z(\mathbf{H}) = (1/g)\sum_C h_C(t_{a1}{}^{i_1}t_{a2}{}^{i_2}\cdots t_{ap}{}^{i_p})(t_{b1}{}^{j_1}t_{b2}{}^{j_2}\cdots t_{bq}{}^{j_q}), \quad (5)$$

wherein the other characters have the same meanings as stated above.

In order to obtain an RG-counting polynomial series, suppose that t_{ar} is a bond-figure inventory of the first orbit (a) and t_{br} is another bond-figure inventory of the second orbit (b):

$$t_{ar} = 1 + x_1{}^r \quad (6)$$

$$t_{br} = 1 + x_1{}^r + x_2{}^r \quad (7)$$

We obtain the polynomial $G_b(x_1, x_2)$ (Eq. 8) for counting RGs by introducing t_{ar} (Eq. 6) and t_{br} (Eq. 7) into the cycle index (Eq. 6):

$$G_b(x_1, x_2) = Z(\mathbf{H}, 1 + x_1, 1 + x_1 + x_2) = \sum B(l_1 l_2) x_1{}^{l_1} x_2{}^{l_2} \quad (8)$$

The coefficient $B(l_1 l_2)$ of $x_1{}^{l_1}x_2{}^{l_2}$ gives the number of RGs in which l_1 of single par-bonds and l_2 of double par-bonds are attached to the edges of the parent BRG.

In the second step of the two-step method, we select an appropriate parent RG that has been derived at the first step described above. Suppose that p and q vertices of a parent RG belong to the two different orbits of a permutation group **H** (degree: $p+q$ and order: g), respectively. The p of the vertices of the first orbit can be substituted by n_1 kinds of atoms. On the other hand, q of the vertices of the second orbit can be substituted by n_2 kinds of atoms. Two different variables, S_{ar} and s_{br}, are assigned to the respective orbits. We then obtain the following cycle index:

$$Z(\mathbf{H}) = (1/g)\sum_C h_C(s_{a1}{}^{i_1}s_{a2}{}^{i_2}\cdots s_{ap}{}^{i_p})(s_{b1}{}^{j_1}s_{b2}{}^{j_2}\cdots s_{bq}{}^{j_q}), \quad (9)$$

wherein the other characters have the same meanings as stated above.

Let s_{ar} and s_{br} be the respective atom-figure inventories for orbits a and b and be defined as

$$s_{ar} = 1 + u_1{}^r + \cdots + u_{n1}{}^r \quad (10)$$

and

$$s_{br} = 1 + u_1{}^r + \cdots + u_{n2}{}^r \quad (11)$$

These equations are introduced to the cycle index (Eq. 9), which is, in turn, expanded into a generating function. An RCG-counting polynomial series $G_a(u_1, u_2, \cdots)$ is thus obtained:

$$G_a(u_1, u_2, \cdots) = Z(\mathbf{H}, 1 + u_1 + \cdots + u_{n1}, 1 + u_1 + \cdots + u_{n2}) = \sum C(k_1 k_2 \cdots)\,(u_1{}^{k_1}u_2{}^{k_2}\cdots). \quad (12)$$

The coefficient $C(k_1 k_2 \cdots)$ of the term $u_1{}^{k_1}u_2{}^{k_2}\cdots$ gives the number of RC graphs in which k_1 atoms of a first kind, k_2 of a second kind and so on are introduced to the vertices of the parent RG.

Results and Discussion

Enumeration of RC Graphs Based on a Parent Basic Reaction Graph. Examples of the One-Step Method. Table 1 summarizes representative BRGs selected as parent graphs and the corresponding cycle indices for the counting of RCGs and/or RCG pairs. These results have been obtained by applying Eq. 1 to the respective cases in accord with their permutation groups. The number of RCGs in each case is obtained where variables s_r and t_r of the cycle index collected in Table 1 are substituted by the figure-counting series (Eqs. 2 and 3).

To exemplify the derivation of cycle indices and of RCG-counting polynomial series, we examine the counting of isomers of hexagonal reaction graphs (Table 2).[21] Suppose that a parent BRG (**11**) is substituted by l_1 single par-bonds on its edges and attached by k_1 nitrogen atoms and k_2 oxygen atoms (and $6-k_1-k_2$ of implicit carbon or other atoms) on its vertices. The vertices of **11** are numbered as 1, 2, ··· 6 and the edges are designated as a, b, ··· f.

The symmetry of **11** is $\mathbf{D}_3$ (order 6). Hence, the permutation corresponding to each symmetry operation is obtained, as shown in Table 2, which permutation is represented by the product of cycles, e.g.,

$$C_{2(1)} \sim \begin{pmatrix} 1 & 2 & 3 & 4 & 5 & 6 & a & b & c & d & e & f \\ 2 & 1 & 6 & 5 & 4 & 3 & a & f & e & d & c & b \end{pmatrix} = (1\ 2)\,(3\ 6)\,(4\ 5)\,(a)\,(d)\,(b\ f)\,(c\ e).$$

Table 1. Parent Basic Reaction Graphs and Cycle Indices for the One-Step Enumeration[a)]

BRG	Symmetry	Cycle indes[b,c)]	Eq.
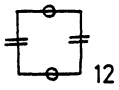 12	D_2	G: $(1/4)(s_1^4t_1^4+2s_2^2t_1^2t_2+s_2^2t_2^2)$	13
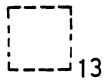 13	D_4	P: $(1/8)(s_1^4t_1^4+2s_1^2s_2t_2^2+2s_2^2t_1^2t_2+s_2^2t_2^2+2s_4t_4)$	14
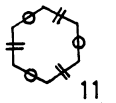 11	D_3	G: $(1/6)(s_1^6t_1^6+3s_2^3t_1^2t_2^2+2s_3^2t_3^2)$	15
14	D_6	P: $(1/12)(s_1^6t_1^6+s_2^3t_2^3+3s_1^2s_2^2t_2^3+3s_2^3t_1^2t_2^2+2s_3^2t_3^2+2s_6t_6)$	16
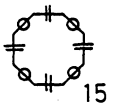 15	D_4	G: $(1/8)(s_1^8t_1^8+4s_2^4t_1^2t_2^3+s_2^4t_2^4+2s_4^2t_4^2)$	17
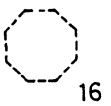 16	D_8	P: $(1/16)(s_1^8t_1^8+4s_2^4t_1^2t_2^3+s_2^4t_2^4+2s_4^2t_4^2+4s_1^2s_2^3t_2^4+4s_8t_8)$	18
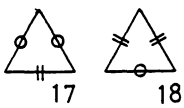 17 18	C_2	G: $(1/2)(s_1^3t_1^3+s_1s_2t_1t_2)$	19
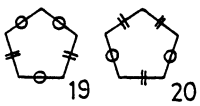 19 20	C_2	G: $(1/2)(s_1^5t_1^5+s_1s_2^2t_1t_2^2)$	20
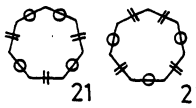 21 22	C_2	G: $(1/2)(s_1^7t_1^7+s_1s_2^3t_1t_2^3)$	21

a) The cycle indices are obtained by applying Eq. 1 to the respective BRGs. b) A variable s_r is assigned to the cycle of length r which is concerned with a permutation of the vertices. On the other hand, a variable t_r is with respect to a permutation of the edges. c) G: a cycle index for counting RCGs. P: a cycle index for counting RCG pairs.

Table 2. A Permutation Group Based on a Parent BRG (**11**)

Parent BRG: 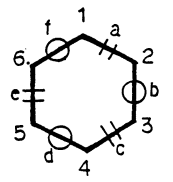

11 (D_3)

Symmetry operation	Permutation	Variable[a)] assigned
I	(1)(2)(3)(4)(5)(6) (a)(b)(c)(d)(e)(f)	$s_1^6t_1^6$
$C_{2(1)}$	(1 2)(3 6)(4 5) (a)(d)(b f)(c e)	$s_2^3t_1^2t_2^2$
$C_{2(2)}$	(1 6)(2 5)(3 4) (c)(f)(a e)(b d)	
$C_{2(3)}$	(1 4)(2 3)(5 6) (b)(e)(a c)(d f)	
C_3	(1 5 3)(2 6 4) (a e c)(b f d)	$s_3^2t_3^2$
C_3^2	(1 3 5)(2 4 6) (a c e)(b d f)	

a) A variable is assigned to each permutation in acord with the cycle structure wherein s_r and t_r are concerned with vertices and edges, respectively. Strictly speaking, this example has three orbits, i.e., (1,2,···6), (a,c,e), and (b,d,f). However, the same variable t_r can be assigned to the latter two orbits without losing generality.

Let us consider a permutation group of degree 12 (=6+6) that is isomorphic to the symmetry of the parent BRG. Obviously, the set of the six vertices and that of the six edges construct different orbits. In other words, the six vertices and six edges are not interchanged with each other by any permutation collected in Table 2. Hence, we introduce different variables, s_r and t_r, to the respective orbits. The assigned variables collected in Table 2 are derived from the cycle structures of the permutations. Upon collecting these assigned variables over all the permutations, we found that the corresponding cycle index (Eq. 15 of Table 1) is a specific case of Eq. 1. Therefore, the variables of Eq. 15 are replaced by atom-figure and bond-figure inventories:

$$s_r = 1 + u^r + v^r \tag{22}$$

and

$$t_r = 1 + x^r. \tag{23}$$

As a result, the following equation is derived as a

generating function called an RCG-counting polynomial series:

$$G(u, v, x)=(1/6)\ \{(1+u+v)^6(1+x)^6+ 3(1+u^2+v^2)^3(1+x)^2(1+x^2)^2+ 2(1+u^3+v^3)^2(1+x^2)^2\}. \quad (24)$$

Since the parent BRG (**11**) is a self-reaction pair, the set of isomers counted by Eq. 24 contains one or more self-reaction pairs. The next problem is the counting of reaction pairs. The corresponding parent graph (**14**) has $\mathbf{D}_6$ symmetry (order 12) and affords the cycle index (Eq. 16) as collected in Table 1. Then, an RCG pair-counting polynomial $P(u, v, x)$ (Eq. 25) is derived by the introduction of Eqs. 22 and 23 into Eq. 16:

$$P(u, v, x) =(1/12)\ \{(1+u+v)^6(1+x)^6+(1+u^2+v^2)^3(1+x^2)^3+ 3(1+u+v)^2(1+u^2+v^2)^2(1+x^2)^3+ 3(1+u^2+v^2)^3(1+x)^2(1+x^2)^2+ 2(1+u^3+v^3)^2(1+x^3)^2+ 2(1+u^6+v^6)(1+x^6)\}. \quad (25)$$

The expansion of Eq. 24 gives a polynomial series in which the coefficient of the term $u^{k_1}v^{k_2}x^l$ indicates the number or isomers derived from the parent BRG (**11**) with l single par-bonds on the edges along with k_1 of nitrogen and k_2 of oxygen atoms. Similarly, an expansion of Eq. 25 affords a polynomial series, the coefficients of which show the numbers of the corresponding RCG pairs. The coefficients derived from Eqs. 24 and 25 are found in Table 3.

Table 3. Enumeration of Reaction Types Based on BRG (**11**)[a]

k_1k_2	Number of RCGs (RCG pairs)			
	l=0 or 6	l=1 or 5	l=2 or 4	l=3
0 0	1 (1)	2 (1)	4 (3)	6 (3)
1 0	1 (1)	6 (3)	15 (9)	20 (10)
0 1	1 (1)	6 (3)	15 (9)	20 (10)
2 0	4 (3)	18 (9)	42 (24)	56 (28)
1 1	5 (3)	30 (15)	75 (39)	100 (50)
0 2	4 (3)	18 (9)	42 (24)	56 (28)
3 0	4 (3)	20 (10)	50 (28)	68 (34)
2 1	10 (6)	60 (30)	150 (78)	200 (100)
1 2	10 (6)	60 (30)	150 (78)	200 (100)
0 3	4 (3)	20 (10)	50 (28)	68 (34)
4 0	4 (3)	18 (9)	42 (24)	56 (28)
3 1	10 (6)	60 (30)	150 (78)	200 (100)
2 2	18 (11)	96 (48)	234 (123)	312 (156)
1 3	10 (6)	60 (30)	150 (78)	200 (100)
0 4	4 (3)	18 (9)	42 (24)	56 (28)
5 0	1 (1)	6 (3)	15 (9)	20 (10)
4 1	5 (3)	30 (15)	75 (39)	100 (50)
3 2	10 (6)	60 (30)	150 (78)	200 (100)
1 4	5 (3)	30 (15)	75 (39)	100 (50)
0 5	1 (1)	6 (3)	15 (9)	20 (10)
6 0	1 (1)	2 (1)	4 (3)	6 (3)
5 1	1 (1)	6 (3)	15 (9)	20 (10)
4 2	4 (3)	18 (9)	42 (24)	56 (28)
3 3	4 (3)	20 (10)	50 (28)	68 (34)
2 4	4 (3)	18 (9)	42 (24)	56 (28)
1 5	1 (1)	6 (3)	15 (9)	20 (10)
0 6	1 (1)	1 (1)	4 (3)	6 (3)

a) The numbers of RCGs with k_1 or nitrogens, k_2 of oxygens and one single par-bond are obtained as the coefficients of $u^{k_1}v^{k_2}x^l$ in Eq. 24. The numbers in the parentheses indicate the number of RCG pairs which are obtained by the expansion or Eq. 25.

The results of Table 3 have been obtained by a mathematical treatment and, hence, affords a good probe to test the validity of manual enumeration. From this point of view, let us examine several examples derived from the parent BRG (**11**). Table 4 collects isomers with one nitrogen and one oxygen and no par-bonds ($k_1=k_2=1$, $l=0$) as well as isomers with two nitrogen ($k_1=2$, $k_2=l=0$).[22] Each couple of the RCGs linked with a brace (Table 4) is a reaction pair. An isolated one is a self reaction pair. The number of NO isomers is 5; this number is obtained as the coefficient of the term uv ($=u^1v^1x^0$) of Eq. 24 (Table 3, $k_1=k_2=1$, $l=0$). The number of RCG pairs is 3, which is obtained from Eq. 25 (the data in parentheses of Table 3 at $k_1=k_2=1$, $l=0$). The latter N_2 case affords 4 for RCGs and 3 for RCG pairs as the respective coefficients of the term u^2 ($=u^2v^0x^0$) in Eqs. 24 and 25 (Table 3). The results shown in Table 4 are, thus, confirmed by the values of Table 3.

A comparison between the NO and N_2 substitutions (Table 4) reveals that the RCG pair of the former NO case (marked by an asterisk) is degenerated to a self RCG pair in the latter N_2 case. This fact reflects the symmetries of the RCGs, which determine the values of the coefficients.

Table 5 shows the case of $k_1=k_2=l=1$. The number of isomers of RC graphs is 30 and that of RCG pairs is 15, which are in accord with the results obtained from the generating functions (Table 3).

It must be emphasized that *the number of reaction types is given in the form of the coefficient of a generating function such as Eq. 24 but not as a result of manual enumeration.* Therefore, the present method

Table 4. Isomeric RCGs with NO or N_2 on the Vertices but No Par-Bonds on the Edges[a]

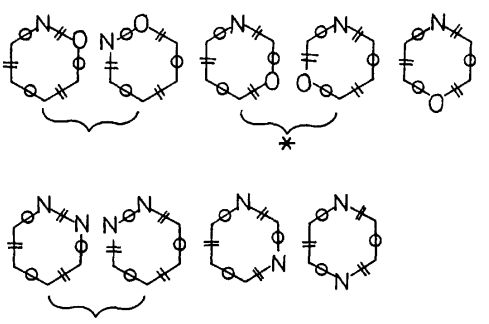

a) Each couple of RCGs linked with a brace is a reaction pair. An isolated RCG is a self-reaction pair. The number of RCGs and that of RCG pairs are obtained as the coefficients of the respective generating functions (Eqs. 24 and 25). These numbers are listed in Table 3 ($k_1=k_2=1$, $l=0$; and $k_1=2$, $k_2=l=0$).

affords an assurance of the validity to a computer program for the enumeration of reaction types or for generating new reactions.

Table 5. Isomeric RCGs Substituted by One Nitrogen and One Oxygen on the Vertices and by One Single Par-Bond on the Edge[a)]

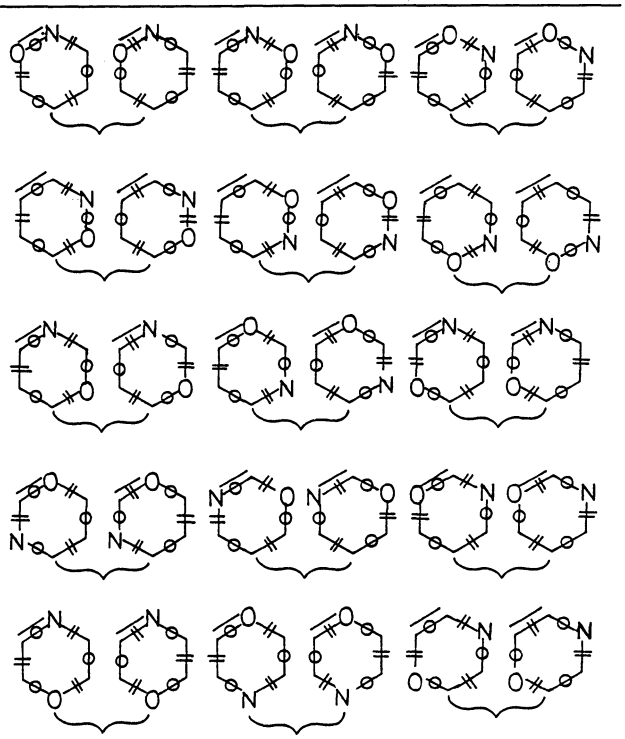

a) Each couple or RCGs linked with a brace is a reaction pair. The number of RCGs and that of RCG pairs are obtained as the coefficients of $u^1v^1l^1$ of Eqs. 24 and 25, respectively (Table 3, $k_1=k_2=l=1$).

Enumeration of RC Graphs Based on a Parent Reaction Graph. The 2nd Step of the Two-Step Method. The number of isomers obtained in the last section contains that of several RCGs in which the valency of the atoms exceeds chemically reasonable values. Hence, a more specific treatment than that mentioned above is necessary in order to avoid counting chemically unreasonable isomers. This approach starts from an appropriate reaction graph (RG) in place of the BRG described above.

Table 6 summarizes parent RGs of the hexagonal class having 0 to 6 single par-bonds along with the respective cycle indices for counting RCGs and/or RCG pairs. The two parent RGs in alignment are a reaction pair with one another (e.g. **23** and **24**). Contrarily, the RG coupled with a broken-lined graph is a self-reaction pair (e.g. **11** followed by **14**). The two cases are slightly different in a practical treatment, although the results are obtained by applying Eq. 9 to each of the parent RGs in a similar manner. In the former case, the number of RCGs derived from a parent RG is equal to the value based on the corresponding reverse RG. Hence, the number of RCG pairs is always half of the total number of RCGs, based on the RG and the reverse RG as parents. On the other hand, the latter case requires a separate treatment of counting the RCG pairs, since the parent RG is a self-reaction pair.

To exemplify the method of enumeration, let us work out the RG (**9**) as a parent and count the isomers having k_1 nitrogen and k_2 oxygen atoms. The six vertices, whose numbering is shown, are divided into three classes by the corresponding permutation group ($\mathbf{C}_2$), i.e., 1, 2; 3, 4; and 5, 6 (Table 7). The cycle index for **9** (Eq. 39) is obtained, as collected in Table 6, when we

Table 6. Hexagonal RGs as Parent Graphs and Their Cycle Indices[a,b)]

RG	Symmetry	Cycle index	Eq.
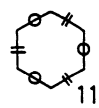 11	$\mathbf{D}_3$	G: $(1/6)(s_{b1}^6+3s_{b2}^3+2s_{b3}^2)$	26
14	$\mathbf{D}_6$	P: $(1/12)(s_{b1}^6+3s_{b1}^2s_{b2}^2+4s_{b2}^3+2s_{b3}^2+2s_{b6})$	27
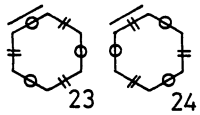 23 24	$\mathbf{C}_2$	G: $(1/2)(s_{b1}^6+s_{b2}^3)$	28
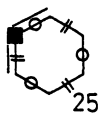 25	$\mathbf{C}_1$	G: $s_{a1}s_{b1}^5$	29
26	$\mathbf{C}_2$	P: $(1/2)(s_{a1}s_{b1}^5+s_{a1}s_{b1}s_{b2}^2)$	30

Table 6. (Continued)

RG	Symmetry	Cycle index	Eq.
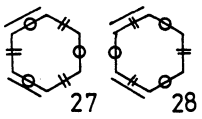 27 28	C_2	G: $(1/2)(s_{b1}^6+s_{b2}^3)$	31
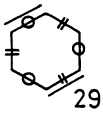 29	C_2	G: $(1/2)(s_{b1}^6+s_{b2}^3)$	32
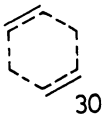 30	D_2	P: $(1/4)(s_{b1}^6+s_{b1}^2s_{b2}^2+2s_{b2}^3)$	33
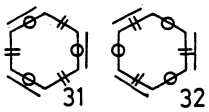 31 32	D_3	G: $(1/6)(s_{b1}^6+3s_{b2}^3+2s_{b3}^2)$	34
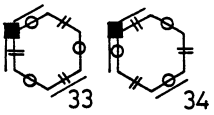 33 34	C_1	G: $s_{a1}s_{b1}^5$	35
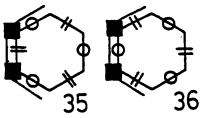 35 36	C_2	G: $(1/2)(s_{a1}^2s_{b1}^4+s_{a2}s_{b2}^2)$	36
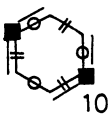 10	C_2	G: $(1/2)(s_{a1}^2s_{b1}^4+s_{a2}s_{b2}^2)$	37
37	D_2	P: $(1/4)(s_{a1}^2s_{b1}^4+s_{a1}^2s_{b2}^2+2s_{a2}s_{b2}^2)$	38
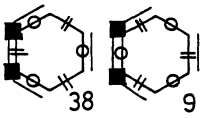 38 9	C_2	G: $(1/2)(s_{a1}^2s_{b1}^4+s_{a2}s_{b2}^2)$	39
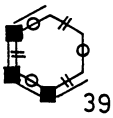 39	C_1	G: $s_{a1}^3s_{b1}^3$	40
40	C_2	P: $(1/2)(s_{a1}^3s_{b1}^3+s_{a1}s_{a2}s_{b1}s_{b2})$	41
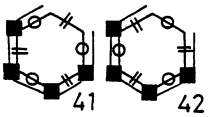 41 42	C_2	G: $(1/2)(s_{a1}^4s_{b1}^2+s_{a2}^2s_{b2})$	42
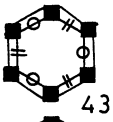 43	D_3	G: $(1/6)(s_{a1}^6+3s_{a2}^3+2s_{a3}^2)$	43
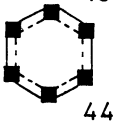 44	D_6	P: $(1/12)(s_{a1}^6+3s_{a1}^2s_{a2}^2+4s_{a2}^3+2s_{a3}^2+2s_{a6})$	44

a) The cycle indices are obtained by applying Eq. 9 to the respective RGs. A variable s_{ar} is assigned to the cycle of length r which is concerned with a permutation of the restricted vertices (■). A variable s_{br} is with respect to a permutation of the unmarked vertices. b) G: a cycle index for counting RCGs. P: a cycle index for counting RCG pairs.

Table 7. Permutation Group Based on a Parent RG (**9**)

Parent RG: 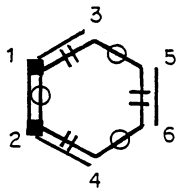

9 (C_2)

Symmetry operation	Permutation	Variable[a] assigned
I	(1)(2) (3)(4) (5)(6)	$s_{a1}^2 s_{b1}^4$
C_2	(1 2) (3 4) (5 6)	$s_{a2} s_{b2}^2$

a) The vertices, 1 and 2, are distinguished from the others because of limitation of valency. The variable s_{br} is given to the former vertices (marked by ■). The other vertices are assigned to s_{br}.

give a variable s_{ar} to the first class and s_{br} to the 2nd and 3rd classes. This treatment stems from the facts that vertices 1 and 2 (marked by boldface squares) are unable to be substituted by oxygen atoms due to a valency limitation and that the substituents on vertices 3 to 6 can be selected freely from a set of nitrogen, oxygen, and implicit carbon atoms.

We then introduce two kinds of atom-figure inventories:

$$s_{ar} = 1 + u^r \tag{45}$$

and

$$s_{br} = 1 + u^r + v^r, \tag{46}$$

the first of which is used for a substitution only by nitrogen atoms and the 2nd of which is used for a substitution by nitrogen and oxygen atoms. The variables of Eq. 39 are substituted by Eqs. 45 and 46 to afford an RCG-counting polynomial series (Eq. 47):

$$G(u, v) = (1/2)\{(1+u)^2(1+u+v)^4 + (1+u^2)(1+u^2+v^2)^2\}. \tag{47}$$

The expanded equation from Eq. 47 is a generating function in which the coefficient of $u^{k_1}v^{k_2}$ is the number of isomers with k_1 nitrogen and k_2 oxygen atoms.

Table 8 shows isomers in which one nitrogen and one oxygen atom substitute the vertices of the parent RG (**9**). The number of isomers collected is 10, the number of which is equal to the coefficient of the term u^1v^1 of Eq. 47. Table 8 also contains isomers having two nitrogen substituents on the RG (**9**). This list contains the isomers of the RCG (**6**) shown in Scheme 2. The number of N_2 isomers is 9, which is, again, confirmed by a comparison with the coefficient of u^2v^0 in Eq. 47.

The parent RG (**9**) is not a self-reaction pair and the TRR operation affords RG (**38**) of the reverse reaction (the retro Diels-Alder reaction). The enumeration of isomers based on RG (**38**) gives the same results as those of RG (**9**).

Table 8. Isomeric RCGs Derived by NO and N_2 Substitution on the Parent RG (**9**)[a]

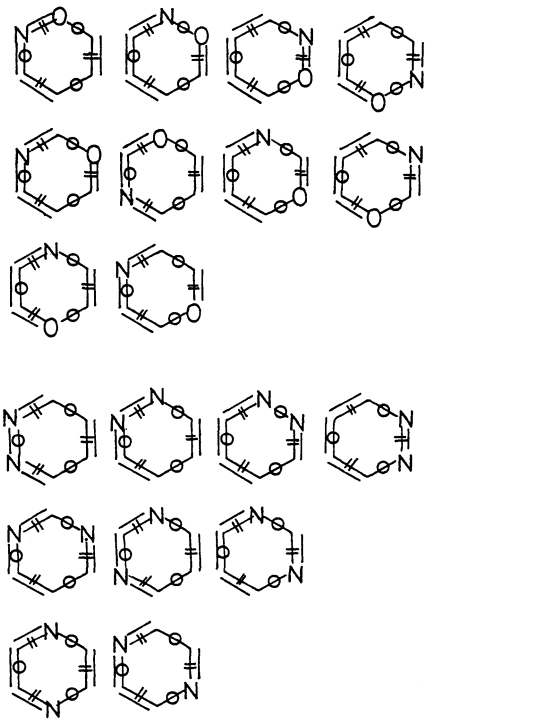

a) The numbers of RCGs are obtained as the coefficients of uv for NO substitution (Table 9, **9**, $k_1=k_2=1$) and of u^2 for N_2 substitution (Table 9, **9**, $k_1=2$, $k_2=0$). See Appendix 2.

The Diels-Alder type addition of a triple bond is represented by the RG (**45**) that also has three classes of vertices (1, 2; 3, 4; and 5, 6). Since vertices 1, 2, 5, and 6 are unable to have oxygen substituents, the cycle index (Eq. 48) is different from Eq. 39.

$$Z(\mathbf{C}_2) = (1/2)(s_{a1}^4 s_{b1}^2 + s_{a2}^2 s_{b2}) \tag{48}$$

By applying Eqs. 45 and 46 to Eq. 48, we obtain the following RCG-counting polynomial series (Eq. 49):

$$G(u, v) = (1/2)\{(1+u)^4(1+u+v)^2 + (1+u^2)^2(1+u^2+v^2)\}. \tag{49}$$

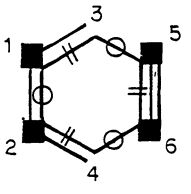

45 (C_2)

Let us next consider a case in which a parent RG is a self-reaction pair. The representative example is the RG (**10**) that has $\mathbf{C}_2$ symmetry (Table 6). The six vertices are divided into three orbits. The vertices of the first orbit (marked by heavy squares) can take only C and N as a substituent because of a valency limitation.

Table 9. Enumeration of Reaction Types Based on Various Parent RGs[a]

k_1k_2	Parent RG: **11 (14)**	**23 25 (26) 24**	**27 29 (30) 28**	**31 33 35 10 (37) 32 34 36**	**38[b] 39 (40) 9**	**41 43 (44) 42**
	number of RCG's (RCG pairs)					
0 0	1 (1)	1 1 (1)	1 1 (1)	1 1 1 1 (1)	1 1 (1)	1 1 (1)
1 0	1 (1)	3 6 (4)	3 3 (2)	1 6 3 3 (2)	3 6 (4)	3 1 (1)
0 1	1 (1)	3 5 (3)	3 3 (2)	1 5 2 2 (1)	2 3 (2)	1 0 (0)
2 0	4 (3)	9 15 (9)	9 9 (6)	4 15 9 9 (6)	9 15 (9)	9 4 (3)
1 1	5 (3)	15 25(13)	15 15 (8)	5 25 10 10 (5)	10 15 (8)	5 0 (0)
0 2	4 (3)	9 10 (6)	9 9 (6)	4 10 4 4 (3)	4 3 (2)	1 0 (0)
3 0	4 (3)	10 20(12)	10 10 (6)	4 20 10 10 (6)	10 20(12)	10 4 (3)
2 1	10 (6)	30 50(26)	30 30(16)	10 50 20 20(10)	20 30(16)	10 0 (0)
1 2	10 (6)	30 40(22)	30 30(16)	10 40 12 12 (7)	12 12 (7)	2 0 (0)
0 3	4 (3)	10 10 (6)	10 10 (6)	4 10 2 2 (1)	2 1 (1)	0 0 (0)
4 0	4 (3)	9 15 (9)	9 9 (6)	4 15 9 9 (6)	9 15 (9)	9 4 (3)
3 1	10 (6)	30 50(26)	30 30(16)	10 50 20 20(10)	20 30(16)	10 0 (0)
2 2	18(11)	48 60(32)	48 48(27)	18 60 20 20(12)	20 18(10)	4 0 (0)
1 3	10 (6)	30 30(16)	30 30(16)	10 30 6 6 (3)	6 3 (2)	0 0 (0)
0 4	4 (3)	9 5 (3)	9 9 (6)	4 5 1 1 (1)	1 0 (0)	0 0 (0)
5 0	1 (1)	3 6 (4)	3 3 (2)	1 6 3 3 (2)	3 6 (4)	3 1 (1)
4 1	5 (3)	15 25(13)	15 15 (8)	5 25 10 10 (5)	10 15 (8)	5 0 (0)
3 2	10 (6)	30 40(22)	30 30(16)	10 40 12 12 (7)	12 12 (7)	2 0 (0)
2 3	10 (6)	30 30(16)	30 30(16)	10 30 6 6 (3)	6 3 (2)	0 0 (0)
1 4	5 (3)	15 10 (6)	15 15 (8)	5 10 1 1 (1)	1 0 (0)	0 0 (0)
0 5	1 (1)	3 1 (1)	3 3 (2)	1 1 0 0 (0)	0 0 (0)	0 0 (0)
6 0	1 (1)	1 1 (1)	1 1 (1)	1 1 1 1 (1)	1 1 (1)	1 1 (1)
5 1	1 (1)	3 5 (3)	3 3 (2)	1 5 2 2 (1)	2 3 (2)	1 0 (0)
4 2	4 (3)	9 10 (6)	9 9 (6)	4 10 4 4 (3)	4 3 (2)	1 0 (0)
3 3	4 (3)	10 10 (6)	10 10 (6)	4 10 2 2 (1)	2 1 (1)	0 0 (0)
2 4	4 (3)	9 5 (3)	9 9 (6)	4 5 1 1 (1)	1 0 (0)	0 0 (0)
1 5	1 (1)	3 1 (1)	3 3 (2)	1 1 0 0 (0)	0 0 (0)	0 0 (0)
0 6	1 (1)	1 0 (0)	1 1 (1)	1 0 0 0 (0)	0 0 (0)	0 0 (0)

a) The coefficients of $u^{k1}v^{k2}$ indicate the numbers of isomeric RCG with k_1 of nitrogens and k_2 of oxygens on each of parent RG. These values are obtained by introducing Eqs. 45 and 46 to each of the cycle indices (Table 4). b) Obtained by the expansion of Eq. 47.

The other vertices are capable of taking a C, N, or O substituent. The cycle index for the parent RG (**10**) is obtained, as shown in Table 6 (Eq. 37), when we introduce a variable s_{ar} to the first orbit and s_{br} to the 2nd and 3rd orbits. In order to obtain an RCG-counting polynomial series, two kinds of atom-figure inventories (Eqs. 45 and 46) are introduced into the cycle index (Eq. 37). The result of the expansion of this polynomial is listed in Table 9.

Since the parent RG (**10**) is a self-reaction pair, the resulting set of isomers contains one or more self RCG pairs. The next problem is counting the RCG pairs. A parent graph (**37**) for counting RCG pairs is obtained by equalizing the in- and out-bonds of RG (**10**). This graph has $\mathbf{D}_2$ symmetry. The six vertices are divided into two orbits by this symmetry. We then obtain the cycle index of Eq. 38 (Table 6), in which two variables (s_{ar} and s_{br}) are assigned to the orbits in accord with their limitation (maked by ■). The expansion of this polynomial gives a generating function that affords the number of RCG pairs with k_1 of oxygen and k_2 of nitrogen atoms as the coefficient of $u^{k_1}v^{k_2}$. The results are listed also in Table 9.

Table 10 lists the isomers of $k_1=0$, $k_2=1$ (O substitution) and of $k_1=1$, $k_2=0$ (N substitution). The number of RCGs in the former case is 2 and that of RCG pairs is 1. These values are equal to the coefficients of the term u^0v^1 listed in Table 9. On making a substitution of one nitrogen, we obtain 3 isomers of RCG and 2

Table 10. Isomeric RCGs with O and N Substitution on the Parent RG (**10**)[a,b]

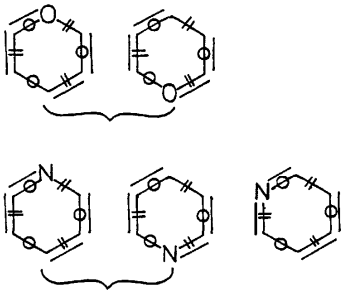

a) The number of the O isomers is the coefficient of v (Table 9, **10**, $k_1=0$, $k_2=1$). The number of RCG pairs is shown also in Table 9 (**37**, $k_1=0$, $k_2=1$). b) The number of the N isomers is the coefficient of u (Table 9, **10**, $k_1=1$, $k_2=0$). The number of RCG pairs is found Table 9 (**37**, $k_1=1$, $k_2=0$). See Appendix 2.

RCG pairs. These numbers are the same values as the coefficients of u^1v^0 collected in Table 9.

Table 9 also lists the other results that are obtained by applying atom-figure inventories (Eqs. 45 and 46) to the cycle indices shown in Table 6. When a parent RG is a self-reaction pair, the isomers, therefrom, contain one or more self-RCG pairs. In this case, Table 9 indicates the results of counting RCG-pairs as well as those of counting RCGs.[23]

In this section, we have dealt only with parent RGs of the hexagonal class. The method discussed, however, is applicable to the other types of parent RGs which are derived from the respective parent BRGs given in Table 1. Although the detailed results are abbreviated, full lists of the latter cases would be of essential importance for didactic and taxonomic purposes.

Enumeration of RGs Based on a Fused BRG. Improved Examples of the First Step of the Two-Step Method. In a previous paper,[17g] we reported an enumeration of RGs in which they are considered to be the isomers of basic reaction graphs given in Table 11. The previous treatment has not differenciated the fused bonds from the other pericyclic bonds. In light of the extension described in this paper, this subject can be discussed in a more detailed fashion.

Suppose that the fused positions can be attached only by a single par-bond and other pericyclic edges can be substituted by a singe or double par-bond. This formulation allows Eq. 5 to be applied to the various parent BRGs given in Table 11, in which the corresponding cycle indices are listed. Upon making the substitution $t_{ar}=1+x^r$ and $t_{br}=1+x^r+y^r$ and collecting like powers of xy, the coefficients of term $x^{l_1}y^{l_2}$ are obtained in order to indicate the number of isomers with l_1 single par-bonds and l_2 double par-bonds.

Enumeration of RGs with Cross-Bonds. Extended Examples of the First Step of the Two-Step Method. The above-mentioned treatment presumes that only in-bonds and out-bonds on edges are the positions of substitution. However, a more general enumeration is sometimes desirable. For example, tetra-*t*-butyltetrahedrane (**56**) and tetra-*t*-butylcyclobutadiene (**57**) have been reported to be interconvertible (Scheme 5).[24] The ITSs (**58** and **59**) represent these reactions. The corresponding reaction graphs (RGs) contain cross-bonds. The final problem discussed in this article is counting this type of reaction graph.

We select a basic reaction graph (**60**) as a parent, which has 4 usual edges and 2 phantom edges (cross-

Table 11. Fused BRG as Parent Graphs and Their Cycle Indices[a]

Fused BRG	Symmetry	Cycle index[b]	Eq.
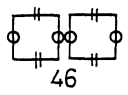 46 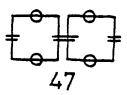 47	D_2	G: $(1/4)(t_{a1}t_{b1}^6+2t_{a1}t_{b2}^3+t_{a1}t_{b1}^2t_{b2}^2)$	50
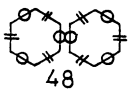 48 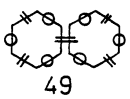 49	D_2	G: $(1/4)(t_{a1}t_{b1}^{10}+2t_{a1}t_{b2}^5+t_{a1}t_{b1}^2t_{b2}^4)$	51
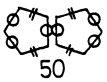 50 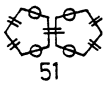 51	D_2	G: $(1/4)(t_{a1}t_{b1}^8+3t_{a1}t_{b2}^4)$	52
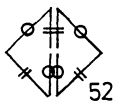 52	C_2	G: $(1/2)(t_{a1}^2t_{b1}^4+t_{a1}^2t_{b2}^2)$	53
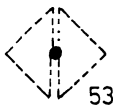 53	D_2	P: $(1/4)(t_{a1}^2t_{b1}^4+2t_{a2}t_{b2}^2+t_{a1}^2t_{b2}^2)$	54
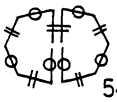 54	C_2	G: $(1/2)(t_{a1}^2t_{b1}^8+t_{a1}^2t_{b2}^4)$	55
55	D_2	P: $(1/4)(t_{a1}^2t_{b1}^8+2t_{a2}t_{b2}^4+t_{a1}^2t_{b2}^4)$	56

a) The cycle indices are obtained by applying Eq. 5 to the respective BRGs. b) A variable t_{ar} is respect to the fused edges, whereas t_{br} is assigned to the pericyclic edges.

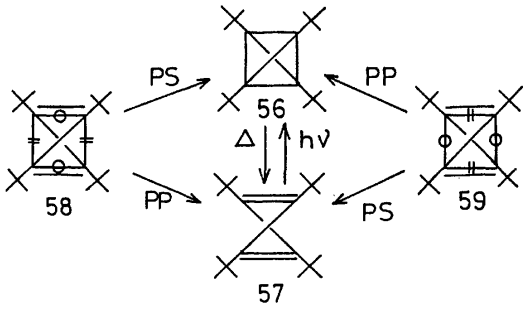

Scheme 5.

linkages of broken lines) as the positions of substitution (Table 12). The consideration of phantom edges is a new matter, compared with the previous enumeration.[17b] When the six edges are marked as above, the 4 permutations of $\mathbf{D}_2$ group (degree 6) are easily obtained (Table 12). The edges are divided into three orbits, i.e., a, c; b, d; and e, f. The edges of the first and 2nd orbits are unable to have a triple par-bond (≡) as a substituent. On the other hand, the phantom edges of the 3rd orbit can be attached by either single, double or triple par-bond. Hence, we introduce a variable t_{ar} to the former and another variable t_{br} to the latter orbits. We thereby obtain a cycle index (Eq. 57), as shown in Table 13.

Table 12. Permutation Group Based on a Parent BRG (**60**)[a]

Parent BRG:

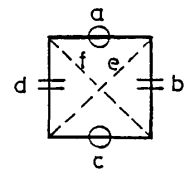

60 (D_2)

Symmetry operation	Permutation	Variable assigned[b]
I	(a)(c) (b)(d) (e)(f)	$t_{a1}^4 t_{b1}^2$
$C_{2(1)}$	(a)(c) (b d) (e f)	$t_{a1}^2 t_{a2} t_{b2}$
$C_{2(2)}$	(a c) (b)(d) (e f)	$t_{a1}^2 t_{a2} t_{b2}$
$C_{2(3)}$	(a c) (b d) (e)(f)	$t_{a2}^2 t_{b1}^2$

a) A broken line indicates a phontom edge which can be substituted by a single, double, or triple par-bond. b) The pericyclic edges have a variable t_{ar}. A variable t_{br} is respect to the phontom edges.

In order to obtain an RG-counting polynomial series $G(x, y, z)$, the variables of Eq. 57 are substituted by the following two kinds of bond-figure inventories:

$$t_{ar} = 1 + x^r + y^r \tag{61}$$

and

$$t_{br} = 1 + x^r + y^r + z^r, \tag{62}$$

wherein t_{ar} is used for a substitution by a single or double par-bond and t_{br} for a substitution by a single, double, or triple par-bond. The expansion of the polynomial affords the following generating function for the counting of RGs:

$$\begin{aligned} G(x, y, z) &= (1 + 3x + 3y + 6x^2 + 9xy + 6y^2 + 8x^3 + 18x^2y + 18xy^2 + \\ &\quad 8y^3 + 6x^4 + 18x^3y + 27x^2y^2 + 18xy^3 + 6y^4 + \cdots) + \\ &\quad z(1 + 3x + 3y + 6x^2 + 10xy + 6y^2 + \cdots) + \\ &\quad z^2(1 + 2x + 2y + 3x^2 + 4xy + 3y^2 + \cdots). \end{aligned} \tag{63}$$

The coefficient of $x^{l_1}y^{l_2}z^{l_3}$ of Eq. 63 is the number of RGs having l_1 single, l_2 double, and l_3 triple par-bonds on the edges.

Table 14 collects RGs of $l_1=3$, $l_2=l_3=0$ as an example. The number of the isomeric RGs is 6, which number is the coefficient of the term $x^3y^0y^0$ of the Eq. 63. Table 14 also shows isomeric RGs of $l_1=4$, $l_2=l_3=0$, the number of which is found as the coefficient of $x^4y^0z^0$ of Eq. 63. The two RGs connected with a brace construct a reaction pair and the isolated ones are self reaction pairs, respectively. The number of reaction pairs can be obtained by using the cycle index (Eq. 58) and the bond-figure inventories (Eqs. 61 and 62).

The BRG (**9**) has 9 additional phantom edges in light of the approach taken in this section. Hence we obtain the cycle index (Eq. 59) shown in Table 13. The degree and order of the permutation group obtained are 15 and 6, respectively. The cycle index (Eq. 60) for counting the corresponding reaction pairs

Table 13. Parent BRGs with Phantom Edges and Their Cycle Indices[a]

BRG	Symmetry	Cycle index[b,c]	Eq.
60	$\mathbf{D}_2$	G: $(1/4)(t_{a1}^2t_{b1}^2+2t_{a1}^2t_{a2}t_{b2}+t_{a2}^2t_{b1}^2)$	57
	$\mathbf{D}_4$	P: $(1/8)(t_{a1}^4t_{b1}^2+2t_{a1}^2t_{a2}t_{b2}+3t_{a2}^2t_{b1}^2+2t_{a4}t_{a2})$	58
61	$\mathbf{D}_3$	G: $(1/6)(t_{a1}^6t_{b1}^9+3t_{a1}^2t_{a2}^2t_{b1}t_{b2}^4+2t_{a3}^2t_{b3}^3)$	59
	$\mathbf{D}_6$	P: $(1/12)(t_{a1}^6t_{b1}^9+3t_{a1}^2t_{a2}^2t_{b1}t_{a2}^4+2t_{a3}^2t_{b3}^2+3t_{a2}^3t_{b1}^3t_{b2}^3+t_{a2}^3t_{b1}^3t_{b2}^3+2t_{a6}t_{b3}t_{b6})$	60

a) The cycle indices are obtained by applying Eq. 5 to the respective BRGs having phantom edges. b) A variable t_{ar} is assigned to the pericyclic edges. The phantom edges have a variable t_{br} assigned. c) G; a cycle index for counting RGs. P: a cycle index counting RG pairs.

Table 14. Isomeric RGs with Cross-Bonds[a)]

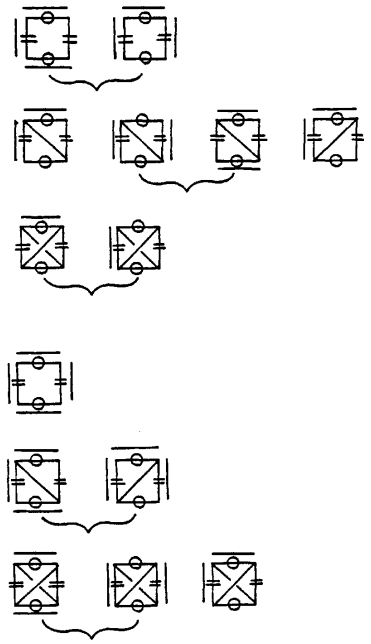

a) Out- and in-bonds are presumed to take pericyclic positions and thus the cross-bonds always consist of par-bonds. This table contains only two types of isomers, i.e. $l_1=3$, $l_2=l_3=0$, and $l_1=4$, $l_2=l_3=0$.

is also found in Table 13. When we introduced bond-figure inventories (Eqs. 61 and 62) to these cycle indices, we obtain generating functions for counting RGs and RG pairs, respectively, of hexagonal class.

Conclusion

We have formulated an enumeration of reaction types as a counting of reaction graphs (RG) and of reaction-center graphs (RCG). The problem has been solved by applying Pólya's theorem in which different variables are introduced to different intransitive orbits of the graph in order to afford a cycle index. Various atom-figure inventories and bond-figure inventories are described for counting the isomers of RG and of RCG. Since the number of isomeric RCGs (or RGs) is obtained by such a mathematical equation as a generating function, the present approach affords a versatile probe for testifying the manual enumeration of reaction types.

Appendix 1

This appendix is dovoted to a derivation of a generating function which enumerates the number of equivalence classes of configurations under the conditions of the present article.

1. Let **D** be a domain which consists of $p+q$ elements called *positions*. Let **H** (order $|\mathbf{H}|$) be a permutation group which acts on a domain **D**. Suppose that **D** is partitioned by **H** into two orbits:

$$\mathbf{D}_1=\{d_{11}, d_{12}, \cdots d_{1p}\} \text{ and } \mathbf{D}_2=\{d_{21}, d_{22}, \cdots d_{2q}\}.$$

Let **X** be a codomain which contains m elements called *figures*:

$$\mathbf{X}=\{X_1, X_2, \cdots X_m\}.$$

Let f_α and f_β be two functions from the domain **D** to the codomain **X**, i.e., f_α: $\mathbf{D}\rightarrow\mathbf{X}$ and f_β: $\mathbf{D}\rightarrow\mathbf{X}$, wherein the functions are called *configurations*.

Definition 1. (binary relation). A relationship between f_α and f_β is defined as a binary relation ($f_\alpha \sim f_\beta$), if the following equation is fulfilled for $^{\exists}H$ ($\in\mathbf{H}$):

$$f_\alpha(d)=f_\beta(H(d)) \quad \text{for } {}^{\forall}d\in\mathbf{D}.$$

Theorem 1. (The proof is abbreviated). The binary relation defined above is an equivalence relation. Therefore, the set of the functions are partitioned into equivalence classes by this relation.

2. We use the terms and notations defined in Definition 1. This section deals with the weight of a function (configuration).

Defenition 2. (the weight of a function). Suppose that two types of weights, $w_1(X_r)$ and $w_2(X_r)$ are assigned to each element (X_r) of the codomain **X**. We then define the weight $W(f)$ for each function (f: $\mathbf{D}\rightarrow X$) as follows:

$$W(f)=\prod_{d\in\mathbf{D}_1} w_1(f(d)) \prod_{d\in\mathbf{D}_2} w_2(f(d)).$$

Theorem 2. Let f_α: $\mathbf{D}\rightarrow\mathbf{X}$ and f_β: $\mathbf{D}\rightarrow\mathbf{X}$ be equivalent. Then,

$$W(f_\alpha)=W(f_\beta).$$

Proof. Since $f_\alpha\sim f_\beta$, an appropriate H ($\in\mathbf{H}$) is present which satisfies the follwing relationship:

$$f_\alpha(d)=f_\beta(H(d)) \text{ for } {}^{\forall}d\in\mathbf{D}.$$

Then,

$$W(f_\alpha)=\prod_{d\in\mathbf{D}_1} w_1(f_\alpha(d)) \prod_{d\in\mathbf{D}_2} w_2(f_\alpha(d))$$
$$=\prod_{d\in\mathbf{D}_1} w_1(f_\beta(H(d))) \prod_{d\in\mathbf{D}_2} w_2(f_\beta(H(d))). \quad \text{(a)}$$

Because of Definition 2,

$$W(f_\beta)=\prod_{d\in\mathbf{D}_1} w_1(f_\beta(d)) \prod_{d\in\mathbf{D}_2} w_2(f_\beta(d)). \quad \text{(b)}$$

A comparison of the right-hand side of (a) with that of (b) shows their equality, since a set of $H(d)$'s is the same as that of d's, except for the sequence. Hence, $W(f_\alpha)=W(f_\beta)$.

It should be noted that the converse of Theorem 2 is not always true: two functions (configurations) having the same weight do not always belong to the same equivalence class. Therefore, our goal is to obtain the number of equivalence classes having the same weight in the form of a generating function based on $W(f)$.

3. Let $\mathbf{F}_\mu$ is a set of functions (f: $\mathbf{D}\rightarrow\mathbf{X}$), all of which have the same weight $W_\mu(f)$. Let H be a permutation of **H** on **D**. This section shows that there is a permutation group on $\mathbf{F}_\mu$ onto which **H** is homomorphic.

Theorem 3. A function $H^{(\mu)}$: $\mathbf{F}_\mu\rightarrow\mathbf{F}_\mu$ is defined in accord with H as follows:

$$H^{(\mu)}(f(d))=f(H(d)) \text{ for } {}^{\forall}d\in\mathbf{D} \text{ and } {}^{\forall}f\in\mathbf{F}_\mu.$$

Then,

(1) The function $H^{(\mu)}$ is a permutation on the set of $\mathbf{F}_\mu$.

(2) The mapping of $\mathbf{H}$ onto $\mathbf{H}^{(\mu)}$ defined above is homomorphic, wherein $\mathbf{H}^{(\mu)}$ is the set of all $H^{(\mu)}$.

Proof. (1) Suppose that both f_α and f_β of $\mathbf{F}_\mu$ ($f_\alpha \neq f_\beta$) are mapped by $H^{(\mu)}$ to the same function, i.e.,

$$H^{(\mu)}(f_\alpha(d)) = H^{(\mu)}(f_\beta(d)) \text{ for } {}^\forall d \in \mathbf{D}.$$

Because of the above definition,

$$H^{(\mu)}(f_\alpha(d)) = f_\alpha(H(d)) \text{ and } H^{(\mu)}(f_\beta(d)) = f_\beta(H(d)).$$

Hence, $f_\alpha(H(d)) = f_\beta(H(d))$. This equation indicates that $f_\alpha = f_\beta$. This is contrary to the presumption. Thererore, ${}^\forall f_\alpha$ ($\in \mathbf{F}_\mu$) is transformed by $H^{(\mu)}$ into a function different from itself. This fact shows that $H^{(\mu)}$ is a permutation on the set of $\mathbf{F}_\mu$.

(2) Let $H_\delta^{(\mu)}$ and $H_\varepsilon^{(\mu)}$ be the permutations on $\mathbf{F}_\mu$. They correspond to H_δ and H_ε ($\in \mathbf{H}$), respectively. Then the following equations are obtained in the light of the definition:

$$H_\delta^{(\mu)}(f(d)) = f(H_\delta(d)) \tag{a}$$

and

$$H_\varepsilon^{(\mu)}(f(d)) = f(H_\varepsilon(d)). \tag{b}$$

Since $\mathbf{H}$ is a permutation group,

$$H_{\varepsilon\delta} = H_\varepsilon H_\delta. \tag{c}$$

Let $H_{\varepsilon\delta}^{(\mu)}$ correspond to $H_{\varepsilon\delta}$ ($\in \mathbf{H}$). Then,

$$H_{\varepsilon\delta}^{(\mu)}(f(d)) = f(H_{\varepsilon\delta}(d)) \overset{c}{=} f(H_\varepsilon H_\delta(d)) = f(H_\varepsilon(H_\delta(d)) \overset{b}{=} H_\varepsilon^{(\mu)}(f(H_\delta(d))) \overset{a}{=} H_\varepsilon^{(\mu)} H_\delta^{(\mu)}(f(d)).$$

That is, $H_{\varepsilon\delta}^{(\mu)} = H_\varepsilon^{(\mu)} H_\delta^{(\mu)}$, which indicates that the mapping of $\mathbf{H}$ onto $\mathbf{H}^{(\mu)}$ is homomorphic.

This theorem shows that $\mathbf{H}^{(\mu)} = \{H^{(\mu)}\}$ is a permutation group on $\mathbf{F}_\mu$ onto which the original permutation group $\mathbf{H}$ on $\mathbf{D}$ is homomorphic.

4. According to Definition 1, the domain $\mathbf{D}$ is partitioned by $\mathbf{H}$ into two orbits $\mathbf{D}_1$ and $\mathbf{D}_2$. Suppose that H ($\in \mathbf{H}$) has the following cycle structure:

$[i_1, i_2, \cdots i_p]$ for a permutation of $\mathbf{D}_1$ part, and
$[j_1, j_2, \cdots j_q]$ for a permutation of $\mathbf{D}_2$ part, wherein
$i_1 + 2i_2 + \cdots + pi_p = p$ and
$j_1 + 2j_2 + \cdots + qj_q = q$.

The function f: $\mathbf{D} \to \mathbf{X}$, which has a weight defined in Definition 2, affords a configuration in which the orbit $\mathbf{D}_1$ has p_1 X_1, p_2 X_2, $\cdots$, and $p_m X_m$ on its positions and the orbit $\mathbf{D}_2$ has q_1 X_1, q_2 X_2, $\cdots$, and q_m X_m on its positions, wherein

$$p_1 + p_2 + \cdots + p_m = p \text{ and}$$
$$q_1 + q_2 + \cdots + q_m = q.$$

Then, the weight of the function $W(f)$ is obtained by Definition 2:

$$W(f) = [w_1(X_1)^{p_1} w_1(X_2)^{p_2} \cdots w_1(X_m)^{p_m}] \cdot [w_2(X_1)^{q_1} w_2(X_2)^{q_2} \cdots w_2(X_m)^{q_m}].$$

Let $A_{p_1, \cdots p_m, q_1, \cdots q_m}$ be the total number of such functions (configurations) which are invariant on a permutation (H) of $\mathbf{H}$ and has $W(f)$ as the weight. Let $B_{p_1, \cdots p_m, q_1, \cdots q_m}$ be the total number of different classes of configurations which have the same weight $W(f)$. To begin with, let us examine the total number of functions.

Theorem 4. A generating function for counting $A_{p_1, \cdots p_m, q_1, \cdots q_m}$ is represented by:

$$\sum A_{p_1, \cdots p_m, q_1, \cdots q_m} [w_1(X_1)^{p_1} \cdots w_1(X_m)^{p_m}] \cdot [w_2(X_1)^{q_1} \cdots w_2(X_m)^{q_m}] = (s_1^{i_1} s_2^{i_2} \cdots s_p^{i_p})(t_1^{j_1} t_2^{j_2} \cdots t_q^{j_q}),$$

wherein $s_r = w_1(X_1)^r + w_1(X_2)^r + \cdots + w_1(X_m)^r$ and
$t_r = w_2(X_1)^r + w_2(X_2)^r + \cdots + w_2(X_m)^r$.

The summation is taken over all the partitions of p ($p_1 + p_2 + \cdots + p_m = p$) and of q ($q_1 + q_2 + \cdots + q_m = q$).

Proof. Let π_1 is a cycle of length r_1 which is involved in H ($\in \mathbf{H}$) and is concerned with the permutation of $\mathbf{D}_1$. Let π_2 be a cycle of length r_2 which is contained in H ($\in \mathbf{H}$) and is concerned with $\mathbf{D}_2$. When a function (configuration) is invariant on the permutation H, it is also invariant on the operations by π_1 and π_2. Then, the r_1 positions of $\mathbf{D}_1$ concerning with π_1 should have r_1 of the same figures, i.e., $r_1 X_1$ or $r_1 X_2 \cdots$ or $r_1 X_m$. Similarly, the r_2 positions of $\mathbf{D}_2$ should have $r_2 X_1$ or $r_2 X_2 \cdots$ or $r_2 X_m$. Hence, the corresponding generating function are represented by:

$$s_{r_1} = \sum_{k=1}^{m} w_1(X_k)^{r_1} \text{ and}$$

$$t_{r_2} = \sum_{k=1}^{m} w_2(X_k)^{r_2}$$

The same kinds of generating functions are obtained for all of the cycles involved in the permutation H. Therefore, a generating function for counting $A_{p_1, \cdots p_m, q_1, \cdots q_m}$ is obtained as follows:

$$\sum A_{p_1, \cdots p_m, q_1, \cdots q_m} [w_1(X_1)^{p_1} \cdots w_1(X_m)^{p_m}] \cdot [w_2(X_1)^{q_1} \cdots w_2(X_m)^{q_m}] = (s_1^{i_1} s_2^{i_2} \cdots s_p^{i_p})(t_1^{j_1} t_2^{j_2} \cdots t_q^{j_q}) = \prod_{r=1}^{p} (\sum_{k=1}^{m} w_1(X_k)^r)^{i_r} \cdot \prod_{r=1}^{p} (\sum_{k=1}^{m} w_2(X_k)^r)^{j_r},$$

which is in accord with the cycle structure of H. When this polynomial is expanded, we obtained a generating function.

We call such summations as s_r and t_r figure inventories.

5. Let us work out H ($\in \mathbf{H}$) which has been defined in Section 4. We introduced a formal variable s_r which corresponds to a cycle of length r of $\mathbf{D}_1$ part. Similarly, a variable t_r is concerned with a cycle of lengh r of $\mathbf{D}_2$ part. We then obtain the following product for H:

$$(s_1^{i_1} s_2^{i_2} \cdots s_p^{i_p})(t_1^{j_1} t_2^{j_2} \cdots t_q^{j_q}).$$

Since the same kind of products can be obtained for all the permutation of $\mathbf{H}$, these products are summed over $\mathbf{H}$.

Definition 3. (cycle index). The following equation is defined as a *cycle index* for $\mathbf{H}$:

$$Z(\mathbf{H}) = \frac{1}{|\mathbf{H}|} \sum_{H \in \mathbf{H}} (s_1^{i_1} s_2^{i_2} \cdots s_p^{i_p})(t_1^{j_1} t_2^{j_2} \cdots t_q^{j_q}).$$

6. We used the terms and notations described in Section 4. The purpose of this section is to derive a generating function of $B_{p_1, \cdots p_m, q_1, \cdots q_m}$.

Theorem 5. A generating function of counting $B_{p_1, \cdots p_m, q_1, \cdots q_m}$ which concerns with the total number of equivalence classes is represented by:

$$\sum B_{p_1, \cdots p_m, q_1, \cdots q_m} [w_1(X_1)^{p_1} \cdots w_1(X_m)^{p_m}] \cdot [w_2(X_1)^{q_1} \cdots w_2(X_m)^{q_m}] = Z(\mathbf{H}; \sum_{k=1}^{m} w_1(X_k)^r, \sum_{k=1}^{m} w_2(X_k)^r),$$

wherein the right-hand side indicates that the two terms denoted by the summations should be introduced to s_r and t_r of $Z(\mathbf{H})$ (Definition 3), respectively. The summation of the left-hand side is taken over all the partitions of p ($p_1+p_2+\cdots+p_m=p$) and of q ($q_1+q_2+\cdots+q_m=q$).

Proof. Let $\mathbf{F}_\mu$ be a set of functions which have the same weight

$$W_\mu=[w_1(X_1)^{p_1}\cdots w_1(X_m)^{p_m}]\cdot[w_2(X_1)^{q_1}\cdots w_2(X_m)^{q_m}]. \quad \text{(a)}$$

Let δ_μ be the number of equivalent classes contained in $\mathbf{F}_\mu$. Then, a generating function for counting equivalence cases is obviously as follows:

$$\sum_\mu \delta_\mu W_\mu .$$

Since $\mathbf{H}_\mu$ is homomorphic to $\mathbf{H}$ (Theroem 3), the number δ_μ is obtained by Burnside's lemma:[19c]

$$\delta_\mu = \frac{1}{|\mathbf{H}|}\sum_{H\in\mathbf{H}} \psi(H^{(\mu)}).$$

wherein $\psi(H^{(\mu)})$ is the number of invariant functions (configurations) of $\mathbf{F}_\mu$ on the operation of $H^{(\mu)}$. Since this lemma is true for all μ,

$$\sum_\mu \delta_\mu W_\mu = \sum_\mu \left(\frac{1}{|\mathbf{H}|}\sum_{H\in\mathbf{H}} \psi(H^{(\mu)})\right) W_\mu$$

$$= \frac{1}{|\mathbf{H}|}\sum_{H\in\mathbf{H}}\sum_\mu \psi(H^{(\mu)})W_\mu . \quad \text{(b)}$$

Because of the definition of $\psi(H^{(\mu)})$ and W_μ, the term

$$\sum_\mu \psi(H^{(\mu)})W_\mu$$

indicates the total number of functions invariant on the permutation H which corresponds to each $H^{(\mu)}$. The term is thus equal to the equation proved in Theorem 4. Therefore,

$$\sum_\mu \psi(H^{(\mu)})W_\mu$$

$$=\sum A_{p_1,\cdots p_m,q_1,\cdots q_m}[w_1(X_1)^{p_1}\cdots w_1(X_m)^{p_m}]\cdot[w_2(X_1)^{q_1}\cdots w_2(X_m)^{q_m}]$$

$$= (s_1^{i_1}s_2^{i_2}\cdots s_p^{i_p})(t_1^{j_1}t_2^{j_2}\cdots t_q^{j_q}), \quad \text{(c)}$$

wherein the summation of the second equation is taken over all the partitions of p ($p_1+p_2+\cdots+p_m=p$) and of q ($q_1+q_2+\cdots+q_m=q$); and the variables s_r and t_r of the 3rd equation are represented by:

$$s_r = \sum_{k=1}^{m} w_1(X_k)^r$$

and

$$t_r = \sum_{k=1}^{m} w_2(X_k)^r.$$

Since Eq. (c) can be established for each H corresponding to $H^{(\mu)}$, the following equation is obtained by the substitution of Eq. (b) by Eq. (c):

$$\sum_\mu \delta_\mu W_\mu = \frac{1}{|\mathbf{H}|}\sum_{H\in\mathbf{H}}(s_1^{i_1}s_2^{i_2}\cdots s_p^{i_p})(t_1^{j_1}t_2^{j_2}\cdots t_q^{j_q})$$

$$= Z(\mathbf{H}; \sum_{k=1}^{m} w_1(X_k)^r , \sum_{k=1}^{m} w_2(X_k)^r),$$

wherein the latter relationship comes from Definition 3. Since

$$\sum_\mu \delta_\mu W_\mu =$$

$$\sum B_{p_1,\cdots p_m,q_1,\cdots q_m}[w_1(X_1)^{p_1}\cdots w_1(X_m)^{p_m}]\cdot[w_2(X_1)^{q_1}\cdots w_2(X_m)^{q_m}],$$

we obtain the relationship to be proved.

7. The weights $w_j(X_k)$ (k=1, 2, ···, m) for $\mathbf{D}_j$ are determined in accord with the restrictive conditions, which are concerned with bond multiplicity (or complex bond number) or the valency of atoms in the present chemical application. The following examples show the effectiveness of Theorem 5.

Example 1. (the derivation of Eq. 4 of the text). The present domain **D** consists of edges and nodes which construct two different orbits on the operation of **H**. Then, Eq. 1 of the text is easily obtained in the light of Definition 3. The codomain **X** contains atom-figures (A, B, C, ···) and bond-figures (ϕ, −, =), i,e.,

$$\mathbf{X}=\{\text{A, B, C, }\cdots;\ \phi, -, =\},$$

wherein the symbol (ϕ) indicates no substitution of bonds on the edges, and the symbols, − and =, denote single and double par-bonds, respectively. Then the weights of them are given as follows:

$$w_1(\text{A})=1,\quad w_1(\text{B})=u_1,\ w_1(\text{C})=u_2,\ \cdots;$$
$$w_1(\phi)=0,\ w_1(-)=0,\ w_1(=)=0 \text{ and}$$
$$w_2(\text{A})=0,\quad w_2(\text{B})=0,\ w_2(\text{C})=0,\ \cdots;$$
$$w_2(\phi)=1,\ w_2(-)=x_1,\ w_2(=)=x_2.$$

Hence, Eqs. 2 and 3 of the text are obtained easily:

$$s_r = \sum_{k=1}^{m} w_1(X_k)^r = 1+u_1^r+u_2^r+\cdots \quad (2)$$

and

$$t_r = \sum_{k=1}^{3} w_2(X_k)^r = 1+x_1^r+x_2^r. \quad (3)$$

Equation 4 is then derived by means of Theorem 5.

Example 2. (the derivation of Eq. 8 of the text). Equation 5 of the text is obtained easily by Definition 3. The codomain **X** contains bond-figures:

$$\mathbf{X}=\{\phi, -, =\}.$$

The weights of them are given as follows:

$$w_1(\phi)=1,\ w_1(-)=x_1,\ w_1(=)=0 \text{ and}$$
$$w_2(\phi)=1,\ w_2(-)=x_1,\ w_2(=)=x_2.$$

Hence, two type of bond-figure inventories are easily obtained:

$$s_r = \sum_{k=1}^{3} w_1(X_k)^r = 1+x_1^r \quad (6)$$

and

$$t_r = \sum_{k=1}^{3} w_2(X_k)^r = 1+x_1^r+x_2^r. \quad (7)$$

In the text, s_r and t_r are denoted as t_{ar} and t_{br}, respectively. Theorem 5 gives Eq. 8 in this case.

8. Theorem 5 can be easily extended to the case in which the domain **D** has three or more orbits. All the proofs described above hold the generality in the extended case. Such extended items are given below:

Domain: $\mathbf{D}=(\mathbf{D}_j)$ for j=1, 2, ··· n.

Orbits of the domain:

$\mathbf{D}_j=\{d_{jk}\}$ for $k=1, 2, \cdots|\mathbf{D}_j|$, $j=1, 2, \cdots n$.
Codomain: $\mathbf{X}=\{X_k\}$ for $k=1, 2, \cdots m$.
Function (Configuration): f: $\mathbf{D}\rightarrow\mathbf{X}$.
Weight of a function (conriguration):

$$W(f) = \prod_{j=1}^{n} \left(\prod_{d\in\mathbf{D}} w_j(f(d)) \right).$$

Cycle structure of **H**:

$$[i_{jk}]\ (k=1 \text{ to } |\mathbf{D}_j|) \text{ for } \mathbf{D}_j\ (j=1 \text{ to } n),$$

wherein

$$\sum_{k=1}^{|\mathbf{D}_j|} k i_{jk} = |\mathbf{D}_j| \quad (j=1, 2, \cdots n).$$

Cycle index of **H**:

$$Z(\mathbf{H}) = \frac{1}{|\mathbf{H}|} \sum_{H\in\mathbf{H}} \left(\prod_{j=1}^{n} \left(\prod_{r=1}^{|\mathbf{D}_j|} s_{jr}^{i_{jr}} \right) \right).$$

Counting polynomial:

$$\sum_{(p_{jk})} B_{(p_{jk})} \left(\prod_{j=1}^{n} \left(\prod_{k=1}^{m} w_j (X_k)^{p_{jk}} \right) \right)$$

$$= Z\left(\mathbf{H}, \sum_{k=1}^{m} w_j (X_k)^r \text{ (for all } j)\right).$$

The summation concerned with (p_{jk}) is taken over all partitions of $|\mathbf{D}_j|$ represented by:

$$\sum_{k=1}^{m} p_{jk} = |\mathbf{D}_j| \text{ for } j = 1, 2, \cdots |\mathbf{D}_j|.$$

Appendix 2

This appendix collects several reactions reported in the literature in order to exemplify the RC graphs of Tables 8 and 10. The examples have been taken from D. L. Boger, *Tetrahedron*, **39**, 2869 (1983); S. B. Needleman and M. C. C. Kuo, *Chem. Rev.*, **62**, 405 (1962); and some original articles. This list contains imaginary transition structures and RC graphs along with conventional reaction diagrams.

The RC graphs which do not appear in this list, but in Table 10, provide us with useful suggestions that would help in the development of new reactions. For example, the

(1-1) Cycloaddition of a vinylnitroso compound with an enamine. (T. L. Gilchrist, D. A. Lingham, and T. G. Roberts, *J. Chem. Soc., Chem. Commun.*, **1979**, 1089).

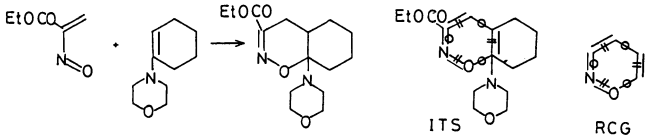

(1-2) Cycloadition of a diene with a nitroso compound. (G. Kreeze and J. Firl, *Tetrahedron Lett.*, **1965**, 1163).

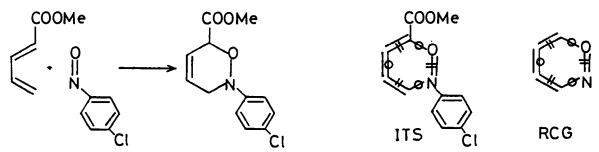

(1-3) Cycloaddition of a reactive *o*-quinone methide ketene with phenyl isocyanate. (H. Herlinger, *Angew. Chem.*, **76**, 437 (1964)).

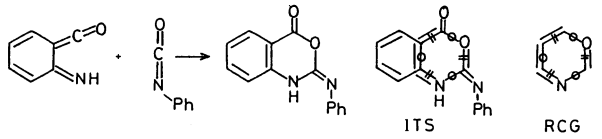

(1-4) Cycloaddition of a hydrazone with diphenylketene. (R. Gommper, *Angew. Chem., Int. Ed. Engl.*, **8**, 312 (1969)).

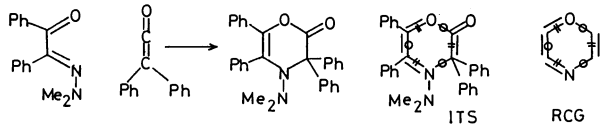

(1-5) The reaction of a 1,2,4,5-tetrazine with cyclohexene. (M. G. Barlow, R. N. Haszeldine, and J. A. Pickett, *J. Chem. Soc., Perkin Trans. 1*, **1978**, 378).

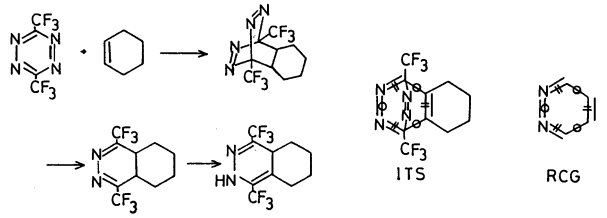

(1-6) Cycloaddition of 1-phenylazocyclohexene with a dienophile. (L. Caglioli, G. Rosini, P. Tundo, and A. Vigevari, *Tetrahedron Lett.*, **1970**, 2349).

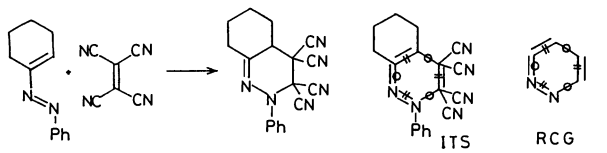

(1-7) Cycloaddition of *N*-ethoxycarbonyl-1,2-dihydropyridine with 4-phenyl-4*H*-1,2,4,-triazole-3,5-dione. (E. E. Knaus, F. M. Pasutto, C. S. Giam, and E. A. Swinyard, *J. Heterocycl. Chem.*, **13**, 481 (1976)).

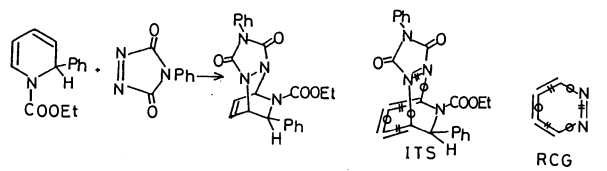

(1-8) The reaction of an imidoyl isothiocyanate with an enamine. (H. M. Blatter and H. Lukaszewski, *J. Org. Chem.*, **31**, 722 (1966)).

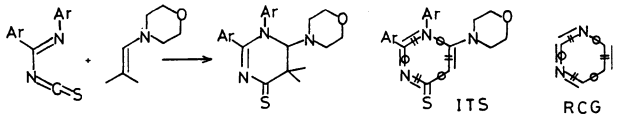

(1-9) Cycloaddition of 2-isopropenyl-2-oxazoline with phenylisocyanate. (A. E. Seelinger, W. Diepers, R. Feinauer, R. Nehring, W. Thier, and H. Hellmann, *Angew. Chem., Int. Ed. Engl.*, **5**, 875 (1966)).

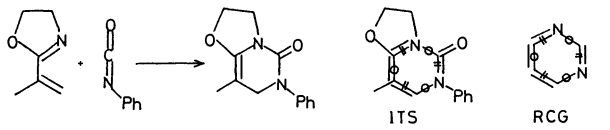

(1-10) Cycloaddition of dehydroindigo with an olefin. (R. Pummerer and E. Stieglitz, *Ber.*, **75**, 1072 (1942)).

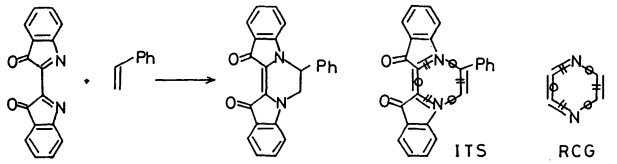

(2-1) The alicyclic Claisen rearrangement. (R. L. Funk and J. D. Munger, Jr., *J. Org. Chem.*, **50**, 707 (1985); A. G. Cameron and D. W. Knight *Tetrahedron Lett.*, **26**, 3503 (1985)).

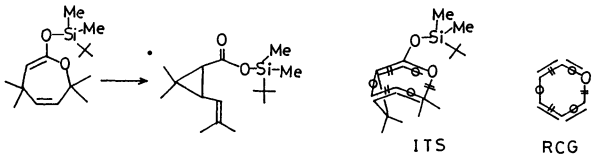

(2-2) The retro-Claisen rearrangement. (R. K. Boeckman, C. J. Flann, and K. M. Poss, *J. Am. Chem. Soc.*, **107**, 4359 (1985)).

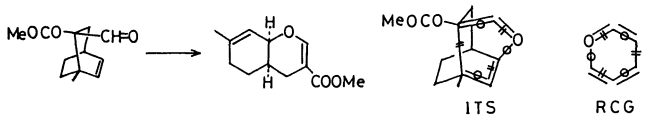

(2-3) The Claisen rearrangement of a ketene *N*-allyl-*N*,*O*-acetal. (H. Hope and M. D. Yanuck, *J. Am. Chem. Soc.*, **107**, 443 (1985)).

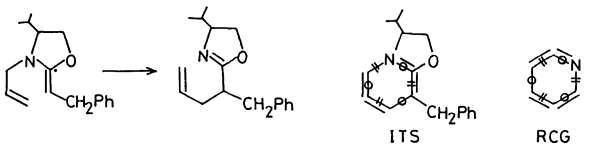

(2-4) The rearrangement of a cyclopropane derivative. (E. Vogel and R. Erb, *Angew. Chem.*, **74**, 76 (1962)).

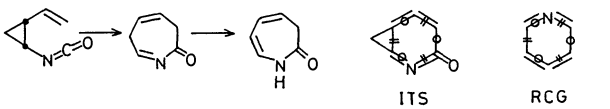

Claisen rearrangement (2-1) and the retro one (2-2) have already been investigated. Although the N-analog of the Claisen rearrangement is a known reaction (2-3), a retro-rearrangement has never been reported, to the best of our knowledge.

References

1) a) E. J. Corey, R. D. Cramer III, and W. J. Howe, *J. Am. Chem. Soc.*, **94**, 440 (1972); b) E. J. Corey and W. T. Wipke, *Science*, **166**, 178 (1969); c) E. J. Corey, A. K. Long, and S. D. Rubenstein, *Science*, **228**, 408 (1985).

2) a) I. Ugi, J. Bauer, J. Brandt, J. Friedrich, J. Gasteiger, C. Jochum, and W. Schubert, *Angew. Chem., Int. Ed. Engl.*, **18**, 111 (1979); b) J. Brandt, J. Bauer, R. M. Frank, and A. von Scholley, *Chem. Scripta*, **18**, 53 (1981); c) J. Bauer, R. Herges, E. Fontain, and I. Ugi, *Chimia*, **39**, 43 (1985).

3) a) J. B. Hendrickson, *Angew. Chem., Int. Ed. Engl.*, **13**, 47 (1974); b) J. B. Hendrickson, *J. Am. Chem. Soc.*, **108**, 6748 (1986); c) J. B. Hendrickson, *J. Chem. Inf. Comput. Sci.*, **19**, 129 (1979); d) J. B. Hendrickson, *Acc. Chem. Res.*, **19**, 274 (1986).

4) J. Mathieu and J. Valls, *Bull. Soc. Chim. Fr.*, **1957**, 1509.

5) J. F. Arens, *Rec. Trav. Chim. Pays-Bas*, **98**, 155 (1979).

6) B. J. Cohen, *J. Chem. Inf. Comput. Sci.*, **22**, 195 (1982).

7) J. S. Litters, *J. Org. Chem.*, **44**, 4657 (1979).

8) D. C. Roberts, *J. Org. Chem.*, **43**, 1473 (1978).

9) a) N. S. Zefirov, *Acc. Chem. Res.*, **20**, 237 (1987) and references cited therein; b) N. S. Zefirov and S. S. Tratch, *Chem. Scripta*, **15**, 4 (1980); c) N. S. Zefirov and S. S. Tratch, *Zhur. Org. Khim.*, **17**, 2465 (1981).

10) V. Kvasnicka, *Coll. Czech. Chem. Commun.*, **49**, 1090 (1984).

11) C. S. Willcox and R. A. Levinson, *ACS Symposium Series*, **306**, 209 (1986).

12) G. Vledutz, "Modern Approach to Chemical Reaction Searching," ed by P. Willet, Gower Publishing Co. Ltd., England (1986), p. 202.

13) J. E. Ash, D. A. Chubb, S. E. Ward, S. M. Weford, and P. Willet, "Communication, Storage, and Retrieval of Chemical Information," Ellis Horwood Ltd., Chichester, U. K. (1985), Chap. 8.

14) J. B. Hendrickson, *J. Chem. Ed.*, **55**, 216 (1978).

15) R. Borone and M. Chanon, "Computer Aids to Chemistry," ed by Vernin, G.; Chanon, M. Ellis Horwood Ltd., Chichester, U.K. (1986), Chap. I, pp. 82—84.

16) S. Fujita, *Yuki Gosei Kagaku Kyokai Shi*, **44**, 354 (1986).

17) a) S. Fujita, *J. Chem. Inf. Comput. Sci.*, **26**, 205 (1986). See also *Chem. Eng. News.* (Sept. 29), 75 (1986); b) S. Fujita, *J. Chem. Inf. Comput. Sci.*, **26**, 212 (1986); c) S. Fujita, *J. Chem. Inf. Comput. Sci.*, **26**, 224 (1986); d) S. Fujita, *J. Chem. Inf. Comput. Sci.*, **26**, 231 (1986); e) S. Fujita, *J. Chem. Inf. Comput. Sci.*, **26**, 238 (1986); f) S. Fujita, *J. Chem. Inf. Comput. Sci.*, **27**, 99 (1987); g) S. Fujita, *J. Chem. Inf. Comput. Sci.*, **27**, 104 (1987); h) S. Fujita, *J. Chem. Inf. Comput. Sci.*, **27**, 111 (1987); i) S. Fujita, *J. Chem. Inf. Comput. Sci.*, **27**, 115 (1987); j) S. Fujita, *J. Chem. Inf. Comput. Sci.*, **27**, 120 (1987); k) S. Fujita, *J. Chem. Soc., Perkin Trans. 2*, **1988**, 597.

18) An additional approach is possible in which the two steps are conducted in the reverse order described. However, the order described in the text is fruitful in a chemical sense.

19) a) G. Pólya, *Acta Math.*, **68**, 145 (1937); b) G. Pólya, R. E. Tarjan, and D. R. Woods, "Notes on Introductory Combinatorics," Birkhaeuser Boston Inc., Boston, Chap. 6 (1983); c) C. L. Liu, "Introduction to Combinatorial Mathematics,"

McGraw-Hill, New York (1969); d) K. Balasubramanian, *Chem. Rev.*, **85**, 599 (1985).

20) For the examples of reaction pairs, see Ref. 17b.

21) For the treatment in which only edges are considered in the same parent BRG, see Ref. 17b.

22) The equivalent problem has been dealt with previously by a difrerent approach,[3a] but the result is different from ours.

23) Hendrickson's manual enumeration of reaction types (Table 1 of Ref. 3a) corresponds to the cases of k_1=0—3, k_2=0—3 collected in Table 9. His enumeration is limited only to that of RCG pairs in the present sense. Although his approach has introduced a σ-shell as a novel concept to solve the problem, a manual enumeration tends to overlook several possible reaction types. In fact, his list (Table 1) contains different values from the results of our work at B=0, NO, C_4Z_2(O); B=2 (O), O, C_3Z_3(V); B=2 (P), N_2O and NO_2(V); B=3 (Δ), N and O, C_4Z_2 (O); B=3 (Δ), NO C_4Z_2 (M); and B=3 (Δ), N and O, C_3Z_3 (L). As a result, the total number of reaction types listed in Table 1 (Ref. 3a) is 957, although the corresponding number of RCG pairs in our result (Table 9) is calculated to be 964.

24) G. Maier, S. Pfriem, U. Schaefer, K.-D. Malsch, and R. Matusch, *Chem. Ber.*, **114**, 3965 (1981).

Structure and Optical Properties of a Thermochromic Schiff Base. Thermally Induced Intramolecular Proton Transfer in the *N,N'*-Bis(salicylidene)-*p*-phenylenediamine Crystals

Naomi HOSHINO,† Tamotsu INABE,* Tadaoki MITANI, and Yusei MARUYAMA*
Institute for Molecular Science, Myodaiji, Okazaki 444
(Received April 9, 1988)

A thermochromic derivative of salicylideneaniline, *N,N'*-bis(salicylidene)-*p*-phenylenediamine (BSP), has been prepared and subjected to structural and optical studies in the crystalline state. An X-ray crystallographic analysis has shown that the molecules are planar and are stacked in a parallel fashion to form one-dimensional columns. The interplanar spacing has been found to be quite short, suggesting the existence of an intermolecular charge-transfer interaction. The molecule contains fairly short O-H ··· N hydrogen bonds, the strength of which is manifested in an OH stretching absorption band in the infrared region, showing considerable broadening and a low-frequency shift. The BSP crystals are remarkably thermochromic, and visible absorption and emission spectral changes with temperature have been interpreted in terms of an intramolecular proton transfer from the hydroxyl oxygen to imine nitrogen through the O-H ··· N hydrogen bond. The emission spectra have also been examined under high pressures.

N-Salicylideneaniline and its derivatives have long been known to show photochromism in the solid state,[1] and a number of studies have revealed that the chromism is produced by intramolecular proton transfer associated with a change in the π-electron configuration and, subsequently, in a molecular conformation (Scheme 1; the nonplanar moleoule undergoes the geometric isomerization, i.e., cis-trans isomerization, following the proton transfer reaction[2]). On the other hand, crystals of some other salicylideneaniline derivatives are thermochromic.[3] This chromism is also due to a change in the π-electron configuration induced by a proton transfer (Scheme 2). In this case, the proton transfer can occur in the ground state. On the basis of comparative structural studies on photochromic and thermochromic salicylideneaniline derivatives, Bregman et al. have concluded that the significant difference lies in the manner of molecular packing in the lattice.[4,5] Namely, photochromic salicylideneanilines are packed rather loosely in the crystal, in which nonplanar molecules may undergo some conformational changes, while thermochromic salicylideneanilines are planar and packed tightly to form one-dimensional columns. It should be noted that this planar structure makes it possible for the proton to transfer through the hydrogen bond in the ground state with a small energy requirement. The title compound is also one of the thermochromic derivatives of salicylideneaniline.

The thermochromic salicylideneanilines, which have attracted less attention, have proved to be interesting to us in that they may be a candidate to construct a novel type of conductive organic material in which the proton motion is essentially correlated to the electron conduction. Particularly favorable features are (1) the proton transfer inevitably involves a π-electron con-

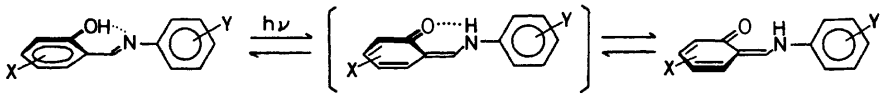

Scheme 1.

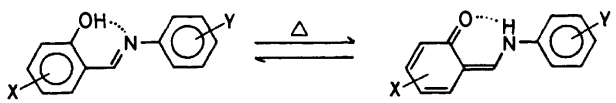

Scheme 2.

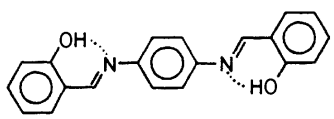

N,N'-bis(salicylidene)-p-phenylenediamine
(BSP)

† Present address: Department of Chemistry, Faculty of Science, Hokkaido University, Sapporo 060.

figurational change, (2) two interconvertible molecules which have different energy levels are thermally distributed, (3) the planar conjugated systems are stacked one-dimensionally, and (4) the π-electron system can be easily extended by chemical modification. When conduction electrons are introduced into these systems, which seems possible because of the one-dimensional stacking nature and the ease of extension of the conjugated system, one would expect that the proton motion would couple to the conduction electron motion. Consequently the proton transfer could operate as a kind of "phonon." Apparently this "phonon" is quite different from the normal variety since the mass of proton is extremely light compared with the whole mass of the molecule. The possibility of this type of "electron-phonon coupling" has never been examined experimentally.

Bearing in mind a subsequent extension to systems furnished with conduction electrons, this study has been initiated by investigating the basic nature of proton transfer of the title compound. Little has been reported on the thermochromism, even for such a simple derivative of salicylideneaniline. In this paper are described the crystal and molecular structures and the single crystal optical properties of the *N,N'*-bis(salicylidene)-*p*-phenylenediamine (BSP). Especially noted is that in the infrared region the OH stretching absorption band was clearly observed for the first time for salicylideneaniline analogues by using a single crystal.

Experimental

Materials. A conventional synthetic method for Schiff base compounds was applied for the preparation of BSP. A methanolic solution containing *p*-phenylenediamine and salicylaldehyde at 1 : 2 molar ratio was refluxed for a couple of hours. Orange microcrystals formed upon cooling, which were then recrystallized from benzene. Slow evaporation of the solvent resulted in the formation of orange platelets of 1×1.5×0.03 mm^3 size. The preparation of the deuterated analogue, BSP-d_2, was carried out by refluxing 40 mg of the above product in a mixture of 10 ml of methanol-d_1 and 10 ml of benzene-d_6 for 25 hours. Slow evaporation of the solvent under an argon flow over a period of one week yielded orange platelets typically of 1×1×0.02 mm^3 size. Mass spectral analysis confirmed completion (>90%) of the deuteration reaction.

Optical Measurements. Single-crystal infrared absorption spectra were measured using an assembled optical system that consisted of a JASCO infrared radiation source, a JASCO CT-25C monochromator, an SBRC HgCdTe detector, and a PAR Model 124A lock-in amplifier. Visible absorption spectra were obtained with a similar system comprising a halogen-gas-filled tungsten incandescent lamp, an ISA Jobin Yvon Type HR1000 monochromator, and a HAMAMATSU R376 photomultiplier. Emission spectra were recorded using the same optical components, except that the light source was replaced by a sample crystal which was irradiated with an argon laser (457.9 nm, 50 mW). The Air-Products HELI-TRAN cryostat was used for variable-temperature measurements. The flat (100) face of the crystals was irradiated with incident light throughout the optical measurements. Emission spectra under high pressures were obtained using a diamond anvil cell with an 0.50-mm aperture. Pressures were monitored by the shift of the ruby R_1 fluorescence line using the linear pressure scale (+0.365 Å $kbar^{-1}$).

X-Ray Measurements. An automated RIGAKU AFC-5R diffractometer with graphite monochromatized Mo $K\alpha$ radiation was used for data collection. Twenty-five reflections with $20°<2\theta<30°$ were used to determine the lattice parameters. Crystal data; monoclinic, space group $P2_1/c$, a=14.643(3), b=4.573(1), c=12.224(3) Å, β=112.04(1)°, V=758.8 (3) $Å^3$, Z=2, and D_c=1.385 g cm^{-3}. The intensity data was collected in the region of $2\theta<60°$ in θ-2θ mode at scan rate of 6° min^{-1}; three standard reflections, −1 −1 5, 6 1 −2, and 2 −1 4, were monitored every 100 reflections. Then, 1428 independent reflections with $|F_o|>3\sigma(F_o)$ were used for structure analysis. The structure solution was obtained by a direct method with MULTAN-71 in the UNICS III[6] computer program system at IMS. An anisotropic block-diagonal least-squares refinement for non-hydrogen atoms and isotropic refinement for hydrogen atoms gave the final R value (weighting scheme, $1/w=\sigma^2+(0.015\,|F_o|)^2$), R=0.059, for the 1428 reflections.

Results and Discussion

Molecular and Crystal Structures. The atomic parameters obtained by the X-ray structure analysis are listed in Table 1,[6] and the molecular geometry is illustrated in Fig. 1. The molecule is located on the center of inversion so that half of molecule is crystallographically independent. Attention was focused first on the equilibrium position of the proton. As revealed by the optical measurements (vide infra), the proton-transferred state of BSP is populated to some extent at

Table 1. Atomic Parameters for BSP

Atom	x	y	z	B_{eq}[a]
O	0.7933(1)	−0.2668(4)	0.1408(1)	4.2
N	0.8640(1)	−0.5744(3)	0.0111(1)	2.4
C1	0.7344(1)	−0.2258(4)	−0.0700(2)	2.4
C2	0.7305(1)	−0.1485(4)	0.0393(2)	2.8
C3	0.6605(1)	0.0535(5)	0.0439(2)	3.8
C4	0.5963(2)	0.1790(5)	−0.0583(2)	3.9
C5	0.6002(1)	0.1099(5)	−0.1669(2)	3.6
C6	0.6691(1)	−0.0895(4)	−0.1720(2)	3.0
C7	0.8043(1)	−0.4388(4)	−0.0795(2)	2.4
C8	0.9311(1)	−0.7866(4)	0.0008(1)	2.2
C9	0.9957(1)	−0.9095(4)	0.1053(2)	2.6
C10	1.0639(1)	−1.1186(4)	0.1052(2)	2.7
H3	0.661(2)	0.093(5)	0.121(2)	4.7
H4	0.547(1)	0.319(5)	−0.051(2)	5.1
H5	0.558(1)	0.201(5)	−0.237(2)	4.5
H6	0.675(1)	−0.142(5)	−0.249(2)	4.8
H7	0.802(1)	−0.484(4)	−0.159(2)	4.3
H9	0.991(1)	−0.840(4)	0.181(1)	3.2
H10	1.109(1)	−1.187(4)	0.177(2)	3.4
H11	0.833(2)	−0.396(6)	0.113(2)	6.6

a) Thermal parameters of the non-hydrogen atoms are given by the equivalent isotropic temperature factors ($Å^2$).

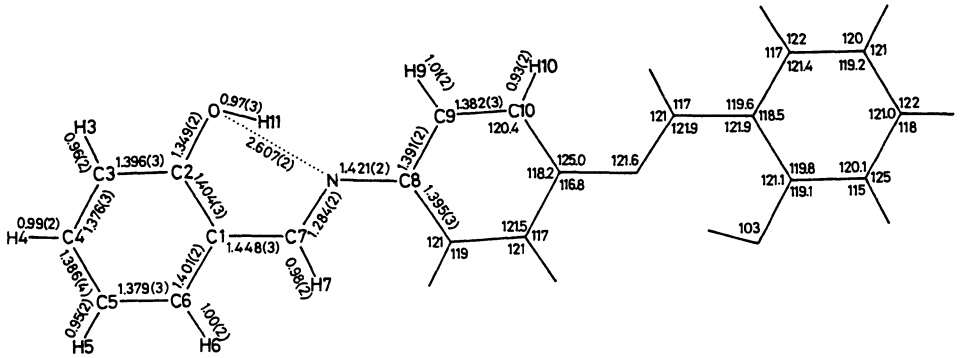

Fig. 1. Bond lengths (Å) and bond angles (degree, standard diviations are 1° for the angles including bond with hydrogen and 0.2° for the other angles).

room temperature. The bond length between O and H11 atoms is still normal as an ordinary hydroxyl group, although the H11 atom has a relatively large thermal parameter (see Table 1).[7] The distance between O and N atoms, which are intramolecularly hydrogen bonded, is 2.607(2) Å and is comparable to those observed for the thermochromic *N*-5-chlorosalicylideneaniline (2.584 Å)[4,8] and the photochromic 2-chloro-*N*-salicylideneaniline (2.609 Å).[8] It is notable that the C3–C4 and C5–C6 bond lengths are considerably shortened. This is a characteristic feature observed among most of the thermochromic salicylideneanilines.[4,8,9] As shown schematically in Scheme 2, the phenol moiety is converted into the *o*-quinoid structure upon proton transfer and the shortening of C3–C4 and C5–C6 bonds should reflect the resonance contribution from the quinoid structure. Such a quinoid contribution is not observed in 2-chloro-*N*-salicylideneaniline, which is photochromic.[8] A reduction in the bond length was also observed for the C2–O bond (1.349 Å), compared with 2-chloro-*N*-salicylideneaniline (1.365 Å); this is due to a contribution from the C2=O quinoid structure.

The dihedral angle between the central and terminal benzene rings is only 2.9° and the molecule is practically planar; the deviation from the mean plane, consisting of three benzene rings, is less than 0.06 Å for nonhydrogen atoms. The crystal structure is shown in Fig. 2. The planar molecules are stacked one-dimensionally along the *b*-axis with an interplanar distance of 3.29 Å. This value appears to be small compared with aromatic hydrocarbons and also with other thermochromic salicylideneanilines, e.g. 3.4 Å for *N*-5-chlorosalicylideneaniline,[8] 3.50 Å for *N*-salicylidene-2-aminopyridine and 3-methyl-*N*-(3-methoxysalicylidene)-2-aminopyridine,[9] 3.42 Å for *N*-(5-bromosalicylidene)-2-aminopyridine,[9] and 3.43 Å for 5-chloro-*N*-(5-methoxysalicylidene)-2-aminopyridine.[9] There must be some intermolecular interaction in BSP; the most probable is that due to charge transfer. It should be recalled that the molecular structure after the proton transfer consists of the *o*-benzoquinone and the aromatic amine moieties. The

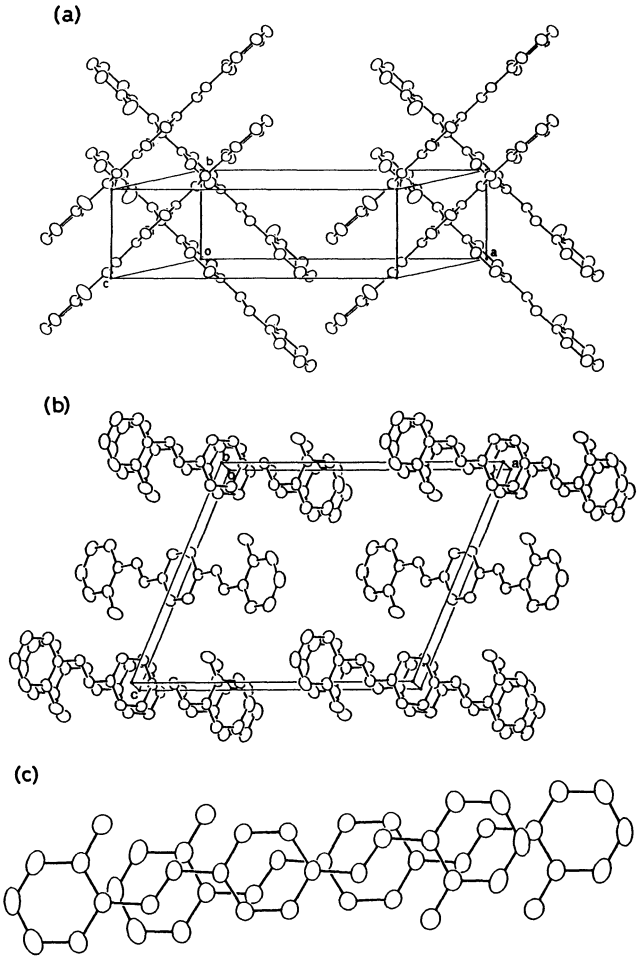

Fig. 2. Crystal structure of BSP (a), (b), and molecular overlap (c).

former is a particularly well-known electron acceptor. Thus, the molecule contains both acceptor and donor portions and the proton transferred species can be an intramolecular charge-transfer compound. The optical studies by Cohen et al.[10] revealed that the thermochromic electronic transition is polarized along the long axis in the molecular plane. Since the intermolecular charge-transfer interaction in their system is not so strong, it is likely that the intramolecular

charge-transfer absorption mainly occurs. In the case of BSP one donor portion carries two acceptor portions. By considering the packing arrangement, a more effective donor-acceptor overlap is seen in BSP (Fig. 2(c)). It should also be noted that the effective overlap between the azomethine groups and the benzene rings may produce intermolecular charge-transfer interactions in the stack of enol form molecules. The contribution from these charge-transfer interactions may lead to a contraction of the interplanar spacing. In order to generate a conduction electron system, the existence of intermolecular interactions in solids is essential. Attempts have been made to extend the system to those which have a stronger charge-transfer interaction; the results will be published elsewhere.[11]

Vibrational Spectra of BSP. The short O···N distance indicated by the crystal structure should be advantageous for the intramolecular proton transfer and an optical study in the infrared spectral region was made in order to obtain information on the vibrational states. Although a few infrared spectroscopic studies of salicylideneanilines to investigate the proton transferring behavior have so far been reported,[12-14] none of the reports has mentioned the OH stretching mode. The infrared measurements with solution,[12] polycrystalline thin film,[14] or KBr disc[12,13] specimens are apparently not adequate for detecting this particular mode. Preliminary experiments using a conventional Nujol mull also faced the same difficulty. However, in this study the OH stretching band was clearly observed for the first time when the spectra were taken using a single crystal specimen. The spectra, thus obtained, are shown in Fig. 3. A broad absorption centered at 2620 cm^{-1} (half width, $\nu_{1/2}$, ca. 550 cm^{-1}) with some subband structure is assigned to the OH stretching mode. A deuteration experiment clearly confirmed this assignment; the absorption band shifts to 2050 cm^{-1} on deuteration, as shown in Fig. 3, with the isotopic frequency ratio ν_{OH}/ν_{OD} of 1.28. The band observed at around 3040 cm^{-1}, which does not shift by deuteration, is assignable to the ν_{CH} band. Changes are also observed in the range below 1600 cm^{-1} upon deuteration. Another pronounced change on deuteration is the disappearance of the band at 1200 cm^{-1}, which is reasonably assigned to the OH in-plane bending mode. The band at 1370 cm^{-1}, which is not influenced by deuteration, can be assigned to the C-O stretching mode. A bunch of bands between 1500 and 1650 cm^{-1} which are slightly affected by deuteration, are assigned to the overlapping bands of the aromatic ring vibration and the C=N stretching. Further assignments have not been attempted.

The broadening and low-frequency shift of this OH stretching absorption band, compared with the free OH group, are characteristic of fairly strongly hydrogen-bonded hydroxyl groups. Novak established a relationship between ν_{OH} frequency and O···O distances for a number of systems involving linear O-H···O hydrogen bonds.[15] Decreasing the O···O distance results in decreasing ν_{OH} and the dependence of the O···O distance on ν_{OH} varies with the hydrogen-bond strength. On the other hand, Wood et al. conducted an IR spectroscopic study on β-diketones and found that the prediction of O···O distances (2.6—2.7 Å) from ν_{OH}, γ_{OH}, and their isotopic frequency ratios based on the Novak's relationship did not coincide with the observed distances (2.42—2.55 Å).[16] These authors suggested that the discrepancy comes from a bent configuration of the O-H···O bond in β-diketones. In the case of BSP, the O-H···N bond is indeed non-linear (O-H···N angle, ca. 155°). However, the observed frequency, 2620 cm^{-1}, predicts the O···N distance as 2.6—2.7 Å on the basis of Novak's relationship (taking into account the larger van der

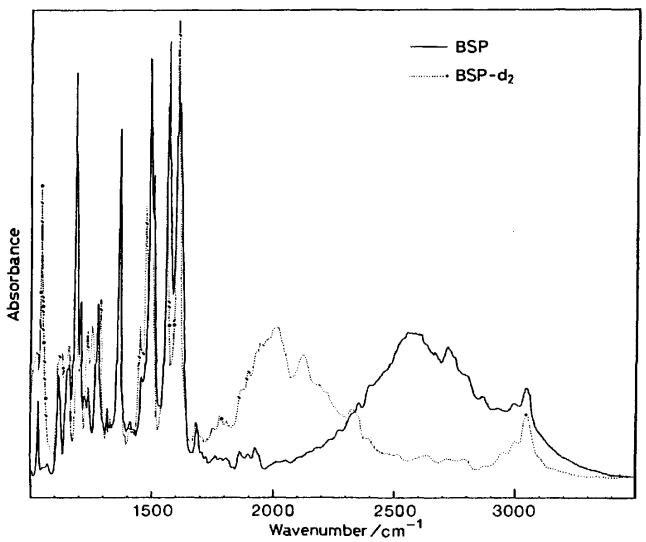

Fig. 3. Single-crystal infrared spectra for BSP and BSP-d_2 recorded at room temperature.

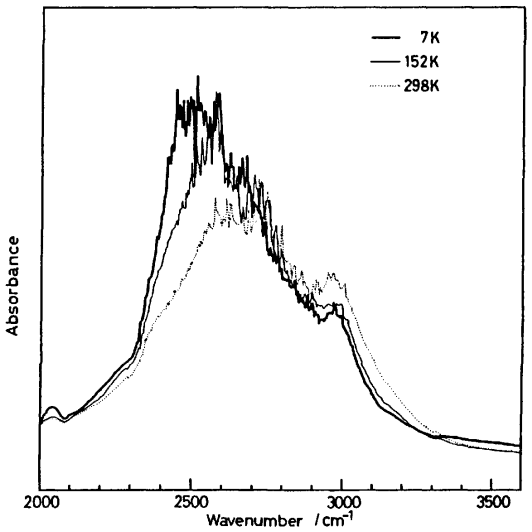

Fig. 4. Single-crystal infrared spectral change of the ν_{OH} band with temperature. The hump near 3000 cm^{-1} is the ν_{CH} band.

Waals radius of nitrogen), which is in good agreement with the observed distance, 2.607 Å. The structural situation of the present system lies between the above two cases of linear and bent hydrogen bond configurations. However, it is found that the small deviation from the linear hydrogen bond configuration does not influence the ν_{OH} frequency.

As shown in the following section, the BSP crystal exhibits an electronic absorption spectral change with a temperature in accord with the π-electron structural change induced by a proton transfer from the hydroxyl oxygen to the imine nitrogen. This self-isomerization process is believed to have some effect on the OH stretching band. In order to investigate this effect, the temperature dependence of the infrared spectra has been measured (Fig. 4). At low temperatures the population of proton-transferred species can be ignored and the crystal is regarded to contain only a single component with all protons bound to the oxygen atoms. At the lowest temperature, the band is still broad ($\nu_{1/2}$ 460 cm^{-1}) and asymmetric. Factors affecting the ν_{OH} band profile may include anharmonic coupling between the ν_{OH} and ν_{OH-N} modes, Fermi resonances between ν_{OH} and combinations or overtones involving δ_{OH} and γ_{OH} modes, and an anharmonicity in the ν_{OH} mode itself. Other factors specific to the solid state, such as Davidov coupling and structural disorder, cannot be ignored.[17] In the case of BSP the primary factor which causes the band to be broad seems to be the anharmonic coupling between the ν_{OH} and ν_{OH-N} modes. Far-infrared spectra[18] have also been measured in order to search for the ν_{OH-N} frequency and, indeed, the spectrum observed at 8 K has exhibited a single peak at 240 cm^{-1}, which can be assigned to the ν_{OH-N} mode. Other peaks in the spectrum are located below 100 cm^{-1}. Then the broad ν_{OH} band observed at 7 K can be fitted to the progression of several bands separated by 240 cm^{-1} (Fig. 5). It can be seen that each of the bands is still broad, suggesting the additional anharmonic coupling with lower-energy phonon modes and/or anharmonicity in the ν_{OH} mode itself.

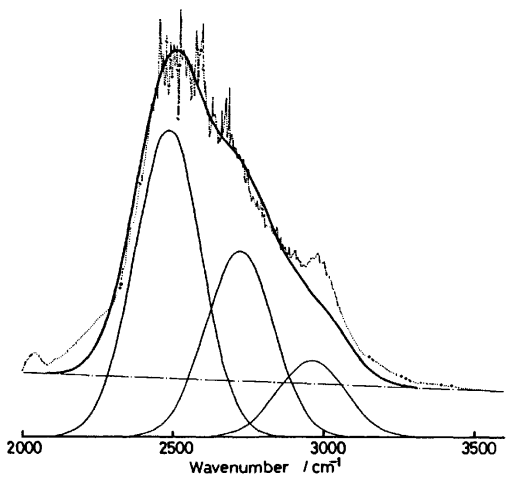

Fig. 5. Simulated infrared band profile as a progression of Gaussian bands equally separated by 240 cm^{-1} (solid line) and the observed OH stretching band at 7 K (dotted line).

With increasing temperature the intensity of the low-energy side of the band decreases, while the high-energy side changes slightly in the opposite way. Below 80 K the ν_{OH} band shows almost no change (for clarity the band observed at 72 K is not presented in Fig. 4). These changes parallel the visible spectral changes (vide infra). The ν_{OH} band profile at 298 K is not satisfactorily explained merely by the progression of bands due to the coupling with the ν_{OH-N} mode, which is observed at 230 cm^{-1} at 323 K in the far-infrared spectra. This must be a consequence, at least partly, of the proton transfer. In the simplest case the two tautomers are distributed statistically as observed in NQR measurements of salicylideneanilines.[19] In the ^{14}N NQR spectra of thermochromic salicylideneanilines, growth of a pair of new absorption peaks which corresponds to the thermally induced species has been observed by increasing temperature, as the original pair of peaks diminishes. Thus, the two chemical species are separable on an NQR time scale. However, the time scale is several orders greater in the infrared experiment. If the dynamic or resonance effect is to be considered, the band profile should not be thought of as a simple superimposition of two components. Furthermore, if the chemical species are interacting with each other in the crystal, which is very likely, the situation becomes more complicated. In any case the band profile cannot be considered as being due to a simple local mode and more information on dynamic and microscopic aspects is required to understand the situation completely.

Electronic Absorption and Emission Spectra of BSP. Crystals of BSP are an orange color at room temperature and turn yellow upon cooling in liquid nitrogen. This thermochromic change was followed spectrophotometrically over a wide temperature range (4—293 K); the results are given in Fig. 6. At the lowest temperature an absorption edge is observed rising sharply around 2.8 eV and tailing down to 2.4 eV; the former is assigned to the π-π^* transition in the enol form. The latter tail has some structure; the slope changes in two regions, 2.42—2.61 and 2.61—2.80 eV. The width of both ranges is 0.19 eV. We feel that this tailing is due to the non-Franck-Condon type absorption and that the appearance of two different slopes is due to the coupling with the CN or CO stretching mode. Up to 80 K practically no temperature effect on the spectra was observed, which agrees well with the observation of the temperature dependence of the ν_{OH} band profile as mentioned in the previous section.

As the temperature rises above 80 K, the absorption band at 2.4 eV grows in and at room temperature this band shows its edge at 2.26 eV. With this band assigned to the keto isomer, the energy difference

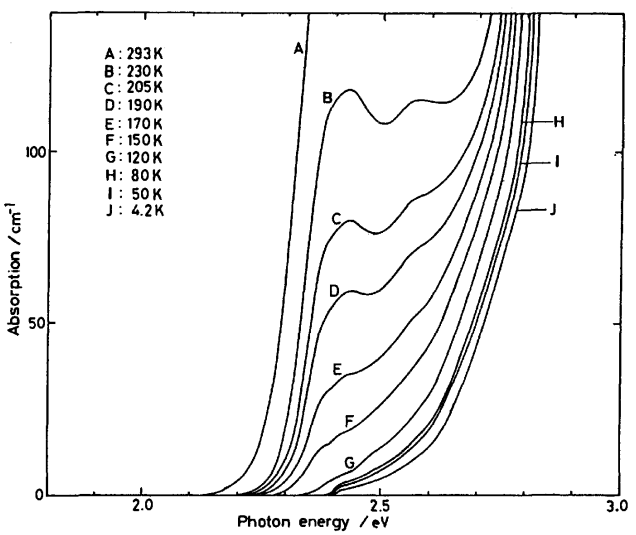

Fig. 6. Single crystal absorption spectral changes with temperature for BSP.

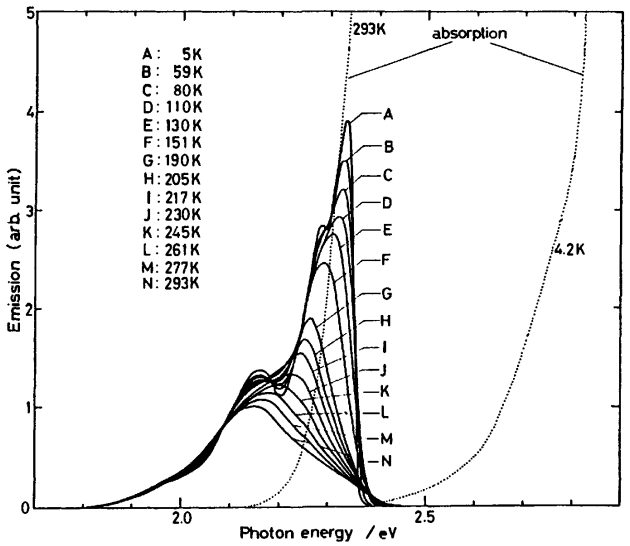

Fig. 7. Single crystal emission spectral changes with temperature for BSP.

between the two tautomers in Scheme 2 is evaluated to be ca. 0.1 eV, which is comparable to that observed for *N*-5-chlorosalicylideneaniline (0.08 eV).[3] The electronic absorption spectral change with temperature indicates that a substantial amount of the proton-transferred species is present at room temperature. The relative population of the enol and keto species has been estimated to be about 50 : 1 at room temperature by assuming that the system is followed by the Boltzmann-type distribution. It is noticed that the absorption band of the keto isomer shows some vibrational structure with an energy difference of ca. 0.14 eV and a shoulder near the absorption edge.

An observation of emission spectra, shown in Fig. 7, gives support for the above explanation of the thermochromism as caused by the proton transfer. It should be noted that the emission spectrum A at 2.33 eV recorded at 5 K shows a large Stokes shift (ca. 0.4 eV) from the corresponding absorption. This is one of the characteristic features of the proton-transfer reactions in salicylideneaniline derivatives.[2] It can be seen that the emission band has some fine structure; humps appear at around 2.33, 2.29, 2.15, 1.97 eV. The separation between the first and the second peaks is small, and this detailed structure could be assigned to the ν_{OH-N} vibrational fine structure. The energy differences between the first and the third and between the third and the fourth are equally 0.18 eV. This energy may correspond to the CN or CO stretching mode. It may be noticed that this fine structure well corresponds to the structure observed in the thermochromic band. The energy of 0.14 eV, which is the energy difference between the second and the third peaks of emission at 5 K, is exactly the energy difference between the two peaks observed in the thermochromic band. The small energy difference between the first and the second peaks of the emission may correspond to that between the shoulder and the first peak of the thermochromic band. Consequently, the emission band can be regarded as a mirror image of the thermochromic band. Cohen and Flavian studied the emission and absorption spectra of several thermochromic salicylideneanilines including BSP in the solid state,[20] and they concluded that the emission is due to deactivation from the same excited state to the same ground state as those involved in the thermochromic absorption. Our results are clearly consistent with their interpretation. Especially, low-temperature emission experiments have confirmed the origin of the largely shifted emission band. The emission gradually diminishes at elevated temperatures, the fine structure becoming less noticeable. At room temperature a broadened emission centered around 2.15 eV remains (spectrum N). The temperature dependence of the emission spectra is better explained by reabsorption by the thermally induced species as discussed in Ref. 19, since the emission intensity changes only at the high energy side where the absorption grows with increasing temperature. The reabsorption effect on the emission band is also reflected in spectral difference between the emissions from different crystal faces; when the (100) face is irradiated, a shoulder-like band observed at 2.25 eV on the higher-energy side in the emission from the flat (100) face is absent in the emission from the lateral (001) face, which reflects the longer penetration depth of this emitted light in this direction.

Since our interest lies in the extent of intermolecular interaction, we examined the pressure effect on the optical properties. Drickamer et al. extensively used high pressures to investigate intra- and intermolecular interactions in molecular crystals.[21] They also examined the pressure effect on the electronic spectra of several thermochromic derivatives of salicylideneani-

line both in the crystalline state[22] and in solid dispersions.[23] According to these authors, thermochromic crystals of *N*-5-bromosalicylideneaniline, for instance, exhibit piezochromic absorption in the visible region, which shifts to lower energy and intensifies with increasing pressure in compensation for the original ultraviolet absorption band. They identified this piezochromic peak as the thermochromic peak under atmospheric pressure, thus describing the pressure effect as a driving force for the proton-transfer equilibrium towards the keto form.

In the case of BSP, the shift in the absorption edge with pressure was also observed. However, the magnitude (0.17 eV by 33 kbar) was larger than that observed for the systems studied by Hockert and Drickamer (less than 0.1 eV by 30 kbar for the absorption peak). On the other hand, the emission spectral changes with pressure for BSP (Fig. 8) indicate only a small maximum shift to lower energy. This is in contrast to the finding of the above-mentioned authors that the energy difference between the piezochromic band and the emission band for *N*-5-bromosalicylideneaniline remains fairly constant over a wider pressure range. It is also noticed that the pressure dependence of the emission intensity of BSP is different from that of other derivatives studied by Hockert and Drickamer[23] and by ourselves;[11] the pressure dependence of the intensity cannot be fitted by a single exponential function in the case of BSP. Thus, the apparent emission spectral changes can only be qualitatively accounted for by an increase in the probability of quenching due to the level crossing resulting from the change of potential surface and/or increase of the reabsorption accompanied by the red shift of absorption. At any rate, the distinctive behavior of BSP must be associated with the existence of a stronger intermolecular interaction in this compound.

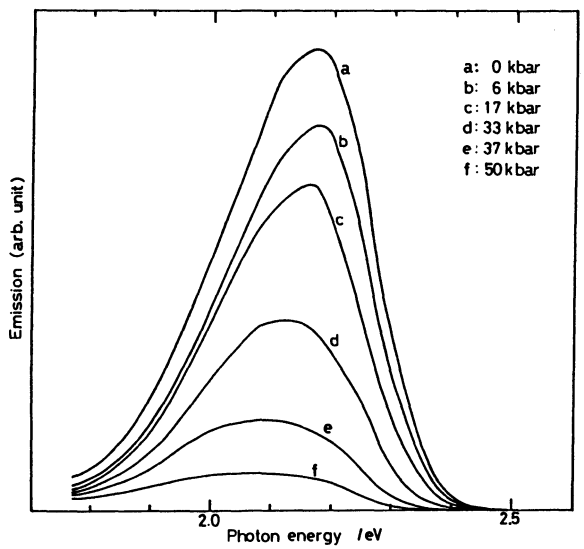

Fig. 8. Single crystal emission spectral changes with pressure for BSP.

Summary

Thermochromic BSP single crystals have been studied both structurally and optically. From the structural study it has been found that the interplanar distance is shorter than in other thermochromic salicylideneanilines, while retaining the normal one-dimensional packing of molecules. Since the keto form of the BSP molecule consists of donor and acceptor portions, it is suggested that the charge-transfer interaction operates in the crystalline state as an intermolecular interaction. The infrared spectroscopic study clearly demonstrates the presence of OH stretching absorption for the first time among the salicylideneanilines and is interpreted in the regime of strong hydrogen bonds. The effect of the thermal proton transfer on the proton vibrational spectra has not been characterized, but additional information on microscopic or dynamic aspects will facilitate the understanding.

The visible absorption and emission spectra are basically understandable in terms of the ground state and the excited-state proton transfer, respectively, as for other salicylideneanilines previously studied. We would like to point out, however, that unconventional interpretations are possible for some detailed aspects noted in this study. Firstly, the absorption band has a long low-energy tail at temperatures below ca. 80 K where thermochromic absorption is not highly visible. Secondly, the emission band edge coincides the edge of this absorption tail edge at 2.4 eV, where the thermochromic absorption also shows up. With regard to the low-energy absorption tail, it is possible that quantum mixing of enol and keto ground states due to proton tunneling results in a significant amount of the population in the latter, even at low temperatures. Another possibility is that this weak absorption is due to non-Frank-Condon type transitions from the enol ground state to the keto excited state cannot be ruled out. This would mean that the optical electronic excitation simultaneously causes the proton transfer, and implies that the excited state of this system has a potential surface close to a single minimum well. Another interesting feature observed in the absorption and emission spectra of BSP is that all spectra related to the proton transfer have phonon structures due to the coupling with the vibrational modes involved in the skeleton of the hydrogen-bonded chelate ring. This becomes particularly important when the coupling between the electronic properties of solids and proton transfer is to be considered. Further studies on extended systems which are designed to introduce the stronger intermolecular charge-transfer interaction are being made, and preliminary results indicate that the equilibrium position of hydrogen atoms is fairly sensitive to the electronic state of the system. Systematic studies of the structure and optical properties of extended systems should help clarify the nature of the

proton transfer and, especially, its coupling with the electronic state.

We are grateful to Dr. Yoshiki Wada for his assistance in optical measurements. This work was partly supported by Scientific Research Grants-in-Aid No. 6155027 from the Ministry of Education, Science and Culture.

References

1) M. D. Cohen and G. M. J. Schmidt, *J. Phys. Chem.*, **66**, 2442 (1962).

2) P. F. Barbara, P. M. Rentzepis, and L. E. Brus, *J. Am. Chem. Soc.*, **102**, 2786 (1980); E. Hadjoudis, *J. Photochem.*, **17**, 355 (1981); D. Higelin and H. Sixl, *Chem. Phys.*, **77**, 391 (1983).

3) M. D. Cohen, G. M. J. Schmidt, and S. Flavian, *J. Chem. Soc.*, **1964**, 2041.

4) J. Bregman, L. Leiserowitz, and G. M. J. Schmidt, *J. Chem. Soc.*, **1964**, 2068.

5) T. Sakurai and K. Kobayashi, *Rep. Inst. Phys. Chem. Res.*, **55**, 69 (1979).

6) The lists of structure factors and anisotropic thermal parameters for non-hydrogen atoms are deposited at Bull. Chem. Soc. Jpn. (Document No. 8835).

7) The difference syntheses based on all atoms except for the hydroxyl hydrogen indicate two peaks in the hydrogen bond region, and the larger peak (0.6 e $Å^{-3}$) corresponds to the hydrogen bound to the oxygen atom. The smaller peak (0.3 e $Å^{-3}$) is reasonably assigned to the NH hydrogen. The details and the low temperature structure will be published soon.

8) J. Bregman, L. Leiserowitz, and K. Osaki, *J. Chem. Soc.*, **1964**, 2086.

9) I. Moustakali-Mavridis, E. Hadjoudis, and A. Marvidis, *Acta Crystallogr., Sect. B*, **34**, 3709 (1978).

10) M. D. Cohen, S. Flavian, and L. Leiserowitz, *J. Chem. Soc. B*, **1967**, 329.

11) T. Inabe, N. Hoshino, T. Mitani, and Y. Maruyama, to be published.

12) J. W. Ledbetter, Jr., *J. Phys. Chem.*, **81**, 54 (1977).

13) R. Nakagaki, T. Kobayashi, J. Nakamura, and S. Nagakura, *Bull. Chem. Soc. Jpn.*, **50**, 1909 (1977).

14) J. W. Lewis and C. Sandorfy, *Can. J. Chem.*, **60**, 1738 (1982).

15) A. Novak, *Struct. Bonding*, **18**, 177 (1974).

16) S. F. Tayyari, Th. Zeegers-Huyskens, and J. L. Wood, *Spectrochim. Acta*, **35A**, 1289 (1979).

17) S. Bratos, J. Lascombe, and A. Novak, "Molecular Interactions," ed by H. Ratajezak and W. J. Orville-Thomas, Wiley & Sons, New York (1980), Vol. 1.

18) T. Mitani, unpublished results.

19) E. Hadjoudis, F. Milia, J. Seliger, R. Blinc, and V. Zagar, *Chem. Phys.*, **47**, 105 (1980).

20) M. D. Cohen and S. Flavian, *J. Chem. Soc. B*, **1967**, 334.

21) H. G. Drickamer, *Acc. Chem. Res.*, **19**, 329 (1986), and references therein.

22) E. N. Hockert and H. G. Drickamer, *J. Chem. Phys.*, **67**, 5178 (1977).

23) E. N. Hockert and H. G. Drickamer, *J. Chem. Phys.*, **67**, 5189 (1977).

Charge Transfer Complexes Based on the Twin-TCNQ-Type Acceptor 11,11,12,12,13,13,14,14-Octacyano-1,4:5,8-anthradiquinotetramethane (OCNAQ)

Tamotsu INABE,* Tsutomu MITSUHASHI,† and Yusei MARUYAMA*
Institute for Molecular Science, Myodaiji, Okazaki 444
†Department of Chemistry, Faculty of Science, The University of Tokyo, Bunkyo-ku, Tokyo 113
(Received May 13, 1988)

Charge transfer complexes of OCNAQ with pyrene, PT (phenothiazine), TMTTF (tetramethyltetrathiafulvalene), TTT (5,6:11,12-bis(epidithio)naphthacene), and TTF (tetrathiafulvalene) have been prepared. The pyrene and PT complexes are electrically insulating and the ground state is neutral. In most of the other complexes OCNAQ is fully charged. One of the TTT complexes, $(TTT)_2$OCNAQ(DMF), where DMF is *N,N*-dimethylformamide, has been found to show metallic conductivity. A structural study has revealed that short S···N contacts exist between TTT and OCNAQ, in addition to one-dimensional TTT stacks. This transverse interaction has been demonstrated by the small anisotropy of the conductivity. The 2:1 TTF complex is also metallic down to 43 K, at which point a metal-to-insulator transition occurs. A structure analysis and thermoelectric power data suggest that the charge conduction in this crystal takes place not only through the TTF stacks but also through a two-dimensional network of the OCNAQ molecules.

Recently, a synthesis and characterization of the title compound OCNAQ (systematic name: 1,4,5,8-tetrakis(dicyanomethylene)anthracene), a twin-TCNQ-type acceptor, has been reported.[1,2] From its molecular structure it is expected that the on-site Coulomb repulsion should be reduced compared with TCNQ. In fact, a cyclic voltammogram shows that the first and second redox waves are closely located.[1,2] Furthermore, the monovalent tetraethylammonium salt $Et_4N \cdot$ OCNAQ exhibits a rather high conductivity[2] as a simple salt. The molecular shape of OCNAQ is nonplanar due to a steric interaction between the cyano groups. The nonplanarity is not advantageous for high electrical conduction through the molecular stacks, since insufficient overlapping between the molecules in a stack causes a small transfer integral and, consequently, a partial reduction state cannot be sufficiently stabilized. Actually, the approaches to obtain any fractionally reduced OCNAQ salts with closed-shell cationic species have so far failed, and only monoanionic and dianionic OCNAQ salts have been obtained.

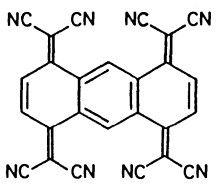

OCNAQ

As a next step toward achieving higher conductivity based on OCNAQ, complexes with various donor molecules, instead of closed-shell cationic species, have been investigated, and the metallic properties of $(TTT)_2$OCNAQ(DMF) have recently been reported.[3] In this compound OCNAQ interacts transversely with the TTT stacks. In this paper the preparation, structures, and charge transport properties of the OCNAQ complexes with pyrene, PT, TMTTF, TTT, and TTF are described. Among them, one of the TTF complexes has been found to be metallic, in which the OCNAQ molecules form a two-dimensional network. A twin-type molecular structure may be responsible for this stacking nature.

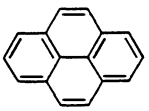
pyrene

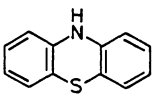

PT

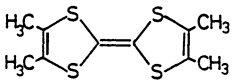

TMTTF

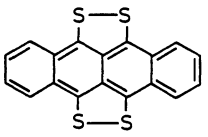

TTT

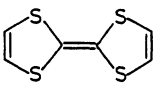

TTF

Experimental

Materials. OCNAQ was synthesized by the same method reported previously.[2] DMF used as a solvent was dried with Molecular Sieve 4A and distilled under reduced pressure. Acetonitrile was dried before distillation with P_2O_5 and repeated with K_2CO_3. 1,2-Dichlorobenzene was used without purification. All donors were purified by recrystallization or sublimation.

Pyrene-OCNAQ: Slow cooling of a hot acetonitrile solution containing pyrene and OCNAQ with a molar ratio of 3:1 yielded black needle-like crystals. Solvent inclusion was found by elemental analysis. Found: C, 78.48; H, 2.79; N, 18.57%. Calcd for $C_{44}H_{19}N_9$ (pyrene·OCNAQ(CH_3CN)): C, 78.45; H, 2.84; N, 18.70%.

PT-OCNAQ: The complex was prepared by slow cooling of a hot acetonitrile solution, including PT and OCNAQ, with a molar ratio of 4:1. The precipitate was found to be a mixture of two kinds of crystals; one is a black needle-like crystal and another is a brown plate-like crystal. One polymorph is PT·OCNAQ(CH_3CN) and the other is PT·OCNAQ. Found: C, 72.06; H, 2.46; N, 20.21%. Calcd

for 2:3 weight fraction of PT·OCNAQ and PT·OCNAQ-(CH_3CN): C, 71.98; H, 2.59; N, 20.53%.

TMTTF-OCNAQ: A powdered material was prepared by mixing TMTTF in hot acetonitrile and OCNAQ in the same solvent with a molar ratio of 2:1. The elemental analysis indicated the 1:1 stoichiometry. Found: C, 62.48; H, 2.68; N, 16.30%. Calcd for $C_{36}H_{18}N_8S_4$: C, 62.59; H, 2.63; N, 16.21%. The same material was obtained in a fine needle-like shape by conventional electrocrystallization using Et_4N·OCNAQ as a supporting electrolyte.

TTT-OCNAQ: Slow cooling of a hot 1,2-dichlorobenzene solution containing TTT and OCNAQ with a molar ratio of 1:1 gave black plate-like crystals. An elemental analysis shows that the composition is $(TTT)_3(OCNAQ)_2$-(dichlorobenzene)$_2$, abbreviated TTT-OCNAQ(I). Found: C, 64.26; H, 1.85; N, 10.40; S, 17.21%. Calcd for $C_{94}H_{44}Cl_4N_{16}S_{12}$: C, 64.06; H, 2.19, N, 10.13; S, 17.40%.

When the complex was prepared electrochemically in DMF, the obtained crystal was found to contain DMF molecules. The composition confirmed by an X-ray structure analysis was $(TTT)_2$OCNAQ(DMF), abbreviated TTT-OCNAQ(II).

TTF-OCNAQ: The complexes were prepared by the following three methods: (1) mixing of the TTF and OCNAQ solutions, and (2) mixing of the $(TTF)_3(BF_4)_2$ and Et_4N·OCNAQ solutions, (3) electrocrystallization. Acetonitril was used as a solvent. Microcrystals were obtained by the first and second methods. An elemental analysis of these materials always showed a slight deviation from the 1:1 stoichiometry, i.e., an excess content of TTF.[1] This small deviation is due to the coexistence of a 1:1 phase and a donor-rich phase. In fact, the stoichiometry of the minor product obtained by the third method was found to be 2:1 by X-ray structure analysis. The correspondence of the major products in all methods was confirmed by optical and electrical measurements. Hereafter, the 1:1 complex is abbreviated TTF-OCNAQ(I) and the 2:1 complex TTF-OCNAQ(II).

Measurements. Infrared spectra were taken by a HITACHI 295 spectrometer by using a Nujol mull specimen. Electrical conductivity measurements were carried out by a conventional four-probe or two-probe method. Thermoelectric power measurements were performed by a method similar to that reported by Chaikin and Kwak.[4]

X-Ray Structure Analyses. The computer program system used was UNICSIII[5] run on a HITACHI M680 at IMS.**

TTT-OCNAQ(II): A black plate-like crystal having approximate dimensions of 0.40×0.15×0.05 mm^3 was used for the crystallographic study. Diffraction data were collected at room temperature using an automated RIGAKU AFC-5R fourcircle diffractometer with graphite monochromatized Mo $K\alpha$ radiation. Fifty reflections with $20°<\theta<30°$ were used to determine the lattice parameters. Crystal data; chemical formula $C_{65}H_{29}N_9OS_8$, formula weight M=1208.51, triclinic, space group $P\bar{1}$, a=11.522(2), b=16.406(3), c=7.942(1) Å, α=94.23(2), β=95.13(2), γ=116.51(1)°, V=1327.0(4) Å^3, Z=1, D_c=1.51 g cm^{-3}, and μ=3.77 cm^{-1}. The intensity data were collected in the region $2\theta<60°$ in the θ-2θ mode at a scan rate of 6° min^{-1}. 3716 independent reflections with $|F_o|>3\sigma(F_o)$ were used for a structure analysis. The structure was solved by the Patterson method. An anisotropic block-diagonal least-squares refinement for non-hydrogen atoms with isotropic hydrogen atoms gave a final R value of 0.063.

TTF-OCNAQ(III): A black plate-like crystal having approximate dimensions of 0.33×0.15×0.05 mm^3 was used for the crystallographic study. The data collection and structure analysis were performed using the same procedure as TTT-OCNAQ(II), except for the diffractometer (RIGAKU AFC-5) and scan rate (3° min^{-1}). Crystal data; chemical formula $C_{38}H_{14}N_8S_8$, formula weight M=839.04, triclinic, space group $P\bar{1}$, a=6.702(6), b=19.302(8), c=7.239(5) Å, α=86.69(5), β=109.22(8), γ=93.64(6)°, V=882(1) Å^3, Z=1, D_c=1.58 g cm^{-3} and μ=5.29 cm^{-1} The intensiy data were collected in the region $2\theta<50°$; 1126 independent reflections with $|F_o|>3\sigma(F_o)$ were used for a structure analysis. The final R value was 0.061.

Results and Discussion

Infrared Spectra. Chapell et al. showed that the reduction state of TCNQ could be estimated from the frequency of the C≡N stretching mode.[6] For OCNAQ, a similar dependence of the frequency of the C≡N stretching mode on the reduction state is expected, since the same type LUMO as TCNQ was obtained by calculation.[2] Figure 1 shows the C≡N stretching bands for OCNAQ, Et_4N·OCNAQ, and $(Et_4N)_2$-OCNAQ. The frequency is 2214, 2186, and 2170 cm^{-1}, respectively; thus, a similar charge dependence of the frequency can be obtained. However, the frequency

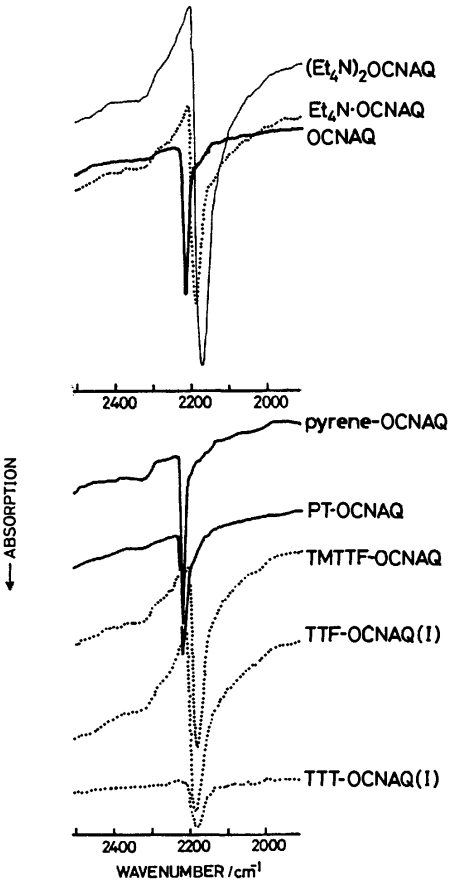

Fig. 1. Infrared spectra of OCNAQ and the OCNAQ complexes.

** IMS: Institute for Molecular Science.

shift by charge is not as large as that of TCNQ (frequency shift $\Delta\nu$ for TCNQ→TCNQ$^-$, 44 cm^{-1}; $\Delta\nu$ for OCNAQ→OCNAQ$^-$, 28 cm^{-1}). This seems to arise from the main characteristics of OCNAQ, namely a twin-TCNQ-type nature. Indeed, the shift from OCNAQ to OCNAQ^{2-} amounts to 44 cm^{-1}, which is exactly the same as that from TCNQ to TCNQ$^-$.

The C≡N stretching bands in the infrared spectra for pyrene-OCNAQ, PT-OCNAQ, TMTTF-OCNAQ, TTF-OCNAQ(I), and TTT-OCNAQ(I) are also shown in Fig. 1. Owing to an electronic transition, which extends in this region in TTT-OCNAQ(II), the infrared spectrum did not provide any useful information about the ionicity of this compound. Data for TTF-OCNAQ(II) are also absent, because the sample amount was insufficient to examine the infrared spectrum. From the position of the C≡N stretching mode a neutral nature was found for the pyrene and PT complexes. Since the ionization potentials of pyrene and PT are relatively high compared with the other donor molecules, a neutral nature for the ground state is reasonable. In the other complexes the OCNAQ molecules are fully ionized, and the electronic structures are represented as (TMTTF$^+$)(OCNAQ$^-$), (TTF$^+$)-(OCNAQ$^-$) for TTF-OCNAQ(I), and $(TTT_3)^{2+}$-$(OCNAQ^-)_2$(dichlorobenzene)$_2$ for TTT-OCNAQ(I).

Crystal Structure. TTT-OCNAQ(II): The molecular structures of TTT and OCNAQ in this compound, obtained by X-ray analysis, are shown in Fig. 2 and the atomic parameters are listed in Table 1.[7] The TTT molecule is essentially planar (deviations from the mean plane are less than 0.15 Å for non-hydrogen atoms). On the other hand, the OCNAQ molecule is largely deformed from the planar structure. The deformation pattern is the same as that observed in

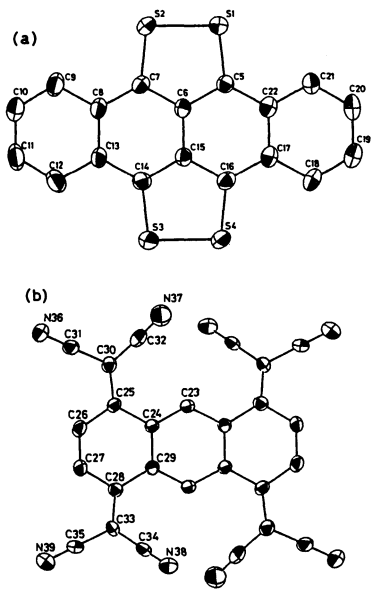

Fig. 2. ORTEP drawing[15] of TTT (a) and OCNAQ (b) in TTT-OCNAQ(II) showing the atom numbering scheme.

Table 1. Atomic Parameters of TTT-OCNAQ(II) (×10^4)

	x	y	z	B_{eq}/Å^2
S1	2245(2)	2234(1)	4723(3)	3.0
S2	1200(2)	2800(1)	3424(3)	3.2
S3	−2816(2)	−1120(1)	−153(3)	3.4
S4	−1754(2)	−1681(1)	1132(3)	3.3
C5	1313(7)	1129(5)	3726(9)	2.2
C6	239(7)	1018(5)	2577(9)	2.2
C7	49(8)	1781(5)	2261(10)	2.3
C8	−1035(8)	1680(5)	1108(10)	2.6
C9	−1203(9)	2466(6)	720(11)	3.5
C10	−2292(9)	2334(6)	−356(12)	3.9
C11	−3217(9)	1459(7)	−1069(12)	4.1
C12	−3087(9)	690(8)	−745(11)	3.5
C13	−1979(8)	784(5)	336(10)	2.4
C14	−1772(8)	16(5)	685(10)	2.4
C15	−667(7)	127(5)	1769(10)	2.3
C16	−498(8)	−643(5)	2121(10)	2.4
C17	601(8)	−545(5)	3242(10)	2.4
C18	811(8)	−1314(5)	3590(10)	2.9
C19	1875(9)	−1191(6)	4691(11)	3.3
C20	2780(9)	−305(6)	5475(11)	3.4
C21	2622(8)	456(6)	5189(11)	2.9
C22	1528(8)	366(5)	4053(10)	2.4
C23	−4335(7)	−5362(5)	−4043(9)	2.2
C24	−4453(7)	−4624(5)	−3274(9)	1.9
C25	−3992(7)	−4277(5)	−1481(9)	2.1
C26	−4520(8)	−3710(5)	−737(9)	2.4
C27	−5140(8)	−3333(5)	−1693(9)	2.4
C28	−5312(7)	−3476(5)	−3517(9)	2.0
C29	−5138(7)	−4237(5)	−4271(9)	1.9
C30	−3097(8)	−4446(5)	−440(10)	2.5
C31	−2796(8)	−4116(5)	1332(10)	2.7
C32	−2359(9)	−4888(7)	−964(11)	4.1
C33	−5561(7)	−2866(5)	−4432(9)	2.2
C34	−5463(8)	−2801(5)	−6182(10)	2.6
C35	−5696(8)	−2132(6)	−3575(10)	2.8
N36	−2534(8)	−3858(5)	2759(9)	4.2
N37	−1732(10)	−5226(8)	−1307(12)	7.6
N38	−5325(8)	−2706(5)	−7578(9)	3.9
N39	−5747(9)	−1508(5)	−2904(10)	4.5
N40	−9861(24)	−4726(12)	−5110(38)	5.5
C41	−9006(16)	−4663(13)	−3833(25)	12.6
C42	−9511(24)	−4032(17)	−5799(40)	8.3
O43	−8525(23)	−3338(14)	−5280(34)	12.0

$Et_4N \cdot OCNAQ$,[2] namely the TCNQ nuclei are distorted into boat forms and the two TCNQ boats are linked by two methylidine groups upside-down with each other.

Since the electronic structure cannot be determined by the infrared spectra, the bond lengths of the molecules were carefully examined by X-ray structure analysis in order to elucidate the charge on the molecules. The mean dimensions of TTT are listed in Table 2 along with data for TTT^0, TTT$^{1/2+}$ (TTT_2I_3), and TTT$^+$ ($TTT(TCNQ)_2$). Major structural differences between TTT^0 and TTT$^{1/2+}$ appear in the bond lengths of A, B, E, and F in Table 2, whereas those between TTT$^{1/2+}$ and TTT$^+$ appear in bond C. By a comparison with these data it is favorable to assign the TTT molecule in TTT-OCNAQ(II) to TTT$^{1/2+}$. The same kind of information can be obtained from the molecular structure of OCNAQ, of which bond

Table 2. Mean Dimensions of TTT (Å)

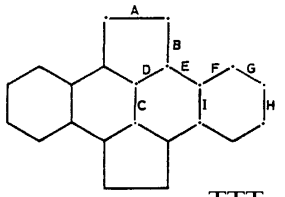

	TTT[a]	TTT_2I_3[a]	TTT-$(TCNQ)_2$[a]	TTT-OCNAQ(II)
A	2.100(2)	2.078(2)	2.082(2)	2.074(4)
B	1.781(6)	1.738(3)	1.732(7)	1.731(10)
C	1.422(13)	1.429(8)	1.375(15)	1.420(9)
D	1.406(7)	1.390(4)	1.401(8)	1.403(13)
E	1.374(7)	1.414(4)	1.431(8)	1.421(12)
F	1.450(7)	1.410(5)	1.426(8)	1.427(14)
G	1.367(7)	1.358(5)	1.360(8)	1.372(15)
H	1.421(11)	1.404(8)	1.401(12)	1.398(12)
I	1.455(9)	1.444(6)	1.413(12)	1.439(11)

a) After Smith and Luth;[8] originally Ref. 9 for TTT and Ref. 10 for $TTT(TCNQ)_2$

Table 3. Bond Lengths of OCNAQ (Å)

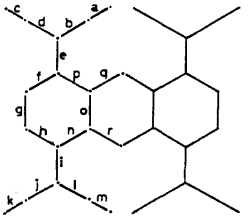

	Et_4N·OCNAQ[a]	$(Et_4N)_2$-OCNAQ	TTT-OCNAQ(II)	TTF-OCNAQ(II)
a	1.146(15)	1.144(17)	1.130(19)	1.148(15)
b	1.423(15)	1.420(17)	1.411(16)	1.402(15)
c	1.141(13)	1.130(15)	1.144(10)	1.140(15)
d	1.441(19)	1.394(16)	1.423(11)	1.439(15)
e	1.398(11)	1.433(14)	1.401(13)	1.406(15)
f	1.425(15)	1.430(14)	1.440(14)	1.430(14)
g	1.333(13)	1.368(13)	1.354(13)	1.362(15)
h	1.436(13)	1.402(15)	1.432(10)	1.415(15)
i	1.388(11)	1.443(11)	1.392(13)	1.406(15)
j	1.435(14)	1.433(18)	1.416(13)	1.415(15)
k	1.144(15)	1.157(19)	1.146(14)	1.138(15)
l	1.420(14)	1.374(14)	1.413(11)	1.425(18)
m	1.143(13)	1.157(14)	1.146(11)	1.149(17)
n	1.459(13)	1.458(15)	1.445(12)	1.472(14)
o	1.429(11)	1.472(13)	1.436(12)	1.440(14)
p	1.464(12)	1.400(17)	1.452(10)	1.441(13)
q	1.391(13)	1.389(18)	1.384(12)	1.410(14)
r	1.404(13)	1.351(21)	1.400(9)	1.371(14)

a) Averaged values.

lengths are listed in Table 3. Unfortunately, the structure of neutral OCNAQ has not been obtained. However, the molecular dimensions of $OCNAQ^-$ and $OCNAQ^{2-}$ are known[2] and are listed in Table 3. The differences between $OCNAQ^-$ and $OCNAQ^{2-}$ appear in the C=C bond length between dicyanomethylene and the ring carbon (e and i in Table 3). Judging from these bond lengths the charge of OCNAQ in TTT-OCNAQ(II) has been assigned as −1. This assignment is consistent with the charge of TTT, and the electronic structure of this compound is represented as $(TTT)_2^+OCNAQ^-(DMF)$.

The crystal structure is shown in Fig. 3. The TTT molecules form one-dimensional columns along the *c*-axis, while the OCNAQ molecules overlap only partly with each other. The DMF molecule is positionally disordered, i.e., one DMF molecule can occupy two positions which are related to each other by an inversion center. Molecular overlapping patterns between the TTT molecules in the stack and between the OCNAQ molecules are shown in Fig. 4. The interplanar and short interatomic distances between the molecules are listed in Table 4. There are

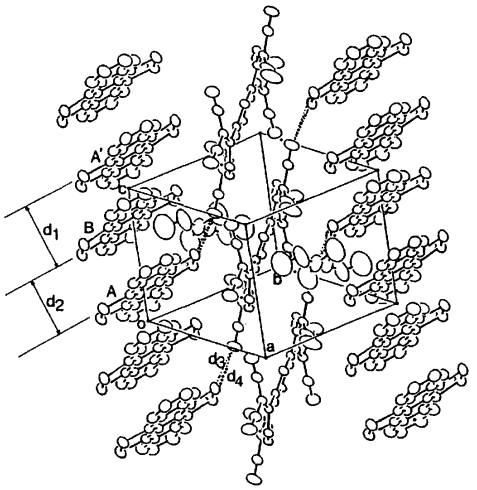

Fig. 3. Crystal structure of TTT-OCNAQ(II).

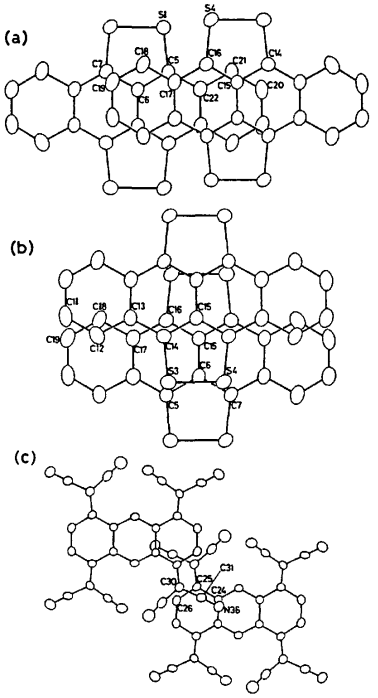

Fig. 4. Molecular overlapping between the TTT molecules; between A and B (a), and between B and A′ (b) in Fig. 3, and between the OCNAQ molecules (c).

Table 4. Interplanar and Interatomic Distances (Å) of TTT-OCNAQ(II): between A and B (a) and between B and A′ (b) in Fig. 4, between the OCNAQ Molecules (c), and Distances Shown in Fig. 3 (d)

(a)	S1-S4	3.506(3)
	S1-C18	3.587(9)
	C5-C17	3.315(11)
	C6-C18	3.454(12)
	C7-C19	3.332(13)
	C14-C20	3.433(13)
	C15-C21	3.349(12)
	C16-C22	3.431(12)
(b)	S3-C5	3.456(9)
	S4-C6	3.550(8)
	S4-C7	3.509(9)
	C11-C19	3.475(15)
	C12-C18	3.470(13)
	C13-C17	3.456(12)
	C14-C16	3.441(12)
	C15-C15	3.408(12)
(c)	C24-N36	3.333(10)
	C25-C31	3.474(10)
	C26-C30	3.320(10)
(d)	d_1	3.38
	d_2	3.26
	d_3	3.084(9)
	d_4	3.252(7)

two kinds of interplanar spacings between the TTT molecules. Spacing between A and B (3.26 Å; d_2 in Fig. 3) is shorter than that between B and A′ (3.38 Å; d_1 in Fig. 3) by 0.12 Å. The molecular overlapping pattern between A and B is the same as that observed in TTT_2I_3,[8] and there are short contacts between sulfur atoms (3.506(3) Å). On the other hand the molecular overlapping between B and A′ is not the same as the pattern reported so far, and there are no effective S ··· S contacts (>3.9 Å). Consequently, TTT is weakly dimerized between A and B in the stack. As can be seen from Fig. 4(c), the overlap between the OCNAQ molecules is only partial; therefore, the interaction is supposed to be weak. The shortest contact between the OCNAQ molecules (3.33(1) Å) are actually larger than those observed in $Et_4N \cdot$OCNAQ (3.05(1) and 3.14(1) Å).[2] Interestingly, a rather strong interaction of OCNAQ exists in the direction toward the donor molecules. As shown in Fig. 3, two nitrogen atoms of OCNAQ strongly interact with the sulfur atoms of TTT. The distances of d_3 (3.084(9) Å) and d_4 (3.252(7) Å) are less than the sum of the van der Waals radii, 3.35 Å. Consequently, the interactions between the molecules in this system are rather two-dimensional.

TTF-OCNAQ(II): The molecular structures of TTF and OCNAQ in this compound are shown in Fig. 5, and the atomic parameters are listed in Table 5.[7] The TTF molecule is perfectly planar (deviations from the mean plane are less than 0.05 Å for the non-hydrogen atoms). The structure of OCNAQ is practically the same as that in TTT-OCNAQ(II). As listed in Table 3 the bond lengths of OCNAQ are close to the values observed for $OCNAQ^-$. The mean dimensions of TTF (Table 6) are closer to those observed in TTF-TCNQ, in which the oxidation state of TTF is +0.59, than those of TTF^0. Therefore, the electronic structure of this complex is supposed to be near $(TTF)_2^+OCNAQ^-$, although there remains some ambiguity (vide infra).

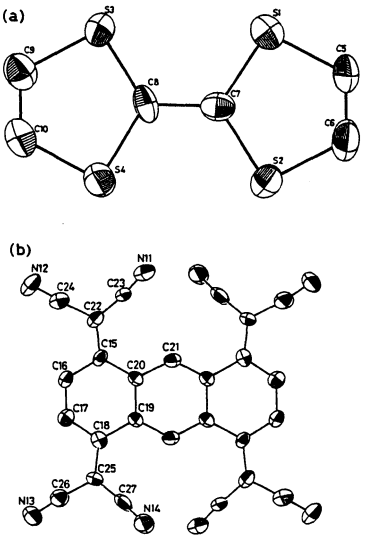

Fig. 5. ORTEP drawing of TTF (a) and OCNAQ (b) in TTF-OCNAQ(II) showing the atom numbering scheme.

Table 5. Atomic Parameter of TTF-OCNAQ(II) (×10⁴)

	x	y	z	B_{eq}(Å²)
S1	−3650(5)	1130(2)	7841(5)	4.1
S2	727(5)	1557(2)	8228(5)	3.8
S3	−2770(5)	−453(2)	7189(5)	3.4
S4	1624(5)	−25(2)	7597(5)	3.5
C5	−2805(20)	1979(6)	8431(19)	4.4
C6	−841(21)	2173(6)	8613(19)	4.6
C7	−1171(17)	883(6)	7839(16)	3.0
C8	−858(18)	196(6)	7559(15)	2.9
C9	−1140(19)	−1077(6)	6902(17)	3.8
C10	809(19)	−884(6)	7112(17)	3.8
N11	−3420(16)	6940(5)	1348(17)	5.1
N12	−9303(15)	5894(6)	330(16)	5.2
N13	−4643(16)	2036(5)	2940(16)	4.8
N14	1591(16)	2739(5)	4124(19)	5.8
C15	−4380(16)	5166(5)	2792(15)	2.4
C16	−5763(16)	4559(5)	2560(15)	2.6
C17	−4987(17)	3914(6)	3063(16)	3.0
C18	−2801(17)	3790(5)	3732(15)	2.6
C19	−1362(16)	4403(5)	4360(15)	2.2
C20	−2167(16)	5087(5)	3844(14)	2.2
C21	−725(17)	5652(5)	4537(16)	2.6
C22	−5274(16)	5791(6)	1902(16)	2.9
C23	−4200(17)	6415(5)	1621(17)	3.2
C24	−7528(18)	5833(6)	1034(16)	3.4
C25	−2148(17)	3111(5)	3736(17)	2.9
C26	−3603(19)	2532(6)	3289(18)	3.6
C27	−50(20)	2933(6)	3951(19)	3.7

Table 6. Mean Dimensions of TTF (Å)

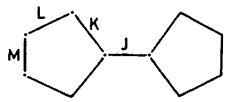

	TTF[a)]	TTF-TCNQ[b)]	TTF-OCNAQ(II)
J	1.349(3)	1.372(4)	1.392(16)
K	1.757(2)	1.745(3)	1.730(16)
L	1.726(2)	1.739(3)	1.733(13)
M	1.314(3)	1.326(4)	1.305(19)

a) Ref. 11. b) Ref. 12.

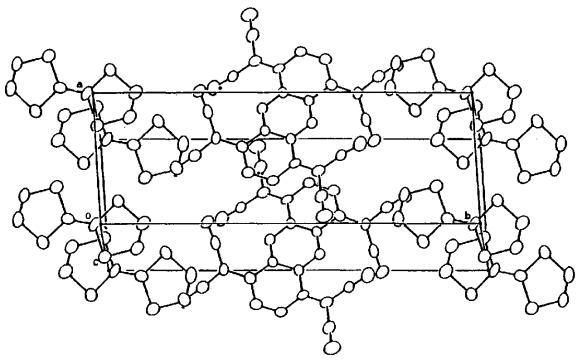

Fig. 6. Crystal structure of TTF-OCNAQ(II).

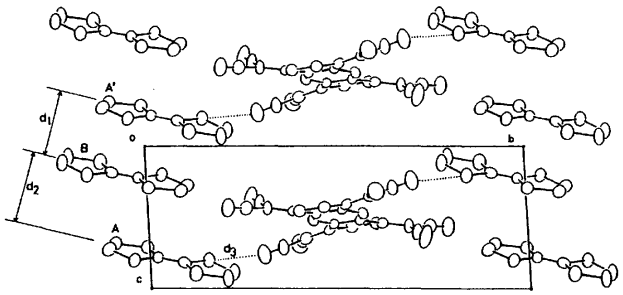

Fig. 7. Donor and acceptor arrangement in TTF-OCNAQ(II) in the (100) plane.

The crystal structure is shown in Figs. 6 and 7. The TTF molecule forms one-dimensional columns along the *c*-axis, and there are no effective intermolecular contacts between the columns. Molecular overlapping patterns between the TTF molecules and between the OCNAQ molecules are shown in Figs. 8 and 9, respectively, and the interplanar and interatomic distances are listed in Table 7. The overlapping pattern between the TTF molecules of B and A′ is similar to that of TTF-TCNQ,[12] in which the intermolecular S ··· S distances are rather large (>3.70 Å). On the other hand, in the overlapping pattern between A and B there is a shorter S ··· S contact (S4 ··· S4; 3.671(5) Å). However, this distance is still longer than those observed for the eclipsed-type stacking of TTF in $TTF \cdot X_y$ (3.55—3.60 Å; where X=Cl, Br, I, and etc.).[13]

In contrast with the case of TTT-OCNAQ(II), efficient stacking of OCNAQ in TTF-OCNAQ(II) can be seen from Fig. 6. There are two kinds of overlapping

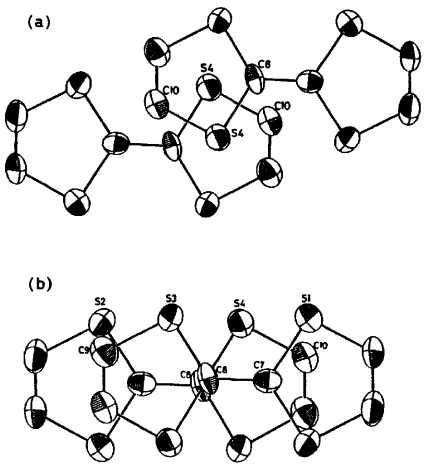

Fig. 8. Molecular overlapping between the TTF molecules; between A and B (a), and between B and A′ (b) in Fig. 7.

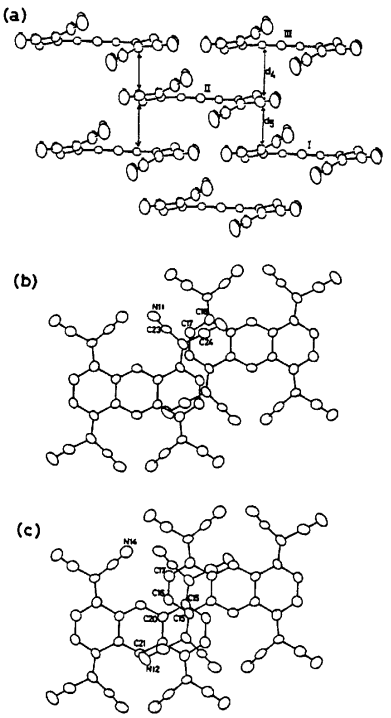

Fig. 9. Molecular overlapping between the OCNAQ molecules; side view of the OCNAQ stack (a), between I and II (b), and between II and III (c) in (a).

patterns and one OCNAQ moleoule interacts with four OCNAQ molecules (Fig. 9). The interplanar distances listed in Table 7 are the distances between the mean planes, calculated for the anthracene framework. Although one of the interplanar distances is large (3.82 Å vs. 3.30 Å), the cyano groups, which are largely deviated from the plane, make the interatomic distances short (e.g., 3.345(17) Å for C17 ··· C23). Therefore, the OCNAQ molecules effectively form a two-dimensional network in the (010) plane. In similarity to the TTT-OCNAQ(II) system, an extra interaction between nitrogen atoms of OCNAQ and a sulfur atom

Table 7. Interplanar and Interatomic Distances (Å) of TTF-OCNAQ(II); between A and B (a) and between B and A′ (b) in Fig. 8, between I and II (c) and between II and III (d) in Fig. 9, and Distances Shown in Figs. 7 and 9 (e)

(a)	S4-S4	3.671(5)
	S4-C8	3.628(12)
	S4-C10	3.657(12)
	C8-C10	3.571(17)
(b)	S1-S4	3.717(6)
	S2-S3	3.740(5)
	S3-S4	3.754(5)
	S1-C10	3.540(12)
	S2-C9	3.518(13)
	C7-C10	3.582(17)
	C8-C8	3.393(15)
(c)	N11-C17	3.492(16)
	C17-C23	3.345(17)
	C18-C24	3.560(17)
(d)	N12-C21	3.478(18)
	N14-C17	3.360(16)
	C15-C15	3.573(17)
	C15-C16	3.406(16)
	C16-C20	3.446(17)
(e)	d_1	3.42
	d_2	3.38
	d_3	3.292(11)
	d_4	3.30
	d_5	3.82

of TTF exists. However, the distance, 3.292(11) Å, is not as short as those observed in TTT-OCNAQ(II).

Charge Transport. The electrical resistivities of the OCNAQ complexes are shown in Fig. 10, except for pyrene-OCNAQ and PT-OCNAQ, which are electrically insulating. The data shown in Fig. 10 were obtained along the long axis of the crystal.

TMTTF-OCNAQ and TTF-OCNAQ(I): As revealed by the infrared spectra, TMTTF-OCNAQ and TTF-OCNAQ(I) are simple salts. The temperature dependence of the resistivities shows a semiconducting behavior with activation energies of 0.14 eV for TMTTF-OCNAQ and 0.15 eV for TTF-OCNAQ-(I). The resistivities at room temperature, 10^2—10^3 Ω cm, are rather small compared with those of usual simple radical salts. This supposedly reflects the main effect produced by the twin-type structure, i.e., a reduced on-site Coulomb repulsion. Indeed, the resistivity at room temperature of $Et_4N \cdot OCNAQ$ is of the same order (2.5×10^3 Ω cm).[2)]

The thermoelectric power (TEP) data are shown in Fig. 11. For a simple salt the energy gap is usually related to the on-site Coulomb repulsion. In these systems the on-site Coulomb repulsion of a donor molecule is much larger than that of OCNAQ, and the charge transport of these systems should be largely governed by OCNAQ. The observed large negative values are consistent with electron conduction through OCNAQ.

TTT-OCNAQ(I): Since the electronic structure of this complex is $(TTT_3)^{+2}(OCNAQ^-)_2$(dichlorobenzene)$_2$, the TTT molecule is formally charged by +2/3. Thus, the resistivity of this compound is expected to be lower than those of simple salts. In fact the resistivity is lower compared with TMTTF-OCNAQ and TTF-OCNAQ(I), although the temperature dependence is semiconducting (Fig. 10). The TEP data shown in Fig. 11 are consistent with TTT based hole conduction. In this compound OCNAQ simply acts as a

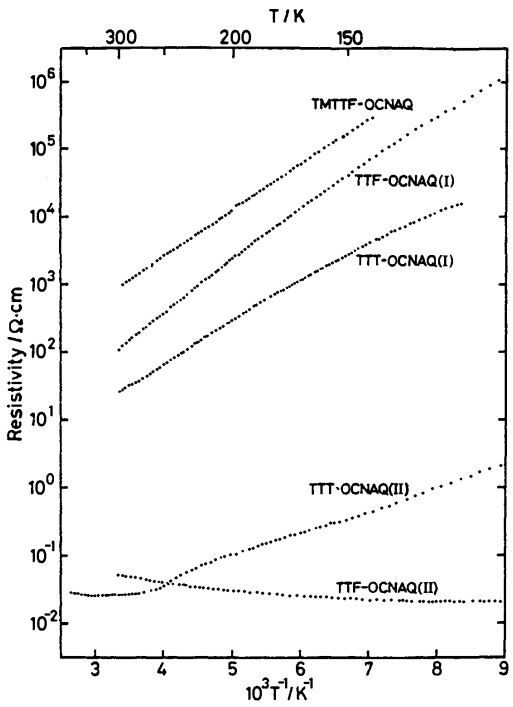

Fig. 10. Electrical resistivities of the OCNAQ complexes.

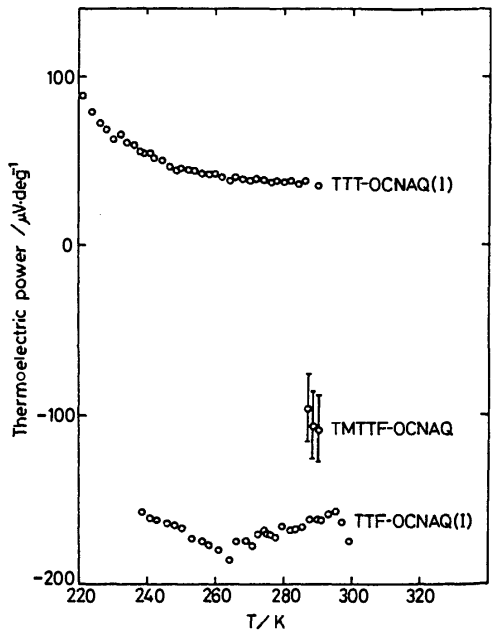

Fig. 11. Thermoelectric power of the OCNAQ complexes.

counterion, and makes no contribution to the charge transport.

TTT-OCNAQ(II): This compound shows a weak metallic behavior down to 250 K, at which point the material turns to the semiconducting state with an activation energy of 0.05 eV. As suggested by the structure analysis, there is a transverse interaction between the TTT columns through the OCNAQ molecules. In order to see this structural peculiarity the conduction was measured not only along the TTT stacking direction but also in the direction corresponding to the transverse interaction. The results are shown in Fig. 12. The anisotropy of the conduction, $\rho(\perp c)/\rho(/\!/c)$, was found to be 30. This value is the smallest among the TTT complexes so far reported.

The TEP measurements were also carried out for both directions, and the results are shown in Fig. 13. The TEP is linearly correlated to the temperature in both directions above 250 K, which corresponds to the metallic state of this compound observed by the conduction measurements. The positive slope suggests that the major charge carrier is a hole in the TTT stacks. However, the TEP crosses zero in the metallic region and becomes negative below the anomaly at 250 K. This behavior is not a typical one of low-dimensional radical cation salt-type conductors, such as D_2X, where D is a donor and X is a counterion, in which the conduction occurs only through the donor stacks. In such compounds the TEP usually decreases towards zero in the metallic region. The deviation from the typical behavior in TTT-OCNAQ(II) is, thus, caused by the structural peculiarity of this compound, i.e., the existence of a transverse interaction between the TTT columns through OCNAQ. When the interaction between the TTT molecules in the stack is large, the total interaction between the donor and acceptor molecules in the system is nearly two-dimensional in the ($\bar{1}10$) plane. However, even at room temperature the TTT molecules are not stacked uniformly, and are weakly dimerized between molecules A and B in Fig. 3. If the dimerization of TTT becomes more developed with decreasing temperature, an energy gap is opened along the stacking direction. However, the interaction along the [112] direction, which corresponds to the $(TTT)_2\cdots OCNAQ\cdots (TTT)_2$ chain, will remain. The charge transport along this chain below 250 K is supposed to be governed by OCNAQ, since the sign of TEP is changed. The additional anomaly at 140 K, which is detectable in the resistivity data, may be related to this chain.

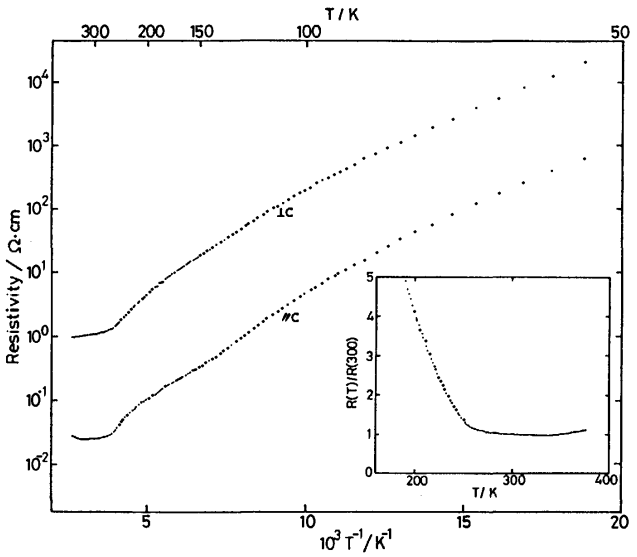

Fig. 12. Electrical resistivities of TTT-OCNAQ(II).

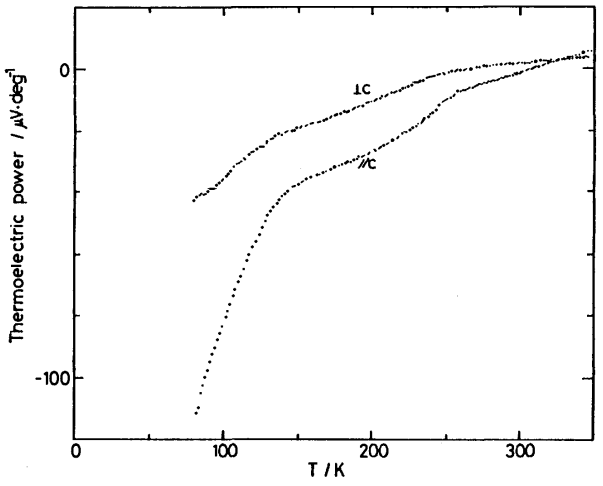

Fig. 13. Thermoelectric power of TTT-OCNAQ(II).

The structure of this compound has some similarities to HMTSF-TCNQ,[14] where HMTSF is bis(trimethylene)tetraselenafulvalene, in which short Se···N contacts between the donor and acceptor molecules exist. The anisotropy of conduction of this material is also 30. The most remarkable characteristic of this material is that the metallic state is stabilized at very low temperature. Comparing this system to TTT-OCNAQ(II), two structural differences can be noted. First, the interaction between the acceptor molecules: in HMTSF-TCNQ a rather strong interaction between the TCNQ molecules exists, while in TTT-OCNAQ(II) the interaction between the OCNAQ molecules is quite weak. Secondly, the pattern of the interaction between the donor and acceptor molecules is different. In HMTSF-TCNQ all the nitrogen atoms of TCNQ interact with all the selenium atoms of HMTSF so that a uniform stacking of the donor (acceptor) is maintained by the transverse interaction with the neighboring acceptor (donor) stacks. On the other hand, in TTT-OCNAQ(II) only two of the eight nitrogen atoms of OCNAQ interact with two of the four sulfur atoms of TTT. This type of transverse interaction is not sufficient to prevent the deformation of the donor stack. These structural differences may cause the difference in the physical properties.

TTF-OCNAQ(II): The temperature dependence of the conductivity is shown in Fig. 14. The conduc-

tivity increases with decreasing temperature down to ca. 90 K then gradually decreases; at 43 K, where the conductivity is still as high as that observed at room temperature, a sharp drop occurs. The temperature dependence of the TEP is shown in Fig. 15. The TEP decreases linearly down to 90 K, and then starts to increase. If this anomaly is due to a metal-to-insulator transition, this upturn is assumed to be caused by a gap formation of the donor stack. However, the TEP below 90 K does not fit a simple activation behavior. Furthermore, for simple hole conduction the zero crossing at 160 K cannot be explained. The TEP rather increases linearly towards zero. This means that the charge transport is metallic and that the major charge carrier is an electron in this region. As discussed in the structure analysis, a crystal of this material consists of TTF and OCNAQ stacks. Thus, the major route of conduction is the TTF stacks above 90 K; it changes to OCNAQ stacks in the region between 43 and 90 K. The material is essentially in a semimetal state. The anomaly at 43 K is assumed to be a normal metal-to-insulator transition.

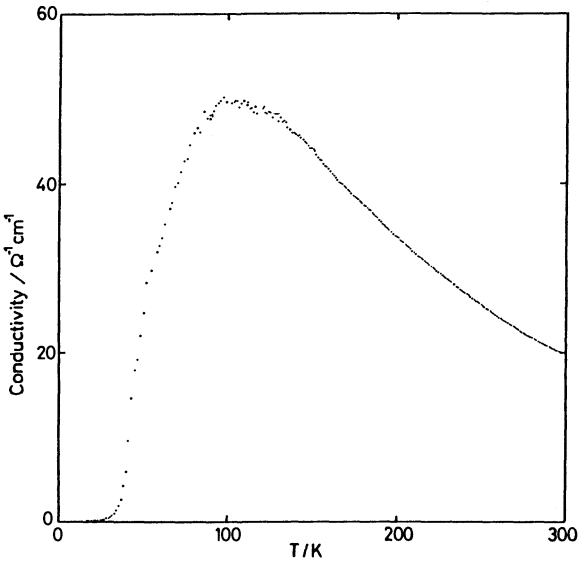

Fig. 14. Electrical conductivity of TTF-OCNAQ(II).

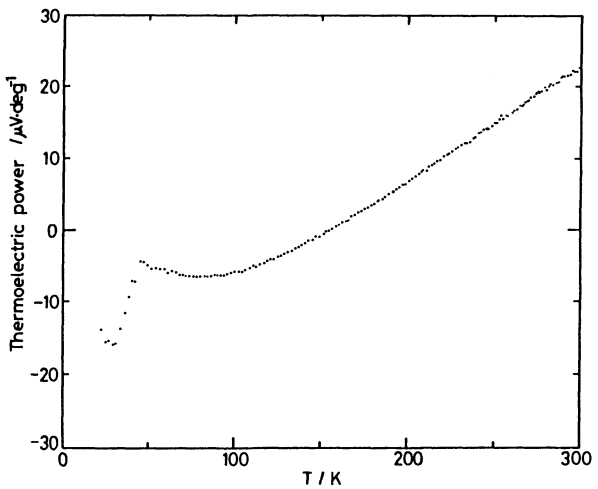

Fig. 15. Thermoelectric power of TTF-OCNAQ(II).

It is noteworthy that conduction through the OCNAQ stacks is realized in this system. This fact suggests that the reduction state of OCNAQ is slightly deviated from an integral value. Such a fractional charge is stabilized only if considerable electron transfer interaction between molecules exists. Although the OCNAQ molecule is not planar, the existence of an intermolecular interaction between the OCNAQ molecules is indicated by an X-ray structure analysis, and the charge transport properties of this material strongly suggests that the interaction is sufficient enough to stabilize the metallic character of the OCNAQ stacks.

Remarks

In the present paper various aspects of OCNAQ are reported. The reduced on-site Coulomb repulsion is manifested in the electrical properties of simple salts. In TTT-OCNAQ(II) a unique transverse interaction through OCNAQ molecules has been found. In TTF-OCNAQ(II) the metallic character of OCNAQ stacks has been observed. Of further interest is the stacking pattern of the OCNAQ molecules in TTF-OCNAQ-(II), in which one OCNAQ undergoes interactions with four OCNAQ molecules. Therefore, this interaction is completely two-dimensional. This stacking pattern is the type expected for a molecule having a twin-type structure. Unfortunately, in this system the stabilization of the metallic state at low temperatures is not realized, since the transfer integral is not sufficiently large to maintain the metallic nature at low temperatures, due to the nonplanarity of the molecule. However, it should be pointed out that one promising approach to design two-dimensional systems is to use such twin-type donor or acceptor molecules.

We are grateful to Dr. Takehiko Mori and Mr. Kenichi Imaeda for helpful discussions and assistance in measurements.

References

1) T. Mitsuhashi, M. Goto, K. Honda, Y. Maruyama, T. Sugawara, T. Inabe, and T. Watanabe, *J. Chem. Soc., Chem. Commun.*, **1987**, 810.

2) T. Mitsuhashi, M. Goto, K. Honda, Y. Maruyama, T. Inabe, T. Sugawara, and T. Watanabe, *Bull. Chem. Soc. Jpn.*, **61**, 261 (1988).

3) T. Inabe, T. Mitsuhashi, and Y. Maruyama, *Chem. Lett.*, **1988**, 429.

4) P. M. Chaikin and J. F. Kwak, *Rev. Sci. Instrum.*, **46**, 218 (1975).

5) T. Sakurai and K. Kobayashi, *Rep. Inst. Phys. Chem. Res.*, **55**, 69 (1979).

6) J. S. Chapell, A. N. Bloch, W. A. Bryden, M. Maxfield, T. O. Poehler, and D. O. Cowan, *J. Am. Chem. Soc.*, **103**,

2442 (1981).

7) The lists of structure factors, atomic parameters for hydrogen atoms, and anisotropic thermal parameters for non-hydrogen atoms are deposited at Bull. Chem. Soc. Jpn. (Document No. 8843).

8) D. L. Smith and H. R. Luss, *Acta Crystallogr., Sect. B*, **33**, 1744 (1977).

9) O. Dideberg and J. Toussaint, *Acta Crystallogr., Sect. B*, **30**, 2481 (1974).

10) R. P. Shibaeva and L. P. Rozenberg, *Sov. Phys. Crystallogr.*, **20**, 581 (1976).

11) W. F. Cooper, N. C. Kenney, J. W. Edmonds, A. Nagel, F. Wudl, and P. Coppens, *Chem. Commun.*, **1971**, 889.

12) T. J. Kistenmacher, T. E. Phillips, and D. O. Cowan, *Acta Crystallogr., Sect. B*, **30**, 763 (1974).

13) C. K. Johnson and C. R. Watson, Jr., *J. Chem. Phys.*, **64**, 2271 (1976); B. A. Scott, S. J. Laplaca, J. B. Torrance, B. D. Silverman, and B. Welber, *J. Am. Chem. Soc.*, **99**, 6631 (1977).

14) J. R. Cooper, M. Weger, D. Jerome, D. Lefur, K. Bechgaard, A. N. Bloch, and D. O. Cowan, *Solid State Commun.*, **19**, 749 (1976).

15) C. K. Johnson, ORTEP, Report ORNL-3794, Oak Ridge National Laboratory, Tennessee (1976).

A Molecular Orbital Study of Cyclodextrin Inclusion Complexes. I. The Calculation of the Dipole Moments of α-Cyclodextrin-Aromatic Guest Complexes

Masaki KITAGAWA, Hajime HOSHI, Minoru SAKURAI,* Yoshio INOUE, and Riichirô CHÛJÔ
Department of Biomolecular Engineering, Tokyo Institute of Technology,
12-1 O-okayama 2-chome, Meguro-ku, Tokyo 152
(Received May 9, 1988)

The dipole moments of α-cyclodextrin(α-CD)-aromatic guest systems have been calculated by means of the CNDO/2 molecular orbital (MO) method in order to investigate the role of electrostatic interaction in the stabilization of the inclusion complexes. It is found that α-CD has a remarkably large dipole moment which amounts to 13.5 D and is directed from its secondary hydroxyl side (the wider rim) towards the primary hydroxyl side (the narrower rim). The dipole moments of the guests, benzene derivatives, run antiparallel to that of α-CD in the complexed state. The MO total energy of the α-CD-guest supermolecular complexes shows that these antiparallel-orientations are energitically more favorable than the reversed one. It is concluded that the electrostatic interaction, mainly dipole-dipole interaction, between the α-CD and the guest molecules plays an essential role in determining the guest orientation. On the basis of these results, it is deduced that during complexation the CD molecule undergoes appreciable amount of conformational change, suggesting that the "induced-fit" mechanism is operating when the guest molecule is admitted into the host cavity.

Cyclodextrin (cycloamylose, CD) is a cyclic oligosaccharide composed of at least six α-1,4-linked D-glucose residues. CD has an intramolecular cavity and forms inclusion complexes with a variety of guest molecules. Much attention has been paid to this property of CD, since CD catalyzes various organic reactions via the formation of host-guest complexes in a way similar to that of enzymes. The mechanism of complex formation must be elucidated for a better understanding of the catalytic behavior of CD. A variety of physicochemical models for CD-guest interactions has been proposed.[1-4] Usually, the driving forces for complexation are attributed to the following interactions: van der Waals interaction,[5-9] hydrogen bonding,[10,11] hydrophobic interaction,[12] release of high-energy cavity water,[13,14] release of macrocyclic ring strain,[15,16] and effects of solvent-surface tension.[17] In spite of much effort, there is no general agreement as to the main force stabilizing the inclusion complexes at present.

From the standpoint of intermolecular interaction theory,[18] long-range types of interaction, especially electrostatic interaction, should be primarily important for stabilizing such non-covalent types of molecular complexes. However, there have been no explicit studies on electrostatic properties of CD, e.g., its dipole moment or electronic distribution. Recently, the importance of the dipole-dipole interaction between CD and guest molecules has been pointed out on the basis of NMR measurements of α-CD-aromatic guest complexes.[19,20] Therefore it is of mechanistic interest to study more extensively and directly the CD-guest inclusion phenomena. Quantum-chemical approaches may be suitable for this purpose. We have already confirmed that the CNDO calculation provides valuable information on the geometry of CD-guest complexes.[21,22]

In this paper we calculate the dipole moments of α-CD (composed of six glucose units) and some guest molecules in their complexed states using the CNDO/2 molecular orbital (MO) method. Here *p*-nitrophenol (PNP), *p*-hydroxybenzoic acid (PHBA), benzoic acid (BA), and water are selected as guest molecules because the α-CD inclusion complexes with them have been extensively studied in both solution and crystal.[19-26] On the basis of the calculated results, we discuss the role of dipole-dipole interaction, the leading term of electrostatic interaction, in stabilizing the inclusion complexes. It is suggested that α-CD has a large dipole moment and the dipole-dipole interaction plays a key role in determining the guest-orientation in each complex. Finally, the mechanism of the inclusion process is discussed. The preliminary results have been already reported.[27]

Methods

The dipole moments of the host and guest molecules were calculated using the CNDO/2 method.[28] Each molecular geometry was derived from the X-ray data for the corresponding inclusion complexes: α-CD-water,[25] α-CD-PNP,[26] and α-CD-PHBA.[26] Figure 1 schematically shows the geometries of α-CD-PNP and α-CD-PHBA complexes determined by the X-ray method. The dipole moments of the host α-CD and guest molecules were calculated separately. The three geometries of α-CD derived from these X-ray data are different from each other. The standard geometrical values by Pople and Beveridge[28] were used for BA molecule because of the lack of the crystalline data by X-ray diffraction.

For the α-CD-PNP complex, the dipole moments of the six glucose residues constructing the α-CD molecule were also estimated separately. Here, the C1 and C4 positions of each glucose residue were terminated by the substitution of hydroxyl groups and the geometry of the residual part remains to be identical with that of the X-ray data.

The MO total energies of the α-CD-PNP and -PHBA supermolecuar complexes were obtained for two modes of

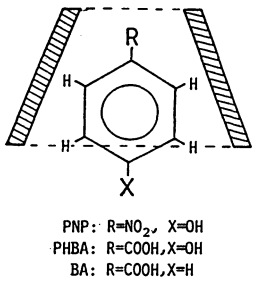

PNP: R=NO_2, X=OH
PHBA: R=COOH, X=OH
BA: R=COOH, X=H

Fig. 1. Schematic representation of the inclusion complex between α-CD and some benzene derivatives. The α-CD has a bucket-like cavity; the diameter on the wider-rim side is 8.8 Å and that on the narrower-rim side is 5.6 Å. Due to the bulkiness of the substituents, the orientational freedom of the guest molecule in the cavity is restrained. Usually, two modes of orientations are descriminated according to which substituent is inserted into the cavity. Here the experimentally determined-orientation is shown for each α-CD-guest complex.

guest-orientations (see Fig. 1): i) the nitro or carboxyl group is included in the α-CD cavity, and ii) the phenolic hydroxyl group is in the α-CD cavity. The former corresponds to the X-ray structure. The geometry of the latter was determined on the assumption that the position of the benzene ring relative to the CD-cavity is kept constant against the inversion of the guest-orientation.

Results and Discussion

Dipole Moment of Host and Guest Molecules. The values of dipole moments for the host molecules are shown in Table 1, together with those for the guest molecules. It is apparent that the host α-CD in all the complexes has a remarkably large dipole moment. The direction of the α-CD dipole moment in each complex runs from the side of the secondary hydroxyl groups to the side of the primary hydroxyl groups of α-CD, although it is not exactly parallel to the apparent cavity axis of α-CD.

It has been confirmed that for a variety of small molecules the values of dipole moments based on the CNDO/2 method are in fairly good agreement with the observed data.[1] However, the dipole momens of the α-CDs are too large in comparison with those of ordinary standard molecules. Thus in order to support the above finding, we again attempted to calculate the dipole moment of the α-CDs by means of the MM2 molecular mechanics method.[29] In this method molecular dipole moments are estimated as the sum of bond dipoles, and the accuracy of the computation would not appreciably depend on the size of molecules. As a result the dipole moment of α-CD in the α-CD-PNP complex is evaluated to be 12.4 D,[30] which is sufficiently close to the CNDO-value (13.5 D).

Moreover, the dipole moments of the glucose residues constructing α-CD were calculated in order to investigate the origin of the large dipole moment of α-CD. For the α-CD-PNP complex, the respective glucose units have diverse values of the dipole moments from 1.8 to 5.1 D, as shown in Table 2. According to the X-ray data for this complex,[26] there are some conformational diffrences among these six residues, which should be responsible for the diversity of the dipole moments. Here we could not find explicit correlations between structural parameters and the magnitudes of dipole moments obtained. The dipole moment averaged over all the residues amounts to 3.4 D. The sum of the contributions from all the residues is not less than the apparent dipole moment of the parent molecule. Therefore it is reasonable that the α-CD molecule has the large dipole moment as shown in Table 1.[31]

Table 1. The Dipole Moments of the Host α-CD and the Guests in Their Inclusion Complexes

Guest	Magnitude/D		Direction[a]/degree			
	host	guest	θ	ϕ	ψ	ω
PNP	13.5	5.0	31	19	22	152
PHBA	10.7	2.3	32	41	9	116
BA[b]	—	1.5	—	44	—	—
$(H_2O)_2$	9.5	1.1	80	—	—	138

a) The definitions of θ, ϕ, and ψ are given in Fig. 2. ω indicates the angle between the dipole moment vectors of the host and the guest. Its value was derived from θ, ϕ, and ψ. b) X-Ray data are unavailable.

Table 2. The Dipole Moments of Glucose Residues of α-CD

Glucose No.[a]	Dipole moment/D
1	1.8
2	5.1
3	4.4
4	4.1
5	2.3
6	2.6

a) Each No. of glucose units corresponds to that found in Ref. 13.

The angle ω between the two dipole moment vectors of the host and the guest was derived from the three tilting angles θ, ϕ, and ψ described in Fig. 2. The results (the last column of Table 1) show that in the complexed state the dipole moment of the guest is nearly antiparallel to that of the hosts. The guest orientations in these complexes are schematically shown in Fig. 1. It has been found that the orientations of the guests in aqueous solution[8,15,16] are the same as those in the crystalline state for the α-CD-PNP and the α-CD-PHBA complexes.

For the α-CD-BA complex, it is difficult to estimate the angle ω, since its crystalline structure has not been published. It has been found that the carboxyl-side of BA is located in the α-CD cavity in solution,[17] as also shown in Fig. 1. The calculated dipole moment of BA runs from the carboxyl group to its para position. As in the previous cases, the two dipole moments of the

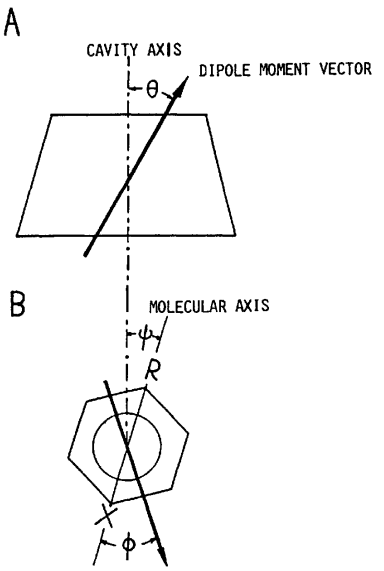

Fig. 2. Definition of the direction in the dipole moment vectors of α-CD and the guest molecules. **A.** The dipole moment of α-CD runs from the wider-rim side to the narrower-rim one. Its direction is defined as the tilting angle θ against the cavity (pseudo-six fold) axis. The angle θ varies dramatically and depends on the type of guest molecule included with concomitant variations in the magnitude of dipole moment. This suggests the conformational change in the macrocyclic ring. **B.** The direction in the dipole moment of the guest molecule is defined as the tilting angle ϕ against its molecular axis. In the crystalline state, the axis is tilted by $\psi°$ against the cavity axis. The angle ψ is estimated from the X-ray data for each complex. Thus, the angle ω between the dipole moment vectors of α-CD and the guest can be derived from θ, ϕ, and ψ. In the complexed state, the dipole moment of the guest is nearly antiparallel to that of the host. The numerical values for the angles defined here are summarized in Table 1.

host and the guest again run antiparallel each other.

Therefore, the antiparallel relationship between the host- and guest-dipole moments holds for all the α-CD complexes studied here, which suggests that electrostatic interaction, chiefly dipole-dipole interaction, is a main contributor stabilizing their complex and thus determines the guest-orientation.

Total Energy of the α-CD-PNP Complex. The MO total energies of the α-CD-guest supermolecular complexes are summarized in Table 3. The total energy of the α-CD-PNP complex with experimentally determined geometry, in which the nitrophenyl group is included in the cavity, is 45 kJ mol^{-1} lower than the sum of the host's and guest's total energies, while that of the complex with the reversed guest-orientation, namely, in the case that the hydroxyphenyl group is in the cavity, is 96 kJ mol^{-1} higher than the sum. Thus, the former orientation is 141 kJ mol^{-1} more stable than the latter. That is, the complex state, in which the nitrophenyl group is included in the cavity, is more stable than the isolated state of

Table 3. The Energy Difference of α-CD-PNP and α-CD-PHBA Complexes for Two Modes of the Guest Orientation

	Energy difference[a]/kJ mol^{-1}	
	PNP	PHBA
Complex[b]	−45	−31
Complex[c]	96	−13

a) Energy difference is calculated from the equation, $E=E_{complex}-E_{host}-E_{guest}$, where $E_{complex}$, E_{host}, and E_{guest} are the total energies for the complex, the host, and the guest, respectively. b) The nitrophenyl and carboxylphenyl groups are located in the α-CD cavity for α-CD-PNP and α-CD-PHBA complexes, respectively. c) The hydroxylphenyl group is located in the cavity.

the two partners, and than the complex state for the reversed guest-orientation. Similarly, in the case of the CD-PHBA complex the experimentally-determined orientation is again more stable. These results imply that the guest-orientations are determined by the electronic interactions, including electrostatic interactions, between the host and the guest molecules.

According to the X-ray data for these complexes, the nitro or carboxyl group is located in the vicinity of the primary hydroxyl groups of CD, but is not hydrogen-bonded with them. Thus, in both cases hydrogen bonding is a less important factor for stabilizing the complexes. However, the polar groups of the guests participate in other hydrogen-bonding networks. The phenolic hydroxyl group protrudes from the CD-cavity, and forms the hydrogen bond with the oxygen atom of the neighboring CD in crystal. Similarly, this group could be hydrogen-bonded with solvent molecules in solution. The effects of such hydrogen bonds, formed with molecules other than the host, on the stabilization of the complexes may be nonnegligible. However, they are not main factors determining the guest-orientation, because for the reversed guest-orientation similar hydrogen-bonding networks in which the newly protruded groups participate are also possible.

On the basis of molecular mechanics calculation, Tabushi et al.[8] have shown that van der Waals interaction is a major contributor for stabilizing α-CD-aromatic guest complexes, and supported the idea that the specificity of substrate binding by CD is mainly related to the extent of host-guest fitting. Mastui[7] has determined the geometry of the some α-CD-guest complexes using Hill's potential,[32] which is an emprical equation evaluating van der Waals interaction. Accoding to his results for the α-CD-PNP complex, the stabilization energy due to van der Waals interaction is 52.26 kJ mol^{-1} for experimentaly determined guest-orientation, and 41.17 kJ mol^{-1} for the reverse guest-orientation. The former is comparable to the stabilization energy estimated from the MO total energy (Table 3). As shown in Table 3, the interaction energy based on the CNDO calculations dramatically

changes depending on the guest-orientation. The energy-difference (141 kJ mol^{-1}) between the two orientations is fairly large compared with that from Mastui's data (11 kJ mol^{-1}).[1] In other words, the van der Waals (dispersion) interactions are less important for determining the guest-orientation than the electronic interaction.

The Formation-Mechanism of α-CD Inclusion Complexes with Aromatic Guests. When two water molecules are included in the α-CD cavity (α-CD-water complex), the dipole moment vector of α-CD considerably deviates from the cavity axis; the θ value in Fig. 2 A is 80°. This finding reflects the fact that the macrocyclic ring of α-CD including two water molecules is highly distorted, as is indicated by Manor and Saenger.[25] On the other hand, in both the α-CD-PNP and α-CD-PHBA complexes, the macrocyclic ring shows a slightly distorted hexagon,[26] corresponding to the smaller tilting angle (θ=30°) of the dipole moment vector.

It is apparent from Table 1 that the values of dipole moment of α-CD in the α-CD-PNP and α-CD-PHBA complexes are larger than that for the α-CD-water complex. Namely, when α-CD accommodates the aromatic guest instead of the two water molecules, its dipole moment becomes larger. Here it is convenient to introduce the induced dipole moment defined as the difference in the dipole moments (magnitudes) between in the α-CD-water and in the α-CD-aromatic guest complexes. The induced dipole moments are evaluated to be 4.0 and 1.2 D for α-CD for the inclusion of PNP and PHBA, respectively. The larger the dipole moment of the guest is, the larger is the induced dipole moment of the α-CD. As described above, the guest-dependence of dipole moment should be related to the conformational changes of the host molecule. Therefore, this finding suggests that on complexation the α-CD molecule undergoes the appreciable extent of conformational changes to strengthen the dipole-dipole interaction with the guest molecules.

If a guest molecule approaches a CD cavity in solution so that its dipole moment would run antiparallel to that of the CD after complexation, the dipole-dipole interaction should produce an energy barrier for complexation and makes it rather difficult to penetrate the guest into the α-CD cavity. This difficulty could be partially removed if the α-CD molecule changes its conformation depending on its relative position to the guest molecules. As described above, the skeleton of α-CD is flexible enough to respond to the perturbation from guest molecules. Thus during the release of included waters and the subsequent inclusion of the guest, the macrocyclic ring of α-CD may take another conformation[34] giving a smaller dipole moment. It is then possible that the conformational change causes the energy barrier to be lower, and thus a guest molecule penetrates into the α-CD cavity more easily. After complexation, α-CD again changes its conformation so that it would make its dipole moment larger to form a more stable complex. The flexibility of the CD macrocycle in aqueous solution has been confirmed by the measurements of ^{13}C spin-lattice relaxation time.[35,36]

More extensive study on the electronic structure of α-CD is required to confirm the above model about the complexation process. At present stage other factors driving the complexation should not be excluded. A thermodynamic study[37] on CD-apolar guest complexation has shown the importance of hydrophobic interaction (apolar binding), which originates from the breakdown of the structural water molecules around an apolar guest. According to this report, a favorable entropy change due to hydrophobic interaction is largely responsible when a guest molecule approaches a CD-cavity from their isolated state. On the other hand, after inclusion of the guest the complex can be stabilized by other factors providing favorable enthalpy change. It is, therefore, natural to say that owing to the hydrophobicity of the aromatic ring PNP is driven into the α-CD cavity with the aid of the hydrophobic interaction. Once the guest is trapped into the α-CD cavity, the complex is predominantly stabilized in terms of the dipole-dipole interaction as is described above.

In conclusion, α-CD has a remarkably large dipole moment so that the host-guest electrostatic interaction can determine a guest orientation in the complexed state. The dipole moment of α-CD varies depending on the type of guest molecule, which reflects the conformational change of the macrocyclic ring of α-CD. On the basis of these results, we conclude that the "induced-fit" mechanism effectively operates on α-CD-guest complex formation and the conformational change of α-CD is caused by the dipole-dipole interaction between the host and the guest molecules. The CD molecule serves a highly electrically anisotropic medium to the guest molecules. The term like a "hydrophobic pocket" is insufficient to describe the character of CD-cavity. We are currently investigating whether these results are applicable to other types of guest molecules like aliphatic compounds.

The authors thank the Computer Center, Institute for Molecular Science, Okazaki National Research Institutes, Japan, for the use of the HITAC M-680H and S-810/10 computer.

One (Y.I.) of authors wishes to thank for the partial support by a Grant-in-Aid for Scientific Research on Priority Area, "Dynamic Interaction and Electronic Processes of Macromolecular Complexes," (1987), from the Ministry of Education, Science and Culture.

References

1) M. L. Bender and M. Komiyama, "Cyclodextrin Chemistry," Spinger-Verlag, New York (1978).

2) W. Saenger, *Angew. Chem., Int. Ed. Engl.*, **19**, 344

(1980).
3) I. Tabushi and Y. Kuroda, *Adv. Catal.*, **32**, 417 (1983).
4) Y. Matsui, T. Nishioka, and T. Fujita, *Top. Curr. Chem.*, **128**, 61 (1985).
5) F. Cramer, *Angew. Chem.*, **68**, 115 (1956).
6) K. Harata, *Bull. Chem. Soc. Jpn.*, **49**, 2066 (1976).
7) Y. Matsui, *Bull. Chem. Soc. Jpn.*, **55**, 1246 (1982).
8) I. Tabushi, Y. Kiyosuke, T. Sugimoto, and R. Yamamura, *J. Am. Chem. Soc.*, **100**, 916 (1978).
9) R. J. Bergeron, D. M. Pillor, G. Gibeily, and W. P. Robert, *Bioorg. Chem.*, **7**, 263 (1978).
10) J. Cohen and J. L. Lach, *J. Pharm. Sci.*, **52**, 132 (1963).
11) F. Cramer and W. Kampe, *J. Am. Chem. Soc.*, **87**, 1115 (1965).
12) D. E. Tutt and M. A. Schwartz, *Chem. Commun.*, **1970**, 113.
13) R. L. VanEtten, J. F. Sebastian, G. A. Clowes, and M. A. Bender, *J. Am. Chem. Soc.*, **89**, 3242 (1967).
14) R. Bergeron and R. Rowan, III, *Bioorg. Chem.*, **5**, 425 (1976).
15) P. C. Manor and W. Saenger, *Nature (London)*, **237**, 392 (1972).
16) W. Saenger and M. Naltemeyer, *Angew. Chem., Int. Ed. Engl.*, **13**, 552 (1974).
17) A. Orstan and J. B. A. Ross, *J. Phys. Chem.*, **91**, 2739 (1987).
18) A. D. Buckingham, P. Claverie, R. Rein, and P. Schuster, "Intermolecular Interactions: From Diatomic to Biopolymers," ed by B. Pullman, Wiley, (1978).
19) R. J. Bergeron, M. A. Channing, and K. A. McGovern, *J. Am. Chem. Soc.*, **100**, 2878 (1978).
20) R. I. Gelb, L. M. Schwartz, B. Cardelino, H. S. Fuhrman, R. F. Johnson, and D. A. Laufer, *J. Am. Chem. Soc.*, **103**, 1750 (1981).
21) Y. Inoue, H. Hoshi, M. Sakurai, and R. Chûjô, *J. Am. Chem. Soc.*, **107**, 2319 (1985).
22) Y. Inoue, M. Kitagawa, H. Hoshi, M. Sakurai, and R. Chûjô, *J. Inclusion Phenomena*, **5**, 55 (1987).
23) R. J. Bergeron, M. A. Channing, G. J. Gibeily, and D. M. Pillor, *J. Am. Chem. Soc.*, **99**, 5146 (1977).
24) Y. Inoue, T. Okuda, Y. Miyata, and R. Chûjô, *Carbohydr. Res.*, **125**, 65 (1984).
25) P. C. Manor and W. Saenger, *J. Am. Chem. Soc.*, **96**, 3630 (1974).
26) K. Harata, *Bull. Chem. Soc. Jpn.*, **50**, 1416 (1977).
27) M. Kitagawa, H. Hoshi, M. Sakurai, Y. Inoue, and R. Chûjô, *Carbohydr. Res.*, **163**, c1 (1987).
28) J. A. Pople and D. A. Beveridge, "Approximate Molecular Orbital Theory," McGraw-Hill, New York (1970).
29) N. L. Allinger and Y. H. Yuh, Quantum Chemistry Program Exchange No. 395, Chemistry Department, Indiana University, U.S.A.
30) M. Kitagawa, M. Sakurai, Y. Inoue, and R. Chûjô, unpublished results.
31) The feature of the electronic distribution in α-CD can be seen from its electrostatic potential maps. Recently we have found that the side of the secondary hydroxyl groups of the CD has positive potentials, while the side of the primary hydroxyl groups does negative ones. Therefore, a very large separation of charges is caused along the CD-cavity axis, resulting in the large dipole moment. This preliminary result has been already accepted for publication (M. Sakurai et al., *Chem. Lett.*, **1988**, 895).
32) T. L. Hill, *J. Chem. Phys.*, **16**, 399 (1948).
33) The geometry for the reversed guest-orientation used here does not necessarily correspond to the energitically optimized one. Thus our calculation should underestimate the stabilization energy for this case. However it is known that the position of the aromatic ring in the cavity, namely the depth of inclusion, is almost independent of the type of substituent (see Ref. 26). It seems that the main conclusions obtained here are no problem.
34) A possible candidate of this transition state is the form III complex found by Chacko and Saenger (*J. Am. Chem. Soc.*, **103**, 1708 (1981)).
35) Y. Inoue, Y. Katono, and R. Chûjô, *Bull. Chem. Soc. Jpn.*, **52**, 1692 (1979).
36) Y. Inoue and Y. Miyata, *Bull. Chem. Soc. Jpn.*, **54**, 809 (1981).
37) M. Komiyama and M. L. Bender, *J. Am. Chem. Soc.*, **100**, 2259 (1978).

The Model Compounds and Conformational Analysis of Poly(thiotrimethylene) Using Molecular Mechanics Method

Taira MIYASAKA* and Takaichi YOSHIDA
Department of Dental Materials Science, School of Dentistry at Tokyo, The Nippon Dental University, 1-9-20, Fujimi, Chiyoda-ku, Tokyo 102
(Received May 19, 1988)

Several model compounds of poly(thiotrimethylene), including one to four thiotrimethylene units, were studied by means of a molecular mechanics method. The geometric and statistical weight parameters were directly derived from the results of molecular mechanics calculations concerning several conformers of these model compounds. Although the first-order interactions of poly(thiotrimethylene) were significantly larger than those of poly(oxyalkylenes), the second-order interactions of this polymer were much smaller. The "gauche effect" by sulfur atoms seemed to be mainly caused by small second-order interactions. By means of the model, compounds including more than three repeating units, the calculated configuration-dependent properties were in better agreement with the experimental ones than that calculated earlier. The better agreement was obtained by varying some of the geometric parameters. Compounds including more than three repeating units of the polymer were available as model compounds. Since this was also true in poly(oxyalkylenes), it was found that a combination of the methods of molecular and statistical mechanics was sufficiently effective to investigate the configurational properties of poly(thiotrimethylene).

Poly(thioalkylenes) have been investigated[1-8] with regard to their configurational properties in comparison with the analogous poly(oxyalkylenes),[9-13] because of their similarity in structure. In the case of poly(oxyalkylenes), it has been shown that the gauche conformations, which are associated with the O-CH_2 interactions, are much preferred to the trans state. This anomalous gauche preference is called the "oxygen gauche effect." Earlier semiempirical calculations[9] of the conformational energies for the model compounds of poly(oxyalkylenes) could not succeed in providing proper interpretations of such anomalous gauche preference, although structural studies in crystal[14,15] or vibrational spectroscopic studies[16] have been well established. In previous studies,[10-13] we undertook the first attempts to combine the molecular mechanics method[17] with the calculations involving statistical mechanics. When the lone-pair electrons on an oxygen atom were taken into consideration, molecular mechanics calculations on the model compounds of poly(oxyalkylenes) prevailed to estimate the proper amount of the gauche oxygen effect. The configuration-dependent properties of poly(oxyalkylenes), which were calculated by means of the rotational isomeric states approximations directly obtained from the results of molecular mechanics on the model compounds, were in fairly good agreement with the experimental ones.

In analogy to the poly(oxyalkylenes), it was found that poly(thioalkylenes) had a similar gauche effect,[1-8] although it was different in amount. Similarly, in poly(oxyalkylenes), earlier conformational energy calculations[6-8] of the model compounds of poly(thioalkylenes) also could not provide proper interpretations of the rotational isomeric states approximations. Moreover, molecular mechanics, which provided successful interpretations of the rotational states approximations for the model compounds of poly(oxyalkylenes), had as yet never been applied to the model compounds of poly(thioalkylenes) for such approximations, except regarding the conformational and packing stability in crystal[18] or the vibrational spectra analysis using the group coordinate force field.[19-21] Poly(thioalkylenes), which included one or two methylene groups in their repeating units, had not been experimentally investigated with regard to the configuration-dependent properties, because of their high melting points and poor solubility in solvents. The simplest poly(thioalkylenes), whose configuration-dependent properties have been experimentally observed, is poly(thiotrimethylene).[8] Therefore, in this study, molecular mechanics were applied to the model compounds of poly(thiotrimethylene), which have various chain lengths. By means of these results, the configuration-dependent properties of this polymer could be estimated. The calculated values were compared with the experimentally observed ones. Then, the most suitable length of the model compound of poly(thiotrimethylene) could be determined. Here, the propriety of the application of the molecular mechanics to the poly(thioalkylenes) is also discussed.

Theoretical

Molecular Mechanics Calculation. Molecular mechanics[17] (or force field method) is a method that allows calculations of the structure and energy of a molecule by means of several potential functions (bending, stretching, torsional, van der Waals, electrostatic, their cross terms) and their experimentally derived parameters. Then the energy is minimized. In recent years, molecular mechanics has become one of the most popular methods, occupying a significant position in the field of computer chemistry, called "applied theoretical chemistry".[22] Although many force fields have been suggested, each force field has a different object to simulate a molecule. The force

fields of Scheraga[23] or Kallman[24] shows fine performances for calculations of the molecular structure of polypeptide or nucleic acids. That of Lifson/Warshel[25,26] has proven to be highly efficient for calculations of the packing of molecules in a crystal, and that of Tadokoro[27] or Williams[28] aim at estimations of crystalline structures. Matsuura et al.[18,19] developed a group coordinate force field, which had been initiated by Shimanouchi et al.,[29] and proved to be suitable for treating the vibrations of molecules. For the general force fields aimed at hydrocarbons, Schleyer's,[30] Boyd's,[31] and Allinger's[32] are very famous. Among them, Allinger's force field is available for a wide range of the problems concerning organic chemistry, since the parameters of hydrocarbons and those of various heteroatoms are made courteously. The use of this method has spread remarkably around world. In this study, the force field of Allinger[32] was selected, because of this remarkably wide spread usage and the reliability of parameters for heteroatoms. Another positive point is that a satisfactory estimation of the rotational isomeric states of poly(oxyalkylenes) had been obtained by the previous force field of Allinger, i.e. MMI;[17,33] therefore, the calculated results of poly(thioalkylenes) can be directly compared with the previous results of poly(oxyalkylenes). More recently, since computer programs for molecular mechanics, which can run on a microcomputer, have become available,[33] molecular mechanics has become easier to use. In this study we used a molecular mechanics program which was reported in 1977 by Allinger et al. (MM2[32]). This program could execute under MS-DOS[34] and be transformed so as to be able to run on a PC-9801 microcomputer.[35]

Considering structural symmetry, and for the purpose of deriving the geometric and statistical weight parameters in order to calculate the configuration-dependent properties of poly(thiotrimethylene), the following model compounds, including one to four thiotrimethylene units $CH_2CH_2CH_2S$ with terminal methyl or ethyl groups, were studied; i.e. 2,6-dithiaheptane (**4T**) $CH_3SCH_2CH_2CH_2SCH_3$, 3,7-dithianonane (**6T**) $CH_3CH_2SCH_2CH_2CH_2SCH_2CH_3$, 2,6,10-trithiaundecane (**8T**) $CH_3S\text{-}(CH_2CH_2CH_2S\text{-})_2\text{-}CH_3$, 3,7,11-trithiatridecane (**10T**) $CH_3CH_2S\text{-}(CH_2CH_2CH_2S)_2CH_2CH_3$, 2,6,10,14-tetrathiapentadecane (**12T**) $CH_3S(CH_2CH_2CH_2S)_3CH_3$, 2,6,10,14,18-pentathianonadecane (**16T**) $CH_3S(CH_2CH_2CH_2S)_4\text{-}CH_3$. The numbers with **T** in parentheses denote the number of skeletal bonds whose rotations experience a first-order interaction between CH_2 and CH_2, or CH_2 and S atoms; these abbreviations are used here instead of the full names of model compounds. Regarding these model compounds, the all-trans conformer, the conformers including one gauche state and those including consecutive two gauche states, were calculated by molecular mechanics. In molecular mechanics, the effect of any solvent was taken into account by considering the solvent as an isotropic continuum having a macroscopic dielectric constant. Under such conditions, the rotational states of molecules have a preference for gauche states as the polarity of solvents increases. The configuration-dependent properties of this polymer, which were to be compared with the results of molecular mechanics, were obtained in a nonpolar solvent, i.e. benzene.[8] Moreover, the configuration-dependent properties of the polymer were studied under an unperturbed state; therefore, no additional treatment was made regarding the effect of a solvent.

Results and Discussion

Results of Molecular Mechanics Calculations on the Model Compounds of Poly(thiotrimethylene). As the model compounds of poly(thiotrimethylene), the six compounds described in the previous section were used in molecular mechanics calculations, in which the dipole-dipole interactions with common atoms were taken into consideration. The calculated energy differences between corresponding an all-trans conformer and several conformers of each model compound are listed in Table 1.

With respect to compound **4T**, the all-trans conformer has the lowest energy and a TTTG conformer with a rotational state of CC-SC is gauche, has secondly low energy. Concerning the derivation of the statistical-weight parameters of poly(thiotrimethylene), **4T** is too short to derive all of the parameters (eight kinds of parameters are needed, although only six are obtained from **4T**).

The **6T** is the smallest model compound of poly(thiotrimethylene), which can be used to derive all of the eight statistical-weight parameters required for a calculation of the configuration-dependent properties of the polymer. The all-trans conformer of **6T** also has the lowest energy; a TTTTGT conformer with a rotational state of CC-SC is gauche, has the second lowest energy.

Throughout the calculated results of all the model compounds, the gauche state about CC-SC is lower in energy than that about SC-CC. In poly(oxytrimethylene), the gauche state about the central bond in the sequence CC-CO has been found to be lower in energy than that in the sequence CC-OC. This is caused by the fact that a C-O bond (1.407 Å) is considerably shorter than a C-C bond; therefore, the van der Waals interactions of a gauche in CC-OC become larger than those in CC-CO and is caused by the large electrostatic attractions of a gauche in CC-CO. On the contrary, the gauche of poly(thiotrimethylene) in CC-SC has been found to be lower in energy than that in CC-CS. The preference of the former is mainly due to stabilizations by van der Waals and torsional interactions owing to the long bond length of C-S, i.e. $l_{C\text{-}S}$=1.815 Å. These contributions to the steric energy are larger

Table 1. The Results of Molecular Mechanics Calculations on Several Model Compounds of Poly(thiotrimethylene)

2,6-Dithiaheptane		3,7-Dithianonane		2,6,10-Trithiaundecane		3,7,11-Trithiatridecane	
Conformer	ΔE / kJ mol^{-1}	Conformer	ΔE / kJ mol^{-1}	Conformer	ΔE / kJ mol^{-1}	Conformer	ΔE / kJ mol^{-1}
TTTT	0.0	TTTTTT	0.0	TTTTTTTT	0.0	TTTTTTTTTT	0.0
TTTG	0.406	TTTTTG	0.603	TTTTTTTG	0.398	TTTTTTTTTG	0.544
TTGT	1.506	TTTTGT	0.297	TTTTTTGT	1.389	TTTTTTTTGT	0.360
TTGG	1.481	TTTGTT	1.439	TTTTTGTT	1.410	TTTTTTTGTT	1.289
TGGT	3.155	TTTTGG	0.598	TTTTGTTT	0.084	TTTTTTGTTT	1.552
TTG$\bar{G}$	10.694	TTTGGT	1.234	TTTTTTGG	1.272	TTTTTGTTTT	0.038
TG$\bar{G}$T	12.381	TTGGTT	2.983	TTTTTGGT	2.808	TTTTTTTTGG	0.510
		TTTTG$\bar{G}$	4.301	TTTTGGTT	0.854	TTTTTTTGGT	0.967
		TTTG$\bar{G}$T	10.523	TTTGGTTT	−0.557	TTTTTTGGTT	2.715
		TTG$\bar{G}$TT	12.021	TTTTTTG$\bar{G}$	6.134	TTTTTGGTTT	0.854
				TTTTTG$\bar{G}$T	12.209	TTTTGGTTTT	−0.615
				TTTTG$\bar{G}$TT	5.594	TTTTTTTTG$\bar{G}$	4.356
				TTTG$\bar{G}$TTT	3.523	TTTTTTTG$\bar{G}$T	10.590
						TTTTTTG$\bar{G}$TT	12.021
						TTTTTG$\bar{G}$TTT	146.633
						TTTTG$\bar{G}$TTTT	3.498

2,6,10,14-Tetrathiapentadecane		2,6,10,14,18-Pentathianonadecane	
Conformer	ΔE / kJ mol^{-1}	Conformer	ΔE / kJ mol^{-1}
TTTTTTTTTTTT	0.0	TTTTTTTTTTTTTTTT	0.0
TTTTTTTTTTTG	0.389	TTTTTTTTTTTTTTTG	0.406
TTTTTTTTTTGT	1.398	TTTTTTTTTTTTTTGT	1.385
TTTTTTTTTGTT	1.418	TTTTTTTTTTTTTGTT	1.460
TTTTTTTTGTTT	0.280	TTTTTTTTTTTTGTTT	0.389
TTTTTTTGTTTT	0.239	TTTTTTTTTTTGTTTT	0.481
TTTTTTGTTTTT	1.460	TTTTTTTTTTGTTTTT	1.615
TTTTTTTTTTGG	1.222	TTTTTTTTTGTTTTTT	1.598
TTTTTTTTTGGT	2.728	TTTTTTTTGTTTTTTT	0.921
TTTTTTTTGGTT	0.921	TTTTTTTTTTTTTTGG	1.197
TTTTTTTGGTTT	−0.561	TTTTTTTTTTTTTGGT	2.703
TTTTTTGGTTTT	0.741	TTTTTTTTTTTTGGTT	0.866
TTTTTGGTTTTT	2.678	TTTTTTTTTTTGGTTT	−0.594
TTTTTTTTTTG$\bar{G}$	6.347	TTTTTTTTTTGGTTTT	0.703
TTTTTTTTTG$\bar{G}$T	12.368	TTTTTTTTTGGTTTTT	2.523
TTTTTTTTG$\bar{G}$TT	10.297	TTTTTTTTGGTTTTTT	1.013
TTTTTTTG$\bar{G}$TTT	91.994	TTTTTTTGGTTTTTTT	−0.398
TTTTTTG$\bar{G}$TTTT	15.414	TTTTTTTTTTTTTTG$\bar{G}$	6.343
TTTTTG$\bar{G}$TTTTT	12.339	TTTTTTTTTTTTTG$\bar{G}$T	12.397
		TTTTTTTTTTTTG$\bar{G}$TT	10.531
		TTTTTTTTTTTG$\bar{G}$TTT	83.881
		TTTTTTTTTTG$\bar{G}$TTTT	12.347
		TTTTTTTTTG$\bar{G}$TTTTT	13.021
		TTTTTTTTG$\bar{G}$TTTTTT	8.046
		TTTTTTTG$\bar{G}$TTTTTTT	4.356

than those from electrostatic interactions in these conformers.

A similar tendency was also found in a report by Tai et al.[18] Their conformational analysis of the crystal states of poly(oxytrimethylene) showed that the molecular chain, consisting of the sequence $C\overset{O}{\overset{\diagdown}{\tau_1}}\ \tau_2 C \tau_3\ \overset{C}{\overset{\diagdown}{\tau_4}}C$, was stable when the C-O bonds were trans and the C-C bonds were gauche, namely $(T_2G_2)_2$ helix ($\tau_1=\tau_2\simeq180°$ and $\tau_3=\tau_3\simeq60°$). It emphasized the preference of GG of the $O\diagdown C\diagup C\diagdown C\diagup O$ bond and coincided with our previous results. The same report also showed that the conformations in the crystal states of poly(thiotrimethylene) about the molecular chain consisted of the sequence $C\diagdown S\diagup C\diagdown C\diagup C$. It showed that the lowest energy conformation was the $(G_2T_2)_2$-type helix, though it has not yet been observed. The next lowest energy conformation was the G_4-type of

the actual existence. The following low-energy conformations were T_4 planar zigzag and a $(T_2G_2)_2$ helix. It demonstrated that the conformer which contained the two consecutive gauche in the bond sequence C\C/S\C/C was the most stable. This result is coincident with the present study, though details are somewhat different because of the premises of the molecular state, namely in the crystal state and in a dilute solution. More recently, Matsuura et al.[20] studied the vibrational spectra of the model compound of poly(thiotrimethylene), $CH_3S(CH_2)_3SCH_3$, by a normal coordinate calculation. This study had helped to clarify that the terminal GT+ and GG+ conformations, namely gauche about the CH_3S-CH_2 axis, were more stable than the TT+ and TG+ conformations, namely trans about the same axis (in the liquid state). Our results are contrary to these owing to a different assumption concerning the molecular state (in crystal or liquid against in gaseous or isolated molecule in some solvent). The propriety of our results were examined in terms of the configuration-dependent properties, which are discussed in following sections.

In the case of model compounds which are longer than **6T**, conformers with rotational states of CC-S-CC in the central positions are two consecutive gauche of the same sign ($G^{\pm}G^{\pm}$), are the lowest in energy among the respective conformers; for example, TTTGGTTT of **8T**, TTTTGGTTTT of **10T**, TTTTTTTGGTTT of **12T**, TTTTTTTTTTTGGTTT and TTTTTTTGGTTTTTTT of **16T**. Because these conformers which include two consecutive gauche of same signs, form a helical structure, the steric repulsions between bulky terminal groups are greatly reduced. Therefore, the van der Waals, torsional and electrostatic interaction energies of these conformers are much smaller than those of others. Contrary to this, the conformers which include two successive gauche about CC-S-CC in the terminal position are not so stable; i.e. TTTTGG of **6T** or TTTTTTTTGG of **10T**. It seems that the helix formation with the terminal part of these conformers does not cause a large reduction in the energy since one of the terminal groups is much larger than the previously mentioned conformers. The conformers containing two successive gauche of the opposite signs about CC-S-CC ($G^{\pm}G^{\mp}$) are also lower in energy than other consecutive gauche of the opposite signs with some exceptions.

Geometric and Statistical Weight Parameters of Poly(thiotrimethylene). From the results of molecular mechanics calculations on the model compounds of poly(thiotrimethylene), the geometric parameters obtained by Boltzmann averaged values over each conformer in Table 1 are shown in Table 2. In any case, the bond lengths are stretched and the bond angles are widened from those in a state of equilibrium, i.e. $l_{C\text{-}S}$=1.815 Å, $l_{C\text{-}C}$=1.523 Å, ∠CSC=96.3°, ∠SCC=109.0°, ∠CCC=109.5°. The bond angle of CSC is especially widened. In this study, the dihedral angles are defined as zero when the rotational state of a skeleton is in an ideal trans state. It is clear from Table 2 that the amount of twisting from the original trans position is small; on the other hand, those from gauche are somewhat large. The differences of the geometric parameters among the model compounds are slight.

The statistical-weight parameters of poly(thiotrimethylene) are constructed by two kinds of first-order interactions and six kinds of second-order interactions (Fig. 1). The skeleton of a repeating unit of poly(thiotrimethylene) consists of four kinds of bonds; each bond is distinguished by an alphabetic notation. Namely, σ and σ' are defined for a first-order interaction due to a rotation around the C-C (*b* and *c*) and C-S (*a* and *d*) bond, respectively. When the gauche sequence of the same sign, $G^{\pm}G^{\pm}$, are consecutive, the second-order interaction parameter ϕ is defined for *bc*, ϕ' for *ab* and *cd*, ϕ'' for *da*. For the consecutive gauche sequence of opposite sign, $G^{\pm}G^{\mp}$, ω with a corresponding number of primes are defined in the same way as ϕ.

For each model compound, the conformers listed in

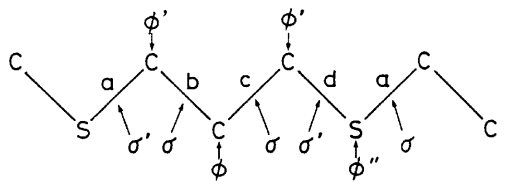

Fig. 1. Alphabetical notation of the skeletal bond and the statistical weight parameters of poly(thiotrimethylene).

Table 2. Geometric Parameters of Poly(thiotrimethylene) Obtained from Various Model Compounds; for Abbreviations of Compounds See Text

Compound	$l_{C\text{-}S}$/Å	$l_{C\text{-}C}$/Å	∠CSC/°	∠SCC/°	∠CCC/°	$\psi_{CC\text{-}SC}$/°		$\psi_{SC\text{-}CC}$/°	
						T	G	T	G
4T	1.829	1.539	101.4	109.9	112.5	−0.1	112.7	2.6	112.8
6T	1.832	1.536	101.6	109.5	111.9	1.0	114.0	1.8	115.0
8T	1.830	1.539	101.3	109.5	111.8	0.3	111.9	1.0	115.0
10T	1.833	1.537	101.2	109.4	111.6	0.2	114.7	0.7	116.0
12T	1.831	1.538	101.2	109.5	111.5	0.0	114.3	0.6	115.4
16T	1.831	1.538	101.0	109.5	111.4	−0.3	114.4	0.3	115.4

Table 1 and include the same first- or second-order interactions are averaged: for example, $E_\sigma+E_{\sigma'}+E_{\phi'}=$ 1.063 kJ mol^{-1} is obtained from TTTTTTGG and TTTTGGTT of **8T**, etc.; then, the obtained simultaneous equations containing eight variables are solved.[10] The obtained statistical-weight parameters are listed in Table 3. Figure 2 shows the variation of E_σ and E_ϕ with no or one prime, and E_ϕ with two primes against the chain length of the model compounds. From Table 3 and Fig. 2, it is clear that the averaged values of first-order interactions, E_σ and $E_{\sigma'}$, assume minima in **8T**; these values increase gradually. This may be caused by a progressive increase of the steric repulsions between bulky substituents when the sole gauche happens to appear in the inner position of the chains. The second-order interaction parameters, E_ϕ, $E_{\phi'}$, and $E_{\phi''}$, decrease with an increase in the chain length with some vibrations. Comparing the first-order interaction energies of poly(oxytrimethylene), i.e. $E_\sigma=-1.67$, $E_{\sigma'}=3.26$ kJ mol^{-1},[13] they are significantly different from those of poly(thiotrimethylene). Even the sequence of E_σ and $E_{\sigma'}$, is reverse. This is due to the same reason mentioned in the previous section. These results show the characteristic fact that the "sulfur gauche effect" is significantly different from the "oxygen gauche effect." The "oxygen gauche effect" causes gauche states about the central bond of CC-CO to be much lower in energy than trans. Compared with this, the "gauche effect" by a sulfur atom seems to be diminished. The second-order interaction energies of poly(oxytrimethylene), i.e. $E_\phi=1.09$, $E_{\phi'}=-0.63$, $E_{\phi''}=0.46$, $E_\omega=9.87$, $E_{\omega'}=6.65$, and $E_{\omega''}=3.22$ kJ mol^{-1},[13] are also different from those of poly(thiotrimethylene). The second-order interaction energies for $G^\pm G^\pm$ of poly(thiotrimethylene), i.e. E_ϕ, $E_{\phi'}$, and $E_{\phi''}$, are all smaller and almost all have negative values. The small values of the second-order interaction energies are caused by the long bond length of C-S, and the stabilization by the helical structure formation (as mentioned before). These small second-order interaction energies are regarded as a metamorphosed "gauche effect." Namely, although an isolate gauche of poly(thiotrimethylene) is unstable, the conformers which include consecutive gauche states lower the conformation energy. These results are strongly supported by the fact that the crystalline-state configuration of poly(thiotrimethylene) has been reported to be $[G^\pm G^\pm G^\pm G^\pm]$.[36]

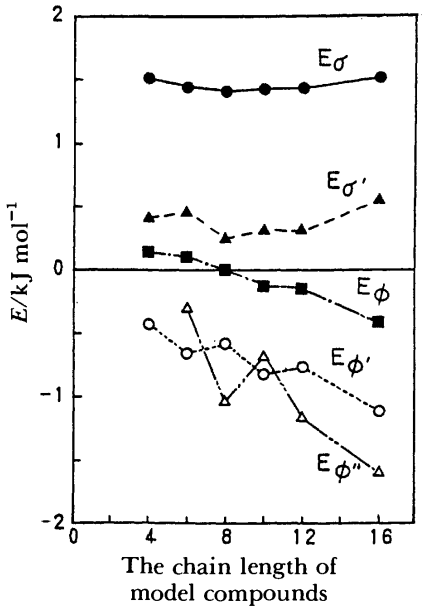

Fig. 2. The variation of statistical weight parameters plotted against the chain length of model compounds of poly(thiotrimethylene).

Unperturbed Dimensions and Dipole Moment. The characteristic ratios, dipole moment ratios and their temperature coefficients, which are calculated by means of the geometric and statistical weight parameters listed in Tables 2 and 3, are plotted in Figs. 3 and 4 against the chain length of the model compounds. Figure 3 shows the unperturbed dimension and its temperature coefficient of poly(thiotrimethylene) with infinite chain length; i.e. more than 500 in degree of polymerization. Figure 4 shows the dipole moment ratio and its temperature coefficient. The characteristic ratio takes a minimum at **8T**, then increases until **12T** and remains on the same level at **16T**. Although its temperature coefficient also takes a minimum at **8T** and shows a similar tendency, its variation with the chain length is larger than that of the characteristic ratio. Because these configuration-dependent properties have not been observed experimentally, the quality of the calculated results could not be ascertained. The

Table 3. Statistical Weight Parameters of Poly(thiotrimethylene) Obtained from Various Model Compounds; for Notation of Statistical Weight Parameters E_σ, E_ϕ, E_ω with and without Primes, See Text

Compound	E_σ	$E_{\sigma'}$	E_ϕ	E_ω	$E_{\phi'}$	$E_{\omega'}$	$E_{\phi''}$	$E_{\omega''}$
	kJ mol^{-1}	kJ mol^{-1}	kJ mol^{-1}	kJ mol^{-1}	kJ mol^{-1}	kJ mol^{-1}	kJ mol^{-1}	kJ mol^{-1}
4T	1.506	0.406	0.142	9.368	−0.431	8.782	—	—
6T	1.439	0.452	0.150	9.142	−0.657	8.632	−0.305	3.397
8T	1.402	0.243	−0.004	9.406	−0.582	4.222	−1.042	3.050
10T	1.423	0.314	−0.130	9.176	−0.824	76.877	−0.682	3.301
12T	1.427	0.301	−0.151	9.502	−0.766	8.958	−1.163	91.391
16T	1.515	0.548	−0.414	9.681	−1.117	7.255	−1.594	43.024

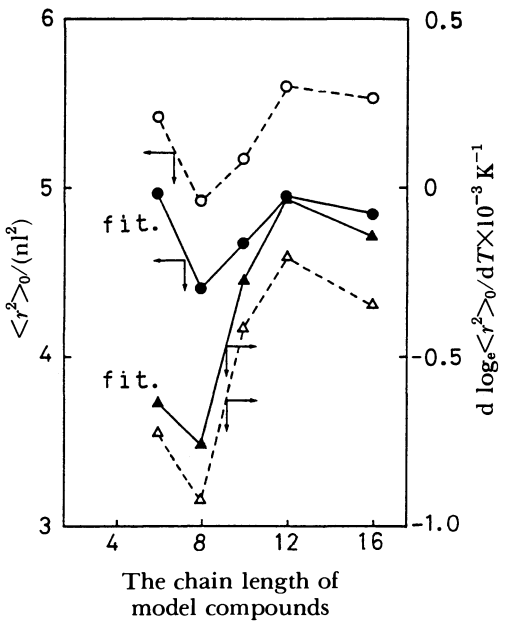

Fig. 3. The dependence of the characteristic ratio and its temperature coefficient of poly(thiotrimethylene) on the chain length of model compounds. Filled circles and filled triangles denote the results after fitting procedure, see text.

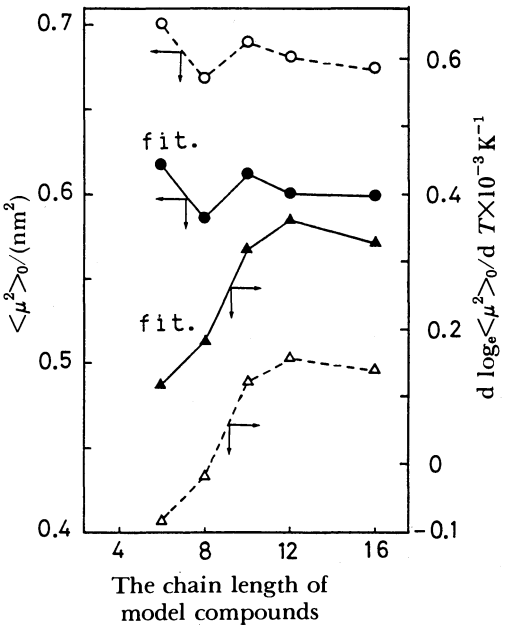

Fig. 4. The dependence of the dipole moment ratio and its temperature coefficient of poly(thiotrimethylene) on the chain length of model compounds. Filled circles and filled triangles denote the results after fitting procedure, see text.

dipole moment ratio becomes minimum at **8T** and increases at **10T**, then slightly decreases with an increase in the chain length to **16T**. Although its temperature coefficient increases from **6T** to **12T**, and remains on the same level at **16T**, the differences between the model compounds from **10T** to **16T** are small. From the variation of configuration-dependent properties with the chain length of model compounds, because these values become almost same at more than **10T** or **12T** and near to observed values, such sizes of molecules seem to be appropriate to the model compound of poly(thiotrimethylene).

In earlier calculations, Guzman et al.[8] obtained $\langle\mu^2\rangle_0/(\mathrm{nm}^2)=0.691$ and $d\log_e(\langle\mu^2\rangle_0)/dT=-0.08\times10^{-3}$ K^{-1} by means of a three-state approximation and $\langle\mu^2\rangle_0/(\mathrm{nm}^2)=0.63$, $d\log_e(\langle\mu^2\rangle_0)/dT=-0.2\times10^{-3}$ K^{-1} by means of a five-state approximation. Although the dipole moment ratio $\langle\mu^2\rangle_0/(\mathrm{nm}^2)$ calculated by means of the five-state approximation is closer to the observed value, i.e. $\langle\mu^2\rangle_0/(\mathrm{nm}^2)=0.598$ (at 20 °C), than that calculated by their three-state approximation, the temperature dependence of the dipole moment by five-state is more different from the observed value ($d\log_e(\langle\mu^2\rangle_0)/dT=1.2\times10^{-3}$ K^{-1}) than that by their three-state. Their first-order interaction energies are $E_\sigma=0.38$ and $E_{\sigma'}=0.46$ kJ mol^{-1}, which had been derived by Welsh et al.[2] They had concluded that all of the skeletal bonds of poly(thiotrimethylene) should have gauche and trans states of essentially the same energy (within 0.4 kJ mol^{-1}); therefore, this molecule may be an interesting approximation to the "freely-rotating" chain used as a highly idealized reference state in configurational analysis.[2] If this polymer is regarded as an ideal "freely-rotating" chain, the temperature coefficients of square moments should be almost zero because of an equal probability of rotational states about the skeletal bonds. The observed temperature coefficient of the dipole moment is, however, too large to regard this polymer as such a chain. Thus, the discrepancy between the observed and their calculated temperature coefficients (almost zero in their three-state approximation) are large.

In contrast to these results, the values of the dipole moment ratio calculated in this study lies between the value calculated by the earlier three-state approximation and that by the five-state calculation. These calculated ratios agree better than that of the previous three-state. The temperature coefficients calculated by the earlier three- and five-state approximations are different, even in the sign. On the other hand, the calculated values in this study become close to the observed one. Considering that the dipole moments are not experimentally observed in the exact unperturbed state, and comparing the results obtained in this study with those obtained by an earlier three- or five-state approximation, the calculations in this study give much more satisfactory results.

As a trial, the geometric parameters obtained from the model compound **8T** were changed while seeking a parameter set which gives a better agreement with the experimentally observed configuration-dependent properties. The bond angles and the dihedral angles of trans and gauche are changed alone or in combination with them by ±5° or ±10° from the original angles

of Table 2, respectively. When the bond angle of CCS decrease by 5° and the torsional angles of CC-SC with both trans and gauche increase by 10°, the best agreement is obtained. Likewise by adding 5° to the bond angle of CCS and 10° to the torsional angles of the trans and gauche of CC-SC, the dipole moment ratios and the temperature coefficients of each model compound calculated by the new geometric parameters and are also shown in Fig. 4. The characteristic ratio and its temperature coefficient are shown in Fig. 3. The calculated values using revised geometric parameters are denoted by *"fit."* in Figs. 3 and 4. Although the general tendencies are similar to those obtained by unchanged geometric parameters, the characteristic ratios and dipole moment ratios become small and their temperature coefficients become large. Using the parameters obtained from the model compounds which are longer than **12T**, the calculated dipole moment ratios, i.e. $\langle\mu^2\rangle_0/(nm^2)=0.612$ at **10T**, 0.600 at **12T** and 0.599 at **16T**, are in fairly good agreement with the observed value of 0.598 at 20 °C and 0.608 at 30 °C. Although the temperature coefficients of the dipole moment, $d\log_e\langle\mu^2\rangle_0/dT=0.32\times10^{-3}K^{-1}$ at **10T**, 0.36×10^{-3} K^{-1} at **12T**, and 0.33×10^{-3} K^{-1} at **16T** are even smaller than the experimentally obtained value of 1.2×10^{-3} K^{-1}, they are much larger and closer to the experimental value than that previously calculated. It is noteworthy that the statistical weight parameters are left unchanged throughout this rough fitting procedure. In this case, the model compounds of **10T** to **16T** also seems to be suitable; especially the model compound of **12T** gives the best results. The model compound of **10T** includes two thiotrimethylene units with terminal ethyl groups. Model compounds **12T** and **16T** include, respectively, three and four repeating units with terminal methyl groups. Therefore, model compounds of the polymer containing more than three repeating units are available. When model compounds containing two repeating units are used, the larger terminal groups are recommended. From these discussions, it is found that the parameters directly derived from the results of molecular mechanics calculations on the model compounds lead to a good agreement between experimental and calculated configuration-dependent properties. Also, a better agreement is obtained by varying the geometric parameters to fit the calculated configuration-dependent properties to the experimental values. Then, a method combining molecular and statistical mechanics is successful for poly(thioalkylenes), just as is the case for poly(oxyalkylenes).

The authors wish to thank Prof. Dr. Eiji Osawa of Hokkaido University for a kind gift of the MM2 program. They also wish to thank Prof. Dr. Yoshio Imamura of the Science University of Tokyo for his valuable advice and guidance.

References

1) E. Riande, S. Boileau, P. Hemery, and J.E. Mark, *J. Chem. Phys.*, **71**, 4206 (1979).
2) W. J. Welsh, J. E. Mark, and E. Riande, *Polym. J.*, **12**, 467 (1980).
3) A. Abe, *Macromolecules*, **13**, 541 (1980).
4) A. Abe, *Macromolecules*, **13**, 546 (1980).
5) E. Riande and J. Guzman, *Macromolecules*, **14**, 1234 (1981).
6) E. Riande, J. Guzman, W. J. Welsh, and J. E. Mark, *Makromol. Chem.*, **183**, 2555 (1982).
7) W. J. Welsh, J. E. Mark, J. Guzman, and E. Riande, *Makromol. Chem.*, **182**, 2565 (1982).
8) J. Guzman, E. Riande, W. J. Welsh, and J. E. Mark, *Makromol. Chem.*, **183**, 2573 (1982).
9) A. Abe and J. E. Mark, *J. Am. Chem. Soc.*, **98**, 6468 (1976).
10) T. Miyasaka, Y. Kinai, and Y. Imamura, *Makromol. Chem.*, **182**, 3533 (1981).
11) T. Miyasaka, T. Yoshida, and Y. Imamura, *Rep. Prog. Polym. Phys. Jpn.*, **25**, 47 (1982).
12) T. Miyasaka, T. Yoshida, and Y. Imamura, *Makromol. Chem.*, **184**, 1285 (1983).
13) T. Miyasaka, T. Yoshida, and Y. Imamura, *Makromol. Chem.*, **187**, 1515 (1986).
14) T. Uchida and H. Tadokoro, *J. Polym. Sci., A-2: Polym. Phys.*, **5**, 63 (1967).
15) H. Kakida, D. Makino, Y. Chatani, M. Kobayashi, and H. Tadokoro, *Macromolecules*, **3**, 569 (1970).
16) H. Matsuura and K. Fukuhara, *J. Polym. Sci., B: Polym. Phys.*, **24**, 1383 (1986).
17) N. L. Allinger and D. Y. Chung, *J. Am. Chem. Soc.*, **98**, 6798 (1976).
18) K. Tai and H. Tadokoro, *Macromolecules*, **7**, 507 (1974).
19) H. Matsuura and H. Murata, *Bull. Chem. Soc. Jpn.*, **55**, 2835 (1982).
20) H. Matsuura, J. Matsumoto, and H. Murata, *Spectrochim. Acta, Part A*, **36A**, 291 (1980).
21) Y. Ogawa, M. Ohta, M. Sakakibara, H. Matsuura, I. Harada, and T. Shimanouchi, *Bull. Chem. Soc. Jpn.*, **50**, 650 (1977).
22) E. Osawa and Y. Mochizuki, *Kagaku*, **40**, 703 (1985).
23) H. A. Scheraga, *Adv. Phys. Org. Chem.*, **6**,103 (1968).
24) D. Hall and N. Pavitt, *J. Comput. Chem.*, **5**, 441 (1984).
25) A. T. Hageler and S. Lifson, *Acta Crystallogr., Sect. B*, **30**, 1336 (1974).
26) A. Warshel, E. Huler, D. Rabinovich, and Z. Shakked, *J. Mol. Struct.*, **23**, 175 (1974).
27) H. Tadokoro, K. Tai, M. Yokoyama, and M. Kobayashi, *J. Polym. Sci., Polym. Phys. Ed.*, **11**, 825 (1973).
28) D. E. Williams, *Acta Crystallogr., Sect. A*, **36**, 715 (1980).
29) T. Shimanouchi, "The Molecular Force Field" in "Physical Chemistry, An Advanced Treatise," ed. by H. Eyring, D. Henderson, and W. Jost, Academic Press, New York (1970), Vol. IV, Chap. 6, pp. 233—306.
30) E. M. Engler, J. D. Andose, and P. von R. Schleyer, *J. Am. Chem. Soc.*, **95**, 8005 (1973).
31) S. Chang, D. McNally, S. SharyTehrany, M. J. Hickey, and R. H. Boyd, *J. Am. Chem. Soc.*, **92**, 3109 (1970).

32) N. L. Allinger, *J. Am. Chem. Soc.*, **99**, 8127 (1977).
33) Quantum Chemistry Program Exchange, Department of Chemistry, Indiana University, Blomington, Indiana, 47405, U.S.A.
34) Microsoft Disk Operation System. MS is a registered trademark of Microsoft Corporation.
35) This revised program was provided us by Prof. Dr. Eiji Osawa of Hokkaido University.
36) H. Sakakihara, Y. Takahashi, and H. Tadokoro, Preprints, SPSJ Symposium on Macromol., The Soc. of Polym. Sci., Jpn. Tokyo, November 11—13, **1969**, 11B11, p. 407.

Possibility of Superconducting and Other Phases in Organic High Polymers of Polyacene Carbon Skeletons. I. Screened Electron-Electron Interaction—Random Phase Approximation—

Minoru KIMURA,* Hiroyuki KAWABE,† Akihiko NAKAJIMA,† Kiyoshi NISHIKAWA,† and Shigeyuki AONO†
Department of Physics, Faculty of Science, Kanazawa University, Marunouchi, Kanazawa, Ishikawa 920
†Department of Chemistry, Faculty of Science, Kanazawa University, Marunouchi, Kanazawa, Ishikawa 920
(Received June 20, 1988)

The effective electron-electron interaction in the high polymers of polyacene carbon skeleton is investigated. The appearance of various phases in this system depends on associated parameters characterizing the electron-electron interactions near the Fermi level. The main purpose of this work is to estimate these parameters under the random phase approximation and to presume whether this polymer may or may not be superconductor at room temperature.

In studies of the high temperature superconductivity, many one- or two-dimensional models have been proposed and the probability of it was discussed.[1,2] We also studied, in our previous reports,[3,4] various phases of polyacene, especially its superconducting phase, which is quasi-one-dimensional system. We have stressed that a characteristic band structure near the Fermi surface of the present system leads to preferable properties to usual one-dimensional models in some points. For example, the gap and the transition temperature are proportional to the exponential of coupling constants in the BCS model for metal:[5]

$$\Delta = \omega_D \exp\left(\frac{-1}{\nu_F |g|}\right), \tag{1}$$

$$T_c = \omega_D \frac{\gamma}{\pi} \exp\left(\frac{-1}{\nu_F |g|}\right). \tag{2}$$

These are due to the linear dispersion of band structure near the Fermi surface. On the other hand, the quadratic dispersion of band structure in polyacene yields,[4]

$$\Delta = \frac{K^2}{4\pi^2 t} \lambda^2, \tag{3}$$

$$T_c = \frac{Z^2}{4t} \lambda^2, \tag{4}$$

where t is the transfer integral between adjacent sites, λ the characteristic parameter responsible for the phase transition (see Eq. 22), K and Z being the positive numerical factors of order 1 (the precise form is given in Ref. 4). The relations, (3) and (4) suggest that polyacene has a more extended region of superconducting phase than that in metal.

We have applied g-ology to our system, which parametrizes the interaction matrix elements near the Fermi momentum ($k=\pi$). In the present work, we estimate the g value numerically and wish to determine the phases of polyacene. In the BCS theory the superconducting phase occurs for negative g value, arising from the electron-phonon interaction. If the latter be replaced by any electronic process, even in the BCS superconductor, the Debye frequency in Eq. 2 is replaced by the associated electronic frequency, so that the critical temperature would be expected to be ten or hundred times larger. To make this be realized, we consider the system composed of the side chains attached to the both sides of polyacene skeleton (Fig 1). This is nothing but the idea proposed by Little.[8]

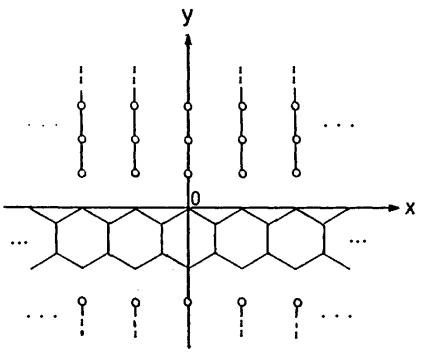

Fig. 1. Polyacene with side chains.

Single Particle States of Polyacene

We consider the transfer integral t between only the adjacent sites. In the case without bond alternation, the Hamiltonian is

$$H_0 = t\sum_n (a_{n1}^+ a_{n2} + a_{n2}^+ a_{n3} + a_{n4}^+ a_{n3} + \text{h.c.}) + t\sum_n (a_{n+1,1}^+ a_{n2} + a_{n+1,4}^+ a_{n3} + \text{h.c.}). \tag{5}$$

Here a_{nr}^+ (a_{nr}) is the creation (annihilation) operator of an electron at r-site of n-th unit cell (see Fig. 2). Because of the periodic property of polymer, the Born

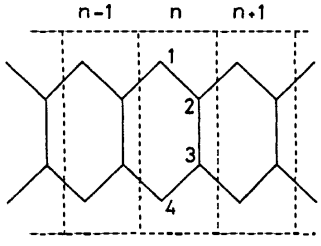

Fig. 2. Polyacene skeleton with the site and cell numbers.

von-Karman condition leads to

$$H_0 = t\sum_k \{(1+e^{-ik})\,(a_{k1}^+ a_{k2} + a_{k4}^+ a_{k3}) + a_{k2}^+ a_{k3} + \text{h.c.}\}, \tag{6}$$

where, for example, a_{ki} is the Fourier transform of a_{ni}:

$$a_{ki} = \sum_n e^{-ikn}\, a_{ni}. \tag{7}$$

The spectrum is composed of four bands given by

$$\begin{aligned}
\varepsilon_{c'}(k) &= \frac{-t}{2}\{1 + s(k)\}\ , \\
\varepsilon_{c}(k) &= \frac{t}{2}\{1 - s(k)\}\ , \\
\varepsilon_{v}(k) &= \frac{-t}{2}\{1 - s(k)\}\ , \\
\varepsilon_{v'}(k) &= \frac{t}{2}\{1 + s(k)\}\ ,
\end{aligned} \tag{8}$$

with

$$s(k) = \sqrt{9 + 8\cos k}\ , \tag{9}$$

and LCAO coefficients for atomic sites are

$$\|U_{rb}(k)\| = \begin{bmatrix} N_{c'} & N_c & N_v & N_{v'} \\ -N_{c'}\varepsilon_{c'}/\tilde{t}_k & -N_c\varepsilon_c/\tilde{t}_k & -N_v\varepsilon_v/\tilde{t}_k & -N_{v'}\varepsilon_{v'}/\tilde{t}_k \\ N_{c'}\varepsilon_{c'}/\tilde{t}_k & -N_c\varepsilon_c/\tilde{t}_k & N_v\varepsilon_v/\tilde{t}_k & -N_{v'}\varepsilon_{v'}/\tilde{t}_k \\ -N_{c'} & N_c & -N_v & N_{v'} \end{bmatrix}, \tag{10}$$

where

$$N_b^2 = \frac{|\tilde{t}_k|^2}{2[|\tilde{t}_k|^2 + \varepsilon_b^2]}\ ,\quad \tilde{t}_k^{-1} = \frac{e^{ik/2}}{2t\cos(k/2)}\ . \tag{11}$$

In the above the column refers to the site, while the row to the level.

Instability

The interaction Hamiltonian H_{int} is written as

$$H_{\text{int}} = \frac{1}{4}\sum_{ijkl}\sum_{\alpha\beta\gamma\delta} \Gamma_{\alpha\beta\gamma\delta}^{ijkl}\, a_{i\alpha}^+ a_{j\beta}^+ a_{k\gamma} a_{l\delta}, \tag{12}$$

where Γ is the bare vertex part:

$$\Gamma_{\alpha\beta\gamma\delta}^{ijkl} = \langle i_\alpha j_\beta | k_\gamma l_\delta\rangle \delta_{\alpha\delta}\delta_{\beta\gamma} - \langle i_\alpha j_\beta | l_\delta k_\gamma\rangle \delta_{\alpha\gamma}\delta_{\beta\delta}, \tag{13}$$

with

$$\langle i_\alpha j_\beta\, | k_\beta l_\alpha\rangle = \int d r_1\, d r_2 \phi_{i\alpha}^*(r_1)\phi_{j\beta}^*(r_2) V(r_1, r_2)\phi_{k\beta}(r_2)\phi_{l\alpha}(r_1)\,. \tag{13a}$$

In order to consider the phase transition, we take into account only of v (the highest valence) and c (the lowest conduction) bands. Thus we obtain

$$\begin{aligned}
H_{int} = \frac{1}{4}\sum_{p_1p_2p_3p_4} \delta(p_1+p_2, p_3+p_4)[&\Gamma_{\alpha\beta\gamma\delta}^{vvvv} a_{vp_1\alpha}^+ a_{vp_2\beta}^+ a_{vp_3\gamma} a_{vp_4\delta} \\
&+ \Gamma_{\alpha\beta\gamma\delta}^{vvcc} a_{vp_1\alpha}^+ a_{vp_2\beta}^+ a_{cp_3\gamma} a_{cp_4\delta} \\
&+ 2\Gamma_{\alpha\beta\gamma\delta}^{vcvc} a_{vp_1\alpha}^+ a_{cp_2\beta}^+ a_{vp_3\gamma} a_{cp_4\delta} + (v\leftrightarrow c)].
\end{aligned} \tag{14}$$

Γ's are given by

$$\begin{aligned}
\Gamma_{\alpha\beta\gamma\delta}^{vvvv} &= \Gamma_{\alpha\beta\gamma\delta}^{cccc} = g_1(\delta_{\alpha\delta}\delta_{\beta\gamma} - \delta_{\alpha\gamma}\delta_{\beta\delta}), \\
\Gamma_{\alpha\beta\gamma\delta}^{vvcc} &= \Gamma_{\alpha\beta\gamma\delta}^{ccvv} = g_2(\delta_{\alpha\delta}\delta_{\beta\gamma} - \delta_{\alpha\gamma}\delta_{\beta\delta}), \\
\Gamma_{\alpha\beta\gamma\delta}^{vcvc} &= \Gamma_{\alpha\beta\gamma\delta}^{cvcv} = g_3\delta_{\alpha\delta}\delta_{\beta\gamma} - g_4\delta_{\alpha\gamma}\delta_{\beta\delta},
\end{aligned} \tag{15}$$

with

$$\begin{aligned}
g_1 &= \langle vv|vv\rangle = \langle cc|cc\rangle, \\
g_2 &= \langle vv|cc\rangle = \langle cc|vv\rangle, \\
g_3 &= \langle vc|vc\rangle = \langle cv|cv\rangle, \\
g_4 &= \langle vc|cv\rangle = \langle cv|vc\rangle.
\end{aligned} \tag{16}$$

Since two-body collisions near the Fermi surface play an important role, we have, in the above, constant matrix elements at the Fermi surface. For example, g_1 is given by

$$g_1 = \int d r_1 d r_2 \phi_{vk_F}^*(r_1)\phi_{vk_F}^*(r_2) V(r_1, r_2)\phi_{vk_F}(r_2)\phi_{vk_F}(r_1)\,, \tag{17}$$

where ϕ_{vk_F} is a single-particle wave function for the valence band at the Fermi surface. As will be seen in the following, electrons near Fermi level localize almost at the 1- or 4-site. Therefore it is expected that electrons passing along edges of skeleton are strongly influenced by the polarized side chains around the spine (see Fig. 1). When $k=k_F=\pi$, Eq. 10 leads for ϕ_{vk} and ϕ_{ck} to

$$\begin{aligned}
\phi_{vk} &= 2^{-1/2}(\chi_{k1} - \chi_{k4}), \\
\phi_{ck} &= 2^{-1/2}(\chi_{k1} + \chi_{k4}),
\end{aligned} \tag{18}$$

where χ_{k1} is the Fourier transform of the Wanier function at site-1 of n-th cell. Namely,

$$\begin{aligned}
\phi_{vk} &= (2L)^{-1/2}\sum_n (x_{n1} - x_{n4})\, e^{ikn}, \\
\phi_{ck} &= (2L)^{-1/2}\sum_n (x_{n1} + x_{n4})\, e^{ikn}.
\end{aligned} \tag{19}$$

Moreover we neglect all differential overlaps. As a result, Eq. 17 turns out to be

$$\begin{aligned}
g_1 &= \frac{1}{(2L)^2}\int d r_1 d r_2 \sum_{m,n} V(r_1, r_2) \\
&\quad \times [\,|x_{m1}(r_1)|^2 + |x_{m4}(r_1)|^2\,][\,|x_{n1}(r_2)|^2 + |x_{n4}(r_2)|^2\,] \\
&= \frac{1}{(2L)^2}\sum_{m,n}(V_{m1,n1} + V_{m1,n4} + V_{m4,n1} + V_{m4,n4})\,.
\end{aligned} \tag{20}$$

Each matrix element depends on the difference, $m-n$, so that we give

$$\begin{aligned}
g_1 &= \frac{1}{2L}\sum_n (V_{01,n1} + V_{01,n4}), \\
g_2 &= \frac{1}{2L}\sum_n (V_{01,n1} - V_{01,n4}), \\
g_3 &= \frac{1}{2L}\sum_n (V_{01,n1} - V_{01,n4}), \\
g_4 &= \frac{1}{2L}\sum_n (V_{01,n1} + V_{01,n4}).
\end{aligned} \tag{21}$$

Let us denote that[4]

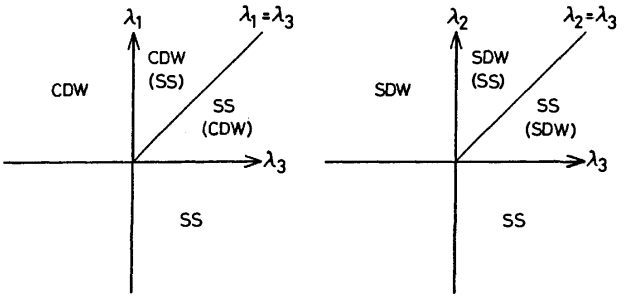

Fig. 3. Phase diagrams for polyacene.

$$\lambda_1 = -g_2 - 2g_3 + g_4,$$
$$\lambda_2 = g_2 + g_4,$$
$$\lambda_3 = -g_1 - g_2. \tag{22}$$

In the previous paper,[4] we have derived the phase diagram versus λ_1, λ_2, and λ_3 on the basis of simple mean field theory as shown in Fig. 3. Positive values of them correspond to appearance of CDW, SDW, and the singlet superconductivity (SS) phases, respectively. The figure suggests that the most possible ordered phase has the largest positive value of λ. Although the theory neglects the interference between various singular channels, we tentatively apply this result to the discussion about the model proposed by Little. In the following sections we calculate these parameters numerically.

Effective Interaction

The screening effect for the electron-electron interaction in the spine near the Fermi surface by electrons in the spine and in the polarized side chains is treated by the perturbation method as shown in Fig. 4. The double wavy line describes the effective interaction, $\tilde{V}_{\text{eff}}$, and the sigle wavy line the bare interation, V_{bare}. For V_{bare}, we adopt the Nishimoto-Mataga potential:

$$V_{\text{bare}} = \frac{14.40}{R_{rs}(n) + 1.33}\ (\text{eV}), \tag{23}$$

where $R_{rs}(n)$ is the distance from r-site of 0-th cell to s-site of n-th cell (in the unit of Å). The calculations were carried out using the following units: the bond length of benzene, 1.4 Å, for distances and the absolute value of the transfer integral, 2.5 eV, for energies. The shaded part of Fig. 4 displays the proper polarization part which includes various processes. We approximate it by the first two diagrams as shown in Fig. 4.

The Dyson equation for $\tilde{V}_{\text{eff}}$ is an integral equation in the coordinate space and is difficult to solve, but is easily manipulated in the momentum space. We take the Fourier transform of $V_{0r,ns} = V_{rs}(n)$ as

$$V_{rs}(n) = \frac{1}{L}\sum_k e^{ikn} v_{rs}(k) \tag{24}$$

and its inverse transform is

$$v_{rs}(k) = \sum_{n=-N}^{N} e^{-ikn} V_{rs}(n). \tag{25}$$

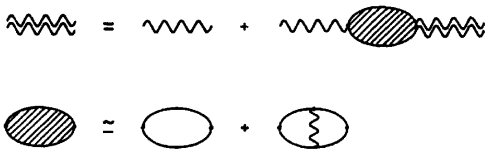

Fig. 4. The Dyson equation for electron-electron interaction and the approximation for the polarization part.

Thus the effective interaction is written in k pace as

$$\tilde{v}(k) = [1 - v(k)\Pi(k)]^{-1} v(k), \tag{26}$$

where $\tilde{v}$ and v are the effective and bare potentials, respectively. Note that each term is a matrix with respect to the atomic sites in the unit cell. We divide this into two parts, P and Q. The former refers to the spine and the latter to the side chain. Then Eq. 26 becomes[6]

$$\begin{bmatrix} \tilde{v}_{PP} & \tilde{v}_{PQ} \\ \tilde{v}_{QP} & \tilde{v}_{QQ} \end{bmatrix} = \left\{1 - \begin{bmatrix} v_{PP} & v_{PQ} \\ v_{QP} & v_{QQ} \end{bmatrix} \begin{bmatrix} \Pi_{PP} & \Pi_{PQ} \\ \Pi_{QP} & \Pi_{QQ} \end{bmatrix}\right\}^{-1} \begin{bmatrix} v_{PP} & v_{PQ} \\ v_{QP} & v_{QQ} \end{bmatrix}. \tag{27}$$

In order to proceed further, we assume $\Pi_{PQ} = \Pi_{QP} = 0$, which implies that the charge transfer between the spine and the side chain is neglected, i.e., there is a single bond between them. Thus we get

$$\tilde{v}_{PP} = [1 - v_{PP}\Pi_{PP} - v_{QP}\Pi_{QQ}(1 - v_{QQ}\Pi_{QQ})^{-1} v_{QP}\Pi_{PP}]^{-1} \times [v_{PP} + v_{PQ}\Pi_{QQ}(1 - v_{QQ}\Pi_{QQ})^{-1} v_{QP}]. \tag{28}$$

If we restrict ourselves to retain the first order term with respect to Π_{QQ}, we get

$$\tilde{v}_{\text{Little}} = (1 - v_{PP}\Pi_{PP})^{-1} v_{PP} + v_{PQ}\Pi_{QQ}v_{QP}, \tag{29}$$

which is the Little's approximation.[6]

If we employ the random phase approximation for the proper polarization part, Π, which is given by the ring diagram in Fig. 4 and denoted by Π^0, it follows that

$$\Pi^0_{sr}(k, \omega) = 2\int \frac{d\nu}{2\pi i} \frac{1}{L}\sum_q G_{sr}(k+q, \omega+\nu) G_{rs}(q, \nu). \tag{30}$$

Using the representation diagonalizing the Hamiltonian (5) and carrying out the integration, we can get

$$\Pi^0_{sr}(k, \omega) = \frac{4}{L}\sum_q \sum_b^{un} \sum_{b'}^{occ} \frac{\langle s|b, k+q\rangle\langle b, k+q|r\rangle\langle r|b', q\rangle\langle b', q|s\rangle}{\omega - \varepsilon_b(k+q) + \varepsilon_{b'}(q)}. \tag{31}$$

In the above, we consider the symmetry property of each band to the Fermi surface. In carrying out the summation with respect to q we make a small cut-off around the Fermi momentum, because electrons in this small region are responsible for the instabilities associated with phase transitions.

In order to improve the random phase approximation for the polarization part, we take into accout the oyster diagram, the second one in the right hand side

of Fig. 4. This involves four Green's functions in the integral the calculation of which requires enormous machine time. Then we are obliged to use an approximation in which the bare electron-electron interaction is restricted only to the one-center type. Thus we get

$$\Pi^1_{sr}(k) = \frac{-1}{2}\sum_t \Pi^0_{st}(k)\, v_{tt}(k)\, \Pi^0_{tr}(k)\,. \qquad (32)$$

It is said that this approximation amounts to 70—80% of the full contribution.[8]

In the following, we use the static approximation, as with $\omega=0$ in Eq. 31.

Side Chain

Since, in the present case, the polarization of the side chain plays a role of the phonon part in the ususal superconductor, it is crucial to choose a suitable side chain. We proceed our consideration along the Salem's idea.[9]

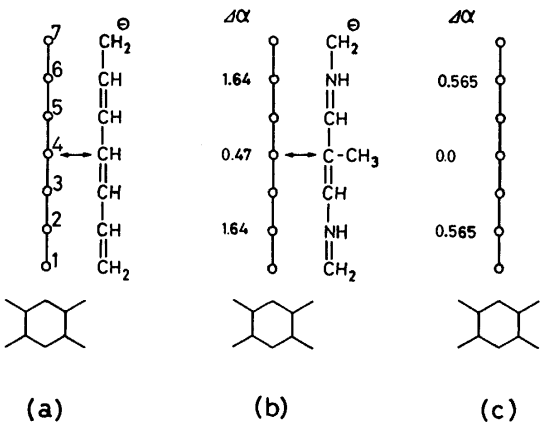

Fig. 5. Side chains. $\delta\alpha_s$ is given in the unit t. (a) Unoptimized, (b) optimized by Salem, and (c) optimized perturbatively.

As the simplest case, we take a dye molecule which is, as shown in Fig. 5a, a conjugated hydrocarbon with eight π-electrons and seven atomic sites. In this molecule, the polarization spreads all over the molecule, so that it is not so effective to reduce the electron-electron interaction on the spine. In order to make it efficient, one can introduce some substituents. Due to the well known symmetry properties of the alternant hydrocarbon, the nonbonding molecular orbital, say the 4-th one in this case, has vanishing amplitude on the even-numbered sites (called the unstarred sites). Even if we put substituents on these sites, this orbital is not affected. Therefore we can design these substituents so that the transition amplitude to the next higher level, which is expected to be most effective for polarization, shall be considerably small except for the both molecular ends.

Following this idea, Salem has obtained the one shown in Fig. 5b, exactly in the frame-work of the Hückel theory. Note that this is not unrealistic from the experimental view-points.

What mentioned above is well understood by the elementary perturbation theory, too.[7] A small perturbation at s-th site, $\delta\alpha_s$ changes the amplitude, $\langle r|i\rangle$ to $\langle r|\tilde{i}\rangle$ as

$$\langle r|\tilde{i}\rangle = \langle r|i\rangle + \sum_{j,s} \frac{\langle r|j\rangle\langle j|s\rangle\delta\alpha_s\langle s|i\rangle}{\varepsilon_i - \varepsilon_j}\,, \qquad (33)$$

where r refers to the site except the two ends, s to unstarred one and i to the lowest vacant level. The optimizing condition for the substituents is found by putting the left hand side of Eq. 33 equal to zero. The coditions obtained by the perturbation analysis are more general but less accurate than the Salem's ones. $\delta\alpha_4=0$ at the beginning, then we obtain a result given in Fig. 5c.

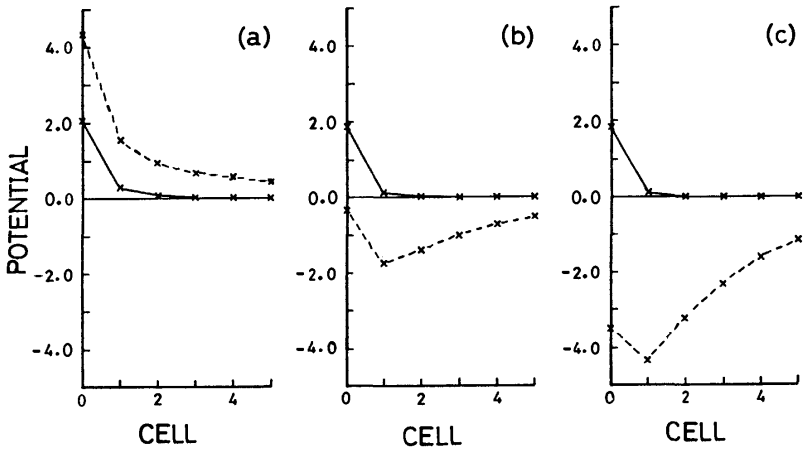

Fig. 6. The screened potential for various cases. (a) Only the spine. Dotted line is for the bare interaction and the solid line for the screened one. (b) The spine with unoptimized side chains. (c) The spine with optimized side chains by Salem. In the cases of (b) and (c), the dotted lines refer to the Little's approximation, and the solid ones to ours. For all cases, the cut-off is 0.01.

Results and Discussion

We should like to mention a little about the numerical procedures. Our final object is to get the coupling constants g_1—g_4. Since these (see Eq. 21) are the components with $k=0$ in the momentum representation, we can get them as the simple sums of coupling constants in the space representation, of course, the latters being renormalized. Suppose that we use two hundred cells in the practical calculation. Since each cell contains four atomic sites, the procedure for getting the screening effect becomes a problem of 800×800 matrix manipulation. This is considerably tedious. In the momentum space, one needs 200 4×4 matrix manipulations. In order to evaluate each term in the right hand side of Eq. 21, the inverse-Fourier transform is used.

The values of $V_{1,1}(n)$ thus obtained are shown in Fig. 6. In Fig. 6a, the screened potential (the solid line) decays very fast and becomes almost zero at the next neighbor cell. This result contrasts with that obtained by Schug et al.[10] They calculated the screened potential for $C_{57}H_{59}$ molecule only within the random phase approximation and obtained the potential which is screened in short-range region but is enhanced in long range region. This shows that for the screening effect in conjugated molecules the Π^1 effect is impotant as well as the Π^0 one. The Little's approximation (dotted lines in Figs. 6b and c) tells us that the side chain works very well to get attractive interactions, while in our higher approximation (solid lines) the potential is not attractive. The modification for the side chain does not affect the behavior qualitatively.

The above trends are shown in more detail in Table 1. It is noted that results are almost independent of cut-off parameters. In the table, every case has two lines, the upper is carried out by including Π^0 only, while the lower by including Π^0 and Π^1. The Π^1 effect is not so significant. Look at the final group. Little's approximation suggests the spine be superconducting at 900 K or higher. But our more elaborate calculation denies his conclusion. As to the side chain effect, the first order effect which is described by the Little's approximation for the polarization part in the side chain gives a considerable effect to the spine, but the higher order effects which are something like the back flows, cancel the first order effect.

We have made several trials for the shape of the side chains, e.g., some networks of the above mentioned side chains, which are constructed by introducing appropriate transfers between them. However, everything has been in vain to make the potential attractive.

Finally, our result is shown in Table 2 for the case of the spine with unoptimized side chains (other models also give qulitatively the same results.). Present result predicts that the SS state is not likely since $\lambda_3<0$ and the SDW state is more favorable than the CDW state since $\lambda_2>\lambda_1$.

Table 2. The Coupling Parameters

g_1	g_2	g_3	g_4	λ_1	λ_2	λ_3
0.059	0.004	0.004	0.059	0.046	0.063	−0.063

These are calculated for the case of the spine with unoptimized side chains. For the treatment of the side chain polarization, of course, ours is adopted. The cut-off parameter is 0.010.

Table 1. Possibility of Superconducting State

Model		Cut 0.005 λ_3	0.005 T_c	0.010 λ_3	0.010 T_c	0.015 λ_3	0.015 T_c
Only spine		−0.037		−0.038		−0.038	
		−0.068		−0.070		−0.070	
Spine with unoptimized side chain	Little	0.313	401	0.312	400	0.312	400
		0.284	364	0.283	363	0.283	363
	ours	−0.033		−0.034		−0.034	
		−0.062		−0.063		−0.063	
Spine with optimized side chain (perturbative)	Little	0.474	607	0.473	606	0.473	606
		0.452	579	0.451	578	0.451	578
	ours	−0.033		−0.034		−0.034	
		−0.062		−0.063		−0.063	
Spine with optimized side chain (Salem)	Little	0.735	941	0.734	940	0.734	940
		0.724	927	0.722	926	0.722	926
	ours	−0.033		−0.034		−0.034	
		−0.061		−0.063		−0.063	

Data of λ_3 and T_c for various models and cut-off parameters. (1) Only the spine. (2) The spine with unoptimized side chains. (3) The spine with side chains optimized perturbatively. (4) The spine with side chain optimized by Salem. Each case is separated into two treatments: Little's approximation and ours. Every one has two lines, the upper in carried out by including Π^0 only, while the lower by including Π^0 and Π^1. The unit for cut and λ_3 is t, and that for T_c is degree.

References

1) "Highly Conducting One-Dimensional Solid," ed.by J. T. Devreese, R. P. Evrard, and V. E. van Doren, Plenum, New York (1979).
2) V. L. Ginzburg, *Ann. Rev. Mater. Sci.*, **2**, 663 (1968).
3) M. Kimura, H. Kawabe, K. Nishikawa, and S. Aono, *J. Chem. Phys.*, **85**, 3090 (1986).
4) M. Kimura, H. Kawabe, K. Nishikawa, and S. Aono, *J. Chem. Phys.*, **85**, 3097 (1986).
5) J. R. Schrieffer, "Theory of Superconductivity," Benjamin, New York (1964).
6) W. A. Little, *Phys. Rev.*, **134**, A1415 (1964).
7) J. Yoshida, K. Nishikawa, and S. Aono, *Prog. Thoret. Phys.*, **50**, 830 (1973).
8) H. Gutfreund and W. A. Little, *Phys. Rev.*, **183**, 68 (1969).
9) L. Salem. *Mol. Phys.*, **11**, 499 (1966).
10) J. C. Schug, R. D. Reid, A. C. Lilly, and R. W. Dwyer, *Chem. Phys. Lett.*, **128**, 5 (1986).

 © 1988 The Chemical Society of Japan Bull. Chem. Soc. Jpn., 61, 4245—4252 (1988)

Possibility of Superconducting and Other Phases in Organic High Polymers of Polyacene Carbon Skeletons. II. Screened Electron-Electron Interaction —Method of Renormalization Group—

Minoru KIMURA,* Hiroyuki KAWABE,† Kiyoshi NISHIKAWA,† and Shigeyuki AONO†
Department of Physics, Faculty of Science, Kanazawa University, Marunouchi, Kanazawa, Ishikawa 920
†Department of Chemistry, Faculty of Science, Kanazawa University, Marunouchi, Kanazawa, Ishikawa 920
(Received June 20, 1988)

The electron-electron interaction which is crucial in determining whether new phases will arise or not in polyacene is investigated by means of the renormalization group. This approach is valuable to effectively include, from the view-point of the group theory, the higher order diagrams not taken into account in the random phase approximation of the previous work. It is found that there is a range of coupling constants where the singlet superconducting phase without simultaneous CDW ordering can be expected.

In the previous papers,[1] we have treated the electron-electron interactions in polyacene from the view-point of the random phase approximation. The system under consideration is, concretely speaking, composed of the one-dimensional polyacene skeleton (called spine) with suitable side chains. These are composed of, for instance, the dye molecules with several carbon atoms and several π-electrons.

The mechanism of phase change in our case is manipulated in terms of the highest valence band (v) and the lowest conduction band (c). The electron-electron interactions in these bands are treated to be screened as follows. We must consider two sources of screening. One is due to the excitation from the lower valence bands to the higher conduction bands inside the spine. The other is due to the excitation in the side chain. The former plays a role to reduce the long range Coulomb repulsion to a short range potential, while the latter produces attractive interaction in the spine. We assume that these two mechanisms of screening can be treated independently. In order to make the superconductivity advantageous, we attempt to optimize the side chain composition in the following manner. Replacing the carbon in the side chain by nitrogen, or replacing hydrogen by a suitable substituent group, we can make the transition amplitude between the highest occupied and lowest vacant orbitals as large as possible. This procedure leads possibly to the largest attractive interaction in the spine as expected.

Thus we might conclude that the superconducting phase be possible in this system, though an anxiety that other phases of CDW or SDW ordering overwhelm the superconducting phase remains.

As is mentioned above, the screening effect inside the spine is independent of that of the side chain, so that interference between them is disregarded. This last phenomenon seems to work unfavorably for the screening. One of the traditional approaches relies on the random phase approximation. It adopts only the ring diagrams, treating that various processes of scattering channels independently. In order to make up for these imperfections, we employ the method of renormalization group,[2,3] as one of the exellent techniques to consider the interfering channels self consistently.

This method will be, in a considerably detail, explained in Appendix and expressed in a form suitable for the present problem. Here we outline the result, which is enough to proceed with the following analysis.

The Dyson equation is invariant under a multiple renormalization of Green's function and coupling parameter (see Eq. A.3). Due to this invariance a complicated scaling procedure leads to a concept of the invariant coupling satisfying a functional equation,

$$\tilde{g}_i(y, u, g)=\tilde{g}_i(y/t, u/t, \tilde{g}(t, u, g)), \tag{1}$$

where y and u are parameters with the dimension of energy, and g is the set of original couplings, $\{g_i\}$. In order to provide practical facilities, Eq. 1 is translated to a differential equation,

$$y\frac{\partial}{\partial y}\tilde{g}_i(y,u,g)=\frac{\partial}{\partial \xi}\tilde{g}_i(\xi, u/y, \tilde{g}(t,u,g))|_{\xi=1}. \tag{2}$$

To solve the above equation, we begin with estimating the right-hand side of Eq. 2 by means of the perturbation theory. Then, if $\tilde{g}_i$ is obtained as a solution of Eq. 2, it must satisfy the group theoretical condition of the renormalization group. We can convince that through this procedure the renormalized coupling parameters are improved better than in the simple random phase approximation. These in turn provide various response functions within the same renormalization scheme.

$$y\frac{\partial}{\partial y}\ln \Lambda(y,u,g)=\frac{\partial}{\partial \xi}\ln \Lambda(\xi, u/y, \tilde{g}(y,u,g))|_{\xi=1}, \tag{3}$$

where Λ is the external vertex.

Invariant Coupling, Application to the Case of Polyacene

Preliminarily, we observe the singular behaviour of the perturbation series in the case of polyacetylene and compare it with that of polyacene, which plays an important role in discussing the ground state of the

systems. As is well known,[4,5] the terms in the perturbation series which become divergently large as the temperature is lowered are, in the case of polyacetylene:

$$\begin{aligned}&\text{I.}\quad g\ln(T/D),\ \{g\ln(T/D)\}^2,\ \cdots,\ \{g\ln(T/D)\}^n,\ \cdots,\\ &\text{II.}\quad g^2\ln(T/D),\ g\{g\ln(T/D)\}^2,\ \cdots,\\ &\text{III.}\quad g^3\ln(T/D),\ g^2\{g\ln(T/D)\}^2,\ \cdots,\\ &\cdots\cdots,\end{aligned}\tag{4}$$

where D is the band width of the conducting π-electrons. The series I is the most divergent terms, II and III, $\cdots$ being the next and further lower divergent terms. Similar behaviours of the perturbation series are well-known in another field of physics, e.g., in the case of the Kondo effect[6,7] and QED.[2] If we take into account only the most divergent series (I), the summation of series diverges at the mean-field critical temperature, T_c. If we do the next divergent series (II), the sum diverges only at the temperature of absolute zero.[5] This aspect is consistent with the theorem of absence of any phase change in a purely one-dimensional system at a finite temperature.

In the case of polyacene, however, the divergent series are not logarithmic but are classified as[1]

$$\begin{aligned}&\text{I.}\quad g(T/t)^{-1/2},\ \cdots,\ \{g(T/t)^{-1/2}\}^n,\ \cdots,\\ &\text{II.}\quad g^2(T/t)^{-1/2},\ \cdots,\ g\{g(T/t)^{-1/2}\}^n,\ \cdots,\\ &\cdots\cdots.\end{aligned}\tag{5}$$

The divergent character of this series are governed by the power law thus stronger than in the case of polyacetylene. The perturbation calculation based on the above classification becomes less accurate than the logarithmic problem. However, the renormalization group theory is still a convenient method to improve the perturbation method and obtain a qualitatively correct result.

It is noted that the most divergent series arises only in the correction of the vertex function, Γ. Zeroth order vertices are given by,[1]

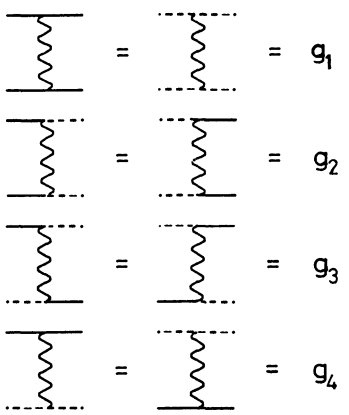

Fig. 1. Various electron–electron scattering amplitudes. The solid line represents the v-state, the dotted line the c-state and the wavy line the electron–electron interaction.

$$\begin{aligned}\Gamma^{(0)vvvv}_{\alpha\beta\gamma\delta}&=g_1(\delta_{\alpha\delta}\delta_{\beta\gamma}-\delta_{\alpha\gamma}\delta_{\beta\delta}),\\ \Gamma^{(0)vvcc}_{\alpha\beta\gamma\delta}&=g_2(\delta_{\alpha\delta}\delta_{\beta\gamma}-\delta_{\alpha\gamma}\delta_{\beta\delta}),\\ \Gamma^{(0)vcvc}_{\alpha\beta\gamma\delta}&=2(g_3\delta_{\alpha\delta}\delta_{\beta\gamma}-g_4\delta_{\alpha\gamma}\delta_{\beta\delta}),\end{aligned}\tag{6}$$

where v and c denote valence and conduction bands lying closest to the Fermi surface, respectively. α—δ are spin indices. The electron-electron interactions g_1—g_4 are shown schematically in Fig. 1.

The complete vertex function, Γ is defined in terms of the two-particle Green's function as

$$\begin{aligned}&G^{II}_{\alpha\beta\gamma\delta}(x_1,x_2,x_3,x_4)\\ &=-<T\psi_\alpha(x_1)\psi_\beta(x_2)\psi^+_\gamma(x_3)\psi^+_\delta(x_4)S>_{conn}\\ &=G_{\alpha\gamma}(x_1,x_3)G_{\beta\delta}(x_2,x_4)-G_{\alpha\delta}(x_1,x_4)G_{\beta\gamma}(x_2,x_3)\\ &\quad+\int dx_{1'}-dx_{4'}\sum_{\alpha'\beta'\gamma'\delta'}G_{\alpha\alpha'}(x_1,x_{1'})G_{\beta\beta'}(x_2,x_{2'})\\ &\quad\times\Gamma_{\alpha'\beta'\gamma'\delta'}(x_{1'},x_{2'},x_{3'},x_{4'})G_{\gamma'\gamma}(x_{3'},x_3)G_{\delta'\delta}(x_{4'},x_4),\end{aligned}\tag{7}$$

where $G_{\alpha\alpha'}$ is the electron propagator and

$$G_{\alpha\alpha'}=\delta_{\alpha\alpha'}G.\tag{8}$$

As the lowest order correction, the renormalized Γ involves the contributions described by (a)—(j) in Fig. 2. Here we present in detail, as an example, a derivation of (a) type correction in Fig. 2: Consider the second order term in the expansion of S in Eq. 7, and take the constructions which give the diagram of Fig. 2(a). Then, we have

$$\begin{aligned}&\delta G^{II}(p_1,p_2,p_3,p_4)\\ &=-\frac{1}{2}\left(-\frac{1}{4}\right)^2\int dt'dt'\Gamma^{(0)vvvv}_{\alpha'\beta'\gamma'\delta'}\Gamma^{(0)vvvv}_{\alpha''\beta''\gamma''\delta''}\\ &\quad\times<Ta_{vp_1\alpha}(t_1)a_{vp_2\beta}(t_2)\\ &\quad\times a^+_{vp_1'\alpha'}(t')a^+_{vp_2'\beta'}(t')a_{vp_3'\gamma'}(t')a_{vp_4'\delta'}(t')\\ &\quad\times a^+_{vp_1''\alpha''}(t'')a^+_{vp_2''\beta''}(t'')a_{vp_3''\gamma''}(t'')a_{vp_4''\delta''}(t'')\\ &\quad\times a^+_{vp_3\gamma}(t_3)a^+_{vp_4\delta}(t_4)>\end{aligned}\tag{9}$$

$$\begin{aligned}&=\frac{1}{2}\int dt'dt''\Gamma^{(0)vvvv}_{\alpha\beta\gamma'\delta'}\Gamma^{(0)vvvv}_{\alpha'\beta'\gamma\delta}\delta_{\alpha'\gamma'}\delta_{\beta'\delta'}\\ &\quad\times G_{vq_1}(t'-t'')G_{vq_2}(t'-t'')\\ &\quad\times G_{vp_1}(t_1-t')G_{vp_2}(t_2-t')G_{vp_3}(t''-t_3)G_{vp_4}(t''-t_4).\end{aligned}\tag{9a}$$

In Eq. 9, the summation with respect to primed variables are implied. The unprimed momentum variables are subjected to the condition of the conservation. In order to get Eq. 9a four procedures (i)—(iv) are needed. (i) Two annihilation operators representing incoming lines are combined with the succeeding creation operators to yield propagators. (ii) The last four propagators yield propagators similarly. These four propagators expressed in the last line of Eq. 9a correspond to the external four lines in Fig. 2(a). (iii) The two propagators with momenta, q_1 and q_2 are constructed from the remaining four operators (The summation with respect to q_1 and q_2 is also omitted for simplicity.). (iv)

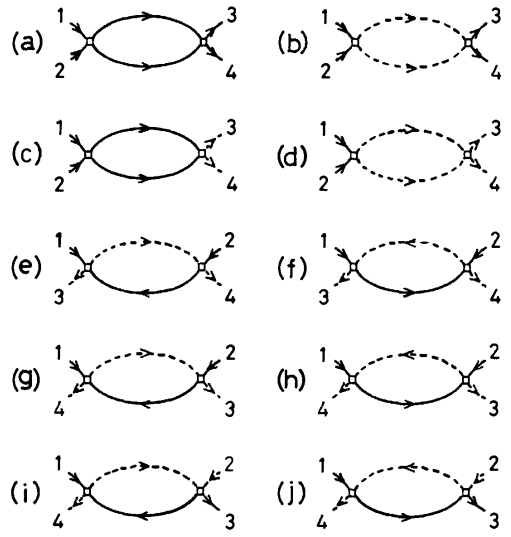

Fig. 2. Various second order corrections to Γ.

The equivalent terms are counted in following manner. The procedures (i)—(iii) are doubly possible, and further we can exchange wholly the singly primed terms for the doubly primed terms. These four procedures result in yielding sixteen equivalent terms. If we insert, in the integrand, $\delta(t_{2'}-t_{1'})$ together with an integration with respect to $t_{2'}$, we can arrange Eq. 9a in the form of Eq. 7, obtaining

$$\Gamma^{vvvv}_{\alpha\beta\gamma\delta}(a) = \frac{1}{2} T\sum G_v(q_1)G_v(q_2)\Gamma^{(0)vvvv}_{\alpha\beta\alpha'\beta'}\Gamma^{(0)vvvv}_{\alpha'\beta'\gamma\delta}$$
$$= -(\delta_{\alpha\delta}\delta_{\beta\gamma}-\delta_{\alpha\gamma}\delta_{\beta\delta})g_1^2\Pi^{vv} \tag{10a}$$

where, for example, q_1 denotes both frequency and momentum in short.

Other contributions denoted by Fig. 2 (b)—(j) are given in the following:

$$\Gamma^{vvvv}_{\alpha\beta\gamma\delta}(\mathrm{b}) = \frac{1}{2} T\sum G_c(q_1)G_c(q_2)\Gamma^{(0)vvcc}_{\alpha\beta\alpha'\beta'}\Gamma^{(0)cc\,vv}_{\alpha'\beta'\gamma\delta}$$
$$= -(\delta_{\alpha\delta}\delta_{\beta\gamma}-\delta_{\alpha\gamma}\delta_{\beta\delta})g_2^2\Pi^{vv}, \tag{10b}$$

$$\Gamma^{vvcc}_{\alpha\beta\gamma\delta}(\mathrm{c}) = \frac{1}{2} T\sum G_v(q_1)G_v(q_2)\Gamma^{(0)vvvv}_{\alpha\beta\alpha'\beta'}\Gamma^{(0)vvcc}_{\alpha'\beta'\gamma\delta}$$
$$= -(\delta_{\alpha\delta}\delta_{\beta\gamma}-\delta_{\alpha\gamma}\delta_{\beta\delta})g_1g_2\Pi^{vv}, \tag{10c}$$

$$\Gamma^{vvcc}_{\alpha\beta\gamma\delta}(\mathrm{d}) = \frac{1}{2} T\sum G_c(q_1)G_c(q_2)\Gamma^{(0)vvcc}_{\alpha\beta\alpha'\beta'}\Gamma^{(0)vvvv}_{\alpha'\beta'\gamma\delta}$$
$$= -(\delta_{\alpha\delta}\delta_{\beta\gamma}-\delta_{\alpha\gamma}\delta_{\beta\delta})g_1g_2\Pi^{vv}, \tag{10d}$$

$$\Gamma^{vvcc}_{\alpha\beta\gamma\delta}(\mathrm{e}) = \frac{1}{2} T\sum G_c(q_1)G_v(q_2)\Gamma^{(0)vvcc}_{\alpha\gamma'\gamma\beta'}\Gamma^{(0)vcvc}_{\beta\beta'\gamma'\delta}$$
$$= -\frac{1}{2}\{g_2g_3\delta_{\alpha\gamma}\delta_{\beta\delta}+g_2g_4(\delta_{\alpha\delta}\delta_{\beta\gamma}-\delta_{\alpha\gamma}\delta_{\beta\delta})\}\Pi^{vc}, \tag{10e}$$

$$\Gamma^{vvcc}_{\alpha\beta\gamma\delta}(\mathrm{f}) = \Gamma^{vvcc}_{\alpha\beta\gamma\delta}(\mathrm{e}), \tag{10f}$$

$$\Gamma^{vvcc}_{\alpha\beta\gamma\delta}(\mathrm{g}) = \frac{1}{2} T\sum G_c(q_1)G_v(q_2)\Gamma^{(0)vvcc}_{\alpha\gamma'\delta\beta'}\Gamma^{(0)vcvc}_{\beta\beta'\gamma'\gamma}$$
$$= \frac{1}{2}\{g_2g_3\delta_{\alpha\delta}\delta_{\beta\gamma}-g_2g_4(\delta_{\alpha\delta}\delta_{\beta\gamma}-\delta_{\alpha\gamma}\delta_{\beta\delta})\}\Pi^{vc}, \tag{10g}$$

$$\Gamma^{vvcc}_{\alpha\beta\gamma\delta}(\mathrm{h}) = \Gamma^{vvcc}_{\alpha\beta\gamma\delta}(\mathrm{g}), \tag{10h}$$

$$\Gamma^{vcvc}_{\alpha\beta\gamma\delta}(\mathrm{i}) = T\sum G_v(q_1)G_c(q_2)\Gamma^{(0)vvcc}_{\alpha\beta'\alpha'\delta}\Gamma^{(0)vvcc}_{\alpha'\beta\gamma\beta'}$$
$$= g_2^2\delta_{\alpha\gamma}\delta_{\beta\delta}\Pi^{vc}, \tag{10i}$$

$$\Gamma^{vcvc}_{\alpha\beta\gamma\delta}(\mathrm{j}) = T\sum G_c(q_1)G_v(q_2)\Gamma^{(0)vcvc}_{\alpha\beta'\alpha'\delta}\Gamma^{(0)vcvc}_{\alpha'\beta\gamma\beta'}$$
$$= \{2g_3(g_3-g_4)\delta_{\alpha\delta}\delta_{\beta\gamma}+g_4^2\delta_{\alpha\gamma}\delta_{\beta\delta}\}\Pi^{vc}, \tag{10j}$$

It can be shown that Γ's given in the above equations depend not only on frequency and momentum of the external line but also on temperature in general. But if every momentum and frequency concerned are much smaller than temperature, Γ's are allowed to be functions only of temperature. We are concerned with this special case in the following analysis. Whence

$$\Pi^{vv} = -\Pi^{vc} \equiv L(T) \tag{11}$$

with

$$L(T) = \frac{Z}{2(tT)^{1/2}} - \frac{1}{2\pi t p_c}, \tag{12}$$

where

$$Z = \frac{1}{(2\pi)^{1/2}}\int_0^\infty \frac{dx}{x^{1/2}\cosh^2 x}. \tag{13}$$

In Eq. 12, p_c is the cut off momentum which is smaller than the Fermi momentum (namely $tp_c \fallingdotseq t$). If temperature is smaller than any of the other variables, T in Eqs. 11 and 12 must be understood as the largest of them. At $T \fallingdotseq t$, we can see

$$L(T) \fallingdotseq 0. \tag{14}$$

Contrariwise, we should in advance adjust p_c so that Eq. 14 is held. As the contribution from the region, $|p|>p_c$, is nonsingular, we can start with the initial coupling parameter g.

Thus we can express the coupling terms, corresponding to those in Eq. 6, as

$$\Gamma^{vvvv}_{\alpha\beta\gamma\delta} = g_1\Gamma_1(\delta_{\alpha\beta}\delta_{\beta\gamma}-\delta_{\alpha\gamma}\delta_{\beta\delta}),$$
$$\Gamma^{vvcc}_{\alpha\beta\gamma\delta} = g_2\Gamma_2(\delta_{\alpha\beta}\delta_{\beta\gamma}-\delta_{\alpha\gamma}\delta_{\beta\delta}),$$
$$\Gamma^{vcvc}_{\alpha\beta\gamma\delta} = g_3\Gamma_3\delta_{\alpha\delta}\delta_{\beta\gamma}-g_4\Gamma_4\delta_{\alpha\gamma}\delta_{\beta\delta}. \tag{15}$$

In Table 1, we have tabulated the contributions of Fig. 2(a)—(j).

For the sake of convenience, we express every g_i in unit of the transfer integral t:

$$g_i/t \to g_i. \tag{16}$$

Then we have

$$L(T) \to \frac{Z}{2}\sqrt{t/T} - \frac{1}{2\pi}\sqrt{t/D} \tag{17}$$

$L(T)$ vanishes at $T=t$ as required by Eq. 14. The condition leads to

$$D = t/(\pi Z)^2. \tag{18}$$

If we remember $D=tp_c^2$, the above requirement determines the cut-off parameter p_c. For the later conven-

Table 1. Coupling Terms Versus Diagrams

$g\Gamma$	Diagram	Contribution	Total
$g_1\Gamma_1$	(a)	$-g_1^2L(T)$	$-(g_1^2+g_2^2)L(T)$
	(b)	$-g_2^2L(T)$	
$g_2\Gamma_2$	(c)	$-g_1g_2L(T)$	$g_2(-2g_1-g_3+2g_4)L(T)$
	(d)	$-g_1g_2L(T)$	
	(e)	$-g_2(g_3-2g_4)L(T)$	
	(f)		
	(g)		
	(h)		
$g_3\Gamma_3$	(j)	$-2g_3(g_3-g_4)L(T)$	$-2g_3(g_3-g_4)L(T)$
$g_4\Gamma_4$	(i)	$g_2^2L(T)$	$(g_2^2+g_4^2)L(T)$
	(j)	$g_4^2L(T)$	

ience, it is better to introduce a parameter κ to rewrite Eq. 17 as

$$L(T)=\frac{1}{2\pi}\{\sqrt{t/(\kappa T)}-\sqrt{t/D}\}, \tag{19}$$

with

$$L(t)=0. \tag{20}$$

Now we try to get the invariant coupling $\tilde{g}_i$. As long as we work within the most divergent approximation, the Green's functions are not renormalized (d=1 in Eq. A.4). But the electron-electron interaction should be:

$$\bar{g}_i=g_i\Gamma_i(y, u, g) \tag{21}$$

where, as mentioned in the previous section,

$$y=T/\lambda,\ u=t/\lambda. \tag{22}$$

As to g_1, consulting Table 1, we have

$$\bar{g}_1=g_1-(g_1^2+g_2^2)L(y, u, g) \tag{23}$$

with

$$L(y, u, g)=\frac{1}{2\pi}\{\sqrt{u/(\kappa y)}-\sqrt{u/u'}\}, \tag{24}$$

where

$$u'=D/\lambda. \tag{25}$$

Thus we have an explicit expression for the differential equation of the renormalization group, Eq. 2. Its right-hand side is

$$\begin{aligned}&\frac{\partial}{\partial\xi}\tilde{g}_1(\xi, u/y, \tilde{g}(y, u, g))\\&=\frac{\partial}{\partial\xi}[\tilde{g}_1-(\tilde{g}_1^2+\tilde{g}_2^2)\frac{1}{2\pi}\{\sqrt{(u/y)/(\kappa\xi)}-\sqrt{u/u'}\}]|_{\xi=1}\\&=\frac{1}{4\pi}\sqrt{u/(\kappa y)}\,(\tilde{g}_1^2+\tilde{g}_2^2).\end{aligned} \tag{26}$$

Then Eq. 2 becomes

$$y\frac{\partial}{\partial y}\tilde{g}_1=\frac{1}{4\pi}\sqrt{u/(\kappa y)}\,(\tilde{g}_1^2+\tilde{g}_2^2). \tag{27}$$

Transforming the variable as

$$\frac{1}{2\pi}\sqrt{u/(\kappa y)}=x, \tag{28}$$

we can rewrite Eq. 27 as

$$\frac{\partial}{\partial x}\tilde{g}_1=-(\tilde{g}_1^2+\tilde{g}_2^2). \tag{29}$$

Similar procedures are applicable to $\tilde{g}_2$—$\tilde{g}_4$ to lead to

$$\frac{\partial}{\partial x}\tilde{g}_2=\tilde{g}_2(-2\tilde{g}_1-\tilde{g}_3+2\tilde{g}_4), \tag{30}$$

$$\frac{\partial}{\partial x}\tilde{g}_3=-2\tilde{g}_3(\tilde{g}_3-\tilde{g}_4), \tag{31}$$

$$\frac{\partial}{\partial x}\tilde{g}_4=\tilde{g}_2^2+\tilde{g}_4^2 \tag{32}$$

Instabily in Polyacene, Renormalization of the External Vertex

The external vertices in the case of polyacene are corrected, up to the first order of H_{int}, as[1]

$$\begin{aligned}&\Lambda_1=1+(-g_2-2g_3+g_4)L(T),\\&\Lambda_2=1+(g_2+g_4)L(T),\\&\Lambda_3=1-(g_1+g_2)L(T),\end{aligned} \tag{33}$$

where Λ_1 refers to CDW, Λ_2 to SDW, and Λ_3 to the singlet superconductivity (SS). If we use Eq. 33 for Λ_i of the right-hand side of Eq. 3, it follows that within the most divergent approximation

$$\Lambda_1(\xi, u/y, \tilde{g}(y, u, g))=1+(-\tilde{g}_2-2\tilde{g}_3+\tilde{g}_4)L(\xi, u/y), \tag{34}$$

and from Eq. 24

$$L(\xi, u/y)=\frac{1}{2\pi}\{\sqrt{u/(\kappa y)}-\sqrt{u/u'}\}. \tag{35}$$

Since we have set L as Eq. 14, it is seen that

$$L(1, u/y)=0, \tag{36}$$

or from Eq. 35

$$L(1, u/y)=\frac{1}{2\pi}\{\sqrt{u/(\kappa y)}-\sqrt{u/u'}\}. \tag{37}$$

Thus Eq. 3 becomes

$$y\frac{\partial}{\partial y}\ln\Lambda_1=\frac{1}{4\pi}\sqrt{u/(\kappa y)}\,(\tilde{g}_2+2\tilde{g}_3-\tilde{g}_4). \tag{38}$$

Changing the variables as in Eq. 28, we get

$$\frac{\partial}{\partial x}\ln\Lambda_1=-\tilde{g}_2-2\tilde{g}_3+\tilde{g}_4. \tag{39}$$

In a similar way, we have

$$\frac{\partial}{\partial x}\ln\Lambda_2=\tilde{g}_2+\tilde{g}_4, \tag{40}$$

$$\frac{\partial}{\partial x}\ln\Lambda_3=-\tilde{g}_1-\tilde{g}_2. \tag{41}$$

Relations obtained in Eqs. 29—32 and in Eqs. 39—41 are the same as those obtained by Kimura and Mishima[8] by means of the parquet diagram sum.

Finally we should like to add a few comments about approximations employed in the present treatment. The typical higher order corrections not taken into

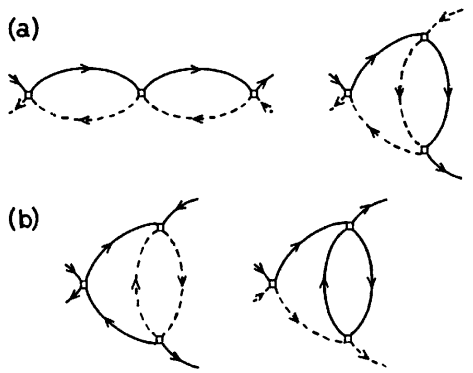

Fig. 3. Typical higher order corrections to Γ.

consideration can be expressed diagrammatically as shown in Figs. 3(a) and (b). The diagrams in Fig. 3(a) involve Π^{vc} twice (called overlap divergence), but those in Fig. 3(b) only once. Therefore, their contributions are proportional to $g^3L^2(T)$ in the former and are proportional to $g^3L(T)$ in the latter. If we use these diagrams to evaluate the right-hand side of Eq. 1, we obtain (with some constants, a and b)

$$\frac{\partial}{\partial\xi}\{\cdots + a\tilde{g}^3L^2(\xi, u/y, g) + b\tilde{g}^3L(\xi, u/y, g)\}|_{\xi=1}$$
$$= 2a\tilde{g}^3L(1, n/y, g)\frac{\partial}{\partial\xi}L(\xi, u/y, g)|_{\xi=1}$$
$$+ b\tilde{g}^3\frac{\partial}{\partial\xi}L(\xi, u/y, g)|_{\xi=1}. \tag{42}$$

Here we use Eq. 36 to get

$$\text{Eq. 42} = b\tilde{g}^3\frac{\partial}{\partial\xi}L(\xi, u/y, g)|_{\xi=1}. \tag{43}$$

Namely, the terms of overlap divergence, g^nL^m ($m\geqq 2$) have no effect on the renormalization equation (Eq. 1). These have been implicitly taken into account when the elementary divergent term ($\propto L$) is input as an initial term.

Next, we examine the approximation arising from the condition that the cut-off parameter p_c is set so that the relation (36) is held. The polarization part is expressed more exactly as

$$\Pi^{vv} = \int_{-\pi}^{\pi}\frac{dq}{2\pi}\frac{1}{2\varepsilon_q^v}\tanh\frac{\varepsilon_q^v}{2T}$$
$$\equiv L(T) + L'(T), \tag{44}$$

where

$$L(T) = \int_{-p_c}^{p_c}\frac{dq}{2\pi}\frac{1}{2\varepsilon_q^0}\tanh\frac{\varepsilon_q^0}{2T} \tag{45}$$

with

$$\varepsilon_p^0(\doteqdot\varepsilon_p^v) = tp^2, \tag{46}$$

and the residual part, L' is analyzed as

$$L'(T) = \int_{-\pi}^{\pi}\frac{dq}{2\pi}\frac{1}{2\varepsilon_q^v}\tanh\frac{\varepsilon_q^v}{2T} - \int_{-p_c}^{p_c}\frac{dq}{2\pi}\frac{1}{2\varepsilon_q^0}\tanh\frac{\varepsilon_q^0}{2T}$$
$$= \int_{-p_c}^{p_c}\frac{dq}{2\pi}\left(\frac{1}{2\varepsilon_q^v}\tanh\frac{\varepsilon_q^v}{2T} - \frac{1}{2\varepsilon_q^0}\tanh\frac{\varepsilon_q^0}{2T}\right)$$
$$+ 2\int_{p_c}^{\pi}\frac{dq}{2\pi}\frac{1}{2\varepsilon_q^v}\tanh\frac{\varepsilon_q^v}{2T}. \tag{47}$$

We can see that from the above expression, L' is regular and a slowly varying function with respect to T. Therefore, since it might be possible for us to choose g, at the beginning, so as to include the effect from L', Π in Eq. 44 is well approximated only by $L(T)$.

Solutions of Renormalization Equation

Our basic equations to look for the low-temperature phases are Eqs. 29—32 for g_i's, and Eqs. 39—41 for Λ_i's.

First, we observe that the equations are invariant under the transformations

$$\tilde{g}_i\to\lambda\tilde{g}_i,\ x\to x/\lambda, \tag{48}$$

where λ is an arbitrary constant.

The initial condition for $\tilde{g}_i$'s and Λ_i's is given at temperature $T=t$

$$\tilde{g}_i = g_i, \text{ and } \Lambda_i = 1, \tag{49}$$

according to Eq. 14. Because of the transformation property, Eq. 48, any solution for a given set of the values of g_i can be scaled into the solutions for another set of initial values λg_i.

We can obtain an analytic solution for Eqs. 29—32 only for the special case of $g_2=0$.

$$\tilde{g}_1 = \frac{1}{x + g_1^{-1}},$$
$$\tilde{g}_2 = 0,$$
$$\tilde{g}_3 = \frac{\tilde{g}_4^2}{2\tilde{g}_4 - Cg_4},$$
$$\tilde{g}_4 = \frac{-1}{x - g_4^{-1}}, \tag{50}$$

where

$$C = 2 - \frac{g_4}{g_3}. \tag{51}$$

Substituting the above into Eqs. 39—41, we obtain

$$\Lambda_1 = \frac{1}{Cg_3x + 1},$$
$$\Lambda_2 = \frac{-1}{g_4x - 1},$$
$$\Lambda_3 = \frac{1}{g_1x + 1}. \tag{52}$$

The phase diagrams corresponding to the case are shown in Figs. 4(a) and (b).

For the case of $g_2\neq 0$, the renormalization equations must be solved numerically. The resulting phase diagrams are shown in Figs. 4(c)—(i).

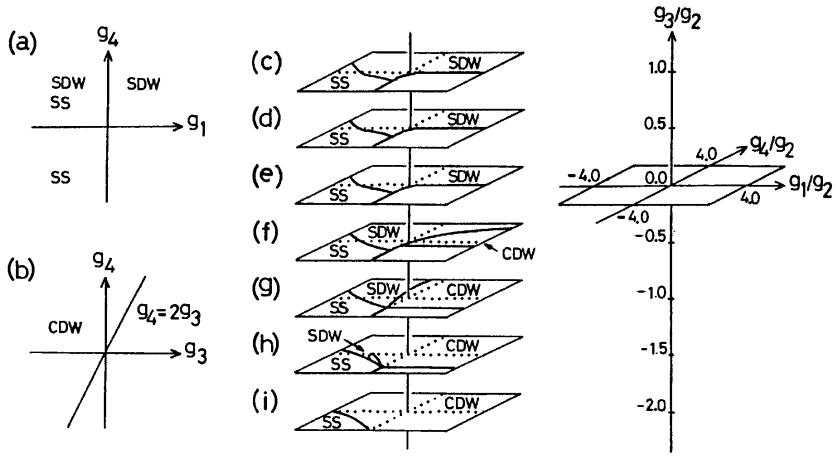

Fig. 4. Phase diagrams for various sets of g_j. (a) and (b): Those for the case of $g_2=0$. (c)—(i): Those for $g_2\neq 0$, and g_3/g_2 is 1.0, 0.5, 0.0, −0.5, −1.0, −1.5, and −2.0, respectively. The coordinate axis for them is shown on their right.

Conclusion

We have discussed the phase diagrams of the polyacene molecules in the framework of renormalization group theory within the most divergent approximation. Under this approximation the instability of the normal electronic state appears at a finite temperature.

Here, we must add some arguments for the justification of the present method. One may take a skeptical view about the validitiy of our results, considering that the renormalization group method is applicable only to a logarithmic singularity but not to a power low case. Indeed, the applications of this method thus far worked out have been fully successful for logarithmic problems.[2-5] However, we stress that the procedure to obtain the fundamental renormalization group equations is not grounded on or restricted within the logarithmic behaviour of the perturbation series, as reviewed in Appendix at some length. In the present problem, the singular terms in the perturbation series for the coupling constants are of the form

$$\tilde{g}=g+Ag^2L+Bg^3L^2+Cg^3L+\cdots, \tag{53}$$

where L is given by Eq. 19 and A, B, and C are constants. In our present analysis, we have taken only the second term of the right hand side of Eq. 53. The next order perturbation will give the third and fourth terms. The third B-term belongs to the most singular class, but does not contribute to the renormalization group equation due to the condition, Eq. 20. The effect has been included in the resultant solutions of that equation. Therefore, an overcounting of divergent diagrams does not occur. The situation is the same as in the logarithmic case. Thus the present results are justifiable within the most divergent approximation. A practical difficulty will arise to obtain the less divergent series, the C and further terms. As discussed in Ref. 1, the next divergent terms would lower the transition temperature to the absolute zero and shift the phase boundary to some extent. The correct estimation of these higher order terms is hard to manipulate because of the stronger singularity in the present problem than the logarithmic case.

The most divergent approximation gives correctly the behaviour of the dominant instabilities in the temperature region higher than the mean field transition temperatre. As for the phase diagram the present results are considered to be reliable at least qualitatively. In usual one-dimensional metals, it was found that superconductivity and CDW tend to appear simultaneously for the negative backward scattering. In the present case, however, the result shows that there is a wide range where nagative constants lead to only the superconductivity phase. In this respect the present system is expected to be more suitable to design for superconductivity.

In conclusion, the electron-electron interaction can lead to various type of ordered phases in the ground state. Such a variety of ordered phases has been observed in recent experiments about conducting organic materials such as TTF-TCNQ and BEDT-TTF where the states of superconductivity, CDW and SDW are mutually correlated and competing. Our result sheds some light on these phenomena. In this connection, we note the overlapping or adjacent appearance of superconducting and SDW states in our phase diagram, which has been discussed as the paramagnon effect in usual texts. By using the renormalization group method within g-ology, we can predict what kind of phase occurs for given interaction parameters. In the present paper, we have considered the interaction constants on the spine as parameters, which are influenced by various complex effects such as the screening by the σ-electron on the spine of polyacene and possibly, the interaction through the side-chain which may be synthesized with various

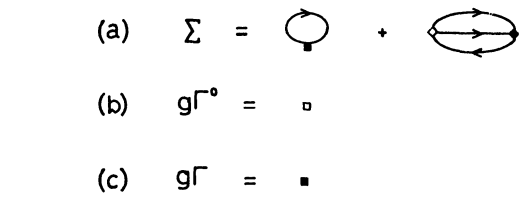

Fig. 5. Diagrammatic expressions for the self-energy and vertices. (a) Self-energy. (b) Bare vertex. (c) Full vertex.

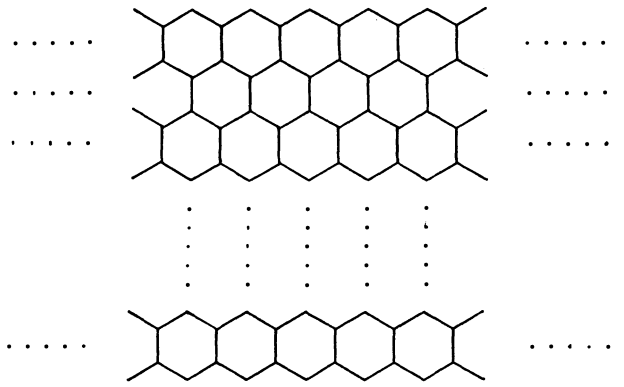

Fig. 6. Polyacene carbone skeleton.

designs. Therefore we can hope to get any phases in the ground state, if side-chains are suitably modified. The problem to analyze the effective interactions including a screening effect and an excitonic processes was discussed in our separate paper.[9]

As pointed earlier,[1,10] the π-electron energy spectrum is similar for polymers with a bridged array of an arbitrary number of polyacene skeletons (Fig. 6), i.e., the conduction- and valence bands are degenerate (or almost degenerate) at the points $k=\pm\pi$. The present theory applies equally to such a system. In the limit of an infinite number of such skeletons, however, the polymer tends to be system with a planar carbon lattice. Even in this two-dimensional lattice the degeneracy of two bands remains, but the one dimensional van Hove singularity as treated here disappears, so that $T^{-1/2}$ singularity will be weakened to the one of ln T. For the latter case many of the qualitative features of the present results remain unaltered. The detailed analysis will be reported elsewhere.

Appendix. Renormalization Group

In this appendix we reformulate the renormalization equations used in the text in a form suitable for the present analysis.[2,3] The Dyson equation for the Green's function G is written symbolically as

$$G=G^0+G^0\Sigma G, \tag{A. 1}$$

which is a matrix notation, and G^0 is for one without interaction. The self-energy part, Σ is

$$\Sigma=g\Gamma G+g\Gamma^0GGGg\Gamma, \tag{A. 2}$$

and it can be expressed diagrammatically as shown in Fig. 5(a), where we extract the coupling g from the vertex part, say, the bare vertex, $g\Gamma^0$ and the full vertex, $g\Gamma$ corresponds to Figs. 5(b) and (c), respectively.

Relations (A. 1) and (A. 2) are invariant under the multiple renormalization such as

$$G \to \frac{1}{Z_1}G, \quad G^0 \to \frac{1}{Z_1}G^0,$$

$$\Gamma_i \to \frac{1}{Z_{i,2}}\Gamma_i, \quad \Gamma_i^0 \to \frac{1}{Z_{i,2}}\Gamma_i^0,$$

$$g_i \to Z_1^2 Z_{i,2} g_i, \tag{A.3}$$

where the index i refers to the i-th element.

The Green's function G is formally written as

$$G(p) = \frac{d(p)}{\varepsilon - \varepsilon_p}, \tag{A.4}$$

for which the transformation (A. 3) is interpreted in such manner,

$$d(T/\lambda_2,\ t/\lambda_2, g_{\lambda_2}) = \frac{1}{Z_1} d(T/\lambda_1, t/\lambda_1, g_{\lambda_1}). \tag{A.5}$$

Strictly speaking, G and Γ depend on quantities with the dimension of energy, i.e., on ε, ε_p, T (temperature) and t (transfer integral). However, we note explicitly only T and t.

We are allowed to set, without loss of generality, as

$$d(1,\ t/\lambda,\ g_\lambda)=1. \tag{A. 6}$$

Then, putting $T=\lambda_2$ in Eq. A. 5, we get

$$Z_1=d(\lambda_2/\lambda_1,\ t/\lambda_1,\ g_{\lambda_1}), \tag{A. 7}$$

and similarly

$$\Gamma_i(T/\lambda_2, t/\lambda_2, g_{\lambda_2}) = \frac{1}{Z_{i,2}}\Gamma_i(T/\lambda_1, t/\lambda_1, g_{\lambda_1}). \tag{A.8}$$

Putting $T=\lambda_2$ in Eq. A. 8, we obtain

$$Z_{i,2} = \frac{\Gamma_i(\lambda_2/\lambda_1, t/\lambda_1, g_{\lambda_1})}{\Gamma_i(1, t/\lambda_2, g_{\lambda_2})}. \tag{A.9}$$

Relations (A. 7) and (A. 9) enable us to lead

$$g_{i,\lambda_2} = g_{i,\lambda_1} d^2(\lambda_2/\lambda_1, t/\lambda_1, g_{\lambda_1}) \frac{\Gamma_i(\lambda_2/\lambda_1, t/\lambda_1, g_{\lambda_1})}{\Gamma_i(1, t/\lambda_2, g_{\lambda_2})}. \tag{A.10}$$

What we want to prove is invariant character of the right-hand side of Eq. A. 10 under a scale transformation. To this end, inserting Eq. A. 7 into Eq. A. 5, and also Eq. A. 8 into Eq. A. 9, we obtain

$$d(T/\lambda_2,\ t/\lambda_2,\ g_{\lambda_2}) = \frac{d(T/\lambda_1, t/\lambda_1, g_{\lambda_1})}{d(\lambda_2/\lambda_1, t/\lambda_1, g_{\lambda_1})}, \tag{A.11}$$

$$\frac{\Gamma_i(T/\lambda_2, t/\lambda_2, g_{\lambda_2})}{\Gamma_i(1, t/\lambda_2,\ g_{\lambda_2})} = \frac{\Gamma_i(T/\lambda_1, t/\lambda_1, g_{\lambda_1})}{\Gamma_i(\lambda_2/\lambda_1, t/\lambda_1, g_{\lambda_1})}. \tag{A.12}$$

Here we put

$$\Gamma_i(1, t/\lambda, g_\lambda)=1. \tag{A. 13}$$

This assumption is not always necessary, but will be met in practical cases. From Eqs. A. 11 and A. 12, we obtain

$$d^2(T/\lambda_2,\ t/\lambda_2,\ g_{\lambda_2})\,\Gamma_i(T/\lambda_2,\ t/\lambda_2,\ g_{\lambda_2}) \times d^2(\lambda_2/\lambda_1,\ t/\lambda_1,\ g_{\lambda_1})\,\Gamma_i(\lambda_2/\lambda_1,\ t/\lambda_1,\ g_{\lambda_1}) g_{i,\lambda_1} = g_{i,\lambda_1} d^2(T/\lambda_1,\ t/\lambda_1,\ g_{\lambda_1})\Gamma_i(T/\lambda_1,\ t/\lambda_1,\ g_{\lambda_1}). \tag{A. 14}$$

If we use Eq. A. 10 in the left-hand side of Eq. A. 14, we have

$$g_{i,\lambda_2}d^2(T/\lambda_2, t/\lambda_2, g_{\lambda_2})\Gamma_i(T/\lambda_2, t/\lambda_2, g_{\lambda_2}) = g_{i,\lambda_1}d^2(T/\lambda_1, t/\lambda_1, g_{\lambda_1})\Gamma_i(T/\lambda_1, t/\lambda_1, g_{\lambda_1}). \quad \text{(A. 15)}$$

This relation is nothing but the invariant character which we have intended to show. We call the above quantity the *invariant coupling*:

$$\bar{g}_i(T/\lambda, t/\lambda, g_\lambda) = d^2(T/\lambda, t/\lambda, g_\lambda)\Gamma_i(T/\lambda, t/\lambda, g_\lambda)g_{i,\lambda}. \quad \text{(A. 16)}$$

Now introducing new variables:

$$y = T/\lambda_1, \quad u = t/\lambda_1, \quad t = \lambda_2/\lambda_1, \quad \text{(A. 17)}$$

we get from Eq. A. 15,

$$\begin{aligned}\bar{g}_i(y, u, g) &= d^2(y, u, g)\Gamma_i(y, u, g)g_i \\ &= d^2(y/t, u/t, g_{\lambda_2})\Gamma_i(y/t, u/t, g_{\lambda_2})g_{i,\lambda_2}, \quad \text{(A. 18)}\end{aligned}$$

where we put

$$g_{\lambda_1} = g. \quad \text{(A. 19)}$$

Since we can rewrite g_{i,λ_2} in Eq. A. 18, by the use of Eq. A. 10, as

$$\begin{aligned}g_{i,\lambda_2} &= g_i d^2(t, u, g)\Gamma_i(t, u, g) \\ &= \bar{g}_i(t, u, g), \quad \text{(A. 20)}\end{aligned}$$

substituting this into Eq. A. 18, we can obtain

$$\bar{g}_i(y, u, g) = d^2(y/t, u/t, \tilde{g}(t, u, g))\Gamma_i(y/t, u/t, \tilde{g}(t, u, g)) \times \tilde{g}_i(t, u, g). \quad \text{(A. 21)}$$

Observing Eq. A. 16, we can rewrite the above as

$$\bar{g}_i(y, u, g) = \bar{g}_i(y/t, u/t, \tilde{g}_i(t, u, g)). \quad \text{(A. 22)}$$

This is a really beautiful functional equation.

In view of a practical use, a form of differential equation is preferable: Differentiating Eq. A. 22 with respect to y, followed by putting $t=y$, we obtain

$$y\frac{\partial}{\partial y}\tilde{g}_i(y,u,g) = \frac{\partial}{\partial \xi}\tilde{g}_i(\xi, u/y, \tilde{g}(y,u,g))\,|_{\xi=1} \quad \text{(A.23)}$$

with the boundary condition, Eq. A. 19. In order to get $\bar{g}_i$ through Eq. A. 23, we begin with calculating $\tilde{g}$ in the right-hand side by the perturbation method. Then solving the differential equation Eq. A. 23, we get $\bar{g}_i$ being improved to be invariant under the operations of the renormalization group.

Another differential equation satisfying $\tilde{g}_i$ is obtained by differentiating Eq. A. 22 with respect to t, followed by putting $t=1$:

$$\left\{y\frac{\partial}{\partial y} + u\frac{\partial}{\partial u} - \sum_j \frac{\partial \tilde{g}_j(t,u,g)}{\partial t}|_{t=1}\frac{\partial}{\partial g_j}\right\}\tilde{g}_i(y,u,g) = 0\,. \quad \text{(A.24)}$$

Similar treatments are possible for d and Γ. From Eqs. A. 11, A. 12, and A. 13 we obtain

$$d(y, u, g) = d(y/t, u/t, \tilde{g}(t, u, g))d(t, u, g) \quad \text{(A. 25)}$$

and

$$\Gamma_i d(y, u, g) = \Gamma_i(y/t, u/t, \tilde{g}(t, u, g))\Gamma_i(t, u, g). \quad \text{(A. 26)}$$

If we differentiate logarithms of both side of Eq. A. 26 with respect to t, and then put $t=y$, the results are

$$y\frac{\partial}{\partial y}\ln d(y,u,g) = \frac{\partial}{\partial \xi}\ln d(\xi, u/y, \tilde{g}(y,u,g))\,|_{\xi=1} \quad \text{(A.27)}$$

and

$$y\frac{\partial}{\partial y}\ln \Gamma_i(y,u,g) = \frac{\partial}{\partial \xi}\ln \Gamma_i(\xi, u/y, \tilde{g}(y,u,g))\,|_{\xi=1}\,. \quad \text{(A.28)}$$

An entirely analogous analysis will be done for the external vertices. These will be transformed, together with ones in Eq. A. 3, as

$$\Lambda_i \to \frac{1}{Z_{i,3}}\Lambda_i\,, \quad \text{(A.29)}$$

which is interpreted as a scale transformation:

$$\Lambda_i(T/\lambda_2, t/\lambda_2, g_{\lambda_2}) = \frac{1}{Z_{i,3}}\Lambda_i(T/\lambda_1, t/\lambda_1, g_{\lambda_1})\,. \quad \text{(A.30)}$$

In the same way as in Eq. A. 13, we assume

$$\Lambda_i(1, t/\lambda, g_\lambda) = 1. \quad \text{(A. 31)}$$

If we put $T=\lambda_2$ in Eq. A. 30, and use Eq. A. 31, it follows that

$$Z_{i,3} = \Lambda_i(\lambda_2/\lambda_1, t/\lambda_1, g_{\lambda_1}). \quad \text{(A. 32)}$$

Substituting this in Eq. A. 30, we obtain

$$\Lambda_i(T/\lambda_1, t/\lambda_1, g_{\lambda_1}) = \Lambda_i(T/\lambda_2, t/\lambda_2, g_{\lambda_2})\Lambda_i(\lambda_2/\lambda_1, t/\lambda_1, g_{\lambda_1}). \quad \text{(A. 33)}$$

By the use of Eqs. A. 17, A. 19, and A. 20, we can rewrite Eq. A. 33 as

$$\Lambda_i(y, u, g) = \Lambda_i(y/t, u/t, \tilde{g}(t, u, g))\Lambda_i(t, u, g). \quad \text{(A. 34)}$$

If we differentiate this with respect to y and put $t=y$, we obtain the result similar to Eqs. A. 27 and A. 28,

$$y\frac{\partial}{\partial y}\ln \Lambda_i(y, u, g) = \frac{\partial}{\partial \xi}\ln \Lambda_i(\xi, u/y, \tilde{g}(y,u,g))\,|_{\xi=1}\,. \quad \text{(A.35)}$$

We can easily realize the transformation characters given by Eqs. A. 3 and A. 29 by use of the perturbation expansions of the correponding quantities.

References

1) M. Kimura, H. Kawabe, K. Nishikawa, and S. Aono, *J. Chem. Phys.*, **85**, 3090 (1986); **85**, 3097 (1986).

2) N. N. Bogoliubov and D. V. Shirkov, "Introduction to the Theory of Quantized Fields," Interscience Publishers Inc., New York (1959).

3) R. D. Mattack, "A Guide to Feynman diagrams in the many-body problem," 2nd ed., McGraw-Hill, New York (1976).

4) M. Kimura, *Prog. Theor. Phys.*, **53**, 955 (1975).

5) J. Sólyom, *Adv. Phys.*, **28**, 201 (1979).

6) M. Fowler and A. Zawadowski, *Solid St. Commun.*, **18**, 241 (1976).

7) P. W. Anderson, *J. Phys.*, **C3**, 2346 (1970).

8) M. Kimura and A. Mishima, *Prog. Theor. Phys.*, **73**, 822 (1985).

9) M. Kimura, H. Kawabe, A. Nakajima, K. Nishikawa, and S. Aono, *Bull. Chem. Soc. Jpn.*, **61**, 4239 (1988).

10) M. H. Wangbo, R. Hoffmann, and R. B. Woodward, *Proc. R. Soc. London, Ser. A*, **366**, 23 (1979).

ESR Studies of Solvent and Pressure Effects on Spin Exchange of Nitroxide Radicals in Solution

Yoshimi SUEISHI,* Norio NISHIMURA, Koichi HIRATA,† and Keiji KUWATA†
Department of Chemistry, Faculty of Science, Okayama University, Okayama 700
†Department of Chemistry, Faculty of Science, Osaka University, Toyonaka, Osaka 560
(Received April 12, 1988)

The rate constants of spin exchange for 2,2,6,6-tetramethyl-4-oxo-1-piperidinyloxyl (Tanone) in various solvents at high pressures were estimated from the line-broadening in ESR spectra. The rate constants of the spin exchange were in the range of 10^9—10^{10} M^{-1} s^{-1} and were compared with the calculated ones on the basis of the Smoluchowski-Stokes-Einstein equation. A significant disagreement between them was observed as the solvent viscosity decreased. The activation volumes estimated from the pressure dependence of the rate constant for the spin exchange were slightly smaller than those for diffusive processes. These findings suggest that the rate process for the spin exchange is virtually a diffusion-controlled one. An interpretation of activation volumes for diffusive process of spin exchange is given.

Recently, the usefulness of the examination of kinetic pressure effects has become recognized in mechanistic studies on the chemical reactions taking place near the diffusion-controlled limit. In particular, such studies have been made actively in the field of photochemistry. Interesting reports on the dynamic measurements of transient fluorescence for some exciplex-formation systems have been put forward,[1-3] and the mechanism of the exciplex-formation reaction has been explained in terms of diffusion-controlled encounters. The physical meaning of the activation volume which is formally obtained from the pressure dependence on the diffusion-controlled rate constants, however, has not yet been well established.

The rate constants of the spin exchange can be easily estimated from the line-broadening of ESR-spectra of radicals.[4] The spin exchange reaction can be regarded as a simplified model of a complex chemical reaction. Up to the present, few ESR studies at high pressures have been done, mainly due to the technical difficulty.

Plachy and Schaafsma[5] used a vessel containing a microwave helix and the field-modulation coils for the measurement of ESR signals at high pressures, and such a vessel can withstand pressures of several thousand atmospheres. It, however, is unsuitable for ESR measurements in polar solvents. Böddeker et al.[6] designed a high-pressure glass cell which could be pressurized to 405 bar.

In the present report, a study on the spin exchange reaction in the solvents of various polarities was carried out at various pressures using a newly designed high-pressure cell for ESR measurements. From the pressure dependence on the rate constant of the spin exchange the activation volumes were estimated, and the results were discussed on the basis of the volume change associated with diffusive processes.

Experimental

Materials. 2,2,6,6-Tetramethyl-4-oxo-1-piperidinyloxyl (Tanone) was purchased from Wako Pure Chemicals, and used without further purification. Toluene, acetone, 2-propanol, methanol, and nitrobenzene are of guaranteed grade and were purified in the usual manner.

High-Pressure ESR Cell. The high-pressure vessel, which is made of copper-beryllium alloy and equipped with a stop valve, is shown in Fig. 1. The sample cell for ESR measurements was composed of a Pyrex glass capillary and its top was bound to the high-pressure vessel by epoxy resin. The glass parts, which were hand-made in our laboratory, were sealed at an open end, annealed, and washed with the 5% aqueous hydrogen fluoride solution at room temperature. In preliminary tests, the cell was designed to be repeatedly pressurized up to 588 bar, however, it was broken at 883 bar as an example (1 bar=0.1 MPa).

Procedures. Pressures were generated by means of a plunger pump, and the pressure was measured by a Haise Bourdon gauge. The sample solution was purged by bubbling nitrogen for ca. 30 min and charged into the pressure cell under a nitrogen atmosphere. After a required pressure

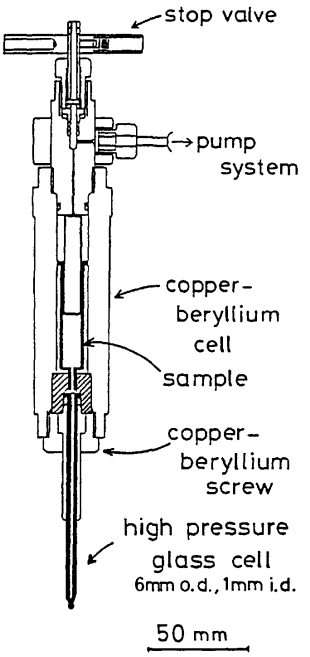

Fig. 1. High pressure cell for use in standard ESR spectrometer.

was established the stop valve was closed, and the pressure vessel separated from the pump system and placed in the ESR cavity.

ESR measurements were performed using a home-made X-band spectrometer with a 100-kHz field modulation. The peak-to-peak width of the central component of the hyperfine structure of the nitroxide radical was measured. The accuracy of the linewidth thus obtained was ±1.5%.

Results

Spin Exchange at High Pressures. The second-order rate constant k_e for the spin exchange process has been estimated easily from the dependence of line-broadening on the concentration of radicals.[4]

$$k_e = A(\Delta H - \Delta H_0)/C, \quad (1)$$

where ΔH_0/mT and ΔH/mT are linewidths in the absence and presence of spin exchange, respectively. C is a radical concentration. A is a constant and its value for the spin exchange of nitroxide radicals has been given to be 2.28×10^8 mT^{-1} s^{-1}.[4] The linear relationships between the linewidths ΔH and the concentrations of the Tanone radical in toluene at different pressures are shown in Fig. 2. This linear relationship shows that the spin exchange makes the major contribution to line-broadening in the concentration range from 10^{-3} to 10^{-2} M (1M=1 mol dm^{-3}) at high pressures as well as at 1 bar. Thus the rate constants k_e for the spin exchange of the Tanone radicals could be estimated by Eq. 1 in various solvents and those values are listed in Table 1.

In Fig. 3, the rate constants of the spin exchange are plotted against the applied pressures. Each plot is seen to be almost linear in the pressure range up to 588 bar. It is noted that the slope is positive in water due to the viscosity decrease with increase of pressure in this pressure range at 288 K (Table 1).

The second-order rate constant of the diffusive processes is given by the Smoluchowski expression,[7] namely

$$k_{diff} = 4\pi aD = (8000\,RT)(3\eta)^{-1}/M^{-1}\,s^{-1}, \quad (2)$$

where a is the sum of the radii of the diffusive molecules, D is the sum of the Stokes-Einstein diffusion

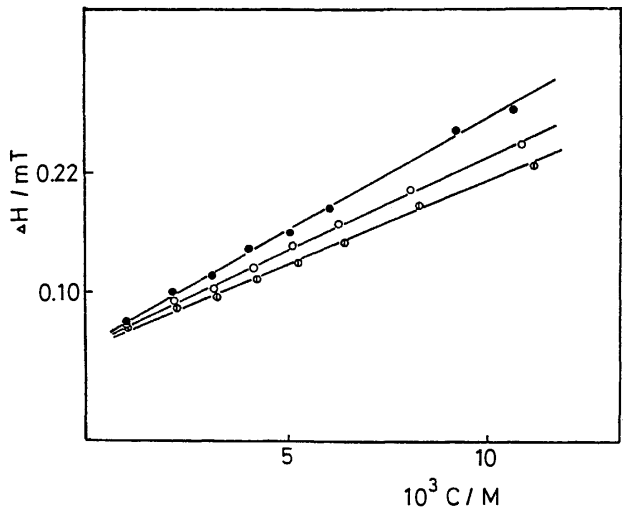

Fig. 2. Concentration dependence of ESR linewidth for Tanone radical in toluene at 1 (●), 294 (○), and 588 (⦶) bars.

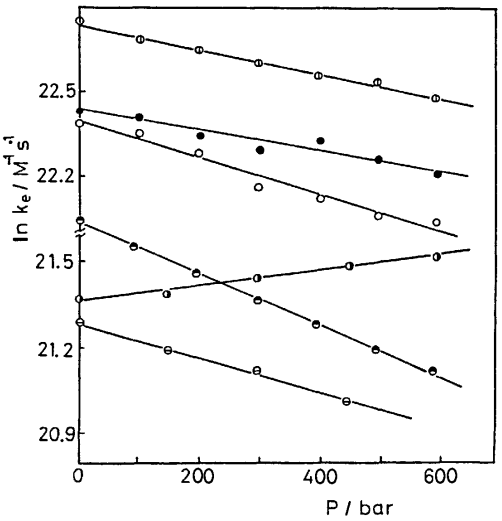

Fig. 3. Pressure effects on the spin exchange reaction between Tanone radicals; (⦶) in acetone, (●) in methanol, (○) in toluene, (⊖) in 2-propanol, (◑) in water, (⊖) in nitrobenzene.

Table 1. Rate Constants (k_e) for Spin Exchange of Tanone Radicals and Diffusion-Controlled Rate Constants (k_{diff}) in Various Solvents at Different Pressures

Solvent	T	1 bar			588 bar		
		η[a]	$10^{-9}k_{diff}$	$10^{-9}k_e$	η[a]	$10^{-9}k_{diff}$	$10^{-9}k_e$
	K	mPa·s	M^{-1} s^{-1}	M^{-1} s^{-1}	mPa·s	M^{-1} s^{-1}	M^{-1} s^{-1}
Toluene	296	0.570	11.6	5.27±0.09	0.848	7.74	3.74±0.07
Nitrobenzene	293	2.01	3.24	1.77±0.11	2.65[b]	2.45[b]	1.35±0.07[b]
Acetone	303	0.285	23.6	7.61±0.22	0.409	16.4	5.81±0.27
2-Propanol	298	2.07	3.19	2.83±0.11	3.34	1.98	1.87±0.06
Methanol	298	0.556	11.9	5.52±0.21	0.718	9.24	4.42±0.16
Water	288	1.40	4.57	1.91±0.10	1.35	4.74	2.21±0.07

a) The viscosities for toluene, 2-propanol, and methanol were estimated from the data at 30 and 75 °C according to $\ln\eta = A + B/T$, and the viscosity of water at 15 °C was estimated from the data at 0, 10.3, and 30 °C. The viscosity of nitrobenzene is the data at 30 °C. b) At 441 bar.

coefficients, and η/Pa·s is the viscosity coefficient of the medium. By this equation and using available data[8] for viscosity, k_{diff}-values were estimated and are given in Table 1.

Discussion

Spin Exchange of Tanone Radicals. As seen in Table 1, the rate constants k_e for the spin exchange in various solvents almost reach the diffusion-controlled limit k_{diff}. As far as our data are concerned, no correlation between the k_e-value and the dielectric constant ε of solvent is observed. This could be accepted when we recall that Tanone is not a polar species. The rate of the spin exchange, however, is invariably retarded by the increase in the solvent viscosity, as predicted by Eq. 2. The rate constant is plotted as a function of inverse viscosity in Fig. 4, where two remarkable features are seen. One is that k_e deviates more and more from that predicted for the diffusive process (Eq. 2) as the solvent viscosity decreases. Another is that the plots of k_e against inverse viscosity seem to fall roughly on a same curve irrespective of solvent, temperature, and pressure. These findings strongly indicate that the spin exchange is controlled by the diffusive processes. At a solvent viscosity $\eta>0.3$ mPa·s the discrepancy between the rate constants of the diffusion collisions calculated according to Eq. 2 and those obtained from the spin exchange amounts to about two-fold, which may be attributed to the discrepancy between the measured diffusion coefficient D[9,10] and the calculated one. At low viscosity $\eta<0.3$ mPa·s the large deviation may be due to transition into the region of weak exchange[4] as well as above.

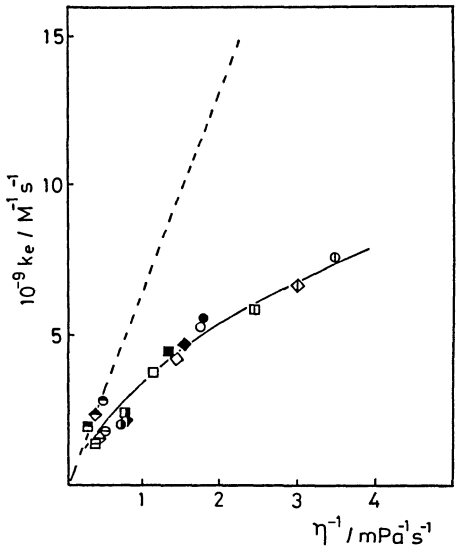

Fig. 4. Plots of k_e against η^{-1} in various solvents, and at various temperatures and pressures; ○ at 1 bar, ◇ at 288 bar, □ at 588 bar. Dashed line; calculated from Eq. 2. The key is shown in Fig. 3.

Comparison of $\Delta V^{\neq}_{obs}$ with $\Delta V^{\neq}_{diff}$. The solid lines in Fig. 3 represent the following linear regression equation.

$$\ln k_e = ap + b \tag{3}$$

The activation volumes $\Delta V^{\neq}_{obs}$ at 1 bar were estimated as

$$RT(\partial \ln k_e/\partial p)_T = aRT = -\Delta V^{\neq}_{obs} + \Delta n^{\neq} \kappa_T RT \tag{4}$$

where $\Delta V^{\neq}_{obs}$ is the partial molar volume change that occurs when a molecule passes from an initial state into a transition state, $\Delta n^{\neq}$ (=−1 in the present case) is the difference in number of species between the activated and initial states, and κ_T is the isothermal compressibility of the solvent. The values of $\kappa_T RT$ at 1 bar were calculated from available data.[8] The values of $\Delta V^{\neq}_{obs}$ are given in the third column of Table 2. The apparent activation volume for this process $\Delta V^{\neq}_{diff}$ can be calculated by

$$RT(\partial \ln k_{diff}/\partial p)_T = -RT(\partial \ln \eta/\partial p)_T = -\Delta V^{\neq}_{diff} - \kappa_T RT \tag{5}$$

The calculated values $\Delta V^{\neq}_{obs}$ are given in the fourth column of Table 2.

It is interesting to examine how $\Delta V^{\neq}_{obs}$ relates to $\Delta V^{\neq}_{diff}$. The observed activation volumes $\Delta V^{\neq}_{obs}$ were in the range from −7.6 to 15.4 $cm^3\ mol^{-1}$ and no systematic solvent dependency was observed (Table 2). On the other hand, the values of $\Delta V^{\neq}_{obs} - \Delta V^{\neq}_{diff}$ in Table 2 are small and all negative. The present values of $\Delta V^{\neq}_{obs} - \Delta V^{\neq}_{diff}$ seem to be classified with regard to viscosity of solvent and difference in solvation; $\Delta V^{\neq}_{obs} - \Delta V^{\neq}_{diff} \approx 0$ $cm^3\ mol^{-1}$ in aprotic solvents, −4.6 $cm^3\ mol^{-1}$ in acetone, a solvent of low viscosity, and ca.−4 $cm^3\ mol^{-1}$ in protic solvents. $\Delta V^{\neq}_{obs}$ in aprotic solvents (toluene and nitrobenzene) are almost equal to $\Delta V^{\neq}_{diff}$, indicating that the spin exchange in such solvents is governed by diffusion of the Tanone radicals. The relatively large difference between $\Delta V^{\neq}_{obs}$ and $\Delta V^{\neq}_{diff}$ was found in protic solvents (methanol, 2-propanol, and water). When we examined the relationship between $\Delta V^{\neq}_{obs}$ and $\Delta V^{\neq}_{diff}$ in protic solvents, a plot of $\Delta V^{\neq}_{obs}$ against $\Delta V^{\neq}_{diff}$ was found to be almost linear; a slope of 1.0±0.1 and intercept of −4.2±1.1. For reactions governed by a diffusive process, the slope and intercept are expected to be ca. 1 and ca. 0, respectively. An appar-

Table 2. Activation Volumes ($cm^3\ mol^{-1}$) for Spin Exchange of Tanone Radicals in Various Solvents

Solvent	T/K	$\Delta V^{\neq}_{obs}$	$\Delta V^{\neq}_{diff}$	$\Delta V^{\neq}_{obs} - \Delta V^{\neq}_{diff}$
Toluene	296	13.7±0.9	14.2	−0.5
Nitrobenzene	293	13.3±0.7	14.1	−0.8
Acetone	303	7.7±0.4	12.3	−4.6
2-Propanol	298	15.4±0.9	19.5	−4.1
Methanol	298	6.7±1.1	8.8	−2.1
Water	288	−7.6±0.4	−2.5	−5.1

ent disagreement between the intercept obtained in protic solvents and that expected for the diffusion-controlled reactions was found and this finding may be ascribed to specific solvation of alcohols to nitroxide radicals. In fact, the observations of large hyperfine coupling constants and g-values of nitroxide radical in protic solvents compared with those in aprotic solvents have been reported.[11] The present value (-4.6 cm^3 mol^{-1}) in acetone is probably to be attributed to weak exchange.[4]

Value of the Activation Volume for Diffusive Processes. Although $\Delta V^{\neq}_{\text{diff}}$ is formally obtainted from the pressure dependence of viscosity (Eq. 2), no clear-cut interpretation of its physical meanings has been put forward so far. In this section, we would like to try to explain the physical meanings of the activation volume of the diffusion process and to estimate its value.

According to the theory of rate processes,[12] the flow of a molecule in the liquid phase can be treated as a rate process. The jump of a molecule from its equilibrium site to the neighboring site is described as a passage over a potential energy surface. The number of times that a molecule passes over the barrier per second is given by

$$k=(kT/h)(q^{\neq}/q)\exp(-\varepsilon_0/kT), \tag{6}$$

where q's are the partition functions and the other notations have their usual meanings. If the passage is to occur, the generation of a hole is necessary, and the excavation of such a hole requires the expenditure of energy. According to this model,[12] the potential energy ε_0 can approximately be related to the viscosity coefficient η of the medium such as

$$\eta=(hL/V)(q/q^{\neq})\exp(\varepsilon_0/kT), \tag{7}$$

where L is the Avogadro number and V the partial molar volume of the molecule. Combining Eq. 6 with Eq. 7, k is given by

$$k=(RT/V)/\eta. \tag{8}$$

Thus the number of passages over the barrier is inversely proportional to η. If we tentatively set $\eta=10^{-3}$/Pa·s (the order of viscosities for most solvents under ordinary conditions), $V=10^{-4}$/m^3 mol^{-1}, and $RT=2.5\times10^3$/J mol^{-1}, then we have $k=2.5\times10^{10}$/s^{-1}, in a reasonable order of magnitude.

It follows from Eq. 8 that

$$RT(\partial \ln\eta/\partial p)_T=\kappa_T RT+\Delta V^{\neq}_{\text{diff}} \tag{9}$$

This is formally the same as Eq. 5. Thus the process for a particle to move from the initial state to the activated state is deduced to require two kinds of energies. The first term comes from the kinetic energy even for a point particle. On the theoretical basis, this term has been predicted[13,14] and has been verified recently.[15] For most liquids, $\kappa_T RT$ is an order of a few cm^3 mol^{-1}.

The second term is considered to be associated with the work to generate a hole as stated above. The volume of this hole is predicted to be a fraction of the molecular volume of the solvent.[12] This could be justified as follows: Let λ be the distance between two equilibrium positions in the direction of motion. The potential energy barrier is assumed to be symmetric. The distance between the initial and the activated state position is $\lambda/2$, thus the ratio of the volume of the molecule to that of the hole may be ca. 8 ($=\lambda^3/(\lambda/2)^3$). Therefore, the predicted $\Delta V^{\neq}_{\text{diff}}$-value is an order of 12—25 cm^3 mol^{-1} since the partial molar volume of most solvents are between 100 and 200 cm^3 mol^{-1}. This is in agreement with available data for $\Delta V^{\neq}_{\text{diff}}$ estimated from the pressure dependence of the viscosity.[2,3] It is noted that the reported $\Delta V^{\neq}_{\text{diff}}$-values are almost independent of the size of the diffusing molecules. For instance, the $\Delta V^{\neq}_{\text{diff}}$-values for the termination constants of free radical polymerization of vinyl monomers are between 13 and 21 cm^3 mol^{-1}.[16] In this case only work to make a hole for the terminal radical segment to move need be necessary.

Concluding Remarks

We estimated the rate constant for the spin exchange reaction of Tanone at high pressures by means of linewidth measurement. The rate was well correlated to the applied pressure. By comparing the rate constant and the activation volume with those for diffusive processes, the conclusion that the rate of the spin exchange is virtually governed by a diffusive process is given. An interpretation for the activation volume associated with the diffusive process is also given.

This work was supported by a Grant-in-Aid for Encouragement of Young Scientist from the Ministry of Education of Japan (No. 62740259).

References

1) W. D. Turley and H. W. Offen, *J. Phys. Chem.*, **88**, 3605 (1984).
2) M. Okamoto, F. Tanaka, and H. Teranishi, *J. Phys. Chem.*, **90**, 1055 (1986).
3) P. C. Johnson and H. W. Offen, *J. Chem. Phys.*, **56**, 1638 (1972).
4) Yu. N. Molin, K. M. Salikhov, and K. I. Zamaraev, "Spin Exchange," Springer-Verlag, Berlin, Heidelberg, New York (1980).
5) W. Z. Plachy and T. J. Schaafsma, *Rev. Sci. Instrum.*, **40**, 1590 (1969).
6) K. W. Böddeker, G. Long, and U. Schindewolf, *Angew. Chem., Int. Ed. Engl.*, **8**, 138 (1969).
7) M. Smoluchowski, *Z. Physik. Chem.*, **92**, 129 (1917).
8) "International Critical Tables," McGraw-Hill, (1928).
9) D. W. McCall, D. C. Douglass, and E. W. Anderson, *J. Chem. Phys.*, **31**, 1555 (1959).
10) A. L. Kovarskii, A. M. Wasserman, and A. L. Buchachenko, *J. Magn. Reson.*, **7**, 225 (1972).
11) T. Kawamura, S. Matsunami, and T. Yonezawa, *Bull.*

Chem. Soc. Jpn., **40**, 1111 (1967).
12) S. Glasstone, K. J. Laidler, and H. Eyring, "The Theory of Rate Processes," McGraw-Hill Book Company, Inc., New York (1941).
13) F. H. Stillinger, *J. Solution Chem.*, **2**, 141 (1973).
14) Y. Yoshimura and M. Nakahara, *J. Chem. Phys.*, **81**, 4080 (1984).
15) N. Nishimura, T. Tanaka, and T. Motoyama, *Can. J. Chem.*, **65**, 2248 (1987).
16) M. Yokawa, J. Yoshida, and Y. Ogo, *Makromol. Chem.*, **178**, 443 (1977) and references therein.

 © 1988 The Chemical Society of Japan Bull. Chem. Soc. Jpn., 61, 4259—4263 (1988)

Potentiometric Studies on Sulfato Complex of Aluminium(III) in Aqueous Solution at Elevated Temperatures

Yoshiyuki MATSUSHIMA, Akio MATSUNAGA, Kazuhiro SAKAI, and Akitsugu OKUWAKI*
Department of Molecular Chemistry and Engineering, Faculty of Engineering, Tohoku University, Sendai 980
(Received April 1, 1988)

Equilibria in aluminium sulfate solutions with a 1 mol kg^{-1} KCl medium and low pH range have been investigated by means of acidity measurements with a hydrogen ion concentration cell from 25 to 125 °C. The results were treated with a nonlinear least squares computer program to analyze the equilibrium constants for aluminium complexes by using a single parameter type of Debye-Hückel equation. The log(K/mol^{-1} kg) values of the formation constant for the reaction, $Al^{3+}+SO_4^{2-} \rightleftarrows [AlSO_4]^+$ varied from 3.35 at 25 °C to 5.34 at 125 °C and were formulated as a function of temperature. The standard enthalpy and entropy of the complex formation computed from the variation of the formation constant with temperature are presented over the experimental temperature range. The species $[Al(SO_4)_2]^-$ was not detected under the present conditions.

Sulfate ion affects the hydrolysis and the precipitation of polyvalent metal ions considerably through complex formation at elevated temperatures and much evidence has been reported for the interaction of sulfate ion with metal ions such as aluminium(III)[1] and iron(III).[2]

Izatt et al. have reported a large number of formation constants for sulfato complexes at 25 °C as determined by calorimetry.[3] Those values become greater with the charge of metal ion.

However, those data are very limited even at moderate temperatures because the hydrolysis of metal ions is too complicated to allow satisfactory analysis of the equilibrium in the solution. Nikolaeva has measured the formation constants of sulfato complexes of bivalent metal ions up to 90 °C by the conductometric method.[4] With regards to tervalent metal ions, only Matijević et al. have investigated sulfato complexes of iron(III)[5] and aluminium(III)[6] ions up to 100 °C with respect to the preparation of monodispersed particles of the hydrous oxides of the metal ions.

At elevated temperatures, Marshall et al. studied the formation of $[MgSO_4]$[7] and $[CaSO_4]$[8] by solubility measurements.

Akitt and his co-workers have studied the complex formation in aqueous aluminium sulfate solution by aluminium-27 NMR spectroscopy.[9] The spectrum of aluminium sulfate solution contains two resonances, one due to the hexa-aqua cation and the other due to the inner sphere sulfato complex. This result showed direct evidence of the existence of sulfato complex of aluminium ion. Unfortunately, an increase in the temperature caused broadening of the two signals and prevented accurate measurements. In a previous study,[10] we have evaluated the second dissociation constant of sulfuric acid up to 200 °C using a hydrogen-ion concentration cell with a view to determining the formation constants for sulfato complexes of multivalent metal ions such as Al^{3+} and Fe^{3+}, because those values are especially important for quantitative analysis of the precipitation of nickel sulfide from the sulfate solutions and the removal of Fe^{3+} from the sulfate solutions at elevated temperatures.

The present study has been undertaken to determine the formation constant for sulfato complexes of aluminium ion in aluminium sulfate solutions using the hydrogen-ion concentration cell at elevated temperatures. It is favorable to study aluminium ion since the solubility of aluminium sulfate is relatively high even at elevated temperatures and aluminium hydrolysis products have been extensively studied.[11]

Experimental

Materials: All aluminium solutions were prepared by dissolving reagent grade aluminium chloride in dilute hydrochloric acid to suppress the hydrolysis of aluminium ion. The total concentration of aluminium ions was determined by back titration of an excess of EDTA with a standard Zn^{2+} solution. The total equivalent cation concentration was determined by using ion exchange resin Amberlite IR-120B(H) in the hydrogen form, followed by titration of the eluate with a 0.1 M (M=mol dm^{-3}) NaOH solution. A stock solution of a 0.1 M HCl was prepared from analytical grade hydrochloric acid diluted with doubly distilled water. Reagent grade KCl and K_2SO_4 were used without further purification. Ultrapure H_2 (99.99999%) was used.

Potentiometric Apparatus and Procedures: The hydrogen ion concentration cell is shown in Fig. 1. The apparatus and the procedure were first developed by Le Peintre[12] and later, Mesmer[13] and MacDonald[14] made similar measurements with some modifications. It consists of a titanium autoclave housing an outer glass beaker and an inner PTFE cup containing matched hydrogen electrodes. These two compartments were connected through the fluid phase by a porous PTFE disk,[10] and vapor space was interconnected via a 0.7 mm pin hole which allowed rapid pressure equilibration of hydrogen gas, yet was small enough to minimize the distillation of hydrochloric acid. The reversible hydrogen electrodes consisting of pure platinum were insulated from the autoclave body and were lightly platinized by electrolysis in a dilute solution of hexachloroplatinic acid before use. A porous PTFE disk (pore size, 0.2 μm; thickness 1 mm), which replaced air in the pores with a saturated KCl solution, was employed for the liquid junction. The treatment of the porous PTFE has been described previously.[10]

The cell representation is:

$$\mathrm{Pt},\ \mathrm{H_2}\ \left|\begin{array}{ll}\mathrm{AlCl_3} & (m_1)\\ \mathrm{HCl} & (m_2)\\ \mathrm{K_2SO_4} & (m_3)\\ \mathrm{KCl} & (m_5=1)\end{array}\right\|\left|\begin{array}{ll}\mathrm{HCl} & (m_4=0.001)\\ \mathrm{KCl} & (m_5=1)\end{array}\right|\ \mathrm{H_2},\ \mathrm{Pt} \qquad \text{(I)}$$

where m represents molality. The right hand (inner cup) of the cell (I) contains the reference electrode. Solution compositions in the test solutions are listed in Table 1. In order to suppress hydrolysis of aluminium ion, the test solutions were acidified (pH<3). The concentration of hydrochloric acid in the reference solution was 0.001 mol kg^{-1}. To minimize the liquid junction potential and to keep the ionic strength constant, KCl was added as a supporting electrolyte in both solutions (1 mol kg^{-1}).

After assembly the gas in the cell was exchanged by alternatively pressurizing it with hydrogen gas to 1.0 MPa and by venting it to an atmospheric pressure five times. Finally, the cell was pressurized to about 0.5 MPa with the hydrogen.

The entire autoclave was immersed in an oil bath. Potentials were measured successively from 25 to 125 °C at 25 °C intervals with a digital voltmeter and were recorded after they had reached a stable value within 0.1 mV for a few minutes.

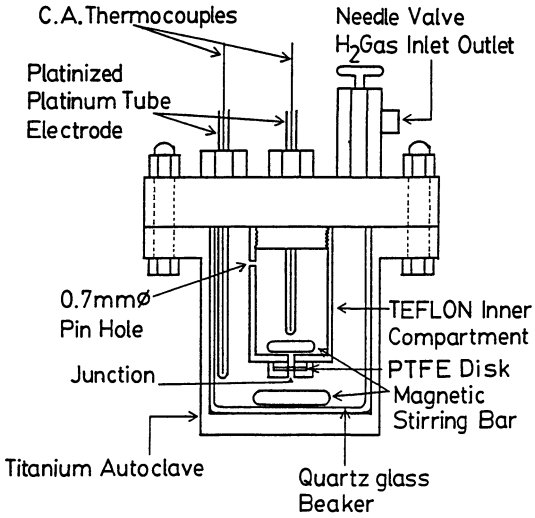

Fig. 1. E.M.F. apparatus for high temperature concentration cell.

Table 1. Initial Concentrations of Each Component at Various Runs

Run No.	$AlCl_3$	K_2SO_4	HCl
	mol kg^{-1}	mol kg^{-1}	mol kg^{-1}
1	0.020	0.020	0.016
2	0.020	0.020	0.018
3	0.020	0.020	0.022
4	0.020	0.020	0.025
5	0.020	0.020	0.027
6	0.020	0.030	0.030
7	0.020	0.032	0.032
8	0.020	0.034	0.034
9	0.020	0.036	0.036
10	0.020	0.038	0.038
11	0.020	0.040	0.040
12	0.020	0.020	0.020
13	0.022	0.022	0.022
14	0.020	0.027	0.027
15	0.030	0.027	0.027

1 mol kg^{-1} KCl as a supporting electrolyte.

Results and Discussion

The results of the potentiometric measurements are summarized in Table 2.

The potentials E (V) for the cell (I) are given by the expression:

$$E=(RT/F)\ln(a_{H^+,t}/a_{H^+,r})+E_j \qquad (1)$$

where a_{H^+} represents the activity of hydrogen ion and subscripts t and r denote the test and reference solutions, respectively. The second term in Eq. 1 represents the liquid junction potential, which can be estimated using the Henderson equation:[13]

$$E_j=-\sum D_i(m_{i,t}-m_{i,r}) \qquad (2)$$

$$D_i=(RT/F)(|Z_i|/Z_i)\lambda_i/\sum(|Z_i|\bar{m}_i\lambda_i) \qquad (3)$$

where $\bar{m}_i$ denotes the average concentration of species i in the two compartments, Z_i is the ionic charge, and λ_i is the limiting equivalent conductance of the i th ion. Values of λ_i have been reported by Quist and Marshall,[15] but that of Al^{3+} was calculated from the Stokes's law:

$$\lambda_i=0.820|z_i|r_s\eta \qquad (4)$$

where r_s is the "Stokes radius" taken as 3.95 Å for aluminium(III) ion[16] and η is the viscosity of water. Since the molal ratio of supporting electrolyte to total aluminium was large, the liquid junction term in Eq. 1 rarely exceeded 1 mV.

It has been recognized that the activity coefficients for uni- and bivalent[17–19] ionic species are expressed

Table 2. Electromotive Force (mV) of the Cell at Each Run

Run No.	Temperature/K				
	298	323	348	373	398
1	64.64	66.97	67.91	69.84	77.80
2	69.00	71.94	73.37	75.57	82.13
3	74.17	77.88	79.71	82.19	87.94
4	77.41	81.35	84.29	87.01	92.56
5	80.00	84.12	87.19	90.26	96.18
6	80.71	84.01	85.84	87.35	92.08
7	81.90	85.22	86.81	88.32	92.55
8	83.29	86.52	88.38	89.71	93.77
9	84.61	87.88	89.60	90.96	94.87
10	86.19	89.45	91.25	92.66	96.25
11	87.39	90.61	92.73	93.79	97.23
12	71.02	74.14	75.99	78.43	84.87
13	73.21	76.48	78.58	81.03	87.48
14	79.37	82.61	84.36	86.05	90.78
15	79.91	83.30	85.83	88.91	96.14

sufficiently to 1 molal 1-1 electrolyte solutions by the single parameter type of Debye-Hückel equation and to 5 molal solutions by the extended Debye-Hückel equation. Although those of the highly charged ions can be estimated only very poorly, Lietzke and Stoughton,[20] and Marshall and Slusher[21] have proved the efficacy of applying the equation to the extent of tervalent ion in the solubility measurement of lanthanum sulfate and samarium sulfate, respectively. Therefore, we used a Debye-Hückel equation to calculate the activity coefficients for ionic species at elevated temperatures:

$$\log \gamma_i = -Z_i{}^2 S\sqrt{I}/(1+A\sqrt{I}) \quad (5)$$

where I is the ionic strength and, S is the Debye-Hückel limiting slope given by:

$$S = 1.824\times10^6\, \rho^{1/2}/(\varepsilon T)^{3/2}\ (\mathrm{kg}^{1/2}\,\mathrm{mol}^{-1/2}) \quad (6)$$

Dielectric constant of water ε is available up to 640 K by Akerlof and Oshry[22] and ρ is the density of water. The adjustable parameter A was experimentally determined from the solubility measurements of various sulfates,[17-19] i.e. A varies from 1.5 at 25 °C to 1.6 at 125 °C.

The principal equilibrium reactions governing the thermodynamic behavior of aluminium sulfate solution at elevated temperatures are assumed to be:

$$Al^{3+} + SO_4^{2-} \rightleftharpoons [AlSO_4]^+ \quad (7)$$

$$2Al^{3+} + 2H_2O \rightleftharpoons [Al_2(OH)_2]^{4+} + 2H^+ \quad (8)$$

$$HSO_4^- \rightleftharpoons H^+ + SO_4^{2-} \quad (9)$$

$$K^+ + SO_4^{2-} \rightleftharpoons KSO_4^- \quad (10)$$

Aluminium ion is extensively hydrolyzed at elevated temperatures and produces various hydroxo complexes.[23] Under the present conditions we assume only one hydrolyzed product, $[Al_2(OH)_2]^{4+}$, reported by MacDonald et al., because the present experimental conditions of hydrothermal hydrolysis (pH, ionic strength, and aluminium concentration) were similar to their ones.

Equilibrium constants for above reactions are expressed as follows:

$$K_f = a_{[AlSO_4]^+}/a_{Al^{3+}}\, a_{SO_4^{2-}} \quad (11)$$

$$= (\gamma_{[AlSO_4]^+}/\gamma_{Al^{3+}}\, \gamma_{SO_4^{2-}})(m_{[AlSO_4]^+}/m_{Al^{3+}}\, m_{SO_4^{2-}}) \quad (11')$$

$$K_h = a_{[Al_2(OH)_2]^{4+}} a_{H^+}^2/a_{Al^{3+}}^2 \quad (12)$$

$$= (\gamma_{[Al_2(OH)_2]^{4+}}\gamma_{H^+}^2/\gamma_{Al^{3+}}^2)(m_{[Al_2(OH)_2]^{4+}} m_{H^+}^2/m_{Al^{3+}}^2) \quad (12')$$

$$K_2 = a_{H^+} a_{SO_4^{2-}}/a_{HSO_4^-} \quad (13)$$

$$= (\gamma_{H^+}\gamma_{SO_4^{2-}}/\gamma_{HSO_4^-})(m_{H^+} m_{SO_4^{2-}}/m_{HSO_4^-}) \quad (13')$$

$$K_k = a_{KSO_4^-}/a_{K^+}\, a_{SO_4^{2-}} \quad (14)$$

$$= (\gamma_{KSO_4^-}/\gamma_{K^+}\gamma_{SO_4^{2-}})(m_{KSO_4^-}/m_{K^+} m_{SO_4^{2-}}) \quad (14')$$

The values of K_2 and K_k were determined previously at temperatures up to 200 °C.[10]

Total analytical concentrations of Al^{3+}, H^+, K^+, and SO_4^{2-} ions are given by:

$$m_{Al^{3+}} + m_{[AlSO_4]^+} + 2m_{[Al_2(OH)_2]^{4+}} = m_1 \quad (15)$$

$$m_{H^+} + m_{HSO_4^-} - 2m_{[Al_2(OH)_2]^{4+}} = m_2 \quad (16)$$

$$m_{K^+} + m_{KSO_4^-} = 2m_3 + m_5 \quad (17)$$

$$m_{[AlSO_4]^+} + m_{HSO_4^-} + m_{KSO_4^-} + m_{SO_4^{2-}} = m_3 \quad (18)$$

And the ionic charge balance in the solution is:

$$3m_{Al^{3+}} + m_{[AlSO_4]^+} + 4m_{[Al_2(OH)_2]^{4+}} + m_{H^+} + m_{K^+} = 2m_{SO_4^{2-}} + m_{HSO_4^-} + m_{KSO_4^-} + m_{Cl^-} \quad (19)$$

If a, h, and s are taken as the Al^{3+}, H^+, and SO_4^{2-} concentrations, the solution of Eqs. 11—19 can be obtained by the following simultaneous equations:

$$a + h + \gamma^{12}K_f as + \gamma^4 hs/K_2 - m_1 - m_2 = 0 \quad (20)$$

$$s + \gamma^{12}K_f as + \gamma^4 hs/K_2 + \gamma^4 K_k(1+2m_3)s/(1+\gamma^4 K_k s) - m_2 = 0 \quad (21)$$

$$h + 3a + \gamma^{12}K_f as + 4K_h a^2/h^2 - (1+3m_1+m_2) - \gamma^4 hs/K_2 - 2s + (1+2m_3)(1-\gamma^4 K_k s)/(1+\gamma^4 K_k s) = 0 \quad (22)$$

The computer program employed to carry out the calculation of K_f and K_h was described below. First, a preliminary value of ionic strength was assumed and was substituted into Eq. 5 to yield the activity coefficients. The concentrations of each ionic species was determined by simultaneous solution of Eqs. 20—22 by the Newton-Raphson method. The ionic strength of the solutions was calculated from the concentrations of each kind of ions and determined by the method of successive approximations. Thus, the activity of hydrogen ion, a_{H^+}, was determined and combined with Eq. 1, and the calculated value of potential was obtained. Then the experimental data were treated with a nonlinear least squares method to analyze the most appropriate set of K_f and K_k, i.e., to minimize the summation of the square difference of observed and calculated values of the potential. The computations were carried out for each system from 25 to 125 °C at 25 °C intervals. The formation constants of aluminium sulfate obtained by the above procedure are presented in Table 3 and illustrated in Fig. 2. Their change with temperature shows that the association of aluminium ion and sulfate ion increases strongly with temperature. Potentials measured at temperatures higher than 125 °C increased gradually, presumably due to the hydrolysis of aluminium ion, followed by precipitation. Therefore it was difficult to deter-

Table 3. Thermodynamic Quantities for the Formation of $AlSO_4^+$

T / K	log (K/mol^{-1}kg)	$\Delta G°$ / kJ mol^{-1}	$\Delta H°$ / kJ mol^{-1}	$\Delta S°$ / J mol^{-1} K^{-1}
298	3.35	−19.1	6.61	86.2
	3.01	−17.2	9.58	89.5[a]
323	3.59	−22.2	30.3	162
348	4.08	−27.2	50.9	224
373	4.66	−33.3	68.6	273
398	5.34	−40.7	83.3	312

a) Ref. 3.

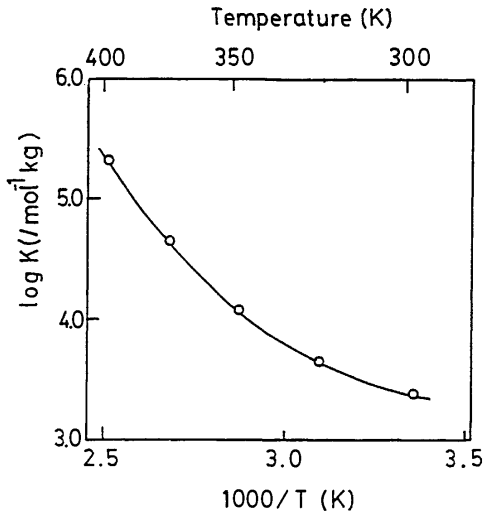

Fig. 2. The formation constant of $AlSO_4^+$ from 25 °C to 125 °C.

mine the association constant of the $[AlSO_4]^+$ ion pair at temperatures above 125 °C. The X-ray diffraction patterns of the precipitate showed that the major constituent was alunite, $KAl_3(SO_4)_2(OH)_6$. Lines assignable to aluminium oxides, hydroxides, and oxychlorides were not observed.

Essentially, the equilibrium constant obtained by the e.m.f. measurements is a sum of the equilibrium constants for the inner-sphere complex, $[Al(SO_4)(OH_2)_{6-x}]^+$ and the outer-sphere one, $[Al(OH_2)_6(SO_4)]^+$. These constants were determined by the pressure jump method up to 40 °C[25] and the inner-sphere complex occupies 17% at 25 °C. The NMR measurements of aluminium sulfate solutions show that the ratio of the inner-sphere complex to the outer one increases with an increase in temperature.[9]

Although the disulfato complex, $[Al(SO_4)_2]^-$, has been reported by other authors[3,6,26] we could not find evidence of its existence. It is supposed that the experimental conditions of both low pH level and small ratio of $[SO_4^{2-}]/[Al^{3+}]$ are unfavorable to the formation of the disulfato complex. If we take into account the precipitation of alunite above 125 °C, it seems that the disulfato or hydroxodisulfato complex may be formed at higher temperatures because aluminium ion in the crystal of alunite is hexa-coordinated with two oxygen atoms of SO_4^{2-} ions and four OH^- ions.[27]

From the formation constant obtained in this work, it is possible to compute the composition of the aluminium sulfate solutions. Some examples are shown in Table 4. As has been pointed out by Akitt et al.,[9] HCl suppresses the formation of $[AlSO_4]^+$, due to the formation of HSO_4^- over the pH range examined at all temperatures.

On the assumption of the linear dependency of ΔC_p° over the temperature range of 25 to 125 °C, the present values of the formation constant were fitted by a method of least squares to yield the four-parameter

Table 4. Molalities of Various Species Present in a Solution Containing 0.020 m in $AlCl_3$ and 0.032 m in K_2SO_4, and 0.032 m in HCl at Various Temperatures

Species	Temperature		
	298 K	348 K	398 K
Al^{3+}	1.78×10^{-2}	1.61×10^{-2}	1.08×10^{-2}
$AlSO_4^+$	2.19×10^{-3}	3.87×10^{-3}	8.32×10^{-3}
$Al_2(OH)_2^{4+}$	—	—	4.53×10^{-4}
SO_4^{2-}	1.80×10^{-2}	1.14×10^{-2}	4.54×10^{-3}
HSO_4^-	6.51×10^{-3}	1.33×10^{-2}	1.77×10^{-2}
KSO_4^-	5.26×10^{-3}	3.44×10^{-3}	1.46×10^{-3}
H^+	2.55×10^{-2}	1.87×10^{-2}	1.52×10^{-2}

1 m=1 mol kg^{-1}.

equation as a function of temperature (K):

$$\log(K_f/\text{mol}^{-1}\,\text{kg}) = -765.90 + 290.1611\log(T/\text{K}) + 26255/(T/\text{K}) - 0.1234(T/\text{K}) \quad (23)$$

From the treatment of Eq. 23, thermodynamic functions for the standard Gibbs energy (ΔG°), enthalpy (ΔH°), and entropy (ΔS°) were obtained from 25 to 125 °C. The values are given in Table 3. At 25 °C the values ΔG°, ΔH°, and ΔS° in this table were compared reasonably with those of Izatt et al.[3]

Another equation for $\log K_f$ was obtained by assuming that ΔC_p° varied as quadratic function of temperature. This equation is given as follows:

$$\log(K_f/\text{mol}^{-1}\,\text{kg}) = -14847.75 + 6358.721\log(T/\text{K}) + 328608/(T/\text{K}) - 7.75167(T/\text{K}) + 3.66574\times10^{-3}(T/\text{K})^2 \quad (24)$$

The thermodynamic quantities derived from Eq. 24 at 25 °C showed unreasonably low values. Therefore, the four-parameter equation (Eq. 23) is believed to yield a better description of the present equilibrium from 25 to 125 °C.

Because all of the test solutions were fairly acidic (pH<3), hydrolysis of Al^{3+} ion at moderate temperatures was suppressed, and consequently, the formation constant for the hydrolyzed product, $[Al_2(OH)_2]^{4+}$, was ill-defined. The hydrolysis occurred with an increase in temperature, and $\log(K_h/\text{mol}\,\text{kg}^{-1}) = -3.0$ was determined for the formation of $[Al_2(OH)_2]^{4+}$ at 125 °C.

We wish to thank Sumitomo Electric Industries, Ltd. for supplying the porous PTFE disks.

References

1) A. Okuwaki, O. Kanome, and T. Okabe, *Metal. Trans.*, **15B**, 609 (1984).

2) H. Kubo, M. Kawahara, and Y. Shirane, *J. Min. Met. Inst. Jpn.*, **98**, 1257 (1987).

3) R. M. Izatt, D. Eatough, J. J. Christensen, and C. H. Bartholomew, *J. Chem. Soc. A*, **1969**, 47.

4) N. M. Nikolaeva, "High Temperature High Pressure Electro-Chemistry in Aqueous Solutions," NACE 4 (1973), p. 146.

5) R. S. Sapieszko, R. C. Patel, and E. Matijevic, *J. Phys. Chem.*, **81**, 1061 (1977).
6) C. C. Lo, L. Meites, and E. Matijevic, *Anal. Chim. Acta*, **139**, 197 (1982).
7) W. L. Marshall, *J. Phys. Chem.*, **71**, 3584 (1967).
8) L. B. Yeatts and W. L. Marshall, *J. Phys. Chem.*, **73**, 81 (1969).
9) J. W. Akitt, N. N. Greenwood, and B. L. Khandelwal, *J. Chem. Soc., Dalton Trans.*, **1972**, 1226; J. W. Akitt, J. A. Farnsworth, and P. Letellier, *J. Chem. Soc., Faraday Trans. 1*, **81**, 193 (1985).
10) Y. Matsushima, and A. Okuwaki, *Bull. Chem. Soc. Jpn.*, **61**, 3344 (1988).
11) C. F. Baes, Jr., and R. E. Mesmer, "The Hydrolysis of Cations," Wiley, New York (1976), p. 112.
12) M. Le Peintre, C. Mahieu, and R. Fournie, Comm. energie at. (France), Rappt. No. 1951, 9p (1961).
13) R. E. Mesmer, C. F. Baes, Jr., and F. H. Sweeton, *J. Phys. Chem.*, **74**, 1937 (1970).
14) D. D. MacDonald, P. Butler, and D. Owen, *Can. J. Chem.*, **51**, 2590 (1973).
15) A. S. Quist and W. L. Marshall, *J. Phys. Chem.*, **69**, 2984 (1965).
16) R. A. Robinson and R. H. Stokes, "Electrolyte Solutions," Butterworths, London (1955), p. 113.
17) L. B. Yeatts and W. L. Marshall, *J. Phys. Chem.*, **71**, 2641 (1967).
18) W. L. Marshall and R. Slusher, *J. Phys. Chem.*, **70**, 4015 (1966).
19) W. Marshall and R. Slusher, *J. Chem. Thermodyn.*, **5**, 189 (1973).
20) M. H. Lietzke and R. W. Stoughton, *J. Inorg. Nucl. Chem.*, **28**, 1063 (1966).
21) W. L. Marshall and R. Slusher, *J. Phys. Chem.*, **70**, 4015 (1966).
22) G. C. Akerlof and H. I. Oshry, *J. Am. Chem. Soc.*, **72**, 2844 (1950).
23) R. E. Mesmer and C. F. Baes, Jr., *Inorg. Chem.*, **10**, 2290 (1971).
24) D. D. MacDonald, P. Butler, and D. Owen, *J. Phys. Chem.*, **77**, 2474 (1973).
25) C. Kalidas, W. Knoche, and D. Papadopoulos, *Ber. Bunsenges. Phys. Chem.*, **75**, 106 (1971).
26) L. Sharma and B. Prasad, *J. Indian Chem. Soc.*, **47**, 693 (1970).
27) S. B. Hendricks, *Am. Mineral.*, **22**, 773 (1937); R. Wang. W. F. Bradley, and H. Steinfink, *Acta Crystallogr.*, **18**, 249 (1965).

 © 1988 The Chemical Society of Japan Bull. Chem. Soc. Jpn., 61, 4265—4268 (1988)

^{81}Br NQR and ^{119}Sn Mössbauer Study for $MSnBr_3$ (M=Cs and CH_3NH_3)

Koji YAMADA,* Sayuri NOSE, Takako UMEHARA, Tsutomu OKUDA, and Sumio ICHIBA
Department of Chemistry, Faculty of Science, Hiroshima University, Higashisenda-machi, Naka-ku, Hiroshima 730
(Received April 8, 1988)

Successive phase transitions were observed for $CsSnBr_3$ and $CH_3NH_3SnBr_3$ by means of ^{81}Br NQR and DTA. These compounds are isomorphous with each other and have typical cubic perovskite structures at room temperature. However, with decreasing temperature both compounds showed successive phase transitions and complex ^{81}Br NQR spectra at 77 K. In the case of $CH_3NH_3SnBr_3$, both ^{81}Br NQR and ^{119}Sn Mössbauer spectra changed markedly with decreasing temperature from those at room temperature. These findings suggested a large distortion of the $SnBr_6$ octahedron from the regular one and were interpreted on the basis of the three-center-four-electron bond model. In relation to these structural changes, a broad-line ^{1}H NMR experiment on $CH_3NH_3SnBr_3$ was also observed in order to determine the effect of the dynamic properties of the cation.

Trihalostannate anions, SnX_3^- (X=Cl, Br, and I), in the solid state still provide us with interesting problems, since the anion changes its structure variously with the replacement of the counter cation. Furthermore, drastic changes of the ^{81}Br NQR spectra accompanied by phase transitions have been reported with decreasing temperature.[1] The structural variety of the SnX_3^- anion has been understood on the basis of the stereochemical activity (or nonactivity) of the nonbonding pair of s-electrons.[2] In the series of our NQR and Mössbauer studies on SnX_3^- anions, however, the structural variety and phase transitions have been disscused on the basis of the hypervalent character of the central metal.[3] In other words, the trans Br-Sn-Br bond is described as a three-center-four-electron (3c-4e) bond.[4] This bond changes continuously from a symmetric X-Sn-X to an asymmetric X-Sn···X, as has been observed for the trans Br-Sb-Br bond in $(C_5H_5NH)SbBr_4$.[5] In this model an inter anionic interaction, such as X-Sn···X, can also be regarded as an extremely asymmetric case of the 3c-4e bond. According to the crystal structures containing SnX_3^- anions, the tin atom forms regular or distorted octahedron with six nearest-neighbor halogens. Therefore, four structural models shown in Fig. 1 can be systematically understandable in terms of whether the trans X-Sn-X bond is a symmetric or asymmetric in each of the three orthogonal directions.[1] The appearance of models (B), (C), and (D) can be interpreted as being a result of a displacement of the central metal in the three different directions shown in model (A). The model (A) structure has been reported for $CsSnBr_3$,[6,7] model (B) for $KSnF_3\cdot(1/2)H_2O$,[8] model (C) for $CsSnI_3$[9] and $(NH_4)SnBr_3\cdot H_2O$,[1,10] and model (D) for $CsSnCl_3$.[11] In our previous paper model (C) anions in $MSnBr_3\cdot H_2O$ (M=K and NH_4) changed their structure with decreasing temperature toward model (D), at which the ^{81}Br NQR frequencies assigned to the basal plane increased enormously.[1]

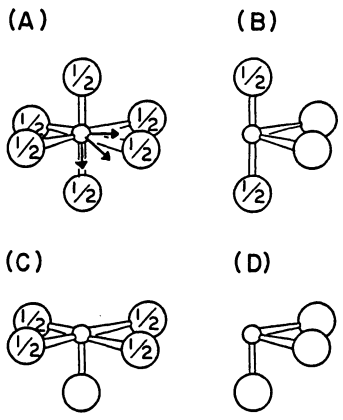

Fig. 1. Structural models for SnX_3^- anion on the basis of octahedral environment around the Sn.

In this paper the structural phase transitions for $CsSnBr_3$ and $CH_3NH_3SnBr_3$ were studied by means of ^{81}Br NQR, DTA, ^{119}Sn Mössbauer effect, and ^{1}H NMR. Especially in the $CH_3NH_3^+$ analogue, the tin environment changed from a regular octahedron at room temperature to a markedly distorted one at 77 K, as was expected from the 3c-4e bond. Furthermore, an interesting problem is the relationship between the 3c-4e bond model and the semimetallic conductivity of the perovskite structure. For the Cs analogue, both experimental and theoretical studies concerning the electric structure have been reported.[12]

Experimental

$CH_3NH_3SnBr_3$ was crystallized as red crystals from ethanol containing stoichiometric amounts of $SnBr_2$ and CH_3NH_3Br. This compound is unstable in air, especially if there exists a trace of hydrobromic acid. $CsSnBr_3$ was obtained from a melt using a Bridgman furnace. These two compounds were identified to be isomorphous with each other at room temperature using powder X-ray diffraction. The cell constants of the cubic perovskite were determined to be a=5.808 and 5.901 Å for Cs and CH_3NH_3 salts, respectively. The former lattice constant agreed well with the value reported previously, a=5.804 Å.[6]

^{79,81}Br NQR was detected with a pulsed spectrometer and was assigned using the quadrupole moment ratio, $Q(^{79}Br)/Q(^{81}Br)$=1.1971. At low temperature, owing to their large line width (ca. 100 KHz), only spin echo signals could be detected using 90°—180° pulses. ^{119}Sn Mössbauer spectra were recorded by means of a constant acceleration type spec-

trometer, using $Ca^{119m}SnO_3$ as a gamma-ray source. The velocity was calibrated with Sn and $BaSnO_3$.

Results and Discussion

^{81}Br NQR and DTA. Figure 2 shows the temperature dependence of the ^{81}Br NQR frequency for $CsSnBr_3$. The phase transition temperatures were determined to be 290±1 and 85±2 K, the former agreeing well with the value reported previously by Scaife et al.[13] Both transitions were accompanied by a continuous temperature dependence of the NQR frequency and no thermal hysteresis, characteristics of a second-order transition. A preliminary experiment concerning the NQR spin-lattice relaxation times also showed a character of the second-order type phase transition; steep minima in the T_1 vs. temperature curve near the phase-transition temperatures. The intermediate phase II has two NQR lines with intensity ratio 2:1, from the highest, suggesting a tetragonally distortion of the perovskite. As Fig. 3 shows, however, the spectra at 77 K is complicated. At least seven ^{81}Br lines could be detected separately, though the exact number of nonequivalent Br sites could not be determined due to the broad linewidth. However, the distortion of the $SnBr_6$ octahedra from a regular form is considered to be only slight because of the small splitting of the NQR frequencies. This was also supported by the ^{119}Sn Mössbauer spectrum, which had no quadrupole splitting (as described later).

Figure 4 shows the temperature dependence of the ^{81}Br NQR frequency for $CH_3NH_3SnBr_3$. One ^{81}Br NQR line was observed near 66 MHz at room temperature, as was expected from the cubic perovskite structure. This NQR signal disappeared at 232 K with decreasing temperature and six new lines appeared at about 180 K, as shown in Fig. 4. Because of the wide distribution of the spectra at 77 K, one part of the ^{79,81}Br NQR spec-

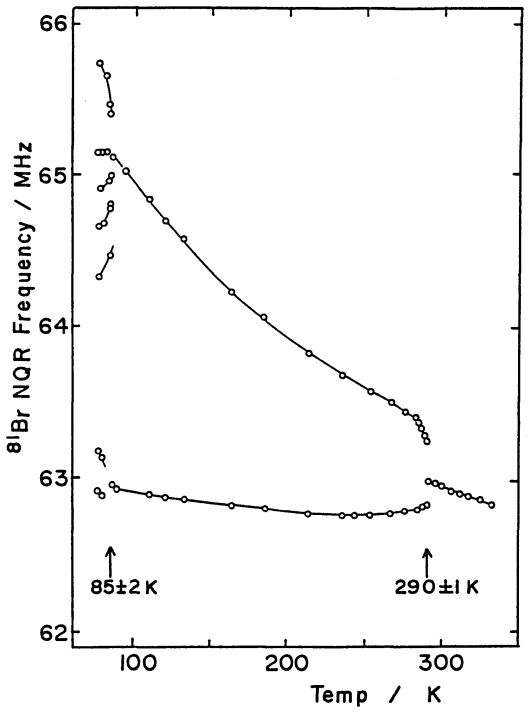

Fig. 2. Temperature dependence of the ^{81}Br NQR frequencies for $CsSnBr_3$. Three phases I, II, and III exist betwen 77 and 330 K from the lowest.

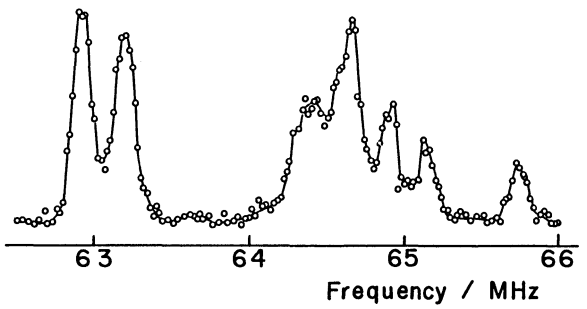

Fig. 3. ^{81}Br NQR spectrum for $CsSnBr_3$ at 77 K using a spin-echo method.

Table 1. ^{81}Br NQR Frequencies for $MSnBr_3$(M=Cs and CH_3NH_3)[a]

Compounds	Frequency/MHz	
	77 K	296 K
$CsSnBr_3$	65.72, 65.13, 64.90, 64.65 64.39, 63.18, 62.92	62.970
$CH_3NH_3SnBr_3$	74.95, 72.83, 71.93 67.15, 65.85, 61.85	65.766

a) Estimated errors ±0.05 and ±0.005 MHz at 77 and 296 K, respectively.

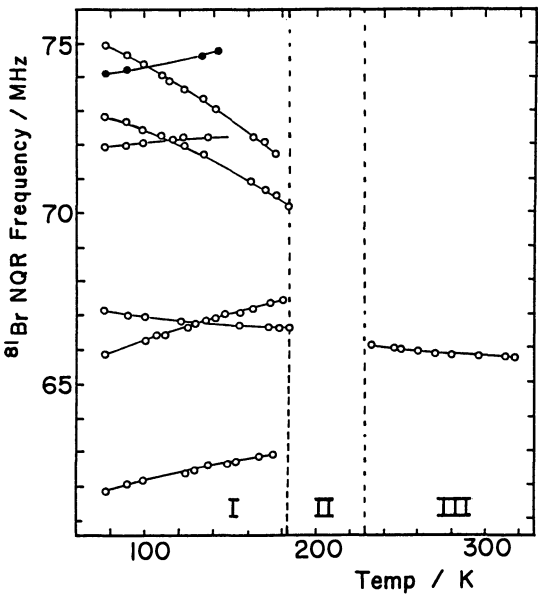

Fig. 4. Temperature dependence of the ^{81}Br NQR frequencies for $CH_3NH_3SnBr_3$. A part of the ^{79}Br NQR line was also observed in the same frequency range because of the wide distribution of the spectrum. Dotted lines show the averaged phase transition temperatures determined by the DTA.

tra overlapped with each other, as shown in Fig. 4. The DTA measurements for this compound are shown in Fig. 5 in the temperature range 160—280 K. Two large peaks corresponding to solid-solid phase transitions appeared with several degrees of hysteresis. Between these two peaks a very small one appeared, though it could not be confirmed by the NQR because of there being no signal in this intermediate phase. Therefore, at least three phases (I, II, and III) exist between 300 and 77 K. Associated with the phase transition between II↔III, the color changed drastically from red to yellow, suggesting a significant structural change. In relation to these successive phase transitions, it is particularly interesting that the splitting of the NQR frequency at 77 K is considerably larger for $CH_3NH_3SnBr_3$ than that expected from the crystal field effect. That is, the highest frequency, about 75 MHz, is comparable to that of a discrete pyramidal $SnBr_3^-$ anion having model (D);[1] the lowest one, about 62 MHz, is lower than that of a room-temperature perovskite structure having model (A). These findings suggest that there are at least two different $SnBr_3^-$ anions having distorted $SnBr_6$ octahedra (such as model (B), (C), or (D)) in the phase I.

Recently, in the course of this study, similar structural phase transitions from model (A) to (D) were reported for a series of $CsGeX_3$ (X=Cl, Br, and I)[14] in which the GeX_3^- anions have the same valence electron configuration as that of SnX_3^-. The high-temperature phase of these compounds belongs to a cubic perovskite, so that the trans Br-Ge-Br bond is symmetric. In the low-temperature phase, however, the Ge atom in the halogen octahedral is considerably displaced from the center of the octahedra along the three-fold axis and the octahedra becomes distorted rhombohedrally. Hence, three trans X-Ge-X bonds become asymmetric X-Ge··· X and the anion can also be regarded as an isolated anion. These structural changes are expected for a main-group element having a valence state with an s-electron lone pair, such as Sn(II), Ge(II), As(III), Sb(III), and Te(IV). The nuclear quadruple resonance of halogens is a useful technique for this problem and drastic NQR frequency shifts have been observed for $MSnBr_3 \cdot H_2O$[1] and $(C_5H_5NH)SbBr_4$.[5]

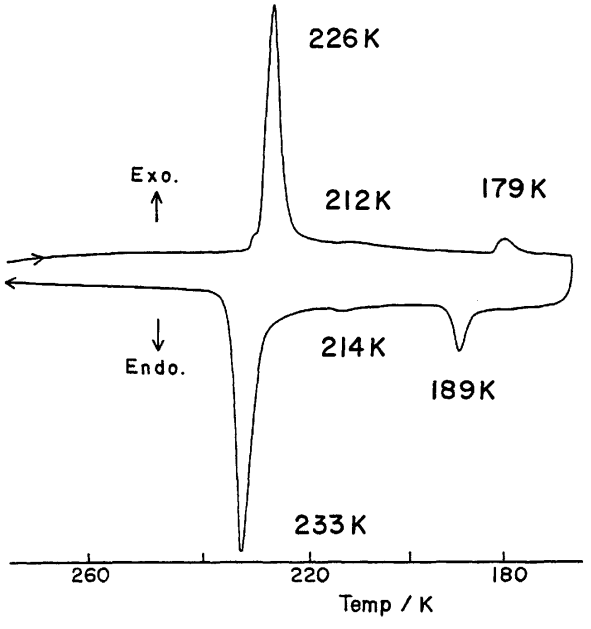

Fig. 5. DTA curve for $CH_3NH_3SnBr_3$ in the temperature range 280—160 K. The transition temperatures, which were determined at the peak positions, show several degrees of hysteresis.

The ^{119}Sn Mössbauer Effect for the $MSnBr_3$ (M=Cs and CH_3NH_3). ^{119}Sn Mössbauer spectra at 93 K are shown in Fig. 6. A quadrupole splitting appears only for $CH_3NH_3SnBr_3$, as was expected from the ^{81}Br NQR. On the other hand, the spectra at 293 K are very weak single Lorentzian, having ca. 1% relative absorption. ^{119}Sn Mössbauer parameters at 293 and 93 K are summarized in Table 2. It is particularly significant that not only the quadrupole splitting but also the isomer shift changed drastically only for the $CH_3NH_3^+$ analog with decreasing temperature. These results suggest that the symmetry at the Sn site lowered and the s-electron density decreased accompanied by structural phase transitions. This large change of the Mössbauer parameters is reasonable if some structural change

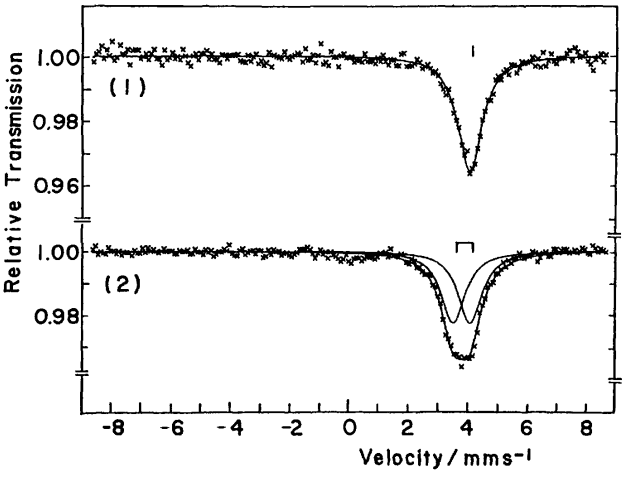

Fig. 6. ^{119}Sn Mössbauer spectra for $CsSnBr_3$ (1) and $CH_3NH_3SnBr_3$ (2) at 93 K.

Table 2. ^{119}Sn Mössbauer Parameters for $MSnBr_3$ (M=Cs and CH_3NH_3)[a]

Compound	Temp / K	I.S. / mm s^{-1}	Q.S. / mm s^{-1}	Line width / mm s^{-1}
$CsSnBr_3$	293	4.00	0	0.84
	93	4.01	0	0.91
	80[b]	3.98	0	0.84
$CH_3NH_3SnBr_3$	293	3.98	0	1.05
	93	3.81	0.54	0.99

a) Estimated error ±0.03 m s^{-1}. b) Ref. 23.

from model (A) to (D) or (B) takes place. In the case of model (A), the tin atom forms symmetric 3c-4e bonds in three orthogonal directions, so that there is no s-orbital hybridization to the bonds. On the other hand, in the model (D) or (B) structure, the bond angle of the $SnBr_3^-$ anion (Br-Sn-Br) becomes slightly larger than 90 degrees and, hence, a hybridization of the s-orbital to the p-orbitals takes place.[15] Thus, the smaller isomer shifts at 93 K than 293 K can be attributed to a decrease in the s-electron density due to a hybridization of the s-orbital to the pure p-orbital bonding.

^{1}H NMR for $CH_3NH_3SnBr_3$. In order to examine the relationship between these phase transitions and the dynamical property of the cation, the ^{1}H NMR was observed as a function of temperature (Fig. 7). The calculated second moments in phases I and III were almost constant and were 8±0.5 and 0.5±0.1 G^2(1G= 10^{-4} T), respectively. According to the previous ^{1}H NMR studies containing the same cation, the second moment of about 7—8 G^2 corresponds to the reorientational motion of the cation around its C_3 axis.[16-19] The second moment of about 0.5 G^2 corresponds to an interionic contribution, indicating that an overall rotation of the cation takes place at a rate higher than ca. $10^5\,s^{-1}$. These phase transitions take place at almost the same temperature at which the 2nd moment changed stepwise. These results suggest that the phase transitions are largely affected by the dynamical properties of the $CH_3NH_3^+$ cation. Many structural phase transitions containing the $CH_3NH_3^+$ cation have been reported, partly because of a change in the effective volume and partly because of a breakdown of the hydrogen-bonding networks.[20-22] In this case, it is particularly noteworthy that the structure and the bonding of the anion are also affected associated with these phase transitions due to the nature of the 3c-4e bond.

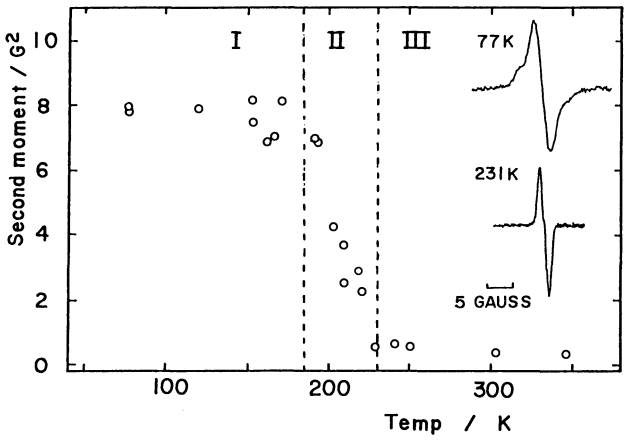

Fig. 7. Temperature dependence of the ^{1}H NMR second moment for $CH_3NH_3SnBr_3$.

References

1) K. Yamada, T. Hayashi, T. Umehara, T. Okuda, and S. Ichiba, *Bull. Chem. Soc. Jpn.*, **60**, 4203 (1987).
2) N. N. Greenwood and A. Earnshaw, "Chemistry of the elements," Pergamon Press (1984), p. 439.
3) T. A. Albright, J. K. Burdett, and M. H. Whangbo, "Orbital Interactions in Chemistry," John Wiley & Sons, New York (1985), p. 258.
4) G. C. Pimentel, *J. Chem. Phys.*, **19**, 446 (1951).
5) T. Okuda, K. Yamada, H. Ishihara, M. Hiura, S. Gima, and H. Negita, *J. Chem. Soc., Chem. Commun.*, **1981**, 979.
6) J. Barrett, S. R. A. Bird, J. D. Donaldson, and J. Silver, *J. Chem. Soc. A*, **1971**, 3105.
7) J. D. Donaldson, J. Silver, S. Hadjiminolis, and S. D. Poss, *J. Chem. Soc., Dalton Trans.*, **1974**, 1500.
8) V. G. Bergerhoff, L. Goost, and E. Shultze-Rhonhof *Acta Crystallogr., Sect. B*, **24**, 803 (1968).
9) P. Mauersberger and F. Huber, *Acta Crystallogr., Sect. B*, **36**, 683 (1980).
10) J. Andersson, *Acta Chem. Scand., Ser. A*, **30**, 229 (1976).
11) F. R. Poulsen and S. E. Rasumussen, *Acta Chem. Scand.*, **24**, 150 (1970).
12) D. E. Parry, M. J. Tricker, and J. D. Donaldson, *J. Solid State Chem.*, **28**, 401 (1979).
13) D. E. Scaife, P. F. Weller, and W. G. Fisher, *J. Solid State Chem.*, **9**, 308 (1974).
14) G. Thiele,. H. W. Rotter, and K. D. Schmidt, *Z. Anorg. Allg. Chem.*, **545**, 148 (1987).
15) M. J. Tricker and J. D. Donaldson, *Inorg. Chem. Acta*, **31**, L445 (1978).
16) R. Ikeda, Y. Kume, and D. Nakamura, *J. Magn. Reson.*, **24**, 9 (1976).
17) Y. Kume, R. Ikeda, and D. Nakamura, *J. Phys. Chem.*, **82**, 1926 (1978).
18) R. Jakubas, Z. Czapla, Z. Galewski, L. Sobczyk, O. J. Zogal, and T. Lis, *Phys. Status Solid A*, **93**, 449 (1986).
19) Y. Kume, R. Ikeda, and D. Nakamura, *J. Magn. Reson.*, **20**, 276 (1975).
20) F. Milia, *Solid State Commun.*, **51**, 625 (1984).
21) H. Fuess, M. Korfer, H. Arend, and R. Kind, *Solid State Commun.*, **56**, 137 (1985).
22) H. Ishida, R. Ikeda, and D. Nakamura, *J. Chem. Soc., Faraday Trans. 2*, **81**, 963 (1985).
23) J. D. Donaldson, R. M. A. Grimsey, and S. J. Clark, *J. Phys. (Paris)*, **40**, C2-289 (1979).

 © 1988 The Chemical Society of Japan Bull. Chem. Soc. Jpn., 61, 4269—4275 (1988)

Study of Polarographic Anodic Wave in the Presence of Sulfate Ions by a Numerical Method

Kenji KIKUCHI* and Teisuke MURAYAMA†
Shiga Prefectural Junior College, Hikone, Shiga 522
†Department of Applied Chemistry, Faculty of Engineering, Shizuoka University, Johoku, Hamamatsu 432
(Received April 27, 1988)

A polarographic anodic wave in the presence of sulfate ions increases with any increase in the concentration of sulfate ions, contrary to the expectation based on a free dissolution of electrode mercury. It does not show any diffusion current plateau. The precipitation of mercury(I) sulfate, the product of an electrode reaction, does not take place within a dropping time. An analysis using a new numerical method previously reported proved that the wave is caused by the formation of a mercury(I) complex, $[Hg_2(SO_4)]$, with a stability constant of 150 $mol^{-1}\,dm^3$.

Kolthoff and Miller reported that an anodic process involving the electrooxidation of mercury appeared as a free dissolution wave in a solution of 0.1 mol dm^{-3} potassium nitrate, since nitrate ions do not depolarize a mercury electrode.[1)]

When sulfate ions are added into the solution, the anodic wave is expected to remain unchanged as long as the concentration of the mercury(I) sulfate produced is below its solubility. This means that the current-potential curve should be written as

$$E=E^0+(RT/2F)\ln \bar{i}. \quad (1)$$

In the above, E is the electrode potential of the dropping mercury electrode, E^0 the standard electrode potential, $\bar{i}$ the average current, and F is the Faraday constant. Equation 1 says that the anodic current is independent of the concentration of sulfate ions. This is not the case, however. The anodic current any increases with increase in the concentration of sulfate ions, as shown in Fig. 1. This fact contradicts Eq. 1.

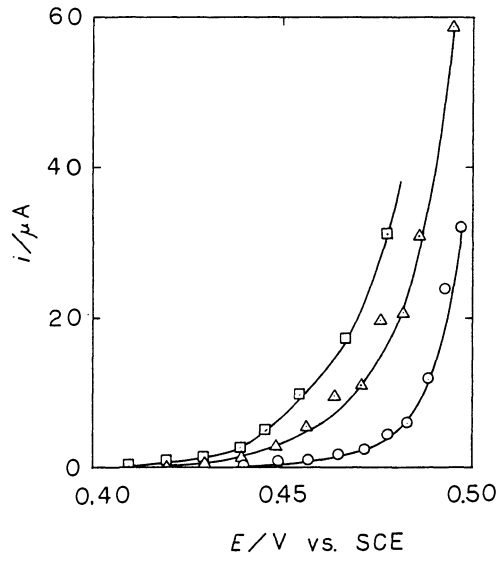

Fig. 1. Effect of the concentration of sulfate ions on the anodic current in a solution of pH 1.93. Concentration of a sodium sulfate, ○; 2 mmol dm^{-3}, △; 10 mmol dm^{-3}, □; 20 mmol dm^{-3}.

Figure 1 also shows that the anodic current does not attain the diffusion current plateau as expected for the anodic current with precipitate formation, of which a treatment was described in a previous paper.[2)]

The purpose of this paper is to clarify processes involving the anodic wave in the presence of sulfate ions by applying a numerical method which was developed in previous reports.[2,3)]

Theory

In the anodic process, mercury is dissolved into solution as a mercury(I) ion; a mercury(I) ion reacts with a sulfate ion to produce a mercury(I) sulfate complex. When the concentration of the complex exceeds its solubility, precipitate particles of mercury(I) sulfate appear in the solution. The sequence of the reactions can be written as follows:

$$2Hg \rightleftharpoons Hg_2^{2+} + 2e^- \quad (2)$$

$$HSO_4^- \underset{k_{-2}}{\overset{k_2}{\rightleftharpoons}} H^+ + SO_4^{2-} \quad (3)$$

$$Hg_2^{2+} + SO_4^{2-} \underset{k_{-3}}{\overset{k_3}{\rightleftharpoons}} Hg_2SO_4 \quad (4)$$

$$Hg_2SO_4 \underset{k_{-4}}{\overset{k_4}{\rightleftharpoons}} \text{precipitate} \quad (5)$$

In the above, k_2, k_{-2}, k_3, k_{-3}, k_4, and k_{-4} are the rate constants of Reactions 3—5. The rate of dissolution of precipitate particles in Reaction 5 is nil in the absence of a precipitate.

An analysis of the anodic current is carried out with using two alternative assumptions.

(1) The first assumption is that the mercury(I) sulfate precipitate particles are produced when the concentration of a mercury(I) sulfate complex exceeds its solubility.

When precipitate particles exist in a volume element or the concentration of the complex exceeds its solubility in it, the simultaneous equations governing the concentrations of species in the sequence of Reactions 2—5 are

$$\frac{\partial C_A}{\partial t} = D_A\left(\frac{\partial^2 C_A}{\partial r^2}\right) + \left(\frac{2}{r}D_A - u\right)\frac{\partial C_A}{\partial r} - k_3 C_A C_B + k_{-3} C_C, \quad (6)$$

$$\frac{\partial C_B}{\partial t} = D_B\left(\frac{\partial^2 C_B}{\partial r^2}\right) + \left(\frac{2}{r}D_B - u\right)\frac{\partial C_B}{\partial r} + k_2 C_D - k_{-2} C_H C_B - k_3 C_A C_B + k_{-3} C_C \ , \quad (7)$$

$$\frac{\partial C_C}{\partial t} = D_C\left(\frac{\partial^2 C_C}{\partial r^2}\right) + \left(\frac{2}{r}D_C - u\right)\frac{\partial C_C}{\partial r} + k_3 C_A C_B - k_{-3} C_C - k_4 C_C + k_{-4} \ , \quad (8)$$

$$\frac{\partial C_D}{\partial t} = D_D\left(\frac{\partial^2 C_D}{\partial r^2}\right) + \left(\frac{2}{r}D_D - u\right)\frac{\partial C_D}{\partial r} - k_2 C_D + k_{-2} C_H C_B \ , \quad (9)$$

and

$$\frac{\partial C_P}{\partial t} = -u\frac{\partial C_P}{\partial r} + k_4 C_C - k_{-4} \ . \quad (10)$$

In the above

$$u = m/(4\pi\rho r^2), \quad (11)$$

where C_h is the concentration of species h, r the distance from the center of the electrode mercury drop, m the flow rate of mercury, and ρ the density of mercury. As for the subscript, A denotes the mercury(I) ion, B the sulfate ion, C the mercury(I) sulfate complex, D the hydrogen sulfate ion, and P the mercury(I) sulfate precipitate.

When the precipitate particles do not exist in a volume element, or the concentration of the complex is below its solubility, partial derivatives in Eq. 10 become zero. This results in the relation $k_4 C_C = k_{-4}$. Using this relation, Eqs. 6—9 become

$$\frac{\partial C_A}{\partial t} = D_A\left(\frac{\partial^2 C_A}{\partial r^2}\right) + \left(\frac{2}{r}D_A - u\right)\frac{\partial C_A}{\partial r} - k_3 C_A C_B + k_{-3} C_C \quad (12)$$

$$\frac{\partial C_B}{\partial t} = D_B\left(\frac{\partial^2 C_B}{\partial r^2}\right) + \left(\frac{2}{r}D_B - u\right)\frac{\partial C_B}{\partial r} + k_2 C_D - k_{-2} C_H C_B - k_3 C_A C_B + k_{-3} C_C \ , \quad (13)$$

$$\frac{\partial C_C}{\partial t} = D_C\left(\frac{\partial^2 C_C}{\partial r^2}\right) + \left(\frac{2}{r}D_C - u\right)\frac{\partial C_C}{\partial r} + k_3 C_A C_B - k_{-3} C_C \ , \quad (14)$$

and

$$\frac{\partial C_D}{\partial t} = D_D\left(\frac{\partial^2 C_D}{\partial r^2}\right) + \left(\frac{2}{r}D_D - u\right)\frac{\partial C_D}{\partial r} - k_2 C_D + k_{-2} C_H C_B . \quad (15)$$

The initial conditions are

$$C_A = 0,\ C_B = C^*_B,\ C_C = 0,\ C_D = C^*_D,\ C_P = 0 \ (t = 0,\ r = a), \quad (16)$$

and the boundary conditions are

$$C_A = C_{A0} = \exp\{2F(E - E^0)/RT\}/\gamma_A,\ (\partial C_B/\partial r)_{r=a} = 0,\ (\partial C_C/\partial r)_{r=a} = 0,\ (\partial C_D/\partial r)_{r=a} = 0 \ (t > 0,\ r = a) \quad (17)$$

$$C_A = 0,\ C_B = C^*_B,\ C_C = 0,\ C_D = C^*_D \text{ and } C_P = 0 \ (t > 0,\ r = \infty). \quad (18)$$

In the above, C_{A0} is the concentration of mercury(I) ions at the surface of the mercury electrode and γ_A is the activity coefficient of mercury(I) ions.

The relation between the concentration of hydrogen sulfate and sulfate ions is expressed by

$$C_F = C_D + C_B$$

and

$$(C_H + K_{a2})C_B/K_{a2} = (C_H + K_{a2})C_D/C_H. \quad (19)$$

In the above, C_H is the concentration of hydrogen ions, and K_{a2} the dissociation constant of the hydrogen sulfate ion. Equations 6—9 and 12—15 can be rewritten using Eq. 19. The following equations are derived from Eqs. 6—9 and 12—15:

$$\frac{\partial C_A}{\partial t} = D_A\left(\frac{\partial^2 C_A}{\partial r^2}\right) + \left(\frac{2}{r}D_A - u\right)\frac{\partial C_A}{\partial r} - \frac{k_3 C_A C_F K_{a2}}{C_H + K_{a2}} + k_{-3} C_C, \quad (20)$$

$$\frac{\partial C_F}{\partial t} = D_F\left(\frac{\partial^2 C_F}{\partial r^2}\right) + \left(\frac{2}{r}D_F - u\right)\frac{\partial C_F}{\partial r} - \frac{k_3 C_A C_F K_{a2}}{C_H + K_{a2}} + k_{-3} C_C \ , \quad (21)$$

$$\frac{\partial C_C}{\partial t} = D_C\left(\frac{\partial^2 C_C}{\partial r^2}\right) + \left(\frac{2}{r}D_C - u\right)\frac{\partial C_C}{\partial r} + \frac{k_3 C_A C_F K_{a2}}{C_H + K_{a2}} - k_{-3} C_C - k_4 C_C + k_{-4} \ , \quad (22)$$

and

$$\frac{\partial C_C}{\partial t} = D_C\left(\frac{\partial^2 C_C}{\partial r^2}\right) + \left(\frac{2}{r}D_C - u\right)\frac{\partial C_C}{\partial r} + \frac{k_3 C_A C_F K_{a2}}{C_H + K_{a2}} - k_{-3} C_C \quad (23)$$

The initial conditions are transformed as

$$C_A = 0,\ C_F = C^*_F,\ C_C = 0,\ C_P = 0 \ (t = 0,\ r = a). \quad (24)$$

The boundary conditions are

$$C_A = C_{A0},\ (\partial C_F/\partial r)_{r=a} = 0,\ (\partial C_C/\partial r)_{r=a} = 0 \ (t > 0,\ r = a) \quad (25)$$

$$C_A = 0,\ C_F = C^*_F,\ C_C = 0,\ C_P = 0 \ (t > 0,\ r = \infty). \quad (26)$$

The instantaneous current, i, is given by

$$i = 2FD_A S(\partial C_A/\partial r)_{r=a}, \quad (27)$$

where S is the surface area of the electrode mercury drop.

The following parameters are used to simplify the description of the simultaneous equations:

$$y_A = C_A/C^*_F,\ y_F = C_F/C^*_F,\ y_C = C_C/C^*_F,\ y_P = C_P/C^*_F,\ y_H = C_H/C^*_F,\ d_A = D_A/D_F,\ d_F = D_F/D_F,\ d_C = D_C/D_F,\ x = (r - a)/L,\ s = 1 - 1/\{1 + (r - a)H/L\},\ T = D_F t/L^2,\ U = Lur^2/D_F a^2 \text{ and } K^*_{a2} = K_{a2}/C^*_F. \quad (28)$$

An introduction of the above parameters into Eq. 20 results in

$$\frac{\partial y_A}{\partial T} = d_A H^2(1 - s)^4\frac{\partial^2 y_A}{\partial s^2} + \left\{\frac{2d_A}{x + a/L} + \frac{x(x + 2a/L)}{(x + a/L)^2}U - 2d_A H(1 - s)\right\}H(1 - s)^2\frac{\partial y_A}{\partial s} - \frac{L^2 C^*_F k_3 y_A y_F K^*_{a2}}{D_F(y_H + K^*_{a2})} + k_{-3} y_C L^2/D_F \ . \quad (29)$$

The space and time coordinates are expressed as

$$s_i = i\Delta s,\ T_j = j\Delta T,\ x_i = i\Delta s/H(1+i\Delta s)$$

and

$$y_A(s,\ t) = y_A(s_i,\ T_j) = y_{A,i,j}. \tag{30}$$

The reaction rate constants are replaced by following parameters:

$$k^*_3 = \Delta TL^2C^*_F K^*_{a2}k_3/D_F(y_H + K^*_{a2}),$$
$$k^*_{-3} = \Delta TL^2k_{-3}/D_F,\ k^*_4 = \Delta TL^2k_4/D_F,$$

and

$$k^*_{-4} = \Delta TL^2k_{-4}/D_FC^*_F. \tag{31}$$

The centered space difference method and the forward time method are used for converting the diffusion equations, except for one involving the concentration of precipitate particles.[3]

By using a method reported by Morihara and Cheng,[4] the chemical kinetics term involving the concentration of mercury(I) sulfate complex can be reformulated as

$$k^*_3(y_{A,i,j+1}y_{F,i,j+1} + y_{A,i,j}y_{F,i,j})/2 = k^*_3(y_{A,i,j+1}y_{F,i,j} + y_{A,i,j}y_{F,i,j+1})/2. \tag{32}$$

The introduction of Eqs. 30, 31, and 32 to Eq. 29 gives the following equations:

$$(E_{A,i} + k^*_3y_{F,i,j}/2)y_{A,i,j+1} = F_{A,i,j+1}y_{A,i+1,j+1} + G_{A,i,j+1}y_{A,i-1,j+1} + D_{A,i,j} - k^*_3y_{F,i,j+1}y_{A,i,j}/2 + k^*_{-3}(y_{C,i,j+1} + y_{C,i,j})/2, \tag{33}$$

$$E_{A,i} = 1 + \Delta TH(1-s_i)^4/(\Delta s)^2, \tag{34}$$

$$F_{A,i,j+1} = \Delta TH(1-s_i)^2\{d_AH(1-s_i)^2/\Delta s + d_A/(x_i+a_{j+1}/L) + x_i(x_i+2a_{j+1}/L)U_{j+1}/2(x_i+a_{j+1}/L)^2 - d_AH(1-s_i)\}/2\Delta s, \tag{35}$$

$$G_{A,i,j+1} = \Delta TH(1-s_i)^2\{d_AH(1-s_i)^2/\Delta s - d_A/(x_i+a_{j+1}/L) - x_i(x_i+2a_{j+1}/L)U_{j+1}/2(x_i+a_{j+1}/L)^2 + d_AH(1-s_i)\}/2\Delta s, \tag{36}$$

and

$$D_{A,i,j} = F_{A,i,j+1}y_{A,i+1,j} + G_{A,i,j+1}y_{A,i-1,j} + \{1-\Delta Td_AH^2(1-s_i)^4/\Delta s^2\}y_{A,i,j}. \tag{37}$$

In much the same way, Eq. 22 is transformed as

$$(E_{F,i} + k^*_3y_{A,i,j}/2)y_{F,i,j+1} = F_{F,i,j+1}y_{F,i+1,j+1} + G_{F,i,j+1}y_{F,i-1,j+1} + D_{F,i,j} - k^*_3y_{A,i,j+1}y_{F,i,j}/2 + k^*_{-3}(y_{C,i,j+1} + y_{C,i,j})/2. \tag{38}$$

The following equations are derived from Eqs. 22 and 23:

$$\{E_{C,i} - (k^*_{-3} - k^*_4)/2\}y_{C,i,j+1} = F_{C,i,j+1}y_{C,i+1,j+1} + G_{C,i,j+1}y_{C,i-1,j+1} + D_{C,i,j} - k^*_3(y_{A,i,j+1}y_{F,i,j}/2 + y_{A,i,j}y_{F,i,j+1})/2 + (k^*_{-3} - k^*_4)y_{C,i,j}/2, \tag{39}$$

and

$$(E_{C,i} - k^*_{-3}/2)y_{C,i,j+1} = F_{C,i,j+1}y_{C,i+1,j+1} + G_{C,i,j+1}y_{C,i-1,j+1} + D_{C,i,j} - k^*_3(y_{A,i,j+1}y_{F,i,j}/2 + y_{A,i,j}y_{F,i,j+1})/2 + k^*_{-3}y_{C,i,j}/2. \tag{40}$$

The backward space difference method must be used in order to obtain the difference equations of Eq. 10 for a precipitate, as was done in a previous study.[2] Equation 10 is transformed as follows. For i=1, the difference equation is expressed with concentrations at nodes (1, j), (2, j), (3, j), (4, j), (1, j+1), (2, j+1), (3, j+1), and (4, j+1).

$$(1+11M_{P,1,j+1})y_{P,1,j+1} = M_{P,1,j+1}(18y_{P,2,j+1} - 9y_{P,3,j+1} + 2y_{P,4,j+1}) + M_{P,1,j+1}(-11y_{P,1,j} + 18y_{P,2,j} - 9y_{P,3,j} + 2y_{P,4,j}) + y_{P,1,j} + k^*_4(y_{C,1,j+1} + y_{C,1,j})/2 - k^*_{-4} \tag{41}$$

For $1<i<99$, the difference equation is expressed with concentrations at nodes (i−1, j), (i, j), (i+1, j), (i+2, j), (i−1, j+1), (i, j+1), (i+1, j+1), and (i+2, j+1).

$$(1+3M_{P,i,j+1})y_{P,i,j+1} = M_{P,i,j+1}(-2y_{P,i-1,j+1} + 6y_{P,i+1,j+1} - y_{P,i+2,j+1}) + M_{P,i,j+1}(-2y_{P,i-1,j} - 3y_{P,i,j} + 6y_{P,i+1,j} - y_{P,i+2,j}) + y_{P,i,j} + k^*_4(y_{C,i,j+1} + y_{C,i,j})/2 - k^*_{-4} \tag{42}$$

For a node with i=99, only an outer node is a node with i=100. Therefore, the backward space difference method is not applicable for a transformation; thus, the forward space difference method is used for this purpose. The difference equation is expressed with the concentrations at nodes (97, j), (98, j), (99, j), (100, j), (97, j+1), (98, j+1), (99, j+1), and (100, j+1).

$$(1-3M_{P,99,j+1})y_{P,99,j+1} = M_{P,99,j+1}(y_{P,97,j+1} - 6y_{P,98,j+1} + 2y_{P,100,j+1}) + M_{P,99,j+1}(y_{P,97,j} - 6y_{P,98,j} + 3y_{P,99,j} + 2y_{P,100,j}) + y_{P,99,j} + k^*_4(y_{C,99,j+1} + y_{C,99,j})/2 - k^*_{-4} \tag{43}$$

$$M_{P,i,j+1} = \Delta TH(1-s_i)^2U_{j+1}x_i(x_i+2a_{j+1}/L)/6\Delta s(x_i+a_{j+1}/L)^2 \tag{44}$$

The derived expression of the boundary condition in Eq. 25 can be rewritten with concentrations at nodes (0, j), (1, j), (2, j), (3, j), (0, j+1), (1, j+1), (2, j+1), and (3, j+1) by a previously reported procedure:[2]

$$y_{F,0,j+1} = (18y_{F,1,j+1} - 9y_{F,2,j+1} + 2y_{F,3,j+1})/11 \tag{45}$$

$$y_{C,0,j+1} = (18y_{C,1,j+1} - 9y_{C,2,j+1} + 2y_{C,3,j+1})/11 \tag{46}$$

Values of $y_{A,i,j+1}$, $y_{C,i,j+1}$, and $y_{F,i,j+1}$ are calculated by using Eqs. 33, 38, 40, 45, and 46 when precipitate particles do not exist in a volume element; these and the value of $y_{P,i,j+1}$ are calculated by using Eqs. 33, 39, 41, 42, 43, 45, and 46 when precipitate particles exist in a volume element.

(2) The second alternative assumption consists of two parts. The first part is that the concentration of the mercury(I) sulfate complex is negligible compared with the concentrations of the mercury(I) and sulfate

ions. A corollary to this is that derivatives in Eqs. 8 and 14 are zero. The second part is that the reaction rates of Reactions 4 and 5 are so large that reactions attains equilibrium within the dropping time. This latter condition is usually assumed for an analysis of a wave involving a precipitation reaction.

When precipitate particles exist in a volume element, Eq. 47 can be derived from Eq. 8:

$$C_C=(k_3C_AC_B+k_{-4})/(k_{-3}+k_4) \tag{47}$$

By the introduction of Eq. 47 to Eqs. 6, 7, 9, and 10, the following equations are obtained:

$$\frac{\partial C_A}{\partial t}=D_A\left(\frac{\partial^2 C_A}{\partial r^2}\right)+\left(\frac{2}{r}D_A-u\right)\frac{\partial C_A}{\partial r}-\frac{k_3k_4C_AC_B-k_{-3}k_{-4}}{k_{-3}+k_4}, \tag{48}$$

$$\frac{\partial C_B}{\partial t}=D_B\left(\frac{\partial^2 C_B}{\partial r^2}\right)+\left(\frac{2}{r}D_B-u\right)\frac{\partial C_B}{\partial r}+k_2C_D-k_{-2}C_HC_B-\frac{k_3k_4C_AC_B-k_{-3}k_{-4}}{k_{-3}+k_4}, \tag{49}$$

$$\frac{\partial C_D}{\partial t}=D_D\left(\frac{\partial^2 C_D}{\partial r^2}\right)+\left(\frac{2}{r}D_D-u\right)\frac{\partial C_D}{\partial r}-k_2C_D+k_{-2}C_HC_B, \tag{50}$$

and

$$\frac{\partial C_P}{\partial t}=-u\frac{\partial C_P}{\partial r}+\frac{k_3k_4C_AC_B-k_{-3}k_{-4}}{k_{-3}+k_4}. \tag{51}$$

The solubility product is related to the reaction rate constants by

$$K_{sp}=C_AC_B=k_{-3}k_{-4}/k_3k_4. \tag{52}$$

When precipitate particles do not exist in a volume element, the simultaneous equations governing the concentration of species involving Reactions 2 and 3 are given as

$$\frac{\partial C_A}{\partial t}=D_A\left(\frac{\partial^2 C_A}{\partial r^2}\right)+\left(\frac{2}{r}D_A-u\right)\frac{\partial C_A}{\partial r}, \tag{53}$$

$$\frac{\partial C_B}{\partial t}=D_B\left(\frac{\partial^2 C_B}{\partial r^2}\right)+\left(\frac{2}{r}D_B-u\right)\frac{\partial C_B}{\partial r}+k_2C_D-k_{-2}C_HC_B, \tag{54}$$

and

$$\frac{\partial C_D}{\partial t}=D_D\left(\frac{\partial^2 C_D}{\partial r^2}\right)+\left(\frac{2}{r}D_D-u\right)\frac{\partial C_D}{\partial r}-k_2C_D+k_{-2}C_HC_B. \tag{55}$$

Equations 48—51 and 53—55 are rewritten by use of Eq. 19:

$$\frac{\partial C_A}{\partial t}=D_A\left(\frac{\partial^2 C_A}{\partial r^2}\right)+\left(\frac{2}{r}D_A-u\right)\frac{\partial C_A}{\partial r}-\frac{k_3k_4C_AC_FK_{a2}}{(k_{-3}+k_4)(C_H+K_{a2})}+\frac{k_{-3}k_{-4}}{k_{-3}+k_4}, \tag{56}$$

$$\frac{\partial C_F}{\partial t}=D_F\left(\frac{\partial^2 C_F}{\partial r^2}\right)+\left(\frac{2}{r}D_F-u\right)\frac{\partial C_F}{\partial r}-\frac{k_3k_4C_AC_FK_{a2}}{(k_{-3}+k_4)(C_H+K_{a2})}+\frac{k_{-3}k_{-4}}{k_{-3}+k_4}, \tag{57}$$

$$\frac{\partial C_P}{\partial t}=-u\frac{\partial C_P}{\partial r}+\frac{k_3k_4C_AC_FK_{a2}}{(k_{-3}+k_4)(C_H+K_{a2})}-\frac{k_{-3}k_{-4}}{k_{-3}+k_4}, \tag{58}$$

$$\frac{\partial C_A}{\partial t}=D_A\left(\frac{\partial^2 C_A}{\partial r^2}\right)+\left(\frac{2}{r}D_A-u\right)\frac{\partial C_A}{\partial r}, \tag{59}$$

and

$$\frac{\partial C_F}{\partial t}=D_F\left(\frac{\partial^2 C_F}{\partial r^2}\right)+\left(\frac{2}{r}D_F-u\right)\frac{\partial C_F}{\partial r}. \tag{60}$$

In much the same way as Eq. 20 was transformed to a difference equation, Eqs. 56, 57, 58, and 60 can be transformed as follows:

$$\{E_{A,i}+k^*_3k^*_4y_{F,i,j}/2(k^*_{-3}+k^*_4)\}y_{A,i,j+1}=F_{A,i,j+1}y_{A,i+1,j+1}+G_{A,i,j+1}y_{A,i-1,j+1}+D_{A,i,j}-k^*_3k^*_4y_{A,i,j}y_{F,i,j+1}/2(k^*_{-3}+k^*_4)+k^*_{-3}k^*_{-4}/(k^*_{-3}+k^*_4), \tag{61}$$

$$\{E_{F,i}+k^*_3k^*_4y_{A,i,j}/2(k^*_{-3}+k^*_4)\}y_{F,i,j+1}=F_{F,i,j+1}y_{F,i+1,j+1}+G_{F,i,j+1}y_{F,i-1,j+1}+D_{F,i,j}-k^*_3k^*_4y_{A,i,j+1}y_{F,i,j}/2(k^*_{-3}+k^*_4)+k^*_{-3}k^*_{-4}/(k^*_{-3}+k^*_4), \tag{62}$$

$$E_{A,i}y_{A,i,j+1}=F_{A,i,j+1}y_{A,i+1,j+1}+G_{A,i,j+1}y_{A,i-1,j+1}+D_{A,i,j}, \tag{63}$$

and

$$E_{F,i}y_{F,i,j+1}=F_{F,i,j+1}y_{F,i+1,j+1}+G_{F,i,j+1}y_{F,i-1,j+1}+D_{F,i,j}. \tag{64}$$

The following equation is derived from Eq. 58 by the same procedure as applied Eq. 10:

$i=1$

$$(1+11M_{P,1,j+1})y_{P,1,j+1}=M_{P,1,j+1}(18y_{P,2,j+1}-9y_{P,3,j+1}+2y_{P,4,j+1})+M_{P,1,j+1}(-11y_{P,1,j}+18y_{P,2,j}-9y_{P,3,j}+2y_{P,4,j})+y_{P,1,j}+k^*_3k^*_4(y_{A,1,j+1}y_{F,1,j}+y_{A,1,j}y_{F,1,j+1})/2(k^*_{-3}+k^*_4)-k^*_{-3}k^*_{-4}/(k^*_{-3}+k^*_4), \tag{65}$$

$1<i<99$

$$(1+3M_{P,i,j+1})y_{P,i,j+1}=M_{P,i,j+1}(-2y_{P,i-1,j+1}+6y_{P,i+1,j+1}-y_{P,i+2,j+1})+M_{P,i,j+1}(-2y_{P,i-1,j}-3y_{P,i,j}+6y_{P,i+1,j}-y_{P,i+1,j})+y_{P,i,j}+k^*_3k^*_4(y_{A,i,j+1}y_{F,i,j}+y_{A,i,j}y_{F,i,j+1})/2(k^*_{-3}+k^*_4)-k^*_{-3}k^*_{-4}/(k^*_{-3}+k^*_4), \tag{66}$$

and

$i=99$

$$(1-3M_{P,99,j+1})y_{P,99,j+1}=M_{P,99,j+1}(y_{P,97,j+1}-6y_{P,98,j+1}+2y_{P,100,j+1})+M_{P,99,j+1}(y_{P,97,j}-6y_{P,98,j}+3y_{P,99,j}+2y_{P,100,j})+y_{P,99,j}+k^*_3k^*_4(y_{A,99,j+1}y_{F,99,j}+y_{A,99,j}y_{F,99,j+1})/2(k^*_{-3}+k^*_4)-k^*_{-3}k^*_{-4}/(k^*_{-3}+k^*_4), \tag{67}$$

When precipitate particles exist in a volume element, the values of $y_{A,i,j+1}$, $y_{F,i,j+1}$ and $y_{P,i,j+1}$ are calculated from Eqs. 45, 46, 61, 62, 65, and 66. When the precipitate particles do not exist in a volume ele-

ment, the values of $y_{A,i,j+1}$ and $y_{F,i,j+1}$ are calculated from Eqs. 45, 46, 63, and 64.

The observed corrected anodic current is obtained by subtracting the anodic current in the absence of sulfate ions from one in the presence of a sulfate ion. A numerical method to calculate an anodic current of mercury in the absence of sulfate ion will now be described.

The differential equation governing the concentration of the mercury(I) ion is given as

$$\frac{\partial C_A}{\partial t} = D_A\left(\frac{\partial^2 C_A}{\partial r^2}\right) + \left(\frac{2}{r}D_A - u\right)\frac{\partial C_A}{\partial r}. \quad (68)$$

The initial condition is

$$C_A = 0 \qquad (t=0, r=a). \quad (69)$$

The boundary conditions are

$$C_{A0} = C_{A0} \qquad (t=0, r=a), \text{ and} \quad (70)$$

$$C_A = 0 \qquad (t>0, r=\infty). \quad (71)$$

The difference equation form of Eq. 68 is

$$E_{A,i}y_{A,i,j+1} = F_{A,i,j+1}y_{A,i+1,j+1} + G_{A,i,j+1}y_{A,i,j+1} + D_{A,i,j}. \quad (72)$$

The instantaneous anodic current in the absence of a sulfate ion, i_r, is given by

$$i_r = 2FD_AS(\partial C_A/\partial_r)_{r=a}. \quad (73)$$

The corrected anodic current, i_C, is obtained by

$$i_C = i - i_r. \quad (74)$$

The corrected current is the current mainly caused by either a complex formation reaction or a precipitation reaction.

Experimental

The chemicals used were of reagent grade. The concentration of sodium sulfate in the stock solution was calculated from a weighed amount of anhydrous sodium sulfate after drying 150 °C for 2 h. The concentration of hydrogen ions in the test solution was controlled with sodium carbonate and perchloric acid. The ionic strength of the solution was also adjusted to 0.1 mol dm^{-3}.

Measurements were carried out using a Hokuto Denko Model HA-104 Potentio-Galvanostat in conjunction with the three-electrode method. Precautions were taken in order to prevent any permeation of both chloride and potassium ions from the salt bridges.

The electric resistance of the test solution in the electrolytic system was determined from the free dissolution wave of electrode mercury. The method used was as follows. The value of the resistance was assumed and the electrode potential (E) was corrected by subtracting the iR drop. The corrected electrode potential was plotted against log i. Such a plot does not necessarily produce a straight line. When the assumed value of the resistance is incorrect, the plot is curved. In this case, plotting is repeated with a slightly different value of resistance. This procedure was repeated until the plotting produced a straight line. When plotting produces a straight line, the value of resistance used is the correct value of the resistance of the circuit. This procedure gave 200 Ω for the corrected value of the resistance. The value of the slope of the straight line, ranging from 32.5 mV/unit to 33.0 mV/unit,[1] agrees with the value reported by Kolthoff and Miller. All potentials reported in this paper were corrected for the iR drop and all polarographic currents were corrected for the residual current.

The dropping mercury electrode used had the following characteristics (in 0.1 mol dm^{-3} sodium perchlorate at zero applied potential vs. SCE, and at a mercury head of 80.0 cm): a flow rate of mercury (m) of 1.86 mg s^{-1}, a drop time (t) of 3.20 s, and a capillary constant ($m^{2/3}t^{1/6}$) of 1.846 mg$^{2/3}$ s$^{-1/2}$.

Results and Discussion

The anodic current in a solution of sulfate ion was examined by our numerical method.

The value of the diffusion coefficient of the mercury(I) ion was chosen so as to give the smallest difference between the calculated diffusion currents and the observed ones.[3] This procedure gave a value of 0.847×10^{-5} cm^2 s^{-1}. A value of 1.08×10^{-5} cm^2 s^{-1} for a sulfate ion was taken from Ref. 5. The value of the diffusion coefficient of a mercury(I) complex is assumed to be equal to that for mercury(I) ion. Values of pK_{a2} and K_{sp} used are 1.99 and 7.4×10^{-7} mol^2 dm^{-6}.[6,7]

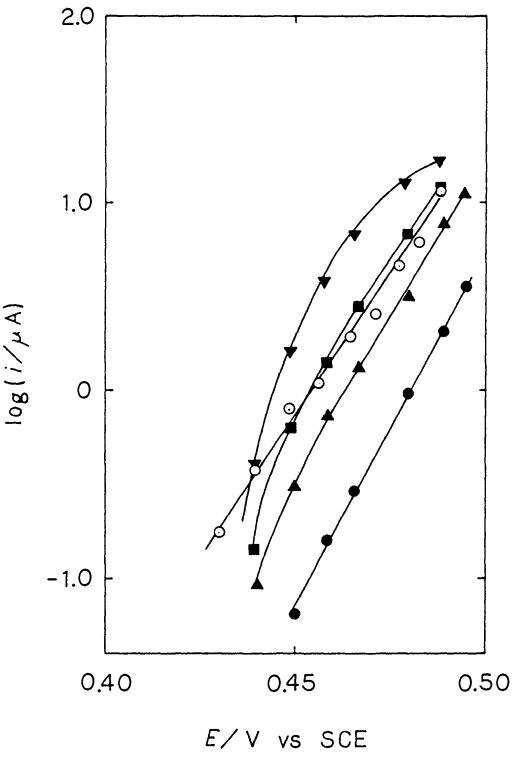

Fig. 2. Effect of the dissolution rate constant on the logarithmic plot in a solution of 2×10^{-3} mol dm^{-3} sodium sulfate and pH 1.93. Computation was carried out using the second alternative assumption. The value of K_{sp} is 0.25×10^{-7} mol^{2}dm^{-6}. ○; observed. Precipitation reaction rate constant (mol^{-1}dm^3 s^{-1}), ●; 10, ▲; 50, ■; 100, ▼; 300.

At first, the anodic current was analyzed using the second assumption, that the concentration of mercury-(I) sulfate complex is negligible compared with the concentrations of mercury(I) and sulfate ions. The observed anodic current does not show any diffusion current plateau. It was shown in a previous report[2] that a diffusion current plateau is observed in the case of a large precipitation rate, even with a large value of K_{sp}. Hence, the absence of a plateau indicates that the rate of Reaction 5 is not so large.

Figure 2 shows the effect of the precipitation reaction rate k_4 on the plots of log i against E, constructed from observed and computed polarograms. The anodic current increased with an increase in the value of k_4. For a value of 100 mol^{-1} dm^3 s^{-1} for k_4, the difference between the calculated and observed current at 0.47 V vs. SCE is smallest compared with other values. However, this value is not sufficiently large to give a plateau.

Figure 3 shows plots of log i against E, constructed from observed and computed polarograms. The observed polarograms give straight lines, of which slope is 30—32 mV/unit. The calculated points approach to the observed points with a decrease in K_{sp}. A fair agreement between the calculated and observed points was obtained with a value of K_{sp} which was smaller than 1/50 of the accepted value.[7] This shows that the second assumption is in contradiction with the observed polarograms.

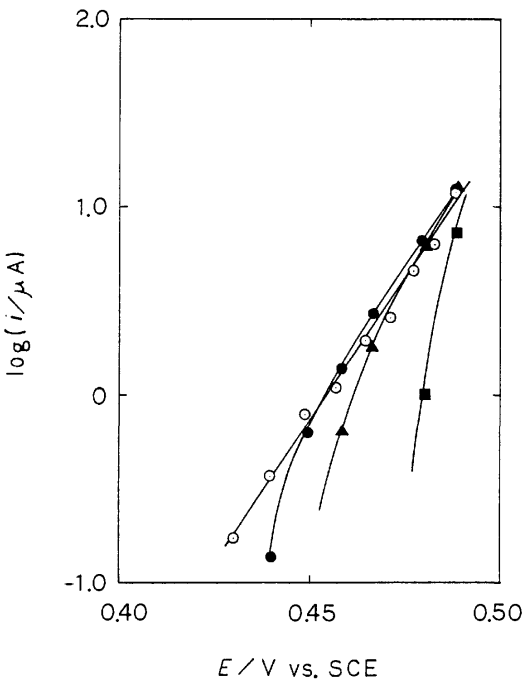

Fig. 3. Logarithmic plots of the anodic current in the solution of 2×10^{-3} mol dm^{-3} sodium sulfate and pH 1.93. Computation was carried out using the second assumption. The value of precipitation reaction rate is 100 mol^{-1} dm^3 s^{-1}. O; observed data. The value of K_{sp} ($mol^2 dm^{-6}$), ●; 0.25×10^{-7}, ▲; 0.93×10^{-7}, 7.40×10^{-7}.

Table 1. The Time Necessary for Appearance of Precipitate Particles after Mixing of Solution of Mercury(I) and Sulfate Ions. The Appearance was Observed Visually

$[Hg_2^{2+}][SO_4^{2-}]$ / 1×10^{-5} mol^2 dm^{-6}	$[Hg_2^{2+}][SO_4^{2-}]/K_{sp}$	Time / min
1.5	2.54	150
3.0	5.08	20
4.5	7.62	1
7.5	12.7	0.5
15.0	25.4	0.5

The solutions of sulfate ion in pH 1.93 are mixed with a solution of 8.03 mM mercury(I) ion in pH 1.93.

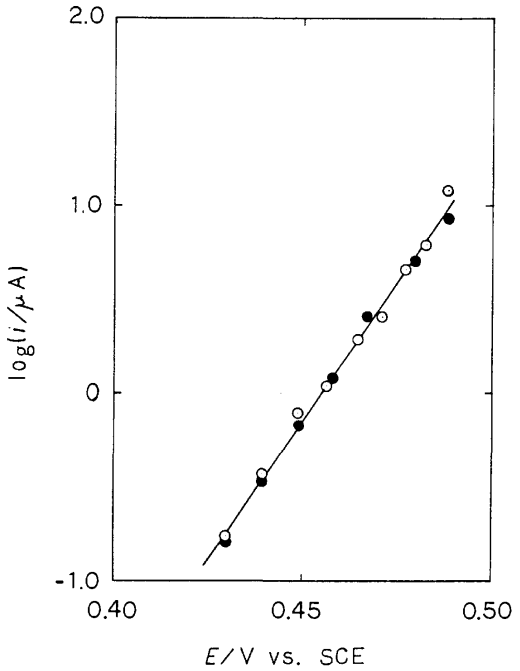

Fig. 4. Logarithmic plots of the anodic current in the solution of 2×10^{-3} mol dm^{-3} soddium sulfate and pH 1.93. Computation was carried out using the first assumptions.
O; observed data, ●; calculated data.

Table 1 shows the time necessary for the appearance of precipitate particles after mixing of solutions of mercury(I) and sulfate ions. The appearance was observed visually. It has been found that the time necessary for the appearance of precipitate particles is too large compared with the dropping time. This means that the values of k_4 and k_{-4} are nearly equal to zero.

Figure 4 shows the anodic current computed by using the first assumption that the mercury(I) sulfate precipitate is produced when the concentration of the mercury(I) sulfate complex exceeds its solubility. The calculated anodic currents are in fair agreement with the observed values. Calculated points were computed with a value of 150 $mol^{-1}dm^3$ for the equilibrium constant of Reaction 4.

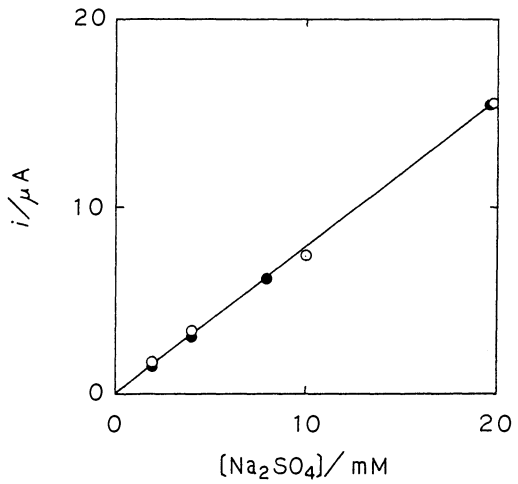

Fig. 5. Effect of the concentration of sodium sulfate on the anodic current at 0.46 V vs. SCE in the solution of pH 1.93. O; observed data, ●; calculated data.

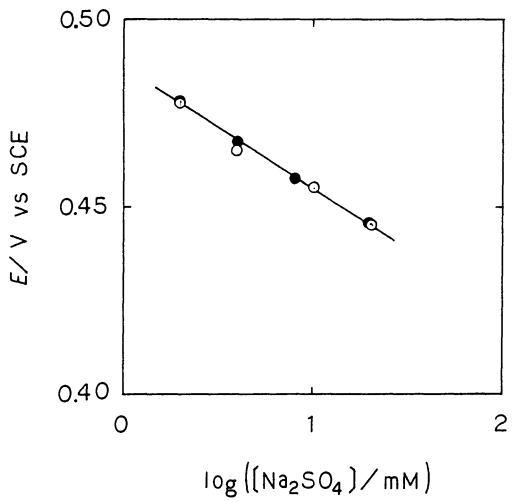

Fig. 6. Effect of the concentration of sodium sulfate on the electrode potential with the value of 5 μA for anodic current in the solution of pH 1.93. O ; observed data, ●; calculated data.

Figure 5 shows the relation between the concentration of the sulfate ions and the anodic current at 0.46 V vs. SCE. It shows that the observed currents agree well with calculated values, and that both are proportional to the concentration of sulfate ions.

Figure 6 shows the relation between the concentration of sulfate ions and the electrode potential where the anodic current is 5 μA. The calculated values agree well with the observed ones.

From the above discussion, it is certain that the anodic current is caused by the formation of a mercury(I) sulfate complex and that the precipitation reaction is slow and negligible within the dropping time.

Conclusion

An anodic wave in the presence of sulfate ions has been studied by a new numerical method. It was found that the value of the anodic current increases with an increase in the concentration of sulfate ions, and that the current is caused by the formation reaction of a mercury(I) sulfate complex. It has been confirmed by a numerical method that the precipitation reaction of mercury(I) sulfate does not take place within a dropping time. The value of the stability constant of a mercury(I) sulfate complex has been determined to be 150 $mol^{-1} dm^3$.

References

1) I. M. Kolthoff and C. S. Miller, *J. Am. Chem. Soc.*, **63**, 1405 (1941).

2) K. Kikuchi and T. Murayama, *Bull. Chem. Soc. Jpn.*, **61**, 3159 (1988).

3) K. Kikuchi, *Bull. Chem. Soc. Jpn.*, **60**, 903 (1987).

4) H. Morihara and R. T. Cheng, *J. Compu. Phys.*, **11**, 550 (1973).

5) I. M. Kolthoff and J. J. Lingane, "Polarography," Interscience Publishers (1965), Vol. 1, p. 52.

6) A. E. Martell and R. M. Smith, "Critical Stability Constants," Plenum Publishers (1976), Vol. 4, p. 79.

7) A. E. Martell and R. M. Smith, "Critical Stability Constants," Plenum Publishers (1976), Vol. 4, p. 83.

Intercalation of a Triethylenetetraminated Cyclodextrin by Na-, Ca-, Zn-, and Cu-Montmorillonites

Tsuyoshi KIJIMA,* Hiromoto NAKAZAWA, and Michiko KOBAYASHI
National Institute for Research in Inorganic Materials, Tsukuba-City, Ibaraki 305
(Received June 3, 1988)

The uptake of mono[6-[(8-amino-3,6-diazaoctyl)amino]-6-deoxy]-β-cyclodextrin (CDtrien) by Na-, Ca-, Zn-, and Cu-montmorillonites has been examined at 25 °C. All of the minerals form only one intercalated phase in which the CDtrien molecules are arranged as a bilayer with their cavity axes perpendicular to the silicate layers. The modes of intercalation for Na- and Ca-montmorillonites are explained differently by an ion exchange of the interlayer Na^+ ions with the divalent cationic forms of CDtrien and by the formation of CDtrien$(H_2O)_2$-Ca complexes, respectively. The intercalation by Zn- and Cu-montmorillonites proceeds by complexation at low uptakes and by the combined modes of ion exchange and complexation at higher loadings.

Inclusion phenomena have aroused increasing interest in the field of organic and inorganic chemistry, but little attention has been paid to the complexation of two or more kinds of host components. Recently, we have prepared several intercalates of layered montmorillonites and zirconium phosphate with α-, β-, and γ-cyclodextrins and their derivatives containing methoxyl or 2-aminoethylamino (en) substituents.[1-5] Some models have been proposed for the arrangement of intercalated cyclodextrin molecules in the interlayer space of the layered crystals. It was also suggested that a family of cyclodextrin intercalates may be useful as artificial enzymes, solid supports in gas or liquid chromatography and as micro-encapsulating agents of unstable substances. In order to develop these functional possibilities, further studies would be required for similar intercalates with cyclodextrin derivatives having longer chain or polyfunctional substituents. Cyclodextrins functionalized with polyamines interact with such metal ions as Cu^{2+} or Zn^{2+} in aqueous solution and the resultant cyclodextrin-metal complexes act as a metal enzyme model endowed with specific metal-substrate binding interaction.[6] If similar complexes are formed in the interlayer space of Cu- or Zn-monlmorillonite, any intercalation effect may be added to their catalytic properties.

We have, thus, attempted to prepare the intercalates of montmorillonite with mono[6-[(8-amino-3,6-diazaoctyl)amino]-6-deoxy]-β-cyclodextrin (CDtrien). This paper reports on the intercatation behavior of CDtrien for Na-, Ca-, Zn-, and Cu-montmorillonites.

Experimental

The Na-, Ca-, Zn-, and Cu-montmorillonite samples used were the same as those used in the preceding studies.[2-5] CDtrien was prepared by a manner similar to that reported for mono[6-(2-aminoethylamino)-6-deoxy]-β-cyclodextrin (CDen).[1,5] β-CD was tosylated with 0.5 equivalent of *p*-toluenesulfonyl chloride in dry pyridine at 5 °C for 2 days. The resulting mono[6-*O*-(*p*-toluenesulfonyl)]-β-CD (CDts) was dissolved in water and recrystallized. The CDts was reacted with triethylenetetramine (trien) at 70 °C for 5 h under nitrogen atmosphere. The crude product was purified by chromatography, using a carboxymethylcellulose column with 0.1 mol dm^{-3} ammonium hydrogencarbonate as an eluent, followed by repeated evaporation of the elute in the presence of a small amount of ammonia, and CDtrien was obtained in a 17% yield based on CDts. The montmorillonite sample was soaked in an aqueous solution containing various amounts of CDtrien at 25 °C for 10 days, centrifuged, fully washed with water, and air-dried at 40 °C.

Results

The uplakes of CDtrien for Na-, Ca-, Zn-, and Cu-montmorillonites are plotted against the amount of CDtrien added in Fig. 1, along with the amount of metal ion released into solution in the intercalation process. Figure 2 shows the variation of the CDtrien concentration and pH of the equilibrated solution in the uptake process.

The interlayer spacings of the dried forms of the resulting complexes were determined from the 001

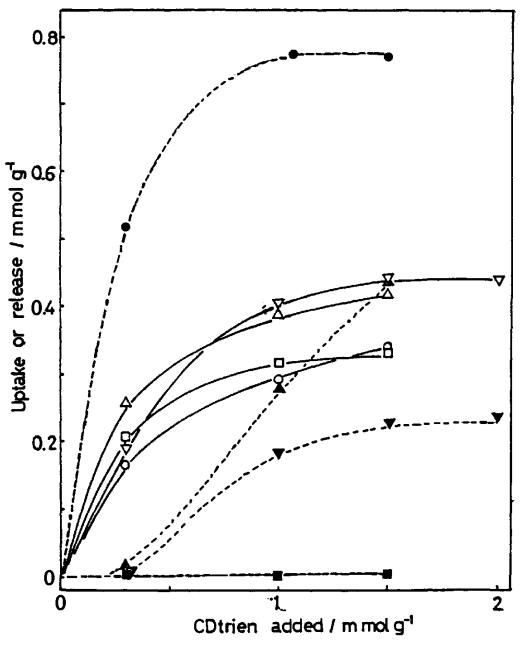

Fig. 1. CDtrien taken up by (○) Na-, (□) Ca-, (△) Zn-, and (▽) Cu-montmorillontes and release of (●) Na^+, (■) Ca^{2+}, (▲) Zn^{2+}, and (▼) Cu^{2+} ions as a function of CDtrien added.

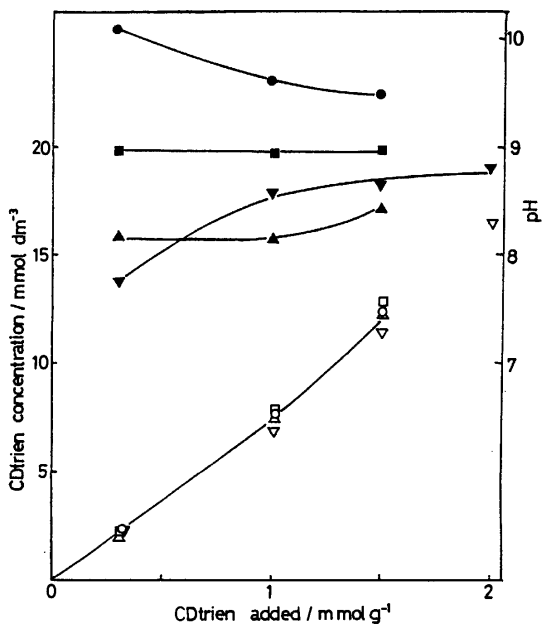

Fig. 2. Plots of the CDtrien concentration (open) and pH (closed) of equilibrated solution against CDtrien added. Key as in Fig. 1.

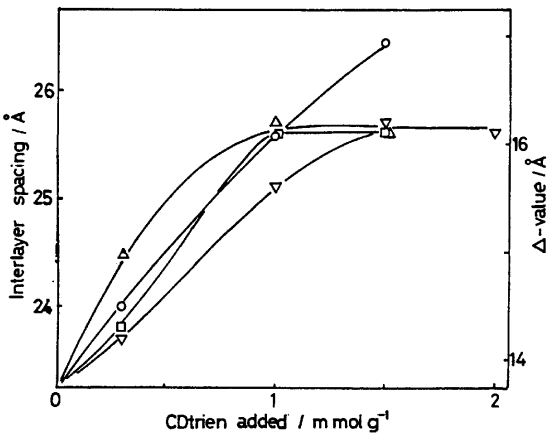

Flg. 3. Interlayer spacing or Δ value (see text) as a function of CDtrien added for the CDtrien intercalates of Na-, Ca-, Zn-, and Cu-montmorillonites. Key as in Fig. 1.

reflections in the X-ray diffraction patterns. The results are shown in Fig. 3, where the Δ values on the right ordinate indicate the thickness of the intercalated layer obtained by subtracting the thickness of the silicate layers, 9.5 Å, from the observed spacings. At a level of 0.3 mmol CDtrien added per gram of each clay, a phase with a Δ value of 14.2—14.7 Å appeared and coexisted with a small amount of its parent host phase. At a level of 1.5 mmol g^{-1}, the solid was totally converted to a single phase with a Δ value of 16.9 Å for the Na-complex and 16.1 Å for the others, and the uplake level of CDtrien became almost constant.

Table 1 summarizes the interlayer spacing and composition of intercalates of Na-, Ca-, Zn-, and Cu-montmorillonites with CDtrien at its full loadings. Our previous study[2] revealed that the content of releasable metal ions in Na-riched montmorillonite was comparable to that of interlayer cations compensating the negative charge of the silicate layers, while the Cu-exchanged mineral possesses two types of copper ions, one held as interlayer ions and one adsorbed as any neutralized species on the external surface of crystals. It was also conceivably possible that the cupric ions in the latter mineral are assigned to $[CuOH]^+$ ions as well as Cu^{2+}. This assignment, however, was inconsistent with the data for the amount of cupric ion desorbed in the intercalation of CDen by the Cu-exchanged mineral. Ca- and Zn-montmorillonites also contained releasable metal ions in some amount exceeding that of interlayer cations.[5] The excess amount of these divalent metal ions also probably exists as any neutralized species with low solubilities. The initial amounts of the interlayer cationic and the neutralized forms of metal ions in montmorillonites are thus evaluated and listed in Table 1 as v_{1i}° and v_{1e}°, respectively. In Tables 1 and 2, the sub- and superscripts are 1=releasable metal ion, 2=CDtrien, i=interlayer, e=external, °=initial, d=desorbed, and r=remaining.

Discussion

CDtrien Uptake Mechanism. As can be seen in Fig. 1, the uptake of CDtrien for Na-montmorillonite is

Table 1. Characterization of Intercalates of Na-, Ca-, Zn-, and Cu-Monmorillonites with CDtrien at Its Full Loadings

Interlayer metal ion	Interlayer spacing/Å	Δ Value/Å	Amount of CDtrien/mmol g^{-1} clay[a] v_2	Amount of releasable metal ion/mmol g^{-1} clay[a]				
				Initial			Desorbed	Remaining
				total v_1°	int[b] v_{1i}°	ext[b] v_{1e}°	v_1^{d}	v_1^{r}
Na	26.4	16.9	0.34	0.91	0.91	0	0.77	0.14
Ca	25.6	16.1	0.33	0.74	0.54	0.20	0.02	0.72
Zn	25.6	16.1	0.42	0.66	0.54	0.12	0.44	0.22
Cu	25.6	16.1	0.44	0.63	0.54	0.09	0.24	0.38

a) Anhydrous form of clay. b) v_{1i}° is the amount of exchangeable cation held as interlayer counter ions for the negatively charged silicate layers and v_{1e}° is that of adsorbed as any neutralized species on the external surface of crystals.

accompanied by the release of Na^+ ions of about twice the CDtrien uptake or more in molar amount on the entire range of CDtrien added. On the other hand, the Ca^{2+} release for Ca-montmorillonite is kept at a level as low as 0.02 mmol g^{-1}. The release of Zn^{2+} or Cu^{2+} ions from Zn- and Cu-analogues at low addition levels of CDtrien remains at an extremely low value, but increases remarkably with any further addition of CDtrien. The pK_{a_i} (i=1—4) values for trien are 3.32, 6.67, 9.20, and 9.92,[7] which are likely to be close to those for CDtrien. The uptake reaction for Na-montmorillonite takes place in the pH range of 9.5—10.1, while that for the others occurs below 9. In these two pH ranges the molecules of CDtrien would exist predominantly as CD-$NH(CH_2)_2NH(CH_2)_2NH(CH_2)_2$-$NH_2$(CDtrien) and CD-$NH(CH_2)_2NH(CH_2)_2$ $H(CH_2)_2$-NH_3^+ (CDtrienH$^+$) and as CDtrienH$^+$ and CD-$NH_2^+(CH_2)_2NH(CH_2)_2NH(CH_2)_2NH_3^+$ (CDtrien2H$^+$), respectively. The CDtrien uptake data are, thus, explained as follows: Na-montmorillonite takes up CDtrien by a two-step reaction. In the first step one mole of CDtrien is taken up as monovalent cation CDtrienH$^+$ by ion exchange with one mole of Na^+ ions. This ion exchange would be followed by the protonation of the CDtrienH$^+$ into CDtrien2H$^+$ in the interlayer medium, with an accompanying release of Na^+ and OH^- ions. On the other hand, Ca-montmorillonite intercalates neutral CDtrien molecules to form complexes with intercayer Ca^{2+} ions over the entire range of CDtrien added. Zn- and Cu-analogues also form similar complexes allow addition levels. The intercalation of CDtrien by Zn- and Cu-montmorillonites with an accompanying release of interlayer metal ion could be interpreted in terms of the combined modes of complexation and an ion exchange of Zn^{2+} or Cu^{2+}/CDtrien2H$^+$.

According to previous studies,[2,5] the neutral species on the external surface of Cu-monlmorillonite are feasibly desorbed in a CDen solution of low concentration, while those for Ca- and Zn-montmorillonites remain undissolved, even at high concentration. The dissolution of the neutral copper(II) species are probably caused by the high stability of a CDen-Cu^{2+} complex in solution. The stability constant of $10^{10.7}$ $mol^{-1}dm^3$ for a 1 : 1 CDen-Cu^{2+} complex in solution is comparable to $10^{10.72}$ for a 1 : 1 en-Cu^{2+} complex.[8] Therefore, the stability constants of 1 : 1 CDtrien-Cu^{2+} and 1 : 1 CDtrien-Zn^{2+} complexes would be as high as close to $10^{20.4}$ for trien-Cu^{2+} and $10^{12.1}$ for trien-Zn^{2+},[9] respectively. This leads us to predict that the extremely high stability of CDtrien-Cu^{2+} and CDtrien-Zn^{2+} complexes would cause not only a dissolution of the copper(II) and zinc species adsorbed on the external surface of montmorillonite crystals, but also the succeeding desorption of interlayer Cu^{2+} and Zn^{2+} ions by an ion exchange with ionized CDtrien. The amount of interlayer metal ion desorbed in the intercalation process, v_{1i}^d, can be estimated by $v_{1i}^d = v_1^d - v_{1e}^\circ$ for the case of $v_1^d > v_{1e}^\circ$. Results are listed in Table 2. The v_{1i}^d data give an expected value for the amount of the ionized form of CDtrien taken up by ion exchange. The v_2 value of 0.34 mmol g^{-1} for the sodium complex is close to an expected value of 0.385 mmol g^{-1} for the ion exchange of two moles of interlayer Na^+ ion with one mole of divalent cation CDtrien2H$^+$. Furthermore, the observed value of 0.42 mmol g^{-1} of CDtrien intercalated by Zn-montmorillonite is more than the 0.32 mmol expected for the interlayer ion exchange of Zn^{2+}/CDtrien2H$^+$ and much less than 0.64 CDtrien mmol g^{-1} expected for that of Zn^{2+}/CDtrienH$^+$. This fact indicates that CDtrien acts as a divaent cation CDtrien2H$^+$ for ion exchanges with interlayer Zn^{2+} ions in montmorillonite crystals. A similar mechanism would also be applicable to Cu-montmorillonite. These considerations enabe us to evaluate the amounts of both neutral and ionized forms of intercalated CDtrien (Table 2).

Arrangement of Intercalated CDtrien. The interlayer thickness (Δ value) of the CDtrien-montmorillonite complex is independent of the interlayer metal ions, except for the sodium complex: the Δ value of the sodium complex is also only slightly larger than that of the others. The Δ value of 16.1 Å for the calcium, zinc, and copper(II) complexes is in good agreement with twice the 8.0 Å for the van der Waals thickness of torus-shaped parent molecule. This suggests that the CDtrien molecules would be arranged as a bilayer with their cavity axes perpendicular to the silicate layers and with trien groups alternatively pointing up- and downward. The lateral packing of the CDtrien mole-

Table 2. Parameters for the Full Uptakes of CDtrien by Na-, Ca-, Zn-, and Cu-Montmorillonites

Interlayer metal ion	Amount of interlayer metal ion released/mmol g^{-1} v_{1i}^d	Amount of CDtrien/mmol g^{-1}[a]			ξ/Å[b]	Mode of intercalation[c]
		Total	Neutral form	Divalent cationic form		
Na	0.77	0.34	0 (0)	0.34(100)	5.1	E
Ca	0	0.33	0.33(100)	0 (0)	5.3	C
Zn	0.32	0.42	0.10(23.8)	0.32(76.2)	2.9	E+C
Cu	0.15	0.44	0.29(65.9)	0.15(34.1)	2.5	E+C

a) Contents in mol% are given in parentheses. b) See text. c) E, ion exchange; C, complexation.

cules in the interlayer may be drawn by the following estimation. If we assume that CDtrien molecules, each 15.4 Å in diameter, are hexagonally packed at a distance of $15.4+\xi$ in Å (center to center), the effective area per molecule is given by $(\sqrt{3}/2)(15.4+\xi)^2$ in Å^2. As the surface area of one face of the unit cell of montmorillonite is estimated as being 46 Å^2,[10] the CDtrien content, v_2, is represented by $v_2=2\times46/\{(\sqrt{3}/2)(15.4+\xi)^2w_0\}$, where w_0 is the unit-cell weight of the host montmorillonite. The ξ values evaluated using the v_2 data are listed in Table 2. Referring to the structural characteristics of well-known complexes of Ca, Zn, and Cu(II),[11] the interlayer Ca^{2+}, Zn^{2+}, and Cu^{2+} ions in the CDtrien intercalates are likely to form coordination groups $[Ca(trien)(H_2O)_2]^{2+}$, $[Zn(trien)]^{2+}$, and $[Cu(trien)]^{2+}$ which are octahedral, tetrahedral and square planar in the atomic configuration, respectively, as illustrated in Fig. 4(a). Thus, models are proposed for the packing of CDtrien moecules in the interlayer space of montmorillonite, as exemplified for the copper complex in Fig. 4(b). The order of the CDtrien content in the resulting complexes is Ca~Na<Zn~Cu. This may be tentatively explained as follows. The relation of Ca<Cu is probably due to the octahedral coordination group $[Ca(trien)(H_2O)_2]^{2+}$ in the calcium complex being more voluminous than the planar $[Cu(trien)]^{2+}$ in the copper one. The v_2 value for the sodium complex is as small as that for the calcium one, suggesting that, in the sodium complex, the trien groups in divalent cationic forms woud largely attract water molecules which would results in the loose packing of CDtrien molecules. Although three quarters of the CDtrien molecules in the zinc complex exist in the same form as in the sodium complex, the CDtrien content in the former is close to that in the copper complex. A possible explanation of this may be that the uptake of CDtrien by Zn-monlmorillonite occurs initially by complexation, followed by the release of Zn^{2+} ion induced by the ionization of the trien group in the interlayer space.

Previously, we reported the CDen intercalates of Cu- and Zn-montmorillonites in which the CDen molecules form a bilayer with a thicknesses of 23.9 or 25.2 Å. The bilayered structure was attributed to a dimerization of pairs of 1:1 $CDen(H_2O)_2$-Cu^{2+} or CDen-$(H_2O)_2$-Zn^{2+} complexes with a tail-to-tail arrangement in the interlayer space. The present observations, on the other hand, indicated that the molecules of CDtrien are also placed as a bilayer, but that the bilayered molecules are in contact with each other in

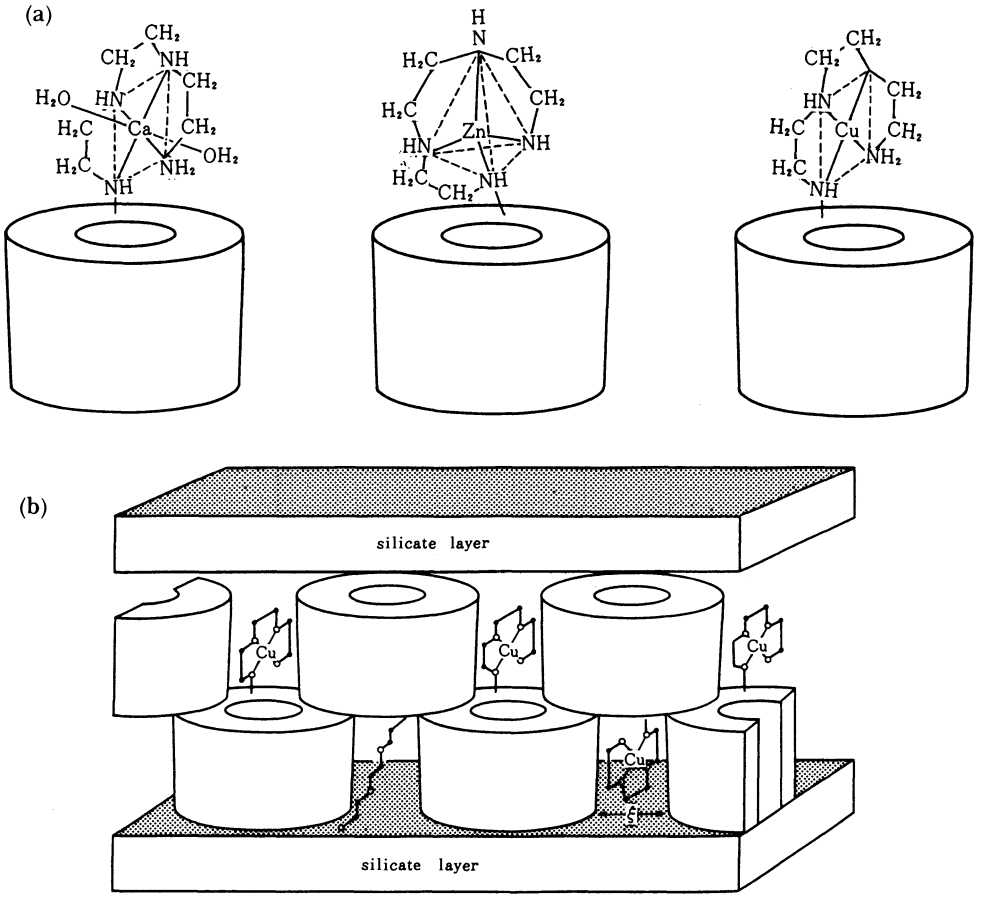

Fig. 4. Models proposed for (a) the atomic configuration of $CDtrien(H_2O)_2$-Ca^{2+}, CDtrien-Zn^{2+}, and CDtrien-Cu^{2+} complexes in montmorillonite and (b) the packing of CDtrien molecules in the interlayer space of Cu-montmorillonite. ●, C; ○, N.

the van der Waals distance. The distinct difference between the thicknesses of the cyclodextrin layers may be explained by referring to Fig. 4: Cu^{2+} or Zn^{2+} ions make a complex with the tail of CDtrien or CDen, as shown in Fig. 4(a). In the present case, the tails and the bodies of CDtrien-Cu^{2+} or CDtrien-Zn^{2+} complexes are arranged in an interfingered manner, as shown in Fig. 4(b), while they are faced and dimeraized in the previous case of CDen. The dimerization in the CDen intercalates is essentially due to a hydrogen bond by which one of the two water molecules associated with one CDen molecule is linked to one of the seven primary hydroxyl groups in the other CDen molecule faced.

The authors wish to thank Dr. Haruo Ohashi and Dr. Yu Komatsu for their helpful discussions.

References

1) T. Kijima, J. Tanaka, M. Goto, and Y. Matsui, *Nature (London)*, **310**, 45 (1984); **316**, 280 (1985).

2) T. Kijima, M. Kobayashi, and Y. Matsui, *J. Inclusion Phenom.*, **2**, 807 (1985).

3) T. Kijima and Y. Matsui, *Nature (London)*, **322**, 533 (1986).

4) T. Kijima, *J. Inclusion Phenom.*, **4**, 333 (1986).

5) T. Kijima, S. Takenouchi, and Y. Matsui, *J. Inclusion Phenom.*, **5**, 469 (1987).

6) I. Tabushi, N. Shimizu, T. Sugimoto, M. Shiozuka, and K. Yamamura, *J. Am. Chem. Soc.*, **99**, 7100 (1977).

7) Lange's Handbook of Chemistry 11th ed., ed. by J. A. Dean, McGraw-Hill Book Comp., New York (1973) pp. 5—38.

8) Y. Matsui, T. Yokoi, and K. Mochida, *Chem. Lett.*, **1976**, 1037.

9) N. Nakasuga and K. Doi, "Complexation Reaction," ed. by The Japan Society for Analytical Chemistry, Maruzen, Tokyo (1974), p. 42.

10) D. J. Greenland, R. H. Raby, and J. P. Quirk, *Trans. Faraday Soc.*, **1962**, 829.

11) K. Ueno, "Introduccton to Chelate Chemistry," Nankodo, Tokyo-Kyoto (1969), Chap. 4.

Resonance Raman Spectroscopic Studies of Electrogenerated Cation Radicals by Column-Electrolytic Continuous-Flow Method

Munetaka Oyama, Koichi Nozaki, Hiroyuki Hatano, and Satoshi Okazaki*
Department of Chemistry, Faculty of Science, Kyoto University, Sakyo-ku, Kyoto 606
(Received June 22, 1988)

For the measurement of resonance Raman (RR) spectra of electrogenerated cation radicals in solution, a column-electrolytic continuous-flow method has been developed. This method has the advantage that the concentration of cation radicals can be easily varied by controlling the applied current. The RR spectra of the thianthrene cation radical ($TH^{+\cdot}$) have been successfully observed. The structure of $TH^{+\cdot}$ is discussed, based on the assignment of the RR band. The RR spectra of the oxidized solutions of three aromatic amines have also been measured. These spectra were assigned not due to those of cation radicals but to those of dimer cation radicals produced in the consecutive reactions.

The resonance effect in Raman spectroscopy has permitted analysis of structural and electronic changes in transient intermediates of organic compounds. These changes in many ion radicals have been studied using this technique. In most of these studies, radical anions and cations were generated by chemical and/or photochemical methods.[1-10]

In the field of electrochemistry, surface enhancement Raman scattering (SERS) and/or surface enhancement resonance Raman scattering (SERRS) have been studied extensively. A potential modulation Raman spectroscopy (PMRS) is also useful for in situ observation of electrode/electrolyte interface.[11,12] With this technique, the change in spectra of surface species with potential was obtained. In these cases, the subjects were restricted to adsorbed species on the electrode surface and/or species near electrodes. To investigate the structure of electrogenerated intermediates in dynamic state, e.g. on their chemical reactions, it is also necessary to observe their Raman spectra in bulk solution. There have been few studies, however, on electrochemically generated ion radicals in solution using resonance Raman spectroscopy (RRS).[13]

In the resonance Raman (RR) measurement of solutions by using a conventional Raman spectrophotometer with 90° scattering geometry, there are two major experimental problems as follows: (1) The concentration of a substrate must be adjusted to optimum condition.[14] (2) Decomposition and thermal absorption of the substrate by excitation laser light must be avoided. As to substrate concentration, it must be high enough to permit the RR spectrum observation. As the concentration increases, however, loss of excitation light and/or scattering light due to the absorption of a substrate also increases. So the concentration of a substrate must be adjusted carefully to the optimum range for RR measurement.

We have therefore developed a column-electrolytic continuous-flow system for Raman spectroscopy to obtain the RR spectra of electrochemically generated ion radicals in homogeneous solutions. The column electrolysis flow-cell and related techniques developed by the author (S.O.)[15,16] has been widely utilized in the preparation of organic ion radicals for their ESR,[17,18] or stopped-flow spectroscopic studies.[19,20] With this technique, it becomes easy to generate ion radicals at high concentration and vary their concentration by controlling the electrolysis current and flow rate. The second problem, decomposition and thermal absorption, can be avoided using the flow system. Thus, this method will provide the vibrational information of electrogenerated intermediates in bulk solution without any influence of the electrode conditions, such as electrode materials, pretreatments, adsorption phenomena, etc.

The present paper first describes the measurement of the resonance Raman spectra of the thianthrene (TH) cation radical ($TH^{+\cdot}$) by using this method. $TH^{+\cdot}$, one of the most stable cation radicals in acetonitrile (AN), has been the subject of a number of electrochemical studies. Recently, Jørgensen clarified its structure as being very similar to the parent molecule via ab initio MO calculation;[21] the present study also shed some light on the structure.

Also measured were the RR spectra of the oxidized AN solutions of aromatic amines such as triphenylamine (TPA), *N*-methyl-*N*-phenylaniline (MPA), and *N*,*N*-dimethylaniline (DMA). In these cases, the cation radicals of aromatic amines are unstable and dimerize rapidly. Thus we obtained the RR spectra not of monomer cation radicals but dimer cation radicals. The observed RR spectra in the flow system are discussed in connection with the absorption spectra and their consecutive reactions.

Experimental

Apparatus and Method. Visible absorption spectra were measured by a Unisoku USP-500 spectrophotometer equipped with a multichannel photodiode array detector. Raman spectra were recorded on a JEOL 400 D Raman spectrophotometer with an argon ion laser excitation source. A Toho Giken 2020 galvanostat was used for constant current electrolysis.

The outline of a column-electrolytic continuous-flow cell for Raman spectroscopy is shown in Fig. 1. The solution containing the parent molecules and supporting electrolyte

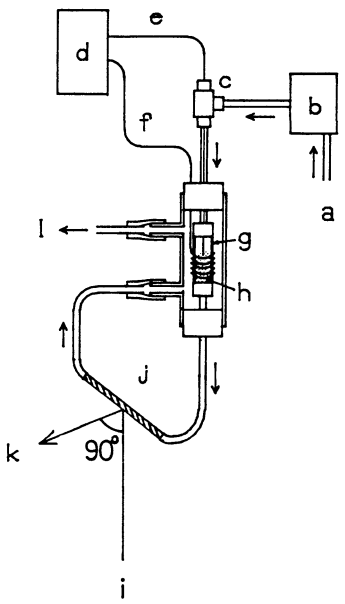

Fig. 1. Outline of the column-electrolytic continuous-flow cell for Raman spectroscopy. (a) reservoir, (b) peristaltic pump, (c) T-joint, (d) galvanostat, (e) Pt-lead to working electrode, (f) Pt-lead to counter electrode, (g) porous glass diaphragm tube, (h) carbon wool working electrode, (i) laser source, (j) capillary cell, (k) detector, (l) drain.

was sent to the column-electrolytic cell by a peristaltic pump at a constant flow rate. Acetonitrile (AN) solvent was used to acquire the RR spectra of electrogenerated cation radicals because: (1) Cation radicals are rather stable in AN. (2) AN shows relatively fewer Raman peaks than other aprotic solvents. The supporting electrolyte used was tetraethylammonium perchlorate (TEAP). The column-electrolytic cell consisted of a carbon wool working electrode which was tightly filled in a porous glass diaphragm tube (i.d. 4 mm, 3 cm length), with a platinum wire (0.3 mm) counter electrode wound outside the tube. The parent molecules were electrooxidized in the course of passing through the cell. The electrolyzed solution was then sent to a capillary cell, where the Raman spectrum was observed. The excitation light was focused from below to the capillary and the scattering light was collected at a 90° angle to the excitation light beam. The solution was then sent to the outer chamber of the cell, to serve as counter electrolyte solution and was then drained.

During measurement of a Raman spectrum, the solution flowed at a constant rate and the parent molecules were electrooxidized by constant current electrolysis. The concentration of electrogenerated cation radicals could be easily adjusted by controlling the electrolysis current and/or the sample flow rate. If the lifetime of a cation radical is sufficiently long to make the concentration decay negligible, concentration at the capillary cell can be estimated as follows:

For a simple one-electron oxidation process, the concentration of the electrogenerated cation radical, c, is given by Eq. 1,

$$c/\text{mol dm}^{-3} = \frac{\text{i/A}}{(F/\text{C mol}^{-1})\,(\text{v/dm}^3\,\text{s}^{-1})} \qquad (1)$$

or Eq. 2 using practical units.

$$c/\text{mol dm}^{-3} = 6.22 \times 10^{-4}\ \frac{i/\text{mA}}{v/\text{ml min}^{-1}} \qquad (2)$$

Where i, i are electrolysis current, v, v are the flow rate, and F is the Faraday constant.

Reagents. Thianthrene (Tokyo Kasei GR grade), triphenylamine, *N*-methyl-*N*-phenylaniline, and *N*,*N*-dimethylaniline (Nacalai tesque GR grade) were used without further purification. AN was twice distilled over P_2O_5. The supporting electrolyte, TEAP, was prepared by adding tetraethylammonium bromide to the aqueous solution of sodium perchlorate, recrystallizing it four times from water and drying over P_2O_5 in vacuo at 80 °C overnight before use.

The sample solutions used were 2.5 mM (1 M=1 mol dm^{-3}) TH with 0.05 M TEAP in AN and 10 mM aromatic amines with 0.1 M TEAP in AN.

Results and Discussion

Acquisition of RR Spectra of TH$^{+\cdot}$. Without the electrolysis current, the Raman spectra show only some peaks due to AN solvent, as shown in Fig. 2a, over all excitation wavelengths of the Ar^+ laser (between 457.9 and 514.5 nm). The Raman peaks of TH in AN were not observed, because (1) TH has no absorption in the region between 457.9 and 514.5 nm and (2) its concentration (2.5 mM) was too low for normal Raman measurement.

Under applied electrolysis current, by contrast, several additional Raman peaks appeared, as shown in Figs. 2b—g. These peaks were identified as the resonance Raman peaks of electrogenerated TH$^{+\cdot}$, based on

Fig. 2. Raman spectra without electrolysis current (a) and resonance Raman spectra of TH$^{+\cdot}$ (b—g) recorded between 300 and 1600 cm^{-1} using (b) 457.9, (c) 476.5, (d) 488.0, (e) 496.5, (f) 501.7, and (g) 514.5 nm excitation. Electrolysis current: 1.5 mA; flow rate: 1.1 ml min^{-1}. Solvent bands are marked with S.

the facts that (1) these peaks were observed only when the electrolysis current was applied, (2) the electrooxidized solution of TH has absorption in the Ar^+ excitation range as shown in Fig. 3; arrows indicate wavelengths of various excitation lines of the Ar^+ laser used, and (3) the absorption spectrum in Fig. 3 is in good agreement with the reported spectrum of $TH^{+\cdot}$.[22] Figures 2b—g show the effect of excitation laser wavelengths on the resonance Raman spectra of $TH^{+\cdot}$. The concentration of $TH^{+\cdot}$ was kept constant in all measurements by controlling the applied current and flow rate as the same.

Raman intensity was proportional to the excitation light intensity and the four powers of an absolute wavenumber of the peak. In the case of resonance Raman spectroscopy, excitation and scattering light were decreased by the absorption of the species. Thus, in considering the excitation profiles, we normalized the Raman peak intensities using the AN band at 920 cm^{-1}. Figure 4 shows the excitation profiles of resonance Raman peaks of $TH^{+\cdot}$. The relative intensities of all Raman bands in Fig. 4 depend on the wavelengths of the excitation laser lines and exhibit the same profile as the absorption spectrum of $TH^{+\cdot}$. This also indicates that these observed peaks are the RR peaks of $TH^{+\cdot}$.

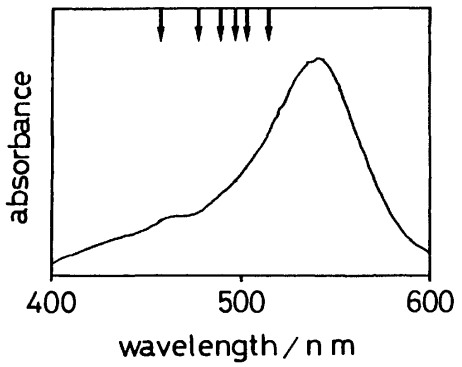

Fig. 3. Visible absorption spectrum of oxidized solution of TH. Arrows show laser lines used.

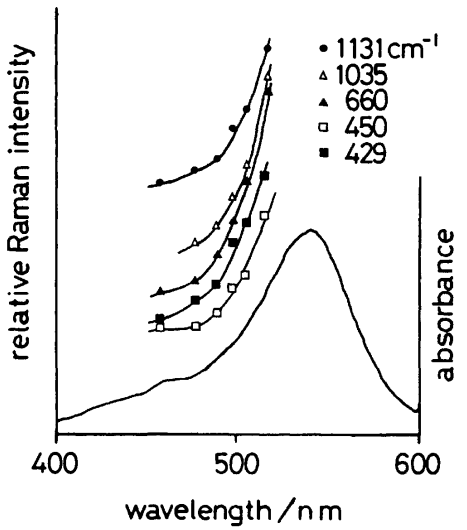

Fig. 4. Visible absorption spectrum of $TH^{+\cdot}$ and excitation profiles of resonance Raman bands, calculated using AN band at 920 cm^{-1} as internal standard.

Control of the $TH^{+\cdot}$ Concentration. Resonance Raman spectra of $TH^{+\cdot}$ were observed under various applied currents and flow rates. Table 1 summarizes the relative intensities of these $TH^{+\cdot}$ bands, normalized with the AN band at 920 cm^{-1}. The concentration of $TH^{+\cdot}$ at each run was calculated using Eq. 2. It was found that the normalized peak intensity is roughly proportional to the molar concentration of $TH^{+\cdot}$.

Figure 5 shows the effect of the electrolysis current (i.e. the concentration of $TH^{+\cdot}$) on absolute Raman intensities. In this figure, the Raman peak of AN at 381 cm^{-1} (a) and the RR peak of $TH^{+\cdot}$ at 429 cm^{-1} (b), under various applied currents at the same flow rate are shown. If there is no loss of light due to absorption by the substrate, the Raman peak of AN should have a constant intensity, while that of $TH^{+\cdot}$ should increase. The result showed, however, that the intensity of the AN band decreased and that of $TH^{+\cdot}$ band did not increase uniformly with increasing electrolysis current, owing to the absorption of the increasing $TH^{+\cdot}$. Thus, the higher concentration is not necessarily the better conditions for measurement, because the scattered light is absorbed to a great extent by the substrate itself in the 90° scattering geometry measurement.

Table 1. Relative Raman Intensities of $TH^{+\cdot}$ under Various Applied Currents and Flow Rates

Current	Flow rate	$[TH^{+\cdot}]$	Relative intensity					
			Raman sifts of $TH^{+\cdot}/cm^{-1}$					
mA	ml min^{-1}	mM	429	450	660	1035	1136	920(AN)
0.5	1.1	0.28	9	6	11	7	33	100
1.0	1.1	0.57	15	7	21	10	51	100
1.5	1.1	0.85	42	24	41	20	99	100
2.0	1.1	1.13	58	31	62	35	146	100
1.0	0.66	0.94	24	11	25	18	74	100
1.0	2.5	0.25	7	4	7	4	23	100

Excitation wavelength: 497.5 nm.

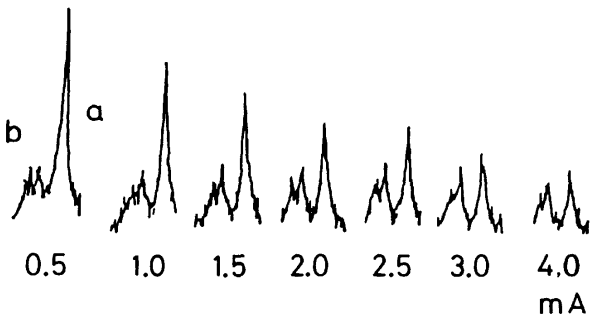

Fig. 5. Changes in intensities of AN solvent 381 cm^{-1} band (a) and $TH^{+\cdot}$ 429 cm^{-1} band (b) by applied currents. Flow rate: 1.7 ml min^{-1}; excitation wavelength: 514.5 nm.

With the electrolysis current of 4.0 mA, the RR peak of $TH^{+\cdot}$ and the Raman peak of AN became rather weak owing to the light loss due to $TH^{+\cdot}$ absorption. As a result, applied current range of 2.5 to 3.0 mA (i.e. the concentration of $TH^{+\cdot}$ was from 0.92 to 1.1 mM) was preferable for obtaining RR spectra of $TH^{+\cdot}$ with high peak intensity. Thus, it was concluded that the optimal concentration of $TH^{+\cdot}$ for the RR measurement was ca. 1.0 mM in this experiment.

Though the flow rate employed in this study was slower than 2.5 ml min^{-1} for the observation of RR spectra of very stable $TH^{+\cdot}$, faster flow-rates, up to 10 ml min^{-1}, can be applied for the acquisition of RR spectra of less short-lived species.

Comparison between the RR Spectrum of $TH^{+\cdot}$ and the Raman Spectrum of TH. The RR spectrum of $TH^{+\cdot}$ in AN (a) and the Raman spectrum of solid TH (b) are shown in Fig. 6. The Raman spectrum of TH powder was observed by the conventional procedure with a capillary cell. Vibrational modes were assigned using the reported Raman spectra of analogous molecules such as phenothiazine,[23] its cation radical,[6] and 5,10-dihydrophenazine cation radical.[8] The results are summarized in Table 2. In the case of $TH^{+\cdot}$, only nine bands were observed in this study. It seems only the most enhanced Raman bands are observed because of self-absorption.

In considering the structural difference between TH and $TH^{+\cdot}$, the significant feature is the change in its dihedral angle (θ in Fig. 7). The structure of TH has been the subject in the fields of X-ray diffraction[24] and electron diffraction.[25] It was revealed that the molecule has a folded C_{2v} conformation with a dihedral angle of 131°. Whereas, as for the structure of $TH^{+\cdot}$, it has been recently clarified by ab initio MO calculation that $TH^{+\cdot}$ is very similar in structure to TH.[21]

Hester et al. analyzed the change in dihedral angles between the phenothiazine derivatives and their cation radicals by comparing their Raman spectra.[6] In the case of phenothiazine, its dihedral angle changes in the cation radical from that of the parent molecule. This change in dihedral angle is thought to appear as the remarkable shifts in the Raman bands of the C-S-C and C-N-C skeletal deformation bands.

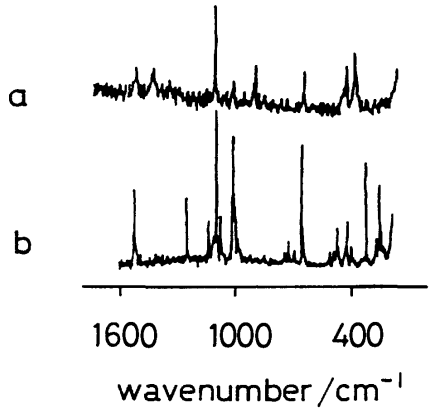

Fig. 6. Resonance Raman spectrum of $TH^{+\cdot}$ in AN (a) and Raman spectrum of solid TH (b). Excitation wavelength: 514.5 nm.

Table 2. Raman Shifts of TH and $TH^{+\cdot}$

TH[a]	$TH^{+\cdot}$ [b]	Assignment
1560 s	1560 m	Ring C-C stretching
	1468 w	Riing C-C stretching
	1329 w	Riing C-C stretching
1280 s		
1160 m		
1138 w		
1118 s	1136 vs	Ring C-S-C stretching
1100 m		
1034 s	1035 m	C-H in-plane bending
1021 s		
1007 m		
	875 w	
759 w		
737 m		
704 w		
662 s	660 s	C-S stretching
516 w		
491 w		
479 m		
469 m	450 m	C-C-C in-plane skeletal deformation
428 w		
419 m	429 s	C-S-C skeletal deformation
399 w		
314 s		

Numerical data denote wavenumbers of Raman shifts (cm^{-1}). a) Solid state. b) AN solution.
Key: s=strong, v=very, m=medium, w=weak.

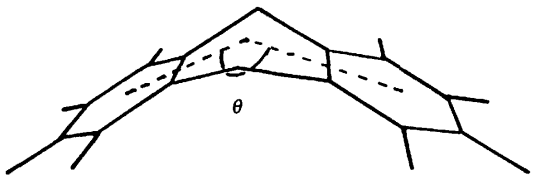

Fig. 7. Structure of $TH^{+\cdot}$. θ: dihedral angle.

In the present study, the C-S-C skeletal deformation band is assumed to correspond with the shift from 419 cm^{-1} in TH to 429 cm^{-1} in $TH^{+\cdot}$. This value is rather smaller than that of phenothiazine. It is therefore surmised that the dihedral angle of $TH^{+\cdot}$ is almost the same as that of TH, as the MO calculations predicted that the structure of $TH^{+\cdot}$ would be very similar to that of TH. However, comparison was made between TH in solid state and $TH^{+\cdot}$ in solution, since the Raman spectrum of TH could not be observed in AN owing to its poor solubility therein (10 mM). So the frequency shifts of Raman bands on dissolution of TH in AN could not be estimated. Moreover, in the short wavenumber range, the Raman spectra in the solution cannot be observed so clearly as in the solid. At present, there are still some experimental difficulties for further discussion as to the structural change in $TH^{+\cdot}$, i.e. the AN peak at 380 cm^{-1} interferes with observa-

tion of the RR spectrum of $TH^{+\cdot}$. Further investigations using other methods are needed for assessing the structural change of TH to $TH^{+\cdot}$.

RR Spectra of the Oxidized Solutions of Aromatic Amines. The RR spectra of electrooxidized solutions of the three aromatic amines TPA, MPA, and DMA were also observed by this method. Table 3 summarizes their RR shifts. For the assignment of those spectra, the reactivities of their cation radicals must be considered; that is because they dimerize rapidly and produce dimer cation radicals and/or dimer dications.

For example, on anodic oxidation of TPA, the reaction proceeds under the following schemes.[26] Here, TPB denotes *N,N,N′,N′*-tetraphenylbenzidine.

$$TPA - e^- \rightarrow TPA^{+\cdot} \quad (3)$$
$$2TPA^{+\cdot} \rightarrow TPB + 2H^+ \quad (4)$$
$$TPB - e^- \rightarrow TPB^{+\cdot} \quad (5)$$
$$TPB^{+\cdot} - e^- \rightarrow TPB^{2+} \quad (6)$$

Hinoue et al. observed in situ absorption spectra in the course of their reactions by means of internal reflection spectroscopy with an optically transparent electrode.[27]

Table 3. Raman Shifts of the Oxidized Solution of Three Aromatic Amines (a—c)[a] and $TMB^{+\cdot}$ (d)[b]

(a) TPA[a]	(b) MPA[a]	(c) DMA[a]	(d) $TMB^{+\cdot}$[b]	Assignment[b]
	1610 s		1627 w	Ring C-C str.
1579 s	1591 s	1588 vs	1602 vs	Ring C-C str.
1573 s	1560 m			
1535 m	1539 w	1555 w		
	1485 w	1489 m	1496 mw	Ring C-N str.
	1475 w	1462 w		
	1415 w	1439 w		
	1408 w	1411 m		
1324 s	1340 m	1340 m	1343 s	Inter ring C-C str.
1211 s	1241 m	1239 s	1241 s	Ring C-H i.p.b
1181 s	1224 s	1179 s	1179 m	Ring C-H i.p.b
1170 m	1129 w			
	1059 w			
994 m	995 m	989 m	991 s	Ring C-H o.p.b
935 m		941 m	941 s	Ring NX_2 wag.
901 s	879 s			
			820 m	Ring C-C str.
		808 w	807 m	Ring C-C str.
775 s	770 s	781 s	780 vvs	Ring brething
753 s	749 w	761 s	759 wm	C-H o.p.b
	660 w	634 m		
541 w				
			551 m	Ring def.
		447 w	479 m	I.p ring def.
410 w			415 m	O.p ring def.
379.w			361 w	Inter ring def.
			284 w	Inter ring def.
			252 w	Inter ring tortion
		232 m	229 m	Inter ring tortion

Numerical data denote wavenumbers of Raman shifts (cm^{-1}). a) This work. b) From Hester et al. s=strong, v=very, m=medium, w=weak, str., stretching. wag., wagging. def., deformation. i.p.b., in-plane bending. o.p.b., out of plane bending. i.p., in-plane. o.p., out of plane.

Though the absorption spectra of $TPA^{+\cdot}$ and $TPB^{+\cdot}$ could be observed, $DMA^{+\cdot}$ seemed to be so unstable and to dimerize so rapidly (within 1 ms) that the detectable species was *N,N,N′,N′*-tetramethylbenzidine (TMB) cation radical ($TMB^{+\cdot}$) or dication (TMB^{2+}).

Hester et al. obtained the RR spectrum of $TMB^{+\cdot}$ by the photoionization of TMB in a glassy ethanol matrix at 77 K (Table 3 d).[9] The obtained RR spectrum in the oxidized solution of DMA showed quite similar results in comparison with the RR spectrum of $TMB^{+\cdot}$ (Table 3 c). Furthermore, as previously reported,[28] the Raman spectrum of dimer dication differs from that of the cation radical. In the case of dianions, the Raman spectra also differed from those of anion radicals.[1] Therefore, the observed RR spectrum of the oxidized solution of DMA was assigned to $TMB^{+\cdot}$ This indicates the possibility of identifying intermediates in the course of electrochemical reactions by comparison with results from other methods.

The RR spectra of the oxidized solutions of MPA and TPA were also observed (see Table 3 a,b). In the case of MPA, the RR spectrum was assigned to *N,N′*-dimethyl-*N,N′*-diphenylbenzidine cation radical ($MPB^{+\cdot}$), considering its stability and the result of DMA. As $TPA^{+\cdot}$ is much more stable than $MPA^{+\cdot}$, $TPA^{+\cdot}$ and dimer cation radicals ($TPB^{+\cdot}$) were assumed to coexist in the capillary cell where the RR spectra were observed. The time resolved visible absorption spectra of the oxidized TPA solution were observed by column-electrolytic stopped-flow spectroscopy,[19,20] where the electrogenerated intermediate was sent rapidly to the optical flow cell and the absorption spectra at every 50 ms were observed by a multichannel photodiode array detector. The results are shown in Fig. 8, in which the decreasing peak at 651 nm was assigned to $TPA^{+\cdot}$ and the increasing peak at 464 nm was that of $TPB^{+\cdot}$. The absorption spectrum of the electrooxidized solution also indicated that $TPA^{+\cdot}$ and $TPB^{+\cdot}$ were present in the flowing solution. Though there were two species, on the basis

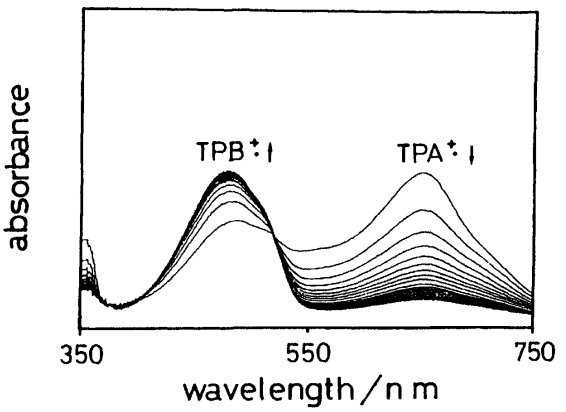

Fig. 8. Time-resolved visible absorption spectra of oxidized solution of TPA by column-electrolytic stopped-flow method.
Observation interval: 50 ms.

of the excitation wavelength (488.0 nm) the observed RR spectrum was assigned not to $TPA^{+\cdot}$ but to $TPB^{+\cdot}$. As well, the observed Raman shift of inter-ring C-C stretching band at 1324 cm^{-1} indicated that the source species is the dimer cation radical.

Though the excitation laser lines were restricted to the range between 457.9 and 514.5 nm in this study, it is very interesting that the RR spectrum of short-lived $TPA^{+\cdot}$ can be observed separately from $TPB^{+\cdot}$ using the excitation lines around 650 nm. This indicates the possibility of selective observation of the RR spectra of substances coexisting in the solution.

In conclusion, the RR spectra of electrogenerated cation radicals have been successfully measured using this method. The great feature of this method is the ease of controlling the concentration of the species, which makes the method a powerful tool for the resonance Raman study of electrogenerated intermediates in a free state, apart from electrodes.

The authors express their gratitude to Prof. Kazuhiro Maruyama for providing the Raman spectrophotometer. This work was supported in part by a Grant-in-Aid for Scientific Research, No 63470029 from the Ministry of Education, Science and Culture.

References

1) C.Takahashi and S. Maeda, *Chem. Phys. Lett.*, **22**, 364 (1973); **24**, 584 (1974); **28**, 22 (1974).
2) S. Yamaguchi, K. Yokoyama, and S. Maeda, *Bull. Chem. Soc. Jpn.*, **51**, 3193 (1978).
3) H. Kihara and Y. Gondo, *J. Raman Spectrosc.*, **17**, 263 (1986).
4) S. M. Beck and L. E. Brus, *J. Am. Chem. Soc.*, **104**, 4789 (1982).
5) G. N. P. Tripathi, D. M. Chipman, C. A. Miderski, H. Floyddavis, and R. W. Fessenden, *J. Phys. Chem.*, **90**, 3968 (1986).
6) R. E. Hester and K. P. J. Williams, *J. Chem. Soc., Parkin Trans. 2*, **1981**, 852.
7) R. E. Hester and K. P. J. Williams, *J. Chem. Soc., Parkin Trans. 2*, **1982**, 559.
8) R. E. Hester and K. P. J. Williams, *J. Raman Spectrosc.*, **13**, 91 (1982).
9) R. E. Hester and K. P. J. Williams, *J. Chem. Soc., Faraday Trans. 2*, **77**, 541 (1981).
10) R. E. Hester and K. P. J. Williams, *J. Chem. Soc., Faraday Trans. 2*, **78**, 573 (1982).
11) R. P. Van Duyne, "Chemical and Biochemical Applications of Lasers," ed by C. B. Moore, Academic Press, New York (1979), Vol. 4.
12) M. Ohsawa, K. Nisijima, and W. Suëtaka, *Surface Sci.* **104**, 270 (1981).
13) D. L. Jeanmaire and R. P. Van Duyne, *J. Am. Chem. Soc.*, **98**, 4043 (1976).
14) T. C. Strekas, D. H. Adams, A. Packer, and T. G. Spiro, *Appl. Spectrosc.*, **28**, 324 (1974).
15) S. Okazaki, *Rev. Polarogr.*, **15**, 154 (1968).
16) T. Fujinaga, T. Yamada, and S. Okazaki, *Chem. Lett.*, **1972**, 863.
17) T. Fujinaga, S. Okazaki, and T. Nagaoka, *Bull. Chem. Soc. Jpn.*, **53**, 2241 (1980).
18) T. Nagaoka, S. Okazaki, and T. Fujinaga, *J. Electroanal. Chem.*, **127**, 289 (1981).
19) M. Oyama, K. Nozaki, T. Nagaoka, H. Hatano, and S. Okazaki, *J. Chem. Soc., Perkin Trans. 2* (submitted for publication).
20) M. Oyama, K. Nozaki, H. Hatano, S. Okazaki, and T. Nagamura, 172nd meeting of the Electrochemical Soc., Honolulu, October 1987, Abstr., No. 1644.
21) K. A. Jørgensen, *Tetrahedron*, **42**, 3707 (1986).
22) E. A. C. Lucken, *J. Chem. Soc.*, **1962**, 4963.
23) B. Kure and M. D. Morris, *Talanta*, **23**, 398 (1976).
24) K. L. Gallaher and S. H. Bauer, *J. Chem. Soc., Faraday Trans. 2*, **71**, 1173 (1975).
25) I. Rowe and B. Poss, *Acta Crystallogr.*, **11**, 372 (1958).
26) E. T. Seo, R. F. Nelson, J. M. Fritsch, L. S. Marcoux, D. W. Leedy, and R. N. Adams, *J. Am. Chem. Soc.*, **88**, 3498 (1966).
27) T. Hinoue, S. Okazaki, and T. Fujinaga, *Anal. Chim. Acta*, **139**, 341 (1982).
28) D. J. Barker, R. P. Cooney, and L. A. Summer, *J. Raman Spectrosc.*, **16**, 265 (1985).

 © 1988 The Chemical Society of Japan Bull. Chem. Soc. Jpn., 61, 4289—4294 (1988)

Kinetic Study on the Reaction of *p*-Nitrophenyl Acetate with 6-Substituted 2,4-Diamino-1,3,5-triazines

Takeo KONAKAHARA,* Koji KISHIMOTO, Hiroyuki SATO, Yasushi TAKAGI, and Kenji SATO
Department of Industrial and Engineering Chemistry, Faculty of Science and Technology, Science University of Tokyo, Noda, Chiba 278
(Received March 2, 1988)

The reactions of *p*-nitrophenyl acetate (**1**) with six 6-substituted 2,4-diamino-1,3,5-triazines, (**2a—2f**), were kinetically investigated in aqueous DMSO or in water at 30 °C. It was found that the reaction rate R could be expressed according to the equation $R=(k_0+k_N[\mathbf{2}])[\mathbf{1}]$, and that Brönsted-type plots for the k_N-reaction give a straight line with a slope (β) of 1.05. The solvent deuterium isotope effect was not observed in this reaction [$k_N(H)/k_N(D)=1.0—1.15$]. Furthermore, the isolated reaction product was 2-acetylamino-4-amino-6-methyl-1,3,5-triazine (**4c**), which was formed by a nucleophilic attack of **2c** to **1**. From these results, the mechanism for this nucleophilic reaction is discussed.

The structure-reactivity relationship in acyl transfer reactions has been investigated by many workers.[1] Among these reactions, nucleophilic reactions of tertiary amines, pyridines, or imidazoles are especially useful in the preparation of acylated compounds[2,3] and in the catalytic hydrolyses of esters.[1] Furthermore, nucleophilic catalyses of secondary or primary amines in acyl transfer reactions are important as a model of enzymatic reactions.[1] It is therefore worthwhile studying the reaction of an ambident nucleophile, such as a 2-aminopolyazine, with carbonyl compounds. It has been reported that 2-aminopyridines[4] or 2-aminopolyazines, such as 2-aminopyrimidines[5] and 2-amino-1,3,5-triazines,[6,7] react with formaldehyde to give 2-(hydroxymethylamino)pyridines or 2-(hydroxymethylamino)polyazines. In addition, 2-aminopyridines and/or 2-aminopyrimidines react with picryl chloride and/or fluoride to give 2-picrylamino derivatives by initial formation and subsequent rearrangement of 1-picryl-2-imino-1,2-dihydro derivatives.[8,9] That is to say, the reacting site in the initial step of this reaction is not the amino-nitrogen atom, but the ring-nitrogen atom of this ambident nucleophile. Since we have been investigating kinetics for the reaction of 2,4,6-triamino-1,3,5-triazine (melamine) with formaldehyde,[10] it is very interesting for us to determine the actual nucleophilic site of this ambident nucleophile.

In this paper, we wish to report on the reaction of *p*-nitrophenyl acetate (**1**) with 6-substituted 2,4-diamino-1,3,5-triazines (**2a—2f**) in aqueous DMSO or water, as an extension of our above-mentioned study or in connection with an investigation regarding the model of enzymatic reactions. The reaction was kinetically investigated by the aid of Brönsted-type plots, the solvent deuterium isotope effect, and product analyses by HPLC.

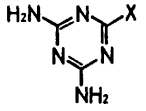

2a; X=N(CH$_3$)$_2$, **b**; X=NH$_2$, **c**; X=CH$_3$, **d**; X=H, **e**; X=OCH(CH$_3$)$_2$, **f**; X=OCH$_3$

Results and Discussion

Kinetics. When *p*-nitrophenyl acetate (**1**) was treated with the 1,3,5-triazines (**2a—2f**) in the presence of phosphate buffers at 30 °C in aqueous DMSO [DMSO : water=3 : 7 (v/v)] or in water, *p*-nitrophenol was generated according to the reaction rate R expressed by Eqs. 1 and 2,

$$R=k_{obsd}[\mathbf{1}] \quad (1)$$

$$k_{obsd}=k_0+k_N[\mathbf{2}] \quad (2)$$

where k_0 is a rate constant for a reaction in the absence of **2** in the buffered media, and k_N is a rate constant for a nucleophilic attack of the 1,3,5-triazines (**2**) to the ester (**1**) (described later). The second-order rate constants (k_N) for the reaction were obtained as slopes of plots of $[\mathbf{2}]_0$ against the observed pseudo first-order rate constants, k_{obsd} (Table 1), at constant pH, buffer concentration, and ionic strength (Eq. 2). Typical examples of the plots are shown in Fig. 1; the k_N values, thus obtained, were not affected by the pH in the medium. Therefore, the mean values are shown in Table 2 together with each pK_a of the conjugate acid of **2**.

Mechanism. The rate constants for the formation of *p*-nitrophenol catalyzed by both water (the spontaneous formation) and phosphate buffers are included in the k_0 term. Since the rate constant k_{obsd} is proportional to the concentration of the 1,3,5-triazine (**2**), as shown in Eq. 2, the following three mechanisms, expressed by Schemes 1—3, are conceivable, where HA and A$^-$ are the acid and base components of the phosphate buffer.

The rate laws of all these three mechanisms are given by Eq. 2. Generally, the solvent isotope effects, k_H/k_D, for the first mechanism shown in Scheme 1 is in the range 2 to 4 when a proton is being transferred in the transition state.[11] However, the observed $k_N(H)/k_N(D)$ values for the reactions of **1** with **2a**, **2c**, and **2e** are 1.0—1.15 in aqueous DMSO or in water (Table 3). Therefore, the first mechanism (Scheme 1) would be ruled out; it is expected that the 1,3,5-triazine (**2**)

Table 1. Experimental Conditions for the Determination of the Rate Constants, k_{obsd}, for the Reaction of *p*-Nitrophenyl Acetate (**1**) with the 1,3,5-Triazine (**2a—2f**) in Aqueous DMSO in the Presence of Phosphate Buffers at 30 °C, Ionic Strength of 0.3 (KCl)[a]

2	[2]/mol·l^{-1}	*br*[b]	pH[c]	k_{obsd}/min^{-1}[d]	No. of run
a	0—1.00×10^{-3}	0.6	8.13	(7.55—8.33)×10^{-4}	10
		0.4	8.32	(8.13—8.99)×10^{-4}	12
		0.2	8.74	(1.21—8.99)×10^{-3}	12
b	0—1.0 ×10^{-3}	0.6	8.23	(7.58—8.05)×10^{-4}	10
		0.4	8.36	(8.13—8.52)×10^{-4}	12
		0.2	8.73	(1.21—1.26)×10^{-3}	12
c	0—1.00×10^{-2}	0.4	8.29	(8.13—8.99)×10^{-4}	14
		0.2	8.71	(1.23—1.31)×10^{-3}	15
		[0.04	8.46	(3.95—4.09)×10^{-3}	10[e]]
d	0—2.01×10^{-2}	0.6	8.17	(7.58—8.13)×10^{-4}	12
		0.4	8.34	(8.13—8.71)×10^{-4}	10
		0.2	8.71	(1.21—1.27)×10^{-3}	12
e	0—6.00×10^{-2}	0.6	8.17	(7.58—7.92)×10^{-4}	11
		0.4	8.33	(8.13—8.50)×10^{-4}	11
		0.2	8.66	(1.21—1.25)×10^{-3}	12
f	0—2.00×10^{-2}	0.4	8.34	(8.13—8.23)×10^{-4}	16
		0.2	8.69	(1.21—1.22)×10^{-3}	20

a) DMSO:H_2O=3:7 (v/v). b) *br*=[$H_2PO_4^-$]/[HPO_4^{2-}]; [HPO_4^{2-}]=1.25×10^{-2} mol·l^{-1}. c) The mean value (standard deviation ≤0.01). d) The observed pseudo-first-order rate constant (correlation coefficients *r* were larger than 0.999 for all runs). In all cases, the initial concentration of **1** was 5×10^{-5} mol·l^{-1}. e) The reaction in water.

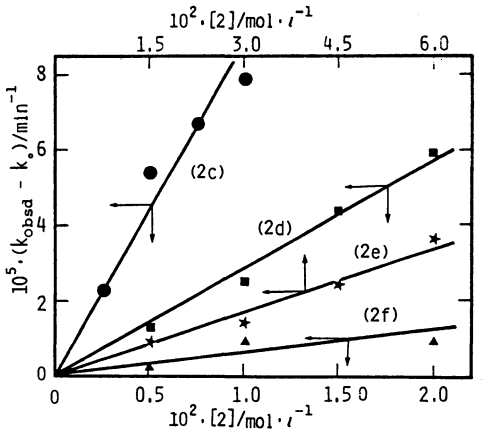

Fig. 1. Plots of ($k_{obsd} - k_0$) against the initial concentration of the 6-substituted 2,4-diamino-1,3,5-triazines (**2**) for the reaction with *p*-nitrophenyl acetate (**1**, 5×10^{-5} mol·l^{-1}) in the presence of phosphate buffers (pH 8.7, *br*=0.2) in aqueous DMSO at 30 °C and ionic strength of 0.3 (KCl).

Table 2. Second-Order Rate Constants, k_N, for the Reaction of *p*-Nitrophenyl Acetate (**1**) with the 1,3,5-Triazine (**2a—2f**) in Aqueous DMSO in the Presence of Phosphate Buffers at 30 °C, Ionic Strength of 0.3 (KCl)[a]

2	pK_a[b]	k_N/l·mol^{-1}·min^{-1}[c]
a	5.50	(8.2±0.4)×10^{-2}
b	5.15	(4.4±0.3)×10^{-2}
c	4.45	(8.8±0.2)×10^{-3}
d	4.00	(2.84±0.02)×10^{-3}
e	3.87	(5.9±0.2)×10^{-4}
f	3.47	(5.7±0.7)×10^{-4}

a) DMSO: H_2O=3:7 (v/v). b) The value of the conjugate acid of **2** was determined by a titrimetric method in aqueous DMSO at 30 °C and ionic strength of 0.3 with KCl. c) The pH's in the medium did not affect on the k_N values, and the error shown is standard deviation of the slope, by least-squares analysis, for the plots of Eq. 2.

nucleophilically attacks the carbonyl carbon of *p*-nitrophenyl acetate (**1**) to form the acetylated compound[12] through a tetrahedral intermediate, as shown in Scheme 2 or 3, like a reaction of 2,4-dinitrophenyl acetate with pyridine,[13] or a reaction of **1** with imidazoles.[14]

In order to determine the reacting site of this ambident nucleophile **2**, the log k_N's for the reactions of the six 1,3,5-triazines (**2a—2f**) in aqueous DMSO were plotted against the pK_a's of their conjugate acids (the Brönsted-type plots). A good linear relationship (the slope, β=1.05) was obtained (Fig. 2). The deviation of **2e** from the line is suggestive that the 1-N atom is the actual nucleophilic site in the reaction of **2e**, because the deviation must result from a steric hindrance by the relatively bulky isopropoxy group adjacent to the 1-N atom[15,16] (Scheme 2). When the log k_N values were statistically corrected, **2b** also showed a large negative deviation from a line like **2e**. This deviation of **2b** and **2e** from statistically corrected Brönsted-type plots is not explicable by the third mechanism (Scheme 3), in which the substituent X does not sterically hinder a carbonyl attack of the amino group. Furthermore, the 1,3,5-triazine **2** is not protonated at the amino group but at the ring-nitrogen,[16] and the basicity or electron density (nucleophilicity) of the amino-nitrogen is extremely diminished by the electron-withdrawing 1,3,5-triazine ring[17] compared

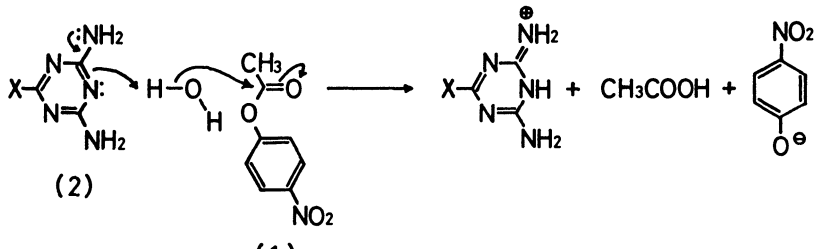

Scheme 1.

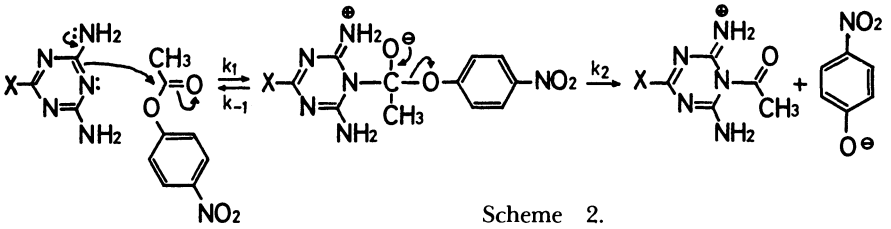

Scheme 2.

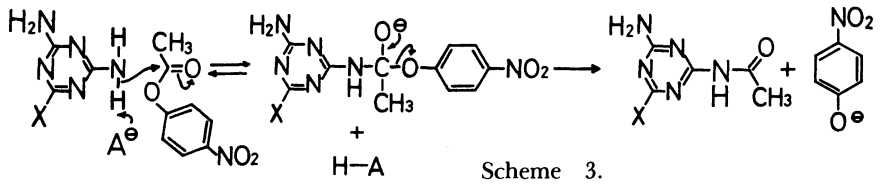

Scheme 3.

Table 3. Solvent Deuterium Isotope Effect in the Reaction of *p*-Nitrophenyl Acetate (**1**) with 6-Substituted 2,4-Diamino-1,3,5-triazines (**2a**, **c**, and **e**) in the Presence of Phosphate Buffers at 30 °C and Ionic Strength of 0.3 (KCl)

2	Solvent	pH or pD[a]	k_N	$k_N(H)$
			$l \cdot mol^{-1} \cdot min^{-1}$	$k_N(D)$
a	DMSO-H_2O[b]	8.34	8.2×10^{-2}	1.0
	DMSO-D_2O[b]	9.24	8.3×10^{-2}	
c	DMSO-H_2O[b]	8.71	8.8×10^{-3}	1.1
	DMSO-D_2O[b]	9.26	8.3×10^{-3}	
c	H_2O	8.46	1.50×10^{-2}	1.15
	D_2O	8.84	1.30×10^{-2}	
e	DMSO-H_2O[b]	8.66	5.9×10^{-4}	1.1
	DMSO-D_2O[b]	9.22	5.3×10^{-4}	

a) pD="meter pH"+0.40 (see Ref. 30). b) DMSO: H_2O (or D_2O)=3 : 7 (v/v).

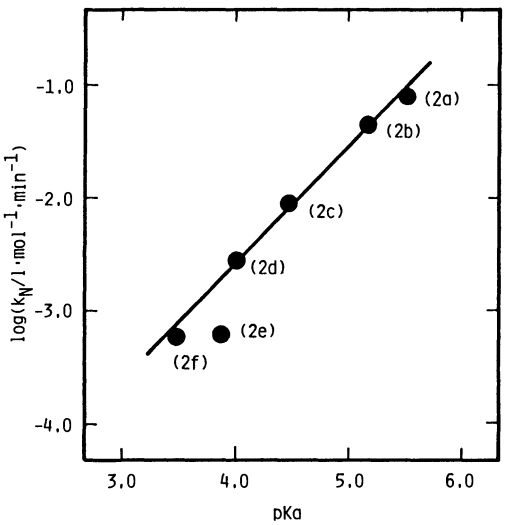

Fig. 2. The Brönsted-type plots for the reaction of *p*-nitrophenyl acetate (**1**, 5×10^{-5} mol·l^{-1}) with the 6-substituted 2,4-diamino-1,3,5-triazines (**2a—2f**) in the presence of phosphate buffers (pH 8.7) in aqueous DMSO at 30 °C and ionic strength of 0.3 (KCl); the slope β=1.05 and correlation coefficient r=0.99. When the k_N values were corrected by statistical factors in order to explain the third mechanism in Scheme 3, **2b** showed a large negative deviation from a line like **2e**.

with the amides[18] or urea (pK_b=13.8).[19] This low nucleophilicity of the amino-nitrogen of **2** was demonstrated by lack of reactivity of **2c** against picryl fluoride (**3**), as described later. From these results, it is

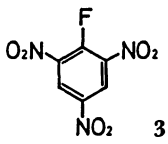

3

inferred that the reaction proceeds through an initially formed unstable acetyl adduct (**6**). In other words, the second mechanism (Scheme 2) is more probable as the main reaction in our system than the third (Scheme 3).

The slope (β=1.05) of the Brönsted-type plots (Fig. 2) is nearly equal to those for aminolysis reactions of activated carbonyl compounds[13] such as 2,4-dinitrophenyl acetate (β=0.85) and methyl chloroformate (β=0.93). If the result of Castro and Freudenberg[13] is applicable to our system, the 1,3,5-triazine leaves more

easily from the tetrahedral intermediate than the *p*-nitrophenoxy group ($k_{-1} \gg k_2$); that is, the second step (the k_2-reaction) would be rate determining in Scheme 2.

We now give another conceivable mechanism (the fourth mechanism). It has been reported by Okano and Ogata[20] that the hydroxymethylation of melamine (**2b**) with formaldehyde in the presence of a basic catalyst takes place by a consecutive mechanism, including a carbonyl attack by a conjugate base of **2b**, which is generated from **2b** by the action of a basic catalyst. However, an analogous mechanism for the reaction of **2** with **1** (the fourth mechanism) would also be ruled out[17] because the amino-hydrogen of **2** (pK_a of **2b**, 36)[17] is not acidic enough to be abstructed by the basic component of the buffer (hydrogenphosphate, pK_a of the conjugate acid,[21] 7.63).

Reaction of *p*-Nitrophenyl Acetate (1) or Picryl Fluoride (3) with 2,4-Diamino-6-methyl-1,3,5-triazine (2c). In order to determine the structure of the product in the reaction of the ester (**1**) with the 1,3,5-triazine (**2**), **1** or **3** was treated with one of the 1,3,5-triazines, **2c**, in dry DMSO, which was employed as a solvent instead of aqueous DMSO to minimize the hydrolysis of **1** or **3** and to increase the solubility of **2c** in the medium.

First, 2,4-diamino-6-methyl-1,3,5-triazine (**2c**) was heated with *p*-nitrophenyl acetate (**1**) in dry DMSO at 100 °C for 17.5 h to afford 2-acetylamino-4-amino-6-methyl-1,3,5-triazine (**4c**) in 60% yield as colorless crystals. The formation of this compound **4c** looks strange in comparison with the result from the Brönsted-type plots (Fig. 2), which supports the second mechanism illustrated in Scheme 2. This discrepancy may be interpreted by the hypothesis that the 1,3,5-triazine (**2**) attacks the ester (**1**) to afford, ultimately, the acetylamino derivative (**4**) by initial formation and subsequent fast rearrangement of 3-acetyl-4-amino-2-imino-2,3-dihydro-1,3,5-triazine derivatives (**6**) or the corresponding 1-acetyl derivatives[16] (Scheme 4). In fact, it has been reported that 2-aminopyridines analogously react with picryl chloride or **3**.[8,9] Accordingly, the 1,3,5-triazine (**2c**) was treated with **3** in dry DMSO at 80 °C. However, neither the corresponding 3-picryl product nor the 2-picrylamino-6-methyl-1,3,5-triazine obtained, and most of the unreacted **2c** was recovered as the picrate. This result indicates that the sterically crowded ring-nitrogen of **2c** is not able to attack the 1-C atom of **3**, which is more crowded than the carbonyl carbon of **1**, and that the acetylation of **2** with **1** must proceed through the pathway illustrated in Schemes 2 and 4.

The acetylated product **4c** was considerably stable under the kinetic conditions in this study, and it was identical with the product in the kinetic runs (by HPLC).

The structure of **4c** was determined by its spectroscopic data. The MS of **4c** showed a molecular ion (M^+) peak at m/z 167 (molecular weight of **4c**; $C_6H_9N_5O$= 167.18), and the IR spectrum, measured in a KBr disk, suggested that the acetylated product was a tautomeric mixture of **4c** and **5c** (Scheme 4). That is to say, absorption bands assignable to the acetylamino form (**4c**) were observed at 3300 (ν_{NH} of the secondary amide), 1680 ($\nu_{C=O}$, amide I band), 1540 (amide II band), 1315 (amide III band), and 815 cm^{-1} (medium, 1,3,5-triazine ring) in addition to those of acetylimino form **5c** at 3230 (ν_{NH} of the ring), 1615 ($\nu_{C=N}$), 1375 (δ_{NH} of the ring), and 760 cm^{-1} (very weak, 2,3-dihydro-1,3,5-triazine ring).[22] Analogous tautomerization was observed in 2,4-diamino-6-cyanoamino-1,3,5-triazine.[22] However, the equilibrium would lie to the left (as discussed below regarding to UV and ^1H and ^{13}C NMR spectra).

Compound **6** is not expected to have a UV absorption maximum in the wavelength region 220 to 280 nm,[23,24] whereas product **4c** shows absorption maxima at 223, 260, and 326 nm. The ^1H NMR spectrum of **4c** consists of two methyl protons (δ 2.4 and 2.7) and the NH protons of NH_2 (δ 7.7) and NH groups (δ 7.1), and ^{13}C NMR of **4c** in acetic acid exhibited a signal at δ 166.9 for the ring-carbon 2-C which was attached to the acetylamino group. This low-field shift of 2-C, compared with 4-C (δ 163.1), must result from the acetyl group. If the structure of the acetylated product is **6**, the ring-carbons would resonate at a higher magnetic field than δ 163.1. Signals assignable to the tautomeric isomer (**5c**) were not observed in the spectrum.

Experimental

All melting and boiling points are uncorrected. The UV spectra were recorded on a JASCO UVIDEC-505 spectrophotometer, and the IR spectra on a Hitachi model 260-50 spectrophotometer. The ^1H NMR spectra were recorded with a JEOL PMX-60SI spectrometer for solutions in DMSO-d_6 or

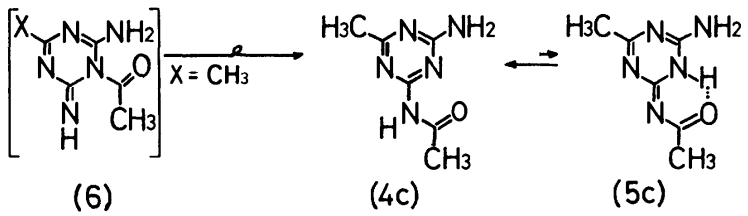

Scheme 4.

CF_3COOH, and ^{13}C and ^{19}F NMR spectra with a JEOL FX-90Q spectrometer in acetic acid. The chemical shifts are reported in δ (internal standard Me_4Si or $CFCl_3$). The MS were determined with a Hitachi M-80 double-focusing mass spectrometer at 70 eV. The pH was measured with a Toa model HM-5ES pH meter. The analytical HPLC determination was carried out with a JASCO TWINCLE apparatus equipped with a UV detector.

Materials. Commercially available 2,4,6-triamino-1,3,5-triazine (**2b**) and 2,4-diamino-6-methyl-1,3,5-triazine (**2c**) were recrystallized from water. 2,4-Diamino-1,3,5-triazine (**2d**) was kindly presented by Dr. E. Ichikawa (Tokyo Institute of Technology) and recrystallized from water, mp 322.3—324.0 °C (lit,[25] 329 °C). The other 6-substituted 2,4-diamino-1,3,5-triazines, (**2a**, **e**, and f), were prepared by methods in literature,[26,27] and recrystallized from water, **2a**; mp 310—312 °C (lit,[28] 307—308 °C), **2e**; mp 168.5—169.5 °C (lit,[27] 172 °C), **2f**; mp 237—238 °C (lit, [27] 229—230 °C). All the 1,3,5-triazines, (**2a—2f**), were dried at 50 °C for one day, and then at room temperature for three days under reduced pressure (5 mmHg; 1 mmHg=133.322 Pa) after recrystallization. ^1H NMR (DMSO-d_6) **2a**, δ=5.97 (4H, s, NH_2), 3.02 (6H, s, CH_3); **2b**, 6.02 (s, NH_2); **2c**, 6.45 (4H, s, NH_2), 1.88 (3H, s, CH_3); **2d**, 6.61 (4H, s, NH_2), 7.91 (1H, s, H); **2e**, 6.63 (4H, s, NH_2), 5.28 (1H, se, J=7 Hz, CH), 1.43 (6H, d, J=7 Hz, CH_3); **2f**, 6.62 (4H, s, NH_2), 3.73 (3H, s, CH_3); ^{13}C NMR (CH_3COOH) **2c**, δ=173.5 (CH_3-C-ring), 164.0 (C-NH_2), 21.7 (CH_3). Picryl fluoride (**3**) was also prepared by a method in literature[29] and recrystallized from carbon tetrachloride. Yield 60—70%, mp 122—123 °C (lit,[29] 122—123 °C). ^1H NMR ($CDCl_3$) δ=8.95 (d, J=5.6 Hz); ^{19}F NMR (84.31 MHz, $CDCl_3$) δ=−116.36 (t, J=5.49 Hz).

Kinetics. Rates of the reaction of **1** with **2a—2f** were followed on a spectrophotometer equipped with an isothermal cell holder (30±0.2 °C) and 1-cm cells by observing the appearance of *p*-nitrophenolate at 408 [in aqueous DMSO, DMSO : H_2O=3 : 7 (v/v)] or 400 nm (in water). The reaction was initiated by stirring the buffer solution with a Teflon rod, on which 30 μl of a stock solution (5.05×10^{-3} mol·l^{-1}) of **1** in DMSO (or in acetonitrile for the reaction in water) was put with a Gilmont micrometer buret. The buffer solution (KH_2PO_4/Na_2HPO_4, [Na_2HPO_4]=1.25×10^{-2} mol·l^{-1}) contained the 1,3,5-triazine (**2**), and the ionic strength was maintained at 0.3 with potassium chloride. The final concentration of acetonitrile, which was introduced with solutions of **2**, in the reaction mixture did not exceed 1%. The initial rate, R_0, was proportional to $[\mathbf{1}]_0$ at constant $[\mathbf{2}]_0$ (5×10^{-5} mol·l^{-1}) and pH (8.7), and a slope of $\log R_0$ vs. $\log[\mathbf{1}]_0$ plots is 1.0. Furthermore, (R_0-R_{00}) was proportional to $[\mathbf{2}]_0$ at constant $[\mathbf{1}]_0$ (5×10^{-5} mol·l^{-1}) and pH (8.7), and a slope of $\log(R_0-R_{00})$ vs. $\log[\mathbf{2}]_0$ plots was also 1.0, where R_{00} is the initial rate in the absence of **2**.

The observed pseudo first-order rate constants, k_{obsd}, were calculated from the spectrometric data by the use of the usual first-order equation (correlation coefficient r is larger than 0.999 for each run), and are summarized in Table 1 along with the reaction conditions. The concentration of (**1**), 5×10^{-5} mol·l^{-1}, was ordinarily used to determine the rate constants k_N by using Eq. 2. The reaction product in the kinetic run of **2c** was found to be identical to the acetylamino derivative **4c** by means of HPLC [column, 4.6×250 mm, Finepak Sil C_{18}, 5 μm; eluent, 0.02 mol·l^{-1} K_2HPO_4/NaH_2PO_4 buffer (pH 6.8) in 10% (v/v) aqueous MeOH; flow rate, 0.5 ml·min^{-1}; detection, 260 nm; retention time of **2c** and **4c**, 23.5 and 25.6 min].

Solvent isotope effect experiments were performed in DMSO-D_2O for **2a**, **2c**, and **2e** and in D_2O for **2c** in the presence of the deuterated phosphate buffers under a nitrogen atmosphere (over a more restricted pD range). The results are summarized in Table 3. The pD values were calculated by adding 0.4 unit to the pH value obtained by using a conventional pH meter.[30]

Reaction of *p*-Nitrophenyl Acetate (1) with 2,4-Diamino-6-methyl-1,3,5-triazine (2c); Preparation of 2-Acetylamino-4-amino-6-methyl-1,3,5-triazine (4c). The 1,3,5-triazine (**2c**) (1.25 g, 0.01 mol) and **1** (3.6 g, 0.02 mol) were heated in dry DMSO (20 ml) at 100 °C for 17.5 h. After cooling, the reaction mixture was poured into 200 ml of water containing crashed ice to afford a crystalline product, which was washed with carbon tetrachloride to give the pure product **4c** in 60% yield. Its homogeneity was established by HPLC (conditions are shown above). Mp 271.0—272.5 °C; UV(EtOH) λ_{max} 223 (ε 2800), 260 (5500), and 326 nm (850); IR(KBr) 3300, 3230, 3140, 1690, 1680, 1615, 1540, 1375, 1315, 815, and 760 cm^{-1}; ^1H NMR(CF_3COOH) δ=7.7 (2H, b, NH_2), 7.1 (1H, b, NH), 2.7 (3H, s, $COCH_3$), 2.4 (3H, s, ring-CH_3); ^{13}C NMR (CH_3COOH) δ=176.6 (CO), 173.1 (CH_3-C-ring), 166.9 (N=C-NH-Ac), 163.1 (C-NH_2), 25.2 (CH_3CO), 22.9 (CH_3-ring); MS m/z (rel intensity in %) 169 (2), 168 (8), 167 (M^+, 80), 139 (19), 126 (10), 125 (M − CH_2=C=O, 97), 110 (13), 98 (42), 85 (11), 84 (27), 83 (22), 68 (24), 43 (100), 42 (59).

Found: C, 42.83; H, 5.37; N, 41.61%. Calcd for $C_6H_9N_5O$: C, 43.11; H, 5.43; N, 41.90%.

Reaction of 2c with Picryl Fluoride (3). A mixture of **2c** (1.25 g, 0.01 mol) and **3** (4.6 g, 0.02 mol) was heated in dry DMSO at 80 °C for 48 h. After cooling, the reaction mixture was poured into 200 ml of water containing crashed ice to afford the corresponding crude picrate (99.6% yield), which was recrystallized from tetrahydrofuran (73% yield, Found: C, 34.23; H, 2.92; N, 31.04%), and it was identical to an authentic sample. Mp 277—278 °C (decomp., browned at 259—260 °C; lit,[31] 275 °C). UV(EtOH) λ_{max} 250 (sh), 360 (ε 1400), 410 nm (sh); IR (KBr) 3430, 3340, 3260, 3120, 1700, 1645, 1625, 1600, 1570, 1545, 1360, 1325, and 790 cm^{-1}; MS m/z (rel intensity in %) 229 [27, 228.9962 (+0.9 mu, $C_6H_3N_3O_7$)], 125 [100, 125.0698 (−0.2 mu, $C_4H_7N_5$)], 62 (10), 42 (28).

Stability of 4c. A solution of the compound **4c** (5×10^{-3} mol·l^{-1}) in aqueous DMSO was maintained at 30 °C under the same conditions used in the kinetic runs. Aliquots were periodically removed, and the amount of unreacted **4c** was determined by HPLC (conditions are shown above). After 1 h, compound **4c** was still unchanged but 5—10% of **4c** was decomposed after 2 h.

We are indebted to Mr. Yuichi Sugiura for his assistance in the experimental work and to Dr. Eiichi Ichikawa (Tokyo Institute of Technology) for his kind gift of 2,4-diamino-1,3,5-triazine (**2d**).

References

1) W. P. Jencks, "Catalysis in Chemistry and Enzymology," McGraw-Hill, New York (1969), Chaps. 2 and 10.

2) A. Williams and K. T. Douglas, *Chem. Rev.*, **75**, 627 (1975).

3) G. Höfle, W. Steglich, and H. Vorbrüggen, *Angew. Chem., Int. Ed. Engl.*, **17**, 569 (1978).
4) B. Skowronska-Serafinowa, *Roczniki Chemii*, **29**, 932 (1955).
5) G. L. MoLeod, *J. Res. Nat. Bureau Stand. (A) Phys. Chem.*, **66**, 65 (1962).
6) H. P. Wohnsiedler, *Ind. Eng. Chem.*, **45**, 2307 (1953).
7) D. Braun and V. Legradić, *Angew. Makromol. Chem.*, **34**, 35 (1973).
8) J. Elguero, C. Marzin, A. R. Katritzky, and P. Linda, "The Tautomerism of Heterocycles," Academic Press, New York (1976), p. 154.
9) W. Harris, J. L. Singleton, and M. D. Coburn, *J. Heterocycl. Chem.*, **10**, 166 (1973).
10) T. Yoshii, T. Konakahara, and K. Sato, *Makromol. Chem.*, **188**, 1683 (1987).
11) R. A. Y. Jones, "Physical and Mechanistic Organic Chemistry," Cambridge University Press, London (1979), p. 243.
12) According to a HPLC analysis of the reaction mixture in the kinetic run, the compound **6** was not detected but a small amount of **4c** was detected.
13) E. A. Castro and M. Freudenberg, *J. Org. Chem.*, **45**, 906 (1980), and references cited therein.
14) M. L. Bender, *Chem. Rev.*, **60**, 82 (1960).
15) R. F. Hudson, "Chemical Reactivity and Reaction Paths," G. Klopman, John-Wiley, New York (1974), Chap. 5.
16) It has been reported that the 1,3,5-triazine **2c** is protonated at the 3-N atom while **2e** and **2f** are protonated at 1-N atom [R. C. Hert and R. G. Schmitt, *Spectrochim. Acta*, **12**, 127 (1958)].
17) The pK_b value of the amino group of **2** may be larger than 13 [V. Novák and I. Dobás, *Collect. Czechoslov. Chem. Commun.*, **41**, 3378 (1976)].
18) K. Sato, T. Konakahara, and M. Kawashima, *Makromol. Chem.*, **183**, 875 (1982).
19) E. P. Parry, D. H. Hern, and J. G. Burr, *Biochim. Biophys. Acta*, **182**, 570 (1969).
20) M. Okano and Y. Ogata, *J. Am. Chem. Soc.*, **74**, 5728 (1953).
21) D. D. Perin, "Ionization Constants of Inorganic Acids and Bases in Aqueous Solution," 2nd ed, Pergamon, New York (1982), p. 87.
22) M. Takimoto, *Nippon Kagaku Zasshi*, **85**, 168 (1964).
23) D. J. Brown and T. England, *J. Chem. Soc. C*, **1971**, 425.
24) I. M. Klotz and T. Askounis, *J. Am. Chem. Soc.*, **69**, 801 (1947).
25) Beilsteins Handbuch der Organischen Chemie, Springer-Verlag, Berlin (1937), Vol. 26, Hauptwerk p. 225.
26) J. T. Thurston, J. R. Dudley, D. W. Kaser, I. Hechenbleikner, F. S. Schaefer, and D. Holm-Hansen, *J. Am. Chem. Soc.*, **73**, 2981, 2984 (1951).
27) J. Contronlis and C. K. Banks, *J. Am. Chem. Soc.*, **67**, 1946 (1945).
28) D. W. Kaiser, U. S. Patent 2567847 (1951); *Chem. Abstr.*, **46**, 2587c (1952).
29) G. C. Shaw, III, and D. L. Seaton, *J. Org. Chem.*, **26**, 5227 (1961).
30) P. K. Glasoe and F. A. Long, *J. Phys. Chem.*, **64**, 188 (1960).
31) Beilsteins Handbuch der Organischen Chemie, Springer-Verlag, Berlin (1937), Vol. 26, Hauptwerk, p. 229.

Rotamer Populations and Molecular Structure of 9-Isobutyl-1,4-dimethoxytriptycene: Further Evidence for the Presence of CH_3···O Hydrogen Bond

Michinori Ōki,*,† Naoyoshi Takiguchi, Shinji Toyota, Gaku Yamamoto, and Shigeru Murata††
Department of Chemistry, Faculty of Science, The University of Tokyo, Bunkyo-ku, Tokyo 113
††Department of Industiral Chemistry, Faculty of Engineering, Mie University, Tsu, Mie 514
(Received March 18, 1988)

^{1}H NMR spectra of the title compound at low temperatures show the presence of the *sc* conformer as a major constituent: $\Delta H°=0.9\pm0.3$ kcal mol^{-1}, $\Delta S°=5\pm2$ cal mol^{-1} for the $sc \rightleftarrows ap$ equilibrium. The line shape analysis of the spectra at various temperatures afforded the following activation parameters for the internal rotation about the C_9-$C_{i\text{-}Bu}$ bond: $\Delta H^*=8.8\pm0.3$ kcal mol^{-1}, $\Delta S^*=-5.0\pm1.2$ cal mol^{-1} K^{-1} for the $ap \rightarrow sc$ process. X-Ray crystallography of the compound revealed that the molecule exists as *sc* conformers in the crystal. One of the methyl groups of the isobutyl group that directs inward relative to the triptycene skeleton, is placed very closely to the 1-methoxy-oxygen to indicate the presence of the CH_3···O hydrogen bond. Implications of other structural parameters are also discussed.

While we have reported that the presence of CH_3··· O hydrogen bond can be detected as the population ratios of rotamers in appropriately substituted triptycenes, the population of the *sc* isomer has never overwhelmed that of the *ap* isomer, although the former is stabilized by the presence of the hydrogen bond.[1,2] The results have been attributed to the weakness of the hydrogen bond that competes with other repulsive forces like van der Waals repulsion in determining the population ratios. Indeed, it has been pointed out that the ρ value in the Hammett plot of the population ratios against the substituent constants for the series of 9-(aryloxymethyl)-1,4-dimethyltriptycenes is unusually small, -0.114,[1] for the interaction involving an atom that is directly attached to the aromatic ring.[3]

This reluctance of showing the electronic effect of the substituent on the rotamer populations is attributed to the steric effect that destabilizes the *sc* form of 1,9-disubstituted triptycenes, although that form is stabilized by the hydrogen bond. Although the β atom in the 9-substituent is close enough to the unsubstituted peri-positions of the triptycene skeleton, when it takes the *ap* position relative to the 1-substituent, the distance is still larger than that between the 1-substituent and the β atom of the 9-substituent when it takes the *sc* position. The situation is clear when one considers the cases in which no strong interactions between the 1- and 9-substituents are expected. 1-Substituted 9-isopropyltriptycenes are known to exist exclusively as the *sc* isomer except for the 1-fluoro derivative.[4] So are 9-allyl-1,4-dimethyltriptycene,[5] 9-(formylmethyl)-1,4-dimethyltriptycene,[5] and 9-(2-acetoxyethyl)-1,2,3,4-tetrachlorotriptycene.[6]

We have been interested in manifesting the overwhelming population of *sc* isomers due to the weak interactions. To this end, it is necessary to lessen the difference in the steric situations of the *sc* and *ap* conformers of the 1,9-disubstituted triptycenes relative to the cases cited. This must be accomplished by destabilizing the *ap* form, while the ground state of the *sc* form is destabilized little, by a modification of the molecule. As one of the candidates of this technique, introduction of a substituent in the β position of the 9-substituent has been tried for the following reasons. Introduction of a methyl group to an *o*-position of the benzyl-phenyl group in 9-benzyltriptycenes raises the ground state energy, if the methyl group directs inward, and the molecule resides in the conformation only for a short time.[7] This idea led to the finding that the molecular gears with two- and three-toothed wheels[8] and two three-toothed wheels[9] could be made. Although the β-carbon in the substituent in the former is sp^2-hybridized, that in the latter is sp^3-hybridized. There is a good reason to expect that the introduction of a substituent there manifests the desired effect.

Following these considerations, we decided to prepare 9-isobutyl-1,4-dimethoxytriptycene (**1**). There are two rotational axes in the 9-substituent of this molecule: C_9-C_α and C_α-C_β. Although there is limited freedom of rotation in the C_9-C_α bond if we consider only stable conformations, namely *ap* and $\pm sc$ only, there are varieties of conformations we must take into account about the C_α-C_β axis.

If the molecule takes the *ap* conformation about the C_α-C_β axis (Fig. 1a), the steric interactions between the peri-CH groups and the isopropyl-methyl groups are too severe to allow the conformation to exist. If the molecule takes the *sc* conformation about the same axis (Fig. 1b), one of the isopropyl-methyl groups is still too close to the peri-CH group to be stable. If this conformation is to exist, it may be necessary to rotate this part slightly so that the repulsive interactions concerned become smaller.

If the molecule has to take a conformation twisted slightly from the normal staggerred form, it will also be possible to take a conformation that is twisted

† Present address: Department of Chemistry, Faculty of Science, Okayama University of Science, Ridaicho, Okayama 700.

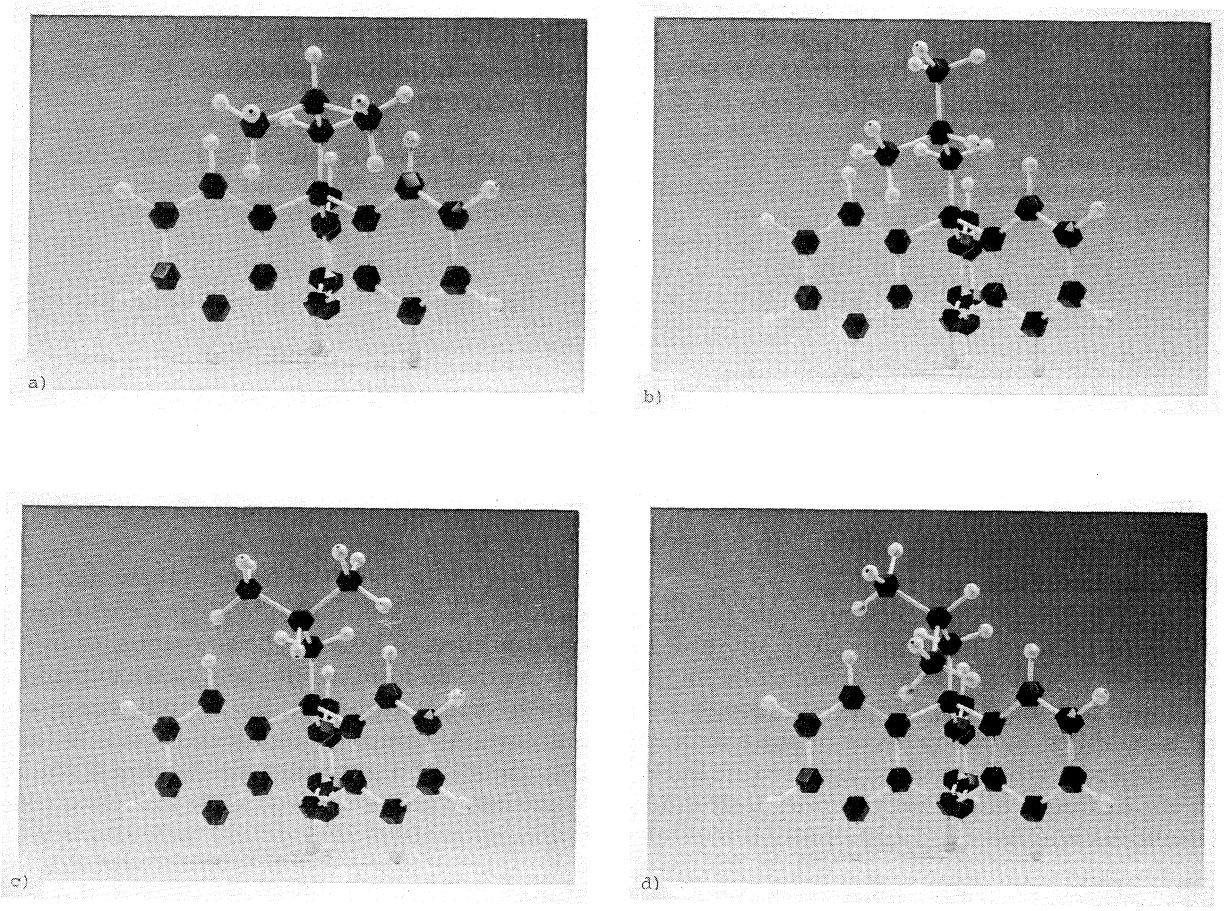

Fig 1. Some extreme conformations of 9-isobutyltriptycene: for clarity, two methoxyl groups at 1 and 4 positions are removed. a) *ap* conformation, b) $+sc$ conformation, c) *sp* conformation, d) $+ac$ conformation.

slightly from the eclipsed conformations. The *sp* conformation (Fig. 1c) may be stabilized by rotating the isopropyl group to some extent about the C_α-C_β bond, because the strain due to eclipsing is eased by doing so. However, this twisting causes another strain between the isopropyl-methyl group and the peri-CH group. It is unlikely that the molecule takes a conformation that is close to the *sp*. In the $\pm 120°$ conformations (Fig. 1d), the repulsive interactions between the two benzeno bridges and the isopropyl-methyl group, which is directing inward relative to the triptycene skeleton, will be minimal. However, the molecule has to avoid the eclipsing interactions of the groups concerned. Although this twisting about the isopropyl-to-methylene bond in the isobutyl group necessarily increases the steric repulsions between the benzeno bridge and the inside-methyl group, these interactions might not be so severe as are expected from the molecular models, because, in the molecular structures of 9-(prim. alkyl)triptycenes, it is known that the dihedral angles made by the two benzeno bridges which flank the β-atom of the substituent is larger than the normal one.[5,10]

In the conformation which is $\pm sc$ about the C_9-C_α bond and is a little twisted from the $\pm 120°$ form about the C_α-C_β bond in 9-isobutyl-1,4-dimethoxytriptycene, the $CH_3 \cdots O$ hydrogen bond is possible, while the $CH \cdots O$ hydrogen bond may have to be between the β-CH and the methoxy-oxygen in the conformation which is $\pm sc$ about the C_9-C_α and is a little twisted from the $\mp 120°$ form about the C_α-C_β bond, if one considers the steric effects caused by the methyl groups by proximating one of them to the 1-methoxy-oxygen. Therefore, if the molecule takes this type of conformation, at the equilibrium between the rotamers, the *sc* conformation may be favored relative to the *ap* owing to the presence of the $CH_3 \cdots O$ hydrogen bond, because the steric effect given by the inward-methyl group will be severe not only in the *sc* conformation but also in the *ap*.

It is not possible to decide which of the two possible conformations discussed above, nearly $\pm sc$ and nearly $\pm ac$ conformations about the C_α-C_β bond, is more stable from the molecular models. In order to find the experimental results, the synthesis of 9-isobutyl-1,4-dimethoxytriptycene (**1**) was undertaken in the following way. Deprotonation of 9,10-dihydroanthracene (**2**) with butyllithium followed by alkylation with iso-

butyl bromide afforded 9-isobutyl-9,10-dihydroanthracene, of which dehydrogenation with 2,3-dichloro-5,6-dicyano-*p*-benzoquinone afforded 9-isobutylanthracene (**3**). The reaction of **3** with *p*-benzoquinone in the presence of boron trifluoride afforded a Diels-Alder adduct which was treated with aqueous sodium hydroxide and dimethyl sulfate to give the desired compound (**1**).

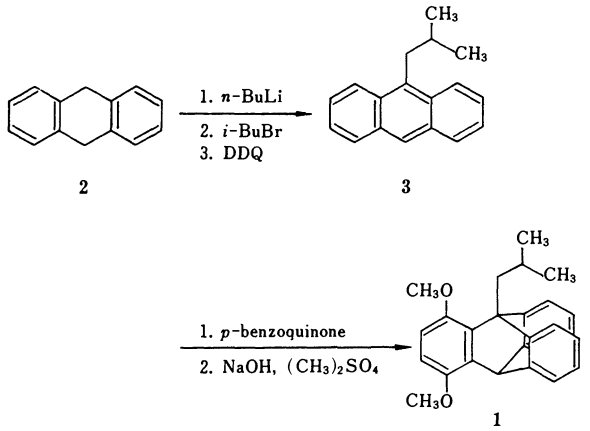

2 3 1

In accordance with the expectation, the barrier to rotation in compound **1** about the C_9-C_α bond is lowered considerably, as evidenced by the fact that the ^{1}H NMR spectrum of the compound in chloroform-*d* did not show decoalescence of any signals, although broadened, at the lowest temperature attainable for the solvent at 270 MHz: The barrier to rotation about the C_9-C_α bond in 1-substituted 9-(prim. alkyl)triptycenes is normally 12—16 kcal mol^{-1} (1 cal=4.184 J) and decoalescence of various signals is complete at about -20 °C.[11-13]

We thus measured the ^{1}H NMR spectra of compound **1** in CD_2Cl_2-CS_2 at 400 MHz. At this magnetic field, the rotation about the C_9-C_α bond was negligibly slow at or below -90 °C. The population ratios were determined at these temperatures and the differences in standard enthalpy and entropy were obtained. The results are shown in Table 1.

Assignment of the signals to *ap* and *sc* conformers was accomplished by finding that, in the 400 MHz ^{1}H NMR spectra at low temperatures, an AB quartet and a singlet,[14] each of which showed further coupling with the methine proton, were separated. In those spectra, the two-proton signals due to the aromatic protons of the dimethoxybenzeno bridge appeared as AB quartets; one at the lower field showed a larger chemical shift difference than that at the higher magnetic field, indicating that the signals at the lower field should be ascribed to the *sc* isomer. The intensity ratios of the proton signals due to the aromatic ring and the α-methylene of the 9-substitutent agreed satisfactorily. Due to the overlaps, however, the determination of the populations was made with the use of the isopropyl-methyl signals.

Table 1. Population Ratios of Rotameric 9-Isobutyl-1,4-dimethoxytriptycene and Differences in Standard Enthalpy and Entropy of the Rotamers in 1 : 1 CD_2Cl_2-CS_2 for the $sc \rightleftarrows ap$ Equilibrium

Temp/°C	−110.6	−100.5	−95.5	−90.5	−85.4
ap/*sc*	0.33	0.37	0.41	0.43	0.48

$\Delta H°$=0.87±0.28 kcal mol^{-1}
$\Delta S°$=4.5±1.6 cal mol^{-1} K^{-1}

Clearly the majority is the *sc* conformation at or below -85 °C. The population of the *sc* form is more than the statistical one and suggests the presence of a kind of stabilizing effects in that form, because no apparent destabilization of the *ap* form is expected. According to the discussion (vide supra), this effect is very likely to be the $CH_3\cdots O$ hydrogen bond. Of another interest is that the preference of the *sc* form over the *ap* diminishes when the temperature is raised: although the low correlation coefficient, 0.984, in the statistical treatment of the equilibrium constants precludes the detailed discussion of the difference in standard entropy, it is tempting to consider that the entropy increases in the process *sc*-**1**→*ap*-**1**, as it appears in the numerical value. This is consistent with the idea that the $CH_3\cdots O$ hydrogen bond reduces the freedom of rotation of the methyl group concerned.

The chemical shift differences between the protons due to isopropyl-methyls are interesting. Whereas that due to the *ap* form gives a simple doublet, the chemical shift differences for the diastereotopic methyl groups in the *sc* form is very large. As is already discussed, there are two conformations of the isobutyl in each rotamer about the C_α-C_β bond. If the rotation of the isopropyl group is slow on the NMR time scale, the chemical shift differences between the two methyl-protons should be large even in the *ap* form because of the anisotropy effect of the benzene ring. The simple doublet signal for these two methyls in the *ap* means that the rotation is fast on the NMR time scale. It is tempting to consider that the large chemical shift difference between the methyl-protons in the *sc* form means that one of the conformers is stabilized relative to the other to make the life-time long, because otherwise the chemical shift differences may be reduced due to the fact that the inside-methyl group in one form is outside in another.

Total line shape analysis of the isopropyl-methyl proton signals was performed with the use of DNMR3 program.[15] Here the rotation of the isobutyl group, in which the isopropyl group passes over the 1-methoxyl group, is assumed not taking place because of the large chemical shift difference between the two methyl signals of the *sc* form: if this rotation takes place, the inside methyl group exchanges the site with the outer methyl even in the absence of rotation about the C_α-C_β bond. The results are shown in Table 2. The low barrier to rotation in compound **1** is clearly derived by

Table 2. Rates of Isomerization ($ap \rightarrow sc$) of Rotameric 9-Isobutyl-1,4-dimethoxytriptycene and Kinetic Parameters for the Isomerization in 1 : 1 CD_2Cl_2-CS_2

Temp/°C	−85.4	−80.4	−75.4	−70.4	−65.4	−60.3	−49.8
k/s^{-1}	20.0	37.5	65	116	205	370	980

$\Delta H^{\ddagger}$=8.8±0.3 kcal mol
$\Delta S^{\ddagger}$=−5.0±1.2 cal mol^{-1} K^{-1}
$\Delta G^{\ddagger}_{200}$=9.8 kcal mol^{-1}

Table 3. Atomic Positional Parameters (×10^4) with Estimated Deviations in Parentheses and Equivalent Isotropic Thermal Parameters of 9-Isobutyl-1,4-dimethoxytriptycene

Atom	x	y	z	B_{eq}[a]
C(1)	3284(1)	5019(2)	7197(1)	2.78
C(2)	3515(1)	4121(2)	6532(1)	3.28
C(3)	2919(1)	3682(2)	5806(1)	3.29
C(4)	2075(1)	4207(2)	5714(1)	2.71
C(4a)	1835(1)	5079(2)	6392(1)	2.37
C(5)	−203(1)	4564(2)	7063(1)	3.54
C(6)	−493(1)	4223(3)	7822(2)	4.53
C(7)	16(1)	4598(3)	8606(2)	4.61
C(8)	832(1)	5274(3)	8654(1)	3.59
C(8a)	1140(1)	5582(2)	7898(1)	2.60
C(9)	2006(1)	6402(2)	7828(1)	2.38
C(9a)	2413(1)	5419(2)	7158(1)	2.36
C(10)	956(1)	5869(2)	6334(1)	2.49
C(10a)	599(1)	5264(2)	7104(1)	2.65
C(11)	1153(1)	7658(2)	6510(1)	2.53
C(12)	1708(1)	7953(2)	7302(1)	2.50
C(13)	1947(1)	9528(2)	7543(1)	3.34
C(14)	1625(1)	10791(2)	6984(1)	4.15
C(15)	1081(1)	10501(2)	6209(1)	4.05
C(16)	835(1)	8917(2)	5963(1)	3.23
C(17)	2584(1)	6771(2)	8706(1)	3.13
C(18)	2873(1)	5408(3)	9387(1)	4.00
C(19)	2921(1)	3690(3)	9049(1)	5.03
C(20)	3717(2)	5904(4)	9968(2)	6.25
C(21)	4759(1)	5482(3)	7872(2)	5.31
C(22)	1681(2)	3060(3)	4304(1)	5.28
O(1)	3875(1)	5584(2)	7889(1)	4.25
O(2)	1440(1)	3953(2)	4996(1)	3.57

a) Equivalent isotropic temperature factor defined by Hamilton.[16]

Table 4. Selected Bond Distances in 9-Isobutyl-1,4-dimethoxytritpycene with Standard Deviations in Parentheses

Atom(1)-Atom(2)	Distance/Å
C(1)-O(1)	1.371(2)
C(21)-O(1)	1.405(3)
C(4)-O(2)	1.375(2)
C(22)-O(2)	1.426(3)
C(4a)-C(10)	1.523(2)
C(10)-C(11)	1.528(2)
C(10)-C(10a)	1.513(3)
C(9)-C(9a)	1.564(2)
C(9)-C(8a)	1.550(2)
C(9)-C(12)	1.551(2)
C(9)-C(17)	1.533(2)
C(17)-C(18)	1.561(3)
C(18)-C(19)	1.524(3)
C(18)-C(20)	1.521(3)

Table 5. Selected Bond Angles in 9-Isobutyl-1,4-dimethoxytriptycene with Standard Deviations in Parentheses

Atom(1)-Atom(2)-Atom(3)	θ/°
C(9a)-C(1)-O(1)	117.8(2)
C(2)-C(1)-O(1)	122.9(2)
C(1)-O(1)-C(21)	119.6(2)
C(3)-C(4)-O(2)	125.1(2)
C(4a)-C(4)-O(2)	116.3(2)
C(4)-O(2)-C(22)	116.5(2)
C(4a)-C(10)-C(10a)	106.6(1)
C(4a)-C(10)-C(11)	104.6(1)
C(10a)-C(10)-C(11)	105.7(1)
C(8a)-C(9)-C(9a)	107.6(1)
C(8a)-C(9)-C(12)	102.6(1)
C(8a)-C(9)-C(17)	114.0(1)
C(9a)-C(9)-C(17)	117.3(1)
C(12)-C(9)-C(17)	112.5(1)
C(9)-C(17)-C(18)	121.2(2)
C(17)-C(18)-C(19)	117.6(2)
C(17)-C(18)-C(20)	108.9(2)
C(19)-C(18)-C(20)	111.4(2)

the relatively unstable ground state. The same reason may apply for the lower barrier to rotation in 9-benzyl-1,4-dimethoxytriptycene[11] than those in 9-ethyl-1,4-dimethoxytriptycene[12] and 9,10-bis(chloromethyl)-triptycene.[13]

The results presented here are all in accordance with the presence of the $CH_3 \cdots O$ hydrogen bond in the *sc* form of compound **1**. However, the results do neither guarantee that the real conformation about the isobutyl group is nearly 120°, nor tell which of the two isopropyl-methyl groups forms the $CH_3 \cdots O$ hydrogen bond with the 1-methoxy-oxygen atom. In order to get further into insight, we decided to perform X-ray crystallographic study of the molecular structure of **1**.

The atomic coordinates, selected bond distances, selected bond angles, selected torsion angles, selected nonbonding distances, and deviations of carbon atoms comprising three benzene rings from the mean plane of the rings are compiled in Tables 3—8, respectively. An ORTEP diagram is shown in Fig. 2 together with numbering of atoms and designation of rings.

The crystallography clearly shows that the molecules are packed in the crystals as *sc* forms. This is quite fortunate, because the molecular structural parameters give information about the $CH_3 \cdots O$ hydrogen bond, but is quite unusual. We have shown that a compound which exhibits the presence of *ap* conformation only gives crystals of *ap* conformation,[5]

Table 6. Selected Torsion Angles in 9-Isobutyl-1,4-dimethoxytriptycene with Standard Deviations in Parentheses

Atom(1)-Atom(2)-Atom(3)-Atom(4)	ϕ/°
C(2)-C(1)-O(1)-C(21)	10.2(3)
C(3)-C(4)-O(2)-C(22)	0.8(3)
C(8)-C(8a)-C(9)-C(9a)	136.6(2)
C(8a)-C(9)-C(9a)-C(1)	140.4(2)
C(12)-C(9)-C(9a)-C(1)	112.4(2)
C(9a)-C(9)-C(12)-C(13)	123.0(2)
C(8)-C(8a)-C(9)-C(12)	117.2(2)
C(8a)-C(9)-C(12)-C(13)	125.8(2)
C(4)-C(4a)-C(10)-C(11)	121.7(2)
C(4a)-C(10)-C(11)-C(16)	123.3(2)
C(11)-C(10)-C(10a)-C(5)	121.6(2)
C(10a)-C(10)-C(11)-C(16)	124.4(2)
C(4)-C(4a)-C(10)-C(10a)	126,7(2)
C(4a)-C(10)-C(10a)-C(5)	127,5(2)
C(10)-C(4a)-C(9a)-C(1)	167.6(1)
C(8)-C(8a)-C(10a)-C(10)	171.8(2)
C(10)-C(11)-C(12)-C(13)	179.5(2)
C(4)-C(4a)-C(9a)-C(9)	179.7(1)
C(9)-C(8a)-C(10a)-C(5)	178.7(2)
C(16)-C(11)-C(12)-C(9)	179.6(2)
C(8a)-C(9)-C(17)-C(18)	56.7(2)
C(9a)-C(9)-C(17)-C(18)	70.3(2)
C(9)-C(17)-C(18)-C(19)	26.5(3)
C(9)-C(17)-C(18)-C(20)	154.4(2)

Table 7. Selected Nonbonding Distances in 9-Isobutyl-1,4-dimethoxytriptycene with Standard Deviations in Parentheses

Atom(1)-Atom(2)	Distance/Å
O(1)-C(17)	2.788(2)
O(1)-C(18)	3.080(3)
O(1)-C(19)	3.017(3)
O(1)-C(20)	3.334(3)
C(1)-C(19)	3.262(3)
C(1)-C(20)	4.337(3)
C(8)-C(18)	3.213(3)
C(8)-C(19)	3.495(3)

Table 8. Atomic Shifts from the Least-Squares Planes in the Benzene Rings of 9-Isobutyl-1,4-dimethoxytriptycene

Ring A		Ring B		Ring C	
Carbon	d/Å	Carbon	d/Å	Carbon	d/Å
C(1)	0.041	C(5)	−0.006	C(11)	−0.001
C(2)	0.004	C(6)	−0.015	C(12)	0.000
C(3)	−0.038	C(7)	0.012	C(13)	0.001
C(4)	0.017	C(8)	0.009	C(14)	−0.001
C(4a)	0.022	C(8a)	−0.018	C(15)	−0.001
C(9a)	−0.044	C(10a)	0.017	C(16)	0.002

and that even a compound which exists solely as *sc* conformation in solution gives crystals which contain both *ap* and *sc* conformations.[10] We believe the reasons for this phenomenon that compound **1** crystallizes in the *sc* form should include the factor that the *sc* form is more stable than the *ap*.

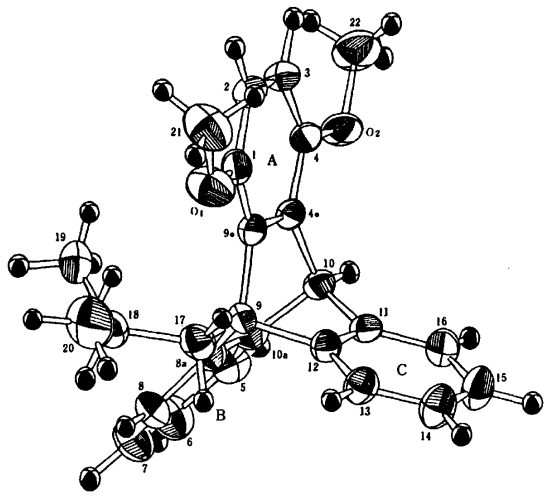

Fig. 2. An ORTEP diagram of 9-isobutyl-1,4-dimethoxytriptycene with numberings of atoms and designation of rings.

As all the data suggest, the structure around the C(10), that is the opposite side of the 9-substituent in the triptycene skeleton, is nearly normal, whereas abnormal are the atomic positions comprising the 9-substituent and the peri-positions which are close to the 9-substituent. We can point out some of the common features of 9-substituted triptycenes[5,10] which are also seen in this compound. The bonds connecting the C(9) and the benzene rings are long, especially long being that between C(9) and the aromatic ring which carries two methoxyl groups. The pyramid made by C(8a), C(9a), C(12), and C(9) has very small C-C-C apex angles at C(9) and correspondingly the angles C(17)-C(9)-C(n), where C(n) is the carbon atom of the aromatic rings, are large. These features are derived to relieve the steric strain formed by the 1- and 9-substituents.

One of the methyl groups in the 9-substituent directs inward relative to the triptycene skeleton, as was expected from the model study, and the eclipsing strain is relieved by rotating 26.5° from the eclipsing position. To accommodate the inward-directing methyl group, the C(8a)-C(9)-C(9a) angle is widened considerably relative to other apex angles and the torsion angles consisting this notch, i.e. C(8)-C(8a)-C(9)-C(9a) and C(8a)-C(9)-C(9a)-C(1), are very large. These are reflected in the dihedral angles made by two average planes of the benzene rings: A and B 132.7°, A and C 112.3°, B and C 114.9°. The difference in the torsion angles involving the same notch is due to the twisting of the benzene rings at the peri-carbons: the peri-carbons flanking the 9-substituent are dislocated from the average plane of the benzene rings away from the substituent, whereas another peri-carbon, C(13), is closely in the average plane of the benzene ring. This situation is clearly seen by the torsion angles involving the axes of bridge carbons of the benzeno moiety.

Whereas the torsion angle, C(10)-C(11)-C(12)-C(13), is very close to 180°, those that involve the peri-carbons flanking the 9-substituent, C(10)-C(4a)-C(9a)-C(1) and C(8)-C(8a)-C(10a)-C(10), are much smaller than 180°. The corresponding torsion angles about the bridge carbon-carbon axis involving the C(9) and the peri-carbon that is in the opposite side of the triptycene skeleton relative to the 9-substituent are again very close to 180°.

Deformation of the benzene rings in the molecule deserves special mention. As are shown in Table 8, while ring C is practically planar and ring B is slightly distorted, deviations of atoms comprising ring A from the average plane are rather large. The situation of ring A is more distinct if one takes deviations of atoms from the mean plane formed by atoms C(3), C(4), C(4a), and C(9a): these atoms comprise a fairly good plane, the atomic shifts being less than 0.003 Å, though that does not mean that these atoms are located normally because, whereas C(9) is in this plane, C(10) is out of this plane by 0.142 Å. C(1) is out of this plane away from the 9-substituent by 0.144 Å and so is C(2) by 0.106 Å. These deformations must be due to the severe steric interactions of the methyl group in the 9-substituent and the atoms of the ring concerned.

The torsion angle at the C_α-C_β axis of the 9-substituent indicates that the substituent is tilted toward the benzene ring which does not carry the methoxyl groups. This is considered to avoid the steric interactions between the 1-methoxyl group and the 9-substituent. The C_α-C_β bond in the substituent is unusually long as an sp^3-sp^3 carbon bond and the bond angle C(9)-C(17)-C(18) is very large. These should be the results of relieving the strain caused by the inside-methyl group and the benzeno bridges that form the notch.

The inside-methyl group is very close to the 1-methoxy-oxygen, the distance being 3.017 Å, well within the sum of the van der Waals radii of the groups concerned. Of course, this distance alone cannot be taken as evidence for the presence of the $CH_3 \cdots O$ hydrogen bond, because the intramolecular nonbonding distance can be very small,[17] especially in congested molecules. However, if one compares the distances, C(19)-O(1) and C(20)-O(1), there is a significant difference between them. This may well support the presence of the $CH_3 \cdots O$ hydrogen bond.

There is another interesting feature in the molecular structure of **1**. That is the 1-methoxyl group is twisted to make the methoxy-methyl group out of the plane of the average benzene ring. Since anisole and related compounds are believed to be stable at a planar structure[18] and the 4-methoxyl group in **1** is indeed in the plane of the benzene ring, there must be a reason for this nonplanar conformation of the 1-methoxyl group. We should tentatively like to attribute this structure to being favorable for forming the $CH_3 \cdots O$ hydrogen bond. If the 1-methoxy-oxygen is sp^2-hybridized, both the direction of the orbital of the oxygen lone pair, of which ionization potential is minimum, and the high ionization potential of the electrons in the orbital, of which axis is parallel to the p-orbitals of the benzene ring, are not favorable for the hydrogen bond. Thus although energetically unfavorable from the view point of conjugation with the benzene ring, the 1-methoxyl group rotates to a small extent about the C(1)-O(1) bond to make the $CH_3 \cdots O$ interaction favorable.

The structure around the methoxy-oxygen is of interest in another point. That is, the C(1)-O(1) bond is bent out of the average plane of ring A and the O(1) atom is shifted from the C(3)-C(4)-C(4a)-C(9a) plane by 0.359 Å away from the 9-substituent. The reason for this deformation is not clear at present, but we believe both the steric and $CH_3 \cdots O$ hydrogen-bond effects are responsible for this unusual structure.

In conclusion, all the data presented in this paper suggest that there is $CH_3 \cdots O$ hydrogen bond in compound **1** both in solution and in the solid state. The technique of introducing a substituent to the β-position of the 9-substituent to lessen the steric energy gap between the *sc* and the *ap* forms may find other uses in manifestation of weak molecular interactions.

Experimental

Material. The sythesis of the compound was carried out as follows.

9-Isobutylanthracene (3). To a solution of 5.4 g (30 mmol) of 9,10-dihydroanthracene (**2**) in 75 mL of tetrahydrofuran, was slowly added 13.5 mL (32 mmol) of butyllithium in hexane at ca. −45 °C under a nitrogen atmosphere. Stirring was continued for further 30 min and then the solution was added to 3.6 mL (33 mmol) of isobutyl bromide in 10 mL of tetrahydrofuran at −30 °C under a nitrogen atmosphere. The mixture was allowed to warm up and then stirred overnight at room temperature. The mixture was treated with water and extracted with benzene. After evaporation of the solvent, the residue was taken up in 30 mL of benzene and heated at 40—60 °C for 1 h with 6.81 g (30 mmol) of 2,3-dichloro-5,6-dicyano-*p*-benzoquinone. The precipitate was filtered off and the solvent was evaporated from the filtrate. The residue was submitted to chromatography on silica gel (hexane eluent) to afford 2.79 g (40%) of the desired product, mp 66—67 °C (lit,[19] mp 57 °C). ^{1}H NMR ($CDCl_3$) δ=0.98 (6H, d, J=6.3 Hz), 2.19 (1H, nonet, J=6.3 Hz), 3.47 (2H, J=6.3 Hz), 7.3—7.8 (9H, m).

9-Isopropyl-1,4-dimethoxytriptycene (1). A solution of 980 mg (4.2 mmol) of 9-isobutylanthracene and 710 mg (6.6 mmol) of *p*-benzoquinone in 7.5 mL of ether was mixed with 1.1 mL of boron trifluoride-etherate and the mixture was stirred for 1 h under a nitrogen atmosphere at room temperature. The produced precipitate was collected by filtration to yield 970 mg of a Diels-Alder adduct. The adduct (670 mg or 2.0 mmol) was dissolved in 22 mL of dioxane and treated with aqueous sodium hydroxide and dimethyl sulfate by adding them alternatively in small portions. In total, 2.0 g of sodium hydroxide (500 mmol) in 20 mL of water and 7.0 mL (75 mmol) of dimethyl sulfate were used. The precipi-

tate was collected and submitted to chromatography on silica gel (5:1 hexane-dichloromethane eluent) to afford 260 mg (36%) of **1**, mp 188.5—189.5 °C. Found: C, 84.30; H, 7.08%. Calcd for $C_{26}H_{26}O_2$: C, 84.29; H, 7.07%. ^{1}H NMR ($CDCl_3$, 270 MHz, room temperature): δ=1.19 (6H, d, J=6.6 Hz), 2.76 (1H, m), 3.31 (2H, d, J=7.7 Hz), 3.70 (3H, s), 3.78 (3H, s), 5.83 (1H, s), 6.45 and 6.49 (2H, ABq, J=9.0 Hz), 6.98 (4H, m), 7.38 (2H, m), 7.59 (2H, m). ^{1}H NMR (CD_2Cl_2-CS_2, δ, 400 MHz, −100 °C): *ap*-form 1.20 (6H, d, J=6.6 Hz), 2.49 (1H, m), 3.36 (2H, d, J=6.6 Hz), 3.68 (3H, s), 3.75 (3H, s), 5.77 (1H, s), 6.41 (2H, br s), 6.87 (2H, t, J=7.1 Hz), 6.97 (2H, t, J=7.5 Hz), 7.25 (2H, d, J=7.3 Hz), 7.60 (2H, m); *sc*-form 0.80 (3H, d, J=6.6 Hz), 1.28 (3H, d, J=6.6 Hz), 2.87 (1H, m), 3.00 and 3.32 (2H, AB of ABX, J=14.3 and 8.8 Hz), 3.70 (3H, s), 3.80 (3H, s), 5.79 (1H, s), 6.52 and 6.57 (2H, ABq, J=9.2 Hz), 7.06 (4H, m), 7.33 (1H, d, J=7.3 Hz), 7.41 (2H, m), 7.73 (1H, d, J=7.0 Hz).

NMR Spectroscopy at Low Temperatures. Compound **1** was dissolved in 1:1 (v/v) carbon disulfide and dichloromethane-d_2 to make up a 19 mmol L^{-1} solution. The spectra at various temperatures were obtained with a JEOL GX400 spectrometer, the temperature being calibrated with a thermocouple. The populations, chemical shift differences, and the coupling constants were checked at 4 temperatures in the slow exchange limit. For the determination of the populations of rotamers, the signals due to the isopropyl-methyl protons were used for the following reasons. Although there was an overlap of the signal due to the α-methylene protons of the 9-substituent in the *ap* form with the lower signal of the two due to the α-CH_2 (AB) protons of the *sc* form, clearly the signals due to the *sc* form were more intense than that due to the *ap* at −100 °C and the assignment of the signals due to the isopropyl-methyl protons was possible by comparing the intensities of the two. The signals due to the isopropyl-methyl protons were found to give more accurate populations than those due to the α-CH_2 protons. The spectra were simulated with the use of the signals due to the isopropyl-methyl protons by the DNMR3 program.[15]

Logarithms of the popultaiton ratios shown in Table 1, when plotted gainst $1/T$(K), afforded the difference in standard enthalpy and entropy, which were used to estimate the populations of the rotamers at temperatures where the change in the line shapes was observed. The coupling constants were constant in the temperature range examined, whereas the chemical shift differences changed linearly with temperature. A straight line was drawn by the least squares method to correlate the chemical shift difference ($\Delta\nu$/Hz) with temperature (t/ °C). The following equations were obtained, where A is the chemical shift at a lower magnetic field than the counterpart B of the AB protons and C denotes the chemical shift of the protons due to the *ap* form: $\Delta\nu_{AC}$=−0.21110t+13.63 Hz, $\Delta\nu_{AB}$=−8.287t+109.70 Hz. These lines were used for the calculation of the chemical shift differences at a given temperature. The chemical shift of the X proton was used as observed at low temperatures. T_2 was estimated as 0.10 s from the line width due to other protons and this value was used throughout the line shape simulation. It was assumed that the observed process was $A_3B_3X \rightleftarrows C_6X \rightleftarrows B_3A_3X$, the direct exchange $A_3B_3X \rightleftarrows B_3A_3X$ being negligibly slow, and could be approximated by $ABX \rightleftarrows C_2X \rightleftarrows BAX$.

X-Ray Crystallography. Crystals were grown from a tetrahydrofuran-hexane solution. The colorless crystal with dimensions 0.6×0.6×0.2 mm was mounted on a Rigaku AFC-5R four-circle diffractometer and the intensity data were collected using Mo$K\alpha$ radiation (λ=0.71073 Å). The ω-2θ scan technique was employed at a scan rate of 4° min^{-1} in ω, and the scan range was calculated by 1.2°+0.5° tanθ. A total of 6644 independent reflections within the 2θ<60° were measured, and 3364 reflections with $|F_o| \geq 3\sigma|F_o|$ were regarded as observed reflections and used for the structure determination and refinement.

The crystal data are as follows: $C_{26}H_{26}O_2$, F.W.=370.47, monoclinic, space group $P2_1/a$, a=15.803(3), b=8.276(1), c=15.706(3) Å, β=101.02(2)°, V=2016.2 Å^3, Z=4, D_c=1.22 g cm^{-3}, μ=0.816 cm^{-1}. The structure was solved by direct methods (MULTAN 78) and refined by the block-diagonal least-squares technique with anisotropic thermal parameters for non-hydrogen atoms and isotropic for hydrogens. All the hydrogen atoms were located on a difference map but their positional parameters were not refined. The atomic scattering factors were taken from International Tables for X-Ray Crystallography.[20] The weighting scheme $w=[\sigma_c^2+(0.03F_o^2)]^{-1}$ was employed. The final R and R_w values were 4.93 and 6.08%, respectively.

All the calculations were carried out on a HITAC M-200H computer with crystallographic computation program systems, MULTAN and UNICS III, filed at the Computer Center of the Institute for Molecular Science. The complete F_o−F_c data are deposited as Document No. 8838 at the Office of the Editor of the Bulletin of the Chemical Society of Japan.

The ^{1}H NMR spectra at 400 MHz were obtained at the JEOL laboratory. We wish to thank for the assistance and the permission of the use of the spectrometer.

References

1) Y. Tamura, G. Yamamoto, and M. Ōki, *Bull. Chem. Soc. Jpn.*, **60**, 1781 (1987).
2) Y. Tamura, G. Yamamoto, and M. Ōki, *Bull. Chem. Soc. Jpn.*, **60**, 3789 (1987).
3) H. H. Jaffé, *Chem. Rev.*, **53**, 191 (1953).
4) F. Suzuki, M. Ōki, and H. Nakanishi, *Bull. Chem. Soc. Jpn.*, **47**, 3114 (1974); G. Yamamoto and M. Ōki, *ibid.*, **56**, 2082 (1983).
5) M. Ōki, G. Izumi, G. Yamamoto, and N. Nakamura, *Bull. Chem. Soc. Jpn.*, **55**, 159 (1982).
6) G. Izumi, G. Yamamoto, and M. Ōki, *Bull. Chem. Soc. Jpn.*, **54**, 3064 (1981).
7) G. Yamamoto and M. Ōki, *Bull. Chem. Soc. Jpn.*, **54**, 481 (1981).
8) R. B. Nachbar, Jr., W. D. Hounshell, V. A. Naman, O. Wennerström, A. Guenzi, and K. Mislow, *J. Org. Chem.*, **48**, 1227 (1983); G. Yamamoto and M. Ōki, *ibid.*, **48**, 1233 (1983).
9) F. Cozzi, A. Guenzi, C. A. Johnson, K. Mislow, W. D. Hounshell, and J. F. Blount, *J. Am. Chem. Soc.*, **103**, 957 (1981); Y. Kawada and H. Iwamura, *ibid.*, **103**, 958 (1981).
10) N. Nogami, M. Ōki, S. Sato, and Y. Saito, *Bull. Chem. Soc. Jpn.*, **55**, 3580 (1982).
11) M. Kono, H. Kihara, N. Nakamura, F. Suzuki, and M. Ōki, *Bull. Chem. Soc. Jpn.*, **52**, 1682 (1979).
12) H. Nakanishi and O. Yamamoto, *Bull. Chem. Soc. Jpn.*, **51**, 1777 (1978).
13) Y. K. Grishin, N. M. Sergeyev, O. A. Subbotin, and Y.

A. Ustynyuk, *Mol. Phys.*, **25**, 297 (1973).
14) F. Suzuki and M. Ōki, *Tetrahedron Lett.*, **1974**, 2845.
15) G. Binsch, *Top. Stereochem.*, **3**, 97 (1968).
16) W. C. Hamilton, *Acta Crystallogr.*, **12**, 609 (1959).
17) R. Taylor and O. Kennard, *J. Am. Chem. Soc.*, **104**, 5063 (1982).
18) H. Dodziuk, H. von Voithenberg, and N. L. Allinger, *Tetrahedron*, **38**, 2811 (1982).
19) C. Liebermann, *Justus Liebigs Ann. Chem.*, **212**, 1 (1882).
20) International Tables for X-Ray Crystallography (1974), Vol. IV, Kynoch Press, Birmingham.

Reactivities of Stable Rotamers. XXIII. Some Addition Reactions toward the Vinyl Group in 9-(2-Vinyl-1-naphthyl)-fluorene Rotamers[1)]

Michinori Ōki,*,† Jiro Tsukahara, Yoriko Sonoda, Kazuhiro Moriyama, and Nobuo Nakamura
Department of Chemistry, Faculty of Science, The University of Tokyo, Bunkyo-ku, Tokyo 113
(Received March 18, 1988)

Addition reactions to the vinyl group of the *ap* and the *sp* rotamers of 9-(2-vinyl-1-naphthyl)fluorene were carried out. Whereas action of sulfuric acid on the *sp* rotamer caused a cyclization reaction, the *ap* isomer was recovered under the conditions. While addition of bromine afforded normal products for both the isomers, reaction of chlorine afforded chlorine-substituted products (chloro olefins) in addition to the normal adduct, the formation of the former being predominant, in the *sp* form. The slightly enhanced reactivity of the *sp* form relative to the *ap* in bromination together with the formation of the chloro olefin and the behavior of the *sp* form in the treatment with sulfuric acid are attributed to the stabilization of the intermediates by the π-participation of the fluorene ring. Other addition reactions, epoxidation, hydrogenation, hydroboration, osmium tetraoxide oxidation, chlorination with (dichloroiodo)benzene, and diimide reduction, which are believed to proceed through a cyclic transition state, have also been studied to show that the rates of the reactions of one isomer are not much different from those of another. Spectroscopic data suggest that the conformation of the vinylnaphthalene portion in both isomers are similar. Little difference in the reaction rates of the two rotamers are attributed to the possible transition state conformation which may not be affected by the steric hindrance of the fluorene ring.

In previous papers of this series, we have pointed out that, in 9-(2-substituted 1-naphthyl)fluorene derivatives (**1**), reactions which occur over the fluorene ring with bulky transition states can be much slower than those which occur in the remote sites from the fluorene moiety.[2,3)] Thus the reactions that occur in the X group of the *ap* conformer (*ap*-**1**) are much

ap-1 *sp*-1

(if X precedes C_{8a} of naphthalene in the sequence rule)

slower than those occurring in the X of the *sp* conformer (*sp*-**1**), the k_{sp}/k_{ap} values exceeding 30 in some cases.

Based on these generallizations, we see that addition reactions of 9-(2-formyl-1-naphthyl)fluorenes (**1**: X= CHO) are on the border line, because the following relative rates, k_{sp}/k_{ap}, are obtained: sodium tetrahydroborate reduction 7.6, oxime formation 3.7, addition of Gringard reagents ca. 1.8.[2)] In view of these results, it will be worthwhile to examine some other reactions that would give similar situations in the transition states of reactions to that of the aldehyde. Since a vinyl group has a similar bulkiness with a formyl group as far as we consider the CH= group that should give important steric interactions with the fluorene moiety, 9-(2-vinyl-1-naphthyl)fluorene (**2**) is a good model to further the understanding of the steric effects in some reactions of this type of compounds. In addition, various types of addition reactions to an olefin which proceed with cyclic and consequently bulky transition states are known. This paper discusses the results of some addition reactions of **2**.

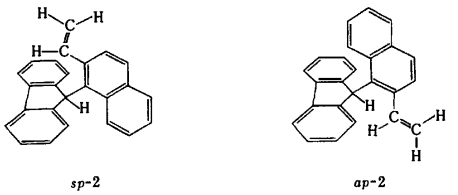

sp-2 *ap*-2

Rotational Barriers and Equilibrium Constant. In order to avoid complexity arising from isomerization of one rotamer to another, it is desirable to run reactions under conditions that do not permit contamination of one isomer by another produced by isomerization. Thus at the outset of the investigation we undertook the measurement of the rates of isomerization of these isomers. *ap*-**2** in toluene-d_8 exhibited the equilibrium constant (*sp*/*ap*) of 0.47 and the rate constant of isomerization of 8.48×10^{-6} s^{-1} at 80 °C. Similarly, the *sp* isomer gave the following results: *ap*/*sp* 2.1, *k*(isomerization) 1.95×10^{-5} s^{-1}. These results agree quite well. The free energy ef activation for rotation is 28.9 kcal mol^{-1} (1 cal=4.184 J) for the *ap*→*sp* process, and is 28.4 kcal mol^{-1} for the *sp*→*ap* process at 80 °C.

The barriers to rotation in these olefins are appreciably higher than those in the aldehyde (**1**: X=CHO), 26.8 kcal mol^{-1} at 80 °C.[2)] The equilibrium constant, 2.1, is significantly larger than the corresponding value, 1.5, for the aldehyde.[2)] The difference cannot be attributed to the difference in the ground state conformations, because both the aldehyde[4)] and the olefins (**2**), for which evidence is described in Experimental section, are coplanar with the naphthalene nucleus.

We attribute the difference in the equilibrium con-

† Present address: Department of Chemistry, Faculty of Science, Okayama University of Science, Ridaicho, Okayama 700.

stants between the aldehyde (**1**: X=CHO) and the olefin (**2**) to the difference in the solvents, hexachlorobutadiene for the aldehyde and toluene-d_8 for the olefin.

Addition Reactions of Cationic Species. Treatment of *sp*-**2** with concentrated sulfuric acid afforded *trans*-8-methyl-8,14c-dihydrodibenz[*a*,*l*]aceanthrylene (**3**) smoothly which was identical with the authentic specimen reported in a previous paper.[5] The result unambiguously shows that the benzylic cation formed by addition of a proton to the vinyl group can attack the aromatic ring of the fluorene moiety if the conformation of the starting olefin is *sp*. By contrast, we recovered *ap*-**2** after the same treatment for 60 days. Thus it is extremely difficult to get a cyclized product from a cation produced in the benzylic position of *ap*-**2**, as reported for another case of dehydration reaction of *sp*-9-[2-(1-hydroxyethyl)-1-naphthyl]fluorene.[6]

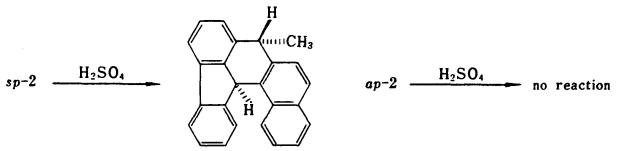

3

Addition of bromine to the olefinic bond is usually assumed to proceed through a bridged bromonium ion because of the stereospecificity of the reaction.[7] However, the stereospecificity is lost in the addition of bromine to *cis*- and *trans*-1-propenylbenzene.[8] Since the compounds we are concerned here are styrene derivatives, the reaction might be assumed to follow the path where an open-chain cation intervenes. If the intermediate is distinctly a cation, then we might expect to obtain a cyclized product from *sp*-**2** as was the case for the sulfuric acid treatment.

In the actual reaction, no anomaly was observed not only for *ap*-**2** but also for *sp*-**2**: normal addition reaction products (**4**) were obtained. This would mean that the cationic species formed during the reaction is not a naked cation but is stabilized by the participation of the bromine atom beta to the cationic center. The nonstereospecificity of the bromine addition[8] is not inconsistent with this interpretation but would mean that, due to the weak participation of the bromine atom, the bond between the cationic center and the bromine atom breaks and reforms rapidly under the conditions, when stereochemistry is reversed. This result is consistent with the finding that, in the addition reaction of bromine to 1-propenylbenzene, partial stereoselectivity is observed.[8,9]

The relative rate (k_{ap}/k_{sp}) of the bromine addition was 0.80 in carbon tetrachloride. It is rather surprising to note that the reaction which occurs at a crowded site is faster than that in a less crowded site. It is especially so when we compare the results with those of addition reactions to the formyl group: although the relative rates vary from reaction to reaction, the reactions that occur in a less crowded site are always faster than those in a crowded site.[2] We wish to attribute this apparently anomalous relative rate to the participation of the π-system of the fluorene ring. Namely the cationic species formed by addition of a cationic bromine is partly stabilized by the π-participation. In agreement with this interpretation, we found that the same reaction in acetonitrile prefers the *ap*-olefin, although the degree of the preference is rather small, k_{ap}/k_{sp}=1.2. It has been found that solvation shell around the cationic species formed over the fluorene ring is completed by involving the participation of the fluorene ring.[6] Thus, if the solvent molecules are good nucleophiles, the cation formed from *ap*-**2** must be more stable than that from *sp*-**2**, because the solvation shell is completed by solvent molecules alone in the *ap*-**2** case.

2 4

The reactions of the olefin (**2**) with chlorine were rather surprising: while the *ap*-form afforded the chlorine-addition product (**5**), as the normal olefin, in addition to a small amount of an unidentified material, the ratio of the addition product (**5**) to a chlorine-substitution product (**6**) was 1.0 : 1.4 in the case of *sp*-**2**. Compound **6** is not the secondary product from **5**, because the formation ratio, **5**/**6**, at the later stage of the reaction was the same with that at the earlier stage and **6** was not converted practically to **5** under the reaction conditions in a separate experiment.

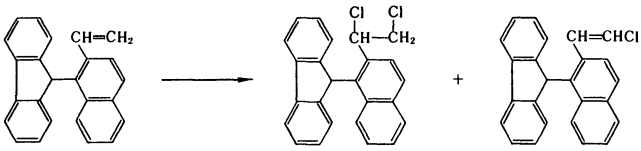

2 5 6

The mechanism of the formation of **6** is assumed to be that the intervening cation (**7**) which is stabilized, though weak, by the participation of the chlorine atom in the β-position suffers from deprotonation more preferably than the attack of the chloride ion at the α-position. The preferred formation of **6** in the case of *sp*-**2** must be derived from the facts that the vinyl group is situated in the sterically more hindered site and that the ionic character of the intervening **7** is more significant than that of the *ap*-form because of the π-participation. It might be argued that the chloronium ion is possible only in aliphatic β-chloro carbocations and not for the benzylic cation.[10] In the addition of chlorine to an olefinic bond in compounds of styrene type, open-chain β-chloro cations which form ion-pairs are postulated.[11] However, the postulate cannot accommodate the difference in the reactivities

of the rotamers observed here. We prefer, therefore, that the chlorine participation is significant in this case, though the C-Cl bond may break and form rapidly because the participation is weak. The formation of the chloro-olefin which is also observed in other cases is attributed to deprotonation from either the weakly chloro-participated **7** or transitionally formed open-chain cation.

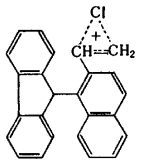

7

Addition Reactions with Cyclic Transition States. Relative rates (k_{ap}/k_{sp}) are given in Scheme 1 for various addition reactions of which transition states are cyclic, together with some related reactions.

Epoxidation of olefins with peroxycarboxylic acids is known to proceed stereospecifically.[12] Even *cis*-stilbene gives a stereospecific addition product, *cis*-2,3-diphenyloxirane.[13] Thus in the formation of epoxides, the transition state may be unequivocally assumed to be a three-membered cycle. Both *ap*-**2** and *sp*-**2** reacted smoothly with *m*-chloroperbenzoic acid to give epoxides (**8**). The relative rate was very close to unity but the reaction of *sp*-**2** was significantly favored over that of *ap*-**2**.

Four-membered cyclic transition states are assumed for catalytic hydrogenation[14] and addition of borane.[15] Hydrogenation of *ap*-**2** and *sp*-**2** over palladium on carbon proceeded smoothly to afford *ap*- and *sp*-9-(2-ethyl-1-naphthyl)fluorene (**9**), respectively. The relative rate was ca. 2. Addition of borane to *sp*-**2** in tetrahydrofuran, followed by oxidation with alkaline hydrogen peroxide, afforded 9-[2-(2-hydroxyethyl)-1-naphthyl]fluorene (**10**) and 9-[2-(1-hydroxyethyl)-1-naphthyl]fluorene (**11**) in 7:3 ratio, whereas *ap*-**2** afforded the corresponding **10** and **11** in 5:2 ratio. This poor regioselectivity in the borane addition was also reported in the literature for the case of styrene.[15,16] Strictly speaking, therefore, we observed two reactions, which differ in the rate constants, to make the comparison of the reactivities of the rotamers very difficult. However, since the product ratios due to the regiochemically different additions in both rotamers are not far from each other and the rates of the additions to the two olefinic substrates are comparable, we may compare the reactivity of the rotamers, as a rule of thumb, by taking the rates of decrease in the amount of the starting materials, *sp*-**2** and *ap*-**2**. These results are shown in Scheme 1. This reaction is the one among those examined in this work, that shows the highest reactivity of the *ap*-isomer relative to the *sp*. Although we tried to add 9-borabicyclo[3.3.1]nonane, which should give distinct steric effects,[17] to the olefin, isomers failed to give products.

Cis-addition, though not exclusive, of chlorine to olefins was first established by Barton and Miller[18] when (dichloroiodo)benzene was used. Although this addition reaction has a complicated nature,[19] it will be worthwhile to try the reaction as an example of a five-membered cyclic transition state. The reaction of (dichloroiodo)benzene with *ap*-**2** and *sp*-**2** proceeded smoothly to give the corresponding dichlorides (**5**). The relative rate was 0.66. Although this reaction can involve ionic, radical, and cyclic intermediates (or transition state), details are not known. However, the results suggest that the mechanism of the reaction of **2** with this reagent is different from the addition reaction of chlorine, because the product ratios were different.

A five-membered cyclic transition state is also expected for the oxidation of the olefin with osmium tetraoxide.[20] Addition of the reagent gave the corresponding diols (**12**). The relative rate was 0.90.

Diimide addition to olefins is also stereospecific and

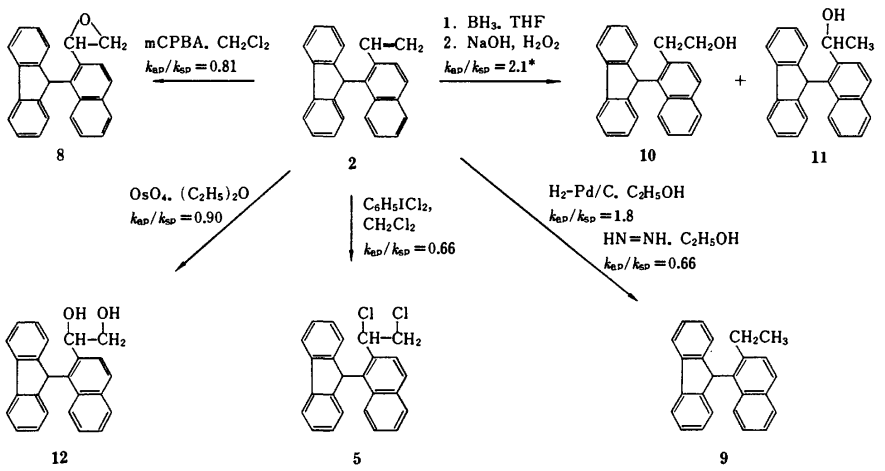

Scheme 1. Reactions of *ap*- and *sp*-9-(2-vinyl-1-naphthyl)fluorene rotamers, products, and relative reactivities (k_{ap}/k_{sp}).
* For k_{ap}/k_{sp} here, see the text.

a six-membered cyclic transition state is involved.[21] Since the isomerization of the rotamers of **2** can occur under the alkaline conditions, we used the method of generation of diimide under neutral conditions.[22] The reduction of **2** took place smoothly to afford 9-(2-ethyl-1-naphthyl)fluorene (**9**). The relative reactivity is less than unity to mean that the vinyl group over the fluorene ring is more vulnerable to the reaction.

Summarizing these results, we notice that the rates of addition reactions of various reagents to the olefinic bond of compound **2** do not differ to a large extent from the *ap* to the *sp* rotamer, even though we selected various space-demanding reactions with cyclic transition states from a three membered to a six-membered ring.

Although the ground state conformations of the vinylnaphthalene moieties are planar, the rotamers cannot react in the conformations as such, because the bulky transition state must be taken that should strongly interfere with the fluorene ring in the *sp* rotamer. Therefore, a strong possibility is that the vinyl group rotates from the naphthalene plane to permit the access of the reagent. This rotation will occur in both conformers, *ap*-**2** and *sp*-**2**, because the reactions of *ap*-**2**, especially those which are not electron-demanding, must be faster than those of *sp*-**2**, to an extent that is determined by the energy required for the rotation, if *ap*-**2** reacts in the planar conformation. Though the electron density in the vinyl group should increase by taking the nonplanar structure, this effect on the reaction rate may be neglected.

If the vinyl group takes the nonplanar conformation invoked above, in the transition state of addition reactions where the benzylic carbon must approach the sp^3-hybridized geometry, the hydrogen on the benzylic carbon will direct toward the fluorene moiety to make the steric interaction energy minimum. We conclude therefore, that in this kind of transition state conformations the steric hindrance is minimum and the transition state energy is by and large the same for the two rotamers to make the relative reaction rates close to unity.

Close examination of the results in Scheme 1 reveals that in nonpolar solvent the reactions in which electron-demanding reagents are used tend to give smaller values of k_{ap}/k_{sp} than unity except for hydroboration. Although we should not overlook solvent effects, it is tempting to consider that the π-participation from the fluorene system is accelerating the reactions of *sp*-**2**.

Borane will not be an adding species as such: it should be accompanied by solvent molecule(s) because of its high Lewis acidity. This steric effect may be the reason why borane gives a k_{ap}/k_{sp} value of more than one. We do not have a good explanation for the results of diimide reduction at present. Probably the solvent effect is important because we used strongly polar and hydrogen-bonding ethanol as a solvent.

Coming back to the situation of addition reactions to the aldehyde (**1**: X=CHO), we now believe that, since the steric situation of it is very close to the olefin (**2**), the k_{sp}/k_{ap} value which is close to unity is normal. Those reactions which give large k_{sp}/k_{ap} values for the aldehyde may involve factors of solvation.

Experimental

^{1}H NMR spectra were recorded on either a Varian EM390 spectrometer which operates at 90 MHz or a JEOL GX270 machine which operates at 270 MHz. Melting points are not corrected.

Infrared Spectra. They were recorded on a Hitachi IR-260-30 spectrophotometer with a thalium(I) chloride cell of 0.1 mm path length. The solutions were prepared by dissolving the sample in carbon tetrachloride to make up 1.04 mol L^{-1} solutions for both isomers. Both isomers exhibited absorptions due to C=C stretching at the identical wavenumber, 1620 cm^{-1}.

Ultraviolet Absorption Spectra. They were recorded on a Hitachi-UV-340 spectrophotometer with a silica cell of 1.0 cm in length. Samples were dissolved in methanol and the concentrations of **2** were ca. 1×10^{-5} mol L^{-1} for the short wavelength region (<300 nm) and ca. 6×10^{-4} mol L^{-1} for the long wavelength region (>300 nm). The spectrum of 2-vinylnaphthalene was recorded for only the long wavelength region with 7.79×10^{-4} mol L^{-1} concentration in methanol because absorptions at the shorter wavelength region have been reported.[23] The following absorption maxima were recorded (wavelength in nm and log ε parentheses given):

sp-**2**:[5] 249 (4.59), 293 (4.09), 303 (4.09), 328 (sh), 346 (1.86).
ap-**2**:[5] 242 (4.65), 267 (sh), 280 (sh), 290 (4.19), 302 (4.17), 320 (sh), 344 (1.69).
2-vinylnaphthalene: 323 (2.69), 331 (2.41), 340 (2.50).

***trans*-8-Methyl-8,14c-dihydrodibenz[*a,l*]aceanthrylene (3).** A solution of 1.0 g of *sp*-**2** in 10 mL of 1,2-dimethoxyethane was mixed with a mixture of 30 mL of 1,2-dimethoxyethane and 30 mL of concentrated sulfuric acid and stirred overnight at room temperature. The mixture was poured into water and extracted with ether. The ethereal extract was washed with aqueous sodium hydrogencarbonate and dried over magnesium sulfate. The solvent was evaporated and the residue was chromatographed on silica gel (hexane eluent) to afford the cyclic compund (**3**), mp 173.0—174.0 °C, in 90% yield. The compound was identical with that previously reported.[5]

9-[2-(1,2-Dibromoethyl)-1-naphthyl]fluorene (4). A solution of 1.0 g (3.1 mmol) of the *ap*-olefin in 150 mL of carbon tetrachloride was mixed with 510 mg (3.2 mmol) of bromine in 50 mL of carbon tetrachloride, by adding the latter gradually at 0 °C. The solvent was evaporated after 30 min and the residue was chromatographed through a short column of silica gel. The *sp*-dibromide was obtained in 1.4 g (93%) yield, mp 173.0—174.0 °C. Found: C, 62.64; H, 3.80; Br, 33.83%. Calcd for $C_{25}H_{18}Br_2$: C, 62.77; H, 3.80; Br, 33.43%. ^{1}H NMR ($CDCl_3$) δ=4.1—4.6 (2H, m), 5.81 (1H, s), 6.0—6.3 (1H, m), 6.4—8.0 (14H, m).

Similarly the *sp*-olefin gave *ap*-dibromide, mp 137.5—138.5 °C. Found: C, 62.69; H, 3.67; Br, 33.71%. Calcd for $C_{25}H_{18}Br_2$: C, 62.77; H, 3.80; Br, 33.43%. ^{1}H NMR ($CDCl_3$) δ=3.2—3.5 (2H, m), 4.0—4.3 (1H, m), 6.17 (1H, s), 7.0—8.0

(13H, m), 8.4—8.6 (1H, m).

Reaction of Olefin 2 with Chlorine. A solution of 50 mg (0.16 mmol) of the olefin (**2**) in 50 mL of carbon tetrachloride was mixed with 8.3 mL of ca. 20 mmol L^{-1} solution of chlorine in carbon tetrachloride at 0 °C and the mixture was stirred for 3.5 h at the temperature. From the reaction mixture, the solvent and other volatile materials were evaporated and the residue was chromatographed on silica gel with 5 : 1 hexane-dichloromethane as an eluent.

ap-**2** afforded the dichloride (*sp*-**5**), mp 150—151 °C, and a small amount of an unidentified by-product. Found: C, 77.41; H, 4.76; Cl, 17.92%. Calcd for $C_{20}H_{18}Cl_2$: C, 77.13; H, 4.66; Cl, 18.21%. ^{1}H NMR ($CDCl_3$) δ=4.25—4.42 (2H, m), 5.83 (1H, s), 5.96—6.06 (1H, m), 6.46—8.00 (14H, m).

sp-**2** afforded the dichloride (*ap*-**5**) and the olefin (*sp*-**6**) in 1.0 : 1.4 ratio. *ap*-**5** was identical with the product obtained from the reaction of *sp*-**2** with (dichloroiodo)benzene which is described later but decomposed on standing to give *sp*-**2** and *sp*-**6**. The olefin originally contained ca. 11 : 1 trans and cis olefins as judged by ^{1}H NMR spectra and gave trans-olefin (*sp-trans*-**6**) on recrystallization from ethanol, mp 134.0—135.0 °C. Found: C, 85.25; H, 5.03%. Calcd for $C_{25}H_{17}Cl$: C, 85.10; H, 4.86%. ^{1}H NMR ($CDCl_3$) δ=5.68 (1H, d, J=14 Hz), 5.90 (1H, d, J=14 Hz), 6.14 (1H, s), 7.11—7.98 (13H, m), 8.53—8.60 (1H, m). The following ^{1}H NMR data ($CDCl_3$, δ) for the *cis*-chloro olefin (*sp-cis*-**6**) were collected: 5.38 (1H, d, J=9 Hz), 5.46 (1H, d, J=9 Hz), 6.12 (1H, s), 7.11—7.98 (13H, m), 8.53—8.60 (1H, m).

9-[2-(1,2-Epoxyethyl)-1-naphthyl]fluorene (8). To a solution of 150 mg (0.47 mmol) of the *ap*-olefin (**2**) in 30 mL of chloroform, was added 110.0 mg (0.64 mmol) of *m*-chloroperbenzoic acid which had been washed with a buffer solution of pH 7.6 to remove any acidic materials.[24] The mixture was stirred for a week at room temperature and the mixture was directly submitted to chromatography on silica gel with 1 : 1 hexane-dichloromethane eluent to give 95% *sp*-epoxy compound. The compound was purified by recrystallization from benzene-hexane, mp 144.0—145.0 °C. Found: C, 89.55; H, 5.16%. Calcd for $C_{25}H_{18}O$: C, 89.79; H, 5.43%. ^{1}H NMR ($CDCl_3$) δ=2.95—3.32 (2H, m), 4.55—4.60 (1H, m), 5.90 (1H, s), 6.40—8.00 (14H, m).

Similar treatment of the *sp*-olefin with stirring for 22 h afforded 70% *ap*-epoxy compound (*ap*-**8**), mp 134.0—135.0 °C, after recrystallization from benzene-hexane. Found: C, 89.67; H, 5.14%. Calcd for $C_{25}H_{18}O$: C, 89.79; H, 5.43%. ^{1}H NMR ($CDCl_3$) δ=1.83—1.95 (2H, m), 2.64—2.68 (1H, m), 6.17 (1H, s), 7.05—8.05 (13H, m), 8.46—8.55 (1H, m). The yield was not improved after stirring for 7 d: unreacted material was detected.

Hydroboration of 2. A solution of 100 mg (0.31 mmol) of *ap*-**2** in 40 mL of tetrahydrofuran, which was freshly distilled from lithium tetrahydridoaluminate, was mixed with 1.4 mL of 1 mol L^{-1} solution of borane in tetrahydrofuran and the mixture was stirred for 2.5 h under a nitrogen atmosphere. To the reaction mixture diluted with 50 mL of tetrahydrofuran, were added 1.5 mL of 30% hydrogen peroxide and 1.5 mL of 3 mol L^{-1} aqueous sodium hydroxide and the whole was stirred for 1.5 h under a nitrogen atmosphere. The mixture was poured into water and extracted with ether. The ether layer was dried over magnesium sulfate and the solvent was evaporated. Chromatography of the residue on silica gel under medium pressure, with 1 : 4 hexane-ether eluent, afforded 1.0 : 2.5 *sp*-1-ol (**11**) and *ap*-2-ol(**10**). The former was identical with that reported[2,5] and the latter was recrystallized from dichloromethane-pentane, mp 110.0—111.5 °C. High resolution MS: m/z 336.1553. Calcd for $C_{25}H_{20}O$: M, 336.1515. ^{1}H NMR ($CDCl_3$) δ=3.44 (2H, t, J=9 Hz), 4.13 (2H, t, J=9 Hz), 5.77 (1H, s), 6.40—7.98 (14H, m). The OH proton was not detected.

Similarly the *sp*-olefin gave 42% *sp*-2-ol (**10**) and 18% *ap*-1-ol (**11**), which was identical with authentic specimen.[2,5]

sp-2-Ol (**10**), mp 115.5—117.5 °C. Found: C, 89.16; H, 6.23%. Calcd for $C_{25}H_{20}O$: C, 89.25; H, 5.99%. ^{1}H NMR ($CDCl_3$) δ=1.91 (2H, t, J=7 Hz), 3.00 (2H, t, J=7 Hz), 6.15 (1H, s), 7.0—8.0 (13H, m), 8.4—8.6 (1H, m). The OH proton was not detected.

9-(2-Ethyl-1-naphthyl)fluorene (9). a) Catalytic Hydrogenation of 2. A solution of 60 mg of the *sp*-olefin in 80 mL of ethanol was added to 10 mg of 5% palladium on carbon, which was activated by shaking with hydrogen and 20 mL of ethanol, and the whole was stirred under a hydrogen atmosphere. The hydrogen absorption was completed after 20 h. The product was recrystallized from ethanol, mp 118.8—119.5 °C. The yield was 99%. Found: C, 93.46; H, 6.11%. Calcd for $C_{25}H_{20}$: C, 93.71; H, 6.29%. ^{1}H NMR ($CDCl_3$) δ=0.48 (3H, t, J=7 Hz), 1.65 (2H, q, J=7 Hz), 6.15 (1H, s), 7.12—7.97 (13H, m), 8.52 (1H, m).

Similarly *ap*-**9**, mp 107.5—108.0 °C, was obtained in 99% yield. Found: C, 93.41; H, 6.19%. Calcd for $C_{25}H_{20}$: C, 93.71; H, 6.29%. ^{1}H NMR ($CDCl_3$) δ=1.40 (3H, t, J=8 Hz), 3.10 (2H, q, J=8 Hz), 5.69 (1H, s), 6.35—7.92 (14H, m).

b) Diimide Reduction of 2. A solution of 100 mg (0.31 mmol) of *sp*-**2** in 100 mL of ethanol was mixed with 0.5 mL (8.6 mmol) of hydrazine hydrate and 1 drop of 1% aqueous copper(II) sulfate. To the mixture was slowly added 2.0 mL (17 mmol) of 30% aqueous hydrogen peroxide with ice-cooling. After 30 min, the mixture was poured into water and extracted with ether. The ethereal extract was dried over magnesium sulfate and the solvent was evaporated to give 95% *sp*-**9** which was identical with the compound obtained above.

Similarly *ap*-**2** afforded *ap*-**9**, identical with the compound described above, in almost quantitative yield.

Reaction of (Dichloroiodo)benzene with 2. To a solution of 40 mg (0.12 mmol) of *ap*-**2** in 35 mL of dichloromethane was added 35 mg (0.12 mmol) of (dichloroiodo)benzene[25] and the mixture was stirred for 23 h at room temperature. The solvent and the volatile materials were removed by distillation in vacuo and the residue was recrystallized from hexane to give *sp*-**5** in almost quantitative yield.

Similarly, the reaction of *sp*-**2** with (dichloroiodo)benzene afforded *ap*-**5**, mp 90—95 °C (decomp). This compound decomposed on attempted recrystallization from pentane to yield *sp*-**2** and *sp*-**6**, though it was stable at 0 °C. It also decomposed slowly at room temperature even in the solid state on standing. The yield was ca. 80%. High resolution MS: m/z 388.0742 and 390.0701. Calcd for $C_{25}H_{16}{}^{35}Cl_2$ and $C_{25}H_{16}{}^{35}Cl^{37}Cl$: M, 388.0784 and 390.0754. ^{1}H NMR ($CDCl_3$) δ=3.05—3.40 (2H, m), 4.04—4.12 (1H, m), 6.22 (1H, s), 7.08—8.02 (13H, m), 8.52—8.64 (1H, m).

Reaction of 2 with Osmium Tetraoxide. To a solution of 70 mg (0.22 mmol) of **2** in 50 mL of ether, was added a solution of ca. 60 mg (0.24 mmol) of osmium tetraoxide in 4.0 mL of ether under an argon atmosphere and the whole was stirred for 24 h at room temperature. To the solution was added 2.5 g of sodium hydrogensulfite, 10 mL of water

and 10 mL of ethanol and the mixture was heated at 60 °C with stirring for 24 h. The mixture was poured into water and the ether layer was separated. The aqueous layer was extracted with ether and the combined extracts were dried over magnesium sulfate. The solvent was evaporated to give the diol (**12**) in ca. 70% yields. The following ^{1}H NMR data were collected ($CDCl_3$, δ). *sp*-**12**: 3.91—4.15 (2H, m), 5.63—5.72 (1H, m), 5.79 (1H, s), 6.40—8.02 (14H, m). The OH protons were not detected. *ap*-**12**: 2.60—3.24 (2H, m), 3.70—3.80 (1H, m), 6.20 (1H, s), 7.13—8.01 (13H, m), 8.52—8.59 (1H, m).

These diols were characterized by converting them to acetonides through treatment of the diols with acetone and *p*-toluenesulfonic acid.

***sp*-Diol Acetonide:** Mp 151.5—152.0 °C, after recrystallization from hexane. High resolution MS: *m/z* 392.1741. Calcd for $C_{28}H_{24}O_2$: M, 392.1775. ^{1}H NMR ($CDCl_3$) δ=1.54 (3H, s), 1.67 (3H, s), 3.96—4.58 (2H, m), 5.64 (1H, s), 5.90—5.96 (1H, m), 6.41—7.95 (14H, m).

***ap*-Diol Acetonide:** oil. High resolution MS: *m/z* 392.1739. Calcd for $C_{28}H_{24}O_2$: M, 392.1775. ^{1}H NMR ($CDCl_3$) δ=0.80 (3H, s), 1.37 (3H, s), 2.56—3.07 (2H, m), 4.07—4.12 (1H, m), 6.18 (1H, s), 7.04—7.97 (13H, m), 8.53—8.56 (1H, m).

Competitive Addition Reactions. Two rotational isomers (10 mg each or 0.03 mmol) of **2** were dissolved in an appropriate solvent with a small amount of fluorene which served as a reference. The appropriate reagent (0.03 mmol or less) in an appropriate solvent was added to the solution and the decrease in the amount of each rotamer was recorded with the use of either integration of ^{1}H NMR signals or calibration curves for the amounts of the olefins drawn by using the UV absorption at 254 nm which was used for the detection in HPLC. The reaction conditions were similar to those described above for the individual rotamers except for the addition of bromine and chlorine, when a dilute solution (ca. 0.1 mmol L^{-1}) of the halogen in carbon tetrachloride was added to the solution of **2**. The results given in Scheme 1 are averages of 2—3 runs which were terminated before 50% completion of the reactions.

Determination of Barriers to Rotation in 9-(2-Vinyl-1-naphthyl)fluorene (2). A solution of 40 mg of the *ap* isomer in 0.5 mL of toluene-d_8 was sealed in an NMR tube. The tube was immersed in a boiling benzene bath. The rotation was quenched by cooling rapidly with an ice-water bath at a given time and the isomer ratio was determined by ^{1}H NMR spectroscopy. The equilibrium constant was obtained by heating the sample tube as above for 48 h. The isomer ratio did not change after heating for further 12 h. The data were treated by assuming a first order reversible reaction.

The *sp*-isomer was treated similarly. It gave the same equilibrium constant that was obtained form the *ap* isomer.

This work was supported by a Grant-in-Aid (No. 62124035) for Fundamental Scientific Research of the Ministry of Education, Science and Culture, to which our thanks are due.

References

1) For Part XXII, see T. Tanaka, K. Yonemoto, Y. Nakai, G. Yamamoto, and M. Ōki, *Bull. Chem. Soc. Jpn.*, **61**, 3239 (1988).
2) M. Ōki and R. Saito, *Chem. Lett.*, **1981**, 649; R. Saito and M. Ōki, *Bull. Chem. Soc. Jpn.*, **55**, 3267 (1982).
3) S. Murata, S. Kanno, Y. Tanabe, M. Nakamura, and M. Ōki, *Angew. Chem., Int. Ed. Engl.*, **20**, 606 (1981); *Bull. Chem. Soc. Jpn.*, **57**, 525 (1984).
4) R. Saito and M. Ōki, *Bull. Chem. Soc. Jpn.*, **55**, 3273 (1982).
5) M. Ōki, J. Tsukahara, K. Moriyama, and N. Nakamura, *Bull. Chem. Soc. Jpn.*, **60**, 1781 (1987).
6) S. Murata, S. Kanno, Y. Tanabe, M. Nakamura, and M. Ōki, *Bull. Chem. Soc. Jpn.*, **55**, 1522 (1982).
7) I. Roberts and G. E. Kimball, *J. Am. Chem. Soc.*, **59**, 947 (1937); J. G. Traynham, *J. Chem. Educ.*, **40**, 392 (1963).
8) R. C. Fahey and H.-J. Schneider, *J. Am. Chem. Soc.*, **90**, 4429 (1968).
9) J. H. Rolston and K. Yates, *J. Am. Chem. Soc.*, **91**, 1467 (1969).
10) R. A. Y. Jones, "Physical and Mechanistic Organic Chemistry," 2nd ed, Cambridge University Press, Cambridge (1984), p. 202.
11) R. C. Fahey and C. Schubert, *J. Am. Chem. Soc.*, **87**, 5172 (1965); K. Yates and H. W. Leung, *J. Org. Chem.*, **45**, 1401 (1980).
12) D. Swern, *J. Am. Chem. Soc.*, **70**, 1235 (1948); B. M. Lynch and K. H. Pausacker, *J. Chem. Soc.*, **1955**, 1525.
13) D. Y. Curtin and D. B. Kellom, *J. Am. Chem. Soc.*, **75**, 6011 (1953).
14) S. Mitsui and A. Kasahara, "Hydrogenation of Alkenes," in "The Chemistry of Alkenes," Vol. 2 ed by J. Zabicky, Interscience Publishers, London (1970), pp. 175—214.
15) H. C. Brown and G. Zweifel, *J. Am. Chem. Soc.*, **82**, 4708 (1960).
16) H. C. Brown and R. L. Sharp, *J. Am. Chem. Soc.*, **88**, 5851 (1966).
17) H. C. Brown, E. F. Nights, and C. G. Souten, *J. Am. Chem. Soc.*, **96**, 7765 (1974).
18) D. H. R. Barton and E. Miller, *J. Am. Chem. Soc.*, **72**, 370 (1950).
19) D. T. Tanner and G. C. Gidley, *J. Org. Chem.*, **33**, 38 (1968).
20) R. Criegee, *Justus Liebigs Ann. Chem.*, **522**, 75 (1936); M. Schröder, *Chem. Rev.*, **81**, 187 (1981).
21) E. M. Garbisch, Jr., S. M. Schildcrout, D. B. Patterson, and C. M. Sprecher, *J. Am. Chem. Soc.*, **87**, 2932 (1965).
22) L. F. Fieser and K. L. Williamson, "Organic Experiments," 3rd ed, D. C. Heath & Co., Letington, Massachusetts (1975), p. 234.
23) H. A. Laitinen, F. A. Miller, and T. D. Parks, *J. Am. Chem. Soc.*, **69**, 2707 (1947).
24) N. N. Schwartz and J. H. Blumbergs, *J. Org. Chem.*, **29**, 1976 (1964).
25) H. J. Lucas and E. R. Kennedy, *Org. Synth.*, Coll. Vol. **3**, 482 (1955).

Reactivities of Stable Rotamers. XXIV. Formation of Isomeric Ketones by Cyclization of Rotameric 3-Methyl-3-(1,2,3,4-tetrahalo-9-triptycyl)butanoyl Chloride and Barriers to Isomerization of the Ketones[1)]

Michinori Ōki,*,† Toshihiro Tanuma, Yasuhiro Tanaka, and Gaku Yamamoto
Department of Chemistry, Faculty of Science, The University of Tokyo, Bunkyo-ku, Tokyo 113
(Received March 29, 1988)

Rotational isomers of 3-methyl-3-(1,2,3,4-tetrahalo-9-triptycyl)butanoic acid, where the halo is either fluoro or chloro have been prepared. Cyclization of their acid chlorides afforded *ap*- and *sc*-ketones from *ap*- and *sc*-isomers, respectively. The barriers to isomerization were 29.9 and 26.8 kcal mol^{-1} at 363 K, for the fluoro and the chloro ketones, respectively, for the $ap \rightarrow \pm sc$ process. The equilibrium constants (*sc*/*ap*) at 363 K were 2.34 and 18.5 for the fluoro and the chloro compounds respectively. The barriers to isomerization and the relative stabilities of the isomeric ketones were discussed based on the MMP2(NONPLANAR) calculation results and the steric congestion in the ground state.

While we have reported interesting differences in reactivities of 3-(1,4-disubstituted 9-triptycyl)-3-methylbutanoyl chloride rotamers, when they were treated with Lewis acids, and isomerization kinetics of the ketones obtained from the respective rotamers,[2)] it is hoped to increase the number of data to discuss the general trends in reactivities, equilibrium constants, and barriers to isomerization. We thus prepared 3-methyl-3-(1,2,3,4-tetrahalo-9-triptycyl)butanoic acid rotamers, and then examined their reactivities, the barriers to isomerization of the ketones derived from them, and the equilibrium constants of the ketones. This paper reports and discusses results of such investigations.

The 3-methyl-3-(1,2,3,4-tetrahalo-9-triptycyl)butanoic acid rotamers (**5**) were prepared in the following ways. Addition of tetrahalobenzyne to 9-(1,1-dimethyl-3-butenyl)anthracene (**1**)[2)] afforded a mixture of rotamers of 9-(1,1-dimethyl-3-butenyl)-1,2,3,4-tetrahalotriptycene (**2**) which contained *ap*-rotamers predominantly. The mixture was heated in boiling 1-chloronaphthalene to enrich *sc*-isomers by isomerization and the resulted mixture of rotamers was separated by chromatography on silver nitrate-impregnated silica gel. The olefins were oxidized with trimethylamine oxide in the presence of osmium tetraoxide[3)] to produce the corresponding diols (**3**) which were further oxidized with periodic acid to afford the aldehydes (**4**).[4)] The aldehydes were finally oxidized with potassium permanganate to produce the desired carboxylic acids (**5**).

The individual rotamers of the carboxylic acids were converted to the corresponding acid chlorides (**6**) by the treatment with oxalyl dichloride, and the acid chlorides were treated with titanium(IV) chloride to produce the ketones (**7**). As expected, due to the low

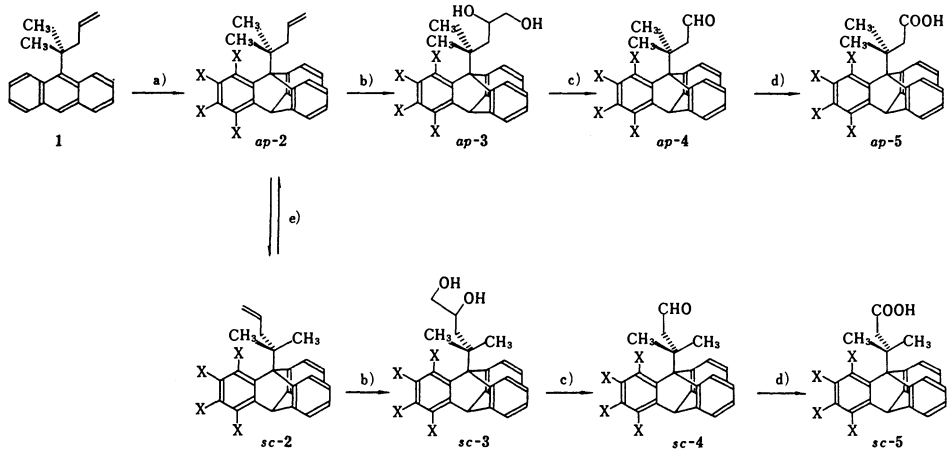

Scheme 1. Synthetic routes to 3-methyl-3-(1,2,3,4-tetrahalo-9-triptycyl)butanoic acid rotamers: a series X=F, b series X=Cl. a) Tetrahalobenzyne, b) OsO_4-$(CH_3)_3NO$, c) HIO_4, e) heating and chromatography on SiO_2–$AgNO_3$. Only one of the *sc*-forms is shown.

† Present address: Department of Chemistry, Faculty of Science, Okayama University of Science, Ridaicho, Okayama 700.

electron density at the 1-position of these compounds (**6**), no ipso attack by the intervening acylium cation was apparent. The corresponding ketones (**7**) were the exclusive products: even the *sc*-isomers afforded **7** only, though in other instances *sc*-isomers gave products of different types.

Although the difference in the reactivities of the rotamers of the chloro compound (**6b**) was not apparent, we noticed a difference in the fluoro compound (**6a**): whereas the reaction of **6b** with titanium(IV) chloride in benzene for 3 hours at room temperature afforded the corresponding cyclic ketones (**7**) of both isomers in good yields, the same treatment of *sc*-**6a** for 4 hours gave back some unreacted compound which was recovered as *sc*-**5a** in addition to the ketone (**7**) (31 and 58% yields, respectively). The incomplete reaction of *sc*-**6a** under the conditions was not due to the hydrolysis of *sc*-**6a** to *sc*-**5a** but slowness of the cyclization reaction. This was checked in two ways. Firstly, ^{1}H NMR spectra did not show any signals due to the hyrolyzed product in the reaction mixture. Secondly, treatment of (*sc*-**6a**) for 6 hours gave the ketones as sole products and no acid *sc*-**5a** was recovered.

It may be argued that the formation of a cation in the vicinity of the fluoro substituent was slow because, in cases where a chloronium or fluoronium ion of a three-membered ring could be formed in competition, only the former was formed.[6,7] However, we believe the results are better interpreted by considering the fact that there are two benzene rings in the *ap*-form (*ap*-**6a**) to react with the acylium ion, whereas there is only one such ring in *sc*-**6a**, because *ap*-**6a** gave 10% recovered acid after 2 hour treatment. The slow reaction in both isomers in **6a** relative to **6b** may be attributed to the stronger electron-withdrawing effect of the fluorine atom than the chlorine.

Ketones, *ap*-**7′** and *sc*-**7′**, obtained from *ap*-**6** and *sc*-**6**, respectively, were different compounds and could be isomerized with each other on heating. The barriers to the isomerization and the equilibrium constants between the isomers are listed in Tables 1 and 2, for the fluoro and the chloro compounds, respectively. The interesting trends seen in these tables are that the isomerization is easier in the chloro compound than in the fluoro compound and the equilibrium constant (*sc*/*ap*) is larger in the chloro compound than in the fluoro compound.

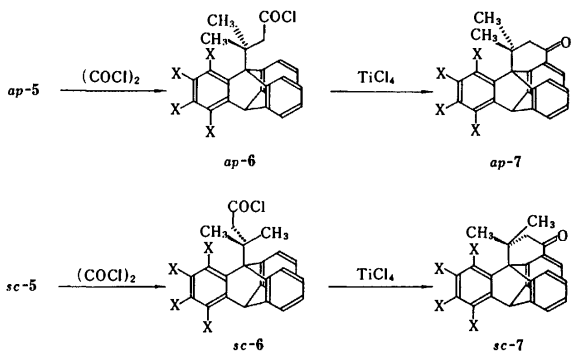

Scheme 2. Formation of isomeric ketones from rotamers of **5**.

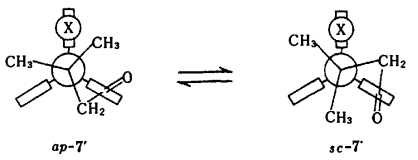

Scheme 3. Isomerization of the ketones (**7**).

Table 1. Rate Constants for Isomerization, *ap* → *sc*, Equilibrium Constants, Thermodynamic Parameters, and Kinetic Parameters for Compound **7a** in Toluene-d_8

Temperature/°C	$k\times10^5$/s^{-1}	K(*sc*/*ap*)
81	0.287	2.39
90	0.729	2.34
100	2.40	2.29
110	6.61	2.25

$\Delta H^{\ddagger}$=28.7±3.1 kcal mol^{-1},[a] $\Delta S^{\ddagger}$=−3±9 cal mol^{-1} K^{-1},
ΔH°=0.6±0.1 kcal mol^{-1}, ΔS°=0.2±0.2 cal mol^{-1} K^{-1}.

a) 1 cal=4.184 J.

Table 2. Rate Constants for Isomerization, *ap* → *sc*, Equilibrium Constants, Thermodynamic Parameters, and Kinetic Parameters for Compound **7b** in Toluene-d_8

Temperature/°C	$k\times10^5$/s^{-1}	K(*sc*/*ap*)
60	2.27	22.6
70	7.02	21.2
80	21.8	20.4
90	52.8	18.5

$\Delta H^{\ddagger}$=24.8±2.8 kcal mol^{-1},[a] $\Delta S^{\ddagger}$=−6±8 cal mol^{-1} K^{-1},
ΔH°=−1.4±0.1 kcal mol^{-1}, ΔS°=2±3 cal mol^{-1} K^{-1}.

In order to see the effects of the 1-substituent on the barriers to isomerization and on the equilibrium constants, the data are summarized in Table 3 together with those of 8,11-dimethyl and 8,11-dimethoxy compounds (**8**). Generally speaking, the bulkier the 1-substituent, the lower the barrier to isomerization and the larger the equilibrium constant. This means that the ground state energy is more effectively raised than the transition state energy for isomerization by introducing a bulky substituent at the 11-position. It is especially so for the *ap*-ketones. The trend observed in the barriers to isomerization is parallel to that observed in 1,2,3,4-tetra- or 1,4-disubstituted 9-(1,1-dimethyl-2-phenylethyl)triptycenes (**9**),[8] open-chain analogs of the ketones.

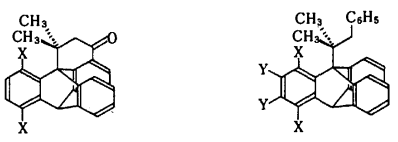

Table 3. Comparison of Free Energies of Activation for Isomerization, $ap \rightarrow sc$, and Equilibrium Constants of Ketones in Toluene-d_8 at 90 °C

Compound	1-Substituent	$\Delta G^{\ddagger}_{363}$ / kcal mol^{-1}	K(sc/ap)	Reference
8b	CH_3	26.0	17.2	2
7b	Cl	27.0	18.5	This work
8a	CH_3O	29.4	6.0	2
7a	F	29.8	2.29	This work

Table 4. Steric Energies and Dissected Energies of Ketones as Calculated by MMP2(NONPLANAR) Method

Conformation		**7a**		**7b**	
		ap	*sc*	*ap*	*sc*
Steric energy		36.375	35.584	49.337	47.896
Compression		3.463	3.358	5.291	5.489
Bending		12.363	12.446	14.138	15.432
Stretch-Bend		0.040	0.024	0.128	0.143
van der Waals	a)	21.574	21.596	27.186	27.677
	b)	−2.600	−2.737	−1.938	−0.763
Torsional		−9.027	−9.690	−4.659	−9.315
Dipole		10.561	10.588	9.192	9.234

a) 1,4 energy. b) Others.

Since single crystals of these compounds have not been obtained yet, we performed molecular mechanics MMP2(NONPLANAR) calculations, in order to get further into insight. The results are shown in Table 4. This program seems to yield more realistic results than MM2 or MMP2 programs, of which results were previously reported.[2,9] As were the cases previously reported, the total energies indicate that *sc*-**7** is always more stable than *ap*-**7** and the main difference in the total energies is attributed to the difference in the torsion terms: *ap*-**7** suffers from severer torsion than the *sc* form and the difference is larger in the case of a bulky 11-substituent than in the case of a less bulky substituent.

Although the reliability of the MM2 calculation results for this kind of highly congested molecules might be argued, we believe, as discussed in the previous paper,[2] that the results are supported by the following ^{1}H NMR data. Namely, there is a methyl group, of which protons give a ^{1}H NMR signal at a considerably high magnetic field, in each of the isomers of **7a** and **7b**. These signals show coupling with a small coupling constant to indicate that there is a long range coupling with a proton. MMP2-(NONPLANAR) calculations show that the −*sc*-methyl in *ap*-**7′** and the *ap*-methyl in *sc*-**7′** are located in the shielding zone of the distorted benzene ring. The *ap*-methyl in *sc*-**7′** suffers from additional shielding of the carbonyl moiety. These methyl groups are exactly antiperiplanar with one of the methylene protons, thus forming a W-letter skeleton that is favorable for the long range coupling.[10]

The spin-couplings between the 1-fluorine and the methyl-protons in *ap*- and *sc*-**7a** are also consistent with the calculated structures. The *ap*-methyl-protons in *sc*-**7′** fail to show coupling with the fluorine but there is a distinct coupling observed with the methylene proton. The distance between the +*sc*-methyl and 1-F in *sc*-**7′** and that between the +*sc*-methyl and 1-F in *ap*-**7′**, 2.73 and 2.71 Å, respectively, are almost the same in agreement with almost the same F-H coupling constants, 7.9 and 8.1 Hz, respectively, for the former and the latter. The distance between the −*sc*-methyl and the 1-F in *ap*-**7′** is much longer than that between the +*sc*-methyl and the 1-F in *ap*-**7′**, 2.99 and 2.71 Å, respectively, justifying the observed coupling constants of 2.6 Hz for the former and 8.1 Hz for the latter. These distances between the methyls and the 1-F would not have been expected from the molecular models.

Experimental

^{1}H NMR spectra were recorded with a JEOL GX-270 spectrometer and infrared spectra with a Hitachi IR-260-30 spectrometer. Freshly distilled benzene was used for the Friedel-Crafts reaction. Others were of commerical origin.

1,2,3,4-Tetrafluoro-9-(1,1-dimethyl-3-butenyl)triptycene (2a). To a solution of 9.92 g (49.1 mmol) of chloropentafluorobenzene in 100 mL of dry ether, cooled with Dry Ice-acetone, was added slowly 32.6 mL (49.1 mmol) of butyllithium in hexane under a nitrogen atmosphere and the mixture was stirred at that temperature for 6 h. To this mixture was added 2.55 g (9.81 mmol) of 9-(1,1-dimethyl-3-butenyl)anthracene (**1**)[2] in 10 mL of ether from a syringe. The whole was stirred for 2 h at −78 °C, for 2 h at 0 °C, and then for 60 h at 13 °C. The reaction was completed by heating under reflux for 2 h and the mixture was washed with dilute hydrochloric acid and then with water. The ether layer was dried over magnesium sulfate and the solvent was evaporated. Chromatography of the residue on silica gel (hexane eluent) afforded a mixture of *ap*-**2a** and *sc*-**2a**, which was contaminated with a 1,4-adduct of the benzyne to the anthracene. The ratio of *ap*-**2a**, *sc*-**2a**, and the 1,4-adduct was 7 : 3 : 1.

The mixture, which weighed 2.5 g at this stage, was dissolved in a small amount of 1-chloronaphthalene and heated under reflux for 50 h under a nitrogen atmosphere. Rough chromatography of the product on silica gel (hexane eluent) afforded a mixture which contained *ap*-**2a** and *sc*-**2a** in 1 : 2 ratio. The mixture was separated by chromatography on silica gel impregnated ca. 10% silver nitrate with the use of 5 : 1 hexane-dichloromethane as an eluent. The order of elution was *sc*-**2a**, *ap*-**2a**, and the 1,4-adduct.

***ap*-2a**, mp 163—164 °C, yield, 3.6%. It was recrystallized from hexane. Found: C, 76.54; H, 5.00%. Calcd for $C_{26}H_{20}F_4$: C, 76.46; H, 4.94%. ^{1}H NMR ($CDCl_3$) δ=2.00 (6H, d, J=8.9 Hz), 3.29 (2H, d, J=7.1 Hz), 5.20—5.36 (2H, m), 5.69 (1H, d. J=1.0 Hz), 6.18—6.37 (1H, m), 7.00—7.12 (4H, m), 7.38—7.48 (2H, m), 7.81—7.90 (2H, m).

***sc*-2a**, caramel, yield 6.7%. ^{1}H NMR ($CDCl_3$) δ=1.93 (3H, d, J=8.1 Hz), 2.05 (3H, s), 3.01 (1H, dd, J=14.5 and 7.2 Hz), 3.31 (1H, dd, J=14.5 and 6.8 Hz), 5.20—5.36 (2H, m), 5.69 (1H, d, J=1.0 Hz), 6.15—6.35 (1H, m), 6.99—7.12 (4H, m), 7.36—7.48 (2H, m), 7.79—7.95 (2H, m).

1,2,3,4-Tetrachloro-9-(1,1-dimethyl-3-butenyl)triptycene (2b). This compound was prepared similarly as described above for the tetrafluoro compound (**2a**) from **1** and hexachlorobenzene, except the followings. The lithiation of hexachlorobenzene was carried out at −30 °C and the generation of the benzyne by stirring for 5—6 h with gradual raise of temperature to −10 °C and then stirring overnight in an ice-bath, during which time the temperature was allowed to rise to room temperautre. A product which contained *ap*-**2b**, *sc*-**2b**, and a 1,4-adduct in 7 : 3 : 5 ratio was obtained in ca. 20% yield. The *ap*-olefin could be isolated by recrystallization of the mixture from hexane-dichloromethane. The separation of the *sc*-isomer from others was carried out by chromatography on SiO_2-$AgNO_3$, after isomerization by heating a 1-chloronaphthalene solution for 20 h, which gave a ca. 1 : 1 *ap*-**2b** and *sc*-**2b** mixture.

ap-**2b**, mp 230.5—231.0 °C. Found: C, 65.99: H, 4.10; Cl, 29.85%. Calcd for $C_{26}H_{20}Cl_4$: C, 65.85; H, 4.25; Cl, 29.90%. ^{1}H NMR ($CDCl_3$) δ=2.29 (6H, s), 3.24 (2H, d, J=7 Hz), 5.22—5.28 (2H, m), 6.07 (1H, s), 6.17—6.32 (1H, m), 7.03—7.11 (4H, m), 7.44—7.47 (2H, m), 7.92—7.95 (2H, m).

sc-**2b**, caramel. ^{1}H NMR ($CDCl_3$) δ=2.60 (3H, s), 2.18 (3H, s), 3.49 (1H, dd, J=15.2 and 6.2 Hz), 3.65 (1H, dd, J=15.2 and 8.1 Hz), 5.26—5.32 (2H, m), 6.09 (1H, s), 6.19—6.34 (1H, m), 7.03—7.11 (4H, m), 7.42—7.48 (2H, m), 7.93—7.98 (1H, m), 8.02—8.05 (1H, m).

***ap*-4-Methyl-4-(1,2,3,4-tetrafluoro-9-triptycyl)-1,2-pentanediol (3a).** To a solution of 251 mg (0.615 mmol) of the olefin (**2a**) in 50 mL of *t*-butyl alcohol, were added 3.76 g (33.8 mmol) of trimethylamine oxide dihydrate, 2 mL of pyridine, and 15 mL of water. To the solution under an argon atmosphere, was added ca. 20 mg of osmium tetraoxide in 1 mL of *t*-butyl alcohol, and the whole was heated for 24 h. The mixture was treated with 20 mL of 20% aqueous sodium hydrogensulfite and then most of *t*-butyl alcohol was evaporated. The residue was extracted with dichloromethane or ether and the extract was washed with saturated aqueous sodium chloride and dilute hydrochloric acid. Evaporation of the solvent afforded the desired product as caramel, which was used directly for the next reaction. The following ^{1}H NMR data ($CDCl_3$, δ) were recorded: 2.03 (3H, d, J=8.1 Hz), 2.13 (3H, d, J=8.8 Hz), 2.66 (1H, dd, J=15.1 and 2.7 Hz), 2.89 (1H, dd, J=15.1 and 7.5 Hz), 3.59 (1H, t, J=8.0 Hz), 4.27 (1H, dd, J=8.0 and 6.0 Hz), 4.63—4.79 (1H, m), 5.69 (1H, br s), 7.02—7.11 (4H, m), 7.39—7.47 (2H, m), 7.69—7.76 (1H, m), 8.03—8.09 (1H, m).

The *sc*-diol (*sc*-**3a**) was prepared similarly and used for the next reaction. The crude product contained two diastereomers due to the presence of a new chiral center in addition to the chirality of being the *sc* form. Due to the complexity of the ^{1}H NMR spectra, only the signals due to methyl protons were recorded ($CDCl_3$, δ): 2.02 (3H, d, J=7.0 Hz), 2.11 (3H, d, J=7.7 Hz), 2.12 (3H, s), 2.24 (3H, s). The formation ratio of the two isomers was 4 : 3.

***ap*-4-Methyl-4-(1,2,3,4-tetrachloro-9-triptycyl)-1,2-pentanediol (3b).** This compound was prepared similarly as above. ^{1}H NMR ($CDCl_3$) δ=2.34 (3H, s), 2.48 (3H, s), 2.63—2.73 (1H, m), 3.45—3.54 (1H, m), 3.68—3.77 (1H, m), 4.33—4.47 (1H, m), 6.07 (1H, s), 7.03—7.10 (4H, m), 7.43—7.46 (2H, m), 7.75—7.79 (1H, m), 8.06—8.10 (1H, m). In addition, a very broad peak at δ 2.1—2.6 was observed.

***sc*-Diol (*sc*-3b).** ^{1}H NMR ($CDCl_3$, δ): *sc*-**3b**(I), 2.20 (3H, s) and 2.25 (3H, s); *sc*-**3b**(II), 2.08 (3H, s) and 2.38 (3H, s). The ratio of *sc*-**3b**(I) and *sc*-**3b**(II) was 4 : 3.

***ap*-3-Methyl-3-(1,2,3,4-tetrafluoro-9-triptycyl)butanal (4a).** The product obtained by the dihydroxylation described above was dissolved in 10 mL of tetrahydrofuran and stirred with 0.46 g (2.0 mmol) of periodic acid dihydrate in 3 mL of water for 3 h at room temperature. The mixture was diluted with 100 mL of water and extracted with dichloromethane. Evaporation of the solvent afforded a crude product which was used directly for the next reaction. The following ^{1}H NMR data ($CDCl_3$, δ) were recorded: 2.22 (6H, d, J=9.2 Hz), 3.66 (2H, d, J=2.2 Hz), 5.70 (1H, d, J=1.0 Hz), 7.04—7.13 (4H, m), 7.42—7.49 (2H, m), 7.75—7.83 (2H, m), 10.23 (1H, t, J=2.6 Hz).

sc-**4a**. ^{1}H NMR ($CDCl_3$) δ=2.19 (3H, d, J=7.9 Hz), 2.25 (3H, d, J=0.7 Hz), 3.47 (1H, br dd, J=16.5 Hz), 3.63 (1H, br dt, J=16.5 and 2.9 Hz), 5.70 (1H, d, J=1.3 Hz), 7.02—7.11 (4H, m), 7.38—7.48 (2H, m), 7.73—7.84 (2H, m), 10.22 (1H, t, J=2.1 Hz).

***ap*-3-Methyl-3-(1,2,3,4-tetrachloro-9-triptycyl)butanal (4b).** This compound was prepared similar as above. ^{1}H NMR ($CDCl_3$) δ=2.49 (6H, s), 3.64 (2H, d, J=2.0 Hz), 6.08 (1H, s), 7.04—7.11 (4H, m), 7.45—7.49 (2H, m), 7.84—7.88 (2H, m), 10.16 (1H, t, J=2.0 Hz).

sc-**4b**. ^{1}H NMR ($CDCl_3$) δ=2.28 (3H, s), 2.42 (3H, s) 3.72 (1H, dd, J=17.0 and 1.8 Hz), 4.16 (1H, dd, J=17.0 and 2.9 Hz), 6.10 (1H, s), 7.07—7.10 (4H, m), 7.44—7.49 (2H, m), 7.83—7.92 (2H, m), 10.20 (1H, dd, J=2.9 and 1.8 Hz).

***ap*-3-Methyl-3-(1,2,3,4-tetrafluoro-9-triptycyl)butanoic Acid (5a).** The aldehyde (*ap*-**4a**) obtained above was dissolved in 22 mL of acetone and stirred for 2 h with 0.29 g (1.8 mmol) of potassium permanganate in 5 mL of water and a small amount of sodium hydrogencarbonate at room temperature. The mixture was acidified with dilute sulfuric acid and the excess of the permanganate was destroyed with 20% aqueous sodium hydrogensulfite. The mixture was extracted with dichloromethane and the solvent was evaporated. The residue was purified by preparative TLC on silica gel (11 : 1 dichloromethane-ether eluent). An analytical sample was obtained by recrystallization of the product from tetrahydrofuran-pentane, mp 282—284 °C (decomp). The yield was 68% based on the olefin (*ap*-**2a**). Found: C, 70.20; H, 4.07%. Calcd for $C_{25}H_{18}F_4O_2$: C, 70.42; H, 4.25%. ^{1}H NMR ($CDCl_3$) δ=2.21 (6H, d, J=8.4 Hz), 3.62 (2H, s), 5.71 (1H, br s), 7.05—7.17 (4H, m), 7.41—7.50 (2H, m), 7.80-7.95 (2H, m), 10.4—11.1 (1H, br s).

sc-**5a**, mp 285—287 °C (decomp), was prepared similarly from the corresponding aldehyde and purified by recrystallization from dichloromethane-hexane. The yield was 67% based on the olefin (*sc*-**2a**). Found: C, 70.14; H, 4.37%. Calcd for $C_{25}H_{18}F_4O_2$: C, 70.42; H, 4.25%. ^{1}H NMR ($CDCl_3$) δ=2.20 (3H, d, J=8.1 Hz), 2.25 (3H, s), 3.46 (1H, dd, J=15.3 and 2.0 Hz), 3.70 (1H, d, J=15.3 Hz), 5.71 (1H, br s), 7.02—7.17 (4H, m), 7.37—7.50 (2H, m), 7.77—7.88 (1H, m), 7.88—7.98 (1H, m), 10.8—11.8 (1H, br s).

***ap*-3-Methyl-3-(1,2,3,4-tetrachloro-9-triptycyl)butanoic Acid (5b).** This compound was prepared similarly as above, the yield being 70% based on the olefin (*ap*-**2b**), and purified by recrystallization from dichloromethane-hexane. The melting point was 254—256 °C (decomp). This compound failed to give correct analytical data but the corresponding methyl ester did. ^{1}H NMR ($CDCl_3$) δ=3.49 (6H, s), 3.60 (2H, s), 6.09 (1H, s), 7.09—7.13 (4H, m), 7.46—7.50 (2H, m), 7.92—7.97 (2H, m).

The methyl ester, mp 209—211 °C. Found: C, 61.75; H, 4.11; Cl, 28.08%. Calcd for $C_{26}H_{20}Cl_4O_2$: C, 61.69; H, 3.98; Cl, 28.01%. ^{1}H NMR ($CDCl_3$) δ=2.44 (6H, s), 3.51 (2H, s), 3.82 (3H, s), 6.08 (1H, s), 7.08—7.13 (4H, m), 7.43—7.50 (2H, m), 7.91—7.95 (1H, m), 8.01—8.05 (1H, m).

***sc*-5b**, mp 286—287 °C (decomp), was similarly prepared in 65% yield based on the olefin (*sc*-**2b**) and purified by recrystallization from dichloromethane-hexane. This compound failed to give correct analytical data but the methyl ester did. ^{1}H NMR ($CDCl_3$) δ=2.24 (3H, s), 2.46 (3H, s), 3.84 and 4.22 (2H, ABq, J=15 Hz), 6.10 (1H, s), 7.07—7.13 (4H, m), 7.43—7.50 (2H, m), 7.91—7.95 (1H, m), 8.01—8.05 (1H, m).

The methyl ester, mp 206—208 °C. Found: C, 61.49; H, 4.28; Cl, 27.98%. Calcd for $C_{26}H_{20}Cl_4O_2$: C, 61.69; H, 3.98; Cl, 28.01%. ^{1}H NMR ($CDCl_3$) δ=2.15 (3H, s), 2.40 (3H, s), 3.84 (3H, s), 3.76 and 4.14 (2H, ABq, J=15.2 Hz), 6.08 (1H, s), 7.06—7.11 (4H, m), 7.42—7.48 (2H, m), 7.90—7.93 (1H, m), 8.03—8.06 (1H, m).

Intramolecular Friedel-Crafts Reaction of the Acid Chloride (6) Derived from 5. The typical reaction is described with the use of *ap*-**5a**. To a solution of 52 mg (0.12 mmol) of *ap*-**5a** in 10 mL of benzene was added 0.1 mL (1.2 mmol) of oxalyl dichloride under a nitrogen atmosphere and the whole was stirred for 4 h at room temperature. The excess of oxalyl dichloride and the solvent were removed in vacuo. The residue showed the following signals in ^{1}H NMR ($CDCl_3$, δ): 2.20 (6H, d, J=9.2 Hz), 4.26 (2H, s), 5.71 (1H, br s), 7.04—7.16 (4H, m), 7.41—7.51 (2H, m). 7.72—7.81 (2H, m). The residue was taken up in 10 mL of benzene and was mixed with 0.2 mL (1.8 mmol) of titanium(IV) chloride. The mixture was stirred for 3 h at room temperature and then treated with water. The organic layer was separated and the aqueous layer was extracted with dichloromethane. The combined organic layers were dried over magnesium sulfate and the solvent was evaporated. The residue was purified by preparative TLC on silica gel (dichloromethane eluent) to give 78% *ap*-8,9,10,11-tetrafluoro-1,1-dimethyl-1,2-dihydro-7*H*-7,11b-*o*-benzeno-3*H*-benz[*dl*]anthracen-3-one (**7a**). The pure sample, mp 176—177 °C, was obtained by recrystallization from hexane. Found: C, 73.62; H, 3.99%. Calcd for $C_{25}H_{16}F_4O$: C, 73.53; H, 3.95%. ^{1}H NMR ($CDCl_3$) δ=1.63 (3H, dd, J=2.6 and 1.4 Hz), 2.03 (3H, d, J=8.1 Hz), 2.78 (1H, d, J=15 Hz), 3.36 (1H, dd, J=15 and 1.4 Hz), 5.76 (1H, d, J=1.5 Hz), 6.95—7.11 (2H, m), 7.15—7.29 (1H, m), 7.33—7.41 (1H, m), 7.58—7.72 (1H, m), 7.77—7.85 (1H, m). IR (Nujol mull): 1695 cm^{-1}. The same treatment for 2 h gave 65% *ap*-**7a** and 10% recovered *ap*-**5a**.

The following ^{1}H NMR data ($CDCl_3$, δ) of *sc*-**6a** were recorded: 2.17 (3H, d, J=8.6 Hz), 2.25 (3H, s), 4.06 (1H, dd, J=18.1 and 4.3 Hz), 4.34 (1H, d, J=18.1 Hz), 5.71 (1H, br d, J=1.3 Hz), 7.01—7.16 (4H, m), 7.38—7.52 (2H, m), 7.70—7.81 (2H, m).

***sc*-7a**, mp 196—197 °C was similarly prepared from the acid chloride (*sc*-**6a**) and purified by recrystallization from hexane. However, the reaction of the acid chloride was slow in this case: after 4 h stirring at room temperature, the ketone was obtained in 58% yield, whereas 31% acid *sc*-**5a** was recovered. When the reaction was continued for 6 h, the ketone was obtained in 87% yield and no acid was recovered. Found: C, 73.78; H, 4.24%. Calcd for $C_{25}H_{16}F_4O$: C, 73.53; H, 3.95%. ^{1}H NMR ($CDCl_3$) δ=1.68 (3H, d, J=1.3 Hz), 2.06 (3H, d, J=7.9 Hz), 2.75 (1H, d, J=15.8 Hz), 3.55 (1H, br d, J=15.8 Hz), 5.81 (1H, d, J=1.3 Hz), 7.13—7.25 (3H, m), 7.50—7.57 (1H, m), 7.58—7.64 (1H, m), 7.67—7.74 (1H, m), 7.86—7.93 (1H, m). IR (Nujol mull): 1690 cm^{-1}.

ap-8,9,10,11-Tetrachloro-1,1-dimethyl-1,2-dihydro-7*H*-7,11b-*o*-benzeno-3*H*-benz[*dl*]anthracen-3-one (**7b**), mp 257—259 °C, when recrystallized from dichloromethane-hexane, was similarly obtained from the corresponding tetrachloro acid (*ap*-**5b**) in 70% yield. Since this compound failed to give the correct analytical data, high resolution mass spectrum was recorded. Found: m/z 471.9970, 473.9988, 475.9924, and 477.9817. Calcd for $C_{25}H_{16}{}^{35}Cl_4O$, $C_{25}H_{16}{}^{35}Cl_3{}^{37}ClO$, $C_{25}H_{16}{}^{35}Cl_2{}^{37}Cl_2O$, and $C_{25}H_{16}{}^{35}Cl^{37}Cl_3O$: 471.9955, 473.9926, 475.9897, and 477.9865. The intensity ratios of the signals agreed with those expected from the natural abundances of ^{35}Cl and ^{37}Cl. ^{1}H NMR ($CDCl_3$) δ=1.83 (3H, d, J=1.5 Hz), 2.34 (3H, s), 2.78 (1H, d, J=15 Hz), 3.31 (1H, dd, J=15 and 1.5 Hz), 6.09 (1H, s), 7.00—7.12 (2H, m), 7.18—7.23 (1H, m), 7.38—7.41 (1H, m), 7.63—7.66 (1H, m), 7.67—7.71 (1H, m), 7.87—7.90 (1H, m). IR (KBr disc): 1690 cm^{-1}.

***sc*-7b**, mp 258—260 °C, was similarly prepared from the corresponding acid (*sc*-**5b**) in 70% yield. Recrystallization of the compound from dichloromethane-hexane afforded the analytical sample. Found: C, 63.36; H, 3.51; Cl, 29.61%. Calcd for $C_{25}H_{16}Cl_4O$: C, 63.32; H, 3.40; Cl, 29.90%. ^{1}H NMR ($CDCl_3$) δ=1.64 (3H, d, J=1.5 Hz), 2.31 (3H, s), 2.78 (1H, d, J=16 Hz), 4.20 (1H, dd. J=16 and 1.5 Hz), 6.14 (1H, s), 7.15—7.23 (3H, m), 7.53—7.56 (1H, m), 7.63—7.66 (1H, m), 7.74—7.77 (1H, m), 7.90—7.93 (1H, m). IR (KBr disc): 1690 cm^{-1}.

Kinetics of Isomerization of Ketones (7). The *ap*-ketone was dissolved in toluene-d_8 to make up a ca. 20 mmol L^{-1} solution. The sample solution was placed in a thermostatted bath, except for one case where a boiling benzene bath was used. The rates of isomerization were followed by the change in intensities of ^{1}H NMR signals due to the methyl protons or the 7-proton. The data were treated by assuming the reversible first order reactions. The rate constants thus obtained were put into the Eyring equation to produce kinetic parameters.

Comparison of the Kinetic and Thermodynamic Parameters. The parameters shown in Table 3 were obtained by extrapolation of the thermodynamic and kinetic parameters obtained in the temperature ranges other than the given temperature. The thermodynamic parameters may include large errors, especially for those which give large K values.

Molecular Mechanics Calculations. Molecular mechanics calculations were performed using the MMP2(82) program[11] at the Computer Center of the University of Tokyo, assuming a "nonplanar" π-system for each compound. As the force field does not contain parameters for halogen atoms attached to an sp^2 carbon atom, several necessary parameters were added. The equilibrium bond length (Å) and stretching force constant (md Å^{-1}) for C(sp^2)-X were assumed to be 1.715 and 2.66, respectively, when X=Cl, and 1.330 and 5.10, respectively, when X=F. The equilibrium bond angle (deg) and bending force constant (md Å rad^{-2}) were 120.0 and 0.40, when X=Cl, for C(sp^2)-C(sp^2)-X, and 120.0 and 0.65, respectively, for X=F. Torsional constants, V_1 and V_2, of −0.93, and 9.0 kcal mol^{-1}, respectively, for X-C(sp^2)-R, where R is any atom, were used. The out-of-plane bending parameter of 0.05 md Å rad^{-1} was used for both the cases where X=Cl and F.

This work was supported by a Grant-in-Aid (No.

62124035) for Fundamental Scientific Research of the Ministry of Education, Science and Culture.

References

1) For Part XXIII of the series, see M. Ōki, J. Tsukahara, Y. Sonoda, K. Moriyama, and N. Nakamura, *Bull. Chem. Soc. Jpn.*, **61**, 4303 (1988).

2) T. Tanaka, K. Yonemoto, Y. Nakai, G. Yamamoto, and M. Ōki, *Bull. Chem. Soc. Jpn.*, **61**, 3239 (1988).

3) R. Ray and D. S. Matteson, *Tetrahedron Lett.*, **21**, 449 (1980).

4) E. L. Jackson, *Org. React.*, **2**, 341 (1944).

5) R. Adams and L. H. Ulich, *J. Am. Chem. Soc.*, **42**, 599 (1920).

6) G. A. Olah and J. M. Bollinger, *J. Am. Chem. Soc.*, **90**, 947 (1968).

7) A referee suggested that, since addition of a cation to fluoro-olefins was much easier than to chloro-olefins [G. A. Olah and Y. K. Mo, *Adv. Fluorine Chem.*, **7**, 69 (1973): W. S. Johnson, G. W. Daub, T. A. Lyle, and M. Niwa, *J. Am. Chem. Soc.*, **102**, 7800 (1980)], the argument would not hold. However, the results of Ref. 6 clearly indicates that a three-membered fluoronium ion is very reluctantly formed. We believe these two cases must be considered separately.

8) G. Yamamoto, M. Suzuki, and M. Ōki, *Bull. Chem. Soc. Jpn.*, **56**, 306 (1983).

9) K. Yonemoto, Y. Nakai, G. Yamamoto, and M. Ōki, *Chem. Lett.*, **1985**, 1739.

10) K. B. Wiberg, G. M. Lampman, R. P. Ciura, D. S. Connor, P. Schertler, and J. Lavanish, *Tetrahedron*, **21**, 2749 (1965) and papers cited therein.

11) N. L. Allinger and H. L. Flanagan, *J. Comput. Chem.*, **4**, 399 (1983).

 © 1988 The Chemical Society of Japan Bull. Chem. Soc. Jpn., 61, 4315—4321 (1988)

Synthesis of Fluorescent Amino Acids and Peptides with 2-Aminopyridine at the Carboxyl or Amino Terminus

Tomohiro MEGA,* Yasuki HAMAZUME, and Tokuji IKENAKA
Department of Chemistry, Osaka University College of Science, Toyonaka, Osaka 560
(Received April 16, 1988)

N-(2-Pyridyl) derivatives of glycine (**1**), DL-alanine (**2**), DL-valine (**3**), and DL-norleucine (**4**) were synthesized as fluorescence labeled amino acids. These amino acids were used for the synthesis of N-terminal fluorescence-labeled peptides. *N*-(2-Pyridyl)-1,2-ethanediamine (**7**) was synthesized and used for the C-terminal labeling of amino acids and peptides. With these amino acid derivatives, some peptides labeled with 2-aminopyridine were synthesized and their spectroscopic characteristics were examined.

Fluorescent labeling of the reducing ends of sugars with 2-aminopyridine has become a useful method in the structure analyses of the sugar moiety of glycoconjugates.[1] This is because of the stability of the 2-pyridylamino group against acid, alkaline, and other reagents, and also the facility both for the detection and purification of 2-pyridylaminosugars during electrophoresis or in several chromatographies including HPLC, owing to its positive charge in acidic conditions or the hydrophobic nature in alkaline conditions. Fluorescence-labeled sugars has been used as substrates for some carbohydrases[2] and glycosyltransferases.[3] This labeling can be employed in the preparation of fluorescent amino acids and peptides that can be used as substrates for enzymes participating in the post-translational modification of the proteins or peptides. Labelling of the N-terminus, C-terminus, or both termini of a peptide may protect the molecule against exopeptidase digestion and serve as the fluorescence marker for the compound. No peptide with 2-aminopyridine has been synthesized. This prompts us to synthesize the *N*-2-pyridylamino peptides. *N*-(2-Pyridyl)glycine (**1**), the sole amino acid reported as a 2-pyridylamino derivative, seemed to be a suitable compound for use in the synthesis of N-terminal and C-terminal fluorescence-labeled peptides, but it was found not to be suitable for the labeling of the C-terminus of peptides because of the low reactivity of its imino group to acylation and because acylation causes the loss of its fluorescence. We then selected *N*-(2-pyridyl)-1,2-ethane diamine (**7**) as a reagent for C-terminal fluorescence-labeling of amino acids and peptides, and found **1** is synthesized by the reduction of *N*-(2-pyridylamino)acetaldehyde oxime with $LiAlH_4$. Here, we develop a new easy route for the preparation of **7**, synthesize some fluorescent peptides with **7** at the C-terminal together with peptides with **1** or **2** at their N-terminal, and examine their fluorescent and UV spectra at different pH's.

Results and Discussion

Four methods have been reported for the synthesis of **1**.[4] We synthesized **1** from formaldehyde via its nitrile by the method of Ohta and Masaki.[4b] This method could be applied to the synthesis of other *N*-(2-pyridyl) derivatives of DL-alanine (**2**), DL-valine (**3**), and DL-norleucine (**4**) using acetaldehyde, isobutyraldehyde, and valeraldehyde as the starting material, respectively. These four *N*-(2-pyridyl) α-amino acids can be used similarly for the syntheses of N-terminal fluorescence-labeled peptides. Here, the synthesis of some peptides starting from **1** and **2** and the characteristics of the peptides were examined.

Blocking the imino group of **1** or **2** by a benzyloxycarbonyl or *t*-butoxycarbonyl group was unsuccessful. *N*-Acetylation of **1** by acetic anhydride in pyridine gave a green by-product, which was not identified, but seemed to be mesomethyloxonol, because **1** is reported to give a green dye with the structure shown below when treated with hot acetic anhydride.[5]

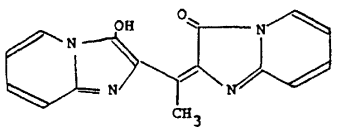

Accordingly, the coupling of **1** to amino acids or peptides was done without blocking the imino group in chloroform with dicyclohexylcarbodiimide (DCC) or in water with water soluble carbodiimide (WSC). When peptide synthesis was carried out in chloroform or methylene dichloride, powdered **1** was used because of the low solubility of **1** in the solvents. The reaction solution of **1** became greenish in a few minutes, and the color increased to dark green or dark purple depending upon the pH of the solution. The yield of the desired peptide was about 50—60% on several conditions and did not exceed 70%. The synthesis of active esters of **1** was unsuccessful, because the active ester may be unstable and convert to 1,3a-diazaindan-3-one.[5]

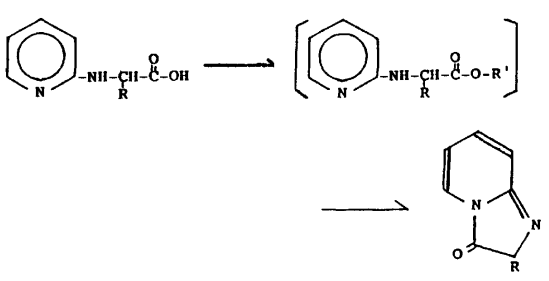

The coupling reaction with **2** proceeded like that with **1**, but the reaction solution turned yellow, because of the formation of unknown by-products.

N-(2-Pyridyl)-1,2-ethanediamine (**7**) has been synthesized from *N*-(2-pyridylamino)acetaldehyde oxime by reduction with $LiAlH_4$.[4a] We found that **7** could be prepared by heating a mixture of 2-chloropyridine and ethylenediamine in a good yield.

Coupling of **7** to carboxyl components proceeded with a good yield in the presence of DCC or WSC without formation of the colored by-products. The 2-pyridylamino derivatives were usually soluble in water at acidic pH and in organic solvents at alkaline pH. These characteristics were sometimes useful and sometimes disadvantageous in the purification of the product. As a whole, the synthesis of 2-pyridylamino peptides was more troublesome than the normal peptide synthesis.

Since the spectroscopic characteristics of *N*-2-pyridyl amino acids or peptides have not been reported, the effect of pH on the UV and fluorescence spectra of these compounds was examined first. Figures 2-A and 2-B present the emission and excitation spectra of **1** at different pH's. The figures show that the fluorescence intensity of **1** is influenced strongly by pH, but the maximum wavelengths for excitation and emission are not influenced. Figure 2-C shows the emission spectra of the four compounds **1**, **2**, **5**, and **7** under the same conditions. The fluorescence intensity decreased in the order of **5**>**7**>**1**>**2**. Compound **2** seems not to be very useful for the synthesis of fluorescent peptides because of its low fluorescence intensity. But the peptide produced from **2** had the normal fluorescence intensity (as shown in Fig. 3-B).

Figure 3 shows the pH dependence of the fluorescence intensities of nine compounds. The fluorescence intensities of these compounds were lowest at around pH 5, and high at around pH 10—11, becoming very low above pH 12. These characteristics were common to all of the 2-pyridylamino derivatives examined. The fluorescence intensities of the *N*-2-pyridylamino acids **2** (Fig. 3-B), **3** (Fig. 3-C), and **4** (data not shown) were weaker than those of the other 2-pyridylamino compounds, but gradually increased when **2** and **3**

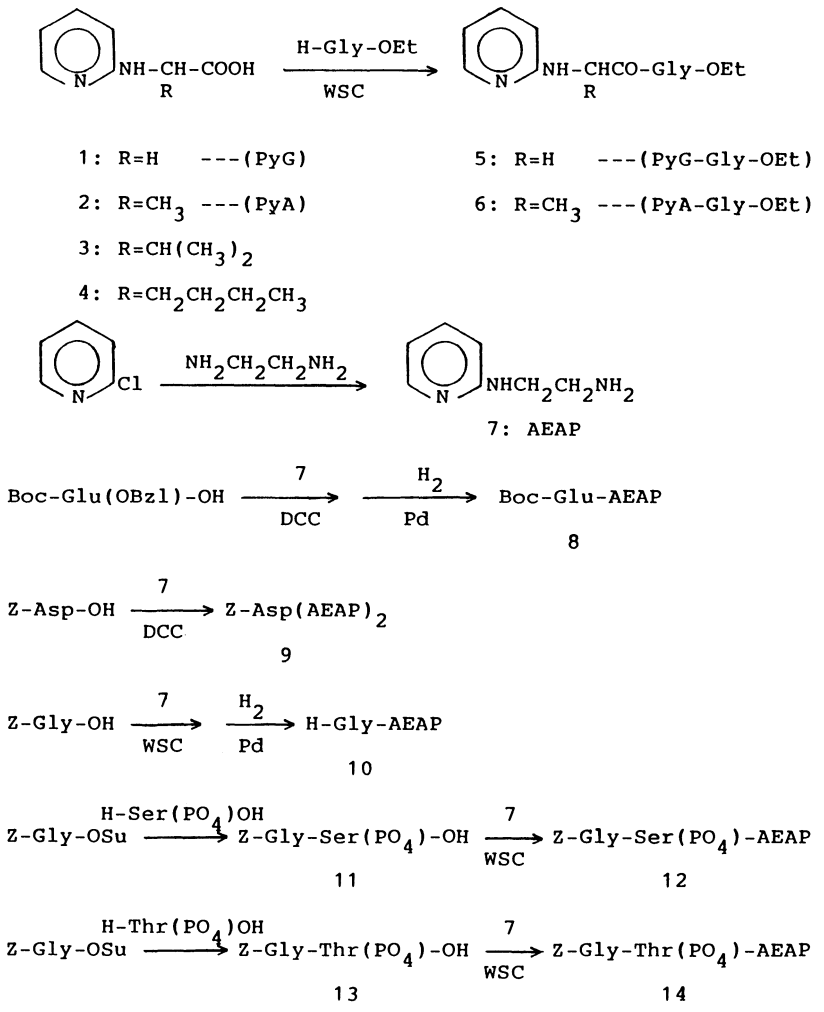

Fig. 1. Structures and syntheses of several fluorescent amino acids and peptides labeled with 2-aminopyridine.

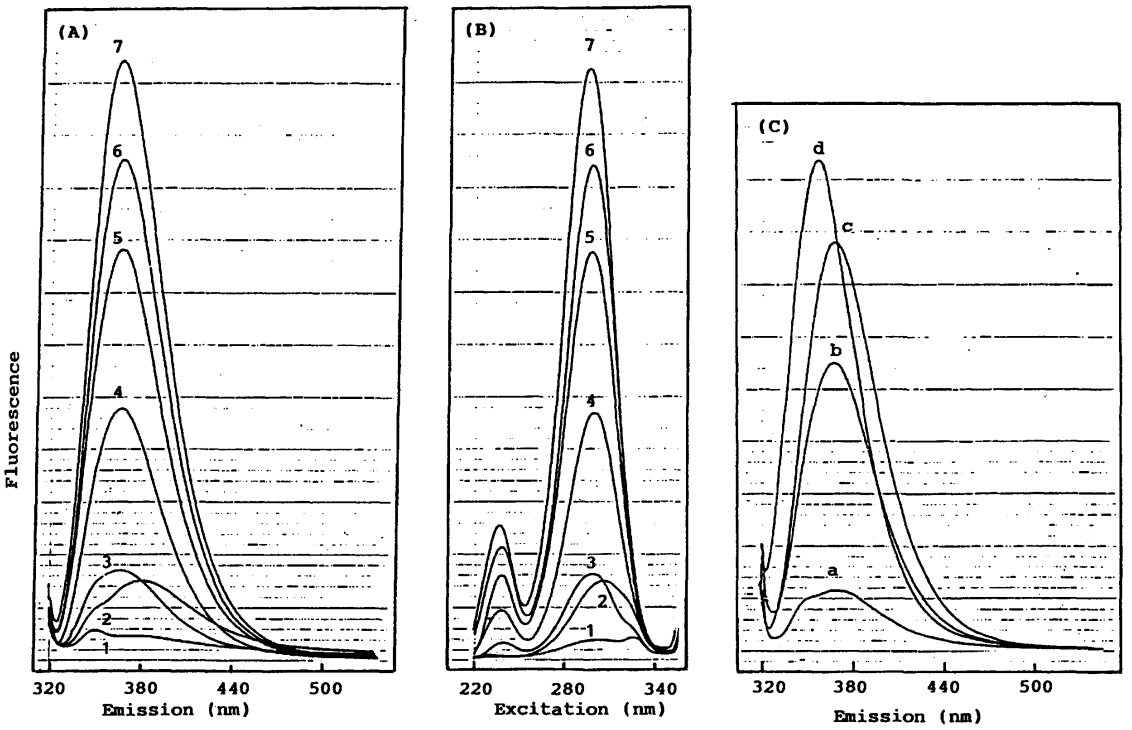

Fig. 2. (A) Emission spectra of **1** in different buffers.
Fluorescence was measured at the excitation wavelength of 304 nm and at the concentration of 2.4 μM. Solvents used were: 1, pH 5 (acetate); 2, 0.1 M HCl; 3, pH 6 (acetate); 4, 0.1 M NaOH; 5, pH 7 (acetate); 6, pH 8 (borate); 7, pH 10 (borate).
(B) Excitation spectra of **1** at the emission wavelength of 375 nm in different solvents. Solvents used were the same as those in A.
(C) Emission spectra of some 2-pyridylamino derivatives measured in borate buffer, pH 10, at the excitaton wavelength of 304 nm and at the concentration of 1.2 μM. Compounds were as follows: a, *N*-(2-pyridyl)-DL-alanine; b, *N*-(2-pyridyl)glycine; c, *N*-(2-pyridyl)-1,2-ethanediamine, and d, PyG-Gly-OEt.

were kept acidic.

The fluorescent intensities of N-terminal-labeled peptides (**5** and **6**) were higher than those of the component amino acids **1** or **2** (Fig. 3-A or 3-B). Fluorescence intensities of the C-terminal-labeled amino acids **8** (Fig. 3-E) and **10** (Fig. 3-D) were higher than those of N-terminal-labeled derivatives.

Figure 4 shows the absorption spectra of **1** in 0.1 M HCl (1 M=1 mol dm^{-3}), 0.1 M NaOH, and acetate buffer, pH 5. Compound **1** had two maxima around 240 and 306 nm. The absorbance at 306 nm in acidic pH was higher than in alkaline pH. The absorption maxima and molar extinction coefficients of compounds **2** and **3** in either 0.1 M HCl or 0.1 M NaOH were almost the same as those of **1** (Table 1). Compounds **6**, **7**, and **8** also had similar UV absorption spectra.

These spectroscopic characteristics were convenient for the detection of the 2-pyridylamino derivatives by TLC and HPLC.

Compound PyG-Gly-OEt (**5**), DL-PyA-Gly-OEt (**6**), Boc-Glu-AEAP (**8**), and Z-Asp(AEAP)$_2$ (**9**) were synthesized to test the coupling reaction and to use as starting materials for the synthesis of many fluorescent peptides. We also synthesized fluorescent phosphopeptides Z-Gly-Ser(PO_4)-AEAP and Z-Gly-Thr(PO_4)-AEAP to study the β-elimination reaction of phosphoserine and phosphothreonine peptides and as substrates for phosphatases. In the coupling of Z-Gly-Ser(PO_4)-OH (**11**) and **7** with WSC, one main product (peak c) appeared (Fig. 5), it was found to be **12**, Z-Gly-Ser(PO_4)-AEAP. Peaks a and b were **7** and **11**, respectively. This shows that *N*-blocked phosphoserine or phosphothreonine could be used as an acid component without blocking the phosphate. The reaction was completed in 2 h and the product (peak c) was isolated using HPLC.

In a study of hen riboflavin-binding protein (RBP), we have found that RBP in hen blood, the precursor of RBP in egg yolk, was 11 or 13 amino acid residues longer than the protein in egg yolk.[6] It is likely that the C-terminal part is removed by protease(s) in the oocyte membrane during the incorporation of RBP from the blood to the oocyte (egg yolk). To search for a specific protease that modifies the C-terminal of the protein, a fluorescent peptide (**15**), PyG-Gln-Lys-Lys-Leu-Leu-Lys-Phe-Glu-βAla having a similar amino acid sequence to that of the C-terminal part was

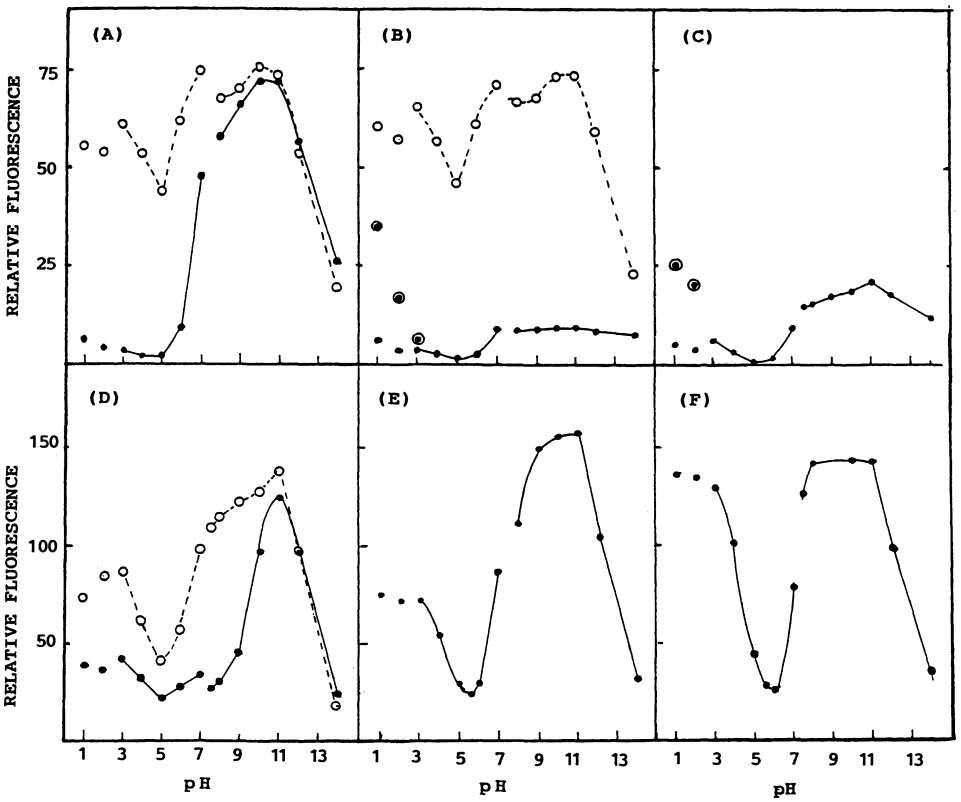

Fig. 3. Relationship of fluorescence and pH for some 2-pyridylamino derivatives at the concentration of 1.2 μM.
(A), **1** (●) and **5** (○); (B), **2** (●) and **6** (○); (C), **4**; (D),**7** (●) and **10** (○); (E), **8** and (F), **9**. The marks (○) in (B) and (C) were the values after 24 h. The excitation wavelength was 304 nm and the emission wavelength was 375 nm. Solvents were: pH 1, 0.1 M HCl; pH 2, 0.02% TFA; pH 3—7, 0.1 M acetate buffer; pH 7.5—12, 0.1 M borate buffer; pH 13, 0.1 M NaOH.

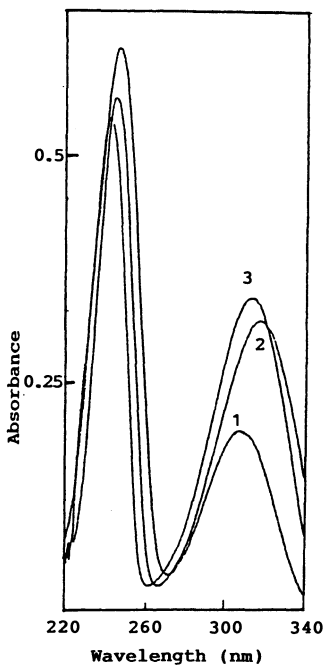

Fig. 4. Absorption spectra of **1** in 0.1 M NaOH (1), 0.1 M acetate buffer (pH 5) (2), and 0.1 M HCl (3) at the concentration of 50 μM.

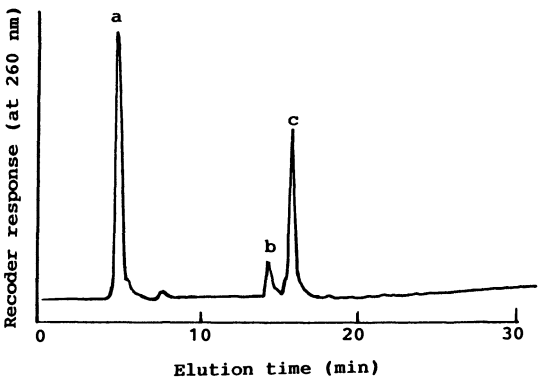

Fig. 5. HPLC of the reaction mixture of **11** and **7** with WSC. Peaks a, b, and c were **7**, **11**, and **12**. Elution was with an exponential gradient of CH_3CN from 0% to 50% in 0.05% TFA, and the starting volume was 50 ml. Column, ODS-120 T (7×250 mm); flow rate, 3 ml min^{-1}.

synthesized. The synthesis of **15** was performed by the solid phase peptide synthesis. In the coupling of **1** with peptides on the resin, the reaction was performed in the CH_2Cl_2 with the suspension of **1** because of its low solubility in the solvent. The reaction solution

Table 1. UV-Spectra of 2-Pyridylamino Derivatives

Compound	Solvent (0.1 M)	λ_{max}	ε_{max}[a]	λ_{max}	ε_{max}[a]
		nm	$l\,mol^{-1}cm^{-1}$	nm	$l\,mol^{-1}cm^{-1}$
1	HCl	308	7200	237	11400
	NaOH	302	4300	242	13200
	pH 5[b]	316	6500	244	11500
2	HCl	308	7200	237	11700
	NaOH	302	4100	242	12700
3	HCl	307	7300	235	12000
	NaOH	302	3800	240	13400
5	HCl	308	7100	238	11100
	NaOH	304	4200	245	12300
7	HCl	308	7200	237	11800
	NaOH	302	4100	243	13200
8	HCl	310	6400	238	11300
	NaOH	307	3800	248	12300
9	HCl	312	12600	242	22100
	NaOH	308	7500	248	24100
10	HCl	308	6400	236	11600
	NaOH	301	3600	239	12200

a) The value is at its maximum wavelength. b) Sodium acetate.

colored dark purple and the resin was stained with the same color. In spite of the strong staining of the resin and using the suspension of **1**, the yield of the coupling was fairly good.

Since fluorescence labeled peptides with 2-aminopyridine can be synthesized by the usual method or with reagents as described above, the labeled peptides are expected to work as useful compounds for the analyses of some enzymes or some reactions owing to its unique spectroscopic characteristics.

Experimental

General. Melting points were measured on a Yanagimoto melting point apparatus and were uncorrected. ^1H NMR spectra were recorded on a Varian XL-100 (100 MHz) or a JEOL FX-90 (90 MHz) spectrometer with Me_4Si as an internal standard, unless otherwise stated.

TLC was done on silica-gel plates (Merck Kieselgel 60 F254). The solvent system was *n*-BuOH-AcOH-H_2O (4 : 1 : 1) unless otherwise stated. HPLC conditions were as follows: column, TSK ODS-120T (7×250 mm); flow rate, 3 ml min^{-1}; detection of pyridylamino compounds at 310 nm or of benzyloxycarbonyl compounds at 260 nm; elution systems; (1), exponential or linear gradient of 0.05% TFA and 50% CH_3CN-0.05% TFA; (2) several isocratic conditions. Fluorescence was measured by a Hitachi spectrophotometer 650-10S.

N-(2-Pyridyl)glycine (**1**) and 2-(2-pyridylamino)propionitrile were synthesized by the method of Ohta and Masaki.[4b]

***N*-(2-Pyridyl)-DL-alanine (2):** A solution of 2-(2-pyridylamino) propionitrile (7 g) in 6 M HCl (100 ml) was refluxed for 5 h and concentrated. Crystals (NH_4Cl) that appeared were filtered off and washed with ethanol. The washings and filtrate were combined and concentrated. The crystals that appeared were filtered off. The filtrate was applied to a Dowex 50 H^+ column (2×12 cm). Compound **2** was eluted with 0.2 M ammonium acetate as a yellow fraction. The solution was concentrated and **2** was crystallized with ethanol; yield 4.7 g (59%); mp 153 °C; pale yellow needles; ^1H NMR (D_2O) δ=1.48 (3H, d, CH_3), 4.0—4.2 (1H, q, CH), 6.8—7.0 (2H, m, pyridine), 7.7—8.0 (2H, m, pyridine). Found: C, 57.82; H, 6.07; N, 16.86%. Calcd for $C_8H_{10}O_2N_2$: C, 57.73; H, 6.10; N, 16.65%.

***N*-(2-Pyridyl)-DL-alanine (2):** A solution of 2-(2-pyridylamino) propionitrile (7 g) in 6 M HCl (100 ml) was refluxed for 5 h and concentrated. Crystals (NH_4Cl) that appeared were filtered off and washed with ethanol. The washings and filtrate were combined and concentrated. The crystals that appeared were filtered off. The filtrate was applied to a Dowex 50 H^+ column (2×12 cm). Compound **2** was eluted with 0.2 M ammonium acetate as a yellow fraction. The solution was concentrated and **2** was crystallized with ethanol; yield 4.7 g (59%); mp 153 °C; pale yellow needles; ^1H NMR (D_2O) δ=1.48 (3H, d, CH_3), 4.0—4.2 (1H, q, CH), 6.8—7.0 (2H, m, pyridine), 7.7—8.0 (2H, m, pyridine). Found: C, 57.82; H, 6.07; N, 16.86%. Calcd for $C_8H_{10}O_2N_2$: C, 57.73; H, 6.10; N, 16.65%.

***N*-(2-Pyridyl)-DL-alaline Hydrochloride:** Mp 160—161 °C. Found: C, 47.42; H, 5.47; N, 13.83; Cl, 17.50%. Calcd for $C_8H_{10}O_2N_2HCl$: C, 47.27; H, 5.46; N, 13.69; Cl, 17.48%.

***N*-(2-Pyridyl)-DL-valine Hydrochloride (3):** Isobutyraldehyde (7.2 g) was mixed with an aqueous solution of $NaHSO_3$ (10 g in 10 ml H_2O) and warmed (60—70 °C) for 0.5 h. 2-Aminopyridine (9.4 g) was added and warmed 0.5 h more. Finally NaCN (7.6 g in 16 ml of water) was added and the mixture was heated under continuous stirring in a boiling water bath for 6 h. The dark brown product of the nitrile (α-(2-pyridylamino)isovaleronitrile) was extracted with 40 ml of chloroform five times, and the organic layer dried over $MgSO_4$ and concentrated. The nitrile was directly hydrolyzed in 6 M HCl (400 ml) under reflux for 6 h. The hydrolysate was concentrated to remove NH_4Cl as crystals and filtered. The filtrate was neutralized with 4 M NaOH, washed with chloroform, and evaporated. The residue was dissolved in water, acidified with 6 M HCl, and concentrated. The crystals that appeared (NaCl) were removed by filtration and washed with acetone. The filtrate and washings were combined and concentrated, giving the desired product in crystalline form. The product was recrystallized from water: Yield, 7.2 g (62%); mp 151—152 °C; ^1H NMR (D_2O) δ=1.7 (6H, d, 2×CH_3), 2.28—2.62 (1H, m, CH), 4.39 (1H, d, CH), 6.9—7.2 (2H, m, pyridine), 7.8—8.1 (2H, m, pyridine). Found: C, 51.94; H, 6.53; N, 12.14%. Calcd for $C_{10}H_{14}N_2O_2HCl$: C, 52.06; H, 6.55; N, 12.14%.

***N*-(2-Pyridyl)-DL-norleucine Hydrochloride (4):** Compound **4** was synthesized similarly as **3** from valeraldehyde. Mp 132—134 °C; ^1H NMR (D_2O) δ=0.9 (3H, t, CH_3), 4.4—5.6 (1H, m, CH), 6.9—7.2 (2H, m, pyridine), 7.8—8.2 (2H, m, pyridine). Found: C, 53.91; H, 6.96; N, 11.42%. Calcd for $C_{11}H_{16}N_2O_2HCl$: C, 53.99; H, 7.00; N, 11.45%.

PyG-Gly-OEt (5): To a solution of **1** (1.9 g), glycine ethyl ester hydrochloride (2.8 g), triethylamine (2 ml) in $CHCl_3$ (80 ml) and DMF (20 ml), and WSC (2.1 g) were added. The mixture was stirred for 2 days at room temperature. The dark green reaction mixture was diluted with 0.1 M HCl, washed with $CHCl_3$ twice and neutralized with triethylamine to pH 7.5. The product was extracted 4 time with $CHCl_3$. The extracts were combined, dried over $MgSO_4$, and concentrated, giving crystalline **5**. The crystals were washed with ethyl acetate. The yield was 1.4 g (61%). Recrystallization was done with ethanol: mp 121.5—122 °C.

^{1}H NMR ($CDCl_3$) δ=1.2—1.34 (3H, t, CH_3), 5.47 (1H, br, NH), 6.4—6.8 (2H, m, pyridine), 7.4—7.6 (1H, m, pyridine), 8.08—8.16 (1H, m, pyridine). Found: C, 55.65; H, 6.38; N, 17.76%. Calcd for $C_{11}H_{15}N_3O_3$: C, 55.69; H, 6.37; N, 17.71%.

DL-PyA-Gly-OEt: WSC (21 mg) was added to a cooled mixture of **2** (17 mg), glycine ethyl ester hydrochloride (28 mg), triethylamine (15 μl), DMF (0.1 ml), and $CHCl_3$ (0.9 ml). The mixture was stirred for 3 h at room temperature. Product **6** was isolated by HPLC with a C_{18}-column. The peak around 7 min on isocratic elution with 25% acetonitrile- 0.01 M NH_4OAc buffer (pH 5.6) was collected, concentrated, and crystallized with ethanol: Yield, 12 mg (48%), mp 109—110 °C. ^{1}H NMR ($CDCl_3$) δ=1.24 (3H, t, $CH_2C\underline{H}_3$), 1.51 (3H, d, $CHC\underline{H}_3$), 5.8 (1H, br, NH), 6.4—6.72 (2H, m, pyridine), 7.3—7.6 (1H, m, pyridine), and 8.08—8.16 (1H, m, pyridine). Found: C, 57.47; H, 6.82; N, 16.78%. Calcd for $C_{12}H_{17}N_3O_3$: C, 57.36; H, 6.82; N, 16.72%.

***N*-(2-Pyridyl)-1,2-ethanediamine Dihydrochloride (7):** A mixture of 1,2-ethanediamine (100 ml) and 2-chloropyridine (10 g) was refluxed for 8 h and concentrated to remove as much of the unreacted 1,2-ethanediamine as possible under reduced pressure. Then 2 M NaOH (40 ml) was added to the residue and the product extracted 8 times with 50 ml of $CHCl_3$ each time. The extracts were evaporated under reduced pressure. Hydrochloric acid was added to the residue and concentrated to crystallize **7**. Recrystallization from a mixture of water and ethanol after charcoal treatment gave **7** as faintly yellow needles: yield 11 g (62%); mp 215—216 °C; ^{1}H NMR (D_2O) δ=3.35 (2H, t, CH_2), 3.79 (2H, t, CH_2), 6.9—7.2 (2H, m, pyridine), and 7.8—8.1 (2H, m, pyridine). Found: C, 39.04; H, 6.22; N, 19.95%. Calcd for $C_7H_{11}N_3$, 2HCl : C, 40.02; H, 6.24; N, 20.00%.

Boc-Glu(OBzl)-AEAP: A solution of Boc-Glu(OBzl)-OH (1.6 g, 5 mmol) in chloroform (20 ml) was mixed with a solution of **7** (1.0 g) in 20 ml of chloroform and 0.7 ml of triethylamine. DCC (1.0 g) was added to the cooled upper solution. After 3 h, the reaction mixture was filtered and evaporated. Ethyl acetate (40 ml) was added to the residue and insoluble materials were removed by filtration. The filtrate was washed twice with 2.5% Na_2CO_3 and then with water, dried over Na_2SO_4, and concentrated to a syrup. The yield was about 80% from the absorbance at 310 nm, the purity was confirmed by TLC (*n*-BuOH-AcOH-H_2O, 4 : 1 : 1) and the compound was used for the next step without further purification.

Boc-Glu-AEAP Acetate (8): The *O*-benzyl group of Boc-Glu(OBzl)-AEAP was removed by hydrogenation over Pd-black in methanol-acetic acid (10 : 1). After filtration and evaporation of the reaction solution, the product was crystallized as acetate from methanol-ethyl acetate: mp 136—137 °C. Found: C, 53.15; H, 7.04; N, 13.14%. Calcd for $C_{19}H_{30}N_4O_7$: C, 53.51; H, 7.09; N, 13.14%.

Z-Asp(AEAP)$_2$ (9): Z-Asp (0.62 g, 2.3 mmol), **7** (1.0 g, 5 mmol), and triethylamine (0.8 ml) were dissolved in a mixture of 5 ml of H_2O and 10 ml of dioxane. WSC (1.1 g, 5.5 mmol) was added to the mixture at 0 °C. After 2 h, the reaction mixture was evaporated; the residue was dissolved in 0.1 M HCl and washed three times with chloroform. After the addition of a sat. $NaHCO_3$ solution to the aqueous layer, the product was extracted twice with $CHCl_3$. The chloroform layer was dried over $MgSO_4$ and concentrated. Compound **9** was crystallized by the addition of ethyl acetate; yield, 0.7 g (60%); mp 103—104 °C; ^{1}H NMR ($CDCl_3$) δ= 2.57—2.72 (2H, m, CH_2), 3.36 (8H, s, 2×CH_2-CH_2), 4.4—4.6 (1H, m, CH), 5.02 (2H, s, $C\underline{H}_2$Ph), 5.5 (2H, br, NH), 6.3—6.7 (4H, m, pyridine), 7.3 (5H, s, Ph), 7.3—7.32 (2H, m, pyridine), 7.5 (1H, s, NH), 7.7 (1H, s, NH), and 7.9—7.96 (2H, m, pyridine). Found: C, 61.22; H, 6.11; N, 19.30%. Calcd for $C_{26}H_{31}N_7O_4$: C, 61.77; H, 6.18; N, 19.39%.

Gly-AEAP (10): WSC (192 mg) was added to a cooled solution of Z-Gly (209 mg), **7** (210 mg), triethylamine (150 μl), chloroform (18 ml), and DMF (2 ml) and stirred for 3 h at room temperature. The product was extracted with 0.1 M HCl, and washed with chloroform. Saturated $NaHCO_3$ was added, and the mixture was extracted with chloroform. The organic layer was concentrated and hydrogenated over Pd-black in 0.1 M HCl to give **10**. Compound **10** was crystallized with ethanol: yield 163 mg (61%); mp 190—192 °C; ^{1}H NMR (D_2O) δ=3.62 (4H, s, CH_2-CH_2), 3.89 (2H, s, CH_2), 6.9—7.2 (2H, m, pyridine), and 7.8—8.1 (2H, m, pyridine). Found: C, 37.78; H, 6.45; N, 19.67%. Calcd for $C_9H_{14}N_4O$, 2HCl, H_2O: C, 37.91; H, 6.36; N, 19.65%.

Z-Gly-Ser(P)OH (11): A solution of Z-Gly-OSu (400 mg) in 2 ml of dioxane was added with stirring to the phosphoserine solution (200 mg) in 4 ml of water and 2 ml of dioxane, the pH of which had been adjusted to 8.5. The mixture was stirred at room temperature for 8 h and concentrated under reduced pressure. The residue was dissolved in water, washed with ethyl acetate three times, and applied to HPLC to purify **11**. Compound **11** was eluted around 13 min, concentrated, and crystallized with chloroform: 246 mg (58%); mp 164—165 °C. ^{1}H NMR (D_2O) δ=3.80 (2H, s, NCH_2), 4.1—4.3 (2H, m, CH_2OP), 5.0 (2H, s, CH_2-O), and 7.26 (5H, s, Ph). Found: C, 41.38; H, 4.43; N, 7.39%. Calcd for $C_{13}H_{17}N_2O_9P$: C, 41.49; H, 4.56; N, 7.44%.

Z-Gly-Thr(P)OH (13): Compound **13** was synthesized in a similar way to **11** with 90 mg (0.45 mmol) of phosphothreonine and 300 mg (0.98 mmol) of Z-Gly-OSu. Compound **13** could not be obtained as a crystal even after purification by HPLC: Yield, 143 mg (78%); ^{1}H NMR (D_2O) δ=1.06 (3H, d, CH_3), 3.74 (2H, s, $NHC\underline{H}_2CO$), 4.42—4.56 (1H, m, CHOP), 4.86 (2H, s, $C\underline{H}_2$Ph), 7.12 (5H, m, Ph).

Z-Gly-Ser(P)-AEAP (12): To a solution of **11** (19.6 mg) and **7** (20.6 mg) in water (0.5 ml), the pH of which had been adjusted to 6, WSC (9.5 mg) was added. The reaction was monitored by the use of HPLC (Fig. 5) to confirm the production of **12** (elution time, 15.5 min). The reaction was completed in 2 h and **12** was isolated by HPLC: Yield, 18 mg (62%); ^{1}H NMR (D_2O) δ=3.48 (4H, s, 2×CH_2), 3.91 (2H, s, NCHCO), 4.4—4.2 (1H, m, CHOP), 5.12 (2H, s, CH_2Ph), 6.28—7.06 (2H, m, pyridine), 7.37 (5H, s, Ph), and 7.76—8.0 (2H, m, pyridine).

Z-Gly-Thr(P)-AEAP (14): Compound **14** was synthesized in a similar way to **12**. The elution time of **14** on HPLC was 15.6 min: Yield, 66%; ^{1}H NMR (D_2O) δ=1.26 (3H, d, CH_3), 3.45 (4H, s, 2×CH_2), 3.92 (2H, s, NCH_2CO), 5.21 (2H, s, $C\underline{H}_2$Ph), 6.8—7.06 (2H, m, pyridine), 7.38 (5H, s, Ph), and 7.7—8.0 (2H, m, pyridine).

PyG-Gln-Lys-Lys-Leu-Leu-Lys-Phe-Glu-βAla (15): Compound **15** was synthesized by the solid phase peptide synthesis.[7] Boc-β-alanine (5 mmol) was coupled to 10 g of chloromethylated polystyrene resin (Peptide Institute, Inc.) according to the method of Gisin[8] and obtained a β-alanyl resin (0.25 mmol g^{-1}). Three fold of Boc-amino acid (26 mmol) was coupled to the resin (3.5 g) stepwise with DCC. The coupling reaction was repeated in the introduction of

Boc-Phe-DCAA and Boc-Gln. In the introduction of *N*-(2-pyridyl)glycine, **1** was powdered in a mortar because of its low solubility in methylene dichloride.

Peptide **15** was purified by HPLC after HF treatment (0 °C, 1 h). The yield was about 55% from the β-alanyl resine. The structure of **15** was confirmed by FAB-mass,[9] (Found: *m/z* 1238.8. Calcd for the structure: M, 1238) and also by amino acid analysis of the peptide. The amino acid composition of **15** was $Glu_{2.1}$ $Leu_{2.0}$ $Phe_{1.0}$ $Lys_{3.0}$ β-$Ala_{1.2}$. PyG could not be analyzed under ordinary analysis conditions.

The authors are grateful to Prof. Yasutsugu Shimonishi, Dr. Toshifumi Takao, and Mr. Hiroyuki Watanabe, Institute for Protein Research, Osaka University, for technical help in the solid phase peptide synthesis and for the FAB-MS measurements.

References

1) a) S. Hase, T. Ikenaka, and Y. Matsushima, *Biochem. Biophys. Res. Commun.*, **85**, 257 (1978); b) H. Takemoto, S. Hase, and T. Ikenaka, *Anal. Biochem.*, **145**, 245 (1985); c) S. Koyama, H. Daiyasu, S. Hase, Y. Kobayashi, Y. Kyogoku, and T. Ikenaka, *FEBS Lett.*, **299**, 265 (1986); d) S. Natsuka, S. Hase, and T. Ikenaka, *Anal. Biochem.*, **167**, 154 and 321 (1987).

2) K. Omichi and T. Ikenaka, *J. Biochem.*, **97**, 977 (1985), **99**, 291 and 1245 (1986), **100**, 1353 (1986).

3) a) N. Morita, S. Hase, K. Ikenaka, K. Mikoshiba, and T. Ikenaka, *J. Biochem.*, **103**, 332 (1988). b) T. Sato, K. Omichi, and T. Ikenaka, *ibid.*, **104**, 18 (1988).

4) a) P. Reynaud, T. Tupin, and R. Delaby, *Bull. Soc. Chim. Fr.*, **1957**, 718; b) M. Ohta and M. Masaki, *Bull. Chem. Soc. Jpn.*, **33**, 1392 (1960); c) M. Augustin and H. Dehne, *J. Prakt. Chem.*, **13**, 118 (1961); d) B. Domu, B. Vercek, B. Stanovnik, and M. Tister, *Chimia*, **28**, 235 (1974).

5) E. B. Knott, *J. Chem. Soc.*, **1956**, 1360.

6) N. Norioka, T. Okada, Y. Hamazume, T. Mega, and T. Ikenaka, *J. Biochem.*, **97**, 19 (1985).

7) D. Yamashiro and C. H. Li, *J. Am. Chem. Soc.*, **95**, 1310 (1973).

8) B. F. Gisin, *Helv. Chim. Acta*, **56**, 1476 (1973).

9) H. Watanabe, K. Takiguchi, S. Aimoto, and Y. Shimonishi, *Peptid. Chem.*, **1985**, 91.

 © 1988 The Chemical Society of Japan Bull. Chem. Soc. Jpn., 61, 4323—4327 (1988)

Reactions of Wittig Reagents with Episulfides or Elemental Sulfur

Kentaro OKUMA,* Yuji TACHIBANA, Jun-ichi SAKATA, Takashi KOMIYA, Isao KANEKO, Yasuo KOMIYA, Yusuke YAMASAKI, Shin-ichi YAMAMOTO, and Hiroshi OHTA
Department of Chemistry, Faculty of Science, Fukuoka University, Jonan-ku, Fukuoka 814-01
(Received April 25, 1988)

The reactions of Wittig reagents with episulfides gave symmetrical olefins and triphenylphosphine sulfide in moderate yields. The same olefins were obtained by reactions of Wittig reagents with elemental sulfur. These reactions might proceed through thiocarbonyl intermediates, the existence of which was confirmed by Diels-Alder reactions with dienes.

The Wittig reaction has been widely adopted for the synthesis of olefins.[1] During the past decade, several authors have reported on the reactions of Wittig reagents (**1**) with epoxides to afford cyclopropane derivatives.[2] Corey and Kang also reported that the reaction of the methylenetriphenylphosphorane anion with epoxides, followed by the addition of carbonyl compounds, gave 2-hydroxy olefin derivatives.[3] One of the methods for the synthesis of thioketones is the reaction of phosphonium ylides with elemental sulfur.[4] In a previous communication, we reported that the reactions of stable Wittig reagents with episulfides (**2**) afforded olefins (**3**) via thiocarbonyl intermediates in moderate yields.[5] Recently, we also found that the reaction of Wittig reagents with elemental selenium gave the corresponding olefins via selenocarbonyl intermediates.[6] This consideration, in turn, prompted us to investigate the possibility of the formation of **3** and thioaldehydes (**4**) by reactions of elemental sulfur with Wittig reagents. In this paper, we would like to report that the reaction of **1** with **2** or elemental sulfur produced **3** via thioaldehyde intermediates.

Results and Discussion

We first tried the reaction of **1** with **2**. A treatment of carbomethoxymethylenetriphenylphosphorane (**1a**) with styrene sulfide (**2a**) in toluene afforded styrene, dimethyl fumarate (**3a**), dimethyl maleate (**3a'**), and triphenylphosphine sulfide (**5**) in 20, 42.5, 9.5, and 74% yields, respectively. It took 2 days of refluxing to complete this reaction. We then carried out this reaction in refluxing benzene as a solvent. However, the yields of the products were lowered less than half, even after refluxing for 8 days. As shown in Table 1, other dialkyl fumarates and maleates were prepared in a similar manner.

Benzylidenetriphenylphosphorane (**1f**) was thermally decomposed at temperatures over 240 °C to give symmetrical olefins via carbene intermediates.[7] In this case, the reaction might proceed through similar carbene intermediates, as shown in Scheme 2. However, the thermolysis of **1a** in refluxing toluene without episulfide did not afford the olefins, but only the recovered starting materials, even after refluxing for 8 days. This result showed that the above-mentioned mechanism was not correct.

It is well-known that the reaction of benzhydrylidenetriphenylphosphorane with elemental sulfur affords thiobenzophenone, which changes to tetraphenylethylene upon heating at temperatures over 200 °C.[4a] Fluorenylidenetriphenylphosphorane was also found to react with sulfur to give thiofluore-

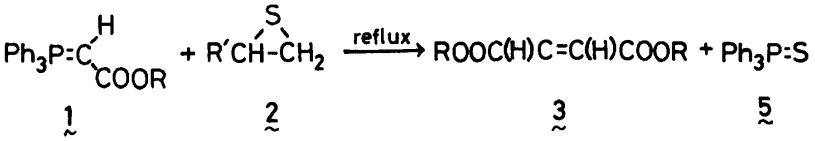

Scheme 1.

Table 1. Reaction of **1** with Episulfides

Compounds				Conditions		Products (Yields/%)		
1	R	**2**	R'	Solvent	Time/day	$Ph_3P=S$	**3**	Trans/Cis[a]
a	Me	**a**	Ph	Toluene	2	74	52	4.5
a	Me	**a**	Ph	Benzene	8	27	14	9.0[b]
a	Me	**b**	Me	Toluene	4	12	6	5.0[b]
a	Me	**c**	Et	Benzene	8	33	11	9.0[b]
b	Et	**a**	Ph	Toluene	2	74	58	3.5
c	*i*-Ph	**a**	Ph	Toluene	2	78	62	5.0

a) The ratio was determined by their ^1H NMR spectra or capillary GC. b) Starting **1a** was recovered in 50, 55, and 50% yields respectively.

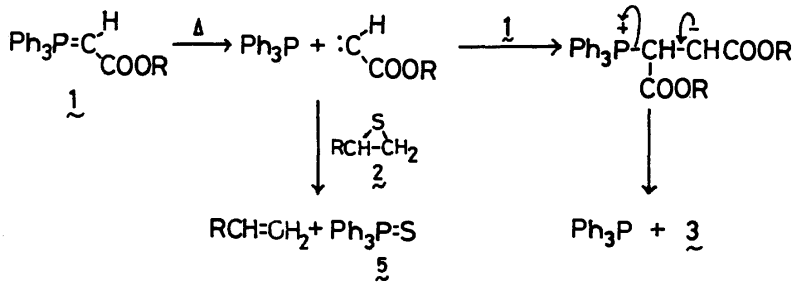

Scheme 2.

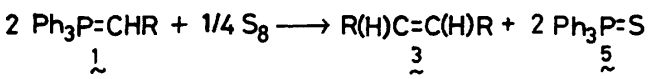

Scheme 3.

Table 2. Reaction of **1** with Elemental Sulfur

Compound		Conditions		Products (Yield/%)		
1	R	Solvent	Time/h	Sulfide **5**	Olefin **3**	Trans/Cis
a	COOMe	Toluene	3	79	76	5.0[a]
b	COOEt	Toluene	3	98	96	4.0[a]
d	CN	Toluene	3	86	60	Trans only[b]
e	COMe	Toluene	3	60	44	Trans only[b]
f	Ph	Benzene	8[c]	55	38	Trans only[b]
f	Ph	Benzene	3	86	60	150[b]

a) The ratio was determined by ^{1}H NMR. b) The ratio was determined by capillary GC. c) The reaction was carried out at room temperature.

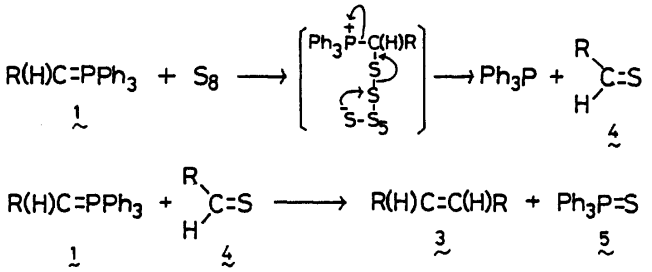

Scheme 4.

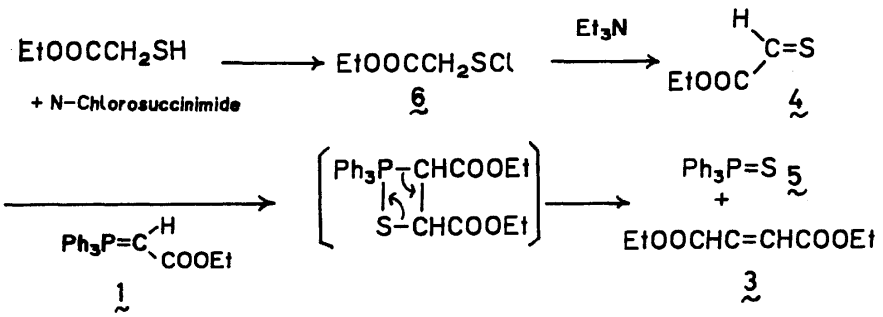

Scheme 5.

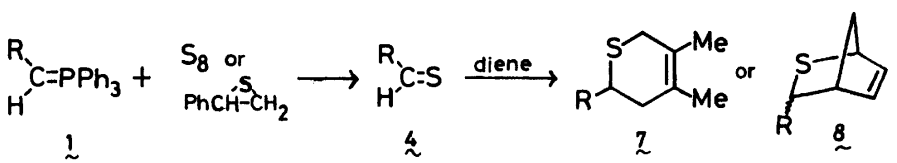

Scheme 6.

Table 3. Reaction of Thioaldehydes with Dienes

Compounds			Diene	Adducts (Yield/%)		
1	R					Endo : Exo[a]
a	COOMe	Sulfur	2,3-Dimethylbutadiene	**7a**	56[10b]	
a	COOMe	Styrene sulfide	2,3-Dimethylbutadiene	**7a**	38	
a	COOMe	Sulfur	Cyclopentadiene	**8a**	64	4 : 3
b	COOEt	Sulfur	2,3-Dimethylbutadiene	**7b**	49[12]	
b	COOEt	Sulfur	Cyclopentadiene	**8b**	84[12]	3 : 2
d	CN	Sulfur	2,3-Dimethylbutadiene	**7d**	35[12]	
d	CN	Sulfur	Cyclopentadiene	**8d**	46[12]	3 : 2
f	Ph	Sulfur	2,3-Dimethylbutadiene	**7f**	60[13]	
f	Ph	Sulfur	Cyclopentadiene	**8f**	66[10a,14]	3 : 1

a) The ratio was determined by their ^{1}H NMR spectra.

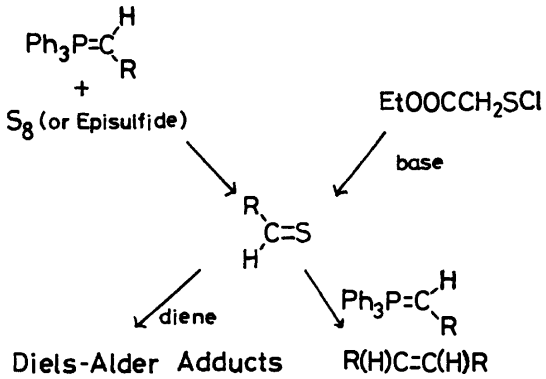

Scheme 7.

none.[4b] Tokunaga and coworkers reported that the reaction of **1f** with sulfur afforded cyclic pentasulfide and a very small amount of stilbene.[8] We therefore tried a reaction of **1** with sulfur in refluxing toluene. A treatment of **1a** with elemental sulfur gave **3a**, **3a'**, and **5** in 63, 13, and 79% yields, respectively. The reaction was faster than that of **2**. As shown in Table 2, olefins **3** and **5** were obtained in good yields. Mägerlein and Meyer reported the same reaction in the case of **1f** in refluxing toluene.[9] They also found that only *trans*-stilbene was obtained in this reaction. These results suggested that a reaction of **1** with **2** or sulfur might proceed through thioaldehyde intermediates. The ylide carbanion attacks episulfide sulfur or sulfur to give the corresponding **4**. The resulting thioaldehyde **4** further reacts with the phosphonium ylide to afford olefins via a Wittig-like reaction. Recently, Kirby and coworkers reported the generation of **4b** by the reaction of ethoxycarbonylmethanesulfenyl chloride (**6**) with triethylamine.[10a] To confirm this mechanism, we tried a similar reaction by using **6**, triethylamine, and **1b**. As shown in Scheme 5, the corresponding **3** and **5** were obtained in good yields (75%, trans/cis=4.5). Compounds **4** were recently prepared by several groups: photolysis of phenacyl sulfide derivatives;[11] reaction of sulfenylchlorides with bases;[10a] reaction of Bunte salts with bases;[12] thermolysis of thiolsulfinates;[13,14] catalytic base abstraction of trimethylsilyl derivatives.[15] While most of thioaldehydes were trapped by dienes, Okazaki and coworkers isolated aromatic and aliphatic thioaldehydes.[16] To confirm the formation of **4** in our case, we carried out a Diels-Alder reaction. A treatment of **1** and elemental sulfur (or styrene sulfide) resulted in the formation of thioaldehydes, which further reacted with dienes to give the corresponding adducts (**7** and **8**) in moderate yields. This result provides another possibility to produce **4**.

In summary, the reaction of **1** with **2** gave symmetrical **3** and **5** in moderate yields. Similarly, the reaction of **1** with elemental sulfur afforded symmetrical **3** and **5** in good yields. Both reactions might proceed through thioaldehyde intermediates, the existence of which was confirmed by a Diels-Alder reaction. We also confirmed that the reaction of thioaldehydes with Wittig reagents gave the corresponding olefins.

Experimental

General Methods. Melting points are uncorrected. NMR spectra were obtained by using JEOL PMX-60 and FX-90Q spectrometers. IR spectra were recorded on a Hitachi IR-345 spectrometer.

Materials. Compounds **1** were prepared by a method mentioned in the literature.[1,3] Compounds **2** were prepared by reactions of epoxides with KSCN or thiourea.[17] Cyclopentadiene was obtained from dicyclopentadiene by distillation. 2,3-Dimethyl-1,3-butadiene was obtained from Aldrich Chem. and used without further purification. Authentic alkyl maleates or fumarates were purchased from Wako Pure Chemicals.

Reaction of 1a with 2a in Benzene. To a solution of **2a** (0.68 g, 5.0 mmol) in benzene (30 ml) was added **1a** (1.67 g, 5.0 mmol) in one portion. After refluxing for eight days, the reaction mixture was evaporated and extracted three times with hexane (30 ml×3). The residue was a mixture (1.19 g) of **1a** (50%) and **5** (24%, yields were determined by its NMR spectrum). The combined extracts were subjected to column chromatography (silica gel). Five components were obtained: styrene (0.05 g, 0.5 mmol) was eluted first (eluant, hexane). A complex mixture of unidentified products (0.03 g) was obtained second (eluant, 80% hexane-dichloromethane). A mixture of dimethyl fumarate and dimethyl maleate (0.05 g, 0.35 mmol, 14%, yields were determined by its NMR spectrum) was further eluted (eluant, 50% hexane-

dichloromethane). A small amount of **5** (0.05 g, 0.17 mmol, 3%) was eluted last (eluant, dichloromethane).

Other reactions were carried out in a similar manner.

Reaction of 1a with Elemental Sulfur. To a solution of **1a** (3.34 g, 10 mmol) in toluene (100 ml) was added a suspension of sulfur (0.38 g, 12 mmol) in toluene (15 ml). After refluxing for 3 h, the solvent was evaporated from the reaction mixture and the remaining oil was extracted three times with hexane (50 ml×3). The residue was mainly triphenylphosphine sulfide, which was purified by recrystallization with benzene-hexane (2.32 g, 7.9 mmol, 79%). The combined extracts were evaporated and chromatographed over silica gel by elution with hexane-dichloromethane (2:1) to give a mixture of dimethyl fumarate and dimethyl maleate in 76% yields (0.51 g, 3.8 mmol, 5:1 ratio by NMR).

Other reactions were carried out in a similar manner.

Reaction of Wittig Reagent with Thioaldehyde (4b) Derived from 6. To a suspension of *N*-chlorosuccinimide (0.93 g, 7.0 mmol) in toluene (20 ml) was added dropwise a solution of ethyl thioglycolate (0.72 g, 6.0 mmol) in toluene (10 ml) at room temperature. After stirring for 2 h, the reaction mixture was filtered to give a yellow solution of the corresponding sulfenyl chloride. This solution was added dropwise to a refluxing solution of **1b** (1.74 g, 5.0 mmol) and triethylamine (0.71 g, 7.0 mmol) in toluene (20 ml). After refluxing for 3 h, the reaction mixture was washed with water (20 ml×3), dried over $MgSO_4$, and evaporated to give pale brown oil which was extracted with pentane (20 ml× 3). The combined extract was evaporated to give a crude mixture of olefins (0.54 g, 3.75 mmol, 75% trans/cis=4.5 by NMR). The resulting oil was chromatographed over silica gel by elution with hexane-dichloromethne (5:1) to give a mixture of diethyl maleate and diethyl fumarate (0.37 g, 2.6 mmol, 52%).

Reaction of Wittig Reagent with Styrene Sulfide in the Presence of 2,3-Dimethylbutadiene. To a solution of **1a** (1.68 g, 5.0 mmol) and 2,3-dimethyl-1,3-butadiene (2 ml, 20 mmol) in toluene (30 ml) was added a solution of styrene sulfide (2.04 g, 15 mmol) in toluene (15 ml). After refluxing for 30 h, the resulting mixture was evaporated to give pale brown oily crystals, which were chromatographed over silica gel by elution of hexane-dichloromethane (1:1) to give adduct **7a** (0.36 g, 1.9 mmol, 38%). ^{1}H NMR ($CDCl_3$) δ=1.73 (6H, s, Me), 2.33—2.47 (2H, br.), 2.98—3.27 (2H, br.), 3.67 (1H, t, J=6.3 Hz), 3.77 (3H, s, Me).

Reactions of 1a with Sulfur in the Presence of Diene. To a solution of **1a** (1.68 g, 5.0 mmol) and 2,3-dimethyl-1,3-butadiene (2 ml, 20 mmol) in toluene (40 ml) was added elemental sulfur (0.64 g, 20 mmol). After refluxing for 20 h, the resulting mixture was evaporated to give reddish-brown oily crystals. This mixture was extracted with methanol (30 ml×2). The combined extracts were evaporated to give a reddish-brown oil, which was chromatographed over silica gel by elution with hexane-dichloromethane (3:1) to give adduct **7a** (0.52 g, 2.8 mmol, 56%). Other reactions were carried out in a similar manner. **8a**; 0.54 g (3.2 mmol, 64%). ^{1}H NMR ($CDCl_3$) (Endo) δ=1.66 (br s, CH_2), 3.65 (s, Me), 3.75 (br s, CH), 4.18 (br, CH), 4.44 (d, CH, J=3.9 Hz), 5.73 (dd,=CH, J=3.3 and 5.1 Hz), 6.49 (dd, =CH, J=3.0 and 5.1 Hz); (Exo) δ=1.84 (br s, CH_2), 3.29 (s, CH), 3.54 (br, CH), 3.86 (s, Me), 4.07 (br, CH), 5.91 (dd, =CH, J=3.2 and 6.2 Hz), 6.36 (dd, =CH, J=3.2 and 4.8 Hz). **7b**; 0.49 g, (2.45 mmol, 49%). ^{1}H NMR ($CDCl_3$) δ=1.27 (t, Me, J=7.5 Hz), 1.74 (s, Me), 2.46 (br, CH_2), 3.06 (br, CH_2), 3.62 (t, CH, J=6.0 Hz), 4.19 (q, CH_2, J=7.5 Hz). **8b**; 0.92 g (4.2 mmol, 84%). ^{1}H NMR ($CDCl_3$) (Endo) δ=1.22 (t, Me, J=7.0 Hz), 1.65 (m, CH_2), 3.75 (br, CH), 4.07 (br s, CH), 4.12 (q, CH_2, J=7.0 Hz), 4.42 (d, CH, J=3.6 Hz), 5.70 (dd, =CH, J=5.4 and 2.6 Hz), 6.45 (dd, =CH, J=3.0 and 5.4 Hz). (Exo) δ=1.25 (t, Me, J=7.2 Hz), 1.77 (m, CH_2), 3.27 (s, CH), 3.50 (br s, CH), 4.08 (br, CH), 4.17 (q, CH_2, J=7.2 Hz), 5.92 (dd, =CH, J=3.2 and 5.4 Hz), 6.33 (dd, =CH, J=2.8 and 5.4 Hz). **7d**; 0.27 g (1.76 mmol, 35%). ^{1}H NMR ($CDCl_3$) δ=1.75 (m, Me), 2.47 (br, CH_2), 3.18 (m, CH_2), 3.73 (t, CH, J=2.5 Hz). **8d**; 0.32 g (2.3 mmol, 46%). ^{1}H NMR ($CDCl_3$) (Endo) δ=1.75 (d, CH_2), 3.74 (br s, CH), 4.20 (br s, CH), 4.23 (d, CH, J=3.4 Hz), 6.03 (dd, =CH), 6.57 (dd, =CH). Minor exo product could not be isolated. **7f**; 0.61 g (3.0 mmol, 60%). ^{1}H NMR ($CDCl_3$) δ=1.71 (s, Me), 2.33—2.67 (br m, CH_2), 2.97 (br s, CH_2), 3.31 (br s, CH_2), 3.94 (dd, CH, J=6.0 and 8.0 Hz), 7.27 (br s, Ar). **8f**; 0.58 g, (3.3 mmol, 66%). ^{1}H NMR ($CDCl_3$) (Endo) δ=1.75 (br s, CH_2), 3.38 (br, CH), 4.12 (br, CH), 4.92 (d, CH, J=3.9 Hz), 5.53 (dd, =CH, J=2.9 and 5.4 Hz), 6.47 (dd, =CH, J=2.8 and 4.8 Hz), 7.22 (s, Ar). Minor exo product could not be isolated.

References

1) G. Wittig and U. Schollkopf, *Chem. Ber.*, **87**, 1318 (1954). For reviews, see J. Emsley and D. Hall, "The Chemistry of Phosphorus," Harper & Row Ltd., London (1976), pp. 274—298; A. W. Johnson, "Ylid Chemistry," Academic Press, New York (1966), pp. 132—147; A. Maercker, "Org. Reactions," ed by R. Adams, John Wiley & Sons, Inc., New York (1965), Vol. 14, Chap. 3.

2) D. B. Denney, J. J. Vill, and M. J. Boskin, *J. Am. Chem. Soc.*, **84**, 3944 (1962); A. Turcant and M. Le Corre, *Tetrahedron Lett.*, **1976**, 1277; W. E. McEwen and A. P. Wolf, *J. Am. Chem. Soc.*, **84**, 676 (1962); W. E. McEwen A. Blade-Font, and C. A. Vanderwelf, *ibid.*, **84**, 677 (1962).

3) E. J. Corey and J. Kang, *J. Am. Chem. Soc.*, **104**, 4724 (1982).

4) a) H. Staudinger and J. Meyer, *Helv. Chim. Acta*, **2**, 635 (1919). b) A. Schönberg, K-H Brosowski, and E. Singer, *Chem. Ber.*, **95**, 2144 (1962).

5) K. Okuma, Y. Yamasaki, T. Komiya, Y. Kodera, and H. Ohta, *Chem. Lett.*, **1987**, 357.

6) K. Okuma, J. Sakata, Y. Tachibana, T. Honda, and H. Ohta, *Tetrahedron Lett.*, **28**, 6659 (1987). Recently, Elker and coworkers reported a similar reaction; G. Elker R. Hock, and R. Nolte, *J. Am. Chem. Soc.*, **110**, 624 (1988).

7) S. Tripett, *Proc. Chem. Soc.*, **1963**, 19.

8) H. Tokunaga, K. Akiba, and N. Inamoto, *Bull. Chem. Soc. Jpn.*, **45**, 506 (1972).

9) H. Mägerlein and G. Meyer, *Chem. Ber.*, **103**, 2995 (1970).

10) a) C. M. Bladen, I. E. G. Fergguson, G. W. Kirby, A. W. Lochead, and D. C. McDougall, *J. Chem. Soc., Chem. Commun.*, **1983**, 423. b) They also generated **4** by base catalyzed cleavage of *N*-(alkoxycarbonylmethylthio)phthalimides. G. W. Kirby and A. W. Lochead, *J. Chem. Soc., Chem. Commun.*, **1983**, 1325.

11) E. Vedejs and D. A. Perry, *J. Am. Chem. Soc.*, **105**, 1683 (1983); E. Vedejs, D. A. Perry, and R. G. Wilde, *J. Am. Chem. Soc.*, **108**, 2985 (1986); E. Vedejs, T. H. Eberlein, D. J. Mazur, C. K. McClure, D. A. Perry, R. Ruggeri, E. Schwartz, J. S. Stults, D. L. Varie, and S. Wittenberger, *J. Org. Chem.*, **51**, 1556 (1986).

12) G. W. Kirby, A. W. Lochead, and G. N. Sheldrake, *J. Chem. Soc., Chem. Commun.*, **1984**, 922.
13) J. E. Baldwin and R. C. Gerald Lopez, *J. Chem. Soc., Chem. Commun.*, **1982**, 1029; *Tetrahedron*, **39**, 1487 (1983); E. Block and S. Ahmad, *J. Am. Chem. Soc.*, **106**, 8295 (1984).
14) G. A. Krafft and P. T. Meinke, *Tetrahedron Lett.*, **26**, 1947 (1985).
15) M. Segi, T. Nakajima, S. Suga, S. Murai, I. Ryu, A. Ogawa, and N. Sonoda, *J. Am. Chem. Soc.*, **110**, 1976 (1988).
16) R. Okazaki, A. Ishii, and N. Inamoto, *J. Chem. Soc., Chem. Commun.*, **1982**, 1187; R. Okazaki, A. Ishii, and N. Inamoto, *J. Am. Chem. Soc.*, **109**, 279 (1987).
17) J. M. Stewart, *J. Org. Chem.*, **28**, 596 (1963); F. K. Lautenschlaeger and N. V. Schwartz, *ibid.*, **34**, 3991 (1969).

Oxidation of Coals in Liquid Phases. IX. Kinetics of the Base-Catalyzed Oxidation of Acetate Ion by Oxygen at Elevated Temperatures

Takayoshi WAKABAYASHI† and Akitsugu OKUWAKI*
Department of Molecular Chemistry and Engineering, Faculty of Engineering, Tohoku University, Sendai 980
(Received March 26, 1988)

The kinetics of the oxidation of the acetate ion by oxygen have been studied to clarify the mechanism of the formation of oxalate from coal in concentrated alkaline solutions at elevated temperatures. The rate for the oxidation in a nickel reactor in the presence of 3 g of iron powder was expressed as $-dm_{Ac}/dt=k' m_{Ac}m_{OH}{}^2P_{O_2}$, where k' is the apparent rate constant, m_{Ac} is the molality of acetate ion, m_{OH} is molality of the hydroxide ion, and P_{O_2} is the partial pressure of oxygen. This result indicates that the oxidation of the acetate ion proceeds according to a base-catalyzed mechanism. The activation energy was 160 kJ mol^{-1}. In addition, the rate of oxidation was affected by the coexistence of the metal powder and the oxidation activity in the order Cu > Ni > Co > Mn ≒ Fe > Cr. The catalytic effect of metal oxides on the rate is discussed.

Oxalate ion is formed with a 30—50% yield of carbon in the oxidation of coal by oxygen in concentrated NaOH solutions at 498—523 K.[1,2] The yield of oxalate ion increases with increasing concentration of NaOH. Essentially, the oxidation of coal may take place via a base-catalyzed oxidation mechanism, since similar yields of oxalate have been obtained in the oxidation of various model compounds such as phenols and carboxylates including acetate.[3]

In spite of the importance of this reaction mechanism for increasing the yield of oxalate from coal, the mechanism of the oxidation of carbonaceous materials under alkaline conditions has not been investigated kinetically in detail. In the present work, kinetic studies have been carried out to clarify the mechanism of the formation of oxalate and to improve the yield of oxalate from coal using acetate ion as the simplest model compound. This is one of the important intermediates in the oxidation of coal in alkaline solutions.

Experimental

A beaker made of nickel or carbon steel was set in a 1 dm^3 SUS 316 autoclave; the stirrer and sampling tube were of the same material as the beaker. Water (550 g), sodium acetate (0.08 mol kg^{-1} H_2O), NaOH, and Na_2CO_3, and metal powder (under 100 mesh), were put into the autoclave, and the amount of Na_2CO_3 was adjusted to coincide with the ionic strength of a 5 molal NaOH solution. The NaOH and Na_2CO_3 concentrations (molal) were 2, 0.253; 3, 0.171; and 4, 0.083; respectively. After replacement of air with N_2 three times, the autoclave was heated to a temperature 20 K below the reaction temperature. The sample solution was withdrawn immediately after oxygen was introduced during stirring at 500—800 rpm (reaction time of 0). The temperature rapidly rose on pressurization of oxygen, reaching the final reaction temperature in 15 min. A sample solution (8—15 cm^3) was then withdrawn at 30-min intervals. The volume of each sample was calculated from its weight and the density of the solution corresponding to the same NaOH concentration. The concentrations of acetate and oxalate ions were determined by ion chromatography after sodium/hydrogen ion exchange.

† Present address: Sumitomo Electric Corp., Itami 664.

Results and Discussion

Oxalate and carbonate ions are formed by the oxidation of acetate ion in the reaction, and the ratio of oxalate to carbonate has been found to vary extensively with the reactor materials. We have not succeeded in finding any corrosion-resistant material under such corrosive conditions and have been obliged to use stainless steels or nickel as the reactor material. Even these metals were corroded considerably to form metal oxides during the reaction time under the present conditions, and the resulting metal oxides affected the rate of the oxidation and the selectivity. The selectivity of the oxalate ion was highest in the presence of iron powder using the nickel beaker.[4]

Catalytic Effect of Various Metals Contained in Stainless Steels. The following preliminary experiments have been carried out to elucidate the significance of adding iron powder.

Activity of Metals: The first order plots of the concentration of acetate ion in the reaction with 3 g of various metal powders in the nickel beaker are shown in Fig. 1. The rate of oxidation of the acetate ion was approximately proportional to the acetate ion concentration and nearly the same in the presence of Cr, Mn, and Fe, all of which have standard electrode potentials lower than that of Ni. On the other hand, the rate of oxidation was accelerated slightly in the presence of Ni the standard electrode potential of which is higher than those of Cr, Mn, and Fe. The first order plots shifted gradually upward with reaction time as was observed in the absence of Ni. Cobalt only slightly affected the rate of oxidation. Copper, the standard electrode potential of which is higher than that of Ni, promoted the reaction remarkably. These results indicate that Cr, Mn, and Fe inhibit the effect of nickel on the reaction rate which was used as the reactor material whereas Cu promotes the reaction. This is an interesting phenomenon suggesting the promotion of the oxidation of coal by the addition of copper oxide.

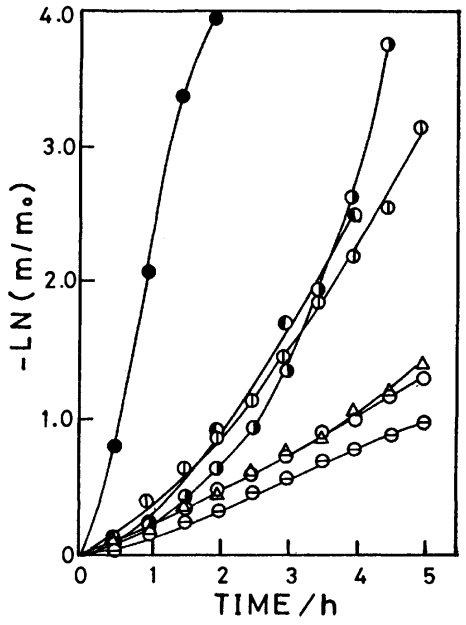

Fig. 1. Effect of metal powders on the rate of oxidation of acetate ion in a Ni reactor at 523 K, 5 mol NaOH/kg H_2O, and P_{O_2} 5 MPa.
●: Cu, ◑: Ni, Φ: Co, ○: Fe, ⊖: Cr, △: Mn, ◐: none.

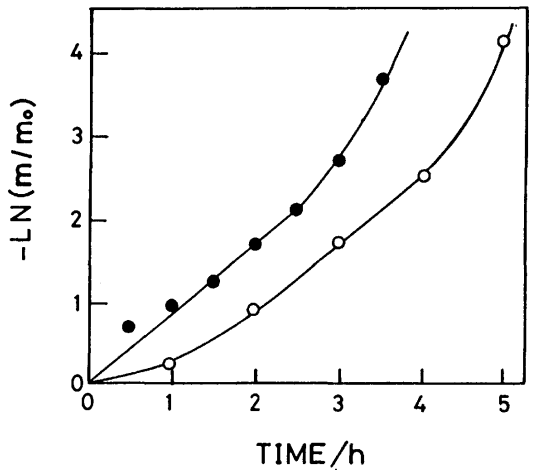

Fig. 2. First order plots of concentration of acetate ion in a Fe and a Ni reactors at 523 K and P_{O_2} 5 MPa.
●: Fe, ○: Ni.

This effect has been confirmed for the oxidation of lignite.[5]

Effect of Reactor Material: Figure 2 demonstrates the first order plots of concentration of acetate ion in nickel and carbon steel reactors without metal powder. The initial rate of oxidation in the steel reactor was obviously greater than that in the nickel reactor. The reason is that in the case of the steel reactor the temperature of the solution rose rapidly up to 540 K, 17 K higher than the reaction temperature of 523 K due to the heat of extreme oxidation of the steel, and it took 30 min until the temperature decreased to 523 K. After the temperature rise had settled, the rate of oxidation

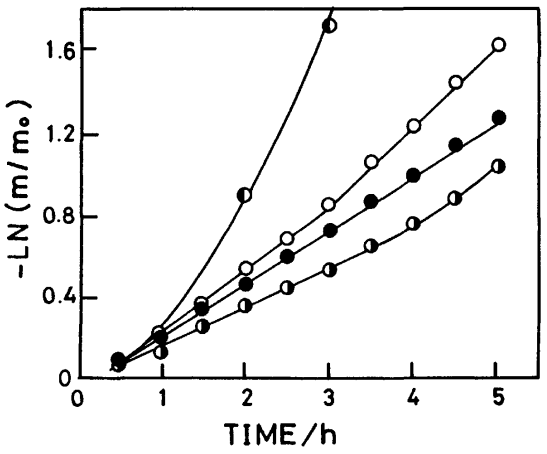

Fig. 3. Effect of Fe powder and Fe_2O_3 on the rate of oxidation in a Ni reactor at 523 K and P_{O_2} 5 MPa.
◑: Fe 1 g, ●: Fe 3 g, ○: Fe_2O_3 4.3 g, ◐: none .

in the steel reactor approached that in the nickel reactor and the two became approximately equal between 1.5 and 3 h. A large amount of Fe_2O_3, haematite, was produced by corrosion of the steel.

Effect of the Amount of Iron Powder on the Reaction in the Nickel Reactor: Figure 3 shows the effects of the amount of iron powder and reagent haematite on the rate of oxidation. Only 1g of iron powder retarded the oxidation of acetate ion in the nickel reactor, but the rate of oxidation was slightly increased in the presence of 3 g of iron powder. This indicates that 1 g of iron powder is enough to control the activity of the nickel reactor. On the other hand, excessive Fe_2O_3 formed by the oxidation of an additional 3 g of iron powder begins to promote the oxidation of the acetate ion. The fact that the rate of oxidation in the steel reactor was approximately equal to that in the nickel reactor under the steady state, supports the hypothesis that Fe_2O_3 promotes the oxidation as oxides of nickel. Namely, the role of iron powder in the nickel reactor seems to change from that of depressor to that of catalyst when increasing amounts of iron powder are added.

The rate of the oxidation of acetate ion with the addition of haematite corresponding to 3 g of iron powder was apparently greater than that with the addition of 3 g of iron powder. This result also supports the hypothesis that excessive Fe_2O_3 accelerates oxidation, since in this case, a large amount of haematite is present from the beginning of the oxidation. This is different from the case of the oxidation with iron powder where Fe_2O_3 is produced gradually with increase in the reaction time. In addition, the first order plot shifted gradually upward compared to that of the iron powder. Thus, iron powder is required to maintain the linearity of the first order plot. With an addition of 1 g of iron powder, however, the first order plot shifted upward during the course of the reaction as shown in Fig. 3. This shows that the oxidation of

acetate ion had begun to be accelerated due to complete consumption of the metallic iron. Consequently, 3 g of iron powder is necessary to maintain the linearity of the first order plot at least for 6 h. Under such reaction conditions, the effects of various parameters on the rate of oxidation of the acetate ion can easily be observed. It is especially important to elucidate the dependency of the rate of the oxidation of the acetate ion on the hydroxide ion concentration to confirm if the oxidation of acetate ion proceeds by a base-catalyzed mechanism. Thus, the kinetic study was just carried out in the presence of 3 g of iron powder in the nickel reactor.

The Rate Equation of the Oxidation of Acetate Ion with 3 g of Iron Powder. The effects of NaOH concentration, partial pressure of oxygen, and temperature have been measured; this system is written below as Ni(Fe).

Effect of NaOH Concentration: Figure 4 shows the first order plots of the concentration of the acetate ion with varying NaOH concentration. It shows that the reaction is first order with respect to acetate ion. The reason why the first order plots do not pass through the origin is that the initial temperature was lower than the reaction temperature in the steady state. The hydroxide ion concentration was calculated using the pK_b (1.07 at 523 K[6]) and an extended Debye-Hückel equation as set forth below since NaOH does not dissociate completely at elevated temperatures.

The following reactions can be assumed at $t=0$:

$$NaOH \overset{K_b}{\rightleftharpoons} Na^+ + OH^- \quad (1)$$

$$NaAc \longrightarrow Na^+ + Ac^- \quad (2)$$

$$Na_2CO_3 \longrightarrow 2Na^+ + CO_3^{2-} \quad (3)$$

$$K_b = a_{Na}a_{OH}/a_{NaOH} \quad (4)$$

a: activity of the corresponding species

The dissociation constant of NaOH, K_b, can be expressed by the molalities of the sodium ion, m_{Na}, the acetate ion, m_{Ac}, the carbonate ion, m_c, the total NaOH, m_o, the undissociated NaOH, m_{NaOH}, and the hydroxide ion, m_{OH}, the degree of dissociation of NaOH, α, and the activity coefficient for monovalent ion, γ, respectively.

$$K_b = \gamma^2 m_{Na} m_{OH}/m_{NaOH} \quad (5)$$

$$= \gamma^2\alpha\,(m_{Ac}+\alpha m_o+2m_c)/(1-\alpha) \quad (5')$$

The ionic strength, I, is given by Eq. 6. Activity coefficients

$$I = m_{Ac}+\alpha m_o+2m_c \quad (6)$$

are expressed by Eq. 7 in the measurement of the solubility of $CaSO_4$ up to 623 K and 5 molal NaCl solutions.[7]

$$\log\gamma = -Z_i^2 S I^{1/2}/(1+A_k I^{1/2}) \quad (7)$$

Z_i: charge of ion i, S: limiting slope of the Debye-Hückel Eq. (0.9785 at 523 K),[8] A_k: 1.74 at 523 K.[7]

The hydroxide ion concentration (αm_o) was obtained by calculating the degree of dissociation in each condition using Eqs. 5′—7.

The relationship between the apparent rate constant and calculated hydroxide ion concentration is shown in Fig. 5. The rate of oxidation of the acetate ion was approximately proportional to the second order in hydroxide ion concentration.

Effect of Partial Pressure of Oxygen: Figure 6 shows the effect of the partial pressure of oxygen on the apparent rate of oxidation. The rate of oxidation was proportional to the partial pressure of oxygen.

Effect of Temperature: The activation energy of the oxidation obtained from the Arrhenius plot of the

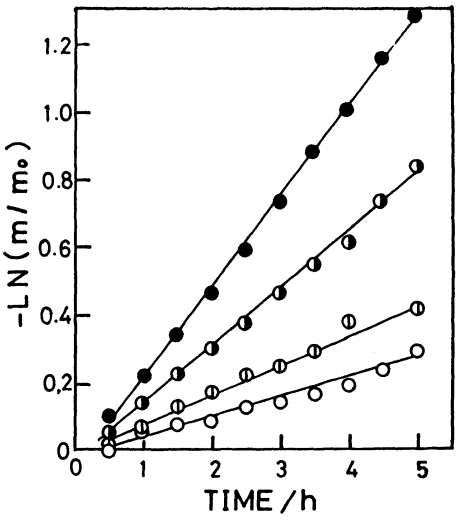

Fig. 4. Effect of NaOH concentration on the rate of oxidation in Ni(Fe) at 523 K and P_{O_2} 5 MPa.
NaOH concn (mol kg^{-1} H_2O) ○: 2.00, ◐: 3.00, ◑: 4.00, ●: 5.00.

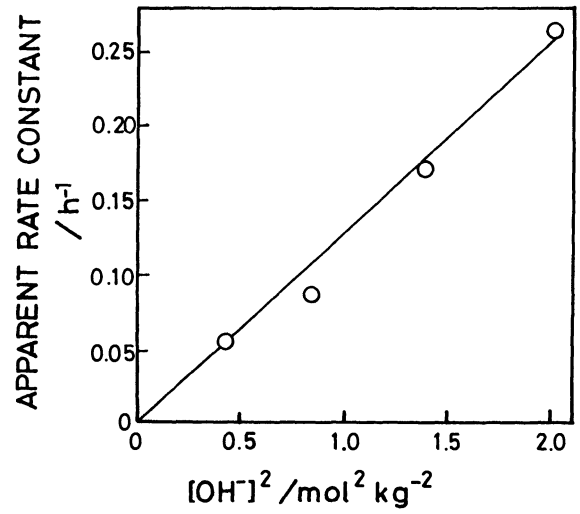

Fig. 5. Relationship between the apparent rate constant and hydroxide ion concentration in Ni(Fe) at 523 K and P_{O_2} 5 MPa.

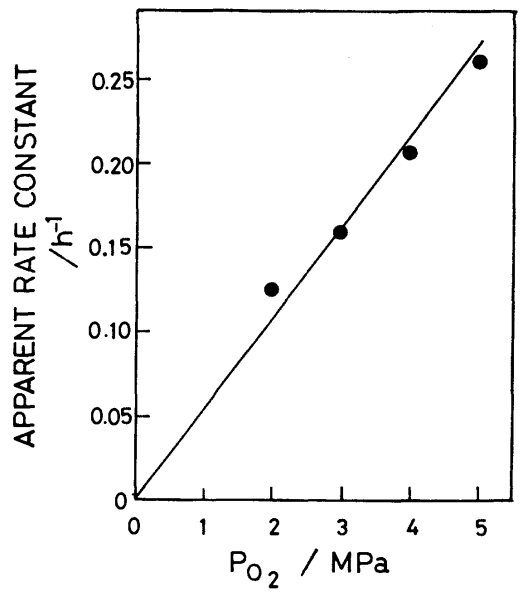

Fig. 6. Effect of partial pressure of oxygen on the rate of oxidation in Ni(Fe) at 523 K and 5 mol kg^{-1} H_2O.

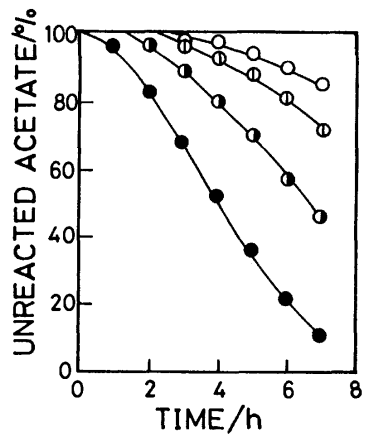

Fig. 7. Effect of NaOH concentration on the rate of oxidation in Ni(R) at 503 K and P_{O_2} 5 M Pa. NaOH concn (mol kg^{-1} H_2O) ○: 2.00, ⊕: 3.00, ◑: 4.00, ●: 5.00.

apparent rate constants at 503, 513, and 523 K was 160 kJ mol^{-1}. This value clearly shows that the rate-determining step is a chemical reaction process.

Rate Equation of the Oxidation: Finally from the above results, the rate of the oxidation of the acetate ion in the presence of 3 g of iron powder in the nickel reactor can be expressed by Eq. 8.

$$-dm_{Ac}/dt = k' m_{Ac} m_{OH}^2 P_{O_2} \quad (8)$$

k': the apparent rate constant, m_{Ac}: molality of the acetate ion, the m_{OH}: molality of the hydroxide ion, P_{O_2}: partial pressure of oxygen.

Oxidation of Acetate Ion without Iron Powder. This system is written as Ni(R) below.

Effect of NaOH Concentration: The first order relationship was not obtained at 523 K, since the rate of the oxidation increased exponentially with the reaction time in the beginning. This tendency is more evident at 503 K as is shown in Fig. 7. This may indicate that some oxide of nickel is involved in the rate-determining step of the reaction and that its amount increases exponentially with the reaction time, since the acetate ion concentration changes slightly in the beginning.

Effect of Partial Pressure of Oxygen: In this case, the effect appeared only in the beginning, and the rate of the oxidation became constant independent of the pressure of oxygen as is shown in Fig. 8. This may indicate that the amount of the oxide of nickel formed is little affected by the partial pressure of the oxygen.

Effect of Initial Concentration of Sodium Acetate: In the case of Ni(Fe), naturally, the initial concentration did not affect the rate of oxidation as it was first order with respect to the acetate ion concentration. However, the rate of oxidation of the acetate ion in Ni(R) at 503 K became constant after 2 h and was proportional to the initial concentration of the acetate ion as is shown in Fig. 9.

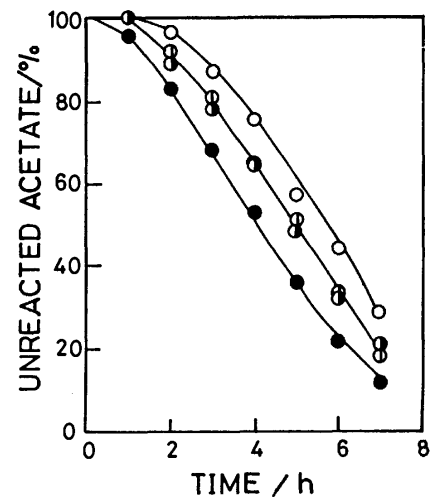

Fig. 8. Effect of partial pressure of oxygen on the rate of oxidation in Ni(R) at 503 K and 5 mol NaOH/kg H_2O. P_{O_2}(MPa) ○: 2.0, ⊕: 3.0, ◑: 4.0, ●: 5.0.

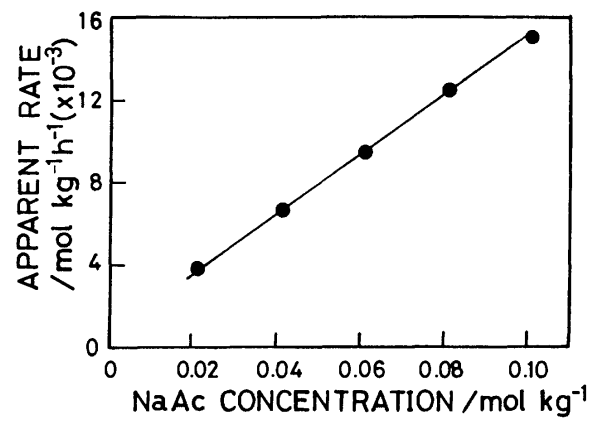

Fig. 9. Effect of initial concentration of acetate ion on the apparent rate constant in Ni(R) at 503 K and P_{O_2} 5 MPa.

The difference in the cases of Ni(Fe) and Ni(R) is discussed in the following mechanism.

Mechanism of the Oxidation of Acetate Ion. Base and Metal Oxide-Catalyzed Oxidation Mechanism: It is thought that this oxidation reaction involves a base-catalyzed oxidation mechanism[9] as follows:

$$XCH_3 + OH^- \overset{K}{\rightleftharpoons} XCH_2^- + H_2O \ (X=COO^-) \quad (9)$$

$$XCH_2^- + O_2 \xrightarrow[(MeO)]{k} XCH_2\cdot + O_2^- \quad (10)$$

$$XCH_2\cdot + O_2 \longrightarrow XCH_2OO\cdot \quad (11)$$

$$XCH_2OO\cdot + XCH_2^- \longrightarrow XCH_2OO^- + XCH_2\cdot \quad (12)$$

$$XCH_2OO\cdot + O_2^- \longrightarrow XCH_2OO^- + O_2 \quad (13)$$

K: equilibrium constant, k: rate constant, MeO: metal oxide

The peroxoanion formed from the oxidation of the carbanion, XCH_2OO^-, is easily oxidized further to oxalate ion.

In Ni(Fe), acetate and hydroxide ions increase the concentration of the carbanion, which is a reactant in the rate-determining step, according to the first order dependence of its formation on the concentrations of acetate and hydroxide ions, as shown by Eq. 9. We may assume Henry's law for the solubility of oxygen in the solutions at constant NaOH concentration and temperature. Thus, the concentration of oxygen should be proportional to its partial pressure. In this case, however, the reaction mechanism seems to be a base-catalyzed oxidation reaction involving the iron oxide catalyst as shown in Eq. 10. There are two results supporting this. Firstly, the rate of the oxidation is proportional to the second order in the concentration of hydroxide ion. This seems to indicate that the rate of formation of a catalyst, the iron oxide, is proportional to the concentration of the hydroxide ion. Although such measurements have not been carried out in the present work or found in the literature, in the anodic oxidation of iron in a 1 mol kg^{-1} LiOH solution at 473 K, oxoanions of iron are formed by the reaction of iron and hydroxide ion.[10] Secondly, the rate of oxidation increased with increasing amount of iron powder as shown in Fig. 3. This means that the soluble species of iron can not be the major oxidizing species, since the solubilities of iron oxides in alkaline solutions are very low[11] and the reaction solutions should be saturated with iron ion even with the addition of 1 g of iron powder. Consequently, the oxidation of acetate ion in Ni(Fe) proceeds on the surface of the iron oxide due to a base-catalyzed and iron oxide-catalyzed oxidation mechanism as shown in Eq. 10.

The mechanism in Ni(R) should be similar to that in the above-mentioned case. A distinct difference is that the rate of reaction in Ni(R) increased exponentially with the reaction time in the initial stage; it then became constant as is shown in Figs. 7 and 8. The rate of reaction is proportional with respect to the initial acetate ion concentration as is shown in Fig. 9. These results may be boldly explained as follows. The amount of nickel oxide formed by corrosion of the reactor material increases exponentially with the reaction time. By analogy with the mechanism of the oxidation of acetate ion in Ni(Fe), the rate in Ni(R) should also be proportional to the products of the concentration of the carbanion and amount of nickel oxide. If the concentration of the carbanion decreases exponentially with the reaction time and both rates compensate each other, the rate of oxidation of the acetate ion becomes constant and is approximately proportional to the initial concentration of acetate ion.

Figure 10 shows the effect of the amount of nickel powder on the oxidation of acetate ion in Ni(R) at 503 K. The rate of the oxidation increases with increasing amounts of nickel. Clearly, these results support the hypothesis that the nickel oxide formed by the corrosion acts as a catalyst since nickel powder is easily oxidized under the reaction conditions. It seems that the hydroxide ion concentration accelerates mainly the formation of the catalyst compared to the amount of nickel powder or partial pressure of oxygen.

The Valency of Nickel in the Oxides Formed in Ni(R): When the Ni(R) run has finished, a greenish white precipitate and a small amount of a black substance are suspended in the solution. Two peaks were observed in the ESCA spectra of the precipitate at 857.8 and 856.4 eV for Ni $2p_{3/2}$ which may correspond to 856.2 and 855.2 eV for reagent Ni_2O_3, respectively. This indicates that Ni^{3+} is contained in the precipitates. There are many types of oxide of nickel having excess oxygen.[12] Only NiO, however, was identified in the precipitates by XRD. According to the

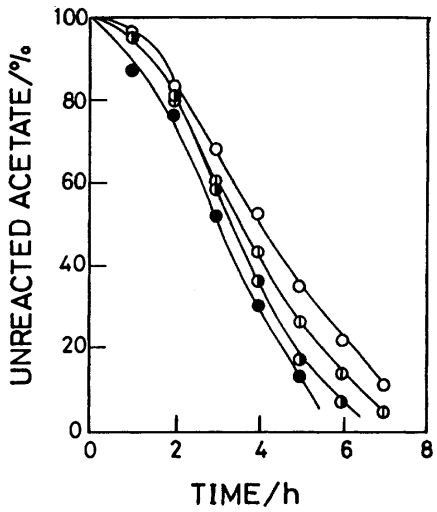

Fig. 10. Effect of amount of Ni powder on the oxidation in Ni(R) at 503 K and P_{O_2} 5 MPa. Amount of Ni(g) ○: 0, ◑: 2, ◑: 4, ●: 6.

potential-pH diagram of a Ni-water system at 523 K,[13-16] even Ni_2O_3 can be formed under the reaction conditions, at a calculated pH of 10.8 (2 mol kg^{-1}) −11.2 (5 mol kg^{-1}) and P_{O_2} 5 MPa. However, in Ni(R), Ni^{3+} probably is not the catalyst but the reactant which directly oxidizes the carbanion, since the partial pressure of oxygen only slightly affected the rate of oxidation as is shown in Fig. 8, in contrast to the case for Ni(Fe) shown in Fig. 6.

Retardation Mechanism of the Oxidation in Ni(Fe): This mechanism can be reasonably explained by the action of metals or Fe_2O_3 added on Ni^{3+} formed by the corrosion of the nickel reactor. There are two factors which cause this phenomenon. One is an electrochemical effect and the other is a mechanical effect.

The former occurs when a metal whose electrode potential is lower than that of nickel is present in the solution as is shown in Fig. 1. According to the mechanism of oxidation in Ni(R), this effect brings about protection of the formation of Ni^{3+} because of the cathodic polarization of the nickel surface covered by iron powder in alkaline solutions or the reduction of Ni^{3+} by iron powder and FeO as shown in Eqs. 14 and 15.

$$2Ni^{3+} + Fe + 6OH^- \longrightarrow 2NiO + FeO + 3H_2O \quad (14)$$

$$2Ni^{3+} + 2FeO + 6OH^- \longrightarrow 2NiO + Fe_2O_3 + 3H_2O \quad (15)$$

The retardation seems to take place without adherence of oxides since it was recognized in Ni(Cr) in which soluble chromate was formed instead of Cr_2O_3. The sole suspension of haematite in the oxidation with the carbon steel reactor does not seem to retard the rate as shown in Fig. 3. In the case of Ni(Fe_2O_3), however, retardation was also observed. This may be caused by the nickel surface being covered with haematite since the electrochemical effect can not take place in this case. Actually, haematite adhered tightly to every part of the nickel reactor in contact with the solution and could not be removed easily by brushing. Consequently, haematite adhering to the nickel surface inhibits the formation of Ni^{3+} by preventing the nickel surface from coming in contact with the solution. Haematite, however, seems not to control the formation of Ni^{3+} completely as it can not reduce Ni^{3+} like iron does. Thus, Ni^{3+}, which forms gradually, accelerates the rate of oxidation.

Copper accelerated the oxidation and this mechanism should be further studied.

Conclusion

In the kinetics of the oxidation of acetate ion by oxygen in strong alkaline solutions at elevated temperatures, the following results have been obtained. In the case of Ni(Fe), the first order plots of acetate ion concentration remain approximately linear while metallic iron remains in the solution. This is realized by the inhibition of the formation of Ni^{3+} by the metallic iron. The rate equation of the oxidation in Ni(Fe) can be expressed as follows: $-dm_{Ac}/dt = k' m_{Ac} m_{OH}^2 P_{O_2}$ where k' is the apparent rate constant. This equation shows quantitatively that the oxidation of acetate ion in alkaline solutions proceeds by a base-catalyzed mechanism. The activation energy is 160 kJ mol^{-1}. In the case of Ni(R), the Ni^{3+} species formed by the oxidation of the nickel reactor was thought to be the reactant which oxidizes the carbanion and increases with the reaction time. In the presence of metal powder, the rate of oxidation in a nickel reactor is in the following order: Cu>Ni>Co>Mn≒Fe>Cr. The effect of metals on the oxidation is also discussed.

This study was supported by the Asahi Glass Foundations for Industrial Technology, 1987—1988.

References

1) A. Okuwaki, N. Sutoh, H. Furuya, A. Amano, and T. Okabe, *Ind. Eng. Chem. Prod. Res. Develop.*, **23**, 648 (1984).
2) N. Sutoh, M. Kato, T. Ikegami, A. Okuwaki, A. Amano, and T. Okabe, *Nippon Kagaku Kaishi*, **1983**, 690.
3) H. Furuya, R. Uwabe, N. Sutoh, A. Okuwaki, A. Amano, and T. Okabe, *Bull. Chem. Soc. Jpn.*, **58**, 3016 (1985).
4) T. Wakabayashi, A. Okuwaki, and T. Okabe, *Nippon Kagaku Kaishi*, **1987**, 299.
5) Unpublished data.
6) O. V. Bryzgalin, *Geokhimiya*, **1985**, 1184.
7) W. L. Marshall and E. V. Jones, *J. Phys. Chem.*, **70**, 4028 (1966).
8) H. C. Helgeson and D. H. Kirkham, *Am. J. Sci.*, **274**, 1199 (1974).
9) T. Matsuura, "Oxygen-oxidation Reaction," Maruzen, Tokyo (1977), p. 165.
10) D. D. Mcdonald and D. Owen, *J. Electrochem. Soc.*, **120**, 317 (1973).
11) P. E. Tremaine and J. C. Leblanc, *J. Chem. Thermodyn.*, **12**, 521 (1980).
12) Gmelins Handbook, 57, Ni[B], Verlag Chem., Weinheim, p. 465 (1966).
13) M. Pourbaix, "Altas of Electrochemical Equilibria in Aqueous Solutions," Pergamon Press, New York (1966), p. 330.
14) C. M. Criss and J. W. Cobble, *J. Am. Chem. Soc.*, **86**, 5385 (1964).
15) C. M. Criss and J. W. Cobble, *J. Am. Chem, Soc.*, **86**, 5390 (1964).
16) J. W. Cobble, *J. Am. Chem. Soc.*, **86**, 5396 (1964).

Regioselective 6-Amination and 6-Arylation of 5,8-Quinolinedione Promoted by Metal Ions

Katsuhira YOSHIDA,* Miwa ISHIGURO, Hiroyuki HONDA, Mayumi YAMAMOTO, and Yuji KUBO
Department of Chemistry, Faculty of Science, Kochi University, Akebono-cho, Kochi 780
(Received May 6, 1988)

The effects of some metal ions on the amination and arylation of 5,8-quinolinedione (**1**) and on the amine displacement of 6-piperidino-5,8-quinolinedione have been investigated. The reaction of **1** with various amines in chloroform or ethanol was specifically promoted by Ni(II) ions to give selectively the corresponding 6-(substituted amino)-5,8-quinolinediones. With *N,N*-dialkylanilines in acetic acid the reaction was strongly promoted by Cu(II) ions to give exclusively 6-arylated products, 6-[*p*-(dialkylamino)phenyl]-5,8-quinolinediones. The metal chelate complex was proposed as an activated intermediate.

It is generally known that the reactivities and electronic structures of organic ligands are affected by coordination to metal ions. In recent papers, we have reported novel direct alkylaminations of various α-substituted anthraquinones in the presence of metal ions.[1] The formation of a metal chelate complex, in which the α-substituent and the neighboring oxygen atom of the quinone carbonyl group coordinate to the metal ion, was proposed to increase the electrophilicity of the anthraquinone nucleus and to facilitate the ocurrence of direct alkylamination.

A strong activation effect induced by metal chelate formation has also been found in the reactions of various amines with 5,8-quinolinedione (**1**), giving 6-aminated and 6-arylated products selectively.[2] In this paper, we report on details of the effect of metal ions on the reaction of 5,8-quinolinediones with various amines. The spectral features for metal chelate formation upon the addition of the metal salts to solutions of substituted 5,8-quinolinediones were also investigated.

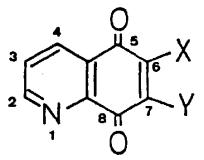

	X	Y
1	H	H
2	Piperidino	H
3	H	Piperidino
4	*n*-BuNH	H
5	H	*n*-BuNH
6	*p*-$(CH_3)_2N$-C_6H_4-NH	H
7	H	*p*-$(CH_3)_2N$-C_6H_4-NH
8	*p*-CH_3O-C_6H_4-NH	H
9	H	*p*-CH_3O-C_6H_4-NH
10	*p*-Cl-C_6H_4-NH	H
11	*p*-O_2N-C_6H_4-NH	H
12	*p*-$(CH_3)_2N$-C_6H_4-	H
13	H	*p*-$(CH_3)_2N$-C_6H_4-
14	*p*-$(C_2H_5)_2N$-C_6H_4-	H
15	*p*-$(CH_3)NH$-C_6H_4-	H
16	*p*-$(C_4H_9)NH$-C_6H_4-	H
17	C_6H_5-$N(CH_3)$-	H
18	C_6H_5-$N(C_4H_9)$-	H

Results and Discussion

Amine Displacement of 6-Piperidino-5,8-quinolinedione (2) Catalyzed by Metal Ions. The reaction of 6-piperidino-5,8-quinolinedione (**2**) with butylamine was found to be catalyzed by some metal ions. As shown in Table 1, the reaction of **2** with butylamine gave 6-butylamino-5,8-quinolinedione (**4**); the amine exchange reaction proceeded at 30 °C in the presence of metal salts (Runs 2—7), but did not proceed at all in the absence of metal salt (Run 1). The catalytic activity of metal chlorides was found to be in the following order: Ni(II)≫Cu(II)>Co(II)>Al(III), Ce(III). The activity of Ni(II) ion was particularly superior to those of other metal ions. In the presence of 0.1 mole ratio of nickel(II) chloride, an 83% yield of **4** was obtained after 2.5 h (Run 5). Copper(II) chloride was less active than nickel(II) chloride; however, the yield of **4** was greatly improved and the reaction proceeded more rapidly with an increase in the amount of catalyst (Runs 2 and 3). Though the displacement of the piperidino group of **2** by butylamine proceeded smoothly in the presence of Ni(II) ions, an amine exchange reaction was not observed when 7-piperidino-5,8-quinolinedione (**3**) and 2-piperidino-1,4-naphthoquinone (**19**) were used instead of **2**, and the starting materials (**3** and **19**) were recovered.

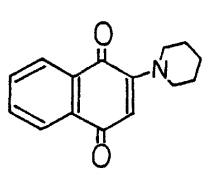

19

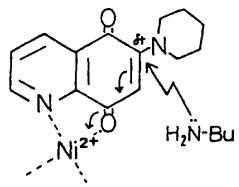

20

Figure 1 shows the spectral changes observed upon an addition of nickel(II) chloride to a chloroform (10 vol% DMF) solutions of **2**. In the case of **2** the absorption maximum around 470 nm, due to a free ligand, was shifted to a longer wavelength with an increase in the absorption intensity. The maximum and constant absorbance were obtained over the range of the mole ratio of [Ni(II)]/[**2**]=0.8—2.0. We tested other metal

Table 1. Effect of Metal Chlorides on the Reaction of **2** with Butylamine[a)]

Run	Metal salt	Mole ratio [Metal salt]/[**2**]	Time h	Recovery/%[b)] **2**	Yield/%[b)] **4**
1	None	—	50	86	0
2	$CuCl_2$	0.1	25	Trace	43
3	$CuCl_2$	1.0	1	0	73
4	$CoCl_2$	0.1	45	4	43
5	$NiCl_2$	0.1	2.5	0	83
6	$AlCl_3$	0.1	25	Trace	7
7	$CeCl_3 \cdot 7H_2O$	0.1	33	Trace	19

a) Reactant **2** (0.5 g) was stirred in pyridine (15 ml) with butylamine (5 ml) and metal salt at 30 °C. b) Isolated yield after column chromatography.

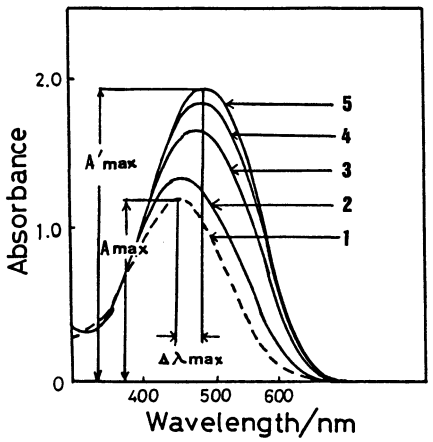

Fig. 1. Influence of added $NiCl_2$ on the absorption spectra of **2** in chloroform (10 vol% DMF) at 25 °C. $[\mathbf{2}]_t=2.5\times10^{-4}$ M ([ ]$_t$ denotes the total concentration; 1 M=1 mol dm^{-3}); $[Ni(II)]_t=0.00$ (1), 5.0×10^{-5} (2), 1.0×10^{-4} (3), 1.5×10^{-4} (4), 2.0×10^{-4}—5.0×10^{-4} M (5).

Table 2. Influence of Added Metal Ions on the Absorption Spectra of **2** in Chloroform (10 vol% DMF) at 25 °C[a)]

Metal salt	Mole ratio [Metal salt]/[**2**]	λ'_{max} nm	$\Delta\lambda_{max}$[b)] nm	RA_{max}[c)]
None	—	470[a)]	—	—
$NiCl_2$	1.0	503	33	1.66
$CuCl_2$	1.0	500	30	1.64
$CoCl_2$	1.0	500	30	1.52

a) $[\mathbf{2}]=2.5\times10^{-4}$ M; λ_{max}(free ligand)=470 nm, A_{max}(free ligand)= 1.206. b) $\Delta\lambda_{max}=\lambda'_{max}$(complex)$-\lambda_{max}$(free ligand). c) $RA_{max}=A'_{max}$(complex)$/A_{max}$(free ligand).

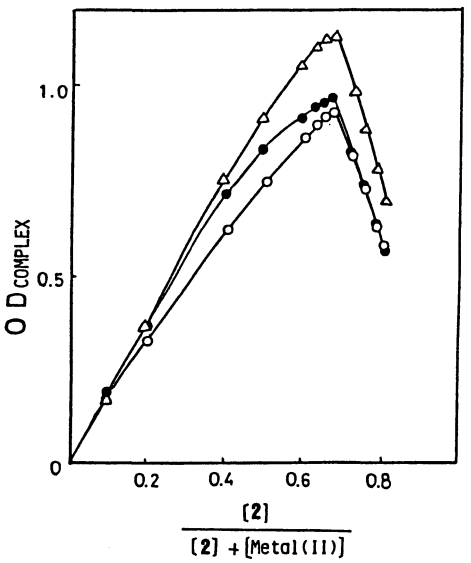

Fig. 2. Continuous variation plots at [**2**]+[Metal(II)]=2.5×10^{-4} M in chloroform(10 vol% DMF) at 25 °C.
—△—; $NiCl_2$, —●—; $CuCl_2$,—○—; $CoCl_2$.

ions (Cu(II) and Co(II)) and observed similar spectral changes. Table 2 summarizes the values of the bathochromic shift, $\Delta\lambda_{max}=\lambda'_{max}$ (complex)$-\lambda_{max}$ (free ligand), and the relative ratio of the absorption intensity, $RA_{max}=A'_{max}$ (complex)$/A_{max}$ (free ligand), calculated on the basis of spectral data. The values of $\Delta\lambda_{max}$ and RA_{max} for the metal ions are compatible with the order of catalytic activity in the amine exchange reaction. In Fig. 2, continuous-variation plots at [**2**]+[Metal(II)]=2.50×10^{-4} mol dm^{-3} are illustrated. The wavelengths (≈500 nm) at the absorption maxima of the metal complexes were employed. Figure 2 clearly shows that maxima appear at [**2**]/([**2**]+[Metal(II)])= 0.67, supporting the formation of 2:1 (Compound (**2**): Metal(II)) chelate complexes.

On the other hand, the spectral changes of compound **3** were fairly smaller than those of **2**, and the pattern of the changes was quite different from that observed in Fig. 1. Furthermore, in the case of **19** the absorption spectrum was not affected at all by the addition of nickel(II) salt. These results suggest that the formation of a metal chelate (**20**), in which the 1-nitrogen atom and the oxygen atom of the 8-carbonyl group of **2** coordinate to the metal ion, probably increases the electrophilicity of the 6-carbon atom and facilitates a nucleophilic substitution of the 6-piperidino group by butylamine. However, the formation of a similar metal chelate of **3** could not facilitate the displacement of the 7-piperidino group, probably because the electron density of the 7-carbon atom is not affected so much by metal chelate formation.

Regioselective 6-Amination of 5,8-Quinolinedione

(1) Catalyzed by Nickel(II) Ion. From the results of the catalytic action of metal ions in the amine exchange reaction of **2**, it is expected that nickel(II) ions can well catalyze the amination of **1** and the amino group would be preferentially introduced onto the 6-position of **1**. Therefore, we examined the reaction of **1** with various amines in the presence of nickel(II) chloride under atmospheric oxygen. The reaction of **1** with aromatic amines is already known to produce a mixture of 6- and 7-arylaminated products;[3,4] however, a reaction with aliphatic amines has not yet been reported. As shown in Table 3, in the absence of metal salt the reactions gave isomeric mixtures of the products, 6- and 7-amino derivatives of **1** (Runs 8, 10, 12, and 15). However, in the presence of nickel(II) chloride the regioselective and the regiospecific 6-amination of **1** were achieved in reactions with the aliphatic and primary aromatic amines, respectively (Runs 9, 11 and 13, 16, 17, 19). The reaction was considerably affected by the amounts of nickel(II) chloride, especially when strong electron-donating amino groups were introduced, more than a half molar ratio of the metal salt to **1** was needed. This suggests that the metal ion is preferentially combined with the aminated product rather than with **1** and that, consequently, the catalytic action of the metal ion is prohibited. When the reaction was conducted under anaerobic conditions, the amination was suppressed considerably (Runs 13 and 14). Atmospheric oxygen plays an important role as an oxidizing agent for the completion of the amination of **1**; the adducts formed by a Michael-type addition of amines to **1** can be dehydrogenated by both the unchanged **1** and atmospheric oxygen to give aminated products. The electrophilicity of 6-position of **1** would be so strongly increased by the formation of nickel(II) chelate that the 6-amination of **1** can proceed even in a reaction with *p*-nitroaniline (Runs 18 and 19). From the results described above, the mechanism of the regioselective 6-amination of **1** was proposed, as shown in Scheme 1.

Table 3. Effect of Added $NiCl_2$ on the Amination of 5,8-Quinolinedione (**1**)

Run	Amine	Mole ratio	Time	Product and yield/%[f]	
		$[Ni^{2+}]/[1]$	h	6-amino isomer	7-amino isomer
8[a]	Piperidine	None[d]	2.0[e]	**2** 48	**3** 10
9[a]	Piperidine	1.0	1.5[e]	**2** 75	**3** 6
10[b]	Butylamine	None[d]	2.0[e]	**4** 30	**5** 26
11[b]	Butylamine	0.5	1.5[e]	**4** 45	**5** 15
12[b]	*p*-(Dimethylamino)aniline	None[d]	6.0[e]	**6** 43	**7** 37
13[b]	*p*-(Dimethylamino)aniline	0.5	2.0	**6** 71	**7** 0
14[c]	*p*-(Dimethylamino)aniline	0.5	2.0[e]	**6** 32	**7** 0
15[b]	*p*-Methoxyaniline	None[d]	7.0[e]	**8** 28	**9** 28
16[b]	*p*-Methoxyaniline	0.5	2.0[e]	**8** 60	**9** 0
17[b]	*p*-Chloroaniline	0.5	3.0[e]	**10** 47	
18[b]	*p*-Nitroaniline	None[d]	15.0	No reaction	
19[b]	*p*-Nitroanilne	0.1	7.0[e]	**11** 36	

a) Reactant **1** (3.14 mmol) was stirred in chloroform (70 ml) at 0 °C with piperidine (9.42 mmol) and $NiCl_2$ under air atmosphere. b) Reactant **1** (3.14 mmol) was stirred in 95% ethanol (150 ml) at 30 °C with the substituted aniline (9.42 mmol) and $NiCl_2$ under air atmosphere. c) Reaction was conducted under argon atmosphere. d) Reactions were conducted without $NiCl_2$. e) Times for the whole starting material **1** was consumed. f) Isolated yield after column chromatography.

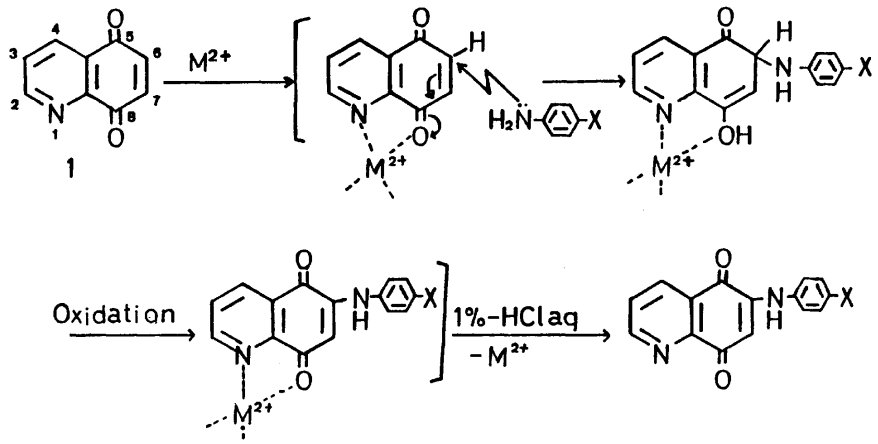

Scheme 1.

Table 4. Reaction of 5,8-Quinolinedione (**1**) with *N*-Alkyl- and *N,N*-Dialkylanilines in the Presence of Metal Salts[a)]

Run	Amine	Metal salt	Mole ratio [Metal salt]/[1]	Solvent	Time h	Product and yield/%[b)] 6-aryl isomer	7-aryl isomer	6-amino isomer
20	*N,N*-Dimethylaniline	None	—	AcOH	94.0	**12** 18	**13** 6	
21	*N,N*-Dimethylaniline	$NiCl_2$	0.5	EtOH	4.0	**12** 2.4	**13** 0	
22	*N N*-Dimethylaniline	$NiCl_2$	0.5	$CHCl_3$	7.5	**12** 2.4	**13** 0	
23	*N,N*-Dimethylaniline	$NiCl_2$	0.5	Pyridine	9.0	**12** Trace	**13** 0	
24	*N,N*-Dimethylaniline	$Ni(OAc)_2 \cdot 4H_2O$	0.5	AcOH	1.0	**12** 51	**13** 0	
25	*N,N*-Dimethylaniline	$Ni(OAc)_2 \cdot 4H_2O$	1.0	AcOH	1.0	**12** 62	**13** 0	
26	*N,N*-Dimethylaniline	$Cu(OAc)_2 \cdot H_2O$	1.0	AcOH	0.5	**12** 80	**13** 0	
27	*N,N*-Dimethylaniline	$Co(OAc)_2 \cdot 4H_2O$	1.0	AcOH	1.5	**12** 48	**13** 0	
28	*N,N*-Dimethylaniline	$Zn(OAc)_2 \cdot 2H_2O$	1.0	AcOH	5.5	**12** 32	**13** 0	
29	*N,N*-Dimethylaniline	$Ce(OAc)_3 \cdot H_2O$	1.0	AcOH	30.1	**12** 24	**13** 0	
30	*N,N*-Diethylaniline	$Cu(OAc)_2 \cdot H_2O$	1.0	AcOH	2.0	**14** 56		
31	*N*-Methylaniline	$Cu(OAc)_2 \cdot H_2O$	1.0	AcOH	0.5	**15** 12		**17** 61
32	*N*-Butylaniline	$Cu(OAc)_2 \cdot H_2O$	1.0	AcOH	1.0	**16** 40		**18** 29

a) Reactant **1** (1.0 g, 6.28 mmol) was stirred in the solvent (100 ml) with the amine (18.8 mmol) and metal salt at 30 °C. b) Isolated yields after column chromatography.

Regioselective 6-Arylation of 5,8-Quinolinedione (1) with *N*-Alkyl- and *N,N*-Dialkylanilines Promoted by Metal Ions. Griffiths et al. found that the reaction of 1,4-naphthoquinone with *N,N*-dialkylarylamines in acetic acid gave 2-[*p*-(dialkylamino)aryl]-1,4-naphthoquinones in 10—66% yields.[5)] As the structure of **1** is analogous to that of 1,4-naphthoquinone, **1** was expected to undergo the arylation by the reaction with *N,N*-dialkylarylamines. Hence, we examined the effects of metal ions on the reaction of **1** with some *N,N*-dialkyl- and *N*-alkylanilines in organic solvents. As shown in Table 4, in the absence of metal salt, the reaction of **1** with *N,N*-dimethylaniline in acetic acid proceeded slowly to give a mixture of 6- and 7-[*p*-(dimethylamino)phenyl]-5,8-quinolinediones (**12** and **13**) in low yields (Run 20). However, the reaction was strongly promoted by some metal ions and gave exclusively the 6-arylated products (Runs 24—29). Metal acetates were arranged in the order of activity as follows: Cu(II)>Ni(II)>Co(II)>Zn(II)≫Ce(III). The activity of Cu(II) ion was particularly superior to those of other metal ions in the arylation. The reaction was also drastically affected by the kind of solvent. The arylation hardly proceeded when ethanol, chloroform, or pyridine was used instead of acetic acid (Runs 21—23). In these solvents, **1** and *N,N*-dimethylaniline immediately formed a reddish purpule charge-transfer complex having an absorption maximum at ca. 510 nm, which was hardly affected by prolonged reaction time. On the contrary, in acetic acid the two reagents hardly form a charge-transfer complex, and gradually reacts to give arylated products. Similar solvent effects were also observed in the arylation of 1,4-naphthoquinone.[5)]

With *N*-alkylanilines, the reaction was also affected by the kind of solvent and metal salt. Pratt has already reported that the reaction of **1** with *N*-methylaniline in an alcohol solution gave a mixture of 6- and 7-(*N*-methylanilino)-5,8-quinolinediones in low yields, but in the presence of cerium(III) chloride the 6-amino isomer (**17**) was obtained exclusively in satisfactory yield.[3c)] In our case of using copper(II) acetate in acetic acid, however, the corresponding reaction gave the 6-arylated product,6-[*p*-(methylamino)phenyl]-5,8-quinolinedione (**15**), together with the 6-aminated product (**17**): the ratio of the yields was abuot 1 : 5 (Run 31). However, in a reaction with *N*-butylaniline the yield of the 6-arylated product (**16**) was higher than that of the corresponding 6-aminated product (**18**): the ratio was about 4 : 3 (Run 32). These results reveal that in a reaction of **1** with *N*-alkylanilines in acetic acid the regioselective 6-arylation competes with the 6-amination, and that the former proceeds predominantly along with an increase in the size of the alkyl residue of *N*-alkylaniline. The nucleophilic attack of the nitrogen atom of *N*-butylaniline would cause a considerable steric crowding in the transient state. The 6-arylation was presumably initiated by a nucleophilic attack of para-position of the benzene ring of the arylamine onto the electron deficient 6-position of **1** complexed with the metal ion, giving the 1,4-adduct and was completed by a subsequent oxidation of the adduct as the similar mechanism shown in Scheme 1.

Experimental

Measurements. All the melting points are uncorrected. The visible spectra were measured using a Hitachi 220A spectrometer. The ^1H NMR spectra were taken on a JEOL Model MH-100 spectrometer with TMS as the internal standard. The elemental analyses were measured on a Yanaco CHN recoder MT-2. Thin-layer chromatography was performed on silica gel (Merk Kieselgel 60) and the resulting chromatograms were measured on a chromatoscanner (Shimadzu CS-900).

Materials. 5,8-Quinolinedione (**1**) was prepared according to a procedure described in the literature.[6)] All of the metal chlorides and the metal acetates were reagent-grade and were used without further purification. All of the metal

perchlorate hexahydrates were prepared according to methods described in the literature.[7] The amines and the solvents were purified by ordinary methods.[8]

Reaction of 2 with Butylamine. The general procedure was as follows. To a solution of **2** (0.5 g, 2.06 mmol) and metal chloride (0—2.06 mmol) in 15 ml of pyridine was added 5 ml of butylamine dropwise with stirring at 30 °C. The reaction was monitored by TLC analysis. (silica gel/ethyl acetate); **2**: R_f=0.25, **4**: R_f=0.35. After the reaction, the solvent was removed under reduced pressure. To the residue was added a cold 1% hydrochloric acid solution; the product was then extracted with chloroform. The chloroform layer was washed with water, dried (Na_2SO_4), and then concentrated. The crude products were separated by column chromatography (silica gel: Wakogel C-300) using ethyl acetate as an eluent. The yields are summarized in Table 1.

Reaction of 1 with Various Amines. The general procedure was as follows. A solution of **1** (1 g, 6.28 mmol) in 100 ml of 95% ethanol was added to a solution of the amine (18.8 mmol) and $NiCl_2$ (0—6.28 mmol) in 50 ml of 95% ethanol with stirring in an open flask at 30 °C. The reaction was monitored by TLC analysis. After the reaction, the solvent was removed under reduced pressure. A cold 1% hydrochloric acid solution was added to the residue in order to decompose the nickel chelate complex of the aminated 5,8-quinolinediones. The aminated products were extracted with chloroform from an acidic solution containing a fine dispersed precipitate. The extraction was repeated several times. After the combined chloroform extracts had been washed with water, dried (Na_2SO_4), and concentrated, the crude products were separated by column chromatography (silica gel: Wakogel C-300) using ethyl acetate and/or chloroform as eluents. The yields are summarized in Table 3.

Reaction of 1 with *N*-Alkyl- and *N,N*-Dialkylanilines. A solution of **1** (1 g, 6.28 mmol) in 80 ml of acetic acid was slowly added to a solution of the *N*-substituted aniline (18.84 mmol) and metal salt (6.28 mmol) in 20 ml of acetic acid with stirring in an open flask at 30 °C. The reaction was monitored by TLC analysis. After the starting material **1** was consumed, the products were extracted with chloroform from the reaction solution. The extraction was repeated several times. After the combined chloroform extracts were washed with saturated sodium carbonate aqueous solution, washed further with water, dried (Na_2SO_4) and then concentrated in vacuo. The crude products were separated by column chromatography (silica gel: Wakogel C-300) using chloroform or ethyl acetate as eluents. The yields are summarized in Table 4.

Characterization and Identification of Products. Some properties of the compounds (**2**,[9] **10**,[3c] and **17**[3c]), were already known; these were identified by data described in the literature, together with the following additional data.

6-Piperidino-5,8-quinolinedione (2): mp 147—148 °C (lit,[9] 146—148 °C). λ_{max} (benzene) 462 nm (ε 3600). ^{1}H NMR ($CDCl_3$) δ=1.6—1.9 (6H, m, $(CH_2)_3$), 3.4—3.7 (4H, m, N-CH_2×2), 6.16 (1H, s, H^7), 7.54 (1H, dd, H^3), 8.30 (1H, dd, H^4), 8.95 (1H, dd, H^2). Found: C, 69.42; H, 6.09; N, 11.48%. Calcd for $C_{14}H_{14}N_2O_2$: C, 69.41; H, 5.82; N, 11.56%.

7-Piperidino-5,8-quinolinedione (3): mp 93—95 °C. λ_{max} (benzene) 465 nm (ε 3400). ^{1}H NMR ($CDCl_3$) δ=1.6—1.9 (6H, m, $(CH_2)_3$), 3.4—3.7 (4H, m, N-CH_2×2), 6.01 (1H, s, H^6), 7.55 (1H, dd, H^3), 8.33 (1H, dd, H^4), 8.86 (1H, dd, H^2). Found: C, 69.18; H, 6.03; N, 11.46%. Calcd for $C_{14}H_{14}N_2O_2$: C, 69.41; H, 5.82; N, 11.56%.

6-Butylamino-5,8-quinolinedione (4): mp 148—150 °C. λ_{max} (benzene) 446 nm (ε 3450). ^{1}H NMR ($CDCl_3$) δ=0.98 (3H, t, CH_3), 1.1—1.9 (4H, m, $(CH_2)_2$), 3.21 (2H, q, NH-CH_2), 5.86 (1H, b, NH), 5.90 (1H, s, H^7), 7.53 (1H, dd, H^3), 8.34 (1H, dd, H^4), 8.97 (1H, dd, H^2). Found: C, 68.17; H, 6.42; N, 12.19%. Calcd for $C_{13}H_{14}N_2O_2$: C, 67.81; H, 6.13; N, 12.17%.

7-Butylamino-5,8-quinolinedione (5): mp 139—141 °C. λ_{max} (benzene) 447 nm (ε 3100). ^{1}H NMR ($CDCl_3$) δ=0.98 (3H, t, CH_3), 1.1—1.9 (4H, m, $(CH_2)_2$), 3.22 (2H, q, NH-CH_2), 5.76 (1H, s, H^6), 6.10 (1H, b, NH), 7.63 (1H, dd, H^3), 8.43 (1H, dd, H^4), 8.89 (1H, dd, H^2). Found: C, 67.58; H, 6.35; N, 12.20%. Calcd for $C_{13}H_{14}N_2O_2$: C, 67.81; H, 6.13; N, 12.17%.

6-[*p*-(Dimethylamino)anilino]-5,8-quinolinedione (6): mp 207—209 °C. λ_{max} (benzene) 543 nm (ε 3800). ^{1}H NMR ($CDCl_3$) δ=2.94 (6H, s, CH_3×2), 6.40 (1H, s, H^7), 6.70 (2H, d, benzene ring), 7.12 (2H, d, benzene ring), 7.40 (1H, b, NH), 7.54 (1H, dd, H^3), 8.39 (1H, dd, H^4), 8.99 (1H, dd, H^2). Found: C, 69.41; H, 5.41; N, 14.57%. Calcd for $C_{17}H_{15}N_3O_2$: C, 69.61; H, 5.15; N, 14.33%.

7-[*p*-(Dimethylamino)anilino]-5,8-quinolinedione (7): mp 223—225 °C. λ_{max} (benzene) 542 nm (ε 3700). ^{1}H NMR ($CDCl_3$) δ=2.95 (6H, s, CH_3×2), 6.25 (1H, s, H^6), 6.71 (2H, d, benzene ring), 7.14 (2H, d, benzene ring), 7.60 (1H, b, NH), 7.63 (1H, dd, H^3), 8.40 (1H, dd, H^4), 8.92 (1H, dd, H^2). Found: C, 69.57; H, 5.36; N, 14.17%. Calcd for $C_{17}H_{15}N_3O_2$: C, 69.61; H, 5.15; N, 14.33%.

6-(*p*-Anisidino)-5,8-quinolinedione (8): mp 256—259 °C. λ_{max} (benzene) 483 nm (ε 4500). ^{1}H NMR ($CDCl_3$) δ=3.78 (3H, s, OCH_3), 6.35 (1H, s, H^7), 6.87 (2H, d, benzene ring), 7.14 (2H, d, benzene ring), 7.35 (1H, b, NH), 7.54 (1H, dd, H^3), 8.34 (1H, dd, H^4), 8.95 (1H, dd, H^2). Found: C, 68.50; H, 4.51; N, 10.02%. Calcd for $C_{16}H_{12}N_2O_3$: C, 68.57; H, 4.32; N, 9.99%.

7-(*p*-Anisidino)-5,8-quinolinedione (9): mp 200—203 °C. λ_{max} (benzene) 483 nm (ε 3600). ^{1}H NMR ($CDCl_3$) δ=3.79 (3H, s, OCH_3), 6.18 (1H, s, H^6), 6.88 (2H, d, benzene ring), 7.15 (2H, d, benzene ring), 7.52 (1H, b, NH), 7.60 (1H, dd, H^3), 8.36 (1H, dd, H^4), 8.88 (1H, dd, H^2). Found: C, 68.47; H, 4.55; N, 10.15%. Calcd for $C_{16}H_{12}N_2O_3$: C, 68.57; H, 4.32; N, 9.99%.

6-(*p*-Chloroanilino)-5,8-quinolinedione (10): mp 239—240 °C (lit,[3c] 237—238 °C). λ_{max} (benzene) 466 nm (ε 3900). ^{1}H NMR (DMSO-d_6) δ=6.16 (1H, s, H^7), 7.38 (4H, s, benzene ring), 7.51 (1H, dd, H^3), 8.35 (1H, dd, H^4), 8.93 (1H, dd, H^2), 9.24 (1H, b, NH). Found: C, 63.87; H, 3.55; N, 9.78%. Calcd for $C_{15}H_9N_2O_2Cl$: C, 63.28; H, 3.19, N, 9.84%.

6-(*p*-Nitroanilino)-5,8-quinolinedione (11): mp 278 °C (decomp). λ_{max} (benzene) 447 nm (ε 6500). ^{1}H NMR (CF_3COOD) δ=6.93 (1H, s, H^7), 7.66 (2H, d, benzene ring), 8.45 (2H, d, benzene ring), 8.50 (1H, dd, H^3), 9.25 (1H, dd, H^4), 9.35 (1H, dd, H^2). Found: C, 61.06; H, 3.39; N, 14.24%. Calcd for $C_{15}H_9N_3O_4$: C, 61.02; H, 3.07; N, 14.23%.

6-[*p*-(Dimethylamino)phenyl]-5,8-quinolinedione (12): mp 204—206 °C. λ_{max} (benzene) 535 nm (ε 7800). ^{1}H NMR ($CDCl_3$) δ=3.02 (6H, s, CH_3×2), 6.70 (2H, d, benzene ring), 7.12 (1H, s, H^7), 7.56 (2H, d, benzene ring), 7.62 (1H, dd, H^3), 8.41 (1H, dd, H^4), 8.98 (1H, dd, H^2). Found: C, 73.60; H, 4.78; N, 10.14%. Calcd for $C_{17}H_{14}N_2O_2$: C, 73.37; H, 5.07; N, 10.07%.

7-[*p*-(Dimethylamino)phenyl]-5,8-quinolinedione (13):

λ_{max} (benzene) 536 nm (ε 7760). ^{1}H NMR ($CDCl_3$) δ=3.06 (6H, s, CH_3×2), 6.76 (2H, d, benzene ring), 7.09 (1H, s, H^6), 7.66 (2H, d, benzene ring), 7.66 (1H, dd, H^3), 8.42 (1H, dd, H^4), 9.055 (1H, dd, H^2). Found: C, 73.19; H, 4.91; N, 9.89%. Calcd for $C_{17}H_{14}N_2O_2$: C, 73.37; H, 5.07; N, 10.07%.

6-[*p*-(Diethylamino)phenyl]-5,8-quinolinedione (14): mp 136—137 °C. λ_{max} (benzene) 551 nm (ε 8700). ^{1}H NMR ($CDCl_3$) δ=1.20 (6H, t, CH_3×2), 3.44 (4H, q, CH_2×2), 6.72 (2H, d, benzene ring), 7.18 (1H, s, H^7), 7.62 (2H, d, benzene ring), 7.62 (1H, dd, H^3), 8.50 (1H, dd, H^4), 9.04 (1H, dd, H^2). Found: C, 74.20: H, 5.50; N, 8.57%. Calcd for $C_{19}H_{18}N_2O_2$: C, 74.23; H, 5.90; N, 9.14%.

6-[*p*-(Methylamino)phenyl]-5,8-quinolinedione (15): mp 248—250 °C. λ_{max} (benzene) 511 nm (ε 7410). ^{1}H NMR ($CDCl_3$) δ=2.88 (3H, s, CH_3), 4.13 (1H, b, NH), 6.65 (2H, d, benzene ring), 7.18 (1H, s, H^7), 7.57 (2H, d, benzene ring), 7.66 (1H, dd, H^3), 8.49 (1H, dd, H^4), 9.03 (1H, dd, H^2).

6-[*p*-(Butylamino)phenyl]-5,8-quinolinedione (16): mp 141—142 °C. λ_{max} (benzene) 515 nm (ε 7300). ^{1}H NMR ($CDCl_3$) δ=0.96 (3H, t, CH_3), 1.2—1.8 (4H, m, $(CH_2)_2$), 3.18 (2H, t, NH-CH_2), 4.16 (1H, b, NH), 6.65 (2H, d, benzene ring), 7.16 (1H, s, H^7), 7.57 (2H, d, benzene ring), 7.69 (1H, dd, H^3), 8.48 (1H, dd, H^4), 9.04 (1H, dd, H^2). Found: C, 74.20, H, 5.73; N, 8.65%. Calcd for $C_{19}H_{18}N_2O_2$: C, 74.49; H, 5.92; N, 9.14%.

6-(*N*-Methylanilino)-5,8-quinolinedione (17): mp 178—180 °C (lit,[3c] 181—182 °C). λ_{max} (benzene) 460 nm (ε 3800). ^{1}H NMR ($CDCl_3$) δ=3.44 (3H, s, CH_3), 6.23 (1H, s, H^7), 7.05—7.5 (5H, m, benzene ring), 7.56 (1H, dd, H^3), 8.21 (1H, dd, H^4), 8.98 (1H, dd, H^2). Found: C, 72.74; H, 4.29; N, 10.49%. Calcd for $C_{16}H_{12}N_2O_2$: C. 72.72; H, 4.58; N, 10.60%.

6-(*N*-Butylanilino)-5,8-quinolinedione (18): mp 141—143 °C. λ_{max} (benzene) 470 nm (ε 3600). ^{1}H NMR ($CDCl_3$) δ=0.93 (3H, t, CH_3), 1.1—1.9 (4H, m, $(CH_2)_2$), 3.79 (2H, t, N-CH_2), 6.21 (1H, s, H^7), 7.0—7.5 (5H, m, benzene ring), 7.53 (1H, dd, H^3), 8.23 (1H, dd, H^4), 8.96 (1H, dd, H^2).

The present work was partially supported by a Grant-in-Aid for Encouragement of Young Scientists (No. 60750806) and for Scientific Research (No. 61550641) from the Ministry of Education, Science and Culture.

References

1) K. Yoshida, M. Matsuoka, Y. Yamashita, and T. Kitao, *Bull. Chem. Soc. Jpn.*, **53**, 2552 (1980); K. Yoshida, M. Matsuoka, Y. Yamashita, S. Nagamori, and T, Kitao, *ibid.*, **53**, 3725 (1980); M, Matsuoka, K. Yoshida, Y. Makino, and T. Kitao, *Dyes and Pigments*, **1**, 27 (1980); M. Matsuoka, T. Takei, I. Nakamura, K. Yoshida, and T. Kitao, *Bull. Chem. Soc. Jpn.*, **54**, 2225 (1981); K. Yoshida, T. Fujiwara, and Y. Yamashita, *Chem. Express*, **1**, 595 (1986); K. Yoshida, K. Kitano, K. Takagishi, and Y. Kubo, *ibid.*, **2**, 735 (1987).

2) K. Yoshida, M. Yamamoto, and M. Ishiguro, *Chem. Lett.*, **1986**, 1059; K. Yoshida, M. Ishiguro, H. Honda, and Y. Kubo, *ibid.*, **1987**, 1191.

3) a) R. Long and K. Schofield, *J. Chem. Soc.*, **1953**, 3919; b) V. Petrow and B. Sturgeon, *ibid.*, **1954**, 570; c) Y. T. Pratt, *J. Org. Chem.*, **27**, 3905 (1962).

4) Y. T. Pratt has found that cerium(III) ion catalyzes the reaction and the 6-arylamino isomers are preferentially obtained.[3c]

5) C. Blackburn and J. Griffiths, *J. Chem. Res. (S)*, **1982**, 320.

6) Y. T. Pratt and N. L. Drake, *J. Am. Chem. Soc.*, **82**, 1155 (1960).

7) H. Ito, *Nippon Kagaku Zasshi*, **77**, 1383 (1956).

8) D. D. Perrin, W. L. F. Armarego, and D. R. Perrin, "Purification of Laboratory Chemicals," 2nd ed, Pergamon Press Ltd., (1980).

9) H. Kuo and S. Yoshina, *Yakugaku Zasshi*, **97**, 827 (1977).

Regioselective Ring Opening Reactions of 1-Aminocyclopropenes via Carbenium Ion and Carbene Intermediates

Hiroshi YOSHIDA,* Hiroe SANO,† Tsuyoshi OGATA, and Kiyoshi MATSUMOTO††
Department of Applied Chemistry, Faculty of Engineering, Shizuoka University, Hamamatsu 432
††College of Liberal Arts and Sciences, Kyoto University, Kyoto 606
(Received May 9, 1988)

The reaction of 1-(disubstituted amino)-2,3-diphenylcyclopropenium salt with phenyl- and alkylmagnesium halides afforded, regioselectively, 1-aminocyclopropenes in good yields. The reactions of these 1-aminocyclopropenes were studied under acidic and nonacidic conditions to yield regioselective ring-opening products (C_2-C_3 and C_1-C_3 bond fissions of the cyclopropene) associated with the carbenium ions and carbene intermediates, respectively.

The chemistry of cyclopropene derivatives has attracted considerable interest due to the high strain energy associated with the unsaturated three-membered ring. A number of studies on the photochemical and thermal ring-opening reactions of cyclopropenes have appeared in recent years.[1-3] In a continuation of our studies on the cyclopropenes substituted with heteroatom groups, we have shown, for example, that a facile ring opening of 1-(methylthio)-2,3,3-triphenylcyclopropene via vinylcarbene intermediate at 50 °C, while 3-(methylthio)-1,2,3-triphenylcyclopropene is stable under similar reaction conditions (Scheme 1).[2a]

Here, we report on the preparation and regioselective acid-catalyzed and thermal ring-opening reactions of 1-aminocyclopropenes.

1-Aminocyclopropenium tetrafluoroborates **1a—e** were prepared in moderate-to-good yields by the reaction of diphenylcyclopropenone with triethyloxonium tetrafluoroborate, followed by treatments with secondary amines.[4-6] To a solution of phenylmagnesium bromide **2a** in tetrahydrofuran (THF) at room temperature was added 1-(diphenylamino)-2,3-diphenylcyclopropenium tetrafluoroborate **1a** in one portion; the mixture was stirred, giving a clean solution. After 10 min the resulting solution was poured on ice water and extracted with ether to give 1-(diphenylamino)-2,3,3-triphenylcyclopropene (**3a**) in a 92% yield. The structure **3a** was unambigously evident from its IR (1820 cm^{-1}) and ^{13}C NMR (s at δ=41.3 of sp^3 carbon of

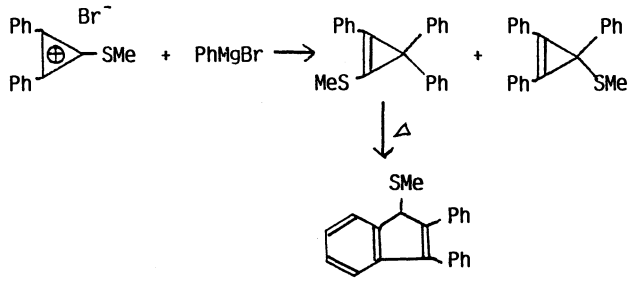

Scheme 1.

Table 1. The Reaction of **1** with **2**

Reaction Conditions						Products (Yield/%)		
1	**2**	Solvent	Temp/°C	Time/h	Extr. Sol.[a]	**3**	**4**	**5**
1a	**2a**	THF	25	0.1	B, E	**3a**(98)		
	2a	THF	25	0.1	C		**4a**(87)	
	2a	THF	60	1.0	B, E	**3a**(45)		**5a**(30)
	2a	THF	60	7.0	B			**5a**(84)
	2b	THF	25	0.1	B, C, E	**3b**(58)		
	2c	THF	25	0.1	B, C, E	**3c**(82)		
	2d	THF	25	0.1	B, C	**3d**(93)		
1b	**2a**	Ether	25	1.0	E, C		**4e**(19)	
	2a	THF	25	0.1	B, C, E		**4e**(69)	
	2a	THF	25	1.0	B, C, E		**4e**(41)	**5e**(11)
	2a	THF	60	0.1	B, C		**4e**(9)	**5e**(23)
	2a	THF	60	0.1	B, C			**5e**(58)
1c	**2a**	THF	25	0.1	B, C		**4f**(40)	
	2a	THF	60	1.0	B, C			**5f**(25)
1d	**2a**	THF	25	0.1	B, C		**4g**(69)	
	2a	THF	60	1.0	B, C			**5g**(80)
1e	**2a**	THF	25	0.1	B, C		**4h**(58)	
	2a	THF	60	1.0	B, C			**5h**(78)

a) Extraction solvent after the aqueous treatment. B: benzene, C: chloroform, and E: ether.

† Present address: Research Center, Polyplastics Co. Ltd., Fuji 416.

C_3) spectra and comparisons of the data with those of the isomer 3-diphenylamino-1,2,3-triphenylcyclopropene (**6a**) prepared from triphenylcyclopropenium perchlorate[5] with diphenylamine (Scheme 3). None of the isomer **6a** was found in the Grignard reaction mixtures, indicating a regioselective nucleophilic attack of Grignard reagent **2a** to **1a**.

The reaction of **1a** with methyl-, ethyl-, and isopropylmagnesium halides **2b—d** yielded cyclopropenes **3b—d** in good yields. In contrast, the reactions of **2a** and the salt **1b—e** yielded two types of products, depending on the reaction conditions employed. Although the reaction of **1b** with **2a** in ether afforded 2-morpholinoindene **4e** in low yield, the use of THF as the reaction medium raised the yield of **4e** up to 41%, together with 1-morpholinoindene **5e**. The reaction at 60 °C afforded **5e**, exclusively, in moderate yield. Similar results were observed for the reaction of **1c—e** with **2a** (Table 1). Attempts to isolate cyclopropenes **3e—h** at low temperature, or direct isolation from the Grignard mixture without aqueous workup, failed, yielding 2-aminoindenes **4e—h** as sole reaction products. These results seem to indicate that the cyclopropenes substituted with relatively basic amino groups undergo a facile ring opening.

The cyclopropenes **3a—d** are relatively stable at room temperature in crystalline form. However, in a chloroform solution at room temperature **3a** afforded **4a** quantitatively, and upon refluxing in benzene for 5 h **5a** in 79% yield. The effect of hydrochloric acid formed from chloroform on the ring opening via the C_2–C_3 bond fission was proven by the conversion of **3a** to **4a** in benzene upon the addition of a small amount of concd HCl, trifluoroacetic acid, or even Lewis acids (Table 2).

Upon heating at reflux in methanol **3a** gave a mixture of aminal **9** and acetal **10** (failed to separate), both of which were converted to aldehyde **11**.[8] The formations of **9** and **10** are supposed to proceed by an insertion of a vinylcarbene to the OH bond of methanol,[2a] followed by methanolysis to yield **10**. A treatment of **3a** in methanol in the presence of acetic acid yielded only **4a** in a good yield.

The structures of indenes **4a** and **5a** were confirmed on the basis of their spectroscopic data as well as converting to 2-indanone **7** and 1*H*-inden-1-one **8**[7] by

Table 2. Ring Opening of **3a**

Reaction conditions				Product(yield/%)
Solvent	Additive(mol)[a]	Temp/°C	Time/h	
PhH	—	70	5	**5a**(79)
THF	—	60	10	**5a**(85)
$CHCl_3$	—	25	1	**4a**(96)
PhH	AcOH(10)	25	5	**4a**(50)
	CF_3CO_2H(1)	25	0.1	**4a**(90)
	HCl(1)	25	1	**4a**(95)
	$MgBr_2$(1)	25	1	**4a**(90)
	BF_3 · ether(1)	25	0.5	**4a**(96)
MeOH	—	60	140	**9** and **10**(75)[b]
	NaOH(3)	60	140	**9** and **10**(68)[b]
	AcOH(10)	60	24	**4a**(93)

a) A mixture of **3a** (1 mmol), and additive (mmol) in a solvent (10 cm^3) was reacted under respective reaction conditions. b) Yield of **11** obtained by the hydrolysis of the crude reaction mixture of **9** and **10**.

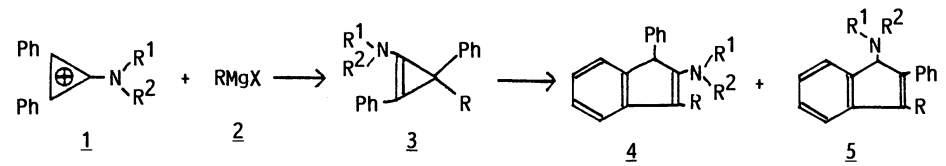

1	R^1	R^2
a	Ph	Ph
b	$(CH_2)_2O(CH_2)_2$	
c	$(CH_2)_5$	
d	Me	Ph
e	$PhCH_2$	Ph

2	R
a	Ph
b	Me
c	Et
d	i-Pr

3,4,5	R^1	R^2	R
a	Ph	Ph	Ph
b	Ph	Ph	Me
c	Ph	Ph	Et
d	Ph	Ph	i-Pr
e	$(CH_2)_2O(CH_2)_2$		Ph
f	$(CH_2)_5$		Ph
g	Me	Ph	Ph
h	$PhCH_2$	Ph	Ph

Scheme 2.

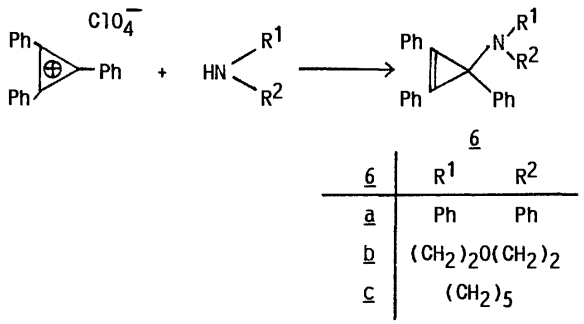

6	R^1	R^2
a	Ph	Ph
b	$(CH_2)_2O(CH_2)_2$	
c	$(CH_2)_5$	

Scheme 3.

hydrolysis or oxidation (Scheme 4). Similar spectra were obtained for all indenes **4** and **5**.

These two types of ring openings were also observed for cyclopropenes **3b—d** substituted with alkyl groups (Scheme 5 and Table 3). Although an addition of trifluoroacetic acid to solutions of **3b** and **3c** in benzene accelerated the ring opening to yield tarry mixtures, treatments of **3b** and **3c** in chloroform at room temperature yielded butadienes **12** in good yields. The isomer **3d** gave a resinous material under similar conditions. In contrast, upon heating in benzene at reflux **3b—d** afforded a mixture of 1-aminoindene **5** and butadiene derivative **14**. Aminobutadienes **12** and **14** were converted to the carbonyl derivatives, **13** and **15**, respectively, by acidic hydrolyses and their structures were confirmed. Ultraviolet irradiation of **15** gave a new set of ^{1}H NMR absorption corresponding to the stereo-

Table 3. Ring Opening Reaction of Alkyl-Substituted Cyclopropenones **3b**, **3c**, and **3d**

	Reaction conditions			Products(Yield/%)
	Solvent	Temp/°C	Time/d	
3b	$CHCl_3$	25	7	**12a**(100)
	PhH	80	4	**5b**(29), **14a**(10)
3c	$CHCl_3$	25	10	**12b**(69)
	PhH	80	5	**5c**(14), **14b**(25)
3d	$CHCl_3$	25	10	Unknown mixture
	PhH	80	7	**14c**(54)

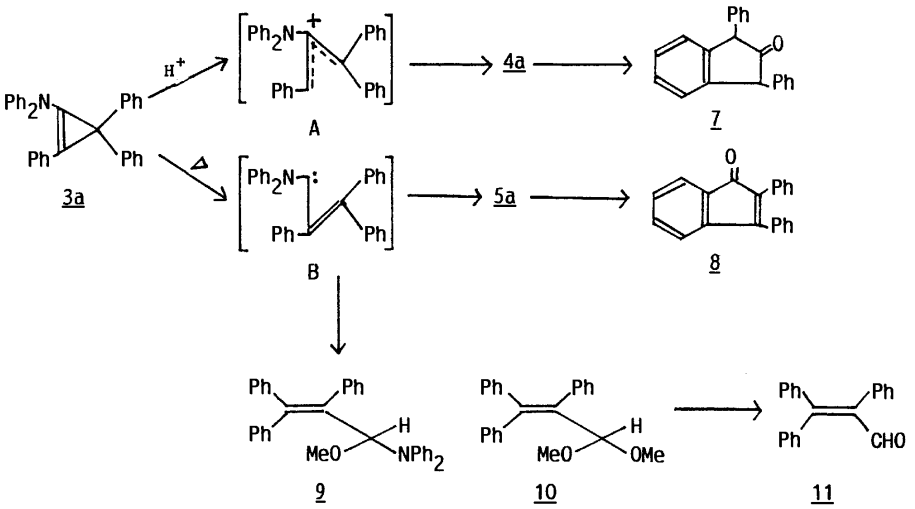

Scheme 4.

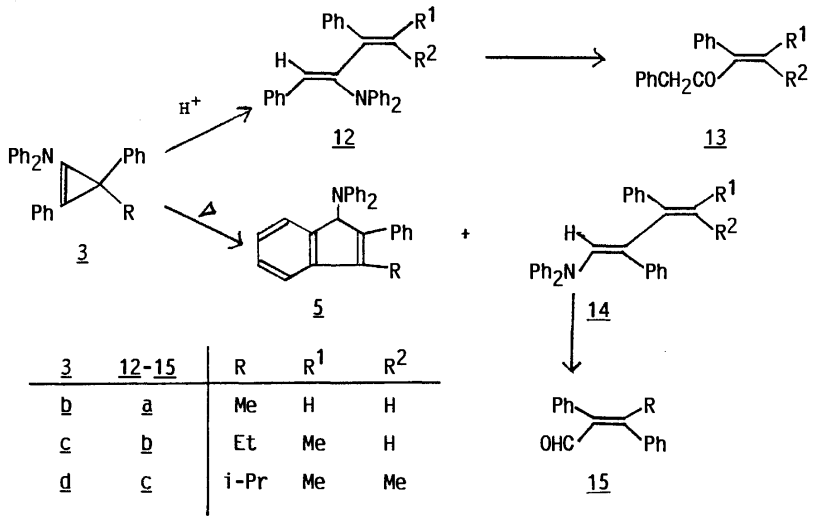

3	12-15	R	R^1	R^2
b	a	Me	H	H
c	b	Et	Me	H
d	c	i-Pr	Me	Me

Scheme 5.

isomer of **15**. A shielding effect of the phenyl groups and NOE studies revealed the stereochemistry of **15** to be the *Z*-form.

These results indicate that two routes are possible for the ring opening of 1-amino-substituted cyclopropenes **3**, involving either a carbenium ion or carbene intermediates (Scheme 4). The protonation of **3a** and the fission of the C_2-C_3 bond via a well-known thermally allowed disrotatory ring opening might give a vinylcarbenium ion **A** stabilized by the neighbouring amino group,[9] followed by cyclization[10] to yield **4a**. The higher reactivity of **3e—h** (not isolated), whose amino groups are stronger bases than that of **3a**, seems to furnish intermediate **A**. Another process is the scission of the C_1-C_3 bond of **3a** to give the vinylcarbene intermediate **B**. Stabilization of the carbene by the contiguous amino group might facilitate the ring opening,[11] since tetraphenylcyclopropene rearranges at temperatures over 200 °C,[12] isomer **6** was recovered unchanged upon prolonged heating in refluxing benzene. Thus, the selection of the reaction conditions controls the regioselective ring opening of 1-aminocyclopropenes **3**. The facile ring opening found for phenylcyclopropenes (**3**: R=Ph), rather than alkylcyclopropenes **3b—d**, could be explained in terms of the resonance stabilization of intermediates **A** and **B** by the phenyl group.

Experimental

General. Melting points were uncorrected. The ^{13}C NMR spectra were recorded either on a JEOL JMN FX-60 spectrometer (15.04 MHz) or JEOL JNM FX-90Q (22.49 MHz) and ^1H NMR spectra on a Hitachi R-24B (60 MHz). The IR spectra were recorded on a JASCO A-3 spectrometer.

Preparation of 1-Amino-2,3-diphenylcyclopropenium Tetrafluoroborates (1). The salts **1** were prepared by a known method.[4-6]

The Reaction of 1 with Grignard Reagents 2. General Procedure. To a solution of phenylmagnesium bromide **2a** (3 mmol) in THF (20 cm^3) was added **1a** (1 mmol) in one portion; the mixture was stirred at room temperature for 10 min to yield a clear solution. The resulting solution was poured into cold water containing 1% of KH_2PO_4 and extracted with an appropriate solvent. The extract was dried over sodium carbonate, condensed in vacuo, and recrystallization from 2-propanol afforded the cyclopropene **3a** (extraction by ether or benzene) or 2-diphenylaminoindene **4a** (extraction by chloroform). Upon refluxing for 1 h, the Grignard reaction mixture yielded 1-diphenylaminoindene **5a** after a similar treatment as mentioned above. **3a**: mp 145—147 °C; IR (KBr) 1820 cm^{-1}; ^1H NMR ($CDCl_3$) δ=6.7—7.5 (m, 25H, 5Ph). ^{13}C NMR ($CDCl_3$) δ=41.7(s), 88.8(s), 120.4(s), 123.8(d), 124.7(d), 125.5(d), 125.9(d), 127.9(d), 128.3(d),128.4(d), 128.5(d), 128.7(d), 129.2(d), 144.2(s), and 145.1(s). Found: C, 90.82; H, 5.62; N, 3.22%; M^+ 435. Calcd for $C_{33}H_{25}N$: C, 91.03; H, 5.75; N, 3.22%; M, 435. **4a**: mp 203—205 °C; IR (KBr) 1600 cm^{-1}; ^1H NMR ($CDCl_3$) δ=6.12 (s, 1H, CH) and 6.5—7.6 (m, 24H, Arom). ^{13}C NMR ($CDCl_3$): δ=68.6 (d, CH), 120.9(d), 121.7(d), 121.8(d), 123.6(d), 126.0(d), 126.9(d), 127.6(d), 127.8(d), 128.0(d), 128.6(d), 128.9(d), 129.2(d), 129.5(d), 135.0(s), 135.1(s), 140.2(s), 143.6(s), 144.1(s), and 147.3(s). Found: C, 91.07; H, 5.72; H, 3.10%; M^+ 435. Calcd for $C_{33}H_{25}N$: C, 91.03; H, 5.75; N, 3.22%; M, 435. **5a**: mp 190—191 °C; IR(KBr) 1600 cm^{-1}; ^1H NMR ($CDCl_3$) δ=5.03 (s, 1H, CH), and 6.5—7.5 (m, 24H, Arom). ^{13}C NMR ($CDCl_3$) δ=55.6(d), 120.6(d), 121.2(d), 122.0(d), 124.0(d), 125.9(d), 126.7(d), 127.0(d), 127.7(d), 127.9(d), 128.1(d), 128.3(d), 128.7(d), 129.0(d), 133.8(s), 140.1(s), 140.7(s), 142.0(s), 145.3(s), and 147.1(s). Found: C, 90.96; H, 5.77; N, 3.02%; M^+, 435. Calcd for $C_{33}H_{25}N$: C, 91.03; H, 5.75; N, 3.22%; M, 435.

Hydrolysis of indene **4a** gave 2-indanone **7** in 70%. A suspension of **4a** in aqueous hydrochloric acid (3 mol dm^{-3}) was srirred at room temperature for 15 h, yielding a clean solution. The chloroform extract gave **7**: mp 150—152 °C; IR (KBr) 1760 cm^{-1}; ^1H NMR ($CDCl_3$) δ=4.78 (s, 2H, 2CH) and 6.9—7.5 (m, 14H, Arom). ^{13}C NMR ($CDCl_3$) δ=59.0(d), 125.8(d), 127.3(d), 128.3(d), 128.9(d), 138.1(s), 140.9(s), and 212.7(s). Found: C, 88.28; H, 5.73%; M^+, 284. Calcd for $C_{21}H_{16}O$: C, 88.73; H, 5.63%; M, 284.

Indene **5a** was stable to acid hydrolysis. Upon treatment with aqueous hydrogen peroxide in a solution of benzene for one day **5a** gave 1*H*-inden-1-one **8** in 20% yield by crystallization from chloroform-ethanol. **8**: mp 152—153 °C (lit,[7] mp 152—152.5 °C).

The reaction of **1b—e** with Grignard reagents yielded **3—5**, as summarized in Table 1. **3b**: mp 110—111 °C; IR(KBr) 1830 cm^{-1}; ^1H NMR ($CDCl_3$) δ=1.85 (s, 3H, Me) and 6.6—7.3 (m, 20H, 4Ph). ^{13}C NMR ($CDCl_3$) δ=22.6(q), 32.2(s), 88.8(s), 123.3(d), 124.5(d), 125.1(d), 125.3(d), 126.4(d), 128.0(d), 128.3(s), 129.3(d), 144.5(s), and 146.8(s). Found: C, 89.46; H, 6.17; N, 3.74%; M^+, 373. Calcd for $C_{28}H_{23}N$: C, 90.08; H, 6.17; N, 3.75%; M, 373. **3c**: mp 120—121 °C; IR (KBr) 1840 cm^{-1}; ^1H NMR ($CDCl_3$) δ=0.82 (t, J=7 Hz, 3H, Me), 2.20 (oct, J=7 Hz, 2H, CH_2), and 6.7—7.5 (m, 20H, 4Ph). ^{13}C NMR ($CDCl_3$) δ=11.4(q), 26.4(t), 37.9(s), 85.4(s), 121.5(s), 123.2(d), 124.5(d), 125.4(d), 126.7(d), 128.0(d), 128.3(d), 129.2(d), 129.9(s), 144.5(s), and 146.6(s). Found: C, 89.40; H, 6.57; N, 3.58%; M^+, 387. Calcd for $C_{29}H_{25}N$: C, 89.92; H, 6.46; N, 3.62%; M, 387. **3d**: mp 158—160 °C; IR (KBr) 1830 cm^{-1}; ^1H NMR ($CDCl_3$) δ=0.85 (d, J=7Hz, 3H, Me), 1.11 (d, J=7Hz, Me), 2.28 (sept, J=7 Hz, CH), and 6.7—7.5 (m, 20H, 4Ph). ^{13}C NMR ($CDCl_3$) δ=21.9(q), 23.4(q), 31.7(d), 44.4(s), 83.8(s), 123.7(d), 123.9(s), 124.6(d), 124.8(d), 125.4(d), 127.6(d), 127.9(d), 128.2(d), 128.3(d), 128.6(d), 129.2(d), 130.3(s), 144.7(s), and 145.7(s). Found: C, 89.52; H, 6.77; N, 3.40%; M^+, 401. Calcd for $C_{30}H_{27}N$: C, 89.78; H, 6.73; N, 3.49%; M, 401. **4e**: mp 130—132 °C; IR (KBr) 1600 cm^{-1}; ^1H NMR ($CDCl_3$) δ=2.3—3.0 (m, 4H, CH_2NCH_2), 3.48 (t, J=5 Hz, 4H, CH_2OCH_2), 4.80 (s, 1H, OH), and 7.0—7.8 (m, 14H, Arom). ^{13}C NMR ($CDCl_3$) δ=49.2(t), 67.6(t), 73.1(d), 120.5(d), 124.6(d), 125.3(d), 126.8(d), 127.4(d), 127.7(d), 128.5(d), 129.3(d), 129.5(d), 135.1(s), 136.0(s), 140.7(s), 142.9(s), 143.1(s), and 144.9(s). Found: C, 85.03; H, 6.56; N, 4.11%; M^+, 353. Calcd for $C_{25}H_{23}NO$: C, 84.93; H, 6.52; N, 3.97%; M, 353. **4f**: mp 94—96 °C; IR (KBr) 1600 cm^{-1}; ^1H NMR ($CDCl_3$) δ=1.2—1.6 (m, 6H, $3CH_2$), 2.3—3.0 (m, 4H, CH_2NCH_2), 4.83 (s, 1H, CH), and 7.1—7.7 (m, 14H, Arom). ^{13}C NMR ($CDCl_3$) δ=24.7(t), 26.7(t), 50.1(t), 73.8(d), 120.3(d), 124.5(d), 125.0(d), 126.6(d), 127.2(d), 127.4(d), 127.5(d), 128.0(d), 128.5(d), 129.4(d), 129.6(d), 129.9(d), 135.4(s), 136.3(s), 140.1(s), 143.8(s), 143.9(s), and 144.9(s). Found: C, 88.82; H, 7.06; N, 4.12%; M^+, 351. Calcd for $C_{26}H_{25}N$: C, 88.89; H, 7.12;

N, 3.99%; M, 351. **4g**: mp 153—155 °C IR (KBr) 1660 cm^{-1}; ^1H NMR ($CDCl_3$) δ=2.30 (s, 3H, Me), 5.93 (s, 1H, CH), and 6.6—7.5 (m, 19H, Arom). ^{13}C NMR ($CDCl_3$) δ=31.9(q), 67.5(d), 113.2(d), 116.9(d), 120.7(d), 123.3(d), 125.8(d), 127.0(d), 127.7(d), 128.0(d), 128.8(d), 129.1(d), 129.3(d), 129.4(d), 134.5(s), 135.2(s), 140.4(s), 143.1(s), 143.4(s), 144.5(s), and 150.4(s). Found: C, 89.99; H, 6.20; N, 3.68%; M^+, 373. Calcd for $C_{28}H_{23}N$: C, 90.08; H, 6.17; N, 3.75%; M, 373. **4h**: mp 158—160 °C; IR (KBr) 1590 cm^{-1}; ^1H NMR ($CDCl_3$) δ=3.96 (s, 2H, CH_2), 6.20 (s, 1H, CH), and 6.7—7.6 (m, 19H, Arom). ^{13}C NMR ($CDCl_3$) δ=50.5(t), 68.7(d), 115.1(d), 117.7(d), 120.8(d), 123.6(d), 125.8(d), 126.0(d), 126.7(d), 126.9(d), 127.6(d), 127.9(d), 128.0(d), 128.1(d), 128.3(d), 128.6(d), 129.1(d), 129.3(d), 129.5(d), 134.6(s), 134.8(s), 138.8(s), 140.4(s), 143.5(s), 143.6(s), 144.4(s), and 149.5(s). Found: C, 90.77; H, 6.12; N, 3.13%; M^+, 449. Calcd for $C_{34}H_{27}N$: C, 90.83; H, 6.05; N, 3.11%; M, 449. **5b**: mp 157—160 °C; IR(KBr) 1590 cm^{-1}; ^1H NMR ($CDCl_3$) δ=2.11 (d, 3H, J=2Hz, Me), 5.9—6.1 (q, J=2Hz, CH), and 6.5—7.6 (m, 19H, Arom). ^{13}C NMR ($CDCl_3$) δ=11.7(q), 68.4(d), 119.5(d), 121.4(d), 121.6(d), 123.1(d), 125.7(d), 126.7(d), 127.9(d), 128.0(d), 128.8(d), 129.2(d), 135.1(s), 135.6(s), 142.7(s), 143.6(s), 144.7(s), and 147.3(s). Found: C, 89.98; H, 6.21; N, 3.81%; M^+, 373. Calcd for $C_{28}H_{23}N$: C, 90.08; H, 6.17; N, 3.74%; M, 373. **5c**: mp 119—120 °C; IR (KBr) 1600 cm^{-1}; ^1H NMR ($CDCl_3$) δ=1.10 (t, J=7Hz, 3H, Me), 2.56 (q, J=7Hz, 2H, CH_2), 5.98 (s, 1H, CH), and 6.5—7.6 (m, 19H, Arom). ^{13}C NMR ($CDCl_3$) δ=13.3(q), 19.1(t), 68.7(d), 119.9(d), 121.4(d), 121.6(d), 123.4(d), 125.6(d), 126.8(d), 127.8(d), 128.0(d), 128.8(d), 129.0(d), 135.7(s), 141.2(s), 142.1(s), 143.5(s), 144.2(s), and 147.3(s). Found: C, 89.97; H, 6.47; N, 3.76%; M^+, 387. Calcd for $C_{29}H_{25}NO_2$: C, 89.77; H, 6.46; N, 3.62%; M, 387. **5e**: mp 170—173 °C; IR (KBr) 1600 cm^{-1}; ^1H NMR ($CDCl_3$) δ=2.8—3.2 (m, 4H, CH_2NCH_2), 3.2—3.5 (m, 4H, CH_2OCH_2), 4.70 (s, 1H, CH), and 6.8—7.6 (m, 14H, Arom). ^{13}C NMR ($CDCl_3$) δ=50.1(t), 55,4(d), 66.6(t), 116.4(s), 116.9(d), 122.3(d), 122.9(d), 126.6(d), 126.8(d), 127.8(d), 128.2(d), 128.9(d), 130.0(d), 136.6(s), 140.5(s), 142,1(s), 146.5(s), and 154.0(s). Found: C, 85.08; H, 6.51; N, 3.88%; M^+, 353. Calcd for $C_{25}H_{23}NO$: C, 84.99; H, 6.52; N, 3.97%; M, 353. **5f**: mp 95—97 °C; IR (KBr) 1620 cm^{-1}; ^1H NMR ($CDCl_3$) δ=0.9—1.6 (m, 6H, $3CH_2$), 2.8—3.1 (m, 4H, CH_2NCH_2), 4.71 (s, 1H, CH), and 6.8—7.6 (m, 14H, Arom). ^{13}C NMR ($CDCl_3$) 24.1(t), 25.8(t), 51.1(t), 55.6(d), 114.3(s), 116.3(d), 121.6(d), 122.7(d), 126.1(d), 126.5(d), 126.7(d), 127.5(d), 128.0(d), 128.5(d), 128.6(d), 129.4(d), 129.6(d), 129.9(d), 137.3(s), 141.0(s), 142.0(s), 147.0(s), and 155.4(s). Found: C, 88.81; H, 7.14; N, 3.78%; M^+, 351. Calcd for $C_{26}H_{25}N$: C, 88.89; H, 7.12; N, 3.99%; M, 351. **5g**: mp 162—164 °C; IR (KBr) 1600 cm^{-1}; ^1H NMR ($CDCl_3$) δ=2.67 (s, 3H, CH_3), 5.05 (s, 1H, CH), and 6.5—7.5 (m, 19H, Arom). ^{13}C NMR ($CDCl_3$) δ=40.0(q), 54.5(d), 117.1(d), 119.0(d), 124.1(d), 124.8(d), 126.6(d), 126.9(d), 127.3(d), 128.2(d), 128.5(d), 128.6(d), 128.7(d), 129.8(s), 134.5(s), 139.1(s), 144.1(s), 144.6(s), 148.2(s), and 153.0(s). Found: C, 89.81; H, 6.20; N, 3.61%; M^+, 373. Calcd for $C_{28}H_{23}N$: C, 90.08; H, 6.17; N, 3.75%; M, 373. **5h**: mp 121—123 °C; IR (KBr) 1590 cm^{-1}; ^1H NMR ($CDCl_3$) δ=4.22 and 4.58 (ABq, J=17 Hz, 2H, CH_2), 5.05 (s, 1H, CH), and 6.5—7.5 (m, 19H, Arom). ^{13}C NMR ($CDCl_3$) δ=55.1(q), 57.4(t), 118.6(d), 119.5(d), 120.5(d), 123.7(d), 124.3(d), 126.5(d), 126.7(s), 126.9(s), 127.0(s), 127.1(s), 128.2(s), 128.3(s), 128.6(d), 128.7(d), 129.0(d), 134.7(s), 139.0(s), 139.4(s), 143.8(s), 145.2(s), 147.9(s), and 151.3(s). Found: C, 90.51; H, 5.98; N, 3.08%; M^+, 449. Calcd for $C_{34}H_{27}N$: C, 90.83; H, 6.05; N, 3.11%; M, 449.

Ring-Opening Reactions of 3. Cyclopropene **3a** was treated under various reaction conditions while checking the mixture by TLC at suitable time intervals. The usual treatment of the reaction mixture afforded crystalline products **4a** or **5a**. Reactions in methanol afforded resinous mass. The ^1H NMR spectra of the products indicated the presence of aminal **9** and acetal **10**. Attempts to separate these products by fractional crystallization, TLC, and CC failed. The hydrolysis of the crude mixture by aqueous hydrochloride (3 mol dm^{-3}) yielded 2,3,3-triphenylpropenal **11**: mp 176—178 °C (lit,[8] mp 175 °C); ^1H NMR ($CDCl_3$) 6.8—7.6 (m, 15H, 3Ph) and 9.65 (s, 1H, CHO); MS m/z 284(M^+).

Cyclopropenes **3b, c** were treated as follows.

(i) A solution of **3** (1 mmol) in chloroform (5 cm^3) was allowed to stay at room temperature. After the reaction, the crude product was chromatographed over silica gel or recrystallized. The results are given in Table 3. **12a**: oil; IR (KBr) 1600 cm^{-1}; ^1H NMR ($CDCl_3$) δ=5.19 (s, 1H, CH), 5.50 (s, 1H, CH), 6.40 (s, 1H, CH), and 6.7—7.5 (m, 20H, Arom). ^{13}C NMR ($CDCl_3$) δ=117.9(t), 120.9(d), 121.1, 121.6, 122.8, 125.2, 127.0, 127.3(d), 127.5(d), 127.8(d), 128.1(d), 128.5(d), 128.8(d), 129.2, 135.1(s), 141.1(s), 143.2(s), 145.3(s), and 148.1(s). Found: C, 90.01; H, 6.13; N, 3.86%; M^+, 373. Calcd for $C_{28}H_{23}N$: C, 90.08; H, 6.17; N, 3.74%; M, 373. **12b**: mp 115—116 °C; IR (KBr) 1570 cm^{-1}; ^1H NMR ($CDCl_3$) δ=1.95 (d, J=7 Hz, 3H, Me), 6.11 (s, 1H, =CH), 6.12 (q, J=7 Hz, =CHMe), and 6.6—7.5 (m, 20H, 4Ph). ^{13}C NMR ($CDCl_3$) δ=15.4(q), 16.1(q), 119.4, 121.3(d), 122.1, 123.1, 125.4, 125.6(d), 126.8, 126.9(d), 127.0(d), 127.1(d), 127.4, 127.6(d), 127.8(d), 127.9(d), 128.0(d), 128.1(d), 128.2(d), 128.5(d), 128.7(d), 129.7(d), 131.4, 135.4(s), 136.8, 138.1, 139.0(s), 140.6(s), 141.5, 142.1, 144.7(s), 145.4(s), and 146.6. Found: C, 89.98; H, 6.51; N, 3.51%; M^+, 387. Calcd for $C_{29}H_{25}N$: C, 89.92; H, 6.46; N, 3.62%; M, 387.

Acidic hydrolyses of **12** afforded vinyl ketones **13** in quantitative yields. **13a**: oil; IR(neat) 1690 cm^{-1}; ^1H NMR ($CDCl_3$) δ=3.95 (s, 2H, CH_2), 5.80 (s, 1H, =CH), 6.05 (s, 1H, =CH), 6.6—8.0 (m, 10H, 2Ph). Found: C, 86.33; H, 6.32%; M^+, 222. Calcd for $C_{16}H_{14}O$: C, 86.45; H, 6.35%; M, 222. **13b**: oil; IR (neat) 1680 cm^{-1}; ^1H NMR ($CDCl_3$) δ=1.65 (d, J=7 Hz, 3H, Me), 3.80 (s, 2H, CH_2), and 6.7—7.6 (m, 10H, 2Ph). Found: C, 86.36; H, 6.89%; M^+, 236. Calcd for $C_{17}H_{16}O$: C, 86.40; H, 6.82%; M, 236.

(ii) A solution of **3** (1 mmol) in benzene (10 cm^3) was heated at reflux until the disappearance of the absorption at around 1800 cm^{-1} in IR spectrum. Evaporation of the solvent under reduced pressure and trituration with cold ethanol afforded crystalline 1-aminoindene **5** and oily 1-aminobutadiene **14**. The former product was recrystallized from ethanol. The latter oil was hydrolyzed with aqueous hydrochloric acid (3 mol dm^{-3}) at room temperature for one day. The chloroform extract gave crystalline aldehyde **15** from ethanol. The results are collected in Table 3. **14c**: mp 103—105 °C; IR (KBr) 1590 cm^{-1}; ^1H NMR ($CDCl_3$) δ=1.75 (s, 3H, Me), 2.08 (s, 3H, Me), 6.40 (s, 1H, CH), and 6.5—7.5 (m, 20H, 4Ph). ^{13}C NMR ($CDCl_3$) δ=22.5(q), 23.1(q), 122.3(d), 122.4(d), 125.7(d), 125.9(d), 127.0(d), 127.6(d), 128.4(d), 128.7(d), 129.6(d), 130.4(s), 132.3(s), 132.4(d), 137.2(s), 138.1(s), 142.4(s), and 145.9(s). Found: C, 89.54; H, 6.75; N, 3.71%; M^+, 401. Calcd for $C_{30}H_{27}N$: C, 89.78; H, 6.73; N, 3.49%; M, 401. **15a**: mp 128—130 °C; IR (KBr) 1660 cm^{-1};

^{1}H NMR ($CDCl_3$) 2.18 (s, 3H, Me), 7.0—7.7 (m, 10H, 2Ph), and 9.61 (s, 1H, CHO). Found: *m/z* 222.1039. Calcd for $C_{16}H_{14}O$: M, 222.1045. **15b**: mp 105—106 °C; IR (KBr) 1660 cm^{-1}; ^{1}H NMR ($CDCl_3$) δ=0.90 (t, *J*=7 Hz, 3H, Me), 2.51 (q, *J*=7Hz, 2H, CH_2), 7.0—7.6 (m, 10H, 2Ph), and 9.58 (1H, s, CHO). ^{13}C NMR ($CDCl_3$) δ=12.7(q), 30.2(t), 127.6(d), 128.3 (d), 128.7(d), 129.2(d), 129.7(d), 135.3(s), 137.8(s), 139.9(s), 165.0(s), and 193.2(s). Found: *m/z* 236.1181. Calcd for $C_{17}H_{16}O$: M, 236.1202.

Irradiation of **15a** in benzene with a high-pressure mercury lamp for 8 h gave an equilibrium mixture of two isomers (6:5). New signals ($CDCl_3$) were 2.57 (s, 3H, Me) and 10.35 (s, 1H, CHO). Similarly **15b** gave 1.18 (t, *J*=7 Hz, 3H, Me), 3.09 (q, *J*=7Hz, 2H, CH_2), and 10.37 (s, 1H, CHO) in 7:5.

Preparation of 3-Amino-1,2,3-triphenylcyclopropenes (6). A mixture of triphenylcyclopropenium perchlorate (2 mmol) and secondary amine (6 mmol) in benzene (30 cm^3) was stirred at room temperature for 2 h. In the reaction of diphenylamine 2 mmol of triethylamine was added. The product was recrystallized from benzene-petroleum ether. **6a** in 15% yield: mp 218—220 °C; IR (Nujol) 1810 cm^{-1}; ^{1}H NMR ($CDCl_3$) δ=6.5—8.2 (m, 25H, 5Ph). ^{13}C NMR (C_6D_6) δ=53.0(s), 118.0(s), 121.9(d), 123.5(d), 126.1(d), 128.1(d), 128.3(d), 128.5(s), 129.1(d), and 146.9(s). Found: C, 91.23; H, 5.79; N, 2.97%; M^+, 435. Calcd for $C_{33}H_{25}N$: C, 91.03; H, 5.75; N, 3.22%; M, 435. **6b** in 56% yield: mp 150—151 °C; IR (KBr) 1810 cm^{-1}; ^{1}H NMR ($CDCl_3$) δ=2.5—2.8 (m, 4H, CH_2NCH_2), 3.6—3.9 (m, 4H, CH_2OCH_2), and 7.1—7.9 (m, 15H, 3Ph). ^{13}C NMR ($CDCl_3$) δ=50.9(t), 54.4(s), 67.3(t), 119.5(s), 126.0(d), 127.2(d), 128.3(d), 128.9(d), 129.2(s), 129.8(d), and 144.1(s). Found: C, 85.26; H, 6.54; N, 3.99%; M^+, 353. Calcd for $C_{25}H_{23}NO$: C, 84.99; H, 6.52; N, 3.97%; M, 353. **6c**: in 65% yield: mp 128—130 °C; IR (KBr) 1800 cm^{-1}; ^{1}H NMR ($CDCl_3$) 1.3—1.9 (m, 6H, $(CH_2)_3$), 2.4—2.7 (m, 4H, CH_2NCH_2), and 7.0—7.8 (m, 15H, 3Ph). ^{13}C NMR ($CDCl_3$) δ=24.7(t), 26.8(t), 51.8(t), 54.9(s), 119.5(s), 125.8(d), 127.2(d), 128.3(d), 128.6(d), 128.9(d), 129.6(s), 129.8(d), and 145.0(s). Found: C, 88.59; H, 7.15; N, 3.82%; M^+, 351. Calcd for $C_{26}H_{25}N$: C, 88.89; H, 7.12; N, 3.99%; M, 351.

References

1) H. Heydt, P. Eisenbarth, K. Feith, K. Urgast, G. Maas, and M. Regitz, *Israel. J. Chem.*, **27**, 96 (1986) and references cited therein.

2) a) H. Yoshida, H. Sano, M. Kato, T. Ogata, and K. Matsumoto, *Bull. Chem. Soc. Jpn.*, **59**, 2833 (1986) and references cited therein. b) H. Yoshida, T. Tamai, T. Ogata, and K. Matsumoto, *Bull. Chem. Soc. Jpn.*, **61**, 2891 (1988).

3) M. G. Steinmetz and R. T. Mayers, *J. Am. Chem. Soc.*, **107**, 2111 (1985).

4) R. Breslow, T. Eicher, A. Krebs, R. A. Peterson, and J. Posner, *J. Am. Chem. Soc.*, **87**, 1320 (1965).

5) R. C. Kerber and C. Hsu, *J. Am. Chem. Soc.*, **95**, 3239 (1973).

6) H. Yoshida, K. Yagi, T. Tamai, H. Sano, T. Ogata, and K. Matsumoto, *Bull. Chem. Soc. Jpn.*, **58**, 1073 (1985).

7) A. Lowenbein and G. Ulich, *Chem. Ber.*, **58**, 2662 (1925).

8) H. Staudinger, *Ber.*, **42**, 4249 (1910).

9) F. L. Scott and R. N. Butler, "Carbonium Ions," ed by G. A. Olah and P. R. von Schleyer, Wiley-Interscience, New York (1973), Vol. IV, p. 1643.

10) T. S. Sorensen, "Carbonium Ions," ed by G. A. Olah and P. R. von Schleyer, Wiley-Interscience, New York (1973), Vol. II, p. 807.

11) R. A. Moss, *Acc. Chem. Res.*, **13**, 58 (1980).

12) M. A. Battiste, B. Halton, and R. H. Grubbs, *Chem. Commun.*, **1967**, 907.

Cyclopropenone Oximes: Preparation and Reaction with Isocyanates

Hiroshi YOSHIDA,* Hideki OHTSUKA, Keisuke YOSHIDA, Yoshiyuki TOTANI, Tsuyoshi OGATA, and Kiyoshi MATSUMOTO†
Department of Applied Chemistry, Faculty of Engineering, Shizuoka University, Hamamatsu 432
†College of Liberal Arts and Sciences, Kyoto University, Kyoto 606
(Received June 8, 1988)

2,3-Diphenyl-, 2-methyl-3-phenyl-, and 2-methyl-3-(4-methylphenyl)cyclopropenone oxime hydrochlorides (**3**) were prepared in good yields from the corresponding cyclopropenones and hydroxylamine hydrochloride in methanol. The salts **3** reacted with alkyl and aryl isocyanates in the presence of triethylamine to afford 1:2 addition products 4,6-diazaspiro[2.3]hexenones in moderate yields. In contrast, acetone, acetophenone, and cyclohexanone oximes reacted with twice excess of methyl isocyanates to give linear 1:2 addition products and benzophenone oxime yielded only 1:1 addition product.

The physical and chemical properties of cyclopropenones, cyclopropenium ions, and triafulvenes have been of great interest and are currently being investigated[1] as microcyclic aromatics. In a continuation of our studies on the chemistry of cyclopropenium salts possesing heteroatom substituents[2] we have found an easy route for the preparation of cyclopropenone oximes; however, their chemical properties have not yet been well-explored.

Several studies have been repored on the reaction of diphenylcyclopropenone (**1a**) with hydroxylamine. Breslow[3] has shown that a reaction of **1a** with hydroxylamine hydrochloride **2** in aqueous ethanol yields deoxybenzoin oxime and diphenylisoxazolone. Kitahara[4] has obtained diphenylcyclopropenone oxime (**4a**) as colorless needles from **1a** and **2** in methanol, followed by treating with aqueous sodium hydrogencarbonate. On the other hand, Eicher has prepared 1-hydroxyamino-2,3-diphenylcyclopropenium tetrafluoroborate (**3a** as BF_4 salt) from 1-ethoxy-2,3-diphenylcyclopropenium salt and hydroxylamine.[5] However, only the reaction of **4a** with secondary amines has been shown.[6]

2,3-Diphenyl-, 2-methyl-3-phenyl-, and 2-methyl-3-(4-methylphenyl)cyclopropenone (**1a—c**) reacted easily with hydroxylamine hydrochloride **2** in methanol at room temperature for one day. The hydrochloride **3a** precipitated from the reaction mixture and the salts **3b, c** were obtained as a dichloromethane soluble products. The salts **3a—c** were colorless and stable at room temperature. Upon treating with aqueous sodium hydrogen carbonate or triethylamine yielded free diphenylcyclopropenone oxime **4a** as yellow needles in quantitative yield which were stable for a long-time storage at room temperature. However, the free oximes **4b, c** turned brown and decomposed at room temperature within one hour while giving a resinous mass. The structures of **3a—c** and **4a** were confirmed by IR, ^1H and ^{13}C NMR and mass spectroscopic studies. The NMR spectra ($CDCl_3$+CF_3CO_2H, 10:1) of **3b, c**, as shown in Table 1, revealed the presence of two isomers, corresponding to *E*- and *Z*-form, in nearly

Table 1. Yields and Physical Properties of Cyclopropenone Oxime Derivatives **3** and **4**

	Yield	Mp	IR(KBr)	MS	^1H NMR[a]	^{13}C NMR[a]	Found(Calcd)/%		
	%	θ_m/°C	cm^{-1}	M^+			C	H	N
3a	83	198—202	2940 2740 1920	221	7.8—8.6(m, 15H, Ph)	119.1(s), 119.2(s), 129.9(d), 130.3(d), 133.6(d), 136.2(d), 139.5(s)	69.98 (69.90)	4.53 (4.69)	5.34 (5.43)
4	98[b]	133—136[c]	3150 1880 1850	221	d)	d)	81.32 (81.43)	4.94 (5.01)	6.49 (6.63)
3b	76	137—141	2980 2720 1940	159	2.75 and 2.80(2s, 3H, Me), 7.1—8.3(m, 6H, Arom and NH)	10.1(q), 10.3(q), 118.8(s), 118.9(s), 129.8(d), 133.3(d), 134.2(d), 135.0(d), 135.3(d), 135.5(s), 136.0(d), 136.5(d), 142.4(d), 143.2(s)	61.49 (61.39)	5.01 (5.15)	6.98 (7.15)
3c	69	148—152	2980 2720 1940	173	2.50(s, 3H, Me), 2.70 and 2.75 (2s, 3H, Me), 7.8—8.6 (m, 4H, Arom)	10.0(q), 10.3(q), 20.9(q), 115.9(s), 116.0(s), 130.6(d), 132.6(s), 133.3(d), 133.4(d), 135.9(s), 137.4(s), 142.9(s), 147.2(s), 147.4(s)	62.94 (63.01)	5.88 (5.76)	6.73 (6.68)

a) In a mixture of $CDCl_3$ and CF_3CO_2H (10:1). b) Yield from **3a**. c) Lit,[5] mp 116—116.5 °C. d) Insoluble in $CDCl_3$, methanol-d_4, or CD_2Cl_2.

equal amounts.

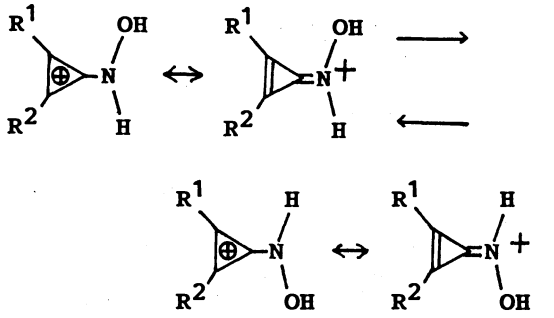

An equimolar reaction of **3a** with methyl isocyanate **5a** in the presence of triethylamine at room temperature gave 4-methyl-6-methylcarbamoyloxy-1,2-diphenyl-4,6-diazaspiro[2.3]hex-1-en-5-one (**6aa**) in a 40% yield. The use of twice excess moles of **5a** yielded **6aa** in a 75% yield. The structure of **6aa** was assigned from its ^{1}H and $^{13}CNMR$, and mass spectroscopic studies and chemical transformations. Thus, upon treating with potassium methoxide in methanol **6aa** afforded 3,3-diaminocyclopropene **7** in a 61% yield. An acidic hydrolysis of **7** gave **1a**, indicating the presence of the cyclopropene ring in **6aa** and **7** (Schemes 2 and 3). A similar treatment of **3a** at room temperature or **3b** at a lower temperature with two moles of **5** yielded spiro compounds **6** in moderate yields, as listed in Table 2. No 1 : 1 addition product could be isolated by us.

It has been well-known that aldoximes and ketoximes react with isocyanates **5** to yield carbamates.[7] To check these results the reaction of ketoximes **8** and **5a** was studied in the presence of triethylamine. The reactions of acetone oxime **8a** with **5a** in 1 : 1 and 1 : 2 molar ratios afforded carbamate-type products **9a** and **10a**, respectively, in moderate yields. Similarly, acetophenone oxime **8b** and cyclohexanone oxime **8d**

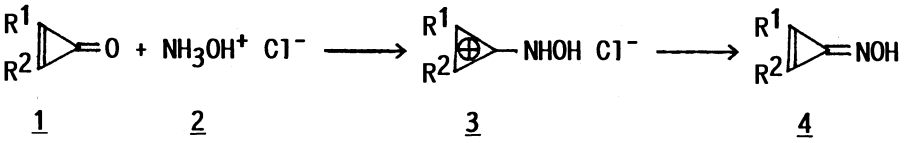

1, 3, 4	R^1	R^2
a	Ph	Ph
b	Me	Ph
c	Me	4-MeC_6H_4

Scheme 1.

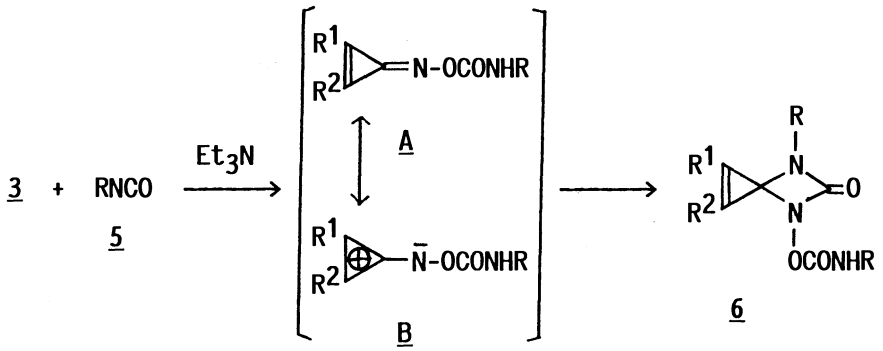

5	R
a	Me
b	n-C_3H_7
c	t-C_4H_9
d	Ph
e	3-MeC_6H_4
f	4-ClC_6H_4

6	R^1	R^2	R
aa	Ph	Ph	Me
ab	Ph	Ph	n-C_3H_7
ac	Ph	Ph	t-C_4H_9
ad	Ph	Ph	Ph
ae	Ph	Ph	3-MeC_6H_4
af	Ph	Ph	4-ClC_6H_4

6	R^1	R^2	R
ba	Me	Ph	Me
bd	Me	Ph	Ph
be	Me	Ph	3-MeC_6H_4
bf	Me	Ph	4-ClC_6H_4

Scheme 2.

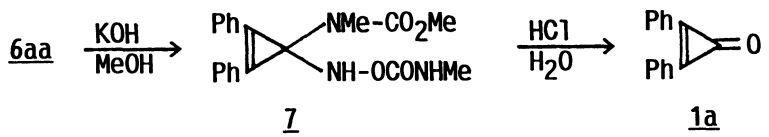

7 1a

Scheme 3.

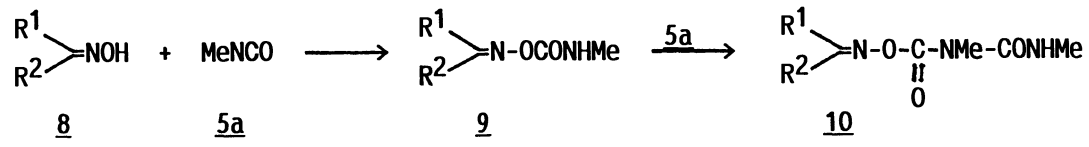

8 5a 9 10

8, 9, 10	R^1	R^2
a	Me	Me
b	Me	Ph
c	Ph	Ph
d	$(CH_2)_5$	

Scheme 4.

Table 2. The Reaction of Oximes **3** or **8** with Isocyanates **5**

Reactants		Reaction conditions			Products	
3	**5**	Mole ratio	Temp/°C	Time/d	(Yield/%)	
3a	**5a**	1 : 1	20	1	**6aa**	(40)
		1 : 2	20	1	**6aa**	(75)
	5b	1 : 2	20	1	**6ab**	(63)
	5c	1 : 2	20	1	**6ac**	(69)
	5d	1 : 2	20	1	**6ad**	(71)
	5e	1 : 2	20	1	**6ae**	(67)
	5f	1 : 2	20	1	**6af**	(48)
3b	**5a**	1 : 2	5	1	**6ba**	(27)
	5d	1 : 2	5	1	**6bd**	(42)
	5e	1 : 2	5	1	**6de**	(38)
	5f	1 : 2	5	1	**6bf**	(32)
8a	**5a**	1 : 1	20	2	**9a**	(85)
		1 : 2	20	2	**10a**	(64)
8b	**5a**	1 : 1	20	1	**9b**	(63)
		1 : 2	20	2	**10b**	(28)
9b	**5a**	1 : 1	20	1	**10b**	(45)
8c	**5a**	1 : 2	20	3	**9c**	(57)
8d	**5a**	1 : 2	20	2	**10d**	(56)

yielded the open-chain 1 : 2 addition products **10b, d**. However, the bulky benzophenone oxime **8c** gave no 1 : 2 addition product under similar reaction conditions (Scheme 4 and Table 2). None of the cyclic product was obtained from reactions of these oxime **8** with **5a**.

Although the isolation of (carbamoyloxyimino)cyclopropene **A**, a 1 : 1 addition product, failed, the intermediacy of **A** was clear from the final product **6**. The reaction of the highly polarized form **B** with **5** would be faster than that of **4** with **5**. Although it has been shown that some C=N derivatives react with **5** to afford the 1 : 1 cycloaddition products, 1,3-diazetidines,[6-8] to our knowledge no spiro derivatives, like **6**, have been reported. The marked difference in the products between **6** from **3** and **10** from **9** can be explained in terms of the polarization of imino nitrogens of oximes **B** and **9**. The highly polarized imino nitrogen of **B** facilitate the formation of **6**, while such activation was not observed for **9**.

Experimental

General. Melting points were uncorrected. The ^{13}C NMR spectra were recorded either on a JEOL JMN FX-60 spectrometer (15.04 MHz) or JEOL JNM FX-90Q (22.49 MHz) and ^1H NMR spectra on a Hitachi R-24B (60 MHz). The IR spectra were recorded on a JASCO A-3 spectrometer.

Preparation of 1-Hydroxyamino-2,3-diphenylcyclopropenium Chloride 3a and 4a. A solution of diphenylcyclopropenone **1a** (5.26 g, 25 mmol) and hydroxylamine

hydrochloride **2** (5.30 g, 76 mmol) in 30 cm^3 of methanol was allowed to stay at room temperature for a day. The precipitated salt **3a** was collected and washed with a small amount of cold methanol and dried under reduced pressure. The salt **3a** was treated with aqueous sodium hydrogencarbonate and extracted with dichloromethane. The extract was dried over sodium carbonate, condensed in vacuo, and recrystallization from methanol yielded diphenylcyclopropenone oxime **4a**. The physical properties are shown in Table 1.

Preparations of 3b and 3c. A solution of **1b** or **1c** (10 mmol) and **2** (10.5 mmol) in methanol (6 cm^3) was reacted at room temperature for one day. The solvent was removed in vacuo and the dichloromethane soluble product was separated. Trituration of the dichloromethane soluble mass with benzene afforded pure cyclopropenone oxime hydrochloride **3b** or **3c** (Table 1).

The Reaction of 3 with Isocyanates 5. A General Procedure. A mixture of **3** (2 mmol), **5** (2 mmol), and triethylamine (4 mmol) in dichloromethane (15 cm^3) was stirred well at appropriate temperature. The resulting solution was poured into cold water and an organic layer was separated. The extract was dried over sodium carbonate, condensed in vacuo, and recrystallized from ether-petroleum ether to give the spiro derivative **6**. **6aa**: mp 135—137 °C; IR (KBr) 3430, 1780, and 1720 cm^{-1}; ^1H NMR ($CDCl_3$) δ=2.59 (s, 3H, CNMe), 2.85 (d, J=6 Hz, 3H, NHMe), 6.13 (bs, 1H, NH), and 7.2—7.9 (m, 10H, 2Ph); ^{13}C NMR ($CDCl_3$) δ=26.5(q), 26.6(q), 65.7(s), 118.4(s), 125.9(s), 128.9(d), 129.9(d), 130.4(d), 155.4(s), and 160.0(s). Found: C, 68.23; H, 4.93; N, 12.64%; M^+, 335. Calcd for $C_{19}H_{17}N_3O_3$: C, 68.05; H, 5.11; N, 12.53%; M, 335. **6ab**: mp 118—122 °C; IR(KBr) 3370, 1770, and 1700 cm^{-1}; ^1H NMR ($CDCl_3$) δ=0.72 (t, J=6Hz, 3H, CH_3), 0.90 (t, J=6Hz, 3H, CH_3), 1.43 (sext, J=6Hz, 4H, $2CH_2CH_3$), 2.45 (t, J=6 Hz, 2H, NCH_2), 3.24 (q, J=6 Hz, 2H, NCH_2), 6.05 (bs, 1H, NH), and 7.2—8.0 (m, 10H, 2Ph). Found: C, 70.58; H, 6.72; N, 10.89%; M^+ 391. Calcd for $C_{23}H_{25}N_3O_3$: C, 70.56; H, 6.43; N, 10.73%; M, 391. **6ac**: mp 142—143 °C; IR (KBr) 3380, 1750, and 1680 cm^{-1}; ^1H NMR ($CDCl_3$) δ=1.29 (s, 9H, t-Bu), 1.40 (s, 9H, t-Bu), 6.0 (bs, 1H, NH), and 7.4—8.1 (m, 10H, 2Ph). Found: C, 71.43; H, 6.79; N, 10.21%; MS, 320 (M^+—t-BuNCO). Calcd for $C_{25}H_{29}N_3O_3$: C, 71.57; H, 6.96; N, 10.01%; M, 419. **6ad**: mp 142—145 °C; IR (KBr) 3330, 1770, and 1710 cm^{-1}; ^1H NMR ($CDCl_3$) δ=7.2—7.7 (m, 21H, 4Ph and NH). Found: C, 75.91; H, 4.32; N, 9.02%; M^+, 459. Calcd for $C_{29}H_{21}N_3O_3$: C, 75.80; H, 4.60; N, 9.14%; M, 459. **6ae**: mp 142—145 °C; IR (KBr) 3330, 1770, and 1710 cm^{-1}; ^1H NMR ($CDCl_3$) δ=2.05 (s, 3H, Me), 2.30 (s, 3H, Me), and 6.8—7.6 (m, 19H, Arom+NH). Found: C, 76.15; H, 5.01; N, 8.73%; MS, 354 (M^+—4-MeC_6H_4NCO). Calcd for $C_{31}H_{25}N_3O_3$: C, 76.36; H, 5.16; N, 8.61%; M, 487. **6af**: mp 146—148 °C; IR (KBr) 3330, 1770, and 1710 cm^{-1}; ^1H NMR ($CDCl_3$) δ=7.1—8.0 (m, 19H, Arom and NH). Found: C, 67.13; H, 4.32; N, 7.82%; M^+, 556. Calcd for $C_{31}H_{23}Cl_2N_3O_3$: C, 66.91; H, 4.16; N, 7.55%; M, 556. **6ba**: mp 135—138 °C; IR (KBr) 3370, 1780, and 1700 cm^{-1}; ^1H NMR ($CDCl_3$) δ=2.45 (s, 3H, Me), 2.55 (s, 3H, Me), 2.85 (d, J=6Hz, 3H, NHMe), 6.1 (bs. 1H, NH), and 7.2—7.8 (m, 5H, Arom). ^{13}C NMR ($CDCl_3$) δ=11.0(q), 26.4(t), 26.6(d), 66.1(s), 115.7(s), 122.7(d), 125.1(s), 128.8(d), 129.3(d), 130.1(d), 155.7(s), and 160.6(s). Found: C, 61.26; H, 5.46; N, 15.09%; M^+, 273. Calcd for $C_{14}H_{15}N_3O_3$: C, 61.55; H, 5.49; N, 15.37%; M, 273. **6bd**: mp 125—128 °C; IR (KBr) 3350, 1770, and 1710 cm^{-1}; ^1H NMR ($CDCl_3$) δ=2.35 (s, 3H, Me) and 6.9—8.1 (m, 16H, Arom and NH). Found: C, 72.67; H, 4.55; N, 10.68%; M^+, 397. Calcd for $C_{24}H_{19}N_3O_3$: C, 72.56; H, 4.78; N, 10.57%; M, 397. **6be**: mp 98—102 °C; IR (KBr) 3050, 1780, and 1720 cm^{-1}; ^1H NMR ($CDCl_3$) δ=2.25 (s, 3H, Me), 2.35 (s, 6H, 2Me), and 6.8—8.1 (m, 14H, Arom). Found: C, 73.25; H, 5.67; N, 9.58%; M^+, 425. Calcd for $C_{26}H_{23}N_3O_3$: C, 73.42; H, 5.40; N, 9.87%; M, 425. **6bf**: mp 141—143 °C; IR (KBr) 3350, 1770, and 1720 cm^{-1}; ^1H NMR ($CDCl_3$) δ=2.85 (s, 3H, Me) and 6.9—8.1 (m, 14H, Arom and NH). Found: C, 61.89; H, 3.52; N, 9.31%; M^+, 474. Calcd for $C_{24}H_{17}Cl_2N_3O_3$: C, 61.83; H, 3.64; N, 9.01%; M, 474.

Methanolysis of 6aa. A solution of **6aa** (1 mmol) and KOH (3 mmol) in methanol (10 cm^3) was stirred at room temperature for 1 h. The mixture was poured into water and extracted with benzene. The benzene extract was dried over sodium carbonate, condensed in vacuo, and recrystallized from petroleum ether to yield the gem-diamine **7**: 61%; mp 122—125 °C; IR (KBr) 3340, 1820, 1770, and 1680 cm^{-1}; ^1H NMR ($CDCl_3$) δ=2.60 (d, J=6Hz, 3H, MeNH), 2.76 (s, 3H, MeN), 3.56 (s, 3H, MeO), 5.72 (bs, 1H, NH), 7.0—8.1 (m, 10H, 2Ph), and 9.52 (bs, 1H, NHO). ^{13}C NMR ($CDCl_3$) δ=26.5(q), 33.9(q), 53.1(q), 58.9(s), 116.1(s), 126.1(s), 128.8(d), 129.7(d), 130.5(d), 159.1(s), and 159.9(s). Found: C, 65.55; H, 5.73; N, 11.23%. M^+, 367. Calcd for $C_{20}H_{21}N_3O_4$: C, 65.38; N, 5.76; N, 11.43%. M, 367. A mixture of **7** (1 mmol), concd HCl (0.3 cm^3), chloroform (3 cm^3), and water (1 cm^3) was stirred well at room temperature for 1 h. The organic extract yielded **1a** in an 89% yield.

The Reaction of Ketoximes 8 with 5a. General Procedure. A solution of **8** (1 mmol), **5a** (1.1 or 2.2 mmol), and triethylamine (1 mmol) in dichloromethane (5 cm^3) was allowed to react at room temperature until the disappearance of **8** by checking the reaction mixture with TLC. The solution was poured into water and an organic layer was separated. The extract was dried over sodium carbonate, condensed, and recrystallized from benzene or ether. The results are listed in Table 2. The physical properties are as follows. **9a**: mp 48—50 °C; IR (KBr) 3350, 1720, and 1700 cm^{-1}; ^1H NMR ($CDCl_3$) δ=1.93 (s, 3H, Me), 1.94 (s, 3H, Me), 2.86 (d, J=6 Hz, NHMe), and 6.40 (bs, 1H, NH). MS m/z 130 (M^+). **10a**: mp 180—183 °C; IR (KBr) 3350, 1720, and 1690 cm^{-1}; ^1H NMR ($CDCl_3$) δ=2.06 (s, 3H, Me), 2.09 (s, 3H, Me), 2.87 (d, J=6 Hz, 3H, NHMe), and 3.28 (s, 3H, CONMe). Found: C, 44.53; H, 7.21; N, 22.48%; M^+, 187. Calcd for $C_7H_{13}N_3O_3$: C, 44.91; H, 6.99; N, 22.44%; M, 187. **9b**: mp 96—98 °C; IR (KBr) 3350 and 1710 cm^{-1}; ^1H NMR ($CDCl_3$) δ=2.38 (s, 3H, MeC=N), 2.91 (d, J=6 Hz, 3H, NHMe), 6.5 (bs, 1H, NH), and 7.2—7.8 (m, 5H, Ph). MS m/z 192 (M^+). **10b**: mp 134—136 °C; IR (KBr) 3370, 1740, and 1690 cm^{-1}; ^1H NMR ($CDCl_3$) δ=2.42 (s, 3H, MeC=N), 2.91 (d, J=6Hz, 3H, NHMe), 3.40 (s, 3H, CONMe), and 7.3—7.9 (m, 5H, Ph). ^{13}C NMR ($CDCl_3$) δ=14.7(q), 27.2(q), 30.3(q), 126.9(d), 128.5(d), 130.7(d), 134.2(s), 154.5(s), 154.8(s), and 163.3(s). Found: C, 57.72; H, 5.87; N, 16.48%; M^+, 249. Calcd for $C_{12}H_{15}N_3O_3$: C, 57.82; H, 6.06; N, 16.85%; M, 249. **9c**: mp 162—164 °C; IR (KBr) 3370, 1740, and 1720 cm^{-1}; ^1H NMR ($CDCl_3$) δ=2.95 (d, J=3 Hz, 3H, NHMe), 6.35 (bs, 1H, NH), and 7.2—7.6 (m, 10H, 2Ph). MS m/z 254 (M^+). **10d**: mp 134—137 °C; IR (KBr) 3350, 1720, and 1690 cm^{-1}; ^1H NMR ($CDCl_3$) 1.5—2.7 (m, 10H, $(CH_2)_5$), 2.93 (d, J=6 Hz, 3H, NHMe), and 3.28 (s, 3H, CONMeCO). Found: C, 52.63; H, 7.49; N, 18.11%. Calcd for $C_{10}H_{17}N_3O_3$: C, 52.85; H, 7.53; N, 18.48%.

References

1) Recent examples: R. A. Moss, S. Shen, K. Krogh-Jespersen, J. A. Potenza, H. J. Schugar, and R. C. Munjal, *J. Am. Chem. Soc.*, **108**, 134 (1986); F. J. Kaiser, G. Offermann, and G. Seitz, *Chem. Ber.*, **119**, 2141 (1986); T. Sugimoto, M. Shibata, S. Yoneda, Z. Yoshida, Y. Kai, K. Miki, N. Kasai, and T. Kobayashi, *J. Am. Chem. Soc.*, **108**, 7032 (1986); W. Sander and O. L. Chapman, *Angew. Chem., Int. Ed. Engl.*, **27**, 398 (1988).

2) H. Yoshida, H. Ohtsuka, T. Ogata, and K. Matsumoto, *Chem. Lett.*, **1987**, 659.

3) R. Breslow, T. Eicher, A. Krebs, R. A. Peterson, and J. Posner, *J. Am. Chem. Soc.*, **87**, 1320 (1965).

4) Y. Kitahara and M. Funamizu, *Bull. Chem. Soc. Jpn.*, **37**, 1897 (1964).

5) T. Eicher and G. Frenzel, *Z. Naturforsch., B*, **20**, 274 (1965).

6) T. Eicher, S. Boehm, H. Eherhaldt, R. Harth, and D. Lerch, *Liebigs Ann. Chem.*, **1981**, 765.

7) R. Richter and H. Ulrich, "The Chemistry of Cyanates and Their Thio Derivatives," ed by S. Patai, John Wiley & Sons, Chichester (1977).

8) H. Ulrich, "Cycloadditon Reactions of Heterocumulenes," Academic Press, New York (1967).

9) J. W. Timberlake and E. S. Elder, "Comprehensive Heterocyclic Chemistry," ed by W. Lwowski, Pergamon Press, Oxford (1984), Vol. 7, p. 449.

Carbonylation of Enynes under Hydroformylation Conditions Catalyzed by Rhodium Carbonyl. A New Method for Synthesis of Cyclic Enones

Kazuo DOYAMA, Takashi JOH, Tomoo SHIOHARA,† and Shigetoshi TAKAHASHI*
The Institute of Scientific and Industrial Research, Osaka University, Ibaraki, Osaka 567
†Central Research Laboratory, Sekisui Chemical Co., Ltd., Mishima-gun, Osaka 618
(Received June 22, 1988)

The reactivities of 1-buten-3-yne derivatives toward hydroformylation were studied using a rhodium catalyst. Unexpectedly, cyclopentenone derivatives were obtained in moderate yields together with formyl-substituted dienes and unsaturated lactones. This reaction offers a new method for the catalytic synthesis of cyclopentenones. A mechanism for the cyclic carbonylation of enynes is also discussed.

The transition-metal-catalyzed carbonylation of unsaturated compounds with carbon monoxide is one of the most important reactions in synthetic organic chemistry, and a number of reports have appeared so far.[1]

Using synthetic gas (H_2/CO), olefins are effectively carbonylated by the catalysis of such transition metal complexes as Co and Rh to yield the hydroformylated products (oxo process).[2] Although this method is applicable to a variety of olefins such as alkenes, acrylates, and dienes, the reports dealing with the hydroformylation of acetylenes are few. It is known that acetylenes show lower reactivities than olefins toward cobalt-catalyzed hydroformylation. This may be attributed to the formation of a stable cobalt-acetylene complex[3] (Eq. 1) resisting hydroformylation

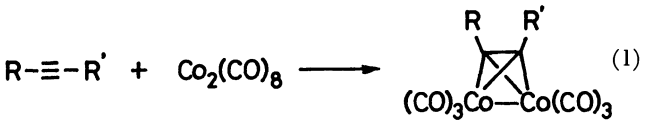

(1)

under usual reaction conditions.[4] Under drastic conditions, i.e., higher reaction temperature and higher CO pressure, acetylenes are converted mainly to saturated aldehydes in analogy with the case of hydroformylation of olefins.[5]

Thus, we attempted to compare the reactivity of carbon-carbon triple bonds with that of double bonds toward hydroformylation. Enynes, R-C≡C-CH=CH-R′, are a suitable candidate for this purpose because they have carbon-carbon triple molecular bonds and double bonds. Moreover, a variety of their derivatives can be conveniently prepared from the palladium-catalyzed reaction (Eq. 2) which we reported previously.[6] Then, we have examined the

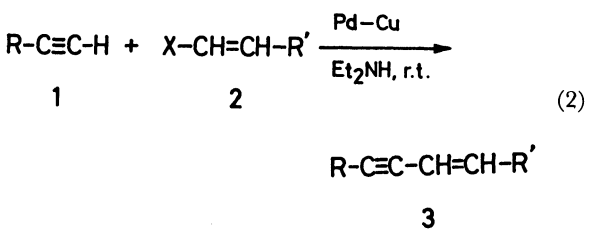

(2)

reactivity of the enynes toward rhodium-catalyzed hydroformylation, and found that the triple bonds are much more reactive than the double bonds and, unexpectedly, the cyclic enones are obtained in moderate yields which might be derived from the hydrocarbonylation of the acetylene group along with the participation of the olefinic part.[7] Here, we wish to report on the results in detail as well as the reaction mechanism.

Results and Discussion

Reactions of 1,4-Diphenyl-1-buten-3-yne (3a) under Hydroformylation Conditions. Enyne **3a** was reacted with carbon monoxide and hydrogen in the presence of a catalytic amount of $Rh_4(CO)_{12}$ at 60 °C. The reaction mixture was concentrated in vacuo and chromatographed on silica. Gradient elution by hexane-benzene gave three carbonylated products, **4a**, **5a**, and

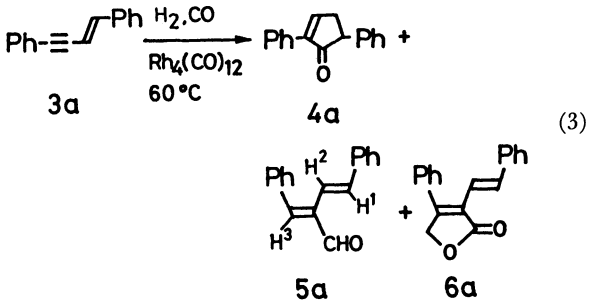

(3)

6a, together with a small amount of the recovered starting material (Eq. 3). One of them was identified as an unexpected cyclocarbonylation product, cyclopentenone **4a**, and others were a normal monoformylated compound **5a** and lactone **6a**. The structure of **4a** was determined by ^{1}H NMR, which showed a characteristic AMX pattern in the aliphatic region and a double-doublet at δ 7.96 (olefinic proton). The parent ion peak at m/z 234 in the mass spectrum and the CO stretching band at 1700 cm^{-1} in the IR spectrum are also consistent with the assigned structure of **4a**. The major product **5a** showed a CO stretch at 1695 cm^{-1} in the IR spectrum and a ^{1}H NMR signal at δ 9.65 (s),

indicating that this compound is α,β-unsaturated aldehyde. To confirm the structure, **5a** was led to 2,4-dinitrophenylhydrazone, which showed ^{1}H NMR signals at δ 7.07 (s) and 7.15 (d, J=16.5 Hz) attributable to H^3 and H^1, respectively. Product **6a** showed a parent ion peak at m/z 262 in the mass spectrum, indicating that two molecules of carbon monoxide and one molecule of hydrogen were introduced to the starting material. The IR spectrum exhibited ν_{CO} at 1760 cm^{-1} and the ^{1}H NMR spectrum signals appeared at δ 5.05 (s, 2H), 7.02 (d, 1H, J=16.3 Hz), and 8.98 (d, 1H, J=16.3 Hz). These spectral data indicate that **6a** has an unsaturated lactone ring and a trans-olefinic part; the structure was then defined as that shown in Eq. 3.

Cyclopentenone derivative **4a** is derived from the hydrocarbonylation of the acetylene group along with a participation of the olefinic part. On the other hand, formyl-substituted diene **5a** and lactone **6a** are formed by the carbonylation of just the acetylene group of **3a**; the olefinic moiety remains intact. This implies that the acetylenic part in the conjugated enynes is more reactive than the olefinic part under the hydroformylation conditions. This idea is also supported by a competitive reaction between diphenylacetylene (**7**) and

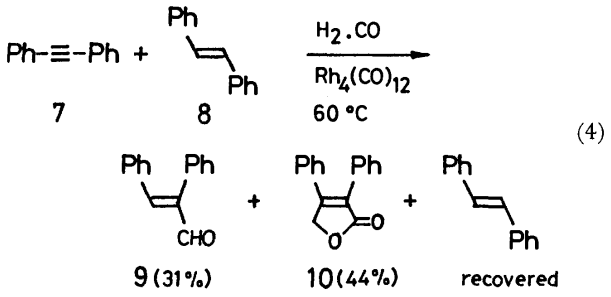

(4)

diphenylethylene (**8**), which gave only the carbonylated product derived from diphenylacetylene, whereas diphenylethylene was recovered, as shown in Eq. 4.

In order to investigate the effect of the partial pressure of carbon monoxide and hydrogen on the product distribution, **3a** was reacted at 60 °C under the conditions shown in Table 1. In these experiments, the total pressure was kept constant at 200 atm and the ratio of carbon monoxide to hydrogen was varied as shown in Table 1. The conversion and the product distribution are plotted against the partial pressure (Fig. 1). As can be seen from Fig. 1, the conversion of **3a** increases with the partial pressure of hydrogen. The selectivities for both **4a** and **5a** have a maximum point around a pressure of H_2/CO=1. Thus, the pressure dependence of the selectivity is commonly observed in hydroformylation reactions.[2] On the other hand, the selectivity of **6a** is almost constant to the H_2/CO ratio. This fact implies that the catalytic cycle producing compounds, **4a** and **5a**, would be different from that of **6a**, which will be discussed later.

In order to obtain further information on the reac-

Table 1. Partial Pressure Dependence of the Reactivity of **3a**[a)]

H_2	CO	Conversion	Selectivity[b)]/%		
atm	atm	%	**4a**	**5a**	**6a**
20	180	29	9	12	11
50	150	57	17	28	13
100	100	91	23	32	9
120	80	97	19	22	23

a) Reaction conditions: **3a**, 4.85 mmol; $Rh_4(CO)_{12}$, 0.027 mmol; benzene, 10 ml; 60 °C; 6 h. b) Isolated yields based on **3a** consumed.

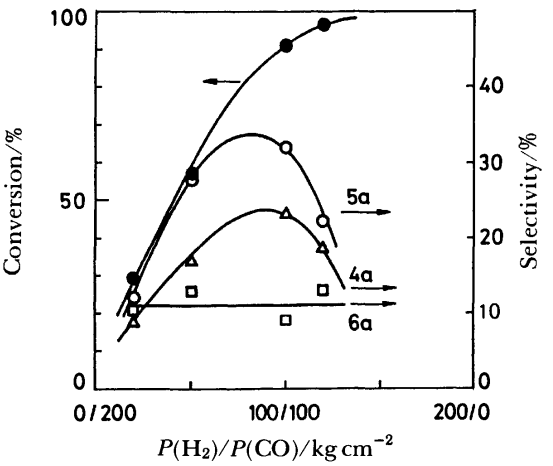

Fig. 1. Partial pressure dependence of conversion (●) and selectivity of **4a** (△), **5a** (○), and **6a** (□).

tion, the reaction temperature was increased to 120 °C. A direct isolation of the carbonylated products was so difficult in this case that the reaction mixture was first led to the stable acetals by treating with ethylene glycol in the presence of a catalytic amount of *p*-toluenesulfonic acid. Then, the resultant products were separated by silica column chromatography, giving four acetals **11a**—**14a** (Eq. 5). Thus, in this reaction at

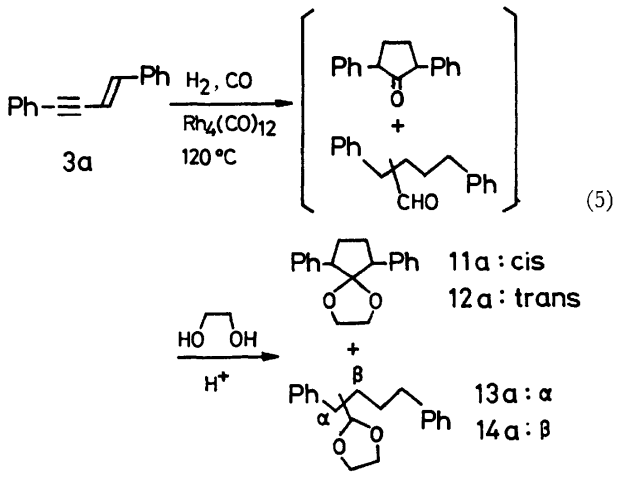

(5)

120 °C, saturated cyclic ketone and aldehyde were formed, meaning that **4a** and **5a** once formed would be hydrogenated at a higher temperature under the

hydroformylation conditions to give saturated aldehydes and kotones. In fact, **4a** was hydrogenated at 120 °C and gave 2,5-diphenylcyclopentanone (**15**) in an almost quantitative yield.

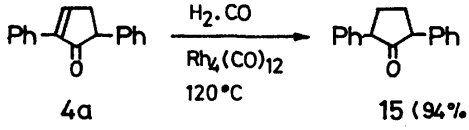

4a 15 (94%) (6)

Reaction of Enynes other than 3a under the Hydroformylation Conditions. In order to examine the scope of the present reaction and to obtain information about the reaction mechanism, the hydroformylation of conjugated enynes **3b**, **3c**, and **3d**, and a nonconjugated enyne **16** was also carried out. The results are summerized in Table 2.

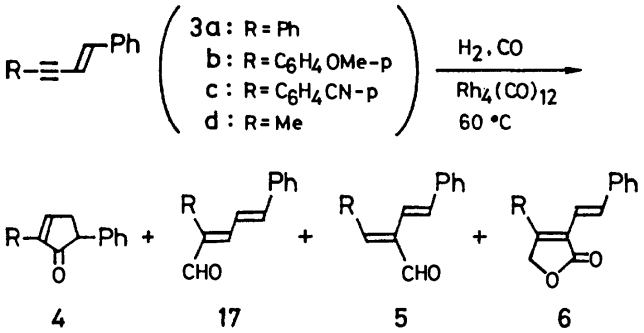

(7)

Of the enynes having aryl substituents at the acetylenic part (**3a**, **3b**, and **3c**), the reactivity increases with increasing the electron density of the acetylenic part: **3c**<**3a**<**3b**. But this electronic effect is not clearly reflected by the product distribution.[8] The methyl-substituted enyne **3d** showed a lower reactivity than the aryl substituted enynes and gave a different result: that not cyclopentenone derivative **4d** but (*E*,*E*)-α-formyldiene **17d** was formed with 19% selectivity. It is noteworthy that the latter **17** was not found among the products from the hydroformylation-yielding cyclopentenones. This phenomenon is discussed later.

On the other hand, a nonconjugated enyne, 1,5-diphenyl-1-penten-3-yne (**16**), showed a similar reactivity to that of the conjugated ones toward hydroformylation, giving cyclohexenone **18**, 2-formyl-1,4-alkadiene **19**, and lactone **20** in 40, 11, and 18% selectivity, respectively (Eq. 8). This result indicates that the formation of cyclic enones does not require the conjugation of unsaturated bonds.

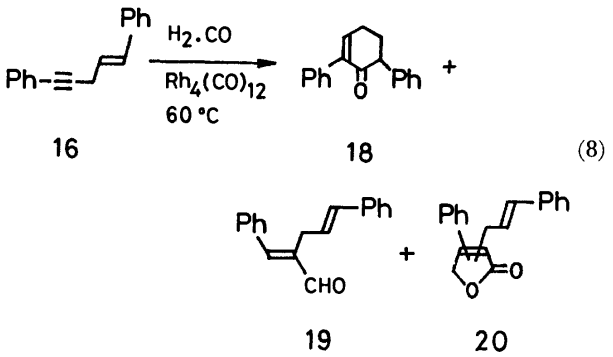

(8)

There are some examples[9–11] of carbonylations of enynes to afford cyclopentenones using cobalt carbonyl. The carbonylation of titana- or zirconacyclopentene complexes, obtained from the reaction of enynes with an equimolar amount of dichlorotitanium or zirconium complexes, also affords cyclopentenones in good yields.[12] With respect to these reactions, all of which being the stoichiometric syntheses from enynes, our method may be characterized in terms of the "catalytic" synthesis of cyclopentenones from the conjugated enynes, though the selectivity is not so high at the present stage.

Reaction Mechanism. First of all, in order to determine whether the formation of cyclic products is characteristic to the enynes, 1,4-diphenyl-1,3-butadiene (**21**), having the same carbon skeleton as enyne **3a**, was reacted under the same conditions as adopted for **3a**. At 60 °C, **21** gave only an α-monoformylated product **22** with 68% selectivity; no cyclization product was formed (Eq. 9). This suggests that the cyclization of

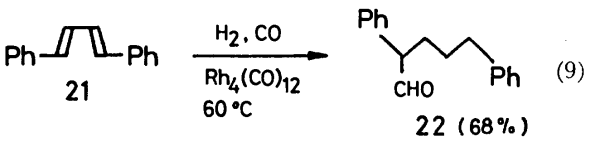

(9)

enynes does not pass through butadiene derivatives which might be formed under the conditions if the addition of hydrogen to the acetylenic part of enynes occurs during the first step. Thus, it should be emphasized that the cyclopentenone derivatives are formed directly from the conjugated enynes by the catalysis of the rhodium complex under the hydroformylation conditions.

As described above, the acetylenic part of enynes is thought to be more reactive than the olefinic one toward the rhodium-catalyzed hydroformylation based on judging the structure of the products. Therefore, the first attack of the rhodium carbonyl hydride species H-[Rh], presumably $HRh(CO)_3$, to the enynes may

Table 2. Conversion and Product Distribution for the Reaction of 3[a]

Enyne	Conversion	Selectivity[b]/%			
	%	4	17	5	6
3a	91	23	0	31	9
3b	100	15	0	20	12
3c	70	17	0	23	6
3d	49	0	19	17	20

a) Reaction conditions: **3**, 4.85 mmol; $Rh_4(CO)_{12}$, 0.027 mmol; benzene, 10 ml; H_2, 100 atm; CO, 100 atm; 60 °C; 6 h. b) Isolated yields based on **3** consumed.

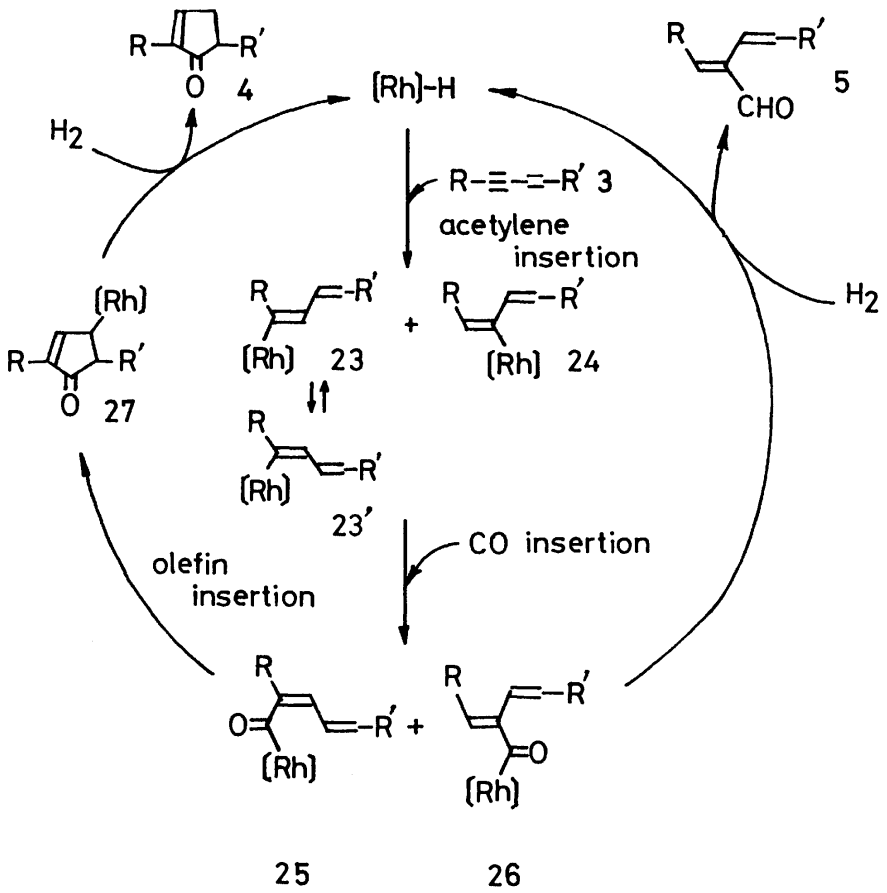

Scheme 1. Proposed reaction mechanism.

occur at the acetylenic part. On the basis of this assumption, a reaction mechanism giving **4** and **5** is proposed in Scheme 1.

The first step may be an insertion of the acetylenic part of the enyne to the Rh-H bond, which gives two η^1-diene intermediates, **23** and **24**, depending on the direction of Rh-H addition to the triple bond. They undergo a CO insertion during the next step, forming an isomeric pair of η^1-acyl intermediates, **25** and **26**. α-Acyl intermediate **25** would cyclize to give **27** by an intramolecular insertion of the olefinic part into the Rh-C bond, followed by a cleavage of the Rh-C bond by hydrogen or H-[Rh] to give cyclopentenone derivative **4**. On the other hand, since β-acyl intermediate **26** wouldn't be able to cyclize, due to the steric factor, it gives β-formyl diene **5** via the direct cleavage of **26** by the action of either H-[Rh] or hydrogen. Under the severer reaction conditions, these unsaturated products would suffer hydrogenation to give saturated products.

The formation of other products may be understood by the following reaction path. Thus, α-formyldiene **17**, which was obtained from the reaction of methyl substituted enyne **3d**, may be formed through intermediate **23** having (*E*,*E*)-diene structure. Whereas, cyclocarbonylation passing through **27** may require (*Z*,*E*)-diene structure **23'**. This suggests the isomerization of (*E*,*E*)-dienyl rhodium intermediate **23** to (*Z*,*E*)-isomer **23'**. Interchanges between (*Z*)- and (*E*)-alkenyl isomers have been reported concerning transition metal-alkenyls such as iron[13] and nickel[14] complexes. On the other hand, a reaction at 120 °C gave both cyclopentanone and saturated aldehyde **13a** (isolated as acetal), which was formed by hydrogenation of α-formyldiene, implying that the olefin insertion step of **25** may compete with the cleavage of the Rh-C bond by either H-[Rh] or hydrogen.

The mechanism yielding unsaturated lactone **6** is not clear at present. But it may be sure that the first step of the lactone formation would not involve an insertion of the acetylenic part to H-[Rh]. The unsaturated lactone ring is constructed by a carbon-carbon triple bond with two molecules of carbon monoxide and one molecule of hydrogen, and the carbon monoxide formally adds to the triple bond in cis-fashion. There are some reports on the formation of lactones from the transition metal-catalyzed carbonylation of acetylenes in alcoholic media.[15]

In the course of our study on the carbonylation of the enynes, we also found that the acetylenes give, selectively, unsaturated lactones under water gas shift conditions.[16] This suggests that the formation of **6** under hydroformylation conditions may be closely related to the presence of a small amount of water in the reaction mixture.

Experimental

General Methods. High-pressure work was carried out by using a stainless-steel autoclave.

Rhodium carbonyl, $Rh_4(CO)_{12}$, was prepared by methods described in the literature.[17] Solvents were distilled before use. The reagents were purified by either distillation or recrystallization.

Melting points were determined by Yanagimoto micro melting point apparatus and are uncorrected. Infrared spectra were recorded on a Hitachi 295 infrared spectrophotometer. Nuclear magnetic resonance spectra were run on a JEOL JNR-PMX 60SI or a Bruker AM-360. Chemical shifts are expressed in parts per million downfield from internal standard, tetramethylsilane. Mass spectra were obtained with JEOL JMS 06. Elemental analyses were performed by the Material Analysis Center, I. S. I. R., Osaka University.

Preparation of Enynes. Conjugated enynes were prepared by a reported method[6] and the preparation of new enynes, **3b** and **3c**, are described below. Non-conjugated enyne **16** was prepared by the reaction of (*E*)-1-phenyl-3-bromopropane with copper(I)-phenylacetylide in the presence of LiBr.[18]

4-(4-Methoxyphenyl)-1-phenyl-1-buten-3-yne (3b). A solution of (4-methoxyphenyl)acetylene (2.0 g, 15.1 mmol), (*E*)-β-bromostyrene (2.8 g, 15.1 mmol), in diethylamine (30 ml) was placed in a 100 ml two-necked round-bottom flask. To the solution were added $PdCl_2(PPh_3)_2$ (35 mg) and CuI (10 mg). Then, the reaction mixture was stirred at room temperature under N_2 for 24 h. The precipitated $Et_2NH \cdot HBr$ was filtered off and washed several times with Et_2NH. The filtrate and the washing were combined and evaporated to dryness. The pale-yellow solid, thus obtained, was dissolved in a small amount of benzene and passed through a short alumina column to remove the catalyst. Elution with benzene gave a crude product, which was recrystallized from EtOH to yield 2.76 g (78%) of **3b**.

3b: Colorless fine needles from EtOH, mp 94—95 °C; ^{1}H NMR (360 MHz, $CDCl_3$) δ=3.81 (s, 3H, CH_3), 6.38 (d, 1H, PhCH=C<u>H</u>, *J*=16.2 Hz), 6.86 (bd, 2H, *o*-H to OCH_3, *J*=8.7 Hz), 6.99 (d, 1H, PhC<u>H</u>=CH, *J*=6.2 Hz), 7.2—7.5 (m, 9H, arom); IR (Nujol) 2190 cm^{-1}; Found: C, 86.89; H, 5.78%. Calcd for $C_{17}H_{14}O$: C, 87.15; H, 6.02%.

4-(4-Cyanophenyl)-1-phenyl-1-buten-3-yne (3c) was prepared similarly from the reaction of (4-cyanophenyl)acetylene with (*E*)-β-bromostyrene in 78% yield.

3c: Colorless needles from EtOH, mp 127—129 °C; ^{1}H NMR (360 MHz, $CDCl_3$) δ=6.37 (d, 1H, PhCH=C<u>H</u>, *J*=16.2 Hz), 7.10 (d, 1H, PhC<u>H</u>=CH, *J*=16.2 Hz), 7.3—7.45 (m, 5H, Ph), 7.5—7.62 (m, 4H, C_6H_4-CN, AA'BB'); IR (Nujol) 3230, 2210, 2095 cm^{-1}; Found: C, 89.28; H, 5.07; N, 6.10%. Calcd for $C_{17}H_{11}N$: C, 89.06; H, 4.84; N, 6.11%.

Reaction of Enynes. For an assignment of the spectra, the protons of cyclopentenones and 2,4-dinitrophenylhydrazone are numbered as shown below.

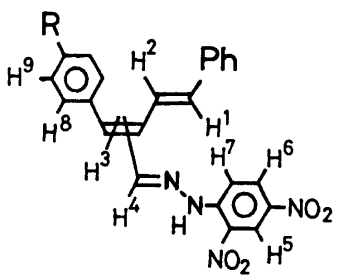

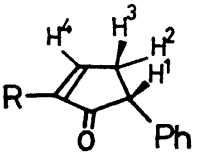

Reaction of 1,4-Diphenyl-1-buten-3-yne (3a) at 60 °C. A solution of **3a** (1.0 g, 4.9 mmol) and $Rh_4(CO)_{12}$ (20 mg, 0.027 mmol) in benzene (10 ml) was put into a 20 ml glass ampule, which was placed in a 100 ml stainless-steel autoclave. The autoclave was charged with 100 atm of carbon monoxide and 100 atm of hydrogen, and then shaken for 6 h at 60 °C. After cooling to room temperature, the reaction mixture was poured onto silica gel (2 g) and evaporated to dryness. It was then placed at the top of a column containing 30 g of silica gel. Gradient elution with hexane-benzene gave three carbonylated products, **4a** (23%), **5a** (32%), and **6a** (9%) together with a small amount of the starting material (90 mg; 91% conversion).

4a: Colorless columns from hexane, mp 75—76 °C; ^{1}H NMR (360 MHz, $CDCl_3$) δ=2.83 (ddd, 1H, H^2, J_{12}=2.8 Hz, J_{24}=2.8 Hz, J_{23}=19.8 Hz), 3.26 (ddd, 1H, H^3, J_{23}=19.8 Hz, J_{13}=7.1 Hz, J_{34}=3.0 Hz), 3.77 (dd, 1H, H^1, J_{12}=2.8 Hz, J_{13}=7.1 Hz), 7.1—7.6 (m, 10H, arom), 7.96 (dd, 1H, H^4, J_{24}=2.8 Hz, J_{34}=3.0 Hz); IR (Nujol) 1700 cm^{-1}; MS, *m/z* 234 (M^+); Found: C, 87.29; H, 5.74%. Calcd for $C_{17}H_{14}O$: C, 87.15; H, 6.02%.

5a: Pale-yellow viscous oil; IR (neat) 1695 cm^{-1}. This was led to 2,4-dinitrophenylhydrazone, **5a-(2,4-D)**, and purified by recrystallization.

5a-(2,4-D): Dark-brown crystals from benzene, mp 221—223 °C; ^{1}H NMR (360 MHz, $CDCl_3$) δ=7.07 (s, 1H, H^3), 7.15 (d, 1H, H^1, J_{12}=16.5 Hz), 7.3—7.5 (m, 11H, H^2 and Ph), 7.98 (d, 1H, H^5, J_{56}=9.6 Hz), 8.06 (s, 1H, H^4), 8.35 (dd, 1H, H^6, J_{67}=2.5 Hz, J_{56}=9.6 Hz), 9.17 (d, 1H, H^7, J_{67}=2.5 Hz), 11.32 (s, 1H, NH); IR (Nujol) 3280 1625, 1590, 1515, 1340, 1305, 745, 690 cm^{-1}; MS, *m/z* 414 (M^+); Found: C, 66.86; H, 4.10; N, 13.47%. Calcd for $C_{23}H_{18}N_4O_4$: C, 66.66; H, 4.38; N, 13.52%.

6a: Pale-yellow crystals from hexane-benzene, mp 114—115 °C; ^{1}H NMR (360 MHz, $CDCl_3$) δ=5.05 (s, 2H, CH_2), 7.02 (d, 1H, PhCH=C<u>H</u>, *J*=16.3 Hz), 7.25—7.5 (m, 10H, arom), 7.99 (d, 1H, PhC<u>H</u>=CH); IR (Nujol) 1760 cm^{-1}; MS, *m/z* 262 (M^+); Found: C, 82.13; H, 5.42%. Calcd for $C_{18}H_{14}O_2$: C, 82 42; H, 5.38%.

Reaction of 1,4-Diphenyl-1-buten-3-yne (3a) at 120 °C. In a similar manner to the procedure adopted for the reaction at 60 °C, **3a** was reacted with carbon monoxide and hydrogen in the presence of a catalytic amount of $Rh_4(CO)_{12}$ at 120 °C for 4 h. The reaction mixture was then placed into a 100 ml flask fitted with a Soxhlet extraction apparatus which was filled with Molecular Sieves 3A. To the solution were added ethylene glycol (0.30 g) and a catalytic amount of *p*-toluenesulfonic acid with an additional 20 ml of benzene. Then, azeotropic dehydration was continued under nitrogen for 4 h. The solution was cooled to room temperature, poured onto silica gel (3 g) and evaporated to dryness. It was then placed at the top of a column containing 30 g of silica gel. Gradient elution with hexane-benzene gave four acetals, in the order of increasing polarity, **11a** (8%), **12a** (7%), **14a** (26%), and **13a** (12%). **11a** and **12a** were further purified by recrystallization and **13a** and **14a** by microdistillation.

11a: Colorless columns from hexane, mp 106—107 °C; ^{1}H NMR (360 MHz, $CDCl_3$) δ=2.0—2.3 (m, 4H, C-CH_2-CH_2-C, A_2B_2), 2.96 (t, 2H, O-CH_2CH_2-O, *J*=6.3 Hz), 3.19 (t, 2H, O-CH_2CH_2-O, *J*=6.3 Hz), 3.42 (bt, 2H, PhC<u>H</u>, *J*=7.0 Hz), 7.2—7.4 (m, 10H, arom); IR (Nujol) 1600, 1200, 1055, 750, 700 cm^{-1}; MS, *m/z* 280 (M^+); Found: C, 81.63; H, 6.90%.

Calcd for $C_{19}H_{20}O_2$: C, 81.40; H, 7.19%.

12a: Colorless needles from hexane, mp 90.5—91.5 °C; ^{1}H NMR (360 MHz, $CDCl_3$) δ=2.06 (m, 2H, C-C$\underline{H}_2$CH$_2$-C), 2.20 (m, 2H, C-CH$_2$C$\underline{H}_2$-C), 2.96 (m, 2H, O-C$\underline{H}$H′), 3.28 (bt, 2H, PhC$\underline{H}$, J=10 Hz), 3.55 (m, 2H, O-CH$\underline{H}$′), 7.2—7.5 (m, 10H, arom); IR (Nujol) 1600, 1180, 1065, 960, 755, 700 cm^{-1}; MS, m/z 280 (M$^+$); Found: C, 81.36; H, 6.92%. Calcd for $C_{19}H_{20}O_2$: C, 81.40; H, 7.19%.

13a: Colorless oil; ^{1}H NMR (360 MHz, $CDCl_3$) δ=1.4—2.0 (m, 4H, PhCH$_2$C$\underline{H}_2$C$\underline{H}_2$-), 2.5—2.7 (m, 2H, PhC$\underline{H}_2$-), 2.83 (dt, 1H, C$\underline{H}$Ph, J=10.8, 4.5 Hz), 3.82 (m, 2H, OC$\underline{H}_2$C$\underline{H}_2$O), 4.98 (d, 1H, OCHO, J=4.5 Hz), 7.0—7.3 (m, 10H, arom); IR (neat) 1600, 1130, 1080, 1050, 1030, 740, 700 cm^{-1}; MS, m/z 282 (M$^+$); Found: C, 80.74; H, 6.88%. Calcd for $C_{19}H_{22}O_2$: C, 80.82; H, 6.78%.

14a: Colorless oil; ^{1}H NMR (360 MHz, $CDCl_3$) δ=1.6—2.1 (m, 3H, PhCH$_2$C$\underline{H}$C$\underline{H}_2$-), 2.6—3.0 (m, 4H, PhC$\underline{H}_2$CH), 3.85, 3.97 (m, 4H, OCH$_2$CH$_2$O), 4.82 (d, 1H, OCHO, J=3.5 Hz), 7.1—7.4 (m, 10H, arom); IR (neat) 1605, 1140, 1080, 1035, 750, 700 cm^{-1}; MS, m/z 282 (M$^+$); Found C, 80.80; H, 6.88%. Calcd for $C_{19}H_{22}O_2$: C, 80.82; H, 6.78%.

Reaction of 4-(4-Methoxyphenyl)-1-phenyl-1-buten-3-yne (3b). 3b was reacted at 60 °C in a similar manner to the procedure for the reaction of **3a**. The products were separated by column chromatography on silica to give three carbonylated products, **4b** (15%), **5b** (20%), and **6b** (12%).

4b: Colorless needles from hexane-benzene, mp 134—136 °C; ^{1}H NMR (360 MHz, $CDCl_3$) δ=2.80 (ddd, 1H, H^2, J_{12}=2.8 Hz, J_{24}=2.8 Hz, J_{23}=19.8 Hz), 3.24 (ddd, 1H, H^3, J_{13}=7.1 Hz, J_{23}=19.8 Hz, J_{34}=3.2 Hz), 3.74 (dd, 1H, H^1, J_{12}=2.4 Hz, J_{13}=7.1 Hz), 3.81 (s, 3H, -CH$_3$), 6.92 (d, 2H, H^6, J=8.7 Hz), 7.15—7.35 (m, 5H, -Ph), 7.73 (d, 2H, H^5, J=8.7 Hz), 7.87 (dd, 1H, H^4, J_{24}=2.8 Hz, J_{34}=3.0 Hz); IR (Nujol) 1700 cm^{-1}; MS, m/z 264 (M$^+$); Found: C, 82.04; H, 5.83%. Calcd for $C_{18}H_{16}O_2$: C, 81.79; H, 6.10%.

5b: Pale-yellow viscous oil; IR (neat) 1695 cm^{-1}. **5b** was led to 2,4-dinitrophenylhydrazone, **5b-(2,4-D)**, and purified by recrystallization.

5b-(2,4-D): Red crystals from benzene, mp 201—204 °C; ^{1}H NMR (360 MHz, $CDCl_3$) δ=3.87 (s, 3H, O-CH$_3$), 6.96 (d, 2H, H^9, J_{89}=8.8 Hz), 7.01 (s, 1H, H^3), 7.14 (d, 1H, H^1, J=16.5 Hz), 7.3—7.5 (m, 8H, -Ph, H^2, and H^8), 7.98 (d, 1H, H^7, J_{67}=9.5 Hz), 8.03 (s, 1H, H^4), 8.34 (dd, 1H, H^6, J_{56}=9.2 Hz, J_{67}=2.3 Hz), 9.17 (d, 1H, H^5, J_{56}=2.3 Hz), 11.3 (bs, 1H, NH); IR (Nujol) 3280, 1615, 1590, 1330, 1305, 1260, 1175, 1130, 755, 735 cm^{-1}; MS, m/z 444 (M$^+$); Found: C, 64.60; H, 4.33; N, 12.42%. Calcd for $C_{24}H_{20}N_4O_5$: C, 64.86; H, 4.54; N, 12.61%.

6b: Pale-yellow crystals from hexane-benzene, mp 123—125 °C; ^{1}H NMR (360 MHz, $CDCl_3$) δ=3.89 (s, 3H, O-CH$_3$), 5.07 (s, 2H, CH$_2$), 7.03 (m, 3H, Ph-CH=C$\underline{H}$ and 2H), 7.2—7.5 (m, 7H, arom), 7.95 (d, 1H, Ph-C$\underline{H}$=CH, J=16.2 Hz); IR (Nujol) 1745 cm^{-1}; MS, m/z 292 (M$^+$); Found: C, 78.05; H, 5.48%. Calcd for $C_{19}H_{16}O_3$: C, 78.06; H, 5.52%.

Reaction of 4-(4-Cyanophenyl)-1-phenyl-1-buten-3-yne (3c). 3c was reacted at 60 °C in a similar manner to the procedure for the reaction of **3a**. The products were separated by column chromatography on silica to give three carbonylated compounds **4c** (17%), **5c** (23%), and **6c** (6%) together with a small amount of the starting material (conversion: 70%).

4c: Pale yellow crystals from hexane-benzene, mp 134—136 °C; ^{1}H NMR (360 MHz, $CDCl_3$) δ=2.81 (m, 1H, H^3), 3.27 (m, 1H, H^2), 3.77 (dd, 1H, H^1, J=7.2, 2.5 Hz), 7.2—7.5 (m, 5H, Ph), 7.6—8.0 (m, 5H, H^4, H^5, and H^6); IR (Nujol) 2220, 1705 cm^{-1}; MS, m/z 259 (M$^+$); Found: C, 82.68; H, 4.73; N, 5.26%. Calcd for $C_{18}H_{13}NO$: C, 83.38; H, 5.05; N, 5.40%.

5c: Pale-yellow viscous oil, IR (neat) 1695 cm^{-1}. **5c** was led to the 2,4-dinitrophenylhydrazone, **5c-(2,4-D)**, and purified by recrystallization.

5c-(2,4-D): Dark-brown powder, mp 233—235 °C; ^{1}H NMR (360 MHz, $CDCl_3$) δ=7.03 (s, 1H, H^3), 7.35—7.5 (m, 6H, -Ph and H^2), 7.58 (d, 2H, H^8, J_{89}=8.4 Hz), 7.70 (d, 2H, H^9, J_{89}=8.4 Hz), 7.98 (d, 1H, H^7, J_{67}=9.6 Hz), 8.05 (s, 1H, H^4), 8.39 (dd, 1H, H^6, J_{67}=9.6 Hz, J_{56}=2.4 Hz), 9.18 (d, 1H, H^5, J_{56}=2.4 Hz), 11.35 (bs, 1H, NH); IR (Nujol) 3280, 2220, 1615, 1330, 1305, 1280, 1140, 1075, 740, 715 cm^{-1}; MS, m/z 439 (M$^+$); Found: C, 65.61; H, 3.98; N, 15.70%. Calcd for $C_{24}H_{17}N_5O_4$: C, 65.60; H, 3.90; N, 15.94%.

6c: Pale-yellow viscous oil; ^{1}H NMR (360 MHz, $CDCl_3$) δ=5.09 (s, 2H, CH$_2$), 6.93 (d, 1H, Ph-CH=C$\underline{H}$, J=16 Hz), 7.2—7.5 (m, 5H, -Ph), 7.61 (m, 2H, o-H to C=C), 7.82 (m, 2H, o-H to CN), 7.92 (d, 1H, Ph-C$\underline{H}$=CH, J=16 Hz); IR (neat) 1765 cm^{-1}; MS, m/z 287 (M$^+$).

Reaction of 1-Phenyl-1-penten-3-yne (3d). 3d was reacted at 60 °C in a similar manner to the procedure for the reaction of **3a**. The products were separated by column chromatography on silica gel to give three carbonylated compounds, **5d** (17%), **17** (19%), and **6d** (20%) together with the unreacted starting material (conversion: 49%).

5d: Pale-yellow viscous oil. **5d** was led to the 2,4-dinitrophenylhydrazone, **5d-(2,4-D)**, and purified by recrystallization.

5d-(2,4-D): Orange powder from benzene, mp 191—193 °C; ^{1}H NMR (360 MHz, $CDCl_3$) δ=2.12 (d, 3H, CH$_3$), 6.25 (q, 1H, H^3, J=7.2 Hz), 7.02 (d, 1H, H^1, J_{12}=16.5 Hz), 7.27 (d, 1H, H^2, J_{12}=16.5 Hz), 7.3—7.53 (m, 5H, Ph), 7.86 (s, 1H, H^4), 7.93 (d, 1H, H^7, J_{67}=9.6 Hz), 8.33 (dd 1H, H^6, J_{56}=2.5 Hz, J_{67}=9.8 Hz), 9.16 (d, 1H, H^5), 11.17 (s, 1H, N); IR (Nujol) 3270, 1620, 1590, 1330, 1305, 1260, 1215, 1115, 755, 745 cm^{-1}; MS, m/z 352 (M$^+$); Found: C, 61.40; H, 4.48; N, 15.65%. Calcd for $C_{18}H_{16}N_4O_4$: C, 61.36; H, 4.58; N, 15.90%.

17: Pale-yellow solid. **17** was led to the 2,4-dinitrophenylhydrazone, **17-(2,4-D)**, and purified by recrystallization.

17-(2,4-D): Dark-red crystals from benzene, mp 232—234 °C; ^{1}H NMR (360 MHz, $CDCl_3$) δ=2.20 (s, 3H, CH$_3$), 6.62 (bd, 1H, H^3, J=10.3, 1 Hz), 6.80 (d, 1H, H^1, J=15.5 Hz), 7.23 (dd, 1H, H^2, J=10.5, 15.4 Hz), 7.3—7.5 (m, 5H, Ph), 7.82 (s, 1H, H^4), 7.99 (d, 1H, H^7, J_{67}=9.6 Hz), 8.33 (dd, 1H, H^6, J_{67}=9.6 Hz), 9.15 (d, 1H, H^5), 11.26 (s, 1H, NH); IR (Nujol) 3280, 1620, 1590, 1330, 1300, 1265, 1205, 1135, 1075, 970, 745 cm^{-1}; MS, m/z 352 (M$^+$); Found: C, 61.02; H, 4.29; N, 15.91%. Calcd for $C_{18}H_{16}N_4O_4$: C, 61.36; H, 4.58; N, 15.90%.

6d: Colorless crystals from hexane-benzene, mp 132.5—133.5 °C; ^{1}H NMR (360 MHz, $CDCl_3$) δ=2.20 (s, 3H, CH$_3$), 4.71 (s, 2H, CH$_2$), 6.79 (d, 1H, C$\underline{H}$=CH-Ph, J=16.3 Hz), 7.2—7.5 (m, 5H, Ph), 7.77 (d, 1H, CH=C$\underline{H}$-Ph, J=16.3 Hz); IR (Nujol) 1750 cm^{-1}; MS, m/z 200 (M$^+$); Found: C, 77.54; H, 6.00%. Calcd for $C_{13}H_{12}O_2$: C, 77.98; H, 6.04%.

Reaction of 1,5-Diphenyl-1-penten-4-yne (16). 16 was reacted at 60 °C in a similar manner to the procedure for the reaction of **3a**. The products were isolated by column chromatography on silica gel to give carbonylated compounds, **18** (40%), **19** (11%), and **20** (18%) together with the unreacted starting material (conversion: 45%).

18: Colorless crystals from hexane, mp 72—74 °C; ^{1}H NMR (360 MHz, $CDCl_3$) δ=2.0—2.2 (m, 1H, Ph-CH-CHH′), 2.5—2.7 (m, 1H, Ph-CH-CHH′), 2.9—3.1 (m, 1H, =CH-CHH′), 3.1—3.2 (m, 1H, =CH-CHH′), 3.61 (dd, 1H, Ph-CH, J=9.7, 10 Hz), 7.2—7.6 (m, 11H, Ph and C=CH); IR (Nujol) 1725 cm^{-1}; MS, m/z 248 (M^+); Found: C, 87.21; H, 6.80%. Calcd for $C_{18}H_{16}O$: C, 87.06; H, 6.49%.

19: Pale-yellow viscous oil; IR (neat) 1685 cm^{-1}. **19** was led to 2,4-dinitrophenylhydrazone, **19-(2,4-D)**, and purified by recrystallization.

19-(2,4-D): Orange-red powder from benzene, mp 218—220 °C; ^{1}H NMR (360 MHz, $CDCl_3$) δ=3.65 (bd, 2H, CH_2, J=5.5 Hz), 6.46 (dt, 1H, H^2, J=5.2, 16 Hz), 6.54 (d, 1H, H^1, J=16 Hz), 7.03 (s, 1H, H^3), 7.2—7.5 (m, 10H, Ph), 7.95 (s, 1H, H^4), 7.95 (d, 1H, H^7, J_{67}=9.5 Hz) 8.29 (dd, 1H, H^6, J_{67}=9.5 Hz, J_{56}=2.3 Hz), 9.14 (d, 1H, H^5), 11.27 (s, 1H, NH); IR (Nujol) 3280, 1610, 1325, 1120, 1085, 750 cm^{-1}; MS, m/z 428 (M^+); Found: C, 67.27; H, 4.64; N, 12.90%. Calcd for $C_{24}H_{22}N_4O_4$: C, 67.28; H, 4.71; N, 13.08%.

20 was a mixture of two isomeric lactones and unable to separate each of the isomers by column chromatography.

20: Pale-yellow viscous oil; ^{1}H NMR (360 MHz, $CDCl_3$) δ=3.43 and 3.49 (d/d, 2H/2H, =C-CH_2-C= for two isomers, J=6.1 Hz/6.7 Hz), 4.85 and 5.09 (s/s, 2H/2H, O-CH_2 for two isomers), 6.18 and 6.32 (dt/dt, 1H/1H, Ph-CH=CH for two isomers, J=15.8, 6.7 Hz/J=15.9, 6.1 Hz), 6.47 and 6.50 (d/d, 1H/1H, Ph-CH for two isomers, J=15.8 Hz/J=15.8 Hz), 7.2—7.6 (m/m, 10H/10H, Ph for two isomers); IR (Nujol) 1770 cm^{-1}; MS, m/z 276 (M^+).

Reaction of 1,4-Diphenyl-1,3-butadiene (21) at 60 °C. 21 (1.0 g, 4.85 mmol) was reacted at 60 °C in a similar manner to the procedure for the reaction of **3a**. After a reaction for 6 h, the reaction mixture was poured to silica gel (1.5 g) and concentrated to dryness. Then, the silica gel was put onto the top of a column containing 20 g of silica gel. Elution by hexane-benzene gave 0.54 g of unreacted **21** (conversion: 46%) and 0.36 g (68% based on **21** consumed) of monoformylated product, **22**.

22: Colorless oil; ^{1}H NMR (60 MHz, $CDCl_3$) δ=1.1—2.1 (m, 4H, Ph-CH_2-(CH_2)$_2$), 2.55 (t, 2H, Ph-CH_2, J=7 Hz), 3.45 (dt, 1H, Ph-CH, J=7, 1 Hz), 7.1—7.5 (m, 10H, Ph), 9.55 (d, 1H, CHO, J=1 Hz); IR (neat) 1735 cm^{-1}. The structure of **22** was also supported by a comparison with the hydrated product of acetal **13a**.

Competitive Reaction between Diphenylacetylene (7) and *trans*-Stilbene (8). An equimolar mixture of **7** (0.86 g, 4.85 mmol) and **8** (0.87 g, 4.85 mmol) was reacted at 60 °C in a similar manner to the procedure for the reaction of **3a**. After a reaction for 6 h, the reaction mixture was evaporated to dryness and chromatographed on silica gel, giving two carbonylated products **9** and **10** in 31 and 44% yields, respectively, which were derived from **7**, while **8** was recovered almost quantatively.

Reaction of Cyclopentenone (4a) at 120 °C. 4a (210 mg) was treated at 120 °C in a similar manner to the procedure for the reaction of **3a**. After a reaction for 4 h, the reaction mixture was passed through a short column of alumina and the eluent was evaporated to dryness, affording 200 mg (94%) of cyclopentanone **15a**.

15a:[19] Colorless crystals from hexane, mp 75—80 °C; *^{1}H NMR (60 MHz, $CDCl_3$) δ=1.9—2.7 (m, 4H, -CH_2-CH_2-),* 3.5 (m, 2H, CH), 7.2—7.5 (m, 10H, Ph); IR (Nujol) 1775 cm^{-1}; MS, m/z 236 (M^+).

The authors wish to express their thanks to Drs. Hiroshi Yamazaki and Pangbu Hong, the Institute of Physical and Chemical Research, for their helpful discussions. We also wish to thank Mr. Osamu Nakanishi, Sekisui Chemical Co. Ltd., for his continuous encouragement. We are grateful to The Material Analysis Center, I. S. I. R., Osaka University, for spectral measurement and microanalysis.

References

1) C. D. Frohning, "New Syntheses with Carbon Monoxide," ed by J. Falbe, Springer Verlag, Berlin (1980); R. P. A. Sneeden, I. Tkatchenko, and C. N. R. S. Villeurbanne, "Comprehensive Organometallic Chemistry," ed by G. Wilkinson, F. G. A. Stone, and E. W. Abel, Pergamon, New York (1982), Vol. 2, p. 19.

2) P. Pino, F. Piacenti, and M. Bianchi, "Organic Synthesis via Metal Carbonyls," ed by I. Wender and P. Pino, Wiley, New York (1977), Vol. 2, p. 43; J. Falbe, "Carbon Monoxide in Organic Synthesis," Springer Verlag, Berlin (1970); R. L. Pruett, *Adv. Organomet. Chem.*, **17**, 1 (1979).

3) R. S. Dickson and P. J. Fraser, *Adv. Oraganomet. Chem.*, **12**, 323 (1974); F. L. Bowden and A. B. P. Lever, *Organomet. Chem. Rev. Sect. A.*, **3**, 227 (1968).

4) H. Greenfield, J. Wotiz, and I. Wender, *J. Org. Chem.*, **22**, 542 (1957).

5) C. K. Brown, D. Georgiou, and G. Wilkinson, *J. Chem. Soc. A*, **1971**, 3120; C. Bolleghi and Ch. Salomon, *Tetrahedron Lett.*, **1974**, 4285; B. Cornils, "New Syntheses with Carbon Monoxide," ed by J. Falbe, Springer Verlag, Berlin (1980), p. 1.

6) K. Sonogashira, Y. Tohda, and N. Hagihara, *Tetrahedron Lett.*, **1975**, 4467; S. Takahashi, Y. Kuroyama, K. Sonogashira, and N. Hagihara, *Synthesis*, **1980**, 627.

7) K. Doyama, T. Joh, S. Takahashi, and T. Shiohara, *Tetrahedron Lett.*, **27**, 4497 (1986).

8) Erratum: Ref. 7, page 4498, in Table 1: The data of **1b** (R=*p*-CH_3O-C_6H_4) should be replaced by those of **1c** (R=*p*-NC-C_6H_4).

9) For recent reports, see: N. E. Shore and M. J. Knudsen, *J. Org. Chem.*, **52**, 569 (1987); V. Sampath, E. C. Lund, M. J. Kundsen, M. M. Olmstead, and N. E. Shore, *ibid.*, **52**, 3595 (1987); N. E. Shore and S. D. Najdi, *ibid.*, **52**, 5298 (1987).

10) For recent reports, see: P. Mugnus, L. M. Principe, and M. J. Slater, *J. Org. Chem.*, **52**, 1483 (1987); P. Mugnus and D. P. Baker, *J. Am. Chem. Soc.*, **109**, 7495 (1987).

11) W. A. Smit, A. S. Gybin, A. S. Shashkov, Y. T. Strychkov, L. G. Kyz'mina, G. S. Mikaelian, R. Caple, and E. D. Swanson, *Tetrahedron Lett.*, **27**, 1241 (1986); S. O. Simonian, W. A. Smit, A. S. Gybin, A. S. Shashkov, G. S. Mikaelian, V. A. Tarasov, I. I. Ibraginov, R. Caple, and D. E. Froen, *ibid.*, **27**, 1245 (1986).

12) E. Negishi, S. J. Holmes, J. M. Tour, and J. A. Miller, *J. Am. Chem. Soc.*, **107**, 2568 (1985); G. W. Parshall, W. A. Nugent, D. M.-T. Chan, and W. Tam, *Pure Appl. Chem.*, **57**, 1809 (1985).

13) D. L. Reger and P. J. McElligott, *J. Am. Chem. Soc.*, ***102**, 5924 (1980).*

14) J. M. Huggins and R. G. Bergman, *J. Am. Chem. Soc.*, **101**, 4410 (1979).

15) J. Tsuji and T. Nogi, *J. Am. Chem. Soc.*, **88**, 1289 (1966); H. Yamazaki and P. Hong, *J. Mol. Catal.*, **21**, 133 (1983).
16) K. Doyama, T. Joh, K. Onitsuka, T. Shiohara, and S. Takahashi, *J. Chem. Soc., Chem. Commun.*, **1987**, 649.
17) S. Martinengo, P. Chini, and G. Giordano, *J. Organomet. Chem.*, **27**, 389 (1971); S. Martinengo, G. Giordano, and P. Chini, *Inorg. Synth.*, **20**, 212 (1980).
18) J. F. Normant, *Synthesis*, **1972**, 63.
19) P. Ruggli and J. Sehmidlin, *Helv. Chim. Acta*, **29**, 396 (1946).

Synthesis and Absolute Configuration of the Acetalic Lignan (+)-Phrymarolin I

Fumito ISHIBASHI and Eiji TANIGUCHI*
Department of Agricultural Chemistry, Faculty of Agriculture, Kyushu University, 6-10-1 Hakozaki, Higashi-ku, Fukuoka 812
(Received June 24, 1988)

The natural (+)-phrymarolin I was stereoselectively synthesized and its absolute configuration was unequivocally determined as being (1*S*,2*S*,5*R*,6*S*)-1-acetoxy-2-(2-methoxy-4,5-methylenedioxyphenoxy)-6-(2-methoxy-4,5-methylenedioxyphenyl)-3,7-dioxabicyclo[3.3.0]octane.

The unique lignans of *Phryma leptostachya* L., phrymarolin I and II, are the first examples of naturally occurring 1,2-dioxygenated 3,7-dioxabicyclo-[3.3.0]octanes.[1] Recently, their congeners, including desacetylphrymarolin III and higher insecticidal sesquilignans,[2] were isolated from the same plant. Concerning the development of new pesticides, we are interested in their absolute configurations and syntheses.

A structure involving the relative configuration of phrymarolin I (**1a**) was proposed on the basis of chemical and spectroscopic information.[1] A total synthesis and a consequent establishment of the whole stereochemistry of (+)-phrymarolin I have recently been communicated.[3] Full details of this work will be described herein.

The strategy for the synthesis is basically the same as that for the syntheses of racemic phrymarolin II and its stereoisomers[4] (Fig. 1); the 1-hydroxy-6-aryl-2-aryloxy-3,7-dioxabicyclo[3.3.0]octane skeleton (**1a**) was constructed from β-vinyl-γ-butyrolactone, 2-methoxy-4,5-methylenedioxybenzaldehyde and 2-methoxy-4,5-methylenedioxyphenol. However, we found that cadmium carbonate-catalyzed condensation[5] of the chloride (**2**) with 2-methoxy-4,5-methylenedioxyphenol (**4**), not as well as sesamol, only gave the undesirable 2α-epimer (**1b**) in low yield (14%). A synthesis of 2β-epimer was achieved by extending the stereocontrolled glycosylation method, developed by Mukaiyama et al., using glycosyl fluoride and tin(II) chloride.[6] The new method improved 2β-isomer production and prevented an epimerization at the C-6 position.

The chiral starting substance, (*S*)-(+)-β-vinyl-γ-butyrolactone, was prepared from its racemate[7] by optical resolution, as shown in Fig. 2. Aminolysis of (±)-**5** with (*S*)-(−)-α-methylbenzylamine in the presence of trimethylaluminium[8] in dichloromethane gave an oily mixture of the hydroxy amides (**7a** and **7b**) in 56% combined yield. The diastereomers were separated by repeated liquid chromatography on silica gel with 3 vol% isopropyl alcohol in benzene as the eluent. Purely isolated **7a** was subjected to alkaline hydrolysis followed by lactonization with an azeotropic removal of the water to afford (+)-**5** in 58% yield. In the same manner as mentioned above, another diastereomer (**7b**) was converted to (−)-**5** in 64% yield. The absolute stereochemistry of the two enantiomeric lactones was unknown at this stage. Hydrogenation of the lactone [(+)-**5**], followed by reduction with lithium aluminium hydride gave the enantiomer, (*R*)-(+)-**8**, $[\alpha]_D$ +14.3° ($CHCl_3$), whereas another lactone [(−)-**5**] led to the opposite enantiomer, (*S*)-(−)-**8**, $[\alpha]_D$ −13.0° ($CHCl_3$). Their absolute configurations were assigned by a comparison of their optical rotations with that of

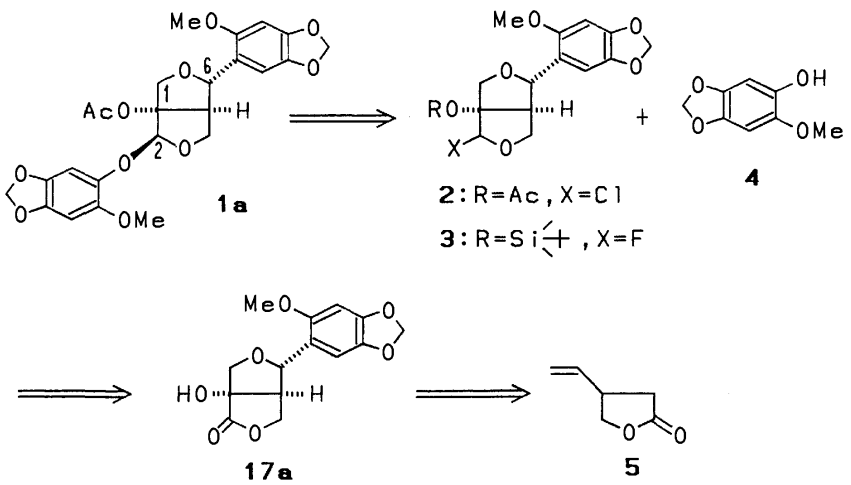

Fig. 1.

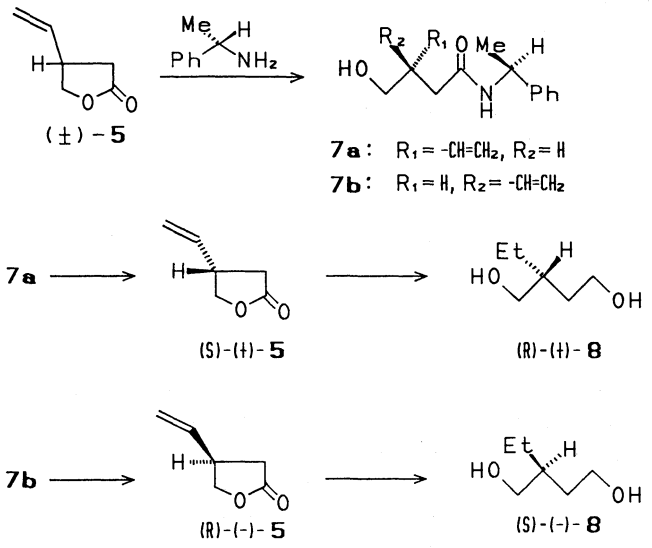

Fig. 2.

the diol (*R*)-(+)-**8** of which configuration was known, $[\alpha]_D$ +7.7° (neat).[9] The stereochemistries of (+)-**5** and (−)-**5** were defined as an (*S*)- and (*R*)-configuration, respectively.

The addition of the lithium enolate of (*S*)-(+)-**5** generated by lithium diisopropylamide (LDA) to 2-methoxy-4,5-methylenedioxybenzaldehyde (**6**) in tetrahydrofuran at −75 °C afforded the erythro and threo aldols (**9**) in 98% yield in the ratio of 65/35 (based on NMR), respectively. Due to the steric repulsion of the vinyl moiety of **5**, the reaction was supposed to be favorable to the (2*R*, 3*S*)-*trans* isomers. Without separation, the mixture was silylated with *t*-butyldimethylsilyl triflate[10] in the presence of 2,6-lutidine in dichloromethane at −30 °C (92% yield), and the silylated lactone was reduced with lithium aluminium hydride in a mixture of ether and tetrahydrofuran (2 : 1) at −10 °C to give the diol (**11**) in 82% yield. The terminal olefin of **11** was oxidized to the carbonyl function by successive oxidation with a catalytic amount of osmium tetraoxide and *N*-methylmorpholine *N*-oxide[11] in a

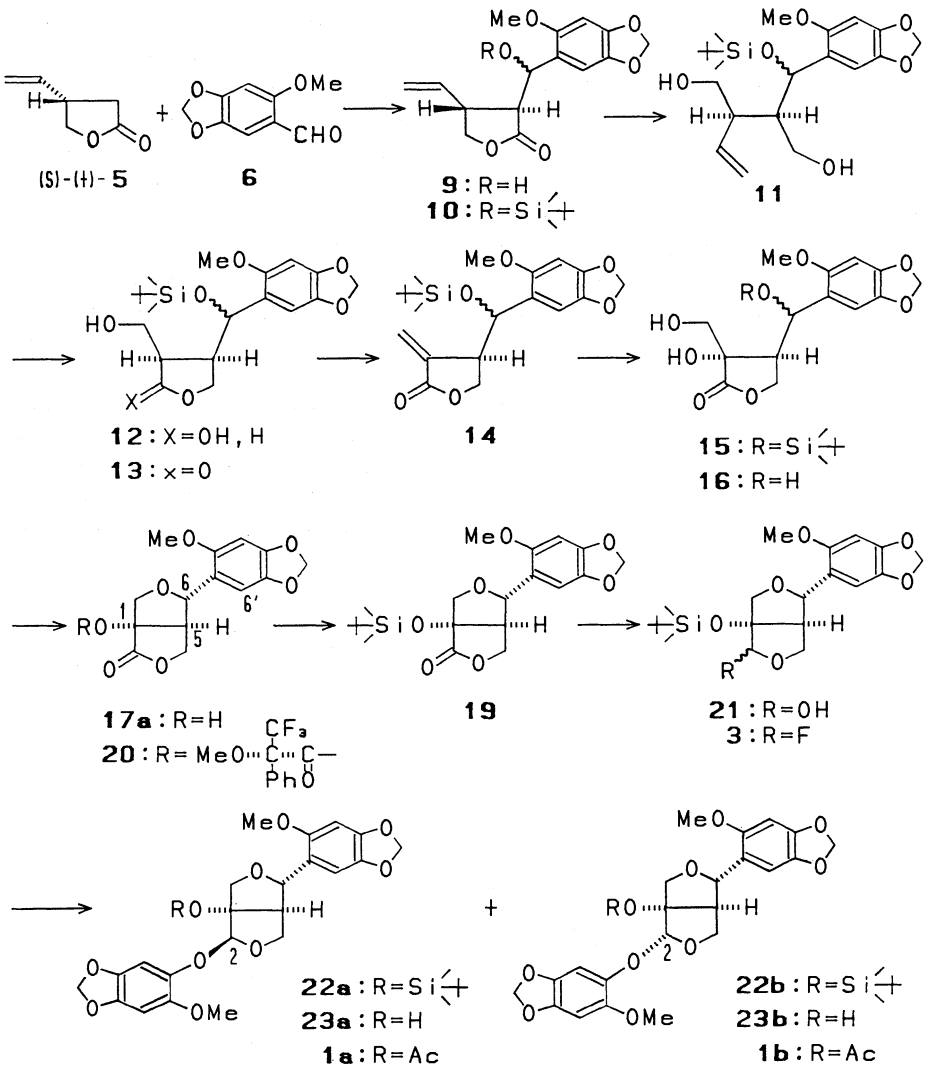

Fig. 3.

mixture of acetone, *t*-butyl alcohol and water at room temperature, followed by sodium periodate in a mixture of ethyl acetate and water. The lactol (**12**) was oxidized to the lactone (**13**) with silver carbonate on Celite in refluxing benzene in 91% overall yield from **11**. After sulfonylation of the primary hydroxyl group in **13** with mesyl chloride, the unstable mesylate was immediately treated with 1,8-diazabicyclo[5.4.0]undec-7-ene (DBU) in benzene at room temperature to furnish the methylene lactone (**14**) in 87% yield. Dihydroxylation with catalytic osmium tetraoxide and *N*-methylmorpholine *N*-oxide[11] in a mixture of acetone, *t*-butyl alcohol and water quantitatively gave the 2α-diol (**15**) in high stereoselectivity, resulting from an exclusive attack of the reagent to the less hindered α-face of the molecule.

After removing the *t*-butyldimethylsilyl group with tetrabutylammonium fluoride in tetrahydrofuran at 0 °C, the resulting triol (**16**) was subjected to dehydrative cyclization with a catalytic amount of 10-camphorsulfonic acid (CSA) in dichloromethane at room temperature to afford the key intermediate (**17a**) in 59% yield, along with a 10% recovery of **15**.

It should be noted that both erythro and threo isomers of **16** afforded **17a** (6α) as the sole product via the thermodynamically preferable common transition state (**18a**), since the alternative transition state (**18b**), leading to **17b** (6β), was destabilized by the 1,3-diaxial interaction between the aromatic ring and the C-4 methylene group (Fig. 4). Under strongly acidic conditions, e.g., with diethyl ether-boron trifluoride (1/1) in dichloromethane or hydrogen chloride in tetrahydrofuran, the cyclization gave a mixture of **17a** and **17b**, probably due to the isomerization of **17a** under the conditions.

After recrystallizing **17a** from a mixture of benzene and diisopropyl ether, the lactone alcohol, $[\alpha]_D$ +67.3° ($CHCl_3$), was derivatized to the ester of α-methoxy-α-(trifluoromethyl)phenylacetic acid (MTPA) according to Mosher et al.[12] The ^{1}H NMR spectrum of the (*S*)-(−)-MTPA ester was measured at 400 MHz; the aromatic proton (6′-H) of the (1*S*, 5*R*, 6*S*)-(*S*)-ester resonated at a higher field (6.73 ppm) than that of the diastereomeric (1*R*, 5*S*, 6*R*)-(S)-ester (6.97 ppm), indicating the optical purity (96% e.e.).

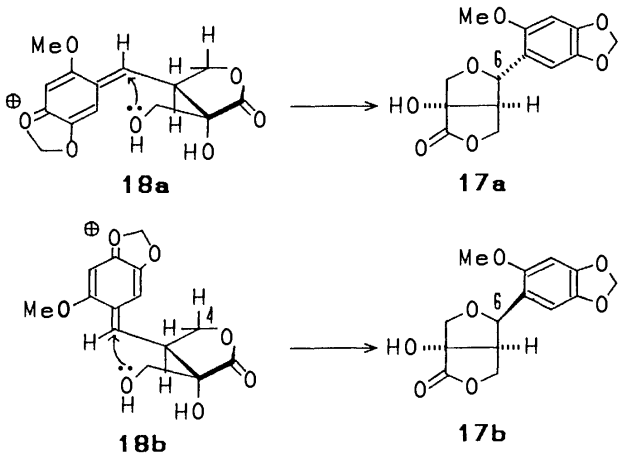

Fig. 4.

The crude sample of (+)-**17a** was treated with *t*-butyldimethylsilyl triflate and 2,6-lutidine[10] in dichloromethane (85% yield), and the resulting silyl ether (**19**) was reduced to the lactol (**21**) in 98% yield with diisobutylaluminium hydride (DIBAL) in toluene at −75 °C. The lactol was fluorinated in 92% yield with 2-fluoro-1-methylpyridinium tosylate and triethylamine[6] in dichloromethane, and the unstable fluoride (**3**) was immediately reacted with 2-methoxy-4,5-methylenedioxyphenol (**4**)[13] in the presence of tin(II) chloride, trityl perchlorate[6] and 4A Molecular Sieves in ether at 0 °C. A mixture of 2β-/2α-isomer, **22a** and **22b**, was obtained in 50% combined yield (**22a**/**22b**= 33/67, based on NMR). Desilylation of the mixture with tetrabutylammonium fluoride in tetrahydrofuran and separation of the products by preparative TLC on silica gel furnished (+)-**23a** and (−)-**23b** in 11 and 29% yields from **3**, respectively (Fig. 3). The optical purity of (+)-**23a** was estimated to be 85% e.e. on the basis of the 400 MHz ^{1}H NMR spectrum of its (*S*)-(−)-MTPA ester.

The rather low optical yield may have resulted from contamination due to the unseparated diastereomer, (2*S*, 3*S*)-*cis*-**9**, produced by the aldol condensation of the benzaldehyde and vinylbutyrolactone during the first step of the synthesis. The (2*S*, 3*S*)-*cis* isomer should give the enantiomeric intermediate, (1*S*, 5*S*, 6*R*)-**17a** and (1*R*, 2*R*, 5*S*, 6*R*)-(−)-phrymarolin I in the following reactions.

Finally, the target molecule (1*S*, 2*S*, 5*R*, 6*S*)-**1a**, $[\alpha]_D$ +106.9° (dioxane), was obtained by acetylation of (+)-**23a** in acetic anhydride containing a small excess of 4-(dimethylamino)pyridine (DMAP). The optical rotation of natural **1a** was $[\alpha]_D$ +131.3° (dioxane). Although the synthesized (+)-**1a** was optically impure, the present synthesis unambiguously established the (1*S*, 2*S*, 5*R*, 6*S*)-configuration of the natural and dextrorotatory phrymarolin I.

Experimental

All melting points and boiling points are uncorrected. IR spectra were determined on a Shimadzu IR-420 spectrophotometer. Unless stated otherwise, ^{1}H NMR spectra were measured in $CDCl_3$ on a JEOL FX-100 spectrometer. Mass spectra were performed by an ESCO FMD-05A spectrometer at 70 ev. Optical rotations were determined on a Union Giken PM-101 polarimeter.

Gravity column chromatography and medium-pressure liquid chromatography were performed with Merck silica gel 60 (70—230 mesh ASTM) and Merck LiChroprep Si 60 (40—63 μm), respectively. TLC was performed on precoated silica-gel plates 60 F_{254} (0.25 mm or 0.5 mm thickness) supplied by E. Merck. Anhydrous sodium sulfate was used for drying solutions.

Optical Resolution of β-Vinyl-γ-butyrolactone. To a solution of (*S*)-(−)-α-methylbenzylamine (10.82 g, 89.2 mmol) in dry CH_2Cl_2 (300 ml) was added a 1 mol dm^{-3} solution of Et_3Al in hexane (90.0 ml, 90.0 mmol). After 30 min, (±)-**5** (10.00 g, 89.2 mmol) was added. The mixture was heated under reflux for 5 h and then poured into a mixture of 2 mol dm^{-3} aqueous HCl and crushed ice. The CH_2Cl_2 layer was separated, washed with water, dried, and concentrated in vacuo. The crude product was purified by medium-pressure liquid chromatography on silica gel eluted with 3 vol% *i*-PrOH in EtOAc to give **7a** (5.38 g, 23.1 mmol) and **7b** (6.37 g, 27.3 mmol) in 56% combined yield. **7a**: mp 97—99 °C; $[\alpha]_D^{14}$ −100.0° (*c* 2.3, $CHCl_3$). **7b**: A viscous oil; $[\alpha]_D^{14}$ −78.2° (*c* 2.2, $CHCl_3$).

A solution of **7a** (5.25 g, 22.5 mmol) in 1 mol dm^{-3} KOH in ethylene glycol (35 ml) was heated at 175 °C under an atmosphere of nitrogen for 10 h. The mixture was then cooled to room temperature, acidified with 2 mol dm^{-3} aqueous HCl (20 ml), diluted with brine, and extracted three times with EtOAc. The organic extracts were combined, dried, and concentrated in vacuo. The crude product was dissolved in benzene (50 ml) and a catalytic amount of *p*-TsOH was added. The resulting solution was heated under reflux with a concominant removal of water. After the mixture had been cooled to room temperature and concentrated in vacuo, the oily residue was chromatographed on silica gel. Elution with hexane–ether (1 : 1) gave crude (+)-**5**, which was distilled using micro Kugelrohr to afford pure (*S*)-(+)-**5** (1.39 g, 58%) as a colorless oil: bp 170 °C (bath)/2666 Pa; $[\alpha]_D^{19}$ +4.9° (*c* 4.3, EtOH). In the same manner as above, the amide (**7b**) gave (*R*)-(−)-**5** in 64% yield: $[\alpha]_D^{22}$ −5.2° (*c* 2.3, EtOH).

A Mixture of (3*R*,4*S*)-4-Ethenyl-3-[(1*R*/*S*)-1-hydroxy-1-(2-methoxy-4,5-methylenedioxyphenyl)methyl]dihydro-2(3*H*)-furanones (9). To a solution of LDA [prepared from butyllithium (15 wt% in hexane, 5.90 ml, 9.5 mmol) and diisopropylamine (1.33 ml, 9.5 mmol) at −10 °C for 15 min in dry THF (30 ml)] was added as drops a solution of (*S*)-(+)-**5** (1.00 g, 8.9 mmol) in dry THF (5 ml) at −75 °C under an atmosphere of dry argon. After 30 min, a solution of 2-methoxy-4,5-methylenedioxybenzaldehyde (1.76 g, 9.8 mmol) in dry THF (20 ml) was added as drops. After 3 h at −75 °C, the reaction was quenched by 10 wt% aqueous NH_4Cl. The solution was then allowed to warm up to room temperature and was extracted twice with ether. The combined organic layers were washed with 5 wt% aqueous $NaHCO_3$ and brine, dried, and evaporated. The crude product was chromatographed on silica gel eluted with EtOAc–benzene (1 : 9) to afford the diastereomeric aldols (**9**) (2.52 g, 8.63 mmol, 97%) as a slightly yellow viscous oil: IR ($CHCl_3$) 1040, 1150, 1185, 1483, 1760, and 3350 cm^{-1}; MS *m*/*z* 292 (M^+), 181, 166, 165, 151, 123, 95, and 53. Found: C, 61.51; H, 5.60%. Calcd for $C_{15}H_{16}O_6$: C, 61.64; H, 5.52%.

A Mixture of (3*R*,4*S*)-3-[(1*R*/*S*)-1-[(*t*-Butyldimethylsilyl)oxy]-1-(2-methoxy-4,5-methylenedioxyphenyl)methyl]-4-ethenyldihydro-2(3*H*)-furanones (10). A solution of *t*-$BuMe_2SiOTf$ (3.0 ml, 12.9 mmol) in dry CH_2Cl_2 (7 ml) was added as drops to a solution of **9** (2.52 g, 8.63 mmol) and 2,6-lutidine (2.0 ml, 17.3 mmol) in the same solvent (30 ml) at −30 °C under an atmosphere of dry argon. After 40 min at that temperature, the mixture was poured into 5 wt% aqueous $NaHCO_3$. The organic layer was separated and the aqueous layer was extracted with ether (75 ml). The combined organic layers were washed successively with 10 wt% aqueous $Cu(NO_3)_2$ and brine, dried, and evaporated. The oily residue was chromatographed on silica gel eluted with hexane–EtOAc (3 : 1) to give the silyl ether (**10**, 3.22 g, 7.93 mmol, 92%) as a mixture of diastereomers. A part of the mixture was separated by medium-pressure liquid chromatography on silica gel with EtOAc–benzene (1 : 19) as the eluant. *erythro*-**10**: A viscous oil; ^{1}H NMR δ=−0.09 (3H, s), 0.12 (3H, s), 0.93 (9H, s), 2.68 (1H, dd, *J*=3 and 8 Hz), 3.06 (1H, m), 3.73 (3H, s), 3.81 (1H, dd, *J*=8 and 9 Hz), 4.21 (1H, dd, *J*=8 and 9 Hz), 5.00—5.30 (3H, m), 5.52—5.84 (1H, m), 5.89 (2H, dd, *J*=3 and 1 Hz), 6.42 (1H, s), and 7.07 (1H, s); IR ($CHCl_3$) 830, 1040, 1150, 1185, 1481, 1762, and 2940 cm^{-1}; MS *m*/*z* 406 (M^+), 350, 349, 295, 169, and 75. *threo*-**10**: White crystals (mp 98—101 °C); ^{1}H NMR δ=−0.06 (3H, s), 0.12 (3H, s), 0.93 (9H, s), 2.81 (1H, dd, *J*=3 and 8 Hz), 3.10—3.48 (1H, m), 3.76 (3H, s), 3.88 (1H, dd, *J*=8 and 9 Hz), 4.38 (1H, t, *J*=8 Hz), 4.52—4.82 (2H, m), 5.12—5.44 (1H, m), 5.65 (1H, d, *J*=2 Hz), 5.89 (2H, q, *J*=1 Hz), 6.44 (1H, s), and 6.93 (1H, s). Found: C, 61.99; H, 7.48%. Calcd for $C_{21}H_{30}O_6Si$: C, 62.04; H, 7.44%.

A Mixture of (2*R*,3*R*)-2-[(1*R*/S)-1-[(*t*-Butyldimethylsilyl)oxy]-1-(2-methoxy-4,5-methylenedioxyphenyl)methyl]-3-vinyl-1,4-butanediols (11). A solution of **10** (3.22 g, 7.93 mmol) in dry THF (25 ml) was added as drops to a stirred slurry of lithium aluminium hydride (0.33 g, 8.68 mmol) in dry ether (50 ml) at −10 °C under an atmosphere of dry argon. After 30 min at −10 °C, the excess reagent was decomposed carefully by the addition of EtOAc followed by 10 wt% aqueous citric acid (100 ml). The organic layer was separated and the aqueous layer was extracted with EtOAc. The two organic extracts were combined, washed with 5 wt% aqueous $NaHCO_3$, dried, and concentrated in vacuo. The oily residue was chromatographed on silica gel eluted with hexane–EtOAc (1 : 1) to give **11** (2.66 g, 6.49 mmol, 82%) as a colorless viscous oil: IR ($CHCl_3$) 835, 1040, 1050, 1070, 1185, 1255, 1462, 1480, 2930, and 3350 cm^{-1}; MS *m*/*z* 295 (M^+ −$SiMe_2Bu$-*t*), 278, 180, 179, 165, 163, 134, and 75. Found: C, 61.30; H, 8.36%. Calcd for $C_{21}H_{34}O_6Si$: C, 61.43; H, 8.34%.

A Mixture of (3*R*,4*R*)-3-Hydroxymethyl-4-[(1*R*/*S*)-1-[(*t*-butyldimethylsilyl)oxy]-1-(2-methoxy-4,5-methylenedioxyphenyl)methyl]dihydro-2(3*H*)-furanones (13). A solution of **11** (2.66 g, 6.49 mmol), *N*-methylmorpholine *N*-oxide monohydrate (0.96 g, 7.10 mmol) and 2 wt% aqueous OsO_4 (1 ml) in a mixture of acetone (30 ml), *t*-BuOH (7 ml), and water (7 ml) was allowed to stand at room temperature under an atmosphere of argon for 15 h. Celite and aqueous $NaHSO_3$ (0.9 g/15 ml) were added and the mixture was filtered. The residue was washed well with acetone, and the filtrate was concentrated in vacuo. The oily residue was taken up in EtOAc and washed with brine.

To the EtOAc extract was added a solution of $NaIO_4$ (1.40 g, 6.55 mmol) in water (100 ml). The resulting two phases were vigorously stirred at room temperature for 3 h. The organic layer was separated and the aqueous layer was extracted with EtOAc. The combined organic layers were dried, and concentrated in vacuo to leave practically pure **12** as a viscous oil, which was used for the next step without further purification.

A mixture of **12** and silver carbonate on Celite (10.0 g, containing ca. 10 mmol of the silver salt) in benzene (75 ml) was heated under reflux for 45 min. After cooling to room temperature, the mixture was filtered through a pad of Celite with more of benzene. After removing the solvent, the oily

residue was chromatographed on silica gel eluted with hexane-EtOAc (1 : 1) to give **13** (2.43 g, 5.93 mmol, 91%) as a viscous oil: IR ($CHCl_3$) 835, 1005, 1040, 1150, 1170, 1185, 1260, 1465, 1482, 1760, 2850, and 3500 cm^{-1}; MS *m/z* 335 (M^+ −Bu-*t*), 295, 278, 268, 259, 208, 165, and 75. Found: C, 58.49; H, 7.36%. Calcd for $C_{20}H_{30}O_7Si$: C, 58.51; H, 7.37%.

A Mixture of (4*R*)-4-[(1*R*/*S*)-1-[(*t*-Butyldimethylsilyl)oxy]-1-(2-methoxy-4,5-methylenedioxyphenyl)methyl]-3-methylenedihydro-2(3*H*)-furanones (14). Methanesulfonyl chloride (0.69 ml, 8.90 mmol) was added to a solution of **13** (2.43 g, 5.93 mmol) and Et_3N (1.65 ml, 11.86 mmol) in dry benzene (50 ml) at ca. 5 °C. The mixture was stirred at room temperature for 4 h before the addition of DBU (1.35 g, 8.90 mmol). After 30 min, the mixture was washed with water and the aqueous layer was extracted with EtOAc. The two organic layers were combined, washed successively with 10 wt% aqueous citric acid and 5 wt% aqueous $NaHCO_3$, and dried. After removing the solvent, the oily residue was chromatographed on silica gel eluted with hexane-EtOAc (4 : 1) to afford **14** (2.02 g, 5.15 mmol, 87%) as a viscous oil: IR ($CHCl_3$) 1040, 1100, 1185, 1480, and 1755 cm^{-1}. Found: C, 61.14; H, 7.18%. Calcd for $C_{20}H_{28}O_6Si$: C, 61.20; H, 7.19%.

A Mixture of (3*S*,4*R*)-4-[(1*S*/*R*)-1-[(*t*-Butyldimethylsilyl)oxy]-1-(2-methoxy-4,5-methylenedioxyphenyl)methyl]-3-hydroxy-3-(hydroxymethyl)dihydro-2(3*H*)-furanones (15). A solution of **14** (2.02 g, 5.15 mmol), *N*-methylmorpholine *N*-oxide monohydrate (0.80 g, 5.92 mmol) and 2 wt% aqueous OsO_4 (1 ml) in a mixture of acetone (30 ml), *t*-BuOH (7 ml) and water (7 ml) was allowed to stand at room temperature under an atmosphere of argon for 12 h. Celite and aqueous $NaHSO_3$ (1.0 g/20 ml) were then added and the mixture was filtered through a pad of Celite. The residue was washed well with acetone, and the filtrate was concentrated in vacuo. The oily residue was taken up in EtOAc and washed with brine. The extract was dried, concentrated in vacuo, and chromatographed on silica gel eluted with hexane-EtOAc (1 : 2) to give **15** (2.12 g, 4.98 mmol, 97%) as a gummy oil: IR ($CHCl_3$) 835, 1040, 1070, 1100, 1150, 1185, 1480, 1600, 1770, and 3350 cm^{-1}; MS *m/z* 369 (M^+−Bu-*t*), 295, 294, 277, 191, 181, 180, 165, 161, 133, and 75. Found: C, 56.41; H, 7.09%. Calcd for $C_{20}H_{30}O_8Si$: C, 56.31; H, 7.09%.

(1*S*,5*R*,6*S*)-(+)-1-Hydroxy-6-(2-methoxy-4,5-methylenedioxyphenyl)-3,7-dioxabicyclo[3.3.0]octan-2-one (17a). A 1 mol dm^{-3} solution of *n*-Bu_4NF in THF (6.00 ml, 6.00 mmol) was added to a solution of **15** (2.12 g, 4.98 mmol) in dry THF (20 ml) at 0 °C. After 2 h at 0 °C the mixture was poured into 10 wt% aqueous NH_4Cl and extracted twice with EtOAc. The extracts were combined, dried, concentrated in vacuo, and chromatographed on silica gel eluted with EtOAc to give **16** as a gummy oil. Found: C, 53.74; H, 5.30%. Calcd for $C_{14}H_{16}O_8$: C, 53.85; H, 5.16%.

The triol **16** was dissolved in dry CH_2Cl_2 (50 ml) containing a catalytic amount of 10-camphorsulfonic acid. The solution was stirred at room temperature for 3 h before being quenched with a few drops of Et_3N. After removing the solvent, the oily residue was chromatographed on silica gel eluted with hexane-EtOAc (1 : 1) to afford **17a** (0.86 g, 2.93 mmol, 59%) as white crystals. An analytically pure sample was obtained by recrystallization from *i*-Pr_2O-benzene: mp 136—137.5 °C; $[\alpha]_D^{25}$ +67.3° (*c* 2.02, $CHCl_3$); ^1H NMR (acetone-d_6) δ=2.84 (1H, s), 2.93 (1H, dt, *J*=8 and 5 Hz), 3.81 (3H, s), 4.11 (2H, s), 4.38 (1H, dd, *J*=5 and 10 Hz), 4.63 (1H, dd, *J*=8 and 10 Hz), 5.07 (1H, d, *J*=5 Hz), 5.92 (2H, s), 6.67 (1H, s), and 6.97 (1H, s); IR ($CHCl_3$) 1040, 1115, 1160, 1187, 1481, 1774, and 3400 cm^{-1}; MS *m/z* 294 (M^+), 277, 180, 165, and 133. Found: C, 57.06; H, 4.81%. Calcd for $C_{14}H_{14}O_7$: C, 57.14; H, 4.80%.

(1*S*,5*R*,6*S*)-1-[(*t*-Butyldimethylsilyl)oxy]-6-(2-methoxy-4,5-methylenedioxyphenyl)-3,7-dioxabicyclo[3.3.0]octan-2-one (19). A solution of *t*-$BuMe_2SiOTf$ (0.70 ml, 2.30 mmol) in dry CH_2Cl_2 (2 ml) was added as drops to a solution of (+)-**17a** (0.48 g, 1.63 mmol) and 2,6-lutidine (0.57 ml, 4.89 mmol) in the same solvent (10 ml) at −10 °C under an atmosphere of dry argon. The reaction mixture was gradually warmed up to room temperature and kept at this temperature for 18 h. The mixture was then diluted with ether (30 ml) and washed successively with 5 wt% aqueous $NaHCO_3$, 20 wt% aqueous $Cu(NO_3)_2$, brine, and again 5 wt% aqueous $NaHCO_3$. The ethereal extract was dried, concentrated in vacuo, and chromatographed on silica gel eluted with hexane-EtOAc (4 : 1) to give **19** (0.57 g, 1.39 mmol, 85%) as a colorless oil: ^1H NMR δ=0.04 (3H, s), 0.17 (3H, s), 0.81 (9H, s), 2.92 (1H, m), 3.76 (3H, s), 4.08 (1H, d, *J*=10 Hz), 4.21 (1H, d, *J*=10 Hz), 4.33 (1H, dd, *J*=5 and 10 Hz), 4.57 (1H, dd, *J*=8 and 10 Hz), 5.05 (1H, d, *J*=5 Hz), 5.90 (2H, s), 6.49 (1H, s), and 6.97 (1H, s); IR ($CHCl_3$) 843, 1043, 1160, 1195, 1487, 1780, and 2960 cm^{-1}; MS *m/z* 408 (M^+), 352, 351, 181, 165, 127 (base), and 75. Found: C, 58.73; H, 6.90%. Calcd for $C_{20}H_{28}O_7Si$: C, 58.80; H, 6.91%.

A Mixture of (1*S*,2*R*/*S*,5*R*,6*S*)-1-[(*t*-Butyldimethylsilyl)oxy]-2-hydroxy-6-(2-methoxy-4,5-methylenedioxyphenyl)-3,7-dioxabicyclo[3.3.0]octanes (21). A 1 mol dm^{-3} solution of DIBAL in toluene (1.60 ml, 1.60 mmol) was added as drops to a solution of **19** (566 mg, 1.39 mmol) in dry toluene (12 ml) at −70 °C under an atmosphere of dry argon. After 1 h at −75 °C, the mixture was diluted with ether and washed successively with 1 mol dm^{-3} aqueous HCl and 5 wt% aqueous $NaHCO_3$. The ethereal extract was dried, concentrated in vacuo, and chromatographed on silica gel eluted with hexane-EtOAc (2 : 1) to give **21** (567 mg, 1.38 mmol, 99%) as a viscous oil: ^1H NMR δ=0.04—0.28 (6H, s×4), 0.84—0.96 (9H, s×2), 2.28—2.68 (1H, m), 3.48—4.32 (5H, m), 3.75 (3H, s), 4.68—4.98 (1H, d×2, *J*=7 and 8 Hz), 5.02—5.24 (1H, d×2, *J*=6 and 8 Hz), 5.91 (2H, s), 6.49 (1H, s), and 6.94—7.06 (1H, s×2); IR ($CHCl_3$), 840, 910, 1045, 1190, 1260, 1487, 2970, and 3150—3650 cm^{-1}; MS *m/z* 410 (M^+), 394, 353, 191, 173, 165 (base), 161, and 75. Found: C, 58.70; H, 6.85%. Calcd for $C_{20}H_{30}O_7Si$: C, 58.51; H, 7.37%.

A Mixture of (1*S*,2*R*/*S*,5*R*,6*S*)-1-[(*t*-Butyldimethylsilyl)oxy]-2-fluoro-6-(2-methoxy-4,5-methylenedioxyphenyl)-3,7-dioxabicyclo[3.3.0]octanes (3). A solution of **21** (146 mg, 0.36 mmol), 2-fluoro-1-methylpyridinium tosylate (150 mg, 0.54 mmol) and Et_3N (0.10 ml, 0.72 mmol) in dry CH_2Cl_2 (3 ml) was stirred at room temperature for 50 min. The mixture was then concentrated in vacuo and the residue was chromatographed on silica gel. Elution with hexane-EtOAc (3 : 1) afforded **3** (134 mg, 0.33 mmol, 92%) as a viscous oil: ^1H NMR δ=0.10 (6H, s), 0.84—0.88 (9H, s×2), 2.36—2.90 (1H, m), 3.48—4.48 (4H, m), 3.74 (3H, s), 4.74—5.06 (1H, d×2, *J*=7 Hz each), 5.06—5.90 (1H, d×2, *J*=64 Hz each), 5.90 (2H, s), 6.47 (1H, s), and 7.00—7.06 (1H, s×2); IR ($CHCl_3$) 838, 1035, 1042, 1105, 1145, 1160, 1190, 1260, 1485, and 2950 cm^{-1}; MS *m/z* 412 (M^+), 355 (base), 191, 175, 165, and 75.

(1*S*,2*S*,5*R*,6*S*)-(+)-1-Hydroxy-2-(2-methoxy-4,5-methylenedioxyphenoxy)-6-(2-methoxy-4,5-methylenedioxyphenyl)-3,7-dioxabicyclo[3.3.0]octane and Its (1*S*,2*R*,5*R*,6*S*)-Isomer [23a (Desacetyl Phrymarolin I) and 23b]. A mixture of

the fluoride **3** (130 mg, 0.32 mmol), 2-methoxy-4,5-methylenedioxyphenol (62 mg, 0.38 mmol), $TrClO_4$ (0.13 g, 0.38 mmol), $SnCl_2$ (0.12 g, 0.64 mmol) and pulverized 4A Molecular Sieve in dry ether (10 ml) was stirred at 0—5 °C for 2.5 h. After the reaction had been quenched by 0.5 mol dm^{-3} aqueous NaOH, the resulting mixture was filtered through a pad of Celite with the aid of ether. The ethereal layer was separated, washed with 0.5 mol dm^{-3} NaOH, dried, and concentrated in vacuo. The crude product was purified by preparative TLC on silica gel developed with benzene-EtOAc (19:1) to give a mixture of **22a** and **22b** (88 mg, 0.16 mmol, 50%).

The crude product was dissolved in dry THF (2 ml) and a 1 mol dm^{-3} solution of n-Bu_4NF in THF (0.35 ml, 0.35 mmol) was added. After 1.5 h at room temperature, the mixture was diluted with CH_2Cl_2, washed with 10 wt% aqueous NH_4Cl, dried, and concentrated in vacuo. The crude product was purified by preparative TLC on silica gel developed with 20 vol% EtOAc in benzene to give **23a** (15.5 mg, 0.034 mmol, 21%) and **23b** (41.6 mg, 0.093 mmol, 58%). **(1*S*,2*S*,5*R*,6*S*)-23a:** mp 133—134 °C (lit. mp 133—134 °C); $[\alpha]_D^{23}$ +128.6° (*c* 0.49, $CHCl_3$); ^1H NMR δ=2.57 (1H, m), 3.72 (1H, d, *J*=10 Hz), 3.74 (3H, s), 3.75 (3H, s), 3.70—3.90 (1H, br), 4.06 (1H, dd, *J*=3 and 10 Hz), 4.31 (1H, d, *J*=10 Hz), 4.40 (1H, dd, *J*=7 and 10 Hz), 4.91 (1H, d, *J*=6 Hz), 5.16 (1H, s), 5.88 (2H, s), 5.89 (2H, s), 6.48 (1H, s), 6.53 (1H, s), 6.76 (1H, s), and 7.12 (1H, s); IR ($CHCl_3$) 1040, 1070, 1165, 1185, 1485, 1503, 2900, and 3150—3650 cm^{-1}; MS *m/z* 446 (M^+), 278, 181, 180, 168 (base), 165, and 153. **(1*S*,2*R*,5*R*,6*S*)-23b:** $[\alpha]_D^{24}$ −38.1° (*c* 1.39, $CHCl_3$); ^1H NMR δ=2.64 (1H, q, *J*=7 Hz), 2.80—3.20 (1H, br), 3.74 (3H, s), 3.78 (3H, s), 4.05 (1H, d, *J*=11 Hz), 4.18 (2H, d, *J*=7 Hz), 4.53 (1H, d, *J*=11 Hz), 5.02 (1H, d, *J*=7 Hz), 5.30 (1H, s), 5.87 (2H, s), 5.89 (2H, s), 6.47 (1H, s), 6.54 (1H, s), 6.74 (1H, s), and 7.05 (1H, s); IR ($CHCl_3$), 865, 940, 1005, 1040, 1162, 1185, 1430, 1483, 1502, 2900, and 3150—3650 cm^{-1}; MS *m/z* 446 (M^+), 278, 181, 180, 168 (base), 165, and 153.

(1*S*,2*S*,5*R*,6*S*)-(+)-1-Acetoxy-2-(2-methoxy-4,5-methylenedioxyphenoxy)-6-(2-methoxy-4,5-methylenedioxyphenyl)-3,7-dioxabicyclo[3.3.0]octane [la (Phrymarolin I)]. A mixture of **23a** and a catalytic amount of DMAP in Ac_2O (ca. 1 ml) was allowed to stand at room temperature for 12 h before being poured onto crushed ice. After the ice had melted, the precipitated solids were collected and dissolved in EtOAc. The extract was washed successively with 1 mol dm^{-3} aqueous HCl and 5 wt% aqueous $NaHCO_3$, dried, and concentrated in vacuo. The crude product was purified by preparative TLC on silica gel developed with benzene-EtOAc (9:1) to give **1a** as white crystals: mp 155—157 °C (lit. mp 155—157 °C); $[\alpha]_D^{25}$ +106.9° (*c* 0.11, dioxane); ^1H NMR δ=2.12 (3H, s), 2.88 (1H, m), 3.73 (3H, s), 3.75 (3H, s), 3.80 (1H, d, *J*=11 Hz), 4.03 (1H, dd, *J*=2 and 9 Hz), 4.49 (1H, dd, *J*=7 and 9 Hz), 4.60 (1H, d, *J*=11 Hz), 4.87 (1H, d, *J*=7 Hz), 5.66 (1H, s), 5.86 (2H, s), 5.91 (2H, s), 6.51 (2H, s), 6.82 (1H, s), and 7.03 (1H, s).

This work was partially supported by a a Grant-in-Aid for Research No. 59470113 from Ministry of Education, Science and Culture.

References

1) E. Taniguchi and Y. Oshima, *Agric. Biol. Chem.*, **36**, 1013 (1972).

2) E. Taniguchi, K. Imamura, and F. Ishibashi, Book of Abstracts, The 1984 International Chemical Congress of Pacific Basin Societies, Honolulu, Hawaii, December 1984, p. 877. Manuscript in preparation.

3) F. Ishibashi and E. Taniguchi, *Chem. Lett.*, **1986**, 1771.

4) F. Ishibashi and E. Taniguchi, *Agric. Biol. Chem.*, **50**, 3119 (1986).

5) R. B. Conrow and S. Bernstein, *J. Org. Chem.*, **36**, 863 (1971).

6) T. Mukaiyama, Y. Hashimoto, and S. Shoda, *Chem. Lett.*, **1983**, 935.

7) K. Kondo and F. Mori, *Chem. Lett.*, **1974**, 741.

8) A. Basha, M. Lipton, and S. M. Weinreb, *Tetrahedron Lett.*, **1977**, 4171.

9) G. Bettoni, C. Cellucci, and F. Berardi, *J. Heterocycl. Chem.*, **17**, 603 (1980).

10) E. J. Corey, H. Cho, C. Rücker, and D. H. Hua, *Tetrahedron Lett.*, **22**, 3455 (1981).

11) V. VanRheenen, R. C. Kelly, and D. Y. Cha, *Tetrahedron Lett.*, **1976**, 1973.

12) J. A. Dale, D. L. Dull, and H. S. Mosher, *J. Org. Chem.*, **34**, 2543 (1969).

13) Compound **4** was synthesized by Baeyer-Villiger oxidation of 2-methoxy-4,5-methylenedioxybenzaldehyde (**6**) with *m*-chloroperbenzoic acid and potassium fluoride in dichloromethane, followed by alkaline hydrolysis.

 © 1988 The Chemical Society of Japan Bull. Chem. Soc. Jpn., 61, 4367—4370 (1988)

Preparation and Properties of Inclusion Compounds of η^3-Allylpalladium Complexes with Cyclodextrins

Akira HARADA,* Mizutomo TAKEUCHI, and Shigetoshi TAKAHASHI*
The Institute of Scientific and Industrial Research, Osaka University, Ibaraki, Osaka 567
(Received June 27, 1988)

Inclusion compounds of di-μ-chloro-bis(η-allyl)dipalladium and its analogues with cyclodextrins (CDs; α-CD, β-CD, and γ-CD) were prepared. One-to-one inclusion compounds were obtained in high yields by the treatment of β- and γ-cyclodextrin with di-μ-chloro-bis(η-allyl)dipalladium and its analogues. The formation of inclusion compounds is selective. β-CD formed inclusion compounds with di-μ-chloro-bis[1-3-η-(2-methylallyl)]dipalladium in high yield, but it did not form any inclusion compounds with di-μ-chloro-bis(1-3-η-2-butenyl)dipalladium. γ-CD formed inclusion compounds with all the η^3-allylpalladium complexes tested in high yields. α-CD did not form inclusion compounds with any η^3-allylpalladium complexes tested. The thermogravimetric measurements show that η^3-allylpalladium complexes are stabilized when they are included in the CD cavity. The inclusion compounds were characterized by ^{1}H NMR, IR, UV, and circular dichroism spectra.

Organotransition metal complexes have been extensively used as homogeneous catalysts in organic reactions and much effort has been paid to improve their activity and selectivity.[1] Meanwhile, cyclodextrins (CDs) have been studied as a model of enzyme for selective catalysts. Therefore to combine the function of organometallic complexes and that of cyclodextrins, we tried to prepare the inclusion compounds of organometallic complexes with cyclodextrins. There are a large number of reports on the inclusion compounds of organic molecules with cyclodextrins.[2,3] In marked contrast, there are only a few reports on the inclusion compounds of organometallic complexes with cyclodextrins.[4,5] We previously reported the preparation and properties of inclusion compounds of ferrocene and its analogues with cyclodextrins as an example of cyclodextrin inclusion compounds of organometallic complexes.[6-9] These observations prompted us to examine the interaction of CD with η^3-allylpalladium complexes which are frequently used in a variety of organic syntheses. Moreover, recently much attention has been devoted to the preparation and properties of inclusion compounds of more than one metal center because of their importance of the cooperative effects.[10] Now we found that β- and γ-cyclodextrin form inclusion compounds with some η^3-allylpalladium complexes and that the formation of the inclusion compounds is selective. In a previous letter,[11] we reported briefly on the preparation of inclusion compounds of π-allyl palladium complexes. We describe here the preparation and properties of inclusion compounds of di-μ-chloro-bis-(η-allyl)dipalladium, $[(\eta\text{-allyl})PdCl]_2$, and its analogues with cyclodextrins in detail and discuss the binding mode. These inclusion compounds are the first inclusion compounds accommodating dinuclear species in a single cavity of CD. We also found that allylpalladium complexes are stabilized when they are included in the CD cavity.

Results and Discussion

Preparation of Inclusion Compounds. Di-μ-chloro-bis(η-allyl)dipalladium, $[(\eta\text{-}C_3H_5)PdCl]_2$, and its analogues are almost insoluble in water. So a co-crystallization method from aqueous solutions, which is usually used to obtain inclusion compounds with water-soluble compounds, cannot be used in this case. We tried to prepare the inclusion compounds by direct addition of fine crystals of π-allylpalladium complexes into a saturated aqueous solution of cyclodextrin at 35 °C. The product precipitated was washed thoroughly with water to remove remaining CD, and dried in vacuo. Unincluded metal complexes were removed by washing with chloroform. During this process, the included guest was not liberated from the CD cavity.

The inclusion compounds are characterized by elemental analysis and their IR, UV, and ^{1}H NMR spectra. Stoichiometries were determined by elemental analysis, including atomic absorption analysis of the metal contents, and from their ^{1}H NMR and UV spectra. All the inclusion compounds obtained in this work were stoichiometric one-to-one complexes. β-CD and γ-CD formed 1 : 1 inclusion compounds even if they were treated with two molar excess of η^3-allylpalladium complexes. This result indicates that the interaction between cyclodextrin and η^3-allylpalladium complexes is a real inclusion phenomenon. Table 1 shows the results on the preparation of inclusion compounds of η^3-allylpalladium complexes with CD. β-CD and γ-CD formed 1 : 1 inclusion compounds with allylpalladium complexes, regardless of the molar ratio of the host to guest in the reaction. γ-CD formed 1 : 1 inclusion compounds with all the η^3-allylpalladium complexes tested in high yields. The inclusion compounds of $[(\eta\text{-allyl})PdCl]_2$ and $[(\eta\text{-allyl})PdBr]_2$ with γ-CD were obtained in quantitative yields. β-CD formed 1 : 1 inclusion compounds with

Table 1. Preparation of Inclusion Compounds of η^3-Allylpalladium Complexes with Cyclodextrins

Guest	CD : Guest	Yield[a] %	Product Pd(%) Found	Calcd
[(η-Allyl)PdCl]$_2$	1 : 2	0	—	—
	1 : 1	21	—	—
	1 : 2	48	12.4	13.2
	1 : 1	68	—	—
	1 : 2	100	11.6	11.9
[1-3-η-(2-Methylallyl)PdCl]$_2$	1 : 2	0	—	—
	1 : 1	61	—	—
	1 : 2	95	14.8	13.0
	1 : 1	58	—	—
	1 : 2	63	9.6	11.7
[1-3-η-(2-Butenyl)PdCl]$_2$	1 : 2	0	—	—
	1 : 2	0	—	—
	1 : 2	96	7.6	11.7
[(η-Allyl)PdBr]$_2$	1 : 2	0	—	—
	1 : 2	23	12.7	12.5
	1 : 2	100	13.2	11.3
[(η-Allyl)PdI]$_2$	1 : 2	0	—	—
	1 : 2	0	—	—
	1 : 2	77	12.5	10.8

a) Calculated from cyclodextrin.

[1-3-η-(2-methylallyl)PdCl]$_2$ in high yield, but it did not form inclusion compounds with [(1-3-η-2-butenyl)PdCl]$_2$ complex. β-CD also formed 1 : 1 inclusion compounds with the chloro- and bromo-bridged complexes in moderate yields but not with the iodo-bridged complex. The yields of the inclusion compounds decreased in the order Cl>Br$\gg$I. β-CD is apparently able to discriminate not only the position of the substituents on the π-allyl ligands but the size of the bridging halogens. α-CD did not form inclusion compounds with any η^3-allylpalladium complexes tested. It is reasonable because the examination of CPK models shows that these allylpalladium complexes are too large to fit in the α-CD cavity.

Properties of Inclusion Compounds. η^3-Allylpalladium complexes are stabilized thermally by the formation of the inclusion compounds with cyclodextrin. Di-μ-chloro-bis(η-allyl)-dipalladium, for example, did not decompose on heating at 170 °C in vacuo when it was included in cyclodextrin. At this temperature the unincluded η^3-allylpalladium complex decomposes to give allyl chloride and palladium metal. Figure 1 shows the results on the thermogravimetric analysis of the inclusion compounds of di-μ-chloro-bis(η-allyl)dipalladium with β-cyclodextrin under nitrogen atmosphere, together with that of the mixture of β-CD and the allylpalladium complex, and that of the free allylpalladium complex. η^3-Allylpalladium complex starts to decompose at 145 °C and shows about 42% weight loss by 190 °C. This weight loss corresponds to 2 moles of allylchloride. In the case of the inclusion compounds there is no significant change until 190 °C except for the weight loss due to the dehydration. Rapid weight loss was observed around 200 °C, probably due to the decomposition of the guest molecule (liberation of allyl ligands). In the case of the mixture the allylpalladium complex decomposes at 145 °C. The decomposition point of π-allylpalladium rose about 50 °C by the formation of inclusion compounds. This is the first observation that metal complex is stabilized by the formation of inclusion compounds with cyclodextrin. γ-CD did not show such a stabilizing effect. On the other hand the decomposition point of β-CD was lowered by the presence of palladium complexes. Uncomplexed β-CD melts and decomposes at about 300 °C, but β-CD

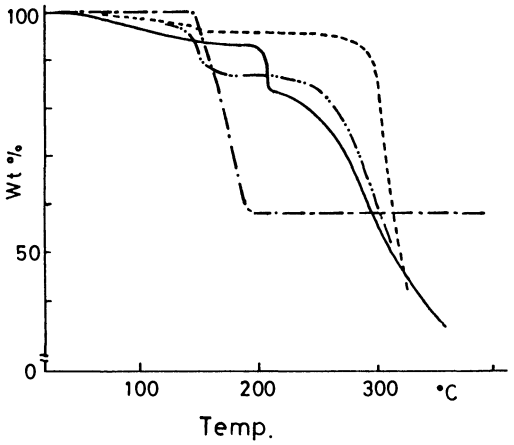

Fig. 1. Thermogravimetric analyses of the inclusion complex of [(η-allyl)PdCl]$_2$ with β-CD (——), the mixture of β-CD and [(η-allyl)PdCl]$_2$ (——·——), [(η-allyl)PdCl]$_2$ (——), and β-CD (-----) in vacuo at 5 °C min^{-1}.

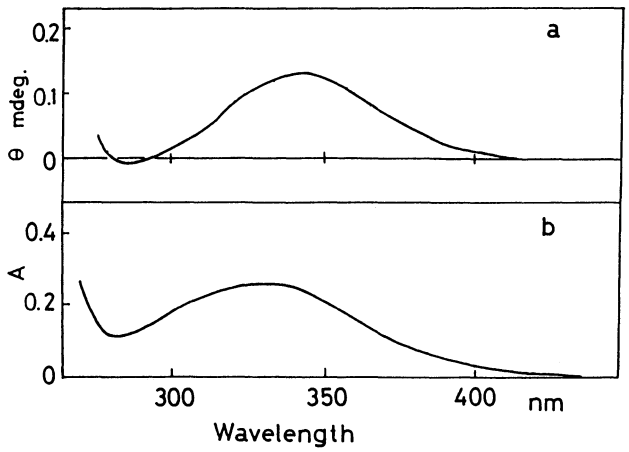

Fig. 2. Circular dichroism spectrum (a) and absorption spectrum (b) of [(η-allyl)PdCl]$_2$ in the presence of β-CD in ethylene glycol at 25 °C. [cyclodextrin] =[(η-allyl)PdCl]$_2$=10^{-3} mol dm^{-3}.

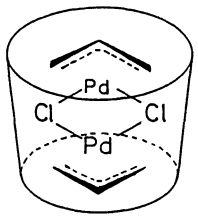

Fig. 3. Proposed structure of the inclusion compound of [(η-allyl)PdCl]$_2$ with β-cyclodextrin.

in the inclusion compound starts to decompose around 200 °C. β-CD also decomposes around 200 °C in the presence of palladium complexes.

The inclusion compounds are insoluble in usual organic solvents such as benzene, hexane, chloroform, and so on. They are soluble in ethylene glycol, dimethyl sulfoxide, and *N,N*-dimethylformamide, and slightly soluble in water. However, the inclusion compounds have been found to dissociate in dimethyl sulfoxide or in *N,N*-dimethylformamide. The inclusion behavior was observed in ethylene glycol solution.

Figure 2 shows the absorption spectra and circular dichroism spectra of [(η-allyl)PdCl]$_2$ in the presence of β-CD in ethylene glycol solution. β-CD causes a positive Cotton effect at about 345 nm with a small negative Cotton effect around shorter wavelength. γ-CD showed no effects. These results indicate that [(η-allyl)PdCl]$_2$ is included in the β-CD cavity with a fixed orientation and are in accordance with those of the inclusion compounds of β-CD–ferrocene and β-CD–arene chromium complexes, which show both positive Cotton effects in the longer wavelength region. This result indicates that π-allylpalldium complexes are included in β-CD cavity with a "perpendicular" manner as shown in Fig. 3 in a similar fashion to those of the ferrocene complex and arene chromium complexes.[7]

According to CPK molecular models, chloro-bridged allylpalladium complexes appear to fit well into the β-CD cavity, whereas bromo-bridged and iodo-bridged complexes are too large to fit in the β-CD cavity. 2-Methyl derivative is symmetric and more compact than 1-methyl derivative. So 2-methyl derivative fits well in the β-CD cavity, but 1-methyl derivative is not able to fit the cavity. Proposed structure for the β-CD–di-μ-chloro-bis(η-allyl)dipalladium is shown in Fig. 3, which could account for the selective inclusion in terms of the steric factor of both the allylic ligands and bridging halogens.

Another feature of these inclusion compounds is their stoichiometry. The inclusion compounds of di-μ-chloro-bis(cyclooctadiene)dirhodium(I) with β-cyclodextrin, which have a similar molecular structure to π-allylpalladium chloride, show 2 : 1 (CD : guest) stoichiometry,[12] whereas the inclusion compounds of π-allylpalladium complexes show 1 : 1 stoichiometry. This result can be interpreted in terms of the bulkiness of the ligands of the metal complexes. Cyclooctadienyl ligand is large enough to fill a single β-CD cavity, whereas π-allyl ligands are too small to fill the cavity which can accommodate the whole molecule of the complex resulting in one to one inclusion compounds. Consequently, the inclusion compounds contain two palladium metals in a single cavity. These inclusion compounds are the first example of those accommodating dinuclear species in a single cyclodextrin ring.

Experimental

All the manipulations were performed under an atmosphere of nitrogen.

Materials. Cyclodextrins (α-CD, β-CD, and γ-CD) were obtained from Hayashibara Biochemical Laboratories Inc. Their purities were checked by elemental analysis and optical rotation. η^3-Allylpalladium complexes were prepared according to the methods described in the literature.[13]

The inclusion compound of di-μ-chloro-bis(η-allyl)dipalladium with β-CD was prepared by adding finely ground crystals of di-μ-chloro-bis(η-allyl)dipalladium complex (0.344 g, 0.95 mmol) to an aqueous solution of β-CD ($10H_2O$ adduct, 0.658 g, 0.50 mmol) at 35 °C with stirring. The product was washed with water to remove remaining CD,

Table 2. Analytical Data of Inclusion Compounds

	Product			
	Found (%)		Calcd (%)	
	C	H	C	H
β-CD-[(η-allyl)PdCl]$_2$	35.91	5.47	35.83	5.76
γ-CD-[(η-allyl)PdCl]$_2$	36.03	5.67	36.25	5.85
β-CD-[1-3-η-(2-methylallyl)PdCl]$_2$	36.43	5.90	36.68	5.91
γ-CD-[1-3-η-(2-methylallyl)PdCl]$_2$	37.27	5.76	37.01	5.99
γ-CD-[1-3-η-(2-butenyl)PdCl]$_2$	36.75	5.44	37.01	5.99
β-CD-[(η-allyl)PdBr]$_2$	35.68	5.28	36.26	5.07
γ-CD-[(η-allyl)PdBr]$_2$	34.81	5.42	34.53	5.58
γ-CD-[(η-allyl)PdI]$_2$	33.28	5.00	32.89	5.31

and dried in vacuum. Nonincluded (η^3-allyl)palladium complex was removed by washing the residue with chloroform. The product was recrystallized from water or aqueous ethanol to give pale yellow crystals. For β-CD ($10H_2O$-dichlorobis(allyl)dipalladium complex: mp 200—205 °C (decomp).

The other inclusion compounds were prepared in a similar way and their analytical data are summarized in Table 2.

Instrumentation. Infrared spectra were taken on a Hitachi 295 spectrometer and UV spectra were recorded on a Shimadzu UV-202 spectrophotometer. ^{1}H NMR spectra were run on a JEOL FX100 spectrometer. Circular dichroism spectra were recorded on a JASCO J-205 spectropolarimeter. Thermogravimetric analysis was made using a Shimadzu thermal analyzer DT-30. Atomic absorption analysis was made using a Shimadzu A-610S atomic absorption/flame spectrophotometer.

References

1) J. P. Collman and L. S. Hegedus, "Principles and Applications of Organotransition Metal Chemistry," University Science Books, Mill Vally, (1980).

2) M. L. Bender and M. Komiyama, "Cyclodextrin Chemistry," Springer-Verlag, Berlin (1977).

3) J. Szejtli, "Cyclodextrin and Their Inclusion Complexes," Akademiai Kiasdo, Butapest (1982).

4) D. R. Alston, A. M. Z. Slawin, J. F. Stoddart, and D. J. William, *Angew. Chem., Int. Ed. Engl.*, **24**, 786 (1985).

5) H. M. Colquhoun, J. F. Stoddart, and D. J. Williams, *Angew. Chem., Int. Ed. Engl.*, **25**, 487 (1986).

6) A. Harada and S. Takahashi, *J. Chem. Soc., Chem. Commun.*, **1984**, 645.

7) A. Harada, K. Saeki, and S. Takahashi, *Chem. Lett.*, **1985**, 1157.

8) A. Harada and S. Takahashi, *J. Incl. Phenomena*, **2**, 791 (1984).

9) A. Harada and S. Takahashi, *J. Chem. Soc., Dalton Trans.*, **1988**, 729.

10) A. Carray and J-M. Lehn, *J. Chem. Soc., Chem. Commun.*, **1986**, 1232.

11) A. Harada, M. Takeuchi, and S. Takahashi, *Chem. Lett.*, **1986**, 1893.

12) A. Harada and S. Takahashi, *J. Chem. Soc., Chem. Commun.*, **1986**, 1229.

13) A. J. Wilkinson, *J. Chem. Soc.*, **1964**, 1585.

The Use of Silica Gel-Supported Ionenes as Reagents and Catalysts for Several Substitution Reactions in Toluene[1)]

Noritaka OHTANI,* Kosaku CHIDA, Hajime SERITA,† Toshiaki MATSUNAGA,† and Chikai KIMURA††
Department of Chemical Engineering for Resources, Mining College, Akita University, Tegata-Gakuencho, Akita 010
†Department of Fuel Chemistry, Mining College, Akita University, Tegata-Gakuencho, Akita 010
(Received July 1, 1988)

Several ionene bromides were used as reagents for the displacement of decyl methanesulfonate into 1-bromodecane. They were very reactive when adsorbed by silica gel. The enhanced activities of the ionenes were hardly dependent on their structures and molecular weights but decreased gradually with increasing the amount of ionene adsorbed by silica gel. Ionene chlorides exhibited a similar enhancement of reactivity when adsorbed by silica gel. However, unlike the ionenes, a large increase in activity due to adsorption was not observed with pendant-type polycations such as poly(4-vinylpyridinium bromide) and poly[(4-vinylbenzyl)tributylammonium chloride]. The silica gel-supported ionenes also exhibited excellent catalytic activities for solid-liquid-solid triphase substitution reactions, particularly for the reactions between 1-bromodecane and such inorganic salts as consisted of relatively hard-basic nucleophilic anions.

It is well-known that lipophilic quaternary ammonium salts are not only good nucleophilic reagents in nonpolar media but also excellent phase-transfer catalysts.[2)] In order to simplify salt recovery and product isolation, the salts have been covalently attached as a pendant group, either to the matrix of swellable cross-linked polymer or to the surface of porous inorganic materials.[3-6)] To those insoluble materials, the salts have been introduced usually at random, which leads to an ambiguous distribution of active sites and an unavoidable assumption about the microenvironment around the active sites. Furthermore, immobilization of the salts gives rise, in most cases, to the reduction of overall activities of the salts, which has been explained in terms of diffusional limitation.[5)]

On the other hand, few reports except two studies[7,8)] have been concerned with reaction and catalysis of the quaternary salts which are adsorbed by inorganic materials. If the quaternary salts are lipophilic, however, this reaction system is likely of little value because the salts are in dynamic equilibrium between adsorbed and desorbed states.[7)] This equilibrium makes it difficult to evaluate the influence of adsorbent unless the adsorption induces a drastic change in activities of the salts. The equilibrium also makes it difficult to accomplish a complete recovery of the salts.

Ionenes are a specific kind of polycations having a definite chemical structure in which quaternary ammonium groups are spaced regularly along the polymer backbone.[9)] Generally, they are quite hydrophilic and easily soluble in water but most of them are neither soluble nor swellable in nonpolar organic solvents. This nature of the ionenes has restricted their use only to aqueous reaction systems. Thus, we have successfully utilized them as catalysts for aqueous interionic reactions[10)] and as flocculants of aqueous kaolin suspension.[11)]

This work demonstrates the applicability of some hydrophilic ionenes, which are shown in Fig. 1(a)—(d), to excellent reagents and catalysts of various substitution reactions in toluene under the conditions where the ionenes are deposited on the surface of silica gel or other inorganic supports. The method is quite simple. After silica gel and a methanol solution of the ionenes (x—y, X) were mixed and equilibrated, the mixture was evaporated to dryness. The obtained silica gel–ionenes complexes (x—y, X/silica gel) were used as reagents of the liquid-solid biphase reactions (Eq. 1) or as catalysts for the solid-liquid-solid triphase catalytic reactions (Eq. 2).

$$n\text{-}C_{10}H_{21}OMs + x\text{-}y,\ X/\text{silica gel} \longrightarrow n\text{-}C_{10}H_{21}X + x\text{-}y,\ OMs/\text{silica gel} \quad (1)$$
$$X = Cl \text{ or } Br,\ OMs = CH_3SO_3$$

$$n\text{-}C_{10}H_{21}X + KY(\text{solid}) \xrightarrow{x\text{-}y,\ Br/\text{silica gel}} n\text{-}C_{10}H_{21}Y + KX(\text{solid}) \quad (2)$$
$$X = OMs \text{ or } Br,\ Y = I,\ CN,\ Br,\ OPh,\ \text{or } OAc$$

The rate enhancement through adsorption has been examined for the ionenes as well as some pendant-type polycations as shown in Fig. 1(e)—(g).

Experimental

Materials. Commercial α,ω-alkanediamines and piperazine were converted to the corresponding α,ω-bis(dimethylamino)alkanes and N,N'-dimethylpiperazine using formalin–formic acid. α,ω-Dihaloalkanes and α,α'-dichloro-p-xylene were purchased and distilled.

Ionene polymers (x—y, X) were prepared from the reaction of the N-methylated diamines with the equimolar dihalides under the conditions previously reported.[11)] 2-Hydroxy-3-ionene chloride, 3-OH, Cl was prepared according to the literature.[12)] The intrinsic viscosities of the ionenes were measured. The data are summarized as follows: x-y, X, $[\eta]/\text{dl g}^{-1}$ (25 °C, aq 0.4 mol dm^{-3} KBr unless otherwise stated); 2-5, Br, 0.12; 3-3, Br, 0.07; 3-4, Br(I), 0.22; 3-4, Br(II), 0.15; 3-4, Br(III), 0.10; 3-6, Br, 0.15; 4-4, Br, 0.05; 6-2, Br,

†† Present address: Tokyo Kasei University, Kaga, Itabashi-ku, Tokyo 173.

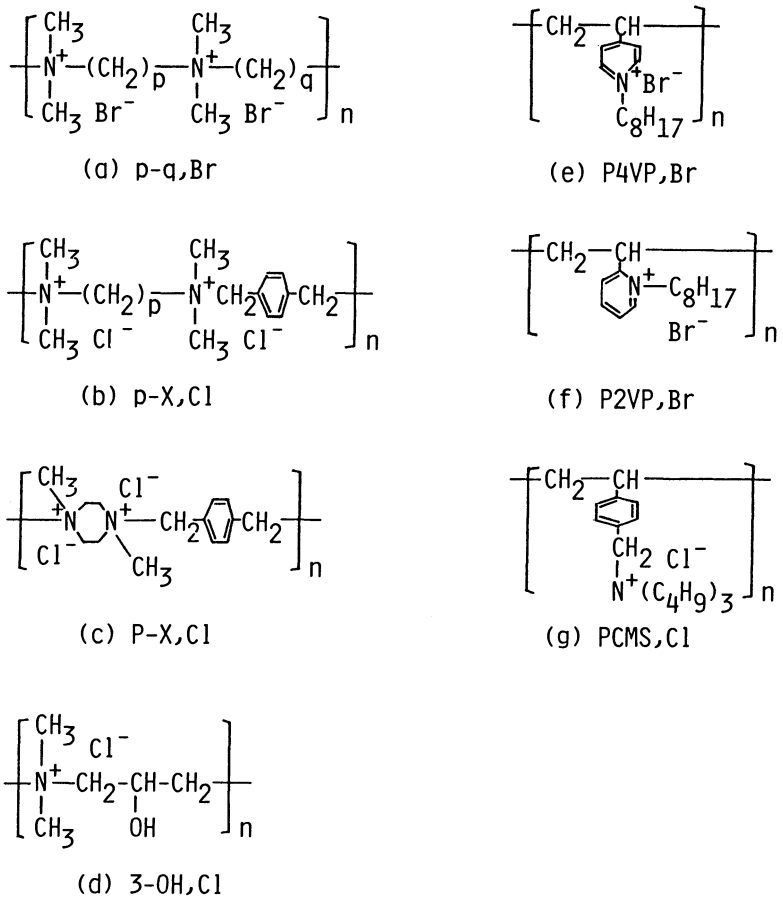

Fig. 1. Ionenes and pendant-type polycations used.

0.09; 6-6, Br, 0.19; 2-X, Cl, 0.18 (0.3 mol dm^{-3} KBr); 3-X, Cl, 0.21; 6-X, Cl, 0.23 (0.3 mol dm^{-3} KBr); P-X, Cl, 0.18 (0.2 mol dm^{-3} KBr); 3-OH, Cl, 0.08. The viscosity-molecular weight relationships for ionenes are available only for 3-4, Br and 6-6, Br.[13] The molecular weights of 3-4, Br(I), 3-4, Br(II), 3-4, Br(III), and 6-6, Br were 40000, 27000, 15000, and 20000, respectively.

Freshly distilled 2- and 4-vinylpyridines were polymerized and then quaternized by 1-bromooctane,[14] to give P2VP, Br and P4VP, Br. Poly[4-(chloromethyl)styrene] was prepared by suspension polymerization of distilled 4-(chloromethyl)-styrene using benzoyl peroxide for 7 h at 80 °C and was purified to remove insoluble crosslinked resins through several reprecipitations using dioxane-methanol. The linear poly[4-(chloromethyl)styrene] was reacted with tributylamine in *N*,*N*-dimethylformamide [14 d, 50 °C] to give the corresponding ammonio-attaching polystyrene, PCMS, Cl. The molecular weight and the degree of quaternization of P2VP, Br, P4VP, Br, and PCMS, Cl were measured according to the literature:[14] Polycation, molecular weight, degree of quaternization; P2VP, Br, 450000, 37.4%; P4VP, Br, 74000, 79.7%; PCMS, Cl, —, 60.0%.

Silica gel (Wakogel C-200, 100—200 mesh), activated alumina (Wako, abt. 200 mesh), neutral alumina (Wako, W-200), and activated carbon powder (Wako, —200 mesh) were dried in vacuo prior to use [3 h, 110 °C]. Molecular Sieves (Wako, 4A 1/16) was ground to a powder and was dried prior to use. The specific surface area of the inorganic supports was measured on Yanagimoto Surface Area Analyzer GSA-10.

Potassium phenoxide, prepared from neutralization of phenol with aqueous potassium hydroxide, and all other commercial solid inorganic reagents were also dried [3 h, 110 °C in vacuo]. Decyl methanesulfonate (abbreviated as decyl mesylate hereinafter) was prepared by the reaction of 1-decanol with methanesulfonyl chloride,[15] and was purified by vacuum distillation.

Silica Gel-Supported Ionenes. A given amount of the pre-dried silica gel was added in one portion to a stirred solution of an ionene in 30 ml of methanol or ethanol. The mixture was stirred for 1 h at room temperature. The solvent was then evaporated and the resulting ionene-silica gel complex (abbreviated as complex hereinafter) was dried in vacuo at 110 °C for 3 h. Other supported polycations were also prepared by the same procedure. Ion content, the ammonium content per gram of the complex, was adjusted to be 0.25 mmol g^{-1} unless stated otherwise. For comparison with the ionenes, potassium bromide and sodium chloride were also supported on silica gel in a manner similar to the literature.[16]

Ionene Halide as a Reagent for Nucleophilic Substitution Reactions. A 25 ml culture tube with a Teflon-lined screw cap was charged with 0.073 mmol of ionene supported or nonsupported plus 1.0 ml of toluene containing pentadecane as an internal standard. The tube was placed in an oil bath maintained at 90 °C and the mixture was stirred for 20 min with a Teflon-coated magnetic stirring bar, followed by injection of 0.073 mmol of decyl mesylate via a syringe.

The disappearance of the mesylate and the appearance of 1-halodecane in the toluene phase were followed by GLC (Hitachi 163 Gas Chromatograph).

Ionene Halides as Solid-Liquid-Solid Triphase Catalysts. To a 25 ml culture tube with a Teflon-lined screw cap was added 5 mmol of solid reagent salt (KBr, NaI, NaCN, KOPh, or KOAc), 0.05 mmol of a polycation supported or nonsupported, and 4.0 ml of toluene containing pentadecane as an internal standard. The mixture was stirred for 1 h at 90 °C, followed by injection of decyl mesylate (0.8 mmol) or 1-bromodecane (0.7 mmol). The substrates and the products were quantitatively analyzed by GLC.

Results and Discussion

Ionene Halide as a Reagent. Nonsupported ionene bromides were all insoluble in toluene. They were very slow to react with the eqimolar amount of decyl mesylate. The results of typical ionene bromides are shown in Fig. 2. The reactions did not follow second-order kinetics. Even after several days, the substantial parts of the bromides were found to remain unreacted.

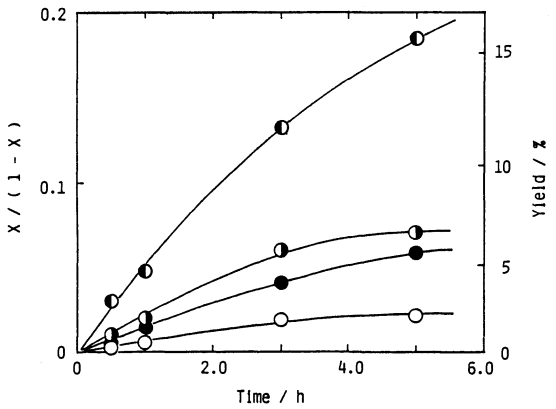

Fig. 2. Reaction of nonsupported ionene bromides with decyl mesylate.
x; yield 1-bromodecane.
●, 3-3, Br; ○, 3-4, Br(I); ◑, 4-4, Br; ◐, 6-6, Br.

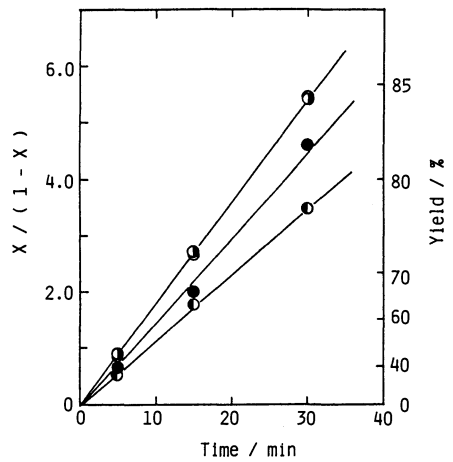

Fig. 3. Reaction of silica gel-supported ionene bromides with decyl mesylate.
●, 3-3, Br; ○, 3-4, Br(I); ◑, 4-4, Br; ◐, 6-6, Br.

When the ionene bromides were supported on silica gel, however, the rates of the substitution were dramatically increased as shown in Fig. 3. The reactions were completed in a few hours. A plot of $x/(1-x)$ vs. reaction time was almost linear for all the supported ionenes, indicating that the reactions were of second order, that is, first order with respect to both decyl mesylate and ammonium bromide. This also indicates that all the ammonium bromides of one ionene have an equal reactivity. The desorption of the ionenes during the reactions was neglected because the weight loss of 3-4, Br complex was not observed after the complex was soaked in toluene for 1 h at 90 °C, separated by filtration, and dried in vacuo. The second-order rate constants calculated from the slopes of the plots are in the narrow range of 2.7×10^{-3} to 4.3×10^{-3} mol^{-1} dm^3 s^{-1}, which are comparable to the reported data for organic-soluble quaternary onium salts.[17] Despite of a polar nature of silica gel surface, the high reactivities observed for the adsorbed ionenes are striking. The results of silica gel-supported and nonsupported ionene bromides are summarized in Table 1 together with the results of P4VP, Br, P2VP, Br, and KBr. It should be noted again that the reactivity of silica gel-supported ionene bromides was hardly dependent on the ionene structure and that the reactivity was much higher than that of nonsupported ionene bromides.

These results clearly indicate that, being adsorbed on silica gel, the ionenes allow decyl mesylate to diffuse easily to active sites and provide an increased number of the active sites. Ionene bromides are crystalline polymers.[9] They have crystalline regions under the nonsupported state. The ammonium bromides in the crystalline region are likely difficult to react. It is therefore assumed that the difference in reactivity of the nonsupported ionenes is attributable partly to the difference in the morphological structure aside from the influence of the powder size.

Table 1. Substitutions of Decyl Mesylate into 1-Bromodecane Using Nonsupported and Silica Gel-Supported Ionene Bromides[a]

Ionene bromide	Yield/%	
	Nonsupported	Supported
2-5, Br	1.4	94.4
3-3, Br	4.0	97.0
3-4, Br(I)	1.7	97.9
3-6, Br	0.1	99.2
4-4, Br	5.6	98.0
6-2, Br	2.2	96.1
6-6, Br	11.9	95.9
P4VP, Br	64.2	86.0
P2VP, Br	3.5	44.2
KBr	1.0[b]	28.9[b]

a) Reactions were carried out in toluene at 90 °C for 3 h: n-$C_{10}H_{21}OMs$, 0.0734 mmol; ammonium bromide, 0.0734 mmol; toluene, 1.0 ml. b) Yield after 20 h.

The adsorption to silica gel possibly induces the destruction of the crystalline region and also weakens the electrostatic interaction among the ammonium bromide ion pairs, so that the formation of aggregates of the ion pairs becomes difficult.

As shown in Fig. 4 (solid line), silica gel-supported 3-4, Br gave an identical reactivity irrespective of molecular weight of the ionene. This fact and the equal reactivity of the ammonium bromides in one ionene strongly suggest uniform and monolayer coverage of ionene over the silica gel surface. The result shown in Fig. 5 supports the validity of the assumption. At low levels of loading on silica gel, 3-4, Br exhibited a constant reactivity. But, beyond 0.5 mmol g^{-1} of ion content, the reactivity of the 3-4, Br complex decreased with increasing loading. The specific surface area of the silica gel was ca. 270 $m^2 g^{-1}$ obtained from BET measurement. Since the maximum cross section per mmol of ammonium unit, estimated from CPK model, is ca. 200 m^2 when 3-4, Br molecule is fully extended, it seems reasonable to assume monolayer adsorption in the case of low ion content.

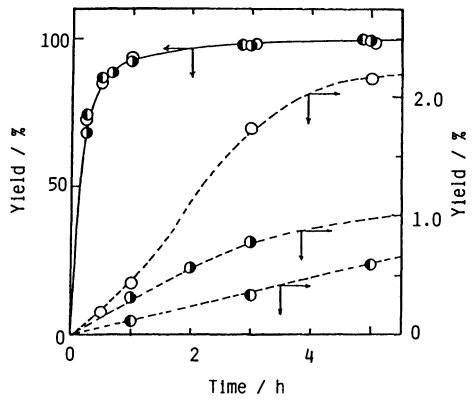

Fig. 4. Effect of molecular weight on the activities of nonsupported and silica gel-supported 3-4, Br toward decyl mesylate.
○, 40000; ◐, 27000; ◑, 15000.——,supported. ----,nonsupported.

P4VP, Br was relatively active without any carrier, whereas P2VP, Br was as poorly active as ionene bromides (Table 1). P4VP, Br swells well in toluene. The high reactivity and swellability imply the absence of the extensive aggregation among the ion pairs of P4VP, Br. Therefore, an increase in activity due to adsorption was not significant for P4VP, Br, while P2VP, Br exhibited a moderate improvement. It is noted that, under the adsorbed state, these pendant-type polycations are not so reactive as ionene bromides. This implies either the relatively weak interaction of the pendant ammonio groups with the silica gel surface or the presence of a dynamic equilibrium of the ammonio groups between adsorbed and desorbed states to form a sort of looped structure of the polymer chains over the silica gel surface. The looped structure is often assumed in the case of the adsorptions of linear polyelectrolytes from aqueous solutions.[18]

As mentioned above, the state of adsorption may be a primary factor to determine the effectiveness of this reaction system. An additional factor to influence the reaction rate is the local concentration of decyl mesylate. Since 0.3 g of uncoated silica gel adsorbs 54% of decyl mesylate from the reaction mixture, decyl mesylate is undoubtly concentrated around the active sites, whereas the adsorption of the product, 1-bromodecane, is as small as 1%.

Figure 6 shows the effect of carriers upon the reactivity of 6-6, Br supported on them. The yield of 1-bromodecane increased in the order of silica gel>activated carbon>Molecular Sieves 4A>activated alumina. This order did not correlate to an ability of carrier to adsorb decyl mesylate from the reaction mixture; silica gel (54%)>activated alumina (34%)>active carbon (8%)>Molecular Sieves 4A (6%). These facts suggest that the interaction between support surface and ammonium bromides is important and that silica gel may attract preferentially ammonium ions to make bromide counter ions somewhat free from the electrostatic restraint of the ammonium ions.

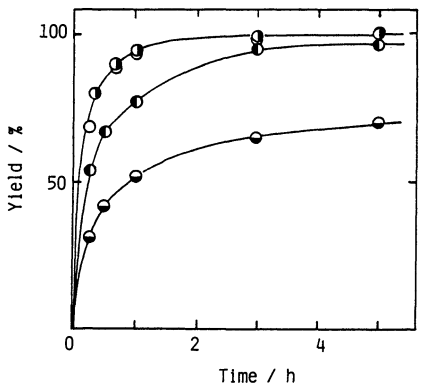

Fig. 5. Effect of ion content on the activity of silica gel-supported 3-4, Br toward decyl mesylate.
○, 0.25; ◑, 0.50; ◐, 1.00; ◒, 2.00 mmol g^{-1}.

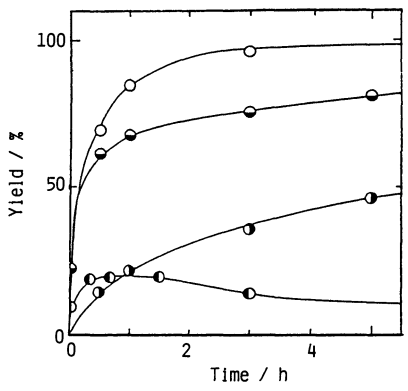

Fig. 6. Effect of carrier on the activity of supported 6-6, Br toward decyl mesylate.
○, silica gel; ◐, activated alumina; ◒, active carbon; ◑, Molecular Sieves 4A.

Table 2. Substitution of Decyl Mesylate into 1-Chlorodecane Using Nonsupported and Silica Gel-Supported Ionene Chlorides[a)]

Ionene Chloride	Yield/%	
	Nonsupported	Supported
2-X, Cl	1.3	74.6
3-X, Cl	0.5	72.0
6-X, Cl	4.1	75.9
P-X, Cl	1.9	79.8
3-OH, Cl	0.0	71.9
PCMS, Cl	66.6	89.2
NaCl	0.0[b)]	16.0[b)]

a) Reactions were carried out in toluene at 90 °C for 3 h: n-$C_{10}H_{21}OMs$, 0.0734 mmol; ammonium chloride, 0.0734 mmol; toluene, 1.0 ml. b) Yield after 20 h.

Contrary to expectation,[7,16,19)] alumina was not only ineffective in this system but also promotive of the hydrolysis of both decyl mesylate and 1-bromodecane. The hydrolysis takes place possibly due to the presence of an irremovable water adsorbed by the alumina. The use of neutral alumina instead of activated alumina brought about any improvement neither on reaction rate nor on product composition. Active carbon also gave the hydrolysis product, 1-decanol, as a by-product, whose yield had reached ca. 25% when the mesylate completely disappeared.

Similarly, ionene chlorides were found to be much more reactive toward decyl mesylate when they were supported on silica gel. The results are summarized in Table 2 together with the results of PCMS, Cl, and NaCl. The reaction rates enhanced by adsorption were very similar for all ionene chrolides, while the rates of nonsupported ionenes differed from each other. PCMS, Cl, which contains pendant ammonio groups, is active without any carrier probably due to its high swellability. Its adsorption onto silica gel, therefore, did not induce a significant increase in activity. This tendency was quite similar to that of P4VP, Br.

Silica Gel-Supported Ionenes as Solid-Liquid-Solid Triphase Catalysts. Silica gel-supported ionenes were found to enhance some substitution reactions between liquid substrates and solid inorganic reagents. Figure 7 shows the results of the reaction between decyl mesylate and potassium bromide. The reaction hardly proceeded either in the absence of catalysts or even in the presence of nonsupported 3-4, Br. The two rates were almost identical. This indicates that the nonsupported 3-4, Br has no catalytic activity.

However silica gel-supported 3-4, Br largely accelerated the reaction. Although uncoated silica gel also promoted the reaction, it was less catalytically active than the 3-4, Br complex. This is consistent with the result that, as reagents, the supported 3-4, Br was much more reactive than the supported KBr (Table 1). Contrary to the lack of catalytic activity of the nonsupported 3-4, Br, the supported 3-4, Br contributes substantially to the rate enhancement. The contribution of the supported 3-4, Br tends to be amplified with decreasing ion content of the complex (Fig. 7).

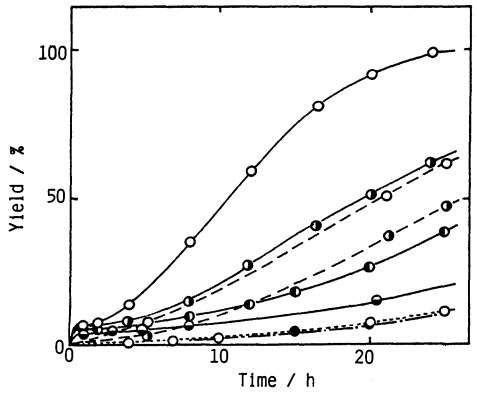

Fig. 7. Catalytic effects of silica gel and 3-4, Br on the solid-liquid-solid triphase reactions between decyl mesylate and potassium bromide.
——, supported 3-4, Br; ion content; ○, 0.25; ◑, 0.50; ◐, 1.00; ◒, 2.00. ---, silica gel; weight/mg; ○, 200; ◑, 100. ------, nonsupported 3-4, Br. —·—, none of catalysts.

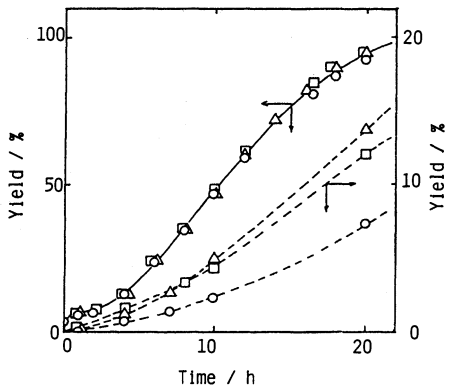

Fig. 8. Solid-liquid-solid triphase catalytic reaction between decyl mesylate and potassium bromide.
○, 3-4, Br; △, 4-4, Br; □, 6-6, Br. ——, supported; ---, nonsupported.

Figure 8 shows the effect of ionene structure on the catalysis. Unlike 3-4, Br, nonsupported 6-6, Br and 4-4, Br, which had relatively high reactivities toward decyl mesylate (Table 1), had minimal catalytic activities. When adsorbed on silica gel, every ionene afforded much higher catalytic efficiency. The enhanced rates were very similar from one ionene to another.

A specific feature of the catalysis of the complexes is the large reaction rates at the initial stage, which is hardly observed either for uncoated silica gel or for nonsupported ionenes. The amount of 1-bromodecane formed within the first one hour approximately corresponded to that of ammonium bromides of the ionene added (Figs. 7 and 8). After the initial stage of the rapid reaction, a rather slow increase in the yield was observed and the time-yield curve presents somewhat autocatalytic feature. These phenomena can be

Table 3. Solid-Liquid-Solid Triphase Reactions Catalyzed by Silica Gel and Silica Gel-Supported 3-4, Br[a)]

Substrate	Solid reagent	Yield/%		
		None	Uncoated silica gel	Supported 3-4, Br[b)]
n-$C_{10}H_{21}OMs$	NaI[c)]	23	23	20
	KCN	65		74
	KOPh[d)]	21	88	87
	KOAc	16	100	96
n-$C_{10}H_{21}Br$	NaI	tr.	5	21
	KCN	0	0	tr.
	KOPh	0	17	48
	KOAc	0	9	35

a) Reactions were carried out in toluene at 90 °C for 25 h: n-$C_{10}H_{21}OMs$, 0.81 mmol ; n-$C_{10}H_{21}Br$, 0.72 mmol; solid reagents, 5.0 mmol; silica gel, 0.2 g. b) Ion content, 0.25 mmol g^{-1}; complex weight, 0.2 g. c) Yield after 1.0 h. d) Yield after 15 min.

accounted for in terms of high reactivity of active sites and slow regeneration of the active sites. Namely, the adsorbed ammonium salts in the form of bromide, which are the active sites in this system, can react immediately with decyl mesylate but ion exchange, which restores the ionene to the original bromide form, is slow compared to the chemical reaction. A clear account has not been given of the mechanism of this sort of ion exchange. There are many possible ways in which the counter ions of the ammonio groups are displaced: exchange by direct contact with the solid KBr, indirect exchange via contact with silica gel-adsorbed KBr, exchange by the trace amounts of KBr salt dissolved in the organic phase, and exchange by the KBr salt dissolved in the minimal amounts of irremovable water. Some discussion on this matter will be done later in this paper.

Table 3 shows the results of other substitution reactions catalyzed by the 3-4, Br complex. Generally, in S_N2 reactions, mesylate is a good leaving group compared to bromide. Hence decyl mesylate underwent rather facile substitutions, particularly with sodium iodide and with potassium phenoxide even in the absence of any catalyst. It was found, however, that the catalytic efficiencies of the complex as well as the uncoated silica gel had no relation to the substrate reactivity, but the efficiencies were determined by the combination of leaving group and attacking nucleophile.

Neither the complex nor the uncoated silica gel facilitated the displacements of decyl mesylate attacked by soft-basic ions, such as iodide and cyanide. In contrast, the displacements of the mesylate by hard-basic ions, acetate and phenoxide, were enhanced both by the complex and by the uncoated silica gel. The catalysis of the complex in these reactions, however, has nothing to do with the supported ionene because the catalytic efficiency of the complex coincides with that of the uncoated silica gel. Interestingly, it is only with bromide ion, a medium-basic nucleophile, that the substitution of decyl mesylate was really catalyzed by the ionene adsorbed on silica gel.

When bromide was a leaving group, the distinct catalytic action of the 3-4, Br complex was observed except for the reaction with sodium cyanide (Table 3), while the nonsupported 3-4, Br hardly catalyzed either reaction. The complex was catalytically more active than the uncoated silica gel, indicating that the adsorbed ionene played a key role in the catalysis. Furthermore, the reaction of 1-bromodecane was fast with hard acetate or phenoxide rather than with soft iodide, though the rates were considerably leveled among these reactions compared to the reactions of decyl mesylate. This fact is consistent with the observations that acetate[8)] and phenoxide[20)] are relatively reactive under anhydrous phase-transfer conditions.

On the basis of all the results, the catalysis of the complex may be summarized as follows. Silica gel undoubtly assists the catalysis through activating the ammonium salts of the ionene. However, the overall rates of the catalytic reactions were controlled by ion-exchange process. Taking into consideration that the uncoated silica gel accelerates the substitutions with hard-basic nucleophiles, silica gel likely facilitates the ion exchange rather selectively of hard-basic anions.

This work was partially supported by Grant-in-Aid for Scientific Research from the Ministry of Education, Science and Culture (No. 57550557).

References

1) This work has been presented in part at the 32nd Annual Meeting of the Society of Polymer Science, Japan, Kyoto, May 1983 (Abstr. No. 1F25).

2) C. M. Starks and C. Liotta, "Phase Transfer Catalysis; Principles and Techniques," Academic Press, New York (1978); E. V. Dehmlow and S. S. Dehmlow, "Phase Transfer Catalysis," 2nd ed, Verlag Chemie, Weinheim (1983); W. P. Weber and G. W. Gokel, "Phase Transfer Catalysis in Organic Synthesis," Springer-Verlag, New York (1977).

3) S. L. Regen, *Angew. Chem., Int. Ed. Engl.*, **18**, 421 (1979).

4) F. Montanari, D. Landini, and F. Rolla, *Top. Curr. Chem.*, **101**, 147 (1982).

5) W. T. Ford and M. Tomoi, *Adv. Polym. Sci.*, **55**, 49 (1984).
6) N. Ohtani, *Yuki Gosei Kagaku Kyokai Shi*, **43**, 313 (1985).
7) P. Tundo, P. Venturello, and E. Angeletti, *J. Am. Chem. Soc.*, **104**, 6551 (1982).
8) G. Bram and G. Decodts, *Tetrahedron Lett.*, **21**, 5011 (1980).
9) L. Holliday, "Ionic Polymers," ed by L. Holliday, Halsted, New York (1975), Chap. 1.
10) N. Ohtani, Y. Tokuta, H. Serita, and C. Kimura, *Polym. Prepr. Am. Chem. Soc. Div. Polym. Chem.*, **20**, 637 (1979).
11) H. Serita, N. Ohtani, and C. Kimura, *Kobunshi Ronbunshu*, **38**, 465 (1981).
12) G. K. Noren, *J. Polym. Sci.*, **31**, 693 (1975).
13) A. Rembaum and H. Noguchi, *Macromolecules*, **5**, 261 (1972).
14) C. Kimura, H. Serita, K. Murai, and Y. Takahashi, *Yukagaku*, **25**, 424 (1976).
15) N. Ohtani, C. A. Wilkie, A. Nigam, and S. L. Regen, *Macromolecules*, **14**, 516 (1981).
16) S. L. Regen, S. Quici, and S. J. Liaw, *J. Org. Chem.*, **44**, 2029 (1979).
17) D. Landini, A. Maia, F. Montanari, *J. Am. Chem. Soc.*, **100**, 2796 (1978).
18) A. Takahashi, *Hyomen*, **23**, 158 (1985); F. R. Eirich, *J. Colloid Interface Sci.*, **58**, 423 (1977).
19) S. Kobayashi, M. Suzuki, and T. Saegusa, *Makromol. Chem.*, **188**, 457 (1987).
20) W. M. McKenzie and D. C. Sherrington, *J. Chem. Soc., Chem. Commun.*, **1978**, 541.

Asymmetric Hydrocyanation of Aldehydes Using Chiral Titanium Reagents

Hiroyuki MINAMIKAWA, Satoshi HAYAKAWA, Tohru YAMADA, Nobuharu IWASAWA, and Koichi NARASAKA*
Department of Chemistry, Faculty of Science, The University of Tokyo, Hongo, Bunkyo-ku, Tokyo 113
(Received July 30, 1988)

Two highly enantioselective methods for hydrocyanation of aldehydes were developed by using chiral alkoxytitanium reagents. Treatment of benzaldehyde with cyanotrimethylsilane in the presence of a chiral alkoxytitanium affords mandelonitrile in good chemical and optical yields. By the use of the chiral cyanotitanium reagent generated in situ from the chiral alkoxytitanium and cyanotrimethylsilane, aliphatic aldehydes are converted into the corresponding cyanohydrins in a highly enantioselective manner.

Asymmetric synthesis of cyanohydrins is an important process in organic synthesis, because cyanohydrins can be easily converted into a variety of valuable synthetic intermediates such as α-hydroxy carboxylic acids, α-hydroxy ketones, and β-amino alcohols. Since the first report by Bredig and Fiske who discovered that chiral mandelonitrile can be obtained by the quinine-catalyzed reaction of hydrogen cyanide and benzaldehyde,[1] a great progress has been made in the asymmetric synthesis of cyanohydrins, and recently several efficient methods have been reported to prepare cyanohydrins in high optical purity. For example, optically active cyanohydrins are obtained with good selectivity by diastereoselective reactions of cyanating reagents with chiral acetals.[2] However, the chiral auxiliaries are destroyed in the process of removing them from the products and not recovered. In the enantioselective reactions using chiral catalysts, such as boryl compounds,[3] D-oxynitrilase,[4] and synthetic peptides,[5] the optical purities of the resulting cyanohydrins are not sufficient except in the case of the preparation of mandelonitrile derivatives.

We reported an enantioselective Diels-Alder reaction by the use of the chiral alkoxytitanium-Molecular Sieves (MS) 4A system.[6] As another utility of this chiral titanium reagent, we examined the asymmetric hydrocyanation of aldehydes.[7]

Firstly, we examined the reaction of 3-phenylpropanal and cyanotrimethylsilane using the chiral alkoxytitanium generated in situ by mixing dichlorodiisopropoxytitanium(IV) and the chiral 1,4-diol, (2*R*,3*R*)-2,3-*O*-(1-phenylethylidene)-1,1,4,4-tetraphenyl-1,2,3,4-butanetetrol (**1**). When 3-phenylpropanal was treated with cyanotrimethylsilane in the presence of the chiral titanium reagent in toluene at −65 °C, the reaction proceeded slowly. On the other hand, by the addition of MS 4A to this solution, the reaction was found to proceed smoothly at the same temperature. Thus, powdered MS 4A were added at room temperature to a toluene solution of dichlorodiisopropoxytitanium(IV), and the chiral diol **1**, then 3-phenylpropanal and excess amounts of cyanotrimethylsilane were added at −65 °C to afford 2-hydroxy-4-phenylbutanenitrile (**3a**, 89% yield, 74% ee). The asymmetric hydrocyanation of 3-phenylpropanal was also investigated in various solvents such as cumene (55% yield, 60% ee, at −65 °C), mesitylene (70% yield, 60% ee, at −45 °C), dichloromethane (23% yield, 72% ee, at −65 °C), acetonitrile (77% yield, 36% ee, at −45 °C), diethyl ether (42% yield, 0% ee, at −65 °C) and tetrahydrofuran (72% yield, 0% ee, at −65 °C): Among them, high enantioselectivity was achieved when the aromatic solvents or dichloromethane was used, but the enantioselectivity decreased when the solvents having

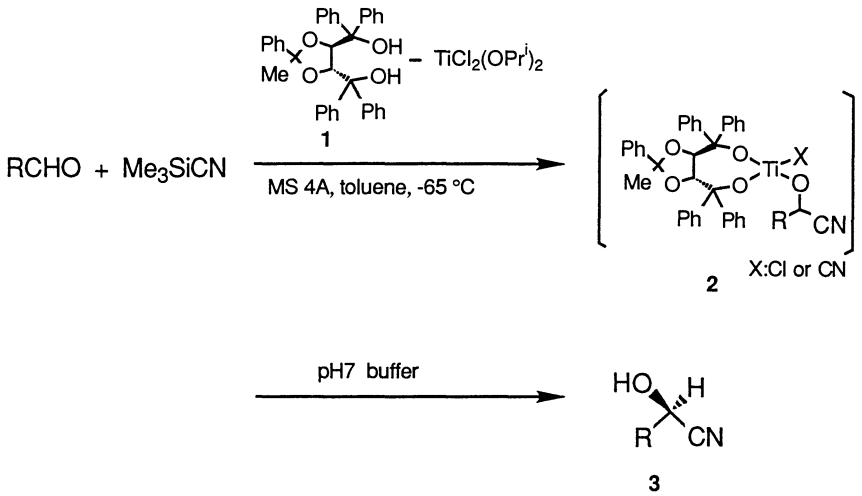

Scheme 1.

Table 1. Asymmetric Hydrocyanation of Aldehydes Using the Chiral Alkoxytitanium and Cyanotrimethylsilane

Entry	Aldehyde R	Reaction time/d	Product	Yield/%	Optical yield/%ee
1	$PhCH_2CH_2$	0.5	**3a**	89	74
2	$PhCH_2$	0.5	**3b**	66	77
3	n-C_8H_{17}	1	**3c**	66	76
4	c-C_6H_{11}	2	**3d**	77	68
5	Ph	0.5	**3e**	79	96

good donor property such as acetonitrile, diethyl ether, and tetrahydrofuran were employed.

It was also found that cyanotrimethylsilane gave the best chemical and optical yields among various cyanating reagents examined: The reaction did not proceed even at room temperature when potassium cyanide with 18-crown-6 or t-butyl isocyanide was employed, and low chiral induction was observed when cyanotributyltin(IV) (52% yield, 0% ee, at −78 °C) or cyanodiethylaluminium (81% yield, 7% ee, at −78 °C) was used as a cyanating reagent. Therefore, the asymmetric hydrocyanation of various aldehydes with cyanotrimethylsilane was examined in toluene at −65 °C (Scheme 1), and the results are summarized in Table 1.

As shown in Table 1, these aldehydes smoothly react with cyanotrimethylsilane to give the optically active cyanohydrins in good optical yield (68—96% ee). Especially, benzaldehyde is converted into (*R*)-mandelonitrile in high optical purity (Entry 5, 96% ee).

When we tried the reaction of 3-phenylpropanal with cyanotrimethylsilane in the presence of a 25% molar amount of the chiral titanium reagent, the chemical yield of the cyanohydrin **3a** was 26%. Furthermore, in every case, no trimethylsilyl ether of a cyanohydrin was detected after the treatment of the reaction mixture with pH 7 phosphate buffer. These results show that cyanohydrins are generated not as silyl ethers but as titanium ethers **2**. The following experiments were carried out in order to examine whether the optically active cyanohydrins were obtained thermodynamically or kinetically. When 3-phenylpropanal was treated with cyanotrimethylsilane in the presence of the chiral titanium reagent and MS 4A at room temperature for 12 h and then the reaction mixture was stirred at −65 °C for 1 d, the optical purity of the resulting cyanohydrin was low (ca. 10% ee). Almost the same level of chiral induction (10% ee) was observed when the above reaction was performed at room temperature for 12 h. These results indicate that the cyanohydrin obtained by the present procedure is not a thermodynamic product but a kinetic product.

In order to get informations on the reaction mechanism, NMR spectrum of cyanotrimethylsilane and the titanium reagent was measured. The ^1H NMR spectrum of the mixture of cyanotrimethylsilane and the chiral alkoxytitanium prepared in situ by mixing the chiral diol **1** and dichlorodiisopropoxytitanium(IV) in toluene-d_8 at −65 °C shows a singlet peak at δ=−0.09 which corresponds to cyanotrimethylsilane, and no absorption is observed at δ=0.20 which corresponds to chlorotrimethylsilane irrespective of the presence or absence of MS 4A. This observation seems to suggest that in the reaction at low temperature the chiral alkoxytitanium reagent activates an aldehyde as a Lewis acid and the activated aldehyde reacts with cyanotrimethylsilane to afford a cyanohydrin. On the other hand, when the mixture of the chiral alkoxytitanium and cyanotrimethylsilane is slowly warmed up to room temperature, the ^1H NMR spectrum indicates the decreasing of the absorption at δ=−0.09 and the appearance of a singlet peak at δ=0.20. This phenomenon is explained by assuming that the ligand-exchange reaction occurs between the chiral alkoxytitanium and cyanotrimethylsilane at room temperature,

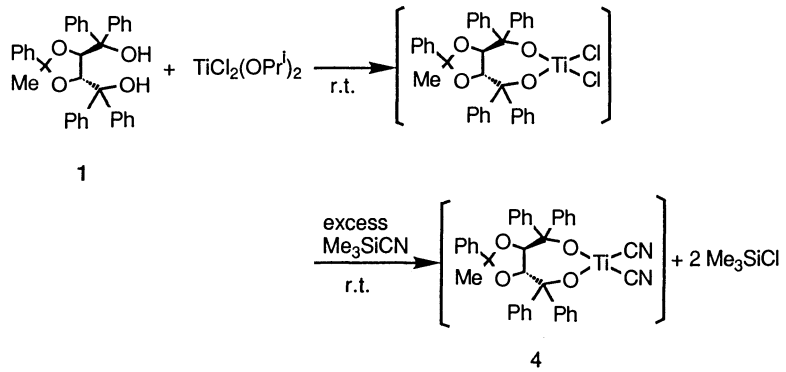

Scheme 2.

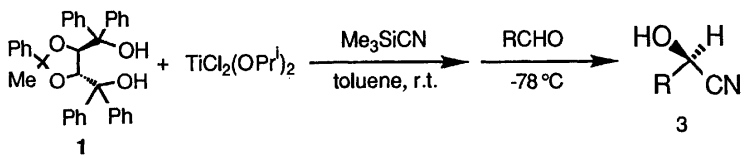

Scheme 3.

Table 2. Asymmetric Hydrocyanation of Aldehydes Using the Chiral Cyanotitanium Reagents

Entry	Aldehyde R	Reaction time/h	Product	Yield/%	Optical yield/%ee
1	$PhCH_2CH_2$	20	**3a**	88	(−)-91
2	$PhCH_2$	12	**3b**	67	(+)-61[a]
3	n-C_8H_{17}	23	**3c**	85	(+)-93
4	n-C_9H_{19}	18	**3f**	83	(+)-85[a]
5	$CH_2=CH(CH_2)_8$	16	**3g**	92	(+)-93
6	Ph	122	**3e**	68	(+)-73

a) Reaction temperature is −65 °C.

resulting in the formation of cyanotitanium species and chlorotrimethylsilane. Integration of the peak at δ=0.20 was attributed to 2 molar amounts of chlorotrimethylsilane, that is, titanium dicyanide species **4** might be generated by the addition of excess (5 molar) amounts of cyanotrimethylsilane (Scheme 2). We were interested in utilizing this chiral cyanotitanium species **4** as a chiral cyanating reagent of aldehydes (Scheme 3). Thus, to a toluene solution of dichlorodiisopropoxytitanium(IV) was added the chiral diol **1** and then cyanotrimethylsilane at 1 hour intervals at room temperature to generate the chiral cyanotitanium reagent. Then 3-phenylpropanal was added at −78 °C and the mixture was further stirred for 20 h. Work-up of the reaction mixture afforded 2-hydroxy-4-phenylbutanenitrile (**3a**) in 88% yield and the optical purity rose up to 91% ee as compared with the result of the previous procedure (74% ee).

The same reactions using various aldehydes were examined in toluene at −78 °C and the results are summarized in Table 2. According to this procedure, the optical purity of aromatic cyanohydrins (Entries 2 and 6) are not sufficiently high, but aliphatic cyanohydrins are prepared in good yield with high optical purity (>85% ee, Entries 3, 4, and 5). The absolute configurations of (+)-2-hydroxy-3-phenylpropanenitrile (**3b**), (+)-mandelonitrile (**3e**), and (+)-2-hydroxyundecanenitrile (**3f**) obtained by employing the (2*R*, 3*R*)-diol **1** were determined to be *R* by the comparison of their rotations with those of the literature.[8] As for (+)-2-hydroxydecanenitrile (**3c**) and (+)-2-hydroxy-11-dodecenenitrile (**3g**), there is no literature concerning the absolute configuration. However, from the analogy that straight-chain aliphatic cyanohydrins such as (*S*)-2-hydroxyhexanenitrile, (*S*)-2-hydroxyheptanenitrile, (*S*)-2-hydroxyoctanenitrile and (*S*)-2-hydroxyundecanenitrile have (−)-rotation,[8] they are assumed to have *R* absolute configuration. Exceptionally 2-hydroxy-4-phenylbutanenitrile (**3a**) was obtained with the opposite (−)-rotation, but the absolute configuration was determined to be *R* after the hydrolysis to the known 2-hydroxy-4-phenylbutanoic acid.[9] These results indicate that cyanide attacks the *si*-face of aldehydes when the (2*R*,3*R*)-diol **1** is employed as a chiral auxiliary.

In conclusion, the optically active cyanohydrins can be obtained not only from aromatic aldehydes but also from aliphatic aldehydes in high optical yields by applying either method. The both enantiomers of cyanohydrins can be prepared in high optical purity since each enantiomer of the chiral 1,4-diol **1** is readily prepared from the commercially available (*R*)- and (*S*)-tartaric acids.

Experimental

General. (a) Spectrometers: IR spectra were measured with a Hitachi Model 260-30 spectrophotometer. ^{1}H NMR spectra were recorded with Hitachi R-24B, JEOL FX90Q and Varian EM390 spectrometers. ^{19}F NMR spectra were taken by using a Varian EM390 spectrometer. High-mass spectra were recorded with a JEOL JMS-D300 mass spectrometer operating at 70 eV. The optical rotations were measured with a JASCO DIP-181 digital polarimeter. (b) Chromatography: Column chromatography was conducted under silica gel (E. Merck, 7734, 70—230 mesh). Preparative TLC was carried out on silica gel (Wakogel B-5F). HPLC was performed using a Waters RESOLVE C_{18} (86016) column. (c) Solvents and Reagents: Toluene was distilled and dried over MS 4A. Dichloromethane was distilled from P_2O_5 then from CaH_2, and was dried over MS 4A. Diethyl ether and tetrahydrofuran were freshly distilled from sodium benzophenone ketyl. Acetonitrile was distilled from P_2O_5, and further distilled from CaH_2, and dried over MS 4A. Mesitylene was distilled and dried over MS 4A. Cumene was distilled from $LiAlH_4$. Dichlorodiisopropoxytitanium(IV) was prepared from titanium(IV) chloride and tetraisopropoxytitanium(IV) according to the literature.[10] Aldehydes

were distilled prior to use. Cyanotrimethylsilane was purified by distillation.

Preparation of (2*R*,3*R*)-2,3-*O*-(1-Phenylethylidene)-1,1,4,4-tetraphenyl-1,2,3,4-butanetetrol (1). Dimethyl (2*R*,3*R*)-2,3-*O*-(1-Phenylethylidene)tartrate. To a benzene solution of dimethyl (2*R*,3*R*)-tartrate (10.7 g, 60 mmol) and acetophenone dimethyl acetal (10.6 g, 60 mmol) was added a catalytic amount of *p*-toluenesulfonic acid, and the mixture was heated to reflux to remove liberated methanol azeotropically with occasional addition of benzene until the boiling point reached 80.5 °C. The mixture was washed with sat. aq. $NaHCO_3$ and then with brine and dried over Na_2SO_4. The solvent was removed under reduced pressure and the residual oil was purified by column chromatography (8:1 hexane/diethyl ether) to afford the product, which was further purified by distillation to give the pure product (10.7 g, 63% yield). Bp 132 °C/0.30 mmHg (1 mmHg≈133.322 Pa); ^1H NMR ($CDCl_3$) δ=1.58 (s, 3H), 3.30 (s, 3H), 3.64 (s, 3H), 4.65 (s, 2H), and 7.0—7.7 (m, 5H); IR (neat) 1740 cm^{-1}; $[\alpha]_D$ +11° (*c* 2.6, CH_2Cl_2).

(2*R*,3*R*)-2,3-*O*-(1-Phenylethylidene)-1,1,4,4-tetraphenyl-1,2,3,4-butanetetrol (1). To a tetrahydrofuran (50 ml) solution of phenylmagnesium bromide (25.0 mmol) was added a tetrahydrofuran (10 ml) solution of dimethyl (2*R*,3*R*)-2,3-*O*-(1-phenylethylidene)tartrate (1.4 g, 5.0 mmol) at 0 °C. After stirring for 4 h at room temperature, the reaction was quenched with sat. aq. NH_4Cl solution. Organic materials were extracted with ethyl acetate, and the combined extracts were washed with brine, and dried over Na_2SO_4. The solvent was removed under reduced pressure and the residue was purified by column chromatography (9:1 hexane/diethyl ether) to afford white amorphous solid. This solid was dissolved in a small amount of hexane, and 2-propanol was added with stirring to afford white crystals. These crystals were recrystallized from 1:1 mixture of hexane and 2-propanol. The crystals thus obtained were a complex of **1** and 2-propanol, and 2-propanol was removed azeotropically with benzene 3 times to afford **1** as white amorphous solid (1.6 g, 60% yield). ^1H NMR ($CDCl_3$) δ=1.30 (s, 3H), 2.32 (s, 1H), 2.45 (s, 1H), 5.04 (d, 1H, *J*=6.0 Hz), 5.08 (d, 1H, *J*=6.0 Hz), and 6.8—7.6 (m, 25H); IR(KBr) 3300, 1490, 1445, and 695 cm^{-1}; $[\alpha]_D^{23}$ +82.9° (*c* 1.3, $CHCl_3$). The elemental analysis was performed after the conversion to the corresponding bis(trimethylsilyl) ether: Found: C, 74.68; H, 7.12%. Calcd for $C_{42}H_{48}O_4Si_2$: C, 74.96; H, 7.19%.

Cyanohydrins: General Procedure for Hydrocyanation of Aldehydes (Method A, Table 1). All reactions were carried out under argon atmosphere. To a toluene (1 ml) solution of dichlorodiisopropoxytitanium(IV) (119 mg, 0.5 mmol) was added a toluene (2 ml) solution of the chiral diol **1** (291 mg, 0.55 mmol) at room temperature. After 1 h, powdered MS 4A (65 mg, heated at 200—300 °C in vacuo prior to use) were added to this solution. Then a toluene (1 ml) solution of aldehyde (0.5 mmol), and a toluene (1 ml) solution of cyanotrimethylsilane (250 mg, 2.5 mmol) were added at −65 °C. After stirring for 0.5—2 d at this temperature, the reaction was quenched with pH 7 phosphate buffer, and the resulting mixture was filtered through Celite. Organic materials were extracted with ethyl acetate, and the combined extracts were washed with brine, and dried over Na_2SO_4. The solvent was removed under reduced pressure and the residue was purified by preparative TLC (hexane/diethyl ether) to afford the corresponding cyanohydrin. The optical purity was assayed by HPLC (40:1 hexane/ethyl acetate) or by ^{19}F NMR analysis of the corresponding (*R*)-(+)-3,3,3-trifluoro-2-methoxy-2-phenylpropionate (MTPA).[11]

General Procedure for Hydrocyanation of Aldehydes Using the Chiral Cyanotitanium(IV) Species (Method B, Table 2). To a toluene (1 ml) solution of dichlorodiisopropoxytitanium(IV) (119 mg, 0.5 mmol) was added a toluene (1 ml) solution of the chiral diol **1** (291 mg, 0.55 mmol) at room temperature. After 1 h, a toluene (1 ml) solution of cyanotrimethylsilane (250 mg, 2.5 mmol) was added at room temperature, and after 1 h, a toluene (1 ml) solution of aldehyde (0.5 mmol) was added at −78 °C. After stirring for 12—122 h at this temperature, the reaction was quenched with pH 7 phosphate buffer, and the resulting cyanohydrin was isolated by the same procedure described above.

2-Hydroxy-4-phenylbutanenitrile (3a). ^1H NMR ($CDCl_3$) δ=1.8—2.2 (m, 2H), 2.6—2.9 (m, 2H), 3.7—4.0 (br, 1H), 4.3 (t, 1H), and 7.1 (s, 5H); IR(CCl_4) 3440, 2930, 1600, 1500, 1450, and 1070 cm^{-1}; $[\alpha]_D^{22}$ −6.79° (*c* 2.04, $CHCl_3$, 89% ee). HRMS Found: *m/z* 161.0873. Calcd for $C_{10}H_{11}NO$: M, 161.0841.

2-Hydroxy-3-phenylpropanenitrile (3b). ^1H NMR ($CDCl_3$) δ=2.9—3.1 (m, 3H), 4.4—4.7 (m, 1H), and 7.3 (s, 5H); IR (CH_2Cl_2) 3430, 3020, 2920, 1600, 1480, and 1050 cm^{-1}; $[\alpha]_D^{26}$ +8.3° (*c* 1.10, $CHCl_3$, 65% ee), lit, $[\alpha]_D^{25}$ −0.5° ($CHCl_3$, 1% ee, (*S*)-form major).[8] HRMS Found: *m/z* 147.0654. Calcd for C_9H_9NO: M, 147.0685.

2-Hydroxydecanenitrile (3c). ^1H NMR (CCl_4) δ=0.8—1.8 (m, 17H), 3.2—3.4 (m, 1H), and 4.3—4.5 (m, 1H); IR (CH_2Cl_2) 3590, 3420, 2940, 2870, 2300, and 1430 cm^{-1}; $[\alpha]_D^{25}$ +12.8° (*c* 2.52, $CHCl_3$, 93% ee).

2-Cyclohexyl-2-hydroxyacetonitrile (3d). ^1H NMR ($CDCl_3$) δ=1.2—1.8 (m, 11H), 3.2—3.5 (br, 1H), and 4.1—4.4 (br, 1H); IR($CHCl_3$) 3600, 3430, 2930, 2860, 1450, and 1040 cm^{-1}; $[\alpha]_D^{25}$ +5.45° (*c* 2.96, $CHCl_3$, 58% ee).

Mandelonitrile (3e). ^1H NMR spectra and IR spectra agreed with those of literatures. $[\alpha]_D^{21}$ +45.5° (*c* 3.53, $CHCl_3$, 96% ee), lit, $[\alpha]_D^{25}$ +43.5° (*c* 5, $CHCl_3$, 92.5% ee, (*R*)-form major).[2a]

2-Hydroxyundecanenitrile (3f). ^1H NMR ($CDCl_3$) δ= 0.8—1.2 (m, 19H), 3.2—3.6 (br, 1H), and 4.4 (t, 1H); IR (CH_2Cl_2) 3580, 3410, 2910, 2850, and 1450 cm^{-1}; $[\alpha]_D^{25}$ +7.9° (*c* 4.03, $CHCl_3$, 85% ee), lit, $[\alpha]_D^{25}$ −2.4° ($CHCl_3$, 16% ee, (*S*)-form major).[8]

2-Hydroxy-11-dodecenenitrile (3g). ^1H NMR ($CDCl_3$) δ= 1.2—2.1 (m, 16H), 3.4—3.6 (br, 1H), 4.4 (t, 1H), 4.8—5.1 (m, 2H), and 5.5—6.1 (m, 1H); IR(CCl_4) 3420, 2900, 2250, and 1640 cm^{-1}; $[\alpha]_D^{21}$ +10.5° (*c* 2.68, $CHCl_3$, 93% ee). HRMS Found: *m/z* 195.1592. Calcd for $C_{12}H_{21}NO$: M, 195.1624.

Hydrolysis of 3a. To **3a** (0.36 mmol, 77% ee, $[\alpha]_D^{23}$ −4.46° (*c* 8.40, $CHCl_3$)) was added 4 ml of concentrated hydrochloric acid. After refluxed for 4 h, 4 ml of water was added and organic materials were extracted with ethyl acetate. The combined extracts were washed with brine, and dried over Na_2SO_4. The solvent was removed under reduced pressure and the residue was recrystallized from benzene to afford white crystals of 2-hydroxy-4-phenylbutanoic acid (59 mg, 91% yield). ^1H NMR ($CDCl_3$) δ=1.7—2.4 (m, 2H), 2.8 (t, 2H), 4.2 (t, 1H), 5.2—6.2 (br, 2H), and 7.2 (s, 5H); IR(KBr) 3470, 2920, 1730, 1600, 1500, 1290, and 1240 cm^{-1}; $[\alpha]_D^{24}$ −6.03° (*c* 1.18, C_2H_5OH), lit, $[\alpha]_D$ −8.6° (*c* 1, C_2H_5OH, (*R*)-form).[9]

This work was partially supported by a Grant-in-Aid for Scientific Research No. 62116003 from the

Ministry of Education, Science and Culture.

References

1) G. Bredig and P. S. Fiske, *Biochem. Z.*, **46**, 7 (1912).

2) a) J. D. Elliott, V. M. F. Choi, and W. S. Johnson, *J. Org. Chem.*, **48**, 2294 (1983); b) V. M. F. Choi, J. D. Elliott, and W. S. Johnson, *Tetrahedron Lett.*, **25**, 591 (1984).

3) M. T. Reetz, F. Kunisch, and P. Heitmann, *Tetrahedron Lett.*, **27**, 4721 (1986).

4) W. Becker, H. Freund, and E. Pfeil, *Angew. Chem.*, **77**, 1139 (1965); F. Effenberger, T. Ziegler, and S. Förster, *Angew. Chem., Int. Ed. Engl.*, **26**, 458 (1987).

5) S. Asada, Y. Kobayashi, and S. Inoue, *Makromol. Chem.*, **186**, 1755 (1985); Y. Kobayashi, S. Asada, I. Watanabe, H. Hayashi, Y. Motoo, and S. Inoue, *Bull. Chem. Soc. Jpn.*, **59**, 893 (1986).

6) K. Narasaka, M. Inoue, and T. Yamada, *Chem. Lett.*, **1986**, 1967.

7) K. Narasaka, T. Yamada, and H. Minamikawa, *Chem. Lett.*, **1987**, 2073.

8) H. Gountzos, W. R. Jackson, and K. J. Harrington, *Aust. J. Chem.*, **39**, 1135 (1986).

9) H. Yanagisawa, S. Ishihara, A. Ando, T. Kanazaki, S. Miyamoto, H. Koike, Y. Iijima, K. Oizumi, Y. Matsushita, and T. Hata, *J. Med. Chem.*, **30**, 1984 (1987).

10) C. Dijkgraaf and J. P. G. Rousseau, *Spectrochim. Acta, Part A.*, **24**, 1213 (1968).

11) J. A. Dale, D. L. Dull, and H. S. Mosher, *J. Org. Chem.*, **34**, 2543 (1969).

 © 1988 The Chemical Society of Japan Bull. Chem. Soc. Jpn., 61, 4385—4388 (1988)

The Redox Reaction by Ferrocene Derivatives Introduced to a Crown Ether in a Liquid Membrane System

Eiichi Ozeki, Shunsaku Kimura, and Yukio Imanishi*
Department of Polymer Chemistry, Kyoto University, Yoshida Honmachi, Sakyo-ku, Kyoto 606
(Received December 26, 1987)

In an organic liquid membrane system, 4′-(ferrocenylcarbonylamino)benzo-18-crown-6 (FCC) dissolved in a dichloromethane membrane was found to reduce hexacyanoferrate(III) ions in the aqueous phase to hexacyanoferrate(II) ions at a rate dependent on the type of metal ion coexisting in the aqueous phase, and bound to the benzo-18-crown-6 unit of FCC.

Transport of electrons, protons, and metal ions across a biological membrane plays an essential role in the transduction of information through the biological membrane. It is known that the transport is mediated by various substances, and furthermore, the different transport systems are frequently coupled with each other.[1]

Recently, several kinds of crown ether derivatives including "antenna" compounds, which respond to light,[2,3] pH,[4,5] redox reagents,[6-8] and electrochemical potential,[9-12] have been synthesized and investigated for the facilitated capture and transport of cations.

In the present study, 4′-(ferrocenylcarbonylamino)-benzo-18-crown-6 (FCC), composed of a ferrocene and a crown ether unit, was synthesized. Ferrocene derivatives are known as electron carriers through a lipid and liquid organic membrane in the presence of lipophilic anions. A ferrocene unit possesses a positive charge in the oxidized state and is neutral in the reduced state.[13] 18-Crown-6 forms a complex with alkali metal ions, especially with a K^+ ion, and it is capable of transporting metal ions through an organic liquid membrane.[14,15]

We examined the redox reaction of FCC solubilized in an organic liquid membrane with a redox reagent dissolved in an aqueous phase containing metal ions. The purpose of the present study is to investigate if the redox reaction of the ferrocene unit of FCC is regulated by the binding of cation with the crown ether unit of FCC, and to examine the possibility of coupled electron and metal-ion transport across an organic liquid membrane.

Experimental

Synthesis. 4′-(Ferrocenylcarbonylamino)benzo-18-crown-6 was prepared according to the scheme shown in Fig. 1. Benzo-18-crown-6 was synthesized from catechol and pentaethylene glycol.[16] An amino group was introduced to the benzene ring of benzo-18-crown-6 by a nitration and reduction reaction.[17] Ferrocenecarbonyl chloride[18] was coupled with 4′-aminobenzo-18-crown-6 in a *N,N*-dimethylformamide (DMF) solution with stirring overnight. DMF was distilled off and the residue was dried under reduced pressure. The crude product obtained was purified by eluting through a silica-gel column (95% $CHCl_3$/5% CH_3OH). Found: C, 59.97; H, 6.27; N, 2.30%. Calcd for $C_{27}H_{33}NO_7Fe$: C, 60.15; H, 6.18; N, 2.60%.

1,1′-Dibutylferrocene (DBF) and dibenzo-18-crown-6 (DBC) were commercially available and used as reference mediators.

Measurement. The electron and cation transport were measured using a U-shaped tube.[19] The aqueous phase I (5 ml) was separated from aqueous phase II (5 ml) by an organic liquid membrane phase (20 ml) containing mediators.

The redox capability of FCC was examined by a two-phase system composed of dichloromethane/water. The aqueous phase (5 ml) contained 1 mM potassium hexacyanoferrate(III) and 54 mM metal chloride, and the dichloromethane phase (10 ml) contained 0.3 mM FCC.

The concentration of hexacyanoferrate(III) ions was determined by measuring the absorption at 420 nm.

The cyclic voltammogram of FCC was measured in an acetonitrile solution containing 0.1 M tetrabutylammonium-hexafluorophosphate.

Results and Discussion

The redox reaction by FCC dissolved in a dichloromethane membrane was examined by using a U-shaped tube system (Fig. 2). It was found that FCC did not extensively reduce hexacyanoferrate(III) ions in the aqueous phase I, before the addition of Na^+ ions. However, the concentration of hexacyanoferrate(III) ions decreased rapidly upon the addition of Na^+ ions to the aqueous phase I. The effect of metal ions on the

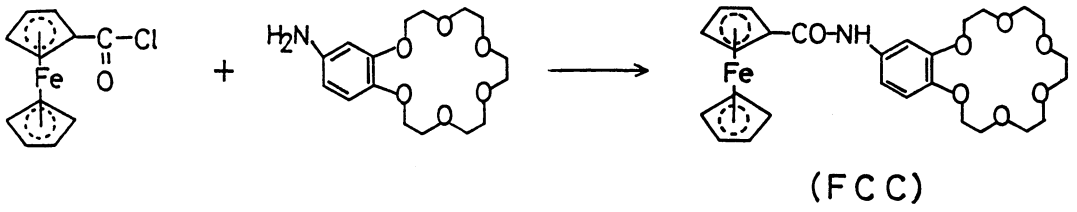

Fig. 1. Synthetic route of FCC.

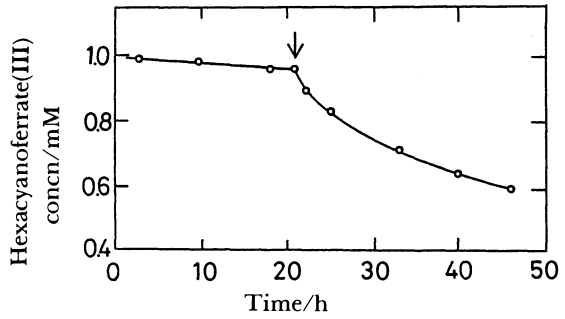

Fig. 2. Change in the concentration of hexacyanoferrate(III) ions against time in the aqueous phase I. Initial composition: aqueous phase I, 1 mM potassium hexacyanoferrate(III); aqueous phase II, 2.5 mM sodium ascorbate; organic phase M, 0.3 mM FCC in DCM. ↓: addition of 1 M NaCl.

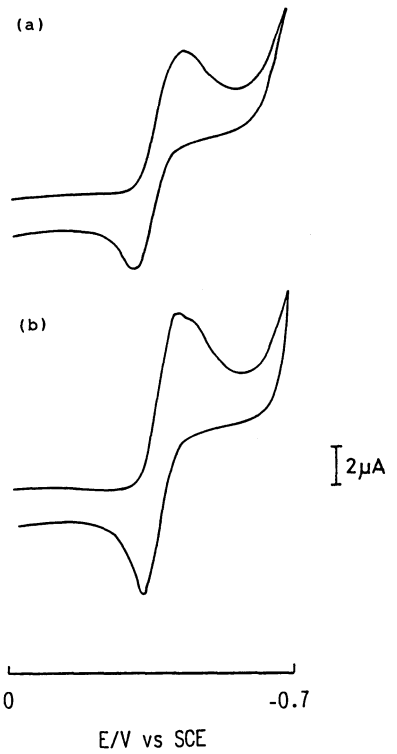

Fig. 3. Cyclic voltammograms in acetonitrile solution of FCC (a) in the absence and (b) in the presence of 1.0 equiv of $KClO_4$.

redox reaction of FCC was examined by a cyclic voltammogram (Fig. 3), and UV and NMR spectroscopies. In these measurements, no significant change was observed on the addition of a metal ion. It is therefore concluded that complexation of the crown ether unit of FCC with a metal ion does not change the redox potential or electron density of the ferrocene unit. Taken together, these experimental results show that the redox reaction by FCC is regulated by the complexation of the crown ether unit of FCC with a metal ion in the aqueous phase. However, the complexation process does not alter the redox potential of the ferrocene unit of FCC.

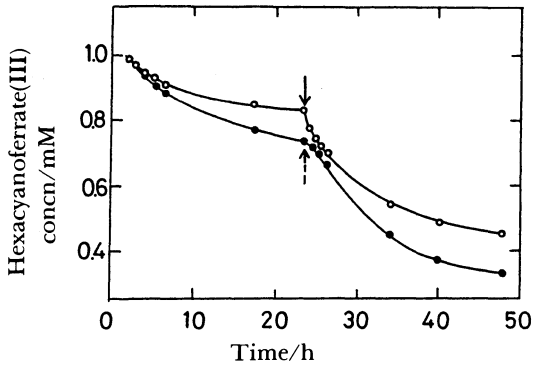

Fig. 4. Change in the concentration of hexacyanoferrate(III) ions against time in aqueous phases I (○) and II (●). Initial composition: aqueous phase I, 1 mM potassium hexacyanoferrate(III), 1 mM potassium hexacyanoferrate(II) and 54 mM $NaClO_4$; aqueous phase II, 1 mM potassium hexacyanoferrate(III), 1 mM potassium hexacyanoferrate(II) and 54 mM $KClO_4$; organic phase, 0.3 mM FCC in DCM .↓: addition of 540 mM NaCl, ↑: addition of 540 mM KCl.

When 1,2-dichloroethane (DCE) was used as an organic liquid membrane, the concentration of hexacyanoferrate(III) ions did not decrease. DCE and DCM have a similar dielectric constant, however, their solubilities in water are different (0.869 g of DCE and 2.0 g of DCM are soluble in 100 g of water).[20] Therefore, the state on the water/DCM boundary region must be different from that of water/DCE, indicating that the nature of the interface between the organic phase and aqueous phase should have a strong influence on the redox reaction by FCC.

An active electron transportation with DBF driven by the different concentration of lipophilic anions between the two aqueous phases has been reported by Sinbo et al.[21] In this study, FCC was examined as a mediator of the active electron transport against redox potential driven by the selective complexation with metal ions and/or the cation transport through an organic membrane. Aqueous phases containing the same concentrations of hexacyanoferrate(III) and hexacyanoferrate(II) ions were separated by a DCM membrane containing FCC. Na^+ ions were added to the aqueous phase I and K^+ ions to the a aqueous phase II. Figure 4 shows the change in the concentration of hexacyanoferrate(III) ions in the aqueous phases I and II. In both phases, concentration of hexacyanoferrate(III) ions decreased. The decrease in the concentration of hexacyanoferrate(III) ion in the aqueous phase II containing K^+ ions was larger than that in the aqueous phase I containing Na^+ ions. This indicates that FCC failed to transport electrons across the DCM membrane.

Reduction of hexacyanoferrate(III) ions by FCC in the DCM solution was examined using a two-phase system (DCM/water). It was found that FCC in the DCM solution reduced hexacyanoferrate(III) ions in

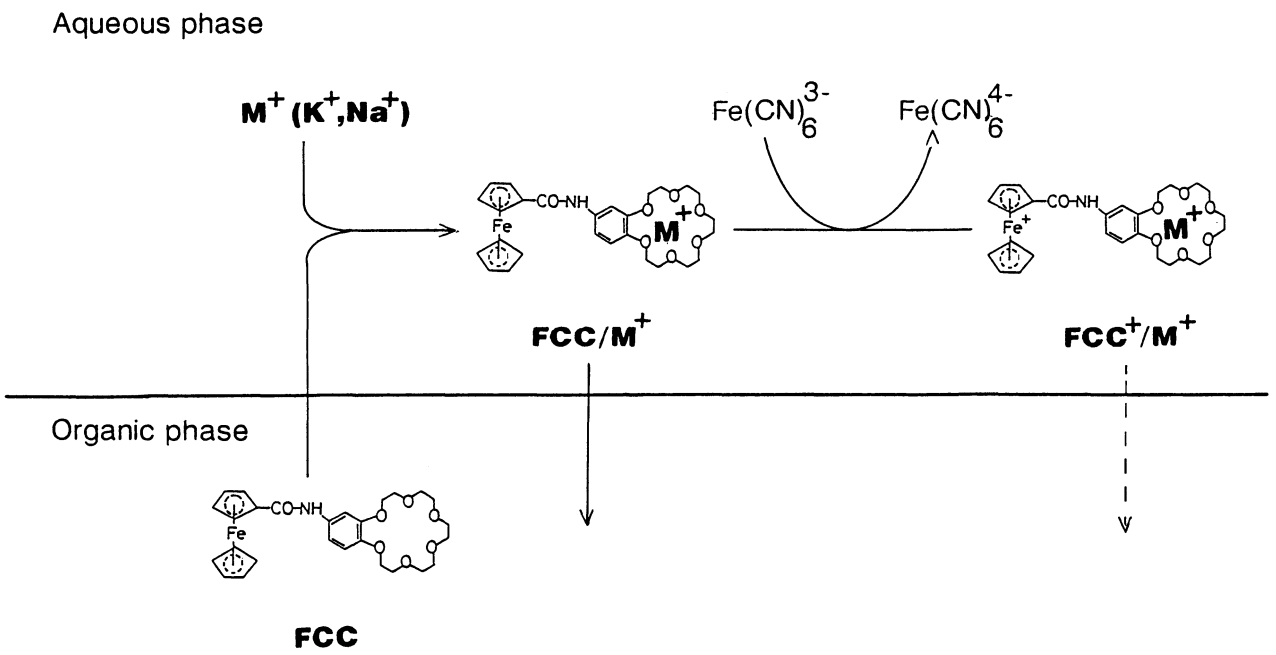

Fig. 5. The diagram of redox behavior of FCC in a liquid organic membrane system with a metal ion.

the aqueous phase containing a high concentration of either K^+ or Na^+ ions. The degree of the reduction of hexacyanoferrate(III) ions by FCC in the aqueous phase was 60% in the presence of K^+ ions, and 45% in the presence of Na^+ ions for 15 h after contacting both phases. These observations indicate that FCC reduces hexacyanoferrate(III) ions to hexacyanoferrate(II) ions in the presence of a metal ion, and that the extent of the reaction is controlled by the type of metal ion in the aqueous phase.

These experimental results can be explained by the mechanism shown in Fig. 5. The ferrocene unit of FCC in DCM solution can not be in contact with hexacyanoferrate(III) ions in the aqueous phase efficiently without metal ions. However, in the presence of metal ions, the ferrocene unit of FCC interacts with hexacyanoferrate(III) ions by complexation of the crown ether unit with a metal ion. FCC was shown to reduce hexacyanoferrate(III) ions more efficiently in the presence of a K^+ ion than in the presence of a Na^+ ion, because 18-crown-6 forms a complex with a K^+ ion more selectively than with a Na^+ ion. However the oxidized FCC (FCC^+) or its complex with a metal ion is so hydrophilic[22,23] that the molecule including an oxidized ferrocene unit can not diffuse freely across a DCM membrane even in the presence of lipophilic anions. This could be the reason for the failure of electron transport by FCC through an organic liquid membrane.

On the other hand, FCC was shown to transport 13.3 μmol of K^+ ions through DCM membrane in 12 h. This was determined by an atomic absorption method. However DBC transported 30.9 μmol of K^+ ions and DBF did not in the experiments using the U-shaped tube system (the aqueous phase I, 0.1 mM potassium hexacyanoferrate(III); the aqueous phase II, 0.1 mM sodium ascorbate and 300 mM KSCN; the DCM phase, 1 mM FCC, DBC, or DBF). This indicates that FCC can transport K^+ ions according to the concentration gradient of K^+ ions, when a metal ion does not exist in the aqueous phase I, in other words, the ferrocene unit of FCC is not oxidized by hexacyanoferrate(III) anions in the aqueous phase I.

Uphill transport of a picrate anion under a concentration gradient of K^+ ions across an organic liquid membrane has been examined using several mediators.[24] It is found that FCC showed an active transport of a picrate anion as in the case of a DBC mediator. This indicates that FCC, which is not oxidised, is active as an ionophore for K^+ ion in the presence of a picrate anion.

We thank Dr. Naoki Kamo, Hokkaido University, for his advice on the transport experiment.

References

1) P. Mitchel, *Nature (London)*, **191**, 144 (1961).
2) S. Shinkai, K. Shigematu, Y. Kusano, and O. Manabe, *J. Chem. Soc., Perkin Trans. 1*, **1987**, 3279.
3) S. Shinkai, K. Inuzuka, O. Miyazaki, and O. Manabe, *J. Am. Chem. Soc.*, **107**, 3950 (1985).
4) R. M. Izatt, J. D. Lamb, R. T. Hawkins, P. R. Brown, S. R. Izatt, and J. J. Christensen, *J. Am. Chem. Soc.*, **105**, 1782 (1983).
5) R. M. Izatt, G. C. Lindh, G. A. Clark, T. S. Bradshaw, Y. Nakatuji, J. D. Lamb, and J. J. Christensen, *J. Chem. Soc., Chem. Commun.*, **1985**, 1676.
6) S. Shinkai, K. Inuzuka, O. Miyazaki, and O. Manabe,

J. Am. Chem. Soc., **107**, 3950 (1985).
7) S. Shinkai, *Pure Appl. Chem.*, **59**, 425 (1987).
8) S. Akabori, Y. Habata, Y. Sakamoto, M. Sato, and S. Ebine, *Bull. Chem. Soc. Jpn.*, **56**, 537 (1983).
9) T. Saji and I. Kinosita, *J. Chem. Soc., Chem. Commun.*, **1986**, 716.
10) L. Echenerria, M. Delgado, V. J. Gatto, G. W. Gokel, and L. Echegoyen, *J. Am. Chem. Soc.*, **108**, 6825 (1986).
11) L. Echegoyen, D. A. Gustowski, V. J. Gatto, and G. W. Gokel, *J. Chem. Soc., Chem. Commun.*, **1986**, 220.
12) A. Kaifer, D. A. Gustowski, L. Echegoyen, V. J. Gatto, R. A. Shultz, T. P. Cleary, C. R. Morgan, D. M. Goli, A. M. Rios, and G. W. Gokel, *J. Am. Chem. Soc.*, **107**, 1958 (1985).
13) P. C. Hinkle, *Federation Proc.*, **32**, 1988 (1973).
14) G. W. Gokel and H. D. Durst, *Synthesis*, **1976**, 168.
15) M. Sugiura and T. Sinbo, *Bull. Chem. Soc. Jpn.*, **52**, 684 (1979).
16) C. J. Pedersen, *J. Am. Chem. Soc.*, **89**, 7017 (1967).
17) R. Ungaro, B. Haj, and J. Smid, *J. Am. Chem. Soc.*, **89**, 5198 (1976).
18) H. Falk, C. Krasa, and K. Schlogel, *Mh. Chem.*, **100**, 1552 (1969).
19) A. Sadakane, T. Iwachido, and T. Toei, *Bull. Chem. Soc. Jpn.*, **48**, 60 (1975).
20) Kirk-Othemer, "Encyclopedia of Chemical Technology," 2nd ed., Vol. **5**, p. 111.
21) T. Sinbo, M. Sugiura, N. Kamo, and Y. Kobatake, *Chem. Lett.*, **1979**, 1177.
22) T. Saji, K. Hoshino, and S. Aoyagui, *J. Am. Chem. Soc.*, **107**, 6865 (1985).
23) T. Saji, K. Hoshino, and S. Aoyagui, *J. Chem. Soc., Chem. Commun.*, **1985**, 865.
24) T. Sinbo, K. Kurihara, Y. Kobatake, and N. Kamo, *Nature (London)*, **270**, 277 (1979).

 © 1988 The Chemical Society of Japan Bull. Chem. Soc. Jpn., 61, 4389—4392 (1988)

Studies on Coupling Reaction of 1-Naphthol. XI.[1] Effect of Additives on the Dissociation Equilibrium of 4-(4-Nitrophenylazo)-1-naphthol in Pyridine

Satoshi KISHIMOTO,* Tsuneo OKUSHI, and Tsuneaki HIRASHIMA
Osaka Municipal Technical Research Institute, Morinomiya, Joto-ku, Osaka-shi 536
(Received January 30, 1988)

The dissociation of 4-(4-nitrophenylazo)-1-naphthol (azo dye) in pyridine was found to be accelerated by the addition of small amounts of quaternary ammonium compounds, $R_4N^+X^-$. The apparent equilibrium constant of the azo dye was influenced enormously by the species of X^-, but was little affected by the structures of R. The effect increased as the X^- became more basic, $ClO_4^- < I^- < BF_4^- < Br^- < HSO_4^- < Cl^-$, in proportion to the ability of X^- to bind with protons formed by dissociated azo dye. The basicity of the X^-, pK_c, was correlated linearly with the variation of the equilibrium constant, owing to the addition of $R_4N^+X^-$, δpK_a. The dissociation of the azo dye in pyridine-water mixtures was also accelerated upon increasing the amount of water (0—10 vol%), correlating with an increase in the basicity of the solution.

The physical properties of azo dyestuffs (e.g., tone, color, crystal form) have been closely related with their dissociation as well as their tautomerism.

4-(4-Nitrophenylazo)-1-naphthol (azo dye) is particularly interesting as the basic structure of the azo compound. The undissociated form of the azo dye, fortunately, exists entirely as a hydrazone form in a solvent such as pyridine, as described in a previous paper.[2] Therefore, the dissociation of azo dye can be described by the equilibrium between the hydrazone form, DH, and the dissociated form, $D^\ominus$, as shown in Eq. 1.

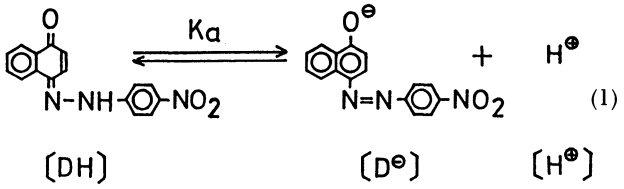

(1)

In polar aprotic solvents, such as dimethyl sulfoxide and *N,N*-dimethylformamide, azo dye exists partly in the dissociated form.[2] In this paper we report that the dissociation of azo dye in pyridine is accelerated by the addition of small amounts of quaternary ammonium compounds, R_4NX. We also describe the relationship between the variation of the equilibrium constant, owing to the addition of R_4NX, and the basicity of the $X^\ominus$.

Experimental

Material. The azo dye, 4-(4-nitrophenylazo)-1-naphthol, was prepared according to a method described in the literature.[3]

Methods. The spectra of the azo dye were taken on a Shimadzu UV-240 spectrometer in a 1.6×10^{-5} M solution (1 M=1 mol dm^{-3}) with 10 mm cuvettes; Beer's law was shown to be obeyed this concentration. The variation of the equilibrium constant, owing to the addition of R_4NX, δpK_a, of azo dye, was estimated in the following way. The absorption maxima for DH and $D^\ominus$ in pyridine are 472 and 655 nm, respectively. If the molar extinction coefficients of DH (or $D^\ominus$) at 472 and 655 nm in pyridine are expressed by ε_{472}^{DH} and ε_{655}^{DH} (or $\varepsilon_{472}^{D^\ominus}$ and $\varepsilon_{655}^{D^\ominus}$), and the mole fractions of DH and $D^\ominus$ by y and x, respectively, then the ratios of the molar extinction coefficients at 472 and 655 nm ($\varepsilon_{472}/\varepsilon_{655}$) should be

$$\frac{\varepsilon_{472}}{\varepsilon_{655}} = \frac{x\varepsilon_{472}^{D^\ominus} + y\varepsilon_{472}^{DH}}{x\varepsilon_{655}^{D^\ominus} + y\varepsilon_{655}^{DH}} \quad (2)$$

Figure 1 shows that the ε_{655}^{DH} is almost zero;[2] therefore, Eq. 2 yields

$$\frac{y}{x} = \frac{\varepsilon_{655}^{D^\ominus}}{\varepsilon_{472}^{DH}} \times \left(\frac{\varepsilon_{472}}{\varepsilon_{655}} - \frac{\varepsilon_{472}^{D^\ominus}}{\varepsilon_{655}^{D^\ominus}}\right) . \quad (3)$$

The ratio $\varepsilon_{472}^{D^\ominus}/\varepsilon_{655}^{D^\ominus} = 2.8/80.3 = 0.035$ was determined by measurements in a pyridine solution saturated with sodium hydroxide; $2.23 (=(80.3-4.1)\times10^3/(36.9-2.8)\times10^3)$ for $\varepsilon_{655}^{D^\ominus}/\varepsilon_{472}^{DH}$ was evaluated by the ratio of the difference in the molar extinction coefficients at 655 and 472 nm between solutions of the azo dye in pyridine and pyridine saturated with sodium hydroxide. From these two ratios Eq. 3 yields

$$\frac{y}{x} = 2.23 \times \left(\frac{\varepsilon_{472}}{\varepsilon_{655}} - 0.035\right) . \quad (4)$$

From the y/x value, the proportions (%) and the concentrations ([DH] and [$D^\ominus$], mol l^{-1}) of DH and $D^\ominus$ can be calculated. When [$H^\oplus$] is equal to [$D^\ominus$] in the dissociation constant (pK_a) of Eq. 5 applied in the equilibrium of Eq. 1, the apparent dissociation constant (pK_a') in the individual solutions containing the quaternary ammonium salts can be represented by the form of Eq. 6, and the difference (δpK_a) between the pK_a and the pK_a' may be expressed as in Eq. 7.

$$pK_a = -\log \frac{[D^\ominus][H^\oplus]}{[DH]} \quad (5)$$

$$pK_a' = -\log \frac{[D^\ominus]^2}{[DH]} \quad (6)$$

$$\delta pK_a = pK_a - pK_a' \quad (7)$$

If the solution of the azo dye is free from the quaternary ammonium salts pK_a' is equal to pK_a.

The pK_a' values in a pyridine-water solution were also estimated by using the same method.

Results and Discussion

Figure 1 shows the electronic spectrum of the azo dye in pure pyridine or pyridine saturated with sodium hydroxide. The band of the undissociated form (hydrazone form, DH) appeared at 472 nm, and that of the dissociated form (phenolate ion, $D^{\ominus}$) at 655 nm.[2] In pyridine, the addition of quaternary ammonium salts (R_4NX) increased the proportion of $D^{\ominus}$, while that of DH decreased. These two bands gave a well-defined isosbestic point at about 520 nm.

Table 1 exhibits the percentage of DH and $D^{\ominus}$ calculated from y/x (Eq. 4), the pK_a' from Eq. 6 and the δpK_a from Eq. 7 together with the molar extinction coefficients (ε_{472} and ε_{655}) at 472 and 655 nm upon the addition of various concentrations of tetrabutylammonium chloride ($(n\text{-}C_4H_9)_4NCl$). Figure 2 exhibits the relation of the δpK_a to the concentration of $(n\text{-}C_4H_9)_4NCl$. The δpK_a increased with increasing concentration of $(n\text{-}C_4H_9)_4NCl$, with the most dramatic effects observed at lower concentrations. Table 2 shows the result for addition of various quaternary ammonium salts (R_4NX) in 8.0×10^{-5} M solution. In all cases the apparent dissociation constant pK_a' for the addition of R_4NX gave a smaller value than the true dissociation constant pK_a (=7.41). The difference (δpK_a) between pK_a and pK_a' was influenced enormously by the species of anion $X^{\ominus}$ in $R_4N^{\oplus}X^{\ominus}$, but was little affected by the structure of an alkyl group R. Table 3 exhibits the dissociation constant pK_{HX}[4] for the conjugated acid HX of the $X^{\ominus}$ together with the δpK_a, and a plot of δpK_a vs. pK_{HX} is shown in Fig. 3. It is apparent from Fig. 3 that δpK_a increases linearly with increasing basicity of $X^{\ominus}$. These results lead to the following

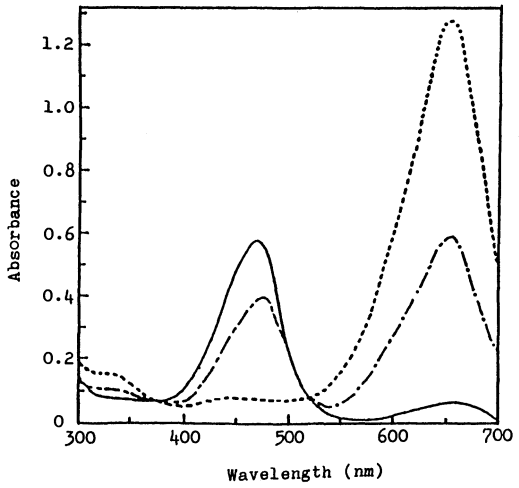

Fig. 1. Absorption spectra of 4-(4-nitrophenylazo)-1-naphthol (1.6×10^{-5} mol l^{-1}).
——: in pyridine. -----: in pyridine saturated with NaOH. -·-·-: +$(n\text{-}C_4H_9)_4NCl$ (2.0×10^{-4} mol l^{-1}) in pyridine.

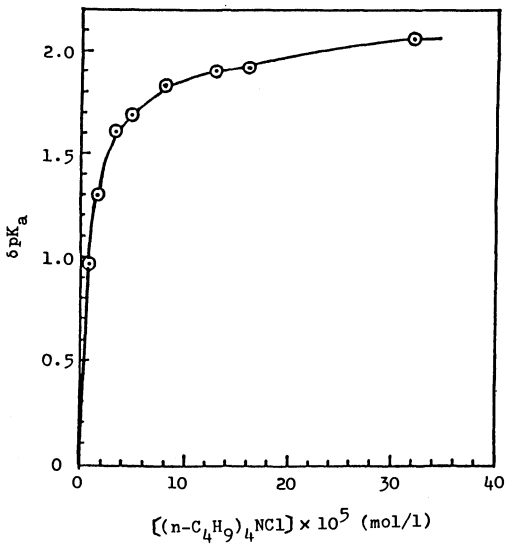

Fig. 2. Plots of δpK_a vs. $[(n\text{-}C_4H_9)_4NCl]$.

Table 1. Molar Extinction Coefficients (ε_{472} and ε_{655}) at the Absorption Maxima of Undissociated and Dissociated Forms (DH and $D^{\ominus}$), Percentage of DH and $D^{\ominus}$, Apparent Dissociation Constant (pK_a') and Difference (δpK_a) between pK_a' and Dissociation Constant (pK_a) on the Addition of Various Concentration of Tetrabutylammonium Chloride ((DH); 4-(4-Nitrophenylazo)-1-naphthol: 1.6×10^{-5} mol l^{-1}. Solvent: Pyridine, T: 25 °C)

No.	$(n\text{-}C_4H_9)_4NCl$ / mol l^{-1}	$\varepsilon_{472}\times10^{-3}$	$\varepsilon_{655}\times10^{-3}$	DH / %	$D^{\ominus}$ / %	pK_a'	δpK_a
1	0	36.9	4.1	95.2	4.8	7.41 (=pK_a)	—
2	8.0×10^{-6}	33.6	12.1	86.0	14.0	6.44	0.97
3	1.6×10^{-5}	31.8	17.2	80.2	19.8	6.11	1.30
4	3.2×10^{-5}	29.2	23.4	73.1	26.9	5.80	1.61
5	4.8×10^{-5}	28.5	25.4	70.8	29.2	5.72	1.69
6	8.0×10^{-5}	27.1	29.0	66.8	33.2	5.58	1.83
7	1.28×10^{-4}	26.7	31.4	64.4	35.4	5.51	1.90
8	1.6×10^{-4}	26.6	32.0	64.0	36.0	5.49	1.92
9	3.2×10^{-4}	25.3	37.5	58.8	41.2	5.34	2.07

Table 2. Molar Extinction Coefficients (ε_{472} and ε_{655}) at the Absorption Maxima of Undissociated and Dissociated Forms (DH and $D^{\ominus}$), Percentage of DH and $D^{\ominus}$, Apparent Dissociation Constant (pK_a') and Difference (δpK_a) between pK_a' and Dissociation Constant (pK_a) on Addition of Various Quaternary Ammonium Compounds ((DH); 4-(4-Nitrophenylazo)-1-naphthol: 1.6×10^{-5} mol l^{-1}, R_4NX: 8.0×10^{-5} mol l^{-1}, Solvent: Pyridine, T: 25 °C)

No.	R_4NX	$\varepsilon_{472}\times10^{-3}$	$\varepsilon_{655}\times10^{-3}$	DH %	$D^{\ominus}$ %	pK_a'	δpK_a
1	—	36.9	4.1	95.2	4.8	7.41 (=pK_a)	—
2	$(CH_3)_4NCl$	28.7	24.9	71.4	28.6	5.74	1.67
3	$(C_2H_5)_4NCl$	28.1	28.1	68.3	31.7	5.63	1.78
4	$(n\text{-}C_4H_9)_4NCl$	27.1	29.0	67.2	32.8	5.58	1.83
5	$[(CH_3)_3NCH_2C_6H_5]Cl$	28.4	24.8	71.3	28.7	5.73	1.68
6	$[(C_2H_5)_3NCH_2C_6H_5]Cl$	27.6	28.6	67.5	32.5	5.60	1.81
7	$[(CH_3)_2C_{16}H_{33}NCH_2C_6H_5]Cl$	29.2	25.3	71.4	28.6	5.74	1.67
8	$(C_2H_5)_4NBr$	32.9	10.6	87.3	12.7	6.53	0.88
9	$[C_5H_5NC_2H_5]Br$	32.7	11.6	86.2	13.8	6.45	0.96
10	$(C_2H_5)_4NI$	34.1	5.0	93.8	6.2	7.19	0.22
11	$(n\text{-}C_3H_7)_4NI$	32.3	5.5	92.9	7.1	7.06	0.35
12	$(n\text{-}C_4H_9)_4NHSO_4$	31.4	14.9	82.2	17.8	6.21	1.20
13	$(n\text{-}C_4H_9)_4NBF_4$	33.9	6.1	92.5	7.5	7.01	0.40
14	$(C_2H_5)_4NClO_4$	34.0	4.9	93.9	6.1	7.19	0.22

Table 3. The Values δpK_a and pK_{HX} to $X^{\ominus}$ in R_4NX ((DH); 4-(4-Nitrophenylazo)-1-naphthol: 1.6×10^{-5}mol l^{-1}, R_4NX: 8.0×10^{-5} mol l^{-1}, Solvent: Pyridine, T: 25 °C)

$X^{\ominus}$	$Cl^{\ominus}$	$HSO_4^{\ominus}$	$Br^{\ominus}$	$BF_4^{\ominus}$	$I^{\ominus}$	$ClO_4^{\ominus}$
δpK_a	1.67—1.83	ca. 1.20	0.96—0.88	ca. 0.40	0.35—0.22	ca. 0.22
pK_{HX}[4]	5.7	—	4.4	—	3.4	3.3

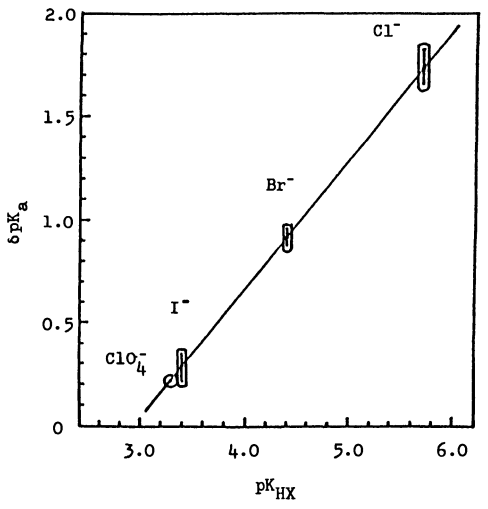

Fig. 3. Relationship between δpK_a and pK_{HX} (pK_a of HX).

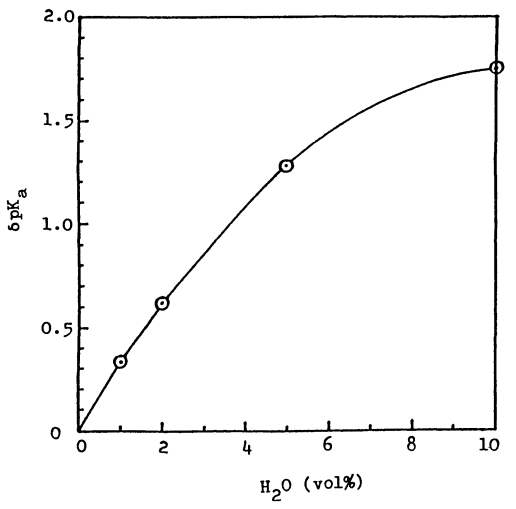

Fig. 4. Plots of δpK_a vs.H_2O (vol%).

discussion. The proton $H^{\oplus}$ formed[5] by the dissociation of azo dye (Eq. 1) reacts with the $X^{\ominus}$ produced in Eq. 8 to give HX (Eq. 9). Therefore, the equilibrium of Eq. 1 is shifted to the right.

$$R_4NX \overset{K_c}{\rightleftharpoons} R_4N^{\oplus} + X^{\ominus} \quad (8)$$

$$HX \overset{K_{HX}}{\rightleftharpoons} H^{\oplus} + X^{\ominus} \quad (9)$$

The above hypothesis can be tested by using the three dissociation constants into Eqs. 1, 8, and 9. Since the pK_a in Eq. 1 is 7.41 ($K_a=3.89\times10^{-8}$), $[H^{\oplus}]$ is equal to 0.077×10^{-5} mol l^{-1} at a total concentration of the azo dye of 1.6×10^{-5} mol l^{-1}; $[X^{\ominus}]$ in Eq. 8 is estimated to be $(7.45—5.25)\times10^{-5}$ mol l^{-1} at an R_4NX concentration of 8×10^{-5} mol l^{-1} because the pK_c[6] is 3—4. Next, we consider the equilibrium of HX, by employing

$[H^{\oplus}]=0.077\times10^{-5}$ and $[X^{\ominus}]=(7.45—5.25)\times10^{-5}$ mol l^{-1} in Eq. 9. If the $X^{\ominus}$ is a strong base, [e.g., the conjugate base of a very weak acid such as HCl in pyridine ($pK_{HCl}=5.7$, $K_{HCl}=2.0\times10^{-6}$)], [HX] becomes $(0.075—0.074)\times10^{-5}$ mol l^{-1}, corresponding to 97—96% of $[H^{\oplus}]=0.077\times10^{-5}$ mol l^{-1}. Therefore, the equilibrium of Eq. 1 may be significantly shifted to the right. On the other hand, if the $X^{\ominus}$ is a weak base [e.g., the conjugate base of a strong acid such as $HClO_4$ in pyridine ($pK_{HClO_4}=3.3$, $K_{HClO_4}=5.0\times10^{-4}$)], [HX] becomes $(0.0100—0.0075)\times10^{-5}$ mol l^{-1}, corresponding to 13—10% of $[H^{\oplus}]$. This means that the equilibrium of Eq. 1 may be only slightly shifted to the right.

The dissociation of azo dye in pyridine is also accelerated by the addition of a large quantity of water. Figure 4 shows the relation of δpK_a to the content of water. The δpK_a for 1 (0.56), 2(1.1), 5(2.8), and 10 vol% (5.6 mol l^{-1}) of water is 0.34, 0.64, 1.28, and 1.75, respectively. This indicates that the hydroxy anion $OH^{\ominus}$ formed in Eq. 10 reacts with a proton $H^{\oplus}$ (in Eq. 1), as shown in Eq. 11, so that the dissociation described in Eq. 1 may be accelerated, and that the basicity in such a solvent system may increase with the water content.

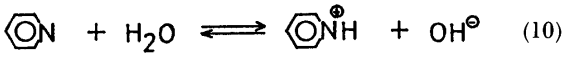

(10)

(11)

This research was supported by a Grant-in-Aid for Scientific Research of Japan (No. 60119007). The author also thanks Prof. Dr. Osamu Manabe (Nagasaki Univ.) for valuable suggestions throughout this work.

References

1) Part X of this series: S. Kishimoto, K. Miyawaki, T. Okushi, and T. Hirashima, *Nippon Kagaku Kaishi*, **1986**, 1778.

2) S. Kishimoto, S. Kitahara, O. Manabe, and H. Hiyama, *J. Org. Chem.*, **43**, 3882 (1978).

3) S. Kishimoto, O. Manabe, H. Hiyama, and N. Hirao, *Nippon Kagaku Kaishi*, **1972**, 2132.

4) Kagaku Binran (Handbook of Chemistry), 3rd ed, Fundamental ed. II, Chemical Society of Japan (1984), p. 343.

5) The proton exists actually in solvated state under these conditions.

6) G. Charlot, B. Trémillon, "Les réactions chimiques dans les solvant et les sels fondus," Gauthier-Villars Paris, (1963), Part II, Chap. 9.

The Chlorination of Vinyl Compounds in Alcohols

Kiyonori SHINODA* and Kensei YASUDA
Toyama National College of Technology, 13 Hongo, Toyama 939
(Received April 25, 1988)

Upon the chlorination of vinyl compounds in alcohols, the reaction products were composed of 2-alkoxy-1-chloro compound (A), 1-alkoxy-2-chloro compound (B) and vicinal dichloride (C). Various vinyl compounds were chlorinated in alcohols at 40 °C in order to elucidate the effect of their molecular structure on the product distribution. The A/(A+B) was inversely proportional to the relative rate of ordinary chlorination in carbon tetrachloride. The A/(A+B) for the chlorination of allyl chloride in methanol was little affected by the reaction conditions: (1) reaction temperature, (2) mole ratio, and (3) elapse of time. However, the A/(A+B) increased with increasing E_s value of the alkyl group of alcohol.

It has been well-known that vicinal dichloride is accompanied by solvent-incorporated products during chlorination in common protic solvents.[1-3] The addition of bromine to olefin in methanol also produces methoxybrominated products.[4,5] The chlorination of various olefins in the protic solvent has been reviewed in detail by de la Mare and Bolton.[6] The kinetic forms, environmental effects, structural effects on the rates of chlorination and products have been described. The solvent-incorporated products for the chlorination of vinyl compound in methanol are composed of 1-methoxy-2-chloro and 2-methoxy-1-chloro compounds. These compounds represent Markownikoff and anti-Markownikoff orientations, respectively.

However, little is known concerning the formation ratio of two solvent-incorporated products. Furthermore, there has been no report on a quantitative examination of the alkoxychlorination of vinyl compounds.

The chlorination of vinyl compounds in various alcohols was carried out in order to elucidate the effect of the molecular structure on alkoxychlorination.

Results and Discussion

The solvent-incorporated products for the chlorination of vinyl compounds in methanol are composed of 1-methoxy-2-chloro and 2-methoxy-1-chloro compounds. The formation ratio of a mixture of two methoxychlorides to dichloride was gradually decreased with the elapse of time in the chlorination of vinyl compounds in methanol. This was because the concentration of methanol decreased as the reaction proceeded. The product composition of the chlorination of allyl cyanide in methanol is illustrated in Table 1.

On the other hand, the proportion of two methoxy chlorides was, roughly, kept constant throughout the reaction. Nevertheless, the formation ratio of two methoxy chlorides was widely changed with the molecular structure of the substrate. The product ratios for the chlorination of various vinyl compounds in methanol at 40 °C are shown in Table 2, together with the rate ratios for chlorination in carbon tetrachloride.[7] Symbols A, B and C represent 2-methoxy-

Table 2. The Effect of the Olefin Structure (CH_2=CH-R) on the Chlorination in Methanol and Carbon Tetrachloride

Substituent (R)	σ^*	A/(A+B) in CH_3OH	k/k_0[6] in CCl_4
-CN	3.64	—	0.00109
-COOH	2.94	—	0.00197
-Br	2.80	92.5	—
$-COOCH_3$	2.00	89.1	0.0181
$-COCH_3$	1.65	81.2	0.0352
$-CHClCH_2Cl$	1.435	81.2	—
$-CH_2CN$	1.300	66.6	0.215
$-CH_2Cl$	1.050	66.1	1.00
$-CH_2Br$	1.000	—	1.40
$-CHClCH_3$	0.950	46.2	2.06
$-CH_2I$	0.85	—	1.63
$-C_6H_5$	0.600	—	2.00
$-CH_2OH$	0.555	32.8	—
$-CH_2CH_2COCH_3$	0.215	22.9	—
$-CH_3$	0	20.9	—
$-CH_2CH(CH_3)_2$	−0.125	27.7	—
$-CH_2CH_2CH_2CH_3$	−0.130	26.1	26.9
$-CH(CH_3)CH_2CH_3$	−0.210	—	35.9
$-C(CH_3)_3$	−0.300	12.4	—

Table 1. Product Composition, A/(A+B) and C/(A+B+C) for the Chlorination of Allyl Cyanide in Methanol at 40 °C

Reaction time	Product composition (%)				A/(A+B)	C/(A+B+C)
min	CH_2:$CHCH_2CN$	A	B	C	(%)*	(%)
5	81.5	11.1	5.5	1.9	66.9	10.3
10	62.2	20.4	12.7	4.7	61.6	12.4
15	41.6	33.4	16.8	8.7	66.5	14.0
20	19.2	44.1	23.4	13.2	65.3	16.5
25	1.8	53.7	26.9	17.6	66.6	17.9

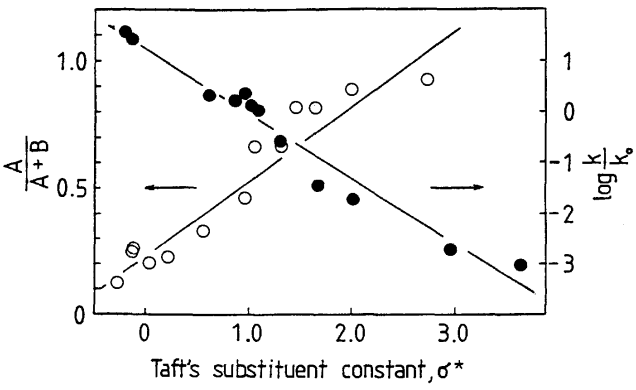

Fig. 1. The plots of A/(A+B) and k/k_0 for the chlorination of various vinyl compounds against σ^*.
○: A/(A+B), ●: k/k_0.

1-chloro, 1-methoxy-2-chloro compounds and vicinal dichloride in the product composition, respectively. Two vinyl compounds were competitively chlorinated in carbon tetrachloride in the presence of oxygen at 30 °C. The value of the relative rate constant was caluculated according to a previously described method.[8] The k/k_0 is the relative rate constant with respect to the standard reaction (allyl chloride in this case). Figure 1 shows the effect of the molecular structure of a vinyl compound upon the formation ratio of two methoxy chlorides [A/(A+B)]. The logarithms of the relative rate constant for the chlorination of a vinyl compound in the presence of oxygen in carbon tetrachloride, as well as the formation ratio of two methoxy chlorides for the chlorination in methanol, are plotted against Taft's substituent constant (σ^*).[9] The data follow two straight lines, though opposite in sign. It is essential that k/k_0 be compared with A/(A+B) in order to consider the reaction mechanism of alkoxychlorination. The general nature of the first stage of attack by chlorine on an unsaturated molecule is established by the effect of the structure on the reaction rate.

As can be seen in Fig. 1, the rate of dark chlorination of a vinyl compound in the presence of oxygen in carbon tetrachloride was increased by the electron-releasing substituent group and decreased by the electron-withdrawing group. The reaction of chlorine with the vinyl compound (Q) in methanol might proceed according to the following mechanism:[2]

$$\mathrm{Q} + \mathrm{Cl_2} \longrightarrow \mathrm{QCl}^{\oplus} \xrightarrow{\mathrm{Cl}^{\ominus}} \mathrm{QCl\text{-}Cl}$$
$$\qquad\qquad\quad \xrightarrow{\mathrm{MeOH}} \mathrm{QCl\text{-}OMe} + \mathrm{H}^{\oplus} \qquad (1)$$

Fahey and Schubert,[1] using a stereochemical criterion, have shown that $QCl^{\oplus}$ may be either bridged or open, depending upon the stability of the open ion. It can be assumed that the intermediates formed in the rate-determining step for chlorination may alternatively be carbonium ion (**1**), carbonium ion (**2**) or bridged chloronium ion (**3**). In view of previous

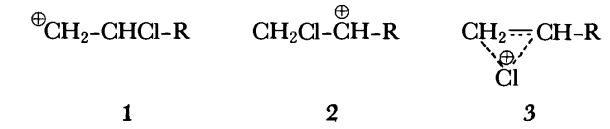

1 **2** **3**

results,[7] the chlorine cation attacks on the carbon which carries an electron-withdrawing substituent to form the carbonium ion (**1**), whereas the substrate, having an electron-releasing group, converts into the carbonium ion (**2**). On the contrary, the bridged chloronium ion (**3**) is formed by the reaction of a chlorine cation with a vinyl compound having a moderate group, such as allyl chloride. While carbonium ion (**2**) is predominantly converted into B by a nucleophilic attack of methanol, carbonium ion (**1**) is transformed into A. It is reasonable to consider that A, B and C are produced by a competitive nucleophilic attack of methanol and a chloride ion to the bridged chloronium ion. That is to say, A/(A+B) is dependent on the carbocationic intermediate, which is controlled by the relative rate constant.

Since allyl chloride could be considered to have a moderate group, allyl chloride was chlorinated in order to investigate the effect of the reaction condition on the A/(A+B) and C/(A+B+C). While the relative rate of chlorination to alkoxychlorination C/(A+B+C) was increased with an increase in the concentration of allyl chloride in methanol, the A/(A+B) was little affected by the concentration of allyl chloride in methanol (Fig. 2) and the reaction temperature. A/(A+B) also remained approximately constant throughout the chlorination, despite the elapse of time. Neither photochemical chlorination under irradiation nor dark chlorination in the presence of oxygen could change A/(A+B). It could be assumed that the chlorination of a vinyl compound in methanol was an ionic reaction.

Since the nucleophilicity and steric hindrance of an alkyl group in a long or bulky chain alcohol were

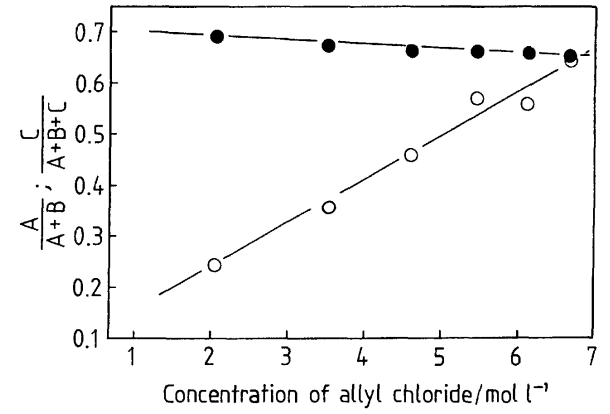

Fig. 2. The plots of A/(A+B) and C/(A+B+C) against concentration of allyl chloride for the chlorination of allyl chloride in methanol at 40 °C.
●: A/(A+B), ○: C/(A+B+C).

Table 3. Effect of E_s Value on A/(A+B) and C/(A+B+C)

Alcohol	E_s[10]	A/(A+B) (%)	C/(A+B+C) (%)
CH_3OH	0.00	66.2	14.2
C_2H_5OH	−0.07	66.5	22.3
n-$C_6H_{13}OH$	−0.34	65.3	36.8
i-$C_5H_{11}OH$	−0.35	66.4	36.5
n-C_3H_7OH	−0.36	63.5	29.7
n-C_4H_9OH	−0.39	64.8	26.8
n-$C_5H_{11}OH$	−0.40	60.1	27.7
i-C_3H_7OH	−0.47	69.0	41.6
i-C_4H_9OH	−0.93	64.4	38.6
$(CH_3)(C_2H_5)CHOH$	−1.13	58.9	50.2
t-C_4H_9OH	−1.54	54.9	82.5

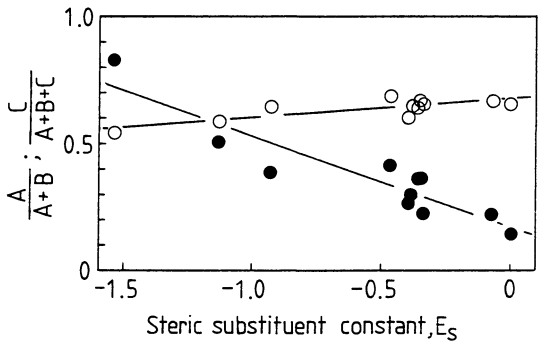

Fig. 3. The relations of A/(A+B) vs. E_s and C/(A+B+C) vs. E_s for the chlorination of allyl chloride in various alcohols at 40 °C.
○: A/(A+B), ●: C/(A+B+C).

compensated for by each other, the variation of A/(A+B) was over a narrow range, even through allyl chloride was chlorinated in several alcohols at 40 °C (Table 3).

The A/(A+B) value for the alkoxychlorination of allyl chloride in various alcohols slightly decreased in the following order:

i-$C_3H_7OH > C_2H_5OH > i$-$C_5H_{11}OH > CH_3OH >$
n-$C_6H_{13}OH > n$-$C_4H_9OH > i$-$C_4H_9OH > n$-$C_3H_7OH >$
n-$C_5H_{11}OH > s$-$C_4H_9OH > t$-C_4H_9OH.

The relations of A/(A+B) and E_s as well as of C/(A+B+C) and E_s are shown in Fig. 3. E_s on the abscissa indicates the steric substituent constants[10] for the alkyl group of alcohol. Since the C/(A+B+C) value increased with the elapse of time, C was obtained by extrapolating the experimental data back to the initial time. The increase in the C/(A+B+C) value with the elapse of time can be explained by using the same reason why the concentration of alcohol in a reaction solution decreases as the reaction proceeds.

It is clear that the rate of a nucleophilic attack on the intermediate was decreased with a long or bulky chain alcohol. On the other hand, the rate of the addition of chloride ion might remain unaltered. Therefore, the C/(A+B+C) value might be changed by the E_s value of the alkyl group of alcohol.

Experimental

Reagents. All the reagents used in this work were purchased from Tokyo Kasei Kogyo Co., except for the alcohols, which were obtained from Wako Pure Chemical Industries. They were not purified further. Chlorine and oxygen were fed from commercial cylinders and were passed through a sulfuric acid trap before use.

Chlorination of Vinyl Compound in Methanol. A 100 ml, flat, cylindrical semibatch Pyrex reactor thermostated at 40 °C was equipped with a Teflon magnetic stirring bar, a gas inlet tube and a reflux condenser. A mixture of 0.1 mol of vinyl compound and 50 ml of methanol was added to the reactor. Chlorine gas was fed into the reactor at the rate of 0.01 mol h^{-1}, until the reaction solution became a pale-yellow color. Chlorination products were analyzed by means of gas chromatography (Shimadzu GC-5A, SDC 550, PEG 6000).

Chlorination of Allyl Chloride in Methanol. Allyl chloride was chlorinated in methanol under various reaction conditions. The photochemical procedure and dark chlorination procedure in the presence of oxygen were similar to those used in the previous study.[7] Furthermore, 30 ml of methanol was mixed with allyl chloride at various volume ratios. The chlorination of this mixture was the same as the preceding techniques.

Chlorination of Allyl Chloride in Various Alcohols. The chlorination procedure was the same as that used in methanol. 30 ml of alcohol was mixed with 0.1 mol allyl chloride and the mixture was then placed in the reactor. The chlorination temperature was maintained at 40 °C. At regular intervals, 1 ml samples were taken from the reaction system and analyzed by gas chromatography.

References

1) R. C. Fahey and C. Schubert, *J. Am. Chem. Soc.*, **87**, 5172 (1965).
2) M. L. Poutsma and J. L. Kartch, *J. Am. Chem. Soc.*, **89**, 6595 (1967).
3) W. M. Baluzow, Ch. Duschek, G. Just, W. Pritzkow, and H. Schmidt, *J. Prakt. Chem.*, **317**, 53 (1975).
4) W. H. Puterbaugh and M. S. Newman, *J. Am. Chem. Soc.*, **79**, 3469 (1957).
5) M. M. Morsumzade, A. S. Kyazimov, A. L. Shabanov, F. G. Ismdilova, and A. A. Babaeva, *Dokl. Akad. Nauk Azerb. SSR*, **29** (5), 29 (1973); *C. A.*, **80**, 59543j (1974).
6) P. B. D. de la Mare and R. Bolton, "Electrophilic Additions to Unsaturated Systems," Elsevier Scientific Pub. Co., Amsterdam (1982), p. 93.
7) K. Shinoda, *Bull. Chem. Soc. Jpn.*, **51**, 913 (1978).
8) K. Shinoda, *Nippon Kagaku Kaishi*, **1973**, 542.
9) M. S. Newman, "Steric Effects in Organic Chemistry," John Wiley & Sons, Inc., New York (1956), p. 618.
10) Ref. 9, p. 598.

 © 1988 The Chemical Society of Japan Bull. Chem. Soc. Jpn., 61, 4397—4400 (1988)

Synthetic Photochemistry. XLV.[1] Photoconversion of 2-Methylenehomobarrelenes to 9-Methylenebarbaralanes

Guan Rong TIAN,† Shigeru SUGIYAMA, Akira MORI, and Hitoshi TAKESHITA*
Institute of Advanced Material Study, 86, Kyushu University, Kasuga-koen, Kasuga, Fukuoka 816
(Received April 27, 1988)

The photolysis of 4-methoxycarbonyl-2-oxatricyclo[6.2.2.0^{1,5}]dodeca-4,6,9,11-tetraen-3-one derivatives yielded 9-methylenebarbaralanes along with 5-methylenetricyclo[4.3.0.0^{2,9}]nonadiene and 1-methyleneindan derivatives. From the benzophenone-sensitization experiments, 9-methylenebarbaralane and 5-methylenetricyclo[4.3.0.0^{2,9}]nonadiene were formed via a triplet excited state, but 1-methyleneindan was formed via a singlet excited state.

Previously, the benzophenone-sensitized irradiation of bicyclo[3.2.2]nona-3,6,8-trien-2-one (homobarrelenone) (**1**) was shown to give a tricyclic ketone (**2**),[2] while direct photolysis afforded the dihydroindenone (**3**).[3] Furthermore, the acetone-sensitized photolysis of 2-methylenehomobarrelene (**4**) resulted in two isomeric products (**5** and **6**) and the direct irradiation of **4** gave methylenedihydroindene (**7**)[4,5] via a concerted [1,3] vinyl shift. Recently, we prepared 2-methylenehomobarrelenes (**8**) from cyclohepta[*b*]furan-2-one derivatives and 2,3-bis(methoxycarbonyl)-7-oxanorbornadiene by a high-pressure cycloaddition-thermal cycloreversion procedure.[6] In this paper we describe the photochemical behaviors of these 2-methylenehomobarrelenes as well as the reaction mechanism.

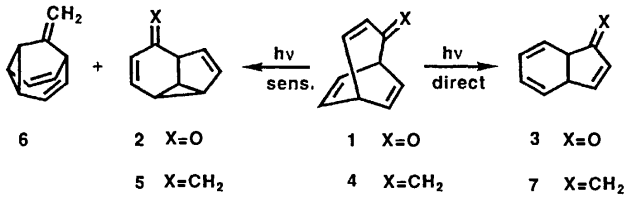

Scheme 1.

Photolysis of 2-Methylenehomobarrelenes. Upon UV-light irradiation by means of a 400-W high-pressure mercury lamp through a Pyrex-glass filter, 4-methoxycarbonyl-2-oxatricyclo[6.2.2.0^{1,5}]dodeca-4,6,9,11-tetraen-3-one (**8a**) furnished three photoproducts (**9a—11a**) in 19, 15, and 25% yields. The structures of these photolysates were determined to be derivatives of a barbaralylidene (type I), a tricyclo[4.3.0.0^{2,9}]nonadiene (type II), and an indanylidene (type III) according to spectral evidence. When the photolysis of **8a** was monitored by ^{1}H NMR spectroscopy, a new set of signals appeared at δ 3.66 (1H, dd, J=11.4, 2.2 Hz), 4.06 (1H, ddq, J=11.4, 4.0, 2.6 Hz), 5.47 (1H, dd, J=6.0, 2.2 Hz), 5.50 (1H, dd, J=9.5, 4.0 Hz), 5.88 (1H, ddd, J=9.5, 6.0, 2.6 Hz), 7.06 (1H, dd, J=5.5, 2.6 Hz), and 7.43 (1H, dd, J=5.5, 2.6 Hz) together with the signals of **9a**, **10a**, and **11a**. These new signals disappeared after silica-gel chromatography. From this evidence, the intermediary product was assigned to be a dihydroindene derivative (**12a**) which isomerized to an indan derivative (**11a**) upon being worked up.

Similarly, the products obtained from 7-chloro-4-methoxycarbonyl-2-oxatricyclo[6.2.2.0^{1,5}]dodeca-4,6,9,11-tetraen-3-one (**8b**) and 7-methoxy-4-methoxycarbonyl-2-oxatricyclo[6.2.2.0^{1,5}]dodeca-4,6,9,11-tetraen-3-one (**8c**) were type I (**9b** and **9c**), type II (**10b** and **10c**), and type III (**11b** and **11c**).

Mechanistic Considerations. In order to determine

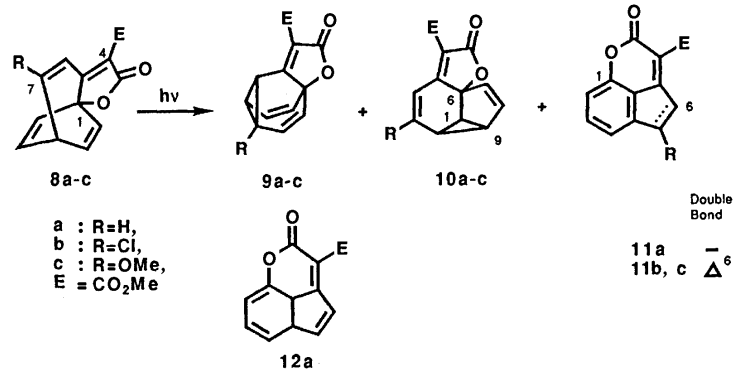

Scheme 2.

† On leave from Yanbian University, Yanji, Jilin, People's Republic of China.

Table 1. Product Distributions of Photolysis in the Presence of 1,3-Pentadiene

Time/min	8a			9a			10a			11a+12a		
	A	B	C	A	B	C	A	B	C	A	B	C
15	85	84	86	3	3	3	4	3	3	9	10	8
30	75	73	74	4	5.5	5	6	6.5	6	15	15	15
45	71	67.5	69	6	6.5	6	7	8	7	16	18	17
60	62	58	61	7	10	8	8	10	9	23	22	22
105	45	43	44	10	12	15	13	15	13	32	30	28
175	29	26	30	15	16	14	17	20	18	39	38	38

Photolysis conditions: A, 0.29 mol dm^{-3} of **8a** in $CDCl_3$. B, 0.29 mol dm^{-3} of **8a** and 0.64 mol dm^{-3} of 1,3-pentadiene in $CDCl_3$. C, 0.29 mol dm^{-3} of **8a** and 1.42 mol dm^{-3} of 1,3-pentadiene in $CDCl_3$.

Table 2. Products Distributions of Photolysis in Acetone

Time/min	8a		9a		10a		11a+12a	
	A	D	A	D	A	D	A	D
10	89	—	—	—	4	—	8	—
25	79	78.5	3	2.5	5	5	12	14
55	65	66	4	4	9	7	22	22.5
115	45	45.5	6	10	14	14.5	35	30
175	28	31.5	9	13	17	18.5	45	37

Photolysis conditions: A, in $CDCl_3$. D, in acetone-d_6.

Table 3. Products Distributions of Benzophenone-Sensitized Photolysis

Time/min	8a		9a		10a		11a+12a	
	A	E	A	E	A	E	A	E
6	88	90	2	3	3	4	7	3
12	80	79	4	6	5	9	11	6
18	70	66	6	10	7	15	17	10
24	69	60	7	13	7	16	18	12
84	22	15	15	25	17	37	46	24

Photolysis conditions: A, 0.21 mol dm^{-3} of **8a** in $CDCl_3$. E, 0.21 mol dm^{-3} of **8a** and 0.24 mol dm^{-3} of benzophenone in $CDCl_3$.

the multiplicity of the excited state, reactions of **8a** with 1,3-pentadiene were traced by means of ^{1}H NMR spectroscopy. Distributions of photolysates, together with results of the photolyses in acetone and of the benzophenone-sensitized photolysis, are summerized in Tables 1—3 and Fig. 1.

As shown in Table 1, product distributions from **8a** were insensitive to the concentrations of 1,3-pentadiene, a triplet quencher. No quenching by 1,3-pentadiene indicates that a singlet state of **8a** can lead to photolysates. However, a triplet intermediate could not be ruled out, since the rate of the intramolecular rearrangements to photolysates could occur more rapidly than a diffusion controlled rate. Product distributions in acetone were almost similar to those in chloroform. The benzophenone-sensitized photolysis of **8a**, however, showed that the yields of **9a** and **10a** increased roughly twice and those of **11a** and **12a** decreased by roughly one half, with a small increasement of the consumption of **8a**. Therefore, **9a** and **10a** formed via a

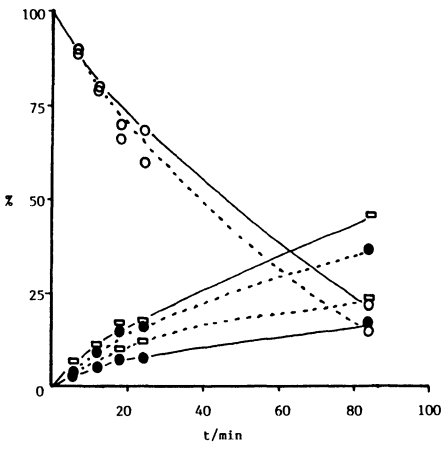

Fig. 1. Time-course of benzophenone-sensitized photolysis of **8a**.
——: in $CDCl_3$, ------: with benzophenone in $CDCl_3$.
○: **8a**, ●: **10a**, □: **11a+12a**.

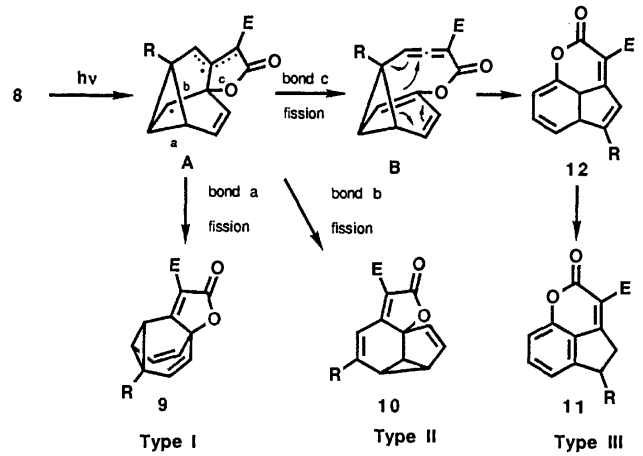

Scheme 3.

triplet excited state and **11a** and **12a** via a singlet excited state.

The formation of photolysates can be explained by di-π-methane rearrangements,[7] as shown in Scheme 3. Bond-a fission in a diradical **A** gave type-I products, while bond-b fission gave type-II products. On the other hand, bond-c fission led to a tricyclic allene derivative (**B**); further, an electrocyclic [4πs+2πa+2σs] path should give a dihydroindan derivative (**12**). Subsequent aromatization and a dehydrogenation of **12** gave type-III products.

These results are as same as those of the previously reported **4**[4,5] and **1**[2,3] in respect to not only the product distributions, but also the multiplicities of the concerned excited state.

Experimental

Elemental analyses were performed by Miss S. Hirashima, of Institute of Advanced Material Study, Kyushu University. The NMR spectra were measured by a JEOL 270 H Spectrometer in a $CDCl_3$ solution, unless otherwise specified, and the chemical shifts expressed were in δ unit. The mass spectra were measured with a JEOL 01SG-2 Spectrometer at 70 eV. The IR spectra were taken in a $CHCl_3$ solution using a Jasco IR-A 102 Spectrometer. The UV spectra were measured by a Hitachi U-3200 Spectrophotometer.

Irradiation of 8. A $CHCl_3$ solution (1 cm^3) of **8** (**8a**, 160 mg; **8b**, 250 mg; **8c**, 223 mg) was irradiated for 3 h with a 400-W high-pressure mercury lamp through a Pyrex filter and the reaction was monitored by ^1H NMR spectroscopy. The solvent was evaporated and the residue was purified by a silica-gel column and HPLC to give products (**9—11**) and the recovered **8** (**8a**, 45.5 mg; **8b**, 116 mg; **8c**, 58 mg).

9a: Colorless crystals, mp 122—123 °C, 22 mg, 19%. Found: C, 67.96; H, 4.14%. Calcd for $C_{13}H_{10}O_4$: C, 67.82; H, 4.38%. ^1H NMR δ=3.0—3.1 (2H, m), 3.87 (3H, s), 4.01 (1H, t, J=7.0 Hz), 5.7 (2H, m), and 6.19 (2H, dm, J=8.8 Hz). ^{13}C NMR δ=22.0, 33.9 (2C), 52.1, 82.0, 112.0, 119.4 (2C), 128.5 (2C), 162.1, 167.3, and 176.2. IR ν: 1785, 1775, 1715, 1660, and 1440 cm^{-1}. UV (MeOH) λ_{max}: 234.0 (ε 11200) and 282.4 nm (4450). MS m/z (%) 230 (M^+, 30), 170 (33), 115 (base), and 91 (74).

10a: Colorless crystals, mp 155—157 °C, 17 mg, 15%. Found: C, 67.59; H, 4.28%. Calcd for $C_{13}H_{10}O_4$: C, 67.82; H, 4.38%. ^1H NMR δ=2.36 (1H, td, J=7.0, 4.4 Hz), 2.94 (1H, ddm, J=7.0, 5.9 Hz), 3.02 (1H, ddd, J=7.0, 5.9, 2.6 Hz), 3.88 (3H, s), 5.33 (1H, dm, J=5.5 Hz), 6.03 (1H, ddd, J=5.5, 2.6, 0.7 Hz), 6.34 (1H, dd, J=9.9, 4.4 Hz), and 7.24 (1H, d, J=9.9 Hz). ^{13}C NMR δ=29.5, 39.1, 43.5, 52.1, 89.6, 111.5, 123.7, 132.2, 133.7, 138.0, 161.8, 167.6, and 172.8. IR ν: 1780, 1715, 1630, and 1440 cm^{-1}. UV (MeOH) λ_{max}: 225.2 (ε 6300), 273.0 (7000), and 314.6 nm (8400). MS m/z (%) 230 (M^+, 24), 202 (32), 198 (65), 170 (55), 142 (40), 131 (33), 115 (base), 114 (40), 89 (32), and 76 (34).

11a: Colorless crystals, mp 172—173 °C, 29.1 mg, 25%. Found: C, 67.87; H, 4.29%. Calcd for $C_{13}H_{10}O_4$: C, 67.82; H, 4.38%. ^1H NMR δ=3.3—3.4 (2H, m), 3.5—3.6 (2H, m), 3.94 (3H, s), 7.10 (1H, d, J=7.7 Hz), 7.23 (1H, d, J=7.0 Hz), and 7.61 (1H, dd, J=7.7, 7.0 Hz). ^{13}C NMR δ=31.4, 33.1, 52.2, 110.8, 112.4, 120.3, 125.5, 135.9, 149.1, 151.9, 158.8, 164.5, and 171.5. IR ν:1755, 1740, and 1600 cm^{-1}. UV (MeOH) λ_{max}: 207.8 (ε 31400), 232.0 (8500 sh), 242.0 (4700 sh), and 309.4 nm (17150). MS m/z (%) 230 (M^+, 42), 199 (49), 198 (base), 170 (34), 115 (52), 114 (45), and 57 (36).

9b: Colorless crystals, mp 124—126 °C, 67 mg, 50%. Found: C, 59.38; H, 3.31%. Calcd for $C_{13}H_9O_4Cl$: C, 59.00; H, 3.43%. ^1H NMR δ=3.36 (1H, ddm, J=7.7, 6.2 Hz), 3.90 (3H, s), 4.29 (1H, d, J=7.7 Hz), 5.76 (1H, d, J=9.1 Hz), 5.87 (1H, dd, J=8.8, 6.2 Hz), 6.18 (1H, d, J=9.1 Hz), and 6.24 (1H, dd, J=8.8, 1.1 Hz). ^{13}C NMR δ=30.9, 43.5, 52.3, 53.3, 81.0, 113.2, 119.6, 123.3, 127.2, 129.2, 161.5, 166.6, and 170.3. IR ν: 1785, 1720, 1665, 1605, and 1440 cm^{-1}. UV (MeOH) λ_{max}: 227.6 (ε 12100) and 279.4 nm (5500).

10b: Colorless crystals, mp 109—110 °C, 23 mg, 17%. Found: C, 59.09; H, 3.19%. Calcd for $C_{13}H_9O_4Cl$: C, 59.00; H, 3.43%. ^1H NMR δ=2.53 (1H, t, J=7.7 Hz), 2.99 (1H, dd, J=7.7, 5.9 Hz), 3.10 (1H, ddd, J=7.7, 5.9, 2.9 Hz), 3.89 (3H, s), 5.39 (1H, dd, J=5.5, 0.7 Hz), 6.15 (1H, ddd, J=5.5, 2.9, 0.8 Hz), and 7.31 (1H, s). ^{13}C NMR δ=34.7, 38.6, 42.4, 52.3, 88.9, 111.6, 121.9, 133.1, 133.3, 143.8, 161.0, 167.1, and 171.5. IR ν: 1780, 1715, 1630, 1540, and 1440 cm^{-1}. UV (MeOH) λ_{max}: 226.0 (ε 5900) and 300.8 nm (9900). MS m/z (%) 266 (M^++2, 9), 264 (M^+, 41), 236 (41), 206 (35), 204 (41), 197 (86), 178 (31), 149 (65), 126 (49), 114 (65), 113 (60), 102 (33), 87 (31), 75 (51), 73 (41), 63 (50), 62 (36), 59 (39), and 42 (base).

11b: Colorless crystals, mp 151 °C, 8.7 mg, 6%. Found: C, 59.70; H, 2.49%. Calcd for $C_{13}H_7O_4Cl$: C, 59.45; H, 2.69%. ^1H NMR δ=3.98 (3H, s), 7.03 (1H, s), 7.16 (1H, d, J=8.4 Hz), 7.26 (1H, d, J=7.0 Hz), and 7.51 (1H, dd, J=8.4, 7.0 Hz). ^{13}C NMR δ=52.9, 114.0, 116.7, 117.1, 118.2, 123.1, 134.1, 137.0, 148.8, 149.4, 152.4, 158.1, and 162.9. IR ν: 1760, 1730, 1665, 1620, 1495, and 1460 cm^{-1}. UV (MeOH) λ_{max}: 246.4 (ε 10600), 290.0 (10600), and 385.4 nm (8300). MS m/z (%) 264 (M^++2, 20), 262 (M^+, 37), 233 (38), 231 (75), 204 (48), 159 (52), 147 (66), 85 (52), 73 (42), and 42 (base).

9c: Colorless crystals, mp 102—104 °C, 56.4 mg, 34%. Found: C, 64.72; H, 4.44%. Calcd for $C_{14}H_{12}O_5$: C, 64.61; H, 4.65%. ^1H NMR δ=3.35 (1H, ddm, J=8.1, 6.2 Hz), 3.55 (3H, s), 3.89 (3H, s), 4.12 (1H, d, J=8.1 Hz), 5.78 (1H, d, J=9.2 Hz), 5.82 (1H, dd, J=8.8, 6.2 Hz), 6.09 (1H, d, J=8.8 Hz), and 6.11 (1H, d, J=9.2 Hz). ^{13}C NMR δ=30.0, 44.5, 52.1, 57.9, 81.8, 82.0, 111.2, 119.2, 119.9, 123.6, 125.4, 162.0, 167.3, and 172.5. IR ν: 1780, 1715, 1655, and 1440 cm^{-1}. UV (MeOH) λ_{max}: 231.6 (ε 11600) and 290.4 nm (7000). MS m/z (%) 260 (M^+, 49), 228 (35), and 121 (base).

10c: Colorless crystals, mp 143—145 °C, 5 mg, 3%. Found: C, 64.62; H, 4.55%. Calcd for $C_{14}H_{12}O_5$: C, 64.61; H, 4.65%. ^{1}H NMR δ=2.31 (1H, t, J=7.7 Hz), 2.9 (2H, m), 3.81 (3H, s), 3.88 (3H, s), 5.35 (1H, d, J=5.9 Hz), 6.05 (1H, ddd, J=5.9, 2.2, 1.1 Hz), and 6.47 (1H, s). ^{13}C NMR δ=29.9, 36.0, 39.7, 51.8, 56.7, 89.1, 96.1, 117.5, 132.2, 134.6, 162.5, 166.3, 168.2, and 177.6. IR ν: 1770, 1705, 1610, and 1560 cm^{-1}. UV (MeOH) λ_{max}: 232.0 (ε 5600) and 329.8 nm (17000). MS m/z (%) 260 (M^+, 21), 73 (base), and 42 (78).

11c: Colorless crystals, mp 197 °C, 6.7 mg, 4%. Found: C, 64.80; H, 3.62%. Calcd for $C_{14}H_{10}O_5$: C, 65.11; H, 3.90%. ^{1}H NMR δ=3.97 (3H, s), 4.11 (3H, s), 6.08 (1H, s), 7.10 (1H, d, J=8.4 Hz), 7.19 (1H, d, J=7.3 Hz), and 7.41 (1H, dd, J=8.4, 7.3 Hz). ^{13}C NMR δ=52.5, 59.3, 96.1, 109.7, 116.8, 117.4, 118.1, 133.1, 134.2, 148.4, 155.5, 158.9, 164.5, and 174.8. IR ν: 1760, 1725, 1620, and 1540 cm^{-1}. UV (MeOH) λ_{max}: 209.8 (ε 30450), 245.6 (7100), 255.0 (7000), 264.6 (6400), 299.0 (10100), and 370.2 nm (10200). MS m/z (%) 258 (M^+, 52), 227 (base), 200 (43), 100 (48), and 74 (39).

References

1) Synthetic Photochemistry. XLIV. N. Kato, H. Takeshita, H. Kataoka, S. Ohbuchi, and S. Tanaka, *J. Chem. Soc., Perkin Trans. 1*, in press.

2) A. S. Kende and Z. Goldschmidt, *Tetrahedron Lett.*, **1970**, 783.

3) M. J. Goldstein and B. G. Odell, *J. Am. Chem. Soc.*, **89**, 6356 (1967).

4) Z. Goldschmidt and A. Worchel, *Tetrahedron Lett.*, **1973**, 3621.

5) Z. Goldschmidt and A. Worchel, *Tetrahedron Lett.*, **1973**, 3623.

6) G. R. Tian, S. Sugiyama, A. Mori, H. Takeshita, M. Higashi, and H. Yamaguchi, *Chem. Lett.*, **1988**, 941.

7) H. E. Zimmerman, *Acc. Chem. Res.*, **15**, 312 (1982).

Rechargeable Lithium Batteries Using Polypyrrole-Poly(styrenesulfonate) Composite as the Cathode-Active Material

Atsushi SHIMIZU,* Kazunori YAMATAKA, and Masashi KOHNO
Division of Chemicals Technology, Asahi Chemical Ind., Co., Ltd.,
Yakoh 1-3-2, Kawasaki-ku, Kawasaki, Kanagawa 210
(Received May 20, 1988)

Polypyrrole-polyelectrolyte composite, obtained by electrochemical polymerization on a vapor-grown carbon fiber (VGCF) electrode, was used as a cathode-active material for a rechargeable lithium battery. Poly(styrensulfonate) ion was suitable as a dopant in terms of rechargeability of the battery. The VGCF, which has a fibrous structure, was effective as a current collector for the polymer electrode. The content of the dopant calculated by the molar ratio of sulfur and nitrogen was ca. 30%. The open-circuit voltage was 3.55 V at the time. A charge-discharge, accompanied by an Li^+ deinsertion-insertion of the composite, was observed. The charge-discharge mechanism is similar to that of inorganic cathode-active materials that show Li^+ intercalation. The battery was cycled stably beyond 30 times between 3.66 and 1.50 V at a constant current of 0.889 mA cm^{-2}. An experimental capacity of 57 Ah kg^{-1} was obtained at the largest value on the basis of the weight of the active material. There is a possibility of developing a light-weight rechargeable battery using the polypyrrole-poly(styrenesulfonate) composite.

A conductive polymer can be used as a cathode-active material for a lithium rechargeable battery.[1-11] A capacity has been reported of more than 100 Ah kg^{-1}, based on the weight of the active material.[2-4,8] The discharge mechanism of a battery using a p-type conductive polymer is shown in Scheme 1. The following problem, however, must be considered for a practical use of the batteries. For instance, 1.0 g of polypyrrole, which has 0.47 g of ClO_4^- (30% doping), needs ca. 5.2 g of propylene carbonate at a minimum to dissolve ClO_4^- at 1.0 mol dm^{-3}. A lot of solvent, which is 5 to 10 times the weight of the active material, is usually necessary to assemble a p-type conductive polymer into a lithium battery. The total weight of the battery will inevitably be heavy, even if the cathode-active material is light. This problem might be solved if an n-type conductive polymer was used, since it could accept Li^+ as the dopant and the electrolyte is only a path for Li^+. The discharge mechanism of a battery using an n-type conductive polymer is shown in Scheme 2. The n-type conductive polymers, however, are usually unstable.[12]

A polypyrrole-polyelectrolyte (PPY-PE) composite that has a charge-discharge property accompanied by Li^+ deinsertion-insertion, despite a p-type conductive polymer, has recently been reported.[13-15] There is a possibility to construct a light-weight rechargeable lithium battery when a PPY-PE composite is used as the cathode-active material. The performance of such a battery (Li|$LiClO_4$|PPY-PE) has been investigated in this study.

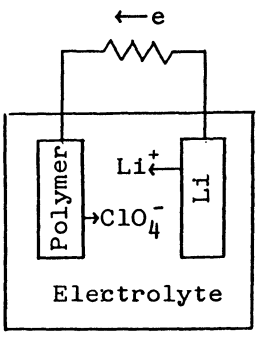

Scheme 1. Discharge mechanism of secondary battery using p-type polymer cathode.

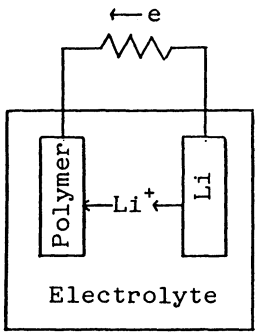

Scheme 2. Discharge mechanism of secondary battery using n-type polymer cathode.

Experimental

Preparation of Polymer Cathode of Rechargeable Batteries. The cathode consisted of a polypyrrole-polyelectrolyte (PPY-PE) composite and a current collector, which is a piece of vapor-grown carbon fiber (VGCF) electrode or a platinum plate. The PPY-PE was prepared by electrochemical polymerization on the current collector from an aqueous solution containing polyanion and pyrrole monomer with a constant-current system (PAB-1A, Kikusui). Reactions were carried out at a constant current density in a 30 ml cell having a VGCF electrode or a Pt electrode, with a working of 15 mm×15 mm, and titanium mesh as the cathode. Pyrrole monomer was dissolved at 6 wt% in 10 wt% of sodium poly(styrenesulfonate) (NaPSS) or sodium poly(ethylenesulfonate) (NaPES) solutions prepared from concentrated solutions of NaPSS or NaPES (Aldrich Chemical). All PPY-PE electrodes were dried in a vacuum oven at 80 °C for 2 h and weighed. All reaction conditions are summarized in Table 1.

Table 1. Conditions of Polymerization Reactions

Run No.	Polymer	Current collector/mg	Reaction conditions			Weight of polymer /mg
			Current/mA	Time/h	Temp/°C	
1	PPY-PSS	Pt plate	0.05—1.0V[a]	5 min	r.t.	—
2	PPY-PSS	Pt plate	10	ca. 2	r.t.	33.9
3	PPY-PSS	VGCF[b] 10.3	10	ca. 3	r.t.	60.8
4		VGCF 33.5				
5	PPY-PSS	VGCF 10.2	10	4	r.t.	79.6
6	PPY-PSS	VGCF 10.0	10	4	r.t.	75.9
7	PPY-PSS	VGCF 10.0	20	2	r.t.	81.3
8	PPY-PSS	VGCF 10.0	5	8	r.t.	76.2
9	PPY-PSS	VGCF 10.4	20	2	56	60.9
10	PPY-PSS	VGCF 10.0	20	2	15	75.9
11	PPY-PSS	VGCF 10.6	20	2	1	89.8
12	PPY-PSS	VGCF 9.6	20	2	−15	71.0
13	PPY-PES	VGCF 9.6	20	2	r.t.	71.1
14	PPY-PSS	VGCF 13.0	10	4	r.t.	76.0

a) Polymerization potential vs. Ag/AgCl. b) VGCF electrode was not shaped into a square.

The VGCF electrode was prepared as follows. 0.05 g of VGCF (Asahi Chemical), which was 0.05—0.1 μm in diameter and 50 μm in length, was suspended in 100 ml of methanol. The suspension was unfolded onto filter paper, which was 35 mm in diameter, through vacuum filtration. After drying, the VGCF felt was cut to a size of 15 mm×20 mm. A platinum plate terminal was bound to the edge of the VGCF felt with a conductive binding agent (Electrodug 504, Acheson Japan). The VGCF electrode was washed with methanol and then with water to become hydrophilic before the polymerization reaction.

The Formation of the Cells and Evaluation of the Batteries. All cells have a PPY-PE cathode, a lithium anode, and a lithium reference electrode. The lithium anode was made by squashing lithium wire on an SUS net. The anode and the cathode were set up at a clearance of 10 mm, and the tip of the reference electrode was set up between the two electrodes in a cylindrical cell. The solvent was propylene carbonate containing 1.0 mol dm^{-3} of $LiClO_4$. This propylene carbonate (exclusive grade for batteries, Mitsubishi Uka) was stored with Molecular Sieves (4Å) and then used. The support electrolyte was dried in a vacuum oven at 50 °C for one day. The amount of solution was 60 ml. Argon gas was filled into the cell, which was made a vacuum in advance. All cells were galvanostatically cycled between two preset voltage limits by a charge-discharge system (HJ-201B, Hokuto Denko). The upper limit was 3.6 or 3.7 V, and the lower limit was 1.5 V.

The Pressing Electrode. Dried PPY-PSS-VGCF electrode was soaked in 6% of a poly(tetrafluoroethylene) dispersion prepared by diluting a 60% dispersion (Polyflon D-2, Daikin), and it was dried for 2 h in a vacuum oven at 80 °C. This material, which was 1 mm thick, was pressed at 50 kg cm^{-2}, and a 0.5 mm thick electrode was obtained.

Results and Discussion

A cyclicvoltamogram of PPY-PSS film on Pt plate (Run 1) showed good reversibility of the redox reaction in an aqueous solution containing 1 mol dm^{-3} of $LiClO_4$, as shown in Fig. 1. A three-volt grade of rechargeable battery was expected in combination with a lithium anode. A cell using a PPY-PSS film

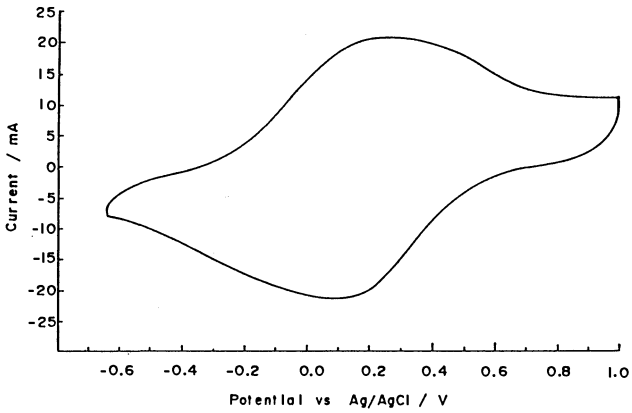

Fig. 1. Cyclic voltamogram of a PPY-PSS film on Pt plate (Run 1). Scan rate: 10 s V^{-1}. Counter electrode: Pt. Reference electrode: Ag/AgCl. Electrolyte: 1 mol dm^{-3} $LiClO_4$ in H_2O.

and a lithium anode was investigated in Run 2. Figure 2-A shows the charge-discharge cycles of this cell at a constant current of 1.0 mA (0.27 mA cm^{-2}). This cell initially showed a 2.80 V of open-circuit voltage, though the cell voltage decreased rapidly during discharge. The capacity was about 1 Ah kg^{-1}. The cause of this low performance was presumed to be the high internal resistance of the active material or the small amount of dopant in the active material. Elemental analysis showed that a SO_3 unit existed at a rate of 1/4—1/5 unit per polypyrrole unit. (Found: C, 55.7; H, 4.3; N, 8.2; S, 4.3%). If the charge had been able to be completely used, the capacity should have been 57 Ah kg^{-1}. It was presumed that an electrode having a fibrous structure, like VGCF felt, would reduce the resistance, since the dense morphology of PPY film probably caused the high Li^+ diffusion resistance.[13] The combination of PPY-PSS and VGCF in Run 3 improved the charge-discharge curve, as shown in Fig. 2-B, according to expectation. The cell had 3.55 V of open-circuit voltage and a flat charge-discharge curve.

The capacity was 42 Ah kg^{-1}, based on the polymer weight. The surface structure of PPY-PSS caused by VGCF surely improved the charge-discharge curve, since VGCF alone did not had a good charge-discharge curve as shown in Fig. 2-C (Run 4). Lithium insertion and deinsertion was confirmed as a result of an elemental analysis after 10 cycles of charge-discharge. (Charged state. Found: C, 58.4; H, 3.2; N, 8.9; S, 6.0; Li, 0.3%. Discharged state. Found: C, 57.0; H, 3.2; N, 8.3; S, 6.0; Li, 1.0%). An energy density of about 40 Ah kg^{-1} was calculated from the lithium content in the charged state. The experimental capacity was in good accordance with the calculated capacity. The cathode reaction is shown as follows:

$$(PPY)(PSS)^{-}\,Li^{+} \rightleftarrows (PPY)^{+}(PSS)^{-} + Li^{+} + e. \quad (1)$$

This mechanism is similar to that of inorganic cathode-active materials that show Li^{+} intercalation.[16,17] The mechanism is very important in terms of setting up a light-weight battery, since the solvent between two electrodes is only a path for lithium ions (Scheme 2) and does not have to exist in large quantities. The degradation of the inorganic active material is accelerated by an excessive discharge, since excessive lithium intercalation causes a destruction of the crystal structure of the active material.[18] The polymer material, which has the mechanism shown by Eq. 1, on the other hand, may have less degradation caused by an excessive discharge, since Li^{+} cannot insert beyond the limit determined by the content of the SO_3 unit.

The battery in Run 5 could be galvanostatically cycled stably over 30 times. The cycles were stopped due to considerable lithium dendrite. Figure 3-A shows the charge-discharge curve. The capacities were about 40 Ah kg^{-1} (including VGCF weight), and the coulombic efficiencies were 100% in each cycle, as shown in Fig. 4. A quick charge seemed possible, since the cell showed a very low overpotential of 0.1 V at the end of the charge. A low overpotential is an important performance factor for practical rechargeable batteries, since it restrains the degradation of both the electrolyte and active material. When the cell was charged under 4 mA (1.78 mA cm^{-2}) in Run 5, it was also cycled stably with 100% coulombic efficiencies and with 42 Ah kg^{-1} of capacity, as shown in Fig. 3-B. The capacities were almost constant under various different discharge currents in Run 6. The results are shown in Fig. 5. The highest capacity was 57 Ah kg^{-1} under 1.0 mA (0.44

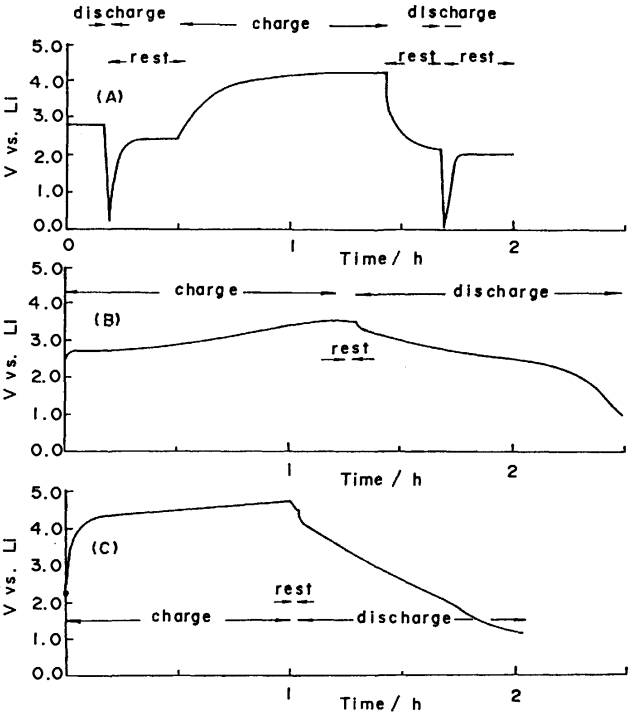

Fig. 2. Charge-discharge curves.
A: PPY-PSS film on Pt, current=1 mA, polymer weight =33.9 mg. B: PPY-PSS-VGCF, current=2 mA, polymer weight=60.8 mg, VGCF weight=10.3 mg. C: VGCF, current=2 mA, VGCF weight=33.5 mg.

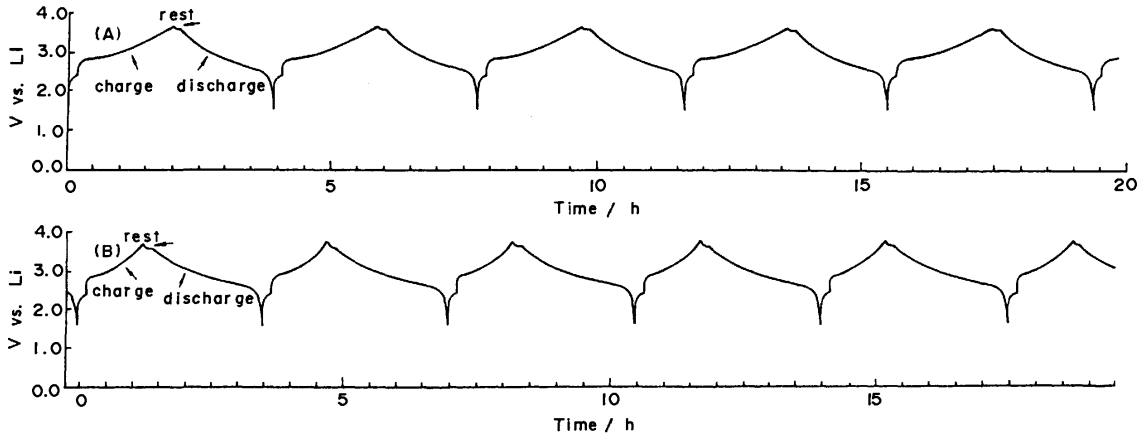

Fig. 3. Charge-discharge cycles.
A: upper limit voltage=3.6 V, lower limit voltage=1.5 V, charge current=2 mA, discharge current=2 mA. B: upper limit voltage=3.7 V. lower limit voltage=1.5 V, charge current=4 mA, discharge current=2 mA.

mA cm^{-2}) of discharge.

The polymerization current of PPY-PSS affected such performances of the cell as the initial cell voltage (just after setting up the cell), the capacity of the cell, the weight of the polymer, and the overpotential at the end of the charge. All results of Runs 6, 7, and 8 are summarized in Fig. 6. The polymerization and oxidation reaction proceeds as follows:

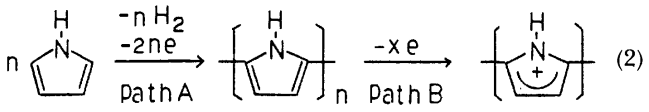

(2)

A large oxidation current probably encouraged path A oxidation, followed by a lack of the charged polymer by path B, from the fact that a large oxidation current caused a lower initial cell voltage just after setting up the cell, as well as a large amount of polymer. A small oxidation current probably made the dense structure of polymer followed by the large diffusion resistance of lithium ions, from the fact that a small oxidation current caused a high overpotential, and a small amount of polymer. The medium-range (10 mA) oxidation reaction probably resulted in the largest capacity of the cell, as a result of these facts.

The effects of temperature at polymerization on the capacities of cells were investigated in Runs 9—12. The charge-discharge properties of these cells are shown in Fig. 7. Polymerization at room temperature afforded the largest capacity.

How are the weight increase and volume increase of PPY-PE, itself, compared with polypyrrole such an incorporating monomer dopant as ClO_4^- ? When polypyrrole is doped with the poly(styrenesulfonate) ion, the poly(ethylenesulfonate) ion, and ClO_4^- at ca. 33.3%, unit structures per one electron are exhibited as follows:

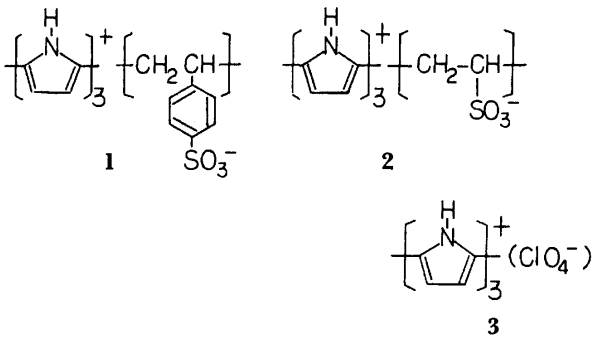

The molecular weights of these units are 378, 302, 294.5, respectively. Although a light-weight unit is

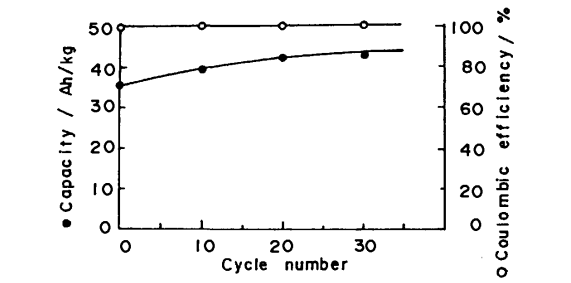

Fig. 4. Capacity vs. cycle number and coulombic efficiency vs. cycle number.

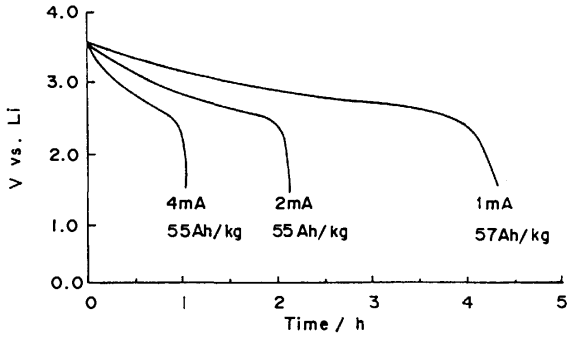

Fig. 5. Discharge curves under 4, 2, and 1 mA discharge current. Capacity were calculated based on PPY-PSS weight.

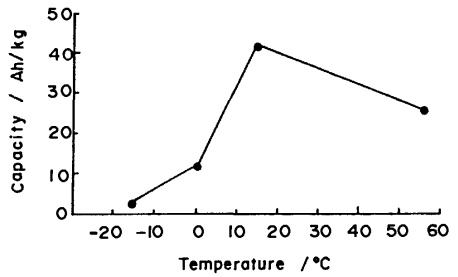

Fig. 7. Effect of polymerization temperature on capacity.

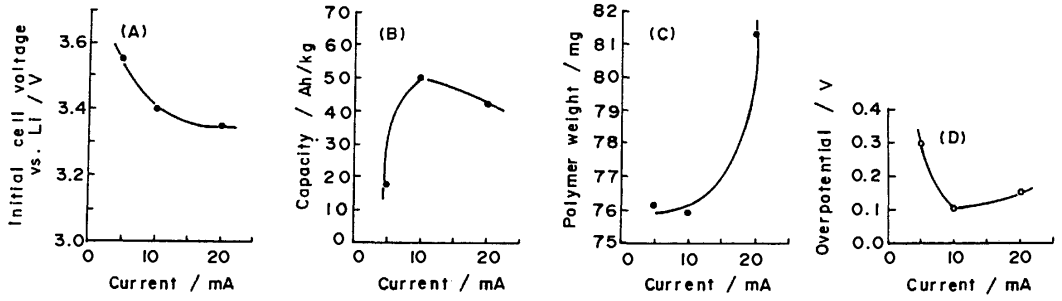

Fig. 6. Polymerization current effects on initial cell voltage, capacity, polymer weight, and overpotential.

desirable for a light-weight battery, a 28% weight excess of unit **1**, compared with unit **3**, is allowable, since the total weight of the battery is not determined only by the cathode active material. The volume of polypyrrole varies with the dopant, and it is not always in direct proportion to the dopant size. It was reported that polypyrrole film incorporating PSS^- had about half the thickness of polypyrrole film incorporating ClO_4^-.[15] This is a suitable performance factor for a compact battery.

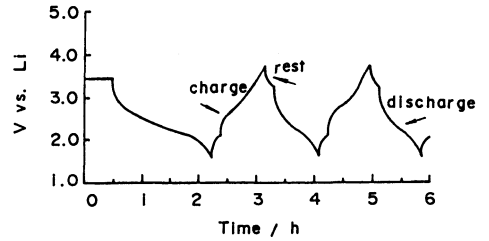

Fig. 8. Charge-discharge curve of PPY-PSS-VGCF cell. Charge current=2 mA. Discharge current=2 mA.

If poly(ethylenesulfonate) ions (**2**) had been capable of being used as a dopant, a very light, active material could have been obtained. However, the performance of the cell using poly(ethylenesulfonate) ions in Run 13 was not very good. Figure 8 shows the charge-discharge curve of the battery. The initial capacity was relatively large (43 Ah kg^{-1}), but the capacity could not be repeated by charging up to 3.7 V.

A pressed cathode was investigated in Run 14, since the capacity of a battery per unit volume is an important performance factor of a battery, as well as the capacity per unit weight. The result of the charge-discharge property is shown in Fig. 9. This approach was useful since the capacity rose to 40 Ah l^{-1} form 20 Ah l^{-1}. On the other hand, an overpotential at the end of the charge increased and the flatness of the curve became reduced. There is room for an improvement in the pressing technique, such as the kinds of binder and the intensities of pressure.

Figures 10-A,B,C, and D are SEM photographs of

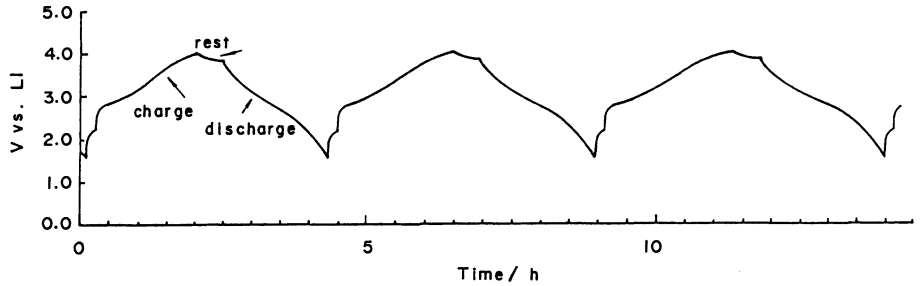

Fig. 9. Charge-discharge curve of pressed electrode. Charge current=2 mA. Discharge current=2 mA.

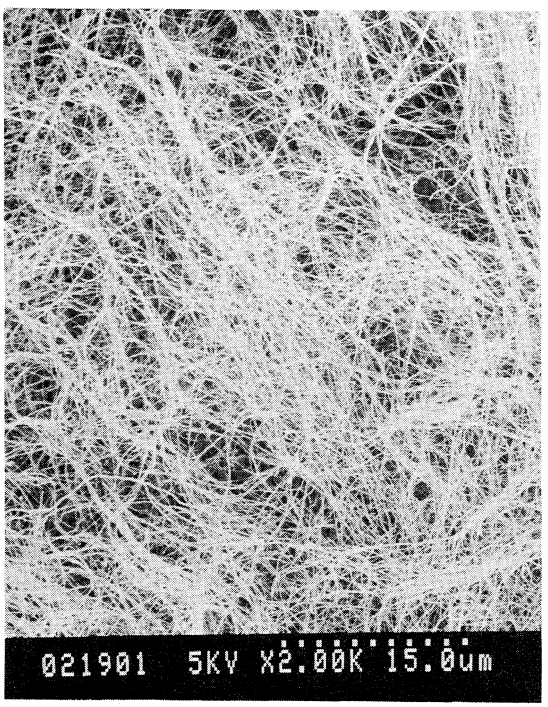

(A)

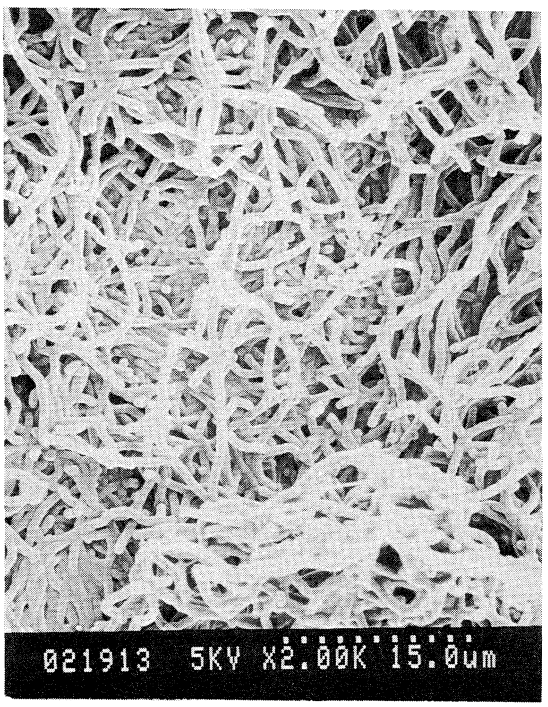

(B)

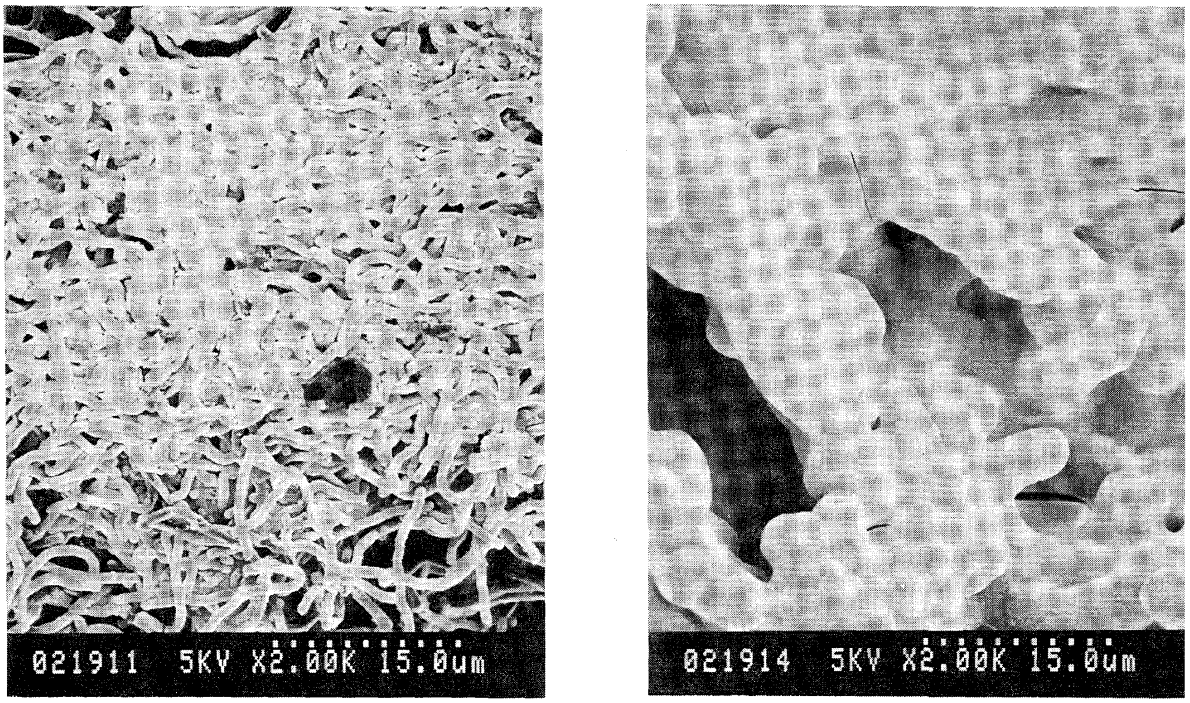

(C) (D)

Fig. 10. SEM photographs of the cathode.
A: VGCF, B: PPY-PSS-VGCF, C: PPY-PSS-VGCF, D: pressed PPY-PSS-VGCF.

the VGCF electrode and the PPY-PSS-VGCF electrode. Samples of the PPY-PSS-VGCF composite maintained a fibrous structure as well as the VGCF current collector. This structure must have encouraged the good charge-discharge property, compared with the PPY-PSS film. There were many fibrils of different diameters. Some were about 0.5 μm (Fig. 10-B), but some were about 5 μm (Fig. 10-D). The samples after pressing were slightly crushed and some fibrils were broken (Fig. 10-C). The lower charge-discharge property compared with the non-pressed sample may be due to this structure.

We conclude that the PPY-PSS-VGCF having a lithium insertion-deinsertion mechanism can be used for a light-weight secondary battery, and that the fibrous structure of PPY-PPS-VGCF is essential for a good performance of the battery. This polymer battery is characterized by a low overpotential at the end of the charge, a stable capacity independent of the charge-discharge current, and a 100% coulombic capacity. These are desirable for a practical secondary battery.

References

1) H. Münstedt, G. Köhler, H. Möhwald, D. Naegel, R. Bitthin, G. Ely, and E. Meissner, *Synthetic Metals*, **18**, 259 (1987).

2) K. Okabayashi, F. Goto, K. Abe, and T. Yoshida, *Synthesic Metals*, **18**, 365 (1987).

3) A. G. MacDiarmid, L. S. Yang, W. S. Huang, and B. D. Humphrey, *Synthetic Metals*, **18**, 393 (1987).

4) L. W. Shacklette, M. Maxfield, S. Gould, J. F. Wolf, T. R. Jow, and R. H. Baughman, *Synthetic Metals*, **18**, 611 (1987).

5) Y. Kobayashi, T. Shishikura, H. Nakamura, H. Konuma, and K. Fugita, *Synthetic Metals*, **18**, 619 (1987).

6) A. Corradini, M. Mastragostino, A. S. Panero, P. Prosperi, and B. Scrosati, *Synthetic Metals*, **18**, 625 (1987).

7) E. M. Genies, M. Lapkowski, C. Santier, and E. Vieil, *Synthetic Metals*, **18**, 631 (1987).

8) F. Passiniemi and J.-E. Österholm, *Synthetic Metals*, **18**, 637 (1987).

9) S. Yata, Y. Hato, K. Sakurai, T. Osaki, K. Tanaka, and T. Yamabe, *Synthetic Metals*, **18**, 645 (1987).

10) T. Nagatomo, C. Ichikawa, and O. Omoto, *Synthetic Metals*, **18**, 649 (1987).

11) P. J. Nigrey, D. MacInnes Jr., D. P. Nairns, A. G. MacDiarmid, and A. J. Heeger, *J. Electrochem. Soc.*, **128**, 1651 (1981).

12) K. Ishida and T. Tanaka, *Mol*, **1986**, 21.

13) T. Iyoda, A. Ohtani, T. Shimidzu, and K. Honda, *Chem. Lett.*, **1986**, 687.

14) D. T. Glatzhofer, J. Ulański, and G. Wegner, *Polymer*, **28**, 449 (1987).

15) L. F. Warren and D. P. Anderson, *J. Electrochem. Soc.*, **134**, 101, (1987).

16) M. Pasquali, G. Pistoia, V. Manev, and R. V. Moshtev, *J. Electrochem. Soc.*, **133**, 2454 (1986).

17) *Nikkei New Material*, **1986**, 33.

18) S. Yoshizawa, "Denchi," Kohdansha, Tokyo (1982), p. 153.

Kinetics of the Oxidation of [*N*-(2-Hydroxyethyl)ethylenediamine-*N*,*N*′,*N*′-triacetato]chromium(III) by Periodate

Ahmed A. ABDEL-KHALEK* and Mahmoud M. ELSEMONGY†
Chemistry Department, Faculty of Science, Cairo University, Beni-Suef City, Egypt
†Chemistry Department, Faculty of Education, Umm Al-Qura University, Al-Taif City, Shihar, Saudi Arabia
(Received November 19, 1987)

The kinetics of oxidation of $[Cr^{III}(H_2O)(TOH)]$, (TOH=*N*-(2-hydroxyethyl)ethylenediamine-*N*,*N*′,*N*′-triacetate) by periodate in aqueous solutions has been found to obey the following equation

$$\text{Rate} = \frac{k_2 K_6 [Cr^{III}]_T [I^{VII}]_T}{1 + [H^+]/K_5 + K_6 [I^{VII}]_T}$$

where k_2 is the rate constant for the electron-transfer process, K_5 is the equilibrium constant for dissociation of $[Cr^{III}(H_2O)(TOH)]$ to $[Cr^{III}(OH)(TOH)]^- + H^+$ and K_6 is the pre-equilibrium formation constant. The activation parameters are reported. It is proposed that electron transfer proceeds via an innersphere mechanism with the hydroxo ligand of the chromium(III) complex bridging the two reactants.

Metal complexes, which are relatively easily oxidized by IO_4^- in aqueous solution, seem to fall into one of two classes: (i) labile complexes[1-6] or (ii) inert complexes that can offer a bridging ligand.[7,8] The mechanism of oxidation of the labile complexes is believed to be of the innersphere type, and in several cases direct evidence in support of this mechanism has been presented.[2-6] Substitution into the inner coordination sphere of the IO_4^- ion, which is labile, is likely.[9] In case of oxidation of $[Cr^{III}(edta)(H_2O)]$ by periodate,[6] it was proposed that the oxidation may proceed via one- or two-electron transfer giving Cr(IV) or Cr(V), respectively, in the rate-determining step, followed by a fast step leading to Cr(VI). An innersphere process is also believed to be operating in the oxidation of inert complexes.[7,8] The unusual second-order dependence on $[Cr(H_2O)_6]^{3+}$ in the chromium(III)-periodate reaction seems to support an innersphere mechanism.[7] The two electron transfer step proposed for this reaction requires this mechanism,[10] where the hydroxo form, $[CrOH]^{2+}$, was considered to be the reactive chromium(III) species.

In particular we have chosen the edta analogues in that it can be supported that some properties of the respective complexes are influenced by the position and number of the functional groups. In this study the kinetics of oxidation of $[Cr^{III}(H_2O)(TOH)]$, where TOH is *N*-(2-hydroxyethyl)ethylenediaminetriacetate, is reported.

Experimental

Reagents. Reagent grade *N*-(2-hydroxyethyl)ethylenediamine-*N*,*N*′,*N*′-triacetic acid, sodium periodate, chromium(III) nitrate hexahydrate, sodium dihydrogenphosphate, sodium hydroxide, and sodium nitrate were used without further purification. Solution of $[Cr^{III}(H_2O)(TOH)]$ was prepared by the method of Wharton and Sykes.[11] Molar absorption coefficients of this complex were calculated on the basis of the chromium concentration which was determined spectrophotometrically as chromate.[12] At the range of pH 6.1—7.3 the species found in the solution have $\varepsilon_{394}=104$ and $\varepsilon_{575}=133$ M^{-1} cm^{-1} (M=mol dm^{-3}) as reported for $[Cr^{III}(OH)(TOH)]^-$.[11] A stock solution of periodate was made up by weight and wrapped with Al foil to avoid photochemical decomposition.[13] Sodium dihydrogenphosphate, sodium hydroxide, and sodium nitrate solutions were made up by weight. Buffer solutions were made up from sodium dihydrogenphosphate-sodium hydroxide mixtures.

Kinetic Measurements. A Unicam SP8000 spectrophotometer, equipped with a thermostated cell holder, was used to monitor the reaction. The reactants in buffer solutions in the two compartments of an intended flask, were thermostated for about 20 minutes. These were thoroughly mixed and quickly transferred to an absorption cell. The formation of the chromium(VI) was followed at a wavelength in the 350—372 nm range where the absorption is maximal at the pH of the reaction. Pseudo-first order conditions were maintained in all runs by using a large excess of periodate concentrations (more than 10-fold) over those of $[Cr^{III}(H_2O)(TOH)]$. The pH of the reaction was measured on a Radiometer digital pH meter model PHM62. The ionic strength was maintained constant by using the appropriate amounts of sodium nitrate solution.

Results and Discussion

The stoichiometry of the $[Cr^{III}(H_2O)(TOH)]$-IO_4^- reaction can be represented by Eq. 1

$$2\,Cr^{III} + 3\,I^{VII} \rightarrow 2\,Cr^{VI} + 3\,IO_3^- \quad (1)$$

where Cr^{III} and I^{VII} represent total chromium(III) and periodate, respectively. The concentration ratio of IO_4^- initially present to Cr^{VI} produced was found to be 1.50±0.04. The stoichiometry is also consistent with the observation that IO_3^- does not oxidize the chromium(III) complex over the pH range where the kinetics was investigated.

At all the chromium(III) complex concentrations used, in presence of vast excess of periodate, plots of $\ln(A_\infty - A_t)$ vs. time, where A_∞ and A_t are the absorbances at infinity and time t, respectively, were linear up to 85% of the reaction. The pseudo-first order rate con-

Table 1. Dependence of the $Cr^{III}(H_2O)(TOH)/IO_4^-$ Reaction Rate on $[Cr^{III}(H_2O)(TOH)]$, $[IO_4^-]$ at pH=7.30 and I=0.5 M,[a] at Different Temperatures

T	$10^2[IO_4^-]$	10^4k_{obs}
°C	M	s^{-1}
20	0.2	8.05±0.12
20	0.3	10.00±0.20
20	0.5	11.60±0.25
20	1.0	12.80±0.31
20	2.0	13.90±0.40
25	0.5	20.80±0.60
25	1.0	24.20±0.70
25	2.0	26.30±0.83
25	2.0	26.40±0.75[b]
25	2.0	26.25±0.80[c]
25	2.0	26.37±0.77[d]
25	3.0	27.02±0.79
25	4.0	27.39±0.85
25	5.0	27.77±0.80
30	0.2	20.80±0.64
30	0.3	25.00±0.81
30	0.5	29.40±0.90
30	1.0	36.60±1.20
30	2.0	40.50±1.34
35	0.5	42.60±1.28
35	1.0	52.60±1.40
35	2.0	60.61±1.43
35	3.0	65.32±1.50
35	5.0	66.70±1.49

a) Unless otherwise stated $[Cr^{III}(H_2O)(TOH)]=1.0\times10^{-4}$ M. For b), c), and d), $[Cr^{III}(H_2O)(TOH)]$ was 2.0×10^{-5} M, 5×10^{-5} M, and 2.0×10^{-4} M respectively.

stant, k_{obs}, was calculated from the slopes of these plots by using a linear least-squares program.

The constancy of k_{obs}, over the complex concentration range $(5.0—20.0)\times10^{-4}$ M under the fixed experimental conditions, shown in Table 1, is in agreement with a first-order dependence on its concentration.

The variation of k_{obs} with periodate concentration, Table 1, exhibits rate saturation at high periodate. Plots of $1/k_{obs}$ versus $1/[IO_4^-]$ were found to be linear with a definite intercept as shown in Fig. 1. The dependence of k_{obs} on periodate concentration is thus described by

$$k_{obs} = \frac{a[IO_4^-]}{1+b[IO_4^-]} \quad (2)$$

or

$$1/k_{obs} = \frac{1}{a[IO_4^-]} + \frac{b}{a}. \quad (3)$$

The values of a and b were obtained from the slope and the intercept as (1.52±0.6) M^{-1} s^{-1} and (529±15) M^{-1}, respectively at 25 °C and pH=7.30.

The effect of hydrogen-ion concentration on the reaction rate was investigated over the pH range 6.10—7.30. Table 2 shows that the rate of reaction increases with increasing pH value.

Table 2. Effect of pH on k_{obs} (s^{-1}) at $[Cr^{III}(H_2O)(TOH)]=1.0\times10^{-4}$ M, I=0.5 M, and T=25 °C

$10^2[IO_4^-]$	$10^4k_{obs}/s^{-1}$			
M	pH=7.30	pH=6.91	pH=6.56	pH=6.10
0.5	20.80±0.60	19.23±0.50	16.95±0.31	12.61±0.60
1.0	24.20±0.70	22.98±0.61	21.74±0.42	17.40±0.56
2.0	26.30±0.83	25.77±0.55	24.39±0.52	21.73±0.47
3.0	27.02±0.77	26.81±0.66	25.64±0.60	24.11±0.63
5.0	27.77±0.80	27.25±0.75	26.67±0.81	25.60±0.71

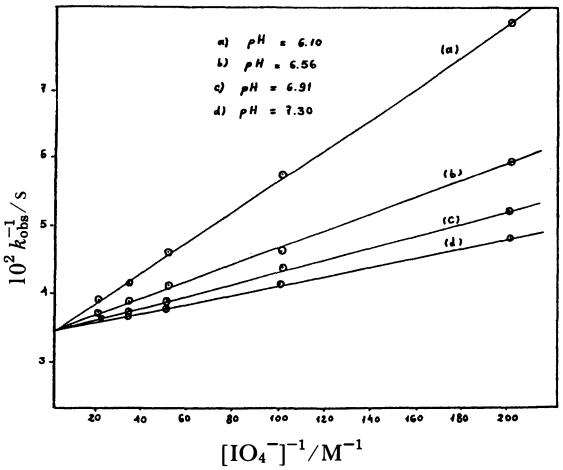

Fig. 1. Plots of k_{obs}^{-1} against $[IO_4^-]^{-1}$.

Bustin and Earley[14] reported that $[Cr^{III}(H_2O)(TOH)]$ undergoes the following equilibria

$$[Cr^{III}(H_2O)(TOH)] \rightleftarrows [Cr^{III}(OH)(TOH)]^- + H^+; K_1 \quad (4)$$

$$[Cr^{III}(OH)(TOH)]^- \rightleftarrows [Cr^{III}(OH)(TO)]^{2-} + H^+; K_2 \quad (5)$$

with K_1 and K_2 having values of 3.63×10^{-7} M and 1.58×10^{-10} M, respectively at 25 °C and I=0.1 M. It is clear from the value of K_2 that $[Cr^{III}(OH)(TO)]^{2-}$ was not present at the employed pH values at the present study. The species present at low pH has the ligand bound in a quinquedentate manner, with the 2-hydroxyethyl group uncoordinated.[14] The absence of an acid dissociation constant at pK_a ca. 3 precludes the presence of any uncomplexed-COO^- groups.[14]

From the reported equilibrium constants of aqueous periodate solutions, it may be concluded that, over the H^+ range used in this study, the periodate species likely to be present are IO_4^-, $H_4IO_6^-$, and $H_3IO_6^{2-}$ [15] which are in the equilibria

$$H_4IO_6^- \rightleftarrows H_3IO_6^{2-} + H^+; K_3 = 5\times10^{-6} \quad (6)$$

$$H_4IO_6^- \rightleftarrows IO_4^- + 2H_2O; K_4 = 40. \quad (7)$$

It is clear from the value of K_4 that IO_4^- is not predominant species (I^{VII} will be used to represent $H_4IO_6^-$ and $H_3IO_6^-$).

The experimental rate equation suggests that a fast equilibrium step precedes the slow intramolecular electron transfer step. A possible mechanism is described by Eqs. 8—12.

$$[Cr^{III}(H_2O)(TOH)] \rightleftarrows [Cr^{III}(OH)(TOH)]^- + H^+; K_5 \quad (8)$$

$$[Cr^{III}(OH)(TOH)]^- + I^{VII} \rightleftarrows [(TOH)Cr^{III}(OH)\text{-}I^{VII}]^-; K_6 \quad (9)$$

$$[(TOH)Cr^{III}(OH)\text{-}I^{VII}]^- \xrightarrow{k_2} Cr^V + IO_3^- + TOH^{3-} \quad (10)$$

$$Cr^V + I^{VII} \xrightarrow{fast} CrO_4^{2-} + I^{VI} \quad (11)$$

$$2\,I^{VI} \xrightarrow{fast} I^{VII} + IO_3^- \quad (12)$$

From the above mechanism, rate of the reaction is given by

$$\begin{aligned} \text{rate} &= k_2[(TOH)Cr^{III}(OH)\text{-}I^{VII}] \\ &= k_2K_6[Cr^{III}(OH)(TOH)^-][I^{VII}]. \end{aligned} \quad (13)$$

If $[Cr^{III}]_T$ represent the total concentrations of Cr^{III} species, then

$$\begin{aligned} [Cr^{III}]_T &= [Cr^{III}(OH)(TOH)^-][H^+]/K_5 \\ &+ [Cr^{III}(OH)(TOH)^-] + K_6[Cr^{III}(OH)(TOH)^-][I^{VII}]. \end{aligned} \quad (14)$$

Substitution for $[Cr^{III}(OH)(TOH)^-]$ from Eq. 14 into Eq. 13, gives

$$\text{rate} = k_2K_6[Cr^{III}]_T[I^{VII}]_T/1 + ([H^+]/K_5) + K_6[I^{VII}]_T \quad (15)$$

and

$$k_{obs} = k_2K_6[I^{VII}]_T/1 + ([H^+]/K_5) + K_6[I^{VII}]_T \quad (16)$$

which on rearrangement, gives

$$1/k_{obs} = K_5 + [H^+]/k_2K_5K_6[I^{VII}]_T + 1/k_2. \quad (17)$$

At constant $[H^+]$ Eq. 18 follows, in which A is a constant

$$1/k_{obs} = A/k_2K_5K_6[I^{VII}]_T + 1/k_2 \quad (18)$$

which is identical to the experimental results shown in Eq. 3, where $a = k_2K_5K_6/A$ and $b = K_5K_6/A$.

Values of k_2 and K_6, at the temperature used, calculated from these relationships, by substitution $K_5 = 3.63\times10^{-7}$ M, are listed in Table 3. The activation parameters obtained from a least-squares' fit to the transition state theory equation are $\Delta H^{\ddagger}_2 = 76.0\pm2.1$ kJ mol^{-1} and $\Delta S^{\ddagger}_2 = -38.7\pm7.1$ J K^{-1} mol^{-1}. The enthalpy of the pre-equilibrium reaction $\Delta H^{\circ}_6 = -32.1\pm1.7$ kJ mol^{-1} is obtained from the temperature variation of K_6. Negative $\Delta S^{\ddagger}$ for the redox reactions between reactants with charges of the same sign were claimed to be largely the result of the charge concentration on encounter complex formation, which causes substantial mutual ordering of the solvated water molecules.[16] Value of $\Delta H^{\ddagger}_6$ indicates that the formation of the precursor complex $[(TOH)Cr^{III}(OH)\text{-}I^{VII}]^-$, is an exothermic process as found in the reaction between $[Co^{II}(edta)^{2-}]$ and IO_4^-.[3] The intramolecular electron transfer step, is endothermic as indicated by the value of $\Delta H^{\ddagger}_2$.

Table 3. Values of k_2 and K_6 at Different Temperatures

T/°C	10^3k_2/s^{-1}	K_6/M^{-1}
20	1.50	751
25	2.95	596
30	4.31	503
35	7.30	414

The contributions of $\Delta H^{\ddagger}$ and $\Delta S^{\ddagger}$ to the rate constant seem to compensate each other. This fact suggests that the factors controlling $\Delta H^{\ddagger}$ must be closely related to those controlling $\Delta S^{\ddagger}$. Therefore, the solvation state of the encounter complex would be important in determining $\Delta H^{\ddagger}$.[16] Thus, the relatively small enthalpy of activation, $\Delta H^{\ddagger}_2$, can be explained in terms of the formation of more solvated complex $[(TOH)\text{-}Cr^{III}(OH)\text{-}I^{VII}]^-$.[17]

From Eq. 17 and Fig. 1, it follows that slopes of the plots can be represented by Eq. 19.

$$\text{slope} = [H^+]/k_2K_5K_6 + 1/k_2K_6 \quad (19)$$

It is obvious, from Eq. 19 that the slope is dependent on $[H^+]$. This plot is shown in Fig. 2 which indicates the validity of our proposed mechanism. Value of K_5 was calculated from Fig. 2, to be 2.70×10^{-7} M. This value is in good agreement with the reported[14] value of $K_5 = 3.63\times10^{-7}$ M at 25 °C. The equilibrium constant K_6 obtained from Eq. 19 and Fig. 2 is 571 M^{-1} which is in a good agreement ($K_6 = 596$ M^{-1}) with that obtained from Eq. 18 and Fig. 1 at 25 °C.

An innersphere mechanism is proposed for the oxidation of $[Cr^{III}(H_2O)(TOH)]^-$ by IO_4^- in which the $[Cr^{III}(OH)(TOH)]^-$ is bridged to IO_4^- through the hydroxo ligand because hydroxide on $[Cr^{III}(OH)\text{-}(TOH)]^-$ is a better bridging ligand than H_2O on $[Cr^{III}(H_2O)(TOH)]$. The assignment of an innersphere mechanism through the hydroxo bridge for this reaction seems to be supported by the following reasons: (i) Periodate ion is capable of acting as a ligand as evidenced from its coordination to copper(III)[18] and nickel(IV).[19] (ii) The hydroxo ligand is a firm ligand bridge. (iii) No reaction was observed at pH below 6.0 where the hydroxo species is not present. (iv) The inverse dependence of $[H^+]$ is usually ascribed to oxidation of the hydroxy species offering a very effective OH bridge in an innersphere process.[20]

The oxidation of $[Cr^{III}(H_2O)(TOH)]$ by IO_4^- may proceed via one- or two-electron transfer giving Cr^{IV} or

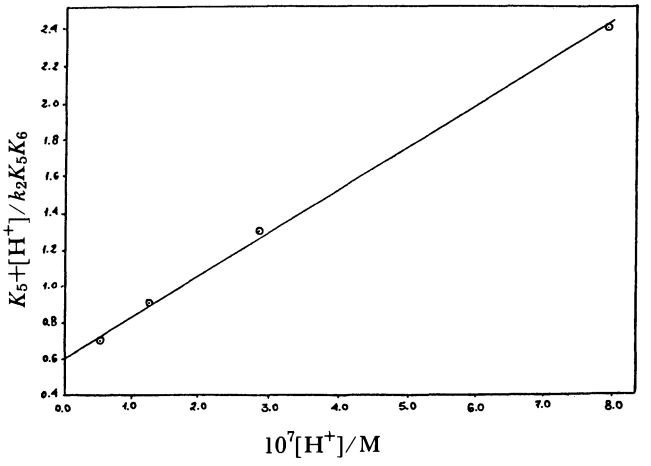

Fig. 2. Plots of $K_5+[H^+]/k_2K_5K_6$ vs. $[H^+]$.

Cr^{V}, respectively in the rate determining step. These may then followed by a fast step leading to Cr^{VI}. The fact that acrylonitrile was not polymerized seems to support two-electron transfer process.

In comparison with oxidation of $[Cr^{III}(edta)(H_2O)]$,[7] under the same conditions, the both hydroxy complexes, $[Cr^{III}(edta)(OH)]^{2-}$ and $[Cr^{III}(OH)(TOH)]^{-}$, are significantly more reactive than their conjugate acids. Value of k_2K_6 (k_2 is the intramolecular transfer rate constant and K_6 is the pre-equilibrium formation constant), for the oxidation of $[Cr^{III}(H_2O)(TOH)]$, is equal to 1.74 at 25 °C. This value is very close to the value of $k^{et}K_4$ (1.81±0.18) for the oxidation of $[Cr^{III}(edta)(H_2O)]$, where $k^{et}K_4$ corresponds to k_2K_6. It would be more informative to compare the intramolecular electron transfer rate constants. However, this is not possible because the value of k^{et} for the edta complex is not known.

It is a great pleasure to acknowledge Prof. Y. Sulfab, Chemistry Department, Faculty of Science, Kuwait University, for his useful ideas.

References

1) Y. Sulfab and A. I. Abu-Shadi, *Inorg. Chim. Acta*, **21**, 115 (1977).
2) A. Y. Kasim and Y. Sulfab, *Inorg. Chim. Acta*, **24**, 247 (1977).
3) F. R. El-Eziri and Y. Sulfab, *Inorg. Chim. Acta*, **25**, 15 (1977).
4) A. A. Abdel-Khalek and Y. Sulfab, *J. Inorg. Nucl. Chem.*, **43**, 3257 (1981).
5) M. A. Hussein, A. A. Abdel-Khalek, and Y. Sulfab, *J. Chem. Soc., Dalton Trans.*, **1983**, 317.
6) N. A. Al-Jallal and Y. Sulfab, *Transition Met. Chem.*, **8**, 51 (1983).
7) A. Y. Kasim and Y. Sulfab, *Inorg. Chem.*, **20**, 506 (1981).
8) P. Guardado, A. Maestra, and M. Baton, *J. Inorg. Nucl. Chem.*, **43**, 1392 (1981).
9) I. Pechet and Z. Luz, *J. Am. Chem. Soc.*, **87**, 4086 (1965).
10) R. Buchacek and G. Gordon, *Inorg. Chem.*, **11**, 2154 (1972).
11) R. K. Wharton and A. G. Sykes, *J. Chem. Soc., Dalton Trans.*, **1972**, 2404.
12) G. W. Haupt, *J. Res. Natl. Bur. Stand. (U.S.)*, **48**, 414 (1952).
13) M. C. R. Symon, *J. Chem. Soc.*, **1955**, 2794.
14) D. I. Bustin and J. E. Earley, *J. Am. Chem. Soc.*, **89**, 1818 (1967).
15) S. H. Laurie, J. M. Williams and C. J. Nyman, *J. Phys. Chem.*, **68**, 1311 (1964).
16) M. J. Weaver and E. L. Yee, *Inorg. Chem.*, **19**, 1936 (1980).
17) Y. Sasaki and R. Kawamura, *Bull. Chem. Soc. Jpn.*, **54**, 3379 (1981).
18) I. Hadinec, L. Jensovsky, A. Linek, and V. Synecek, *Naturwiss*, **47**, 377 (1960).
19) P. Ray, *Inorg. Synth.*, **5**, 201 (1957).
20) R. G. Wilkins, "The Study of Kinetics and Mechanism of Reactions of Transition Metal Complexes," Allyn & Bacon, Boston (1970), p. 262.

 © 1988 The Chemical Society of Japan Bull. Chem. Soc. Jpn., 61, 4411—4416 (1988)

Efficiency of Azodyes in Retarding the Dissolution of Aluminium in Hydrochloric Acid

Abd El-Aziz El-Sayed FOUDA,*,† Hamed ABU-EL-NADER, Mahmoud Nor El-Din MOUSSA, and Ibrahim SHEHATA
Chemistry Department, Faculty of Science, Mansoura University, Mansoura, Egypt
(Received December 11, 1987)

The inhibition of the corrosion of aluminium in hydrochloric acid solution by some 4-(*m*-Substituted phenylazo)pyrazoles has been studied by three different techniques. The inhibitor efficiency calculated from the three techniques are in good agreement. The corrosion rate is a function of temperature, concentration, and nature of the inhibitor. The inhibitors appear to function through general adsorption following the Langmuir adsorption isotherm. Thermodynamic parameters for adsorption of inhibitors have been calculated and discussed.

The industrial importance of corrosion inhibitors is widespread, ranging from pickling to water-cooled systems. The selection of inhibitor for a given system depends on the corrosive medium, the nature of the metal, the magnitude of the charge at the metal-solution interface, and the cathodic reaction.[1] The study of adsorption of organic compounds at electrode-electrolyte interfaces is a subject with pronounced practical significance in view of its relevance to electrochemical energy conversion, electro-organic synthesis, and corrosion inhibition. The latter is most popular since such compounds effectively inhibit the corrosion process even when present in trace amounts.[2] It is known that inhibitor efficiency depends on the mode of adsorption of inhibitor molecule, electron density at the electroactive center[3] and the state of the surface.[4]

Aluminium is extensively used in various industrial operations and the study of its corrosion inhibition is of great importance. Oxygen- and nitrogen-containing organic compounds have been tried as corrosion inhibitors for metals.[2,5-7]

The aim of this article is to throw some light on the mechanism of inhibition of these bulky molecules on the corrosion of aluminium in hydrochloric acid.

4-Phenylazo-1-phenyl-3-methyl-5-chloropyrazole (**1**)

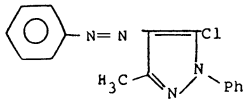

4-(*m*-Tolylazo)-1-phenyl-3-methyl-5-chloropyrazole (**2**)

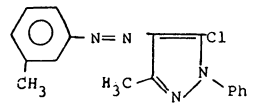

4-(*m*-Chlorophenylazo)-1-phenyl-3-methyl-5-chloropyrazole (**3**)

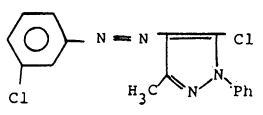

† Present address: Chemistry Department, Faculty of Science, Qatar University, Qatar-DOHA, P.O. Box 2713.

4-(*m*-Methoxyphenylazo)-1-phenyl-3-methyl-5-chloropyrazole (**4**).

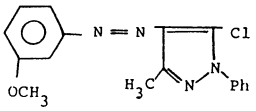

Experimental

Thermometric Method. Chemicals used were of analytical grade and were used without further purifications. The solutions were made from freshly prepared twice distilled water. The procedure for the determination of metal dissolution rate by the thermometric method has been described previously,[8] the reaction tube being placed inside a vacuum flask to minimize heat losses. Aluminium strips measuring 100×10×1 mm were lightly abroaded with 2/0 and 3/0 emery paper, then degreased with alkaline solution ((15 g Na_2CO_3+ 15 g Na_3PO_4)·l^{-1}) and washed with running twice distilled water. The specimens were then dried between two filter papers. Each experiment was carried out with a new Al strip and 15 ml of the corroding solution, and repeated to ensure reproducibility of the results.

The reaction number (RN) is defined as $RN=(T_m-T_i)/t$ °C min^{-1}. T_m, T_i are the maximum and initial temperatures, respectively and t is the time in min, taken to reach T_m. All experiments were started at 25±0.1 °C (T_i). The percentage inhibition, I, is taken as:

$$\%I=(RN_{pure}-RN_{inh})\,100/RN_{pure} \quad (1)$$

Weight Loss Method. The test pieces measuring 20×20×1 mm were prepared as before, weighed, then immersed in 50 ml of the test solution at a temperature of 25±0.1 °C for a period of 15 min. They were then cleaned and washed with distilled water, dried and re-weighed.

$$\%\,I=\frac{\text{Wt. loss}_{pure}-\text{Wt. loss}_{inh}}{\text{Wt. loss}_{pure}}\times 100\,\% \quad (2)$$

Gasometeric Method. The reaction vessel and procedure for determining the rate of dissolution of aluminium in HCl were the same as described before.[9] The test pieces measuring 20×20×1 mm were prepared as before.

The efficiency of the inhibitors used can be evaluated as the percentage reduction in RR, viz.

$$\%\text{ Reduction in RR}=(R_{free}-R_{inh})\,100/R_{free} \quad (3)$$

where R_{free} and R_{inh} are rates of Al dissolution in the absence and presence of the additive, respectively, both measured at the same reaction time.

Results and Discussion

By following the temperature changes of the system in absence and presence of different concentrations of 4-(*m*-substituted phenylazo)pyrazoles, the temperature of the system was found to change slightly during the initial stages of the reaction (due to the originally formed oxide film). After a certain period which depended upon the concentration of the additives, the temperature rose to attain a maximum value. A representative temperature-time relationship obtained in presence of varying concentrations of compound **1** is shown in Fig. 1. The relationship between the reaction number (RN) of the system and the logarithm of the concentration (C) of compound **1** is indicated by the curve shown in Fig. 2. Curves having the same character are obtained with the other tested materials.

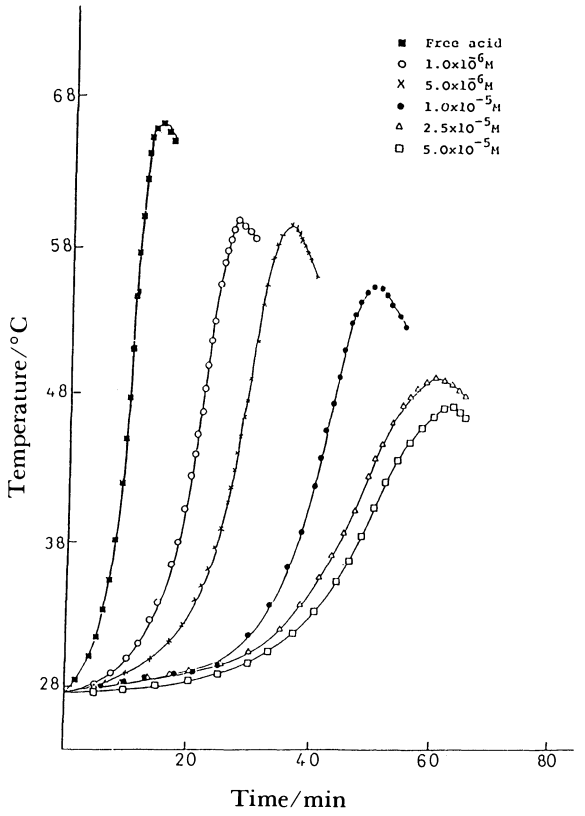

Fig. 1. Temperature-time curves obtained in the absence and presence of varying concentrations of compound **1**.

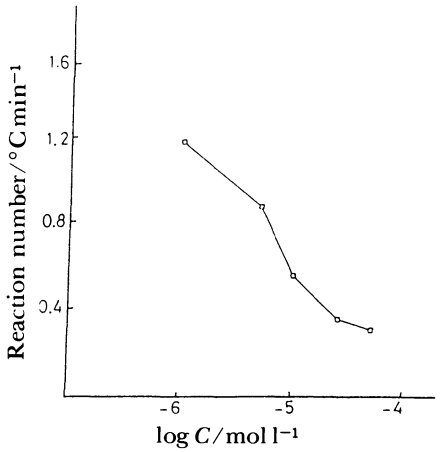

Fig. 2. Variation of the reaction number with the logarithm of concentration of compound **1**.

The reaction number-log C curves consist of an initial descending portion along which RN decreases slowly followed by a sharp descending portion to a certain limit of concentration. On further increase of the concentration of the additive, the values of RN decreases linearly with concentration and then become more or less constant. This behavior is explained on the basis of one-step adsorption process. The inhibiting action of tested compounds on Al dissolution is manifested by a decrease in T and an increase in the incubation period. The increase in the incubation period indicates that the additive acts in the acid solution as a strong cathodic inhibitors[10,11] and the lowering in T_m shows the strong adsorbability of the additive.[11]

The results obtained (Table 1) support the view that tested compounds have an inhibitive effect on the corrosion of Al in HCl. This apparent from the reduction of the values of RN of the metal by increasing the concentration of the additive. The percentage reduction in RN for all tested compounds are presented in Table 2.

Table 1. Efficiency of Corrosion Inhibition of 4-(*m*-Substituted phenylazo)pyrazoles as Determined by Percentage Reduction in Reaction Number in 2 M HCl

Concn of the additive in mol l^{-1}	% Reduction in RN			
	1	**2**	**3**	**4**
1.0×10^{-6}	55.3	50.8	36.0	33.0
2.5×10^{-6}	—	53.6	43.3	36.7
5.0×10^{-6}	67.0	63.4	51.3	48.0
1.0×10^{-5}	70.3	74.8	65.0	60.7
2.5×10^{-5}	86.8	81.2	72.7	68.5
5.0×10^{-5}	88.5	82.6	75.1	69.4

Table 2. Comparison between Efficiency of 4-(*m*-Substituted phenylazo)pyrazoles as Determined by Thermometric Weight Loss and Hydrogen Evolution Techniques in 2 M HCl at 10^{-5} M Inhibitors Concentration

Inhibitor	% Reduction in RN	% Inhibition	Reduction in RR
1	79.3	94.0	70.7
2	74.8	92.4	69.6
3	65.0	89.4	59.0
4	60.7	87.4	48.4

Figure 3 shows the volume of hydrogen evolved in $ml\,cm^{-2}$ vs. the reaction time of compound **1**. The slope of the curve at specified times gives the reaction rate in $1\,m^{-2}\,min^{-1}$. The percentage reduction in RR, after 60 min, for all the studied compounds are presented in Table 2.

Figure 4 represents the relation between the weight loss and time for compound **1**. The inhibition efficiences of the additives after 60 min are included in Table 2. In this table the 4-(*m*-substituted phenylazo)-pyrazoles examined are arranged in the order of decreasing inhibition efficiency. The same order is obtained from both the experimental methods employed.

According to Damaskin[12] the surface coverage (θ) can be determined as follows:

$$\theta = 1 - \frac{I}{I_0} \tag{4}$$

where I and I_0 are the current densities of the given potentials in electrolytes with and without inhibitor, respectively. But Rozenfeld[13] and Gardner[14] replace the current density by the capacitance of the double layer, dissolution rates, adsorption potential, or weight losses. Accordingly, it seemed promising to use U values instead of any of these variables. Equation 4 can thus be written as:

$$\theta = 1 - \frac{U_i}{U} \tag{5}$$

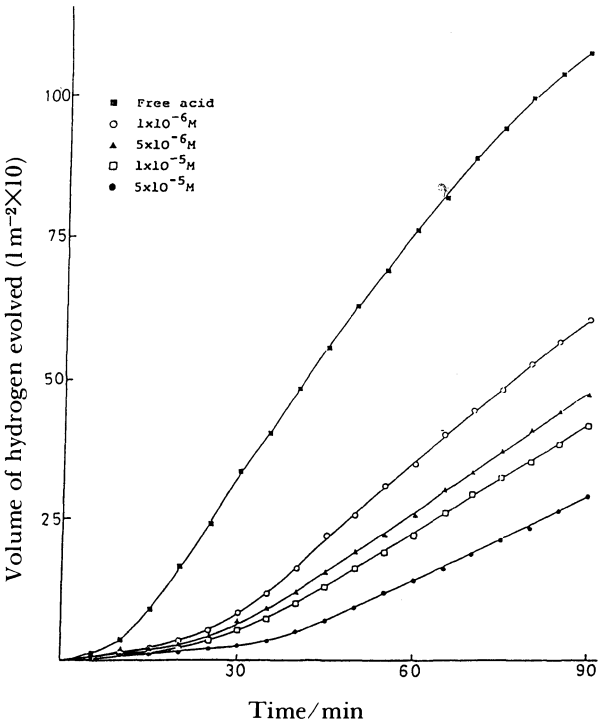

Fig. 3. Volume of hydrogen evolved-time curves obtained in the absence and presence of varying concentrations of compound **1**.

where U_i and U are corrosion rates in solution with and without inhibitor, respectively in case of weight loss method. It is available from the results of the present investigation to calculate the surface coverage, θ. The Langmiur adsorption isotherm may be written in the form:[15]

$$\log \frac{\theta}{1-\theta} = \log BC - G/2.303\,RT \tag{6}$$

where B is the adsorption equilibrium constant and G is the free energy of adsorption. Plotting $\log[\theta/(1-\theta)]$ against $\log C$ of compound **1** gives straight line, Fig. 5,

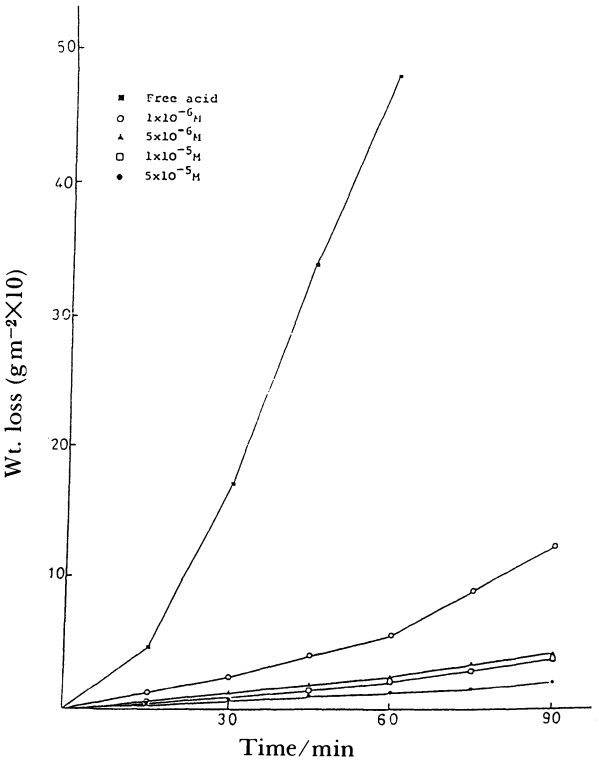

Fig. 4. Weight loss-time curves obtained in the absence and presence of varying concentrations of compound **1**.

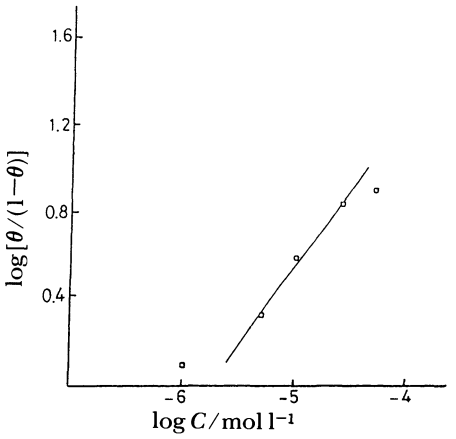

Fig. 5. Dependence of $\log[\theta/(1-\theta)]$ on logarithm of concentration of compound **1**.

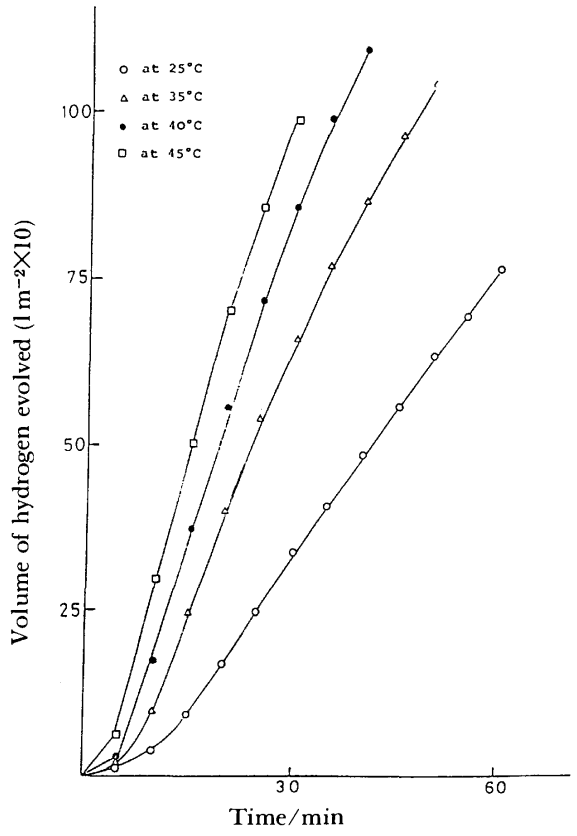

Fig. 6. Volume-time curves for 2 M HCl at different temperatures.

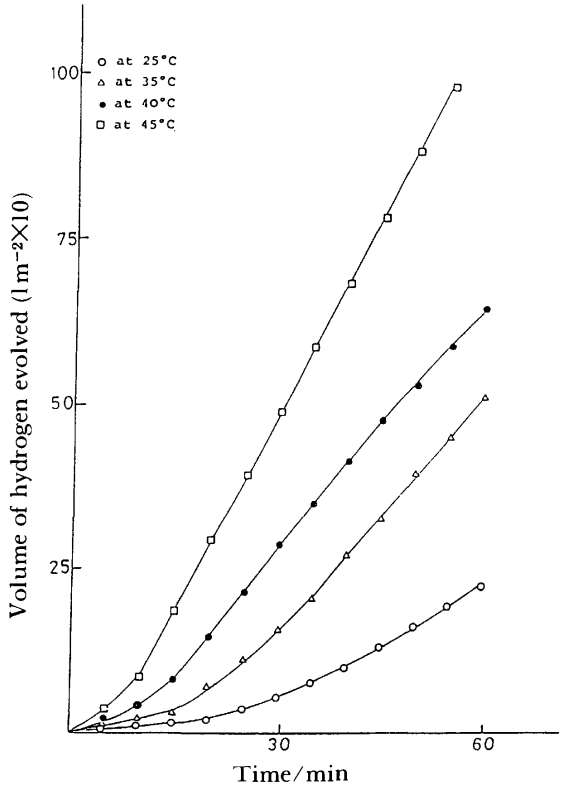

Fig. 7. Volume-time curves for compound **1** at different temperatures.

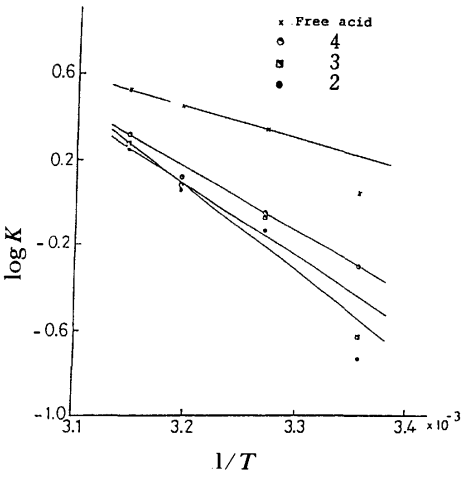

Fig. 8. $\log K$-$1/T$ curves for aluminium dissolution in presence and in absence of 4-(m-substituted phenylazo)pyrazoles.

Table 3. Effect of Temperature on the % Reduction in RR in Presence of 10^{-5} M 4-(m-Substituted phenylazo)pyrazoles at 30 min

Temp/°C	1	2	3	4
25	83.5	82.4	78.8	55.1
35	76.0	66.8	60.4	58.5
40	67.0	59.7	57.2	53.3
45	50.0	45.1	41.2	36.0

indicating almost a general agreement with Langmiur adsorption isotherm.

To study the effect of temperature on the rate of hydrogen evolution, hydrogen evolved was determined in 2 M HCl (1 M=1 mol dm^{-3}) without (Fig. 6) and with 10^{-5} M (Fig. 7) from compound **1** at solution temperatures of 25, 35, 40, and 45 °C. It was observed from the results of Table 3 that the inhibitive efficiency of all tested compounds decreases with the rise in temperature from 25 to 45 °C. This indicates that these compounds are physically adsorbed on aluminium surface.

The values of energy of activation, E, were calculated from the slopes of the Arrhenius plots of $\log k$ vs. $1/T$, where k is the corrosion rate and T the absolute temperature (Fig. 8). The E values are given in Table 4. From Table 4 it is evident that the E values in presence of additives are significantly lower than in its absence. This indicates that the four compounds function as effective inhibitors. The almost similar values of E suggest that the inhibitors are similar in their mechanism of action and the order of efficiency may be related to the preexponential factor A by the equation:

$$\log k = \log A - E/RT \qquad (7)$$

This is further related to concentration, steric effects, metal surface characteristics etc.

For calculating the values of heat of adsorption of the various inhibitors, plots were drawn of log

Table 4. Thermodynamic Parameters for Adsorption of Inhibitors on to an Aluminium Surface in 2 M HCl Containing 10^{-5} M Inhibitors

Inhibitor	E	$-\Delta G^{\circ}_{ads}$	ΔS°_{ads}	$-Q$	Slope of
	kcal mol^{-1}	kcal mol^{-1}	cal K^{-1} mol^{-1}	kcal mol^{-1}	log[θ/(1−θ)]vs.(1/T)
Free acid	6.4	—	—	—	—
4	14.1	10.3	51.6	5.1	1.1
3	17.8	10.4	50.4	4.6	1.0
2	15.5	10.6	49.5	4.2	0.9
1	17.4	10.8	47.1	3.2	0.7

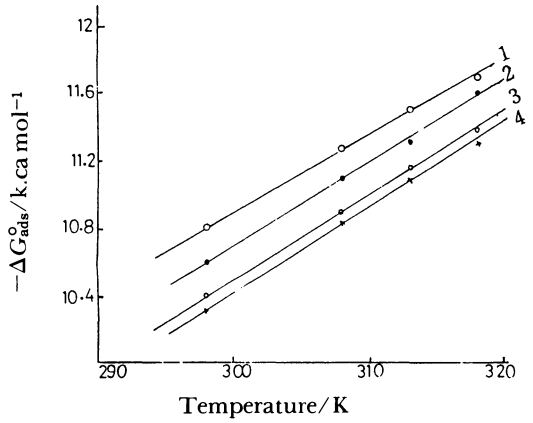

Fig. 9. Relation between $-\Delta G^{\circ}_{ads}$ and temperature for different 4-(m-substituted phenylazo)pyrazoles.

[θ/(1−θ)] vs. 1/T [θ=fraction of the surface covered by the inhibitor=1−μ_i/μ]. The Q values obtained from the slopes of these plots (ranging from 0.7—1.1) are given in Table 4. From the results it may be generalized that the more efficient inhibitor the less value of Q it has and vice versa.

The values of free energy of adsorption ΔG°_{ads}, are given in Table 4 at 25 °C. The results show that compound **1** which gives maximum efficiency shows more negative free energy of adsorption indicating that it is strongly adsorbed on the metal surface. In general, the negative values of free energy of adsorption, ΔG°_{ads}, indicate the spontaneous adsorption of inhibitors on aluminium. Also the entropy of adsorption, ΔS°_{ads}, was calculated[16] from the slopes of Fig. 9 and its values are recorded in Table 4.

Effect of Chemical Constitution on Inhibition Efficiency. The order of decreased inhibition efficiency for 4-(m-substituted phenylazo)pyrazoles **1**, **2**, **3**, and **4** is: H>CH_3>Cl>OCH_3 as indicated by the results in Table 2. Differences in the inhibition efficiency for aluminium corrosion in 2 M HCl as indicated by the above orders probably do not originate from the pyrazole moiety of the molecule, but arise from the substituents in the phenylazo group. It is evident that the electrophilic character of these substituents plays a determining role in imparting inhibition efficiency. Therefore, increase in electron-withdrawing ability of substituents is expected to increase the positive charge on the protonated form (acid form) of the inhibitors

Table 5. Spectroscopic Data for 4-(m-Substituted phenylazo)pyrazoles

Compound	λ_{max}/nm	pK
1	334	12.2
2	336	6.4
3	360	5.8
4	334	5.3

which is adsorbed on the aluminium surface. In strong acid solutions at pH 0 the acid-base equilibrium of the azo inhibitors to consider is as follows:

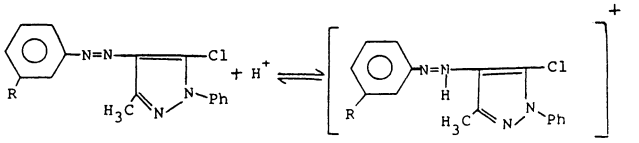

R = H, CH_3, Cl, OCH_3

Moreover, the intensity of the azo bands decreases with increase in pH and isobestic points are observed in the absorption spectra at longer wavelength. This behavior refers to the presence of the acid-base equilibrium and indicates that the acid form is predominant at low pH values. Also pK values were determined spectrophotometrically by well-known procedure.[17] A large value points to the presence of the azo inhibitors more in the acid form. The results of spectrophotometric measurements are summarized in Table 5. The order of decrease of these pK values is: H>CH_3>Cl>OCH_3 which is similar to that of decreased inhibition efficiency.

Fouda[18] and Barradas[19] reported before that the increased protection efficiency for some derivatives of thiophene is due to the presence of electrophilic substituents. This phenomenon was accounted[20] for by the adsorption of the protonated form of the inhibitor species and hence a decrease in the electron density of the functional group leads to an effective increase in its positive charge. Consequently, adsorption is reinforced by electrostatic forces.

The electrophilic character of the substituents used is decreased in the order:[21] Cl>H>CH_3>OCH_3. This order runs parallel to the above mentioned observed sequence of decreased inhibition efficiency of the azo inhibitors (**1**—**4**) with exception of the Cl-substituted one (**3**) which could be accounted for by the operation of a mesomeric effect (+M) involving

electron pairs on Cl which acts in opposite direction to the −I effect and the overall mechanism constitutes electron release which reduces the positive charge on the protonated from of the azo inhibitor **3** in a greater extent than the methyl-substituted compound **2** and renders it less inhibitive. Also the increase in red shift for R=Cl over that for R=CH_3 supports the suggestion that +M effect operates in this case.

References

1) O. L. Riggs, Jr., "Corrosion Inhibitors," ed by C. C. Nathan, NACE, Houston (1973), p. 7.
2) S. M. Mayanna and T. H. V. Setty, *Corros. Sci.*, **15**, 627 (1975).
3) N. Hackerman and R. M. Hurd, 1st Int. Congress on Metallic Corrosion Butterworths, London (1962), p. 166.
4) D. A. Vermilyea, 1st Int. Congress on Metallic Corrosion Butterworths, London (1962), p. 62.
5) S. Nakagawa and G. Hashizume, *Denkikagaku*, **43**, 500 (1975).
6) S. Siddagangappa, S. M. Mayanna, and F. Pushpanaden, *Anticorros.*, **23**, 11 (1978).
7) M. F. Ahmed, S. M. Mayanna, and F. Pushpanaden, *J. Electrochem. Soc.*, **124**, 1667 (1977).
8) K. Aziz and A. M. Shams El Din, *Corros. Sci.*, **5**, 489 (1965).
9) S. M. Hassan, M. N. H. Moussa, F. I. M. Taha, and A. S. Fouda, *Corros. Sci.*, **21**, 439 (1981).
10) J. M. Abd El Kader and A. M. Shams El-Din, *Corros. Sci.*, **10**, 551 (1970).
11) A. M. Shams El Din and J. M. Abd El Kader, *Oberflache Surface*, **1977**, 11.
12) B. B. Damaskin, "Adsorption of Organic Compounds on Electrodes," Plenum Press, New York (1971).
13) I. L. Rozenfeld "Corrosion Inhibitors," McGraw Hill, (1981).
14) G. Gardner, "Corrosion Inhibitors," ed by C. C. Nathan, National Association of Corrosion Engineers, Houston, Texas (1973).
15) T. P. Hoar and R. D. Haliday, *J. Appl. Chem.*, **3**, 502 (1953).
16) H. B. Rudresh and S. M. Mayanna, *J. Electrochem. Soc.*, **124**, 340 (1977).
17) I. M. Issa, R. M. Issa, M. R. Mahmoud, and Y. M. Temerk, *Z. Physik. Chem.*, **253**, 289 (1973).
18) A. S. Fouda, *Monatsh Chem.*, **117**, 159 (1986).
19) B. E. Conzay and R. G. Barradas, *Electrochem. Acta*, **5**, 319, 349 (1961).
20) H. Brandt, M. Fischer, and K. Schwabe, *Corros. Sci.*, **10**, 631 (1970).
21) M. S. Newan, "Steric Effects in Organic Chemistry," John Wiley & Sons, Inc. Revs, London (1956), p. 571.

 © 1988 The Chemical Society of Japan Bull. Chem. Soc. Jpn., 61, 4417—4421 (1988)

1,1′-Bis(selenocyanatomercurio)ferrocene as Ligand towards $M(NCS)_2$ [M=Co(II), Ni(II), and Zn(II)]

Pashupati Prasad SINGH,* Divya SINGH, and Narendra Bahadur SINGH
Chemistry Department, Bareilly College, Bareilly-243001, India
(Received July 27, 1987)

A comparative study of the behaviors of 1,1′-bis(selenocyanatomercurio)ferrocene (FBMS) with those of its thiocyanate analog (FBMT), has been made. Various physicochemical studies indicate that the Lewis acids and the adducts formed by FBMS are less stable than those of FBMT. The D_q values of FBMS adducts are higher, but the β values are lower. The matching constant values of FBMT complexes are higher than their corresponding FBMS complexes. The structures of Lewis acids and the adducts are similar in both the cases.

In our recent communication we have reported on the complexes of 1,1′-bis(thiocyanatomercurio)ferrocene (FBMT).[1] Since selenocyanate derivatives differ in their mode of bonding in certain cases,[2] a comparative study of the complexes of 1,1′-bis(selenocyanatomercurio)ferrocene (FBMS) was done.

Experimental

Material and Manipulation. Reagent grade solvents were purified before use. KSeCN was prepared and recrystallized by the method described elsewhere.[3] Nicotinamide (nia) and 2,2′-bipyridyl (bpy) were used from fresh bottle. 1,1′-Bis(selenocyanatomercurio)ferrocene (FBMS) was prepared as given below.

Preparation of FBMS. 11.5 g of ferrocene was dissolved in 65 ml of benzene. A suspension of 20 g of $Hg(OAc)_2$ in 250 ml of methanol was very slowly added to the solution of ferrocene through a dropping funnel with vigorous stirring. A clear dark brown solution was obtained. To this a solution of 6.5 g KSeCN in 10 ml of water was added with continuous stirring. A yellow precipitate was obtained, which was filtered on a Buchner funnel and washed with petroleum ether. This yellow compound was a mixture of (selenocyanatomercurio)ferrocene and FBMS. The former was removed by repeated extraction with hot 1,2-dichloroethane. FBMS left as insoluble yellow solid was dissolved in DMSO. To the solution a few drops of water were added, and it was left for a few days. Crystals of FBMS formed, were filtered, washed with the solvent and dried in vacuum.

Analytical Data. Mp 115 °C (decomp); Found: N, 6.74; Hg, 50.00; Se, 19.12%; Calcd for $C_{12}N_2H_8Se_2Hg_2Fe$: N, 7.04; Hg, 50.37; Se, 19.89%. IR (Nujol); ν(C-N) 2180(s), 2130(s), 2080 (sh); ν(C-Se) 765(s), 730(s), 680(m); δ(NCSe) 440(s), 420(s). IR(acetone): ν(C-N) 2130(s), 2070(s); ν(C-Se) 760(s), 740(s), 680(s), 660(m); δ(NCSe) 440(s), 510(s).

Preparation of Lewis Acids, $Fe(C_5H_4HgSeCN)_2M(NCS)_2$ [M=Ni(II), Co(II), and Zn(II)]. A calculated amount of FBMS was dissolved in a small quantity of DMSO and diluted to 200 ml of acetone. $M(NCS)_2$ was dissolved either in acetone or DMSO-acetone mixture. The solutions were mixed in 1 : 1 molar ratio and stirred for 24 h or until precipitate appeared. When the quantity of DMSO was too much, the precipitate was obtained by the addition of ethanol. The precipitate was filtered, washed with ethanol and dried in vacuum. The compounds thus obtained were recrystallized from acetone-ethanol mixture.

Preparation of Adducts, $Fe(C_5H_4HgSeCN)_2M(NCS)_2 \cdot L_x$ [M=Ni(II), Co(II), and Zn(II); x=2 when L is nia and one when bpy]. The adducts were prepared by two methods:

1. A suspension or solution of the Lewis acids was prepared in acetone-ethanol mixture and mixed with an ethanol solution of nicotinamide in 1 : 2 molar ratio or with bpy in 1 : 1 molar ratio and stirred for 24 h. In each case precipitate was formed, filtered, washed with ethonal, and dried in vacuum. The compounds were recrystallized from acetone-ethanol mixture.

2. $M(NCS)_2(nia)_2$ were first prepared by reaction of $M(NCS)_2$ with nicotinamide in 1 : 2 molar ratio in ethanol. Precipitate appeared in each case which was filtered, washed with ethanol and dried in vacuum. The complexes were recrystallized from acetone-ethanol mixture. $M(NCS)_2(nia)_2$ was dissolved in acetone and FBMS was dissolved in DMSO-acetone mixture. The solutions of $M(NCS)_2(nia)_2$ and FBMS were mixed in 1 : 1 molar ratio and stirred for 24 h. The precipitate formed was filtered, washed with ethanol and dried in vacuum. The compounds were recrystallized from acetone-ethanol mixture.

Analysis of the Complexes. Selenium was estimated as selenium metal, the other elements (Co, Ni, S, Hg) were analyzed as described.[1]

Physical Measurements. The molar conductance of the complexes were measured in DMSO using a Philips conductivity bridge model PR 9500. The magnetic susceptibility measurements were made at room temperature by Gouy's method using $CoHg(SCN)_4$ as standard. The diamagnetic corrections were made using Pascal's constants. Infrared spectra of the complexes were recorded as Nujol mulls on a Pye Unicam SP3-300 infrared spectrophotometer in the range 4000—200 cm^{-1}. The electronic spectra in DMSO (except FBMS·$Co(NCS)_2$) were recorded on a Cary-14 spectrophotometer. The spectra of FBMS·$Co(NCS)_2$ was recorded in solid phase adopting the procedure of Lee.[10]

Results and Discussion

Lewis Acids, $Fe(C_5H_4HgSeCN)_2M(NCS)_2$ [M= Ni(II), Co(II), and Zn(II)]. Like their SCN analogs[1] these Lewis acids are prepared by direct reaction of FBMS and $M(NCS)_2$. The positions of IR bands in the region of ν(CN), ν(CSe), and δ(NCSe) in FBMS·$Co(NCS)_2$ are basically similar to those of FBMT·$Co(NCS)_2$ except in the number of bands in the ν(CN), ν(CX), and δ(NCX) (X=S or Se) regions (cf. Table 2). This difference is due to the different local symmetries around Co(II), i.e. Td in the former C_{2v} in the latter.

Table 1. Analytical Data of the Complexes

Complex	Colour	Mp	% Sulfur		% Mercury		% Metal		% Nitrogen		% Selenium		Mole conductance
		θ_m/°C	Calcd	Found	Calcd	Found	Calcd	Found	Calcd	Found	Calcd	Found	cm^2 mho mol^{-1}
$Fe(C_5H_4HgSeCN)_2$-$Ni(NCS)_2$	Brown	173(d)	6.61	6.12	41.32	40.20	6.09	5.99	5.78	5.61	16.42	16.14	61.71
$Fe(C_5H_4HgSeCN)_2$-$Co(NCS)_2$	Blue	168(d)	6.61	6.23	41.32	40.12	6.09	5.85	5.78	5.55	16.42	16.23	42.75
$Fe(C_5H_4HgSeCN)_2$-$Zn(NCS)_2$	Grey	140(d)	6.56	6.25	41.02	40.89	6.66	6.32	5.74	5.53	16.30	16.35	58.81
$Fe(C_5H_4HgSeCN)_2$-$Ni(NCS)_2(bpy)$	Brown	190(d)	5.69	5.52	35.58	34.91	5.16	4.98	4.98	4.73	14.05	13.95	60.11
$Fe(C_5H_4HgSeCN)_2$-$Ni(NCS)_2(nia)_2$	Brown	185(d)	5.28	5.19	33.00	32.59	4.78	4.15	4.62	4.42	13.03	12.99	63.23
$Fe(C_5H_4HgSeCN)_2$-$Co(NCS)_2(bpy)$	Brown	180(d)	5.69	5.49	35.58	35.13	5.16	5.01	4.92	4.71	14.05	13.92	41.15
$Fe(C_5H_4HgSeCN)_2$-$Co(NCS)_2(nia)_2$	Brown	170(d)	5.28	5.12	33.00	33.10	4.78	4.32	4.62	4.33	13.03	12.95	43.01
$Fe(C_5H_4HgSeCN)_2$-$Zn(NCS)_2(bpy)$	Dirty white	175(d)	5.65	5.53	35.36	34.93	5.74	5.54	4.95	4.66	13.97	13.82	66.18
$Fe(C_5H_4HgSeCN)_2$-$Zn(NCS)_2(nia)_2$	Dirty white	155(d)	5.24	5.15	32.81	32.13	5.33	5.03	4.59	4.41	12.96	12.82	59.12

d = decomposes.

Table 2. Infrared Spectral and Electronic Spectral Bands with Spectral Parameters

Complex	ν(C-N)	ν(C-X)	δ(NCX)	ν(M-NCX/M-L)	ν_1	ν_2	ν_3	D_q	B'	β	μ_{eff}
	cm^{-1}	cm^{-1}	cm^{-1}	cm^{-1}	cm^{-1}	cm^{-1}	cm^{-1}	cm^{-1}	cm^{-1}		BM
Lewis acid											
$Fe(C_5H_4HgSeCN)_2$-$Ni(NCS)_2$	2180s, 2120m, 2050sh	780s, 750s, 680w, 660s	460s, 410s	250s, 230sh	10010	16800	28200	1031	938	0.96	3.01
$Fe(C_5H_4HgSeCN)_2$-$Co(NCS)_2$	2180m, 2130s, 2090sh	775s, 740sh, 670w, 650m	460s, 410s	310s, 280sh	—	6000	15500	356	721	0.74	4.25
$Fe(C_5H_4HgSeCN)_2$-$Zn(NCS)_2$	2160m, 2120s, 2070sh	730s, 710s, 650w, 630s	400s, 400w	315s, 270sh	—	—	—	—	—	—	—
Adduct											
$Fe(C_5H_4HgSeCN)_2$-$Ni(NCS)_2(nia)_2$	2170s, 2090s, 2050sh	760s, 745w, 695s, 660w	470m, 415s	295s, 230sh	9100	16950	27850	1052	882	0.85	2.99
$Fe(C_5H_4HgSeCN)_2$-$Ni(NCS)_2(bpy)$	2160s, 2100s, 2060sh	760s, 740s, 690s, 665m	470s, 420w	275s, 225sh	9500	16700	28000	1025	930	0.90	3.02
$Fe(C_5H_4HgSeCN)_2$-$Co(NCS)_2(nia)_2$	2160w, 2090s, 2050s	660s, 750m, 690s,660s	460s, 410w	280s, 215sh	10450	17700	20800	944	914	0.94	5.14
$Fe(C_5H_4HgSeCN)_2$-$Co(NCS)_2(bpy)$	2155s, 2090b, 2040s	760s, 735sh, 680s, 650s	466w, 420s	270s, 210sh	10500	15870	19230	866	898	0.92	5.06
$Fe(C_5H_4HgSeCN)_2$-$Zn(NCS)_2(nia)_2$	2160s, 2110w, 2040sh	740s, 720sh, 670s, 730m	450m, 400s	275s, 210sh	—	—	—	—	—	—	—
$Fe(C_5H_4HgSeCN)_2$-$Zn(NCS)_2(bpy)$	2140s, 2110w, 2030sh	730m, 715s, 670s, 635w	445s, 425s	270s, 220sh	—	—	—	—	—	—	—

s=strong, sh=shoulder, b=broad, m=medium, w=weak; X=S or Se.

This increase of number of bands is due to the presence of ν(CN), ν(CS), ν(CSe), δ(NCS), and δ(NCSe) bands. The IR spectra show the presence of both bridged and terminal NCX groups (Table 1).

The magnetic moment values show close resemblance with the SCN analogs. The electronic spectral bands positions and the spectral parameters of FBMS·$Co(NCS)_2$ are presented in Table 2. Two intense bands (Fig. 5) observed in the region 15500 and 6000 cm^{-1} are assigned to $^4A_2 \rightarrow {}^4T_2(F)$ (ν_3) and $^4A_2 \rightarrow {}^4T_1(P)$ ($\nu 2$). These bands, D_q and magnetic moment values show that cobalt is in tetrahedral geometry. The compound is non-conducting but is dissociated significantly. The following structure (Fig. 1) can thus be proposed for the Lewis acids where M is Co(II), and also for Zn(II) which is very similar.

The electronic spectra of Lewis acid with Ni(II) show three bands in the region 28200, 16800, and 10010 cm^{-1} which are assigned to $^3A_{2g} \rightarrow {}^3T_{1g}$ (P) (ν_3), $^3A_{2g} \rightarrow {}^3T_{1g}$ (F) (ν_2), and $^3A_{2g} \rightarrow {}^3T_{2g}$ (F) (ν_1), respectively. Various spectral parameters have been calculated with the help of ν_2 and ν_3 bands using the secular equation

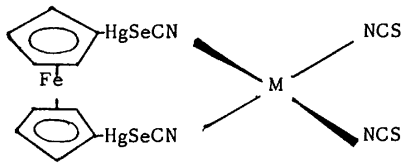

M = Co(II) and Zn(II)

Fig. 1.

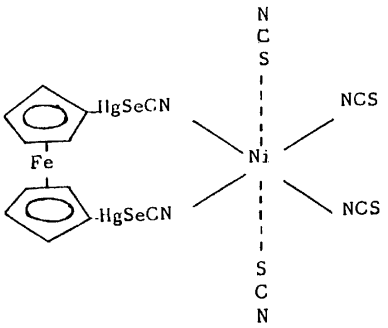

Fig. 2.

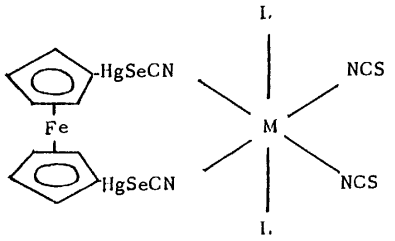

[M= Co(II), Ni(II) and Zn (II); L= nicotinamide (nia)]

Fig. 3.

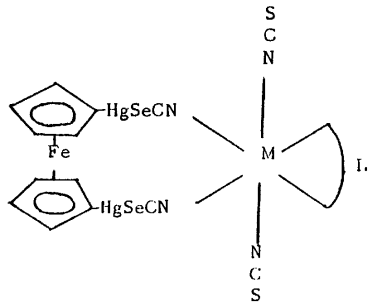

[M= Co(II), Ni(II) and Zn (II); L= 2,2′-bipyridyl (bpy)]

Fig. 4.

of Tanabe and Sugano[4] and the results are included in Table 2. The electronic spectra and magnetic moment values for FBMS·Ni(NCS)$_2$ are indicative of octahedral coordination geometry around Ni(II), which is achieved by axial coordination from adjacent layer. On the basis of these results the structure in Fig. 2 can be proposed for it.

The D_q values of the FBMT Lewis acids are lower than those of FBMS Lewis acids. This indicates that FBMS exerts stronger ligand field than FBMT.[5] The B' value shows a decrease on changing from FBMT to FBMS indicating greater orbital overlap. The D_q, B', and β values of different series are presented in Table 2.

Adducts. Fe(C$_5$H$_4$HgSeCN)$_2$M(NCS)$_2$L$_x$ [M= Co(II), Ni(II), Zn(II); x=2 when L is nia and one when bpy]. In FBMS-M(NCS)$_2$ the coordination number of Co(II) and Zn(II) is four, against the maximum of six, hence they can be treated as Lewis acids. In case of the Ni(II) analogs the weak axial NCS ligands can easily be replaced by any strong base. Accordingly, when all the Lewis acids were treated with nicotinamide and 2,2′-bipyridyl, adducts of general formula FBMS·M(NCS)$_2$·L$_x$ were formed. The molar conductance values of these complexes in DMSO are in the range 40 to 63 cm^2 mho mol^{-1} (Table 1) showing that they are dissociated significantly.

IR spectra show that the positions of ν(CN), ν(CS), ν(CSe), δ(NCS), and δ(NCSe) bands of the Lewis acids are not significantly changed on adduct formation. The slight changes observed are due to, the change in stereochemistry around M. This reveals that the original structure of the Lewis acids is retained and only the coordination geometry of M changes on account of linkage of ligands. On adduct formation there is a slight change in ν(M-NCS) band in the case of Co and Zn. While, there is almost no change in ν(M-NCS) band in the case of Ni. The negative shifts in the case of Co and Zn are due to the change from tetrahedral geometry around M in the Lewis acids to octahedral in the adducts.[6,7] Such a change is not observed in Ni adduct because of the presence of octahedral configuration in the Lewis acids and the adducts as well. The electronic spectra of FBMS·Co(SCN)$_2$L$_x$ show the presence of three bands in the regions 19230—20800, 15870—17700, and 10450—10500 cm^{-1} which are assigned to $^4T_{1g}\rightarrow{}^4T_{1g}(P)$ (ν_3), $^4T_{1g}\rightarrow{}^4A_{2g}$ (ν_2), and $^4T_{1g}\rightarrow{}^4T_{2g}$ (ν_1) transitions respectively. The electronic spectra of Ni complexes show the presence of three bands in the regions 27850—28000, 16700—16950, and 9100—9500 cm^{-1} which are assigned just as in the case of the parent Lewis acid. The D_q values calculated from ν_2 and ν_3 are presented in Table 2. The structure as in Figs. 3 and 4 can be proposed for the adducts. Though a trans structure has been shown in Fig. 3, yet the possibility of cis structure is not ruled out.

Comparison with the Complexes of FBMT.

1. The Lewis acids and the adducts formed by FBMS are less stable than those formed by FBMT. The former complexes start decomposing after a month giving selenium metal.

2. Molar conductance values of FBMS complexes are slightly lower than those of FBMT analog, indicating that their dissociation in solution is less.

3. Complexes of FBMS are less soluble in DMSO than those of FBMT.

4. Three bands are present in ν(CN) region in the Lewis acids and adducts of FBMS series against two in FBMT analog. This is due to the difference in local symmetry around M.

5. The ν(M-NCSe) bands in the Lewis acid appear at lower frequency as compared with ν(M-NCS) band.

6. The D_q values of FBMS adducts are higher than their FBMT analogs. The β values show a decrease on changing from the latter to the former, indicating greater orbital overlap.

Quantitative Softness. The softness value of a metal ion has been denoted by $E_n^{\ddagger}$ and that of a base ion by $E_m^{\ddagger}$ and the difference between the two by $\Delta E_{nm}^{\ddagger}$.[8] The softness value of any metal in different compounds has been expressed by effective softness and denoted by $E_{n(eff)}^{\ddagger}$, similarly the softness of any atom in a neutral base such as nitrogen in nicotinamide and 2,2′-bipyridyl has been denoted by $E_{m(eff)}^{\ddagger}$ the difference between the two is denoted by $\Delta E_{nm(eff)}^{\ddagger}$. This is described as matching. A higher value of $\Delta E_{nm}^{\ddagger}$ indicates better matching. This can be represented by the following equation. The detail description of estimation of various softness parameters is given in Ref. 9.

$$\Delta E_{nm(eff)}^{\ddagger}\,(\text{Matching}) = |E_{n(eff)}^{\ddagger} - E_{m(eff)}^{\ddagger}| + \text{CFSE}$$

The $\Delta E_{nm}^{\ddagger}$ values in the Table 3 indicate that FBMT show better match with various $M(NCS)_2$ than FBMS. The effective softness of ligands and of M in the Lewis acids have also been calculated. The matching between the two has been derived and is presented in Table 4. A reference to Table 4 shows that 2,2′-

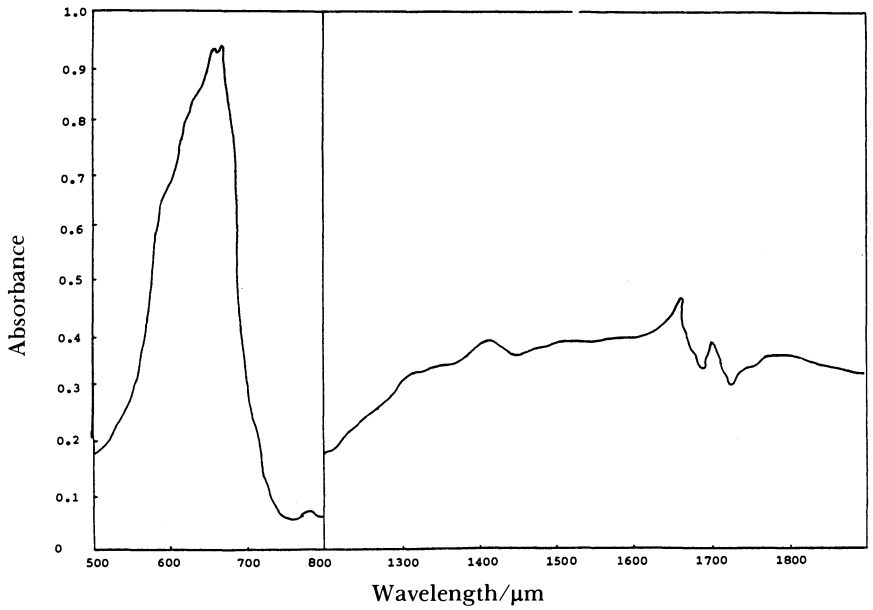

Fig. 5. Electronic spectra of FBMS·Co(NCS)$_2$.

Table 3. $\Delta E_{nm}^{\ddagger}$ Derived from $E_{n(eff)}^{\ddagger}$ of M in $M(NCS)_2$ and $E_{m(eff)}^{\ddagger}$ of FBMS in the Formation of Lewis Acids

Lewis acid	$E_{n(eff)}^{\ddagger}$ of M in $M(NCS)_2$	$E_{m(eff)}^{\ddagger}$ of FBMS	$\Delta E_{nm}^{\ddagger}$	CFSE	Matching constant $\Delta E_{nm}^{\ddagger}$+CFSE
$Fe(C_5H_4HgSeCN)_2Ni(NCS)_2$	−3.10	−11.14	8.04	6.41	14.45
$Fe(C_5H_4HgSeCN)_2Co(NCS)_2$	−3.56	−11.14	7.58	4.68	12.19
$Fe(C_5H_4HgSeCN)_2Zn(NCS)_2$	−4.92	−11.14	6.22	—	6.22

Table 4. $\Delta E_{nm}^{\ddagger}$ Derived from $E_{n(eff)}^{\ddagger}$ of M in FBMS·$M(NCS)_2$ and $E_{m(eff)}^{\ddagger}$ of the Ligand in the Formation of Adducts

Complex	$E_{n(eff)}^{\ddagger}$ of M in Lewis acids	$E_{m(eff)}^{\ddagger}$	$\Delta E_{nm}^{\ddagger}$	CFSE	Matching constant
$Fe(C_5H_4HgSeCN)_2Ni(NCS)_2(nia)_2$	−2.29	13.86	11.57	6.39	17.96
$Fe(C_5H_4HgSeCN)_2Ni(NCS)_2(bpy)$	−2.29	24.08	19.14	6.42	25.56
$Fe(C_5H_4HgSeCN)_2Co(NCS)_2(nia)_2$	−2.85	13.86	11.01	4.22	15.23
$Fe(C_5H_4HgSeCN)_2Co(NCS)_2(bpy)$	−2.85	24.08	18.38	4.29	22.67
$Fe(C_5H_4HgSeCN)_2Zn(NCS)_2(nia)_2$	−4.13	13.86	9.73	—	9.73
$Fe(C_5H_4HgSeCN)_2Zn(NCS)_2(bpy)$	−4.13	24.08	15.82	—	15.82

bipyridyl forms more stable M-L bond than nicotinamide agreeing with the established fact. $\Delta E^{\ddagger}_{nm(eff)}$ values are highest when M=Ni(II) and lowest when M=Zn(II). The sequence with other M is as follows:

Nickel > Cobalt > Zinc.

On changing organomercury thiocyanate part of the Lewis acid with organomercury selenocyanate, the M becomes slightly more soft and accordingly $\Delta E^{\ddagger}_{nm}$ values also become lower. Thus the complexes of FBMT are more stable than those of FBMS.

The authors gratefully acknowledge the financial support received from Council of Scientific and Industrial Research, New Delhi.

References

1) P. P. Singh and Meena Singh, *Bull. Chem. Soc. Jpn.*, **59**, 1219 (1986).
2) P. P. Singh and S. B. Sharma. *J. Coord. Chem.*, **7**, 213 (1978).
3) G. R. Waitkins, *Inorg. Synth.*, Vol. II, 186 (1946).
4) Y. Tanabe and S. Sugano, *J. Phys. Soc. Jpn.*, **9**, 753 (1954).
5) J. L. Burmeister, *Coord. Chem. Rev.*, **1**, 205 (1960).
6) Kurt Dehnicke, *J. Organomet. Chem.*, **9**, 11 (1967).
7) R. J. H. Clark and C. S. Williams, *Spectrochim. Acta* **22**, 1081 (1966).
8) G. Klopman, *J. Am. Chem. Soc.*, **90**, 223 (1968).
9) P. P. Singh, S. K. Srivastava, and A. K. Srivastava, *J. Inorg. Nucl. Chem.*, **42**, 521 (1980).
10) R. H. Lee, G. Griswold, and J. Kleinberg, *Inorg. Chem.*, **5**, 1662 (1966).

 © 1988 The Chemical Society of Japan Bull. Chem. Soc. Jpn., 61, 4423—4426 (1988)

Solvent and Reversed-Phase Extraction Chromatographic Separation of Niobium, Zirconium, and Hafnium with Aliquat 336

Nitya Ranjan Das* and Putul Chattopadhyay
Nuclear Chemistry Division, Saha Institute of Nuclear Physics, Sector-1, Block-'AF',
Bidhannagar, Calcutta-700 064, India
(Received December 10, 1987)

Aliquat 336 has been employed as an effective anionic extractant for the radiochemical separation of niobium, zirconium, and hafnium in mixtures using solvent extraction and reversed phase extraction chromatography (RPEC). In solvent extraction, niobium and zirconium are extracted with reagent solutions in the respective concentration ranges <0.001—0.04 mol dm^{-3} and 0.5 mol dm^{-3} leaving hafnium in the aqueous phase. In RPEC, niobium and zirconium are extracted by the reagent impregnated column and hafnium is completely eluted with water. Zirconium and niobium subsequently are eluted successively with 0.5 mol dm^{-3} HNO_3 and 1 mol dm^{-3} HF solutions. Distribution studies indicate that the extracted species for niobium and zirconium are respectively mono- and dinegative in charge. The extent of separation and the purity of the separated species were verified by means of gamma-ray spectrometry.

Zirconium and hafnium constitute the most important congeneric pair of elements in the periodic system and their similarity, both in the metallic state and in their compounds, is greater than that of any other homologous elements. It is not surprising that they invariably accompany each other in nature. With respect to elemental purity, their mutual separation has always been problem for analytical chemists. Moreover, in radiochemical separations of zirconium from hafnium, the presence of niobium must be taken into account since ^{95}Zr always occurs in equilibrium with its daughter isotope, ^{95}Nb.

Amongst the analytical procedures generally used in their separation study, solvent extraction[1-6] and reversed-phase extraction chromatography (RPEC) using various organic extractants[7,8] are found to be very effective. Survey of literature[9] reveals that the liquid exchangers, namely, the high-molecular-weight organonitrogenous compounds, in general, show very promising features in liquid-liquid extraction applications[10-13,14a] such as nuclear fuel processing and fission product recovery.[14b] Similarly, in RPEC[15-17] also, the column loaded with strong organic base is mainly devoted to the use of quaternary ammonium compounds as the stationary phase for various separation studies. In this regard, the quaternary ammonium salt, Aliquat 336 (tricaprylmethylammonium chloride), although displaying very high selectivity for different elements under specific experimental conditions as an anion exchanger involving solvent extraction as well as RPEC, it has not yet been fruitfully utilized for the individual separation of the concerned elements in a mixture.

With these facts in view, in the present study, attempts have been made to develop effective solvent extraction and RPEC procedures for tracer scale separation of the critical element pair, zirconium-hafnium, in admixture with niobium using the quaternary ammonium compound, Aliquat 336, as the liquid anion exchanger.

Experimental

Reagents. Aliquat 336 of molecular weight 404.17 was procured from Aldrich Chemical Co., Inc. USA. All other reagents used were of analytical grade. The carrier-free radioisotopes, ^{95}Zr (65d) and ^{95}Nb (35d) in hydrochloric acid solution and ^{181}Hf (44.6d) as HfO_2 of high specific activity were supplied by BARC, Trombay, India. HfO_2 powder was dissolved in the minimum quantity of a mixture of hydrofluoric and nitric acids and then diluted with water as required.

Solvent Extraction. Extractant stock solutions of desired concentrations were prepared by adding the necessary amount of Aliquat 336 to the nonpolar diluent cyclohexane, together with 3% (v/v) octanol as phase modifier. About 20 ml of the aqueous feed containing the mixture of the radiotracers, ^{95}Zr-^{95}Nb and ^{181}Hf ($<10^{-7}$ mol dm^{-3}) in acid medium were shaken with equal volumes of the extractant solution for ten minutes. Following separation, elements present in both phases were measured radiometrically. The optimal condition for complete separation of the tracers were such that niobium was first extracted from 9 mol dm^{-3} HCl solution with Aliquat 336 in cyclohexane in the concentration range <0.001—0.04 mol dm^{-3} leaving zirconium and hafnium in the aqueous phase. In the second stage, zirconium was separated from hafnium with 0.5 mol dm^{-3} extractant solution, whereby hafnium remained entirely in the aqueous phase.

RPEC. For the separation of the tracer mixture, the extraction column of hydrophobised kieselguhr impregnated with the exchanger, Aliquat 336, was prepared and preconditioned.[18,19] When the tracer species, i.e., ^{95}Zr-^{95}Nb and ^{181}Hf in dilute hydrochloric acid solution was loaded on the top of the column, hafnium emerged without being extracted by the reagent, whereas zirconium and niobium remained completely absorbed on the column. Subsequently, zirconium and niobium were successively separated by elution with nitric (0.5 mol dm^{-3}) and hydrofluoric (1 mol dm^{-3}) acids respectively. A flow rate of 10—12 drops per minute was maintained with the aid of a peristaltic pump. Radioactivity present in different fractions of the effluents was measured by means of a GM counter.

In both methods, the extraction or elution of each species

was first tested with individual tracers under identical experimental conditions.

Results and Discussion

Solvent extraction and RPEC procedures, though independent, appear to be inter-related in that they follow similar types of extraction mechanisms. In solvent extraction, elements which have a higher affinity for the extractant are easily extracted in the organic phase, leaving others in the aqueous phase. In the RPEC system, a mixture of metal ions is percolated through the column of inert material impregnated with an organic exchanger, and elements which are readily bound to the extractant molecules are extracted in the column by the extractant and subsequently eluted by means of suitable agents. Elements with low affinity for the reagent come out of the column by simple washing with water. Depending on experimental conditions, both procedures may thus be applied to the separation of the critical pair of elements, zirconium and hafnium in the presence of niobium.

Aliquat 336 is amphiphilic in nature, i.e., the molecule has a polar end and a long hydrophobic alkyl chain. The simultaneously hydrophobic-hydrophilic nature of the extractant is essential in maintaining both a high solubility in diluents with low dielectric constant and a high complexing power with respect to inorganic metal species. These reagents are accordingly characterized by high interfacial activity and enhanced extracting power. Reaction of the surface-active reagent with the metal ion takes place at the interface. The nonpolar alkyl groups surround the metal complex formed at the interface and solubilize it in the bulk organic phase. In this case the extractant and the extractant metal complex can undergo aggregation and disaggregation processes which can affect the distribution ratio value appreciably.

The higher efficiency of the quaternary salts is understandable for conditions under which the extraction mechanism is of the ion-association or ion-exchange type; in such instances, the charge of the metal anionic complexes in aqueous medium is balanced by salts which results in the formation of neutral species.[20]

Niobium and zirconium, unlike hafnium, tend to form negatively charged species in the acidic medium and are extracted to a different extent by Aliquat 336, depending upon the types of the acids and their acidities. In the present study, it was observed that the difference in the extent of extraction is especially pronounced in hydrochloric acid medium. It is also evident from Fig. 1 that the extent of extraction of zirconium along with its niobium daughter increases with increasing acid concentration, complete extraction occurring at 9 mol dm^{-3} HCl. However, hafnium has a lower tendency to form anionic complexes under these conditions, and remains unextracted by Aliquat 336 in the concentration region where niobium and zirconium are extracted. At higher acid concentrations viz., at about 10 mol dm^{-3} HCl, hafnium is extracted to a slight extent.

The concentration of the reagent is important, 0.5 mol dm^{-3} reagent solution extracting both niobium and zirconium completely from the aqueous solution and leaving hafnium in the aqueous phase. Niobium can be separated from the mixture with a lower concentration of the reagent. Extraction of niobium begins at <0.001 mol dm^{-3} reagent and is complete at 0.04 mol dm^{-3} reagent. Whereas the extraction of zirconium starts at about 0.05 mol dm^{-3} reagent, other conditions remaining same (Fig. 2).

It is evident from Fig. 3 that under conditions of RPEC, the extractional behavior of these elements corresponds closely to that of the solvent extraction. When the mixture is absorbed on the column impregnated with Aliquat 336, hafnium elutes quantitatively

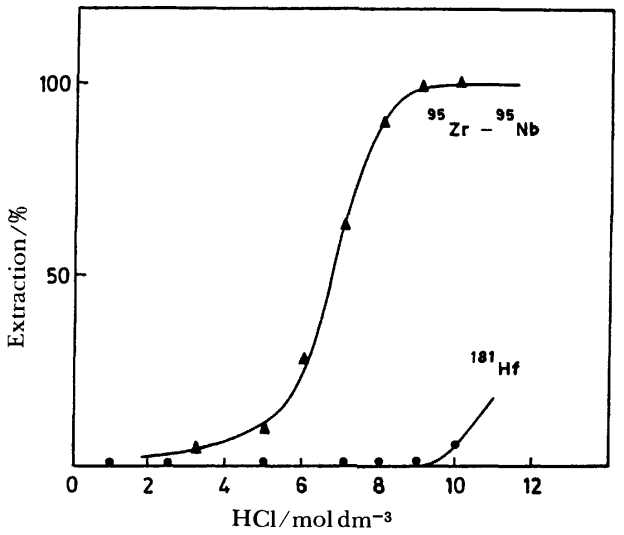

Fig. 1. Extraction dependence of ^{95}Zr–^{95}Nb and ^{181}Hf on HCl concentration using 0.5 mol dm^{-3} Aliquat 336 solution.

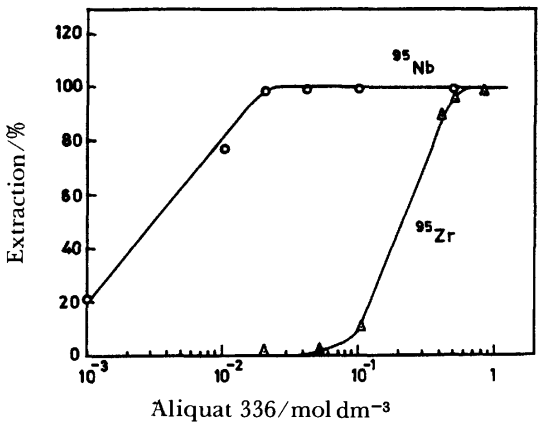

Fig. 2. Extraction dependence of ^{95}Nb and ^{95}Zr on Aliquat 336 concentration in 9 mol dm^{-3} HCl solution.

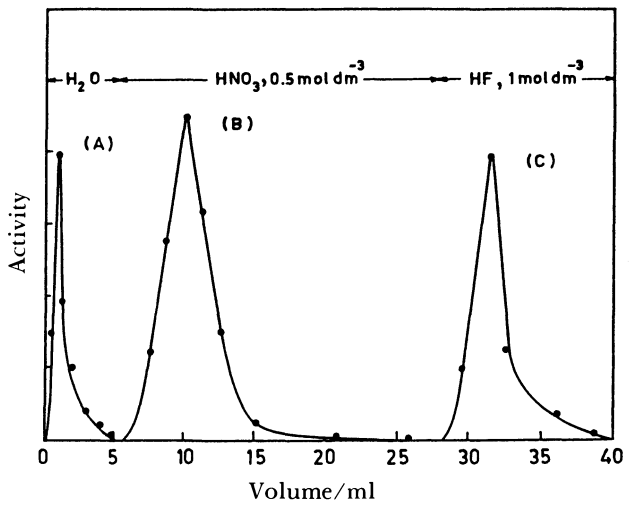

Fig. 3. Separation of ^{95}Zr, ^{95}Nb, and ^{181}Hf in the RPEC method (A) ^{181}Hf by water, (B) ^{95}Zr by 0.5 mol dm^{-3} HNO_3, and (C) ^{95}Nb by 1 mol dm^{-3} HF.

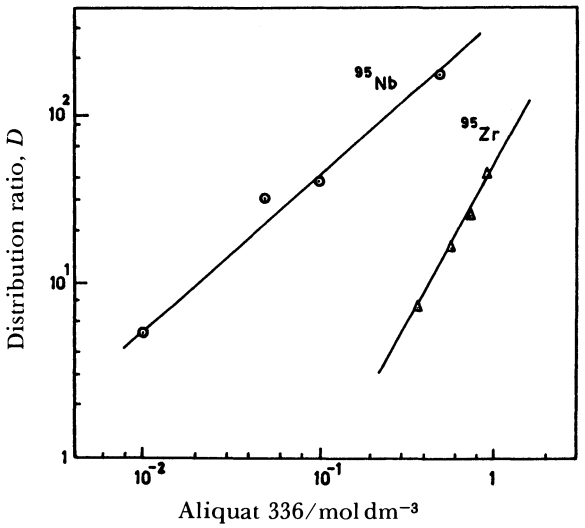

Fig. 4. Distribution ratio, D, of ^{95}Nb and ^{95}Zr as a function of Aliquat 336 concentration in 9 mol dm^{-3} HCl.

since it does not form anionic species in this case. Zirconium can be eluted with dilute nitric acid since it is bound by the reagent less firmly than niobium, which is finally eluted with dilute hydrofluoric acid.

Although both niobium and zirconium can form anionic species in aqueous medium, the difference in extraction of these species results from their competitive association with the bulky reagent cation. The preferential extraction of niobium with respect to zirconium may be attributed to the fact that the former primarily forms singly charged oxo- and hydroxychlorocomplexes such as $NbOCl_4^-$, $Nb(OH)_2Cl_4^-$,[21] etc., which are readily extracted by the reagent. Zirconium in aqueous solution generally forms dinegative species like $ZrCl_6^{2-}$ and hence it requires two molecules of the reagent to form a neutral complex. Moreover, it tends to form polymerized species[22,23] of the form $(ZrOCl_4)_n^{2-}$ resulting in an overall hindrance in its extraction.

This behavior is evident from the results shown in Fig. 4 for which the values of the distribution ratio for niobium and zirconium were measured at various concentrations of Aliquat 336 in the organic phase. For niobium, it is observed that D values increase with increasing extractant concentrations, and the slope of this increment is 1. It follows that niobium forms uninegative species in the aqueous phase, and is easily extracted into the organic phase. In the case of zirconium, however, the increment in D-values with the increase in concentration of Aliquat 336 is characterized by a slope of about 2, indicating that zirconium forms dinegative species in the aqueous phase. Hence, the mechanism of extraction of niobium and zirconium may be represented as

$$R_3R'\overset{+}{N}\,Cl^-_{org} + NbOCl_{4aq} \longrightarrow R_3R'N\,NbOCl_{4org} + Cl^-_{aq}$$

and

$$2R_3R'\overset{+}{N}\,Cl^-_{org} + ZrCl^{2-}_{6aq} \longrightarrow (R_3R'N)_2ZrCl_{6org} + 2Cl^-_{aq}$$

where,

R = capryl (C_8—C_{10}-alkyl) group,
R′ = methyl group.

The absence of any anionic species of hafnium as indicated by its extraction behavior towards the anionic extractant may be attributed to its electronic configuration. Hafnium ions are very weakly polarizing and as a result the formation of the complex compounds is very unusual.

The purity of the separated elements in both methods was monitored by gamma ray spectrometry at each stage of separation. The elements were identified by their characteristic gamma ray spectral lines using the following energies, 765.8 keV for ^{95}Nb, 724.0 and 756.6 keV for ^{95}Zr and 133.1, 345.7, and 482.2 keV for ^{181}Hf (Fig. 5).

In RPEC, kieselguhr was selected as a support because of its high resistance to nuclear radiation. This property is essential for radiochemical studies[24,25] of this kind. Moreover, kieselguhr is sufficiently porous, has a large capacity for absorbing the organic extractant with which it is impregnated and is chemically inert.

It is considered that the RPEC procedure is preferable to solvent extraction owing to its simplicity and selectivity. In liquid-liquid extraction, fresh portions of the reagent are repeatedly necessary, whereas in RPEC, the column can be impregnated with the reagent and used for several runs. In liquid-liquid extraction sometimes a phase modifier is required to prevent the formation of emulsions. But in RPEC, where the extractant is used as a stationary phase in the extraction columns the addition of the phase modifier is not required. Furthermore, the latter process is less time-consuming and results in a quantitative and

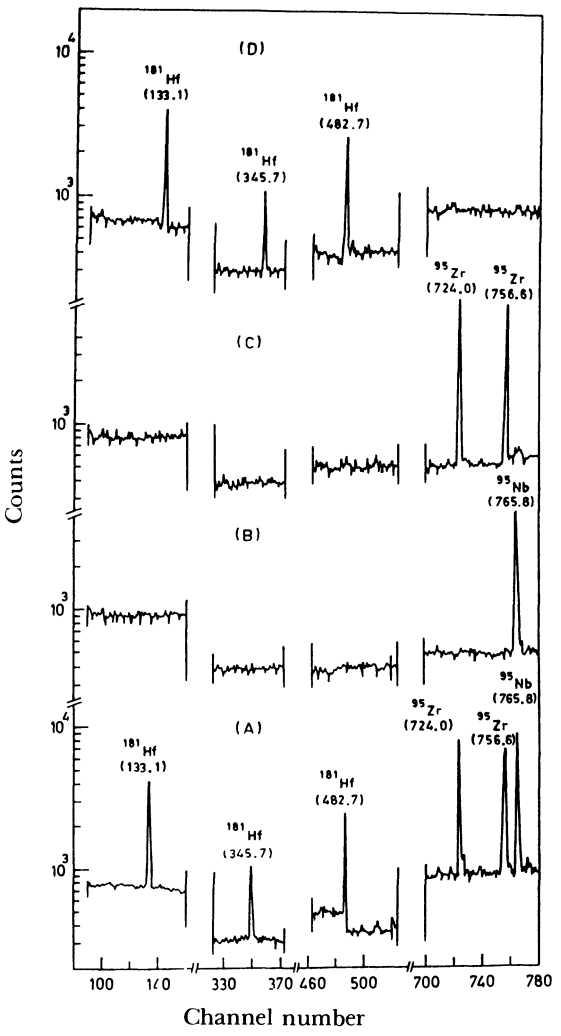

Fig. 5. Gamma spectra of ^{95}Nb, ^{95}Zr, and ^{181}Hf separated by solvent extraction. (A) Mixture of ^{95}Nb, ^{95}Zr, and ^{181}Hf before separation (B) ^{95}Nb separated in Aliquat 336 (0.02 mol dm^{-3}) (C) ^{95}Zr separated in Aliquat 336 (0.5 mol dm^{-3}) and (D) ^{181}Hf in aqueous phase.

clear-cut separation with minimal contamination.

Grateful acknowledgement is due to Professor S. N. Bhattacharyya, Head, Nuclear Chemistry Division, for his encouragement in the work.

References

1) B. Nandi, N. R. Das, and S. N. Bhattacharyya, *Solv. Extrn. and Ion Exch.*, **2**, 699 (1984).
2) N. R. Das, B. Nandi, and S. N. Bhattacharyya, *J. Radioanal. Chem.*, **62**, 53, (1981).
3) I. M. Gibalo, N. A. Mymsik (Moscow State Univ.) pp. 206—210 of Uspekhi Analiticheskoshimii, Solotov. Yu. A. (Ed.), Moscow: Izdatel'stovo Nauka (1974), Russ.
4) Solvent Extraction, London Society of Chemical Industry (1974), International Solvent Extraction Conference, Lyon-France, pp. 2185—2196 (8 Sept. 1976).
5) T. Sato, S. Ikoma, and T. Nakamura, *J. Inorg. Nucl. Chem.*, **39**, 395, (1977).
6) G. M. Vol'dman, O. A. Sotnikova, E. A. Mironova, and N. I. Gavrilov, *Russ. J. Inorg. Chem.*, **29**, 1175 (1984).
7) J. S. Fritz and R. T. Frazee, *Anal. Chem.*, **37**, 1358 (1965).
8) R. H. A. Crawley, *Nature (London)*, **197**, 377 (1963).
9) H. Green, *Talanta*, **20**, 158 (1973).
10) T. Sato and H. Watanabe, *Anal. Chim. Acta*, **49**, 463 (1970).
11) T. Sato and H. Watanabe, *Anal. Chim. Acta*, **54**, 439 (1971).
12) I. S. El-Yamani, M. Y. Farah, and F. A. Abd El-Aleim, *J. Radioanal. Chem.*, **45**, 125 (1978).
13) I. S. El-Yamani, M. Y. Farah, and F. A. Abd El-Aleim, *Talanta*, **25**, 714 (1978).
14) a) K. Grudpan and C. G. Taylor, *Analyst*, **109**, 585 (1984); b) T. Braun and G. Ghersini, "Extraction Chromatography," Elsevier Scientific Publishing Company, Amsterdam (1975).
15) C. A. Colvin, Atlantic Richland Hanford Co., Richland, Wash., USA, ASH-SA-28. 1969, 12 p. CONF-690606-2.
16) P. G. Barbano and L. Rigali, *J. Chromatogr.*, **29**, 309 (1967).
17) E. P. Horwitz, K. A. Orlandini, and C. A. A. Bloomquist, *Inorg. Nucl. Chem. Lett.*, **2**, 87 (1966).
18) N. R. Das and P. Chattopadhyay, *J. Radioanal. Nucl. Chem. Articles*, **109**, 1 (1987).
19) S. N. Bhattacharyya and S. Sarkar, *J. Inorg. Nucl. Chem.*, **41**, 755, 1979.
20) A. K. De, S. M. Khopkar, and R. A. Chalmers, "Solvent Extraction of Metals," Van Nostrand Reinhold Company, London (1970), p. 25.
21) T. Omori and N. Suzuki, *Bull. Chem. Soc. Jpn.*, **35**, 1633 (1962).
22) A. K. Mukherjee, "Analytical Chemistry of Zirconium and Hafnium," Pergamon Press, Oxford (1970).
23) "Comprehensive Inorganic Chemistry," ed by A. F. Trotman-Dickenson, Pergamon Press, NY (1970), Vol. 3, Chap. 33.
24) J. Kooi, *Radiochim. Acta*, **5**, 91 (1966).
25) E. P. Horwitz, C. A. A. Bloomquist, and H. E. Griffin, US. At. Energy Comm. Rept. ANL-7569, (1969).

 © 1988 The Chemical Society of Japan Bull. Chem. Soc. Jpn., 61, 4427—4430 (1988)

Synthesis of γ-Butyrolactones, Quinoxalines, and Azauracils from 4-Aryl-2-oxobutanoic Acid Derivatives[1)]

G. H. Labib, M. Abdel Rahman, Y. El-Kilany, A. I. El-Massry, and E. S. H. El-Ashry*
Chemistry Department, Faculty of Science, Alexandria University, Alexandria, Egypt (A. R. E.)
(Received November 26, 1987)

4-Aralkyl-5-aryl-3-hydroxy-2(5*H*)-furanones (**2**) have been prepared from the corresponding 4-aryl-2-oxobutanoic acids (**1**). The anticipated products from the reaction of the furanones (**2**) with *o*-phenylenediamine (**3**) have not been isolated, but products resulting from the condensation followed by retro-aldol type of reaction are obtained and determined as 3-(2-arylethyl)-2(1*H*)-quinoxalinones (**4**). Compounds **4** could be readily obtained by the condensation of **3** with **1**. 4-Aryl-2-oxobutanoic acid thiosemicarbazones (**5**) have been cyclized to 5-(2-arylethyl)-6-azauracils (**6**).

Butyrolactones are one of the integral building blocks of many natural products.[2)] Moreover, they exhibit a wide range of biological activities.[3)] The antitumour properties of lignans and the identification of a butyrolactone, with *m*-hydroxybenzyl residues in the urine of certain mammals have attracted much interest in their physiological activities and consequently, in their synthesis.[4)] In the present report, as a continuation of our work[5)] on lactones and vitamin C, we have prepared a number of unsaturated γ-butyrolactones possessing aralkyl residues. Having the above aspects in mind, the prepared lactones are of potential value as precursors for the synthesis of biologically important functionalized lactones. Moreover, their conversion into heterocyclic compounds of potential chemotherapeutic interest, such as quinoxalines and azauracils, have been investigated.

Results and Discussion

The 4-aryl-2-oxobutanoic acids (**1**) were prepared by the reductive rearrangement of the corresponding 4-aryl-2-oxo-3-butenoic acids; the preparation[6)] of which was carried out by the condensation of pyruvic acid with aromatic aldehydes in alkaline medium followed by acidification.

The condensation of the keto acids **1** with aromatic aldehydes in a solution of acetic acid and in the presence of hydrogen chloride afforded the corresponding butyrolactones **2**. The structures of **2** were deduced from the mode of their preparation[6)] as well as from their spectral data (Table 1). They exist exclusively in the enolic form in the solid state. This conclusion was based on the absence of carbonyl absorption bands in their IR spectra, whereas they showed absorptions indicating the presence of lactone carbonyl and hydroxyl groups at 1740—1755 and 3210—3350 cm^{-1}, respectively. The ^1H NMR spectrum of **2g** in a solution of $CDCl_3$ showed a broad singlet at δ 6.0 due to the hydroxyl group. The singlet appearing at δ 5.45 was due to H-5 and agreed with the enolic structure, otherwise it would be splitted by a neighboring proton if it existed in the keto form. The methylene protons appeared as two doublets at δ 3.68 and 2.82 (J=16 Hz) indicating their nonequivalence. This may be attributed to the difference in orientation of the two protons with respect to the anisotropic effect of the aromatic residue on position 5.

The reaction of α-keto lactones such as dehydroascorbic acid and its analogues with *o*-phenylenediamine **3** has been investigated extensively[5,7)] in our laboratory. The reaction products were usually of the 2(1*H*)-quinoxalinone type resulting from a direct condensation accompanied by a lactone ring opening. However, the attempted condensation of the lactones **2** with **3** did not similarly afford the anticipated 2(1*H*)-quinoxalinones or even fused furoquinoxaline derivatives. The reaction products were assigned to be the structures **4**. This was apparent from the elemental analysis which indicated the loss of the elements Ar'CHO. The infrared spectra of **4** showed the presence of bands in the carbonyl frequency region at 1665 cm^{-1} indicating the presence of OCN groups, thus, rejecting the structure having the fused heterocyclic ring in agreement with a structure having a quinoxalinone ring. The ^1H NMR spectrum (DMSO-d_6) of **4**, showed a singlet of four-proton intensity at δ=3.10 due to the ethylene group and a singlet of one proton intensity at δ=12.37 due to NH. The aromatic protons appeared as a multiplet at δ=7.0—8.0. Conclusive evidence for the structure to be 3-aralkyl-2(1*H*)-quinoxalinone was provided by their unequivocal synthesis by the reaction of the corresponding 4-aryl-2-

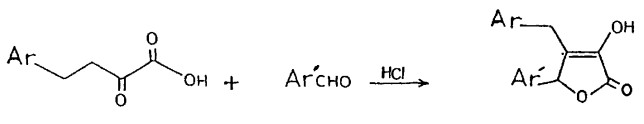

1 2

a) Ar=C_6H_5-, Ar'=CH_3-*p*-C_6H_4-
b) Ar=C_6H_5-, Ar'=CH_3O-*p*-C_6H_4-
c) Ar=CH_3-*p*-C_6H_4-, Ar'=C_6H_5-
d) Ar=CH_3-*p*-C_6H_4-, Ar'=CH_3-*p*-C_6H_4-
e) Ar=CH_3-*p*-C_6H_4-, Ar'=CH_3O-*p*-C_6H_4-
f) Ar=Cl-*p*-C_6H_4-, Ar'=C_6H_5-
g) Ar=Cl-*p*-C_6H_4-, Ar'=CH_3-*p*-C_6H_4-
h) Ar=Cl-*p*-C_6H_4-, Ar'=CH_3O-*p*-C_6H_4-
i) Ar=Cl-*p*-C_6H_4-, Ar'=NO_2-*p*-C_6H_4-

Scheme 1.

Table 1. ^{1}H NMR Spectral Data

Compd. No.	Solvent	Chemical shifts (δ) and assignments
2a	$CDCl_3$	7.00 (m, 9H, Ar), 6.00 (bs, 1H, OH is D_2O exchangeable), 5.45 (s, 1H, -CH-), 3.25 (dd, J=15 Hz, 2H, CH_2), 2.28 (s, 3H, CH_3)
2f	$CDCl_3$	7.10 (m, 10H, Ar, OH), 5.48 (s, 1H, -CH-), 3.43 (dd, J=15 Hz, 2H, CH_2)
2g	DMSO-d_6	10.27 (s, 1H,OH is D_2O exchangeable), 7.15 (m, 8H, Ar), 5.67 (s, 1H, -CH-), 3.40 (dd, J=15 Hz, 2H, CH_2), 2.30 (s, 3H, CH_2)
2h	DMSO-d_6	10.31 (s, 1H, OH is D_2O exchangeable), 7.10 (m, 8H, Ar), 5.70 (s, 1H, -CH-), 3.82 (s, 3H, OCH_3), 3.40 (dd, J=15 Hz, 2H, CH_2)
2i	DMSO-d_6	10.55 (s, 1H, OH is D_2O exchangeable), 7.21, 8.18 (m, d, 8H, Ar), 5.99 (s, 1H, -CH-), 3.43 (dd, J=15 Hz, 2H, CH_2)

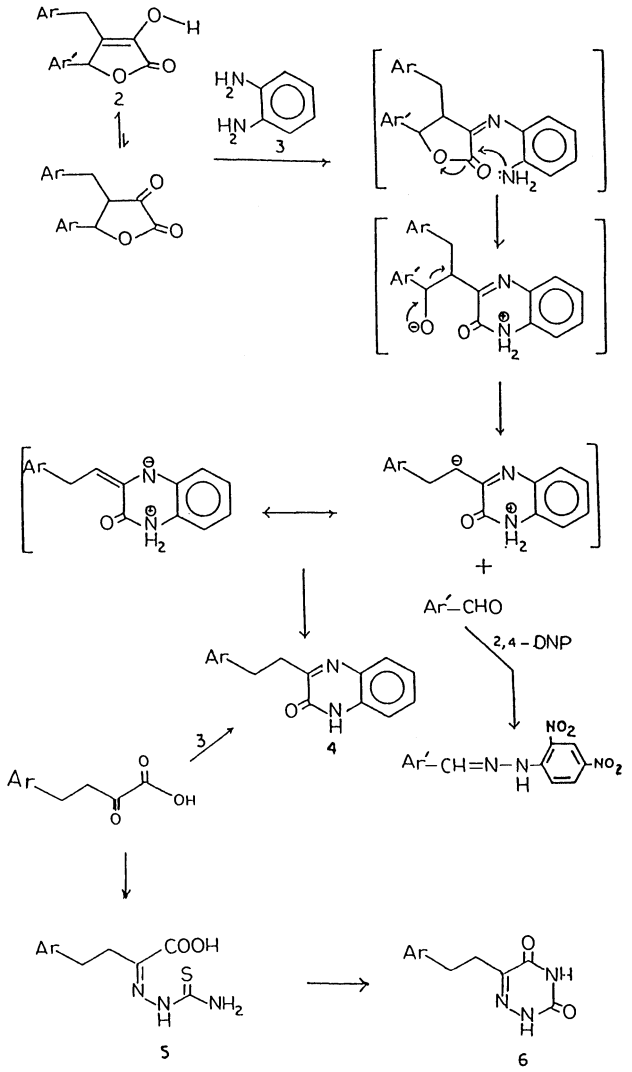

Scheme 2.

oxobutanoic acid **1** with *o*-phenylenediamine.

The formation of **4** from the lactone **2** may be explained as outlined in Scheme 2. The reaction may be started by a nucleophilic attack of the amino group on the α-carbonyl group in the keto form of **2** to give the Schiff base, which was not isolated, followed by the attack of the second amino group on the lactone carbonyl group which caused its ring opening. The final step of the reaction sequence is a retro-aldol condensation in which aldehyde is split off to give the product **4**. The generated aldehyde was trapped and isolated as its 2,4-dinitrophenylhydrazone.

When 4-aryl-2-oxobutanoic acids (**1**) were treated with thiosemicarbazide, they gave the corresponding thiosemicarbazones **5**, which upon boiling with methyl iodide in ethanol afforded colorless products whose elemental analyses and spectroscopic data agreed with the cyclized structures **6**. Their infrared spectra showed bands at 1685—1665 cm^{-1} due to the OCN groups and bands at 3240—3100 cm^{-1} due to NH groups. Their ^{1}H NMR spectra agreed with the assigned structures.

Experimental

Generals. Melting points were determined with Meltemp apparatus with a 76-mm immersion thermometer, and are uncorrected. Infrared spectra were recorded with a pye Unicam SP1025 spectrometer. ^{1}H NMR spectra were taken on a Varian EM-390 spectrometer. Chemical shifts are expressed in δ scale relative to tetramethylsilane as an internal standard. Elemental analyses were performed at Faculty of Science, Cairo University.

4-Aralkyl-5-aryl-3-hydroxy-2(5*H*)-furanone (2). A solution of **1** (5.6 mmol) and the aromatic aldehyde (5.6 mmol) in glacial acetic acid (6 ml) and 18% hydrochloric acid (6 ml) was heated on a water-bath for 4 h. The reaction mixture was poured onto crushed ice. The organic material was extracted with ether and the ether extract was washed with water, 5% sodium hydrogencarbonate solution to separate the unreacted acid, followed by 5% sodium hydroxide solution. The sodium hydroxide extract was cooled, acidified with cold concentrated hydrochloric acid and left overnight. The product was filtered, washed with water, dried, and recrystallized from the indicated solvent (Table 2).

3-(2-Phenylethyl)-2(1*H*)-quinoxalinone (4a). a) A solu-

Table 2. Microanalytical and Infrared Spectral Data of 4-Aralkyl-5-aryl-3-hydroxy-2(5*H*)-furanones (**2**)[a]

Compd. No.	Ar	Ar′	Yield %	Mp °C	Molecular formula	Calcd (Found) (%) C	Calcd (Found) (%) H	ν_{max}^{KBr}/cm^{-1} CO	ν_{max}^{KBr}/cm^{-1} OH
2a	C_6H_5	CH_3-*p*-C_6H_4	19	147—148	$C_{18}H_{16}O_3$	77.1 (76.80)	5.7 (5.8)	1755	3250
2b	C_6H_5	CH_3O-*p*-C_6H_4	24	106	$C_{18}H_{16}O_4$	73.0 (73.1)	5.4 (5.6)	1750	3350
2c	CH_3-*p*-C_6H_4	C_6H_5	42	111—112	$C_{18}H_{16}O_3$	77.1 (76.9)	5.7 (5.5)	1740	3315
2d	CH_3-*p*-C_6H_4	CH_3-*p*-C_6H_4	27	155—156	$C_{19}H_{18}O_3$	77.6 (78.0)	6.1 (6.2)	1745	3300
2e	CH_3-*p*-C_6H_4	CH_3O-*p*-C_6H_4	19	102	$C_{19}H_{18}O_4$	73.6 (73.7)	5.8 (5.7)	1755	3300
2f	Cl-*p*-C_6H_4	C_6H_5	32	142—144	$C_{17}H_{13}ClO_3$	67.9 (67.9)	4.3 (4.5)	1745	3350
2g	Cl-*p*-C_6H_4	CH_3-*p*-C_6H_4	35	130—132	$C_{18}H_{15}ClO_3$	68.7 (69.0)	4.8 (4.5)	1755	3210
2h	Cl-*p*-C_6H_4	CH_3O-*p*-C_6H_4	32	118—120	$C_{18}H_{15}ClO_4$	65.6 (65.2)	4.5 (4.6)	1750	3340
2i	Cl-*p*-C_6H_4	NO_2-*p*-C_6H_4	41	156—158	$C_{17}H_{12}ClNO_5$	59.1 (59.1)	3.5 (3.7)	1755	3320

a) Recrystallized from petroleum ether except **a** from carbon tetrachloride-petroleum ether; **b**, **d**, and **h** from benzene-petroleum ether; **i** from carbon tetrachloride.

tion of **2a** (1.12 g, 4 mmol), *o*-phenylenediamine (0.43 g, 4 mmol) and drops of acetic acid in ethanol (25 ml) was heated on a water-bath for 4 h. It was then concentrated and the product (yield 0.4 g, 40%) was crystallized from ethanol as colorless needles, mp 207—209 °C; ν_{max}^{KBr} 1665 (OCN) and 3140 (NH) cm^{-1}. ^{1}H NMR (DMSO-d_6): δ=3.10 (s, 4H, $2CH_2$), 7.33, 7.74 (m, d, 9H, Ar), 12.37 (s, 1H, NH is D_2O exchangeable).

Found: C, 77.1; H, 5.7; N, 11.1%. Calcd, for $C_{16}H_{14}N_2O$: C, 76.8; H, 5.6; N, 11.2%.

The *p*-methylbenzaldehyde which splitted out from the reaction was trapped as *p*-methylbenzaldehyde 2,4-dinitrophenylhydrazone.

b) A solution of **1a** (0.78 g, 4.4 mmol), and *o*-phenylenediamine (0.47 g, 4.4 mmol) in ethanol (20 ml) was heated under reflux on a water-bath for 1 h, and the product (yield 0.3 g, 27%) was found to be identical with the one obtained by method a.

3-[2-(*p*-Chlorophenyl)ethyl]-2(1*H*)-quinoxalinone (4g). a) A solution of **2g** (0.6 g, 1.9 mmol), *o*-phenylenediamine (0.2 g, 1.9 mmol) and drops of acetic acid in ethanol (18 ml) was processed as above to give the title compound (yield 0.35 g, 65%) as pale yellow needles; mp 218—220 °C; ν_{max}^{KBr} 1665 (OCN) and 3140 (NH) cm^{-1}. ^{1}H NMR (DMSO-d_6): δ=3.10 (s, 4H, $2CH_2$), 7.33, 7.76 (m, d, 8H, Ar), 12.36 (s, 1H, NH is D_2O exchangeable).

Found: C, 67.3; H, 4.9; N, 9.8%. Calcd for $C_{16}H_{13}Cl\ N_2O$: C, 67.5; H, 4.6; N, 9.8%.

The *p*-methylbenzaldehyde which splitted out from the reaction was trapped as *p*-methylbenzaldehyde 2,4-dinitrophenylhydrazone.

b) A solution of 4-(*p*-chlorophenyl)-2-oxobutanoic acid (**1f**, 0.12 g, 0.6 mmol), and *o*-phenylenediamine (0.06 g, 0.6 mmol) in ethanol (10 ml) was processed as before to give a product (yield 0.1 g, 63%) identical with that obtained by method a.

4-(*p*-Methylphenyl)-2-oxobutanoic Acid Thiosemicarbazone (5c). A solution of **1c** (1.92 g, 10 mmol) and thiosemicarbazide (0.91 g, 10 mmol) in ethanol (50 ml) was heated under reflux on a water-bath for 1 h. The product was crystallized from water as colorless crystals; mp 174—175 °C; ν_{max}^{KBr} 1680 (COOH), 3200, 3280, 3440 (NH, NH_2, OH) cm^{-1}.

Found: C, 54.6; H, 5.9; N, 15.8%. Calcd. for $C_{12}H_{15}N_3O_2S$: C, 54.3; H, 5.7; N, 15.9%.

4-(*p*-Chlorophenyl)-2-oxobutanoic Acid Thiosemicarbazone (5f). A solution of **1f** (1.06 g, 5 mmol) and thiosemicarbazide (0.45 g, 5 mmol) in ethanol (25 ml) was processed as above to give the title compound (yield 0.8 g, 56%) as colorless crystals; mp 178—179 °C; ν_{max}^{KBr} 1687 (COOH), 3200, 3290, 3470 (NH, NH2, OH) cm^{-1}.

Found: C, 46.6; H, 4.3; N, 14.5%. Calcd for $C_{11}H_{12}ClN_3O_2S$: C, 46.2; H, 4.2; N, 14.7%.

5-[2-(*p*-Methylphenyl)ethyl]-6-azauracil (6c). A solution of **5c** (0.27 g, 1 mmol) in ethanol (5 ml) was treated with methyl iodide (0.15 ml) and the reaction mixture was heated under reflux on a water bath for 3 h. The product (yield 0.15 g, 65%) was crystallized from ethanol as colorless crystals; mp 207—208 °C; ν_{max}^{KBr} 1685 (OCN) and 3240 (NH) cm^{-1}. ^{1}H NMR (DMSO-d_6): δ=2.17 (s, 3H, CH_3), 2.67 (s, 4H, $2CH_2$), 6.90 (m, 4H, Ar), 11.80 (s, 2H, 2NH are D_2O exchangeable).

Found: C, 62.0; H, 5.6; N, 18.4%. Calcd for $C_{12}H_{13}N_3O_2$: C, 62.3; H, 5.6; N, 18.2%.

5-[2-(*p*-Chlorophenyl)ethyl]-6-azauracil (6f). A solution of **5f** (0.29 g, 1 mmol) in ethanol (10 ml) was treated with methyl iodide (0.15 ml) and the reaction mixture was processed as above to give the product (yield 0.17 g, 68%); mp 229—230 °C; ν_{max}^{KBr} 1665 (OCN) and 3100 (NH) cm^{-1}. ^{1}H NMR (DMSO-d_6): δ=2.81 (s, 4H, $2CH_2$), 7.22 (m, 4H, Ar), 11.93 (s, 2H, 2NH are D_2O exchangeable).

Found: C, 52.4; H, 4.0; N, 16.6%. Calcd. for $C_{11}H_{10}ClN_3O_2$: C, 52.5; H, 4.0; N, 16.7%.

References

1) Ketoacids and lactones, Part 2. For part 1, see E. S. H. El Ashry, A. Amer, G. Labib, A. Abdel Rahman, and A. El Massry, *J. Heterocycl. Chem.*, **24**, 63 (1987). A part in the series "Scope of the Reactions of Hydrazines and Hydrazones," Abstracted from the M. Sc. (1981) and Ph. D. (1984) Theseses of A. El Massry.

2) Y. S. Rao, *Chem. Rev.*, **76**, 625 (1976); R. McCrindle and E. Nakamura, *Can. J. Chem.*, **52**, 2029 (1974); L. J. Haynes and J. R. Plimmer, *Quart. Rev. Chem. Soc.*, **14**, 292 (1960); T. C. McMorris and A. W. Barksdales, *Nature (London)*, **215**, 5098 (1967); H. M. R. Hoffman and J. Rape, *Angew. Chem., Int. Ed. Engl.*, **214**, 94 (1985); N. Petragnani, H. M. C. Ferraz, and G. V. J. Silva, *Synthesis*, **1986**, 157.

3) L. J. Haynes, *Quart. Rev. London*, **2**, 46 (1948); F. Dickens, *Brit. Med. Bull.*, **20**, 96 (1964); J. H. Hartwell, *Cancer Treat. Rep.*, **60**, 1031 (1976); A. H. Barclay and R. E. Perdue, Jr., *Cancer Treat. Rep.*, **60**, 1081 (1976).

4) G. Cooley, R. D. Farrant, D. N. Kirk, and S. Wynn, *Tetrahedron Lett.*, **22**, 349 (1981); A. Pelter, P. Satyanarayana, and R. S. Ward, *Tetrahedron Lett.*, **22**, 1549 (1981).

5) E. S. H. El Ashry, *Advan. Chem. Ser. (ACS)*, **200**, 179 (1982).

6) P. Cordier and S. Jung, *C. R. Acad. Sci.*, **252**, 3199 (1960); P. Cordier and A. Haberzettl, *C. R. Acad. Sci., Ser. C*, **254**, 699 (1962).

7) E. S. H. El Ashry, M. A. Abdel Rahman, Y. El. Kilany, and N. Rashed, *Carbohydr. Res.*, **153**, 146 (1986); E. S. H. El Ashry, Y. El Kilany, N. El Shimy, and T. N. Huckerby, *Sci. Pharm.*, **54**, 121 (1986); E. S. H. El Ashry, Y. El Kilany, and H. Abdel Hamid, *Gazz. Chim. Ital.*, **116**, 721 (1986); H. Zimmer and A. Amer, *J. Heterocycl. Chem.*, **20**, 359 (1983).

α,β-Unsaturated Nitriles in Heterocyclic Synthesis. Novel Synthesis of Pyridines and Thieno[2,3-*b*]pyridine Derivatives

Galal E. H. ELGEMEIE,* Hassan A. ELFAHHAM,† and Hesham A. NABEY†
Chemistry Department, Faculty of Science, Bani Suef, Egypt
†Chemistry Department, Faculty of Science, Minia University, Minia, Egypt
(Received February 15, 1988)

Arylmethylenecyanothioacetamide reacts with ethyl acetoacetate and acetylacetone to give the corresponding 3-cyano-2(1*H*)-pyridinethione derivatives, which can be alkylated at sulfur atom and cyclized into the corresponding thieno[2,3-*b*]pyridine derivatives.

α,β-Unsaturated nitriles are versatile reagents that have been extensively utilized in heterocyclic synthesis.[1-3] We have previously reported several novel syntheses of azoles,[4] azines,[5] and azoloazines[6] utilizing α,β-unsaturated nitriles as starting components. In continuation of this work, we report here the results of our investigation into the utility of the readily obtainable arylmethylenecyanothioacetamide in heterocyclic synthesis. The investigation have resulted in the development of a novel procedure for the synthesis of pyridines and thieno[2,3-*b*]pyridine derivatives. The compounds obtained seem promising for further chemical transformations and for biological evaluation studies.

Thus, it has been found that benzylidencyanothioacetamide (**1a**) reacted with acetylacetone (**2a**) in boiling ethanol containing catalytic ammounts of piperidine to yield a product with the molecular formula $C_{15}H_{12}N_2OS$ (M^+ 268). Structure **4a** was considered for the product. ^1H NMR spectroscopy was used to confirm this structure for the product. Thus, ^1H NMR revealed two singlets at δ 1.90 and 2.55 assignable for two methyl groups, a broad band at δ 13.86 assignable to NH group, and a multiplet at δ 6.24—

Table 1. Analytical Data of Compounds **4**, **5**, and **6**

Compound	Ar	X	R	Yield %	Mp θ_m/°C	Found/Calcd (%) C	H	N	*m/z*
4a	C_6H_5	$COCH_3$		75	198—199	67.6	4.1	10.0	268
						67.2	4.5	10.4	
4b	4-$CH_3OC_6H_4$	$COCH_3$		70	235—237	64.0	4.5	9.0	
						64.4	4.7	9.4	
4c	4-$(CH_3)_2NC_6H_4$	$COCH_3$		80	248—250	65.8	5.8	13.2	311
						65.6	5.5	13.5	
4b	2-Furanyl	$COCH_3$		72	145	60.8	3.6	10.6	258
						60.5	3.9	10.9	
4e	C_6H_5	CO_2Et		70	180—182	64.3	4.5	9.0	
						64.4	4.7	9.4	
4f	4-$CH_3OC_6H_4$	CO_2Et		75	193—195	62.1	4.5	8.1	328
						62.2	4.9	8.5	
4g	4-$(CH_3)_2NC_6H_4$	CO_2Et		70	244—245	63.8	5.9	12.0	341
						63.3	5.6	12.3	
4h	2-Furanyl	CO_2Et		80	238—240	58.2	4.4	9.5	288
						58.3	4.2	9.7	
5a	C_6H_5	$COCH_3$	H	77	120—122	67.8	4.9	9.5	
						68.1	5.0	9.9	
5b	4-$CH_3OC_6H_4$	$COCH_3$	H	75	135—136	65.6	5.3	8.6	312
						65.4	5.1	9.0	
5c	4-$(CH_3)_2NC_6H_4$	$COCH_3$	H	75	116—117	66.6	5.5	12.5	
						66.5	5.8	12 9	
5d	2-Furanyl	$COCH_3$	H	70	90—92	62.0	4.0	9.9	
						61.8	4.4	10.3	
5e	C_6H_5	CO_2Et	H	70	87—88	65.7	5.3	8.6	
						65.4	5.1	9.0	
5f	4-$CH_3OC_6H_4$	CO_2Et	H	73	80—82	62.9	5.0	7.8	
						63.2	5.3	8.2	
5g	4-$(CH_3)_2NC_6H_4$	CO_2Et	H	80	138—140	63.8	5.5	11.5	355
						64.2	5.9	11.8	
5h	2-Furanyl	CO_2Et	H	72	85	59.4	4.8	9.6	
						59.6	4.6	9.3	

Table 1. (Continued)

Compound	Ar	X	R	Yield %	Mp θ_m/°C	Found/Calcd (%) C	H	N	m/z
6a	C_6H_5	$COCH_3$	COC_6H_5	70	143—145	71.2	4.5	6.9	
						71.5	4.7	7.2	
6b	4-$CH_3OC_6H_4$	$COCH_3$	COC_6H_5	70	150	69.0	4.7	6.5	416
						69.2	4.8	6.7	
6c	4-$(CH_3)_2NC_6H_4$	$COCH_3$	COC_6H_5	73	190	69.5	5.0	9.5	
						69.9	5.4	9.8	
6d	2-Furanyl	$COCH_3$	COC_6H_5	70	138—140	66.8	4.8	7.2	
						67.0	4.3	7.4	
6e	C_6H_5	CO_2Et	COC_6H_5	75	108—110	69.0	4.5	6.5	
						69.2	4.8	6.7	
6f	4-$CH_3OC_6H_4$	CO_2Et	COC_6H_5	65	99—100	67.0	5.3	6.2	
						67.3	5.3	6.3	
6g	4-$(CH_3)_2NC_6H_4$	CO_2Et	COC_6H_5	60	163—165	68.2	5.0	9.1	
						68.0	5.4	9.2	
6h	2-Furanyl	CO_2Et	COC_6H_5	67	82—83	64.8	4.2	6.6	
						65.0	4.4	6.9	

Table 2. Spectral Data of Compounds **4**, **5**, and **6**

Compound	IR (KBr)/cm^{-1}	^1H NMR (DMSO) δ/ppm
4b	3450 (NH); 2225 (CN); 1700 (CO)	1.92 (s, 3H, CH_3); 2.52 (s, 3H, CH_3); 3.80 (s, 3H OCH_3); 6.32—6.92 (m, 4H, C_6H_4); 13.95 (s, br 1H, NH)
4e	3300—3200 (NH); 2220 (CN); 1680 (CO)	0.92 (t, J=7 Hz, 3H, CH_3); 2.66 (s, 3H, CH_3); 4.00 (q, J=7 Hz, 2H, CH_2); 7.27—7.56 (m, 5H, C_6H_5); 13.98 (s, br, 1H, NH)
4f	3400 (NH); 2215 (CN); 1720 (CO)	0.89 (t, J=7 Hz, 3H, CH_3); 2.22 (s, 3H, CH_3); 3.82 (s, 3H, OCH_3); 3.99 (q, J=7 Hz, 2H, CH_2); 7.02—7.42 (m,4H, C_6H_4); 13.8 (s, br 1H, NH)
4h	3250 (NH); 2215 (CN); 1730 (CO)	1.1 (t, J=7 Hz, 3H, CH_3); 2.42 (s, 3H, CH_3); 4.18 (q, J=7 Hz, 2H, CH_2); 6.82 (m, 1H furan H-3); 7.42 (d, J=6 Hz, 1H, furan H-4); 8.18 (d, J=6 Hz, 1H, furan H-5); 13.88 (s, br, 1H, NH)
5a	2220 (CN); 1700 (CO)	1.85 (s, 3H, CH_3); 2.55 (s, 3H, CH_3); 2.65 (s, 3H, SCH_3); 7.32—7.60 (m, 5H, C_6H_5)
5b	2220 (CN); 1690 (CO)	1.66 (s, 3H CH_3); 2.22 (s, 3H, CH_3); 2.68 (s, 3H, SCH_3); 3.42 (s, 3H, OCH_3); 6.5—6.8 (m, 4H, C_6H_4)
5d	2220 (CN); 1700 (CO)	2.22 (s, 3H, CH_3); 2.55 (s, 3H, SCH_3); 2.66 (s, 3H, CH_3), 6.68 (m, 1H, furan H-3); 7.22 (d, J=6 Hz, 1H furan H-4); 7.65 (d, J=6 Hz, 1H, furan H-5)
5f	2220 (CN); 1715 (CO)	0.94 (t, J=7.5 Hz, 3H, CH_3); 2.33 (s, 3H, CH_3); 2.41 (s, 3H, SCH_3); 3.40 (s, 3H, OCH_3); 3.81 (q, J=7.5 Hz, 2H, CH_2); 6.32—6.88 (m, 4H, C_6H_4)
5g	2220 (CN); 1715 (CO)	0.96 (t, J=7.5 Hz, 3H, CH_3); 2.30 (s, 3H, CH_3); 2.35 (s, 3H, SCH_3); 2.68 (s, 6H, $N(CH_3)_2$); 3.88 (q, J=7.5 Hz, 2H, CH_2); 6.44—678 (m, 4H, C_6H_4)
5h	2220 (CN); 1730 (CO)	1.25 (t, J=7.5 Hz, 3H, CH_3); 2.62 (s, 3H, CH_3); 2.68 (s, 3H, SCH_3); 4.22 (q, J=7.5 Hz, 2H, CH_2); 6.60 (m, 1H, furan 3-H); 7.25 (d, J=6 Hz, 1H, furan 4-H); 7.64 (d, J=6 Hz, 1H, furan 5-H)
6a	3400, 3200 (NH_2); 1700 (CO)	2.00 (s, 3H, CH_3); 2.26 (s, 3H, CH_3); 6.66 (s, br, 2H, NH_2); 7.22—7.88 (m, 10H, $2C_6H_5$)
6b	3500, 3200 (NH_2); 1700 (CO)	2.00 (s, 3H, CH_3); 2.32 (s, 3H, CH_3); 3.8 (s, 3H, OCH_3); 6.06—7.23 (m, 11H, C_6H_5, C_6H_4 and NH_2)
6d	3400—3200 (NH_2); 1710 (CO)	2.08 (s, 3H, CH_3); 2.58 (s, 3H, CH_3); 6.68 (m, 2H, furan 3,4-H); 7.08 (s, br, 2H, NH_2); 7.42 (d, J=6.5 Hz, 1H, furan 5-H); 7.48—7.92 (m, 5H, C_6H_5)
6g	3450 (NH_2); 1718 (CO)	1.1 (t, J=7.5 Hz, 3H, CH_3); 2.62 (s, 3H, CH_3); 3.08 (s, 6H, $N(CH_3)_2$); 4.20 (q, J=7.5 Hz, 2H, CH_2); 6.7—7.88 (m, 11H, C_6H_5, C_6H_4 and NH_2)

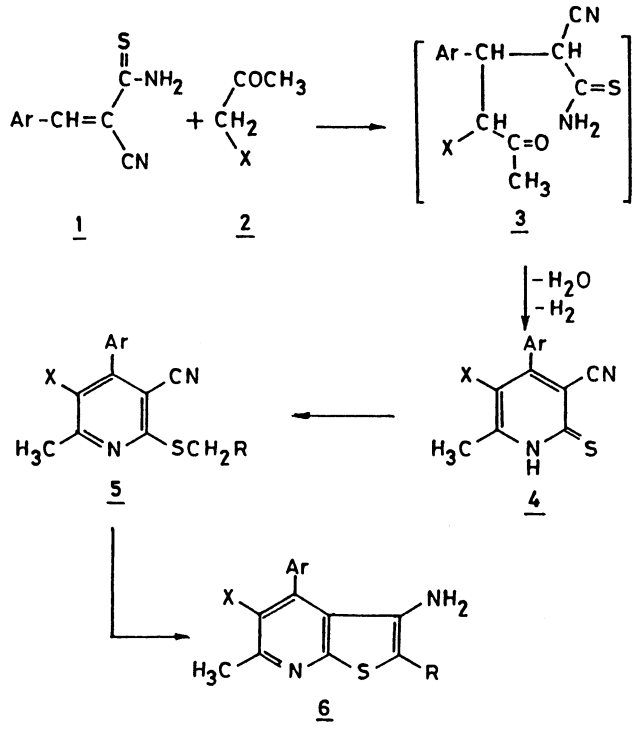

7.00 assigned for aromatic protons (cf. Table 2). The formation of **4** from the reaction of **1** with **2** is assumed to proceed via Michael type addition of the methylene function in **2** to the activated double bond in **1** to yield acyclic Michael adducts **3** which then loses H_2O and cyclizes into the final isolable stable compounds **4**.

Subjecting the potassium salts of **4** to the action of alkylating agents such as methyl iodide afforded the corresponding *S*-alkyl derivatives **5**. The sturcture of **5** was inferred from analysis, MS and ^{1}H NMR. When using phenacyl bromide as alkylating agent, the *S*-alkylated derivative can not be isolated, but cyclized into thieno[2,3-*b*]pyridines **6**. The structure of **6a** could be established for the reaction product based on the absence of a CN absorption in the IR spectrum and on ^{1}H NMR which revealed two singlets at δ 2.00 and 2.26 assignable for two methyl groups, a broad band at δ 6.66 assignable to amino group, and a multiplet at δ 7.22—7.88 assigned for aromatic protons (cf. Table 2). The formation of **6** from reaction of **4** with phenacyl bromide constitutes a new synthesis of thieno[2,3-*b*]pyridine derivatives.

Experimental

All melting points are uncorrected. Analytical data were obtained from the Microanalytical Data Unit at Cairo University. The IR spectra were obtained on a Pye-Unicam SP-1000 spectrophotometer. ^{1}H NMR spectra were measured in DMSO or $CDCl_3$ on a Varian EM-360-60 MHz using TMS as internal standard and chemical shifts are expressed as δ ppm. Mass spectra were recorded on a Varian MAT 112 spectrometer.

Compounds **1a—d** were prepared following literature procedure.[7]

5-Substituted 4-Aryl-3-cyano-6-methyl-2(1*H*)-pyridinethione (4a—d). General Procedure: To a mixture of arylmethylenecyanothioacetamide **1** (0.01 mol) and acetylacetone **2a** or ethyl acetacetate **2b** (0.01 mol) in ethanol (50 ml), piperidine (a few drops) is added. The mixture is heated under reflux for 3 h, and then allowed to stand overnight. The resultant precipitate is isolated by suction and crystallized.

5-Substituted 4-Aryl-3-cyano-6-methyl-2-(methylthio)pyridines (5a—d). General Procedure. A mixture of **4** (0.01 mol), KOH powder (0.02 mol), and MeI (0.02 mol) in dry CH_2Cl_2 (50 ml) was stirred at room temperature for 3 h and then diluted with cold water (100 ml). The dichloromethane layer was washed several times with water, dried and then evaporated. The resulting solid product was collected by filteration and crystallized.

Thieno[2,3-*b*]pyridine Derivatives (6a—d). General Procedure: A mixture of **4** (0.01 mol), K_2CO_3 (0.02 mol), and phenacyl bromide (0.01 mol) in dry DMF (50 ml) was stirred at room temperature for 3 h and then diluted with cold water (50 ml). The resulting solid product was collected by filteration and crystallized.

References

1) G. E. H. Elgemeie and F. A. Aal, *Heterocycles*, **24**, 349 (1986).

2) G. E. H. Elgemeie, M. M. Sallam, S. M. Sherif, and M. H. Elnagdi, *Heterocycles*, **23**, 3107 (1985).

3) G. E. H. Elgemeie, A. M. Gohar, H. A. Regaila, and H. A. Elfahham, *Arch. Pharm. (Weinheim)*, **331**, 131 (1988).

4) G. E. H. Elgemeie, H. A. Elfahham, S. M. Hassan, and M. H. Elngadi, *Z. Naturforsch.*, **38b**, 781 (1983).

5) G. E. H. Elgemeie, H. A. Elfahham, S. Elgamal, and M. H. Elnagdi, *Heterocycles*, **23**, 1999 (1985).

6) G. E. H. Elgemeie, B. Y. Riad, G. A. Nawwar, and S. Elgamal, *Arch. Pharm. (Weinheim)*, **320**, 223 (1987).

7) J. S. A. Brunskill and Asish De, *J. Chem. Soc., Perkin Trans. 1*, **1978**, 629.

 © 1988 The Chemical Society of Japan Bull. Chem. Soc. Jpn., 61, 4435—4437 (1988)

Synthesis and Structure of the Diterpenoid Peucelinendiol

Joaquín R. Moran, Victoria Alcazar, and Manuel Grande*
Department of Organic Chemistry, F. C. Químicas, University of Salamanca, 37008 Salamanca, Spain
(Received March 19, 1988)

The synthesis of peucelinendiol has been carried out starting from geraniol, and using as a key intermediates the anion of phenylthiogeraniol and (−)-geraniol epoxide obtained by the Sharpless procedure. Its structure was stablished as (6*S*,7*R*)-7-hydroxymethyl-2,6,10,14-tetramethylpentadeca-2,9,13-trien-6-ol. Isopeucelinendiol, epipeucelinendiol, and epiisopeucelinendiol were also synthesized.

Some years ago we isolated from *Magydaris panacifolia* (Umbelliferae) a new diterpenoid named magydardiendiol,[1] for which the irregular isoprenoid structure **1** was recently proposed.[2] The structure of this diol seems to be the result of a head to head coupling of two monoterpene units, i.e. two geranyl units linked through C_1-C_2' and C_3-C_4'.

Although the head to head coupling is normal in the biogenesis of triterpenoids and carotenoids, it is quite unusual in the case of lower terpenoids. We have only found two more diterpenoids with a head to head skeleton, namely digeranyl[3] and peucelinendiol **2**.[4] Moreover the C_1-C_2' union between isoprenoid chains, quite uncommon, is also present for instance in lavandulol and in tetraterpenes like that one isolated from *Elodea canadensis*.[5]

We were interested in peucelinendiol, because it could be a biogenetic precursor of **1**, and the fact that neither the absolute nor the relative stereochemistry for **2** were given, encouraged us to accomplish the total asymmetric synthesis of peucelinendiol.

Peucelinendiol can be envisaged as the product from the attack of anion **A** on the epoxide **B**, both materials easily available from geraniol. The synthesis of each one of the two possible diastereomers for **2** can be done if the suitable cis or trans epoxide **B** is used as starting material.

The nucleophile **A** can be prepared as a magnesium derivative, a cuprate or a sulfur-stabilized anion. However the high nucleophilicity of stabilized sulfur anions allows to carry out the displacement reactions under very mild conditions and formation of secondary by-products (rearrangement, allylic attack, halohydrine formation···) is minimized. Also good yields are reported in the reaction of allylic sulfur-stabilized anions and epoxides.[6,7] We chose the geranyl phenyl sulfide **4**, as a synthetic equivalent of carbanion **A**.

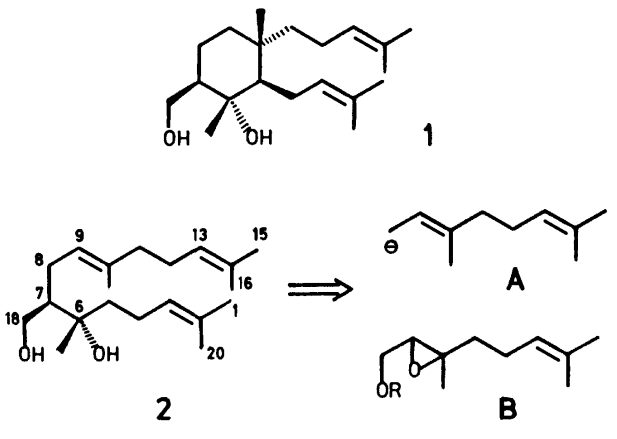

Chart 1.

Treatment of geraniol with 2,4-dinitro-1-fluorobenzene[8] yielded the aromatic ether **3**, which on reaction with potassium benzenethiolate gave the expected allylic sulfide **4** whose physical properties are in good agreement with those reported.[6]

It is known that the hydroxyl group in allylic alcohols can induce the selective epoxidation of the β,γ-double bond in the presence of other olefins. Furthermore, it is possible the asymmetric epoxidation of allylic alcohols with *t*-butyl hydroperoxide, (+)-diethyl tartrate and titanium(IV) isopropoxide.[9] We used this method to prepare the epoxidic substrate **B**. In our hands, the asymmetric epoxidation of geraniol proceeded smoothly to yield the optically active geranyl epoxide **5** in 80% e.e.

The free hydroxyl group of **5** is not compatible with the strong basic conditions needed to the coupling with the anion **A**, so that protection either with butyl vinyl ether, or with methyl isopropenyl ether was used, to give the respective acetal derivatives **6** or **7** in high yield.

Metallation of the allylic sulfide **4** (BuLi, DABCO/THF −25 °C), followed by addition of the protected alcohol epoxide **6** gave in a fast and clean reaction, after deprotection, a single mixture of the phenylthio isomers **8**.

Desulfuration of this material was accomplished either with Raney Ni, or with $Li/NH_3/Et_2NH$. In both cases mixtures of constitutional isomers **2** and **9** were obtained. Although the ratio **2**/**9** was higher when the desulfurization was carried out with $Li/NH_3/Et_2NH$, the product distribution was difficult to control. Chromatography on SiO_2 allowed us to separate both compounds. The physical constants of the diol with the three trisubstituted double bonds were in good agreement with the previously reported for peucelinendiol, and also the optical activity ($[\alpha]_D$+4.4°) was the expected for an 80% e.e. (reported $[\alpha]_D$+5.4°).[4]

According to the stereochemistry of the reactions

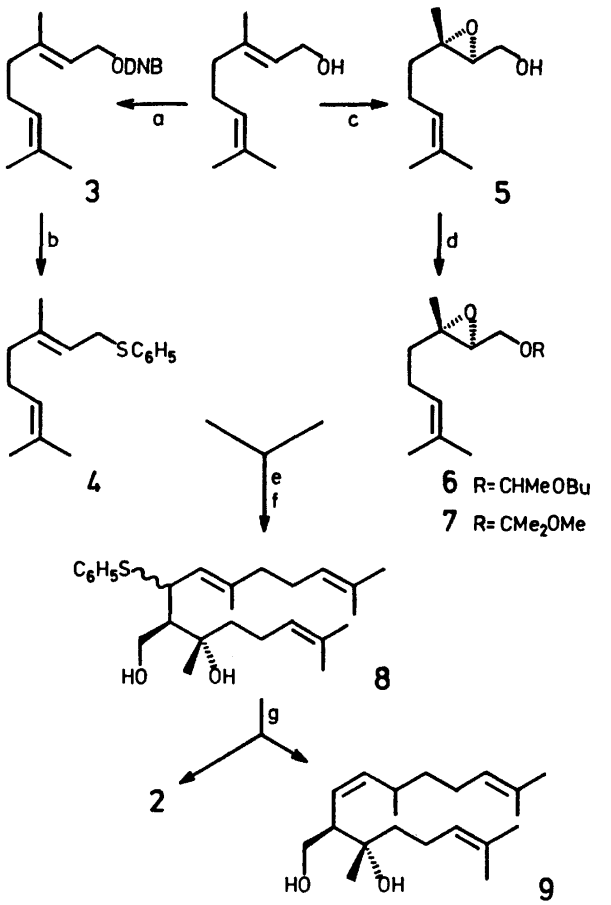

Chart 2.

a) 2,4-DNFB/NEt_3, b) C_6H_5SH, K/EtOH, c) $Ti(OPr)_4$, (+)-DET, THBP/CH_2Cl_2 −20°C, d) BuO-CH=CH_2 or MeOCMe=CH_2/TsOH, e) BuLi, DABCO/THF −25°C, f) HCl 0.5 M, g) Li, NH_3/Et_2NH.

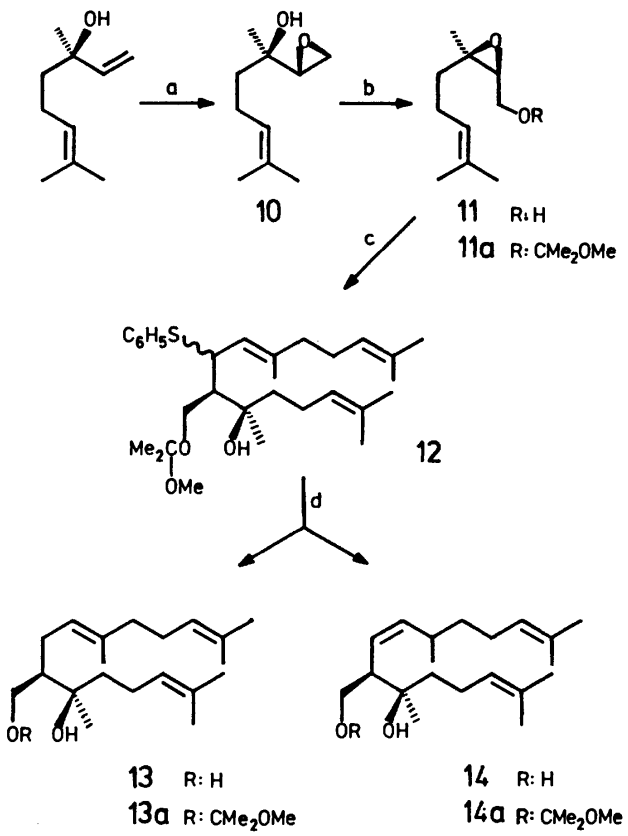

Chart 3.

a) *t*-BuOOH, $VO(acac)_2/C_6H_6$, b) KOH/H_2O, c) MeOCMe=CH_2/C_6H_6 (TsOH); BuLi, DABCO/THF −25°C; **4**, d) Li, NH_3/Et_2NH.

described, we consequently propose for compound **2** the absolute configuration 6*S*, 7*R*.

However to rule out definitively the alternative stereochemistry, we repeated the reaction with the isomeric epoxide **11**. The synthesis of this compound was accomplished starting from (−)-linalool, using *t*-butyl hydroperoxide and $VO(acac)_2$, to get the epoxidation product **10**. This material rearranged cleanly into the trisubstituted epoxide **11** when handled with aqueous KOH.[10] Protection of the hydroxyl group with methyl isopropenyl ether (**11a**), and reaction with the foregoing anion **4**, produced the expected epimeric mixture **12** which upon hydrolysis and desulfurization with $Li/NH_3/Et_2NH$ led to epipeucelinendiol **13** ($[\alpha]_D$−7.5°) and its isomer with the disubstituted double bond **14**.

Comparison of the ^{13}C NMR spectra, specially the signals at 5-C (39.8 vs. 41.6), 7-C (49.6 vs. 47.7), 11-C (38.3 vs. 39.9), and 19-C (26.4 vs. 23.4) of epipeucelinendiol and the already described peucelinendiol, led no doubt about their different structures. As a conclusion we propose the structure **2** for natural peucelinendiol.

Experimental

Optical rotations were measured on a polarimeter Perkin-Elmer 241. IR spectra were recorded on a Beckman Acculab II. NMR were recorded on a Bruker WP 200 SY (200 MHz ^1H, 50.3 MHz ^{13}C).

Protection of Geranyl Epoxide. The alcohol **5** (2.6 g), prepared as described in Ref. 9, was dissolved in ether (30 ml) and reacted with methyl isopropenyl ether or with butyl vinyl ether (5 ml) and a trace of TsOH. After 30 minutes at room temperature, ether and aqueous Na_2CO_3 (4%) were added, the organic layer was dried and the solvent removed in vacuo to yield a crude material (3.2 g) which was used without further purification.

8-Phenylthiopeucelinendiol (8). The sulfide **4** (1.5 g), prepared as described in Ref. 6 in THF (60 ml) and DABCO (750 mg) was cooled down to −20 °C. An excess of BuLi (5 ml, 1.6 M in hexane; 1 M=1 mol dm^{-3}) was then added. The reaction mixture turns then into orange. After 5 minutes, the epoxide **6** (or **7**) was slowly dropped, and the mixture was allowed to warm up to room temperature. Work up, hydrolysis (0.5 M HCl) and chromatography on SiO_2 (60 g, hexane/ether, 6:3) rendered 2.05 g (80%) of a 1:1 mixture of the epimeric hydroxy sulfides **8**. ^1H NMR ($CDCl_3$) δ=7.30 (10H, m), 5.25 (6H, m), 4.10 (6H, m), 1.62 (6H, s), 1.60 (6H, s), 1.56 (6H, s), 1.52 (6H, s), 1.34 (3H, s), 0.95 (3H, s).

Peucelinendiol (2) and Isopeucelinendiol (9). Desulfurization of the foregoing mixture was carried out as follows: over the stirred sulfide mixture (380 mg) in diethylamine (3 ml), was condensed NH_3 (30 ml). Li (100 mg) was added in small pieces and the blue solution was kept at reflux temperature for 30 minutes. MeOH was then dropped in until the blue color vanished and NH_3 was allowed to evaporate. Work up with ether and aqueous HCl (0.5 M) yielded a mixture (280 mg) of two compounds which could be separated on a SiO_2 column (60 g, hexane/ether, 7 : 3) affording 175 mg of peucelinendiol **2** ($[\alpha]_D$ +4.4° *c* 3, $CHCl_3$) and isopeucelinendiol **9** (60 mg), which showed the following physical data: $[\alpha]_D$ −11.0° (*c* 3.3, $CHCl_3$). IR (film) 3400, 2950, 1450, 1380, 1200, 1040, 990 cm^{-1}. ^1H NMR ($CDCl_3$) δ=5.37 (1H, dd *J*=15 and 7 Hz, 9-H), 5.07 (1H, dd, *J*=15 and 9 Hz, 8-H), 5.03 (2H, m, 3-H, 13-H), 3.78 (1H, dd, *J*=9 and 8 Hz, 18-H_A), 3.55 (1H, dd, *J*=9 and 6 Hz, 18-H_B), 2.35 (1H, m, 7-H), 1.60 (6H, s, 1-CH_3, 15-CH_3), 1.54 (3H, s, 16-CH_3), 1.50 (3H, s, 20-CH_3), 1.10 (3H, s, 19-CH_3), 0.89 (3H, d, *J*=7 Hz, 17-CH_3). ^{13}C NMR ($CDCl_3$) δ=140.9 (d, 8-C), 131.7 (s, 2-C), 131.2 (s, 14-C), 125.4 (d, 9-C), 124.6 (d, 3-C), 124.5 (d, 13-C), 75.4 (s, 6-C), 64.2 (t, 18-C), 52.8 (d, 7-C), 4.16 (t, 5-C), 37.1 (t, 11-C), 36.6 (d, 10-C), 25.8 (t, 12-C), 25.6 (q, 1-C, 15-C), 23.5 (q, 19-C), 21.7 (t, 4-C), 20.6 (q, 17-C), 17.6 (q, 16-C, 20-C).

8-(Phenylthio)epipeucelinendiol (12). The alcohol **11** (710 mg) prepared according to Ref. 10, in ether (5 ml) was protected by reacting it with 2 ml of 2-methoxy propene and a trace of pyridinium tosylate during 10 minutes. Work up with aqueous Na_2CO_3 (4%) and ether produced 750 mg of the epoxy acetal **11a** which was used without purification in the next reaction. The sulfide **4** (500 mg) and DABCO (200 mg) in THF (20 ml) at −20 °C were treated with BuLi in hexane (2 ml, 1.6 M). After 5 minutes the epoxy acetal **11a** (400 mg) in THF (10 ml) was added and the reaction was allowed to warm up to room temperature. Usual work up followed by chromatography on SiO_2 (50 g, hexane/ether, 95 : 5) afforded 650 mg of an epimeric sulfide mixture **12** which was further reacted by dissolving it in 6 ml of diethylamine and 50 ml of refluxing NH_3. Li (200 mg) was then added with strong stirring and the reaction mixture was allowed to stand for 30 minutes more. After this time MeOH was added until the blue color disappeared. Evaporation of the NH_3 and usual work up with aqueous HCl (0.5 M) and ether produced a mixture (420 mg) which could be resolved on a SiO_2 column (80 g, hexane/ether, 9 : 1) to yield epipeucelinendiol acetal **13a** (85 mg) and epiisopeucelinendiol acetal **14a** (210 mg).

Epipeucelinendiol Acetal 13a. Oily, $[\alpha]_D$ −11.0° (*c* 0.9, $CHCl_3$). IR (firm) 3400, 2950, 1460, 1380, 1220, 1090, 1050 cm^{-1}. ^1H NMR ($CDCl_3$) δ=5.10 (3H, m, 3-H, 9-H, 13-H), 3.55 (2H, m, 18-H), 3.16 (3H, s, OCH_3), 1.64 (6H, s, 1-CH_3, 15-CH_3), 1.57 (9H, s, 15-CH_3, 17-CH_3, 20-CH_3), 1.30 (3H, s, CH_3), 1.29 (3H, s, CH_3), 1.20 (3H, s, 19-CH_3). ^{13}C NMR ($CDCl_3$) δ=136.1 (s, 10-C), 131.3 (s, 2-C), 131.2 (s, 14-C), 124.9 (d, 3-C), 124.2 (d, 13-C), 123.5 (d, 9-C), 100.3 (s, O-C-O), 74.8 (s, 6-C), 61.1 (t, 18-C), 48.8 (q, OCH_3), 47.9 (d, 7-C), 39.8 (t, 5-C), 38.6 (t, 11-C), 26.7 (t, 8-C), 25.9 (q, 19-CH_3), 25.5 (q, 1-CH_3, 15-CH_3), 25.5 (t, 12-C), 24.3 (q, 2CH_3), 22.4 (t, 4-C), 17.5 (q, 16-CH_3, 20-CH_3), 16.2 (q, 17-CH_3).

Epipeucelinendiol (13). The acetal **13a** (110 mg) was hydrolyzed in MeOH (8 ml) with aqueous HCl (1 ml, 0.5 M) for ten minutes. Work up with aqueous Na_2CO_3 (4%), yielded 81 mg of the compound **13**. Colorless oil. $[\alpha]_D$ −7.5° (*c* 0.8, $CHCl_3$). IR (film) 3400, 2950, 1450, 1380, 1150, 1050, cm^{-1}. ^1H NMR ($CDCl_3$) δ=5.05 (3H, m, 3-H, 9-H, 13-H), 3.75 (2H, m, 18-H), 1.65 (6H, s, 1-CH_3, 15-CH_3), 1.58 (9H, s, 16-CH_3, 17-CH_3, 20-CH_3), 1.26 (3H, 19-CH_3). ^{13}C NMR ($CDCl_3$) δ=136.5 (s, 10-C), 131.8 (s, 2-C), 131.6 (s, 14-C), 124.5 (d, 13-C), 124.3 (d, 3-C), 123.3 (d, 9-C), 76.2 (s, 6-C), 63.1 (t, 18-C), 49.6 (d, 7-C), 39.8 (t, 5-C), 38.3 (t, 11-C), 26.7 (t, 8-C), 26.4 (q, 19-C), 25.6 (q, 1-C, 15-C), 25.3 (t, 12-C), 22.4 (t, 4-C), 17.6 (q, 16-C, 20-C), 16.1 (q, 17-C).

Epiisopeucelinendiol Acetal (14a). Oily, IR (film) 3400, 2950, 1450, 1380, 1200, 1090, 980 cm^{-1}. ^1H NMR ($CDCl_3$) δ=5.05 (2H, m, 3-H, 13-H), 3.55 (2H, m, 18-H), 3.16 (3H, s, OCH_3), 1.63 (6H, s, 1-CH_3, 15-CH_3), 1.57 (3H, s, 16-CH_3), 1.54 (3H, s, 20-CH_3), 1.30 (6H, s, 2 CH_3), 1.14 (3H, d, *J*=7 Hz, 17-CH_3). ^{13}C NMR ($CDCl_3$) δ=140.0 (d, 8-C), 131.1 (s, 2-C), 131.0 (s, 14-C), 126.4 (d, 9-C), 100.3 (s, O-C-O), 74.0 (s, 6-C), 63.0 (t, 18-C), 52.1 (q, OCH_3), 48.7 (d, 7-C), 38.8 (t, 5-C), 37.2 (t, 11-C), 36.7 (d, 10-C), 25.9 (t, 12-C), 25.6 (q, 19-C), 25.5 (q, 1-C, 15-C), 24.3 (q, 2 CH_3), 22.1 (t, 4-C), 20.7 (q, 17-C), 17.6 (q, 16-C, 20-C).

We wish to thank Mr. A. Zarzo, University of Alicante, for the synthesis of **4** and Dr. Cambronero, ACEDESA, El Palmar, Murcia (Spain) for samples of geraniol and (−)-linalool.

References

1) J. de Pascual Teresa, C. Grande, and M. Grande, *Tetrahedron Lett*, **1978**, 4563.

2) J. de Pascual Teresa, C. Grande, J. R. Morán, and M. Grande, *Chem. Lett.*, **1984**, 247; J. de Pascual Teresa, J. R. Morán, J. J. Blanco, A. F. Mateos, and M. Grande, *An. Quim.*, **82C**, 183 (1986).

3) M. Souček, V. Herout, and F. Šorm, *Collect. Czech. Chem. Commun.*, **26**, 2551 (1961).

4) E. Lemmich, *Phytochemistry*, **18**, 1195 (1979).

5) L. Mangoni, D. Merola, P. Monaco, M. Parrilli, and L. Previtera, *Tetrahedron Lett.*, **25**, 2597 (1984).

6) J. F. Biellmann and J. B. Ducep, *Tetrahedron*, **27**, 5861 (1971).

7) M. Kodama, Y. Matsuki, and S. Ito, *Tetrahedron Lett.*, **1975**, 3065.

8) H. L. Goering and W. I. Kimoto, *J. Am. Chem. Soc.*, **87**, 1748 (1965).

9) T. Katsuki and K. B. Sharpless, *J. Am. Chem. Soc.*, **102**, 5974 (1980).

10) G. Ohloff, W. Giersch, K. H. Schulte-Elte, P. Enggist, and E. Demole, *Helv. Chim. Acta*, **63**, 1582 (1980).

The Magnetic Properties of Copper(II) Alkanoate Adducts with Pyridine and Quinoline Analogues

Shuji EMORI,* Katsuko OHISHI, Hikari KURIHARA, and Yoneichiro MUTO
Department of Chemistry, Faculty of Science and Engineering, Saga University, Honjo-machi, Saga 840
(Received June 24, 1988)

Synopsis. Various copper(II) alkanoate adducts with pyridine and quinoline analogues have been prepared, and characterized by means of magnetic susceptibility and IR measurements. The effects of axial ligands on the magnetic moments are discussed on the basis of their basicities and steric requirements.

In most dinuclear copper(II) carboxylate adducts, the coordination geometry is essentially five-coordinate tetragonal pyramidal.[1-5] The addend donor occupies the apical site (axial position) and affects the strength of the spin-exchange coupling within the dinuclear complex.[2] For adducts with σ-donor ligands, which exhibit no steric hindrance to an axial coordination, the room-temperature magnetic moments (BM) can be expressed according to Eq. 1:

$$\mu_{eff} = -0.052(pK_a - 0.068pK_a' - 4.56) + \Delta\mu_\alpha + 1.38_5, \quad (1)$$

where pK_a and pK_a' are the acidities of the conjugate acids of alkanoate and axial ligands, respectively.[6] $\Delta\mu_\alpha$ is the correction term for the substitution in the methyl group of acetic acid (-0.05_8 and -0.07_0 for the series of mono- and disubstituted acetates, respectively), including corrections for the steric strain, field effect, and hyperconjugation.[6] On the other hand, for adducts with *N*-heteroaromatic (pyridine-type) donors, the magnetic moments are, more or less, lower than those of the adducts with alkyl-[6,7] and arylamines,[8] owing to a steric hindrance to their axial coordination.[9-11] In order to investigate these steric effects quantitatively, we prepared several copper(II) alkanoate adducts with pyridine (py), 3-chloropyridine (3-Clpy), 3-bromopyridine (3-Brpy), 3,5-dichloropyridine (3,5-Cl_2py), 3-ethylpyridine (3-Etpy), 4-methylpyridine (4-Mepy), pyrazine (pyz), quinoline (quin), 4-methylquinoline (4-Mequin), and quinoxaline (quix), and measured their magnetic susceptibilities at room temperature.

The adducts were obtained, except for the cyclohexanecarboxylates, by standard procedures,[12] and recrystallized from chloroform whenever possible. The cyclohexanecarboxylates were prepared in a similar way, using dioxane as a solvent.[13] The effective magnetic moments of these compounds (Table 1) were evaluated from the room-temperature magnetic susceptibilities, which were corrected for the diamagnetic contribution (χ_{dia}) using Pascal constants[14] and for temperature-independent paramagnetism ($N\alpha$) using the value of 60×10^{-6} emu mol^{-1} (1 emu$=4\pi\times10^{-6}$ m^3). Although a number of copper(II) alkanoate adducts with various pyridine-type donors have been already studied magnetically,[2,15-17] their magnetic moments were reevaluated in order to avoid any errors derived from differences in the standard samples used for susceptibility measurement and in the correction values for χ_{dia} and $N\alpha$. The IR spectra of the solid compounds show characteristic bands connected with unsymmetric and symmetric carboxyl stretching vibrations, the latter with a variable intensity.[18] The magnetic and IR spectral data indicate that the present compounds have a bridged dinuclear structure similar to that of copper(II) acetate monohydrate.[2]

Although a pyridine-type donor can function as a π-acceptor in some circumstances, it functions here almost entirely as a σ-donor base,[5] because X-ray crystallographic analyses indicate that a pyridine or quinoline analogues adopts a staggered orientation with respect to the planes of carboxylato groups.[1-5] By analogy with Eq. 1, the magnetic moments of the present adducts may be expressed as

$$\mu_{eff} = -0.052(pK_a - 0.068pK_a' - 4.56) + \Delta\mu_\alpha + \Delta\mu_{ST} + 1.38_5, \quad (2)$$

where the correction term $\Delta\mu_{ST}$ depends on the steric hindrance to an axial coordination; its value can be evaluated from the graphic interpolation shown in Fig. 1. In this series of axial ligands, the pK_a' value varies from -2.60 for 1/2quix to -2.10, 0.67, 0.72, 2.89, 3.16, 4.94, 5.23, 5.73, 5.89, and 6.04 for 1/2pyz, 3,5-Cl_2py, quix, 3-Brpy, 3-Clpy, quin, py, 4-Mequin, 3-Etpy, and 4-Mepy, respectively. To plot the points for the 1/2pyz and 1/2quix adducts, the first dissociation constants of pyrazine and quinoxaline are selected, since their

Table 1. Effective Magnetic Moments (BM) at 20 °C for $[Cu(RCOO)_2 \cdot L]_2$ Compounds

L\R	CH_3	C_2H_5	C_3H_7	$ClCH_2CH_2$	$ClCH_2$	$(CH_3)_2CH$	C_6H_{11}	CH_3CHCl	Cl_2CH
1/2pyz	1.32	1.30	1.27	1.30	1.37	1.28			
3,5-Cl_2py	1.35	1.29	1.30	1.33	1.38	1.28	1.24	1.38	1.44
3-Brpy	1.34	1.31	1.29	1.36	1.39	1.29	1.28	1.37	
3-Clpy	1.35	1.30	1.29	1.32	1.39	1.29	1.29	1.37	
py	1.35	1.32	1.32	1.36	1.38	1.28	1.29	1.42	1.47
3-Etpy	1.37	1.32	1.31	1.36	1.40	1.30	1.30	1.41	
4-Mepy	1.36	1.32	1.33	1.36	1.43	1.32	1.29	1.43	
1/2quix					1.38			1.34	
quix	1.37	1.29		1.31		1.28	1.26	1.37	1.45
quin	1.39	1.33	1.33	1.36	1.41	1.32	1.28	1.41	1.48
4-Mequin	1.37	1.33	1.32	1.36	1.41	1.29	1.28	1.39	

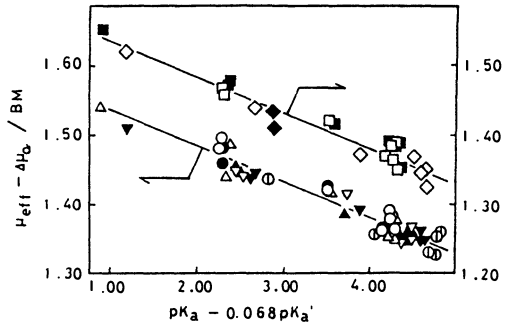

Fig. 1. The corrected magnetic moments at 20°C plotted against the acidities of the ligands for the copper(II) alkanoate adducts with 1/2quix (◆), 1/2pyz (Φ), 3,5-Cl_2py (▼), quix (◇), 3-Brpy (▽), 3-Clpy (▲), quin (■), py (△), 4-Mequin (□), 3-Etpy (●), and 4-Mepy (○).

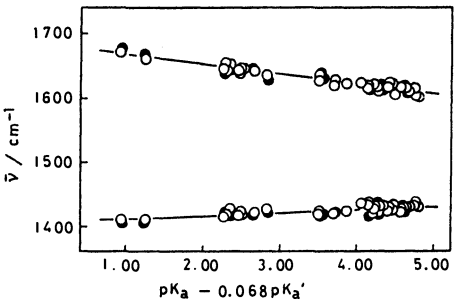

Fig. 2. The carboxyl stretching frequencies plotted against the acidities of the ligands for the copper(II) alkanoate adducts with pyridine analogues (○) and quinoline analogues (●).

second coordination abilities must be reduced by the first coordination on the other sites. The obtained slope of −0.052 BM is exactly the same as that shown in Eq. 2, indicating the validity of the equation, although we disregard interactions between different dinuclear complexes,[19] the presence of modifications,[2] and crystallographically independent dinuclear complexes,[1,4] and packing effects. The obtained values of $\Delta\mu_{ST}$ are -0.03_3 BM for the adducts with pyridine analogues (py, 3-Clpy, 3-Brpy, 3,5-Cl_2py, 3-Etpy, 4-Mepy, and pyz) and -0.03_4BM for those with quinoline analogues (quin, 4-Mequin, and quix), being almost the same with each other. This fact is consistent with the coincidence of the singlet-triplet separation values for the copper(II) acetate adducts with pyridine and quinoline,[20] and should be attributed to a similarity of the steric interferences hindering their axial coordination; a mutual repulsion between the adjacent Cu-O and N-C bonding electron pairs may be taken as such a steric hindrance.[21]

The correlation between the magnetic moments and the acidities of the parent carboxlic acids (Eq. 2) suggests that the magnitude of spin-exchange coupling is closely related to the nature of Cu-O bonds. It has been pointed out that, for carboxylate compounds with the same structure, the frequency shift of the carboxyl stretching vibrations can be used as a measure of the relative strengths of the metal-oxygen bonds.[22] Systematic shifts of the carboxyl frequencies against the acidities of the parent carboxylic acids (Fig. 2), which can also be demonstrated for the dimeric aliphatic[23] and arenecarboxylic asids,[24] indicate that an increase in the acidity of the parent carboxylic acid leads to a more asymmetric structure of the carboxyl group, thereby resulting in an increase in the frequency separation of the two carboxyl bands. The slopes and intercepts found here −15.0 and 1682 cm^{-1} for unsymmetric and +4.9 and 1407 cm^{-1} for symmetric vibrations. These slopes are almost the same with those found for the adducts with unhindered σ-donors ($\tilde{\nu}_{unsym}$=1692−15.1(pK_a−0.068pK_a'))[6] and for the dimeric arenecarboxylic acids ($\tilde{\nu}_{unsym}$=1760−14.7pK_a).[24] On the other hand, the difference in the values of the intercept between the adducts with unhindered σ-donors and the present adducts indicates the existence of a steric hindrance to the axial coordination of pyridine-type donors.

References

1) L. K. Minocheva, T. S. Khodashova, M. A. Porai-Koshits, and Y. A. Tsivadze, *Koord. Khim.*, **7**, 455 (1981).
2) M. Melnik, *Coord. Chem. Rev.*, **42**, 259 (1982).
3) V. Mohan Rao, D. N. Sathyanarayana, and H. Monohar, *J. Chem. Soc., Dalton Trans.*, **1983**, 2167.
4) K. Smolander and M. Melnik, *Acta Chem. Scand.*, **A38**, 619 (1984).
5) M. Melnik, K. Smolander, and P. Sharrock, *Inorg. Chim. Acta*, **103**, 187 (1985).
6) S. Emori, H. Nonaka, N. Ikeda, and Y. Muto, *Bull. Chem. Soc. Jpn.*, **61**, 1812 (1988).
7) J. Bera and D. Sen, *J. Chem. Soc., Dalton Trans.*, **1977**, 18.
8) F. G. Herring, B. Landa, R. C. Thompson, and C. F. Schwerdtfeger, *J. Chem. Soc. A*, **1971**, 528.
9) J. Lewis, Y. C. Lin, L. K. Royston, and R. C. Thompson, *J. Chem. Soc.*, **1965**, 6464.
10) W. E. Marsh, G. O. Carlisle, and M. V. Hanson, *J. Inorg. Nucl. Chem.*, **39**, 1839 (1977).
11) Y. Muto, N. Hirashima, T. Tokii, M. Kato, and I. Suzuki, *Bull. Chem. Soc. Jpn.*, **59**, 3672 (1986).
12) E. Kokot and R. L. Martin, *Inorg. Chem.*, **3**, 1306 (1964).
13) P. O. Ikekwere and K. S. Patel, *J. Inorg. Nucl. Chem.*, **43**, 1085 (1981).
14) G. Foex, "Constants Sélectionées, Diamagnétisme et Paramagnétisme," Masson Paris (1957).
15) Yu. V. Jablokov, L. V. Mosina, Yu. A. Simonov, L. N. Milkova, A. V. Ablov, and V. I. Ivanov, *Zh. Strukt. Khim.*, **19**, 42 (1978).
16) M. Melnik, *Finn. Chem. Lett.*, **1980**, 177.
17) Y. Muto, T. Tokii, K. Chijiwa, and M. Kato, *Bull. Chem. Soc. Jpn.*, **57**, 1008 (1984).
18) L. J. Bellamy, "The Infrared Spectra of Complex Molecules," 3rd ed., Chapman and Hall, London (1975).
19) J. S. Valentine, A. J. Silverstein, and Z. G. Soos, *J. Am. Chem. Soc.*, **96**, 97 (1974).
20) R. J. Doedence, *Prog. Inorg. Chem.*, **21**, 209 (1976); and refs. therein.
21) S. Wolfe, *Acc. Chem. Res.*, **5**, 102 (1972).
22) K. Nakamoto, Y. Morimoto, and A. E. Martell, *J. Am. Chem. Soc.*, **83**, 4528 (1961).
23) J. Guilleme, M. Chabanel, and B. Wojtkowiak, *Spectrochim. Acta*, **27A**, 2335 (1971).
24) C. J. W. Brooks, G. Eglinton, and J. F. Morman, *J. Chem. Soc.*, **1961**, 106.

The Preparation and the Structure of Bis(1,3-dimethylureido)methane

Toichi EBISUNO,* Michiaki TAKIMOTO, Miyuki TAKAHASHI,† and Ryuichi SHIBA†
Department of Chemistry, Faculty of Science, Toho University, Miyama 2-2-1, Funabashi, Chiba 274
†Department of Applied Science, Faculty of Technology, Tokyo Denki University, Kanda Chiyoda-ku, Tokyo 101
(Received March 26, 1988)

Synopsis. A new 1,3-dimethylurea-formaldehyde condensate, bis(1,3-dimethylureido)methane, was prepared and the molecular structure, as determined by X-ray analysis, and possible specific interaction to alkaline metal ions were compared with those of 1,3,5,7-tetramethyltetrahydro-1,3,5,7-tetrazocine-2,6(1*H*,3*H*)-dione. Although both structures are different from each other, their UV spectra in aqueous solution show that alkaline metal ions, Li^+ and Na^+, are caught by both of them.

In a previous paper,[1] 1,3,5,7-tetramethyltetrahydro-1,3,5,7-tetrazocine-2,6(1*H*, 3*H*)-dione (tetramethyldimethylenediurea: TMDMU) was reported to have a hole of 0.5—1.6 Å in the interior of the ring structure. When TMDMU was added to an aqueous solution of the lithium or sodium salt of phenol, a discernible shoulder at 225 nm characteristic to alkaline metal salts of phenol disappeared and the absorption spectrum in the UV region changed to that of phenol.[1]

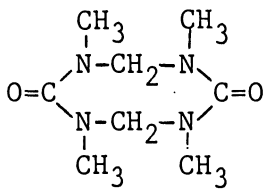
(TMDMU)

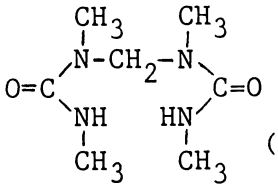
(BDMUM)

A new 1,3-dimethylurea-formaldehyde condensation product, bis(1,3-dimethylureido)methane (BDMUM), was prepared and its molecular structure was determined by X-ray analysis. Possible specific interactions to alkaline metal ions in aqueous solution were compared with those of TMDMU.

Experimental

The Preparation of BDMUM. Ten grams of 1,3-dimethylurea were dissolved in 23.5 g of formalin and the pH of the solution was adjusted to 8.8 by successive additions of 20% NaOH aqueous solution. The reaction was carried out at 50 °C for 30 min. The reaction solution was evaporated to dryness under reduced pressure at 18—25 °C. A few ml of concd HCl was added as an acid catalyst to the desiccated residue in a large excess of MeOH. Keeping the temperature of the solution at 0—5 °C for 30 min, the reaction solution was neutralized with 20% NaOH aqueous solution at below −15 °C. After evaporation of the solvent, the methoxymethylated products were extracted with CH_2Cl_2, then with diethyl ether. After a viscous solution was evaporated under reduced pressure, the residue was distilled at 95—99 °C/1—2 Torr (1 Torr=133.322 Pa) to give 1-methoxymethyl-1,3-dimethylurea (yield 71%).

As an acid catalyst, 100 mg of *p*-toluenesulfonic acid was added to a mixture of 5 g of 1-methoxymethyl-1,3-dimethylurea and 3.3 g of 1,3-dimethylurea. The mixture was stirred for 30 min at 110 °C using an oil bath. Upon cooling, deposited white crystals were separated by filtration. Recrystallization from CH_2Cl_2 gave white rod-like crystals (Yield 82%), mp 145.0—146.2 °C. BDMUM was assigned by elemental analysis, ^1H and ^{13}C NMR and FD-MS spectrometry. ^1H and ^{13}C NMR spectra were measured in a $CDCl_3$, with TMS as the internal standard, at 90 MHz on a JEOL FX90Q instrument. Found: C, 44.57; H, 8.60; N, 29.72%: Calcd for $C_7H_{16}N_4O_2$: C, 44.68; H, 8.51; N, 29.79%: ^1H NMR, δ=6.32 (2H, q, J=4Hz, -NH-), 4.79 (2H, s, -CH_2-), 3.00 (6H, s, -CH_3), 2.78 (6H, d, J=4.5 Hz, -CH_3): ^{13}C NMR, δ=159.47 (>C=O), 63.07(-CH_2-), 34.90 (-CH_3), 27.50 (-CH_3): MS(FD); m/z=188(M^+).

X-Ray Analysis. A colorless single crystal with dimensions of ca. 0.1×0.2×0.2 mm^3 was mounted on a Rigaku AFC-6S diffractometer. The lattice parameters were determined by least-squares from 18 reflections in the 2θ range 20—30°. Systematic absences $0kl$ for k odd, $h0l$ for l odd, $hk0$ for h odd. Intensity data were measured by means of the ω-2θ scan mode (scan speed 4° min^{-1} in ω) up to 2θ of 45° by using graphite-monochromated Mo $K\alpha$ radiation (λ=0.7107 Å). A deterioration of the crystal was not observed during measurements. Lorentz and polarization corrections were made, but no correction was made for absorption. 1008 independent reflections with $|F_o|>3\sigma(|F_o|)$ were used for a structure determination.

Crystal data for $C_7H_{16}N_4O_2$: M.W.=188.23, orthorhombic, space group Pbca, a=14.350(5), b=12.115(4), c=12.015(5) Å; V=2089(1) $Å^3$: Z=8; D_m=1.199, D_c=1.197 $g\cdot cm^{-3}$; μ(Mo $K\alpha$)=0.9 cm^{-1}.

The structure of BDMUM was solved by a direct method (MULTAN78[2]). The positions of H atoms were determined

Table 1. Final Atomic Parameters (Positional ×10^4) and Equivalent Isotropic Temperature Parameters (B_{eq} ×10) for Non-H Atoms with Their e.s.d.'s in Parentheses

Atom	x	y	z	B_{eq}/Å$^{2\,a)}$
C(1)	1064(6)	3705(7)	−347(7)	50(4)
C(2)	881(5)	4001(6)	1659(6)	34(3)
C(3)	2304(6)	4499(9)	2745(7)	62(5)
C(4)	733(5)	4469(6)	3635(5)	36(3)
C(5)	−120(6)	6186(7)	3145(6)	49(4)
C(6)	1126(5)	6164(6)	4585(5)	31(3)
C(7)	1557(6)	7906(7)	5459(7)	54(5)
N(1)	1443(4)	3910(5)	767(5)	41(3)
N(2)	1302(4)	4241(5)	2660(5)	37(3)
N(3)	579(4)	5610(5)	3843(5)	35(3)
N(4)	1035(4)	7265(5)	4635(5)	40(3)
O(1)	24(3)	3883(4)	1594(4)	41(2)
O(2)	1671(3)	5653(4)	5211(4)	41(2)

a) The equivalent temperature parameters are defined by Hamilton.[6]

Table 2. Bond Lengths and Angles

Bond length	l/Å	Bond angle	ϕ/°
C(1)-N(1)	1.466(10)	C(1)-N(1)-C(2)	121.3(6)
C(2)-N(1)	1.345(9)	N(1)-C(2)-O(1)	122.3(6)
C(2)-N(2)	1.377(9)	N(1)-C(2)-N(2)	116.7(6)
C(2)-O(1)	1.241(8)	N(2)-C(2)-O(1)	121.0(6)
C(3)-N(2)	1.475(10)	C(2)-N(2)-C(3)	122.2(6)
C(4)-N(2)	1.455(9)	C(2)-N(2)-C(4)	119.8(6)
C(4)-N(3)	1.422(9)	C(3)-N(2)-C(4)	116.8(6)
C(5)-N(3)	1.482(10)	N(2)-C(4)-N(3)	114.5(6)
C(6)-N(3)	1.364(9)	C(4)-N(3)-C(5)	117.6(6)
C(6)-N(4)	1.342(9)	C(4)-N(3)-C(6)	120.2(6)
C(6)-O(2)	1.250(8)	C(5)-N(3)-C(6)	121.8(6)
C(7)-N(4)	1.465(10)	N(3)-C(6)-N(4)	117.5(6)
		N(3)-C(6)-O(2)	120.7(6)
		N(4)-C(6)-O(2)	121.8(6)
		C(6)-N(4)-C(7)	120.4(6)

from a difference Fourier map. The structure was refined anisotropically for non-H atoms and isotropically for H atoms by a block-diagonal least-squares method. The final R was 0.087 and R_w was 0.082 (w=unit wt) (s=2.3), $(\Delta/\sigma)_{max}$ in final refinement cycle was 0.103 for non-H atoms, max. and min. $\Delta\rho$ in the final difference map were +0.3 and −0.4 e Å^{-3}. The atomic scattering factors were taken from Ref. 3. Calculations were carried out on a HITAC M-680H computer at the Computer Center of The University of Tokyo, using the local version of UNICS III.[4] The final atomic parameters are given in Table 1.[5] Bond lengths and angles are given in Table 2.

Results and Discussion

A view of the molecule with atomic numbering is shown in Fig. 1. O(1), C(2), N(1), and N(2) lie on a plane, which makes an angle of 98° with the other plane composed of O(2), C(6), N(3), and N(4). While two ureido groups are substantially on a plane in TMDMU, forming a ring with a hole of 0.5—1.6 Å, the BDMUM molecule has no such ring structure in the crystalline state. In spite of the difference in the molecular structures of TMDMU and BDMUM, a possible specific interaction with Li^+ or Na^+ was observed for both compounds. K^+, however, was apparently caught by BDMUM, but not by TMDMU. These facts suggest that BDMUM takes a similar structure to TMDMU by capturing alkaline metal ions in solutions, though the former is more flexible to catch metal ions than the latter. The possibility of interactions of metal ions with carbonyl anions can be ruled out. That is, the extent of resonance of the ureido groups in urea,[7] BDMUM, and TMDMU decreases in this order since the C=O bond lengths of these are 1.262, 1.241(8), and 1.250(8), and 1.216 Å respectively, and the C-N bond lengths adjacent to the carbonyl groups are 1.335 Å in urea, 1.342(9), 1.345(9), 1.364(9), and 1.377(9) Å in BDMUM, and 1.377 and 1.378 Å in TMDMU. Even though the differences in the C=O bond lengths are partly due to the presence and absence of the hydrogen bonds involving the C=O bonds (urea has 4, BDMUM has 1 and TMDMU has no hydrogen bonds), the conclusion described above can hold. None of the urea, bis(ureido)methane, and bis(1-methylureido)methane showed any effect on the UV spectra of the solutions of phenol-alkaline metal salts.[1] Thus, interactions between alkaline metal ions and BDMUM or TMDMU are possibly correlated to the localized electron densities of four nitrogen atoms donated by the methyl groups.

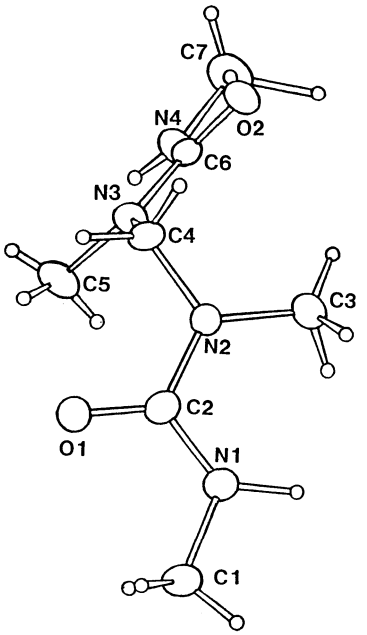

Fig. 1. The view of the molecule with atomic numbering.

The authors wish to express their hearty thanks to Prof. Hayao Kobayashi of Toho University, for his kind support in the data collection on Rigaku AFC-6S diffractometer at Toho Unversity and regarding computation.

References

1) T. Ebisuno, M. Takimoto, M. Takahashi, and R. Shiba, *Bull. Chem. Soc. Jpn.*, **61**, 2191 (1988).

2) P. Main, S. E. Hull, L. Lessinger, G. Germain, J. P. Declercq, and M. M. Woolfson, MULTAN 78. "A System of Computer Programs for Automatic Solution of Crystal Structures from X-Ray Diffraction Data," Univ. of York, England and Louvain, Belgium (1978).

3) "International Tables for X-Ray Crystallography," Kynoch Press, Birmingham (1974), Vol. IV.

4) T. Sakurai and K. Kobayashi, *Rikagaku Kenkyusho Hokoku*, **55**, 69 (1979).

5) The coordinates and isotropic temperature parameters of H atoms, the anisotropic temperature parameters of non-H atoms and F_o—F_c tables have been deposited as Document No. 8839 at the Office of Editor.

6) W. C. Hamilton, *Acta Crystallogr.*, **12**, 609 (1959).

7) P. Vaughan and J. Donohue, *Acta Crystallogr.*, **5**, 530 (1952).

The Synthesis of 5-(*p*-Bromophenacylthio)- and 5-(Carbamoylthio)isothiazoles

Naoaki FUKADA,* Toshihisa MORI, Motomu MURAOKA,† Tatsuo YAMAMOTO,† and Tatsuo TAKESHIMA
Department of Chemistry, Faculty of Science, Chiba University, Yayoicho, Chiba 260
†Department of Chemistry, Faculty of Science, Josai University, Keyakidai, Sakado 350-02
(Received May 11, 1988)

Synopsis. The reaction of the ammonium salts of 5(2*H*)-isothiazolethiones with *p*-bromophenacyl bromide, and methyl and phenyl isocyanates afforded 5-(*p*-bromophenacylthio)-, and 5-(carbamoylthio)isothiazoles. From phenyl isothiocyanate and hydrazine, 2,4-pyrimidinedithione, and 3*H*-pyrazole-3-thione derivatives were obtained, respectively.

Previously, we have reported on a new zwitterion, *N*-(1-ammoniocyclohexyl)-1,4,5,6-tetrahydro-2,1-benzisothiazole-3-thiolate, obtained through a reaction of cyclohexanone with carbon disulfide in the presence of aqueous ammonia and sulfur.[1] Under similar conditions, cyclopentanone gave 1,4,5,6-tetrahydro-3*H*-cyclopent[*c*]isothiazole-3-thione(**2a**),[1] which was the cyclo-oxidation product of 2-iminocyclopentanecarbodithioic acid.[2] Although many 5-substituted isothiazole derivatives have been reported, there are few 5(2*H*)- and 5(4*H*)-isothiazolethiones, and 5-alkylthioisothiazoles mentioned in the literature.[3] In this note, we wish to report on a new synthesis of 5-(*p*-bromophenacylthio)- (**3**), and 5-(carbamoylthio)isothiazoles (**4** and **5**) by a reaction of ammonium salts

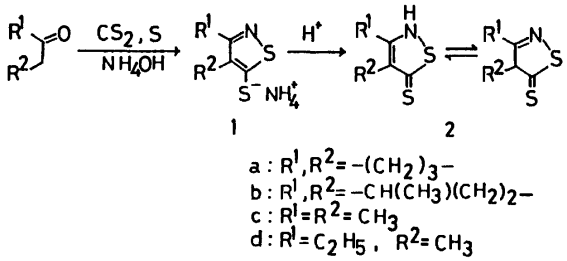

Scheme 1.

1a—d with *p*-bromophenacyl bromide, and methyl and phenyl isocyanates.

Salts **1b—d** were obtained from 2-methylcyclopentanone, ethyl methyl ketone, and diethyl ketone, respectively, in lower yields in a similar manner as described for the preparation of **1a**.[1] A treatment of **1** with hydrochloric acid gave 5(2*H*)-isothiazolethiones **2**. Salts **1** reacted with *p*-bromophenacyl bromide to give 5-(*p*-bromophenacylthio)isothiazoles **3**, whereas it was difficult to obtain crystalline products by a reac-

Table 1. Physical Properties and Spectral Data

Compd	Yield %	Mp θ_m/°C	IR spectra in KBr(cm^{-1})	UV spectra in EtOH (nm) (log ε)	Molecular formula	Found(Calcd)(%) C	H	N	S
2b	79	123—125	3250—3180(s) 1615(vs)	279(3.74), 298sh(3.72), 395(4.13)	$C_7H_9NS_2$	48.89 (49.12)	5.23 (5.30)	7.90 (8.18)	37.00 (37.39)
2c	94	113—115 (decomp)	1515(vs)	256(3.80), 307(3.70), 357(3.75)	$C_5H_7NS_2$	41.57 (41.38)	4.79 (4.86)	9.71 (9.65)	44.15 (44.10)
3a	83	123—125	1688(vs)	263(4.36)	$C_{14}H_{12}NOS_2Br$	47.57 (47.46)	3.45 (3.41)	3.73 (3.95)	17.90 (18.10)
3b	23	95—97	1680(vs)	263(4.69)	$C_{15}H_{14}NOS_2Br$	48.99 (48.92)	3.72 (3.83)	4.05 (3.80)	17.81 (17.41)
4a	85	149	3180(s) 1695(vs)	270(3.99), 311sh(2.97)	$C_8H_{10}N_2OS_2$	44.99 (44.86)	4.70 (4.71)	12.95 (13.08)	29.72 (29.88)
4b	26	96—97	3160(s) 1695(vs)	269(4.28), 310sh(3.33)	$C_9H_{12}N_2OS_2$	47.22 (47.37)	5.29 (5.30)	12.26 (12.28)	28.10 (28.05)
4c	70	143—145	3205(s) 1680(vs)	259(3.88), 266(3.88), 306(3.57)	$C_7H_{10}N_2OS_2$	41.85 (41.58)	4.99 (4.99)	13.97 (13.86)	31.90 (31.66)
4d	42	103—104	3212(s) 1685(vs)	258(3.85), 264(3.84), 306(3.60)	$C_8H_{12}N_2OS_2$	44.18 (44.44)	5.44 (5.60)	12.87 (12.96)	29.60 (29.60)
5a	59	166	3155(m) 1688(vs)	245(4.17), 277(4.14), 310sh(3.39)	$C_{13}H_{12}N_2OS_2$	56.57 (56.52)	4.55 (4.38)	9.97 (10.14)	23.54 (23.17)
5b	48	143—144	3175(m) 1690(vs)	246(4.16), 255sh(4.14), 277(4.11), 308sh(3.67)	$C_{14}H_{14}N_2OS_2$	58.19 (57.93)	4.83 (4.86)	9.67 (9.65)	21.88 (22.05)
5c	86	180—184	3200(m) 1695(vs)	236(3.90), 253sh(3.44), 306(3.62)	$C_{12}H_{12}N_2OS_2$	54.32 (54.54)	4.41 (4.58)	10.49 (10.60)	24.02 24.22)
5d	35	140—141	3200(m) 1702(vs)	239(4.23), 255sh(4.07), 276(3.99), 306(3.77)	$C_{13}H_{14}N_2OS_2$	56.11 (56.11)	5.10 (5.07)	10.07 (10.07)	23.38 (23.00)
6	35	116	3220(vs)	230sh(3.98), 268(4.23)	$C_8H_{10}N_2S_3$	41.95 (41.74)	4.48 (4.38)	12.21 (12.17)	41.55 (41.71)
7	32	ca. 190 (decomp)	3230—3150(m) 1610(vs)	264(4.38), 295sh(4.00), 432(4.32)	$C_{13}H_{12}N_2S_2$	59.95 (59.99)	4.58 (4.65)	10.79 (10.77)	24.59 (24.59)
9	83	ca. 190	3250—3170(m) 1715(vs)	240(4.06), 271(3.73), 337(3.69), 415(4.19)	$C_{13}H_{12}N_2OS_2$	56.80 (56.52)	4.66 (4.38)	10.32 (10.14)	23.59 (23.17)

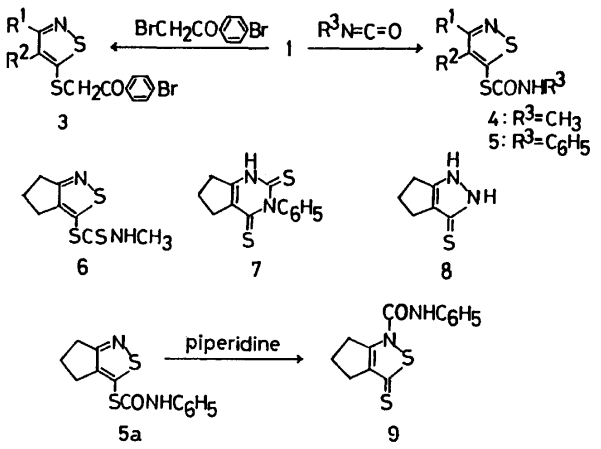

Scheme 2.

tion with methyl iodide.

Reaction of **1** with methyl and phenyl isocyanates gave the corresponding addition compounds, 5-(carbamoylthio)isothiazoles **4** and **5**. Although the expected adduct, 5-(thiocarbamoylthio)isothiazole **6**, was obtained from methyl isothiocyanate, the reaction of **1a** with phenyl isothiocyanate afforded a ring-expanded compound **7**. The structure of **7** was judged from the microanalysis, and mass (M^+ 260) and UV spectra (432 nm). Salt **1a** reacted with hydrazine hydrate to give the pyrazole derivative **8**, which we had previously prepared from 2-imino-[4] or 2-oxocyclopentanecarbodithioic acid.[5] Perhaps the mechanism of the reaction leading to **7** or **8** involves a replacement of either the sulfur atom of **1a** by a nitrogen atom of isothiocyanate or hydrazine. It is of interest that a treatment of **5a** with piperidine afforded isomer **9**. The UV spectrum of **9** showed a red shift due to the thione-type structure (Table 1). A rearrangement, however, did not occur in **5b—d**.

Experimental

The Ammonium Salts (1) and 5(2*H*)-Isothiazolethiones (2). General Procedure. A mixture of ketone (0.25 mol), carbon disulfide (38 g, 0.5 mol), aqueous ammonia (28%; 70 ml), and sulfur (10 g, 0.31 mol) was stirred for 6 h—2 days at 0 °C. The mixture was kept for 2—7 days at 0—4 °C. The solid product was collected, and washed with carbon disulfide and ether. The crude salt was dissolved in water; the solution was then filtered and saturated with ammonium chloride to give practically pure crystals for use in reactions. The yields and melting points (from ethanol-hexane) of the salts were: **1a**, 61%, 145—146 °C;[1] **1b**, 30%, 93—95 °C; **1c**, 6%, 158—159 °C (decomp); **1d**, 3%, 97—99 °C. The salt **1** was dissolved in water and acidified with dilute hydrochloric acid to give yellow crystals, 1,4,5,6-tetrahydro-3*H*-cyclopent-[*c*]isothiazole-3-thione (**2a**),[1] 6-methyl-1,4,5,6-tetrahydro-3*H*-cyclopent[*c*]isothiazole-3-thione (**2b**), or 3,4-dimethyl-5(2*H*)-isothiazole-5-thione (**2c**). Compound **2d**, an oil, was not analyzed.

3-(*p*-Bromophenacylthio)-5,6-dihydro-4*H*-cyclopent[*c*]isothiazole (3a) and 3-(*p*-Bromophenacylthio)-6-methyl-5,6-dihydro-4*H*-cyclopent[*c*]isothiazole (3b). To a solution of **1** (0.003 mol) in ethanol (3 ml) was added a solution of *p*-bromophenacyl bromide (1.3 g, 0.005 mol) in ethanol (2 ml) with stirring at room temperature. The solid product was collected, washed with ether, and recrystallized from ethanol.

3-(Methylcarbamoylthio)-5,6-dihydro-4*H*-cyclopent[*c*]isothiazole (4a), 6-Methyl-3-(methylcarbamoylthio)-5,6-dihydro-4*H*-cyclopent[*c*]isothiazole (4b), 3,4-Dimethyl-5-(methylcarbamoylthio)isothiazole (4c), and 3-Ethyl-4-methyl-5-(methylcarbamoylthio)isothiazole (4d). To a solution or suspension of **1** (0.002 mol) in ethanol (2 ml) was added an excess of methyl isocyanate (0.004—0.005 mol); the mixture was kept for 2 days at 4—20 °C. In the case of **4a** or **4b**, the mixture was warmed at 60 °C for 20 min, and then kept for 3 days at 4 °C. The solid product was collected, washed with carbon disulfide and ethanol, and recrystallized from ethanol.

3-(Phenylcarbamoylthio)-5,6-dihydro-4*H*-cyclopent[*c*]isothiazole (5a), 6-Methyl-3-(phenylcarbamoylthio)-5,6-dihydro-4*H*-cyclopent[*c*]isothiazole (5b), 3,4-Dimethyl-5-(phenylcarbamoylthio)isothiazole (5c), and 3-Ethyl-4-methyl-5-(phenylcarbamoylthio)isothiazole (5d). Compounds **5b—d** were prepared by the method used for **4c** and **4d**, and recrystallized from methanol. In the case of **5a**, **1a** (0.35 g, 0.002 mol) was dissolved in ethanol (3.5 ml) at 50 °C, and to the warm solution was added phenyl isocyanate (0.6 g, 0.005 mol). When a large excess of phenyl isocyante was used, needles of *N,N'*-diphenylurea (mp 238 °C) were obtained together with **5**.

3-(Methylthiocarbamoylthio)-5,6-dihydro-4*H*-cyclopent[*c*]-isothiazole (6). To a suspension of **1a** (0.5 g, 0.0029 mol) in ethanol (3 ml) were added methyl isothiocyanate (0.4 g, 0.0055 mol) and acetic acid (0.12 ml), and the mixture was warmed for 10 min at 60 °C. The solid product was collected and washed with ethanol and carbon disulfide.

3-Phenyl-6,7-dihydro-1*H*-cyclopentapyrimidine-2,4(3*H*, 5*H*)-dithione (7). A mixture of **1a** (0.5 g, 0.0029 mol) and phenyl isothiocyanate (0.8 g, 0.0059 mol) was kept for 4 days at room temperature. The solid product was collected, washed with ethanol and carbon disulfide, and recrystallized from methanol.

1,4,5,6-Tetrahydrocyclopenta[*c*]pyrazole-3(2*H*)-thione (8). To a suspension of **1a**(0.5 g, 0.0029 mol) in ethanol (3 ml) was added 80% hydrazine hydrate (0.5 g, 0.008 mol). The mixture was warmed for 3 min at 60 °C and cooled to room temperature. Acetic acid (1 ml) was then added dropwise, and the solid product was collected, washed with water and ethanol, and recrystallized from ethylene glycol; mp 230 °C (decomp). The IR spectrum was identical with that reported.[4,5]

1-(Phenylcarbamoyl)-1,4,5,6-tetrahydro-3*H*-cyclopent[*c*]isothiazole-3-thione (9). A mixture of **5a** (0.1 g, 0.00036 mol), ethanol (3 ml), and piperidine (0.04 ml) was warmed for 10 min at 60 °C and kept overnight at room temperature. The solid product was collected and recrystallized from ethanol-pyridine.

References

1) T. Takeshima, K. Tazaki, N. Fukada, and M. Muraoka, *J. Chem. Res.* (*S*), **1979**, 410.

2) Preparation of the dithio acid, see: T. Takeshima, M. Muraoka, N. Fukada, A. Takayama, and T. Yamamoto, *J. Org. Chem.*, **42**, 3383 (1977).

3) R. Slack and K. R. H. Wooldridge, "Advances in Heterocyclic Chemistry," ed by A. R. Katritzky, Academic Press, New York and London (1965), Vol. 4, p. 107; K. R. H. Wooldridge, *ibid.*, ed by A. R. Katritzky and A. J. Boulton, Academic Press, New York and London (1972), Vol. 14, p. 1.

4) T. Takeshima, T. Miyauchi, N. Fukada, S. Koshizawa, and M. Muraoka, *J. Chem. Soc., Perkin Trans. 1*, **1973**, 1009.

5) T. Takeshima, N. Fukada, E. Okabe, F. Mineshima, and M. Muraoka, *J. Chem. Soc., Perkin Trans. 1*, **1975**, 1277.

Resolution of Hosoya's Mystery?

Sven J. CYVIN
Division of Physical Chemistry, The University of Trondheim, N-7034, Trondheim-NTH, Norway
(Received December 26, 1987)

Synopsis. Three classes of polynomials for conjugated hydrocarbons are studied: characteristic polynomials (Hückel determinants) for cyclic polyenes, and combinatorial formulas for Kekulé structure counts of two classes of circulenes.

In the present communication three classes of polynomials are discussed, which all have relevance to molecular topology of conjugated hydrocarbons.

The characteristic polynomial of a conjugated system is very similar to the well-known Hückel determinant in the chemical context; see, e.g.[1] The simple Hückel molecular orbital theory is recognized as a part of molecular topology or graph theory.[2,3] In modern times these mathematical methods seem to penetrate into organic chemistry to a high degree.[4]

The two other classes of polynomials considered here describe the Kekulé structure counts (K) for classes of circulenes, which have counterparts in a new class of polycyclic aromatic hydrocarbons called cycloarenes.[5] Kekulene is a famous member of this class. The number K=200 for this molecule was probably given for the first time by Aihara.[6]

The present article is formulated as a comment on a remark by Hosoya,[7] who observed a coincidence between the forms of two polynomials, which are found in Table 1 under the designations $\phi_6(x)$ and $K_1(x, 6)$. In Hosoya's wording: "The reason for this mystic coincidence, however, is not known."[7] During the attempts to shed some light into this matter it was found that the coincidence is more far-reaching than the single example of Hosoya indicates.

The scope of the present work is, however, considerably broader than an attempt to resolve "Hosoya's mystery." It was aimed at a more general insight into the topological properties of circulene systems.

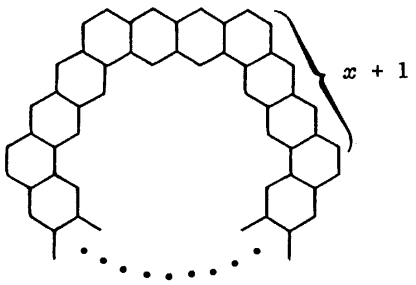

Fig. 1. Definition of a circulene. For N segments the number of hexagons is Nx.

Characteristic Polynomials. The class of characteristic polynomials for the cyclic polyacene systems (cyclopropenyl, cyclobutadiene, cyclopentadienyl, benzene,···) are considered and denoted $\phi_N(x)$ for N vertices (or N carbon atoms). An alternative to the well-known Hückel determinant is another standard formula, which reads

$$\phi_N(x)=\prod_k[x-2\cos(2k\pi/N)];$$
$$k=0, \pm1, \pm2, \cdots, \begin{cases} \pm(N-1)/2;\ N=3, 5, 7, \cdots \\ \pm(N-2)/2,\ N/2;\ N=4, 6, 8, \cdots. \end{cases} \quad (1)$$

Perhaps somewhat less known is the explicit formula

$$\phi_N(x)=2^{-N}[x+(x^2-4)^{1/2}]^N+2^{-N}[x-(x^2-4)^{1/2}]^N-2 \quad (2)$$

and the accompanying recurrence relation:

$$\phi_{N+3}=(x+1)(\phi_{N+2}-\phi_{N+1})+\phi_N \quad (3)$$

A special treatment of recurrence relations for characteristic (and other) polynomials is found in a paper of Hosoya and Ohkami,[8] which also may be consulted for some key references to this topic.

Cycloarenes with N Segments. Consider the class of circulenes consisting of N linear segments of x+1 hexagons each; see Fig. 1. The number of Kekulé structures is[9]

$$K_1(x, N)=2^{-N}[x+(x^2+4)^{1/2}]^N + 2^{-N}[x-(x^2+4)^{1/2}]^N+1+(-1)^N. \quad (4)$$

We find a striking similarity between Eqs. 2 and 4, which were derived from two apparently disconnected phenomena. The K formula for the class of circulenes considered by Hosoya,[7] and independently by others,[10,11] corresponds to N=6 in Eq. 4. The constant (x-independent) terms are somewhat elaborate. In the expanded polynomials (cf. Table 1) they manifest themselves in a repeating sequence (−2, 0, −2, −4) for $\phi_N(x)$ and (0, 4) for $K_1(x, N)$. Otherwise we find the same terms for a given N in the two polynomials, with the difference that they have alternating signs in ϕ, but

Table 1. Three Classes of Polynomials in Expanded Form for Some Values of N

N	$\phi_N(x)$	$K_1(x, N)$	$K_2(x, N)$
3	x^3-3x-2	x^3+3x	x^3-3x+2
4	x^4-4x^2	x^4+4x^2+4	x^4-4x^2+4
5	x^5-5x^3+5x-2	x^5+5x^3+5x	x^5-5x^3+5x+2
6	$x^6-6x^4+9x^2-4$	$x^6+6x^4+9x^2+4$	$x^6-6x^4+9x^2$
7	$x^7-7x^5+14x^3-7x-2$	$x^7+7x^5+14x^3+7x$	$x^7-7x^5+14x^3-7x+2$
8	$x^8-8x^6+20x^4-16x^2$	$x^8+8x^6+20x^4+16x^2+4$	$x^8-8x^6+20x^4-16x^2+4$

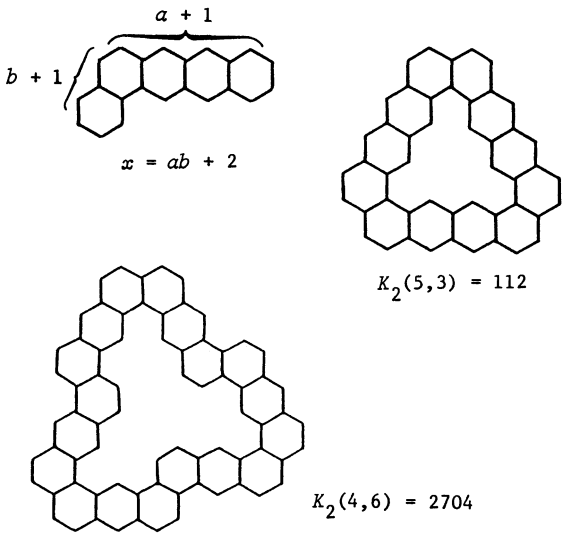

Fig. 2. Another class of circulenes. For N units the number of hexagons is $N(a+b)$. Two examples of complete systems are shown, and their K numbers are indicated.

are all positive in K_1. This feature is a consequence of the different signs in the square roots of Eqs. 2 and 4.

The function $K_1(x, N)$ may, as an alternative to Eq. 4, be expressed in terms of an $N \times N$ determinant as:

$$K_1(x, N)=(-1)^N \begin{vmatrix} -x & 1 & 0 & \cdots & 0 & 1 \\ -1 & -x & 1 & \cdots & 0 & 0 \\ 0 & -1 & -x & \cdots & 0 & 0 \\ \cdot & \cdot & \cdot & \cdots & \cdot & \cdot \\ 0 & 0 & 0 & \cdots & -x & 1 \\ -1 & 0 & 0 & \cdots & -1 & -x \end{vmatrix} \quad (5)$$

Cycloarenes with 2*N* Segments. We wish to show a modification of the system in Fig. 2 so that the K formula becomes a polynomial with alternating signs as in Eq. 2; it will in fact be identical with Eq. 2 apart from the constant term.

Consider a circulene with N units, each of them being a chain with two linear segments as shown in Fig. 2. The variable x, as determined by the two segments of one unit, is specified in the figure. An explicit equation for the K numbers was derived and reads

$$K_2(x, N)=2^{-N}[x+(x^2-4)^{1/2}]^N + 2^{-N}[x-(x^2-4)^{1/2}]^N+2. \quad (6)$$

It should be compared with Eq. 2. The sequence for constant terms of the polynomial $K_2(x, N)$ is (2, 4, 2, 0); cf. Table 1.

We give also a determinant formula for $K_2(x, N)$, which may be related to the characteristic polynomial of a Möbius ring.[12]

$$K_2(x, N)=(-1)^N \begin{vmatrix} -x & 1 & 0 & \cdots & 0 & -1 \\ 1 & -x & 1 & \cdots & 0 & 0 \\ 0 & 1 & -x & \cdots & 0 & 0 \\ \cdot & \cdot & \cdot & \cdots & \cdot & \cdot \\ 0 & 0 & 0 & \cdots & -x & 1 \\ -1 & 0 & 0 & \cdots & 1 & -x \end{vmatrix} \quad (7)$$

Conclusion

In the present note some similarities are pointed out for a class of characteristic polynomials and formulas for Kekulé structure counts of certain classes of circulenes. The results have bearings on a coincidence between the forms of two polynomials, viz. $\phi_6(x)$ and $K_1(x, 6)$, which Hosoya[7] observed and characterized as a mystery. The present work does not pretend to give a complete resolution, since it is still unknown, in a deeper sense, why these coincidences should appear.

References

1) A. Streitwieser, "Molecular Orbital Theory for Organic Chemists," Wiley, New York (1961).
2) A. Graovac, I. Gutman, and N. Trinajstić, "Topological Approach to the Chemistry of Conjugated Molecules," Lecture Notes in Chemistry 4, Springer-Verlag, Berlin (1977).
3) N. Trinajstić, "Chemical Graph Theory," CRC Press, Boca Raton, Florida (1983), Vols. I and II.
4) I. Gutman and O. E. Polansky, "Mathematical Concepts in Organic Chemistry," Springer-Verlag, Berlin (1986).
5) H. A. Staab and F. Diederich, *Chem. Ber.*, **116**, 3487 (1983).
6) J. Aihara, *Bull. Chem. Soc. Jpn.*, **49**, 1429 (1976).
7) H. Hosoya, *Comp. and Maths. with Appls.*, **12B**, 271 (1986).
8) H. Hosoya and N. Ohkami, *J. Comput. Chem.*, **4**, 585 (1983).
9) J. L. Bergan, B. N. Cyvin, and S. J. Cyvin, *Acta Chim. Hung.*, **124**, 299 (1987).
10) D. Babić and A. Graovac, *Croat. Chem. Acta*, **59**, 731 (1986).
11) J. L. Bergan, S. J. Cyvin, and B. N. Cyvin, *Chem. Phys. Lett.*, **125**, 218 (1986).
12) N. Mizoguchi, *J. Am. Chem. Soc.*, **107**, 4419 (1985).

Organophosphorus Analogues and Derivatives of the Natural L-Amino Carboxylic Acids and Peptides. IV.[1] A Phospha^{C}-Peptide Analogue of Plumbemycin A

Ivan A. NATCHEV
Research Centre Konstrukcionni Polymeri, 5-003 Gara Iskar, 1528 Sofia, Bulgaria
(Received October 3, 1987)

Synopsis. A condensation of 1,2-azaphosphorine **1** and the dipeptide **2** to the entirely protected phospha^{C}-tripeptide **3** was carried out by the DCC method. A high selectivity was achieved in the enzyme-catalyzed hydrolysis of the ethoxycarbonyl groups with alkaline mesintericopeptidase to **4** and of the peptide bond Ala-Asp with α-chymotrypsin to **5**, which in acid-catalyzed hydrolysis releases the norvaline **6**. Antitumor activity of the phospha^{C}-peptides **4** and **5** was found.

The tripeptide antibiotic Plumbemycin A was isolated from *Streptomices plumbeus* by Hirota and Sakai.[2,3] Its physiological activity was also studied.[4]

With a view to studying the relationship between the chemical structure and the physiological activity, in the present note the synthesis of phospha^{C}-peptide analogue of the above mentioned antibiotic is discussed.

Cyclic analogue of C-terminal-phosphonylated amino acid-3,4-didehydro-5-phosphono-L-norvaline= (*S*)-(6-ethoxycarbonyl-2-hydroxy-1,2,3,6-tetrahydro-1,2-azaphosphorine 2-oxide (**1**) recently synthesized (cf. later commun. of the same author) by us and the commercially available dipeptide H-Ala-Asp(OEt)-OEt (**2**) were chosen as starting substances. The condensation was carried out by DCC method. After the usual work-up of the reaction mixture, the fully protected phospha^{C}-tripeptide **3** was isolated with a yield of about 70%. At "mild" acid-catalyzed hydrolysis, the simultaneous hydrolytic cleavage of both PO-NH bonds (cyclic and exocyclic) was attained and the following products were obtained: 3,4-didehydro-5-phosphono-L-norvaline ethyl ester and the dipeptide H-Ala-Asp (OEt)-OEt (**2**) (see Scheme 1).

To ensure selective hydrolysis of the ethoxycarbonyl groups of the dipeptide **3** the alkaline mesintericopeptidase was used. Under the optimum conditions,[5] namely, 20 g substrate **3**, 5 mg enzyme in an aqueous buffer (500 ml, pH 7.8), stirring at 25 °C to a ninhydrin positive detection, the phospha^{C}-tripeptide **4** was isolated in about 90% yield.

The second enzyme we employed was α-chymotrypsin. Under the usual conditions (25 °C, pH 7.8) this enzyme enhances the hydrolysis of the peptide bond Ala-Asp selectively with no effect on the two PO-NH bonds. Thus, using 20 g substrate **4** and 5 mg enzyme α-chymotrypsin, the phospha^{C}-dipeptide **5** was isolated in about 70% yield. A "mild" acid hydrolysis (0.5 M HCl, 50 °C, 30 min) of the product **5** liberated the norvaline **6**.

The enzymes phosphodiesterase I and alkaline phosphatase did not exhibit enzyme-substrate interaction with the synthesized phospha^{C}-peptide analogues of Plumbemycin A.

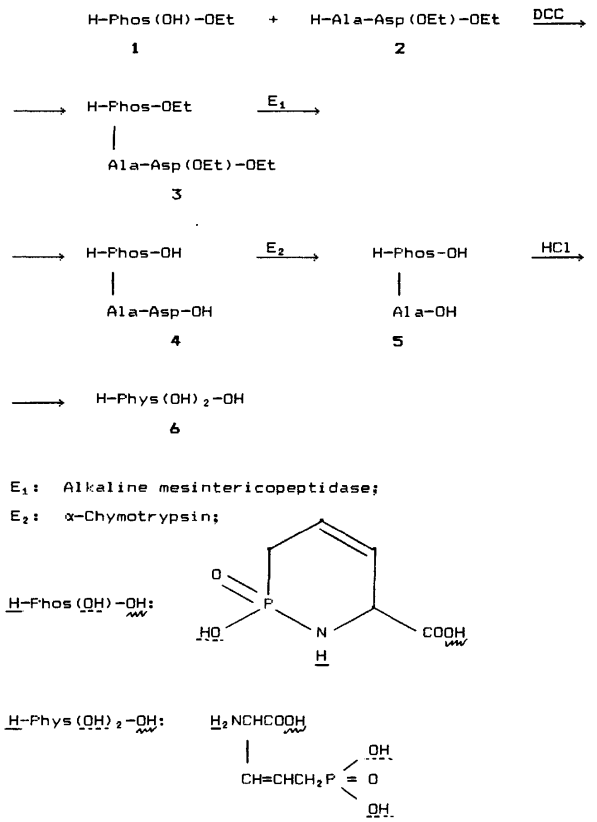

Scheme 1.

Preliminary physiological tests with the phospha^{C}-tri- and dipeptides **4** and **5** have been carried out. When applied to an experimental tumor L1210 in mice in doses of 20 and 28 mg/kg per day for 5 consecutive days, the T/L (T/L% is the ratio of the mean survival time, expressed as a percentage of untreated controls) was 184% and 172% for the tripeptide **4** and for the dipeptide **5**, respectively. The insecticidal activity of the two peptides was also studied and it has been established that the tripeptide **5** is the stronger. It is of interest to point out the following observation: when the tripeptide **5**, Plumbemycin A, L-norvaline **6**, and its cyclic analogue (*S*)-1,2,3,6-tetrahydro-1,2-azaphosphorine-6-carboxylic acid were compared, it was found that the 1,2-azaphosphorine analogue had the highest insecticidal activity, whereas in the L-norvaline **6** and in Plumbemycin A, it was entirely missing.

Detailed investigations on the insecticidal activity are now under way and the results will be published soon.

Experimental

General. IR spectra, elemental analysis, mp, Mw, $[\alpha]_D^{22}$ on Perkin-Elmer instruments; ^{1}H NMR—JEOL 100 MHz and Brucker 250 MHz; Mass spectra—LKB 900 and Barian; reagents and solvents from "Aldrich," and "Merck"; α-chymotrypsin—from Pharmachim, Bulgaria; alkaline mesintericopeptidase—Inst. Org. Chem., Bulg. Acad. Sci.; TLC-silica gel film—molybdophosphate or ninhydrin detection.

***N*-[(*S*)-(6-Ethoxycarbonyl-1,2,3,6-tetrahydro-1,2-azaphosphorin-2-yl)]alanylaspartic Acid α,β-Diethyl Ester (3).** A mixture of 1,2-azaphosphorine (**1**) (20.52 g, 0.1 mol), the dipeptide (**2**) (26.03 g, 0.1 mol) and DCC (22.69 g, 0.11 mol) in dry ethyl acetate (300 ml) was stirred in a closed Erlenmeyer flask at room temperature for 24 h. After filtration, the reaction mixture was washed consecutively with water, 5% aqueous sodium carbonate, water, 0.5% hydrochloric acid, water, and then dried over anhydrous $MgSO_4$. After distillation under vacuum to dryness, the oily residue was taken into a silica-gel column and eluted with chloroform: methanol from 9 : 1 to 7 : 3 v/v. The product was dissolved in cold dry ethyl acetate (250 ml) and dry hexane was added until it becomes turbid. After rubbing to the flask walls with a glass stick and after a continuous stay in refrigerator at −5 °C, the product **3** was slowly crystallized.

Compound 3: Yield, 29.17 g (67.3%); mp 78—81 °C (EtOAc/*n*-C_6H_{14}); IR (KBr) cm^{-1}; 1755—1730, 1640, 1520, 1330—1300, 1200; R_f: 0.68 ($CHCl_3$: MeOH=9 : 1); $[\alpha]_D^{20}$ −46.4° (*c* 1, MeOH).

Found: C, 48.60; H, 6.86; N, 9.07%. Calcd for $C_{18}H_{30}N_3O_8P$: C, 48,32; H, 6.76; N, 9.39%. Mw, Found/Calcd, 443/447.427.

The substance is soluble in the usual organic solvents and insoluble in water. When **3** (4.47 g, 0.01 mol) was heated in 0.5 M HCl (25 ml) at 50 °C for 30 min, the products isolated were: H-Ala-Asp(OEt)-OEt (**2**) in a yield of 2.11 g (81.2%) and 3,4-didehydro-5-phosphono-L-norvaline ethyl ester: yield 1.58 g (77.7% as HCl salt); mp 210 °C (decomp); IR (KBr) cm^{-1}: 1750, 1550, 1240, 1010, 970; ^{1}H NMR (DMSO-d_6, δ, free basse) δ=1.26 (3H, t, $OCH_2C\underline{H}_3$), 2.75 (2H, dd, $J_{P\text{-}C\underline{H}_2}$=8.6 and 23 Hz), 4.03 (2H, q, $OC\underline{H}_2CH_3$), 4.80 (1H, d, *J*=8 Hz, CH), 5.65 (1H, m, C<u>H</u>=CH), 6.13 (1H, m, CH=C<u>H</u>CH_2), 10.4—10.8 (2H, br, s, PO_3H_2); MS-free base, *m/z*, Found/Calcd, 223 (18%)/223.166; R_f: 0.33 (*n*-BuOH : AcOH : H_2O=3 : 1 : 1); $[\alpha]_D^{20}$ −56.3° (*c* 1, 0.1 M NaOH).

Found: C, 32.71; H, 5.61; N, 5.42%. Calcd for $C_7H_{14}NO_5P \cdot HCl$: C, 32.38; H, 5.82; N, 5.40%.

***N*-[(*S*)-(6-Carboxyl-1,2,3,6-tetrahydro-1,2-azaphosphorin-2-yl)]alanylaspartic Acid (4).** A mixture of the tripeptide **3** (20 g, 0.04 mol) homogenized with 3—4 drops of "Tween-8-", and the enzyme alkaline mesintericopeptidase (5 mg) in an aqueous buffer [tris(hydroxymethyl)aminomethane-(Trisma^R), 500 ml, 0.05 M, pH 7.8 at 25 °C] was stirred until it gave a positive test on ninhydrin. After acidification (pH 6.5) and distillation under vacuum to dryness, the organic mass was extracted with boiling ethanol. After cooling, the product **4** was filtered.

Compound 4: Yield, 14.18 g (87.3%); mp 162—165 °C (EtOH); IR (KBr) cm^{-1}; 3860—2800, 1760, 1640, 1520, 1340, 1265, 970—840, 630; ^{1}H NMR (D_2O+Na_2CO_3) δ=1.52 (3H, d, *J*=8 Hz, $CHC\underline{H}_3$), 2.26 (2H, d, CH_2CO), 4.2—4.6 (3H, m, 3×CH), 2.72 (2H, m, PCH_2), 5.68 and 6.21 (2H, m, C<u>H</u>=C<u>H</u>), R_f: 0.56 (DMF: dioxane: $CHCl_3$=9 : 1 : 1); $[\alpha]_D^{20}$ 63.8° (*c* 0.1, 0.1 M NaOH).

Found: C, 40.00; H, 5.11; N, 11.38%. Calcd for $C_{12}H_{18}N_3O_8P$: C, 39,67; H, 4.99; N, 11.57%. Mw, Found/Calcd, 360/363.327.

The substance is highly soluble in DMF, DMSO, hexamethylphosphoric triamide, and water, less in dioxane and ethanol and is insoluble in chloroform, ether, and hexane. When **4** (3.60 g, 0.01 mol) was heated in 0.5 M HCl (25 ml) at 50 °C for 30 min, the following products were isolated: the dipeptide H-Ala-Asp-OH (1.70 g, 83.4%) and 3,4-didehydro-5-phosphono-L-norvaline (**6**): yield 1.52 g (78.3%) mp 188—190 °C (decomp) [for the D-form mp: 183—185 °C[1]]; IR (KBr) cm^{-1}: 1735, 1630, 1520, 1240, 1150 1040, 930, 860, 725, 630; ^{1}H NMR (D_2O+NaOD) δ=2.75 (2H, dd, $J_{P\text{-}CH_2}$=8.3 and 23 Hz), 4.03 (2H, q, $OC\underline{H}_2CH_3$), 4.81 (1H, d, *J*=8 Hz, CH), 5.66 (1H, m, C<u>H</u>=CH), 6.12 (1H, m, CH=C<u>H</u>CH_2) and five exchangeable protons NH_2, COOH, PO_3H_2; MS, *m/z*, Found/Calcd, 195/195.112; R_f: 0.33 (*n*-BuOH : Pyr : AcOH : H_2O=15 : 12 : 3 : 10) and 0.10 (*n*-BuOH : AcOH : H_2O=3 : 1 : 1); $[\alpha]_D^{20}$ −53.2° (*c* 1, H_2O).

Found: C, 30.53; H, 5.28; N, 7.06%. Calcd for $C_5H_{10}NO_5P \cdot HCl$: C, 30.78; H, 5.17; N, 7.18%.

***N*-[(*S*)-(6-Carboxyl-1,2,3,6-tetrahydro-1,2-azaphosphorin-2-yl)]alanine (5).** A mixture of the tripeptide **4** (20 g, 0.55 mol) and α-chymotrypsin (5 mg) in an aqueous buffer [tris-(hydroxymethyl)aminomethane(Trisma^R), 500 ml, 0.05 M, pH 7.8 at 25 °C] was stirred for 6 h. After acidification (pH 5.8) and vacuum distillation to dryness, the organic residue was extracted with boiling ethanol. After cooling, the product **5** was filtered.

Compound 5: Yield, 11.04 g (82.8%); mp approx. 200 °C (decomp); IR (KBr) cm^{-1}; 3800—3000, 1750—1725, 1360, 1280, 960, 840, 720, 630; ^{1}H NMR (D_2O+Na_2CO_3) δ=1.48 (3H, d, *J*=8 Hz, $CHC\underline{H}_3$), 4.18 and 4.42 (2H, m, 2×CH), 2.77 (2H, m, PCH_2), 5.72 and 6.33 (2H, m, C<u>H</u>=C<u>H</u>), and four exchangeable protons; MS, *m/z*: Found/Calcd, 248 (18%)/248.175; R_f: 0.68 (DMF: dioxane: $CHCl_3$=9 : 1 : 3); $[\alpha]_D^{20}$ −63.7° (*c* 1, H_2O).

Found: C, 38.66; H, 5.41; N, 11.36%. Calcd for $C_8H_{13}N_2O_8P$: C, 37,72; H, 5.28; N, 11.29%. Mw, Found/Calcd, 251/248.175.

The substance is very soluble in DMF, DMSO, hexamethylphosphoric triamide, comparatively in dioxane and ethanol and is insoluble in chloroform, ether and hexane. When **5** (2.51 g, 0.01 mol) was heated in 0.5 M HCl (25 ml) at 50 °C for 30 min, the product 3,4-didehydro-5-phosphono-L-norvaline (**6**) (1.74 g, 89.1%) was isolated and has spectral data identical with those obtained by based-hydrolysis of the peptide **4** (cf. the above section).

References

1) Part III: I. A. Natchev, *Bull. Chem. Soc. Jpn.*, **61**, 3711 (1988).

2) B. Park, A. Hirota, and H. Sakai, *Agric. Biol. Chem.*, **40**, 1505 (1976).

3) T. Boku, A. Hirota, and H. Sakai, *Jpn. Kokai*, **77**, 108904.

4) H. Doddens, M. Dorgerleh, and H. Zocher, *J. Antibiot.*, **32**, 87 (1979).

5) I. Natchev, *Synthesis*, **1987**, 1079.

A Theoretical Study on Bromochlorination

Shinichi YAMABE* and Tsutomu MINATO†,††
Department of Chemistry, Nara University of Education, Takabatake-cho, Nara 630
†Yuge Mercantile Marine College, Yuge-cho, Ochi-gun, Ehime 794-25
(Received January 23, 1988)

Synopsis. The bromochlorination to ethylene is studied by ab initio MO calculations. The presence of the bridge ion is verified by a transition state (TS) search. The TS geometry is represented as an ion pair. Two mechanistic questions, orientation of Br-Cl and the anti Cl^- addition, are discussed in terms of the frontier-orbital theory.

Additions of bromine chloride (BrCl) in CCl_4 or CH_2Cl_2 have been investigated extensively.[1,2] The regioselectivity of the bromochlorination may be explained by the AD_E (electrophilic addition) mechanism, where a bridged bromonium ion intermediate is attacked by a chloride ion.[1] This scheme is based on the product analysis of 1-hexene in a nonpolar solvent (CCl_4) and a protic solvent (methanol).

n-BuCH=CH_2 + BrCl → n-BuCHCl-CH_2Br + Others (in CCl_4)

n-BuCH=CH_2 + BrCl → n-BuCH(OMe)-CH_2Br + Others (in MeOH)

Two mechanistic questions emerge.

(1) Why is no chloronium ion intermediate formed in the electrophilic attack of BrCl on a double bond?

(2) What is the driving force for anti addition of a nucleophile to a bridged bromonium ion in Fig. 1? In a cyclic intermediate, the cationic nature is retained in the bromine atom, and two carbon atoms are somewhat anionic (see Fig. 4).

To solve these problems, ab initio MO calculations were made with 3-21G and 3-21G(*) basis sets,[3] using the GAUSSIAN 82 program.[4]

MO Calculations of the BrCl Addition to Ethylene

In Fig. 2, two TS structures are shown. The two geometries are found to be similar. Bromide and chloride ions are remote from the cyclic chloronium and bromonium ions, respectively. It is noteworthy that

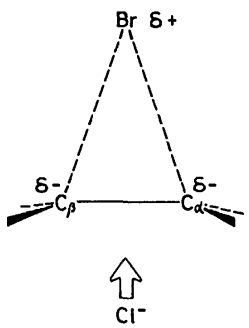

Fig. 1. Schematic presentation of the anti attack of Cl^- to the cyclic bromonium ion.

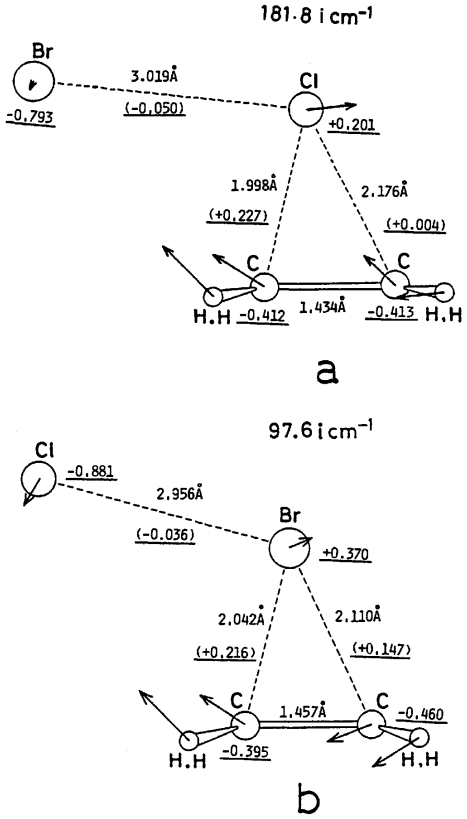

Fig. 2. Transition-state geometries of the bromochlorination to ethylene obtained with the 3-21G optimization. The imaginary-frequency vibrational mode showing the reaction path is sketched with arrows. The 3-21G(*)//3-21G total energies are −3095.12477 a.u. (a) and −3095.17221 a.u. (b). 1 a.u.=627.566 kcal mol^{-1}=2625.736 k J mol^{-1}.
The underlined numbers denote the 3-21G(*) atomic net charges (negative, anionic) and those in parentheses are atom-atom bond populations.

bridged halonium ions are almost formed at TS. The ion-pair formation is more complete in TS *b* ($Br^{+0.370}$ vs. $Cl^{-0.881}$) than in TS *a* ($Cl^{+0.201}$ vs. $Br^{-0.793}$). Also, there is a noticeable difference in the bonding nature between the C··· Br bonds and the C··· Cl bonds. While the C··· Br bonds have large bonding populations (+0.216 and +0.147), one of the C··· Cl bonds has a small bonding population (+0.004). These results of the electron population indicate that TS *b* is more favorable for the formation of a bridged intermediate plus an anion than TS *a*. In fact, the activation energy of TS *b* [=44.6 kcal mol^{-1} (1 cal mol^{-1}=4.184 J mol^{-1}), 3-21G(*)//3-21G relative to the energy of the C_{2v} π complex, C_2H_4 ··· BrCl] is much smaller than that of TS *a* [=71.9 kcal mol^{-1}]. Thus, the present calculation

†† Present address: Institute for Natural Science, Nara University, 1500 Misasagi-cho, Nara 631.

shows that a bromonium ion intermediate is formed in the bromochlorination.[1)]

The ease of the cyclic bromonium ion formation in the BrCl addition is explicable by the shape of the lowest unoccupied MO (LUMO) of Br-Cl. The ionization potential of the chlorine atom (=12. 976 eV) is larger than that of the bromine atom (=11.814 eV). The difference leads to the asymmetric orbital extension. The energy of the LUMO of BrCl is close to that of the Br atomic orbital, and the LUMO has a bromine $4p_\sigma$ character. Therefore. the electrophilicity is larger at the bromine site, and the charge transfer (CT) from the ethylene π MO to the LUMO is effective in $C_2H_4 \rightarrow$BrCl coordination as is shown in Fig. 3. Thus, the first question of the bromonium ion selectivity has been answered by the frontier orbital theory. [5)]

The Origin of the Anti Nucleophilic Addition

After the cyclic bromonium ion is formed, how is the anti addition of the chloride ion brought about? In Fig. 4, the optimized structure of the cyclic bromonium ion is shown. It is realized that the geometry is close to that at TS *b* in Fig. 2. The b_2 in-plane antisymmetric vibrational mode is also shown in Fig. 4 and it has the lowest value among the 15 (=3×7 atoms−6) harmonic frequencies. This mode indicates that the "b_2 spring" is the most fragile (C··· Br bond cleaved) against the external fluctuation (i.e., the Cl^- attack). When the C_{2v} geometry is deformed along the b_2 vibration, two low-lying vacant MO's mix with each other. The mixing leads to the lowering of the energy level of the LUMO and consequently to higher reactivity against the nucleophilic attack. The mixing also causes a change in the shape of the MO's as is shown in Fig. 5. The α carbon atom has the larger lobe of the LUMO and is ready to catch Cl^- in syn and anti directions (two bold empty arrows). The syn direction is apparently more favorable than the anti one, because there is a larger lobe of the LUMO along the C··· Br bond. However, a crucial factor of making the syn attack unfavorable is the nodal property of the LUMO. Although the magnitude of the spatial extension of the LUMO is larger at the syn site than the anti site, the presence of the distinct node prohibits the effective CT from the chloride ion. The anti attack is not prohibited by the nodal property of the LUMO and may cause the larger CT. Thus, the second question is answered. The anti attack shown by the lower arrow is initiated by the geometric distortion along the lowest-frequency vibration and the resultant MO mixing. The Cl^- orientation is determined not by the electrostatic force but by the shape of the frontier orbital, the LUMO. To prove this prediction, the partial geometric optimizations for syn and anti attacks were made with the $Cl^- \cdots C_\alpha$ distance fixed to 2.3 Å. The

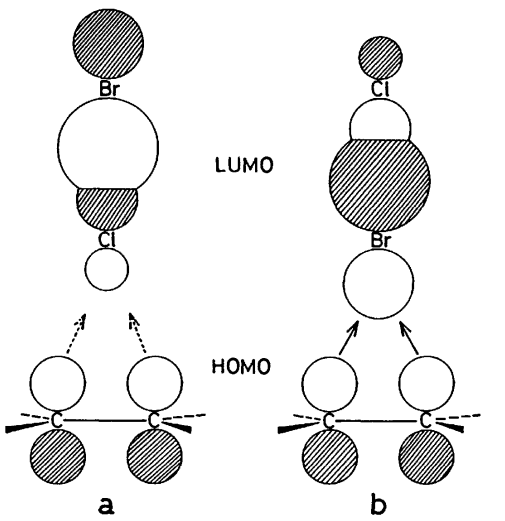

Fig. 3. $C_2H_4 \rightarrow$ClBr(a) and $C_2H_4 \rightarrow$BrCl(b) charge-transfer interactions.

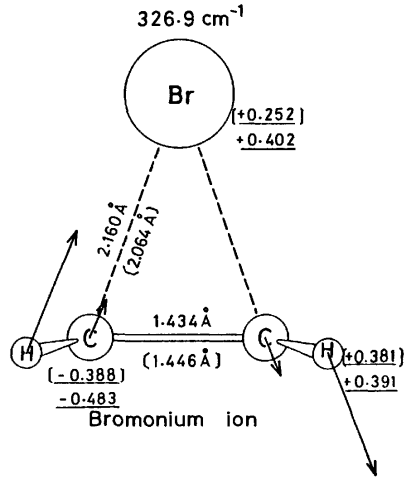

Fig. 4. The geometry of the bridged bromonium ion intermediate ($C_2H_4Br^+$) and the lowest-frequency vibrational mode. Numbers in brackets denote the 3-21G(*) optimized distances and the net charges. The C_{2v} geometry was also obtained by Poirier et al. with a somewhat different basis set.[6)] The 3-21(*)//3-21G total energy is −2637.57871 a.u.

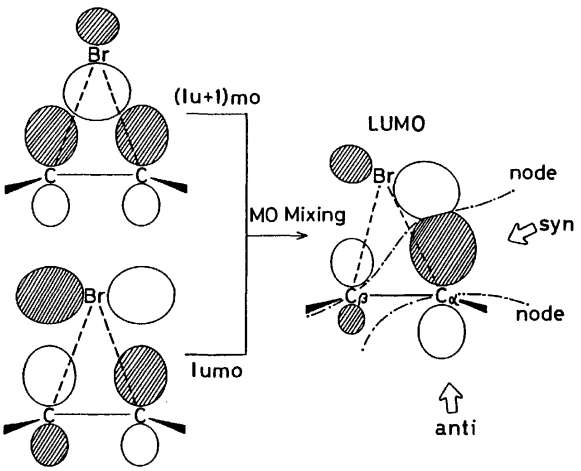

Fig. 5. The mixing of two low-lying vacant MO's, lumo and (lu+1)mo, to give LUMO through the geometric distortion along the harmonic vibration of the smallest frequency. LUMO and lumo are the lowest unoccupied MO's. The (lu+1)mo is the next lowest unoccupied one. Bold empty arrows indicate possible directions of the Cl^- attack.

distance is thought to correspond approximately to the transition state of the nucleophilic Cl^- addition. The anti attack is calculated to be 12.3 kcal mol^{-1} more stable (smaller activation-energy barrier) than the syn attack. This result supports the above prediction.

In Fig. 4, the 3-21G and 3-21G(*) bond distances are found to be similar. Therefore, the basis set dependence of the geometry seems not to be so significant as that of the electron distributions (underlined numbers), and the 3-21G(*)//3-21G calculation may be appropriate to the present discussion.

Concludig Remarks

In this work, an electrophilic addition of bromine chloride to ethylene is investigated theoretically. Two mechanistic questions are solved by the frontier orbital theory. The first is the orientation of Br-Cl toward the double bond of ethylene. The softer atom, bromine, gets the larger lobe in the LUMO and is directed to ethylene. Activation energies for two models of the BrCl approach are compared, and the predicted orientation is confirmed. Noteworthy is the TS geometry in Fig. 2(b), where the cyclic bromonium ion intermediate and the chloride ion are almost separated. The formation of the ion pair is found to be possible without the assistance of a polar solvent. The second question is concerned with the theoretical origin of the Cl^- anti addition. The nucleophilic attack becomes likely through the coupling of the fragle b_2 in-plane vibration and the MO mixing. In spite of the anionic nature of the ethylenic carbon atom, C_α, it accepts the Cl^- attack through the LUMO.

The authors thank the Institute for Molecular Science for the allotment of the CPU time of the HITAC S-810 computer.

References

1) V. L. Heasley, D. F. Shellhamerm, J. A. Iskikian, D. L. Street, and G. E. Heasley, *J. Org. Chem.*, **43**, 3139 (1978); V. L. Heasley, D. W. Spaite, D. F. Shellhamer, and G. E. Heasley, *ibid.*, **44**, 2608 (1979).

2) T. Negoro and Y. Ikeda, *Bull. Chem. Soc. Jpn.*, **57**, 2111 (1984); **57**, 2116 (1984); **58**, 3655 (1985); **59**, 2547 (1986).

3) J. S. Binkley, J. A. Pople, and W. J. Hehre, *J. Am. Chem. Soc.*, **102**, 939 (1980); K. D. Dobbs and W. J. Hehre, *J. Compt. Chem.*, **7**, 359 (1986).

4) J. S. Binkley, M. J. Frisch, D. J. DeFrees, K. Raghavachari, R. A. Whiteside, H. B. Schlegel, and J. A. Pople, "GAUSSIAN 82 Program Package," Carnegie-Mellon Chemistry Publishing Unit, Pittsburgh, USA (1982).

5) K. Fukui, "Theory of Orientation and Stereoselection," Springer-Verlag, Heidelberg (1970).

6) R. A. Poirier, R. G. Mezey, K. Yates, and I. G. Csizmadia, *J. Mol. Struct. (THEOCHEM)*, **85**, 153 (1981)

Phospholipid Inverted Micellar Aggregate as an Ionophore in Liquid Membrane System

Kozue KAIBARA,* Keiko ITO, and Kenji MIYAKAWA†
Department of Chemistry, Faculty of Science, Kyushu University, Hakozaki, Higashi-ku, Fukuoka 812
†Department of Applied Physics, Faculty of Science, Fukuoka University, Nanakuma, Jonan-ku, Fukuoka 814
(Received July 11, 1988)

Synopsis. Electrochemical, thermochemical, and light scattering investigations were performed on the 1-octanol liquid membrane systems containing dipalmitoyl-DL-phosphatidylcholine (DPPC) as an ionophore. It was suggested that DPPC molecules form inverted micellar aggregate in water saturated 1-octanol and that the membrane processes can be regulated by an endothermic phase transition of the DPPC multimolecular cation carrier.

Phospholipids, as an essential constituent of the biological systems, are important to assemble a bimolecular layer structure of the biomembrane. Bimolecular membrane structure of lipids observed in the artificial planar membrane or liposome has long been a useful model to investigate the biological membrane-related processes. On the other hand, it has been demonstrated that phospholipids dissolved in organic solvent with trace water content form inverted micellar aggregates.[1-5] There is interest in inverted micelles in these days as a mediator of the specific chemical reactions relating to a water pool trapped inside the micelle phase. In the present study, the ionophoretic capabilities of the inverted micellar aggregates of phospholipid in liquid membrane systems were investigated.

Experimental

Liquid membranes were prepared by dissolving dipalmitoyl-DL-phosphatidylcholine (DPPC), purchased from Sigma Chemical Co. and used without further purification, into 1-octanol saturated with water or 10^{-2} mol dm^{-3} aqueous NaCl solution by applying the ultrasonic irradiation above the main transition temperature of DPPC-water system. Three types of experiments, electrochemical, thermochemical, and photon correlation spectroscopic measurements, were carried out: (A) Transmembrane potentials and conductances were measured with varying temperature, 0—50 °C, in an immobilized liquid membrane-aqueous NaCl system to estimate the ion selectivity parameters. The immobilized liquid membrane systems consisted of solution phase I, where NaCl concentration was varied from 10^{-1} to 10^{-3} mol dm^{-3}, and phase II with a fixed NaCl concentration of 10^{-2} mol dm^{-3} separated a poly(tetrafluoroethylene) membrane filter (Fluoropore FP100, pore size: 1.00 μm, Sumitomo Electric Co.) impregnated with a 1-octanol solution of 10^{-2} mol dm^{-3} DPPC saturated with 10^{-2} mol dm^{-3} NaCl solution. (B) A differential scanning calorimeter (SSC/560U, Dainiseikosha Co.) was employed to observe thermal behavior of DPPC molecules using a 50 μl liquid membrane sample containing 1 mg DPPC sealed in a silver pan with a main scanning rate at 1 °C min^{-1}. (C) Laser light scattering equipments and measuring conditions were the same as used in the previous experiments.[6] The liquid membrane samples were illuminated by an argon laser operated in the TEM_{00} mode at 514.5 nm, at a power 100 mW. Providing that autocorrelation function, $C(t)$, in the heterodyne regime has a single exponential decay mode, the relaxation time, τ, was determined from a nonlinear least-squares fit to the relation as:

$$C(t)=A+B\exp(-t/\tau) \quad (1)$$

where A is the background part of $C(t)$ and B is a constant.

Results and Discussion

Figure 1 summarizes the experimental data and the estimated parameters as a function of temperature. The observed membrane potential data indicated that DPPC in the 1-octanol liquid membrane phase acts as a cation carrier with a transport number to Na^+, 0.82—0.92. The transport number to Na^+ increased with raising temperature and decreasing NaCl concentration in phase I. Systematic investigations by Green et al.[7-9] demonstrated that phospholipids function as an ionophore and, in some cases, ionophoretic capabilities are comparable to those of authentic antibiotic ionophores. Highly selective and specific biomembrane transport processes are considered nowadays to be determined by proteinic materials embedded in the phospholipid bilayers such as ionophoretic substances and transport enzymes. However, phospholipids still play some roles in the broad spectrum of biomembrane transport capabilities. In the context of a possible physiological significance of the ionophoretic activities of phospholipids, involvements to the energy coupling process were suggested.[7]

As can be seen in Fig. 1-A, the curve relating the membrane conductance, G_m, with temperature shows a change of gradient at around 18 °C. And, the curve relating the membrane permeabilities to Na^+ and Cl^-, P_{Na} and P_{Cl}, with temperature in Fig. 1-B shows a change of gradient as corresponding with the membrane conductance change as a function of temperature. P_{Na} and P_{Cl}, indicating the membrane permselectivities by referring to the permeating speed of respective ions, can be calculated from the membrane potential and conductance data based on the preceding membrane theory.[10,11] The membrane permeability ratio, P_{Cl}/P_{Na}, decreased slightly with raising temperature.

It is a well-known fact that the conductance of phospholipid bilayer membrane changes drastically at the temperature corresponding to the gel-liquid crystal phase transition temperature observed in phospholipid-water system. Differential scanning calorimetry (DSC) measurements on the DPPC-1-octanol liquid membrane were carried out to examine a phase behavior of DPPC molecule at around 18 °C where the temperature-dependent characteristics of membrane transport altered. Examples of the DSC thermogram of the DPPC-1-octanol liquid membrane fluid are

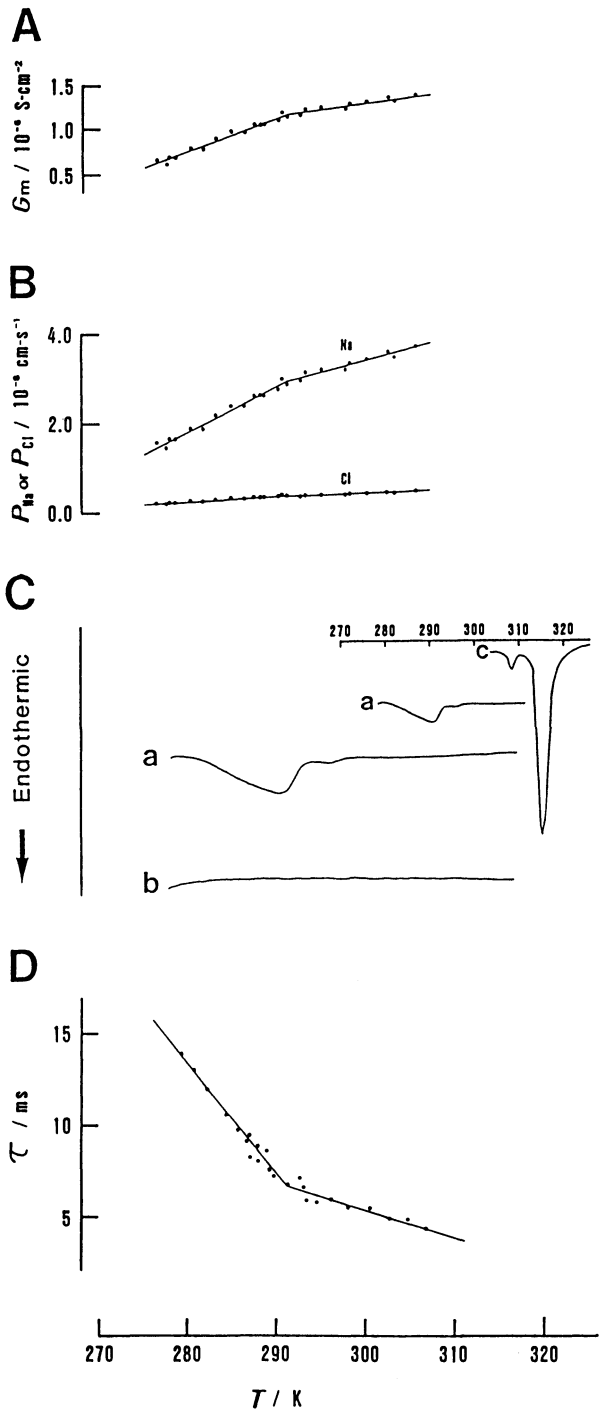

Fig. 1. Membrane conductance [A], membrane permeabilities to Na^+(●) and Cl^-(○) [B], DSC thermogram [C], and relaxation time obtained by the light scattering study [D] as a function of temperature. The membrane conductance and permeability values were obtained for 10^{-2} mol dm^{-3} NaCl(I)-10^{-2} mol dm^{-3} NaCl(II) system. In Fig. 1-C, thermograms a, b, and c were recorded for the systems in which DPPC dissolved in 1-octanol saturated with 10^{-2} mol dm^{-3} NaCl aqueous solution, in pure 1-octanol, and in 10^{-2} mol dm^{-3} NaCl aqueous solution, respectively. The scale of the upperright frame comparing the thermograms a and c is reduced to 1/2 of the original scale for the thermograms a and b.

shown in Fig. 1-C. As illustrated in the thermogram a, an endothermic peak was detected at around 18 °C in 1-octanol solution of DPPC saturated with water or aqueous NaCl solution. None of the detectable thermal changes were observed, on the contrary, in the pure 1-octanol solution of DPPC (thermogram b) and in the system without DPPC. Up to 80—90 °C, additional thermal changes were not observed in these systems. The peak height of the thermogram a is approximately 1/10 of that of the established endothermic changes for the gel-liquid crystal transition of DPPC-water system (compare the thermograms a and c). The thermograms a, b, and c were recorded from the samples containin 20 mg ml^{-1} DPPC dissolved into respective solvents. The present DSC results suggest that the changes in mode of the DPPC-mediated cation transport at critical temperature, 18 °C, are related in some way to endothermic phase transitions of DPPC in the liquid membrane phase.

It is also a common observation that addition of short-chain normal alkanols cause broadening of the thermal peak and lowering of the temperature for the endothermic gel-liquid crystal transition of phospholipid-water system.[12,13] These alterations in the endothermic behavior were suggested to be due to the penetrations of additives into the phospholipid bilayer structure. The present DPPC-1-octanol liquid membrane systems are different definitely in 1-octanol/water ratio from these phospholipid-excess water system with adding alcohols. It is expected, accordingly, in the present DPPC-1-octanol with trace water system (solubility of water in 1-octanol at 25 °C: ca. 3.5 wt%)[14] that the DPPC molecules form inverted micellar aggregates trapping a pool water phase. The formation of micelles in nonaqueous solvent is suggested to be affected by a trace amount of water existing in the solvent.[2,3] In the present system, appearance and peak height of the endothermic change illustrated in the DSC thermogram Fig. 1-C-a were quite sensitive to water content in the 1-octanol liquid membrane phase (unpublished observations).

To confirm the participations of DPPC inverted micellar aggregate in the cation transport across liquid membrane, the micelle formation was detected directly by means of the photon correlation spectroscopy. The mode of temperature dependences of the relaxation time constant obtained from the analyses of laser light scattering measurements on the DPPC-1-octanol membrane fluid samples saturated with water or aqueous NaCl solution is shown in Fig. 1-D. In case of the samples with pure 1-octanol as well as the samples without DPPC, none of the evidence indicating aggregate formations was obtained. The DPPC inverted micellar diameter at 18 °C can be estimated approximately at 0.1 μm, on the assumption of a formation of spherical aggregates. As illustrated in Fig. 1-D, the curve relating the relaxation time constant with temperature shows a distinct change of slope, and, accordingly, indicates an alteration of the temperature dependences of diffusion coefficient of the DPPC aggregate at around 18 °C. Possible mechanisms to decrease the diffusion coefficient of DPPC inverted micellar aggregate in lower temperature

region are increases in micellar diameter, changes in micellar shape, fusion of micellar aggregate, etc. It was reported that the inverted micellar size increases with decreasing solvent dielectric constant and with lowering temperature.[1,15] An increase in micellar diameter due to the fusion of DPPC aggregates is possible in relation to the decrease in water solubility into 1-octanol. Changes in the surface charge conditions of DPPC aggregates are also possible in addition to these mechanisms.

The present results, especially the DSC and light scattering investigations demonstrating the importance of trace water content in the present liquid membrane system, suggest that the DPPC molecules form inverted micellar aggregates and function as a multimolecular cation carrier across the liquid membrane phase. Cations are thought to be transported by means of the trapping into a pool water phase as well as of the binding to the phosphate charges on the inverted micellar surface. The multimolecular ion carrier is expected to serve more possibilities to regulate membrane transport processes than the usual unimolecular ion carrier as shown in the present results, in which the effects of temperature on membrane permeability to Na^+ are demonstrated based on the endothermic phase transition of the DPPC inverted micellar aggregates. A detailed description of the phase behavior of the DPPC-1-octanol-trace water system requires further careful experiments, since the contents of trace amount of water seem to play a critical role for the phase behavior and the contributions to the liquid membrane transport. These experiments are also required for more direct evidence indicating the existence of the DPPC inverted micellar aggregates in the liquid membrane phase. The phase behavior studies of phospholipid-water system with and without addition of organic substances have been carried out extensively. For better understanding of the biological importance of phospholipids, however, systematic investigations on the phase behavior of phospholipid-organic solvent with trace water system are required. In the context of an existence of trace amount of water within membrane phase, the liquid membrane systems containing inverted micellar aggregates as an ion carrier provide an interesting model system to analyze the ion transport mechanisms of highly hydrophobic fluorinated ion-exchange membrane,[16,17] of which technological importance in membrane utilizing process is recognized in these days.

The authors wish to thank Prof. Shoji Kaneshina of Tokushima University for facilities for the DSC measurements. The authors are grateful to the Ministry of Education, Science and Culture of Japan for a Grant-in-Aid for Scientific Research on Priority Areas and one of the authors (K.K.) is also grateful to the Kurata Foundation for the research grant support.

References

1) P. H. Elworthy and D. S. McIntosh, *J. Pharm. Pharmacol.*, **13**, 663 (1961).
2) R. Kanamoto, Y. Wada, G. Miyajima, and M. Kito, *J. Am. Oil Chem. Soc.*, **58**, 1050 (1981).
3) M. Hayashi, K. Fukushima, and A. Kitamura, *Chem. Phys. Lipids*, **33**, 1 (1983).
4) V. V. Kumar, C. Kumar, and P. Raghunathan, *J. Colloid Interface Sci.*, **99**, 315 (1984).
5) M. Hayashi and Y. Maeda, *J. Jpn. Oil Chem. Soc.*, **34**, 758 (1985).
6) K. Miyakawa, T. Hirakawa, and S. Yamashita, *J. Phys. Soc. Jpn.*, **54**, 445 (1985).
7) D. E. Green, *Ann. N. Y. Acad. Sci.*, **264**, 61 (1975).
8) C. A. Tyson, H. Vande Zande, and D. E. Green, *J. Biol. Chem.*, **251**, 1326 (1976).
9) D. E. Green, M. Fry, and G. A. Blondin, *Proc. Natl. Acad. Sci. U.S.A.*, **77**, 257 (1980).
10) K. Kaibara, H. Sonoda, Y. Nagata, and H. Kimizuka, *Bull. Chem. Soc. Jpn.*, **56**, 1346 (1983).
11) K. Kaibara, Y. Nagata. T. Kimotsuki, and H. Kimizuka, *J. Membr. Sci.*, **29**, 37 (1986).
12) A. W. Eliasz, D. Chapman, and D. F. Ewing, *Biochim. Biophys. Acta*, **448**, 220 (1976).
13) E.S. Rowe, *Mol. Pharmacol.*, **22**, 130 (1982).
14) J. M. Sørensen and W. Arlt, "Liquid-Liquid Equilibrium Data Collection, Binary Systems," Deutschen Gesellschaft für Chemisches Apparatewesen, Frankfurt (1979).
15) N. Muller, "Micellization, Solubilization and Microemulsions," ed by K. L. Mittal, Plenum Press, New York (1977), Vol. 1, p. 229.
16) T. G. Gierke and W. H. Hsu, "Perfluorinated Ionomer Membranes," American Chemical Society, Washington, DC (1982), p. 283.
17) R. Wódzky, A. Narebska, and W. K. Nioch, *J. Appl. Polym. Sci.*, **30**, 769 (1985).

Crystal Structure of $K_4[H_2P_2Mo_5O_{21}]\cdot 2H_2O$

Tomoji OZEKI, Hikaru ICHIDA, Hiroshi MIYAMAE,† and Yukiyoshi SASAKI*
Department of Chemistry, Faculty of Science, The University of Tokyo, Hongo, Tokyo 113
†Department of Chemistry, Faculty of Science, Josai University, Keyakidai, Sakado-shi 350-02
(Received April 16, 1988)

Synopsis. $K_4[H_2P_2Mo_5O_{21}]\cdot 2H_2O$ crystallizes in monoclinic system, $P2_1/a$ with a=13.648(4), b=15.591(7), c=10.889(4) Å, β=94.21(2)°, U=2311(1) Å^3, Z=4. It contains a discrete pentamolybdodiphosphite anion, $[H_2P_2Mo_5O_{21}]^{4-}$, which has, approximately, a C_{2v} symmetry. Its framework is the same as those found in the pentamolybdodiphosphate and the pentamolybdodiphosphonate anions. The P-O and Mo-O distances are 1.49—1.55 and 1.69—2.46 Å, respectively.

It has been known since early this century that trivalent phosphorus forms heteropolymolybdates.[1] Kwak et al.[2] reported the synthesis and characterization of a series of anions $[(RP)_2Mo_5O_{21}]^{4-}$, where R=H, CH_3, C_2H_5, C_6H_5, $C_2H_4NH_3^+$, and p-$CH_2C_6H_4NH_3^+$. Stalik and Quicksall[3] carried out X-ray structure analyses of complexes with R=CH_3 and $C_2H_4NH_3^+$. They have identical oxometalate structures as those of the pentamolybdodiphosphate anion[4] and its protonated species[5] containing pentavalent P atoms: $[(HOP)_n(OP)_{2-n}Mo_5O_{21}]^{(6-n)-}$ where n=0, 1, 2. We have investigated the crystal structure of $[(HP)_2Mo_5O_{21}]^{4-}$, which turned out to have the same framework as those of pentamolybdodiphosphate and pentamolybdodiphosphonate anions.

Experimental

Colorless tabular crystals of the title compound were obtained by mixing a K_2MoO_4 solution (3.0 g in 20 ml H_2O) and a H_3PO_3 solution (0.4 g in 10 ml H_2O), followed by the addition of 2.0 ml of acetic acid to adjust the pH to ca. 7. A single crystal (0.05×0.08×0.18 mm^3) was mounted on a RIGAKU AFC-5 diffractometer and intensity data were collected using graphite monochromatized Mo$K\alpha$ radiation (λ=0.71069 Å). The lattice parameters were obtained by least-squares from 40 reflections with 2θ ranging from 30° to 40°. Crystal data are as follows: $K_4[H_2P_2Mo_5O_{21}]\cdot 2H_2O$; Mr=1072.1; monoclinic; space group $P2_1/a$; a=13.648(4), b=15.591(7), c=10.889(4) Å, β=94.21(2)°, U=2311(1) Å^3; Z=4; $F(000)$=2024; D_x=3.08 g cm^{-3}; μ(Mo $K\alpha$)=3.53 mm^{-1}. A total of 7335 reflections ($2\theta\leqq 60°$) were collected by the ω-2θ scan method with the scan rate of 3° min^{-1} in ω. The ranges of the indices were $0\leqq h\leqq 19$, $0\leqq k\leqq 21$, $-15\leqq l\leqq 15$. Three standard reflections were monitored every 100 reflections. Their intensity variations were within ±3%. The intensity data were corrected for the Lorentz-polarization effect. Absorption correction was not applied. 3433 independent reflections with $|F_o|\geqq 3\sigma(|F_o|)$ and $|F_o|\geqq 8.0$ were used for a structure determination and refinement. The Weissenberg photograph of the $h0l$ layer showed some reflections with $h=2n+1$, breaking the extinction rule for the space group $P2_1/a$. However, most of them were not observed. Assuming the space group to be $P2_1$, the Patterson function was analysed to give the positions of ten Mo atoms, followed by Fourier syntheses which were used to locate the P and O atoms of the two independent $[H_2P_2Mo_5O_{21}]^{4-}$ anions. These positional parameters indicated that these two anions are related to each other by a center of symmetry; also, a full-matrix least-squares refinement showed a strong correlation between the parameters related by the center of symmetry. Therefore, the space group was assumed to be $P2_1/a$ and the atomic parameters of these atoms were refined. The difference Fourier map calculated at this stage showed the peaks assigned to the K atoms and O atoms of the water of crystallization. The heights of these peaks and the distances between them indicated that some of them are disordered. The appearance of $h0l$ reflections with $h=2n+1$ is due to the partial order of these groups. These groups tend to keep the 2_1 symmetry rather than the a-glide. The site occupancies of these disordered atoms were fixed to 0.5, and the average structure, based on the centric space group, was refined with

Table 1. Positional Parameters (×10^4) and Thermal Parameters (Å^2) with e. s. d.'s in Parentheses
$B_{eq}=8/3\pi^2\sum_i\sum_j U_{ij}a^*_i a^*_j a_i a_j$

Atom	x	y	z	B_{eq}
Mo(1)	853(1)	1322(1)	1124(1)	1.4
Mo(2)	2064(1)	1303(1)	3983(1)	1.4
Mo(3)	2160(1)	3346(1)	5070(1)	1.4
Mo(4)	1463(1)	4718(1)	2355(1)	1.4
Mo(5)	280(1)	3351(1)	319(1)	1.4
P(6)	158(3)	2799(3)	3368(4)	1.2
P(7)	2554(3)	2868(3)	1898(4)	1.2
Ot(1a)	66(11)	493(9)	1429(12)	2.4
Ot(1b)	1271(11)	1048(9)	−245(12)	2.5
Ot(2a)	1317(10)	533(9)	4526(12)	2.3
Ot(2b)	3245(11)	931(9)	4255(14)	2.6
Ot(3a)	1808(10)	3735(9)	6462(12)	2.1
Ot(3b)	3438(10)	3428(9)	5207(13)	2.3
Ot(4a)	424(11)	5259(10)	2723(13)	2.6
Ot(4b)	2287(10)	5522(9)	2228(14)	2.6
Ot(5a)	−885(10)	3766(10)	197(14)	2.6
Ot(5b)	631(11)	3269(10)	−1148(13)	2.6
Op(36)	531(8)	3143(8)	4595(12)	1.7
Op(456)	388(10)	3449(8)	2350(11)	1.6
Op(126)	536(8)	1900(8)	3113(10)	1.3
Op(47)	2732(8)	3825(8)	1899(11)	1.2
Op(157)	1690(8)	2599(8)	1021(12)	1.5
Op(237)	2405(9)	2577(8)	3216(11)	1.6
Ob(12)	1965(9)	1050(8)	2244(11)	1.3
Ob(23)	2025(10)	2111(8)	5325(11)	1.8
Ob(24)	1839(9)	4274(9)	3970(10)	1.7
Ob(45)	1053(10)	4361(8)	728(12)	1.9
Ob(15)	−82(9)	2175(8)	654(11)	1.4
K(1)	3411(3)	−83(3)	1601(4)	2.4
K(2)	4147(4)	4559(3)	3524(5)	2.9
K(3)[a]	0	5000	5000	4.1
K(4)[a]	3687(9)	6981(7)	2419(9)	3.8
K(5)[a]	641(9)	7034(7)	3346(9)	3.4
K(6)[a]	2594(17)	7248(10)	1662(19)	10.0
O(aq1)	3239(14)	4050(15)	9381(21)	6.5
O(aq2)[a]	4852(36)	3941(29)	7076(31)	7.2
O(aq3)[a]	3224(26)	2511(21)	8321(33)	4.0

a) Multiplicities of these atoms are 0.5.

the block-diagonal least-squares method on F with anisotropic temperature factors for all atoms by using UNICSIII program system.[6] The final refinement converged at $R(=\sum||F_o|-|F_c||/\sum|F_o|)=0.072$, $wR(=[\sum w(|F_o|-|F_c|)^2/\sum w|F_o|^2]^{1/2})=0.092$ and $S(=[\sum w(|F_o|-|F_c|)^2/(m-n)^{1/2}])=1.55$. The weighting scheme employed was $w^{-1}=\sigma^2(|F_o|)+(0.03|F_o|)^2$. All of the calculations were carried out on HITAC M680-H computers at the Computer Centre of the University of Tokyo. The complex atomic scattering factors were taken from the International Tables for X-Ray Crystallography.[7] The H atoms, which are supposed to be attached to the P atoms, were not found by this X-ray analysis. The final atomic parameters are given in Table 1.[††] The notation of the O atoms in the anion is as follows: Ot for the terminal O atoms, Op for the O atoms shared by one P atom and one or two Mo atoms, and Ob for those shared by two Mo atoms, with appended numerals in the following parentheses representing the numbers of the Mo and/or P atoms to which they are bound.

Results and Discussion

Figure 1 shows an ORTEP[8] view of the $[H_2P_2Mo_5O_{21}]^{4-}$ anion with the Mo-O and P-O bond distances in it. The anion consists of five MoO_6 octahedra which form a ring. These octahedra are joined together by sharing edges, except at one contact (Mo(3)-Mo(4)), where they share only one corner. Two P atoms are attached to this ring, one above and the other below, each having three O atoms in common with the ring and forming a PO_3 trigonal pyramid. This anion nearly possesses a twofold rotation axis running through the Mo(1) and Ob(34) atoms.

The Mo-Mo, Mo-P, and P-P distances are listed in Table 2. The Mo-Mo distances for the edge shared octahedra are 3.360—3.397 Å (av. 3.39(2) Å while that for the corner shared octahedra is 3.716 Å. The deviations of the P-Mo distances are explained by the shifts of the Mo atoms from the least-squares plane calculated for the five Mo atoms which crosses the P(6)-P(7) vector with the angle of 86.8°. Mo(1) lies almost on the plane, Mo(3) and Mo(5) are displaced toward the same direction with P(6), and Mo(2) and Mo(4) to the opposite side, thus forming a skew conformation of the Mo_5 ring.

The O-P-O angles in the PO_3 pyramids are listed in Table 3. These angles agree well with those found in the simple salts containing HPO_3^{2-} anions.[9] The P-O distances for the Op atoms doubly shared by one P and one Mo atoms (Op(36) and Op(47)) are 1.49 and 1.51 Å, while they are 1.52—1.55 Å (av. 1.53(2) Å) for those triply shared by one P and two Mo atoms. However, the O-P-O angles are not affected by the differences of the coordination around the O atoms. In the penta-

Table 2. Interatomic Distances (Å) between Mo and P Atoms with e.s.d.'s in Parentheses

Mo(1)-Mo(2)	3.416(2)	P(6)-Mo(1)	3.538(5)
Mo(2)-Mo(3)	3.397(2)	P(6)-Mo(2)	3.520(5)
Mo(3)-Mo(4)	3.716(2)	P(6)-Mo(3)	3.300(5)
Mo(4)-Mo(5)	3.397(2)	P(6)-Mo(4)	3.692(5)
Mo(5)-Mo(1)	3.360(2)	P(6)-Mo(5)	3.446(5)
Mo(1)-Mo(3)	5.521(2)	P(7)-Mo(1)	3.410(5)
Mo(2)-Mo(4)	5.652(2)	P(7)-Mo(2)	3.432(5)
Mo(3)-Mo(5)	5.604(2)	P(7)-Mo(3)	3.612(5)
Mo(4)-Mo(1)	5.511(2)	P(7)-Mo(4)	3.300(5)
Mo(5)-Mo(2)	5.533(2)	P(7)-Mo(5)	3.518(5)
		P(6)-P(7)	3.930(6)

Table 3. O-P-O Angles(°) in the PO_3 Moieties with e.s.d.'s in Parentheses

Op(36)-P(6)-Op(456)	109.3(7)
Op(456)-P(6)-Op(126)	112.4(7)
Op(126)-P(6)-Op(36)	113.3(7)
Op(47)-P(7)-Op(157)	113.0(7)
Op(157)-P(7)-Op(237)	110.8(7)
Op(237)-P(7)-Op(47)	108.9(7)

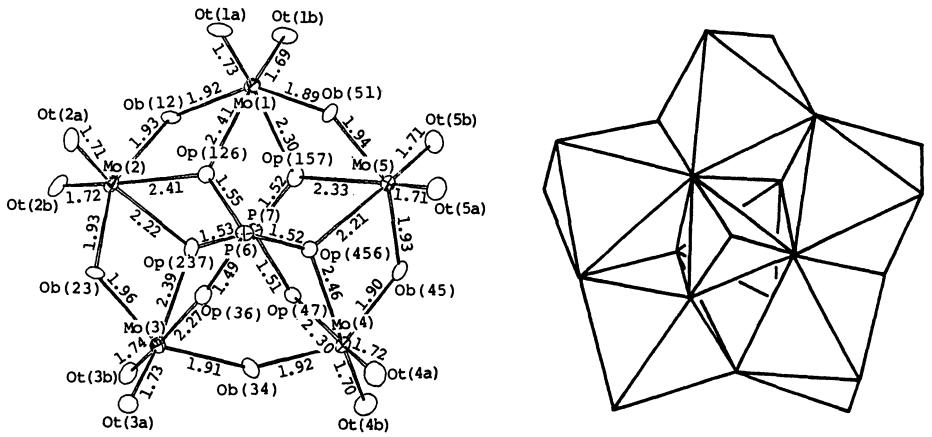

Fig. 1. The structure of the $[H_2P_2Mo_5O_{21}]^{4-}$ anion by the ORTEP[8] drawing and the polyhedra representation. The P-O and Mo-O distances are given in Å. Their e.s.d.'s are 0.02 Å for Mo(4)-Ot(4a) and 0.01 Å elsewhere. Thermal ellipsoids are scaled to enclose 30% probability level.

†† Lists of the structure factors and the anisotropic thermal parameters are deposited at the office of the Chemical Society of Japan as Document No. 8842.

molybdodiphosphonate anions, the P–O distances for doubly shared Op atoms are 1.52(1) Å, for triply shared Op atoms 1.54(1) Å, and the O–P–O angles are 111(1)°. This shows that the organic groups covalently bonded to the P atoms have only a little influence on the coordination of the PO_3 trigonal pyramids.

The MoO_6 octahedra are highly distorted in forming this polyanion. Each Mo atom is surrounded by six O atoms which are divided into three groups: two Ot's in the *cis* position relative to each other, two Op's each of which is in the *trans* position to an Ot atom. and two Ob's in the *trans* position to each other. The average Mo–O distances are 1.72(1), 2.38(8), and 1.92(2) Å, for Mo–Ot, Mo–Ob, and Mo–Ob, respectively. These values agree well with those of the pentamolybdodiphosphate and pentamolybdodiphosphonate anions.

This work was partly supported by Grant-in-Aid for Scientific Resarch (No. 62470038) from the Ministry of Education, Science and Culture.

References

1) A. Rosenheim, W. Weinberg, and J. Pinsker, *Z. Anorg. Chem.*, **84**, 217 (1914); A. Rosenheim and M. Schapiro, *Z. Anorg. Allg. Chem.*, **129**, 196 (1923).

2) W. Kwak, M. T. Pope, and T. F. Scully, *J. Am. Chem. Soc.*, **97**, 5753 (1975).

3) J. K. Stalick and C. O. Quicksall, *Inorg. Chem.*, **15**, 1577 (1976).

4) R. Strandberg, *Acta Chem. Scand.*, **27**, 1004 (1973).

5) B. Hedman, *Acta Chem. Scand.*, **27**, 3335 (1973); B. Hedman and R. Strandberg, *Acta Crystallogr., Sect. B*, **35**, 278 (1979).

6) T. Sakurai and K. Kobayashi, *Rikagaku Kenkyusho Hokoku*, **55**, 69 (1979).

7) "International Tables for X-Ray Crystallography," Birmingham, Kynoch Press (1974), Vol. IV.

8) C. K. Johnson, ORTEPII, Report ORNL-5138, Oak Ridge National Laboratory, Tennessee, USA (1976).

9) M. Handlovič, *Acta Crystallogr., Sect. B*, **25**, 227 (1969); D. E. C. Corbridge, *Acta Crystallogr.*, **9**, 991 (1956).

Ferrocene-Mediated Enzyme Electrode for Glucose with the Use of Conducting Polymer Support

Fumio MIZUTANI* and Michihiko ASAI
Research Institute for Polymers and Textiles, 1-1-4 Higashi, Tsukuba, Ibaraki 305
(Received April 20, 1988)

Synopsis. An amperometric glucose-sensing electrode has been constructed by immobilizing glucose oxidase and fine particles of ferrocene in a photo-crosslinked poly(vinyl alcohol) layer. The magnitude of the response of the ferrocene-mediated electrode to glucose (0.5—50 mmol dm^{-3}) increases when polypyrrole, an electrically conducting polymer, is incorporated into the poly(vinyl alcohol) support.

Much effort has been directed at devising an amperometric electrode for glucose by combining immobilized glucose oxidase (GOD) with immobilized electroactive molecules that mediate the electron transfer between the enzyme and an electrode:[1-4]

$$\text{glucose} + \text{GOD/FAD} \rightarrow \text{gluconolactone} + \text{GOD/FADH}_2$$
$$\text{GOD/FADH}_2 + 2\text{M}^+ \rightarrow \text{GOD/FAD} + 2\text{M} + 2\text{H}^+$$
$$2\text{M} \rightarrow 2\text{M}^+ + 2\text{e (at the electrode)}$$

In this scheme, GOD/FAD and $GOD/FADH_2$ represent the oxidized and reduced forms of flavin adenine dinucleotide within GOD, respectively, and M^+/M, the mediator which is assumed to be a one-electron couple. One of the most convenient ways for preparing such a mediator-based glucose electrode is the use of a membrane-type polymer containing an immobilized GOD/mediator-couple. However, the rate of charge transport through the nonconducting layer is much lower than desired,[5] which seriously limits the application of the layer system.

The use of an electrically conducting polymer as the support seems to be a suitable approach, since the conducting support is expected to enhance the effectiveness of the mediator by providing a larger microscopic electrode surface area and a larger percentage of active centers than the case of nonconducting support being used.[6-9] We report here on the construction and preliminary testing of a ferrocene (bis(cyclopentadienyl)iron, abbreviated FcH)-mediated glucose electrode. Two kinds of polymer supports, an insulator and a conductor, were employed for the construction of the glucose electrode with the use of the GOD/FcH-couple; the current response to the substrate was examined in connection with the electrical conductivity of the support.

Experimental

A type-I layer, a poly(vinyl alcohol) (PVA)-based one, was prepared from a mixture of GOD (Sigma Chemical Co., Type X), FcH (Aldrich Chemical Co., ground to a powder with a diameter less than 1 μm), and a photo-crosslinkable PVA (generous gift from Dr. K. Ichimura of this Institute, 8 wt. % aqueous solution, pH 7), 1 : 3 : 30 by weight, according to a procedure similar to that described previously.[10-12] In the type-I layer, GOD was physically entrapped in the crosslinked PVA matrix and FcH was embedded in the matrix. The thickness of the prepared type-I layer was about 20 μm. A type-II layer, with a matrix comprising a polymer mixture of crosslinked PVA and polypyrrole (PPy), was prepared by incorporating PPy into the type-I layer. The incorporation of PPy was performed through the oxidative polymerization of pyrrole with $K_2S_2O_8$ as follows. The type-I layer was placed so as to be in contact with a monomer-containing solution from one side and an oxidant-containing solution from the other side (for 30 min at 25 °C):

aqueous solution containing 0.1 mol dm^{-3} pyrrole, 0.05 mol dm^{-3} $KClO_4$, and 0.1 mol dm^{-3} phosphate buffer (pH 7)/type I layer/aqueous solution containing 0.1 mol dm^{-3} $K_2S_2O_8$, 0.05 mol dm^{-3} $KClO_4$, and 0.1 mol dm^{-3} phosphate buffer (pH 7)

The type-II layer, thus prepared, was thoroughly washed with 0.1 mol dm^{-3} phosphate buffer (pH 7).

The type-I or -II layer was separately placed on a platinum disk electrode (diameter, 5 mm) and covered with a polyester mesh (diameter, 20 mm). The mesh was held in place with rubber rings so that the layer was directly in contact with the electrode surface. The test solution used was a phosphate buffer (0.1 mol dm^{-3}, pH 7, 30 °C), being saturated with argon, unless otherwise stated. A saturated calomel electrode (SCE) and a platinum wire were used as reference and auxiliary electrodes, respectively. All potentials given in the present paper were measured against an SCE. The layer-attached electrodes were stored in a phosphate buffer (0.1 mol dm^{-3}, pH 7) at 4 °C when not in use.

The GOD activities in the layers were measured by using the 4-aminoantipyrine/phenol/peroxidase color-generating system[13] at a glucose concentration of 0.1 mol dm^{-3}. The diffusion coefficients of glucose in the layers, D's, were determined by applying a method similar to that described elsewhere.[12] The electrical conductivities of the layers were measured by using a two-point probe method, after a thorough washing of the samples with distilled water and drying under a vacuum below 10^{-1} Pa.

Results and Discussion

The parameters measured for the type-I and -II layers are given in Table 1. As shown in Table 1, the incorporation of PPy into the PVA matrix brought about a slight decrease in the GOD activity and a little decrease in the D-value, but a remarkable increase in the electric conductivity, as expected. However, the

Table 1. Parameters Obtained for the Type I and II Layers

Type of layer	GOD activity in the layer	Diffusion coefficient of glucose, D	Electrical conductivity
	U cm^{-3}	cm^2 s^{-1}	s cm^{-1}
I	135	4×10^{-7}	$<10^{-8}$
II	125	1×10^{-7}	2×10^{-4}

conductivity of the type-II layer, 2×10^{-4} S cm^{-1}, was still lower than that of a PPy-containing polymer mixture obtained under appropriate conditions.[8,9,14-16] Further examinations for obtaining the PPy/PVA mixture with a higher conductivity are in progress.

Nevertheless, the increase in the conductivity of the support was effective for enhancing the electron transferability between the mediator and the electrode. Figure 1 shows cyclic voltammograms on the layer-attached electrodes for the immobilized redox system of ferricinium ion (FcH^+) and FcH. The electrode coated with the type-II layer exhibited much larger current peaks than that with the type-I layer.

It is expected that the enhanced electron transferability of the FcH^+/FcH system in the type-II layer results in an increased current response to glucose, compared with the case of the type-I layer. Figure 2 shows the response/time curves. The electrode potential, 0.25 V, was sufficient for the oxidation of FcH to form FcH^+ (Fig. 1). The electrode with the type-II layer gave a larger current response, as expected, than that with the type-I layer.

A few additional characteristics of the electrode with the type-II layer, as a glucose-sensing one, were then examined. Figure 3 shows calibration curves of the electrode obtained in argon-saturated and air-saturated solutions. The introduction of air into the test solution brought about a decrease in the current response by ca. 5% at all the glucose concentrations examined (0.5—50 mmol dm^{-3}). The decrease in the response is considered to be caused by interference with oxygen in the air: oxygen reacts with GOD/$FADH_2$ to form GOD/FAD and hydrogen peroxide, and the electrode potential was not sufficiently positive to reoxidize the hydrogen peroxide produced. However, in each solution, the electrode gave a linear current response in the range of 0.5—8 mmol dm^{-3} glucose and a discernible increase in the response with an increase in the glucose concentration above 8 mmol dm^{-3}. These results indicated that the electrode could be used for a determination of glucose in the high concentration range (e.g., blood glucose concentration range), even in an air-saturated buffer. Subsequent experiments were, therefore, performed in air-saturated buffers. The relative standard deviations were ca. 1.5 and 2.5% for 10 successive measurements of 4 and 15 mmol dm^{-3} of glucose, respectively. The long-term stability of the electrode was examined as follows: the determination of 4 mmol dm^{-3} glucose was carried out 10 times a day, every day for one month. The average value of the measurement on each day did not virtually change during this period.

Recently, another method involving the use of PPy for the construction of glucose-sensing electrodes has been reported: GOD was entrapped in a PPy layer on an electrode by the electrolytic polymerization of pyrrole in the presence of the enzyme.[17-19] The procedure for the preparation of the glucose electrode seems to be of particular interest due to its simplicity. However, the resulting GOD/PPy electrode, unfortunately, showed a rather poor stability.[17] The current response of the electrode to glucose diminished within a few days owing to the leaching of GOD out of the PPy

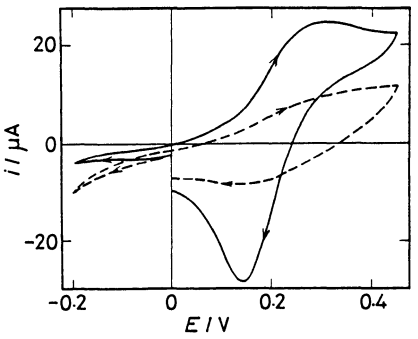

Fig. 1. Cyclic voltammograms on the electrode covered with the type-I layer (----) and with the type-II (——) layer. Potential sweep rate, 50 mV s^{-1}; solution, argon-saturated phosphate buffer (not containing glucose).

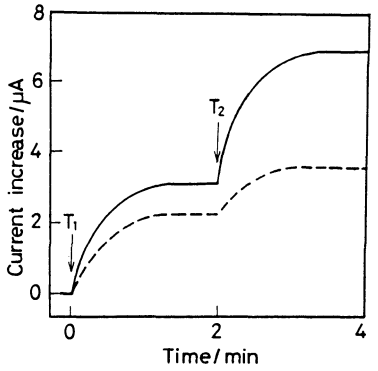

Fig. 2. Response/time curves of the electrodes using type-I (----) and type-II (——) layers to glucose. Electrode potential, 0.25 V; rotating rate of the layer-attached electrode, 20 Hz. T_1 and T_2 are the time points when glucose is added into the argon-saturated buffer to be 5 mmol dm^{-3} and 20 mmol dm^{-3}, respectively.

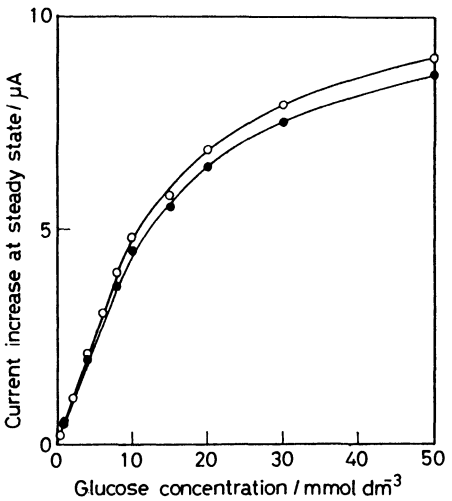

Fig. 3. Calibration curves for glucose of the electrode with the type-II layer in argon (—○—) and air (—●—) saturated buffers. Electrode potential, 0.25 V; rotating rate of the electrode, 20 Hz.

matrix and to the chemical and/or electrochemical decomposition of PPy during the measurement of hydrogen peroxide, the product of the GOD-catalyzed reaction in the absence of the non-physiological mediator such as FcH^+/FcH couple. On the other hand, the present electrode was essentially free from these problems, which resulted in the higher stability of the electrode, although the procedure for its construction was more complicated. The approach to obtain a glucose electrode having a high performance by a simpler process is in progress, with the use of the conducting support system.

References

1) A. E. G. Cass, G. Davis, G. D. Francis, H. A. O. Hill, W. J. Aston, I. J. Higgins, E. V. Plotokin, L. D. L. Scott, and A. P. F. Turner, *Anal. Chem.*, **56**, 667 (1984).
2) H. A. Lange and J. Q. Chambers, *Anal. Chim. Acta*, **175**, 89 (1985).
3) G. Jonsson and L. Gorton, *Biosensors*, **1**, 355 (1985).
4) G. Davis, *Biosensors*, **1**, 161 (1985).
5) K. Doblhofer, W. Durr, and M. Jauch, *Electrochim. Acta*, **27**, 677 (1982).
6) K. Okabayashi, O. Ikeda, and H. Tamura, *J. Chem. Soc., Chem. Commun.*, **1983**, 684.
7) R. A. Bull, F. R. Fan, and A. J. Bard, *J. Electrochem. Soc.*, **131**, 687 (1984).
8) F. Mizutani, S. Iijima, Y. Tanabe, and K. Tsuda, *J. Chem. Soc., Chem. Commun.*, **1985**, 1728.
9) T. Shimidzu and T. Iyoda, *Membrane*, **11**(2), 71 (1986).
10) K. Ichimura, *J. Polym. Sci., Polym. Chem. Ed.*, **22**, 2817 (1984).
11) K. Matsumoto, H. Mizuguchi, and K. Ichimura, *Kobunshi Ronbunshu*, **41**, 221 (1984).
12) F. Mizutani, T. Yamanaka, Y. Tanabe, and K. Tsuda, *Anal. Chim. Acta*, **177**, 153 (1985).
13) G. A. Hamilton, *Adv. Enzymol.*, **32**, 55 (1969).
14) O. Niwa and T. Tamamura, *J. Chem. Soc., Chem. Commun.*, **1984**, 817.
15) M. A. de Paoli, R. J. Waltman, and A. F. Diaz, *J. Chem. Soc., Chem. Commun.*, **1985**, 1015.
16) T. Ojio and S. Miyata, *Polym. J.*, **18**, 95 (1986).
17) M. Umana and J. Waller, *Anal. Chem.*, **58**, 2979 (1986).
18) N. C. Foulds and C. R. Lowe, *J. Chem. Soc., Faraday Trans. 1*, **82**, 1259 (1986).
19) H. Shinohara, T. Chiba, and M. Aizawa, Proc. 6th Sensor Sym., Tsukuba, Japan, 207 (1986).

Crystal Structure of 1:2 Charge Transfer Complex of 2,7-Bis(methylthio)-1,6-dithiapyrene (MTDTPY) and Tetrahydrobarreleno-tetracyanoquinodimethane (THBTCNQ)

Kazuhiro NAKASUJI,* Mitsuru SASAKI, Ichiro MURATA,* Atsushi KAWAMOTO,† and Jiro TANAKA†
Department of Chemistry, Faculty of Science, Osaka University, Toyonaka, Osaka 560
†Department of Chemistry, Faculty of Science, Nagoya University, Chikusa-ku, Nagoya 464
(Received May 24, 1988)

Synopsis. The crystal structure of a 1:2 complex of bis(methylthio)dithiapyrene and tetrahydrobarreleno-TCNQ contained face-to-face packings of acceptor-donor-acceptor units which are isolated from each other. The IR spectrum, geometry, and absorption spectrum showed the neutral nature of this complex.

Recently, we reported the synthesis and properties of three-dimensionally modified tetracyanoquinodimethanes (TCNQ's). An interesting result was the formation of relatively highly conducting charge transfer (CT) complexes.[1] More recently, we have explored new donor molecules, such as 2,7-bis(methylthio)-1,6-dithiapyrene (MTDTPY) and 2,3:7,8-bis(ethylenedithio)-1,6-dithiapyrene (ETDTPY), which are classified into peri-condensed Weitz-type donors[2] having alkylthio substituents. MTDTPY produced metallic CT complexes with TCNQ, chloranil, and bromanil.[3] In this report, we present the crystal structure and some physical properties of the title 1:2 CT complex, which is composed of MTDTPY and one of the three-dimensionally modified TCNQ derivatives, tetrahydrobarreleno-TCNQ (THBTCNQ).

Experimental

Preparation of Single Crystals of MTDTPY-(THBTCNQ)$_2$ Complex. A solution of the donor and the acceptor in dichloromethane (ca. 0.02 M) was allowed to evaporate at room temperature. After several days, black prisms of MTDTPY-(THBTCNQ)$_2$ were grown: mp 202—204 °C. The stoichiometry was deduced from an X-ray analysis.

Crystal Structure Analysis. Crystal data: $C_{52}H_{36}S_4N_8$, FW =901.15, triclinic, space group $P\bar{1}$, a=14.589 (3), b= 15.4421 (3), c=7.367 (1) Å, α=93.32 (2), β=92.50 (2), γ=139.22 (1), V=1072.3 Å^3, d_{obs}=1.400 g cm^{-3}, d_{calc}=1.396 g cm^{-3}, Z=1. A prism-like crystal with dimensions of 0.5×0.5×0.3 mm was used for data collection on a Rigaku automated four-circle diffractometer (AFC-5) using graphite-monochromated Cu $K\alpha$ radiation (λ=1.5418 Å). 2θ-ω scan mode was employed ($2\theta_{max}$=126°). The structures were solved by the Monte-Carlo direct method[4] with a MULTAN-78[5] program system using 3061 non-zero unique reflections and refined on F^2 by a full-matrix least-squares program with absorption corrections made by an analytical method.[6] The donor molecule turned out to contain an orientational disorder. The occupancy ratio for disordered sulfur and carbon atoms of SC1 and SC2 was assumed to be 1:1. Anisotropic temperature factors were used for the refinement of non-H atoms. The final R value ($R=\sum||F_o|-|F_c||/\sum|F_o|$) is 0.057. Atomic scattering factors were taken from International Tables for X-ray Crystallography.[7] All calculations were made on FACOM M-382 computer at the computer center of Nagoya University. The complete F_o-F_c data and the temperature parameters are deposited as Document No. 8845 at the Office of the Editor of Bull. Chem. Soc. Jpn.

Results and Discussion

The atomic coordinates as well as the bond lengths and angles are listed in Tables 1—3, respectively. An ORTEP drawing of the molecular structures and numbering schemes are shown in Fig. 1. As shown in the crystal structures (Figs. 2 and 3), the donor (D) and the acceptor (A) form an ADA-type arrangement in which each donor molecule lies on an inversion center. The interplanar spacing between D and A is 3.5 Å. One of the C≡N bonds is tilted away from the quinodimethane moiety (Fig. 3): the deviation from the plane of the six-membered ring is 0.446 Å for C19 and 0.701 Å for N3. Methylthio groups also deviate from

Table 1. Atomic Coordinates and Equivalent Isotropic Temperature Parameters[a] with Estimated Standard Deviations in Parentheses for MTDTPY-(THBTCNQ)$_2$

Atom	x	y	z	B_{eq}/Å^2
SC1	0.2186(2)	0.9986(2)	0.8704(2)	9.2(1)
SC2	−0.0597(1)	0.7390(1)	0.9799(2)	6.5(1)
S2	0.1549(1)	0.7770(1)	0.8517(1)	8.0(1)
N1	0.5028(4)	1.0582(3)	0.7452(5)	9.3(2)
N2	0.9226(3)	1.3211(3)	0.6568(5)	7.7(2)
N3	0.5271(3)	0.4804(2)	0.7486(4)	6.2(2)
N4	0.9008(3)	0.7852(3)	0.5201(4)	6.9(2)
C2	0.0976(3)	0.8415(3)	0.9021(4)	5.3(2)
C3	−0.0765(3)	0.8340(3)	1.0159(4)	5.1(2)
C4	0.0185(3)	0.9693(3)	0.9818(3)	4.3(2)
C5	0.1485(3)	1.0429(3)	0.9125(3)	5.1(2)
C6	0.2353(3)	1.1718(3)	0.8770(4)	5.1(2)
C7	−0.2002(3)	0.7674(3)	1.0871(4)	5.3(2)
C8	−0.0027(5)	0.6002(4)	0.8442(8)	9.0(3)
C9	0.6748(3)	0.9759(3)	0.6717(4)	4.8(2)
C10	0.5497(3)	0.8368(3)	0.6940(4)	5.0(2)
C11	0.5499(3)	0.7480(3)	0.6788(4)	4.6(2)
C12	0.6756(3)	0.7908(3)	0.6426(3)	4.2(2)
C13	0.7953(3)	0.9269(3)	0.6062(4)	5.0(2)
C14	0.7956(3)	1.0140(3)	0.6227(4)	4.8(2)
C15	0.6888(3)	1.0753(3)	0.6890(4)	5.1(2)
C16	0.5818(3)	1.0602(3)	0.7240(4)	6.1(2)
C17	0.8199(3)	1.2110(3)	0.6706(4)	6.0(2)
C18	0.6893(3)	0.7109(3)	0.6407(3)	4.3(2)
C19	0.5947(3)	0.5827(3)	0.7007(4)	4.9(2)
C20	0.8093(3)	0.7553(3)	0.5756(4)	5.0(2)
C21	0.4068(3)	0.6060(3)	0.6883(5)	5.7(2)
C22	0.4070(3)	0.7704(3)	0.7267(6)	7.3(2)
C23	0.3007(4)	0.5662(4)	0.5348(6)	7.4(2)
C24	0.2990(4)	0.6633(4)	0.5613(7)	7.3(2)
C25	0.3596(4)	0.5987(4)	0.8732(6)	9.2(3)
C26	0.3672(5)	0.7042(4)	0.9017(7)	9.0(3)

a) $B_{eq}=8/3\pi^2\sum_i\sum_j U_{ij}a^*_i a^*_j a_i a_j$.

Table 2. Bond Distances with Estimated Standard Deviations in Parentheses for MTDTPY-(THBTCNQ)$_2$

Bond	l/Å	Bond	l/Å
SC1-C2	1.635(3)	C11-C21	1.506(3)
SC1-C5	1.635(7)	C12-C13	1.444(3)
SC2-C2	1.678(3)	C12-C18	1.391(7)
SC2-C3	1.671(6)	C13-C14	1.340(7)
C2-S2	1.753(6)	C15-C16	1.432(8)
C3-C4	1.433(4)	C15-C17	1.433(3)
C3-C7	1.387(5)	N1-C16	1.146(9)
C4-C5	1.427(5)	N2-C17	1.149(4)
C4-C4′	1.423(10)	C18-C19	1.426(4)
C5-C6	1.380(5)	C18-C20	1.436(6)
C6-C7′	1.387(8)	N3-C19	1.152(5)
S2-C8	1.791(4)	N4-C20	1.140(6)
C9-C10	1.449(4)	C21-C23	1.542(7)
C9-C14	1.447(6)	C21-C25	1.525(7)
C9-C15	1.384(7)	C22-C24	1.535(5)
C10-C11	1.371(7)	C22-C26	1.538(7)
C10-C22	1.512(6)	C23-C24	1.520(10)
C11-C12	1.448(6)	C25-C26	1.547(11)

Table 3. Selected Bond Angles with Estimated Standard Deviations for MTDTPY-(THBTCNQ)$_2$

Angle	ϕ/°	Angle	ϕ/°
C2-SC1-C5	104.7(3)	C10-C11-C12	121.0(3)
C2-SC2-C3	103.6(2)	C11-C12-C13	117.2(4)
C2-S2-C8	103.1(3)	C11-C12-C18	124.9(3)
SC1-C2-SC2	132.7(4)	C13-C12-C18	117.9(4)
SC2-C3-C4	128.0(3)	C12-C13-C14	121.6(4)
C4-C3-C7	119.5(5)	C9-C14-C13	122.0(3)
C3-C4-C5	121.6(5)	C9-C15-C16	127.0(3)
C3-C4-C4′	118.8(4)	C9-C15-C17	121.3(4)
C5-C4-C4′	119.6(3)	C16-C15-C17	111.7(5)
SC1-C5-C4	129.0(3)	N1-C16-C15	174.0(4)
C4-C5-C6	119.7(5)	N2-C17-C15	177.4(7)
C5-C6-C7′	121.0(4)	C12-C18-C19	127.1(4)
C3-C7-C6′	121.3(3)	C12-C18-C20	120.6(3)
C10-C9-C14	117.0(4)	C19-C18-C20	112.4(4)
C10-C9-C15	126.3(4)	N3-C19-C18	174.3(5)
C14-C9-C15	116.7(3)	N4-C20-C18	177.1(3)
C9-C10-C11	121.0(4)		

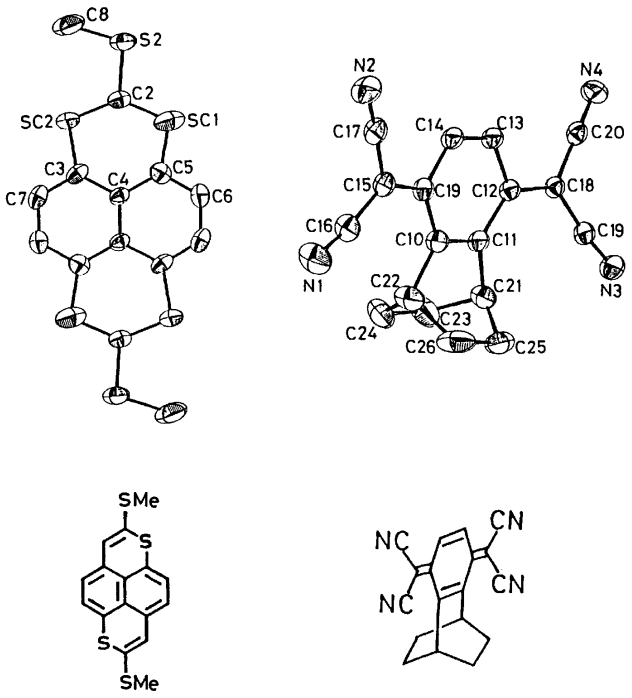

Fig. 1. ORTEP drawings and atomic numbering schemes of MTDTPY and THBTCNQ.

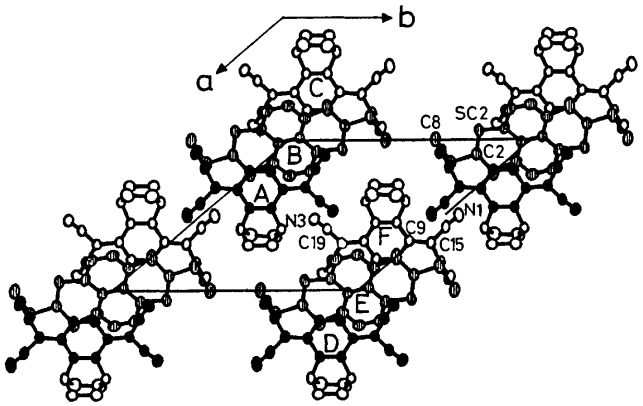

Fig. 2. Crystal structure of MTDTPY-(THBTCNQ)$_2$ viewed along the c axis.

the almost planar DTPY skeleton: 0.508 Å for C8. The molecular overlap mode is shown in Fig. 4. There are no shorter intermolecular distances between ADA units than the van der Waals contacts. In this sense, ADA units are isolated from each other.

This complex can be classified into a neutral complex, as inferred from the following evidence. The stretching frequency of the C≡N bonds for the complex appeared at 2219 cm^{-1}, which is almost the same as that of the neutral THBTCNQ, itself (2213 cm^{-1}).[1] From the bond-length-ratio procedure of Kistenmacher et al.,[8] the degree of CT was calculated to be 0.25 by using the average bond lengths of the assumed *mmm* molecular symmetry. Although such a calculation is too primitive to draw a precise ionicity, both the stretching frequency and the molecular geometry show the neutral nature of the complex.

The ionicity of CT complexes can be conveniently predicted from $\Delta E^{o,r}$ which denotes the difference between the oxidation potential of the donor and the reduction potential of the acceptor. The value of $\Delta E^{o,r}$ for MTDTPY and THBTCNQ is 0.23 eV, which falls within the range of neutral to partial-ionic complexes. Therefore, the neutral nature of the complex is consistent with such a prediction. $\Delta E^{o,r}$ exhibits a further utility when the CT transition energy is taken into account for discussion. Torrance et al. reported a simple V-shape correlation between the energy of the CT absorption band ($h\nu_{CT}$) and $\Delta E^{o,r}$ for mixed stacking complexes. In the electronic spectrum of this complex dispersed in KBr, a strong absorption band at 23900 cm^{-1} and a weak band at 5800 cm^{-1} are assignable to the molecular absorption band of both neutral THBTCNQ[1] and MTDTPY,[3] and a CT band

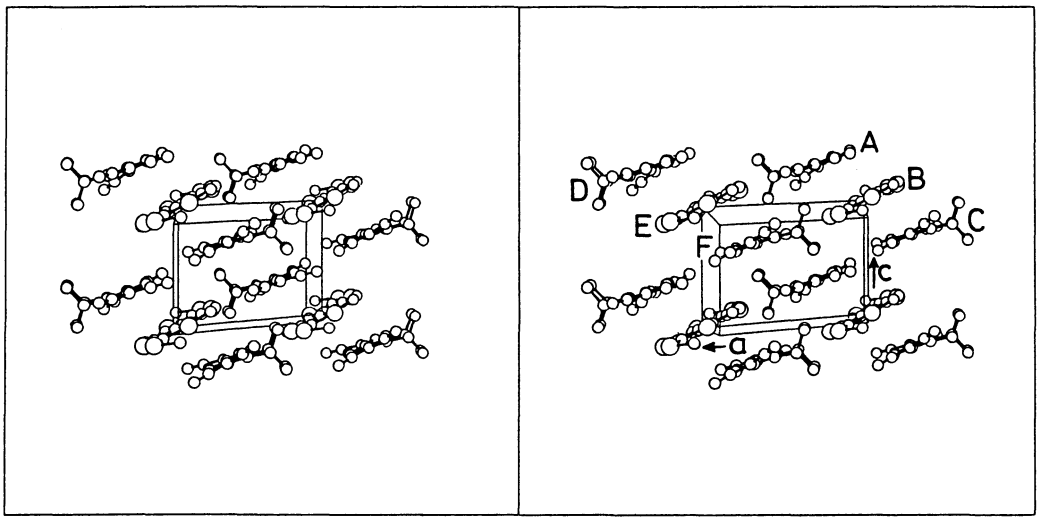

Fig. 3. Stereoview of the crystal packing viewed along the b axis.

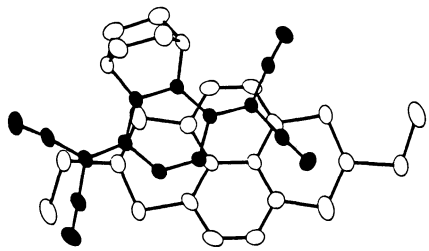

Fig. 4. The mode of molecular overlap between the donor and the acceptor.

between two component molecules, respectively. Although this complex cannot be classified into the usual mixed stacking complexes, it essentially contains a DA-type overlap mode. Therefore, we could estimate the CT transition energy for the complex by the empirical formula,[1,10] $h\nu_{CT,N}=\Delta E^{o,r}+0.5$ (eV), deduced from the V-shape correlation. The estimated value, 0.73 eV, is very close to the observed one, 0.72 eV (5800 cm^{-1}). Such a result suggests the potential applicability of the V-shape correlation to a wider range of CT complexes with DA-type overlap modes, although more data are needed to make this argument conclusive. However, such rough information regarding the electronic structure, which can be obtained readily from 1 mg of powdered sample, is especially valuable for chemists exploring new component molecules of organic conductors.

References

1) K. Nakasuji, M. Nakatsuka, H. Yamochi, I. Murata, S. Harada, N. Kasai, K. Yamamura, J. Tanaka, G. Saito, T. Enoki, and H. Inokuchi, *Bull. Chem. Soc. Jpn.*, **59**, 207 (1986).

2) K. Nakasuji, H. Kubota, T. Kotani, I. Murata, G. Saito, T. Enoki, K. Imaeda, H. Inokuchi, M. Honda, C. Katayama, and J. Tanaka, *J. Am. Chem. Soc.*, **108**, 3460 (1986).

3) K. Nakasuji, M. Sasaki, T. Kotani, I. Murata, T. Enoki, K. Imaeda, H. Inokuchi, A. Kawamoto, and J. Tanaka, *J. Am. Chem. Soc.*, **109**, 6970 (1987).

4) A. Furusaki and A. Furusaki, *Acta Crystallogr., Sect. A*, **35**, 220 (1979).

5) P. Main, S. E. Hull, L. Lessinger, G. Germain, J. P. Declercq, and M. M. Woolfson, MULTAN-78, University of York, York, England and Louvain, Belgium, (1978).

6) C. Katayama, N. Sakabe, and K. Sakabe, *Acta Crystallogr., Sect. A*, **28**, S207 (1972).

7) "International Tables for X-ray Crystallography," Kynoch Press, Birmingham, 1974, Vol. IV.

8) T. J. Kistenmacher, T. J. Emge, A. N. Bloch, and D. O. Cowan, *Acta Crystallogr., Sect. B*, **38**, 1193 (1982).

9) a) R. C. Wheland and J. L. Gillson, *J. Am. Chem. Soc.*, **98**, 3916 (1976); b) J. B. Torrance, *Acc. Chem. Res.*, **12**, 79 (1979); c) G. Saito and J. P. Ferraris, *Bull. Chem. Soc. Jpn.*, **53**, 2141 (1980).

10) J. B. Torrance, J. E. Vazquez, J. J. Mayerle, and V. Y. Lee, *Phys. Rev. Lett.*, **46**, 253 (1981).

The Baeyer-Villiger Reaction of Polycyclic Aromatic Aldehydes: Preparation of Polycyclic Phenols

Koichi FUJISHIRO and Shuichi MITAMURA*
Chemicals Research Laboratory, R & D Laboratories-1, Nippon Steel Corporation, 1618 Ida, Nakahara-ku, Kawasaki 211
(Received May 10, 1988)

Synopsis. Baeyer-Villiger reactions of such polycyclic aromatic aldehydes as 2-dibenzofurancarbaldehyde with various peroxy compounds have been studied in detail, giving predominantly the corresponding phenols.

In contrast to simple benzenoid aromatics, only a little attention has been paid to such polycyclic aromatic compounds as naphthalene, dibenzofuran, anthracene and so on, though they have attractive attributes, i.e., their rigid ring skeletons and rich π-electron systems. We have been interested in the reaction characteristic of the polycyclic aromatic systems to provide a variety of useful derivatives. In this paper, we wish to report on the Baeyer-Villiger reaction (B-V reaction)[1] of polycyclic aromatic aldehydes yielding a series of polycyclic phenols.

Table 1. B-V Reaction of Polycyclic Aromatic Aldehydes with MCPBA

Run No.	Ar	X[a] / %	Yield/% ArOH	Yield/% ArCOOH
1	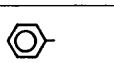	81	32	42
2	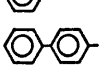	95	80	2
3		75	48	16
4		97	79	2
5	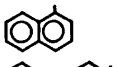	94	85	2
6	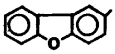	97	86	1
7	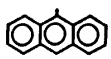	99	92	2

a) X is the conversion of the aldehyde.

Several kinds of polycyclic aromatic aldehydes[2] were allowed to react with *m*-chloroperbenzoic acid (MCPBA) in dry dichloromethane at room temperature under an argon atmosphere. The results are shown in Table 1. Polycyclic aromatic aldehydes gave the corresponding phenols predominantly, while benzaldehyde yielded a mixture of phenol and benzoic acid. This difference can be attributed to a difference in the electron-donative nature between the polycyclic aromatic ring and the benzene ring. The mechanism shown in Scheme 1 is generally proposed.[3] A peroxy compound (ROOH) attacks the carbonyl group of an aldehyde (ArCHO) to afford an intermediate **1**, followed by a migration of the aryl group, Ar, (path a) or the hydride, H, (path b). The relative migratory aptitude of Ar and H depends on their electron-donative nature, so that the more electron-donative polycyclic aromatic ring migrates predominantly to give the formate, which is transformed into the phenol, ArOH, by alkaline hydrolysis. Thus, this work presents a new synthetic method regarding polycyclic phenols.

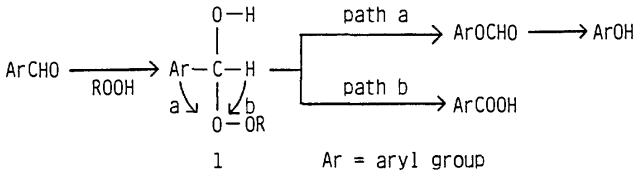

Scheme 1.

Many kinds of peroxy compounds were examined as oxidants instead of MCPBA in this B-V reaction of 2-dibenzofurancarbaldehyde (**2**). Table 2 shows the results of a reaction of **2** with aqueous hydrogen peroxide (30 wt%) in the presence of various acids to yield 2-dibenzofuranol (**3**) and 2-dibenzofurancarboxylic acid (**4**). The reaction was strongly affected by the

Table 2. B-V Reaction of **2** with Aqueous Hydrogen Peroxide

Run No.	H_2O_2/**2** mol/mol	Solvent	T[a] °C	t[b] h	X[c] %	Yield/% **3**	Yield/% **4**
8	2.0	CH_3COOH	40	168	50	2	47
9	1.3	HCOOH	20	20	98	76	3
10	1.0	HCOOH	20	20	95	81	1
11	1.2	CF_3COOH	20	20	85	13	1
12	1.2	CH_3COOH-H_2SO_4 (5%)[d]	40	24	86	49	4
13	1.1	CH_3COOH-$CH_2ClCOOH$ (5%)[d]	40	20	80	66	7
14	1.2	CH_3COOH-CF_3COOH (5%)[d]	40	20	60	34	13
15	2.0	CH_3OH-HCOOH (30%)[d]	40	24	41	2	22
16	1.2	CH_3OH-H_2SO_4 (5%)[d]	40	48	100	36	64
17	1.3	$(CH_3)_2CO$-H_2SO_4 (5%)[d]	40	24	78	1	55

a) T is the reaction temperature. b) t is the reaction time. c) X is the conversion of **2**. d) The concentration of the second material.

Table 3. B-V Reaction of **2** with Various Peroxy Compounds

Run No.	Peroxy Compound[a]	Solvent	T °C	t h	X %	Yield/% **3**	Yield/% **4**
18	*t*-BuOOH	HCOOH	40	48	11	3	0.2
19	*t*-BuOOH	CH_3OH-H_2SO_4[b]	40	48	90	61	15
20	*t*-BuOO-$COCH_3$	CH_3OH-H_2SO_4[b]	40	24	43	29	9
21	*t*-BuOO-C(CH_3)$_2$-OO-*t*-Bu	CH_3OH-H_2SO_4[b]	40	24	52	17	17
22	$(PhCO)_2O_2$	CH_3OH-H_2SO_4[b]	40	48	92	—	85
23	$K_2S_2O_8$	CH_3OH-H_2SO_4[b]	40	24	56	9	29
24	CH_3CO_3H	$(CH_3CO)_2O$	40	24	97	2	68

a) The molar ratio of the peroxy compound to **2** is 1.2. b) The concentration of H_2SO_4 is 5 wt%.

acidity of the acid used. The reaction in formic acid gave **3** in high yield (81%, Run 10) and high selectivity, while the reaction in acetic acid proceeded slowly and gave **4** (47%, Run 8). When the reaction was carried out in trifluoroacetic acid, the yield of **3** was low (13%) and tarry materials were obtained (Run 11). Acid catalysts yield the conjugate acids of aldehydes and accelerate the nucleophilic additions of peroxides to the protonated carbonyl groups (Scheme 1).[3] The acidity of formic acid (pK_a=3.75 at 25 °C) is stronger than that of acetic acid (pK_a=4.76); thus, a reaction in formic acid gives **3** predominantly. In the case of trifluoroacetic acid (pK_a=0.23), its acidity is so strong that **2** and products would be further converted to tarry materials. When sulfuric acid (pK_a=1.99, Run 12) or chloroacetic acid (pK_a=2.87, Run13) was added to acetic acid solvent, the yield of **3** increased, while the addition of formic acid or sulfuric acid in methanol (Runs 15, 16) and acetone (Run 17) did not improve the yield of **3**.

Table 3 shows the results of a reaction of **2** with several kinds of peroxy compounds. The reaction of **2** with *t*-butyl hydroperoxide (*t*-BuOOH) in methanol-sulfuric acid (Run 19) proceeded more rapidly and gave **3** more dominantly than that in formic acid (Run 18). When *t*-butyl peracetate (Run 20) and 2,2-bis(*t*-butyldioxy)propane (Run 21) were used as oxidants, **3** was also obtained more than **4**. On the other hand, other peroxy compounds such as dibenzoyl peroxide (Run 22), potassium peroxodisulfate (Run 23) and peracetic acid (Run 24) gave **4** predominantly. These results indicate that the nature of the leaving group of the intermediate **1** may affect the relative migratory tendency of the aryl and the hydride groups.

To sum up, polycyclic phenols were obtained from the corresponding aldehydes under the system of MCPBA-CH_2Cl_2, H_2O_2-HCOOH, H_2O_2-CH_3COOH-$CH_2ClCOOH$ or *t*-BuOOH-CH_3OH-H_2SO_4. This reaction provides a new method for the preparation of polycyclic phenols.

Experimental

All melting points were measured by a Yanagimoto micro melting point apparatus and were uncorrected. NMR spectra were taken on a JEOL JMN-FX90 spectrometer. Mass spectra were obtained with a Shimadzu QP-1000 spectrometer. Gas chromatographs were obtained with a Shimadzu GC-9A. All aldehydes, except for **2**, were commercially available and purified by a column chromatography on silica gel with dichloromethane as the eluent. Solvents such as benzene and dichloromethane were dried on Molecular Sieves 3A. All peroxy compounds and acids, except for peracetic acid, were purchased commercially and were used without purification. Peracetic acid was prepared in situ by the reaction of acetic anhydride with aqueous hydrogen peroxide.[4]

Preparation of 2-Dibenzofurancarbaldehyde (2). To a solution of 21.4 g (127 mmol) of dibenzofuran in 40 cm^3 of dry benzene was added 38.3 g (287 mmol) of aluminum chloride and 1.2 g (12 mmol) of copper(I) chloride in a 200 cm^3 autoclave. It was filled with carbon monoxide until the pressure reached 4.9 MPa; the mixture was then stirred at 40 °C for 3 h maintaining the pressure at 4.9 MPa. The mixture was poured onto 500 g of ice to hydrolyze the complex of the product and aluminum chloride. The aqueous layer was removed; then, the organic layer was washed with 100 cm^3 of water and dried (magnesium sulfate). After evaporation in vacuo, the residue was purified by a column chromatography (silica gel, dichloromethane). The eluent was evaporated, and the residual solid was recrystallyzed from petroleum ether to afford 17.4 g of **2** (70% yield).

2-Dibenzofurancarbaldehyde (2): Mp 61—63 °C; ^1H NMR ($CDCl_3$) δ=7.1—7.4 (4H, m), 7.6—7.8 (2H, m), 8.09 (1H, d, J=2 Hz) and 9.90 (1H, s, CHO); ^{13}C NMR ($CDCl_3$) δ=111.71, 111.81, 120.75, 122.54, 123.14, 123.30, 124.71, 127.96, 128.66, 131.91, 156.62, 159.27, and 190.69; MS (70 eV) m/z (rel intensity) 196 (M^+; 90), 195 (100), 167 (30), and 139 (58); Found: C, 79.62; H, 4.08%; Calcd for $C_{13}H_8O_2$: C, 79.61; H, 4.08%.

B-V Reaction of 2 with MCPBA. To a solution of 392 mg (2 mmol) of **2** in 5 cm^3 of dry dichloromethane was added 414 mg (2.4 mmol) of MCPBA. The mixture was stirred at room temperature under an argon atmosphere for 20 h. An excessive amount of aqueous sodium thiosulfate solution was added to the reaction mixture and no remains of MCPBA were checked by potassium iodide-starch paper. After an addition of 10 cm^3 of 2 mol dm^{-3} NaOH and 10 cm^3 of methanol, the mixture was stirred for 0.5 h and neutralized to pH 7—8 with 1 mol dm^{-3} HCl and aqueous sodium hydrogencarbonate solution, then extracted with 30 cm^3 of dichloromethane. The amounts of **2** and **3** in the organic layer were determined by gas chromatography (200 °C, Fuloxylate-K, 3 mm×2 m) using dimethyl 2,6-naphthalenedicarboxylate as an internal standard. After the organic layer was evaporated, **3** was isolated from the residue by column chromatography (silica gel, dichloromethane) and recrystallization from ethanol.

2-Dibenzofuranol (3): Mp 136—137 °C; ^{1}H NMR ($CDCl_3$) δ=4.82 (1H, s, OH), 6.95 (1H, dd, J=9 Hz, 3 Hz), 7.1—7.7 (5H, m), and 7.90 (1H, dd, J=9 Hz, 2 Hz); MS (70 eV) m/z (rel intensity) 184 (M^+; 100), 155 (9), 128 (17), and 127 (10); Found: C, 78.07; H, 4.35%; Calcd for $C_{12}H_8O_2$: C, 78.28, H, 4.34%.

The aqueous layer, which contained **4**, was acidified with concentrated HCl and extracted with 30 cm^3 of ethyl acetate. A diazomethane-ether solution was added to the organic layer to convert **4** into the methyl ester; then, the amount of the methyl ester was measured by gas chromatography. The methyl ester was isolated by column chromatography (silica gel, dichloromethane).

Methyl 2-Dibenzofurancarboxylate: ^{1}H NMR ($CDCl_3$) δ=3.97 (3H, s), 7.3—7.7 (4H, m), 7.9—8.2 (3H, m), and 8.60 (1H, d, J=2Hz); MS (70 eV) m/z (rel intensity) 226 (M^+; 66), 195 (100), 167 (25), and 139 (31); Found: C, 74.30; H, 4.48%; Calcd for $C_{14}H_{10}O_3$: C, 74.33; H, 4.46%.

The products of the B-V reaction of other aldehydes (Table 1) were analyzed using the same method, except for the reaction of 9-anthracenecarbaldehyde. They were identified through a comparison of their respective retention times in gas chromatography and the mass spectra with those of commercially available chemicals. 9-Anthryl formate was isolated by column chromatography (silica gel, dichloromethane) without an alkaline hydrolysis of the reaction mixture.

9-Anthryl Formate: Mp 90—91 °C; ^{1}H NMR ($CDCl_3$) δ= 7.4—7.7 (4H, m), 7.9—8.2 (4H, m), 8.41 (1H, s), and 8.66 (1H, s); MS (70 eV) m/z (rel intensity) 222 (M^+; 20), 195 (16), 194 (100), 193 (18), 165 (75), and 163 (14); Found: C, 81.11; H, 4.66%; Calcd for $C_{15}H_{10}O_2$:C, 81.10; H, 4.50%.

References

1) The B-V reactions of ketones and aldehydes have been extensively studied, but there are only a few reports on the similar reactions of polycyclic aromatic compounds. a) Y. Ogata and Y. Sawaki, *J. Org. Chem.*, **34**, 3985 (1969). b) M. F. Hawthorne, W. D. Emmons, and K. S. McCallum, *J. Am. Chem. Soc.*, **80**, 6393 (1958). c) Y. Ogata and Y. Sawaki, *ibid.*, **94**, 4189 (1972).

2) Polycyclic aromatic hydrocarbons react with carbon monoxide in the presence of aluminum chloride and hydrogen chloride to yield the corresponding aromatic aldehydes. N. N. Crounse, "Organic Reactions," John Wiley & Sons, Inc., New York (1949), Vol. 5, Chap. 6, pp. 290—300.

3) H. O. House, "Modern Synthetic Reactions," W. A. Benjamin, Inc., California (1972), Chap. 6, pp. 321—329.

4) D. Swern, "Organic Reactions," John Wiley & Sons, Inc., New York (1953), Vol. 7, Chap. 7, p. 378.

New Synthetic Methods and Reagents for Complex Carbohydrates. II. Synthesis of 2-Acylamino-2-deoxy-D-glucopyranose Derivatives by Dimethylphosphinothioic Mixed Anhydride Method

Toshiyuki INAZU,* Hideaki HOSOKAWA, and Masahide AMEMIYA
The Noguchi Institute, 1-8-1, Kaga, Itabashi-ku, Tokyo 173
(Received May 28, 1988)

Synopsis. Dimethylphosphinothioic (Mpt) mixed anhydrides of carboxylic acids were found to be useful for *N*-acylation of 2-amino-2-deoxy-D-glucopyranose derivatives without protecting the hydroxyl functions. By this method, *N*-acylation of 2-amino-2-deoxy-D-glucopyranose hydrochloride in methanol was also found to be possible.

In recent years, *N*-acyl derivatives of amino sugars became interesting substances in biochemical studies. In order to study their structure-activity relationship etc., analogs of amino sugars which have various acyl group are desired. Symmetrical anhydrides are widely used for the *N*-acylation of amino sugars.[1,2] However, it seems difficult to introduce various acyl groups into the amino group without protecting the hydroxyl functions in sugars and acyl groups. For example, it was reported that 2-acetamido-3,4,6-tri-*O*-benzyl-2-deoxy-D-glucopyranose (**2**) was prepared by the deprotection of *O*-acetyl group from *N*,*O*-diacetate which was derived from 2-amino-3,4,6-tri-*O*-benzyl-2-deoxy-D-glucopyranose (**1**) and acetic anhydride.[2]

Recently, it has been reported that the dimethylphosphinothioic (Mpt) mixed anhydride method is useful for the synthesis of peptides containing hydroxyamino acids without protecting the hydroxyl functions.[3] In this paper, we wish to describe an efficient and general *N*-acylation of 2-amino-2-deoxy-D-glucopyranose derivatives by Mpt mixed anhydrides which were derived from the corresponding carboxylic acids and dimethylphosphinothioyl chloride (Mpt-Cl).[4]

Results and Discussion

First, the reactivity of the Mpt mixed anhydride with hemiacetal hydroxyl group, which had not been previously reported, was investigated by the *N*-acylation of **1**. Mpt acetic anhydride was synthesized from Mpt-Cl and acetic acid in the presence of triethylamine in dichloromethane. It could be detected by silica-gel thin-layer chromatography (TLC). To this reaction mixture, compound **1** and 2 equiv of triethylamine were added and the resulting solution was stirred overnight at room temperature. The usual work-up gave the desired *N*-acetyl derivative (**2**) in quantitative yield. Similarly, the *N*-benzoyl derivative (**3**) was obtained in 86% yield. During these reactions no 1-*O*-acyl derivative could be detected by TLC.

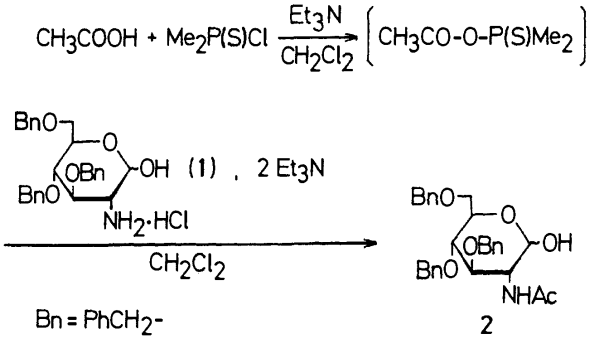

Next, we studied *N*-hydroxyacylation of **1** using Mpt mixed anhydrides according to a procedure similar to those described above. *N*-Hydroxyacyl amino sugars are found in complex carbohydrates, such as lipid A, *N*-glycoloyl neuraminic acid. Usually for the *N*-hydroxyacylation, *O*-protected acylation reagents were used.[5,6] However, by the Mpt mixed anhydride method *N*-hydroxyacylation without protecting the hydroxyl function in the acyl group was anticipated to occur.

In spite of the poor reactivity of Mpt-Cl with alcohol,[3] the mixture of the desired *N*-hydroxyacyl derivatives (**4**, **5**) and the corresponding *O*-dimethylphosphinothioyl derivatives (**6**, **7**) were obtained unexpectedly in the case of glycolic acid and 3-hydroxypropanoic acid in accord with following equation.

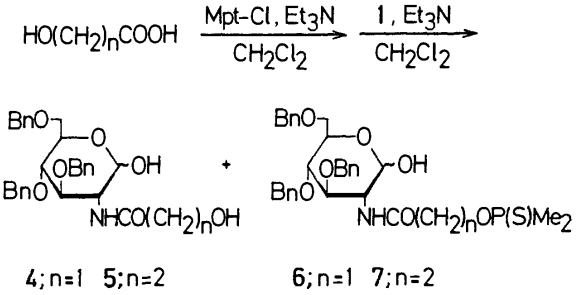

This side reaction suggested that Mpt-Cl might react with the hydroxyl group in carboxylic acid, which was activated by the formation of intramolecular hydrogen bond, to give two mixed anhydrides. In fact, these two mixed anhydrides could be detected by TLC. Therefore, we expected that this side reaction could be overcome if a polar solvent and a low nucleophilic base were used.

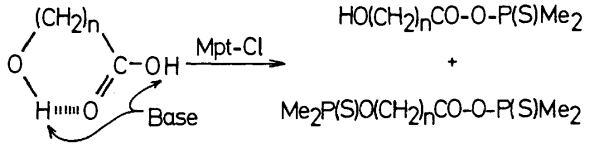

Based on this hypothesis, we studied the *N*-glycoloylation of **1**, and found *N*,*N*-diisopropylethylamine (DIEA) in tetrahydrofuran (THF) effective to promote selective *N*-acylation. On the other hand, we also found that the *N*-glycoloyl derivatives (**4**) could not be obtained in good yield by the reaction of gly-

Table 1. *N*-Glycoloylation of **1** by Mpt Mixed Anhydride

Base	Solvent	Yield/%	
		3	**5**
Et_3N	CH_2Cl_2	Mixture	
Et_3N	THF	87	Trace
DIEA	CH_2Cl_2	84	Trace
DIEA	THF	84	0

Table 2. *N*-Acylation of **1** by Mpt Mixed Anhydride

Acyl group	Yield/%
Ac-	quant.
Bz-	86
$HOCH_2CO$-	84
$HO(CH_2)_2CO$-	68
$HO(CH_2)_{15}CO$-	78

colic acid and **1** using dicyclohexylcarbodiimide (DCC). To clarify this point, we attempted the synthesis of the symmetrical anhydride of glycolic acid by DCC according to the literature[5] and found that 1,4-dioxane-2,5-dione (**8**) was obtained as the main product.

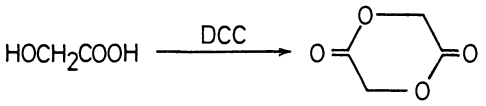

8

In a similar manner using Mpt mixed anhydrides, *N*-(3-hydroxypropanoyl) and *N*-(16-hydroxyhexadecanoyl) derivatives (**5**, **9**) were obtained in good yields. The results described above are summarized in Tables 1 and 2.

Finally, we applied this method to the *N*-benzoylation of 2-amino-2-deoxy-D-glucopyranose hydrochloride (**10**) in methanol. In order to simplify the reaction system the benzoyl Mpt mixed anhydride was purified by means of silica-gel flash-column chromatography to give colorless crystals **11** in 93% yield. The reaction of compound **10** and Mpt mixed anhydride **11** in the presence of various bases in methanol was tried. The desired 2-benzamido-2-deoxy-D-glucopyranose (**12**) was obtained in 76% yield as colorless crystals by using of DIEA. On the contrary, in the case of 1,8-diazabicyclo[5.4.0]undec-7-ene (DBU), only benzoic acid was obtained. These results suggested that the nucleophilicity of the base might be an important factor for this reaction.

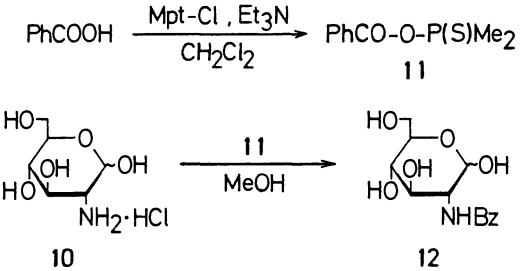

10 **12**

According to the present method, various *N*-acyl derivatives of 2-amino-2-deoxy-D-glucopyranose could be synthesized in good yields. It should be noted that the protection of the hydroxyl functions in acyl groups and sugars was not necessary and further, this *N*-acylation could be carried out in an alcoholic solvent, such as methanol.

Experimental

Mp's were uncorrected. Optical rotations were measured at 26—29 °C after being kept overnight at room temperature.

Typical Procedure for *N*-Acylation of 1. To a mixture of carboxylic acid (0.2 mmol) and 0.2 mmol of base (triethylamine or DIEA) in dichloromethane or THF (1 mL) was added a solution of Mpt-Cl (25.7 mg; 0.2 mmol) in the solvent (1 mL) under ice-cooling. After stirring for 30 min, the formation of Mpt mixed anhydride could be confirmed by TLC, then compound **1** (97.2 mg; 0.2 mmol) and the base (0.4 mmol) were added to it. The resulting mixture was stirred overnight at room temperature. Usual work-up followed by evaporation and preparative thin-layer chromatography gave the desired *N*-acyl derivatives in good yield.

2-Acetamido-3,4,6-tri-*O*-benzyl-2-deoxy-D-glucopyranose (2). 98.3 mg (100%): Mp 216—217 °C (lit; 216—219 °C);[7] $[\alpha]_D$ +67.2° (*c* 1.08, $CHCl_3$) (lit; +71.3° (*c* 1.08, $CHCl_3$)).[2]

2-Benzamido-3,4,6-tri-*O*-benzyl-2-deoxy-D-glucopyranose (3). 95.2 mg (86%): Mp 215—217 °C (lit; 215—217 °C);[8] $[\alpha]_D$ +80.8° (*c* 0.48, pyridine) (lit; +88.6° (*c* 0.48, pyridine)).[8]

3,4,6-Tri-*O*-benzyl-2-deoxy-2-glycoloylamino-D-glucopyranose (4). 84.8 mg (84%): Mp 204—206 °C; $[\alpha]_D$ 40.0° (*c* 0.4, 10% MeOH/$CHCl_3$). Found: C, 67.08; H, 6.46; N, 2.65%. Calcd for $C_{29}H_{33}NO_7 \cdot 1/2H_2O$: C, 67.43; H, 6.63; N, 2.71%.

3,4,6-Tri-*O*-benzyl-2-deoxy-2-(3-hydroxypropanoylamino)-D-glucopyranose (5). 70.0 mg (68%): Mp 191—194 °C; $[\alpha]_D$ +51.2 (*c* 1, $CHCl_3$). Found: C, 68.23; H, 6.70; N, 2.66%. Calcd for $C_{30}H_{35}NO_7 \cdot 1/2H_2O$: C, 67.91; H, 6.84; N, 2.64%.

3,4,6-Tri-*O*-benzyl-2-deoxy-2-(16-hydroxyhexadecanoylamino)-D-glucopyranose (9). 109.5 mg (78%): Amor.; $[\alpha]_D$ +20.0° (*c* 0.4, 20% $CHCl_3$/MeOH). Found: C, 72.14; H, 8.69; N, 2.08%. Calcd for $C_{43}H_{61}NO_7 \cdot 1/2H_2O$: C, 72.44; H, 8.77; N, 1.96%.

2-Benzamido-2-deoxy-D-glucopyranose (12). To the mixture of compound **10** (107.8 mg; 0.5 mmol) and DIEA (0.19 mL; 1.5 mmol) in methanol (4 mL) was added the solution of benzoic Mpt mixed anhydride (160.7 mg; 0.75 mmol) in 1 mL of methanol. After stirring overnight at room temperature, the methanol was evaporated in vacuo. The residue was dissoleved in water and adsorbed on Dia-ion HP-20. The resin was washed with water and eluted with methanol and evaporated. The residue was purified by preparative thin-layer chromatography using the chloroform-methanol-acetic acid (85 : 25 : 20) solvent system. The desired band was eluted with methanol and evaporated in vacuo. The residue was dissolved in methanol, placed in a Sephadex LH-20 column (2×100 cm), and eluted with methanol. The desired fractions were collected to yield **10** as colorless crystals (107.6 mg, 76%). Mp 198 °C (decomp) (lit; 198—200 °C);[9] $[\alpha]_D$ +29.2° (*c* 1, H_2O) (lit; +35.0° (*c* 2, H_2O)).[9] The similar procedure using 1 equiv of **11** in the presence of 2 equiv of Et_3N or DIEA gave **12** in 58, 62% yield, respectively. On the other hand, when 2 equiv of DBU was used only benzoic acid was recovered.

We are deeply indebted to Profs. Teruaki Mukaiyama and Hidefumi Hirai, the Science University of Tokyo, for their helpful discussions.

References

1) Y. Inouye, K. Onodera, S. Kitaoka, and S. Hirano, *J. Am. Chem. Soc.*, **78**, 4722 (1956).
2) R. Harrison and H. G. Fletcher, Jr., *J. Org. Chem.*, **30**, 2317 (1965).
3) M. Ueki and T. Inazu, *Chem. Lett.*, **1982**, 45.
4) M. Ueki, T. Inazu, and S. Ikeda, *Bull. Chem. Soc. Jpn.*, **52**, 2424 (1979).
5) D. Charon, M. Mordange, and L. Szabo, *J. Chem. Soc., Perkin Trans. 1*, **1984**, 2291.
6) M. Inage, H. Chaki, M. Imoto, T. Shimamoto, S. Kusumoto, and T. Shiba, *Tetrahedron Lett.*, **24**, 2011 (1983).
7) C. D. Warren, M. A. E. Shaban, and R. W. Jeanloz, *Carbohydr. Res.*, **59**, 427 (1977).
8) P. A. Gent, R. Gigg, and R. Conant, *J. Chem. Soc., Perkin Trans. 1*, **1972**, 1535.
9) H. Mukerjee, *J. Org. Chem.*, **35**, 2042 (1970).

Preparation of Pyrroles Having Long Alkyl Chains from Nitroalkenes

Noboru ONO* and Kazuhiro MARUYAMA
Department of Chemistry, Faculty of Science, Kyoto University, Kyoto 606
(Received June 16, 1988)

Synopsis. Pyrroles having long alkyl chains at the 3- and/or 4-positions are readily prepared by the reaction of ethyl isocyanoacetate with nitroalkenes having long alkyl chains.

As pyrroles having long alkyl chains at the 3- and/or 4-positions are important intermediates for the synthesis of lipophilic polypyrroles and porphyrins, synthesis of such pyrroles is becoming important in recent years.[1] Acylation of pyrroles followed by the reduction of the carbonyl group[2] or the Wittig type reaction of 3-formyl pyrroles followed by hydrogenation of the double bond has been used for the introduction of long chains at the 3-position.[3] However, they require tedious procedures and can not be applied to the synthesis of pyrroles having two long alkyl groups at the 3- and 4-positions. In connection with our study of porphyrin model systems, we need a more simple and effective method for the preparation of pyrroles having long alkyl chains. In this paper we wish to report the preparation of hitherto unfamiliar nitroalkenes having long alkyl chains and their conversion into the corresponding pyrroles by the reaction with isocyanides.[4]

Results and Discussion

The requisite nitroalkenes were prepared by dehydration of the corresponding nitro alcohols (**1**) on treatment with dicyclohexylcarbodiimide (DCC) in the presence of copper(I) chlorid.[5] Nitro alcohols (**1**)

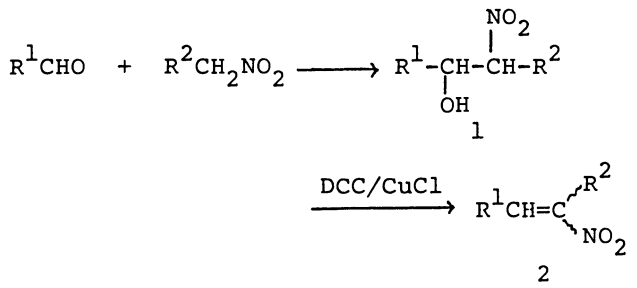

were prepared by the nitro aldol condensation of higher alkanals with higher nitroalkanes. A strong base such as 1,8-diazabicyclo[5.4.0]undec-7-ene (DBU) was required for this step.[6] Althogh many methods are available for the conversion of **1** into nitroalkenes (**2**)[7] the formation of nonconjugated nitroalkenes is a serious problem for higher nitroalkenes. In fact, the most widely used method consisted of methansulfonylation and the effecting elimination on treatment with a base[8] gave a mixture of **2** and the nonconjugated nitroalkenes whose ratio was about 7 : 3. Dehydration with DCC in the presence of copper(I) chloride gave **2** in good yields without formation of nonconjugated nitroalkenes. The results are summarized in Table 1.

Nitroalkenes **2** were converted into pyrroles on treatment with ethyl isocyanoacetate in the presence of a base.[4] The reaction was carried out by stirring a mixture of **2**, ethyl isocyanoacetate, and DBU in tetrahydrofuran (THF) at room temperature. 2-Ethoxycarbonyl-3,4-dialkylpyrroles (**3**) and 2,4-bis(ethoxycarbonyl)-3-alkylpyrroles (**4**) were obtained in 70—80% and 5—10% yields, respectively. They are readily separated by column chromatography (silica gel/benzene) to afford pure **3** and **4**. The results are summarized in Table 2. Formation of **4** has not been reported

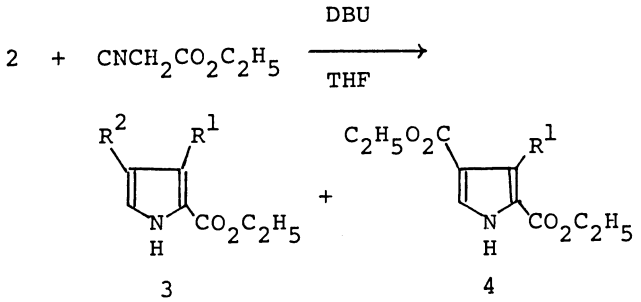

in the literature,[4] but it is unavoidable in the preparation of pyrroles using nitroalkenes. The possible route for the formation of **3** and **4** is shown in Scheme 1. The intermediate **5** undergoes either cyclization to give **3** or elimination of the anion of nitro compounds to give **6** which reacts with ethyl isocyanoacrtate to give **4**.[9]

Table 1. Preparation of Nitro Alcohols (**1**) and Nitroalkenes (**2**) Having Long Alkyl Chains

R^1	R^2	Base (equiv)	Method[a]	**1**, Yield/%	**2**, Yield/% (*E*/*Z*)[b]
n-C_6H_{13}	CH_3	DBU (0.1)	A	**1a**, 90	**2a**, 85 (63/37)
n-C_9H_{19}	CH_3	DBU (0.1)	A	**1b**, 95	**2b**, 80 (65/35)
n-C_5H_{11}	*n*-C_7H_{15}	DBU (0.3)	B	**1c**, 98	**2c**, 88 (60/40)
n-C_7H_{15}	*n*-C_7H_{15}	DBU (0.3)	B	**1d**, 95	**2d**, 80 (57/43)
n-C_8H_{17}	*n*-C_8H_{17}	DBU (0.3)	B	**1e**, 90	**2e**, 85 (57/43)
n-C_5H_{11}	$CH_2CH_2CO_2CH_3$	DBU (0.3)	B	**1f**, 94	**2f**, 76 (55/45)

a) Method A: The reaction was carried out in acetonitrile at room temperature. Method B: the reaction was carried out without solvents at room temperature. b) The *E*/*Z* ratio was determined by NMR and HPLC.

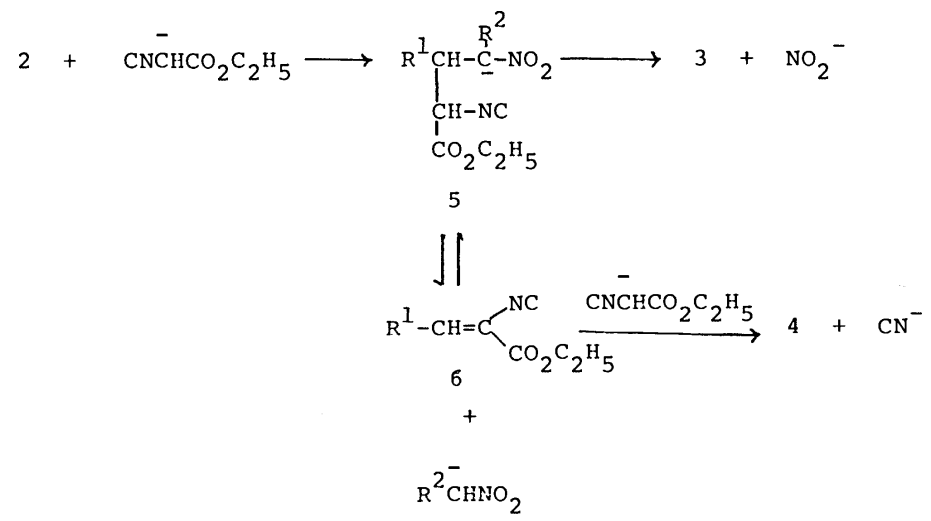

Scheme 1.

Table 2. Preparation of Pyrroles **3** and **4**[a]

R^1	R^2	Time h	**3**, yield %	**4**, yield %
n-C_6H_{13}	CH_3	15	**3a**, 78	**4a**, 8
n-C_9H_{19}	CH_3	20	**3b**, 80	**4b**, 5
n-C_5H_{11}	n-C_7H_{15}	20	**3c**, 80	**4c**, 8
n-C_7H_{15}	n-C_7H_{15}	20	**3d**, 77	**4d**, 6
n-C_8H_{17}	n-C_8H_{17}	20	**3e**, 85	**4e**, 5
n-C_5H_{11}	$CH_2CH_2CO_2CH_3$	20	**3f**, 70	**4c**, 5

(a) The reaction was carried out by stirring amixture of **2** (10 mmol), ethyl isocyanoacetate (10 mmol), and DBU (10 mmol) in THF (20 ml). The separation of **3** was carried out by column chromatography (silica gel/benzene).

Thus, pyrroles having long alkyl chains are conveniently prepared from nitroalkenes. Pyrroles **3** are useful for the synthesis of lipophilic porphyrins.[1]

Experimental

Nitroalkanes were prepared by the reaction of the corresponding alkyl bromides with sodium nitrite in dimethyl sulfoxide,[10] or the Michael addition of nitrometane to methyl acrylate.[11] Aldehydes were used after distillation of commercially available materials. Ethyl isocyanoacetate was prepared according to the literature.[12]

Preparation of β-Nitro Alcohols. Method A: A mixture of nitroethane (8.3 g, 0.11 mol), heptanal (11.4 g, 0.10 mol), and DBU (0.15 g, 0.01 mol) in acetonitrile (10 ml) was stirred at room temperature for 24 h and then diluted with water (50 ml) containing 1 M HCl (10 ml; 1 M=1 mol dm^{-3}), and extracted with ethyl acetate. The extracts were washed with water and dried with anhydrous magnesium sulfate. The solvent was removed under reduced pressure, and the residue was distilled to give 2-nitro-3-nonanol (**1a**), 16 g (90%), bp 100—105 °C/1 mmHg (1 mmHg=133.32 Pa); lit.,[11] 110 °C/1.5 mmHg. 2-Nitro-3-dodecanol (**1b**): bp 110—115 °C/1 mmHg.

Method B: A mixture of 1-nitrooctane (3.2 g, 20 mmol), hexanal (2.0 g, 20 mmol), and DBU (0.45 g, 2 mmol) was stirred at room temperature for 24 h and then diluted with ethyl acetate (20 ml). The resulting solution was poured into 1 M HCl (100 ml) and extracted with ethyl acetate. The extracts were washed with water and the solvent was removed to give 7-nitro-6-tetradecanol (**1c**), which was pure enough to use for the next step; 4.9 g (98%).

Preparation of Nitroalkenes (2). A mixture of **1c** (3.68 g, 14.2 mmol), copper(I) chloride (34 mg, 3.4 mmol), and DCC (3.50 g, 17.1 mmol) in dioxane (40 ml) was stirred at room temperature for 48 h. The precipitated solid was removed by filtration and washed with hexane. The filtrate and washings were combined, and washed with 1 M HCl and water. The solvent was removed after drying with anhydrous magnesium sulfate. The residue was subjected to column chromatography (silica gel/ benzene-hexane) to give **2c**, 3.01 g (88%). ^{1}H NMR ($CDCl_3$) δ=0.87 (t, 6 H, J=7 Hz), 1.00—1.60 (m, 16 H), 1.64—1.98 (m, 2 H), 2.04—2.68 (m, 2 H), 5.63 (t, Z-CH=C), and 6.98 (t, E-CH=C). IR (neat) 1360, 1530, and 1670 cm^{-1}. Found: m/z 241.2064. Calcd for $C_{14}H_{27}NO_2$: M, 241.2042.

Following nitroalkenes were prepared by this procedure.

2a: ^{1}H NMR ($CDCl_3$) δ=0.90 (t, 3 H, J= 7 Hz), 1.10—1.70 (m, 8 H), 2.10 (s, 3 H), 2.28—2.45 (m, 2 H), 5.83 (t, Z-CH=C), and 7.07 (t, E-CH=C). IR (neat) 1360, 1530, and 1650 cm^{-1}. Found: m/z 171.1138. Calcd for $C_9H_{17}NO_2$: M, 171.1145.

2b: ^{1}H NMR ($CDCl_3$) δ=0.90 (t, 3 H, J= 7 Hz), 1.05—1.75 (m, 14 H), 2.08 (s, 3 H), 2.20—2.50 (m, 2 H), 5.83 (t, Z-CH=C), and 7.02 (t, E-CH=C). IR (neat) 1360, 1530, and 1650 cm^{-1}. Found: m/z 230.1932. Calcd for $C_{12}H_{23}NO_2$: M, 230.1934.

2d: ^{1}H NMR ($CDCl_3$) δ=0.85 (t, 6 H, J=7 Hz), 1.04—1.78 (m, 20 H), 2.05—2.74 (m, 4 H), 5.64 (t, Z-CH=C), and 7.00 (t, E-CH=C). IR (neat) 1360, 1530, and 1650 cm^{-1}. Found: m/z 269.2348. Calcd for $C_{16}H_{31}NO_2$: M, 269.2354.

2e: ^{1}H NMR ($CDCl_3$) δ=0.85 (t, 6 H, J=7 Hz), 1.02—1.78 (m, 24 H), 2.10—2.65 (m, 4 H), 5.62 (t, Z-CH=C), 7.02 (t, E-CH=C). IR (neat) 1360, 1530, and 1650 cm^{-1}. Found: m/z 297.2876. Calcd for $C_{18}H_{35}NO_2$: M, 297.2886.

2f: ^{1}H NMR ($CDCl_3$) δ=0.89 (t, 3 H, J=7 Hz), 1.10—1.80 (m, 6 H), 2.12—2.82 (m, 4 H), 2.85 (q, 2 H, J=8 Hz), 3.64 (s, 3 H), 5.91 (t, Z-CH=C), and 7.13 (t, E-CH=C). IR (neat) 1360, 1530, 1650, and 1730 cm^{-1}. Found: m/z 229.1314. Calcd for $C_{11}H_{19}NO_4$: M, 229.1314.

Preparation of Pyrroles. Typical Procedure: A mixture of **2a** (1.71 g, 10 mmol), ethyl isocyanoacetate, and DBU (1.52 g, 10 mmol) in THF (20 ml) was stirred at room temperature for 15 h. The reaction mixture was poured into water (100 ml) containing 1 M HCl (10 ml) and extracted with ethyl acetate (3×50 ml). The extracts were washed with water and dried with anhydrous magnesium sulfate, The solvent was

removed under reduced pressure, and the reside was subjected to column chromatography (silica gel/benzene) to give **3a** (1.85 g, 78%) and **4a** (0.24 g, 8%). **3a**: mp 55—56 °C. IR (KBr) 3340 and 1680 cm^{-1}. ^1H NMR ($CDCl_3$) δ=0.95 (t, 3 H, J=7 Hz), 1.2—1.8 (m, 11 H), 2.02 (s, 3 H), 2.70 (q, 2 H, J=7 Hz), 4.25 (q, 2 H, J=7 Hz), 6.70 (d, 1 H, J=3 Hz), and 9.45 (br s, 1 H). Found: C, 70.76; H, 9.87; N, 5.93%. Calcd for $C_{14}H_{23}NO_2$: C, 70.84; H, 9.77; N, 5.90%. **4a**: oil. IR (neat) 3340, 1620, and 1680 cm^{-1}. ^1H NMR ($CDCl_3$) δ=0.95 (t, 3 H, J=7 Hz), 1.2—1.7 (m, 14 H), 3.10 (q, 2 H, J=7 Hz), 4.28 (q, 2 H, J=7 Hz), 4.35 (q, 2 H, J=7 Hz), 7.45 (d, 1 H, J=2 Hz), and 9.28 (br s, 1 H). Found: C, 65.14; H, 8.39; N, 4.68%. Calcd for $C_{16}H_{25}NO_4$: C, 65.06; H, 8.53; N, 4.74%. Following pyrroles were prepared by this procedure.

3b: Oil. IR (neat) 3340 and 1685 cm^{-1}. ^1H NMR ($CDCl_3$) δ=0.90 (t, 3 H, J=7 Hz), 1.1—1.8 (m, 17 H), 2.0 (s, 3 H), 2.69 (q, 2 H, J=7 Hz), 4.25 (q, 2 H, J=7 Hz), 6.68 (d, 1 H, J=3 Hz), and 9.40 (br s, 1 H). Found: C, 75.51; H, 10.78; N, 5.13%. Calcd for $C_{17}H_{29}NO_2$: C, 75.79; H, 10.85; N, 5.20%.

3c: Oil. IR (neat) 3340 and 1680 cm^{-1}. ^1H NMR ($CDCl_3$) δ=0.90 (t, 6 H, J=7 Hz), 1.1—1.8 (m, 19 H), 2.36 (q, 2 H, J=7 Hz), 2.70 (q, 2 H, J=7 Hz), 4.25 (d, 2 H, J=7 Hz), 6.66 (d, 1 H, J=3 Hz), and 9.20 (br s, 1 H). Found: C, 74.38; H, 10.78; N, 4.79%. Calcd for $C_{19}H_{33}NO_2$: C, 74.22; H, 10.82; N, 4.56%.

3d: Oil. IR (neat) 3320 and 1680 cm^{-1}. ^1H NMR ($CDCl_3$) δ=0.90 (t, 6 H, J=7 Hz), 1.1—1.8 (m, 23 H), 2.38 (q, 2 H, J=7 Hz), 2.70 (q, 2 H, J=7 Hz), 4.25 (q, 2 H, J=2 H), 6.62 (d, 1 H, J=3 Hz), and 8.98 (br s, 1 H). Found: C, 75.25; H, 11.28; N, 4.28%. Calcd for $C_{21}H_{37}NO_2$: C, 75.17; H, 11.12; N, 4.18%.

3e: Oil. IR (neat) 3320 and 1680 cm^{-1}. ^1H NMR ($CDCl_3$) δ=0.90 (t, 6 H, J=7 Hz), 1.1—1.8 (m, 27 H), 2.40 (q, 2 H, J=7 Hz), 2.72 (q, 2 H, J= 7 Hz), 4.26 (q, 2 H, J=7 Hz), 6.62 (d, 1 H, J=3 Hz), and 9.90 (br s, 1 H). Found: C, 75.89; H, 12.57; N, 3.74%. Calcd for $C_{23}H_{41}NO_2$: C, 75.98; H, 12.32; N, 3.85%.

3f: Oil. IR (neat) 1680, 1730, and 3340 cm^{-1}. ^1H NMR ($CDCl_3$) δ=0.97 (t, 3 H, J=7 Hz), 1.2—2.0 (m, 11 H), 2.64 (q, 2 H, J=7 Hz), 2.86 (q, 2 H, J=7 Hz), 3.64 (s, 3 H), 4.28 (q, 2 H, J=7 Hz), 6.78 (d, 1 H, J=3 Hz), and 9.90 (br s, 1 H). Found: C, 65.28; H, 8.38; N, 4.57%. Calcd for $C_{16}H_{25}NO_4$: C, 65.06; H, 8.53; N, 4.74%.

4b: Oil. IR (neat) 3340, 1640, and 1680 cm^{-1}. H NMR ($CDCl_3$) δ=0.95 (t, 3 H, J=7 Hz), 1.2—1.8 (m, 20 H), 3.12 (q, 2 H), J=7 Hz), 4.26 (q, 2 H, J=7 Hz), 4.36 (q, 2 H, J=7 Hz), 7.35 (d, 1 H, J= 2 Hz), and 9.26 (br s, 1 H). Found: C, 67.73; H, 9.12; N, 4.27%. Calcd for $C_{19}H_{31}NO_4$: C, 67.62; H, 9.26; N, 4.15%.

4c: Oil. IR (neat) 3340, 1640, and 1680 cm^{-1}. ^1H NMR ($CDCl_3$) δ=0.95 (t, 3 H, J=7 Hz), 1.2—1.8 (m, 12 H), 3.20 (q, 2 H, J=7 Hz), 4.25 (q, 2 H, J=7 Hz), 4.36 (q, 2 H, J=7 Hz), 7.40 (d, 1 H, J=2 Hz), and 9.30 (br s, 1 H). Found: C, 64.17; H, 8.13; N, 4.78%. Calcd for $C_{15}H_{23}NO_4$: C, 64.04; H, 8.24; N, 4.92%.

4d: Oil. IR (neat) 3340, 1640, and 1680 cm^{-1}. ^1H NMR ($CDCl_3$) δ= 0.95 (t, 3 H, J=7 Hz), 1.2—1.8 (m, 16 H), 3.12 (q, 2 H, J=7 Hz), 4.25 (q, 2 H, J=7 Hz), 4.36 (q, 2 H, J=7 Hz), 7.32 (d, 1 H, J= 2 Hz), and 9.25 (br s, 1 H). Found: C, 66.17; H, 8.89; N, 4.40%. Calcd for $C_{17}H_{27}NO_4$: C, 65.99; H, 8.80; N, 4.53%.

4e: Oil. IR (neat) 3340, and 1680 cm^{-1}. ^1H NMR ($CDCl_3$) δ=0.95 (t, 3 H, J=7 Hz), 1.2—1.8 (m, 18 H), 3.12 (q, 2 H, J=7 Hz), 4.25 (q, 2 H, J=7 Hz), 4.36 (q, 2 H, J=7 Hz), 7.37 (d, 1 H, J=2 Hz), and 9.25 (br s, 1 H). Found: C, 66.79; H, 9.23; N, 4.15%. Calcd for $C_{18}H_{29}NO_4$: C, 66.84; H, 9.04; N, 4.33%.

References

1) C. K. Chang, *J. Am. Chem. Soc.*, **99**, 2819 (1977); H. Nishide, H. Maeda, S. Wong, and E. Tsuchida, *J. Chem. Soc., Chem. Commun.*, **1985**, 573; K. Maruyama, F. Kobayashi, and A. Osuka, *Chem. Lett.*, **1984**, 821; "The Porphyrins" ed by D. Dolphin, Vol. I, Part A, Academic Press, New York (1978).

2) H. Diekmann, C. K. Chang, and T. G. Traylor, *J. Am. Chem. Soc.*, **93**, 4068 (1971) and Ref. 1.

3) K. M. Smith and G. M. F. Bisset, *J. Org. Chem.*, **44**, 2077 (1979).

4) A. M. Van Leusen, H. Siderius, R. E. Hoogenboom, and D. Von Leusen, *Tetrahedron Lett.*, **1972**, 5337; S. Halazy and P. Magnus, *ibid.*, **25**, 1421 (1984); D. H. R. Barton and S. Z. Zard, *J. Chem. Soc., Chem. Commun.*, **1985**, 1098, in which the reaction of nitroalkenes with ethyl isocyanoacetate was reported.

5) P. Knochel and D. Seebach, *Synthesis*, **1982**, 1017.

6) Triethylamine, KF, or NaOH is generally used as a base for the nitro aldol condensation reaction. However, these bases are not effective to induce the reaction of higher nitroalkanes with higher alkanals.

7) A. G. M. Barrett and G. G. Graboski, *Chem. Rev.*, **66**, 751 (1986) and references therein.

8) J. Melton and J. E. McMurry, *J. Org. Chem.*, **40**, 2138 (1975).

9) M. Suzuki, M. Miyoshi, and K. Matsumoto, *J. Org. Chem.*, **39**, 1980 (1974).

10) N. Kornblum, *Org. React.*, **12**, 101 (1962).

11) "Houben Weyl, Methoden der Organischen Chemie, 4th ed." ed by E. Muller, George Thieme Verlag, Stuttgart, 1971.

12) G. D. Hartmann and L. M. Weinstock, *Org. Synth.*, Coll. Vol. 6, 620 (1988); I. Ugi, V. Fetzer, H. Knupfer, and K. Offermann, *Angew. Chem., Int. Ed. Engl.*, **4**, 472 (1965).

Hexacarbonylmolybdenum-Induced N-N Bond Cleavage of Pyrazoles. Conversion of 1-Acylpyrazoles to Pyrimidines

Makoto NITTA,* Tatsuo HAMAMATSU, and Hiroyuki MIYANO
Department of Chemistry, School of Science and Engineering, Waseda University, Shinjuku-ku, Tokyo 160
(Received June 17, 1988)

Synopsis. [$Mo(CO)_6$]-induced reactions of 1-acyl-3,5-disubstituted pyrazoles underwent N-N bond cleavage and subsequent cyclocondensation to give pyrimidines as well as deacylation to give 3,5-disubstituted pyrazoles. Under similar conditions, 1,3,5-trisubstituted pyrazoles, which have no electron-withdrawing substituent on N1, gave no product, except for the starting materials.

Previous studies in this series have included papers involving a system which formally contains a C=N-O group. The reaction of substituted 2-isoxazolines with [$Mo(CO)_6$], [$Fe_2(CO)_9$], or [$Fe(CO)_5$] under thermal conditions or photo-irradiations has been shown to undergo N-O and C4-C5 bond cleavages to give two fragments of aldehydes (or ketones) and complexed vinylnitrenes, which could collapse to ketones in a protic media.[1,2] Similarly substituted isoxazoles underwent a reductive cleavage of the N-O bond to give β-amino enones in good yields.[3] The *N*-complexed isoxazole has been isolated as a reasonable intermediate in the reaction.[3] The easy, metal-carbonyl prompted N-O bond cleavage has a strong resemblance to the photochemically induced N-O bond cleavage of isoxazoles to give oxoazirines.[4] The photochemical reaction of a pyrazole has also been known to undergo a possible N-N bond cleavage to give an imidazole.[5] In pyrazoles the nitrogen-nitrogen linkage appears to be antibonding in character

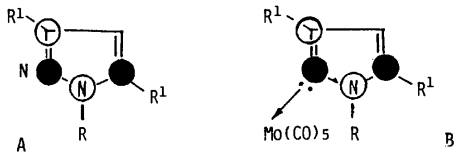

(LUMO shown as **A** in the Figure), and this seems to cause a possible photochemical N-N bond cleavage. Considering the pyrazoles *N*-complexed **B** to a [$Mo(CO)_5$] species, a possible delocalization of a π-d electron from the central metal to the π* (LUMO) of the pyrazole is expected to facilitate an N-N bond cleavage. This paper describes the [$Mo(CO)_6$]-induced N-N bond cleavage of 1-acetyl- and 1-benzoyl-3,5-disubstituted pyrazoles and a subsequent cyclocondensation to give 2,4,6-trisubstituted pyrimidines.

The thermal reaction of 1-acetyl-3,5-diphenyl-, 1-benzoyl-3,5-diphenyl-, and 1-benzoyl-3,5-dimethylpyrazoles (**1a—c**) with [$Mo(CO)_6$] in dry 1,2-dimethylbenzene underwent an N-N bond cleavage and a subsequent cyclocondensation to give pyrimidine derivatives **2a—c** as well as deacylation to give 3,5-disubstituted pyrazoles **3a, c** (Scheme 1). The detailed

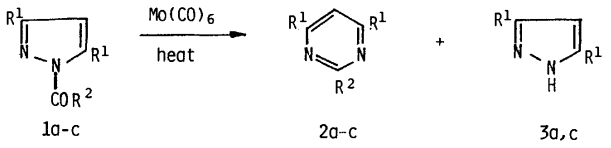

a: R^1 = Ph; R^2 = Me, b: R^1 = R^2 = Ph, c: R^1 = Me; R^2 = Ph

Scheme 1.

reaction conditions and the yields of the products are summarized in Table 1 (Entries 1—3). Since compound **1a** underwent no reaction under heating in the absence of [$Mo(CO)_6$], [$Mo(CO)_6$] is indispensable for the formation of **2** and **3**. The structures of the pyrimidines **3a**,[6] **3b**,[7] and **3c**[6] were confirmed by comparisons of their physical data with those found in the literature. On the other hand, reactions proceeded slowly in dry toluene or acetonitrile in place of 1,2-dimethylbenzene, and gave pyrimidines **2a—c** as well as pyrazoles **3a,c**, in addition to the unreacted starting materials **1a—c** (Table 1, Entries 4—7). Compound **1c** does not seem to be labile, as compound with **1a,b**, in N-N cleavage reactions (Entries 3 and 7).

The formation of pyrimidines **2a—c** and pyrazoles **3a, c** can be explained as follows. Since [$Mo(CO)_6$] has been shown to give an *N*-complexed isoxazoles, the

Table 1. Experimental Results Obtained in the Reaction of **1a—c** with [$Mo(CO)_6$][a]

Entry	Pyrazole			Solvent	Product (yield/%)		Recovery (%)
	1	R^1	R^2		2	3	1
1	**1a**	Ph	Me	DMB[b]	**2a** (30)	**3a** (37)	(0)
2[c]	**1b**	Ph	Ph	DMB[b]	**2b** (30)	**3a** (40)	(0)
3[c]	**1c**	Me	Ph	DMB[b]	**2c** (12)	**3c** (34)	(0)
4	**1a**			Toluene	**2a** (18)	**3a** (47)	**1a** (8)
5	**1a**			CH_3CN	**2a** (9)	**3a** (60)	**1a** (10)
6[c]	**1b**			CH_3CH	**2b** (5)	**3a** (47)	**1b** (45)
7[c]	**1c**			CH_3CN	**2c** (0)	**3c** (82)	**1c** (15)

a) A molar equivalent amount of [$Mo(CO)_6$] was used, being heated under reflux for 24 h. b) DMB denotes 1,2-dimethylbenzene. c) Benzoic acid was isolated as ethyl benzoate albeit in low yields (ca. 1—12 %) (see Experimental).

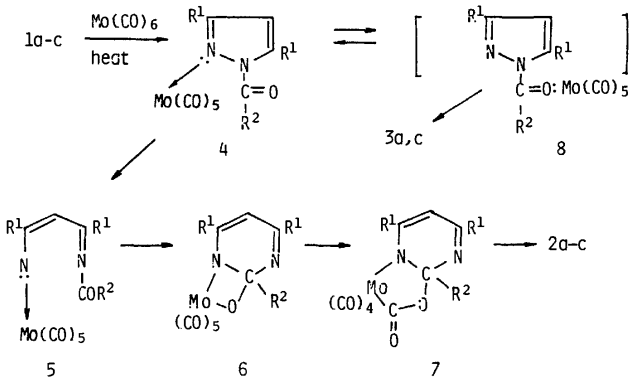

Scheme 2.

initial step is a complexation of **1** to give **4**.[3] The following N-N bond cleavage of **4** gives complexed nitrene **5**. The intermediate **5** can cyclize to give **6**, a ligand migration of which is followed by decomplexation would give pyrimidines **2a—c**.[8] Although isolated yields of benzoic acid (Entries 2,3,6, and 7) were very low, pyrazoles **3a,c** presumably originate from the formally postulated complex **8**, which undergoes deacylation with contaminated water or under workup conditions. Even a reaction in a dry solvent can not eliminate the possibility of stray water. In a deacylation reaction, a molybdenum moiety seems to act as a Lewis acid. The carbonyl ligand of $[Mo(CO)_6]$ is easily substituted by acetonitrile,[3,9] several carbonyl ligands in each of the postulated complexes **4—8** are possibly exchanged with acetonitrile in the reactions of Entries 5—7. The formation of pyrazoles **3a, c** predominates over pyrimidines **2a—c**. This fact is suggestive of a high energy barrier of N-N bond cleavage, as compared to that of deacylation, and a possible existence of equilibrium between **4** and **8**. Although the N-N bond cleavage of **1a—c** was enhanced by $[Mo(CO)_6]$, the reaction seems to require a higher temperature, compared to that of isoxazoles.[3] This fact is ascribed to the large resonance energy of pyrazole, as compared to that of isoxazole.[10] Thus, the appreciable delocalization of a d electron from the central metal to the π^* (LUMO) of the pyrazole is actually suggested by the present reactions (figure).

Similarly, a reaction of 1-phenyl-3,5-dimethyl- and 1,3,5-triphenylpyrazoles (**9a, b**), both of which have no electron-withdrawing substituent at N1, was studied (Scheme 3). In this case, the expected vinylnitrene complex **11** can not collapse to pyrimidine. Thus, reactions expected N-N bond cleavage in moist solvents to give such products as **12** (and/or **13**) were carried out as in reactions of isoxazoles to give β-amino enones.[3] However, the reactions gave no product, except for the starting materials (see Experimental). This fact is suggestive of an enhanced resonance energy and a strong N-N bond of **9a, b**, compared to those of 1-acyl-substituted pyrazoles **1a—c**.

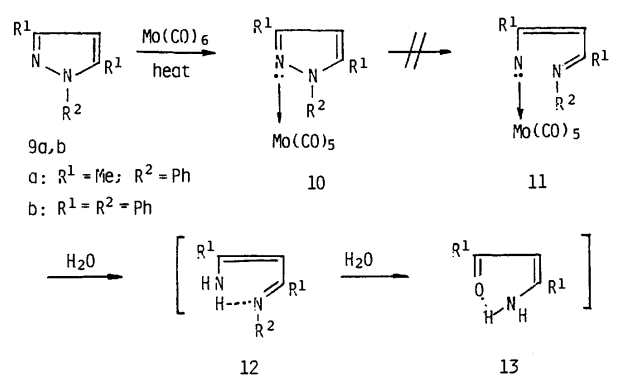

Scheme 3.

Experimental

The ^1H NMR spectra were recorded on a Hitachi R-24 spectrometer and the chemical shifts are given in ppm (δ) relative to the internal $SiMe_4$ standard. The desired compounds, 1-acylpyrazole derivatives **1a—c**, 1-phenyl-3,5-dimethylpyrazole (**9a**), and 1,3,5-triphenylpyrazole (**9b**), were prepared according to methods described in the literature.[11] All of the reactions were carried out under a dry nitrogen atmosphere.

General Procedure for the Reaction of Acylpyrazoles 1a—c with $[Mo(CO)_6]$ in 1,2-Dimethylbenzene. A solution of **1** (0.5 mmol) and $[Mo(CO)_6]$ (133 mg, 0.5 mmol) in 1,2-dimethylbenzene (5 cm^3) was refluxed for 24 h. After the solvent was evaporated, the residue was dissolved in chloroform (10 cm^3); it was then filtered through Celite to remove insoluble materials. After the filtrate was concentrated, the residue was separated by TLC on silica gel. In the reaction of **1a**, the first band (R_f 0.3) from the TLC plates developed by hexane-chloroform (1/3) gave pyrimidine **2**. The second band (R_f 0.1) gave **3a**. In reactions of **1b, c**, the first band (R_f 0.8 for **2b**; 0.6 for **2c**) from the TLC plates developed by hexane-AcOEt (6/1) gave pyrimidine **2b,c**. The second band (R_f 0.3 for **3b**; 0.2 for **3c**) gave a mixture containing **3b,c**. This mixture was heated in ethanol (5 cm^3) and H_2SO_4 (0.2 cm^3) for 3.5 h. After the usual workup, the pyrazole and ethyl benzoate (ca. 7%) were obtained. The yields of the products are summarized in Table 1. For **2a**: mp 91—92 °C (lit, mp 96—97 °C); ^1H NMR ($CDCl_3$) δ=2.83 (3H, s), 7.3—7.6 (6H, m), 7.79 (1H, s), 7.9—8.0 (4H, m).[6] For **2b**: mp 183—184 °C (lit, mp 183—184 °C); ^1H NMR ($CDCl_3$) δ=7.3—7.7 (9H, m), 7.98 (1H, s), 8.0—8.5 (4H, m), 8.5—8.9 (2H, m).[7] For **2c**: mp 74—78 °C (lit, mp 81—83 °C); ^1H NMR ($CDCl_3$) δ=2.62 (6H, s), 6.95 (1H, s), 7.3—7.7 (3H, m), 8.3—8.7 (2H, m).[6]

Thermal Reaction of 1-Acetyl-3,5-diphenylpyrazole 1a in 1,2-Dimethylbenzene. A solution of **1a** (131 mg, 0.5 mmol) in 1,2-dimethylbenzene (5 cm^3) was heated under reflux for 24 h. After the solvent was evaporated, the residue was purified by TLC on silica gel using hexane-AcOEt (5/1) as a developer to give **1a** (111 mg, 85%).

Reaction of 1-Acetyl-3,5-diphenylpyrazole 1a with $[Mo(CO)_6]$ in Toluene. A solution of **1a** (132 mg, 0.5 mmol) and $[Mo(CO)_6]$ (133 mg, 0.5 mmol) in dry toluene (5 cm^3) was heated under reflux for 24 h. After the solvent was evaporated, the residue was dissolved in dichloromethane (10 cm^3), and the solution was filtered through Celite to remove insoluble materials. The filtrate was concentrated and the resulting residue was separated by TLC on silica gel using hexane-chloroform (1/2) as a developer. The first band (R_f 0.6) from the TLC plates gave the starting material **1a**. The second band (R_f 0.2) gave the pyrimidine **2a**. The third band (R_f 0.1) gave the pyrazole **3a**. The yields are summarized in Table 1.

General Procedure for the Reaction of 1a—c with $[Mo(CO)_6]$ in Acetonitrile. A solution of **1** (1 mmol) and $[Mo(CO)_6]$ (266 mg, 1 mmol) in dry acetonitrile (5 cm^3) was

heated under reflux for 24 h. The acetonitrile was evaporated and the residue was dissolved in dichloromethane (10 cm^3). After the solution was filtered through Celite to remove insoluble materials, the filtrate was concentrated and the residue was separated by TLC on silica gel. In the reaction of **1a**, the first band (R_f 0.6) from the TLC plates developed by hexane-chloroform (1/3) gave **1a**. The second band (R_f 0.3) gave pyrimidine **2a**. The third band (R_f 0.1) gave pyrazole **3a**. In reactions of **1b, c**, the first band (R_f 0.6 for **1b**; 0.7 for **1c**) from the TLC plates developed by hexane-AcOEt (6/1) gave **1b, c**. The second band (R_f 0.3 for **2b**) gave pyrimidine **2b**. The third band (R_f 0.3 for **3b**; 0.2 for **3c**) gave a mixture containing **3b,c**. This mixture was then heated in ethanol (5 cm^3) and H_2SO_4 (0.2 cm^3) under reflux. The usual workup afforded pyrazole **2** and ethyl benzoate (ca. 1—12%).

General Procedure for the Reaction of Pyrazoles 9a, b with [Mo(CO)$_6$] in Moist Toluene and/or Acetonitrile. A solution of **9** (0.5 mmol) and [$Mo(CO)_6$] (133 mg, 0.5 mmol) in moist toluene (5 cm^3) and/or acetonitrile (5 cm^3) was heated under reflux for 24 h. After the reaction mixture was concentrated, the resulting residue was purified by TLC on silica gel using hexane-AcOEt (3/1) as a developer to give the starting material: **9a** (84% in acetonitrile); **9b** (96% in acetonitrile and 94% in toluene).

References

1) M. Nitta and T. Kobayashi, *Chem. Lett.*, **1983**, 51; M. Nitta and T. Kobayashi, *J. Chem. Soc., Perkin Trans. 1*, **1984**, 2103.

2) M. Nitta, A. Yi, and T. Kobayashi, *Bull. Chem. Soc. Jpn.*, **58**, 991 (1985).

3) M. Nitta and T. Kobayashi, *J. Chem. Soc., Perkin Trans. 1*, **1985**, 1401.

4) E. F. Ullman and B. Singh, *J. Am. Chem. Soc.*, **88**, 1844 (1966); B. Singh and E. F. Ullman, *J. Am. Chem. Soc.*, **89**, 6911 (1967).

5) P. Beak, J. L. Miesel, and W. R. Messer, *Tetrahedron Lett.*, **1967**, 5315.

6) H. Yamanaka, K. Edo, F. Shoji, S. Konno, T. Sakamoto, and M. Mizugaki, *Chem. Pharm. Bull.*, **26**, 2160 (1978); T. Nishio, T. Tokunaga, and Y. Omote, *J. Heterocycl. Chem.*, **22**, 405 (1985).

7) A. L. Weis and V. Rosenbach, *Tetrahedron Lett.*, **22**, 1453 (1981); A. -A. Pourzal, *Synthesis*, **1983**, 717.

8) T. Kobayashi and M. Nitta, *Bull. Chem. Soc. Jpn.*, **58**, 1057 (1985); T. Kobayashi and M. Nitta, *Bull. Chem. Soc. Jpn.*, **58**, 3099 (1985); and references cited therein.

9) D. P. Tate, W. R. Knipple, and J. M. Augl, *Inorg. Chem.*, **1**, 433 (1962).

10) A. G. Anastassiou, S. W. Eachus, R. P. Cellura, and J. H. Gebrian, *J. Chem. Soc., Chem. Commun.*, **1970**, 1133; A. V. Chapman, M. J. Cook, A. R. Katritzky, M. H. Abraham, A. F. Danil DE Namor, L. Dumont, and J. Reisse, *Tetrahedron*, **34**, 1571 (1978).

11) K. T. Potts, "Comprehensive Heterocyclic Chemistry," Vol. 5, Pergamon Press, Oxford, New York, Toronto, Sydney, Paris, and Frankfurt; and references cited therein.

General Synthesis of 2-, 3-, and 4-Hydroxyalkylphosphonium Salts by the Reaction of Triphenylphosphine with Cyclic Ethers in the Presence of Strong Acids

Shin-ichi YAMAMOTO (formerly NAKAMURA), Kentaro OKUMA,* and Hiroshi OHTA
Department of Chemistry, Faculty of Science, Fukuoka University, Jonan-ku, Fukuoka 814-01
(Received June 20, 1988)

Synopsis. Cyclic ethers were efficiently converted to the corresponding hydroxyalkylphosphonium salts by the reaction with triphenylphosphine and trifluoromethanesulfonic or trifluoroacetic acid. The reaction of these salts with bases afforded the corresponding phosphonium inner salts which reacted with carbonyl compounds to give homoallylic alcohols.

2-Hydroxyalkylphosphonium salts (**1**) are an important class of compounds because of their use in the mechanistic investigation of the Wittig reaction and their versatile synthetic utility.[1] However, there are only a few reports regarding the synthesis of **1**.[2-4] While triphenylposphine (**2**) has been found to react with epoxides (**3**) to afford olefins via betaine intermediates,[5] there is, to our knowledge, no report on the synthesis of **1** from epoxides and triphenylphosphine. Recently, we reported the convenient synthesis of (hydroxyalkyl)dimethylsulfonium salts from cyclic ethers, acid, and dimethyl sulfide.[6] This result, in turn, prompted us to investigate the possibility of the synthesis of hydroxyalkylphosphonium salts. We report here a new general and convenient method for the preparation of **1**, 3- (**4**), and 4-hydroxyalkylphosphonium salts (**5**) by the reaction of **2** with **3**, oxetane (**6**), or tetrahydrofuran (**7**) in the presence of trifluoromethanesulfonic acid (**8a**) or trifluoroacetic acid (**8b**).

Results and Discussion

We first tried the reaction of epoxides with triphenylphosphine. Treatment of 1,2-epoxycyclohexane (**3a**) with **2** in the presence of **8a** afforded corresponding 2-hydroxycyclohexylphosphonium triflate (**1a**) in 65.0% yields. As shown in Table 1, phosphonium salts **1** were prepared in good yields. Previously, com-

Table 1. Preparation of Hydroxyalkylphosphonium Salts

Cyclic ether	Acid		Phosphonium salt[a]	Anion	Yield/%	Mp/°C
1,2-Epoxycyclohexane	**8a**	**1a**	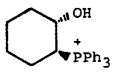	$^-$OTf	65.0	184—185
	8b	**1a′**		$^-$BPh$_4$	37.8[b]	219—220
2-Metyloxirane	**8a**	**1b**	$Ph_3\overset{+}{P}$-$CH_2CH(Me)OH$	$^-$BPh$_4$	78.0	172—173
	8b	**1b**			80.4	
2-Ethyloxirane	**8a**	**1c**	$Ph_3\overset{+}{P}$-$CH_2CH(Et)OH$	$^-$BPh$_4$	75.7	161—162
	8b	**1c**			69.5	
Oxetane	**8a**	**4**	$Ph_3\overset{+}{P}$-$CH_2CH_2CH_2OH$	$^-$BPh$_4$	90.0	178—179
	8b	**4′**		$^-$OCOCF$_3$	84.3	162—163
Tetrahydrofuran	**8a**	**5**	$Ph_3\overset{+}{P}$-$CH_2CH_2CH_2CH_2OH$	$^-$BPh$_4$	65.0	197—198

a) Since most of the products were oils, yields and elemental analyses were determined by their tetraphenylborates except **1a** and **4′**. When styrene oxide was used as epoxide, corresponding phosphonium salt could not be isolated. b) Triphenylphosphine was recovered in 34% yield

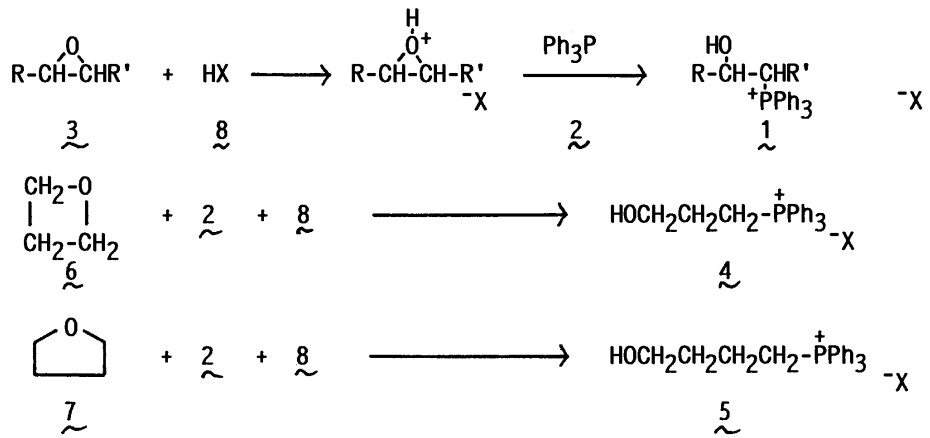

Scheme 1.

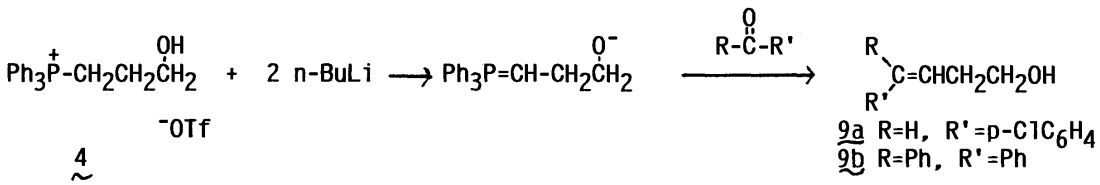

Scheme 2.

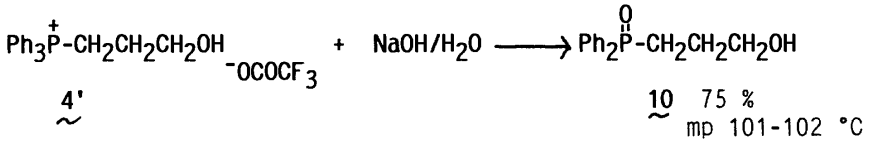

Scheme 3.

pounds **1** were obtained from the corresponding 2-hydroxyalkyl halides and triphenylphosphine,[2] by the reaction of the more nucleophilic 2,6-disubstituted triphenylphosphine with epoxides,[3] or by the reaction of phosphonium ylides with aldehydes followed by the addition of acids.[7] The reaction is stereospecific and regiospecific. The present method requires only one step and good yields were generally obtained.

Reactions of **2** with **3** have long been known to demand much more severe conditions. Products of these reactions in protic solvents are complex mixtures of triphenylphosphine oxide and alkenes formed directly from betaine or oxaphosphetane intermediates.[5] The present method will provide a much more precise mechanistic view of these reactions.

Corey and Yamamoto reported that the reaction of Wittig reagents with aldehydes gave the corresponding adducts at low temperature, which further reacted with a base to afford 2-phosphonio-1-alkanolates.[8] They also reported the reaction of phosphonium ylide anions with epoxides to give 3-phosphino-1-alkanolates.[9] Schlosser et al. and Maryanoff et al. also reported the stereoselective synthesis of alkenols from **1**.[10] The present method may be an alternative approach for the synthesis of the above alcohols. To confirm this possibility, we investigated the reaction of **4** with two equivalents of a base followed by the addition of carbonyl compounds. As expected, the corresponding homoallyl alcohols (**9a**, **b**) were obtained in good yields.

Recently, Warren and co-workers reported the stereoselective synthesis of homoallylic alcohols by the reactions of (hydroxyalkyl)diphenylphosphine oxide (**10**) with aldehydes.[11] So, we tried the preparation of **10** from **4**. As shown in Scheme 3, compound **10** was obtained in good yields.[12]

Within the current synthetic effort in organic chemistry, hydroxyalkylphosphonium salts play an important role in the total synthesis of many conventional natural products containing double bonds.[13] There is therefore a requirement for a simple preparative method for this key intermediate. This synthesis should afford many applications in olefin synthesis.

Experimental

General Methods. Melting points are uncorrected. ^{1}H NMR spectra were recorded on a JEOL JNM-90Q and a JEOL JNM-60 SI spectrometers with Me_4Si as the internal standard.

Synthesis of 1 and 4. General Procedure. To a solution of triphenylphosphine (**2**) (5 mmol) and a solution of corresponding acids (**8**) (5.2 mmol) in dichloromethane (10 mL) was added a solution of cyclic ether (**3**, **6**) (5.5 mmol) in dichloromethane (10 mL) at room temperature. After refluxing for 8 h, the reaction mixture was evaporated to give a pale yellow oil. The residue was washed with ether (20 mL) for several times to yield color less crystals. Recrystallization from dichloromethane-ether gave pure salts. **1a**: mp 184—185 °C. ^{1}H NMR ($CDCl_3$) δ=3.42 (1H, m, CH), 4.00 (1H, m, CH), 4,87 (1H, d, OH), 7.78 (15H, m, Ph). Calcd for $C_{25}H_{24}F_3O_4PS$: C, 59.05; H, 4.76%. Found: C, 59.05; H, 5.01%. **4'**: mp 162—163 °C. ^{1}H NMR ($CDCl_3$) δ=1.83 (2H, m, CH_2), 3.53 (2H, m, CH_2), 3.78 (2H, t, CH_2), 5.64 (1H, br, OH) 7.76 (15H, d, Ph). Calcd for $C_{23}H_{22}F_3O_3P$: C, 63.59; H, 5.10%. Found: C, 63.98; H, 4.80%.

Other salts were obtained as colorless oils. These compounds were converted to their tetraphenylborates for elemental analysis: To a solution of the resulting oil in acetone (5 mL) was added a solution of sodium tetraphenylborate (5.20 mmol) in acetone (5 mL). Colorless crystals of tertaphenylborates were precipitated by addition of ether (50 mL). Recrystallization from dichloromethane gave pure tetraphenylborate salts. **1a'**: mp 219—220 °C. ^{1}H NMR (DMSO-d_6) δ=3.52 (1H, m, CH), 4.76 (1H, m, CH), 5.12 (1H, br, OH), 7.66 (15H, m, Ph). Calcd for $C_{48}H_{46}BOP$: C, 84.70; H, 6.81%. Found: C, 84.90; H, 6.96%. **1b**: mp 172—173 °C. ^{1}H NMR (DMSO-d_6) δ=0.95 (3H, t, CH_3), 3.95 (3H, m, CH-CH_2), 4.70 (1H, d, OH), 7.73 (15H, m, Ph). Calcd for $C_{43}H_{42}BOP$: C, 84.37; H, 6.61%. Found: C, 84.74; H, 6.36%. **1c**: mp 161—162 °C. ^{1}H NMR (DMSO-d_6) δ=0.92 (3H, q, CH_3), 1.59 (2H, m, CH_2), 3.68 (3H, m, CH-CH_2), 5.32 (1H, br, OH), 7.72 (15H, m, Ph). Calcd for $C_{44}H_{44}BOP$: C, 84.40; H, 6.77%. Found: C, 84.78; H, 6.48%. **4**: mp 178—179 °C. ^{1}H NMR (DMSO-d_6) δ=1.64 (2H, m, CH_2), 3.51 (2H, t, CH_2), 3.72 (1H, br, OH), 7.72 (15H, m, Ph). Calcd for $C_{43}H_{42}BOP$: C, 84.37; H, 6.61%. Found: C, 84.26; H, 6.81%.

Synthesis of 5. To a solution of triphenylphosphine (**2**) (1.32 g, 5.03 mmol) in THF (10 mL) was added trifluoromethanesulfonic acid (**8a**) (0.787 g, 5.25 mmol) at room temperature. After refluxing for 8 h, reaction mixture was evaporated to give a pale yellow oil. A solution of sodium tetraphenylborate (1.80 g, 5.25 mmol) in acetone (5 mL) was added to a solution of this oil in acetone (5 mL). When ether (50 mL) was added to the mixture, colorless crystals were precipitated. Recrystallization from dichloromethane gave pure phosphonium salts (2.20 g, 65.0%). Mp 197—198 °C. ^{1}H NMR δ=1.59 (4H, m, CH_2-CH_2), 3.18 (2H, m, CH_2), 3.39

(2H, m, CH_2), 4.46 (1H, br, OH), 7.74 (15H, d, Ph). Calcd for $C_{46}H_{44}BOP$: C, 84.40; H, 6.77%. Found: C, 84.29; H, 6.87%.

Synthesis of 9. To a suspension of **4** (2.35 g, 5.00 mmol) in THF (15 mL) was added a solution of two equimolar amounts of butyllithium in THF (5 mL) at −78 °C. After stirring for 1 h, a solution of *p*-chlorobenzaldehyde (0.744 g, 5.29 mmol) or benzophenone (1.00 g, 5.47 mmol) in THF (10 mL) was added to the mixture at 0 °C. After stirring for 10 h at 30 °C, water (5 mL) was added to the mixture and the solvent was evaporated. Aq. NH_4Cl was added to neutralize the mixture. The aqueous mixture was extracted with dichloromethane (25 mL×2). The combined extracts were dried over $MgSO_4$ and evaporated to give a pale yellow oil. The resulting residue was extracted with hexane (20 mL×3). The combined extracts were evaporated to give a yellow oil. The corresponding homoallyl alcohol **9** was isolated from this oil by column chromatography on silica gel by elution with dichloromethane. **9a** was obtained as a mixture of *E*- and *Z*-isomers. Yield 74% (0.673 g). ^{1}H NMR ($CDCl_3$) δ=2.47 (2H, q, CH_2), 3.74 (2H, t, CH_2), 4.63 (1H, br, OH), 5.97—6.53 (2H, m, CH=CH), 7.25 (4H, s Ph). M^+_{found}=182.0497, $C_{11}H_{11}OCl$ (^{35}Cl) requires 182.0498. **9b**: Yield 56% (0.627 g). ^{1}H NMR ($CDCl_3$) δ=2.39 (2H, q, CH_2), 3.50 (2H, t, CH_2), 3.71 (1H, br, OH), 6.12 (1H, t, CH), 7.21 (10H, s, PH). M^+_{found}=224.1181, $C_{16}H_{16}O$ requires 224.1201.

Synthesis of 10. A suspension of **4'** (1.30 g, 3.00 mmol) in 30% aqueous NaOH (20 mL) was refluxed for 3 h. The reaction mixture was extracted with 20 mL of dichloromethane for three times. The combined extracts was dried over $MgSO_4$ and evaporated to give yellow oil. When the yellow oil was washed with ether (20 mL×3), the crystals were obtained. Recrystallization from ethyl acetate gave pure crystals (0.585 g, 2.25 mmol, 75%). Mp 101—102 °C. ^{1}H NMR ($CDCl_3$) δ=1.85 (2H, m, CH_2), 2.36 (2H, m, CH_2), 3.68 (2H, q, CH_2), 4.38 (1H, t, OH), 7.48 (10H, m, Ph). Calcd for $C_{15}H_{17}O_2P$: C, 69.22; H, 6.58%. Found: C, 69.14; H, 7.07%.

This work was partly supported by the Central Research Institute of Fukuoka University. We are grateful to Dr. Haruo Matsuyama at Tokyo Metropolitan University for the high-resolution mass spectroscopic analysis.

References

1) For a review; see J. March, "Advanced Organic Chemistry," John Wiley & Sons, New York (1985), pp. 849—851; E. Vedejs, G. P. Meier, and K. A. J. Snoble, *J. Am. Chem. Soc.*, **103**, 2823 (1981); F. C-Rouhou, Y. L. Bigot, R. E. Gharbi, M. Delmas, and A. Gaset, *Synthetic Commun.*, **16**, 1739 (1986).

2) G. Aksnes, *Acta Chem. Scand.*, **15**, 438 (1961).

3) M. Wada and A. Tsuboi, *J. Chem. Soc., Perkin Trans. 1*, **1987**, 151.

4) G. Wittig, H.-D. Weigmann, and M. Schlosser, *Chem. Ber.*, **94**, 676 (1961); M. Schlosser and K. F. Christmann, *Justus Liebigs Ann. Chem.*, **708**, 1 (1967); J. M. McIntosh and R. S. Stevensz, *Can. J. Chem.*, **55**, 2442 (1977).

5) G. Wittig and W. Haag, *Chem. Ber.*, **88**, 1654 (1955).

6) K. Okuma, S. Nakamura, and H. Ohta, *Heterocycles*, **26**, 2343 (1987).

7) E. M. Richards and J. C. Tebby, *J. Chem. Soc., C*, **1971**, 1059.

8) E. J. Corey and H. Yamamoto, *J. Am. Chem. Soc.*, **92**, 226 (1970); E. J. Corey and H. Yamamoto, *ibid.*, **92**, 6636 (1970).

9) E. J. Corey and J. Kang, *J. Am. Chem. Soc.*, **104**, 4724 (1982).

10) B. Schaub, G. Blaser, and M. Schlosser, *Tetrahedron Lett.*, **26**, 307 (1985); M. Schlosser, H. B. Tuong, and B. Schaub, *ibid.*, **26**, 311 (1985); B. E. Maryanoff, A. B. Reiz, and B. A. Duhl-Emswiller, *J. Am. Chem. Soc.*, **107**, 217 (1985).

11) A. D. Buss, N. Greeves, D. Levin, P. Wallace, and S. Warren, *Tetrahedron Lett.*, **25**, 357 (1984) and references cited there in.

12) Formerly, compound **10** was prepared from methyldiphenylphosphine oxide, butyllithium, and ethylene oxide,[a] or by the reaction of diphenylphosphine oxide with 3-chloro-1-propanol in the presence of KOH.[b] a) I. Fleming and C. D. Floyd, *J. Chem. Soc., Perkin Trans. 1*, **1981**, 969; b) E. N. Tsvetkov, N. A. Bondarenko, I. G. Malakhova, and M. I. Kabachinik, *Synthesis*, **1986**, 198.

13) G. W. J. Fleet and T. K. M. Shing, *Tetrahedron Lett.*, **24**, 3657 (1983); R. Zambani and J. Rokath, *Tetrahedron Lett.*, **23**, 4751 (1982); Teikoku Chemical Industry Co., Japan Kokai Tokkyo Koho, J. Patent 8345230 (*Chem. Abstr.*, **99**, 123124v, (1983).

Withacoagin, a New Withanolide from *Withania coagulans* Roots

Partha NEOGI, Masao KAWAI, Yasuo BUTSUGAN,* Yuji MORI,† and Makoto SUZUKI†
Department of Applied Chemistry, Nagoya Institute of Technology, Showa-ku, Nagoya 466
†Faculty of Pharmacy, Meijo University, Tenpaku-ku, Nagoya 468
(Received July 14, 1988)

Synopsis. The structure of withacoagin, a new withanolide isolated from *Withania coagulans*, has been elucidated as (20*R*,22*R*)-5α,20-dihydroxy-1-oxowitha-2,6,24-trienolide by spectral analysis and chemical transformation to a known compound. This is the second report of a Δ^6-withanolide. Isolation of three known compounds, (20*R*,22*R*)-6α,7α-epoxy-5α,20-dihydroxy-1-oxowitha-2,24-dienolide, (20*S*, 22*R*)-6α,7α-epoxy-5α-hydroxy-1-oxowitha-2,24-dienolide, and withaferin A, are also reported.

Withanolides[1] are a group of ergostanolides, generally having a δ-lactone in the side chain and a 2-en-1-one system in the A ring. These are exclusive to the family *Solanaceae*[2-6] and withaferin A,[1] the first withanolide, was isolated from *Withania somnifera* L. Dun. Withanolides are interesting because they show antitumorous[2,5] antibacterial,[7] antiinflammatory,[8] and immunosupressive[9] activities.

W. coagulans Dunal, which grows widely in India and West Pakistan, is used in the Indian indigenous system of medicine[10] and fruits of the plant have milk coagulating properties.[11] In addition to a biogenetically important precursor of withanolides,[12] four withanolides from the roots,[13] two from the leaves,[14] and two from the fruits[12,15] of this plant were reported. Here we will describe the isolation from the roots of *W. coagulans* and the structure elucidation of a new withanolide (**1**), named withacoagin, as well as the isolation and characterization of three known withanolides.

Dried roots of *W. coagulans* were defatted with hexane and extracted with methanol. The extract was subjected to silica gel column chromatography and the major component **2** was characterized as the known (20*R*,22*R*)-6α,7α-epoxy-5α,20-dihydroxy-1-oxowitha-2,24-dienolide[13a] by ^{1}H and ^{13}C NMR spectra (Tables 1 and 2).

Withacoagin (**1**), also isolated from the methanol extract as colorless crystals (mp 230—232 °C), showed a molecular peak at *m/z* 454. The M^+-H_2O peak in the high-resolution mass spectrum established its molecular formula as $C_{28}H_{38}O_5$. The IR spectrum showed

Table 1. ^{1}H NMR Data of Compounds **1**, **2**, and **3** in $CDCl_3$ Solution (Chemical shift in δ and multiplicity with coupling constants in Hz in parentheses)

Assignment	1	2	3
2	5.89, dd (10.0, 2.4)	5.85, dd (10.1, 2.3)	5.85, dd (10.1, 2.7)
3	6.58, ddd (10.0, 5.2, 2.2)	6.59, ddd (10.1, 5.1, 2.2)	6.59, ddd (10.1, 5.1, 2.2)
4α	2.36, dd (19.0, 5.2)	2.53, dd (19.0, 5.1)	2.53, dd (19.0, 5.1)
4β	2.63, dt (19.0, ca. 2.3)	2.68, br d (19.0)	2.69, br d (19.0)
6	5.73, dd (9.9, 1.7)	3.04, d (3.7)	3.04, d (3.7)
7	5.57, dd (9.9, 2.7)	3.32, m	3.31, m
18	0.95, s	0.96, s	0.77s
19	1.20, s	1.18, s	1.18s
21	1.32, s	1.32, s	1.02, d (6.6)
22	4.21, dd (13.3, 3.5)	4.21, dd (13.3, 3.5)	4.38, dt (13.2, 3.4)
23α	2.10, dd (16.8, 3.5)	2.12, dd (17.1, 3.0)	1.97 (overlapped)
23β	2.40, br t (ca. 15)	2.39, br t (ca. 15)	2.45, br t (ca. 15)
27	1.89, s	1.89, s	1.89, s
28	1.95, s	1.95, s	1.95, s

Table 2. ^{13}C NMR Data (δ) of Compounds **1**, **2**, and **3** in $CDCl_3$ Solution[a,b]

Assignment	1	2	3	Assignment	1	2	3
1	203.8	203.1	203.1	15	23.6	23.3	23.6
2	129.6[a1]	129.1	129.1	16	21.9	21.9[a2]	27.3
3	140.4	139.6	139.6	17	54.7[a3]	54.6	51.5[a2]
4	36.5	36.8	36.8	18	13.8	13.8	12.1
5	74.9[a2]	73.3	73.3	19	14.6	14.8	14.7
6	133.3	56.4	56.4	20	75.2[a2]	75.1	39.0
7	129.4[a1]	57.3	57.3	21	21.0	21.2	13.3
8	37.5	35.2[a1]	35.8[a1]	22	81.0	81.0	78.3
9	41.5	35.7[a1]	35.6[a1]	23	31.7	31.7	29.7
10	51.4	51.1	51.0	24	148.7	148.8	149.1
11	22.4	21.9[a2]	21.9	25	122.1	122.1	122.0
12	40.7	40.5	39.9	26	166.0	166.0	167.0
13	44.1	43.9	43.5	27	12.5	12.5	12.5
14	54.3[a3]	50.2	51.9[a2]	28	20.5	20.5	20.5

a) Superscripts a1, a2, and a3 refer to interchangeable data. b) Assignments are based on Ref. 23.

absorption bands for hydroxyl (3435 cm^{-1}), cyclohexenone (1672 cm^{-1}), and α,β-unsaturated δ-lactone (1716 cm^{-1}). The ultraviolet spectrum showed absorption maximum at 225 nm (ε 12000) characteristic of summation of absorptions of the conjugated enone and the conjugated δ-lactone chromophores[16] which are commonly present in withanolides. The fragment ion peaks at m/z 169 and 125 in its mass spectrum suggested that **1** is a 20-hydroxywithanolide.[17]

The ^1H NMR spectrum of **1** showed three singlets at δ 0.95, 1.20, and 1.32 which were assigned to C(18)-, C(19)-, and C(21)-methyl groups, respectively. The chemical shift of the deshielded C(21)-methyl singlet and the appearance of the C(22)-methine signal (δ 4.21) as a double doublet (J=13.3 and 3.5 Hz) also supported the presence of an OH group at C(20)-position. The two vinylic methyl singlets at δ 1.89 and 1.95 were assigned to the methyl groups attached to the conjugated lactone group in the side chain. The ^1H signals assignable to the hydrogens at C(18), C(21), C(22), C(27), and C(28) of **1** resembled closely to those of **2** as shown in Table 1, which suggested the identity of substitution pattern of the D ring and the side chain in **1** and **2**. Dependence of the chemical shifts of the methyl peaks upon the stereochemistry of the hydroxyl group at C(20) was already documented.[18]

The α- and β-hydrogen signals of the conjugated enone system at the A ring were observed at δ 5.89 (dd, J=10.0 and 2.4 Hz) and 6.58 (ddd, J=10.0, 5.2, and 2.2 Hz), respectively. The allylic methylene signals at δ 2.36 (dd, J=19.0 and 5.2 Hz) and 2.63 (dt, J=19.0 and 2.3 Hz) indicated that C(4) is unsubstituted and that C(5) bears no hydrogen atom. Thus, hydroxyl group can be located at the C(5)-position. Unlike the common withanolides it showed an additional set of mutually coupled olefinic proton signals at δ 5.57 (dd, J=9.9 and 2.7 Hz) and 5.73 (dd, J=9.9 and 1.7 Hz) indicating the presence of a cis-disubstituted double bond. The cis-double bond can be located either at C(6)-C(7), at C(11)-C(12), or at C(15)-C(16) position. The comparison of ^{13}C NMR spectral data of **1** and **2** given in Table 2 revealed their close resemblance except the resonances assignable to C(6) and C(7). Thus, the Δ^6-structure has been assigned to **1**. All of the 28 carbon resonance signals of **1** are consistent with the 5,20-dihydroxy-Δ^6-withanolide structure.

Stereochemistry of **1** was studied by the CD spectrum measured in methanol solution. A negative Cotton effect ([θ] −5200) at 333 nm observed for **1** revealed the trans juncture of the A/B ring moiety,[19] and a positive Cotton effect ([θ] +7000) at 250 nm suggested the R-configuration at C(22).[20]

Withacoagin (**1**) has been found to differ from **2** only at the moiety of C(6) and C(7), i.e., while a double bond is present in the former, the latter possesses an α-epoxide group in the corresponding position. So a chemical transformation of **1** to **2** was then attempted to prove the structure of **1**. Epoxidation of **1** with m-choloroperbenzoic acid yielded an epoxide which was identical in all respects with the naturally occuring **2**. Thus, structure of **1** was established unambiguously as (20R,22R)-5α,20-dihydroxy-1-oxowitha-2,6,24-trienolide. This compound constitutes the second example of a Δ^6-withanolide.[17]

The third compound (**3**) isolated from the roots, mp 254—255 °C, was found to be isomeric with **1** and showed close resemblance in spectral properties to its congener **2**. Detailed analysis of the ^1H and ^{13}C NMR spectral data revealed that **3** is a 20-dehydroxy analog of **2**. The compound **3**, namely (20S,22R)-6α,7α-epoxy-5α-hydroxy-1-oxowitha-2,24-dienolide, is known as lycium substance B, isolated earlier from *Lycium chinense* and *Datura* species,[21,22] but this is the first report of the isolation of **3** from a *Withania*

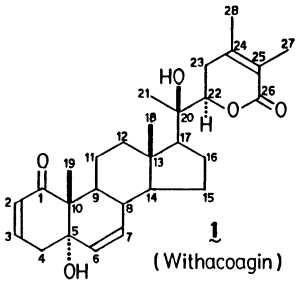

1 (Withacoagin)

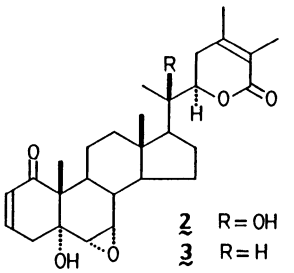

2 R=OH
3 R=H

species. The study of ^{13}C NMR spectra with DEPT method indicated that the assignments of C(10) and C(17) resonances in the original paper[21a] should be interchanged as shown in Table 2.

In addition to the three withanolides **1**, **2**, and **3** described above, withaferin A was also isolated, though only in minor quantity, from the extracts of *W. coagulans* and was characterized by ^1H NMR spectroscopy.

Withanolides are significant for displaying antitumour activity. Withacoagin (**1**), compound **2**, and lycium substance B (**3**) were studied for their cytotoxicity against HeLa cells. All the three compounds, however, did not show significant antitumour activity, i.e., inhibitory concentrations of **1**, **2**, and **3** to the proliferation of HeLa cells were 84, 87, and >100 $\mu g\,ml^{-1}$, respectively. While these impotent withanolides contain a 5α-hydroxyl and/or a 6α,7α-epoxy group, the cytotoxic withanolides possess a 5α,6β-epoxy group.[2,5] In the case of physalins, cytotoxic steroids from *Physalis* plants having highly oxygenated ergostane skeleton, it was proposed that α-hydroxyl and α-epoxy groups at ring A or ring B markedly decrease the cytotoxicity and that β-hydroxyl and β-epoxy groups increase or do not affect the activity.[24]

Experimental

Melting points are uncorrected. Optical rotation was measured using a JASCO DIP-4 digital polarimeter. IR

spectra were recorded as KBr discs on a JASCO IRA-1 spectrometer and FT-IR on a JEOL JIR-100 instrument using a diffuse reflectance accessory. NMR spectra were run on a JEOL JNM-GX 400 spectrometer at 400 MHz for ^{1}H NMR and at 100 MHz for ^{13}C NMR with $CDCl_3$ solutions. UV, CD, and mass spectra were measured on HITACHI 124, JASCO J-40C, and HITACHI M 2000 spectrometers, respectively. Column chromatography was performed using SiO_2 (Merck, Silicagel 60, 7734). Precoated SiO_2 plates (Merck, Silica Gel 60 F_{254}) were used for TLC analysis and R_f values with $CHCl_3$-MeOH (19 : 1) system are given.

Plant Material. The roots of *W. coagulans* Dunal were purchased from United Chemicals and Allied Products, Calcutta, India and a specimen sample is being preserved.

Isolation. The air-dried roots (3.0 kg) were powdered, defatted with hexane, and extracted twice with cold MeOH. The MeOH extract was chromatographed over SiO_2 and the column was eluted with hexane-AcOEt (1 : 0, 3 : 1, 1 : 1, 1 : 2, and 0 : 1). The eluates with hexane-AcOEt (1 : 1 and 1 : 2) were pooled together and subjected to repeated chromatography using $CHCl_3$-MeOH as eluent to yield **1** (62 mg), **2** (650 mg), **3** (40 mg), and withaferin A (43 mg).

Withacoagin (1). Colorless needles from $CHCl_3$; mp 230—232 °C; R_f 0.29; $[\alpha]_D^{24}$ +114° (*c* 0.19, $CHCl_3$); IR (KBr) 3435, 1716, and 1672 cm^{-1}; UV (MeOH) 225 nm (ε 12000); MS (70 eV) *m/z* (rel intensity) 454 (M+; 0.2), 436 (M^+-H_2O; 5), 421 (2), 311 (57), 269 (15), 171 (25), 169 (16), 148 (16), 134 (18), 125 (100), 85 (15), and 69 (12); CD (MeOH) $[\theta]_{333}$ −5200, $[\theta]_{268}$ 0, and $[\theta]_{251}$ +7000. Found: *m/z* 436.2576. Calcd for $C_{28}H_{36}O_4$: M−H_2O, 436.2611.

Compound 2. Colorless needles from $CHCl_3$; mp 282—285 °C (decomp) (lit,[13] mp 282—284 °C); R_f 0.36.

Compound 3. Colorless plates from $CHCl_3$; mp 252—254 °C (lit,[21b] mp 260—65 °C); R_f 0.55.

Withaferin A. Colorless needles from $CHCl_3$; mp 241—243 °C (lit,[1] mp 243—245 °C); R_f 0.35.

Epoxidation of 1. To a solution of **1** (10 mg) in $CHCl_3$ was added *m*-chloroperbenzoic acid (10 mg) and stirred at room temperature for 26 h. Usual workup and SiO_2 column chromatography ($CHCl_3$) yielded a solid (7.6 mg), which crystallized from $CHCl_3$ as fine needles, mp 286—289 °C; FT-IR (KBr) 3456, 3429, 1716, 1683, 1373, and 1344 cm^{-1}. The FT-IR spectrum of this epoxide was found to be indistinguishable with that of **2**.

The authors are grateful to Mr. Jun'ichi Ohya of Pharmaceuticals Laboratory, Mitsubishi Chemical Industries Ltd. for the assay of cytotoxic activity and to Instrument Center, Nagoya Institute of Technology for mass spectra and FT-IR measurements.

References

1) D. Lavie, S. Greenfield, and E. Glotter, *J. Chem. Soc. C*, **1966**, 1753.
2) E. Glotter, I. Kirson, D. Lavie, and A. Abraham, "Bio-Organic Chemistry," ed by E. E. van Tamelen (1978), Vol. 2, p. 57.
3) R. N. Tursunova, V. A. Maslennikova, and N. K. Abubakirov, *Khim. Prir. Soedin.*, **1977**, 147.
4) A. V. Kamernitskii, I. G. Reshetova, and V. A. Krivoruchko, *Khim. Prir. Soedin.*, **1977**, 156.
5) I. Kirson and E. Glotter, *J. Nat. Prod.*, **44**, 633 (1981).
6) O. E. Vasina, V. A. Maslennikova, and N. K. Abubakirov, *Khim. Prir. Soedin.*, **1986**, 243.
7) a) P. A. Kurup, *Curr. Sci.*, **25**, 57 (1956); b) S. Kohlmuenzer and J. Krupinska, *Diss. Pharm.*, **14**, 501 (1963).
8) R. D. Budhiraja, S. Sudhir, and K. N. Garg, *Planta Medica*, **50**, 134 (1984).
9) B. Shohat, I. Kirson, and D. Lavie, *Biomedicine*, **28**, 18 (1978).
10) K. R. Kirtikar and B. D. Basu, "Indian Medicinal Plants," 2nd ed, ed by L. M. Basu, Allahabad (1933), Vol. 3, p. 1777.
11) C. K. Atal and P. D. Sethi, *Ind. J. Pharm.*, **25**, 163 (1963).
12) V. Vande Velde, D. Lavie, R. D. Budhiraja, S. Sudhir, and K. N. Garg, *Phytochemistry*, **22**, 2253 (1983).
13) a) S. S. Subramanian, P. D. Sethi, E. Glotter, I. Kirson, and D. Lavie, *Phytochemistry*, **10**, 685 (1971); b) P. D. Sethi and S. S. Subramanian, *Ind. J. Pharm.*, **38**, 22 (1976).
14) S. S. Subramanian and P. D. Sethi, *Ind. J. Pharm.*, **33**, 40 (1971).
15) P. A. Ramaiah, D. Lavie, R. D. Budhiraja, S. Sudhir, and K. N. Garg, *Phytochemistry*, **23**, 143 (1984).
16) A. Bagchi, P. Neogi, M. Sahai, A. B. Ray, Y. Oshima, and H. Hikino, *Phytochemistry*, **23**, 853 (1984).
17) I. Kirson, E. Glotter, D. Lavie, and A. Abraham, *J. Chem. Soc. C*, **1971**, 2032.
18) A. Mijares, D. I. Cargill, J. A. Glasel, and S. Lieberman, *J. Org. Chem.*, **32**, 810 (1967).
19) R. Tschesche, M. Baumgarth, and P. Welzel, *Tetrahedron*, **24**, 5169 (1968).
20) R. Tschesche, H. Schwang, H. W. Fehlhaber, and G. Snatzke, *Tetrahedron*, **22**, 1129 (1966).
21) a) W. C. Evans, R. J. Grout, and M. L. K. Mensah, *Phytochemistry*, **23**, 1717 (1984); b) R. Hansel, J. T. Huang, and D. Rosenberg, *Arch. Pharm.*, **1975**, 653.
22) In Ref. 21a the structural formula of lycium substance B possesses *S*-configuration at C(20) while in the text the absolute configuration at C(20) is erroneously designated as *R*. Detailed comparison of the ^{13}C NMR spectral data of **3** and lycium substance B with those of the C(20)-unsubstituted compounds given in Ref. 23 indicated that the two compounds are identical with each other possessing *S*-configuration at C(20).
23) H. E. Gottlieb and I. Kirson, *Org. Magn. Reson.*, **16**, 20 (1981).
24) M. Kawai, T. Ogura, M. Nakanishi, Y. Butsugan, T. Matsuura, R. Nakashima, and L. R. Ramachandran, 16th International Symposium on the Chemistry of Natural Products, Kyoto, May 1988, Abstr., No. PC26.

Carbonyl Fluoride of Molybdenum (Synthesis and Structural Investigation)

Sudhindra N. MISRA* and K. VENKATASUBRAMANIAN†
Department of Chemistry, Bhavnagar University, Bhavnagar 364002, Gujarat, India
†Central Salt and Marine Chemicals Research Institute, Bhavnagar 364002, Gujarat, India
(Received October 19, 1987)

Synopsis. Difluorotricarbonylmolybdenum $MoF_2(CO)_3$ has been synthesized by selective fluorination of molybdenum carbonyl by xenon difluoride in perfluoro solvents as well as in anhydrous hydrogen fluoride. The titled compound was isolated as an orange yellow solid and its composition was established by elemental analysis. It decomposes very slowly at room temperature, but on heating at 100 °C it decomposes completely to yield molybdenum carbonyl, molybdenum fluoride oxide and molybdenum fluoride. The compound was structurally characterized using IR, mass spectral, and X-ray powder diffraction analysis.

Sharp in 1960 reported[1] the preparation of dicarbonyl octafluoro platinum $PtF_8(CO)_2$ and dicarbonyl trifluoro rhodium $RhF_3(CO)_2$, though the existence of these compounds is still considered to be doubtful. Haig[2] later proved that dicarbonyl octafluoro platinum was nothing but dibromo dicarbonyl platinum. O'Donnell and Phillips[3] reported the isolation of $MoF_4(CO)_4$ from the reaction mixture of molybdenum hexacarbonyl and molybdenum hexafluoride in Kel-F system. The product obtained by Donnell and Phillips,[3] was however, contaminated with molybdenum tetrafluoride oxide and unreacted molybdenum carbonyl as well molybdenum pentafluoride. The same authors[4] also studied the fluorination of rhenium carbonyl by rhenium fluoride and have isolated a compound which was formulated to be $ReF_3(CO)_3$. Bruce and coworkers[5] have made a systematic study of the reaction of rhenium carbonyl with rhenium hexafluoride in anhydrous hydrogen fluoride and have isolated two types of products: orange presin and green platelets in very high yield. O'Donnell and Phillips[6] later modified their version and have reported the formation of $ReF(CO)_5$ from the reaction between rhenium carbonyl and rhenium hexafluoride; further reaction of $ReF(CO)_5$ with XeF_2, they asserted yielded $ReF_3(CO)_3$. One of the authors (SNM) attempted the selective fluorination of rhenium carbonyl by xenon difluoride in perfluoro solvents and had isolated a complex having the composition $3[ReF_2(CO)_3]\cdot ReF_5$. Similar interesting results were obtained when iridium system was studied. In view of this we have tried to prepare difluorotricarbonyl molybdenum; isolation and structural characterization of this compound are reported in this paper.

Experimental

Reaction of Molybdenum Carbonyl and Xenon Difluoride in Inert Solvent Genetron/Perfluoro Hydrocarbons Like PP-3 (Perfluoro-1,3-dimethylcyclohexane) and PP-9 (Perfluoro-1-methyldecaline). The apparatus used is shown in Fig. 1. Hexacarbonyl molybdenum (0.360 g) was transferred to the reaction flask and it was connected to the vacuum line and evacuated. The glass vacuum line was evacuated to exclude moisture and air. Perfluoro hydrocarbons or genetron was condensed in the reaction flask by the help of Taps T_1, T_2, T_3. All the taps were closed and the delicate glass seal of xenon difluoride tube was broken by dropping nickel balls through a magnet and xenon difluoride was condensed in the reaction flasks maintained at liquid oxygen temperature. The reaction was exothermic and resulted in the isolation of orange solid. Excess solvent was then distilled out and the

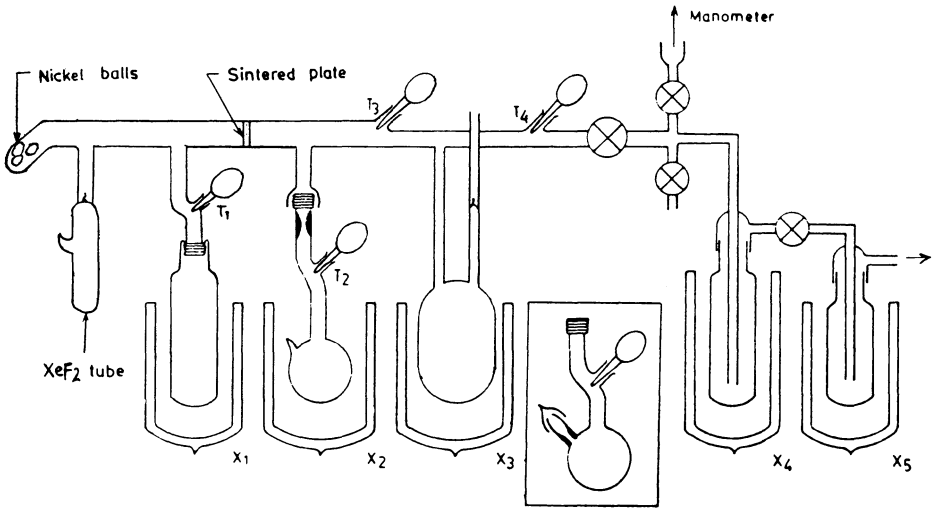

T_1—T_4: Rotoflow taps.
X_1—X_5: Dewar flask kept at liquid oxygen temperature.
Inset showing reaction vessel.

Fig. 1. An assembly used for the synthesis of carbonyl fluorides of molybdenum, tungsten, and rhenium.

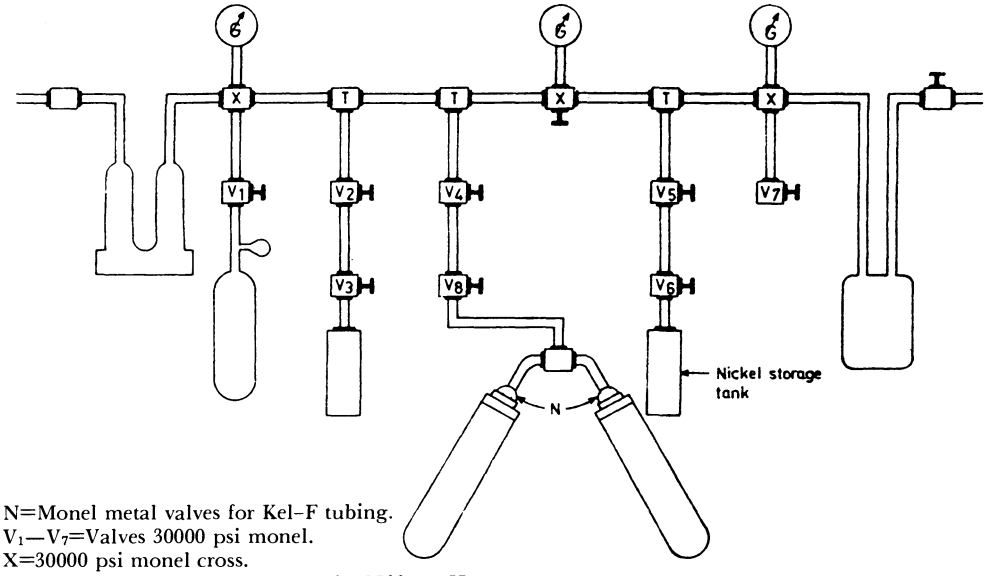

N=Monel metal valves for Kel-F tubing.
V_1—V_7=Valves 30000 psi monel.
X=30000 psi monel cross.
G=Welded monel bourdon gauge 0—1500 mmHg.

Fig. 2. Metal vacuum line with Kel-F reaction vessel.

system was pumped for overnight to remove unreacted xenon difluoride and other volatile contaminant. The reaction vessel was then disconnected from the line by sealing off its narrow end and immediately transferred to the inert box (yield 63%). Found: Mo, 43.6; C, 15.8; F, 18.4%. Calcd for $MoC_3O_3F_2$: Mo, 44.5; C, 16.3; F, 17.2%.

Reaction of Molybdenum Carbonyl and Xenon Difluoride in Stoichiometric Ratio 1:2 in Anhydrous Hydrogen Fluoride in Metal Vacuum Line. The reaction was carried out in assembly shown in the Fig 2. Both Kel-F tubes were first seasoned with hydrogen fluoride overnight. One of the tubes was removed from the line and placed in the dry box. A weighed amount of molybdenum carbonyl (0.4 g) was then transferred to the tube and the tube was connected to the vacuum line and evacuated. Anhydrous hydrogen difluoride (0.5 g) was condensed in another Kel-F tube which already had xenon difluoride. Both the tubes were then connected by opening the values in between them so that xenon difluoride hydrogen fluoride mixture slowly gets condensed in the tube containing molybdenum carbonyl. This assembly was left as such overnight. An orange crystalline solid separated out from the resulting orange solution. The solvent was then removed with the isolation of more and more solid. The product was purified by repeated washing with anhydrous hydrogen fluoride in the vacuum line. Found: Mo, 44.0; F, 18.0%. Calcd for $MoC_3O_3F_2$: Mo, 44.5; F, 17.2%.

Purification of Carbonyl Fluoro Molybdenum. Tricarbonyl difluoro molybdenum was taken in quartz tube B in the inert box and the assembly was evacuated by attaching it to the vacuum line. Tungsten hexafluoride was condensed at tube B by cooling it at liquid air temperature. After collecting sufficient amount of WF_6 the tube B was warmed up to the room temperature and left for two hours. The whole assembly was then rotated by 180° so that insoluble carbonyl fluoro molybdenum remained in the tube B while soluble fluorides of molybdenum collected in the tube A. Excess WF_6 was pumped back to the storage tube and the product in the tube B was dried in vacuo and characterized by analysis and IR.

Molybdenum in this complex was estimated by fusing with NaOH and Na_2O_2 mixture followed by precipitating metal gravimetrically as 8-hydroxy quinolinate. Fluorine in this compound was estimated by Seels' method.

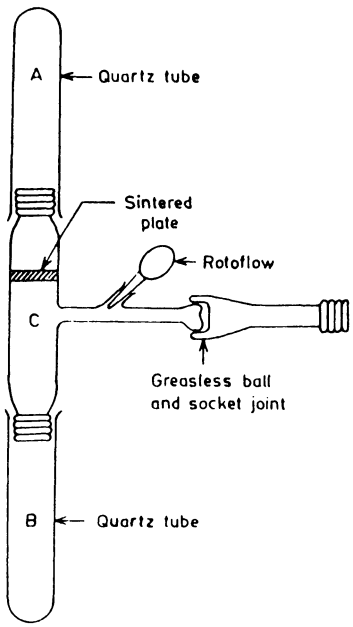

Fig. 3. Assembly used for the purification of cabonyl fluoride.

The molecular weight of carbonylfluoromolybdenum was determined in anhydrous hydrogen fluoride cryoscopically; this revealed a molecular complexity of around 4, thus indicating the molecules to be a tetramer, having the composition $[MoF_2(CO)_3]_4$.

Results and Discussion

O'Donnell and Phillips claimed to have isolated a polymeric dicarbonyltrifluoromolybdenum(III)[6] from the reaction mixture of molybdenum hexafluoride and hexacarbonyl molybdenum(0) in Kel-F apparatus. However, an attempt made by Edward and coworkers[8] to study the same reaction in glass apparatus resulted in the formation of fluorides of molybdenum and with

no evidence for the formation of any other compounds. O'Donell's samples were invariably contaminated with molybdenum pentafluoride and molybdenum tetrafluoride oxide.

Holloway and Szary[9] have made a systematic study of molybdenum carbonyl molydbenum pentafluoride system in genetron and in anhydrous hydrogen fluoride in the stoichiometric ratio of 1 : 1. They have observed that the reaction was slow in genetron but faster in anhydrous hydrogen fluoride. The product showed carbonyl stretching at 2145 (s) and 2060 (s) cm^{-1}. This compound was neither molybdenum pentafluoride nor carbonylfluoro complex, which is generally formed in xenon difluoride reaction. The resulting product was identical with the one isolated by O'Donnell; however, Holloway and Szary have proposed the following formulation for the resulting compound:

$[Mo(CO)_6]^+[MoF_6]$ or $[Mo(CO)_6]^+[Mo_2F_{11}]$ or $[Mo(CO)_5]^+[Mo_3F_{16}]$ or $[Mo(CO)_4F_2][Mo_2F_{11}]$

Elemental analyses of the products obtained in our reactions established the stoichiometry unequivocally as $Mo(CO)_3F_2$. The bands observed in the region 2200—1900 cm^{-1} in the infrared spectrum of carbonylfluoromolybdenum are typical of terminal carbonyl ligands [ν_{CO} at 2125(s), 2085(s), 2035(s), 1980(s), 1950(s)]. Since the carbonyl fluoride contains highly electronegative fluorine as substituent, it is not surprising that the carbonyl frequencies are also observed at higher wavenumber than the parent carbonyl complex. A comparison of the infrared spectra of the carbonylhalogeno complexes of molybdenum [$MoCl_2(CO)_3$ ν_{CO} at 2100(s), 2050(s), 1980(s), 1956(s), and $MoBr_2(CO)_3$ ν_{CO} at 2098(s), 2080(s), 2007(s), 1958(s)] confirm that these shift to lower wavenumber as the substituent changes from fluorine to bromine.

The Mo-F stretching frequencies were observed at 660 (w), 620 (w), 600 (w), and 560 (w) cm^{-1} indicating terminal and bridging fluoride ligands.

In the tricarbonyldifluoromolybdenum, the metal has d^4 configuration, which is quite susceptible to Jahn Teller distortion to one of the lower states, which will destroy the electronic degeneracy. When the distortion energy is comparable to the energy of the relevant vibration mode, no static distortion will be observed; however, certain abnormalities in the electronic spectra are expected as a result of electronic coupling.

The mass spectrum of tricarbonyl difluoromolybdenum indicated the presence of some fragments with dimeric units such as $[MoF_2(CO)_2]^+$, $[MoF_2(CO)_3]^+$, and $[MoF_4(CO)_4]^+$ along with several monomeric units, suggesting the molecular complexity to be more than two.

Our efforts to grow single crystals suitable for a detailed X-ray diffraction study were met with no success. However, a decent powder pattern of the substance could be recorded with Ni filtered Cu $K\alpha$ radiation. The analysis of this photograph showed that though the compound gives a pattern similar to that of tricarbonyl difluororuthenium, for which a detailed X-ray study has been carried out by Peacock et al.,[10] the intensities differ somewhat. The powder pattern could be indexed on an orthorhombic cell of dimensions a=11.221, b=10.742, and c=9.384 Å. The density calculated on the basis of 8 formula units per unit cell is 2.560 g cm^{-1}. The study on the ruthenium[10] compound also indicated that it exists as a tetrameric unit with fluorides in cis arrangement and in bridging positions.

A mechanistic study on the structural arrangement can be attempted on the following lines. The formation of 'cis' isomer from hexacarbonyl complex and fluorine can be tentatively explained by assuming simultaneous attack of hexacarbonyl complex by two atoms of the fluorine molecule. The alternate possibility of heterocyclic cleavage of fluorine molecule to give the nucleophilic fluorine would result in the preliminary introduction of the 'first fluorine'; entry of the second fluorine in the cis position would certainly be statistically favored and most probably electronically favoured too in view of the strong 'trans' effect of the carbon monoxide ligand.

One of the authors (S.N.M.) is extremely grateful to Prof. R. D. Peacock of Leicester University for providing a Senior Research Fellowship (1970—72) and his keen interest in this field.

References

1) D. W. A. Sharp, *Proc. Chem. Soc.*, **1960**, 317.
2) I. Haig, M. Sc. Thesis, Leicester University, Leicester, U. K. (1971).
3) T. A. O'Donnell and K. A. Phillips, *Inorg. Chem.*, **9**, 2611 (1970).
4) T. A. O'Donnell and K. A. Phillips, *Inorg. Chem.*, **11**, 2563 (1972).
5) D. M. Bruce, J. H. Holloway, and D. R. Russell, *Chem. Commun.*, **1973**, 321.
6) T. A. O'Donnell and K. A. Phillips, *Inorg. Chem.*, **12**, 1437 (1973).
7) S. N. Misra, *Indian J. Chem.*, **17A**, 101 (1979); *J. Sci. Ind. Res.*, **40**, 709 (1981).
8) A. Edward, R. D. Peacock, and R. W. H. Small, *J. Chem. Soc.*, **1962**, 4486.
9) J. H. Holloway and A. Szary, private communication.
10) R. D. W. Kemmitt, R. D. Peacock, and I. L. Wilson, *Chem. Commun.*, **1968**, 772.

Synthesis, Characterization, and the Thermal Decomposition of Copper(II) Bis(oxalato)cuprate(II) Dihydrate

Nidhuban Deb, Pradip K. Gogoi, and Narendra N. Dass*
Department of Chemistry, Dibrugarh University, Dibrugarh 786004 (Assam), India
(Received January 14, 1988)

Synopsis. Copper(II) bis(oxalato)cuprate(II) dihydrate, $Cu[Cu(C_2O_4)_2]\cdot 2H_2O$, has been synthesized and characterized by elemental analysis, magnetic moment measurement, and IR, electronic and ESR spectral studies. The low value of magnetic moment (1.57 B.M.) from spin-only value is indicative of the antiferromagnetic spin pairing between two paramagnetic copper(II) ions. The ESR spectrum of the powder showed a single signal with a g value of 2.1. The thermal decomposition in air and nitrogen media was investigated by TG, DTG, and DSC. Some of the decomposition products were identified by spectral, analytical and X-ray powder diffraction studies.

There has been a considerable interest in the study of oxalato complexes of transition metals[1-10] and much of the work have been periodically reviewed.[11] Binuclear complexes of Cu(II) with oxygen donor ligands involving metal-metal bonding have been reported.[12-16] However, studies on the compounds of the type $M[M(C_2O_4)_n]\cdot xH_2O$, [where M=same metal] are still rare.[17] The synthesis of copper(II) bis(oxalato)-cuprate(II) dihydrate, has not been reported so far. Here we are reporting the synthesis and characterization of copper(II) bis(oxalato)cuprate(II) dihydrate, $Cu[Cu(C_2O_4)_2]\cdot 2H_2O$. The thermal decomposition was also investigated and a tentative mechanism of thermal decomposition has been proposed.

Experimental

Materials. Copper(II) hydroxide, prepared from copper(II) chloride was made free from chloride. It was dissolved in glacial acetic acid and the mixture was heated on a steam bath. A light blue compound was precipitated by dropwise addition of a saturated solution of oxalic acid in glacial acetic acid. The compound was filtered off and purified by standard procedure.[17] The compound was insoluble in common organic solvents, however, decomposes in presence of acid or alkali. The water content was determined thermogravimetrically, while copper content was determined iodometrically. The percentages of carbon and hydrogen were estimated with Thomas CH analyzer. Found: C, 14.42; H, 1.13; Cu, 37.62; H_2O, 10.56%. Calcd for $C_4H_4O_{10}Cu_2$: C, 14.17; H, 1.19; Cu, 37.48; H_2O, 10.61%.

Measurements. IR spectra of the gases evolved were recorded by the reported method[17] and those of the complex and the intermediates were recorded on a Perkin-Elmer 781 spectrophotometer in CsI as well as in Nujol. The low frequency IR spectrum (600—100 cm^{-1}) of the complex was obtained using a Polytec FIR-30 instrument. Diffuse reflectance spectrum was recorded with a Shimadzu UV-240 spectrophotometer using $BaSO_4$ as the reference material. ESR spectrum at liquid nitrogen temperature was obtained on a Varian E-line century series ESR spectrometer with TCNE as marker. The magnetic moment of the complex was measured as described earlier.[17] The thermogravimetric (TG) and derivative thermogravimetric (DTG) curves were obtained in the range from room temperature to 800 °C with a Perkin-Elmer thermal analyzer at a heating rate of 10 °C min^{-1}. Differential scanning calorimetric (DSC) screen was performed using a Mettler TA 3000. The experiment was carried out in air purged at a rate of 30 cm^3 min^{-1} with a heating rate of 10 °C min^{-1}. X-Ray powder diffraction patterns of the decomposition products were taken using Cu $K\alpha$ radiation. The time of exposure was 4 h. The residues were identified by direct comparison with photograph of standard materials. For decomposition the complex was heated in a tube as described earlier.[17]

Results and Discussion

Spectral and Magnetic Studies. The room temperature magnetic moment of the compound was 1.57 B.M. The considerable lowering on μ_{eff} from the spin-only value may be attributed to extreme distortion or partial quenching of the spin moment of the copper ions[18] or may be due to the presence of intramolecular exchange interaction between adjacent copper atoms.[19] In the ESR spectrum of the powdered compound at liquid nitrogen temperature, a strong signal with a g value of 2.1 was obtained. From the above results a binuclear configuration of the compound with antiferromagnetic spin pairing between two paramagnetic copper(II) ions could be suggested.[12,20] Further, the electronic spectrum of the solid sample (Fig. 1) showed bands around 13260 sh, 15500, 20200, 33100, and 40800 cm^{-1}, of which the bands around 13000—20000 cm^{-1} are d-d transitions. The shoulder at 13260 cm^{-1} and the band at 15500 cm^{-1} are tentatively assigned to $\delta\rightarrow\sigma(d_{x^2-y^2}\rightarrow d_{z^2})$ and $\delta\rightarrow\pi$ or $\delta'[d_{x^2-y^2}\rightarrow d_{zx}, d_{yz}, \text{or } d_{xy}]$ respectively.[16] The intense bands observed at higher frequencies are L→M or M→L charge transfer, of which the band at 33100 cm^{-1} could be possibly due to transition involving the Cu-Cu bond.[21] The two

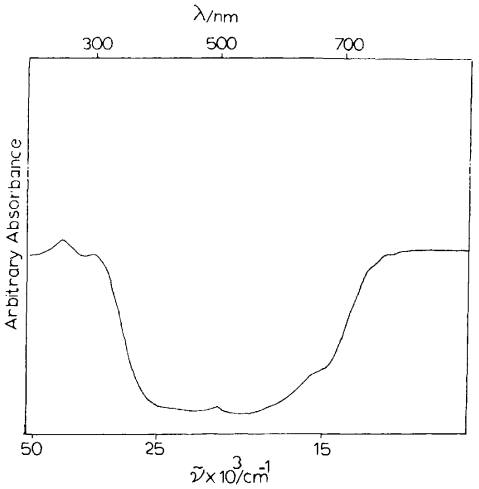

Fig. 1. Reflectance spectrum of $Cu[Cu(C_2O_4)_2]\cdot 2H_2O$.

copper atoms may be linked by either a δ bond (by lateral overlap of two $d_{x^2-y^2}$ orbitals with their lobes parallel) or σ bond due to end to end on overlap of d_{z^2} orbitals. In view of the g value of 2.1 and on the basis of valance bond and molecular orbital arguments[12,16] the nature of the Cu-Cu covalent bond is likely to be δ-type. The chelating character of the oxalato group was identified by IR spectroscopy[22] as shown in Table 1. In the farinfrared region a sharp peak at 188 cm^{-1} is due to Cu-Cu stretching vibrations[23] which further substantiated the presence of metal-metal bond.

TG, DTG, and DSC Studies. In the TG plot of the complex in nitrogen and air media (Fig. 2) the respective weight losses of 5.2% (at 292 °C) and 5% (at 298 °C) indicated the removal of one molecule of water. The calculated mass loss for this is 5.3%. Removal of this water at high temperature is suggestive of coordination with the metal ion with possible hydrogen bonding with the chelated oxalato group. Beyond 292 °C in nitrogen a steep slope up to 322 °C with a weight loss (Found 56.79%; Calcd 57.80%) indicated the formation of a mixture of Cu and CuO. The formation of a mixture of Cu and CuC_2O_4 as an unstable intermediate cannot be ruled out as CuC_2O_4 decomposes immediately to CuO at about 310 °C.[1,8] Corresponding to this overall decomposition a sharp peak ranging between 246—322 °C with a ΔT_{max} of 309 °C was obtained in DTG curve. The activation energy and order of reaction of the overall decomposition stage were computed on the basis of the Freeman and Carroll's equation[24] and were found to be 348.14 kJ mol^{-1} and 1.5 respectively. The rise in the TG curve beyond 322 °C and stabilization around 483 °C with a net gain of weight by 3.79% and overall weight loss (Found 53%; Calcd 53.08%) indicated the formation of a probable stable compound like 2CuO. The gain in weight may be due to the presence of carbon formed during disproportionation of some CO(g) to C and CO_2(g), due to catalytic activity of CuO.[25] The reduction of some amount of CuO to elementary copper by CO(g) cannot be ruled out.[7] In air medium beyond 298 °C a steep slope up to 310 °C in TG curve with a weight loss 84.75% apparently indicated the formation of metallic copper. This was confirmed as the positions and number of lines in the X-ray diffraction powder photograph exactly coincide with that obtained from pure copper wire. The activation energy and order of decomposition were calculated to be 503.63 kJ mol^{-1} and 1 (unity) respectively. In the DSC curve recorded in air (Fig. 3), the presence of two overlapping exotherm indicated that the complex decomposes via two stages. The first exotherm at 260.3—312 °C with a ΔT_{max} of 295.7 °C with activation energy and enthalpy change 252.79±10.38 and 155.09 kJ mol^{-1} respectively. The second exotherm at 312—329 °C with a ΔT_{max} of 323.4 °C with respective activation energy and enthalpy change 412.51±16.64 and 99.17 kJ mol^{-1}. The intermediate compound formed corresponding to first exotherm could not be identified by the temperature arrest technique as it was immediately decomposed to subsequent product and is suggestive of the removal of coordinated water molecule. The weight loss (Found 53%; Calcd 53.08%) after complete decomposition indicated the compound to be 2CuO. The residue gave an analysis, Cu, 80.15% compared to the calculated value of 79.88%. The X-ray

Table 1. Selected Bands in the Infrared Spectrum of the Complex $Cu[Cu(C_2O_4)_2]\cdot 2H_2O$

IR band/cm^{-1}	Assignment
3200—3660b	ν_{sy}(O-H)+ν_{asy}(O-H)
1610s	δ_{sy}(H-O-H)
1500—1750b	ν_{asy}(C=O)
ca. 1390m	ν(C-O) and/or ν(C-C)
ca. 1350s, ca.1305s, and ca. 1265m	ν(C-O) and/or δ(O-C=O)
810s	ν(Cu-O) and/or δ(O-C=O)
470—500b (split into two peeks)	ring deformation and/or δ(O-C=O)
365s	δ(O-C=O)
317m	out of plane bending
188 (sharp)	ν(Cu-Cu)

b=broad, m=medium, and s=strong.

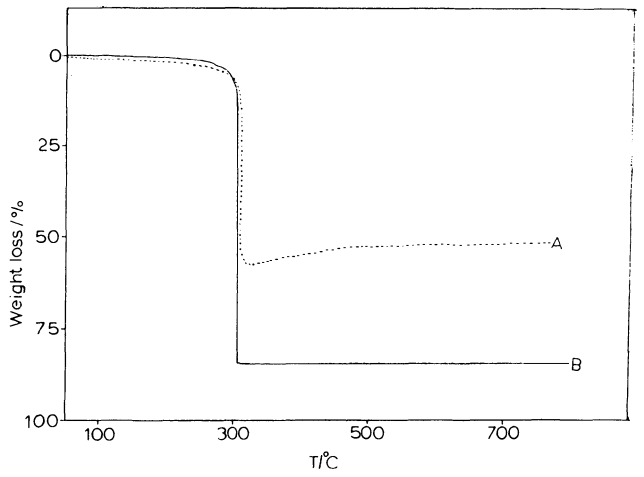

Fig. 2. A: TG curve of $Cu[Cu(C_2O_4)_2]\cdot 2H_2O$ in a flowing nitrogen atmosphere. B: TG curve of $Cu[Cu(C_2O_4)_2]\cdot 2H_2O$ in a flowing air atmosphere.

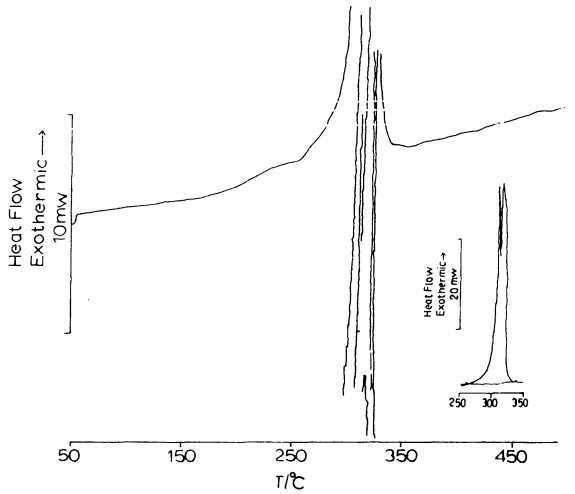

Fig. 3. DSC curve of $Cu[Cu(C_2O_4)_2]\cdot 2H_2O$ in a flowing air atmosphere.

powder diffraction photograph is similar to that of pure CuO which confirmed the black residue to be 2CuO. In the farinfrared absorption spectrum of the residue the presence of band around 600, 540, 410, and 310 (strong) cm^{-1} further substantiated the compound to be 2CuO.[26] In comparison with TG in air discussed above, the corresponding weight loss in DSC is 53% instead of 84.75% and apparently this could be due to the escape of CO(g) through the pan hole before reducing CuO. X-Ray powder diffraction analysis of the product obtained on heating beyond 310 °C in a closed vessel suggested the reduction of CuO to metallic copper.[27] The infrared spectral analysis[22] of the gaseous products confirmed the evaluation of both carbon monoxide and carbon dioxide.

On the basis of above results the following thermal decomposition processes in nitrogen medium may be suggested.

$$Cu[Cu(C_2O_4)_2]\cdot 2H_2O \xrightarrow{\text{ca. } 292\,^\circ C} Cu[Cu(C_2O_4)_2]\cdot H_2O$$

$$+ H_2O(v) \xrightarrow{322\,^\circ C} Cu + CuO + H_2O(v) + CO_2(g)$$

$$+ CO(g) \xrightarrow{\text{ca. } 483\,^\circ C} 2CuO \text{ (stable)}.$$

We thank the RSIC, CDRI, Lucknow for C, H analysis and IR spectra, RSIC, IIT, Madras for low frequency IR spectra, RSIC, IIT, Bombay for the ESR spectra, RSIC, Nagpur University for TG and DTG and Dr. S. K. Datta of Forensic Science Laboratory, Gauhati, Assam for DSC.

References

1) D. Dollimore, D. L. Griffiths, and D. Nicholson, *J. Chem. Soc.*, **1963**, 2617.
2) D. Dollimore and D. Nicholson, *J. Chem. Soc.*, **1962**, 960.
3) D. Dollimore, J. Dollimore, and J. Little, *J. Chem Soc. A*, **1969**, 2946.
4) K. Nagase, K. Sato, and N. Tanaka, *Bull. Chem. Soc. Jpn.*, **48**, 439 (1975).
5) K. Nagase, K. Sato, and N. Tanaka, *Bull. Chem. Soc. Jpn.*, **48**, 868 (1975).
6) K. Nagase, *Bull. Chem. Soc. Jpn.*, **46**, 144 (1973).
7) D. Krug and W. Haedrich, Experientia Suppl, 37 (Angew. Chem. Thermodyn. Thermoanal), (1979) p. 54.
8) D. Broadbent, D. Dollimore, and J. Dollimore, "Thermal Analysis," Academic Press, New York (1969), Vol. 2, p. 739.
9) M. G. Usha, M. Subba Rao, and T. R. N. Kutty, *Indian J. Chem.*, **20A**, 319 (1981).
10) S. K. Awasthi, K. L. Chawla, and D. M. Chackraburthy, *J. Inorg. Nucl. Chem.*, **35**, 3805 (1973).
11) K. V. Krishnamurty and G. M. Harris, *Chem. Rev.*, **61**, 213 (1961).
12) B. N. Figgis and R. L. Martin, *J. Chem. Soc.*, **1956**, 3837.
13) A. E. Hansen and C. J. Ballhausen, *Trans. Faraday Soc.*, **61**, 631 (1965).
14) L. S. Forster and C. J. Ballhausen, *Acta Chem. Scand.*, **16**, 1385 (1962).
15) I. G. Ross, *Trans. Faraday Soc.*, **55**, 1057 (1959).
16) M. L. Tonnet, S. Yamada, and I. G. Ross, *Trans. Faraday Soc.*, **60**, 840 (1964).
17) T. K. Sanyal and N. N. Dass, *J. Inorg. Nucl. Chem.*, **42**, 811 (1980).
18) J. Lewis, Y. C. Lin, L. K. Royston, and R. C. Thomson, *J. Chem. Soc*, **1965**, 6464.
19) R. L. Martin and A. Whitley, *J. Chem. Soc.*, **1958**, 1394.
20) P. S. Zacharias and N. K. Reddy, *Indian J. Chem.*, **25A**, 243 (1986).
21) M. G. B. Drew, A. Lavery, V. Mckee, and S. M. Nelson, *J. Chem. Soc.*, **1985**, 1771.
22) K. Nakamoto, "Infrared Spectra of Inorganic and Coordination Compounds," 2nd ed, Wiley-Interscience, New York (1969), pp. 83, 89, 219, 245.
23) J. D. Corbett, *Inorg. Chem.*, **1**, 700 (1962).
24) E. S. Freeman and B. Carroll, *J. Phys. Chem.*, **62**, 394 (1958).
25) P. K. Gallagher, "Thermal Analysis, Comparative Studies on Materials," ed by H. Kambe and P. D. Garn, Halsted Press, Tokyo (1974), p. 23.
26) F. F. Bentley, L. D. Smithson, and A. L. Rozek, "Infrared Spectra and Characteristic Frequencies 700—300 cm^{-1}," Wiley-Interscience, New York (1968), p. 103.
27) N. N. Dass, P. K. Gogoi, and N. Deb, "Proceedings of the National Symposium on Unusual Valency States in Coordination Compounds," Bhabha Atomic Research Centre, Bombay, India, 12 Nov. 1987.

Organophosphorus Analogues and Derivatives of the Natural L-Amino Carboxylic Acids and Peptides. V.[1] Synthesis of Analogues of Plumbemycin A

Ivan A. NATCHEV
Research Centre Konstrukcionni Polymeri, 5-003 Gara Iskar, 1528 Sofia, Bulgaria
(Received October 3, 1987)

Synopsis. Analogues of antibiotic Plumbemycin A were synthesized by an exchange of D-norvaline residue with 1,2,3,6-tetrahydro-1,2-azaphosphorine and by coupling of alanylaspartic acid with N-terminal norvaline. The protecting groups were released by highly selective enzyme hydrolysis.

With a view to studying the relationship between the structure and the physiological activity, we wish to report some of the chemical modifications of the tripeptide antibiotic Plumbemycin A.[2,3]

As a starting substance for the first modification, we have selected (*R*)-2-ethoxy-1,2,3,6-tetrahydro-1,2-azaphosphorine-6-carboxylic acid 2-oxide (**1**) [H-Phos(OEt)-OH] recently synthesized by us. The condensation with H-Ala-Asp(OEt)-OEt (**2**)[4] was carried out by the usual DCC method for peptide synthesis to give H-D-Phos(OEt)-Ala-Asp(OEt)-OEt in a yield of 72—75%.

As the tetrahydro-1,2-azaphosphorine ring is very unstable under the conditions of both base- and acid-catalyzed hydrolysis, we have chosen the method[5] of enzyme-catalyzed hydrolysis of substrates containing organophosphorus groups.

It was found that the enzyme phosphodiesterase I hydrolyzes only the ethoxyphosphinylidene group of **3** to give the corresponding free cyclic derivative **4** quantitatively.

The hydrolysis of the *O*-protected groups of **4** can not be carried out by conventional methods of base- or acid-hydrolysis,because the 1,2-azaphosphorine ring is easily hydrolyzed in the bond PO-NH. The ester hydrolysis of **4** with alkaline mesintericopeptidase was applied successfully to give the corresponding free tripeptide **5**.

When the treatment of **5** with α-chymotrypsin is carried out, only the hydrolysis of the peptide bond in Ala-Asp sequence took place to give H-D-Phos(OH)-Ala-OH (**6**) (see Scheme 1) due to the D-tetrahydro-1,2-azaphosphorine ring. It is worthwhile noting that the catalytic activity of phosphodiesterase I is quite independent on the optical form of 2-ethoxy-1,2,3,6-tetrahydro-1,2-azaphosphorine 2-oxide.

An analogous scheme was applied for the synthesis of the other possible modified peptide with C-terminal Ala residue. The condensation of **1** with H-Asp(OEt)-Ala-OEt (**7**)[6] was carried out by the DCC method described above to give the expected tripeptide **8** obtained in ca. 75% yield. The subsequent enzyme-catalyzed hydrolysis of the ethoxyphosphinylidene group of **8** with phosphodiesterase I was similarly worked up under the above conditions to give the corresponding tripeptide **9**. The two ethylesters of **9** were hydrolyzed with alkaline mesintericopeptidase to give the free tripeptide **10**.

Following Scheme 1, we subjected **10** to a treatment similar to that employed for α-chymotripsin. As was expected, enzyme-substrate interaction took place to give H-D-Phos(OH)-Asp-OH (**11**) in about 90% yield (Scheme 2).

The marked difference in the case of hydrolysis of the peptide bond on the one hand and the 1,2,3,6-tetrahydro-1,2-azaphosphorine ring on the ether makes it possible to be "soft" base-catalyzed hydrolysis and to obtain Plumbemycin A analogues, which L-amino acids were arranged each other. However, heating **5** and **10** in 0.1 M NaOH (1 M=1 mol dm^{-3}), the

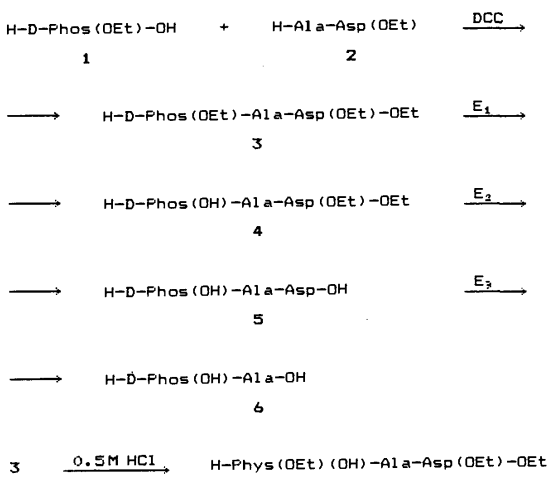

Scheme 1.

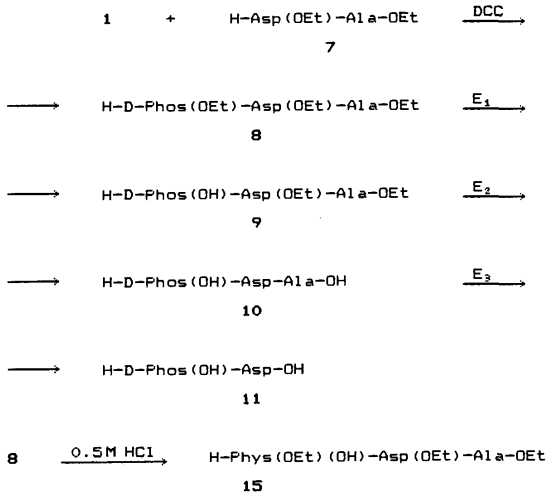

Scheme 2.

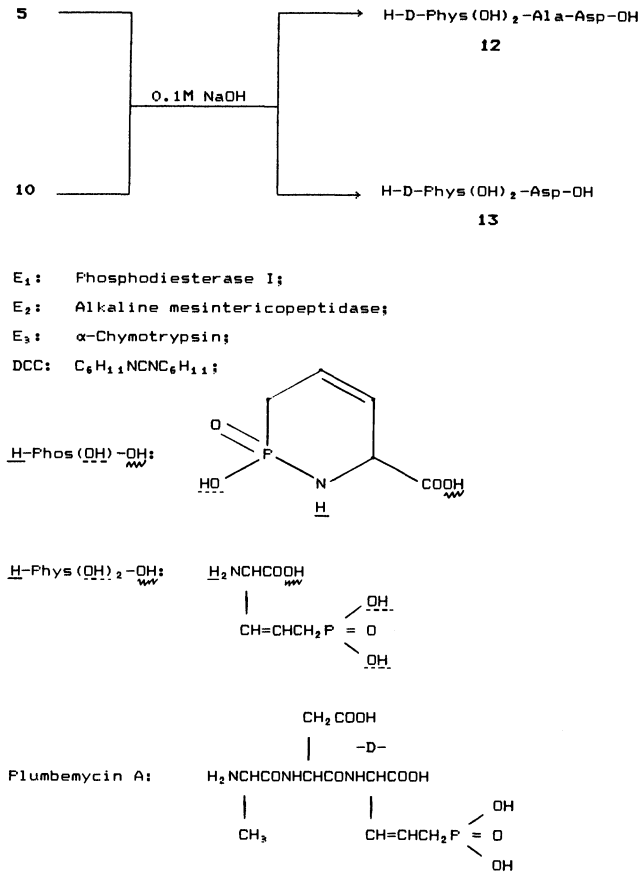

Scheme 3.

H-D-Phys(OH)$_2$-Ala-Asp-OH (**12**) and H-D-Phys-(OH)$_2$-Asp-OH (**13**) were obtained in about 90% yields, respectively (Scheme 3).

The facile hydrolysis of PO-NH bond also occured when compounds **3** and **8** were treated with dilute hydrochloric aicd. As a result, the protected tripeptides **14** and **15**, in which ethoxyl groups remain unchanged, were obtained in about 80% yields in both cases.

Preliminary tests for physiological activity point to some interesting problems with structure changes of the studied compounds. Thus, the modified tripeptides **5** and **10** were found to have a more pronounced bactericidal activity than Plumbemycin A, whereas that of three tripeptides **12**, **13**, and Plumbemycin A is almost the same. The modified aspertic acid **11** was proved to possess the highest bactericidal activity, while that of the modified alanine **6** is much weaker, though still better pronounced than that of Plumbemycin A. A detailed study of the discussed activities is now under way and will be published separately.

Experimental

General. IR spectra, elemental analysis, mp, HPLC, and $[\alpha]_D^{20}$ were measured with Perkin-Elmer instruments; TLC-molybdophosphate acid or ninhydrin detection; enzymes and buffers from "Signa."

H-D-Phos(OEt)-Ala-Asp(OEt)-OEt (3) and H-D-Phos-(OEt)-Asp(OEt)-Ala-OEt (8). A mixture of **1** (20.52 g, 0.12 mol) and dipeptides **2** (26.03 g, 0.10 mol) or **7** (22.70 g, 0.11 mol) and DCC (22.70 g, 0.11 mol) in dry ethyl acetate (250 ml) was stirred at room temperature for 12 h. After filtration, the filtrate is washed consecutively with 5% aqueous sodium carbonate, water, 5% hydrochloric acid, water, and finally dried over anhydrous $MgSO_4$ and distilled. The oily residue was purified on a silica-gel column using a mixture of chloroform and methanol (9:1). After evaporation under vacuum the residue was dissolved in dry ethyl acetate (200 ml) and cooled to −5 °C and then hexane was added until the mixture became turbid. The mixture was left overnight in refrigerator and products precipitated were collected.

Compound 3: Yield, 32.71 g (73.1%); mp 73—75 °C (EtOAc/*n*-C_6H_{14}); R_f: 0.76 (DMF:$CHCl_3$:MeOH=2:8:1); $[\alpha]_D^{20}$ 78.3° (*c* 1, MeOH).

Found: C, 48.66; H, 6.52; N, 9.38%. Calcd for $C_{18}H_{30}N_3O_9P$: C, 48.31; H, 6.76; N, 9.39%.

Compound 8: Yield, 34.14 g (76.3%); mp 98—101 °C (EtOAc/*n*-C_6H_{14}); R_f: 0.80 (DMF:$CHCl_3$:MeOH=2:8:1); $[\alpha]_D^{20}$ 79.1° (*c* 1, MeOH).

Found: C, 48.11; H, 6.93; N, 9.61%. Calcd for $C_{18}H_{30}N_3O_8P$: C, 48.31; H, 6.76; N, 9.39%.

H-Phys(OEt)(OH)-Ala-Asp(OEt)-OEt (14) and H-D-Phys(OEt)(OH)-Asp(OEt)-Ala-OEt (15). A suspension of **3** or **8** (4.47 g, 0.01 mol) in 0.5 M HCl (50 ml) was heated with stirring at 45 °C for 30 min. A homogeneous solution obtained was cooled and neutralized with 1% aqueous sodium carbonate. After extraction with ethyl acetate (3×20 ml) the combined organic extracts were dried over anhydrous $MgSO_4$ and distilled under vacuum to dryness. The residue was dissolved in chilled ethyl acetate (25 ml) and hexane was added until it became turbid. After standing overnight in refrigerator, the tripeptides **14** and **15** were collected, respectively.

Compound 14: Yield, 4.13 g (88.7%); mp 102—104 °C (EtOAc/*n*-C_6H_{14}); R_f: 0.81 (DMF:$CHCl_3$:MeOH=2:1:3); $[\alpha]_D^{20}$ 69.7° (*c* 1, MeOH).

Found: C, 46.31; H, 7.11; N, 8.77%. Calcd for $C_{18}H_{32}N_3O_9P$: C, 46.45; H, 6.93; N, 9.03%.

Compound 15: Yield, 3.83 g (76.3%); mp 111—114 °C (EtOAc/*n*-C_6H_{14}); R_f: 0.80 (DMF:$CHCl_3$:MeOH=2:1:3); $[\alpha]_D^{20}$ 77.7° (*c* 1, MeOH).

Found: C, 46.66; H, 6.76; N, 9.17%. Calcd for $C_{18}H_{32}N_3O_9P$: C, 46.45; H, 6.93; N, 9.03%.

Enzyme-Catalyzed Hydrolysis of 3 and 8. A mixture of the corresponding substrates **3** and **8** (each 20 g), phosphodiesterase I (5 mg or 10—15 mg in case that it is spread on a polymer carrier) in aqueous buffer (500 ml, pH 8.8) was stirred at 37 °C for 6 h. After removal of the enzyme acidification and concentration, the reaction mixture is extracted with diisopropyl ether (3×50 ml). The organic extracts collected are dried over anhydrous $MgSO_4$ and distilled to dryness. The residue was dissolved in dry ethyl acetate (200 ml) and hexane was added until the solution became turbid. After overnight in refrigerator, the products **4** and **9** were filtered.

***N*-[(*R*)-(2-Hydroxy-1,2,3,6-tetrahydro-1,2-azaphosphorin-6-yl)carbonyl]alanylaspartic Acid α,β-Diethyl Ester (4):** Yield, 15.27 g (81.6%); mp 92—94 °C (EtOAc/*n*-C_6H_{14}); IR (KBr) cm^{-1}: 2840—2320, 1760—1735, 1640, 1550, 1250, 1100, 930, 810, 720, 630; R_f: 0.61 (DMF:$CHCl_3$:MeOH=2:8:1); $[\alpha]_D^{20}$ 80.4° (*c* 1, MeOH).

Found: C, 46.00; H, 6.18; N, 9.73%. Calcd for $C_{16}H_{26}N_3O_8P$: C, 45.82; H, 6.25; N, 10.02%.

***N*-[(*R*)-(2-Hydroxy-1,2,3,6-tetrahydro-1,2-azaphosphorin-6-yl)carbonyl]aspartylalanine Asp$^{\beta}$, Ala-Diethyl Ester (9):** Yield, 14.95 g (79.9%); mp approx. 100 °C (decomp); IR (KBr) cm^{-1}: 2840—2350, 1765—1725, 1645, 1250, 1100—930, 815, 770, 635; R_f: 0.66 (DMF:$CHCl_3$:MeOH=2:8:1); $[\alpha]_D^{20}$ 84.2° (*c* 1, MeOH).

Found: C, 45.62; H, 6.33; N, 9.90%. Calcd for $C_{16}H_{26}N_3O_8P$: C, 45.82; H, 6.25; N, 10.02%.

Enzyme-Catalyzed Hydrolysis of 4 and 9. A mixture of the corresponding substrates **4** and **9** (each 20 g), the enzyme alkaline mesintericopeptidase (8 mg) in aqueous buffer (500 ml, pH 7.8) was stirred at 27 °C for 4 h until a ninhydrin-positive detection was observed. After acidification and evaporation of the reaction mixture to dryness, the amorphous residue was extracted with boiling ethanol. After cooling, the corresponding **5** and **10** were filtered.

***N*-[(*R*)-(2-Hydroxy-1,2,3,6-tetrahydro-1,2-azaphosphorin-6-yl)carbonyl]alanylaspartic Acid (5):** Yield, 13.91 g (80.3%); mp 182—186 °C (EtOH); IR (KBr) cm^{-1}: 3855—3200, 2850—2430, 1750, 1640, 1520, 1305, 1255, 985, 840, 720, 630; R_f: 0.61 (dioxane: 25% aqueous ammonia=4:1); $[\alpha]_D^{20}$ 72.6° (*c* 1, NaOH).

Found: C, 39.81; H, 4.71; N, 11.44%. Calcd for $C_{12}H_{18}N_3O_8P$: C, 39.67; H, 11.57; N, 11.57%.

***N*-[(*R*)-(2-Hydroxy-1,2,3,6-tetrahydro-1,2-azaphosphorin-6-yl)carbonyl]aspartylalanine (10):** Yield, 13.20 g (76.2%); mp about 186 °C (decomp) (EtOH); IR (KBr) cm^{-4}: 3620—3200, 2855—2430, 1755, 1640, 1525, 1300, 1250, 980, 845, 715, 630; R_f: 0.61 (dioxane: 25% aqueous ammonia=4:1); $[\alpha]_D^{20}$ 82.3° (*c* 1, 0.1 M NaOH).

Found: C, 39.91; H, 4.76; N, 11.52%. Calcd for $C_{12}H_{18}N_3O_8P$: C, 39.67; H, 11.57; N, 11.57%.

Enzyme-Catalyzed Hydrolysis of 5 and 10. A mixture of the corresponding substrates **5** and **10** (each 20 g), and α-chymotrypsin (5 ml) in aqueous buffer (500 ml, pH 7.8) was stirred at 25 °C for 6 h. After acidification and evaporation under vacuum to dryness, the amorphous residue was extracted with boiling ethanol. After cooling, the corresponding products **6** and **11** were filtered.

***N*-[(*R*)-(2-Hydroxy-1,2,3,6-tetrahydro-1,2-azaphosphorin-6-yl)carbonyl]alanine (6):** Yield, 12.12 g (88.7%); mp about 200 °C (decomp) (EtOH); IR (KBr) cm^{-1}: 3540—3200, 2840—2460, 1755, 1640, 1525, 1300, 1250, 970; ^1H NMR (D_2O, TMS, δ, ppm) 1.38 (3H, d, *J*=8 Hz, $CHC\underline{H}_3$), 2.76 (2H, m, CH_2), 4.2—4.4 (2H, m, 2×CH), 5.55 and 6.28 (2H, m, $C\underline{H}$=$C\underline{H}$) and four exchangeable protons; MS, *m/z*: Found/Calcd, 248/248.1; R_f: 0.66 (*n*-BuOH: AcOH: H_2O=9:1:1); $[\alpha]_D^{20}$ 69.3° (*c* 0.1, 0.1 M NaOH).

Found: C, 38.66; H, 5.35; N, 11.41%. Calcd for $C_8H_{13}N_2O_5P$: C, 38.72; H, 5.28; N, 11.29%.

***N*-[(*R*)-(2-Hydroxy-1,2,3,6-tetrahydro-1,2-azaphosphorin-6-yl)carbonyl]aspartic Acid (11):** Yield, 14.85 g (92.3%); mp, not defined, the substance is gradually decomposing with the melting; IR (KBr) cm^{-1}; 3845—3200, 2850—2420, 1750, 1640, 1525, 1300, 1250, 975, 840, 630; MS, *m/z*: Found/Calcd, 292/292.186; R_f: 0.72 (dioxane: 25% aqueous ammonia=9:1); $[\alpha]_D^{20}$ 83.4° (*c* 1, 0.1 M NaOH).

Found: C, 37.11; H, 4.21; N, 9.66%. Calcd for $C_9H_{13}N_2O_7P$: C, 37.00; H, 4.48; N, 9.56%.

Base-Catalyzed Hydrolysis of 5 and 10. A solution of **5** or **10** (0.1 mol each) in 0.1 M NaOH (100 ml) is heated to 50—60 °C for 30 min. After acidification and vacuum distillation to dryness, the amorphous residue was extracted with boiling ethanol. After cooling, the following products **12** and **13** are filtered:

***N*-(3,4-Didehydro-5-phosphono-D-norvalyl)alanylaspartic Acid (12):** Yield, 35.19 g (92.3%); mp about 220 °C (decomp); IR (KBr) cm^{-1}: 3845—3200, 2840—2395, 1750, 1640, 1520, 1255, 970, 720, 630; R_f: 0.50 (dioxane: 25% aqueous ammonia=4:1); $[\alpha]_D^{20}$ 79.3° (*c* 0.1, 0.1 M NaOH).

Found: C, 37.62; H, 5.44; N, 11.11%. Calcd for $C_{12}H_{20}N_3O_9P$: C, 37.80; 5.29; N, 11.02%.

***N*-(3,4-Didehydro-5-phosphono-D-norvalyl)aspartic Acid (13):** Yield, 33.97 g (89.1%); mp about 200 °C (decomp); IR (KBr) cm^{-1}: 3850—3200, 2850—2400, 1750, 1650, 1520, 1300, 1250; R_f: 0.50 (dioxane: 25% aqueous ammonia=4:1); $[\alpha]_D^{20}$ 72.4° (*c* 0.1, 0.1 M NaOH).

Found: C, 38.09; H, 5.00; N, 10.92%. Calcd for $C_{12}H_{20}N_3O_9P$: C, 37.80; H, 5.29; N, 11.02%.

References

1) Part IV: I. A. Natchev, *Bull. Chem. Soc. Jpn.*, **61**, 4447 (1988).

2) B. Park, A. Hirota, and H. Sakai, *Agric. Biol. Chem.*, **40**, 1505 (1976).

3) T. Boku, A. Hirota, and H. Sakai, *Jpn. Kokai*, **77** 108904; CA, 89: p1952.

4) S. Terashima, M. Wagatsuma, and S. Yamada, *Tetrahedron*, **79**, 1487 (1973).

5) I. Natchev, *Synthesis*, **1987**, 1079.

6) M. Wagatsuma, S. Terashima, and S. Yamada, *Tetrahedron*, **79**, 1497 (1973).

Organophosphorus Analogues and Derivatives of the Natural L-Amino Carboxylic Acids and Peptides. VI.[1] A Phospha^C-Peptide Analogue of Plumbemycin A

Ivan A. NATCHEV
Research Centre Konstrukcionni Polymeri, 5-003 Gara Iskar, 1528 Sofia, Bulgaria
(Received October 3, 1987)

Synopsis. A phospha^C-peptide of Plumbemycin A has been studied. Condensation of *N*-trifluoroacetyl-3,4-didehydro-5-(ethoxyhydroxyphosphinyl)norvaline (**1**) and L-analyl-L-aspartic acid diethyl ester (**2**) is carried out by the DCC method to give the entirely protected phospha^C-tripeptide (**3**). Conditions for the enzyme-catalyzed hydrolysis of the ester groups with alkaline mesintericopeptidase, phosphodiesterase I, and α-chymotrypsin and the removal of the trifluoroacetyl group with an aqueous ammonia solution has been achieved.

Phospha^C-peptides (the CO-NH group is exchanged for PO-NH) were first synthesized by Imoto et al.[2] and Martell et al.[3] The protected phospha^C-peptide [[(benzyloxycarbonyl)amino]methylphosphinyl]phenylalanine[4] has been synthesized and studied as inhibitor of enzyme carboxypeptidase. A. Yamauchi et al.[5] synthesized *N*-[(2-aminoethyl)ethoxyphosphinyl]glycine ethyl ester. This compound is a phospha^C-peptide, in which a hydroxyl group in the phosphoryl group is protected as an ester. The major problem in the synthesis of "pure" phospha^C-peptides (without protected groups) is its highly sensitive nature upon hydrolysis to even mild acids and bases.[3] Campbell et al.,[6] recommend for removal of two *O*-ethyl groups in diethyl phosphonate ($-PO(OEt)_2 \rightarrow -PO_3H_2$) to use HBr/AcOH or to carry out treatment of $-PO(OSiMe_3)_2$, which are more readily hydrolyzable with Me_3SiBr. The last possibility was explored by Issleib et al.[7] to obtain "pure" phospha^C-peptides. Our attempts to apply these methods to the synthesis of phospha^C-peptides analogues of Plumbemycin were unsuccessful due to the rather sensitive olefinic bond of 3,4-didehydronorvaline. Our studies directed toward the synthesis of methylphosphoryl analogue of Plumbemycin A,[8] methylphosphoryl- and phosphono analogues of gluthathion[9,10] and phospha^C-peptide analogue of Bialaphos (SF-1923)[11] showed as a most promising method for the synthesis of "pure" phospha^C-peptides, the one developed in our laboratory[12] which makes possible the use of highly selective enzymes to catalyze the hydrolysis of the blocking groups.

The condensation of *N*-trifluoroacetyl-3,4-didehydro-5-(ethoxyhydroxyphosphinyl)norvaline ethyl ester (**1**) synthesized by us (cf. later communication from the same author) and L-alanyl-L-aspartic acid diethyl ester (**2**) was carried out by the DCC method. When we used *N*-TFA-3,4-didehydro-5-phosphono-L-norvaline ethyl ester free phosphono groups, extra products were obtained and the yield of the protected phospha^C-peptide **3** was much lower.

A mixture of molar equivalent amounts of components **1** and **2** and a 10% excess of DCC in dry ethyl acetate at room temperature was stirred for 12 h and after the usual work-up, the phospha^C-tripeptide **3** was isolated in about 70% yield.

An attempt at the base- or acid-catalyzed hydrolysis of the ethoxycarbonyl groups of **3** afforded the hydrolytic decomposition of PO-NH.

When the enzyme alkaline mesintericopeptidase was applied under the most favorable conditions established by us [20 g substrate **3**, 6—7 mg enzyme in aqueous buffer (500 ml, pH 7.8), stirring at 25 °C to a ninhydrin-positive detection], selective hydrolysis of the ethoxycarbonyl groups proceeded to give the *N*- and *P*-protected phospha^C-tripeptide **4**.

The enzyme phosphodiesterase I, free or spread on a polymer carrier, contributed to the hydrolysis of the ethoxyphosphonyl group to afford phospha^C-tripeptide acid *N*-trifluoroacetyl **5**, which was isolated in almost quantitative yield. Naturally, the previously established amount of 5 mg phosphodiesterase I for 20 g substrate can be varied, but the enzyme/substrate ratio must be within the prescribed limits. The experimental technique was much simplified when the enzyme was spread on a polymer carrier. In that case 10—15

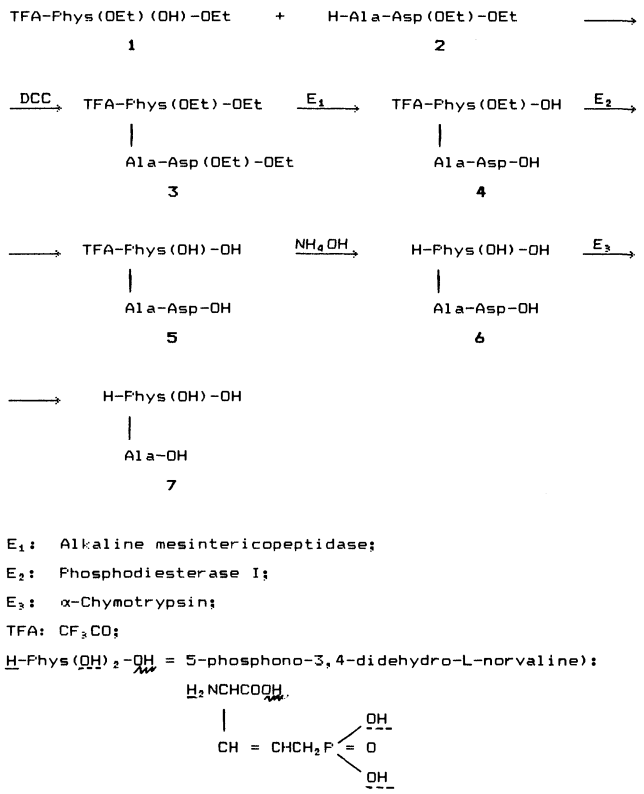

Scheme 1.

mg enzyme was used for 20 g of the substrate and continuous stirring of the reaction mixture was necessary. The enzyme spread on a polymer carrier can be used at least in twelve consecutive experiments without losing its activity towards the standard substrate bis(4-nitrophenyl) hydrogenphosphate.

It is of interest to note that none of the substrates with PO-NH bond studied in our laboratory underwent hydrolytic cleavage of PO-NH bonds with phosphodiesterase I.

On the other hand alkaline phosphatase with closely related activity has a catalytic effect towards neither ethoxyphosphinyl, nor aminophosphinyl groups.

The main problem in the synthesis of "pure" phospha^{C}-peptide analogue of Plumbemycin A is the removal of the *N*-protective group. Unfortunately, positive results were not obtained for the samples studied here. Thus, the test for selective hydrolysis of *N*-acetyl group with the proteolytic enzymes resulted in decomposition of the peptide bond Ala-Asp. The catalytic hydrogenation, the treatment with HBr/AcOH or the base- or acid-catalyzed hydrolysis of other *N*-protective groups were also unsuitable due to lability of the PO-NH group and the olefinic bond. The optimum conditions were found by using the *N*-trifluoroacetyl protective group, which could be removed in about 45% yield with aqueous ammonia-dioxane solution (pH 10) at 30—40 °C for 1 h to afford phospha^{C}-peptide analogue **6** of Plumbemycin A.

Base-catalyzed hydrolysis of **6** liberates, 3,4-didehydro-5-phosphono-L-norvaline[12] and the dipeptide alanyl-aspartic acid.

Under the optimum conditions[12] [20 g substrate **6**, 5 mg α-chymotrypsin in an aqueous buffer medium (500 ml, pH 7.8), stirring at 25 °C for 6 h] the dipeptide **7** was isolated in about 85% yield.

Studies of the physiological activity of the newly snythesized phospha^{C}-peptides **6** and **7** are under way and will be published in due course.

Experimental

General. IR spectra, elemental analysis, mp, Mw, HPLC, $[\alpha]_D^{22}$ on Perkin-Elmer instruments; reagents and solvents from "Fluka", "Aldrich", and "Merck"; phosphodiesterase I-"Sigma"; α-chymotrypsin—Pharmachim, Bulgaria; alkaline mesintericopeptidase—Inst. Org. Chem., Bulg. Acad. Sci.; TLC—silica-gel film "Merck"-molibdophosphate or ninhydrin detection.

Synthesis of the *N*-[(*S*)-(4-Ethoxycarbonyl-4-trifluoroacetamido-2-butenyl)ethoxyphosphinyl]alanylaspartic Acid α,β-Diethyl Ester (3). A mixture of *N*-trifluoroacetyl-1-L-3,4-didehydro-(*S*)-(ethoxyhydroxyphosphinyl)norvaline ethyl ester **1** (34.72 g, 0.1 mol), alanylaspartic acid diethyl ester **2** (26.03 g 0.1 mol) and DCC (22.69 g, 0.11 mol) in dry ethyl acetate (300 ml) is stirred at room temperature for 12 h. After filtration, the reaction mixture is washed consecutively with water, 5% aqueous sodium carbonate solution, water, 5% hydrochloric acid, water, and dried over anhydrous $MgSO_4$, and concentrated under vacuum to dryness. The light yellow viscous oil is loaded on a silica-gel column, which is eluted with chloroform : methanol (9 : 1).

Compound 3: Yield, 41.38 g (70.2%); mp 73—75 °C (after a continuous stay of the obtained oil in EtOAc/*n*-C_6H_{14} at −5 °C in refrigerator); IR (KBr) cm^{-1}: 1750—1720, 1670—1620, 1550, 1310, 1210, 1000, 960, 855, 730, 635; R_f: 0.75 ($CHCl_3$: MeOH=9 : 1); $[\alpha]_D^{20}$ −96.3° (*c* 1, MeOH).

Found: C, 44.61; H, 6.11; N, 6.96%. Calcd for $C_{22}H_{35}F_3N_3O_{10}P$: C, 44.82; H, 5.98; N, 7.13%. Mw, Found/Calcd, 587/589.503.

The substance is soluble in most organic solvents and is insoluble in water. Heating of **3** (5.88 g, 0.01 mol) in 0.2 M HCl (25 ml) (1M=1 mol dm^{-3}) at 50 °C for 30 min gives the starting norvaline (**1**) (2.99 g, 86.3%) and the dipeptide (**2**) (1.93 g, 73.4%).

***N*-[(*S*)-(4-Carboxy-4-trifluoroacetamido-2-butenyl)ethoxyphosphinyl]alanylaspartic Acid (4).** A mixture of the tripeptide **3** (20 g, 0.034 mol), alkaline mesintericopeptidase (8 mg), 3—4 drops of "Tween-80" (beforehand homogenized with **3** in 200 ml of water) in an aqueous buffer (500 ml, pH 7.8) is stirred at 25 °C to a ninhydrin-positive detection. After acidification (pH 6.5) and evaporation to dryness, the amorphous residue is extracted with boiling ethanol. After cooling, the tripeptide **4** is filtered.

Compound 4: Yield, 15.19 g (88.6%); mp 182—186 °C (EtOH); IR (KBr) cm^{-1}: 3750—2840, 1760, 1640, 1520, 1370, 1250, 1100—940, 870, 630; R_f: 0.62 (*n*-BuOH: 25% NH_3aq= 6 : 1); $[\alpha]_D^{20}$ −83.6° (*c* 0.1, 0.1 M NaOH);

Found: C, 44.61; H, 6.11; N, 6.96%. Calcd for $C_{22}H_{35}F_3N_3O_{10}P$: C, 44.82; H, 5.98; N, 7.13%. Mw, Found/Calcd, 587/589.503.

***N*-[(*S*)-(4-Carboxy-4-trifluoroacetamido-2-butenyl)hydroxyphosphinyl]alanylaspartic Acid (5).** A mixture of the tripeptide **4** (20 g, 0.039 mol) and phosphodiesterase I (5 mg or 10—15 mg, if spread on a polymer carrier) is stirred at 37 °C for 6 h. After removal of the enzyme by ultrafiltration or centrifugation (in case the enzyme is spread on a polymer carrier), the reaction mixture is acidified (pH 6.0) and evaporated under vacuum to dryness. The amorphous residue is extracted with boiling ethanol and after cooling, the product **5** is filtered.

Compound 5: Yield, 18.38 g, (97.3%); mp about 200 °C (decomp); IR (KBr) cm^{-1}: 3480—2860, 2840—2460, 1760, 1640, 1520, 1320, 1250, 980—840, 630; R_f: 0.39 (*n*-BuOH: 25% NH_3aq=6 : 1); $[\alpha]_D^{20}$ −83.6° (*c* 0.1, 0.1 M NaOH).

Found: C, 35.46; H, 3.88; N, 8.91%. Calcd for $C_{14}H_{19}F_3N_3O_{10}P$: C, 35.27; H, 4.01; H, 8.80%. Mw, Found/Calcd, 481/477.287.

***N*-[(*S*)-(4-Carboxy-4-amino-2-butenyl)hydroxyphosphinyl]-alanylaspartic Acid (6).** A solution of the tripeptide **5** (23.86 g, 0.05 mol) in a mixture of dioxane: 25%. aq. ammonia (150 ml, pH 10.0) is heated at 35—40 °C for 1 h. After evaporation under vacuum to dryness and additon of 200 ml of water, the solution is once again evaporated under vacuum. The product **6** is isolated by fractional crystallization.

Compound 6: Yield, 9.38 g (49.2%); mp 163—165 °C (decomp); IR (KBr) cm^{-1}: 3480—2860, 2460—2120, 1750—1720, 1640, 1520, 1310, 1200; R_f: 0.66 (DMF : $CHCl_3$: MeOH= 9 : 2 : 3); $[\alpha]_D^{20}$ −93.3° (*c* 0.1, 0.1 M NaOH).

Found: C, 38.01; H, 5.11; N, 10.93%. Calcd for $C_{12}H_{20}N_3O_9P$: C, 37.80; H, 5.29; N, 11.02%. Mw, Found/Calcd, 380/381.279.

The substance is quite soluble in DMF, DMSO, hexamethylphosphoric triamide, less in dioxane, and is insoluble in ethanol, ethyl acetate, ether, chloroform, and hexane. When **6** (3.81 g, 0.01 mol) is heated in 0.1 M NaOH (20 ml) at 50 °C for 30 min, the dipeptide H-Ala-Asp-OH (1.74 g, 85.3%) and 3,4-didehydro-5-phosphono-L-norvaline is isolated: yield 1.48 g (76.1%); mp 188—190 °C (decomp) [for the D-form 183—185 °C (decomp)];[12] IR (KBr) cm^{-1}: 1735, 1630, 1520, 1240, 1150, 1040, 930, 860, 775, 630; ^1H NMR (D_2O+NaOD, δ, ppm): 2.75 (2H, dd, $J_{P\text{-}CH_2}$=8.3, and 23 Hz), 4.81 (1H, d, *J*=9 Hz), 5.66 (1H, m, C<u>H</u>C<u>H</u>), 6.12 (1H, m, CH=C<u>H</u>CH_2)

and five exchangeable protons NH_2, COOH, PO_3H_2; R_f: 0.24 (*n*-BuOH : Pyr : AcOH : H_2O=15 : 12 : 3 : 10) and 0.10 (*n*-BuOH : AcOH : H_2O=3 : 1 : 1); $[\alpha]_D^{20}$ −53.2° (*c* 1, H_2O).

Found: C, 30.87; H, 4.93; N, 7.33%. Calcd for $C_5H_{10}NO_5P$: C, 30.78; H, 5.17; N, 7.18%. Mw, Found/Calcd, 197/195.112.

***N*-[(*S*)-(4-Carboxy-4-amino-2-butenyl)hydroxyphosphinyl]-alanine (7).** A mixture of the tripeptide **6** (20 g, 0.071 mol) and α-chymotrypsin (5 mg) in an aqueous buffer (500 ml, pH 7.8) is stirred at 25 °C for 6 h. After acidification and evaporation under vacuum to dryness, the amorphous residue is extracted with hot dioxane. After cooling, the dipeptide **7** is filtered.

Compound 7: Yield, 12.01 g (86.1%); mp about 200 °C (decomp); IR (KBr) cm^{-1}: 3450—2920, 2840—2460, 1750, 1640, 1520, 1320, 980—740, 635; R_f: 0.62 (*n*-BuOH : AcOH : H_2O=9 : 1 : 1); $[\alpha]_D^{20}$ −63.4° (*c* 0.1, 0.1 M NaOH).

Found: C, 36.18; H, 5.41; N, 10.41%. Calcd for $C_8H_{15}N_2O_6P$: C, 36.09; H, 5.68; N, 10.52%. Mw, Found/Calcd, 263/266.206.

References

1) Part V: I. A. Natchev, *Bull. Chem. Soc. Jpn.*, **61**, 4488 (1988).
2) K. Yamauchi, M. Kinoshita, and M. Imoto, *Bull. Chem. Soc. Jpn.*, **45**, 2528 and 2531 (1972).
3) M. Hariharau, S. Cheberek, and A. Martell, *Syntetic Commun.*, **3**, 375 (1973).
4) N. Jacobsen and P. Bartlet, ACS Symp. Ser. (Phosphorus Chem.), 171 and 221 (1981).
5) K. Yamauchi, S. Ohtsuki, and M. Kinoshita, *Pept. Chem.*, **19**, 53 (1981).
6) M. Campbell, N. Carruthers, and S. Mickel, *Tetrahedron*, **38**, 2513 (1982).
7) K. Issleib, A. Balszuweit, and K. Doepter, DDR. Pat. 212 739; *Chem. Abst.*, p. 167 (1985).
8) I. Natchev, 31st Congress IUPAC, 1987 Sofia, Congress Papers v. 2, p. 4.90.
9) I. Natchev, International Symposium, Present state and Perspectives in Application of Inhibitors of Nucleic Acid and Protein Synthesis, Varna 1985, Symp. Papers. p. 68.
10) I. Natchev, Third Intern. Conf. F.E.C.S., 1985-Sofia, Conf. Papers, v. 4, p. 414.
11) I. Natchev, Third intern. Conf. F.E.C.S., 1985-Sofia, Conf. Papers, v. 4, p. 421.
12) I. Natchev, *Synthesis*, **1987**, 1079.
13) B. Park, A. Hirota, and H. Sakai, *Agric. Biol. Chem.*, **40**, 1505 (1976).

Spectral and Biological Studies on Organotin(IV) Complexes of Heterocyclic Benzothiazolines

Kiran SINGH, Ranvir SINGH, and Jagdish Prasad TANDON*
Department of Chemistry, University of Rajasthan, Jaipur-302004, India
(Received January 25, 1988)

Synopsis. The monobasic bidentate benzothiazolines, which were produced by the reaction of 2-mercaptoaniline and the heterocyclic aldehydes e.g., 2-furaldehyde, 2-thiophenecarbaldehyde, 2-pyridinecarbaldehyde, and 3-indolecarbaldehyde, have reacted with dialkyltin dichloride to give colored compounds. These compounds were characterized on the basis of elemental analyses, molar conductance, molecular weight determination, electronic and infrared spectral studies. Multinuclear NMR(^{1}H, ^{13}C, and ^{119}Sn) data suggest trigonal bipyramidal and octahedral geometries for the resulting $Me_2Sn\widehat{Cl(NS)}$ and $Me_2Sn(\widehat{NS})_2$ type complexes where $\widehat{NS}$ indicates benzothiazoline ligand, respectively. The fungitoxicity of 2-(2-thienyl)benzothiazoline and its complexes has been evaluated on pathogenic fungi.

During the recent years, much interest has been shown in the synthesis of metal chelates with sulfur containing ligands due to their different biological applications.[1,2] It has, however, been reported that on complexation[3,4] the activity of sulfur-containing ligands increases still further. Our continuing interest in the synthesis of biologically active complexes have led us to prepare and study the structures as well as other features of organotin complexes of heterocyclic benzothiazolines. The equilibrium forms of the ligands used during these investigations are shown below:

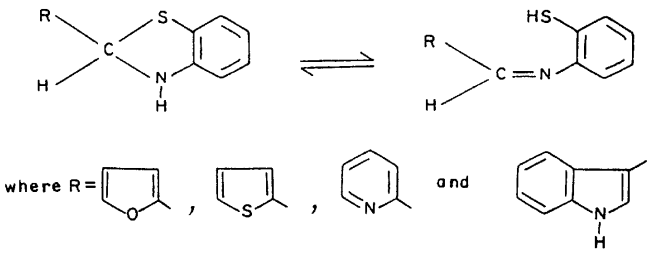

Experimental

Chemicals and solvents used were dried and purified by standard methods and moisture was excluded from the glass apparatus using $CaCl_2$ guard tubes. The ligands were prepared as reported in our earlier publication.[5]

Preparation of Complexes. To a weighed amount of dimethyltin dichloride in ca. 30 cm^3 of dry methanol in 100 cm^3 R.B. flask, was added the calculated amount of sodium salt of the ligand in 1 : 1 and 1 : 2 molar ratios. The mixture was heated under reflux for about 6 hours and the precipitate of sodium chloride so formed was filtered off. The solvent was removed and the product dried in vacuo. It was repeatedly washed with dry cyclohexane and again dried in vacuo. The physical properties and analytical data of these complexes are recorded in Table 1.

^{1}H NMR spectra were recorded on a JEOL FX 90Q spectrometer in DMSO-d_6 at 89.55 MHz, and ^{13}C and ^{119}Sn NMR spectra in methanol at 22.49 MHz and 33.35 MHz, respectively. Other methods of analyses and physical measurements are same as reported earlier.[5,6]

Results and Discussion

The reactions of dimethyltin dichloride with benzothiazolines (abbrev. to $\widehat{NS}$) in 1 : 1 and 1 : 2 molar ratios proceed as follows:

$$Me_2SnCl_2 + \widehat{NS}Na \xrightarrow[1:1]{MeOH} Me_2SnCl(\widehat{NS}) + NaCl$$

$$Me_2SnCl_2 + \widehat{NS}Na \xrightarrow[1:2]{MeOH} Me_2SnCl(\widehat{NS})_2 + NaCl$$

All the newly synthesized complexes are colored solids and soluble in most of the common organic solvents. The low values of molar conductance (15—20 ohm^{-1} cm^2 mol^{-1}) in anhydrous *N,N*-dimethylformamide show them to be nonelectrolytic in nature. The molecular weight determinations show them to be monomeric.

The electronic spectra of the ligands consist of two bands around 250 nm and 315 nm characteristic of benzothiazolines.[8] These bands arise out of θ-θ^* and π-π^* benzenoid[8] transitions and which remain almost unchanged in all the tin complexes. However, an additional band is also observed in the region 390—410 nm due to n-π^* electronic transitions of the azomethine[8] and which indicates rearrangement of the ligands to the imine on complexation.

In the IR spectra of the ligands strong bands in the regions 3370—3200 cm^{-1} and 1670—1705 cm^{-1} due to NH stretching and deformation vibrations, respectively are observed. The absence of ν(SH) at 2500—2600 cm^{-1} and ν(C=N) at 1600—1650 cm^{-1} is indicative of the benzothiazolines.[9] In complexes, the bands due to NH vibrations are not observed and this indicates the chelation of nitrogen with the tin atom. A new band at ca. 1600 cm^{-1} in the spectra of complexes due to ν(C=N) vibrations suggests that the complexes are metal-Schiff base derivatives as the benzothiazoline ring rearranges to give the Schiff base derivatives in the presence of metal ion.[8] Several new bands in the spectra of tin complexes[6] in the regions 390—450, 325±20, and 280±15 cm^{-1} may be assigned to ν Sn←N, ν Sn-S, and ν Sn-Cl respectively, and this lends further support to the proposed coordication in these complexes.

^{1}H NMR spectral studies further support the bonding pattern as discussed above. The N-H proton signals at δ 4.20 (2-furyl-BztH) and δ 4.36 (2-thienyl-BztH) in the spectra of benzothiazolines disappear in the corresponding tin complexes. The azomethine proton signal shifts down field in the spectra of complexes due to the formation of a coordinate linkage

Table 1. Analyses and Physical Characterics of Organotin Complexes

Compound[a]	Color and state	Mp θ_m/°C	Yield %	Analysis/% C Found (Calcd)	H Found (Calcd)	N Found (Calcd)	S Found (Calcd)	Cl Found (Calcd)	Sn Found (Calcd)
Me_2SnCl(2-furyl-Bzt)	Yellow solid	190	73	40.15 (40.39)	3.32 (3.63)	3.24 (3.63)	8.03 (8.29)	8.95 (9.19)	30.30 (30.73)
Me_2Sn(2-furyl-Bzt)$_2$	Yellow solid	198	72	45.01 (49.26)	3.46 (3.76)	4.52 (4.79)	10.53 (10.95)	—	19.89 (20.29)
Me_2SnCl(2-thienyl-Bzt)	Green solid	240d[b]	78	38.55 (38.79)	3.23 (3.48)	3.15 (3.48)	15.63 (15.91)	8.52 (8.83)	29.27 (29.51)
Me_2Sn(2-thienyl-Bzt)$_2$	Yellowish brown solid	235	75	49.00 (49.26)	3.45 (3.76)	4.38 (4.79)	21.56 (21.89)	—	20.00 (20.31)
Me_2SnCl(3-indolyl-Bzt)	Brown solid	115d	71	46.65 (46.88)	3.66 (3.91)	6.23 (6.43)	7.10 (7.35)	7.88 (8.15)	26.95 (27.27)
Me_2Sn(3-indolyl-Bzt)$_2$	Dark brown solid	133	69	58.81 (59.01)	4.01 (4.30)	8.30 (8.61)	9.71 (9.84)	—	18.00 (18.24)
Me_2SnCl(2-pyridyl-Bzt)	Grey solid	232	78	41.85 (42.29)	3.53 (3.78)	6.81 (7.05)	7.95 (8.06)	8.54 (8.94)	29.57 (29.88)
Me_2Sn(2-pyridyl-Bzt)$_2$	Dark yellow solid	215d	77	53.92 (54.29)	4.00 (4.18)	9.42 (9.74)	10.94 (11.14)	—	20.31 (20.65)

a) Benzothiazoline is abbreviated to Bzt which are 2-(2-furyl)benzothiazoline, 2-(2-thienyl)benzothiazoline, 2-(3-indolyl)benzothiazoline, and 2-(2-pyridyl)benzothiazoline. b) d=decomp.

Table 2. ^{13}C NMR Spectral Data for Benzothiazoline and Its Corresponding Tin Complexes

	1	2	3	4	5	6	7	8	9	10	11	12	Sn-C
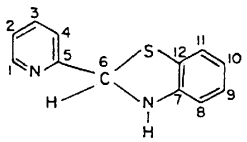	123.46	121.89	120.64	121.19	125.52	149.57	126.17	125.95	125.61	125.42	126.77	136.92	—
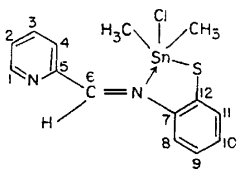	123.64	121.92	120.72	121.23	125.83	151.32	126.71	126.12	126.43	126.59	127.13	139.24	17.92
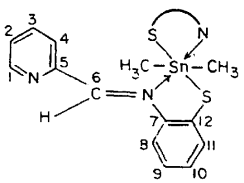	123.72	121.90	120.87	121.22	125.85	153.32	126.75	126.31	126.32	126.42	127.82	140.23	16.85

Table 3. Fungicidal Screening Data of Ligand and Its Complexes

Compound	Average percentage inhibition after 96 h: Organism Helminthosporium gramineum concn used 0.01%	0.1%	Organism Rhizopus oryzae concn used 0.01%	0.1%	Organism Aspergillus concn used 0.01%	0.1%
2-Thienyl-BztH	37	41	34	46	41	53
Me_2SnCl(2-thienyl-Bzt)	58	68	65	85	70	84
Me_2Sn(2-thienyl-Bzt)$_2$	56	71	60	79	63	85

between nitrogen and tin atoms. The protons of the methyl groups appear at δ 1.12, 1.34, 1.08, and 1.33 in the tin complexes.

^{13}C NMR spectra of 2-(2-pyridyl)benzothiazoline and its 1 : 1 and 1 : 2 tin complexes were also recorded (Table 2). The considerable shifts in the positions of carbons of the tin complexes marked by (6) and (12) attached to N and S, respectively, clearly indicate that

the nitrogen and sulfur of the mercapto group participate in complexation reaction as discussed earlier.

The compound Me_2SnCl(2-pyridyl-Bzt) gives a signal at −147 ppm in the ^{119}Sn NMR indicative of five-coordination around the tin atom as it is in agreement with the previously reported values.[10]

On the basis of the foregoing discussions, trigonal bipyramidal and octahedral geometries around the tin atom have been proposed in 1:1 and 1:2 tin complexes, respectively.

Evaluation of the Antifungal Activity. Helminthosporium gramineum, Rhizopus oryzae and Aspergillus flavus were employed to check the antifungal activity of the benzothiazoline and its 1:1 and 1:2 complexes. The results of the antifungal activity given in Table 3 show that Me_2Sn(2-thienyl-Bzt)$_2$ shows almost complete inhibition in higher concentration. As compared to 2-(2-thienyl)benzothiazoline, Me_2SnCl(2-thienyl-Bzt) and Me_2Sn(2-thienyl-Bzt)$_2$ exhibit greater fungitoxicity against all the fungi. The fungitoxicity of ligand and its complexes decreases on lowering the concentration. The increased fungitoxicity of the complexes as compared to the ligand may be due to chelation as the polarity of the metal ion in the complexes which reduces considerably due to the partial sharing of its positive charge with the donor groups and possible π-electron delocalization over the whole chelate ring system. This in turn increases the hydrophobic character of the metal favoring its permeation through the lipoid layers of the fungal membranes.[11]

One of us (Mrs.) Kiran Singh is thankful to the CSIR, New Delhi for the financial assistance.

References

1) N. P. Buu-Hoi, T. B. Voc, and N. D. Xuong, *Bull. Soc. Chim. Fr.*, **1955**, 694.
2) B. G. Benns, B. A. Gingras, and C. H. Bayley, *App. Microbiol.*, **8**, 353 (1960).
3) Y. Skada, Jpn. Patent 7017189 (1970); *Chem. Abstr.*, **73**, 77252y (1970).
4) R. S. Srivastava, *J. Inorg. Nucl. Chem.*, **42**, 1526 (1980).
5) Mrs. K. Singh, R. V. Singh, and J. P. Tandon, *Inorg. Chim. Acta*, **151**, 179 (1988).
6) Mrs. K. Singh, R. V. Singh, and J. P. Tandon, *Synth. React. Inorg. Met-Org. Chem.*, **16**, 1341 (1986) and references therein.
7) J. G. Horsfall, *Bot. Rev.*, **11**, 357 (1945).
8) R. V. Singh and J. P. Tandon, *Synth. React. Inorg. Met-Org. Chem.*, **11**, 109 (1981).
9) H. Jadamus, Q. Fernando, and H. Freiser, *J. Am. Chem. Soc.*, **86**, 3056 (1964).
10) S. J. Blunden and P. J. Smith, *J. Organomet. Chem.*, **157**, 226 (1982).
11) R. S. Srivastava, *Inorg. Chim. Acta*, **56**, 165 (1981).

Studies in the Extraction of Metals with 3-Phenyl-4-acetyl-5-isoxazolone

A. JYOTHI and G. N. RAO*
Chemistry Department, Indian Institute of Technology, Hauzkhas, New Delhi-110016, India
(Received February 22, 1988)

Synopsis. Extraction of manganese(II), iron(II), cobalt(II), nickel(II), copper(II), zinc(II), and cadmium(II) from aqueous solution with 3-phenyl-4-acetyl-5-isoxazolone (HPAI) in 4-methyl-2-pentanone (MIBK) has been studied and the extraction constants have been calculated for all the systems except cadmium(II). Separation factors have been calculated for the separation of metals.

In the extraction of metals, β-diketones such as thenoyltrifluoroacetone (HTTA)[1] are extensively used. Acylpyrazolones have been proved promising reagents for the extraction of metals from acidic media.[2-8] In our previous paper,[9] we have reported the extraction of iron(II), manganese(II), cobalt(II), nickel(II), zinc(II), cadmium(II), and lead(II) with 3-phenyl-4-benzoyl-5-isoxazolone (HPBI), a new chelating ligand in which the β-diketone moiety is fused to a heterocyclic ring. In continuation of this work, 3-phenyl-4-acetyl-5-isoxazolone (HPAI) has been used to evaluate the potential of this reagent for the extraction of metals. Solid complexes of these metals with HPAI have also been isolated and studied.[10] In common with other β-diketones (like acylpyrazolones) HPAI exists in keto and enol forms (Fig. 1). It has been confirmed by the presence of an enolic peak at δ 12 relative to TMS in the ^{1}H NMR spectrum of ligand HPAI. The present paper deals with the extraction of iron(II), manganese(II), cobalt(II), nickel(II), copper(II), zinc(II), and cadmium(II) into MIBK and the effectiveness of the ligand HPAI in the separation of metals. 4-Methyl-2-pentanone was used as solvent as it is commonly employed in atomic absorption studies and the ligand was soluble to a greater extent in this solvent than other solvents like toluene or chloroform.

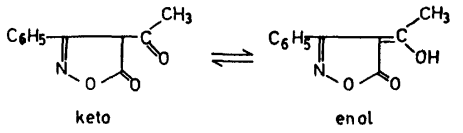

Fig. 1. The enolic and keto forms of the 3-phenyl-4-acetyl-5-isoxazolone.

Experimental

Reagents. Ethyl benzoylacetate (Fluka), acetic anhydride (Merck), sodium acetate (Merck), and hydroxylamine hydrochloride (Sarabhai) were used for the preparation of ligand. MIBK (BDH) was used as solvent for the extraction. The pH of the aqueous phase was maintained by using mixtures of potassium chloride and hydrochloric acid for pH 1—3, sodium acetate-acetic acid for pH 4—6, acetic acid-ammonia for pH 6—8 and ammonium chloride-ammonia for pH 8—10. A constant ionic strengths of 0.1 mol dm^{-3} was maintained by using potassium nitrate solution. Stock solutions were prepared by using AR grade chemicals.

Preparation of the Ligand. The ligand 3-phenyl-4-acetyl-5-isoxazolone (HPAI) was prepared by using 3-phenyl-5-isoxazolone and acetic anhydride in the presence of sodium acetate as described by Korte and Storiko.[11] Mp 140±2 °C, Calcd for $C_{11}H_9O_3N$: C, 65.02; H, 4.43; N, 6.89%. Found: C, 64.86; H, 4.48; N, 6.95%. The UV spectrum of the ligand in 95% ethanol showed two absorption maxima at 285 and 232 nm.

Extraction Procedure. Ten ml of the aqueous solution containing an aliquot of metal solution, five ml of the buffer solution and one ml of 1 mol dm^{-3} KNO_3 solution was equilibrated with ten ml of organic phase containing the required amount of the ligand in a stoppered bottle. The mixture was shaken on a mechanical shaker for one hour at 25±1 °C. After equilibration, the aqueous phase was separated from the organic layer and its pH was measured by using an expanded scale pH meter (ECIL India). The concentration of metal ion was monitored using atomic absorption spectrophotometer. A Pye-Unicam SP-191 unit with air-acetylene burner and the required hollow cathode lamps was utilized in this study. Distribution coefficient K_d (defined as the total concentration of metal in organic phase divided over the total concentration of metal in aqueous phase) was calculated.

Results and Discussion

The extraction curves of each element as a function of pH of the aqueous solution are shown in Fig. 2. Quantitative extraction of iron(II) was observed in the pH range 1.5 to 8.0. Above pH 8.0, the extraction registered a sharp drop and at pH 9.5 iron(II) showed only 90% extraction. Nickel(II) and cobalt(II) were extracted quantitatively from pH 3.0 to 9.0. Between

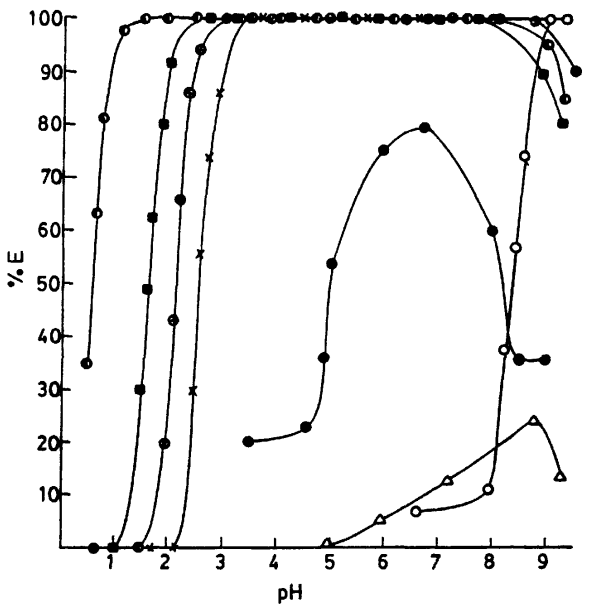

Fig. 2. Plot of %E vs. pH. ○=Mn(II); ◐=Fe(II); ■=Cu(II); ⊗=Ni(II); ×=Co(II); ●=Zn(II); △=Cd(II); HPAI 0.01 mol dm^{-3} in MIBK.

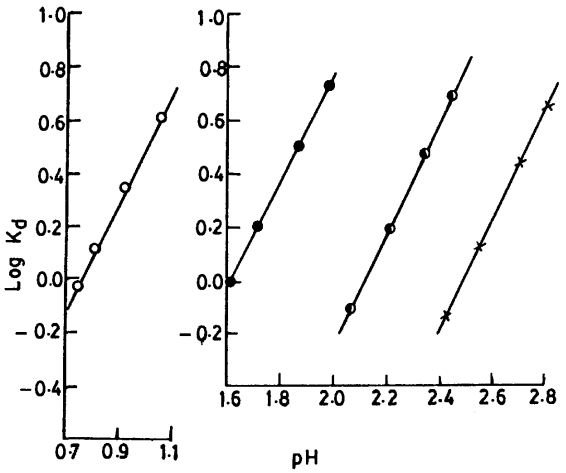

Fig. 3. Plots of log K_d vs. pH. ○=Fe(II); ●=Cu(II); ◐=Ni(II); ×=Co(II); HPAI 0.01 mol dm^{-3} in MIBK.

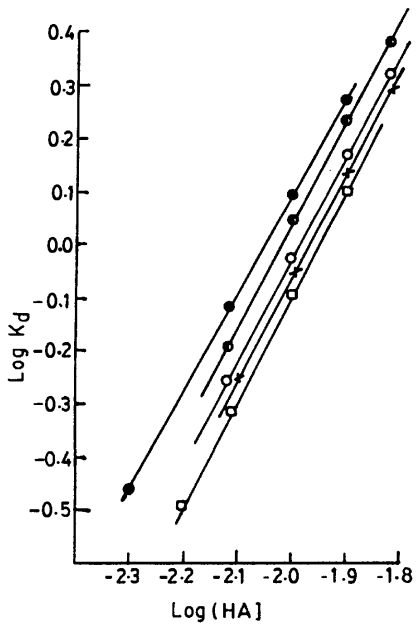

Fig. 4. Plot of log K_d vs. log[HA]. ○=Mn(II) (pH 8.4); ●=Zn(II) (pH 5.0); ×=Cu(II) (pH 1.55); ◐=Fe(II) (pH 0.75); □=Ni(II) (pH 2.05).

pH 9.0 and 9.5 the % extraction dropped to 90%. The extraction of copper(II) was quantitative in the pH range 2.5 to 8.0, then the extraction decreased at higher pH values and at pH 9.0 only 80% of copper(II) was extracted. Maximum extraction of zinc(II) (80%) was observed over the pH range 6.0 to 7.0, then the extraction decreased at higher pH up to 9.0, where only 35% zinc(II) was extracted. Figure 2 shows a sharp rise in the extraction of manganese(II) from pH 8.0 and the quantitative extraction of manganese(II) into the organic phase was observed at pH 9.0. Below pH 6.0 no appreciable quantity of manganese(II) was extracted. Maximum extraction shown by cadmium-(II) was only 25% at a pH of 8.8.

In order to understand the extraction behavior in more detail, log of distribution coefficient K_d was plotted against pH and log of ligand concentration at fixed ligand concentration and pH respectively (Figs. 3 and 4). The plots were linear with a slope of ca. 2 indicating the release of two H^+ ions and involvement of two molecules of ligand (HPAI) during the extraction process. It can be inferred from these results that the main equilibrium involved in the extraction process is

$$M^{2+} + 2HPAI_{(org)} \rightleftharpoons M(PAI)_{2(org)} + 2H^+ \quad (1)$$

where, PAI=anion of 3-phenyl-4-acetyl-5-isoxazolone.

The extraction constant values (log K_{ex}) in Eq. 1 were calculated for manganese(II), iron(II), nickel(II), cobalt(II), copper(II), and zinc(II) systems and are given in Table 1. The $pH_{1/2}$ values (pH at which 50% of the metal ion is extracted) for the extracted metals are compared with those of the corresponding systems using thenoyltrifluoroacetone (HTTA) (Table 1). It is evident from the table that the extraction of copper(II), iron(II), cobalt(II), nickel(II), and zinc(II) occurs in the acidic medium as in HTTA. Manganese(II) is extracted from slightly acidic medium with HTTA, whereas with HPAI it is extracted from rather alkaline medium. In case of cadmium(II), quantitative extraction is accomplished from the alkaline medium with HTTA,[12] in contrast to its partial extraction (25%) with HPAI at higher pH values.

The possibility of utilizing this reagent HPAI for the separation of metals has been investigated by calculating the separation factor S which is the ratio of the distribution coefficients of the elements to be separated.[16] A separation in which not more than 1% of one element is coextracted will be obtained if $S \geqslant 10^4$ and the product of distribution coefficients is unity. The separation factors calculated are given in Table 2. It can be concluded from the table that the reagent

Table 1. Extraction Data of Some Metals Using 0.01 mol dm^{-3} HPAI in MIBK

Metal	$pH_{1/2}$(50% extraction)	log K_{ex}	$pH_{1/2}$, 0.15 mol dm^{-3} HTTA in benzene[a]
Mn(II)	8.4	−12.63	6.05
Fe(II)	0.6	+ 2.57	—
Co(II)	2.6	− 1.10	4.1
Ni(II)	2.1	− 0.51	5.0
Cu(II)	1.6	+ 0.75	1.34
Zn(II)	5.0	− 5.89	5.10
Cd(II)	Only 25% extraction	—	8.0

a) Refs. 12—15.

Table 2. Separation Factors for the Separation of Metals Using 0.01 mol dm^{-3} HPAI in MIBK

Metals to be separated	Separation factor	Metals to be separated	Separation factor
Fe(II)-Mn(II)	1.5×10^{15}	Mn(II)-Cu(II)	2.3×10^{13}
Fe(II)-Co(II)	4.6×10^{3}	Mn(II)-Zn(II)	5.4×10^{6}
Fe(II)-Ni(II)	1.2×10^{3}	Co(II)-Ni(II)	4
Fe(II)-Cu(II)	66	Co(II)-Cu(II)	70
Fe(II)-Zn(II)	2.8×10^{8}	Co(II)-Zn(II)	6.1×10^{4}
Mn(II)-Co(II)	3.3×10^{11}	Ni(II)-Cu(II)	18
Mn(II)-Ni(II)	1.3×10^{12}	Cu(II)-Zn(II)	4.3×10^{6}

HPAI would be useful for the separation of manganese(II), and zinc(II) from the other metals reported here. In conclusion, like HTTA and acylpyrazolones, these acylisoxazolones represent a new group of versatile chelating agents with great potential in solvent extraction.

The authors wish to thank CSIR (India) for financial support.

References

1) A. K. De, S. M. Khopkar, and R. A. Chalmers, "Solvent Extraction of Metals," Von Nostrand Reinhold, London (1970), p. 56.
2) B. S. Jensen, *Acta Chem. Scand.*, **13**, 1958 (1959).
3) B. S. Jensen, *Acta Chem. Scand.*, **13**, 1890 (1959).
4) G. N. Rao and V. S. Chouhan, *Bull. Chem. Soc. Jpn.*, **55**, 301 (1982).
5) G. N. Rao and H. C. Arora, *J. Inorg. Nucl. Chem.*, **39**, 2057 (1977).
6) Yu. A. Zolotov and V. G. Lambrev, *Zh. Anal. Khim.*, **20**, 659 (1965).
7) O. Navratil and B. S. Jensen, *J. Radioanal. Chem.*, **5**, 313 (1970).
8) M. K. Chmutova, G. A. Pribylova, and B. F. Myasoldov, *Zh. Anal. Khim.*, **28**, 2340 (1973).
9) A. Jyothi and G. N. Rao, *Chemica Scripta*, **27**, 367 (1987).
10) A. Jyothi and G. N. Rao, *Spectrochim. Acta*, **43A**, 517 (1987).
11) F. Korte and K. Storiko, *Chem. Ber.*, **94**, 1956 (1961).
12) A. K. Schmeitzer and D. R. Randolph, *Anal. Chim. Acta*, **26**, 567 (1962).
13) H. M. Poskanzer and B. M. Foreman, *J. Inorg. Nucl. Chem.*, **16**, 323 (1961).
14) T. Sekine and D. Dyrssen, *J. Inorg. Nucl. Chem.*, **26**, 1727 (1964).
15) H. M. N. H. Irwing and D. N. Edgington, *J. Inorg. Nucl. Chem.*, **27**, 1359 (1965).
16) Yu. A. Zolotov, "Extraction of Chelate Compounds," Humphrey Science publishers, INC., Ann Arbor, Michigan (1970), pp. 152—154.